Polyhedron Vol. 5, No. 1/2, p. 1, 1986
Pergamon Press Ltd. Printed in Great Britain

FOREWORD

E. R. BRAITHWAITE

This publication contains lectures and posters presented at the Climax Fifth International Conference on the Chemistry and Uses of Molybdenum held at the University of Newcastle, 1–5 July 1985. Two hundred and sixty participants from 26 countries attended the meeting and have provided an update on current research into molybdenum chemistry and the important uses of molybdenum compounds.

The conference was sponsored by Climax Molybdenum Co. Ltd, an affiliate of AMAX, and the Dalton Division of The Royal Society of Chemistry.

The interdisciplinary nature of previous conferences was preserved, though one was aware of the increased interest in the application of solid-state chemistry to heterogeneous catalysis.

I would like to thank the Chairmen of the sessions and all who helped with the conference, including the Managing Committee consisting of Professor A. G. Sykes, Professor C. D. Garner, Dr M. L. H. Green, FRS, and Dr P. C. H. Mitchell, without whose help the conference would not have been possible. Especially I would like to thank Professor Sykes, who was responsible for all the domestic arrangements and the academic programme. A very special thank you is also due to Mrs Rhoda Stafford for her invaluable secretarial help and constant good humour which helped to preserve our equanimity.

This special journal issue has been edited jointly by Professor Sykes and Dr Mitchell, an onerous task for which I am duly grateful.

Polyhedron Vol. 5, No. 1/2, pp. 3–14, 1986
Printed in Great Britain

0277–5387/86 $3.00 + .00
© 1986 Pergamon Press Ltd

HIGHLIGHTS OF RECENT RESEARCH ON COMPOUNDS WITH Mo–Mo BONDS

F. ALBERT COTTON

Department of Chemistry and Laboratory for Molecular Structure and Bonding, Texas A&M University, College Station, TX 77843, U.S.A.

(*Received* 26 *June* 1985)

Abstract—Research during the period 1981 to the present in two areas of molybdenum chemistry is surveyed. The first area is that of equilateral triangular cluster compounds. Some very new work, such as that on the $Mo_3S_4^{4+}$ aquo ion, will also be mentioned. The second area is that of Mo–Mo triple and quadruple bonds. Several ways in which quadruply bonded Mo_2 compounds have been used to investigate the properties of strong metal–metal bonds in general will be emphasized.

The chemistry of molybdenum is so extensive and diverse as to discourage any effort by one person to survey it broadly. It is to be hoped that the combined efforts of those participating in this conference will add up to such a broad review. For my own part, I have elected to focus on two areas in which my research group has been especially active in the past few years. While our own work will feature prominently in this paper, I shall endeavor to cite some important contributions from other laboratories. My topics will be: (1) triangular trinuclear molybdenum compounds with Mo–Mo bonds, and (2) binuclear molybdenum complexes with strong Mo–Mo bonds. Even after so limiting my purview, I can still offer no warrant of completeness.

TRIANGULAR TRINUCLEAR COMPOUNDS WITH Mo–Mo BONDS

Back in 1980 we knew that two general types of trimolybdenum cluster compounds existed, those shown as (a) and (b) in Fig. 1. Rather little was known about either type. With regard to type (a), there was, in fact, only one publication in which, as we now know, there was an error.[1] This error is of little importance when measured against the major contribution which that publication made, namely, showing what happens to most of the molybdenum when $Mo(CO)_6$ is refluxed with a mixture of CH_3CO_2H and $(CH_3CO)_2O$. In that reaction, as first reported by Bannister and Wilkinson[2] years before, dimolybdenum tetraacetate appears as a beautiful yellow crystalline product. The yield of this product based on molybdenum is at best around 20% (although it can be made much higher by using other solvents such as diglyme) but strangely, for about 15 years, no one found out what became of the rest of the molybdenum. It is interesting to note that the analogous reaction of $W(CO)_6$ with CH_3CO_2H–$(CH_3CO)_2O$ produces *no* $W_2(O_2CCH_3)_4$, and nobody had correctly identified the products that were formed. It was into this state of virtually total ignorance that the 1976 paper by Bino *et al.*[3] shone a prescient beam of light. The ability of these workers to make a major advance was due to the fact that they used a technique no one had used before in addressing this problem, namely, ion exchange chromatography. Attempts to obtain characterizable substances by other, conventional techniques (e.g. crystallization and extraction) had always failed. Ion exchange chromatography has

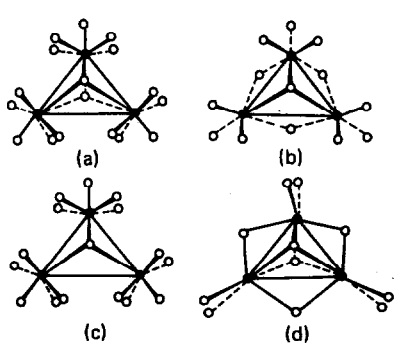


Fig. 1. Schematic drawings of four types of equilateral trinuclear metal cluster compounds.

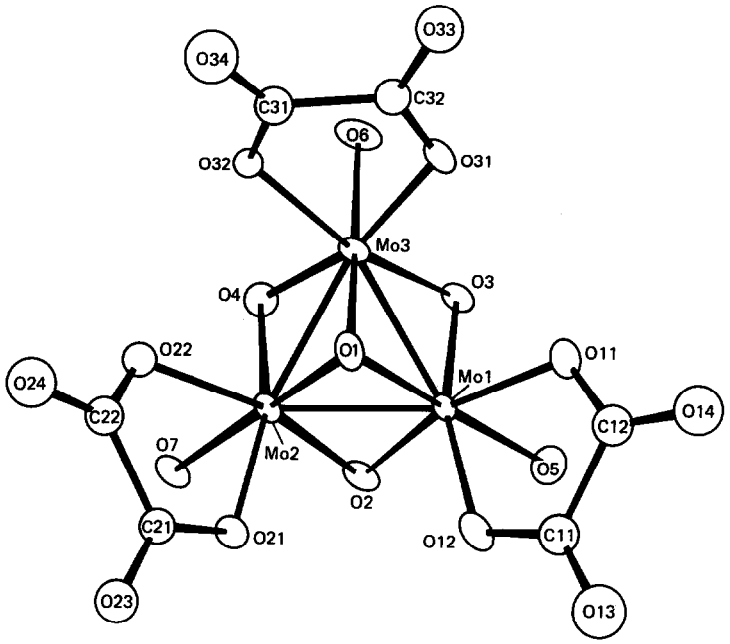


Fig. 2. Structure of $[Mo_3O_4(C_2O_4)_3(H_2O)_3]^{2-}$.

been the key to success in this type of chemistry ever since.

With regard to species of type (b) a bit more was known in 1980. Bino *et al.*[3] showed in 1978 that from solutions of the aquo molybdenum(IV) ion (about the nature of which great controversy still raged) one could isolate the oxalato anion

$$[Mo_3O_4(C_2O_4)_3(H_2O)_3]^{2-},$$

whose structure is shown in Fig. 2. This work established for the first time that this type of cluster can occur as a discrete entity in solution and crystals (it was previously known only in the solid state as a part of a continuous, fused array). Equally important, it provided a wholly new idea of what the aquo molybdenum(IV) ion might be: neither a monomer nor a dimer, but a trimer, with a central $Mo_3O_4^{4+}$ core surrounded by nine water molecules. This notion was soon strongly supported by our isolation[4] of an EDTA complex in which the central $Mo_3O_4^{4+}$ core was present.

An attempt in 1979 to check this by EXAFS study of the solution was inconclusive,[5] although this sort of study was later carried out much more thoroughly and did afford conformation.[6]

Also prior to 1981 was a preliminary report of an isotopic exchange study by Murmann and Shelton[7] (the full report of which appeared only recently[8]) which provided another completely independent line of very convincing evidence that the aquo molybdenum(IV) ion is trinuclear. Indeed, from Murmann's detailed report[8] we now know that the exchange rates for the four types of oxygen atoms in the $[Mo_3O_4(H_2O)_9]^{4+}$ ion vary from >3 years (27°C) for the three μ_2-O atoms to *ca* 5 days (27°C) for the μ_3-O atom, to *ca* 1 h (27°C) for the three H_2Os *trans* to μ_3-O, and to 20 months (0°C) for the other six outer H_2O molecules.

Several other points ought to be mentioned to round out the pre-1981 picture. There is no doubt that a *very* long time ago[9] Spittle and Wardlaw (1929) had isolated molybdenum(IV) complexes containing the $Mo_3O_4^{4+}$ core, which they formulated as "$R_2[Mo_3O_4(C_2O_4)_3 \cdot 5H_2O]$, where R = K, NH_4 or C_5H_6N". These workers even surmised that the complex anion was triangular, but without X-ray crystallography they could go no further. I became cognizent of their paper only a few years ago, and I don't think that anyone else working in this field in the late 1970s was aware of it.

In 1979, Bino *et al.*[10] showed that the structure of type (b) is a theme that can accommodate many variations by preparing and characterizing the $[Mo_3OCl_3(O_2CCH_3)_3(H_2O)_3]^{2+}$ ion, which differs from derivatives of the $Mo_3O_4^{4+}$ species in two ways: the three μ-O atoms are replaced by μ-Cl atoms and there are eight rather than six electrons in the Mo_3 core.

It is also noteworthy that the reaction of $W(CO)_6$ with CH_3CO_2H–$(CH_3CO)_2O$ was shown[11,12] to generate exclusively $W_3(\mu_3\text{-}O)_2(O_2CCH_3)_6L_3$ species; the tungsten chemistry is thus very similar to the molybdenum chemistry except that no

$W_2(O_2CCH_3)_4$ can be made under these acid conditions.

Finally, there was some important work done in the later 1970s, mainly by Achim Müller and his school,[12] that led to the characterization of the $[Mo_3(\mu_3\text{-}S)(S_2)_6]^{2-}$ ion. While this ion has certain obvious superficial differences from the complexes of the $Mo_3O_4^{4+}$ ion, it is, as we shall later see clearly, closely allied.

Let us now turn to a selective review of some of the progress that has been made since 1980. Much of this progress has been with the bicapped structures of type (a). As clearly noted, prior to the period under review, 1981 to the present, there was only one short publication[1] dealing with them as well as one fairly extensive paper[11] on the bioxocapped tritungsten compounds.

During 1981, the fundamental point was established[13–15] that, by appropriate control of the reaction conditions, the reaction of a CH_3CO_2H–$(CH_3CO)_2O$ mixture with molybdenum hexacarbonyl could give rise to three types of compounds, all having a structure of the bicapped type, namely (a) in Fig. 1. The ones with two capping oxygen atoms were not surprising, especially in view of the ease with which the tungsten analogs can be made under similar conditions.[11] Subsequently, there have been a number of studies of these bioxocapped molybdenum compounds[16–20] in which many of their properties have been established and methods for their preparation have been diversified. One of their most remarkable properties is the stability of the entire $Mo_3O_2(O_2CR)_6L_3$ unit, which we attribute, at least in part, to the fact that each metal atom is forming nine bonds and thus utilizing fully its valence shell orbitals. A striking example of this stability is provided by the

$$[Mo_3O_2(O_2CPh)_6(H_2O)_3]^{2+} \text{ ion,}^{19}$$

which can be fully nitrated in all phenyl groups under the usual aromatic nitration conditions (1 : 1 mixture of conc. H_2SO_4 and conc. HNO_3 at 45°C) without observable decomposition.

Perhaps the biggest surprise in this chemistry has been that there are $Mo_3(\mu_3\text{-}X)_2(O_2CR)_6L_3$ species in which one or both capping groups, μ_3-X, are alkylidyne groups.[13–15,21,22] The

$$[Mo_3(CCH_3)_2(O_2CCH_3)_6(H_2O)_3]^{2+}$$

ion, shown in Fig. 3, is of special interest since it is the species originally[1] thought to be

$$[Mo_3(OCH_2CH_3)_2(O_2CCH_3)_6(H_2O)_3]^{2+}.$$

Figure 4 shows the mixed-cap species,

$$[Mo_3O(CCH_3)(O_2CCH_3)_6(H_2O)_3]^{+}.$$

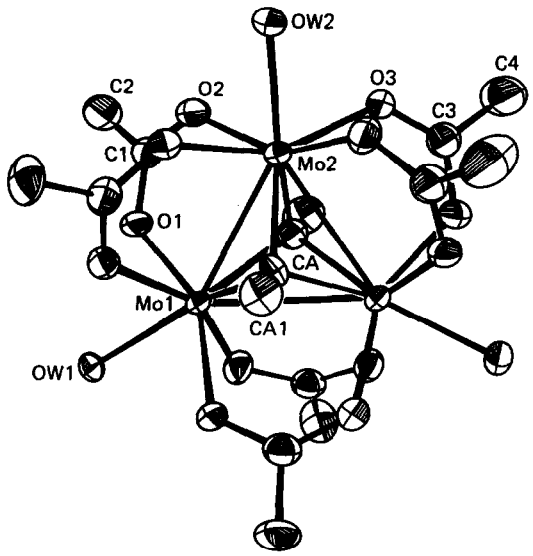


Fig. 3. Structure of $[Mo_3(CCH_3)_2(O_2CCH_3)_6(H_2O)_3]^{2+}$ ion.

Considering that these compounds are all very stable toward oxygen, aqueous acids, and even toward permanganate (which does, however, oxidize the core, see below), it is quite amazing that they contain metal–carbon bonds. Presumably, the stability of these Mo–C bonds towards oxidative and hydrolytic attack is kinetic in nature. It may be noted that, while no bi-alkylidyne capped tritungsten species have yet been observed, the

$$[W_3(\mu_3\text{-}O)(\mu_3\text{-}CCH_3)(O_2CCH_3)_6(H_2O)_3]^{+}$$

ion[23] has been made.

The electronic structures of both the type (a) and type (b) triangular species have been analyzed by molecular-orbital methods and a basic understanding of the metal–metal bonding has been achieved.[24] The bi-capped clusters can accommodate a maximum of six cluster electrons, whereby three M–M single bonds are formed. In several compounds there are only five or four such electrons and the M–M bond orders are then only $\frac{5}{6}$ and $\frac{2}{3}$, respectively. Reasonable increases in the bond lengths (*ca* 0.06 Å) accompany each decrease of $\frac{1}{6}$ in the bond order. The type (b) clusters can accommodate six M–M bonding electrons but also one or two more that can enter an orbital that has little if any M–M antibonding character. The

$$[Mo_3(\mu_3\text{-}O)(\mu_2\text{-}Cl)_3(O_2CCH_3)_3(H_2O)_3]^{2+}$$

ion mentioned earlier[10] is an example (the first) of an eight-electron cluster of this type. Very recently, we have provided another example of such an eight-electron species,[25] which is perhaps even more interesting because it is also the first example of a

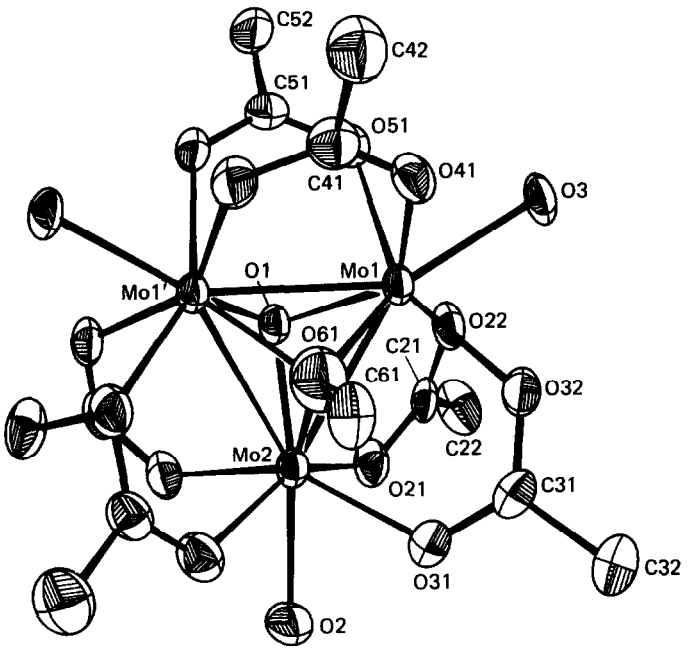


Fig. 4. Structure of $[Mo_3O(CCH_3)(O_2CCH_3)_6(H_2O)_3]^+$ ion.

type (b) structure in which the capping group is an alkylidyne. The species in question is

$$[Mo_3(\mu_3\text{-}CCH_3)(\mu_2\text{-}Br)_3(O_2CCH_3)_3(H_2O)_3]^+.$$

It is also pertinent to note here that niobium analogs of the bioxo-capped trimolybdenum compounds have recently been made.[26] These are of the type $[Nb_3O_2(O_2CR)_6(THF)_3]^+$ and they have four cluster electrons. They therefore have triplet ground states ($a_1^2e^2$) with bond orders of $\frac{2}{3}$ and Nb—Nb distances of *ca* 2.84 Å.

In the case of tungsten, one compound with the hemicapped structure [type (c) in Fig. 1] has been prepared and characterized.[27] We are still trying to learn how to obtain the molybdenum analog of this $[W_3(\mu_3\text{-}O)(O_2CCH_3)_6(H_2O)_3]^{2+}$ ion. At the time of writing, we believe that we may have done so, but disclosure of our results would be premature.

It is noteworthy that the

$$[M_3O_2(O_2CR)_6(H_2O)_3]^{2+}$$

ions are distinctly acidic; protons from the outer water molecules may be ionized leaving species with a mixture of H_2O and OH ligands in these positions. As Bino and Gibson[28] have shown, these mixed species associate with each other through

$$M—O(H)\cdots H\cdots O(H)—M$$

bridges, which are, in effect hydrated hydroxide ions, $HOHOH^-$.

Still a fourth type of equilateral triangular molybdenum cluster has been reported by Chisholm *et al.*[29] This is represented schematically by (d) in Fig. 1, and real examples are

$$[Mo_3(\mu_3\text{-}O)(\mu_3\text{-}OR)(\mu\text{-}OR)_3(OR)_6],$$

where $R = (CH_3)_2CH$ or $(CH_3)_3CCH_2$. The electronic and spectroscopic properties of such compounds have been elucidated by physical and theoretical studies.[30]

To conclude this section I wish to return to the species of type (b) in Fig. 1, of which the aquo ion, $Mo_3O_4^{4+}(aq)$, and its complexes are probably the most important examples so far. I have already mentioned several early publications in which these complexes were isolated in crystalline form, thus providing clear indications that the core of the aquo molybdenum(IV) ion is the $Mo_3O_4^{4+}$ unit. There have been several other reports of such isolated and crystallographically characterized complexes[31–34] as well as further studies of the aquo ion in solution.[32,35,36] For obvious reasons, a chemist might naturally wonder about the possibility of replacing one, three or all four of the oxygen atoms in the $Mo_3O_4^{4+}$ ion by sulfur atoms. In fact, a number of workers in addition to me and my coworkers[37,38] have been attracted by this possibility, and some interesting progress has been made.[39–43]

Müller and Reinsch[39] were by far the first (1980) to isolate a derivative of $Mo_3S_4^{4+}$, which they did by treating the $[Mo_3S(S_2)_6]^{2-}$ ion with excess aqueous KCN. The cyanide ions convert S_2^{2-} ions to $S^{2-} + SCN^-$ and then also occupy positions in the coordination sphere, thus giving the

$[Mo_3S_4(CN)_9]^{5-}$ ion. The same species has also been described (1983) by another group,[40] and has been further studied by Wieghardt *et al.*[41] In this case, three outer coordination positions on each Mo atom of $Mo_3S_4^{4+}$ are occupied, as would be expected by analogy to the stereochemistry around the $Mo_3O_4^{4+}$ ion.

In another synthetic procedure[42] that begins with the $[Mo_3S(S_2)_6]^{2-}$ ion, an excess of $Na_2(SCH_2CH_2S)$ and $(NEt_4)Br$ were used and the product was $(NEt_4)_2[Mo_3S_4(SCH_2CH_2S)_3]$. It was found that treatment of this with elemental sulfur converts it to $[Mo_3S(S_2)_3(SCH_2CH_2S)_3]^{2-}$, from which the $[Mo_3S_4(SCH_2CH_2S)_3]^{2-}$ ion can again be obtained by treatment with more $Na_2(SCH_2CH_2S)$, PPh_3 or CN^- in acetonitrile. Clearly, we are again dealing with reactions in which sulfur atoms are extracted from S_2^{2-} ions to give S^{2-} ions plus appropriate other products such as $[S_2CH_2CH_2S]^{2-}$, Ph_3PS or SCN^-. It is noteworthy that in the $[Mo_3S_4(SCH_2CH_2S)_3]^{2-}$ ion there are only two outer ligand positions occupied on each metal atom rather than three.

Japanese workers have reported the only example of a mixed sulfur–oxygen species, $Ba[Mo_3(\mu_3\text{-}S)O_3(HNTA)_3]$, were H_3NTA = nitrilotriacetic acid.[43] They prepared this in about 20% yield by heating the μ-S–μ-O binuclear complex $Mg[Mo_2O_3S(EDTA)]$ with aqueous K_2CO_3 followed by neutralization, cation exchange chromatography and addition of H_3NTA and $BaCl_2$.

Our own work in this area also began with $(NH_4)_2[Mo_3S(S_2)_6]$, which we call Müller's compound. We first found[37] that it is not necessary to add any reagent to serve as a sulfur atom acceptor. Simply by treatment of Müller's compound with a large excess of either oxalic acid or H_3NTA under reflux, the color changes from red to green and it is possible to isolate products containing the

$$[Mo_3S_4(HNTA)_3]^{2-}$$

and

$$[Mo_3S_4(C_2O_4)_3(H_2O)_3]^{2-}$$

ions. We believe that the expulsion of S and S_2^{2-} simply leads to formation of species such as S_3^{2-}.

In order to simplify and diversify this chemistry efficiently, we have sought to obtain aqueous solutions of the $Mo_3S_4^{4+}$(aq) ion, and we have been successful.[38] One way to do it is to hydrolyze the $[Mo_3S_4(HNTA)_3]^{2-}$ complex in 2 M HCl for 8 h, from which a clear green solution is obtained. From this the $Mo_3S_4^{4+}$ ion can be caught on a cation exchange column and solutions prepared by elution with various acids such as 2 M $HClO_4$. These solutions are stable in air for at least 2 weeks and allow the preparation of a variety of complexes, including those previously known.

Of far more interest, however, is a new and much superior way to obtain solutions of the $Mo_3S_4^{4+}$(aq) ion. To do this, $Mo(CO)_6$ is refluxed in $(CH_3CO)_2O$ containing dry Na_2S, under nitrogen, and the cooled reaction mixture hydrolyzed with water. This solution deposits a green band at the top of a Dowex 50W × 2 cation exchange column. The $Mo_3S_4^{4+}$(aq) ion can be eluted with 1 M $HClO_4$. A second green species, which elutes only with much more concentrated acid, is still under investigation.* We have also obtained solutions of the $W_3S_4^{4+}$(aq) ion by a similar procedure. Figure 5 shows the structure of the oxalato complex,

$$[Mo_3S_4(C_2O_4)_3(H_2O)_3]^{2-},$$

* This is now known to be the $Mo_4S_4^{5+}$ ion.

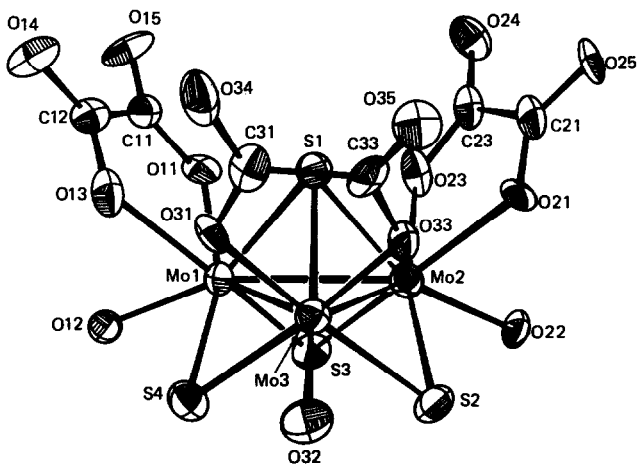


Fig. 5. $[Mo_3S_4(C_2O_4)_3(H_2O)_3]^{2-}$ ion as prepared by addition of oxalate ions to a solution of the $Mo_3S_4^{4+}$(aq) ion.

obtained from an aqueous solution of the $Mo_3S_4^{4+}$(aq) ion.

QUADRUPLE BONDS IN DIMOLYBDENUM COMPOUNDS

The level of activity in research on multiple bonds between metal atoms continues to be very high. The 1982 book *Multiple Bonds between Metal Atoms*, by Walton and me,[44] covered the literature to about the end of 1980, with most citations being to a period of *ca* 16 years immediately preceding 1980. In the years 1981–1984 there have been roughly half as many publications as in all of the previous years. Of that number (*ca* 450 publications) about 40% have dealt with dimolybdenum compounds. Clearly, the Mo–Mo triple and quadruple bonds have been the chief testing grounds for ideas and experiments on M–M multiple bonds. This is because molybdenum is relatively inexpensive and readily forms a great variety of compounds, many of which are fairly easy to handle.

It is symptomatic of how much work has been done on the chemistry of compounds with Mo–Mo quadruple bonds that during the four year period 1981–1984 67 new molecular structures have been determined by X-ray crystallography, and one by gas-phase electron diffraction. These are listed in Table 1 in the same way as earlier structures were listed in Table 3.1.1 of Ref. 44. The number of structures in the earlier table, which covers all those done prior to 1981, is only 71. The compounds listed in Table 1 are a rather diverse lot: although they are not necessarily a random sampling of all the compounds that have been studied in the four year period, they are probably indicative of the directions research on Mo–Mo quadruple bonds has been taking.

Table 1. Structures of compounds with Mo–Mo quadruple bonds, 1981–1984[a]

Compound	X'tal symmetry	Virtual symmetry	Mo–Mo	χ	Reference[b]
$[Mo_2(O_2CH)_4]$	$\bar{1}$	D_{4h}	2.091(1)	0	1
$[Mo_2(O_2CH)_4(H_2O)_2]$	$\bar{1}$	D_{4h}	2.100(1)	0	1
$Mo_2(O_2CCH_3)_4 \cdot Na(CH_3CO)_2H$	$\bar{1}$	D_{4h}	2.0926(10)	0	2
$Mo_2Me_4(PMe_3)_4$	C_2	D_{2d}	2.153(1)	0	3
$Mo_2(O_2CCH_3)_2[Al(OPr^i)_4]_2$	$\bar{1}$	D_{4h}	2.079(1)	0	4
$[C_4H_{10}NO]_2[Mo_2Cl_6(H_2O)_2]$	$\bar{1}$	C_{2h}	2.118(1)	0	5
$[C_4H_{10}NO]_2[Mo_2Br_6(H_2O)_2]$	$\bar{1}$	C_{2h}	2.114(2)	0	5
$Mo_2(\mu\text{-}O_2CCH_3)_2(OSiMe_3)_2(PMe_3)_2$	1	C_{2h}	2.114(1)	N rep[c]	6
$Mo_2(O_2CCH_3)_4$(g)	—	D_{4h}	2.079(3)	0	7
$Mo_2(\mu\text{-}O_2CCH_3)_2Cl_2(PBu^n_3)_2$	$\bar{1}$	C_{2h}	2.099(1)	0	8
cis-$Mo_2(\mu\text{-}O_2CMe_3)_2Cl_2(PEt_3)_2$	$\bar{1}$	C_2	2.113(1)	N rep	9
trans-$Mo_2(\mu\text{-}O_2CMe_3)_2Cl_2(PEt_3)_2$	$\bar{1}$	C_{2h}	2.0984(4)	N rep	9
$Mo_2(\mu\text{-}S_2PEt_2)_4THF$	1	C_{4v}	2.123(1)	N rep	10
$Mo_2(\mu\text{-}S_2PEt_2)_2(S_2PEt_2)_2$	1	C_{2v}	2.137(1)	N rep	10
			2.124(11)	N rep	10
$Mo_2(\mu\text{-}PBu^t_2)_2(PBu^t_2)_2$	*m*	C_{2v}	2.209(1)	R rel[d]	11
$[C_3N_2H_5]^+\{Mo_2(O_2CCH_3)$ $[CH_3Ga(C_3N_2H_3)O]_4\}$	*mm*	C_{2v}	2.127(1)	0	12
$Mo_2(OPr^i)_4py_4$	N rep	D_{2d}	2.195(1)	N rep	13
$Mo_2(OCH_2CMe_3)_4(PMe_3)_4$	N rep	D_{2d}	2.209(1)	N rep	13
$Mo_2(OPr^i)_4(Pr^iOH)_4$	N rep	D_{2d}	2.110(3)	N rep	13
$Mo_2(OCH_2CMe_3)_4(Me_2NH)_4$	N rep	D_{2d}	2.133(2)	N rep	13
$(pipH)_4[Mo_2Cl_8] \cdot 4H_2O$	$\bar{1}$	D_{4h}	2.1293(3)	0	14
β-$Mo_2(O_2CH)_4$	$\bar{1}$	D_{4h}	2.093(1)	0	15
	1	D_{4h}	2.0916(9)	N rep	15
γ-$Mo_2(O_2CH)_4$	$\bar{1}$	D_{4h}	2.0910(8)	0	15
$Mo_2(O_2CH)_4 \cdot KCl$	$\bar{1}$	D_{4h}	2.109(2)	0	15
	$\bar{1}$	D_{4h}	2.102(2)	0	15

(*Contd.*)

Table 1. (*Contd.*)

Compound	X'tal symmetry	Virtual symmetry	Mo–Mo	χ	Reference[b]
$[Mo_2(D\text{-phe})_2(L\text{-phe})_2I_2]I_2 \cdot 6H_2O$	$\bar{1}$	D_{4h}	2.114(1)	0	16
$[Mo_2(D\text{-tyr})_2(L\text{-tyr})_2I_2]I_2 \cdot 6H_2O$	$\bar{1}$	D_{4h}	2.116(1)	0	16
$[Mo_2(D\text{-phgly})_2(L\text{-phgly})_2](PTS)_4 \cdot 4H_2O$	$\bar{1}$	D_{4h}	2.113(1)	0	16
$Mo_2(O_2CCH_3)(ambt)_3 \cdot 2THF$	1	m	2.093(3)	1.9	17
$Mo_2(ambt)_4 \cdot THF$	$\bar{1}$	C_{2h}	2.103(1)	0	17
$Mo_2(acbt)_4 \cdot 2THF$	$\bar{1}$	C_{2h}	2.117(1)	0	17
Hambt = 2-NH_4-4-Me benzothiazole					
Hacbt = 2-NH_2-4-Cl benzothiazole					
$Mo_2(O_2CCH_3)_2\{[(xylyl)N]_2CCH_3\}_2 \cdot 4THF$	$\bar{1}$	D_{2h}	2.107(1)	0	18
$Mo_2(O_2CCH_3)[(PhN)_2CCH_3]_3$	1	C_{2v}	2.082(1)	~0	18
$Mo_2(\mu\text{-}O_2CCF_3)_2(O_2CCF_3)_2(PPhEt_2)_2$	$\bar{1}$	C_{2h}	2.100(1)	0	19
$Mo_2(\mu\text{-}O_2CCF_3)_2(O_2CCF_3)_2(PPh_2Me)_2$	$\bar{1}$	C_{2h}	2.107(2)	0	19
$Mo_2(\mu\text{-}O_2CCF_3)_4(PPh_2Me)_2$	1	D_{4h}	2.128(2)	~0	20
$Mo_2Cl_4(PMe_3)_4$	C_2	D_{2d}	2.130(0)	~0	21
$Mo_2[O_2CC_6H_4(2\text{-}C_6H_5)]_4$	$\bar{1}$	D_{4h}	2.082(1)	0	22
$Mo_2(Et_tBpz_2)_2[Et_2B(O)pz]_2$	1	C_2	2.156(1)	15.3	23
$Mo_2(o\text{-}Me_2NC_6H_4)_4$	1	C_2	2.145(1)	11	24
$Mo_2(O_2CCH_3)_2(o\text{-}Me_2NC_6H_4CH_2)_2$	$\bar{1}$	i	2.065(1)	0	25
$Mo_2[(xylyl)NC(CH_3)O]_4(THF)_2$	1	C_{2v}	2.097(3)	~0	26
	C_2	C_{2v}	2.093(2)	~0	26
$Mo_2[(xylyl)NC(CH_3)O]_4py$	1	C_{2v}	2.101(1)	~0	26
$Mo_2[(xylyl)NC(CH_3)O]_4NC_6H_4CH_3$	C_2	C_{2v}	2.102(1)	~0	26
$Mo_2(O_2CC_6H_4OH)_4[Me(OC_2H_4)_2OMe]_2$	$\bar{1}$	C_{2h}	2.101(1)	0	27
$Mo_2(O_2CC_6H_4OH)_4$	$\bar{1}$	C_{2h}	2.092(1)	0	27
	$\bar{1}$	C_{2h}	2.094(1)	0	27
$Mo_2[O_2CCH(OH)C_6H_5]_4$	1	C_4	2.104(1)	~0	28
	1	C_4	2.101(1)	~0	28
$[NBu_4]_2[Mo_2(O_2CCF_3)_4Br_2]$	$\bar{1}$	D_{4h}	2.134(2)	0	29
$[NBu_4]_2[Mo_2(O_2CCF_3)_4I_2]$	$\bar{1}$	D_{4h}	2.140(2)	0	29
	$\bar{1}$	D_{2h}	2.136(2)	0	29
$[NBu_4]_2[Mo_2(O_2CCF_3)_2Br_4]$	$\bar{1}$	D_{2h}	2.098(1)	0	29
$\beta\text{-}Mo_2Cl_4(dmpe)_2$	C_2	D_2	2.183(3)	40.0	30
$\beta\text{-}Mo_2Cl_4(dppe)_2$	1	D_2	2.183(3)	30.5	31
$Mo_2(6\text{-}F\text{-}2\text{-}O\text{-}C_5NH_3)_4(THF)$	1	C_{4v}	2.092(1)	~0	32
$Mo_2(\mu\text{-}O_2CCF_3)_2Cl_2(C_2H_5CN)_2$	1	C_2	2.134(2)	~0	33
$Mo_2(\mu\text{-}O_2CCF_3)_3Cl(C_2H_5CN)$	1	C_s	2.127(2)	~0	33
$Mo_2[MeNC(PPh_2)S]_4$	1	D_{2d}	2.083(1)	~0	34
$Mo_2[MeNC(PPh_2)S]_2[MeNC(S)PPh_2]_2$	$\bar{1}$	i	2.104(2)	~0	34
$Mo_2(SO_4)_2(py)_4(ax\text{-}py)_2 \cdot 2py$	$\bar{1}$	D_{2h}	2.134(2)	0	35
$Mo_2(o\text{-}C_6H_5NC_5H_4N)_4$	$\bar{1}$	C_{2h}	2.073(2)	0	36
	$\bar{1}$	C_{2h}	2.068(2)	0	36
$Mo_2Br_4(dppm)_2 \cdot 2THF$	$\bar{1}$	C_{2h}	2.138(1)	0	37
$Mo_2Cl_4[(Ph_2P)_3CH]_2 \cdot 2CH_2Cl_2$	1	C_2	2.148(1)	20	37
$(pyH)_2[Mo_2(O_2CCH_3)_4Br_2]$	$\bar{1}$		2.010(1)	0	38
$(pyH)_2[Mo_2(O_2CCH_3)_4I_2]$	$\bar{1}$		2.103(1)	0	38
	$\bar{1}$		2.103(1)	0	38
	$\bar{1}$		2.102(1)	0	38

[a] See Table 3.1.1 of Ref. 44 for a list of earlier structures and definitions.
[b] The list of references to this table is given in the Appendix.
[c] Not reported.
[d] Not relevant.

The two alkoxide compounds, $Mo_2(OPr^i)_4py_4$ and $Mo_2(OCH_2CMe_3)_4(PMe_3)_4$, contain the longest Mo–Mo quadruple bonds yet reported, 2.195(1) and 2.209(1) Å, respectively. These are about as long as most Mo–Mo triple bonds and thus clearly illustrate the fact that bond order and bond length are not as simply related in the realm of metal–metal bonds as in the traditional chemistry of the light elements.

Another record established by one of the structures listed is that of the shortest bond length for the $Mo_2Cl_8^{4-}$ ion, viz. 2.129 Å in the piperidinium salt $(pipH)_4[Mo_2Cl_8]\cdot 4H_2O$.

Because of the time limitation on this lecture, I shall restrict myself to just three lines of work that have been carried out on Mo–Mo quadruple bonds: All three concern the response of a quadruple bond when the molecule containing it is caused to twist away from its preferred conformation, namely, that in which it is eclipsed. The three important responses are: (1) a lengthening of the bond, (2) a change in the energy of the $\delta \rightarrow \delta^*$ transition, and (3) the development of optical activity.

Bond lengthening

The notion that a quadruple bond should weaken and therefore lengthen as the molecular conformation changes from eclipsed to staggered is well known. Qualitatively, this is due to the dependence of the δ-component of the bond on the degree of staggering. Quantitatively, the strength of the δ-bond should vary with cos 2χ, where χ is the angle of internal rotation, taken as zero in the eclipsed conformation.[45] The way in which χ is caused to change from zero in a generally homologous series of compounds is to employ compounds of the type

$$Mo_2X_4[R_2P(CH_2)_{1,2}PR_2]_2,$$

in which the diphosphine ligands bridge the metal atoms. A representative compound is shown in Fig. 6. Both the angle of twist and the Mo–Mo distance are ascertained by X-ray crystallography. If it is then assumed that the bond length will be linearly proportional to the strength of the δ-bond, and further that no other factors (e.g. electronic or steric properties of the R groups) are important, one might expect an inverse linear relationship between the Mo–Mo bond lengths and cos 2χ.

First with three compounds,[46] and later with 10,[47] the approximate validity of such a relationship was demonstrated. However, because of concern about some unexpected scatter, we have recently been led to take into account the possible effect of a systematic difference between alkyl and aryl groups in the diphosphine. A way to make an empirical correction for this (employing dirhenium compounds in which there are no delta bonds) has been found, and in this way the correlation shown in Fig. 7 has been obtained.[48] This seems to be about as far as this general concept can be developed, and it gives the result that complete loss of the δ-bond from a Mo–Mo quadruple bond causes an increase of $\sim$0.10 Å in the bond length.

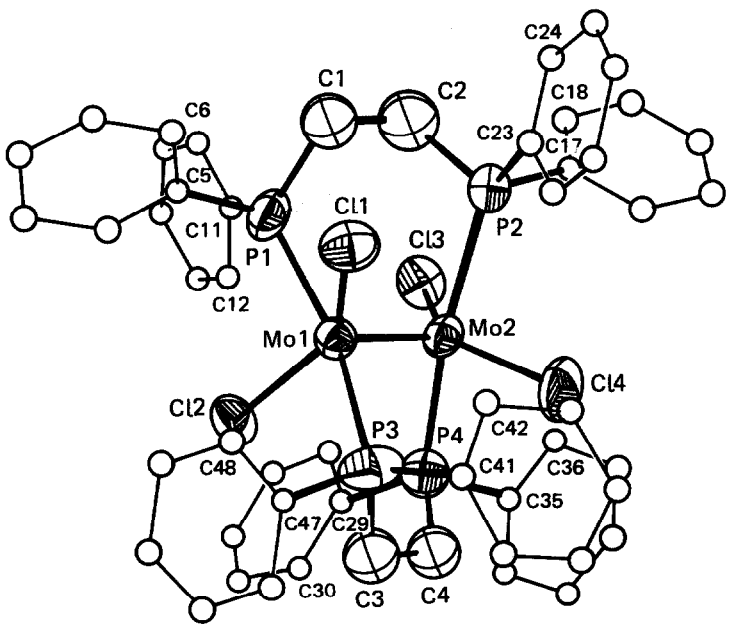


Fig. 6. $Mo_2Cl_4(Ph_2PCH_2CH_2PPh_2)_2$ molecule.

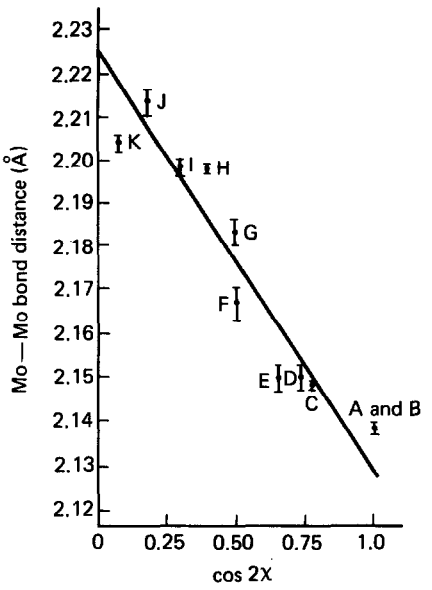


Fig. 7. Plot of Mo–Mo bond length vs cos 2χ for 11 compounds of the type $Mo_2X_4[R_2P(CH_2)_{1,2}PR_2]_2$, where an empirical correction has been applied to combine data for R = alkyl and aryl.

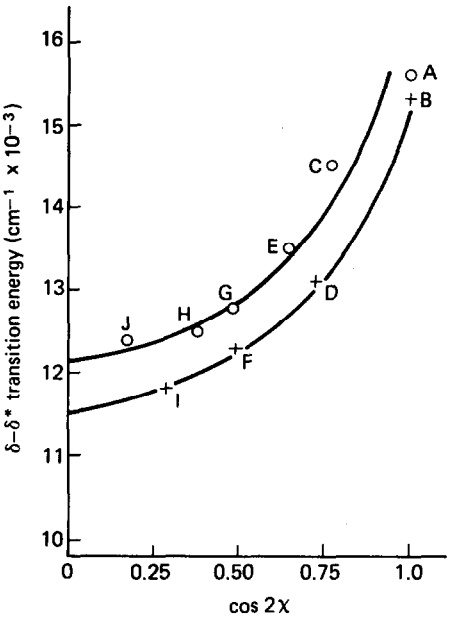


Fig. 8. $\delta \rightarrow \delta^*$ transition energies vs cos 2χ for 10 compounds of the type $Mo_2X_4[R_2P(CH_2)_{1,2}PR_2]_2$. The upper curve is for compounds with X = Cl and the lower one for X = Br.

The $\delta \rightarrow \delta^*$ transition energy

As the strength of the δ-interaction is decreased by twisting a quadruple bond, the energy of the electronic absorption band assignable to the $A_{1g}(\delta^2) \rightarrow A_{2u}(\delta\delta^*)$ transition (normally called, simply, the $\delta \rightarrow \delta^*$ transition) should become lower. The same set of compounds used to study the relationship between metal–metal bond length and cos 2χ can be used to establish the dependence of the energy of the $\delta \rightarrow \delta^*$ transition on cos 2χ. The relationship found[49] is shown in Fig. 8. The fact that the transition energy tends not to zero but to an extrapolated limit in the neighborhood of 12,000 cm^{-1} confirms that, for this weakly bonded δ-manifold, the correlation energy makes a large contribution to the energies of the states. It suggests that this energy contributes around 12,000 cm^{-1} to the transition energy, which is in reasonable agreement with theoretical estimates of about 10,000 cm^{-1}.

Optical activity

A twisted molecule such as that shown in Fig. 6 is, of course, chiral. However, the enantiomers interconvert rather rapidly in solution, and in order to observe the optical consequences of this chirality (e.g. CD or ORD spectra) it is necessary to employ a ligand, such as *S,S*-$Ph_2PCH(CH_3)CH(CH_3)PPh_2$, that locks the molecule into one enantiomer, as shown in Fig. 9. When this is done, a beautiful CD spectrum (Fig. 10), can then be observed.

The one feature of this CD spectrum that will be discussed here is the negative feature at *ca* 730 nm.

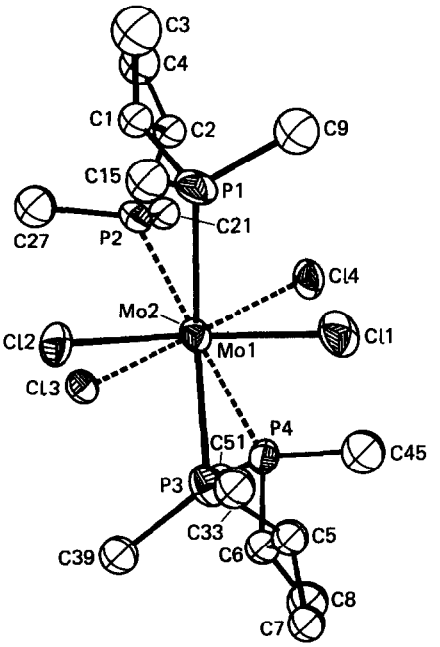


Fig. 9. View down the Mo–Mo axis of the $Mo_2Cl_4[S,S\text{-}Ph_2PCH(CH_3)CH(CH_3)PPh_2]_2$ molecule, showing its absolute conformation, which is Γ (a counterclockwise helix).

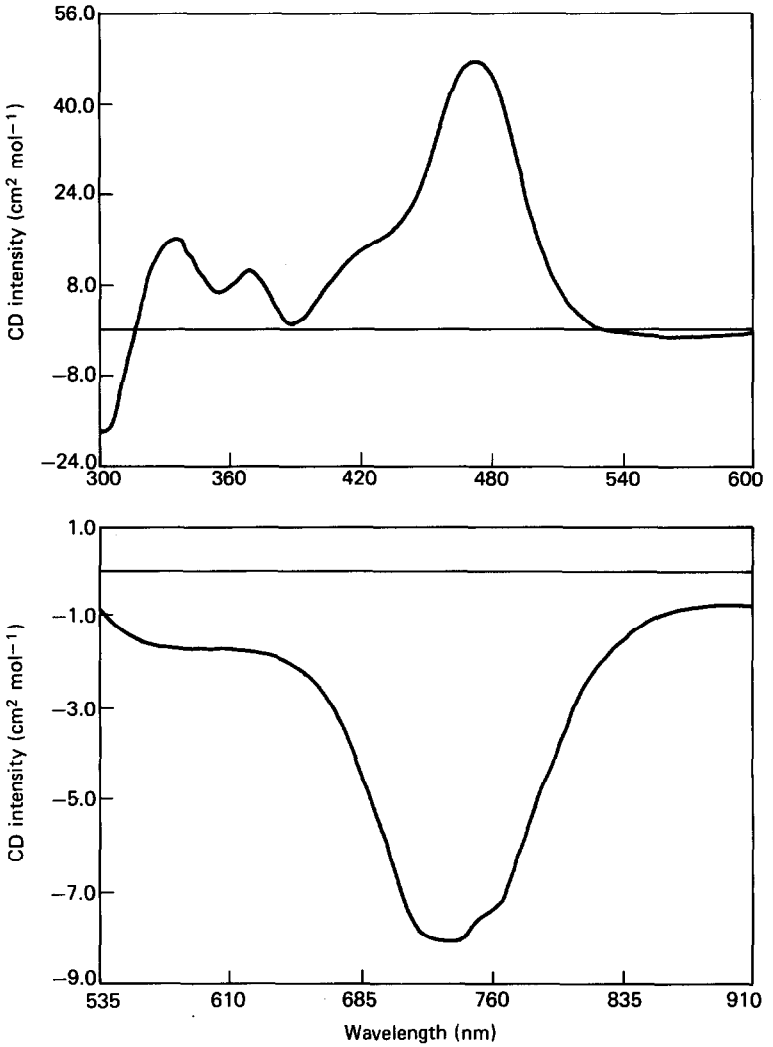


Fig. 10. Circular dichroism spectrum of $Mo_2Cl_4[S,S\text{-}Ph_2PCH(CH_3)CH(CH_3)PPh_2]_2$.

This corresponds to the $\delta \rightarrow \delta^*$ transition. By an unequivocal, qualitative argument it can be shown[50] that for the direction and magnitude of the angle of twist (Fig. 9) a negative CD must be expected for the $\delta \rightarrow \delta^*$ transition. We thus have a powerful piece of evidence that the generally accepted picture of the quadruple bond in Mo_2^{4+} systems is correct.

Acknowledgements—I wish to acknowledge the tremendous contributions made by a number of coworkers to the work done in my laboratory. Their names will be found in the references, but I must make special mention of Professor Zvi Dori, of The Technion, Haifa, Israel, who could not attend this meeting. Zvi Dori has been not only a fountain of good ideas, a masterful laboratory chemist and the man who put me in touch with all of my other Israeli coworkers, but a friend of rare qualities. The National Science Foundation has been the principal supporter of our work, but assistance from the US–Israel Science Foundation, The Robert A. Welch Foundation and the Texas A&M University is also gratefully acknowledged.

REFERENCES

1. A. Bino, M. Ardon, I. Maor, M. Kaftory and Z. Dori, *J. Am. Chem. Soc.* 1976, **98**, 7093.
2. E. Bannister and G. Wilkinson, *Chem. Ind. (London)* 1968, 349.
3. A. Bino, F. A. Cotton and Z. Dori, *J. Am. Chem. Soc.* 1978, **100**, 5252.
4. A. Bino, F. A. Cotton and Z. Dori, *J. Am. Chem. Soc.* 1979, **101**, 3842.
5. S. Cramer, H. B. Gray, Z. Dori and A. Bino, *J. Am. Chem. Soc.* 1979, **101**, 2770.
6. S. P. Cramer, P. K. Eidem, M. T. Paffett, J. R. Winkler, Z. Dori and H. B. Gray, *J. Am. Chem. Soc.* 1983, **105**, 799.
7. R. K. Murmann and M. E. Shelton, *J. Am. Chem. Soc.* 1980, **102**, 3984.
8. *K. R. Rogers, R. K. Murmann, E. O. Schlemper and M. E. Shelton, Inorg. Chem.* 1985, **24**, 1313.
9. H. M. Spittle and W. Wardlaw, *J. Chem. Soc.* 1929, 792.

10. A. Bino, F. A. Cotton and Z. Dori, *Inorg. Chim. Acta* 1979, **33**, L133.
11. A. Bino, F. A. Cotton, Z. Dori, S. Koch, H. Küppers, M. Millar and J. C. Sekutowski, *Inorg. Chem.* 1978, **17**, 3245.
12. See, for example, A Müller, S. Pohl, M. Dartmann, J. P. Cohen, J. M. Bennet and R. M. Kirchner, *Z. Naturforsch.* 1979, **34B**, 434.
13. A. Bino, F. A. Cotton and Z. Dori, *J. Am. Chem. Soc.* 1981, **103**, 243.
14. A. Bino, F. A. Cotton, Z. Dori and B. W. S. Kolthammer, *J. Am. Chem. Soc.* 1981, **103**, 5779.
15. M. Ardon, A. Bino, F. A. Cotton, Z. Dori, M. Kaftory, B. W. S. Kolthammer, M. Kapon and G. Reisner, *Inorg. Chem.* 1981, **20**, 4083.
16. M. Ardon, A. Bino, F. A. Cotton, Z. Dori, M. Kaftory and G. Reisner, *Inorg. Chem.* 1982, **21**, 1912.
17. F. A. Cotton, Z. Dori, D. O. Marler and W. Schwotzer, *Inorg. Chem.* 1983, **22**, 3104.
18. A. Birnbaum, F. A. Cotton, Z. Dori and M. Kapon, *Inorg. Chem.* 1984, **23**, 1617.
19. F. A. Cotton, Z. Dori, D. O. Marler and W. Schwotzer, *Inorg. Chem.* 1984, **23**, 4033.
20. F. A. Cotton, Z. Dori, D. O. Marler and W. Schwotzer, *Inorg. Chem.* 1984, **23**, 4738.
21. A. Bino, F. A. Cotton, Z. Dori, L. R. Falvello and G. M. Reisner, *Inorg. Chem.* 1982, **21**, 3750.
22. A Bino and D. Gibson, *Inorg. Chim. Acta* 1982, **65**, L37.
23. F. A. Cotton *et al.*, unpublished.
24. B. E. Bursten, F. A. Cotton, M. B. Hall and R. C. Najjar, *Inorg. Chem.* 1982, **21**, 302.
25. A. Birnbaum, F. A. Cotton, Z. Dori, M. Kapon, D. O. Marler, G. M. Reisner and W. Schwotzer, *J. Am. Chem. Soc.* 1985, **107**, 2405.
26. F. A. Cotton, S. A. Duraj and W. J. Roth, *J. Am. Chem. Soc.* 1984, **106**, 3527.
27. M. Ardon, F. A. Cotton, Z. Dori, A. Fang, M. Kapon, G. M. Reisner and M. Shaia, *J. Am. Chem. Soc.* 1982, **104**, 5394.
28. A. Bino and D. Gibson, *J. Am. Chem. Soc.* 1982, **104**, 4383.
29. M. H. Chisholm, K. Folting, J. C. Huffman and C. C. Kirkpatrick, *J. Am. Chem. Soc.* 1981, **103**, 5967.
30. M. H. Chisholm, F. A. Cotton, A. Fang and E. M. Kober, *Inorg. Chem.* 1984, **23**, 749.
31. A. Müller, A. Ruck, M. Dartmann and U. Reinsch-Vogell, *Angew. Chem., Int. Ed. Engl.* 1981, **20**, 483.
32. S. F. Geller, T. W. Hambley, R. T. C. Brownleee, M. J. O'Connor, M. R. Snow and A. G. Wedd, *J. Am. Chem. Soc.* 1983, **105**, 1527.
33. E. O. Schlemper, M. S. Hussain and R. K. Murmann, *Cryst. Struct. Commun.* 1982, **11**, 89.
34. E. Benory, A. Bino, D. Gibson, F. A. Cotton and Z. Dori, *Inorg. Chim. Acta* 1985, **99**, 137.
35. M. A. Harmer, D. T. Richens, A. B. Soares, A. J. Thornton and A. G. Sykes, *Inorg. Chem.* 1981, **20**, 4155.
36. M. T. Paffett and F. C. Anson, *Inorg. Chem.* 1983, **22**, 1347.
37. F. A. Cotton, Z. Dori, R. Llusar, D. O. Marler and W. Schwotzer, *Inorg. Chem.* 1985, **102**, L25.
38. F. A. Cotton, Z. Dori, R. Llusar and W. Schwotzer, submitted for publication.
39. A. Müller and U. Reinsch, *Angew. Chem., Int. Ed. Engl.* 1980, **19**, 72.
40. N. C. Howlader, G. P. Haight, Jr, T. W. Hambley, G. A. Lawrance, K. M. Rahmoeller and M. R. Snow, *Aust. J. Chem.* 1983, **36**, 377.
41. K. Wieghardt, W. Herrmann, A. Müller, W. Eltzner and M. Zimmermann, *Z. Naturforsch.* 1984, **39B**, 876.
42. T. R. Halbert, K. McGauley, W. H. Pan, R. S. Czernuszewicz and E. I. Stiefel, *J. Am. Chem. Soc.* 1984, **106**, 1849.
43. T. Shibata, H. Hattori and H. Kuroya, *J. Am. Chem. Soc.* 1984, **106**, 2710.
44. F. A. Cotton and R. A. Walton, *Multiple Bonds between Metal Atoms.* John Wiley, New York (1982).
45. F. A. Cotton, *Chem. Soc. Rev.* 1983, **12**, 35.
46. F. A. Cotton and G. L. Powell, *Inorg. Chem.* 1983, **22**, 1507.
47. F. L. Campbell III, F. A. Cotton and G. L. Powell, *Inorg. Chem.* 1984, **23**, 4222.
48. F. L. Campbell III, F. A. Cotton and G. L. Powell, to be published.
49. F. L. Campbell III, F. A. Cotton and G. L. Powell, *Inorg. Chem.* 1985, **24**, 177.
50. P. A. Agaskar, F. A. Cotton, I. F. Fraser and R. D. Peacock, *J. Am. Chem. Soc.* 1984, **106**, 1851.

APPENDIX: REFERENCES TO TABLE 1

1. P. A. Koz'min, M. D. Surazhskaya and T. B. Larina, *Russ. J. Inorg. Chem.* 1980, **25**, 702.
2. D. L. Kepert, B. W. Skelton and A. H. White, *Aust. J. Chem.* 1980, **25**, 1847.
3. G. S. Girolami, V. V. Mainz, R. A. Andersen, S. H. Vollmer and V. W. Day, *J. Am. Chem. Soc.* 1981, **103**, 3953.
4. J. Lamotte, O. Dideberg, L. Dupont and P. Durbut, *Cryst. Struct. Commun.* 1981, **10**, 59.
5. J. V. Brencic, L. Golic and P. Segedin, *Inorg. Chim. Acta* 1982, **57**, 247.
6. G. S. Girolami, V. V. Mainz and R. A. Andersen, *J. Am. Chem. Soc.* 1982, **104**, 2041.
7. M. H. Kelley and M. Fink, *J. Chem. Phys.* 1982, **76**, 1407.
8. M. L. H. Green, G. Parkin, J. Bashkin, J. Fail and K. Prout, *J. Chem. Soc., Dalton Trans.* 1982, 2519.
9. J. D. Arenivar, V. V. Mainz, H. Ruben, R. A. Andersen and A. Zalkin, *Inorg. Chem.* 1982, **21**, 2649.
10. J. H. Burk, G. E. Whitwell II, J. T. Lemley and J. M. Burlitch, *Inorg. Chem.* 1982, **22**, 1306.
11. R. A. Jones, J. G. Lasch, N. C. Norman, B. R. Whittlesey and T. C. Wright, *J. Am. Chem. Soc.* 1983, **105**, 6184.
12. K. R. Breakell, S. J. Rettig, A. Storr and J. Trotter, *Can. J. Chem.* 1983, **61**, 1659.

13. M. H. Chisholm, K. Folting, J. C. Huffman and R. J. Tatz, *J. Am. Chem. Soc.* 1984, **106**, 1153.
14. I. Leban and P. Segedin, *Inorg. Chim. Acta* 1984, **85**, 181.
15. G. A. Robbins and D. S. Martin, *Inorg. Chem.* 1984, **23**, 2086.
16. A. Bino, *Inorg. Chem.* 1984, **23**, 2902.
17. F. A. Cotton and W. H. Ilsley, *Inorg. Chem.* 1981, **20**, 572.
18. F. A. Cotton, W. H. Ilsley and W. Kaim, *Inorg. Chem.* 1981, **20**, 930.
19. F. A. Cotton and D. G. Lay, *Inorg. Chem.* 1981, **20**, 935.
20. G. S. Girolami and R. A. Andersen, *Inorg. Chem.* 1982, **21**, 1318.
21. F. A. Cotton, M. W. Extine, T. R. Felthouse, B. W. S. Kolthammer and D. G. Lay, *J. Am. Chem. Soc.* 1981, **103**, 4040.
22. F. A. Cotton and J. L. Thompson, *Inorg. Chem.* 1981, **20**, 3887.
23. F. A. Cotton, B. W. S. Kolthammer and G. N. Mott, *Inorg. Chem.* 1981, **20**, 3890.
24. F. A. Cotton and G. N. Mott, *Inorg. Chem.* 1981, **20**, 3896.
25. F. A. Cotton and G. N. Mott, *Organometallics* 1982, **1**, 302.
26. S. Baral, F. A. Cotton, W. H. Ilsley and W. Kaim, *Inorg. Chem.* 1982, **21**, 1644.
27. F. A. Cotton and G. N. Mott, *Inorg. Chim. Acta* 1983, **70**, 159.
28. F. A. Cotton, L. R. Falvello and C. A. Murillo, *Inorg. Chem.* 1983, **22**, 382.
29. F. A. Cotton and P. E. Fanwick, *Inorg. Chem.* 1983, **22**, 1327.
30. F. A. Cotton and G. L. Powell, *Inorg. Chem.* 1983, **22**, 1507.
31. P. A. Agaskar and F. A. Cotton, *Inorg. Chem.* 1984, **23**, 3383.
32. F. A. Cotton, L. R. Falvello, S. Han and W. Wang, *Inorg. Chem.* 1983, **22**, 4106.
33. P. Agaskar and F. A. Cotton, *Inorg. Chim. Acta* 1984, **83**, 33.
34. H. P. M. M. Ambrosius, F. A. Cotton, L. R. Falvello, H. T. J. M. Hintzen, T. J. Melton, W. Schwotzer, M. Tomas and J. G. M. van der Linden, *Inorg. Chem.* 1984, **23**, 1611.
35. F. A. Cotton and A. H. Reid, Jr, *Nouv. J. Chim.* 1984, **8**, 203.
36. A. R. Chakravarty, F. A. Cotton and E. S. Shamshoum, *Inorg. Chem.* 1984, **23**, 4216.
37. F. L. Campbell III, F. A. Cotton and G. L. Powell, *Inorg. Chem.* 1984, **23**, 4222.
38. L. Golic, I. Leban and P. Segedin, *Croat. Chem. Acta* 1984, **57**, 565.

Polyhedron Vol. 5, No. 1/2, pp. 15–23, 1986
Printed in Great Britain

0277–5387/86 $3.00 + .00
© 1986 Pergamon Press Ltd

REACTIVITY OF QUADRUPLY BONDED DIMOLYBDENUM(II) COMPLEXES WITH ALKYL ISOCYANIDES: Mo–Mo BOND CLEAVAGE OR RETENTION?

W. S. HARWOOD, JU-SHENG QI and R. A. WALTON*

Department of Chemistry, Purdue University, West Lafayette, IN 47907, U.S.A.

(*Received* 14 *June* 1985)

Abstract—The quadruply-bonded dimolybdenum(II) complexes $Mo_2(\mu\text{-dppm})_2X_4$ (X = Br or I) can be prepared in high yield from $Mo_2(\mu\text{-dppm})_2Cl_4$ (dppm = $Ph_2PCH_2PPh_2$) via simple halide-exchange reactions (using NaX in acetone). The complexes $Mo_2(\mu\text{-dppm})_2X_4$ (X = Cl, Br or I) react with one equivalent of RNC (R = *i*-Pr or *t*-Bu) in the presence of $TlPF_6$ (in THF) or KPF_6 (in acetone) to give $[Mo_2X_3(dppm)_2(CNR)]PF_6$, the first examples of multiply bonded Mo_2^{4+} complexes that contain coordinated π-acceptor RNC ligands. The reactions of $Mo_2(\mu\text{-dppm})_2X_4$ with an excess of RNC lead to seven-coordinate mononuclear cations $[MoX(dppm)(CNR)_4]^+$, which are in turn converted into $[Mo(CNR)_5(dppm)]^{2+}$ and thence $[Mo(CNR)_7]^{2+}$. The significance of these results, insofar as they relate to the cleavage of mixed halide–phosphine complexes of dimolybdenum(II) by isocyanides and the substitution chemistry of $[Mo(CNR)_7](PF_6)_2$ by phosphine ligands, are discussed. Comparisons are made with related chemistry of dinuclear and mononuclear molybdenum(II) complexes that contain bidentate nitrogen donors such as 2,2′-bipyridine, 1,10-phenanthroline and 1,4-disubstituted diaza-1,3-butadienes. The reactions between *cis*-$Mo_2(mhp)_2Cl_2(PMePh_2)_2$ (mhp is the anion of 2-hydroxy-6-methylpyridine) and *t*-BuNC (in the presence of KPF_6) result in the formation of mixtures of $Mo_2(mhp)_4$ and $[Mo(CN\text{-}t\text{-}Bu)_5(PMePh_2)_2](PF_6)_2$

The cleavage of multiply bonded dimetal units in M_2L_8 systems (especially when M = Mo, W, Re or Ru; L represents a conventional σ-donor ligand) by π-acceptor ligands such as CO and RNC (R = alkyl or aryl) has provided a convenient and important synthetic route to a variety of mononuclear complexes.[1,2] Little is known, however, about the mechanisms of these cleavage reactions although recent studies on dirhenium(II) complexes that contain stable intramolecular phosphine-ligand bridges, e.g. $Re_2Cl_4(dppm)_2$ (dppm = $Ph_2PCH_2PPh_2$), have, for the first time, allowed for the stabilization of multiply bonded species that contain CO and/or RNC ligands, e.g. $Re_2Cl_4(dppm)_2(CO)_n$ ($n = 1$ or 2).[3] These compounds can be viewed as intermediates in the cleavage process.

In the present report we address the situation as it pertains to the quadruply bonded $(Mo{\equiv}Mo)^{4+}$ core. The results of previous studies, which have led to the formation of mononuclear molybdenum isocyanide complexes, are briefly reviewed and new data are described which provide evidence for the formation of the multiply bonded dimolybdenum(II) complexes $[Mo_2X_3(dppm)_2(CNR)]PF_6$ (X = Cl, Br or I; R = *i*-Pr or *t*-Bu).

EXPERIMENTAL

Starting materials

The following compounds were prepared by standard literature procedures: *iso*-propyl isocyanide (*i*-PrNC),[4] *tert*-butyl isocyanide (*t*-BuNC),[4] $Mo_2(\mu\text{-dppm})_2X_4$ (X = Cl or Br)[5,6]† and

* Author to whom correspondence should be addressed.

† This procedure involves the reaction between $(NH_4)_4Mo_2Br_8$ and dppm in refluxing methanol. Full details are provided elsewhere[7] and are available upon request from Dr T. J. Smith.

$Mo_2Cl_4(PMePh_2)_4$.[8] Samples of thallium(I) hexafluorophosphate ($TlPF_6$) and dppm, which were obtained from Strem Chemical Co., and 2-hydroxy-6-methylpyridine (Hmhp), obtained from Aldrich Chemical Co., were used without further purification.

Reaction procedures

All reactions were carried out under a dry nitrogen atmosphere, and all reaction solvents were dried and deoxygenated prior to use by purging with N_2 gas for 15 min. In those cases where compounds were prepared by very similar procedures, details of representative recipes only are given. In those instances where microanalytical data are not given, identification of products is based upon their spectroscopic and electrochemical properties which showed the samples to be pure.

A. *Preparation of* $Mo_2(\mu\text{-dppm})_2X_4$. (i) $Mo_2(\mu\text{-dppm})_2I_4 \cdot 1.5C_3H_6O$. A 50-$cm^3$ round-bottom flask was charged with a mixture comprising $Mo_2(\mu\text{-dppm})_2Cl_4$ (0.505 g, 0.46 mmol), NaI (1.04 g, 6.93 mmol) and 20 cm^3 of acetone. The reaction mixture was refluxed for 12 h, cooled and then filtered in air. The green precipitate was washed with water, ethanol and pentane, and then vacuum dried: yield 0.55 g (77%). Calc. for $C_{54.5}H_{53}I_4Mo_2O_{1.5}P_4$: C, 42.1; H, 3.4; I, 32.6%. Found: C, 42.1; H, 3.6; I, 32.2%. The presence of lattice acetone was confirmed by IR spectroscopy [Nujol mull, ν(CO) at 1705s cm^{-1}] and ^1H NMR spectroscopy (CD_2Cl_2 solvent, δ +2.12 ppm for CH_3 of acetone: integration showed dppm: acetone $\simeq$ 4:3).

(ii) $Mo_2(\mu\text{-dppm})_2Br_4 \cdot 2C_3H_6O$. A procedure similar to A(i) was used but with NaBr in place of NaI: yield 81%. It was obtained as its bis-acetone solvate as shown by IR spectroscopy [Nujol mull, ν(CO) at 1705s cm^{-1}] and ^1H NMR spectroscopy (CD_2Cl_2 solvent, δ +2.14 ppm for CH_3 of acetone: integration showed dppm: acetone = 1:1).

B. *Reactions of* $Mo_2(\mu\text{-dppm})_2X_4$ *with alkyl isocyanides.*

(i) $[Mo_2Cl_3(dppm)_2(CNCMe_3)]PF_6 \cdot CH_2Cl_2$.

A 100-cm^3 three-neck round-bottom flask was charged with $Mo_2(\mu\text{-dppm})_2Cl_4$ (0.40 g, 0.36 mmol) and $TlPF_6$ (0.156 g, 0.45 mmol). A quantity of THF (50 ml) was syringed into the flask, followed by 46 μl (0.44 mmol) of *t*-BuNC, and the resulting green suspension was stirred at room temperature for 7 h. The precipitate was collected by filtration and washed with THF (3 × 5 ml) and then with pentane (5 ml). The product was extracted into dry, freshly distilled CH_2Cl_2 and the extract filtered from the insoluble residue and then evaporated to dryness. The green solid was washed with 10 cm^3 of a CH_2Cl_2–pentane mixture (1:3) and vacuum dried: yield 0.25 g (50%). Calc. for $C_{56}H_{55}Cl_5F_6Mo_2NP_5$: C, 48.7; H, 4.0; Cl, 12.8%. Found: C, 49.0; H, 4.1; Cl, 12.2%. The presence of lattice CH_2Cl_2 was confirmed by ^1H NMR spectroscopy ($CDCl_3$ solvent, δ +5.28 ppm). This complex could be obtained as an acetone solvate [ν(CO) at 1709s cm^{-1}] when acetone was used as the reaction solvent.

(ii) $[Mo_2Cl_3(dppm)_2(CNCHMe_2)]PF_6$. This complex was prepared from the reaction between $Mo_2(\mu\text{-dppm})_2Cl_4$ (0.24 g, 0.22 mmol), *i*-PrNC (21 μl, 0.23 mmol) and KPF_6 (0.39 g, 2.12 mmol) in 10 cm^3 of refluxing acetone for 6–8 h. The reaction mixture was then cooled to room temperature, filtered, and the solid washed with acetone and then very sparingly with CH_2Cl_2. The solid product was dissolved in the minimum volume of dry, freshly distilled CH_2Cl_2 (100–120 ml), filtered, and the filtrate evaporated under a blanket of nitrogen. The solid residue was washed with pentane and cold CH_2Cl_2 (3 × 5 ml), and then vacuum dried: yield 0.17 g (63%). Calc. for $C_{54}H_{51}Cl_3F_6Mo_2NP_5$: C, 50.6; H, 4.0; Cl, 8.3%. Found: C, 49.5; H, 4.2; Cl, 8.1%. The microanalytical data are consistent with the presence of a trace of lattice CH_2Cl_2.

(iii) $[Mo_2Br_3(dppm)_2(CNCMe_3)]PF_6$. This complex was prepared from $Mo_2(\mu\text{-dppm})_2Br_4$, $TlPF_6$ and *t*-BuNC using a procedure similar to that described in B(i): yield 50%. Calc. for $C_{55}H_{53}Br_3F_6Mo_2NP_5$: C, 46.2; H, 3.7; Br, 16.8%. Found: C, 46.1; H, 3.6; Br, 17.8%. The somewhat high halogen microanalysis probably reflects the presence of a trace of lattice CH_2Cl_2. Unfortunately, the poor solubility properties of this complex (in solvents other than CH_2Cl_2) precluded the measurement of a ^1H NMR spectrum that would confirm the presence of CH_2Cl_2. This complex could be obtained as an acetone solvate [ν(CO) at 1705s cm^{-1}] when acetone was used as the reaction solvent.

(iv) $[Mo_2Br_3(dppm)_2(CNCHMe_2)]PF_6$. This was prepared as described in B(iii): yield 44%. Calc. for $C_{54}H_{51}Br_3F_6Mo_2NP_5$: C, 45.8; H, 3.6%. Found: C, 44.8; H, 3.6%.

(v) $[Mo_2I_3(dppm)_2(CNCMe_3)]PF_6 \cdot C_3H_6O$. A mixture comprising $Mo_2(\mu\text{-dppm})_2I_4 \cdot 1.5C_3H_6O$ (0.39 g, 0.25 mmol) and KPF_6 (0.51 g, 2.77 mmol) was brought to reflux in acetone (15 ml). A small quantity of *t*-BuNC (28 μl, 0.27 mmol) was added and reflux continued for 4 h. The reaction mixture was cooled, stirring continued overnight, and the insoluble green product filtered off, washed with water, ethanol, THF and pentane, and finally vacuum dried: yield 0.33 g (81%). Calc. for $C_{58}H_{59}F_6I_3Mo_2NOP_5$:

C, 42.8; H, 3.7; I, 23.4%. Found: C, 42.8; H, 4.2; I, 23.4%. IR spectroscopy confirmed the presence of lattice acetone [Nujol mull, ν(CO) at 1707s cm^{-1}].

(vi) $[Mo_2I_3(dppm)_2(CNCHMe_2)]PF_6$. This complex was prepared from $Mo_2(\mu\text{-dppm})_2I_4$, $TlPF_6$ and *i*-PrNC using THF as solvent [see B(i)]: yield 41%. Calc. for $C_{54}H_{51}F_6I_3Mo_2NP_5$: C, 41.7; H, 3.3%. Found: C, 41.5; H, 3.4%.

(vii) $[MoCl(dppm)(CNCMe_3)_4]PF_6 \cdot 0.25CH_2Cl_2$. The complex $Mo_2(\mu\text{-dppm})_2Cl_4$ (0.70 g, 0.64 mmol) was treated with an excess of *t*-BuNC (0.40 cm^3, 3.79 mmol) and this mixture refluxed in 40 cm^3 of CH_2Cl_2 for 6 h. The reaction solution was then evaporated to dryness, 0.3 g of KPF_6 added, and the residue dissolved in a small volume of methanol. This was stirred for 15 min, 100 cm^3 of diethyl ether was added, and the KPF_6 that precipitated was filtered off. The filtrate was evaporated to dryness and the residue dissolved in a minimum volume of CH_2Cl_2. Diethyl ether was carefully layered over this solution which was allowed to slowly evaporate under a stream of nitrogen to give small orange-yellow crystals: yield 0.55 g (43%). Calc. for $C_{45.25}H_{58.5}Cl_{1.5}F_6MoN_4P_3$: C, 53.6; H, 5.8; Cl, 5.2%. Found: C, 53.7; H, 5.9; Cl, 5.1%. The micro-analytical data and ^1H NMR spectroscopy (acetone-d_6 solvent, δ +5.34 ppm) indicated the presence of a small amount of lattice CH_2Cl_2.

(viii) $[MoBr(dppm)(CNCMe_3)_4]PF_6$. This complex was prepared from $Mo_2(\mu\text{-dppm})_2Br_4$ as described in B(vii): yield 49%. Calc. for $C_{45}H_{58}BrF_6MoN_4P_3$: C, 52.1; H, 5.6; Br, 7.7%. Found: C, 52.0; H, 5.7; Br, 7.7%.

(ix) $[MoI(dppm)(CNCMe_3)_4]PF_6$. A procedure similar to B(vii) was used with $Mo_2(\mu\text{-dppm})_2I_4$ in place of $Mo_2(\mu\text{-dppm})_2Cl_4$: yield 50%. This complex was identified on the basis of its spectroscopic properties which were very similar to those of its chloride and bromide analogues.

C. *Preparation of* $Mo_2(\mu\text{-mhp})_2Cl_2(PMePh_2)_2$. The reaction between $Mo_2Cl_4(PMePh_2)_4$ (1.21 g, 1.07 mmol) and 2-hydroxy-6-methylpyridine (0.23 g, 2.15 mmol) was carried out in 20 cm^3 of refluxing toluene for 16 h. The red mixture was concentrated to half volume under a stream of dry nitrogen gas, filtered, and the insoluble red product washed with methanol (5 cm^3) and vacuum dried: yield 0.77 g (82%), Calc. for $C_{38}H_{38}Cl_2Mo_2N_2O_2P_2$: C, 51.9; H, 4.4%. Found: C, 51.2; H, 4.1%.

D. *Reactions of* $Mo_2(\mu\text{-mhp})_2Cl_2(PMePh_2)_2$ *with* *t*-BuNC. The reactions between $Mo_2(\mu\text{-mhp})_2Cl_2(PMePh_2)_2$ and *t*-BuNC (2–12 equivalents) were carried out in hot methanol. After a reaction time of *ca* 18 h, the reaction mixture was cooled and then filtered. The precipitate (if present) was identified as $Mo_2(mhp)_4$ on the basis of its electrochemical and spectroscopic properties.[9] The orange colored reaction filtrate was treated with an excess of KPF_6, stirred for 1 h, evaporated to dryness, and the residue extracted into CH_2Cl_2. The extract was filtered and added dropwise with stirring to either diethyl ether or diethyl ether–petroleum ether mixtures. The orange solid was shown to be $[Mo(CNCMe_3)_5(PMePh_2)_2](PF_6)_2$: it possessed an identical cyclic voltammogram, and IR and ^{31}P NMR spectral properties to those exhibited by an authentic sample of this complex.[10] Further details concerning these reactions are given in Results and Discussion.

Physical measurements

IR spectra were recorded on KBr plates in the region 4800–400 cm^{-1} and on polyethylene plates in the region 500–50 cm^{-1} using IBM Instruments IR/32 and IR/98 FTIR spectrometers, respectively. Electronic absorption spectra were recorded as CH_2Cl_2 solutions on an IBM 9420 (350–900 nm) UV–visible spectrophotometer. Conductivity measurements were performed on 1×10^{-3} M acetonitrile solutions using an Industrial Instruments Inc. Model RC-16B2 conductivity bridge. Electrochemical measurements were made in CH_2Cl_2 containing 0.1 M tetra-*n*-butyl ammonium hexafluorophosphate (TBAH) as supporting electrolyte. $E_{1/2}$ values were determined as $(E_{p,a} + E_{p,c})/2$ and referenced to the silver–silver chloride (Ag–AgCl) electrode at room temperature and are uncorrected for junction potentials. Voltammetric experiments were performed using a Bioanalytical Systems Inc. Model CV-1A instrument in conjunction with a Hewlett–Packard model 7035 x–y recorder. ^1H NMR and ^{31}P–$\{^1H\}$ NMR spectra were recorded on a Varian XL-200 spectrometer operated at 200.0 and 80.98 MHz, respectively. ^{31}P resonances were referenced to an external standard of aqueous 85% H_3PO_4 and ^1H NMR spectra were referenced to the residual protons of the solvent [$CDCl_3$, $\delta = +7.24$ ppm; CD_2Cl_2, $\delta = +5.32$ ppm; $(CD_3)_2CO$, $\delta = +2.04$ ppm]. Microanalyses were performed by Dr H. D. Lee of the Purdue University micro-analytical laboratory.

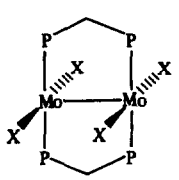
RESULTS AND DISCUSSION

Dinuclear and mononuclear molybdenum(II) complexes containing isocyanide and phosphine ligands

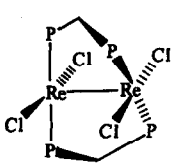
The ease with which multiply bonded dimolybdenum species are cleaved by π-acceptor ligands is

exemplified by the conversion of the quadruply bonded complexes $Mo_2Cl_4(dppm)_2$, $Mo_2Cl_4(dppe)_2$ and $Mo_2Cl_4(PR_3)_4$ (dppe = $Ph_2PCH_2CH_2PPh_2$, and PR_3 = PEt_3, P-*n*-Pr_3 or $PEtPh_2$) by isocyanide ligands RNC (R = Me, *t*-Bu or C_6H_{11}) to the mononuclear species $[Mo(CNR)_5(dppm)]^{2+}$, $[Mo(CNR)_5(dppe)]^{2+}$, $[Mo(CNR)_5(PR_3)_2]^{2+}$ or $[Mo(CNR)_6(PR_3)]^{2+}$ when a large excess of isocyanide is used.[10] In some instances, the seven-coordinate homoleptic species $[Mo(CNR)_7]^{2+}$ can be generated in these reactions, and it is the primary product when $Mo_2(O_2CCH_3)_4$ and $K_4Mo_2Cl_8$ are reacted with an excess of RNC in hot methanol.[11] Upon reaction of $[Mo(CNR)_7]^{2+}$ with an excess of dppm, dppe or PR_3, the preceding mixed phosphine–isocyanide complexes can be produced in high yield.[10] In contrast to these non-redox cleavage reactions, aryl isocyanide ligands (ArNC) react with $Mo_2(O_2CCH_3)_4$ to give the homoleptic Mo(0) complexes $Mo(CNAr)_6$.[12,13]

While $Mo_2(\mu\text{-dppm})_2X_4$ are very easily converted into $[Mo(CNR)_5(dppm)]^{2+}$,[10] the related dirhenium(II) complex, $Re_2(\mu\text{-dppm})_2Cl_4$, forms stable dinuclear complexes with isocyanide ligands and also with CO.[3] The complexes $Mo_2(\mu\text{-dppm})_2X_4$ (X = Cl or Br) and $Re_2(\mu\text{-dppm})_2Cl_4$ have similar molecular structures (**I** and **II**, respectively) in which the dppm ligands form



I



(P ⌒ P = dppm)

II

intramolecular bridges. However, they differ in that the dimolybdenum complex, which possess a Mo–Mo quadruple bond ($\sigma^2\pi^4\delta^2$ configuration), has an eclipsed rotational geometry[14,15] while the triply bonded dirhenium complex ($\sigma^2\pi^4\delta^2\delta^{*2}$ configuration) is staggered.[16]

The preceding structural difference not withstanding, we wondered whether intermediates in this cleavage process might not be isolated in the case of $Mo_2(\mu\text{-dppm})_2X_4$ (X = halide) with a judicious choice of mild reaction conditions. This possibility first led us to develope a procedure for the preparation of the iodo derivative $Mo_2(\mu\text{-dppm})_2I_4$ via a halide exchange reaction [eqn (1)]:

$$Mo_2(\mu\text{-dppm})_2Cl_4 + 4NaI \xrightarrow{\text{acetone}} Mo_2(\mu\text{-dppm})_2I_4 + 4NaCl. \quad (1)$$

This procedure works equally well for the preparation of $Mo_2(\mu\text{-dppm})_2Br_4$ (using NaBr), and provides a fourth method for preparing the latter complex: others are: (i) the reaction of $Mo_2Br_4(PEt_3)_4$ with dppm in methanol;[5] (ii) the reaction of $(NH_4)_4Mo_2Br_8$ with dppm in methanol;[6] and (iii) the reaction between $Mo_2(O_2CCH_3)_4$, Me_3SiBr and dppm in THF.[15] The procedure we used affords the iodo the bromo derivatives as their acetone solvates. The propensity of $Mo_2(\mu\text{-dppm})_2X_4$ to form solvates has been well documented previously.[14,15]

A comparison of the far-IR spectra of $Mo_2(\mu\text{-dppm})_2X_4$ (recorded as Nujol mulls) shows the expected shift in the ν(Mo—X) modes [338s (X = Cl), 259m (X = Br), and 214m-w (X = I) cm^{-1}].* The ratios ν(Mo—Br)/ν(Mo—Cl) = 0.77 and ν(Mo—I)/ν(Mo—Cl) = 0.63 are in good agreement with those reported for other terminal metal–halogen stretching modes.[17] In the case of their electronic absorption spectra (Table 1), these complexes display a smooth trend in the position of the $\delta \rightarrow \delta^*$ transition (λ_{max} = 634, 650 and 684 nm for X = Cl, Br and I, respectively). The intense absorptions at 360 and 429 nm in the case of the bromo and iodo derivatives are tentatively assigned to allowed halogen (π) → Mo transitions. The ^1H NMR spectra show the expected pentet for the methylene protons of the dppm ligands (Table 1), while the $^{31}P\text{–}\{^1H\}$ NMR spectra are characterized by singlets for the chemically and magnetically equivalent phosphorus atoms.

The electrochemical properties of these complexes were studied using the cyclic voltammetric technique. The measured half-wave or peak potentials vs Ag–AgCl for 0.1 M TBAH–CH_2Cl_2 solutions of $Mo_2(\mu\text{-dppm})_2X_4$ are listed in Table 1 (see also Fig. 1). Each complex exhibits a process at *ca* +0.7 V. In the case of X = Cl or Br this process is reversible and corresponds to a one-electron oxidation (as determined by coulometry). The couple is characterized by $i_{p,a}/i_{p,c} = 1$ and a constant $i_p/v^{1/2}$ ratio for sweep rates between 50 and 400 mV s^{-1}. The potential separation between the anodic and cathodic peaks, ΔE_p, was between 100 and 120 mV for a sweep rate of 200 mV s^{-1} and increased slightly with increase in sweep rate. These properties are (with our cell configuration) consistent with a reversible electron-transfer process or one that approaches reversibility.[18] This behavior resembles closely that of other dimolybdenum(II) complexes

*Similar data for the chloride and bromide were reported earlier in Ref. 5 (viz. 340s and 260w cm^{-1}, respectively).

Table 1. Spectroscopic and electrochemical properties of $Mo_2(\mu\text{-dppm})_2X_4$ (X = Cl, Br or I)

Complex	Electronic absorption spectra[a] (nm)	NMR (δ)		Voltammetric half-wave potentials[d]		
		^1H[b]	$^{31}P-\{^1H\}$[c]	$E_{p,a}$	$E_{1/2}$(ox)	$E_{p,c}$
$Mo_2(\mu\text{-dppm})_2Cl_4$	634 (2100), 462 (600), ~ 360sh	4.35p (J_{P-H} = 5.0 Hz)	+16.14s		+0.66 (100)	~ −1.50
$Mo_2(\mu\text{-dppm})_2Br_4$	650 (2600), 480 (1000), 360	4.44p (J_{P-H} = 4.4 Hz)	+14.85s		+0.71 (120)	−1.28
$Mo_2(\mu\text{-dppm})_2I_4$	684 (3000), 499 (720), 480sh 429 (3800), 400sh	4.54p (J_{P-H} = 4.6 Hz)	+12.43s	+1.21	+0.77[e]	−1.03

[a] Recorded in CH_2Cl_2 solutions in the region 900–350 nm: ε_{max} values are given in parentheses.
[b] Recorded in CD_2Cl_2: each resonance is a pentet.
[c] Recorded in CH_2Cl_2. Positive values are downfield of 85% H_3PO_4.
[d] In V (Ag–AgCl). Recorded on solutions in 0.1 M TBAH–CH_2Cl_2 using a Pt-bead electrode. Data obtained at v = 200 mV s^{-1}. $E_{p,a}-E_{p,c}$ values are given in parentheses.
[e] Irreversible process: $E_{p,a}$ value given.

that contain halide and phosphine ligands, all of which show a reversible oxidation in the vicinity of +0.5 V.[18] In the case of the iodide complex $Mo_2(\mu\text{-dppm})_2I_4$, a second well-defined oxidation process is seen in the single-scan cyclic voltammogram at $E_{p,a}$ = +1.21 V.

While $Mo_2(\mu\text{-dppm})_2X_4$ reacts with an excess of RNC (R = Me, *t*-Bu or C_6H_{11}) to give $[Mo(CNR)_5(dppm)]^{2+}$ and, in some instances, $[Mo(CNR)_7]^{2+}$,[10] we find that the use of a much smaller amount of RNC (five–six equivalents) gives the mononuclear complexes [MoX(CN-*t*-Bu)$_4$(dppm)]PF_6 (X = Cl, Br or I) as the major products. With this "deficiency" of *t*-BuNC, the yields of [MoX(CN-*t*-Bu)$_4$(dppm)]PF_6 do not (as expected) exceed *ca* 50%. An increase in the amount of RNC (up to eight equivalents) leads to the formation of appreciable quantities of [Mo(CN-*t*-Bu)$_5$(dppm)]$(PF_6)_2$. Indeed, the reaction of [MoCl(CN-*t*-Bu)$_4$(dppm)]PF_6 with one–three equivalents of *t*-BuNC (in the presence of KPF_6) in refluxing methanol gives [Mo(CN-*t*-Bu)$_5$(dppm)]$(PF_6)_2$ in high yield (up to *ca* 80%), a result which implies that [MoX(CN-*t*-Bu)$_4$(dppm)]PF_6 is a precursor to [Mo(CN-*t*-Bu)$_5$(dppm)]$(PF_6)_2$, and that this is in turn converted into [Mo(CN-*t*-Bu)$_7$]$(PF_6)_2$ in the presence of a sufficient excess of *t*-BuNC.

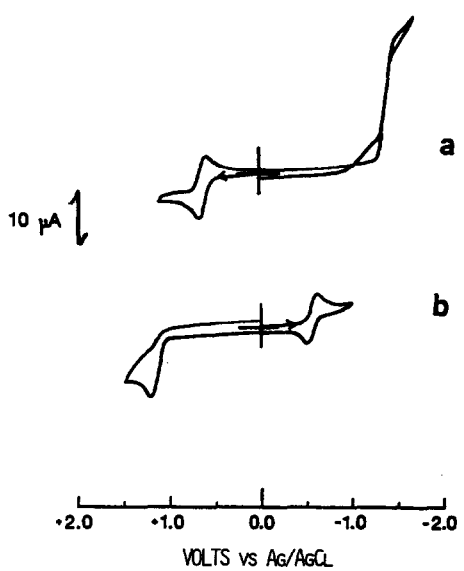


Fig. 1. Cyclic voltammograms (scan rate 200 mV s^{-1} at a Pt-bead electrode) in 0.1 M TBAH–CH_2Cl_2 of: (a) $Mo_2(\mu\text{-dppm})_2Cl_4$, and (b) $[Mo_2Cl_3(dppm)_2(CN\text{-}t\text{-}Bu)]PF_6$.

The pertinent spectroscopic properties of these monohalide complexes are summarized in Table 2. The simplicity of the $^{31}P-\{^1H\}$ and ^1H NMR spectra signify that these complexes are stereochemically non-rigid in solution at ambient temperatures. These complexes dissolve in acetonitrile to give solutions (*ca* 10^{-3} M) that have conductivities ($\Lambda_M \simeq 130\,\Omega^{-1}$ cm^2 mol^{-1}) which are in the range expected for 1:1 electrolytes (120–160 Ω^{-1} cm^2 mol^{-1}).[19] The electrochemical properties of [MoX(CN-*t*-Bu)$_4$(dppm)]PF_6 (Table 2) are characterized by a reversible one-electron (by coulometry) oxidation at $E_{1/2} \simeq$ +0.5 V (Ag–AgCl). The comparable redox process in the cyclic voltammograms of $[Mo(CNR)_5(dppm)](PF_6)_2$ (R = Me or C_6H_{11}) is at *ca* +1.0 V (SCE).[10] This shift (of *ca* 0.5 V) to more negative potentials upon replacing a RNC ligand by a halide, is similar to that found between the corresponding redox processes (one-electron oxida-

Table 2. Spectroscopic and electrochemical properties of $[MoX(CN\text{-}t\text{-}Bu)_4(dppm)]PF_6$ (X = Cl, Br or I)

Complex	IR spectra (cm^{-1})[a]	NMR (δ)		Voltammetric half-wave potentials[d]		
	ν(CN)	^1H[b]	$^{31}P-\{^1H\}$[c]	$E_{p,a}$	$E_{1/2}$(ox)	$E_{p,c}$
X = Cl	2176s, 2098vs, 2052sh	1.30s,[e] 4.56t[f]	+7.32s[g]	~ +1.6	+0.48 (100)	−2.00
X = Br	2170s, 2137m-w, 2099vs, 2058sh	1.30s,[e] 4.56t[f]	+3.23s	+1.56	+0.51 (100)	−1.83
X = I	2158m, ~2125vs,br, 2051s	1.27s,[e] 4.51t[f]	+2.22s	~ +1.6	+0.58 (130)	−1.89

[a] Nujol mull spectra.
[b] Recorded in acetone-d_6.
[c] Recorded in acetone. Positive values are downfield of 85% H_3PO_4.
[d] In V (Ag–AgCl). Recorded on solutions in 0.1 M TBAH–CH_2Cl_2 using a Pt-bead electrode. Data obtained at ν = 200 mV s^{-1}. $E_{p,a}-E_{p,c}$ values are given in parentheses.
[e] Singlet due to Me_3CNC ligands.
[f] Triplet due to —CH_2— of the dppm ligand (J_{P-H} ~ 10 Hz).
[g] This resonance is at δ +5.05 ppm in CH_2Cl_2 solution.

tion) of $[Re(CNAr)_6]^+$ and $Re(CNAr)_5X$,[20,21] and betwween those of $[Mo(CNR)_7]^{2+}$ and $[Mo(CNR)_6Cl]^+$.[22]

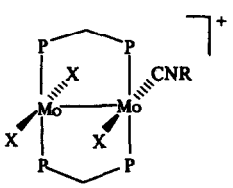
Although we found no evidence for multiply bonded dimolybdenum intermediates in the reactions between $Mo_2(\mu\text{-dppm})_2X_4$ and RNC when these reactions were carried out in CH_2Cl_2, we were eventually able to modify the reaction procedure to give such species. The reaction of $Mo_2(\mu\text{-dppm})_2X_4$ with one equivalent of RNC (R = *i*-Pr or *t*-Bu) in THF in the presence of $TlPF_6$, or in acetone with excess KPF_6 present, gives the monoisocyanide complexes $[Mo_2X_3(dppm)_2(CNR)]PF_6$. These complexes behave as 1 : 1 electrolytes in acetonitrile ($\Lambda_M \simeq 130\ \Omega^{-1}\ cm^2\ mol^{-1}$ for $C_m \simeq 10^{-3}$ M) and display a single sharp ν(CN) band in their IR spectra at 2170(±5) cm^{-1}. Unfortunately, these complexes have low solubility in polar solvents, and in halogenated hydrocarbons, in which they are most soluble, the solutions decompose on standing. However, freshly prepared solutions in CH_2Cl_2 have the spectroscopic and electrochemical properties given in Table 3. Each complex displays an intense transition (tentatively assigned as $\delta \rightarrow \delta^*$) in the

Table 3. Spectroscopic and electrochemical properties of $[Mo_2X_3(dppm)_2(CNR)]PF_6$ (X = Cl, Br or I; R = *i*-Pr or *t*-Bu)

Complex	Electronic absorption spectra[a] (nm)	^1H NMR (δ)[b]		Voltammetric half-wave potentials[c]	
	$\delta \rightarrow \delta^*$ transition	RNC	—CH_2—(dppm)	$E_{p,a}$	$E_{1/2}$(red)
X = Cl					
R = *i*-Pr	730 (1800)	1.34d[d]	4.35m, 4.66m	+1.21	−0.55 (100)
R = *t*-Bu	718 (1800)	1.12s	4.19m, 4.62m	+1.26	−0.54 (100)
X = Br					
R = *i*-Pr	733 (2200)			+1.24	−0.48 (100)
R = *t*-Bu	730 (2000)	1.02s	4.20m, 4.63m	+1.26	−0.52 (100)
X = I					
R = *i*-Pr	791 (2800)			+1.21	−0.40 (100)
R = *t*-Bu	749 (3100)	0.94s	4.25m, 4.55m	+1.22	−0.48 (100)

[a] Recorded in CH_2Cl_2: ε_{max} values are given in parentheses.
[b] Recorded in CD_2Cl_2. Abbreviations are as follows: d, doublet; m, multiplet; s, singlet.
[c] In V (Ag–AgCl). Recorded on solutions in 0.1 M TBAH–CH_2Cl_2 using a Pt-bead electrode. Data obtained at ν = 200 mV s^{-1}. $E_{p,a}-E_{p,c}$ values are given in parentheses.
[d] CH_3 resonance of the *i*-Pr group: the unique methine proton is located at δ ~ +3.7 as a broad septet.

region 715–790 nm, the energy of which decreases in the order Cl ≳ Br > I. The electrochemical properties of $[Mo_2X_3(dppm)_2(CNR)]PF_6$ are quite different from those of the parent complexes $Mo_2(\mu\text{-dppm})_2X_4$ (compare Tables 1 and 3 and Fig. 1). Once again, the replacement of an isocyanide ligand by halide makes the complex much easier to oxidize and, consequently, harder to reduce. In all instances the monoisocyanide complexes are characterized by an irreversible oxidation at $E_{p,a} \simeq +1.2$ V and a reversible process at $E_{1/2} \simeq -0.5$ V (Ag–AgCl) that corresponds to a one-electron reduction (Table 3 and Fig. 1). The poor solubility properties of these complexes precluded us from obtaining high-quality NMR spectra. The ^1H NMR spectra (recorded in CD_2Cl_2) show an AB pattern, with superimposed P–H coupling, for the $-CH_2-$ protons of the bridging dppm ligands. This inequivalence of the protons of the bridgehead methylene groups (H_α and H_β) implies the presence of an asymmetric structure. This conclusion is supported by the $^{31}P-\{^1H\}$ NMR spectrum of $[Mo_2Cl_3(dppm)_2(CN\text{-}t\text{-}Bu)]PF_6$ which exhibits an AA'BB' pattern ($\delta_A = +20.82$, $\delta_B = +11.51$) of a type that is commonly encountered in asymmetric multiply bonded dimetal species that contain two bridging dppm ligands.[23] While we have been unable as yet to obtain single crystals of any of the derivatives $[Mo_2X_3(dppm)_2(CNR)]PF_6$ that are suitable for a single-crystal X-ray structure analysis, the available evidence supports their possessing structure **III**, although we have not been able to



III

establish the rotational geometry (eclipsed or staggered).

On the basis of the aforementioned results we can represent the sequence of reactions that lead to the conversion of $Mo_2(\mu\text{-dppm})_2X_4$ to $[Mo(CNR)_7]^{2+}$ in terms of the following steps [(1)–(5)]:

$$Mo_2(\mu\text{-dppm})_2X_4$$

$$\xrightarrow[(1)]{RNC} [Mo_2X_3(dppm)_2(CNR)]^+$$

$$\xrightarrow[(2)]{RNC} \{[Mo_2X_3(dppm)_2(CNR)_n]^+\}$$

$$\xrightarrow[(3)]{RNC} [MoX(CNR)_4(dppm)]^+$$

$$\xrightarrow[(4)]{RNC} [Mo(CNR)_5(dppm)]^{2+}$$

$$\xrightarrow[(5)]{RNC} [Mo(CNR)_7]^{2+}.$$

The details of step (2), in which other isocyanide containing multiply bonded dimolybdenum(II) species are presumably formed, have not yet been delineated, although we do have evidence that the reaction of $[Mo_2Cl_3(dppm)_2(CN\text{-}t\text{-}Bu)]PF_6$ with one equivalent of *t*-BuNC in THF gives the analogous *bis*-isocyanide complex, albeit somewhat impure.* This complex is analogous to the dirhenium(II) complexes of stoichiometry $[Re_2Cl_3(dppm)_2(CNR)_2]PF_6$.[23]

We have also studied the reactivity of other dimolybdenum(II) species towards RNC ligands. Of special note are the species *cis*-$Mo_2(mhp)_2Cl_2(PR_3)_2$, whose preparation and spectroscopic and electrochemical properties [along with those of $Mo_2(mhp)Cl_3(PR_3)_3$ and $Mo_2(mhp)_3Cl(PR_3)$] will be the subject of a future detailed report.[24] The structure of this group of molecules has been established by a single-crystal X-ray analysis of *cis*-$Mo_2(mhp)_2Cl_2(PEt_3)_2$.[25] A study of the reactions of its $PMePh_2$ analogue towards various amounts of *t*-BuNC did not afford us any isocyanide-containing dimolybdenum species. No products were isolated from the reaction of *cis*-$Mo_2(mhp)_2Cl_2(PMePh_2)_2$ with one equivalent of *t*-BuNC in the presence of $T1PF_6$ or KPF_6. Reactions using 2–12 equivalents of *t*-BuNC in acetone gave $Mo_2(mhp)_4$ and $[Mo(CN\text{-}t\text{-}Bu)_5(PMePh_2)_2](PF_6)_2$ as the only identifiable products. It seems likely that cleavage of the dimolybdenum complex occurs with concomitant loss of mhp ligand which in turn attacks unreacted (or partially reacted) starting material to give $Mo_2(mhp)_4$. The $PMePh_2$ so released then reacts with mononuclear cleavage products to give stable $[Mo(CN\text{-}t\text{-}Bu)_5(PMePh_2)_2](PF_6)_2$. Whereas very little $Mo_2(mhp)_4$ is produced with a $Mo_2(mhp)_2Cl_2(PMePh_2)_2$: *t*-BuNC stoichiometric ratio of 1:2 or 1:4, the yields of $Mo_2(mhp)_4$ and $[Mo(CN\text{-}t\text{-}Bu)_5(PMePh_2)_2](PF_6)_2$ are 17 and 26%, respectively, with a 1:6 ratio. Thereafter, the yield of

* Preliminary spectroscopic and electrochemical characterizations of this green 1:2 complex are as follows: IR (Nujol) ν(CN) 2182sh and 2164s cm^{-1}; ^1H NMR (CD_2Cl_2) δ +1.52 (s, Me_3CNC, 18H), δ +4.55 (p, $-CH_2-$ of dppm, 4H, $J_{P-H} = 4.8$ Hz); CV (in 0.1 M TBAH–CH_2Cl_2): $E_{p,a} = +1.22$ V, $E_{1/2}$(red) = −0.32 V, and $E_{1/2}$(red) = −1.28 V (Ag–AgCl).

the former decreases while the latter increases (e.g. a 1:12 ratio gives 7 and 51% of isolated products, respectively).

Mixed isocyanide–nitrogen donor complexes of molybdenum(II)

The detailed study of the reactions between $Mo_2(\mu\text{-dppm})_2X_4$ and RNC has provided insights into the reaction pathway involved in the cleavage of the Mo≡Mo bond by the π-acceptor ligands. In the case of the corresponding reaction chemistry involving dimolybdenum compounds that contain heterocyclic amine ligands, we have found that both similarities and some striking differences exist. Thus $Mo_2Cl_4(bpy)_2$ and $Mo_2Cl_4(py)_4$ (bpy = 2,2′-bipyridine and py = pyridine) are converted into mononuclear $[MoCl(CN\text{-}t\text{-}Bu)_4(bpy)]PF_6$ and $[Mo(CN\text{-}t\text{-}Bu)_6(py)](PF_6)_2$, respectively.[26] On the other hand, the reactions of mononuclear $[Mo(CNR)_7](PF_6)_2$ with the bidentate nitrogen donors (abbreviated N–N) bpy, 4,4′-dimethyl-2,2′-bipyridine (Me_2bpy) and 1,10-phenanthroline (phen) show an interesting dependence upon the nature of the RNC ligand. In the case of $[Mo(CNR)_7](PF_6)_2$, where R = Me, Me_2CH or C_6H_{11}, dark red-purple complexes of the type $[Mo(CNR)_5(N\text{–}N)](PF_6)_2$ are formed in high yield when the reactions are carried out in refluxing 1-propanol.[26] However, $[Mo(CN\text{-}t\text{-}Bu)_7](PF_6)_2$ reacts with bpy, Me_2bpy and phen under these same conditions to produce the cyano-bridged complexes $\{[Mo(CN\text{-}t\text{-}Bu)_4(N\text{–}N)]_2(\mu\text{-}CN)\}(PF_6)_3$, through dealkylation of a *t*-BuNC ligand.[26] The crystal structure of $\{[Mo(CN\text{-}t\text{-}Bu)_4(bpy)]_2(\mu\text{-}CN)\}(PF_6)_3$ has been determined and shows the presence of seven-coordinate molybdenum atoms and an essentially linear Mo—N≡C—Mo bridge. However, the mononuclear complex $[Mo(CN\text{-}t\text{-}Bu)_5(bpy)](PF_6)_2$ can be prepared from $\{[Mo(CN\text{-}t\text{-}Bu)_4(bpy)]_2(\mu\text{-}CN)\}(PF_6)_3$, as shown in eqn (2):

$$\{[Mo(CN\text{-}t\text{-}Bu)_4(bpy)]_2(\mu\text{-}CN)\}(PF_6)_3$$

$$\xrightarrow[\text{heat}]{t\text{-BuCl, MeOH}} [Mo(CN\text{-}t\text{-}Bu)_4(bpy)Cl]PF_6$$

$$\xrightarrow[\text{heat}]{t\text{-BuNC, KPF}_6\text{, MeOH}} [Mo(CN\text{-}t\text{-}Bu)_5(bpy)](PF_6)_2$$

$$\xrightarrow[\text{reflux, 1}\tfrac{1}{2}\text{ h}]{\text{1-propanol}} \{[Mo(CN\text{-}t\text{-}Bu)_4(bpy)]_2(\mu\text{-}CN)\}(PF_6)_3 \qquad (2)$$

and it can in turn be converted back to the cyano-bridged species thermally.[26]

An alternative procedure for synthesizing the mononuclear molybdenum complexes $[Mo(CNR)_5(N\text{–}N)](PF_6)_2$ {which is, incidentally, also applicable to the tungsten(II) analogues $[W(CNR)_5(N\text{–}N)](PF_6)_2$} involves the $PhICl_2$ oxidation of $Mo(CO)_4(N\text{–}N)$ in the presence of a stoichiometric quantity of RNC [eqn (3)].[27]

$$Mo(CO)_4(N\text{–}N) \xrightarrow[\text{(2) RNC (six equivalents), KPF}_6]{\text{(1) PhICl}_2\text{, MeOH, RT}} [Mo(CNR)_5(N\text{–}N)](PF_6)_2. \qquad (3)$$

These one-pot syntheses, using readily available starting materials, offer advantages over the somewhat more elaborate procedure used previously to prepare the EtNC complex $[Mo(CNEt)_5(bpy)](BF_4)_2$.[28]

A variation of the reaction depicted in eqn (3) has been used to prepare the mononuclear complexes

$$[Mo(CNR)_5(R'\text{-DAB})](PF_6)_2$$

$$(R'\text{-DAB} = R'\text{—N=CH—CH=N—}R')$$

which cannot be generated by the direct reaction of $[Mo(CNR)_7](PF_6)_2$ with the bidentate 1,4-di-substituted diaza-1,3-butadiene ligands R′-DAB (R′ = *i*-Pr, *t*-Bu or C_6H_{11}).[26] We have found that the reactions of the molybdenum(II) species

$$Mo(CO)_3(R'\text{-DAB})(SnCl_3)Cl$$

[which are themselves prepared by treating $Mo(CO)_4(R'\text{-DAB})$ with $SnCl_4$ in CH_2Cl_2] with RNC (R = *i*-Pr, *t*-Bu or C_6H_{11}) in the presence of KPF_6 lead to the formation of

$$[MoCl(CNR)_4(R'\text{-DAB})]PF_6$$

or

$$[Mo(CNR)_5(R'\text{-DAB})](PF_6)_2$$

(R′ = *i*-Pr or Cy) depending upon the reaction stoichiometry and reaction conditions.[29] The monocationic chloro species are converted into

$$[Mo(CNR)_5(R'\text{-DAB})](PF_6)_2$$

upon heating with the stoichiometric amount of RNC. Under similar reaction conditions $Mo(CO)_3(t\text{-Bu-DAB})(SnCl_3)Cl$ (i.e. R′ = *t*-Bu) reacts with RNC with the reductive-elimination of the elements of $SnCl_4$ and the formation of octahedral $Mo(CO)_3(CNR)(t\text{-Bu-DAB})$.[29] The latter compounds represent a class of mixed carbonyl–isocyanide complexes of molybdenum(0) for which other preparative procedures have recently been devised, and for which an interesting and quite extensive redox chemistry has been uncovered.[30]

Acknowledgement—We thank the National 'Science Foundation for support of this work through grant No. CHE82-06117.

REFERENCES

1. F. A. Cotton and R. A. Walton, *Multiple Bonds between Metal Atoms*. John Wiley, New York (1982) (and references cited therein).
2. R. A. Walton, *Am. Chem. Soc. Symp. Ser.* 1981, **155**, 207 (and references cited therein).
3. For selected key references, see, L. B. Anderson, T. J. Barder and R. A. Walton, *Inorg. Chem.* 1985, **24**, 1421; F. A. Cotton, L. M. Daniels, K. R. Dunbar, L. R. Falvello, S. M. Tetrick and R. A. Walton, *J. Am. Chem. Soc.* 1985, **107**, 3524; F. A. Cotton, K. R. Dunbar, L. R. Falvello and R. A. Walton, *Inorg. Chem.* (accepted for publication).
4. W. D. Weber, G. W. Gokel and I. K. Ubi, *Angew. Chem., Int. Ed. Engl.* 1972, **11**, 530.
5. S. A. Best, T. J. Smith and R. A. Walton, *Inorg. Chem.* 1978, **17**, 99.
6. T. J. Smith and D. R. Root, unpublished results.
7. D. R. Root, Undergraduate Research Project Report, Kalamazoo College, Kalamazoo, MI (1983).
8. (a) J. San Fillipo, Jr, H. J. Sniadoch and R. L. Grayson, *Inorg. Chem.* 1974, **13**, 2121; (b) H. D. Glicksman, A. D. Hamer, T. J. Smith and R. A. Walton, *Inorg. Chem.* 1976, **15**, 2205.
9. B. E. Bursten, F. A. Cotton, A. H. Cowley, B. E. Hansen, M. Lattman and G. G. Stanley, *J. Am. Chem. Soc.* 1979, **101**, 6244.
10. T. E. Wood, J. C. Deaton, J. Corning, R. E. Wild and R. A. Walton, *Inorg. Chem.* 1980, **19**, 2614.
11. P. Brant, F. A. Cotton, J. C. Sekutowski, T. E. Wood and R. A. Walton, *J. Am. Chem. Soc.* 1979, **101**, 6588.
12. K. R. Mann, M. Cimolino, G. L. Geoffroy, G. S. Hammond, A. A. Orio, G. Albertin and H. B. Gray, *Inorg. Chim. Acta* 1976, **16**, 97.
13. D. A. Bohling, K. R. Mann, S. Enger, T. Gennett, M. J. Weaver and R. A. Walton, *Inorg. Chim. Acta* 1985, **97**, L51.
14. E. H. Abbott, K. S. Bose, F. A. Cotton, W. T. Hall and J. C. Sekutowski, *Inorg. Chem.* 1978, **17**, 3240.
15. F. L. Campbell III, F. A. Cotton and G. L. Powell, *Inorg. Chem.* 1984, **23**, 4222.
16. T. J. Barder, F. A. Cotton, K. R. Dunbar, G. L. Powell, W. Schwotzer and R. A. Walton, *Inorg. Chem.* 1985, **24**, 2550.
17. K. Nakamoto, *Infrared and Raman Spectra of Inorganic and Coordination Compounds*, 3rd Edn, p. 317. John Wiley, New York (1978).
18. T. C. Zietlow, D. D. Klendworth, T. Nimry, D. J. Salmon and R. A. Walton, *Inorg. Chem.* 1981, **20**, 947.
19. W. J. Geary, *Coord. Chem. Rev.* 1971, **7**, 81.
20. C. J. Cameron, S. M. Tetrick and R. A. Walton, *Organometallics* 1984, **3**, 240.
21. K. A. Conner and R. A. Walton, unpublished results.
22. A. Bell, D. D. Klendworth, R. E. Wild and R. A. Walton, *Inorg. Chem.* 1981, **20**, 4456.
23. L. B. Anderson, T. J. Barder and R. A. Walton, *Inorg. Chem.* 1985, **24**, 1421.
24. P. E. Fanwick, W. S. Harwood, Ju-sheng Qi and R. A. Walton, manuscript in preparation.
25. P. E. Fanwick, *Inorg. Chem.* 1985, **24**, 258.
26. A. Bell, S. J. Lippard, M. Roberts and R. A. Walton, *Organometallics* 1983, **2**, 1562.
27. A. Bell and R. A. Walton, *J. Organomet. Chem.* 1984, **263**, 359.
28. J. A. Connor, E. J. James, C. Overton and N. El Murr, *J. Chem. Soc., Dalton Trans.* 1984, 255.
29. A. Bell and R. A. Walton, *J. Organomet. Chem.* 1985, **290**, 341.
30. A. Bell and R. A. Walton, *Polyhedron* (in press).

Polyhedron Vol. 5, No. 1/2, pp. 25–30, 1986
Printed in Great Britain

0277–5387/86 $3.00 + .00
© 1986 Pergamon Press Ltd

INTERCONVERTING MULTIPLE BONDS BETWEEN MOLYBDENUM AND TUNGSTEN ATOMS: OXIDATIVE-ADDITIONS AND REDUCTIVE-ELIMINATIONS FROM DINUCLEAR CENTERS

MALCOLM H. CHISHOLM

Department of Chemistry, Indiana University, Bloomington, IN 47405, U.S.A.

(*Received* 18 *June* 1985)

Abstract—Analogies between the chemistry of mononuclear group 8, 9 and 10 transition elements and the chemistry of dinuclear molybdenum and tungsten compounds are noted. Just as the d^8- and d^6-configurations determine preferred coordination numbers, geometries, substitution patterns and the propensity for oxidative-addition or reductive-elimination, so does the M–M bonding configuration influence the coordination chemistry and reactivity of dinuclear compounds. The presence of two metal atoms united by a multiple bond provides an electron source or sink for multi-electron redox reactions and a template for substrate assembly and coupling. The presence of two metal centers poses fascinating mechanistic questions concerning cooperative interactions between the metal atoms and the detailed reaction profile for even simple addition–elimination sequences. These general principles are illustrated in studies of the formation of M–M quadruple bonds by reductive-elimination from $(M{\equiv}M)^{6+}$ centers and oxidative-additions leading to $(M{=}M)^{8+}$ and $(M{-}M)^{10+}$ centers.

Several years ago I began to speculate about the reactivity of compounds containing M–M multiple bonds[1] and started a systematic search for reactions leading to stepwise changes in bond order akin to those well known in organic chemistry. In particular, redox reactions involving dinuclear compounds should find many parallels with mononuclear chemistry. Oxidative-additions and reductive-eliminations interconverting d^8 and d^6 transition-metal-containing complexes are well-documented and provide fundamental steps in numerous homogeneous catalytic or stoichiometric reactions.[2,3] Although the intimate mechanism of a given reaction may vary from metal to metal and substrate to substrate, the general concept of reactivity based on d^n-configuration, coordination geometry and ligand substitution lability are relatively well-advanced for mononuclear metal centers.[4,5] Surely we can extend these principles to dinuclear compounds where the M–M bonding electronic configuration takes the place of the ligand field stabilized d^n set of electrons? Walton, Cotton and coworkers[6,7] were the first to show that simple electrochemical oxidations and reductions could interconvert M–M bonds of order 4, 3.5 and 3 by feeding electrons in and out of δ- and δ^*-orbitals. Our work has focused attention on chemical reactions wherein the ligands are intimately involved in the redox process.

FORMING QUADRUPLE BONDS, $\sigma^2\pi^4\delta^2$, BY REDUCTIVE-ELIMINATIONS FROM COMPOUNDS CONTAINING TRIPLE BONDS, $\sigma^2\pi^4$

Our initial strategy was to devise routes to thermodynamically stable quadruply bonded compounds by elimination of kinetically labile organic molecules (fragments). Suitable precursor compounds were the 1,2-diorgano-dimetal-tetraamides which can readily be prepared according to the reaction sequence outlined in eqn (1):

$$M_2(NMe_2)_6 + 2Me_3SiCl \rightarrow 1,2\text{-}M_2Cl_2(NMe_2)_4 + 2Me_3SiNMe_2, \quad (1i)$$

$$1,2\text{-}M_2Cl_2(NMe_2)_4 + 2LiR \rightarrow 1,2\text{-}M_2R_2(NMe_2)_4 + 2LiCl. \quad (1ii)$$

Largely through the work of Chetcuti and Haitko, a wide variety of R groups have been attached to the dinuclear metal center including Me, Et, Pr (*n* and *i*), Bu (*n*, *i*, *s* and *t*), Ph, *o*- and *p*-tolyl, CH_2Ph, CH_2CMe_3 and CH_2SiMe_3.[8,9] More recently the dimetallacycles, where $R = (CH_2)_4$, have been prepared.[10]

A common structural feature of these compounds is a central ethane-like $M_2N_4C_2$ core with M≡M distances in the range 2.2 (M = Mo)–2.3 Å (M = W). In the solid state either *anti* or *gauche* rotamers may be found and in solution there is generally a mixture of the two with the equilibrium being in favor of the *gauche*. These compounds are thermally stable at room temperature and may be sublimed *in vacuo* at *ca* 80–120°C, 10^{-4} torr, with little decomposition. The reluctance of these compounds to undergo facile β-hydrogen elimination can be understood in terms of the existence of: (i) the M≡M bond, and (ii) the strong Me_2N–M π-bonding. Quite simply metal *d*-orbitals are not available for M–H–C interactions. On thermodynamic grounds we also would not expect the formation of an M–M quadruply bonded compound to be favored by either C–C or C–N coupling reactions. The inorganic residue formed by such an elimination, $Mo_2(NMe_2)_4$ or $Mo_2R(NMe_2)_3$, has no known analogue and might be expected to be a relatively high energy species.

Since CO_2 is known to react with M–NMe_2 bonds to generate, by a formal insertion process,[11] carbamate ligands,[12] O_2CNMe_2, a reaction between $M_2R_2(NMe_2)_4$ compounds and CO_2 was expected to yield a route to $M_2(O_2CNMe_2)_4$ compounds, analogues of the well-known carboxylates of formula $Mo_2(O_2CR)_4$ (M≡M),[6] providing that the organo ligands, R, yielded a kinetically labile elimination pathway.

This expectation was realized in the chemistry of 1,2-$Mo_2R_2(NMe_2)_4$ compounds where R = an alkyl containing a β-hydrogen atom. These react with CO_2 according to the reaction shown in eqn (2):[13]

$$Mo_2R_2(NMe_2)_4 + CO_2 \rightarrow Mo_2(O_2CNMe_2)_4 + \text{alkene} + \text{alkane}. \quad (2)$$

Similarly reactions involving 1,3-diaryltriazines led to elimination from the dimolybdenum center and formation of quadruply bonded compounds of formula $Mo_2(ArN_3Ar)_4$ [eqn (3)]:[13]

$$1,2\text{-}Mo_2R_2(NMe_2)_4 + 4ArNNNHAr \rightarrow Mo_2(ArN_3Ar)_4 + 4HNMe_2 + \text{alkene} + \text{alkane}. \quad (3)$$

Rather interestingly, reactions employing $W_2R_2(NMe_2)_4$ compounds (R = an alkyl ligand containing β-hydrogen atoms) do not react similarly to their molybdenum analogues in eqns (2) and (3), though a general procedure for the formation of quadruple bonds has been devised. This involves the addition of carboxylic anhydrides to $M_2R_2(NMe_2)_4$ compounds [eqn (4)]:[14,15]

$$1,2\text{-}M_2R_2(NMe_2)_4 + 4R'COOCOR' \rightarrow M_2(O_2CR')_4 + 4R'CONMe_2 + \text{alkene} + \text{alkane}. \quad (4)$$

The reaction shown in eqn (4) has proven general for R' = Me, Et, Bu^t and Ph.

From labelling studies involving the alkyl ligands in the $M_2R_2(NMe_2)_4$ compounds, we have found that the β-hydrogen atom of one alkyl ligand is transferred to the α-carbon atom of the other in the elimination process, e.g. as shown in eqn (5):

$$CD_3CH_2M{\equiv}MCH_2CD_3 \rightarrow M{\equiv}M + CD_3CH_2D + CD_2{=}CH_2. \quad (5)$$

In reactions involving the metallacyclic compound $Mo_2(CH_2)_2(NMe_2)_4$, the formation of the Mo–Mo quadruple bond is accompanied by the liberation of 2 equivalents of ethylene.[15]

Reactions employing $M_2R_2(NMe_2)_4$ compounds where R = an alkyl ligand lacking β-hydrogen atoms, e.g. Me, CH_2Ph or CH_2CMe_3, cannot undergo this type of reductive-elimination (alkyl group disproportionation) and compounds of the type $M_2R_2(O_2CX)_4$, where X = NMe_2[16] or R',[17,18] have been isolated. Reductive-elimination is still possible and may occur by a radical pathway which may be promoted either thermally or photochemically.[17–19] The ease of reductive-elimination follows the order Mo > W and $PhCH_2$ > Bu^tCH_2. An extension of this type of reductive-elimination involves reactions of

$$(L_nM')(Me_2N)_2M{\equiv}M(NMe_2)_2(M'L_n),$$

where L_nM' = $CpFe(CO)_2$ or $(Me_3Sn)_3Sn$ [eqn (6)]:[20,21]

$$(L_nM')(Me_2N)_2Mo{\equiv}Mo(NMe_2)_2(M'L_n) + CO_2 \rightarrow Mo_2(O_2CNMe_2)_4 + 2L_nM''. \quad (6)$$

The fate of the L_nM'' radicals, as with R$^{\cdot}$, depends upon its relative reactivity. For $CpFe(CO)_2^{\cdot}$ coupling to the dimer is favored as for $PhCH_2^{\cdot}$ in aromatic solvents. For $(Me_3Sn)_3Sn^{\cdot}$ a decomposition to Me_4Sn and Sn(metal) occurs while for R = *t*-$BuCH_2^{\cdot}$, hydrogen–deuterium atom abstraction from the solvent is favored.[15,18]

OXIDATIVE-ADDITIONS TO $(M{\equiv}M)^{6+}$ CENTERS LEADING TO $(M{=}M)^{8+}$ AND $(M{-}M)^{10+}$

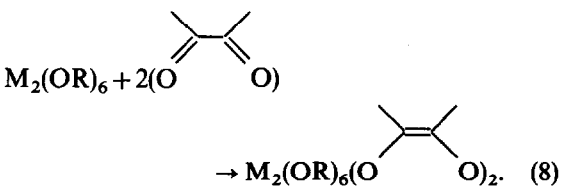
Our initial approach was to start with a $(M{\equiv}M)^{6+}$ compound and convert this to a known

compound containing either an $(M{=}M)^{8+}$ or an $(M{-}M)^{10+}$ center. The dinuclear alkoxide $Mo_2(OPr^i)_6$[22] was converted to $Mo_2(OPr^i)_8$[23] by reaction with Pr^iOOPr^i [eqn (7)]:[24]

$$Mo_2(OPr^i)_6 + Pr^iOOPr^i \rightarrow Mo_2(OPr^i)_8. \quad (7)$$

Steric considerations are apparently important in reactions of type(7) since attempted reactions employing Bu^tO ligands and/or Bu^tOOBu^t failed to react.

Additions of the halogens, X_2, to solutions of $Mo_2(OPr^i)_6$ proceed directly to $Mo_2X_4(OPr^i)_6$ (M—M) compounds (X = Cl, Br and I)[24] and only in the case of I_2 is there any evidence for the formation of an intermediate. Similarly reactions involving a variety of substituted (H, alkyl and Cl) ortho-quinones with $M_2(OR)_6$ compounds yield 2:1 adducts,[25,26] as do α-diketones.[27] These reactions can be summarized by eqn (8) in which each ligand is reduced by two electrons upon complexation to the dimetal center:



$$M_2(OR)_6 + 2(O\!=\!\!-\!\!-\!\!=O) \rightarrow M_2(OR)_6(O\!=\!\!-\!\!-\!\!=O)_2. \quad (8)$$

In the reaction between $Mo_2(OPr^i)_6$ and 1,4-diisopropyl-1,4-diaza-1,3-butadiene a 1:1 adduct is formed, $Mo_2(OPr^i)_6(Pr^iNCH{=}CHNPr^i)$ (M=M).[28] Formally this may be viewed as a Diels–Alder type of addition to the Mo≡Mo bond, though the structure in the solid state reveals that the bis-amide ligand is chelated to one metal atom.

The $M_2(OR)_6$ compounds also react with π-acceptor ligands such as CO and acetylenes to form 1:1 adducts which may be viewed in terms of redox reactions between the π-acceptor ligand and the M≡M bond as the donor.[29] From studies of these reactions it is clear that the reducing power of the M≡M bond follows the order W > Mo. Within this context the remarkable metathesis reactions involving $W_2(OBu^t)_6$ and alkynes[30,31] or nitriles,[30] [eqns (9) and (10)] may be viewed as oxidative-cleavages which are favorable for W but not Mo:*

$$W_2(OBu^t)_6 + RC{\equiv}CR \rightarrow 2(Bu^tO)_3W{\equiv}CR, \quad (9)$$

$$W_2(OBu^t)_6 + RC{\equiv}N \rightarrow (Bu^tO)_3W{\equiv}CR + (Bu^tO)_3W{\equiv}N. \quad (10)$$

These redox reactions [(7)–(10)] are synergistic. The ligand is reduced by the metal and the metal receives electrons from the ligand in forming new metal–ligand bonds.

The reactions between $W_2(NMe_2)_6$ and alcohols have proved to yield a variety of products depending upon the reaction conditions and the alcohol. For the not so sterically demanding alcohols oxidative-addition is commonly observed. For example, the reaction involving Pr^iOH yields $W_4(H)_2(OPr^i)_{14}$ which may be viewed as a dimer of dinuclear compounds, $[W_2(H)(OPr^i)_7]_2$.[33] The reaction sequence leading to this product has proved to be quite fascinating. Formally the reaction represents the simple addition of Pr^iOH across the W≡W bond. Mechanistically the path is much more complex since a direct alcoholysis involving $W_2(OBu^t)_6$ and Pr^iOH yields only $[W(OPr^i)_3]_4$.[34] Moreover, $W_2(OPr^i)_6(HNMe_2)_2$, which is the major product formed in the reaction between $W_2(NMe_2)_6$ and Pr^iOH (excess) in hexane or toluene at short reaction times, fails to react further with Pr^iOH. However, the addition of base ($HNMe_2$, NEt_3, NMe_3 or proton sponge) to a hydrocarbon solution of $W_2(OPr^i)_6(HNMe_2)_2$ in the presence of Pr^iOH does yield $W_4(H)_2(OPr^i)_{14}$. Also reactions involving either $W_2(OBu^t)_6$ or $W_2(OPr^i)_6(HNMe_2)_2$ in hexane–Pr^iOH solvent with $NaOPr^i$ yield $NaW_2(H)(OPr^i)_8$ which can be isolated in crystalline form as a diglyme adduct.[34] A subsequent reaction with a mild proton source in hexane–Pr^iOH yields essentially quantitative formation of $W_4(H)_2(OPr^i)_{14}$, while treatment of the latter compound with $NaOPr^i$ regenerates the mixed metal hydrido alkoxide.[34] This overall sequence is summarized by the reactions shown in eqns (11)–(13):

$$W_2(OBu^t)_6 + NaOPr^i \xrightarrow[\text{hexane–}Pr^iOH]{25^\circ C} NaW_2(H)(OPr^i)_8, \quad (11)$$

$$NaW_2(H)(OPr^i)_8 + Me_2NH_2^+I^- \xrightarrow[\text{hexane–}Pr^iOH]{25^\circ C} \tfrac{1}{2}W_4(H)_2(OPr^i)_{14} + NaI + Me_2NH, \quad (12)$$

$$W_4(H)_2(OPr^i)_{14} + 2NaOPr^i \rightarrow 2NaW_2(H)(OPr^i)_8. \quad (13)$$

From these studies it seems likely that the role of the base in the oxidative-addition of Pr^iOH to the W_2^{6+} center involves the initial conversion of an unbridged to a bridged d^3–d^3 dimer, perhaps in a manner akin to that seen by Rothwell and coworkers[35] in the reaction between *p*-cresol and $Mo_2(NMe_2)_6$ which yields the salt $Me_2NH_2^+Mo_2(OAr)_7(HNMe_2)_2^-$.

* Cleavage of the Mo≡Mo bond in the reaction between $Mo_2(OBu^t)_6$ and PhC≡CH (*ca* 15-fold excess) has been noted but it is clear from this and other studies that the Mo≡Mo bond is less reducing. See Refs 29 and 32.

COUPLED ADDITION–ELIMINATION SEQUENCES

Essential to many catalytic or stoichiometric reactions involving mononuclear metal centers is the coupling of addition–elimination sequences and such reaction sequences hold great promise for dinuclear compounds with M–M bonds. A very facile example is seen in the alcoholyses of 1,2-$Mo_2R_2(NMe_2)_4$ compounds where the alkyl group R contains β-hydrogen atoms. These reactions yield $Mo_2R''(OR')_5$ compounds according to eqn (14) (R = Et, Pr or Bu):[36]

$$1,2\text{-}Mo_2R_2(NMe_2)_4 + R'OH \rightarrow Mo_2R''(OR')_5 + 4HNMe_2 + RH. \quad (14)$$

Reaction (14) contrasts with reactions involving β-hydrogen-lacking alkyl ligands, R, which give 1,2-$Mo_2R_2(OR')_4$ compounds according to eqn (15) (R = Me, R' = Bu^t; R = CH_2CMe_3 or CH_2Ph; R' = Pr^i, Bu^t or Et):[36]

$$1,2\text{-}Mo_2R_2(NMe_2)_4 + R'OH \rightarrow 1,2\text{-}Mo_2R_2(OR')_4 + 4HNMe_2. \quad (15)$$

Studies of reaction (14) employing labelled alkyl ligands show that elimination of alkane involves a β-hydrogen atom transfer akin to that shown in eqn (5) and furthermore that the alkyl group results from the hydroxyl proton of the alcohol and the liberated alkene [eqn (5)].[36] The sequence thus involves: (i) reductive-elimination from the $(Mo{\equiv}Mo)^{6+}$ center generating a reactive $(Mo{\equiv}Mo)^{4+}$ species, and (ii) oxidative-addition of R'OH followed by insertion of alkene to a metal hydride. Evidence in support of this pathway includes the isolation of a quadruply bonded compound, $Mo_2(OPr^i)_4(HOPr^i)_4$,[37] in reaction (16):

$$1,2\text{-}Mo_2(Bu^i)_2(NMe_2)_4 + Pr^iOH \rightarrow Mo_2(OPr^i)_4(HOPr^i)_4 + 4HNMe_2 + Bu^iH + Me_2C{=}CH_2, \quad (16)$$

and its conversion to the ethyl compound in reaction (17):[37]

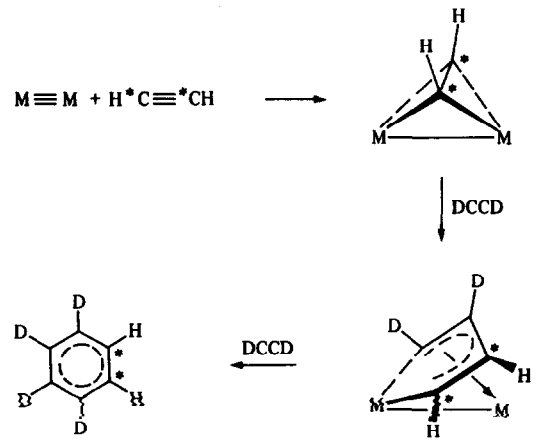
$$Mo_2(OPr^i)_4(HOPr^i)_4 + C_2H_4 \rightarrow Mo_2Et(OPr^i)_5 + 3Pr^iOH. \quad (17)$$

The regeneration of the alkyl ligand in eqn (14) occurs such that the most sterically hindered ligand is kinetically favored, e.g. if R = Pr^n then R'' = Pr^i, and if R = Bu^i than R'' = Bu^t. A subsequent isomerization of R'' to the least sterically encumbered alkyl ligand (e.g. Pr^i to Pr^n) is promoted by Lewis bases such as pyridine or PMe_3.[36,38]

Another sequence in which addition–elimination reactions involve use of the M—M bond as a reservoir of electrons is the catalytic cyclization of alkynes (C_2H_2 and C_2Me_2) by $Mo_2(OR)_6$ compounds.[39] The initial step in the reaction involves the formation of 1:1 alkyne adducts. The alkyne is bonded in the perpendicular mode with C—C = *ca* 1.40 Å and Mo—Mo = *ca* 2.60 Å for the central $Mo_2(\mu\text{-}C_2)$ moiety. These distances may be viewed as somewhere between M–M and C–C double- and single-bond distances. The next step in the reaction involves the coupling of two alkyne units at the dimetal center to give a $Mo_2(\mu\text{-}C_4R_4)$ moiety which may be viewed as one metallacyclopentadiene unit π-bonded to the other metal atom. A further reaction with acetylene promotes benzene elimination and the cycle is repeated. This sequence involves only the linking of C_2 units; this has been determined from labelling studies* (see Scheme 1). Rather interestingly, $W_2(OR)_6$ compounds are not catalysts for cyclotrimerization of alkynes because the hydrocarbon fragments attached to the dimetal center are not readily released.[41] This provides yet another example of the ease of reductive-elimination, Mo > W, which is the converse of the order of oxidative-addition at the dinuclear centers. Though tungsten is not catalytic in cyclotrimerization of alkynes, stable compounds of formula

$$W_2(OPr^i)_6(\mu\text{-}C_4R_4)(\eta^2\text{-}C_2R_2),$$

where R = H or Me, have been isolated.[40] These provide models for reactive intermediates in the $Mo_2(OR)_6$-catalyzed sequence. The W—W distances are *ca* 2.8 Å, representing weak single bonds.



Scheme 1. Cyclotrimerization of ethyne molecules at the dinuclear center. The specific combination of labels shown here involved $Mo_2(OCH_2Bu^t)_6(py)_2$ in [$^2H_8$]toluene at room temperature.

* The labelling experiments shown in the scheme were performed by Dr David Hoffman.

CONCLUDING REMARKS

Oxidative-additions and reductive-eliminations at dimolybdenum and ditungsten centers can lead to stepwise changes in M–M bond order. There are notable parallels in these reactions at dinuclear metal centers with those well documented for the group 8, 9 and 10 transition elements. We have not yet noted the facile oxidative-addition of molecular hydrogen or alkyl halides,[41] reactions which are common to the later mononuclear transition-metal complexes. This may merely reflect unsuitable orbital energetics in our compounds and this may be markedly influenced by the ligand set attached to the dinuclear center. However, working with alkoxide ligands we have found a number of reactions which have no parallel in mononuclear chemistry. The redox power of the M–M multiple bond and the template action of the metal atoms may be extended when two dinuclear compounds act in consort. One spectacular example of this is seen in the reaction between $W_2(OPr^i)_6(py)_2$ and acetone [eqn (18)]:[42]

$$2W_2(OPr^i)_6(py)_2 + 2Me_2C{=}O \rightarrow W_4O_2(OPr^i)_{12} + Me_2C{=}CMe_2 + 4py. \quad (18)$$

This provides us with a molecular model for the McMurray reagent[43] which is now believed to involve finely divided Ti metal.[45,46]

The detailed reaction pathways of these transformations at dinuclear metal centers remain to be elucidated and should provide a fertile area for future work.

Acknowledgements—I thank my many talented coworkers cited in the text and the National Science Foundation, the Office of Naval Research, the Department of Energy, Office of Basic Chemical Sciences, Chemistry Division and the Petroleum Research Fund administered by the American Chemical Society for financial support of various aspects of this work.

REFERENCES

1. M. H. Chisholm, *Adv. Chem. Ser.* 1979, **173**, 396.
2. J. K. Kochi, *Organometallic Mechanisms and Catalysis*. Academic Press, New York (1978).
3. C. A. Tolman, *Chem. Soc. Rev.* 1972, **1**, 337.
4. F. A. Cotton and G. Wilkinson, *Advanced Inorganic Chemistry*, 4th edn. John Wiley, New York (1980).
5. F. Basolo and R. G. Pearson, *Mechanisms of Inorganic Reactions, A Study of Metal Complexes in Solution*, 2nd edn. John Wiley, New York (1968).
6. F. A. Cotton and R. A. Walton, *Multiple Bonds between Metal Atoms*. John Wiley, New York (1982).
7. R. A. Walton, *Am. Chem. Soc. Symp. Ser.* 1981, **155**, 207.
8. M. H. Chisholm, D. A. Haitko and J. C. Huffman, *J. Am. Chem. Soc.* 1983, **103**, 4046.
9. M. J. Chetcuti, M. H. Chisholm, K. Folting, D. A. Haitko, J. C. Huffman and J. Janos, *J. Am. Chem. Soc.* 1983, **105**, 1163.
10. M. J. Chetcuti, M. H. Chisholm, H. T. Chiu and J. C. Huffman, *Polyhedron* 1985, **4**, 1213.
11. M. H. Chisholm and M. W. Extine, *J. Am. Chem. Soc.* 1977, **99**, 792.
12. M. H. Chisholm and M. W. Extine, *J. Am. Chem. Soc.* 1977, **99**, 782.
13. M. J. Chetcuti, M. H. Chisholm, K. Folting, D. A. Haitko and J. C. Huffman, *J. Am. Chem. Soc.* 1982, **104**, 2138.
14. M. H. Chisholm, H. T. Chiu and J. C. Huffman, *Polyhedron* 1984, **3**, 759.
15. M. H. Chisholm and H. T. Chiu, unpublished observations.
16. M. H. Chisholm, F. A. Cotton, M. W. Extine and B. R. Stults, *Inorg. Chem.* 1977, **16**, 603.
17. M. H. Chisholm, D. M. Hoffman, J. C. Huffman, W. G. Van Der Sluys and S. Russo, *J. Am. Chem. Soc.* 1984, **106**, 5386.
18. M. H. Chisholm, J. C. Huffman and W. G. Van Der Sluys, unpublished observations.
19. M. J. Chetcuti, M. H. Chisholm, K. Folting, J. C. Huffman and J. Janos, *J. Am. Chem. Soc.* 1982, **104**, 4684.
20. M. J. Chetcuti, M. H. Chisholm, H. T. Chiu and J. C. Huffman, *J. Am. Chem. Soc.* 1983, **105**, 1060.
21. M. H. Chisholm, H. T. Chiu, K. Folting and J. C. Huffman, *Inorg. Chem.* 1984, **23**, 4097.
22. M. H. Chisholm, F. A. Cotton, C. A. Murillo and W. W. Reichert, *Inorg. Chem.* 1977, **16**, 1801.
23. M. H. Chisholm, F. A. Cotton, M. W. Extine and W. W. Reichert, *Inorg. Chem.* 1978, **17**, 2944.
24. M. H. Chisholm, C. C. Kirkpatrick and J. C. Huffman, *Inorg. Chem.* 1981, **20**, 871.
25. T. B. Blatchford and M. H. Chisholm, unpublished observations.
26. M. H. Chisholm, *Polyhedron* 1983, **2**, 681.
27. M. H. Chisholm, J. C. Huffman and A. L. Ratermann, *Inorg. Chem.* 1983, **22**, 4100.
28. M. H. Chisholm, J. C. Huffman and J. J. Koh, unpublished observations.
29. M. H. Chisholm, *Chem. Soc. Rev.* 1985, **14**, 69 (and references cited therein).
30. R. R. Schrock, M. L. Listemann and L. G. Sturgeoff, *J. Am. Chem. Soc.* 1982, **104**, 4291.
31. M. L. Listemann and R. R. Schrock, *Organometallics* 1985, **4**, 74.
32. H. Strutz and R. R. Schrock, *Organometallics* 1984, **3**, 1600.
33. M. Akiyama, M. H. Chisholm, F. A. Cotton, M. W. Extine, D. A. Haitko, J. Leonelli and D. Little, *J. Am. Chem. Soc.* 1981, **103**, 779.
34. M. H. Chisholm, J. C. Huffman and C. A. Smith, *J. Am. Chem. Soc.* 1986 (in press).
35. T. W. Coffindaffer, J. C. Huffman and I. P. Rothwell, *Inorg. Chem.* 1983, **22**, 3178.
36. M. H. Chisholm, J. C. Huffman and R. J. Tatz, *J. Am. Chem. Soc.* 1983, **105**, 2075.
37. M. H. Chisholm, K. Folting, J. C. Huffman and R. J. Tatz, *J. Am. Chem. Soc.* 1984, **106**, 1153.

38. R. J. Tatz, Ph.D. thesis, Indiana University, Bloomington, Indiana (1984).
39. M. H. Chisholm, K. Folting, J. C. Huffman and I. P. Rothwell, *J. Am. Chem. Soc.* 1982, **104**, 4389.
40. M. H. Chisholm, D. M. Hoffman and J. C. Huffman, *J. Am. Chem. Soc.* 1984, **106**, 6806.
41. M. H. Chisholm, J. C. Huffman, A. L. Ratermann and C. A. Smith, *Inorg. Chem.* 1984, **23**, 1596.
42. T. P. Blatchford, M. H. Chisholm, K. Folting and J. C. Huffman, *J. Chem. Soc., Chem. Commun.* 1984, 1295.
43. J. E. McMurray, *Acc. Chem. Res.* 1983, **16**, 405.
44. R. Dams, M. Malinowski, I. Westdorp and H. Y. Geise, *J. Org. Chem.* 1982, **47**, 248.
45. H. Ledon, D. Young and I. Tatchenko, *Tetrahedron Lett.* 1979, 173.

Polyhedron Vol. 5, No. 1/2, pp. 31–33, 1986
Printed in Great Britain

0277–5387/86 $3.00 + .00
© 1986 Pergamon Press Ltd

REMOVAL OF ACETATE BRIDGES FROM $Mo_2(O_2CMe)_4$: CHARACTERIZATION OF $[Mo_2(O_2CMe)_2(NCMe)_6][BF_4]_2$

WILLIAM CLEGG*

Department of Inorganic Chemistry, The University, Newcastle upon Tyne NE1 7RU, U.K.

and

GILLIAN PIMBLETT and C. DAVID GARNER*

Chemistry Department, Manchester University, Manchester M13 9PL, U.K.

(*Received* 14 *June* 1985)

Abstract—Reaction of $Mo_2(O_2CMe)_4$ with $[Me_3O][BF_4]$ in MeCN solution at room temperature produces red crystals of $[Mo_2(O_2CMe)_2(NCMe)_6][BF_4]_2$, which have been characterized by X-ray crystallography and NMR spectroscopy. The central $[Mo_2(O_2CMe)_2]^{2+}$ core, with a quadruple Mo–Mo bond of length 2.136(1) Å, has two acetate bridges in *cis* positions. Octahedral coordination of each Mo atom is completed by two equatorial and one axial MeCN ligand, with the axial Mo—N much longer than the equatorial Mo—N. The MeCN ligands are labile in MeCN solution, giving complete scrambling on the NMR time-scale.

Reactions of dimolybdenum tetracarboxylates with a strong acid (CF_3SO_3H or $HBF_4 \cdot Et_2O$) in acetonitrile solution have recently been shown to produce derivatives of the $[Mo_2(O_2CR)_2]^{2+}$ core; products were formulated as, *inter alia*,

$$[Mo_2(O_2CMe)_2(NCMe)_4][CF_3SO_2]_2$$

and

$$[Mo_2(O_2CMe)_2(NCMe)_5][BF_3OH]_2$$

on the basis of elemental analysis and spectroscopic investigations.[1] We have found that treatment of $Mo_2(O_2CMe)_4$ with $[Me_3O][BF_4]$ in MeCN at room temperature gives red crystals of $[Mo_2(O_2CMe)_2(NCMe)_6][BF_4]_2$, which have been characterized by X-ray crystallography and NMR spectroscopy.

EXPERIMENTAL

Preparation

Manipulations were performed under an atmosphere of dinitrogen, with freshly dried and distilled solvents. $Mo_2(O_2CMe)_4$ (1.12 g, 2.62 mmol) was added to a stirred solution of $[Me_3O][BF_4]$ (1.55 g, 10 mmol) in MeCN (50 cm^3), and the mixture stirred at room temperature for 30 min, to produce a red solution. Concentration of the solution by evaporation, followed by slow cooling, gave red crystals of the product, which was recrystallized from MeCN. Yield *ca* 1.5 g (84%). Found: C, 26.3; H, 3.3; N, 10.9; Mo, 25.7%. Calc: C, 26.3; H, 3.3; N, 11.5; Mo, 26.3%.

Spectroscopy

^1H NMR: Perkin–Elmer R34 (220 MHz) and Varian SC300 (300 MHz) FT spectrometers. ^{13}C NMR: Bruker WP-80 FT spectrometer at 20.1 MHz. CD_3CN solutions, TMS standard.

Crystallography

$M_r = 729.9$, $P2_1/m$, $a = 7.160(1)$ Å, $b = 10.642(1)$ Å, $c = 19.402(2)$ Å, $\beta = 99.47(1)°$, $V = 1458.2$ Å^3, $Z = 2$, $D_x = 1.662$ g cm^{-3}, $F(000) = 720$, λ(Mo-K_α) = 0.71069 Å, $\mu = 0.92$ mm^{-1}. Of 3753 reflections measured with a Stoe–Siemens AED diffractometer[2] ($2\theta_{max} = 55°$), 3524 were unique, and 2774 with $F > 4\sigma(F)$ were used for structure solution by Patterson and difference syntheses.[3] Blocked-

*Authors to whom correspondence should be addressed.

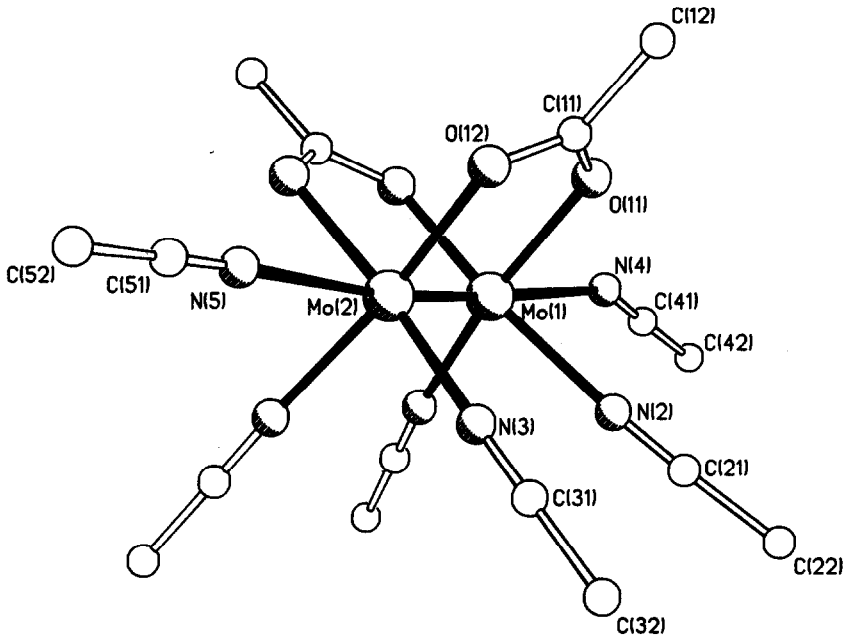


Fig. 1. Structure of the cation, showing the numbering scheme.

cascade least-squares refinement on F with $w^{-1} = \sigma^2(F) + 0.00068F^2$, anisotropic thermal parameters, no hydrogen atoms, and a disordered anion, gave $R = 0.053$ and $R_w = 0.055$.

RESULTS AND DISCUSSION

In the crystal structure, the cation and both anions lie on mirror planes. One anion is disordered; both show high thermal motion. The mirror plane in the cation passes through both Mo atoms and between the acetate bridges (Fig. 1). These two bridges occupy *cis* positions, and an essentially octahedral coordination of each Mo atom is completed by two equatorial and one axial MeCN ligands (Table 1).

The length of the Mo–Mo quadruple bond [2.136(1) Å] is typical of Mo_2^{4+} complexes with two carboxylate bridges, and is intermediate in length

Table 1. Coordination geometry[a]

Bond length (Å)			
Mo(1)—Mo(2)	2.136(1)	Mo(1)—O(11)	2.075(4)
Mo(1)—N(2)	2.148(4)	Mo(1)—N(4)	2.772(8)
Mo(2)—O(12)	2.093(4)	Mo(2)—N(3)	2.147(4)
Mo(2)—N(5)	2.745(10)		
Bond angle (°)			
Mo(2)—Mo(1)—O(11)	91.0(1)	Mo(2)—Mo(1)—N(2)	104.0(1)
O(11)—Mo(1)—N(2)	88.5(1)	Mo(2)—Mo(1)—N(4)	177.9(2)
O(11)—Mo(1)—N(4)	87.5(1)	N(2)—Mo(1)—N(4)	77.5(2)
O(11)—Mo(1)—O(11a)	91.5(2)	N(2)—Mo(1)—O(11a)	165.0(2)
N(2)—Mo(1)—N(2a)	87.7(2)	Mo(1)—Mo(2)—O(12)	91.1(1)
M(1)—Mo(2)—N(3)	100.0(1)	O(12)—Mo(2)—N(3)	89.2(2)
Mo(1)—Mo(2)—N(5)	173.6(2)	O(12)—Mo(2)—N(5)	84.4(2)
N(3)—Mo(2)—N(5)	84.5(2)	O(12)—Mo(2)—O(12a)	89.9(2)
N(3)—Mo(2)—O(12a)	168.8(2)	N(3)—Mo(2)—N(3a)	89.6(2)

[a] The suffix a on an atom number indicates an atom generated by reflection in the mirror plane.

between those in $[Mo_2(O_2CR)_4 \cdot 2L]$ and $[Mo_2X_4(NCMe)_4]$ complexes with four and no carboxylate bridges, respectively.[4–6] The axial Mo—N bonds are considerably longer than the equatorial bonds, by about 0.6 Å.

In the ^1H NMR spectrum (CD_3CN solution) one signal is observed for the acetate and one for the acetonitrile ligands. Thus, on the NMR time-scale, all the acetonitrile ligands are equivalent. The signal due to the acetonitrile ligand protons is at the same chemical shift as for free MeCN, indicating labile ligands. This is supported by the ^{13}C NMR spectrum (CD_3CN solution), which shows two signals for the acetate carbon atoms, and only two peaks for acetonitrile. This behaviour contrasts sharply with that of the corresponding Rh(II) complex, $[Rh_2(O_2CMe)_2(NCMe)_6]^{2+}$, in which axial and equatorial ligands can be distinguished by NMR.[7]

A pink solution of the Mo complex in methanol slowly turns yellow, more quickly on direct exposure to the atmosphere. An aqueous solution is yellow, but addition of acetonitrile turns it pink. The reversibility of this ligand exchange is gradually lost on prolonged exposure to water or moist air. The displacement of the labile MeCN ligands provides a route to other complexes of the $[Mo_2(O_2CMe)_2]^{2+}$ core.

REFERENCES

1. J. Telser and R. S. Drago, *Inorg. Chem.* 1984, **23**, 1798.
2. W. Clegg, *Acta Cryst.* 1981, **A37**, 22.
3. G. M. Sheldrick, *SHELXTL: an Integrated System for Solving, Refining and Displaying Crystal Structures from Diffraction Data.* University of Göttingen, F.R.G. (1978).
4. F. A. Cotton and J. G. Norman, Jr, *J. Am. Chem. Soc.* 1972, **94**, 5697.
5. J. San Filippo, Jr and H. J. Snaidoch, *Inorg. Chem.* 1976, **15**, 2209.
6. J. San Filippo, Jr, H. J. Snaidoch and R. L. Grayson, *Inorg. Chem.* 1974, **13**, 2121.
7. G. Pimblett, C. D. Garner and W. Clegg, *J. Chem. Soc., Dalton Trans.* (in press).

Polyhedron Vol. 5, No. 1/2, pp. 35–37, 1986
Printed in Great Britain

0277–5387/86 $3.00 + .00
© 1986 Pergamon Press Ltd

ISOMERIZATION REACTIONS OF BRIDGED AND CHELATED DIMOLYBDENUM COMPLEXES

SHEENA CHRISTIE, IAIN F. FRASER, ANDREW McVITIE and ROBERT D. PEACOCK†

Department of Chemistry, The University, Glasgow G12 8QQ, U.K.

(*Received* 14 *June* 1985)

Abstract—The isomerization reactions of complexes of general formula $Mo_2Cl_4(P\frown P)_2$, where $P\frown P$ is a diphosphine, are considered. Such complexes can exist as chelated or bridged isomers. When the diphosphine has a C_2 backbone the chelated isomer spontaneously isomerizes to the bridged complex. With diphosphines with a C_3 backbone, however, it is possible to stabilize the chelated isomer in certain solvents and, indeed, for bridged → chelated isomerization to occur.

Dimolybdenum complexes of general formula $Mo_2X_4(P\frown P)_2$, where $P\frown P$ is a diphosphine ligand,‡ can exist in two isomeric forms (Fig. 1). In the α or chelated isomer the bidentate ligands chelate both molybdenum atoms, the chelate rings are *trans* to each other and the ligators are eclipsed. In the structurally characterized complexes with ethane backbone ligands the rings are in the "envelope" conformation with the carbon backbone lying above the Mo—Mo bond and in close proximity to the halide atoms.[1] In the β or bridged isomers the ligands bridge between two molybdenum atoms and, when the ligand has two or more carbon atoms in the backbone, the two sets of ligators are twisted with respect to each other. This twist angle is, for example, 60° in $Mo_2Cl_4(dppe)_2$[2] and 23° in $Mo_2Cl_4(S,S\text{-dppb})_2$.[3]

We have recently shown[4] for a number of complexes with C_2 backbone ligands that the α-isomer spontaneously isomerizes to the corresponding β-isomer with first-order kinetics and a rate constant in the range 10^{-3}–10^{-6} s^{-1} (Table 1). We concluded that the rate-determining step was most likely to involve a rotation about the Mo—Mo bond since only this geometric change would lead to the observed changes in the energy and intensity of the $\delta \rightarrow \delta^*$ transition. It is unfortunately difficult to ascribe much meaning to the Arrhenius factors which are, in some cases, the major cause of isomerization rate differences between complexes. However, if we compare the rates for the isomerization of α-$Mo_2Cl_4(dppe)_2$ and α-$Mo_2Cl_4(R\text{-dppp})_2$ where the Arrhenius factors are essentially identical, we can see that the faster isomerization of the latter complex is largely accounted for by the smaller activation energy. The fact that α-$Mo_2Cl_4(S,S\text{-dppb})_2$ cannot (easily?) be prepared may be simply a consequence of an even lower activation energy (E_a) in this case (an

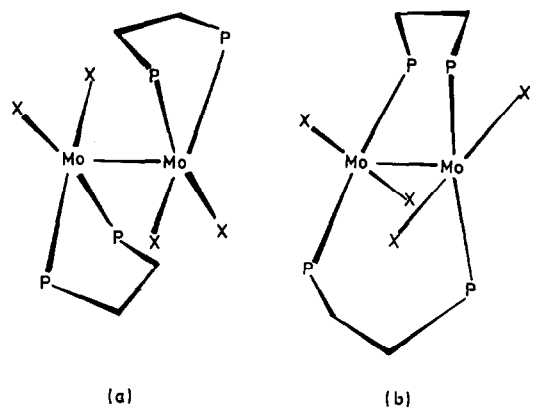


Fig. 1. Schematic structures of: (a) the chelated and, (b) the bridged isomer of $Mo_2Cl_4(P\frown P)_2$.

† Author to whom correspondence should be addressed.

‡ Ligand abbreviations: dppe, 1,2-bis(diphenylphosphino)ethane; *R*-dppp, (*R*)-1,2-bis(diphenylphosphino)propane; *S,S*-dppb, (*S,S*)-2,3-bis(diphenylphosphino)butane; *R*-phenphos, (*R*)-1-phenyl-1,2-bis(diphenyl)phosphino)ethane; dppp, 1,3-bis(diphenylphosphino)propane; *S*-chairphos, (*S*)-1,3-bis(diphenylphosphino)butane; *S,S*-skewphos, (*S,S*)-2,4-bis(diphenylphosphino)pentane.

Table 1. Kinetic parameters for the isomerization of the chelated isomers to the corresponding bridged isomers in dry dichloromethane solution[a]

	k (298 K) (s^{-1})	$t_{1/2}$ (298 K)	E_a (kJ mol^{-1})	log A
$Mo_2Cl_4(dptpe)_2$	$(8.1\pm0.4)\times10^{-6}$	24 h	133 ± 5	14.7
$Mo_2Cl_4(dppe)_2$	$(1.8\pm0.1)\times10^{-5}$	10.7 h	121 ± 5	16.5
$Mo_2Cl_4(R\text{-dppp})_2$	$(1.5\pm0.1)\times10^{-3}$	7.7 min	107 ± 5	16.0
$Mo_2Cl_4(dppp)_2$	$(2.5\pm0.2)\times10^{-4}$	46 min	96 ± 5	13.3

[a] k, rate constant; $t_{1/2}$, half-life; E_a, activation energy.

E_a of 93 kJ mol^{-1} and log A of 16 would give a half-life of less than a second). We have now prepared β-$Mo_2Cl_4(R\text{-phenphos})_2$ but find that the α-isomer either cannot be prepared or has a very short half-life. The absorption and circular dichroism (CD) of the bridged isomer are extremely similar to those of β-$Mo_2Cl_4(R\text{-dppp})_2$, which suggests that the twist angles of the complexes and so, probably, the conformations of the ligands are nearly identical. The much faster isomerization rate of α-$Mo_2Cl_4(R\text{-phenphos})_2$ is probably due, therefore, to the very unfavourable interaction of the phenyl group on the backbone with the halide atoms on the adjacent molybdenum.

We have recently begun to study the chemistry of dimolybdenum complexes with diphosphine ligands which have three carbon atoms in the backbone and we present some preliminary results. Figure 2 shows the change in absorption spectrum as α-$Mo_2Cl_4(dppp)_2$ isomerizes to the β-form. The reaction is first order in the α-isomer and the rate constant and E_a are in the same range as the other complexes we have studied (Table 1). The $\delta \rightarrow \delta^*$ transition of the bridged isomer comes at a much higher energy than those of any of the bridged complexes with dppe-type ligands and indeed is close to that of the α-isomer. This suggests that the ligators in β-$Mo_2Cl_4(dppp)_2$ are nearly eclipsed, a structure most likely achieved by a twist angle of close to 90°.

Perhaps the most interesting chemistry which we have discovered among complexes with propane backbone diphosphine ligands is the isomerization behaviour of $Mo_2Cl_4(S\text{-chairphos})_2$. Here we find that whether the α- or the β-isomer is thermodyn-

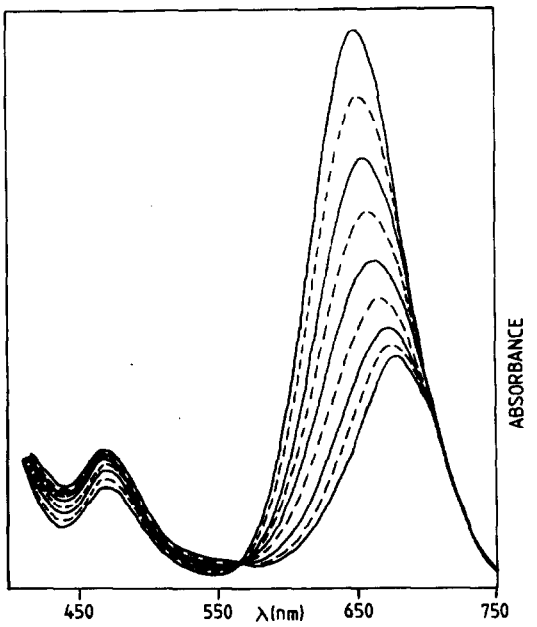


Fig. 2. Change in the electronic spectrum with time as α-$Mo_2Cl_4(dppp)_2$ isomerizes to β-$Mo_2Cl_4(dppp)_2$ in dry dichloromethane solution.

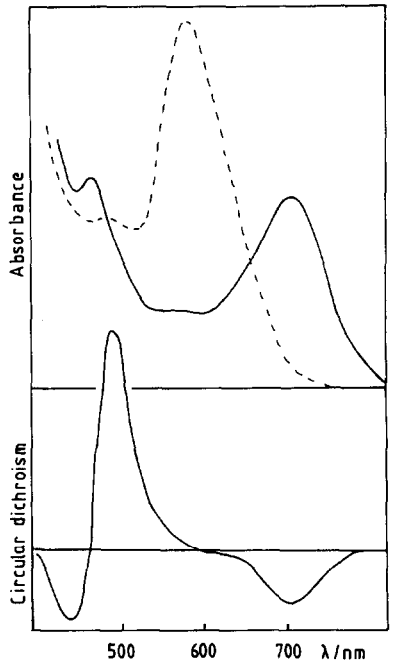


Fig. 3. Absorption spectrum of α- (dashed line, acetonitrile solution), and absorption and CD spectra of β- (full line, benzene solution) $Mo_2Cl_4(S\text{-chairphos})_2$.

amically more stable depends upon the solvent. Preparation of the complex from $K_4Mo_2Cl_8$ and the ligand in methanol gives the α-isomer. This is stable in methanol, ethanol, acetonitrile and methylene chloride which is in direct contrast to the behaviour of all of the other chelated isomers we have studied. On dissolving the solid in benzene or toluene at room temperature, however, the β-isomer is immediately formed. The absorption spectrum of the α-isomer and the absorption and CD spectra of the β-isomer are shown in Fig. 3. This $\alpha \rightleftarrows \beta$ interconversion is reversible in both directions, although a little decomposition usually occurs even when solvents are dried and degassed on a vacuum line. The isomerization rate is comparable with the rate of solution at room temperature, but we know that the reaction is a true solution isomerization because the rate is sufficiently slow at the freezing point of acetonitrile for the colour change to be followed as the solution warms up. Inspection of the crystal structure of α-$Re_2Cl_4(dppp)_2$ shows that the interactions of the carbon backbone with the opposite chlorine atoms are less severe than in the chelated complexes with dppe-type ligands. Also, in this complex, the phenyl groups are quite close together in parallel pairs, suggesting strong hydrophobic interactions and reminiscent of "charge-transfer" complexes. It may be that these phenyl interactions produce an extra stability which can only be overcome by an aromatic solvent. Work on this system, and on complexes with *S,S*-skewphos, is continuing.

REFERENCES

1. F. A. Cotton and R. A. Walton, *Multiple Bonds between Metal Atoms*. John Wiley, New York (1982).
2. P. A. Agaskar and F. A. Cotton, *Inorg. Chem.* 1984, **23**, 3883.
3. P. A. Agaskar, F. A. Cotton, I. F. Fraser and R. D. Peacock, *J. Am. Chem. Soc.* 1984, **106**, 1851.
4. I. F. Fraser, A. McVitie and R. D. Peacock, *J. Chem. Res. (S)* 1984, 420.
5. N. F. Cole, F. A. Cotton, G. L. Powell and T. J. Smith, *Inorg. Chem.* 1983, **22**, 2618.

Polyhedron Vol. 5, No. 1/2, pp. 39–45, 1986
Printed in Great Britain

0277–5387/86 $3.00 + .00
© 1986 Pergamon Press Ltd

CIRCULAR DICHROISM OF CONFIGURATIONALLY CHIRAL DIMOLYBDENUM COMPLEXES

IAIN F. FRASER, ANDREW McVITIE and ROBERT D. PEACOCK*

Department of Chemistry, The University, Glasgow G12 8QQ, U.K.

(*Received* 14 *June* 1985)

Abstract—We present an account of the preparation, structure and circular dichroism spectra of configurationally chiral quadruply bonded dimolybdenum complexes. A simple metal-localized model for the optical activity is described which provides a correlation between the stereochemistry of the complexes and the signs of both the $\delta \rightarrow \delta^*$ and $\delta \rightarrow x^2 - y^2$ transitions.

Chiral complexes may be divided into two general types: those in which the chromophore is dissymmetric (configurational chirality) and those in which the chromophore is symmetric, the overall molecular chirality arising from chiral substituents or ligands attached to the chromophore (conformational or vicinal chirality). Examples of a symmetric chromophore in a chiral environment include the carbonyl group in optically active ketones or the NiN_4 chromophore in square planar $[Ni(R\text{-pn})_2]^{2+}$;† examples of intrinsically dissymmetric chromophores include twisted chiral olefins or tris-chelate complexes such as Λ-$[Co(en)_3]^{3+}$, where the two triangles of ligating nitrogen atoms are twisted with respect to each other about the C_3-axis.

Most quadruply bonded dimolybdenum complexes contain eclipsed Mo_2L_8 or $Mo_2L_4L'_4$ chromophores and so are not configurationally chiral even if the co-ordinated ligands are themselves chiral. Complexes containing chiral monodentate phosphines, for example, come into this category. The simplest method of producing a twisted chromophore of D_4- or D_2-symmetry is to involve ligands having two or more carbon atoms separating the ligators, for example dppe. Such ligands can co-ordinate to the Mo_2 unit in two ways (Fig. 1) giving chelated (α) isomers of C_{2h} chromophoric symmetry and bridged (β) isomers of D_2-symmetry. The bridged isomer is in many cases the one which is thermodynamically more stable.[1]

In this paper we discuss a range of complexes of general formula $Mo_2X_4(P\frown P)_2$ [X = Cl or Br, P⌒P is a chiral bis(diphenyl)diphosphine ligand] or $[Mo_2(N\frown N)_4]^{4+}$ (where N⌒N is a chiral diamine). We present an account of the circular dichroism (CD) spectra of these complexes and show how the CD spectra may be used, in favourable cases, to make structural assignments.

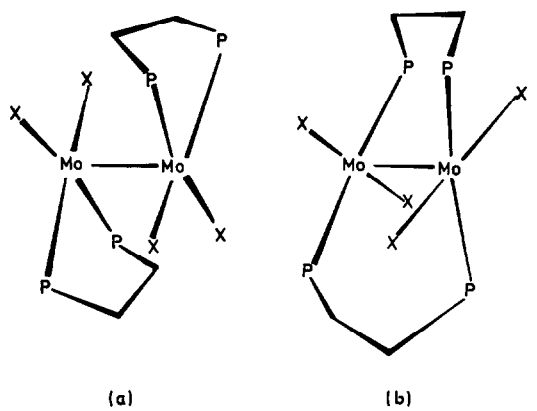


Fig. 1. Schematic diagrams of the structures of: (a) α-$Mo_2X_4(P\frown P)_2$, and (b) β-$Mo_2X_4(P\frown P)_2$.

* Author to whom correspondence should be addressed.

† Ligand abbreviations: en, 1,2-diaminoethane; *R*-pn, (*R*)-1,2-diaminopropane; *S,S*-bn, (*S,S*)-2,3-diaminobutane; dppe, 1,2-bis(diphenylphosphino)ethane; arphos, 1-(diphenylphosphino)-2-(diphenylarsino)ethane; *R*-dppp, (*R*)-1,2-bis(diphenylphosphino)propane; *S,S*-dppb, (*S,S*)-2,3-bis(diphenylphosphino)butane; *S*-chairphos, (*S*)-1,3-bis(diphenylphosphino)butane; *S,S*-skewphos, (*S,S*)-2,4-bis(diphenylphosphino)pentane; *R*-phenphos, (*R*)-1-phenyl-1,2-bis(diphenylphosphino)ethane.

CD of quadruply bonded dimolybdenum complexes

It is generally accepted[2] that the lowest energy absorption band in the electronic spectrum of quadruply bonded dimolybdenum complexes is due to the $\delta \rightarrow \delta^*$ ($b_{2g} \rightarrow b_{2u}$ in D_{4h}-symmetry) transition. This generally occurs between 12,000 and 17,000 cm^{-1} for the $Mo_2X_4P_4$ (X = Cl or Br) chromophore and around 20,000 cm^{-1} for the Mo_2N_8 chromophore. An experimental correlation between the energy of the $\delta \rightarrow \delta^*$ transition and the twist angle (χ) between the two MoX_2P_2 units has been published[3] for the phosphine complexes. The $\delta \rightarrow \delta^*$ transition is electric dipole allowed in a direction parallel to the Mo—Mo bond. This is shown in Fig. 2 which also serves to illustrate the method of orbital phase multiplication[4] which enables one to obtain the transient charge distribution accompanying the electronic excitation. This pictorial method is particularly useful for illustrating the transient charge distribution for the $\delta \rightarrow \delta^*$ transition when the chromophore is twisted. Figure 3 shows the product of the δ- and δ^*-orbital phases looking along the Mo—Mo bond for a twisted chromophore with the Λ absolute configuration in which the twist is between 0 and 45° [Fig. 3(a)] and between 45 and 90° [Fig. 3(b)]. The direction of charge movement accompanying the excitation is obtained, as in Fig. 2, by following the positive to negative phases *through the shortest distance*. Thus, in Fig. 3(a) the electron can be considered to take a left-handed helical path along and around the Mo—Mo bond, and in Fig. 3(b) a right-handed helical path. The former gives rise to a negative CD or Cotton effect and the latter to a positive CD or Cotton effect.[5] At a twist of 45° the simple metal-localized model described above predicts zero intensity for both the absorption and CD of the $\delta \rightarrow \delta^*$ transition. The signs of the Cotton effects are reversed for the Δ absolute configuration. The net result is the sign rule shown in Fig. 4 in which the sign of the CD associated with the $\delta \rightarrow \delta^*$ transition is given by the signs within the segments containing the rear set of ligators.

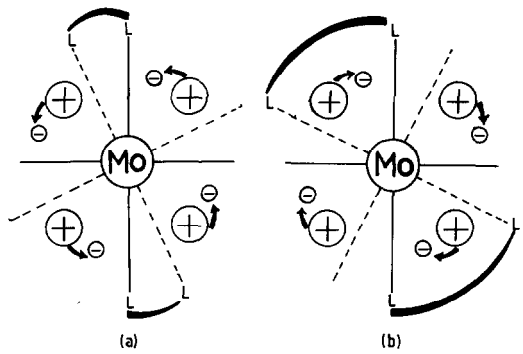


Fig. 3. The transient charge distribution for the $\delta \rightarrow \delta^*$ transition of the twisted $Mo_2L_4L'_4$ chromophore. (a) On rotating the rear set of ligators through an angle of less than 45° in the counterclockwise direction the transient charge distribution is that of a left-handed helix. (b) On rotating counterclockwise through an angle of greater than 45° the transition gives rise to a right-handed helical charge displacement.

The helical charge displacement can be decomposed into the product of a translation along (electric dipole transition) and a rotation about (magnetic dipole transition) the Mo—Mo bond. Both of these may be quantified within the metal-localized model as follows. The electric dipole transition moment, $\hat{\mu}$, has its maximum values at 0 and 90° and is zero for a twist of 45°:

$$\hat{\mu}(\chi) = \hat{\mu}_{max} \cos 2\chi.$$

The magnetic dipole transition moment, $\hat{m}$, on the

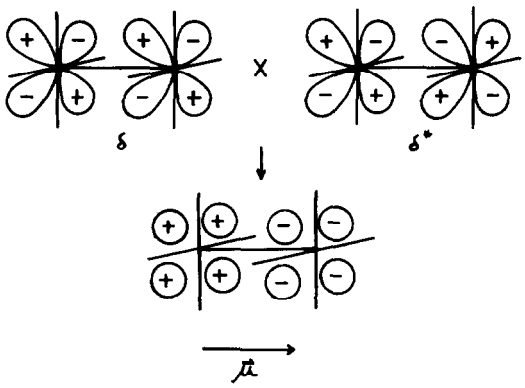


Fig. 2. The transient charge distribution for the $\delta \rightarrow \delta^*$ transition of an eclipsed chromophore obtained by multiplying the phases of the δ- and δ^*-orbitals.

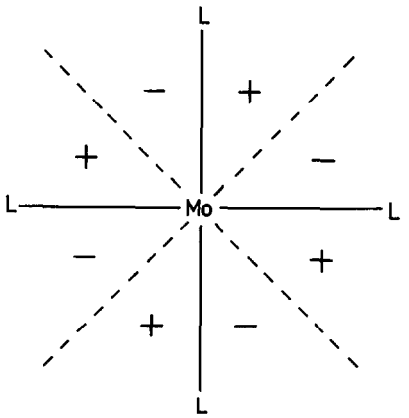


Fig. 4. Sign rule for the CD of the $\delta \rightarrow \delta^*$ transition. The sign of the CD is that of the sectors containing the rear set of ligating atoms.

other hand, is at a maximum for a twist of 45° and is zero for the eclipsed configurations:

$$\hat{m}(\chi) = \hat{m}_{max} \sin 2\chi.$$

Thus, the dipole strength (D), which is proportional to $|\hat{\mu}|^2$ and the rotational strength (R), which is proportional to $\hat{\mu} \times \hat{m}$, may be written as:

$$D(\chi) = D_{max} \cos^2 2\chi,$$

$$R(\chi) = R_{max} \cos 2\chi \sin 2\chi.$$

Finally the dissymmetry factor, $g\,(= \Delta\varepsilon/\varepsilon)$, which is a measure of the ratio of the magnetic to the electric dipole strength of the transition may be written as:

$$g(\chi) = g_{max} \tan 2\chi.$$

These relationships are summarized in Fig. 5 for the Δ absolute configuration.

Calculations[6] on the $[Mo_2Cl_8]^{4-}$ ion assign the next highest absorption after the $\delta \rightarrow \delta^*$ transition to a pair of magnetic dipole transitions, $\delta \rightarrow x^2-y^2$ ($b_{2g} \rightarrow b_{1g}$), which involves a rotation of charge about the Mo—Mo bond and $\pi \rightarrow \delta^*$ ($e_u \rightarrow b_{1u}$) which involves rotation of charge about the metal–ligand axes. The absorption which occurs at around 21,000 cm^{-1} in the phosphine complexes and around 27,000 cm^{-1} in the diamine complexes must be characterized as magnetic dipole in the parent chromophoric symmetry because of the magnitude of its dissymmetry factor. We have attempted to assign the transition causing this absorption by measuring the m.c.d. spectrum of $[Mo_2(en)_4]^{4+}$. Irrespective of whether the ligands are chelating or bridging in this complex the symmetry cannot be lower than D_4 and so the double degeneracy of the ^1E excited state of the $\pi \rightarrow \delta^*$ transition should be preserved. Were the absorption due to this transition we would expect to see an A term in the m.c.d. spectrum whereas only very weak B terms were observed. We therefore assign the 27,000-cm^{-1} absorption in the diamine complexes to $\delta \rightarrow x^2-y^2$. The strong similarity between the absorption and CD spectra of the diamine and phosphine complexes makes this assignment likely in the latter species also. A recent calculation[7] on the twisted diphosphine complexes has confirmed the assignment and has also assigned the higher energy transitions observed in their spectra.

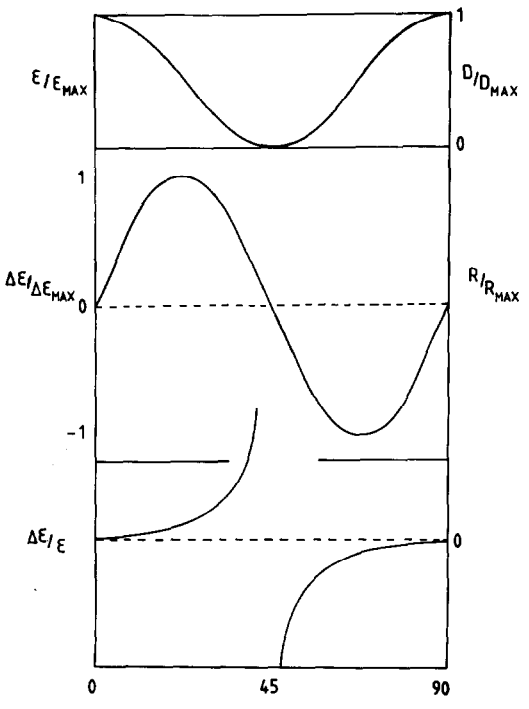


Fig. 5. The variation of dipole strength (D) (and ε), rotational strength (R) (and $\Delta\varepsilon$) and the dissymmetry factor ($\Delta\varepsilon/\varepsilon$) with twist angle χ (for the $\delta \rightarrow \delta^*$ transition of a complex with the Δ absolute configuration).

Having assigned the $\delta \rightarrow x^2-y^2$ transition we may construct a sign rule for its CD in the same way as was done for the $\delta \rightarrow \delta^*$ transition. The product of the phases of the δ-orbital and the x^2-y^2 orbital leads to a rotation of charge about the Mo—Mo bond (Fig. 6). Displacement of the rear set of ligators (Λ absolute configuration) of between 0 and 45° introduces a linear displacement of charge along the Mo—Mo bond and inspection of Fig. 7(a) shows that the net helical displacement is in the clockwise direction, thus giving a positive CD. At an angle of 45° the transition becomes magnetic dipole forbidden and in the twist range 45–90° the helical displacement is counterclockwise [Fig. 7(b)]. The sign rule for the $\delta \rightarrow x^2-y^2$ transition has therefore

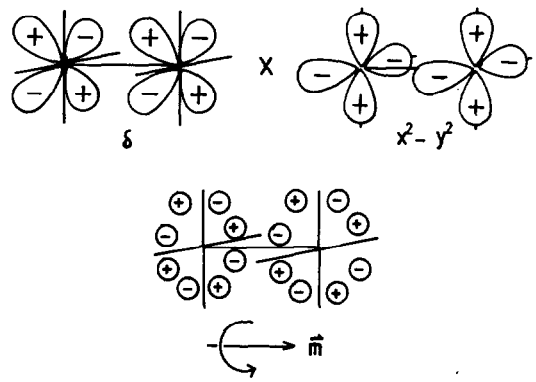


Fig. 6. The transient charge distribution for the $\delta \rightarrow x^2-y^2$ transition of an eclipsed chromophore obtained by multiplying the phases of the δ and x^2-y^2 orbitals.

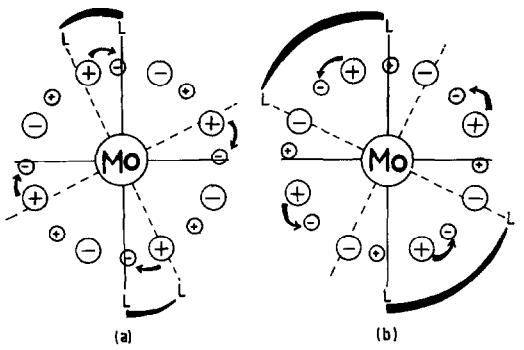


Fig. 7. The transient charge distribution for the $\delta \rightarrow x^2-y^2$ transition of the twisted $Mo_2L_4L'_4$ chromophore. (a) On rotating the rear set of ligators through an angle of less than 45° in the counterclockwise direction the transient charge distribution is that of a right-handed helix. (b) On rotating counterclockwise through an angle of greater than 45° the transition gives rise to a left-handed helical charge displacement.

the same nodal planes but opposite signs to that obtained for the $\delta \rightarrow \delta^*$ transition.

In summary, our metal-localized picture predicts that the $\delta \rightarrow \delta^*$ transition and the $\delta \rightarrow x^2-y^2$ transition should show a CD of opposite sign and that this CD should have, for the $\delta \rightarrow \delta^*$ transition, a negative R for a counterclockwise twist of between 0 and 45° and a positive R for a twist of between 45 and 90° in the same direction. Since the $\delta \rightarrow x^2-y^2$ transition is magnetic and the $\delta \rightarrow \delta^*$ transition is electric dipole allowed in the untwisted chromophore we expect the g value of the former to be considerably larger than that of the latter.

COMPLEXES WITH CHIRAL DIPHOSPHINE LIGANDS

There are two ways of obtaining one enantiomer of a chiral complex: one is to resolve the racemate [of, for example, $Mo_2Cl_4(dppe)_2$], the other to perform an asymmetric synthesis. Resolution of neutral species is especially difficult and requires special methods, e.g. HPLC on chiral columns, chiral clatheration or (if one is lucky) spontaneous enantiomorphic crystallization. We chose, therefore, to synthesize complexes using resolved chiral phosphines in the hope that they would force the complex to take up only one absolute configuration. Scale models suggest that a substituent with R-configuration on the ethane backbone of a diphosphine ligand, for example, would force the molecule to adopt the Λ absolute configuration if the substituent is to be in the equatorial plane of the $Mo_2P_2C_2$ ring.

The absorption and CD spectra of $Mo_2Cl_4(R\text{-dppp})_2$ and $Mo_2Cl_4(S,S\text{-dppb})_2$ are shown in Fig. 8. Apart from slight energy and intensity differences due to the complexes having slightly different torsion angles, the CD spectra have a mirror-image relationship to each other. The g values for both transitions are large, being at the upper end of the range observed for electric- and magnetic-dipole transitions, respectively, of configurationally chiral metal complexes, and we concluded that an essentially complete asymmetric synthesis had been achieved.

Given the conformational requirement that the S,S-dppb ligands should force a Λ and the R-dppp ligands a Δ configuration on the complexes, we concluded that the twist between the two sets of ligators is in the range 0–45°. When these spectra were first obtained the only crystal structures available of quadruply bonded bridged complexes were of $W_2Cl_4(dppe)_2$ and $Mo_2Br_4(arphos)_2$, where the twist angles were greater than 45° [59° for $W_2Cl_4(dppe)_2$[8] and 61° for $Mo_2Br_4(arphos)_2$[9]]. This cast some doubt upon our analysis and we felt that the crystal structure of one of our chiral complexes was necessary. Fortunately $Mo_2Cl_4(S,S\text{-dppb})_2$ forms suitable quality single crystals from a number of solvents and we were able to have the structure of

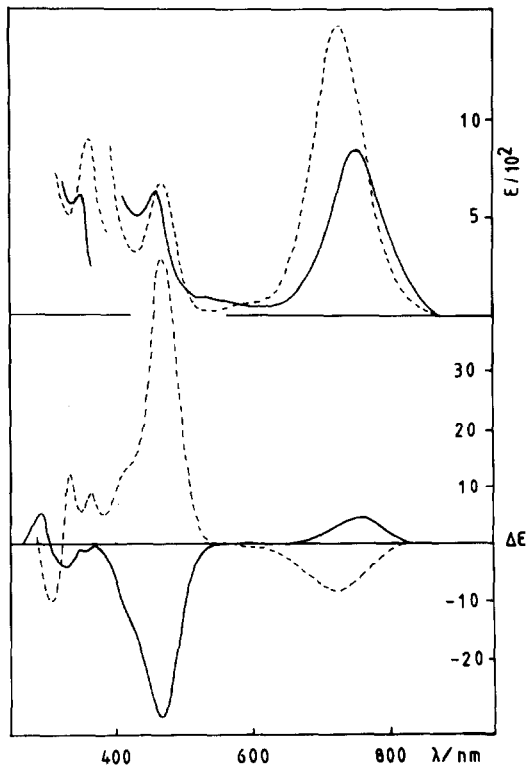


Fig. 8. Absorption and CD spectra of $Mo_2Cl_4(R\text{-dppp})_2$ (full line) and $Mo_2Cl_4(S,S\text{-dppb})_2$, all in dichloromethane solution.

the acetonitrile solvate determined by Manojlovic-Muir and Muir. The structure of the THF solvate was solved independently by Agaskar and Cotton and the results of the two determinations are in complete agreement.[10,11] Mo_2Cl_4(*S,S*-dppb)$_2$ does indeed have the Λ absolute configuration with an average twist angle of 23° in the counterclockwise direction. This confirms our analysis of the CD spectra and our sign rule. The evidence of two independent crystal structures giving the Λ configuration together with the large g values (which are identical in solution and the solid state) leads us to believe that, for the six-membered complexes at least, the syntheses are entirely stereospecific and this in turn gives us confidence in our application of conformational analysis to the six-membered $Mo_2P_2C_2$ rings.

Table 1 contains a summary of the energies and g values for the $\delta \rightarrow \delta^*$ and $\delta \rightarrow x^2-y^2$ transitions of the various chiral complexes that we have synthesized.[10,12–14] The complexes of *R*-phenphos were prepared in the hope that their isomerization kinetics could be compared with those of the *R*-dppp complexes:[1] unfortunately we have been able to synthesize only β-isomers of the former. A comparison of the CD spectrum of Mo_2Cl_4(*R*-phenphos)$_2$ with that of Mo_2Cl_4(*R*-dppp)$_2$ shows that the effect on the conformation of the $Mo_2P_2C_2$ ring of replacing methyl by the phenyl group is negligible. The crystal structure of β-Mo_2Cl_4(dppe)$_2$ has now been determined[15] and shows the complex to have a twist angle of 60°. Successive substitution of the ethane backbone causes the angle to "tighten" from 60° when the ligand is dppe, through ~27° for *R*-dppp and *R*-phenphos (interpolated using Campbell *et al*'s plot[3]) to 23° for *S,S*-dppb. The bromide complexes have very similar spectra to their chloride analogues, with slightly smaller g values which may be due to more metal–ligand mixing in the former species. The crystal structure of Mo_2Br_4(*S,S*-dppb)$_2$ has been determined.[7,11] The complex has the expected Λ configuration with a twist angle of 21°. We have prepared β-Mo_2I_4(dppe)$_2$ but have had no success in obtaining analogous complexes with the chiral diphosphine ligands.

We have recently turned our attention to chiral diphosphine ligands with three carbon atoms in their backbones, *S*-chairphos and *S,S*-skewphos, and present some preliminary results. The first point to be made is that complexes with these ligands are much less stable than those with the ethane backbone diphosphines. Both α- and β-Mo_2Cl_4(*S*-chairphos)$_2$ and β-Mo_2Cl_4(*S,S*-skewphos)$_2$ have been synthesized by refluxing the appropriate ligand with $K_4Mo_2Cl_8$ in methanol. The solids so obtained give satisfactory analyses but redissolving the solids always causes some decomposition even when the solvents are thoroughly dried and degassed on a vacuum line. The spectra of α- and β-Mo_2Cl_4(*S*-chairphos)$_2$ are shown in Fig. 9. The α-isomer has a CD which is too weak to be measured on our apparatus ($g < 5 \times 10^{-5}$). The g value of the bridged isomer [and that of β-Mo_2Cl_4(*S,S*-skewphos)$_2$] is somewhat lower than that found for the ethane backbone diphosphine complexes. This may reflect the smaller twist angle in the seven-membered ring complexes but may also indicate an incomplete asymmetric synthesis. The $\delta \rightarrow \delta^*$ transition energies are somewhat higher than those of the six-membered ring complexes. Interpolating the energies into Campbell *et al*'s curve[3] leads to twist angles of 18 or 72° for β-Mo_2Cl_4(*S*-chairphos)$_2$ and 22 or 68° for β-Mo_2Cl_4(*S,S*-skewphos)$_2$. The smaller twist angle does not seem to be acceptable since it is extremely

Table 1. Energies ($\tilde{\nu}$) and dissymmetry factors ($\Delta\varepsilon/\varepsilon$) for the $\delta \rightarrow \delta^*$ and $\delta \rightarrow x^2-y^2$ transitions of chiral dimolybdenum complexes

	$\delta \rightarrow \delta^*$		$\delta \rightarrow x^2-y^2$	
	($\times 10^{-3}$ $\tilde{\nu}$ cm^{-1})	$\Delta\varepsilon/\varepsilon$ ($\times 10^3$)	($\times 10^{-3}$ $\tilde{\nu}$ cm^{-1})	$\Delta\varepsilon/\varepsilon$ ($\times 10^2$)
Mo_2Cl_4(*S,S*-dppb)$_2$	13.70	−5.8	21.05	+7.3
Mo_2Cl_4(*R*-dppp)$_2$	13.33	+7.5	21.74	−6.7
Mo_2Cl_4(*R*-phenphos)$_2$	13.20	+6.0	21.51	−6.2
Mo_2Cl_4(*S*-chairphos)$_2$	14.33	−2.0	21.28	+1.1
Mo_2Cl_4(*S,S*-skewphos)$_2$	13.89	−10.8	20.83	+3.7
Mo_2Br_4(*S,S*-dppb)$_2$	13.24	−3.2	20.70	+8.5
Mo_2Br_4(*R*-dppp)$_2$	12.82	+3.0	20.83	−4.5
$[Mo_2$(*R*-pn)$_4]^{4+}$	20.96	−9.1	27.78	+17.0

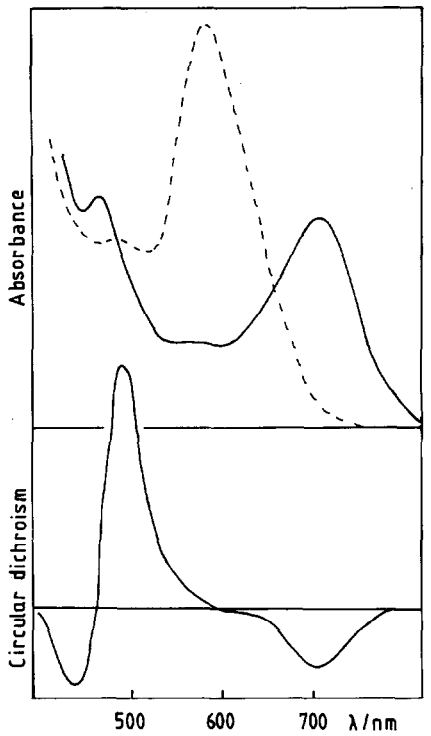


Fig. 9. Absorption spectrum of α- (dashed line, acetonitrile solution) and absorption and CD spectra of β- (full line, benzene solution) Mo_2Cl_4(*S*-chairphos)$_2$.

unlikely that the seven-membered $Mo_2P_2C_3$ rings could have smaller torsion angles than the six-membered $Mo_2P_2C_2$ ones. We therefore suggest that the complexes have the larger twist angle in each case. This, together with the sign of the CD spectra, leads to a Δ absolute configuration for both complexes. This is also the structure which conformational analysis of the seven-membered heterocyclic rings suggests is most favourable.

COMPLEXES OF CHIRAL DIAMINE LIGANDS

Some years ago Bowen and Taube reported[16] the preparation of $[Mo_2(en)_4]^{4+}$. Until our present work[14] this was the sole example of a dimolybdenum complex with aliphatic amine ligands and it is interesting to contrast the paucity of such complexes with their dominant rôle in mononuclear co-ordination chemistry. The structure of $[Mo_2(en)_4]^{4+}$ has not been determined. We, and doubtless others, have attempted to obtain single crystals but without success.

It was a logical extension of our work with chiral diphosphine complexes to prepare analogues of $[Mo_2(en)_4]^{4+}$ with the chiral diamines *R*-pn and *S,S*-bn. Both the complexes $[Mo_2(R\text{-pn})_4]^{4+}$ and $[Mo_2(S,S\text{-bn})_4]^{4+}$ are prepared in an analogous way to the ethylenediamine complex although the *S,S*-bn complex is difficult to purify. The absorption and CD spectrum of $[Mo_2(R\text{-pn})_4]^{4+}$ is shown in Fig. 10. Apart from a blue shift in the energy and a reduction in intensity the spectra clearly show a strong similarity to those of the diphosphine complexes shown in Fig. 8. The complex with *S,S*-bn has an essentially identical absorption spectrum and an enantiomeric CD to that with *R*-pn.

The g values for both the $\delta \rightarrow \delta^*$ and the $\delta \rightarrow x^2 - y^2$ transition are larger than in the phosphine complexes. Indeed that for the $\delta \rightarrow x^2 - y^2$ transition of $[Mo_2(R\text{-pn})_4]^{4+}$ (17×10^{-2}) is among the largest ever recorded for a solution CD and is comparable to even the largest single-crystal g values. This, and the fact that the eclipsed chelated isomers of Mo_2Cl_4(*R*-dppp)$_2$ and Mo_2Cl_4(*S*-chairphos)$_2$ have g values of less than 5×10^{-5}, provides conclusive evidence that the Mo_2N_8 chromophore is configurationally chiral. Since all chelated dimolybdenum complexes so far characterized have eclipsed chromophores, we conclude that the two chiral diamine complexes and, by extension, $[Mo_2(en)_4]^{4+}$ have bridging diamine ligands.

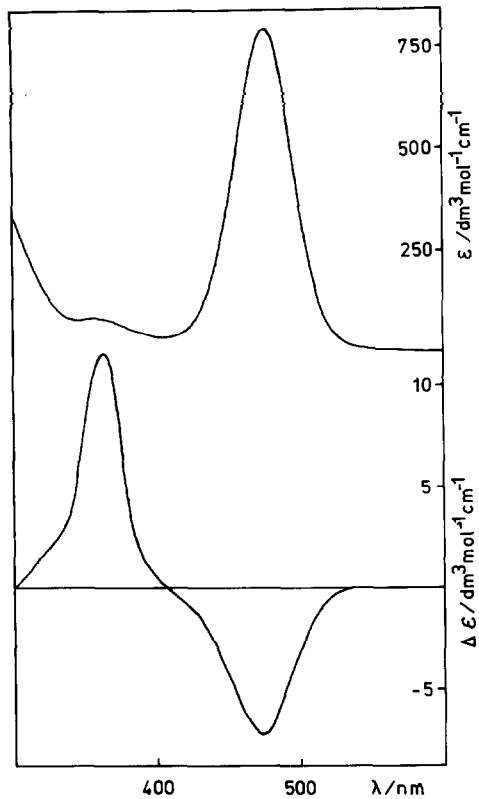


Fig. 10. Absorption and CD spectra of $[Mo_2(R\text{-pn})_4]^{4+}$ as the chloride salt in 10^{-2} mol l^{-1} HCl.

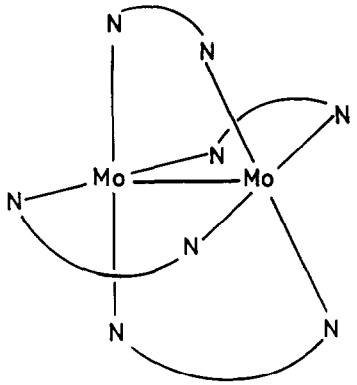


Fig. 11. Schematic diagram of the suggested structure of $[Mo_2(en)_4]^{4+}$.

The conformational preference of *R*-pn is the same as that of *R*-dppp and yet $[Mo_2(R\text{-pn})_4]^{4+}$ has a CD of opposite sign to that of $Mo_2Cl_4(R\text{-dppp})_2$. This implies that the diamine complex has a twist angle of between 45 and 90° in contrast to the diphosphine complexes. This is illustrated schematically in Fig. 11.

REFERENCES

1. I. F. Fraser, A. McVitie and R. D. Peacock, *J. Chem. Res. (S)* 1984, 420.
2. F. A. Cotton and R. A. Walton, *Multiple Bonds between Metal Atoms*. John Wiley, New York (1982).
3. F. L. Campbell III, F. A. Cotton and G. L. Powell, *Inorg. Chem.* 1985, **24**, 117.
4. See, for example, G. Snatzke, U. Wagner and H. P. Wolff, *Tetrahedron* 1981, **37**, 349.
5. S. F. Mason, *Optical Activity and the Chiral Discriminations*. Cambridge University Press, New York (1983).
6. J. G. Norman, Jr and H. J. Kolari, *J. Am. Chem. Soc.* 1975, **97**, 33.
7. P. A. Agaskar, Ph.D. dissertation, Texas A&M University (1985).
8. F. A. Cotton, T. R. Felthouse and D. G. Lay, *J. Am. Chem. Soc.* 1980, **102**, 1431.
9. F. A. Cotton, P. E. Fanwick, J. W. Fitch, H. D. Glicksman and R. A. Walton, *J. Am. Chem. Soc.* 1979, **101**, 1752.
10. P. A. Agaskar, F. A. Cotton, I. F. Fraser and R. D. Peacock, *J. Am. Chem. Soc.* 1984, **106**, 1851.
11. P. A. Agaskar, F. A. Cotton, I. F. Fraser, Lj. Manojilovic-Muir, K. W. Muir and R. D. Peacock, *J. Am. Chem. Soc.* (to be published).
12. I. F. Fraser, Ph.D. thesis, University of Glasgow (1985).
13. S. C. Christie, A. McVitie and R. D. Peacock, unpublished work.
14. I. F. Fraser and R. D. Peacock, *Inorg. Chem.* 1985, **24**, 989.
15. P. A. Agaskar and F. A. Cotton, *Inorg. Chem.* 1984, **23**, 3883.
16. A. R. Bowen and H. Taube, *Inorg. Chem.* 1974, **13**, 2245.

Polyhedron Vol. 5, No. 1/2, pp. 47–50, 1986
Printed in Great Britain

0277–5387/86 $3.00 + .00
© 1986 Pergamon Press Ltd

ELECTROGENERATED CHEMILUMINESCENCE OF $Mo_6Cl_{14}^{2-}$: FREE-ENERGY EFFECTS ON CHEMILUMINESCENCE REACTIVITY

R. D. MUSSELL and D. G. NOCERA†

Department of Chemistry, Michigan State University, East Lansing, MI 48824, U.S.A.

(*Received* 15 *June* 1985)

Abstract—Electrogenerated $Mo_6Cl_{14}^{-}$ and $Mo_6Cl_{14}^{3-}$ react with electroactive donors (D^-s) (nitroaromatic radical anions) and acceptors (A^+s) (aromatic amine radical cations), respectively, to produce the luminescent excited state of $Mo_6Cl_{14}^{2-}$. The dependence of the electrogenerated chemiluminescence (ecl) reactivity on the free-energy driving force of the $Mo_6Cl_{14}^{3-}$–A^+ and $Mo_6Cl_{14}^{-}$–D^- annihilation reactions has systematically been probed by varying the $A^{+/0}$ and $D^{0/-}$ reduction potentials. The $Mo_6Cl_{14}^{3-}$–A^+ reaction exhibits an ecl threshold free energy 0.18 V more positive than that of the $Mo_6Cl_{14}^{-}$–D^- reaction, suggesting that electron transfer between $Mo_6Cl_{14}^{-}$ and D^- to produce electronically excited cluster confronts a larger reorganizational barrier than the $Mo_6Cl_{14}^{3-}$–A^+ system.

The lower-halide clusters of molybdenum and tungsten [$M_6X_{14}^{2-}$: M = Mo(II) or W(II); X = Cl, Br or I] constitute an exciting new class of inorganic reagents for redox-induced chemiluminescent reactions. For the molybdenum chloride cluster, reaction of electrogenerated intermediates, $Mo_6Cl_{14}^{-}$ and $Mo_6Cl_{14}^{3-}$, yields a red luminescence attributable to an electronically excited ion ($Mo_6Cl_{14}^{2-}$*: $\tau_o = 180$ μs, $\phi_e = 0.20$, $\lambda_{em,max} = 805$ nm in CH_3CN at 25°C).[1] Observation of electrogenerated chemiluminescence (ecl) from $M_6X_{14}^{2-}$ ions is of interest because ecl chemistry of inorganic complexes is limited to only a few transition-metal systems: Ru(II)- and Os(II)–polypyridyl chelates,[2] Pd(II) and Pt(II) metalloporphyrins,[3] Re(I)–phenanthroline complexes,[4] and Pt(II) pyrophosphite dimer.[5] Potentially high electrical efficiencies, coupled with visible and near-IR chemiluminescence, have suggested the application of inorganic ecl systems to the design of light-emitting devices.[6] In addition, ecl reactions can provide insight into fundamental processes of electron-transfer reactions in highly exothermic regimes.[7]

Our studies are centered on elucidating the factors fundamental to the ecl reactivity of the $M_6X_{14}^{2-}$ ions. We report here investigations on the energy dynamics of the $Mo_6Cl_{14}^{2-}$ ecl process. The approach we have taken is centered on the oxidation–reduction reactions of $Mo_6Cl_{14}^{-}$ and $Mo_6Cl_{14}^{3-}$ with electroactive donor (D^-) and acceptor (A^+), respectively:

$$Mo_6Cl_{14}^{-} + D^- \rightarrow Mo_6Cl_{14}^{2-} + D \quad (1a)$$

$$Mo_6Cl_{14}^{-} + D^- \rightarrow Mo_6Cl_{14}^{2-}{}^* + D \quad (1b)$$

$$Mo_6Cl_{14}^{3-} + A^+ \rightarrow Mo_6Cl_{14}^{2-} + A \quad (2a)$$

$$Mo_6Cl_{14}^{3-} + A^+ \rightarrow Mo_6Cl_{14}^{2-}{}^* + A \quad (2b)$$

By tuning the free-energy driving force of reactions (1) and (2) with the respective $D^{0/-}$ and $A^{+/0}$ reduction potentials, the energy dependence of $Mo_6Cl_{14}^{2-}$ ecl can conveniently be monitored. The magnitude of the $Mo_6Cl_{14}^{-/2-}$ and $Mo_6Cl_{14}^{2-/3-}$ reduction couples in conjunction with the low energy of the $Mo_6Cl_{14}^{2-}$ emissive excited state has allowed us to systematically probe the ecl chemistry of $Mo_6Cl_{14}^{2-}$ over a wide potential-energy range.

EXPERIMENTAL

CH_2Cl_2, obtained from Burdick and Jackson Laboratories, was degassed by seven freeze–pump–thaw (fpt) cycles and then vacuum distilled onto activated 4-Å molecular sieves. The sieves were contained in a 1-liter flask equipped with a high-vacuum Teflon valve. Solutions for electrochemical, spectroscopic and quenching experiments were prepared on a high-vacuum manifold and were

† Author to whom correspondence should be addressed.

degassed by an additional three fpt cycles prior to measurements.

Tetrabutylammonium perchlorate (TBAP: Southwestern Analytical Chemicals) was recrystallized from a pentane–ethyl acetate solution and dried *in vacuo* for 12 h at 60°C. Preceding all electrochemical and quenching experiments, the TBAP salt was heated for an additional 4 h at 100°C. Molybdenum dichloride was purchased from Cerac Inc. and converted to the acid salt by established procedures.[8] Addition of tetrabutylammonium chloride to 6 M HCl solutions of the hydronium salt afforded $(NBu_4)_2Mo_6Cl_{14}$. The yellow powder was taken up in CH_2Cl_2 and the solution was dried over $MgSO_4$, filtered, and evaporated in air to yield large yellow-orange crystals. Nitroaromatics and aromatic amines were purchased from Aldrich except 10-methylphenothiazine (Pfaltz and Bauer), 4,4′-dimethoxydiphenylamine (Alfa Products) and tris-(*p*-tolyl)amine, which was synthesized using a published procedure.[9] Solids were purified by multiple sublimations and liquids by fractional distillation.

Electrochemical measurements were obtained with a Princeton Applied Research (PAR) 173 potentiostat/galvanostat driven by a PAR 175 universal programmer and a PAR 179 digital coulometer. Experiments were performed in CH_2Cl_2 ($\mu = 0.1$ M TBAP) using a three-electrode system: Pt wire or button working, Pt mesh auxiliary and Ag wire reference electrodes. A conventional H-cell design was used for determination of D and A redox couples. Potentials were referenced to a ferrocene internal standard and related to the SCE reference scale with a value of 0.31 V vs SCE for the ferricinium–ferrocene couple.[10] Ecl experiments utilized a high-vacuum electrochemical cell which permitted all sample manipulations and solvent transfers to be performed in the absence of oxygen and moisture. A triple-step square wave potential program was employed to generate ecl transients. Chemiluminescence was sought by interfacing the high-vacuum cell to the detection side of a red-sensitive emission spectrometer built at MSU.

Stern–Volmer quenching experiments were performed on CH_2Cl_2 solutions ($[(NBu_4)_2Mo_6Cl_{14}] = 3$ mM, $\mu = 0.1$ M TBAP) contained in high-vacuum cells, consisting of a 10-ml round bottom connected to a 1-cm quartz cuvette sidearm. Quencher concentrations spanned a 10^{-3}–10^{-2} M range; quencher additions were made under high-vacuum conditions. Luminescence intensities were measured on the MSU-constructed emission spectrometer. Quenching rate constants were determined from plots of I_o/I vs $[Q]$ using τ_o ($Mo_6Cl_{14}^{2-}$*) = 160 μs in CH_2Cl_2 at 25°C.

RESULTS AND DISCUSSION

Ds and As suitable for reactions (1) and (2) should fulfill several criteria for their successful application as probes of $Mo_6Cl_{14}^{2-}$ ecl: (i) the lowest-energy excited states of Ds and As should be energetically inaccessible, thereby ensuring that the electrochemical excitation energy is channelled via the cluster's excited state; (ii) Ds and As should be inefficient quenchers of $Mo_6Cl_{14}^{2-}$ luminescence since ensuing electron- or energy-transfer reactions between $Mo_6Cl_{14}^{2-}$* and the D or A will modulate ecl intensity; and (iii) Ds and As must exhibit reversible electrochemistry. Finally, structurally and electronically related Ds and As will facilitate the comparison of the ecl chemistry between the series.

Table 1 collects the spectroscopic, electrochemical and quenching data for electroactive Ds and As employed in our ecl studies. Cyclic voltammograms show reversible oxidation and reduction waves for Ds and As, respectively, in CH_2Cl_2 solutions; $E_{1/2}$ values are listed in Table 1 as reduction potentials vs the SCE reference. From these data, and $Mo_6Cl_{14}^{2-}$ redox couples, reaction free energies for electron-transfer reactions (1a) and (2a) may be calculated. Comparison of these energies ($\Delta G_r^{o'}$ in Table 1) with the lowest-energy D and A excited states indicates that production of electronically excited Ds and As is an unimportant electron-transfer reaction pathway. Additionally, the quenching rate constants shown in Table 1 are well below the diffusion-controlled limit and indicate that the Ds and As are inefficient quenchers of $Mo_6Cl_{14}^{2-}$ luminescence.

Ecl experiments were performed on CH_2Cl_2 solutions containing equimolar concentrations of $Mo_6Cl_{14}^{2-}$ and electroactive species. Reactions (1) and (2) were established upon pulsing a Pt working electrode with potentials appropriate to ensure production of electrogenerated species in the mass-controlled region. D and A systems exhibiting ecl are indicated in Table 2. For systems yielding chemiluminescence, the ecl spectrum is identical to the emission spectrum of $Mo_6Cl_{14}^{2-}$ in CH_2Cl_2. As originally inferred from spectroscopic data, the absence of D and A emission for all systems listed in Table 1 confirms that the population of D or A electronic excited states is not an energetically favorable process. That luminescence is observed only when the potentials applied to the Pt working electrode are stepped into the oxidation–reduction waves of the electroactive species establishes that ecl results from annihilation of the electrogenerated products.

Inspection of the calculated free energies for reactions (1b) and (2b), listed in Table 2, clearly reveals an energy dependence for the ecl chemistry of

Table 1. Spectroscopic, electrochemical and quenching data for Ds and As used in ecl threshold experiments

D	$E_{1/2}$[a] (V)	$\Delta G_r^{o'}$[b] (V)	E_T[c] (V)	k_q[d] ($M^{-1}\,s^{-1}$)
2,6-Dimethyl-*p*-benzoquinone	−0.85	−2.21	2.32[e]	1.9×10^5
p-Dinitrobenzene	−0.86	−2.22	2.54[f]	1.1×10^6
o-Dinitrobenzene	−0.97	−2.33	2.55[f]	7.9×10^3
p-Nitrobenzaldehyde	−1.03	−2.39	—	1.6×10^4
m-Nitrobenzaldehyde	−1.17	−2.53	—	$<10^3$
1-Chloro-4-nitrobenzene	−1.23	−2.59	—	8.1×10^3
5-Nitro-*m*-xylene	−1.30	−2.66	—	1.7×10^3
3-Nitro-*o*-xylene	−1.51	−2.87	—	3.0×10^4
2-Nitro-*m*-xylene	−1.65	−3.01	—	2.1×10^4
A				
Dimethoxydiphenylamine	+0.43	−2.13	—	1.7×10^7
Phenothiazine	+0.45	−2.15	2.62[g]	1.1×10^7
N,N-dimethyl-*p*-toluidine	+0.51	−2.21	—	1.9×10^6
10-Methylphenothiazine	+0.58	−2.28	2.66[h]	2.9×10^6
Tris(*p*-tolyl)amine	+0.67	−2.37	3.0[i]	1.4×10^6
Tris(4-bromophenyl)amine	+1.04	−2.74	>3.1[j]	6.9×10^4

[a] As reduction potentials for $D^{0/-}$ and $A^{+/0}$ couples in CH_2Cl_2 (μ = 0.1 M NBu_4ClO_4, 23 ± 1°C) vs SCE.

[b] For Ds: $\Delta G_r^{o'} = -[E_{1/2}(Mo_6Cl_{14}^{-/2-}) - E_{1/2}(D^{0/-})]$; and, for As: $\Delta G_r^{o'} = -[E_{1/2}(A^{+/0}) - E_{1/2}(Mo_6Cl_{14}^{2-/3-})]$. In CH_2Cl_2, $E_{1/2}(Mo_6Cl_{14}^{-/2-}) = 1.36$ V and $E_{1/2}(Mo_6Cl_{14}^{2-/3-}) = -1.70$ V vs SCE.

[c] Lowest excited-state energies of Ds and As.

[d] Stern–Volmer quenching constants in CH_2Cl_2 (μ = 0.1 M NBu_4ClO_4, 23 ± 1°C).

[e] H. P. Trommsdorf, *J. Chem Phys.* 1972, **56**, 5358.

[f] R. G. Brown, A. Harriman and L. Harris, *J. Chem. Soc., Faraday Trans.* 2 1978, **74**, 1193.

[g] S. A. Alkaitis, M. Grätzel and A. Henglein, *Berg. Bunsenges. Phys. Chem.* 1975, **79**, 541.

[h] G. Rothenberge, P. P. Infelta and M. Grätzel, *J. Phys. Chem.* 1979, **83**, 1871.

[i] K. A. Zachariasse, Ph.D. Thesis, Free University, Amsterdam (1972).

[j] A. Terenin and V. Ermolaev, *Sov. Phys.—Dokl.* 1967, **6**, 600.

the $Mo_6Cl_{14}^{2-}$ ion. While both reactions yield the same excited state species, annihilation between $Mo_6Cl_{14}^{-}$ and D^- to produce chemiluminescence requires a driving force 0.18 V in excess of the chemiluminescence threshold free energy of the $Mo_6Cl_{14}^{3-}$–A^+ system.

The difference in D and A ecl threshold free energies can be appreciated from a simple electron-transfer analysis of the $Mo_6Cl_{14}^{-}$–D^- and $Mo_6Cl_{14}^{3-}$–A^+ annihilation reactions. Figure 1 illustrates chemiluminescence in terms of a potential-energy surface for reactants, one for products in their ground states, and a potential surface in which one or more products are electronically excited. High exergonicities of chemiluminescence reactions can cause the reactant well to become imbedded in the ground-state well.[11] In this case, electron transfer to excited-state species will be more favorable than direct reaction to the ground state. From Marcus theory,[11(b),12] the rate for electron transfer to

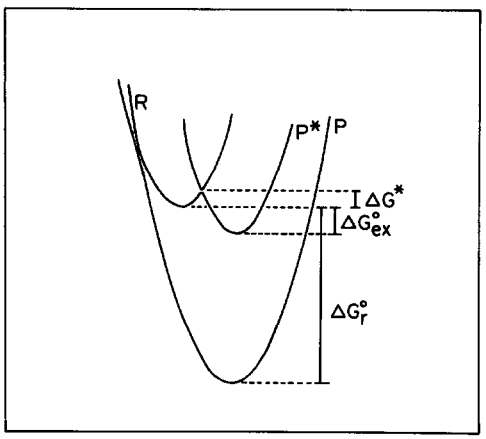


Fig. 1. Profile of potential-energy surfaces for reactants (R), products in their ground states (P), and products which are electronically excited (P*). ΔG_{ex}^{o} and ΔG_r^{o} are reaction free energies for electron transfer to produce excited- and ground-state products, respectively, and ΔG^* is the activation energy for the excited-state reaction.

Table 2. Summary of ecl threshold experiments

D	ΔG^o_{ex} (V)	Ecl?
2,6-Dimethyl-*p*-benzoquinone	−0.21	No
p-Dinitrobenzene	−0.22	No
o-Dinitrobenzene	−0.33	No
p-Nitrobenzaldehyde	−0.39	Yes
m-Nitrobenzaldehyde	−0.53	Yes
1-Chloro-4-nitrobenzene	−0.59	Yes
5-Nitro-*m*-xylene	−0.66	Yes
3-Nitro-*o*-xylene	−0.87	Yes
2-Nitro-*m*-xylene	−1.01	Yes
A		
Dimethoxydiphenylamine	−0.13	No
Phenothiazine	−0.15	No
N,*N*-dimethyl-*p*-toluidine	−0.21	Yes
10-Methylphenothiazine	−0.28	Yes
Tris(*p*-tolyl)amine	−0.37	Yes
Tris(4-bromophenyl)amine	−0.74	Yes

[a] $\Delta G^o_{ex} = \Delta G^{o'}_r - \Delta G^o_{ES}$, where ΔG^o_{ES} is the free-energy content of electronically excited $Mo_6Cl^{2-}_{14}$ over the ground state. ΔG^o_{ES} may be determined from the energy of the 0,0 transition (1.9 eV) with corrections for entropic contributions ($T\Delta S$ = 0.1 V; C. P. Bock, J. A. Connor, A. R. Gutierrez, T. J. Meyer, D. G. Whitten, B. P. Sullivan and J. K. Nagle, *J. Am. Chem. Soc.* 1979, **101**, 4815).

excited-state products is given by:

$$k_{et} = \kappa(k_B T/h)\exp(-\Delta G^*/RT), \quad (3)$$

$$\Delta G^* = w_r + \frac{(\lambda + \Delta G^{o'}_r)^2}{4\lambda}, \quad (4)$$

$$\Delta G^o_r = \Delta G^{o'}_r + w_p - w_r. \quad (5)$$

In the above expressions, ΔG^* is the free energy required to reach the activated complex, κ is the probability for electron transfer within the activated complex, w_r is the work required to bring reactants together, w_p is the corresponding product work term, λ is the reorganizational energy for electron transfer, and $\Delta G^{o'}_r$ is the standard free-energy change of the reaction. The vertical displacement of the potential-energy surfaces for products relative to the reactant well is defined by ΔG^o_r. For the $Mo_6Cl^{3-}_{14}$–A^+ system, $w_p = 0$, giving an effective ecl threshold free energy, $\Delta G^o_{ecl}(Mo_6Cl^{3-}_{14}\text{–}A^+) = -0.21\text{ V} - w_r$. Because w_r is a negative quantity, $\Delta G^o_{ecl}(Mo_6Cl^{3-}_{14}\text{–}A^+)$ is > -0.21 V. Likewise, $w_p = 0$ for the electron-transfer reaction between $Mo_6Cl^{-}_{14}$ and D^-; however, w_r is >0 and, therefore, $\Delta G^o_{ecl}(Mo_6Cl^{-}_{14}\text{–}D^-)$ is < -0.39 V. Thus, the 0.18 V difference between the ecl threshold free energies of the D and A series represents a lower limit. According to eqn (3), the more exothermic ecl threshold free energy for the D series suggests that the reaction of $Mo_6Cl^{-}_{14}$ and D^- to produce electronically excited $Mo_6Cl^{2-}_{14}$ confronts a larger activation barrier and, therefore, a greater reorganizational energy than the chemiluminescent reaction between $Mo_6Cl^{3-}_{14}$ and A^+. Studies currently underway in our laboratories are directed toward defining the nature of the reorganizational barriers confronting $Mo_6Cl^{2-}_{14}$ ecl pathways and toward assessing the importance of nonadiabatic electron transfer on the overall ecl efficiency of the $Mo_6Cl^{2-}_{14}$ system.

Acknowledgement—This work was financially supported by grants from the Amax Foundation and Research Corporation.

REFERENCES

1. D. G. Nocera and H. B. Gray, *J. Am. Chem. Soc.* 1984, **106**, 824.
2. (a) N. E. Tokel-Takvoryan, R. E. Hemingway and A. J. Bard, *J. Am. Chem. Soc.* 1973, **95**, 6582; (b) J. Gonzales-Velasco, I. Rubinstein, R. J. Crutchley, A. B. P. Lever and A. J. Bard, *Inorg. Chem.* 1983, **22**, 822; (c) H. D. Abruna, *J. Electroanal. Chem. Interfacial Electrochem.* 1984, **175**, 321; (d) H. D. Abruna, *J. Electrochem. Soc.* 1985, **132**, 842.
3. N. E. Tokel-Takvoryan and A. J. Bard, *Chem. Phys. Lett.* 1974, **25**, 235.
4. J. C. Luong, L. Nadjo and M. S. Wrighton, *J. Am. Chem. Soc.* 1978, **100**, 5790.
5. A. Vogler and H. Kunklay, *Angew. Chem., Int. Ed. Engl.* 1984, **23**, 316.
6. (a) W. L. Wallace and A. J. Bard, *J. Phys. Chem.* 1979, **83**, 1350; (b) H. Schaper and E. J. Schnedler, *J. Phys. Chem.* 1982, **86**, 4380; (c) H. Schaper, H. Koestlin and E. Schnedler, *Philips Tech. Rev.* 1982, **40**, 69.
7. (a) L. R. Faulkner, *Int. Rev. Sci., Phys. Chem. Ser. Two* 1975, **9**, 213; (b) L. R. Faulkner and R. S. Glass, In *Chemical and Biological Generation of Excited States* (Edited by W. Adams and G. Gilento), p. 191. Academic Press, New York (1982).
8. J. C. Sheldon, *J. Chem. Soc.* 1960, 1007.
9. R. I. Walter, *J. Am. Chem. Soc.* 1955, **77**, 5999.
10. A. J. Bard and L. R. Faulkner, *Electrochemical Methods*, p. 701. John Wiley, New York (1980).
11. (a) R. A. Marcus, *J. Chem. Phys.* 1965, **43**, 2654; (b) T. J. Meyer, *Prog. Inorg. Chem.* 1983, **30**, 389.
12. N. Sutin, *Prog. Inorg. Chem.* 1983, **30**, 441.

Polyhedron Vol. 5, No. 1/2, pp. 51–61, 1986
Printed in Great Britain

0277-5387/86 $3.00 + .00
© 1986 Pergamon Press Ltd

SOME STRUCTURE–BONDING CORRELATIONS IN REDUCED TERNARY MOLYBDENUM OXIDES WITH INFINITE CHAINS OF EDGE-SHARED OCTAHEDRAL CLUSTER UNITS

R. E. McCARLEY

Ames Laboratory, U.S.D.O.E., and Department of Chemistry, Iowa State University, Ames, IA 50011, U.S.A.

(*Received* 18 *June* 1985)

Abstract—The work reported here is concerned with the structure–bonding relationships among compounds belonging to the structure types $NaMo_4O_6$, $Sc_{0.75}Zn_{1.25}Mo_4O_7$, $Mn_{1.5}Mo_8O_{11}$, $Ca_{5.45}Mo_{18}O_{32}$ and $LiMo_8O_{10}$. Each of these structures is dominated by Mo–Mo bonding in infinite chains composed of edge-shared octahedral cluster repeat units. It is shown that the application of both Mo–O and Mo–Mo bond distance–bond order equations can provide useful information about the bonding in these chains. In both simple and complex structures reasonable estimates have been obtained for valence of Mo atoms, net charges on cluster anion repeat units, and numbers of electrons actually involved in the Mo–Mo bonding.

During the past few years the synthesis, structure and properties of many different metal–metal-bonded oxide compounds having molybdenum in oxidation states lower than 4+ have been studied in this laboratory.[1–6] Because of the complexity of the structures involved even the matter of counting electrons available for construction of the various metal–metal-bonded units may be obscure. Beyond the matter of simply counting the number of electrons which are formally available for participation in metal–metal bonding there is the further problem of assessing the relative number of electrons which really contribute to the bonding (reside in bonding states), as opposed to the number which may reside in nonbonding or antibonding states.

This paper is concerned with the application of bond distance–bond order relations to these ternary molybdenum oxide compounds to derive both Mo–O and Mo–Mo bond orders, and subsequently the use of these bond orders to estimate oxidation states of the Mo atoms, formal anion charges, and number of electrons available for Mo–Mo bonding. In the materials to be discussed here this approach has been so successful that even the relative numbers of electrons in bonding and antibonding states may be estimated. A description of the structure types containing infinite chains of edge-shared octahedral cluster units will be given first, and then the application of the bond distance–bond order relations will be discussed.

OXIDE COMPOUNDS HAVING INFINITE CHAINS OF CONDENSED OCTAHEDRAL CLUSTER UNITS

Up to the present time five different crystallographic structure types have been identified as belonging to this class of compounds. Some crystallographic information, and members of each type for which accurate structural data are available, are listed in Table 1. Type 1, $M_xMo_4O_6$, is characterized by $[Mo_4O_6]$ infinite octahedral cluster chains extended along the tetragonal *c*-axis.[1] These chains are then coupled through Mo–O–Mo interchain linkage to weave a square pattern and forming tunnels parallel to *c* in which the ternary metal ions are located. A view of this structure as projected down the *c*-axis is provided in Fig. 1 and a view of one cluster chain perpendicular to the direction of chain growth is given in Fig. 2. Unshared Mo atoms [Mo(a)] occupy apex positions in the cluster repeat units, while Mo atoms [Mo(w)] on the shared edges occupy waist positions along the chain.

Table 1. Molybdenum oxide compounds having edge-shared octahedral cluster chains

Structure type	Crystal class	Lattice constants	Space group	Isomorphous members	Reference
1 $NaMo_4O_6$	Tetragonal	$a = 9.570(3)$ Å $c = 2.8634(8)$ Å	*P4/mbm*	$InMo_4O_6$ $Sn_{0.9}Mo_4O_6$, $Pb_{0.8}Mo_4O_6$	1 7
2 $Zn_{1.25}Sc_{0.75}Mo_4O_7$	Orthorhombic	$a = 6.085(1)$ Å $b = 17.002(4)$ Å $c = 5.764(1)$ Å	*Imam*	$M_xM'_{2-x}Mo_4O_7$ [$MM' = Ti_{0.5}Zn_{1.5}$, $Sc_{0.5}Fe_{1.5}$, $Fe(Fe_{0.89}Mo_{0.11})$, $Zn(Zn_{0.4}Al_{0.5}Mo_{0.1})$, $(Al_{0.4}Fe_{1.5}Mo_{0.1})$	4, 5 8 8 8
3 $Mn_{1.5}Mo_8O_{11}$	Monoclinic	$a = 9.859(3)$ Å $b = 16.921(4)$ Å $c = 2.846(1)$ Å $\beta = 94.94(4)°$	$P2_1/a$	None	9
4 $Ca_{5.45}Mo_{18}O_{32}$	Monoclinic	$a = 24.234(7)$ Å $b = 2.8503(7)$ Å $c = 9.875(7)$ Å $\beta = 109.82(4)°$	$C2/m$	None	6
5 $ZnMo_8O_{10}$	Tetragonal	$a = 5.8961(4)$ Å $c = 24.840(3)$ Å	$I4_1md$	$LiMo_8O_{10}$	8

Both intra- and intercluster sharing of atoms is represented in the connectivity formula

$$Na^+[(Mo_2Mo_{4/2}O_{8/2}O_{2/2})O_{2/2}]^-.$$

All Mo atoms are found with coordination number 11 [Mo(a), 5O + 6Mo; Mo(w), 4O + 7Mo), and within each Mo_4O_6 repeat unit there is a total of 13 Mo–Mo bonds, with distances in $NaMo_4O_6$ ranging from 2.75 to 2.86 Å. Based on M–O bond distances for the ternary metal ions located in the tunnel sites it appears that these have the respective valences: Na and In,[6] +1; Pb and Sn,[7] +2. The coordination number and geometries are: Na, 8, compressed cube; In and Pb, 4, square pyramidal; Sn, 4, square planar.

Compounds of type **2**, with $Sc_{0.75}Zn_{1.25}Mo_4O_7$ as prototype,[4,5] are orthorhombic with the infinite cluster chains extending along the *c*-axis. The repeat unit along the chains is doubled compared to that in

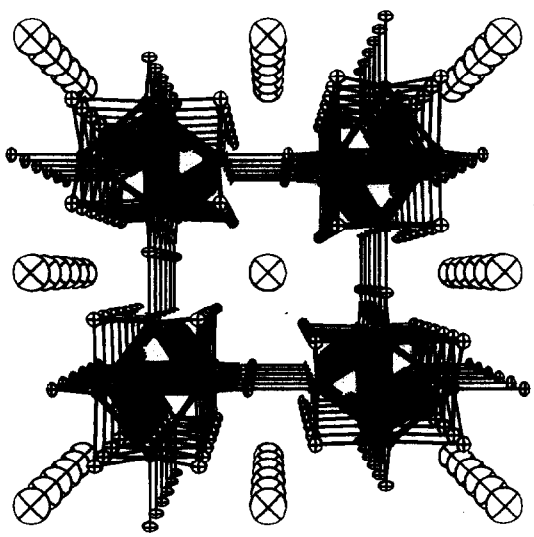


Fig. 1. The structure of $NaMo_4O_6$ as viewed down the tetragonal *c*-axis. Mo–Mo bonds in the octahedral cluster units are shown by heavy filled lines. Mo–O bonds are shown by light unfilled lines. Unconnected ellipsoids represent the Na atoms.

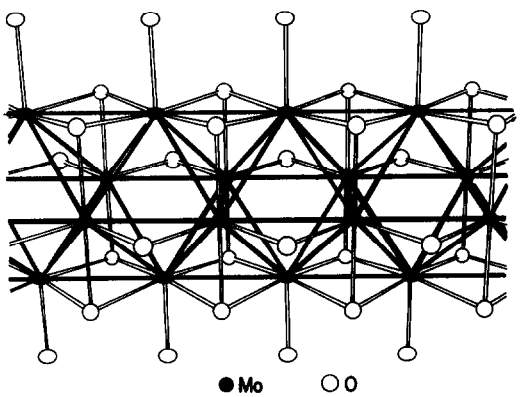


Fig. 2. The structure of a segment of one chain from $NaMo_4O_6$ as viewed perpendicular to the chain axis. The O atoms connected to the apex Mo atoms above and below the chain also form the Mo–O–Mo links to neighboring chains.

compounds of type **1**. A consequence of this doubling is that the octahedral cluster units may be tilted slightly about the edge-shared Mo–Mo bonds. This tilting of units results in alternately long and short Mo(a)–Mo(a) bonds along the chain, i.e. pairwise joining of the apex atoms. The three-dimensional structure can be viewed as formed from the stacking of layers perpendicular to the *b*-axis, with the infinite chains of one layer shifted by $\frac{1}{2}a$ with respect to the layers above and below. Within a given layer the infinite chains are linked together through unique O atoms having square planar geometry and forming bonds to two Mo(w) atoms of each adjacent chain. The ternary metal ions are located in both tetrahedral (M^t) and octahedral (M^o) coordination sites formed by the stacking of the layers. The number of M^t and M^o sites is each equal to one per formula unit $M^tM^oMo_4O_7$. Stability of this structure apparently demands that the average valences of M^t and M^o be in the range 2.3–2.5. This requires either mixed valency for one ternary element, or two elements, M(2+) and M′(3+). Examples are $Fe_{1.89}Mo_{4.11}O_7$ and $Fe_{1.5}Sc_{0.5}Mo_4O_7$, where the occupation of tetrahedral and octahedral sites is, respectively,

$$Fe^t_1(Fe^o_{0.89}Mo^o_{0.11})Mo_4O_7$$

and

$$Fe^t_1(Fe^o_{0.5}Sc^o_{0.5})Mo_4O_7.^8$$

With the exception of $Fe_{1.5}Sc_{0.5}Mo_4O_7$ all members of this family appear to have about 10 atom % of Mo in the octahedral sites, a phenomenon which is not understood at the present time. Because of the presence of this Mo in an undetermined oxidation state in the octahedral sites, and the evident mixed valency of other atoms (e.g. Fe and Ti) in the ternary metal ion sites, the anion charge and metal-centered electrons (MCE) available for Mo–Mo bonding in the infinite chains is difficult to assess from the formula alone. However it is obvious that in compounds of type **2** the MCE per cluster unit is higher than that in the compounds of type **1**, *ca* 14.5–14.75 in the former and 13.0–14.0 in the latter.

Compounds of type **3** are represented by the formula $M_xMo_8O_{11}$ of which $Mn_{1.5}Mo_8O_{11}$ is the sole member known to date.[9] In this monoclinic structure the infinite chains, composed of $Mo_4O_{5.5}$ repeat units, run parallel to the *c*-axis. This structure as viewed along the *c*-axis is shown in Fig. 3. The odd stoichiometry is introduced by the unique coupling of adjacent chains in the lattice as represented by the connective formula for the $Mo_4O_{5.5}$ repeat unit,

$$[(Mo_2Mo_{4/2}O_{6/2}O_{2/3}O_{2/2})O_{1/2}O_{1/3}].$$

Of special note are the unusual geometries around two sets of the O atoms involved in the intercluster Mo–O–Mo linkages. One set of O atoms has distorted square planar bonding, and another set, observed also in structure types **2** and **5**, exhibits a bond configuration about oxygen like that about sulfur in SF_4. The unique coupling of the chains in this compound provides channels with coordination spaces surrounded by six O atoms in a distorted trigonal prismatic geometry. Upon occupation of these spaces the Mn atoms seek sites of lower coordination number which is achieved by moving out of the center of the prismatic site. Two sites are thus occupied with about equal population, one having coordination number 4, and the other 5. Because of their close proximity within the same cavity these two sites cannot be simultaneously

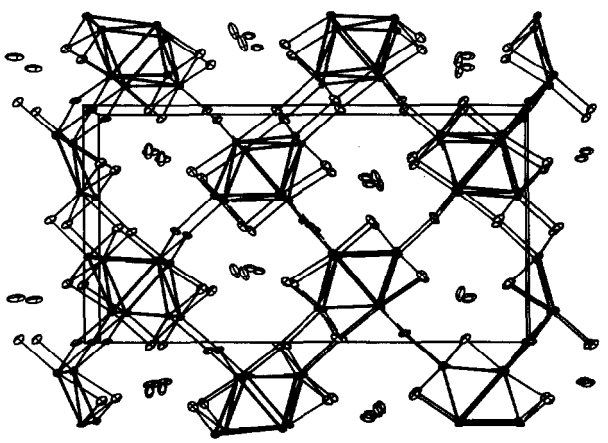


Fig. 3. A projection of the structure of $Mn_{1.5}Mo_8O_{11}$ as viewed down the monoclinic *c*-axis. The infinite cluster chains are paralled to the direction of view, and the unit cell is outlined. Mo atoms, filled ellipsoids; O atoms, connected, open ellipsoids; Mn atoms, open, unconnected ellipsoids.

occupied. It is probable that these sites are occupied in an ordered fashion because oscillation photographs show superstructure reflections indicating the true unit cell is some (as yet undetermined) multiple of the subcell in the *c* direction. Magnetic susceptibility results show that the Mn is present as high-spin Mn^{2+}, as should be expected in such a highly reduced compound.

Structure type **4** is represented by the compound $Ca_{5.45}Mo_{18}O_{32}$,[6] for which a projection of the unit cell along the *b*-axis is given in Fig. 4. This compound is unique among those discussed here in having three kinds of infinite chains, each of which runs parallel to the *b*-axis with repeat distance of 2.8503(7) Å. The three kinds of chains are indicated by the formula

$$Ca_{5.45}(MoO_3)_2(Mo_2O_{3.5})_4(Mo_4O_6)_2,$$

with repeat units (MoO_3) consisting of single Mo atom chains like those found parallel to the *c*-axis in the rutile structure, repeat units $(Mo_2O_{3.5})$ composed of *trans* edge-shared rhomboidal clusters like those found in $NaMo_2O_4$,[6] and repeat units Mo_4O_6 like those in $NaMo_4O_6$ (**1**).[1] Within this complex framework the Ca atoms are located in tunnels formed along the *b* direction, in eight-coordinate sites having six O atoms in roughly trigonal prismatic array and two additional bonds to O atoms located outside the square faces of the prism. Each site is only partially occupied such that on the average 5.45 atoms reside in the eight sites available in the unit cell. No evidence of superstructure reflections has been found in single-crystal oscillation photographs of this compound; thus the Ca sites appear to be randomly occuped. As noted in the following section an assessment of anion charges from bond length–bond strength calculations provided the formula

$$Ca_{5.45}(MoO_3^{2.2-})_2(Mo_2O_{3.5}^{0.24-})_4(Mo_4O_6^{2.6-})_2.$$

In the subsequent section only the $Mo_4O_6^{2.6-}$ cluster chains will be of interest for further discussion.

Only two compounds, $LiMo_8O_{10}$ and $ZnMo_8O_{10}$, having structure type **5** have been discovered so far.[8] The outstanding feature of this structure type is that the infinite octahedral cluster chains run in two orthogonal directions, parallel to the *a* and *b* tetragonal axes. A schematic representation of this structure is shown in Fig. 5. The structure may be regarded as a cross-wise stacking of layers perpendicular to the *c*-axis, each layer composed of infinite chains oriented with their axes orthogonal to those of the chains in adjacent layers. The mode of interchain coupling through Mo–O–Mo linkages is shown in Fig. 5. Within the layers the bridging O atoms again have square planar bond configuration, and the O atoms which provide the links between chains in two different layers again show "sawhorse" geometry (as in SF_4). The small cavities resulting from the cross-wise layer stacking provide coordination sites of tetrahedral (actually C_{2v}) symmetry which appear to be fully occupied by Li^+ or Zn^{2+} cations. Another interesting feature of this structure is that it may be conceptually obtained from the $M^IM^oMo_4O_7$ structure by substituting an octahedral cluster chain for the M^o atoms, which themselves form a chain (nonbonded) parallel to the *a*-axis of structure type **2**. This may be represented more clearly by rewriting the formula of **2** as $M^I(M^oO_2)(Mo_4O_5)$ and then replacing the M^oO_2 unit with a second Mo_4O_5 unit,

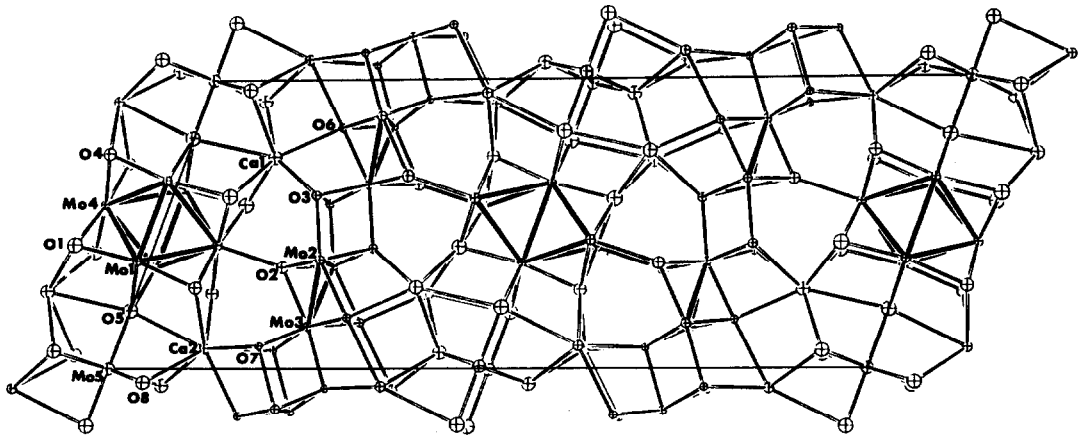


Fig. 4. The contents of one unit cell of $Ca_{5.45}Mo_{18}O_{32}$ as viewed down the monoclinic *b*-axis parallel to the direction of chain growth. Mo1 and Mo4 belong to edge-shared octahedral cluster chains, Mo2 and Mo3 belong to edge-shared rhomboidal cluster chains, and Mo5 belongs to single-atom chains like those in rutile.

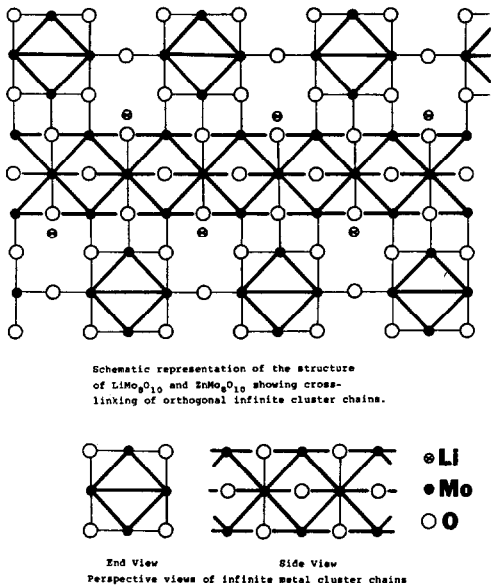


Fig. 5. Schematic representation of the structure of $LiMo_8O_{10}$ or $ZnMo_8O_{10}$ as viewed down the *a* tetragonal axis.

$M^I(Mo_4O_5)(Mo_4O_5)$. Finally, it should be noted that $ZnMo_8O_{10}$ is the most reduced molybdenum oxide compound currently known, and indeed it attains the highest MCE per cluster unit, 15, of any compound containing the condensed octahedral cluster units.

APPLICATION OF BOND LENGTH–BOND ORDER RELATIONS

The relation between bond distance and bond order for metal–metal bonds in metallic elements and their compounds has been given by Pauling[10] as:

$$d(n) = d(1) - 0.6 \log n, \qquad (1)$$

where $d(n)$ and $d(1)$ are the bond distances for bonds of order n and 1, respectively, and n is the bond order. Recently Corbett[11] has shown, for reduced halides and chalcides of the early transition metals, that Pauling bond order (PBO) sums for metal–metal-bonded compounds correlate well with the number of electrons available. The number of electrons available are those remaining on the metal atom after subtraction of those transferred to or shared with the nonmetal atoms, which thereby achieve a closed-shell configuration. Generally the correlation works very well in compounds where the nonmetal/metal ratio is less than 2 and the coordination number of the metal atom (with respect to nonmetal atoms) is less than 6. In this context "very well" means that the PBO sum divided by the number of MCE (PBO/e) falls in the range 0.8–1.0. Exceptions to this occur when "matrix effects"[11] become important, as for example when nonmetal–nonmetal spacings dictate weakened metal–metal bonds, or when the metal–metal bonding must take place through shared edges or faces of polyhedra formed by the nonmetal coordination sphere around the metal atom.

In the compounds discussed here we find that the PBO/e values, calculated from the observed Mo–Mo distances, without exception fall in the range 0.9–1.0 *when the counting of MCE is unambiguous.* This result is not really surprising in view of a number of factors which are particularly favorable in these structures. (1) The O/Mo ratios are < 2.0 and coordination numbers of the metal atoms towards oxygen are < 6. (2) Because of the small radius of the oxide ion [$r(O^{2-}) = 1.38$ Å][12] O–O nonbonded contacts are sufficiently short that Mo–Mo bonds formed at the same distance are still reasonably strong. (This is important for bonding along infinite chains where M–M bond distances parallel to the chain direction are dictated by and must be the same as the nonbonded O–O distance.) (3) The structures feature high total coordination numbers, M–M + M–O, about the metal atoms. Thus the bonding environment is similar to that found in the metal itself, from which the parameters of the PBO equation were established.[12] It is well known that the PBO equation works best for cases where the individual M–M bond orders are $\leqslant 1$.

Our encounter with the compound $Ca_{5.45}Mo_{18}O_{32}$[6] stimulated a further consideration of the bond length–bond order relations. In this compound the structure is built up from *three* types of metal–metal-bonded chains, as reflected in the formula $Ca_{5.45}(MoO_3^{m-})_2(Mo_2O_{3.5}^{n-})_4(Mo_4O_6^{p-})_2$. Assuming that each Ca transfers two electrons to the molybdenum oxide framework we see that

$$2m + 4n + 2p = 2(5.45) = 10.9.$$

Thus the important question concerns the evaluation of the individual anion charges m, n and p and simultaneously the correct MCE to be assigned to each kind of metal cluster repeat unit in the infinite chains. Fortunately a method to evaluate this electron distribution is provided by the M–O bond length–bond strength relations,[13] which permits evaluation of the net oxidation state of the individual metal atoms in the structure. The latter corresponds to the number of MCE given to M–O bonding, and hence the anion charge (assuming all oxygen atoms are always O^{2-}) and the MCE available for M–M bonding may be computed.

For most metal atoms reasonably reliable

empirical relations have been established for assessment of M–O bond strengths (synonymous with bond order) in oxide compounds. For this purpose equations of the general type

$$s(\text{M–O}) = [d(\text{M–O})/d_1(\text{M–O})]^{-n}$$

have been used,[13] where s = bond strength in valence units (v.u.), d(M–O) = observed M–O bond distance (Å), d_1(M–O) = M–O single bond distance (Å), and n is an exponential parameter having a value characteristic of each metal atom. The best values of the parameters d_1(M–O) and n have been derived for most metallic elements from fitting data for many oxide structures where accurate bond distances are known and the oxidation state of the M atom is unambiguous. The parameters in this equation perhaps have been established with greater confidence for molybdenum than for any other element. In particular, Bart and Ragaini[14] have arrived at "best" parameters by examining data for a wide variety of oxygen-ligated molybdenum compounds with molybdenum in oxidation states from 2+ to 6+. They find d_1(Mo–O) = 1.882 and n = 6.0 provide the best results for calculating the valence of molybdenum in the broad range of compounds from binary oxides (Mo_xO_y) to complexes like $Mo_2(O_2CMe)_4$. In this paper all calculations of individual Mo–O bond orders are thus made with the equation:

$$s(\text{Mo–O}) = [d(\text{Mo–O})/1.882]^{-6.0}. \quad (2)$$

Since s(Mo–O) is given in v.u. the sum of all Mo–O bond orders about a given Mo atom gives the valence of that atom [eqn (3)]:

$$\sum s(\text{Mo–O}) = v(\text{valence}) \quad (3)$$

and the anion charge on a unit $Mo_xO_y^{q-}$ in the lattice is given by:

$$q^- = xv - 2y. \quad (4)$$

In cases where several crystallographically distinct metal atoms exist in the structure, e.g. as in $NaMo_4O_6$ with Mo(1) and Mo(2), the sum over all metal atoms must be taken [eqn (5)]:

$$q^- = \sum_i x_i v_i - 2y, \quad (5)$$

where x_i represents the number of equivalent atoms Mo(i) having valence v_i in the formula unit.

These calculations are given in detail for $NaMo_4O_6$ in Table 2. In the infinite chain structure of this compound there are two distinct kinds of Mo atoms in the Mo_4O_6 repeat units, viz. the Mo(a) and Mo(w), each occurring twice in the formula unit, $NaMo(a)_2Mo(w)_2O_6$. We expect that the Na atoms transfer their valence electrons to the oxide framework, hence the formulation $Na^+Mo_4O_6^-$ and q^- (expected) = −1.00. From the values of s(Mo–O) given in Table 2 we obtain

$$q^-(\text{calc.}) = [2(3.13)+2(2.46)]-6(2) = -0.82 \pm 0.20.$$

The error of ±0.2 in this calculated value for q^- is the *maximum* error produced by an error of one standard deviation in all of the Mo–O bond distances used to compute the Mo–O bond strengths. Within this error limit the agreement between the expected and calculated anion charge is satisfactory. Thus in a case where we can be confident of the correct anion charge the procedure based on Mo–O bond strengths does indeed provide a reliable result.

Application of this procedure to the compound $Ca_{5.45}Mo_{18}O_{32}$ should then provide estimates of the anion charges for the three types of anion chains found in the structure. The pertinent Mo–O bond distances and bond strengths are given in Table 3. From these results, values of the individual anion charges have been calculated as shown in Table 3. The sum over all anion units gives the total anion charge

$$q^- = 2(-2.2)+4(-0.24)+2(-2.6) = -10.6.$$

Within the expected error the latter is in good agreement with the total cation charge arising from Ca^{2+}, $q^+ = 2(5.45) = 10.9$. Furthermore, the MCE derived from these individual anion charges for each kind of repeat unit are in agreement with those found in related compounds having only one of the corresponding structural repeat units. For example, the $Mo_2O_{3.5}^{0.24-}$ repeat units compose infinite chains of edge-fused rhomboidal clusters like those found in $NaMo_2O_4$.[6] The MCE/repeat unit is 5.24 in the former and 5.0 in the latter. A comparison of the $Mo_4O_6^{2.6-}$ repeat units with those in many other compounds having the same edge-fused octahedral cluster chains is given in the following section.

ELECTRON-COUNTING SCHEMES

We wish to relate here how further use of the bond length–bond order (bond strength) empirical relations can be applied to derive useful estimates of the numbers of electrons involved in M–O and M–M bonding, and even to estimate whether any electrons enter antibonding states with respect to the M–M interactions. Although extended Hückel band structure calculations[15] have been made for structure types **1** and **2** these do not have sufficient accuracy to provide a complete understanding of the three-dimensional band structure in these complex materials. The placement of bands near the Fermi

Table 2. Bond distances and bond orders in $NaMo_4O_6$

Bond type	d(Mo–O) (Å)	s(Mo–O)	f[a]	fs
Mo–O bonds				
Mo(a)–O	2.024(11)[b]	0.65(2)[c]	1	0.65(2)[c]
Mo(a)–O	2.040(6)	0.62(1)	4	2.48(4)
				$v = \sum s = 3.13(6)$
Mo(w)–O	2.068(8)	0.57(1)	2	1.14(2)
Mo(w)–O	2.015(8)	0.66(1)	2	1.32(2)
				$v = \sum s = 2.46(4)$
Mo–Mo bonds				
	d(Mo–Mo) (Å)	n(Mo–Mo)		fn
Mo(a)–Mo(a)	2.8618(2)[b]	0.386(0)[c]	2	0.77(0)[c]
Mo(a)–Mo(w)	2.780(2)	0.529(4)	4	2.12(2)
				$\sum n = 2.89(2)$
Mo(w)–Mo(w)	2.753(3)	0.587(7)	1	0.59(1)
Mo(w)–Mo(w)	2.8618(2)	0.386(0)	2	0.77(0)
Mo(w)–Mo(a)	2.780(2)	0.529(4)	4	2.12(2)
				$\sum n = 3.48(3)$

[a] Number of times each bond type occurs.

[b] Number in parentheses indicates estimated standard deviation in least significant digit.

[c] Number in parentheses indicates maximum error produced by change in bond distance of one standard deviation.

level is especially important in accurately predicting the electron occupation number and bonding or antibonding character of the occupied states. These calculations however do provide valuable insights about the nature of the orbital overlaps, which M–M interactions are most important, and how the interactions are changed or adapt upon change of structure type.

A very important point which must be established first is in regard to the degree of participation of the metal valence electrons in M–M interactions. For example, in the compound $NaMo_4O_6$ we can deduce readily from the average oxidation state of the Mo atoms of 2.75 that 3.25 e/Mo are left for potential involvement in Mo–Mo bonding. However, in the absence of persuasive evidence to the contrary we cannot state with confidence that all of these electrons will indeed enter into M–M bonding. Localization of electrons in essentially nonbonding orbitals is of course always possible in suitable structure types and becomes increasingly favored for elements occurring later in the transition series.

If the bond length–bond order expressions work correctly, for a given metal atom the number of electrons devoted to M–O bonding is given by eqn (6):

$$n_e(\text{M–O}) = v = \sum S(\text{M–O}) \tag{6}$$

and the number of electrons devoted to M–M bonding is given by eqn (7):

$$n_e(\text{M–M}) = \sum n(\text{M–M}). \tag{7}$$

Thus, if all electrons in the valence shell of the metal atom are involved in bonding the sum of n_e(M–O) and n_e(M–M) should equal the periodic group number. For Mo we have the condition:

$$N_e = n_e(\text{Mo–O}) + n_e(\text{Mo–Mo}) = 6. \tag{8}$$

Calculations for all compounds where accurate structural refinements have been performed are

Table 3. Mo–O bond distance–bond strength calculations for structural components of $Ca_{5.45}Mo_{18}O_{32}$

	d(Mo–O) (Å)	s(Mo–O)	f^a	fs
		MoO_3^{m-} units		
Mo(5)	2.004(13)[b]	0.69(3)[c]	2	1.38(6)[c]
	1.971(10)	0.76(2)	2	1.52(4)
	2.169(10)	0.43(1)	2	0.86(2)
				$v = \sum s = 3.76(12)$
	$m^- = 3.8(1) - 2(3) = -2.2(1)$			
		$Mo_2O_{3.5}^{n-}$ units		
Mo(2)	2.058(10)	0.58(1)	2	1.16(2)
	2.033(12)	0.63(2)	1	0.63(2)
	2.089(9)	0.53(1)	2	1.06(2)
	2.079(13)	0.55(2)	1	0.55(2)
				$v = \sum s = 3.40(8)$
Mo(3)	2.073(8)	0.56(1)	2	1.12(2)
	2.090(12)	0.53(1)	1	0.53(1)
	2.054(8)	0.59(1)	2	1.18(2)
	2.095(15)	0.53(3)	1	0.53(3)
				$v = \sum s = 3.36(8)$
	$n^- = (3.40 + 3.36) - 2(3.5) = -0.24(6)$			
		$Mo_4O_6^{p-}$ units		
Mo(4)	2.095(10)	0.53(2)	2	1.06(4)
(apex)	2.097(11)	0.52(2)	2	1.04(4)
	2.213(14)	0.38(2)	1	0.38(2)
				$v = \sum s = 2.48(10)$
Mo(1)	2.116(10)	0.50(2)	2	1.00(4)
(waist)	2.049(11)	0.60(2)	1	0.60(2)
	2.043(11)	0.61(2)	1	0.61(2)
				$v = \sum s = 2.21(8)$
	$p^- = [2(2.48) + 2(2.21)] - 2(6) = -2.6(4)$			

[a] Number of times each bond type occurs.

[b] Number in parentheses indicates estimated standard deviation in least significant digit.

[a] Number in parentheses indicates maximum error produced by change in bond distance of one standard deviation.

Table 4. Metal-centered electron (MCE) counts for compounds containing edge-shared octahedral cluster chains

Compound	N_e/Mo[b]	MCE count[a]			Δ[f]	n_a	n_b
		$\sum s$[c]	$\sum n$[d]	Formula[e]			
$NaMo_4O_6$	6.0	12.8(2)[g]	12.7(1)[g]	13.0	0.3	0.2	12.8
$InMo_4O_6$	5.8	13.1(2)	12.3(1)	13.0	0.7	0.4	12.6
$Pb_{0.8}Mo_4O_6$	5.9	13.3(2)	12.7(1)	13.5	0.8	0.4	13.1
$Sn_{0.9}Mo_4O_6$	5.8	13.4(2)	13.3(1)	13.8	0.5	0.3	13.5
$Sc_{0.75}Zn_{1.25}Mo_4O_7$	5.8	14.5(2)	13.6(1)	$\geqslant$14.7	$\geqslant$1.1	0.6	14.1
$Ti_{0.5}Zn_{1.5}Mo_4O_7$	5.8	14.4(2)	13.4(1)	$\geqslant$14.5	$\geqslant$1.1	0.6	14.0
$Sc_{0.5}Fe_{1.5}Mo_4O_7$	5.8	14.3(2)	13.5(1)	$\geqslant$14.5	$\geqslant$1.0	0.5	14.0
$Fe(Fe_{0.89}Mo_{0.11})Mo_4O_7$	5.8	14.3(2)	13.5(1)	$\geqslant$14.5	$\geqslant$1.0	0.5	14.0
$Mn_{1.5}Mo_8O_{11}$	5.9	14.0(2)	13.4(1)	14.5	1.1	0.6	13.9
$Ca_{5.45}Mo_{18}O_{32}$	5.8	14.6(2)	13.6(1)	$\sim$14.6	$\sim$1.0	0.5	14.1
$LiMo_8O_{10}$	5.9	14.3(2)	13.9(1)	14.5	0.6	0.3	14.2
$ZnMo_8O_{10}$	5.9	14.7(2)	14.1(1)	15.0	0.9	0.4	14.6

[a] Per octahedral cluster unit.
[b] Total valence electrons per Mo atom from $N_e = \sum s(\text{Mo–O}) + \sum n(\text{Mo–Mo})$.
[c] MCE count derived from Mo–O bond order sums.
[d] MCE count derived from Mo–Mo bond order sums.
[e] MCE count derived from formula of compound.
[f] MCE(Formula) − MCE($\sum n$).
[g] Numbers in parentheses are estimated maximum error in least significant digit.

listed in Table 4.* The results for N_e given in column 1 confirm that essentially in all cases the valence electrons of Mo are completely utilized in bonding according to this criterion.

From this point we can proceed in three ways to obtain the MCE/repeat unit for metal–metal bonding. First, from a summation of all Mo–Mo bond orders around each Mo atom in the repeat unit we get directly the total MCE/unit. We will designate this estimate MCE ($\sum n$). Second, we may obtain the valence of each Mo atom in the repeat unit via summation of Mo–O bond orders. The MCE/Mo is then obtained from the relation MCE = $6-v$, and the total MCE/repeat unit is MCE($\sum s$) = $\sum_i$ MCE$_i$(Mo$_i$). Third, if the average valence of the Mo can be reliably determined from the formula, as in cases where the valence of all other elements can be assigned with confidence, the MCE/repeat unit can be determined from MCE(Formula) = $x(6-\bar{v})$, where x is the number of Mo atoms and $\bar{v}$ is the average valence. This method of course is not subject to uncertainties introduced by errors in the bond distances, but does rest on the assumption that all valence electrons are involved in the bonding, i.e. there are no localized nonbonding electrons.

Estimates of the MCE/repeat unit by each of these methods is given in Table 4 for all compounds containing the condensed octahedral cluster repeat units. It is notable that the three methods are in essential agreement for the simplest of these compounds, $NaMo_4O_6$. This may be interpreted as an indication that $NaMo_4O_6$ is perfectly bonded with all valence electrons of the Mo atoms in either Mo–Mo or Mo–O bonding states. Accordingly we conclude that nonbonding and antibonding states are essentially unoccupied. Extended Hückel calculations[15] corroborate this result and place the Mo–O valence band well below the bands derived from Mo–Mo interactions. The density of states at the Fermi level also is predicted to be quite low, and this is consistent with resistivity measurements, which indicate that $NaMo_4O_6$ passes through a metal–semiconductor transition at low temperatures. This implies that antibonding states are separated from the filled bonding states by a small energy gap at low temperature. In this structure type

* All Mo–Mo bond orders have been calculated using the single-bond distance d_1(Mo–Mo) = 2.614 Å. This value is slightly different from the value of 2.592 Å given by Pauling's[10] single-bond radius, R_1(Mo) (1.296 Å). The value of d_1 = 2.614 Å was calculated from the nearest neighbor [d(n.n)] and next nearest neighbor [d(n.n.n.)] distances in bcc Mo–metal by solving the three equations based on the PBO equations for the two distances and the condition that $8n$(n.n.) + $6n$(n.n.n.) = 6, where n(n.n.) and n(n.n.n.) are the bond orders for nearest neighbor and next nearest neighbor Mo–Mo bonds, respectively.

apparently 13 e/repeat unit are required for complete occupation of the bonding states.

If the above conclusions are correct one may ask, what are the consequences of adding additional electrons to this structure? The answer is not easily obtained because synthesis of compounds having M^{2+} in the ternary cation sites leads to: (a) incomplete occupation of the metal ion sites with consequent superstructure effects, and/or (b) involvement of the ternary metal *s* and *p* valence orbitals in the valence and conduction bands. Both of these effects are important with the compounds $Sn_{0.9}Mo_4O_6$ and $Pb_{0.8}Mo_4O_6$, while only the latter is involved in the case of $InMo_4O_6$. In contrast to $NaMo_4O_6$ both $Sn_{0.9}Mo_4O_6$ and $InMo_4O_6$[7] are metallic conductors, with a normal temperature dependence of their resistivity down to 2 K. Thus the structure of the conduction band is different for the latter pair, even though $InMo_4O_6$ appears to be isoelectronic with $NaMo_4O_6$. As shown by the data in Table 4 the difference in MCE($\sum s$) and MCE($\sum n$) for $InMo_4O_6$ is quite significant. Because MCE($\sum n$) is low the Mo–Mo bonding is evidently weaker than in $NaMo_4O_6$. Weaker Mo–Mo bonding could result either from a lower population of electrons in the bonding states, inferring that In transfers fewer electrons to the Mo_4O_6 units, or from the population of antibonding levels, inferring that In transfers more electrons and adopts an average valence >1.0. The result MCE($\sum s$) = 13.1(2) seemingly negates both of these possibilities. A third possibility is that mixing of the In *s*-orbitals (which have lower energy) with the Mo4*d* orbitals in the conduction band results in lifting some of the *d*-states to antibonding character. Since the *s*-orbitals of In^+ remain occupied this would result in the occupation of some antibonding *d*-states and a consequent lowering of the Mo–Mo bond orders.

The results given in Table 4 reveal an obvious trend that, with the exception of the numbers for $NaMo_4O_6$, all MCE($\sum n$) are significantly lower than MCE($\sum s$) or MCE(Formula), with differences, Δ, [MCE(Formula) − MCE($\sum n$)], of 0.6–1.1 e/repeat unit. A plausible explanation for this behavior concerns the limiting MCE based on occupation of only bonding states in the undistorted chains (as in $NaMo_4O_6$) and the interplay between occupation of antibonding states and stabilizing distortions of the cluster units with increasing MCE. Distortions of the cluster units can result in the creation of additional bonding states via band splitting and lowering resulting from reduced symmetry. This effect has been treated and discussed by Hughbanks and Hoffmann[15] for compounds of type **2**. However, their study did not permit a reliable estimate of the total occupied states at the Fermi energy because of the complicated band structure. Consequently, a reliable estimate of the MCE/repeat unit was not derived from their calculations. It can be stated with confidence however that the doubling of the cluster repeat unit and the pairwise Mo(a)–Mo(a) interactions resulting from the tilting of adjacent octahedral units does indeed create additional bonding states. Thus it can be asserted that the observed distortion is electronically driven and the net Mo–Mo bonding within the chains is thereby enhanced for MCE > 13.

Notably, the widest range of Mo–Mo bond distances is found within the cluster units of $LiMo_8O_{10}$ and $ZnMo_8O_{10}$, having MCE of 14.5 and 15.0, respectively. In these compounds the true repeat unit is again doubled and even more drastic pairwise coupling of adjacent atoms is observed, except that these occur in a less understandable fashion than in compounds of type **2**. Some shortened Mo–Mo distances in $ZnMo_8O_{10}$ are 2.581(2), 2.680(2) and 2.694(2) Å, and some lengthened distances are 3.246(2), 3.202(2) and 2.952(2) Å, all relative to the averaged Mo–Mo bond distance of 2.809 Å. The latter average bond distance differs little from the corresponding average distance of 2.803 Å in $NaMo_4O_6$, whereas the values of MCE($\sum n$) are 14.1 and 12.7 for $ZnMo_8O_{10}$ and $NaMo_4O_6$, respectively. This large difference in MCE($\sum n$) illustrates dramatically the effect that distortions can have on the net metal–metal bond orders within cluster units. For example, the PBO equation gives a lower $\sum n$ for two bonds of equal length than that for the same bonds, one lengthened and the other shortened by the same increment. This simply reflects the well-known fact that bond energies and bond orders increase exponentially with decreasing bond distance. In this connection we note that important distortions occur in the cluster units of all structure types having MCE $\geqslant 14$. The particular form of the cluster distortion is governed by symmetry constraints of the lattice and metal positions, which in turn are determined by the ternary metal ions through their direction of the structure type adopted.

ESTIMATION OF MCE IN ANTIBONDING STATES

The basis for this approach is suggested by the results given in Table 4 and discussed in the previous section. Namely, since $\sum s + \sum n$ approach 6.0 in all cases there is valid reason to believe that all Mo valence electrons are involved in bonding interactions. Why then do the values MCE($\sum n$) consistently fall below those of either MCE($\sum s$) or MCE(Formula)? If the latter arises because some

electrons enter antibonding states which then weaken the Mo–Mo bonding, the number of such electrons may then be estimated from the results of the bond order summations. In order to derive an expression for this purpose we need to make the assumption that the number of electrons in nonbonding states is negligibly small compared to those in bonding or antibonding states. If we take MCE(Formula), given below as MCE(F), as the true measure of the total number of cluster electrons, and define n_b and n_a as the number of bonding and antibonding electrons, respectively, we get eqns (9) and (10):

$$\mathrm{MCE}(F) = n_b + n_a, \tag{9}$$

$$\sum n = (n_b - n_a)/2, \tag{10}$$

where $\sum n^*$ is the PBO sum over all M–M bonds in the repeat unit. These equations yield the solutions:

$$n_b = \mathrm{MCE}(F)/2 + \sum n, \tag{11}$$

$$n_a = \mathrm{MCE}(F) - n_b. \tag{12}$$

Noting that $2\sum n = \mathrm{MCE}(\sum n)$ and defining the quantity Δ as

$$\mathrm{MCE}(F) - 2\sum n = \mathrm{MCE}(F) - \mathrm{MCE}(\sum n)$$

we get the final equations:

$$n_a = \Delta/2, \tag{13}$$

$$n_b = \mathrm{MCE}(F) - \Delta/2. \tag{14}$$

The results Δ, n_b and n_a for all of the compounds are listed in Table 4. With the exception of $NaMo_4O_6$ the values of Δ are rather significant for all compounds, but still the number of antibonding electrons is small for all structures. Within the limits of error $NaMo_4O_6$ has no electrons in antibonding states. Again, the small range of 0.3–0.6 antibonding electrons for the range of MCE from 13 to 15 e/cluster unit illustrates the effectiveness of internal distortions and adaptation of Mo–Mo bonding in avoiding the population of antibonding states. It will be interesting to see if MCE = 15 represents an upper limit for structures derived from the edge-shared octahedral cluster chains, or if new compounds having higher MCE may be prepared. Based on the correlations presented here it appears that the cluster units in the edge-shared octahedral cluster chains are likely to suffer such severe distortions for MCE > 15 that alternate modes of cluster condensation will be favored for higher e/M ratios than those observed in these structures.

* Note here that $\sum n$ represents the sum over *individual Mo–Mo bonds*, rather than over the individual Mo atoms, of the cluster repeat unit. By taking the sum over atoms each bond is counted twice, thus $\sum n(\text{bonds}) = \sum n(\text{atoms})/2$.

Acknowledgements—I am indebted to J. D. Corbett, H. F. Franzen and K.-H. Lii for valuable discussions. The continuing support of the U.S. Department of Energy, Division of Basic Energy Sciences, for this research is also gratefully acknowledged. This work was supported by the U.S. Department of Energy through Ames Laboratory, which is operated by Iowa State University under Contract No. W-7405-Eng-82. This research was supported by the Assistant Secretary for Energy Research, Office of Basic Energy Sciences.

REFERENCES

1. C. C. Torardi and R. E. McCarley, *J. Am. Chem. Soc.* 1979, **101**, 3963.
2. C. C. Torardi and R. E. McCarley, *J. Solid State Chem.* 1981, **37**, 393.
3. R. E. McCarley, T. R. Ryan and C. C. Torardi, *Am. Chem. Soc. Symp. Ser.* 1981, **155**, 41.
4. R. E. McCarley, *Am. Chem. Soc. Symp. Ser.* 1983, **211**, 273.
5. R. E. McCarley, *Philos. Trans. R. Soc. London A* 1982, **308**, 141.
6. R. E. McCarley, K.-H. Lii, P. A. Edwards and L. F. Brough, *J. Solid State Chem.* 1985, **57**, 17.
7. K.-H. Lii, B. A. Aufdembrink and R. E. McCarley, unpublished research.
8. K.-H. Lii and R. E. McCarley, unpublished research.
9. C. D. Carlson, L. F. Brough, P. A. Edwards and R. E. McCarley, unpublished research.
10. L. Pauling, *The Nature of the Chemical Bond*, 3rd Edn, p. 400. Cornell University Press, Ithaca, NY (1960).
11. J. D. Corbett, *J. Solid State Chem.* 1981, **37**, 335.
12. R. D. Shannon, *Acta Cryst.* 1976, **A32**, 751.
13. I. D. Brown, In *Structure and Bonding in Crystals* (Edited by M. O'Keefe and A. Navrotsky), Vol. 2, p. 1. Academic Press, New York (1981).
14. J. C. J. Bart and V. Ragaini, *Inorg. Chim. Acta* 1979, **36**, 261.
15. T. Hughbanks and R. Hoffmann, *J. Am. Chem. Soc.* 1983, **105**, 3528.

Polyhedron Vol. 5, No. 1/2, pp. 63–66, 1986
Printed in Great Britain

0277–5387/86 $3.00 + .00
© 1986 Pergamon Press Ltd

HYDROGEN INSERTION COMPOUNDS OF THE MOLYBDIC ACIDS

S. CROUCH-BAKER and P. G. DICKENS*

Inorganic Chemistry Laboratory, South Parks Road, Oxford OX1 3QR, U.K.

(*Received* 26 *June* 1985)

Abstract—This paper describes the structural and thermodynamic characterization of hydrogen insertion compounds of the molybdic acids, $H_xMoO_3 \cdot nH_2O$, comparing, where possible, the properties of this system with those of the hydrogen insertion compounds of MoO_3 itself.

The three compounds $MoO_3 \cdot 2H_2O$, yellow (or β-) $MoO_3 \cdot H_2O$ and white (or α-) $MoO_3 \cdot H_2O$, known as the molybdic acids, constitute the three stoichiometric, well-characterized hydrates of MoO_3. The dihydrate consists of infinite layers of vertex-sharing MoO_6 octahedra;[1,2] one terminal oxygen in each octahedron forms a short Mo—O bond while the opposite oxygen is replaced by a coordinated water molecule. There are also discrete water molecules between the layers.[3] The yellow monohydrate is formed by the topotactic loss of the interlayer water molecules on dehydration of the dihydrate while retaining the $MoO_5(OH_2)$ layer structure.[4] In the white monohydrate there are isolated double chains of edge-sharing octahedra with each molybdenum atom bearing a coordinated water molecule.[5]

Hydrogen insertion into MoO_3[6] produces four phases of H_xMoO_3 in the range $0 < x \leqslant 2$. This paper describes the characterization of corresponding insertion compounds of the molybdic acids.

REDUCED MOLYBDIC ACIDS

Recently, the preparation of hydrogen insertion compounds of $MoO_3 \cdot 2H_2O$ and yellow $MoO_3 \cdot H_2O$ by catalytic hydrogenation has been described by the authors[7,8] leading to materials of composition $H_{1.0}MoO_3 \cdot 2H_2O$ and $H_{1.0}MoO_3 \cdot H_2O$. Further, it has been noted that the white monohydrate shows no reaction under similar conditions.[7]

Initial characterization by the authors[8] showed these hydrogen insertion compounds to be metallic with insignificant long-range proton mobility. Further structural and thermodynamic characterization has been carried out using the following techniques.

IR spectroscopy

The IR spectrum of $H_{1.0}MoO_3 \cdot H_2O$ is shown in Fig. 1 compared with that of yellow $MoO_3 \cdot H_2O$. A new absorption band is found in the spectrum of the reduced material at 1200 cm^{-1}. This is assigned to the bend of an Mo—O—H group.[9,10] A similar assignment has been made in the case of $H_{0.36}MoO_3$ on the basis of inelastic neutron-scattering data.[11] An identical band appears in the IR spectrum of the reduced dihydrate and is assigned similarly.

Single-crystal X-ray diffraction

A single crystal of $H_xMoO_3 \cdot 2H_2O$ was prepared by exposing a single crystal of $MoO_3 \cdot 2H_2O$ to gaseous hydrogen at room temperature in the presence of a platinized silica catalyst. Analysis of single-crystal diffraction data collected at room temperature showed there is no major structural rearrangement of the dihydrate on hydrogen insertion. Significant changes were revealed, however, in the immediate coordination environment of each molybdenum atom, in particular in the arrangement of bridging oxygen atoms. In $MoO_3 \cdot 2H_2O$ itself the four bridging oxygen atoms around each molybdenum atom are arranged in two sets of two (at ~1.75–1.80 and ~2.05–2.18 Å from the molybdenum), whereas in the reduced material

* Author to whom correspondence should be addressed.

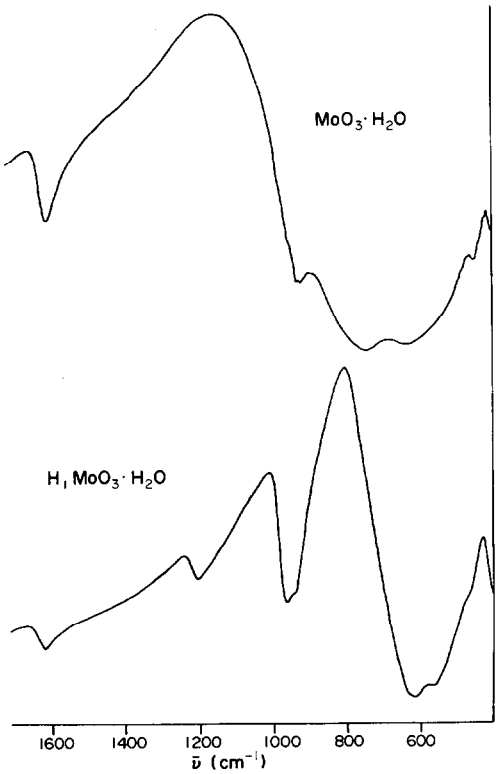


Fig. 1. IR spectra.

this distinction is removed and the oxygen atoms lie at intermediate distances from the molybdenum (at ~1.85–2.05 Å).

The reduction of MoO_3 to give $H_{0.36}MoO_3$ has been studied by powder neutron diffraction.[11] It was found that the inserted hydrogen atoms are attached to the oxygen atoms which bridge two molybdenum atoms in MoO_3 as OH groups. It was also shown that, on hydrogen insertion, the distances from the molybdenum atom to the bridging oxygen atoms, which are very different in MoO_3 itself, become equal. Hence it is proposed that the inserted hydrogen atoms in $H_xMoO_3 \cdot 2H_2O$ are attached, as part of OH groups, to the bridging oxygen atoms in the molybdic acid structure. The resulting hydrogen-bonding arrangement is shown in Fig. 2. Along each O---O line (approximately 3 Å long) there will be two possible hydrogen atom positions, only one of which may be occupied. This gives a maximum hydrogen content of $x = 1.0$, as is observed experimentally. Such an arrangement of hydrogen atoms is compatible with the extremely low rate of proton diffusion observed in the reduced molybdic acids.[8] The rigidity of the molybdic acid layer dictates that the only motion available to a proton is hopping between the two available sites along its own O---O lines. In the case of $H_{1.68}MoO_3$, a good proton conductor, diffusion probably takes place between the MoO_3 layers. The hydrogen atoms are attached to the terminal oxygen atom in MoO_3 as either OH_2 or OH groups; protons may be transferred from one site to another via a Grotthus type mechanism involving reorientation of the coordinated OH_2 groups.

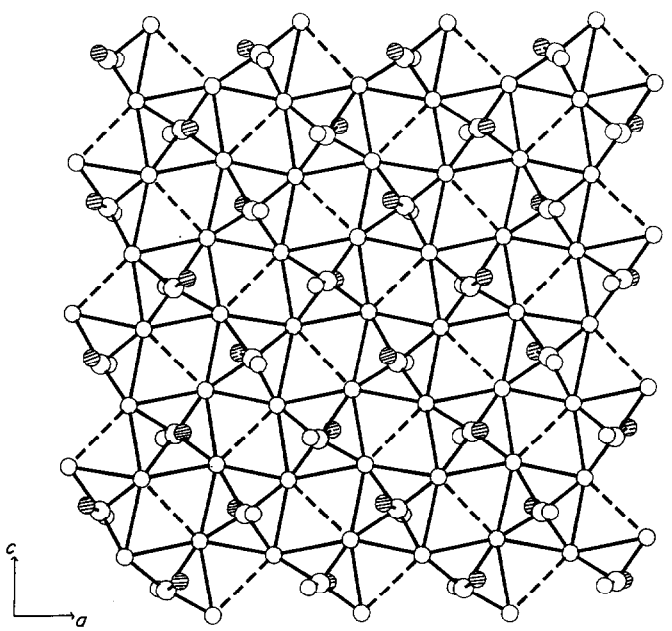


Fig. 2. Arrangement of hydrogen-bonds in $H_xMoO_3 \cdot 2H_2O$. For convenience the interlayer water molecules are not shown. Coordinated OH_2 groups are represented by shaded circles. A broken line between oxygen atoms indicates the unit O—H---O.

Solution calorimetry

The enthalpy change of the reaction

$$\frac{1}{2}H_2(g)+\frac{1}{x}MoO_3\cdot H_2O(s)=\frac{1}{x}H_xMoO_3\cdot H_2O(s)$$

at $x = 1.04$ has been determined[12] as $\Delta H = -43.9$ kJ mol^{-1}. This gives the mean O—H bond energy associated with the guest hydrogen atoms (ignoring the effects of any hydrogen-bonding) as approximately 470 kJ mol^{-1}, a value very similar to those quoted for OH groups in other solids, e.g. 486 kJ mol^{-1} in $H_{0.34}MoO_3$ and 470 kJ mol^{-1} in $H_{1.68}MoO_3$.[13]

Thermogravimetric analysis

The thermogravimetric decomposition curve for $H_{1.0}MoO_3\cdot 2H_2O$ is shown in Fig. 3 compared with that of the unreduced dihydrate. The decomposition curve of the latter shows two sharp weight losses corresponding to the two steps:[4]

$$MoO_3\cdot 2H_2O \overset{323\ K}{=\!=} MoO_3\cdot H_2O \overset{383\ K}{=\!=} MoO_3.$$

In the case of the decomposition of the reduced dihydrate (in an inert atmosphere), two similar dehydration steps are observed, analogous to those in the parent, leading to the formation of a material of composition $H_{1.0}MoO_3$. At approximately 473 K this material undergoes another dehydration step, distinctly less sharp than the previous two, removing constitutional oxygen and hydrogen to leave a material of composition $MoO_{2.5}$, the composition of which was confirmed thermogravimetrically by oxidation to MoO_3. The material $MoO_{2.5}$ was deep purple in colour and largely amorphous to X-rays. However, a powder X-ray pattern did contain the two strongest peaks due to MoO_2. Similar results were found for the reduced monohydrate without, of course, the initial dehydration at 323 K.

The thermal decomposition *in vacuo* of $H_{0.36}MoO_3$ has also been investigated.[14,15] The conclusions obtained are the same as those reached here, i.e. that thermal decomposition proceeds via dehydration giving materials of composition $MoO_{3-x/2}$.

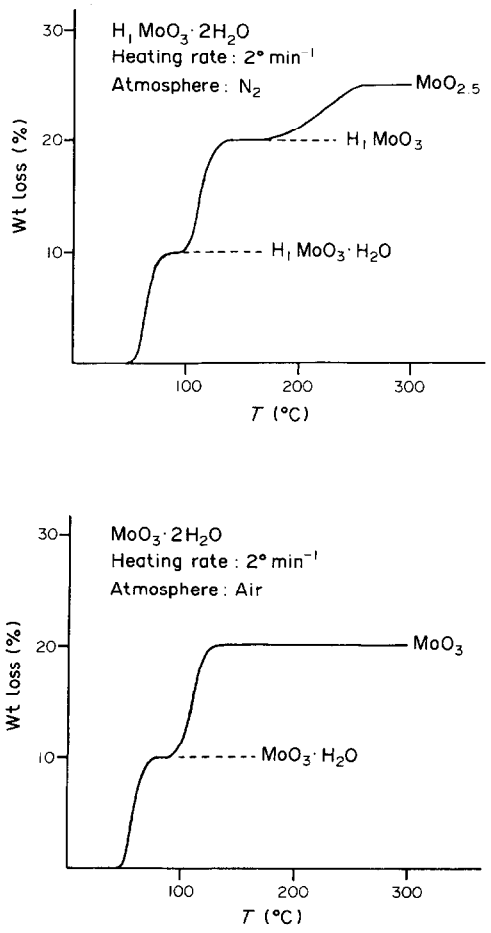


Fig. 3. Thermogravimetric decomposition curves.

CONCLUSION

Based on the results quoted here, and those stated previously,[7,8] it is concluded that hydrogen insertion into $MoO_3\cdot 2H_2O$ and yellow $MoO_3\cdot H_2O$ proceeds to give hydrogen insertion compounds closely analogous to $H_{0.36}MoO_3$, with the inserted hydrogen bound to bridging oxygen atoms as OH groups.

Acknowledgements—We would like to thank the Chemical Crystallography Department, Oxford, for use of their equipment and, in particular, D. M. Thomas for help with single-crystal data collection. We further wish to thank the U.S.A.F. Office of Scientific Research for sponsorship under Grant AFOSR-83-0052.

REFERENCES

1. B. Krebs, *Acta Cryst.* 1972, **B28**, 2222.
2. S. Asbrink and B. G. Brandt, *Chem. Scr.* 1971, **1**, 169.
3. S. Crouch-Baker and P. G. Dickens, *Acta Cryst.* 1984, **C40**, 1121.
4. J. R. Gunter, *J. Solid State Chem.* 1972, **5**, 354.
5. I. Boschen and B. Krebs, *Acta Cryst.* 1974, **B30**, 1795.
6. J. J. Birtill and P. G. Dickens, *Mater. Res. Bull.* 1978, **13**, 311.
7. S. Crouch-Baker and P. G. Dickens, *Mater. Res. Bull.* 1984, **19**, 1457.

8. S. Crouch-Baker and P. G. Dickens, *Solid State Protonic Conductors III*, p. 275. Odense University Press, Denmark (1985).
9. K. Nakamoto, *Infrared Spectra of Inorganic and Coordination Compounds*. John Wiley, New York (1963).
10. E. Hartert and O. Glemser, *Z. Elektrochem.* 1956, **60**, 746.
11. P. G. Dickens, J. J. Birtill and C. J. Wright, *J. Solid State Chem.* 1979, **28**, 185.
12. S. Crouch-Baker, P. G. Dickens and S. A. Kay, to be published.
13. P. G. Dickens, R. H. Jarman, R. C. T. Slade and C. J. Wright, *J. Chem. Phys.* 1982, **77**, 575.
14. N. Sotani, Y. Kawamoto and M. Inui, *Mater. Res. Bull.* 1983, **18**, 797.
15. N. Sotani, M. Kunimoto and M. Hasegawa, *Chem. Lett.* 1983, 647.

Polyhedron Vol. 5, No. 1/2, pp. 67–69, 1986
Printed in Great Britain

0277–5387/86 $3.00 + .00
© 1986 Pergamon Press Ltd

STRUCTURAL AND COMPOSITIONAL CHANGES IN A HYDROGEN MOLYBDENUM BRONZE, $H_{0.83}MoO_3$, BY VACUUM HEATING

NORIYUKI SOTANI

College of Liberal Arts, Kobe University, Tsurukabuto, Nada, Kobe 657, Japan

(*Received* 18 *June* 1985)

Abstract—$H_{0.83}MoO_3$ was a mixture of blue orthorhombic and blue monoclinic phases and decomposed, accompanied by structural and compositional changes, as follows:

$$H_{0.83}MoO_3 \xrightarrow{\sim 232°C} H_{0.58}MoO_{2.88} \xrightarrow{\sim 290°C} H_{0.21}MoO_{2.69} \xrightarrow{\sim 375°C} H_{0.02}MoO_{2.60} \xrightarrow{\sim 378°C} MoO_{2.59}.$$

It was reported by Birtill and Dickens[1] that a hydrogen molybdenum bronze, H_xMoO_3 ($0 < x \leqslant 2$) has four phases. Among them, many studies on a blue orthorhombic phase ($0.23 < x < 0.40$) by means of X-ray diffraction analysis,[2] neutron diffraction analysis,[3] IR spectroscopy[4] and NMR spectroscopy[5] have been reported. The others studied[6–8] the thermal stability of the orthorhombic bronze, $H_{0.30}MoO_3$, when it was treated *in vacuo* and in various gases by isothermal heat treatment and by heat treatment with increasing temperature, and its structural and compositional change was also studied. Since a bronze with higher hydrogen contents was obtained, the author tried to characterize this bronze as in the case of $H_{0.30}MoO_3$.

EXPERIMENTAL

The sample was prepared by the Glemser's method.[9,10] The composition was $H_{0.83}MoO_3$ by chemical analysis[11] and thermogravimetry.[7] $H_{0.83}MoO_3$ was composed of a mixture of blue orthorhombic and blue monoclinic ($0.85 < x < 1.04$) phases. A conventional high-vacuum system equipped with a Cahn electromicrobalance was used for measurements of weight changes. Samples after heat treatment *in vacuo* were studied by X-ray diffraction analysis and IR spectroscopy.

RESULTS AND DISCUSSION

Samples were heated isothermally at various temperatures (101–444°C) after pretreatment for 1 h in a vacuum of 10^{-4} torr. When the sample was treated at 373°C the fraction reacted, α, reached 1 within 20 min. On the other hand, when it was heated at 332°C for more than 3 h, α increased gradually, but did not reach 1.

Figure 1 shows X-ray patterns of samples heated isothermally at various temperatures. The X-ray result gave four kinds of patterns. Pattern (A) is due

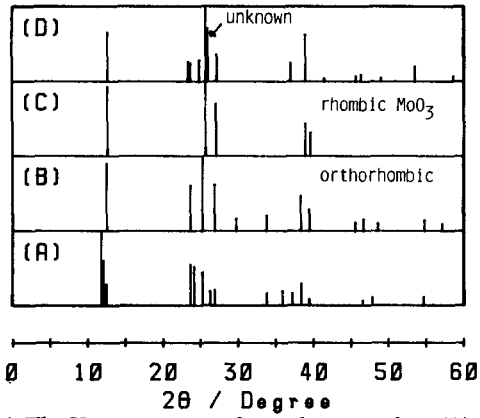


Fig. 1. The X-ray patterns of samples treated at: (A) room temperature–202°C, (B) 250°C, (C) 299–332°C, and (D) above 373°C.

to an original sample and samples heated below 202°C, and shows a mixture of orthorhombic and monoclinic phases. Pattern (B) is due to the sample heated at 250°C and shows only the orthorhombic phase. Patterns (C) and (D) of samples treated above 299°C show the rhombic MoO_3 phase, but, in addition to this phase, samples treated above 373°C gave an unknown phase.

The original sample and samples heated below 202°C show bands at 1004, 986, 942, 641 and 559 cm^{-1}, and the sample heated at 250°C shows bands at 1004, 975, 830, 631 and 559 cm^{-1}. Samples treated above 299°C show bands at 969, 830 and 559 cm^{-1}. According to the literature, bands due to the orthorhombic bronze[6,12] appeared at 1004 (835), 626 and 569 cm^{-1}, and those due to the rhombic MoO_3[13–15] at 998, 878, 820 and 557 cm^{-1}. As described above, bands for the original sample agree with those for the orthorhombic phase except for the band at 942 cm^{-1}. This suggests that the band at 942 cm^{-1} should be a characteristic band for the blue monoclinic bronze. On the other hand, bands of the samples treated above 299°C are for the rhombic MoO_3 but there is a small difference. As mentioned above, X-ray and thermogravimetric data proved that samples treated above 299°C were composed of a nonstoichiometric compound with a rhombic MoO_3 phase. It is, therefore, assumed that small shifts in frequencies resulted from this nonstoichiometry.

The gas eliminated from the sample was confirmed to be only H_2O and no other gas was detected. As in the case of $H_{0.30}MoO_3$,[8] this means that hydrogen atoms reacted with lattice oxygen and H_2O was produced.

Figure 2 shows plots of α against temperature. Curve I is the change in α at the isothermal-heating temperature and curve II that in α obtained from the weight loss by increasing temperature with a heating rate of 1.6°C min^{-1}. There is little difference in α over a temperature range of 100–300°C between samples obtained by isothermal treatment and by treatment by increasing temperature. In this range curve II could be expected to approach curve I if samples were heated at a heating rate slower than 1.6°C min^{-1}. Curve II shows discontinuity at points A, B and C. The change in α from C to D was small but steep. Considering X-ray and thermogravimetric results, α and the corresponded temperature were estimated as follows: (A) $\alpha = 0.30$ (232°C), (B) $\alpha = 0.75$ (290°C), (C) $\alpha = 0.98$ (375°C), and (D) $\alpha = 1.00$ (378°C). Consequently, the hydrogen content could be calculated from these values, and the composition of the stable phase at each point was also determined. Therefore, it is concluded that the decomposition of $H_{0.83}MoO_3$ proceeds by four steps as follows:

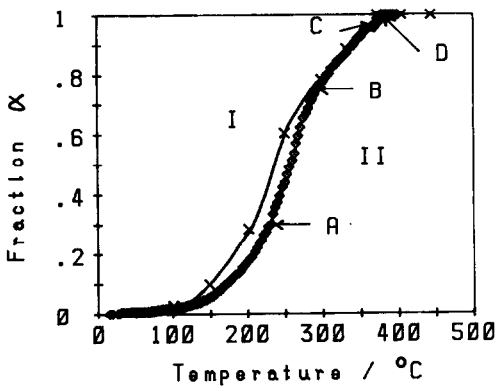


Fig. 2. Plot of α against temperature. Curve I = isothermal heat treatment, and curve II = heat treatment by increasing temperature.

$$H_{0.83}MoO_3 \xrightarrow{\sim 232°C} H_{0.58}MoO_{2.88},^{*} \quad (1)$$

$$H_{0.58}MoO_{2.88} \xrightarrow{\sim 290°C} H_{0.21}MoO_{2.69},^{\dagger} \quad (2)$$

$$H_{0.21}MoO_{2.69} \xrightarrow{\sim 375°C} H_{0.02}MoO_{2.60},^{\ddagger} \quad (3)$$

$$H_{0.02}MoO_{2.60} \xrightarrow{\sim 378°C} MoO_{2.59}.^{\S} \quad (4)$$

Processes (1) and (2) are the decomposition from the mixture of orthorhombic and monoclinic phases to the orthorhombic phase. This means that decomposition from the monoclinic to the orthorhombic phase occurs and hydrogen reacts easily with lattice oxygen. As reported previously,[8] the blue orthombic bronze decomposed through the isomorphous compound with a rhombic MoO_3 phase to the nonstoichiometric compound with a rhombic MoO_3 phase. In the present work, processes (3) and (4) correspond to these processes and complete removal of hydrogens, which should be distributed sparsely, takes place without any structural change.

Acknowledgement—This work was partly supported by the Hyogo Prefecture Foundation for Promotion of Science and Technology, for which I am thankful.

* Mixture of orthorhombic and monoclinic phases.

† Orthorhombic phase.

‡ Isomorphous with the rhombic MoO_3 phase.

§ Nonstoichiometric compound with rhombic MoO_3 and unknown phases.

REFERENCES

1. J. J. Birtill and P. G. Dickens, *Mater. Res. Bull.* 1978, **13**, 311.
2. K. A. Wilhelm, *Acta Chem. Scand.* 1969, **23**, 419.

3. P. G. Dickens, J. J. Birtill and C. J. Wright, *J. Solid State Chem.* 1979, **28**, 185.
4. F. A. Schroeder and H. Weizel, *Z. Anorg. Allg. Chem.* 1977, **435**, 247.
5. R. C. Slade, T. K. Halstead and P. G. Dickens, *J. Solid State Chem.* 1980, **34**, 183.
6. N. Sotani, Y. Kawamoto and M. Inui, *Mater. Res. Bull.* 1983, **18**, 797.
7. N. Sotani, M. Kunitomo and M. Hasegawa, *Chem. Lett.* 1983, 647.
8. N. Sotani, N. Yoshida, Y. Kawamoto, S. Kishimoto and M. Hasegawa, *Bull. Chem. Soc. Jpn* 1984, **57**, 3032.
9. O. Glemser and G. Lutz, *Z. Anorg. Allg. Chem.* 1951, **264**, 17; 1956, **285**, 173.
10. O. Glemser and G. Lutz, *Z. Anorg. Allg. Chem.* 1952, **269**, 93.
11. C. Choain and F. Marion, *Bull. Chem. Soc. Fr.* 1963, 212.
12. N. Sotani, Y. Yoshida, Y. Yoshioka and S. Kishimoto, *Bull. Chem. Soc. Jpn* 1985, **58**, 1626.
13. N. Sotani, Y. Saito, M. Oita and M. Hasegawa, *Nippon Kagaku Kaishi* 1974, 673.
14. K. Nakamoto, *Infrared Spectra of Inorganic and Coordination Compounds.* John Wiley, New York (1971).
15. J. R. Feraro, *Low Frequency Vibration of Inorganic Compounds.* Plenum Press, New York (1971).

Polyhedron Vol. 5, No. 1/2, pp. 71–73, 1986
Printed in Great Britain

0277–5387/86 $3.00 + .00
© 1986 Pergamon Press Ltd

TEMPERATURE-PROGRAMMED DECOMPOSITION STUDIES OF A HYDROGEN MOLYBDENUM BRONZE, $H_{0.83}MoO_3$

NORIYUKI SOTANI* and MASATOMO HASEGAWA

College of Liberal Arts, Kobe University, Tsurukabuto, Nada, Kobe 657, Japan

(*Received* 18 *June* 1985)

Abstract—A temperature-programmed decomposition (TPD) study of a hydrogen molybdenum bronze, $H_{0.83}MoO_3$, is reported. TPD spectra obtained from changes in pressure showed four bands (PI, PII, PIII and PIV); activation energies, E_a, determined from the shifts in maximum peak temperatures were 23.8 (PI), 106.7 (PII), 118.6 (PIII) and 164.3 (PIV) kJ mol^{-1}. E_as obtained from thermogravimetric data varied from 52.7 to 153.2 kJ mol^{-1} as the fraction reacted increased. E_as obtained from both methods were in good agreement.

It is reported in this issue[1] that the thermal decomposition of a hydrogen molybdenum bronze, $H_{0.83}MoO_3$, took place by four steps as follows:

$$H_{0.83}MoO_3 \xrightarrow{\sim 232°C} H_{0.58}MoO_{2.88}$$
$$\xrightarrow{\sim 290°C} H_{0.21}MoO_{2.69}$$
$$\xrightarrow{\sim 375°C} H_{0.02}MoO_{2.60}$$
$$\xrightarrow{\sim 378°C} MoO_{2.59}.$$

$H_{0.83}MoO_3$ is a mixture of orthorhombic and monoclinic phases and it decomposes to $MoO_{2.59}$, a nonstoichiometric compound with a rhombic MoO_3 phase through the orthorhombic phase. During the decomposition, hydrogens in the bronze reacted with lattice oxygen and H_2O was, therefore, produced. In the present work, the bronze was studied by a temperature-programmed decomposition (TPD) technique and the authors tried to compare the results obtained for changes in pressure and weight.

EXPERIMENTAL

A hydrogen molybdenum bronze, $H_{0.83}MoO_3$, was prepared by Glemser's method,[2] and was a mixture of blue orthorhombic and blue monoclinic phases.[1]

A high-vacuum line was used for the experiment.[3] Samples were studied by the TPD technique. The TPD spectrum was obtained from the change in pressure by using a Pirani gauge and thermogravimetric data were obtained by using a Cahn electromicrobalance. The rate of heating was controlled by a temperature-programmed controller.

RESULTS AND DISCUSSION

The bronze $H_{0.83}MoO_3$ was degassed at room temperautre in a vacuum of 10^{-4} torr for 1 h and then heated at various heating rates (βs) (1.6–6.9°C min^{-1}). The change in pressure was recorded with a Pirani gauge. Figure 1 shows TPD spectra at β 1.6, 3.4, 4.5 and 6.9°C min^{-1}. A small band appeared below 150°C, but above 150°C the TPD spectrum showed two distinct peaks at around 300 and 400°C, and two shoulders at around 200 and 350°C. This suggests that the spectrum may be composed of four bands and the line shape of each band may be symmetrical. Therefore, the spectra above 150°C could be analysed by using a computer.[3] One of the results is shown in Fig. 2. This shows that the spectrum above 150°C consists of four bands (PI, PII, PIII and PIV). The peak temperatures are denoted as T_m(I), T_m(II), T_m(III) and T_m(IV) in order from the lowest temperature. All spectra in Fig. 1 were analyzed by the same technique. Shifts in each peak temperature to a higher temperature were observed when β was increased. The T_m(I) appeared over a temperature range of 198–281°C and the

* Author to whom correspondence should be addressed.

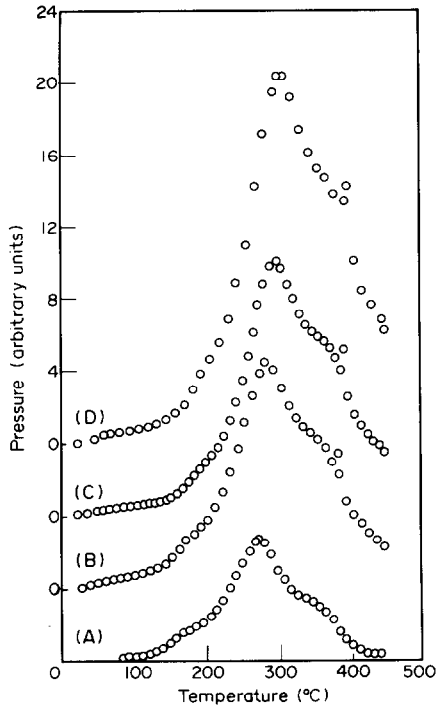


Fig. 1. TPD spectra of the samples heated at various heating rates: (A) 1.6, (B) 3.4, (C) 4.5, and (D) 6.9°C min^{-1}.

T_m(II) at 270–299°C. The T_m(III) and T_m(IV) appeared at 331–362 and 369–400°C, respectively.

The activation energy, E_a, can be estimated from the shift in the peak temperatures.[4] The plot of $-\ln(\beta T_m^{-2})$ vs $1/T_m$ is a straight line and the slope corresponds to E_a/R, where R is constant. From the slope, E_a was determined to be 23.8 (PI), 106.7 (PII), 118.6 (PIII) and 164.3 (PIV) kJ mol^{-1}, respectively.

The rising-temperature technique has been widely used in kinetic investigation of thermal decomposition and other reactions of solids.[4–7] Applying this technique, Ozawa[7] proposed a simple and useful method to analyze thermogravimetric data and determine the E_a of the decomposition of calcium oxalate and the degradation of Nylon 6. According to his technique, E_a can be easily determined as follows: initially the fraction reacted, α, is plotted against the reciprocal absolute temperature ($1/T$), and the value of $1/T$ corresponding to the $1-\alpha$ of each β curve can be estimated. Secondly, E_a can be determined from the plot of log β vs $1/T$ obtained from the above plot. If the decomposition proceeds in one step, E_a estimated from plots of log β vs $1/T$ should be equal at every α.

Figure 3 shows plots of E_a at every 0.05 of $1-\alpha$. Vertical arrows indicate the $1-\alpha$ which corresponds to stable phases in the decomposition process as described previously.[1] E_a varies greatly, from 52.7 to 153.2 kJ mol^{-1}, with the increase in α. Analysing in detail, E_a increases gradually at first, is constant over the range of $\alpha = 0.45$–0.85, and finally increases steeply. Also in Fig. 3 the ranges of $1-\alpha$ corresponding to the peaks of the TPD spectra are indicated by horizontal bidirectional arrows. As mentioned previously, T_m(I) appeared over a very wide range and over that range E_a also varied widely as shown in Fig. 3. Considering these results, it is reasonable that disagreement exists on the E_a obtained from the change in pressure and weight loss. On the other hand, E_as of PII, PIII and PIV are a

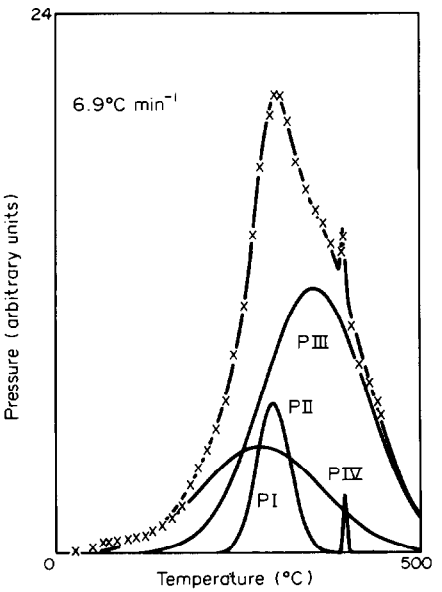


Fig. 2. Analysis of TPD spectrum of the sample treated at a heating rate of 6.9°C min^{-1}. (×) Observed, and (—) calculated.

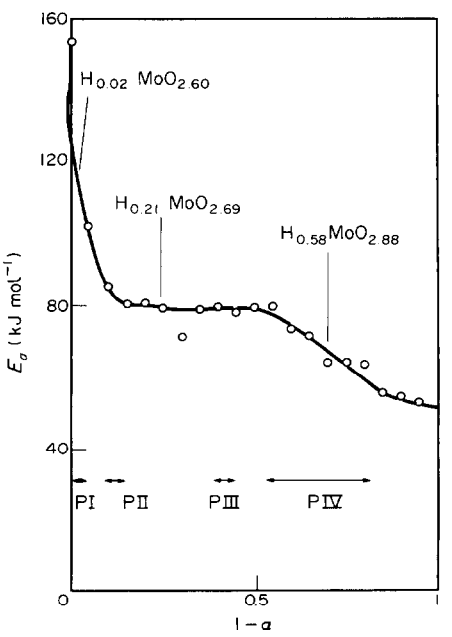


Fig. 3. Plot of E_a vs $1-\alpha$.

little larger than that in Fig. 3, but they agree well with each other.

Acknowledgement—This work was partly supported by the Hyogo Prefecture Foundation for Promotion of Science and Technology, for which we are thankful.

REFERENCES

1. N. Sotani, *Polyhedron* 1986, **5**, 67.
2. O. Glemser and G. Lutz, *Z. Anorg. Allg. Chem.* 1951, **264**, 17; 1956, **285**, 173.
3. N. Sotani, N. Yoshida, Y. Kawamoto, S. Kishimoto and M. Hasegawa, *Bull. Chem. Soc. Jpn* 1984, **57**, 3032.
4. C. H. Banford and C. F. H. Tipper (Eds) *Comprehensive Chemical Kinetics*, Vol. 22. Elsevier, Amsterdam (1980).
5. P. Murray and J. White, *Trans. Br. Ceram. Soc.* 1955, **54**, 202.
6. C. D. Doyle, *J. Appl. Polym. Sci.* 1961, **5**, 285; 1962, **6**, 639.
7. T. Ozawa, *Bull. Chem. Soc. Jpn* 1965, **38**, 1881.

Polyhedron Vol. 5, No. 1/2, pp. 75–78, 1986
Printed in Great Britain

0277-5387/86 $3.00 + .00
© 1986 Pergamon Press Ltd

THE ADSORPTION OF HEPTAMOLYBDATE IONS ON OXIDIC SURFACES

J. A. R. VAN VEEN* and P. A. J. M. HENDRIKS

Koninklijke/Shell-Laboratorium, Amsterdam (Shell Research B.V.), P.O. Box 3003, 1003 AA Amsterdam, The Netherlands

(*Received* 19 *June* 1985)

Abstract—The adsorption of ammonium heptamolybdate (AHM) on γ-Al_2O_3 is governed by the basic surface hydroxyl groups. Having determined the number of these groups on the γ-Al_2O_3 used, we can give a quantitative description of the adsorption isotherm. When too highly concentrated AHM solutions are used, a (surface) precipitate is formed as well. On TiO_2, only the formation of a surface precipitate is observed, even at low [AHM]; this effect is probably due to the acidic surface OH groups. On SiO_2, not much adsorption takes place, but AHM reacts with the oxide to form a molybdosilicate solution species.

The qualitative features of the interaction of aqueous ammonium heptamolybdate (AHM) solutions with γ-Al_2O_3 are well known:[1] important are those OH groups on the γ-Al_2O_3 surface which can be released into solution as OH^- ions, and the reaction between these OH^- ions and heptamolybdate to form MoO_4^{2-}. Adsorption occurs through electrostatic attraction between the positively charged Al_2O_3 surface and the molybdate ions in solution:

$$Al_s—OH \rightleftarrows Al_s^+ + OH^-, \quad (1)$$

$$Mo_7O_{24}^{6-} + 8OH^- \rightleftarrows 7MoO_4^{2-} + 4H_2O, \quad (2)$$

$$2Al_s^+ + MoO_4^{2-} \rightleftarrows (Al_s)_2MoO_4, \quad (3)$$

$$6Al_s^+ + Mo_7O_{24}^{6-} \rightleftarrows (Al_s)_6Mo_7O_{24}, \quad (4)$$

where the subscript s denotes surface species. As to the shape of the AHM–γ-Al_2O_3 adsorption isotherm and the limiting adsorption level, no unanimity exists, no less than five different isotherms having been reported.[1–5] Interestingly, the maximum Mo uptake is found to increase with increasing ratio of the weight of γ-Al_2O_3 to the volume of the AHM solution used in the adsorption experiments. Also, some isotherms show only one plateau region, while others show two. We have attempted to resolve this problem, and in this poster we will: (i) describe what we think is the true adsorption isotherm, (ii) offer an explanation of its form and the limiting adsorption capacity observed, (iii) indicate under which conditions deviations from this isotherm may occur, and (iv) describe some results concerning the adsorption of AHM on TiO_2 and SiO_2, and compare them with those obtained for γ-Al_2O_3.

EXPERIMENTAL

Adsorption isotherms were determined as follows. The oxide was contacted with aqueous AHM solutions in various ratios (standard 2g/100 cm^3) and the mixture shaken occasionally. After the desired adsorption time, 1–14 days, the Mo uptake was determined by measuring the Mo concentration left in solution (atomic absorption spectrometry) and/or the Mo content of the solid (X-ray fluorescence). To gauge the stability of AHM solutions, blank experiments were performed. The number of basic hydroxyl groups on γ-Al_2O_3 was determined through adsorption of $MoO_2(acac)_2$, a complex extremely sensitive to OH^-, from a methanolic solution.[6] IR spectra of γ-Al_2O_3 before and after AHM adsorption were recorded on a Digilab FT instrument. Raman spectra were determined with a Spex Ramalog spectrometer and TPR profiles were measured on a laboratory-built instrument.

The oxides used were: γ-Al_2O_3, AC 300 (Shell) (250 $m^2\ g^{-1}$); TiO_2, P25 (ex Degussa) (50 $m^2\ g^{-1}$); and SiO_2 spheres (Shell) (285 $m^2\ g^{-1}$).

* Author to whom correspondence should be addressed.

RESULTS AND DISCUSSION

The AHM–γ-Al_2O_3 adsorption isotherm, obtained under conditions such that no precipitates develop in solution on a time scale comparable to that of the adsorption experiment and that a true equilibrium has been reached (cf. below), is shown in Fig. 1. To see whether the shape and the limiting Mo uptake are explicable in terms of eqns (1)–(4), we need an independent measurement of the number of surface OH groups that can react according to eqn (1). For our γ-Al_2O_3 sample, $MoO_2(acac)_2$ adsorption leads to a value of 0.80 mmol g^{-1}. That in fact only the basic OH groups are involved in the adsorption of $MoO_2(acac)_2$ as well as of AHM follows from the observation that, as expected,[7] in both cases only the high-frequency band in the OH stretch region of the IR spectrum of γ-Al_2O_3 had disappeared. The quantitative description of the isotherm is now easy.

At low [AHM], i.e. when the [AHM]/basic OH molar ratio in the system is smaller than 8, there are sufficient hydroxyl ions to depolymerize all heptamolybdate (HM) ions [eqn (2)], and the adsorption reaction proceeds, in the first instance, according to eqns (1)–(3):

$$8Al_s\text{—}OH + Mo_7O_{24}^{6-} \rightarrow 4(Al_s)_2MoO_4 + 3MoO_4^{2-}. \quad (5)$$

However, there are still some basic OH groups left, and if the pH of the solution is lower than the isoelectric point (IEP) of the solid, these will start dissociating, which will in turn lead to adsorption of some of the MoO_4^{2-} ions still left in solution. That is, more Mo will be adsorbed than follows from eqn (5) and the deviation will be larger the lower the Mo loading (IEP of our γ-Al_2O_3 sample is about 8.2, it decreases with increasing Mo loading; the pH of an AHM solution is around 5). When the [AHM] and the amount of OH groups just balance, eqn (5) predicts an adsorption of 0.038 g Mo $(g\ Al_2O_3)^{-1}$ at $c' = 0.86 \times 10^{-3}$ M AHM. The actual isotherm and that predicted by eqn (5) do indeed meet at this point (Fig. 1). Thus, the first part of the adsorption isotherm can be accounted for in terms of eqns (1), (3) and (5).

At higher [AHM], there are not sufficient OH^- ions to depolymerize all the HM ions, and so, after all basic OH groups have reacted, we are left with a mixture of MoO_4^{2-} and $Mo_7O_{24}^{6-}$ ions, the latter increasingly predominating as [AHM] increases. Adsorption now occurs according to eqns (3) and (4). In the limit [AHM] $\rightarrow \infty$, eqn (4) predicts an adsorption of 0.090 g Mo $(g\ Al_2O_3)^{-1}$, and so, after the first plateau, the isotherm will rise again and strive towards this limiting value, as observed (Fig. 1).

Under which conditions can isotherms be obtained that deviate from the one just discussed? Isotherms without the first plateau are obtained when the adsorption time is too short. This is due to the fact that splitting off OH^- ions to increase the pH towards the IEP value is a very slow process, as is also observed in the absence of AHM (it takes about a week to reach equilibrium). This state of affairs is reflected in the pH of the AHM solution after the adsorption experiment: while adsorption occurs according to eqn (5) the pH does not rise above 6; only after all the AHM has reacted and the second process comes into play [eqns (1) and (3)] does the pH slowly rise to reach, at lower [AHM], 7.8 at equilibrium.

Sometimes[2,3] rather high ratios of the weight of Al_2O_3 to the volume of AHM solution are used in the determination of the adsorption isotherm. Under these conditions, much higher loadings of Mo can be achieved, as we have verified. However, rather concentrated AHM solutions have to be applied here, and these tend to be unstable, developing a precipitate {presumably[8] $[(NH_4)_6Mo_8O_{27}]_n$} in a matter of hours at the highest concentration (2.2 M in Mo). In other words, the high Mo loadings are not so much due to adsorption as to precipitation (see below). We have found that where the adsorption time is much shorter than the time needed for a precipitate to develop in solution, no precipitated phase is present on the Al_2O_3 surface.

We propose, then, the existence of three surface

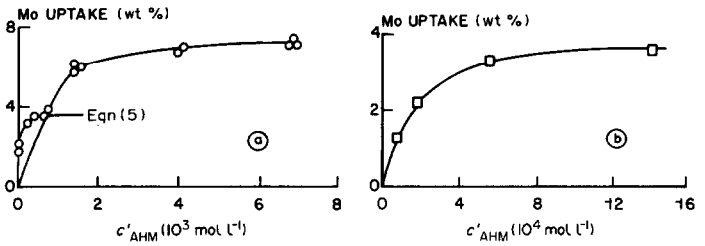


Fig. 1. Adsorption isotherms of AHM on γ-Al_2O_3 (a) and TiO_2 (b).

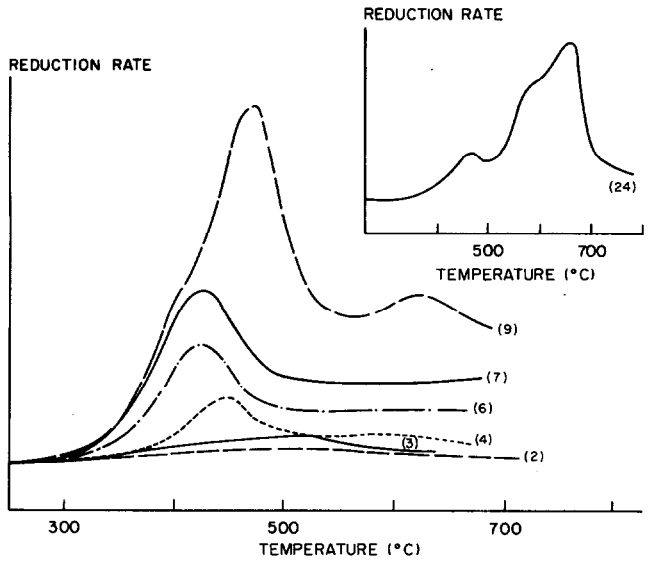


Fig. 2. TPR profiles of AHM–γ-Al_2O_3 catalysts (numbers in parentheses give the wt % Mo in the samples).

species: (i) adsorbed monomolybdate, (ii) adsorbed HM, and (iii) a precipitate. It turns out that these three species can be distinguished by TPR and Raman spectroscopy. Typical TPR profiles are shown in Fig. 2. A sample is first calcined at 600°C in 5% O_2 in He, and after cooling down a TPR is run using 5% H_2 in N_2 (heating rate 5°C min^{-1}; gas flow 6 cm^3 min^{-1}). It is apparent that at low loadings a Mo species is present which is difficult to reduce (T_{max} about 530°C, amount of H_2 consumed per Mo in the temperature interval 200–665°C, H_2/Mo, about 0.2), and that between 4 and 7% wt Mo, a more easily reducible species becomes dominant (T_{max} about 425°C, H_2/Mo increases to 0.37), corresponding to (the calcination products of) adsorbed monomolybdate and HM, respectively. At still higher loadings (9 and 24 wt % in Fig. 2) a third feature develops, which is due to the (surface) precipitate, and is characterized by a relatively high T_{max} and high H_2/Mo (around 1.0).

Raman spectroscopy of the dried samples also shows the existence of three different species: at low Mo loadings we observe a small, broad band at about 965 cm^{-1}, above 4% Mo a second broad band appears centred at about 995 cm^{-1}, while the precipitates are characterized by two sharp bands at 995 and 955 cm^{-1}, and a broad feature at 635 cm^{-1}. In sum, the TPR and Raman data are fully consistent with the adsorption scheme proposed here. Thus, the true AHM–γ-Al_2O_3 adsorption isotherm is the one shown in Fig. 1; it can be explained in terms of eqns (1)–(5), and deviations can occur, at low loadings, when the adsorption time is too short, and at high loadings when the AHM solutions used are not stable enough.

TiO_2

Since TiO_2 also contains basic surface OH groups—in the case of our sample 0.14 mmol g^{-1} (determined by F^- exchange[9])—an adsorption behaviour similar to that of γ-Al_2O_3 might have been expected. However, much more Mo is adsorbed than can be accounted for in terms of the basic OH groups [max. 1.6 wt % Mo (Fig. 1b)]. Since TiO_2 contains quite a few fairly acidic surface OH groups as well (in the present case, 0.33 mmol g^{-1}, determined by NaOH adsorption[9]), and since insoluble species tend to form in AHM solution when it is acidified,[8] we suggest that TiO_2 does not really adsorb a Mo species, but that it catalyses the formation of a surface precipitate. TPR results, in showing a highly reducible species (H_2/Mo about 0.8), and the Raman spectrum of the 3.7% Mo–TiO_2 sample, being similar to that of the precipitate referred to above (although shifted to higher wavenumbers, the doublet now appearing at 1057 and 1044 cm^{-1}), do not disagree with this suggestion.

SiO_2

Silica does not posses basic surface hydroxyl groups and so eqns (1)–(4) will not be appropriate. On the other hand, although many acidic silanol groups are present, a surface precipitate does not form either. Instead, $Mo_7O_{24}^{6-}$ ions react with SiO_2

to form $[SiMo_{12}O_{40}]^{4-}$ ions, which are subsequently released into solution [little Mo is left on the SiO_2 surface (less than 1 wt %)]. The occurrence of this reaction has been suggested before.[10]

Acknowledgements—We would like to thank Mr E. J. G. M. Romers for the TPR experiments, Dr C. A. Emeis for the IR measurements, and Dr C. A. Emeis and Mr H. de Wit for the Raman work.

REFERENCES

1. See, for example, A. Iannibello and P. C. H. Mitchell, In *Preparation of Catalysts. II* (Edited by B. Delmon, P. Grange, P. Jacobs and G. Poncelet), p. 469. Elsevier, Amsterdam (1979).
2. M. A. Aulmann, G. J. Siri, M. N. Blanco, C. V. Caceres and H. J. Thomas, *Appl. Catal.* 1983, **7**, 139.
3. G. A. Tsigdinos, H. Y. Chen and B. J. Streusand, *Ind. Eng. Chem. Prod. Res. Dev.* 1981, **20**, 619.
4. L. Wang and W. K. Hall, *J. Catal.* 1982, **77**, 232.
5. N. P. Martinez, P. C. H. Mitchell and P. Chiplunker, *J. Less-Common Met.* 1977, **54**, 33.
6. J. A. R. van Veen, to be published.
7. H. Knözinger and P. Ratnasamy, *Catal. Rev.—Sci. Eng.* 1978, **17**, 31.
8. K.-H. Tytko and O. Glemser, *Adv. Inorg. Chem. Radiochem.* 1976, **19**, 239.
9. J. A. R. van Veen, F. T. G. Veltmaat and G. Jonkers, submitted to *J. Chem. Soc., Chem. Commun.*
10. N. N. Chumachenko, T. M. Yurieva, D. V. Tarasova and G. I. Aleshina, *React. Kinet. Catal. Lett.* 1980, **14**, 87.

Polyhedron Vol. 5, No. 1/2, pp. 79–86, 1986
Printed in Great Britain

0277-5387/86 $3.00 + .00
© 1986 Pergamon Press Ltd

MULTI-ELECTRON REDUCTION SITES OF POLYMOLYBDATES AS PHOTOREDOX CATALYSTS

TOSHIHIRO YAMASE

Research Laboratory of Resources Utilization, Tokyo Institute of Technology, 4259 Nagatsuta, Midori-ku, Yokohama 227, Japan

(*Received* 14 *June* 1985)

Abstract—During our studies on the photochemistry of polyoxometalates we have found that the polyoxometalates are potential photosensitizers and electron relay species in redox cycles for chemical conversion of light energy. This paper describes the characterization of multi-electron reduction sites in $[Mo_8O_{26}(MoO_4)_2]^{8-}$ and $[Mo_7O_{24}]^{6-}$, based on the analysis of ESR spectra for UV-irradiated $[NH_3Me]_8[Mo_8O_{26}(MoO_4)_2]\cdot 2H_2O$ and $[NH_3Pr^i]_6[Mo_7O_{24}]\cdot 3H_2O$ single crystals. The ESR spectra show the formation of two distinct localized $Mo(V)O_5(OH)$ sites in the lattice. The analysis of the ESR parameters g, $^{95,97}Mo$ hyperfine structure, and ^1H superhyperfine structure indicates the direct participation of H1*s* in the half-occupied molecular orbital. From the direction of the maximum principal value of the ^1H superhyperfine tensor, which lies close to the Mo(V) . . . $H^+(O)$ direction, two paramagnetic sites in the anion can be determined. The results show that the multi-electron photoreduction consists of separate and independent one-electron reductions at four and two octahedral sites in $[Mo_8O_{26}(MoO_4)_2]^{8-}$ and $[Mo_7O_{24}]^{6-}$, respectively. On the other hand, a single crystal of $[NH_2Pr^i_2]_4[H_{1.5}W_{10}O_{32}]\cdot 8H_2O$, which was a photochemically 1.5-electron reduced species, exhibits extensive delocalization of the paramagnetic electron (around $g = 1.84$) interacting with eight equivalent hydrogen-bonding protons.

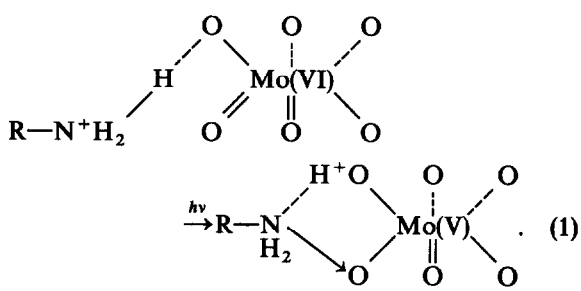
During our studies of the photoredox reactions of polyoxometalates with water,[1] carboxylic acids,[2] alcohols,[3] alkynes[4] and alkenes,[5] photoreactive centers of the alkylammonium polymolybdates

$$[NH_3Pr^i]_6[Mo_8O_{26}(OH)_2]\cdot 2H_2O$$

and

$$[NH_3Pr]_6[Mo_7O_{24}]\cdot 3H_2O$$

have been investigated by single-crystal ESR.[6,7] The reduction of Mo(VI) to Mo(V) proceeds via photoexcitation of the oxygen-to-molybdenum charge-transfer band in a terminal Mo=O bond with an accompanying transfer of a hydrogen-bonding proton from alkylammonium nitrogen to a bridging oxygen atom, followed by an interaction of the nonbonding electrons of the amino nitrogen with the terminal oxo-group leading to a charge-transfer complex (**I**) as shown in reaction (1):



(1)

I

Single-crystal ESR spectra of the UV-irradiated alkylammonium polyoxomolybdates at room temperature shows the formation of a localized Mo(V) site. Based on the analysis of ESR parameters, the paramagnetic site in the anion has been determined in correlation with the X-ray crystal structure data.

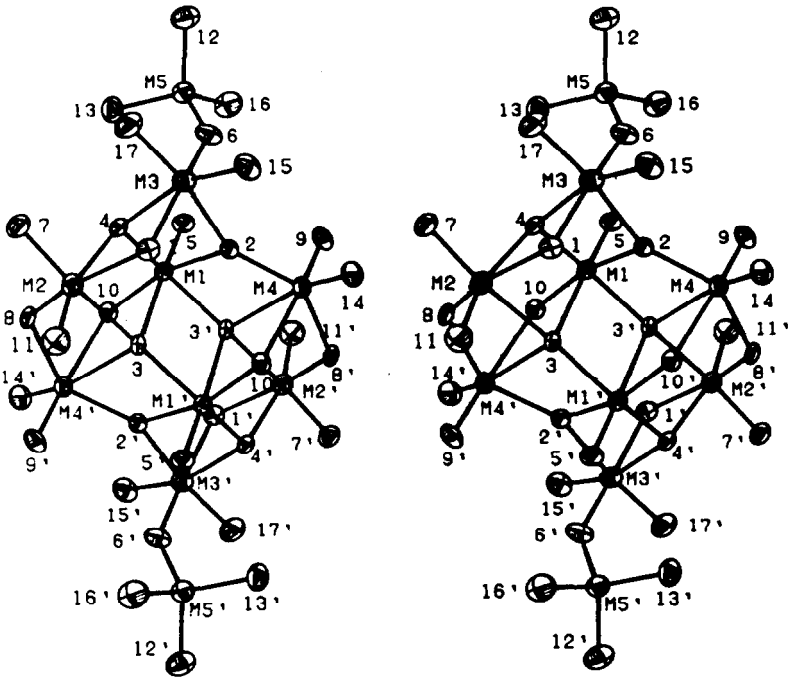


Fig. 1. Stereoscopic drawing of $[Mo_{10}O_{34}]^{8-}$. M represents an Mo atom.

The Mo(V) site in the $[Mo_8O_{26}(OH)_2]^{6-}$ lattice has been observed at the octahedral site where the molybdenum atom originally co-ordinates a hydroxide group.[6] The Mo(V) formation in the $[Mo_7O_{24}]^{6-}$ lattice occurs at the end of three octahedra in a line in the central horizontal level of the $[Mo_7O_{24}]^{6-}$ polyhedral configuration.[7] Studies of the paramagnetic sites in the polyoxoanions have been extended to the decamolybdate $[Mo_{10}O_{34}]^{8-}$ and decatungstate $[W_{10}O_{32}]^{4-}$. The structural configuration of the

$$[Mo_{10}O_{34}]^{8-} \equiv [Mo_8O_{26}(MoO_4)_2]^{8-}$$

lattice,[8] having an arrangement of eight edge-shared distorted MoO_6 octahedra linked by a pair of distorted MoO_4 tetrahedra as shown in Fig. 1, is the same as that of dihydrogen octamolybdate $[Mo_8O_{26}(OH)_2]^{6-}$ as found by us.[9] Although structurally very similar, $[Mo_8O_{26}(MoO_4)_2]^{8-}$ in this work is a linkage isomer of the decamolybdate reported by Fuchs *et al.*[10] These two decamolybdates can be distinguished by a different linkage of the MoO_4 groups.

EXPERIMENTAL

Octakis (methylammonium) decamolybdate (VI) dihydrate, $[NH_3Me]_8[Mo_{10}O_{34}]\cdot 2H_2O$, was obtained by the method previously described.[11]* Single crystals were grown by slow evaporation from aqueous solutions at room temperature. Well-developed colorless crystals of approximate dimensions $3 \times 2 \times 1$ mm were obtained. The crystal is monoclinic with $a = 12.596$ Å, $b = 17.175$ Å, $c = 10.653$ Å, $\beta = 91.40°$, $Z = 2$, $R = 0.041$ and space group $P2_1/n$. The two molecules in the unit cell, being related by a center of inversion, are magnetically equivalent. A crystal was irradiated at room temperature with UV light of $\lambda \geqslant 313$ nm from a 500-W super-high-pressure mercury lamp in conjunction with filters. After about 30 min of irradiation, the crystal, which is reddish brown, was mounted on a quartz rod for the ESR study.

Blue single crystals of

$$[NH_2Pr^i_2]_4[H_{1.5}W_{10}O_{32}]\cdot 8H_2O$$

were prepared by irradiating the deaerated aqueous solution of $[NH_2Pr^i_2]_4[W_{10}O_{32}]$ at pH 2 with

* MAM, IPAM, PAM and 6IAP8M2 in Ref. 11 must be rewritten as

$[NH_3Me]_8[Mo_{10}O_{34}]\cdot 2H_2O$,

$[NH_3Pr^i]_6[Mo_7O_{24}]\cdot 3H_2O$,

$[NH_3Pr]_6[Mo_7O_{24}]\cdot 3H_2O$

and

$[NH_3Pr^i]_6[Mo_8O_{26}(OH)_2]\cdot 2H_2O$,

respectively.

UV light. The crystal is monoclinic with $a = 11.48$ Å, $b = 12.22$ Å, $c = 10.79$ Å, $\beta = 100.3°$, $Z = 2$, $R = 0.12$ and space group $P2_1/n$. Analysis of W(V) in the crystal was carried out at room temperature by titration of $KMnO_4$ for the aqueous solution of the blue crystal under an atmosphere of nitrogen, which resulted in the disappearance of the blue color due to W(V). Blue crystals consisted of one- and two-electron reduction species in *ca* 1:1 molar ratio, since the absorption spectrum of the deaerated aqueous solution of the blue crystal exhibited absorption maxima at 780 and 630 nm due to one- and two-electron reduced species, respectively.[3]

ESR experiments were performed on a Varian E-12 spectrometer with *X*-band (100-kHz field modulation). DPPH was used as a field marker. Spectra were recorded at intervals of 10°, as the magnet was rotated about each of the orthogonal *X*-, *Y*- and *Z*-axes to which our results were referred. After completion of ESR measurements the orientation of the body-fixed orthogonal *X*-, *Y*- and *Z*-axes with respect to the crystallographic axes was determined by both oscillation and Weissenberg photographs.

RESULTS AND DISCUSSION

Multi-electron reduction sites in $[Mo_8O_{26}(MoO_4)_2]^{8-}$ *and* $[Mo_7O_{24}]^{6-}$

The spectrum obtained with the UV-irradiated

$$[NH_3Me]_8[Mo_{10}O_{34}]\cdot 2H_2O$$

single crystal reveals the presence of two paramagnetic Mo(V)(OH) sites, A and B, as shown in Fig. 2. The spectrum of each Mo(V) center consists of two sets of lines, a doublet and a sextet of doublet. The first set of lines is attributed to the interaction (*ca* 10 G) of the unpaired electron with a ^1H which has a nuclear spin (I) of $\frac{1}{2}$. The nature of this more intense set of lines corresponds to the zero nuclear spin ^{96}Mo atom. The second set of lines, of less intensity, characterizes the hyperfine spectrum of ^{95}Mo and ^{97}Mo further split by the same superhyperfine interaction of the first set of lines. The relative intensity of the two sets of lines agrees well with the molybdenum isotopic composition. The spectrum has been interpreted using the spin Hamiltonian [eqn (2)] with $S = \frac{1}{2}$, $I_{Mo} = \frac{5}{2}$ and $I_H = \frac{1}{2}$:

$$\mathcal{H} = \beta g \cdot H \cdot S + A_{Mo} \cdot I_{Mo} \cdot S + A_H \cdot I_H \cdot S. \quad (2)$$

ESR parameters g, A_{Mo} and A_H tensors have been obtained using successively a least-squares fitting subroutine and performing a direct diagonalization of the Hamiltonian. We have previously described this procedure elsewhere.[6,7] The results are given in Table 1. Two sets of tensor, g, A_{Mo} and A_H, can be referred to two magnetically inequivalent paramagnetic sites A and B in the unit cell, where two molecules are magnetically equivalent related to a center of inversion.[8] It is interesting that the parameters found in the present work are quite compatible with those for the octahedral Mo(V) site in $[Mo_8O_{26}(OH)_2]^{6-}$ or $[Mo_7O_{24}]^{6-}$.[6,7] This indicates that the sign choice for the tensor components of sites A and B is the same as that for the Mo(V) site in $[Mo_7O_{24}]^{6-}$, which gives the total spin density closest to unity. It is this which we report in Table 1. The non-coincidence of principal axes of the g- and A-tensors originates in the extensive d-orbital mixing allowed by the low-symmetry ligand field in the site, indicating the displacement of the directions of the principal g values from the Mo—O axes.

The principal values of $^{95,97}Mo$ hyperfine tensors in units of 10^{-4} cm^{-1} are 23.7, 40.2 and 73.5 for site A (28.0, 41.8 and 76.8 for site B). To an approximation,

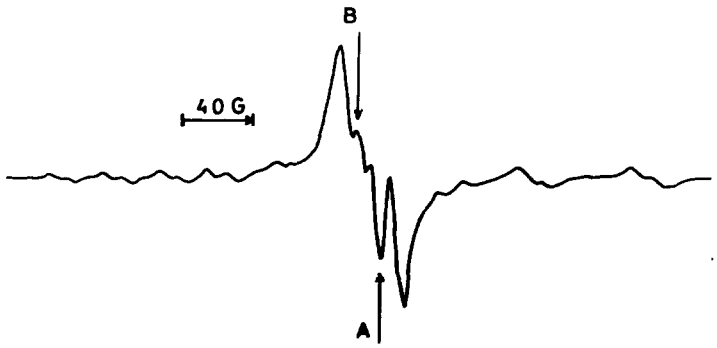


Fig. 2. Example of ESR spectrum obtained with an UV-irradiated crystal of $[NH_3Me]_8[Mo_{10}O_{34}]\cdot 2H_2O$ at room temperature. H_0 is in the ZX plane at an angle of 20° to the X-axis. A and B correspond to the two paramagnetic sites.

Table 1. ESR parameters of Mo(V) centers in polyoxomolybdates

Principal value		$[NH_3Me]_8[Mo_{10}O_{26}(MoO_4)_2]\cdot 2H_2O$ Site A	Site B	$[NH_3Pr^i]_6[Mo_8O_{26}(OH)_2]\cdot 2H_2O$[6]	$[NH_3Pr]_6[Mo_7O_{24}]\cdot 3H_2O$[7]	$[NH_3Pr^i]_6[Mo_7O_{24}]\cdot 3H_2O$[1] Site A	Site B
g[a]	g_1	1.899	1.899	1.897	1.895	1.899	1.898
	g_2	1.930	1.930	1.941	1.925	1.924	1.922
	g_3	1.949	1.949	1.955	1.937	1.935	1.936
	g_0	1.926	1.926	1.931	1.919	1.919	1.919
A_{Mo}[b]	A_{Mo1}	23.7	28.0	—[c]	23.4	30.7	28.5
	A_{Mo2}	40.2	41.8	—	42.0	34.0	37.1
	A_{Mo3}	73.5	76.8	—	69.9	74.5	74.7
	A_{Mo0}	45.8	48.9	—	45.1	46.4	45.8
A_H[d]	A_{H1}	6.57	6.87	8.69[e]	8.15	6.36	5.98
	A_{H2}	10.7	9.69	9.28	9.14	8.63	9.39
	A_{H3}	12.4	12.3	10.1	12.5	11.85	11.58
	A_{H0}	9.86	9.63	9.37	9.93	8.95	8.98

[a] $g_0 = (g_1+g_2+g_3)/3$.
[b] Units in 10^{-4} cm^{-1}, $A_{Mo0} = (A_{Mo1}+A_{Mo2}+A_{Mo3})/3$.
[c] The signals due to ^{95,97}Mo hyperfine structure were too weak to analyse at all orientations.
[d] Units in 10^{-4} cm^{-1}, $A_{H0} = (A_{H1}+A_{H2}+A_{H3})/3$.
[e] In Ref. 6 a choice of signs for ^{1}H tensors was not decided.

therefore, the hyperfine tensors are axial with $A_{Mo\parallel} = 73.5 \times 10^{-4}$ cm^{-1} (76.8×10^{-4} cm^{-1} for site B) and $A_{Mo\perp} = 31.9 \times 10^{-4}$ cm^{-1} (34.9×10^{-4} cm^{-1}). Defining an anisotropic hyperfine parameter for *d*-orbitals as $\frac{2}{7}(A_{Mo\parallel} - A_{Mo\perp})$ and dividing its value, 48.3×10^{-4} cm^{-1} (49.0×10^{-4} cm^{-1}), by $P = g\beta\gamma_{Mo}\langle r^{-3}\rangle_{4d}$ for ^{95,97}Mo (150.7 MHz[12] = 50.3×10^{-4} cm^{-1}) gives an estimate of 0.96 (0.97 for site B) for the spin population in Mo4*d* orbitals, when $A_{Mo\parallel}$ and $A_{Mo\perp}$ have the same sign. If $A_{Mo\parallel}$ and $A_{Mo\perp}$ are assumed to have opposite signs one obtains an estimated Mo4*d* contribution of 2.55. This constitutes an unacceptably large total spin density and strongly implies that $A_{Mo\parallel}$ and $A_{Mo\perp}$ have the same sign. The ^{95,97}Mo isotropic hyperfine interaction is equal to 45.8×10^{-4} cm^{-1} for site A (48.9×10^{-4} cm^{-1} for site B). The isotropic hyperfine interaction for unit spin density in the Mo5*s* orbital, which is obtained by computing $A = (8\pi g\beta\gamma/3)\psi^2(0)$, is 66.2×10^{-3} cm^{-1};[7,12] hence an Mo5*s* contribution of 0.07 for each of two sites is indicated. Since the physically most reasonable sign choice for ^{1}H superhyperfine tensor components is the positive sign, as discussed in a previous paper,[7] an H1*s* contribution of 0.02 may be derived from dividing $A_{H0} = 9.86 \times 10^{-4}$ cm^{-1} (9.63×10^{-4} cm^{-1} for site B) by the isotropic hyperfine interaction 474 $\times 10^{-4}$ cm^{-1}[13] for unit spin density in the 1*s* orbital of the H atom. The total spin density for site A is therefore $0.96 + 0.07 + 0.02 = 1.05$ (1.06 for site B), a reasonably satisfactory result.

The positive sign of the ^{1}H superhyperfine tensors indicates that H1*s* participates directly in the half occupied molecular orbital and that the highest of the principal values $A_{H3} = 12.4 \times 10^{-4}$ cm^{-1} for site A (12.3×10^{-4} cm^{-1} for site B) is approximately parallel to the Mo(V) . . . H$^+$(O) direction.[7] The proton at the photoreduced MoO_6 site in the UV-irradiated specimen of

$$[NH_3Pr^i]_6[Mo_8O_{26}(OH)_2]\cdot 2H_2O$$

and

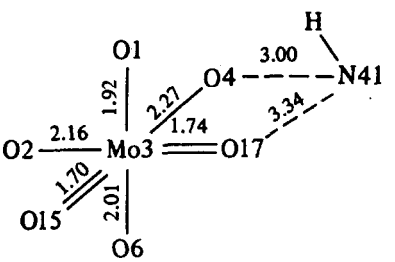
$$[NH_3Pr]_6[Mo_7O_{24}]\cdot 3H_2O$$

was derived from the transfer of the alkylammonium hydrogen-bonding proton to the bridging oxygen atom, which resulted from the photoexcitation of the l.m.c.t. band of the terminal Mo=O bond [eqn (1)].[6,7] The hydrogen-bonding proton at the Mo(V) site of the photoreduced $[Mo_{10}O_{34}]^{8-}$ would be situated around the N . . . O line in range of one-fourth to three-fourths of the N . . . O distance (2.77–3.20 Å)[8] from the oxygen atom, in conjunction with the fact that methylammonium N$^+$—H and hydroxide O—H distances are 0.68–0.83[8] and 0.82 Å, respectively. Since there was no significant change in both IR spectra and X-ray diffraction powder patterns between non-irradiated and irradiated samples, it is assumed that the structure of the parent oxidized form is retained upon irradiation, as proposed in the solid-state photochemistry of

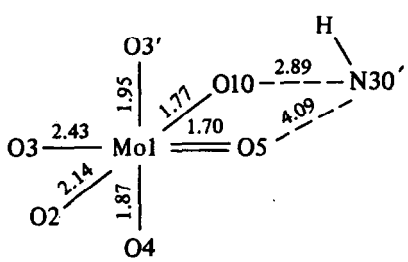
$$[NH_3Pr]_6[Mo_7O_{24}]\cdot 3H_2O.^7$$

Thus, the present ESR results are in agreement with the site symmetry determined for $[Mo_{10}O_{34}]^{8-}$. This enables us to determine the paramagnetic sites in the anion.

The molecule viewed in projection along the *Z*-axis is represented together with the principal A_{H3} directions in Fig. 3, where dotted lines indicate the N . . . O distance of 2.77–3.20 Å, with the involvement of a hydrogen-bonding proton. The Mo sites, in which the Mo . . . H$^+$(O) direction seems to accord well with the direction of the A_{H3} for each of molecular views projected along the *X*-, *Y*- and *Z*-axes, are determined. Thus, we can assign the paramagnetic site A to Mo3 . . . H$^+$ (O4 . . . N41) and site B to Mo1 . . . H$^+$ (O10 . . . N30′). Any other Mo sites are extremely improbable. As shown in (3) the Mo3 atom is surrounded by a distorted octahedral set of six O atoms, two of which belong to the terminal doubly bonded *cis*-dioxo group and four are bridging. This arrangement resembles the photoreducible MoO_6 sites in two anions, $[Mo_7O_{24}]^{6-}$ and $[Mo_8O_{26}(OH)_2]^{6-}$. On the other hand, Mo1 is surrounded by one terminal doubly bonded oxygen (O5) and five bridging oxygen atoms, as shown in (4).



(3)



(4)

ESR signals (Fig. 2) showed both ^{95,97}Mo hyperfine and ^{1}H superhyperfine structures without any exchange broadening, which were characteristic of the unpaired electron localized on one Mo site only. Therefore, the signals indicate the small extent

of antiferromagnetic coupling of the two electrons at the adjacent edge-shared octahedral sites of Mo(V)1 and Mo(V)3 (Fig. 1). This may be attributed to the significant departure of both Mo1—O2—Mo3 (103.3°) and Mo1—O4—Mo3 (108.7°) angles[8] from linearity. The conclusion that both Mo1 and Mo3 sites are photoreducible gives also paramagnetic sites at both Mo1′ and Mo3′, since the arrangement of polyhedra can be related to the inversion center in the anion (Fig. 1). This implies the occurrence of four separate and independent one-electron photoreductions at Mo1, Mo1′, Mo3 and Mo3′ in $[Mo_{10}O_{34}]^{8-}$. The nonlinear arrangement of Mo1—O3—Mo1′ (104.3°)[8] seems to be a factor for the localization of the unpaired electron at each Mo(V) site of Mo1 and Mo1′, showing that there are two distinct sites for four-electron reduction of the anion.

In the light of the ESR signals from the Mo(V)1 and Mo(V)3 sites in $[Mo_{10}O_{34}]^{8-}$, one may state the alternative possibility that the ESR signals belong to the one-electron reduction at either the Mo1 or the Mo3 site in the anion. In this case, the two kinds of species of Mo(V)1 and Mo(V)3 must be randomly distributed over the whole lattice, since there was no significant difference in the signal intensities between the two sites. It must be recalled that the rate of the UV-induced coloration due to Mo(V) formation for the $[Mo_{10}O_{34}]^{8-}$ lattice was a few times higher than that of $[Mo_8O_{26}(OH)_2]^{6-}$ or $[Mo_7O_{24}]^{6-}$.[11] In conjunction with the similarity of the absorption spectra ($\lambda_{max} = 480 \sim 510$ nm) among these UV-irradiated polyoxomolybdates solids,[11] a high efficiency of the rate of photocoloration of the

$$[NH_3Me]_8[Mo_{10}O_{32}]\cdot 2H_2O$$

solid strongly supports four separate and independent one-electron reductions of $[Mo_{10}O_{34}]^{8-}$. Failure to observe the tetrahedral Mo(V)5 site can be explained by the electrostatic repulsion between the proton and the hole photogenerated at the terminal O12, O13 and O16 atoms (Fig. 3), which gives little possibility of a proton transfer at the Mo5 site resulting in thermal deactivation to the original Mo=O state without any formation of the charge-transfer complex (I).

Two distinct paramagnetic centers have also been observed for the UV-irradiated

$$[NH_3Pr^i]_6[Mo_7O_{24}]\cdot 3H_2O$$

single crystal.[1] Unfortunately, the final R value of 0.060 for the crystal structure data made interatomic distances and angles of the hydrogen bonds uncertain,[14] and resulted in the difficulty in assigning the photoreducible Mo site. On the other hand, the Mo(V) formation in the

$$[NH_3Pr]_6[Mo_7O_{24}]\cdot 3H_2O$$

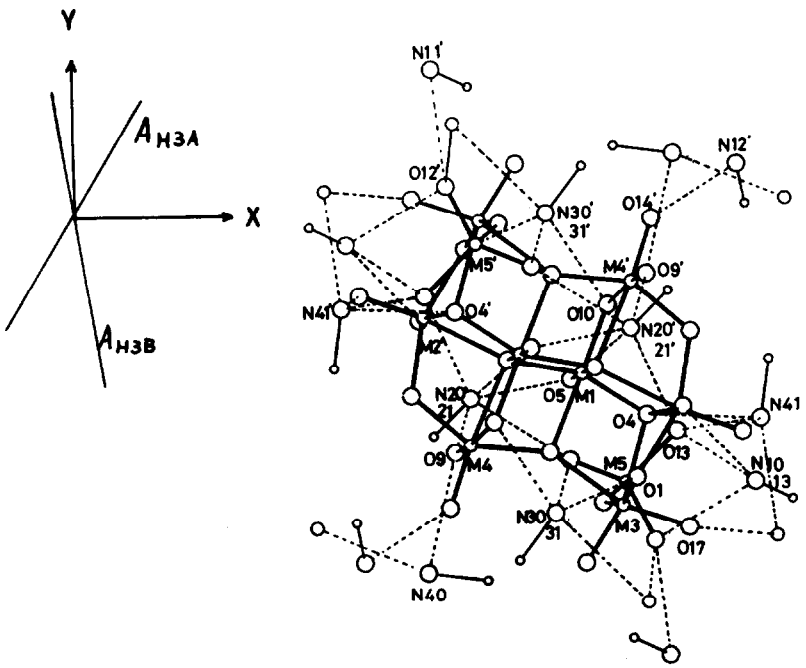


Fig. 3. Drawing of the molecular structure, viewed in projection along the Z-axis. A_{H3A} and A_{H3B} denote the principal A_{H3} directions of sites A and B, respectively, in the XY plane.

crystal occurred at an end of three octahedra in a line in the central horizontal level of the $[Mo_7O_{24}]^{6-}$ configuration.[7] Therefore, it is suggested that the two paramagnetic Mo(V) sites in the $[NH_3Pr^i]_6[Mo_7O_{24}]\cdot 3H_2O$ (space group $P2/n$, $Z = 4$)[14] belong to two ends (two-electron reduction) of three octahedra in the central level of $[Mo_7O_{24}]^{6-}$ or one at alternate ends (one-electron reduction), which must be randomly distributed over the lattice. Figure 4 shows photoreducible octahedra sites for multi-electron reduction sites in $[Mo_8O_{26}(MoO_4)_2]^{8-}$ and $[Mo_7O_{24}]^{6-}$.

Photoreduction of $[W_{10}O_{32}]^{4-}$

The structure of $[W_{10}O_{32}]^{4-}$ is shown in Fig. 5.[15] The photolysis of $[NH_2Pr^i_2]_4[W_{10}O_{32}]$ in aqueous solution led to the formation of one- and two-electron reduced decatungstate anions, which were coupled with the oxidation of water (to $^{\cdot}OH$) and $[NH_2Pr^i_2]^+$ (to acetone).[1,3] The photolyte exhibited an ESR signal at 77 K due to W(V), which consisted of a singlet isotropic line ($g = 1.84$, $\Delta H_{ms} = 20$ G) without a hyperfine structure. During the photolysis process leading to the formation of the two-electron reduced species, the signal intensity decreased steadily without a change in the g value, suggesting that the two-electron reduction species is diamagnetic.[3] There was no significant difference in W—O distances and W—O—W angles between the oxidized and photoreduced decatungstates crystals. A typical ESR spectrum of the

$$[NH_2Pr^i_2]_4[H_{1.5}W_{10}O_{32}]\cdot 8H_2O$$

crystal, recorded at 77 K, is shown in Fig. 6. The increasing number of lines around $g = 1.84$ is attributed to interaction of the unpaired electron with the protons. The superhyperfine structure can be fairly well accounted for if we assume eight

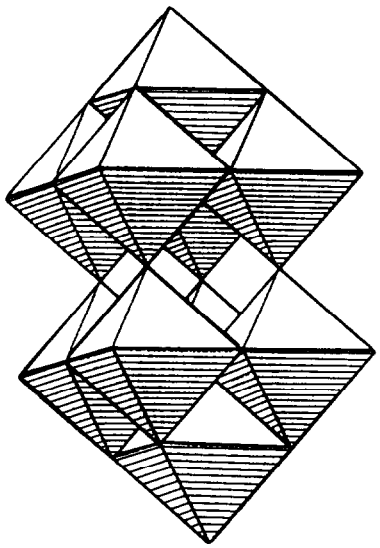


Fig. 5. Structure of $[W_{10}O_{32}]^{4-}$.

equivalent protons. Obviously these eight equivalent protons, giving nine lines with intensities in ratio 1:8:28:56:70:56:28:8:1, must be hydrogen-bonding protons at WO_6 sites in the anions. It is unlikely that the side signal corresponds to ^{183}W ($I = \frac{1}{2}$) hyperfine line, since the natural abundance (14.28%) of ^{183}W is low. Both g and superhyperfine tensors exhibited little anisotropy. The results indicate a complete delocalization of the unpaired electron over 10 tungsten atoms. Therefore, it is concluded that the protonation induced by the photoreduction of $[W_{10}O_{32}]^{4-}$ is not constrained at a peculiar octahedron site but delocalized over 10 WO_6 sites, different from the photoreductions of the above isopolymolybdates. The difference in the localization of the unpaired electron between the molybdate and tungsten isopolyanions is probably due to the larger extension of the W5*d* orbitals.

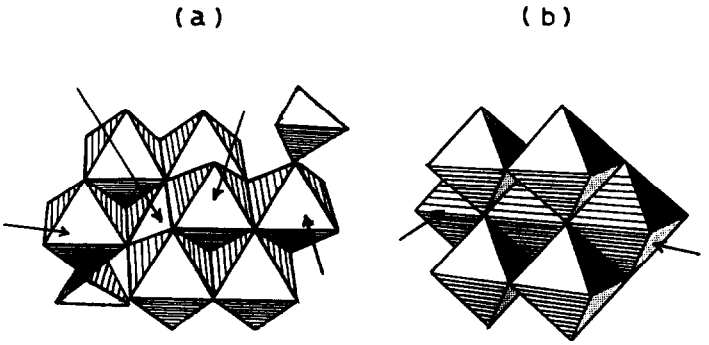


Fig. 4. Photoreducible sites (shown by arrow) for multi-electron reduction in $[Mo_8O_{26}(MoO_4)_2]^{8-}$ (a) and $[Mo_7O_{24}]^{6-}$ (b) lattices.

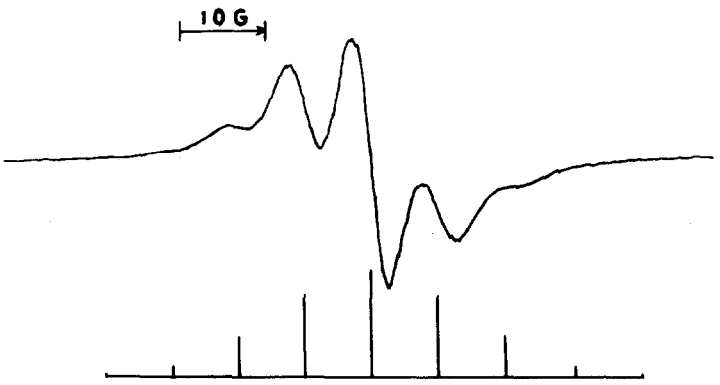


Fig. 6. Example of ESR spectrum obtained with $[NH_2Pr^i_2]_4[H_{1.5}W_{10}O_{32}] \cdot 8H_2O$ crystal at 77 K. H_0 is in the XY plane along the X-axis.

REFERENCES

1. T. Yamase, R. Sasaki and T. Ikawa, *J. Chem. Soc., Dalton Trans.* 1981, 628; T. Yamase, *Inorg. Chim. Acta* 1981, **54**, L207; T. Yamase and T. Ikawa, *ibid.* 1979, **37**, L529; 1980, **45**, L55; T. Yamase, *ibid.* 1983, **76**, L25; 1982, **64**, L155; 1981, **54**, L165.
2. T. Yamase and T. Kurozumi, *J. Chem. Soc., Dalton Trans.* 1983, 2205.
3. T. Yamase, N. Takabayashi and M. Kaji, *J. Chem. Soc., Dalton Trans.* 1984, 793.
4. T. Yamase and T. Kurozumi, *Inorg. Chim. Acta* 1984, **83**, L25.
5. T. Yamase, *J. Synth. Org. Chem. Jpn* 1985, **43**, 249.
6. T. Yamase, *J. Chem. Soc., Dalton Trans.* 1978, 283.
7. T. Yamase, *J. Chem. Soc., Dalton Trans.* 1982, 1987.
8. Y. Sasaki, T. Yamase, P. K. Bharadwaj, Y. Ohashi and Y. Sasada, *Acta Cryst., Sect. C* (in press).
9. M. Isobe, F. Marumo, T. Yamase and Y. Ikawa, *Acta Cryst.* 1978, **B34**, 2728.
10. J. Fuchs, H. Hartl, W.-D. Hunnius and S. Mahjour, *Angew. Chem.* 1975, **87**, 634.
11. T. Yamase and T. Ikawa, *Bull. Chem. Soc. Jpn* 1977, **50**, 746.
12. J. R. Morton and K. F. Preston, *J. Magn. Reson.* 1978, **30**, 577.
13. J. R. Morton, *Chem. Rev.* 1964, **64**, 453; P. W. Atkins and M. C. R. Symons, *The Structure of Inorganic Radicals*, p. 24. Elsevier, Amsterdam (1967).
14. Y. Ohashi, K. Yanagi, Y. Sasada and T. Yamase, *Bull. Chem. Soc. Jpn* 1982, **55**, 1254.
15. J. Fuchs, H. Hartl and W. Schiller, *Angew. Chem., Int. Ed. Engl.* 1973, **12**, 420.

Polyhedron Vol. 5, No. 1/2, pp. 87–94, 1986
Printed in Great Britain

0277–5387/86 $3.00 + .00
© 1986 Pergamon Press Ltd

SUPERCONDUCTING CHEVREL PHASES: PROSPECTS AND PERSPECTIVES

R. CHEVREL,* M. HIRRIEN and M. SERGENT

Université de Rennes-Beaulieu, Laboratoire de Chimie Minérale B, UA CNRS No. 254, Avenue du Géneral Leclerc, 35042 Rennes, France

(*Received* 4 *July* 1985)

Abstract—Research on superconducting Chevrel phases and other properties is reviewed: the impact of this large family of compounds on solid-state cluster chemistry, their novel pseudo-molecular structures with a new manner of coupling the clusters producing some outstanding physical properties: ternary superconductors, high T_c and H_{c_2} superconductors, interplay between superconductivity and long-range magnetic order, magnetic-field induced superconductivity and potential developement of superconducting wires are described; the electron donor–acceptor role of the Mo_6 cluster and cation donor–acceptor role of the channels of the structure of the quasi rigid Mo_6X_8 building blocks provide potential for cationic electrodes for secondary batteries.

STRUCTURAL OVERVIEW: CHEVREL PHASES AND SOLID-STATE CLUSTER CHEMISTRY

"*First comes synthesis*"

For over a decade, the outstanding superconducting properties of the ternary Mo chalcogenides, so-called Chevrel phases,[1] have stimulated a great amount of interest in the scientific community. These materials can be described by the formula $M_xMo_6X_8$, where M = Pb, Sn, Ln (lanthanon), K, Ca, Cu, Li . . . , $\simeq$40 different elements, and X is usually S, Se or Te (and occasionally Br or I). They are prepared at high temperatures (1000–1100°C) as black polycrystalline powders or single crystals.

Some of the highlights of this research will be described in this paper.

Certain ternary Mo chalcogenides have relatively high superconducting temperatures, as high as 15 K for $PbMo_6S_8$,[2] with an extremely high upper critical field approaching 60 T or more,[3] others with lanthanides[4] provide a unique opportunity to study the competition between superconductivity and long-range magnetic order.[5] Another property is the high reversible mobility of the counterions M^{n+}, e.g. lithium, copper and nickel ions, in these compounds allowing us to envisage cationic electrodes in secondary batteries.[6,7]

A great surprise was the discovery of the superconductivity of these sulfur- or selenium-based materials because superconductivity was until then exclusive to metals, alloys or intermetallic compounds [Pb, (Nb, Ti), Nb_3Sn]. The interest of these phases is that they are new ternary mineral-based cluster superconductors. So, the "ternary-superconductors" era began.[8] It was a breakthrough in superconductivity and the starting point for an intensive research on new ternary-cluster-based materials (borides, stannides, germanides, silicides and other chalcogenides).[5] Actually, it seems that the clustering of the transition-metal atoms has been found to be a feature common to ternary high-T_c superconductors.

Why do these materials which are bad conductors become very good superconductors? The answer is in the structural feature of the material: it contains Mo_6 octahedral clusters, "little bits of metal".

After the report of the discovery of Chevrel phases (over 100 Mo chalcogenides), parallel and subsequent synthetic efforts have led to the identification of many metal-rich halides, oxides and other ligands that possess a related, though unique, structural chemistry of considerable novelty. These are new and unusual compounds that lie at the interface between metal and molecular compounds.

* Author to whom correspondence should be addressed.

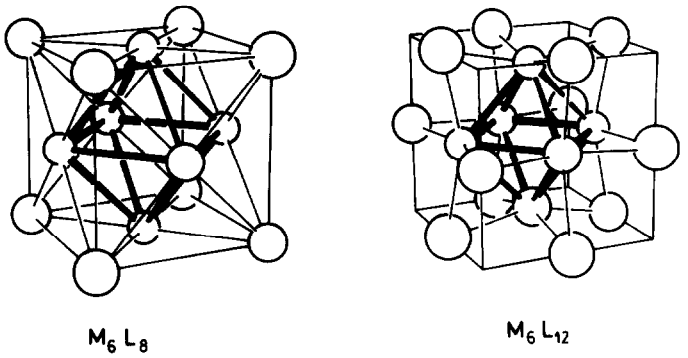


Fig. 1. Environment of the octahedral M_6 clusters (outlined in bold) in the M_6L_8 and M_6L_{12} units.

The novelty of most of these materials is due to the presence of one of the two fundamental cubic structural units, M_6L_8 and M_6L_{12}, which form the framework of their structure. The cubic block units containing octahedral clusters of the M_6L_8 type consist of eight non-metal atoms which lie above the triangular faces of the metal octahedron (μ_3-ligand), while, in the M_6L_{12} type, 12 non-metal atoms bridge the edges of the metal octahedron (μ_2-ligand) (Fig. 1).

A classification of most of these materials can be based on, first, progressive condensation of ligands (terminal *a*, bridging *a–a*, inner *i* and mixed *i–a*) and, second, condensation of clusters (apex, edge and face-sharing).

A basic structural principle apparently always applies to the bonding between isolated Mo_6 clusters throughout the solid. The empty region that otherwise lies outward (apical or exo position) from the metal vertex in each cluster is invariably occupied by a fifth non-metal neighbor. This leads to an $(M_6X_8)X_6$ pseudo-group. For instance, the additional six chlorine atoms that serve only to complete the clusters in $PbMo_6Cl_{14}$ are terminal $Pb(Mo_6Cl_8^i)Cl_6^a$. The discrete molecules $(Mo_6Cl_8)Cl_6^{2-}$ are linked together via the Pb^{2+} ions. On contrary, the exo atoms can serve to bridge the clusters between them in a three-dimensional solid as in Nb_6I_{11} or $Mo_6Cl_{10}S$: $(M_6X_8^i)X_{6/2}^{a-a}$, or both at once as in $MoCl_2$: $(Mo_6Cl_8^i)Cl_{4/2}^{a-a}Cl_2^a$. There are no direct metal–metal intercluster interactions. In other cases, some inner (*i*) atoms must also function as exo (*a*) atoms to vertices in other clusters. This occurs with Zr_6I_{12} where the connectivity is $(Zr_6I_6^iI_{6/2}^{i-a})I_{6/2}^{a-i}$.[9] A higher condensation is the cluster condensation, for instance the M_6X_{12} unit found in niobium monoxide, where the Nb atoms of the Nb_6 cluster are all connected in three dimensions, forms a framework of three-dimensional vertex-linked M_6 octahedra giving metallic properties.

Another type of condensation of M_6X_{12} units via edge-sharing Mo_6 clusters is described by McCarley[10] in $NaMo_4O_6$ compound. The $M_xMo_6X_8$ phases are the last step between the condensed-cluster phases and discrete clusters. They contain Mo_6X_8 building blocks but lack additional anions for the exo sites; they fill exo positions with six out of eight inner chalcogens from six other clusters: $(Mo_6X_{6/2}^{i-a}X_2^i)X_{6/2}^{a-i}$ (Fig. 2). The structure appears to be the face-capped equivalent of the edge-bridged Zr_6I_{12}.

Owing to the strength of these (MoX^{a-i}) intercluster bridges, the metal–metal intercluster interactions become important and are essential for understanding the striking physical properties of these materials. The Mo—Mo intercluster distance can vary between 3.1 and 3.6 Å; it depends on the nature of the chalcogen and the M-intercalated counterion. The average Mo—Mo intracluster distance is about 2.7 Å.[11]

In conclusion, it is a new manner of coupling Mo_6 clusters and Mo_6X_8 units. This intercluster metal–metal bonding persists, though often at longer distances in two dimensions for $Re_6Se_8Cl_2$,[12] where

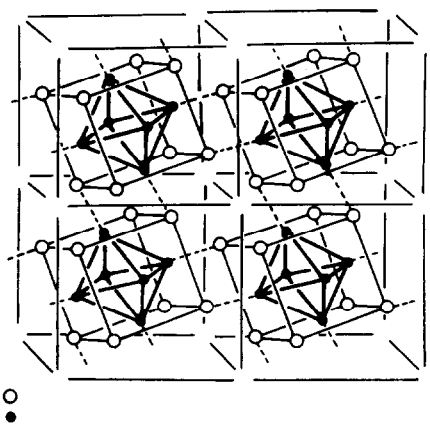


Fig. 2. A new way of stacking M_6L_8 cluster units: view of the rhombohedral structure of Mo_6X_8 binary compounds (X = S or Se).

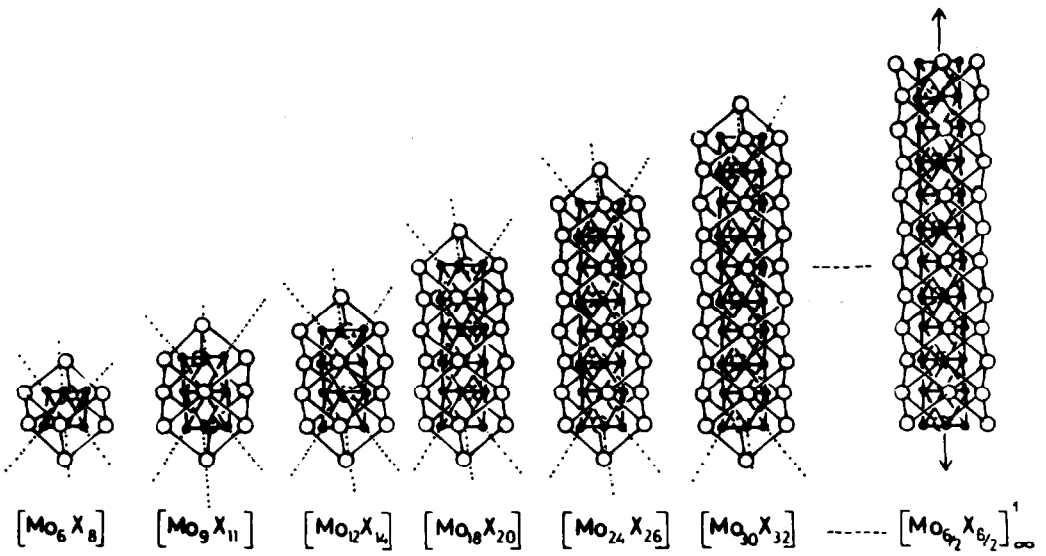


Fig. 3. Face-sharing Mo_6 cluster condensation.

the two additional chlorines cap two apices, and, in one dimension, in some of the derivatives, such as $Mo_6Br_6S_3$[13] and $Mo_6I_8Se_2$.[14]

FACE-SHARING OCTAHEDRAL CLUSTERS

It is natural that a non-metal : metal ratio below 8 : 6 leads to cluster condensation if the above concepts regarding face capping and exo bonding are maintained. Fortunately, the bonding is favorable and large extended clusters are formed by the face sharing of six–eight groups, namely the Mo_9X_{11}, $Mo_{12}X_{14}$, $Mo_{18}X_{20}$, $Mo_{24}X_{26}$ and $Mo_{30}X_{32}$ clusters shown in Fig. 3 along with the Mo_6X_8 cluster. The Mo_9X_{11} and $Mo_{12}X_{14}$ units were first discovered crystallizing with Mo_6X_8 clusters, but have recently been found alone. If we omit the Mo_9X_{11} unit, these new condensed clusters crystallize alone in a new large series, $M_{2n-2}Mo_{6n}X_{6n+2}$.[15]

The central units of these condensed clusters are planar Mo_3X_3 groups, while exo-bridging groups are far away at the ends of the extended clusters where pairs of intercluster Mo—X bonds again generate intercluster Mo—Mo bonds. The limit for this type of condensation is found in the $M_2Mo_6X_6$ phases. Here, the infinite chains $^1_\infty|Mo_3X_3^{-1}|$ have the same structure[16] as the central part of the discrete condensed clusters but without any interchain bonding (except that provided by the M^+ cations). The chains separated by the ternary element have a large intercluster Mo—Mo distance (6.4 Å) compared to 3.4 Å commonly observed for the Chevrel phases.

An interesting product would be the oxidized and cation-free material with presumably weak interchain interaction, Van der Waals' bonds only, in two dimensions. Actually, the metastable $(Mo_3Se_3)^1_\infty$ compound has been synthesized by deintercalation of the M^+ cation by an HCl flow at about 400°C.[17] So the fact of very weak interaction between the linear, one-dimensional chains allows us to think of separating the different molecular fibers in solution (Fig. 4). Tarascon and Di Salvo[18] have succeeded in obtaining the first example of monodispersed $(Mo_3X_3)^1_\infty$ clusters. The pseudo-one-dimensional compounds ($M_2Mo_6X_6$; X = Se or Te, M = Li or Na) can be dissolved in highly polar solvents such as DMSO and NMF. These solutions contain individual $(Mo_3X_3)^1_\infty$ chains; they are the first examples of purely inorganic transition-metal polymer solutions.

ELECTRONIC STRUCTURE AND PROPERTIES

It is generally agreed that the origin of superconductivity in Chevrel phases is the Mo4*d* electrons which are strongly localized at the Mo_6 octahedra because the Mo—Mo intercluster distance (3.3 Å) is about 10–20% larger than the Mo—Mo intracluster distance (2.7 Å). This gives rise to very narrow bands and high, needle-shaped peaks in the density of states $N(E_F)$. This picture is supported by several band structure calculations[19] which also show the common feature of a gap in $N(E)$ corresponding to 24 electrons per Mo_6 cluster or two electrons per Mo—Mo bond (as for $MoCl_2$).

Another idea concerning cluster atoms is the

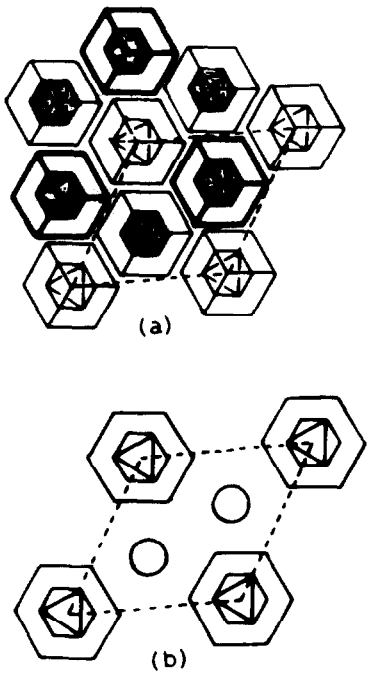


Fig. 4. Schematic projection onto the (001) basal hexagonal plane. (a) $M_xMo_6X_8$ and $M_{2n-2}Mo_{6n}X_{6n+2}$. For clarity, the M ions have been omitted. (b) $M_2Mo_6X_6$. Open circles are the M ions.

addition of interstitial atoms (or molecular units). Actually, the intercalation of e^- donors (metal M between the clusters) adds electrons to the clusters and leads to their stabilization. In Chevrel phases, the Mo_6S_8 binary phase cannot be prepared by high-temperature synthesis like the $M_xMo_6X_8$ phases but only by deintercalation of $M_xMo_6S_8$ (M = Fe, Co, Ni, Cu . . .) in dilute HCl.[20] Mo_6S_8 is a metastable compound containing only 20 electrons per Mo_6 cluster; it is the most electron-poor compound with electron-deficient Mo—Mo bond. So, the addition of metal atoms like copper atoms in the three-dimensional channels between the Mo_6S_8 units adds electrons to the cluster and stabilizes the cluster unit. The Mo—Mo intracluster bond becomes shorter (mainly d_1 Mo—Mo intracluster distance parallel to the three-fold axis of the hexagonal cell) and the octahedron becomes regular for 24 e^- per cluster. The Mo_6 cluster most oxidized is the largest cluster (20 e^-) and becomes smaller (24 e^-) when it is reduced.

The Mo_6 cluster plays the electron donor–acceptor role. That explains why a large variety of ions can be intercalated into the channels (Na^+, Pb^{2+}, Ln^{3+}, U^{4+} or Cu_x^+, $1 < x < 4$).

Curiously, it looks like the iron–sulfur cluster of the ferredoxin in the chloroplasts of the green plants which plays the e^- acceptor or donor role related to the symmetry and bonds of the cluster.[21]

Furthermore, M_6 metal cluster complex ions in homogeneous solutions are well known to be able to undergo redox reactions (one–four electrons) owing to the fact that the M_6 clusters are stable in electron-deficient states (delocalized e^--deficient bonding). It was shown some time ago[6] that the Mo cluster chalcogenides Mo_6X_8 (X = S or Se) with a framework lattice have a similar electronic flexibility and are able to undergo reversible topotactic electron–ion transfer reactions. These solid-state reactions are able to proceed:

$$xA^+ + xe^- + Mo_6X_8 \leftrightarrows A_x^+Mo_6X_8^{x-},$$

since the lattice provides, in addition to suitable electronic properties, an intersecting network of empty channels that can be occupied by ions of appropriate size and charge. Recently, a rechargeable non aqueous lithium–Mo_6S_8 battery has been investigated.[7]

The extreme flexibility of the structure allows us to synthesize, at high temperatures, the pseudo-binaries $Mo_6S_6Br_2$ and $Mo_6S_6I_2$, stabilized with 22 e^- per Mo_6 cluster. These compounds are very high T_c superconductors (T_c = 13.8 and 14 K, respectively) like the best $SnMo_6S_8$ and $PbMo_6S_8$ superconducting Chevrel phases (22 e^- per cluster).[22] The gradual filling of the conduction bands gives a gap for 24 e^- per Mo_6 cluster. So, the semiconducting pseudo-binary $(Mo_2Re_4)S_8$ with 24 e^- per cluster has been synthesized.[23]

Another interesting property is the ability to obtain at low temperatures new metastable ternary compounds by intercalation.[17] For instance, a $TlMo_6Se_8$ metastable compound is found superconducting at 12.2 K.[24] Likewise, activity and selectivity of Chevrel phase catalysts were further investigated.[25]

COEXISTENCE OR INTERPLAY BETWEEN MAGNETISM AND SUPERCONDUCTIVITY

Usually, small quantities of magnetic impurities in a metal will destroy its superconducting properties completely. Likewise, the addition of 3*d* elements (Fe, Mn . . .) ($\simeq$0.5 atom %) to $SnMo_6S_8$ or $PbMo_6S_8$ destroys superconductivity completely because the magnetic ions are distributed at random throughout the channels.

The fact that the Mo4*d* electrons are responsible for the superconductivity of these materials led us to think that a magnetic M element added to the channels of the structure, with a weak exchange interaction between e^- conduction and magnetic

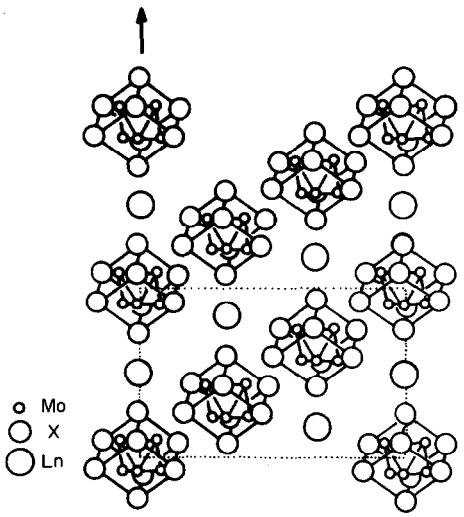


Fig. 5. Projection onto the $(11\bar{2}0)$ hexagonal plane of the $LnMo_6X_8$ chalcogenides. The Ln ions are about 6.5 Å apart. Ln is a lanthanide.

moment, i.e. a large M—Mo distance, would not affect the superconductivity too much; for instance large cations in origin site like Ln ions.

The Ln ions in the ternary $LnMo_6X_8$ compounds form a regular (nearly cubic) array and are screened from the Mo atoms (Ln—Mo > 4.10 Å) (Fig. 5).

Most of the $LnMo_6X_8$ chalcogenides become superconducting (except Ce and Eu) well above their magnetic ordering temperatures (very weak *d–f* exchange). In fact, it is a completely new situation: it was the first time that a system containing a regular lattice of magnetic ions was found to be superconducting. The question then arises: what does the superconducting state become when the magnetic order appears? Most $LnMo_6X_8$ compounds are found to order antiferromagnetically (Dy, Pr, Gd, Tb...) and it is now well established that superconductivity coexists with long-range antiferromagnetism.*

The $HoMo_6S_8$ compound becomes superconducting at 1.2 K, but becomes normal again below 0.65 K; this state is called reentrant superconductivity. At this temperature, the superconducting state is practically destroyed by the onset of the ferromagnetic order. Recently, a "domain walls" superconductivity has been discovered in the ferromagnetic state.[26]

Likewise, in a narrow temperature range near the ferromagnetic transition temperature, a sinusoidally magnetic state with a wavelength of about 250 Å coexists with a superconducting state.

As a result of the discovery of these compounds, research activity is very intense in cluster chemistry to solve the problem of the coexistence of superconductivity and magnetism, research on new materials and the manufacture of large single crystals.

MAGNETIC FIELD INDUCED SUPERCONDUCTIVITY

It is well known that a magnetic field tends to destroy superconductivity [curve $H(T)$]. So, a completely new situation occurs in a series $Sn_{1-x}Eu_xMo_6(S,Se)_8$. For $x \simeq 0.8$ and $T < 1$ K, superconductivity is destroyed at low magnetic field (0.6–1.0 T) and, in a striking manner, appears again around 8 T and finally disappears only above 20 T[27] (Fig. 6). Here, superconductivity appears with a magnetic field.

This phenomenon is explained by the exchange field compensation effect proposed by Jaccarino and Peter. The exchange field created by the 4*f* electrons of europium is opposite to the applied field. The conduction *d*-electrons "see" only the difference between the applied field and the internal exchange field. Previously, this two-domain superconductivity had never been seen in spite of a negative exchange interaction observed in many compounds

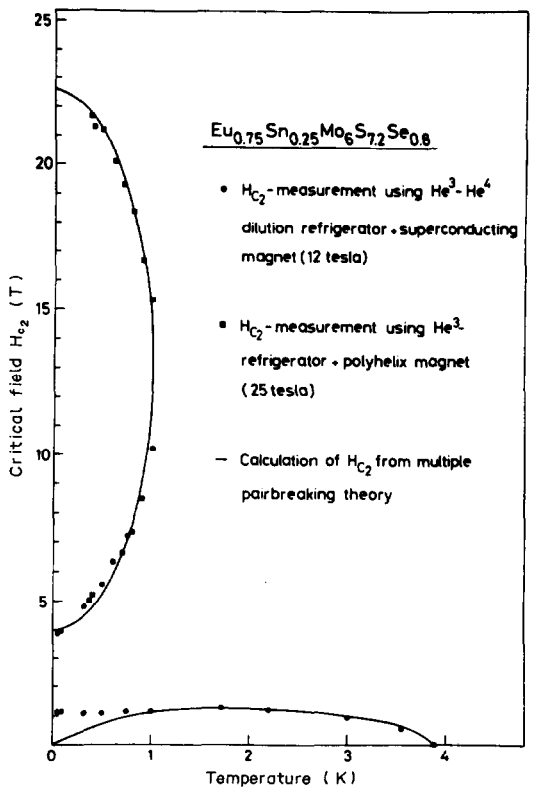


Fig. 6. First example of magnetic field induced superconductivity (from Ref. 28).

* This aspect is reviewed in Ref. 5.

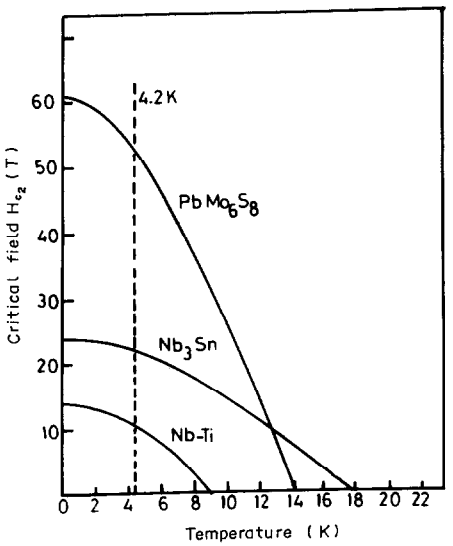


Fig. 7. Upper critical field H_{c_2} vs temperature. NbTi is a technical superconductor.

because of the coherence length, ξ, was too large ($H_{c_2} = \phi_o/2\pi\xi^2$) or the observed critical field was too low.

POTENTIAL FOR TECHNICAL APPLICATIONS

The compounds $PbMo_6S_8$, $PbGd_xMo_6S_8$, $SnMo_6S_8$ and $SnAl_xMo_6S_8$ were found to be the best superconductors in the Chevrel phases. The compounds were synthesized from mixed elemental powders by reaction in evacuated quartz ampoules heated to various temperatures for 24 h and then slowly cooled. $PbGd_xMo_6S_8$ gave the maximum T_c of 14.4 K, dH_{c_2}/dT of 6 T K^{-1}, H_{c_2} (4.2 K) higher than 51 T and estimated $H_{c_2}(0)$ of 60 T. This is of course the highest critical field of any bulk superconductor. It exceeds the highest value reported for the best binary compound, Nb_3Ge, by more than 20 T in spite of the fact that lead molysulfide has a much lower T_c.

The technical superconducting material NbTi has a T_c of 9 K and a H_{c_2} (4.2 K) of 10 T (Fig. 7). So, the ternary molybdenum sulfide $PbMo_6S_8$ is a very interesting candidate for future applications because of its high critical field, connected with a pseudo-molecular structure. But, this compound, like an A15 compound (for instance Nb_3Sn), is a brittle material,

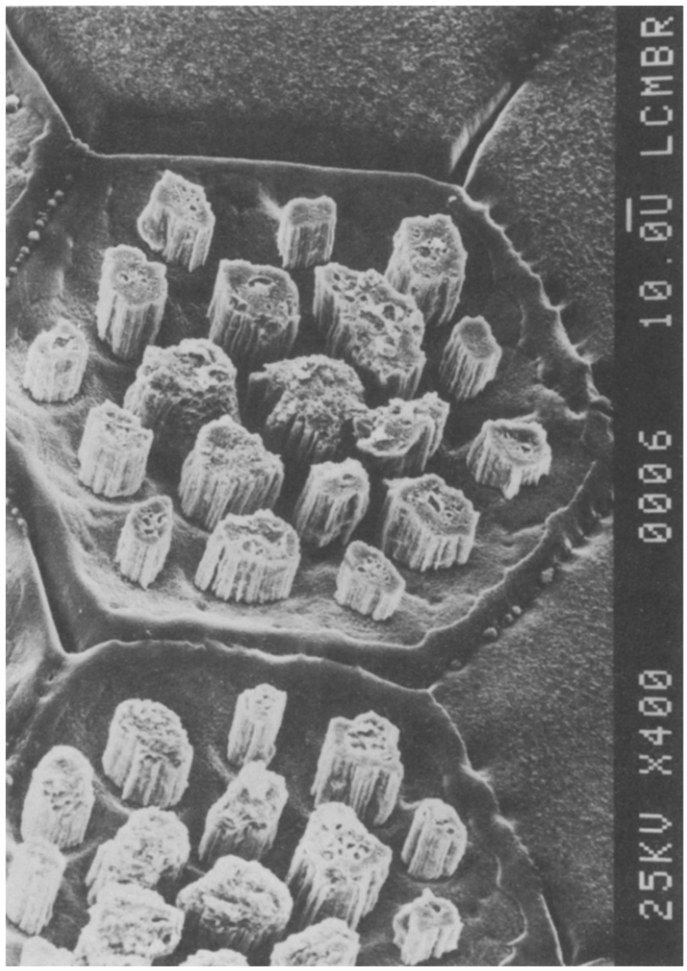


Plate 1. Details of the strands of Chevrel phase in a copper matrix (285 filaments in a 1-mm diameter wire).

whereas NbTi is a ductible alloy. Thus, this material cannot be manufactured easily into wires or ribbons.

The first results ($2–5 \times 10^7$ A m^{-2} at 4.2 K) were relatively low[28] but further results on bulk samples allow us to hope for the improvement of critical current densities: 3×10^8 A m^{-2} in a 10-T field[29] and 10^8 A m^{-2} at 14 T.[30] Investigations on thin films [31] and new progress in the processing of wires have revealed substantially higher critical current densities, J_c. Special technology has to be used to make wires. Two problems arise, the manufacture of wires and the current-carrying capacity. $PbMo_6S_8$ monofilamentary wires were fabricated by a powder process using Ta and Mo as sheath material.[32,33] The value of J_c is about 2×10^8 A m^{-2} at 6 T and more recently 10^8 A m^{-2} at 10 T.

The first attempt at multifilamentary feasibility has been performed by cold hydrostatic extrusion of powder-metallurgy-processed superconducting Chevrel phases. Hydrostatically extruded multifilamentary composites of $PbMo_6S_8$ powder in a copper billet were drawn into fine wires without intermediate annealing. The powder was isostatically compacted in the form of a cylinder. A less than 1-mm wire with 285 filaments of $PbMo_6S_8$ has been made.

The average filament is about 10–30 μm in diameter (Plate 1). The first superconducting characteristics of such monofilamentary wires exhibit T_c of 14 K, dH_{c_2}/dT of about 4 T K^{-1} and critical current densities at 4.2 K of about 10^8 A m^{-2} at 5 T.[34]

These results show promise for large-scale fabrication of powder-metallurgy processed superconductors.

It is clear that Chevrel phase material is capable of further improvement. The increase of one order of magnitude of critical current densities would make this new superconducting material competitive with respect to other technical superconductors (NbTi and Nb_3Sn). The range of fields where these materials will become interesting is between 15 and 40 T for the production of ultra-high static magnetic fields. Another problem will arise concerning degradation of the superconducting properties of the wires under mechanical strains due to magnetic forces.

Much remains to be done on basic and applied research on Chevrel phases.

REFERENCES

1. R. Chevrel, M. Sergent and J. Prigent, *J. Solid State Chem.* 1971, **3**, 515; Ø. Fischer, *Appl. Phys.* 1978, **16**.
2. B. T. Matthias, M. Marezio, E. Corenzwit, A. S. Cooper and H. E. Barz, *Science* 1972, **175**, 1465.
3. Ø. Fischer, H. Jones, G. Bongi, M. Sergent and R. Chevrel, *J. Phys.* 1974, **C7**, L450; R. Odermatt, Ø. Fischer, H. Jones and G. Bongi, *J. Phys.* 1974, **C7**, L13; S. Foner, E. J. McNiff, Jr and E. J. Alexander, *Phys. Lett.* 1974, **49A**, 269.
4. Ø. Fischer, A. Treyvaud, R. Chevrel and M. Sergent, *Solid State Commun.* 1975, **17**, 721.
5. Ø. Fischer and M. B. Maple (Eds), *Superconductivity in Ternary Compounds I and II. Top. Curr. Phys.* **32** and **34**. Springer, Berlin (1982).
6. R. Schollhorn, M. Kumpers and J. O. Besenhard, *Mater. Res. Bull.* 1977, **12**, 781.
7. P. J. Mulhern and R. R. Haering, *Can. J. Phys.* 1984, **62**, 527.
8. G. K. Shenoy, B. D. Dunlap and F. Y. Fradin (Eds), *Ternary Superconductors.* North-Holland, Amsterdam (1981).
9. J. D. Corbett, *Pure Appl. Chem.* 1984, **56**, 1527.
10. R. E. McCarley, *Polyhedron* 1986, **5**, 51.
11. R. Chevrel and M. Sergent, In *Superconductivity in Ternary Compounds I* (Edited by Ø. Fischer and M. B. Maple), *Top. Curr. Phys.* **32**, 25. Springer, Heidelberg (1982).
12. L. Leduc, A. Perrin and M. Sergent, *Acta Cryst.* 1983, **C39**, 1503.
13. C. Perrin, M. Potel and M. Sergent, *Acta Cryst.* 1983, **C39**, 415.
14. C. Perrin and M. Sergent, *J. Chem. Res. (S)* 1983, **2**, 38.
15. P. Gougeon, thesis, Rennes (1984); M. Potel, thesis, Rennes (1981); R. Chevrel, P. Gougeon, M. Potel and M. Sergent, *J. Solid State Chem.* 1985, **57**, 25.
16. M. Potel, R. Chevrel and M. Sergent, *Acta Cryst.* 1980, **B36**, 1545.
17. M. Potel, P. Gougeon, R. Chevrel and M. Sergent, *Rev. Chim. Miner.* 1984, **21**, 509.
18. J. M. Tarascon and F. J. Di Salvo, personal communication.
19. Papers are cited in Ref. 5; H. Nohl, W. Klose and O. K. Andersen, In *Superconductivity in Ternary Compounds I* (Edited by Ø. Fischer and M. B. Maple), *Top. Curr. Phys.* **32**, 165. Springer, Heidelberg (1982); T. Hughbanks and R. Hoffmann, *J. Am. Chem. Soc.* 1983, **105**, 1150.
20. R. Chevrel, M. Sergent and J. Prigent, *Mater. Res. Bull.* 1974, **9**, 1487.
21. F. A. Cotton and G. Wilkinson (Eds), *Advanced Inorganic Chemistry*, 4th edn. John Wiley, New York (1980).
22. M. Sergent, Ø. Fischer, M. Decroux, C. Perrin and R. Chevrel, *J. Solid State Chem.* 1977, **22**, 87.
23. A. Perrin, M. Sergent and Ø. Fischer, *Mater. Res. Bull.* 1978, **13**, 259.
24. J. M. Tarascon, F. J. Di Salvo, D. W. Murphy, G. Hull and J. V. Waszczak, *Phys. Rev.* 1984, **B29**, 172.
25. K. F. MacCarty and G. L. Schrader, *Ind. Eng. Chem. Proc. Res. Dev.* 1984, **23**, 519; K. F. MacCarty, J. W. Anderegg and G. L. Schrader, *J. Catal.* 1985, **93**.
26. J. L. Genicon, J. P. Modon Danon, R. Tournier, O. Pena, R. Horyn and M. Sergent, *J. Phys. Lett.* 1984, **45**, L1175; *Ann. Chim. Fr.* 1984, **9**, 1019.

27. H. W. Meul, C. Rossel, M. Decroux, Ø. Fischer, G. Remenyi and A. Briggs, *Phys. Rev. Lett.* 1984, **53**, 497; Ø. Fischer, *Ann. Chim. Fr.* 1984, **9**, 867.
28. N. E. Alekseevskii, M. Glinski, N. M. Dobrovolskii and V. I. Tsebro, *JETP Lett.* 1976, **23**, 412; M. Decroux, Ø. Fischer and R. Chevrel, *Cryogenics* 1977, **17**, 291; T. Luhman and D. Dew-Hughes, *J. Appl. Phys.* 1979, **34**, 409.
29. V. R. Karasik, E. V. Karyaev, M. O. Rikel' and V. I. Tsebro, *Sov. Phys.—JETP* 1982, **56**, 881.
30. C. Rossel and Ø. Fischer, *J. Phys. F* 1984, **14**, 455.
31. K. Hamasaki, T. Inoue, T. Yamashita, T. Komata and T. Sasaki, *Appl. Phys. Lett.* 1982, 41, 667.
32. B. Seeber, C. Rossel and Ø. Fischer, *Ternary Superconductors*, p. 119. Elsevier–North-Holland, Amsterdam (1981); B. Seeber, C. Rossel, Ø. Fischer and W. Glaetze, *IEEE Trans Magn.* 1983, **19**, 402.
33. H. Yamasaki and Y. Kimura, In *Proceedings, Applied Superconductivity, San Diego, August* 1984.
34. M. Sergent, R. Chevrel, J. Padiou, O. Pena, R. Barathe, M. Hirrien, H. Massat, T. Pech, B. Turck, P. Dubots and M. Couach, *Ann. Chim. Fr.* 1984, **9**, 1069.

Polyhedron Vol. 5, No. 1/2, pp. 95–102, 1986
Printed in Great Britain

0277–5387/86 $3.00 + .00
© 1986 Pergamon Press Ltd

γ–γ-CORRELATION SPECTROSCOPY OF ^{99}Mo-LABELLED PROTONATED "MoS_2"

C. VOGDT,*† T. BUTZ*†‡ and A. LERF†

*Physik-Department der Technischen Universität München, 8046 Garching, F.R.G.; and †Walther-Meißner-Institut für Tieftemperaturforschung, 8046 Garching, F.R.G.

and

H. KNÖZINGER

Physikalisch-Chemisches Institut der Universität München, 8000 München, F.R.G.

(*Received* 18 *June* 1985)

Abstract—Nuclear quadrupole interactions as measured by time differential perturbed angular correlation on ^{99}Tc have been used to characterize molybdenum sulfides and an Al_2O_3-supported Mo catalyst. The technique proved successful for the detection of anion vacancies and hydrogen uptake in highly disperse unsupported MoS_2. The results obtained for the supported catalyst suggest the presence of non-stoichiometric MoS_2-like species with a high density of anion vacancies and presumably containing appreciable amounts of hydrogen.

The investigation of the ^{99}Tc (daughter of ^{99}Mo, $T_{1/2} = 66$ h) nuclear quadrupole interaction (NQI) on Mo sites in molybdates proved very useful for the differentiation between isolated and condensed Mo polyhedra in crystalline solids,[1] frozen molybdate solutions[2] and surface adsorbates.[3] The principle is as follows: isolated polyhedra are essentially undistorted and lead to a vanishing NQI at the Mo site: on the contrary, the condensation of polyhedra leads to a considerable distortion and hence to a well-defined non-zero NQI. Both the strength and symmetry of the electric field gradient (EFG) tensor are used as fingerprints to characterize a specific compound. In this contribution we report on the application of γ–γ-correlation spectroscopy of ^{99}Mo labels [TDPAC (time-differential perturbed angular correlation)] to protonated "MoS_2" species. "MoS_2" species appear to be very important in Mo-based supported catalysts.[4,5] The mode of hydrogen activation under catalytic conditions is not clear at present, although hydrogen uptake in MoS_2 has been clearly established.[6–8] On the basis of neutron-scattering data, the formation of SH groups during H_2 uptake has been suggested.[6,7] The proton uptake is expected to modify both the strength and symmetry of the EFG, even in cases where structural changes are minute. Therefore we performed TDPAC experiments to distinguish between ordinary MoS_2 and protonated forms.

EXPERIMENTAL

Spectrometer

The TDPAC spectrometer was a conventional fast–slow four-detector set-up with NaI(Tl) scintillation crystals mounted on RCA 8850 photomultipliers. The experimental time resolution (τ_{res}) was typically 2.2 ns. The four detectors are mounted in a plane at 90° intervals. Since each detector served as a start-and-a-stop detector eight out of 12 possible coincidences (four × 180°, four × 90°) were stored simultaneously.

TDPAC and nuclear quadrupole interaction

The coincidence count rate between two successively emitted γ-quanta in a nuclear γ–γ-cascade can be written as:[9]

$$W(t, \theta) = e^{-t/\tau_N}[1 + A_{22} G_{22}(t)(P_2 \cos \theta)], \quad (1)$$

‡ Author to whom correspondence should be addressed.

where τ_N = the nuclear lifetime of the intermediate nuclear state of the cascade, A_{22} = anisotropy of the cascade (depends on nuclear properties only), $P_2 \cos\theta$ = Legendre polynomial, θ = angle between emission direction of the first and second γ-quantum, and $G_{22}(t)$ = perturbation function (contains all information on the NQI).

In the present experiment, we use the 740–181 keV cascade in ^{99}Tc which is fed via β-decay from ^{99}Mo ($T_{1/2}$ = 66 h). For this cascade we have τ_N = 5.05 ns, $A_{22} \cong +0.1$ and spin $I = \frac{5}{2}$ for the intermediate (181-keV) state. The NQI leads to a splitting of the $\frac{5}{2}$ state into three substates with quantum numbers (m) of $\pm\frac{5}{2}$, $\pm\frac{3}{2}$ and $\pm\frac{1}{2}$. For an axial EFG tensor, the energy differences $E_{\pm 3/2} - E_{\pm 1/2}$, $E_{\pm 5/2} - E_{\pm 3/2}$ and $E_{\pm 5/2} - E_{\pm 1/2}$ are $\hbar\omega$, $2\hbar\omega$ and $3\hbar\omega$, respectively, where $\omega = 3\pi\nu_Q/10$ with the quadrupole frequency:

$$\nu_Q = e^2qQ/h. \tag{2}$$

eQ denotes the nuclear quadrupole moment, eq is the largest component of the EFG tensor (V_{zz}), and h is Planck's constant. For this case the perturbation function reads for a polycrystalline (random powder) sample:

$$G_{22}(t) = 0.2 + 0.371 \cos\omega t + 0.286 \cos 2\omega t + 0.143 \cos 3\omega t. \tag{3}$$

If the EFG tensor deviates from axial symmetry, both the frequency (ω), its harmonics, and the coefficients in front of the cosine terms depend on the asymmetry parameter (η):

$$\eta = \left(\frac{V_{xx} - V_{yy}}{V_{zz}}\right), \tag{4}$$

with V_{ii} being the EFG tensor components in the principal-coordinate system. The expression of eqn (1) with eqn (3) has to be convoluted with the experimental time resolution. The difficulty for practical applications with this γ–γ-cascade lies in the fact, that τ_N is rather short, not much larger than our experimental time resolution. Furthermore, eQ is presumably small and hence typically one precession period (T) ($= 2\pi/\omega$) or less can only be observed.

Sample preparation

In all cases ^{99}Mo ($T_{1/2}$ = 66 h) was obtained by irradiating Mo-containing samples with natural isotopic abundance in a thermal neutron flux of 10^{13} n cm^{-2} s for a few hours. In some cases radiation damage occurs and has to be considered. In the following we list the important aspects of all samples used.

MoO_3. This was used in neutron-irradiated form: irradiation causes oxygen vacancies (colour centers);[10] the disappearance of these colour centers with time was monitored.

MoS_2. This was prepared by iodine vapour transport from the elements; used in neutron-irradiated form since no radiation damage was detected; in one case it was subsequently treated in an H_2 atmosphere.

$Li_{1.1}(NH)_3)_{0.6}MoS_2$: This was prepared by reaction of neutron-irradiated MoS_2 in excess Li dispersed in liquid NH_3 at -60°C for $\frac{1}{2}$ h.[11]

$(NH_4)_2MoS_4$. This was prepared by passing gaseous H_2S through an ammoniacal ammonium paramolybdate (APM) solution,[12] neutron irradiated, dissolved in water and subsequently precipitated with butanol–acetone to eliminate radiation damage.

Amorphous MoS_3 (a-MoS_3). This was prepared from neutron-irradiated $(NH_4)_2MoS_4$ by thermal decomposition at 473 K.[13]

"H_xMoS_2". This was prepared from radioactive a-MoS_3 by H_2 treatment at 673 K for 48 h.[13]

"MoS_2" (*highly disperse*). This was prepared as "H_xMoS_2" but stored in air for at least half a year, and therefore assumed to be substantially oxidized: it was neutron irradiated, and reduced and sulfided in H_2–H_2S (9 : 1) at 623 K for 18 h; subsequently it was annealed at Ar at 623 K for 40 h, and subsequently treated with H_2 at 623 K for 120 h.

Mo12Al. Al_2O_3 (BET surface area 148 m^2 g^{-1}), obtained from CONDEA PURAL SB by calcination in air at 1023 K for 16 h without further preactivation before use, was impregnated with neutron-irradiated APM solution (12% MoO_3 equivalent) by a pore-filling method, dried, calcined at 773 K for 2 h in air, sulfided in H_2–H_2S (9 : 1) at 623 K for 18 h, and subsequently treated with H_2 at 623 K for 18 h.

RESULTS AND DISCUSSION

In the following we use ω, η and the possible population in multicomponent spectra to characterize and identify Mo species.

Colour centers in MoO_3

The NQI at ^{99}Tc on Mo sites in MoO_3 has been studied previously[1] and will not be discussed here. Of interest in the present paper is the NQI associated with the colour centers which are due to oxygen vacancies.[10] These lead to a rather high ω of the order of 1.0–1.2 GRad s^{-1} as compared to the undistorted Mo environment with ω = 210 MRad s^{-1} and η = 1.0. In Fig. 1 we show the time evolution of this high-frequency component. ω first shifts from almost 1.2 to 1.0 GRad s^{-1} and finally disappears. This is

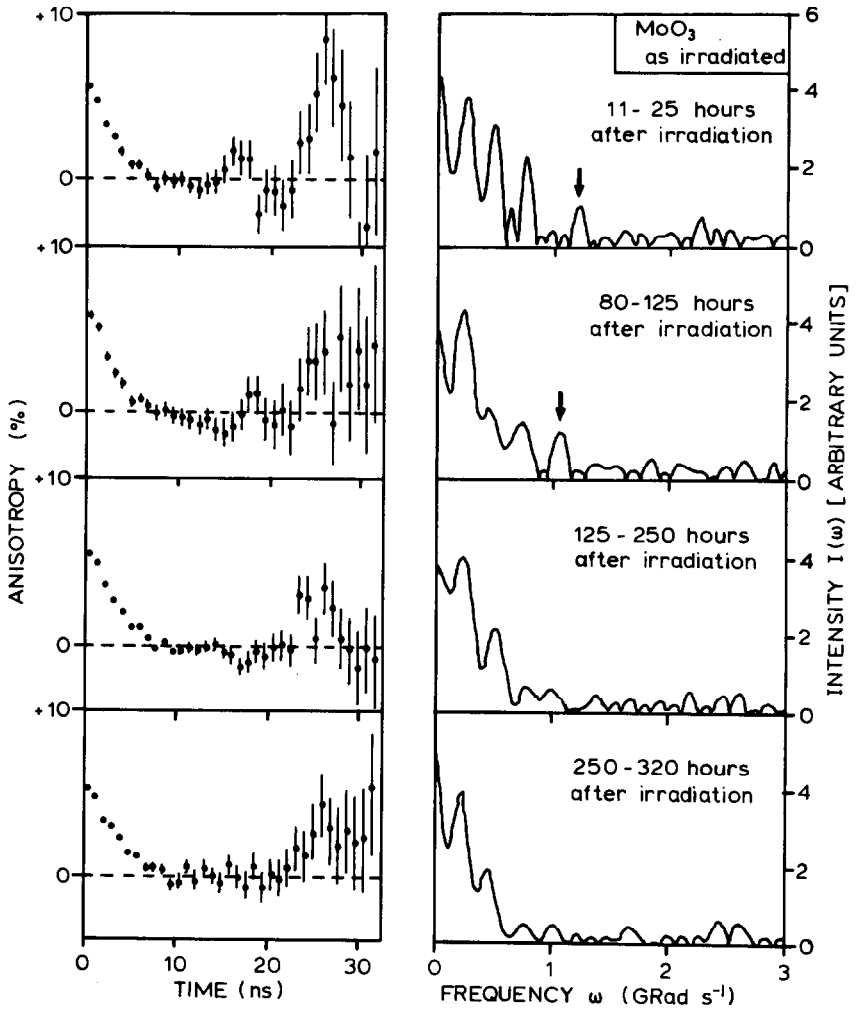


Fig. 1. TDPAC spectra (left) and their Fourier transforms (right) for neutron-irradiated MoO_3 at 300 K. The high-frequency components around $\omega = 1.0 \ldots 1.2$ GRad s^{-1}, marked by arrows, are attributed to colour centers (oxygen vacancies) and disappear gradually with time due to oxygen vacancy recombination.

interpreted to be the consequence of oxygen vacancy recombination. We report such high-frequency components in catalytically relevant materials below.

Bulk MoS_2

Since MoS_2-like species are generally assumed for the surface species of Al_2O_3-supported sulfided Mo-based catalysts[4,5] a study of bulk MoS_2 seemed appropriate. Both a polycrystalline powder and a single crystal in several orientations were studied and yielded practically identical results: $\omega = 112$ MRad s^{-1} and $\eta = 0.0$. A typical TDPAC spectrum for a single crystal averaged over three different orientations is shown in Fig. 2 (top). Axial symmetry is required because MoS_2 has a three-fold rotation axis around Mo sites. Powder samples at various temperatures from 77 up to 673 K showed that the temperature variation of the EFG is negligible. Furthermore, radiation damage appeared to be unimportant, since annealing at 673 K yielded no change. Interestingly enough, treatment in H_2 for at least 48 h did not show any change in ω and η. Hence, there was no indication of hydrogen uptake in bulk MoS_2. The results of least-squares fits like eqn (3) to the data points are summarized in Table 1.

"H_xMoS_2"

A TDPAC spectrum for the starting material $(NH_4)_2MoS_4$ is shown in Fig. 3. Apart from the small fraction of a high-frequency component with $\omega =$ 341 MRad s^{-1} (with $\eta = 0.0$ assumed), the main

Table 1. Nuclear quadrupole interaction for various molybdenum–sulfur compounds[a]

Sample	Treatment	Temperature (K)	Site 1 Fraction (%)	Site 1 ω_1 (MRad s^{-1})	Site 2 Fraction (%)	Site 2 ω_2 (MRad s^{-1})	Comments
MoS_2 powder	As irradiated	77	100	124(6)	—	—	$\eta = 0$
MoS_2 powder	As irradiated	300	100	112(2)	—	—	$\eta = 0$
MoS_2 powder	As irradiated	623	100	113(4)	—	—	$\eta = 0$
MoS_2 powder	As irradiated	673	100	110(3)	—	—	$\eta = 0$
MoS_2 single crystal	As irradiated	300	100	109(7)	—	—	$\eta = 0$, 25% spread in ω_1
MoS_2 powder	During H_2 exposure	623	100	113(3)	—	—	$\eta = 0$
$(NH_4)_2MoS_4$	Precipitated	300	67(7)	0	33(7)	341(5)	$\Gamma = 35(1)$ MRad s^{-1} around $\omega_1 = 0$
a-MoS_3	From above, thermal decomposition	300	52(5)	93(5)	48(5)	194(8)	Two sites, texture
"H_xMoS_2"	MoS_3 reduced in H_2	300	89(2)	153(8)	11(2)	630(25)	$x \approx 0.1$, texture
$Li_{1.1}(NH_3)_{0.6}MoS_2$	Intercalation from Li–NH_3(liq.) at 195 K	195	65(2)	119(4)	20(3)	485(22)	Incomplete reaction, 15% with $\omega_3 = 0$
"MoS_2" disperse	As irradiated	300	100	134(5)	—	—	
"MoS_2" disperse	During H_2 exposure	623	93(2)	75(2)	7(2)	1200(130)	
"MoS_2" disperse	Reduced and sulfided	300	100	115(3)	—	—	
"MoS_2" disperse	Reduced and sulfided during Ar exposure	623	69(4)	204(1)	31(4)	943(34)	During first 24 h of Ar exposure
"MoS_2" disperse	Reduced and sulfided during Ar exposure	623	92(5)	153(6)	8(5)	930(10)	During last 24 h after 8 days of Ar exposure
"MoS_2" disperse	Reduced and sulfided, Ar exposed, during H_2 exposure	623	65(2)	123(5)	35(2)	870(20)	During first 24 h of H_2 exposure
"MoS_2" disperse	Reduced and sulfided, Ar exposed, during H_2 exposure	623	100	62(2)	—	—	Averaged over the second–eighth day of H_2 exposure
Mo12Al	Reduced and sulfided	300	71(3)	262(8)	29(3)	1240(60)	
Mo12Al	Reduced and sulfided, H_2 exposed	300	70(2)	221(6)	30(2)	1010(25)	

[a] If no error limits are quoted the corresponding quantity was not treated as an adjustable parameter. Unless stated otherwise we assumed $\eta = 0$ and a negligible spread in ω.

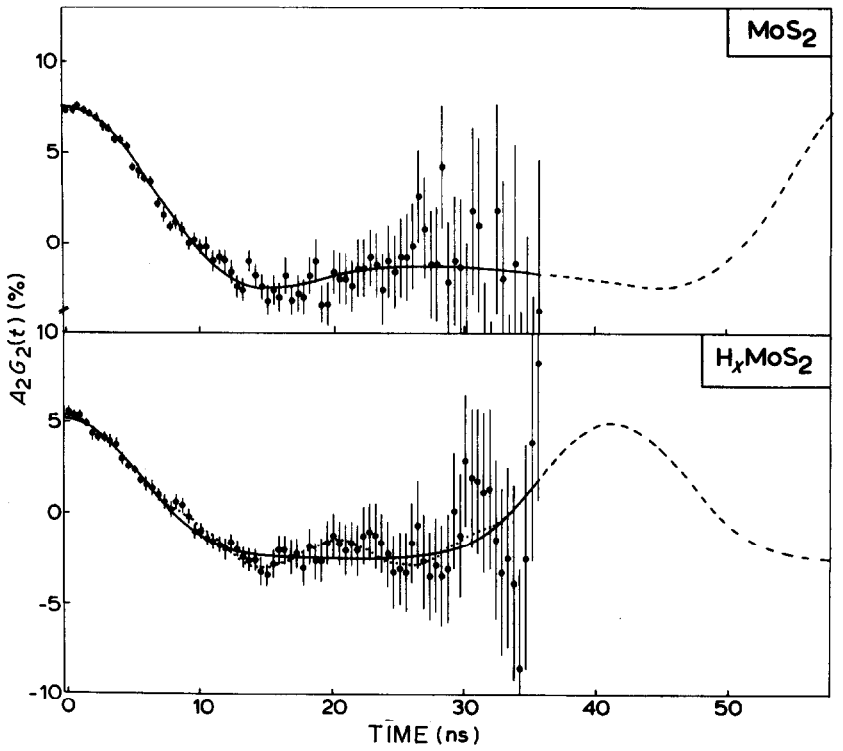


Fig. 2. TDPAC spectrum for a MoS_2 single crystal (averaged over three different orientations) at 300 K (top) compared to "H_xMoS_2" obtained by treating amorphous MoS_3 in H_2 at 673 K for 40 h (bottom). The dotted line in the lower picture represents an improved fit allowing for a second, high-frequency site.

interaction can be described as a distribution with a width (Γ) (35 MRad s^{-1}) centered around a mean value of $\omega = 0$ MRad s^{-1}. This is in good agreement with earlier observations for compounds with isolated Mo–O tetrahedra.[1,2] Apparently, the MoS_4 tetrahedron is only weakly deformed. The small component with $\omega = 341$ MRad s^{-1} is ascribed to Mo sites with a defective environment which could be a consequence of the precipitation procedure. The spectrum, taken *in situ* for a-MoS_3, obtained by thermal decomposition of $(NH_4)_2MoS_4$, is shown in Fig. 4. One clearly observes a main-frequency component of $\omega = 93$ MRad s^{-1} and $\eta = 0.0$, and

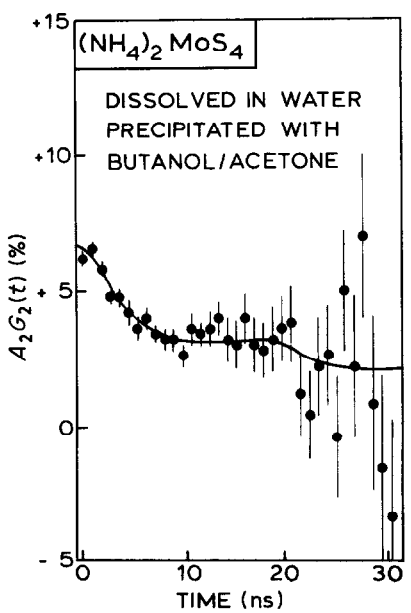


Fig. 3. TDPAC spectrum for $(NH_4)_2MoS_4$ at 300 K.

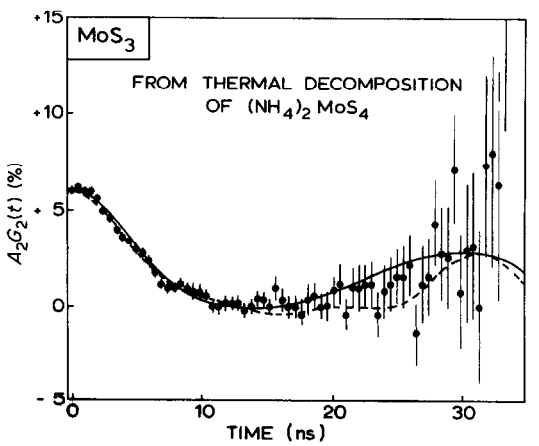


Fig. 4. TDPAC spectrum for a-MoS_3 at 300 K. Solid line: single site with a broad frequency distribution; dashed line: two equally populated sites with sharp frequencies.

another high-frequency component with $\omega = 194$ MRad s^{-1} ($\eta = 0$ assumed) with about equal populations. It appears that in a-MoS_3 two inequivalent Mo sites occur. The recently proposed structure models[14] would be consistent with two inequivalent Mo sites. The TDPAC spectrum for hydrogen treated a-MoS_3 is shown in Fig. 2 (bottom). A comparison with the spectrum for bulk MoS_2 [Fig. 2 (top)] shows that a different compound, denoted "H_xMoS_2", has been formed rather than MoS_2. The results of least-squares fits for all three compounds discussed above are listed in Table 1. In order to characterize this "H_xMoS_2" compound further, we studied the effect of charge transfer on the NQI in the intercalation compound $Li_{1.1}(NH_3)_{0.6}MoS_2$. This compound seemed most appropriate because the Li uptake and consequently the charge transfer is extremely large. The cointercalation of NH_3 ensures a high intercalate mobility and the solvent NH_3 is thought to prevent the reduction to Mo metal. The measurements were performed at 195 K to minimize amide formation. Unfortunately we did not observe a single-frequency component as expected for this compound. Rather we observed a smaller fraction (20%) with $\omega = 485$ MRad s^{-1} ($\eta = 0.0$ is assumed), a larger fraction (65%) with $\omega = 119$ MRad s^{-1} and $\eta = 0.0$, and the remainder with $\omega = 0$ MRad s^{-1}. If we identify the high-frequency signal with the maximum possible uptake of Li, i.e. a charge transfer of 1.1 e^-/MoS_2, we can quote a frequency increase with charge transfer of 340 MRad s^{-1} per e^-. This compares qualitatively with our previous observations in MoO_3 and $Na_{1/2}(H_2O)_xMoO_3$.[1] The larger part of the signal may be identified with either unreacted MoS_2, with a subsequent decomposition product, or both. The least-squares fit parameters for $Li_{1.1}(NH_3)_{0.6}MoS_2$ are also listed in Table 1. Since the protons in H_xMoS_2 are known to reside in the van der Waals' gap and to form S—H bonds[6] we can derive a value of $x = 0.12(2)$ for the hydrogen uptake in our "H_xMoS_2". Of course, this number has to be used with precautions because the comparison with just a single intercalation compound could be dangerous. However, previous experience with the rather extensively studied intercalation compounds of 2H-TaS_2[15] showed that a rather universal correlation between the NQI at Ta sites and the charge transfer exists, and we suggest that this holds true for MoS_2, too. The above estimate is in agreement with the values derived from ^1H NMR[16] and volumetric measurements.[6–8,17] Since bulk MoS_2 does not take up hydrogen we consider the reduction process from a-MoS_3 to "H_xMoS_2" and its high degree of dispersion essential for the H_2 dissociation and uptake in the form of protons.

Highly disperse "MoS_2"

The behaviour of highly disperse "MoS_2" which was partially oxidized was found to be quite different compared to "H_xMoS_2" freshly prepared by reduction in H_2 of a-MoS_3. This material was studied after various treatments: (a) as irradiated, (b) during H_2 treatment, (c) after reduction and sulfidation in H_2–H_2S, (d) during Ar treatment following (c), and (e) during H_2 exposure following (d). All procedures were performed *in situ*. The results for these samples from least-squares fits are summarized in Table 1.

First, we note that the frequency for the compound measured as irradiated, $\omega = 134$ MRad s^{-1}, disagrees with that for bulk MoS_2. We tend to attribute this to the partial oxidation rather than to the disperse nature because the NQI is a very short-range interaction and the ratio of surface/volume is still large for our material with a surface area of approximately 50 m^2 g^{-1}. Second, the interaction frequency decreases considerably to $\omega = 75$ MRad s^{-1} ($\eta = 0.0$ is assumed) upon H_2 treatment. Simultaneously, a second rather high frequency component with $\omega = 1.2$ GRad s^{-1} ($\eta = 0.0$ is assumed) shows up. The low-frequency component cannot be assigned at present. The high-frequency component is considered to be due to the formation of a substantial fraction of anion vacancies ($\sim$2–3%, if each vacancy is assumed to be signalized by three Mo neighbours), in analogy to the O vacancies in the MoO_3. With regard to the presumably very small quadrupole moment of the 5/2 state in ^{99}Tc these high frequencies imply very high EFGs which can hardly be produced in the presently studied compounds without defects in the first coordination shell.

When the starting "MoS_2" was reduced and sulfided initially we observe $\omega = 115$ MRad s^{-1} and $\eta = 0.0$, quite comparable with the results for bulk MoS_2. There are no vacancy type frequency components. It is, however, dangerous to conclude that O has been substituted quantitatively by S and that no proton uptake has occurred. This is borne out by subsequent treatments. First, treating such a sample in Ar at 623 K leads to dramatic changes: within the first 24 h ω increased to 204 MRad s^{-1} and a vacancy type frequency at $\omega \sim 950$ MRad s^{-1} with a fraction of 31% shows up (see Table 1). During prolonged Ar treatment ω decreases to 153 MRad s^{-1} and the high-frequency component gradually disappears. It is difficult to understand that the Ar treatment causes such drastic changes unless the preceeding reduction and sulfidation was incomplete and hydrogen uptake had occurred. In this case a partial release of H_2 could lead to H_2S and H_2O

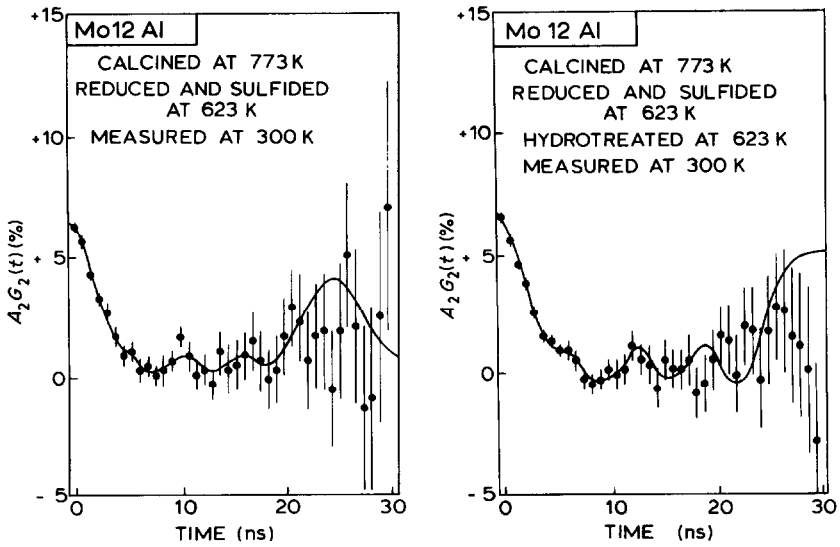


Fig. 5. TDPAC spectra for a reduced–sulfided Mo12Al catalyst (left) and after subsequent H_2 treatment (right).

formation and hence create anion vacancies. A further hint of an incomplete reduction and sulfidation follows from the fact that a subsequent H_2 treatment of the Ar-treated sample yields $\omega = 62$ MRad s^{-1}, in very close agreement with the results for the starting material which was H_2 treated only. During the first 24 h vacancy type high-frequency components reappear, which later vanish. Whereas the appearance of defect sites is very likely related to sulfur loss, their disappearance with time can tentatively be connected with lattice relaxation or self-intercalation. It is, however, not understood why these self-intercalates do not show up in the spectra as a new distinct-frequency component.

Mo12Al *catalysts*

We are now in a position to attack the final goal: the characterization of the surface species on sulfided Mo-based supported catalysts. Typical TDPAC spectra taken for a reduced and sulfided Mo12Al catalyst and after a subsequent H_2 treatment are shown in Fig. 5. The results derived from least-squares fits are listed in Table 1. We note that in both spectra the main component has $\omega \sim 220$–260 MRad s^{-1}; a further characteristic high-frequency component of $\omega = 1.2$ GRad s^{-1} (before H_2 treatment) and $\omega = 1.0$ GRad s^{-1} (after H_2 treatment) shows up. Both observations resemble those made for highly disperse, partially oxidized, reduced and sulfided and Ar-treated "MoS_2", especially for the spectra taken during the first 24 h. The high-frequency components around $\omega = 1.0$–1.2 GRad s^{-1} show that a large fraction ($\sim 10\%$) of anion vacancies is produced during reduction and sulfidation.

CONCLUSIONS

It has been shown that hydrogen uptake in MoS_2 and anion vacancy formation can be monitored via the ^{99}Tc NQI by TDPAC. The results obtained for unsupported "MoS_2" can be used as reference data for the interpretation of the results obtained for sulfided Mo12Al catalysts. Bulk MoS_2 or "$H_{0.12}MoS_2$" cannot be detected on Mo12Al after the sulfidation conditions applied in this study. The comparison with unsupported highly disperse "MoS_2" suggests that, during reduction and sulfidation of the oxidic precursor, a non-stoichiometric MoS_2-like species with a high concentration of anion vacancies ($\sim 10\%$) is formed which presumably has taken up a fair amount of hydrogen. Our data do not allow us to draw a conclusion concerning the completeness of the sulfidation. Experiments addressing the question whether there is a correlation between the catalytic activity of Mo-based supported catalysts and the anion vacancy concentration are presently under way.

Acknowledgements—We are grateful to Prof. W. K. Hall for valuable discussion during the course of this work and for providing the highly disperse MoS_2 powder. We thank Prof. A. Wold for an MoS_2 single crystal. The irradiation of the samples was kindly performed at the Forschungsreaktor Garching. This work was supported by the Deutsche Forschungsgemeinschaft and the Deutsche Gesellschaft für Mineralölwissenschaft und Kohlechemie e.V.

REFERENCES

1. T. Butz, A. Lerf, C. Vogdt and A. M. M. Eid, *Hyperfine Interactions* 1983, **15/16**, 915.
2. A. Lerf, C. Vogdt, T. Butz, A. M. M. Eid and H. Knözinger, *Hyperfine Interactions* 1983 **15/16**, 921.
3. C. Vogdt, T. Butz, A. Lerf and H. Knözinger, In *Proceedings of the 8th International Congress on Catalysis, Berlin*, 1984, Vol. 3, p. 117.
4. R. R. Chianelli, *Catal. Rev.—Sci. Eng.* 1984, **26**, 361.
5. P. C. H. Mitchell, Catalysis. Specialist Periodical Report No. 4, p. 175. Royal Society of Chemistry, London (1981).
6. C. J. Wright, C. Sampson, D. Fraser, R. B. Moyes, P. B. Wells and C. Riekel, *J. Chem. Soc., Faraday Trans.* 1 1980, **76**, 1585.
7. C. Sampson, J. M. Thomas, S. Vasudevan and C. J. Wright, *Bull. Soc. Chim. Belg.* 1981, **90**, 1215.
8. A. Blackburn and P. A. Sermon, *J. Chem. Technol. Biotechnol.* 1983, **33A**, 120.
9. H. H. Frauenfelder and R. M. Steffen, In *Alpha-, Beta-, Gamma-Ray Spectroscopy* (Edited by K. Siegbahn), Vol. 2, p. 997. North-Holland, Amsterdam (1965).
10. M. R. Tubbs, *Physica Status Solidi A* 1974, **21**, 253.
11. W. Rüdorff, *Angew. Chem.* 1959, **71**, 487.
12. G. Brauer (Ed.), *Handbuch der Präparativen Anorganischen Chemie*, Vol 3, p. 1551. Enke, Stuttgart (1981).
13. E. M. M. Badger, R. M. Griffith and W. B. S. Newling, *Proc. R. Soc. London* 1949, **197**, 184; J. C. Wildervanck and F. Jellinek, *Z. Anorg. Allg. Chem.* 1964, **328**, 309.
14. F. Z. Chien, S. C. Moss, K. S. Liang and R. R. Chianelli, *Phys. Rev.* 1984, **29**, 4606.
15. T. Butz and A. Lerf, *Rev. Chim. Miner.* 1982, **19**, 496.
16. H. Jeziorowski, H. Knözinger and W. K. Hall, unpublished data.
17. G. Ledezma and H. Knözinger, unpublished data.

Polyhedron Vol. 5, No. 1/2, pp. 103–105, 1986
Printed in Great Britain

0277-5387/86 $3.00 + .00
© 1986 Pergamon Press Ltd

EFFECT OF PHOSPHORUS ON THE OXIDATION SELECTIVITY OF MoO_3-BASED CATALYSTS

M. AI

Research Laboratory of Resources Utilization, Tokyo Institute of Technology, 4259 Nagatsuta, Midori-ku, Yokohama 227, Japan

(*Received* 7 *June* 1985)

Abstract—Vapor-phase air oxidation of propylene, 1-butene, propionic acid and isobutyric acid was performed with a variety of MoO_3-based mixed oxides and heteropoly compounds. The results indicate that the selectivity is not fully explained by the difference in the reactivities between the reactant and the product because the oxidation reaction is accompanied by C—C bond fission. A remarkable increase in the selectivity was observed by the addition of phosphorus. It is proposed that phosphorus plays a role in eliminating the basic sites which promote the C—C bond fission.

MoO_3 and V_2O_5 are fundamental components of selective oxidation catalysts because both oxides possess acidic and, at the same time, redox[1] properties. The oxidation activity of metal-oxide catalysts has been studied mainly in connection with their redox function. However, such data are not sufficient to explain the catalytic activity and selectivity in the case of mild oxidation, though the possession of a redox function is undoubtedly one of the necessary conditions for an oxidation catalyst.

Recently, it has been proposed that, in the case of mild oxidation, the catalytic activity is governed by the activation of the reactant molecule, which is attributed to an acid–base-type interaction between the catalyst surface and the reactant to be oxidized, rather than by the activation of oxygen, and that the selectivity is brought about by the difference in the mode or degree of reactant activation.[2]

The presence of a large difference in reactivities between the reactant and the product is surely a necessary condition to achieve a high selectivity, but it is not always a sufficient condition. For example, oxidation catalysts effective for production of acidic products are, without exception, strongly acidic oxides, e.g. MoO_3- or V_2O_5-based oxides. However, it is still difficult to explain the selectivities only by the possession of a sufficiently acidic property in the case of certain partial oxidations, such as formation of maleic anhydride from butene or butane, of acrylic acid from propylene, and of methacrylic acid from methacrolein or isobutyric acid.

In this connection, it is also proposed that the oxidation reaction is sometimes accompanied by a side pathway consisting of C—C bond fission, which is considered to be promoted by the action of acidic sites, much as the oxidation reations.[3]

EXPERIMENTAL

In view of this, and to extract some new rules effective for a better understanding of the selectivity of MoO_3-based catalysts for an acid formation reaction, the following four reactions were studied as models of competitive reactions between oxidation and C—C bond fission:

$$CH_3CH_2COOH \begin{cases} \nearrow CH_2{=}CHCOOH \\ \searrow CH_3CHO \text{ or } CH_3COOH + CO_x \end{cases} \quad (1)$$

$$CH_3CH(CH_3)COOH \begin{cases} \nearrow CH_2{=}C(CH_3)COOH \\ \searrow CH_3COCH_3 \text{ or } CH_2{=}CHCH_3 + CO_x \end{cases} \quad (2)$$

$$CH_2{=}CHCH_3 \begin{cases} \nearrow CH_2{=}CHCOOH \\ \searrow CH_3COOH + CO_x \rightarrow CO_x \end{cases} \quad (3)$$

$$CH_2{=}CHCH_2CH_3 \begin{cases} \nearrow \text{maleic anhydride} \\ \searrow 2CH_3COOH \end{cases} \quad (4)$$

RESULTS AND DISCUSSION

The selectivities of each reaction at a fixed conversion are listed in Table 1.

The results may be summarized as follows:

(i) The reactants in the four reactions are much more reactive than the corresponding acidic products,[3] indicating that the selectivities cannot be explained by differences in reactivities between the reactant and the product.

(ii) The addition of V_2O_5 or amphoteric oxides such as TiO_2, SnO_2, Fe_2O_3, and Co_3O_4 enhances the oxidation activity, but it cannot suppress the C—C bond fission.

(iii) A remarkable increase in the selectivities for partial oxidation is brought about by the addition of phosphorus.

As for the role of phosphorus, it may be possible to connect the high selectivity with some structural aspects commonly observed in phosphorus-containing catalysts, but we would like to ascribe the high selectivity to some chemical property of phosphorus. As chemical factors, (i) an acidic property, and (ii) a basic property are presented as possibilities.

The addition of phosphorus to MoO_3 or V_2O_5 causes a marked increase in the acidic property,[4] but the addition of V_2O_5 to MoO_3 and that of amphoteric oxides to MoO_3 or V_2O_5 also causes a marked increase in the acidic property.[2] On the other hand, it is unlikely that the acidic sites promote the oxidation reaction in preference to the C—C bond fission. Therefore, the selectivity may not be related to the acidic property.

Accordingly, the view that the addition of phosphorus plays a role in eliminating the basic sites seems to be probable. This leads us to assume that the C—C bond fission is promoted by a cooperative action of the acid and base. Indeed, it has already been pointed out that the C—C bond fission in the oxidation of butene is ascribed to the action of basic sites at the step

$$CH_3CH(OH)CH_2CH_3 \rightarrow CH_3COCH_2CH_3,$$

and that methylethylketone is susceptible to decomposition.[5] The situation may be the same in the case of the oxidation of propylene; the

$$CH_3CH(OH)CH_3 \rightarrow CH_3COCH_3$$

step is promoted by the action of a base, and acetone is decomposed to acetic acid and CO_x.[6] However, it is still unsolved whether the C—C bond fission of the carboxylic acids proceeds in the same manner. Further studies are needed.

It should be noted that, if the basic property is eliminated completely by the addition of acidic compounds such as phosphorus, the catalyst surely loses its oxidation activity, because the oxidizing sites are closely related to the basic sites.[2,7] It may be most important for the selective-oxidation catalysts that the basic sites are suppressed just sufficiently not to eliminate completely the oxidizing function. We consider at present that phosphorus is best for this

Table 1. Selectivities between oxidation and C—C fission[a]

Reactant	CH_3CH_2COOH			$CH_3CH(CH_3)COOH$			$CH_2=CHCH_3$			$CH_2=CHCH_2CH_3$		
Conversion (%)	50			50			50			98		
	AcH			Acetone								
Product	AA	AcOH	CO_x	MAA	C_3H_6	CO_x	AA	AcOH	CO_x	MA	AcOH	CO_x
Mo–V 8–2	7	51	42	23	45	32	5	10	85	9	40	51
Mo–Ti 6–4	10	61	29	21	41	38	8	1	91	8	24	68
Mo–Sn 7–3	15	55	30	20	52	28	4	29	67	8	33	59
Mo–Fe 7–3	9	70	21	7	84	9	3	0	97	2	18	80
Mo–Co 8–2	9	81	10	9	73	8	—	—	—	7	16	77
PMo_{12}	24	43	33	62	29	19	20	41	39	33	19	48
$PMo_{10}V_2$	20	30	50	60	33	7	21	29	50	30	24	46
Cs_2PMo_{12}	31	37	32	69	27	4	20	31	49	35	26	49
$Cs_{2.5}PMo_{10}V_2$	31	38	31	55	38	7	22	35	43	33	29	38
V	3	82	15	12	72	16	0	60	40	1	31	68
V–P 1–1.6	17	59	24	57	36	7	32	16	52	33	18	49

[a] AA, acrylic acid; MAA, methacrylic acid; MA, maleic anhydride; PMo_{12}, $H_3PMo_{12}O_{40}$; $PMo_{10}V_2$, $H_5PMo_{10}V_2O_{40}$.

purpose because of its mild acidic character, and that the appropriate extent of base suppression is achieved by catalysts having a special structure, for example heteropoly compounds and B-phase, i.e. $(VO)_2P_2O_7$.[8]

REFERENCES

1. P. Mars and D. W. Van Krevelen, *Chem. Eng. Sci.* Suppl. 1954, **3**, 41.
2. M. Ai, *J. Synth. Org. Chem. Jpn* **35**, 201; In *Proceedings of the 7th International Congress on Catalysis, Tokyo*, p. 1060. Elsevier, Amsterdam (1981).
3. M. Ai, In *Proceedings of the 9th Iberoamerican Symposium on Catalysis, Lisbon*, Vol. 2, p. 836 (1984).
4. M. Ai, submitted for publication.
5. M. Ai, *J. Catal.* 1984, **85**, 324.
6. M. Ai and A. Ozaki, *Bull. Chem. Soc. Jpn* 1979, **52**, 1454.
7. M. Ai, *J. Catal.* 1978, **54**, 223; *ibid.* 1979, **60**, 306.
8. R. A. Schneider (to Chevron Research Co.), U.S. Patent 3,864,280 (1975).

Polyhedron Vol. 5, No. 1/2, pp. 107–109, 1986
Printed in Great Britain

0277-5387/86 $3.00 + .00
© 1986 Pergamon Press Ltd

SURFACE STRUCTURE AND REACTIVITY OF MoO_3

JERZY HABER and EWA SERWICKA*

Institute of Catalysis and Surface Chemistry, Polish Academy of Sciences,
30-239 Krakow, ul. Niezapominajek 1, Poland

(*Received* 18 *June* 1985)

Abstract—Interaction of propene and diallyloxalate vapour with MoO_3 specimens of different crystallite habits was studied by ESR. The reducibility of a sample whose surface was predominantly the (010) crystal plane increased greatly when the diallyloxalate was used. The results indicate that the selective insertion of lattice oxygen into the hydrocarbon molecule occurs at the (010) basal plane, whereas the side crystal faces are responsible for the activation of a propene molecule.

It is now well-established that in molybdate catalysts it is the molybdenum–oxygen sublattice that is responsible for the insertion of oxygen into the organic molecule in the selective oxidation of hydrocarbons. When an organic molecule is activated by some other route, pure MoO_3 performs the insertion of oxygen very efficiently.[1] In an extensive catalytic study Brückman *et al.*[2] reported that the yield of acrolein from allylic compounds was linearly dependent on the surface area of the (010) face, showing that only this plane was responsible for insertion of oxygen into the activated hydrocarbon molecule. On the other hand, the product distribution in propene oxidation could be explained by assuming that its activation took place at the side (100) and (101) faces, and total oxidation occurred at all faces of the MoO_3 catalyst.

In order to elucidate this point further, the ESR study reported here on the interaction of MoO_3 specimens of different crystallite habits with propene and diallyloxalate was undertaken.

EXPERIMENTAL

Two polycrystalline MoO_3 materials of different crystal habits were used:

(a) Climax Molybdenum Co. product with plate-like crystallites exposing predominantly the (010) face, BET surface area 0.6 $m^2 g^{-1}$, denoted MoO_3(p).

(b) Climax Molybdenum Co. product with needle-like crystallites and no preference for any particular crystal face, BET surface area 2.7 $m^2 g^{-1}$, denoted MoO_3(n).

Both materials were subjected to standard oxidizing pretreatment in air at 620 K for 24 h in order to remove possible organic impurities, and to assure sample stoichiometry. Subsequently approximately 0.05 g of the MoO_3 samples were placed in quartz ESR tubes, connected to the vacuum line, outgassed at room temperature for 0.5 h *in vacuo* at 10^{-3} Pa and subjected to reduction with propene or diallyloxalate in the temperature range 400–570 K for different periods. After each stage of reduction the ESR spectrum was recorded. Propene and diallyloxalate used were purified by repeated freeze–thaw pump cycles.

ESR spectra were recorded at 77 and 293 K by using an ESR X-band spectrometer type SE/X produced by the Technical University, Wroclaw, equipped with a magnetometer. Spin densities were estimated by use of a $VOSO_4$ standard. A DPPH sample ($g = 2.0036$) was used for determination of g values.

RESULTS AND DISCUSSION

After the standard pretreatment in air, both the MoO_3(p) and MoO_3(n) were white and, according to ESR analysis, contained negligible amounts of Mo^{5+} ions (0.0002%).

Upon heating in an atmosphere of C_3H_6 at 1.3×10^4 Pa the specimens of different crystal habit showed different behaviour. The MoO_3(n) sample

* Author to whom correspondence should be addressed.

changed colour to white-greyish at 400 K, and simultaneously a strong signal appeared in the ESR spectrum (Fig. 1). The main ESR absorption was characterized by $g_x = 1.943$, $g_y = 1.954$, and $g_z = 1.878$, and a well-resolved hyperfine pattern due to the 25% abundant ^{95}Mo and ^{97}Mo isotopes ($A_x = 3.2$ mT, $A_y = 3.0$ mT, and $A_z = 7.0$ mT). A similar spectrum was reported by us for the first time for polycrystalline MoO_3 reduced with atomic hydrogen at room temperature.[3] There the experimental conditions ensured samples with fully occupied anionic sites resulting in an octahedral environment of Mo^{5+}. Hence the above signal can be ascribed to an hexacoordinated Mo^{5+} ion forming a molybdenyl bond with one of the surrounding oxygens.

The signal intensity normalized to surface area increased with time and temperature of the reducing treatment (Table 1). Simultaneously disappearance of the hyperfine pattern and loss of resolution of the perpendicular g factor components due to dipolar broadening effects were observed.

The MoO_3(p) sample treated with propene under similar conditions showed slightly poorer reducibility when compared to MoO_3(n) (Table 1). As in the former case the ESR spectrum consisted of a well-resolved signal characteristic of the hexacoordinated Mo^{5+} ion.

In both samples the appearance of a singlet line at $g = 2.003$ was observed, in addition to the Mo^{5+} signal. Similar signals have been observed previously for various oxides subjected to the reducing

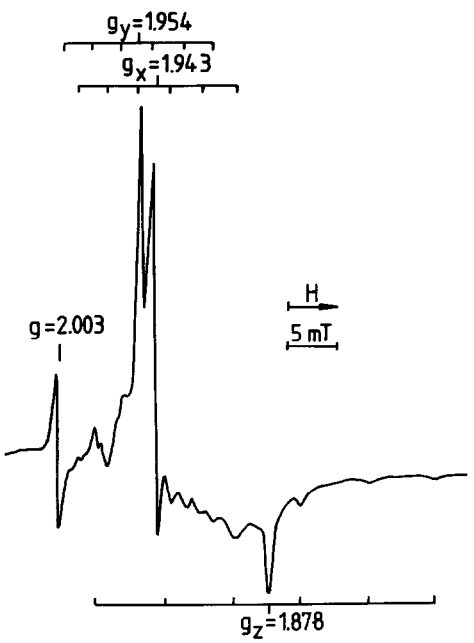


Fig. 1. ESR spectrum of MoO_3(n) reduced with propene at 400 K. Spectrum recorded at 77 K.

Table 1. Mo^{5+} concentration in the MoO_3(n) and MoO_3(p) samples after reduction with C_3H_6, determined from the ESR spectra

Temperature (K)	Time (min)	Mo^{5+} concentration (spin $m^{-2} \times 10^{17}$)	
		MoO_3(n)	MoO_3(p)
400	20	0.5	—
	80	1.6	—
470	5	1.4	0.7
	30	2.9	1.6

treatment.[4–8] There is no unequivocal interpretation of this absorption; F centres, carbon impurities or organic radicals could be responsible. The exact nature of this signal is currently being studied and the results will be published in a separate paper.

It is known that the activation of a propene molecule over molybdena catalysts consists of a hydrogen atom abstraction to form the allyl radical, which in turn undergoes further transformation by incorporation of the lattice oxygen. The results of reduction experiments with propene are consistent with the assumption, based on the catalytic tests, that the side crystal planes perpendicular to the (010) face are responsible for the propene activation. Obviously, the catalyst reduction occurs on account of both the activation and the oxidation processes. This explains the enhanced reducibility of the MoO_3(n) specimen, where the (100) and (101) planes are present in high abundance.

Further evidence for the mechanism of lattice oxygen insertion into the hydrocarbon molecule was found in experiments in which MoO_3(n) and MoO_3(p) were subjected to reduction by diallyloxalate vapour. This substance decomposes readily to yield free allyl radicals which are the intermediate species necessary for the selective pathway of propene oxidation.

The experiments showed that both samples were readily reduced by diallyloxalate vapour at 400 K (Table 2). The ESR spectra revealed the formation of Mo^{5+} species similar to those observed in the case of propene reduction. From Table 2 it can be seen that the rate of the reduction is much higher for the MoO_3(p) sample than for the MoO_3(n) catalyst. It is evident that here the experimental conditions, i.e. the supply of allyl species, enhances the formation of Mo^{5+} ions in the MoO_3(p) sample. Obviously, when the selective oxidation pathway is favoured, it is the abundance of the (010) plane which controls the catalyst reducibility. This indicates that the insertion

Table 2. Mo^{5+} concentration in the MoO_3(n) and MoO_3(p) samples after reduction with diallyloxalate vapour, determined from the ESR spectra

Temperature (K)	Time (min)	Mo^{5+} concentration (spin $m^{-2} \times 10^{17}$)	
		MoO_3(n)	MoO_3(p)
400	5	0.2	1.0
	20	0.3	1.3
470	3	0.5	2.8
	10	0.8	3.7
	30	1.3	6.7

of the lattice oxygen into the hydrocarbon molecule takes place at the (010) basal plane of MoO_3.

The ESR parameters of the Mo^{5+} spectra produced in the course of reduction with propene and diallyloxalate vapour show that the molybdenyl bond is preserved. This indicates that the reduction occurs at the expense of bridging oxygen atoms, possibly those most nucleophilic in "*trans*" position to the molybdenyl bond. Strong evidence supporting this model is provided by our study of the vacuum-reduced MoO_3.[9] Analysis of the values of the g tensor revealed the appearance of two different Mo^{5+} centres: one formed at an early stage of reduction and assigned to square pyramidal surrounding with the $\sigma\pi$-double bonded oxygen, and the second appearing in the later stages of the reduction and due to Mo^{5+} in octahedra along the shear planes. Similar behaviour was observed for the hydrogen-reduced MoO_3 samples.[10] Comparison with the situation at the surface of MoO_3 crystallites leads to the conclusion that it is the surface oxygen ion bridging two adjacent octahedra in the double string of edge-linked Mo–O octahedra which is removed on reduction of MoO_3. When the concentration of vacancies increases, a crystallographic shear takes place and Mo^{5+} cations assume an octahedral coordination along the shear planes.

We could not detect the pentacoordinated Mo^{5+} species in the samples reduced with propene and diallyloxalate. The ESR spectra showed only the presence of octahedrally coordinated Mo^{5+} ions. This might be due either to the immediate rearrangement of the surface polyhedra, resulting in the elimination of the oxygen vacancies, or to the completion of the coordination sphere of the $(MoO_5)^{5-}$ cluster by the product of propene or allyl oxidation, to form hexacoordinated Mo^{5+} species.

REFERENCES

1. B. Grzybowska, J. Haber and J. Janas, *J. Catal.* 1977, **49**, 150.
2. K. Brückman, R. Grabowski, J. Haber, A. Mazurkiewicz, J. Sloczyński and T. Wiltowski, *J. Catal.* (in press).
3. E. Serwicka and R. N. Schindler, *Z. Phys. Chem. N.F.* 1982, **133**, 175.
4. J. H. C. van Hoof, *J. Catal.* 1968, **11**, 277.
5. C. Naccache, P. Meriaudeau, M. Che and A. J. Tench, *Trans. Faraday Soc.* 1971, **57**, 506.
6. D. J. Miller and D. Haneman, *Surf. Sci.* 1971, **24**, 639.
7. L. Burlamacchi, G. Martini, F. Trifiro and G. Caputo, *J. Chem. Soc., Faraday Trans.* 1 1975, **71**, 209.
8. E. Serwicka, M. W. Schlierkamp and R. N. Schindler, *Z. Naturforsch.* 1981, **36A**, 226.
9. E. Serwicka, *J. Solid State Chem.* 1984, **51**, 300.
10. J. Haber and E. Serwicka, in preparation.

Polyhedron Vol. 5, No. 1/2, pp. 111–117, 1986
Printed in Great Britain

0277–5387/86 $3.00 + .00
© 1986 Pergamon Press Ltd

ACIDIC PROPERTIES OF MOLYBDATE-BASED CATALYSTS FOR PROPYLENE OXIDATION

I. MATSUURA,* S. MIZUNO and H. HASHIBA

Faculty of Science, Toyama University, Toyama 930, Japan

(*Received* 15 *June* 1985)

Abstract—Propylene oxidation on Bi- and Fe-doped molybdate ($MMoO_4$)-based catalysts proceeds to acrylic acid via acrolein utilizing their bifunctional properties. The first step of acrolein formation occurs on the surface of Bi molybdate; acrolein is subsequently oxidized to acrylic acid on the acid sites. The acidic site is related to the coordinatively unsaturated Mo ion in the surface Mo oxide coordinated with $MMoO_4$.

Many of catalysts for selective oxidation of hydrocarbons to unsaturated aldehydes, acids or acidic anhydrides are constructed with molybdate-based complex solid oxides that are either converted into a solid solution or remain polyphase. The industrial development of oxidation catalysts started with the report of Hearne and Adams[1] in 1948 that acrolein could be produced from propylene by the use of a mixed Cu–Mo oxide as oxidant. Around 1960 Veach *et al.*[2] reported the use of Bi molybdate with a composition $Bi_9PMo_{12}O_{52}$ for propylene oxidation to acrolein and for the conversion of propylene, ammonia and oxygen to acrylonitrile. This latter process was commercialized by SOHIO. Today this catalyst has been replaced by the so-called "multicomponent molybdate catalysts" that are composed of a variety of elements such as Ni, Co, Fe, Mg, P and K but always contain Bi and Mo. The principal advantages of the multicomponent molybdate catalysts are a low content of expensive Bi, somewhat higher conversions and specially a high yield of acrolein at low reaction temperature.

One of us[3] reported X-ray photoelectron spectroscopy (XPS) measurements on the multicomponent molybdate catalysts, and proposed a skin model consisting of a core of a molybdate matrix material, $MMoO_4$ (where M is a divalent cation, commonly Co, Ni, Mg or Mn) covered by successive layers of Fe(III) and Bi molybdates. Later this model was improved by more accurate measurements.[4] The surface was supposed to be Bi molybdate enclosed in Mo oxide. SOHIO[5] reported that $MMoO_4$ impregnated with a small amount of Fe and Bi gave high activity and selectivity for propylene ammoxidation to acrylonitrile. The composition is $(M_{11}Mo_{12}O_x)Fe_{0.3}Bi_{0.1}$, where M is Co, Ni, Mg, Mn, Fe and/or a mixture of them.

On the other hand, Pb and Ca molybdate having the Scheelite structure are active for propylene oxidation to acrolein via simultaneous incorporation of Bi ions and cation vacancies.[6] The limiting composition of this catalyst system is $Bi_2Mo_3O_{12}$. The $MMoO_4$-related α-$CoMoO_4$, α-$MnMoO_4$ and Scheelite structures with incorporation of Bi ions make a catalyst for selective oxidation of hydrocarbons.

In the presence of water, propylene or acrolein is oxidized to acrylic acid over Co, Va and Tl molybdate[7–9] and heteropoly compounds of Mo.[10] The so-called "multicomponent molybdate catalysts" have an activity in the oxidation of propylene to acrolein but also to acrylic acid as a subsequent product in the chain of the oxidation reaction. An important feature of these catalysts is that they might have acidic sites. These acidic sites may consist of surface hydroxyl groups and they can promote the formation of propene-diol as a reaction intermediate in the formation of acrylic acid.[11]

The present work is an attempt to study the structure and acidity of $MMoO_4$ system catalysts with the addition of Bi in selective oxidation of propylene to acrolein and acrylic acid, and to discuss

* Author to whom correspondence should be addressed.

the results in terms of current hypotheses on the mechanism of propylene oxidation.

EXPERIMENTAL

The catalysts used in this work are listed in Table 1. To prepare $CoMo_4$, powdered H_2MoO_4 was added to a stirred hot solution of $Co(NO_3)_2 \cdot 6H_2O$; the atomic ratio Co:Mo was 10:12. Dilute ammonia was then added until the pH was 5. The mixture was dried and freed of NH_4NO_3 by spraying on a hot plate at 350°C. The collected powder was further calcinated at 520°C for 2 h. Other samples were prepared by the same procedure. A sample was impregnated with Fe and Bi by slowly adding a solution of Fe and Bi in nitric acid and drying and calcining at 520°C for 2 h. Most samples were impregnated with 3% Fe and 1% Bi. Bi_2MoO_6 was prepared as follows. Solid basic Bi nitrate, $BiO(NO_3)$, and molybdic acid, H_2MoO_4, were powdered, slurried in water, and boiled with stirring 16 h. Then, the solid material was filtered and dried. The initial Bi:Mo ratio was 2:1.02 for the synthesis of active γ-Bi_2MoO_6.

The catalytic activity of the various samples for the oxidation of propylene to acrolein and acrylic acid was measured using a flow system at atmospheric pressure at 340°C. In each experiment samples (0.2–4 g) were used, the gas flows were 10 $cm^3\ min^{-1}$ of propylene and 100 $cm^3\ min^{-1}$ of air containing 10% water vapor. Dehydration of iso-propyl alcohol was also measured on 1 g of catalyst at 180°C.

^{18}O-exchange experiments between $H_2{}^{18}O$ and acrolein and acrylic acid were carried out by a pulse method at 340°C; a quadrupole mass spectrometer, ULVAC-190, was connected directly to the outlet of the pulse reactor containing 1 g of catalyst.

Table 1. Rate of propylene oxidation and iso-propyl alcohol dehydration[a]

Catalyst	k_{AL} (l min^{-1} m^{-2})	k_{AA} (l min^{-1} m^{-2})	k_{IP} (l min^{-1} m^{-2})
$NiMoO_4$	0.145	0.175	0.22
$Ni_{0.5}Co_{0.5}MoO_4$	0.225	0.23	0.18
$CoMoO_4$	0.240	0.200	0.16
$CoMoO_4$ (1% KOH)	0.230	0.045	—
$Co_{0.7}Fe_{0.3}MoO_4$	0.230	0.175	0.14
$FeMoO_4$	0.195	0.135	0.12
$MgMoO_4$	0.075	0.075	0.06
$MnMoO_4$	0.060	0.055	0.04
$PbMoO_4$	0.060	0.031	—
Bi_2MoO_6	0.075	0.030	—

[a] AL, C_3H_4O; AA, C_3H_3OOH; IP, iso-C_3H_7OH.

X-ray diffraction measurements were performed on a Shimazu XD7A spectrometer with Cu-K_α radiation and Ni filter.

XPS measurements were performed using an AEI ES200 spectrometer with Mg-K_α radiation. The power supply was run at 12 kV and 15 mA, the spectra being collected with a PPDS computer and stored in a 32 K disc. The powder sample was pressed on a sample holder covered with indium.

The IR spectra of samples were recorded with a JASCO IRA-2 spectrometer in the range 1250–400 cm^{-1} using the conventional KBr disk techniques. The Raman spectra of powders from 1200 to 0 cm^{-1} were measured on a rotating disk at liquid-nitrogen temperature.

RESULTS

Figure 1 shows the results of propylene oxidation on the $CoMoO_4$-based catalysts and Bi_2MoO_6. The $CoMoO_4$-based catalyst shows a high activity for propylene oxidation and subsequent acrolein oxidation to acrylic acid [Fig. 1(a)]. However, after

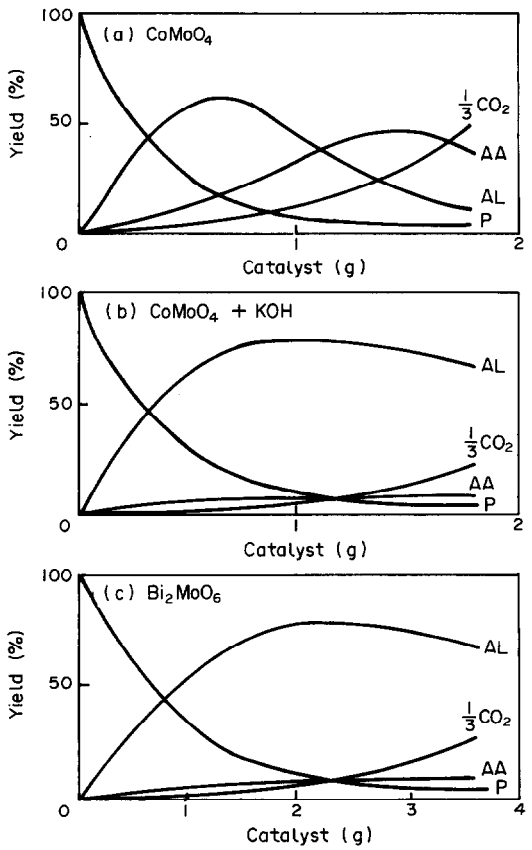


Fig. 1. Propylene oxidation on different amounts of catalyst. Abbreviations: P, propylene; AA, acrylic acid; AL, acrolein.

Table 2. X-ray diffraction pattern of $MMoO_4$-based catalyst: *d*-values (Å)

$NiMoO_4$	$Co_{0.5}Ni_{0.5}MoO_4$	$CoMoO_4$	$Co_{0.7}Fe_{0.3}MoO_4$	$FeMoO_4$	α-$CoMoO_4$ (*h* *k* *l*)
6.139	6.226	6.248	6.310	6.325	1 1 0
3.723	3.754	3.770	3.770	3.769	0 2 1
3.516	3.534	3.540	3.527	3.519	0 0 2[a]
3.339	3.376	3.389			2 0 1[b]
3.100	3.132	3.150	3.156	3.164	2 2 0
2.747	2.753	2.781	2.782	2.789	0 2 2[c]
2.323	2.323	2.338	2.350	2.353	1 3 2[d]
2.192	2.212	2.222		2.238	2 2 $\bar{3}$
2.062	2.080	2.097	2.100		0 2 $\bar{3}$[e]

[a] {1 1 $\bar{2}$; 2 0 $\bar{2}$. [b] 2 2 $\bar{1}$. [c] {1 1 2 ; 2 2 $\bar{2}$. ; 3 1 $\bar{2}$ [d] {2 0 2 ; 4 0 $\bar{2}$. [e] 4 0 $\bar{3}$.

the addition of KOH to the $CoMoO_4$-based catalyst, propylene oxidation stayed at the same level of activity but acrylic acid formation was suppressed [Fig. 1(b)]. Bi_2MoO_6 was not so active and we found a low conversion to acrylic acid from propylene [Fig. 1(c)]. The results suggest the oxidation of propylene to acrylic acid through acrolein with the successive first-order reaction. Table 1 shows the rate of overall propylene oxidation and acrylic acid formation. The rate of iso-propyl alcohol dehydration as an indicator of the catalyst acidity is also shown in Table 1.

$NiMoO_4$, $CoMoO_4$ and $FeMoO_4$ have two different phases. One is a high-temperature modification of the α-$MnMoO_4$ type and the other is a low-temperature modification of α-$CoMoO_4$-type. The X-ray diffraction lines of $MMoO_4$-based catalysts having α-$CoMoO_4$-type structure are listed in Table 2. Our samples of $NiMoO_4$ and $CoMoO_4$ show the α-$CoMoO_4$ structure as described by Smith and Ibers.[12,13] The mixed Ni–Co and Co–Fe molybdates show that these X-ray diffraction lines shift from one molybdate to the other systematically. This observation indicates that the mixed molybdates form a solid solution. The unit cell dimensions of the samples of α-$CoMoO_4$ structure are shown in Table 3.

Table 3. Lattice constants of α-$CoMoO_4$-structure molybdates

	a (Å)	*b* (Å)	*c* (Å)	*β* (°)
$NiMoO_4$	9.592	8.765	7.665	114.25
$Ni_{0.5}Co_{0.5}MoO_4$	9.652	8.765	7.665	114.25
$CoMoO_4$	9.712	8.865	7.666	114.15
$Co_{0.7}Fe_{0.3}MoO_4$	9.749	8.903	7.664	114.03
$FeMoO_4$	9.805	8.950	7.660	114.05

The IR and Raman frequencies of the samples examined are listed in Table 4 for the α-$CoMoO_4$ and α-$MnMoO_4$-structure molybdates. These two structures have the same space group ($C2/m$) and similar cell dimensions. The basic difference between the two structures is the coordination of Mo by oxygen which is octahedral in α-$CoMoO_4$ and tetrahedral in α-$MnMoO_4$. In the structures there are two crystallographically independent Mo atoms which are displaced from the center of their octahedra with Mo—O distances ranging from 1.73 to 2.31 Å and from 1.72 to 2.33 in α-$CoMoO_4$, and from their tetrahedra with Mo—O distances ranging from 1.731 to 1.795 and from 1.724 to 1.851 Å in α-$MnMoO_4$. We assume that for both symmetries the base structural unit is the system of tetrahedra in the C_2- and C_s-lattices and the space group has C^3_{2h}-symmetry. In Table 4 we give a description of normal modes for MoO_4 in lattice modes C_2 and C_s for our samples.

XPS was performed on our catalysts. The method gives information about the outermost 15–40 Å of the particles. Quantitative analysis of metal ions from XPS was calculated the method proposed by Carter *et al.*[14] who applied the photoelectron cross-sections of Scofield.[15] The results are shown in Table 5. Comparison with the bulk compositions shows the surfaces to be covered by MoO_3 with Bi ions appearing in the surface MoO_3 layer. On the contrary, the $PbMoO_4$-based catalyst has a surface composition nearly equal to that of the bulk composition.

Results of ^{18}O-exchange between $H_2{}^{18}O$ and

Table 4. Raman and IR spectra of $MMoO_4$[a]

α-$CoMoO_4$ type						α-$MnMoO_4$ type					
$NiMoO_4$		$Ni_{0.5}Co_{0.5}MoO_4$		$CoMoO_4$		$Co_{0.7}Fe_{0.3}MoO_4$		$FeMoO_4$		$MgMoO_4$		$MnMoO_4$		Mode
Raman	IR	Raman	IR	Raman	IR	Raman	IR	Raman	IR	Raman	IR	Raman	IR	
964vs	960vs	950vs	950vs	946vs	945vs	936vs	932vs	925vs	920vs	955s	945s	930s	928s	B_g, A_u (C_s)
915m	935sh	904m	924sh	882w	880sh	876w	884sh	875m		906s	890s	880s	870s	A_g, B_u (C_2)
821m	830w	819w	820w	814m	810sh	809s	793sh	805w	795sh	855s	780s	821s	800s	B_g, A_u (C_s)
712m	720m	704s	715m	701s	710sh	695m	710sh	700m	716w		735s	703w	725s	A_g, B_u (C_2), B_u (C_s)
	685sh		667sh		675sh		668sh		665sh					
	640s		640s		655s		652s		650s					
	450m		440sh		435sh		432sh		432sh	425w	440sh		403sh	
	415m		410m		410m		408m		408m	405w	420s	404w	400s	(MO_6)
387w		380w		380w										

[a] Band positions (cm^{-1}) and relative intensities (vs, very strong; s, strong; m, medium; w, weak; sh, shoulder).

acrolein and acrylic acid are given in Table 6. For the ^{18}O-exchange between $H_2{}^{18}O$ and acrolein during the oxidation reaction it was found that the ^{18}O content of unreacted acrolein and the reaction products was very high over the $CoMoO_4$-based catalyst but not over the $PbMoO_4$-based catalyst or Bi_2MoO_6.

DISCUSSION

Our XPS experiments on $MMoO_4$-based catalysts show that the surface is mainly covered by MoO_3 and Bi ions dispersed in the MoO_3 surface layer over the core of $MMoO_4$. The solid-state reaction between MoO_3 and Bi_2O_3 forms Bi molybdate. It confirms the model of Bi molybdate enclosed in the MoO_3 surface layer on a core of $MMoO_4$. It is known that the Bi molybdates are good catalyst for propylene oxidation to acrolein. On the $MMoO_4$-based catalysts propylene oxidation to acrolein proceeds on the surface Bi molybdate enclosed in the MoO_3 surface layer. However, acrylic acid formation occurs only on the $MMoO_4$-based catalysts and not on Bi molybdates. Our experimental result shows propylene oxidized successively to acrylic acid through acrolein on the $MMoO_4$-based catalysts. Moro-oka *et al.*[16] studied propylene oxidation on mixed Co and Mo oxides. They found that when the atomic ratio of Co/Mo was higher than 1 the main oxidation product was acetone; when the ratio was near 1, acrylic acid was observed in the oxidation products. It is known that V and Tl molybdate and also heteropoly compounds of Mo are good catalysts for acrylic acid formation by acrolein oxidation. The acidic property of these catalysts is an important factor for the reaction. The $MMoO_4$-based catalysts have acidic sites because they have a catalytic activity for iso-propyl alcohol dehydration. When the $CoMoO_4$-based catalyst was treated with KOH, the catalyst lost its activity for iso-propyl alcohol dehydration and acrylic acid formation from propylene oxidation was also suppressed. There is no doubt that the acidic sites on $MMoO_4$-based catalysts are necessary for acrylic acid formation from propylene oxidation. Figure 2 shows the rate of iso-propyl alcohol dehydration as an indication of acidity against the rate of acrylic acid formation on the $MMoO_4$-based catalysts. Increasing the rate of iso-propyl alcohol dehydration leads to an increase in the rate of acrylic acid formation.

There are three different structures for $MMoO_4$ compounds, viz. α-$CoMoO_4$, α-$MnMoO_4$ and the Scheelite structure which depends on the M^{2+} cation size in the molybdate. The first two structures have the same space group ($C2/m$) and similar cell

Table 5. Surface composition of metal ions for catalysts[a]

Catalyst	M/Σ	Mo/Σ	Bi/Σ	Fe/Σ
$NiMoO_4$	7 (47)	77 (51)	14 (0.5)	2 (1.5)
$Ni_{0.5}Co_{0.5}MoO_4$	8 (47)	76 (51)	14 (0.5)	2 (1.5)
$CoMoO_4$	8 (47)	79 (51)	11 (0.5)	2 (1.5)
$Co_{0.7}Fe_{0.3}MoO_4$	5 (33)	78 (51)	11 (0.5)	6 (15.5)
$FeMoO_4$		76 (51)	9 (0.5)	15 (48.5)
$MgMoO_4$	14 (47)	74 (51)	9 (0.5)	3 (1.5)
$MnMoO_4$	17 (47)	71 (51)	9 (0.5)	3 (1.5)
$PbMoO_4$	48 (45.5)	50 (50)	5 (4.5)	
Bi_2MoO_6		54 (33.3)	46 (66.7)	

[a] $\Sigma = M^{2+} + Mo + Fe + Bi$. Figures in parentheses are the bulk compositions of metal ions in wt %.

Table 6. ^{18}O-exchange between $H_2{}^{18}O$ and acrolein and acrylic acid

Catalyst	Reaction	Conversion (%)	^{18}O content (%)			
			H_2O	C_3H_4O	C_3H_3OOH	CO_2
$CoMoO_4$	$C_3H_4O + H_2{}^{18}O$	42	36	32	30	13
	$C_3H_3OOH + H_2{}^{18}O$	4	46		28	11
$PbMoO_4$	$C_3H_4O + H_2{}^{18}O$	18	78	3	5	6
	$C_3H_3OOH + H_2{}^{18}O$	5	81		6	5
Bi_2MoO_6	$C_3H_4O + H_2{}^{18}O$	22	72	3	4	4
	$C_3H_3OOH + H_2{}^{18}O$	6	76		8	7

dimensions. The basic difference between the two structures is the coordination of Mo by oxygen which is octahedral in α-$CoMoO_4$ and essentially tetrahedral in α-$MnMoO_4$. The M^{2+} cations coordinate six oxygens in both structures. The high-temperature form is always found to have the α-$MnMoO_4$ structure, while the low-temperature form is found to have the α-$CoMoO_4$ structure. Under our experimental conditions for propylene oxidation, these catalysts have the α-$CoMoO_4$ structure. Figure 3(a) shows the basic structure of α-$CoMoO_4$ in which infinite chains formed by Mo and Co edge-sharing octahedra parallel to the *c*-axis are surrounded by other chains. The distances between cations in α-$CoMoO_4$ are close to those found in the complex Mo oxides Mo_8O_{23} and Mo_9O_{26} or $(Mo_7O_{24})^{6-}$ and $(Mo_8O_{24})^{4-}$ ions.[17,18] Figure 3(b) shows MoO_3 have a layer structure in which some oxygen atoms are three-coordinate whilst others are two-coordinate or terminal. The Raman spectra of MoO_3 shows frequencies at 999s, 821vs and 668w cm^{-1}. If the surface of the $MMoO_4$-based catalyst is covered by MoO_3, the Raman bands should be observed. We observed the typical band at 999 cm^{-1} of MoO_3 in the $MnMoO_4$-based catalyst but no MoO_3 bands in the $CoMoO_4$-based catalyst. We suggest that the surface MoO_3 on the α-$CoMoO_4$-based catalyst is strongly coordinated with octahedral Mo ions in α-$CoMoO_4$ as shown in Fig. 3(c).

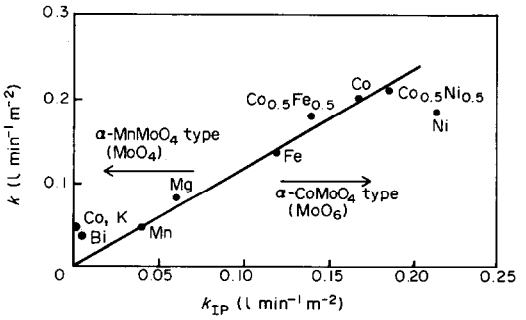


Fig. 2. Correlation of the rate of iso-propyl alcohol dehydration (k_{IP}) with the rate of acrylic acid formation (k) on $MMoO_4$-based catalysts.

The acidic sites of the $MMoO_4$-based catalysts may be their coordinatively unsaturated surface Mo ions connected with the surface MoO_3 layer. Figure 4 shows the relation between the rate of iso-propyl alcohol dehydration and the square of the frequency

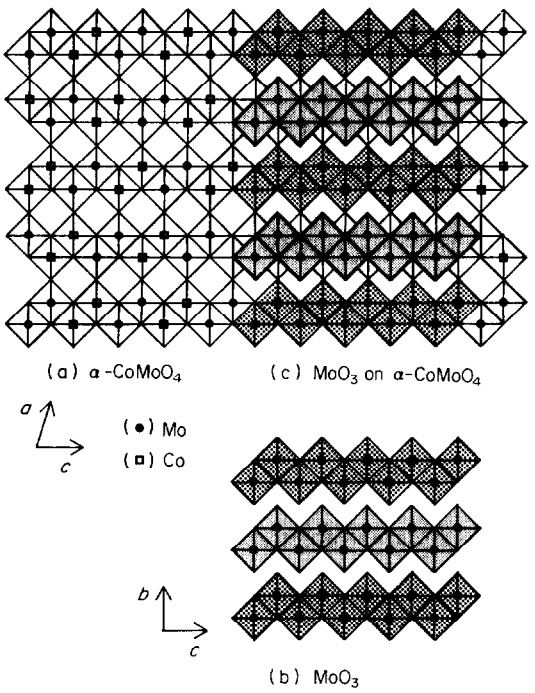
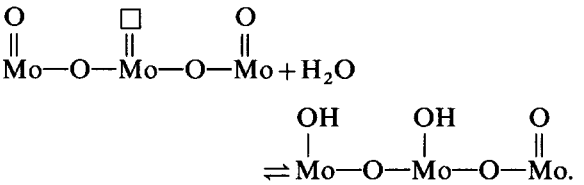


Fig. 3. Postulated surface state of an α-$CoMoO_4$-based catalyst.

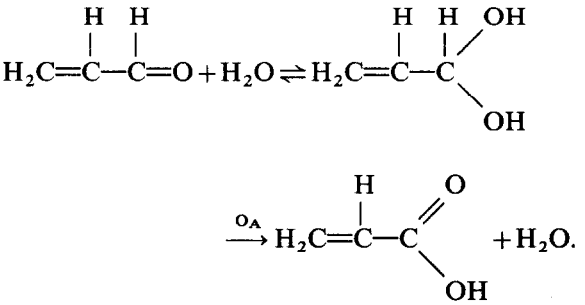
for Mo—O stretching in the C_2-mode in $MMoO_4$. The coordinatively unsaturated surface Mo ions of the α-$CoMoO_4$ structure have more acidic properties than the Mo ions of the α-$MnMoO_4$ structure. Scheelite molybdate and Bi_2MoO_6 have no acidic sites.

In the ^{18}O-exchange between $H_2{}^{18}O$ and acrolein during the oxidation reaction it was found that the ^{18}O content of unreacted acrolein and the reaction products was very high on $CoMoO_4$-based catalysts but not on $PbMoO_4$-based catalysts and Bi_2MoO_6 as shown in Table 6. A similar result for the exchange reaction between $H_2{}^{18}O$ and acrylic acid was found. These results indicate that the acid sites are important for the oxidation of acrolein to acrylic acid. Acrylic acid formation from acrolein oxidation on $MMoO_4$-based catalysts proceeds by oxidative dehydrogenation with H_2O.

The coordinatively unsaturated surface Mo ions forms hydroxyl groups by H_2O adsorption:



Then acrolein forms propenediol as a reaction intermediate. Thereafter oxidative dehydrogenation proceeds:



We propose that the $MMoO_4$-based catalysts have bifunctional catalytic properties, one yielding acrolein from propylene oxidation on the surface Bi molybdate and another oxidizing acrolein to acrylic acid on the acidic sites of coordinatively unsaturated surface Mo ions. The reaction model is shown in Fig. 5.

A small amount of acrylic acid forms during propylene oxidation on Bi_2MoO_6 and the $PbMoO_4$-based catalyst even though they have no acidic sites. The mechanism of acrylic acid formation should be different from the propenediol intermediate mechanism because no ^{18}O-exchange between H_2O and acrolein was observed on these catalysts. One of us has studied the adsorption of acrolein on Bi_2MoO_6.[19] The adsorption of acrolein was explained by assuming that the hydrogen from the COH group is dissociated and donated to a surface O atom while the residual carbonyl group occupies a surface anion vacancy with its oxygen atom, thereby becoming bonded to a neighboring

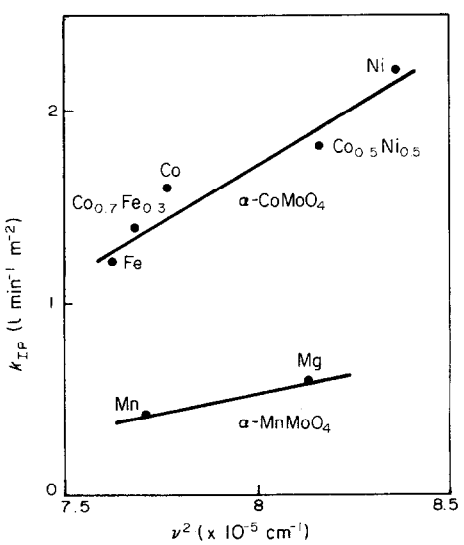


Fig. 4. Relation between the rate of iso-propyl alcohol dehydration and the square of the frequency of Mo—O stretching in the C_2-mode in $MMoO_4$.

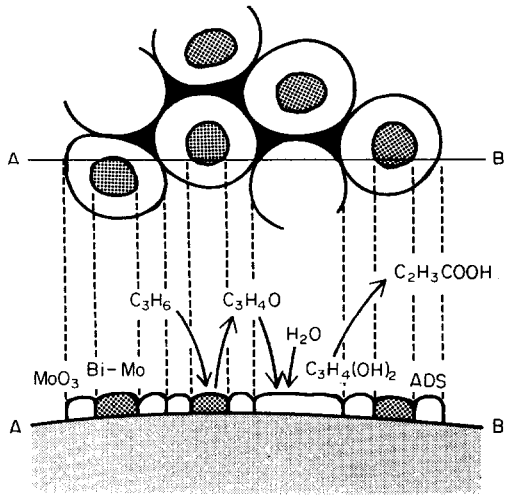
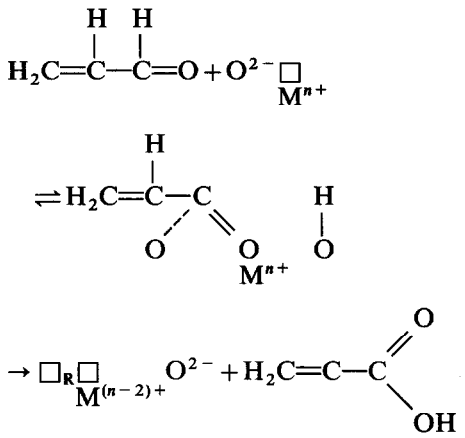


Fig. 5. Active surface model and reaction scheme.

surface oxygen:



The hydrogen donated to a surface O atom transfers to the adsorbed carbonyl. After desorption acrylic acid is formed and the adsorption site is reduced.

REFERENCES

1. G. W. Hearne and M. L. Adams, U.S. Patent 2,451,485 (1948).
2. F. Veach, J. L. Callahan and E. C. Milberger, *Chem. Eng. Prog.* 1960, **5b**, 65.
3. I. Matsuura and M. W. J. Wolfs, *J. Catal.* 1974, **37**, 174.
4. I. Matsuura, In *Proceedings of the 7th International Conference on Catalysis, Tokyo* (Edited by T. Seiyama and K. Tanabe), p. B-1099. Kodansha Ltd, Tokyo (1981).
5. SOHIO, Dutch Patent 7006454 (1970); Offenlegungsschrift 2203710 (1972).
6. K. Aykan, D. Halvorson, A. W. Sleight and D. B. Rogers, *J. Catal.* 1974, **35**, 401.
7. Distillers, British Patent 915799 (1961).
8. Nippon Kayaku, Japanese Patent 91014 (1973).
9. Distillers, Japanese Patent 21348 (1964).
10. T. Ohara, *Shokubai* 1977, **19**, 157.
11. M. Misono, K. Sakate and Y. Yoneda, In *Proceedings of the 7th International Congress on Catalysis, Tokyo* (Edited by T. Seiyama and K. Tanabe), p. B-1047. Kodansha Ltd, Tokyo (1981).
12. G. W. Smith, *Acta Cryst.* 1962, **15**, 1054.
13. G. W. Smith and J. A. Ibers, *Acta Cryst.* 1965, **19**, 269.
14. W. J. Carter, G. K. Schweitzer, A. Carlson and J. Thomas, *J. Electron Spectrosc. Relat. Phenom.* 1974, **5**, 827.
15. J. H. Schofield, Laurence Livermore Laboratory Report UCRL-51326 (1973).
16. Y. Moro-oka, S. Tan and A. Ozaki, *J. Catal.* 1968, **12**, 291.
17. A. Magneli, *Acta Chem. Scand.* 1948, **2**, 501.
18. I. Lindquist, *Ark. Kemi* 1950, **2**, 325, 349.
19. I. Matsuura, *J. Catal.* 1974, **33**, 420.

Polyhedron Vol. 5, No. 1/2, pp. 119–121, 1986
Printed in Great Britain

0277–5387/86 $3.00 + .00
© 1986 Pergamon Press Ltd

MECHANISM OF OXIDATIVE DEHYDROGENATION OF 1-BUTENE OVER BISMUTH MOLYBDATE

M. F. PORTELA,* M. M. OLIVEIRA and M. J. PIRES

Centro de Processos Químicos (INIC), Technical University of Lisbon, Instituto Superior Técnico, Aven. Rovisco Pais, 1096 Lisboa Codex, Portugal

(*Received* 20 *June* 1985)

Abstract—The oxygen reaction rate and the amount of retained oxygen, when mixtures of 1-butene and oxygen are pulsed over the low-temperature Bi_2O_3, MoO_3 (γ) pure phase, were recorded as a function of the pulse number. Results provided direct evidence that the sites at which oxygen enters the catalyst and the sites at which oxygen is used for oxidation reactions are separate and also of an inhibiting competitive adsorption of 1-butene over the reduced sites.

In previous studies of the oxidative dehydrogenation of 1-butene:

$$C_4H_8 + \tfrac{1}{2}O_2 \rightarrow C_4H_6 + H_2O$$

over bismuth molybdates, carried out by the continuous-flow method and using the initial-rate approach, it was observed that, keeping the oxygen partial pressure constant, the rate of butadiene formation, after a pseudo-linear initial increase with the butene partial pressure, attains a maximum and decreases afterwards with increasing olefin pressure.[1–3] This decrease for the higher butene pressures was interpreted as being due to an inhibiting competitive adsorption of the olefin over the reduced sites. On the other hand, it was reported that reoxidation of the catalyst occurs at surface sites which are separate from the olefin activation sites.[4] However no direct evidence of such phenomena have been provided. Such evidence clearly emerges from the results reported in this paper.

EXPERIMENTAL

The unsupported low-temperature Bi_2O_3, MoO_3 (γ) pure phase was prepared by a reproducible coprecipitation technique.[5] X-ray diffraction and IR and Raman spectroscopies did not show traces of impurities. Analysis by XPS confirmed the right Bi/Mo atomic ratio. The BET surface area was 1.0 $m^2\ g^{-1}$.

For the catalytic tests, the classical pulse method was used with a Pyrex reactor. The operating pressure was 4 bar (absolute). The catalyst was diluted with quartz of the same grain size (0.50–0.63 mm) whose inertness had been checked. Pulses of 2 standard cm^3 were used.

The experiments were performed at 280 and 350°C, with reaction mixtures of constant butene partial pressure (42 kPa) and variable oxygen pressure (2–72 kPa) with nitrogen. They were carried out so as to obtain differential conversions, adjusting the catalyst charge in order to eliminate the influence of the reaction products. The degradation to CO_2, although detectable, was negligible.

The reactants and reaction products were analyzed by a 3920 Perkin–Elmer gas chromatograph with a hot wire detector and 2,4-dimethylsulpholane (for CO_2 and hydrocarbons) and 13X molecular sieve (for O_2 and N_2) columns.

Other details of the experimental techniques are given elsewhere.[1]

RESULTS AND DISCUSSION

Figure 1 shows that the oxygen reaction rates decrease with the pulse number and tend to level off. At 280°C the curves are practically independent of the oxygen content in the reaction mixture, indicating a zero order in oxygen. However, at 350°C the reaction rates are practically equal after the first pulse and when activity levels off are lower the lower the oxygen pressure, showing a pressure dependence with respect to oxygen. It is obvious that in both

* Author to whom correspondence should be addressed.

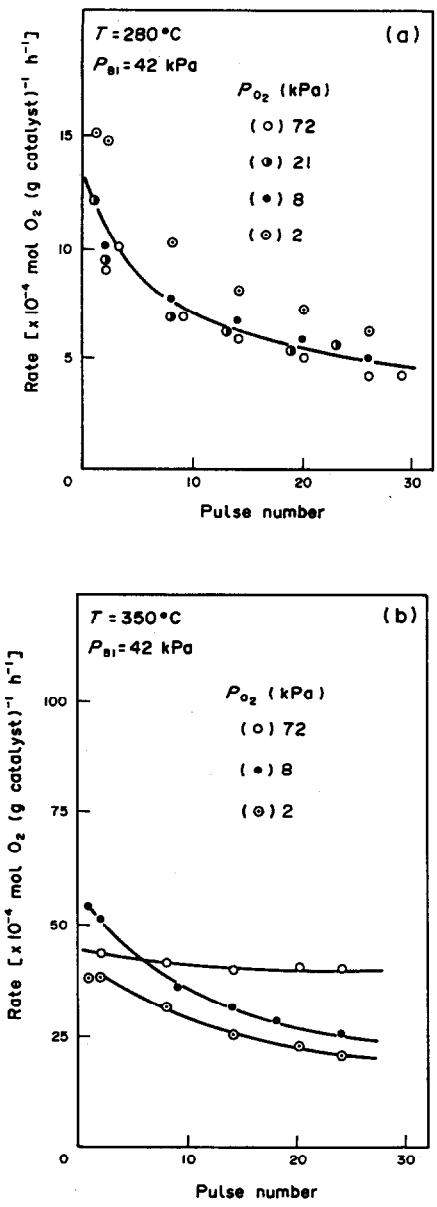


Fig. 1. Oxygen reaction rate vs pulse number at: (a) 280, and (b) 350°C. The oxygen reaction rate is half the butadiene formation rate.

cases activity tends to level off when the catalyst reduction rate is equal to its reoxidation rate. The data in Fig. 1 for lower oxygen partial pressures correspond to a butene partial pressure higher than the one which gives a rise to the previously mentioned maximum in the butadiene formation rate in continuous-flow experiments.[2,3]

To understand better the above results, we investigated the change with pulse number of the amount of oxygen retained by the catalyst after each pulse, and the balance of oxygen retained less oxygen consumed in the olefin oxidative dehydrogenation. The results are given in Table 1.

Table 1. Oxygen retained and oxygen balance as a function of pulse number[a]

Oxygen pressure (kPa)	Pulse number	Oxygen retained ($\times 10^{-6}$ mol O_2 g^{-1})	Oxygen balance ($\times 10^{-6}$ mol O_2 g^{-1})
	Temperature = 280°C		
2	1	1.44	−0.42
	2	1.60	−0.23
	8	1.15	−0.12
	14	0.67	−0.31
	20	0.44	−0.45
	26	0	−0.76
8	1	0.98	—
	2	0.98	−0.17
	8	1.06	0.17
	14	1.02	0.24
	20	0.91	0.22
	26	0.80	0.21
	Temperature = 350°C		
2	1	0.86	−3.7
	2	0.79	−3.8
	8	0.49	−3.4
	14	0.28	−2.8
	20	0.16	−2.6
	26	0.12	−2.4
8	1	5.9	−0.51
	2	5.6	−0.46
	9	4.6	0.28
	14	4.6	0.88
	19	4.5	1.04
	24	5.0	1.98
	25	4.6	1.39

[a] Butene partial pressure = 42 kPa.

We see that at the lowest oxygen pressure the catalyst is progressively reduced with successive pulses, but the amount of retained oxygen decreases with the pulse number, and a stage is reached in which the oxygen of the reaction mixture is not able to reoxidize the reduced catalyst. Increasing the oxygen pressure, we observe a negative balance of oxygen with the first pulses, indicating reduction of the catalyst, but a positive balance is recorded later, although data in Fig. 1 show that catalyst reduction occurs.

We conclude that the sites of catalyst reduction and reoxidation are different, and that reoxidation is progressively inhibited by the butene remaining adsorbed over the reduced sites of the catalyst after each pulse.

REFERENCES

1. M. Oliveira, M. F. Portela, M. J. Pires and F. R. Ribeiro, *Can. J. Chem. Eng.* 1983, **61**, 87.
2. M. F. Portela, M. J. Pires and M. Oliveira, In *Proceedings of the 8th Iberoamerican Symposium on Catalysis, Huelva*, 1982, Vol. 1, p. 374.
3. M. F. Portela, M. M. Oliveira, M. J. Pires, F. M. S. Lemos and L. Ferreira, In *Proceedings of the 8th International Congress on Catalysis, Berlin*, 1984, Vol. 2, p. 533.
4. R. K. Grasselli, In *Proceedings of the 9th Iberoamerican Symposium on Catalysis, Lisbon*, 1984, Vol. 1, p. 106.
5. M. J. Pires, M. F. Portela, M. M. Oliveira, A. Saraiva and T. Miranda, In *Proceedings of the 7th Iberoamerican Symposium on Catalysis, La Plata*, 1980, p. 189.

Polyhedron Vol. 5, No. 1/2, pp. 123–128, 1986
Printed in Great Britain

0277–5387/86 $3.00 + .00
© 1986 Pergamon Press Ltd

INFLUENCE OF Mo–SiO_2 CATALYST PREPARATION ON MOLYBDENUM COORDINATION AND CATALYTIC PROPERTIES

M. CHE,* C. LOUIS*† and J. M. TATIBOUËT‡

*Laboratoire de Réactivité de Surface et Structure, UA CNRS 1106, Université P. et M. Curie, 4 Place Jussieu, 75230 Paris Cedex 05, France; and ‡Laboratoire de Catalyse Organique, LA CNRS 231, Université Lyon I, 43 Bd du 11 novembre 1918, 69622 Villeurbanne Cedex, France

(*Received* 18 *June* 1985)

Abstract—Mo–SiO_2 catalysts were prepared by grafting, i.e. by reacting $MoCl_5$ with the hydroxyl groups of silica. The analysis of the Mo coordination sphere during grafting by reflectance spectroscopy and EPR indicates that grafting occurs probably through the following mechanism: $MoCl_5 + SiOH \rightarrow SiOMoCl_4 + HCl$. Grafted Mo–$SiO_2$ catalysts differ from Mo–SiO_2 catalysts prepared by impregnation by the presence of a tetracoordinated Mo^{5+} species (identified by EPR after thermal activation), a better molybdenum dispersion and stronger Mo–silica interactions. The methanol oxidation reaction was found to be sensitive to molybdenum dispersion and this might be an appropriate way to evaluate the dispersion of supported oxides.

The slower progress towards understanding catalysis on supported oxides compared to catalysis on supported metals arises from the difficulty of preparing well-dispersed oxides and from the lack of a reliable method of measuring the dispersion, similar to that of hydrogen chemisorption for supported metals. The aim of this work is to investigate the influence of molybdenum dispersion of various Mo–SiO_2 catalysts on both the coordination sphere of molybdenum ions and their catalytic properties.

EXPERIMENTAL

Two preparation methods were used:

(1) classical impregnation of silica with an aqueous solution of ammonium heptamolybdate; and

(2) grafting of $MoCl_5$ onto dehydrated silica via its silanol groups in strict absence of air and water. The grafting is performed either with $MoCl_5$ dissolved in cyclohexane[1,2] or with $MoCl_5$ vapour at 200°C.[2] The advantage of using $MoCl_5$ vapour is that the grafting can be monitored by EPR and UV spectroscopies.[2]

RESULTS AND DISCUSSION

Dehydrated silica at 400°C exhibits a charge-transfer band at about 260 nm in the UV region and two vibration bands at 1365 and 2190 nm in the near IR, assigned to SiOH groups[3] (Fig. 1).

When silica is heated in the presence of $MoCl_5$ at 200°C, a decrease in intensity of the near-IR bands is observed, indicating that $MoCl_5$ reacted with the silanol groups. Simultaneously, bands appear in the UV–visible region and an EPR signal is observed (Fig. 2). The EPR parameters ($g_\perp = 1.952$ and $g_\parallel = 1.968$, $A_\perp = 37$ G and $A_\parallel = 70$ G) and the presence of a hyperfine structure in the signal obtained after grafting, due to interaction with the nuclear spins ($I = 5/2$) of the ^{95}Mo and ^{97}Mo isotopes (natural abundance 25%), show that this signal arises from Mo^{5+} ions. The EPR signal possesses axial symmetry whereas that of $MoCl_5$ in cyclohexane is isotropic at 77 K.[2] The change of symmetry indicates that the Mo^{5+} coordination sphere is affected on grafting and confirms the

† Author to whom correspondence should be addressed.

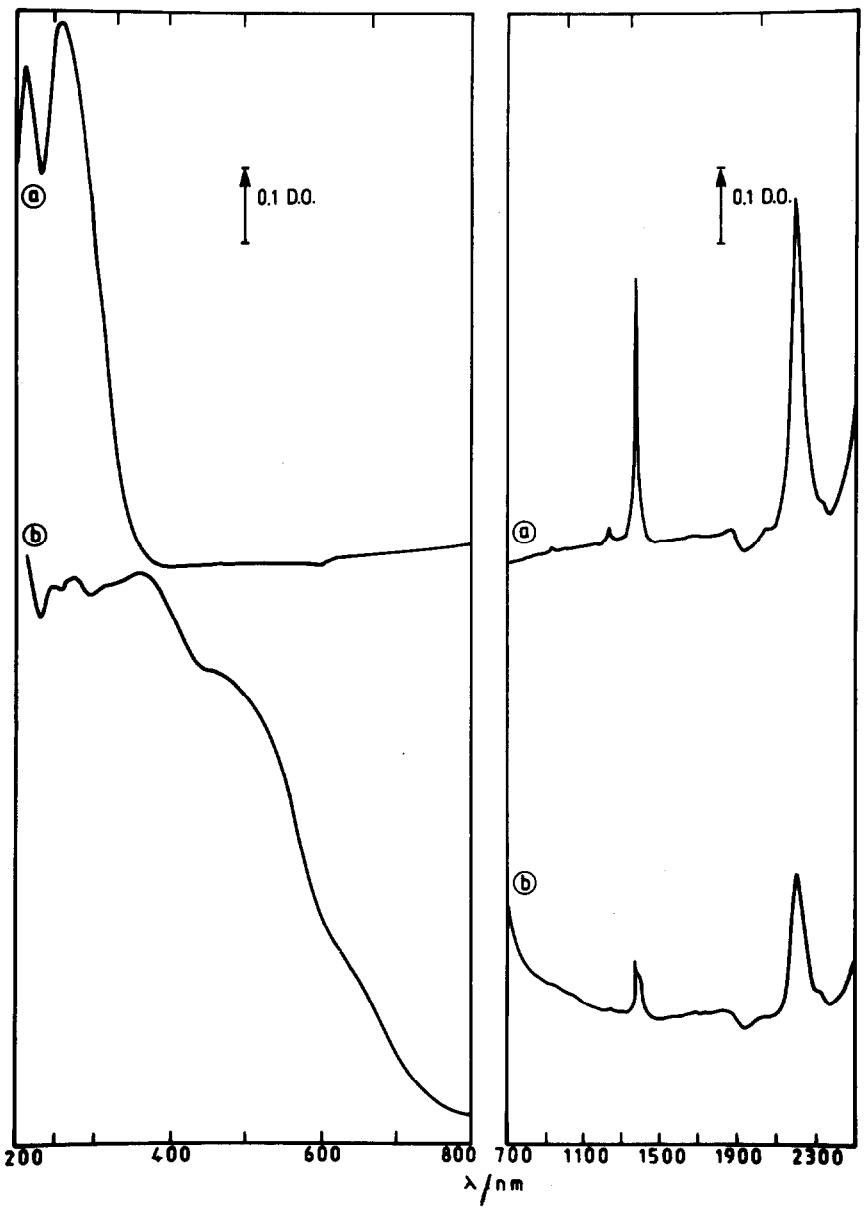


Fig. 1. UV–visible–near-IR reflectance spectra: (a) dehydrated silica at 400°C, and (b) silica after grafting with $MoCl_5$ vapour at 200°C.

formation of bonds with silica. Finally, the parameters of the EPR signal and of the UV spectrum of Mo after grafting have been compared, respectively, with those of $MoCl_5$,[2,4] $[MoOCl_4]^-$[5] and $[MoOCl_5]^{2-}$[6,7] and found to be very similar to those of the $[MoOCl_4]^-$ ion.

The previous results can be interpreted in terms of the following grafting reaction:

$$MoCl_5 + SiOH \rightarrow SiOMoCl_4 + HCl.$$

It is also observed that a part of $MoCl_5$ does not react and is only adsorbed on the silica support in a dimer state, Mo_2Cl_{10}, which does not exhibit an EPR signal, due to electron pairing. This adsorbed molybdenum is evidenced as follows. When exposed to air, the catalyst, which was red-brown, instantaneously turns blue because of hydrolysis and partial oxidation of Mo_2Cl_{10} to molybdenum blues[8,9] (mixed Mo^{5+}–Mo^{6+} hydroxides). Its UV–visible spectrum is then similar to that of molybdenum blues,[10] i.e. an intervalence band around 900–1000 nm is observed, which arises from electron hopping between Mo^{5+} and Mo^{6+} ions. The molybdenum blues can be eliminated by washing with water or ammonia solutions and the sample turns greyish brown which is the colour

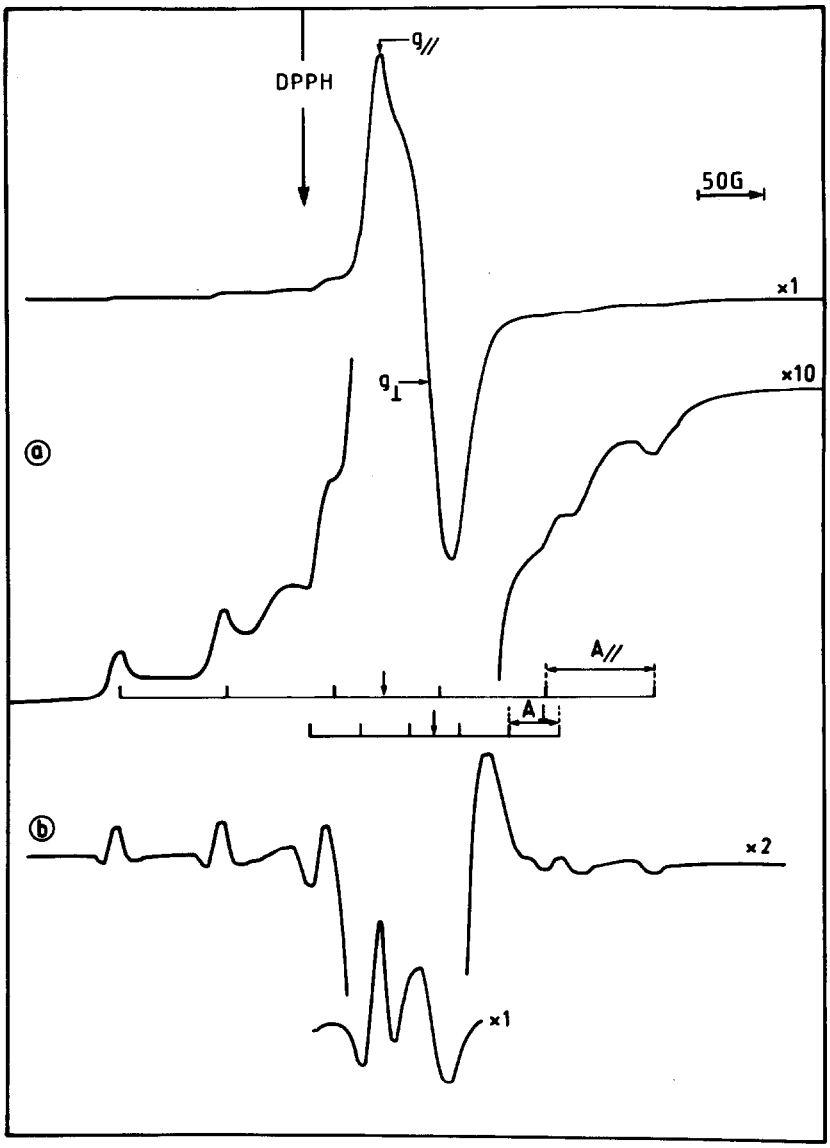


Fig. 2. EPR spectra recorded at 77 K of Mo–SiO_2 catalysts obtained after grafting with $MoCl_5$ vapour at 200°C: (a) first derivative, and (b) third derivative.

characteristic of grafted molybdenum remaining on silica. The intervalence band is no longer present whereas a *d–d* band of Mo^{5+} around 450 nm and a charge-transfer band of Mo^{6+} around 280 nm are observed. These facts suggest that the Mo^{5+} and Mo^{6+} ions are isolated from each other. In the following, the term "grafted" refers to samples which have been washed in order to eliminate the adsorbed molybdenum.

When, after grafting, the sample is directly evacuated at increasing temperatures, without any intermediate contact with air or water, the following changes are observed: at around 200°C, the relative values of the g components are reversed with $g_\perp$ becoming larger than $g_\parallel$ (Fig. 3). At 300°C, a second Mo^{5+} signal with $g_\perp > g_\parallel$ appears and, at 500°C, three different signals corresponding to three types of Mo^{5+} ions in axial symmetry are clearly visible ($g_\perp = 1.944$ and $g_\parallel = 1.892$, $g_\perp = 1.957$ and $g_\parallel = 1.866$, and $g_\perp = 1.926$ and $g_\parallel = 1.755$, referred to as Mo^{5+}_{6c}, Mo^{5+}_{5c} and Mo^{5+}_{4c}, respectively). During evacuation of the sample at increasing temperatures, the spin concentration measurements indicate that the number of Mo^{5+} ions remains constant, suggesting that the spectral changes arise only from modification within the Mo^{5+} coordination sphere.

The spectrum observed after evacuation at 500°C is also detected for the grafted catalyst after washing and thermal activation (oxidation, reduction under H_2 at 500°C and evacuation at the same

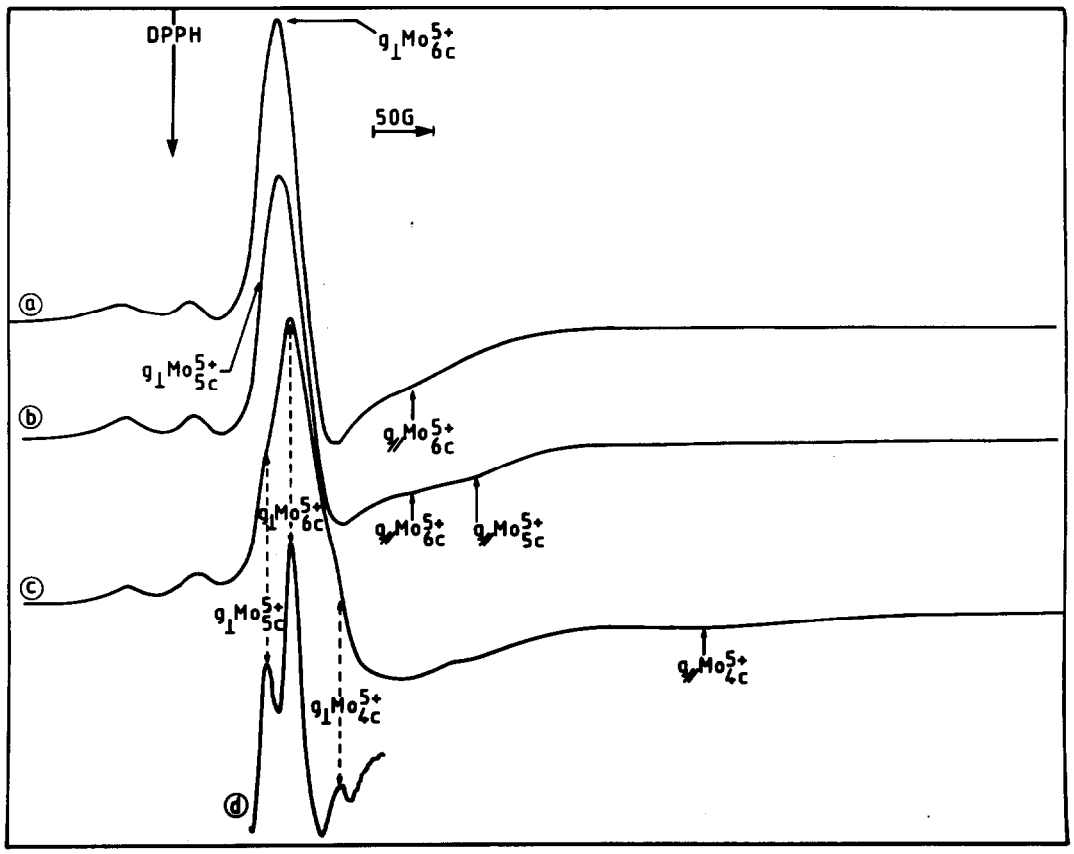
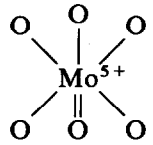


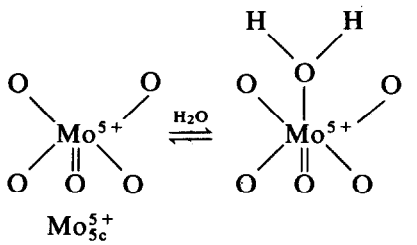
Fig. 3. EPR spectra recorded at 77 K of the Mo–SiO_2 catalysts prepared by grafting with $MoCl_5$ vapour at 200°C, followed by evacuation: (a) at 200°C for 30 min, (b) at 300°C for 30 min, and (c) at 500°C for 30 min; and (d) third-derivative spectrum of (c).

temperature). It should be noted that impregnated Mo–SiO_2 catalysts possess only two Mo^{5+} species (Mo^{5+}_{5c} and Mo^{5+}_{6c}) and exhibit a spectrum analogous to that obtained after grafting and evacuation at 300°C. One of these common species (Mo^{5+}_{6c}) possesses EPR parameters very close to those of $[Mo_6O_{19}]^{3-}$.[11] This polyanion is composed of six molybdenum ions (one Mo^{5+} and five Mo^{6+}) in octahedral symmetry. Each molybdenum ion is surrounded itself by an octahedron of O^{2-} ions and possesses one molybdenum–oxygen bond of molybdenyl type.[11] It is deduced that Mo^{5+}_{6c} is hexacoordinated with one molybdenyl bond:



Mo^{5+}_{6c}

The coordination of the two other species (Mo^{5+}_{4c} and Mo^{5+}_{5c}) has been determined using probe molecules. On impregnated catalysts, adsorption of water transforms the Mo^{5+}_{5c} EPR signal into Mo^{5+}_{6c}, due to the introduction of one water molecule into the coordination sphere, according to the following reaction:[11]

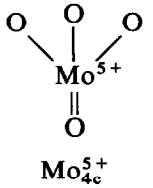


Mo^{5+}_{5c}

Adsorption of water at room temperature and increasing pressures is found to transform the third species (Mo^{5+}_{4c}) observed on grafted Mo–SiO_2 into Mo^{5+}_{5c} and then into Mo^{5+}_{6c}.[2] It suggests that Mo^{5+}_{4c} is less coordinated than Mo^{5+}_{5c}, i.e. with more than one vacancy in its coordination sphere. During adsorption, the spin concentration is found to remain constant, showing that water acts only as a ligand and not as a redox agent. This is reasonable owing to the temperatures (25°C) and the pressures (1–18 torr) involved. Since the species obtained after water adsorption have a molybdenyl character, it

can be deduced that the starting Mo_{4c}^{5+} species also possesses a molybdenyl character.

In order to determine the number of vacancies within its coordination sphere, adsorptions of CO and ^{13}CO have been performed onto the Mo_{4c}^{5+} species. The analysis of the new signal obtained ($g_1 = 1.965$, $g_2 = 1.969$, g_3 not resolved), and of the superhyperfine structure due to interaction between the unpaired electron of Mo^{5+} and the nuclear spin ($I = \frac{1}{2}$) of ^{13}C (one set of three lines for each g value of the new signal, with relative intensity 1:2:1 and a coupling constant $A = 7.5$ G), reveals that two CO molecules can enter into the Mo_{4c}^{5+} coordination sphere. Hence, Mo_{4c}^{5+} possesses two vacancies in its coordination sphere and the following model for this species can be proposed:



Mo_{4c}^{5+}

The changes described above, when a catalyst after grafting is evacuated at increasing temperatures, may be interpreted on the basis of the previous results. At 200°C, the change of the g components from $g_{\parallel} > g_{\perp}$ to $g_{\perp} > g_{\parallel}$ involves the replacement of chlorine by oxygen ligands in the Mo^{5+} coordination sphere, leading to the Mo_{6c}^{5+} signal. At 300°C, a part of the Mo_{6c}^{5+} species is transformed into Mo_{5c}^{5+} owing to the formation of one vacancy within the coordination sphere. Above 500°C, a second vacancy is created, leading to the Mo_{4c}^{5+} signal. Hence, increasing the temperature causes the formation of vacancies within the Mo^{5+} coordination sphere. The Mo_{4c}^{5+} signal seems to be characteristic of grafted samples.

The grafted and impregnated Mo–SiO_2 samples differ from each other in several other ways. It was also found[1] that grafted molybdenum interacts more strongly with silica than impregnated molybdenum: whereas impregnated molybdenum is easily dissolved in water, grafted molybdenum remains fixed on silica. More drastic tests in hot HF–H_2SO_4 solutions show that, for the grafted sample, molybdenum and silica dissolve very little while they completely dissolve in the case of impregnated catalysts. On the other hand, grafted molybdenum is found to be less reducible than impregnated molybdenum. Thermogravimetric and micromanometric measurements have allowed us to derive the mean oxidation state of molybdenum at the end of a reduction step performed under hydrogen at 600°C: it is 4 for grafted samples instead of 2–3 for impregnated ones. The increased resistance to reduction of grafted molybdenum may be interpreted in terms of a stronger interaction with silica which would limit reduction or/and a better dispersion of molybdenum. The molybdenum behaves more as bulk molybdenum oxide on impregnated catalysts than on grafted ones and can thus be viewed as aggregates of molybdenum oxide on the former catalysts.

The electron-transfer reaction $Mo^{5+} + O_2 \rightarrow Mo^{6+}–O_2^-$ was used to measure the Mo^{5+} dispersion by EPR spectroscopy.[1,2] In conditions precluding bulk oxidation (77 K, 10^{-1} torr), O_2 is adsorbed on catalysts previously thermally reduced by H_2. The Mo^{5+} signal decreases as the O_2^- signal appears. The Mo^{5+} dispersion can be calculated from the ratio of the integrated intensities of the Mo^{5+} EPR signal:

$$\frac{I_i(Mo^{5+}) - I_f(Mo^{5+})}{I_i(Mo^{5+})},$$

where $I_i(Mo^{5+})$ is determined before O_2 adsorption and $I_f(Mo^{5+})$ after. For example, for Mo–SiO_2 samples containing 1% of Mo by weight, the calculated Mo^{5+} dispersion is found to be 80% for the grafted sample against 30% for the impregnated one.

The reaction of methanol partial oxidation is known to be structure-sensitive.[12] Whereas, on polycrystalline MoO_3 oxide, it essentially produces formaldehyde, on orientated crystallites the selectivity to formaldehyde, methylal or dimethylether depends on the exposed face. The same reaction performed over an Mo–SiO_2-supported catalyst leads essentially to formaldehyde and methylformate. On grafted catalysts, methylformate is the principal product, whereas on impregnated ones it is formaldehyde. For example, for 1% molybdenum loading, the selectivity towards methylformate is equal to 90% for grafted catalysts and only 20% for the impregnated ones. For smaller molybdenum loadings, as the Mo^{5+} dispersion increases, the selectivity to methylformate also increases. For molybdenum loadings between 1 and 0.07%, the Mo^{5+} dispersion of grafted catalysts varies from 80 to 100% and their selectivity (at 230°C) from 90 to 95%, whereas for impregnated samples the Mo^{5+} dispersion varies from 30 to 100% and the selectivity from 20 to 91%. These results indicate that a correlation exists between the molybdenum dispersion and the selectivity in methanol oxidation, and that this reaction is not only structure-sensitive but also dispersion-sensitive.

The mechanism for the formation of methylformate may be summarized as follows. Formaldehyde is produced on molybdenum of Mo–SiO_2 catalysts in the same way as for polycrystalline

bulk MoO_3. However, instead of desorbing, formaldehyde migrates onto silica and reacts with methoxy group arising from dehydration between methanol and silanol surface group. A hemiacetal intermediate can be formed to lead to methylformate. The same type of mechanism has been recently proposed by Cant *et al.*[13] using various deuterated compounds on copper-based catalysts.

CONCLUSION

The absence of any intervalence Mo^{5+}–Mo^{6+} band, the high dispersion of Mo^{5+} ions, and the significant selectivity in methylformate, lead us to conclude that the grafting method using $MoCl_5$, is suitable for preparing highly dispersed molybdenum. The methanol oxidation appears to be a good reaction to compare the dispersion of supported molybdenum catalysts prepared differently. The grafted catalysts differ from the impregnated ones by the presence of the Mo^{5+}_{4c} tetracoordinated species detected by EPR, a stronger Mo–silica interaction and a better molybdenum dispersion connected with the significant selectivity to methylformate in methanol oxidation.

Acknowledgements—We wish to acknowledge M. Fournier (Laboratoire de physico-chimie inorganique, UA 419, CNRS, Université P. et M. Curie) for helpful discussions concerning the chemistry of molybdenum. We gratefully acknowledge P. Gihr and F. Delvalle who kindly prepared the poster connected with this note (presented to the Fifth International Mo Conference, Newcastle upon Tyne, 1–5 July 1985). M. Che dedicates the work he has performed in this study to Y. Tarnopolsky, and to Y. Kukk, Estonian Professor of Chemistry, who died in a Soviet labour camp on 27 March 1981 at the age of 40.

REFERENCES

1. C. Louis, M. Che and F. Bozon-Verduraz, *J. Chim. Phys.* 1982, **79**, 803.
2. C. Louis, Thesis, Paris (1985).
3. J. H. Anderson and K. A. Wickersheim, *Surf. Sci.* 1964, **2**, 252.
4. R. F. W. Bader and A. D. Westland, *Can. J. Chem.* 1961, **39**, 2309.
5. C. D. Garner, L. H. Hill, F. E. Mabbs, D. L. McFadden and A. T. McPhail, *J. Chem. Soc., Dalton Trans.* 1977, 853.
6. P. T. Manoharan and M. T. Rogers, *J. Chem. Phys.* 1968, **49**, 5510.
7. H. B. Gray and C. R. Hare, *Inorg. Chem.* 1962, **1**, 363.
8. Climax Molybdenum Co., Chemical Data Series, Bulletin Cdb-3A (1969).
9. Climax Molybdenum Co., Experimental Molybdenum Chemicals Data Sheets, EX-6 (1965).
10. C. Heitner-Wirguin and D. Hall, *J. Inorg. Nucl. Chem.* 1974, **36**, 3870.
11. M. Che, M. Fournier and J. C. Launay, *J. Chem. Phys.* 1979, **71**, 1954.
12. (a) J. M. Tatibouët and J. E. Germain, *J. Catal.* 1981, **72**, 375; (b) J. M. Tatibouët, J. E. Germain and J. C. Volta, *J. Catal.* 1983, **82**, 240.
13. N. W. Cant, S. P. Tonner, D. L. Trimm and M. S. Wainwright, *J. Catal.* 1985, **91**, 197.

Polyhedron Vol. 5, No. 1/2, pp. 129–139, 1986
Printed in Great Britain

0277–5387/86 $3.00 + .00
© 1986 Pergamon Press Ltd

OXY-METHOXY COMPOUNDS OF MOLYBDENUM(VI) AND THEIR RELATIONSHIP TO THE SELECTIVE OXIDATION OF METHANOL OVER MOLYBDATE CATALYSTS

E. M. McCARRON III* and A. W. SLEIGHT

Central Research and Development Department, E.I. du Pont de Nemours and Co., Experimental Station, Wilmington, DE 19898, U.S.A.

(*Received* 18 *June* 1985)

Abstract—The selective oxidation of methanol to formaldehyde over molybdate catalysts has been modeled synthetically by the formation of oxy-methoxy compounds of molybdenum(VI). The formation, decomposition and reoxidation of the compound $Mo_2O_5(OCH_3)_2$ are found to correspond remarkably well with the three elementary steps of the catalytic cycle. Thermal decomposition experiments performed on the compounds

$$Mo_2O_5(OCH_3)_2,\ Mo_2O_5(OCD_3)_2,\ Mo_2O_5(OCH_3)_2 \cdot 2CH_3OH$$

and $Na_4[Mo_8O_{24}(OCH_3)_4] \cdot 8CH_3OH$ imply that C—H bond breaking is rate-limiting in accord with the kinetically determined catalytic result. The nature of the catalytic site, inhibition of the reaction by water, and poisoning of the catalyst by pyridine are also adequately modeled. The structure of $Na_4[Mo_8O_{24}(OCH_3)_4] \cdot 8CH_3OH$ is seen as a model for coordination geometry of the molybdenum–methoxy interaction at the catalyst surface.

In our laboratory much effort has been directed at understanding the mechanism of the selective oxidation of methanol to formaldehyde over molybdate catalysts.[1] While much of the work has involved reactor studies, surface science, and numerous physical techniques, a small but no less important effort has been aimed at synthesizing model compounds, i.e. compounds which mimic the chemistry of the catalytic process. In this paper we present the results of our model-compound studies and discuss how these compounds either helped to provide us with new insight or served to reinforce our earlier conclusions regarding methanol oxidation. The compounds to be discussed are

$$Mo_2O_5(OCH_3)_2,\ Mo_2O_5(OCD_3)_2,$$
$$Mo_2O_5(OCH_3)_2 \cdot 2CH_3OH,$$
$$Na_4[Mo_8O_{24}(OCH_3)_4] \cdot 8CH_3OH$$

and

$$(C_5H_5NH)_4[Mo_8O_{26}(C_5H_5N)_2] \cdot 2(CH_3)_2SO.$$

METHANOL OXIDATION

What follows is a brief, general overview of the selective oxidation of methanol to formaldehyde over molybdate catalysts. For a detailed account of how these conclusions were reached see the review of Cheng *et al.*[1]

Methanol reacts with molybdate surfaces at room temperature forming methoxy groups and liberating water. As the temperature is raised the methoxy groups begin to decompose forming formaldehyde and more water. These products rapidly desorb from the surface leaving the molybdate phase reduced. Rapid reoxidation of the catalyst takes place to complete the catalytic cycle. The rate-limiting step in this process is the abstraction of a methoxy hydrogen. The reaction is highly selective towards formaldehyde, with water found to be an inhibitor.

* Author to whom correspondence should be addressed.

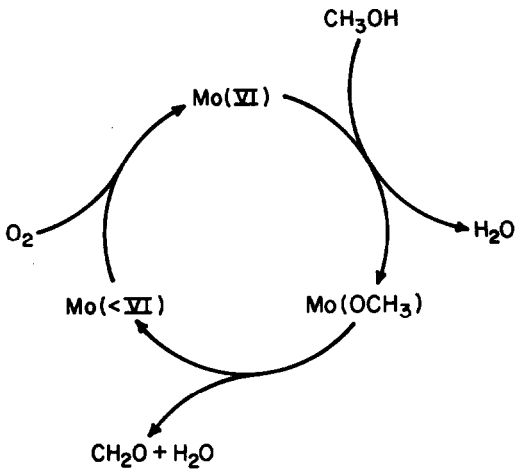


Fig. 1. Schematic diagram for the selective oxidation of methanol to formaldehyde over molybdate catalysts.

The active sites are determined to be coordinatively unsaturated molybdenum atoms.

The rest of this paper will deal with how the study of model compounds has either influenced or confirmed many of these above conclusions.

REACTIONS

A schematic diagram of the conversion of methanol to formaldehyde at a molybdate site is given in Fig. 1. The mechanism is seen to involve three elementary steps.[2] Parallels between each of the individual steps and the chemistry of the model compound, $Mo_2O_5(OCH_3)_2$, are given below.

Step 1

The uptake of methanol by MoO_3 at room temperature has been quantified by adsorption studies[2] and the formation of methoxy groups on the surface confirmed by IR measurements.[3] Less than monolayer coverage implies that MoO_3 is not very reactive towards methanol at low temperatures. This lack of reactivity can be attributed to the layer structure of MoO_3,[4] the surface of which consists predominantly of coordinatively saturated molybdenum atoms.

Fortunately, $MoO_3 \cdot 2H_2O$[5] is more reactive than MoO_3 at low temperatures. This enhanced reactivity is a result of the lability of the water molecule bound directly to molybdenum.[6]* A comparison of the layer structures of MoO_3 and $MoO_3 \cdot 2H_2O$ is given in Fig. 2.

In the case of $MoO_3 \cdot 2H_2O$, water loss makes coordinatively unsaturated molybdenum sites available for reaction:

$$MoO_{1/1}O_{4/2}H_2O_{1/1} \cdot H_2O \rightarrow MoO_{1/1}O_{4/2}\square_{1/1} + 2H_2O. \quad (1)$$

As a result, $MoO_3 \cdot 2H_2O$ reacts in absolute methanol as follows:[7]

$$2MoO_3 \cdot 2H_2O + 2CH_3OH \xrightarrow{60°C} Mo_2O_5(OCH_3)_2 + 5H_2O, \quad (2)$$

$$2MoO_3 \cdot 2H_2O + 4CH_3OH \xrightarrow{0°C} Mo_2O_5(OCH_3)_2 \cdot 2CH_3OH + 5H_2O. \quad (3)$$

Both reaction products are white microcrystalline powders with plate-like habits. The dimethanolate [eqn (3)] loses methanol at roughly 100°C

* The bond strength, s, of the Mo—OH_2 bond is 0.31, as calculated from the expression $s = (d/1.882)^{-6.0.24}$

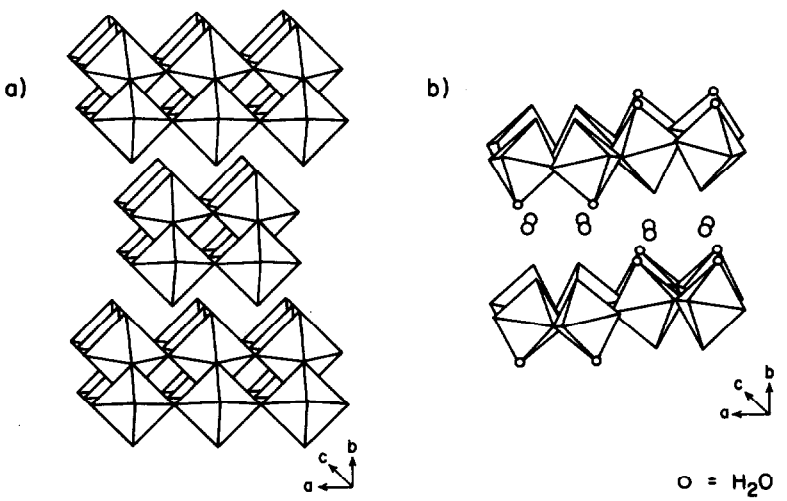


Fig. 2. The layer structures of: (a) MoO_3, and (b) $MoO_3 \cdot 2H_2O$.

converting to the simple dimethoxide [eqn (2)]. Hydrolysis of the dimethoxide gives the hemihydrate:[8]

$$Mo_2O_5(OCH_3)_2 + 2H_2O \rightarrow 2MoO_3 \cdot \tfrac{1}{2}H_2O + 2CH_3OH. \quad (4)$$

Hydrolysis may account for the inhibiting effect which water displays in the catalytic reaction.[9]

As yet the actual structure of $Mo_2O_5(OCH_3)_2$ is unknown, but a structure can be proposed consistent with the following observations: (1) $Mo_2O_5(OCH_3)_2$ exhibits a single-line solid-state ^{13}C NMR spectrum (Fig. 3), implying that all carbon environments are equivalent; and (2) $Mo_2O_5(OCH_3)_2$ adopts a plate-like crystal habit, suggesting that the structure is layered. The proposed structure, shown in Fig. 4, is based on stacked double layers (ReO_3-type) of $MoO_{5/2}(OCH_3)_{1/1}$ corner-sharing octahedra.

A comparison of the IR spectra of methoxy groups bound to the surface of MoO_3 and $Mo_2O_5(OCH_3)_2$ is shown in Fig. 5. The similarity of the IR data led us to conclude that the chemistry taking place in both cases is essentially equivalent. This apparent chemical equivalence, when coupled with the seeming necessity that coordinatively unsaturated molybdenum atoms be present for reaction to occur [from eqn (1)], led us to speculate that the *010* surface of MoO_3 would be inactive with respect to methanol chemisorption. In fact, it has been shown that, in the case of oriented single crystals, methanol adsorbs intact on the *010* surface but does not dissociatively chemisorb.[10] Therefore, methanol oxidation must take place on non-*010* surfaces ($\sim 10\%$ of the total surface area of a typical MoO_3 sample). Subsequent temperature-programmed desorption experiments have shown that only 12% of the surface molybdenum sites are catalytically active, further supporting this hypothesis.[11]

Step 2

The rate-limiting step in methanol oxidation, as determined by kinetic studies,[12] is the transfer of a

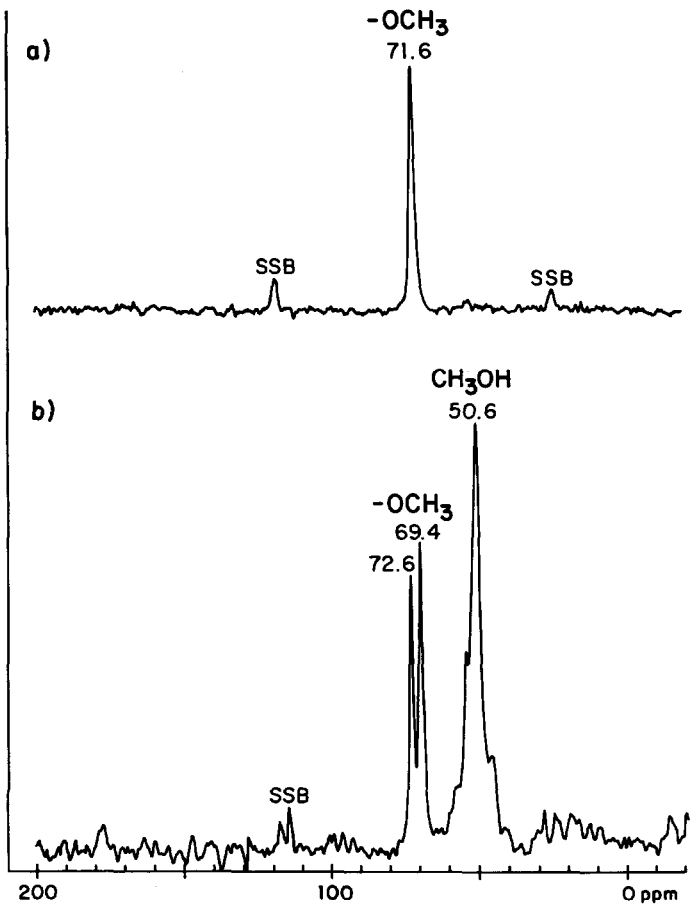


Fig. 3. Solid-state ^{13}C NMR spectra (^{13}C CP-MAS, 75 MHz) for: (a) $Mo_2O_5(OCH_3)_2$, and (b) $Na_4[Mo_8O_{24}(OCH_3)_4] \cdot 8CH_3OH$.

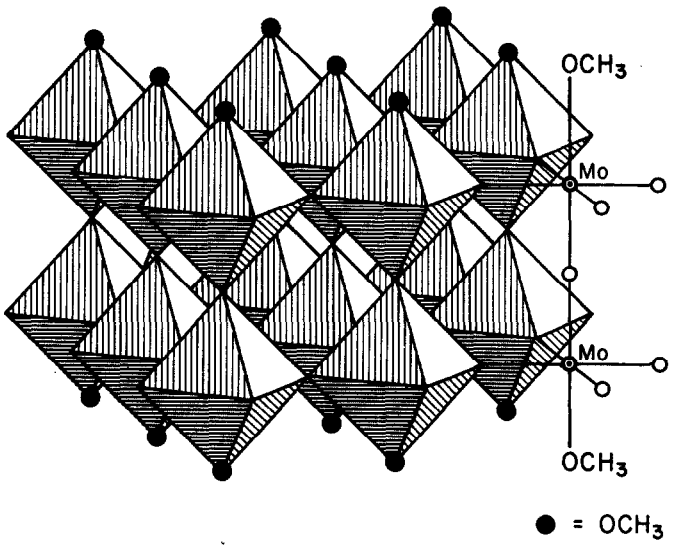


Fig. 4. Proposed structure for $Mo_2O_5(OCH_3)_2$.

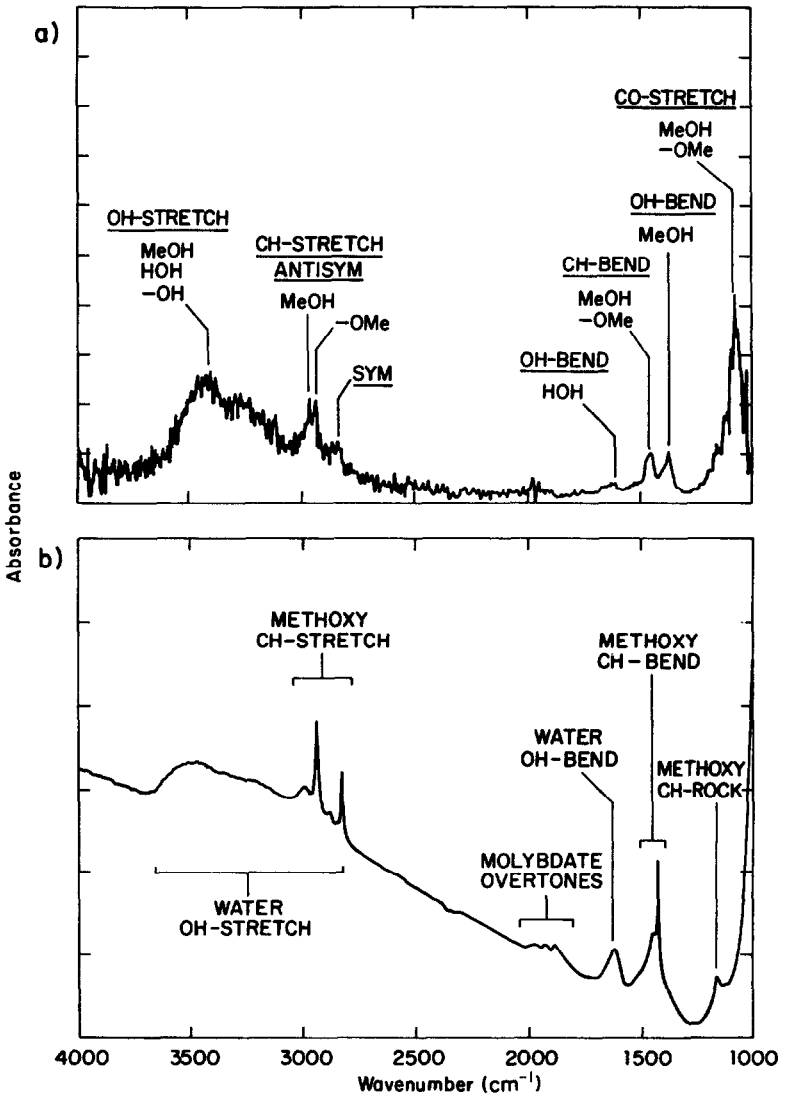


Fig. 5. A comparison of the FTIR spectra (MoO_3–CH_3OH—reflectance IR; $Mo_2O_5(OCH_3)_2$—transmission IR) of: (a) MoO_3–CH_3OH surface species, and (b) $Mo_2O_5(OCH_3)_2$.

hydrogen from a methoxy group to a surface oxygen. Coupled to the hydrogen transfer is the rapid loss of formaldehyde and water, with concomitant reduction of the molybdate catalyst.

$Mo_2O_5(OCH_3)_2$ is also observed to undergo redox chemistry. When exposed to sunlight, white $Mo_2O_5(OCH_3)_2$ photodecomposes leaving a blue-colored, amorphous residue. Subsequent photolysis experiments, monitored by mass spectroscopy, revealed that, in the initial stages of decomposition, roughly equal amounts of formaldehyde and methanol were produced:

$$Mo_2O_5(OCH_3)_2 \rightarrow [Mo_2O_5] + CH_2O + CH_3OH. \quad (5)$$

This result is consistant with either photon-assisted C—H bond breaking[13] or photo-generation of methoxy radicals.[14] However, an observed increase in the formaldehyde:methanol ratio with time suggests that C—H bond activation is indeed responsible—as photodecomposition decreases the number of methoxy groups available for reaction with photo-liberated hydrogen:

$$—OCH_3 \rightarrow CH_2O + —H, \quad (6)$$

the probability of forming methanol:

$$—H + —OCH_3 \xrightarrow{-2\bar{e}} CH_3OH \quad (7)$$

must also decrease.

This leads to a build-up of hydrogen in the reduced molybdate residue. In the limit that no methanol is formed, the reaction becomes:

$$Mo_2O_5(OCH_3)_2 \rightarrow [H_2Mo_2O_5] + 2CH_2O. \quad (8)$$

The extent of reduction, x [a measure of the relative rates of eqns (5) and (8)], of the molybdate phase has never been quantitatively determined, but could be measured in principle by monitoring either the quantities of the gases evolved or by counting the residual protons [combining eqns (5) and (8)]:

$$Mo_2O_5(OCH_3)_2 \rightarrow [H_{2x}Mo_2O_5] + (1+x)CH_2O + (1-x)CH_3OH, \quad (9)$$

where x will have a value between 0 and 1.

Step 3

The reoxidation of the reduced molybdate catalyst phase is fast under catalytic condition owing to the high surface oxygen mobility and high electronic conductivity of the reduced phase at temperatures above 200°C. At room temperature, as in the case of photochemically decomposed $Mo_2O_5(OCH_3)_2$, reoxidation of the residue is found to be slow. However, thermogravimetric analysis has shown that reoxidation of the photochemically reduced residue is complete at 350°C, the normal operating temperature of the catalytic reaction:[15]

$$[H_{2x}Mo_2O_5] + \left(\frac{1+x}{2}\right)O_2 \rightarrow 2MoO_3 + xH_2O. \quad (10)$$

THERMAL-DECOMPOSITION EXPERIMENTS

$Mo_2O_5(OCH_3)_2$

The nature of the photolysis experiments is such that complete decomposition of $Mo_2O_5(OCH_3)_2$ is never certain. Therefore, the thermal decomposition of $Mo_2O_5(OCH)_3)_2$ was investigated as a means of determining the full extent of the redox chemistry.

Thermogravimetric curves for $Mo_2O_5(OCH_3)_2$ both *in vacuo* and in oxygen are shown in Fig. 6. The general observations to note are the following: (1) $Mo_2O_5(OCH_3)_2$ decomposes sharply at ~225°C; (2) *in vacuo*, a second sharp decomposition takes place at ~325°C; and (3) in oxygen, decomposition and reoxidation of the molybdenum oxide residue appear to occur simultaneously. Additionally, it was noted that the degree of reduction of the residue (maximum weight loss *in vacuo*) was dependent upon the heating rate, with faster rates leading to deeper reduction. A series of experiments was performed in an attempt to sort out the effect of thermal treatment upon $Mo_2O_5(OCH_3)_2$ decomposition.

A typical decomposition experiment involved the rapid heating of $Mo_2O_5(OCH_3)_2$ *in vacuo* to a given temperature and holding it there until gas evolution ceased. Evolved gases were monitored by mass spectroscopy and the decomposition residues characterized by powder X-ray diffraction. Experiments run in a flowing helium atmosphere allowed for the quantitative analysis of the evolved gases by gas chromatography. After annealing at 500°C *in vacuo* to remove water, the relative degree of reduction of molybdenum oxide residue was measured thermogravimetrically by uptake of oxygen [see eqns (11) and (13) below].

All thermal-decomposition experiments resulted in the production of the following gaseous products: formaldehyde, water, methanol and dimethyl ether. Changes in the product distribution, reflected by changes in the O/Mo ratio of the residues, were monitored over the temperature range 200–400°C, at roughly 50°C intervals. Table 1 lists the results.

A gross change in the nature of the product distribution is seen to occur at ~325°C, the

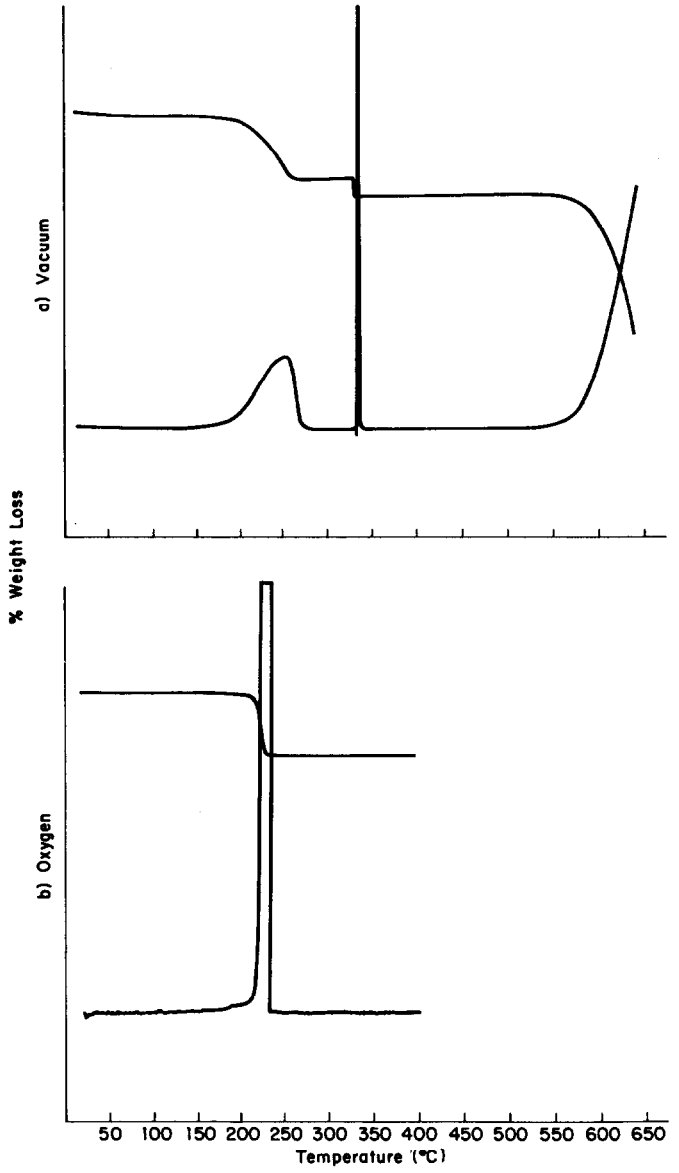


Fig. 6. TGA data (Du Pont 951-990 instrument at a heating rate of 5°C min^{-1}) for $Mo_2O_5(OCH_3)_2$: (a) *in vacuo*, and (b) in oxygen.

temperature of the sharp decomposition in the vacuum TGA data (Fig. 6). Below 325°C the distribution of the products was such that, as the reaction temperature at which the $Mo_2O_5(OCH_3)_2$ sample was decomposed was increased, the amounts of formaldehyde and water produced increased at the expense of methanol and dimethyl ether. At all temperatures above 325°C, the product distribution remained constant. Closer examination of this 325°C event revealed that it coincided with an abrupt water loss and a change in the molybdate residue from an amorphous to a crystalline state. The crystalline material was determined to be a mixture of MoO_2 and Mo_4O_{11}. Following from eqn (9):

$$3[H_{2x}Mo_2O_5] \xrightarrow{325°C} (2+4x)MoO_2 + (1-x)Mo_4O_{11} + 3xH_2O. \quad (11)$$

Apparently, above 325°C, water formation [following from eqn (6)]:

$$2(\text{—H}) + O^{2-} \xrightarrow{-4\bar{e}} H_2O \quad (12)$$

is facile and controls the product distribution by competing successfully with methanol formation [eqn (7)].

Table 1. Temperature dependence of the thermal decomposition of $Mo_2O_5(OCH_3)_2$

Decomposition temperature (°C)	$MoO_2 : Mo_4O_{11}$ ratio[a]	O/Mo[b]	Product formation trend			
			CH_2O	H_2O	CH_3OH	$(CH_3)_2O$
150	Trace MoO_2	2.75	↓	↓	↑	↑
200	~1:2	2.68				
250	~1:1	2.60				
300	~3:2	2.54				
350[c]	~2:1	2.50				
400[c]	~2:1	2.50				

[a] Determined by a comparison of the relative X-ray powder diffraction peak intensities of the individual molybdenum oxide phases of the residue [see eqn (9)] with those observed for simple physical mixtures of the phases.

[b] O/Mo for the molybdenum oxide residues was determined thermogravimetrically by weight gain in oxygen, in accordance with eqn (13). Deeper reduction corresponds to lower O/Mo values.

[c] Above ~325°C, O/Mo is observed to be constant.

Oxygen uptake measurements on samples decomposed at temperatures above 325°C indicate that $x = 0$ [O/Mo = 2.5 (Table 1)] for eqn (13):

$$(2+4x)MoO_2 + (1-x)Mo_4O_{11} + \tfrac{3}{2}(1+x)O_2 \xrightarrow{500°C} 6MoO_3. \quad (13)$$

This implies that $x = 0$ for eqn (11) also, which is at odds with the observed water loss. In fact, for decompositions run at lower temperatures, x appeared to be negative {O/Mo > 2.5 [$x = 5 - 2$(O/Mo)] (see Table 1)}. These apparent contradictions can be attributed to the production of dimethyl ether:

$$Mo_2O_5(OCH_3)_2 \rightarrow 2MoO_3 + (CH_3)_2O. \quad (14)$$

The production of dimethyl ether does not involve the reduction of Mo(VI). This leads to an anomalously low x value as measured by oxygen uptake. Therefore, the true measure of the extent of the reduction of $Mo_2O_5(OCH_3)_2$ would involve quantifying the water formed [eqn (11)].

Regarding dimethyl ether formation, it should be noted that the steady-state catalytic reaction of methanol on MoO_3 can produce significant quantities of dimethyl ether under low-conversion conditions where the surface concentration of methoxy groups is expected to be greatest.[9] This is in qualitative agreement with the $Mo_2O_5(OCH_3)_2$ results embodied in eqn (14).

Table 1 indicates that dimethyl ether formation is favored at lower reaction temperatures. This result can be understood as being a result of the fact that C—H bond breaking is rate-limiting. Thus, at lower temperatures, where the energy for C—H bond breaking is less, the rate of methoxy decomposition is slow. This allows for intact methoxy groups to react with liberated methanol [eqns (6) and (7)] to produce hydroxyl groups and form dimethyl ether:

$$—OCH_3 + CH_3OH \rightarrow —OH + (CH_3)_2O. \quad (15)$$

As the reaction temperature is increased, the rate of methoxy decomposition increases and, as a result, the number of methoxy groups available for reaction with methanol must decrease, suppressing the formation of $(CH_3)_2O$. Furthermore, the increased rate of methoxy decomposition [eqn (6)] makes available more hydroxyl groups:

$$—H + O^{2-} \xrightarrow{-2\bar{e}} —OH \quad (16)$$

for recombination with any liberated methanol:

$$—OH + CH_3OH \rightarrow —OCH_3 + H_2O, \quad (17)$$

which, in turn, leads to further reduction:

$$2(—OCH_3) \xrightarrow{-(2+2x)\bar{e}} 2x(—H) + (1+x)CH_2O + (1-x)CH_3OH. \quad (18)$$

The net result is that increasing the reaction temperature leads to increased formaldehyde formation and, consequently, deeper reduction of the molybdenum oxide residue. Further evidence for this line of thinking will be presented in the next two sections and the section on $[Mo_8O_{24}(OCH_3)_4]^{4-}$.

For the most part the thermal-decomposition results are similar to those observed for photodecomposition. The major difference lies in the formation of dimethyl ether. That dimethyl ether formation is absent during the room-temperature photodecomposition experiments implies that the reaction mechanism which leads to dimethyl ether

has a thermal-activation threshold somewhat above ambient conditions.

$Mo_2O_5(OCH_3)_2 \cdot 2CH_3OH$

With respect to thermal decomposition, the additional two methanol molecules of the dimethanolate, $Mo_2O_5(OCH_3)_2 \cdot 2CH_3OH$, should promote the formation of dimethyl ether as indicated by eqn (15). This has been observed experimentally; for a given reaction temperature, the degree of reduction of the residue is found to be less for

$$Mo_2O_5(OCH_3)_2 \cdot 2CH_3OH$$

than for $Mo_2O_5(OCH_3)_2$ (see Table 2).

Deuteration

$MoO_3 \cdot 2H_2O$ was reacted with CD_3OH to produce $Mo_2O_5(OCD_3)_2$. In a gross demonstration of the kinetic isotope effect, it was observed that, for a given reaction temperature, the degree of reduction of the residue of $Mo_2O_5(OCD_3)_2$ was less than that of the undeuterated material (see Table 2). Again the suppression of C—H bond breaking, this time by the kinetic isotope effect, slows the rate of methoxy decomposition and enhances the probability that liberated methanol will combine with intact methoxy groups to produce dimethyl ether [eqn (15)].

Additionally, it was noted that the photodecomposition of the deuterated material was not as rapid as that of $Mo_2O_5(OCH_3)_2$ under similar conditions.

ISOPOLYMOLYBDATES

Unfortunately, the state of surface science at present does not allow for a direct, detailed examination of the surface molybdenum–methoxy coordination geometry. Therefore, the only hope of inferring the structure of the surface species lies in making analogies with model compounds.

Although the correspondence between the chemistry of $Mo_2O_5(OCH_3)_2$ and the surface chemistry of MoO_3 is clearly evident from the above discussions, the lack of structural details for $Mo_2O_5(OCH_3)_2$ was particularly distressing, since, given the chemical similarity, a structural similarity was most probable.

$[Mo_8O_{24}(OCH_3)_4]^{4-}$

Fortunately, on the basis of the work of Klemperer and co-workers[16–18] and the work of Knoth and Harlow,[19] it appeared that chemistry similar to that described for the $Mo_2O_5(OCH_3)_2$ system could be performed on isopolymolybdate anions.

The compound

$$Na_4[Mo_8O_{24}(OCH_3)_4] \cdot 8CH_3OH,^{20}$$

can be produced by any of the following reactions:

$$2Na_2MoO_4 + 6MoO_3 + 12CH_3OH \xrightarrow[CH_3OH]{abs.} Na_4[Mo_8O_{24}(OCH_3)_4 + 8CH_3OH + 2H_2O, \quad (19)$$

$$4NaOCH_3 + 8MoO_3 + 8CH_3OH \xrightarrow[CH_3OH]{abs.} Na_4[Mo_8O_{24}(OCH_3)_4] + 8CH_3OH, \quad (20)$$

$$8MoO_3 \cdot 2H_2O + 12CH_3OH + 4Na^+ \xrightarrow[CH_3OH]{abs.} Na_4[Mo_8O_{24}(OCH_3)_4] + 8CH_3OH + 18H_2O + 4H^+. \quad (21)$$

Table 2. Comparison of the degree of reduction (as measured by the O/Mo of the molybdenum oxide residues)[a] of the compounds $Mo_2O_5(OCH_3)_2$, $Mo_2O_5(OCD_3)_2$ and $Mo_2O_5(OCH_3)_2 \cdot 2CH_3OH$ as a function of temperature

Decomposition temperature (°C)	O/Mo[b]		
	$Mo_2O_5(OCH_3)_2$	$Mo_2O_5(OCD_3)_2$	$Mo_2O_5(OCH_3)_2 \cdot 2CH_3OH$
150	2.75	2.88	2.94
250	2.60	2.73	2.80
350	2.50	2.61	2.71

[a] The degree of reduction is inversely proportional to O/Mo, with deeper reduction corresponding to lower O/Mo values.

[b] O/Mo determined thermogravimetrically by weight gain in oxygen, in accordance with eqn (13).

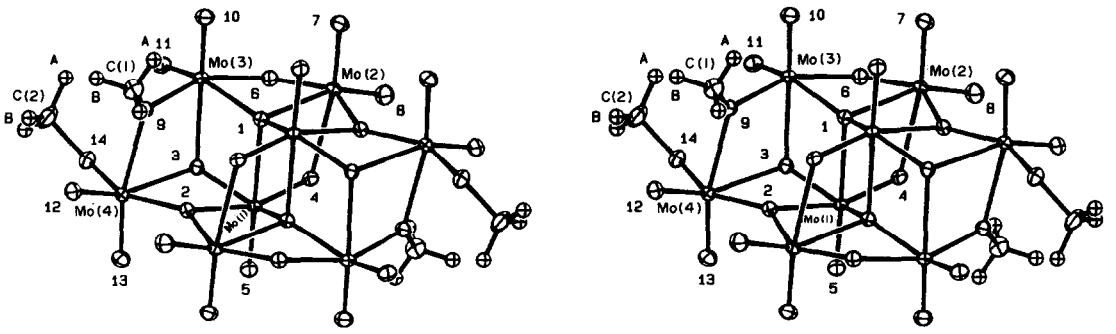


Fig. 7. Stereoscopic view of the $[Mo_8O_{24}(OCH_3)_4]^{4-}$ anion.

$Na_4[Mo_8O_{24}(OCH_3)_4]\cdot 8CH_3OH$ is soluble in methanol and is readily recrystallized from it. Absolute methanol also acts as a drying agent preventing hydrolysis:[21]

$$Na_4[Mo_8O_{24}(OCH_3)_4]\cdot 8CH_3OH + 4H_2O \rightarrow Na_4[Mo_8O_{26}]\cdot 2H_2O\cdot 8CH_3OH + 4CH_3OH. \quad (22)$$

The structure of the $[Mo_8O_{24}(OCH_3)_4]^{4-}$ anion is shown in Fig. 7. Both terminal and bridging methoxy groups are present and resonances for each have been identified in the solid-state ^{13}C NMR spectrum (Fig. 3). Presumably both types of methoxy group may be present on the surface of the MoO_3 catalyst, but so far attempts to probe the surface species by NMR techniques have been unsuccessful.

The structural details of the molybdenum–methoxy interactions are presented in Table 3. The Mo—O bond lengths and calculated bond strengths along with the Mo—O—C bond angles clearly indicate that the Mo—OCH_3 bond is of order 1, and not a molybdenyl type of interaction, Mo=OCH_3, for which a shorter Mo—O bond length and a more nearly linear Mo—O—C bond angle would be expected.

Photolysis of $Na_4[Mo_8O_{24}(OCH_3)_4]\cdot 8CH_3OH$ generates formaldehyde. There is one short intermolecular C—H—O contact for each of the two types of methoxy groups. Additionally, there is one short intramolecular C—H—O contact involving the terminal methoxy group. Table 4 lists the short C—H—O contacts which presumably are the sites of hydrogen transfer. A theoretical model for this photon-assisted C—H bond activation has recently been proposed by Anderson and Ray.[13]

In contrast, the thermal decomposition of $Na_4[Mo_8O_{24}(OCH_3)_4]\cdot 8CH_3OH$ generates primarily dimethyl ether. This is seen as a natural extension of eqn (15), since there are two coordinated methanol molecules for each methoxy group in the structure. Consequently, as more of the coordinated methanol is removed by gentle heating in a vacuum, more formaldehyde is detected as a decomposition product.

$[Mo_8O_{26}(C_5H_5N)_2]^{4-}$

The determination of the number of catalytically active sites on the surface of molybdates typically involves selective poisoning. A base which binds

Table 3. Structural details of the Mo–OCH_3 interactions of $Na_4[Mo_8O_{24}(OCH_3)_4]\cdot 8CH_3OH$

Methoxy group[a]	Mo—O (Å)	s^b	Mo—O—C (°)	O—C (Å)
Terminal				
[Mo(4)—O(14)—C(2)]	1.904	0.93	126.1	1.440
Bridging				
[Mo(3)—O(9)—C(1)]	1.993	0.71	124.9	1.438
[Mo(4)—O(9)—C(1)]	2.261	0.33	120.9	—

[a] Atom labels refer to Fig. 7.
[b] Bonds strengths calculated as in Ref. 24.

Table 4. Short C—H—O distances in the $Na_4[Mo_8O_{24}(OCH_3)_4]\cdot 8CH_3OH$ structure

Atoms[a]	O—H (Å)	C—H—O (°)	H—O—Mo (°)
C(1)—H(1)A—O(10)	2.49	116	90
C(2)—H(2)A—O(11)	2.48	120	109
C(2)—H(2)A—O(8″)	2.47	123	126

[a] Atom labels refer to Fig. 7.

more strongly to the molybdate surface than methanol is reacted with the molybdate in gradually increasing amounts. The base acts so as to block sites and inhibit methanol chemisorption. Just at the point where base addition effectively inhibits methanol chemisorption, the number of base molecules are counted and taken as a measure of the number of catalytically active sites. Pyridine is the base of choice for this selective poisoning. Accordingly, $MoO_3\cdot C_5H_5N$[22] does not react with methanol, whereas $MoO_3\cdot 2H_2O$ does.

The structure of $MoO_3\cdot C_5H_5N$ had not been solved completely and therefore the nature of the molybdenum(VI)–pyridine interaction was not known in detail. However, $MoO_3\cdot 2H_2O$ is observed to react with pyridine as follows:[23]

$$8MoO_3\cdot 2H_2O + 6C_5H_5N \xrightarrow{45°C} (C_5H_5NH)_4[Mo_8O_{26}(C_5H_5N)_2] + 14H_2O. \quad (23)$$

The product was recrystallized from dimethyl sulfoxide to give

$$(C_5H_5NH)_4[Mo_8O_{26}(C_5H_5N)_2]\cdot 2(CH_3)_2SO.$$

The structure of the anion is shown in Fig. 8. The strength of the Mo–N interaction is compared with other molybdenum–base interactions in Table 5.

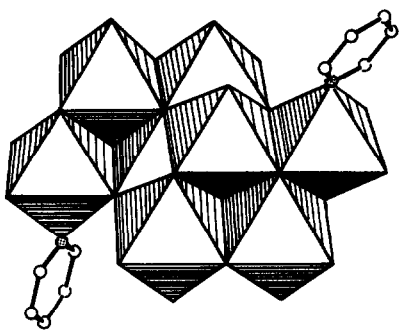


Fig. 8. The structure of the $[Mo_8O_{26}(C_5H_5N)_2]^{4-}$ anion.

Table 5. Comparison of molybdenum–base (Mo–X) interactions in various molybdenum(VI) oxide structures

X	d (Å)	s[a]	Dissociation temperature (°C)	Reference
H_2O	2.293	0.31	~120	6
C_5H_5N	2.279	0.32	~150	23
$(CH_3)_2SO$	2.245	0.35	~180	25

[a] Bond strengths calculated as in Ref. 24.

Once formed, the molybdenum–pyridine interaction cannot be displaced by the weaker base methanol even though the chemisorption of methanol would result in the formation of the stronger molybdenum–methanol interaction (Table 3).

CONCLUSIONS

The chemistry of the selective oxidation of methanol to formaldehyde over molybdate catalysts has been shown to be adequately modeled by both molybdenum oxy-methoxides and methoxy-containing isopolymolybdates. Formaldehyde formation, kinetics (rate-limiting C—H bond breaking and water inhibition), and the nature of the catalytically active sites are accounted for by analogy with the model compounds. Additionally, structural studies of the isopolymolybdates have provided coordination geometries which could not be determined by surface science.

Acknowledgements—We would like to acknowledge the contributions of all those associated with the methanol oxidation program at Du Pont: W.-H. Cheng, U. Chowdhry, W. E. Farneth, A. Ferretti, L. E. Firment, R. P. Groff, F. Hong, C. J. Machiels, F. Ohuchi and R. H. Staley. D. B. Chase and R. D. Farlee are acknowledged for providing, respectively, the IR and NMR spectral data; and R. L. Harlow and J. F. Whitney for the structural solutions.

REFERENCES

1. W.-H. Cheng, U. Chowdhry, A. Ferretti, L. E. Firment, R. P. Groff, C. J. Machiels, E. M. McCarron, F. Ohuchi, R. H. Staley and A. W. Sleight, In *Heterogeneous Catalysis, Proceedings of the 2nd Symposium of IUCCP of Department of Chemistry, Texas A&M* (Edited by B. L. Sharpiro), p. 165. Texas A&M University Press, College Station, TX (1984).
2. W. E. Farneth, F. Ohuchi, R. H. Staley, U. Chowdhry and A. W. Sleight, *J. Phys. Chem.* 1985, **89**, 2493.
3. R. P. Groff, *J. Catal.* 1984, **86**, 215.
4. L. Kihlborg, *Ark. Kemi* 1963, **21**, 357.
5. G. Brauer (Ed.), *Handbook of Preparative Inorganic Chemistry*, 2nd edn, p. 1412. Academic Press, New York (1965).
6. B. Krebs, *Chem. Commun.* 1970, 50; *Acta Cryst.* 1972, **B28**, 2222.
7. E. M. McCarron III, R. H. Staley and A. W. Sleight, *Inorg. Chem.* 1984, **23**, 1043.
8. R. L. Fellows, M. H. Lloyd, J. F. Knight and H. L. Yakel, *Inorg. Chem.* 1983, **22**, 2468.
9. C. J. Machiels and A. W. Sleight, In *Proceedings of the Fourth International Conference on the Chemistry and Uses of Molybdenum* (Edited by H. F. Barry and P. C. H. Mitchell), p. 411. Climax Molybdenum Co., Ann Arbor, MI (1982).
10. F. Ohuchi, L. E. Firment, U. Chowdhry and A. Ferretti, *J. Vac. Sci. Technol.* 1984, **A2**, 1022.
11. U. Chowdhry, A. Ferretti, L. E. Firment, C. J. Machiels, F. Ohuchi, A. W. Sleight and R. H. Staley, *Appl. Surf. Sci.* 1984, **19**, 360.
12. C. J. Machiels and A. W. Sleight, *J. Catal.* 1982, **76**, 238; C. J. Machiels, *Am. Chem. Soc. Symp. Ser.* 1982, **178**, 239.
13. A. B. Anderson and N. K. Ray, *J. Am. Chem. Soc.* 1985, **107**, 253.
14. E. A. Cueller, S. S. Miller, T. J. Marks and E. Weitz, *J. Am. Chem. Soc.* 1983, **105**, 4580 (and references therein).
15. C. J. Machiels, U. Chowdhry, R. H. Staley, F. Ohuchi and A. W. Sleight, In *Catalytic Conversions for Synthesis Gas and Alcohols to Chemicals* (Edited by R. G. Harman), p. 413. Plenum, New York (1984).
16. R. D. Adams, W. G. Klemperer and R.-S. Liu, *J. Am. Chem. Soc., Chem. Commun.* 1979, 256.
17. V. W. Day, M. F. Fredrich, W. G. Klemperer and R.-S. Liu, *J. Am. Chem. Soc.* 1979, **101**, 491.
18. V. W. Day, M. R. Thompson, C. S. Day, W. G. Klemperer and R.-S. Liu, *J. Am. Chem. Soc.* 1980, **102**, 5973.
19. W. H. Knoth and R. L. Harlow, *J. Am. Chem. Soc.* 1981, **103**, 4265.
20. E. M. McCarron III and R. L. Harlow, *J. Am. Chem. Soc.* 1983, **105**, 6179.
21. E. M. McCarron III and R. L. Harlow, *Acta Cryst.* 1984, **C40**, 1140.
22. J. W. Johnson, A. J. Jacobson, S. M. Rich and J. F. Brody, *J. Am. Chem. Soc.* 1981, **103**, 5246; *Rev. Chim. Miner.* 1982, **19**, 420.
23. E. M. McCarron III, J. F. Whitney and D. B. Chase, *Inorg. Chem.* 1984, **23**, 3275.
24. J. C. J. Bart and V. Ragaini, In *Proceedings of the Third International Conference on the Chemistry and Uses of Molybdenum* (Edited by H. F. Barry and P. C. H. Mitchell), p. 19. Climax Molybdenum Co., Ann Arbor, MI (1979).
25. E. M. McCarron III and R. L. Harlow, *J. Chem. Soc., Chem. Commun.* 1983, 90.

Polyhedron Vol. 5, No. 1/2, pp. 141–144, 1986
Printed in Great Britain

0277-5387/86 $3.00+.00
© 1986 Pergamon Press Ltd

OXIDATION OF ACROLEIN OVER PHOSPHOPOLYMOLYBDATES: STRUCTURE OF THE CATALYST

J. B. BLACK,* E. SERWICKA,† N. J. CLAYDEN and J. B. GOODENOUGH

Inorganic Chemistry Laboratory, University of Oxford, South Parks Road, Oxford OX1 3QR, U.K.

and

J. D. SCOTT

ICI Mond Division, The Heath, Runcorn, Cheshire WA7 4QF, U.K.

(*Received* 15 *June* 1985)

Abstract—Catalysts from the series $K_xH_{3-x}PMo_{12}O_{40}$ have been characterized by X-ray diffraction, solid-state NMR, TGA–DTA and ESR, and the selectivity of this and similar systems in acrolein oxidation is discussed in the light of their multiphase nature.

Catalysts based on 12-molybdophosphoric acid have been shown to be highly selective in the oxidation of unsaturated aldehydes, such as acrolein and methacrolein, to the corresponding acids.[1,2] Several authors have investigated the effect of partial or total proton substitution by different cations on the catalytic performance, and the formation of the corresponding acid salts of the form

$$(M^+)_x(H_3O^+)_{3-x}PMo_{12}O_{40}$$

is usually assumed.[3–7]

In this note we report results indicating that in the case of the $K_xH_{3-x}PMo_{12}O_{40}$ series ($0 < x < 3$) the working catalysts are complex, multiphase systems; consequently simple correlations lose their significance.

EXPERIMENTAL

Materials

The catalysts were prepared by previously described procedures.[5,8] $H_3PMo_{12}O_{40} \cdot 28H_2O$ (ex BDH Ltd, "AnalaR" grade) was dissolved in water and the required quantities of K_2CO_3 (ex BDH Ltd, "AnalaR" grade) were added to the solution. The final product was obtained by evaporation to dryness under reduced pressure at 353 K. Fresh catalysts were calcined in air at 673 K.

Thermogravimetric analysis was carried out in static air in a Stanton–Redcroft STA-780 thermal analyser. Samples of around 150 mg (TGA only) or 15 mg (simultaneous TGA–DTA) were heated at 10 K min^{-1} up to 873 K.

Powder X-ray diffraction data were obtained with a Phillips PW-1720 diffractometer and a Guiner–Haag focusing camera.

A JEOL FX-200 spectrometer operating at 80.9 MHz was used to acquire ^{31}P solid-state NMR spectra. Magic angle sample spinning in Delrin rotors at 4 kHz was employed, and all spectra were referenced externally to 85% orthophosphoric acid.

ESR spectra were recorded at room temperature and at 77 K with a Varian E-112 century-line spectrometer equipped with a fieldial, operating in the *X*-band. DPPH ($g = 2.0036$) was used as a standard for the determination of *g*-factors.

Catalyst testing was carried out in a continuous flow microreactor at 623 K in an atmosphere of 4.5% acrolein and 10.5% oxygen in nitrogen. Organic products were detected with a flame ionization detector, and carbon oxides with a katharometer. Catalyst charges were between 0.3 and 1.0 g, and selectivity–conversion curves were obtained by varying the overall flow rate over the catalyst between 60 and 7.5 ml min^{-1}.

* Author to whom correspondence should be addressed.

† On leave from Institute of Catalysis and Surface Chemistry, Polish Academy of Sciences, 30-239 Krakow, ul. Niezapominajek, Poland.

RESULTS AND DISCUSSION

The presence of more than one phase in the freshly prepared catalysts was initially detected by X-ray diffraction. A pattern characteristic of the cubic lattice of $K_3PMo_{12}O_{40}$ was detected in all potassium-containing samples. Extra peaks belonging to some of the hydrates of $H_3PMo_{12}O_{40}$ could be detected for compositions with $x < 2$.

Further evidence was supplied by the ^{31}P solid-state NMR spectra of the fresh catalysts shown in Fig. 1. The resonance at $\sigma = 4.3$ ppm is characteristic of $K_3PMo_{12}O_{40}$,[9] and the resonance at $\sigma = 3.9$ ppm is found in spectra of the free acids $H_3PMo_{12}O_{40} \cdot nH_2O$ with $n = 30$ and 9, but not with $n = 0$. This latter resonance also agrees well with the solution resonance of the $[PMo_{12}O_{40}]^{3-}$ anion ($\delta = -3.9$ ppm).[10]

The thermogravimetric results provide evidence that there is no solid solution range as x approaches 3. The only feature in the TGA curve for fresh $K_3PMo_{12}O_{40}$ [Fig. 2(a)] is the loss of physisorbed water below 500 K: otherwise it is thermally stable up to 873 K. On the other hand, the $H_3PMo_{12}O_{40}$ sample [Fig. 2(b)] loses its water of crystallization by 450 K, and the weight loss observed in the range 500–700 K corresponds exactly to the weight loss expected on complete decomposition of the acid (1.5 water molecules per Keggin anion). TGA profiles for the catalysts with intermediate values of x up to 2.75 were obtained, and all samples behaved as mixtures of the end members of the series, $H_3PMo_{12}O_{40}$ and $K_3PMo_{12}O_{40}$. The curve for $K_{2.5}H_{0.5}PMo_{12}O_{40}$ is presented as an example in Fig. 2(c). In particular, the weight loss between 500 and 750 K was consistent

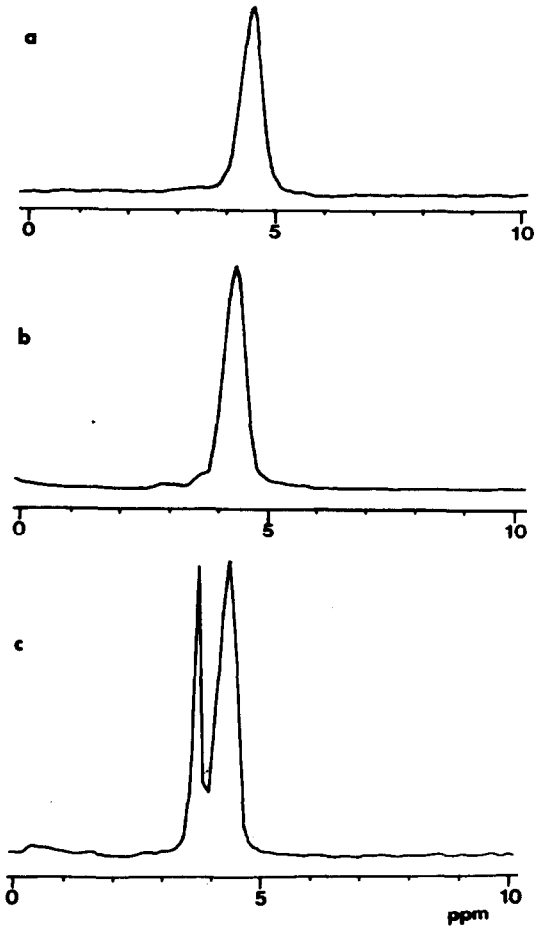


Fig. 1. Solid-state ^{31}P NMR spectra of: (a) $K_3PMo_{12}O_{40}$, (b) $K_2H_1PMo_{12}O_{40}$, and (c) $K_1H_2PMo_{12}O_{40}$.

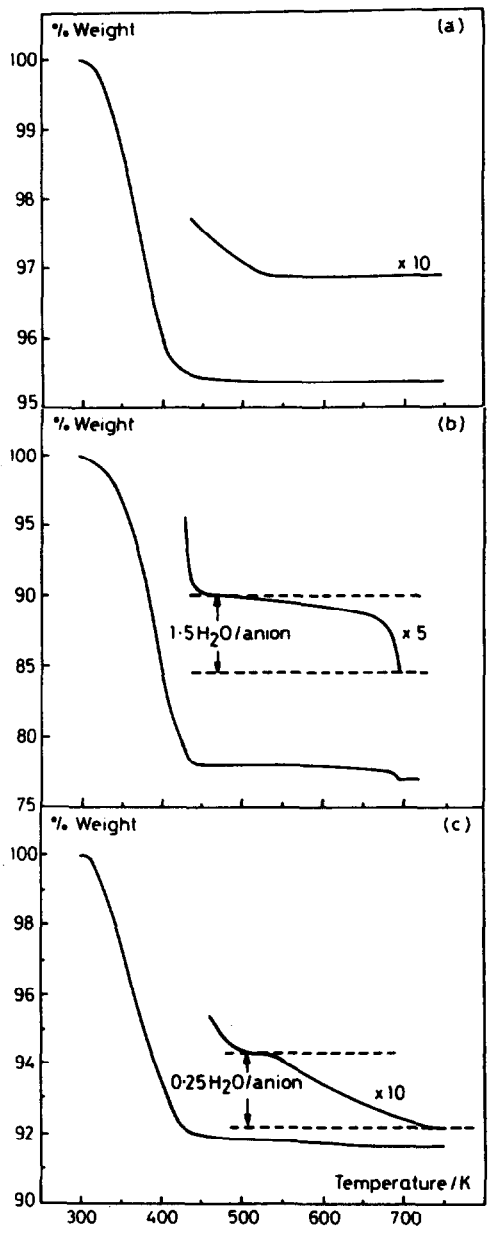


Fig. 2. TGA traces for: (a) $K_3PMo_{12}O_{40}$, (b) $H_3PMo_{12}O_{40} \cdot 28H_2O$, and (c) $K_{2.5}H_{0.5}PMo_{12}O_{40}$.

with the formulation $(x/3)K_3PMo_{12}O_{40}+(3-x)/3H_3PMo_{12}O_{40}$, but not with the solid solution stoichiometry

$$(M^+)_x(H_3O^+)_{3-x}PMo_{12}O_{40}^{3-}.$$

In addition, the features observed in the DTA curve for $H_3PMo_{12}O_{40}$ are reproduced at the same temperatures in all samples with $x < 3$.

Decomposition of $H_3PMo_{12}O_{40}$ begins by 500 K; although it only becomes rapid above 675 K, the thermal instability of this component in all of the catalysts means that the calcined catalysts must have an even more complex phase composition.

X-ray diffraction of the calcined $H_3PMo_{12}O_{40}$ catalyst showed the presence of MoO_3, indicating that at least part of the acid component undergoes complete decomposition on calcination. ESR investigation of the calcined samples showed that the MoO_3 formed is slightly oxygen-deficient, since the Mo(V) signal characteristic of the $[(MoO)O_4]^{5-}$ could be identified (Fig. 3).[11] This signal could be

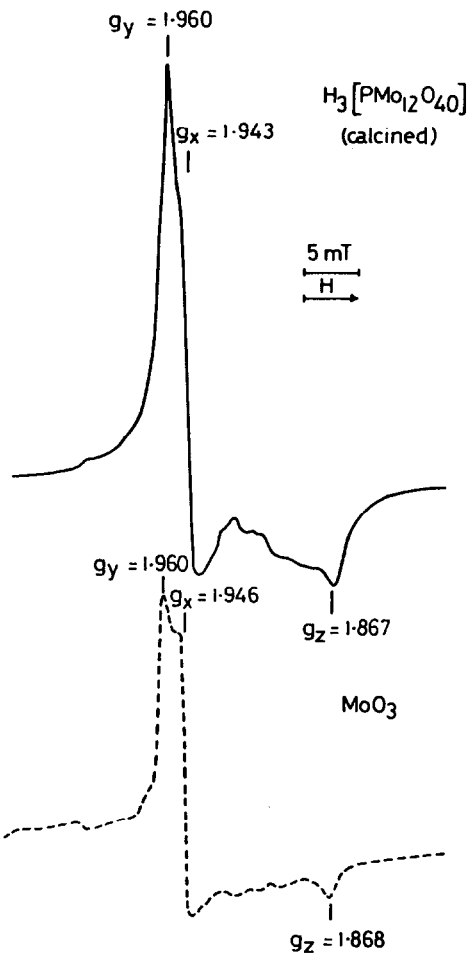


Fig. 3. ESR spectra of calcined $H_3PMo_{12}O_{40}$ and $[(MoO)O_4]^{5-}$ in MoO_3.

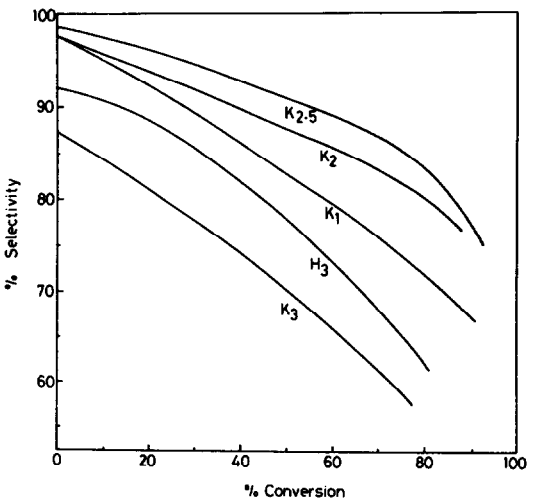


Fig. 4. Selectivity–conversion curves for catalysts from the series $K_xH_{3-x}PMo_{12}O_{40}$ in acrolein oxidation.

detected, in decreasing intensity, across the entire composition range up to (but not including) $x = 3$. Since MoO_3 is known to have a significant catalytic activity in many oxidation reactions, any discussion of catalytic results must take into account its presence as part of the multiphase working catalyst.

Figure 4 shows selectivity–conversion profiles for the oxidation of acrolein over the whole series of calcined catalysts. It can be seen that the maximum efficiency is achieved for $K_{2.5}H_{0.5}PMo_{12}O_{40}$. The catalytic performance of MoO_3 supported on Al_2O_3 was checked for comparison; MoO_3 was found to be active but non-selective in acrolein oxidation. In view of this we associate the steady fall in selectivity for $x < 2.5$ with the increasing amount of MoO_3 and possibly other decomposition products of $H_3PMo_{12}O_{40}$ in the calcined catalysts. The poorer selectivity of $K_3PMo_{12}O_{40}$ is thought to be due to the lack of sufficient Bronsted acidity necessary for desorption of the reaction product.

In conclusion, it is clear that the $K_xH_{3-x}PMo_{12}O_{40}$ system is a complex multiphase mixture, and this must be appreciated in interpreting the catalytic data. Other 12-molybdophosphate systems prepared in a similar manner, such as $Cs_xH_{3-x}PMo_{12}O_{40}$ and $(NH_4)_xH_{3-x}PMo_{12}O_{40}$, are most probably multiphase mixtures as well, contrary to the accepted view representing them as acid salts. Their catalytic properties, which correspond closely to those reported here for the potassium-based series,[12,13] must be reinterpreted in the light of this finding.

Acknowledgements—J.B.B. and E.S. thank ICI Mond Division and the SERC for support.

REFERENCES

1. M. Otake and T. Oneda, *Shokubai* 1976, **18**, 169.
2. T. Ohara, *Shokubai* 1977, **19**, 157.
3. T. Komaya and M. Misono, *Chem. Lett.* 1983, 1177.
4. N. Mizuno and M. Misono, *Chem. Lett.* 1984, 669.
5. M. Ai, *J. Catal.* 1981, **71**, 88.
6. M. Ai, *Appl. Catal.* 1982, **4**, 245.
7. M. Akimoto, Y. Tsuchida, K. Sato and E. Echigoya, *J. Catal.* 1981, **72**, 83.
8. G. A. Tsigdinos, *Ind. Eng. Chem., Prod. Res. Dev.* 1974, **13**, 267.
9. J. B. Black, N. J. Clayden, L. Griffiths and J. D. Scott, *J. Chem. Soc., Dalton Trans.* 1984, 2765.
10. L. P. Kazanskii, M. A. Fedotov, I. V. Potapova and V. I. Spitsyn, *Dokl. Chem.* 1979, **224**, 1029.
11. E. Serwicka, *J. Solid State Chem.* 1984, **51**, 300.
12. J. D. Scott, unpublished work.
13. S. Nakamura and H. Ichichihashi, In *Proceedings of the 7th International Congress on Catalysis, Tokyo*, p. 755. Elsevier, Amsterdam (1981).

Polyhedron Vol. 5, No. 1/2, pp. 145–150, 1986
Printed in Great Britain

0277–5387/86 $3.00 + .00
© 1986 Pergamon Press Ltd

DEFECT STRUCTURE AND CATALYTIC PROPERTIES OF MOLYBDENUM SULFIDE

HENRY WISE

Materials Research Laboratory, SRI International, Menlo Park, CA 94025, U.S.A.; and Department of Materials Science and Engineering, Stanford University, Stanford, CA 94305, U.S.A.

(*Received in revised form* 26 *June* 1985)

The physical properties of layered transition-metal chalcogenides have been studied in considerable detail. The work has led to a basic understanding of the relationships between their structural, optical, magnetic, superconductive and electrical properties.[1–3] Among these compounds the group VI dichalcogenides MoS_2 and WS_2 are of special interest because of their wide range of catalytic properties, extending from hydrodesulfurization (HDS) and hydrodenitrogenation to hydrogenation, isomerization and methanation.

Thus it is timely to inquire into the relationships which may exist between the electronic properties of these materials and their catalytic behavior.

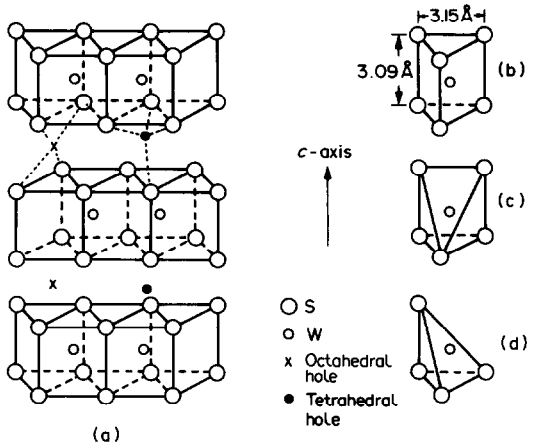


Fig. 1. Crystal structure of MoS_2.

PHYSICAL PROPERTIES

Crystal structure

Molybdenum sulfide, as well as tungsten sulfide, exhibits a hexagonal or rhombohedral crystal structure, in which one cation layer is sandwiched between two anion layers. Bonding of each metal atom to six sulfur atoms is covalent with trigonal prismatic coordination. Each of the three-layer slabs is stacked in the z-direction and held together by weak van der Waals' (vdW) forces (Fig. 1). As a result cleavage between the slabs is readily achieved. Two-dimensional projections of the hexagonal and rhombohedral polymorphs of MoS_2, designated by 2H-MoS_2 and 3R-MoS_2, are indicated in Fig. 2. (The prefixes indicate the number of metal atoms in each unit cell.) Empty octahedral and tetrahedral sites are found in the vdW gap, which can be filled by intercalation with foreign metal atoms.[4] This process is to be distinguished from substitutional or interstitial doping.

Band structure and electronic properties

Based on electrical and optical measurements, band diagrams[5] have been constructed for the dichalcogenides (Fig. 3). For the group VI sulfides with d^2-configuration on the metal atom, as for MoS_2, the overlap of the d_{z^2}-orbitals results in the formation of a full d_{z^2} band. As a result MoS_2 is a semiconductor. For the group V compounds with d^1-configuration, such as NbS_2, the d_{z^2} band is half filled. As a result metallic properties are exhibited by this material. For the group IV compounds with d^0-configuration, such as ZrS_2, the d_{z^2} band is empty and insulator properties are observed. In MoS_2 the conduction band (Fig. 4), made up of the Mo4d orbitals ($4d_{xy}$ and $4d_{x^2-y^2}$), is about 3 eV wide. The

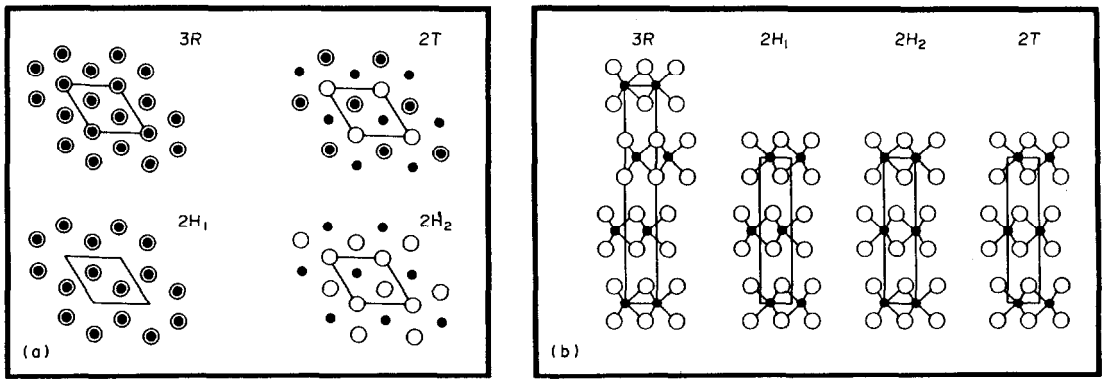


Fig. 2. MoS_2 crystal polytypes (from *Bull. CDB* 1973, **17**, 5, Climax Molybdenum Co.). (a) Along *c*-axis, and (b) along a_2-axis. (●) Mo, and (○) S: Mo and S atoms located one above the other.

non-bonding $4d_{z^2}$ orbitals are 1.75–2 eV below the conduction band. Overlapping with the $Mo4d_{z^2}$ band is the S3*p* valence band, approximately 5 eV wide. The narrow $Mo4d_{z^2}$ band near the valence band allows *d–d* transitions. Both *p*- and *n*-type conductivity are exhibited by molybdenum sulfide as a result of: (1) doping with foreign cations[6] with valence states different from that of Mo^{4+}, or (2) by adjusting the ratio S^{2-}/Mo^{4+} in the material. For $Mo_{1\pm x}S_2$ the stability range appears to be quite large.

For a single crystal of molybdenum sulfide the defects associated with a range of sulfur activities were evaluated from equilibrium conductivity studies in the presence of H_2S–H_2 gas mixtures of different composition. The catalyst, in the form of a small single crystal ($1 \times 1 \times 0.1$ cm), was cut from a larger crystal of naturally occurring molybdenite* [hexagonal crystal structure (C7)]. It was mounted in a quartz reactor provided with Pt feedthroughs for electrical conductivity measurements by the four-probe technique. The electrical conductors were made of Pt wire (0.075 cm in thickness) and attached to the four corners of the crystals. Good electrical contact was achieved by drilling a small hole in each corner of the crystal and tightly looping the Pt wire through the opening and around the crystal. The resistivity of the original crystal was measured and found to be comparable to that reported for molybdenum sulfide.[7]

The layer structure of MoS_2 favors rapid transport of ionic species within the lattice at elevated temperatures. Also measurements of the Hall coefficient, after establishment of equilibrium at the gas–solid interface, permit identification of the type of lattice defects.

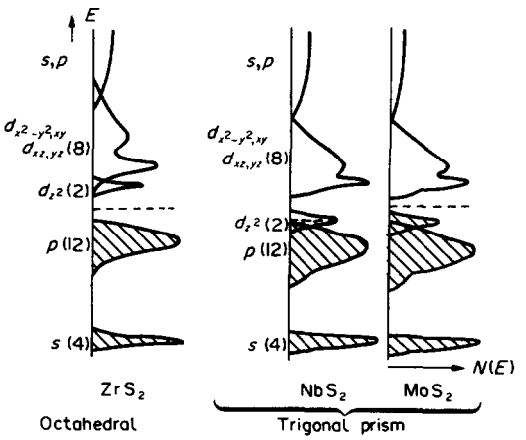


Fig. 3. Band structure of dichalcogenides (from A. D. Yoffe, *Chem. Soc. Rev.* 1976, **5**, 51).

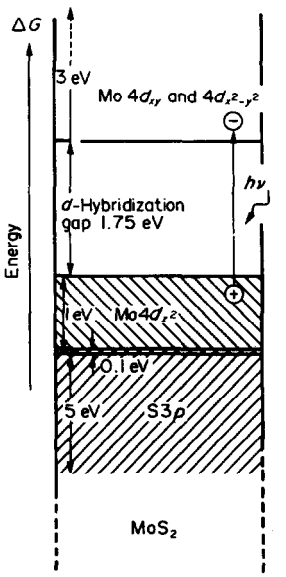


Fig. 4. Band structure of MoS_2 (from A. D. Tributsch, *Ber. Bunsenges.* 1977, **81**, 361).

*This material was kindly provided by Climax Molybdenum Co. of Michigan.

For *n*-type molybdenum sulfide,* the starting material in our studies, the interaction with a sulfur-containing atmosphere may be formulated as:

$$S_2(g) + 4e + 2V_a \rightleftarrows 2S^{2-}, \quad (1)$$

where e represents an electron and V_a an unoccupied anion vacancy, with an effective charge of +2 relative to the normal lattice since it can trap one or two electrons. Reaction (1) in the forward direction describes the addition of sulfur to the lattice with depletion of electrons and anion vacancies.

For low vacancy concentrations, the law of mass action yields at equilibrium:

$$K = 1/p_{S_2}[n_e]^4[V_a]^2, \quad (2)$$

where $[n_e]$ denotes the electron density and $[V_a]$ the anion vacancy density. Since the electrons and vacancies contribute to conduction, the electrical conductivity is given by:

$$\sigma \propto (Kp_{S_2})^{-1/6}, \quad (3)$$

i.e. the conductivity is inversely proportional to the sulfur pressure raised to the $\frac{1}{6}$th power. By analogous reasoning the prevalence of singly charged lattice defects (V_a^-) would yield a conductivity dependence on sulfur pressure of:

$$\sigma \propto (K'p_{S_2})^{-1/4} \quad (4)$$

and for doubly charged imperfections (V_a^{2-}):

$$\sigma \propto (K''p_{S_2})^{-1/2}. \quad (5)$$

Thus, measurement of the electrical conductivity as a function of sulfur pressure allows identification of the type of anion vacancy constituting the lattice defect in the catalyst.

For sulfur pressures of less than 10^{-8} atm, a decline in electrical conductivity was observed with increasing sulfur pressure (Fig. 5). The conductivity data exhibit a sulfur pressure exponent of about $-\frac{1}{8}$, somewhat less than the value derived from the equilibrium given by eqn (2). This discrepancy may be associated with inadequate quenching of the equilibrium composition and/or the presence of impurities in the crystal.

At a partial pressure of S_2 near 10^{-8} atm the conductivity passes through a minimum and the semiconductor becomes intrinsic, with equal concentration of electron and hole carriers. Because of variations in mobility of the carriers this condition does not coincide with the ideal stoichiometry of MoS_2 (i.e. $S^{2-}/Mo^{4+} = 2$). At higher sulfur activities

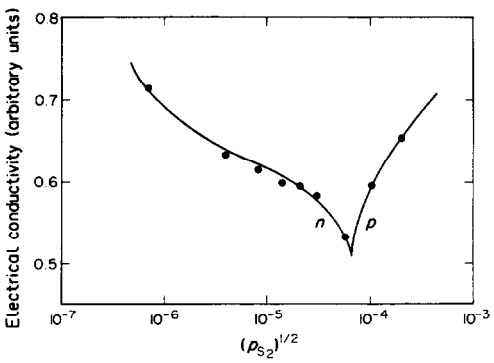


Fig. 5. Electrical conductivity of molybdenum sulfide equilibrated with sulfur at 893 K and quenched to 300 K.

an increase in conductivity is observed with a transition from *n*- to *p*-type behavior. In this region the predominant process of sulfur addition to the crystal proceeds by way of

$$S_2(g) \rightleftarrows 2S^{2-} + 4p + V_c,$$

where V_c represents a cation vacancy and p an electron hole.

Over the range of sulfur activities used in the conductivity measurements, the carrier density is estimated to vary from 10^{16} to 10^{18} cm^{-3} based on available mobility data.[7]

An alternative method for changing the electronic carrier density and carrier type in molybdenum sulfide is the introduction of foreign cations with different valence states from that of Mo^{4+}. In this case the use of Co^{2+} is of special interest because of its prevalent use as a promoter in various catalysts based on molybdenum sulfide. Based on the principle of "controlled conductivity", the incorporation of a foreign divalent cation will result in the formation of Mo^{4+} cation vacancies and hole conduction.

The introduction of Co^{2+} into MoS_2 was achieved by exposure of the crystal to an aqueous 0.1 M solution of $Co(NO_3)_2$, followed by evaporation of the solvent, sintering and exposure to H_2S. As detailed in Table 1, the doping process was monitored by electrical conductivity and Hall coefficient measurements. Both an increase in conductivity and change in carrier type from *n*- to *p*-type were observed (Table 1). Based on the conductivity data, the doping level was estimated to be of the order of 10–100 ppm.

CHARGE TRANSFER DURING SURFACE CATALYSIS

A series of HDS experiments were performed in which pulses of gaseous butyl mercaptan were

*As determined in separate Hall coefficient measurements.

Table 1. Electronic properties of doped MoS_2 crystal with Co^{2+}

Treatment	Electrical conductivity[a] (mho cm^{-1})	Electronic carrier type
Before doping	0.17	*n*
After doping[b]	0.47	*p*

[a] Measured at 300 K.

[b] Heated in He at 900 K for 18 h, in H_2 at 800 K for 12 h, and in H_2S–H_2 (1000 ppm) at 880 K for 4 h.

injected into the carrier stream of H_2 which passed over the single crystal of molybdenum sulfide at a flow rate of 2 cm^3 s^{-1}, at 760 torr. After leaving the reactor the gas mixture entered the gas chromatograph for quantiative determination of the products (butene, butane, H_2S and butyl mercaptan). Provisions were made for pretreatment of the crystal with H_2 or H_2S–H_2 at elevated temperatures (850–900 K). In addition the conductivity of the crystal was monitored during passage of the butyl mercaptan pulse. The electrical responses observed were found to be strongly dependent on the type and concentration of defects in the crystal. For *n*-type material containing more than 10^{18} electrons cm^{-3}, the charge exchange at the gas–crystal interface was of the type shown in Fig. 6. The transient electrical response during the pulsed HDS reaction was accompanied by a rapid decline in conductivity followed by a recovery to less than the initial value. Subsequent pulses, as shown for pulse numbers 3 and 15, continued to show the same pattern of conductivity response. The time between pulses was varied from 5 to 10 min during which the catalyst crystal was exposed to the flowing H_2 carrier gas. With each pulse of butyl mercaptan the electron density of the crystal was reduced. Most likely this

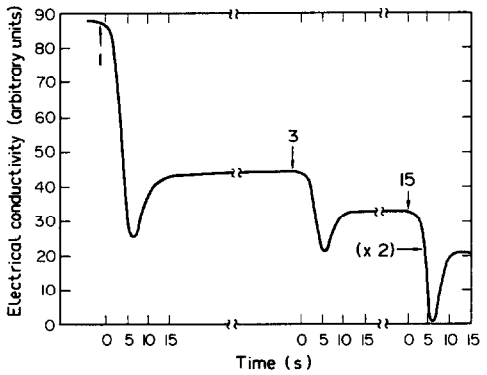


Fig. 6. Conductivity change of molybdenum sulfide crystal at 530 K during passage of reactant pulse.

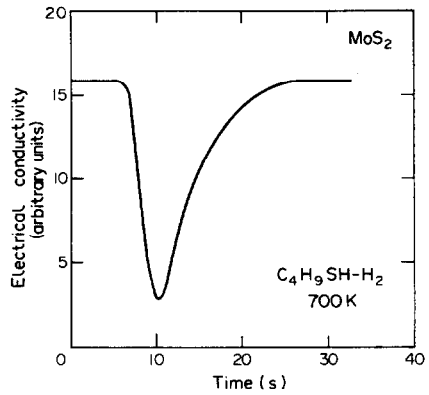


Fig. 7. Electrical response of MoS_2 crystal to passage of reactant pulse.

effect was accompanied by the incorporation of sulfur from the reactant pulse into the anion vacancies of the crystal. In accordance with eqn (1) the process results in a decrease in conductivity. On the other hand, for a catalyst with significantly lower anion vacancies, brought about by pretreatment in 4000 ppm H_2S (in H_2), the electrical response was entirely different (Fig. 7). Exposure to a pulse of butyl mercaptan caused a transient conductivity change with complete recovery to its initial value. The electron injection rate during the pulse was estimated to be about 10^{15}–10^{16} electrons cm^{-3} s^{-1}.

As shown by the results presented in Fig. 8, both the conversion of butyl mercaptan and the distribution of products were a function of the defect structure. At high concentrations of anion vacancies (high conductivity) the conversion of reactant was

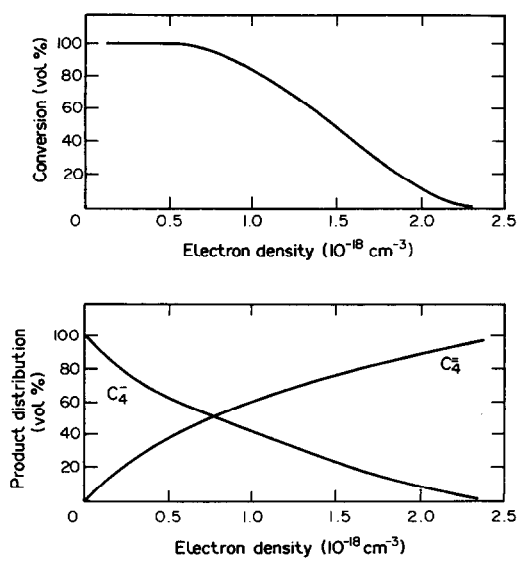


Fig. 8. HDS activity and product distribution at 700 K (C_4H_9SH).

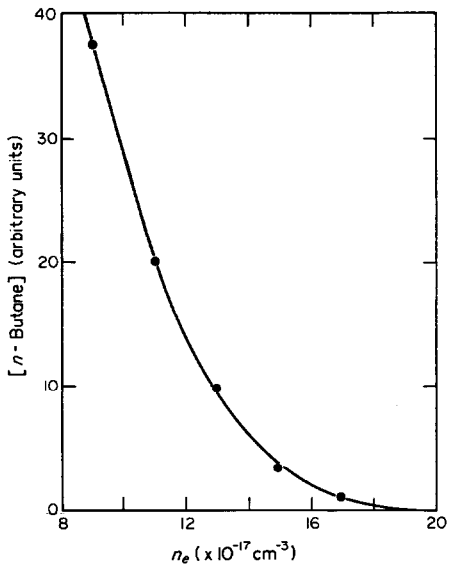


Fig. 9. Catalytic activity of molybdenum sulfide for 1-butene hydrogenation at 623 K.

relatively low and the major C_4 product was butene. However with decreasing anion vacancies, the conversion grew and butane predominated. In separate experiments of 1-butene hydrogenation the electron density was observed to control the conversion of the olefin to the alkane (Fig. 9). The results suggest that, during HDS of butyl mercaptan, the initial step involves the formation of butene which can be hydrogenated subsequently to butane if the catalyst exhibits *p*-type conductivity.

The results clearly demonstrate the close relationship between defect structure, catalytic activity and product specificity. This effect is further exemplified by the HDS properties of the cobalt-doped molybdenum sulfide crystal. In continuous flow experiments the steady-state conversion of butyl mercaptan was examined at 700 K at a feed mixture ratio of $H_2/C_4H_9SH = 1$ and compared to that of undoped molybdenum sulfide (Table 2) the data show the superior properties of the *p*-type crystal for HDS as compared to that of the *n*-type crystal. Of special interest is the formation of butane as a product in the case of electron holes as majority carriers.

This aspect is related to the high rate of hydrogen adsorption exhibited by the *p*-type catalyst and its high equilibrium coverage with chemisorbed hydrogen. For a highly dispersed molybdenum sulfide sample made from ammonium thiomolybdate[8] and pretreated at 800 K in H_2S–H_2 gas mixtures, the amount of H_2 adsorbed at different sulfur activities is shown in Fig. 10. It attains a value corresponding to a stoichiometry of $H_{0.039}MoS_2$. This value corresponds very closely to the saturation coverage of $H_{0.04}WS_2$ recently reported[9] from inelastic neutron-scattering experiments. For molybdenum sulfide the stoichiometry $H_{0.067}MoS_2$ was measured by the same authors.[10] The chemisorbed hydrogen is bonded to sulfur atoms. As a matter of fact the acidic nature of the SH group formed can be titrated with ammonia.[11]

In the presence of electron hole as majority carriers the adsorption of hydrogen may be facilitated by a process, such as:

$$\tfrac{1}{2}H_2(g) + p \rightleftarrows H^+(a).$$

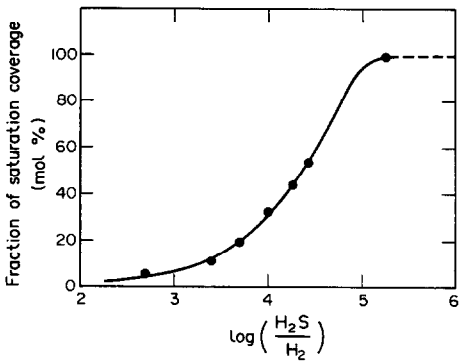


Fig. 10. Fractional surface coverage with H_2 of catalyst A at 475 K [saturation coverage = 123×10^{-6} mol (g catalyst)$^{-1}$ at $H_2S/H_2 > 10^5$ ppm].

Table 2. HDS activity and product distribution at 700 K

Catalyst	Electronic carrier type	Density ($\times 10^{-17}$ cm^{-3})	Conversions (vol %)	C_4H_{10} specificity (vol %)
MoS_2	*n*	17	8	30
	n	10	70	50
$MoS_2(Co^{2+})$	*p*	2.5	87	100
	p	1.9	68	100

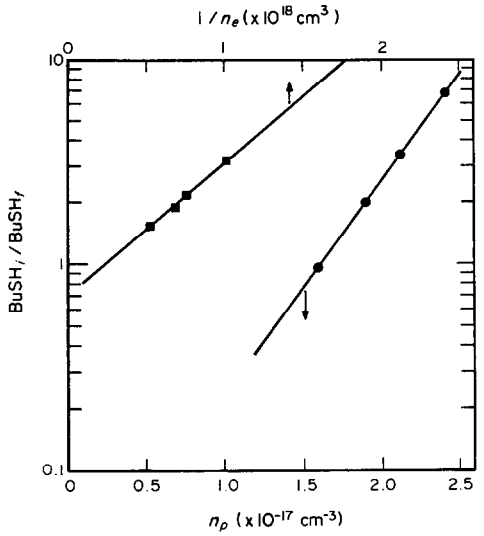


Fig. 11. HDS activity as a function of electronic carrier density: (●) *p*-type, (■) *n*-type.

Thus *p*-type conductivity induced by pretreatment at high H_2S levels or by doping with Co^{2+} provide a suitable path for chemisorption of hydrogen. Its presence explains the versatility of the molybdenum sulfide catalyst for such a range of catalytic processes extending from olefin hydrogenation to HDS, each of which requires hydrogen addition as a step in the reaction sequence.

For HDS of butyl mercaptan (BuSH) in the presence of a large excess of H_2 (H_2 : RSH > 40 : 1) the rate equation for this process may be expressed as a product of a first-order dependency on mercaptan concentration and the electron hole carrier density:

$$-d(\text{BuSH})/dt = k_p n_p(\text{BuSH}). \quad (6)$$

At constant space velocity, i.e. contact time with the single-crystal catalyst, one obtains on integration of eqn (3):

$$\ln [(\text{BuSH})_i/(\text{BuSH})_f] = k'_p n_p, \quad (7)$$

where the subscripts *i* and *f* represent the initial and final concentrations of reactant and *k'* the product of the rate constant and contact time (*kt*). Indeed the dependency of HDS on hole density, as given by eqn (7) is exhibited by the data presented in Fig. 11. On the other hand, for *n*-type molybdenum sulfide, with electrons as majority carriers, the HDS rate exhibits an inverse dependency on n_e:

$$-d(\text{BuSH})/dt = k'_e(\text{BuSH})/n_e. \quad (8)$$

as shown in Fig. 11.

Under equilibrium conditions

$$K_i = n_e n_p = N_c V_v \exp(-E_i/kT),$$

where K_i is the equilibrium constant, n_e and n_p the electron and hole densities, N_c the number of available states in the conduction band, N_v that in the valence band, and E_i is the band-gap energy ($E_c - E_v$). In view of the fact that $n_p = K_i/n_e$, it is apparent that the functional relationship between n_e and n_p exhibited by the data in Fig. 11 is to be expected on the basis of solid-state theory.

REFERENCES

1. J. A. Wilson and A. D. Yoffee, *Adv. Phys.* 1969, **18**, 193.
2. A. A. Balchin, In *Physics and Chemistry of Materials with Layered Structure* (Edited by F. Lévy), p. 200. Reidel, Dordrecht (1976).
3. C. N. Rao and K. P. R. Pisbarod, *Prog. Solid State Chem.* 1975, **10**, 107.
4. G. V. S. Rao and M. W. Shafer, In *Intercalated Layer Materials* (Edited by F. Lévy), p. 99. Reidel, Dordrecht (1979).
5. A. D. Yoffe, *Chem. Soc. Rev.* 1976, **5**, 51.
6. F. Lévy, P. Schmid and H. Berge, *Philos. Mag.* 1976, **34**, 1129.
7. R. Fivaz and E. Mooser, *Phys. Rev.* 1967, **163**, 743.
8. T. T. Eggersten and R. M. Roberts, *J. Phys. Chem.* 1959, **63**, 1981.
9. C. J. Wright, D. Fraser, R. B. Moyes and P. B. Wells, *J. Appl. Catal.* 1981, **1**, 48.
10. C. J. Wright, D. Fraser, R. B. Moyes and P. B. Wells, *J. Chem. Soc., Faraday Trans.* 1 1980, **76**, 1585.
11. P. Hou and H. Wise, *J. Catal.* 1982, **78**, 469.

Polyhedron Vol. 5, No. 1/2, pp. 151–155, 1986
Printed in Great Britain

0277-5387/86 $3.00 + .00
© 1986 Pergamon Press Ltd

THE RELATION BETWEEN ELECTRONIC TRENDS AND THE PROMOTER EFFECT ON CATALYTIC ACTIVITY OF HYDRODESULFURIZATION CATALYSTS

SUZANNE HARRIS

Exxon Research and Engineering Co., Route 22 East, Clinton Township, Annandale, NJ 08801, U.S.A.

(*Received* 1 *July* 1985)

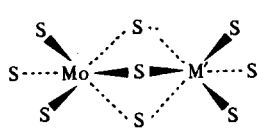
Abstract—The origin of the promoting effect of certain first-row transition metals on the hydrodesulfurization (HDS) activity of MoS_2 is not well understood. We have carried out a systematic theoretical study of the electronic structure of simple clusters which model these catalyst systems and have used the results of these calculations to establish an electronic basis for the trends in promotion effects observed in the MoS_2 systems. Both Co and Ni, which serve as promoters, have the ability to donate electrons to Mo, while Cu, which serves as a poison, withdraws electrons from Mo. The other first-row transition metals, which have little effect on the HDS activity of MoS_2, do not have the ability to donate to or accept electrons from Mo. Thus promotion is associated with an increase in electron density on Mo while poisoning is associated with a decrease in electron density. These results are consistent with previous results for binary catalysts which related particular electronic factors to the HDS activity of the sulfide.

Recently, we described a relation between trends in the calculated electronic structure of the transition-metal sulfides (TMS) and trends in the measured hydrodesulfurization (HDS) activity of these materials.[1] The experimental trends in the activities of the unsupported TMS had been previously measured using the HDS of dibenzothiophene as a model reaction,[2] and a theoretical basis for understanding these experimental trends had been initiated by studying the electronic structure of the first- and second-row TMS.[3] Calculations were carried out for a group of octahedral MS_6^{n-} clusters, where the transition metal M was varied systematically across both the first and second transition series, and based on these calculations it was shown[1] that a relation exists betwen the calculated electronic structure of the sulfides and their activity as HDS catalysts. Several electronic factors were identified which appear to be related to catalytic activity, and these factors were incorporated into a calculated activity parameter which correlates with the observed catalytic activity of the sulfides. We have now extended this combined theoretical and experimental approach to study the promoted or "synergic" MoS_2 catalyst systems, and in this paper we show that there is an electronic basis for the promotion effect observed in MoS_2-based catalysts.

Although it is well known that the addition of a second transition metal such as Co or Ni to a binary sulfide such as MoS_2 or WS_2 brings about an increase in HDS activity, the basis for this promotion effect is certainly not well understood. Work from numerous laboratories[4–6] has established, however, that the promoter atoms are associated with the edge planes of the layered compounds MoS_2 and WS_2, in close proximity to the Mo or W atoms. Several studies[7,8] also suggest that the effect of this edge promoter is electronic rather than structural (i.e. the promoter influences the quality of the active site rather than altering the number of active sites). In order to further explore the idea that the basis for promotion is electronic in nature, a systematic study of the promoting effect of the first-row transition metals V–Zn on the HDS activity of MoS_2 was carried out in our laboratory.[9] In this study the activities of unsupported MS_x–MoS_2 (M = V, Cr, Mn, Fe, Co, Ni, Cu or Zn) catalysts in the HDS of

DBT were measured. It was found that: (1) V, Cr, Mn, Fe and Zn have little or no effect on the HDS activity of MoS_2; (2) Co and Ni, in agreement with previous literature, act as strong promoters; and (3) Cu acts as a poison, serving to decrease the activity of MoS_2. In order to understand these effects we have carried out a systematic theoretical study of the electronic structure of simple clusters which model these promoted catalyst systems. As mentioned above, the importance of the edge planes and the proximity of the promoter and Mo atoms in MoS_2-based catalyst systems has been previously established, and we have chosen the model clusters so that their structure is consistent with this established information.

Calculations were carried out for a group of clusters $MoM'S_9^{n-}$, where the first-row transition metal M′ was varied systematically across the series from V to Zn. Each cluster carries a negative charge $(n-)$ because enough electrons were included in each cluster so that each sulfur is formally S^{2-}, the molybdenum is formally Mo^{4+}, and the first-row metal M′ has the formal oxidation state appropriate for the corresponding metal sulfide stable under reactor conditions. The geometry of the cluster can be seen in Fig. 1. Both metals are octahedrally coordinated by six sulfurs, three of which are shared between the two metals. Thus the model cluster is composed of two face-sharing octahedra. Within each cluster, all of the metal–sulfur bond distances were taken to be equal. These distances were determined for each cluster by averaging 2.42 Å, the Mo—S distance in MoS_2, and the M′—S distance in the corresponding first-row transition-metal sulfide. The choice of octahedral coordination around Mo allowed us to compare the Mo–S bonding and Mo electronic configuration in these model clusters with that in the simple binary clusters used previously. If the first-row transition metal M′ occupies sites around the edges of MoS_2, an examination of a model of MoS_2 suggests that M′ might occupy either octahedral or tetrahedral sites and share sulfurs with an adjacent Mo. Once again, we chose to use octahedral coordination for M′ because it allows us to make comparisons readily with our earlier



M′ = V,Cr,Mn,Fe,Co,Ni,Cu or Zn

Fig. 1. Geometry of a model cluster $MoM'S_9^{n-}$ used for the molecular-orbital calculations.

calculations. We verified with selected calculations using tetrahedrally coordinated M′ that a change in geometry would not change the major conclusions of our calculations using octahedrally coordinated M′. As in our previous work[1,3] all the calculations on these clusters were carried out using the SCF-$X\alpha$ scattered wave method with tangent spheres.[10] The atomic sphere radii were chosen according to Norman's criteria.[11] The atomic exchange parameter α values for the regions within the metal and sulfur spheres are those of Schwarz.[12] A weighted average of these atomic α values was used for the intersphere and outersphere region.

In our previous reports we described in detail the electronic structure and bonding in the model octahedral first- and second-row transition-metal–sulfur clusters. Figure 2(a) shows a schematic diagram of the valance energy levels calculated for those clusters. Each group of levels, except for those corresponding to the metal *d*-orbitals, is represented by a block which is labelled according to the atomic orbital making the major contribution to these levels. There is of course some mixing between the metal and sulfur orbitals, but this mixing is not important for this discussion. Lying at the lowest energy is a group of levels arising from the sulfur 3*s* orbitals. The next group of levels arises primarily from combinations of sulfur 3*p* orbitals. At the top of this group of sulfur levels is the $1t_{1g}$ level, a nonbonding combination of sulfur 3*p* orbitals. Finally, at the highest energy (in most of the clusters) are the $2t_{2g}$ and $3e_g$ levels. These levels correspond primarily to the metal 3*d* or 4*d* orbitals. We found that a major effect of varying the transition metal in these octahedral clusters is a shift in the energy of the metal *d*-orbitals relative to the energy of the sulfur 3*p* orbitals. As measured by the difference in energy between the $2t_{2g}$ and $1t_{1g}$ orbitals, it was found that from Ti to Ni in the first transition series the energy of the 3*d* orbitals shifts downward in energy (i.e. closer in energy to the sulfur 3*p* orbitals) by about 1.5 eV. This shift is expected when moving from left to right in the transition series and is confirmed by available photoelectron spectra of the TMS.[3]

For the face-sharing octahedral clusters considered here, we can also draw a schematic energy level diagram showing the main features and patterns of the energy levels resulting from the calculations. It should be noted that the point group symmetry of the face-shared cluster is C_{3v} (as compared to O_h in the octahedral clusters). Since in the C_{3v} point group there are no triply degenerate representations, the set of 3*d* or 4*d* orbitals which in O_h-symmetry transform as the t_{2g} representation are no longer degenerate in these clusters. The remnants of the octahedral splitting between the t_{2g}- and e_g-

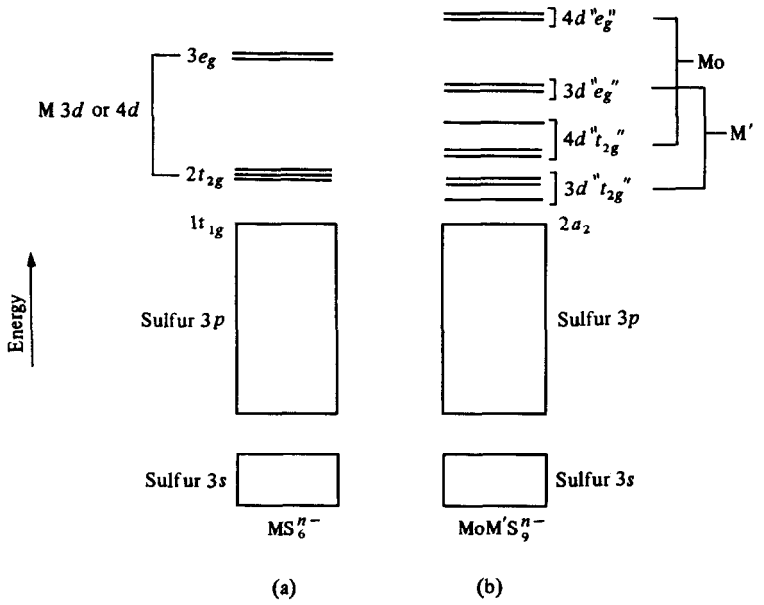


Fig. 2. Schematic valence energy level diagrams for: (a) an octahedral MS_6^{n-} cluster, and (b) an $MoM'S_9^{n-}$ cluster made up of two face-sharing octahedra. The ordering of 3*d* and 4*d* levels is for M′ = Co or Ni.

orbitals are still apparent in these lower-symmetry clusters, however, so that we continue to label "t_{2g}" and "e_g" sets of metal *d*-orbitals. A schematic level diagram for a $MoM'S_9^{n-}$ cluster is shown in Fig. 2(b). Once again, the sulfur 3*s* levels lie below the broader group of levels resulting from the sulfur 3*p* levels. The top of the sulfur 3*p* group of levels is once again delineated by a nonbonding combination of sulfur 3*p* orbitals, in this case the $2a_2$ level as shown in the diagram. The really notable feature of this level diagram is the presence, above the sulfur 3*p* levels, of levels resulting from both the Mo 4*d* and M′ 3*d* metals. Each set of five *d*-orbitals forms "t_{2g}" and "e_g" sets of levels, so on the diagram we see a "t_{2g}" and "e_g" set of levels for both the metal 3*d* and 4*d* orbitals. The schematic diagram in Fig. 2(b) would correspond to the case where the M′ levels lie low enough in energy that the M′ 3*d* "t_{2g}" and "e_g" sets of levels each lie below the corresponding Mo 4*d* sets of orbitals but not so low in energy that the entire 3*d* manifold of levels lies below the 4*d* levels. This relative energy separation applies to most of the clusters considered here. The relative energies of these levels and the numbers of electrons and their distributions within these levels both depend on M′. We will see below that it is these quantities which are related to the ability of the 3*d* metal M′ to serve as a promoter.

As we noted earlier, the metal 3*d* orbitals become more stable upon proceeding from the left to the right side of the transition series, i.e. dropping in energy relative to the sulfur 3*p* orbitals. This means that in these clusters, which contain both a 3*d* metal and Mo, the metal 3*d* orbitals also drop in energy relative to the Mo 4*d* orbitals. Proceeding across the 3*d* series from V to Zn this drop in energy is quite large. For V, Cr and Mn the 3*d* and Mo 4*d* "t_{2g}" sets of levels are very close in energy. Moving to the right, however, the 3*d* levels shift lower in energy so that the 3*d* and 4*d* sets of levels lie in the order illustrated in Fig. 2(b). Finally, for Cu and Zn the shift in energy becomes large enough that the entire set of 3*d* levels lies below the Mo 4*d* levels. At the same time that the 3*d* levels decrease in energy, the number of 3*d* electrons occupying the orbitals increases. For all the clusters, Mo contributes two "*d*"-electrons while the number of "*d*"-electrons contributed by the first-row metal depends on the metal. Thus the total number of "*d*"-electrons in the clusters varies from four in the V–Mo cluster all the way up to 12 in the Zn–Mo cluster. The distribution of electrons among the metal orbtitals depends on the relative energies of the orbitals, and an examination of the metal orbital occupations reveals an important difference between the clusters containing 3*d* metals which are known to promote or poison the activity of MoS_2 and the clusters containing those 3*d* metals which have no effect on the activity.

In the clusters containing Co or Ni, the two metals which can act as promoters, we find that Co and Ni donate electrons to Mo so that Mo is formally reduced relative to the Mo present in MoS_2. This occurs because Co and Ni provide seven and eight "*d*"-electrons, respectively, to the cluster. In a pure Co–S or Ni–S cluster, the 3*d* "e_g" orbitals would be occupied. In these clusters containing Mo, however, the lower energy Mo "t_{2g}" orbitals are available so

that a net transfer of charge from Co or Ni to Mo occurs. This is a result of the Mo "t_{2g}" orbitals lying energetically between the 3*d* "t_{2g}" and "e_g" orbitals and Co and Ni having a high eneough *d*-electron count that the 3*d* "e_g" orbitals would normally be partially occupied. The electron transfer of this type only occurs because both of these effects are present. In both the Co–Mo and Ni–Mo clusters, the Mo is thus formally reduced relative to the Mo present in MoS_2. In the cluster containing Cu, a metal which poisons the activity of MoS_2, we find that Mo is formally oxidized relative to the Mo in MoS_2. This occurs because, while all five of the Cu 3*d* orbitals now lie well below the Mo 4*d* levels, Cu contributes only nine "*d*"-electrons to the cluster. As a result there is a net transfer of electrons from Mo to Cu. This is not entirely surprising because it is known that in CuS[13] (which contains nominally Cu^{2+} and S^{2-}) the Cu 4*d* levels lie low enough in energy that some of the Cus are reduced to Cu^{+}, while some sulfurs are oxidized to S_2^{2-}. In our Cu–Mo cluster the Mo electrons are even more available than the sulfur 3*p* electrons and thus the Mo is oxidized relative to the Mo in MoS_2. In all the other clusters (those containing V, Cr, Mn, Fe and Zn) there is no such clear transfer of electrons between the Mo and the 3*d* metal, and the electronic state of Mo is similar to the Mo in MoS_2. For these metals the relative energies of the 3*d* and Mo 4*d* orbitals and/or the number of 3*d* electrons are not appropriate for electron transfer.

In summary, when the first-row transition metal M′ is varied in these Mo–M′ clusters, the changes in electronic structure depend on changes in both the relative energies of the Mo 4*d* and M′ 3*d* orbitals and the number of "*d*"-electrons which M′ contributes to the cluster. As the 3*d* levels drop in energy across the first transition series, the number of 3*d* electrons occupying these levels increases. It is only when M′ is Co, Ni or Cu, however, that these effects combine in such a way that the electronic state of Mo is formally affected. Since it is these three first-row metals which have a measurable effect on the HDS activity of MoS_2, we associate their ability to reduce or oxidize Mo with their promoting or poisoning effect.

Not only do these results identify an electronic origin for the promotion effect, but they are also consistent with our earlier theory relating catalytic activity to several electronic factors for the binary sulfides. One of those factors is the ability of the transition metal to bond covalently, in both a sigma and pi fashion, to the 3*p* orbitals of sulfur. This factor serves to differentiate the 3*d* from the 4*d* transition metals, since the 3*d* metals covalently bond much less effectively to sulfur than do the 4*d* metals. We defined a quantity, called *B*, which measures the covalent contribution to the metal–sulfur bond strength and found that a large value of *B*, and thus a strong covalent contribution to the metal–sulfur bonding, correlates with high activity. Another important factor is *n*, the number of "*d*"-electrons in the highest occupied orbital. We saw that a large value of *n* also correlates with high activity. Thus the most active catalysts have large values of *n* and/or *B*. We combined these quantities to form an activity parameter "A_2", where:

$$A_2 = nB.$$

This parameter provided us with a simple quantiative relationship between the calculated electronic structure and the HDS catalytic activity of the TMS. A metal sulfide with a large value of A_2 will have a high HDS activity.

Our model cluster calculations indicate that in the promoted Co–Mo and Ni–Mo systems one of these electronic factors for Mo, *n*, the number of electrons in the HOMO, is increased by the presence of the promoter. Since these extra electrons occupy an antibonding orbital, the Mo—S bonds are somewhat weakened. Thus the factor *B* which enters the activity parameter and measures the relative Mo—S covalent bond strength decreases in the presence of the promoter. On the other hand, the presence of a poison such as Cu has just the opposite effect. To a first approximation, for all the other systems considered here the two electronic factors *n* and *B* for Mo are unaffected by the presence of the 3*d* transition metal. We can calculate an activity parameter for the Mo portion of the model clusters treated here. This activity parameter, along with the experimental HDS activities of the real catalyst systems, is plotted in Fig. 3, and from this figure we see that the trends in activity are reproduced by the

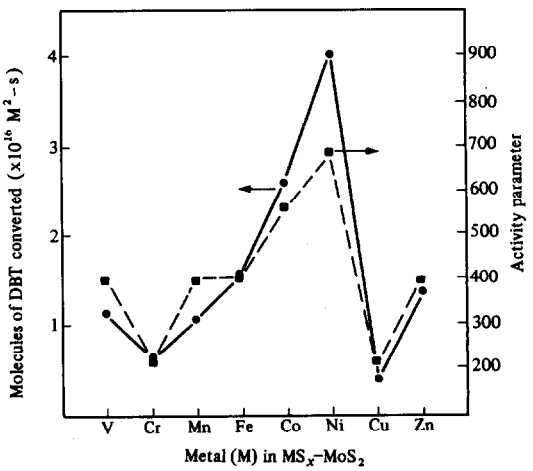


Fig. 3. Calculated activity parameter for each mixed-metal sulfide system (right-hand scale). Shown for comparison, using the left-hand scale, are the measured HDS activities.[9]

trends in the value of the activity parameters. The qualitative correlations obtained here thus indicate that the electronic factors identified earlier in our study of the binary sulfides are influenced by the presence of a promoter. It should be noted that the variations in the activity parameter are dominated by changes in n rather than B, and it appears that the dominant electronic factor related to promotion of MoS_2 is the increase in the number of "d"-electrons on Mo. This result is consistent with the physical picture and model for thiophene binding which we described earlier for the binary sulfide systems. We suggested that these active catalysts can bind to the ring sulfur atom in thiophene and donate electron density into an empty thiophene pi* orbital. It is reasonable, then, that in the promoted MoS_2 catalysts an increase in the number of electrons occupying the Mo 4d orbitals will result in an increase in catalytic activity, since an increase in d-electron density on Mo would strengthen the interaction between Mo and the ring sulfur atom in thiophene.

In conclusion, by combining measured trends in the HDS activity of promoted MoS_2 catalysts with calculated trends in the electronic structure of cluster models of these catalyst systems, we have established that there is an electronic basis for the promotion effects observed in MoS_2-based HDS catalysts. The calculated electronic structure of the cluster models of the promoted catalyst systems indicates that Co and Ni have the ability to formally reduce Mo in these systems, while Cu has the ability to formally oxidize Mo. None of the other 3d metals have this ability. The number of 3d electrons which Co, Ni or Cu contribute to the cluster and the energies of their 3d orbitals relative to the Mo 4d orbitals make these metals unique when combined with Mo. These results are consistent with our earlier identification of electronic factors which are related to the HDS activity of binary sulfide catalysts and with our model for thiophene binding to the catalyst.

REFERENCES

1. S. Harris and R. R. Chianelli, *J. Catal.* 1984, **86**, 400.
2. T. A. Pecoraro and R. R. Chianelli, *J. Catal.* 1981, **67**, 430.
3. S. Harris, *Chem. Phys.* 1982, **67**, 229.
4. R. J. H. Voorhoeve and J. C. M. Stuiver, *J. Catal.* 1971, **23**, 228, 243.
5. A. L. Farragher and P. Cossee, In *Proceedings of the 5th International Congress on Catalysis* (Edited by J. J. Hightower), p. 1301. North-Holland, Amsterdam (1973).
6. C. Wivel, R. Candia, B. S. Clausen, S. Mørup and H. Topsøe, *J. Catal.* 1981, **68**, 453.
7. S. Kasztelan, H. Toulhoat, J. Grimblot and J. P. Bonnelle, *Bull. Soc. Chim. Belg.* 1984, **89**, 807.
8. R. R. Chianelli, T. A. Pecoraro, T. R. Halbert, W.-H. Pan and E. I. Stiefel, *J. Catal.* 1984, **86**, 226.
9. S. Harris and R. R. Chianelli, *J. Catal.* (in press).
10. K. H. Johnson, *Adv. Quantum. Chem.* 1973, **7**, 143.
11. J. G. Norman, *Mol. Phys.* 1973, **31**, 1191.
12. K. Schwarz, *Phys. Rev. B* 1972, **5**, 2466; *Theor. Chim. Acta* 1974, **34**, 225.
13. J. C. W. Folmer, Ph.D. Thesis, Rijksuniversiteit te Groningen (1981).

Polyhedron Vol. 5, No. 1/2, pp. 157–167, 1986
Printed in Great Britain

0277–5387/86 $3.00 + .00
© 1986 Pergamon Press Ltd

INDUSTRIAL MoO_3–PROMOTER OXIDE–γ-Al_2O_3 HYDROTREATING CATALYSTS: GENESIS AND ARCHITECTURE DESCRIPTION

S. KASZTELAN,* E. PAYEN,† H. TOULHOAT,‡
J. GRIMBLOT* and J. P. BONNELLE*§

* UA CNRS 402, Laboratoire de Catalyse Hétérogène et Homogène, Université de Lille I, Bât. C.3, 59655 Villeneuve d'Ascq Cedex, France; † L.A.S.I.R. (LP, 2641 CNRS), Université de Lille 1, Bât. C.5, 59655 Villeneuve d'Ascq Cedex, France; and ‡ I.F.P., B.P. 311, 92506 Rueil Malmaison Cedex, France

(*Received* 14 *June* 1985)

Abstract—The catalytic performances (activity, selectivity, deactivation by phase transformation . . .) of hydrotreating catalysts composed of supported Mo associated with a promoter (Co or Ni) and working in a sulphided state are greatly dependent on the sequences and conditions of the preparation process. A large number of works dealing with the description of one or several steps in the catalyst elaboration have been already published, specially in the previous Molybdenum Conference in which review articles can be found. However, in these works, all the preparations sequences are not always considered and some experimental conditions are far from those used in *industrial catalyst preparation* in the oxide or commercial form. In this paper we report new results about the architecture of oxide precursors of series of Mo-based catalysts prepared according to industrial conditions. These results will be compared and discussed with other descriptions already published. Starting with the support and commercial products chosen because they are very soluble in water, easily decomposed and less expensive [ammonium heptamolybdate (AHM), and cobalt or nickel nitrate], six steps, viz. molybdate impregnation, intermediate drying and calcination, impregnation of the promoter solution, drying and final calcination, are necessary to obtain the final or commercial catalyst. Moreover after the intermediate or final calcination, the samples prepared can be modified by aging during storage in the laboratory atmosphere. The nature and quantity of the supported species, their structure and size, the chemical state of the elements, their dispersion on the support, the interaction between the molybdate entities, with the support or with the promoter, are among the main aspects, considered in this investigation for which we used techniques dealing with surface characterization X-ray photoelectron spectroscopy (XPS) and ion-scattering spectroscopy (ISS)] and a vibrational technique such as laser Raman spectroscopy (LRS). During the first impregnation step, an electrostatic interaction between the ionized surface species of the support and the molybdate ions in solution occurs. The subsequent drying and calcination steps induce formation of strong chemical bonds between the supported molybdate species and the carrier. After this step, the species are well dispersed on the support as proved by XPS and ISS. The second impregnation transforms the molecular aggregates previously created by (partial) hydrolysis and therefore gives back the initial species. The added promoter is then interacting with the polymolybdate or the support. Calcination can provoke a partial incorporation of the promoter into the support but bilayers in which the promoter is between the molybdate phase and the support are not detected. Aging of the catalyst after the calcination step is a hydration process. Reverse dehydration can be achieved by a new calcination step.

A large number of studies of the preparation, surface characterization, activation (sulphidation) and catalytic performance with model molecules and real feeds of MoO_3–γ-Al_2O_3 catalysts, with which a promoter (CoO or NiO) can be associated, have been published in recent years. Those catalysts are generally used in hydrotreatment, namely hydrodesulfurization (HDS), hydrodenitrogenation

§ Author to whom correspondence should be addressed.

(HDN), hydrodemetallation (HDM) and hydrodeoxygenation (HDO), of petroleum fractions, heavy residues or coal liquids. They represent a large proportion of catalysts used in modern petrochemistry and, according to Jacobsen,[1] the hydroprocessing catalyst market is about 25,000–30,000 tons year^{-1} at a value of the order of 250 million \$ year^{-1}.

Even though commercial catalysts exist and work well, there is a challenge to improve them by considering in particular the relations which should exist between the genesis stage leading to the commercial precursor oxides and the working state in which the active components are sulphided. As a matter of fact, in the previous Molybdenum Conferences several papers concerned with this objective can be found. In particular in the review of Delmon,[2] a description of the species present in the oxide form of CoO–MoO_3–γ-Al_2O_3 catalysts and their localization is given and it is shown how the oxide precursor determines the nature and dispersion of the species in the active form. Hall[3] related the preparation and properties of molybdena–alumina catalysts obtained by using an equilibrium adsorption method from a polymolybdate solution. These catalysts can be described as small islands containing seven or more Mo atoms and perhaps two layers thick. However, in both cases, all the preparation sequences were not always considered and, in Hall's work,[3] the impregnation method is quite different from that generally used in industrial catalyst preparations.

Therefore, in this paper we report results about the genesis and architecture of oxide precursors of Mo-based catalysts prepared in six elementary steps, viz. (i) molybdate impregnation, (ii) drying, (iii) intermediate calcination, (iv) promoter impregnation, (v) drying, and (vi) final calcination. For each step, we took care to simulate conditions as close as possible to industrial operations. The six-step procedure is in some cases applied on the large scale. We will show also that aging of the catalysts, after calcination, in the laboratory atmosphere can modify the structure of the supported phase. In this investigation, we will not consider the problem of support choice as we always used well-defined γ-Al_2O_3 extrudates nor the activation or sulphidation step which generally takes place before the catalytic run and transforms the catalyst into supported sulphides.

EXPERIMENTAL

Sample preparation

The support, as extrudates 1.2 mm in diameter, is γ-Al_2O_3 of high purity which has a surface area of 246 $m^2\,g^{-1}$ and a total pore volume (v_p) of 0.50 $cm^3\,g^{-1}$. In industrial preparations, the chosen impregnating compounds must be very soluble in water, easily decomposed and less expensive. Therefore, we used ammonium heptamolybdate (AHM), $(NH_4)_6Mo_7O_{24}\cdot 4H_2O$, from Merck and cobalt or nickel nitrate hexahydrate from Prolabo.

The alumina extrudates were impregnated by the pore-filling (or incipient wetness impregnation) method. Solutions containing the exact amount of Mo (or Co or Ni) to yield catalysts of desired composition were prepared. The alumina extrudates were gently agitated in a rotating drum, and the freshly prepared solution was slowly added in order to ensure a good distribution and elimination of wetting heat. The volume of the solution corresponded exactly to the v_p of the carrier. The wet samples were left at room temperature in closed flasks (maturation) for a few hours to obtain equilibrium in the pores and then dried at 110°C overnight. Note that the wet samples examined by laser Raman (LR) spectroscopy (LRS) after impregnation had been left at room temperature for a longer time as the preparation was performed in the IFP laboratories and the characterization at Lille University. Then the samples were calcined in air at various temperatures (up to 900°C for 2 h) for the intermediate calcination or at 500°C for 2 h for the final calcination. After each preparation step a small sample was left out for characterization. The MoO_3 loading of the samples [x (in % by weight of MoO_3)] varies between 2 and 24%.

Characterization

The samples were characterized by LRS and XPS for which the procedures have been given.[4] ISS measurements were also performed on the same spectrometer as used for XPS using He^+ ions as projectiles. The experimental conditions have been fully described previously.[5]

RESULTS AND DISCUSSION

MoO_3–γ-Al_2O_3 *preparation and characterization*

Impregnation. When impregnating molybdate solutions on γ-Al_2O_3, both pH and Mo concentration can modify the nature of the adsorbed species. γ-Al_2O_3, among other mineral oxides in suspension in aqueous solution, tends to be electrically charged[6] and the isoelectric point (IEP) is about pH 8. Therefore, in acidic medium (pH < 8), the γ-Al_2O_3 particles, positively charged, are surrounded by anions, whereas, at pH > 8, the inverse situation

occurs, according to eqns (1) and (2):

$$Al—OH + H^+,A^- \rightleftarrows Al—OH_2^+,A^-, \quad pH < IEP, \quad (1)$$

$$Al—OH + B^+,A^- \rightleftarrows Al—O,B^+ + H_2O, \quad pH > IEP, \quad (2)$$

$$IEP(\gamma\text{-}Al_2O_3): pH \simeq 8.$$

As molybdates in solution are always negatively charged (except at very low pH), the impregnation step should preferably occur at pH < IEP (Al_2O_3). This was experimentally shown by an equilibrium adsorption process with solutions at various pH: for pH $\gtrsim$ 8, the amount of Mo adsorbed is very small.[7] This result can be extended to other anionic species.[8]

In the pore-filling method, as adsorption of Mo is forced (it can be, in fact, Mo deposition rather adsorption) during water elimination (drying and calcination stages) it is not necessary, *a priori*, to adjust the pH of the solution to obtain MoO_3–γ-Al_2O_3 catalysts. However, the real nature of the molybdate ions starting from the heptamolybdate (HM) in solution is a function of the Mo concentration and pH according to eqn (3):

$$Mo_7O_{24}^{6-} + 4H_2O \underset{K}{\rightleftarrows} 7MoO_4^{2-} + 8H^+. \quad (3)$$

(In this investigation we will not consider $Mo_8O_{26}^{4-}$, which is only detected at low pH.)

The equilibrium constant K ($[HM]/[M][H^+]^8$) was reported to be $10^{57.7}$ in 3 M $NaClO_4$ at 25°C.[9] The AHM concentration, C_{AHM}, of the impregnating solution depends on the desired MoO_3 loading, x, of the final catalyst [eqn (4)]:

$$C_{AHM} = \frac{x}{100-x} \times \frac{1}{v_p} \times 0.992 \text{ mol } l^{-1}. \quad (4)$$

The ratio [M]/[HM] in solution changes when x increases (Fig. 1) (M represents the monomer species MoO_4^{2-} and HM $Mo_7O_{24}^{6-}$).

From Tsigdinos *et al.*,[9] the pH of the AHM solution varies from 5.1 to ~5.5 when C_{AHM} increases so that in the impregnating solution [M]/[HM] is between $\sim 9.10^{-2}$ ($x = 2$, pH → 5.1) and $\sim 1.8\ 10^{-2}$ ($x = 24$, pH → 5.5) and, as a consequence, HM is the major species when using solutions with their "natural" pH.

Due to the amphoteric character of γ-Al_2O_3, the dispersion can be changed when the impregnating solution fills the pores of the support. LRS is a suitable technique to follow the evolution of the species in contact with γ-Al_2O_3 as M and HM have quite different Raman spectra.[4,10,11] M, a perfect tetrahedral species (T_d) in solution, has the major Raman band at 898 cm^{-1}, whereas the main band of HM is at 941 cm^{-1}. In the low-wavenumber region,

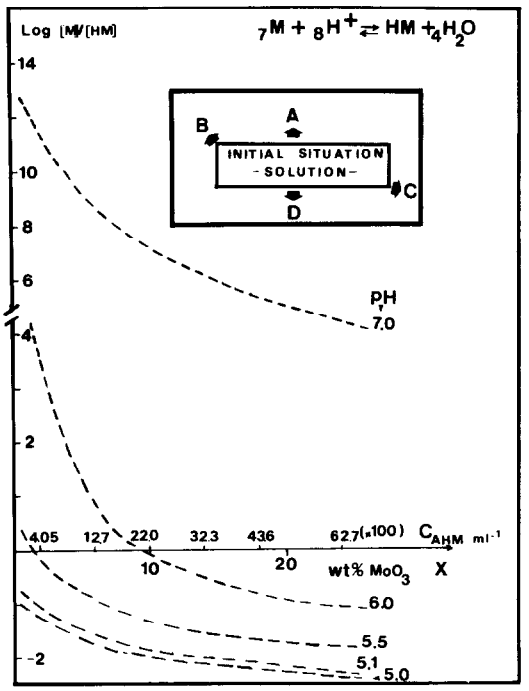


Fig. 1. Variation of $\log_{10}$ [M]/[HM] as a function of the HM concentration, C_{AHM}, of the impregnating solution which determines the final Mo loading x (% MoO_3 by weight). log $K = 10^{57.7}$ is taken from Ref. 9. In the insert at the corner are schematically shown the trends which could occur, if, starting from a given situation in solution: (A) interaction with γ-Al_2O_3 is effective, pH increases; (B) there is a concentration gradient from outside to inside the pores and an interaction with γ-Al_2O_3 as in A; (C) water is eliminated during drying and calcination at moderate temperature (no interaction with γ-Al_2O_3); and (D) NH_4^+ is decomposed into NH_3 and H^+ ads during calcination.

there is also some difference: 316 cm^{-1} for M, 357 and 217 cm^{-1} for HM. In Fig. 2(a), the Raman spectra in the 700–1000-cm^{-1} region obtained on the impregnated samples maintained at room temperature are reported. Four bands at 860 (a broad shoulder), 898, 925 and 947 cm^{-1} are clearly detected. For low Mo loading samples ($x = 2.6$), the M characteristic band (898 cm^{-1}) only is present with two shoulders at 860 and 925 cm^{-1}. As the loading increases, the 947-cm^{-1} line assigned to HM appears and becomes the major band at $x = 18$ and 24 whereas the 860-cm^{-1} shoulder seems to decrease and even disappears for $x = 24$. Due to the overlap or broadening of the 898- and 947-cm^{-1} lines, the presence of the 925-cm^{-1} band is not obvious for high-x samples. Although the HM anion is the major species in solution, its presence is not detected in impregnated samples corresponding to low Mo loading. Therefore, as already reported,[12] γ-Al_2O_3 causes a pH increase which, by consuming H_3O^+, transforms HM into M (see Fig. 1, arrows A and B if

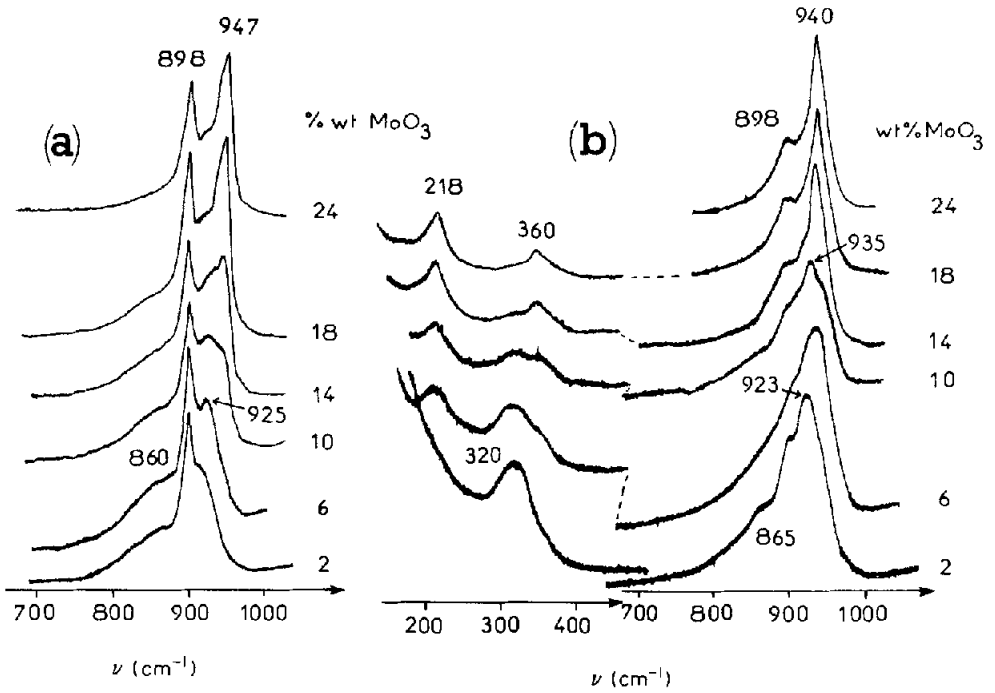
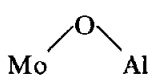


Fig. 2. Raman spectra of: (a) "wet" samples, and (b) samples after drying (110°C overnight).

there is also a concentration gradient into the pores of Al_2O_3). As C_{AHM} increases for higher-x samples, one can see from Fig. 1 that a small local pH increase is not enough to produce high amounts of M and in this case HM remains the predominant species. Although the LRS information is not quantitative because: (i) the scattering Raman cross-sections of these species can be different in solution and in contact with or adsorbed on a solid, and (ii) the spectra result both from the solution remaining in the pores and from adsorbed species, it appears that, for concentrated solutions, the pH shift due to γ-Al_2O_3 is not sufficient to completely transform HM into M.

We propose that the 925- and 860-cm^{-1} bands, which are not present in solutions (only for M is a very weak and broad band detected[11] at 846 cm^{-1}) can be assigned to vibrational modes of, respectively, Mo=O(t) (symmetric stretching) and Mo—O—Al bridges of adsorbed species M whose tetrahedral symmetry is distorted by interaction with the support. This first point is in agreement with Iannibello *et al.*,[13] who suggested that the shift to higher wavenumber of MoO_4^{2-} in tetrahedral coordination reflects the distortion from T_d symmetry and increases the Mo(VI)=O double bond character. Note that HM does not seem to be strongly shifted (941–947 cm^{-1}) when in contact or adsorbed on γ-Al_2O_3 at high x. For this larger-size anion, γ-Al_2O_3 has probably no distortion effect so that the Mo=O(t) stretching vibration is not really affected. The



bond with the support, vibrations of which should be detected in the 900-cm^{-1} region,[14] is not seen because of the presence of the remaining line of M.

All this information on wet samples can be compared with results already published. Those of Jeziorowski and Knözinger[11] at pH = 6 using a pore-filling method are in complete agreement with ours as they found lines at 918 and 894 cm^{-1} on a 3% MoO_3 sample and at 938 and 921 cm^{-1} on an 8% MoO_3 sample. In addition, a broad tail is observed at wavenumbers below 900 cm^{-1}. Their conclusion was that HM is degraded by interaction with Al_2O_3 and M is the initial adsorbed species. However even with 8% MoO_3 some HM remains (938-cm^{-1} line). No higher Mo loading samples were investigated. Comparison with Hall's work,[3,10] who reached different conclusions, is more difficult as: (i) the impregnation method is different, and (ii) the pH of the solution chosen (and imposed) are lower (1.0 or 3.9) or higher (8.6).

Drying. In Fig. 2(b) we report the Raman spectra of the dried samples. For low x values, the 920-cm^{-1} line is prominent whereas the 898-cm^{-1} line has completely disappeared. All the M ions are in

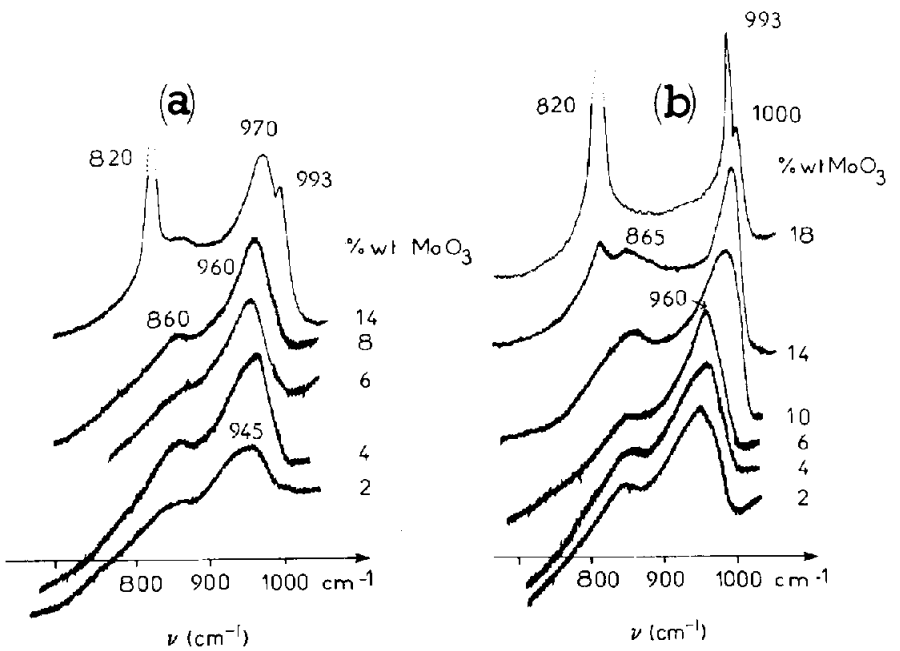


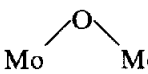
Fig. 3. Raman spectra of samples calcined in air (500°C for 2 h) by using: (a) a low laser power (~40 mW), and (b) a high laser power (~300 mW).

chemical interaction with Al_2O_3 according to eqn (5):

$$MoO_4^{2-} + Al{-}OH_2^+ \rightarrow Al{-}O{-}MoO_3^- + H_2O. \quad (5)$$

$$898\ cm^{-1} \qquad \sim 860 \quad 920\ cm^{-1}$$

We will see later that the species on the right-hand side of eqn (5) is hydrated (if samples are not sufficiently calcined) and should be written as Al—O—MoO_3...H. To confirm that the 920-cm^{-1} vibration is not a result of the polymerization of M, note the absence in the low-wavenumber region of the (360- and 220-cm^{-1} bands characteristic of polymolybdate species



For high x values, water elimination by a concentration effect should locally slightly decrease the pH inside the pores (arrow C in Fig. 1) which is not favorable for producing M. However, when interaction with Al_2O_3 occurs, the trend is along arrow A so that drying of a high-x sample might result in combination of arrows C and A. However, as the H^+ exchange of Al_2O_3 appears limited, the trend is not sufficient to see the complete transformation of HM into M during drying. Note also that during drying (and more probably during calcination), NH_4^+ in solution can be decomposed which leaves H^+ adsorbed on Al_2O_3 (arrow D in Fig. 1). All these arguments favor the conclusion that the ~940-cm^{-1} line is characteristic of HM (hydrated form, as we will see later) bound to Al_2O_3 probably through a few Mo—O—Al bonds which are not perturbing the whole anion (no or small shift with HM in solution). However, perturbed M anions (898 cm^{-1}, not or weakly adsorbed) are not detected: water elimination seems incomplete in the pores.

Calcination: standard conditions. In Fig. 3 we report the Raman spectra of samples after standard calcination (500°C for 2 h in air) recorded: (i) at low laser power which does not modify the nature of the supported species, and (ii) at high laser power which can be considered as an additional calcination.[14]

On the 14 and 18% MoO_3 samples, the bands at 993 and 820 cm^{-1} are assigned to bulk MoO_3 which means that all the HM anions are not really bound to γ-Al_2O_3 even in the drying step. These free HM species decompose to MoO_3.

So except for these two bands, the Raman features in the 800–1000-cm^{-1} region appear very similar. In particular the Mo=O(t) stretching vibration is always at 940–1000 cm^{-1}, as already reported,[4,15–19] and depends on both the Mo content (higher degree of aggregation of Mo species) and the extent of hydration of the supported molybdate. So in order to choose among the following hypotheses: (i) the initial adsorbed species are maintained "intact", (ii) the initial adsorbed species are transformed by surface polymerization, and (iii) the initial adsorbed

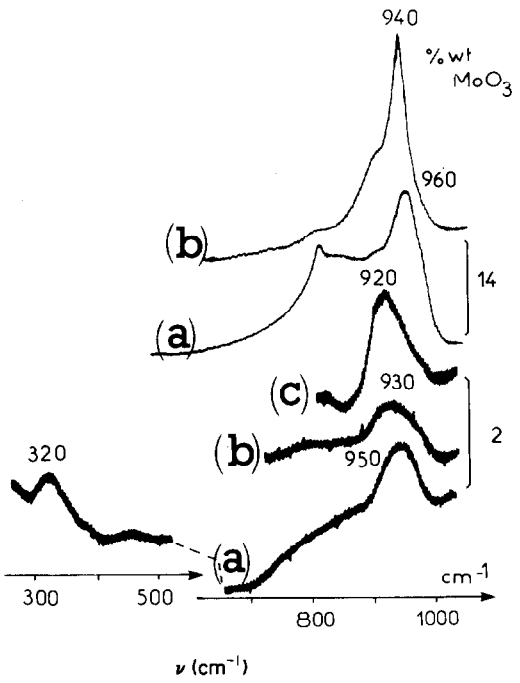


Fig. 4. Raman spectra of MoO_3–γ-Al_2O_3 samples with two Mo loadings ($x = 2$ and 14): (a) just calcined, and (b) and (c) after more or less prolonged aging (laboratory atmosphere).

species are transformed by surface depolymerization which will correspond to a sample of a given Mo loading, both the Raman spectra of the samples in the (freshly) calcined state [Fig. 3(a) and (b)] and after aging (which produces surface hydration) (Fig. 4) will be considered.

The molybdate species, which gives a band at 920 cm^{-1} after adsorption is rather isolated on the support (6% MoO_3 corresponds to ~ 1 Mo nm^{-2}) and polymerization is highly improbable during calcination. This treatment only reinforces the bonds with γ-Al_2O_3 (shift to 945 cm^{-1}, a value which has already been reported[11–13]), according to eqn (6):

$$\text{Al—O—MoO}_3\ldots\text{H} + \text{Al—OH} \underset{\text{aging}}{\overset{\text{calcination}}{\rightleftharpoons}} (\text{Al—O})_2\text{MoO(OH)}_2 \rightleftarrows \cdots \quad (6)$$

This 945-cm^{-1} line can be shifted to higher-wavenumber values if more severe treatments are performed[14] (i.e. *in vacuo* at 700°C) to provoke complete dehydration. However these reactions are reversible if the samples are aging in (wet) air as seen in Fig. 4. Obtaining lines at 930–920 cm^{-1} after aging is significantly in favor of the presence of monomer species in the calcined state for low-x samples.

For the HM species, it is much more difficult to determine the transformation upon calcination. For x from 6 to 24 wt% MoO_3, the adsorbed HM species can be considered isolated: one Mo occupies ~ 1–~ 0.20 nm^2, but HM (seven Mo atoms) adsorbed as a whole according to the Hall's hypothesis[3] occupies ~ 7–~ 1.40 nm^2. Then, if the adsorbed HM is not mobile within the standard calcination conditions, polymerization is highly improbable. The shifts observed in Fig. 3(b) are then more suggestive of a different dehydration level with an increasing number of links with Al_2O_3 than of HM aggregation. By aging (Fig. 4), a shift from 960 to 940 cm^{-1} is observed which once again confirms our hypothesis that HM is maintained "intact" during calcination.

Calcination: effect of temperature. The effect of the calcination temperature has been investigated on the $x = 14MoO_3$–γ-Al_2O_3 sample whose color changes: white from 25 to 100°C, yellow to 200°C, heterogeneous white and dark blue at 350°C, pale green from 450 to 700°C and white-blue at 900°C. In that case, sintering due to γ-Al_2O_3 transformation is observed. The LR spectra and X-ray photoelectron spectroscopy (XPS)–ion-scattering spectroscopy (ISS) intensity ratios are reported in Figs 5 and 6. In the Raman spectrum of the sample calcined at 900°C, the characteristic bands of $Al_2(MoO_4)_3$ are observed,[14,20,21] which are absent at lower temperatures. Note also that the 820- and 995-cm^{-1} bands of MoO_3, present at 500°C, disappeared at higher temperatures and probably by sublimation of MoO_3, unless, as in the case of WO_3–γ-Al_2O_3 samples,[22] bulk MoO_3 reacts with Al_2O_3 to give $Al_2(MoO_4)_3$.

The XPS Mo/Al (Mo3*d* and Al2*p* peaks) ratio is indicative of a small change of dispersion between 100 and 350°C as already pointed out by Houalla *et al.*,[23] whereas the O/Al ratio (O1*s*–Al2*p* peaks) considerably decreases at 900°C, which is again indicative of γ-Al_2O_3 transformation. The ISS results give similar conclusions but sensitivity is much better when the ion incident energy used is the lowest (500 eV). By LRS one can see that: (i) the dispersion effect observed by XPS–ISS corresponds to transformation of the adsorbed species "wet state" to molybdate species really bound to Al_2O_3, and (ii) the 950–980-cm^{-1} line observed at low laser power is shifted to ~ 1000 cm^{-1} when high laser power is used (*in situ* dehydration). The 860-cm^{-1} line, still present in the wet state, increases up to 350°C and then appears slightly constant with respect to the major line. As a consequence, the interaction between species in solution with Al_2O_3 occurs mainly between 25 and 350°C, this last temperature corresponding to salt decomposition. Therefore, from this study it appears that the lower limit for calcination is 350°C and $Al_2(MoO_4)_3$ should not be formed during standard calcination (500°C for 2 h).

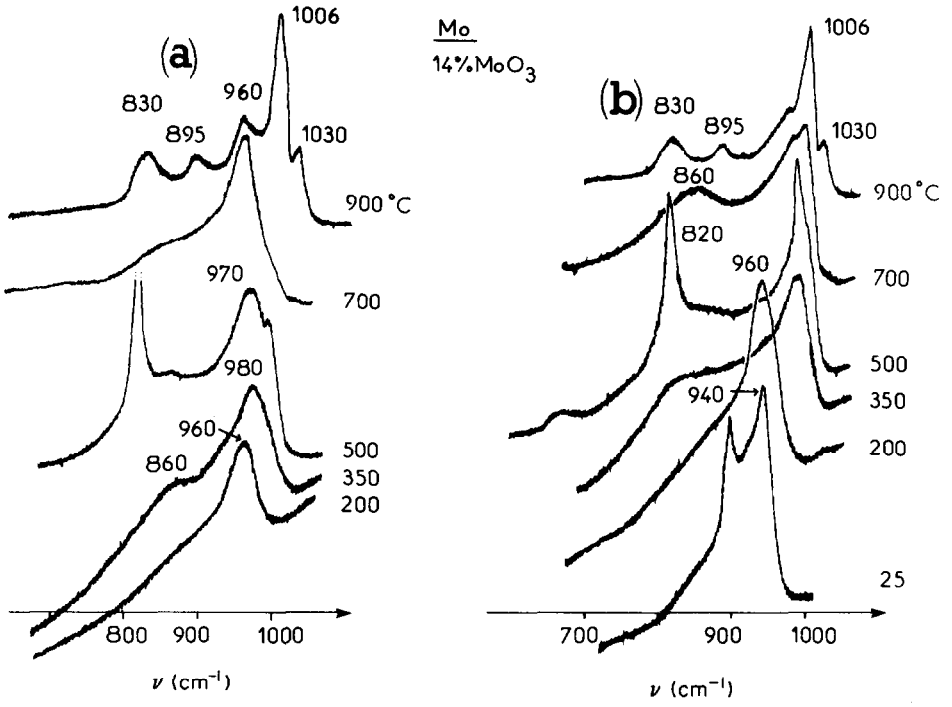


Fig. 5. Raman spectra of a 14 wt % MoO_3 sample calcined at different temperatures (2 h): (a) low laser power (~40 mW), and (b) high laser power (~300 mW).

14% MoO_3–3% promoter oxide–γ-Al_2O_3: characterization

Special attention is given to this system with a promoter/(Mo + promoter) atomic ratio close to 0.3 (promoter is Co or Ni) as this composition is generally found to provide the best synergy for optimum catalytic performance.[2,24] Hence, the majority of commercial catalysts have relative compositions similar to that considered here.

Aging of the calcined MoO_3–γ-Al_2O_3, in which the main supported species are HM in interaction with γ-Al_2O_3, provokes (partial) hydrolysis of the Al—O—Mo bonds; then during the promoter solution impregnation, an interaction of the Co^{2+} or Ni^{2+} cations may occur with HM weakly bound to

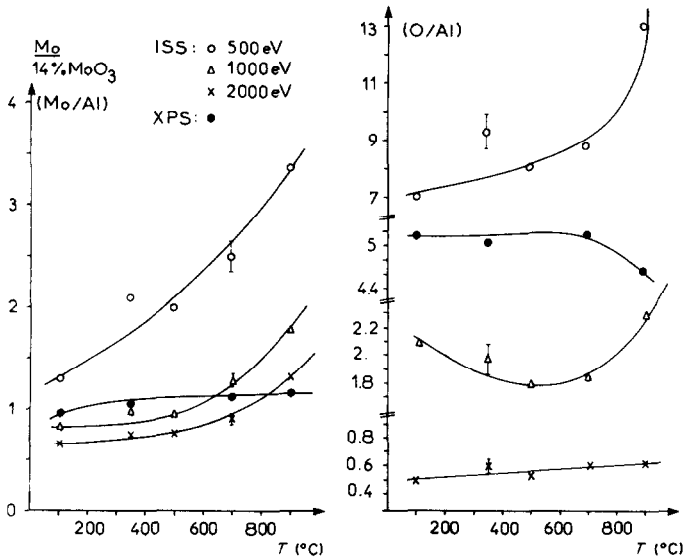


Fig. 6. XPS and ISS intensity ratios as a function of the calcination temperature of the 14 wt % MoO_3 sample.

alumina. However Co^{2+} or Ni^{2+} cations may also interact with the free surface of Al_2O_3. On drying, no discernible reaction occurred between Ni^{2+} or Co^{2+} with HM as evidenced by Raman spectra in Fig. 7. The 950-cm^{-1} line still characterizes the HM species which is weakly bound to Al_2O_3 because the 860-cm^{-1} broad band is almost absent. The 1050-cm^{-1} line is assigned to NO_3^- which is not decomposed at this stage. On *in situ* calcination, the Raman features change: the 1050-cm^{-1} line disappeared and the 1000-cm^{-1} band, characteristic of the dehydrated supported molybdate,[14] is prominent. On the low-wavenumber tail, maxima at 860 and ~930 cm^{-1} can be distinguished. The presence of the latter band can be due to incomplete dehydration which is not really controlled in these experiments. At this step, the main point, perhaps, emerging from this analysis is the absence of a detectable effect of the promoter on the 1000-cm^{-1} Mo=O(t) stretching vibration.

During the sequences of drying and calcination, after the promoter impregnation, the Mo and promoter dispersion changes have been followed by ISS and XPS and, for Mo compared with the results obtained before impregnation (Fig. 8). As already discussed in the preceding paragraph, calcination of the impregnated Mo–Al_2O_3 sample slightly improves Mo dispersion by eliminating residual water

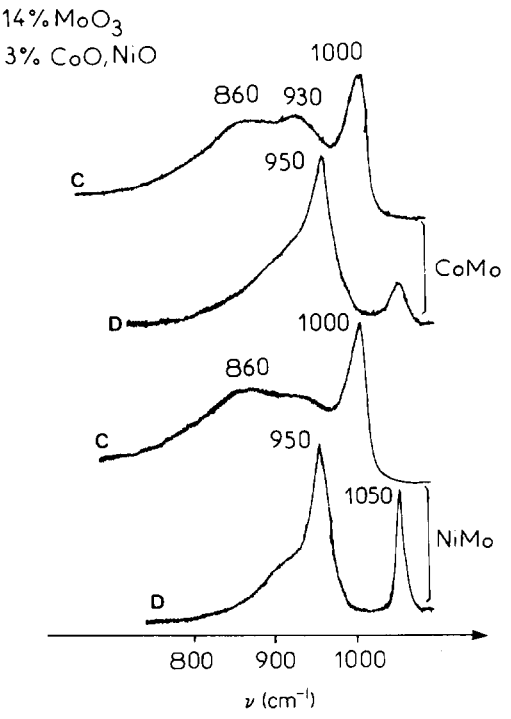


Fig. 7. Raman spectra of dry (D) and calcined (C) (by laser beam) MoO_3–promoter oxide–γ-Al_2O_3 samples. The MoO_3–γ-Al_2O_3 precursor was prepared by AHM impregnation at pH = 2[4] which leads to only HM species in solution.

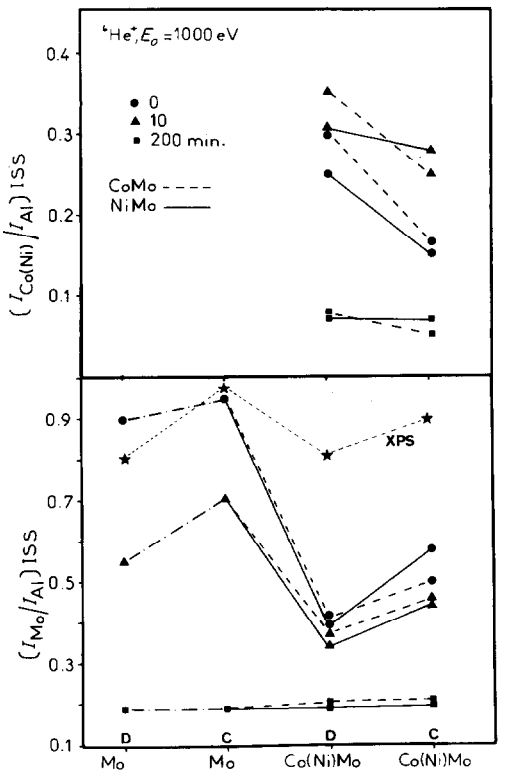


Fig. 8. Variation of the Mo/Al and Co(Ni)/Al intensity ratios as a function of the step of preparation. The XPS results, presented in the bottom part, have been previously reported[4] and concern a MoO_3–γ-Al_2O_3 sample prepared at pH = 2. All the drying and calcination parameters are the same.

and NH_4^+. The reverse trend is observed when the promoter solution is added. The relative Mo/Al ratio decrease is much more pronounced for ISS than for XPS, which means that, on the atomic scale, in addition to remaining water and other species, the promoter ions Co^{2+} and Ni^{2+} partly block the supported molybdate. After the final calcination, a small increase in the Mo signal relative to Al is detected but the initial value is not restored. As H_2O and NO_3^- are eliminated (see the Raman results) only the promoter ions can have a shadowing effect on the Mo phase which is therefore (partly) covered by Co or Ni. On the other hand, the relative promoter intensity slightly decreases. This can be interpreted by diffusion of the promoter ions into Al_2O_3 (this diffusion appears to be more easy with Co than with Ni). This was already evidenced by Jeziorowski *et al.*[25] using ISS and this effect is much more important when the calcination temperature increases.

MoO_3–*promoter oxide*–γ-Al_2O_3 *of other compositions: characterization*

To achieve this investigation, MoO_3–CoO (or NiO)–γ-Al_2O_3 samples of various compositions

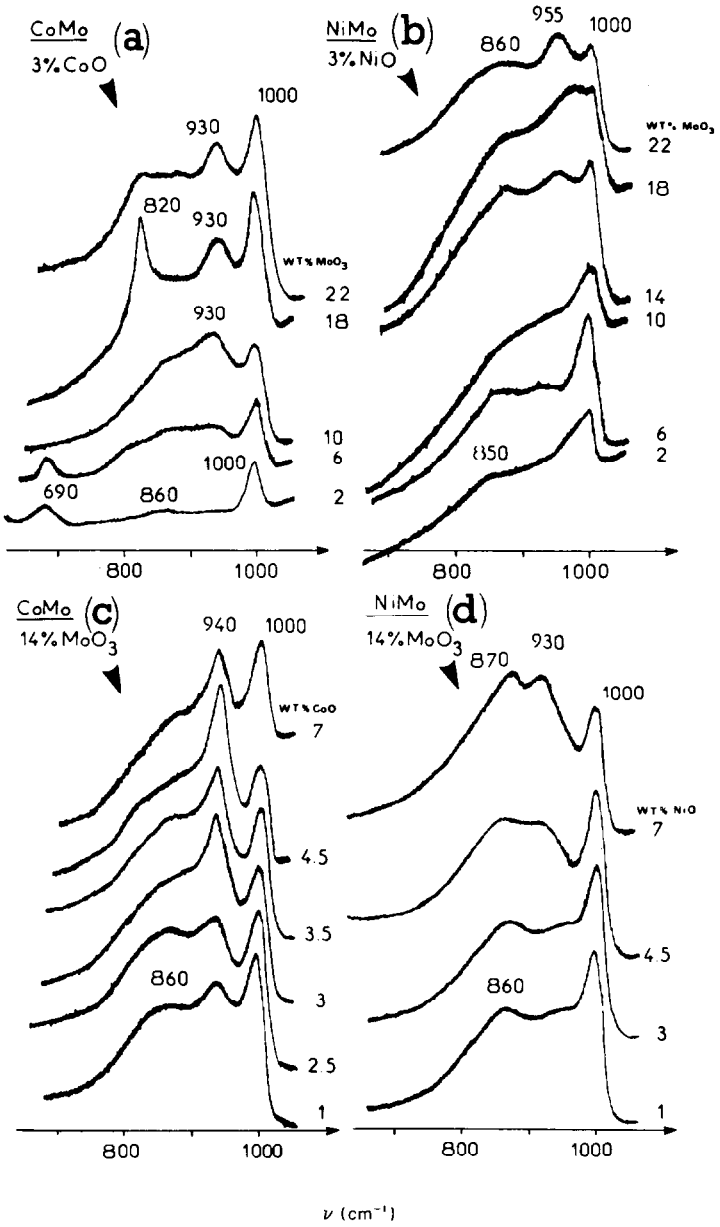


Fig. 9. Raman spectra (high laser power ≃ 300 mW) of Co–Mo and Ni–Mo samples calcined in air (500°C, 2 h): (a) constant Co content (3% CoO), (b) constant Ni content (3% NiO), and (c) and (d) constant Mo content (14% MoO_3).

have been characterized by LRS after a final calcination at 500°C for 2 h. In Fig. 9 are reported the main Raman features in the ~700–1000-cm^{-1} region obtained by using a high laser power (~300 mW). However, dehydration of the supported molybdate is not proven to be complete in all the examined samples as local temperature at the sample, light focusing etc . . . are not always reproducible. Nevertheless, the effect of promoter is clearly detected. The 1000-cm^{-1} line is easily obtained on the low MoO_3 loading samples when the promoter, Co or Ni, is present [Fig. 9(a) and (b)], whereas, in the same recording conditions, this line is not visible on the sample without promoter [Fig. 3(b)]. A more severe treatment (i.e. *in vacuo* at 700°C,[14]) is necessary to obtain this line. It therefore appears that dehydration is favored by the presence of a promoter whose location might be close to the adsorbed molybdate. On the Co–Mo samples at low Mo loading [Fig. 9(a)], the 690-cm^{-1} line is assigned to the presence of $CoAl_2O_4$ and/or Co_3O_4.[26] For such low Mo loadings, the uncovered surface of Al_2O_3 is quite large so that Co (or Ni) may easily interact with the support. By subsequent heating,

some of the promoter then diffuses into the Al_2O_3 as already shown by XPS–ISS.

As the Mo loading increases, the broad feature between 800 and 1000 cm^{-1} increases [Fig. 9(a) and (b)] and the bands at 930–950 cm^{-1}, characteristic of hydrated supported molybdate still remain, which means that the presence of the promoter influences the extent of hydration or makes the dehydration reaction incomplete. Analysis of a series of samples with constant MoO_3 loading (14 wt %) and increasing amount of promoter complements this observation. As the promoter loading increases, the relative intensity of the 940-cm^{-1} line increases [Fig. 9(c) and (d)]. Even for 1% CoO, this 940-cm^{-1} line remains. Comparison of Fig. 9(c) and (d) shows that presence of Ni favors the 860-cm^{-1} band relative to the 930–940- and 1000-cm^{-1} lines. No definitive explanation can be given at the moment to take into account this difference; it may be suggested that the Ni–molybdate interaction is stronger than the Co–molybdate one. Within this hypothesis, formation of a surface like Ni–heteropolymolybdate bound to the alumina surface, as already postulated by Knözinger,[27] is possible.

CONCLUSIONS

Starting with a well-defined γ-Al_2O_3 support, the whole sequence of the preparation of MoO_3–CoO or NiO–γ-Al_2O_3 hydrotreating catalysts have been studied and the following conclusions can be drawn.

(i) Although the main species in the impregnating solution with natural pH are HM anions, in the low Mo loading samples the major species are M.

(ii) By adsorption on γ-Al_2O_3, M species are distorted.

(iii) For higher Mo loading samples, HM species are also adsorbed. Bonds with the support do not appreciably modify the Mo=O(t) stretching vibration of HM.

(iv) Standard calcination (500°C, for 2 h) reinforces the links between M and/or HM with the support. Polymerization of HM on the γ-Al_2O_3 surface to form a supported polymolybdate phase of higher Mo number seems improbable unless, during calcination, adsorbed HM is mobile.

(v) Calcination at higher temperature forms $Al_2(MoO_4)_3$. Thus, to obtain optimum Mo dispersion, calcination between ~350 and ~500°C is preferred.

(vi) Aging of the catalyst is shown by hydration of the supported molybdate. This reaction modifies the bonds of the supported species with Al_2O_3 by hydrolysis. Calcination and aging are therefore two antagonistic reactions; only NH_3 desorption during calcination is an irreversible step.

(vii) The promoter added to the MoO_3–γ-Al_2O_3 samples may be close to or on the supported molybdate and on the free surface of Al_2O_3.

(viii) By calcination, some of the promoter diffuses into the support. The rest, in a strong interaction with the supported molybdate, modifies its hydration dehydration properties.

(ix) The exact location of the promoter in contact with the supported molybdate phase is not defined for the moment but it can be assumed that this promoter–molybdate entity is the precursor of the small MoS_2 patches "decorated" at the edge sites by Co or Ni.[28]

Acknowledgements—This work is part of S.K.'s thesis (Lille, 1984) and S.K., J.G. and J.P.B. are indebted to the Institut Français du Pétrole for a financial support.

REFERENCES

1. A. C. Jacobsen, In *Surface Properties and Catalysis by Non-metals* (Edited by J. P. Bonnelle *et al.*), p. 305. D. Reidel, Dordrecht (1983).
2. B. Delmon, In *Proceedings of the Third International Conference on the Chemistry and Uses of Molybdenum* (Edited by H. F. Barry and P. C. H. Mitchell), p. 73. Climax Molybdenum Co., Ann Arbor, MI (1979).
3. W. K. Hall, In *Proceedings of the Fourth International Conference on the Chemistry and Uses of Molybdenum* (Edited by H. F. Barry and P. C. H. Mitchell), p. 224. Climax Molybdenum Co., Ann Arbor, MI (1982).
4. S. Kasztelan, J. Grimblot, J. P. Bonnelle, E. Payen, H. Toulhoat and Y. Jacquin, *Appl. Catal.* 1983, **7**, 91.
5. S. Kasztelan, J. Grimblot and J. P. Bonnelle, *J. Chim. Phys.* 1983, **80**, 793.
6. J. P. Brunnelle, *Pure Appl. Chem.* 1978, **50**, 1211.
7. L. Wang and W. K. Hall, *J. Catal.* 1982, **77**, 232.
8. M. J. D'Aniello, Jr, *J. Catal.* 1981, **69**, 9.
9. G. A. Tsigdinos, H. Y. Chen and B. J. Streusand, *Ind. Eng. Chem., Prod. Res. Dev.* 1981, **20**, 619.
10. L. Wang and W. K. Hall, *J. Catal.* 1980, **66**, 251.
11. H. Jeziorowski and H. Knözinger, *J. Phys. Chem.* 1979, **83**, 1166.
12. A. Iannibello, S. Marengo, P. Tittarelli, G. Morelli and A. Zecchina, *J. Chem. Soc., Faraday Trans* 1 1984, **80**, 2209.
13. A. Iannibello, S. Marengo, F. Trifiro and P. L. Villa, In *Preparation of Catalysts II. Scientific Bases for the Preparation of Heterogeneous Catalysts* (Edited by B. Delmon, P. Grange, P. Jacobs and G. Poncelet), p. 65. Elsevier, Amsterdam (1979).
14. E. Payen, S. Kaztelan, J. Grimblot and J. P. Bonnelle, *J. Raman Spectrosc.*, (in press).
15. H. Knözinger and H. Jeziorowski, *J. Phys. Chem.* 1978, **82**, 2002.
16. B. Sombret, P. Dhamelincourt, F. Wallart, A. C. Muller, M. Bouquet and J. Grosmangin, *J. Raman Spectrosc.* 1980, **9**, 291.

17. R. Thomas, M. C. Mittelmeyer-Hazeleger, F. P. J. M. Kerkhof, J. A. Moulijn, J. Medema and V. H. J. de Beer, In *Proceedings of the Third International Conference on the Chemistry and Uses of Molybdenum* (Edited by H. F. Barry and P. C. H. Mitchell), p. 85. Climax Molybdenum Co, Ann Arbor, MI (1979).
18. J. M. Stencel, L. E. Makovsky, T. A. Sarkus, J. de Vries, R. Thomas and J. A. Moulijn, *J. Catal.* 1984, **90**, 314.
19. S. S. Chan, I. E. Wachs, L. L. Murrell, L. Wang and W. K. Hall, *J. Phys. Chem.* 1984, **88**, 5831.
20. J. Medema, C. van Stam, V. H. J. de Beer, A. J. A. Konings and D. C. Koningsberger, *J. Catal.* 1978, **53**, 386.
21. D. S. Zingg, L. E. Makovsky, R. E. Tischer, F. R. Brown and D. M. Hercules, *J. Phys. Chem.* 1980, **84**, 2898.
22. S. S. Chan, I. E. Wachs, L. L. Murrell and N. C. Dispenziere, Jr, *J. Catal.* 1985, **92**, 1.
23. M. Houalla, C. L. Kibby, L. Petrakis and D. M. Hercules, *J. Catal.* 1983, **83**, 50.
24. J. F. Lepage *et al.*, In *Catalyse de contact*, p. 441. Editions Technip, Paris (1978).
25. H. Jeziorowski, H. Knözinger, E. Taglauer and C. Vogdt, *J. Catal.* 1983, **80**, 286.
26. E. Payen, J. Barbillat, J. Grimblot and J. P. Bonnelle, *Spectrosc. Lett.* 1978, **11**, 997.
27. B. Canosa-Rodriguo, H. Jeziorowski, H. Knözinger, X. Wang and E. Taglauer, *Bull. Soc. Chim. Belg.* 1981, **90**, 1339.
28. S. Kasztelan, H. Toulhoat, J. Grimblot and J. P. Bonnelle, *Appl. Catal.* 1984, **13**, 127; *Bull. Soc. Chim. Belg.* 1984, **93**, 807.

Polyhedron Vol. 5, No. 1/2, pp. 169–177, 1986
Printed in Great Britain

0277–5387/86 $3.00 + .00
© 1986 Pergamon Press Ltd

A COMPARISON OF THE SURFACE CHEMISTRY AND CATALYTIC PROPERTIES OF REDUCED VS SULFIDED MOLYBDENA–ALUMINA CATALYSTS

WILLIAM S. MILLMAN, KOH-ICHI SEGAWA,* DALE SMRZ and W. KEITH HALL†

Department of Chemistry, Laboratory of Surface Studies, University of Wisconsin—Milwaukee, Milwaukee, WI 53201, U.S.A.; and * Department of Chemistry, Sophia University, 7-1 Kioicho Chiyoda-ku, Tokyo 102, Japan

(*Received* 15 *June* 1985)

Abstract—Molybdena–alumina catalysts have been studied by both chemisorption and spectroscopic methods to relate their surface properties to catalytic function. IR studies of the OH region and CO_2 chemisorption have been used to determine the variation in the exposed alumina surface area as a function of Mo loading, and of the extent of reduction. NO chemisortion has been used as a selective probe of the molybdena portion of the surface. The data show that H_2 reduction decreases the coverage with molybdena and suggests that this phase undergoes a surface rearrangement with concomitant agglomeration. These processes are accentuated by sulfiding. The effects of loading on the ease of reduction and sulfiding were characterized and found to be different. The NO data show little change in the nature of the sites upon sulfiding. Catalytic reactions of ethene, propene and 1,3-butadiene with H_2 or D_2 were studied. Although changes in rate occurred on reduction or sulfiding, tracer experiments revealed that these changes did not alter the reaction mechanisms. The changes in the activity of the catalysts could be entirely attributed to changes in the active-site concentration rather than to the nature of the catalytic sites.

Molybdena–alumina catalysts are used industrially in both the reduced (oxidic) and sulfided forms. Because they are good hydrogenation catalysts which are relatively tolerant to sulfur and nitrogen compounds, they have attracted increasing interest in recent years. Both their surface chemistry and their catalytic properties are here compared for the two kinds of catalysts (oxide vs sulfide anions).

At a previous Molybdenum Chemistry Conference, Hall[1] reviewed progress in understanding the surface chemistry of the oxidic forms. During preparation molybdena becomes bound to the alumina surface as polymeric clusters as $H_6Mo_7O_{24}$ undergoes condensation with (replaces) alumina surface OH groups. On reduction with H_2, the Al—O—Mo bonds are attacked, regenerating (partially) the surface OH groups. More and more surface OH reappear as the catalysts are reduced more and more extensively. On reduction with CO, CO_2 is produced,[2] and such preparations have been reported[3] to have catalytic properties similar to the H_2-reduced forms.

The EXAFS studies of Clausen *et al.*[4] have indicated that the small cluster size (seven or eight Mo/cluster) is maintained on mild reduction although sintering and recrystallization into larger units (bound, oxygen-deficient MoO_2 crystallites) may occur under more severe conditions. A similar chemistry is now known for the sulfided catalysts. During sulfiding, recrystallization into sulfur-deficient surface-bound MoS_2 occurs.[5–7]

In the present paper important aspects of the surface chemistry and catalytic properties of reduced catalysts are compared with those of the sulfided ones. Attention is focused on the hydrogenation of simple olefins and diolefins, and on the development and assay of the catalytic centers. The chemistry over both catalysts is believed to center around alkyl,

† Author to whom correspondence should be addressed. Present address: P.O. Box 102, Chemistry Building, University of Pittsburgh, PA 15260, U.S.A.

alkylidene and allylic intermediates, with the ability of the latter to convert into metallocyclobutanes. Thus, it is noteworthy that olefin metathesis is not observed over the sulfided catalysts, but is facile over the oxidic one.[8]

EXPERIMENTAL

Catalysts

These were prepared either by the incipient wetness technique or by the equilibrium adsorption method. The source of Mo was ammonium heptamolybdate. Two nearly identical aluminas were used in this study. The first was Ketjen CK-300 and the second was JRC-ALO-4. Both had surface areas of about 185 $m^2\ g^{-1}$ with pore volumes of about 0.50 ml g^{-1}. The impurity levels were very low, particularly for transition metals, and the IR spectra showed nearly identical OH regions. All catalysts were dried at 110°C before calcining in air to 500°C.

Pretreatment of the catalysts involved, first, evacuation or flushing with purified He for 2 h at 500°C, or at the final reduction temperature, whichever has higher. Following this procedure they were treated with dry O_2 overnight at a reduction temperature of 500°C as described above. The He was purified by passing through a charcoal trap thermostatted at −195°C. The O_2 was passed through a column of anhydrous magnesium perchlorate to remove water.

Activation of the catalysts in H_2 *(reduction)*

This was carried out either in a recirculation system (500 torr initial pressure) with an in-line trap thermostatted at −195°C to remove water or in flowing H_2 (at 60 $cm^3\ min^{-1}$) for 1 h. Typically the reduction temperature was 500°C. Other temperatures, when used, are noted in the text. Following reduction, the catalyst was either evacuated or flushed with He at the same temperature before cooling *in vacuo* or in He flow.

Alternatively, the catalysts were sulfided. The oxidized catalysts were purged with purified He flowing at 75 $cm^3\ min^{-1}$ for 20 min at 500°C. The temperature was then lowered to 350°C where the He was replaced for 4 h with a preblended 10:1 H_2–H_2S mixture flowing at 80 $cm^3\ min^{-1}$. The gas stream was then switched back to He and the catalyst flushed for 20 min before raising the temperature to 500°C where the He was flow maintained for an additional hour to equilibrate the surface to the same OH content used for the reduced catalysts and in other studies[2] where actual H_2 contents were determined by isotope dilution methods.

Temperature-programmed reduction (TPR)

TPR experiments were carried out with a linear temperature programmer linked to a gold reflective furnace (Trans Temp Co, Type C). With this furnace, a uniform temperature was maintained to within 1″ from each end. The typical procedure was to treat the catalyst with pure dry O_2 overnight at 600°C before flushing with pure He for an additional hour during which it was cooled to ambient temperature. The He was then replaced with 5% H_2 in N_2 flowing at 75 $cm^3\ min^{-1}$. This gas was passed through a glass wool trap thermostatted with an *n*-hexane slush bath (~ −95°C) prior to entry into the thermal conductivity detector. After a stable baseline was obtained, the temperature program was started at 2.5° min. Upon reaching 600°C, the temperature was held constant until the baseline was again reached. Then the reductive gas was replaced with He. The sample was cooled to ambient conditions and the reactor sealed so it could be transferred to an all-glass recirculation system for quantitative reoxidation with O_2 to independently measure the extent of reduction achieved in the TPR experiment.

IR experiments

These were carried out using a Nicolet MX-1 Fourier Transform spectrometer using the absorbance mode. The resolution was controlled at 2 cm^{-1} by the spectrometer software. The cell design used has been reported previously.[9]

Reaction studies

These were carried out in an all-glass recirculation system as before.[3] The propene hydrogenations were carried out using 22 cm^3 (NTP) of propene and 110 cm^3 (NTP) of H_2. The total system volume was about 500. The products were separated on a $4' \times \frac{1}{4}''$ GLC column filled with 80–100-mesh Durapak at 0°C. For ethene hydrogenation a 1:1 mixture of ethene and D_2 [130 cm^3 (NTP)] was employed. The same column could be used for the separation of the products from these experiments by lowering the column temperature to −20°C. D_2 distributions in the several products were analyzed by mass spectrometry. The 1,3-butadiene experiments were carried out in a similar way using 100 torr of 1,3-butadiene [60 cm^3 (NTP)] and 200 torr of D_2. These products were separated on two columns in series. The first $15' \times \frac{1}{4}''$ column contained 40% dimethylsulfolane on Anakrom C22A held at 25°C; the second was a $10' \times \frac{1}{4}''$ column containing 30% propylene carbonate on Chromosorb P thermostatted at 20°C. The He flow rate used was 85 $cm^3\ min^{-1}$. The latter

column was needed only to obtain a quantitative separation of *cis*-2-butene from *trans*-2-butene. Isotopic analyses were made using a Hitachi Model RMU-6 magnetic sector mass spectrometer. The D distributions and the average D content were derived. The ionization voltage used was between 9.8 and 12 eV depending on the appearance potential of the individual molecule. The location of the deuterium within the molecules was determined using a Bruker WM-250 Fourier transform NMR equipped with an Aspect 2000 data system and a multinuclear probe. The deuterium was located by examining the ^2H NMR spectrum which was broad band decoupled from the ^1H nuclei. Typical pulse delay times of 25 ms were required, as determined experimentally from the perhydro standard, to obtain correct integrations. The amount of D in each position was then determined by normalizing the NMR integrated area to the average D content from the mass spectral data. This was then distributed about the molecular positions according to the integration for each unique resonance.

RESULTS AND DISCUSSION

IR and chemisorption studies

These were carried out to look for differences and/or similarities in the surface chemistry of reduced vs sulfided molybdena–alumina catalysts. In Fig. 1A, the OH spectra from the oxidized, reduced and sulfided forms of a catalyst loaded with $\sim 5 \times 10^{20}$ Mo g^{-1} are compared with that for the parent alumina. The corresponding spectra for the OD region, shown in Fig. 1B, were obtained from

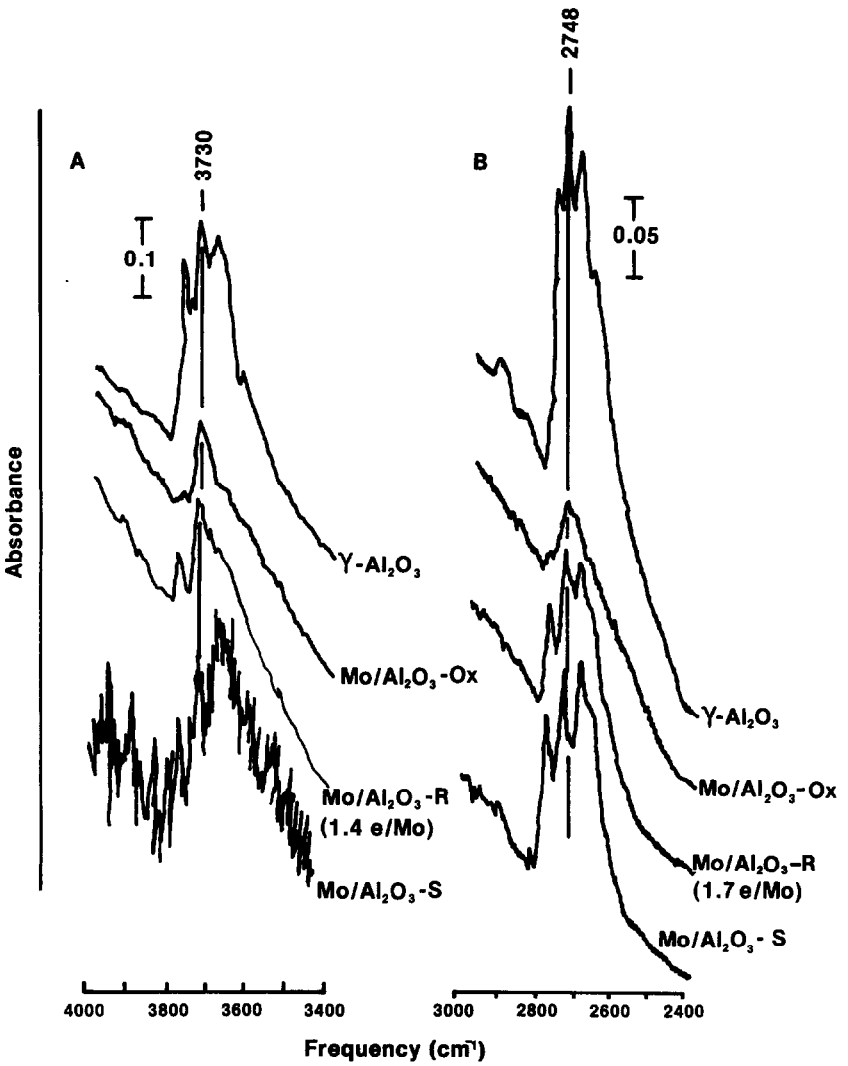


Fig. 1. IR spectra of: (A) the OH, and (B) the OD stretching regions from the parent alumina, and the catalyst in its oxidized, reduced and sulfided forms. In all cases the catalysts were evacuated at 500°C as the final step in preparation. The activation procedures are given in the text.

samples prepared as those in Fig. 1A following exhaustive exchange with D_2O or D_2. As reported earlier,[5] the OH spectrum from the sulfided preparation was very noisy; it was much cleaner in the OD region. Otherwise the two sets of spectra were in good general agreement. The alumina OH bands appeared in all of the spectra, but they were very weak in the oxidized form of the catalyst because of the well-known[1,2,10] bonding of molybdena to alumina by replacement of the surface OH groups. The regeneration of these bands as the catalyst was reduced[1,2,10] or sulfided[5] has also been reported previously. On sulfiding, the integrated intensity in the OH region appeared to be somewhat higher than with the reduced catalyst, but this was difficult to assess because of the noise. The OD spectra were taken to check this point. The increase, if real, was not large enough to be significant. Differences in relative intensity, particularly for the high-frequency band near 3785 cm^{-1}, may be noted, but like the low-frequency shoulder apparent in the spectrum from the deuterated sulfided preparation cannot be presently interpreted.

It is by now well established that NO and O_2 are absorbed selectively by the molybdena portion of the surface, apparently on the catalytically active CUS (coordinatively unsaturated sites). Moreover, evidence has been presented[9] suggesting that CO_2 is adsorbed selectively by the exposed alumina portions of the surface. As shown in Fig. 2, the two

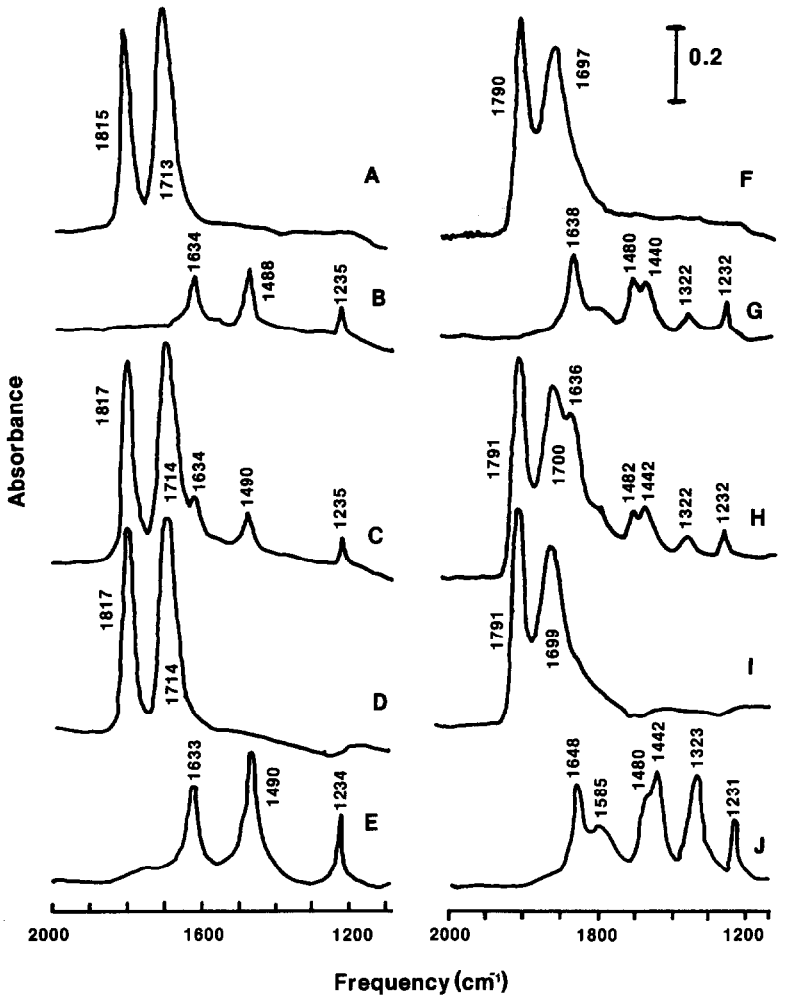


Fig. 2. IR spectra showing the independent chemisorption of CO_2 and NO on reduced (e/Mo = 1.8) molybdena–alumina catalyst (5×10^{20} g^{-1}): (A) NO on reduced catalyst, (B) CO_2 on reduced catalyst, (C) NO adsorbed on top of CO_2 on preparation shown in spectrum B, (D) spectrum C minus spectrum B (by computer subtraction), and (E) CO_2 adsorbed on parent alumina pretreated as was the reduced catalyst. IR spectra for comparable sulfided preparations are shown side by side: (F) NO on same catalyst sulfided, (G) CO_2 on sulfided catalyst, (H) NO adsorbed on top of CO_2 on preparation in spectrum G, (I) spectrum H minus spectrum G (by computer subtraction), and (J) CO_2 on parent alumina after same sulfiding pretreatment used with the molybdena–alumina catalyst.

adsorbed molecules do not interfere with each other as judged by the ability of either to be adsorbed after the other without altering the intensity of the IR bands, e.g. compare Fig. 2A and D; the latter spectrum was obtained by computer subtraction of spectrum B from C, i.e. by subtraction of the CO_2 bands from the spectrum having both NO and CO_2 bands. Note that spectrum D is in all respects identical with Fig. 2A which was obtained from the freshly reduced preparation. The reverse experiment,[9] where NO was adsorbed first and CO_2 was adsorbed second, produced the same CO_2 spectrum as if CO_2 was adsorbed alone, after the NO spectrum was subtracted. Results from sulfided catalysts (Fig. 2F–J) may be compared with those from reduced catalysts (Fig. 2A–E). The same pattern of behavior was obtained for both kinds of preparations, the sole difference being in the CO_2 spectrum from the sulfided preparations. On treatment with H_2S–H_2, alumina undergoes a change leading to extra bands at 1323, 1442 and 1585 cm^{-1} not present in the unsulfided material (Fig. 2E and J). When this has been taken into account, the NO spectrum (Fig. 2I) obtained by subtraction is in all respects identical to the one obtained from the clean catalyst (Fig. 2F). The spectra for NO adsorbed on the reduced and sulfided catalysts may be compared side by side in Fig. 2A and F; the similarity is striking. Dinitrosyl species are formed on both surfaces, although the frequencies for the sulfided catalyst were lower by from 15 to 25 cm^{-1}. Thus, except for an unidentified change in the alumina portion of the surface, the surface chemistry of reduced vs sulfided catalysts appears remarkably similar. Delgado *et al.*[11] have found, however, significant changes in the spectra from CO adsorbed at subzero temperatures on similar preparations, which they attributed to lower-valence states in the sulfided preparation.

The chemisorption of CO_2 may be used to assay the extent of exposed alumina surface. The irreversible chemisorption for a series of catalysts of increasing loading (made by the equilibrium adsorption method[1] using JRC-ALO-4 alumina) was determined. These data, together with the surface areas of the catalysts, are plotted in Fig. 3. The data show the chemisorption falling, as the uncovered alumina surface decreases with increasing loading, to zero at about 12% MoO_3 where monolayer coverage is expected. The corresponding decrease in intensities in the OH region with increasing loading has been noted previously.[1,2,10,12]

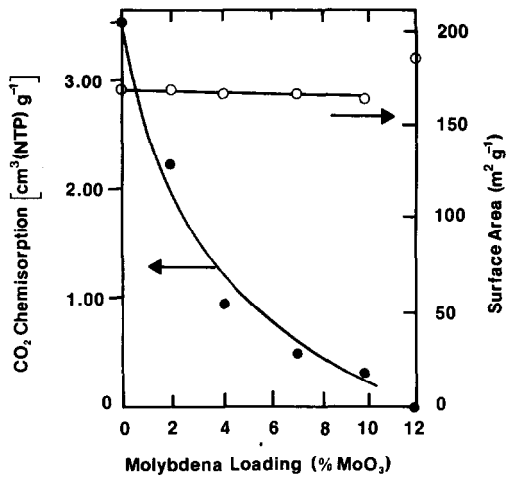


Fig. 3. CO_2 chemisorption as a function of loading for a series of calcined molybdena–alumina catalysts after evacuation at 500°C. Adsorption was carried out for 30 min (to saturation) at room temperature and the preparations were then evacuated for 30 min. The irreversible chemisorption is plotted. Surface areas per gram of the alumina support are also shown.

Extent of reduction

The changes in the extent of alumina surface as the catalyst is reduced can similarly be deduced.[9] Figure 4A demonstrates that the extent of free alumina surface increases about linearly with increasing extent of reduction, e/Mo (defined as the average number of electrons the Mo^{6+} ions have been reduced). For reference, the parent alumina chemisorbed about 3.5 cm^3 (NTP) g^{-1} (Fig. 3): thus, the maximum chemisorption for the catalyst loaded to 5×10^{20} Mo g^{-1} (8% Mo or 2.5×10^{14} cm^{-2}) when fully reduced was about 50% of that for the parent alumina, a value which is in good agreement with the fractional increase in surface OH concentration[9] or as estimated from Fig. 4B. These data suggest a doubling of cluster thickness. They are plotted in another way in Fig. 5 where the fraction of the total surface which is uncovered alumina is plotted as a function of the extent of reduction. The 12% MoO_3–Al_2O_3 catalyst was selected for this demonstration since in its oxidized state it was the one which had just about a completely covered the free alumina surface (see Fig. 3). They show that the free alumina surface starts to appear at about e/Mo = 0.5. This intercept is reminiscent of similar ones for O_2, NO and H_2 chemisorption[13,14] and the data are in general agreement with our earlier ^1H NMR work.[15] These results illustrate the hazards of taking correlations to imply relationships. As demonstrated by Fig. 2, these molecules do not chemisorb on alumina, but on CUS of molybdena which are formed concomitantly. The solid square of Fig. 5 is datum from the same catalyst after sulfiding. It demonstrates the continuity of system. As shown previously,[5] the sulfided catalyst is

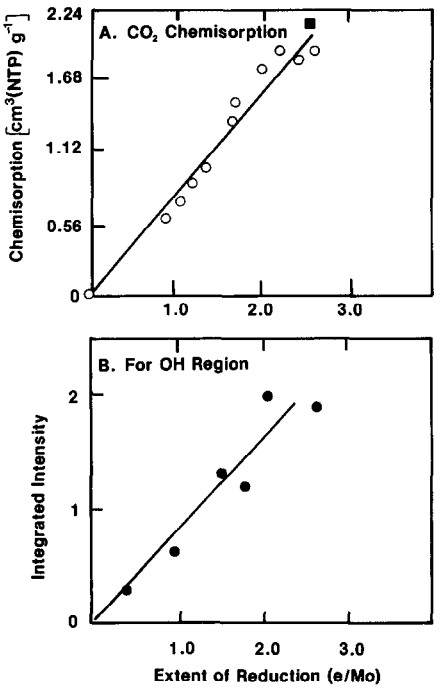


Fig. 4. Estimation of free alumina surface for the 12% MoO_3–Al_2O_3 catalyst. (A) Variation in CO_2 chemisorption as a function of the extent of reduction; the open circles are from the reduced oxidic form, and the solid square from the sulfided form of the catalyst; (B) variation of the integrated intensity of the OH groups as a function of the extent of reduction. Data are the increases in integrated intensity over that of the oxidized catalyst.

generally more deeply reduced (to e/Mo ~ 2.5), is a bit better crystallized, and therefore has a slightly higher fraction of exposed alumina surface than the reduced form. Noteworthy is the fact that a substantial fraction of the molybdenum ions have valence states *lower* than Mo^{4+}.

Another interesting feature of these systems is shown in Fig. 6. These data confirm the well-known fact that molybdena–alumina catalysts become easier to reduce with H_2 as the loading increases, or conversely. They also show that the reverse is true when the reducing agent is H_2–H_2S. Two sets of experiments are shown for H_2 reduction which, although they varied in several details, showed the same trend in e/Mo with increasing loading. The solid circles are data taken from Ref. 1 for a series of catalysts made by the equilibrium adsorption method[16] using Ketjen CK-300 alumina. The reductions were carried out by TPR, with a gradient of 5° min^{-1} up to 600°C, where a flow of 17% H_2 of 60 cm^3 min^{-1} was continued for an additional 2 h. The open circles are new data obtained from a similar set of preparations made using the Japanese JRC-ALO-4 alumina (177 m^2 g^{-1}). The temperature gradient in these experiments was 2.5° min^{-1} and the reducing gas was 5% H_2 in N_2; the program was stopped at 600°C where the catalysts were purged with He. They were then cooled to room temperature and the sealed tubes were removed to a volumetric apparatus and the e/Mo values measured[17] volumetrically from the O_2 consumed for complete reoxidation. The older data were values calculated from the consumption of H_2 during reduction corrected for the H_R (a high-temperature form of adsorbed H_2[1,17]) determined separately. Although the two sets of results are not in quantitative agreement, the trends are the same and the differences may be attributed to the different catalyst preparation and other experimental variables (time at high temperatures etc.) as well as the uncertainties in the evaluation of H_R.[1] The really significant difference is the reverse trend found on sulfiding. These data (squares) were obtained from sulfided preparations made from the same set of catalysts[1] shown as solid circles by reoxidation.[5] The salient feature is that the low-loading catalysts,

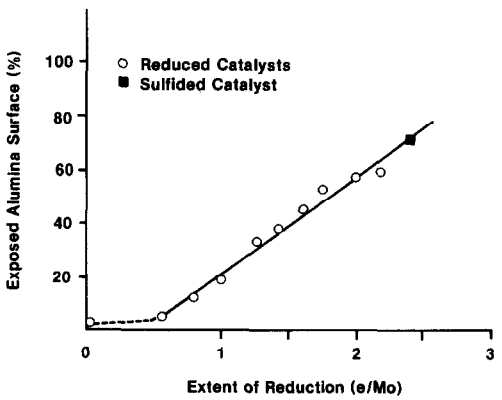


Fig. 5. Percentage of free alumina surface as a function of the extent of reduction of the standard 8% Mo catalyst. Data were calculated from the CO_2 chemisorptions on a per unit weight of alumina (metal free) basis.

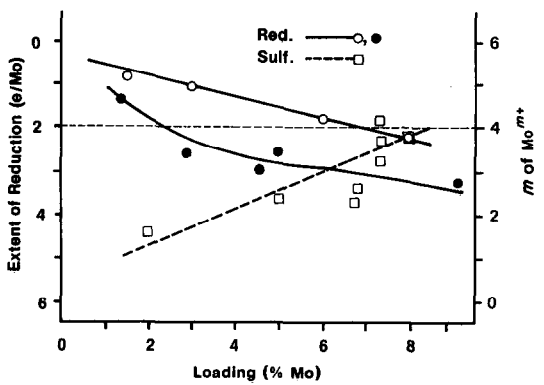


Fig. 6. Variation in the average valence state of Mo^{m+} in reduced and sulfided catalysts as a function of Mo loading; see text for details. Note that $m = 6 - e/Mo$.

which contained predominantly tetrahedral monomeric surface-bound molybdena, stubbornly resist attack by H_2, whereas these same species appear to be easily destroyed in the presence of H_2S. Note also that valence states below Mo^{4+} are common in these preparations, i.e. all the points which fall below the dashed line of Fig. 6 have average values, e/Mo $\geqslant 2$, i.e. higher than that required for stoichiometric MoS_2 or MoO_2. That metallic molybdenum is not a likely source for these low values is shown by the work of Burwell and Brenner[18] who reported that Mo(0), freed by decomposition of $Mo(CO)_6$ on alumina surfaces, becomes spontaneously oxidized by reaction with surface OH groups, freeing H_2. Recently, we have presented evidence that the active centers (CUS) may be Mo^{2+}.[5,19,20]

Relationships with catalysis

This is the ultimate goal of much research in the area of surface chemistry. We have fixed our attention on hydrogenation of olefins and butadiene in an effort to link the foregoing surface chemistry to catalytic function. Data obtained for the reactions of ethane with D_2 are listed in Table 1. Only a little exchange into the unreacted ethene was observed at low conversions over the reduced catalyst and the principal product was ethane-d_2. With increasing conversion the extent of exchange into the olefin (with the resulting production of ethane-d_1 and ethane-d_3) was more extensive than reported earlier.[21] The reasons for this are not known, but may reflect differences in the extent of reduction or other experimental variables. Nevertheless, these effects are secondary and provide some perspective in looking at the existing literature. In agreement with the data of Tanaka and Okuhara,[22] exchange was more important with the sulfided catalysts than with the reduced ones, and this was reflected in a further spreading of the distribution in the ethanes. Ethane-d_2 remained the most important product, but the d_1 and d_3 paraffins increased substantially. Thus, a continuous gradation of behavior exists with ZnO[23] and chromia[24] catalysts at one extreme yielding only ethane-d_2 and ethene-d_0 (no alkyl reversal), to sulfided molybdena–alumina and MoS_2, where substantial back-exchange was observed into the reactant olefin. The reduced preparations appeared to be intermediate cases with the importance of aklyl reversal depending on the extent of reduction, temperature, type of reactor used etc. As shown earlier,[21] HD formed by exchange of D_2 with the reactant olefin rapidly reacted with ethene forming ethane-d_1; similarly, ethane-d_3 was formed efficiently by reaction of ethene-d_1, already held on the catalyst surface with D_2.

The D distributions in the products of deuteration of olefins over oxides and sulfides differ dramatically from those obtained over metals.[25] This difference may be attributed to the ease with which the olefin interacts reversibly with the catalytic sites relative to hydrogenation. Thus, for metals the chemistry is commonly written:

$$D_2(g) + C_2H_4(g) \underset{k_d}{\overset{k_a}{\rightleftharpoons}} \underset{*}{CH_2}\text{—}\underset{*}{CH_2} + \underset{*}{2D}$$

$$\underset{k_{-1}}{\overset{k_1}{\rightleftharpoons}} DCH_2\text{—}\underset{*}{CH_2} + \underset{*}{D} \xrightarrow{k_2} C_2H_{6-x}D_x,$$

where * is taken to mean a surface metal atom. In these cases, $k_{-1} \gg k_2$, leading to both exchanged ethene and a broad binomial deuterium distribution in the ethanes. With ZnO and chromia $k_2 \gg k_{-1}$ and so only ethane-d_2 is produced. The reversibility is somewhat higher over reduced (even more so over sulfided) molybdena–alumina and the distribution in the ethanes starts to broaden, but to nowhere near the extent found for metals. In all these cases, alkyl reversal (the half-hydrogenated state) is either slow or zero. Even at high conversions, the deuteration appears to be limited to ethane-d_4. It was for this reason that we previously suggested[21] that exchange might occur by a reversible interconversion of the alkyl into ethylidene carbene.

Table 1. Deuterium distributions from the reaction of ethene with deuterium over molybdena–alumina catalysts

Catalyst preparation	Conversion (%)	Ethene					Ethane						
		d_0	d_1	d_2	d_3	d_4	d_0	d_1	d_2	d_3	d_4	d_5	d_6
Reduced	9	95	4	1	—	—	—	11	89	—	—	—	—
	28	91	7	2	—	—	—	16	79	5	—	—	—
	35	86	11	3	—	—	—	18	76	6	—	—	—
Sulfided	25	87	12	2	—	—	—	30	61	8	1	—	—
	45	81	16	2	—	—	—	36	53	10	1	—	—
	66	67	29	5	—	—	—	38	50	11	1	—	—

The reaction of propene with D_2 was studied earlier.[3] These results fit neatly into the picture. The propene-d_0 concentration decreased about linearly with per cent conversion while the propene-d_1 and propene-d_2 increased from zero. Propene-d_3 also formed, but appeared as a product of secondary reaction. These results should be compared with those of Table 1. As with ethene the exchange into the paraffin appeared to be limited to propane-d_4.

The hydrogenation rate for propene was slower, other things being equal, than for ethene. This may be attributed to additional chemistry which becomes possible with propene due to its allylic hydrogen. Thus, sites which chemisorb H_2 with which olefins react to form bound alkyls, may be occupied by the allylic species characterized for ZnO,[26] or metallocyclobutane complexes. In the present work, 1-butene was found to react quite similarly.

Rates of hydrogenation of propene are presented in Fig. 7. The open circles are data for reduced catalysts reported earlier;[3] the open squares are new data for the same catalyst repeated in the present work for comparison with sulfided catalysts (open and filled triangles). The extents of reduction for the latter were determined by reoxidation.[5] These data fit nicely onto the upper end of the curve for the reduced catalysts, demonstrating that no basic differences exist except for higher rates because of the lower average valence states of the sulfided catalysts.

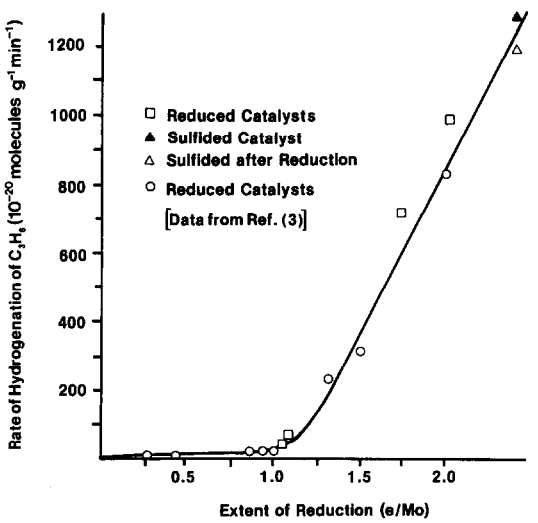


Fig. 7. Rates of propene hydrogenation as a function of the extent of reduction for H_2 and H_2–H_2S reduced catalysts. Rates reported were measured at −27°C in a recirculation BET system. The data are based on GLC analyses of the products. Data points for e/Mo $\leqslant$ 1.0 were taken using 1 g of catalyst and those for e/Mo $\geqslant$ 1.0 using 0.1 g to avoid pump limitation.

This observation is in agreement with the recent observations of Burwell *et al.*[27]

Because of the additional complications introduced with propylene due to its allylic hydrogen, some studies of the reactions of butadiene with deuterium were made to complete the picture. This conjugated diolefin reacted more slowly than propene, and was slower over sulfided catalysts than over reduced ones. Although a detailed study of the kinetics was not made, the rate was strongly inhibited by increase in diolefin pressure, more strongly so with the sulfided catalysts, and $k_H/k_D \simeq 1.4$ for hydrogenation vs deuteration, respectively. These facts suggested that the diolefin interacted strongly with the hydrogenation sites and that the hydrogenation rate was limited by the adsorption of H_2 (D_2).

The dominant primary product of hydrogenation was 1-butene, although smaller amounts of 2-butene were also formed. Exchange of butadiene with D_2 was competitive with deuteration. The distribution of D in the separated reaction products was determined in the usual way[3] by mass spectrometry, i.e. the mole fractions, N_i, of the particular hydrocarbon containing i deuterium atoms were determined. The distribution of D in each molecule was then derived from ^2H resonance spectra of each product molecule. Some results of this work are shown in Fig. 8. Butadiene exchanged at all positions, but was faster at the terminal vinyl positions than at the internal ones. Presumably, the former resulted from formation of the secondary, and the latter from the primary alkylidene. The addition of a second D would lead to 1-butene in each case, while exchange would result from reversal to the diolefin. The relatively small extents of exchange at ~20% conversion suggests that this reversal is slow with butadiene, as with monoolefins. The 1-butene formed reflects this underlying exchange and in addition clearly shows the saturation of one double bond producing (approximately) 1-butene-3,4-d_2.

The average compositions of the 1-butene product and the remaining butadiene for the reduced and sulfided catalyst at a similar conversion level may be compared in Fig. 8A and B, respectively. The close correspondence of the data demonstrates clearly that the catalytic sites on the two forms of the catalyst are virtually the same.

Sufficient data now exist to define the primary reaction centers as low-valent Mo^{n+} ions with multiple coordinative unsaturation. H_2 is dissociated at such sites and this chemisorption may be competitive with hydrocarbons. The hydrogen, so dissociated may spill over into the bulk-forming bronzes of composition such as $H_{0.1}MoS_2$,[28]

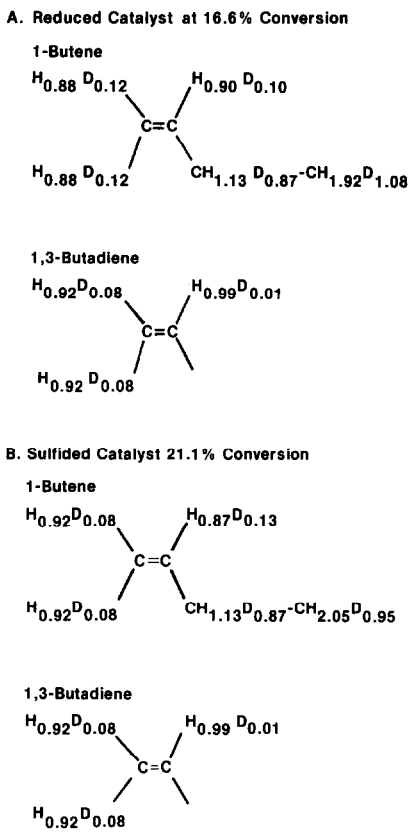


Fig. 8. Quantities of deuterium incorporated into 1-butene and 1,3-butadiene over: (A) reduced catalysts, and (B) sulfided ones. These evaluations were obtained by combining mass spectrometric and ^2H NMR results (see text).

inducing as yet unrecognized catalytic effects. Conceivably, this ability to travel may make possible the catalysis of certain reactions on the basal planes as well as the CUS. The structure of MoS_2, and the present knowledge that the active component of sulfided molybdena catalysts has a similar structure, strongly suggests that these CUS must be at the edges and corners of the chalcogenite wafers. Moreover, whatever the exact nature of these centers, they must be closely similar for both reduced and sulfided catalysts. It seems unlikely, therefore, that these active centers could be Mo^{4+} for reduced catalysts and Mo^{2+} for sulfided ones as suggested recently by Delgado *et al.*[11]

Acknowledgements—This work was supported by the National Science Foundation under Grant CHE-8317606, for which we wish to express our gratitude. One of us (WSM) wishes to express his thanks to the Union Oil Foundation for their support.

REFERENCES

1. W. K. Hall, In *Proceedings of the Fourth International Conference on the Chemistry and Uses of Molybdenum* (Edited by H. F. Barry and P. C. H. Mitchell), p. 224. Climax Molybdenum Co., Ann Arbor, MI (1982).
2. W. S. Millman, M. Crespin, A. C. Cirillo, S. Abdo and W. K. Hall, *J. Catal.* 1979, **60**, 404.
3. E. A. Lombardo, M. LoJacono and W. K. Hall, *J. Catal.* 1978, **51**, 243.
4. B. S. Clausen, H. Topsøe, R. Candia, J. Villadsen, R. Lingler, J. Als-Nielsen and F. Christensen, *J. Phys. Chem.* 1981, **85**, 3868.
5. J. Valyon and W. K. Hall, *J. Catal.* 1985, **92**, 155.
6. D. R. Huntley, T. G. Parnham, R. P. Merrill and M. J. Sienko, *Inorg. Chem.* 1983, **22**, 4244.
7. H. Topsøe, B. S. Clausen, R. Candia, C. Wivel and S. Mørup, *J. Catal.* 1981, **68**, 433.
8. W. K. Hall, R. L. Schneider and J. Goldwasser, In *Proceedings of the 8th International Congress on Catalysis, Berlin*, Vol. 4, p. 273. DECHEMA, Frankfurt am Main, F.R.G. (1984).
9. K. Segawa and W. K. Hall, *J. Catal.* 1982, **77**, 221.
10. T. Fransen, O. van der Meer and P. Mars, *J. Catal.* 1976, **42**, 791.
11. E. Delgado, G. A. Fuentes, C. Herman, G. Kunzman and H. Knözinger, *Bull. Soc. Chim. Belg.* 1984, **93**, 735.
12. K. Segawa and W. K. Hall, *J. Catal.* 1982, **76**, 133; J. Valyon, R. L. Schneider and W. K. Hall, *ibid.* 1984, **85**, 277.
13. W. S. Millman and W. K. Hall, *J. Catal.* 1979, **59**, 311.
14. W. K. Hall and W. S. Millman, *Proceedings of the 7th International Congress on Catalysis, Tokyo* (Edited by T. Seiyama and K. Tanabe), p. B-1304. Kodansha Ltd., Tokyo (1981).
15. A. C. Cirillo, F. R. Dollish and W. K. Hall, *J. Catal.* 1980, **62**, 379.
16. L. Wang and W. K. Hall, *J. Catal.* 1980, **66**, 251; 1982, **77**, 232.
17. W. K. Hall and F. E. Massoth, *J. Catal.* 1974, **34**, 41.
18. R. L. Burwell and A. Brenner, *J. Catal.* 1978, **52**, 353.
19. J. Valyon and W. K. Hall, *J. Catal.* 1983, **84**, 216.
20. R. P. Rosen, K. Segawa, W. S. Millman and W. K. Hall, *J. Catal.* 1984, **90**, 368.
21. E. A. Lombardo, M. Houalla and W. K. Hall, *J. Catal.* 1978, **51**, 256.
22. K. I. Tanaka and T. Okuhara, *Catal. Rev.—Sci. Eng.* 1977, **15**, 249.
23. A. L. Dent and R. J. Kokes, *J. Phys. Chem.* 1969, **73**, 3772, 3781; W. C. Conner and R. J. Kokes, *ibid.* 1969, **73**, 2436.
24. R. L. Burwell, A. B. Littlewood, M. Cardew, G. Pas and C. T. H. Stoddard, *J. Am. Chem. Soc.* 1960, **82**, 6272.
25. G. C. Bond, *Catalysis by Metals*, p. 252. Academic Press, New York (1962).
26. R. J. Kokes and A. L. Dent, *Adv. Catal.* 1972, **22**, 1.
27. R. Nakamura, D. Pioch, R. G. Bowman and R. L. Burwell, *J. Catal.* 1985, **93**, 388.
28. A. Blackburn and P. A. Sermon, *J. Chem. Technol. Biotechnol.* 1983, **33A**, 120 (and earlier references cited therein).

Polyhedron Vol. 5, No. 1/2, pp. 179–182, 1986
Printed in Great Britain

0277–5387/86 $3.00 + .00
© 1986 Pergamon Press Ltd

CHARACTERIZATION OF SUPPORTED MoO_3 BY TEMPERATURE-PROGRAMMED REDUCTION

JOAQUÍN BRITO and JORGE LAINE*

Laboratorio de Catálisis Heterogénea, Centro de Química, I.V.I.C., Apartado 1827, Caracas 1010-A, Venezuela

(*Received* 17 *June* 1985)

Abstract—Temperature-programmed reduction (TPR) was employed for the characterization of molybdena catalysts. The effect of several variables on reduction of the supported catalysts was determined. The TPR spectra changed significantly with both the amount of MoO_3, from 5 to 80 wt %, and the type of support, several silica–alumina carriers, of compositions ranging from pure SiO_2 to pure Al_2O_3. The peak assigned to buildup of multilayers of molybdena on the γ-Al_2O_3 supports was affected by the calcination temperature and by the amount of promoter (0–5 wt % NiO). Nickel-promoted catalysts activated hydrogen easier than both cobalt-promoted and unpromoted catalysts.

The activation of molybdena-based hydrotreating catalysts is brought about by reductive processes, which occur mainly during pretreatments or during the first stages of the catalytic reaction, the role of hydrogen being still imperfectly understood.

Classical work on reduction of catalysts has been carried out by using conventional, static or dynamic adsorption and reaction studies (mainly by means of gravimetric or volumetric techniques), or by characterizing the catalysts during or after the reductive treatment. Currently, there have been an increasing number of papers aiming at similar goals by means of transient temperature-programmed reduction (TPR) techniques,[1] whose various advantages (high sensitivity to hydrogen, readiness and low cost) compensate the complexity of the interpretation of the TPR spectra.

Most of the early reports (up to about 1977) concerning reduction of molybdena catalysts and of their assumed components, have been reviewed by Massoth.[2] More recent work, introducing the use of TPR to the characterization of hydrotreatment catalysts, includes that of Thomas *et al.*,[3] Nag *et al.*[4] and Yao.[5]

In this paper, the effects of several variables such as type of support, calcination temperature, and amount of Mo and promoters upon the reduction characteristics of supported MoO_3 are investigated using TPR.

* Author to whom correspondence should be addressed.

EXPERIMENTAL

Catalysts

Three series of catalysts were prepared by the method of incipient wetness ("dry") impregnation, followed by drying (at 120°C), and firing at various temperatures. In one series (MoAlSi), commercial silica (Merck) was first impregnated with $Al(NO_3)_3$ solutions, dried and calcined at 550°C, in order to obtain six carriers (0, 5, 15, 25, 75 and 100 wt % Al_2O_3, the remainder SiO_2), which were impregnated with ammonium heptamolybdate (AHM) solutions, dried and calcined again at 550°C, resulting in solids with 5, 10, 30 and 80 wt % MoO_3.

In another series of catalysts (NiMoAl), commercial γ-Al_2O_3 (Filtrol) was impregnated with an AHM solution, dried and calcined at 400°C (12 wt % MoO_3). Afterwards, it was impregnated with $Ni(NO_3)_2$ solutions, in order to obtain catalysts with 0, 1, 3 and 5 wt % NiO. Portions of these solids were calcined at 400, 500, 600, 660 and 800°C.

The third series (CoNiMoAl) was prepared by impregnating another commercial γ-Al_2O_3 (Akzo Ketjen) with an AHM solution, and then with $Ni(NO_3)_2$ and $Co(NO_3)_2$ solutions, to give a composition of 10.4 wt % MoO_3 and 3.5 wt % (CoO + NiO), the atomic ratio r [Co/(Co + Ni)] varying between 0 and 1. The samples were divided in two parts and calcined at 500 and 600°C. Further details of the preparation of these catalysts have been given elsewhere.[6]

TPR apparatus

It consisted of a quartz tube with an intern frit which supported the samples. Heating was effected by means of a tubular furnace and a temperature programmer. Gas purity was assured by using molecular sieves, deoxo and liquid nitrogen traps for collecting traces of water and other impurities. The flow of gases was controlled with electronic mass flowmeters. A thermal conductivity detector allowed monitoring of the changes in the composition of the reductive gas.

Experimental conditions

Reducing gas: 15 vol% H_2 in N_2, flowing at 40 cm^3 min^{-1}. The samples were not pretreated, and were heated at 20°C min^{-1} from 190 to 910°C. The typical sample weight was 100 mg, except for the highest MoO_3 content catalysts (80 wt %), where it was 50 mg. The attenuation of the detector was varied in order to obtain spectra of similar size.

The samples were introduced to the quartz reactor, positioned in the furnace and, after stabilization of the baseline (usually several minutes), the run was started. A liquid nitrogen trap after the reactor removed the H_2O produced during the reduction. Thus, the TCD signal was proportional to the H_2 concentration. The TPR traces, which were perfectly reproducible, consisted of various peaks; we define a quantity T_m for each peak as the temperature of the maximum rate of H_2 consumption.

RESULTS AND DISCUSSION

MoAlSi *series*

Figure 1 shows the spectra of the MoO_3–SiO_2–Al_2O_3 catalysts. From 5 to 30 wt% MoO_3 the shape of the TPR spectra is strongly dependent on the type of carrier. The 100:0 and 75:25 supports give solids with the characteristic, two-peaks pattern which has been observed previously for MoO_3–Al_2O_3.[3,5] The first peak (lower T_m) has been attributed to Mo multilayers,[3(a)] which appears to be reasonable as the size of this peak increases with increasing Mo content. In particular, for the 5 wt% MoO_3 catalysts the ratio of the second to the first peak is high, which suggests a good dispersion, though not as a monolayer. The dispersion becomes poorer as the Mo content becomes higher. The silica (0:100)-supported catalysts also show two peaks, but closer than the alumina-rich solids. In this case it is the first peak which has been assigned to a single Mo monolayer,[3(b)] and our results agree, as the size of the second peak increases with higher Mo content. The peaks of MoO_3 supported on SiO_2 are sharper than on Al_2O_3, suggesting either a better crystallinity or more homogeneity of the reducible phases. The fact that the peak for the monolayer of MoO_3 supported on Al_2O_3 appears at a much higher T_m agrees with the stronger interaction of MoO_3 with this support compared to silica.

The lower T_m of the peak assigned to MoO_3 multilayers relative to the monolayer signal in Al_2O_3-rich catalysts could be explained as a stabilization effect of the neighbouring Mo cations upon the one which undergoes reduction. Several Mo atoms bridged by O anions should share better the excess negative charge than single molybdate groups directly mounted on the support, as Al is less capable of changing its oxidation state than Mo. In the case of the silica support, apparently there is no formation of multilayers but nucleation leading to MoO_3 microcrystallites, because the second peak of MoO_3–SiO_2 has a T_m similar to bulk MoO_3 (not shown).

Mo supported on the intermediate, silica-rich carriers gave ill-defined traces, with single but broad and highly complex bands, which seem to be composed of the superposition of various peaks. This may be related to the high heterogeneity of MoO_3–SiO_2–Al_2O_3. Indeed, by means of ammonia adsorption measurements we have shown[7] that this kind of catalyst is both more acidic and more heterogeneous (from the point of view of acid-site distribution) than either MoO_3–SiO_2 or MoO_3–Al_2O_3.

The catalysts with the highest MoO_3 content have spectra whose shapes are quite similar, except for

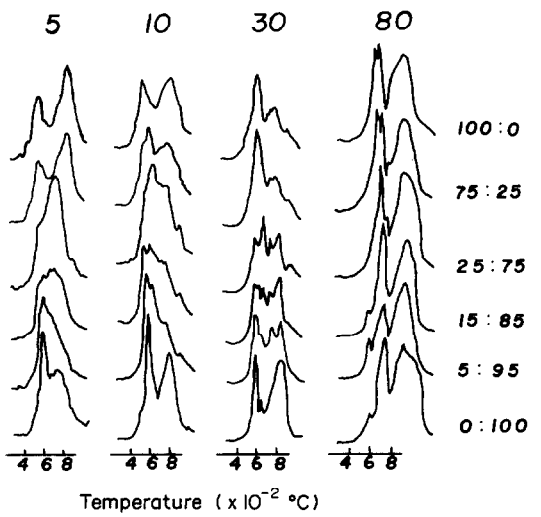


Fig. 1. TPR spectra of MoAlSi catalysts. Each row corresponds to a type of support, indicated on the right as wt % Al_2O_3: wt % SiO_2. The MoO_3 content varies from column to column, and is indicated over each as wt %.

some fine details, regardless of the carrier composition. However, this similarity is only apparent, as the T_m value of the lower-temperature peaks varies smoothly in a wide range from the 0 : 100 carrier (single peak, $T_m = 760°C$) to the 100:0 support (two close peaks, $T_m = 680$ and 710°C). This reveals that even at high Mo concentration the interaction with the support (or, in this case, modifier) may bring about significant differences between the catalysts' reducibilities.

NiMoAl *series*

The most conspicuous change in the TPR spectra of MoO_3–Al_2O_3 catalysts brought about by the incorporation of Ni (Fig. 2) is the appearance of a broad band, with a T_m intermediate between the two peaks of the unpromoted catalyst. This extra signal, however, is only well defined in the patterns of catalysts with high Ni contents and lower firing temperatures. It is evident that the position of this band changes with increasing calcination temperature, being superimposed on the second Mo peak at >600°C, as reflected in the higher size of this peak with increasing Ni concentration. Conversely, contrary to a previous suggestion,[4] the size of the first peak does not change with Ni content, showing that this promoter does not affect the dispersion of MoO_3 in the oxidic precursors.

TPR spectra of bulk NiO (single sharp peak at about 300°C) and of Ni–Al_2O_3 (broad band appearing at >700°C, see also below), allow us to suggest that the extra peak is probably due to a spinel-like surface phase, and that the movement to higher T_m is due to increasing interaction of Ni with the support.

Although the size of the first peak does not change with Ni content, the T_m decreases with increasing concentration of the promoter (Fig. 3). This suggests that, while Ni does not change the nature of MoO_3 multilayers, it favours their reduction. It may also be appreciated in Fig. 3 that, at the lower calcination temperatures, the 3 wt % NiO catalyst is similar to the 5 wt % NiO-promoted catalyst, but, as the firing temperature increases, it becomes similar to the 1 wt % NiO one. As Ni cations tend to enter the alumina lattice with increasing calcination temperature, it may be inferred that the effect of Ni on the reducibility of the MoO_3 multilayers is related to its presence on the catalyst surface, and could be attributed to a spill-over of hydrogen from Ni-reduced centers to the molybdena surface.

CoNiMoAl *series*

In Fig. 4a, we show the TPR spectra of these solids. Once again, Ni lowers the T_m of the first peaks with respect to the unpromoted catalysts (from 480 to 430°C when calcined at 500°C, and from 480 to 455°C at a firing temperature of 600°C). Incorporation of Co in the MoO_3–Al_2O_3 system causes an increase in the size of both peaks, though a slight one in the first peak. No extra bands, as in the case of Ni, are observed, even at the lowest calcination temperature. This was unexpected, as the TPR trace of a Co–Al_2O_3 catalyst of similar Co content has a peak with lower T_m than Ni–Al_2O_3. The possible explanation is that Co interacts more with Mo than Ni does or that the presence of Mo promotes the interaction between Co and the support. The T_m of both Co–Mo–Al_2O_3 peaks are similar to those

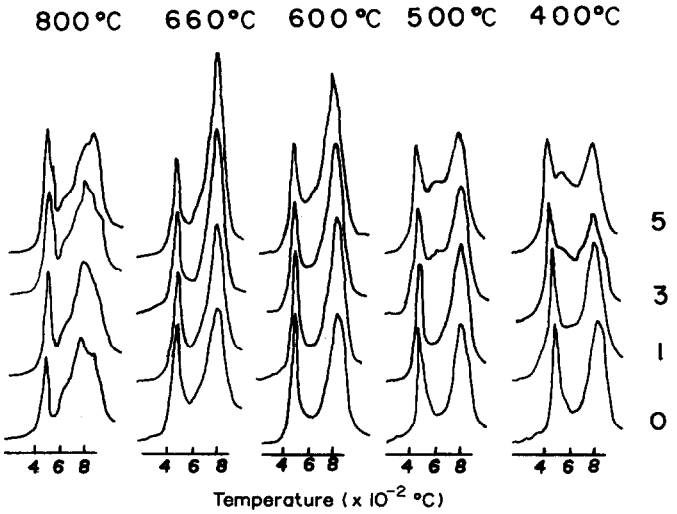


Fig. 2. TPR spectra of the NiMoAl catalysts. The calcination temperature is given over the corresponding column. Each row corresponds to a Ni content, displayed on the right as wt % NiO.

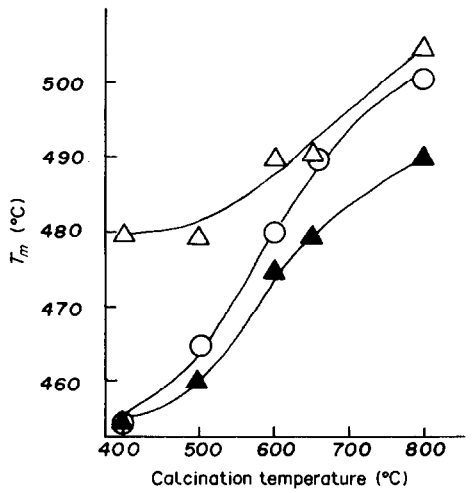


Fig. 3. Dependence of the T_m value for the first TPR peak of the NiMoAl catalysts on their calcination temperature. (△) 1 wt % NiO, (○) 3 wt % NiO, and (▲) 5 wt % NiO.

for Mo–Al_2O_3, showing that Co does not favour hydrogen activation as Ni does.

As commented above, the patterns of Co–Al_2O_3 show peaks with lower T_m than those of Ni–Al_2O_3. Also, these peaks are sharper. Both these facts may suggest that, in the Co catalyst, there are bulk-like cobalt oxide phases, contrary to the case of Ni–Al_2O_3 (as discussed above). This possibility is being examined at present by obtaining TPR spectra of bulk compounds: $CoAl_2O_4$, $NiAl_2O_4$, CoO and Co_3O_4.

The trimetallic catalysts show a gradual change of the T_m of the first peak, from 430 (only Ni) to 480°C (only Co), whereas the second peak vary more abruptly: its T_m is 800°C between $r = 0$ and $r = 0.6$, and then it changes to 825–830°C. It has been reported[6] that this trimetallic system has an optimum composition for the best hydrodesulfurization activity, but no features of the TPR spectra have been found that correlate with that activity behaviour.

Acknowledgement—We thank the Consejo Nacional de Investigaciones Científicas y Tecnológicas for financial assistance.

REFERENCES

1. N. W. Hurst, S. J. Gentry, A. Jones and B. D. McNicol, *Catal. Rev.—Sci. Eng.* 1982, **24**, 233.
2. F. E. Massoth, *Adv. Catal.* 1978, **27**, 265.
3. (a) R. Thomas, E. M. van Oers, V. H. J. de Beer, J. Medema and J. A. Moulijn, *J. Catal.* 1982, **76**, 241; (b) R. Thomas, E. M., van Oers, V. H. J. de Beer and J. A. Moulijn, *J. Catal.* 1983, **84**, 275.
4. N. K. Nag, D. Frankel, J. A. Moulijn and B. C. Gates, *J. Catal.* 1980, **66**, 162.
5. H. C. Yao, *J. Catal.* 1981, **70**, 440.
6. J. Laine, F. Severino and R. Golding, *J. Chem. Technol. Biotechnol.* 1984, **33A**, 387.
7. (a) J. Laine, S. Yunes, J. Brito and P. Andréu, *J. Catal.* 1980, **62**, 157; (b) J. Laine, J. Brito, S. Yunes and P. Andréu, *React. Kinet. Catal. Lett.* 1984, **25**, 5.

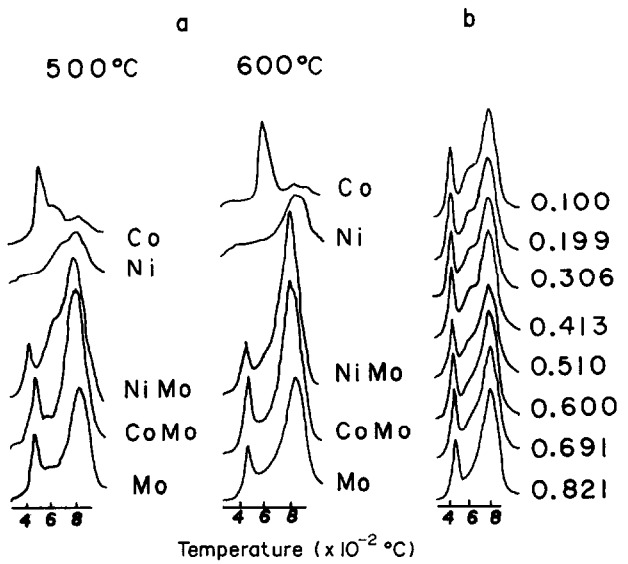


Fig. 4. TPR spectra of NiCoMoAl catalysts. (a) Mono- and bimetallic catalysts supported on γ-Al_2O_3. Type of catalyst, indicated beside its spectrum; calcination temperature above the column. (b) Trimetallic catalysts, calcined at 500°C. Co/(Co + Ni) is given on the right of the spectra.

Polyhedron Vol. 5, No. 1/2, pp. 183–186, 1986
Printed in Great Britain

0277-5387/86 $3.00 + .00
© 1986 Pergamon Press Ltd

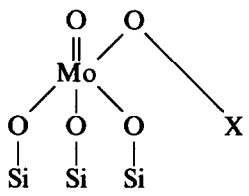
STRUCTURE OF Mo CATALYSTS SUPPORTED ON SILICA: IR AND GRAVIMETRIC RESULTS

M. CORNAC, A. JANIN and J. C. LAVALLEY*

UA 414, Laboratoire de Spectrochimie, I.S.M.Ra, Université de Caen, 14032 Caen Cedex, France

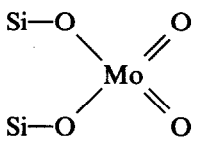
(*Received* 18 *June* 1985)

Abstract—Isotopic exchange with $H_2{}^{18}O$ followed by IR spectroscopy, and H_2S chemisorption followed by gravimetry, show that the species formed on MoO_3–SiO_2 at low loading is:



(X = Si or Mo). O atoms of the Mo=O bond and the Mo—O—X bridge are exchangeable by ^{18}O or S atoms.

The MoO_3–SiO_2 system is of interest for catalyzing oxidation[1] or ammoxidation reactions. FTIR spectroscopy has enabled us to determine the stepwise appearance on MoO_3–SiO_2 samples of at least three species,[2] depending on the Mo loading. The species formed at low loading (species **I**) has been assigned[3] a tetrahedral structure by comparison with work on MoO_3–Al_2O_3:[4]



This species is the active one in the selective oxidation of methanol to acetaldehyde.[5]

To clarify the nature of this surface phase, we have studied the isotopic exchange $^{16}O \rightarrow {}^{18}O$ by IR spectroscopy.

Also, as our system is close to precursors of HDS catalysts, which are used in sulfided form, we have followed the action of H_2S by IR spectroscopy and gravimetry. The results enable us to specify the nature of species **I** and to propose a model of interaction between the Mo phase and the surface.

EXPERIMENTAL

The preparation of catalysts, sulfidation method and IR measurements have been described elsewhere.[2] The isotopic exchange was performed by repeated cycles of hydration by $H_2{}^{18}O$ at 150°C and dehydration at 400°C. The labelled water was 98% enriched, from CEA-ORIS. Weight changes have been followed with a McBain microbalance,[6] for the following sulfidation method: $H_2S + H_2$ introduction at room temperature, equilibration, and evacuation at temperatures increasing from 20 to 300°C.

RESULTS

In a previous study,[2] we showed the presence of three species on MoO_3–SiO_2 catalysts, depending on the Mo loading:

(i) species **I**, appearing at low loading, characterized by IR bands at 990 and 920 cm^{-1};

(ii) species **II**, for medium-loading samples, IR band at 970 cm^{-1}, probably a polymer phase [Fig. 1(a)];

* Author to whom correspondence should be addressed.

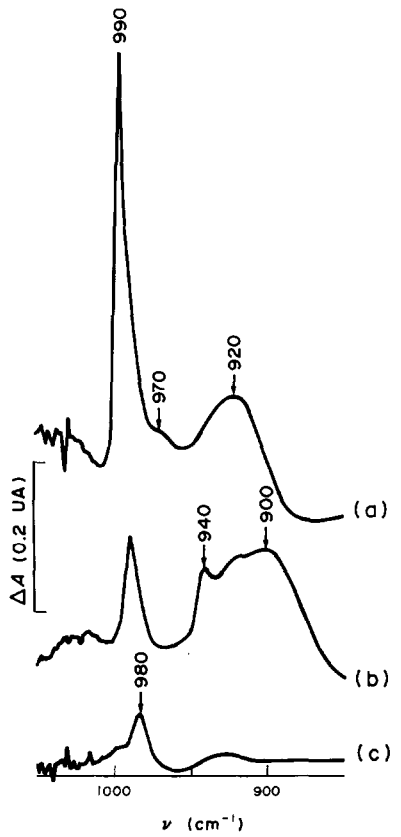


Fig. 1. IR spectra of oxymolybdenum species (obtained by subtraction of the spectrum of the same amount of pure silica): (a) Mo-8–SiO_2, O_2 calcined at 400°C; (b) after isotopic exchange with $H_2{}^{18}O$ at 150°C and dehydration at 400°C; and (c) effect of the addition of 5-torr H_2O on (a).

(iii) species **III**, at high loading, IR bands at 875, 820 and 670 cm^{-1}, a pseudo-MoO_3 phase.

Progressive addition of water at room temperature to the different calcined samples decreases the intensity of the 990- and 920-cm^{-1} bands while the 990-cm^{-1} band continuously shifts to 980 cm^{-1} [Fig. 1(c)]. Complete disappearance of the bands is obtained by heating at 400°C for 20 min (P_{H_2O} = 10 torr). Heating *in vacuo* at 400°C regenerates the initial bands. The 970-cm^{-1} band, characteristic of species **II** in Mo-8 and Mo-14 samples, disappears completely with the addition of even a small amount of water at room temperature.

On all the catalysts, water addition creates a broad band at 3550 cm^{-1}, which shifts to 3450 cm^{-1} on further water addition. Corresponding to this band is another band at 1615 cm^{-1}, characteristic of the water bending vibration. We assign these bands to molecular water adsorption.

We observe the same phenomena using $H_2{}^{18}O$. However after the final dehydration at 400°C, we observe that each of the two bands of species **I** (990 and 920 cm^{-1}) has decreased in intensity and is accompanied by a second band at lower wavenumber (940 and 900 cm^{-1}, respectively) [Fig. 1(b)]. We deduce that an isotopic exchange $^{16}O(Mo) \rightarrow {}^{18}O(Mo)$ has occurred. The 970-cm^{-1} band is also decreased in intensity but, because of its low intensity, we are not able to observe the shifted band.

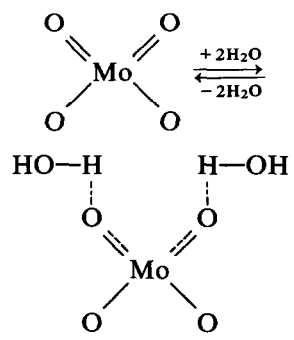
An experiment was also carried out using H_2S. We have reported before[2] the effects of $H_2 + H_2S$ addition on the IR spectra of MoO_3–SiO_2 samples. The same results are observed using H_2S alone: the intensity of the 990- and 920-cm^{-1} bands, and eventually of the 970-cm^{-1} band, decreases even at room temperature, and a broad band at 3550 cm^{-1} and a sharp band at 1615 cm^{-1} appear, showing the formation of water. By gravimetric measurements we found that the calcined Mo-2 sample, which contains 136 μmol g^{-1} of Mo as species **I**, chemisorbs irreversibly 280 μmol g^{-1} of H_2S at room temperature, i.e. $2H_2S$ per 1 Mo. Evacuation from 20 to 300°C removed the water formed, approximately 270 μmol g^{-1} in agreement with the equation

$$2H_2S + 2O(Mo) \rightarrow 2H_2O + 2S(Mo).$$

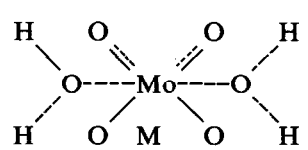
The ultimate weight increase corresponds to the replacement of 2O per Mo atom by 2S.

DISCUSSION

Raman studies have shown that the vibrational spectra of the Mo or W surface species in MoO_3– or WO_3–Al_2O_3 catalysts are influenced by the water content of the samples.[7,8] In particular, Stencel *et al.*[7] have reported that the Mo=O band at 1000 cm^{-1} was progressively shifted to 950 cm^{-1} by water exposure; repeated H_2O exposure and O_2 calcination cycles showed that this shift was reversible. It has been explained by the following equilibria:



or



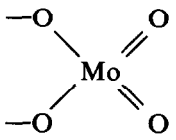
The present study shows that the IR bands characteristic of species **I** and **II** disappear with water addition. By isotopic $^{16}O \rightarrow {}^{18}O$ exchange, the shift, $\Delta\nu$, is 50 cm^{-1} for the 990-cm^{-1} band, and only 20 cm^{-1} for the 920-cm^{-1} band (species **I**).

At first approximation a band characteristic of an Mo—O simple oscillator is expected to lead to an isotopic ratio of:

$$\frac{\nu(\text{Mo}-{}^{16}\text{O})}{\nu(\text{Mo}-{}^{18}\text{O})} = \left(\frac{\frac{1}{96}+\frac{1}{18}}{\frac{1}{96}+\frac{1}{16}}\right)^{1/2} = 0.951.$$

The observed isotopic shift on the high-frequency band of species **I** (50 cm^{-1}) is almost exactly equal to the theoretical shift (49 cm^{-1}). Therefore, the 990-cm^{-1} band is assigned to a terminal Mo=O bond.

In a

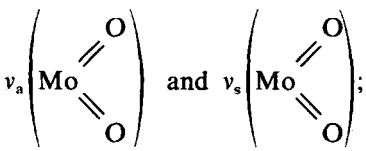


species with C_{2v}-symmetry the two Mo=O vibrations should be coupled

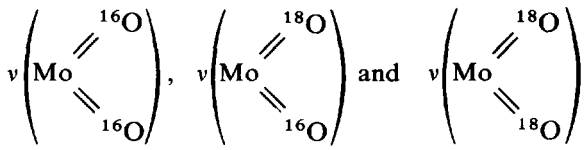


(unless the M=O angle is 90°),

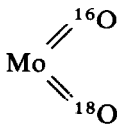
giving antisymmetric (a) and symmetric (s) modes



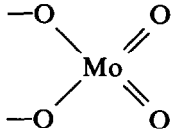
each mode would be affected by the $^{16}O \rightarrow {}^{18}O$ exchange, and would lead to three bands, i.e.



When the isotopic exchange is incomplete, the



band is expected to be predominant. In the present study, we were unable to detect any intermediate band between 990 and 945 and 920 and 900 cm^{-1}, respectively. So we discard a species of the



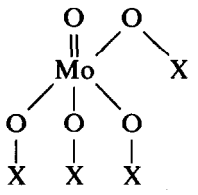
type.

Our results are more in favour of a species with a single Mo=O bond.

The frequency shift of the low-wavenumber band (920 cm^{-1}) of species **I** is smaller ($\Delta\nu$ = 20 cm^{-1}). Therefore this band does not correspond to a terminal Mo=O bond. In the previous paper,[2] we assigned it to the vibration of a Si—O—Mo group in agreement with Ref. 9. It has a particular character as we find that the oxygen is exchangeable by $H_2{}^{18}O$ at room temperature.

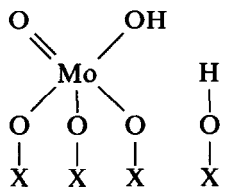
We deduce that the 2O per Mo that are exchangeable by S through H_2S adsorption at room temperature are the oxygen of the terminal Mo=O bond and the oxygen in the particular X—O—Mo bridge.

Our results agree with the conclusions of a Raman study of Kasztelan on MoO_3–Al_2O_3.[10] Structure **A**



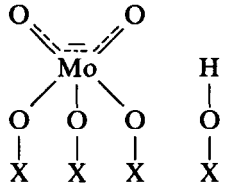
A

(X = Al or Mo) was proposed for calcined MoO_3–Al_2O_3; the particular Mo—O—X bridge is sensitive to H_2O addition. This species would be formed by dehydration of **B**:



B

H^+



C

Addition of H_2O to **A** (with X = Si or Mo in our case) leads to species **B** in equilibrium with **C**. The reversibility of the process explains why after dehydration the O atoms of the Mo=O bond and the X—O—Mo bridge are exchanged. These two particular O atoms are certainly those replaced by S atoms in the H_2S reaction. Experiments are in

progress to determine the nature and structure of the sulfided species formed.

REFERENCES

1. H. F. Liu, R. S. Liu, K. Y. Liew, R. E. Johnson and J. H. Lundsford, *J. Am. Chem. Soc.* 1984, **106**, 4117.
2. M. Cornac, A. Janin and J. C. Lavalley, *Infrared Phys.* 1984, **24**, 143.
3. A. Castellan, J. C. J. Bart, A. Vaghi and N. Giordano, *J. Catal.* 1976, **42**, 162.
4. F. E. Massoth, In *Advances in Catalysis* (Edited by D. D. Elez, H. Pines and P. G. Weige), Vol. 27, p. 265. Academic Press, New York (1978).
5. Y. Iwasawa, Y. Nakano and S. Ogasawara, *J. Chem. Soc., Faraday Trans* 1 1978, **74**, 2968.
6. D. Ouafi, A. Janin and J. C. Lavalley, *X Symposium International sur la Réactivité des Solides*, 27-08/1-09 1984, *Dijon* (*France*) (in press).
7. J. M. Stencel, L. E. Makovsky, T. A. Sarkus, T. de Vries, R. Thomas and J. A. Moulijn, *J. Catal.* 1984, **90**, 314.
8. J. M. Stencel, L. E. Makovsky, J. R. Diehl and T. A. Sarkus, *J. Raman Spectrosc.* 1984, **15**, 282.
9. S. R. Seyedmonir, S. Abdo and R. F. Howe, *J. Phys. Chem.* 1982, **86**, 1233.
10. S. Kasztelan, Thèse, Université de Lille (1984).

Polyhedron Vol. 5, No. 1/2, pp. 187–190, 1986
Printed in Great Britain

0277–5387/86 $3.00 + .00
© 1986 Pergamon Press Ltd

STABILITY AND CATALYTIC PROPERTIES OF Mo-CONTAINING Y-TYPE ZEOLITE CATALYSTS CALCINED BY AN ISOBARIC THERMAL DECOMPOSITION PROCEDURE

ANTONIO LÓPEZ AGUDO,* RUBY CID,† FRESIA ORELLANA† and JOSÉ LUIS G. FIERRO

Instituto de Catálisis y Petroleoquímica, C.S.I.C., Madrid, Spain; and † Facultad de Ciencias, Universidad de Concepción, Concepción, Chile

(*Received* 15 *June* 1985)

Abstract—A study has been made of the effect of calcination temperature, under isobaric thermal conditions, on the structural stability and catalytic activity for thiophene conversion of Mo-impregnated NaY and NH_4NaY zeolite catalysts. The IR spectra, X-ray diffraction, BET surface area and sorption capacity results indicated that catalyst crystallinity was largely preserved after treatment at 110°C, and decreased substantially after calcination at over 350°C. All Mo-containing zeolite catalysts remained stable in air.

Interest in the preparation of stable Mo-containing zeolite catalysts has increased in recent years.[1–6] However, there is not general agreement about the stability of the zeolite, even using the same forms of zeolites and similar methods to incorporate Mo,[4,5] as well as the effect of the activation conditions on its stability.

The present work was undertaken to study the effect of calcination temperature under isobaric conditions on the stability of the Na- and NH_4-forms of zeolite Y impregnated with ammonium heptamolybdate (AHM). Several physico-chemical techniques, viz. IR spectroscopy, X-ray diffraction (XRD), BET surface area (S_{BET}) and sorption capacity, including catalytic-activity measurements, have been used to characterize these catalysts.

EXPERIMENTAL

The NaY parent zeolite was LZ-Y52 from Union Carbide. The 0.68-NH_4NaY zeolite (denoted as HNaY) was prepared by repeated ion exchange of the NaY with 0.5 M ammonium acetate solution at 20°C for 4 h. Both NaY and HNaY zeolites were impregnated with aqueous solutions of AHM of the appropriate concentration to obtain a nominal loading of 10 wt % MoO_3. The slurry was stirred for about 2 h and then the excess of water was evaporated under vacuum in a rotary evaporator. The resulting precursor was calcined gradually from room temperature to 520°C at a constant decomposition rate using an isobaric (8×10^{-2} torr) thermal procedure (ITD). Portions of the sample were withdrawn at 110, 350, 440 and 520°C; they are denoted as Mo–NaY(x) or Mo–HNaY(x), where x is the calcination temperature. Additionally, two samples, Mo–NaY(520)F and Mo–HNaY(520)F, were prepared by fast calcination at 520°C in air, in a current furnace, of aliquots of the hydrate Mo-impregnated NaY and HNaY zeolites, respectively. IR spectra were recorded in a Perkin–Elmer 580 B spectrophotometer by the KBr technique (1/100). Sorption capacities of catalysts thoroughly outgassed at 350°C were measured using a Setaram microbalance. XRD patterns were obtained on a Philips PW-1010 diffractometer using Cu-K_α radiation. S_{BET}s were measured at −195°C with N_2. Catalytic activity for thiophene conversion was measured at 340°C and atmospheric pressure in a flow microreactor, using 0.3 g catalyst and 30 cm^3 min^{-1} of H_2 saturated with 10 mol % thiophene–methylcyclohexane mixture at 0°C. Catalysts were pre-sulfided "*in situ*" at 320°C in 10% H_2S–H_2 mixture at 18 cm^3 min^{-1} for 5 h. Reaction products were analyzed by gas chromatography.

* Author to whom correspondence should be addressed.

RESULTS

Figure 1 shows that the intensities of the framework vibration bands of the Mo-impregnated zeolites calcined at 110 and 350°C decreased only slightly in comparison with those of the NaY and HNaY zeolites. Calcination at higher temperature resulted in a gradual decrease in band intensity and some band broadening, which was relatively more pronounced for the Mo–HNaY series. Comparison between catalysts calcined at 520°C in air (spectra f and f') and by using the ITD procedure (spectra e and e') showed that the former exhibited less intense bands than the latter. A shoulder (or small band) gradually appeared in the region 900–920 cm^{-1} with increasing calcination temperature, which was clearly present in the catalysts calcined at 520°C, as observed previously.[2,4–6]

The position of the bands in general did not change with calcination, except for the catalysts Mo–NaY(520) and Mo–HNaY(520) (spectra e and e', respectively) in which various bands (~1000, 800 and 585 cm^{-1}) were slightly shifted to higher frequencies. These shifts, accompanied by a marked decrease in band intensities, are indicative of a loss of crystallinity rather than dealumination.

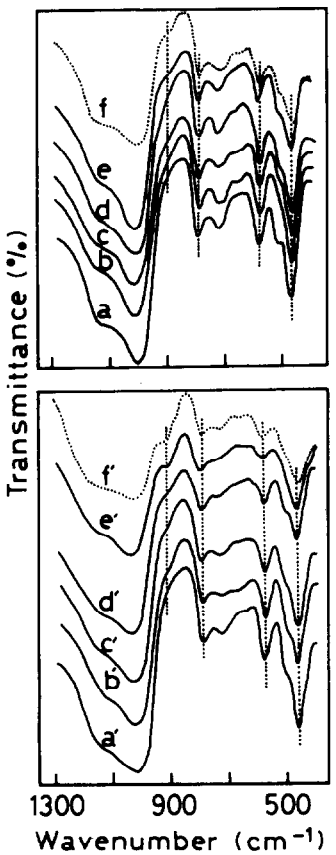


Fig. 1. IR spectra in the mid-frequency region of: (a) NaY, (b) Mo–NaY(110), (c) Mo–NaY(350), (d) Mo–NaY(440), and (e) Mo–NaY(520)F. Primes denote the same treatments on the Mo–HNaY series.

The relative adsorption capacities (from isotherms not shown here) of both adsorbates for the Mo-impregnated zeolites when compared with those for the NaY and HNaY decreased gradually with increasing calcination temperature (Fig. 2). The relative change was significantly larger in the Mo–HNaY than in the Mo–NaY series.

The XRD patterns (not shown here) of all the Mo-impregnated zeolite catalysts were similar to that for the NaY parent zeolite, except for the peak intensities, which decreased slightly after impregnation with AHM and more markedly with increasing calcination temperature. Relative crystallinities compared to the NaY or NaHY zeolites decreased (Fig. 2) generally with increasing calcination temperature. It is interesting to note that the relative crystallinities for the samples calcined in air by a conventional procedure (series F) were much lower than the corresponding catalysts calcined by the ITD procedure.

In Fig. 2 it can be seen that the relative change in S_{BET} of all Mo-impregnated zeolite catalysts (identically outgassed) with respect to the parent NaY or HNaY zeolites decreased also with calcination temperature, in parallel with crystallinity as determined by XRD.

The variations with reaction time of the thiophene conversion at 340°C on catalysts calcined at 350, 440 and 520°C are shown in Fig. 3. A rapid catalyst decay, more marked for the Mo–HNaY series, was initially observed. The reaction products on all the catalysts consisted mainly of butenes and traces of *n*-butane; propylene was also produced in appreciable amounts (~7% conversion of thiophene) on the Mo–HNaY series, and generally as traces on the Mo–NaY series. Complementary activity measurements on NaY and HNaY revealed that the former initially was slightly active to convert thiophene, while the latter initially showed an overall activity comparable to that of the Mo–HNaY catalysts, but on both NaY and HNaY catalysts activity decreased dramatically throughout the experiment, in such a way that after 100 min the catalysts were nearly inactive.

DISCUSSION

When NaY and HNaY were impregnated with AHM and then calcined by the ITD procedure at 110°C their crystallinity was largely maintained (> 90%) according to the IR spectra, and slightly decreased (80–90%) according to the XRD or the S_{BET} results. The lower values of crystallinity for

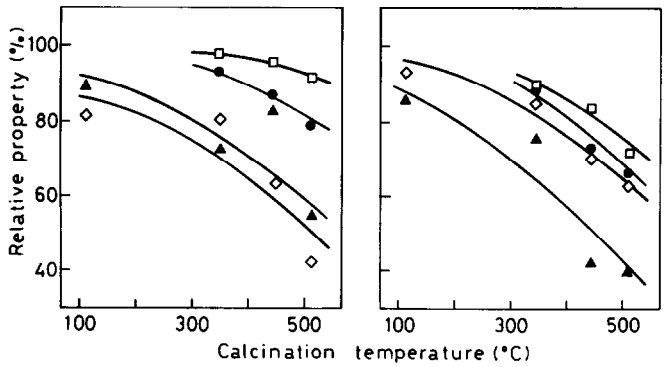


Fig. 2. Relative variation of XRD crystallinity (▲), S_{BET} (◇) and H_2O (□) and *n*-hexane (●) sorption capacity as a function of calcination temperature of Mo-impregnated zeolites. Values for NaY and HNaY taken as references (100%).

XRD and S_{BET} were probably due to the dilution effect caused by the incorporation of molybdate and some blocking of the zeolite cavities by molybdate, respectively. By calcining at 350°C an additional slight loss in both crystallinity (XRD) and S_{BET} occurred. However, the sorption capacities of such calcined catalysts and their structure-sensitive band intensities varied insignificantly, particularly for the Mo–NaY(350) catalyst. It is then interpreted that at 350°C the samples still retain a high degree of crystallinity, but the zeolite lattice may present some partial breakdown and/or distortion caused by some interaction of the molybdate anions with the oxygen of the zeolite lattice. This interaction may occur when dehydration takes place. A further increase in the calcination temperature up to 440 and 520°C led to substantial loss of crystallinity and sorption capacity of both zeolites (more pronounced in the HNaY series) which is related to complete dehydration and partial dehydroxylation of the zeolites, and the following bonding of Mo to the zeolite framework. This was supported by the appearance of a band at about 900 cm^{-1} clearly present in the Mo–HNaY(520) catalyst, which is usually attributed to an Mo—O or Mo=O vibration.[1,2,4–6] It seens that the presence of hydroxyl groups, as in the HNaY zeolite, favoured the bonding of molybdate anions to the zeolite framework and then caused the loss of crystallinity.

The decrease in activity (steady-state values) of the Mo–NaY catalysts series with increasing calcination temperature (Fig. 3) is in agreement with the loss of crystallinity and surface area of the zeolite, as a result probably of the decreasing dispersion of the accessible Mo-active phase on the zeolite support. Since Mo migration from the external surface of the zeolite to inside the cavities has been observed by XPS analysis,[7] the possibility that differences in accesibility of Mo to the reactant could also contribute to the decrease in activity must not be excluded. In the case of the Mo–HNaY catalysts, we cannot separate rigorously the contribution of the Mo-active phase from that of the HNaY zeolite support, which showed increasing thiophene conversion with increasing preactivation temperature of the HNaY zeolite.

Finally, on comparing the catalyst calcined under the ITD procedure and in air at 520°C, it is evident, as shown by IR and XRD, that the former maintained a higher level of crystallinity than the latter. Thus, the ITD is a useful method to prepare stable calcined Mo-containing zeolites with crystallinity > 50%.

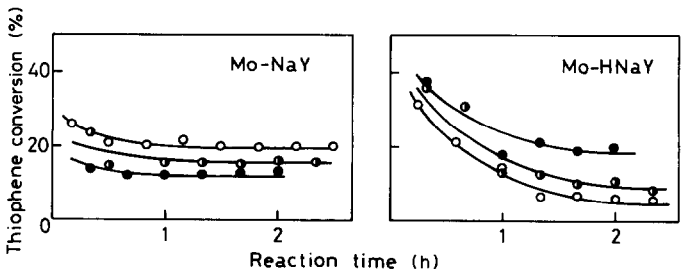


Fig. 3. Thiophene conversion at 340°C vs reaction time on Mo-impregnated zeolites calcined at: (○) 350, (◑) 440, and (●) 520°C.

REFERENCES

1. P. Gallezot, G. Coudurier, M. Primet and B. Imelik, *Am. Chem. Soc. Symp. Ser.* 1977, **40**, 144.
2. P. E. Dai and J. H. Lunsford, *J. Catal.* 1980, **64**, 173.
3. E. L. Moorehead, U.S. Patent 4,297,243 (1981).
4. S. Abdo and R. F. Howe, *J. Phys. Chem.* 1983, **87**, 1713; *ibid.* 1983, **87**, 1722.
5. M. B. Ward and J. H. Lunsford, In *Proceedings of the Sixth International Conference on Molecular Sieves* (Edited by D. Olmon and A. Bisio), p. 405. Butterworths, London (1984).
6. R. Cid, F. J. Gil Llambías, J. L. G. Fierro, A. López Agudo and J. Villaseñor, *J. Catal.* 1984, **89**, 478.
7. J. L. G. Fierro, R. Cid and A. López Agudo, unpublished results.

Polyhedron Vol. 5, No. 1/2, pp. 191–194, 1986
Printed in Great Britain

0277-5387/86 $3.00+.00
© 1986 Pergamon Press Ltd

ESR, OXYGEN CHEMISORPTION AND ACTIVITY STUDIES ON MoO_3–ZrO_2 CATALYSTS

B. M. REDDY, K. V. R. CHARY, B. RAMA RAO, V. S. SUBRAHMANYAM* and C. S. SUNANDANA†

Regional Research Laboratory, Hyderabad 500 009, India; and †University of Hyderabad, Hyderabad 500 137, India

and

NABIN K. NAG*

Fuels Engineering Department, University of Utah, Salt Lake City, UT 84112, U.S.A.

(*Received* 15 *June* 1985)

Abstract—ESR studies on ZrO_2-supported Mo oxide catalysts indicate the presence of two types of paramagnetic Mo^{5+} species on the support surface. The oxygen uptake capacities (at −78°C), as well as the hydrodesulfurization and hydrogenation activities of the catalysts are found to correlate with the Mo loadings on the support. The results are explained with the help of a "patch" model of the Mo oxide phase.

Supported Mo-containing catalysts are used in many important reactions including hydroprocessing, coal liquefaction, hydrogenation (HYD), polymerization and metathesis of olefins. Numerous studies have been devoted towards understanding of the surface structure of the supported Mo oxide phase and its consequence upon the resulting activity and selectivity for certain reactions.[1,2] Pursuant to our earlier ESR[3] and oxygen chemisorption[4] studies on V_2O_5–Al_2O_3 catalysts an investigation has been made with the Mo–ZrO_2 system by these techniques in order to gain some information on the surface structure of the Mo oxide phase and its relevance to probe reactions like hydrodesulfurization (HDS) of thiophene and HYD of cyclohexene.

EXPERIMENTAL

Catalyst preparation

The ZrO_2 support was prepared by precipitating Zr hydroxide from $ZrOCl_2 \cdot 8H_2O$ by dilute ammonia solution. The precipitate was freed from chloride ions, dried at 120°C for 24 h and finally calcined at 540°C for 4 h in air. The supported Mo oxide catalysts were prepared by an incipient wetting technique: a calculated amount of ammonium heptamolybdate (spectroscopic grade, Baker) corresponding to the desired Mo loading on the support was dissolved in that volume of water which corresponded exactly to the total pore volume of the quantity of support used for impregnation. The support was then uniformly wetted by the solution, stirred well for 30 min and allowed to stand for 1 h. The impregnated sample thus obtained was dried at 120°C for 16 h and then calcined in air for 12 h at 540°C.

Chemisorption measurements

A conventional static high-vacuum (up to 10^{-6} torr) system, with the facility for reducing the catalysts *in situ* by flowing hydrogen, was used for oxygen chemisorption, which was performed at −78°C, following the procedure of Parekh and Weller.[5] The same system was used to measure the BET surface areas of the catalysts by N_2 (0.162 nm^2) adsorption at −196°C. The details of the experimental set-up and chemisorption procedure have been given elsewhere.[4]

* Authors to whom correspondence should be addressed.

Activity measurements

Thiophene HDS and cyclohexene HYD were chosen as the model reactions for testing the activities of the catalysts which were sulfided at 400°C for 2 h in a flow of a purified hydrogen and CS_2 mixture before the reactions. For this purpose, a fixed-bed differential flow microreactor operating under normal atmospheric pressure and interfaced with a gas chromatograph by a six-way sampling valve for product analysis was used. The conversions were kept within 10%. The experimental procedure and method of activity calculation have been described elsewhere.[6]

ESR and XRD measurements

The ESR spectra of the catalysts were recorded *in vacuo* (10^{-6} torr) and at 25°C on a JEOL FE 3X X-band spectrometer with 100-KHz modulation. The details of sample preparation and the experimental procedure have been elaborated in a previous paper.[3] The X-ray diffractograms were recorded on a Philips PW 1051 diffractometer by using Ni-filtered Cu-K_α radiation.

RESULTS AND DISCUSSION

Representative ESR spectra of the unreduced [(a) and (b)] and the reduced [(c)] catalysts are shown in Fig. 1. A comparison of these spectra with those of Mo–SiO_2 catalysts[7,8] shows that for the 1% Mo–ZrO_2 catalyst the ESR spectrum due to Mo^{5+} represents a "solution-like" behaviour due to incomplete removal of water ($g_{iso} = 1.975$). For the catalysts with Mo contents higher than 1%, an axially symmetric spectrum appears at the centre of the pattern [Fig. 1(b)] with $g_{\|} = 1.910$ and $g_{\perp} = 1.932$ ($g_{\|} < g_{\perp}$). The intensity of the anisotropic spectrum increased with increasing Mo loading. Upon reduction, the "solution-like" behaviour almost disappears, while an anisotropic spectrum appeared with maximum intensity for the sample

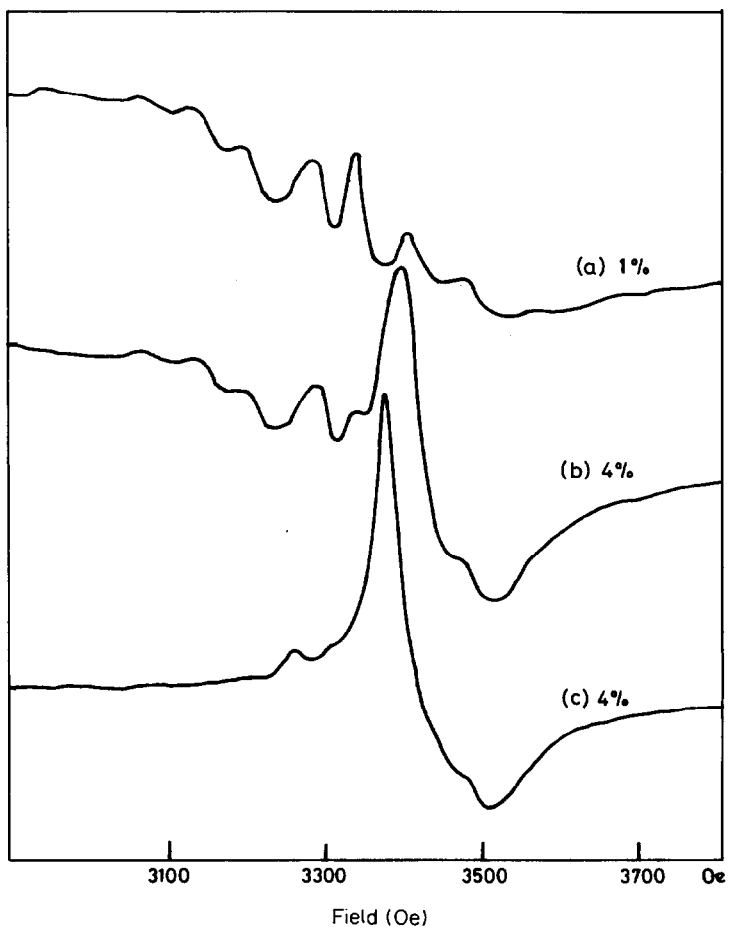


Fig. 1. ESR spectra of unreduced [(a) and (b)] and reduced [(c)] Mo–ZrO_2 catalysts recorded at 27°C and 10^{-6} torr.

with 1% Mo loading (not shown in Fig. 1). The intensity of this spectrum, unlike in the case of the unreduced catalysts, decreased rapidly with increasing Mo loading and became asymptotic just above 4% Mo loading.

The oxygen uptake capacities, HDS and HYD activities of the reduced catalysts are given as a function of Mo loading on ZrO_2 in Fig. 2. The oxygen chemisorption (at −78°C) behaviour of the Mo–ZrO_2 catalysts shows a similarity with that of the well-studied Mo–Al_2O_3 catalysts.[9] As observed from Fig. 2, the oxygen uptake increases as a function of Mo loading up to about 3.5% and then levels off. This saturation level indicates the completion of a monolayer coverage of the "active" ZrO_2 surface by Mo oxide. The monolayer corresponds to about 10 μmol Mo m^{-2} of the support surface. This value is about twice as high as the corresponding value for Mo–Al_2O_3 catalysts. The maximum oxygen uptake by the Mo–ZrO_2 catalysts is found to be about 3 μmol m^{-2} compared to about 0.3 μmol m^{-2} for Mo–Al_2O_3 catalysts. These results therefore, indicate that the Mo oxide is dispersed better on ZrO_2 than on Al_2O_3. This conclusion is made from the higher surface coverage and higher oxygen uptake capacity at the monolayer level of the Mo–ZrO_2 catalysts.

The HDS and HYD activities of the catalysts [curves (b) and (c) of Fig. 2] show a sharp rise as a function of Mo loading upto the monolayer level. Beyond this level, the activities show a very slow rise as a function of Mo loading. A closer look at Fig. 2 also reveals a good correlation of both HDS and HYD activities with the oxygen uptake capacities of the catalysts. These results indicate, therefore, that: (1) the HDS and HYD active sites, i.e. the coordinatively unsaturated sites (CUS), are titrable by oxygen chemisorbed at low temperatures; and (2) beyond the monolayer coverage, further addition of the active component, i.e. Mo oxide, does not contribute to the generation of active CUS upon which oxygen chemisorption, HDS and HYD reactions can take place.

Based on the "patch" model of Hall,[2] the nature of the oxygen chemisorption sites on Mo–Al_2O_3 catalysts has recently been discussed by Nag.[9] It has been envisaged that at lower Mo loadings small patches of Mo oxide, two layers thick and with Mo in an octahedral coordination, are formed on the support surface. Upon reduction, CUS are generated by the removal of oxygen from the edge and corner sites of the patches. These are the sites upon which oxygen chemisorption, HDS and HYD reactions

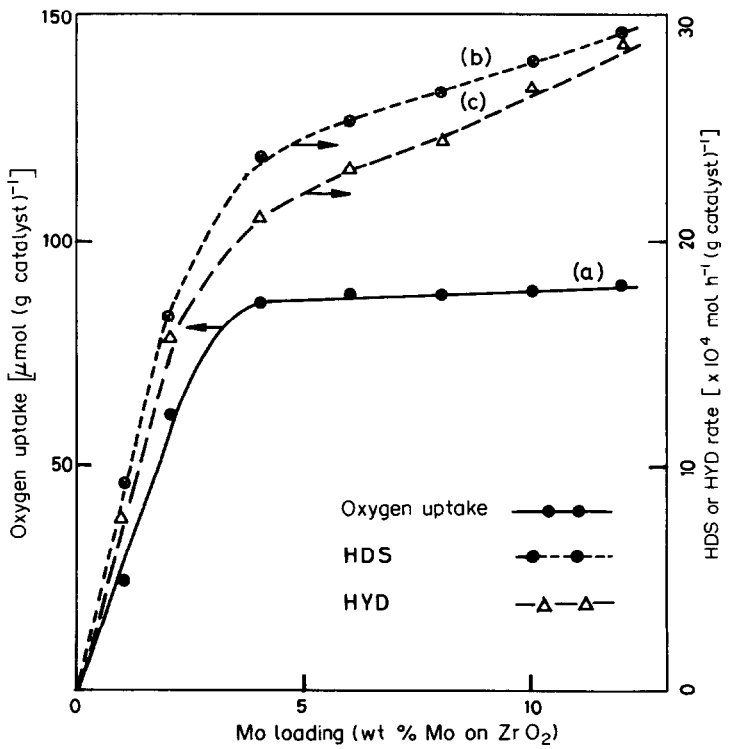


Fig. 2. Oxygen uptake at −78°C (a), hydrodesulfurization (HDS) of thiophene at 420°C (b) and hydrogenation (HYD) of cyclohexene at 400°C (c). Activities as a function of Mo loading. All the data are corrected for the contributions by the support.

take place. It has also been proposed that as the Mo loading increases the number of these patches increases with attendant increase in the number of CUS up to the monolayer level. Beyond the monolayer level the patches grow three-dimensionally, thus decreasing the dispersion of Mo oxide. It is proposed that a similar mechanism operates in the Mo–ZrO_2 system, and the present results can be explained with the help of the above concepts. Thus the initial increase and subsequent levelling off in the oxygen uptake capacity of the catalysts as a function of Mo loading are due to generation of new CUS up to the monolayer level and a subsequent decrease in the edge and corner CUS beyond the monolayer level due to crystal growth. Since the HYD and HDS activities are correlated with the CUS, their initial increase and subsequent levelling off tendencies can be understood by the same mechanism. It is worth mentioning here that, indeed, XRD lines of reduced Mo oxide were detectable only with samples containing Mo oxide at greater than the monolayer level.

Several conclusions can be derived from this present work: (1) as in the case of the Mo–Al_2O_3 system, the CUS of highly dispersed Mo oxide on ZrO_2 responsible for HDS and HYD reactions can be titrated by low-temperature oxygen chemisorption; (2) low-temperature oxygen chemisorption data can precisely determine the Mo level where the formation of a monolayer reaches completion; and (3) Mo oxide is dispersed better on the ZrO_2 support than on the Al_2O_3 support.

Acknowledgement—We are thankful to the Director, Regional Research Laboratory, Hyderabad, for permission to publish this paper.

REFERENCES

1. F. E. Massoth and G. Muralidhar, In *Proceedings of the Fourth International Conference on the Chemistry and Uses of Molybdenum* (Edited by H. F. Barry and P. C. H. Mitchell), p. 343. Climax Molybdenum Co., Ann Arbor, MI (1982).
2. W. K. Hall, In *Proceedings of the Fourth International Conference on the Chemistry and Uses of Molybdenum* (Edited by H. F. Barry and P. C. H. Mitchell), p. 224. Climax Molybdenum Co., Ann Arbor, MI (1982).
3. K. V. R. Chary, B. M. Reddy, N. K. Nag, V. S. Subrahmanyam and C. S. Sunandana, *J. Phys. Chem.* 1984, **88**, 2622.
4. N. K. Nag, K. V. R. Chary, B. M. Reddy, B. Rama Rao and V. S. Subrahmanyam, *Appl. Catal.* 1984, **9**, 225.
5. B. S. Parekh and S. W. Weller, *J. Catal.* 1977, **47**, 100.
6. B. M. Reddy, K. V. R. Chary, V. S. Subrahmanyam and N. K. Nag, *J. Chem. Soc., Faraday Trans.* 1985, **81**, 1655.
7. R. Fricke, W. Hanke and G. Ohlmann, *J. Catal.* 1983, **79**, 1.
8. M. Narayana, R. Y. Zhan and L. Kevan, *J. Phys. Chem.* 1985, **89**, 636.
9. N. K. Nag, *J. Catal.* 1985, **92**, 432.

Polyhedron Vol. 5, No. 1/2, pp. 195–198, 1986
Printed in Great Britain

0277–5387/86 $3.00 + .00
© 1986 Pergamon Press Ltd

EFFECT OF THE ACTIVATION CONDITIONS ON THE STRUCTURE AND CATALYTIC ACTIVITY OF A Co–Mo–γ-Al_2O_3 HYDRODESULFURIZATION CATALYST

R. PRADA SILVY,* F. DELANNAY, P. GRANGE and B. DELMON

Groupe de Physico-Chimie Minérale et de Catalyse, Université Catholique de Louvain, Place Croix du Sud, 1, B-1348 Louvain-la-Neuve, Belgium

(*Received* 13 *June* 1985)

Abstract—A Co–Mo–γ-Al_2O_3 hydrodesulfurization catalyst was activated under an H_2S–H_2 mixture at temperatures ranging from 673 to 1073 K using two different procedures. The samples were characterized by ion-scattering spectrometry (ISS), dynamic O_2 chemisorption (DOC) and dynamic NO chemisorption (DNOC). Comparison of ISS and DOC indicates that the decrease in activity with increasing activation temperature could be due to the sintering of MoS_2 but also to an incomplete sulfuration of molybdenum due to the formation of difficultly sulfidable MoO_2. Comparison of DOC and DNOC suggests that the amount of sulfided cobalt increases with increasing activation temperature up to 923 K. This phenomenon was confirmed by diffuse-reflectance spectroscopy, which revealed a drastic decrease in tetrahedral Co^{2+} species (cobalt pseudo aluminate) with increasing activation temperature.

This poster reports some new results of a research program aimed at a systematic investigation of the influence of the conditions of pretreatment and activation on the structure and catalytic activity of a Co–Mo–γ-Al_2O_3 hydrodesulfurization (HDS) catalyst.

We have previously studied how activity and selectivity are affected by the nature of the sulfiding molecules.[1] We have also reported preliminary results about the dependence of the activity on the activation temperature under an H_2S–H_2 mixture.[2] Optimum HDS activity was observed after activation in the range 673–803 K. Characterization of the activated samples by high-resolution electron microscopy (HREM), X-ray photoelectron spectroscopy (XPS), ion-scattering spectroscopy (ISS) and dynamic O_2 chemisorption (DOC) indicated that optimum activity corresponded to an optimum dispersion of MoS_2-like crystallites. The activity decrease at high sulfidation temperature accompanies a sintering of these crystallites.

The results presented in this poster complement this latter investigation in three directions: (i) it is shown that the activity of the samples sulfided at high temperature may be improved by some modification of the activation procedure, (ii) comparison of O_2 and NO chemisorption highlights the higher sensitivity of the latter molecules toward the active sites and suggests an increasing sulfidation of cobalt with increasing activation temperature, and (iii) characterization by diffuse reflectance spectroscopy and XPS of catalysts reoxidized in air at 673 K after activation gives evidence that part of the cobalt initially entrapped in the alumina lattice as cobalt aluminate migrates back toward the surface during activation at high temperature.

The Co–Mo–γ-Al_2O_3 catalyst used in this study is the commercial precursor (namely before reduction sulfidation) HR 306 from Procatalyse (3% CoO, 14% MoO_3, 195 $m^2\ g^{-1}$). In the previous study,[2] the activation procedure consisted in heating 2 g of this precursor in Ar up to the sulfidation temperature (673, 803, 923 or 1073 K) and then sulfiding them at this temperature for 4 h in a flow of an H_2S–H_2 (15% H_2S) mixture at atmospheric pressure. In the present work, an alternative activation procedure was used for sulfidation temperatures higher than 673 K: the sample was heated in Ar up to 673 K, it was then exposed to the H_2S–H_2 mixture, heating was continued at the same rate up to the final sulfidation temperature (803, 923 or 1073 K), and the activation was completed for 4 h at this temperature with the

* Author to whom correspondence should be addressed.

Table 1. Variation in the MoO_3 content and the BET surface area (S_{BET}) as a function of sulfidation temperature

Pretreatment temperature (K)	% MoO_3	S_{BET} ($m^2\ g^{-1}$)
673	13.5	198
803	—	195
923	13.3	170
1073	13.1	130

same H_2S–H_2 mixture. These activation procedures will be called, in the following, the first and the second procedure, respectively.

Table 1 presents the molybdenum content (measured as equivalent MoO_3 by atomic absorption spectrometry) and the BET surface area (S_{BET}) of the catalysts activated following the second procedure. These results do not differ significantly for the two procedures. The molybdenum content did not change during the heating but sintering of alumina occurred during activation at 923 and 1073 K.

After introduction in the high-pressure catalytic reactor, the samples were resulfided for 2 h at 673 K in 4% H_2S in H_2 at 2 MPa. Their activities for the HDS of thiophene and hydrogenation (HYD) of cyclohexene were measured at 510 K under a total pressure of 3 MPa using the same conditions as described previously,[2] in the test reaction using, as a feed, a mixture of 0.5% thiophene, 30% cyclohexene and 69.5% cyclohexane.

Figure 1 shows the variations in HDS and HYD conversion as a function of the activation temperature for both pretreatments: heating under Ar (full circles) and under an H_2S–H_2 mixture (open circles). It is shown that the second activation procedure gives a higher activity after activation at high temperature. The optimum temperature range extends in this case from 673 up to 923 K.

The experimental conditions for ISS measurements have been described previously.[2] All samples have been protected from oxidation by keeping them under a meniscus of iso-octane which evaporated during pumping of the spectrometer chamber. The ISS peak intensity ratio $(I_{Mo}/I_{Al})_{ISS}$ is, to a first approximation, proportional to the ratio of the surface area of the phases containing molybdenum and aluminium. As the S_{BET} is essentially equal to the surface area of alumina alone, the product $(I_{Mo}/I_{Al})_{ISS} \cdot S_{BET}$ should be approximately proportional to the dispersion of the molybdenum species.

Figure 2(a) presents the variation of this expression for catalysts pretreated following the

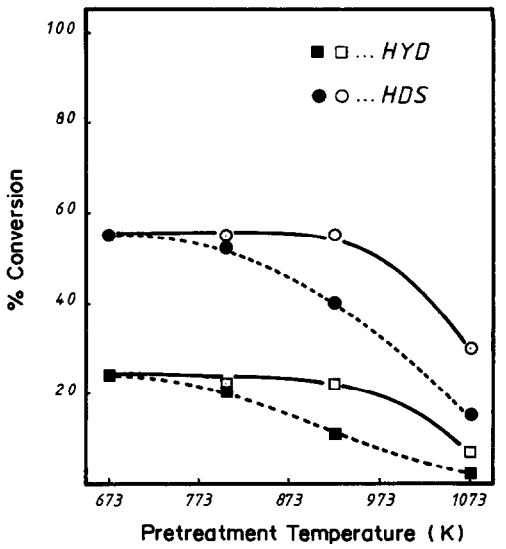


Fig. 1. Variation in HDS and HYD conversions as a function of activation conditions. (■) and (●) heating in Ar ("first procedure"), and (□) and (○) heating under a H_2S–H_2 mixture ("second procedure").

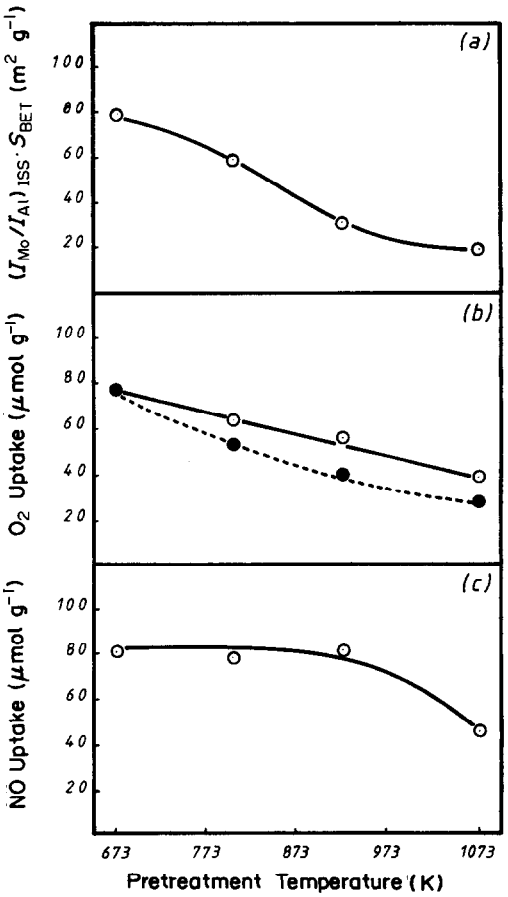


Fig. 2. Variation as a function of activation conditions of: (a) $(I_{Mo}/I_{Al})_{ISS} \cdot S_{BET}$, (b) oxygen uptake, and (c) NO uptake. (●) Heating in Ar ("first procedure"), and (○) heating under a H_2S–H_2 mixture ("second procedure").

second procedure as a function of the sulfiding temperature. The values do not differ significantly for the two procedures. A decrease in molybdenum dispersion is observed with increasing sulfiding temperature.

DOC and dynamic NO chemisorption (DNOC) at room temperature were measured using a pulse technique.[3] The samples activated by both procedures were resulfided in a U-pyrex tube reactor in a flow of H_2S–H_2 (15% H_2S) at 673 K, atmospheric pressure, for 2 h and flushed in Ar for 0.5 h at this temperature. The catalysts were then maintained in a flow of He at 293 K and 2-ml pulses of 5% O_2 or NO in He were injected until equilibrium was reached. Results are expressed as μmols of gas adsorbed per gram of catalyst.

Figure 2(b) shows the O_2 chemisorption results for catalysts activated following both procedures: heating in Ar (full circles) and heating in an H_2S–H_2 mixture (open circles). In both procedures, the O_2 uptake decreases continuously with increasing sulfidation temperature. However, the O_2 uptake decreases more for catalysts pretreated following the first procedure.

Figure 2(c) shows the NO chemisorption results for the samples sulfided using the second procedure. It shows that the NO uptake remains constant for the catalysts sulfided up to 923 K and decreases strongly for the sample activated at 1073 K. This variation is conspicuously similar to the variation of the catalytic activity (Fig. 1). For samples sulfided using the first procedure, NO uptake measurements have not been made.

From an investigation involving HREM, DOC and ISS, it was previously concluded that the loss of activity observed when increasing the activation temperature (using the first procedure) should be mainly ascribed to the sintering of the active phase. It is thus tempting to explain the dependence of activity on the activation procedure (Fig. 1) by involving a different degree of sintering. Indeed, one might speculate that sintering is greater when the catalyst is suddenly exposed to the H_2S–H_2 mixture after having been heated under Ar than when it is exposed to the H_2S–H_2 mixture from 673 K. This explanation is only partly supported by experiment: the lower O_2 uptake after the first procedure suggests a lower dispersion of the active phase [Fig. 1(b)]; however, ISS was unable to detect a significant difference in the dispersion of molybdenum after the two procedures. This disagreement points toward more subtle differences between the samples. An explanation based on the present knowledge on the chemistry of reduction–sulfidation of Mo–Co catalysts[4,5] is the following; when exposing the sample suddenly to the H_2S–H_2 mixture at high temperature (first procedure), the rate of reduction (by H_2) could be too high in comparison with the rate of sulfidation, so that MoO_2 could be formed. As MoO_2 cannot be easily sulfided, incomplete sulfurization of molybdenum would result.[4] Such a phenomenon might explain the differences between the ISS and the DOC results.

In Fig. 2, the different variations in ISS, DOC and DNOC results as a function of activation temperature indicate strikingly that each technique is sensitive to a different type of "surface species". Only DNOC appears to be sensitive to the type of species which is responsible for the HDS activity. It has been reported in the literature that NO adsorbs on both cobalt and molybdenum in the sulfided state, whereas the O_2 uptake is not modified when the ratio Co/Mo or Ni/Mo in the catalyst is below 0.5.[6–8] The fact that the NO uptake remains constant up to 923 K, whereas O_2 uptake decreases monotonously with increasing temperature may thus suggest that, up to 923 K, the decrease in the dispersion of MoS_2 is compensated for by an increase in the amount of sulfided cobalt. The strong decrease in the NO uptake at 1073 K would be due to the sintering of both cobalt sulfide and molybdenum sulfide.

The increase in the amount of sulfided cobalt suggested by DNOC could simply originate from the increasing sulfidation of cobalt entrapped in the alumina lattice in the form of cobalt aluminate. In order to check this hypothesis, the catalysts activated by the second procedure were reoxidized by calcination in a flow of air at 673 K for 15 h. The mere

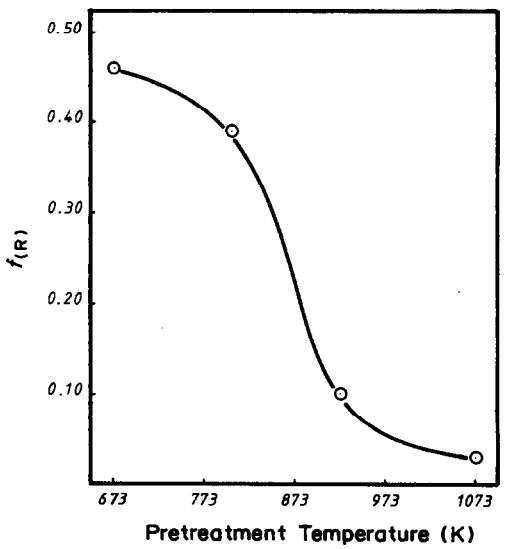


Fig. 3. Dependence of the Kubelka–Munk function [$f_{(R)}$] for the cobalt species as a function of sulfidation temperature.

change of colour (blue to green) with increasing sulfidation temperature suggested a diminution in the amount of cobalt aluminate after activation at higher temperatures. The samples were analyzed by diffuse-reflectance spectroscopy (DRS). Figure 3 shows the dependence of the Kubelka–Munk function for the cobalt species in tetrahedral coordination [$Co^{2+}_{(tet)}$] as a function of sulfidation temperature. The strong decrease in these $Co^{2+}_{(tet)}$ species indicates the migration of an increasing amount of these species toward the surface where they can become sulfided. Hence, this observation supports the conclusion drawn from the DNOC results. A more in-depth investigation of this phenomenon by Mössbauer emission spectroscopy, DRS, XPS and IR spectroscopy will be published elsewhere.[9]

Acknowledgements—R. Prada Silvy thanks the Centro de Formación y Adiestramiento Petrolero y Petroquímico (CEPET), Venezuela, for a grant. We are indebted to Mr J. M. Beuken and Dr P. Bertrand from the Laboratoire de Physico-Chimie et Physique de l'Etat Solide, Louvain-la-Neuve, for the ISS measurements and to Dr J. L. G. Fierro for fruitful discussions. We also thank Mrs M. E. Prada for typing this poster.

REFERENCES

1. R. Prada Silvy, P. Grange, F. Delannay and B. Delmon, In *Proceedings of the 9th Iberoamerican Symposium on Catalysis, Lisbon*, p. 1141 (1984).
2. R. Prada Silvy, J. M. Beuken, P. Bertrand, B. K. Hodnett, F. Delannay and B. Delmon, *Bull. Soc. Chim. Belg.* 1984, **93**, 775.
3. T. Bodrero and C. Bartholomew, *J. Catal.* 1983, **84**, 145.
4. J. J. M. Zabala, Thesis, Université Catholique de Louvain (1976).
5. R. Prada Silvy, J. L. G. Fierro, P. Grange and B. Delmon, in preparation.
6. R. Candia, O. Sørensen, J. Villadsen, N. Y. Topsøe, B. Clausen and H. Topsøe, *Bull. Soc. Chim. Belg.* 1984, **93**, 763.
7. J. Bachelier, M. J. Tilliette, M. Cornac, J. C. Duchet, J. C. Lavalley and D. Cornet, *Bull. Soc. Chim. Belg.* 1984, **93**, 743.
8. A. Lopez Agudo, F. J. Gil Llambias, J. M. D. Tascon and J. L. G. Fierro, *Bull. Soc. Chim. Belg.* 1984, **93**, 719.
9. R. Prada Silvy, J. L. G. Fierro, J. Ladriere, P. Grange and B. Delmon, in preparation.

Polyhedron Vol. 5, No. 1/2, pp. 199–202, 1986
Printed in Great Britain

0277-5387/86 $3.00 + .00
© 1986 Pergamon Press Ltd

X-RAY ABSORPTION SPECTROSCOPY STUDIES OF CALCINED $Mo-Al_2O_3$ AND $Co-Mo-Al_2O_3$ HYDRODESULFURIZATION CATALYSTS

BJERNE S. CLAUSEN,*† BRUNO LENGELER‡ and HENRIK TOPSØE*

*Haldor Topsøe Research Laboratories, DK-2800 Lyngby, Denmark; and ‡Institut für Festkörperforschung, Kernforschungsanlage Jülich, D-5170 Jülich, F.R.G.

(*Received* 1 *July* 1985)

Abstract—X-ray absorption spectroscopy has been used to obtain information on the Co and Mo structures present in calcined $Co-Mo-Al_2O_3$ and $Mo-Al_2O_3$ catalysts. The results indicate that the elements are present in disordered structures. From a detailed analysis of the X-ray absorption fine structure (EXAFS), information on the oxygen coordination around Co and Mo is obtained. An apparent decrease in the oxygen coordination number around Mo with increasing Mo loading is explained by a change in the Debye–Waller factor, presumably due to a decrease in the support interactions. The presence of Co in the catalysts is found to have very little effect on the local structure around the Mo atoms. The Co EXAFS results indicate that Co is predominantly octahedrally coordinated.

X-ray absorption spectroscopy, and, in particular, extended X-ray absorption fine structure (EXAFS), has become an important and widely used probe of short-range order in many different catalyst systems (see, for example, Refs 1 and 2). Previous EXAFS studies combined with studies using a variety of other techniques have given detailed insight into the structure and catalytic properties of the sulfided state of Co–Mo hydrodesulfurization (HDS) catalysts (see, for example, Ref. 3). As a result the structure of the sulfided catalysts is now quite well understood. However, the structure of the Co and Mo phases in the calcined precursor state is still open to discussion in the literature. There is some evidence that the Mo atoms are present in both tetrahedrally and octahedrally coordinated environments[4–6] with the latter species being favored at high Mo loadings. Although EXAFS should be an ideal tool for such studies, the previous EXAFS results have been interpreted in quite different ways.[7–10]

Regarding the state of Co in the calcined catalyst, it has been generally accepted that Co may be present in tetrahedral coordination in the alumina lattice. Recent studies show, however, that octahedrally coordinated Co may also be present.[11–13] Furthermore, this Co species was found to be precursor for the active Co–Mo–S phase.[11,14]

† Author to whom correspondence should be addressed.

In order to obtain more information on the local structure (e.g. bond lengths and coordination numbers) around the Co and Mo atoms we have studied the EXAFS of both the Co and Mo absorption *K*-edges.

EXPERIMENTAL

The preparation of the HDS catalysts has been reported previously.[15] Calcination of the catalysts was carried out at 775 K for 2 h. The various model compounds

$$[MoO_3,\ MoO_2,\ Al_2(MoO_4)_3,$$
$$CoMoO_4,\ K_2MoO_4,\ Na_2MoO_4 \cdot 2H_2O,$$
$$Ba_2CaMoO_6,\ Co_3O_4,\ CoO \text{ and } CoAl_2O_4]$$

were either obtained commercially or synthesized in the laboratory. The phase purity of all the samples was checked by X-ray diffraction.

The X-ray absorption spectra were recorded by placing appropriate mixtures of the catalysts and boron nitride in thin aluminum frames equipped with Kapton windows. The absorber thickness, x, of all the samples was chosen such that $\mu x \sim 1$ (μ is the linear absorption coefficient), on the high-energy side of the absorption edge, and great care was taken in

order to make samples of homogeneous thickness. The experiments were performed at DESY in Hamburg using the synchrotron radiation from the DORIS storage ring and the experimental RÖMO set-up. The X-rays were monochromatized by two single crystals [Si(111) for the Co *K*-edge and Si(311) for the Mo *K*-edge], and the incident and transmitted intensity were recorded by use of two ionization chambers [filled with N_2 (Co *K*-edge) or Ar (Mo *K*-edge)]. The calibration of the energy scale is essential for the determination of the small changes in the core level threshold occurring when the chemical state of the absorbing atom changes. Therefore, a third ionization chamber was placed after a thin foil of the absorbing atoms in the metallic state in order to have an "internal energy calibration". The EXAFS oscillations were analyzed according to the procedure described in detail in Refs 16 and 17. This procedure involves a background subtraction by means of cubic spline functions, multiplication of the EXAFS by a factor k^2, and normalization by the jump height at the *K*-edge. All the data reported in this paper were obtained at liquid-nitrogen temperature.

RESULTS AND DISCUSSION

The Fourier transform of the Mo EXAFS for both $Mo–Al_2O_3$ and $Co–Mo–Al_2O_3$ catalysts in the calcined (oxidic) state shows only a single strong backscatter peak due to oxygen atoms present in the nearest neighbor shell (Fig. 1). The apparent absence of more distinct peaks suggests that a well-defined Mo-containing compound is not present in any appreciable amounts. Rather the structures are amorphous, disordered, or consist of extremely small entities. From a fit of the contribution to the EXAFS due to the first shell (using the phase and

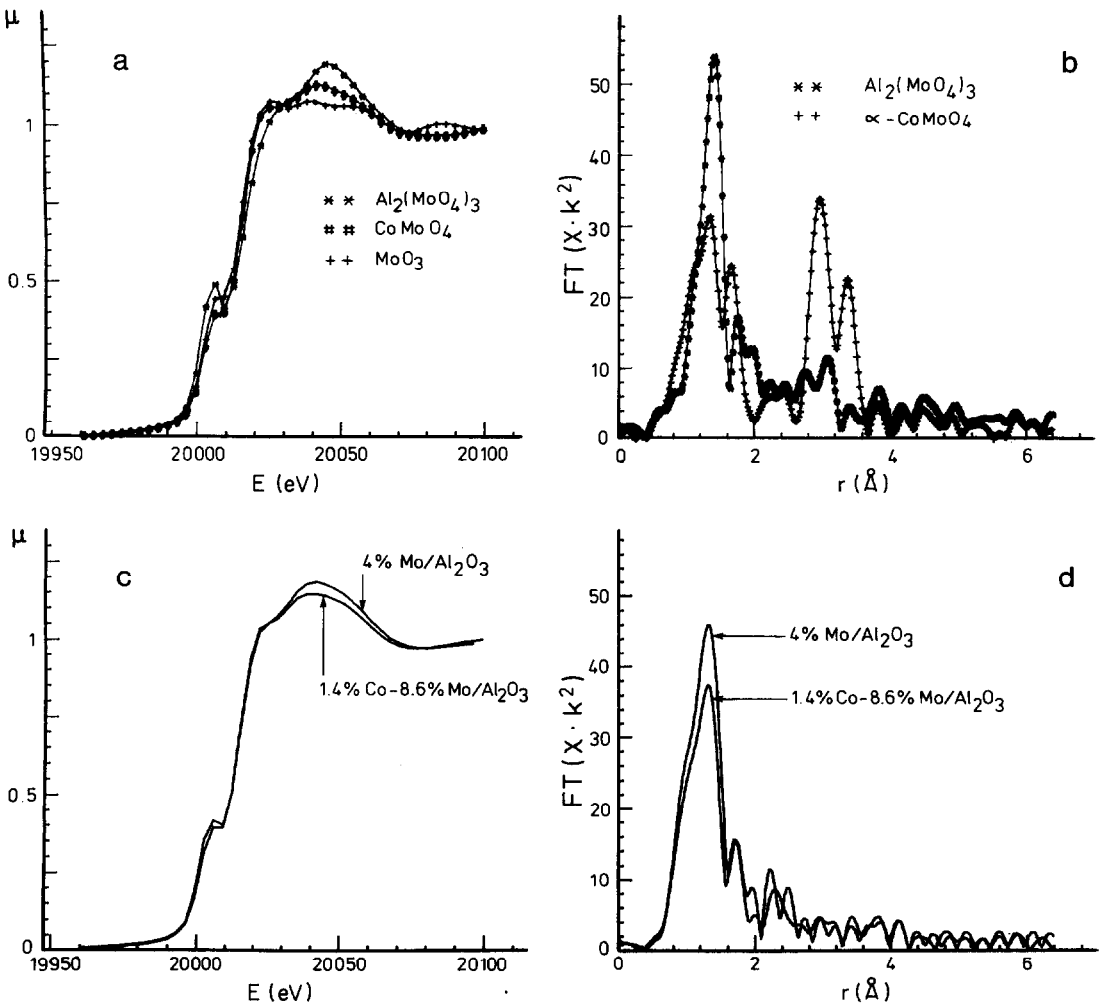


Fig. 1. Examples of X-ray absorption results of some model compounds and catalysts. Mo *K*-edge absorption spectra (a and c), and Fourier transforms of the Mo EXAFS (b and d). μ is the linear absorption coefficient of the sample, and χ is the normalized EXAFS.

Table 1. Bond lengths, R, and coordination numbers, N, obtained by fitting the Fourier-filtered Mo EXAFS of calcined catalysts

Catalyst	R (Å)	N
4% $Mo–Al_2O_3$	1.76	3.3
8.6% $Mo–Al_2O_3$	1.73	2.8
11.5% $Mo–Al_2O_3$	1.73	2.4
1.4% Co–8.6% $Mo–Al_2O_3$	1.74	3.0

amplitude functions of K_2MoO_4), the Mo—O bond lengths and coordination numbers listed in Table 1 were estimated for the calcined catalysts. The presence of Co was not observed to influence these parameters significantly, whereas the Mo loading is seen to have a small effect on the coordination number, the apparent value of which seems to decrease slightly with increasing Mo loading (Table 1).

Recent results by Chiu *et al.*[9] show the same trend and they interpreted their results in terms of an increased distortion of MoO_6 octahedra with increasing Mo loading. It should be stressed that, for disordered systems, the true coordination number is not trivial to obtain. Contrary to well-ordered compounds, where this parameter may be determined to an accuracy of about 10%, the uncertainty may be much larger in distorted systems due to the presence of non-Gaussian thermal as well as static disorder. Furthermore, since the Debye–Waller factor and the coordination number enter as a product in the expression used to fit the EXAFS, a change in the apparent coordination number may also be due to a change in the Debye–Waller factor. The apparent decrease in the observed coordination number with increasing Mo loading may therefore originate from the presence of larger entities of Mo species which have less interaction (and thus a smaller Debye–Waller factor) with the alumina support. This interpretation is in accordance with the observations[4–6] that by increasing the Mo loading the coordination changes from tetrahedral to octahedral, since the tetrahedrally coordinated Mo is generally believed to be bonded to the alumina surface via two oxygen atoms, whereas the octahedrally coordinated Mo atoms are assumed to be predominantly bridged to each other. The latter type of Mo species will presumably have less support interaction than the former.

The shape of the absorption edge itself also gives information on the local structure around the Mo atoms, although an unambiguous distinction between tetrahedral and octahedral coordination is not possible. The edge spectra of all the calcined catalysts show a weak peak or "shoulder" on the low-energy side of the edge. This peak is assigned to a $1s \rightarrow 4d$ transition which is allowed for Mo in a tetrahedral field but is also observed in compounds with Mo in a distorted octahedron of oxygen atoms.[9,18] Thus we can rule out the presence of Mo in a strictly octahedral field in these catalysts. It has recently been proposed that the relative intensity of another transition ($1s \rightarrow 5p$) can be used as a measure of the degree of distortion.[9]

The Fourier transform of the Co EXAFS for the calcined $Co–Mo–Al_2O_3$ catalyst shows only one strong peak. The absence of well-defined peaks outside the first coordination shell of oxygen atoms suggests that cobalt in the present calcined catalysts is not located in well-ordered surroundings like, for example, those found in Co_3O_4, CoO, $CoAl_2O_4$ or $CoMoO_4$. Rather, the results suggest that the Co atoms are present in a disordered phase. These results are in agreement with Mössbauer emission spectroscopy results.[11] From an analysis of the present EXAFS data, a Co—O bond length of about 1.99 Å and a coordination number of about 6 are found. In Ref. 10 a bond length identical to the above was reported, but a coordination number of 4 was given. The coordination number found presently is consistent with recent Mössbauer emission, magnetic and IR results,[11–13] which show that in the present catalysts (which have been calcined at rather low temperatures), the majority of Co atoms are present in octahedral surroundings probably in the surface layers of the alumina. The observed bond length of 1.99 Å is also in accordance with an octahedral location in the alumina [radius of holes in alumina: $(Me—O)_{oct} \sim 1.98$ Å and $(Me—O)_{tet} \sim 1.71$ Å].

Acknowledgements—We are grateful to HASYLAB for offering beam time on the synchroton radiation facility of DESY and for providing access to the EXAFS spectrometer at RÖMO.

REFERENCES

1. F. W. Lytle, G. H. Via and J. H. Sinfelt, In *Synchrotron Radiation Research* (Edited by H. Winick and S. Doniach), Chap. 12. Plenum Press, New York (1980).
2. P. Gallezot, In *Catalysis—Science and Technology* (Edited by J. R. Anderson and M. Boudart), Vol. 5, Chap. 4. Springer, Berlin (1984).
3. H. Topsøe and B. S. Clausen, *Catal. Rev.—Sci. Eng.* 1984, **26**, 395.
4. N. Giordano, J. C. J. Bart, A. Vaghi, A. Castellan and G. Martinotti, *J. Catal.* 1975, **36**, 81.
5. H. Knözinger and H. Jeziorowski, *J. Phys. Chem.* 1978, **82**, 2002.

6. J. Medema, C. van Stam, V. H. J. de Beer, A. J. A. Konings and D. C. Koninsberger, *J. Catal.* 1978, **53**, 386.
7. B. S. Clausen, H. Topsøe, R. Candia, J. Villadsen, B. Lengeler, J. Als-Nielsen and F. Christensen, *J. Phys. Chem.* 1981, **85**, 3868.
8. T. G. Parham and R. P. Merrill, *J. Catal.* 1984, **85**, 295.
9. N.-S. Chiu, S. H. Bauer and M. F. L. Johnson, *J. Catal.* 1984, **89**, 226.
10. G. Sankar, P. R. Sarode, A. Srinivasan, C. N. R. Rao, S. Vasudevan and J. M. Thomas, *Proc. Indian Acad. Sci. (Chem. Sci.)* 1984, **93**, 321.
11. C. Wivel, B. S. Clausen, R. Candia, S. Mørup and H. Topsøe, *J. Catal.* 1984, **87**, 497.
12. N.-Y. Topsøe and H. Topsøe, *J. Catal.* 1982, **75**, 354.
13. R. Candia, N.-Y. Topsøe, B. S. Clausen, C. Wivel, R. Nevald, S. Mørup and H. Topsøe, In *Proceedings of the Fourth International Conference on the Chemistry and Uses of Molybdenum* (Edited by H. F. Barry and P. C. H. Mitchell), p. 374. Climax Molybdenum Co., Ann Arbor, MI (1982).
14. N.-Y. Topsøe and H. Topsøe, *J. Catal.* 1982, **77**, 293.
15. C. Wivel, R. Candia, B. S. Clausen, S. Mørup and H. Topsøe, *J. Catal.* 1981, **68**, 453.
16. B. Lengeler and P. Eisenberger, *Phys. Rev.* 1980, **B21**, 4507.
17. B. Lengeler and R. Zeller, *J. Less-Common Met.* 1984, **103**, 337.
18. R. G. Shulman, Y. Yafet, P. Eisenberger and W. E. Blumberg, *Proc. Nat. Acad. Sci. U.S.A.* 1976, **73**, 1384.

Polyhedron Vol. 5, No. 1/2, pp. 203–210, 1986
Printed in Great Britain

0277-5387/86 $3.00 + .00
© 1986 Pergamon Press Ltd

INORGANIC-CHEMISTRY APPROACH TO THE PREPARATION OF SULFIDED "MIXED-PHASE" HYDROTREATING CATALYSTS USING THIOMETALATES AS PRECURSORS

W. ELTZNER, M. BREYSSE,* M. LACROIX and M. VRINAT

Institut de Recherches sur la Catalyse, Laboratoire Propre du CNRS, Conventionné à l'Université Claude Bernard, Lyon I, 2 Avenue Albert Einstein, 69626 Villeurbanne Cedex, France

(*Received* 17 *June* 1985)

Abstract—The application of bisthiometalato complexes of the type $[M'(MS_4)_2]^{n-}$ ($n = 2$ or 3, M' = Co or Ni, and M = Mo or W) as precursors for the preparation of hydrotreating catalysts was investigated. The thermal decomposition of the tetraethylammonium salts of these complexes in an H_2–H_2S atmosphere at 400°C leads to the formation of catalytically active materials which were characterized by physico-chemical methods and their catalytic activities in biphenyl hydrogenation. As the molecular structures of the starting complexes are known, the resulting catalysts can be discussed as "modified precursors". Structural models of these catalysts have been developed on the basis of this assumption and the present results.

In recent years discussion of the structure of the active centers in unsupported promoted group VI sulfides has gained special interest. This problem is still a matter of controversy in the literature and has led to the development of different models.[1–3] The CoMo-based catalysts have received the largest attention because of their widespread industrial application as HDS catalysts. The extensive work of Topsøe's group on this system has shown that a mixed "CoMoS phase" is present in unsupported and supported catalysts.[4,5]

The appearance of a "mixed phase" is discussed for catalysts prepared also by the "comaceration" method (CM),[6] as for those prepared by "homogeneous sulfide precipitation" (HSP).[4] Interesting results concerning the structure of the "mixed phase" have been found by the use of Mössbauer emission spectroscopy and EXAFS on unsupported samples,[7] suggesting that the CoMoS phase could be regarded as an MoS_2 structure with Co atoms located at the edge positions. Nevertheless the discussion about the composition and constitution of CoMoS, CoWS, NiMoS and NiWS "mixed phases" has not yet led to a complete description. A reason for this may be the insufficiently well characterized precursor states of these catalysts. As in both preparation methods (CM and HSP) a great part of aqueous solution chemistry is involved, it is surprising that little is known concerning the chemistry of aqueous M', M and S^{2-} mixtures. With the CM method the formation of a large variety of species is limited by the "insolubility" of Co_3O_4 in this medium, whereas, in the case of the HSP method, depending on the pH of the metal salt solution, the formation of several different species (e.g. heteropolyanions, thioanions and metal sulfur clusters) besides M' or M sulfides come into consideration.

Our new approach to this problem consists in using well-defined tetraethylammonium salts of $[M'(MS_4)_2]^{n-}$ ($n = 2$ or 3) complexes as precursors which can be easily synthesized in each combination of M' = Co or Ni with M = Mo or W. The tetraethylammonium cation was choosen as its facile decomposition into volatile products on heating could be assumed.[8]

All these complexes isolated from aqueous or organic solutions can be obtained pure and in high yields (70–95%).

As already mentioned, almost all of these complexes are structurally characterized by single-crystal X-ray analysis.[9,10] Two representative examples of the structure are given in Fig. 1.

Interestingly the Co—S distance in

* Author to whom correspondence should be addressed.

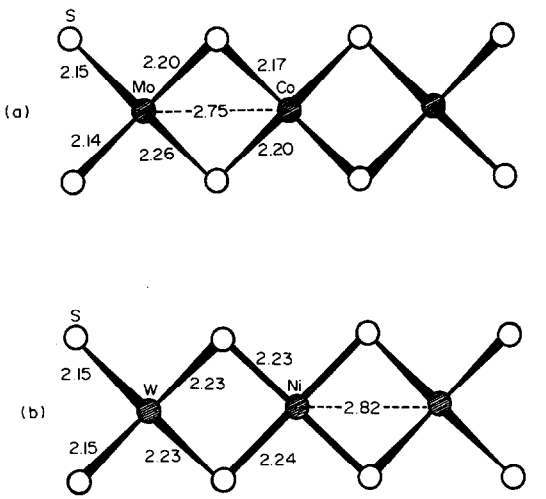


Fig. 1. Schematic representation of the structures of: (a) $[Co(MoS_4)_2]^{3-}$,[9] and (b) $[Ni(WS_4)_2]^{2-}$.[10]

$[Co(MoS_4)_2]^{3-}$ (~2.2 Å) is of the same order as the one found by EXAFS spectroscopy (Co-K_α edge) in CoMoS catalysts (~2.3 Å), and also the coordination number around Co in the first shell (4.6)[7] is almost equal to the molecular model. These structural similarities and the recent patent claims[11] gave rise to the investigation of bisthiometalato complexes as catalyst precursors. In order to obtain comparable catalysts, the tetraethylammonium salts were decomposed thermally in a flow of H_2–H_2S (15%) at 400°C. The decomposition was controlled by DTA–TG and the solid products were characterized by XRD, XPS, VIS spectroscopy and catalytic tests of biphenyl hydrogenation.

EXPERIMENTAL

Preparation of the complexes

According to the general equation:

$$2(Et_4N)^+ + M'^{2+} + 2MS_4^{2-} \rightarrow (Et_4N)_2[M'(MS_4)_2] \quad (1)$$

bisthiometalato complexes with M' = Ni and M = Mo or W can be isolated from aqueous solutions.[10] $(Et_4N)_3[Co(MoS_4)_2]$ (**1**) was prepared in an organic solvent (CH_3CN) using thiophenol as reducing agent.[12] The syntheses of $(Et_4N)_2[Co(WS_4)_2]$ (**2**), $(Et_4N)_2[Ni(MoS_4)_2]$ (**3**) and $(Et_4N)_2[Ni(WS_4)_2]$ (**4**) were carried out in deoxygenated water under an argon atmosphere. All chemicals used were of p.a. quality. Organic solvents used were of reagent grade, dried using standard procedures. $(NH_4)_2MoS_4$ and $(NH_4)_2WS_4$ were prepared by literature methods.[13,14] As an example, the preparation of **3** is given:

Preparation of **3**. To an aqueous solution (150 cm^3) of $Ni(NO_3)_2 \cdot 6H_2O$ (2.91 g, 10 mmol) and Et_4NBr (4.20 g, 20 mmol) an aqueous solution (150 cm^3) of $(NH_4)_2MoS_4$ (5.20 g, 20 mmol) was added dropwise under stirring. The dark-brown precipitate was washed with water, ethanol and ether, and dried *in vacuo* over P_4O_{10}.

2 and **4** were synthesized similarly.

Pretreatment of the precursor

The complexes obtained by the described procedures were decomposed under a reducing atmosphere [H_2–H_2S(15%)] during 4 h at 400°C. After cooling to room temperature under the same atmosphere, the catalysts were purged with N_2 and stored in sealed bottles under argon. This procedure was chosen in order to treat the complexes in the same manner as the HSP precursor.

Physico-chemical and catalytic measurements

Thermogravimetric experiments were performed using a Sartorius 4102 Microbalance and the DTA measurements were obtained against γ-Al_2O_3 as reference.

Electronic spectra of solutions and the solids (using an integrating sphere) were recorded with a Varian Carry 219 spectrometer.

XPS measurements were carried out with a Hewlett–Packard spectrometer using monochromatic Al-K_α radiation. Charge compensation on the complex precursor was effected by an electron floodgun and the values were calibrated to C1*s* = 284.5 eV as internal standard.

XRD experiments on powdered samples were performed using Co-K_α radiation (λ = 1.54178 Å).

The catalytic activities were determined during the hydrogenation of biphenyl (BP). This reaction test was carried out in the vapour phase using a dynamic high-pressure microreactor working at 22.5 $\times 10^5$ Pa. The partial pressure of BP was 8×10^2 Pa. A small amount of H_2S ($P_{H_2S} = 4.5 \times 10^2$ Pa) was added to the gas flow in order to maintain the sulfidation degree of the catalyst. The specific rate A_s is calculated using the following equation:

$$A_s = Q \cdot \frac{\tau}{m} \text{ (mol s}^{-1}\text{ g}^{-1}\text{)}, \quad (2)$$

with Q = BP flow (mol s^{-1}), τ = conversion, and m = weight of catalyst (g).

The intrinsic rate, A_i, is defined by A_s/S, in which S is the surface area of the sample. In a typical run the

specific rate was determined at 257°C in the pseudo-stationary state.

In order to estimate the stability of the catalyst, a catalytic run was performed at 400°C. After 16 h on stream, the reaction temperature was decreased to 257°C and the percentage of activity loss observed was calculated by eqn (3):

$$\Delta r = \frac{A_b - A_a}{A_b} \quad \text{(at 257°C)}, \qquad (3)$$

with A_b = BP hydrogenation rate at 257°C before the test at 400°C, and A_a = BP hydrogenation rate at 257°C after the test at 400°C.

RESULTS AND DISCUSSION

Thermal analysis

The thermal decomposition of the $(Et_4N)_n[M'(MS_4)_2]$ ($n = 2$ or 3) salts were studied in the range of 25–600°C under an inert gas atmosphere. The results given in Table 1 show that decomposition steps occur between 200 and 300°C in connection with endothermic reactions.

In the cases of **2–4** the total weight losses obtained at 400°C correspond to the loss of 2 mol triethylamine and 1 mol diethylsulfide (**2** and **3**) or diethyldisulfide (**4**) which could also be identified chemically. The same decomposition products were also obtained by the thermal decomposition of simple tetraethylammonium tetrathiomolybdates.[8] Therefore the general equation for the thermal decomposition of **2–4** can be given as follows:

$$(Et_4N)_2[M'(MS_4)_2] \xrightarrow{\Delta T} 2Et_3N + Et_2S \text{ (or } Et_2S_2) + M'M_2S_{6-7}. \qquad (4)$$

From chemical analysis and the TG experiments we deduce the following reaction scheme for the decomposition of **1** in an N_2 atmosphere:

$$(Et_4N)_3[Co(MoS_4)_2] \xrightarrow{\Delta T} 3Et_3N + Et_2S + \tfrac{1}{2}Et_2S_2 + CoMo_2S_6. \qquad (5)$$

The same experiments were also performed under an H_2–H_2S (15%) atmosphere. As in these cases the weight losses at 400°C are slightly higher, the loss of 1 mol H_2S in addition to the above-mentioned products had to be assumed. These treatments led to solids with the analytical composition $M'M_2S_{5-6}$.

The results show that these compounds decompose at moderate temperatures under the formation of volatile products which mainly originate from the quaternary alkylammonium cation.

Catalytic activities

Table 2 presents the activities of the different catalysts prepared either by decomposition of the complexes or by using the HSP method. Both kind of catalysts present the same deactivation curve but their extent is much lower than the one previously reported for unpromoted catalysts prepared by the decomposition of ammonium thiometalates.[15] As for these unpromoted samples, a large part of the deactivation has been attributed to catalyst sintering. Surface areas have been measured after the catalytic run.

From the results reported in Table 2 the following conclusions can be drawn:

(a) independently of the preparation method, the

Table 1. TG–DTA results of the thermal decomposition of the $(Et_4N)_n[M'(MS_4)_2]$ salts ($n = 2$ or 3, M' = Co or Ni, M = Mo or W) in an N_2 atmosphere

Complex[a]	Decomposition step (°C)	Total weight loss at 400°C[b] (%)	Assignment of decomposition products
1	220 (endo) 260 (endo)	51.0 (50.7)	$3Et_3N + Et_2S + \frac{1}{2}Et_2S_2$
2	215 (endo) 230 (endo)	31.0 (31.0)	$2Et_3N + Et_2S$
3	210 (endo)	37.5 (38.1)	$2Et_3N + Et_2S$
4	260 (endo)	32.5 (31.0)	$2Et_3N + Et_2S$

[a] **1**, $(Et_4N)_3[Co(MoS_4)_2]$; **2**, $(Et_4N)_2[Co(WS_4)_2]$: **3**, $(Et_4N)_2[Ni(MoS_4)_2]$; **4**, $(Et_4N)_2[Ni(WS_4)_2]$.

[b] Values given in parentheses are calculated according to eqns (4) and (5).

Table 2. Activity measurements for biphenyl hydrogenation[a]

Catalyst[b]	S ($m^2\ g^{-1}$)	A_s (10^8 mol $s^{-1}\ g^{-1}$)	A_i (10^8 mol $s^{-1}\ m^{-2}$)	Δr (%)
CoMoS (e.c.)	47	22.5	0.5	58
CoMoS (HSP)	22	6.3	0.28	50
NiMoS (e.c.)	1	1.6	1.6	68
NiMoS (HSP)	14	19.0	1.3	78
NiWS (e.c.)	3	10.2	3.4	23
NiWS (HSP)	10	14.0	1.4	25
MoS_2[c]	—	—	0.16	—
WS_2[c]	—	—	0.21	—

[a] S, surface area: A_s, specific rate of biphenyl hydrogenation; A_i, intrinsic rate ($=A_s/S$); Δr, activity loss according to eqn (3).

[b] e.c., catalysts obtained from bisthiometalato complexes; HSP, catalysts prepared by the HSP method.

[c] See Ref. 15.

hydrogenation activities follow the order NiWS > NiMoS ≫ CoMoS;

(b) the presence of Ni greatly promotes the hydrogenation function, whatever the preparation method;

(c) the decomposed bisthiometalato complexes lead to catalysts having an activity 2–3 times higher than the corresponding HSP samples; and

(d) for a given MM′ system, the same activity loss is observed after a catalytic test at 400°C.

The former observation refers to the stability of the active species under hydrogen atmosphere. Breysse *et al.*[16] have shown on HSP samples that, for example, the active "CoMoS phase" segregates into Co_9S_8 and MoS_2 under the applied conditions of high temperature, pressure and a reducing atmosphere. This phase segregation decreases drastically the amount of active sites and consequently the catalytic activity.

Recently we have also evidenced the same trend for a series of NiWS catalysts[17] in which the nickel concentration, defined by the atomic ratio Ni/(Ni + W), varied from 0.1 to 0.8.

This phase segregation is not surprising, as, according to Topsøe's model, the promoter atoms (Co or Ni) are located at the edge planes of lamellar MoS_2 or WS_2. The similar kinetic results obtained on samples with different precursors (HSP and complexes) suggest that the same kinds of active centers are responsible for the catalytic activity. The higher efficiency observed with the ex complex samples favors a higher amount of Co or Ni involved in the "mixed phase", meaning most probably that the promoter atoms are not only located at the edge positions of MoS_2 but are also distributed throughout the "entire" structure of the group VI sulfide.

X-ray analysis

The samples obtained after thermal decomposition of the complexes in an H_2–H_2S (15%) atmosphere and after the catalytic test were investigated by X-ray powder diffraction. Generally, the curves of the decomposed complexes resemble the results obtained on thermally decomposed diammonium tetrathiomolybdate[18] and -tungstate.[19]

Two examples of X-ray intensity curves of the CoMoS and NiWS catalysts before and after a catalytic run are presented in Fig. 2.

For the decomposed complexes (upper curves) the scattering curves of both samples show the same features as almost completely X-ray amorphous group VI disulfides. Only very broad maxima at about 14, 33 and 58° (2θ) are observed, which correspond well with those obtained on a-MoS_2 and a-WS_2. In the case of crystalline group VI disulfides these maxima can be attributed to the (002), (100, 101) and (110) Bragg reflections, respectively. Several attempts have been made to get more structural information on CoMoS[7] and also NiWS[20] "mixed phases" by the use of EXAFS spectroscopy and RDF calculations. The EXAFS investigations of Topsøe *et al.*[3] showed that the presence of the promoter atom Co in the CoMoS "mixed phase" was indicated by a peak at $r \sim 2.3$ Å, which was assigned to a Co—S distance, but also that, in spite of the presence of Co, the MoS_2 structure dominates.

Contrary to this, a comparison with the X-ray

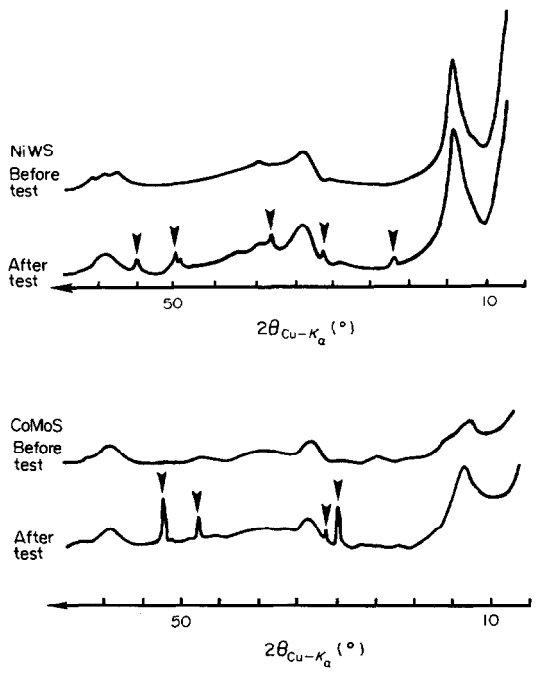


Fig. 2. X-ray intensity curves of NiWS and CoMoS ex complex samples before and after catalytic test (the arrows indicate the reflexions of Ni_3S_2 and Co_9S_8).

patterns of the corresponding binary sulfides showed that "badly crystalline" molybdenum disulfide and tungsten disulfide and crystalline Co_9S_8 or Ni_3S_2 were present in the samples after a catalytic test. Co_9S_8 and Ni_3S_2 are the thermodynamically most stable sulfides of these metals under these conditions[21,22] ($T = 400°C$, $P_{H_2} = 23 \times 10^5$ Pa). This behavior was in accordance with the observed activity loss and showed that severe structural changes occur, i.e. a partial destruction of the active phase.

Electron spectroscopy

Diffuse-reflectance spectra. Complexes of the type $[M'(MS_4)_2]^{n-}$ possess unique electronic properties characterized by a strong $M' \rightarrow MS_4$ electron delocalization.[10] The deeply coloured tetrathiometalates show electron absorption bands in the visible region where the lowest-energy bands were assigned to a $T_1 \rightarrow 2E$, i.e. $L \rightarrow M$, charge-transfer transition. It could be shown that, on co-ordination to a heterometal center, mainly the lowest-energy band, ν_1, of the free tetrathiometalato ligand was affected. For example a splitting into two bands at higher and lower energies compared to ν_1 could be obtained in the spectra of $[M'(MS_4)_2]^{n-}$ complexes which was proposed to be due to the non-equivalence of the sulfur atoms in the complexes.[23] The diffuse-reflectance spectra recorded from the complex precursor and the catalysts before test of the CoMoS and NiWS samples (Fig. 3) showed also the predicted splitting of the ν_1 charge-transfer band.

Surprisingly the catalysts before testing present a similar splitting (more pronounced in the spectrum of the NiWS sample) which cannot be easily explained but may also be due to the different $S(3p) \rightarrow M(nd)$ transitions.

XPS measurements. In order to get more insight into the electronic properties, especially of the NiWS system, the XPS of the starting complex and the catalysts before and after testing were taken. These results were compared with those obtained for a

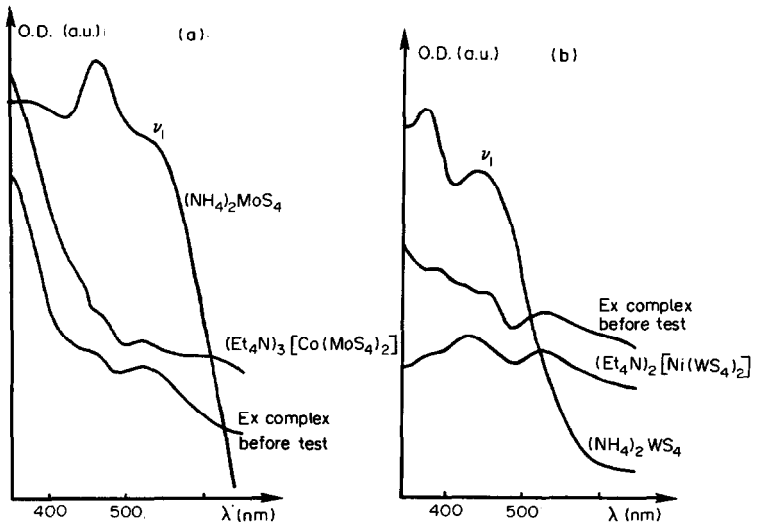


Fig. 3. Diffuse-reflectance spectra of: (a) CoMoS samples, and (b) NiWS samples in comparison with the corresponding tetrathiometalates (MgO reference).

Table 3. XPS data

Compound	Binding energy (eV)[a]		
	$S2p_{3/2}$	$W4f_{7/2}$	$Ni2p_{3/2}$
$(Et_4N)_2[Ni(WS_4)_2]$	161.5[b]	32.9	853.9
Ex complex, before test	161.9	32.3	854.1
Ex complex, after test	162.0	32.4	854.7
NiWS (HSP)	161.9	32.3	854.3
NiS	161.6	—	853.3
Ni_3S_2	161.8	—	853.0
WS_2	161.9	32.4	—

[a] Relative to C1s = 285.0 eV of the Et_4N^+ cation.
[b] Broad; no resolution of $S2p_{1/2}$ and $S2p_{3/2}$ levels.

NiWS sample prepared by the HSP method, WS_2 and NiS (Table 3).

Concerning the S2p binding energies (BEs) no large deviations from the mean value of $S2p_{3/2} \simeq$ 161.9 eV were measured for the different samples except for the complex precursor **4** ($S2p_{3/2}$ = 161.5 eV). The value of $S2p_{3/2} \simeq$ 161.9 eV is characteristic for S^{2-} ligands with a high co-ordination number whereas in **4** two different types of S^{2-} ligands (μ_2-S^{2-} and $S^{2-}_{term.}$) exist. (A dependence of the BE of S^{2-} ligands on the co-ordination number was shown recently in a series of molybdenum–sulfur complexes.[24]) This situation may be responsible for the fact that only a broad band at 161.5 eV without the typical resolution into the $S2p_{1/2}$ and $S2p_{3/2}$ levels could be measured.

Again the BE measured for the $W4f_{7/2}$ levels (~32.4 eV) of all compounds except for **4** [formally W(VI)], are representative for a W(IV) oxidation state. Similar results and also a higher value for **4** $W4f_{7/2}$ BE = 32.9 eV) were published recently.[25]

Interestingly the trend observed for S2p and W4f electron BEs is not as straight concerning the $Ni2p_{3/2}$ core levels (Table 2 and Fig. 4).

NiS serves as a reference for a compound with only Ni(II) in a sulfur environment ($Ni2p_{3/2}$ BE = 853.3 eV). As **4** ($Ni2p_{3/2}$ BE = 853.9 eV) reflects a situation of $M' \rightarrow MS_4$ electron delocalisation this fact seems to be also valid for the catalyst before testing ($Ni2p_{3/2}$ BE = 854.1 eV). Even in the case of the catalyst after testing, where the presence of Ni_3S_2 was detected by X-ray methods, the unexpectedly high value of $Ni2p_{3/2}$ (854.7 eV) and the large half-width of the peak probably indicate the existence of Ni in several oxidation states. Contrary to this the catalyst before test shows a half-width of the band which is comparable to that found in NiS.

The valence band spectra given in Fig. 5 will be discussed only qualitatively as no exact estimation of

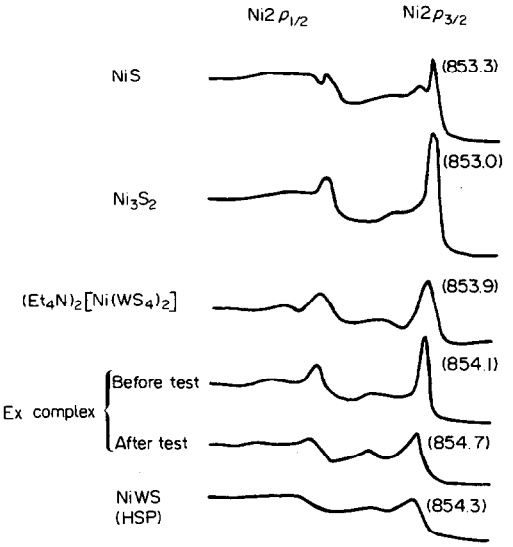


Fig. 4. XPS of different NiWS catalysts and Ni sulfides in the region of Ni2p electron energy levels. Binding energies are given in parentheses.

the Fermi level was performed. In the case of NiS and WS_2 we found, according to the literature,[26,27] a pronounced separation of the highest Mnd band from the bands arising from Mnd–S3p MOs and S3p levels, which again are separated from the S3s bands. The catalyst before test presents an almost unique valence band spectrum. No distinct separations of the bands are observed, but only an envelope type curve between 0 and 10 eV. This high density of states

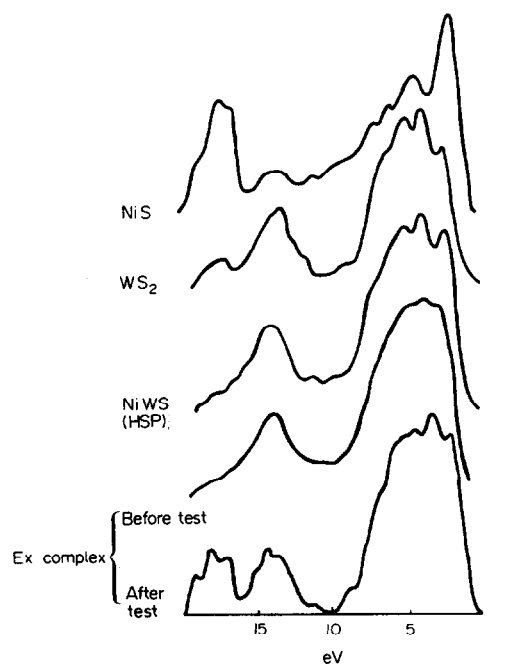


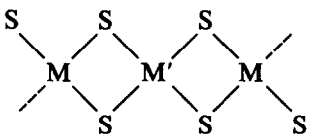
Fig. 5. XP valence band spectra.

may be discussed as a consequence of the mixing of Ni3*d* energy levels into the W4*d*–S3*p* band. The valence band spectrum of the sample after testing is almost identical to that of NiWS (HSP). Interestingly both samples possess the same catalytic activity.

Generally the features of the valence band spectra of transition-metal sulfides can be approximately represented by the use of simple MO considerations on the basis of an $[MS_6]^{n-}$ model in which the metal is octahedrally co-ordinated by six sulfur atoms.[28] In the spectra of simple 3*d* transition-metal sulfides the tendency of a decreasing gap (going from left to right in the 3*d* period) between the bands corresponding to the HOMO (mainly M*nd*-localized) and the sulfur π-band (nonbonding Sπ-orbitals) occurs, whereas the gap between the bands arising from nonbonding Sπ-orbitals and mixing of M*nd*–Sπ orbitals is always very narrow. If one treats the mixed-sulfide systems (CoMoS, NiWS etc.) as if the MOs of an $[MS_6]^{n-}$ (M = Mo or W) complex are perturbed by M'3*d* (M' = Co or Ni) levels, one can easily imagine that a higher density of states and a mixing of M'3*d* orbitals into M4*d*–S3*p* orbitals may occur. The envelop type curve in the region between 0 and 10 eV of the NiWS (ex complex) system seems to indicate this possibility. One short comment will be given on the presence of peaks with varying intensity in the region of 17–18 eV in NiS, WS_2 and the catalyst after testing. A plausible explanation may be the presence of S_2^{2-} groups.[29] As the penetration of the radiation used several Ångströms, S_2^{2-} groups may be present at the surface of the solids.

Structural models

Regarding the results obtained on the catalysts with complex precursor, a structural model of the "mixed-phase" M'MS, containing "paradigmatic"



units, already present in the precursor state, was developed.

For two models the X-ray intensity curves were calculated[30] using Debye's equation. The calculation of the X-ray curve of a given model is in principle the reverse procedure as the calculation of the radial distribution function from an experimental curve.

Our calculations were performed on the NiWS system as this catalyst showed the highest catalytic activity and the atomic co-ordinates of the complex $[Ni(WS_4)_2]^{2-}$ were available.[31] The results obtained on this system may be also valid for the NiMoS and CoMoS catalysts.

Model a consists of 10 units as drawn above, arranged in a chain-like manner. In order to have a "realistic" co-ordination number on tungsten the model was modified in the way that between each W–W pair an S_2^{2-} group was introduced. The following distances were taken from the single-crystal X-ray structure of **4**: d(M—M') = 2.82, d(M—M) = 2.96, d(M—S) and d(M'—S) = 2.24,[10] and $d(S—S)_{S_2^{2-}}$ = 2.00 Å.

The second model (b) consists of two parallel chains (d_{ch-ch} = 6.5 Å) of model a, where the chains are shifted against each other by about 4.3 Å. This type of arrangement represents a part of a WS_2 layer structure, in which certain positions of W atoms are substituted by Ni. The calculated X-ray intensity curves of the models a and b together with the experimental curves of the NiWS catalyst before testing and amorphous WS_2 are given in Fig. 6.

The difference between the single-chain model (a) (curve a) and model b (curve b) is demonstrated by an enhancement of the maximum at $2\theta \sim 14°$. The fact that curve b shows a better correlation with the experimental curve c, and the similarity of curves c and d suggests that some type of substituted WS_2 layer structure is present in the catalyst.

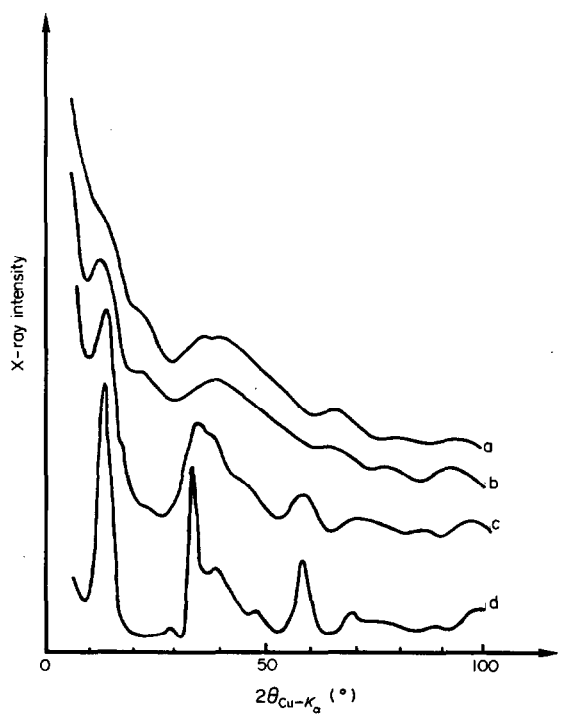


Fig. 6. X-ray intensity curves of: (a) model a (see text), (b) model b (see text), (c) NiWS ex complex before test, and (d) amorphous WS_2.

CONCLUSIONS

From the physico-chemical and catalytic results the following conclusions can be drawn:

(a) Concerning the different precursor preparation methods (CM, HSP or complexes) of unsupported, promoted hydrotreating catalysts, undoubtedly the bisthiometalato complexes are the best defined ones. They can be isolated as the *only* species from simple procedures.

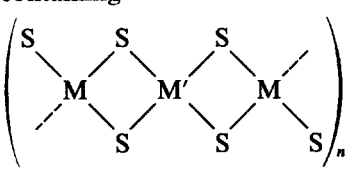
(b) The catalysts obtained after thermal decomposition of the complexes in an H_2–H_2S atmosphere show a catalytic activity in the hydrogeneration of BP, which is 2–3 times higher than those prepared by the HSP method.

(c) As the deactivation behavior of these catalysts is similar to those prepared by conventional methods, the same nature for the catalytic active sites is suggested.

(d) The XRD results show the amorphous character of the active catalysts. Under the conditions of a catalytic test, "crystallization" occurs, and simultaneously the activity decreases.

(e) The electronic properties of the catalysts resemble those of the complex precursor, i.e. of electron-delocalized systems $M' \rightarrow MS_n$, which was evidenced by the unique features of the VIS, XPS and valence band spectra.

(f) The fact that not only the final states (after a catalytic test) but also the precursor states are structurally characterized enables us to propose a model of the intermediate states (catalysts before testing). This model is related to the structure of the precursor containing



units supposed to be characteristic of the bulk catalyst.

Acknowledgements—W.E. is grateful to the CNRS for financial support. We thank Dr R. Jostes for carrying out the calculations on the NiWS model.

REFERENCES

1. A. L. Farragher and P. Cossee, In *Proceedings of the 5th International Congress on Catalysis* (Edited by J. W. Hightower). Elsevier, Amsterdam (1973).
2. B. Delmon, *Am. Chem. Soc., Div. Pet. Chem.* 1977, 503.
3. H. Topsøe, B. S. Clausen, R. Candia, C. Wivel and S. Mørup, *J. Catal.* 1981, **68**, 433.
4. R. Candia, B. S. Clausen and H. Topsøe, *Bull. Soc. Chim. Belg.* 1981, **90**, 1225.
5. H. Topsøe, B. S. Clausen, R. Candia, C. Wivel and S. Mørup, *J. Catal.* 1981, **68**, 453.
6. C. Hagenbach, P. Courty and B. Delmon, *J. Catal.* 1971, **23**, 259.
7. B. S. Clausen, H. Topsøe, R. Candia and B. Lengeler, *Am. Chem. Soc. Symp. Ser.* 1984, **248**.
8. M. J. F. Leroy, G. Kaufmann, R. Charlionet and R. Rohmer, *C. R. Acad. Sci., Ser. C* 1966, **263**, 601.
9. A. Müller, W. Hellmann, C. Römer, M. Römer, H. Bögge, R. Jostes and U. Schimanski, *Inorg. Chim. Acta* 1984, **83**, L75.
10. A. Müller, E. Diemann, R. Jostes and H. Bögge, *Angew. Chem., Int. Ed. Engl.* 1981, **20**, 934 (and literature cited therein).
11. European Patent 124-344-A (1983).
12. W.-H. Pan, D. C. Johnston, S. T. McKenna, R. R. Chianelli, T. R. Halbert, L. L. Hutchings and E. I. Stiefel, *Inorg. Chim. Acta* 1985, **97**, L17.
13. G. Krüss, *Justus Liebigs Ann. Chem.* 1884, **225**, 6.
14. E. Corleis, *Justus Liebigs Ann. Chem.* 1886, **232**, 264.
15. R. Fréty, M. Breysse, M. Lacroix and M. Vrinat, *Bull. Soc. Chim. Belg.* 1984, **93**, 663.
16. M. Breysse, R. Fréty, M. Vrinat, P. Grange and M. Genet, *Appl. Catal.* 1984, **12**, 165.
17. M. Lacroix, M. Vrinat and M. Breysse, submitted for publication.
18. J. C. Wildervank and F. Jellinek, *Z. Anorg. Allg. Chem.* 1964, **328**. 309.
19. R. J. H. Voorhoeve and H. B. M. Wolters, *Z. Anorg. Allg. Chem.* 1970, **376**, 165.
20. E. A. Moroz, S. V. Bogdanov, S. V. Tsybulya, V. A. Burmistov, A. N. Startsev and Yu. I. Yermakov, *Appl. Catal.* 1984, **11**, 173.
21. E. Dönges, *Z. Anorg. Chem.* 1947, **254**, 267.
22. R. H. Griffith and S. G. Hill, *J. Chem. Soc.* 1938, 717.
23. R. Jostes, Dissertation, Universität Bielefeld (1984).
24. W. Eltzner, Neue Aspekte der Komplexchemie des Molybdäns, Wissenschafl. Reihe, Bd. 23, B. Kleine, Bielefeld (1984).
25. A. P. Shepelin, P. A. Zhdan, V. A. Burmistov, A. N. Startsev and Yu. I. Yermakov, *Appl. Catal.* 1984, **11**, 29.
26. J. Gopalakrishnan, T. Murugesan, M. S. Hedge and C. N. R. Rao, *J. Phys. C* 1979, **12**, 5255.
27. G. K. Wertheim, F. J. Di Salvo and D. N. E. Buchanan, *Solid State Commun.* 1973, **13**, 1225.
28. S. Harris, *Chem. Phys.* 1982, **67**, 229.
29. H. van der Heide, R. Hemmel, C. F. van Bruggen and C. Haas, *J. Solid State Chem.* 1980, **33**, 17.
30. E. Diemann and R. Jostes, DEBYE, Fortran IV program, unpublished.
31. A. Müller, personal communication.

Polyhedron Vol. 5, No. 1/2, pp. 211–217, 1986
Printed in Great Britain

0277-5387/86 $3.00 + .00
© 1986 Pergamon Press Ltd

LOW-TEMPERATURE SYNTHESIS OF MIXED NiMo SULFIDES: STRUCTURAL, TEXTURAL AND CATALYTIC PROPERTIES

F. B. GARREAU and H. TOULHOAT*

Institut Français du Petrole, B.P. 311, 92506 Rueil Malmaison Cedex, France

S. KASZTELAN

Laboratoire de Catalyse Homogène et Hétérogène, UA CNRS 402, Université des Sciences et Techniques de Lille, 59655 Villeneuve d'Ascq Cedex, France

and

R. PAULUS†

Institut de Recherche sur la Catalyse, CNRS, 2 Avenue Albert Einstein, 69026 Villeurbanne Cedex, France

(*Received* 18 *June* 1985)

Abstract—Unsupported NiMo sulfide catalysts are prepared by an original coprecipitation technique performed at low temperature. Studies by several surface investigation techniques (X-ray diffraction, electron microscopy, O_2-chemisorption, and X-ray photoelectron and ion-scattering spectroscopy) provide a good qualitative picture of these catalysts. The existence of an Ni–Mo–S mixed phase is observed over the whole range of composition. This MoS_2-like structure is supported on Ni_xS_y if $Ni/(Ni+Mo) > 0.25$, resulting in an enhancement of catalytic activities (on hydrogenolysis and hydrogenation). These results are discussed with respect to the geometrical model of hydrotreating catalysts. This work points out the extreme importance of the degree of exposure of active edges of the Ni–Mo–S phase on the overall activity.

Even if unsupported catalysts have much less industrial application than supported catalysts, studies on these materials are of great interest because the active-phase characterization is not modified by the presence of the support.

Different authors have prepared mixed-sulfide catalysts by several methods: sulfidation of coprecipitated oxides,[1,2] the comaceration method described by Hagenbach *et al.*,[3,4] or homogeneous sulfide precipitation (HSP) described by Candia *et al.*[5]

With these various preparation techniques, the authors obtained different results, but, generally, complete structural descriptions of their samples are not available, and unitary interpretation of their activity results is not possible. In order to study the state of Ni in unsupported catalysts, we have developed a new method of preparation,[6–8] which is to some extent similar to the HSP method. This paper deals with catalytic results obtained on that new generation of unsupported catalysts, related to their structure; new aspects of the phase relationships in the metastable low-temperature ternary Ni–Mo–S system are demonstrated.

EXPERIMENTAL

Catalysts of various atomic ratios {r [Ni/(Ni + Mo)] = 0–1} obtained directly in sulfided forms, at low temperature, were subjected to a multi-technique analysis approach:

(a) catalytic-activity determinations for the

* Author to whom correspondence should be addressed.
† Present address: Société des Electrodes et Réfractaires de Savoie, 73260 Aigueblanche, France.

following reactions: (i) atmospheric-pressure hydrogenolysis of dibenzothiophene (DBT) at 513 K,[6] (ii) high-pressure hydrogenolysis of DBT at 24×10^5 Pa and 530 K,[6] and (iii) high-pressure hydrogenation of toluene at 60×10^5 Pa and 623 K.

(b) textural measurements (porosity and BET).

(c) physical investigations using various surface techniques: high-resolution electron microscopy (HREM) (JEOL 120X), analytical electron microscopy (AEM) (VG HB5), X-ray diffraction (XRD), X-ray photoelectron spectroscopy (ESCA) (AEI ES 200B spectrometer), ion-scattering spectroscopy (ISS) (LEYBOLD LH-S10), and O_2-chemisorption.

CATALYTIC RESULTS

Specific activity patterns of our mixed NiMo sulfides are shown in Fig. 1 for atmospheric-pressure HDS of DBT, high-pressure HDS or DBT and toluene hydrogenation. Reference activities of an industrial NiMo catalyst are reported for each reaction.

A maximum activity is obtained for $r = 0.7$. This ratio is unusual for such catalysts. On the three reaction diagrams, Mo efficiency increases with the increase in Ni content. However, the variation is not linear and we can consider two catalytic regions: the Mo-rich region, $r < 0.3$, for which all activities are low, and the Ni-rich region for which activities are high.

The comparison with the commercial NiMo–Al_2O_3 catalyst (Fig. 1) shows two different activity behaviours for unsupported catalysts, one for hydrogenolysis reactions, and one for the hydrogenation reaction.

Although our unsupported NiMo catalysts have a low activity in DBT hydrogenolysis our Ni-rich catalysts are more active in toluene hydrogenation than the industrial NiMo–Al_2O_3 catalyst [Fig. 1(c)]. The activities in toluene hydrogenation of the industrial catalyst and our NiMo catalyst of the

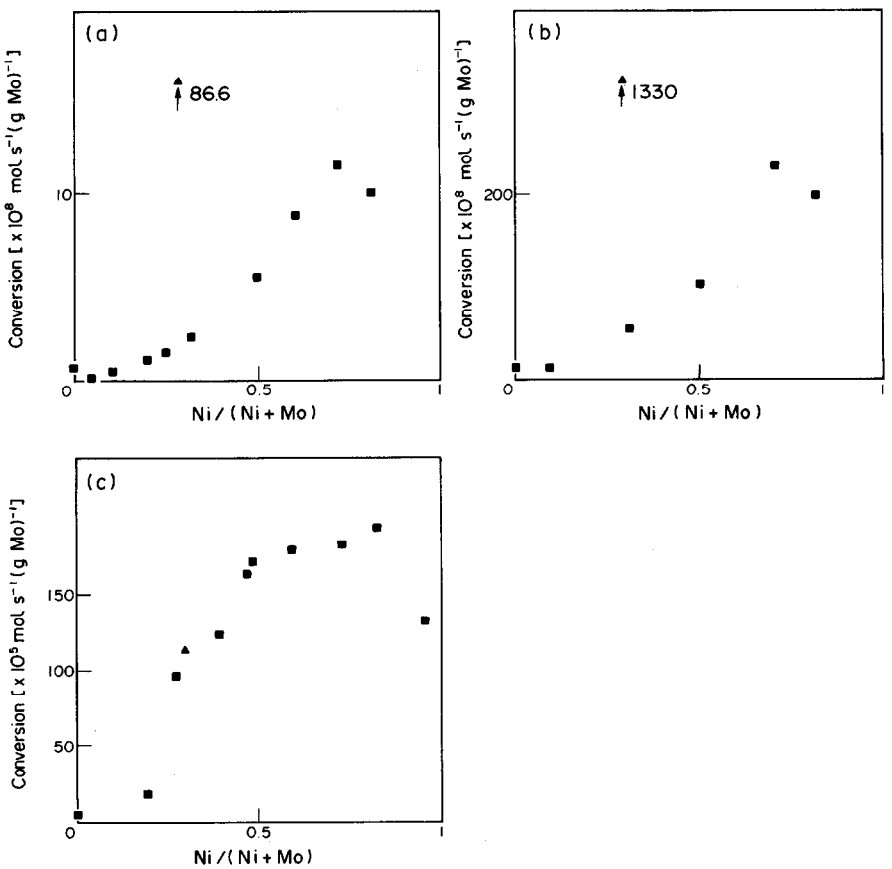


Fig. 1. Catalytic activities of NiMo catalysts. Conversion vs mole fraction Ni for: (a) dibenzothiophene HDS at 1 atm, 513 K; (b) dibenzothiophene HDS at 24×10^5 Pa, 530 K; and (c) toluene hydrogenation at 60×10^5 Pa, 623 K. Symbols: (■) our unsupported catalysts, and (▲) γ-alumina-supported industrial NiMo–Al_2O_3 catalyst.

same composition are similar. This suggests that the active sites are the same in the two types of catalyst.

STRUCTURAL RESULTS

Textural results

The distinction between two regions observed for catalytic activities is also observed if we consider porosities of the catalysts. In the Mo-rich region, catalysts are microporous with small crystallites (average diameter 5 nm); with increase of total Ni content, macroporosity appears, suggesting the presence of large crystallites (average diameter 100–200 nm) in the catalysts, together with smaller ones.

The BET specific surface is greater for Mo-rich catalysts than for Ni-rich catalysts. The average value, 50 $m^2\ g^{-1}$, is important for such catalysts.

XRD

Figure 2 shows XRD patterns of catalysts before catalytic experiments. No nickel sulfides are present in the Mo-rich region, where a MoS_2-like phase only is apparent, whereas nickel sulfides are present in the Ni-rich region, in various crystalline forms, such as NiS or NiS_2.

Ni_3S_2 is the thermodynamically stable nickel sulfide under our catalytic working conditions. We verified that Ni_3S_2 was present in the mixed catalysts after testing.[6,8] However, after catalytic runs the catalysts were not a simple mixture of MoS_2 and Ni_3S_2. Post-run sulfur analysis[6] showed a gap between observed sulfur content and theoretical content for mixtures of MoS_2 and Ni_3S_2. In the Mo-rich region S/(Ni + Mo) was constant at about 1.8–1.9; in the Ni-rich region the linear variation of S/(Ni + Mo) was consistent with the presence of a mixture of the Ni–Mo–S phase and Ni_3S_2.[6,8]

ESCA

ESCA is a well-known surface investigation technique, and is of great interest in approaching the surface composition of the catalysts specially in the Mo-rich region.

Figure 3 is a plot of the composition "seen" by ESCA expressed as the ratio of the intensity of the Ni2$p_{3/2}$ peak to the sum of the intensities of the Mo3d and Ni2$p_{3/2}$ peak vs bulk composition of our materials. These results show the same difference between two composition regions. For Mo-rich catalysts, the overall composition is the same as the ESCA composition; the surface composition is the same as the bulk. However, at higher Ni content, a Mo enrichment of the crystallite surfaces is clear.

ISS

The enrichment of the surface with Mo is confirmed by ISS experiments.

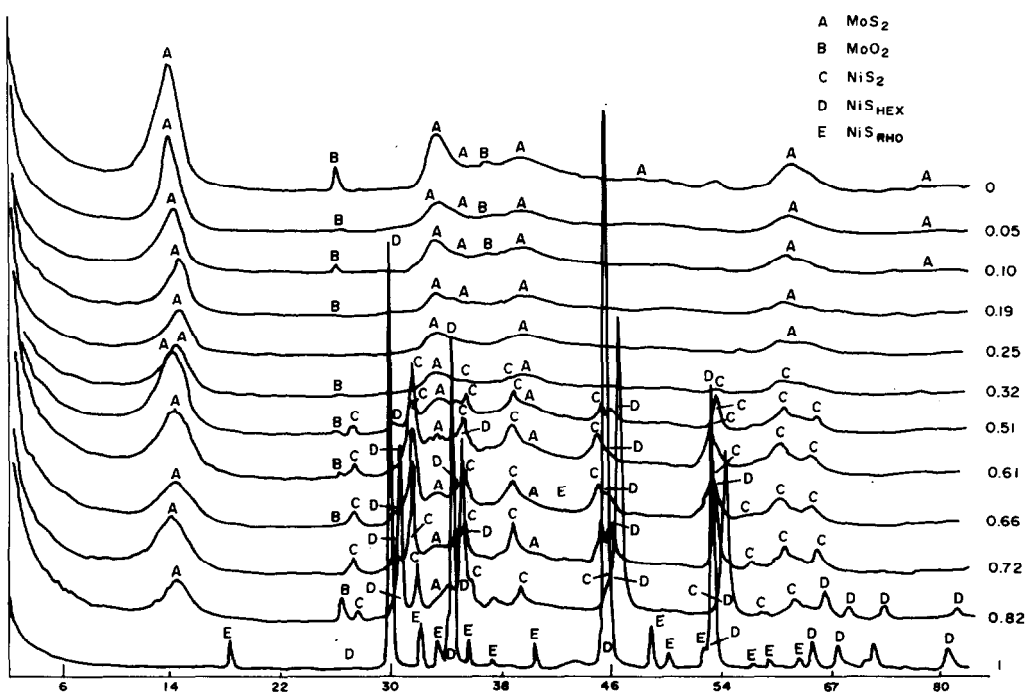


Fig. 2. XRD patterns before testing.

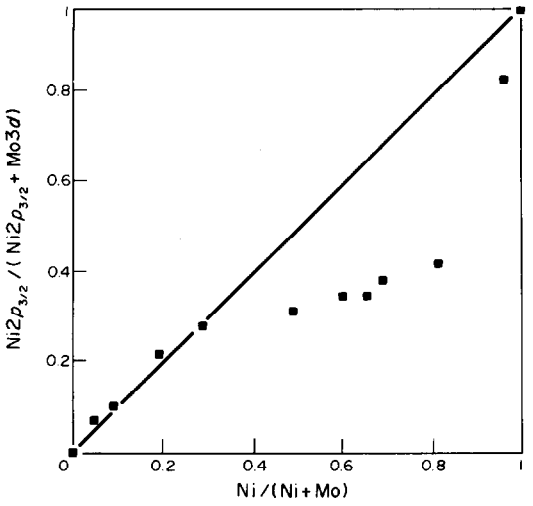


Fig. 3. ESCA results.

ESCA and ISS do not provide in this case an unambiguous location of Ni in the catalysts; but they do show a certain disposition of phases. The only way to have more Mo located at the surface of a catalyst than in the bulk is to support the Mo-containing phase on Ni sulfides since solid solutions of Mo in Ni sulfides are not known. The other important point is that Mo is always associated with Ni in ISS experiments. We know, however, that pure Mo sulfide is not present in the catalysts; but association of Ni with the MoS_2 structure is possible, giving a mixed Ni–Mo–S phase with a similar structure.

Electron microscopy

In order to visualize the catalysts, high-resolution transmission electron microscopy was performed. We produce two typical pictures to illustrate our results. In the Mo-rich region, only one phase is observed, with the typical "fingerprint" structure attributed to MoS_2.[1,2] For an Ni content with $r > 0.25$, large crystallites of different Ni sulfides appear and coating of the MoS_2-like structure is evident.

AEM analysis did not enable us to find any Ni-free zones in the MoS_2-like structure.

Figure 4(1) is a high-resolution photograph of $r = 0.2$ catalyst. We see that incorporation of nickel in an MoS_2 catalyst does not change drastically the well-known structure of MoS_2. In Fig. 4(2), representing $r = 0.6$ catalyst, coating of the mixed Ni–Mo–S phase on an NiS_2 large crystallite is very well displayed.

It is worth emphasizing what appears as an essential difference between Ni–Mo–S phase morphology in our "supported" unsupported catalysts and in an industrial alumina-based catalyst. In the former, five or six Ni–Mo–S slabs are stacked along the (002) axis for $r < 0.25$, against four or five for $r > 0.25$, as shown by the (002) XRD peak analysis and HREM micrographs, whereas in the latter single slabs only (and very rarely two or three stacked slabs) are visible by HREM, according to our results[9,10] and many others reported elsewhere.[11]

O_2-chemisorption

Dynamic O_2-chemisorption experiments performed for the catalysts at 333 K show a poor uptake ($0.05–0.5 \times 10^{-4}$ O_2-mol g^{-1}) compared to the industrial catalyst (1.8×10^{-4} O_2-mol g^{-1}), except at high Ni content, where some oxidation begins to occur with the Ni sulfides. These results tend to prove that the active phase is less dispersed in unsupported mixed sulfides than in the commercial catalyst, a result in agreement with the description obtained by all other investigation techniques.

DISCUSSION

The results show that our Ni–Mo–S system is quite unusual compared to all unsupported NiMo catalysts described in the literature.

First, activities in both hydrogenation and hydrogenolysis reactions are a maximum at $r = 0.7$. Pratt *et al.*[2] obtained comparable results for atmospheric thiophene hydrogenolysis on unsupported NiMo catalysts.

Second, the system shows two regions with different characteristics; for r between 0 and 0.25, activities are not very high. Catalysts are composed of monophasic small crystallites. This unique phase is an MoS_2-like structure phase containing Ni. The incorporation of Ni in the structure goes along with some changes in the structure, as apparent diminution of the c parameter corresponding to the (002) broad peak in the MoS_2 XRD diagram. In the first composition region the parameter decreases. When Ni sulfides appear, for $r > 0.25$, the parameter begins to increase up to its original value (Fig. 5).

We cannot relate these variations to a precise change in the structure of the MoS_2-like phase. The effect can be due simply to the changes in the crystallinity of the mixed Ni–Mo–S phase. Electron microscopy studies seem to prove that the mixed phase is better organized with the incorporation of Ni; better crystallinity, larger crystallites. . . .

The novelty of our catalysts is the structure found at high Ni content. Catalysts are made of a mixed Ni–Mo–S phase coated onto Ni sulfides crystallites. All

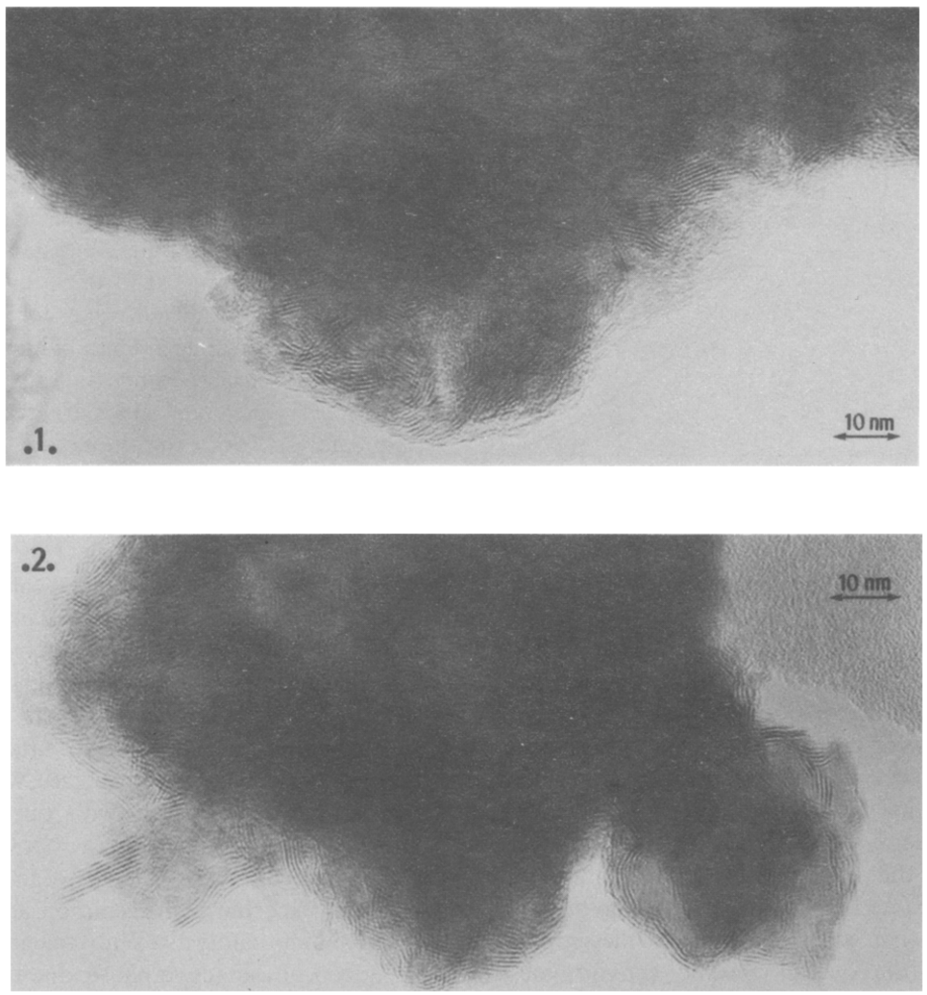


Fig. 4. CTEM images of the catalysts. The pictures show the MoS_2-like structure of the Ni–Mo–S phase (1) and its coating on NiS_2 (2) at high Ni content. (1) Ni/(Ni + Mo) = 0.2; (2) Ni/(Ni + Mo) = 0.60.

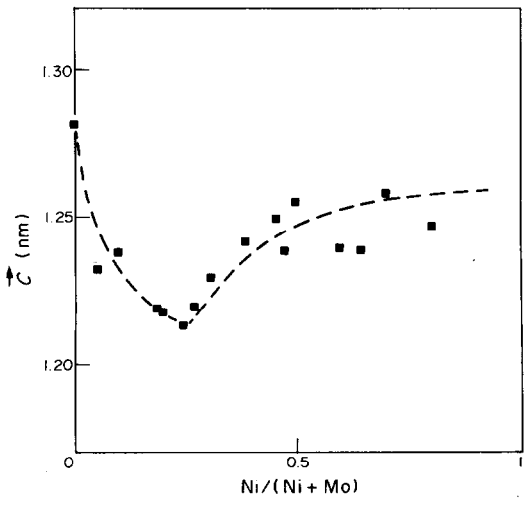


Fig. 5. Evolution of MoS_2 (002) parameter.

experimental results (stoichiometry and ESCA results) suggest that Ni sulfides, specially Ni_3S_2, which is thermodynamically stable under catalytic conditions, are really the support of the mixed phase, which is the active phase in all reactions (an Ni-only catalyst is poorly active for all reactions).

For $r = 0$–0.25, all the nickel is incorporated in the MoS_2 structure. After this value the mixed phase does not incorporate more Ni and its composition seems to be constant. This fact was verified[6] using selective extractions of the mixed phase in the Ni-rich catalysts.

For $r > 0.25$, the excess of Ni segregates into large Ni sulfide crystallites. The role of these large crystallites is to support the mixed phase, and the major consequence is to enhance the catalytic activities.

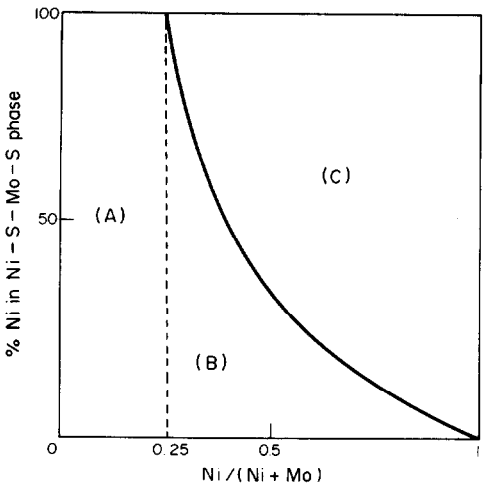


Fig. 6. Pseudo-phase diagram: (a) solid solution of NiSMoS phase in MoS_2, (B) NisSMoS phase supported on Ni_xS_y, and (C) Ni_xS_y.

These considerations enable us to build a "pseudo-phase diagram" for our Ni–Mo–S system. In the region between pure MoS_2 and $r = 0.25$ catalyst, all the Ni is incorporated in the MoS_2 structure. For $r > 0.25$, the Ni_3S_2 phase appears, and the mixed phase does not accept more Ni in its structure. The amount of the active phase then decreases with the Ni content (see Fig. 6).

The fact that, when the amount of the active phase decreases, the overall specific activity goes on increasing proves that the number of active sites is closely connected with the dispersion of the mixed phase.

It is of a great interest to connect these results with the geometrical model for hydrotreating catalysts proposed by Kasztelan.[12] In this theory, the activity of catalysts can be related to crystallite geometry by postulating that active sites are the Mo edge atoms in MoS_2 crystallites. From this point of view, an optimum size of crystallite is obvious for a given number of Mo atoms, in order to get the maximum specific activity. The role of the promoter, assumed to decorate MoS_2 crystallites (that is to say, Ni atoms placed in the Mo plane at the edge), is in this model to enhance the catalytic activity of each active site. We can understand, that for a given number of Mo atoms, and a given form for MoS_2 crystallites, a number of active sites (edge Mo atoms) and an optimum Ni : Mo ratio exist for which the catalytic activity is a maximum. All results for this theory are consistent with independent experimental results, activities, O_2-chemisorption, sulfur content measurements etc.

For instance, with a rhombohedral form for MoS_2 crystallites, an optimum r of 0.33 is found.

It is possible to apply the geometrical model of a hydrotreating catalyst to our system, even if the model refers to supported catalysts. In a sense Ni_3S_2 is a support for the Ni–Mo–S active phase in our "unsupported" catalysts. We can say that there is no contradiction between our results and the geometrical model. In fact, Paulus' results show that the mixed phase exhibits a quasi constant r for high Ni content, in the range 0.20–0.25, a value in good agreement with predicted values for rhombohedral slab sizes in the range 5–8 nm (which are observed values in HREM experiments) [Fig. 4(2)].

Another interesting fact is the agreement between our catalysts and the industrial reference for hydrogenation activity. In Fig. 1(c), the specific activity for the commercial catalyst lies on the curve obtained for unsupported mixed NiMo sulfide catalysts.

We think that the differences between the two kinds of material essentially consist in the dispersion of the active phase, and that the active phase is the same for all catalysts (and is a mixed Ni–Mo–S phase with the MoS_2 structure).

On the commercial catalyst surface, the active phase is known to be well-dispersed, which is not the case to the same extent with our unsupported materials. The consequence is a poor O_2 uptake and a poor specific hydrogenolysis activity, but an equivalent specific hydrogenation activity, for the mixed-sulfide catalysts. With the increase in the dispersion of the active phase, due to a less active phase for more Ni sulfides as a support in the catalyst (see Fig. 6), all specific activities increase, but electron microscopy shows that the dispersion remains poor, compared to commercial catalysts, even when activities are maximum. For these reasons, we think that hydrogenolysis sites and hydrogenation sites are different.

All sites are sensitive to the active-phase dispersion, but in different ways. We may assume that a good hydrogenolysis activity needs a significant dispersion of the Ni–Mo–S structure and a good aromatic hydrogenation needs stacked active-phase slabs. If both reactions take place on the edge sites of decorated MoS_2 slabs, (according to Kasztelan's model), the effect of stacking seems to be predominant particularly for aromatic hydrogenation, even if supports' influences, on industrial or in our "unsupported" catalysts, are not very well defined.

In conclusion, it is possible to say that we elucidated the structure of this system involving Ni, Mo and sulfur in a very fine mixture. The preparation method leads to catalysts with significant hydrogenation activities (the efficiency of Mo is better in most of our materials than in a commercial catalyst).

The structure resolved by our investigation techniques is new, and promises developments for this class of materials.

Acknowledgements—O_2-chemisorption experiments were performed at Caen (ISMRA) and ESCA and ISS at Lille (UST) University. We are grateful to Dr Bachelier and Pr Duchet (CAEN), to Dr Grimblot and Pr Bonnelle (Lille), to Dr Gachet (IRC-Lyon) and to Dr Durand (IFP) for fruitful discussions.

REFERENCES

1. J. V. Sanders and K. C. Pratt, *J. Catal.* 1981, **67**, 331.
2. K. C. Pratt, J. V. Sanders and N. Tamp, *J. Catal.* 1980, **66**, 82.
3. G. Hagenbach, P. Courty and B. Delmon, *J. Catal.* 1971, **23**, 205.
4. G. Hagenbach, P. Courty and B. Delmon, *J. Catal.* 1973, **31**, 264.
5. R. Candia, B. J. Clausen and H. Topsøe, *Bull. Soc. Chim. Belg.* 1981, **90**, 1271.
6. R. Paulus, Thèse de Docteur-Ingénieur, Lyon (1984).
7. French Patent F8316944.
8. C. Gachet, R. Paulus, L. de Mourgues, C. Durand and H. Toulhoat, *Bull. Soc. Chim. Belg.* 1984, **93**, 681.
9. F. Garreau and H. Toulhoat, Colloque Franco-Vénézuélien de Catalyse, Rueil Malmaison, 22–26 avril 1985.
10. S. Kasztelan, H. Toulhoat, J. Grimblot and J. P. Bonnelle, *Bull. Soc. Chim. Belg.* 1984, **93**, 807.
11. G. R. Millward and J. M. Thomas, in *Surface Properties and Catalysis by Non-metals* (Edited by J. P. Bonnelle, B. Delmon and E. Derouane), p. 197. D. Reidel, Dordrecht (1983).
12. S. Kasztelan, H. Toulhoat, J. Grimblot and J. P. Bonnelle, *C. R. Acad. Sci.* 1981, **299**, 289; S. Kasztelan, H. Toulhoat, J. Grimblot and J. P. Bonnelle, *Appl. Catal.* 1984, **13**, 127.

Polyhedron Vol. 5, No. 1/2, pp. 219–224, 1986
Printed in Great Britain

0277–5387/86 $3.00 + .00
Pergamon Press Ltd

THE REACTIVITY AND STABILITY OF MIXED-SULFIDE STRUCTURES IN UNSUPPORTED MoS_2-BASED HYDRODESULFURIZATION CATALYSTS PROMOTED BY GROUP VIII METALS

S. GŐBÖLÖS,* Q. WU,† F. DELANNAY, P. GRANGE and B. DELMON‡

Groupe de Physico-Chimie Minérale et de Catalyse, Université Catholique de Louvain, Place Croix du Sud, 1, B-1348 Louvain-la-Neuve, Belgium

and

J. LADRIÈRE

Laboratoire de Chimie Inorganique et Nucléaire, Université Catholique de Louvain, Chemin du Cyclotron, 2, B-1348 Louvain-la-Neuve, Belgium

(*Received* 1 *July* 1985)

Abstract—Unsupported CoMo, NiMo and FeMo catalysts have been prepared by the homogeneous sulfide precipitation method and the coprecipitation method. The presence of a group VIII metal (Me) causes a decrease in the reactivity with O_2 and an increase in the reducibility in H_2. These effects are correlated with the increase in the catalytic activity. The stability of cobalt and iron sulfide species in CoMo and FeMo catalysts was studied by Mössbauer spectroscopy. A significant amount of Me–Mo–S structure remains stable after strong reducing treatment. Catalysts contain also sulfur-rich group VIII metal sulfide species which appear stabilized by MoS_2. The role of these species in promoting HDS activity is evaluated.

The optimum activity of hydrodesulfurization (HDS) catalysts based on Mo is usually achieved with the addition of a proportion of group VIII metal (Me) (Co, Ni or Fe) corresponding to an atomic ratio (r) [Me/(Me + Mo)] of $\simeq 0.3$. The central question remains the chemical nature of this group VIII metal under catalytic conditions.[1] The compounds Co_9S_8, Ni_3S_2 and FeS should be the only stable phases from the thermodynamic point of view. However, analysis of CoMo and FeMo catalysts by Mössbauer spectroscopy shows the presence of cobalt and iron species other than these stable phases.[2,3] Much interest has been concentrated recently in the so-called Me–Mo–S structure proposed by Topsøe and coworkers.[4,5] This structure would consist of the coverage of the edges of MoS_2 crystal flakes by some mixed MeMo sulfide species.

In order to learn more about the nature and stability of group VIII metal species in HDS catalysts, we have prepared unsupported MeMo catalysts by methods reported to maximize the formation of Me–Mo–S structures. We have studied the reactivity of these catalysts with H_2 and O_2 by temperature-programmed methods. Mössbauer spectroscopy was used to characterize the group VIII metal species in CoMo and FeMo catalysts and to investigate their stability under various reducing treatments. We evaluate the correlations between these results and the activity of the samples in the HDS of thiophene.

* Present address: Central Research Institute for Chemistry of the Hungarian Academy of Sciences, 1025 Budapest, Pusztaszeri út 59-67, Hungary.

† Present address: Beijing Municipal Chemical Industry Research Institute, Cheng Fu, Haidian, Beijing P.B. 2653, People's Republic of China.

‡ Author to whom correspondence should be addressed.

EXPERIMENTAL

Sample preparation

Unsupported CoMo and NiMo catalyst precursors with $r = 0.3$ were prepared by the so-called homogeneous sulfide precipitation (HSP) method.[6] Briefly, this method consists in adding a solution of Co or Ni nitrate and ammonium heptamolybdate (AHM) slowly to a solution of $(NH_4)_2S$. The atomic ratio S/(Me+4Mo) in the final mixture was larger than 1.5 (i.e. more than 1.5 times the ratio needed for the complete sulfuration of Me and Mo into MeS and MoS_4^{2-}). The solid precursor is obtained by allowing the mixture to evaporate to dryness.

For the Mössbauer emission spectroscopy (MES) measurements, a ^{57}Co-labelled precursor with $r = 0.3$ was prepared under identical conditions, using about 1 mCi of ^{57}Co per 0.5 g of sample.

A FeMo precursor with $r = 0.3$ was prepared by the HSP method, using $FeCl_2 \cdot 4H_2O$ instead of nitrate.

A FeMo precursor with $r = 0.15$ was prepared by the so-called coprecipitation (CP) method,[7] which consists in adding slowly a solution of $Fe(NO_3)_3 \cdot 9H_2O$ to a solution of ammonium thiomolybdate. In this case, the atomic ratio S/(Fe+4Mo) was 1.03. This mixed slurry was evaporated to dryness.

A precursor containing only molybdenum was prepared following the HSP method by adding a solution of AHM to a solution of $(NH_4)_2S$. More details about the preparation of samples are in Refs 7 and 8.

The precursors are named by the metal(s) present, followed by the method of preparation and the composition ratio r (e.g. Mo–HSP–0.0, CoMo–HSP–0.3 and FeMo–CP–0.15).

Reduction–sulfidation treatments

The precursors were converted into active catalysts by a standard activation by reduction–sulfidation. This activation consists in heating the samples for 4 h at 653 K in a flow of 15% H_2S–H_2 and cooling them thereafter to room temperature under argon. Catalysts obtained after this standard activation will be designated by adding the letter S to the name of the precursor.

Some of these catalysts were thereafter submitted to various reducing treatments designed to test their stability. These treatments are listed in Table 1 in order of increasing reducing strength. Except for treatment C, all treatments consist of a reduction in pure H_2 followed by resulfuration in H_2S–H_2 mixture.

Table 1. Reducing treatments

Name	Gas	P (MPa)	T (K)	Time (h)
A	H_2	0.1	573	6
	15% H_2S–H_2	0.1	573	1
B	H_2	0.1	723	6
	15% H_2S–H_2	0.1	723	2
C	0.1% H_2S–H_2	3.0	723	6
D	H_2	3.0	723	6
	5% H_2S–H_2	3.0	723	2
E	H_2	3.0	723	6
	0.1% H_2S–H_2	3.0	723	2

Catalytic-activity measurements

The activity in the HDS of thiophene and hydrogenation of cyclohexene was measured at 573 K on 0.5 g of catalyst under 3 MPa, using a feed containing 69.5 wt % cyclohexane, 30.0 wt % cyclohexene and 0.5 wt % thiophene. The mass flow rate of the liquid feed was 48 g h^{-1}. As exposure to air could not be avoided during the transfer of the sample in the reactor, the catalysts were exposed *in situ* to 4% H_2S–H_2 at 573 K under 3 MPa for 1 h prior to the catalytic reaction. The intrinsic HDS activities at steady state (i.e. after 8 h of reaction) are expressed as the amount of thiophene converted per second and per unit surface area of the catalyst.

Temperature-programmed oxidation (TPO)

The reactivity of the catalysts under air was studied by differential thermal analysis. Three hundred milligrams of precursor were first sulfided by heating at a constant rate of 11 K min^{-1} from 373 to 703–723 K under 15% H_2S–H_2 mixture at atmospheric pressure. The sample was then kept at 673 K for 2 h under the same atmosphere and allowed to cool down to room temperature under argon. (One may consider that this pretreatment is nearly equivalent to the standard activation treatment S.) This sample was then heated under air at a rate of 11 K min^{-1}. The thermal effects during the oxidation in air were monitored by measuring the temperature difference between the sample and a 300-mg SiO_2 reference. More details about the TPO measurements may be found in Ref. 8.

Temperature-programmed reduction (TPR)

The experiment was carried out at atmospheric pressure in a flow reactor.[9,10] Two hundred

milligrams of catalyst were first resulfided *in situ* under 15% H_2S–H_2, at 673 K, for 2 h. After purging with argon and cooling to room temperature, the sample was heated to 773 K at a rate of 0.17 K s^{-1} in a flow of 0.5 cm^3 s^{-1} of pure H_2. The H_2S evolving from the reactor was measured by a thermal conductivity detector.

Mössbauer spectroscopy

The Mössbauer spectra were recorded at 298 K using a constant-acceleration spectrometer. MES of CoMo samples enriched in ^{57}Co was performed by use of a moving single line absorber of $K_4Fe(CN)_6 \cdot 3H_2O$ enriched with ^{57}Fe. For Mössbauer absorption spectrometry (MAS) of the FeMo samples, use was made of a moving ^{57}Co source in a Rh matrix. All isomer shifts were referred to pure α-iron. The experimental spectra were fitted by a sum of Lorentzian lines using an iterative non-linear least-squares program. The relative amounts of the components were computed from the peak areas assuming that all species have an identical f factor. The estimated error is ±5%. More details about the Mössbauer measurements may be found in Refs 9, 11 and 12.

RESULTS

Figure 1 presents, as an illustration, the DTA curves recorded during the TPO of samples Mo–HSP–0.0–S and NiMo–HSP–0.3–S. The major feature common to all samples is the broad exothermic effect starting at a temperature (T_0) between 600 and 700 K. The reactivity of the samples in air is less, the higher the T_0 of the start of the exothermic effect.

Figure 2 (right-hand side) presents the values of T_0 for four samples of MeMo–HSP–0.3–S as a function of the intrinsic HDS activity of the samples. As a rule, T_0 increases with increasing amount of group VIII metal and this effect is the strongest for Ni and the weakest for Fe. The HDS activity increases with increasing T_0.

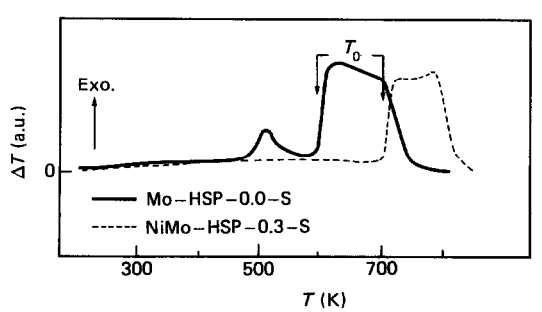


Fig. 1. TPO curves for samples Mo–HSP–0.0–S and NiMo–HSP–0.3–S.

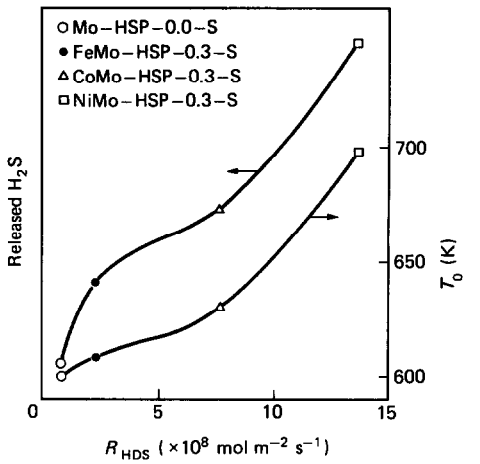


Fig. 2. Correlation between the intrinsic HDS activity and (right-hand side) the temperature T_0 of the onset of oxidation in TPO, or (left-hand side) the amount of H_2S released during TPR.

Figure 2 (left-hand side) also presents the total amount of H_2S released during TPR (up to 773 K) of the same samples of MeMo–HSP–0.3–S. The increase in HDS activity correlates well with the increase in the amount of released H_2S.

Owing to the low crystallinity of the samples, Mössbauer spectroscopy is usually the only method of studying the nature and stability of group VIII metal species in the catalysts. The decomposition of the MES spectra of the CoMo samples (enriched with ^{57}Co) enabled us to distinguish three types of cobalt species in three different environments: Co_9S_8, CoS_{1+x} and the Co–Mo–S structure described by Topsøe *et al.*[2] (More details about the decomposition of the MES spectra may be found in Ref. 11.) We made use of MES to investigate the stability of these three cobalt species in a catalyst, CoMo–HSP–0.3–S, exposed to treatments A and B (described in Table 1). The results are given in Table 1 together with the HDS activity of three samples. It is noteworthy that the HDS activity increases when the amount of cobalt in Co–Mo–S decreases.

Three types of Fe species were distinguished in the MAS spectra of FeMo catalysts: FeS, FeS_2 and Fe–Mo–S. (More details about the decomposition of the MAS spectra may be found in Ref. 12.) Table 2 gives the variation of the amount of these three Fe species in a catalyst, FeMo–CP–0.15–S, subjected to treatments B, C, D and E. The amount of Fe in Fe–Mo–S remains unaffected by the treatments. Except for the untreated sample, the HDS activity appears to decrease with decreasing amount of FeS_2 (or with increasing amount of FeS).

Table 2. Effect of reducing treatments on the distribution of Fe species and catalytic activity for catalyst FeMo–CP–0.15–S

Treatment	% Fe[a] in FeS	% Fe[a] in FeS_2	% Fe[a] in Fe–Mo–S	R_{HDS} ($\times 10^{-8}$ mol m^{-2} s^{-1})
None	—	77	23	1.8
B	17	60	23	2.6
C	26	50	24	1.9
D	37	41	22	1.9
E	41	37	22	1.4

[a] Determined by MAS after catalytic test, except for the untreated sample (first line).

DISCUSSION

The results summarized in Fig. 2 indicate a direct correlation between catalytic activity and reducibility of the catalyst by H_2, and an inverse correlation between activity and reactivity with O_2. The correlation between catalytic activity and reducibility is not too surprising. Indeed, it is widely believed that active sites in HDS are located at sulfur vacancies at the surface of the catalyst. The role of group VIII metal in promoting the release of sulfur may be due either to a weaker bonding of sulfur at the surface or to the "activation" of H_2 by some sort of spill-over effect according to the remote-control hypothesis.[13] Correlation between HDS activity and reducibility was previously reported by Hoodless *et al.*[14]

The broad exothermic effect at high temperature in the TPO curves (Fig. 1) corresponds to the oxidation of MoS_2 with formation of MoO_2 and SO_2.[15] The presence of a group VIII metal brings about a lower reactivity of MoS_2 with O_2 so that a higher temperature is needed for the onset of the reaction. As the edges of MoS_2 crystals are much more reactive than the basal planes, it is generally assumed that oxidation proceeds from the edges.[16] (It is known that oxygen adsorbs preferentially on the edges.[17]) It may thus be concluded that group VIII metal modifies the nature of the edges. Such a modification could involve the formation of the Me–Mo–S structure proposed by Topsøe and coworkers.[4,5] It has been proposed that the bond strength of sulfur exposed on the edges is weaker in the Me–Mo–S structure than in MoS_2.[4,18] This would justify the higher release of H_2S in TPR. One may speculate that the adsorption of oxygen on such a structure creates a "passivating" layer which hinders the further oxidation of the crystal.

In the case of CoMo catalysts, it was shown that the temperature of the onset of oxidation of the catalyst was similar to the temperature of the onset of oxidation of pure cobalt sulfide.[8] Instead of postulating the presence of a Me–Mo–S structure, the change of reactivity with oxygen could thus be also explained by the presence of a layer of group VIII metal sulfide covering the edge of MoS_2 and protecting it from oxidation.

The MES and MAS results presented in Tables 2 and 3 reveal the presence of two different cobalt or iron sulfide phases beside the Me–Mo–S structure. Thermodynamically, Co_9S_8 and FeS should be the only stable phases under the conditions of the catalytic reaction.[19] It could thus be expected that the Me–Mo–S structures and the sulfur-rich CoS_{1+x} and FeS_2 phases would decompose after prolonged exposure to the reducing conditions prevalent during the reaction.

In the catalyst CoMo–HSP–0.3–S (Table 2), it is found that the amount of cobalt in Co–Mo–S decreases after increasingly severe reducing treatment. However, a significant amount of Co–Mo–S remains even after 6 h of exposure to pure H_2 at 723 K. The sulfur-rich CoS_{1+x} phase also remains abundant and even increases after exposure to H_2 at 723 K. (This may be caused by the resulfidation in 15% H_2S–H_2 at 723 K.) The thermodynamically unstable phase CoS_{1+x} appears to be stabilized by the presence of MoS_2. This stabilizing effect is supported by the appearance of peaks attributed to the phase β'-$CoS_{1.097}$ in X-ray diffractograms of unsupported CoMo catalysts.[9]

In the catalyst FeMo–CP–0.15–S, the amount of iron in Fe–Mo–S seems unaffected by the reducing treatments. The amount of sulfur-rich sulfide FeS_2 decreases progressively when increasing the strength of the reducing treatment (or when decreasing the proportion of H_2S in the H_2S–H_2 mixture). Nevertheless, this amount remains surprisingly

Table 3. Effect of reducing treatments on the distribution of Co species and catalytic activity for catalyst CoMo–HSP–0.3–S

Treatment	% Co[a] in Co_9S_8	% Co[a] in CoS_{1+x}	% Co[a] in Co–Mo–S	R_{HDS} ($\times 10^{-8}$ mol m^{-2} s^{-1})
None	28	30	42	5.0
A	59	18	23	8.7
B	—	—	—	11.9
A+B	45	40	15	—

[a] Determined by MES.

large. This suggests again some sort of stabilizing effect caused by the presence of MoS_2.

It may be suggested that the presence of these sulfur-rich group VIII metal sulfide phases can be related to the increased release of H_2S in TPR and, possibly, to the decreased reactivity of MoS_2 with O_2.

Mössbauer spectroscopy characterizes the nature of the species in the whole bulk of the samples whereas catalytic activity is a property of the accessible surface only. Unsupported catalysts studied in this work have a BET surface area of *ca* 10 m^2 g^{-1}.[9,10] Hence, direct comparison of MES or MAS results and catalytic activity data is dubious. In addition, the reducing treatments bring about some sintering of phases and changes of the distribution of the species between surface and bulk.[9] We notice that Tables 2 and 3 reveal no direct correlation between the amount of Me–Mo–S and the HDS activity of the samples. If one excepts the case of the untreated samples (first line), comparison of the second and fourth columns in Tables 2 and 3 seems to suggest a possible correlation between the catalytic activity and the amount of sulfur-rich group VIII metal sulfide. It is worth mentioning in this context that Vissers[20] has recently concluded that the active sites for HDS in carbon-supported CoMo catalysts are located exclusively on the cobalt atoms.

CONCLUSIONS

The following conclusions may be drawn about unsupported MeMo catalysts.

(1) The higher the HDS activity, the higher the removal of sulfur by H_2 and the lower the reactivity with O_2.

(2) The influences of group VIII metal on the reactivity with O_2 may be due to the coverage of the edges of MoS_2 by the Me–Mo–S structure or by a group VIII metal sulfide.

(3) The Me–Mo–S structure remains present in the catalysts even after drastic reducing treatments.

(4) Sulfur-rich metal sulfide species (CoS_{1+x} and FeS_2) are stabilized by the presence of MoS_2.

(5) It is possible that these sulfur-rich species play an important role in promoting the activity.

Acknowledgements—S. Göbölös thanks the Central Research Institute for Chemistry of the Hungarian Academy of Sciences, and Q. Wu thanks the Beijing Municipal Chemical Industry Research Institute, Cheng Fe, for leaves of absence during which this work was accomplished. The financial support of the Services de Programmation de la Politique Scientifique and FNRS (Belgium) is gratefully acknowledged.

REFERENCES

1. P. Grange, *Catal. Rev.—Sci. Eng.* 1980, **21**, 135.
2. H. Topsøe, B. S. Clausen, R. Candia, C. Wivel and S. Mørup, *J. Catal.* 1981, **68**, 433.
3. B. S. Clausen, S. Mørup, H. Topsøe and R. Candia, *J. Phys. Colloq.* 1976, **37**, C6-249.
4. H. Topsøe, In *Surface Properties and Catalysis by Non-metals* (Edited by J. P. Bonnelle, B. Delmon and E. Derouane, p. 329. D. Reidel, Dordrecht (1983).
5. H. Topsøe, R. Candia, N.-Y. Topsøe and B. S. Clausen, *Bull. Soc. Chim. Belg.* 1984, **93**, 783.
6. R. Candia, B. S. Clausen and H. Topsøe, *Bull. Soc. Chim. Belg.* 1981, **90**, 1225.
7. S. Göbölös, Q. Wu and B. Delmon, *Appl. Catal.* 1984, **13**, 89.
8. Q. Wu, S. Göbölös, P. Grange and F. Delannay, *Thermochim. Acta* 1984, **81**, 281.
9. S. Göbölös, Q. Wu, J. Ladrière, F. Delannay and B. Delmon, *Bull. Soc. Chim. Belg.* 1984, **93**, 687.
10. S. Göbölös, Q. Wu, O. André, F. Delannay and B. Delmon, to be published.
11. J. Ladrière, S. Göbölös, F. Delannay and B. Delmon, to be published.

12. J. Ladrière, S. Gőbölös, D. S. Thakur, Q. Wu and B. Delmon, to be published.
13. B. Delmon, *Bull. Soc. Chim. Belg.* 1979, **88**, 979.
14. R. C. Hoodless, R. B. Moyes and P. B. Wells, *Bull. Soc. Chim. Belg.* 1984, **93**, 673.
15. M. M. Spivak, A. S. Pashinkin, R. A. Isakova and K. S. Amosova, *Zh. Prikl. Khim. (Leningrad)* 1978, **51**, 549.
16. O. P. Bahl, E. L. Evans and J. M. Thomas, *Proc. R. Soc. London, Ser. A* 1968, **306**, 53.
17. S. J. Tauster, T. A. Pecoraro and R. R. Chianelli, *J. Catal.* 1980, **63**, 515.
18. R. R. Chianelli, T. A. Pecoraro, T. R. Halbert, W.-H. Pan and E. I. Stiefel, *J. Catal.* 1984, **86**, 226.
19. J. B. McKinley, In *Catalysis* (Edited by P. B. Emmett), Vol. 5, p. 405. Reinhold, New York (1957).
20. J. P. R. Vissers, Ph.D. Thesis, Technical University of Eindhoven (1985).

Polyhedron Vol. 5, No. 1/2, pp. 225–227, 1986
Printed in Great Britain

0277–5387/86 $3.00 + .00
© 1986 Pergamon Press Ltd

INVESTIGATION OF UNSUPPORTED Co–Mo CATALYSTS IN THEIR OXIDIC STATE AND DURING SULFIDATION BY THIOPHENE

T. I. KORÁNYI, T. SZILÁGYI, I. MANNINGER and Z. PAÁL*

Institute of Isotopes, Hungarian Academy of Sciences, H-1525 Budapest, P.O. Box 77, Hungary

(*Received* 15 *June* 1985)

Abstract—Unsupported Co–Mo oxides of various compositions were investigated by IR, XRD and XPS techniques. They contain $CoMoO_4$ plus the corresponding oxide with slight Mo enrichment on the surface. After reduction with H_2, the changes in their catalytic activity in thiophene HDS were monitored with the reactant itself as the sulfiding agent. Relatively high activities with good C_4-selectivities were observed when the degree of sulfidation of the catalysts was relatively low. Partially sulfided surface species possess the highest activity, especially in hydrogenation.

The structure of Co–Mo–Al_2O_3 catalysts has been studied recently by a large number of surface physico-chemical methods.[1] Their unsupported analogues have also been studied frequently[2] because of the absence of any support effects which—however important in preserving a high activity—may conceal the inherent catalytic properties of Mo and Co species. The present study deals with the structure and surface composition of unsupported Co–Mo catalysts in their oxide forms and also with the changes in yields and product composition in thiophene hydrodesulfurization during a period of sulfidation with the reactant itself. The latter approach permitted us to determine an "activity pattern" characterizing the development of catalytically active sites *by the reaction itself*, although we are not able to identify them with any species seen by surface methods. Few publications relate to the initial period of sulfidation.[3]

CATALYST CHARACTERIZATION

Aqueous solutions of $(NH_4)_6Mo_7O_{24} \cdot 4H_2O$ and $Co(NO_3)_2 \cdot 6H_2O$ were dried in air and calcined for 4 h at 723 K in atomic ratios $\{r\ [Co/(Co+Mo)]\}$ of 0, 0.17, 0.38, 0.50, 0.75 and 1. The calcined, oxidic form of the catalysts contains a-$CoMoO_4$ ($r = 0.5$) mixed with MoO_3 ($r < 0.5$) or with Co_3O_4 ($r > 0.5$) according to XRD, XPS and IR measurements. The interplanar spacings and relative intensities measured by XRD are in accordance with the literature data of the Powder Diffraction File of ICPDS of these compounds. The IR data[4–6] (Fig. 1) clearly show the gradual transition from the bands of MoO_3 through the bands of a-$CoMoO_4$ to the bands of Co_3O_4. The XPS binding energies are in relatively good agreement with literature data,[7,8] taking into account our different reference line (C1*s* = 285.0 eV). The "surface" r atomic ratios seen by XPS were calculated by the method of Grimblot *et al.*[9] A slight surface enrichment in Mo is seen from Table 1 which is in agreement with the results of Okamoto *et al.*[10] Specific surface areas of the calcined (oxidic) catalysts, and those of samples prereduced for 2 h at 673 K in 40 ml min^{-1} H_2, were measured by the BET method with N_2. Prereduction increased greatly the specific surface areas of the catalysts with $r = 0.38$–0.75 (from about 20 to about 100 $m^2\ g^{-1}$).

THIOPHENE CONVERSIONS

The "activity profiles" were determined by injecting 0.5 μl thiophene pulses on to the prereduced catalysts (20 mg weighed in the calcined state, reaction temperature 673 K, H_2 stream: 40 ml min^{-1}). The products were analyzed by gas

* Author to whom correspondence should be addressed.

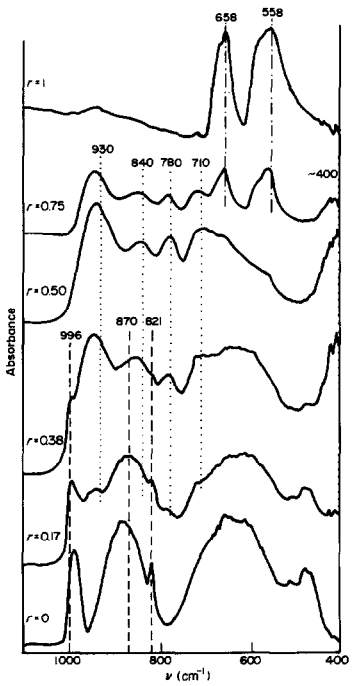


Fig. 1. IR spectra of calcined catalysts. Assignments: MoO_3^4: 996, 870 and 821 cm^{-1}; a-$CoMoO_4^5$: 930, 840, 780, 710 and ~400 cm^{-1}; $Co_3O_4^6$: 658 and 558 cm^{-1}.

chromatography.[11] Two 0.5-μl dimethylsulfoxide (DMSO) pulses were introduced between each two thiophene pulses, in order to accelerate sulfur uptake. DMSO is claimed to decompose on the catalyst giving H_2S.[12]

Thiophene conversions during subsequent pulses show a maximum in the second thiophene pulse with Mo-rich catalysts ($r = 0$ and 0.17) and decrease monotonically with other samples (Fig. 2). The C_4-selectivity in the first pulse decreases gradually with increasing Co content (Table 2). Except for pure Co, it has reached already, however, a rather high value by the second pulse which increases further only slowly. We took the ratio of *n*-butane to the sum of butanes as characteristic of the hydrogenation selectivity (Fig. 3). This has a maximum value for all catalysts (except for $r = 1$). The indication of a maximum between the two pulses is justified by analogous experiments carried out without DMSO pulses where the sulfur uptake should have been slower (Fig. 3, insert). Figures 2 and 3 show also

Table 1. "Surface" compositions of the calcined (oxidic) catalysts as seen by XPS

r (bulk)	0.17	0.38	0.50	0.75
r (surface)	0.15	0.27	0.33	0.60

Table 2. C_4-selectivity of various catalysts

Pulse No.	Catalyst composition *r*					
	0	0.17	0.38	0.50	0.75	1
1	83	83	62	47	24	20
2	92	97	95	97	96	53
5	97	97	96	96	96	43

comparative literature data.[3,11] Here the amount of sulfur introduced was related to a 20 mg Co plus Mo oxide content of the catalyst. The distribution of the fragments shows an excess of CH_4 in the first pulse, and C_3 excess (propane plus propene) in the second and third pulses. The amount of C_2 fragments was always lower than expected on the basis of random rupture of the C_4 hydrocarbon chain.

The activity profiles point to a profound change in the catalytic activity of our unsupported samples during their contact with the first sulphur-containing reactants after reduction. There is disagreement in the literature as far as the chemical state of Mo is concerned after reduction: Mo^{4+} and Mo^{2+} have been proposed.[13,14] They must be surrounded by O-anions which, during sulfidation, are exchanged for S-anions. Our measurements show that maximum activity is reached when this exchange is far from complete. For example, the sulfur atoms from thiophene transformed in the first

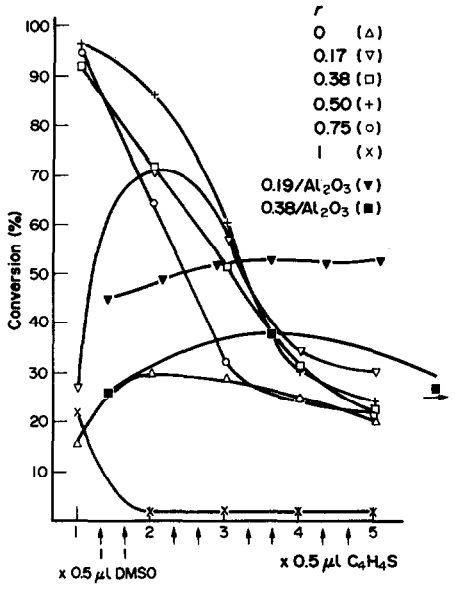


Fig. 2. Thiophene conversions during subsequent pulses on catalysts with different *r* atomic ratios. The amount of sulfur introduced onto supported catalysts was recalculated to 20 mg oxide content: (▼) Ref. 3, and (■) Ref. 11.

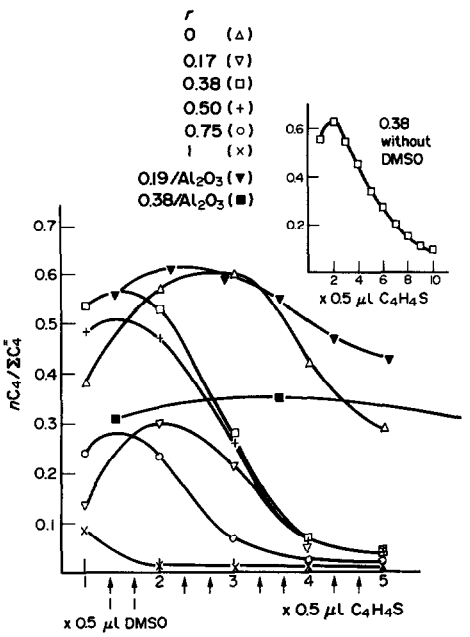


Fig. 3. Butane–butenes ($nC_4/\sum C_4^=$) ratios during subsequent pulses (see also caption to Fig. 2).

pulse would be sufficient to sulfide about 1% of the catalysts and the maximum upper limit of sulfidation at maximum activity—pulse 2—would be 5–10%, even if all the DMSO were used for catalyst sulfidation. This may mean that the most active surface species may be Mo oxysulfides. Delgado *et al.*[15] argue that a further reduction of Mo takes place under sulfidation (perhaps that of Mo^{4+} to Mo^{2+}) and this process can also contribute to the formation of catalytically active sites. Oxidic catalysts produce mainly fragments (pulse 1); upon partial sulfidation (pulses 2 and 3), hydrogenation activity is maximum, whereas HDS activity decreases monotonically during these, as well as subsequent pulses. Accumulation of carbonaceous residues may also occur (cf. the methane deficit in pulses 2 and 3) and this may be the reason why the surface S : Mo ratio was always lower when sulfidation was carried out with thiophene instead of H_2S.[10] Comparison with supported catalysts[11] indicates that the "Mo-type" activity profile having a maximum at low sulfidation levels is characteristic for samples with r between 0 and 0.38. This confirms the strong interaction between the Co–Mo species and the support up to a higher Mo content and also shows that $CoMoO_4$ species—present here in ample amounts—may not be precursors of catalytically active species on an Al_2O_3 support. Supported catalysts show a similar behaviour in hydrogenation selectivities but a much more stable HDS activity.

Acknowledgements—We thank Mr L. Tóth for specific surface area measurements. A valuable discussion with Prof. H. Knözinger is gratefully acknowledged.

REFERENCES

1. E.g. *Bull. Soc. Chim. Belg.* 1984, **93**, No. 8–9.
2. E.g. pp. 663, 673, 681 and 687 in Ref. 1; M. Breysse, R. Frety, M. Vrinat, P. Grange and M. Genet, *Appl. Catal.* 1984, **12**, 165.
3. H. R. Chang and S. W. Weller, *Ind. Eng. Chem. Process Des. Dev.* 1978, **17**, 310.
4. P. C. H. Mitchell and F. Trifiro, *J. Chem. Soc. A* 1970, 3183.
5. F. Trifiro, G. Caputo and P. L. Villa, *J. Less-Common Met.* 1974, **36**, 305.
6. N. V. Kozlova, V. V. Salaginov, V. N. Lomova and D. M. Shub, *Zh. Neorg. Khim.* 1983, **28**, 2455.
7. P. Gajardo, D. Pirotte, C. Defosse, P. Grange and B. Delmon, *J. Electron. Spectrosc. Relat. Phenom.* 1979, **17**, 121.
8. R. L. Chin and D. M. Hercules, *J. Phys. Chem.* 1982, **86**, 3079.
9. J. Grimblot, E. Payen and J. P. Bonnelle, In *Proceedings of the Fourth International Conference on the Chemistry and Uses of Molybdenum* (Edited by H. P. Barry and P. C. H. Mitchell), p. 261. Climax Molybdenum Co., Ann Arbor, MI (1982).
10. Y. Okamoto, T. Shimokawa, T. Imanaka and S. Teranishi, *J. Catal.* 1979, **57**, 153.
11. M. Dobrovolszky, Z. Nagy, Z. Paál and P. Tétényi, *Bull. Soc. Chim. Belg.* 1984, **93**, 659.
12. M. Keck, H. Meye and R. Schödel, Paper No. 8 presented at the yearly meeting of catalytic scientists in the G.D.R., Reinhardsbrunn, March 1983.
13. H. C. Yao, *J. Catal.* 1981, **70**, 440.
14. J. Valyon and W. K. Hall, *J. Catal.* 1983, **84**, 216.
15. E. Delgado, G. A. Fuentes, G. A. Hermann, C. Kunzmann and H. Knözinger, *Bull. Soc. Chim. Belg.* 1984, **93**, 735.

Polyhedron Vol. 5, No. 1/2, pp. 229–232, 1986
Printed in Great Britain

0277–5387/86 $3.00 + .00
© 1986 Pergamon Press Ltd

CATALYTIC PROPERTIES IN HYDROTREATING REACTIONS ON UNSUPPORTED PURE OR PROMOTED MOLYBDENUM SULFIDE

J. L. PORTEFAIX,* M. BREYSSE, M. CATTENOT, R. FRETY, M. LACROIX and M. VRINAT

Institut de Recherches sur la Catalyse, Laboratoire Propre du CNRS, Conventionné à l'Université Claude Bernard, Lyon I, 2 Avenue Albert Einstein, 69626 Villeurbanne Cedex, France

(*Received* 21 *June* 1985)

Abstract—Unsupported MoS_2 samples with surface areas ranging from 1 to 83 $m^2\ g^{-1}$ were prepared by treatment of different precursors in a H_2–H_2S atmosphere at 673 K. Their catalytic properties were determined for several hydrotreating reactions. Dibenzothiophene hydrodesulfurization, and biphenyl and cyclohexene hydrogenations were found to be "texture-insensitive", while pyridine hydrogenation and piperidine hydrodenitrogenation appeared to be "texture-sensitive". It is proposed that the catalytic sites responsible for the reactions involving nitrogen-containing molecules are different from those where other reactions take place. These sites probably contain more atoms and are more dependent on the environment. The peculiar nature of the sites of nitrogen-containing molecule reactions is supported by comparison of the catalytic properties of these MoS_2 samples with those of a cobalt-promoted molybdenum sulfide catalyst.

Recent work has shown the presence of several different functions on hydrotreatment MoS_2-based catalysts, i.e. hydrodesulfurization (HDS), hydrogenation (HN), hydrodenitrogenation (HDN), cracking (CK) etc . . . , and it has been assumed that these reactions utilize distinct sites. This hypothesis rests upon the different responses to preparation and pretreatment methods and to reaction conditions. For example, the presence of H_2S in the reactant flow has a higher negative influence in HDS than in HN, whereas H_2S improves the HDN function.[1]

The question of the nature of these sites is still under discussion. It is generally agreed that HDS reactions take place on sulfur vacancies, but their location is not firmly established, since some authors consider different activities for edge or basal sites in the MoS_2 structure.[2,3] In a recent paper, some of us have shown that the rates for HDS of dibenzothiophene and HN of biphenyl (BP) were proportional to the surface areas of unsupported MoS_2 and WS_2 catalysts. They have proposed that these reactions are "texture-insensitive"; this notion has been preferred to the "structure sensitivity" one because significant modification of H_2S pressure may alter the S/metal ratio which can modify the rate constants.[4]

Moreover, literature data show that it is not certain that HN of aromatics or olefinics implies the same type of sites and their location seems to be different from that of the HDS sites.[5] As a matter of fact, many of the HN studies have been deduced from selectivity measurements during HDS reactions.

Concerning HDN sites, only a few papers deal with their nature. Satterfield and Yang[6] suggest that C—N bond hydrogenolysis occurs on Brönsted acidic sites resulting from the dissociative adsorption of H_2S on anionic vacancies of the sulfide. Laine[7] proposes that the first step of the C—N bond cleavage is the formation of a metalloazocyclic intermediate or an iminium complex on a metallic site of the active phase. However, no information is given about the location and complexity of these sites in the solid structure.

By analogy with the notion of reaction sensitivity

* Author to whom correspondence should be addressed.

on metal catalysts, it seemed useful to investigate simple-model reactions with model catalysts in order to describe the variations of reaction rates with surface areas. Indeed, the existence of a simple proportionality between these parameters ("structure or texture sensitivity") would imply simple and (or) numerous catalytic sites, whereas the contrary would suggest the participation of sites with complex geometry and (or) limited number.

In the present work, a series of unsupported MoS_2 samples of varying surface areas were studied for several hydrotreating catalytic model reactions, viz. HDS of dibenzothiophene (DBT), HN of BP, cyclohexene and pyridine, and HDN of piperidine. For comparison, an unsupported molybdenum sulfide promoted by cobalt was also studied for the same reactions.

EXPERIMENTAL

Catalysts preparation

For the preparation of pure molybdenum catalysts, several precursors were used: (i) ammonium tetrathiomolybdate (ATTM), (ii) ammonium oxothiomolybdate (AOTM), (iii) commercial molybdenum trioxide (MoO_3), (iv) commercial metallic molybdenum (Mo), and (v) commercial molybdenum disulfide (MoS_2).

ATTM and AOTM were prepared by reacting MoO_3 with an aqueous solution of $(NH_4)_2S$ at 343 K. By crystallization at room temperature, the resulting solution led to ATTM; by evaporation to dryness at 343 K in the presence of traces of air, it led to AOTM.

For the preparation of the cobalt–molybdenum sample, the precursor was obtained by the homogeneous sulfide precipitation (HSP) method described by Candia *et al.*[8] The atomic ratio Co/(Co + Mo) was taken as equal to 0.3, which corresponds to the maximum of the synergetic effect in HDS.

The different precursors were heated in a flow of H_2–15% H_2S up to 673 K and kept at this temperature for 4 h. Changes in heating rates allowed us to obtain samples with different surface areas from ATTM and AOTM. After cooling down to room temperature under the sulfiding atmosphere, the samples were flushed with nitrogen and stored under argon in sealed bottles.

Catalytic-activity determination.

The catalytic activities were determined in dynamic microreactors, working in the gaseous phase, at low conversion and under atmospheric or medium high pressure. Rates were measured in the pseudo steady state. The reaction conditions are summarized in Table 1.

Surface-area measurement

The specific surface areas of the different catalysts were determined before and after reaction, since previous results had shown that a drastic decrease occurs during catalytic tests.[4] Measurements were performed gravimetrically (with a Sartorius 4102 microbalance) by the BET method, using argon as absorbent at 77 K. At this temperature, the area of an atom of argon, in the adsorbed state, was taken as equal to 13.4 Å^2. Samples were first treated *in vacuo* (1.3×10^{-3} Pa) at 673 K until a steady weight was obtained.[9]

RESULTS AND DISCUSSION

The initial and final (FSA) surface areas of the catalysts in $m^2\,g^{-1}$, the apparent activation energies in kcal mol^{-1}, and the specific (SR) and intrinsic (SR/FSA) reactions rates, respectively, in 10^{-8} mol $s^{-1}\,g^{-1}$ and 10^{-8} mol $s^{-1}\,m^{-1}$, determined at 530 K for the HDS of DBT and the HN of BP, at 523 K for the HN of cyclohexene and pyridine, and at 548 K for the HDN of piperidine, are given in Tables 2–6.

For HDS of DBT and HN of BP and cyclohexene, the intrinsic reaction rates are constant whatever the

Table 1. Reaction conditions

Reaction	H_2 pressure ($\times 10^5$ Pa)	H_2S pressure ($\times 10^2$ Pa)	Hydrocarbon pressure ($\times 10^2$ Pa)	Temperature range (K)
HDS of DBT	22.5	0.04–1	4	530–590
HN of BP	22.5	4.5	8	500–560
HN of cyclohexene	1	2.2	3.4	480–530
HN of pyridine	20	330	260	500–540
HDN of piperidine	20	330	260	530–570

Table 2. Dibenzothiophene hydrodesulfurization[a]

Catalyst	Precursor	ISA	FSA	AE	SR[b]	IR[b]
MoS_2 1	ATTM	83	30	24	12.8	0.43
MoS_2 2	AOTM	43	20	22	7.8	0.39
MoS_2 3	Mo	7	7	22	2.9	0.41
MoS_2 4	MoS_2	6	6	21	2.3	0.38
MoS_2 5	MoO_3	1	1	23	0.37	0.37

[a] Abbreviations (Tables 2–6): ATTM, $(NH_4)_2MoS_4$; AOTM, $(NH_4)_2MoO_2S_2$; ISA and FSA, initial and final surface areas ($m^2\ g^{-1}$); AE, activation energies (kcal mol^{-1}); SR and IR, specific and intrinsic reaction rates ($\times 10^{-8}$ mol $s^{-1}\ g^{-1}$ or 10^{-8} mol $s^{-1}\ m^{-2}$).
[b] 530 K.

Table 3. Biphenyl hydrogenation[a]

Catalyst	Precursor	ISA	FSA	AE	SR[b]	IR[b]
MoS_2 1	ATTM	83	44	18	6.8	0.15
MoS_2 2	AOTM	43	30	16	4.2	0.14
MoS_2 6	ATTM	54	32	18	5.3	0.17
MoS_2 7	AOTM	5	5	16	0.61	0.12

[a] See Table 2, footnote [a].
[b] 530 K.

Table 4. Cyclohexene hydrogenation[a]

Catalyst	Precursor	ISA	FSA	AE	SR[b]	IR[b]
MoS_2 8	ATTM	75	25	24	4.1	0.16
MoS_2 9	ATTM	73	17	24	3.9	0.23
MoS_2 10	AOTM	40	12	24	2.3	0.19
MoS_2 11	AOTM	12	3	24	0.64	0.21

[a] See Table 2, footnote [a].
[b] 523 K.

Table 5. Pyridine hydrogenation[a]

Catalyst	Precursor	ISA	FSA	AE	SR[b]	IR[b]
MoS_2 6	ATTM	54	20	15	20	1.0
MoS_2 8	ATTM	75	13	14	48	3.7
MoS_2 9	ATTM	73	30	15	24	0.8
MoS_2 12	ATTM	66	29	15	19	0.7
MoS_2 13	AOTM	2	2		3.5	1.8
MoS_2 14	AOTM	18	8	15	38	4.8
CoMo		35	29	14	38	1.3

[a] See Table 2, footnote [a].
[b] 523 K.

Table 6. Piperidine hydrodenitrogenation[a]

Catalyst	Precursor	ISA	FSA	AE	SR[b]	IR[b]
MoS_2 6	ATTM	54	11	24	58	5.3
MoS_2 8	ATTM	75	12		56	4.7
MoS_2 9	ATTM	73	28	25	39	1.4
MoS_2 12	ATTM	66	13	24	36	2.8
MoS_2 13	AOTM	2	2	18	9	4.5
MoS_2 14	AOTM	18	7	25	44	6.3
MoS_2 15	AOTM	31	14	23	22	1.6
CoMo		35	31	22	72	2.3

[a] See Table 2, footnote [a].
[b] 548 K.

nature of the precursor and the range of surface area values. These results are consistent with those of Furimsky and Amberg[10] concerning the HDS of thiophene, and of Thakur *et al.*[11] concerning this latter reaction and the HN of cyclohexene. They do not follow the results of Tauster *et al.*,[3] in which a direct proportionality between surface area and rate constant for HDS of DBT was not found. This discrepancy may arise either from our experimental conditions (low reaction temperatures and low order with respect to hydrocarbons) or from sample purity. One can conclude that these reactions are "texture-insensitive" and that the corresponding catalytic sites are rather simple.

For HN of pyridine and HDN of piperidine, the intrinsic rates are not constant and it was not possible to find a relationship with the nature of the precursor.

A particular behaviour of nitrogen-containing molecules also appears for the CoMo(HSP) catalyst. The activity of this latter sample was found to be 4–7 times higher than that of MoS_2 in HN of BP and HDS of DBT, respectively.[12] In the present work, the promoting effect of cobalt was nil for the reactions with pyridine and piperidine. In that case, however, cobalt has a clear effect on the textural stability of the catalyst. Therefore, we can conclude that the behaviour of reactions involving nitrogen-containing molecules is different from that of other model reactions studied. It must be emphasized that the reactions with nitrogen heterocompounds are performed under rather different experimental conditions. Actually, a high partial pressure of H_2S is necessary to get a measurable HDN rate. On the other hand, during these reactions, heavy by-products are formed and they may remain adsorbed on the surface after the outgassing treatment performed prior to the surface-area determination. Consequently, the values of the FSA have to be considered with caution.

Nevertheless, we believe that these observations are not sufficient to explain the different comportment of nitrogen-containing molecule reactions and, even if the variations in intrinsic rates are lower than one order of magnitude, we proposed that HN of pyridine and HDN of piperidine are "texture-sensitive". They would, therefore, take place on sites which are made up of a large number of atoms and are dependent on their environment.

REFERENCES

1. Y. Liu, F. E. Massoth and J. Shabtai, *Bull. Soc. Chim. Belg.* 1984, **93**, 627.
2. G. C. Stevens and T. Edmonds, *J. Less-Common Met.* 1977, **51**, 321.
3. S. J. Tauster, T. A. Pecoraro and R. R. Chianelli, *J. Catal.* 1980, **63**, 515.
4. R. Fréty, M. Breysse, M. Lacroix and M. Vrinat, *Bull. Soc. Chim. Belg.* 1984, **93**, 663.
5. F. E. Massoth and G. Muralidhar, In *Proceedings of the Fourth International Conference on the Chemistry and Uses of Molybdenum* (Edited by H. F. Barry and P. C. H. Mitchell), p. 343. Climax Molybdenum Co., Ann Arbor, MI (1982).
6. C. N. Satterfield and S. H. Yang, *J. Catal.* 1983, **81**, 335.
7. R. M. Laine, *Catal. Rev.* 1983, **25**, 459.
8. R. Candia, B. J. Clausen and H. Topsøe, *Bull. Soc. Chim. Belg.* 1981, **90**, 1225.
9. R. Fréty and M. Breysse, In *Surface Properties and Catalysis by Non-metals* (Edited by J. P. Bonnelle, B. Delmon and E. Derouane), p. 379. D. Reidel, Dordrecht (1983).
10. E. Furimsky and C. M. Amberg, *Can. J. Chem.* 1975, **53**, 3567.
11. D. S. Thakur, G. C. Stevens, P. Grange, T. Edmonds and B. Delmon, In *Proceedings of the Fourth International Conference on the Chemistry and Uses of Molybdenum* (Edited by H. F. Barry and P. C. H. Mitchell), p. 353. Climax Molybdenum Co., Ann Arbor, MI (1982).
12. M. Vrinat, M. Lacroix, M. Breysse and R. Fréty, *Bull. Soc. Chim. Belg.* 1984, **93**, 697.

Polyhedron Vol. 5, No. 1/2, pp. 233–236, 1986
Printed in Great Britain

0277–5387/86 $3.00 + .00
© 1986 Pergamon Press Ltd

EFFECT OF CATALYST COMPOSITION ON THE HYDROGENOLYSIS OF ANISOLE

M. K. HUUSKA*

Department of Chemistry, Helsinki University of Technology, SF-02150 Espoo 15, Finland

(*Received* 14 *June* 1985)

Abstract—The hydrogenolysis of anisole was studied in a fixed-bed reactor at 300°C and 5 MPa hydrogen pressure on pure carriers and different catalysts containing Mo or Ni. Catalysts based on an acidic carrier gave mainly phenol and methyl-substituted phenols. On catalysts without an acidic support very little methyl substitution occurred and the main products were phenol and cyclic hydrocarbons. Reaction mechanisms and the structure of possible active sites are briefly discussed.

Mo catalysts have been employed in the petroleum industry for hydrodesulfurization (HDS) and hydrotreating processes for a long time.[1,2] More recently, these catalysts have found extensive use in hydrorefining and hydrodeoxygenation (HDO) of shale oils, coal-derived liquids, and other synthetic crudes.[3,4]

The surface of the working molybdena–alumina catalysts can be envisioned to consist of the molybdena portion and the uncovered alumina portion. These parts of the surface can be studied separately by different methods. Gil Llambías *et al.*[5] applied electrophoretic migration and Mo extraction measurements for determination of the apparent surface coverages of differently prepared and treated molybdena–alumina catalysts. They came to the conclusion that the Mo is present on the alumina surface not exclusively as a monolayer but also forming patches in multilayers, even at low loadings. The usual Mo loadings of the industrial HDS catalysts (10–12 wt % of MoO_3) were found to cover up to 60% of the alumina surface. Chemisorption measurements have been widely applied to study the surface portions and active sites of Mo–alumina catalysts. For instance, Segawa and Hall[6] have reported that on a reduced Mo–alumina catalyst, CO_2 adsorbs selectively on the uncovered alumina portion of the surface, whereas NO adsorbs selectively on the molybdena portion, on coordinatively unsaturated sites. On the contrary, NH_3 and pyridine have been found to chemisorb *unselectively* on both the alumina and the molybdena portions of the surface.[7] It is evident that active sites acidic in nature exist on both portions of the catalyst surface.[8] However, the acid strength and character of these sites obviously are quite different due to the chemically different environments that they are located in.

In previous work we studied the hydrogenolytic reactions of anisole and some other oxygen-containing aromatics on a hydrocracking catalyst ($NiMo–SiO_2–Al_2O_3$) and an HDS catalyst ($CoMo–\gamma\text{-}Al_2O_3$).[9,10] It was concluded that the hydrogenolysis of anisole may take place via different reaction routes depending on the nature of the catalytically active sites involved in the reactions. Thus, reaction (1) in Fig. 1 occurs predominantly on acidic sites of the carriers, whereas reactions (2) and (3) are catalyzed by sites which possess some hydrogenation–dehydrogenation activity, i.e. active sites on the metals or metal sulfides.

In the present work simple catalytic materials, including pure carriers and unsupported metal sulfides, were used to study the hydrogenolysis of anisole in order to confirm the reaction pathways proposed in Fig. 1 and to further elucidate the reaction mechanisms.

EXPERIMENTAL

All chemicals were pure or analytical-grade reagents. Hydrogen was laboratory grade and was used without further purification.

* Present address: Chemical Laboratory, Technical Research Centre of Finland, Biologinkuja 7, SF-02150 Espoo 15, Finland.

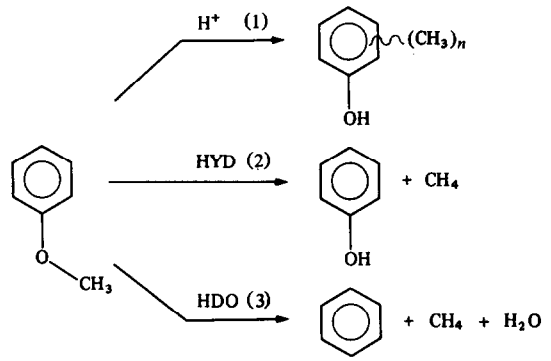


Fig. 1. Reaction pathways in the hydrogenolysis of anisole.[9,10]

The composition and major properties of the catalysts studied are listed in Table 1. Most of the catalysts were commercial samples. Catalyst C, unsupported MoS_2, was prepared by pressing small tablets from a pure MoS_2 powder, followed by crushing and sieving. Catalyst G was prepared by impregnating γ-Al_2O_3 tablets with a dilute nickel acetate solution, drying and calcining at 500°C. Catalysts D–G were sulfided *in situ* at 275°C and 5 MPa hydrogen pressure with a feed containing 0.5 vol % CS_2 in benzene for 4–5 h (LHSV = 2.0 h^{-1}). Catalyst E was studied also in the unsulfided (oxidic) form.

The fixed-bed tubular reactor and its use have been described previously.[9] The catalyst load was usually 5 cm^3 but in the case of the unsupported MoS_2 catalyst 8 cm^3 was used. The feedstock was neat anisole containing 0.05 vol % CS_2 in order to maintain the catalyst in the sulfided state. With catalysts A, B and E in unsulfided form no CS_2 was added to the feed.

Product analysis was carried out with gas chromatography, mainly as described earlier.[9] Some analyses were also done with a HP 5880 A equipment applying silica capillary columns. Water content of the feedstock and the reaction products was analyzed by Karl Fischer titration using an electrometric end-point recognition. Anisole feed was found to contain less than 0.1 wt % water. The reaction products contained up to 6 wt % water depending on the extent of the HDO reaction.

RESULTS AND DISCUSSION

In order to obtain comparable results most of the runs reported in this paper were carried out under fixed reaction conditions: temperature 300°C, pressure 5 MPa of hydrogen, H_2/anisole molar ratio $\simeq$ 100, and LHSV = 2.0 h^{-1}. For catalyst C a lower space velocity of 1.0 h^{-1} was applied due to the low surface area of this catalyst. Normally, over 90% of the reaction product could be accounted for. The selectivities, calculated on the basis of anisole reacted, were normalized to 100% of the conversion. The results are shown in Table 2. On some catalysts a steep decrease in activity was observed at the beginning of a run. To level off this initial high activity and to stabilize the reaction products runs were continued for a few hours before representative samples were taken.

Carrier materials

On the pure carrier materials studied, γ-Al_2O_3 and SiO_2–Al_2O_3, the main reaction products were phenol and methyl-substituted phenols. On SiO_2–Al_2O_3 appreciable amounts of methyl anisoles, *o*-methyl anisole dominating, were also formed. The loss of methyl groups as methane was minor as was the formation of hydrocarbons.

The conversion of anisole dropped quickly. For both carrier materials studied it was approximately halved during the first 4 h on stream.

It can be concluded that in the hydrogenolysis of anisole the acidic carriers exhibit only isomerization and methyl group transferring activity but no

Table 1. Composition and properties of catalysts

Catalyst	Metal content (%)	Carrier material	Surface area ($m^2\ g^{-1}$)	Particle form	Particle size (mm)	Bulk density ($g\ cm^{-3}$)
A	—	γ-Al_2O_3	100	Crushed	0.84–1.0	0.8
B	—	SiO_2–Al_2O_3 (87:13)	100	Crushed	0.84–1.0	0.6
C	Mo 60	—	6.9	Crushed	0.84–1.0	1.7
D	Ni 11	SiO_2	280	Crushed	0.84–1.0	0.6
E	Mo 6.7	γ-Al_2O_3	160	Tablets	3.2 × 3.2	0.9
F	Ni 11	γ-Al_2O_3	65	Tablets	3.2 × 3.2	1.0
G	Ni 0.5	γ-Al_2O_3	100	Tablets	3.2 × 3.2	0.9

Table 2. Reaction of anisole on different catalysts[a]

Catalyst	A	B	C[b]	D	E	E[c]	F	G
Conversion (%)	22.5	10.2	50.0	19.4	74.5	73.7	42.1	90.1
Selectivity (%)								
Phenol	46.8	51.1	63.1	53.8	47.0	46.3	77.1	40.4
o-Cresol	27.9	12.9	1.9	0.8	29.5	28.7	8.6	35.0
2,6-Dimethylphenol	9.7	1.8	—	—	14.8	14.5	+	18.6
Other *O*-compounds	13.1	28.7	0.4	5.1	1.8	1.8	0.6	5.0
Sum of *O*-compounds	97.5	94.5	65.4	59.7	93.1	91.3	86.3	99.0
Benzene	1.9	1.3	27.8	31.4	3.0	5.3	8.3	+
Other hydrocarbons	0.6	4.1	6.8	9.0	3.8	3.4	5.4	1.0
Sum of hydrocarbons	2.5	5.4	34.6	40.4	6.8	8.7	13.7	1.0
Catalyst age (h)	4	4	5	5	6	7	6	7

[a] Reaction conditions: $T = 300°C$, $P = 5$ MPa, H_2/anisole = 100 mol/mol, LHSV = 2.0 h^{-1}.
[b] LHSV = 1.0 h^{-1}.
[c] Unsulfided catalyst E.

hydrogenation or HDO activity. The reactions of the methyl groups proceed most probably through a carbonium ion mechanism.[10] The rapid deactivation of the carriers is obviously due to carbon deposition on the catalyst surface as the coke-forming precursors cannot be hydrogenated to desorbable products.

Unsupported MoS_2

The conversion of anisole was on this catalyst surprisingly high in spite of the very low surface area. The product distribution was simple: mainly phenol and benzene. Only minor amounts of methyl-substituted products were formed. The catalyst was stable and no deactivation could be noted in 5 h. Very similar results have also been obtained on an unsupported WS_2 catalyst (surface area 2.6 m^2 g^{-1}).[11]

It is obvious that on unsupported sulfide catalysts of this kind hydrogenolysis activity is the dominating catalytic function and acidity, if present in any appreciable amount, does not take part in the reactions. It may be envisioned that the radicals, formed through homolytic splitting on the catalyst surface, are immediately hydrogenated by adsorbed hydrogen atoms to products readily desorbable.[10] This scheme explains the high activity of these low-area catalysts: as the adsorbed species stay only for a very short moment on the surface high turnover numbers of individual sites can be reached.

$Ni–SiO_2$

Silica is usually regarded as a rather inactive carrier material for catalysts[12–14] and the results obtained in the present study support this view. The conversion of anisole was very low and the product distribution nearly the same as on the unsupported MoS_2 catalyst. The finding that despite a very large surface area (see Table 1) the activity of the $Ni–SiO_2$ catalyst is low may be due to a very poor dispersion of the metal or to a low activity of the sulfided Ni for this type of reaction. The latter explanation is more probable because the Ni load was quite high (11%).

$Mo–\gamma\text{-}Al_2O_3$

This catalyst gave high conversion of anisole both in the sulfided and unsulfided forms. The sulfided form was found to be more stable but in product distribution no clear differences were noted. It is known that hydrodenitrogenation reactions, in contrast to HDS reactions, take place on the oxidic as well as on the sulfidic forms of the CoMo–alumina catalysts.[15] It has been even reported that in the HDO of 1-naphthol the oxidic forms are, especially initially, more active than the sulfidic forms.[16] Thus the results obtained in the present work are in accordance with previous knowledge.

In addition to the main reaction products, phenol and *o*-cresol, 2,6-dimethylphenol was also formed in appreciable amounts. The share of methylated anisoles was very small, especially compared to that obtained on pure carriers. Nearly similar reaction products have been obtained also on oxidic $Cr–\gamma\text{-}Al_2O_3$ catalysts.[17]

The HDO activity of the $Mo–\gamma\text{-}Al_2O_3$ catalyst was much lower than found previously for sulfided $NiMo–SiO_2–Al_2O_3$ and $CoMo–\gamma\text{-}Al_2O_3$ catalysts.[10] Ni and Co evidently are effective promoters

for the Mo catalysts not only in HDS reactions but also in HDO reactions.

Ni–γ-Al_2O_3

The two Ni–alumina catalysts studied, F and G, contained very different loadings of Ni, viz. 11 and 0.5%. Catalyst G, with the low loading of Ni, surprisingly gave a higher conversion of anisole than any of the other catalysts studied in this work. The reaction product consisted exclusively of phenol and methyl-substituted phenols. This high activity can be explained as follows: the γ-Al_2O_3 carrier is a very active catalyst in isomerization and disproportionation of methylated phenols *initially*, but due to a high rate of coke formation the activity decreases steeply as was noted for catalysts A and B. A small amount of Ni inhibits this deactivation by hydrogenating the coke-forming precursors on the catalyst surface. Some kind of spillover mechanism can be envisioned to transfer hydrogen atoms from the metal to alumina. It is also possible that during the impregnation stage of the catalyst preparation Ni adsorbs mainly on the most active sites which otherwise would form the coke-forming centers.

On catalyst F the main reaction products were phenol and benzene as on catalysts C and D. Thus it may be concluded that a high metal load is essential for HDO of anisole. Catalysts D and F contained equal amounts of Ni (11%) but on different supports. The higher activity of the alumina support is clearly noted. However, the Ni–SiO_2 catalyst is more active in HDO of anisole. It is evident that strong metal–support interactions may play important roles in the catalytic reactions of anisole but these questions are outside the scope of this paper.

Concluding remarks

The results obtained on different catalysts indicate that the reactions proposed in Fig. 1 are characteristic of the catalytic hydrogenolysis of anisole. Whether the HDO reaction takes place directly from anisole or via phenol as an intermediate is not clear. However, if the dissociative adsorption of anisole as a phenoxide ion or a phenoxy radical is accepted,[10] the direct splitting of a methoxy group can be ruled out.

Acknowledgements—I am indebted to Professor J. B. Bredenberg for valuable discussions. Financial support from the Neste Oy Foundation is very gratefully acknowledged.

REFERENCES

1. F. E. Massoth, *Advances in Catalysis*, Vol. 27, p. 265. Academic Press, New York (1978).
2. O. Weisser and S. Landa, *Sulphide Catalysts: Their Properties and Applications*. Pergamon Press, New York (1973).
3. E. Furimsky, *Catal. Rev.—Sci. Eng.* 1983, **25**, 421.
4. C. N. Satterfield and S. H. Yang, *J. Catal.* 1983, **81**, 335.
5. F. J. Gil Llambías, A. M. Escudey-Castro, A. López Agudo and J. L. G. Fierro, *J. Catal.* 1984, **90**, 323.
6. K. Segawa and W. K. Hall, *J. Catal.* 1982, **77**, 221.
7. J. Valyon, R. L. Schneider and W. K. Hall, *J. Catal.* 1984, **85**, 277.
8. F. E. Massoth and G. Muralidhar, In *Proceedings of the Fourth International Conference on the Chemistry and Uses of Molybdenum* (Edited by H. F. Barry and P. C. H. Mitchell), p. 343. Climax Molybdenum Co., Ann Arbor, MI (1982).
9. J. B. Bredenberg, M. Huuska, J. Räty and M. Korpio, *J. Catal.* 1982, **77**, 242.
10. M. Huuska and J. Rintala, *J. Catal.* 1985, **94**, 230.
11. M. Huuska, P. Toropainen and A.-M. Sipilä, unpublished results.
12. C. N. Satterfield, *Heterogeneous Catalysis in Practice*. McGraw-Hill, New York (1980).
13. P. Gajardo, R. I. Declerck-Grimee, G. Delvaux, P. Olodo, J. M. Zabala, P. Canesson, P. Grange and B. Delmon, *J. Less-Common Met.* 1977, **54**, 311.
14. B. Delmon, In *Proceedings of the Third International Conference on the Chemistry and Uses of Molybdenum* (Edited by H. F. Barry and P. C. H. Mitchell), p. 73. Climax Molybdenum Co., Ann Arbor, MI (1979).
15. B. C. Gates, J. R. Katzer and G. C. A. Schuit, *Chemistry of Catalytic Processes*. McGraw-Hill, New York (1979).
16. M. W. Vogelzang, C.-L. Li, G. C. A. Schuit, B. C. Gates and L. Petrakis, *J. Catal.* 1983, **84**, 170.
17. M. Huuska, unpublished results.

Polyhedron Vol. 5, No. 1/2, pp. 237–241, 1986
Printed in Great Britain

0277–5387/86 $3.00 + .00
© 1986 Pergamon Press Ltd

THE INTERACTION OF VANADIUM AND NICKEL PORPHYRINS AND METAL-FREE PORPHYRINS WITH MOLYBDENUM-BASED HYDROPROCESSING CATALYSTS: RELEVANCE TO CATALYST DEACTIVATION AND CATALYTIC DEMETALLIZATION

PHILIP C. H. MITCHELL*

Department of Chemistry, The University, Whiteknights, Reading RG6 2AD, U.K.

and

CARLOS E. SCOTT

Universidad Central de Venezuela, Facultad de Ciencias, Escuela de Quimica, Caracas, Venezuela

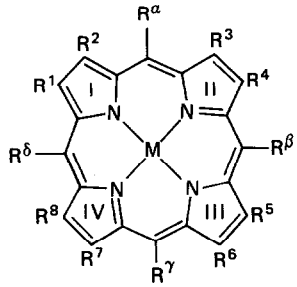
(*Received* 26 *June* 1985)

Abstract—The poisoning of a Co–Mo–alumina hydrodesulphurization (HDS) catalyst by metal-free, vanadium and nickel etio- and tetraphenyl porphyrins and the binding and reactivity of the porphyrins on oxide and sulfide surfaces is described. The surface interactions of porphyrins were studied by adsorption from solution, and UV–visible diffuse-reflectance and ESR spectroscopy. Metalloporphyrins undergo demetallation at acidic sites. The porphyrin ring is oxidized at a *meso*-carbon by oxomolybdenum(VI) species and adsorbed oxygen to a cation radical and an oxophlorin. During HDS porphyrin bound to the catalyst is hydrogenated at the *meso*-carbon to phlorin. Interaction of the porphyrins with surfaces is similar to that of polynuclear aromatic hydrocarbons. The relevance of these results to catalyst deactivation and catalytic demetallation is discussed.

Hydroprocessing catalysts are poisoned by metalloporphyrins in petroleum crudes. In this paper we report a study of the interaction of vanadium and nickel etioporphyrin (ETP) (**1a**) and tetraphenylporphyrin (TPP) (**1b**) and the metal-free porphyrins with molybdenum-based catalysts. Our object was to discover specific interactions between the porphyrins and the molybdenum species in the catalysts.

EXPERIMENTAL

The catalytic hydrodesulphurization (HDS) of thiophene (i.e. reaction with hydrogen with elimination of H_2S) was studied at 250–350°C and 1 atm in a conventional flow microreactor.[1] The catalyst was a commercial Co–Mo–Al_2O_3 catalyst (Co 3.2 and Mo 7.7 wt %, surface area 268 $m^2\ g^{-1}$). The catalyst was presulphided in H_2S/H_2. Thiophene was injected into the inlet dihydrogen. In the poisoning experiments, solutions of porphyrins in dichloromethane were injected in successive por-



1a M = H_2, VO or Ni
$R^1 = R^3 = R^5 = R^7 = CH_3$
$R^2 = R^4 = R^6 = R^8 = C_2H_5$

1b M = H_2, VO or Ni
$R^1 \ldots R^8$ = H; $R^{\alpha-\delta} = C_6H_5$

* Author to whom correspondence should be addressed.

tions onto the catalyst bed. Surface concentrations of the porphyrins were *ca* 10^{-5} mol (g catalyst)$^{-1}$, equivalent to *ca* 0.2 wt % V or Ni.

UV–visible diffuse-reflectance spectra (DRS)[2] and ESR spectra[3] of the supported porphyrins were recorded.

The amount of porphyrin adsorbed by the catalysts was determined from the decrease of light absorbance of porphyrin solutions in dichloromethane contacted with the catalysts.

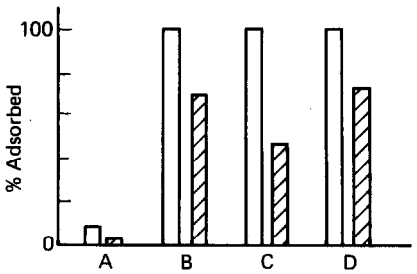


Fig. 2. Adsorption of H_2ETP (open) and VOETP (hatched bars) (10^{-3} mol l^{-1} in CH_2Cl_2) by γ-alumina (A), MoO_3–Al_2O_3 (B), CoO–MoO_3–Al_2O_3 (C) and MoS_2 (D).

RESULTS AND DISCUSSION

Catalyst deactivation

Thiophene conversions at 300°C are plotted against the amount of porphyrin added to the catalyst in Fig. 1. Poisoning of the catalysts is shown by the decrease of thiophene conversion. We observe:

(a) The metal-free porphyrins are initially more severe poisons than the metalloporphyrins. Evidently the whole metalloporphyrin molecule, not just the metal, poisons the catalyst.

(b) The first additions of VOETP increase the catalytic activity. With NiETP the activity is, at first greater, than with the metal-free H_2ETP. Therefore, either the metalloporphyrins are themselves active in HDS or, more likely, they are part demetallated and the metal ions released promote the HDS reaction until the poisoning effect of increasing amounts of porphyrin becomes dominant.

The poisoning and promoter effects imply that the porphyrins bind and decompose at molybdenum sites.

Adsorption of porphyrins by the catalysts

The catalysts, and also γ-alumina and MoS_2 were suspended in solutions of the porphyrins in dichloromethane (10^{-3} mol l^{-1}) and the amount of porphyrin adsorbed was determined from the decrease of light absorbance of the solutions. In Fig. 2 we show the relative amounts of H_2ETP and VOETP adsorbed. We observe:

(a) A strong interaction with the molybdenum-containing catalysts, especially MoS_2. (Note that the surface area of MoS_2 was <10 m^2 g^{-1}.)

(b) The amount of metal-free porphyrin, H_2ETP, adsorbed is greater than that of VOETP; the adsorption of VOETP is greater on MoO_3–Al_2O_3, which is more acidic, than on Al_2O_3. These two observations suggest that acidic sites, Lewis sites or surface protons, may be involved in the adsorption process.

In an earlier paper[3] we suggested, from an analysis of the ESR parameters of adsorbed VO porphyrins, that metalloporphyrins lie flat on the support and bind to the surface via a charge-transfer interaction from the π-system of the porphyrin ring to surface acceptor sites. The fraction of the surface covered when a porphyrin monolayer is established is $<5\%$ of the available surface. Evidently there are preferred binding sites, possibly flat slabs with acidic molybdenum species.

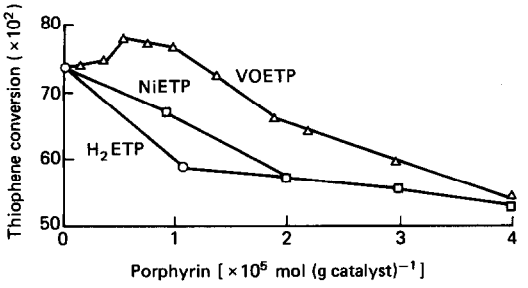


Fig. 1. Poisoning of a Co–Mo–Al_2O_3 catalyst by metal-free (H_2ETP), nickel (NiETP) and vanadyl (VOETP) ETP. Thiophene conversion (300°C, 1 atm) vs porphyrin concentration on the catalyst.

Demetallization

DRS of the porphyrins on the catalysts and acidic supports are shown in Fig. 3. For the more acidic supports, HF–SiO_2 and NiO–MoO_3–Al_2O_3, we see absorption peaks of protonated porphyrins. These peaks are not observed on the less acidic alumina. Demetallization of VOTPP on HF–SiO_2 and NiO–MoO_3–Al_2O_3 is evident from the appearance of a new peak in the spectrum at 650–660 nm assigned to the protonated porphyrin released by demetallization. There is no such peak on alumina. Thus interaction with surface protons causes demetallization of VOTPP. There appears to be no, or much less, decomposition of VOETP. Instead with VOETP a new peak appears near 650 nm; this is discussed later.

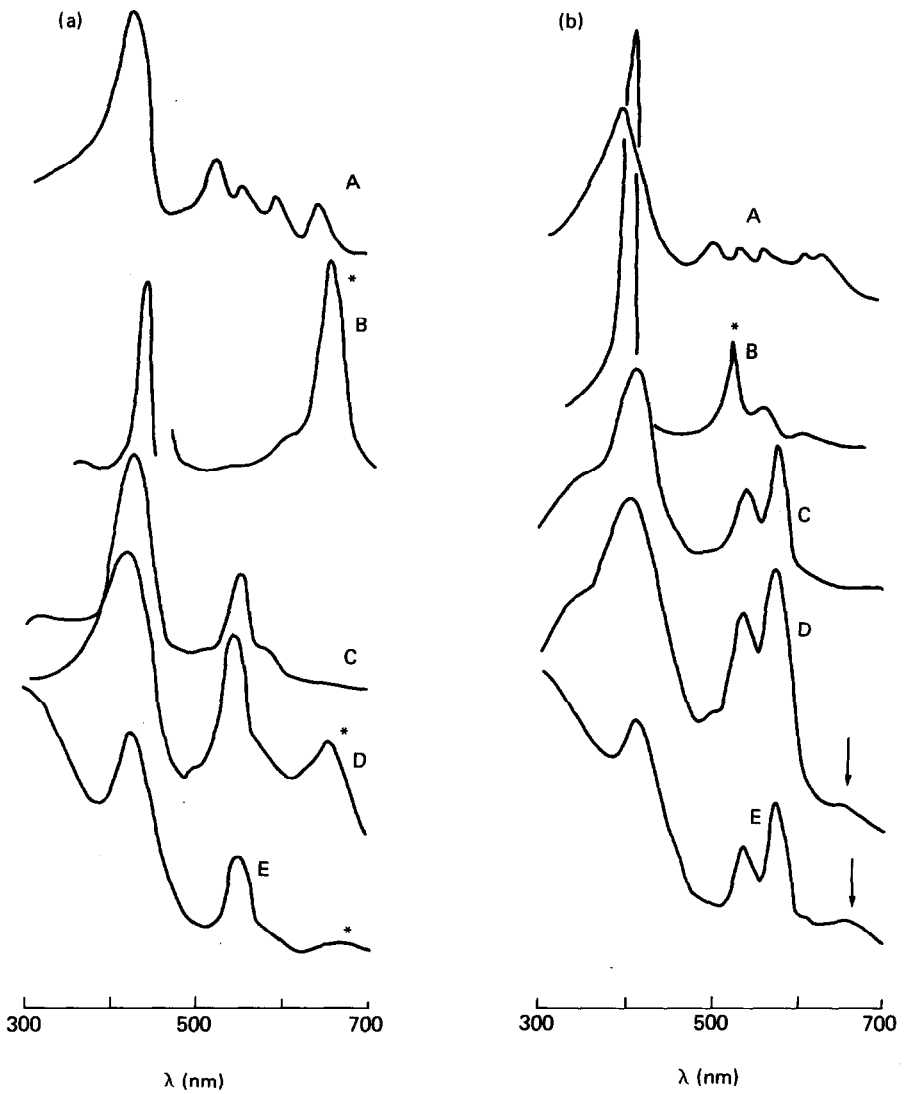


Fig. 3. UV–visible DRS of surface-bound porphyrins [*ca* 5×10^{-6} mol (g catalyst)$^{-1}$]. (a) Tetraphenylporphyrin (TPP): H_2TPP on Al_2O_3 (A) and HF–SiO_2 (B); VOTPP on Al_2O_3 (C), HF–SiO_2 (D) and NiO–MoO_3–Al_2O_3 (E). (b) ETP: H_2ETP on Al_2O_3 (A) and HF–SiO_2 (B); VOETP on Al_2O_3 (C), HF–SiO_2 (D) and NiO–MoO_3–Al_2O_3 (E). Light absorbance increases vertically. Peaks marked (*) characteristic of protonated porphyrin; vertical arrow, oxophlorin.

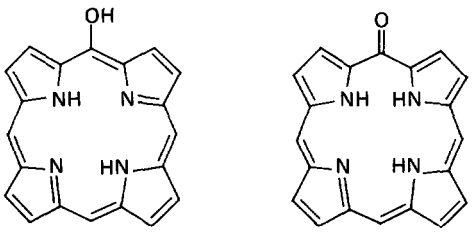
Oxidation of surface-bound porphyrin by oxomolybdenum (VI)

Porphyrins supported on MoO_3–Al_2O_3 and Co–Mo–Al_2O_3 were heated under nitrogen at 300°C. Typical ESR spectra are shown in Fig. 4. In the spectrum of H_2ETP on MoO_3–Al_2O_3 we see lines assigned to oxomolybdenum(V) ($g = 1.928$), oxomolybdenum(V) porphyrin ($g = 1.968$), and a porphyrin radical ($g = 2.003$).[4] Evidently the porphyrin has been oxidized to a cation radical by oxomolybdenum(VI) which has been reduced. The spectrum of VOETP similarly shows the lines of oxomolybdenum(VI) and the porphyrin radical, although not MoOETP. Similar results were obtained with NiETP.

The porphyrin radical was also observed for porphyrins on silica–alumina (but not alumina). Here the porphyrins are apparently behaving in the same way as adsorbed polyaromatic hydrocarbons, the oxidation being effected by adsorbed oxygen and surface protons.[5]

The effect on the UV–visible spectrum of heating the surface-bound metalloporphyrins was to collapse the peaks in the visible region. This change is consistent with formation of a porphyrin cation radical.[6]

We can now explain the new peak at *ca* 650 nm in



2a 2b

the DRS spectrum of VOETP on acidic supports (see Fig. 3). This peak is characteristic of an oxophlorin, i.e. a compound with O or OH at a bridging (*meso*) carbon (**2**).[7] We conclude, then, that surface-bound porphyrins oxidize to a cation radical and an oxophlorin. These reactions are well known in the solution chemistry of porphyrins but have not, as far as we know, been reported previously for surface-bound porphyrins.

Hydrogenation of surface-bound porphyrin

The ESR spectra of VOETP on a sulfided Co–Mo–Al_2O_3 catalyst which had been used for thiophene HDS are shown in Fig. 5. The significant feature is new lines (starred), in addition to those of VOETP, in the spectrum of the catalyst before it had been exposed to air. After exposure to air these new lines disappear and the spectrum is that of VOETP. Evidently the compound responsible for the new lines oxidizes in air. This behaviour is typical of a phlorin, i.e. a compound in which a *meso*-carbon has been hydrogenated (**3**).[8] We suggest, therefore, that during the HDS reaction the bound porphyrin is hydrogenated at a *meso*-carbon. The hydrogenation is presumably catalysed by MoS_2.

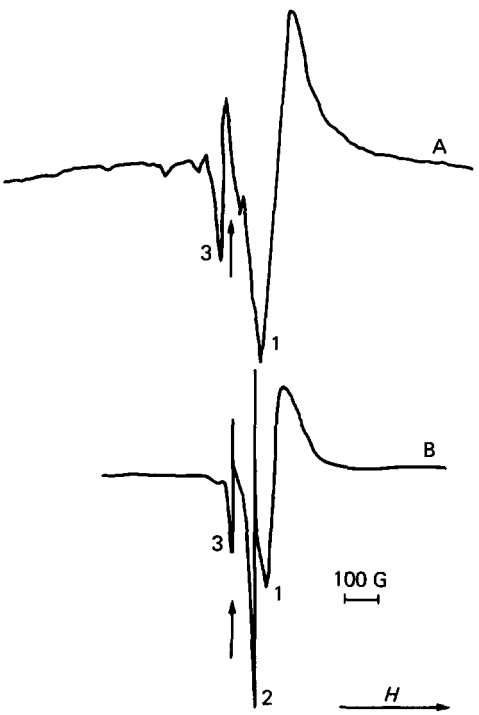


Fig. 4. ESR derivative spectra after heating (300°C, 1 h, under N_2): VOETP on CoO–MoO_3–Al_2O_3 (A) and H_2ETP on MoO_3–Al_2O_3 (B). Line assignments: (1) oxoMo(V) ($g = 1.928$), (2) oxoMo(V) porphyrin ($g = 1.968$), and (3) porphyrin radical ($g = 2.003$). Vertical arrow = DPPH calibrant.

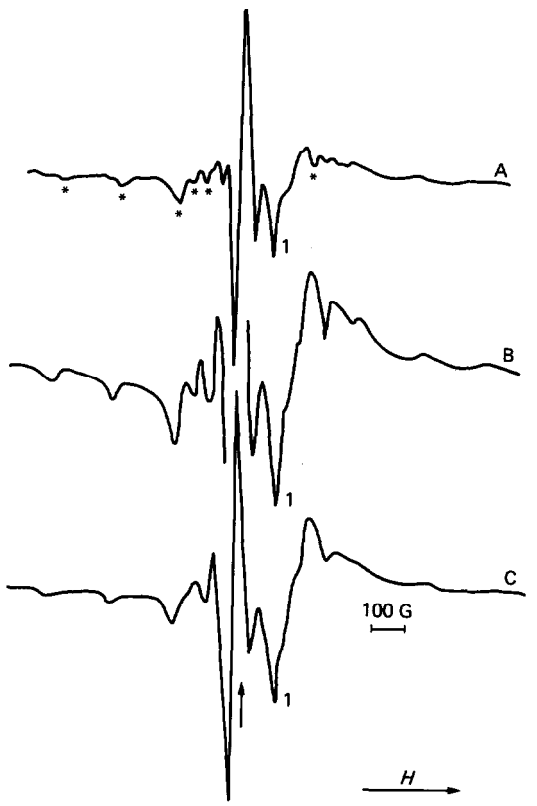
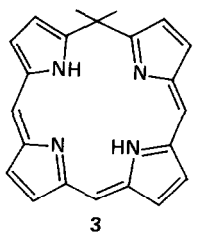


Fig. 5. ESR derivative spectra of VOETP (*ca* 0.2 wt %) on sulfided Co–Mo–Al_2O_3 catalyst after thiophene HDS: sample kept in nitrogen (A), exposed to air (B), and extracted with CH_2Cl_2 (C). Lines marked (*) are additional to those of VOETP and assigned to a VO phlorin; line 1 = oxoMo(V); vertical arrow = DPPH calibrant.



3

CONCLUSIONS

We identify three types of surface reaction of porphyrins with molybdenum-containing catalysts:

(a) demetallization by reaction with protons, (b) oxidation of the porphyrin ring by oxo-molybdenum(VI) at a *meso*-carbon giving a porphyrin radical and an oxophlorin, and (c) hydrogenation of the porphyrin also at a *meso*-carbon giving a phlorin. Further work is in progress to confirm these suggestions through synthesis of metallo-oxophlorins and phlorins and a study of their characteristic properties.

The significance of these observations for catalyst deactivation and demetallization is as follows. The initial poisoning by metalloporphyrins is due to the whole molecule, not just the metal; the porphyrins behave like nitrogen bases. Demetallization of the metalloporphyrins is accomplished by reaction with surface protons of acidic catalysts. Both oxidation and hydrogenation of the porphyrins are likely to increase their binding to acidic sites since oxophlorins and phlorins are more basic than porphyrins.[9] Also, for the oxophlorins, oxo or hydroxo groups in the porphyrin ring provide a further point of attachment to a surface. Increased binding may, of course, be desirable if the object is to prevent the porphyrin from passing through the HDS catalyst. On the other hand increased binding is likely to mean more poisoning. The practical conclusion would seem to be that porphyrin removal, and the accompanying chemistry, is best done before the hydroprocessing stage on, for example, an MoO_3–Al_2O_3 catalyst in a guard reactor.

Acknowledgements—We thank Climax Molybdenum Co. (PCHM) and the Universidad Central de Venezuela (CES) for support.

REFERENCES

1. P. C. H. Mitchell and C. E. Scott, *Bull. Soc. Chim. Belg.* 1984, **93**, 619.
2. P. C. H. Mitchell, C. E. Scott, J. P. Bonnelle and J. G. Grimblot, *J. Chem. Soc., Faraday Trans.* 1 1985, **81**, 1047.
3. P. C. H. Mitchell and C. E. Scott, In *Actas do 9.º Simpósio Iberamericano de Catálise (Proceedings of the 9th Iberoamerican Symposium on Catalysis)* (Edited by M. F. Portela), Vol. 2, p. 1303. Technical University, Lisbon (1984).
4. J. Fajer and M. S. Davis, In *The Porphyrins* (Edited by D. Dolphin), Vol. 4, p. 197. Academic Press, New York (1979).
5. (a) B. D. Flockhart, I. M. Sesay and R. C. Pink, *J. Chem. Soc., Faraday Trans* 1 1983, **79**, 1009; (b) D. Cordischi, V. Indovina and M. Occhiuzzi, *Magnetic Resonance in Surface and Colloid Science*, p. 461. D. Reidel, New York (1980).
6. J. H. Furhop, In *Porphyrins and Metalloporphyrins* (Edited by K. M. Smith), p. 609. Elsevier, Amsterdam (1975).
7. (a) H. Scheer, In *The Porphyrins* (Edited by D. Dolphin), Vol. 2, p. 71. Academic Press, New York (1979). (b) P. S. Clezy, *op. cit.*, p. 103.
8. D. Manzerall, In *The Porphyrins* (Edited by D. Dolphin), Vol. 2, pp. 52 and 92. Academic Press, New York (1979).
9. P. S. Clezy, In *The Porphyrins* (Edited by D. Dolphin), Vol. 2, p. 113. Academic Press, New York (1979).

Polyhedron Vol. 5, No. 1/2, pp. 243–247, 1986
Printed in Great Britain

0277-5387/86 $3.00 + .00
Pergamon Press Ltd

SUPPORT EFFECTS ON HYDROCRACKING AND HYDROGENATION ACTIVITIES OF MOLYBDENUM CATALYSTS USED FOR UPGRADING COAL-DERIVED LIQUIDS

A. NISHIJIMA,* H. SHIMADA, T. SATO, Y. YOSHIMURA and J. HIRAISHI

National Chemical Laboratory for Industry, 1-1, Higashi, Yatabe, Ibaraki 305, Japan

(*Received* 13 *June* 1985)

Abstract—Studies of the effect of supports on the molybdenum catalysts used for upgrading coal-derived liquids showed that hydrocracking and hydrogenation activities are greatly dependent upon their supports. The relation between catalytic selectivities and properties of the molybdenum catalysts were investigated by using an X-ray photoelectron spectrometer and a Raman spectrometer. A TiO_2 support gave the highest hydrocracking activity among simple oxides examined, while a Al_2O_3 support showed the highest hydrogenation activity. Both hydrocracking and hydrogenation activities of the molybdenum catalysts increased when some double oxides such as TiO_2–Al_2O_3 or TiO_2–ZrO_2 were used as catalyst supports.

Molybdenum catalysts have been much used in the petroleum industry for hydrotreating and hydrodesulfurization. Recently, these catalysts have been employed in coal liquefaction and upgrading of coal-derived liquids. However, improvement of the selectivity of the molybdenum catalysts for hydrocracking (HC) and hydrogenation (HY) activities is required for upgrading the coal-derived liquids and producing effective recycle solvents. In this work, the support effect on the selectivity of the molybdenum catalysts was investigated to find the most suitable supports by which higher HC and HY activities of the catalysts could be obtained. The catalysts were characterized using an X-ray photoelectron spectrometer (XPS) and a Raman spectrometer. The reactions of separate model tests, as well as the upgrading of coal-derived liquids, were performed to clarify catalytic functionalities of the catalysts. A high hydrogen pressure was used for the test reactions; experiments in previous studies of the support effects have been undertaken under atmospheric pressure.[1,2]

EXPERIMENTAL

TiO_2 and ZrO_2 supports were prepared by precipitation from aqueous solutions of $Ti(SO_4)_2$ and $ZrOCl_2$, respectively. Some double oxides such as TiO_2–Al_2O_3 or TiO_2–ZrO_2 were also prepared by similar methods. Commercially available supports, such as Al_2O_3 and SiO_2, were used as catalyst supports. A series of Mo and Ni–Mo supported catalysts were prepared by an impregnation method. The supports prepared were impregnated in a solution of ammonium paramolybdate or solutions of ammonium paramolybdate and nickel nitrate.[3] Catalysts were then dried at 110°C for 10 h, and finally calcined at 500°C for 4 h. The catalysts were presulfided in a stream of 10 vol % of H_2S (balance H_2) at 400°C for 2 h before reaction.

The reactions of upgrading of coal-derived liquids and the separate model tests were carried out using batch type reactors (50 cm^3). Ten cubic centimetres of coal-derived liquid and 0.5 g of catalyst were charged into the reactor. After being pressurized with H_2 to 9.8 MPa, the microreactor was injected into an oven heated at 430°C. The temperature of the reactor was kept at 400°C during the 2-h reaction. An initial H_2 pressure of 6.9 MPa was used for HC of diphenylmethane and HY of 1-methylnaphthalene. Reaction products were analyzed by a gas chromatograph and a mass spectrometer. The surface area and the pore volume of each catalyst were measured by a nitrogen adsorption technique and a BET method. Temperature-programmed desorption (TPD) of NH_3 was employed to measure

* Author to whom correspondence should be addressed.

acidic properties of the catalysts. The characterization of the molybdenum catalysts, such as the electronic state or the structure of the molybdenum species, was carried out using XPS, a Raman spectrometer and an X-ray diffractometer.

RESULT AND DISCUSSION

Simple-oxide support

Table 1 shows the catalytic functionalities of the molybdenum catalyst obtained on each support. Among simple oxides examined, the effectiveness order of the support for HC and HY is as follows:

$$\text{HC: } TiO_2 \gg SiO_2 > ZrO_2 > Al_2O_3 \gg MgO,$$

$$\text{HY: } Al_2O_3 > TiO_2 \gg MgO > ZrO_2 > SiO_2.$$

The TiO_2 support gave the highest HC activity, while the MgO support gave no activity for HC. In the case of HY activity, the Al_2O_3 support showed the highest HY activity. The TiO_2 support also gave a higher HY activity compared to other supports. The HY activity increased with the increase in the surface area of the catalyst, when the chemical composition of the support used was the same. The HY activity also increased with the increase in the amount of MoO_3 supported on the carrier. However, after a certain amount of MoO_3, the HY activity remained constant. These results seem to indicate that a highly dispersed state of molybdenum species is required for the HY activity of the catalysts.

Table 1. Hydrocracking and hydrogenation activities of molybdenum catalysts[a]

Support	SA[b] ($m^2\ g^{-1}$)	PV[c] ($cm^3\ g^{-1}$)	HC of DPM[d] (%)[e]	HY of 1-MN[f] (%)[g]
Alumina	170	0.47	2.0	20.3
Titania	66	0.17	27.3	11.8
Silica	266	1.09	5.3	0.8
Magnesia	51	0.16	0.0	3.3
Zirconia	53	0.06	3.6	3.0

[a] 10 wt % of MoO_3 was supported on each carrier. Each catalyst was used as a powder after presulfiding with H_2S before reaction.
[b] Surface area.
[c] Pore volume.
[d] Hydrocracking of diphenylmethane.
[e] Yield of benzene and toluene.
[f] Hydrogenation of 1-methylnaphthalene.
[g] Yield of 1-methyltetralin and 5-methyltetralin.

Characterization of the catalysts

Figure 1 shows Raman spectra of the molybdenum catalysts observed on various supports. In the Raman spectra, the bands between 900 and 1000 cm^{-1}, which were assigned to a Mo—O stretching vibration mode of the molybdenum species on the catalysts, shifted on changing the chemical composition of the support. The sharp bands at 998 and 820 cm^{-1} indicate the presence of crystalline MoO_3. Strong peaks of crystalline MoO_3 were observed on the SiO_2 support, though no peak was detected by the X-ray diffractometer. The poor dispersion of the molybdenum species on SiO_2 might result in a lower HY activity on SiO_2. The broad and intense band at 950 cm^{-1} shifted to 970 cm^{-1} when the support was changed from Al_2O_3 to TiO_2. This result shows the presence of a more highly aggregated molybdenum species on the TiO_2 support.[4] The spectrum of MoO_3–MgO may suggest the formation of a tetrahedral structure of MoO_4^{2-} on MgO.[5] Figure 2 shows Raman spectra of MoO_3–TiO_2 catalysts prepared as a function of Mo loading. At 2 wt % of MoO_3 loading a broad band at 945 cm^{-1} was observed. As the MoO_3 loading increased from 2 to 10 wt %, the band shifted to higher wavenumbers, reaching 970 cm^{-1}. This result shows a lower dispersion of the molybdenum species at a higher loading of MoO_3. After the monolayer coverage was exceeded (calculated to be about 8 wt %), sharp bands at 820 and 998 cm^{-1} ap-

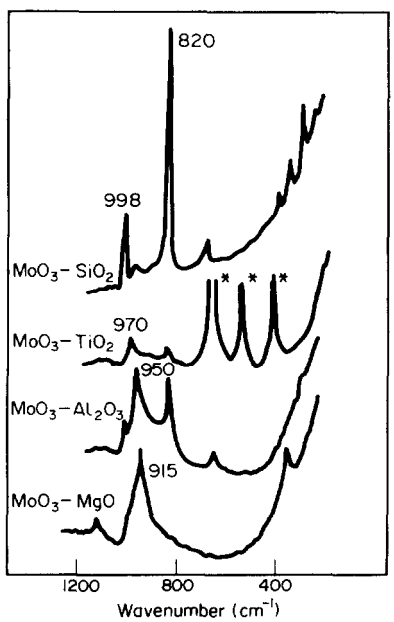


Fig. 1. Raman spectra of molybdenum catalysts. * Bands from TiO_2.

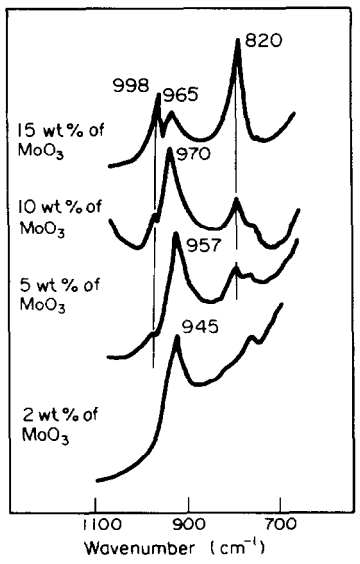


Fig. 2. Raman spectra of MoO_3–TiO_2 catalysts as a function of MoO_3 loading.

peared, indicating the formation of crystalline MoO_3 on the TiO_2 support.

The relevant active sites of the molybdenum catalysts for HC have been considered to be acidic. However, no correlation was obtained under a high pressure of H_2 between HC activities and acidic properties of the catalysts measured by TPD of NH_3. The amount of acid sites on the TiO_2 support was much less than that on Al_2O_3, suggesting that all the acid sites cannot be active for HC. The XPS analyses showed that the binding energy of the Mo3*d* line shifted from 232.6 (MoO_3–Al_2O_3) to 231.8 (MoO_3–TiO_2), while that of the pure MoO_3 appeared at 232.4 eV (Fig. 3). The molybdenum ion on the MgO support was less electronegative (233.0 eV) than that on the Al_2O_3 support. Thus, the interaction between the support and the molybdenum affects the electronic state of the molybdenum ion. An electronegative state of the molybdenum ion will be necessary for the HC activity of the catalyst.

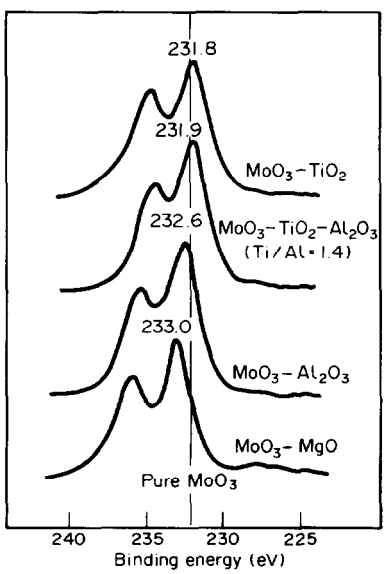


Fig. 3. Mo3*d* photoelectron spectra for molybdenum catalysts.

Double-oxide support

The TiO_2 support gave the highest activity for HC. On the other hand Al_2O_3 showed the highest HY activity. Accordingly, double oxides consisting of TiO_2 and Al_2O_3 were prepared by changing the atomic ratio of Ti/Al. Properties of the TiO_2–Al_2O_3 supports prepared are summarized in Table 2. Figure 4 shows the HC activities of the molybdenum catalysts when TiO_2–Al_2O_3 supports were used instead of simple-oxide supports. Much higher HC activities were obtained on TiO_2–Al_2O_3 supports, indicating a cooperative or a synergistic effect of both component supports. No peak was observed from three kinds of TiO_2–Al_2O_3 supports by the X-ray diffractometer. As shown in Fig. 3, the XPS analyses showed that the electronic state of the molybdenum ions on TiO_2–Al_2O_3 supports was almost the same as that on the TiO_2 support, showing that the molybdenum ions exist in a suitable electronic state for HC. On the other hand, in the case of HY activity, no cooperative effect was obtained on TiO_2–Al_2O_3 supports (Fig. 5).

Similar trends were observed on TiO_2–ZrO_2 supports. Figure 6 shows the effect of the supports on the HY activities of the catalysts. TiO_2–ZrO_2 supports also gave higher HC activities than the simple oxides (TiO_2 and ZrO_2). However, little cooperative effect was observed on TiO_2–MgO supports in the HC of diphenylmethane, though the

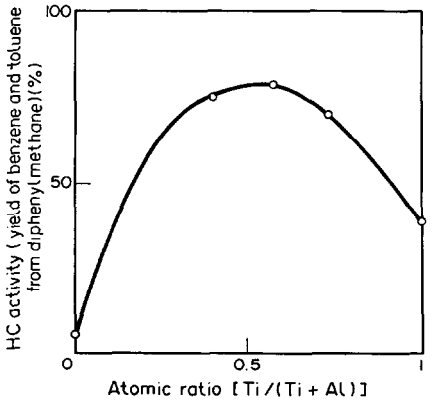


Fig. 4. Effect of support on the HC activities of molybdenum catalysts.

Table 2. Properties of TiO_2–Al_2O_3 supports

Support	TiO_2	TiO_2–Al_2O_3			Al_2O_3
Ti/(Ti+Al)[a]	1.0	0.75	0.60	0.40	0.0
Crystallinity					
XRD[b]	ana.[c]	am.[d]	am.	am.	am.
Raman	ana.	ana.	(ana.)[e]	am.	am.
Porosity					
SA[f] ($m^2\ g^{-1}$)	66	171	287	262	184
PV[g] ($cm^3\ g^{-1}$)	0.17	0.25	0.45	0.42	0.53
APD[h] (nm)	10	5.8	6.3	6.4	12

[a] Atomic ratio.
[b] X-ray diffraction.
[c] Anatase.
[d] Amorphous.
[e] Trace of anatase.
[f] See footnote [b] in Table 1.
[g] See footnote [c] in Table 1.
[h] Apparent pore diameter.

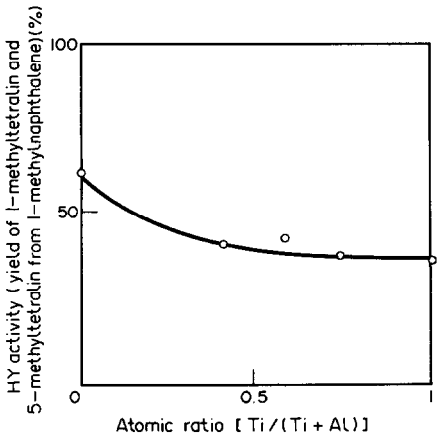


Fig. 5. Effect of support on HY activities of molybdenum catalysts.

HC activities on TiO_2–Fe_2O_3 supports increased to some extent (Fig. 7). These results clearly show that proper combinations of simple oxides, such as the combination of TiO_2 with Al_2O_3, are necessary to design suitable supports for the molybdenum catalysts.

Upgrading of coal-derived liquids

Based on the results obtained from the test reactions on various supports and the characterization of the molybdenum catalysts, some of the molybdenum catalysts were examined for upgrading coal-derived liquids. Middle and heavy distillates obtained from Wandoan coal were used as starting materials. After upgrading the coal-derived liquids, elemental anlyses, such as for nitrogen or sul-

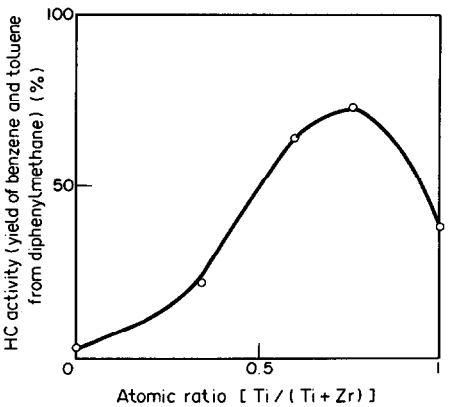


Fig. 6. Effect of TiO_2–ZrO_2 support on HC activities of molybdenum catalysts.

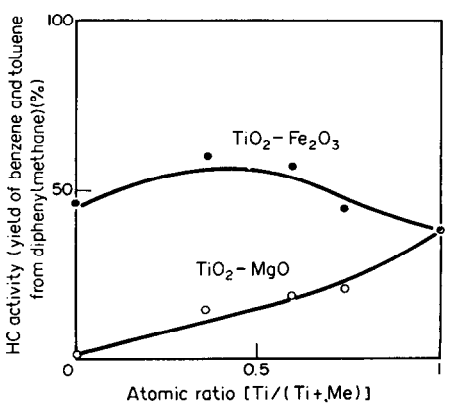


Fig. 7. Effect of double-oxide supports on HC activities of molybdenum catalysts.

Table 3. Upgrading of coal-derived liquids

Catalyst	Middle distillate			Heavy distillate		
	HDN[a] (%)	HY index[b]		HDN (%)	HY index	
		T/N[c]	8HP/P[d]		T/N	8HP/P
Raw material	[e]	0.73	1.66	[f]	0.41	0.30
$Mo-Al_2O_3$[g]	44	1.80	2.67	18	0.74	0.59
$Mo-TiO_2$[g]	45	1.58	2.39	14	0.68	0.54
$Ni-Mo-Al_2O_3$[h]	64	7.9	3.8	10	1.0	0.42
$Ni-Mo-TiO_2-Al_2O_3$[h]	93	9.8	6.0	33	2.4	1.06

[a] Hydrodenitrogenation.
[b] Index of hydrogenation activity.
[c] Ratio of tetralin/naphthalene in each product.
[d] Ratio of octahydrophenanthrene/phenanthrene in each product.
[e] The middle distillate contains 0.34 wt % of nitrogen.
[f] The heavy distillate contains 0.67 wt % of nitrogen.
[g] 10 wt % of MoO_3 was supported. Each catalyst was used as a powder.
[h] 2 wt % of NiO and 7 wt % of MoO_3 were supported. Extrudate catalysts were used.

fur, were performed to determine the hydrodenitrogenation and hydrodesulfurization activities of the catalysts. Ratios of tetralin/naphthalene and octahydrophenanthrene/phenanthrene measured by the gas chromatograph were used as the index of HY activity. The catalytic activities and selectivities of the catalysts used for the upgrading of the coal-derived liquids are summarized in Table 3. For the upgrading of the middle distillate, TiO_2 and Al_2O_3 supports showed higher hydrodenitrogenation (HDN) activities among the simple oxides. When Ni–Mo-supported catalysts were used, the HDN activities of the catalysts increased to a great extent. A $TiO_2-Al_2O_3$ support (Ti/Al = 2.5) gave a much higher HDN activity than the Al_2O_3 support. The effectiveness order of HY activities agreed with that measured in the HY of 1-methylnaphthalene. These results for the upgrading of the middle distillate are compatible with the results obtained from the catalytic functionalities of the catalysts. Similar trends were observed in the upgrading of the heavy distillate, though the HDN and HY activities of the catalysts for the heavy distillate were much lower than those for the middle distillate. Higher amounts of carbonaceous deposits were observed on the catalysts used for upgrading the heavy distillate, indicating deactivation of the catalysts in the early stage of the run.[6] In the upgrading of the heavy distillate, catalyst shapes will also affect the HDN activities of the catalysts because of the pore diffusional limitation. In fact, the powder catalyst ($MoO_3-Al_2O_3$) showed a higher HDN activity than the extrudate catalyst ($NiO-MoO_3-Al_2O_3$), though the pore structure of Al_2O_3 used was the same. The $TiO_2-Al_2O_3$ supports also showed much higher activities for HDN and HY than the Al_2O_3 support in the upgrading of the heavy distillate.

The HDN catalyst requires both HC and HY activities. As shown in Figs 4 and 5, $TiO_2-Al_2O_3$ supports showed higher activities for HC and HY. Moreover, the $TiO_2-Al_2O_3$ support showed excellent activities for HDN and HY of the coal-derived liquids (Table 3). Accordingly, $TiO_2-Al_2O_3$ supports seem to be suitable supports for the molybdenum catalysts used for hydrotreating coal-derived liquids.

REFERENCES

1. F. E. Massoth, G. Muralidhar and J. Shabtai, *J. Catal.* 1984, **85**, 53.
2. G. Muralidhar, F. E. Massoth and J. Shabtai, *J. Catal.* 1984, **85**, 44.
3. H. Shimada, M. Kurita, T. Sato, Y. Yoshimura and A. Nishijima, *Chem. Lett.* 1984, 1861.
4. C. P. Cheng and G. L. Schrader, *J. Catal.* 1979, **60**, 276.
5. W. Ogonowsky, J. Hanuza, B. Jezowska-Trzebiatowska and J. Wrzyszcz, *J. Catal.* 1975, **39**, 161.
6. Y. Yoshimura, K. Hayamizu, T. Sato, H. Shimada and A. Nishijima, In *Proceedings of the 21st Conference on Coal Science, J. Fuel Soc. Jpn.* p. 317 (1984).

Polyhedron Vol. 5, No. 1/2, pp. 249–255, 1986
Printed in Great Britain

0277-5387/86 $3.00 + .00
© 1986 Pergamon Press Ltd

WHEN DOES MOLYBDENUM OXIDE EQUAL MOLYBDENUM HEXACARBONYL?: RELATIONS BETWEEN HETEROGENEOUS AND HOMOGENEOUS MOLYBDENUM CATALYSTS IN SYNGAS CATALYSIS*

R. SAPIENZA,† W. SLEGEIR and D. MAHAJAN

Department of Applied Science, Brookhaven National Laboratory,
Associated Universities, Inc.

(*Received* 26 *June* 1985)

Abstract—Molybdenum provides one of the most versatile sets of materials for synthesis gas catalysis. In its reduced states (Mo^0–Mo^{4+}), molybdenum can act as a "metal" system yielding mainly hydrocarbon products. In its oxidized state, as the trioxide or as a metal molybdate, molybdenum may serve as an alcohol synthesis catalyst or as an alcohol to hydrocarbon conversion system. The oxides can also be used as a support for more typical syngas catalysts. Molydenum hexacarbonyl undergoes chemistry which can be related to these reactions. These relationships offer a frontier between molybdenum homogeneous and heterogeneous catalysis. Literature and mechanistic studies indicate that the formate and formyl intermediates represent the link between homogeneous catalysis by molybdenum carbonyl and oxide catalysis of reactions of carbon monoxide. The formate approach centers on the fact that virtually all catalysts that have a water-gas shift activity will promote, or are themselves, methanol catalysts. It is more than coincidental that these two embodied reactions have been shown to involve a similar type of intermediate, metal formates. This moiety, found in base-promoted molybdenum carbonyl and molybdenum trioxide catalyzed water-gas shift reactions, symbolizes the link between these chemistries and the potential route to developing new methanol catalyst systems. The use of carbon monoxide and water, or low-H_2 : CO ratio syngas, for the direct production of methanol and/or hydrocarbons with heterogeneous molybdenum systems can be explained. The formyl approach is based on a stoichiometric reaction of some main-group hydrides with molybdenum carbonyl to yield methanol. This chemistry is related to metal oxide catalyzed methanol synthesis from high-ratio ($2:1 \leqslant H_2$: CO) syngas. The molybdenum carbonyl or oxide is used to coordinate or fix the carbon monoxide while another metal system functions by activating the hydrogen. This can be pictured as the reduction of a carbonyl group by a complex metal hydride. Initial demonstration of the conceptual basis of each of these approaches has been accomplished at Brookhaven National Laboratory. Concepts for the extension of homogeneous catalysis into these regions of overlap with some examples will be presented.

The chemical versatility of molybdenum can provide a fertile link between homogeneous and heterogeneous catalysis.[1] Connections and similarities in surface molybdenum oxide chemistry and homogeneously catalyzed reactions of molybdenum hexacarbonyl are found for example in olefin metathesis,[2] desulfurization,[3] aqueous coal liquefaction[4] and expoxidation reactions.[5] This paper will emphasize relationships in the synthesis gas reactions of molybdenum oxide and molybdenum hexacarbonyl. Since comparisons of catalytic behavior utilizing the same metal give more insight than comparisons involving different metals, the common features and the similitudes of active species and

*Work done under Contract No. DE-AC02-76CH00016 with the U.S. Department of Energy.

† Author to whom correspondence should be addressed.

elementary steps in these reactions provided a guide for the design of new catalysts for the methanol synthesis.

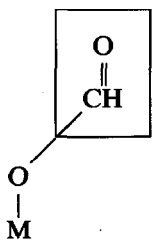
Typically the scientist extracts interpretations of heterogeneous catalytic effects by examining the mechanism of homogeneous catalytic reactions. In this work homogeneous catalytic features were adapted to information concerning the mechanism of the reaction extracted from a variety of catalytic studies of heterogeneous molybdenum and related oxides. These include the water-gas shift reaction, methanol synthesis and the formic acid and methanol decomposition reactions.

BACKGROUND

There are two proposed mechanisms for the heterogeneous methanol synthesis reactions (Fig. 1).[6]

The key intermediates are the initially formed hydrogenated carbon monoxide species; the formyl group (1) in mechanism A and the formate (2) in mechanism B. These species represent the connection between homogeneous catalysis by molybdenum hexacarbonyl and oxide catalysis of reactions of synthesis gas.

Mechanisms A and B are interrelated. If one considers the surface in mechanism A (Fig. 1) to be a metal oxide, the formyl would be coordinated to an oxygen resulting in a metal formate species. In other words, the surface in mechanism B is the metal of the catalytic oxide. The carbon monoxide of mechanism A was activated by oxide coordination as in the carbon monoxide oxidation[7] reaction. Hydrogen is initially activated in a similar manner in mechanism B:



Metal oxides tend to yield methanol rather than hydrocarbons because this formate–oxyformyl "serves" the activated carbon monoxide to a hydrogenation site. The coordination of the carbon monoxide to the oxide inhibits dissociation and therefore hydrocarbon formation.[8]

Other work on the decomposition of metal formates demonstrates this proposition. This decomposition is thought to need vacant sites and is enhanced by the presence of foreign metal ions.[9] A bicoordinated structure is visualized from the "served" carbon monoxide which reacts by one of three pathways (Fig. 2).

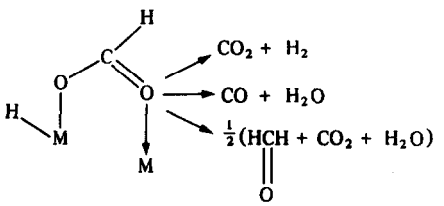


Fig. 2. Formate decomposition.[9]

Most interest in the literature has been focused

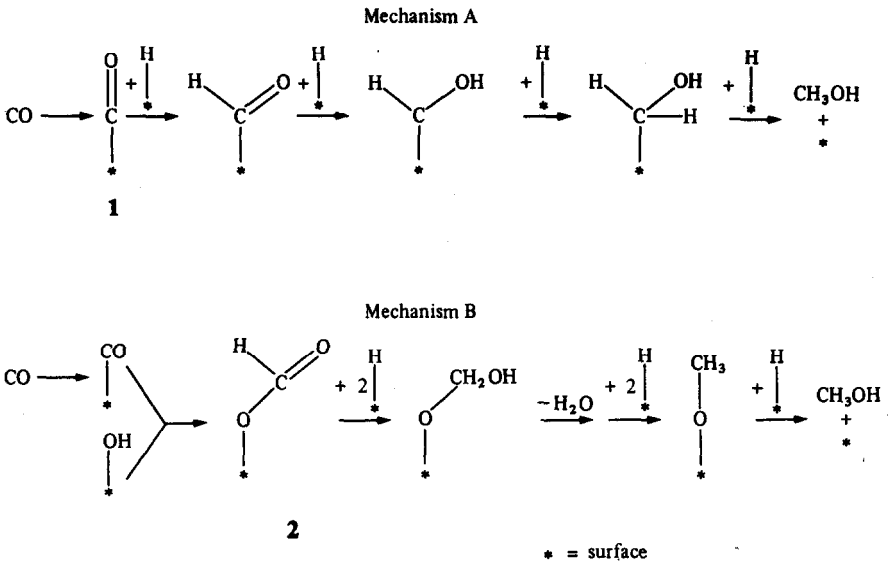


Fig. 1. Current methanol mechanisms.[6]

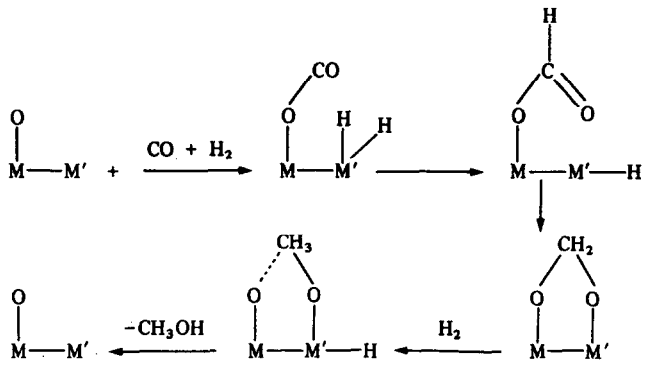


Fig. 3. Proposed methanol mechanism.

upon the dehydrogenation and dehydration reactions, but the minor reaction, which leads to the formation of formaldehyde, became the center of our attention. Although little data on this byproduct are available, and little is known about the mechanism involved, appreciable amounts (~10%) of formaldehyde are formed in formic acid decompositions catalyzed by thoria, molybdena and zinc oxide.[10] In fact, the high yield of formaldehyde (~25%) from the decomposition of zinc formate was the likely cornerstone of the earliest methanol synthesis.[11] If the site receiving the formate has the ability to hydrogenate the formaldehyde intermediate, methanol is generated.

The formaldehyde–formate relationship leads to an encompassing mechanism for the formation of methanol from synthesis gas which integrates identified reaction intermediates (Fig. 3).

With this mechanism as a guide to methanol synthesis, the chemistry of molybdenum offers an interesting model for study.

HETEROGENEOUS MOLYBDENUM AND METHANOL CATALYSIS

The chemical features of molybdenum are relevant to its role in the methanol mechanism described above: (1) In heterogeneous systems, substrates tend to react with oxide ions of the molybdenum oxide lattice. For example oxidation of carbon monoxide proceeds via nucleophilic attack on the lattice oxygen (Fig. 4).

This coordination of carbon monoxide occurs on a strong electron donor (Lewis base) molybdenum oxide surface.[12] (2) Molybdates also form the basis of a family of sulfur-tolerant water-gas shift catalysts. Formate is the intermediate in this chemistry.[13] (3) Formic acid decomposition over molybdenum oxides yields small, but measurable, amounts of formaldehyde.[10] (4) As these points suggest, the synthesis of methanol over complex molybdenum oxides is possible (a sluggish reaction under traditional commercial conditions.[14] Recently an alkali-promoted (which would increase formate) molybdenum on silica was shown to afford a more active system.[15] (5) Finally, most catalysts for the methanol synthesis are oxides developed by studying the methanol decomposition reaction and, although a poor synthesis catalyst, we also felt that the high selectivity molybdenum oxide exhibited for the oxidative dehydrogenation of methanol to formaldehyde could provide a similar model. Mechanistic considerations of this reverse reaction indicate initial dissociation to a surface methoxy species (**a**) followed by rate-determining breakage of the C—H bond of methoxy (**b**). Further reaction yields the formate species (**c**) and eventual decomposition to hydrogen and carbon monoxide (Fig. 5).

Since similar syngas species are found in $Mo(CO)_6$ chemistry, could these intermediates be directed to produce methanol?

Taken together these observations confirmed our mechanistic evaluation of methanol synthesis but, if one also considers homogeneous molybdenum hexacarbonyl chemistry, some interesting approaches to new catalyst design are possible.

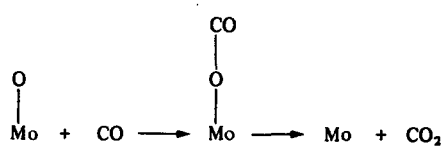


Fig. 4. Carbon monoxide oxidation

MOLYBDENUM HEXACARBONYL AND METHANOL CATALYSIS

To envision the catalytic system based on molybdenum hexacarbonyl for the reduction of carbon monoxide, the $Mo(CO)_6$ was substituted in function for the metal oxide surface (Fig. 6).

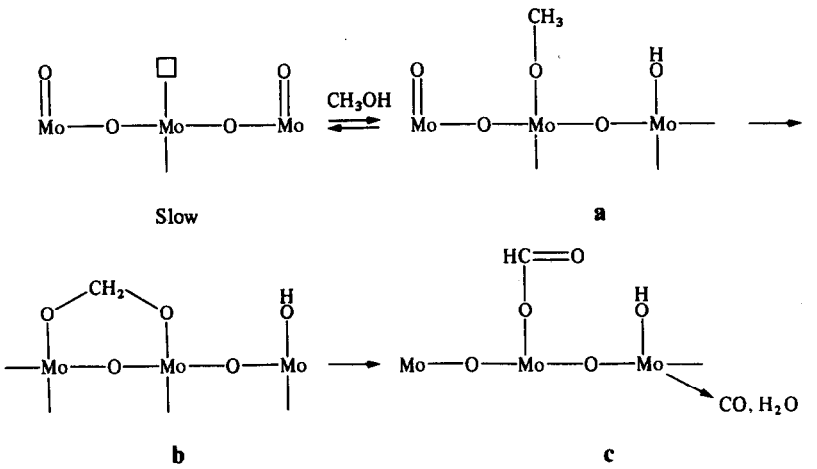


Fig. 5. Methanol dehydrogenation mechanism.[16]

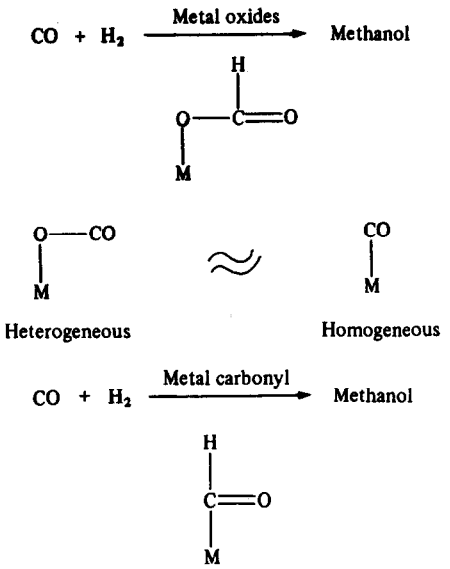


Fig. 6. Homogeneous methanol analogy.

As in the heterogeneous system, to achieve the synthesis of the formyl intermediate a separate metal center would be needed for hydrogenation, e.g. the hydrogen attack must be external from the metal center coordinating the carbon monoxide. Work on stoichiometric reactions of carbon monoxide and metal hydrides provided the clue to this design.

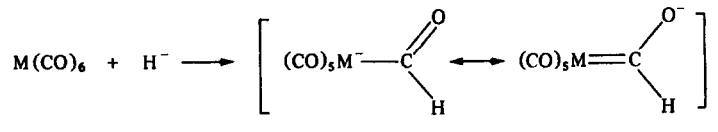
When molybdenum hexacarbonyl was treated with lithium borohydride in wet tetrahydrofuran under carbon monoxide pressure at 70°C, methanol is produced in high yields. A blank reaction showed that the metal carbonyl was catalytic:[18]

$$CO + NaBH_4 \xrightarrow{Mo(CO)_6} CH_3OH.$$

The product arises from a nucleophilic attack by the hydride at the carbonyl carbon and results in the formation of a formyl–metal carbonyl anion (**d**) (Fig. 7). These anions have been isolated in similar reactions.[19]

This result showed that hydride attack upon molybdenum hexacarbonyl may be related to the methanol synthesis. To turn this stoichiometric reaction into a catalytic reaction a replacement for the hydride would be needed. Screening was started using complex transition-metal reducing agents, metal systems formed from salts with complex hydrides. These hydrogenate in a hydride-like manner.

The reducing agent nickel boride, formed from nickel acetate and sodium borohydride,[20] was selected. Indeed a cooperative effect of the heterogeneous nickle boride and molybdenum hexacarbonyl yielded methanol from carbon monoxide and hydrogen in tetrahydrofuran. This



d

Fig. 7. Hydride metal carbonyl reaction.

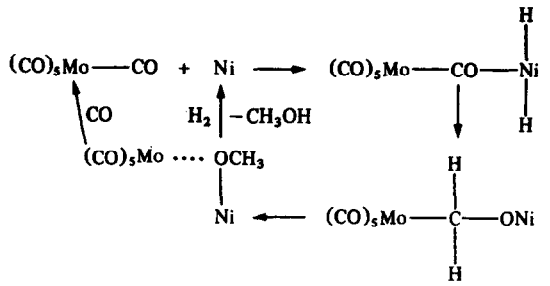


Fig. 8. Proposed reaction sequence.

system, although only very modest in activity, functions similarly to that described for the alkali hydrides but is catalytic in the hydrogenation function. Exploratory work directed toward improved design and formulation has begun.

Other, more active, heterogeneous nickel catalysts have also been developed. These catalytic systems are effective at temperatures below 150°C and have batch-measured volumetric activities equal to or greater than conventional methanol catalysts.[21]

It should be noted that the synergistic relationship of the heterogeneous nickel and homogeneous carbonyl offers a new approach to molecular catalyst design and reaction tailoring which to our knowledge has not been described in the literature. The possibility of reaction control and product selectivity is unique.

The molybdenum carbonyl in this system demonstrates a new mode of reaction in homogeneous catalysis. Normally a homogeneous catalyst must loose a ligand to be effective; an open site must be generated to coordinate the reactant molecule. The molybdenum carbonyl in the described methanol system already carried the activated reactant in a saturated (more stable) state. Upon hydrogenation, the reaction of the carbonyl ligand generates an open site on the catalyst, promoting further reaction. This may account for the activity of the catalyst system since the driving force to form the product is the reforming of the stable carbonyl. This also allows the catalyst to be effective at moderate or industrial pressures.

Another unique and important aspect is that the homogeneous catalyst, the molybdenum carbonyl, "carries" the preactivated carbon monoxide molecule to the heterogeneous nickel surface in a mode that is similar to the metal formate in traditional systems (Fig. 8). Since the reaction temperature is below the dissociation temperature of the metal carbonyl, it is likely that the carbon monoxide molecule is brought to the surface still coordinated and is placed, or "served", in the proper configuration for reaction. This would account for the lower reaction temperature since a lower activation energy is needed to reduce the carbon monoxide. In this configuration the molecule seems to be predisposed to form methanol rather than any other product. Typically, heterogeneous nickel catalysts give methane as the major product in synthesis gas reactions. The preactivated carbon monoxide also negates some of the poisoning effect that carbon monoxide has on hydrogenation catalysts. Since the heterogeneous catalyst is mainly a reducing agent, a great variety of systems are available for study.

The base-promoted molybdenum hexacarbonyl catalyzed water-gas shift reaction gave us an alternative approach to methanol catalysis.[22] The homogeneous mechanism is shown in Fig. 9.

An essential feature of this reaction is the intermediacy of the formate complex, **f**, formed from the reaction of a coordinately unsaturated metal carbonyl complex, **e**, with the formate ion, which in turn is formed by the facile reaction of carbon monoxide with the hydroxide ion.

From earlier discussions regarding heterogeneous catalysts, it is evident that this homogeneous formate complex might be reduced to methanol by the

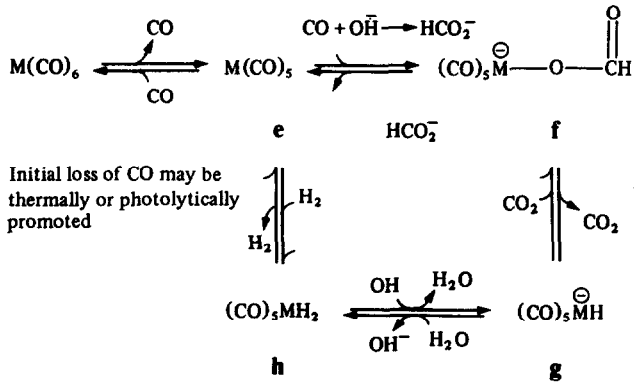


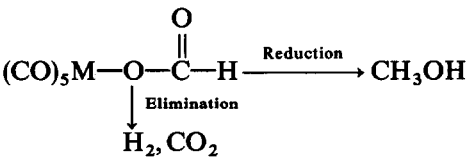
Fig. 9. Homogeneous water-gas shift mechanism.[22]

hydride complexes, **g** and **h**, in this reaction. These intermediates are generated by the base-promoted reaction of carbon monoxide and water so that methanol would be synthesized by the reaction:

$$3CO + 2H_2O \rightarrow CH_3OH + 2CO_2.$$

In fact, molybdenum carbonyl does catalyze the formation of methanol from carbon monoxide and water at temperature below 150°C, making it one of the few effective homogeneous catalysts for methanol synthesis.

In attempting to improve the yields of methanol, several factors warrant particular attention. In this system the water-gas shift reaction competes with methanol formation, with the formate complex being the branch point:



Ideally, it would be desirable to minimize the tendency for carbon dioxide elimination or to enhance the rate of reduction of the formate complex. The molybdenum hydride complexes, **g** and **h** in Fig. 9, are notably poor reducing agents. On the other hand, particular metal carbonyls, notably osmium, form little hydrogen but are highly effective reduction catalysts under conditions comparable to those used. Preliminary experiments indicate that addition of very small quantities of osmium carbonyl afford substantial improvements in the yield of methanol with molybdenum carbonyl as catalyst.

Although this work emphasizes carbon monoxide plus water routes to methanol, the addition of hydrogen to these reactions also proves encouraging:

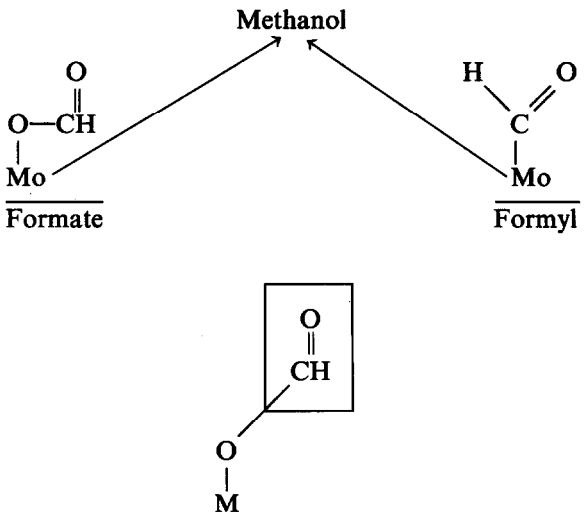
$$2CO + H_2O + H_2 \rightarrow CH_3OH + CO_2.$$

Improved yields of methanol can be achieved by the hydrogenation of formate complex with traditional reducing catalysts (Fig. 10). The experimental embodiment of these reactions was unusual in that, while the metal carbonyl formate complex was in a homogeneous phase, the hydrogenation catalyst was usually a heterogeneous solid.

The mechanism followed (Fig. 10) is similar to that proposed for commercialy heterogeneous catalysts (Fig. 3) in that the formate group delivers carbon monoxide to the hydrogenating center.

CONCLUSION

Connections between molybdenum hexacarbonyl and molybdenum oxide catalyzed synthesis gas reactions offer an interesting insight into the workings of methanol catalysts. Two interrelated routes are available:



and three stoichiometries (Fig. 11).

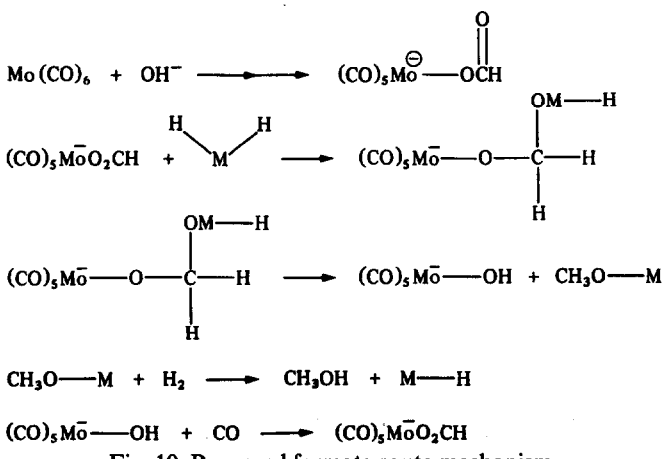


Fig. 10. Proposed formate route mechanism.

Formyl		Formate
$CO + 2H_2$	$2CO + H_2 + H_2O$	$3CO + 2H_2O$
$NiB_2 + Mo(CO)_6$	$Pd-Al_2O_3 + Mo(CO)_6$-base	$Mo(CO)_6$-base

Fig. 11. Routes to methanol.

The unusual features of these reactions may be important in designing, developing and improving new and traditional methanol catalysts.

REFERENCES

1. E.g. P. C. H. Mitchell, *Q. Rev.* 1966, **20**, 103.
2. R. H. Grubbs, *Prog. Inorg. Chem.* 1978, **24**, 1.
3. (a) H. Alper and C. Blais, *Fuel* 1980, **59**, 670; (b) H. Alper and H. N. Paik, *J. Org. Chem.* 1977, **42**, 3522.
4. T. Yoshii and T. Ueda, U.S. Patent 4,467,049 (1984).
5. (a) M. N. Sheng, *Synthesis* 1972, 194; (b) R. A. Sheldon, *Recl Trav. Chim. Pays-Bas* 1973, **92**, 367.
6. H. H. Kung, *Cat. Rev.—Sci. Eng.* 1980, **22**, 235.
7. E.g. (a) J. Happel, S. Kiang, J. L. Spencer, S. Oki and M. A. Hnatow, *J. Catal.* 1977, **50**, 429; (b) Y. Kubokaw, *Bull. Chem. Soc. Jpn* 1960, **33**, 555; (c) D. Brennan, *Proc. R. Soc. A* 1960, **256**, 81.
8. M. Araki and V. Ponec, *J. Catal.* 1976, **44**, 439.
9. E.g. (a) Y. Amenomiya and G. Pleizier, *J. Catal.* 1982, **76**, 345; (b) G. M. Shaborwa, *Dokl. Akad. Nauk SSSR* 1960, **133**, 1375; (c) R. E. Eischens and W. A. Plisken, In *Actes Du Deuxieme Congress International de Catalyse, Paris*, 1960, p. 789. Editions Technip, Paris (1961).
10. P. Sabatier, *Catalysis in Organic Chemistry* (translated by E. E. Reid). Van Nostrand, New York (1923).
11. K. Hofman and H. Schibsted, *Chem. Ber.* 1918, **51**, 1389, 1398.
12. P. C. Stair, Northwestern University Material Research Center, 21st Annual Report.
13. (a) K. Tsuchimoto and Y. Morita, *Kogyo Kagaku Zasshi* 1968, **71**, 1488; (b) G. S. Levinson, J. Ramsbotham and S. T. Sie, German Patent 2,416,351 (1974); (c) D. S. Newsome, *Cat. Rev.—Sci. Eng.* 1966, **21**, 103.
14. A. T. Larson, U.S. Patents 1,844,857 and 1,844,129 (1932); (b) A. T. Larson, U.S. Patent 2,061,470 (1936); (c) A. Mittasch, M. Pier and K. Winkler, U.S. Patent 1,558,559 (1925).
15. T. Tatsumi, A. Muramatsu and H. Tominaga, ICC-PBS Preprints, Appl. 03G25 (1984).
16. C. J. Machiels and A. W. Sleight, In *Proceedings of the Fourth International Conference on the Chemistry and Uses of Molybdenum* (Edited by H. F. Barry and P. C. H. Mitchell), p. 411. Climax Molybdenum Co., Ann Arbor, MI (1982).
17. R. S. Sapienza, L. D. Spaulding, M. J. Sansone and J. F. Lynch, *Am. Chem. Soc., Dis. Pet. Chem., Prepr.* 1978, **23**, 1336.
18. R. S. Sapienza, Ph.D. dissertation, University of Texas (1976).
19. C. P. Casey and S. Neumann, *J. Am. Chem. Soc.* 1976, **98**, 5395.
20. (a) T. W. Russell and R. C. Hoy, *J. Org. Chem.* 1971, **36**, 2018; (b) T. W. Russell, R. C. Hoy and J. E. Cornelius, *J. Org. Chem.* 1972, **37**, 3552; (c) H. Kirita and Y. Tsutsumi, *Nippon Kagaku Zasshi* 1961, **82**, 1461; (d) R. W. Mitchell, L. J. Pandolfi and P. C. Maybury, *J. Chem. Soc., Chem. Commun.* 1976, 172.
21. R. S. Sapienza, W. A. Slegeir, D. Mahajan, M. Foran, T. E. O'Hare and G. T. Skaperdas, *9th Annual EPRI Contractors' Conference on Coal Liquefaction*, May 8–10, 1984, BNL-36282.
22. W. A. Slegeir, R. S. Sapienza and B. Easterling, *In Catalytic Activation of Carbon Monoxide* (Edited by P. C. Ford). ACS Symposium Series No. 152, Washington, DC (1981).

Polyhedron Vol. 5, No. 1/2, pp. 257–260, 1986
Printed in Great Britain

0277-5387/86 $3.00 + .00
© 1986 Pergamon Press Ltd

EFFECTS OF Mo PRECURSORS ON THE ACTIVITY OF ALKALI-PROMOTED Mo CATALYSTS FOR ALCOHOL SYNTHESIS FROM CO–H_2

TAKASHI TATSUMI,* ATSUSHI MURAMATSU, TETSUYA FUKUNAGA and HIRO-O TOMINAGA

Department of Synthetic Chemistry, Faculty of Engineering, University of Tokyo, Hongo, Tokyo 113, Japan

(*Received* 18 *June* 1985)

Abstract—Three Mo precursors, $(NH_4)_6Mo_7O_{24}$, $H_3PMo_{12}O_{40}$ and $MoO_2(acac)_2$ (acacH is acetylacetone), have been used to prepare SiO_2-supported Mo catalysts. SiO_2 was pretreated with either KCl or K_2CO_3. The effects of these Mo precursors on the activity and product selectivity of the Mo catalysts in CO hydrogenation were examined at 16 kg cm^{-2} and 573 K. Selectivity for alcohols vs hydrocarbons was greatly influenced by the precursors and K salts. Catalysts prepared from $(NH_4)_6Mo_7O_{24}$ and supported on KCl-treated SiO_2 had the highest activity and selectivity for alcohols. Catalysts prepared from $MoO_2(acac)_2$ produced mainly hydrocarbons. The observed changes in activity and selectivity with preparation method seem to be governed by the oxidation state of Mo.

The selective production of C_{2+} alcohols remains one of the main goals of syntheses from carbon oxides and hydrogen. The C_2–C_4 alcohols can be easily converted to the corresponding C_2–C_4 olefins to replace the manufacture of these important monomers from petroleum. Furthermore, the mixed alcohols can be used as additives in gasoline to enhance the octane number.[1] Since the use of methanol raises the problem of its solubility in the hydrocarbons, higher alcohols are better additives. While methanol synthesis from CO and H_2 is a mature process, direct synthesis of C_{2+} alcohols is only in the research and development stage. Recently, the Institut Français de Petrole patented a Co–Cu–K catalyst for synthesis of C_1–C_5 alcohols.[2] In the course of our study of the catalysis of supported Mo, we found that SiO_2-supported Mo catalysts, promoted by alkali-metal halides, give C_1–C_5 alcohols with good selectivity.[3] Here we report the effects of molybdenum precursors on the performance of the Mo catalysts.

EXPERIMENTAL

Catalysts (10 wt % Mo) were prepared by impregnating SiO_2 (Fuji Davison ID) with an aqueous solution of $(NH_4)_6Mo_7O_{24}$ or $H_3PMo_{12}O_{40}$ or an acetone solution of $MoO_2(acac)_2$ (acacH = acetylacetone). In most cases 1.67 wt % K^+ (K/Mo molar ratio = 0.4) was added to the silica by impregnation with KCl or K_2CO_3, followed by air calcination at 673 K for 1 h and then impregnation with the molybdenum salts. Catalysts were treated in flowing He at 673 K for 1 h and then reduced in flowing H_2 at 773 K for 12 h. The synthesis reaction was carried out in a stainless steel tubular reactor holding 1.0 g catalyst in a flow system. Reaction products were analyzed by GC using several columns. Details of the reaction and analysis will be published separately.

Catalytic surface areas of reduced, supported Mo catalysts were measured by O_2 adsorption at 195 K.[4,5] Prior to each adsorption measurement 0.4–0.5 g of catalyst was weighed into a Pyrex chemisorption cell. The material was next reduced as previously described and evacuated to 1×10^{-5} torr at 723 K for 2 h and then cooled to 195 K. The adsorption isotherm was measured at 195 K over a pressure range of 50–200 torr. The sample was then evacuated to 1×10^{-5} torr at 195 K and a second isotherm was determined. The difference between the two isotherms after extrapolation to zero pressure was assumed to be the amount which chemisorbed on the surface.

* Author to whom correspondence should be addressed.

The apparent oxidation number of the Mo on various catalysts was assayed by oxygen titration.[6] The reduced catalyst was flushed with He at 723 K and cooled to room temperature. Pulses of O_2 (<0.2 O/Mo) were injected into the He and consumption of O_2 was calculated from the amount which passed the catalyst. The catalyst was then heated stepwise up to 773 K while further pulses of O_2 were passed. The original oxidation number of the Mo could then be calculated from the total amount of O_2 consumed, assuming that Mo(VI) was the final product. X-ray powder diffraction measurements were performed using a Rigaku Denki diffractometer RU-200A with Cu-K_α radiation.

RESULTS AND DISCUSSION

The conversion and product distribution of the various Mo catalysts changed significantly with time on stream. Steady-state activities were reached within 24–100 h on stream, depending on the catalyst, and are summarized in Table 1. As is expected from the CO shift activity of the Mo catalysts, almost all of the oxygen in products leaves the reactor as CO_2 rather than as H_2O.[7–9] For this reason the product distribution is given on a CO_2-free basis.

The CO conversion over the Mo catalysts supported on KCl-treated SiO_2 depended on the Mo precursor in the following order: $H_3PMo_{12}O_{40}$ < $(NH_4)_6Mo_7O_{24}$ < $MoO_2(acac)_2$. However, the sample prepared from $MoO_2(acac)_2$ gave hydrocarbons as the major products. The selectivity for C_1–C_5 alcohols increased in the order

$$MoO_2(acac)_2 < H_3PMo_{12}O_{40} < (NH_4)_6Mo_7O_{24}.$$

Thus the catalyst derived from $(NH_4)_6Mo_7O_{24}$ was the most active in alcohol production. Incidentally, without KCl addition, Mo–SiO_2 gave hardly any alcohols.[3]

When K_2CO_3 was used in place of KCl, the selectivity for alcohols was slightly suppressed for both $(NH_4)_6Mo_7O_{24}$- and $H_3PMo_{12}O_{24}$-derived catalysts; the choice of precursor resulted in no significant difference in the product selectivity. In view of the higher CO conversion, however, $(NH_4)_6Mo_7O_{24}$ was a better precursor than $H_3PMo_{12}O_{40}$. It should be noted that C_{2+} alcohol/methanol ratios were higher for K_2CO_3-treated catalysts than for KCl-treated catalysts. The Mo catalyst derived from $(NH_4)_6Mo_7O_{24}$ and supported on KCl-treated SiO_2 proved to be the best one for alcohol synthesis. The product distribution was greatly dependent on the content of Mo and K and the reaction condition; the best catalyst gave C_1–C_6 alcohols with 80% selectivity by weight of the total product, exclusive of CO_2, and the space–time yield (STY) of the alcohols exceeded 400 g (kg catalyst)$^{-1}$ h^{-1}.[10]

Values of O_2 adsorption uptake following reduction, apparent oxidation number of the Mo and STY of alcohols and hydrocarbons are shown in Table 2 for Mo catalysts supported on KCl-treated SiO_2. There is no apparent correlation between initial CO hydrogenation activity and the quantity of oxygen adsorbed for fresh catalysts. The initial specific activity (CO turnover frequency) was estimated on the basis of site densities measured by O_2 adsorption assuming O/Mo = 1 and then listed in Table 2. The high initial specific activity of the catalyst derived from $MoO_2(acac)_2$ seems to be related to the low apparent oxidation number. The exact oxidation state of the surface Mo is uncertain. There is evidence from previous studies that the activity of reduced Mo for CO hydrogenation producing hydrocarbons increases with decreasing

Table 1. Steady-state activities for CO hydrogenation over SiO_2-supported Mo catalysts[a]

K salt	Mo precursor	CO conversion (%)	CO_2 yield (%)	Selectivity (C atom %)						
				CH_4	C_{2+} hydrocarbons	MeOH	EtOH	PrOH	C_{4+} alcohols	Other oxygens
None	$(NH_4)_6Mo_7O_{24}$	9.7	4.7	35.7	63.3	0.8	0	0	0	0
KCl	$(NH_4)_6Mo_7O_{24}$	5.6	1.8	18.9	30.8	17.7	20.7	7.0	3.2	1.7
	$H_3PMo_{12}O_{40}$	4.0	1.8	25.5	35.0	15.3	15.6	5.2	1.5	2.0
	$MoO_2(acac)_2$[b]	8.9	4.2	32.4	47.7	7.4	8.2	2.5	0.5	1.4
K_2CO_3	$(NH_4)_6Mo_7O_{24}$	6.3	2.9	21.1	44.3	10.9	13.8	5.3	2.1	2.5
	$H_3PMo_{12}O_{40}$	3.5	1.6	22.6	42.9	9.9	13.3	8.7	1.5	1.2

[a] Conditions: 573 K, 16 kg cm^{-2}, H_2/CO = 1, W/F = 10 g catalyst h^{-1} mol^{-1}, K/Mo = 0.4, and Mo = 10 wt %.
[b] acacH = acetylacetone.

Table 2. O_2 adsorption uptakes, apparent oxidation number and initial and steady-state activity of Mo catalysts supported on KCl–SiO_2[a]

Mo precursor	O_2 uptake[b] [μmol (g catalyst)$^{-1}$]	CO TOF[c] (10^3 s^{-1})	Apparent oxidation number[d]	Initial CO conversion (%)	Initial STY[e] [g (kg catalyst)$^{-1}$ h^{-1}]		S.S. CO conversion (%)	S.S. STY[e] [g (kg catalyst)$^{-1}$ h^{-1}]	
					Hydrocarbons	Alcohols		Hydrocarbons	Alcohols
$(NH_4)_6Mo_7O_{24}$	54.2	3.3	4.7	2.6	4.7	5.6	5.6	12.3	21.0
$H_3PMo_{12}O_{40}$	72.9	4.4	4.8	4.6	12.4	7.5	4.0	9.5	10.4
$MoO_2(acac)_2$[f]	46.3	13.8	4.2	9.2	28.7	6.7	8.9	24.1	9.9

[a] Reaction conditions: 573 K, 16 kg cm^{-2}, $H_2/CO = 1$; $W/F = 10$ g catalyst h^{-1} mol^{-1}, K/Mo = 0.4, and Mo = 10 wt%.
[b] O_2 uptake measured at 195 K, corrected for support adsorption.
[c] CO turnover frequency (number of CO molecules converted per site s^{-1}); site densities measured by O_2 adsorption, assuming O/Mo = 1.
[d] Determined by oxygen titration.
[e] Space–time yield.
[f] acacH = acetylacetone.

oxidation state.[8] The lower initial specific activities of the samples prepared from $(NH_4)_6Mo_7O_{24}$ and $H_3PMo_{12}O_{40}$ are consistent with the higher oxidation number. There is no significant difference for the initial alcohol productivity of the three catalysts and no correlation of alcohol yield with oxygen uptake or average oxidation number was observed.

During reaction at 573 K for 50–100 h, the mass-based alcohol production activity of the $(NH_4)_6Mo_7O_{24}$-derived catalyst increased by a factor of 4, while the activities of the other catalysts increased by only 40–50%. The hydrocarbon production over the $(NH_4)_6Mo_7O_{24}$-derived catalyst increased, while the production over the other catalysts decreased slightly. The increase in alcohol yield for the $(NH_4)_6Mo_7O_{24}$-derived catalyst might be explained by formation of active sites induced by reduction with CO or CO–H_2.[10] These sites cannot be brought out by H_2 reduction and should be specific for alcohol synthesis. On the other hand, extensive reduction of Mo with H_2 occurred in the case of the $MoO_2(acac)_2$-derived catalyst, yielding active sites for hydrocarbon formation. Interaction of P and Mo seemingly caused a smaller increase in alcohol formation over the $H_3PMo_{12}O_{24}$-derived catalyst.

X-ray patterns for reduced Mo–SiO_2 contained lines characteristic of MoO_2 and Mo metal. In addition, the presence of KCl was evident for the catalyst derived from $MoO_2(acac)_2$. On the contrary, there was no XRD evidence of KCl for the catalysts prepared from $(NH_4)_6Mo_6O_{24}$ and $H_3PMo_{12}O_{40}$. These findings suggest that the Mo on the $MoO_2(acac)_2$-derived sample is hardly influenced by KCl, leading to a hydrocarbon-forming catalyst. The extensive reduction of molybdenum in this case could be a result of weak $MoO_2(acac)_2$–support interaction. It has been found that $H_3PMo_{12}O_{40}$ is more reducible than $(NH_4)_6Mo_7O_{24}$,[11] but the apparent oxidation number for the $H_3PMo_{12}O_{40}$-derived catalyst was found to be about the same as for the $(NH_4)_6Mo_7O_{24}$-derived catalyst. This behaviour may be explained by formation of K salts of $H_3PMo_{12}O_{40}$, which are much less reducible than $H_3PMo_{12}O_{40}$[12] on the catalyst surface. It is noteworthy that, without K salt addition, supported $H_3PMo_{12}O_{40}$ was a highly active catalyst for hydrocarbon formation.[10]

REFERENCES

1. K. Klier, In *Catalysis of Organic Reactions* (Edited by W. R. Moser), p. 195. Marcel Dekker, New York (1981).

2. A. Sugier and E. Freund, US Patent 4,122,110 (1978).
3. T. Tatsumi, A. Muramatsu and H. Tominaga, *Chem. Lett.* 1984, 685.
4. J. L. G. Fierro, S. Mendioroz, J. A. Pajares and S. W. Weller, *J. Catal.* 1980, **65**, 263.
5. B. E. Concha, G. L. Bartholomew and C. H. Bartholomew, *J. Catal.* 1984, **89**, 536.
6. R. G. Bowman and R. L. Burwell, Jr, *J. Catal.* 1980, **63**, 463.
7. C. B. Murchison and D. A. Murdick, *Hydrocarbon Process.* 1981, **60**, 159; C. B. Murchison, In *Proceedings of the Fourth International Conference on the Chemistry and Uses of Molybdenum* (Edited by H. F. Barry and P. C. H. Mitchell). Climax Molybdenum Co., Ann Arbor, MI (1982).
8. M. Saito and R. B. Anderson, *J. Catal.* 1980, **63**, 438.
9. A. J. Bridgewater, R. Burch and P. C. H. Mitchell, *J. Catal.* 1982, **78**, 116.
10. A. Muramatsu, T. Tatsumi and H. Tominaga, unpublished results.
11. H. Niiyama, H. Tsuneki and E. Echigoya, *Nippon Kagaku Kaishi* 1979, 996.
12. H. Miura, H. Ishiguro, M. Osawa, K. Sasagawa, K. Sugiyama and T. Matsuda, *Bull. Chem. Soc. Jpn* 1985, **58**, 236.

Polyhedron Vol. 5, No. 1/2, pp. 261–269, 1986
Printed in Great Britain

0277–5387/86 $3.00 + .00
© 1986 Pergamon Press Ltd

CATION–ANION EFFECTS IN HETEROPOLY COMPOUNDS WITH KEGGIN STRUCTURES

J. B. MOFFAT

Department of Chemistry and Guelph–Waterloo Centre for Graduate Work in Chemistry, University of Waterloo, Waterloo, Ontario, Canada N2L 3G1

(*Received* 10 *June* 1985)

Abstract—In heteropoly compounds with anions of Keggin structure, the elemental composition of the anion has been shown, through temperature-programmed desorption, photoacoustic FTIR spectroscopy, and extended Hückel calculations, to influence the protonic mobility, the lability of the anionic outer oxygen atoms, and the surface and catalytic properties of these heteropoly solids. The nature and size of the cation, in addition to altering the catalytic activity and selectivity, has been demonstrated to have a significant effect on the pore structures of the heteropoly compounds, with some salts displaying microporosity, tentatively attributed to the shifting of anionic outer oxygen atoms to form channels from interstitial void spaces.

Heterogeneous catalysts have widespread application in industrial chemical processes as a means of directing reactions to the desired products at appreciable rates. Heteropoly compounds offer appealing characteristics as heterogeneous catalysts as a consequence of both their chemical and physical properties.[1–17] These compounds are complex ionic solids with large cage-like anions, the latter containing a minimum of three elements. The heteropoly compounds of interest in the present work have anions with a central atom such as phosphorus, silicon and arsenic, surrounded by four oxygen atoms arranged tetrahedrally. Twelve octahedra with oxygen atoms at their vertices and a peripheral metal atom at each of their centres envelope the central tetrahedron and share oxygen atoms with the latter and with each other (Fig. 1). A number of excellent reviews on heteropoly compounds may be consulted for additional details.[18–23]

Structures

What may well be the most definitive structural information on any heteropoly compound has been provided by Brown *et al.*[24] for 12-tungstophosphoric acid (HPW). Through X-ray and neutron diffraction techniques these workers have shown that the proton is surrounded by and coplanar with four water molecules, each with the oxygen atom pointing toward the proton (Fig. 2). A two-fold thermal disorder exists between the proton and four water molecules, so that the proton is hydrogen-bonded to only two water molecules at a given time. In turn the water molecules are hydrogen-bonded to the terminal oxygen atoms of the heteropoly anion (Fig. 3).

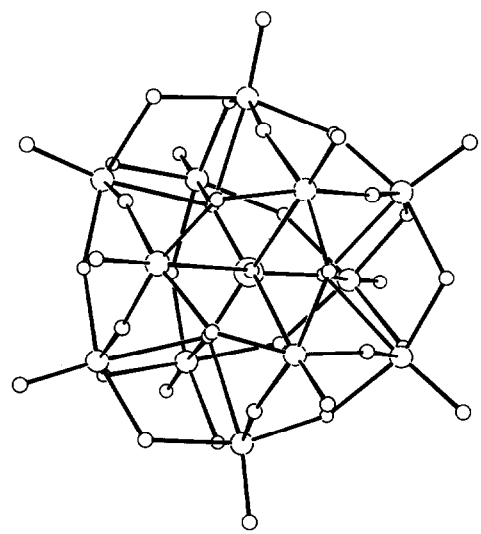


Fig. 1. Anion of 12-molybdosilicic acid ($SiMo_{12}O_{40}^{4-}$).

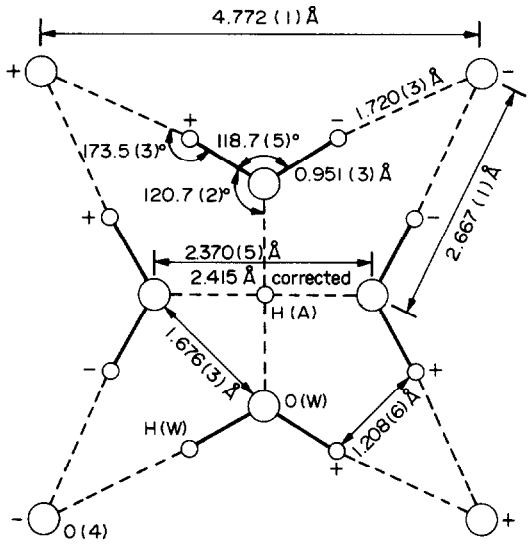


Fig. 2. Structural arrangement of the proton, four water molecules and oxygen atoms of the anions.[24]

Catalytic properties

In earlier work from this laboratory it has been shown that 12-tungstophosphoric acid catalyzes the conversion of methanol to hydrocarbons, although the selectivity is dependent upon both the pretreatment environment and temperature as well as the reaction conditions.[1] Substitution of silicon for phosphorus as the central metal atom in HPW produces a catalyst, 12-tungstosilicic acid (HSiW), which is only slightly reduced in selectivity for methanol conversion. However, 12-molybdophosphoric acid (HPMo), in which tungsten is replaced by molybdenum as the peripheral metal element, converts methanol to oxidation products such as carbon monoxide. Evidently the peripheral metal element is of particular importance in the methanol conversion process.

Loss of water

Temperature-programmed desorption (TPD)[8,11,12,15,16] and photoacoustic FTIR spectroscopy[7,10,11,13–15] have shown that water is eliminated from the aforementioned heteropoly acids at two different temperatures, one at approximately 200°C, the other in the range of 450–500°C, the former due to the desorption of hydrogen-bonded water, the latter apparently resulting from water formed by the acidic protons and anionic oxygen (Fig. 4). Photoacoustic FTIR spectroscopy[7,10] has been employed to identify two bands characteristic of the Keggin structure for the anion, one at 1080 cm^{-1} attributed to the triply degenerate asymmetric stretch of the central XO_4 tetrahedron, and a second at 980 cm^{-1}

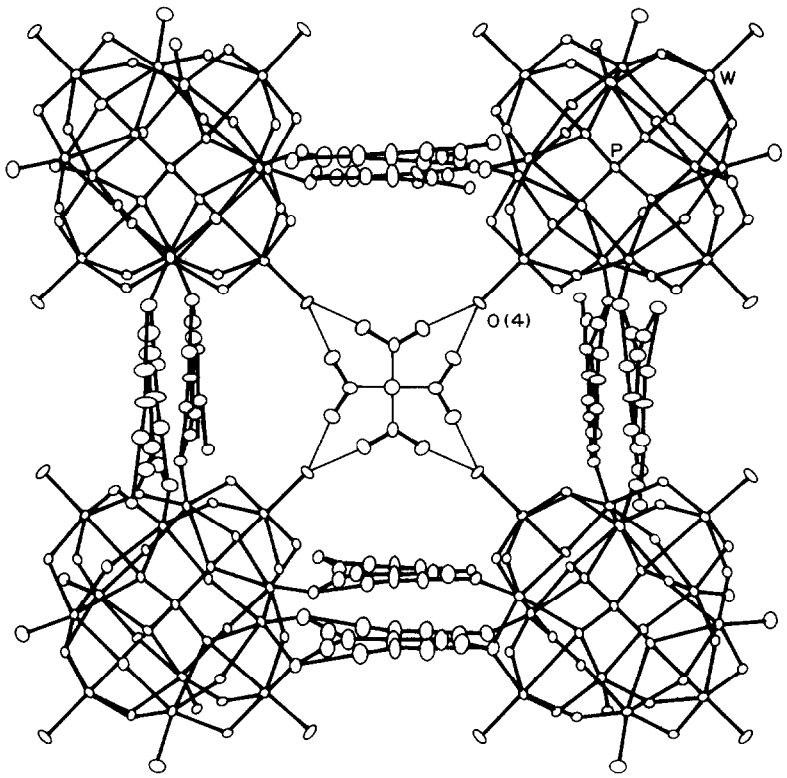


Fig. 3. Structural arrangement of anions, protons and water molecules in HPW.[24]

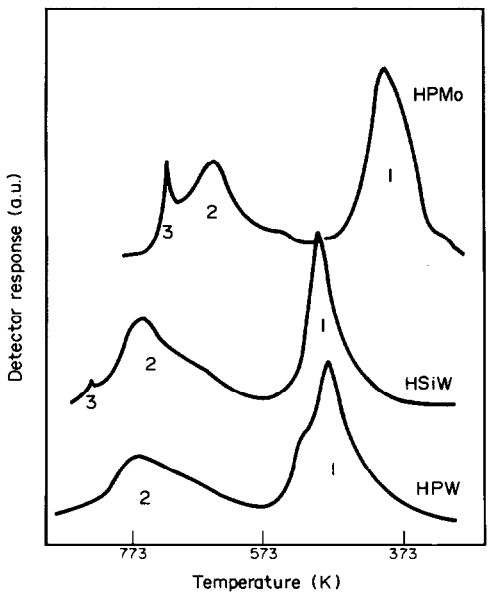


Fig. 4. TPD profiles for HPW, HSiW and HPMo after pretreatment at 298 K for 16 h.

resulting from the stretching vibration of the M—O bond where M is the peripheral metal atom and O is the terminal oxygen atom (Fig. 5). These two bands remain essentially intact after the loss of water at the higher temperature in the TPD studies. Temperature-programmed reduction (TPR) and temperature-programmed exchange (TPE) studies,[16] the former with protium, the latter with deuterium, have provided ancillary information on the subject.

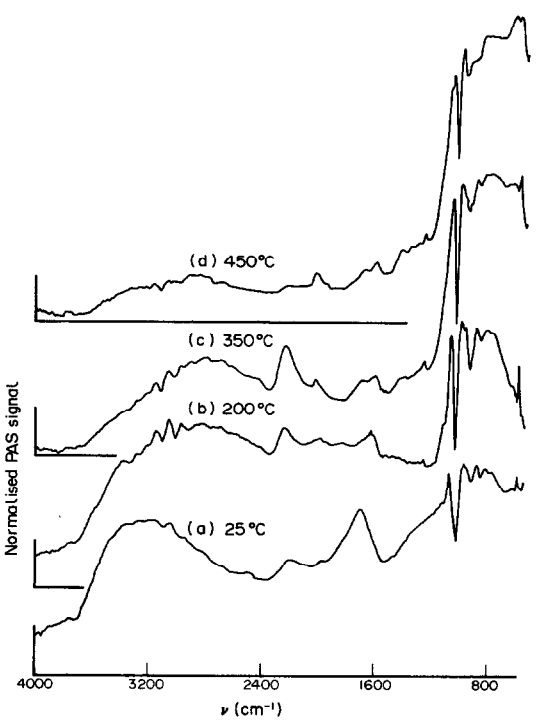


Fig. 5. Photoacoustic FTIR spectra of HPW after heating at various temperatures *in vacuo*.

It is of interest to note that the high-temperature peak in the TPD spectra (Fig. 4) emerges at a lower temperature with HPMo than with either HPW or HSiW, suggesting that the oxygen atoms in the molybdenum-containing anion are more labile than those in the corresponding tungsten species. Such a conclusion presumably implies that the Mo—O_t bond, where O_t refers to a terminal oxygen atom of the heteropoly anion, is weaker than the W—O_t bond, regardless of the nature of the central atom in the anion. Semi-empirical calculations with the extended Hückel technique,[6,11,12,13,15] on a fragment (Fig. 6) consisting of the central tetrahedron and three octahedra of the anion, designed to simulate results expected for the complete anion, show that the magnitude of the charge on the terminal oxygen atoms of the heteropoly anions with a Keggin structure is larger with HPMo than with either HPW or HSiW (Fig. 7). Consequently the protons in the former solid are less mobile and hence less acidic than those in the latter two materials, a conclusion which is consistent with the observations of the catalytic selectivities in the conversion of methanol. In addition, the calculations demonstrate that the M—O_t bond in HPMo is weaker than that in either HPW or HSiW, consistent with the aforementioned conclusions from TPD, TPR and TPE experiments, as well as reaction studies with methanol.

Cation effects

Turning now to cation effects, it has been shown[3] that, although the activity of a variety of metallic salts of HPW in the conversion of methanol is uniformly high, the selectivity to hydrocarbons is markedly dependent on the cation, being lowest for sodium and higher for aluminum. The selectivity to C_4 hydrocarbons, for example, was shown to be inversely proportional to the magnitude of the charge on the terminal oxygen atoms of the anion, a correlation again consistent with the results of TPD, TPR and TPE experiments as well as extended Hückel calculations.

Unexpectedly, however, the ammonium salt of HPW produced the highest yield of all the salts and the parent acid in the methanol conversion process, but particularly surprisingly produced primarily saturated paraffins, unlike the olefinic species found with the aforementioned catalysts[4] (Fig. 8). Most recently it has been shown that, in contrast, the tetramethylammonium salt of HPW is less effective

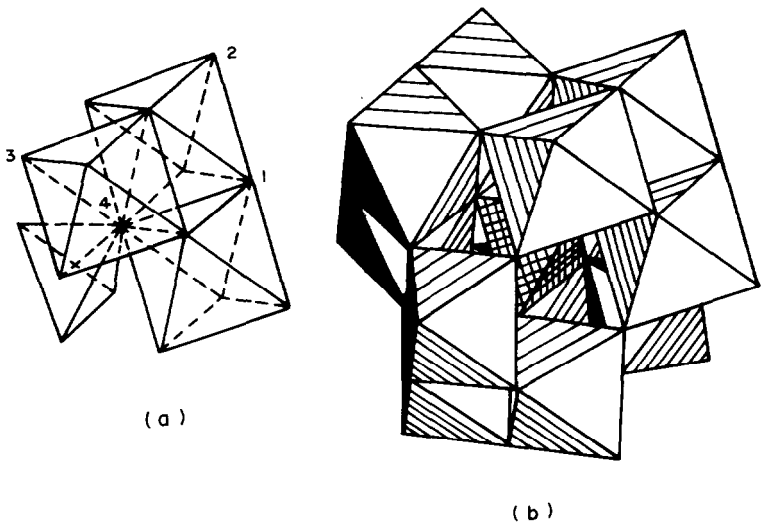


Fig. 6. (a) Fragment $[XM_3O_{16}]^{n-}$ of heteropoly anion; (b) heteropoly anion showing fragment as part of the complete structure.

than the ammonium salt of HPW and even than the parent acid itself.[17]

The present work examines the effect of changes both in the cations and the anions on the pore structures, and in particular the microporosity of heteropoly compounds. The present work is restricted to a series of monovalent cations and the anions of HPW, HPMo and HSiW.

EXPERIMENTAL

The parent acids HPW and HPMo were obtained as Analar grade from BDH and were further purified by recrystallization, where appropriate. The heteropoly acid HSiW was purchased from Baker and was used without further purification. The monovalent heteropoly salts were prepared by

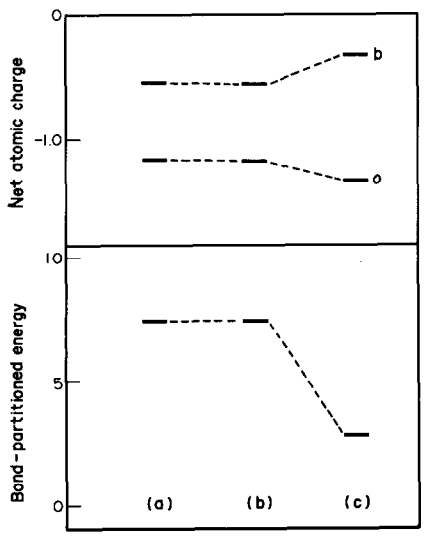


Fig. 7. Net atomic charges on the bridging (b) and outer (o) oxygen atoms, and energies of the M—O (outer) bonds of three heteropoly fragments: (a) $PW_3O_{16}^{9-}$, (b) $SiW_3O_{16}^{10-}$, and (c) $PMo_3O_{16}^{9-}$.

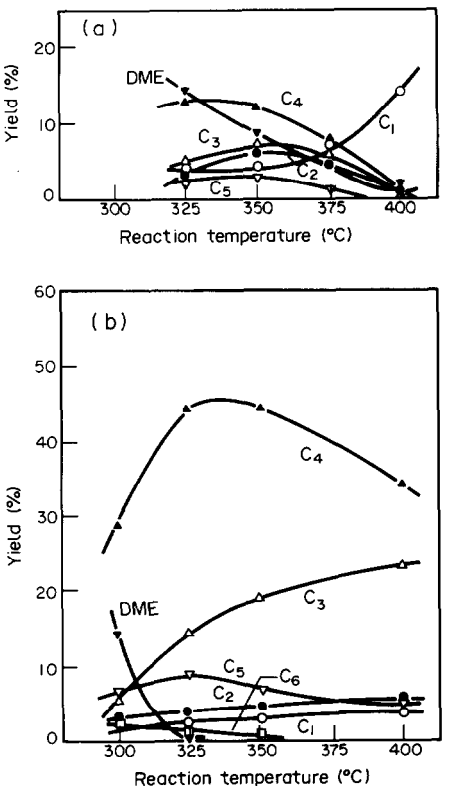


Fig. 8. Product distributions of methanol on HPW (a) and its ammonium salt (b). Catalysts calcined at 400°C in helium for 2 h; W/F = 246 mg catalyst min^{-1} $(cm^3\ He)^{-1}$.

precipitation or crystallization from aqueous solutions.[3]

Adsorption–desorption isotherms were obtained with nitrogen at 77.4 K in a standard glass volumetric system. Samples were evaluated at 10^{-5} torr and 473 K for 2 h prior to adsorption measurements.

Analyses of pore size distributions were obtained for mesopores and micropores with the Roberts[25] and MP[26] methods, respectively. The *t*-plot required with the latter method was generated by employing the C_{BET} matching technique of Lecloux and Pirard.[27]

X-ray powder diffraction patterns were obtained with a Phillips model PW-1011/60 diffractometer with the incident Cu-K_α radiation filtered through nickel.

RESULTS

Surface areas

The BET surface areas for the monovalent salts of HPW, HPMo and HSiW are listed in Table 1 and shown plotted as a function of cation diameter in Fig. 9. For salts such as those of sodium where the cation is relatively small, the surface area is itself small. However, as the size of the cation increases, the surface areas increase markedly, remain high but fall precipitously when the methyl ammonium salts are reached. The adsorption isotherms of all salts with high surface areas show sharp increases in the amount adsorbed at low relative pressures, characteristic of the presence of micropores, and in some cases adsorption–desorption hysteresis is also observed at higher relative pressures. High values (>300) of the *C* parameter in the BET equation, also indicative of the presence of micropores, are found for the large area salts (Table 2). In addition, the salts displaying characteristics expected of microporous substances have reduced ranges of linearity in BET plots (Table 3).

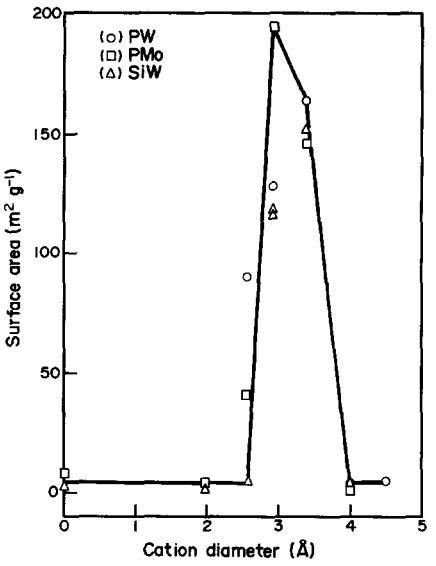


Fig. 9. Surface areas (BET) for monovalent salts of HPW, HPMo and HSiW, as a function of cation diameter.

Microporosity

The C_{BET}-dependent standard isotherms of Lecloux and Pirard[27] were employed, along with the experimental nitrogen adsorption–desorption isotherms to generate *t*-plots for the large-area heteropoly salts. In all such cases these plots could be extrapolated through the origin and displayed negative deviations from linearity, the latter being

Table 1. Surface areas of heteropoly salts of monovalent cations

	BET surface area ($m^2\ g^{-1}$)		
	Salt of		
Cation	HPW	HPMo	HSiW
H	(8)	(8)	3.2
Na	3.7	3.5	1.3
Ag	3.0	—	—
K	90.0	39.9	3.3
NH_4	128.2	193.4	116.9
Rb	—	—	116.3
Cs	162.9	145.5	153.4
$MeNH_3$	3.0	1.3	3.0
Me_4N	4.5	—	—

Table 2. Values of C_{BET} for heteropoly salts

	C_{BET}		
	Salt of		
Cation	HPW	HPMo	HSiW
H	—	—	100
Na	18	142	473
Ag	101	—	—
K	2430	1070	127
NH_4	760	877	1919
Rb	—	—	489
Cs	1720	568	—
$MeNH_3$	261	—	—
Me_4N	113	—	—

Table 3. BET linearity range for microporous compounds

Heteropoly compound	Linearity range (P/P_o)
KPW	0.05–0.1
NH_4PW	0.05–0.1
CsPW	0.05–0.15
KPMo	0.05–0.12
NH_4PMo	0.05–0.18
CsPMo	0.05–0.3
NH_4SiW	0.05–0.12
RbSiW	0.05–0.15
CsSiW	0.05–0.20

further evidence for the presence of a microporous structure. Micropore volumes were estimated by extrapolation of the portion of the t-plot for relative pressures greater than 0.4 to the $t = 0$ axis and converting to a liquid volume. Typical micropore volume distributions as calculated by the MP method[26] are shown in Figs 10–12 for the ammonium salts of HPW, HPMo and HSiW. With all of these solids a maximum in the distribution is found in the region of 8–10 Å, while a second maximum occurs with the ammonium salt in the range of 13–14 Å. The onset of mesoporosity is also evident in the micropore distribution for the latter salt. Satisfactory internal self-consistency is evident from the agreement between the BET surface areas and those from t-plots for the microporous solids (Table 4).

The experimentally measured nitrogen adsorption isotherms were fitted to the n-layer BET equation:[28]

$$n = \frac{Cv_m x[1-(n+1)x^n+nx^{n+1}]}{(1-x)[1+(c-1)x-Cx^{n+1}]},$$

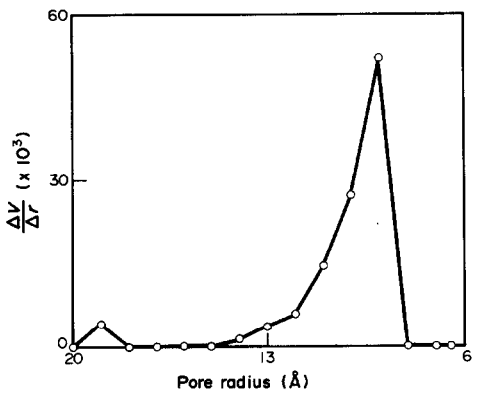


Fig. 10. Micropore volume distribution for ammonium 12-tungstophosphate.

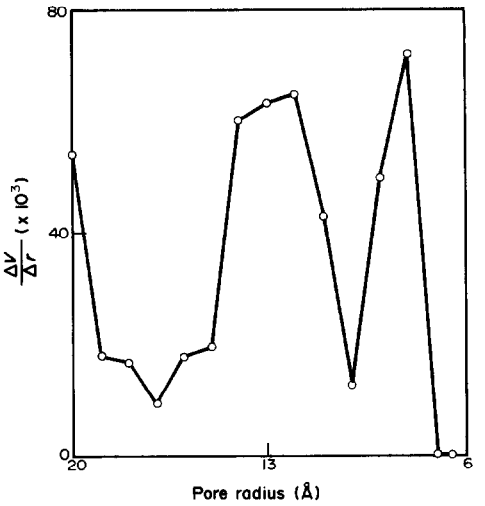


Fig. 11. Micropore volume distribution for ammonium 12-molybdophosphate.

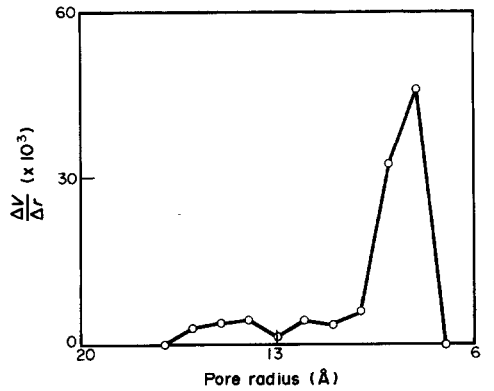


Fig. 12. Micropore volume distribution for ammonium 12-tungstosilicate.

Table 4. Comparison of surface areas

Heteropoly compound	Surface area ($m^2\ g^{-1}$) BET	t-Plot
KPW	90.0	92.8
NH_4PW	128.2	126.7
CsPW	162.9	160.5
KPMo	39.9	40.7
NH_4PMo	193.4	192.9
CsPMo	145.5	136.9
NH_4SiW	116.9	123.1
RbSiW	116.3	114.7
CsSiW	150.4	152.7

where n represents the maximum attainable number of adsorbate layers, by first employing the infinite-layer BET to generate a v_m and C value for each isotherm, followed by trial and error selection of best-fit n values. The optimum n values were found to be small ($\leqslant 5$) for all heteropoly compounds displaying microporosity. The mean micropore radius is found to be a reasonably good linear function of the n value, providing further supporting evidence for the validity of the micropore analysis (Fig. 13).

DISCUSSION

With the three anions PW, PMo and SiW studied in the present work there is a marked similarity between the results obtained for the micropore structures. This is evident in the dependence of surface areas and micropore volumes on cation and cation diameter (Table 1 and Figs 14–16) as well as from the micropore distributions. Although any dependence of micropore structure on the composition of the anion appears to be minimal, one observation should be noted. While KPW and KPMo possess appreciable micropore structure, the corresponding potassium salt of HSiW has little or no microporosity. Additional structural information will be required before a satisfactory explanation of this difference can be offered.

It is of some interest to investigate the relationship between the microporous structures found in the heteropoly salts and relevant structural factors. Both the reproducibility of the results and the internal self-consistency of the data provide assurance that the

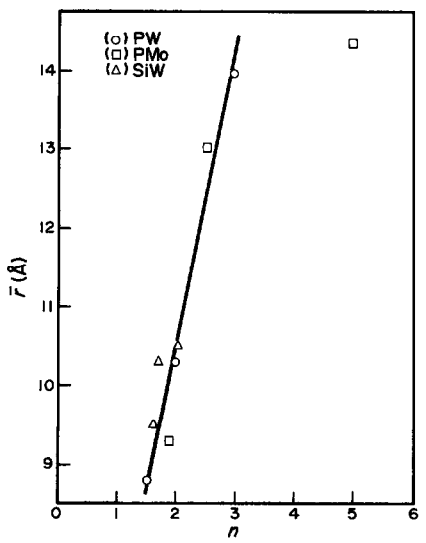


Fig. 13. Mean micropore radius as a function of the n value calculated from the n-layer BET equation for the microporous salts.

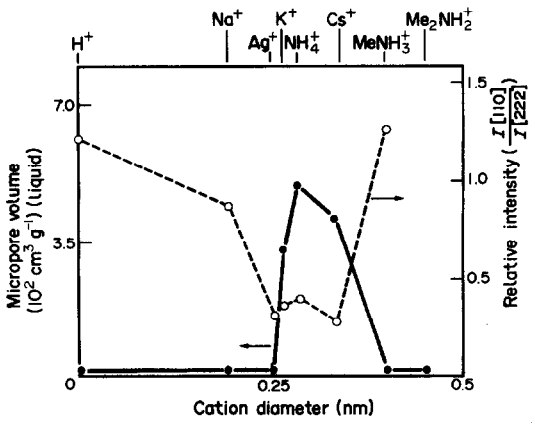


Fig. 14. Micropore volume and XRD [110]/[222] intensity ratio for various monovalent salts of HPW.

observation of microporosity is neither fortuitous nor a function of the preparative methods. In addition, no relationship to the crystal structure is evident. However, data obtained from X-ray diffraction (XRD) analysis has provided an interesting correlation. The intensity of the [110] reflection relative to that of the [222] plane, the latter of which is usually the most intense reflection, shows an approximately inverse relationship to the micropore volume (Figs 14–16). For salts with little or no microporosity the intensity ratio is relatively high, for each of the three anions, while with the microporous salts this ratio has decreased to significantly smaller values, often as much as a factor of three smaller.

An ion-packing model, assuming a cubic structure, demonstrates the presence of interstitial voids apparently separated from one another by the terminal oxygen atoms of the anions and capable of alignment with each other in directions parallel with or normal to the [110] plane of the crystal. Since the

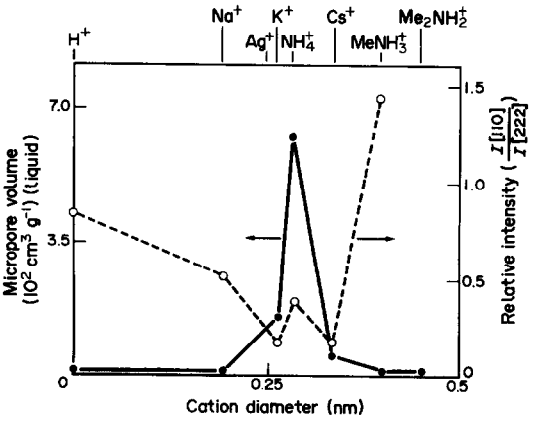


Fig. 15. Micropore volume and XRD [110]/[222] intensity ratio for various monovalent salts of HPMo.

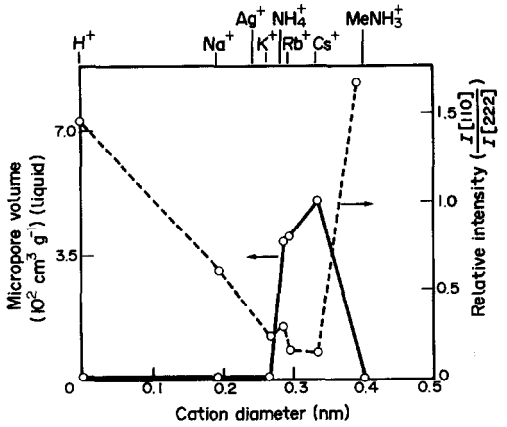


Fig. 16. Micropore volume and XRD [110]/[222] intensity ratio for various monovalent salts of HSiW.

cubic lattice parameter of the heteropoly salts increases with increasing cation size, the separation of the anions which accompanies this increase would be expected to result in widening of the interstitial voids, changes in the anionic bonding pattern, and reorientation of the anions within the secondary structure. This may alter the position of the anionic oxygen atoms so that the XRD intensity of the [110] plane is decreased, the interstitial voids are no longer separated, and channels running both parallel with and normal to this plane are formed. These channels would be observed in the present experiments provided that their diameters are sufficiently large to permit nitrogen molecules to enter. That the pores widen as the cation increases in size is evident from Fig. 13. While the absence of measurable microporosity may be due to the lack of pores of size sufficient to permit entry of nitrogen molecules, it is more probable that the terminal oxygen atoms occupy positions separating interstitial voids from one another.

There are, of course, a number of additional factors which may influence the observation of microporosity. The nature of the cation as well as its shape and size may be important. The absence of microporosity in the methylammonium salts may originate from the nonspherical shape of this cation, the substituent group penetrating into the interstitial void spaces to block the entrance of nitrogen into the [110] plane.

The present work has shown that, in addition to the effects of anion composition on the catalytic activity and selectivity of heteropoly compounds, the cations influence not only such properties but also the morphological structure of the salts in which they are found.

Table 5. Micropore volumes of heteropoly salts

	Micropore volume (10^2 cm^3 liquid g^{-1})		
	Salt of		
Cation	HPW	HPMo	HSiW
K	3.1	1.5	0.1
NH_4	5.0	5.3	4.0
Rb	—	—	4.1
Cs	3.4	0.6	5.2

Acknowledgement—The financial support of the Natural Sciences and Engineering Research Council of Canada is gratefully acknowledged.

REFERENCES

1. H. Hayashi and J. B. Moffat, *J. Catal.* 1982, **77**, 473.
2. H. Hayashi and J. B. Moffat, *Talanta* 1982, **29**, 943.
3. H. Hayashi and J. B. Moffat, *J. Catal.* 1983, **81**, 61.
4. H. Hayashi and J. B. Moffat, *J. Catal.* 1983, **83**, 1982.
5. H. Hayashi and J. B. Moffat, In *Catalytic Conversion of Synthesis Gas and Alcohols to Chemicals* (Edited by R. G. Herman), p. 395. Plenum, New York (1984).
6. J. B. Moffat, *J. Mol. Catal.* 1984, **26**, 385.
7. J. G. Highfield and J. B. Moffat, *J. Catal.* 1984, **88**, 177.
8. B. K. Hodnett and J. B. Moffat, *J. Catal.* 1984, **88**, 253.
9. J. B. McMonagle and J. B. Moffat, *J. Colloid Interface Sci.* 1984, **101**, 479.
10. J. G. Highfield and J. B. Moffat, *J. Catal.* 1984, **89**, 185.
11. J. G. Highfield, B. K. Hodnett, J. B. McMonagle and J. B. Moffat, In *Proceedings of the 8th International Congress on Catalysis* 1984, p. 611. DECHEMA, Frankfurt am Main, F.R.G.
12. J. B. Moffat, In *Proceedings of the 9th Iberoamerican Symposium on Catalysis, Lisbon* (Edited by M. F. Portela), p. 349. Jorge Fernandes, Lisbon (1984).
13. J. B. Moffat, In *Catalysis on the Energy Scene, Studies in Surface Science and Catalysis* (Edited by S. Kaliaguine and A. Mabay), Vol. 19, p. 165. Elsevier, Amsterdam (1984).
14. J. B. Moffat and J. G. Highfield, In *Catalysis on the Energy Scene, Studies in Surface Science and Catalysis* (Edited by S. Kaliaguine and A. Mabay) Vol. 19, p. 77. Elsevier, Amsterdam (1984).
15. J. B. Moffat, In *Catalysis by Acids and Bases* (Edited by B. Imelik, C. Naccache, G. Coudurier, Y. Ben Taarit and J. C. Vedrine), p. 17. Elsevier, Amsterdam (1985).
16. B. K. Hodnett and J. B. Moffat, *J. Catal.* 1985, **91**, 93.
17. J. B. McMonagle and J. B. Moffat, *J. Catal.* 1985, **91**, 132.
18. T. J. R. Weakley, In *Structure and Bonding* (Edited by J. D. Dunitz), Vol. 18. Springer, New York (1974).
19. D. L. Kepert, In *Comprehensive Inorganic Chemistry* (Edited by J. C. Bailar), Vol. 4, Chap. 51. Pergamon Press, New York (1973).

20. H. T. Evans, Jr, In *Perspectives in Structural Chemistry* (Edited by J. D. Dunitz and J. A. Ibers), Vol. 4. John Wiley, New York (1971).
21. G. A. Tsigdinos, In *Methodicum Chimicum* (Edited by F. Korte), Vol. 8, Chap. 32. Academic Press, New York (1976).
22. G. A. Tsigdinos, *Top. Curr. Chem.* 1978, **76**, 1.
23. M. T. Pope, *Heteropoly and Isopoly Oxometalates.* Springer, Berlin (1973).
24. G. M. Brown, M. R. Noe-Spirlet, W. R. Busing and H. A. Levy, *Acta Cryst.* 1977, **B33**, 1038.
25. B. F. Roberts, *J. Colloid Interface Sci.* 1967, **23**, 266.
26. R. Sh. Mikhail, S. Brunauer and E. E. Bodor, *J. Colloid Interface Sci.* 1968, **26**, 45.
27. A. Lecloux and J. P. Pirard, *J. Colloid Interface Sci.* 1979, **70**, 265.
28. S. Brunauer, L. S. Deming, W. E. Deming and E. Teller, *J. Am. Chem. Soc.* 1940, **62**, 1723.

Polyhedron Vol. 5, No. 1/2, pp. 271–275, 1986
Printed in Great Britain

0277–5387/86 $3.00 + .00
© 1986 Pergamon Press Ltd

EPOXIDATION OF ETHYLENE CATALYSED BY MOLYBDENUM COMPLEXES

Z. DAWOODI and R. L. KELLY*

Research and Development Department, BP Chemicals Ltd, Salt End, Hull HU12 8DS, U.K.

(*Received* 24 *June* 1985)

Abstract—A series of MoO_2L_2 (L = N⌒O) complexes has been examined which exhibit activity as catalysts for the epoxidation of ethylene by *t*-butyl hydroperoxide. Improvements in selectivity and reproducibility for these catalysts have been shown to result from the addition of cyclohexene oxide to the reaction mixture. A mechanism which invokes dissociation of an N⌒O ligand is suggested.

Olefin epoxides are intermediates for a wide variety of commercial products based on epoxide polymers and co-polymers. Currently the most important is ethylene oxide with annual production of the order of 4–5 million tonnes. It is produced worldwide by the direct oxidation of ethylene over a heterogeneous silver catalyst. Considerable effort has been directed over a long period towards improving this process which has been optimized at yields between 72 and 78% based on ethylene consumed. The balance of the ethylene is lost as carbon dioxide and water. Increasing costs of the ethylene feedstock dictate improvements in process efficiency and the work reported here has been directed towards developing a homogeneous catalyst for this purpose.

The route investigated proceeds *via* the reaction between ethylene and *t*-butyl hydroperoxide (TBHP), which results in the formation of ethylene oxide and co-product *t*-butanol. This co-product can contribute to the process economics through its market potential as an octane improver in low-lead gasoline. TBHP is accessible by direct aerial oxidation of isobutane via known technology, and an attractive feature of this route is the ready availability of this raw material from gas-condensate fields, including the North Sea.

Homogeneous metal complex catalysts for the epoxidation of olefins other than ethylene are well-known[1] and indeed a major commercial process for the manufacture of propylene oxide employing a homogeneous molybdenum catalyst is operated by the Halcon Corp. and their licencees.[2] However, in the case of ethylene, most systems give a low selectivity to ethylene oxide based on TBHP, with reaction (1) predominating:

$$t\text{-BuOOH} \rightarrow t\text{-BuOH} + \tfrac{1}{2}O_2. \qquad (1)$$

This is consistent with the observation that in general, electron-rich olefins are the more reactive for this particular route.[3]

REACTION MECHANISM

A number of mechanisms have been proposed for transition-metal-catalysed hydroperoxide epoxidation of olefins. These may be separated into two main types, both invoking the initial formation of a catalyst–hydroperoxide complex.

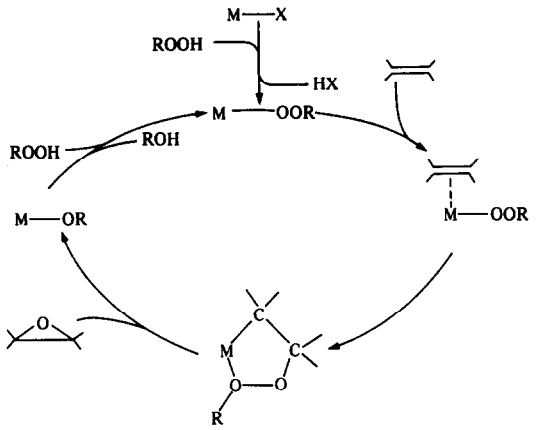
Olefin insertion mechanism

This proceeds via prior co-ordination of the olefin to the metal hydroperoxide, followed by insertion to form a cyclic intermediate and thence elimination of the epoxide as shown in Scheme 1.[4]

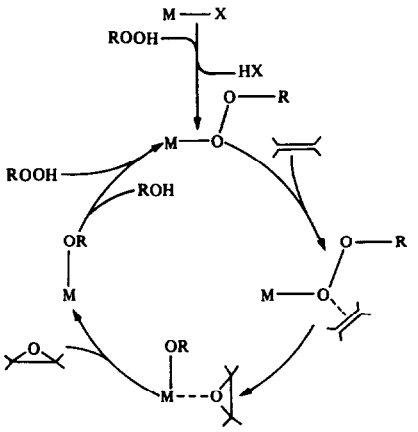
Metal-activated hydroperoxide mechanism

In mechanisms of this type the role of the metal catalyst is that of a Lewis acid which serves to activate by electronic induction the oxygen atoms of the hydroperoxide ligand towards electrophilic attack on olefin substrates.[5] One example is illustrated in Scheme 2.

* Author to whom correspondence should be addressed.



Scheme 1.



Scheme 2.

RESULTS AND DISCUSSION

Sheldon and Kochi[6] have stated that a good catalyst for the hydroperoxide epoxidation of olefins should be both a strong Lewis acid and a poor oxidizing agent. The former characteristic should produce an active catalyst as rationalized above, whilst the latter would be expected to inhibit loss of selectivity resulting from breakdown of the hydroperoxide substrate. Previous work has shown that molybdenum complexes offer the best combination of rate and selectivity.[7] However, because most of this work was carried out on olefins other than ethylene, a preliminary screening of a range of metal complexes was carried out. The results are shown in Table 1 and offer little reason for deviating from molybdenum. Potential catalysts for ethylene epoxidation were selected from complexes possessing robust, non-oxidizable ligands which would be expected to confer stability towards the powerful oxidizing properties of TBHP (Table 2).

The suggested chemistry involved in generating this intermediate is shown in Scheme 3. Addition of the epoxide across a Mo=O bond can generate a relatively unstable 7-coordinate intermediate **A**. On reaction with TBHP this can then eliminate N⌒OH to give the proposed active catalyst for the Sharpless mechanism,[5] **B**. Elimination of the epoxide followed by uptake of ethylene could then give **C** which can be considered as the Mimoun mechanism active catalyst.[4]

Testing was carried out in batch reactions between TBHP and ethylene in toluene solvent typically at 90°C at pressures of 60–90 bar, in a stirred autoclave. Although a number of these catalysts work well for propylene, in general selectivities to ethylene oxide were low. High TBHP conversions were obtained but the product predominating was *t*-butanol.

Significant increases in ethylene oxide yield with respect to TBHP were however obtained when molybdenum dioxo complexes possessing N⌒O donor ligands were employed (Table 3).

The highest ethylene oxide selectivity was obtained with MoO_2(8-hydroxyquinoline)$_2$ which

Table 1. Screening of catalysts for epoxidation of ethylene by TBHP

Catalyst[a]	Ethylene pressure (bar)	Temperature (°C)	Reaction time (h)	Conversion of TBHP (%)	Yield of EO[b] (%)
$VO(acac)_2$	73	90	1	98	0.3
$MoO_2(acac)_2$	75	90	5	94	14
$Rh(acac)_3$	69	90	1	100	1
$Ni(acac)_2$	73	90	2	80	2
$Cu(acetate)_2$	44	90	1	96	0.6
Re_2O_7	72	90	1	20	0
$(NH_4)ReO_4$	80	90	2	3	0

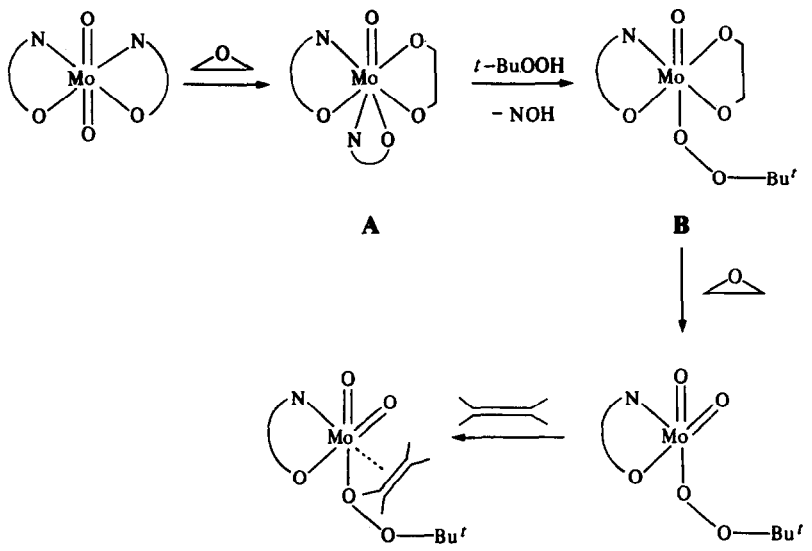
[a] Toluene solvent.
[b] Based on TBHP. EO = ethylene oxide.

Table 2. Molybdenum complexes screened as catalysts for ethylene epoxidation

Ligand type	Catalyst[a]	Ethylene pressure (bar)	Temperature (°C)	Reaction time (h)	Conversion of TBHP (%)	Yield of EO[b] (%)
	$MoO_2(acac)_2$	75	90	5	94	14
	$Mo_2(CF_3CO_2)_4$	52	90	1	85	5
	$MoO_2(OCH_2CH_2OH)_2$	72	90	1	40	6
	$[MoO_2(C_2O_4)]_x$	85	90	2	91	8
	$[MoO_2(SCH_2CO_2)]_x$	83	90	2	1.5	11
CO	$Mo(CO)_6$	52	90	1	84	3
	$[CpMo(CO)_3]_2$	80	90	1.5	93	8
	MoO_2(phthalocyanine)	80	90	2	19	15

[a] Toluene solvent.
[b] Based on TBHP. Yields of EO based on ethylene were 95–100% in all cases.

exhibits TBHP conversion of 42% with 69% selectivity to ethylene oxide. In an effort to improve the yields a small quantity of epoxide, usually cyclohexene oxide for convenience, was added to the reaction mixture at the start of an experiment. This resulted in most cases in increased yields of ethylene oxide. A comparison of some of the most active catalysts with and without the inclusion of starting epoxide is shown in Table 4. Although the yields of ethylene oxide obtained for MoO_2(8-hydroxy-



Scheme 3.

Table 3. Molybdenum complexes containing N⌒O type ligands as catalysts for ethylene epoxidation

Catalyst[ab]	Ethylene pressure (bar)	Temperature (°C)	Time (h)	Conversion of TBHP (%)	Yield of EO[c] (%)
MoO_2(8-hydroxyquinoline)$_2$	90	90	1	42	69
MoO_2(5-nitroso-8-hydroxyquinoline)$_2$	85	90	2	51	61
MoO_2(salen)	83	90	2	4	12
MoO_2(salphen)	81	90	2	60	49
MoO_2(pycarb)$_2$	71	90	3	95	5
MoO_2(salicylaldoxime)$_2$	78	90	2	77	51
MoO_2(SAP)	75	90	2	20	26

[a] Toluene solvent.

[b] Salen = ethylene-1,2-bis-salicylimine, salphen = phenylene-bis-salicylimine, pycarb = pyridine-2-carbinol and SAP = salicylimino phenol.

[c] Based on TBHP. Yields of EO based on ethylene were 95–100% in all cases.

quinoline)$_2$ did not improve, problems with reproducibility which had been a feature of this work were largely alleviated.

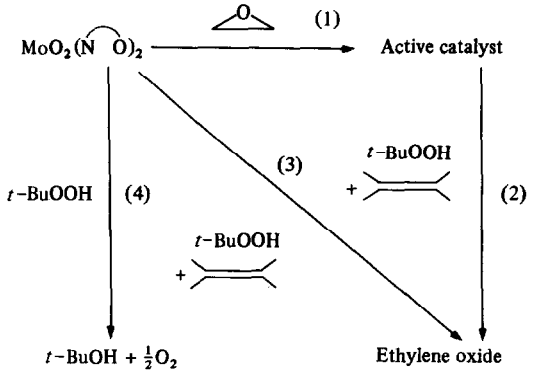
The role of the added epoxide, we believe, is to facilitate rapid formation of the active catalyst for carrying out the epoxidation step. In Scheme 4 if steps (1) and (2) take place faster or in preference to steps (3) and (4), and step (4) is faster than step (3), then on adding cyclohexene oxide the active catalyst is rapidly formed. This can then turn over TBHP and ethylene to autocatalytically generate further active catalyst. If, however, epoxide is not present at the start then decomposition of TBHP results giving the alcohol and oxygen.

Support for this mechanism may be drawn from a series of experiments using dioxomolybdenum bis-salicylimino complexes as epoxidation catalysts (Table 5). The salicylimino ligands were prepared via condensation of salicylaldehyde with the appropriate amine, and the basicity of the imine ligand in each case may be directly linked to the basicity constants (K_b) of the amine precursor. For the series *n*-propylamine to cyclohexylamine all with similar K_b values, it is apparent that the catalysts give higher TBHP conversions according to increasing bulk of the amine precursor of the salicylimino ligand. This is consistent with a mechanism in which formation of the active catalyst occurs via dissociation of a salicylimino ligand. The lower ethylene oxide yields obtained are presumably a result of the tendency

Table 4. Effect of added cyclohexene oxide on molybdenum catalysts

Catalyst[ab]	Time (h)	Conversion of TBHP (%)	Selectivity to EO (%)	Cyclohexene oxide added
MoO_2(salen)	2	4	12	No
	1	29	55	Yes
MoO_2(salphen)	2	60	49	No
	2	34	55	Yes
MoO_2(8-hydroxyquinoline)$_2$	1	42	69	No
	1	42	69	Yes
MoO_2(pycarb)$_2$	3	95	5	No
	2	26	43	Yes
MoO_2(salicylaldoxime)$_2$	2	77	51	No
	2	58	53	Yes
MoO_2(SAP)	2	20	26	No
	2	54	44	Yes

[ab] As for Table 3.



Scheme 4.

for elimination of both the weakly bound ligands. This would generate the bis (diolato) analogue of **B** in Scheme 3, which decomposes TBHP unproductively.

EXPERIMENTAL

t-BHP was supplied by Laporte Industries as an anhydrous solution in toluene. Ethylene used contained maximum levels of water and oxygen of 1 ppm. Toluene was distilled from sodium–benzophenone and stored over molecular sieves.

Catalysts used were either obtained commercially or prepared according to the following procedures.

MoO_2L_2 *complexes*

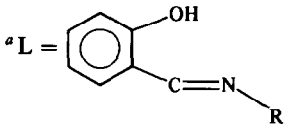
Typically, two molar equivalents of the appropriate ligand (L) were added to a solution of either $MoO_2(acac)_2$ or $MoO_2(OCH_2CH_2OH)_2$ in ethanol or methanol under a nitrogen atmosphere. The mixture was refluxed for 3–6 h and then allowed to reach room temperature. The solution was then filtered and concentrated under reduced pressure to precipitate the crystalline product. The product was then recrystallized from methanol or methanol solution.

$MoO_2(OCH_2CH_2OH)_2$

A slurry of $MoO_2(acac)_2$ (50 g) in ethylene glycol (100 ml) was heated to 80°C under a nitrogen atmosphere for 1 h. Isopropanol (250 ml) was then added and the mixture allowed to reach room temperature. It was then poured into diethyl ether (1 l). The white solid thus formed was filtered off, washed with diethyl ether and then dried *in vacuo*. Yield 30.8 g (80%).

Table 5. MoO_2L_2[a] complexes tested for epoxidation[ab]

Amine precursor H_2NR	K_b amine	Conversion of TBHP (%)	Yield of EO[c] (%)
n-Propylamine	3.8×10^{-4}	55	34
t-Butylamine	4.1×10^{-4}	75	34
Cyclohexylamine	4×10^{-4}	88	28

[a] L = 

Salicylimino

[b] All reactions carried out at 90°C and 80-bar ethylene pressure for 2 h.

[c] As for Table 3.

Epoxidation reactions

Batch reactions between ethylene and TBHP were carried out in Roth magnetically stirred Monel autoclaves at pressures up to 100 bar as follows.

Typically, a 100-ml autoclave was charged with a solution of TBHP in toluene (20 cm^3 of 3.45 M soln, 0.069 mol) and the catalyst (0.12 mmol). The autoclave was sealed and purged twice by pressurizing to 50 bar with ethylene, followed by venting. It was then charged with 90-bar ethylene pressure and heated at 90°C for 1 h. After this time it was allowed to reach room temperature, cooled further in dry ice–acetone and vented. The products were discharged into a cooled vessel and analysed by GC.

REFERENCES

1. See, for example, W. F. Brill, *J. Am. Chem. Soc.* 1963, **85**, 141; W. F. Brill and N. Indictor, *J. Org. Chem.* 1964, **29**, 710; N. Indictor and W. F. Brill, *J. Org. Chem.* 1965, **30**, 2074.
2. J. Kollar, U.S. Patents 3,350,422 and 3,351,635 (1967) to Halcon International.
3. See, for example, R. A. Sheldon, *Recueil* 1973, **92**, 253.
4. H. Mimoun, *J. Mol. Catal.* 1980, **7**, 1 (and references therein).
5. A. O. Chong and K. B. Sharpless, *J. Org. Chem.* 1977, **42**, 1587.
6. R. A. Sheldon and J. K. Kochi, *Adv. Catal.* 1976, **25**, 343; *Oxid. Comb. Rev.* 1973, **5**, 202.
7. R. A. Sheldon, *Aspects of Homogeneous Catalysts*, Vol. 4.

Polyhedron Vol. 5, No. 1/2, pp. 277–279, 1986
Printed in Great Britain

0277–5387/86 $3.00 + .00
© 1986 Pergamon Press Ltd

MOLYBDENUM BIS(DIPHENYLPHOSPHINE)ETHANE COMPLEXES: STRUCTURE AND REACTIVITY IN CATALYTIC EPOXIDATION OF OLEFINS WITH ORGANIC HYDROPEROXIDES

A. HERBOWSKI

Institute of Chemistry, Silesian University, Katowice, Poland

and

J. M. SOBCZAK and J. J. ZIÓŁKOWSKI*

Institute of Chemistry, University of Wrocław, 50-383 Wrocław, Poland

(*Received* 11 *June* 1985)

Abstract—Catalytic activity of molybdenum complexes in different oxidation states with bis(diphenylphosphine)ethane and the related phosphonium cation was examined in olefin epoxidation with organic hydroperoxides.

Mo compounds are well-known, effective catalysts for epoxidation of olefins with organic hydroperoxides.[1] However, only a few literature data on the catalytic activity of Mo phosphine complexes in olefin epoxidation reactions are available, although the transition-metal phosphine complexes are widely applied in numerous catalytic reactions.[2] The possibility of the simple synthesis of Mo complexes in different oxidation states (from +2 to +5) with the same ligand bis(diphenylphosphine)ethane (dppe)[3] gave the chance for studies on correlation between the structure and catalytic reactivity of these compounds in catalytic epoxidation reactions of olefins by the organic hydroperoxides.

The subjects of our studies were: the Mo(V) compounds $(dppeH_2)[MoOCl_5]$,[4] $MoOCl_3(dppe)$ (brown[4] and red[5] isomers) and

$$Mo_2O_{2.5}Cl_5(dppe)_2;^{4}$$

the Mo(IV) compound

$$[MoOCl(dppe)_2]Cl;^{6}$$

the Mo(III) compounds

$$(dppeH_2)_{1.5}[MoCl_8H],^{6}$$

$$(dppeH_2)_{1.5}[MoCl_6]\cdot 6H_2O,^{7}$$

$$(dppeH_2)_2[Mo_2(OH)_2Cl_8]^{3}$$

and

$$Mo_2Cl_6(dppe)_2;^{6}$$

and the Mo(II) compounds $MoCl_2(dppe)_2$ and α-$Mo_2Cl_4(dppe)_2$.[8]

EXPERIMENTAL

The catalytic activities of these complexes were examined in the decomposition reaction of cumene hydroperoxide (ROOH) and in cyclohexene epoxidation. Catalytic decomposition of ROOH was examined in the system: $[ROOH]_o = 0.1–0.35$ M, $[cat.] = 1\times10^{-4}–1\times10^{-3}$ M, temperature = 35–70°C, solvent = PhCl, atmosphere = Ar.

RESULTS AND DISCUSSION

ROOH decomposition is catalyzed by: $(dppeH_2)[MoOCl_5]$ (24.3), $MoOCl_3(dppe)$ [brown (46.4) and red (39.3) isomers], $(dppeH_2)_{1.5}$

* Author to whom correspondence should be addressed.

$[MoCl_8H]$ (35.0) and $(dppeH_2)_2[Mo_2(OH)_2Cl_8]$ (57.2); activation energies in kcal mol^{-1} in the temperature range 35–70°C are given in parentheses. Acetone and phenol are the main cumene hydroperoxide decomposition products in chlorobenzene. Characteristic features of all decomposition reactions are induction time, appearance of a yellow colour during the process, which quickly turned to brown-red, and precipitation of the brown precipitate from post-reaction mixtures. The shape of the kinetic curves, indicating inhibition of the reaction (Fig. 1), points to catalyst deactivation (it was confirmed experimentally by introduction of an additional amount of ROOH to the reaction system). The brown precipitate was carefully examined and the results revealed the complete destruction of the initial Mo catalyst.[9]

Analysis of the catalytic activities of the Mo complexes under study revealed that the induction time and ROOH decomposition rate are functions of the stability of the initial compounds used as catalysts. In the case of the air- and moisture-sensitive compounds, such as

$$(dppeH_2)[Mo_2(OH)_2Cl_8]$$

and

$$(dppeH_2)_{1.5}[Mo_2Cl_8H],$$

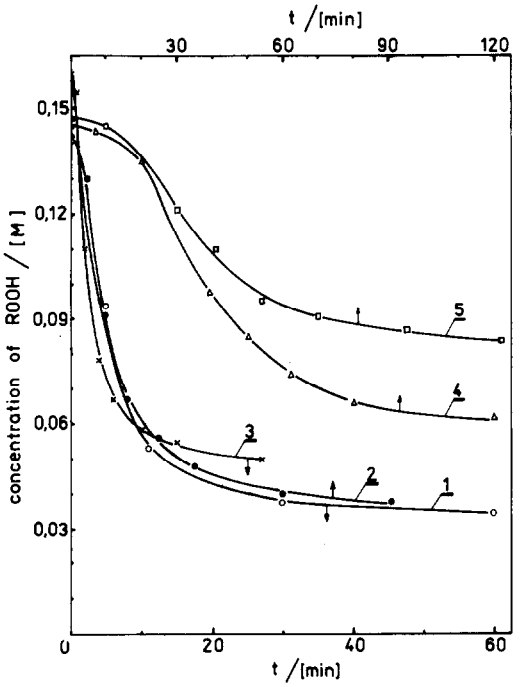


Fig. 1. Cumene hydroperoxide (ROOH) decomposition catalyzed by the Mo complexes $(dppeH_2)_2[Mo_2(OH)_2Cl_8]$ (1), $(dppeH_2)[MoOCl_5]$ (2), $(dppeH_2)_{1.5}[Mo_2Cl_8H]$ (3) and $MoOCl_3(dppe)$ [red (4) and brown (5) isomers]. $[Mo]_o = 1 \times 10^{-4}$ M, PhCl, 50°C, Ar.

the induction times were short and the ROOH decomposition rates were high. For the relatively stable complexes such as $MoOCl_3(dppe)$ isomers, the induction time is much longer (for the brown isomer about 15 min) and the reaction rate is lower. The other complexes, stable in air, are inactive as ROOH catalysts.

All Mo (II, III, IV and V) complexes under study are catalytically active in olefin epoxidation with the organic hydroperoxides. As a model reaction we have chosen cyclohexene epoxidation by ROOH examined in the system: $[cyclohexene]_o = 0.7–2.0$ M, $[ROOH]_o = 0.1–1.0$ M, $[cat.] = 1 \times 10^{-4}–1 \times 10^{-3}$ M, solvent = PhCl, temperature = 50–70°C, neutral atmosphere (Ar). All catalytic reactions have no induction time. Kinetic studies of epoxidation were limited to the initial reaction stage. The reaction orders determined vs olefin ROOH and catalyst are about one. Activation energies determined for that stage can be used as a factor determining the reactivity of the initial form of the molybdenum complex (Table 1).

Generally speaking, for the reactive complexes activation energy values are lower, e.g. for $(dppeH_2)_2[Mo_2(OH)_2Cl_8]$ (17.5). As a rule, for these compounds higher reaction rates were observed. Selectivity of epoxidation with time was examined to conclude that independently of the starting structure of the Mo compound used, selectivity approached a certain limiting value (~82%). This suggests that the Mo complexes used in epoxidation undergo "*in situ*" transformation to one type of compound. Such a statement was confirmed by isolation from the post-reaction mixtures of the compound formulated as $MoO_2(C_6H_{11}O_2)(dppeO_2)$ (analogous to the compound described earlier[9]). This compound exhibits great catalytic activity in epoxidation but does not catalyze ROOH decomposition. Simultaneously the

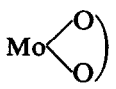
Table 1. Activation energies

Catalyst	E_a (kcal mol^{-1})
$(dppeH_2)[MoOCl_5]$	26.0
$MoOCl_3(dppe)$ red isomer	32.0
$MoOCl_3(dppe)$ brown isomer	43.9
$Mo_2O_{2.5}Cl_5(dppe)_2$	57.7
$[MoOCl(dppe)_2]Cl$	112.3
$(dppeH_2)_{1.5}[Mo_2Cl_8H]$	38.2
$Mo_2Cl_6(dppe)_2$	43.6
$(dppeH_2)_{1.5}[MoCl_6]\cdot 6H_2O$	47.6
$(dppeH_2)_2[Mo_2(OH_2)_2Cl_8]$	17.5

side-product of cyclohexene epoxidation was isolated, i.e. cyclohexanediol-1,2.

The ^1H NMR spectrum (in $CDCl_3$) of this compound (δ3.38; s, 2H from OH; δ3.50 for *trans* isomer) and its melting point 97.7–98.5°C, point to the *cis* isomer.

Formation of *cis*-cyclohexanediol-1,2 suggests its formation within the coordination sphere of the Mo catalyst. Epoxide interaction with the Mo=O group, leading to the formation of



seems to be most likely, whereas liberation of diol from the coordination sphere is realized in the subsequent reaction with ROOH.

REFERENCES

1. R. A. Sheldon, In *Aspects of Homogeneous Catalysis* (Edited by R. Ugo), p. 3. D. Reidel, Dordrecht (1981); J. Sobczak and J. J. Ziółkowski, *J. Mol. Catal.* 1981, **13**, 11.
2. L. Pignolet (Ed.), *Homogeneous Catalysis with Metal Phosphine Complexes.* Plenum, New York (1983).
3. A. Herbowski, J. M. Sobczak and J. J. Ziółkowski, *Polyhedron* 1986, **5**, 399.
4. A. Herbowski, *Inorg. Chim. Acta* 1981, **54**, L121.
5. A. V. Butcher and J. Chatt, *J. Chem. Soc.* (*A*) 1971, 2356.
6. A. Herbowski and J. O. Dzięgielewski, *Chem. Scr.* 1984, **24**, 41.
7. A. Herbowski and T. Lis, *Polyhedron* 1985, **4**, 127.
8. C. Miniscloux, G. Martino and L. Sajus, *Bull. Soc. Chim. Fr.* 1973, **7–8**, 2179.
9. A. Herbowski, J. M. Sobczak and J. J. Ziółkowski, *J. Mol. Catal.* 1983, **19**, 309.

Polyhedron Vol. 5, No. 1/2, pp. 281–287, 1986
Printed in Great Britain

0277–5387/86 $3.00 + .00
Pergamon Press Ltd

SELECTIVE ETHYLENE OXIDE HYDROLYSIS CATALYSED BY OXO-MOLYBDENUM SPECIES*

JOHN R. BRIGGS,† ARNOLD M. HARRISON and JOHN H. ROBSON

Long Range Catalyst Group, Union Carbide Corp., P.O. Box 8361,
South Charleston, WV 25303, U.S.A.

(*Received* 28 *June* 1985)

Abstract—Ortho-molybdate and ortho-tungstate (MO_4^{2-}, M = Mo or W) are selective catalysts for the hydrolysis of ethylene oxide. Model compounds synthesized from epoxides and organic soluble molybdate and tungstate salts of the bis(triphenylphosphine)iminium cation suggest that intermediates in this reaction are anionic molybdenum(VI) or tungsten(VI) alkoxide complexes of type $[MO_2(OCH_2CH_2O)_2]^{2-}$, containing chelating vicinal dialkoxide ligands derived from the epoxide residue. Hydrolysis of an ethylene oxide derived complex has been shown to yield exclusively monoethylene glycol as the organic product, with the regeneration of the metallate dianion (MO_4^{2-}).

Ethylene oxide is a valuable and versatile chemical intermediate. Its synthesis forms the basis of the ethylene-based route to monoethylene glycol, a product which consumes a large portion of the industrial production of this material. We have been interested in the interaction of epoxides with transition-metal complexes, and particularly in the possibility of catalytically transforming epoxides into desirable derivatives. Here we report our investigations into the use of high-valent group 6 oxy-metal anions as catalysts for the selective hydrolysis of epoxides to monoglycols.

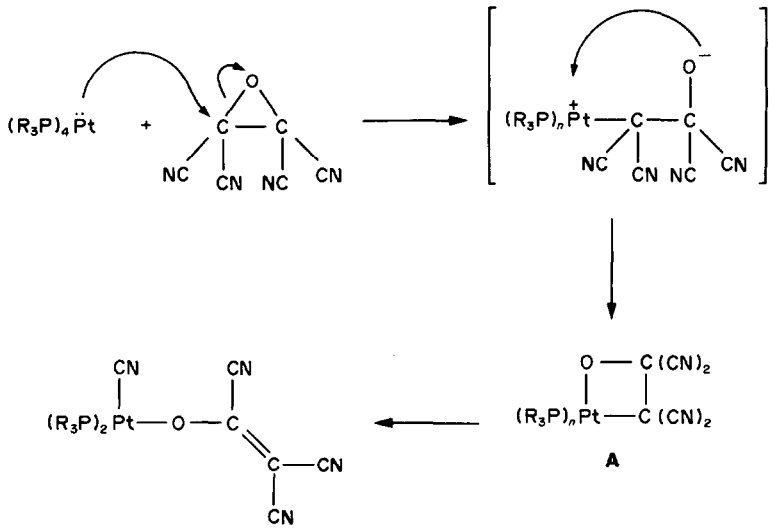
Transition metals are known to catalyze a large number of transformations of epoxides including hydrogenation, hydroformylation, carbonylation and deoxygenation.[1] Some mechanistic information has been inferred from reactions of "model" transition-metal complexes and epoxides, but in general, considering the industrial importance of epoxides as chemical intermediates, their transition-metal-mediated chemistry appears to have been somewhat neglected. The catalytic synthesis of epoxides, on the other hand, has received much study.[2]

A particularly fruitful area involving epoxide transformations has involved the use of low-valent and electron-rich noble-metal complexes and electron-deficient epoxides (for example, often bearing electron-withdrawing cyano groups).[3] A frequently observed feature in these studies is that the low-valent complex oxidatively adds to the C—O bond of the epoxide, resulting in the generation of an oxametallacyclobutane moiety. In many cases, subsequent transformations can lead to the isolation of rearranged products. For example, upon treatment with tetracyanoethylene oxide (Scheme 1), platinum(0) phosphine complexes, $[Pt(PR_3)_n]$, yield bisphosphine oxaplatinacyclobutane complexes, $[(R_3P)_2\overline{PtOC(CN)_2C}(CN)_2]$ (A in Scheme 1). When $R_3P = PPh_2Me$, or with the analogous and kinetically more labile palladium complexes, rearrangement leads to the isolation of tricyanoethanolato complexes. Although ring opening of epoxides usually occurs by C—O bond cleavage, oxidative addition of this type of low-valent complex into the C—C bond of an epoxide has also been reported,[4] but this report is probably erroneous.[3(a)]

The proposed mechanism for the formation of these metallacyclic complexes (Scheme 1) involves initial S_{N^2} type fission of the C—O bond of the epoxide upon nucleophilic attack by the lone pair of electrons on the metal complex. The resulting zwitterionic species, $\overset{+}{Pt}—C—C—\bar{O}$, is not observed, but rapidly recyclizes to yield the observed product. Support for this mechanism is claimed[3(c),5]

* © 1986 Union Carbide Corporation.

† Author to whom correspondence should be addressed.



Scheme 1. Ring-opening of epoxides by low-valent noble-metal phosphine complexes.

in the observation that tricyanoethylene oxide, $(NC)_2\dot{C}—\dot{C}H(CN)\dot{O}$, yields a metallacycle of type $\dot{P}t—\dot{C}(CN)_2\dot{C}H(CN)\dot{O}$, where the hydrogen is located β to the metal, indicative of platinum attacking the more electropositive carbon (bearing two cyano groups). This observation alone, however, does not rule out prior coordination of epoxide through oxygen before ring opening. Much of the above chemistry has been reviewed.[6]

Nucleophilic ring opening of epoxides by anionic transition-metal complexes, e.g. $[CpFe(CO)_2]^-$ (Cp = cyclopentadienyl), has also been proposed.[7] In this case, deoxygenation occurs, ultimately yielding iron(II) olefin complexes. Lack of vacant coordination sites on iron presumably precludes recyclization in this case.

Although most reports detailing this chemistry appear to favor the first step in ring opening as nucleophilic attack of metal complex on epoxide, initial coordination by epoxide through oxygen is a possible first step. However, to our knowledge only a single example of an isolated complex containing an intact epoxide ligand exists, viz. $[CpMo(CO)_3(\dot{O}CH_2\dot{C}H_2)]^+$.[8]

RESULTS AND DISCUSSION

Catalysis

The uncatalysed hydrolysis of ethylene oxide yields a mixture of ethylene glycols (mono-, di-, tri- and higher), the proportions of which depend principally upon the hydrolysis ratio (the weight ratio of water to ethylene oxide used during the hydrolysis reaction). The higher glycols are formed by reaction of product glycols with unreacted epoxide, and consequently a higher hydrolysis ratio enhances the formation of lower molecular weight glycols.

We have found that water-soluble salts of both molybdate and tungstate are effective homogeneous catalysts for the selective hydrolysis of ethylene oxide to monoethylene glycol. Typical plots of monoethylene glycol selectivity against hydrolysis ratio at several sodium molybdate catalyst concentrations are shown in Fig. 1. As can be seen, selectivity is a

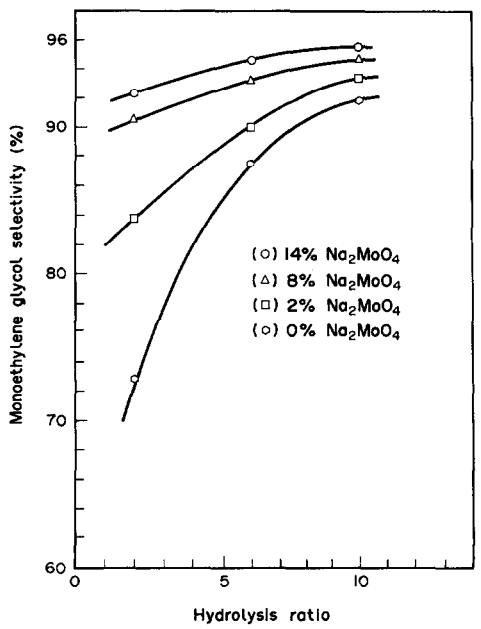


Fig. 1. Monoethylene glycol selectivity as a function of hydrolysis ratio: effect of catalyst concentration.

strong function of hydrolysis ratio and catalyst concentration. Since we are working in aqueous solution, these selectivity curves are a composite of the uncatalyzed and catalyzed routes. Consequently the effect of increasing catalyst concentration is most dramatically seen at low hydrolysis ratio, since, under these conditions, less of the monoglycol selectivity is generated by the uncatalyzed route.

Synthesis of model compounds

Bis(triphenylphosphine)iminium cation, $[(Ph_3P)_2N]^+$ (PPN), metallates. Our main goal in this work was to detail the reaction sequence by attempting to isolate and identify intermediates in the catalytic reaction. Our approach was based upon the use of salts of the metallates (molybdate and tungstate) which were soluble in organic solvents. We thought it unlikely that we would be able to isolate intermediates in the catalytic cycle by working in aqueous solution, since we anticipated that such species would be hydrolytically unstable. Thus, initially, we undertook the synthesis of metallate salts which we hoped would possess the desired solubility characteristics. The metallate salts of PPN proved to be suitable for our studies. Their solubility in dichloromethane of >0.3 mol l^{-1} was sufficient to enable us to obtain good-quality NMR spectra (including ^{95}Mo and ^{183}W), and additionally the proton resonances of the cation proved to be well removed from those of the epoxide residues which we were to study.

The synthesis of these salts is straightforward. They can be prepared most readily by precipitation from stirred hot (60°C) aqueous solutions of sodium metallate and PPN chloride. It is important to maintain the temperature around 60°C, otherwise the desired products are contaminated by precipitated PPN chloride. A second treatment with hot aqueous sodium metallate, although not absolutely necessary when good temperature control is achieved, generally ensures that a substantially chloride-free product is obtained. Additionally, these materials can be synthesized by treating a freshly prepared suspension of silver metallate ($AgNO_3 + Na_2MO_4$) in dichloromethane with PPN chloride. Anion exchange results in the formation of soluble PPN metallate and insoluble silver chloride. Again, a second treatment of the PPN metallate with fresh silver metallate ensures removal of any excess chloride ion. Materials prepared by both routes are identical by IR spectroscopy.

These materials have been characterized by IR and metal NMR spectroscopies. The IR spectra of both the molybdate and tungstate salts contain a band at 830 cm^{-1} arising from the anion, in addition to all the bands present in the spectrum of PPN chloride. This should be compared with bands at 830 cm^{-1} for molybdate and 830 and 850 cm^{-1} for tungstate as hydrated sodium salts (all spectra measured as KBr wafers).

In anhydrous dichloromethane solution, both compounds show a single resonance in their respective metal NMR spectra close to that of our reference samples of aqueous sodium metallate, and we therefore formulate them as tetrahedral MO_4^{2-} species. The sharpness of the molybdenum signal, in particular, suggests that the species is highly symmetric.

In some early experiments, we treated dichloromethane solutions of PPN molybdate in a NMR tube with some of the materials to be found under ethylene oxide hydrolysis reaction conditions, i.e. water, ethylene oxide and ethylene glycol. Addition of small (1–2 mol equivalents) amounts of water results in the broadening of the molybdenum resonance at probe temperature ($\simeq 23$°C), and, upon cooling to -30°C, a second resonance appears several ppm to low field of the original PPN_2MoO_4 resonance. This second, minor resonance can be increased by further addition of water, or by cooling, and can be decreased by warming. Recooling of a warmed solution regenerates the second resonance. These observations can be interpreted in terms of molybdate ligation by water via an equilibrium:

$$MoO_4^{2-} + xH_2O \rightleftharpoons [MoO_4(H_2O)_x]^{2-} \qquad (x = 1 \text{ or } 2).$$

Oxygen atom exchange between ^{17}O-labelled water and molybdate has been previously observed,[9] although species of the type postulated above were not directly identified.

In a similar fashion, we have found that a new, minor resonance to low field of that assigned to MoO_4^{2-} is generated upon addition of 1 mol of ethylene glycol to PPN_2MoO_4 in dichloromethane solution at ambient temperature. We assign this peak to an octahedral $[MoO_4(HOCH_2CH_2OH)]^{2-}$ species containing a chelating glycol ligand. Neither the monomethyl-ether of ethylene glycol, $MeOCH_2CH_2OH$, nor methanol give any indication from the ^{95}Mo spectra of being able to ligate molybdate under these conditions. Presumably the bidentate nature of ethylene glycol makes it the most potent ligand of the three alcohols studied. By these criteria, ethylene oxide shows no indication of being able to ligate molybdate in experiments performed at 23 and -30°C. Analogous experiments have not yet been performed with the corresponding tungstate salts due to the extended length of time required to achieve a good signal : noise ratio in ^{183}W spectra.

Epoxide adducts. We have prepared adducts of

ethylene and styrene oxides with both molybdate and tungstate, but those of styrene oxide have proven most amenable to spectral analysis, and we have done most work with these species. Most of the discussion of spectral properties will be concerned with these adducts, although when relevant we will also discuss ethylene oxide adducts.

Treatment of dichloromethane solutions of the PPN_2MO_4 (M = W or Mo) with an excess of styrene oxide at *ca* 100°C for molybdate, 140°C for tungstate, for *ca* 3 h in a sealed vessel (see Experimental) results in the formation of species of stoichiometry $[MO_4(epoxide)_2]^{2-}$. Removal of volatiles *in vacuo* and repeated washing with ether gives the impure materials (sometimes contaminated with unreacted PPN_2MO_4) as white powders. We have not been able to obtain analytically pure materials from these preparations, but rather our structural assignments are based on the spectroscopic properties of these products.

The proton NMR spectra of the products are essentially identical for molybdate and tungstate, with only minor variations in chemical shifts and coupling constants. A spectrum of the methine–methylene region of the styrene oxide molybdate adduct is shown in Fig. 2, and data are shown in Table 1. The spectra are characterized by an ABX spin system for the methylene–methine protons, and a complex aromatic resonance for cation and styrene phenyl protons. Integration of methylene and methine signals against a combined cation and styrene oxide derived phenyl signals gives a ratio of epoxide to cation of 1 : 1, i.e. two epoxides per metal atom. This ratio is variable from preparation to preparation, but never exceeds two epoxides per metal (integration of resonances of such disparate intensities is somewhat difficult).

The ethylene oxide adducts contain a single resonance in their ^1H NMR spectra in addition to a complex aromatic resonance. Again the tungstate and molybdate adducts are essentially identical. The singlet resonance in the spectra which we assign to the equivalent methylenes occurs very close to those of free glycol, but can be distinguished by spiking a sample of molybdate adduct with free glycol. In this case, two separate signals are observed. Thus, in these complexes, all epoxide-derived protons are equivalent, and for this reason we formulate them and the related styrene oxide derived adduct as *trans*-$[MoO_2(OCH_2CH_2O)_2]^{2-}$ species.

The IR spectrum of the styrene oxide–molybdate adduct, measured as a KBr wafer, shows bands due to PPN. The presence of an epoxide residue is most clearly demonstrated by the presence of weak ν(C—H) bands below 3000 cm^{-1}. The band at 830 cm^{-1} observed in the spectrum of PPN_2MoO_4 had disappeared, and a new band at 870–880 cm^{-1}, presumably due to an Mo—O vibration, has appeared. Definite structural assignment from IR spectra is prevented by the presence of other bands in the metal–oxygen region, and, because some bands may be obscured, we are unable to obtain any conclusive evidence regarding the molybdenum coordination sphere by this technique.

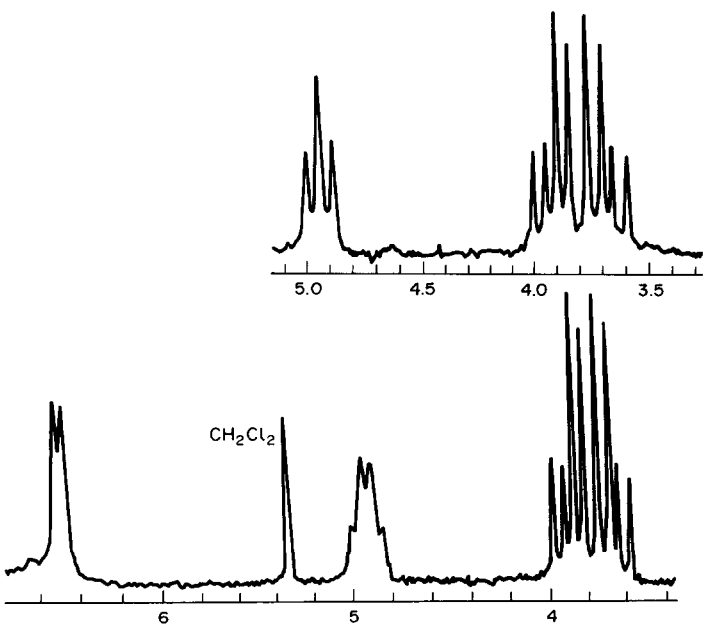
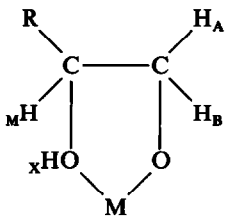


Fig. 2. ^1H NMR spectra (aliphatic region) of $[MoO_2(OCH_2CH(Ph)OH)_2]$ (lower) and $[MoO_2(OCH_2CH(Ph)O)_2]$ (upper).

Table 1. ^{1}H NMR data for epoxide adducts



(R = H or Ph; M = Mo or W)

M	Epoxide	R	Chemical shifts[a] H_A	H_B	H_M	H_X	Coupling constants[b] J_{AB}	J_{AM}	J_{BM}	J_{MX}
Mo	Styrene	[c]	3.88	3.67	4.90	—	10.6	6.5	5.6	—
W	Styrene	[c]	3.89	3.71	4.92	—	10.7	6.5	5.8	—
Mo	Ethylene		—	3.92	—	—	—	—	—	—
W	Ethylene		—	3.95	—	—	—	—	—	—
Mo	Styrene + H^+	[c]	3.88	3.67	4.90	6.48	10.6	6.6	5.6	5.0

[a] In ppm, to low field of TMS, but referenced to residual protons in CD_2Cl_2 solution as 5.32.
[b] In Hz.
[c] Obscured by cation resonance.

Sheldon[10] has reported that complexes of the type *trans*-$[MoO_2(OCH_2CH_2OH)_2]$ have been isolated from reaction mixtures containing molybdenum formulated to perform catalytic epoxidation of olefins. Such species are isolated no matter what the source of molybdenum, and probably arise as a secondary product from reaction of epoxide with molybdenum complexes present in solution. These products are closely related to those which we have isolated, but few spectroscopic details are provided for the complexes with which we are able to compare our results. We believe that similar complexes are formed upon treatment of our anionic epoxide adducts with acids (see later).

Hydrolysis of epoxide adducts

Treatment of an isolated sample of $PPN_2[MoO_2(OCH_2CH_2O)_2]$ in dichloromethane solution with water (4 equivalents), followed by extraction of the organic layer with additional water, and gas chromatographic analysis of the aqueous layer, showed the formation of only monoethylene glycol. No higher glycols were produced. IR analysis of material obtained from the organic layer shows that it contains PPN_2MoO_4. Some information relevant to this hydrolysis can be gained from proton NMR spectra of the styrene oxide adducts.

In some preparations of the styrene epoxide adducts, the low-field triplet, assigned to the methine proton, appears as a broad featureless resonance, while in one preparation it appeared as a quartet (NMR data in Table 1) shown in Fig. 2. In this latter case, an additional resonance appears as a doublet at *ca* δ 6.5 also. This proton is clearly coupled to the methine proton, and to no other (see Fig. 2).

We suggest that this extra resonance and coupling arise from the presence of a scavenged proton which resides upon the oxygen closed to the methine proton. No protonation of the second oxygen is apparent. This proton is probably derived from acidity present in the methylene chloride during the preparation. Intermediate cases where the methine resonance appears broad, probably indicate partial protonation, or a fluxional process. It should be noted that in all these cases, the AB portion of the spectrum remains stoically unchanged. These products are analogous to those reported by Sheldon.

The addition of either solid sodium hydroxide or *p*-toluene sulfonic acid to a CD_2Cl_2 solution of the molybdate–styrene oxide adduct exhibiting a broad methine resonance sharpens up the signal to a sharp triplet. In the former case we believe that the oxygen is deprotonated, while, in the latter, the presence of excess protons moves us into a fast exchange regime.

The addition of water alone, or acid alone does not result in cleavage of styrene glycol from this adduct, as measured by proton NMR, but rather both of these are required to give rapid cleavage of glycol. This is also accompanied by the precipitation of green crystals of a molybdenum-containing material

which we suggest is a condensed polymolybdate. A similar colored material is produced upon addition of acid to solutions of PPN_2MoO_4.

Thus it would seem that protonation of the adducts is the first step in the hydrolysis to give glycol and regenerated metallate.

EXPERIMENTAL

All manipulations were performed under an argon atmosphere using standard techniques unless otherwise stated. Solvents were distilled from appropriate drying agents before use; other reagents were used as received. Ethylene glycol analyses were performed by gas chromatography using a Chromasorb 101 column using 2-ethyl-1,3-hexanediol as internal standard.

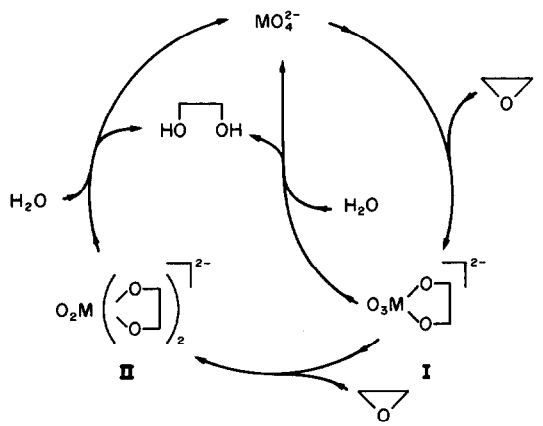
IR spectra were measured on a Perkin–Elmer 683 spectrometer, FT NMR spectra on either a Nicolet NT 200 widebore for ^{95}Mo and ^{183}W or a Varian XL-100-15 with Nicolet data system for ^{1}H.

The preparation of the PPN salts of molybdate and tungstate are essentially the same. That for molybdate, $[(Ph_3P)_2N]_2[MoO_4]$, is given as an example.

Sodium molybdate dihydrate (6.32 g, 26.12 mmol) was dissolved in distilled water (100 cm^3) and heated to 55°C—at this temperature the solution was homogeneous. To this solution was added a solution of $[(Ph_3P)_2N]Cl$ (30.00 g, 52.25 mmol) in distilled water (600 cm^3), also at 55°C. The resulting cloudy solution was stirred at 55°C for 75 min before being allowed to cool to 45°C. At this temperature a precipitate, often very oily, was produced. This generally solidified on stirring at this temperature for a few minutes, and then the product was isolated by filtration. This material was washed with 3 × 100 cm^3 of distilled water at 50°C to remove unchanged $[(Ph_3P)_2N]Cl$. The product contained large quantities of water, which was removed by drying firstly in air, then *in vacuo* over P_2O_5. Yield is typically 60–70%.

The preparation of the epoxide adducts is exemplified by that of the styrene oxide–molybdate adduct, $[PPN]_2[MoO_2(OCH_2CH(Ph)O)_2]$.

PPN_2MoO_4 (10.57 g, 8.55 mmol) was dissolved in dichloromethane (55 cm^3) and this solution dried over activated 4-Å molecular sieves for 3 h. This solution was transferred to a 300-cm^3 Parr stainless steel autoclave. To this, styrene oxide (11.5 g, 96.6 mmol) was added. The mixture was heated to 100°C for 3 h. After cooling, this solution was stripped of volatiles and washed with a total of 400 cm^3 of diethyl ether. The product, in almost quantitative yield, is a white powder.



Scheme 2. Proposed reaction sequence for metallate-catalysed epoxide hydrolysis.

CONCLUSIONS

Aqueous soluble salts of molybdate and tungstate are effective catalysts for selective hydrolysis of ethylene oxide to monoethylene glycol. From studies with model compounds we proposed the catalytic cycle of Scheme 2 as an outline of the reaction mechanism.

We envision the first step as nucleophilic ring opening of epoxide by molybdate followed by recyclization to give species **I**. Further reaction with epoxide giving species **II** may not occur in aqueous solution, since **I** probably is hydrolyzed rapidly. In non-aqueous solution, we isolate species of type **II**. These are hydrolyzed after protonation to complete the catalytic cycle.

Further work to elucidate the mechanism in more detail is being undertaken.

Acknowledgements—We would like to thank O. H. Huffman for excellent technical assistance, Union Carbide Corp. for granting permission to publish, to George O'Connor for continued inspiration, Brian Keen for sharing results, and Kathy Canterbury and Nancy Broyles for obtaining NMR spectra.

REFERENCES

1. See relevant references from D. Milstein and J. C. Calabrese, *J. Am. Chem. Soc.* 1982, **104**, 3773.
2. For a review see P. S. Kilty and W. M. H. Sachtler, *Catal. Rev. —Sci. Eng.* 1974, **10**, 1.
3. (a) R. Schlodder, J. A. Ibers, M. Lenarda and M. Graziani, *J. Am. Chem. Soc.* 1974, **96**, 6893; (b) M. Lenarda, R. Ros, O. Traverso, W. D. Pitts, W. H. Baddley and M. Graziani, *Inorg. Chem.* 1977, **16**, 3178;

(c) R. B. Osborne and J. A. Ibers, *J. Organomet. Chem.* 1982, **232**, 371.
4. M. Lenarda, R. Ros, M. Graziani and U. Belluco, *J. Organomet. Chem.* 1972, **46**, C29.
5. M. Lenarda, N. B. Pahor, M. Calligaris, M. Graziani and L. Randaccio, *J. Chem. Soc., Dalton Trans.* 1978, 279.
6. M. Graziani, M. Lenarda, R. Ros and U. Belluco, *Coord. Chem. Rev.* 1975, **16**, 35.
7. (a) W. P. Giering, M. Rosenblum and J. Tancrede, *J. Am. Chem. Soc.* 1972, **94**, 7170; (b) M. Nitay and M. Rosenblum, *J. Organomet. Chem.* 1977, **136**, C23.
8. K. Schleter and W. Beck, *Z. Naturforsch.* 1980, **35B**, 985.
9. R. R. Vold and R. L. Vold, *J. Magn. Reson.* 1975, **19**, 365.
10. R. A. Sheldon, *Recl Trav. Chim. Pays-Bas* 1973, **92**, 367.

Polyhedron Vol. 5, No. 1/2, pp. 289–296, 1986
Printed in Great Britain

0277–5387/86 $3.00 + .00
© 1986 Pergamon Press Ltd

CATALYSIS BY TETRABROMOOXOMOLYBDATE(V) COMPLEX: OXIDATION OF OLEFINS AND ALCOHOLS WITH *t*-BUTYL HYDROPEROXIDE

YASUHIKO KURUSU* and YOSHIRO MASUYAMA

Department of Chemistry, Faculty of Science and Technology, Sophia University, 7-1 Kioicho, Chiyoda-ku, Tokyo 102, Japan

(*Received* 14 *June* 1985)

Abstract—Molybdenum is a good catalyst for epoxidation of olefins with *t*-butyl hydroperoxide (*t*-BuOOH). However, use of this system for oxidation of alcohols has seldom been reported. Therefore, the catalytic activity of substituted ammonium tetrabromooxomolybdate(V) for *t*-BuOOH oxidation was investigated. The type of substituted ammonium ion used as a counter cation became a dominant factor. The ion with no hydrogen on the nitrogen showed only oxidation of alcohol, but ions with hydrogen on the nitrogen exhibited epoxidation activity. The investigation of oxidation of alcohols and olefins with *t*-BuOOH in the presence of the molybdenum complexes with substituted ammonium ion as a counter cation is described and discussed.

From the point of view of economics, selectivity and safety, *t*-butyl hydroperoxide (*t*-BuOOH) is one of the best sources of oxygen atoms for a variety of organic oxygenations.[1] *t*-BuOOH shows heterolysis of the O—O bond by nucleophilic attack,[2] and we are interested in metal-catalyzed reactions for the activation of *t*-BuOOH. It is well known that molybdenum, vanadium and tungsten are effective as metal catalysts for this reaction. During our investigations of molybdenum catalysts[3] we found that the tetrabromooxomolybdate(V) complex showed a characteristic reactivity. Substituted ammonium as a counter cation (A) of the tetrabromooxomolybdate(V) complex controls catalytic activity for oxidation of alcohols and epoxidation of olefins with *t*-BuOOH.[4,5] The chemoselective oxidation is a very interesting theme in synthetic organic chemistry.

In this paper, we report our results on chemoselective reactions for olefin epoxidation and alcohol oxidation with *t*-BuOOH in the presence of various substituted ammonium tetrabromooxomolybdate(V) complexes.

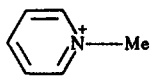
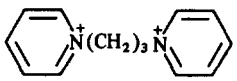
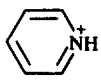
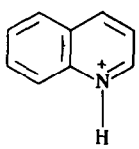
* Author to whom correspondence should be addressed.

RESULTS AND DISCUSSION

Catalytic activity of substituted ammonium tetrabromoxomolybdate(V) complexes

During investigations of the epoxidation of olefins with *t*-BuOOH in the presence of various molybdenum compounds,[6] we found that the reactivity of the complex was dependent on A. In order to clarify this dependency, we prepared tetrabromooxomolybdate(V) complexes with A = benzyltrimethylammonium (**1**), *N*-methylpyridinium (**2**), trimethylenebispyridinium (**3**), pyridinium (**4**), quinolinium (**5**), 1.3-propanediammonium (**6**) and 1,6-hexanediammonium (**7**). The results are shown in Table 1; **1** shows the highest activity in the decomposition of *t*-BuOOH. When the cation A of tetrabromooxomolybdate(V) has no hydrogen on the nitrogen atom (**1–3**) the decomposition of *t*-BuOOH and oxidation of alcohols to carbonyl compounds took place smoothly, but the epoxidation of olefins with *t*-BuOOH did not proceed. On the other hand, decomposition is rarely found in **6** and **7**, but epoxidation occurs in good yield. When an equimolar mixture of cyclohexene and 2-octanol was epoxidized with *t*-BuOOH in the presence of **6**, the

Table 1. Catalytic activity of various substituted ammonium tetrabromooxomolybdates[a]

		Yield (%)		
			Epoxidation of	
		Decomposition of *t*-BuOOH		Oxidation of 2-octanol
$PhCH_2\overset{+}{N}Me_3$	**1**	85	0	80
	**2**	96	0	44
	**3**	91	0	46
	**4**	37	66	78
	**5**	35	68	—
$H_3\overset{+}{N}(CH_2)_3\overset{+}{N}H_3$	**6**	10	78	77
$H_3\overset{+}{N}(CH_2)_6\overset{+}{N}H_3$	**7**	6	85	—

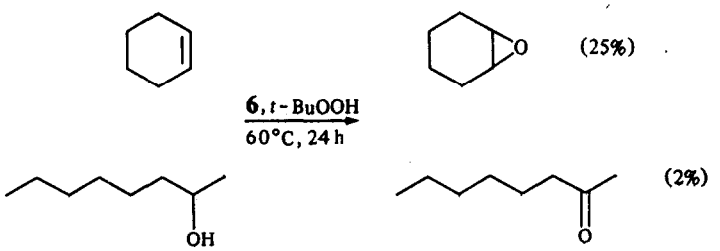
[a] Conditions—decomposition: 0.05 mol *t*-BuOOH, 50 cm^3 benzene, 0.2 mmol molybdenum catalyst, 60°C, 1 h; epoxidation: 0.05 mol cyclohexene, 0.05 mol *t*-BuOOH, 50 cm^3 benzene, 0.2 mmol molybdenum catalyst, 60°C, 1 h; oxidation: 3 mmol 2-octanol, 5 mmol *t*-BuOOH, 3 cm^3 benzene, 0.15 mmol molybdenum catalyst, 60°C, 24 h.

olefin was epoxidized but the alcohol was not oxidized, as shown in eqn (1).

Oxidation of primary and secondary alcohols

The oxidation of various alcohols is shown in Table 2. An equimolar mixture of 1- and 2-octanol under the same conditions leads to complete conversion of the secondary alcohol (80% yield of 2-octanone) and to recovery of the primary alcohol (~100%). This selectivity for a secondary over a primary alcohol is also easily demonstrated in the intermolecular case [eqn (2)].

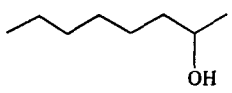
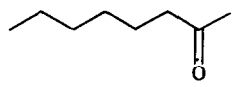
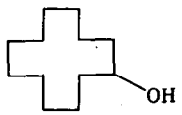
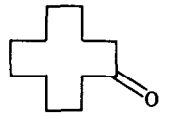
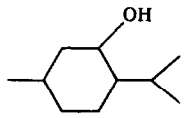
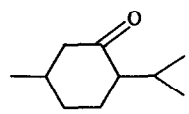
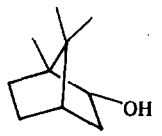
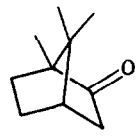
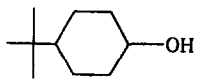
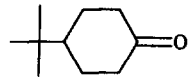
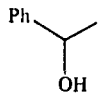
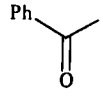
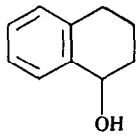
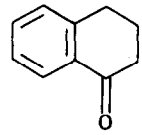
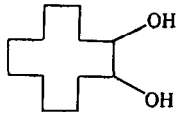
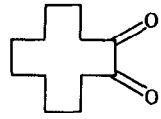
Lengthening the reaction time or a higher reaction



(1)

Conditions: 1 mmol cyclohexene, 1 mmol 2 - octanol, 1 mmol *t* - BuOOH, 0.2 mmol **6**, 2 cm^3 benzene.

Table 2. Oxidation of secondary alcohols[a]

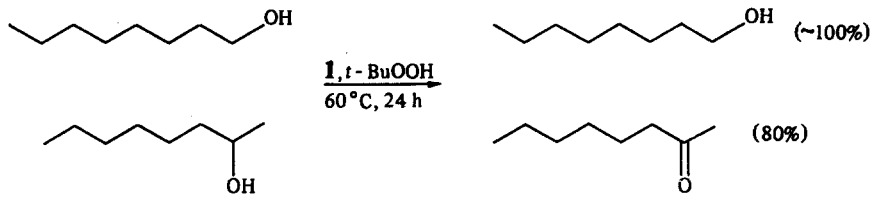
Entry	Alcohol	Time (h)	Product	Yield[b] (%)
1		42		70
2		46		92
3		12		52
4		21		~100
5		72		87
6		24		99
7		24		84[c]
8		12		50[d]

[a] Conditions: 3 mmol alcohol, 4–5 mmol *t*-BuOOH, 0.2 mmol **1**, 2–3 cm^3 benzene.

[b] All yields are for isolated pure products. No by-product was detected under these conditions.

[c] Room temperature.

[d] 1 mmol alcohol, 3 mmol *t*-BuOOH.



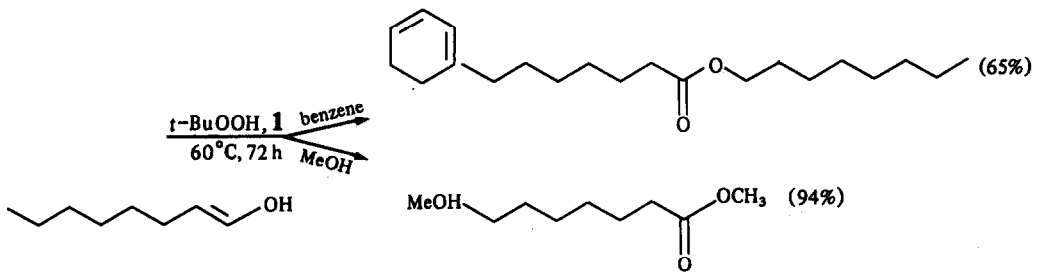
(2)

Conditions: 1 mmol 1 - octanol, 1 mmol 2 - octanol, 1 mmol *t* - BuOOH, 0.2 mmol **1**, 2 cm³ benzene.

temperature causes 1-octanol to oxidize to octyl octanoate via hemiacetal intermediate. The oxidation of 1-octanol in methanol provides methyl octanoate [eqn (3)]. Aldehyde as an intermediate was not observed in this reaction and no by-products were detected. So aldehyde was spontaneously reacted with alcohol to form hemiacetal, which then oxidized to ester, as shown in eqn (4). In the reaction of diol, cyclic ester was obtained in good yield [eqn (5)].

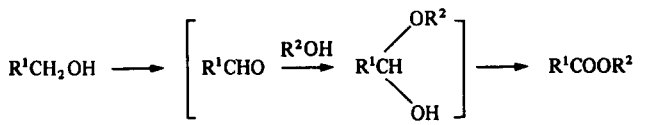
On the other hand, in the case of the diol containing secondary and primary hydroxyl groups, the secondary hydroxyl group was selectively oxidized by this system. A hydroxy ketone was obtained as shown in eqn (6). These reactions are thought to proceed through the abstraction of a hydride ion.

Oxidation of borneol and isoborneol was carried out to investigate the effect of the stereochemical hindrance in the case of hydroxyl group. Our results

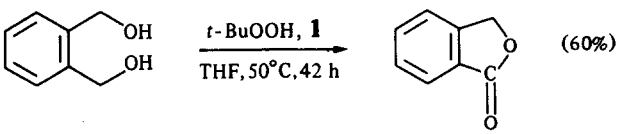


(3)

Conditions: 3 mmol alcohol, 7 mmol *t* - BuOOH, 0.4 mmol **1**, 2 cm³ solvent.

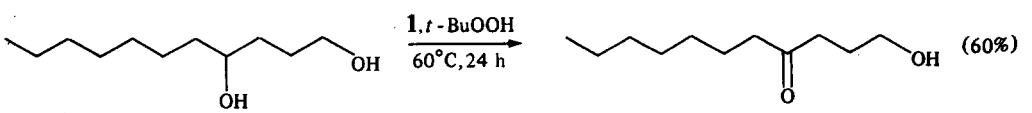


(4)



(5)

Conditions: 2 mmol alcohol, 4 mmol *t* - BuOOH, 0.1 mmol **1**, 3 cm³ THF.



(6)

Conditions: 3 mmol alcohol, 4 mmol *t* - BuOOH, 0.1 mmol **1**, 2 cm³ THF.

Table 3. Oxidation of borneol and isoborneol[a]

Reaction time (min)	Substrate		Product[b]	Substrate		Product[b]
	Isoborneol (%)	Borneol (%)	Camphor (%)	Isoborneol (%)	Borneol (%)	Camphor (%)
0	20	80	0	85	15	0
30	13.4	75.1	11.5	49.1	14.0	36.9
60	1.8	71.6	26.6	5.6	6.1	88.0
120	0	46.4	53.6	0	6.2	92.8
180	0	26.1	73.6	0	2.5	97.5

[a] 3 mmol substrate, 4 mmol *t*-BuOOH, 0.2 mmol **1**, 2 cm^3 benzene, 50°C.
[b] Yield was calculated by GC.

obtained with the molybdenum complex–*t*-BuOOH system are shown in Table 3. Isoborneol is more readily oxidized to the ketone. The reactivity of borneol and isoborneol is the same as that reported by Iwamura and Hirao,[7] who used 2,3-dichloro-5,6-dicyano-1,4-benzoquinone as oxidant. Thus, a reasonable explanation for reactivity in this case can be the strain relief of the sterically hindered hydroxyl group.

The oxidation of 2-octanol in the presence of **1**, which is mixed with an equivalent amount of acid or base, was investigated; the results are shown in Table 4. Acid has no effect, but capric acid was effective in some degree. The effect comes from its hydrophobic character rather than from its acidity. As bases, sodium methoxide and sodium acetate were used but there was no effect.

On the other hand, this reaction was influenced considerably by solvent. These results are shown in Table 5. Polar solvents were effective for the reaction. This showed that the reaction proceeds through an ionic process. This reaction was not affected by a radical scavenger such as 2,6-di-*t*-butyl-4-methylphenol. These results suggest the reaction process shown in eqn (7).

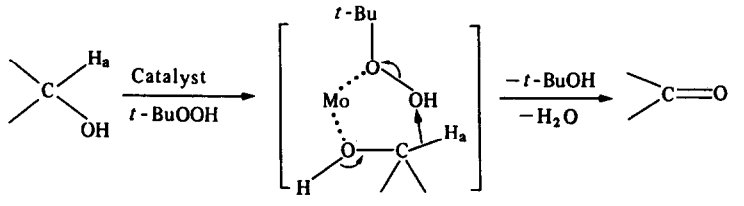
Table 4. Effect of acids on the oxidation of 2-octanol[a]

Reaction time (min)	Yield[b] of 2-octanone (%)			
	Additive			
	—	Capric acid	Acetic acid	Phenol
30	20.0	23.2	19.9	14.1
60	41.4	46.1	36.4	33.1
120	67.0	72.2	60.1	59.4

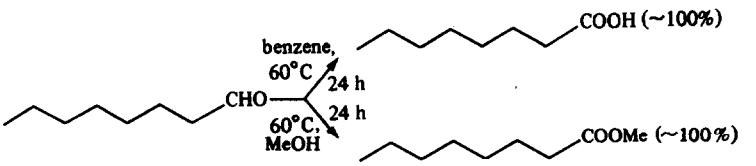
[a] 1 mmol 2-octanol, 2 mmol *t*-BuOOH, 0.1 mmol **1**, 3 cm^3 benzene, 50°C, 0.1 mmol additive.
[b] Yield was calculated by GC.

Oxidation of aldehydes

As mentioned above, aldehydes were not obtained but ester was formed so we think that the oxidation of alchol to aldehyde is the rate-determining step and that the reaction of aldehyde with alcohol proceeds spontaneously. Thus the oxidation of aldehydes was investigated as shown in eqn (8).



(7)



(8)

Conditions: 3 mmol aldehyde, 5 mmol *t*-BuOOH, 0.2 mmol **1**, 5 cm^3 solvent.

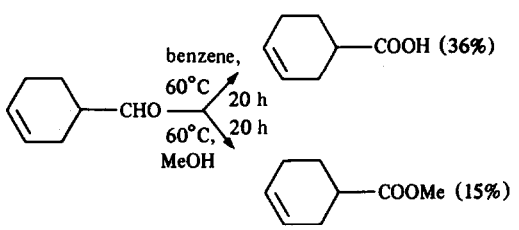
Table 5. Effect of solvent on the oxidation of 2-octanol[a]

Reaction time (min)	Yield[b] of 2-octanone		
	Solvent		
	Benzene	Methanol	Acetonitrile
30	20.0	45.2	87.2
60	41.4	70.2	97.9
120	67.0	91.6	100

[a] 1 mmol 2-octanol, 2 mmol *t*-BuOOH, 0.1 mmol **1**, 3 cm^3 solvent, 50°C.

[b] Yield was calculated by GC.

In benzene the corresponding carboxylic acid was obtained but in methanol a methylester was formed quantitatively. The oxidation of an olefinic aldehyde was more difficult than that of other aldehydes. The results are shown in eqn (9):



(9)

Conditions: 2 mmol aldehyde, 4 mmol *t* - BuOOH, 0.2 mmol **1**, 3 cm^3 solvent.

This low reactivity was caused by the hindrance of oxidation with *t*-BuOOH owing to complex formation between the olefin and the molybdenum complex.

Selective oxidation of alcohol containing carbon–carbon double bond

Olefinic alcohols could be oxidized selectively with *t*-BuOOH in the presence of **3**. The results are shown in Table 6. The hydroxyl group of allylic alcohol was easily oxidized and no epoxidation of olefin was observed. As the hydroxyl group at the allyl position was activated, oxidation occurred easily. However, alcohols with a carbon–carbon double bond at the γ-position were not easily oxidized, because the molybdenum complex and the olefin got close and interacted, and also because of the difficulty of activation at the α-position. In the presence of cyclohexene, oxidation of 2-octanol was disturbed. Lee and Noureldin[8] reported the same reactivity in the presence of $Cu(MnO_4)_2 \cdot 8H_2O$. They proposed π-complex formation between manganese and olefin. Complex formation was also recognized in our case.

Molybdenum complexes are not widely used in the oxidation of alcohols with *t*-BuOOH. Nevertheless, we could find that the molybdenum complex $R_4N^+O^-MoBr_4$ showed a high activity for oxidation with hydroperoxide. In this case, R_4N^+ as the counter cation of the complex exerted an influence upon the chemoselectivity of *t*-BuOOH. When all the R are alkyl groups, alcohol oxidation occurred quantitatively, but when one R is hydrogen, alcohol oxidation and olefin epoxidation were observed at the same time. Thus, chemoselective oxidation of a hydroxyl group in the presence of olefin or a carbon–carbon double bond in the same molecule was observed in the reaction with *t*-BuOOH when we used **1**–**3**.

EXPERIMENTAL

Materials

4 and **5** were prepared according to the procedure of Allen and Neumann.[9] Similar procedures were used for the preparation of other ammonium tetrabromooxomolybdate(V) complexes. The complexes were characterised by elemental analysis (Mo by EDTA and Br by the Volhard method), and spectral measurements. **1**, Found: C, 20.6; H, 2.9; N, 2.43; Mo, 15.8; Br, 54.6%. Calc. for $C_{10}H_{16}Br_4MoNO$: C, 20.6; H, 2.8; N, 2.4; Mo, 16.5; Br, 54.9%. **2**. Found: C, 13.6; H, 1.5; N, 2.9; Mo, 18.2%. Calc. for $C_6H_8Br_4MoNO$: C, 13.7; H, 1.5; N, 2.7; Mo, 18.3%. **3**. Found: Mo, 18.3%. Calc. for $C_{13}H_{16}Br_8Mo_2N_2O_2$: Mo, 18.0%. **6**. Found: Mo, 20.0; Br, 64.0%. Calc. for $C_3H_{12}Br_8Mo_2N_2O_2$: Mo, 20.4; Br, 68.1%. **7**. Found: Mo, 19.0; Br, 63.8%. Calc. for $C_6H_{18}Br_8Mo_2N_2O_2$: Mo, 19.6; Br, 65.1%.

t-BuOOH supplied by Nippon Oils & Fats Co. was used after purification by vacuum distillation.

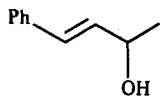
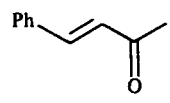
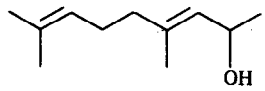
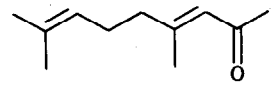
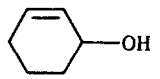
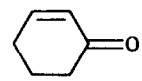
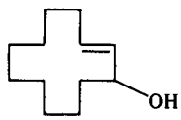
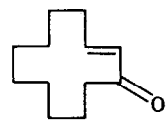
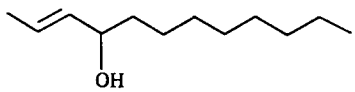
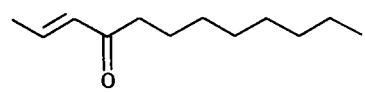
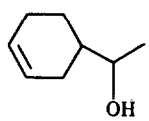
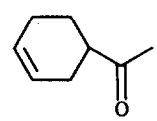
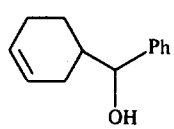
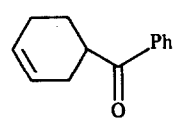
General procedure for decomposition

In a test tube with a screw cap, benzene (50 cm^3) and *t*-BuOOH (0.05 mol) were mixed with a catalytic amount of molybdenum complex (0.2 m-equiv). Then the tube contents were stirred at 60°C for 60 min in an aluminum block thermostat. The products were analyzed by GC: the column packing material was DOP/chromosorb PNAW, carrier gas was hydrogen.

General procedure for epoxidation of olefin

Cyclohexene (0.05 mol) was dissolved in benzene (50 cm^3) and the mixture was stirred at 60°C. Then

Table 6. Oxidation of olefinic alcohols[a]

Entry	Alcohol	Time (h)	Product	Yield[b] (%)
1		72		37[c]
2		20		60
3		48		48(82)[d]
4		48		57
5		72		65
6		24		11(97)[d]
7		24		18(95)[d]

[a] Conditions: 3 mmol alcohol, 3–4 mmol *t*-BuOOH, 0.2 mmol **1**, 3 cm^3 benzene.

[b] Yield was calculated by GC. All yields are for isolated pure products. Yields in parentheses are based on consumed starting material. No by-product was detected under these conditions.

[c] Room temperature.

[d] 1 mmol alcohol, 2 mmol *t*-BuOOH, 0.2 mmol **1**, 3 cm^3 benzene.

molybdenum catalyst (0.2 m-equiv) and *t*-BuOOH (0.05 mol) were added to the solution. The stirring was continued at 60°C for 60 min. Cyclohexene oxide was separated by GC (DOP/chromosorb PNAW, carrier gas nitrogen or helium) and identified by NMR and IR.

General procedure for oxidation of alcohol

A solution of molybdenum complex (0.15 m-equiv) *t*-BuOOH (5 mol) and the alcohol (3 mmol) in benzene (3 cm^3) was stirred at 60°C. The solution was evaporated. After ether extraction and evaporation, the product was purified by distillation or chromatography and identified by NMR and IR.

REFERENCES

1. K. B. Sharpless and T. R. Verhoeven, *Aldrichimica Acta* 1979, **12**, 63; R. A. Sheldon, In *The Chemistry of Functional Groups, Peroxides* (Edited by S. Patai). John Wiley, Chichester (1983); R. A. Sheldon, *J. Mol. Catal.* 1983, **20**, 1.

2. R. Hiatt, In *Organic Peroxides* (Edited by D. Swern), 2nd edn, Chap. 1. Wiley Interscience, New York (1971).
3. Y. Kurusu, *Bull. Chem. Soc. Jpn* 1981, **54**, 293; M. Yamazaki, H. Endo, M. Tomoyama and Y. Kurusu, *ibid.* 1983, **56**, 3523.
4. Y. Masuyama, M. Takahashi and Y. Kurusu, *Tetrahedron Lett.* 1984, **25**, 4417.
5. Y. Kurusu, Y. Masuyama and M. Saita, *Bull. Chem. Soc. Jpn* 1985, **58**, 1065.
6. Y. Kurusu, Y. Masuyama and T. Nishio, In *Proceedings of the Fourth International Conference on the Chemistry and Uses of Molybdenum* (Edited by H. F. Barry and P. C. H. Mitchell), p. 241. Climax Molybdenum Co., Ann Arbor, MI (1982).
7. J. Iwamura and N. Hirao, *Tetrahedron Lett.* 1983, 2447.
8. D. G. Lee and N. A. Noureldin, *J. Am. Chem. Soc.* 1983, **105**, 3188.
9. J. F. Allen and H. M. Neumann, *Inorg. Chem.* 1964, **3**, 1612.

Polyhedron Vol. 5, No. 1/2, pp. 297–299, 1986
Printed in Great Britain

0277-5387/86 $3.00 + .00
© 1986 Pergamon Press Ltd

NEW MONO-DINITROGEN COMPLEXES OF MOLYBDENUM*

T. ADRIAN GEORGE† and ROBERT C. TISDALE
University of Nebraska—Lincoln, Lincoln, NE 68588, U.S.A.

(*Received* 14 *June* 1985)

Abstract—The synthesis is reported of a mono-dinitrogen complex of molybdenum, $Mo(N_2)(triphos)(PMe_2Ph)_2$, where triphos = $PhP(CH_2CH_2PPh_2)_2$, that yields significant yields of ammonia and hydrazine when treated with HCl or HBr in organic solvents. Generally, increasing the temperature increases the combined yield of ammonia and hydrazine.

The bis-dinitrogen complexes of molybdenum (and tungsten) stand out among all the known dinitrogen complexes of transition metals because of the reactivity of coordinated dinitrogen, as exemplified by: (i) alkylation,[2,3(a)] and (ii) protonation.[1,3] This is in dramatic contrast to the general lack of reaction displayed by coordinated dinitrogen in the many mono-dinitrogen complexes of molybdenum.‡ We wish to report one example of an extensive new series of mono-dinitrogen complexes[5] of molybdenum that react with strong acid to form ammonia or ammonia and hydrazine. These complexes contain five group 15 atoms bound to molybdenum. Only one such complex, $Mo(N_2)(PMe_3)_5$, has been reported previously.[6]

EXPERIMENTAL

General procedures

All preparations and reactions were carried out in a dinitrogen atmosphere or *in vacuo*. Compounds were handled using standard inert atmosphere techniques. Elemental analyses were performed by Galbraith Laboratories Inc., Knoxville, TN.

Procedures for acid reactions and analyses of ammonia and hydrazine have been detailed previously.[1]

Reagents and materials. All solvents were reagent grade and dried rigorously by heating at reflux over an appropriate drying agent followed by distillation in a dinitrogen atmosphere and saturated with dinitrogen immediately before use by bubbling the gas through the solvent for up to 3 h. Chemicals were purchased from commercial sources and used without purification. $MoCl_3(triphos)$ (1) was prepared according to a published procedure.[1]

Spectral studies. IR spectra (4000–200 cm^{-1}) were recorded on a Perkin–Elmer 283 or 1430 spectrophotometer as KBr pellets. $^{31}P-\{^1H\}$ NMR spectra were obtained with a Varian XL-200 spectrometer operating at 80.984 MHz. Chemical shifts (ppm) are referenced to 85% H_3PO_4. Triphos-phosphorus atom assignments are: central—PhP_a; terminal—Ph_2P_b and Ph_2P_c.

Preparation of $Mo(N_2)(triphos)(PMe_2Ph)_2$. In a dry box ($N_2$ atmosphere) a 500 cm^3 Fischer–Porter pressure bottle was charged with a magnetic stir-bar, 3.0 g (4.07 mmol) $MoCl_3(triphos)$ and THF (100 cm^3). To this stirred bright yellow suspension was added PMe_2Ph (1.2 cm, 8.43 mmol) by syringe followed by 1% sodium amalgam (0.6 g Na, 26 mmol). Immediately the reaction vessel was sealed (enclosing *ca* 4.2 equiv. of N_2) and transferred to an ice bath before being pressurized to *ca* 75 lb in^{-2} with argon. The reaction was stirred for *ca* 15 h (with reaction reaching room temperature after a few hours). The reaction vessel was transferred to a N_2-filled glove-bag and depressurized. The dark red solution was decanted from the amalgam and filtered through *ca* 1″ celite in a medium-porosity frit. The

* Reactions of coordinated dinitrogen—XIX. For Part XVIII see Ref. 1.

† Author to whom correspondence should be addressed.

‡ A notable exception would be the reaction of $(MeC_6H_5)Mo(PPh_3)_2N_2$ with $[(C_5H_5)Fe(dmpe)(Me_2CO)]BF_4$ to form the {Mo–N_2–Fe} complex.[4]

resultant filtrate was bubbled vigorously with N_2 until the volume of the solvent was reduced to *ca* 35 cm^3 before *ca* 150 cm^3 MeOH was added, while stirring, in 10-cm^3 aliquots to induce precipitation of a bright orange solid. The solid was collected by filtration and washed with MeOH (two 20-cm^3 aliquots) before being dried *in vacuo* (which causes the solid to acquire a dark brown color). Refilling the drying tube with N_2 restores the characteristic bright orange color. The yield of $Mo(N_2)$(triphos)$(PMe_2Ph)_2$ was 3.0 g (78%). Calc. for $C_{50}H_{55}MoN_2P_5$: C, 64.24; H, 5.93; N, 3.00; P, 16.56%. Found: C, 63.56; H, 5.93; N, 2.87; P, 16.28%. ^{31}P NMR (C_6D_6): 85.91 (dd, $^2J_{P_aP_e} = 101.5$, $^2J_{P_aP_d} = 11.5$, $^2J_{P_aP_b} = {}^2J_{P_aP_c} = 0.0$ Hz, P_a), 66.41 (ddd, $^2J_{P_bP_d} = 93.0$, $^2J_{P_bP_c} \approx 4$, $^2J_{P_bP_e} \approx 18$ Hz, P_b), 58.96 (complex t, $^2J_{P_cP_d} \approx {}^2J_{P_cP_e} \approx 18$ Hz, P_c), 1.41 (ddt, P_d), −3.57 (ddt, P_e). IR (KBr): ν(NN) 1978 cm^{-1}.

Preparation of fac-Mo(CO)(triphos)$(PMe_2Ph)_2$. Orange **2A** (0.15 g) was placed in a round-bottom flask (50 cm^3) and subjected to a high vacuum (*ca* 48 h) in room light. The color gradually darkened to give a very dark brown colored solid by which time the pressure was 5×10^{-6} torr or less. Refilling the flask with CO (1 atm) resulted in a rapid (*ca* 20 min) restoration of a bright orange solid. IR (KBr): ν(CO) 1768 cm^{-1}. ^{31}P NMR (C_6D_6): 84.89 (ddd, $^2J_{P_aP_d} = 84.9$, $^2J_{P_aP_e} = 9.8$, $^2J_{P_aP_b} = 4.9$ Hz, P_a), 73.93 (split dt, $^2J_{P_bP_e} = 74.3$, $^2J_{P_bP_c} = 16.2$, $^2J_{P_bP_d} = 3.1$ Hz, P_b), 40.76 (multiplet, P_c), 0.61 (split dq, $^2J_{P_dP_e} = 19.7$ Hz, P_d), −2.28 (split dt, P_e).

Preparation of $Mo(^{15}N_2)$(triphos)$(PMe_2Ph)_2$. This complex was made in an analogous manner to the above carbonyl complex. IR (KBr): ν(NN) 1918 cm^{-1}.

RESULTS AND DISCUSSION

Reduction of $MoCl_3$(triphos) in a large excess of dinitrogen (*ca* 13 equiv.) in the presence of 1 equiv. of monodentate phosphine affords a high yield of the corresponding bis-dinitrogen complex [eqn (1)]:[1,7]

$$MoCl_3(\text{triphos}) + PR_3 \xrightarrow[\text{THF}]{\text{Na–Hg, } N_2} Mo(N_2)_2(\text{triphos})(PR_3), \quad (1)$$

where $PR_3 = PPh_3$ or PPh_2Me. However, when $PR_3 = PMe_2Ph$ an oil rather than a solid was obtained.[8] Similar reactions carried out with only a small excess of dinitrogen (*ca* 4 equiv.) and 2 equiv. of PMe_2Ph or 1 equiv. of a bidentate ligand produced an extensive novel series of mono-dinitrogen complexes [eqn (2)]:[5]

$$MoCl_3(\text{triphos}) + L_2 \text{ (or 2L)} \xrightarrow[\text{THF}]{\text{Na–Hg, } N_2} Mo(N_2)(\text{triphos})(L_2), \quad (2)$$

where L = PMe_2Ph (**2A**), $L_2 = Me_2PCH_2PMe_2$ (**2B**), $L_2 = 1,2\text{-}(Me_2As)_2C_6H_4$ (**2C**), $L_2 = Ph_2PCH_2PPh_2$ (**2D**), $L_2 = Ph_2PCH_2CH_2PPh_2$ (**2E**), or $L_2 = 1,1'\text{-}[Ph_2PC_5H_4]_2Fe$ (**2F**).

Complex **2A**, obtained in 78% yield, gave a first-order spectrum in which four of the phosphorus atoms displayed large *trans* coupling constants, including the PMe_2Ph ligands. Previous work[9] with six-coordinate molybdenum(0) complexes containing the triphos ligand have shown that when triphos adopts a meridional configuration, $J_{P_aP_b} = 0$ Hz, whereas when triphos is facial $J_{P_aP_b} > 0$ Hz. The data clearly show that triphos is facial in **2A** and N_2 is *trans* to a terminal triphos-phosphorus atom, P_c. This is in contrast to the bis-dinitrogen complexes in which triphos is meridional.

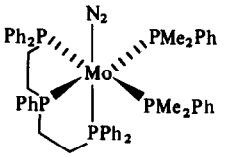


Table 1. Yields of ammonia and hydrazine from $Mo(N_2)$(triphos)$(PMe_2Ph)_2$ and acid

Acid (mol)	Solvent	Time (h)	Temperature (°C)	N_2[ab]	NH_3[a]	N_2H_4[a]
HCl (40)	CH_2Cl_2	64	18	0.28	0.32	0.17
HBr (40)	CH_2Cl_2	36	18	0.35	0.51	0.30
HCl (36)	Toluene	15	61	0.54	0.51	0.29
HBr (40)	Toluene	39	70	0.56	0.36	0.48
HCl (10)	THF	38	55	—[c]	0.10	0.12
HCl (80)	THF	38	55	0.68	0.84	0.41
HBr (20)	THF	96	25	0.82	0.08	0

[a] Mol (mol of **2A**)$^{-1}$.

[b] Also H_2.

[c] Significant H_2 evolution; total gas = 1.30 mol (mol of **2A**)$^{-1}$.

In vacuo, dinitrogen is slowly lost from solid **2A** to produce a dark brown solid. The process appears to be reversible since exposure of this solid to dinitrogen at room temperature spontaneously regenerates orange **2A**. With $^{15}N_2$ and CO, **2A**-($^{15}N_2$) and Mo(CO)(triphos)(PMe_2Ph)$_2$ are produced, respectively. Reaction of **2A** with CO in solution results in the loss of N_2 and PMe_2Ph.

Complex **2A** reacts with anhydrous HCl and HBr in organic solvents to produce ammonia and hydrazine (see Table 1). Generally, increasing the temperature increases the combined yield of ammonia and hydrazine, as well as producing dihydrogen. As far as we know **2A** is the first mono-dinitrogen complex of any metal that affords significant amounts of ammonia and hydrazine.

Acknowledgement—This work was supported by the National Science Foundation through Grant CHE83-05478.

REFERENCES

1. J. A. Baumann, G. E. Bossard, T. A. George, D. B. Howell, L. M. Koczon, R. K. Lester and C. M. Noddings, *Inorg. Chem.* (in press).
2. For example: (a) J. Chatt, R. A. Head, C. J. Leigh and C. J. Pickett, *J. Chem. Soc., Dalton Trans.* 1978, 1638; (b) G. E. Bossard, D. C. Busby, M. Chang, T. A. George and S. D. A. Iske, Jr, *J. Am. Chem. Soc.* 1980, **102**, 1001.
3. For example: (a) J. Chatt, A. A. Diamantis, G. A. Heath, N. E. Hooper and G. J. Leigh, *J. Chem. Soc., Dalton Trans.* 1977, 688; (b) J. Chatt, A. J. Pearman and R. L. Richards, *ibid.* 1977, 1852; (c) T. Takahashi, Y. Mizobe, M. Sato, Y. Uchida and M. Hidai, *J. Am. Chem. Soc.* 1980, **102**, 7461.
4. M. L. H. Green and W. E. Silverthorn, *J. Chem. Soc., Dalton Trans.* 1973, 301.
5. T. A. George and R. C. Tisdale, *J. Am. Chem. Soc.* (in press).
6. (a) M. Brookhardt, K. Cox, F. G. N. Cloke, J. C. Green, M. L. H. Green, P. M. Hare, J. Baskin, A. E. Derome and P. D. Grebenik, *J. Chem. Soc., Dalton Trans.* 1985, 423; (b) F. G. N. Cloke, K. P. Cox, M. L. H. Green, J. Baskin and K. Prout, *J. Chem. Soc., Chem. Commun.* 1982, 393; (c) E. Carmona, J. M. Martin, M. L. Proveda, J. L. Atwood and R. D. Rogers, *J. Am. Chem. Soc.* 1983, **105**, 3014.
7. T. A. George and R. A. Kovar, *Inorg. Chem.* 1981, **20**, 285.
8. R. K. Lester, Ph.D. Thesis, University of Nebraska (1983).
9. M. C. Davies and T. A. George, *J. Organomet. Chem.* 1982, **224**, C25.

Polyhedron Vol. 5, No. 1/2, pp. 301–304, 1986
Printed in Great Britain

0277–5387/86 $3.00 + .00
© 1986 Pergamon Press Ltd

ORGANOIMIDO COMPLEXES OF Mo(IV), Mo(V) AND Mo(VI): PREPARATION, STRUCTURE AND REACTIVITY

C. Y. CHOU, D. D. DEVORE, S. C. HUCKETT and E. A. MAATTA*

Department of Chemistry, Kansas State University, Manhattan, KS 66506, U.S.A.

J. C. HUFFMAN

Molecular Structure Center, Indiana University, Bloomington, IN 47405, U.S.A.

and

F. TAKUSAGAWA

Department of Chemistry, University of Kansas, Lawrence, KS 66045, U.S.A.

(*Received* 12 *June* 1985)

Abstract—Two series of *p*-tolylimido (Ntol) complexes of Mo(VI), Mo(V) and Mo(IV) are described. One series, containing diethyldithiocarbamate ligands, is formed via oxygen atom abstraction from Mo(VI)O(Ntol)$(S_2CNEt_2)_2$ using tertiary phosphines which affords the oxo-bridged Mo(V) dimer $[Mo(Ntol)(S_2CNEt_2)_2]_2O$ and the Mo(IV) species $Mo(Ntol)(S_2CNEt_2)_2$. In solution, the Mo(V) dimer participates in a disproportionation equilibrium affording the Mo(VI) and Mo(IV) complexes. $Mo(Ntol)(S_2CNEt_2)_2$ reacts with O_2 to regenerate $MoO(Ntol)(S_2CNEt_2)_2$, thus completing a catalytic phosphine oxidation cycle. $Mo(Ntol)(S_2CNEt_2)_2$ also reacts with Me_2SO to yield the Mo(VI) complex and Me_2S, and with dimethylacetylenedicarboxylate to yield the alkyne complex, $Mo(Ntol)(DMAC)(S_2CNEt_2)_2$. The second series of *p*-tolylimido complexes contains chloride and phosphine co-ligands and derives from the Mo(VI) species $Mo(Ntol)Cl_4(THF)$. In the presence of tertiary phosphines, this complex undergoes reduction to afford monomeric Mo(V) complexes of the form $Mo(Ntol)Cl_3L_2$ ($L = Ph_3P$, $EtPh_2P$ and Me_3P; $L_2 = Ph_2PC_2H_4PPh_2$). The bis(monodentate phosphine) complexes possess the *trans, mer*-geometry while the diphos complex is assigned the *cis, mer*-configuration. Reduction of $Mo(Ntol)Cl_3(Me_3P)_2$ by Na–Hg in the presence of Me_3P affords the Mo(IV) complex *cis, mer*-$Mo(Ntol)Cl_2(Me_3P)_3$ whose molecular structure is described.

In recent years, an increasing research effort has been focused on transition-metal complexes bearing organoimido ligands (NR), and it is now clear that such species are of importance and utility in a diverse array of processes ranging from synthetic procedures (e.g. the amination,[1] aziridination[2] and metathesis[3] of olefins) to biological functions (e.g. metabolism of certain hydrazines[4]). Molybdenum organoimido complexes are of additional interest in that they may serve as models of the {Mo(NH)} species that are likely intermediates in nitrogen fixation[5] and in the ammoxidation of propylene.[6]

Most of the organoimido molybdenum complexes prepared to date are Mo(VI) species.[7] Herein we describe two series of *p*-tolylimido complexes of Mo(VI), M(V) and Mo(IV). One series, containing diethyldithiocarbamate ligands, displays prominent oxygen atom transfer reactivity; the second series, containing chloride and phosphine ligands, is characterized by facile oxidation and reduction reactions.

* Author to whom correspondence should be addressed.

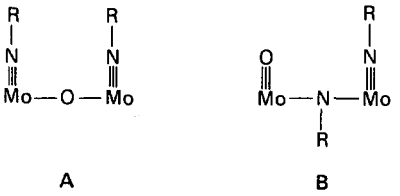
RESULTS AND DISCUSSION

Dithiocarbamate complexes

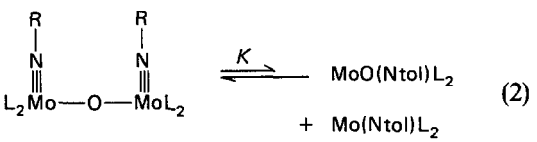
The reaction of the *p*-tolylimido Mo(VI) species $MoO(Ntol)L_2$ ($L = S_2CNEt_2$) with 0.5 equivalents of Ph_3P or $EtPh_2P$ in CH_2Cl_2 produces the corresponding phosphine oxide and a dinuclear Mo(V) complex $Mo_2O(Ntol)_2L_4$ [eqn (1)]:[8]

$$MoO(Ntol)L_2 + 0.5R_3P \rightarrow Mo_2O(Ntol)_2L_4 + 0.5R_3PO. \quad (1)$$

Two core structures, **A** and **B**, are conceivable for the Mo(V) dimer; the oxo-bridged structure **A** is



indicated by IR data [absence of ν(Mo=O)] and ^{17}O NMR studies [$\delta(^{17}O) = 1002$ ppm]. The electronic spectrum of $(Mo(Ntol)L_2)_2O$ in toluene displays an intense absorption at 533 nm, a region characteristic of mono-oxo-bridged Mo(V) dimers.[9] However, this band does not obey Beer's law, a result which by analogy to the behavior of the corresponding $Mo_2O_3L_4$ system,[10] suggests the occurrence of the disproportionation equilibrium shown in eqn (2):

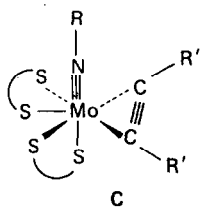


(2)

In support of this proposition, we find that toluene solutions of $[Mo(Ntol)L_2]_2O$ react with $EtPh_2P$ to produce $EtPh_2PO$ and the reactive 16-electron Mo(IV) species $Mo(Ntol)L_2$ [eqn (3)]:

$$[Mo(Ntol)L_2]_2O + EtPh_2P \rightarrow 2Mo(Ntol)L_2 + EtPh_2PO. \quad (3)$$

Although we have not isolated a pure sample of $Mo(Ntol)L_2$, we have been able to probe its reactivity in solution. Thus, when the reaction of eqn (3) is conducted in the presence of an excess of the activated alkyne dimethylacetylenedicarboxylate (DMAC), the bright yellow alkyne complex $Mo(Ntol)(DMAC)L_2$ is formed. Solution ^1H NMR results and an X-ray diffraction study[11] confirm the expected pentagonal bipyramidal geometry for this species (**C**).



Solutions of $Mo(Ntol)L_2$ react rapidly with O_2 (1 atm) at ambient temperature to regenerate $MoO(Ntol)L_2$ [eqn (4)]:

$$Mo(Ntol)L_2 + \tfrac{1}{2}O_2 \rightarrow MoO(Ntol)L_2. \quad (4)$$

Thus, taken collectively, eqns (1), (3) and (4) constitute a catalytic phosphine oxidation cycle. We have observed the oxidation of *ca* 50 equiv. of PPh_3 using this system without any diminution of catalytic activity. $Mo(Ntol)L_2$ solutions also react with dimethylsulfoxide to afford $MoO(Ntol)L_2$ and dimethyl sulfide [eqn (5)]:

$$Mo(Ntol)L_2 + Me_2SO \rightarrow MoO(Ntol)L_2 + Me_2S. \quad (5)$$

Chloride and phosphine species

The reaction of *p*-tolylazide with $MoCl_4(THF)_2$ (THF = tetrahydrofuran) in 1,2-dichloroethane provides the *p*-tolylimido Mo(VI) species $Mo(Ntol)Cl_4(THF)$ in excellent yield [eqn (6)]:[12]

$$MoCl_4(THF)_2 + p\text{-}tolN_3 \rightarrow Mo(Ntol)Cl_4(THF) + N_2. \quad (6)$$

The molecular structure of this 16-electron species features a short Mo—N bond [1.717(3) Å] and a near-linear Mo—N—C bond angle [174.5(3)°], consonant with the presence of a triply-bonded, four-electron donor tolylimido ligand. The Mo—O bond length of 2.234(3) Å for the THF molecule suggests that the tolylimido ligand exerts a *trans*-influence of *ca* 0.2 Å in this complex.

The reaction of $Mo(Ntol)Cl_4(THF)$ with various tertiary phosphines (L) in 1,2-dichloroethene solution induces reduction of the metal and affords *p*-tolylimido Mo(V) complexes of the form $Mo(Ntol)Cl_3L_2$ [eqn (7)]:[13]

$$Mo(Ntol)Cl_4(THF) + 2L \rightarrow Mo(Ntol)Cl_3L_2, \quad (7)$$

where $L = Ph_3P$, $EtPh_2P$ or Me_3P; and $L_2 = Ph_2PC_2H_4PPh_2$. These 17-electron monomeric d^1 complexes are air-stable in the solid state and display magnetic moments near the spin-only value of 1.73 μ_B. The molecular structure of $Mo(Ntol)Cl_3(EtPh_2P)_2$ displays a pseudo-octahedral coordination about the Mo atom, with a

meridional arrangement of the chlorine atoms and a *trans*-disposition of the phosphine ligands. Thus, the overall geometry is similar to that previously found for the analogous Re and W complexes,

$$Re(NMe)Cl_3(EtPh_2P)_2$$[14]

and

$$W(NPh)Cl_3(Ph_3P)_2.$$[15]

Solutions of the $Mo(Ntol)Cl_3L_2$ complexes give rise to sharp ESR spectra at room temperature. The spectra of the Ph_3P, $EtPh_2P$ and Me_3P complexes are very similar and reveal superhyperfine coupling to two equivalent ^{31}P nuclei, consistent with their expected *trans, mer*-geometry. The ESR spectrum of the chelating diphos complex, however, shows strong coupling to only one ^{31}P nucleus: since the unpaired electron is expected to reside in the formally non-bonding Mo d_{xy}-orbital, the *cis, mer*-geometry is indicated for this species.

The phosphine ligands in $Mo(Ntol)Cl_3(EtPh_2P)_2$ can be substituted by the corresponding phosphine oxide [eqn (8)]:

$$Mo(Ntol)Cl_3(EtPh_2P)_2 + 2EtPh_2PO \rightarrow Mo(Ntol)Cl_3(OPEtPh_2)_2. \quad (8)$$

ESR evidence suggests that the *trans, mer*-geometry is maintained for the bis(phosphine oxide) complex. When a toluene solution containing either

$$Mo(Ntol)Cl_3(EtPh_2P)_2$$

or

$$Mo(Ntol)Cl_3(OPEtPh_2)_2$$

is exposed to moist air, crystals of the Mo(VI) complex

$$[MoO_2Cl_2(OPEtPh_2)\cdot\tfrac{1}{2}\text{toluene}]$$

are deposited and the mother liquor is found to contain *p*-toluidine and $EtPh_2PO$. When the preceeding experiment is conducted under an atmosphere of dry O_2, an extremely hydrolytically sensitive intermediate species containing a terminal oxo ligand and a tolylimido group can be identified by IR spectra. We believe this species to be $MoO(Ntol)Cl_2(OPEtPh_2)_2$ by analogy to the known complex $MoO(NH)Cl_2(OPEtPh_2)_2$,[16] which also contains a readily hydrolyzed imido ligand.

Sodium amalgam reduction of

$$Mo(Ntol)Cl_3(Me_3P)_2$$

in toluene in the presence of PMe_3 proceeds cleanly to give a dark green, diamagnetic Mo(IV) species, $Mo(Ntol)Cl_2(Me_3P)_3$ [eqn (9)]:

$$Mo(Ntol)Cl_3(Me_3P)_2 + Me_3P + Na\text{–}Hg \rightarrow Mo(Ntol)Cl_2(Me_3P)_3. \quad (9)$$

A meridional arrangement of the Me_3P ligands is indicated by NMR spectroscopy. In the ^1H spectrum, the methyl protons of the Me_3P groups appear as a triplet (δ 1.42, J_{HP} = 3.6 Hz, 18 H) and a doublet (δ 1.28, J_{HP} = 7.8 Hz, 9 H), while the $^{31}P\text{–}\{^1H\}$ spectrum consists of a triplet at δ 5.38 (J_{pp} = 18.1 Hz; area 1) and a doublet at δ −7.32 [J_{pp} = 18.1 Hz (area 2)].

The molecular structure of $Mo(Ntol)Cl_2(Me_3P)_3$ has been determined. A drawing of the molecule is shown in Fig. 1 and selected bond lengths and angles are given in Table 1. The pseudo-octahedral structure features the expected meridional configuration of the Me_3P ligands with the chlorine atoms occupying mutually *cis*-positions. Perhaps the most salient aspect of the structure is the absence of a *trans*-influence exerted by the tolylimido ligand: the *trans* Mo—Cl(3) bond distance of 2.497(1) Å is in fact *ca* 0.03 Å *shorter* than the *cis* Mo—Cl(2) distance [2.525(1) Å]. This small lengthening of Mo—Cl(2) can be ascribed to the *trans*-influence of the Me_3P ligand which is also evidenced by the Mo—P bond lengths: the pair of mutually *trans* phosphines display identical Mo—P distances of 2.509(1) Å while the Mo—P(4) bond length is *ca* 0.04 Å shorter at 2.471(1) Å.

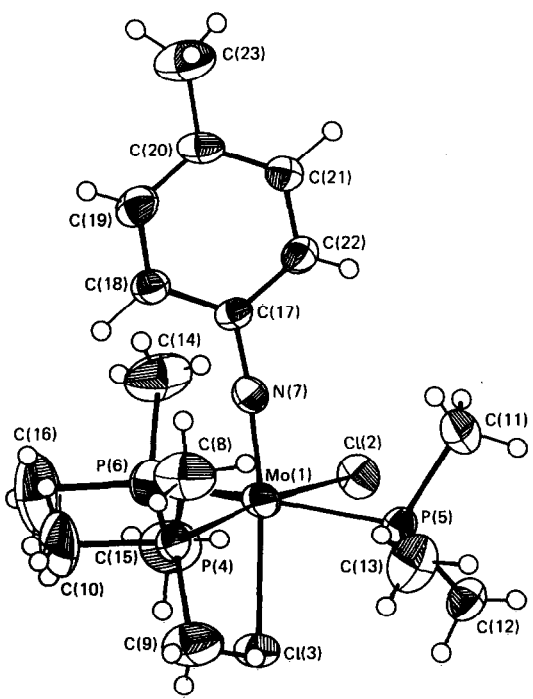


Fig. 1. An ORTEP drawing of $Mo(Ntol)Cl_2(Me_3P)_3$. Thermal ellipsoids are drawn at the 50% probability level.

Table 1. Selected bond distances (Å) and angles (°) in $Mo(Ntol)Cl_2(Me_3P)_3$

Mo(1)—Cl(2)	2.525(1)	Mo(1)—P(5)	2.509(1)
Mo(1)—Cl(3)	2.497(1)	Mo(1)—P(6)	2.509(1)
Mo(1)—P(4)	2.471(1)	Mo(1)—N(7)	1.739(2)
Mo(1)—N(7)—C(17)	175.39(17)	Cl(2)—Mo(1)—P(5)	82.10(3)
N(7)—Mo(1)—Cl(3)	171.78(6)	Cl(2)—Mo(1)—P(6)	81.55(3)
N(7)—Mo(1)—Cl(2)	97.62(6)	P(4)—Mo(1)—P(5)	94.15(3)
N(7)—Mo(1)—P(4)	89.35(6)	P(4)—Mo(1)—P(6)	101.36(3)
N(7)—Mo(1)—P(5)	96.46(6)	P(5)—Mo(1)—P(6)	162.54(3)
N(7)—Mo(1)—P(6)	91.71(6)	Cl(3)—Mo(1)—P(4)	83.61(2)
Cl(2)—Mo(1)—Cl(3)	89.65(2)	Cl(3)—Mo(1)—(5)	88.29(2)
Cl(2)—Mo(1)—P(4)	172.40(2)	Cl(3)—Mo(1)—P(6)	85.56(2)

EXPERIMENTAL

Crystal data for $Mo(Ntol)Cl_2(Me_3P)_3$

$C_{16}H_{34}NCl_2P_3Mo$, $M = 500.22$, monoclinic, $P2_1/n$, $a = 11.214(2)$ Å, $b = 22.371(3)$ Å, $c = 9.525(2)$ Å, $\beta = 94.62(1)°$, $U = 2381.8(5)$ Å^3, $Z = 4$, $D_c = 1.395$, $\mu = 9.63$ cm^{-1}.

Data collection

Syntex $P2_1$ diffractometer, graphite-monochromated Mo-K_α radiation ($\lambda = 0.71069$ Å), θ–2θ technique, scan range 1.0° below $K_{\alpha1}$ and 1.1° above $K_{\alpha2}$, scan speed 1.5–20.0° min^{-1}, $4.0 \leqslant 2\theta \leqslant 45.0°$, 3616 reflections measured, 3134 unique [data with $I_o < 0.2\sigma(I_o)$ reset to $I_o = 0.2\sigma(I_o)$], empirical absorption correction applied.

Structure solution and refinement

Heavy-atom, two block matrix least squares. Non-hydrogen atoms assigned anisotropic thermal parameters, hydrogen atoms isotropic. Anomalous dispersion corrections for Mo, Cl and P. Final agreement factors: $R = 0.032$, and $R_w = 0.036$. Other details as described in Ref. 11.

Acknowledgements—We are grateful to the donors of the Petroleum Research Fund, administered by the American Chemical Society, and to the Bureau of General Research at Kansas State University for support of this research. D.D.D. thanks the Phillips Petroleum Corp. for a fellowship.

REFERENCES

1. D. W. Patrick, L. K. Truesdale, S. A. Biller and K. B. Sharpless, *J. Org. Chem.* 1978, **43**, 2628.
2. (a) J. T. Groves and T. Takahashi, *J. Am. Chem. Soc.* 1983, **105**, 2073; (b) D. Mansuy, J.-P. Mahy, A. Dureault, G. Bedi and P. Battioni, *J. Chem. Soc., Chem. Commun.* 1984, 1161.
3. J. Kress, M. Wesolek, J.-P. LeNy and J. A. Osborn, *J. Chem. Soc., Chem. Commun.* 1981, 1039.
4. (a) R. N. Hines and R. A. Prough, *J. Pharmacol. Exp. Ther.* 1980, **214**, 80; (b) R. A. Prough, P. C. Freeman and R. N. Hines, *J. Biol. Chem.* 1981, **256**, 4178.
5. J. Chatt, J. R. Dilworth and R. L. Richards, *Chem. Rev.* 1978, **78**, 589.
6. J. D. Burrington, C. T. Kartisek and R. K. Grasselli, *J. Catal.* 1983, **81**, 489.
7. W. A. Nugent and B. L. Haymore, *Coord. Chem. Rev.* 1980, 123.
8. D. D. Devore and E. A. Maatta, *Inorg. Chem.* 1985, **24**, 2846.
9. E. I. Stiefel, *Prog. Inorg. Chem.* 1977, **22**, 1.
10. (a) R. Barral, C. Bocard, I. Seree de Roch and L. Sajus, *Tetrahedron Lett.* 1972, 1693; (b) W. E. Newton, J. L. Corbin, D. C. Bravard, J. E. Searles and J. W. McDonald, *Inorg. Chem.* 1974, **13**, 1100.
11. D. D. Devore, F. Takusagawa and E. A. Maatta, *Inorg. Chim. Acta* (in press).
12. C. Y. Chou, J. C. Huffman and E. A. Maatta, *J. Chem. Soc., Chem. Commun.* 1984, 1184.
13. C. Y. Chou, J. C. Huffman and E. A. Maatta, *Inorg. Chem.* (in press).
14. D. Bright and J. A. Ibers, *Inorg. Chem.* 1969, **8**, 703.
15. D. C. Bradley, M. B. Hursthouse, K. M. A. Malik, A. J. Neilson and R. L. Short, *J. Chem. Soc., Dalton Trans.* 1983, 2651.
16. J. Chatt, R. Choukroun, J. R. Dilworth, J. Hyde, P. Vella and J. Zubieta, *Transition Met. Chem.* 1979, **4**, 59.

Polyhedron Vol. 5, No. 1/2, pp. 305–314, 1986
Printed in Great Britain

0277–5387/86 $3.00 + .00
© 1986 Pergamon Press Ltd

SYNTHESIS AND CHEMICAL CHARACTERIZATION OF DIAZENIDO DERIVATIVES OF OXOMOLYBDATE CLUSTERS: THE STRUCTURES OF THE TETRANUCLEAR COMPLEXES $[Mo_4O_8(OR)_2(NNC_6H_5)_4]^{2-}$ (R = CH_3 OR C_2H_5)

T.-C. HSIEH and J. A. ZUBIETA*

Department of Chemistry, State University of New York at Albany,
Albany, NY 12222, U.S.A.

(*Received* 18 *June* 1985)

Abstract—α-$[Mo_8O_{26}]^{4-}$ reacts with phenylhydrazine in alcohols to yield tetranuclear clusters of the type $[Mo_4O_8(OR)_2(NNC_6H_5)_4]^{2-}$, with R = CH_3, C_2H_5 or $CH(CH_3)_2$, depending on the solvent alcohol employed. The crystallizations from alcohol–ether mixtures afford single crystals of the various derivatives. $(HNEt_3)_2[Mo_4O_8(OCH_3)_2(NNC_6H_5)_4]$ (**1**) crystallizes in the triclinic space group $P\bar{1}$, a = 12.326(3) Å, b = 12.799(3) Å, c = 16.190(3) Å, α = 83.56(1)°, β = 83.94(1)°, γ = 83.67(1)°, V = 2521(1) Å^3, Z = 2. Refinement based on 4243 reflections converged at a residual of 0.050. One form of

$$(NBu^n_4)_2[Mo_4O_8(OCH_3)_2(NNC_6H_5)_4]$$

(**1a**) crystallizes in the monoclinic space group $P2_1/c$, a = 19.735(4) Å, b = 16.222(3) Å, c = 23.802(4) Å, β = 111.92(1)°, V = 7069(2) Å^3, Z = 4. Refinement was based on 3390 reflections and converged at a residual of 0.050. One form of

$$(NBu^n_4)_2[Mo_4O_8(OC_2H_5)_2(NNC_6H_5)_4]$$

(**2**) is isomorphous with **1a**, crystallizing in the monoclinic space group $P2_1/c$, a = 19.840(3) Å, b = 16.445(3) Å, c = 24.074(4) Å, β = 112.39(1)°, V = 7264(1) Å^3, Z = 4; refinement converged at a value of 0.060 for the conventional R factor. A second modification of $(NBu^n_4)_2[Mo_4O_8(OC_2H_5)_2(NNC_6H_5)_4]$ crystallizes in the tetragonal space group $I4_1/a$, a = 35.236(6) Å, b = 35.236(6) Å, c = 12.137(4) Å, V = 15066.0(13) Å^3, Z = 8. Refinement based on 1734 reflections converged at a residual of 0.082. The structures consist of discrete tetranuclear units, presenting *cis*-bisdiazenido moieties, $[Mo(NNC_6H_5)_2]^{2+}$, bridged by two alkoxy groups and two tetra-oxomolybdate, $[MoO_4]^{2-}$, fragments.

The polyoxoanions of molybdenum are of fundamental chemical interest as catalysts,[1] as selective labelling and imaging agents for biological systems, as spectroanalytical reagents, and most recently as photosensitizers[2] and as catalysts in the photooxidation of organic compounds.[3] The perceived analogies of the polyoxoanions to metal oxide surfaces and their real and potential catalytic applications[4–6] provide the current focus of attention. The derivative chemistry of heteropolyanions has involved replacement of peripheral metal–oxygen groups by other metal–ligand units,[7] attachment of low-valent transition-metal organometallic fragments to the heteropoly framework,[8] the incorporation of organic groups into the heteropolybackbone,[9] and electrophilic *O*-alkylation of bridging oxygen atoms of the heteropoly anion.[10] Isopolymolybdate chemistry has also been expanded to include coordination chemistry of small organic molecules, as illustrated by the characterization of a formylated derivative, $[(HCO)_2Mo_8O_{28}]^{6-}$,[11] of a methoxy derivative, $[Mo_8O_{24}(OCH_3)_4]^{4-}$,[12] of a species incorporating

* Author to whom correspondence should be addressed.

a methylene group, $[CH_2Mo_4O_{15}H]^{3-}$,[13] and of an octamolybdate containing coordinated pyridine $[(C_5H_5N)_2Mo_8O_{26}]^{4-}$.[14] In each of the examples of derivatized isopolymolybdates cited above, each molybdenum atom is octahedrally coordinated either exclusively to oxygen donors or to five oxygen donors and a single nitrogen donor ligand.

Since the ability of polymolybdates to coordinate nitrogen donors has been established, we sought to extend this chemistry to the organodiazenido group, NNR, a ligand known to form robust complexes with molybdenum by the displacement of *cis*-dioxo groups to give the *cis*-$[Mo(NNR)_2]^{2+}$ structural unit.[15] We report herein the synthesis and structural characterization of a series of tetranuclear dianions, $[Mo_4O_8(OR)_2(NNC_6H_5)_4]^{2-}$ (R = CH_3, C_2H_5 or $CH(CH_3)_2$).*

EXPERIMENTAL

Preparations

All compounds were prepared from commercially available materials. All solvents were degassed, and subsequent reactions were carried out in an atmosphere of purified nitrogen. Microanalyses were performed by MicAnal Laboratories, Tucson, AZ.

Preparation of

$(HNEt_3)_2[Mo_4O_8(OCH_3)_2(NNC_6H_5)_4]$ (**1**).

A mixture of phenylhydrazine (4.32 g) and triethylamine (8.08 g) in methanol (50 cm^3) was added to a refluxing solution of

$[MoO_2(C_4H_9O_2)_2]\cdot 2C_4H_{10}O_2$

(2.43 g)[17] in methanol (200 cm^3). A deep purple color developed immediately. After refluxing for 0.5 h, the solution was allowed to cool to room temperature, whereupon diethylether was carefully layered over the solution. After standing for 1 week at room temperature, lustrous purple-black crystals and a red powder were observed. The crystalline material analysed for

$(HNEt_3)[Mo_2O_4(OCH_3)(NNC_6H_5)_2]$

and conductivity measurements in acetonitrile indicated a 2:1 electrolyte, suggesting the tetranuclear formulation

$(HNEt_3)_2[Mo_4O_8(OCH_3)_2(NNC_6H_5)_4]$.

The crystalline material proved to be neither air- nor moisture-sensitive, requiring no special precautions. Yield 20–25%.

Analysis of the red powder is consistent with the formulation

$[Mo(NNC_6H_5)_2(C_4H_9O_2)_2]\cdot H_2NNHC_6H_5$.

Attempts to confirm the structural identity of this species proved unsuccessful. Yield 30–35%.

Preparation of

$(NBu^n_4)_2[Mo_4O_8(OCH_3)_2(NNC_6H_5)_4]$ (**1a**).

A mixture of phenylhydrazine (12.96 g) and triethylamine (24.24 g) in methanol (150 cm^3) was added to a refluxing solution of

α-$(NBu^n_4)_4[Mo_8O_{26}]$

(3.17 g) in methanol (200 cm^3). The characteristic deep purple color developed after 0.5 h of refluxing. After cooling to room temperature, diethylether was layered carefully over the solution; this mixture was allowed to stand at room temperature for several weeks, whereupon lustrous purple cyrstals were observed growing at the solvent interface. Yield 30–40%.

$(NBu^n_4)_2[Mo_4O_8(OC_2H_5)_2(NNC_6H_5)_4]$ (**2**) and

$(NBu^n_4)_2[Mo_4O_8(OPr^i)_2(NNC_6H_5)_4]$ (**3**)

were synthesized in an anologous manner using the appropriate alcohol as solvent. In the case of the ethoxy derivative, three crystal forms were isolated. The purple-black irregular crystals proved to be

$(NBu^n_4)_2[Mo_4O_8(OC_2H_5)_2(NNC_6H_5)_4]$,

while the lustrous red crystals of hexagonal habit have been identified as

$(NBu^n_4)_4[Mo_8O_{20}(NNC_6H_5)_6]$.[22]

Storage at 4°C for 1 week of the filtrate from which these species were isolated yields crystals of tetragonal habit,

$(NBu^n_4)_2[Mo_4O_8(OC_2H_5)_2(NNC_6H_5)_4]$ (**2a**).

Analytical data are presented in Table 1.

Spectroscopic measurements

Electronic spectra of chloroform solutions were obtained on a Cary 14 spectrophotometer at concentrations of 10^{-3}–10^{-5} M using 1-cm matched quartz cells. IR spectra were taken on a Beckman IR-12 instrument in the range 4000–200 cm^{-1} using KBr pellets. The spectra were calibrated against polystyrene. Table 1 summarizes the relevant spectroscopic data.

*A preliminary report of the structure of $[Mo_4O_8(OCH_3)_2(NNC_6H_5)]^{2-}$ has appeared.[16]

Table 1. Complexes of the type $(NR_4)_2[Mo_4O_8(OR)_2(NNC_6H_5)_4]$

No.	Complex	Color	Analysis (calc.) (%)			IR (cm^{-1})	Electronic spectrum [nm (ε)]
			C	H	N		
1	$(HNEt_3)_2[Mo_4O_8(OCH_3)_2(NNC_6H_5)_4]$	Purple	37.7(38.1)	4.79(4.84)	11.8(11.7)	1632, m, ν(N—N_{asym}) 1576, m, ν(N—N_{sym}) 932, ms ν(Mo—O_t) 887, ms, ν(Mo—O_t) 830, s 803, vs, ν(Mo—O_b) 741, ms, ν(Mo—O_b)	510 (5.5×10^3) 410 (2.5×10^3) 300 (2.8×10^4) 270 (2.9×10^4)
1a	$(NBu^n_4)_2[Mo_4O_8(OCH_3)_2(NNC_6H_5)_4]$	Purple	47.3(47.1)	6.75(6.63)	9.23(9.47)	1615, m, ν(N—N_{asym}) 1562, m, ν(N—N_{sym}) 925, ms, ν(Mo—O_t) 895, s, ν(Mo—O_t) 826, s 796, s, ν(Mo—O_b) 721, m, ν(Mo—O_b)	510 (5.5×10^3) 410 (2.5×10^3) 300 (2.8×10^4) 270 (2.9×10^4)
2	$(NBu^n_4)_2[Mo_4O_8(OC_2H_5)_2(NNC_6H_5)_4]$	Purple	47.7(47.8)	6.65(6.77)	9.20(9.30)	1625, m, ν(N—N_{asym}) 1569, m, ν(N—N_{sym}) 923, sh 891, s, ν(Mo—O_t) 815, s 790, s, ν(Mo—O_b) 724, m, ν(Mo—O_b)	512 (5.6×10^3) 410 (2.0×10^3) 305 (2.8×10^4) 270 (2.9×10^4)
3	$(NBu^n_4)_2[Mo_4O_8(OPr^i)_2(NNC_6H_5)_4]$	Purple	48.2(48.5)	6.90(6.91)	9.02(9.13)	1630, m, ν(N—N_{asym}) 1563, m, ν(N—N_{sym}) 930, ms, ν(Mo—O_t) 890, s, ν(Mo—O_t) 812, s, ν(Mo—O_b) 761, m, ν(Mo—O_b)	510 (5.4×10^3) 405 (2.2×10^3) 295 (2.7×10^4) 270 (2.9×10^4)

X-ray crystallography

The crystal data and experimental details of the structure determinations are given in Table 2. A full description of the experimental details and the methods of structure solution may be found in Ref. 18.

RESULTS AND DISCUSSION

Preparations

In methanolic solution, polyisomolybdate anions react to give a variety of oxy-methoxy species of hexavalent molybdenum, of which

$$[Mo_8O_{24}(OCH_3)_4]^{4-}$$ [12]

and

$$Mo_2O_5(OCH_3)_2 \cdot 2CH_3OH$$ [19]

constitute the major products. The initial step of the synthesis of the diazenido derivatives would appear to be the formation of some equilibrium mixture of these oxy-methoxy species, which subsequently react with phenylhydrazine, with concomitant cluster dissociation and reaggregation [eqns (1) and (2)]:

$$[Mo_8O_{26}]^{4-} + 4CH_3OH \rightarrow [Mo_8O_{24}(OCH_3)_4]^{4-} + 2H_2O, \quad (1)$$

$$[Mo_8O_{24}(OCH_3)_4]^{4-} + 8H_2NNHC_6H_5 \rightarrow 2[Mo_4O_8(OCH_3)_2(NNHC_6H_5)_4]^{2-} + 8H_2O. \quad (2)$$

The reaction with phenylhydrazine may be viewed formally as a simple condensation reaction to yield:

$$-Mo{=}O + H_2NNHR \rightarrow -Mo{=}N{=}N(H)R + H_2O. \quad (3)$$

the Mo=N=NHR unit [eqn (3)], but evidently some internal redox step, perhaps involving Mo—OH, is necessary to remove the remaining hydrogen atom. The deep purple color developed in the methanol solution of the complex is characteristic of the *cis*-bisdiazenido molybdenum unit,[20] a robust chemical core which persists in the reaction chemistry of these species.

The successful syntheses of the analogous ethoxy and isopropoxy derivatives confirms the scope of the general synthetic procedure and the stability of the tetranuclear unit, $[Mo_4O_8(OR)_2(NNC_6H_5)_4]^{2-}$. Attempts to synthesize analogous species from phenol yielded intensely colored oils from which no solid materials were recoverable, although solution IR spectra exhibited bands characteristic of the tetranuclear core.

The reaction of the molybdenum(VI)–diolato complex,

$$[MoO_2(C_4H_9O_2)_2] \cdot 2C_4H_{10}O_2,$$

with phenylhydrazine provides an alternative route to

$$[Mo_4O_8(OR)_2(NNC_6H_5)_4]^{2-}$$

species. The initial step appears to be formation of

$$[Mo(NNC_6H_5)_2(C_4H_9O_2)_2]$$

by the condensation pathway, followed by hydrolysis, proton transfer and rearrangement over the reaction and the recrystallization period. In a purely formal sense, the reaction may be represented by eqns (4) and (5):

$$[MoO_2(C_4H_9O_2)_2] + 2H_2NNHC_6H_5 \rightarrow [Mo(NNC_6H_5)_2(C_4H_9O_2)_2] + 2H_2O, \quad (4)$$

$$2[Mo(NNC_6H_5)_2(C_4H_9O_2)_2] + 2[MoO_2(C_4H_9O_2)_2] + 2CH_3OH + 4H_2O \xrightarrow{NEt_3} [Mo_4O_8(OCH_3)_2(NNC_6H_5)_4]^{2-} + 2(HNEt_3)^+ + 8C_4H_{10}O_2. \quad (5)$$

Under these conditions, two major reaction products are isolated, lustrous purple crystalline **1a** and a dark-red powder analyzing for

$$[Mo(NNH_6H_5)_2(C_4H_9O_6)_2] \cdot H_2NNHC_6H_5.$$

Although this latter complex gives satisfactory analytical results and exhibits IR spectral characteristics consistent with the presence of the *cis*-bisdiazenido unit and with the absence of Mo–oxo groups, molecular-weight data are ambiguous, suggesting some degree of aggregation. Since all attempts to crystallize this species proved futile, its structural identity remains in doubt.

IR and electronic spectroscopy

The IR spectra of the tetranuclear complexes exhibit two bands in the 1560–1640-cm^{-1} region characteristic of the symmetric and antisymmetric

Table 2. Summary of crystal data and experimental details for the structural studies

	Crystal parameters at 23°C[a]			
	1	**1a**	**2**	**2a**
a (Å)	12.326(3)	19.735(3)	19.840(4)	35.236(6)
b (Å)	12.799(3)	16.222(3)	16.445(3)	35.236(6)
c (Å)	16.190(3)	23.802(4)	24.074(4)	12.137(4)
α (°)	86.56(1)	90.00	90.00	90.00
β (°)	83.94(1)	111.92(1)	112.39(1)	90.00
γ (°)	83.67(1)	90.00	90.00	90.00
V (Å^3)	2521(1)	7069(1)	7264(1)	15066(2)
Space group	$P\bar{1}$	$P2_1/c$	$P2_1/c$	$I4_1/a$
Z	2	4	4	8
D_c (g cm^{-3})	1.58	1.39	1.38	1.31
Measurement of intensity data				
Crystal dimensions (mm)	0.24 × 0.26 × 0.22	0.18 × 0.26 × 0.16	0.12 × 0.14 × 0.21	0.16 × 0.18 × 0.16
Instrument	Nicolet R3 m			
Radiation	Mo-K_α, λ = 0.71069 Å			
Scan mode	Coupled θ (crystal)–2θ (counter)			
Scan rate	Variable: 7–30° min^{-1}			
Scan range	$3.0 \leqslant 2\theta \leqslant 45.0°$			
Scan length	From $[2\theta(K_{\alpha_1})-1.0]$ to $[2\theta(K_{\alpha_2})+1.0]$°			
Background measurement	Stationary counter, stationary crystal at the beginning and end of each 2θ scan; each taken for 0.5 of the scan length			
Standards	3 every 200 reflections			
Number of reflections collected	6981	6466	6695	4536
Number of independent reflections used in solution	4243	3390	4035	1744
Reduction of intensity data and summary of structure solution and refinement[b]				
Data reduction	Data corrected for background, attenuators, Lorentz and polarization effects in the usual fashion			
Absorption coefficient (cm^{-1})	10.06	7.31	7.13	6.87
Absorption correction	Based on ψ scans for five medium intensity reflections with χ near 90 or 270°			
Structure solution	Patterson syntheses yielded the Mo atom positions; all remaining non-hydrogen atoms were located on subsequent Fourier maps			
Atom-scattering factors[c]	Neutral atomic scattering factors were used throughout the analysis			
Anomalous dispersion[d]	Applied to all non-hydrogen atoms			
Final discrepancy factor[e]				
R	0.050	0.050	0.060	0.082
R_w	0.052	0.056	0.064	0.078
Goodness of fit[f]	1.58	1.70	1.45	1.68

[a] From a least-squares fitting of the setting angle of 25 reflections.

[b] All calculations were performed on a Data General Nova 3 computer with 32K of 16-bit words using local versions of the Nicolet SHELXTL interactive crystallographic software package as described in G. M. Sheldrick, *Nicolet SHELXTL Operations Manual*, Nicolet XRD Corp., Cupertino, CA (1979).

[c] D. T. Cromer and J. B. Mann, *Acta Cryst.* 1968, **A24**, 321.

[d] *International Tables for X-ray Crystallography*, Vol. 3. Kynoch Press, Birmingham, U.K. (1962).

[e] $R = [\sum |F_o|-|F_c|/\sum |F_o|]$. $R_w = [\sum w(|F_o|-|F_c|)^2/\sum w|F_o|^2]^{1/2}$. $w = 1/\delta^2(F_o)+g^*(F_o)^2$. $g = 0.001$.

[f] $[\sum w(|F_o|-|F_c|)^2/(NO-NV)]^{1/2}$, where NO is the number of observations and NV is the number of variables.

stretching modes of the *cis*-bisdiazenido grouping. In addition, all derivatives display a pattern of five bands in the 720–930-cm^{-1} range attributable to Mo–O modes. Finally, sharp C—H stretch features in the 2950-cm^{-1} region and alkyl CO stretch features at *ca* 1160 cm^{-1} confirm the presence of the coordinated alkoxy groups.

The electronic spectra of the complexes are characterized by intense absorptions in the visible region, at *ca* 510 and 410 nm, and by three absorption bands in the UV range, at *ca* 300 and 270 nm. The electronic spectrum of

$$[Mo_2(SC_6H_5)_5(NNC_6H_5)_4]^-,^{21}$$

an example of a species possessing the *cis*-bisdiazenido-molybdenum core, exhibits intense bands at 515 and 270 nm. Strong absorption bands in the 510–520- and 270-nm regions may be characteristic of the *cis*-bisdiazenido-molybdenum unit. Unambiguous and complete assignment of the spectra of the tetranuclear complexes must await more detailed spectroscopic analysis of additional examples of this structural type.

Solid-state structures

Atomic positional parameters with standard deviations are available as supplementary material from Dr Mitchell. Relevant bond distances and angles are presented in Table 3. Figures 1(a) and (b) show the structures of

$$[Mo_4O_8(OCH_3)_2(NNC_6H_5)_4]^{2-}$$

and

$$[Mo_4O_8(OC_2H_5)_2(NNC_6H_5)_4]^{2-},$$

respectively, and indicate the atom-labelling scheme.

The structure of **1a** consists of two crystallographically independent $(Bu_4N)^+$ cations and a discrete tetranuclear anion

$$[Mo_4O_8(OCH_3)_2(NNC_6H_5)_4]^{2-}.$$

The overall geometry may be viewed as two

$$[Mo(NNC_6H_5)_2]^{2+}$$

units bridged by two methoxy groups and two $[MoO_4]^{2-}$ units, functioning as bidentate bridging ligands. The

$$[Mo_2(OCH_3)_2(NNR)_4]$$

fragment is nearly planar with maximum deviations of *ca* 0.05 Å from the least-squares plane through all atoms. The Mo_4O_4 heterocycle forms a puckered ring, elongated along the Mo2–Mo4 axis, which presents a Mo2—Mo4 distance of 6.08 Å, relative to 3.455 Å for Mo1—Mo3. The

Mo1–Mo3–O1–O2–O3–O4

unit is nearly planar, with Mo4 and Mo2 disposed slightly above and below the plane, respectively. The bridging $[MoO_4]^{2-}$ units display tetrahedral geometry about the Mo atoms with valence angles approaching the ideal tetrahedral limit and average Mo—terminal oxo and Mo—bridging oxo distances of 1.71(1) and 1.80(1) Å, respectively. The diazenido-coordinated Mo atoms enjoy distorted octahedral geometry through ligation to the oxygen atoms of the bridging methoxy groups, to the bridging oxo groups of the $[MoO_4]^{2-}$ units, and to the terminal nitrogens of the diazenido ligands, with average bond distances of 2.14(1), 2.06(1) and 1.81(1) Å, respectively.

Whereas derivatized isopolymolybdate structures previously described exhibit molybdenum atoms that are exclusively pseudooctahedrally coordinated Mo(VI) units, the present structures are characterized by tetrahedral $[MoO_4]^{2-}$ units sharing vertices with each of the Mo1 and Mo3 octahedra, which in turn share an edge defined by the O11–O12 vector.

The linearity of the Mo–N–N linkages, together with the short average Mo—N distance of 1.81(1) Å and the short average N—N distance of 1.25(2) Å, is indicative of extensive delocalization throughout the Mo–N–N unit and significant multiple bond character to the Mo—N and N—N bonds. These metrical parameters are consistent with the description of the phenyldiazo linkage as the three-electron donating N_2R^+ structure.[29] Electron counting is also consistent with this assignment and with the absence of a metal–metal bond, a feature consistent with the observed Mo1—Mo3 distance.

The *cis*-bisdiazenido-molybdenum unit appears to be a persistent theme of the structural chemistry of molybdenum.[20–22] Since the structural parameters associated with the bridging $[MoO_4]^{2-}$ groups are similar to those observed for $Na_2MoO_4 \cdot 2H_2O$,[23] the formal oxidation state of these Mo centers may be assigned as Mo(VI). Thus, the Mo centers of the $[Mo(NNC_6H_5)_2]^{2+}$ units may be described as Mo(0), an assignment also consistent with the presence of the phenyldiazo group, N_2R^+.

Structural parameters for **1** are nearly identical to those discussed for **1a**, as illustrated in Table 4. The ethoxy-bridged derivative exhibits two crystal modifications: **2** which is isomorphous with **1a** and presents analogous structural features, and the tetragonal form **2a**. The structure of **2a** consists of centrosymmetrically generated tetranuclear units

$$[Mo_4O_8(OC_2H_5)_2(NNC_6H_5)_4]^{2-}$$

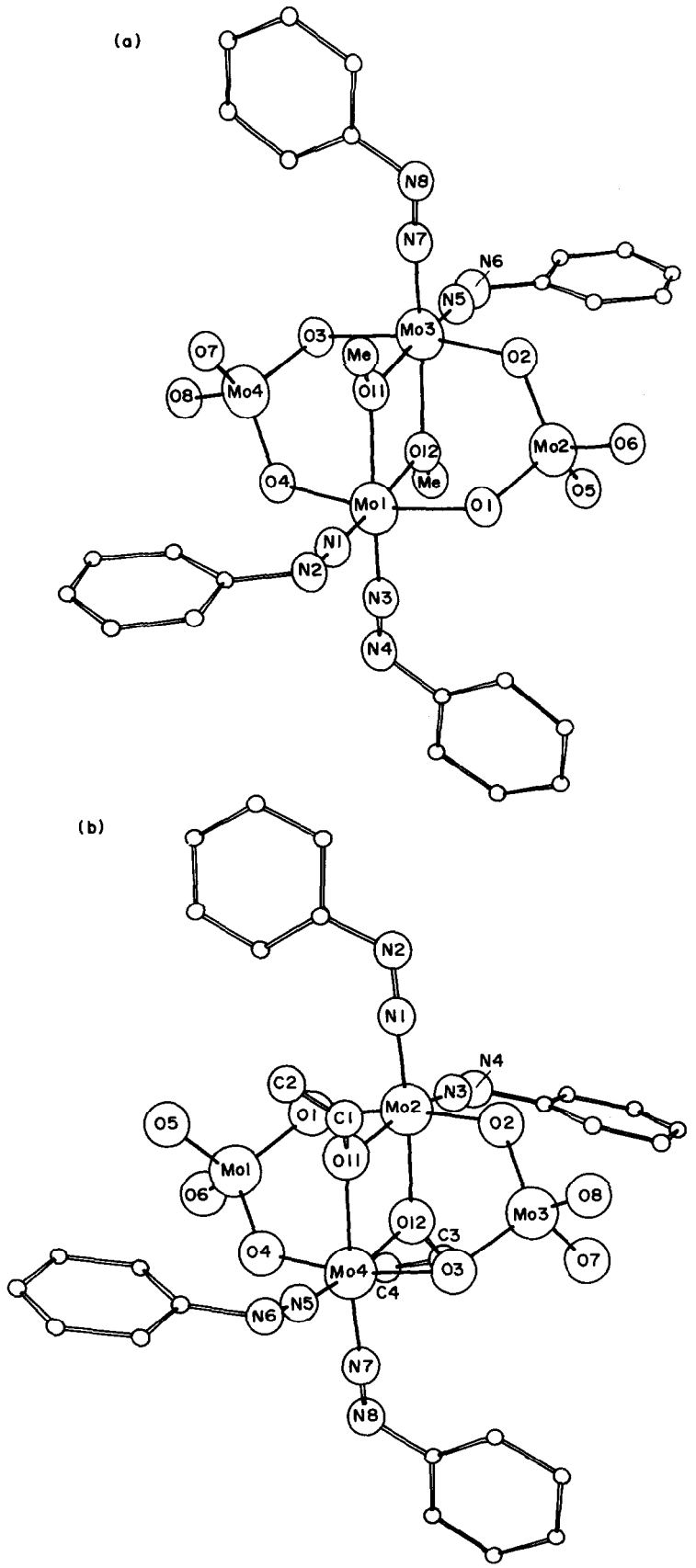


Fig. 1 (a) ORTEP representation of the structure of the tetranuclear dianion $[Mo_4O_8(OCH_3)_2(NNC_6H_5)_4]^{2-}$. (b) Structure of the tetranuclear dianion $[Mo_4O_8(OC_2H_5)_2(NNC_6H_5)_4]^{2-}$.

Table 3. Comparison of selected bond lengths (Å) and angles (°) for the structures of **1**, **1a**, **2** and **2a**

	1	**1a**	**2**	**2a**
Mo1...Mo3(Mo1a)[a]	3.465(2)	3.457(4)	3.455(3)	3.443(3)
Mo1—O1	2.060(6)	2.059(9)	2.06(1)	2.06(1)
Mo1—O4	2.058(6)	2.072(8)	2.05(1)	2.04(1)
Mo1—O11	2.133(6)	2.137(11)	2.16(1)	2.14(1)
Mo1—O12(O11a)	2.144(5)	2.123(7)	2.113(8)	2.13(1)
Mo1—N1	1.816(8)	1.812(10)	1.83(1)	1.74(2)
Mo1—N3	1.832(8)	1.825(13)	1.84(1)	1.71(2)
Mo2—O1	1.803(6)	1.79(1)	1.82(1)	1.82(1)
Mo2—O2(O4a)	1.794(7)	1.793(9)	1.836(9)	1.80(1)
Mo2—O5	1.728(7)	1.69(1)	1.715(9)	1.69(2)
Mo2—O6	1.701(6)	1.70(1)	1.70(1)	1.73(2)
Mo3—O2	2.066(6)	2.050(9)	2.031(9)	—
Mo3—O3	2.067(6)	2.048(8)	2.068(10)	—
Mo3—O11(O12a)	2.147(6)	2.137(8)	2.119(8)	—
Mo3—O12	2.137(6)	2.157(10)	2.14(1)	—
Mo3—N5	1.811(8)	1.798(10)	1.84(1)	—
Mo3—N7	1.833(10)	1.804(14)	1.82(1)	—
N1—N2	1.234(12)	1.27(2)	1.23(1)	1.33(2)
N3—N4	1.234(11)	1.20(2)	1.22(1)	1.29(3)
N5—N6	1.229(12)	1.26(2)	1.24(2)	—
N7—N8	1.211(13)	1.26(2)	1.22(1)	—
O1—Mo1—O4	165.2(2)	165.5(4)	167.2(4)	166.3(5)
O1—Mo1—O11	86.8(2)	83.6(4)	84.2(4)	80.8(6)
O1—Mo1—O12(O11a)	82.0(2)	84.7(3)	86.8(3)	88.1(6)
O1—Mo1—N1	95.6(3)	96.6(4)	95.5(5)	92.1(8)
O1—Mo1—N3	94.2(3)	92.9(5)	93.0(5)	95.3(8)
O4—Mo1—O11	81.6(2)	86.2(4)	85.1(4)	88.3(6)
O4—Mo1—O12(O11a)	85.7(2)	83.8(3)	83.2(3)	80.6(6)
O4—Mo1—N1	93.7(3)	93.3(4)	92.7(5)	97.8(8)
O4—Mo1—N3	96.6(3)	95.0(4)	95.9(5)	94.1(8)
O11—Mo1—O12(O11a)	71.8(2)	72.5(3)	71.5(3)	72.6(6)
O11—Mo1—N1	166.9(3)	96.5(5)	97.2(5)	99.0(7)
O11—Mo1—N3	99.0(3)	168.8(4)	166.9(4)	95.3(8)
O12(O11a)—Mo1—N1	95.7(3)	166.9(4)	168.2(5)	171.5(6)
O12(O11a)—Mo1—N3	170.1(3)	94.6(4)	95.6(4)	98.1(7)
N1—Mo1—N3	93.8(4)	96.4(6)	95.8(6)	90.3(9)
O1—Mo2—O2(O4a)	109.4(3)	110.1(4)	109.6(4)	109.7(6)
O1—Mo2—O5	112.2(3)	109.9(5)	109.2(5)	110.9(10)
O1—Mo2—O6	107.6(3)	109.3(6)	109.5(5)	110.5(8)
O2(O4a)—Mo2—O5	111.5(3)	110.7(6)	110.4(5)	109.7(8)
O2(O4a)—Mo2—O6	107.8(3)	108.4(5)	109.2(4)	108.6(8)
O5—Mo2—O6	108.1(3)	108.3(5)	108.9(5)	107.4(12)
O2—Mo3—O3	165.2(3)	165.9(4)	167.0(4)	—
O2—Mo3—O11(O12a)	81.5(2)	83.1(3)	84.1(4)	—
O2—Mo3—O12	85.8(2)	84.9(4)	86.6(4)	—
O2—Mo3—N5	92.4(3)	93.3(4)	96.2(5)	—
O2—Mo3—N7	93.4(3)	96.2(5)	92.4(4)	—
O3—Mo3—O11(O12a)	85.4(2)	85.6(3)	85.1(4)	—
O3—Mo3—O12	83.4(3)	83.6(4)	83.2(4)	—
O3—Mo3—N5	98.8(3)	95.6(4)	92.7(5)	—
O3—Mo3—N7	95.9(3)	93.5(5)	95.9(5)	—
O11(O12a)—Mo3—O12	71.3(3)	71.9(3)	71.5(3)	—
O11(O12a)—Mo3—N5	166.2(3)	166.4(6)	97.2(5)	—
O11(O12a)—Mo3—N7	100.4(3)	96.5(4)	166.9(4)	—
O12—Mo3—N5	96.0(3)	94.7(5)	168.2(5)	—
O12—Mo3—N7	171.7(3)	168.2(4)	95.6(4)	—

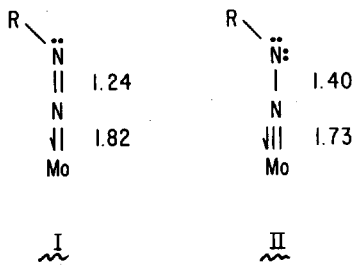
(*Contd.*)

Table 3. (*Contd.*)

	1	1a	2	2a
N5—Mo3—N7	92.3(4)	96.9(6)	95.8(6)	—
O3—Mo4—O4(O3a)	110.4(3)	111.0(4)	111.6(4)	—
O3—Mo4—O7	106.3(3)	110.3(5)	110.4(5)	—
O3—Mo4—O8	112.9(3)	108.5(5)	107.5(5)	—
O4—(O3a)—Mo4—O7	108.8(3)	109.7(5)	111.5(5)	—
O4—(O3a)—Mo4—O8	111.1(2)	107.8(4)	108.2(4)	—
O7—Mo4—O8	107.1(3)	109.7(5)	107.5(5)	—

[a] Atom designators in parentheses refer to the symmetry-generated atoms in structures **1** and **2a**. The structure of **1** consists of two tetranuclear units, each generated from crystallographically independent binuclear units, $[Mo_2O_4(OCH_3)(NNC_6H_5)_2]$, and a center of symmetry located at the mid-point of the Mo1–Mo1a vector. The structure of **2a** consists of a single crystallographically independent $[Mo_2O_4(OC_2H_5)(NNC_6H_5)_2]$ unit.

with an overall geometry similar to that observed for **1**, **1a** and **2**. The interesting structural features are the Mo—N and N—N bond distances which average 1.73 and 1.31 Å, respectively. Although the relatively poor resolution achieved for this structure precludes an unambiguous conclusion, these distances suggest a degree of valence isomerism for the diazenido-molybdenum unit in these structures. The molybdenum–diazenido interaction may be represented by the limiting formalisms **I** and **II**, for which expected bond distances may be estimated.[24]



We see that the bond distances in **1**, **1a** and **2** closely approximate those expected for **I**, while those in **2a** suggest a significant contribution from **II**, representing about a 40:60 mixture of **I** and **II**.

Synthetic investigations

The structural studies reveal that the $[Mo(NNC_6H_5)_2]^{2+}$ core is persistent and displays significant delocalized multiple bond character; in contrast, the bridging $[MoO_4]^{2-}$ units and the alkoxy ligands exhibit relatively long bond distances. Since the relative strengths of the various molybdenum–ligand interactions is reflected in the bond lengths, the bond strengths, s, may be derived from the expression:[25]

$$s = (d/1.882)^{-6.0},$$

where d is the bond length. For diazenido-coordinated molybdenum atom–ligand interactions, average bond strengths of 1.26, 0.58 and 0.46 are calculated for Mo—N, Mo—O(oxo) and Mo—O(alkoxy), respectively. This observation suggests that, whereas the *cis*-bisdiazenido-molybdenum(0) core may be chemically robust, the alkoxy and oxo groups are relatively weakly bonded and may be readily displaced upon reaction with appropriate ligands.

Indeed, the complex anions are reactive toward both oxidation–reduction reactions and substitution reactions at the oxo and alkoxy centers, providing useful synthetic precursors for a variety of complexes incorporating the $[Mo(NNC_6H_5)_2]^{2+}$ core. Thus, reaction with arenethiolate ligands yields binuclear species, $[Mo_2(NNC_6H_5)_4(SAr)_5]^-$:[21]

$$[Mo_4O_8(OR)_2(NNC_6H_5)_4]^{2-} + 15HSAr + NEt_3 \rightarrow (HNEt_3)[Mo_2(NNC_6H_5)_4(SAr)_5] + 2[MoO(SAr)_4]^- + ArSSAr + 6H_2O + 2ROH. \quad (6)$$

The thiolate acts both as ligand and as reducing agent for the Mo(VI) centers. Addition of excess phenylhydrazine to this reaction mixture does not substantially improve the yield of

$$[Mo_2(NNC_6H_5)_4(SAr)_5]^-.$$

The nature of the thiolate ligand does influence the reaction chemistry. Thus, reaction of

$$[Mo_4O_8(OR)_2(NNC_6H_5)_4]^{2-}$$

clusters with ethanedithiol again results in dimer formation, but with displacement of diazenido units and protonation of ligated diazenido groups to yield

the unusual species

$$[Mo_2(SCH_2CH_2S)_3(SCH_2CH_2SH)(NNC_6H_5)(NNHC_6H_5)]^{2-}.$$[26]

Displacement of a diazenido group also occurs upon reaction with sterically-hindered thiolates such as 2,4,6-triisopropylthiophenol (TIPT), where the monomeric species

$$[Mo(NNC_6H_5)(CH_3CN)(TIPT)_3]$$

is isolated.[27] In this and other reactions involving TIPT, steric constraints appear to dominate the course of the reaction.

Reaction with dialcohols in chlorinated solvents invariably results in C—C bond cleavage and the formation of alkoxy-bridged dimers. Thus, reaction of

$$[Mo_4O_8(OR)_2(NNC_6H_5)_4]^{2-}$$

with butane-2,3-diol in CH_2Cl_2 yields

$$[Mo_2Cl_2(OC_2H_5)_2(HOC_2H_5)_2(NNC_6H_5)_4],$$

the chloro ligand presumably extracted from the chlorinated solvent.[28] In this case, the *cis*-bisdiazenido-molybdenum core is retained and appears structurally identical to that reported for **1a**.

Reactions with dithiocarbamates, $^-S_2CNR_2$, and dithiophosphates, $^-S_2P(OR)_2$, yield mononuclear species of the type $[Mo(NNC_6H_5)_2(SS)_2]$, where (SS) is the bidentate 1,1-dithioacid ligand. Likewise, with tetradentate ligands such as

$$HSCH_2CH_2X(CH_2)_nXCH_2CH_2SH, (HSXXSH),$$

[X = S or NR], species of the type

$$[Mo(NNC_6H_5)_2(SXXS)]$$

have been isolated. Both series of complexes display the $[Mo(NNC_6H_5)_2]^{2+}$ core.

The tetranuclear clusters appear to provide useful synthetic precursors. The *cis*-bisdiazenido-molybdenum unit is persistent throughout much of this chemistry, suggesting that it provides a chemically robust core, somewhat reminiscent of the *cis*-$[MoO_2]^{2+}$ unit now well-documented in the structural chemistry of Mo(VI).

REFERENCES

1. I. V. Kozhenikov and K. I. Matveev, *Appl. Catal.* 1983, **5**, 135.
2. R. Ballardini, Q. G. Mulazzani, M. Venturi, F. Bolletta and V. Balzani, *Inorg. Chem.* 1984, **23**, 300.
3. A. Ioannidis and E. Papaconstantinou, *Inorg. Chem.* 1985, **24**, 439.
4. M. T. Pope, *Heteropoly and Isopoly Oxometalates.* Springer, New York (1983).
5. F. Ortega and M. T. Pope, *Inorg. Chem.* 1984, **23**, 3292.
6. M. Misono, In *Proceedings of the Fourth International Conference on the Chemistry and Uses of Molybdenum* (Edited by H. F. Barry and P. C. H. Mitchell), p. 289. Climax Molybdenum Co., Ann Arbor, MI (1982).
7. See, for example, A. Komura, M. Hayashi and H. Imanaga, *Bull. Chem. Soc. Jpn* 1976, **49**, 87; R. K. C. Ho and W. G. Klemperer, *J. Am. Chem. Soc.* 1978, **100**, 6772; W. H. Knoth, *J. Am. Chem. Soc.* 1979, **101**, 759; W. H. Knoth, *J. Am. Chem. Soc.* 1979 **101**, 2211; Ref. 2.
8. C. J. Besecker, V. W. Day, W. G. Klemperer and M. R. Thompson, *Inorg. Chem.* 1985, **24**, 44.
9. K. M. Barkigia, L. M. Rajkovic-Blazer, M. T. Pope and C. O. Quicksall, *Inorg. Chem.* 1981, **20**, 3318 (and references therein).
10. W. H. Knoth and R. L. Harlow, *J. Am. Chem. Soc.* 1981, **103**, 4265.
11. R. D. Adams, W. G. Klemperer and R.-S. Liu, *J. Chem. Soc., Chem. Commun.* 1979, 256.
12. E. M. McCarron III and R. L. Harlow, *J. Am. Chem. Soc.* 1983, **105**, 6179.
13. V. W. Day, M. F. Fredrick, W. G. Klemperer and R.-S. Liu, *J. Am. Chem. Soc.* 1979, **101**, 491.
14. E. M. McCarron III, J. F. Whitney and D. B. Chase, *Inorg. Chem.* 1984, **23**, 3275.
15. P. L. Dahlstrom, J. R. Dilworth, P. Schulman and J. Zubieta, *Inorg. Chem.* 1982, **21**, 933.
16. T.-C. Hsieh and J. Zubieta, *Inorg. Chem.* 1985, **24**, 1287.
17. R. J. Butcher, B. R. Penfold and E. Sinn, *J. Chem. Soc., Dalton Trans.* 1979, 668.
18. A. Bruce, J. L. Corbin, P. D. Dahlstrom, J. R. Hyde, M. Minelli, E. I. Stiefel, J. T. Spence and J. Zubieta, *Inorg. Chem.* 1982, **21**, 917.
19. E. M. McCarron III, R. H. Staley and A. W. Sleight, *Inorg. Chem.* 1984, **23**, 1043.
20. C. Pickett, S. Kumar, P. A. Vella and J. Zubieta, *Inorg. Chem.* 1982, **20**, 908.
21. T.-C. Hsieh and J. Zubieta, *Inorg. Chim. Acta* 1985, **99**, L47.
22. T.-C. Hsieh and J. Zubieta, *J. Chem. Soc., Chem. Commun.*, submitted for publication.
23. K. Matsumoto, A. Kobayashi and Y. Sasaki, *Bull. Chem. Soc. Jpn* 1975, **48**, 1009.
24. G. L. Hillhouse, B. L. Haymore, S. A. Bistram and W. A. Herrmann, *Inorg. Chem.* **22**, 314.
25. J. C. J. Bart and V. Ragaini, In *Proceedings of the Third International Conference on the Chemistry and Uses of Molybdenum* (Edited by H. F. Barry and P. C. H. Mitchell), p. 19. Climax Molybdenum Co., Ann Arbor, MI (1979).
26. T.-C. Hsieh and J. Zubieta, *J. Chem. Soc., Chem. Commun.* 1984, 1172.
27. P. T. Bishop, P. J. Blower, J. R. Dilworth and J. A. Zubieta, *Polyhedron* 1986, **5**, 363.
28. T. Hsieh and J. Zubieta, unpublished results.
29. M. Cowie, B. L. Haymore and J. A. Ibers, *Inorg. Chem.* 1975, **14**, 2617; B. L. Haymore and J. A. Ibers, *Inorg. Chem.* 1979, **18**, 2423; A. P. Gaughan, B. L. Haymore, J. A. Ibers, W. H. Myers, T. E. Nappier and D. W. Meek, *J. Am. Chem. Soc.* 1973, **95**, 6859.

Polyhedron Vol. 5, No. 1/2, pp. 315–317, 1986
Printed in Great Britain

0277–5387/86 $3.00 + .00
© 1986 Pergamon Press Ltd

MOLYBDENUM PHTHALOCYANINE

STEPHEN J. EDMONDSON and PHILIP C. H. MITCHELL*

Department of Chemistry, The University, Whiteknights, Reading RG6 2AD, U.K.

(*Received* 11 *June* 1985)

Abstract—Reaction of ammonium heptamolybdate with fused phthalodinitrile (1,2-dicyanobenzene) gave blue oxomolybdenum(IV) phthalocyanine, $MoO(C_{32}H_{16}N_8)$ (MoOPc). Reactions involved in the preparation are discussed. MoOPc sublimes at 400°C *in vacuo* giving a violet second crystalline form. The IR spectrum showed a characteristic Mo=O vibration at 974 cm^{-1}. The electronic spectrum of MoOPc in 1,2,4-trichlorobenzene showed a characteristic metallophthalocyanine peak at 703 nm and a weaker peak at 643 nm. In pyridine new peaks appeared and the spectrum changed with time. Methods of synthesis and applications of molybdenum phthalocyanines are reviewed.

Phthalocyanines of most of the metallic elements are well-known and well-characterized with, until recently, the notable exception of a molybdenum phthalocyanine, although molybdenum porphyrins are well-known. Molybdenum phthalocyanines have been mentioned in the literature, especially patents, but the nature of the substances is obscure. Compounds claimed include MoPc,[1] MoOPc,[2] MoO_2Pc[3] and $MoClPc_2$.[4] In 1966 Hill and Norgett[2] reported the preparation of oxomolybdenum(IV) phthalocyanine, MoOPc (Pc^{2-} is the phthalocyaninato anion, $C_{32}H_{16}N_8^{2-}$), in very low yield. While our work was in progress Borschel and Strahle[5] reported the preparation of MoOPc, from $Mo(CO)_6$ and phthalodinitrile in a sealed tube, and its crystal structure. The structure of MoOPc is similar to the structure of VOPc. The molybdenum coordination is square pyramidal. The molybdenum atom is located 69 pm above the plane of the four nitrogens of the phthalocyanine and forms a short bond of 166.8 pm to oxygen.

The molybdenum phthalocyanines are potentially interesting and useful. Patents claim applications of molybdenum phthalocyanines as pigments and corrosion inhibitors, as catalysts for the epoxidation of olefins and the electroreduction of oxygen,[6] and as sulphur-resistant catalysts for the hydrogenation of quinoline and coal-derived liquids.[7] The dimeric $MoPc_2Cl$ is said to have "semiconductor properties".[4]

* Author to whom correspondence should be addressed.

The object of our work was to devise syntheses of molybdenum phthalocyanines as a preliminary to studying their properties and applications. Our initial experience was that attempts to repeat preparations described in the literature produced substances of doubtful composition and purity in low yields. Clearly there is a preparative problem. This paper describes a convenient, high-yield synthesis and characterization of MoOPc.

EXPERIMENTAL

Preparation of MoOPc, $MoO(C_{32}H_{16}N_8)$

Ammonium heptamolybdate,

$$(NH_4)_6Mo_7O_{24}\cdot 4H_2O,$$

and phthalodinitrile (PDN), $C_6H_4(CN)_2$, in the ratio 1Mo : 4PDN were ground together and heated in a closed vacuum system at 270°C for 0.75 h. The blue solid formed was washed with potassium hydroxide solution and water to remove any unreacted molybdate or MoO_3 and phthalimide, and then with ethanol and acetone until the washings were colourless. Alternatively, purification could be carried out by Soxhlet extraction with butanone for 6 h.

The reaction can also be carried out in air. When a tube containing phthalodinitrile and ammonium heptamolybdate was heated the PDN melted at

140°C, the liquid turned brown at 200°C, and at 240°C reaction started with vigorous gas evolution.

As much as 50 g of MoOpc in yields > 70% based on molybdenum have been prepared by this method.

Analysis

Routine CHN microanalysis of the sublimed substance corresponded closely to MoOPc. Found: C, 61.5; H, 2.8; N, 18.0%. Calc. for $C_{32}H_{16}MoN_8O$: C, 61.5; H, 2.6; N, 18.0%.

Physical measurements

UV–visible spectra of solutions of the compounds were recorded on a Pye Unicam SP1800 spectrophotometer. IR spectra of compounds in Nujol mulls and KBr discs were recorded on a Perkin–Elmer 983 IR spectrophotometer. X-ray diffraction patterns of powders were recorded on a Phillips PW1710/00 instrument.

RESULTS AND DISCUSSION

Preparative chemistry and reactions

The reaction between ammonium heptamolybdate and fused phthalodinitrile produced MoOPc in high yield. The IR spectrum and X-ray diffraction pattern of the blue product showed the absence of MoO_3, MoO_2, metal-free phthalocyanine and unreacted phthalodinitrile. Some phthalimide was formed by hydrolysis of the phthalodinitrile.

Reduction of molybdenum(VI) is accomplished by ammonia (from ammonium heptamolbydate). When sodium molybdate was used in place of ammonium heptamolybdate there was no reaction.

Properties of MoOPc

Our sample of MoOPc sublimed at 400°C and 10^{-3} torr with some decomposition. The sublimate was violet and appeared to be the same crystalline form as reported by Borschel and Strahle.[5] Grinding

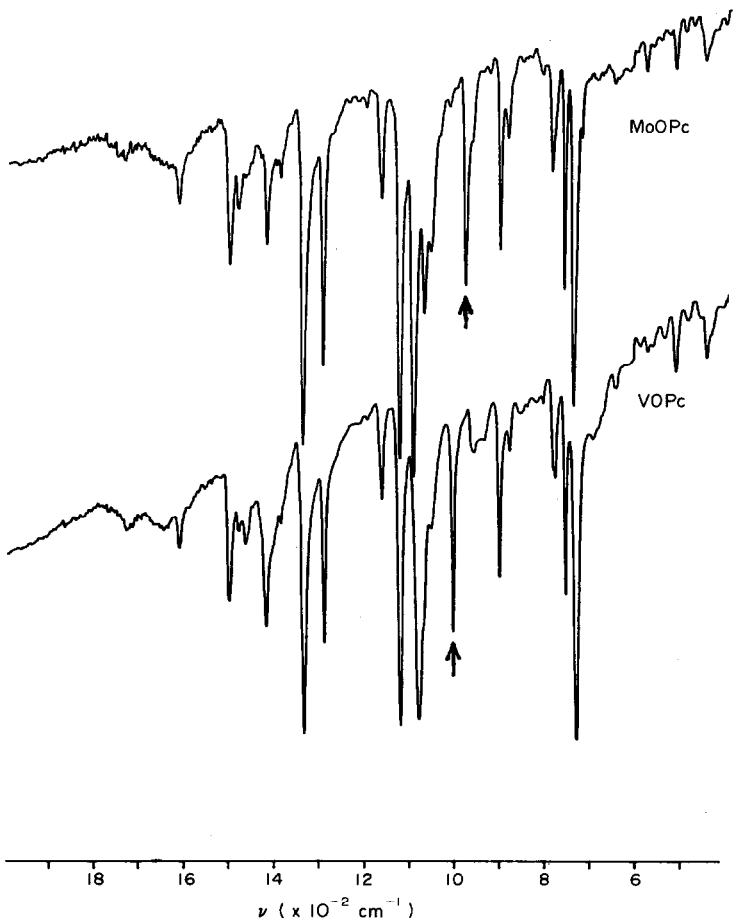


Fig. 1. IR spectra of MoOPc and VOPc in KBr discs. The arrows show the metal–oxygen vibrations.

of the violet form caused a reversion to the blue form. The blue residue remaining from the sublimation was shown to contain the blue form of MoOPc and some MoO_2 by X-ray diffraction.

MoOPc is slightly soluble in chlorobenzenes and chloronaphthalenes and acetone and butanone and rather more soluble in pyridine. It dissolved in concentrated sulphuric acid; reprecipitation at 0°C by addition of water gave a green compound which is still being investigated.

X-ray diffraction powder pattern

The strong diffraction lines were at the following values of $2\theta°$ (relative intensities are in parentheses): 3.1 (2.4), 3.5 (1.4), 3.6 (1.3), 4.0 (2.15), 5.3 (1.0) and 7.0 (1.5). Lines due to metal-free phthalocyanine, phthalodinitrile and MoO_2 were absent from the purified MoOPc. The powder pattern is a useful criterion of purity.

The X-ray diffraction pattern which we calculated from the X-ray crystallographic data of Borschell and Strahle[5] was different from ours; strong lines at our 2θ were not present. This, together with the different colours of the compounds (ours is bluc and theirs violet) suggests that there are two crystal forms of MoOPc, our preparation giving a different crystal form. The existence of different crystal forms is not uncommon with metallophthalocyanines.

IR spectra

The IR spectra of MoOPc and VOPc, which has the same structure, are shown in Fig. 1. The two spectra are similar both in the number and positions of the bands except that the wavenumber of the metal–oxygen vibration is lower for MoOPc (974 cm^{-1}) than for VOPc (1002 cm^{-1}). We estimate the effect of the different atomic masses of molybdenum and vanadium from the simple expression for the vibration frequency (v) [$(k/m)^{0.5}$, where k is the force constant and m is the reduced mass]. The calculated value for MoOPc is 1001 cm^{-1}, nearly 30 cm^{-1} higher than the experimental value. The observed Mo=O vibration frequency is therefore lower than can be accounted for by the mass different; evidently, in the phthalocyanine complexes, the Mo=O force constant is less and the Mo=O bond weaker than the V=O bond.

UV–visible spectrum

The spectrum of MoOPc in 1,2,4-trichlorobenzene shows a characteristic metallophthalocyanine peak at 703 nm and a weaker peak at 643 nm. The corresponding peaks of VOPc are at 700 and 630 nm and of metal-free phthalocyanine at 697 and 659 nm.

The spectrum of MoOPc in pyridine changed with time. The bands shifted to 710 and 652 nm and a new band at 676 nm appeared and grew in intensity with time.

Acknowledgements—We thank Climax Molybdenum Co. (PCHM) and the SERC (SJE) for support, G. A. Paterson of the Geology Department of Reading University for recording X-ray powder patterns, and Prof. J. Strahle (Tubingen) for helpful comments.

REFERENCES

1. J. F. Boas, P. E. Fielding and A. G. Mackay, *Aust. J. Chem.* 1974, **27**, 7.
2. (a) H. A. O. Hill and M. M. Norgett, *J. Chem. Soc. A* 1966, 1476; (b) Tokyo Ink Manufacturing Co., Japanese Patent 12,065 (1982).
3. Yu. A. Zhukov, L. N. Shylapora, I. N. Sokolova and B. D. Berezin, *Tr. Ivanov. Khim.-Tekhnol. Inst.* 1969, **11**, 52.
4. M. I. Federov, V. A. Shorin and L. M. Federov, *Izv. Vyssh. Uchebn. Zaved., Fiz.* 1978, **21**, 158.
5. V. Borschel and J. Strahle, *Z. Naturforsch.* 1984, **39B**, 1664.
6. (a) G. Magner, M. Savy, G. Scarbeck, J. Riga and J. J. Verbist, *J. Electrochem. Soc.* 1981, 1674; (b) J. Riga, M. Savy, J. J. Verbist, J. E. Guerchais and J. Sala-Pala, *J. Chem. Soc., Faraday Trans. 1* 1982, **78**, 2773.
7. L. J. Boucher, N. L. Holy and B. H. Davis, In *New Approaches to Coal Chemistry* (Edited by B. D. Blaustein, B. C. Bockrath and S. Friedman), p. 319. ACS Symposium Series 169, American Chemical Society (1981).

Polyhedron Vol. 5, No. 1/2, pp. 319–321, 1986
Printed in Great Britain

0277–5387/86 $3.00 + .00
© 1986 Pergamon Press Ltd

STRUCTURAL, SPECTROSCOPIC AND ELECTROCHEMICAL STUDIES ON A NEW Mo(VI) CATECHOLATE COMPLEX

STUART BRISTOW, C. DAVID GARNER* and GARETH A. MORRIS

Department of Chemistry, University of Manchester, Manchester M13 9PL, U.K.

and

JOHN H. ENEMARK, MARTIN MINELLI and RICHARD B. ORTEGA

Department of Chemistry, University of Arizona, Tucson, AZ 85721, U.S.A.

(*Received* 17 *June* 1985)

Abstract—The reaction of *cis*-$[MoO_2(C_5H_{10}NO)_2]$ ($C_5H_{10}NOH$ = 1-piperidinol) with benzene 1,2-diol (catechol) in $CHCl_3$ leads to the formation of $[MoO(C_5H_{10}NO)_2(C_6H_4O_2)]$, which has been characterized by X-ray crystallography, NMR spectroscopy and cyclic voltammetry.

We have been interested in developing the chemistry of complexes of the type *cis*-$[MoO_2(R^1R^2NO)_2]$ (R^1R^2NO = *N*,*N*-dialkylhydroxylamido(1−)-*O*,*N*) because they are the only six-coordinate Mo(VI) complexes found to date in which an oxo group can be replaced by a sulphido group.[1–3] The $\{MoOS\}^{2+}$ centre produced by this reaction is thought to be relevant to the nature of the coordination environment about Mo in xanthine oxidase and related enzymes.[4] We report herein that an oxo group in these complexes can also be replaced by a catecholate moiety to give complexes of the type $MoO(R^1R^2NO)_2$(catecholate). The salient properties of the prototypical member of this series, $[MoO(C_5H_{10}NO)_2(C_6H_4O_2)]$ ($C_5H_{10}NOH$ = 1-piperidinol), are described.

EXPERIMENTAL

To a solution of *cis*-$[MoO_2(C_5H_{10}NO)_2]$[1] in $CHCl_3$ was added an equimolar amount of solid catechol. After stirring for *ca* 1 h, the purple solution was evaporated to dryness under reduced pressure, giving analytically pure $[MoO(C_5H_{10}NO)_2(C_6H_4O_2)]$ as a deep purple powder.

* Author to whom correspondence should be addressed.

RESULTS

NMR spectroscopy

The 75 MHz ^{13}C NMR spectrum of the complex dissolved in $CDCl_3$ showed 11 signals: five in the 1-piperidinolate region, and six in the catecholate region. The former implies a symmetry element in the molecule which relates the 1-piperidinolate rings. This cannot be a C_2-axis, because of the six catecholate signals observed, and must, therefore, be a mirror plane. If this plane relates one half of each piperidinolate ring to the other half of the *same* ring, then, given the expected[1,2] mode of coordination of the 1-piperidinolate ligand, this would require all the ligand donor atoms to be coplanar with Mo—a highly unusual and sterically unfavourable arrangement. Thus, we are driven to the conclusion that the molecule possesses C_s point symmetry, with the catecholate ligand lying in the mirror plane.

The detailed assignments of the 300-MHz ^1H and 75-MHz ^{13}C NMR spectra were not trivial: although the ^1H resonances of the aromatic protons are readily interpreted, assignment of the corresponding ^{13}C resonances are equivocal. Conversely, the ^{13}C resonances of the 1-piperidinolate groups are easily elucidated but the methylene proton resonances are very complicated. Therefore, a two-dimensional ^1H–^{13}C chemical-shift correlation (Fig. 1) was used to complete the assignment of

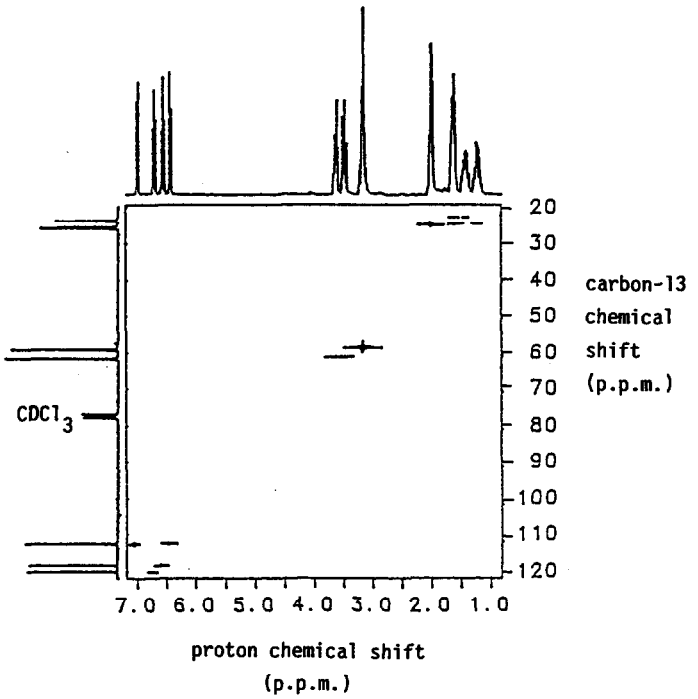


Fig. 1. Two-dimensional proton–carbon chemical-shift correlation for $[MoO(C_5H_{10}NO)_2(C_6H_4O_2)]$ in $CDCl_3$. The corresponding one-dimensional proton and carbon spectra (300- and 75-MHz, respectively) are plotted along the axes.

each spectrum. This two-dimensional technique generates spectra as a function of both the proton and carbon chemical shifts: one peak appears for each distinct CH group. This improves the effective resolution of the spectrum, since it is very rare for both the ^1H and ^{13}C resonances of two CH groups to be accidentally coincident.

X-ray crystallography

A single crystal of $[MoO(C_5H_{10}NO)_2(C_6H_4O_2)]$ was selected from a batch grown by diffusing *n*-heptane into a solution of the complex in $CHBr_3$, and examined by X-ray diffraction techniques.* $[MoO(C_5H_{10}NO)_2(C_6H_4O_2)]$ crystallizes in the tetragonal space group $P\bar{4}2_1/c$ with $a = 14.080(4)$ Å, $c = 18.099(8)$ Å and $Z = 8$. The molecular unit (see Fig. 2) involves the distorted pentagonal bipyramidal arrangement of ligand donor atoms typical of seven-coordinate Mo(VI), with the catecholate ligand spanning an equatorial and an axial site, thus confirming the deductions from NMR spectroscopy. A notable aspect of the molecular structure is that there is no appreciable static trans effect due to Mo—O_t; the lengths of the Mo—O bonds involving the catecholate ligand are 2.016(5) Å (*cis*) and 2.012(5) Å (*trans*). Other important molecular dimensions are: Mo—O1 = 1.688(6) Å, C31—O31 = 1.352(9) Å, C36—O32 = 1.375(9) Å, O1—Mo—O31

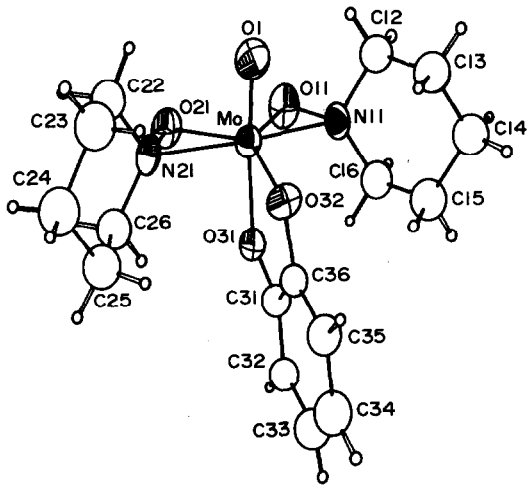


Fig. 2. Molecular structure of $[MoO(C_5H_{10}NO)_2(C_6H_4O_2)]$.

* Mo-K_α radiation, $\mu = 7.4\ cm^{-1}$, $F(000) = 1728$, 1080 reflections for $F_o^2 > 3\sigma(F_o^2)$, Lorentz-polarization and numerical absorption corrections, Patterson solution, H atoms included as fixed contribution to structure factor, full-matrix least-squares refinement, anomalous dispersion effects included for all non-H atoms, $R = 4.0\%$, $R_w = 4.4\%$.

Table 1. Cyclic voltammetric data for $[MoO(C_5H_{10}NO)_2(catecholate)]$ complexes in 0.2 M $[NBu_4][BF_4]$ in MeCN at a Pt electrode

Compound	Reduction potential[a] (V)
$[MoO_2(C_5H_{10}NO)_2]$[3]	−2.5
$[MoO(C_5H_{10}NO)_2$(3,5-di-*t*-butylcatecholate)]	−1.9
$[MoO(C_5H_{10}NO)_2$(catecholate)]	−1.7
$[MoO(C_5H_{10}NO)_2$(4-nitrocatecholate)]	−1.4

[a] Versus the ferricenium–ferrocene couple.

= 163.9(3)°, and O1—Mo—O32 = 87.4(3)°. The Mo atom is displaced 0.14 Å out of the best plane through the equatorial ligand donor atoms towards O1.

Cyclic voltammetry

Cyclic voltammetry at a Pt wire in MeCN indicates that the complex undergoes an irreversible one-electron reduction, deviating towards a two-electron stoichiometry at slow scan rates. This observation is confirmed by controlled-potential electrolysis at a Hg surface, when 2 mol of electrons are consumed per mol of complex. Analogous complexes with 4-*t*-butylcatechol and 3,5-di-*t*-butylcatechol also undergo a reversible one-electron oxidation. The peak potentials for oxidation and reduction vary in the expected manner with substitution of the catecholate ring; in comparison with the electrochemical properties of the parent complex, *cis*-$[MoO_2(C_5H_{10}NO)_2]$,[3] the catecholate ligand imparts a greater facility to reduction of the complex (see Table 1).

Acknowledgements—We thank the U.K. Science and Engineering Research Council, the North Atlantic Treaty Organisation, the U.S. Department of Agriculture, and the U.S. National Institute of Environmental Health Sciences for financial support of this research, and Dr C. J. Pickett for help with electrochemical studies. S.B. thanks the Royal Society of Chemistry, Dalton Division, for a bursary to attend this conference.

REFERENCES

1. K. Wieghardt, M. Hahn, J. Weiss and W. Swiridoff, *Z. Anorg. Allg. Chem.* 1982, **492**, 168.
2. S. Bristow, D. Collison, C. D. Garner and W. Clegg, *J. Chem. Soc., Dalton Trans.* 1983, 2495.
3. S. Bristow, C. D. Garner and C. J. Pickett, *J. Chem. Soc., Dalton Trans.* 1984, 1617.
4. R. C. Bray, *Adv. Enzymol. Relat. Areas Mol. Biol.* 1980, **51**, 107.

Polyhedron Vol. 5, No. 1/2, pp. 323–340, 1986
Printed in Great Britain

0277–5387/86 $3.00 + .00
© 1986 Pergamon Press Ltd

COORDINATION CHEMISTRY OF Mo– AND W–S COMPOUNDS AND SOME ASPECTS OF HYDRODESULFURIZATION CATALYSIS

A. MÜLLER

Faculty of Chemistry, University, 4800 Bielefeld, F.R.G.

(*Received* 4 *July* 1985)

Abstract—The coordination chemistry of Mo– and W–S compounds has been reviewed with emphasis on new results of our laboratory (including a systematic treatment of the compound types with different functional groups and the different reaction types). Molecular models for crystalline MoS_2 and the nitrosylated CoMoS phase as well as for the promoting effect of the Co atoms on hydrodesulfurization catalysis have been discussed.

During the last few years a tremendous amount of material has been collected about Mo– and W–S complexes and clusters. There is no other transition metal for which so many pure and discrete heterometal–S species (with only S_x^{2-} ligands; $x = 1, 2, \ldots$) are known (even more than for Cu). The relevance to the bioinorganic chemistry[1–6] of Mo and also to heterogeneous catalysis [especially hydrodesulfurization (HDS)][7–9] has been stressed several times in the literature. In this article we will develop a systematic treatment of the coordination chemistry of Mo– and W–S compounds with emphasis on new results of our institute (for a recent review of the corresponding solid-state chemistry see Ref. 10). Mo compounds and especially those with only "S ligands" are considered preferable. Representative examples for different types of species regarding molecular and electronic structure are given in Tables 1 and 2.

SURVEY OF COMPOUND TYPES

Simple di-($\{Mo_2S_2\}^{n+}$), *tri-*($\{Mo_3S_4\}^{n+}$) *and tetra-*($\{Mo_4S_4\}^{n+}$) *nuclear* Mo–S *clusters*

Species with different electron populations and with the same central units as the ferredoxins, that means with $\{Mo_2S_2\}^{n+}$, $\{Mo_3S_4\}^{n+}$ and $\{Mo_4S_4\}^{n+}$ {see Fig. 1 for the structure of $[Mo_4S_4(CN)_{12}]^{8-}$}, can be prepared (see Table 1). Cyano derivatives which can be reversibly reduced and oxidized might have been of importance for the evolution of Mo enzymes[12,38] (compound types and references in Table 1).

Species with functional groups of high reactivity

Species with $\{M{=}S_t\}^{n+}$ *groups.* The reactivity of a terminal Mo=S group, for instance, is very high compared to that of a bridging Mo—S—Mo one. Quite a number of species with $\{M{=}S_t\}^{n+}$ units, which are only stable in the higher oxidation states of M, are known (compound types and references in Table 1). Species with the binuclear (central) $\{M_2S_2(X_t)_2\}^{2+}$ (X = O or S) unit have a high formation tendency. For some of those see Fig. 2 and later.

Metal–sulfur aggregates with no metal–metal interactions and μ_n-S^{2-} *ligands.* Metal–sulfur aggregates with no metal–metal interaction exist preferably with strong π-acceptor ligands like NO. $[Mo_4(NO)_4(S_2)_5S_3]^{4-}$, built up by four Mo atoms, contains (besides S_2^{2-} ligands, see next section) two μ_3-S^{2-} and one μ_4-S^{2-} ligand. An interesting species with a bridging Mo=S=Mo group is $[(CN)_6MoSMo(CN)_6]^{6-}$, which was obtained by us by the reaction of molybdate with H_2S in the presence of CN^- (compound types and references in Table 1).

Mono- and polynuclear species with S_x^{2-} *ligands* ($x > 1$). W and (especially) Mo have a very high tendency to form polysulfido compounds with S_2^{2-} and S_4^{2-} ligands. It is worthwhile distinguishing between species with terminal S_x^{2-} ligands [$\{M(S_2)\}^{n+}$ ($n = 4, 3$ or 2) and $\{M(S_4)\}^{n+}$ ($n = 3$ or 2) groups] and those with bridging ones [i.e. with

Table 1. Different types of coordination compounds of Mo and W with M—S bonds (M = Mo or W)

Type		M—M (pm)	M—S (pm)	Reference
$\{Mo_2S_2\}^{n+}$				
$n = 6$, Mo(V)	$[Mo_2O_2S_2(S_2)_2]^{2-}$	282.9(2)	230.4(4)–233.8(4)	11
$n = 4$, Mo(IV)	$[Mo_2S_2(CN)_8]^{4-}$	275.8(7)	229.3(13), 229.8(14)	12
$n = 2$, Mo(III)	$[Mo_2S_2(CN)_8]^{6-}$	264.4(5)	236(1), 237(1)	13
$(n = 2)$, $\{Mo_2S_2(NO)_2\}^{0}$ [a]	$[Mo_2S_2(NO)_2(CN)_6]^{6-}$			14
$\{Mo_3S_4\}^{n+}$				
$n = 4$, Mo(IV)	$[Mo_3S_4(CN)_9]^{5-}$	276.9(1), 278.1(1)	231.2(2)–236.8(3)	12
$n = 3$, (2Mo(IV), 1Mo(III)) [a]	$[Mo_3S_4(cp)_3]$			15
$\{Mo_4S_4\}^{n+}$				
$n = 4$, Mo(III)	$[Mo_4S_4(CN)_{12}]^{8-}$	285.3(1), 235.5(1)	238.1(2), 238.2(2)	16
$n = 5$, (3Mo(III), 1Mo(IV)) [a]	$[Mo_4S_4(C_5H_4i\text{-}Pr)_4]^{+}$	286.0(1)–292.3(1)	234.3(3) } mean values	17
$n = 6$, (2Mo(III)/(IV)) [a]	$[Mo_4S_4(C_5H_4i\text{-}Pr)_4]^{2+}$	279.0(1)–290.2(1)	234.3(2) } mean values	17
$(n = 4)$, $\{Mo_4S_4(NO)_4\}^{0}$	$[Mo_4S_4(NO)_4(CN)_8]^{8-}$	299(3), 367(4)	235(2), 276(2)	18
$\{M = S_t\}^{n+}$				
$n = 4$, Mo(VI)	MoS_4^{2-}		217.1(5)–218.6(6)	19
$n = 3$, M(V)	$[M_2S_4(S_4)_2]^{2-}$, M = Mo	284.6(1)	211.4(2), 212.3(2)	20
	M = W	283.4(2)	208.9(11), 211.7(9)	21
$n = 2$, M(IV)	$[MS(MS_4)_2]^{2-}$, M = Mo	280.2(5)–308.2(6)	208.6(4)	22
	M = W	288.2(1), 304.7(1)	207.0(10)	23, 26
$\{M{=}S{=}M\}^{n+}$				
$n = 6$, Mo(IV)	$[(CN)_6MoSMo(CN)_6]^{6-}$		217.2(1)	12, 24
$\{M(S_2)_t\}^{n+}$				
$n = 4$, Mo(VI)	$[(Cl_2Fe)S_2MoO(S_2)]^{2-}$	[275.2(2)]	239.6(4), 242.1(4)	25
$n = 3$, Mo(V) [b]	$[Mo_2O_2S_2(S_2)_2]^{2-}$	282.9(2)	238.4(6)–242.6(5)	11
$n = 2$, Mo(IV) [a]	$[Mo_3S(S_2)_6]^{2-}$	271.9(2), 272.5(2)	240.3(7)–245.9(6)	29

$\{M(S_4)_t\}^{n+}$				
$n = 3$, W(V)	$[W_2S_4(S_4)_2]^{2-}$	283.4(2)	238.9(8)–243.5(9)	21
$n = 2$, Mo(IV)	$[MoS(S_4)_2]^{2-}$		233.1(1), 238.7(1)	20
$n = 2$, Mo(IV)	$[MoO(S_4)_2]^{2-}$		234.6(6), 238.6(7)	3, 27
$\{M(S_2)M\}^{n+}$				
$n = 8$, Mo(V)	$[Mo_2(S_2)_6]^{2-}$	282.6(2), 282.8(2)	238.2(4)–250.7(3)	28
$n = 6$, Mo(IV)	$[Mo_3S(S_2)_6]^{2-}$	271.9(2), 272.5(2)	241.3(6)–249.0(7)	29
$(n = 6)$, $\{MoNO\}^{3+}$ [a]	$[Mo_4(NO)_4(S_2)_5S_3]^{4-}$	334.2(2)–345.8(2)	244.1(5)–254.7(3)	30, 42
$(n = 6)$, $\{MoNO\}^{3+}$ [a]	$[Mo_4(NO)_4(S_2)_6O]^{2-}$	330.9(1) [b]	244.4(3)–252.4(3) [b]	31
$(n = 6$, Mo(IV)) [a]	$[Mo_2(S_2)(SO_2)(CN)_8]^{4-}$	268.4(1)	242.2(3)–243.7(2)	32
$(n = 5$, Mo(III), Mo(IV)) [a]	$[Mo_2(S_2)(SO_2)(CN)_8]^{5-}$	279.0(1)	243.6(3)–244.8(3)	32
$\{M(S_x)M\}^{n+}$				
$(n = 6)$, $\{MoNO\}^{3+}$ [a]	$[Mo_2(NO)_2(S_2)_3(S_5)(OH)]^{3-}$	341.3(2)	247.5(3), 248.5(3)	33
$\{M(SH)\}^{n+}$				
$n = 5$, W(VI)	$[WS_3(SH)]^-$			34
$n = 3$, W(IV)	$[W(CN)_7(SH)]^{4-}$		262.1(8)	35
$\{M_2S_2(SH)_2\}^{n+}$				
$n = 2$, Mo(IV)	$[Mo_2S_2(SH)_2(cp\text{-}Me_n)_2]$			36, 37

[a] Formal description (ligands considered as NO^- and SO_2^{2-}).

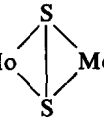
[b] The values refer to the Mo  Mo subunits in the $[Mo_4(NO)_4(S_2)_6O]^{2-}$ anion.

Table 2. Different types of thiometalato complexes with special reference to those existing with different and unusual (trianions) electron populations (averaged distances in pm)

Compound	n_s[a]	n_b[b]	N (μ_N)	M—S_{br}	M—S_t	M...M′	Type, coordination of M′[c]	Reference
$(PPh_4)_2[SW(WS_4)_2]$	2	2	2	225.4	214.2	296.5[d]	Mixed-valence, sp-SWS_4	23
$(PPh_4)_2[OMo(MoS_4)_2]$	2	2	2	224.5	213.7	298.4[d]	Mixed-valence, sp-$OMoS_4$	45
$Cs_2[(H_2O)OW(WS_4)_2]$	2	2	2	225.3	216.4	299.0[d]	Mixed-valence, o-O_2WS_4	23
$(PPh_4)_2[NCCu(MoS_4)]$	2	2	2	224.5	216.3	263.0	tp-$CuNS_2$	42
$(NEt_4)[(NO)_2Co(MoO_2S_2)]$	2	2	2	224.9	(171.9)[e]	282.9	t-CoN_2S_2	43
$(AsPh_4)_2[Ni(WS_4)_2]$	2	2	2	223.2	215.1	181.7	sqp-NiS_4	23
$(PPh_4)_2[(NO)Co(WS_4)_2]$	2	2	2	222.1	213.0	283.9	sp-$CoNS_4$	43
$(NEt_4)_2[(H_2O)_2Fe(WS_4)_2]$	2	2	2	221.9	217.4	301.0	o-FeO_2S_4	45
$(PPh_4)_2[Au_2(WS_4)_2]$	2	2	2	[f]	213.6	316.9	$Au_2W_2S_4$-ring	46
$(PPh_4)_4[Sn_2(WS_4)_4]$	2	2	2	223.1	215.4		Terminal and bridging WS_4^{2-}	47
	3	4	2, 3	219.9	216.8			
$\{Cu_2MoS_3\}(PPh_3)_3O \cdot 0.8CH_2Cl_2$	3	4	2, 3	223.8	(170.0)[e]	271.9	Cubane { }, 2 mc	48
$\{Cu_3MoS_3Br\}(PPh_3)_3 \cdot 0.5Me_2CO$	3	6	3	226.2	(185.3)[e]	271.8	Cubane { }	49
$\{Ag_4Mo_2S_6\}(PPh_3)_4S_2$	3	6	3	222.7	210.8	297.5	Prismane { }	50
$(PPh_4)_2[\{Cu_3MoS_3\}Cl_3O]$	3	6	3	226.3	(169.3)[e]	263.8	Cubane { }, 1 mc	48
$(PEt_3)_2Au_2(MoS_4)$	4	4	2	222.0		281.5	Linear AuMoAu, tp-$AuPS_2$	51
$(NMe_4)_2NCCu(MoS_4)\{CuCN\}$	4	4	2	221.8		268.4	Linear CuMoCu, chain { } tp- and t-$Cu(N,C)S_2$	42
$(PPh_4)_2[(Cl_2Fe)_2(MoS_4)]$	4	4	2	220.4		277.5	Linear FeMoFe, t-$FeCl_2S_2$	52
$(PPh_3)_4Cu_3(VS_4) \cdot 2CH_2Cl_2$	4	6	2, 3	218.5		266.3	Cu_2VCu, T-form structure	53
$(Ph_3PNPPh_3)_2(NEt_4)_2[Fe_2S_2(WS_4)_2] \cdot 3MeCN$	2	2	2	223.4	217.3	281.6	Linear WFeFeW	45
$(PPh_4)(NEt_4)_3[Fe_3S_2(WS_4)_3]$	2	2	2	223.8	215.2	277.4	Planar Fe_3W_3	54
$(Ph_3PNPPh_3)_2(NEt_4)[Fe(MoS_4)_2] \cdot 2DMF$	2	2	2	225.5	217.1	274.0		55
$(Ph_3PNPPh_3)_2(NEt_4)[Co(MoS_4)_2] \cdot 2MeCN$	2	2	2	223	215	275		45, 56
$(Ph_3PNPPh_3)_2(NEt_4)[Fe(WS_4)_2] \cdot 2MeCN$	2	2	2	223.9	216.6	274.9	t-M′S_4	57
$(PPh_4)_2[Co(WS_4)_2]$	2	2	2	221.9	213.9	279.8		58
$(Ph_3PNPPh_3)_2(NEt_4)[Co(WS_4)_2] \cdot 2MeCN$	2	2	2	223.0	217.5	272.7		56, 59

[a] Number of coordinating S-atoms per thiometalate ligand.
[b] Number of M′—S bonds formed per $MS_nO_{4-n}^{2-}$ (n = 2, 3, or 4) ligand.
[c] Abbreviations: sp, square pyramidal; tp, trigonal planar; t, tetrahedral; o, octahedral; sqp, square planar; mc, missing corner(s).
[d] M′ = M.
[e] M–O distance.
[f] Not given because of disorder.
[g] With different electron populations; strongly delocalized MOs (in trianions).

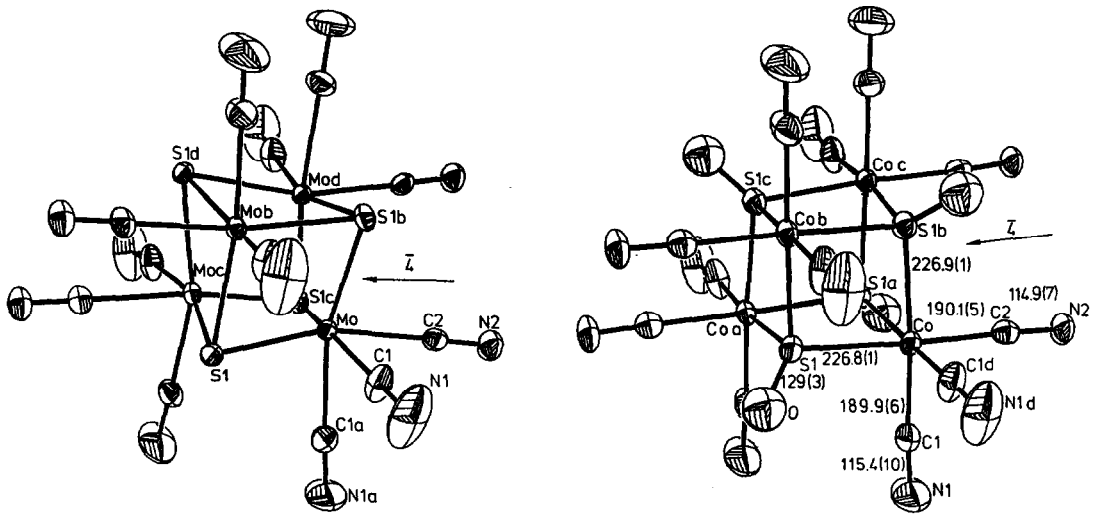


Fig. 1. Structures of $[Mo_4S_4(CN)_{12}]^{8-}$ and $[Co_4S_3(SO)(CN)_{12}]^{8-}$ (see last section) (bond lengths in pm) in crystals of $K_8[Mo_4S_4(CN)_{12}]\cdot 4H_2O$ and $K_8[Co_4S_3(SO)(CN)_{12}]\cdot 4H_2O$.[16,91]

$M(S_x)M$ moieties]. In $[Mo_2(S_2)_6]^{2-}$ and $[Mo_3S(S_2)_6]^{2-}$ (Fig. 3) both types occur. A large variety of different coordination types, especially of S_2^{2-}, exists.[39,40] In the two tetranuclear complexes $[Mo_4(NO)_4(S_2)_5S_3]^{4-}$ and $[Mo_4(NO)_4(S_2)_6O]^{2-}$, which have nearly the same stoichiometry, for instance, four different types of coordinated S_2^{2-} ligands occur (in the nomenclature of Ref. 39 structural types Ia, Ib, IIb and III). In $[Mo_2(NO)_2(S_2)_3(S_5)(OH)]^{3-}$ the doubly bridging S_5^{2-} ligand occurs (compound types and references in Table 1).

Species with SH^- *ligands.* Compounds containing SH^- ligands are interesting with respect to the possible activation of H_2 at the S sites of HDS catalysts. Very few species are known as yet, like

$$[WS_3(SH)]^-, \quad [W(CN)_7(SH)]^{4-}$$

and

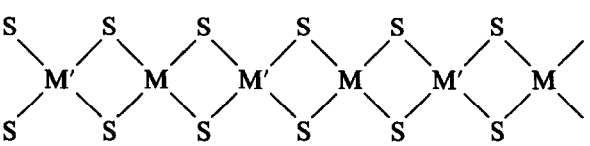
$$[Mo_2S_2(SH)_2(Me_n\text{-cp})_2]^{36,37}$$

(see Table 1 and references, and Fig. 4).

Heterometallic aggregates with thiometalato ligands

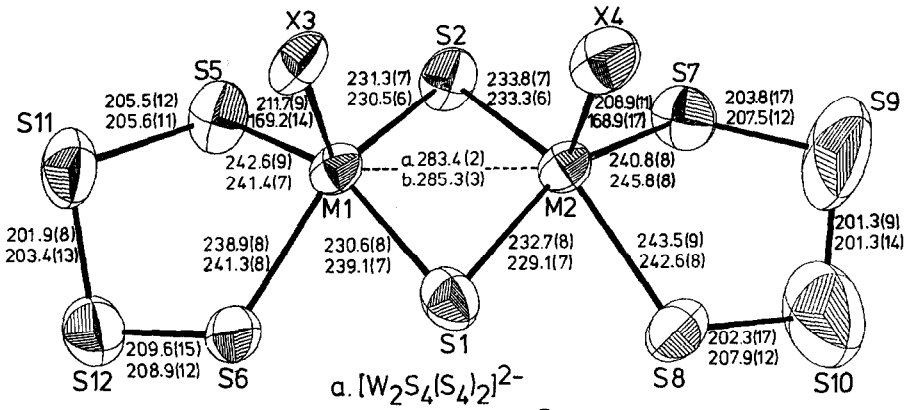
Since the isolation of $[Ni(WS_4)_2]^{2-}$, the first discrete thiometalato complex, in 1971 by us, anions of the type $MO_{4-n}S_n^{2-}$ have gained growing attention in complex chemistry. At present, more than a hundred complexes are known with the following elements: Fe, Co, Ni, Cu, Zn, Mo, Ru, Pd, Ag, Cd, Sn, W, Pt, Au, Hg and Pb. The interest in this class of compounds is mainly due to three reasons: (1) the thiometalates show a versatile coordination behaviour, (2) many of the multi-metal systems possess unique electronic properties (existence of species with different electron populations), and (3) some of the species are of bioinorganic or catalytical interest (for instance the thermal-decomposition products of salts of $[Ni(WS_4)_2]^{2-}$ and $[Co(MoS_4)_2]^{3-}$ act as excellent hydrogenation and HDS catalysts).

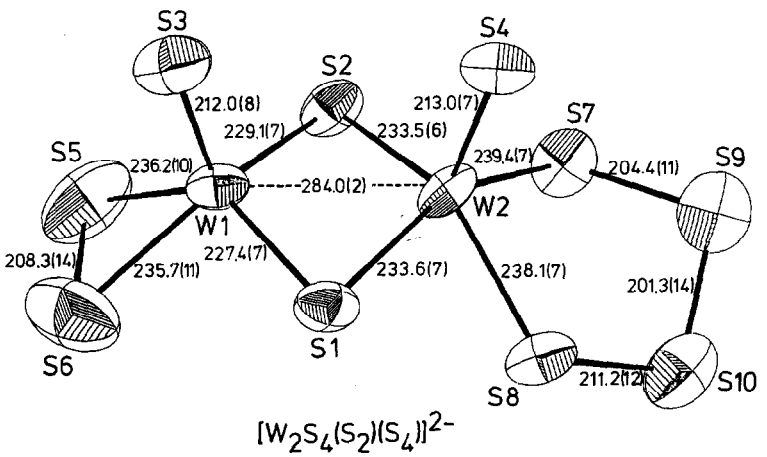
If complexes with univalent (like $[M'(MS_4)_2]^{3-}$, M' = Cu or Ag; for structures see Fig. 5) or formally univalent (like $[Fe(WS_4)_2]^{3-}$) M' cations exist, compounds with a catena structure of the anions like $(PPh_4)Fe(WS_4)$ and $PPh_4Ag(WS_4)$ can be obtained, too. (All corresponding compounds are isostructural.) Though no single-crystal structure determination could be done for the microcrystalline material of the polymeric compounds, vibrational spectroscopy (mainly resonance-Raman), powder diffraction studies and Mössbauer spectroscopy (for the Fe species) suggest strongly the presence of chains ($M'S_4$ and MS_4 tetrahedra sharing edges) in the compounds $(PPh_4)M'(MS_4)$:[60,61]



where M' = Fe, Cu or Ag; M = Mo or W.

The Fe^{n+}–WS_4^{2-} system is, in particular, very interesting. While $[Fe(WS_4)_2]^{2-}$, $[Fe(WS_4)_2]^{3-}$ and $[Fe(H_2O)_2(WS_4)_2]^{2-}$ can be precipitated directly from an aqueous solution,[45]





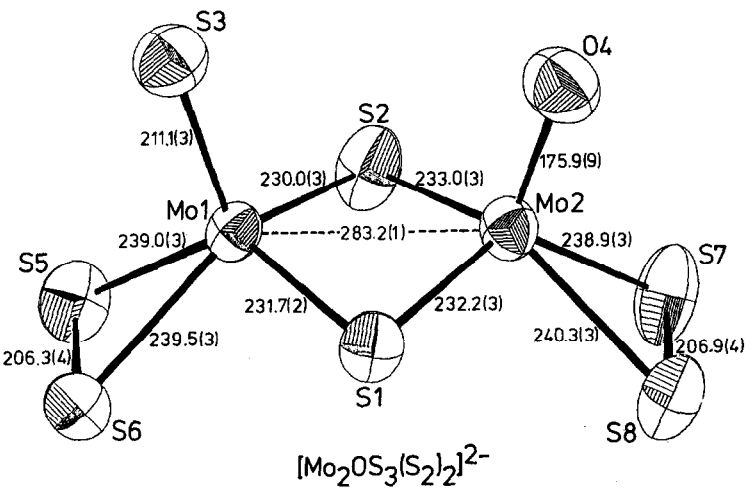
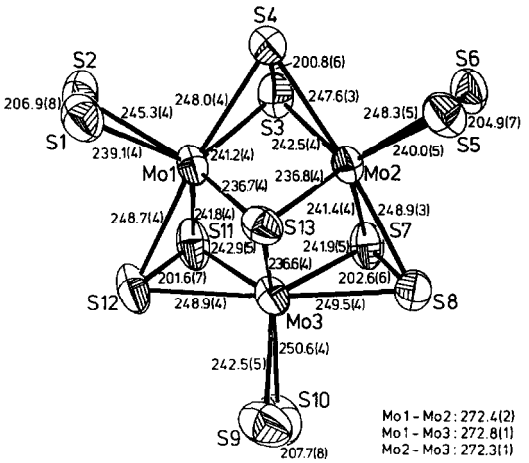
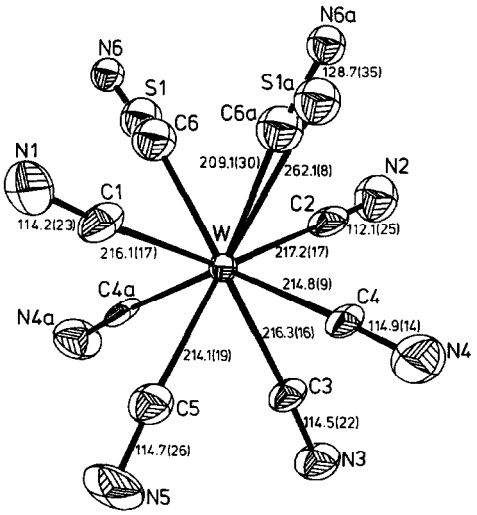


Fig. 2. Structures of $[W_2S_4(S_4)_2]^{2-}$ (with bond lengths (pm) also for $[Mo_2O_2S_2(S_4)_2]^{2-}$), $[W_2S_4(S_2)(S_4)]^{2-}$ and $[Mo_2OS_3(S_2)_2]^{2-}$ in crystals of $(PPh_4)_2[W_2S_4(S_4)_2] \cdot 0.5DMF$, $(PPh_4)_2[Mo_2O_2S_2(S_4)_2]$, $(PPh_4)_2[W_2S_4(S_2)(S_4)] \cdot 0.5DMF$ and $(PPh_4)(NEt_4)[Mo_2OS_3(S_2)_2] \cdot MeCN$.[21]



$[Mo_3S(S_2)_6]^{2-}$ ($AsPh_4^+$-salt)

Fig. 3. Structure of $[Mo_3S(S_2)_6]^{2-}$ in crystals of the new $(AsPh_4)_2[Mo_3S(S_2)_6]\cdot 2MeCN$ [$P\bar{1}$, $a = 1107.5(3)$ pm, $b = 1231.9(3)$ pm, $c = 2443.7(6)$ pm, $\alpha = 94.37(2)°$, $\beta = 103.67(2)°$, $\gamma = 110.49(2)°$, bond lengths in pm].[96]



$[W(CN)_7(SH)]^{4-}$

Fig. 4. Structure of $[W(CN)_7(SH)]^{4-}$ in crystals of $K_4[W(CN)_7(SH)]\cdot 2H_2O$ [*Pnma*, $a = 1657.6(6)$ pm, $b = 1157.8(3)$ pm, $c = 873.2(3)$ pm; bond lengths in pm]. Refinement in space group $Pna2_1$ showed the S atom occupying one position only. However, since, due to correlation effects, the structure could not be refined properly in $Pna2_1$, *Pnma* was chosen even though in this space group a mirror plane through W, Cl, N1, C2, N2, C3, N3, C5 and N5 causes a "disorder" of the SH^- and a CN^- ligand (S1 and C6, N6).[35]

$[Fe_3S_2(WS_4)_3]^{4-}$ [54] and the linear tetranuclear $[Fe_2S_2(WS_4)_2]^{4-}$ [45] (with fully reduced $\{Fe_2S_2\}^o$ core!) can be obtained from organic solvents.

The Fe^{n+}–MoS_4^{2-} solvent system is not as versatile due to the high formation tendency of the reduced $[Fe(MoS_4)_2]^{3-}$ [55] species. (It is formed simply in aqueous solution from Fe(II) and MoS_4^{2-} [60]). The discrete dianion could not be isolated until now, only a polymeric substance with the rough composition $(PPh_4)_2Fe(MoS_4)_2$ showing a powder diffraction pattern characteristic for an X-ray amorphous substance.[62]* All known pure metal–sulfur di- and trianions, which exist with different electron populations, are presented in Table 2.

Several mixed-ligand complexes are known (Table 2). Those with NO ligands with formally very low oxidation states of the central atoms are of interest for the characterization of the HDS catalyst {see Figs 6 and 7 for the structures of $[(NO)_2Co(WS_4)_2]^-$, $[(NO)_2Co(MoO_2S_2)_2]^-$ and $[(NO)Fe(WS_4)_2]^{2-}$, Table 2 and the previous section}.

A detailed report on many Cu complexes has been written by Garner *et al.*[5]

Species with oxidized S_x^{2-} *and organo substituted* S *ligands*

$[Mo_2S_4(S_2)(S_3O)]^{2-}$ and $[Mo_2O_2S_2(S_2)(S_3O_2)]^{2-}$ are examples of complexes in which S_x^{2-} ligands are oxidized (see Fig. 8).[64,65] Three complexes with organo substituted ligands, which have been obtained from pure chalcogeno species should be considered here: $[Mo_2O_2S_2(DMAD)_2]^{2-}$ with an Mo(V)—C bond (obtained from $[Mo_2O_2S_2(S_2)_2]^{2-}$ [66]), $[Mo_2S_4(dtc)_2]$ (from $[Mo_2(S_2)_6]^{2-}$ [67]) and $[Mo_3S_4(SCH_2CH_2S)_3]^{2-}$ (from $[Mo_3S(S_2)_6]^{2-}$).[68]

SYNTHESIS AND REACTIVITY

A tremendous variety of simple species containing only S (and O) and M exist: e.g. MO_3S^{2-}, $MO_2S_2^{2-}$, MOS_3^{2-}, MS_4^{2-}, $[MoS(S_4)_2]^{2-}$, $[MoO(S_4)_2]^{2-}$, $[Mo_2(S_2)_6]^{2-}$, $[Mo_2S_4(S_2)_2]^{2-}$, $[M_2S_4(S_4)_2]^{2-}$, $[M_2S_4(S_2)(S_4)]^{2-}$, $[Mo_2OS_3(S_2)_2]^{2-}$,

$[Mo_2O_2S_2(S_2)(S_x)]^{2-}$ ($x = 2$ or 4),

$[Mo_2O_2S_2(S_2)(S_3O_2)]^{2-}$, $[Mo_2S_4(S_2)(S_3O)]^{2-}$ and $[MX(MS_4)_2]^{2-}$ (X = O or S, M = Mo or W)† (see Tables 1 and 2 as well as different figures).

* Besides Ref. 83 this is the first note on the bioinorganic relevance of the Fe^{n+}–MoS_4^{2-} system.

† In addition, some higher aggregated species like $[Mo_3S(S_2)_6]^{2-}$, $[Mo_2O_2S_2(S_2)(MoS_4)]^{2-}$, $[WS(WS_4)(WS_3(S_2))]^{2-}$ and $[W_2S_4(WS_4)_2]^{2-}$.[64,65,75,100]

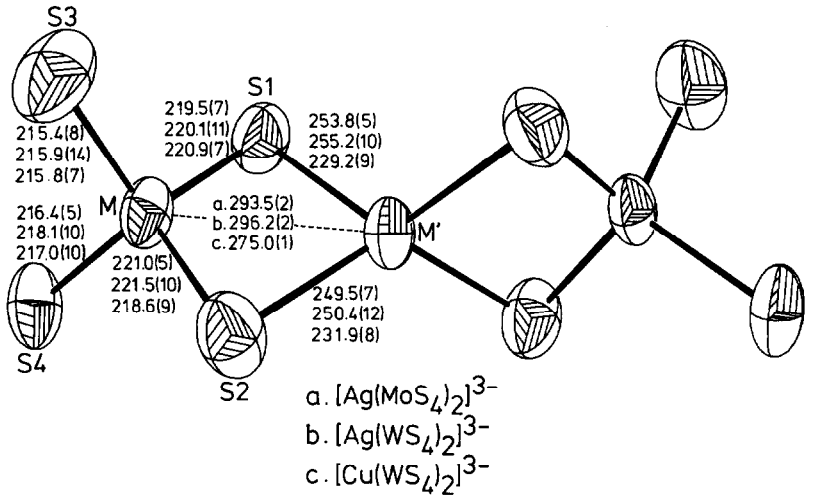


Fig. 5. Structure of $[Ag(MoS_4)_2]^{3-}$ with bond lengths (pm) together with data for $[Ag(WS_4)_2]^{3-}$ and $[Cu(WS_4)_2]^{3-}$ in crystals of $(Ph_3PNPPh_3)_2(NEt_4)[M'(MS_4)_2] \cdot n$MeCN (M = Mo or W, M' = Ag or Cu, $n = 1$ for M' = Ag, $n = 2$ for M' = Cu). All salts crystallize in the space group $P2_12_12$; cell constants for the Ag–Mo compound: $a = 1254.6(5)$ pm, $b = 3431.1(13)$ pm, $c = 1079.0(4)$ pm.[96]

Synthesis of species with S_x^{2-} ligands (x = 1 or 2)

Because of the high affinity, especially of Mo, for S (see the next section), compounds with Mo—S bonds are easily formed. Reagents for the preparation may be S_8, S^{2-}, SH^-, H_2S, S_x^{2-} and organic polysulfides like BzSSSBz. There is a special tendency to form $Mo(S_x)$ ($x = 2$ or 4) units. Even in nearly boiling water containing S_x^{2-} a species is formed which contains only S and no O: $(NH_4)_2[Mo_3S(S_2)_6] \cdot nH_2O$ ($n = 0$–2; the unit cell dimensions vary with the H_2O content[90]).

An example of the variety of Mo–S species in a solution containing Mo^{n+} and S_x^{2-} ions: the Mo^{n+}–S_x^{2-}–H_2O system with special reference to $(NH_4)_2[Mo_3S(S_2)_6] \cdot nH_2O$ (n = 0–2)[30,69,70]

The formation of $[Mo_3S(S_2)_6]^{2-}$ proceeds easily on heating a solution of MoO_4^{2-} [reduction to Mo(IV)] and ammonium polysulfide* ($[Mo_2(S_2)_6]^{2-}$ is formed from the filtrate at room temperature). At a reaction temperature of about 45°C after 16 h mainly the formation of MoS_4^{2-} is observed (the oxothiomolybdates $MoO_nS_{4-n}^{2-}$ are formed correspondingly much faster). At reaction temperatures >95°C after 16 h *only* $(NH_4)_2[Mo_3S(S_2)_6] \cdot nH_2O$ is obtained (if the reaction time is reduced considerably, the yield is also reduced) and from the filtrate $[Mo_2(S_2)_6]^{2-}$ (as NH_4^+ salt) at room temperature. We have also studied the influence of the amount of elemental S used for the preparation of the polysulfide solution. The yield of $[Mo_3S(S_2)_6]^{2-}$

* For its preparation see Ref. 70.

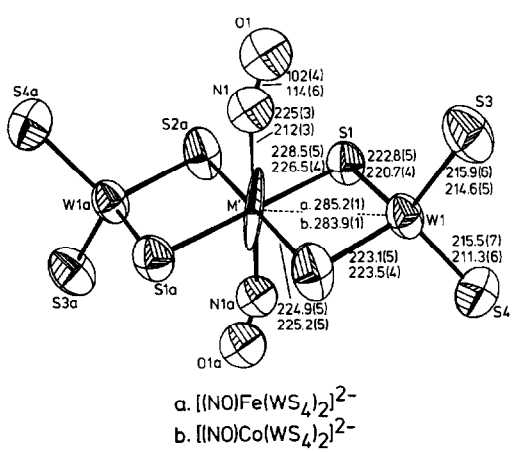


Fig. 6. Structure of disordered $[(NO)Fe(WS_4)_2]^{2-}$ with bond lengths (pm) together with data for $[(NO)Co(WS_4)_2]^{2-}$ in crystals of their PPh_4^+ salts.[43]

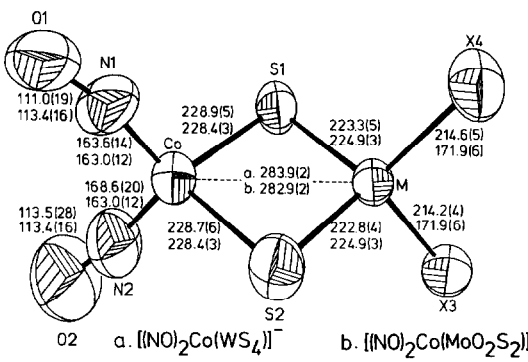
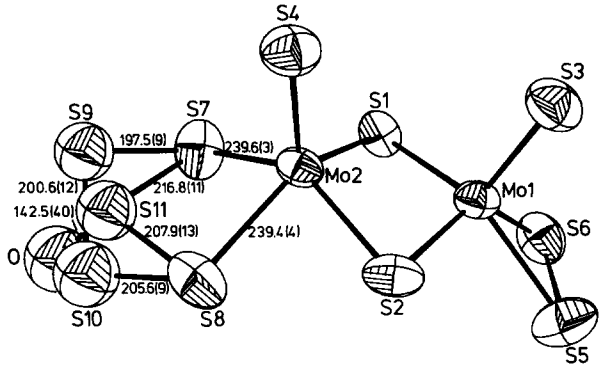
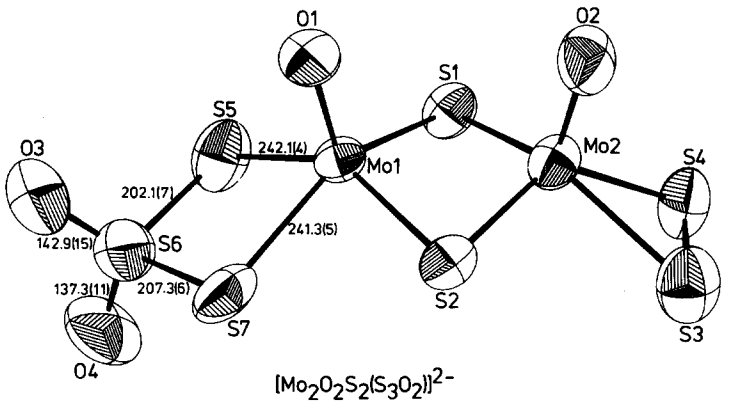


Fig. 7. Structure of $[(NO)_2Co(WS_4)]^-$ with bond lengths (pm) together with data for $[(NO)_2Co(MoO_2S_2)]^-$ in crystals of their PPh_4^+ and NEt_4^+ salts, respectively.[43]



$[Mo_2S_4(S_2)(S_4)]^{2-}_{0.6}$ $[Mo_2S_4(S_2)(S_3O)]^{2-}_{0.4}$



$[Mo_2O_2S_2(S_3O_2)]^{2-}$

Fig. 8. Structures of $[Mo_2S_4(S_2)(S_4)]^{2-}$ (in pure form[97]), $[Mo_2S_4(S_2)(S_3O)]^{2-}$ and $[Mo_2O_2S_2(S_3O_2)]^{2-}$ in crystals of $(PPh_4)_2[Mo_2S_4(S_2)(S_4)]_{0.6}[Mo_2S_4(S_2)(S_3O)]_{0.4}$ [$P\bar{1}$, $a = 1043.0(2)$ pm, $b = 1166.3(2)$ pm, $c = 2212.2(4)$ pm, $\alpha = 76.27(12)°$, $\beta = 85.84(2)°$, $\gamma = 78.23(2)°$] and $(PPh_4)_2[Mo_2O_2S_2(S_3O_2)]$ with bond lengths (pm) of the ligands attached to the $\{Mo_2X_2S_2(S_2)\}$ (X = O or S) fragment.[64,65]

increases strongly with an increasing S content. If S_x^{2-} solutions containing a high amount of S are heated for a long time the yield of $(NH_4)_2[Mo_3S(S_2)_6]\cdot nH_2O$ is nearly quantitative.[30,69]

The cluster anion $[Mo_3S(S_2)_6]^{2-}$ can also be obtained with an organic cation upon heating the reaction mixture of $(NH_4)_2[Mo_3S(S_2)_6]\cdot nH_2O$ and $(AsPh_4)Cl$ in acetonitrile (see structure in Fig. 3).

The high formation tendency of

$$[Mo_3(IV)S(S_2)_6]^{2-}$$

at higher temperatures in solution corresponds to that of $Mo(IV)S_2$ in the solid state (see last section on catalysis).

Reaction types

Electron-transfer processes (mainly intramolecular ones) keep the chemistry in check. Reactions are known where only "S ligands" (type II), only metal centers (type I) or both (types III and IVa–d) show redox processes. No redox process necessarily occurs when the M–S moiety acts as a nucleophile (type V) (see Table 3 for details, examples and references as well as the previous section for a discussion of type II').

Reversible redox processes of type I (leading to "stable" species) preferably occur in cases where clusters have π-acceptor ligands like CN^- and mainly cp^- (contrary to comparable clusters of the 3*d* metals like $[Fe_4S_4X_4]^{n-}$ existing with ligands X = Hal or SR, and also with different electron populations).

If a neutral S atom transfer occurs from an M—S_t bond (abstracted by a nucleophile) the M center is reduced and consequently M—M bonds can be formed[18] (III). However, if the S atom transfer occurs at an $M(S_2)M$ unit there is no change in the oxidation state of M (type II). Processes like III and IV where the oxidation state of M and the "S ligands" change simultaneously (type III with reduction of both) are very important, especially for the relevant chemistry of Mo.

Table 3. Different reaction types of Mo and W complexes with S_x^{2-} ligands ($x = 1, 2, \ldots$)[a]

Type				Reference
I	$\{[M]^{ox}[S]\}$	$\underset{EA}{\overset{ED}{\rightleftharpoons}}$	$\{[M]^{red}[S]\}$	
	$[Mo_2S_2(CN)_8]^{4-}$	$2e^-$	$[Mo_2S_2(CN)_8]^{6-}$	12
	$[Mo_2(S_2)(SO_2)(CN)_8]^{4-}$	e^-	$[Mo_2(S_2)(SO_2)(CN)_8]^{5-}$	32
II	$\{[M][S]^{ox}\}$	$\overset{N}{\longrightarrow}$	$\{[M][S]^{red}\}^b$	
	$[Mo_2(V)(S_2)_6]^{2-}$	dtc^-	$[Mo_2(V)S_4(dtc)_2]$	67
	$[Mo_2(V)(S_2)_6]^{2-}$	OH^-	$[Mo_2(V)O_2S_2(S_2)_2]^{2-}$	71
	$[Mo_3(IV)S(S_2)_6]^{2-}$	CN^-	$[Mo_3(IV)S_4(CN)_9]^{5-}$	72
II′	$\{[M][S]^{ox}\}$	$\longrightarrow$	$\{[M][S]^{red}\} + S_x$	
	$(NH_4)_2[Mo_3(IV)S(S_2)_6]$	T	$Mo(IV)S_2 + S_x$ $(+H_2S + NH_3)$	90
III	$\{[M]^{ox}[S]^{ox}\}$	$\overset{N}{\longrightarrow}$	$\{[M]^{red}[S]^{red}\}^b$	
	$[Mo_2(V)(S_2)_6]^{2-}$	CN^-	$[Mo_2(III)S_2(CN)_8]^{6-c}$	71
	a-MoS_3	CN^-	$[Mo_3(IV)S_4(CN)_9]^{5-c}$	12
	a-MoS_3	CN^-	$[Mo_4(III)S_4(CN)_{12}]^{8-c}$	16
	$[Mo_4(NO)_4(S_2)_6O]^{2-}$	CN^-	$[Mo_4S_4(NO)_4(CN)_8]^{8-c}$	18
IVa	$\{[M]^{ox}[S]^{red}\}$	$\overset{E(EA)}{\longrightarrow}$	$\{[M]^{red}[SE]\}/\{[M]^{red}[S]^{ox}\}^b$	
	$Mo(VI)S_4^{2-}$	S_8	$[Mo(IV)S(S_4)_2]^{2-}$	20
	$Mo(VI)S_4^{2-}$	S_8	$[Mo_2(V)S_4(S_2)(S_4)]^{2-}$	69 (see also 20)
	$W(VI)S_4^{2-}$	S_8	$[W_2(V)S_4(S_4)_2]^{2-}$	21
	$Mo(VI)S_4^{2-}$	O_2	$[Mo_2(V)O_2S_2(S_2)(S_3O_2)]^{2-}$	65
IVb	$\{[M]^{ox}[S]^{red}\}$	$\underset{ED}{\overset{EA}{\rightleftharpoons}}$	$\{[M]^{red}[S]^{ox}\}^b$	
	$Mo(VI)S_4^{2-}$	$RSSR \rightarrow$	$[Mo_2(V)S_4(S_2)_2]^{2-}$	73
	$Mo(VI)S_4^{2-}$	$\leftarrow SR^-$	$[Mo(IV)S(S_4)_2]^{2-}$	6, 69
IVc	$\{[M]^{ox}[S]^{red}\}$	$\overset{(Solvent)}{\longrightarrow}$	$\{[M]^{red}[S]^{ox}\}^b$	
	$W(VI)S_4^{2-}$	(Organic)	$[W(IV)S(WS_4)_2]^{2-d}$	23, 26
	$Mo(VI)O_2S_2^{2-}$	(H_2O)	$[Mo_2(V)O_2S_2(S_2)_2]^{2-}$	11, 74
	$W(VI)S_4^{2-}$	(H_2O)	$[W(IV)O[W(VI)S_4]_2]^{2-d}$	23
IVd	$\{[M]^{ox}[S]\}$	$\overset{T}{\longrightarrow}$	$\{[M]^{red}[S]\} + S_x^{bef}$	
	$Cs_2[Mo_2(V)(S_2)_6]$	200°C	$\{MoS\}$ cluster $+ S_2$	40, 89
	a-MoS_3		$Mo(IV)S_2 + S_x$	63
V	$\{[M][S]\}$	$\overset{E}{\longrightarrow}$	$\{[M][S][E]\}$	

(*Contd.*)

Table 3. (*Contd.*)

Type			Reference
MoS_4^{2-}	CuCN	$[NCCu(MoS_4)]^{2-}$	42
$MoOS_3^{2-}$	CuCl	$[(CuCl)_3(MoOS_3)]^{2-}$	48
MoS_4^{2-}	$FeCl_2$	$[Cl_2Fe(MoS_4)]^{2-}$	1, 95
MS_4^{2-}	$Cu(PPh_3)^+$	See Table 2	

[a] Abbreviations: N, nucleophile; EA, electron acceptor; E, electrophile; ED, electron donor; $[M]^{ox/red}$, metal center(s); [S], S_x^{2-} ligand(s); $[S]^{red}$, S^{2-} ligand(s); $[S]^{ox}$, S_x^{2-} ligand(s) ($x > 1$).

[b] $[S]^{red/ox}$ stands for at least one oxidized or reduced ligand.

[c] First step with abstraction of neutral S according to type II.

[d] Oxidized ligand S_2^{2-} very probably in the intermediate product.

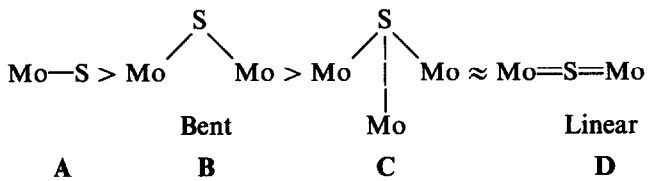
[e] Reductive elimination.

[f] [S] is not defined because of the not exactly defined states of the "S ligands" in a-MoS_3 and the {MoS} cluster; similar to II'.

Quite a number of the intramolecular redox reactions are known. If there is no electron balance for the intramolecular redox process, an electron acceptor (EA) or electron donor (ED) has to be added (IVb). The pathways for reactions IVa (with addition of an electrophile, which may act as an EA, too) and IVc (without addition of a reagent and where the educt or an intermediate may act as an EA) are not completely understood.

If the electron density on S atoms of M—S_t bonds is high, type V reactions can occur. [In this case, interesting oxidations of S_x^{2-} ligands by O_2 are also possible, leading to novel ligands like $S_3O_2^{2-}$ or S_3O^{2-} (see Fig. 8) (type IVa).[64,65]]

An especially remarkable reaction is that of type IVd. For example, $Cs_2[Mo_2(S_2)_6]\cdot nH_2O$ can be used as an S_2 generator at rather low temperatures (reductive-elimination process).[40,89]



CHARACTERIZATION BY PHYSICAL METHODS AND MO CALCULATIONS: ELECTRONIC STRUCTURE AND CHEMICAL BONDING

Several, mostly simple species, have been characterized in detail by physical methods and MO calculations. Typical examples, especially of Mo compounds, are presented in Table 4.

An important feature of Mo—S bonds, in general, is the occurrence of π-bonding over a wide range of bond lengths (*ca* 2.1–2.4 Å) if S3*p* lone-pairs are available. This is strongly supported by the fact that the overlap integral S (Mo4*d*, S3*p*) varies to a relatively small extent with the internuclear distance (compared, for example, to M—O bonds). Besides, the Mo4*d* and S3*p* VOIPs are nearly equal. Thus, very different electron density distributions within the Mo—S bonds are possible (depending on geometry, electron population and additional ligands).

The series

Mo—S > Mo Mo > Mo Mo ≈ Mo=S=Mo

A B C D

is characterized by a decrease in the negative charge on S (large charge separation, for example, in MoS_4^{2-} and almost equal net charges of Mo and S in $[Mo_2S(CN)_{12}]^{6-}$). The facility of charge displacement is important for the properties of Mo–S systems in Mo–S catalysts and enzymes.

Charge-transfer bands of the type S → Mo are observed in compounds with structure types **A** and **B** but not type **C**, whereas the opposite transition (Mo → S) is found for type **D**.

It is interesting that there is no such clear correlation between the oxidation state of Mo and the preferred μ_n-S coordination type found for clusters with weak covalent metal–sulfur bonds (for example $\{Fe_xS_y\}^{n+}$ type clusters). A simplified explanation for this is the following: in Mo–S species, upon reduction, the additional charge "goes into the bonds". Therefore, there is a considerable change in the Mo—Mo and Mo—S bond lengths accompanying the reduction, for example from $[Mo_2S_2(CN)_8]^{4-}$ to $[Mo_2S_2(CN)_8]^{6-}$. In the Fe–S

Table 4. Characterization by physical methods (with major references only)

	Physical method (spectra), procedure	Results	Interpretation, conclusion[a]	Reference
MoS_4^{2-}	(1) IR, normal-coordinate analysis (NCA)	$^{92/100}$Mo isotope frequencies, force constants	Strong π-bonding, high electron density on S, strong σ-acceptor ligand, LUMO 2e with strong contribution from S and Mo AOs	3, 76–80
	(2) Resonance-Raman	Anharmonicity constants, excitation profile		
	(3) Electronic absorption spectrum	Assignment of the S → Mo charge-transfer bands, oscillator strength	$\nu_1 \hat{=} t_1 \rightarrow 2e$, $\nu_2 \hat{=} 3t_2 \rightarrow 2e$, $\nu_3 \hat{=} t_1 \rightarrow 4t_2$[b]	
	(4) mcd	Description of the electronic structure		
	(5) MO calculations			
	(6) Valence band XPS			
$MoOS_3^{2-}$	(1) Resonance-Raman	Progression of only ν_s(MoS) bands (λ_e = 488 nm), assignment of the $a_2 \rightarrow e$ [π(S) → d(Mo)] transition	Weak mixing between MOs with Mo–O and Mo–S character, S → O substitution increases Mo—S bond strength	3, 79, 81, 82
	(2) Valence band XPS	Distinction between MOs with predominantly Mo—S and Mo—O bond character		
	(3) MO calculations			
$[Ni(MoS_4)_2]^{2-}$	(1) IR	$^{64/68}$Ni and $^{92/100}$Mo isotope frequencies, force constants	Partial interligand S—S bond (reduction of Ni center)	83, 84
	(2) MO calculations			
$[Cl_2Fe(MoS_4)]^{2-}$	(1) ^{57}Fe Mössbauer	Very low IS value for Fe(II) (0.48 at RT, α-Fe)	Strong σ-acceptor property of MoS_4^{2-} ligand	84, 85, 99
	(2) MO calculations			
	(3) Magnetic measurement	5.00 μ_B (RT)	Consistent with high-spin Fe(II)–Mo(VI) description	
$(PPh_4)Fe(MoS_4)$	(1) ^{57}Fe Mössbauer	Very low IS value for Fe(II)	Very strong electron delocalization (highly delocalized MOs in the chain)	60, 61, 84
	(2) Resonance-Raman (λ_e = 647.1 nm)	ν_s(WS) + ν_s(FeS) combination band enhanced		

$[Co(WS_4)_2]^{2-/3-}$	(1) Magnetic measurement	Low μ_{eff} values for a $^4A_2$ ground state ($[2^-]$), 4.0 μ_B (RT)	Strong electron delocalization Co → WS_4, upon reduction additional charge mainly on terminal W—S bonds	84, 86
	(2) Cyclic voltammetry	$[2^-] \rightleftharpoons [3^-]$		
	(3) MO calculations			
	(4) Electronic absorption spectrum	"Nonclassical" VIS–NIR bands of high intensity		
$[(CuCl)_3(MoOS_3)]^{2-}$	(1) X-ray	Very short Cu–Mo distances	(Closed shell!) Cu(I) → $MoOS_3^{2-}$ electron delocalization	48, 87
	(2) Resonance-Raman (λ_e = 488 nm)	Enhancement of ν_s(Cu—S) [and not (!) ν_s(Mo—S)] band		
$[Fe_2S_2(WS_4)_2]^{4-}$	(1) Resonance-Raman (λ_e = 488 nm)	Enhanced intensity of $\nu_s(FeS_2Fe)$ + ν_s[Fe—S(W)] band, IS = 0.33 mm s^{-1}	Very strong $\{Fe_2S_2\}^0$ → WS_4^{2-} electron delocalization	61, 84, 87
	(2) Mössbauer			
$[Fe_3S_2(WS_4)_3]^{4-}$	(1) Magnetic measurement	$J = -268$ cm^{-1}	Very strong $\{Fe_3S_2\}^{2+}$ → WS_4^{2-} electron delocalization, strong antiferromagnetic coupling, small repulsive interaction between Fe(II) centers	61, 84, 87
	(2) Mössbauer	IS = 0.30 mm s^{-1} (RT, α-Fe)		
	(3) MO calculations			
$[WS(WS_4)]^{2-}$	(1) Magnetic measurement	Diamagnetic electronic ground state	Mixed-valence species with (approximate) W(IV) and W(VI)	84
	(2) MO calculations			
$[Mo_2S_2(CN)_8]^{4/6-}$	(1) IR, R, NCA		Strong Mo—Mo bonds, strong variation in the electron density distribution in the Mo—S bonds in different species	12
$[Mo_3S_4(CN)_9]^{5-}$	(2) Cyclic voltammetry	Reversible redox processes		
$[Mo_4S_4(CN)_{12}]^{8-}$	(3) ν(CN) IR-band intensities	Strongly dependent on species		
	(4) Resonance-Raman	Identification of bands in the VIS range		
	(5) Electronic absorption spectra			
	(6) MO calculations	Cluster bonding MOs 70–80% Mo4*d*–S3*p* contributions		
	(7) XPS	Distinction between μ_2-S^{2-} and μ_3-S^{2-}		
	(8) Magnetic measurement	All diamagnetic		
$[Mo_2S(CN)_{12}]^{6-}$	(1) Resonance-Raman (λ_e = 647.1)	Enhancement of bands due to *all* ν_s stretchings	Strongly delocalized MOs over the whole system	12
	(2) MO calculations			
$[Mo_2(S_2)(SO_2)(CN)_8]^{4-/5-}$	(1) ESR	g = 2.012, $A(^{95}Mo)$ = 19.2 G ($[5-]$)	The unpaired electron spin of the less stable $[5-]$ ion is strongly delocalized, (approximate) SO_2^{2-} ligand	32
	(2) XPS			
	(3) IR	Low ν(SO) frequencies		
	(4) Magnetic measurement	$S = \frac{1}{2}$($[5-]$)		

(*Contd.*)

Table 4. (*Contd.*)

	Physical method (spectra), procedure	Results	Interpretation, conclusion	Reference
$[Mo_2O_2S_2(S_2)_2]^{2-}$	(1) Electronic absorption spectra	Identification of a $\pi^*(S_2^{2-}) \rightarrow d(Mo)$ transition		40, 88, 89
	(2) Vibrational spectra ($^{92/100}Mo$), NCA	$\nu(MoS_2Mo)$ ring vibrations at 467 (IR) and 428 (R)		
	(3) MO calculations	HOMO: $\pi^*(S_2^{2-})$		
$[Mo_2O_2S_2(S_2)(S_3O_2)]^{2-}$	XPS	Identification of the "S^{6+}" of the dithiosulfate ligand		65

[a] In general obtained from all results!

[b] Improved assignment mainly according to the study of the halfwidth of the charge-transfer bands in species with negligible $M'(d^{10})$–MoS_4^{2-} π-interaction.[2,79]

clusters, the additional charge is mostly stored on the S atoms (which can accommodate charge more easily in the case of "positivation of the sulfurs" as a consequence of their higher coordination numbers in higher aggregated species).

The fact that the Mo4*d* and S3*p* VOIPs are nearly equal has other important consequences: the easy formation of S_x^{2-} ligands attached to Mo (mainly in valence states IV and V) and the tendency of Mo–S compounds towards intramolecular redox reactions in general.

A remarkable aspect of Mo–S and W–S chemistry is the electron-withdrawing power of the MoS_4^{2-} and WS_4^{2-} ligands, with the consequence that species exist with different electron populations like $[Fe(WS_4)_2]^{2-/3-}$ (even the "fully reduced" $\{Fe_2S_2\}^0$ core can be stabilized by WS_4^{2-} ligands in $[Fe_2S_2(WS_4)_2]^{4-}$).[45]

SOME ASPECTS WITH RELEVANCE TO HDS CATALYSIS

HDS involves the conversion of S from crude oil fractions or coal-derived liquids in the presence of H_2 into H_2S. Some aspects of the structure and catalytic activity of MoS_2 and the CoMoS phase[7,8] (present on the industrial catalyst) as well as their model systems should be presented here.

It turns out, from many independent experiments, that MoS_2 is the most stable binary Mo–S compound in the solid state while the $[Mo_3S(S_2)_6]^{2-}$ ion seems to be the corresponding most stable discrete species [both contain Mo(IV)!]. Structurally, both are closely related and can be prepared from each other (cf. Fig. 9). Removing the apical S atom from $[Mo_3S(S_2)_6]^{2-}$, the S_2^{2-} groups can be ordered symmetrically around the Mo_3 triangle (see below). By some variation of the bond distances [*d*(Mo—Mo) from 2.72 to 3.15 Å and *d*(S—S) from 2.0 to 3.6 Å] we have already a complete section from the MoS_2 lattice. On the other hand $[Mo_3S(S_2)_6]^{2-}$ may also be regarded as a model for the surface of MoS_2 crystallites (basal plane with μ_3-S atoms and edges with S_2^{2-} groups).

We have studied earlier the thermal decomposition of $(NH_4)_2[Mo_3S(S_2)_6] \cdot nH_2O$ to MoS_2 by DTA–TG measurements accompanied by a control of the gas phase with a mass spectrometer, by IR spectra and by XRD measurements of intermediate products.[90] Some additional experiments have been carried out and, using Debye's scattering equation, we have also calculated the X-ray scattered intensity for different (short-range order) models.[98] The main features* are shown in

* Formal treatment.

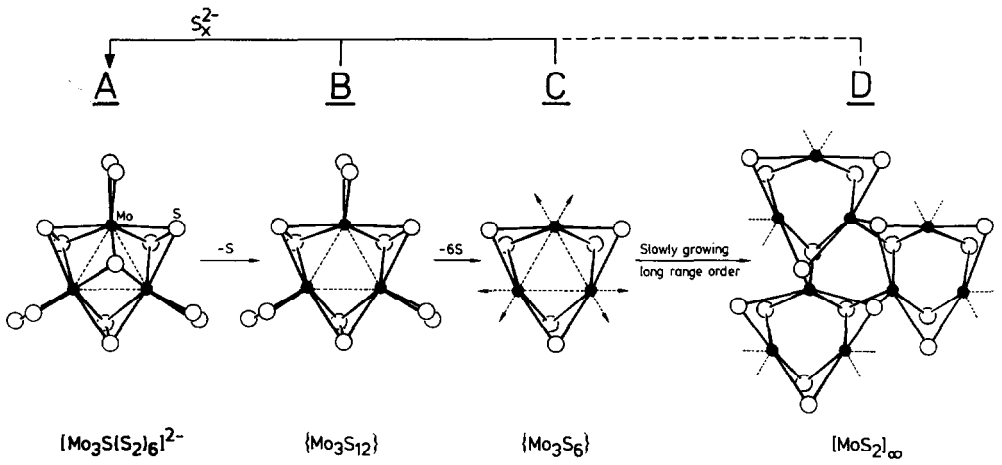


Fig. 9. Schematical representation of the thermal decomposition reaction $(NH_4)_2[Mo_3S(S_2)_6] \rightarrow MoS_2$ (for further details of the overall reaction, see Ref. 98).

Fig. 9. After the loss of the water of crystallization up to 150°C (if $n > 0$) the first reaction of the anion **A** itself is to release the apical S atom (at *ca* 260°C in the form of H_2S, together with some loss of ammonia). The bridging S_2^{2-} groups, which were centered below the Mo_3 plane in structure **A**, can now bind symmetrically (with a mirror plane through the three metal atoms). The metal–metal distance should not change greatly and stays at about 2.7 Å.

Proceeding to higher temperatures, from about 310°C the sample loses continuously up to 6 mol of neutral S, which can formally be released from the terminal S_2^{2-} groups of structure **B**. This reductive-elimination step leaves two electrons per Mo center which can be used to reduce the bridging S_2^{2-} groups to two bridging S^{2-} ligands (the S–S distance changes from 2.0 to 3.6 Å). The resulting unit, **C**, still with short Mo–Mo distances, will not be stable and adds bridging S^{2-} ligands from neighboring triangles to the coordinatively unsaturated Mo sites. As a result, at about 430°C, structure **D** is obtained. Each Mo now has more than two metal neighbors and the Mo–Mo distance should increase to its final value, i.e. 3.15 Å, with six Mo neighbors in the MoS_2 structure.

Since the average number of S atoms in the first coordination shell of Mo does not vary significantly, the major changes in the X-ray scattered intensity of the intermediate products will be mainly due to a variation in the Mo–Mo distances. There should be two diffuse maxima in the scattering curve between 20 and 100° (at $2\theta \approx 42$ and 86° with Cu-K_α radiation for structure **A**, shifting to $2\theta_{max} \approx 36$ and 65° for structure **D**). Although, particularly at lower angles, the experimental-scattering curves are screened by crystalline residues of $(NH_4)_2[Mo_3S(S_2)_6]$ or the beginning of crystallization of MoS_2, respectively, the experimental data show the behavior expected from the computations. The material with the greatest conversion ($T = 450$°C) shows two maxima in the range 60–90°, indicating the presence of both Mo_3 triangles with short and long metal–metal distances, paralleled by a pronounced crystallization in the *ab* plane {increase in the [100] reflection of MoS_2 and a less pronounced growing of the crystallites parallel to the *c*-axis of MoS_2 ([002] reflection)}.

Our investigations regarding the catalytic activity of thermally decomposed $(NH_4)_2[Mo_3S(S_2)_6] \cdot nH_2O$ (and also of the thiometalato complexes of Ni and Co) are promising as expected.[94]

A problem which could not be explained until now is the reason for the promoting effect of Co. We could isolate the "pseudo-isostructural" metal–sulfur cluster anions $[Mo_4S_4(CN)_{12}]^{8-}$ and $[Co_4S_4O(CN)_{12}]^{8-}$[91] (the valence states of the metal atoms in the clusters being comparable to those in the CoMoS phase). An SCCC-MO calculation shows that the electron density at the S atoms in the Co cluster is much higher than in the Mo one. Consequently, it can be understood that the Co cluster species is oxidized in the presence of air (μ_3-$S^{2-} \rightarrow \mu_3$-SO^{2-}) but not $[Mo_4S_4(CN)_{12}]^{8-}$. One influence of Co in the catalyst should definitely be the increase in the electron density at the S atoms, which could improve the activation of H_2 for instance.

IR studies of NO absorption of Al_2O_3-supported and unsupported Co–Mo HDS catalysts have shown that the CoMoS phase consists of Co atoms at the edges of MoS_2. (A high coverage of the MoS_2 edges and a high MoS_2 edge dispersion achieves a large promotion.) The IR spectrum of "NO absorbed" on a sulfided Co–Mo–Al_2O_3 catalyst shows three bands, which can be assigned to Co [ν(NO) 1850 and 1785 cm^{-1}] and Mo [ν(NO) 1785 and 1690 cm^{-1}] sites.[92] As ν(NO) frequencies are

very sensitive to the electronic state of the coordination centers it is worthwhile investigating the corresponding ν(NO) values of model substances[43] like $[(NO)_2Co(MoS_4)]^-$ [ν(NO) 1852 and 1770 cm^{-1}] and $[(NO)_2Co(MoO_2S_2)]^-$ [ν(NO) 1859 and 1781 cm^{-1}] (both with a $\{Co(NO)_2\}^{10}$ configuration which has a very high formation tendency) and $[(NO)_2Mo(NCS)_4]^{2-}$ with an $\{Mo(NO)_2\}^6$ configuration [ν(NO) 1782 and 1661 cm^{-1}].[93] The excellent agreement between the ν(NO) frequencies proves that the electronic environment of the Co and Mo centers in the model systems and the nitrosylated catalyst are comparable. Mononitrosyl complexes of Mo and Co have significant lower ν(NO) frequencies. The $(NO)_2CoS_2Mo$ moiety of the above-mentioned complex should therefore be abundant on the nitrosylated catalyst, too.[94]

Acknowledgements—Our own work cited in this review was supported by the Deutsche Forschungsgemeinschaft, the Fonds der Chemischen Industrie and the Minister für Wissenschaft und Forschung NRW. Thanks are due to Drs H. Bögge, E. Diemann, R. Jostes and H. Topsøe for helpful discussions.

REFERENCES

1. B. A. Averill, *Struct. Bonding (Berlin)* 1983, **53**, 59.
2. R. H. Holm, *Chem. Soc. Rev.* 1981, **10**, 455; D. Coucouvanis, *Acc. Chem. Res.* 1981, **14**, 201.
3. A. Müller, E. Diemann, R. Jostes and H. Bögge, *Angew. Chem., Int. Ed. Engl.* 1981, **20**, 934.
4. Reviews of B. K. Burgess and W. E. Newton, D. Coucouvanis, J. H. Enemark, C. D. Garner as well as E. I. Stiefel and R. R. Chianelli, In *Nitrogen Fixation, The Chemical–Biochemical–Genetic Interface* (Edited by A. Müller and W. E. Newton). Plenum Press, New York (1983).
5. C. D. Garner, J. R. Nicholson, S. K. Hagyard, J. Charnock and C. F. Mills, *Rev. Port. Quim.* 1985, **27**, 78.
6. E. I. Stiefel, In *Proceedings of the Fourth International Conference on the Chemistry and Uses of Molybdenum* (Edited by H. F. Barry and P. C. H. Mitchell), p. 56. Climax Molybdenum Co., Ann Arbor, MI (1982).
7. H. Topsøe and B. S. Clausen, *Catal. Rev.—Sci. Eng.* 1984, **26**, 395; H. Topsøe, R. Candia, N. Y. Topsøe and B. S. Clausen, *Bull. Soc. Chim Belg.* 1984, **93**, 783.
8. H. Topsøe, In *Surface Properties and Catalysis by Non-metals* (Edited by J. P. Bonnelle, B. Delmon and E. Derounane), p. 329. D. Reidel, Dordrecht (1983).
9. R. R. Chianelli, *Catal. Rev.—Sci. Eng.* 1984, **26**, 361.
10. J. B. Goodenough, In *Proceedings of the Fourth International Conference on the Chemistry and Uses of Molybdenum* (Edited by H. F. Barry and P. C. H. Mitchell), p. 1. Climax Molybdenum Co., Ann Arbor, MI (1982).
11. W. Clegg, N. Mohan, A. Müller, A. Neumann, W. Rittner and G. M. Sheldrick, *Inorg. Chem.* 1980, **19**, 2066.
12. A. Müller, R. Jostes, W. Eltzner, Chong-shi Nie, E. Diemann, H. Bögge, M. Zimmermann, M. Dartmann, U. Reinsch-Vogell, Shun Che, S. J. Cyvin and B. N. Cyvin, *Inorg. Chem.* 1985, **19**, 2872; K. Wieghardt, W. Herrmann, A. Müller, W. Eltzner and M. Zimmermann, *Z. Naturforsch.* 1984, **39B**, 876.
13. M. G. B. Drew, P. C. H. Mitchell and C. F. Pygall, *Angew. Chem., Int. Ed. Engl.* 1976, **15**, 784; *J. Chem. Soc., Dalton Trans.* 1979, 1213.
14. A. Müller, W. Eltzner and E. Krickemeyer, to be published; see also Ref. 18.
15. W. Beck, W. Danzer and G. Thiel, *Angew. Chem., Int. Ed. Engl.* 1973, **12**, 582.
16. A. Müller, W. Eltzner, H. Bögge and R. Jostes, *Angew. Chem., Int. Ed. Engl.* 1982, **21**, 795; *Angew. Chem.* Suppl. 1982, 1643.
17. J. A. Bandy, C. E. Davies, J. C. Green, M. L. H. Green, K. Prout and D. P. S. Rodgers, *J. Chem. Soc., Chem. Commun.* 1983, 1395.
18. A. Müller, W. Eltzner, W. Clegg and G. M. Sheldrick, *Angew. Chem., Int. Ed. Engl.* 1982, **21**, 536; *Angew. Chem.* Suppl. 1982, 1177.
19. P. J. Lapasset, N. Chezeau and P. Belougne, *Acta Cryst.* 1976, **B32**, 3087.
20. M. Draganjac, E. Simhon, L. T. Chan, M. Kanatzidis, N. C. Baenziger and D. Coucouvanis, *Inorg. Chem.* 1982, **21**, 3321.
21. A. Müller, M. Römer, C. Römer, U. Reinsch-Vogell, H. Bögge and U. Schimanski, *Monatsh. Chem.* 1985, **116**, 711.
22. W.-H. Pan, M. E. Leonowicz and E. I. Stiefel, *Inorg. Chem.* 1983, **22**, 672.
23. A. Müller, H. Bögge, E. Krickemeyer, G. Henkel and B. Krebs, *Z. Naturforsch.* 1982, **37B**, 1014.
24. A. Müller and P. Christophliemk, *Angew. Chem., Int. Ed. Engl.* 1969, **8**, 753; C. Potvin, J.-M. Manoli, J.-M. Brégeault and G. Chottard, *Inorg. Chim. Acta* 1983, **72**, 103; see also Ref. 13.
25. A. Müller, S. Sarkar, H. Bögge, R. Jostes, A. Trautwein and U. Lauer, *Angew. Chem., Int. Ed. Engl.* 1983, **22**, 561; *Angew Chem.* Suppl. 1983, 747.
26. E. Königer-Ahlborn and A. Müller, *Angew. Chem., Int. Ed. Engl.* 1975, **14**, 574.
27. A. Müller, U. Reinsch-Vogell and H. Bögge, to be published.
28. A. Müller, W. O. Nolte and B. Krebs, *Inorg. Chem.* 1980, **19**, 2835.
29. A. Müller, S. Pohl, M. Dartmann, J. P. Cohen, J. M. Bennett and R. M. Kirchner, *Z. Naturforsch.* 1979, **34B**, 434; see also Ref. 90.
30. A. Müller, R. G. Bhattacharyya, W. Eltzner, N. Mohan, A. Neumann and S. Sarkar, In *Proceedings of the Third International Conference on the Chemistry and Uses of Molybdenum* (Edited by H. F. Barry and P. C. H. Mitchell), p. 59. Climax Molybdenum Co., Ann Arbor, MI (1979).
31. A. Müller, W. Eltzner, H. Bögge and S. Sarkar, *Angew. Chem., Int. Ed. Engl.* 1982, **21**, 535; *Angew. Chem.* Suppl. 1982, 1167.

32. A. Müller, W. Eltzner, R. Jostes, H. Bögge, E. Diemann, J. Schimanski and H. Lueken, *Angew. Chem., Int. Ed. Engl.* 1984, **23**, 389.
33. A. Müller, W. Eltzner, H. Bögge and E. Krickemeyer, *Angew. Chem., Int. Ed. Engl.* 1983, **22**, 884.
34. E. Königer-Ahlborn, H. Schulze and A. Müller, *Z. Anorg. Allg. Chem.* 1977, **428**, 5.
35. A. Müller, J. Schimanski and H. Bögge, to be published.
36. M. Rakowski DuBois, M. C. VanDerveer, D. L. DuBois, R. C. Haltiwanger and W. K. Miller, *J. Am. Chem. Soc.* 1980, **102**, 7456.
37. M. Rakowski DuBois, D. L. DuBois, M. C. VanDerveer and R. C. Haltiwanger, *Inorg. Chem.* 1981, **20**, 3064.
38. P. C. H. Mitchell and C. F. Pygall, *J. Inorg. Biochem.* 1979, **11**, 25.
39. A. Müller and W. Jaegermann, *Inorg. Chem.* 1979, **18**, 2631.
40. A. Müller, W. Jaegermann and J. H. Enemark, *Coord. Chem. Rev.* 1982, **46**, 245.
41. A. Müller, W. Eltzner and N. Mohan, *Angew. Chem., Int. Ed. Engl.* 1979, **18**, 168.
42. A. Müller, M. Dartmann, C. Römer, W. Clegg and G. M. Sheldrick, *Angew. Chem., Int. Ed. Engl.* 1981, **20**, 1060.
43. A. Müller, P. Stolz, H. Bögge, S. Sarkar, K. Schmitz, A. Fangmeier, H. Büker and W. Twistel, *Z. Anorg. Allg.* Chem. (in press); A. Müller *et al.*, to be published.
44. A. Müller, E. Krickemeyer and H. Bögge, to be published.
45. A. Müller, W. Hellmann, C. Römer, M. Römer, H. Bögge, R. Jostes and U. Schimanski, *Inorg. Chim. Acta* 1984, **83**, L75 (and literature cited therein).
46. A. Müller, H. Dornfeld, G. Henkel, B. Krebs and M. P. A. Viegers, *Angew. Chem., Int. Ed. Engl.* 1978, **17**, 52.
47. A. Müller, I. Paulat-Böschen, B. Krebs and H. Dornfeld, *Angew. Chem., Int. Ed. Engl.* 1976, **15**, 633.
48. A. Müller, U. Schimanski and J. Schimanski, *Inorg. Chim. Acta* 1983, **76**, L245.
49. U. Schimanski, PhD Thesis, Bielefeld (1983).
50. A. Müller, H. Bögge, E. Königer-Ahlborn and W. Hellmann, *Inorg. Chem.* 1979, **18**, 2301.
51. E. M. Kinsch and D. W. Stephan, *Inorg. Chim. Acta* 1985, **96**, L87.
52. D. Coucouvanis, N. C. Baenziger, E. D. Simhon, P. Stremple, D. Swenson, A. Simopoulos, A. Kostikas, V. Petrouleas and V. Papaefthymiou, *J. Am. Chem. Soc.* 1980, **102**, 1732.
53. A. Müller, J. Schimanski and H. Bögge, *Z. Anorg. Allg. Chem.* (in press).
54. A. Müller, W. Hellmann, H. Bögge, R. Jostes, M. Römer and U. Schimanski, *Angew. Chem., Int. Ed. Engl.* 1982, **21**, 860; *Angew. Chem.* Suppl. 1982, 1757.
55. D. Coucouvanis, E. D. Simhon and N. C. Baenziger, *J. Am. Chem. Soc.* 1980, **102**, 6644; J. W. McDonald, G. D. Friesen and W. E. Newton, *Inorg. Chim. Acta* 1980, **46**, L79.
56. A. Müller, R. Jostes, W. Hellmann, C. Römer, H. Bögge, U. Schimanski, B. Zhuang, L. D. Rosenheim, J. W. McDonald and W. E. Newton, *Z. Anorg. Allg. Chem.* (in press).
57. J. W. McDonald, D. G. Friesen, W. E. Newton, A. Müller, W. Hellmann, U. Schimanski, A. Trautwein and U. Bender, *Inorg. Chim. Acta* 1983, **76**, L297.
58. A. Müller, N. Mohan and H. Bögge, *Z. Naturforsch.* 1978, **33B**, 978.
59. A. Müller, W. Hellmann, U. Schimanski, R. Jostes and W. E. Newton, *Z. Naturforsch.* 1983, **38B**, 528.
60. A. Müller, W. Hellmann, J. Schneider, U. Schimanski, U. Demmer, A. Trautwein and U. Bender, *Inorg. Chim. Acta* 1982, **65**, L41.
61. A. Müller and W. Hellmann, *Spectrochim. Acta* 1985, **41A**, 359.
62. A. Müller and S. Sarkar, *Angew Chem., Int. Ed. Engl.* 1977, **16**, 705.
63. T. P. Prassad, E. Diemann and A. Müller, *J. Inorg. Nucl. Chem.* 1973, **35**, 1895.
64. A. Müller *et al.*, to be published.
65. A. Müller, U. Reinsch-Vogell, E. Krickemeyer and H. Bögge, *Angew. Chem., Int. Ed. Engl.* 1982, **21**, 796.
66. T. R. Halbert, W.-H. Pan and E. I. Stiefel, *J. Am. Chem. Soc.* 1983, **105**, 5476.
67. A. Müller, R. G. Bhattacharyya, N. Mohan and B. Pfefferkorn, *Z. Anorg. Allg. Chem.* 1979, **454**, 118.
68. T. R. Halbert, K. McGauley, W.-H. Pan, R. S. Czernuszewicz and E. I. Stiefel, *J. Am. Chem. Soc.* 1984, **106**, 1849.
69. A. Müller and E. Krickemeyer, to be published.
70. A. Müller, R. G. Bhattacharyya and B. Pfefferkorn, *Chem. Ber.* 1979, **112**, 778; see also Ref. 30.
71. A. Müller, E. Krickemeyer and U. Reinsch, *Z. Anorg. Allg. Chem.* 1980, **470**, 35.
72. A. Müller and U. Reinsch, *Angew. Chem., Int. Ed. Engl.* 1980, **19**, 72.
73. W.-H. Pan, M. A. Harmer, T. R. Halbert and E. I. Stiefel, *J. Am. Chem. Soc.* 1984, **106**, 459.
74. W. Rittner, A. Müller, A. Neumann, W. Bäther and R. C. Sharma, *Angew. Chem., Int. Ed. Engl.* 1979, **18**, 530.
75. P. Secheresse, J. Lefebvre, J. C. Daran and Y. Jeannin, *Inorg. Chem.* 1982, **21**, 1311.
76. K. H. Schmidt and A. Müller, *Coord. Chem. Rev.* 1974, **14**, 115.
77. A. Müller, W. Jaegermann and W. Hellmann, *J. Mol. Struct.* 1983, **100**, 559.
78. R. J. Clark and T. J. Dines, *Angew Chem., Int. Ed. Engl.* (in press).
79. R. Jostes, A. Müller and E. Diemann, *J. Mol. Struct. Theochem.* (in press). [For older work see: A. Müller, E. Diemann and C. K. Jørgensen, *Struct. Bonding (Berlin)* 1973, **14**, 23; A. Müller and E. Diemann, *Chem. Phys. Lett.* 1971, **9**, 369.]
80. J. Bernholc and E. I. Stiefel, *Inorg. Chem.* 1985, **24**, 1323.
81. E. Diemann and A. Müller, *Chem. Phys. Lett.* 1974, **27**, 351.
82. A. Müller and E. Diemann, *J. Chem. Phys.* 1974, **61**, 5469.
83. E. Königer-Ahlborn, A. Müller, A. D. Cormier, J. D. Brown and K. Nakamoto, *Inorg. Chem.* 1975, **14**, 2009.

84. R. Jostes and A. Müller, to be published.
85. A. Müller, R. Jostes, H. G. Tölle, A. Trautwein and E. Bill, *Inorg. Chim. Acta* 1980, **46**, L121.
86. A. Müller, R. Jostes, V. Flemming and R. Potthast, *Inorg. Chim. Acta* 1980, **44**, L33.
87. W. Hellmann, PhD. Thesis, Bielefeld (1984).
88 J. Bernholc and N. A. W. Holzwarth, *J. Chem. Phys.* 1984, **81**, 3987.
89. W. Jaegermann, PhD Thesis, Bielefeld (1981).
90. E. Diemann, A. Müller and P. J. Aymonino, *Z. Anorg. Allg. Chem.* 1981, **479**, 191.
91. A. Müller, E. Krickemeyer, R. Jostes, H. Bögge, E. Diemann and U. Bergmann, *Z. Naturforsch.* (in press).
92. N. Y. Topsøe and H. Topsøe, *J. Catal.* 1983, **84**, 386; N. Y. Topsøe, H. Topsøe, O. Sørensen, B. S. Clausen and R. Candia, *Bull. Soc. Chim. Belg.* 1984, **93**, 727.
93. A. Müller, W. Eltzner, S. Sarkar, H. Bögge, P. J. Aymonino, N. Mohan, U. Seyer and P. Subramanian, *Z. Anorg. Allg. Chem.* 1983, **503**, 22.
94. A. Müller *et al.*, to be published.
95. R. H. Tieckelmann, H. C. Silvis, T. A. Kent, B. H. Huynh, J. V. Waszczak, B.-K. Teo and B. A. Averill, *J. Am. Chem. Soc.* 1980, **102**, 5550; A. Müller, H.-G. Tölle and H. Bögge, *Z. Anorg. Allg. Chem.* 1980, **471**, 115.
96. A. Müller, H. Bögge and E. Krickemeyer, to be published.
97. W. Clegg, G. Christou, C. D. Garner and G. M. Sheldrick, *Inorg. Chem.* 1981, **20**, 1562.
98. A. Müller and E. Diemann, *Chimia* 1985, **39**, 312.
99. H. Winkler, E. Bill, U. Lauer, A. X. Trautwein, A. Kostikas, V. Papaefthymiou, H. Bögge, A. Müller, E. Gerdau and U. Gonser, *J. Chem. Phys.* 1985, **82**, 3594.
100. Y. Do, E. D. Simhon and R. H. Holm, *Inorg. Chem.* 1985, **24**, 2827.

Polyhedron Vol. 5, No. 1/2, pp. 341–347, 1986
Printed in Great Britain

0277–5387/86 $3.00 + .00
© 1986 Pergamon Press Ltd

LIGAND AND INDUCED INTERNAL REDOX PROCESSES IN Mo– AND W–S SYSTEMS

M. A. HARMER, T. R. HALBERT, W.-H. PAN, C. L. COYLE, S. A. COHEN and E. I. STIEFEL*

Corporate Research Science Laboratories, Exxon Research and Engineering Co., Clinton Township, Route 22, East Annandale, NJ 08801, U.S.A.

(*Received* 5 *August* 1985)

Abstract—This paper reviews recent work from our laboratory on redox chemistry of Mo–S systems. Mo and S are each capable of existing in multiple oxidation states. When found together in the same compound, these elements elicit numerous redox possibilities. The classical situation involving simple changes in the oxidation state of Mo is well known. Recent work has also documented the ability of coordinated S ligands (e.g. S^{2-}, S_2^{2-} and S_4^{2-}) to undergo redox while Mo remains in a given state of oxidation. In this paper cases are presented wherein both the Mo and S oxidation states change. For example, the reaction of the red MoS_4^{2-} ion with organic disulfides gives the purple $Mo_2S_8^{2-}$ ion in high yield. The oxidizing disulfide added to the hexavalent MoS_4^{2-} ion leads quantiatively to the reduced pentavalent dinuclear $Mo_2S_8^{2-}$ ion. Mechanistically, this reaction proceeds in two stages involving a green intermediate of yet unknown structure. The net reaction embodies an induced internal electron transfer from S to Mo in the same sense that Taube *et al.* elucidated in the chemistry of cobalt. Application of the concept of induced internal electron transfer allows access to new low-valent Mo–S systems by adding oxidants to Mo(VI)–S species. For example, the reactions of MoS_4^{2-} with thiuram disulfides give compounds of the form $MoS_2(S_2CNR_2)_3$ (R = Et or *i*-Bu). These are mononuclear EPR-active Mo(V) complexes containing eight-coordinate Mo. As expected, W shows distinctly less reactivity than Mo in S → M redox processes. The ability of S^{2-} ligands to act as donors and Mo and W atoms to act as acceptors of electron density has also been exploited in the synthesis of new heteronuclear "thiocubane" clusters.

Mo and S, in their respective groups VI of the periodic table, are each renowned for their ability to form numerous compounds in relatively large numbers of oxidation states.[1] For Mo, states −II to VI have been reported, and for S the same range is spanned, as exemplified by the inorganic limits, S^{2-} and SO_4^{2-}. Whenever Mo *or* S is present in a compound, redox reactions often play a central role in the chemistry of that compound.

Redox chemistry also plays a potential role in the action of Mo enzymes[2] and Mo-based heterogeneous catalytic systems.[3] In such systems, Mo can span oxidation states IV–VI with the possible presence of trivalent Mo as well. In many of these systems seemingly simple Mo-based redox reactions may be crucial to catalysis and have been proposed as key steps in reaction pathways. However, the assumption of a purely metal-based redox process must always be questioned when the ligand involved is S-containing and thereby has capacity for redox of its own or in conjunction with Mo-based redox.

Although examples are known in which one cannot meaningfully disect the metal or ligand contribution to a given redox process, such ambiguous cases will not be encountered in the present paper. Rather, here we consider cases in which, on chemical or physical grounds, the bulk redox change can be regarded as a discrete combination of metal and ligand-based redox processes. For Mo, these discrete changes interconvert specific *d*-electron configurations which embody characteristic Mo–Mo bonding, structural,

* Author to whom correspondence should be addressed.

spectroscopic and magnetic behavior. For example, Mo(VI), $4d^0$, compounds display no tendency to form Mo–Mo bonds and have no "*d–d*" bands. In contrast, Mo(V), $4d^1$, compounds have a tendency to form dinuclear compounds with a single metal–metal bond or, if mononuclear, show a single unpaired *d*-electron with characteristic EPR signal.

Changes in S oxidation state likewise correlate with distinct structural differences. For example, S^{2-}, the most reduced form of S, tends to multiply bond to Mo, either by forming double or triple bonds to a single Mo atom or by bridging two or three Mo atoms.[4] There is no S—S bonding in this most highly reduced form of the S ligand. However, upon oxidation to S_2^{2-} there is clearly an S–S bond at ~2.05 Å, characteristic of S(−I) containing compounds[5] (analogous to the O–O single bond in the peroxide ion, O_2^{2-}). Even if we restrict our consideration to ligands containing only S, we find an extensive series that includes S_8,[6] S_6^{2-},[7] S_5^{2-},[8] S_4^{2-},[7] S_3^{2-}[9,10] and S_2^{2-}.[11] In this series, the oxidation state of S ranges from 0 to −II. For example, formally, the non-ligating S atoms in a chelating or bridging S_n^{2-} ligand are S(0), while each of the terminal S atoms are S(−I). Clearly, rudimentary inspection of the structural and spectroscopic properties of Mo–S complexes is sufficient to assign oxidation states and corresponding electron configurations. For the purpose of systematizing the chemistry of these and related compounds, it is crucial to make such assignments.

In this paper we review recent work on the redox chemistry of Mo–S systems. We use formal oxidation states to keep track of redox changes and we show that internal electron transfer between S and Mo occurs commonly and can explain seemingly paradoxical redox events.

LIGAND-BASED REDOX

The availability of Mo–S complexes with S_2^{2-} ligands, namely the Mo(V) complex $Mo_2(S_2)_6^{2-}$[12] and the Mo(IV) complex $Mo_3S(S_2)_6^{2-}$,[13] led us to attempt reactions, wherein the disulfido ligands constitute the sites of reactivity. Although the reactions are quite general,[14,15] in the examples below we use only ethane-1,2-dithiolate as our reductant and ligand. The dinuclear complex reacts according to Ref. 14:

$$Mo_2(S_2)_6^{2-} + \text{excess } \begin{matrix} CH_2S^- \\ | \\ CH_2S^- \end{matrix} \rightarrow Mo_2S_4(SCH_2CH_2S)_2^{2-}.$$

The $Mo_2(S_2)_6^{2-}$ starting material[12] is a Mo(V) dinuclear species, as is the $Mo_2S_4(SCH_2CH_2S)_2^{2-}$ product. Although no Mo redox is involved, the reaction nevertheless involves a 12-electron reduction in which the six disulfido ligands are reduced to four sulfido ligands and eight free S^{2-} ions (or HS^- or H_2S, depending on the acidity). Similarly, $Mo_3S(S_2)_6^{2-}$ reacts according to Ref. 15:

$$Mo_3S(S_2)_6^{2-} + \text{excess } \begin{matrix} CH_2S^- \\ | \\ CH_2S^- \end{matrix} \rightarrow Mo_3S_4(SCH_2CH_2S)_3^{2-}.$$

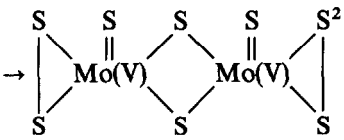
Here the $Mo_3S(S_2)_6^{2-}$[13] starting material is a Mo(IV) trinuclear complex, as is the $Mo_3S_4(SCH_2CH_2S)_3^{2-}$ product. Again, the 12-electron redox reaction involves only the S ligands. Clearly, extensive redox activity is inherent in *S*-donor ligands bound to Mo.

INTERNAL REDOX PROCESSES

The ligand redox activity augments the well-known metal-based redox reactivity, which is characteristic of Mo complexes. In certain cases, both metal and ligand redox can occur during a given reaction. The result is often a seemingly paradoxical redox change. For example, the addition of the oxidant S_8 to the Mo(VI) complex MoS_4^{2-} leads[16,17] to the Mo(IV) complex MoS_9^{2-}, i.e. addition of *oxidant* leads to the *reduction* of the metal center.

A very clear example of this process occurs in the reaction:[18]

$$2Mo(VI)S_4^{2-} + RSSR \rightarrow$$



$$+ 2RS^-.$$

The structure of the $Mo_2S_8^{2-}$ product is shown in Fig. 1. The presence of four sulfido and two disulfido ligands leave no doubt as to the appropriateness of the Mo(V) formulation of the dianionic product. Here, addition of the organic disulfide oxidant,

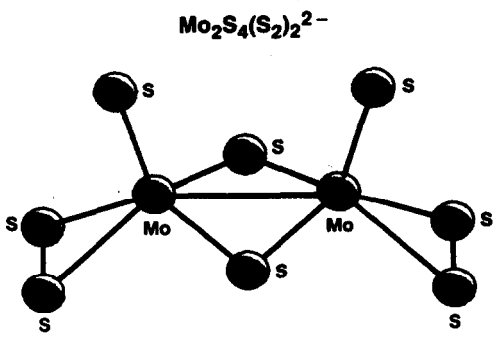


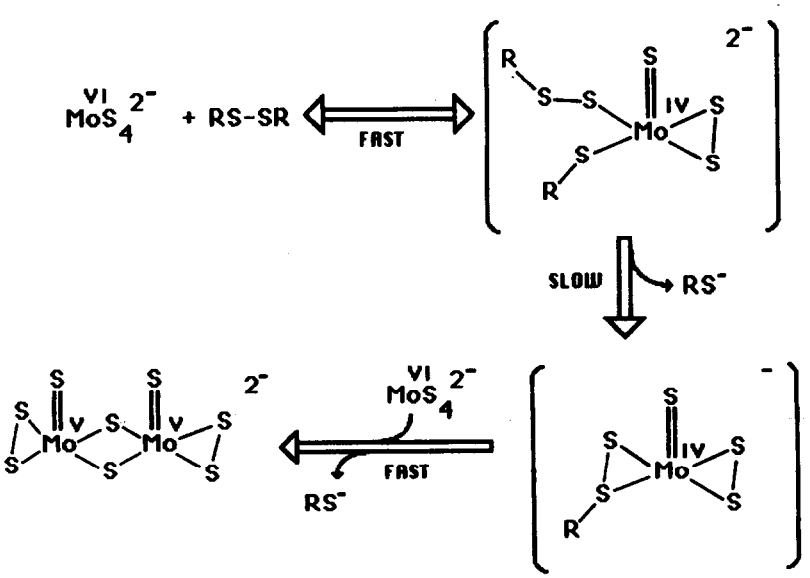
Fig. 1. Structure of $Mo_2S_8^{2-}$.[18]

RSSR, leads to the oxidation of two MoS_4^{2-} ions by two electrons (i.e. $2MoS_4^{2-} \rightarrow Mo_2S_8^{2-} + 2e^-$). Moreover, since $Mo_2S_8^{2-}$ contains Mo in the V oxidation state the external *oxidant* has led to internal *reduction* of the metal center. However, the source of electrons (reductant) is clearly those bound sulfido ligands that are oxidized to disulfido ligands during the reaction. Indeed, the ligands undergo a four-electron oxidation ($4S^{2-} \rightarrow 2S_2^{2-} + 4e^-$). Two of the electrons are transferred to the RSSR oxidant ($RSSR + 2e^- \rightarrow 2RS^-$) while the remaining two go, one each, to the two Mo(VI) ions generating the two Mo(V) ions. The reaction thus involves an internal electron transfer from S → Mo that is induced by the external oxidant RSSR.

Such *induced internal electron transfers* are known in the chemistry of other systems. For example, Taube[19] has shown that the oxalato Co(III) complex $Co(NH_3)_5(C_2O_4)^+$ reacts with one equivalent of the one-electron oxidant Ce^{4+} to generate Ce^{3+} and Co^{2+}. Each metal ion can be reduced by one electron as the coordinated oxalate is oxidized by two electrons to CO_2 ($C_2O_4^{2-} \rightarrow 2CO_2 + 2e^-$). In this case, the external oxidant, Ce^{4+}, induces ligand → Co(III) internal electron transfer. The analogy with MoS_4^{2-} oxidation by RSSR is clear, and the Mo–S reaction is therefore also described as an induced internal electron transfer process.

We have investigated the mechanism of formation of $Mo_2S_8^{2-}$ from $2MoS_4^{2-}$.[20] Reaction of the red MoS_4^{2-} ion with RSSR establishes an equilibrium with the formation of a green intermediate. The rate of formation of this intermediate is first order in both RSSR and MoS_4^{2-} and depends upon the nature of R. Electron-withdrawing R groups cause the intermediate to be formed more rapidly and shift the equilibrium toward more complete reaction. The green intermediate ($\lambda_{max} = 620$) decays by pseudo first-order kinetics to give the purple $Mo_2S_8^{2-}$ product. A sequence of events consistent with the data is shown in Scheme 1. The implied mononuclear, even-electron nature of the intermediate, although not unequivocally established, is consistent with all experimental data obtained to date. The occurrence of a mononuclear intermediate suggests that a mononuclear complex could be trapped if appropriate measures were taken. For example, if the organic disulfide were part of a chelating ligand, the resultant thiolate, i.e. the reduced form of the disulfide oxidant, might remain bound to and stabilize the mononuclear Mo center. Such a strategy has indeed been effective in yielding mononuclear reduced Mo centers.

Reaction of MoS_4^{2-} with tetraethylthiuram disulfide, $(C_2H_5)_2NC(S)S\text{-}SC(S)N(C_2H_5)_2$,[21] leads to the isolation of a mononuclear Mo(V) complex, $MoS_2[S_2CN(C_2H_5)_2]_3$. The structure of this complex and its EPR spectrum are shown in Fig. 2 and Fig. 3, respectively. The EPR spectrum, with its characteristic Mo(V) parameters, illustrates dramatically the $4d^1$ configuration of the Mo(V) complex. This configuration is, of course, unequivocally inferred from the valency of the ligands, i.e. three dtc^- ligands and one S_2^{2-} ligand in this neutral complex. Clearly, in this case the Mo center has been reduced by internal electron transfer from the bound sulfide ligands, while the latter are concomitantly oxidized to bound S_2^{2-} (and to free oxidized S-



Scheme 1.

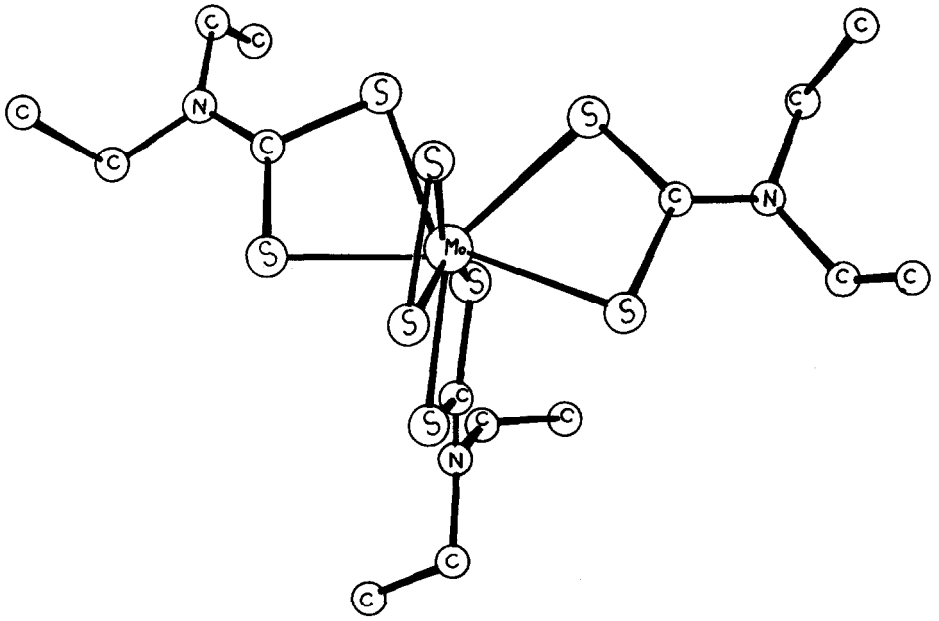


Fig. 2. Structure of $Mo(S_2)[(C_2H_5)_2dtc]_3$.[21]

containing species). Remarkably, it has thus proven possible to produce *new reduced Mo–S complexes* by adding *oxidants* to MoS_4^{2-} which contains Mo in its highest oxidation state (VI). This is a synthetically useful procedure leading to high yields of the new products.

Although this paper concentrates on the chemistry of Mo–S systems, we briefly discuss some W–S chemistry for the purpose of comparison. WS_4^{2-} reacts with S_8 upon heating[22] to produce the $(S_4)W(S)S_2WS(S_4)^{2-}$ ion containing a W(V), $W_2S_4^{2+}$-core and peripheral bidentate tetrasulfide S_4^{2-} ligands. At room temperature, unlike MoS_4^{2-}, which reacts with S_8 to give MoS_9^{2-},[16,17] WS_4^{2-} does not react with S_8. The W(IV) oxidation state required to form WS_9^{2-} may not be attainable. The greater difficulty in reducing W(VI), cf. Mo(VI), is also clearly manifested in the reaction of WS_4^{2-} with the tetraalkylthiuram disulfide. Here, in sharp contrast with the MoS_4^{2-} case (*vide supra*), WS_4^{2-} reacts with $R_2NC(S)S\text{-}SC(S)NR_2$ to yield $WS(S_2)(R_2dtc)_2$, a W(VI) complex, whose structure is shown in Fig. 4.[21] Clearly, while MoS_4^{2-} reacts by internal $S \rightarrow Mo$ redox, WS_4^{2-} reacts via a purely ligand-based redox process in which no $S \rightarrow W$ electron transfer occurs. The reactivity comparison of WS_4^{2-} and MoS_4^{2-} emphasizes the known trend that Mo compounds are more easily reduced than their W analogs.

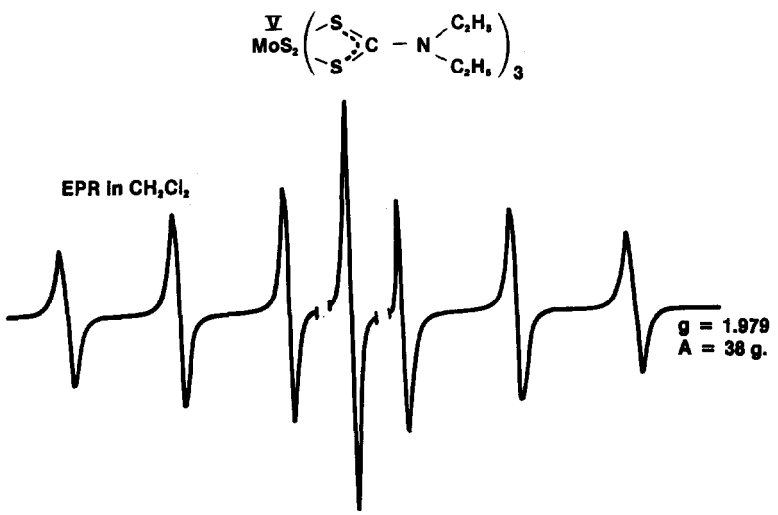


Fig. 3. EPR spectrum of $Mo(S_2)[(C_2H_5)_2dtc]_3$.

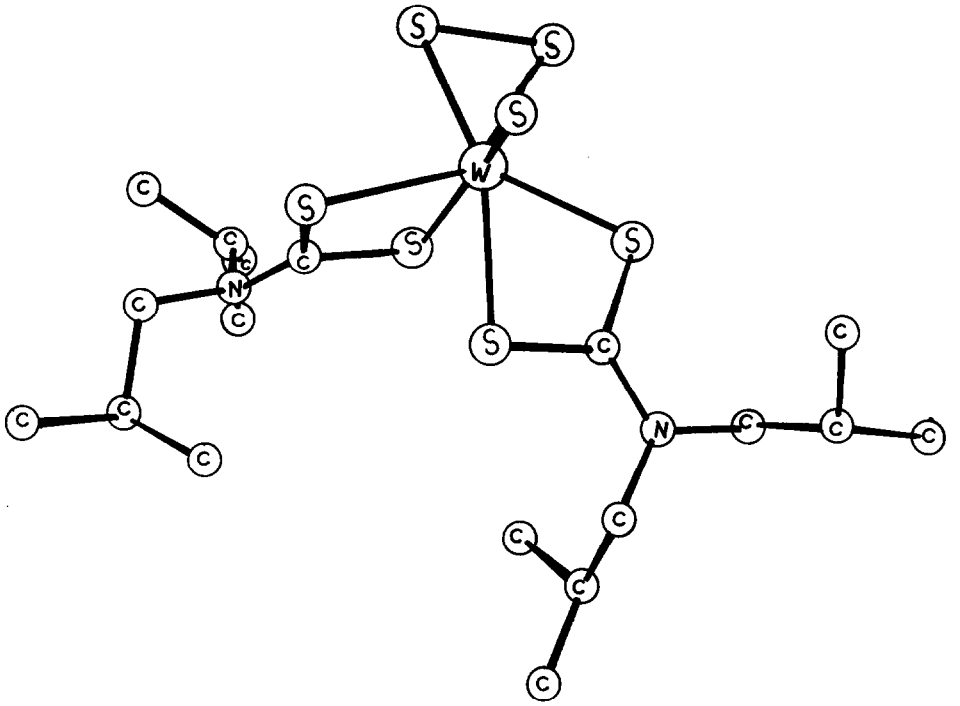


Fig. 4. Structure of $WS(S_2)[(C_4H_9)_2dtc]_2$.[21]

In Mo chemistry it is possible to change the redox tendency of a given complex by changing ligands. In particular, substitution of oxo for sulfido ligands makes it more difficult to reduce the resultant complex. For example, $Mo_2O_2S_2(R_2dtc)_2$ is more difficult to reduce than $Mo_2S_4(R_2dtc)_2$.[23] We therefore tried the reaction of $MoO_2S_2^{2-}$ with the thiuram disulfide to see whether it would undergo S → Mo internal electron transfer, as does MoS_4^{2-}, or purely ligand redox, as does WS_4^{2-}. The product of the reaction of $MoO_2S_2^{2-}$ and thiuram disulfide is the known complex $MoO(S_2)(R_2dtc)_2$,[24] the oxo analog of the W reaction product. Therefore, substitution of oxo for sulfido changes the reaction pathway of the Mo complex from one involving S → M internal electron transfer to one involving simple ligand redox. In a sense substitution of oxo for sulfido causes Mo to behave more like W.

The varied redox reactivity of Mo–S systems is indicative of facile electron transfer between Mo and S components of a given complex. This in turn implies that frontier orbitals which are predominantly "Mo" and "S" in character may lie very close in energy. Therefore, an external agent, e.g. an oxidant, can sufficiently perturb the energy levels to precipitate the internal redox process. Indeed, in other systems, thermal or photochemical activation may also provoke internal redox. For example, the conversion of $(NH_4)_2MoS_4$ to MoS_3[25] upon heating involves metal reduction and ligand oxidation, i.e. the formulation of the amorphous trisulfide as $Mo_2(S_2)(S)_4$, invokes Mo in the V oxidation state. Moreover, the photochemical conversion of $(Cp')_2Mo_2S_4$ to $(Cp')_2Mo_2S_2(S_2)$,[26] involves an Mo(V) sulfido complex converting to an Mo(IV) disulfido complex upon excitation with visible light. Clearly, S → Mo redox can be facilitated by various *physical* or *chemical* stimuli.

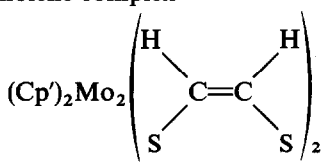
So far we have only considered cases in which internal *S* → *Mo* electron transfer occurs. However, *Mo* → *S* electron transfer is also possible. MoS_9^{2-} contains Mo in the IV oxidation state and tetrasulfide ligands. Addition of ethane-1,2-dithiol to MoS_9^{2-} leads quantitatively to the formation of MoS_4^{2-} containing hexavalent Mo.[18] Since no oxidant was added, the oxidation of Mo(IV) here was undoubtedly internal with S_4^{2-} ligands serving as oxidants for both the Mo by internal redox and the dithiolate ligand by external redox. Clearly, in lower-valent Mo complexes containing oxidized S ligands, Mo → S internal electron transfer processes may also be common.

BONDING, ORGANIC REACTIVITY AND SYNTHONS

The closeness of the energy levels available to Mo(IV), Mo(V) and Mo(VI) and S ligands also manifests itself in highly delocalized bonding in

binary Mo–S systems. For example, recent first-principles molecular orbital calculations on $Mo_3S_9^{2-}$[27] and $Mo_2S_8^{2-}$[28] reveal, respectively, a highly delocalized HOMO and very closely lying S- and Mo-based levels. This delocalized nature and closeness of the HOMOs and LUMOs also influences the reactivity of the complexes in question. We will use the reactivity of acetylenes to illustrate this influence.

Classically, coordination compounds are considered to react most readily at sites of real or potential coordinative unsaturation on their *metal* centers. For example, $MoO(R_2dtc)_2$ reacts with substituted acetylenes ($R'C{\equiv}CR'$, R' = H, C_6H_5 or CO_2CH_3) to produce adducts such as $MoO(R'C{\equiv}CR')(R_2dtc)_2$ where the acetylene is π-bound directly to the metal in the classical manner.[29] In contrast, Rakowski DuBois *et al.*[30] have shown that $(Cp')_2Mo_2S_4$ reacts with acetylene to yield the bridged dithiolene complex



in which the acetylene has reacted solely with the four S^{2-} ligands of the complex. Moreover, we have reported[31] that $Mo_2O_2S_2(S_2)_2^{2-}$ reacts with

$$R'C{\equiv}CR' \ (R' = CO_2CH_3)$$

to yield

$$\{Mo_2O_2S_2[SSC(CO_2CH_3)]_2\}^{2-},$$

a complex containing a vinyl disulfide ligand formed by insertion of the activated acetylene into one Mo—S bond of an MoS_2 linkage. Clearly, in specific circumstances, either metal-based, ligand-based or delocalized reactivity can occur.

Finally, the ability of bound sulfide to donate and high-valent Mo to accept electron density causes high-valent binary Mo–S complexes to act as potent ligands to transition-metal ions in low oxidation states. For example, $Fe(MoS_4)_2^{3-}$,[32] and $Co(MoS_4)_2^{3-}$[33] contain tetrahedral, high-spin Fe(I) and Co(I) ions, respectively, bound to bidentate MoS_4^{2-} ligands. These complexes are stabilized by metal–metal back donation from Fe or Co to Mo. Likewise, $Mo_3S_9^{2-}$, i.e. $MoS(MoS_4)_2^{2-}$, contains an MoS^{2+} thiomolybdenyl core also stabilized by back donation to the chelating bidentate tetrathiomolybdate ligands.[34] Clearly, MoS_4^{2-} is a versatile ligand that serves as a building block for the formation of polynuclear transition-metal sulfide clusters. Similarly, complexes containing the $Mo_2S_4^{2+}$ core can serve as building blocks to tetranuclear clusters. For example, terminal sulfide serves as the donor and Mo as an electron acceptor in the reaction of $Mo_2S_4(R_2dtc)_2$ with $Co_2(CO)_8$ to form a compound containing the thiocubane, $Mo_2Co_2S_4^{2+}$, core structure.[35] Similar reactions[36] indicate the potential utility of a "synthon", i.e. building-block, approach to the planned synthesis of heteronuclear clusters.

CONCLUSIONS

Mo–S complexes display great versatility in redox, bonding and reactivity. This versatility is at least in part due to the closeness of S and Mo energy levels, which leads in turn to facile redox and chemical reactivity. It is perhaps, in part, this type of reactivity that is responsible for the common presence of Mo–S systems in enzymic and industrial catalytic systems.

REFERENCES

1. F. A. Cotton and G. Wilkinson, *Advanced Inorganic Chemistry*, 4th Edn. John Wiley, New York (1980).
2. T. G. Spiro (Ed.), *Molybdenum Enzymes*, p. 89. John Wiley, New York (1985).
3. B. C. Gates, J. R. Katzer and G. C. A. Schuit, *Chemistry of Catalytic Processes*, p. 390. McGraw-Hill, New York (1979).
4. E. I. Stiefel, *Prog. Inorg. Chem.* 1977, **22**, 1.
5. A. Müller, W. Jaegermann and J. H. Enemark, *Coord. Chem. Rev.* 1982, **46**, 245.
6. H. W. Roesky, M. Thomas, J. Schimkowiak, P. G. Jones, W. Pinkert and G. M. Sheldrick, *J. Chem. Soc., Chem. Commun.* 1982, 895.
7. D. Coucouvanis, R. R Patil, M. G. Kanatzidis, B. Petering and N. C. Baenziger, *Inorg. Chem.* 1985, **24**, 24.
8. A. Müller, J. Schimanski and U. Schimanski, *Angew. Chem., Int. Ed. Engl.* 1984, **23**, 159.
9. R. D. G. Hard, F. L. Wimmer and J. P. G. Richards, *J. Chem. Soc., Dalton Trans.* 1985, 253; C. M. Bolinger, T. B. Rauchfuss and S. R. Wilson, *J. Am. Chem. Soc.* 1981, **103**, 5620.
10. A. Shaver and J. M. McCall, *Organometallics* 1984, **3**, 1823.
11. A. Müller, E. Diemann, R. Jostes and H. Bögge, *Angew. Chem., Int. Ed. Engl.* 1981, **20**, 933.
12. A. Müller, W. O. Nolte and B. Krebs, *Angew. Chem., Int. Ed. Engl.* 1978, **17**, 279.
13. A. Müller, S. Sarkar, R. G. Bhattacharyya, S. Pohl and M. Dartmann, *Angew. Chem., Int. Ed. Engl.* 1978, **17**, 535.
14. K. F. Miller, A. E. Bruce, J. L. Corbin, S. Wherland and E. I. Stiefel, *J. Am. Chem. Soc.* 1980, **102**, 5103.
15. T. R. Halbert, K. McGauley, W.-H. Pan, R. S. Czernuszewicz and E. I. Stiefel, *J. Am. Chem. Soc.* 1984, **106**, 1849.
16. M. Draganjac, E. Simhon, L. T. Chan, M. Kanatzidis, N. C. Baenziger and D. Coucouvanis, *J. Am. Chem. Soc.* 1981, **103**, 128.

17. E. D. Simhon, N. C. Baenziger, M. Kanatzidis, M. Draganjac and D. Coucouvanis, *J. Am. Chem. Soc.* 1981, **103**, 128.
18. W.-H. Pan, M. A. Harmer, T. R. Halbert and E. I. Stiefel, *J. Am. Chem. Soc.* 1984, **106**, 459.
19. H. Taube, *Electron Transfer Reactions of Complex Ions in Solution*, p. 73 (and references therein). Academic Press, New York (1970).
20. C. L. Coyle, M. A. Harmer, T. R. Halbert and E. I. Stiefel, in preparation.
21. W.-H. Pan, T. R. Halbert, L. L. Hutchings and E. I. Stiefel, *J. Chem. Soc., Chem. Commun.* 1985, 927.
22. S. A. Cohen and E. I. Stiefel, *Inorg. Chem.* (in press).
23. F. A. Schultz, V. R. Ott, D. S. Rolison, D. C. Bravard, J. W. McDonald and W. E. Newton, *Inorg. Chem.* 1978, **17**, 1758.
24. W. E. Newton, J. W. McDonald, J. L. Corbin, A. Ricard and R. Weiss, *Inorg. Chem.* 1980, **19**, 1997.
25. A. Müller and E. Diemann, *Z. Naturforsch.* 1968, **23B**, 1607; S. P. Cramer, K. S. Liang, A. J. Jacobson, C. H. Chang and R. R. Chianelli, *Inorg. Chem.* 1984, **23**, 1215.
26. A. E. Bruce and D. R. Tyler, *Inorg. Chem.* 1984, **23**, 3433.
27. J. Bernholc and E. I. Stiefel, *Inorg. Chem.* 1985, **24**, 1323.
28. J. Bernholc and E. I. Stiefel, submitted for publication.
29. K. Leonard, K. Plute, R. C. Haltiwanger and M. Rakowski DuBois, *Inorg. Chem.* 1979, **18**, 3246; J. Dirand-Colin, L. Ricard, R. Weiss and M. Schappacher, *J. Less-Common Met.* 1977, **54**, 91; J. Dirand, L. Ricard and R. Weiss, *Inorg. Nucl. Chem. Lett.* 1975, **11**, 661.
30. M. Rakowski DuBois, R. C. Haltiwanger, D. J. Miller and G. J. Glatzmaier, *J. Am. Chem. Soc.* 1979, **101**, 5245.
31. T. R. Halbert, W.-H. Pan and E. I. Stiefel, *J. Am. Chem. Soc.* 1983, **105**, 5476.
32. J. W. MacDonald, G. D. Friesen and W. E. Newton, *Inorg. Chim. Acta* 1980, **46**, L79; D. Coucouvanis, E. D. Simhon and N. C. Baenziger, *J. Am. Chem. Soc.* 1980, **102**, 6644; D. Coucouvanis, N. C. Baenziger, E. D. Simhon, P. Stremple, D. Swenson, A. Kostikas, A. Simopoulos, V. Petroleas and V. Papaefthymiou, *J. Am. Chem. Soc.* 1980, **102**, 1732; A. Müller, S. Sarkar, A. Dommröse and R. Filguera, *Z. Naturforsch.* 1980, **35B**, 1592.
33. W.-H. Pan, S. T. McKenna, R. R. Chianelli, T. R. Halbert, L. L. Hutchings and E. I. Stiefel, *Inorg. Chim. Acta* 1985, **97**, L17.
34. W.-H. Pan, M. E. Leonowicz and E. I. Stiefel, *Inorg. Chem.* 1983, **22**, 672.
35. T. R. Halbert, S. A. Cohen and E. I. Stiefel, *Organometallics* 1985, **4**, 1689.
36. H. Brunner and J. J. Wachter, *J. Organomet. Chem.* 1982, **240**, C41.

Polyhedron Vol. 5, No. 1/2, pp. 349–356, 1986
Printed in Great Britain

0277–5387/86 $3.00 + .00
© 1986 Pergamon Press Ltd

UNIQUE REACTIVITY CHARACTERISTICS OF Mo-COORDINATED S_2^{2-} AND S_4^{2-} LIGANDS

D. COUCOUVANIS,* A. HADJIKYRIACOU, M. DRAGANJAC, M. G. KANATZIDIS and O. ILEPERUMA

Department of Chemistry, University of Michigan, Ann Arbor, MI 48109, U.S.A.

(*Received* 15 *July* 1985)

Abstract—The synthesis of the new dithiolene complexes, $[\{(MeOOC)_2C_2S_2\}_2Mo(\mu_2\text{-}S)]_2^-$ and $[OMo(S_2C_2(COOMe)_2)_2]^{2-}$, is reported. These complexes are obtained by the reaction of dicarbomethoxyacetylene (DMA) with either $[(S_4)Mo(S)(\mu_2\text{-}S)_2Mo(S)(S_4)]^{2-}$ or $[(CS_4)Mo(S)(\mu_2\text{-}S)_2Mo(S)(CS_4)]^{2-}$ and $[OMo(S_4)_2]^{2-}$, respectively. The reaction of $[(S_4)Mo(O)(\mu_2\text{-}S)_2Mo(O)(S_2)]^{2-}$ with DMA results in the new dithiolene complex $[\{(MeOOC)_2C_2S_2\}Mo(O)(\mu_2\text{-}S)]_2^-$, which is the isomeric form of the vinyl disulfide complex obtained in the reaction of the $[(S_2)Mo(O)(\mu_2\text{-}S)_2Mo(O)(S_2)]^{2-}$ complex with DMA. The difference in reactivity between the two complexes that contain the same $[Mo_2O_2S_2]^{2+}$ core is attributed to the intrinsically different reactivity characteristics of the S_4^{2-} and S_2^{2-} ligands. As a result of Mo–S d_π–p_π bonding an alternation in the S—S bond lengths is observed in virtually all of the structurally characterized Mo–S_4 units. The consequent weakening of the S—S bonds adjacent to the Mo—S bonds allows for the ready dissociation of S_2^0 from the Mo-coordinated S_4^{2-} ligands. This weakening also accounts for the facile formation of dithiolenes in cycloaddition reactions of alkynes with the Mo–S_4 units. By comparison, the S—S bond in side-on Mo-coordinated S_2^{2-} ligands is strengthened as a result of depopulation of the ligand π^*-orbitals. Reactions of the latter with alkynes do not proceed by cycloaddition. Instead, insertion into the Mo—S bond has been reported for at least one such reaction. The importance of activated polysulfide ligands in the hydrodesulfurization reaction is discussed.

The extensive chemistry of molecular binary molybdenum sulfide compounds presents a unique opportunity for the study of units which may be structurally and electronically similar to the Mo–S active sites in the catalysts employed in the hydrodesulfurization (HDS) reaction.

The wide variety of binary molybdenum sulfides that have emerged in recent years derives primarily from the reactivity of the MoS_4^{2-} dianion toward sulfur reagents. The complex equilibria and interconversions between Mo thioanions that prevail in MoS_4^{2-}–$(NH_4)_2S_x$ or MoS_4^{2-}–S_8 solutions, in aqueous or non-aqueous media, have been described.[1] Depending on the conditions employed and the nature of the counterions salts of thioanions, such as $[Mo_2(S_2)_6]^{2-}$,[2] $(MoS_9)^{2-}$,[1] $[Mo_2(S)_4(S_2)(S_4)]^{2-}$,[1,3] $[Mo_2(S)_4(S_4)_2]^{2-}$,[1] $[(MoS_4)_2MoS]^{2-}$,[4] $(Mo_3S_{13})^{2-}$[5] and $(Mo_2S_8)^{2-}$,[6] can be isolated from these solutions in crystalline form and their structures have been determined (Fig. 1).

The reaction chemistry of the Mo thioanions with electrophilic reagents is extensive. With electrophiles such as CS_2 and dicarboalcoxyacetylenes the $(MoS_9)^{2-}$ and $[Mo_2(S)_4(S_4)_2]^{2-}$ anions react to form the $[(CS_4)_2MoS]^{2-}$,[7] $[Mo_2(S)_4(CS_4)_2]^{2-}$[7] and $\{Mo[S_2C_2(COOR)_2]_3\}^{2-}$[8] complexes. The CS_4^{2-} and dithiolene ligands in these compounds possibly are generated by cycloaddition reactions to the coordinated S_x^{2-} ligands. The $[Mo_2S_6O_2]^{2-}$ anion displays unique reactivity in its reaction with dicarbomethoxyacetylene and forms the very interesting $\{Mo_2O_2S_2[SSC_2(COOMe)_2]_2\}^{2-}$ complex.[9] In the latter, insertion of the alkyne into the

* Author to whom correspondence should be addressed.

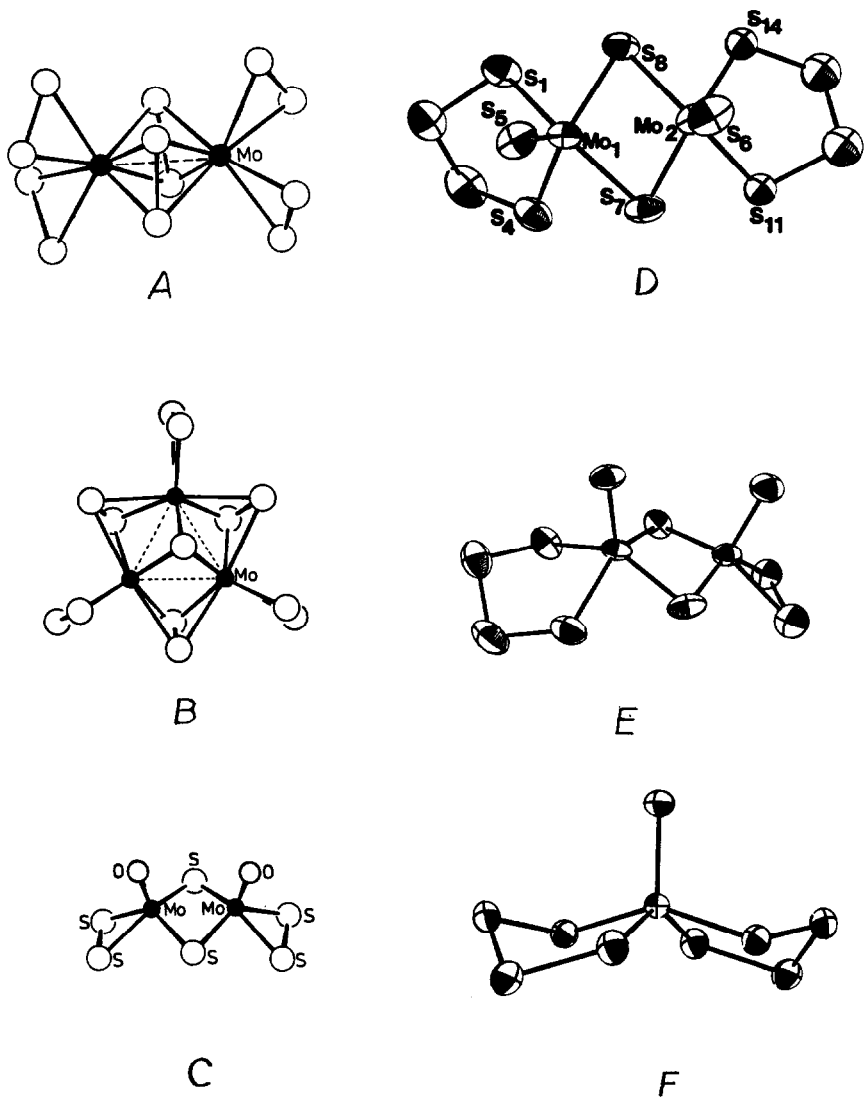


Fig. 1. Structures of: (A) $[Mo_2(S_2)_6]^{2-}$,[2] (B) $(Mo_3S_{13})^{2-}$,[5] (C) $(Mo_2S_8)^{2-}$,[6] (D) $[Mo_2(S)_4(S_4)_2]^{2-}$,[1] (E) $[Mo_2(S)_4(S_2)(S_4)]^{2-}$,[1,3] and (F) $[MoS_9]^{2-}$ and $[MoS_8O]^{2-}$.[1]

Mo—S bond results in the formation of a vinyl disulfide chelate ligand which is S,C bound to the Mo(V) ion.

The reactivity of the Mo thioanions often can be attributed to facile intramolecular charge-transfer or redox processes that activate the Mo–S_x units prior to their reactions with electrophiles.[6] This reactivity depends on the nature of the S_x^{2-} ligand coordinated to the Mo atom and appears to be different for the S_4^{2-} ligands by comparison with the S_2^{2-} ligands. This difference in reactivity reflects the structural and electronic differences between the "side-on" bonded S_2^{2-} ligand and the chelating S_4^{2-} ligands.

The S—S bond in the "side-on" coordinated S_2^{2-} ligand in the Mo–S_2 units is longer than the S—S bond in S_2^0 but shorter than the S–S single bond in S_2^{2-}. By contrast a pronounced lengthening of the S—S bonds adjacent to the Mo atom in the Mo–CS_4 and Mo–S_4 units is readily apparent in virtually all of the structurally characterized complexes that contain these units. This structural effect has been attributed previously to significant S–Mo p_π–d_π bonding[1] and results in an alternation of the S—S bonds lengths within the Mo-coordinated S_4^{2-} ligand.

Recently we have been exploring the comparative reaction chemistry of the Mo–S_2 and Mo–S_4 units. In this paper we present evidence for the difference in the reactivity characteristics of the Mo–S_4 and Mo–S_2 units.

EXPERIMENTAL

Synthesis

The chemicals in this research were used as purchased. Acetonitrile (CH_3CN), dichloromethane (CH_2Cl_2) and diethyl ether were distilled over calcium hydride. Dimethyl acetylene dicarboxylate (DMA) was distilled under reduced pressure at $\sim 50°C$. All syntheses were carried out under a dinitrogen atmosphere.

Physical methods

Visible and UV spectra were obtained on Cary Model 118 and 219 spectrophotometers. A Debye–Scherrer camera with nickel-filtered copper radiation was utilized to obtain X-ray powder diffraction patterns.

Electrochemical measurements were performed with a PAR Model 173 potentiostat/galvanostat and a PAR Model 175 universal programmer. The electrochemical cell used had platinum working and auxiliary electrodes. As the reference electrode a saturated calomel electrode was used. All solvents used in the electrochemical measurements were properly dried and distilled, and tetra-*n*-butylammonium perchlorate was used as the supporting electrolyte. Normal concentrations used were ~ 0.001 M in the electroanalyte and 0.1 M in the supporting electrolyte. Purified dinitrogen was used to purge the solutions prior to the electrochemical measurements.

Preparation of compounds

Bis(tetraphenylphosphonium)bis(μ - thio)(bis - [bis(1,2 - dimethylcarboxylate)dithioethylene) molybdate(V)] $(Ph_4P)_2[Mo_2S_2(S_2C_2(COOMe)_2)_4]$. *Method A.* To a solution of $(Ph_4P)_2Mo_2S_{10}/S_{12} \cdot \frac{1}{2}DMF$[1] (0.52 g, 0.42 mmol) in 300 cm^3 of CH_3CN was added with stirring 0.21 cm^3 (1.67 mmol) of freshly distilled DMA. The ensuing brown solution was refluxed for *ca* 30 min. The color of the solution changed to violet and then to a final green color. Upon cooling to ambient temperature and removing the solvent *in vacuo*, a green residue was obtained. The residue was washed with a 30-cm^3 portion of CH_2Cl_2 and the remaining solid was dissolved in the minimum amount of a DMF–CH_2Cl_2 (6 : 1) mixture. The slow diffusion of diethyl ether resulted in the formation of green crystals. The yield after drying was 0.22 g (26%).

Method B. To a solution of 0.26 g (0.21 mmol) of $(Ph_4P)_2Mo_2S_4(CS_4)_2 \cdot \frac{1}{2}DMF$[7] in the minimum amount of CH_3CN was added 0.10 cm^3 (0.80 mmol) of freshly distilled DMA. After refluxing for *ca* 30 min. the dark solution was allowed to cool to ambient temperature and the solvent was removed under vacuum. A workup procedure similar to the one described in Method A above yielded 0.10 g of product (26% yield). The X-ray powder pattern, electrochemistry and electronic spectrum of this material was identical to the product obtained by Method A. The X-ray powder pattern of the crystalline product is identical to the pattern calculated on the basis of the single-crystal X-ray diffraction data.*

Electronic spectrum

680 nm ($\varepsilon = 10{,}600$); 582 nm ($\varepsilon = 14{,}600$); 430 nm (sh) and 380 nm ($\varepsilon = 20{,}000$).

IR spectrum (selected characteristic vibrations)

ν(C=O): 1705(s), 1675(s) and 1650 cm^{-1}; 1220 cm^{-1} (v.s. broad absorption).

Electrochemical data

The cyclic voltammogram (in CH_3CN) of this material shows a quasireversible reduction at -0.67 V and an irreversible oxidation at $+0.85$ V (vs SCE).

Bis(tetraethylammonium)bis(1,2 - dimethyl - carboxylate)dithioethylene oxomolybdate(IV) $(Et_4N)_2MoO(S_2C_2COOMe)_2)_2$. To a solution of 2.0 g (3.18 mmol) of recrystallized $(Et_4N)_2MoO(S_4)_2$ in *ca* 350 cm^3 of CH_3CN was added 0.9 cm^3 (7.32 mmol) of DMA. The reaction mixture was stirred for 10 min and an orange red solution was obtained. The solution was concentrated to 30 cm^3, by evaporation of the solvent *in vacuo*, and then filtered. To the filtrate was added 100 cm^3 of tetrahydrofuran (THF). Upon standing, a solid deposited, was isolated and washed with three 30-cm^3 portions of THF. The crude product was recrystallized from a concentrated CH_3CN solution upon addition of THF and standing at ambient temperature for *ca* 10 h. Brown red needles formed and were isolated. The yield after drying was 1.20 g (48.1%). The powder pattern of this compound was identical to the pattern calculated on the basis of single-crystal X-ray diffraction data.[10]

* A detailed description of the structures of

$$\{Mo_2S_2[S_2C_2(COOMe)_2]_4\}^{2-}$$

and

$$[OMo(S_2C_2COOMe)_2]^{2-}$$

will be published elsewhere.

RESULTS AND DISCUSSION

Synthetic studies

Our studies of the reactions of the $(MoS_9)^{2-}$, $(Mo_2S_{10})^{2-}$ and $(Mo_2S_{12})^{2-}$ complexes thus far have shown that these anions readily react with CS_2. The crystalline $[(CS_4)_2MoS]^{2-}$, (*cis* or *trans*) and $[(CS_4)_2Mo_2S_4]^{2-}$ anions contain the S–S chelating perthiocarbonate ligand[7] (Fig. 2). The reaction of $(MoS_9)^{2-}$ with 2-butynedimethanoate (DMA) also proceeds smoothly and the $\{Mo[S_2C_2(COOCH_3)_2]_3\}^{2-}$ anion contains the bidentate $[S_2C_2(COOCH_3)]^{2-}$ ligands and a nearly trigonal prismatic MoS_6 core[8] (Fig. 3B). Under the assumption that the $\{Mo[S_2C_2(COOCH_3)_2]_3\}^{2-}$ complex was a final product of a series of intermediate Mo–sulfido-dithiolene complexes we proceeded with a detailed study of the reactions of the Mo thioanions with DMA. The $[(CS_4)_2Mo_2S_4]^{2-}$ and $[(S_4)_2Mo_2S_4]^{2-}$ anions react with DMA in a 1 : 4 molar ratio to afford in modest yields the $\{Mo_2S_2[S_2C_2(COOMe)_2]_4\}^{2-}$ anion[10] (**1**) (Fig. 3A). The synthesis of **1** can also be accomplished by the reaction of $(MoS_9)^{2-}$ with DMA under *aerobic* conditions. The same reaction under a N_2 atmosphere affords the $\{Mo[S_2C_2(COOCH_3)_2]_3\}^{2-}$ complex. A clue regarding the possible reaction pathway toward the synthesis of **1** from $(MoS_9)^{2-}$ is provided by the corresponding reaction of $[MoS_8O]^{2-}$ with DMA. In the latter reaction, the $\{OMo[S_2C_2(COOMe)_2]\}^{2-}$ complex is obtained[10] (Fig. 3C) and contains five-coordinate Mo(IV). By analogy, it is reasonable to assume that the MoS_5^{2-} anion reacts with DMA initially to form the $\{SMo[S_2C_2(COOMe)_2\}^{2-}$ complex. Oxidation

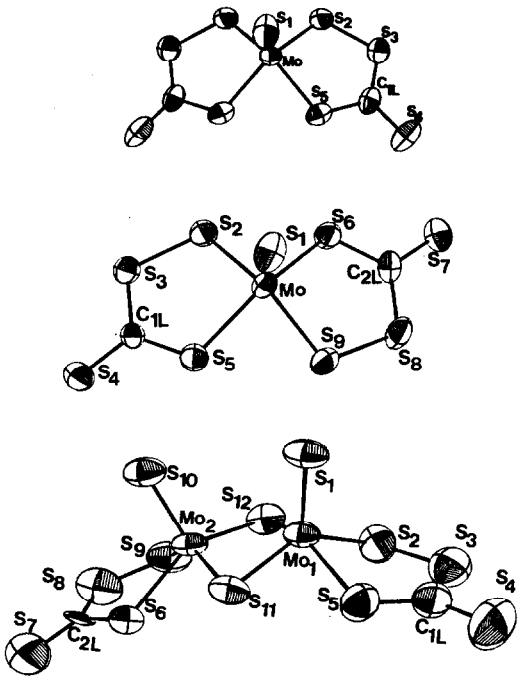


Fig. 2. Structures of *cis*- and *trans*-$[(CS_4)_2MoS]^{2-}$ and of $[(CS_4)_2Mo_2S_4]^{2-}$.[7,19]

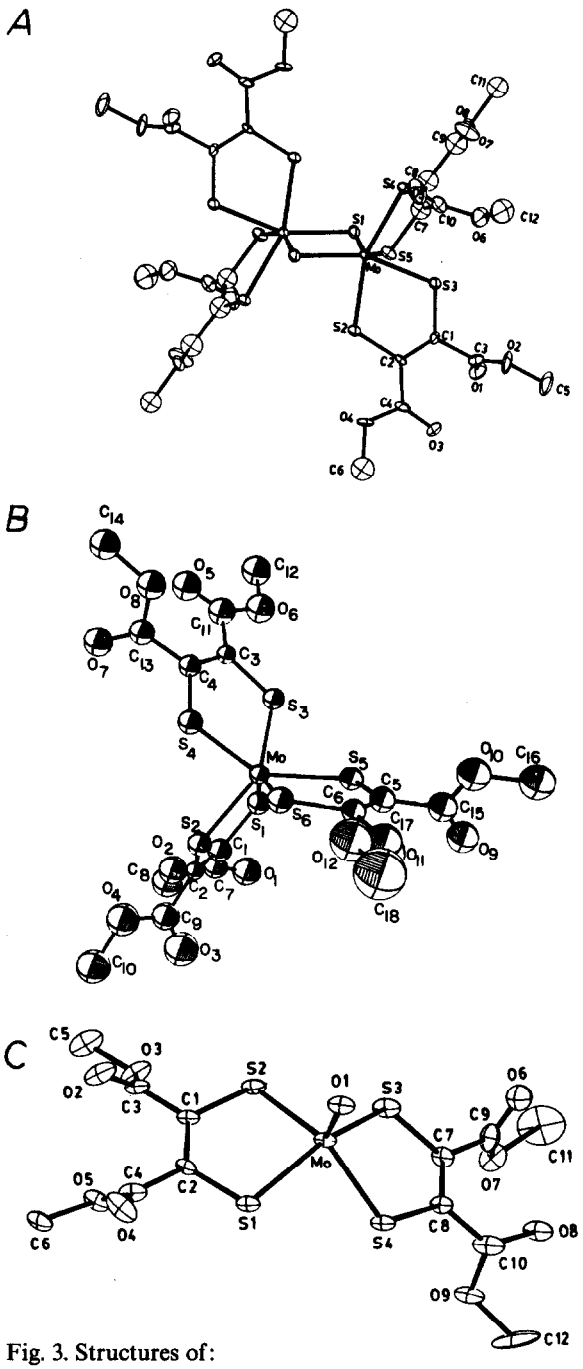


Fig. 3. Structures of:

(A) $\{Mo_2S_2[S_2C_2COOMe)_2]_4\}^{2-}$,[10]

(B) $\{Mo[S_2C_2(COOMe)_2]_3\}^{2-}$,[8]

and

(C) $\{OMo[S_2C_2(COOMe)_2]\}^{2-}$.[10]

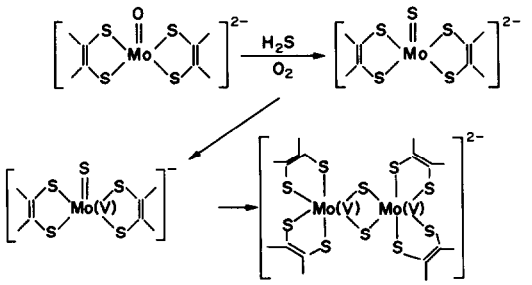


Fig. 4. Reaction of $\{OMo[S_2C_2(COOMe)_2]\}^{2-}$ with H_2S.

of this complex to the monoanion followed by dimerization will result in the formation of **1**. This assumption is supported by the reaction of $\{OMo[S_2C_2(COOMe)_2]\}^{2-}$ with H_2S. The only product that can be isolated from this reaction (Fig. 4) is **I**.

The formation of the $[S_2C_2(COOMe)_2]^{2-}$ ligand in the reactions of Mo-coordinated S_4^{2-} ligands with DMA contrasts with the reaction of the coordinated S_2^{2-} ligand in the $[Mo_2S_6O_2]^{2-}$ anion (Fig. 1C). The latter inserts DMA into the Mo—S bond with formation of a product that contains the S–C-coordinated vinyl disulfide ligand[9] (Fig. 5).

The $[(S_4)MoO(\mu\text{-}S)_2Mo(O)(S_2)]^{2-}$ complex reacts with DMA at ambient temperature to give the same vinyl disulfide complex (Fig. 5). The same reaction under reflux conditions affords the $[(L)Mo(O)(\mu\text{-}S)_2Mo(O)(L)]^{2-}$ dithiolene isomer,[11(a)] $\{L = [S_2C_2(COOR)_2]^{2-}\}$. Apparently, the $[Mo_2S_6O_2]^{2-}$ anion (Fig. 1C), obtained by dissociation of S_2^0 from the $[(S_4)Mo(O)(\mu\text{-}S)_2Mo(O)(S_2)]^{2-}$ complex, reacts rapidly with DMA

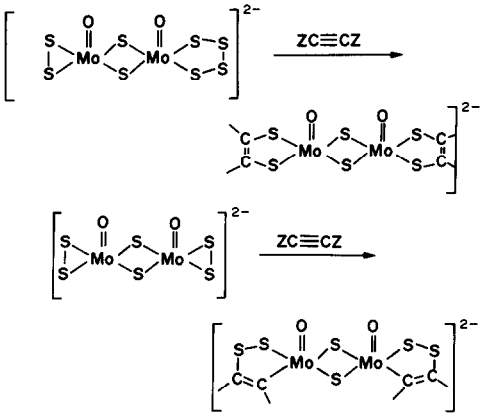
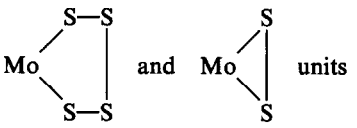


Fig. 5. Reactions of dicarbomethoxyacetylene with the



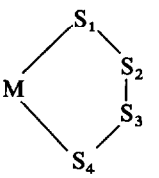
units

to form the vinyl disulfide complex. The latter, as verified by NMR spectral changes, rearranges thermally to the dithiolene dimer (Fig. 5). A similar thermal rearrangement was observed[11(b)] previously in the formation of the $(Cp)_2Ti[S_2C_2(COOR)_2]$ dithiolene complex from the corresponding vinyl disulfide isomer.

Reactivities of the Mo-*coordinated* S_4^{2-} *and* S_2^{2-} *ligands*

An examination of the structural data available for the *Mo-coordinated* S_4^{2-} ligands (Table 1) and the

Table 1. Influence of M–S bonding on the S–S bonding of the coordinated S_4^{2-} ligands



Compound[a]	S(1)—S(2)	S(2)—S(3)	S(3)—S(4)	M—S(1)	M—S(4)	Reference
$(Et_4N)_2Zn(S_4)_2$[b]	2.045(4)	2.044(5)	2.062(5)	2.376(3)	2.331(3)	14
	2.034(5)	2.032(5)	2.056(5)	2.343(2)	2.354(3)	
$(Et_4N)_2Ni(S_4)_2$[c]	2.073(2)	2.037(4)	2.073(2)	2.185(2)	2.185(2)	14, 15
$(Ph_3P)_2PtS_4$	2.024(8)	2.022(10)	2.081(10)	2.360(6)	2.366(5)	16
$(Ph_4P)_2Mo_2S_{10}$[d]	2.093(4)	2.018(4)	2.053(3)	2.399(2)	2.427(2)	1
$(Ph_4As)_2Mo_2S_{10}$[e]	2.019(5)	1.970(6)	2.115(5)	2.409(2)	2.403(3)	3
$(Et_4N)_2MoS_9$	2.107(1)	2.012(1)	2.166(1)	2.387	2.331(1)	1
$(Et_4N)_2MoS_8O$	2.120(3)	2.008(3)	2.159(3)	2.395(2)	2.363(2)	1
$(\eta^5\text{-}C_5H_5)_2Mo(S_4)$	2.081(8)	2.018(9)	2.085(7)			17
$(\eta^5\text{-}C_5H_5)_2W(S_4)$	2.105(7)	2.016(8)	2.116(9)			18

[a] Distances in Å.

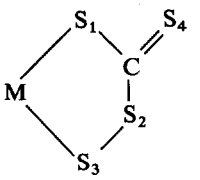
[b] The $[Zn(S_4)_2]^{2-}$ anion contains two crystallographically independent S_4^{2-} ligands.

[c] The $[Ni(S_4)_2]^{2-}$ anion possesses D_2-symmetry.

[d] For the S_4^{2-} ligand not subject to disorder.

[e] From the major component in a disordered structure.

Table 2. Influence of M–S bonding on the structural parameters of the coordinated CS_4^{2-} ligands



Compound[a]	M—S(1)	M—S(3)	S(2)—S(3)	S(1)—C	S(2)—C	S(4)—C	Reference
$(Ph_4P)_2Ni(CS_4)_2$	2.174(2)	2.165(2)	2.064(2)	1.707(4)	1.711(5)	1.678(4)	14
$(Et_4N)_2Mo(S)(CS_4)_2$ (*trans*)[b]	2.386(3)	2.320(3)	2.102(5)	1.735(12)	1.719(12)	1.640(11)	
	2.380(3)	2.333(3)	2.100(5)	1.739(12)	1.709(12)	1.662(11)	7
$(Ph_4P)_2Mo(S)(CS_4)_2$ (*cis*)	2.376(3)	2.320(3)	2.105(4)	1.756(10)	1.726(11)	1.615(9)	19

[a] Distances in Å.

[b] Contains two symmetry-independent CS_4^{2-} ligands.

S_2^{2-} ligands[12] shows that the effect of coordination is quite different for the two ligands. Thus, the S—S bond length in the "side-on" bound S_2^{2-} ligands ranges[12] from 2.03 to 2.074(5) Å and is slightly longer than the S—S bond in elemental S_8. By contrast, an alternation in the S—S bond lengths is apparent in the bidentate S_4^{2-} ligand in complexes that contain the Mo–S_4 unit. The significant elongation of the S—S bonds directly adjacent to the Mo atom correlates directly with a shortening of the corresponding Mo—S bonds and suggests that bonding electrons from the S—S bond are transferred to Mo–S bonding orbitals. The facile transfer of this type most likely arises as a result of the effective energy matching of the appropriate atomic wavefunctions.*

The ease by which the coordinated S_4^{2-} ligands dissociate S_2^0 following interactions with electrophilic molecules such as CS_2 or DMA very likely is due to the proximal S—S bond activation by the Mo atom. It should be emphasized that the S_4^{2-} ligand in the tetrahedral $[Zn(S_4)_2]^{2-}$ complex anion,[14] which contain the d^{10} Zn(II) ion, does not show an alternation of the S—S bond lengths (Table 1).

A lengthening of the S—S bond adjacent to the Mo atom also is apparent in the structures of both the *cis*- and *trans*-$[(Cs_4)_2MoS]^{2-}$ complex anions (Fig. 2) and in the $[(CS_4)Mo(S)(\mu\text{-}S)_2Mo(S)(CS_4)]^{2-}$ complex (Table 2). As observed with the S_4^{2-} ligands, the Mo—S bond directly adjacent to the lengthened S—S bond of the CS_4^{2-} ligand always is significantly shorter than the Mo—S bond with the thiolate sulfur of the ligand. Such differences in M–S bonding, or lengthening of the S—S bond are not apparent in the structure of the $[N_1(CS_4)_2]^{2-}$ complex[14] (Table 2).

With the Mo-"side-on"-bound S_2^{2-} ligand, and in the absence of other activating interactions, the transfer of electron density to the Mo—S bonds would originate from the antibonding π^*-orbital and should result in a strengthening of the S—S bond. A bond order >1 for the "side-on"-coordinated S_2^{2-} ligand is evident in the S—S stretching vibrations (500–600 cm^{-1}) and the S—S bond lengths (2.00–2.10 Å) in these species. The corresponding values for the uncoordinated S_2, S_2^- and S_2^{2-} fragments are: S_2^0, 725 cm^{-1}, 1.89 Å; S_2^-, 589 cm^{-1}, 2.00 Å; S_2^{2-}, 446 cm^{-1}, 2.13 Å. A net depopulation of the S_2^{2-} π^*-orbital in the Mo–S_2 complexes and the π^* nature of the LUMO result in a situation where a cycloaddition of an acetylene or olefin to the Mo-"side-on"-bound S_2^{2-} would be a symmetry-forbidden process, it is not surprising therefore that such cycloaddition reactions with "*pure*" Mo–S_2 units are virtually unknown. In the only well-documented reaction of DMA with such a unit [in the $(Mo_2S_6O_2)^{2-}$ complex], the alkyne has inserted into the Mo—S bond.[9]

The reactions of the Mo-coordinated S_4^{2-} ligands with DMA and the subsequent formation of the dithiolene ligand, are analogous to other reactions of M–S_x units with DMA. Such reactions as the addition of DMA to the Fe–S_5 unit in $(Fe_2S_{12})^{2-}$,[20,21] the addition of DMA to the Ti–S_5 unit in $(Cp)_2TiS_5$ and the V–S_5 unit in $(Cp)_2VS_5$,[22] give rise to dithiolene complexes that contain $M[S_2C_2(COOMe)_2]$ units. An important mechanistic step in these reactions very likely involves the cycloaddition of the electrophilic alkyne to the coordinated S_x^{2-} chelate (Fig. 6). Interactions of the type depicted in Fig. 6 have a precedence in dithiolene chemistry. The addition of alkenes

*For the neutral free atoms, a compilation of Roothaan–Hartree–Fock atomic wavefunctions show the sulfur 3*p* orbitals with an energy of −0.43694 a.u. and the molybdenum $4d(s^1d^5)$ with an energy of −0.34811 a.u. The localization of partial positive charge on the Mo and partial negative charge on the S is expected to bring these energies even closer together.[13]

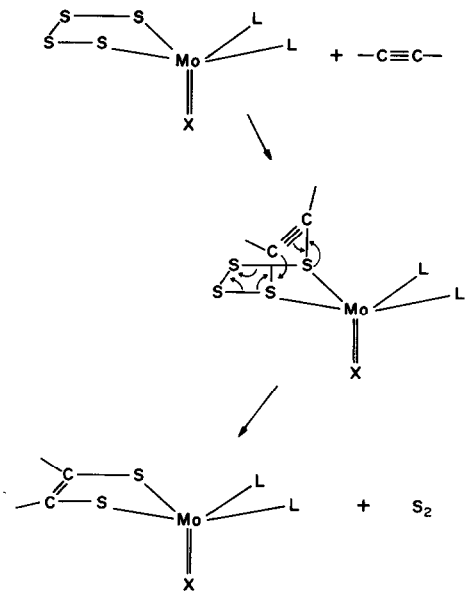


Fig. 6. Cycloaddition of alkynes to the Mo–S_4 unit.

across the coordinated *S*-donor atoms in the $Ni[S_2C_2(Ph)_2]_2$ complexes has been reported by Schrauzer and Mayweg[23] and the norbornadiene adduct of $Ni[S_2C_2(CF_3)_2]_2$ has been obtained and structurally characterized.[24]

The activation, and change in reactivity patterns of the Mo-bound S_2^{2-} ligand, following the addition of elemental sulfur and formation of the Mo–S_4 units, may be of relevance to the HDS reaction. The HDS reaction is important in the catalytic hydrogenolysis of organosulfur compounds, and the heterogeneous catalysts employed in this reaction contain "sulfided" molybdenum and cobalt salts supported on β-alumina.[25] Proposed mechanisms for the HDS reaction[25–27] invariably involve the metals (Mo and Co) directly in the activation of H_2 and the C—S bond cleavage reactions. The suggestion has been advanced[28] that S_2^{2-} pairs, present in the catalyst, may be directly linked with thiophene HDS activity. This suggestion is supported by the pioneering work of Rakowski Dubois, who has demonstrated that appropriately activated S_2^{2-} units in the $(CpMoS_2)_2$ complex are capable of activating H_2[29] and catalyze the reduction of elemental sulfur and the hydrogenation of alkynes.[30] With appropriately activated Mo–S_2 units, in fact, one can envision all of the HDS important reaction steps occurring directly on the S_2 unit (Fig. 7).

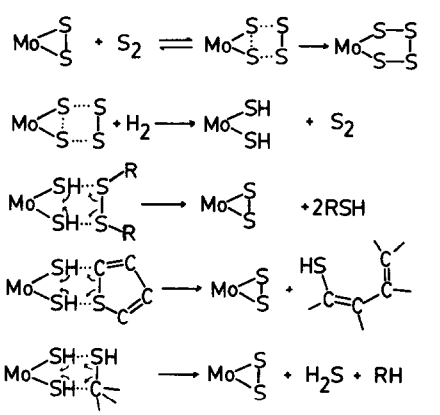


Fig. 7. Possible reactions of the activated S_2^{2-} ligand relevant to the HDS process.

Acknowledgement—This work has been supported generously by a grant from the National Science Foundation (No. CHE-79-0389).

REFERENCES

1. M. Draganjac, E. Simhon, L. T. Chan, M. Kanatzidis, N. C. Baenziger and D. Coucouvanis, *Inorg. Chem.* 1982, **21**, 3321.
2. A. Müller, W. O. Nolte and B. Krebs, *Inorg. Chem.* 1980, **19**, 2835.
3. W. Clegg, G. Christou, C. D. Garner and G. M. Sheldrick, *Inorg. Chem.* 1981, **20**, 1562.
4. (a) E. I. Stiefel, In *Nitrogen Fixation, The Chemical–Biochemical–Genetic Interface* (Edited by A. Müller and W. E. Newton). Plenum Press, New York (1982). (b) W.-H. Pan, M. E. Leonowicz and E. I. Stiefel, *Inorg. Chem.* 1983, **22**, 672.
5. A. Müller, R. G. Bhattacharyya and B. Pfefferkorn, *Chem. Ber.* 1979, **112**, 778.
6. K. F. Miller, A. E. Bruce, J. L. Corbin, S. Wherland and E. I. Stiefel, *J. Am. Chem. Soc.* 1980, **102**, 5102.
7. D. Coucouvanis and M. Draganjac, *J. Am. Chem. Soc.* 1982, **104**, 6820.
8. M. Draganjac and D. Coucouvanis, *J. Am. Chem. Soc.* 1983, **105**, 139.
9. T. R. Halbert, W.-H. Pan and E. I. Stiefel, *J. Am. Chem. Soc.* 1983, **105**, 5476.
10. D. Coucouvanis, A. Hadjikyriacou, M. Kanatzidis and O. Ileperuma, manuscript in preparation.
11. (a) A. Hadjikyriacou and D. Coucouvanis, manuscript in preparation; (b) T. B. Rauchfuss, personal communication.
12. A. Müller and W. Jaegermann, *Inorg. Chem.* 1979, **18**, 2631.
13. E. Clementi and C. Roetti, *At. Data Nucl. Data Tables* 1974, **14**, 3.
14. (a) D. Coucouvanis, P. R. Patil, M. G. Kanatzidis, B. Detering and N. C. Baenziger, *Inorg. Chem.* 1985, **24**, 24; (b) P. D. Williams, Ph.D. thesis, University of Michigan (1985).
15. A. Müller, E. Krickemeyer, H. Bögge, W. Clegg and G. M. Sheldrick, *Angew. Chem., Int. Ed. Engl.* 1982, **22**, 1006.
16. D. Dudis and J. P. Fackler, *Inorg. Chem.* 1982, **12**, 3578 (and references therein).

17. H. D. Block and R. Allman, *Cryst. Struct. Commun.* 1975, **4**, 53.
18. B. R. Davis, I. Bernal and H. Köpf, *Angew. Chem., Int. Ed. Engl.* 1971, **10**, 921.
19. M. Draganjac, Ph.D. Thesis, University of Iowa (1983).
20. D. Coucouvanis, D. Swenson, P. Stremple and N. C. Baenziger, *J. Am. Chem. Soc.* 1979, **101**, 3392.
21. M. G. Kanatzidis and D. Coucouvanis, *Inorg. Chem.* 1984, **23**, 403.
22. C. M. Bolinger and T. B. Rauchfuss, *Inorg. Chem.* 1982, **21**, 3947.
23. G. N. Schrauzer and V. P. Mayweg, *J. Am. Chem. Soc.* 1965, **87**, 1483.
24. R. M. Wing, G. C. Tustin and W. H. Okamura, *J. Am. Chem. Soc.* 1970, **92**, 1935.
25. F. E. Massoth, *Adv. Catal.* 1978, **27**, 265.
26. F. E. Massoth, *J. Catal.* 1975, **36**, 164.
27. H. Topsøe, B. S. Clausen, R. Candia, C. Wivel and S. Mørup, *J. Catal.* 1981, **68**, 433.
28. J. C. Ducket, E. M. Van Oers, H. J. De Beer and R. Prins, *J. Catal.* 1983, **80**, 386.
29. M. Rakowski Dubois, M. C. Van Derveer, D. L. Dubois, R. C. Haltiwanger and W. K. Miller, *J. Am. Chem. Soc.* 1980, **102**, 7456.
30. M. Rakowski Dubois, R. C. Haltiwanger, D. J. Miller and G. Glatzmaier, *J. Am. Chem. Soc.* 1979, **101**, 5245.

Polyhedron Vol. 5, No. 1/2, pp. 357–361, 1986
Printed in Great Britain

0277-5387/86 $3.00 + .00
© 1986 Pergamon Press Ltd

PREPARATION OF TRINUCLEAR MOLYBDENUM(IV) ION, $Mo_3S_4^{4+}$, AND X-RAY STRUCTURE OF $Ca[Mo_3S_4\{HN(CH_2CO_2)_2\}_3]\cdot 11.5H_2O$

TAKASHI SHIBAHARA* and HISAO KUROYA

Department of Chemistry, Okayama University of Science, 1-1 Ridai-cho, Okayama 700, Japan

(*Received* 13 *June* 1985)

Abstract—The equilateral trinuclear Mo(IV) ion of incomplete cubane-type structure, $Mo_3S_4^{4+}$, was prepared by the reduction of $[Mo_2O_2S_2(cys)_2]^{2-}$ with $NaBH_4$ followed by air oxidation and Sephadex G-10 separation. The resultant green solution was analyzed to give S/Mo = 1.33. The spectrum $\{\lambda_{max}[\varepsilon(M^{-1}cm^{-1})]: 367(5190), 500sh(290)$ and $602(351)$ in 2 M HPTS$\}$ remains unchanged in the air. The existence of the Mo_3S_4 core has been confirmed by X-ray structure analysis of $Ca[Mo_3S_4(ida)_3]\cdot 11.5H_2O$ (H_2ida = iminodiacetic acid) which was prepared from the $Mo_3S_4^{4+}$ ion and H_2ida. Crystal data: orthorhombic, $a = 13.815(3)$ Å, $b = 26.189(9)$ Å, $c = 9.447(3)$ Å, $V = 3417.9(17)$ Å^3, $Z = 4$, $D_c = 2.053$ g cm^{-3}, space group $P2_12_12_1$. R value is 0.048 for 3705 reflections $[F_o \geqslant 3\sigma(F_o)]$. The anion $[Mo_3S_4(ida)_3]^{2-}$ has an approximate symmetry of C_{3v} and contains an incomplete cubane-type Mo_3S_4 core. Selected mean bond distances are as follows: Mo—Mo, 2.754 Å, Mo—μ_3-S, 2.349 Å; Mo—μ_2-S, 2.295 Å; Mo—O, 2.167 Å, Mo—N, 2.227 Å. The existence of an $[Mo(IV)]_2Mo(III)$ oxidation state has been indicated for the first time from the cyclic voltammogram and polarogram of the anion.

The presence of equilateral trinuclear Mo(IV) ions of incomplete cubane-type structure, $Mo_3O_4^{4+}$,[1] and sulfur-capped $Mo_3O_3S^{4+}$,[2] has been reported, the latter showing a greater stability toward air oxidation. Several reports on the X-ray structure of the Mo_3O_4 core[3] and a report on that of the Mo_3O_3S core[2] have appeared. We will describe here the preparation and characterization of an incomplete cubane-type Mo(IV) ion, $Mo_3S_4^{4+}$, and the X-ray structure analysis of $Ca[Mo_3S_4(ida)_3]\cdot 11.5H_2O$ (H_2ida = iminodiacetic acid) having the Mo_3S_4 core. Accounts of the electrochemistry and a new oxidation state, $[Mo(IV)]_2Mo(III)$, will be given and the effects of introducing sulfur(s) into the Mo_3O_4 core will be discussed.

* Author to whom correspondence should be addressed.

EXPERIMENTAL

Preparation of $Mo_3S_4^{4+}$ *ion*

Two grams (3.1 mmol) of the di-μ-sulfidomolybdenum(V) dimer, $Na_2[Mo_2O_2S_2(cys)_2]\cdot 4H_2O$[4] dissolved in diluted HCl (0.03 M, 200 cm^3) was transferred into a round-bottom flask containing $NaBH_4$ (1 g, 20 mmol). Concentrated HCl (30 cm^3) was added slowly with stirring to the mixture, which was then kept overnight in a refrigerator. Up to now all operations were performed under an N_2 atmosphere. Air oxidation of the resultant brown solution in a hot bath gave dark green solution, which gave four greenish bands through Sephadex G-10 separation. The species in the last band was purified by the use of ion exchange technique: that is, after dilution with three parts of water, the solution was absorbed on a Dowex 50W-X2 cation

exchanger, and this was washed with 1 M HCl, and the green eluant was obtained by the use of 2 M HCl. The solution was analysed to give S/Mo = 1.33 ±0.02 (three determinations).[5] The yield was ca 15%, based on the starting binuclear complex. The HPTS solution of the ion was obtained by absorption of the ion on the cation exchanger from the HCl solution followed by the elution of it with 2 M HPTS.

Preparation of $Ca[Mo_3S_4(ida)_3]\cdot 11.5H_2O$

H_2ida ($H_2ida/Mo \simeq 10$) dissolved in a minimum amount of concentrated KOH (*ca* 10 M) was added to the $Mo_3S_4^{4+}$ solution in 2 M HCl. Concentrated KOH at first, and then diluted KOH, was added very slowly (in *ca* 4 days) to raise the pH of the solution to *ca* 10. After being diluted, the resultant solution was absorbed on a Dowex 1-X2 anion exchanger, which was washed with 0.05 M $CaCl_2$. Elution with 0.3 M $CaCl_2$ gave two major bands. The solution obtained from the first band was passed through a Sephadex G-10 column for desaltation, after the volume of the solution had been decreased to *ca* one third by the use of a rotary evaporator. The resultant solution was diluted *ca* 10 times, and again absorbed on a Dowex 1-X2 anion exchanger. Green crystals were deposited from the solution obtained by the use of 1 M $CaCl_2$ as an eluent.

Spectrophotometry and electrochemistry

Spectra were recorded with a Hitachi 330 spectrophotometer. Absorption coefficients (ε) recorded are per trimer. Cyclic voltammetry was conducted with a Yanaco Polarographic Analyzer P1100 using a glassy carbon working electrode, a Pt counter electrode, and a saturated calomel electrode (SCE). The polarogram was obtained with the same instrument.

Crystallographic study of $Ca[Mo_3S_4(ida)_3]\cdot 11.5H_2O$

Crystal data: Formula weight = 1056.60, orthorhombic, $a = 13.815(3)$ Å, $b = 26.189(9)$ Å, $c = 9.447(3)$ Å, $V = 3417.9(17)$ Å^3, $Z = 4$, $D_c = 2.053$ g cm^{-3}, space group $P2_12_12_1$, $\lambda(\text{Mo-}K_\alpha) = 0.71073$ Å, $\mu(\text{Mo-}K_\alpha) = 15.27$ cm^{-1}.

Data collection. The crystal employed for data collection was approximately $0.2 \times 0.3 \times 0.4$ mm in dimension with well-defined faces. Intensity data ($2\theta \leqslant 55°$) were collected on a RIGAKU AFC-6A four-circle diffractometer. During data collection, three standard reflections monitored after every 150 reflections did not show any appreciable decay. A total of 4437 reflections were collected, of which 3705 with $F_o \geqslant 3\sigma(F_o)$ were used for the structure analysis. Intensities were corrected for polarization and Lorentz factors, but not for absorption.

Structure solution and refinement. The coordinates of three Mos were determined by means of MALTAN and the remaining non-hydrogen atoms were located from successive difference Fourier maps. The block-diagonal least-squares refinement with anisotropic temperature factors for all non-hydrogen atoms gave $R = 0.048$ and $R'[(\Sigma\omega\Delta F^2/\Sigma\omega F_o^2)^{1/2}] = 0.045$. The function minimized was $\Sigma\omega(F_o - |F_c|)^2$, where $\omega = 1/\sigma^2(F_o)$ was used. No attempt was made to locate hydrogen atoms. A final different Fourier map revealed no peak greater than 1.3 e Å^{-3} in the vicinity of Mo atoms. The computer programs involved have been described before.[6] Atomic coordinates, anisotropic thermal parameters, bond distances, bond angles and a list of F_o and F_c values have been deposited with the Editor as supplementary material.

RESULTS AND DISCUSSION

Preparation of $Mo_3S_4^{4+}$ *and* $[Mo_3S_4(ida)_3]^{2-}$

Four greenish species were prepared by the reduction of the Mo(V) dimer $[Mo_2O_2S_2(cys)_2]^{2-}$ with $NaBH_4$, and the $Mo_3S_4^{4+}$ ion is the fourth species from the Sephadex G-10 column.* The charge of the ion is estimated to be 4+ on the basis of its behavior, similar to those of $Mo_3O_4^{4+}$ and $Mo_3O_3S^{4+}$ ions on the ion exchanger. $Mo_3S_4^{4+}$ ion in 2 M HCl or HPTS is stable toward air oxidation.

The anion exchanger separation of the reaction mixture of $Mo_3S_4^{4+}$ and H_2ida gives two green bands. The green air-stable complex $[Mo_3S_4(ida)_3]^{2-}$ has been obtained as a calcium salt from the first band. The electronic spectrum of the crystals obtained from the second band in a similar manner shows the same peak positions as those of the crystals obtained from the first band, although the peak positions of the solution from the second band are slightly different from those of the solution from the first band. The unit cell dimensions of the crystal from the second band are found to be the same as those of the crystals from the first band.

Electronic spectra

The electronic spectrum of the $Mo_3S_4^{4+}$ ion in 2 M HPTS {$\lambda_{max}[\varepsilon\ (M^{-1}\ cm^{-1})]$: 367(5190), 500sh(290) and 602(351)} is shown in Fig. 1 together with those of the $Mo_3O_4^{4+}$ and $Mo_3O_3S^{4+}$ ions. The spectrum of $[Mo_3S_4(ida)_3]^{2-}$ in water [$\lambda_{max}(\varepsilon)$: 246(21,700),

* Three other species have been characterized and will be reported elsewhere.

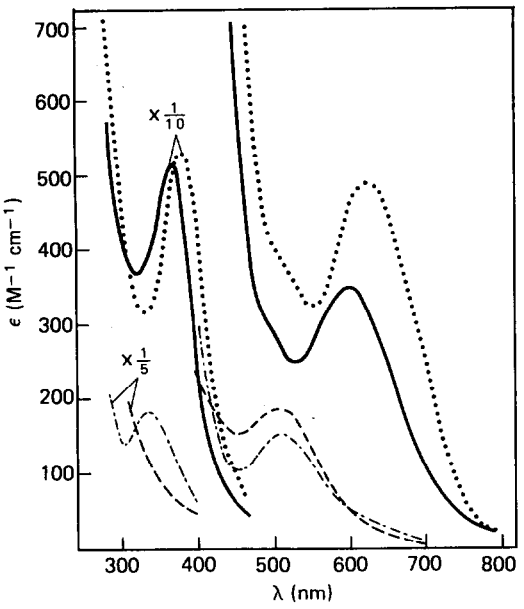


Fig. 1. Electronic spectra of trinuclear Mo(IV) ions in 2 M HPTS except for (d): (a) $Mo_3S_4^{4+}$ (——), (b) $Mo_3O_3S^{4+}$(— - — - —), (c) $Mo_3O_4^{4+}$ (— —), and (d) $[Mo_3S_4(ida)_3]^{2-}$ in water (- - - -).

380(5330), 520sh(374) and 622(494)] is also included in Fig. 1. No peaks appear for the $Mo_3S_4^{4+}$ and $[Mo_3S_4(ida)_3]^{2-}$ ions in the near-IR region. The positions of maximal absorption are shifted toward a longer wavelength upon substitution of sulfur(s) for oxygen(s) in the Mo_3O_4 core: it seems that the influence of μ_2-S on the red shift is larger than that of μ_3-S.

X-ray crystal structure of $Ca[Mo_3S_4(ida)_3]\cdot 11.5H_2O$

A perspective view of the complex anion is given in Fig. 2. The anion has an approximate symmetry of C_{3v} and contains an incomplete cubane-type Mo_3S_4 core. This supports the existence of an $Mo_3S_4^{4+}$ ion (probably $[Mo_3S_4(H_2O)_9]^{4+}$) in solution. Every nitrogen in the ida^{2-} ligands occupies a position *trans* to μ_3-S and every Mo has an octahedral coordination distorted by three S atoms from the core and two O and one N atom from the ida^{2-} ligand. Selected bond distances and angles are listed in Table 1. A comparison of some bond distances is made among clusters with Mo_3S_4, Mo_3O_3S and Mo_3O_4 cores (Table 2). The Mo—Mo distance of $[Mo_3S_4(ida)_3]^{2-}$ is slightly shorter than that of other complexes with an Mo_3S_4 core and is evidently longer than that of complexes with an Mo_3O_3S or Mo_3O_4 core. Mo—μ_2-S and Mo—μ_3-S distances are similar to each other, except for $[Mo_3S_4(h\text{-}C_5H_5)_3]^+$. The calcium ion is surrounded by six water molecules: Ca—O distances range from 2.364(10) to 2.428(15) Å, with a mean value of 2.40(2) Å.

Electrochemistry

The $Mo_3S_4^{4+}$ ion reacts easily with mercury, showing a color change, and, therefore, a definite cyclic voltammogram of this ion at a hanging mercury electrode was not obtained, although sharp reduction and oxidation peaks were seen ($E_{p,c}$ −0.185 and $E_{p,a}$ −0.105 V (SCE)). On the other

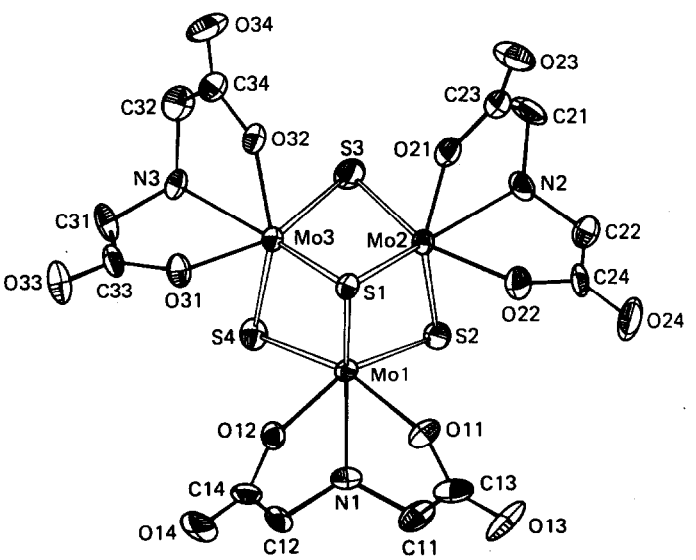


Fig. 2. Perspective view of $[Mo_3S_4(ida)_3]^{2-}$ showing the atom-numbering scheme.

Table 1. Selected bond distances (Å) and angles (°)

Bond distance		Bond angle	
Mo1—Mo2	2.741(2)	Mo3—Mo1—Mo2	60.25(4)
Mo1—Mo3	2.795(2)	Mo1—Mo2—Mo3	60.20(4)
Mo2—Mo3	2.761(2)	Mo1—Mo3—Mo2	59.55(4)
Mo1—S1	2.345(4)	S2—Mo4—S4	94.26(14)
Mo2—S1	2.340(4)	S2—Mo2—S3	94.68(14)
Mo3—S1	2.358(4)	S3—Mo3—S4	96.35(14)
Mo1—S2	2.289(4)	S1—Mo1—S2	106.38(14)
Mo1—S4	2.295(4)	S1—Mo1—S4	105.78(13)
Mo2—S2	2.290(4)	S1—Mo2—S2	106.52(14)
Mo2—S3	2.289(4)	S1—Mo2—S3	106.32(14)
Mo3—S3	2.310(4)	S1—Mo3—S3	105.04(14)
Mo3—S4	2.289(4)	S1—Mo3—S4	105.67(13)
Mo1—O11	2.152(9)	Mo1—S1—Mo2	71.62(11)
Mo1—O12	2.142(9)	Mo2—S1—Mo3	71.98(11)
Mo2—O21	2.170(9)	Mo3—S1—Mo1	71.84(11)
Mo2—O22	2.183(10)	Mo1—S2—Mo2	73.54(12)
Mo3—O31	2.145(10)	Mo2—S3—Mo3	73.77(12)
Mo3—O32	2.201(10)	Mo3—S4—Mo1	74.02(12)
Mo1—N1	2.271(11)		
Mo2—N2	2.279(12)		
Mo3—N3	2.271(11)		

Table 2. Comparison of bond distances (Å) among clusters with Mo_3S_4, Mo_3O_3S and Mo_3O_4 cores[a]

	Mo—Mo	Mo—μ_3-X[X]	Mo—μ_2-Y[Y]	Reference
$[Mo_3S_4(ida)_3]^{2-}$	2.754	2.349[S]	2.295[S]	This work
$[Mo_3S_4(CN)_9]^{5-}$	2.765	2.363[S]	2.312[S]	7
$[Mo_3S_4(SCH_2CH_2S)_3]^{2-}$	2.783	2.345[S]	2.293[S]	8
$[Mo_3S_4(h\text{-}C_5H_5)_3]^{+}$	2.813	2.314[S]	2.293[S]	9
$[Mo_3O_3S(Hnta)_3]^{2-}$	2.589	2.360[S]	1.917[O]	2
$[Mo_3O_4(mida)_3]^{2-}$	2.495	2.043[O]	1.918[O]	3(c)

[a] Mean values.

hand, no peak appeared in the region of 0 to ~ −0.5 V (SCE) at a glassy carbon electrode.

The cyclic voltammogram of $[Mo_3S_4(ida)_3]^{2-}$ (Fig. 3) shows two reversible one-electron waves and an ill-defined one. This clearly indicates the existence of $[Mo(IV)]_2Mo(III)$ and $Mo(IV)[Mo(III)]_2$ oxidation states. The polarogram (Fig. 4) for this compound also supports the existence of both oxidation states. No such an oxidation state of trinuclear molybdenum cluster as

$$[Mo(IV)]_2Mo(III)$$

has been found in the reduction process of $Mo_3O_4^{4+}$ or

$$[Mo_3O_4(C_2O_4)_3(H_2O)_3]^{2-}.^{\text{I(b)-(d)}}$$

The introduction of sulfur into the Mo_3O_4 core can be one of the causes* of the appearance of the $[Mo(IV)]_2Mo(III)$ oxidation state and the presence of aqua ligand(s) may prevent $Mo_3O_4^{4+}$ or

$$[Mo_3O_4(C_2O_4)_3(H_2O)_3]^{2-}$$

from exhibiting the $[Mo(IV)]_2Mo(III)$ oxidation state. Further studies on the electrochemistry of the

* $[Mo_3O_3S(ida)_3]^{2-}$ also shows the $[Mo(IV)]_2Mo(III)$ oxidation state (unpublished data).

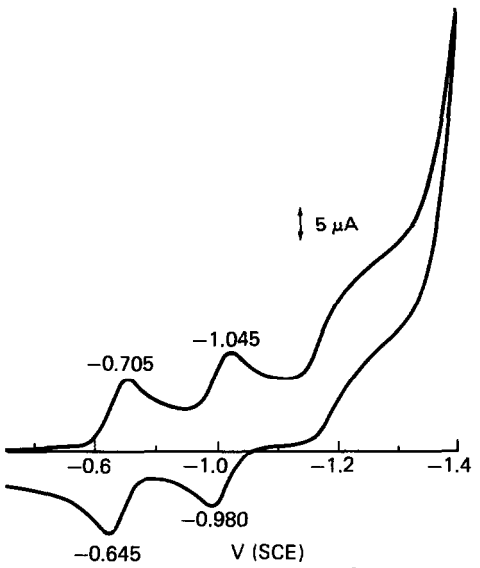


Fig. 3. Cyclic voltammogram of $[Mo_3S_4(ida)_3]^{2-}$ (0.96 mM) in 0.1 M KCl at a glassy carbon electrode: scan rate 100 mV s^{-1}, reference electrode is an SCE; temperature 25°C.

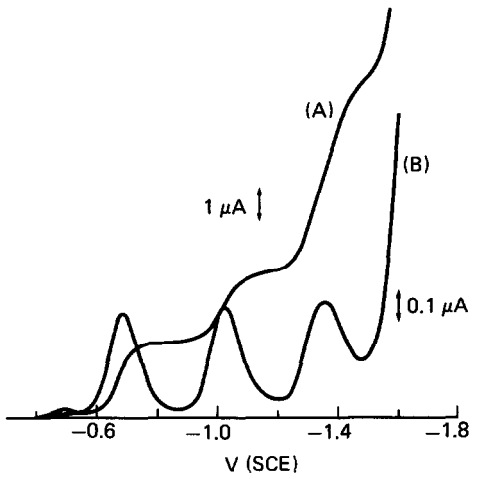


Fig. 4. Polarogram (a) and difference polarogram (b) of $[Mo_3S_4(ida)_3]^{2-}$ (0.96 mM) in 0.1 M KCl.

compounds with an Mo_3S_4 core, as well as those with an Mo_3O_4 core, are to be expected.

Acknowledgement—This work was supported by a Grant-in-Aid for Scientific Research (No. 59470039) from the Ministry of Education, Science and Culture.

REFERENCES

1. (a) R. K. Murmann and M. E. Shelton, *J. Am. Chem. Soc.* 1980, **102**, 3984; (b) D. T. Richens and A. G. Sykes, *Inorg. Chim. Acta* 1981, **54**, L3; (c) D. T. Richens and A. G. Sykes, *Inorg. Chem.* 1982, **21**, 418; (d) M. T. Paffet and F. C. Anson, *Inorg. Chem.* 1983, **22**, 1347; (e) S. P. Cramer, P. K. Eidem, M. T. Paffet, J. R. Winkler, Z. Dori and H. B. Gray, *J. Am. Chem. Soc.* 1983, **105**, 799; (f) D. T. Richens and A. G. Sykes, *Comments Inorg. Chem.* 1981, **1**, 141.
2. T. Shibahara, H. Hattori and H. Kuroya, *J. Am. Chem. Soc.* 1984, **106**, 2710.
3. (a) A. Bino, F. A. Cotton and Z. Dori, *J. Am. Chem. Soc.* 1978, **100**, 5252; (b) *ibid.* 1979, **101**, 3842; (c) S. F. Gheller, T. W. Hambley, R. T. C. Brownlee, M. J. O'Connor, M. R. Snow and A. G. Wedd, *ibid.* 1983, **105**, 1527.
4. V. R. Otto, D. S. Swieter and F. A. Schultz, *Inorg. Chem.* 1977, **16**, 2538.
5. F. A. Armstrong, T. Shibahara and A. G. Sykes, *Inorg. Chem.* 1978, **17**, 189.
6. T. Shibahara, S. Ooi and H. Kuroya, *Bull. Chem. Soc. Jpn* 1982, **55**, 3742.
7. (a) A. Müller and U. Reinsh, *Angew. Chem., Int. Ed. Engl.* 1980, **19**, 72; (b) N. C. Howlader, G. P. Haight, Jr, T. W. Hambly, G. A. Lawrance, K. M. Rahmoeller and M. R. Snow, *Aust. J. Chem.* 1983, **36**, 377.
8. T. R. Halbert, K. McGauley, W.-H. Pan, R. S. Czernuszewicz and E. I. Stiefel, *J. Am. Chem. Soc.* 1984, **106**, 1849.
9. P. J. Vergamini, H. Vahrenkamp and L. F. Dahl, *J. Am. Chem. Soc.* 1971, **93**, 6327.

Polyhedron Vol. 5, No. 1/2, pp. 363–367, 1986
Printed in Great Britain

0277-5387/86 $3.00 + .00
© 1986 Pergamon Press Ltd

COMPLEXES OF MOLYBDENUM WITH STERICALLY HINDERED THIOLATO-LIGANDS

P. T. BISHOP,* P. J. BLOWER and J. R. DILWORTH*†

AFRC Unit of Nitrogen Fixation, University of Sussex, Brighton BN1 9RQ, U.K.

and

J. A. ZUBIETA

Chemistry Department, State University of New York at Albany, Albany, NY 12222, U.S.A.

(*Received* 28 *June* 1985)

Abstract—$[MoBr_2(CO)_4]$ reacts with 2,4,6-$Pr^i_3C_6H_2S^-$ ($TIPT^-$) to give trigonal bipyramidal $[Mo(CO)_2(TIPT)_3]^-$ (**I**). The tungsten and rhenium analogues are isostructural. Complex **I** reacts with neutral donors to give $[Mo(TIPT)_3(CO)L]^-$ (L = MeCN, Bu^tCN, MeNC, Bu^tNC or PMe_2Ph) and with $[PhN_2][BF_4]$ to give $[Mo(N_2Ph)(TIPT)_3(MeCN)]$ (**II**). Complex **II** is also trigonal bipyramidal with axial N_2Ph and MeCN ligands. $[MoCl_3(MeCN)_3]$ reacts with TIPT in MeCN to give "$[Mo(MeCN)(TIPT)_4]$". By contrast, $MoCl_4$ in dimethoxyethane with TIPT gives $[Mo_2(TIPT)_6]$ together with $[MoO(TIPT)_4]^-$. An X-ray crystal structure of $[Mo_2(TIPT)_6]$ revealed an Mo–Mo triple bond analogous to $[Mo_2(OR)_6]$ species. The phenylated thiol, 2,6-$Ph_2C_6H_3S^-$ (DPT^-), reacts with $[MoBr_2(CO)_4]$ in dimethoxyethane to give $[Mo(CO)(DPT)_2]$. One of the *o*-phenyl groups is η^6-bonded to give a distorted piano-stool structure. The η^6-phenyl group is readily displaced by a range of neutral donor ligands to give access to a new series of Mo(II) thiolato-derivatives.

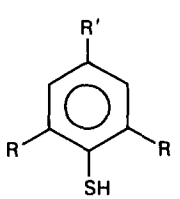
There is now strong evidence from EXAFS studies that the metal ions in nitrogenase are ligated primarily by sulphur. However, there are comparatively few reported examples of molybdenum–sulphur complexes containing small molecules such as CO, H_2 and NO, and none with dinitrogen. In this paper we describe our attempts to prepare reactive monomeric molybdenum complexes using bulky 2,6-disubstituted aryl thiols of the types shown in Fig. 1.

The Mo(IV) complex $[MoCl_4(thf)_2]$ (thf = tetrahydrofuran) reacts with

$$2,4,6\text{-}Pr^i_3C_6H_2S^- \ (TIPT^-)$$

in thf in the presence of CO to give $[Mo(TIPT)_3(CO)_2]^-$ (**I**), isolated as a tetraphenylphosphonium salt. Complex **I** can also be prepared more conveniently by reaction of $[MoCl_2(CO)_4]$ with three equivalents of TIPTH in methanol in the presence of triethylamine. The bright pink complex **I** is diamagnetic and shows ν(CO) at 1860 cm^{-1} in the IR spectrum. An X-ray crystal structure revealed a trigonal bipyramidal structure with axial CO ligands.[1] Reaction with neutral two-electron donor ligands gave purple $[Mo(TIPT)_3(CO)L]$ (L = MeCN, Bu^tCN, MeNC, Bu^tNC or PMe_2Ph).

However, reaction with $[PhN_2][BF_4]$ in aceto-



R' = R = Me or Pr^i
R' = H, R = Ph

Fig. 1. Sterically hindered arylthiolato-ligands.

* Present address: Chemistry Department, University of Essex, Colchester CO4 3SQ, U.K.

† Author to whom correspondence should be addressed.

nitrile occurred rapidly and smoothly to give green $[Mo(N_2Ph)(TIPT)_3(MeCN)]$ (**II**). An X-ray crystal structure of complex **II** again revealed a trigonal bipyramidal structure (Fig. 2) with apical N_2Ph and MeCN groups. The N_2Ph ligand has a linear Mo—N—N— system and the bond lengths are also consistent with the diazenido-ligand functioning as a three-electron donor, giving the metal an overall 14-electron configuration. The complex is isostructural with the closely related nitrosyl derivative $[Mo(TIPT)_3(NO)(NH_3)]$ which contains a nearly linear Mo—N—O moiety. ^{15}N NMR spectra of ^{15}N-labelled complex **II** revealed two resonances for the β-nitrogen consistent with two isomers depending on the concentration of the aryl groups of the thiolate ligands relative to the diazenido-ligand. The shift in the β-nitrogen resonance on addition of acid is consistent with the formation of the hydrazido(2−)-complex $[Mo(NNHPh)(TIPT)_3(MeCN)]^+$.

The reaction of the Mo(IV) precursors with $TIPT^-$ leads to reduction of the molybdenum. By contrast, reaction of $[MoCl_3(MeCN)_3]$ with TIPTH in dry acetonitrile under reflux in the presence of triethylamine gives brown crystalline air-sensitive $[Mo(TIPT)_4(MeCN)]$ (**III**) with nett oxidation of the metal. Suitable crystals for an X-ray structure have not yet been obtained and the formulation is based on elemental analysis, ^1H NMR and molecular-weight determinations. Complex **III** is related to $[Mo(SBu^t)_4]$[2] but is stabilized with respect to C—S bond cleavage which dominates the chemistry of the *t*-butylthiolato-complex.[2] The MeCN is readily displaced by other two-electron donor ligands, providing ready access to a range of Mo(IV) thiolato-derivatives.

The products obtained from the reaction of molybdenum halido-precursors with the sterically demanding thiolates are also highly dependent on the solvent used in the reaction. Thus reaction of $MoCl_4$ with NaTIPT in 1,2-dimethoxyethane gave $[MoO(TIPT)_4]^-$ (**IV**), isolated as a tetraphenylphosphonium salt from methanol (40% yield) and a red crystalline, hexane-soluble complex of empirical formula $Mo(TIPT)_3$ (**V**).

The formation of the Mo(V) oxo-complex (**IV**) demonstrates the high oxygen affinity of these molybdenum thiolato-systems and it is found as a

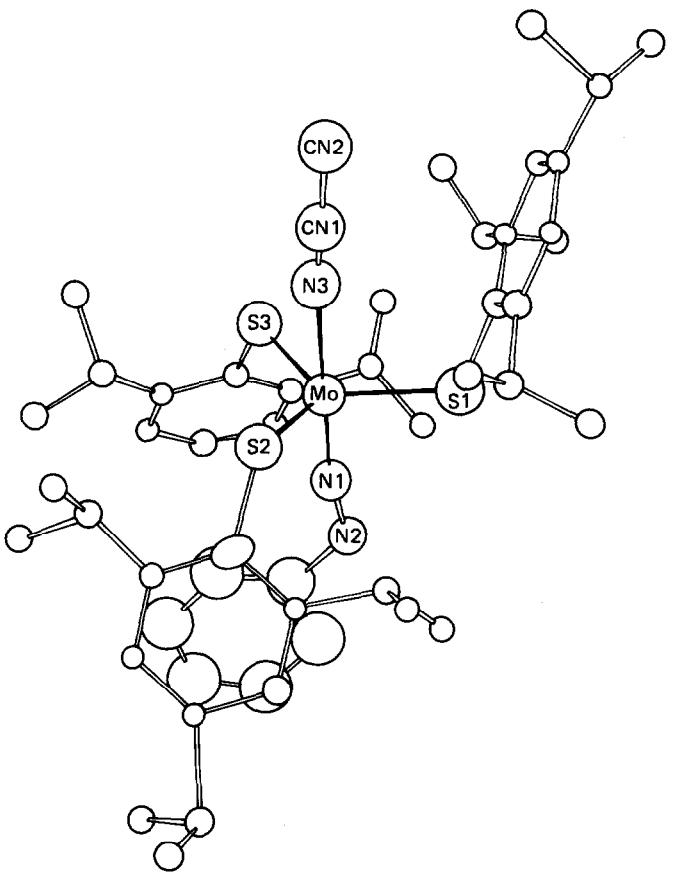


Fig. 2. Structure of $[Mo(NNPh)(TIPT)_3(MeCN)]$.

contaminant in many reactions. The source of the oxygen is not certain but equivalent yields are also produced when the reactions are done in a glove-box at oxygen concentrations of less than 1 ppm O_2. Traces of water in the solvent or the solvent itself may be responsible. The ready formation of the oxo-species is also illustrated by reaction of $[MoCl_4(PPh_3)_2]$ with NaTIPT in toluene under N_2 when the only isolable characterizable product was yellow-orange crystalline $[Mo_2O_4(TIPT)_2(PPh_3)_2]$ (**VI**) shown by an X-ray crystal structure to have both terminal and bridging oxo groups.

The Mo(V) oxo-complexes (**IV**) are deep blue paramagnetic d^1-systems with EPR spectra extremely similar to the known thiophenolato-complex $[MoO(SPh)_4]^-$,[3,4] suggesting an analogous square pyramidal structure with an apical oxo-group. They can be synthesized more systematically by reaction of $[Bu^n_4N][MoOCl_4]$ with NaTIPT in thf in near quantitative yield. The purple tungsten analogue is prepared analogously from $WOCl_4$. Cyclic voltammetric measurements show that, whereas the thiophenolate complex is irreversibly oxidized and quasi-reversibly reduced, complex **IV** is reversibly oxidized and totally irreversibly reduced. This is consistent with facile expulsion of bulky thiolate anion on reduction and stabilization of the Mo(VI) oxo-species formed on oxidation.

The second reaction product (**V**) mentioned above of empirical formula $Mo(TIPT)_3$ was shown to be dimeric by cryoscopic measurements in benzene. An X-ray crystal structure (Fig. 3) revealed a dimeric structure with an Mo–Mo triple bond. The complex has a closely related structure to the complex $[Mo_2(2,4,6\text{-}Me_3C_6H_2S)_6]$ reported earlier by Chisholm *et al.*[5] However, the synthesis we report here is more convenient, proceeding in one step from readily available $MoCl_4$ and avoiding the more difficult preparation of $[Mo_2(NMe_2)_6]$ and several succeeding complex substitution steps. The bulk of the thiolate ligands drastically reduces the reactivity of the complex and there is no sign of the reactions with small molecules such as acetylenes and other multiply bonded species reported for analogous alkoxides such as $[Mo_2(OPr^i)_6]$.

If the sterically hindered thiolates bear phenyl groups in the *ortho*-positions then completely different co-ordination behaviour is observed. Thus the sodium salt of 2,6-diphenylthiophenol (NaDPT) reacts with $[MoBr_2(CO)_4]$ in 1,2-dimethoxyethane

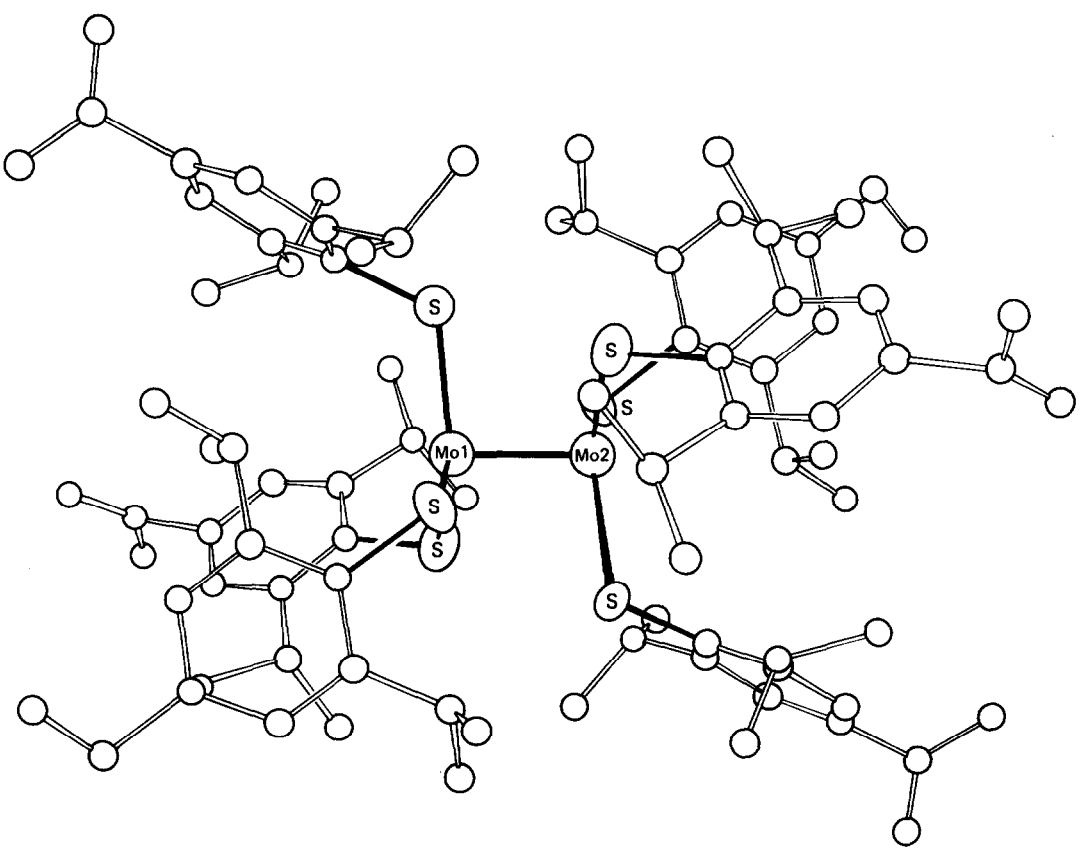


Fig. 3. Structure of $[Mo_2(TIPT)_6]$.

at room temperature to give a green air-stable solid of empirical formula $[Mo(DPT)_2(CO)]$ (**VII**).[6] This complex shows ν(CO) in the IR spectrum at 1915 cm^{-1} and the ^1H NMR spectrum reveals a pattern of resonances in the 5–7-ppm region characteristic of an η^6-bonded phenyl group. This was confirmed by an X-ray crystal structure of complex **VII** shown in Fig. 4 in partial form. The overall structure is best described as a distorted piano-stool with one of the *o*-phenyl substituents of the thiol η^6-bonded to the molybdenum.

The η^6-bonded group is labile and is readily displaced by CO to give a purple polycarbonyl complex. This has not been isolated as it readily loses CO during work up to reform the π-arene complex. Reaction of the arene complex (**VII**) with bipyridyl gives a purple-pink crystalline complex in less than 50% yield which shows two IR bands at 1855 and 1950 cm^{-1} assignable to ν(CO). Elemental analysis and ^1H NMR are consistent with the empirical formulation $[Mo(DPT)_2(bipy)(CO)_2]$ (**VIII**) (bipy = bipyridyl). An X-ray crystal structure of complex **VIII** revealed a pseudo-octahedral *dicarbonyl* complex with *cis* carbonyl groups. The mechanism of formation of the dicarbonyl product from a monocarbonyl precursor is obscure but a bridged carbonyl intermediate could possibly be involved. The remaining molybdenum complex has not yet been identified, but contains no co-ordinated CO groups, as evidenced by IR.

In contrast, the reaction of complex **VII** with $Ph_2PCH_2CH_2PPh_2$ (dppe) gives the pink five-co-ordinate *monocarbonyl* complex $[Mo(DPT)_2(CO)(dppe)]$ (**IX**). Complex **IX** exists in solution as two isomers which are distinguishable by ^{31}P NMR and solution IR spectroscopy.

EXPERIMENTAL

All reactions were carried out under dinitrogen using dry solvents and conventional Schlenk apparatus or in a Faircrest glove-box and recirculator. IR spectra were determined on Pye Unicam SP2000 and Perkin–Elmer 1330 spectrophotometers, and ^1H and ^{31}P NMR spectra on JEOL FX 90Q and Bruker 80 multinuclear instruments. Microanalyses were made by Mrs A. Olney at the University of Sussex. The following materials were synthesized by literature methods: $[MoBr_2(CO)_2]$,[7] $MoCl_4$,[8] $[MoCl_3(MeCN)_3]$[9] and $[Mo(CO)_2(TIPT)_3]^-$ and $WOCl_4$.[10] The thiols TIPTH and DPTH were prepared by slight modifications of reported methods.

Hexakis(2,4,6 - triisopropylbenzenethiolato)dimolybdenum(III), $[Mo_2(TIPT)_6]$

HTIPT (2.1 cm^3, 9.8 mmol) was added to an excess of sodium pieces in 1,2-dimethoxyethane (20 cm^3) and heated under reflux for 2 h. This solution of NaTIPT was added to $MoCl_4$ (0.38 g, 2.0 mmol) in 1,2-dimethoxyethane (15 cm^3), and the solution stirred for 16 h. It was then filtered through Celite, the solvent removed and the residue titrated with hexane (15 cm^3) to give a dark coloured solid. This was washed with dry methanol until the washings were free of blue $[MoO(TIPT)_4]^-$. The pinkish-brown solid was recrystallized as red prisms by diffusion of acetonitrile into a dichloromethane solution which yielded crystals suitable for the X-ray crystal structure. Found: C, 67.2; H, 8.9%. $Mo_2S_6C_{90}H_{138}$ requires: C, 67.4; H, 6.8%.

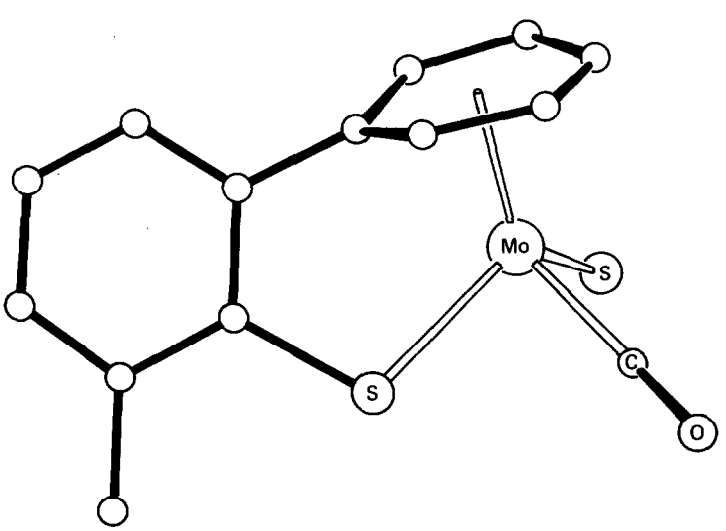


Fig. 4. Partial structure of $[Mo(DPT)_2(CO)]$.

Tetraphenylphosphonium oxotetrakis(2,4,6 - triiso - propylbenzenethiolato)molybdenum(V), $[Ph_4P][MoO(TIPT)_4]$

$[Bu^n_4N][MoOCl_4]$ (1.04 g, 2.1 mmol) was dissolved in acetonitrile (30 cm^3), and HTIPT (2.20 cm^3, 10 mmol) and triethylamine (1.16 cm^3, 8.4 mmol) added. The resulting dark blue solution was evaporated to dryness and the residue extracted with methanol. Addition of $[Ph_4P]Br$ gave the complex (2.8 g). Found: C, 72.1; H, 7.7%. $MoOS_4PC_{84}H_{112}$ requires: C, 72.5; H, 7.7%.

The tungsten analogue $[WO(TIPT)_4]^-$ was prepared similarly using $WOCl_4$.

Acetonitrile(phenyldiazemdo)tris(2,4,6 - triisopropyl - benzenethiolato)molybdenum(II), $[Mo(NNPh)(TIPT)_3(N_2Ph)]$

$[PhN_2][BF_4]$ (0.063 g, 0.33 mmol) in acetonitrile (10 cm^3) was added dropwise to a solution of $[Ph_4P][Mo(TIPT)_3(CO)_2]$ in acetonitrile (25 cm^3). Rapid evolution of CO occurred with formation of a green crystalline precipitate (the complex). Found: C, 66.8; H, 8.0; N, 3.8%. $MoN_3S_3C_{53}H_{77}$ requires: C, 67.2; H, 8.1; N, 4.4%.

[η^6 - 2 - *Phenyl* - 6 - *phenylbenzenethiolato*)(2,6 - *diphenylbenzenethiolato)carbonylmolybdenum(II)*, $[Mo(\eta^6 - Ph)PhC_6H_3S - 2,6)(SC_6H_3Ph_2 - 2,6)(CO)]$

Sodium DPT (2.0 g, 7.1 mmol) dissolved in 1,2-dimethoxyethane (20 cm^3) was added dropwise to a solution of $[MoBr_2(CO)_4]$ (1 g, 3.6 mmol) in 1,2-dimethoxyethane (30 cm^3) and stirred for 12 h. The green-yellow solution was filtered through Celite and the filtrate evaporated to dryness. The resulting green-yellow oil was titrated with warm hexane for 5 min to yield the complex as a green powder. Yield 1.6 g (73.3%). Found: C, 69.0; H, 5.2%. $MoOS_2C_{37}H_{36}$ requires: C, 68.7; H, 4.0%.

Bis(2,6 - diphenylbenzenethiolato)bipyridylbiscarbonylmolybdenum(II), $[Mo(DPT)_2(bipy)(CO)_2]$

Excess bipyridyl (0.1 g) was added to a solution of the π-arenethiolato complex in 1,2-dimethoxyethane giving an immediate dark purple solution. After 3 h the solution was evaporated to dryness and the residue chromatographed on neutral alumina using dichloromethane as solvent. The deep purple band was eluted and collected, evaporated and the residue titrated with diethyl ether to yield the complex as a purple-red powder.

REFERENCES

1. J. R. Dilworth, J. Hutchinson and J. A. Zubieta, *J. Chem. Soc., Chem. Commun.* 1983, 1034.
2. S. Otsuka, M. Kamata, K. Hirotsu and T. Higuchi, *J. Am. Chem. Soc.* 1981, **103**, 3011.
3. I. W. Boyd, I. G. Dance, K. S. Murray and A. G. Weald, *Aust. J. Chem.* 1978, **31**, 279.
4. R. J. Burt, J. R. Dilworth, G. J. Leigh and J. A. Zubieta, *J. Chem. Soc., Dalton Trans.* 1982, 2295.
5. M. H. Chisholm, J. F. Corning and J. C. Huffman, *J. Am. Chem. Soc.* 1983, **105**, 5924.
6. P. T. Bishop, J. R. Dilworth and J. A. Zubieta, *J. Chem. Soc., Chem. Commun.* 1985, 257.
7. R. Colton and I. B. Tomkins, *Aust. J. Chem.* 1966, **19**, 1143.
8. M. L. Larson and F. W. Moore, *Inorg. Chem.* 1964, **3**, 285.
9. J. R. Dilworth and J. A. Zubieta, *J. Chem. Soc., Dalton Trans.* 1982, 397.
10. R. Colton and I. B. Tomkins, *Aust. J. Chem.* 1965, **18**, 447.

Polyhedron Vol. 5, No. 1/2, pp. 369–376, 1986
Printed in Great Britain

0277–5387/86 $3.00 + .00
© 1986 Pergamon Press Ltd

MONONUCLEAR THIOLATE COMPLEXES OF Mo(II) AND Mo(III): X-RAY CRYSTAL STRUCTURE OF *TRANS*-$[Mo(SBu^n)_2(Ph_2PCH_2CH_2PPh_2)_2]$

DAVID C. POVEY

Department of Chemistry, University of Surrey, Guildford GU2 5XH, U.K.

and

RAYMOND L. RICHARDS* and CAROLINE SHORTMAN

AFRC Unit of Nitrogen Fixation, University of Sussex, Brighton BN1 9RQ, U.K.

(*Received* 18 *June* 1985)

Abstract—The complexes *trans*-$[Mo(SR)_2(diphos)_2]$ (A) [R = alkyl, C_6F_5 or C_6H_4X-4, where X = H, F, Cl, CH_3, NH_2 or OCH_3; diphos = $Ph_2PCH_2CH_2PPh_2$ (dppe) or $(C_6H_4CH_3$-$3)_2PCH_2CH_2P(C_6H_4CH_3$-$3)_2$ (dmtpe)] have been prepared by treatment of *trans*-$[Mo(N_2)_2(diphos)_2]$ with RSH. *trans*-$[Mo(SBu^n)_2(dppe)_2]$ crystallizes in the monoclinic space group $C2/c$ with $a = 25.605(5)$ Å, $b = 12.055(2)$ Å, $c = 19.637(4)$ Å, $\beta = 107.08(2)°$ and final $R = 0.041$. The molecule is centrosymmetric with Mo—S = 2.363(1) Å and $Mo—P_{average} = 2.511(1)$ Å. Compounds (A) are diamagnetic and the ^{31}P NMR chemical shifts and $E^{ox}_{1/2}$ values of (A, R = C_6H_4X-4) show a linear dependence upon the Hammett σ function for X. Chemical oxidation ($FeCl_3$ or $CuCl_2$) followed by anion exchange gives the complexes $[Mo(SR)_2(dppe)_2][BPh_4]$, whose ESR spectra show a rhombic signal in frozen solution having hyperfine splitting which is solvent-dependent.

Of relevance to the study of molybdenum enzymes and of nitrogenase in particular is information upon the nature of molybdenum–thiolate bonding, especially in the lower oxidation states of this metal.[1] Whilst pursuing our interest in the reactions of dinitrogen complexes of molybdenum,[2] we obtained a number of thiolate complexes of Mo(II), *trans*-$[Mo(SR)_2(dppe)_2]$, by treatment of *trans*-$[Mo(N_2)_2(dppe)_2]$ with RSH.[3] These compounds have the *trans*-arrangement of groups and thus the tendency of the thiolate ligands to undergo *cis*-elimination, dealkylation or form bridges, which creates difficulties in attempted preparations of mononuclear complexes,[4] are avoided.

The mononuclear series (A) allows us to examine the behaviour of thiolate ligands at a single metal centre by spectroscopic and electrochemical means. In this paper we describe the preparation of an extension of the original series of complexes to include (A, R = C_6H_4X-4), which allows an examination of the electronic effects of the thiolate within the complexes. One-electron oxidation of compound (A) is not only a means of probing such electronic effects, but it has also led to the preparation of a series of Mo(III) complexes, $[Mo(SR)_2(dppe)_2]Y$ (B) (Y = $FeCl_4$ or BPh_4), which show interesting ESR properties.

PREPARATION OF COMPLEXES AND STRUCTURE OF *TRANS*-$[Mo(SBu^n)_2(dppe)_2]$

Complexes (A) were prepared by treating *trans*-$[Mo(N_2)_2(diphos)_2]$ in thf solution with an excess of RSH as described earlier[3] [eqn (1)]:

$$trans\text{-}[Mo(N_2)_2(diphos)_2] + 2RSH \rightleftharpoons trans\text{-}[Mo(SR)_2(diphos)_2] + 2N_2 + H_2 \quad (1)$$

Analytical and other data for these diamagnetic compounds are shown in Table 1. The reaction

* Author to whom correspondence should be addressed.

Table 1. Thiolate complexes of Mo(II) and Mo(III)

Complex[a]	Colour	Yield (%)	Analyses (%)[b] C	H	Other data
$[Mo(SEt)_2(dppe)_2]$[c]	Yellow	70			
$[Mo(SPr^n)_2(dppe)_2]$[c]	Yellow	71			
$[Mo(SBu^n)_2(dppe)_2]$[c]	Yellow	70			
$[Mo(SPh)_2(dppe)_2]$[c]	Red	70	69.0 (69.2)	5.3 (5.3)	
$[Mo(SC_6H_4CH_3\text{-}4)_2(dppe)_2]$	Red	60	67.9 (67.8)	5.9 (6.0)	
$[Mo(SC_6H_4NH_2\text{-}4)_2(dppe)_2]$	Blue	50	65.4 (65.8)	5.6 (5.7)	ν(NH)[d] 1610 cm^{-1}
$[Mo(SC_6H_4OMe\text{-}4)_2(dppe)_2]$	Red	60	67.6 (67.7)	5.7 (5.3)	
$[Mo(SC_6H_4F\text{-}4)_2(dppe)_2]$	Red	60	67.4 (67.0)	4.9 (4.9)	ν(CF)[d] 1220 cm^{-1}
$[Mo(SC_6H_4Cl\text{-}4)_2(dppe)_2]$	Red	60	65.0 (65.1)	5.2 (4.8)	
$[Mo(SC_6F_5)_2(dppe)_2]$	Orange	70	59.0 (59.5)	3.7 (4.1)	ν(CF)[d] 980 and 850 cm^{-1}
$[Mo(SC_6H_5)_2(dmtpe)_2]$	Red	65	69.3 (70.7)	6.1 (6.1)	
$[Mo(SEt)_2(dppe)_2][FeCl_4]$	Brown	75	55.4 (55.5)	5.0 (4.8)	
$[Mo(SEt)_2(dppe)_2][BPh_4]$	Brown	70	71.9 (72.0)	6.3 (5.9)	μ_{eff} = 1.3 BM, Λ_m = 72.5 S cm^2 mol^{-1}[e]
$[Mo(SPr^n)_2(dppe)_2][BPh_4]$	Brown	55	72.6 (72.3)	5.9 (6.1)	
$[Mo(SPr^n)_2(dppe)_2][FeCl_4]$	Brown	75	55.5 (56.2)	5.5 (5.1)	
$[Mo(SBu^n)_2(dppe)_2][FeCl_4]$	Brown	55	72.0 (72.6)	6.5 (6.2)	Λ_m = 70.5 S cm^2 mol^{-1}[f]
$[Mo(SC_6H_5)_2(dppe)_2][BPh_4]$	Purple	65	72.7 (73.4)	5.4 (5.5)	
$[Mo(SC_6H_4Me\text{-}4)_2(dppe)_2][BPh_4]$	Purple	62	73.6 (74.1)	6.5 (5.7)	
$[Mo(SC_6H_4OMe\text{-}4)_2(dppe)_2][BPh_4]$	Purple	60	73.4 (73.6)	5.6 (6.8)	Λ_m = 63.5 S cm^2 mol^{-1}[e]
$[Mo(SC_6H_4F\text{-}4)_2(dppe)_2][FeCl_4]$	Purple	55	56.1 (57.2)	4.5 (4.2)	
$[Mo(SC_6H_4Cl\text{-}4)_2(dppe)_2][FeCl_4]$	Purple	70	55.8 (54.9)	4.1 (4.3)	
$[Mo(SC_6H_4Cl\text{-}4)_2(dppe)_2][BPh_4]$	Purple	70	69.7 (70.5)	4.9 (5.1)	μ_{eff} = 1.3 BM

[a] All complexes have *trans*-configuration.
[b] Calculated values in parentheses.
[c] Taken from Ref. 3.
[d] Nujol mull spectra.
[e] In MeCN solution.
[f] In acetone solution.

proceeds via green intermediates which have been isolated for certain bulky R groups[5] and shown to be the hydrides $[MoH(SR)(dppe)_2]$.

Attempts to carry out the same reaction for *trans*-$[W(N_2)_2(dppe)_2]$ gave only mixtures of products which contained thiolate but could not be purified.

Compound (A, R = Bu^n) forms yellow crystals (thf–Et_2O) in space group $C2/c$ with four molecules in the unit cell. Disordered water molecules are also found which must have arisen adventitiously during the recrystallization process. The molybdenum is surrounded by six ligating atoms in an essentially octahedral array with the equatorial plane defined by the four phosphorus atoms of the chelating diphosphine and the thiolate ligands in the *trans*, *anti*-configuration (Fig. 1). The methylene bridges of the two diphosphine ligands have an eclipsed configuration. Relevant bond distances and angles are in Table 2. The P—phenyl distances range from 1.840(5) to 1.854(4) Å, which is within the usual range[6] of 1.838 ± 0.026 Å for the P—C (sp^3) distance: all the phenyl rings are planar within experimental error.

The butyl groups of the thiolate lie between two $P(C_6H_5)_2$ moieties of the dppe chelate ligands. On the electron-density maps, the rather diffuse electron-density contours in the region of the

Table 2. Selected bond distances (Å) and angles (°) for *trans*-$[Mo(SBu^n)_2(dppe)_2]$

Mo—S(1)	2.361(1)	P(2)—C(2)	1.872(4)
Mo—P(1)	2.521(1)	P(2)—C(3)	1.844(5)
Mo—P(2)	2.500(1)	P(2)—C(9)	1.859(5)
P(1)—C(1)	1.854(4)	P(1)—P(2)	3.885(2)
P(1)—C(15)	1.843(5)	C(1)—C(2)	1.519(7)
P(1)—C(21)	1.840(5)	S(1)—C(27)	1.842(5)

P(1)—Mo—P(2)	78.63(4)
P(1)—Mo—S(1)	93.18(4)
P(2)—Mo—S(1)	92.05(4)
Mo—S(1)—C(27)	120.07(4)

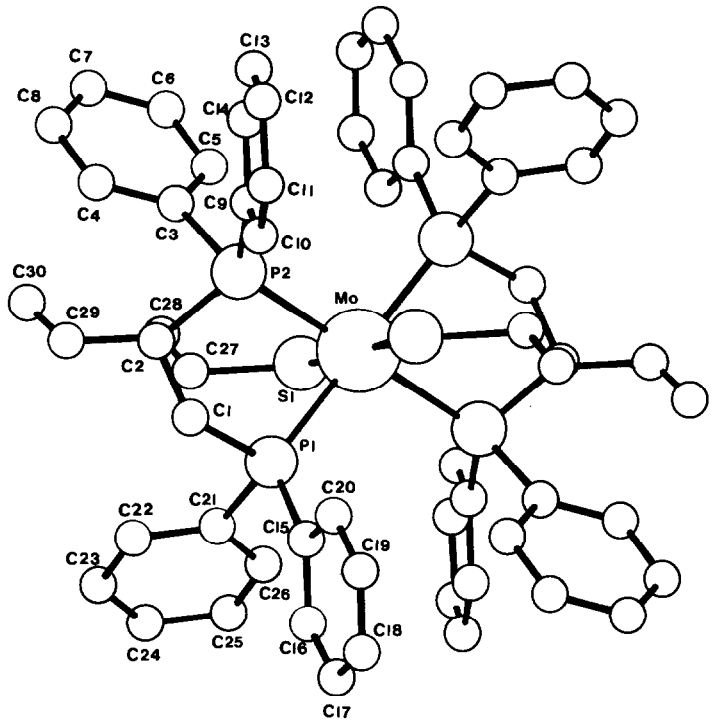


Fig. 1. Molecular structure of *trans*-[Mo(SBu^n)$_2$(dppe)$_2$].

terminal carbon atoms, C(29) and C(30), of the SBu^n moiety suggest some thermal disorder. This is borne out by the high thermal parameters of these two atoms. This might imply a low thermal barrier to isomerization of this group from the observed *anti*-conformation to the *syn*-arrangement. The poor solubility of these compounds has prevented an examination of isomerisation by variable-temperature ^{1}H NMR studies, but a very low barrier to isomerization has been established by NMR for the compound *cis*-[Mo(SBu^t)$_2$(CNBu^t)$_4$].[7]

The structure of (**A**, R = Bu^n) appears to be dominated by the steric constraints imposed by the dppe ligands. As in other [ML$_2$(dppe)$_2$] compounds,[8(a),(b)] a *trans*-octahedral geometry ensures a minimum in steric repulsions, although electronic factors can override this, e.g. in *cis*-[Mo(CO)$_2$(dppe)$_2$].[8(b)]

The phenyl groups in each P(C$_6$H$_5$)$_2$ moiety are nearly mutually perpendicular, and thus direct protons towards the electron-rich centre of a neighbouring phenyl ring, a situation similar to that found in free dppe[9] and in others of its complexes such as *trans*-[MoCl$_2$(dppe)$_2$].[8(a)] The average Mo—P distance, 2.511(1) Å, is in the range normally found for dppe compounds with the P—Mo—P angle, 78.63(4)°, being at the lower end of the expected range.

Since compounds (**A**) are formally 16-electron species it is interesting to consider whether the sulphur atoms are able to release π-electron density to the metal, which might be reflected in the Mo—S distance. It is, however, difficult to decide whether or not the Mo—S distances in *trans*-[Mo(SBu^n)$_2$(dppe)$_2$] are especially short because of the lack of suitable complexes with which to compare them. Table 3 lists mononuclear thiolate compounds of Mo(II) which have been structurally characterized and includes both Mo—S distances and the Mo—S—C angles, which might also be diagnostic of Mo—S π-interaction. These data, although not all pertaining to the same geometry, do not suggest that the Mo—S distance in (**A**, R = Bu^n) is particularly short.

The Mo—S—C angle is at the high end of the observed range, which would be consistent with some interaction of the "lone pair" electrons on sulphur with the metal centre. We note that a π-interaction of chloride lone pair electrons has been suggested to occur in *trans*-[MoCl$_2$(dppe)$_2$] on the basis of the Mo—Cl distance, which is thought to be short by comparison with Mo—Cl distances in a range of other complexes.[8(a)] If this conclusion is correct, one would expect a similar interaction in complexes (**A**). The diamagnetism of the complexes is not unexpected, since their analogue [Mo(SBu^t)$_2$(CNBu^t)$_4$] and other thiolate complexes of Mo(II) are diamagnetic.[10]

Table 3. Mo—S bond lengths (Å) and Mo—Ŝ—C bond angles (°) in various Mo(II) complexes

Complex	Type of co-ordination	Mo—S	M—Ŝ—C	Reference
trans-[Mo(SBu^n)$_2$(dppe)$_2$]	Octahedral	2.364	120.07(4)	This work
cis-[Mo(SBu^t)$_2$(CNBu^t)$_4$]	Octahedral	2.374(3)	119.7(4)	[a]
[Mo(SBu^t)$_2$(CNBu^t)$_2$(PhC≡CPh)]	Trigonal	2.337(3)	120.0(4)	[b]
	Bipyramidal	2.338(3)	120.0(4)	
[Mo(SBu^t)$_2$(CNBu^t)(HC≡CH)]·½C$_6$H$_{14}$	Trigonal	2.321(3)	118.3(4)	[b]
	Bipyramidal	2.305(1)	120.4(6)	
[Mo(HBMe$_2$pz)$_3$(SC$_6$H$_4$Cl-4)(CO)$_2$][c]	Octahedral	2.305(1)	116.5(1)	[d]
[Mo(η^5-C$_5$H$_5$)(SC$_6$F$_5$)(CO)(CF$_3$C≡CCF$_3$)]	Octahedral	2.366(1)	105.7(1)	[e]
[Mo(TIPT)$_3$(NH$_3$)(NO)]	Trigonal	2.318(14)	111.6(15)	[f]
	Bipyramidal	2.350(14)	113.4(18)	
		2.199(26)	110.9(16)	
[Mo(NNPh)(TIPT)$_3$(NCMe)]	Trigonal	2.336(14)	109.7(5)	[g]
	Bipyramidal	2.312(3)	114.6(13)	

[a] M. Kamata, T. Yoshida and S. Otsuka, *J. Am. Chem. Soc.* 1981, **103**, 3572; Ref. 10.

[b] M. Kamata, K. Huotsu, T. Higuchi, M. Kido, K. Tatsumi, Y. Yoshida and S. Otsuka, *Inorg. Chem.* 1983, **22**, 2416.

[c] HBMe$_2$pz = dimethylpyrazolylborate.

[d] T. Begley, D. Condon, G. Ferguson, F. J. Lalor and M. A. Khan, *Inorg. Chem.* 1981, **20**, 3420.

[e] J. A. K. Howard, F. R. D. Stansfield and P. Woodward, *J. Chem. Soc., Dalton Trans.* 1976, 246.

[f] P. T. Bishop, J. R. Dilworth, J. Zubieta and J. Hutchinson, personal communication.

[g] P. J. Blower, D.Phil. Thesis, 1984 (University of Sussex).

SPECTROSCOPIC AND ELECTROCHEMICAL PROPERTIES

The ^{31}P chemical shifts, UV–visible spectroscopic and electrochemical data for compounds (**A**, diphos = dppe) are shown in Table 4. Singlet ^{31}P resonances are expected for these diamagnetic *trans*-complexes and they fall in the range −87.54 to −92.02 ppm [relative to P(OMe)$_3$], to high field of the parent *trans*-[Mo(N$_2$)$_2$(dppe)$_2$], which resonates at −75.3 ppm.

For the series (**A**, R = C$_6$H$_4$X-4), the ^{31}P shift

Table 4. ^{31}P NMR shifts, electronic spectral data and electrochemical data for compounds (**A**)

Compound[a]	^{31}P shift[b] (ppm)	λ_{max}[c] (nm)	$E^{ox}_{1/2}$ primary[d] (V)	$E^{ox}_{1/2}$ secondary[d] (V)	$E^{red}_{1/2}$[d] (V)
[Mo(SEt)$_2$(dppe)$_2$]	−87.75	456.8	—	—	—
[Mo(SPr^n)$_2$(dppe)$_2$]	−87.68	458.3	−0.19[15]	—	−1.96[15]
[Mo(SBu^n)$_2$(dppe)$_2$]	−87.54	457.6	−0.20[15]	—	−1.97[15]
[Mo(SPh)$_2$(dppe)$_2$]	−91.32	524.6	−0.05	+0.82	−1.61
[Mo(SC$_6$H$_4$CH$_3$-4)$_2$(dppe)$_2$]	−91.11	531.0	−0.07	+0.77	−1.68
[Mo(SC$_6$H$_4$NH$_2$-4)$_2$(dppe)$_2$]	−90.06	573.0	−0.24	+0.34	−1.84[e]
[Mo(SC$_6$H$_4$OMe-4)$_2$(dppe)$_2$]	−90.62	543.5	−0.08	+0.72	−1.18
[Mo(SC$_6$H$_4$F-4)$_2$(dppe)$_2$]	−91.32	523.0	+0.01	+0.81	−1.57
[Mo(SC$_6$H$_4$Cl-4)$_2$(dppe)$_2$]	−92.02	526.0	+0.04	+0.84	−1.82
[Mo(SC$_6$F$_5$)$_2$(dppe)$_2$][f]	—	—	+0.3	n.o.[g]	n.o.

[a] *trans*-Configuration.

[b] Relative to P(OMe)$_3$ in thf solution.

[c] thf solution.

[d] Reversible processes unless otherwise stated, scan rates 0.01–2 V s^{-1}, values relative to saturated calomel electrode in thf containing 0.2 M [NBu$_4$][BF$_4$].

[e] Irreversible wave.

[f] Too insoluble for most measurements.

[g] Not observed.

varies with X and a plot of shift against the Hammett σ_p function for X is linear ($r = 0.98$), whereas there is no linear correlation with σ_p^+. This correlation indicates that the ^{31}P shift is influenced by a through inductive effect rather than one involving conjugation of the arene substituent.

The electronic spectra of compounds (**A**) are very similar with dominant, high-intensity charge-transfer bands below 400 nm and an intense peak at 400–580 nm for all complexes (Table 4). Accurate extinction coefficients could not be obtained due to the low solubilities of the complexes, but they are of the order 2×10^4 dm^3 mol^{-1} cm^{-1}, indicative of charge-transfer transitions. These are possibly thiolate-to-metal ($n \rightarrow \pi^*$) in origin due to the electron deficiency of the 16-electron metal centre as discussed earlier. For (**A**, R = C_6H_4X-4) ν_{max} moves to longer wavelengths as X is more electron-donating. A similar trend has been reported for $[MoO(SR)_4]^-$ (R = C_6H_5, $C_6H_4CH_3$-4 or C_6Cl_5) and was considered to involve an S-ligand-to-metal charge transfer.[11]

For (**A**, R = alkyl) ν_{max} is essentially invariant and is at shorter wavelengths than for (**A**, R = aryl) as might be expected since there are no conjugative effects for R = alkyl.

Electrochemical data for (**A**, R = aryl) are shown in Table 4. All complexes show a primary oxidation in the range −0.24 to +0.3 V, which meets the criteria for a diffusion-controlled, reversible, one-electron oxidation.[12] The values of $E_{1/2}^{ox}$ can be considered to be a relative measure of the HOMO in these complexes[13] and, as expected, the more electron-donating thiolate groups form the most easily oxidized complexes. A plot of $E_{1/2}^{ox}$ against Hammett σ_p is linear ($r = 0.99$) with Hammett σ_p^+ giving a poor correlation ($r = 0.95$). Thus the same type of apparently solely inductive correlation is seen for both $E_{1/2}^{ox}$ and ^{31}P shift measurements. This observation does not necessarily exclude an Mo—S π-interaction, however, since the basis of ^{31}P shift correlations in co-ordination complexes is not established and the HOMO, which relates to the value of $E_{1/2}^{ox}$, may be essentially non-bonding and therefore only be affected by the overall charge on the metal and not directly sense a conjugative effect. With regard to the last point, it has been concluded that in the series $[Cr(CO)_5L]$ (L = PR_3, RNC, halide etc.) the ligands influence the energy of the HOMO (and hence $E_{1/2}^{ox}$) mainly by an inductive process, with L not conjugated to the HOMO, although ligands such as RNC are good π-acceptors.[14]

For (**A**, C_6H_4X-4; X = H, CH_3, NH_2. OCH_3, F or Cl) a secondary oxidation is observed in the region +0.34 to +0.84 V, but it is not so reversible as the primary oxidation at slow scan rates. The ease of the second oxidation depends upon the electron release exerted by the thiolate ligands, since, for (**A**, R = C_6F_5), where the thiolate substituent is strongly electron-withdrawing, the second oxidation is not observed within the range afforded by the thf solvent. For comparison, *trans*-$[MoCl_2(dppe)_2]$ oxidizes at −0.05 V (vs SCE in thf–0.2 M $[NBu_4][BF_4]$) which is identical to the value for *trans*-$[Mo(SPh)_2(dppe)_2]$. However, a second oxidative wave is not observed for the chloride species, which suggests that either the thiolate ligands induce stabilization through electron release or possibly the second oxidation is ligand-based. A third oxidation peak is seen for (**A**, R = $C_6H_4NH_2$-4) at +0.74 V. The oxidized species so produced may be stabilized by the electron release of the thiolate or possibly the oxidation is ligand-based, involving the NH_2 group.

It has been shown that the analogue of compounds (**A**), *cis*-$[Mo(SBu^t)_2(CNBu^t)_4]$,[10] undergoes reversible oxidation at +0.4 V in dimethylformamide. Thus this compound is more difficult to oxidize than compounds (**A**), a reflection of the electron-withdrawing properties of the $CNBu^t$ ligands as compared to dppe and possibly the *cis*-geometry.

All complexes of the above series show reduction waves which are partially reversible at a scan rate of 200 mV s^{-1} [except for (**A**, R = $C_6H_4NH_2$-4)], but which tend to irreversibility at slow scan rates ($\sim$10 mV s^{-1}). It has been shown elsewhere[14] that the product of the electron-transfer process is unstable and undergoes loss of SR^-. The species $[MoSR(dppe)_2]$ thus generated react with available substrates.[15]

PREPARATION AND ESR SPECTRA OF *TRANS*-$[Mo(SR)_2(dppe)_2]Y$ (B, Y = $FeCl_4$ OR BPh_4)

Following the observation by electrochemistry of the formation of a stable product by one-electron oxidation of (**A**), it has proved possible to isolate the cationic Mo(III) complexes *trans*-$[Mo(SR)_2(dppe)_2]Y$ (**B**, Y = $FeCl_4$ or BPh_4) by reaction steps (2):

$$\textit{trans}\text{-}[Mo(SR)_2(dppe)_2] + FeCl_3(\text{excess}) \xrightarrow[20°C]{MeOH} [Mo(SR)_2(dppe)_2][FeCl_4]$$

$$\xrightarrow[Na[BPh_4]]{MeOH} [Mo(SR)_2(dppe)_2][BPh_4] \qquad (2)$$

Analytical data and other data for these complexes are shown in Table 1. Compounds (**B**) are sufficiently soluble in acetonitrile for conductivity measurements, which establishes them as 1 : 1 electrolytes in this solvent (Table 1).

Cyclic voltammetry of compounds (**B**) in thf (Pt electrode–0.2 M $[NBu_4][BF_4]$) showed a reversible one-electron reduction, shown by addition of (**A**) to unambiguously correspond to the (**A**)–(**B**) couple. Thus the product of chemical oxidation is the oxidised species observed by voltammetry. The reversibility of the system showed that no gross structural changes had occurred on bulk chemical oxidation, i.e. the *trans*-octahedral geometry is retained on oxidation.

The ESR spectra of compounds (**B**) in frozen solution (approximately 4×10^{-4} M) established that they are low-spin Mo(III) ($S = \frac{1}{2}$) species, of which there are few well-documented cases. One example[16] is $K_4[Mo(CN)_7] \cdot 2H_2O$, which has $g_{\|} = 2.103$ and $g_{\perp} = 1.973$, but its exact geometry is uncertain. Compounds (**B**) have rather low μ_{eff} values [around 1.3 BM (Table 1)].

In CH_2Cl_2 solution at 100 K the ESR spectrum of $[Mo(SBu^n)_2(dppe)_2][BPh_4]$ shows a rhombic signal with no resolved ^{95}Mo or ^{31}P hyperfine coupling [Table 5 and Fig. 2(b)]. In thf solution, however, hyperfine coupling can be seen on the g_2 tensor [Fig. 2(a)] whose resolution depends upon time. Thus, if the spectrum is run immediately on freezing an unresolved spectrum as in Fig. 2(b) is seen. On leaving the sample at 100 K and recording spectra at various times after the initial freezing time, hyperfine structure slowly resolves. If the sample is then allowed to thaw quickly at room temperature and then refrozen, the same time-dependent effect is seen (Fig. 3). This sequence could be repeated many times without significant loss of signal intensity.

A noticeable difference in g_1 is seen between spectra for R = alkyl as opposed to those for R = aryl. For R = C_6H_4X-4, two g_1 values are seen (g_1 and g_1' in Table 5). The ratio of the heights of g_1 and g_1' is not constant. There appears to be no shift of g values with time, solvent or variation of X in C_6H_4X-4.

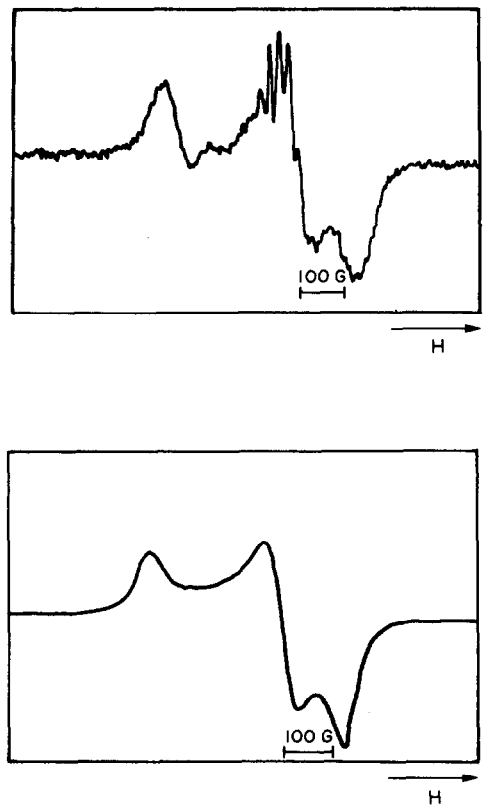


Fig. 2. ESR spectra of *trans*-$[Mo(SBu^n)_2(dppe)_2][BPh_4]$: (a) frozen thf solution, and (b) frozen CH_2Cl_2 solution.

The reason for the solvent dependence of hyperfine coupling is not clear. Possibly there is some distortion of the *trans*-geometry of compounds (**B**) induced by this solvent, but a full explanation requires a much more detailed study.

Table 5. ESR data for compounds (**B**)[a]

Compound[b]	g_1	g_1'	g_2	g_3
$[Mo(SEt)_2(dppe)_2][BPh_4]$	2.180	—	1.993	1.917
$[Mo(SPr^n)_2(dppe)_2][BPh_4]$	2.173	—	1.991	1.914
$[Mo(SBu^n)_2(dppe)_2][BPh_4]$	2.170	—	1.991	1.920
	2.173[c]	—	1.994[c]	1.920[c]
$[Mo(SPh)_2(dppe)_2][BPh_4]$	2.215	2.159	1.988	1.911
$[Mo(SC_6H_4OMe\text{-}4)_2(dppe)_2][BPh_4]$	2.22	2.145	1.997	1.920
$[Mo(SC_6H_4Me\text{-}4)_2(dppe)_2][BPh_4]$	2.223	2.128	1.998	1.914
$[Mo(SC_6H_4Cl\text{-}4)_2(dppe)_2][BPh_4]$	2.241	2.163	1.988	1.909
$[Mo(SC_6H_4F\text{-}4)_2(dppe)_2][BPh_4]$	2.215	2.163	1.988	1.911

[a] Frozen solutions in thf, unless otherwise stated.
[b] *trans*-Configurations.
[c] Frozen solution in CH_2Cl_2.

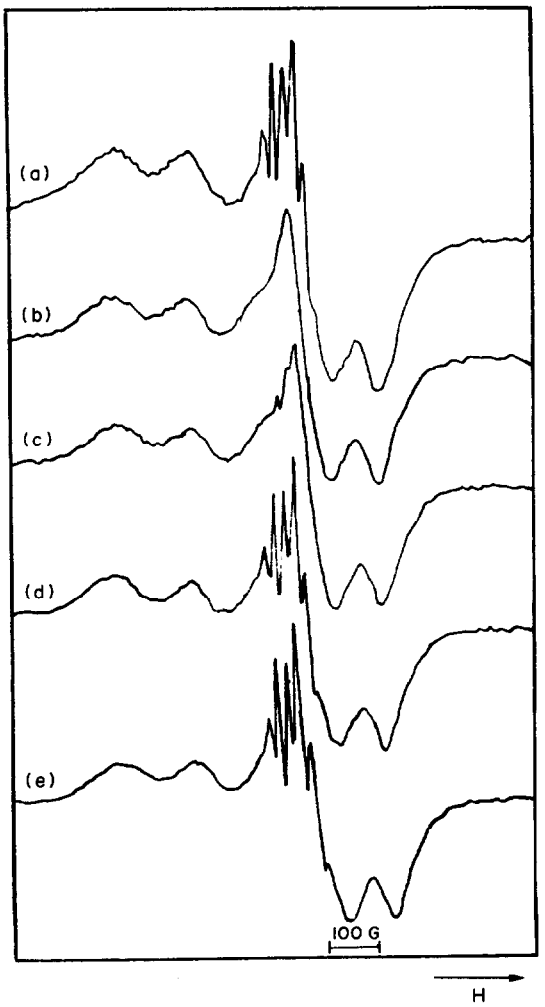


Fig. 3. Time dependence of ESR spectrum of [**B**, R = $C_6H_4CH_3$-4]: (a) resolved spectrum in frozen thf; (b) spectrum after thawing and refreezing, $t = 0.5$ min; (c) $t = 80$ min after refreezing; (d) $t = 185$ min; and (e) $t = 345$ min.

CONCLUSION

The series of thiolate complexes of Mo(II), *trans*-[$Mo(SR)_2(dppe)_2$](**A**) show electronic properties which depend upon the R group of the thiolate and are transmitted primarily by a σ-inductive mechanism, although π-electron release from S cannot be ruled out. One-electron oxidation of compounds (**A**) gives a series of low-spin complexes of Mo(III) which show an unusual solvent dependence in their ESR spectra.

EXPERIMENTAL

All air-sensitive materials were handled using standard Schlenk techniques under pure dinitrogen. All solvents were rigorously dried and distilled under dry dinitrogen prior to use. All other reagents were analytical grade and used without further purification. The complexes *trans*-[$Mo(N_2)_2(diphos)_2$] (diphos = dppe or dmtpe) were prepared by published methods.[1,2,6]

IR spectra were determined by Pye Unicam SP2000 or Perkin–Elmer SP3-200 instruments. NMR spectra were measured on a JEOL FX90Q spectrometer and electronic spectra on a Perkin–Elmer Lambda 5 UV–visible spectrophotometer. Conductivities were obtained with a Portland Electronics P310 conductivity bridge. Magnetic susceptibilities were determined with a Faraday balance. Cyclic voltammetric measurements were made using an EG and G(PAR) Model 174A polarographic analyser in conjunction with a Bryans 2400 XY recorder in a conventional[14,15] three-electrode cell at Pt-wire electrodes in thf–0.2 mol dm^{-3} $[NBu_4][BF_4]$. ESR spectra were recorded by Dr D. Lowe (AFRC, Unit of Nitrogen Fixation) on a Bruker ER200 instrument with an Oxford ESR 900 cooling system using liquid nitrogen as coolant. Microwave power = 2.06 mW, field modulation intensity = 5 G, microwave frequency = 9.45 GHz, and temperature = 125 K with thf or CH_2Cl_2 solutions of *ca* 4×10^{-4} molarity. Micro-analyses were performed by Mrs A. G. Olney (University of Sussex) and Mr C. Macdonald (AFRC, Unit of Nitrogen Fixation). Mr Macdonald also carried out NMR spectroscopic measurements.

Analytical data for the compounds prepared are shown in Table 1. Typical preparations of these compounds are given below.

Bis[*bis*(*diphenylphosphino*)*ethane*]*bis*(4 - *chloro* - *benzenethiolate*)*molybdenum*(*II*) [$Mo(SC_6H_4Cl\text{-}4)_2(dppe)_2$]

The complex *trans*-[$Mo(N_2)_2(dppe)_2$] (0.3 g, 0.32 mmol) and HSC_6H_4Cl-4 (0.14 g, 0.97 mmol) in thf (20 cm^3) were heated to 60°C for 1.5 h under dinitrogen, to give a red solution. Hexane (40 cm^3) was added and the solution left at −4°C for *ca* 3 h to give a red microcrystalline product. The solid was filtered, washed with hexane (3×10 cm^3) and dried *in vacuo*. The product was analytically pure *trans*-[$Mo(SC_6H_4Cl\text{-}4)_2(dppe)_2$] (0.2 g, 0.17 mmol, 54%).

Bis[*bis*(*diphenylphosphino*)*ethane*]*bis*(4 - *chloro* - *benzenethiolate*)*molybdenum*(*III*) *tetraphenylborate*, [$M(SC_6H_44\text{-}Cl)_2(dppe)_2][BPh_4$]

trans-[$Mo(SC_6H_44\text{-}Cl)_2(dppe)_2$] (0.2 g, 0.2 mmol) was suspended in methanol (20 cm^3) and $FeCl_3$ (0.15 g, 0.9 mmol) was added. The purple product, [$Mo(SC_6H_44\text{-}Cl)_2(dppe)_2][FeCl_4$], precipitated and was filtered, washed with methanol (2×10 cm^3) and

dried *in vacuo*. This complex was converted to its tetraphenylborate analogue by suspension in methanol and stirring with $NaBPh_4$ (0.1 g, 0.3 mmol) for *ca* 0.5 h. The resultant purple solid was filtered, washed with methanol (3×10 cm^3) and dried *in vacuo*. Recrystallization from thf–methanol gave purple, microcrystalline $[Mo(SC_6H_4$-$Cl)_2(dppe)_2][BPh_4]$ (0.15 g, 0.1 mmol, 52%).

Crystallographic studies

Crystal data. $C_{60}H_{66}MoP_4S_2 \cdot H_2O$, M = 1089.07, monoclinic, a = 25.605(5) Å, b = 12.055(2) Å, c = 19.637(4) Å, β = 107.08(2)°, U = 5793.4 Å^3, space group $C2/c$ (No. 15), Z = 4, D_c = 1.25 g cm^{-3}, D_m not measured, $F(000)$ = 2280, μ(Mo-K_α) = 4.3 cm^{-1}.

Data collection. Enraf–Nonius CAD4 diffractometer, Mo-K_α radiation, graphite monochromator θ–2θ scan mode, 1.0° < 25°, 10,522 data measured, reduced to 5100 unique reflections, 3671 observed [$I > 2.5\sigma(I)$]; data corrected for absorption and crystal decay (intensity of reference reflection dropped by 9%).

Structure solution and refinement. The structure was solved by the heavy-atom method and refined by full-matrix least squares to a final R factor of 0.041 {weighting scheme used: $\omega = 1/[\sigma^2(F_o) + 0.05F_o^2]$}. Non-hydrogen atoms were assigned anisotropic thermal parameters. The positions of the hydrogen atoms were calculated from geometrical criteria. They were not refined but were included in the structure factor calculations with fixed-temperature factors of 5.0 Å^2. Difference electron density maps revealed a disordered water molecule. The two positions for the oxygen atom were allocated fixed occupancies of 0.5 and the positional and anisotropic thermal parameters were allowed to refine freely. The C(28)—C(29)—C(30) bond lengths together with the high-temperature factors and diffuse electron density indicate severe thermal motion of C(29) and C(30). Attempts to restrict the terminal portion of the chain to a more reasonable geometry resulted in extremely high thermal parameters for C(29) and C(30) and these were therefore allowed to refine freely. Their refined positions are, therefore, ones which produce a minimum R factor.

REFERENCES

1. R. H. Holm, *Chem. Soc. Rev.* 1981, **10**, 455.
2. J. Chatt and R. L. Richards, *J. Organomet. Chem.* 1982, **239**, 65.
3. J. Chatt, J. P. Lloyd and R. L. Richards, *J. Chem. Soc., Dalton Trans.* 1976, 565; D. Povey and R. L. Richards, *J. Chem. Soc., Dalton Trans.* 1984, 2585.
4. P. M. Boorman, T. Chivers, K. N. Mahadev and B. D. O'Dell, *Inorg. Chim. Acta* 1976, **19**, L35 (and references therein).
5. C. Shortman and R. L. Richards, *J. Organomet. Chem.* 1985, **286**, C3.
6. P. B. Hitchcock, C. T. Kan and R. L. Richards, *J. Chem. Soc., Dalton Trans.* 1982, 79 (and references therein).
7. N. C. Payne, N. Okura and S. Otsuka, *J. Am. Chem. Soc.* 1983, **105**, 245.
8. M. Nardelli, G. Pelizzi and G. Predieri, *Gazz. Chim. Ital.* 1980, **110**, 375 (and references therein); (b) L. K. Holden, A. H. Mawby, D. C. Smith and R. Whyman, *J. Organomet. Chem.* 1973, **55**, 343.
9. C. Pelizzi and G. Pelizzi, *Acta Cryst.* 1979, **B35**, 1785.
10. M. Kamata, K. Hirotsu, T. Higuchi, K. Tatsumi, R. Hoffman, T. Yoshida and S. Otsuka, *J. Am. Chem. Soc.* 1981, **103**, 5772.
11. G. R. Hanson, A. A. Brunette, A. C. McDonell, K. S. Murray and A. G. Wedd, *J. Am. Chem. Soc.* 1981, **103**, 1953.
12. D. Pletcher, *Chem. Soc. Rev.* 1975, **4**, 471.
13. J. Chatt, G. J. Leigh, H. Neukomm and C. J. Pickett, *J. Chem. Soc., Dalton Trans.* 1980, 121.
14. J. Chatt, C. T. Kan, G. J. Leigh, C. J. Pickett and D. R. Stanley, *J. Chem. Soc., Dalton Trans.* 1980, 2033.
15. T. L. Al-Salih and C. J. Pickett, *J. Chem. Soc., Dalton Trans* 1985, 1255.
16. G. R. Rossman, F. D. Tsay and H. B. Gray, *Inorg. Chem.* 1973, **12**, 824.

Polyhedron Vol. 5, No. 1/2, pp. 377–379, 1986
Printed in Great Britain

0277-5387/86 $3.00 + .00
© 1986 Pergamon Press Ltd

STRUCTURE AND PROPERTIES OF TRIS(QUINOXALINE-2,3-DITHIOLATO)MOLYBDATE(IV)

S. BOYDE* and C. D. GARNER

Chemistry Department, Manchester University, Manchester M13 9PL, U.K.

and

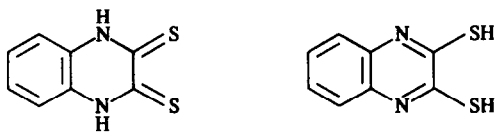
J. H. ENEMARK and R. B. ORTEGA

Department of Chemistry, University of Arizona, Tucson, AZ 85721, U.S.A.

(*Received* 14 *June* 1985)

Abstract—The synthesis, crystal structure, spectroscopic and electrochemical properties of tris(quinoxaline-2,3-dithiolato)molybdate(IV), $[Mo(qdt)_3]^{2-}$, are reported. This complex undergoes reversible protonation on the ligand nitrogen atoms and the triply protonated species $[Mo(Hqdt)_3]^{+}$ has also been isolated and characterized as its chloride salt.

Complexes of quinoxaline-2,3-dithiolate (qdt) with many of the later transition metals have been synthesized.[1,2] However, the only report of qdt complexes of molybdenum merely describes the observation of molybdenum(V) species in solution by EPR spectroscopy; the complexes reported were not isolated.[3]



Dithione Dithiol

Fig. 1. Tautomers of H_2qdt.

EXPERIMENTAL

The ligand 1,4-dihydroquinoxaline-2,3-dithione (H_2qdt) was synthesized by the method of Furst and Morrison.[4] This compound is only sparingly soluble in most organic solvents and is less acidic than normal thiols because it exists as the dithione rather than the dithiol form (Fig. 1).

Addition of H_2qdt to a stirred suspension of $[MoO_2(acac)_2]$[5] (3:1) in 98% H_2SO_4 produced an intensely coloured, bottle green solution. Rapid dilution of this solution with H_2O precipitated a green powder which dissolved in methanolic NaOH to give a purple solution. Addition of $[PPh_4]Br$ to this solution precipitated $[PPh_4]_2[Mo(qdt)_3]\cdot H_2O$ as purple, needle-like crystals in *ca* 50% yield. Recrystallization from MeCN by controlled evaporation in air gave large rectangular crystals which proved suitable for structure determination by X-ray crystallography. $[PPh_4]_2[Mo(qdt)_3]\cdot H_2O$ crystallizes in the monoclinic space group $P2_1/c$ with unit cell dimensions $a = 20.15(2)$ Å, $b = 14.014(5)$ Å, $c = 23.53(2)$ Å, and $Z = 4$. The structure of the anion is shown in Fig. 2.

RESULTS AND DISCUSSION

The geometry about molybdenum is almost perfectly trigonal prismatic; the average Mo—S distance is 2.393 Å, the average intra-ligand S—S distance is 3.127 Å, and the average inter-ligand S–S separation is 3.142 Å. The ligands show only very slight deviations from planarity and the molybdenum atom lies within each of the ligand planes; thus the anion has overall D_{3h}-symmetry. This structure was unexpected as it is unlike that of the valence isoelectronic complex tris(maleonitrile-

* Author to whom correspondence should be addressed.

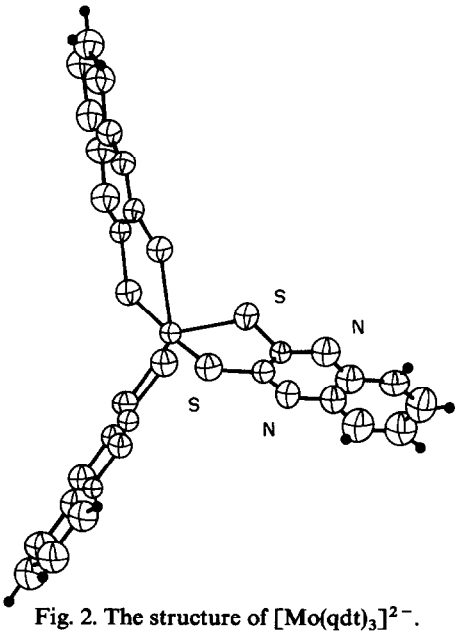


Fig. 2. The structure of $[Mo(qdt)_3]^{2-}$.

Table 1. UV–visible spectra of $[PPh_4]_2[Mo(qdt)_3]\cdot H_2O$ and $[Mo(Hqdt)_3]Cl$

$[PPh_4]_2[Mo(qdt)_3]\cdot H_2O$[ab]	$[Mo(Hqdt)_3]\cdot Cl$[c]
276 (107,000)	450
396 (47,000)	660
561 (55,000)	
770 (1400)	

[a] Wavelength (nm) [extinction coefficient (l mol^{-1} cm^{-1}) in parentheses].
[b] In MeCN solution.
[c] Nujol mull.

dithiolato)molybdate (IV),[6] $[Mo(mnt)_3]^{2-}$, which has an MoS_6 core with a geometry intermediate between that of an octahedron and a trigonal prism. Also, the structure of $[Mo(qdt)_3]^{2-}$ differs from that of the trigonal prismatic dithiolene complex tris(benzene-1,2-dithiolato)molybdate(VI),[7] $[Mo(bdt)_3]$, in which the molybdadithiolene rings are puckered and the molybdenum atom does not lie within the ligand planes.

The electrochemical behaviour of $[Mo(qdt)_3]^{2-}$ in MeCN has been investigated by cyclic voltammetry at a Pt working electrode. The complex undergoes a reversible one-electron oxidation at −0.19 V, an irreversible one-electron oxidation at +0.56 V and a reversible one-electron reduction at −1.70 V. (Potentials are relative to the ferrocene–ferricenium couple at 0.0 V.) The reversible oxidation occurs at a potential at which oxidation should be readily accomplished by chemical oxidants. Thus, addition of iodine to solutions of $[Mo(qdt)_3]^{2-}$ in CH_2Cl_2 or MeCN produces an olive green colouration and a molybdenum(V) EPR signal (g = 2.002, A = 32 G) consistent with the formation of $[Mo(qdt)_3]^{-}$.

Acidification of a solution of $[Mo(qdt)_3]^{2-}$ in MeCN with HCl causes a colour change from purple to turquoise and the immediate precipitation of $[Mo(Hqdt)_3]Cl$. The absorption maxima of the UV–visible spectra of $[Mo(qdt)_3]^{2-}$ and $[Mo(Hqdt)_3]^{+}$ are listed in Table 1 and selected bands from the IR spectra of $[PPh_4]_2[Mo(qdt)_3]\cdot H_2O$ and $[Mo(Hqdt)_3]\cdot Cl$ are given in Table 2. From the IR data and by analogy with the well-characterized nickel complexes of qdt[8,9] it is considered that each

Table 2. IR spectra of $[PPh_4]_2[Mo(qdt)_3]\cdot H_2O$ and $[Mo(Hqdt)_2]\cdot Cl$[a]

$[PPh_4]_2[Mo(qdt)_3]\cdot H_2O$	$[Mo(Hqdt)_3]\cdot Cl$	Assignment[b]
	3110 (w)	ν(N—H)
	1600 (m)	ν(N—C—S)
1540 (m)	1540 (w)	Assymmetric
1360 (m)	1340 (m)	
1170 (s)	1175 (s)	ν(C—C—S)
1120 (s)	1135 (s)	ν(N—C—S)
	1120 (s)	Symmetric
760 (s)	755 (s)	ν(C—S)
	650 (m)	
595 (s)	605 (m)	
430 (m)		
405 (m)	405 (n)	
340 (s)	340 (s)	ν(Mo—S)

[a] Wavenumbers (cm^{-1}) and relative intensitites (s = strong, m = medium, and w = weak).
[b] Ref. 8.

of the qdt ligands in $[Mo(Hqdt)_3]Cl$ is singly protonated at a nitrogen atom.

Acknowledgements—We wish to thank the SERC for provision of a studentship (to SB) and NATO for supporting the collaboration between CDG and JHE.

REFERENCES

1. L. J. Theriot, K. K. Ganguli, S. Kavanos and I. Bernal, *J. Inorg. Nucl. Chem.* 1969, **31**, 3133.
2. K. K. Ganguli, G. O. Carlisle, H. J. Hu, L. J. Theriot and I. Bernal, *J. Inorg. Nucl. Chem.* 1971, **33**, 3579.
3. A. T. Pilipenko, V. V. Trachevskii and N. V. Rusetskaya, *Russ. J. Inorg. Chem.* 1979, **24**, 697.
4. A. Furst and D. C. Morrison, *J. Org. Chem.* 1956, **21**, 470.
5. M. M. Jones, *J. Am. Chem. Soc.* 1959, **81**, 3188.
6. G. F. Brown and E. I. Stiefel, *Inorg. Chem.* 1973, **12**, 2140.
7. M. Cowie and M. J. Bennett, *Inorg. Chem.* 1976, **15**, 1584.
8. A. Pignedoli, G. Peyronel and W. Malawasi, *J. Inorg. Nucl. Chem.* 1976, **38**, 1963.
9. A. Pignedoli and G. Peyronel, *Acta Cryst.* 1977, **B33**, 1439.

Polyhedron Vol. 5, No. 1/2, pp. 381–385, 1986
Printed in Great Britain

0277–5387/86 $3.00+.00
© 1986 Pergamon Press Ltd

COMPLEXES OF Mo(VI) WITH LACTIC, THIOLACTIC AND THIOMALIC ACIDS STUDIED BY NMR SPECTROSCOPY

M. MADALENA CALDEIRA and VICTOR M. S. GIL†

Department of Chemistry, University of Coimbra, Coimbra, Portugal

(*Received* 25 *June* 1985)

Abstract—Proton and ^{13}C evidence is presented on the number, stoichiometry, geometry and relative stability of the complexes formed in the systems Mo(VI) + L-lactic acid, Mo(VI) + D,L-thiolactic acid and Mo(VI) + D,L-thiomalic acid in aqueous solutions at pH values in the range 3–8. In particular, 1:2 complexes are always formed and, in addition, complexes of higher metal content are detected in the case of thiolactic and thiomalic acids.

NMR spectroscopy has proved to be a powerful technique in speciation studies of complexation of oxoions with hydroxycarboxylic acids and related ligands.[1–3] This paper deals with the application of ^{1}H and ^{13}C NMR to the title compounds. Whenever possible, comparison with the corresponding W(VI) systems is also made.

RESULTS AND DISCUSSION

Mo(VI) + L-*lactic acid*

When sodium molybdate is added to an aqueous solution of L-lactic acid, a new set of peaks appear in the ^{1}H NMR spectrum corresponding to bound ligand. The spectra of free and bound ligand are of the A_3X type,

$$\underset{A_3}{CH_3}—\underset{X}{CH(OH)}—CO_2H,$$

with relative shifts that are slightly pH-dependent; for pH* = 5.1 they are $\Delta\delta(X) = 0.740$ and $\Delta\delta(A) = 0.072$ ppm, when going from free to bound lactic acid, with $\delta(X) = 4.12$ and $\delta(A) = 1.34$ ppm. Complexation occurs for pH less than about 8 and its extent increases on lowering the pH. For pH $\lesssim$ 3, the NMR signals broaden, presumably due to extensive polymerization.

The big shift undergone by the X signal is a clear indication of the involvement of the hydroxyl group in chelation to Mo(VI) together wth the CO_2H group. This conclusion is supported by the ^{13}C shifts observed on complexation (Table 1).

The presence of only one complex in the pH range 3–8, irrespective of molar ratios and concentrations (up to 1 M in the complexing species) is supported also by the observation of only one peak of bound molybdenum in the ^{95}Mo NMR spectrum of an aqueous solution of sodium molybdate and L-lactic acid (0.5–0.5 M, pH 5.7).‡ This peak has a linewidth of 80 Hz and lies 84 ppm to high frequency relative to the signal of MoO_4^{2-}(aq) as external reference.

Table 1. ^{13}C chemical shifts (ppm) for Mo(VI) + L-lactic acid (0.5 M–1.0 M, temperature 295 K)

	CH_3	CH(OH)	CO_2H
pH* = 3.0			
Free ligand[a]	19.6	67.4	180.4
Complex[b]	−0.4	13.8	7.0
pH* = 5.0			
Free ligand[a]	20.4	69.2	183.8
Complex[b]	−1.8	12.0	3.9
pH* = 6.9			
Free ligand[a]	20.4	69.2	184.0
Complex[b]	−1.8	12.0	3.6

[a] Referred to TMS, using δ_C(dioxane) = 67.4.
[b] Relative to free ligand.

† Author to whom correspondence should be addressed.

‡ This spectrum was kindly obtained by M. T. Nunes (LNETI, Sacavem, Lisbon) on a Brucker WT-80 FY spectrometer.

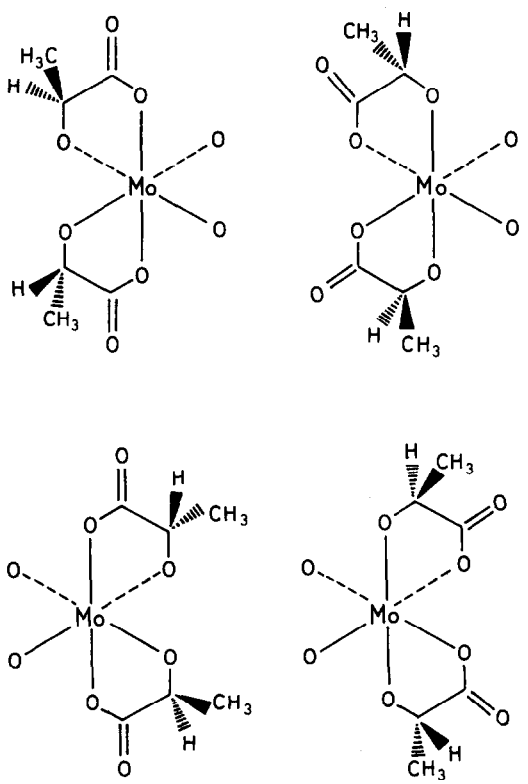
From the relative intensities of the signals in the proton NMR spectra of mixtures of equimolar solutions of sodium molybdate and L-lactic acid, Job's plots for the bound ligand were obtained which clearly show the composition of the complex to be 1 : 2 (metal : ligand) (see also Refs 4–7). Preliminary studies also lead to a 1 : 2 stoichiometry for W(VI)–lactic acid complexation, but now an additional (weaker) complex is also found.

For a pH* = 4.5 and the metal concentrations used (0.01–0.04 M), the main Mo(VI) species present in solution is the heptamolybdate ion $Mo_7O_{24}^{6-}$.[8] We can thus write the following equation for the formation of the complex (the ligand, represented by H_2Y, is almost completely ionized at this pH[9]):

$$Mo_7O_{24}^{6-} + 14HY^- + 6H^+ \rightleftharpoons 7MoO_2Y_2^{2-} + 10H_2O.$$

This equation assumes that the OH group loses H^+ on complexation. A crude estimate based on the NMR spectral intensities leads to a value of −49 for the pK of formation of the complex.

Preliminary Raman spectroscopic evidence[10] shows that the dioxomolybdenum(VI) group, MoO_2, has a *cis* configuration, as expected. The magnetic equivalence of the two ligand molecules requires a C_2-configuration of the complex. The four possible structures are as follows:



Mo(VI) + D,L-*thiolactic acid*

A similar study was performed with D,L-thiolactic acid,

$$\underset{A_3}{CH_3}—\underset{X}{CH(SH)}—CO_2H,$$

as ligand. Again, the extent of complexation decreases upon increasing pH, there being no evidence of complexation for pH above *ca* 8.5. Due to broadening effects and more extensive oxidation of the acid to the disulphide at low pH, the study was limited to the pH range 3–8.5.

Three complexes were detected. The observed proton shifts upon complexation of the acid are, for pH* = 5.6, as follows: $\mathbf{a}_1$, $\Delta\delta(X) = 0.580$ ppm, $\Delta\delta(A) = 0.050$ ppm; $\mathbf{a}_2$, $\Delta\delta(X) = 0.545$ ppm, $\Delta\delta(A) = 0.062$ ppm; **b**, $\Delta\delta(X) = 0.460$ ppm, $\Delta\delta(A) = 0.040$ ppm.

Three different sets of lines due to bound ligand are also observed in the ^{13}C NMR spectrum. The shifts for various pH values are given in Table 2. It is clear that the sulphydryl group is involved in complexation. The carboxyl groups are also bound to the metal in ligands $\mathbf{a}_1$ and $\mathbf{a}_2$, but the small shift observed in **b** seems to indicate the contrary in this case. In addition, there is a much bigger shift of *C*H(SH) than in $\mathbf{a}_1$ and $\mathbf{a}_2$ and an unexpected (low-frequency) shift of the methyl signal of about −5 ppm.

A Job's plot for $\mathbf{a}_1 + \mathbf{a}_2$ (no separate integration of $\mathbf{a}_1$ and $\mathbf{a}_2$ was possible) shows a clear maximum at 1 : 2, which suggests 1 : 2 complexation, as in the case of the Mo(VI)–lactic acid system. Comparison with this system when active and racemic lactic acid are

Table 2. ^{13}C chemical shifts (ppm) for Mo(VI) + D,L-thiolactic acid (0.5 M–1.0 M, temperature 295 K)

	CH_3	CH(SH)	CO_2H
pH* = 3.0			
Free ligand[a]	21.0	36.4	180.2
Bound ligand[b]:			
$\mathbf{a}_1$ and $\mathbf{a}_2$	1.8	6.4	10.0
b	−4.0	13.2	−0.8
pH* = 5.1			
Free ligand[a]	22.2	39.8	183.4
Bound ligand[b]:			
$\mathbf{a}_1$ and $\mathbf{a}_2$	−1.0	5.6	5.2
b	−4.8	12.0	−1.6
pH* = 7.2			
Free ligand[a]	22.2	39.8	183.8
Bound ligand[b]:			
$\mathbf{a}_1$ and $\mathbf{a}_2$	−0.8	5.6	5.2
b	−4.4	12.4	−1.6

[a] Referred to TMS, using δ_C(dioxane) = 67.4.
[b] Relative to free ligand.

used leads us to propose that $\mathbf{a}_1$ and $\mathbf{a}_2$ correspond to DD (or LL) and DL diastereoisomers. As far as complex **b** is concerned, a firm conclusion could not be reached because, when its concentration is a maximum (at 2:1), there is a comparable concentration of the 1:2 complexes present. However, there is little doubt that it has a higher metal content, being either a 1:1 or a 2:1 complex. We recall that the ^{13}C shifts indicate a stronger involvement of the SH group in complex **b** and no participation of CO_2H in complexation. A 2:2 species having two S bridges between the Mo atoms could fit the data, but we can offer no further support for this hypothesis.

Mo(VI)+(D,L)-*thiomalic acid*

The proton NMR spectra are now of the ABX type,

$$\underset{\text{AB}}{\text{CO}_2\text{H—CH}_2\text{—CH(SH)—CO}_2\text{H.}}\quad \underset{\text{X}}{}$$

Depending on pH, four complexes are now detected: one complex (**a**) is only present at pH above *ca* 5, whereas another complex (**c**) only appears at pH less than *ca* 5. Two other (similar) species ($\mathbf{b}_1$ and $\mathbf{b}_2$) occur in the whole pH range covered (2.5–8.5). The chemical shifts of the X proton observed on complexation are 0.5–0.7 ppm, whereas those for the AB part lie between 0.05 and 0.3 ppm.

Table 3 shows the ^{13}C shifts observed for pH* 4.0 and 7.0. The shifts to high frequency of the methyne carbon signal and those of the α-carboxyl group are consistent with the involvement of the S atom and of that carboxyl group in bonding to Mo(IV). A similar shift is also recorded for the β-carboxyl group in the case of complex **c**. It thus seems that in complexes **a**, $\mathbf{b}_1$ and $\mathbf{b}_2$ the ligand acts as bidentate (forming five-membered rings), whereas it has a terdentate function in complex **c**.

Job's curves for complexes **a**, $\mathbf{b}_1+\mathbf{b}_2$ (no separate integration was possible in all solutions) and **c** are shown in Figs 1 and 2. The maximum at the molar ratio 1:2 for $\mathbf{b}_1+\mathbf{b}_2$ suggests a 1:2 composition for these complexes; **a** and **c** are species of higher Mo content, possibly a 1:1 and a 2:1 complex, respectively. These stoichiometries are the same as those that occur in the complexation of Mo(VI) with malic acid.[11–13] They differ from those for W(VI)+thiomalic acid[1] insofar as the complexes in this case are 1:2 at any pH (above 3), only a small concentration of a species involving terdentate ligand being observed.

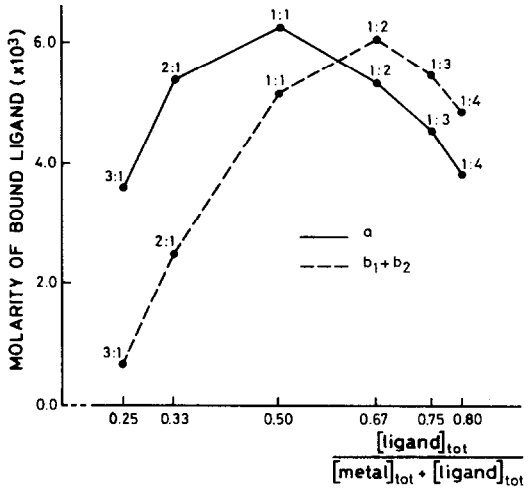


Fig. 1. Job's curves based on proton NMR spectral intensities for the system Mo(VI)+D,L-thiomalic acid. Total concentration of complexing species 0.050 M (D_2O solutions, 1 M in NaCl, pH* 7.0, temperature 275 K).

Table 3. ^{13}C chemical shifts (ppm) for Mo(VI)+D,L-thiomalic acid (0.50 M–0.50 M, temperature 295 K)

	CO_2H	CH_2	CH(SH)	CO_2H
pH* = 4.0				
Free ligand[a]	177.4	41.4	38.8	179.7
Bound ligand[b]: $\mathbf{b}_1$	1.8	1.4	8.6	7.1
$\mathbf{b}_2$				7.2
c	4.2	1.2	9.4	5.3
pH* = 7.0				
Free ligand[a]	180.9	44.8	42.0	182.0
Bound ligand[b]: **a**	0.3	1.0	6.2	4.2
$\mathbf{b}_1$	0.3	−0.6	6.6	5.4
$\mathbf{b}_2$		−0.4		5.2

[a] Referred to TMS, using δ_C(dioxane) = 67.4.
[b] Relative to free ligand.

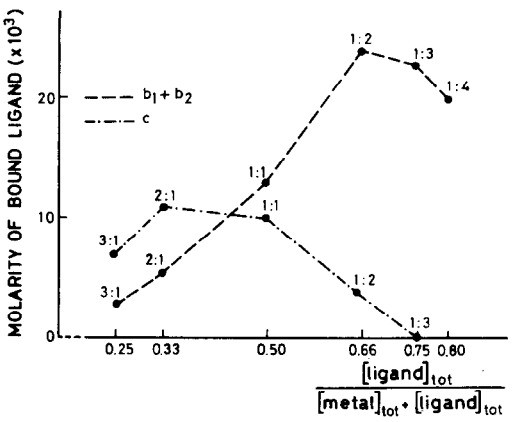
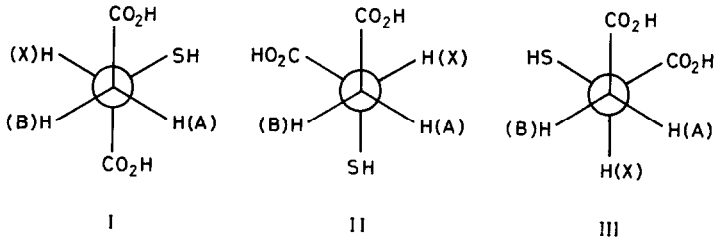


Fig. 2. Same as Fig. 1 with pH* 4.0.

The analysis of the various ABX spectra leads to the coupling constants and chemical shifts given in Table 4. The values of the vicinal coupling constants for **a**, $\mathbf{b_1}$ and $\mathbf{b_2}$ at pH 7.0 show that the rotational isomer **I**, which is the most stable[14,15] for the free acid (in the rotational isomeric state approximation) becomes even more favoured in the complexes; in fact, J_{AX} increases and J_{BX} decreases thus implying an essentially *trans* arrangement of A and X and a *gauche* arrangement of B and X. When lowering the pH, $J_{AX} \simeq J_{BX}$ for thiomalic acid, which means that form **II** is stabilized relative to **I**; however, in complexes **a**, $\mathbf{b_1}$ and $\mathbf{b_2}$ although J_{AX} is smaller than it is at pH 7.0, we have again $J_{AX} > J_{BX}$ in accordance with form **I** being stabilized by complexation. We can thus conclude that in complexes **a**, $\mathbf{b_1}$ and $\mathbf{b_2}$, where the ligand acts as bidentate, the ligand conformation is close to **I** at high pH (the β-carboxyl group is then fully ionized) and undergoes a slight distortion at low pH.

Complex **c**, with $J_{AX} \simeq J_{BX}$ and values typical of a *gauche* arrangement of the vicinal H atoms, has the ligand essentially in conformation **III**. This is the appropriate conformation for a terdentate function of thiomalic acid bonded to a Mo atom, which was independently indicated by the ^{13}C shifts. If complex **c** is a 2:1 species, then it probably is a 4:2 dimer as is the case of a complex of Mo(VI) with L-malic acid characterized by X-ray diffraction.[16] Evidence that it is a polymeric species comes from the fact that dilution of the solutions at pH 4 causes a noticeable decrease in the corresponding relative spectral intensities.



EXPERIMENTAL

D_2O solutions were used throughout. The concentrations of the molybdate solutions were established by weight and the acid solutions were standardized by potentiometry. The pH was

Table 4. ^1H chemical shifts (ppm) and coupling constants (Hz) for Mo(VI) + DL-thiomalic acid (2:1 and 1:2 solutions, temperature 295 K)

	J_{AB}	J_{AX}	J_{BX}	$\delta_B - \delta_A$	$\Delta\delta(X)^a$	$\Delta\delta(B)^a$	$\Delta\delta(A)^a$
pH* = 4.0							
Free ligand	15.9	7.3	7.8	0.204	—	—	—
Bound ligand: $\mathbf{b_1}$	16.1	8.8	4.2	0.233	0.602	0.089	0.059
$\mathbf{b_2}$	16.0	9.0	4.3	0.222	0.579	0.078	0.060
c	18.8	4.4	3.9	0.277	0.509	0.310	0.237
pH* = 7.0							
Free ligand	15.1	9.1	5.9	0.368	—	—	—
Bound ligand: **a**	15.1	11.2	3.7	0.516	0.548	0.110	−0.032
$\mathbf{b_1}$	15.1	10.6	4.0	0.441	0.663	0.124	0.051
$\mathbf{b_2}$	15.2	10.6	3.7	0.429	0.637	0.112	0.052

[a] Relative to free ligand.

adjusted by addition of solutions of DCl and NaOD; the pH* values quoted are the direct pH-meter readings (room temperature) after standardization with aqueous (H_2O) buffers. Whenever necessary (for the application of Job's method) the ionic strength was kept approximately constant by using NaCl. In order to minimize air oxidation of the mercapto acids, N_2 was run through the solutions during preparation and the NMR tubes were sealed under a nitrogen atmosphere.

The ^1H and ^{13}C spectra were obtained on a Varian XL-200 NMR spectrometer. The latter were recorded using proton-decoupling techniques with suppression of the nuclear Overhauser effect; in this manner, temperature fluctuations of the sample were reduced to *ca* $\pm$ 1°C. Most ^1H NMR spectra were run at low temperature (275 K) as signals are sharper than at room temperature, due to slower exchange processes. Dioxane and DSS were used as internal references, respectively, for ^{13}C and ^1H shifts.

Acknowledgements—This work is a contribution of the Centro de Investigação em Química, Coimbra, supported by the Instituto Nacional de Investigação Científica (Portuguese Ministry of Education).

REFERENCES

1. M. M. Caldeira and V. M. S. Gil, *Can. J. Chem.* 1984, **62**, 2094 (and references therein).
2. A. M. S. Cavaleiro, V. M. S. Gil, J. Pedrosa Jesus, R. D. Gillard and P. A. Williams, *Transition Met. Chem.* 1984, **9**, 62.
3. M. T. Nunes, V. M. S. Gil and A. V. Xavier, *Inorg. Chim. Acta* 1984, **95**, 13 (and references therein).
4. W. Voelter, E. Bayer, G. Barth, E. Bunnenberg and C. Djerassi, *Chem. Ber.* 1969, **102**, 2003.
5. L. Davies and E. Richardson, *J. Less-Common Met.* 1962, **4**, 109.
6. E. Mikanova and M. Bartusek, *Scr. Fac. Sci. Nat. Univ. Purkynianae Brun.* 1982, **11**, 439; *Chem. Abstr.* 1982, **96**, 25298y.
7. A. Beltrán-Porter, A. Cervilla, F. Caturla and M. J. Villa, *Transition Met. Chem.* 1983, **8**, 324.
8. C. F. Baes and R. E. Mesmer, In *The Hydrolysis of Cations*, p. 253. John Wiley, New York (1976).
9. L. G. Sillén and A. E. Martell, *Stability Constants of Metal Ion Complexes.* Chemical Society, London (1964).
10. M. M. Caldeira and J. J. C. Teixeira-Dias, unpublished results.
11. M. Cadiot and B. Viossat, *Rev. Chim. Minér.* 1969, **6**, 727.
12. M. M. Caldeira, M. E. T. L. Saraiva and V. M. S. Gil, *Inorg. Nucl. Chem. Lett.* 1981, **17**, 295.
13. C. B. Knobler, A. J. Wilson, R. N. Hider, I. W. Jensen, B. R. Penfold, W. T. Robinson and C. J. Wilkins, *J. Chem. Soc., Dalton Trans.* 1983, 1299.
14. D. E. Leyden and D. B. Walters, *Spectrochim. Acta* 1969, **25A**, 1869.
15. V. M. S. Gil, *Org. Magn. Reson.* 1981, **15**, 96.
16. J. E. Berg, S. Brandange, L. Lindblom and P. E. Werner, *Acta Chem. Scand.* (*A*) 1977, **31**, 325.

Polyhedron Vol. 5, No. 1/2, pp. 387–391, 1986
Printed in Great Britain

0277-5387/86 $3.00 + .00
© 1986 Pergamon Press Ltd

SEVEN- AND EIGHT-COORDINATED COMPLEXES OF Mo(V) AND Mo(IV) WITH 2-AMINO-1-CARBODITHIOATO LIGANDS: SYNTHESIS, SPECTRA AND ELECTROCHEMISTRY

MUKTIMOY CHAUDHURY

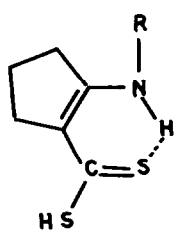
Department of Inorganic Chemistry, Indian Association for the Cultivation of Science, Calcutta 700 032, India

(*Received* 28 *June* 1985)

Abstract—Electrochemical half-wave potentials, charge-transfer absorption, ESR and magnetic properties are reported for a series of seven-coordinated Mo(V) (**1a–d**) and eight-coordinated Mo(IV) (**2a–d**) complexes with 2-alkylaminocyclopent-1-ene-1-dithiocarboxylato ligands (HL). The Mo(IV) compounds constitute the first reported example of a series of complexes with MoS_8 chromophore having a spin-triplet ground state. Electrochemical oxidation of **2c** is quite interesting as it involves a single-step reversible two-electron transfer involving an Mo(IV)–Mo(VI) couple.

A good deal of recent excitement has centered in the area of molybdenum–sulfur coordination chemistry due to some recent interesting results obtained from various chemical and spectroscopic studies[1,2] and Mo-EXAFS data[3–5] which led to a unique delineation for the metal binding sites of different molybdoenzymes. These enzymes are known to catalyse a number of important biological oxo-transfer reactions where valence of molybdenum cycles between Mo(VI) and Mo(IV) states in their reaction with substrates and subsequent reactivation.[6,7] As a part of our systematic approach to study the structure–redox activity relationship of molybdenum compounds with varying degree of sulfur coordination,[8–10] we recently have reported that[9,10] 2-aminocyclopent-1-ene-1-dithiocarboxylic acid (HL^1) binds molybdenum through disulfur chelation, forming a number of monomeric compounds of types $Mo(VI)O_2(L^1)_2$, $Mo(V)O(L^1)_3$ and $Mo(IV)(L^1)_4$, where oxygen atoms are successively removed from the metal's coordination sphere by various oxo-transfer reactions. The electrochemical results clearly indicate that when the same ligand system is used to bind the molybdenum center, oxygen atoms of the oxomolybdenum species have a definite role to play in guiding the nature of the electrode process. The kinetics of electron transfer get increasingly sluggish as more and more oxygen atoms are ligated to the metal center.

In this paper I would like to report the synthesis, spectroscopic and electrochemical studies of some seven- and eight-coordinated monomeric molybdenum complexes in the oxidation states V and IV using 2-alkylaminocyclopent-1-ene-1-dithiocarboxylic acid (HL^2–HL^5) as the $(S,S)^-$ donor metal-binding substrate:



HL

where R = H (HL^1), R = C_2H_5(HL^2), R = C_3H_7 (HL^3), R = C_4H_9 (HL^4) and R = C_6H_{13} (HL^5).

EXPERIMENTAL

Materials

Where available, AR or spectroscopic grade solvents were employed. Standard distillation techniques were employed to further purify and dry

solvents. *n*-Propylamine, *n*-butylamine and *n*-hexylamine were of >99% purity (K. Light) and distilled over KOH prior to use. All other chemicals used were reagent grade unless otherwise noted.

Synthesis

The ligands (HL^1–HL^5) were prepared by known procedure.[11–13] All manipulations involving Mo(V) and Mo(IV) compounds were carried out under an atmosphere of purified dinitrogen. MoO_2L_2[9] and $MoOCl_2L_2$[10] were prepared as described elsewhere.

$MoO(L^2)_2(L^1)$ (**1a**). In a three-necked flask equipped with a reflux condenser and a dropping funnel 0.25 g (0.5 mmol) of $MoO_2(L^2)_2$ was suspended in methanol (30 cm^3). To the stirred suspension was added dropwise a solution of HL^1 (0.18 g, 1.1 mmol) in methanol (20 cm^3) over a period of 45 min. The resulting solution was warmed to 40°C and the stirring was continued for 4h. During this period, the color of the solution changed from red to black through an intermediate red-brown stage. After cooling, the black microcrystalline product was filtered, washed with chloroform–hexane [1 : 2 (v/v)] mixture (4 × 10 cm^3) and finally dried *in vacuo*. The purity of the product was checked by TLC. Yield 65%.

Other $MoO(L)_2(L^1)$ complexes [L = L^3 (**1b**), L^4 (**1c**) and L^5 (**1d**)] were prepared following the same procedure with yields of 50–70%.

$Mo(L^2)_2(L^1)_2$ (**2a**). In a three-necked flask, fitted with a reflux condenser and a dropping funnel, was placed a suspension of finely ground $MoOCl_2(L^2)_2$ (0.28 g, 0.5 mmol) in methanol (30 cm^3). The stirred suspension was warmed to 40°C and a solution of HL^1 (0.35 g, 2.2 mmol) in methanol (40 cm^3) was added dropwise over a period of 45 min. After the end of the addition, the stirring was further continued for 4h. The solution was then cooled to room temperature and the black-violet product formed was filtered, washed with 1 : 3 (v/v) chloroform–hexane mixture (4 × 10 cm^3) and finally dried *in vacuo*. The purity of the product was checked by TLC. Yield 60%.

The complexes (**2b–2d**) with other ligand derivatives (HL^3–HL^5) were synthesized in a similar manner. Yields 55–70%.

All the reported compounds gave satisfactory analytical results.

Physical measurements

Room-temperature EPR spectra for solutions [1 : 10 (v/v) DMF–$CHCl_3$] were recorded at X-band frequency on a Varian E-109 Spectrometer equipped with a 100-kHz field modulation unit. Cyclic voltammetry (CV), differential pulse voltammetry (DPV) and coulometric measurements were made using a PAR model 370-4 electrochemistry systems. A Metrohm E410 hanging mercury drop electrode and a mercury pool electrode were used as the working electrodes for CV and coulometric work, respectively. All measurements were performed for DMF solutions at 298 K. The potentials are referenced to a saturated calomel electrode and are uncorrected for junction potentials. The details of electrochemical and various other physical measurements have been described elsewhere.[9,10]

RESULTS AND DISCUSSION

Using the redox coordinating ability of 2-aminocyclopent-1-ene-1-dithiocarboxylic acid (HL^1),[9,10] various monomeric Mo(V) and Mo(IV) complexes of types $MoO(L)_2(L^1)$ (**1a–1d**) and $Mo(L)_2(L^1)_2$ (**2a–2d**) were prepared from $MoO_2(L)_2$ and $MoOCl_2(L)_2$ (L = L^2–L^5), respectively, by oxo-transfer reactions. Their elemental analyses are in good agreement with the assigned formulations. The compounds are air-stable in the solid state but slowly decompose in solution.

IR spectral features of these compounds are relatively straight forward and almost identical, except in the region 1000–850 cm^{-1}. While for Mo(V) compounds (**1a–1d**) a strong band appears at ~950 cm^{-1} assignable to ν(MO=O) stretching,[14] the absence of similar band in the Mo(IV) compounds suggests complete removal of the oxo group from the metal's coordination sphere. The compounds also show a single sharp carbon–sulfur stretching in the ~830 cm^{-1} region due to ν_{asym}(CSS) with no evidence for splitting indicating a bidentate (*S,S*) mode of chelation by the ligands.[15] The appearance of a low frequency band in the region 350–380 cm^{-1} is attributed to a ν(Mo—S) vibration.[16]

Electronic spectra

An important feature of all these Mo(V) (**1a–1d**) and Mo(IV) (**2a–2d**) compounds is their intense red color in DMF solution, owing to electronic transitions in the region 850–300 nm. Bands occurring below 400 nm are due to internal ligand transitions.[13] Spectral data (Table 1) of $MoO(L)_2(L^1)$ (**1a–1d**) are consistent with the $(4d_{xy})^1$ electronic ground state ($^2B_2$) for Mo(V). Detailed interpretations of these data for similar Mo(V) complexes are given elsewhere.[9,10] Electronic spectra of the Mo(IV) compounds (**2a–2d**) in DMF solution are complex in nature (Table 2), containing

Table 1. Electronic spectral, magnetic and ESR data for the $MoO(L)_2(L^1)$ complexes

Compound	λ_{max} (nm) [ε (M^{-1} cm^{-1})][a]	μ_{BM}	$\langle g \rangle$[b]	$\langle A \rangle$ ($\times 10^4$ cm^{-1})
$MoO(L^2)_2(L^1)$ (**1a**)	808(1150), 652(2500), 538(sh), 380(29,500), 336(18,100)	1.54	1.986	31.1
$MoO(L^3)_2(L^1)$ (**1b**)	812(1050), 648(2360), 538(sh), 382(29,800) 338(15,500)	1.69	1.984	31.5
$MoO(L^4)_2(L^1)$ (**1c**)	808(1250), 652(2530), 538(sh), 382(29,400), 336(17,000)	1.58	1.984	31.5
$MoO(L^5)_2(L^1)$ (**1d**)	813(1330), 656(2670), 540(sh), 386(38,600), 338(18,400)	1.60	1.985	32.0

[a] Spectra recorded in DMF solution.
[b] In 10:1 $CHCl_3$–DMF mixture at room temperature.

five intense bands in addition to the high-energy π–π^* internal ligand transitions.[13] The spectral features are closely comparable to those reported for many Mo(IV) compounds containing the MoS_8 chromophore.[17–20] Most of these transitions are tentatively assigned to the charge-transfer type (L → M) because of their high extinction (ε) values (2000–3700 M^{-1} cm^{-1}).

Magnetic-moment and ESR data

The room-temperature magnetic-moment and ESR data for the Mo(V) compounds are listed in Table 1. The magnetic-moment values ($\mu_{eff} \sim 1.60$ BM) are quite close to the spin-only value for a d^1-system. Their ESR spectra contain a strong central line due to the 75% Mo isotopes with $I = 0$ and six satellite lines arising from the hyperfine interaction of the unpaired electron with ^{95,97}Mo nuclei of spin $\frac{5}{2}$. The observed $\langle g \rangle$ values are somewhat higher and $\langle A \rangle$ values significantly lower compared to those of other Mo(V) complexes with different donor atom sets,[21] the reason for which may be the polarizable nature of sulfur ligands.[22]

So far as the magnetic behavior is concerned, Mo(IV) compounds are really novel because of their spin-triplet ground state. Their room-temperature susceptibilities lie between 2.35 and 2.77 BM (Table 2). Till now, apart from a few scattered examples,[23,24] most of the reported Mo(IV) complexes with MoS_8 chromophore have been diamagnetic.[17–20] Possible reason(s) for this unusual paramagnetism will be described elsewhere.[11]

Electrochemistry

Electrochemical behavior of $Mo(L)_2(L^1)_2$ compounds in DMF–0.1 M TEAP solution are shown in Fig. 1 and the relevant electrochemical data are summarized in Table 2. Apart from **2c** the electrochemical behavior of the other three compounds are almost identical, each involving two nearly reversible waves [Fig. 1(a)], one due to reduction ($E_{1/2}$ −0.42 V) and the other due to oxidation ($E_{1/2}$ −0.2 V). In each case, the scan was initiated from −0.3 V and the nature of the voltammograms remains practically identical, irrespective of the scan direction. The currents observed by DPV or CV for the two steps are of equal height, indicating an identical number of electrons in each step. Reversibility of both the electron-transfer processes [couples (1) and (2)] and single-electron involvement in the reduction process [couple (1)] are confirmed from CV and coulometric measurements (Table 2).[10] The electron stoichiometry determination for the oxidation step [couple (2)] by potentiostatic coulometry did not yield satisfactory results due to constant coulomb counts. However, on the basis of CV, DPV and coulometric results, the following reactions may be assigned:

$$[Mo(III)(L)_2(L^1)_2]^- \overset{e^-}{\rightleftharpoons} [Mo(IV)(L)_2(L^1)_2]^0, \quad (1)$$

$$[Mo(IV)(L)_2(L^1)_2]^0 \overset{e^-}{\rightleftharpoons} [Mo(V)(L)_2(L^1)_2]^+. \quad (2)$$

For **2c** the reduction behavior is essentially identical to other Mo(IV) compounds (Fig. 1), involving a reversible Mo(IV)–Mo(III) single-

Table 2. Electronic spectral, magnetic and electrochemical data for $Mo(L)_2(L^1)_2$ complexes

Compound	λ_{max} (nm) [ε (M^{-1} cm^{-1})][a]	μ_{BM}	Mo(IV)–Mo(III)[b]				Mo(IV)–Mo(V), Mo(VI)[b]		
			$(E_{1/2})_1$, (V)[c]	ΔE_p (mV)[d]	i_{pc}/i_{pa}	n[e]	$(E_{1/2})_2$, (V)[c]	ΔE_p (mV)[d]	i_{pc}/i_{pa}
$Mo(L^2)_2(L^1)_2$ (**2a**)	808(2220), 744(sh), 656(4800), 536(10,300), 454(sh), 382(37,100)	2.46	−0.42	70	1.0	1.05	−0.20	80	1.0
$Mo(L^3)_2(L^1)_2$ (**2b**)	808(2700), 746(sh), 660(6200), 540(13,300), 495(13,000), 382(42,000)	2.50	−0.42	70	0.95	0.98	−0.20	80	1.0
$Mo(L^4)_2(L^1)_2$ (**2c**)	808(2800), 744(sh), 662(6800), 540(14,500), 496(10,100), 386(42,000)	2.35	−0.42	60	0.90	1.10	−0.21	80	0.95
$Mo(L^5)_2(L^1)_2$ (**2d**)	804(2800), 740(sh), 658(6100), 534(13,250), 496(13,500), 387(45,500)	2.77	−0.46	140	0.90	0.95	−0.19	160	1.1

[a] Spectra recorded in DMF solution.
[b] Cyclic voltammograms performed in 0.1 M TEAP–DMF with $\sim 10^{-3}$ M compound at an HMDE working electrode.
[c] Potentials vs SCE and estimated from CV using a scan rate of 50 mV s^{-1}: $E_{1/2} = 0.5(E_{pc} + E_{pa})$.
[d] $\Delta E_p = (E_{pc} - E_{pa})$.
[e] Number of electrons/molecule determined by controlled potential coulometry.

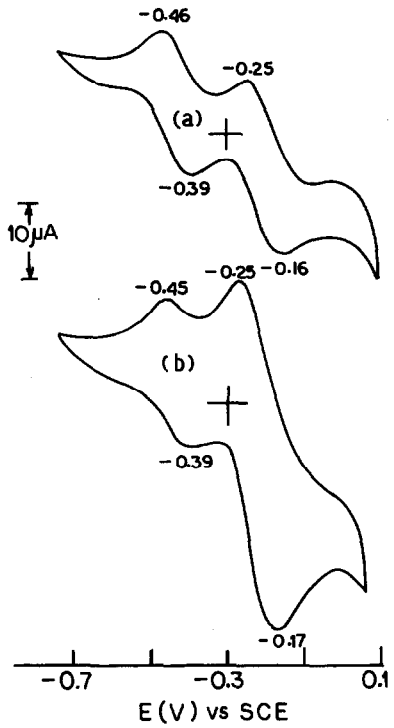


Fig. 1. Cyclic voltammograms (at a hanging mercury drop electrode, $V = 50$ mV s^{-1}) of $Mo(L^2)_2(L^1)_2$ (a) and $Mo(L^4)_2(L^1)_2$ (b). The voltammetric features of **2b** and **d** are almost identical to (a).

electron transfer ($E_{1/2}$ −0.42 V). However, its oxidation behavior is quite unique as it involves a reversible one-step two-electron transfer comprising Mo(IV)–Mo(VI) states {couple (3) [Fig. 1(b)]}. Like other Mo(IV) compounds, a meaningful coulometric result was not obtained for this electron-transfer process. Nevertheless, the CV and DPV current heights for this wave are twice that of the reduction process, indicating that two electrons are transferred in couple (3):

$$[Mo(IV)(L^4)_2(L^1)_2]^0 \overset{2e^-}{\rightleftharpoons} [Mo(VI)(L^4)_2(L^1)_2]^{2+}. \quad (3)$$

Similar redox behavior involving a simultaneous two-electron transfer is well known for many biochemical reactions catalysed by molybdo-enzymes.[6,7]

Acknowledgements—Thanks are due to Dr K. Nag for many helpful suggestions, and to Dr P. Ghosh for assistance in the electrochemical experiments. I am indebted to Professor A. Chakravorty for use of electrochemical equipment.

REFERENCES

1. M. P. Coughlan (Ed.), *Molybdenum and Molybdenum-containing Enzymes*. Pergamon Press, Oxford (1980).
2. W. E. Newton and S. Otsuka (Eds), *Molybdenum Chemistry of Biological Significance*. Plenum Press, New York (1980).
3. J. Bordas, R. C. Bray, C. D. Garner, S. Gutteridge and S. S. Hasnian, *Biochem. J.* 1980, **199**, 499.
4. S. P. Cramer, H. B. Gray and K. V. Rajagopalan, *J. Am. Chem. Soc.* 1979, **101**, 2772.
5. T. D. Tullius, M. Kurtz, Jr, S. D. Conradson and K. O. Hodgson, *J. Am. Chem. Soc.* 1979, **101**, 2776.
6. S. Gutteridge and R. C. Bray, In *Proceedings of the Third International Conference on the Chemistry and Uses of Molybdenum* (Edited by H. F. Barry and P. C. H. Mitchell), p. 275. Climax Molybdenum Co., Ann Arbor, MI (1979).
7. R. H. Holm and J. M. Berg, *Pure Appl. Chem.* 1984, **56**, 1645.
8. M. Chaudhury, *J. Chem. Soc., Dalton Trans.* 1983, 857.
9. M. Chaudhury, *J. Chem. Soc., Dalton Trans.* 1984, 115.
10. M. Chaudhury, *Inorg. Chem.* 1984, **23**, 4434.
11. M. Chaudhury, *Inorg. Chem.* 1985, **24**, 3011.
12. B. Bordas, P. Sohar, G. Matolcsy and P. Berencsi, *J. Org. Chem.* 1972, **37**, 1727.
13. K. Nag and D. S. Joardar, *Inorg. Chim. Acta* 1976, **17**, 111.
14. E. I. Stiefel, *Prog. Inorg. Chem.* 1977, **22**, 1.
15. D. A. Brown, M. A. Burke and W. K. Glass, *Spectrochim. Acta* 1976, **32A**, 137.
16. J. Dirand, L. Ricard and R. Weiss, *J. Chem. Soc., Dalton Trans.* 1976, 278.
17. R. D. Bereman, D. M. Baird, C. T. Vance, J. Hutchinson and J. Zubieta, *Inorg. Chem.* 1983, **22**, 2316.
18. O. Piovesana and L. Sestili, *Inorg. Chem.* 1974, **13**, 2745.
19. A. Nieuwpoort and J. J. Steggerda, *Recl Trav. Chim. Pays-Bas* 1976, **95**, 294.
20. J. Hyde and J. Zubieta, *J. Inorg. Nucl. Chem.* 1977, **39**, 289.
21. J. T. Spence, M. Minelli, C. A. Rice, N. C. Chasteen and M. Scullane, In Ref. 2, p. 263.
22. I. W. Boyd, I. G. Dance, K. S. Murray and A. G. Wedd, *Aust. J. Chem.* 1978, **31**, 279.
23. T. M. Brown and J. N. Smith, *J. Chem. Soc., Dalton Trans.* 1972, 1614.
24. R. N. Jowith and P. C. H. Mitchell, *Inorg. Nucl. Chem. Lett.* 1968, **4**, 39.

Polyhedron Vol. 5, No. 1/2, pp. 393–398, 1986
Printed in Great Britain

0277–5387/86 $3.00 + .00
© 1986 Pergamon Press Ltd

SYNTHESIS OF A NEW CLASS OF Mo–Fe–S CLUSTERS CONTAINING THE MoS_2Fe_2 UNIT

K. S. BOSE,* P. E. LAMBERTY,† J. E. KOVACS,† E. SINN* and B. A. AVERILL*‡

* Department of Chemistry, University of Virginia, Charlottesville, VA 22901, U.S.A.; and
†Department of Chemistry, Michigan State University, East Lansing, MI 48824, U.S.A.

(*Received* 3 *July* 1985)

Abstract—A new synthetic route to Mo–Fe–S clusters related to nitrogenase has been developed, in which the bridging sulfides originate with the iron reagent (rather than with MoS_4^{2-}, as is the case for other known Mo–Fe–S clusters). This route produces clusters containing the novel $Mo(\mu_3\text{-}S)_2Fe_2$ structural unit, which is only the third known type of such a cluster (in addition to those containing the "linear" MoS_2Fe and "cubane" $MoFe_3S_4$ units). Reaction of the $[Fe_2S_2(CO)_6]^{2-}$ dianion with $MoCl_5$ has been found to produce at least four new clusters, including two Fe–S carbonyl clusters and two novel Mo–Fe–S clusters, including **I**. Complex **I**, isolated as the Ph_4As^+ salt, has been identified as the $[MoOFe_5S_6(CO)_{12}]^{2-}$ dianion by a single-crystal structure determination: space group $P2_1/n$, monoclinic, $Z = 4$; $a = 14.127(6)$ Å, $b = 17.818(5)$ Å; $c = 26.802(18)$ Å, $\beta = 94.51(2)°$, $V = 6726$ Å^3; current $R = 8.9\%$, $R_w = 9.4\%$; 2768 unique data with $F^2 > 3\sigma(F^2)$. Complex **I** can also be prepared in higher yield from the reaction of $MoOCl_3 \cdot 2THF$ with excess $[Fe_2S_2(CO)_6]^{2-}$ or $[Fe_4S_4(CO)_{12}]^{2-}$.

Recent efforts in a number of laboratories have been directed at the preparation of synthetic models[1] for the Fe–Mo cofactor (FeMo-co) of nitrogenase.[2] To data, two relevant types of synthetic Mo–Fe–S clusters have been prepared, containing the "cubane" $MoFe_3S_4$[1,3] and "linear" MoS_2Fe[1,4] structural units. The former include both double-[5–7] and single-cubane[8] clusters of stoichiometry $[Mo_2Fe_6S_8(\mu_2\text{-}L)_3(L')_6]^{3-,5-}$ (L = RS^- or RO^-, L′ = RS^- or ArO^-) and $[MoFe_3S_4(cat)(SR)_3L]^{2-,3-}$ (cat = substituted catecholate, L = any of a variety of ligands). Typical examples of the latter include the $[S_2MoS_2FeL_2]^{2-}$ [L = ArS^-,[9(a)–(c)] ArO^-[9(d),(e)] or OAc^-[9(f)]], $[S_2MoS_2FeS_2Fe(SAr)_2]^{3-}$[9(e),10] and $[Cl_2FeS_2MoS_2FeCl_2]^{2-}$[11] ions. Of these, the single cubanes display the most convincing similarity to FeMo-co in electronic properties[2(b),8(b)] and Mo EXAFS spectra,[2(b),5(c),12,13] while certain linear complexes[9(e)] provide the closest approximation to the Fe EXAFS of FeMo-co.[12,14] No synthetic complex yet prepared, however, bears a convincing similarity to FeMo-co in stoichiometry, collective electronic properties, and structural features.

All of the Mo–Fe–S clusters mentioned above are obtained by the reaction of MoS_4^{2-}[15] with various iron salts. Although MoS_4^{2-} is obtained upon acid degradation of the MoFe protein of nitrogenase,[16] its role in the biosynthesis of FeMo-co remains to be demonstrated. Accordingly, we have focussed on the development of new synthetic routes to Mo–Fe–S clusters, utilizing reagents in which the sulfide originates with the Fe species in order to increase the likelihood of obtaining new structural types, rather than variants on familiar systems. We report herein the synthesis and structure of a new type of Mo–Fe–S cluster containing the $Mo(\mu_3\text{-}S)_2Fe_2$ structural unit; it represents the first example of an Mo–Fe–S cluster related to nitrogenase whose synthesis does not require MoS_4^{2-}. While this manuscript was in preparation, a report of the synthesis and structure of a related complex, the $[MoFe_3S_6(CO)_6]^{2-}$ ion, appeared.[17]

EXPERIMENTAL

All operations were carried out under an atmosphere of purified dry dinitrogen.

‡ Author to whom correspondence should be addressed.

$MoOCl_3 \cdot 2THF$ was prepared as described previously.[18]

Preparation of $(Ph_4As)_2[MoOFe_5S_6(CO)_{12}]$, $(Ph_4As)_2I$

Method A. A solution of $Li_2[Fe_2S_2(CO)_6]$[19] was prepared by the addition of 1 M $LiEt_3BH$ (6.0 mmol) in THF to a solution of $Fe_2S_2(CO)_6$[20] (2.91 mmol) in 75 cm^3 THF at −78°C. To the deep green solution at −78°C was slowly added a solution of $MoOCl_3 \cdot 2THF$[18] (0.96 mmol) in 7 cm^3 MeCN. The solution was allowed to warm to room temperature and stirred for 1 h, after which the solvent was removed *in vacuo* at room temperature. The solid residue was dissolved in 10 cm^3 MeCN, $Ph_4As^+Cl^-$ (2.8 mmol) in 50 cm^3 MeOH was added, and the solution was maintained at −20°C overnight. The black microcrystalline solid was separated by filtration, washed with MeOH, and recrystallized by dissolving in 10 cm^3 MeCN or 7 cm^3 DMF, followed by addition of *ca* 50 cm^3 MeOH and cooling to −20°C overnight to afford black crystals of $(Ph_4As)_2[MoOFe_5S_6(CO)_{12}]$ (45% based on Mo). The compound is air-stable in the solid state, but was stored under N_2. Calc. for $C_{60}H_{40}As_2Fe_5MoO_{13}S_6$: C, 42.8; H, 2.4; As, 8.9; Fe, 16.6; Mo, 5.7; S, 11.4%. Found: C, 42.3; H, 2.4; As, 10.0; Fe, 16.6; Mo, 5.7; S, 11.3%.

Method B. A solution of $Li_2[Fe_4S_4(CO)_{12}]$[21] was prepared by addition of 1 M $LiEt_3BH$ (3.0 mmol) in THF to a solution of $Fe_2S_2(CO)_6$[20] (2.91 mmol) in 75 cm^3 THF at −78°C over 10 min, followed by maintaining the deep green solution at 0°C for 1 h, addition of 7 cm^3 DMF, and reduction of the volume *in vacuo* at room temperature to *ca* 20 cm^3. To this solution at room temperature was slowly added a solution of $MoOCl_3 \cdot 2THF$[18] (0.72 mmol) in 10 cm^3 MeCN. After stirring for 1 h, the volume was reduced *in vacuo* at room temperature to *ca* 7 cm^3, $Ph_4As^+Cl^-$ (2.8 mmol) in 50 cm^3 MeOH was added, and the solution was cooled to −20°C overnight. The black crystalline product was isolated and recrystallized as in method A (55% based on Mo). The products obtained via the two methods were identical in all respects. Found: C, 42.6; H, 2.5; Fe, 16.8%.

X-ray structure determination

Crystals of $(Ph_4As)_2I$ were obtained by diffusion of *i*-PrOH into an MeCN–*i*-PrOH solution of $(Ph_4As)_2I$ at room temperature under reduced pressure. Several crystals were mounted and sealed in glass capillaries, and the one giving the best diffraction pattern was used for the data collection.

Table 1. Crystal data and data collection procedures for $(Ph_4As)_2[MoOFe_5S_6(CO)_{12}]$

Formula	$C_{60}H_{40}As_2Fe_5MoO_{13}S_6$
Formula weight (amu)	1686
Crystal form	Monoclinic
Space group	$P2_1/n$
a (Å)	14.127(6)
b (Å)	17.818(5)
c (Å)	26.802(18)
β (°)	94.51(2)
V (Å^3)	6726
Z	4
Temperature (°C)	22
ρ_c (g cm^{-3})	1.67
μ (cm^{-1})	25.2
Radiation	Graphite-monochromated Mo-K_α $\lambda(\alpha_1) = 0.7093$ Å
Scan range	$1.50 < 2\theta < 49.00°$
Scan type	θ–2θ
Unique data	6097
Unique data with $F^2 > 3\sigma(F^2)$	2768

Crystal data and data collection procedures are summarized in Table 1.

Cell dimensions and space group data were obtained by standard methods on an Enraf–Nonius CAD-4 diffractometer. The θ–2θ scan technique[22(a)] was used to record the intensities of all nonequivalent reflections for which $1.5 < 2\theta < 49°$. Scan widths were calculated as $(A + B \tan \theta)°$, where A is estimated from the mosaicity of the crystal and B allows for the increase in peak width due to $K\alpha_1$–$K\alpha_2$ splitting. The values of A and B used were 0.8 and 0.35, respectively.

The intensities of three standard reflections showed a gradual decrease with X-ray exposure to about 63% of the original values. The data set was scaled to correct for this. The raw intensity data were corrected for Lorentz polarization and absorption. Of the 6097 independent reflections, there were 2768 with $F^2 > 3\sigma(F^2)$, where $\sigma(F^2)$ was estimated from counting statistics.[22(b)] These data were used in the final refinement of the structural parameters.

A three-dimension Patterson synthesis was used to determine the heavy-atom positions, which phased the data sufficiently well to permit location of the remaining nonhydrogen atoms from Fourier syntheses. Full-matrix least-squares refinement was carried out as previously described.[22(a)] Anisotropic temperature factors were introduced for the nonhydrogen atoms. Further Fourier difference functions permitted location of the non-methyl hydrogen atoms, which were included in the

$$3[Fe_2S_2(CO)_6]^{2-}\ (THF,\ -78°C) + MoCl_5\ (MeCN,\ \text{room temperature})$$
$$\downarrow$$
$$(Q^+)_2[MoOFe_5S_6(CO)_{12}]\ \textbf{(I)} + (Q^+)_2[Fe_6S_6(CO)_{12}]\ \textbf{(II)}$$
brown xtals purple xtals
$$+(Q^+)_2[Fe_5S_4(CO)_{12}]\ \textbf{(III)} + (Q^+)_2[Mo_2O_4(Fe_2S_2(CO)_6)_2]\ \textbf{(IV)}$$
brown xtals purple xtals

Scheme 1.

refinement for four cycles of least squares and then held fixed.

The model converged with $R = 8.9\%$ and $R_w = 9.4\%$. A final Fourier difference map was featureless. A listing of atomic coordinates and calculated thermal parameters is available as supplementary material.* The principal programs used are as previously described.[22(a)]

RESULTS AND DISCUSSION

Synthesis

Previous studies in our laboratory[23] have demonstrated that the reaction of the $[Fe_2S_2(CO)_6]^{2-}$ dianion with Mo halides is unexpectedly complex. Under conditions similar to those described in method A, at least four new cluster products can be isolated from the reaction of $MoCl_5$ with excess $[Fe_2S_2(CO)_6]^{2-}$, as shown in Scheme 1; similar results are obtained with $MoCl_4$.[23]

The structures of suitable salts of anions **I** and **II**[24] have been solved by single-crystal X-ray structure determinations, while structure determinations on salts of **III** and **IV** are in progress.

Because of the complexity of this reaction mixture, which makes isolation of pure compounds in reasonable yields difficult, alternative syntheses of all four clusters have now been developed.[23–25] The presence of the Mo=O group in **I** suggests that it arises via oxygen abstraction[26] from the THF cosolvent in Scheme 1; consequently, syntheses employing reagents containing the MoO unit were explored. Of the systems examined, the compound $MoOCl_3 \cdot 2THF$[18] is the most promising, due to its solubility in polar organic solvents. Treatment of $MoOCl_3 \cdot 2THF$ in MeCN with a THF solution of 3 equivalents of $[Fe_2S_2(CO)_6]^{2-}$[19] (method A) or 2 equivalents of $[Fe_4S_4(CO)_{12}]^{2-}$[21] (method B) affords salts of anion **I** in 45–55% yield based on Mo. Method A requires generation of the $[Fe_2S_2(CO)_6]^{2-}$ anion *in situ*, while method B utilizes the $[Fe_4S_4(CO)_{12}]^{2-}$ ion, which can be stored as the solid Ph_4As^+ salt for prolonged periods. The latter may therefore be slightly more convenient.

The structure of anion **I** (see below) contains an FeS_2 unit in addition to discrete $[Fe_2S_2(CO)_6]^{2-}$ units. The former must arise from a rearrangement of the $Fe_2S_2(CO)_6$ core. Related rearrangements are required to account for the formation of **II** and **III** as well. Further discussion of the complex solution chemistry leading to the formation of **I–III** is deferred until studies on the latter two compounds are completed.[24,25] Preliminary evidence from elemental analysis and spectroscopic results suggests that complex **IV** contains the $[Mo_2O_4]^{2+}$ core ligated by $[Fe_2S_2(CO)_6]^{2-}$ units similar to that in **I**.

Structure of **I**

The best crystal of $(Ph_4As)_2$**I** available did not diffract well enough to permit a high-resolution structure of the material. One of the two Ph_4As^+ cations was found to be positionally disordered, and the CO groups are more poorly resolved than is usual for such compounds. The latter may be due to disorder or to partial loss of CO during data collection, reducing the coordinated carbonyls to $<100\%$ occupancy. Some of the phenyl group carbon atoms of the disordered Ph_4As^+ were not included in the calculations at the current stage of refinement. The crystallographic results thus suffice for elucidation of the structure of **I**, but bond distances and angles are subject to standard deviations somewhat larger than desirable.

The structure of the $MoOFe_5S_6$ core of **I** is shown in Fig. 1; carbonyl ligands on Fe1, Fe2, Fe4 and Fe5 have been omitted for clarity. Three key structural features are immediately apparent: (i) the novel $Mo(\mu_3\text{-}S)_2Fe_2$ unit (Fig. 1, right-hand side); (ii) the $Fe_3(\mu_3\text{-}S)_2$ unit attached to Mo via two μ_2-sulfides (Fig. 1, left-hand side); and (iii) the Mo=O unit. The overall coordination about Mo is a distorted square

* Atomic positional and thermal parameters, and lists of F_c/F_o, have been deposited as supplementary material with the Editor, from whom copies are available on request. Atomic coordinates have also been deposited with the Cambridge Crystallographic Data Centre.

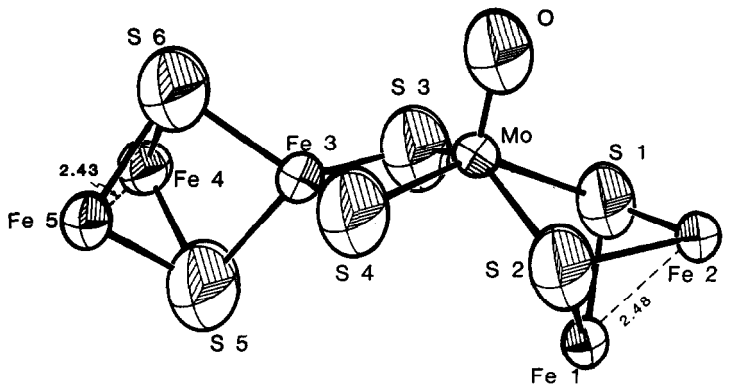


Fig. 1. An ORTEP drawing of the $MoOFe_5S_6$ core of **I**, showing the atomic labelling scheme and selected distances. The carbonyl groups have been omitted for clarity.

pyramidal $MoOS_4$ array. Selected bond distances and angles are given in Table 2.

The $Mo(\mu_3\text{-}S)_2Fe_2$ portion of **I** represents the first example of an Mo–Fe–S cluster related to nitrogenase that does not contain either the $MoFe_3(\mu_3\text{-}S)_4$ (cubane) or $Mo(\mu_2\text{-}S)_2Fe$ (linear) fragments. Within this unit, the Fe—Fe, Fe—S, and S···S distances are comparable to those observed for $Fe_2(\mu\text{-}SEt)_2(CO)_6$,[27] $(\mu\text{-}RS)(\mu\text{-}RHgS)Fe_2(CO)_6$[28] and $[Fe_4S_4(CO)_{12}]^{2-}$.[21] The acute SMoS angle (70.8°) is significantly smaller than that observed in $Ge[S_2Fe_2(CO)_6]_2$[29] (86.4°), the only other structurally characterized $Fe_2S_2(CO)_6$ chelate. It is also substantially smaller than that observed within the $Fe_3S_2(CO)_6$ portions of **I** and $[MoFe_3S_6(CO)_6]^{2-}$ (**V**)[17] (84.2 and 85.6°, respectively), suggesting that coordination to Mo results in a preference for an unusually small bite angle. This indicates that the $[Fe_2S_2(CO)_6]^{2-}$ and dithiocarbamate ($R_2NCS_2^-$) ligands have similar spatial constraints and may result in similar chemistry at the Mo. Attempts to prepare analogs to, for example, $Mo(CO)_2(R_2dtc)_2$,[30(a)] and to explore related ligand binding reactions[30(b)] are underway. The Mo···Fe1,2 distances are >3.3 Å, consistent with the absence of significant metal–metal interactions.

The $Fe_3(\mu_3\text{-}S)_2$ unit in **I** is very similar to that recently reported for **V**.[17] The triply bridging sulfides in **I** are asymmetrically located, with the bonds to Fe3 being slightly (*ca* 0.04 Å) longer than those to Fe4,5. A comparison of the bond distances between the unique iron and the bridging sulfides to Mo in **I** and **V** reveals that those in **I** are ~0.04 Å shorter than those in **V**, consistent with a higher formal valence for the unique Fe in **I** than in **V** (see below). The Mo—Fe3 distance is only 2.72 Å, similar to that found in other MoS_2Fe units,[1,4] and is within the range where direct metal–metal interactions must be considered.

Table 2. Selected bond distances (Å) and angles (°) for $(Ph_4As)_2[MoOFe_5S_6(CO)_{12}]$

Distance			
Mo—O	1.628(4)	Fe3—S3	2.205(5)
Mo—S1	2.458(4)	Fe3—S4	2.203(5)
Mo—S2	2.460(4)	Fe3—S5	2.272(5)
Mo—S3	2.291(4)	Fe3—S6	2.301(5)
Mo—S4	2.299(4)		
Fe1—S1	2.272(5)	Fe4—S5	2.314(5)
Fe1—S2	2.246(5)	Fe4—S6	2.286(5)
Fe2—S1	2.249(5)	Fe5—S5	2.269(5)
Fe2—S2	2.258(5)	Fe5—S6	2.257(5)
Mo---Fe3	2.717(2)	Fe1---Fe2	2.480(3)
Mo---Fe1	3.309(2)	Fe4---Fe5	2.434(3)
Mo---Fe2	3.584(2)	Fe3---Fe5	3.093(3)
S1---S2	2.861(6)	Fe3---Fe4	3.070(3)
S5---S6	3.072(6)		
S3---S4	3.563(6)		
S1---S3	3.064(6)		

Angle			
O—Mo—S1	107.2(3)	S1—Mo—S2	70.8(3)
O—Mo—S2	111.9(3)	S2—Mo—S3	139.4(3)
O—Mo—S3	106.3(3)	S3—Mo—S4	101.9(3)
O—Mo—S4	105.1(3)	S1—Mo—S3	85.3(3)
S1—Fe1—S2	78.2(5)	Fe3—S3—Mo	74.5(4)
S1—Fe2—S2	78.4(5)	Fe3—S4—Mo	74.4(4)
Fe1—S1—Mo	88.9(4)	S3—Fe3—S4	107.9(5)
Fe1—S2—Mo	89.5(4)	S5—Fe3—S6	84.1(5)
Fe2—S1—Mo	98.9(4)	Fe3—S5—Fe5	86.7(5)
Fe2—S2—Mo	98.5(4)	Fe3—S5—Fe4	84.6(5)
Fe1—S1—Fe2	67.1(5)	Fe5—S6—Fe4	66.6(5)
Fe1—S2—Fe2	67.3(5)	Fe5—S5—Fe4	65.9(5)
		S6—Fe5—S5	85.1(5)
		S6—Fe4—S5	83.4(5)

The Mo=O distance of 1.63 Å is one of the shortest reported for any monooxomolybdenum species[31] {cf. $[MoO(SPh)_4]^-$, 1.70 Å;[32] and $MoO(n\text{-}Pr_2dtc)_2$, 1.695 Å[33]}. The distorted square pyramidal coordination and short Mo=O bond are perhaps most consistent with a Mo(V) formulation, but are also consistent with Mo(IV).[31]

Physical and spectroscopic results

Solutions of **I** in polar organic solvents are brown, due to several poorly-resolved absorptions in the UV and visible regions: λ_{max} [ε (M^{-1} cm^{-1})] 330 (1.27×10^4), 459 (8.52×10^3), 544 (sh), 624 (sh) (MeCN). At this time, assignment to specific S → M charge-transfer or *d–d* transitions is not possible.

The IR spectrum of **I** in MeCN solution shows three very strong bands, at 2040, 2005 and 1967 cm^{-1}. These are diagnostic of the presence of the $Fe_2S_2(CO)_6$ unit.[19,21,29] IR spectra of the solid Ph_4As^+ salt of **I** in Nujol mulls show a strong absorption at 924 cm^{-1}. This is attributable to the Mo=O group, and is in the same range as those reported for $[MoO(SPh)_4]^-$ (931–940 cm^{-1})[18] or $MoO(Et_2dtc)_2$ (962 cm^{-1}).[34] It is, however, not consistent with the unusually short Mo=O distance, which would be expected to produce an IR stretch at higher energy.[31]

Room-temperature magnetic susceptibility measurements give a value of $\mu_{eff}^{corr} = 5.20$ BM for solid $(Ph_4As)_2$**I**. This indicates the presence of four unpaired electrons ($S = 2$) and is consistent with either of two possible formulations for the MoS_2Fe unit (assuming that all Fe atoms coordinated to three carbonyl ligands are formally Fe(I)): (a) Mo(VI) (d^0) plus high-spin Fe(II) (d^6), or (b) Mo(V) (d^1) antiferromagnetically coupled to high-spin Fe(III) (d^5).

The question of oxidation states is best addressed by ^{57}Fe Mössbauer spectra, which have been measured for solid $(Ph_4As)_2$**I** at 4.2 K in zero applied field. The spectra consist of two overlapping quadrupole doublets in a 4:1 area ratio: doublet 1 (more intense), $\delta = 0.07$ mm s^{-1}, $\Delta E_Q = 0.70$ mm s^{-1}; doublet 2, $\delta = 0.35$ mm s^{-1}, $\Delta E_Q = 1.6$ mm s^{-1}. Doublet 1 has parameters typical of $Fe_2S_2(CO)_6$ and related compounds.[23,24,35] Doublet 2, on the other hand, has parameters that are more typical of high-spin Fe^{3+} than high-spin Fe^{2+}. For example, the isomer shift* of 0.35 mm s^{-1} is very close to that of oxidized *Clostridium pasteurianum* rubredoxin (0.32 mm s^{-1})[36] and $[Fe_2S_2(S_2\text{-}o\text{-}xyl)_2]^{2-}$ (0.29 mm s^{-1}).[37] In particular, the parameters differ significantly from those observed for

$$[S_2MoS_2Fe(SPh)_2]^{2-}\ ^{9(b),(c)}$$

and

$$[S_2MoS_2FeCl_2]^{2-},^{9(b)}$$

for which a predominantly ferrous description has been suggested, and for the corresponding unique Fe site in **V**.[17]

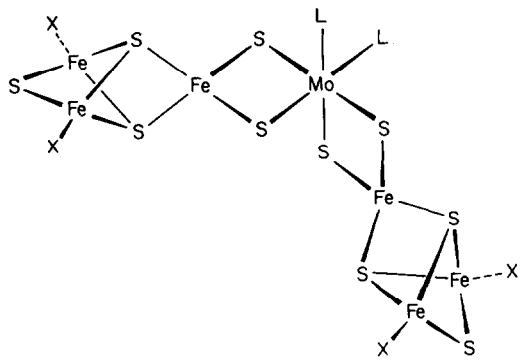


Fig. 2. A possible structure for the FeMo-cofactor of nitrogenase, based on the chemistry described in this paper.

Conclusions

Based on the available data, complex **I** is best formulated as containing a strongly antiferromagnetically coupled Fe(II)(μ-S)$_2$Mo(V)=O core, each metal ion of which is further coordinated by an $[Fe_2S_2(CO)_6]^{2-}$ unit. The resulting complex provides the first structurally characterized example of the novel Mo(μ_3-S)$_2$Fe$_2$ unit, as well as providing an example of an Fe$_3$(μ_3-S)$_2$ unit attached to Mo via bridging sulfides. It also appears to be the most complex oxomolybdenum–Fe–S cluster reported. The stability and ease of formation of the Mo(μ-S)$_2$Fe$_3$(μ_3-S)$_2$ unit, two examples of which, prepared via different synthetic routes, now exist, suggest that it might well be a potential structural fragment in the FeMo-co of nitrogenase; one possible structure for FeMo-co based on this chemistry is shown in Fig. 2. Synthetic efforts aimed at preparing complexes related to this model are in progress.

*The chemical shift data in this work are reported vs metallic Fe at room temperature. The data in Ref. 37 have been corrected by +0.12 mm s^{-1} to correct for the 4.2-K source temperature used in that work.

Acknowledgements—B. A. Averill was an Alfred P. Sloan Fellow, 1981–1985. This work was supported in part by a grant from the U.S. Department of Agriculture Competitive Research Grants Office (82-CRCR-1-1123). We thank Drs T. A. Kent and E. Münck of the Grey

Freshwater Biological Institute, Navarre, MN, for measuring the Mössbauer spectra.

REFERENCES

1. B. A. Averill, *Struct. Bonding (Berlin)* 1983, **53**, 59.
2. (a) V. K. Shah and W. J. Brill, *Proc. Nat. Acad. Sci. U.S.A.* 1977, **74**, 3249; (b) B. K. Burgess and W. E. Newton, In *Nitrogen Fixation, The Chemical–Biochemical–Genetic Interface* (Edited by A. Müller and W. E. Newton), p. 83. Plenum Press, New York (1983).
3. (a) R. H. Holm, *Chem. Soc. Rev.* 1981, **10**, 455; (b) C. D. Garner, S. R. Acott, G. Christou, D. Collison, F. E. Mabbs, V. Petrouleas and C. J. Pickett, In *Nitrogen Fixation, The Chemical–Biochemical–Genetic Interface* (Edited by A. Müller and W. E. Newton), p. 243. Plenum Press, New York (1983).
4. D. Coucouvanis, *Acc. Chem. Res.* 1981, **14**, 201.
5. (a) G. Christou, P. K. Mascharak, W. H. Armstrong, G. C. Papaefthymiou, R. B. Frankel and R. H. Holm, *J. Am. Chem. Soc.* 1982, **104**, 2820; (b) R. E. Palermo, P. P. Power and R. H. Holm, *Inorg. Chem.* 1982, **21**, 173; (c) T. E. Wolff, J. M. Berg, K. O. Hodgson, R. B. Frankel and R. H. Holm, *J. Am. Chem. Soc.* 1979, **101**, 4140.
6. (a) G. Christou, D. Collison, C. D. Garner, S. R. Acott, F. E. Mabbs and V. Petrouleas, *J. Chem. Soc., Dalton Trans.* 1982, 1575; (b) G. Christou, C. D. Garner, R. M. Miller, C. E. Johnson and J. D. Rush, *ibid.* 1980, 2363; (c) G. Christou and C. D. Garner, *ibid.* 1980, 2354.
7. W. E. Cleland and B. A. Averill, *Inorg. Chim. Acta* 1985, **107**, 187.
8. (a) R. E. Palermo, R. Singh, J. K. Bashkin and R. H. Holm, *J. Am. Chem. Soc.* 1984, **106**, 2600; (b) P. K. Mascharak, G. C. Papaefthymiou, W. H. Armstrong, S. Foner, R. B. Frankel and R. H. Holm, *Inorg. Chem.* 1983, **22**, 2851; (c) P. K. Mascharak, W. H. Armstrong, Y. Mizobe and R. H. Holm, *J. Am. Chem. Soc.* 1983, **105**, 475; (d) W. H. Armstrong, P. K. Mascharak and R. H. Holm, *ibid.* 1982, **104**, 4374.
9. (a) D. Coucouvanis, E. D. Simhon, D. Swenson and N. C. Baenziger, *J. Chem. Soc., Chem. Commun.* 1979, 361; (b) R. H. Tieckelmann, H. C. Silvis, T. A. Kent, B. H. Huynh, J. V. Waszczak, B. K. Teo and B. A. Averill, *J. Am. Chem. Soc.* 1980, **102**, 5550; (c) D. Coucouvanis, P. Stremple, E. D. Simhon, D. Swenson, N. C. Baenziger, M. Draganjac, L. T. Chan, A. Simopoulos, V. Papaefthymiou, A. Kostikas and V. Petrouleas, *Inorg. Chem.* 1983, **22**, 293; (d) H. C. Silvis and B. A. Averill, *Inorg. Chim. Acta* 1981, **46**, L57; (e) B. K. Teo, M. R. Antonio, R. H. Tieckelmann, H. C. Silvis and B. A. Averill, *J. Am. Chem. Soc.* 1982, **104**, 6126; (f) B. Zhuang, J. W. McDonald and W. E. Newton, *Inorg. Chim. Acta* 1983, **77**, L221.
10. R. H. Tieckelmann and B. A. Averill, *Inorg. Chim. Acta* 1980, **46**, L35.
11. (a) D. Coucouvanis, N. C. Baenziger, E. D. Simhon, P. Stremple, D. Swenson, A. Simopoulos, A. Kostikas, V. Petrouleas and V. Papaefthymiou, *J. Am. Chem. Soc.* 1980, **102**, 1732; (b) A. Müller, S. Sarkar, A.-M. Dommröse and R. Filgueira, *Z. Naturforsch.* 1980, **35B**, 1592.
12. M. R. Antonio, B. K. Teo, W. E. Cleland and B. A. Averill, *J. Am. Chem. Soc.* 1983, **105**, 3477.
13. (a) S. P. Cramer, K. O. Hodgson, W. O. Gillum and L. E. Mortenson, *J. Am. Chem. Soc.* 1978, **100**, 3398; (b) S. P. Cramer, W. O. Gillum, L. E. Mortenson, E. I. Stiefel, J. R. Chisnell, W. J. Brill and V. K. Shah, *ibid.* 1978, **100**, 3814.
14. M. R. Antonio, B. K. Teo, W. H. Orme-Johnson, M. J. Nelson, S. E. Groh, P. A. Lindahl, S. M. Kauzlarich and B. A. Averill, *J. Am. Chem. Soc.* 1982, **104**, 4703.
15. (a) G. Krüss, *Justus Liebigs Ann. Chem.* 1984, **225**, 6; (b) J. W. McDonald, G. D. Friesen, L. D. Rosenheim and W. E. Newton, *Inorg. Chim. Acta* 1983, **72**, 205.
16. W. G. Zumft, *Eur. J. Biochem.* 1978, **91**, 345.
17. J. A. Kovacs, J. K. Bashkin and R. H. Holm, *J. Am. Chem. Soc.* 1985, **107**, 1784.
18. I. W. Boyd, I. G. Dance, K. S. Murray and A. G. Wedd, *Aust. J. Chem.* 1978, **31**, 279.
19. D. Seyferth, R. S. Henderson and L.-C. Song, *Organometallics* 1982, **1**, 125.
20. W. Hieber and J. Gruber, *Z. Anorg. Allg. Chem.* 1958, **296**, 91.
21. K. S. Bose, E. Sinn and B. A. Averill, *Organometallics* 1984, **3**, 1126.
22. (a) D. P. Freyberg, G. M. Mockler and E. Sinn, *J. Chem. Soc., Dalton Trans.* 1976, 447; (b) P. W. R. Corfield, R. J. Doedens and J. A. Ibers, *Inorg. Chem.* 1967, **6**, 197.
23. K. S. Bose, P. E. Lamberty, J. Kovacs and B. A. Averill, unpublished results.
24. G. L. Lilley, E. Sinn and B. A. Averill, submitted.
25. K. S. Bose and B. A. Averill, unpublished results.
26. H. Funk, F. Schmeil and H. Scholz, *Z. Anorg. Allg. Chem.* 1961, **310**, 86.
27. L. F. Dahl and C.-H. Wei, *Inorg. Chem.* 1963, **2**, 328.
28. C. Chieh, D. Seyferth and L.-C. Song, *Organometallics* 1982, **1**, 473.
29. N. S. Nametkin, V. D. Tyurin, G. G. Aleksandrov, O. V. Kuz'min, A. I. Nekhaev, V. G. Andrianov, M. Mavlonov and Yu. T. Struchkov, *Izv. Akad. Nauk SSSR, Ser. Khim.* 1979, 1353.
30. (a) J. L. Templeton and B. C. Ward, *J. Am. Chem. Soc.* 1980, **102**, 6568; (b) G. J.-J. Chen, R. O. Yelton and J. W. McDonald, *Inorg. Chim. Acta* 1977, **22**, 249.
31. E. I. Stiefel, *Prog. Inorg. Chem.* 1977, **22**, 1.
32. J. R. Bradbury, M. F. MacKay and A. G. Wedd, *Aust. J. Chem.* 1978, **31**, 2423.
33. L. Ricard, J. Estienne, P. Karagiannidis, P. Toledano, A. Mitchell and R. Weiss, *J. Coord. Chem.* 1974, **3**, 277.
34. R. N. Jowitt and P. C. H. Mitchell, *J. Chem. Soc. (A)* 1969, 2632.
35. T. C. Gibb, R. Greatrex and N. N. Greenwood, *J. Chem. Soc. (A)* 1967, 1663.
36. C. Shulz and P. G. Debrunner, *J. Phys. (Paris)* Suppl., 1976, **12**, C6-153.
37. W. O. Gillum, R. B. Frankel, S. Foner and R. H. Holm, *Inorg. Chem.* 1976, **15**, 1095.

Polyhedron Vol. 5, No. 1/2, pp. 399–401, 1986
Printed in Great Britain

0277–5387/86 $3.00 + .00
© 1986 Pergamon Press Ltd

PHOSPHONIUM SALTS OF CHLOROMOLYBDATE ANIONS

A. HERBOWSKI

Institute of Chemistry, Silesian University, Katowice, Poland

and

J. M. SOBCZAK and J. J. ZIÓŁKOWSKI*

Institute of Chemistry, University of Wrocław, 50-383 Wrocław, Poland

(*Received* 11 *June* 1985)

Abstract—Synthesis, properties and application of chloromolybdate anion salts with $[HP(Ph)_2(CH_2)_2P(Ph)_2H]^{2+}$ are described.

Many phosphine complexes are active and specific homogeneous catalysts.[1] Our recent positive results in the application of Mo complexes with bis(diphenylphosphine)ethane (dppe) as homogeneous catalysts of olefin epoxidations with organic hydroperoxides[2] encouraged us to discover new Mo complexes with dppe and to develop a new, simple and effective synthesis route. We present here our new synthesis of Mo complexes with dppe via the phosphonium compound. This method proved to be advantageous. First, synthesis proceeds in an acidic-water medium. Second, the large phosphonium cation, $dppeH_2^{2+}$, precipitates and stabilizes many Mo anions in various oxidation states. Third, phosphonium compounds of $dppeH_2^{2+}$ could easily be converted into phosphine complexes.

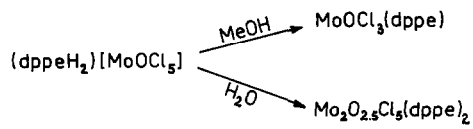
EXPERIMENTAL

A Mo(V) phosphonium salt was obtained by reaction of $[MoOCl_5]^{2-}$ (prepared according to Palmer[3]) with dppe solution in concentrated HCl. The salt, $(dppeH_2)[MoOCl_5]$ (**I**), was isolated as a light-green amorphous powder, stable in dry air, but moisture sensitive. Prolonged storage of this compound (as well as of the others described below) in air, especially under moisture, causes its conversion to the complex with phosphine oxide, in this case to $MoOCl_3(dppeO_2)$.

* Author to whom correspondence should be addressed.

RESULTS AND DISCUSSION

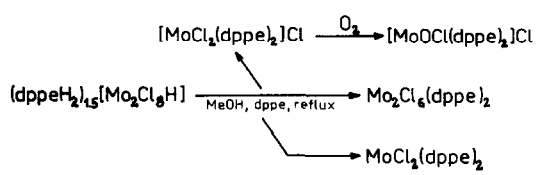
I is paramagnetic (1.74 BM) and insoluble in most solvents. **I** could easily be converted into phosphine complexes[4] (Scheme 1):



Scheme 1.

The quantitatively prepared $MoOCl_3(dppe)$ is the brown isomer of the compound synthesized earlier by another method.[5]

Mo(III) phosphonium salts were obtained by adding dppe solution in concentrated HCl to freshly prepared solutions of $[Mo_2Cl_8H]^{3-}$[6] and $[Mo_2Cl_9]^{3-}$.[7] The salts obtained, $(dppeH_2)_{1.5}[Mo_2Cl_8H]$ (**II**) and $(dppeH_2)_{1.5}[Mo_2Cl_9]$ (**III**), are diamagnetic, insoluble in most solvents, and quite stable in dry air. **II** proved to be a convenient precursor for the synthesis of some Mo phosphine complexes with dppe[8] (Scheme 2):



Scheme 2.

Table 1. Analytical data (wt %)

Compound	Mo		C		Cl	
	Found	Calc.	Found	Calc.	Found	Calc.
I	13.5	13.92	44.7	45.25	25.0	25.74
II	17.7	17.82	43.0	43.47	26.2	26.34
III	17.0	17.27	42.1	42.12	28.4	28.72
IV	9.7	9.43	46.8	46.03	21.3	20.72
V	14.1	14.65	48.0	47.65	21.8	21.66
VI	14.8	15.04	49.1	48.93	21.8	22.24

The above procedure does not yield the analogous phosphonium salt with the $[MoCl_6]^{3-}$ anion. However, we have synthesized crystalline $(dppeH_2)_{1.5}[MoCl_6]\cdot 6H_2O$ (IV) and its crystallographic structure was determined.[9] This structure confirmed the postulated formula for the cation, $[HP(Ph)_2(CH_2)_2P(Ph)_2H]^{2+}$.

Reaction between green Mo(III) solution (prepared according to Palmer[3]) and dppe solution in 8 N HCl produced a sky-blue precipitate of the phosphonium salt $(dppeH_2)_2[Mo_2(OH)_2Cl_8]$ (V), which was oxygen- and moisture-sensitive. This compound, unlike previously described dimeric Mo(III) di-μ-hydroxo complexes[10] is paramagnetic (1.8 BM per Mo atom, practically temperature-independent). This suggests that the structure of the $Mo(OH)_2Mo$ fragment in this complex is not planar. The possibility of such a structure was confirmed by Cramer *et al.*[11]

The freshly precipitated V solvolysed with methanol and ethanol is converted to the pink phosphine complex initially formulated as $Mo_2(OH)_2(dppe)_2Cl_4$.

A Mo(II) phosphonium complex, $(dppeH_2)[Mo_2Cl_8]$ (VI), also air- and moisture-sensitive, was obtained by a similar procedure. During its synthesis in 7–8 N HCl solution, the formation of a green complex, α-$Mo_2Cl_4(dppe)_2$, identical to a compound obtained earlier[12] was observed. This is the first case of the direct synthesis of a phosphine complex from the acidic-water solutions observed by us. Analytical data for the Mo phosphonium complexes are listed in Table 1.

Electronic spectra of isolated phosphonium salts are similar to Mo complexes of similar structure (Table 2).

The IR spectra of these compounds exhibit, besides absorption characteristic of the dppe ligand, bands at 2400 cm^{-1}, assigned to ν(P—H) stretching vibration, and ~900 cm^{-1}, assigned to δ(P—H) deformation vibrations. The IR spectrum of V shows an additional band at ~980 cm^{-1}, typical of the $Mo(OH)_2Mo$ fragment.[13]

Positive results obtained in applying the phosphonium and phosphine Mo complexes as olefin epoxidation catalyst,[2,14] as well as the fact that during this reaction the initial compounds are converted into $MoO_2(diol)(dppeO_2)$, allowed us to expect to obtain effective catalysts heterogenized on polymer carriers, functionalized by the phosphonium groups.

REFERENCES

1. L. Pignolet (Ed.), *Homogeneous Catalysis with Metal Phosphine Complexes*. Plenum, New York (1983).
2. A. Herbowski, J. M. Sobczak and J. J. Ziółkowski, *J. Mol. Catal.* 1983, **19**, 309.
3. W. G. Palmer, *Experimental Inorganic Chemistry*, p. 404. Cambridge (1962).
4. A. Herbowski, *Inorg. Chim. Acta* 1981, **54**, L121.

Table 2. Electronic transitions of Mo phosphonium complexes

Compound	Absorption band [λ (cm^{-1})]
I	22,170 13,600
II	23,530, 19,050, 13,330, 10,530
III	25,530, 19,230, 17,560, 15,150, 13,160, 10,160
IV	23,810, 18,870, 14,925, 10,000
V	27,400, 23,250, 16,150, 13,070
VI	21,500, 13,790

5. A. V. Butcher and J. Chatt, *J. Chem. Soc.* (*A*) 1971, 2356.
6. J. San Filippo, Jr and H. J. Sniadoch, *Inorg. Synth.* **19**, 128.
7. Ref. 3, p. 419.
8. A. Herbowski and J. O. Dzięgielewski, *Chem. Scr.* 1984, **24**, 41.
9. A. Herbowski and T. Lis, *Polyhedron* 1985, **4**, 127.
10. K. Wieghardt, M. Hahn, W. Swiridoff and J. Weiss, *Inorg. Chem.* 1984, **23**, 94.
11. S. P. Cramer, P. K. Eiden, M. T. Paffett, J. R. Winkler, Z. Dori and H. B. Gray, *J. Am. Chem. Soc.* 1983, **105**, 799.
12. S. A. Best, T. J. Smith and R. A. Walton, *Inorg. Chem.* 1978, **17**, 99.
13. H. J. Schugar, G. R. Rossmann and H. B. Gray, *J. Am. Chem. Soc.* 1969, **91**, 4564; G. W. Bushnell, K. R. Dixon, R. G. Hunter and J. J. McFarland, *Can. J. Chem.* 1972, **50**, 3964.
14. A. Herbowski, J. M. Sobczak and J. J. Ziółkowski, *Polyhedron* 1986, **5**, 277.

Polyhedron Vol. 5, No. 1/2, pp. 403–406, 1986
Printed in Great Britain

0277–5387/86 $3.00 + .00
© 1986 Pergamon Press Ltd

^{95}Mo NMR STUDIES OF SOME CARBONYLATE ANIONS

E. C. ALYEA,* A. MALEK and J. MALITO

Guelph–Waterloo Centre for Graduate Work in Chemistry, Guelph Campus, Department of Chemistry and Biochemistry, Guelph, Ontario, Canada N1G 2W1

(*Received* 17 *June* 1985)

Abstract—^{95}Mo NMR chemical shifts are reported for a range of molybdenum(0) carbonylate anions of the type $[Mo(CO)_5X]^-$ (X = halide or pseudohalide). The dimethylsulphoxide solution data substantiate the existence of more than one product, unexpected products and ambidentate pseudohalogen bonding modes. The sensitivity of the ^{95}Mo NMR chemical shifts to the ligand field and polarizability properties of the anions in the $[Mo(CO)_5X]^-$ complexes results in an over 500 ppm range of values (−1980 to −1435 ppm); the shielding order is $H^- > CN^- > I^- > NCO^- > NCS^- > NCSe^- > Br^- > N_3^- > NO_2^- > Cl^- > O_2CH^- > O_2N^- > OCH_3^-$. Species arising from the reaction of $Mo(CO)_6$ with hydroxide ion have been previously implicated in the homogeneous catalysis of the water-gas shift reaction; the utility of ^{95}Mo NMR spectroscopy in identifying some of these products is also described.

^{95}Mo NMR spectroscopy is now well established as a sensitive probe of both electronic and structural effects in diamagnetic molybdenum complexes.[1] The chemical shift range for ^{95}Mo for all oxidation states is *ca* 7000 ppm, with resonances for Mo(0) compounds extending *ca* 2000 ppm to higher frequency from the most shielded value {−2123 ppm for $Na[CpMo(CO)_3]$}. We have previously[2] studied the ^{95}Mo NMR spectra of a series of substituted molybdenum carbonyls, $Mo(CO)_{6-n}L_n$ (n = 1–3, L = N, P, As or Sb donor ligands). Subsequent work[3] demonstrated the usefulness of ^{95}Mo NMR spectroscopy in characterizing a variety of unstable ionic complexes of the type [Cat][$Mo(CO)_5$L] and [Cat][$Mo(CO)_4$L–L] (Cat = NH_4, Na or K; L or L–L = dithiocarbamato, xanthato or phosphorodithioato). The present study extends our identification of molybdenum(0) carbonylate anions to a variety of $[Mo(CO)_5X]^-$ (X = pseudohalide) complexes. Particular interest focuses on the anionic molybdenum carbonyl species generated by the reaction of $Mo(CO)_6$ with hydroxide ion since they have been implicated in the homogeneous catalysis of the water-gas shift reaction (WGSR).[4,5] A preliminary report of this study has been published.[6]

* Author to whom correspondence should be addressed.

EXPERIMENTAL

^{95}Mo NMR spectra were recorded for naturally abundant (15.7 atom %) samples using a Bruker WH-400 NMR spectrometer in the pulsed Fourier transform mode. The spectra were obtained at ambient temperature with the probe specifically tuned for ^{95}Mo at 26.08 MHz using a field strength of 9.3956 T. The external standard was aqueous 2 M K_2MoO_4 at pH 11. The pulse width was normally in the 50–100 μs range for the 90° pulse, but other parameters varied widely, though typically the resolution was better than 5 Hz per point. Parameters used for the observation of the ^{95}Mo NMR spectrum of the possible products arising from the reaction of $Mo(CO)_6$ and $NaBH_4$ in dimethylsulphoxide (DMSO) solution are listed as a typical example: sweep width 29,412 Hz, data points 16 K, pulse width 50 μs, line broadening 25 Hz, number of scans 1871, resolution 3.6 Hz per point; the signal occurring at −1941 ppm (no other peaks were observed) has a linewidth at half height of 50 Hz and a signal-to-noise ratio of 50.

Samples were prepared *in situ* under dinitrogen using *ca* 0.1 mol dm^{-3} DMSO solutions of the alkali metal salt or hydroxide and $Mo(CO)_6$ in 1 : 1 molar ratios. Transfer to septum-sealed 10-mm NMR

tubes via a syringe was effected after warming the solutions at 60–65°C until a colour change and/or IR spectroscopy indicated an appreciable conversion to the carbonylate anion. Both the concentrations and the reaction times (typically ½–5 h) varied considerably for the samples. Solution IR spectra were also normally obtained on diluted samples subsequent to NMR analyses to ensure the integrity of the solutions, which were assumed to be air-sensitive. Matched CaF_2 or KBr sealed cells of 0.2-mm path length were used in conjunction with a Perkin–Elmer 180 grating IR spectrophotometer.

The sodium salts of $[HMo_2(CO)_{10}]^-$, $[HMoCr(CO)_{10}]^-$ and $[HMoW(CO)_{10}]^-$ were produced *in situ* in THF or DMSO following the method of Hayter.[7] The solutions were reduced to near dryness under reduced pressure to remove volatile by-products before dilution for ^{95}Mo NMR and IR measurements.

RESULTS AND DISCUSSION

The molybdenum carbonylate anions $[Mo(CO)_5X]^-$ (X = halide) are stable well-characterized species that have been long used as precursors in the synthesis of $Mo(CO)_5L$ complexes.[8] Earlier ^{95}Mo NMR studies[3,9] established that the chemical shifts of these d^6 species follow a 'normal halogen dependence',[10] in contrast to an inverse correlation observed for the $[MoE_4]^{2-}$ anions (E = O, S or Se) and $[MoO_2]^{2+}$ complexes.[11] Investigations on other $[Mo(CO)_5X]^-$ (X = pseudohalide) species are less extensive, though IR spectroscopy has shown the existence of more than one product with a given anion,[12] unexpected products,[13] and ambidentate pseudohalogen bonding modes.[14] Our success in utilizing ^{95}Mo NMR spectroscopy to identify unstable $[Mo(CO)_5L]^-$ and $[Mo(CO)_4L\text{–}L]^-$ (L or L–L = dithiocarbamato, xanthato or phosphorodithioato) anions, generated *in situ* in warm DMSO solution,[3] led us to this ^{95}Mo NMR investigation of the products formed by reacting $Mo(CO)_6$ with pseudohalides and hydroxide ions under similar conditions. Formation of the anionic products was monitored using the IR carbonyl region since a three-band pattern with a strong band near 1920 cm^{-1} is diagnostic of the presence of these pentacarbonyl species.[3,15] In the case of BH_4^-, CN^-, NCO^- and the halide ions, IR spectroscopy indicates only the pentacarbonyl product in the DMSO reaction mixture, and thus the corresponding observation of just one peak in the ^{95}Mo NMR spectrum leads to a reasonably unambiguous assignment. With the other anions employed in this study, the complexity of the IR spectra of the reaction mixtures showed only that two or more products had formed, and the identification of the species that actually exist in solution was more clearly suggested by observation of the ^{95}Mo resonances. Table 1 lists the ^{95}Mo NMR chemical shifts and their tentative assignments for the carbonylate anions of the type $[Mo(CO)_5X]^-$ formed in this study.

The spread of 545 ppm in the ^{95}Mo chemical shift resonances indicates the high sensitivity of the NMR method to the environment of the pseudooctahedral molybdenum atoms. The nephelauxetic term in the Ramsey expression[1] for the paramagnetic shielding appears to be dominant, since polarizable anions (H, CN or I) give the highest observed shielding whereas the more electronegative or harder anions (oxygen donor ions) lead to molybdenum being deshielded. The importance of the ΔE term was obvious for other series of substituted molybdenum carbonyls[2] and thus the ligand field strength of the anion is surely also an important influence on the observed range of chemical shifts for the present carbonylate anions. For example, although the data clearly differentiates between the NCO, NCS and NCSe anions, the relative contribution of π-acceptor ability and polarizability factors must remain debatable. We include the chemical shifts[3] for the species involving unidentate $S_2P(OEt)_2$, S_2CNPh_2 and S_2CNMe_2 anions in Table 1 for the sake of comparison and note their similarity to the values observed with several *N*-donor anions. We previously assigned a peak at

Table 1. ^{95}Mo NMR chemical shifts for some molybdenum(0) carbonylate anions of the type $[Mo(CO)_5X]^-$

X[a]	$\delta(^{95}Mo)$ (ppm)	X[a]	$\delta(^{95}Mo)$ (ppm)
H	−1980	Br[b]	−1540
CN	−1887	S_2CNMe_2[c]	−1534
I[b]	−1660	N_3	−1523
$S_2P(OEt)_2$[c]	−1626	NO_2	−1514
NCO	−1604	Cl[b]	−1513
NCS	−1596	O_2CH	−1495
S_2CNPh_2[c]	−1596	O_2N	−1435
NCSe[d]	−1590	OCH_3	−1435

[a] Solutions prepared *in situ* in DMSO solution, except Cl (CH_2Cl_2), Br and I (CD_2Cl_2), and OMe (THF).

[b] Previously reported, see Refs 2 and 9.

[c] Previously reported.[3]

[d] The major peak at −1438 ppm is an alternative assignment; other minor peaks occur at −1887, −1867, −1735, −1603, −1590, −1452 and −1360 ppm (see text).

−943 ppm to $[Mo(CO)_5F]^-$ and found that the ^{95}Mo NMR spectrum for the reaction of $NaBF_4$ with $Mo(CO)_6$ in DMSO solution also gave a resonance in the same region. It is more probable that a polynuclear hydroxo-species is responsible for the −943 ppm peak, considering its downfield position as compared to those for the other halide species and the fact that reaction mixtures of hydroxyl ion with $Mo(CO)_6$ always show a peak at −943 ppm.

The existence of more than one product, suggested by the observance of more than three IR carbonyl bands, was verified by the ^{95}Mo NMR data for reactions of $Mo(CO)_6$ with NaN_3, KCNS, KCNSe, NaOMe, $NaNO_2$, NaO_2CH and NaOH or KOH (*vide infra*). The second peak of lower intensity observed for the azide reaction can be attributed to the formation of the isocyanate group since the only peak found in the reaction mixture of NaNCO with $Mo(CO)_6$ also occurs at −1604 ppm; this reaction has previously been followed by IR spectroscopy.[13] Similarly, IR studies suggested that NCS-bridged binuclear species as well as *N*-bonded mononuclear species were formed in the reaction of the thiocyanate ion with $Mo(CO)_6$.[14] We assign the major peak at −1596 ppm to the $[Mo(CO)_5NCS]^-$ ion, whereas the minor peak at −1370 ppm may be due to the bridged species or, alternatively, the *S*-bonded mononuclear isomer. Some of the peaks observed for the DMSO solution containing KSeCN and $Mo(CO)_6$ are reasonably identified as unreacted $Mo(CO)_6$ (−1867 ppm), $[Mo(CO)_5CN]^-$ (−1887 ppm), $[Mo(CO)_5NCSe]^-$ [−1590 ppm or −1438 ppm (the major peak)], $[Mo(CO)_5NCO]^-$ (−1603 ppm); other minor peaks suggest the presence of *Se*-bonded and bridging species (−1438 and −1360 ppm). Whilst the major peak that occurs in the ^{95}Mo NMR spectrum of a THF solution of NaOMe and $Mo(CO)_6$ is assigned to the presence of the $[Mo(CO)_5OMe]^-$ ion, the weak broad peak at −1784 ppm remains unassigned. The two equal intensity peaks found in the case of the reaction of $NaNO_2$ with $Mo(CO)_6$ in warm DMSO solution are assigned to $[Mo(CO)_5NO_2]^-$ (−1514 ppm) and $[Mo(CO)_4O_2N]^-$ (−1435 ppm). The occurrence of bidentate nitrito coordination is suggested by the IR spectrum [peaks at 2050(w), 1970(s), 1925(vs, b) and 1850(s)] but the presence of monodentate *O*-bonded nitrito groups cannot be ruled out.

^{95}Mo NMR chemical shifts for some molybdenum carbonylate anions generated in polar solvents by the addition of hydroxide ion to $Mo(CO)_6$ are listed in Table 2. The $[Mo_2(CO)_{10}H]^-$ species is also the only product of the reaction of $NaBH_4$ with $Mo(CO)_6$ in warm DMSO solution, as previously identified by IR studies.[4,7] Masters *et al.*[16] previously reported the resonance for $[Mo_2(CO)_{10}H]^-$ at −1937 ppm (THF solution). We observe formation of the hydrido-bridged species in reactions of hydroxyl or formate ions with $Mo(CO)_6$. In the case of the reaction of NaO_2CH with $Mo(CO)_6$, the $[Mo(CO)_5O_2CH]^-$ ion is the major species formed, and we note that there is no indication of the presence of $[Mo(CO)_5H]^-$. This was surprising in that recent investigations[4] of these systems (albeit in nonpolar media) suggested that the $[Mo(CO)_5H]^-$ ion was the primary product of the decarboxylation of the $[Mo(CO)_5O_2CH]^-$ ion. Darensbourg and Rokicki[4] showed that the latter ion was readily formed by bubbling CO_2 through a solution of $[Mo(CO)_5H]^-$. We find that $[Mo_2(CO)_{10}H]^-$ generated *in situ*[7] in THF or DMSO solution reacts with CO_2 under ambient conditions to produce $[Mo(CO)_5O_2CH]^-$, identified by IR, ^{1}H and ^{95}Mo NMR spectroscopy. The characteristic IR and ^{1}H NMR peaks due to coordinated formato peaks are observed at 1600 cm^{-1} and 8.55 ppm, respectively.[4,7,17] It is nevertheless interesting to note that the major initial product of the reaction of hydroxyl ion with $Mo(CO)_6$ in DMSO solution is $[Mo(CO)_5H]^-$ {major peak at −1980 ppm; minor peaks at −1940 and −943 ppm are assigned to $[Mo_2(CO)_{10}H]^-$ and a polynuclear hydroxo-species, respectively}. Longer reaction times give rise to peaks at −1544 ppm (unidentified) and at −1495 ppm {$[Mo(CO)_5O_2CH]^-$}. The complexity of the interrelationships of the various species is of current interest[4,5,17] due to the implication of the system in the homogeneous catalysis of the WGSR. Our continuing investigations of these species employing ^{95}Mo NMR spectroscopy will be reported later.

Table 2. ^{95}Mo NMR chemical shifts for some molybdenum(0) carbonylate anions generated in polar media

Anion[a]	$\delta(^{95}Mo)$ (ppm)	Solvent
$[HMo(CO)_5]^-$	−1980	DMSO
$[HMo_2(CO)_{10}]^-$	−1941	DMSO
	−1940	CH_3CN
	−1937[b]	THF
$[HMoW(CO)_{10}]^-$	−1916	THF
$[HMoCr(CO)_{10}]^-$	−1872	THF
$[Mo(CO)_5(O_2CH)]^-$	−1495	DMSO
	−1494	THF
	−1491	CH_3CN

[a] Solutions prepared *in situ* in given solvent.
[b] Previously reported.[16]

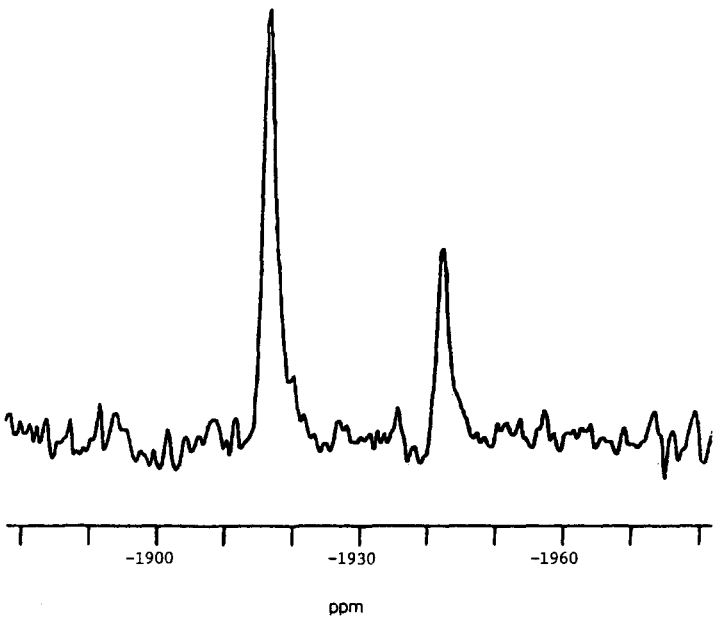


Fig. 1. The ^{95}Mo NMR spectrum of $[HMoW(CO)_{10}]^-$ (−1916 ppm) and $[HMo_2(CO)_{10}]^-$ (−1942 ppm), generated *in situ* in a 2:1 molar ratio in THF solution.[7]

Hayter[7] demonstrated earlier that one molybdenum atom in $[Mo_2(CO)_{10}H]^-$ could be replaced by a W or Cr atom: ^{1}H NMR spectroscopy showed a statistical distribution of homonuclear to heteronuclear species. Observations of the species generated in THF solution by ^{95}Mo NMR spectroscopy shows that the substitution of W or Cr atoms results in the Mo atom being deshielded. The spectrum for the W case is shown in Fig. 1. The trend is consistent with, but opposite to, the order reported[7] for the hydride chemical shifts.

Acknowledgements—Support of this research via an operating grant from the Natural Sciences and Engineering Research Council of Canada and a University Research Grant from Imperial Oil of Canada to E.C.A. is gratefully acknowledged. A.M. was on leave from Dacca University, Bangladesh.

REFERENCES

1. M. Minelli, J. H. Enemark, R. T. C. Brownlee, M. J. O'Connor and A. G. Wedd, *Coord. Chem. Rev.* (in press).
2. E. C. Alyea and A. Somogyvari, In *Proceedings of the Fourth International Conference on the Chemistry and Uses of Molybdenum* (Edited by H. F. Barry and P. C. H. Mitchell), p. 46. Climax Molybdenum Co., Ann Arbor, MI (1983).
3. E. C. Alyea and A. Somogyvari, *Inorg. Chim. Acta* 1984, **83**, L49.
4. D. J. Darensbourg and A. Rokicki, *Organometallics* 1982, **1**, 1685 (and references cited therein).
5. B. H. Weiller, J.-P. Liu and E. R. Grant, *J. Am. Chem. Soc.* 1985, **107**, 1595.
6. E. C. Alyea, A. Malek and J. Malito, *Inorg. Chim. Acta* 1985, **101**, 147.
7. R. G. Hayter, *J. Am. Chem. Soc.* 1966, **88**, 4376.
8. E. W. Abel, I. S. Butler and J. G. Reid, *J. Chem. Soc.* 1963, 2068.
9. S. Dysart, I. Georgii and B. E. Mann, *J. Organomet. Chem.* 1981, 213, C10.
10. R. G. Kidd, *Annu. Rep. NMR Spectrosc.* 1980, **10**, 1.
11. M. Minelli, J. H. Enemark, K. Wieghardt and M. Hahn, *Inorg. Chem.* 1983, **22**, 3953.
12. E. Lindner and H. Behrens, *Spectrochim. Acta* 1967, **23A**, 3025.
13. H. Werner, W. Beck and H. Engelmann, *Inorg. Chim. Acta* 1969, **3**, 331.
14. A. Wojcicki and M. F. Farona, *Inorg. Chem.* 1968, **7**, 1268.
15. C. S. Kraihanzel and F. A. Cotton, *Inorg. Chem.* 1963, **2**, 533.
16. A. F. Masters, G. E. Bossard, T. A. George, R. T. C. Brownlee, M. J. O'Connor and A. G. Wedd, *Inorg. Chem.* 1983, **22**, 908.
17. S. Attali, R. Mathieu and G. J. Leigh, *J. Mol. Catal.* 1982, **14**, 293.

Polyhedron Vol. 5, No. 1/2, pp. 407–413, 1986
Printed in Great Britain

0277–5387/86 $3.00 + .00
© 1986 Pergamon Press Ltd

APPLICATIONS OF ^{95}Mo NMR TO INORGANIC AND BIOINORGANIC CHEMISTRY

CHARLES G. YOUNG, MARTIN MINELLI and JOHN H. ENEMARK*

Department of Chemistry, University of Arizona, Tucson, AZ 85721, U.S.A.

GARY MIESSLER

Department of Chemistry, St. Olaf College, Northfield, MN 55057, U.S.A.

and

NORBERT JANIETZ, HEIKE KAUERMANN and JOACHIM WACHTER

Institut für Anorganische Chemie, Universität Regensburg, Universitätsstrasse 31, D-8400 Regensburg, F.R.G.

(*Received in revised form* 22 *July* 1985)

Abstract—A variety of dinuclear Mo(V), Mo(IV), Mo(III) and Mo(I) complexes, and tri- and tetranuclear homo- and heterometallic complexes of molybdenum have been studied by ^{95}Mo NMR. The Mo(V) complexes, $Cp'_2Mo_2Y_2(\mu\text{-}X)_2$ (Y = O or S, X = S or Se, Cp′ = η^5-C_5Me_5), exhibit resonances in the −93 to 478 ppm region, the chemical shifts being sensitive to changes in the oxygen, sulfur and selenium content of the coordination spheres. The Mo(IV) complexes, $Cp'_2Mo_2(\mu\text{-}X)_2(\mu\text{-}X_2)$ (X = S or Se), and their derivatives exhibit resonances in the 382–790 ppm region: isomers of $Cp'_2Mo_2(\mu\text{-}S)_2(\mu\text{-}SH)_2$ which differ in the arrangement of the bridging ligands were also detected. Dinuclear Mo(III) complexes of the form Mo_2L_6 (L = amido, alkoxy or alkyl ligand) exhibit very deshielded resonances (2430–3624 ppm). The complexes $Cp_2Mo_2\{\mu\text{-}S_2C_2(CF_3)_2\}_2$ and $Cp_2Mo_2(CO)_2\{\mu\text{-}S_2C_2(CF_3)_2\}_2$ (Cp = η^5-C_5H_5) exhibit resonances consistent with their formulation as distinct Mo(III) and mixed-valence Mo(IV–II) complexes, respectively. The Mo(I) complexes exhibit resonances which are very sensitive to the bond order of the Mo–Mo bond: the resonances of the $L_2Mo_2(CO)_6$ complexes (L = Cp, −1856 ppm; L = Cp′, −1701 ppm) are more than 1800 ppm more shielded than the triply metal–metal bonded complexes, $L_2Mo_2(CO)_4$ (L = Cp, 182 ppm; L = Cp′, 133 ppm). The molybdenum containing homo- and heterometallic complexes exhibit resonances in the −133 to −1619 ppm region. The Fe_2Mo_2 cubane complex, $Cp'_2Mo_2Fe_2(\mu_3\text{-}S)_4(CO)_4$, exhibits a resonance at −506 ppm. The ease of observation of the sulfurized complexes suggests that ^{95}Mo NMR may be a valuable technique for the study of hydrodesulfurization processes.

In recent years the characterization of coordination and organometallic complexes of molybdenum by ^{95}Mo NMR spectroscopy has developed rapidly. In general, the measurement of the spectra of Mo(VI), Mo(II) and Mo(0) complexes has become routine, and the chemical-shift ranges and halogen dependencies of such complexes are well-defined.[1] For these oxidation states the ability of ^{95}Mo NMR to monitor solution processes,[2,3] to distinguish diastereomers[4–6] and to aid solid–solution structure correlations[7] has also been demonstrated.

In contrast, the study of Mo(V), Mo(IV), Mo(III) and Mo(I) complexes has been limited or nonexistent. ^{95}Mo NMR investigations of Mo(V),

* Author to whom correspondence should be addressed.

Mo(III) and Mo(I) complexes are restricted to spin-paired $(Mo_2)_n$ species possessing the diamagnetism necessary for NMR observation. Mo(V) complexes possessing *syn*- and *anti*-$[Mo_2O_2(\mu\text{-}X)_2]^{2+}$ (X = O or S) structural cores exhibit resonances in the 320–982-ppm region,[3,8] the chemical shifts being sensitive to changes in the stereochemistry of the core, e.g. *syn*- and *anti*-$[Mo_2O_4L_2]^{2+}$ (L = 1,4,7-triazacyclononane) exhibit resonances at 586 and 342 ppm, respectively.[3] Dinuclear Mo(IV) complexes have not been studied by ^{95}Mo NMR, although an extensive study of complexes possessing the $[Mo_3O_4]^{4+}$ core has been reported.[8,9] Our recent investigation of mononuclear oxo-Mo(IV) complexes by ^{95}Mo NMR[10] has established an enormous range of chemical shifts (3180 to −1309[11] ppm)* and linewidths (80[11] to >5000 Hz) for mononuclear Mo(IV) complexes. To date, complexes of Mo(III) have not been studied by ^{95}Mo NMR, and only one Mo(I) complex, $Cp_2Mo_2(CO)_6$[12] (hereafter, Cp = η^5-C_5H_5, Cp′ = η^5-C_5Me_5), has been investigated by this technique.

Here we report the ^{95}Mo NMR spectra of 22 dinuclear metal–metal bonded complexes of Mo(V), Mo(IV), Mo(III) and Mo(I). This work describes the first ^{95}Mo NMR data for dinuclear complexes of Mo(IV) and Mo(III) and expands upon the single previous result[12] for Mo(I). In addition, preliminary studies on several homo- and heterometallic molybdenum cluster compounds are presented. The compounds investigated are relevant to studies involving hydrodesulfurization and bioinorganic catalysis.

EXPERIMENTAL

Sample preparation

The complexes were prepared by literature methods or slight modifications thereof: a guide to the source of each complex is given in Table 1. Solutions of air-sensitive samples were prepared under anaerobic conditions using dried and deoxygenated solvents. Concentrations in the range 3–100 mM were employed.

Instrumentation

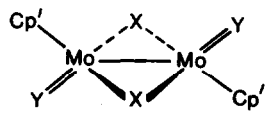
The ^{95}Mo NMR spectra were recorded on a Bruker WM250 spectrometer equipped with a 10-mm molybdenum probe and operating at 16.3 MHz. To reduce the effects of probe ringing[1] a Doty Scientific duplexer and pre-amplifier with a 16 MHz center was inserted between the probe and the Bruker broadband pre-amplifier. The duplexer was gated off during the pulse and for 5 μs thereafter. With this arrangement the pre-acquisition delay was reduced to 100 μs. The transmitter output was amplified with a Heathkit SB-201 (1-kW) linear amplifier. The input was attenuated to give a 26-μs 90° pulse. A 2 M $Na_2[MoO_4]$ solution in D_2O, effective pH 11, was used as external reference.

RESULTS AND DISCUSSION

The ^{95}Mo NMR data are summarized in Table 1, along with a guide to the structure and source of each complex. Structural formulae for the complexes are given in the appropriate sections.

Mo(V) complexes

Singly metal–metal bonded dinuclear Mo(V) complexes possessing the *anti*-$[Mo_2Y_2(\mu\text{-}X)_2]^{2+}$ core[13,14] exhibit resonances in the −93 to 478 ppm region. With the exception of $Cp'_2Mo_2S_2(\mu\text{-}S)_2$ (**2**),[14] these complexes are more shielded than previously



X=S, Y=O (**1**)
X=S, Y=S (**2**)
X=Se, Y=O (**3**)

studied dinuclear Mo(V) analogues.[3,8] The oxo complex, $Cp'_2Mo_2O_2(\mu\text{-}S)_2$ (**1**),[14] exhibits the most shielded resonance of the series at −93 ppm. Considerable deshielding of the ^{95}Mo nuclei occurs upon replacement of the Mo=O_t (t = terminal) groups of **1** by Mo=S_t: the resonance of **2** (478 ppm) is deshielded by 571 ppm compared to the oxo complex **1**. The deshielding influence of the Mo=S_t group has been previously observed in complexes such as $[MoX_4]^{2-}$[15] and $MoX_2(R_2NO)_2^2$ (X = O or S): for these types of complexes, conversion of each Mo=O_t group to Mo=S_t results in a deshielding of *ca* 500 and 700 ppm, respectively. Similarly, a deshielding of *ca* 320 ppm results upon successive replacement of Mo=S_t groups by Mo=Se_t groups.[2,15(b)] However, comparison of **1** and $Cp'_2Mo_2O_2(\mu\text{-}Se)_2$ (**3**) reveals that replacement of the μ-S ligands by μ-Se ligands deshields the ^{95}Mo nuclei by only *ca* 230 ppm. A reduced deshielding effect of 203 ppm has also been observed upon replacement of the μ-O ligands of $[Mo_2O_4(\text{L-cysteinate})_2]^{2-}$ by μ-S ligands.[8] These trends show that the substitution of bridging vs terminal atoms can be readily distinguished by ^{95}Mo NMR.

* The values given in Ref. 11 are for $[Mo(CN)_8]^{4-}$.

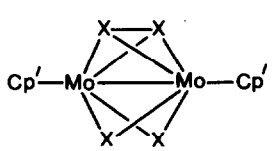
Table 1. ^{95}Mo NMR data[a]

Complex	Chemical shift (ppm)	Linewidth (Hz)	Reference (synthesis)
Mo(V)			
$Cp'_2Mo_2O_2(\mu\text{-}S)_2$ (1)	−93	90	14
$Cp'_2Mo_2S_2(\mu\text{-}S)_2$ (2)	478	260	14
$Cp'_2Mo_2O_2(\mu\text{-}Se)_2$ (3)	131	90	17
Mo(IV)			
$Cp'_2Mo_2(\mu\text{-}S)_2(\mu\text{-}S_2)$ (4)	440	110	16
$Cp'_2Mo_2(\mu\text{-}Se)_2(\mu\text{-}Se_2)$ (5)	770	110	17
$Cp'_2Mo_2(\mu\text{-}S)_2(\mu\text{-}SH)_2$ (6)	714, 728	40, 50 (2:1)	18
$Cp'_2Mo_2(\mu\text{-}S)_2(\mu\text{-}SMe)_2$ (7)	790	70	20
$[Cp'_2Mo_2(\mu\text{-}S)(\mu\text{-}SMe)(\mu\text{-}S_2)]I$ (8)	382	110	18
$Cp'_2Mo_2S_2(\mu\text{-}S_2)$ (9)	756	20	16
$Cp'_2Mo_2OS(\mu\text{-}S_2)$ (10)	−54, 699	100, 100	16
Mo(III)[b]			
$Mo_2(NMe_2)_6$ (11)	2430	1320	21
$Mo_2(OCHMe_2)_6$ (12)	2444	350	22
$Mo_2(OCH_2CMe_3)_6$ (13)	2447	600	22
$Mo_2(OCMe_3)_6$ (14)	2645	120	22
$Mo_2(CH_2SiMe_3)_6$ (15)	3624	500	23
$Cp_2Mo_2\{\mu\text{-}S_2C_2(CF_3)_2\}_2$ (16)	2301	37	25
$Cp_2Mo_2(CO)_2\{\mu\text{-}S_2C_2(CF_3)_2\}_2$ (17)	−789	190	25
Mo(I)			
$Cp_2Mo_2(CO)_6$ (18)	−1856	180	28, 29
$Cp'_2Mo_2(CO)_6$ (19)	−1701	180	29
$Cp_2Mo_2(CO)_4$ (20)	182	160	28
$Cp'_2Mo_2(CO)_4$ (21)	133	150	31
$Cp'_2Mo_2(CO)_3\{P(OMe)_3\}$ (22)[c]	d 373, J = 416 Hz	150	32
	s 154	150	
"Cubanes"			
$Cp'_2Mo_4(\mu_3\text{-}S)_4(CO)_6$ (23)	−558, −1256	15, 74	33
$Cp'_2Mo_2Cr_2(\mu_3\text{-}S)_3(\mu_3\text{-}O)(CO)_6$ (24)	−265, −471	20, 20	20
$Cp_2Cp'_2Mo_4(\mu_3\text{-}S)_4$ (25)	−1444, −1619	64, 230	34
$Cp'_2Mo_2Fe_2(\mu_3\text{-}S)_4(CO)_4$ (26)	−506	25	33
$Cp'_2Mo_2(\mu_2\text{-}S_2CO)(\mu_3\text{-}S)_2Fe(CO)_2$ (27)	−133	70	33

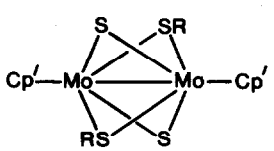
[a] At ambient temperature in CH_2Cl_2 solvent unless otherwise specified.
[b] All Mo(III) complexes, except **16** and **17**, were studied in toluene.
[c] d = doublet, s = singlet.

Mo(IV) complexes

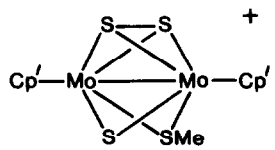
The $Cp'_2Mo_2(\mu\text{-}S)_2(\mu\text{-}S_2)$ complex (**4**)[16] exhibits a resonance at 440 ppm whereas the selenium analogue, $Cp'_2Mo_2(\mu\text{-}Se)_2(\mu\text{-}Se_2)$ (**5**),[17] exhibits a relatively deshielded resonance at 770 ppm. The 330-ppm deshielding observed upon complete replacement of μ-S ligands by μ-Se ligands is also small compared to that expected for the exchange of a similar number and type of terminal ligands (cf. **1** and **3**). Hydrogenation of **4** results in an isomeric mixture of **6**,[18] which exhibits two resonances at 714 and 728 ppm. This is consistent with the previous detection, by ^{1}H NMR, of two isomers in the analogous



X=S (**4**) or Se (**5**)

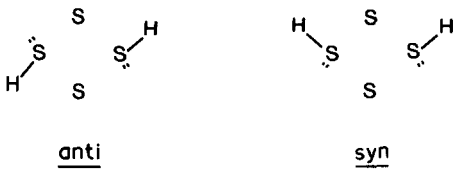


R=H (**6**) or Me (**7**)



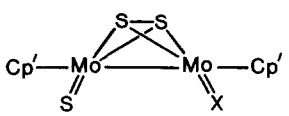
8

$(MeCp)_2Mo_2(\mu\text{-}S)_2(\mu\text{-}SH)_2$ complex.[19] For the *trans* isomer[19] two arrangements of the bridging SH ligands are possible (*anti* and *syn* below). The bis-μ-



methylthiolate complex (**7**), having a chemical shift of 790 ppm, has been crystallographically characterized as the *anti* isomer.[20] The reaction of **4** with methyl iodide results in the methylation of one μ-S group:[18] the resulting cationic complex, **8**, exhibits a slightly shielded resonance at 382 ppm. The chemical shifts of **6** and **7** reflect the opening of the $\mu\text{-}S_2^{2-}$ ligand to form two deshielding $\mu\text{-}S^{2-}$ ligands.

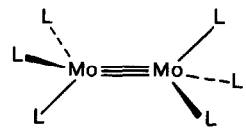
Complex **4** is converted, at 45°C in toluene, to $Cp'_2Mo_2S_2(\mu\text{-}S_2)$ (**9**):[16] the transformation of the



two $\mu\text{-}S^{2-}$ ligands into two terminal S^{2-} ligands leads to a deshielding of the ^{95}Mo nuclei and the observation of a resonance at 756 ppm for **9**. A by-product of this reaction, the unsymmetrical complex $Cp'_2Mo_2OS(\mu\text{-}S_2)$ (**10**),[16] provides a nice example of the deshielding influence of the Mo=S_t group relative to Mo=O_t. For **10**, the two resonances at −54 and 699 ppm may be readily assigned to the Mo=O_t and Mo=S_t centers, respectively. The 753-ppm shielding difference observed here is similar in magnitude to that observed elsewhere.[2]

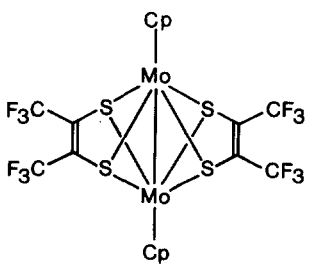
Mo(III) complexes

A wide variety of diamagnetic Mo(III) dimers having general formulae Mo_2L_6 ($L = NR_2^-, OR^-$ or R^-) have been reported by Chisholm[21,22] and Wilkinson:[23] we have initiated a study of these complexes, their derivatives and their tungsten analogues. The complexes Mo_2L_6 [$L = NMe_2^-$ (**11**), $OCHMe_2^-$ (**12**), $OCH_2CMe_3^-$ (**13**), $OCMe_3^-$ (**14**) or $CH_2SiMe_3^-$ (**15**)] exhibit resonances over the chemical-shift range 2430–3624 ppm, a very deshielded portion of the known chemical-shift

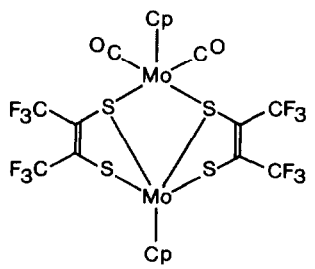


range.[1] Only one other class of metal–metal-bonded complex, quadruply bonded Mo(II) dimers, possesses more deshielded resonances (3227–4148 ppm).[1] The shielding of the ^{95}Mo nuclei increases in the order alkyl < 3°-alkoxide < 1°- and 2°-alkoxide < dialkylamide. The *N*- and *O*-donor ligand complexes exhibit a narrow range of chemical shifts while the chemical shift of the silyl derivative **15**[23] is quite disparate.* Accounting for such observations will provide a critical test for developing theoretical treatments of ^{95}Mo chemical-shift data. The linewidths of the Mo(III) resonances range from 120 to 1320 Hz, contrasting with the generally broad resonances of Mo(II) dimers.[1]

The μ-dithiolene complexes **16** and **17** exhibit readily observable resonances. The singly metal–metal bonded **16** [Mo—Mo = 2.584(1) Å[25]]



16



17

exhibits a deshielded resonance at 2301 ppm ($W_{1/2}$ = 37 Hz). The relatively shielded position compared to the triply metal–metal bonded M_2L_6 complexes is consistent with a similar trend found in the Mo(I)

* The similarly disparate ^{183}W NMR chemical shifts of $W(CXMe_3)(CH_2XMe_3)_3$ (X = C, 2867 ppm; X = Si, 3613 ppm) support a general deshielding influence for β-Si substitution.[24]

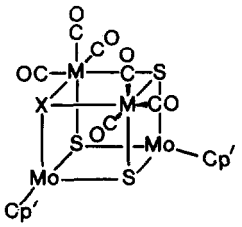
complexes below. A structure determination of **17** revealed two distinctly different molybdenum environments and a Mo... Mo interatomic distance of 3.256(1) Å,[25] indicative of a localized Class I mixed-valence complex in the Robin and Day classification.[26] The ^{95}Mo NMR spectrum of **17** is consistent with this formulation as only one peak at −789 ppm is observed. This peak is likely to be due to the $CpMo(II)(CO)_2$ moiety, while that due to the Mo(IV) fragment remains unobserved due to its rapid relaxation time.[10] Supporting this contention, the complexes

$$CpMo(CO)_2(S_2CNEt_2),\ CpMo(CO)_2(S_2COEt)$$

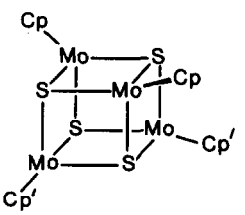
and

$$CpMo(CO)_2\{C(CF_3)=C(CF_3)C(O)SMe\}$$

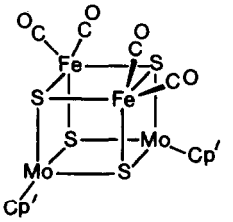
resonate at −544, −559 and −845 ppm, respectively.[27]



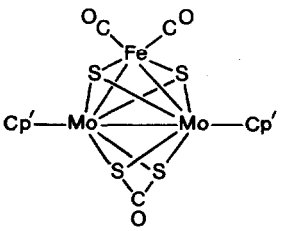
M=Mo, X=S (**23**)
M=Cr, X=O (**24**)



25



26



27

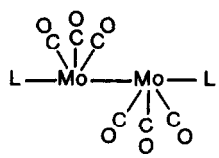
Homo- and heterometallic cubanes and related complexes

We have recently undertaken an NMR investigation of new homo- and heterometallic complexes of molybdenum and catalytically or biologically relevant co-metals such as cobalt, nickel (hydrodesulfurization) and iron (nitrogenase). Complexes **23**–**27** exhibit narrow, readily observable ^{95}Mo NMR resonances in the shielded portion of the chemical-shift range. Complexes **23**–**25** possess two environments for molybdenum and each exhibits two resonances of equal intensity: these have been assigned as described below. The shielded resonances of other carbonylmolybdenum(0) complexes[1] permits the assignment of the −1256 ppm resonance

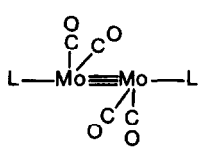
Mo(I) complexes

To date, the ^{95}Mo NMR spectrum of only one Mo(I) complex has been reported: the metal–metal singly bonded species $Cp_2Mo_2(CO)_6$ (**18**) exhibits a relatively shielded resonance at −1856 ppm.[12] In a similar spectral region, we have observed the resonance of $Cp'_2Mo_2(CO)_6$ (**19**)[29] at −1701 ppm. Remarkably, the metal–metal triply bonded complexes, **20** and **21**, exhibit resonances which are deshielded by over 1800 ppm compared to **18** and **19**: the tetracarbonyl complexes, **20**[28] and **21**,[30,31] exhibit resonances at 182 and 133 ppm, respectively. We have also studied the unsymmetrical triply bonded complex **22**,[32] which exhibits two resonances, a doublet (J_{Mo-P} = 412 Hz) at 373 ppm and a singlet at 154 ppm. The J value is *ca* 120 Hz higher than any previously observed value:[1] coupling of the ^{31}P nucleus to both Mo nuclei was not discerned.

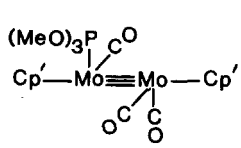
of **23**[33] to the $Mo(CO)_3$ moieties of this complex. The resonance at −558 ppm is therefore due to the Cp'Mo moieties. The μ_3-O ligand in **24**[20] is expected to shield the Mo center to which it is bound (relative to μ_3-S) and thus the −265 and −471 ppm resonances of this complex are assigned to μ_3-S-Mo and μ_3-O-Mo centers, respectively (compare **9** and **10**). The presence of a *ca* −500 ppm resonance attributable to μ_3-S-coordinated Mo in complexes **23** and **26** raises the possibility that the −471-ppm resonance of **24** is due to the μ_3-S-coordinated Mo center. This latter assignment is contrary to all previously observed shielding trends for $Mo{=}X_t$ and μ-X (X = O or S) ligand complexes[2,8,15] and, therefore, seems unlikely. Definitive assignment of the resonances of **24** awaits data for complexes such as $Cp'_2Mo_2Cr_2(\mu_3\text{-}X)_4(CO)_6$ (X = O or S). A



L=Cp (**18**) or Cp' (**19**)



L=Cp (**20**) or Cp' (**21**)



22

shielding effect of Cp relative to Cp′ is observed in resonances in the shielded portion of the chemical shift range (e.g. **18** and **19**) and on this basis the resonances of **25**[34] at −1444 and −1619 ppm are ascribed to Cp′- and Cp-bearing Mo atoms, respectively.

The paramagnetism of most Fe–Mo–S cubane and double-cubane cluster complexes has prevented their study by ^{95}Mo NMR. The diamagnetism of Fe–Mo–S clusters derived from **4** and $Fe_2(CO)_9$ make them attractive candidates for assessing the NMR properties of more biologically pertinent centers. Complex **26**[33] exhibits a single sharp resonance at −506 ppm, 946 ppm more shielded than the precursor **4**. The data for **26** provide evidence that μ_3-S ligands shield the molybdenum nuclei compared to μ-S and S_t ligands. The resonance of **27**[33] at −133 ppm is also shielded due to conversion of the μ-S ligands into μ_3-S ligands.

CONCLUSION

The ability of terminal X^{2-} (X = O or S) ligands to effect predictable changes in the chemical shifts of ^{95}Mo NMR resonances has been confirmed in this study. Moreover, new deshielding trends may be discerned from the data presented herein, e.g. the deshielding ability of bridging ligands involved in this study increase in the order μ-S_2^{2-} < μ-SH < μ-SMe < μ-S < μ-Se and μ_3-O < μ_3-S.

There also appears to be a deshielding effect upon increasing the bond order of the metal–metal bond. While changes in the coordination sphere accompany such reactions, the concomitant change in chemical shift is often not accounted for by these changes alone. The most dramatic example of this effect involves the pairs **18–20** and **19–21** where singly and triply bonded species differ in chemical shift by over 1800 ppm.

The ready detection and differentiation of sulfidomolybdenum complexes by ^{95}Mo NMR provides encouragement for the application of this technique to the study of hydrodesulfurization catalysis. The hydrodesulfurization reaction is an important catalytic process for the purification of petroleum products.[35] The reaction, exemplified by the equation below, involves the

$$RSH + H_2 \rightarrow RH + H_2S$$

hydrogenolysis of organosulfur compounds, and is most often effected by heterogeneous catalysts containing sulfided Mo and Co species supported on alumina. Both metal and sulfide ions have been proposed as active sites in the hydrodesulfurization reaction: the ability of sulfide ligands to react with hydrogen and other small molecules is exemplified by complexes such as **6–8** and **26** and **27**. Species such as **6–8** are important model complexes for reactivity and mechanistic studies of hydrodesulfurization.[19] Due to their narrow linewidths, the resonances of these species are readily detected even at concentrations of ^{95}Mo as low as 0.5 mM. Thus ^{95}Mo NMR may prove valuable in the characterization of solution species and intermediates, and for monitoring the course of homogeneous hydrodesulfurization systems.

Acknowledgements—We thank the U.S. Department of Agriculture for support of this work through grant No. 84-CRCR-1-1416, Dr K. A. Christensen for his technical assistance with the NMR spectrometer, and Dr E. M. Kober for helpful discussions.

REFERENCES

1. M. Minelli, J. H. Enemark, R. T. C. Brownlee, M. J. O'Connor and A. G. Wedd, *Coord. Chem. Rev.* (in press).
2. M. Minelli, J. H. Enemark, K. Wieghardt and M. Hahn, *Inorg. Chem.* 1983, **22**, 3952.
3. K. Wieghardt, M. Guttmann, P. Chaudhuri, W. Gebert, M. Minelli, C. G. Young and J. H. Enemark, *Inorg. Chem.* 1985, **24**, 3151.
4. (a) M. Minelli, T. W. Rockway, J. H. Enemark, H. Brunner and M. Muschiol, *J. Organomet. Chem.* 1981, **217**, C34; (b) H. Brunner, P. Beier, E. Frauendorfer, M. Muschiol, D. K. Rastogi, J. Wachter, M. Minelli and J. H. Enemark, *Inorg. Chim. Acta A* 1985, **96**, L5.
5. I. Buchanan, M. Minelli, M. T. Ashby, T. J. King, J. H. Enemark and C. D. Garner, *Inorg. Chem.* 1984, **23**, 495.
6. I. Buchanan, C. D. Garner and W. Clegg, *J. Chem. Soc., Dalton Trans.* 1984, 1333.
7. M. Minelli, J. H. Enemark, J. R. Nicholson and C. D. Garner, *Inorg. Chem.* 1984, **23**, 4384.
8. S. F. Gheller, T. W. Hambley, R. T. C. Brownlee, M. J. O'Connor, M. R. Snow and A. G. Wedd, *J. Am. Chem. Soc.* 1983, **105**, 1527.
9. S. F. Gheller, R. T. C. Brownlee, M. J. O'Connor and A. G. Wedd, In *Proceedings of the Fourth International Conference on the Chemistry and Uses of Molybdenum* (Edited by H. F. Barry and P. C. H. Mitchell), p. 67. Climax Molybdenum Co., Ann Arbor, MI (1982).
10. C. G. Young and J. H. Enemark, *Inorg. Chem.* (in press).
11. O. Lutz, A. Nolle and P. Kroneck, *Z. Naturforsch.* 1976, **31A**, 454.
12. S. Dysart, I. Georgii and B. E. Mann, *J. Organomet. Chem.* 1981, **213**, C10.
13. W. Danzer, W. P. Fehlhammer, A. T. Liu, G. Thiel and W. Beck, *Chem. Ber.* 1982, **115**, 1682.
14. M. Rakowski DuBois, D. L. DuBois, M. C. VanDerveer and R. C. Haltiwanger, *Inorg. Chem.* 1981, **20**, 3064.
15. (a) O. Lutz, A. Nolle and P. Kroneck, *Z. Naturforsch.*

1977, **32A**, 505; (b) S. F. Gheller, P. A. Gazzana, A. F. Masters, R. T. C. Brownlee, M. J. O'Connor, A. G. Wedd, J. R. Rodgers and M. R. Snow, *Inorg. Chim. Acta* 1981, **54**, L131.
16. H. Brunner, W. Meier, J. Wachter, E. Guggolz, T. Zahn and M. L. Ziegler, *Organometallics* 1982, **1**, 1107.
17. H. Brunner, J. Wachter and H. Wintergerst, *J. Organomet. Chem.* 1982, **235**, 77.
18. H. Brunner, H. Kauermann, W. Meier and J. Wachter, *J. Organomet. Chem.* 1984, **263**, 183.
19. M. Rakowski DuBois, M. C. VanDerveer, D. L. DuBois, R. C. Haltiwanger and W. K. Miller, *J. Am. Chem. Soc.* 1980, **102**, 7456.
20. J. Wachter, unpublished results.
21. M. H. Chisholm, F. A. Cotton, B. A. Frenz, W. W. Reichert, L. W. Shive and R. B. Stults, *J. Am. Chem. Soc.* 1976, **98**, 4469.
22. M. H. Chisholm, F. A. Cotton, C. A. Murillo and W. W. Reichert, *Inorg. Chem.* 1977, **16**, 1801.
23. W. Mowat, A. Shortland, G. Yagupsky, N. J. Hill, M. Yagupsky and G. Wilkinson, *J. Chem. Soc., Dalton Trans.* 1972, 533.
24. C. G. Young, E. M. Kober and J. H. Enemark, unpublished results.
25. G. Miessler, manuscript in prepration.
26. M. B. Robin and P. Day, *Adv. Inorg. Chem. Radiochem.* 1967, **10**, 247.
27. J. Y. LeGall, M. M. Kubicki and F. Y. Petillon, *J. Organomet. Chem.* 1981, **221**, 287.
28. R. J. Klinger, W. Butler and M. D. Curtis, *J. Am. Chem. Soc.* 1975, **97**, 3535 (and references therein).
29. D. S. Ginley and M. S. Wrighton, *J. Am. Chem. Soc.* 1975, **97**, 3533.
30. R. B. King and A. Efraty, *J. Am. Chem. Soc.* 1972, **94**, 3773.
31. R. B. King, M. Z. Iqbal and A. D. King, Jr, *J. Organomet. Chem.* 1979, **171**, 53.
32. J. G. Riess, U. Klement and J. Wachter, *J. Organomet. Chem.* 1985, **280**, 215.
33. H. Brunner, N. Janietz, J. Wachter, T. Zahn and M. L. Ziegler, *Angew. Chem., Int. Ed. Engl.* 1985, **24**, 133.
34. H. Brunner, H. Kauermann and J. Wachter, *J. Organomet. Chem.* 1984, **265**, 189.
35. F. E. Massoth, *Adv. Catal.* 1978, **27**, 265.

Polyhedron Vol. 5, No. 1/2, pp. 415–421, 1986
Printed in Great Britain

0277–5387/86 $3.00 + .00
© 1986 Pergamon Press Ltd

PATTERNS OF ^{95}Mo SHIELDING IN ORGANOMETALLIC AND INORGANIC CHEMISTRY

RUTH A. GRIEVES and JOAN MASON*

Department of Chemistry, The Open University, Milton Keynes MK7 6AA, U.K.

(*Received* 2 *July* 1985)

Abstract—Reasonable ^{95}Mo NMR properties, a good shift dispersion, centrality in the Periodic Table, the great variety of organometallic and inorganic bond types, and comparisons with (electronic) excitation energies and ionization energies, allow in-depth examination of the determinants of the metal nuclear shielding. Exceptions to the normal correlation of decrease in shielding with increase in oxidation number are found at the top of the shielding range {for Mo(VI) in $[MoCp_2H_3]^+$} and at the bottom end [for Mo(II) in quadruply-bonded dimers with axial ligands]. The decrease in shielding with increase in bond order, Mo—Mo > Mo=Mo > Mo≡Mo > Mo≣Mo, contrasts with the sequence C—C < C≡C < C=C in carbon resonance. All these exceptions, however, prove the "spectrochemical" rule of decrease in shielding with decrease in ligand field splitting, with dependence also on nephelauxetic effects. Various sequences of ligand dependence of the ^{95}Mo shift show that nephelauxetic effects may reinforce or oppose spectrochemical influences, both in inorganic compounds (in which the two influences have differing periodicities) and in organometallic compounds.

^{95}Mo has a reasonable natural abundance (15.7%), NMR receptivity (better than for ^{13}C) and quadrupole moment (-0.019×10^{-28} m^2, similar to that for ^{14}N). Only in viscous solutions, large molecules, or unusually unsymmetrical electronic environments (as in some Mo≣Mo compounds), are the lines uncomfortably broad, and a sizeable ^{95}Mo literature has developed within the last 5 years.[1] By comparison ^{183}W, although a spin-$\frac{1}{2}$ nucleus, has a sufficiently low magnetogyric ratio that the lower sensitivity and working frequencies (with attendant problems of probe ringing) have tended to limit NMR studies.[1] We have observed a shift range of 7250 ppm for molybdenum, interestingly with high oxidation numbers at both extremes (as also for ^{183}W, with a shift range of 11,000 ppm[1]). Because of the large shift dispersion, NMR spectroscopy of the metal nucleus can be helpful in preparative and mechanistic work, and the shift relationships contain particularly interesting information on spectrochemical and nephelauxetic effects of the ligands.

RESULTS

Patterns of ^{95}Mo *shielding*

High shielding is often associated conceptually with low oxidation numbers and negative charge, probably as a lingering influence of proton (and ^{13}C) NMR spectroscopy. In fact we have observed the highest recorded ^{95}Mo shielding for the bent sandwich hydride $[MoCp_2H_3]^+$,† in which the metal is Mo(VI), formally d^0, and the complex is positively charged. Somewhat lower shielding is observed for the dihydride $[MoCp_2H_2]$ containing Mo(IV), formally d^2 (cf. Table 1); similarly the highest ^{183}W shielding so far has been observed for $[WCp_2H_2]$.[2] It is a general observation that the effect on the transition-metal nucleus shielding of a small difference in charge on the complex as a whole is relatively small.

As to the overall pattern, high ^{95}Mo shielding is

* Author to whom correspondence should be addressed at: 152 Castelnau, London SW13 9ET, U.K.

† Cp, (η^5-C_5H_5); CpR, (η^5-C_5H_4R); Bz, (η^6-C_6H_6).

Table 1. ^{95}Mo chemical shifts in bent sandwich complexes

Compound	Solvent	$\delta(^{95}Mo)^a$ (ppm)	$W_{1/2}{}^b$ (Hz)
$[MoCp_2H_3]Cl$	Dilute HCl(aq)	−2953	300
$[MoCp_2H_2]$	Toluene	−2507	300
$[MoBzCp(PMe_3)]PF_6$	Acetone	−2170	350
$[MoCp_2CO]$	thf	−1964	150
$[MoBz(Pr^iCp)(MeCN)]BF_4$	Acetone	−1805	550
[MoBzCpCl]	Toluene	−1750	Broad

[a] Relative to 1 M Na_2MoO_4(aq) at pH 11.
[b] Linewidth at half-height (not optimized).

observed[1,3] in piano-stool compounds, complexes with strong ligands such as CO, phosphite, phosphine etc., and sandwich compounds. The shielding then decreases in the ligand sequence[4] $CN^- > N_2 > NO^+ > NNR^+$ (diazenido)[5] > NNR_2^{2-} (hydrazido)[5] > O-ligands > S-ligands (thiolate-bridged dimers,[6] thiomolybdates etc.) > Se ligands etc.[1] In the polyhapto ring compounds (piano-stool or sandwich) the shielding decreases with increase in ring size, with ring alkylation, and from closed to open π systems of the same hapticity.[7] In Mo–Mo bonded compounds, like ligands being compared, the ^{95}Mo shielding decreases in the sequence Mo—Mo > Mo=Mo > Mo≡Mo > Mo≡Mo (Table 4), in contrast to the well-known C—C > C≡C > C=C sequence in carbon shielding.

The very lowest metal shielding has been observed for the quadruply bonded carboxylate dimers, $[M_2(O_2CR)_4]$, for both molybdenum[8] and tungsten.[9] In ^{95}Mo resonance we have found that attachment of an axial ligand such as pyridine to molybdenum in $[Mo_2(O_2CCF_3)_4]$ decreases the shielding further, whereas in quadruply-bonded compounds of molybdenum with phosphine and halide ligands the ^{95}Mo shielding is several hundred ppm greater than in the carboxylates, as shown in Tables 2 and 3.

Table 2. ^{95}Mo and other spectroscopic observations for Mo≡Mo-bonded compounds with phosphine and halide ligands

					UV–vis[e]		IE (eV)			
Compound	Solvent[a]	$\delta(^{95}Mo)^b$ (ppm)	$W_{1/2}{}^c$ (Hz)	$\delta(^{31}P)^d$ (ppm)	λ_{max} (nm)	$10^{-3}\,\varepsilon_{max}$ ($M^{-1}\,cm^{-1}$)	δ	π		Reference
$[Mo_2I_4(PMe_3)_4]$	Toluene	2927	850	−15.3	614	3.5	Decomp.			
					508	0.24				
					397	4.1				
$[Mo_2Br_4(PMe_3)_4]$	thf	2996	800	−11.6	595	3.6	6.6	7.8		[f]
	Toluene	3008	840		463	0.22				
					346	4.0				
$[Mo_2Cl_4(PMe_3)_4]$	Toluene	3008	800	−9.4	583	3.4	6.44	7.70	8.41	[g]
	thf	3021	800		441	0.22			9.98	
					328	3.9				
$[Mo_2Cl_4(dmpe)_2]$	Toluene	n.o.[h]								

[a] Toluene solvent contains 10% (v/v) C_6D_6, thf solvent contains 10% (v/v) $(CD_3)_2CO$.
[bc] As [ab] in Table 1.
[d] Relative to 85% H_3PO_4.
[e] Benzene solvent.[28]
[f] Measured by A. W. Potts.
[g] Reference 29.
[h] Not observed.

Table 3. ^{95}Mo and other spectroscopic observations for Mo≡Mo-bonded compounds with μ_2-carboxylate ligands

Compound	Solvent	$\delta(^{95}Mo)^a$ (ppm)	$W_{1/2}{}^b$ (Hz)	UV–vis λ_{max} (nm)	UV–vis $10^{-3}\,\varepsilon_{max}$ ($M^{-1}\,cm^{-1}$)	UV–vis Reference (UV)	IE^c (eV) δ	IE^c (eV) π	IE^c (eV)
$[Mo_2(O_2CBu^t)_4]$	thf[d]	3667	870	434	0.136	[e]	6.75	8.54	10.22
				~ 326	sh				10.97
				295	10				11.61
$[Mo_2(O_2CPr^n)_4]$	dmf	3730[f]	1400						
$[Mo_2(O_2CH)_4]$	HCO_2H	3768[g]	670	441	0.1	[h]	7.60	9.37	
				327	sh				
$[Mo_2(O_2CCF_3)_4]$	$CDCl_3$	3874	430	430	0.80		8.67	10.44	12.59
	thf[i]	4021	400						
	thf	4026[j]	250	435	0.170	[e]			
				~ 333	sh				
				306	12.1				
$[Mo_2(O_2CCF_3)_4(py)_2]$	CH_2Cl_2 py	4199	320	504	1.125				

[ab] As in Table 1.
[c] Ref. 30.
[d] Containing 10% (v/v) $(CD_3)_2CO$.
[e] thf solvent.[9(a)]
[f] Determined at 70°C.[8]
[g] Weak signal (low solubility).
[h] Low-temperature glass or thin film.[26]
[i] Containing 10% (v/v) $CDCl_3$.
[j] Determined at 55°C.[8]

DISCUSSION

Spectrochemical and nephelauxetic influences on the metal nucleus shielding

The shielding of the transition-metal nucleus can be related to frontier orbital splittings and to nephelauxetic effects by a ligand field "atom-in-a-molecule" formulation of shielding theory.[10,11] In its simplest form, for comparisons of complexes of the same (high) symmetry:

$$\delta \propto \langle r^{-3} \rangle_d / \Delta E,$$

in which the constant of proportionality subsumes the angular momentum terms which depend on the local electronic symmetry (with unquenching by the magnetic field). The effective excitation energy, ΔE, which is the HOMO–LUMO gap for paramagnetic circulations in the magnetic field, is normally the ligand field splitting, the *d–d* excitations being magnetic dipole allowed. For lower symmetries the imbalance of charge in the valence shell augments paramagnetic circulations (and a summation over two or more terms with appropriate ΔE may be necessary). The radial term $\langle r^{-3} \rangle_d$, the inverse cube of the valence *d*-electron radius, is the one appropriate to a dipolar phenomenon such as magnetism.

Thus the energy term gives a spectrochemical ligand dependence to the metal nucleus shift, and the radial term gives a quasi-nephelauxetic dependence: the deshielding is the greater the smaller the excitation energy, and the closer the paramagnetic circulation to the resonant nucleus.

The high metal shielding observed for the cyclopentadienyl hydrides is clearly related to the very strong ligand field. Particularly interesting is the effect of protonation of $[MoCp_2H_2]$, d^2. This increases the metal shielding by 450 ppm, with removal of the relatively low-energy *d–d* circulation as the *d*-electron lone pair forms a bond to hydrogen (cf. the increase in ^{57}Fe shielding by 1109 ppm from ferrocene to $[FeCp_2H]^+$ in $BF_3 \cdot H_2O$ solvent[12]). The increase in metal shielding may be compared with the increase by 100 ppm or more on protonation of nitrogen in a delocalized system (in pyridine, for example) with removal of the low-energy $n \rightarrow \pi^*$ circulation.[13]

Lower oxidation states. For d^6 octahedral complexes of molybdenum, variation of a ligand Y in $[Mo(CO)_5Y]^q$ complexes[1] produces an approxi-

mate sequence of increase in metal shielding:

$$\text{py} < \text{amines} \sim \text{MeCN} < \text{Cl}^- < \text{S-ligands} \sim \text{Br}^- < \text{I}^- < \text{PPh}_3 < \text{AsPh}_3 < \text{PR}_3 \sim \text{CO} < \text{P(OMe)}_3 \sim \text{SbPh}_3 \quad \text{(range 480 ppm).} \quad (1)$$

{The higher symmetry of $[\text{Mo(CO)}_6]$ influences the position of CO in this series: thus molybdenum is deshielded by 500 ppm in $[\text{Mo}\{\text{P(OMe)}_3\}_6]$[2] relative to $[\text{Mo(CO)}_6]$.} Similarly, comparison of *trans* complexes with a $(\text{dppe})_2$ or related P_4 core produces a sequence:

$$=\text{NNR}_2^{2-} < \text{N}{=}\text{NR}^+ < \text{NO}^+ < \text{N}_2 \lesssim \text{PhCN} < \text{C}_2\text{H}_4 < \text{RNC} < \text{CO} \quad \text{(1600 ppm range).} \quad (2)$$

[Again, effects of symmetry are significant: thus the presence of a chelating phosphine such as dppe may increase the metal shielding by 100–300 ppm relative to corresponding monodentate ligands, in this case $(\text{PPh}_2\text{R})_2$.] For anionic *trans*-ligands in hydrazido(2−), diazenido and nitrosyl phosphine complexes the molybdenum shielding increases as:[5]

$$\text{OPh}^- < \text{Br}^- < \text{SPh}^- \lesssim \text{I}^- < \text{OH}^- < \text{N}_3^- \sim \text{NCO}^- \sim \text{NCS}^- < \text{CN}^- \quad \text{(range 285 ppm).} \quad (3)$$

In piano-stool carbonyl complexes of Mo(II),[14,15] $[\text{MoCp(CO)}_3\text{Y}]$ compounds produce the sequence for the Y ligand:

$$(\text{CMe}{=}\text{CMe}_2)^- < \text{Cl}^- < \text{Br}^- < \text{I}^- < \text{Me}^- < (\text{Hg}/2)^- < \text{MoCp(CO)}_3^- < \text{H}^- < \text{SnMe}_3^- \quad \text{(1240 ppm range)} \quad (4)$$

closely resembling the corresponding series in ^{183}W resonance, with 1640 ppm from Cl^- to SnMe_3^-.[2] If we allow for the deshielding of ^{95}Mo with increase in ring size, and with ring alkylation, the bent sandwich Mo(II) compounds in Table 1 give the series:

$$\text{Cl}^- < \text{MeCN} < \text{CO} < \text{PMe}_3 < \text{H}^- \quad \text{over a 750 ppm range.} \quad (5)$$

In each series the ordering shows an overall resemblance to the spectrochemical series (small ΔE corresponding to low shielding) *insofar as ligating atoms from the same row of the Periodic Table are being compared.* A notable difference from the spectrochemical ordering is the high position of ligands from lower rows of the Periodic Table. The metal shielding increases as Cl < Br < I, P < As < Sb, C ≪ Sn etc. (cf. Kidd's "normal halogen dependence"[16]), sequences related to increase in the radial term $\langle r^{-3}\rangle_d$, and to increase in polarizability and nephelauxetic effects with increase in size of the ligating atom. These relationships have been the subject of long discussion for many transition nuclei, notably ^{59}Co, ^{51}V etc.[10,11,16,17] With the heaviest ligating atoms relativistic (spin-polarization) effects are significant, acting in the same direction as nephelauxetic effects.[11]

Within a series for a particular ligating atom, also, a "spectrochemical" sequence may be evident, such as $\text{PPh}_3 < \text{PR}_3 < \text{P(OR)}_3$ (over a range of 120 ppm) in series (1), with increase in π-acceptor ability. The piano-stool $[\text{MoCp(CO)}_2\text{S}\frown\text{S}]$ compounds,[14] however, follow an opposite sequence, $\text{S}_2\text{P(OEt)}_2^- < \text{S}_2\text{CSEt}^- < \text{S}_2\text{CNR}_2 < \text{S}_2\text{COEt}$ (over a range of 220 ppm), perhaps because of an increase in π-donor ability and nephelauxetic effect. A similar sequence is observed for Mo(0) $[\text{Mo(CO)}_4\text{S}\frown\text{S}]^-$ compounds, though with indications of the opposite sequence in the corresponding pentacarbonyl compounds (both over a smaller range).[18]

It needs to be pointed out that effects of the energy term (ligand field splittings, in the present instance) and of the radial term are likely to reinforce, for comparisons of ligating atoms from the same row of the Periodic Table, although (as is better known) they are in opposition for ligating atoms from different rows. Ligand field splittings depend strongly on the ligating atom, increasing as[19] I < Br < Cl < S < F < O < N < C < H, and Se < S < O (although N < P ~ As, since back-bonding increases the splitting). Nephelauxetism in optical spectroscopy is related to decrease in electron repulsion parameters, corresponding to decrease in $\langle r^{-1}\rangle_d$.[19] It tends to increase (with decrease in electronegativity of the ligand) across the row of the ligating atom as F < O < N < C, but down the group, Cl < Br < I etc. The difference in the two periodicities has been obscured by the historical development of the field.[10] The early reports were of linear δ/λ (*d–d*) relationships, and only subsequently was it discovered that heavier ligands gave lines of decreased slope, corresponding to decrease in $\langle r^{-3}\rangle_d$ terms. In practice the slopes of the lines for ligating atoms from the same row are commonly determined by "spectrochemical" effects reinforced by nephelauxetism.[10,11] Some quantification of nephelauxetic effects on ^{59}Co shielding in terms of electron repulsion parameters has now been initiated.[20]

Polyhapto organo-ligands. It would be particularly helpful if light could be thrown on nephelauxetic and spectrochemical effects of polyhapto organic

ligands, since *d–d* bands in the electronic spectra are frequently masked by strong charge-transfer bands. Tsuchida *et al.*[21] derived the sequence of increase in hypsochromic effect (ligand field strength) Bz < Cp^- < CO from the electronic absorption spectra of chromium complexes (also PhNC < MeNC < CN^- < CO). Comparisons of sandwich or piano-stool complexes with a variety of polyhapto ligands shows that the ^{95}Mo shielding decreases with increase in ring size, with alkylation of the ring, from closed to open π systems (with the same hapticity) and with extension of the π-system.[3,7] Further information is available from comparisons of metal and ligand shielding, excitation and ionization energies, substituent effects etc.[3] In some of these comparisons it seems likely that spectrochemical and nephelauxetic effects may be opposed (even though the ligating atom is carbon in each case). Thus increase in ring size disfavours the forward bonding (as the $2p\pi$ HOMO energies drop below *d*-orbital energies), decreasing the ligand field splitting and the metal shielding. On the other hand, ring enlargement favours the back-bonding (as the $2p\pi^*$ LUMO energies approach the *d*-orbital energies) with increased nephelauxetic effect.

Higher oxidation states. Fairly low shielding is observed for Mo(VI) in molybdates, decreasing sharply in the sequence $[MoO_4]^{2-}$ > $[MoS_4]^{2-}$ > $[MoSe_4]^{2-}$ over a range of 3150 ppm, as the low-energy absorption moves to longer wavelengths in the visible spectrum. Although the formal configuration is d^0, the shielding is still dominated by *d–d* circulations, with ligand-to-metal $(\sigma+\pi)$-delocalization (as demonstrated in explanation of the temperature-independent paramagnetism and electronic spectra of $[MnO_4]^-$ and related ions,[22] and the ^{17}O shielding pattern in these tetroxo species[23]). Large differences in shift are commonly found when ΔE values are small, as relatively small differences bulk large.

The very low shielding observed for quadruply-bonded Mo(II), as in Tables 2 and 3, can be related to small *d–d* excitation energies and to considerable asymmetry of charge in the valence shell which also broadens the lines. The decrease in molybdenum shielding from the phosphine halides to the carboxylates follows the "spectrochemical" ordering, as does the deshielding with increase in acid strength. Among the phosphine halides the increase in molybdenum shielding Cl^- < Br^- < I^- (over a range of 90 ppm) is a quasi-nephelauxetic order, but relativistic effects of the heavier halogens are implicated[24] since much of the increase is from the bromide to the iodide. The failure to observe a resonance for $[Mo_2Cl_4(dmpe)_2]$ is explained by the paramagnetism of this compound, in which the small bite of the bridging ligand induces a twist angle of 40° from the eclipsed position.[25]

In the M≡M orbital ladder ($\sigma < \pi < \delta < \delta^* < \pi^* < \sigma^*$) magnetically active excitations are of $\sigma \leftrightarrow \pi$, $\pi \leftrightarrow \delta$ (etc.) type. Rather little is known of these as they are likely to be overlaid by stronger (electric dipole allowed) transitions, but some $\delta \rightarrow \pi^*$ transitions have been assigned.[26,27] At the same time, quite good δ/λ relationships may be found between nuclear magnetic shielding and $(\Delta E)^{-1}$ values for magnetically inactive excitations when these vary in parallel with the active ones (as found for ^{17}O shielding in transition-metal tetroxo compounds.[23]) Such correlations are evident in Tables 2 and 3. As the ^{95}Mo shielding in the phosphine halides decreases, so does the energy of all the electronic spectral bands[28] and of the δ and π p.e. bands,[29] and also the ^{31}P shielding. For the carboxylate dimers the relationships are more complex. The ionization energy of the δ and π bands increases[30] as the ^{95}Mo shielding decreases, both within the series (with increase in inductive effect of the carboxylate) and relative to the phosphine halides. The latter increase is evident also in the SCF-Xα-SW calculated energies, which however indicate a decrease for the σ-Mo—Mo orbital ionization energy from phosphine halide to carboxylate,[27,29] decreasing $\sigma \leftrightarrow \pi$ and $\sigma \leftrightarrow \delta$ excitation energies.

The addition of two axial pyridine ligands to the trifluoroacetate dimer lengthens the Mo≡Mo bond (from 2.09 to 2.13 Å), and lowers the Mo≡Mo stretching frequency (from 397 to 367 cm^{-1}).[31] At the same time the low-energy absorption goes to longer wavelengths as the orbital overlap and splitting are reduced, and the ^{95}Mo shielding decreases by over 300 ppm as shown in Table 3. These are corresponding indications of decrease in ^{95}Mo shielding with better-coordinating solvents, e.g. from chlorinated solvents or toluene to thf.

Deshielding of ^{95}Mo *with increase in metal–metal bond order*

According to Table 4, if due regard is paid to the influence of the ligands in question (albeit bridging[6,32,33] or semi-bridging in some examples), it seems likely that the ^{95}Mo shielding decreases steadily with increase in bond order (from 1 to 4) in metal–metal bonds. This sequence seems reasonable in view of the decrease in overlap from σ- to π- to δ-orbitals, and the decrease in electronic symmetry with increase in multiplicity (indeed, the linewidths tend to increase in this sequence).

Particularly interesting is the contrast with ^{13}C resonance, since alkyne carbon is much more highly shielded than alkene carbon. The chemical shifts are

Table 4. Dependence of ^{95}Mo shielding on Mo–Mo bond order

Compound	Mo–Mo bond order	$\delta(^{95}Mo)$ range	Reference
$[Mo(CpR)(CO)_3]_2$	1	−1700 to −1830	3, 15
$[Mo_2Cp_2(\mu\text{-}C_8Me_8)]$	2	−220 to +580	32
$[Mo(CpR)(\mu\text{-}S)(\mu\text{-}SR)]_2$	2	500–600	6
$[Mo(CpR)(\eta^2\text{-}\mu\text{-}CO)_2]_2$	3	159	
$[Mo_2Cp_2\{(\mu\text{-}PR)_2C_6H_4\}(\mu\text{-}CO)]$	3	1370–1400	33
$[Mo_2X_6]$	3	2420–3620	[a]
$[Mo_2(PMe_3)_4X_4]$	4	2925–3020	[b]
$[Mo_2(O_2CR)_4]$	4	3665–4200	[c]

[a] Unpublished work by M. Minelli, E. M. Kober and J. H. Enemark, mentioned in Ref. 1. X = NMe_2^-, OR^- or $CH_2SiMe_3^-$.
[b] Table 2.
[c] Table 3.

6, 123 and 72 ppm, respectively, for C_2H_6, C_2H_4 and C_2H_2. There is, however, a special reason for high shielding in alkynes, since the C_∞- or D_∞-symmetry allows of free diamagnetic circulation about the bond axis.[34] This is not possible in transition-metal complexes because of the higher coordination number.

EXPERIMENTAL

^{95}Mo measurements were made when possible on a JEOL FX90Q spectrometer, with a pre-acquisition delay of 0.5 ms to reduce the effects of probe ringing. Typical repetition times were of the order of 0.2 s. Higher sensitivity was needed for the quadruply-bonded compounds because of the broader lines and insufficient solubility, and for these a Bruker WH400 spectrometer was used. Manipulation of most of the compounds was carried out in the absence of oxygen, usually under nitrogen.

Acknowledgements—We thank Drs J. N. Verpeaux, V. Patel and A. Izquierdo and Mr S. K. Habron for the loan of samples, Dr J. C. Green for counsel, Drs E. Curzon and O. W. Howarth for spectra run on the WH400 spectrometer at Warwick University, and the S.E.R.C. for the provision of the high-field spectrometer.

REFERENCES

1. M. Minelli, J. H. Enemark, R. T. C. Brownlee, M. J. O'Connor and A. G. Wedd, *Coord. Chem. Rev.* (in press).
2. H. C. E. McFarlane, W. McFarlane and D. S. Rycroft, *J. Chem. Soc., Dalton Trans.* 1976, 1616.
3. R. A. Grieves, unpublished work.
4. S. Donovan-Mtunzi, M. Hughes, G. J. Leigh, H. Modh. Ali, R. L. Richards and J. Mason, *J. Organomet. Chem.* 1983, **246**, C1.
5. M. Hughes, J. Mason and R. L. Richards, unpublished work.
6. Unpublished work with C. J. Casewit and M. Rakowski DuBois.
7. J. C. Green, R. A. Grieves and J. Mason *J. Chem. Soc., Dalton Trans.* (in press).
8. S. F. Gheller, T. W. Hambley, R. T. C. Brownlee, M. J. O'Connor, M. R. Snow and A. G. Wedd, *J. Am. Chem. Soc.* 1983, **105**, 1527.
9. (a) D. J. Santure, J. C. Huffman and A. P. Sattelberger, *J. Am. Chem. Soc.* 1985, **24**, 371; (b) D. J. Santure, K. W. McLaughlin, J. C. Huffman and A. P. Sattelberger, *Inorg. Chem.* 1983, **22**, 1877.
10. J. Mason, *Adv. Inorg. Chem. Radiochem.* 1979, **22**, 199; 1976, **18**, 197.
11. J. Mason and C. J. Jameson, In *Multinuclear NMR* (Edited by J. Mason), Chap. 3. Plenum, New York (1986).
12. A. A. Koridze, P. V. Petrovskii, S. P. Gubin and E. I. Fedin, *J. Organomet. Chem.* 1975, **93**, C26.
13. J. Mason, *Chem. Rev.* 1981, **81**, 205.
14. J.-Y. Le Gall, M. M. Kubicki and F. Y. Petillon, *J. Organomet. Chem.* 1981, **221**, 287.
15. S. Dysart, I. Georgii and B. E. Mann, *J. Organomet. Chem.* 1981, **213**, C10.
16. R. G. Kidd, *Annu. Rep. NMR Spectrosc.* 1980, **10A**, 1.
17. D. Rehder, *Magn. Reson. Rev.* 1984, **9**, 125; In *Multinuclear NMR* (Edited by J. Mason), Chap. 19. Plenum, New York (1986). R. J. Goodfellow, In *Multinuclear NMR* (Edited by J. Mason), Chap. 2. Plenum, New York (1986).
18. E. C. Alyea and A. Somogyvari, *Inorg. Chim. Acta* 1984, **83**, L49.
19. C. K. Jørgensen, *Absorption Spectra and Chemical Bonding.* Pergamon Press, Oxford (1962). C. K. Jørgensen, *Modern Aspects of Ligand Field Theory.* North-Holland, Amsterdam (1971). C. S. G. Phillips

and R. J. P. Williams, *Inorganic Chemistry*. Oxford University Press, Oxford (1965).
20. R. Bramley, M. Brorson, A. M. Sargeson and C. E. Schäffer, *J. Am. Chem. Soc.* 1985, **107**, 2780.
21. S. Yamada, H. Yamazaki, H. Nichikawa and R. Tsuchida, *Bull. Chem. Soc. Jpn* 1960, **33**, 481.
22. A. Carrington, *Mol. Phys.* 1960, **3**, 271; A. Carrington and D. S. Schonland, *Mol. Phys.* 1960, **3**, 331.
23. B. N. Figgis, R. G. Kidd and R. S. Nyholm, *Proc. R. Soc. London, Ser. A* 1962, **269**, 469.
24. A. A. Cheremisin and P. V. Schastnev, *J. Magn. Reson.* 1980, **40**, 459.
25. M. D. Hopkins, T. C. Zietlow, V. M. Miskowski and H. B. Gray, *J. Am. Chem. Soc.* 1985, **107**, 510.
26. W. C. Trogler and H. B. Gray, *Acc. Chem. Res.* 1978, **11**, 232.
27. J. G. Norman, H. J. Kolari, H. B. Gray and W. C. Trogler, *Inorg. Chem.* 1977, **16**, 987.
28. S. K. Habron, Part II thesis, Oxford (1983).
29. F. A. Cotton, J. L. Hubbard, D. L. Lichtenberger and I. Shim, *J. Am. Chem. Soc.* 1982, **104**, 679.
30. A. W. Coleman, J. C. Green, A. J. Hayes, E. A. Seddon, D. R. Lloyd and Y. Niwa, *J. Chem. Soc., Dalton Trans.* 1979, 1057.
31. F. A. Cotton and J. G. Norman, *J. Am. Chem. Soc.* 1972, **94**, 5697; D. S. Martin, R. A. Newman and P. E. Fanwick, *Inorg. Chem.* 1982, **21**, 3400.
32. M. Green, N. C. Norman, A. G. Orpen and C. J. Schaverien, *J. Chem. Soc., Dalton Trans.* 1984, 2455.
33. Unpublished work with E. P. Kyba.
34. J. A. Pople, *Mol. Phys.* 1963–1964, **7**, 301.

Polyhedron Vol. 5, No. 1/2, pp. 423–425, 1986
Printed in Great Britain

0277–5387/86 $3.00 + .00
© 1986 Pergamon Press Ltd

THE EPR SPECTRA AND ELECTRONIC STRUCTURES OF LOW-SYMMETRY OXO-MOLYBDENUM(V) COMPLEXES

D. COLLISON* and F. E. MABBS

Department of Chemistry, University of Manchester, Manchester M13 9PL, U.K.

and

J. H. ENEMARK and W. E. CLELAND, JR

Department of Chemistry, University of Arizona, Tucson, AZ 85721, U.S.A.

(*Received* 17 *June* 1985)

Abstract—EPR spectra of fluid and frozen toluene solutions of $MoOLX_2$, where L = hydrotris(3,5-dimethylpyrazolyl(borate), and X = Cl, SEt, OMe or NCS, at both *X*- and *Q*-band frequencies, have been simulated on the basis of C_s-symmetry for the molecules. The non-coincidence of the *g*- and *A*-tensor axes are discussed in terms of the probable *d*-orbital mixings caused by the low-symmetry ligand fields in these molecules.

The point symmetry of a metal complex determines which metal *d*-orbitals are allowed to intermix. Such intermixing will determine whether or not the principal axes of the *g*- and metal ion *A*-tensors coincide. Complexes with no symmetry elements (C_1) or with an inversion centre (C_i) are *not required* to have any of the principal *g*- or *A*-tensor axes coincident, whilst those with a two-fold axis (C_2), or a mirror plane (C_s) or with C_{2h} point symmetries are *required* to have *one* of the principal *g*- and *A*-tensor axes coincident. A group of complexes which conform, or very closely approximate, to the C_s point group are $MoOLX_2$ where X = Cl, SEt, OMe or NCS, and L = the tridentate anion, hydrotris(3,5-dimethylpyrazolyl)borate. The mirror plane includes the molybdenum, the terminal oxo atom, and the nitrogen atom of the ligand L which is *trans* to the oxo group. The mirror plane bisects the X—Mo—X angle. In the case of X = NCS in the solid state the existence of a mirror plane in the molecule is a crystallographic requirement.[1]

EPR spectra of frozen toluene solutions of each of the above complexes at both *X*- and *Q*-band frequencies have been successfully simulated on the basis of C_s-symmetry. In this symmetry the axes of the coincident *g*- and *A*-tensor elements are *required* to be perpendicular to the mirror plane. The spectrum simulations were achieved via the spin-Hamiltonian eqn [(1)] and using methods based on those outlined previously:[2,3]

$$\mathcal{H} = \beta H(g_{xx}\hat{S}_x + g_{yy}\hat{S}_y + g_{zz}\hat{S}_z) + A_{XX}\hat{S}_X\hat{I}_X + A_{YY}\hat{S}_Y\hat{I}_Y + A_{ZZ}\hat{S}_Z\hat{I}_Z, \quad (1)$$

where the axes of the *g*-tensor (*x*, *y*, *z*) may not coincide with the axes of the *A*-tensor (*X*, *Y*, *Z*). The simulations in general use the parameters g_{xx}, g_{yy}, g_{zz}, A_{XX}, A_{YY} and A_{ZZ}, and the three Euler[4] angles, α, β and γ which are used to transform the *A*-tensor into the *g*-tensor axis system (in the case of C_s-symmetry only α is needed). In addition to the *g* and *A* tensor elements the principal linewidth parameters W_{xx}, W_{yy} and W_{zz} with axes coincident with the *g*-tensor axes are also included. Values of the parameters to give best fits (by eye) are given in Table 1. It should be noted that erroneous values of A_{ii} may be obtained in these low-symmetry compounds if the observed splittings between the hyperfine lines are used directly from either the *X*- or *Q*-band spectra. For example, for $MoOLCl_2$ direct measurement from the *X*-band spectrum gives A_{ZZ} = 74 G and A_{XX} = 76 G, whereas the simulation requires 78 and 42 G, respectively. Thus in this case a casual interpretation of the spectrum suggests that the *A* values are nearly axially symmetric but in a completely different sense from that obtained from the simulated spectrum.

* Author to whom correspondence should be addressed.

Table 1. Parameters required to simulate the frozen solution EPR spectra

Compound	g_{yy}	g_{zz}	g_{xx}	g_{xz}	A_{YY}[a] ($\times 10^4$ cm^{-1})	A_{ZZ}[a] ($\times 10^{-4}$ cm^{-1})	A_{XX}[a] ($\times 10^4$ cm^{-1})	α (°)	β (°)	γ (°)
$MoOLCl_2$	1.941	1.971	1.934	−0.017	18.1	71.4	38.1	33	0	0
					(20)	(78)	(42)			
$MoOL(SEt)_2$	1.952	2.011	1.931	−0.038	27.3	58.2	27.6	39	0	0
					(30)	(63)	(30)			
$MoOL(OMe)_2$	1.942	1.905	1.966	−0.030	13.6	72.0	39.9	38	0	0
					(15)	(80)	(44)			
$MoOL(NCS)_2$	1.943	1.933	1.954	−0.009	30.8	67.8	30.0	27	0	0
					(34)	(75)	(33)			
$MoOCl_3(hmpa)_2$[b]	1.932	1.951	1.928	0.0006	36.1	75.6	35.7	−80.8	21.7	88.4
					(40.1)	(83.2)	(39.6)			

[a] Values in parentheses are in G.
[b] Single-crystal data from Ref. 5.

An example of a complex which only approximates to C_s-symmetry, but which is strictly C_1-symmetry, is $MoOCl_3(hmpa)_2$, where hmpa = tris(dimethylamino)phosphineoxide. Diluted single-crystal EPR studies[5] on this compound revealed a total lack of coincidence between the principal g and A tensor axes (see Table 1). However, the principal values of the A tensor were close to metal ligand directions and in particular the largest value of A, A_{ZZ}, was nearly coincident with the terminal Mo=O vector. For this reason, and also by analogy with higher-symmetry systems,[6,7] in the present compounds we assign the largest hyperfine values to A_{ZZ} with the Z-axis parallel to Mo=O. In Table 1 the direction perpendicular to the mirror plane is chosen as the coincident y- and Y-axes.

In C_s-symmetry, with the y-axis as specified above, the allowed d-orbital mixings are:

$$\begin{aligned}
\phi_1 &= a_1 d_{x^2-y^2} + b_1 d_{xz} + c_1 d_{z^2},\\
\phi_2 &= a_2 d_{x^2-y^2} + b_2 d_{xz} + c_2 d_{z^2},\\
\phi_3 &= e_3 d_{xy} + f_3 d_{yz},\\
\phi_4 &= e_4 d_{xy} + f_4 d_{yz},\\
\phi_5 &= a_5 d_{x^2-y^2} + b_5 d_{xz} + c_5 d_{z^2}.
\end{aligned} \tag{2}$$

Assuming ϕ_1 to be the groundstate for these d^1 systems then the separation between ϕ_1 and any other orbital ϕ_i ($i = 2, 3, 4$ or 5) is defined as Δ_i. The relationship between the orbital mixings and the g- and A-tensor elements can be derived using Abragam and Bleaney's[8] perturbation equation. Working in a diagonal A-tensor axis framework, and ignoring terms in $\xi P/\Delta_i$ in the A-tensor elements, enables us to make a semi-quantitative estimate of some of the orbital mixing coefficients. ξ is the metal single electron spin–orbit coupling constant and $P = g_e g_n \beta_e \beta_n \langle r^{-3} \rangle$. For example, in $MoOL(NCS)_2$ the very small value of g_{xz} (= −0.009) coupled with the near equality of A_{YY} and A_{XX} require c_1 to be essentially zero and $b_1 \ll a_1$. Values of $a_1^2 = 0.9999$, $b_1^2 = 0.0001$ and $c_1^2 = 0.0000$ and $P = -39 \times 10^{-4}$ cm^{-1} give $A_{ZZ} = 67.8(67.8) \times 10^{-4}$ cm^{-1}, $A_{XX} = 33.9(30.0) \times 10^{-4}$ cm^{-1}, $A_{YY} = 34.0(30.8) \times 10^{-4}$ cm^{-1}, $A_{XZ} = -0.016(0.000) \times 10^{-4}$ cm^{-1}, where the values in parentheses are the experimental values. Thus in the case of the thiocyanato compound the groundstate is almost entirely composed of the metal $d_{x^2-y^2}$-orbital. The rotation of the g-tensor axes from those of the A-tensor has its origin in the d-orbital mixing in ϕ_3 and ϕ_4. Under the action of spin–orbit coupling this mixing causes g_{xz} to be non-zero. The mixing in ϕ_3 and ϕ_4 has been related[9] to the angle α. Using the criterion in Ref. 9, and on the basis of the sign of our g_{xz}, we would expect $\phi_3 = 0.891 d_{xy} + 0.454 d_{yz}$ and $\phi_4 = -0.454 d_{xy} + 0.891 d_{yz}$. As pointed out previously[9] this large amount of mixing implies that ϕ_3 and ϕ_4 are fairly close in energy. The similarity in the angle α required in the spectrum simulation for each of the compounds studied suggests a similar degree of d-orbital mixing in ϕ_3 and ϕ_4 in all of them. Furthermore, the relatively small anisotropies in g_{xx} and g_{yy}, and in A_{XX} and A_{YY}, indicate that the groundstate of each compound almost exclusively involves only $d_{x^2-y^2}$ of the metal d-orbitals. These conclusions imply that the MoOL moiety is the dominant factor in determining the part of the electronic structure which influences the EPR behaviour of each of these compounds.

REFERENCES

1. J. H. Enemark and R. B. Ortega, unpublished results.
2. D. Collison and F. E. Mabbs, *J. Chem. Soc., Dalton Trans.* 1982, 1565.

3. B. Gahan and F. E. Mabbs, *J. Chem. Soc., Dalton Trans.* 1983, 1713.
4. H. Goldstein, *Classical Mechanics.* Addison–Wesley, Reading, MA (1950).
5. C. D. Garner, P. Lambert, F. E. Mabbs and T. J. King, *J. Chem. Soc., Dalton Trans.* 1977, 1191.
6. C. D. Garner, L. H. Hill, F. E. Mabbs, D. L. McFadden and A. T. McPhail, *J. Chem. Soc., Dalton Trans.* 1977, 853, 1202.
7. M. J. Nilges and R. L. Belford, *J. Magn. Reson.* 1979, **35**, 259.
8. A. Abragam and B. Bleaney, *Electron Paramagnetic Resonance of Transition Ions.* Clarendon Press, Oxford (1970).
9. M. I. Scullane, R. D. Taylor, M. Minelli, J. T. Spence, K. Yamanouchi, J. H. Enemark and N. D. Chasteen, *Inorg. Chem.* 1979, **18**, 3213.

Polyhedron Vol. 5, No. 1/2, pp. 427–433, 1986
Printed in Great Britain

0277-5387/86 $3.00 + .00
© 1986 Pergamon Press Ltd

MOLYBDENUM-CENTRED CARBON–CARBON BOND FORMATION REACTIONS

MICHAEL GREEN

Department of Inorganic Chemistry, School of Chemistry, University of Bristol, Bristol BS8 1TS, U.K.

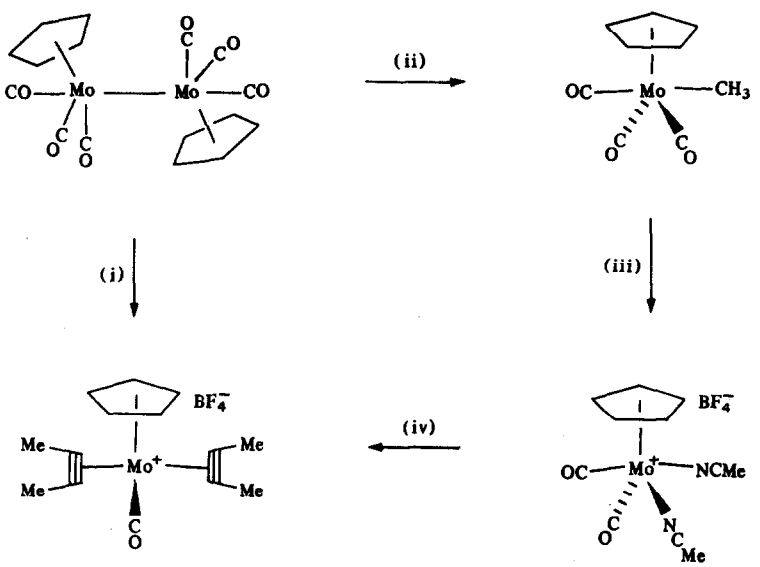
(*Received* 19 *June* 1985)

Abstract—The chemistry of the bisalkyne molybdenum complexes $[Mo(L)(\eta^2\text{-}RC_2R)_2(\eta\text{-}C_5H_5$ or $\eta^5\text{-}C_9H_7)][BF_4]$ (L = CO or MeCN) is described. The reaction of the carbonyl cation with *o*-diphenylphosphinostyrene affords an alkyne–alkene complex which is transformed into a 1,3-diene complex in refluxing MeCN via C—C bond formation and a 1,3-H shift, whereas the acetonitrile species with cyclo-octatetraene and cyclo-heptatriene undergo $(6+2)\pi$ addition reactions with the co-ordinated alkyne. Addition of one electron to the acetonitrile cation leads to novel alkyne-linking reactions at two molybdenum centres.

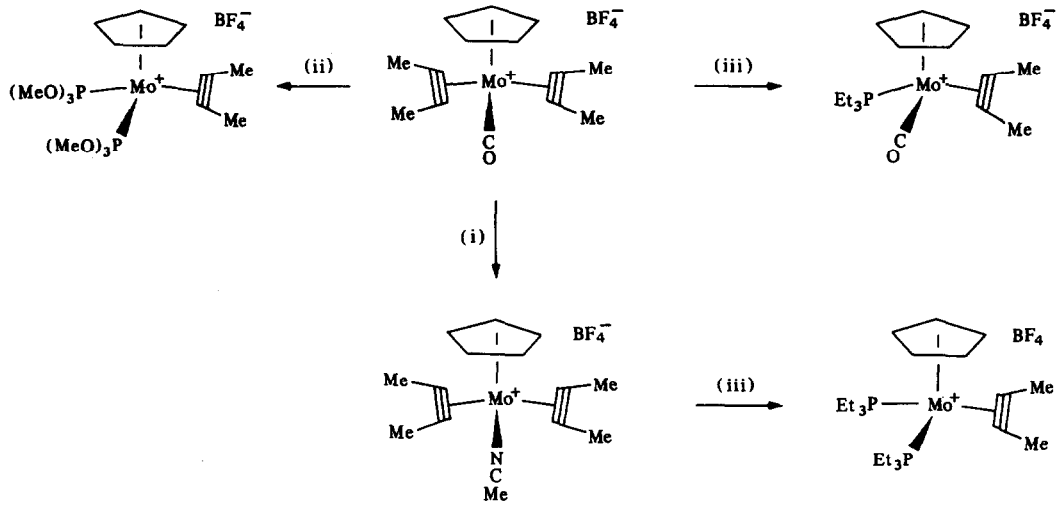
Recently[1] we have been exploring the chemistry of an interesting group of cationic alkyne molybdenum complexes in which the alkyne functions as either a three- or a four-electron donor. The starting point for our investigation was the molecule

$$[Mo(CO)(\eta^2\text{-}MeC_2Me)_2(\eta\text{-}C_5H_5)][BF_4]$$

(Scheme 1), which was readily available from the redox cleavage of the Mo—Mo bond present in $[Mo_2(CO)_6(\eta\text{-}C_5H_5)_2]$ with $AgBF_4$ in the presence of but-2-yne. An alternative synthesis which can be extended to alkynes carrying reactive functional groups such as $SiMe_3$,[2] makes use of the lability of the cation *cis*-$[Mo(NCMe)_2(CO)_2(\eta\text{-}C_5H_5)][BF_4]$, and has the advantage that it avoids the use of expensive silver salts. The methodology can be readily extended to allow easy access to the more reactive corresponding η^5-indenyl complexes.



Scheme 1. (i) $AgBF_4$, CH_2Cl_2, MeC_2Me; (ii) Na–Hg, MeI; (iii) $HBF_4 \cdot Et_2O$, CH_2Cl_2, −78°C, MeCN; (iv) MeC_2Me, CH_2Cl_2.



Scheme 2. (i) Reflux MeCN; (ii) $P(OMe)_3$, CH_2Cl_2; (iii) PEt_3, CH_2Cl_2.

These monocarbonylbis(alkyne) complexes are reactive towards donor ligands. In refluxing acetonitrile in the presence of but-2-yne the remaining carbon monoxide is readily displaced by acetonitrile forming a member of a potentially interesting group of molecules,

$$[Mo(NCMe)(\eta^2\text{-}MeC_2Me)_2(\eta\text{-}C_5H_5)][BF_4]$$

(Scheme 2). Trimethylphosphite also reacts rapidly with this cation at room temperature, but this leads instead to displacement of both carbon monoxide and one of the co-ordinated alkynes: generalization of this reaction provides access to the cations

$$[Mo\{P(OMe)_3\}_2(\eta^2\text{-}RC_2R)(\eta\text{-}C_5H_5$$

or $\eta^5\text{-}C_9H_7)][BF_4]$ where the alkyne is a four-electron donor to the molybdenum centre. The corresponding bisphosphine-substituted monoalkyne cations can only be synthesized by reacting the acetonitrile complexes with a phosphine, the reaction of

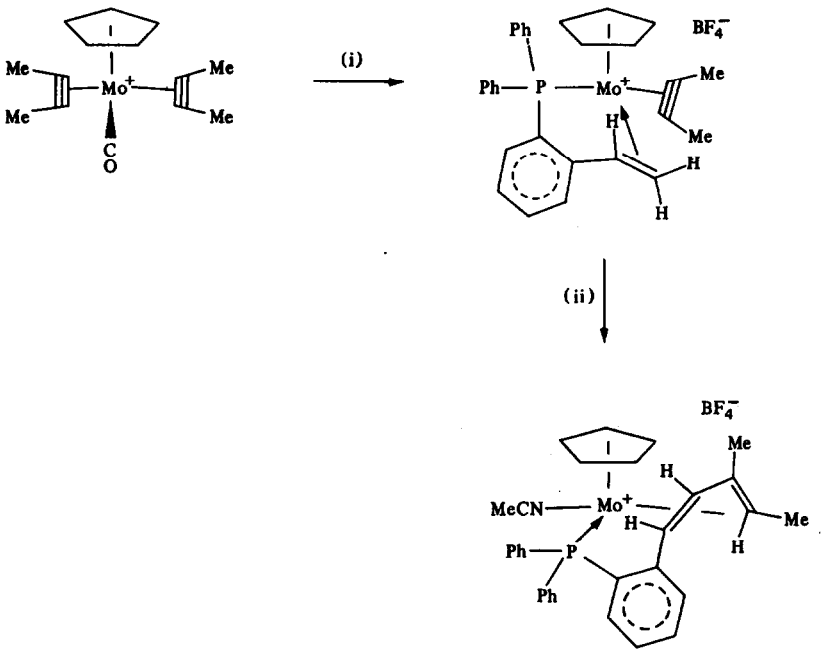
$$[Mo(CO)(\eta^2\text{-}RC_2R)_2(\eta\text{-}C_5H_5)][BF_4]$$

with PR_3 affording the asymmetric cations

$$[Mo(CO)(PR_3)(\eta^2\text{-}RC_2R)(\eta\text{-}C_5H_5)][BF_4].$$

When this type of reaction was extended to *o*-diphenylphosphinostyrene an interesting cation was obtained which was thought from examination of the NMR spectra to contain a co-ordinated alkene and a four-electron alkyne[3] (Scheme 3). This was confirmed by X-ray crystallography which showed that the molybdenum atom is bonded to an $\eta\text{-}C_5H_5$, an η^2-bonded but-2-yne, and a chelating *o*-diphenylphosphinostyrene ligand, where the C—C vectors of the co-ordinated alkyne and alkene lie essentially parallel to the Mo—P axis. This is a potentially interesting molecule since it has been suggested[4–6] that oxidative coupling of co-ordinated alkynes and alkenes to form a metallacyclopenta-2-ene is a key step in the metal-catalysed cyclocotrimerization of alkynes and alkenes. When this cation was heated under reflux in acetonitrile solution an orange crystalline complex was formed, which was identified by X-ray crystallography as the illustrated 1,3-diene complex (Scheme 3). Examination of the solution NMR spectra showed the existence of two conformational isomers differing only in the orientation of the 1,3-diene relative to the $Mo(NCMe)(P)(\eta\text{-}C_5H_5)$ fragment. Thus, co-ordination of acetonitrile appears to promote oxidative coupling of the co-ordinated alkyne and alkene: however, this is then followed by an apparent 1,3-hydrogen shift affording the 1,3-diene cation (Scheme 4). It is interesting to note that some years ago Pauson and Khand[7] reported that alkenes carrying strong electron-withdrawing groups (CN and CO_2Et) react with the transversely bonded alkyne complex $[Co_2(\mu\text{-}PhC_2H)(CO)_6]$ to give conjugated 1,3-dienes, a reaction which resembles in some respects the processes which occur at a molybdenum centre.

In view of these observations we then examined the reaction of the labile bisalkyne acetonitrile molybdenum cations with cyclo-octatetraene and cycloheptatriene in the belief that we might see analogous behaviour to that found with the *o*-diphenylphosphinostyrene system. However, when the cations $[Mo(NCMe)(\eta^2\text{-}PhC_2Ph)_2(\eta\text{-}C_5H_5$ or $\eta^5\text{-}C_9H_7)][BF_4]$ are reacted with an excess of cyclo-octatetraene in refluxing acetonitrile an organic compound is formed which was identified as a

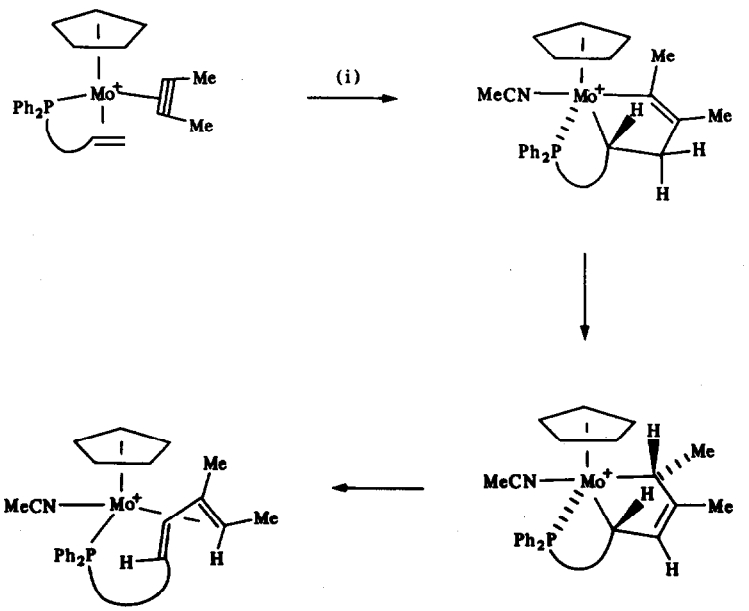


Scheme 3. (i) *o*-Diphenylphosphinostyrene, (ii) reflux MeCN.

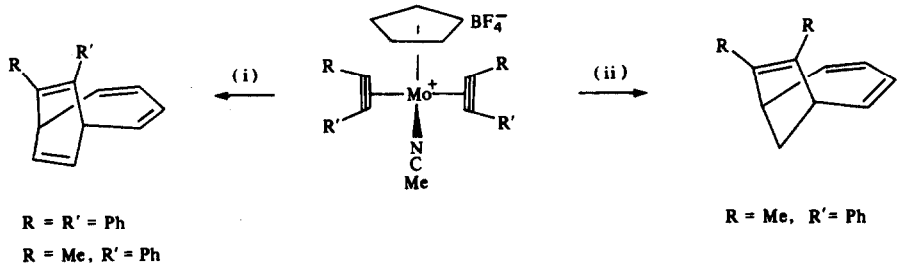
substituted bicyclo[4.2.2]decatetraene.[8] Both the η-cyclopentadienyl and the corresponding η^5-indenyl cations are catalysts for the transformation of diphenylacetylene and cyclo-octatetraene into the decatetraene. The catalytic reaction could also be extended to the synthesis using phenylprop-2-yne, and, significantly, an analogous reaction occurred between

$$[Mo(NCMe)(\eta^2\text{-}PhC_2Me)_2(\eta\text{-}C_5H_5)][BF_4]$$

and cycloheptatriene affording a bicyclo[4.2.1]nona-2,4,7-triene (Scheme 5). Thus, these observations suggest that a formally forbidden $6\pi_s + 2\pi_s$ reaction is occurring at a molybdenum centre, and it is



Scheme 4. (i) Reflux MeCN.



Scheme 5. (i) Alkyne + C_8H_8, reflux MeCN; (ii) alkyne + C_7H_8, reflux MeCN.

possible that this involves a stepwise rather than a concerted addition of the alkyne to co-ordinated C_8H_8 or C_7H_8. Recently, it has been reported[9] that norbornadiene(cycloheptatriene)ruthenium(0) reacts with ethyne in a stoichiometric reaction to afford norbornadiene(bicyclo[4.2.1]nona-2,4,7-triene)ruthenium(0).

In contrast, when the but-2-yne complex

$$[Mo(NCMe)(\eta^2\text{-}MeC_2Me)_2(\eta\text{-}C_5H_5)][BF_4]$$

was reacted in an analogous manner with C_8H_8 in MeCN a *neutral* air-stable crystalline molybdenum complex was formed. An X-ray crystal structure determination revealed that a complex C_{12} ligand had been formed by formal $(6+2)\pi$ addition of but-2-yne to co-ordinated C_8H_8, but, instead of a 7,8-disubstituted bicyclo[4.2.2]decatetraene being displaced, as happens with the corresponding reactions of PhC_2Ph and PhC_2Me, hydrogen migration occurs *via* the metal, followed by proton loss to give a complex containing η^4-1,3-diene and η^3-allyl ligands (Scheme 6).

This type of molecule had not been obtained before and it was obviously interesting to examine the reactivity towards protons. Addition of CF_3SO_3H in CH_2Cl_2 to the η^5-indenyl species gave dark brown crystals of

$$[Mo(C_{12}H_{14})(\eta^5\text{-}C_9H_7)][CF_3SO_3]$$

showing a high-field ^1H NMR signal (−80°C, CD_2Cl_2) at −7.83 ppm. A low-temperature X-ray structural analysis showed the cation geometry illustrated in Scheme 7. Protonation has occurred at one of the terminal allyl carbons transforming the η^3-allyl moiety into an alkene. The resultant unsaturation at the molybdenum centre is then relieved by an agostic *endo*-C–H interaction.[10] This interaction models the initial stage (**B** in Scheme 8) of a metal-assisted 1,3-hydrogen shift.[11] In this context it is interesting to note the shortening of the allylic C–C bond [to 1.471(8) Å] *prior* to C–H bond cleavage, and the non-planar geometry of the four-centre Mo–C_α–C_β–H system [dihedral angle 27(3)°]. This latter feature is in marked contrast to other β-agostic interactions, where M–C_α–C_β–H angles are < 17°, but rather close to that in $[IrCl(PPh_3)_2(\eta^3\text{-}C_3H_4Ph)(H)]$,[12] a model for **C** in Scheme 8. It is interesting that in solution at room temperature a dynamic process occurs, which involves reversible transfer of the agostic hydrogen to an end carbon of the 1,3-diene system (see Scheme 7).

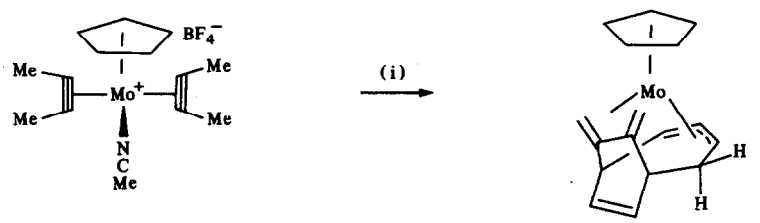
When the cation

$$[Mo(NCMe)(\eta^2\text{-}MeC_2Me)_2(\eta\text{-}C_5H_5)][BF_4]^1$$

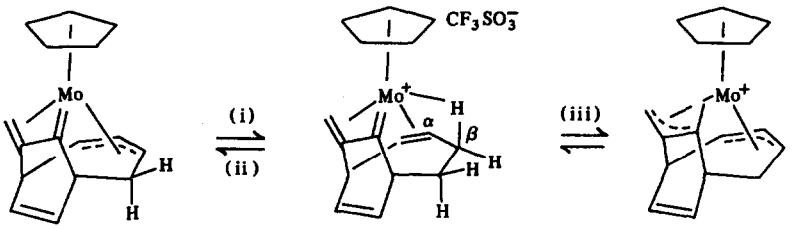
is reacted with Na or Mg amalgam, or $Na[Fe(CO)_2(\eta\text{-}C_5H_5)]$ in tetrahydrofuran (THF) an apparent one-electron reduction occurs, resulting in the formation of an octamethyloctatrienediylidenedimolybdenum complex

$$[Mo_2\{\mu\text{-}(\eta^1,\eta^3,\eta^2,\eta^3,\eta^1\text{-}C_8Me_8)\}(\eta\text{-}C_5H_5)_2]$$

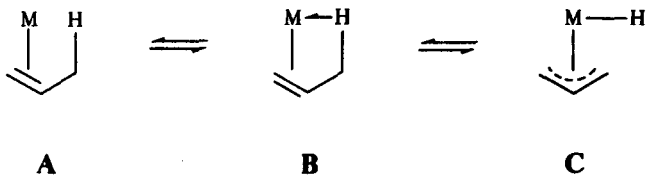
where the C_8 chain begins and ends with σ-bonds to one molybdenum.[13,14] This reaction is interesting in the context of the Reppe synthesis[15] of [8] annulene, cyclo-octatetraene, where a nickel salt catalyses the cyclotetramerization of ethyne. Remarkably, despite the advances which have been made in the last 40 years in organometallic chemistry, we still do not



Scheme 6. (i) + C_8H_8, reflux MeCN.



Scheme 7. (i) CF_3SO_3H, −78°C, CH_2Cl_2; (ii) base; (iii) room temperature.



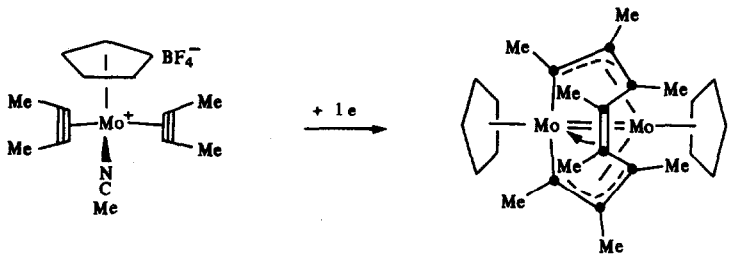
Scheme 8. Metal-mediated alkene isomerization.

understand the mechanism[16] of Reppe's reaction. Recently attention has focused on reaction pathways which involve the linking of ethyne molecules at two adjacent metal centres.[17,18] Hence the interest in the reaction illustrated in Scheme 9.

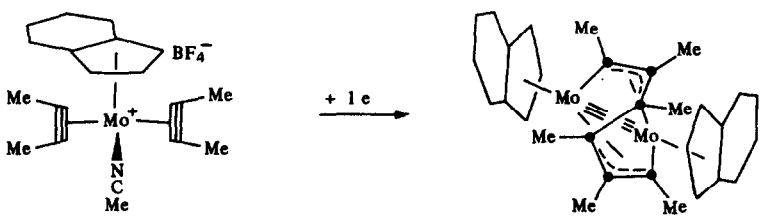
When a THF solution of the indenyl analogue

$[Mo(NCMe)(\eta^2\text{-}MeC_2Me)_2(\eta^5\text{-}C_9H_7)][BF_4]$

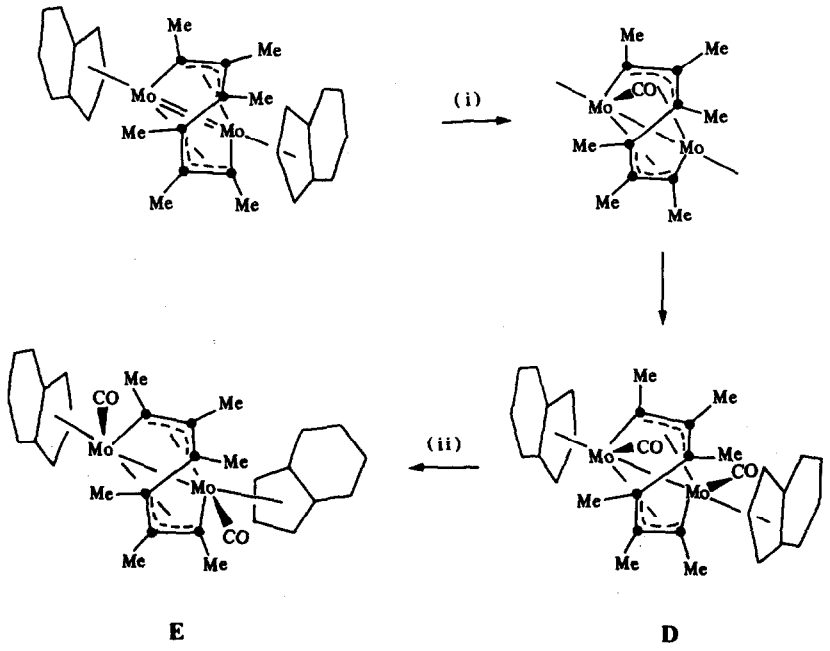
was reacted with a suspension of Na or Mg amalgam a green crystalline air-sensitive material was formed, which was identified by NMR and X-ray crystallography as a three-alkyne "fly-over" complex[19] (Scheme 10) with C_2-symmetry. In contrast, with the molecule $[Mo_2\{\mu\text{-}(\eta^1,\eta^3,\eta^2,\eta^3,\eta^1\text{-}C_8Me_8)\}(\eta\text{-}C_5H_5)_2]$, the three-alkyne "fly-over" complex is reactive towards carbon monoxide, forming a kinetically controlled isomer (**D**) (Scheme 11) at room temperature and the thermodynamic product (**E**) in refluxing hexane. These isomeric dicarbonyl complexes were identified by NMR and X-ray crystallography, and it is interesting that the reaction with carbon monoxide results in a lengthening of the Mo–Mo bond from a triple [Mo(1)–Mo(2) 2.306(2) Å] to a single [Mo(1)–Mo(2) 2.933(1) Å in (**D**)] bond with a consequent uncoiling of the C_6 "fly-over" array.



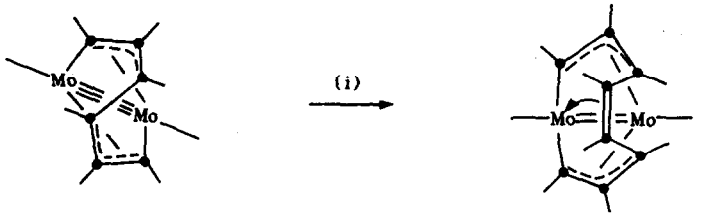
Scheme 9. (i) $NaFe(CO)_2(\eta\text{-}C_5H_5)$–THF or Mg–Hg, THF.



Scheme 10. (i) Mg–Hg, THF, room temperature.



Scheme 11. (i) + CO, room temperature; (ii) + CO, reflux hexane.



Scheme 12. η-C_5H_5 ligands omitted for clarity, (i) + RC_2R.

From studies on the thermal reaction of alkynes with complexes of the type

$$[Mo_2(\mu\text{-alkyne})(CO)_4(\eta\text{-}C_5H_5)_2]$$

it has been suggested that alkynes can sequentially link at two metal centres, and in particular it was proposed that three-alkyne "fly-over" complexes are the immediate precursors of the dinuclear C_8 species.

$$[Mo_2\{\mu\text{-}(\eta^1,\eta^3,\eta^2,\eta^3,\eta^1\text{-}C_8R_8)\}(\eta\text{-}C_5H_5)_2]$$

(R = H, Ph or CO_2Me) (Scheme 12).[18] It was therefore important to examine the reactivity of the structurally characterized three-alkyne "fly-over" complex

$$[Mo_2\{\mu\text{-}(\eta^1,\eta^3,\eta^3,\eta^1\text{-}C_6Me_6)\}(\eta^5\text{-}C_9H_7)_2]$$

towards but-2-yne. Since the octamethyl dimolybdenum complex

$$[Mo_2\{\mu\text{-}(\eta^1,\eta^3,\eta^2,\eta^3,\eta^1\text{-}C_8Me_8)\}(\eta\text{-}C_5H_5)_2]$$

is formed rapidly at room temperature then it might be expected that, if the cyclopentadienyl analogue of the C_6 "fly-over" complex was indeed a precursor of

$$[Mo_2\{\mu\text{-}(\eta^1,\eta^3,\eta^2,\eta^3,\eta^1\text{-}C_8Me_8)\}(\eta\text{-}C_5H_5)_2],$$

then the η^5-indenyl complex should rapidly react with but-2-yne, and it would be expected that this reaction would be facilitated from slippage (η^5 to η^3) of the indenyl ligand. However, the three-alkyne "fly-over" proved to be unreactive towards but-2-yne. Thus suggests that, in the case of the methyl-substituted systems, three-alkyne "fly-over" complexes and octatrienediylidenedimolybdenum species are *not* formed sequentially, but instead arise from competitive reaction pathways which are available to some earlier intermediates in the reaction sequence.

Acknowledgements—I gratefully acknowledge all the intellectual and practical contributions of my co-workers whose names are given in the references. The work was made possible by support from the SERC and the donors of the Petroleum Research Fund administered by the American Chemical Society.

REFERENCES

1. S. R. Allen, P. K. Baker, S. G. Barnes, M. Green, L. Trollope, L. M. Muir and K. W. Muir, *J. Chem. Soc., Dalton Trans.* 1981, 873.
2. S. R. Allen, M. Green, A. G. Orpen and I. D. Williams, *J. Chem. Soc., Chem. Commun.* 1982, 826.
3. S. R. Allen, M. Green, G. Moran, A. G. Orpen and G. E. Taylor, *J. Chem. Soc., Dalton Trans.* 1984, 441.
4. Y. Wakatsuki, K. Aoki and H. Yamazaki, *J. Am. Chem. Soc.* 1979, **101**, 1123.
5. P. Caddy, M. Green, E. O'Brien, L. E. Smart and P. Woodward, *J. Chem. Soc., Dalton Trans.* 1980, 962.
6. L. D. Brown, K. Itoh, H. Susuki, K. Hirai and J. A. Ibers, *J. Am. Chem. Soc.* 1978, **100**, 8232.
7. P. L. Pauson and I. U. Khand, *Ann. N.Y. Acad. Sci.* 1977, **295**, 1.
8. D. G. Bourner, L. Brammer, M. Green, G. Moran, A. G. Orpen, C. Reeve and C. J. Schaverien, *J. Chem. Soc., Chem. Commun.* 1985, 1409.
9. H. Nagashima, H. Matsuda and K. Itoh, *J. Organomet. Chem.* 1983, **258**, C15.
10. M. Brookhart and M. L. H. Green, *J. Organomet. Chem.* 1983, **250**, 395.
11. G. F. Emerson and R. Pettit, *J. Am. Chem. Soc.* 1962, **84**, 4591; C. P. Casey and C. R. Cyr, *J. Am. Chem. Soc.* 1973, **95**, 2248; G. M. Whitesides and J. P. Neilen, *J. Am. Chem. Soc.* 1976, **98**, 63; J. W. Byrne, H. U. Blaser and J. A. Osborn, *J. Am. Chem. Soc.* 1975, **97**, 3871; M. Green and R. P. Hughes, *J. Chem. Soc., Dalton Trans.* 1976, 1907; D. B. Jacobson and B. J. Freiser, *J. Am. Chem. Soc.* 1985, **107**, 72.
12. T. H. Tulip and J. A. Ibers, *J. Am. Chem. Soc.* 1979, **101**, 4201.
13. M. Green, N. C. Norman and A. G. Orpen, *J. Am. Chem. Soc.* 1981, **103**, 1269.
14. M. Green, N. C. Norman, A. G. Orpen and C. J. Schaverien, *J. Chem. Soc., Dalton Trans.* 1984, 2455.
15. W. Reppe, O. Schlichting, K. Klager and T. Toepel, *Liebigs Ann. Chem.* 1948, **560**, 1.
16. R. E. Colborn and K. P. C. Vollhardt, *J. Am. Chem. Soc.* 1981, **103**, 6259 (and references therein).
17. G. Wilke, *Pure Appl. Chem.* 1978, **50**, 677.
18. S. A. R. Knox, R. F. D. Stansfield, F. G. A. Stone, M. J. Winter and P. Woodward, *J. Chem. Soc., Dalton Trans.* 1982, 173.
19. L. Brammer, M. Green, A. G. Orpen, K. E. Paddick and D. R. Saunders, *J. Chem. Soc., Dalton Trans.* (in press).

Polyhedron Vol. 5, No. 1/2, pp. 435–437, 1986
Printed in Great Britain

0277–5387/86 $3.00 + .00
© 1986 Pergamon Press Ltd

CYCLIC CARBENE COMPLEXES OF THE TYPE *cis*-MI[$\overline{CN(Me)(CH_2)_nCH_2}$](CO)$_2$($\eta$-$C_5H_5$) (M = Mo, n = 2 OR 3; M = W, n = 2): THEIR SYNTHESES AND REACTIONS OF THE MOLYBDENUM SYSTEMS WITH $LiEt_3BH$

VALERIE A. OSBORN and MARK J. WINTER*

Department of Chemistry, The University, Sheffield S3 7HF, U.K.

(*Received* 17 *June* 1985)

Abstract—Treatment of [M(CNMe)(CO)$_2$(η-C_5H_5)]$^-$ with I[CH_2]$_{n+1}$I provides the cyclic carbene species *cis*-MI[$\overline{CN(Me)(CH_2)_nCH_2}$](CO)$_2$($\eta$-$C_5H_5$) (M = Mo, n = 2 or 3; M = W, n = 2), the molybdenum examples of which undergo reaction with $LiEt_3BH$, so forming the compounds *cis*-Mo[η^2-$\overline{CH(CH_2)_{n+1}N(Me)}$](CO)$_2$($\eta$-$C_5H_5$).

Cyclic carbene complexes of the 2-oxacyclopentylidene ligand are well known and available by several synthetic strategies,[1–5] in particular through the reaction of N^- with Mo[$(CH_2)_3X$](CO)$_3$(η-C_5H_5) (X = Br or I) which leads to

trans-Mo(N)(CO)$_2$[$\overline{CO(CH_2)_2CH_2}$]($\eta$-$C_5H_5$)

(N = I, CN or SPh).[6] The first step in this reaction is a migratory insertion of the alkyl group $(CH_2)_3X$ to a *cis* carbonyl induced by the nucleophile N^-, this is followed by a ring-closing reaction of the ensuing anionic acyl. Although there are several examples of carbene synthesis by this type of ring closure reaction for molybdenum there are fewer involving tungsten, owing to the relative difficulty of achieving insertion for [WR(CO)$_3$(η-C_5H_5)] systems.[7]

We recently communicated the synthesis of the five-membered cyclic carbene

cis-MoI[$\overline{CN(Me)(CH_2)_2CH_2}$](CO)$_2$($\eta$-$C_5H_5$)

(**1**) through a related process involving migration of the same $(CH_2)_3X$ alkyl group to the isonitrile of an intermediate

Mo[$(CH_2)_3$I](CNMe)(CO)$_2$(η-C_5H_5).[8]

One interesting feature of the molecule and a related acyclic analogue

MoI[C(NHMe)Me](CO)$_2$(η-C_5H_5)[9]

is their *cis* stereochemistry; all the related

MX(CO)$_2$[C(OR^1)R^2](η-C_5H_5)

(M = Mo or W) complexes are *trans*[10–12] and there is a possibility that any *cis–trans* isomerization is sterically blocked by the methyl group although electronic factors also need to be considered. As complexes of the six-membered ring 2-oxacyclohexylidene are few and far between,[4,13] it is normally necessary to induce ring closure through silver cation assisted halide removal at the acyl stage.[13]

We now report a facile six-membered ring carbene molybdenum complex synthesis, facile synthesis of a tungsten carbene complex through an isonitrile insertion reaction, and preliminary results of reactions of some of these carbene complexes with $LiEt_3BH$.

RESULTS AND DISCUSSION

Addition of I[CH_2]$_4$I to a solution containing[14,15] [Mo(CNMe)(CO)$_2$(η-C_5H_5)]$^-$ gives rise to a dark coloured reaction mixture from which the only isolable product is the spectroscopically characterized

cis-MoI[$\overline{CN(Me)(CH_2)_3CH_2}$](CO)$_2$($\eta$-$C_5H_5$)

(**2**) (21%). The IR spectra of **1** and **2** are very similar, while both ^{1}H and ^{13}C NMR spectra suggest that **2** is very closely related to **1**, differing only in the extra CH_2 in the carbene ring. Complex **2** does not crystallize readily, accounting for the low isolated

* Author to whom correspondence should be addressed.

yield, but the reaction itself proceeds rather cleanly, as indicated by the IR spectrum of the reaction mixture. The ease of formation of **2** is accounted for by the ease with which alkyl groups migrate to coordinated isonitrile (Scheme 1).[16–18]

Treatment of a solution containing

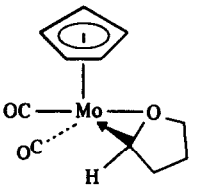
$$[W(CNMe)(CO)_2(\eta\text{-}C_5H_5)]^-$$

with $I[CH_2]_3I$ results in a smooth reaction leading after workup to the single product

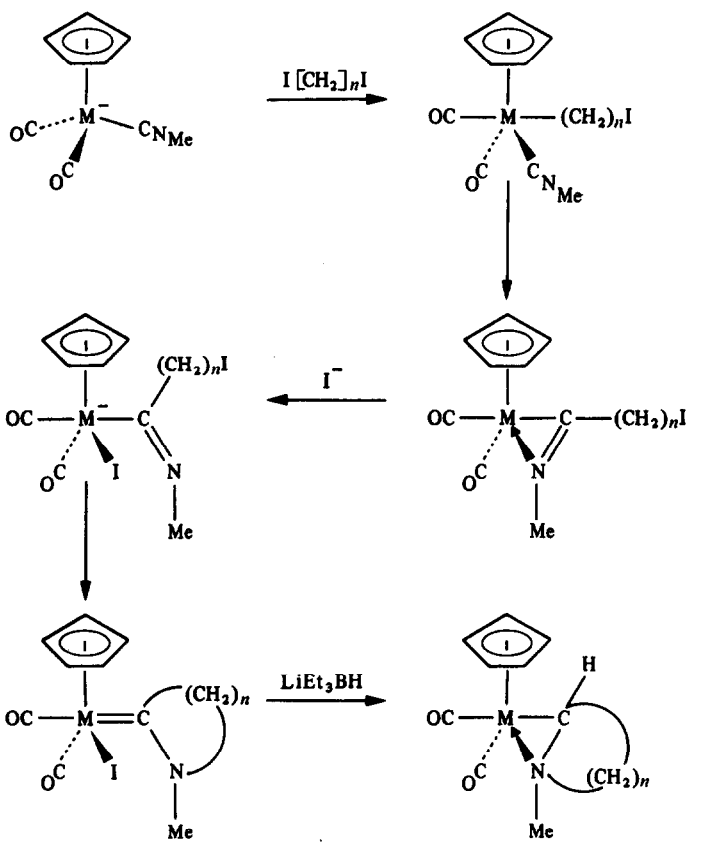
$$cis\text{-}WI[\overline{CN(Me)(CH_2)_2CH_2}](CO)_2(\eta\text{-}C_5H_5)$$

(3) (65%), whose spectroscopic properties are comparable to those of the molybdenum analogue.[8] In common with similar compound systems the chemical shifts of the carbene and carbonyls are at a somewhat higher frequency than those of the molybdenum analogues, that of the carbene by a considerable amount.[19,20] These signals are assigned by inspection of their $^1J(WC)$ couplings; ^{13}C NMR: $\delta(C_6D_5CD_3)$ 245.1 [s, CO, $^1J(WC)$ 146 Hz], 240.9 [s, W=C, $^1J(WC)$ 101 Hz] and 237.1 [s, CO, $^1J(WC)$ 154 Hz]. The two signals with comparable coupling constants are assumed to arise from carbonyls while the unique signal with a low coupling constant is assigned to the carbene.

We recently communicated the structure of an



4



1 M = Mo, $n = 3$
2 M = Mo, $n = 4$
3 M = W, $n = 3$

5 M = Mo, $n = 3$
6 M = Mo, $n = 4$

Scheme 1.

unusual complex (**4**) arising in the reaction of

trans-MoI(CO)$_2$[$\overline{CO(CH_2)_2\overline{CH_2}}$]($\eta$-$C_5H_5$)

with $LiEt_3BH$.[21] Complexes **1** and **2** undergo related reactions with $LiEt_3BH$. Addition of $LiEt_3BH$ to solutions of **1** or **2** leads to the isolation of, respectively,

Mo(CO)$_2$[η^2-$\overline{CH(CH_2)_3\underline{N}(Me)}$]($\eta$-$C_5H_5$)

(**5**) (36%) or

Mo(CO)$_2$[η^2-$\overline{CH(CH_2)_4\underline{N}(Me)}$]($\eta$-$C_5H_5$)

(**6**) (10%). Both these compounds are fully spectroscopically characterized, in particular the J(HH) coupling constants extracted from the ^{1}H NMR spectrum of **5** are virtually identical to those of **4**, indicating a very similar geometry for the ligated ring system. It is likely that formation of **4** proceeds by direct attack of the hydride reagent at the carbene (followed by loss of I^- as the oxygen atom enters the coordination sphere of the metal) rather than initial coordination at the metal or carbonyl followed by an inter- or intramolecular hydride transfer process.[22] Since we have not attempted to spectroscopically identify any intermediates in these reactions we assume a similar mechanism here.

Compound **4** undergoes O—Mo bond cleavage on attack by PPh_3, resulting in

trans-Mo[η^1-$\overline{CH(CH_2)_3\underline{O}}$](CO)$_2$($PPh_3$)($\eta$-$C_5H_5$).[21]

While one might expect a similar lability for the N—Mo bond of **5** and **6**, in the event neither compound undergoes reaction with PPh_3, even during prolonged heating at reflux in tetrahydrofuran. However reaction is observed for both **5** and **6** with H_2SO_4; thus treatment of **5** with acid results in the rapid decomplexation of the cycle as *N*-methyl pyrrolidine, $\overline{CH_2N(Me)[CH_2]_2\overline{CH_2}}$ (43%) (characterized and quantified by GLC and GC–mass spectrometry), together with formation of unidentified metal species. In a similar fashion H_2SO_4 treatment of **6** results in the evolution of *N*-methyl piperidine, $\overline{CH_2N(Me)[CH_2]_3\overline{CH_2}}$ (54%).

REFERENCES

1. C. P. Casey and R. L. Anderson, *J. Organomet. Chem.* 1974, **73**, C28.
2. J. R. Moss, *J. Organomet. Chem.* 1982, **231**, 229.
3. C. P. Casey, *J. Chem. Soc., Chem. Commun.* 1970, 1220.
4. C. H. Game, M. Green, J. R. Moss and F. G. A. Stone, *J. Chem. Soc., Dalton Trans.* 1974, 351.
5. F. A. Cotton and C. M. Lukehart, *J. Am. Chem. Soc.* 1971, **93**, 2672.
6. N. A. Bailey, P. L. Chell, C. P. Manuel, A. Mukhopadhyay, D. Rogers, H. E. Tabbron and M. J. Winter, *J. Chem. Soc., Dalton Trans.* 1983, 2397.
7. A. Wojcicki, *Adv. Organomet. Chem.* 1973, **11**, 87.
8. H. Adams, N. A. Bailey, V. A. Osborn and M. J. Winter, *J. Organomet. Chem.* 1984, **284**, C1.
9. R. D. Adams and D. F. Chodosh, *J. Am. Chem. Soc.* 1977, **99**, 6544.
10. L. Y. Y. Chan, W. K. Dean and W. A. G. Graham, *Inorg. Chem.* 1977, **16**, 1067.
11. W. K. Dean and W. A. G. Graham, *Inorg. Chem.* 1977, **16**, 1061.
12. G. A. Carriedo, D. Hodgson, J. A. K. Howard, K. Marsden, F. G. A. Stone, M. J. Went and P. Woodward, *J. Chem. Soc., Chem. Commun.* 1982, 1006.
13. F. A. Cotton and C. M. Lukehart, *J. Am. Chem. Soc.* 1973, **95**, 3552.
14. R. D. Adams, *J. Organomet. Chem.* 1975, **88**, C38.
15. R. D. Adams, *Inorg. Chem.* 1976, **15**, 169.
16. Y. Yamamoto and H. Yamazaki, *J. Organomet. Chem.* 1975, **90**, 329.
17. R. D. Adams and D. F. Chodosh, *J. Organomet. Chem.* 1976, **122**, C11.
18. R. D. Adams and D. F. Chodosh, *J. Am. Chem. Soc.* 1976, **98**, 5391.
19. B. E. Mann and B. F. Taylor, ^{13}C NMR *Data for Organometallic Compounds*. Academic Press, London (1981).
20. H. Adams, N. A. Bailey and M. J. Winter, *J. Chem. Soc., Dalton Trans.* 1984, 273.
21. H. Adams, N. A. Bailey, P. Cahill, D. Rogers and M. J. Winter, *J. Chem. Soc., Chem. Commun.* 1983, 831.
22. M. J. Winter, unpublished observations.

Polyhedron Vol. 5, No. 1/2, pp. 439–443, 1986
Printed in Great Britain

0277–5387/86 $3.00 + .00
©1986 Pergamon Press Ltd

MOLYBDENUM-MEDIATED CARBON–CARBON BOND FORMATION

B. J. BRISDON, D. W. BROWN and C. R. WILLIS*

School of Chemistry, University of Bath, Claverton Down, Bath BA2 7AY, U.K.

(*Received* 19 *June* 1985)

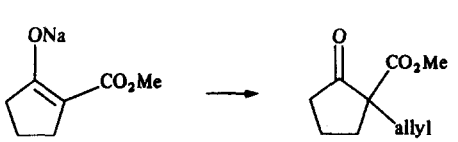
Abstract—Reaction of $(CH_2)_nCH{=}CHCHBr$ (n = 3–5) with sodium pentan-2,4-dionate (Napda) in the presence of catalytic quantities of $Mo(CO)_4$bipyridine leads to high yields of the coupled products $\{(CH_2)_nCH{=}CHCH\}_2$ as mixtures of two diastereoisomers, with little or no alkylated derivative $(CH_2)CH{=}CHCHpda$. Up to 50% of the molybdenum present was recovered as $[MoBr(CO)_2(\eta^3\text{-}CH{\cdots}CH{\cdots}CH(CH_2)_n(bipyridine)]$ in reactions involving 3-bromocyclohexene and 3-bromocycloheptene. η^3-Allyl complexes $[MoX(CO)_2(\eta^3\text{-}C_5H_7O)]$ (where X = Cl or Br), formed by alkoxycarbonylation of the propargyl entity, were also isolated from the reaction of $[MoX(CO)_3(bipyridine)]^-$ anions with propargyl halides in methanol, and yielded dimethyl methylsuccinate on treatment with $NaBH_4$.

Several molybdenum(0) carbonyl derivatives including $Mo(CO)_4$bipy (bipy = bipyridine) have been shown recently to be effective catalysts for allylic alkylation reactions.[1] The intermediacy of metal–allyl species in catalytic cycles has been inferred from the known interaction between allyl halides and some $Mo(CO)_4L_2$ species to yield $[MoX(CO)_2(\eta^3\text{-allyl})L_2]$ (where X = halide)[2] and from stoichiometric reactions, involving attack by a carbon nucleophile on two of these neutral allyl complexes, which yield the same products as the catalytic reactions [eqns (1) and (2)]:

$$Mo(CO)_4L_2 + allylX \rightarrow MoX(CO)_2(\eta^3\text{-allyl})L_2 + 2CO \quad (1)$$

(L_2 = bipy and other N-donor ligands),

$MoCl(CO)_2(\eta^3$-allyl$)L_2$ +



(2)

(L_2 = bipy or bis(diphenylphosphino)ethane).

Although the allyl substituent, the solvent and the nature of L_2 have a marked effect on the reaction in terms of rate and regioselectivity, only alkylated products have been reported as arising from these reactions.[1]

Under only slightly different reaction conditions, we have observed that treatment of $[MoCl(CO)_2(\eta^3\text{-}C_3H_5)bipy]$ with the pentan-2,4-dionate (pda) anion in the presence of pyridine (py) results in ligand exchange with no evidence of nucleophilic attack on the allyl moiety [eqn (3)][3]:

$$[MoCl(CO)_2(\eta^3\text{-}C_3H_5)bipy] + Napda + py \rightarrow [Mo(CO)_2(\eta^3\text{-}C_3H_5)(pda)py] + NaCl. \quad (3)$$

Both the solid-state structure and the dynamic behaviour of the product were reported subsequently.[4] In view of these results, we decided that the generality of the molybdenum-catalysed allylic alkylation reaction required probing. In this paper we describe reactions in which molybdenum catalysed homo coupling rather than alkylation occurs under very similar conditions to those described by Trost and Lautens.[1] We also include a brief account of our preliminary results on the interactions of propargyl halides with molybdenum carbonyl complexes, which also result in new C—C bond formation.

* Author to whom correspondence should be addressed.

RESULTS AND DISCUSSION

In view of the anomolous behaviour of the pda anion, as noted above, we first examined the interaction of this carbanion with the neutral complexes $[MoBr(CO)_2(\eta^3\text{-cyclohexenyl})L_2]$ [L_2 = bipy (**1**) or diphos (**2**)], which were readily prepared by the stoichiometric reaction between $[MoBr(CO)_2(\eta^3\text{-cyclohexenyl})(NCMe)_2]$[5] and the appropriate bidentate ligand in acetonitrile. Using tetrahydrofuran or toluene as solvent, unreacted **1** or **2** could be recovered exchanged even after reaction for several hours under reflux. At higher temperatures (boiling *n*-butylacetate), complex **1** decomposed completely yielding $Mo(CO)_4$bipy and free bipy as isolable products. However, in the presence of py this same complex reacted in boiling tetrahydrofuran to afford $[Mo(CO)_2(\eta^3\text{-cyclohexenyl})(pda)py]$ in high yield. Thus in these stoichiometric reactions between pda and complex **1** or **2**, we obtained no evidence of allylic alkylations resulting from nucleophilic attack on the coordinated cyclic allyl ligand, although attack at the metal centre of **1** could be induced under certain conditions.

We next investigated the reaction of 3-bromocyclohexene with the pda anion both in the presence and absence of $Mo(CO)_4$bipy. In the absence of the molybdenum complex, the expected product 3-(cyclohex-2-enyl)pentan-2,4-dione was formed in *ca* 15% yield after 0.5 h and *ca* 40% yield after 15 h of reaction in refluxing toluene. In the presence of a 10 mol % of $Mo(CO)_4$bipy, reaction in boiling toluene was complete in 0.5 h, but this time the major product (*ca* 60%) was 3,3′-bicyclohexenyl. Reducing the metal complex concentration had no significant effect on the rate or direction of the reaction. Reversed-phase HPLC and ^{13}C NMR spectroscopy established the presence of *dl* and *meso* forms of the bicyclic product, and showed, rather surprisingly, that no significant diastereoselectivity had occurred in the coupling reaction. The alkylated product 3-(cyclohex-2-enyl)pentan-2,4-dione was isolated as a minor component of the reaction mixture. The only inorganic complex which could be recovered from the reaction mixture and identified with certainty was complex **1**, but strong IR evidence for a non-carbonyl-containing molybdenum–pda entity was also obtained. Under similar conditions, but in the absence of Napda, $Mo(CO)_4$bipy reacted with 3-bromocyclohexene to form a complex mixture of organics, together with impure $MoBr_4$bipy. No detectable amount of the allyl complex (**1**) was found in the reaction mixture. Furthermore, reaction of **1** with excess 3-bromocyclohexene in refluxing toluene did not yield 3,3′-bicyclohexenyl, and **1** remained unchanged at the end of the reaction. Thus the pda anion plays a key role in determining both the inorganic and organic products in this molybdenum-catalysed allylic coupling reaction.

In view of the excellent coordinating properties of the pda anion, and the IR evidence referred to above, it is tempting to postulate the intermediacy of metal–pda complex(es) in the catalytic cycle, and indeed greatly reduced yields of 3,3′-bicyclohexenyl were obtained if pda was replaced by a less effective metal-complexing agent such as $[EtO_2CCH_2CO_2]^-$. However, neither $Mo(CO)_4$bipy nor $Mo(CO)_4$ diphos appear to react with Napda in refluxing toluene in the absence of an allyl halide, nor have we been able to isolate a definite pda complex from any of the catalytic reactions. We find that several other molybdenum complexes (Table 1) also catalyse this homo coupling reaction, although less efficiently than $Mo(CO)_4$bipy, and we tentatively suggest that the metal complex facilitates halogen transfer from the cyclohexenyl bromide to the pda anion which is oxidized in the course of the reaction. In most other metal-assisted reductive coupling reactions, the oxidized product is a metal species,[6] although several examples of organic anions acting as a source of hydride in catalytic cycles are documented.[7]

In order to explore the synthetic utility of this facile coupling reaction, we extended our investigations to other cyclic allyl halides, and found that high yields of 3,3′-bicycloalkenes could also be obtained for seven- and eight-membered ring systems (Table 1). As judged by the integrals of well-resolved, like ^{13}C, atoms, the bicycloheptenyl was obtained again as a 1 : 1 mixture of two diastereoisomers, whereas the bicyclooctenyl was isolated in an approximately 5 : 4 mixture. ^{13}C NMR shift values indicate that the double bonds in the latter compound had the *Z*-configuration.

In both the cyclohexenyl- and cycloheptenyl bromide reactions, a significant proportion of the molybdenum present in the reaction mixture (up to 50%) was converted to the $[MoBr(CO)_2(\eta^3\text{-allyl})bipy]$ species. The identity of the allyl complexes (where $n = 3$ or 4) were confirmed by their independent synthesis from $Mo(CO)_3(NCMe)_3$. However, the preformed allyl complex $[MoBr(CO)_2(\eta^3\text{-}\overline{CH\cdots CH\cdots CH(CH_2)_5})(bipy)]$ differed in its spectroscopic properties from those of the molybdenum-containing species isolated after the catalytic cycle involving cyclooctenyl bromide.

In view of the results obtained from $(\overline{CH_2)_n(CH{=}CHCHBr}$ systems, we decided to extend our investigations to $CH{\equiv}CCH_2X$ (X = Cl or Br) in order to determine whether propargyl

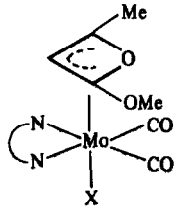
Table 1. Molybdenum-catalysed coupling reactions of $(\overline{CH_2)_nCH{=}CHCH}Br$ (n = 3–5) in the presence of Napda[a]

Metal complex	n	Yield of $\{(CH_2)_nCH{=}CHCH\}_2$ (%)	Yield of $(\overline{CH_2)_nCH{=}CHCH}$pda (%)
$Mo(CO)_4$bipy	3	63	20
$Mo(CO)_6$	3	24	22
[$Mo(CO)_2(\eta^3$-cyclohexenyl)(pda)py]	3	30	23
$Mo(CO)_4$diphos	3	—	45[b]
$Mo(CO)_4$bipy	4	61	12
$Mo(CO)_4$bipy	5	90	—

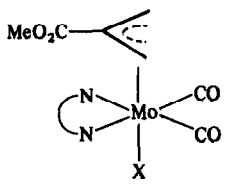
[a] 10 mol % molybdenum complex, 45 mol % Napda and 45 mol % 3-bromocyclohexene in refluxing toluene for 0.5 h.

[b] Reaction time of 2.5 h.

alkylation or coupling reactions could also be effected by molybdenum complexes. Reaction of $CH{\equiv}CCH_2X$ with Napda in the presence of a 10 mol% of $Mo(CO)_4$bipy in refluxing toluene yielded a complex and irreproducible mixture of organics together with molybdenum-containing decomposition products. In the absence of Napda, little reaction occurred in boiling toluene, tetrahydrofuran or dioxan. However, the more nucleophilic $[MoX(CO)_3bipy]^-$ anions reacted cleanly with a methanolic solution of the corresponding propargyl halide to yield a *cis*-dicarbonylmolybdenum complex as an unstable brown solid. Analytical and IR data established that the complex had the composition $[MoX(CO)_2bipy(C_5H_7O_2)]$, and that the coordinated $C_5H_7O_2$ ligand exhibited a strong CO absorption at *ca* 1665 cm^{-1}. It has been shown previously that σ-propargylic molybdenum, tungsten and manganese carbonyl complexes are alkoxycarbonylated in methanol to yield organometallics containing the η^3-2-$MeO_2CC_3H_4$ ligand,[8] but the ^1H NMR data for $[MoCl(CO)_2(bipy)(C_5H_7O_2)]$ (which was of poor quality because of the low solubility of the complex in common solvents), indicate that structure **A** rather than **B** is appropriate for these complexes.



A



B

In an attempt to further define the structure of the $C_5H_7O_2$ ligand, the chloro-complex was reacted with $NaBH_4$ in methanol at −78°C. Column separation of the organic products yielded dimethyl methylsuccinate as the major constituent. Although the mechanism by which this product is formed is unknown, the carbon skeleton of dimethyl methylsuccinate can be readily derived from a complex with structure **A** via hydride attack and CO insertion reactions.

Finally, we would note that, in this two-stage reaction, two new C—C bonds are formed with the overall transformation of a linear three-carbon chain into an isopentane derivative:

$$CH{\equiv}CCH_2X \xrightarrow[NaBH_4 \text{ in MeOH (2)}]{Ph_4P[MoX(CO)_3bipy] \text{ in MeOH (1)}} MeO_2CCH_2CHMeCO_2Me.$$

Further mechanistic and synthetic investigations of this unusual reaction are in progress.

EXPERIMENTAL

All preparations involving metal carbonyl derivatives were performed in an atmosphere of dry N_2 gas using solvents and liquid reagents freed from moisture and oxygen by standard procedures. The starting materials $Mo(CO)_4$bipy, $Mo(CO)_4$diphos, $Ph_4P[MoX(CO)_3(bipy)]$ (where X = Cl or Br) and $(\overline{CH_2)_nCH{=}CHCH}Br$ (where n = 3–5) were prepared by standard literature procedures.[9–11]

IR spectra in the region 200–4000 cm^{-1} were recorded on a Perkin–Elmer 597 spectrophotometer. ^1H and ^{13}C NMR spectra were measured in $CDCl_3$ unless otherwise stated using JEOL PS 100 and FX 90Q FT instruments respectively with $SiMe_4$ as internal standard. Carbon types were identified by the INEPT technique but quoted as if determined by

off-resonance decoupling thus: δ (multiplicity, relative intensity and assignment).

Preparation of

$[MoBr(CO)_2(\eta^3\text{-}\overline{CH{=}CH{=}CH(CH_2)}_n(bipy)]$

(*where* $n = 3$–5)

A solution of $Mo(CO)_6$ (0.528 g, 2×10^{-3} mol) in MeCN (20 cm^3) was heated under reflux for 24 h. To the cooled reaction mixture was added dropwise, with stirring, a solution of the allyl bromide (2×10^{-3} mol) in MeCN (5 cm^3). The resulting suspension of $[MoBr(CO)_2(\eta^3\text{-}\overline{CH\cdots CH\cdots CH(CH_2)}_n)(NCMe)_2]$ was stirred at room temperature with 2,2′-bipy (0.312 g, 2×10^{-3} mol) dissolved in MeCN (5 cm^3). The products were isolated in 64, 77 and 44% yields, respectively, for $n = 3$, 4 or 5 after cooling the reaction mixture in ice for 0.5 h. Found for $[MoBr(CO)_2(\eta^3\text{-}\overline{CH\cdots CH\cdots CH(CH_2)}_3(bipy)]$: C, 46.1; H, 3.8; N, 5.75%. Calc. for $C_{18}H_{17}N_2O_2BrMo$: C, 46.1; H, 3.62; N, 5.97%. ν(CO) (Nujol) 1920 and 1835 cm^{-1}. Found for $[MoBr(CO)_2(\eta^3\text{-}\overline{CH\cdots CH\cdots CH(CH_2)}_4(bipy)]$: C, 47.2; H, 3.80; N, 5.75%. Calc. for $C_{19}H_{19}N_2O_2BrMo$: C, 47.2; H, 3.93; N, 5.80%. ν(CO) (Nujol) 1920 and 1835 cm^{-1}. Found for $[MoBr(CO)_2(\eta^3\text{-}\overline{CH\cdots CH\cdots CH(CH_2)}_5(bipy)]$: C, 48.5; H, 4.40; N, 5.63%. Calc. for $C_{20}H_{21}N_2O_2BrMo$: C, 48.3; H, 4.23; N, 5.63%. ν(CO) (Nujol) 1935 and 1850 cm^{-1}.

Preparation of

$[MoBr(CO)_2(\eta^3\text{-}\overline{CH\cdots CH\cdots CH(CH_2)}_3)(diphos)]$

A mixture of

$[MoBr(CO)_2(\eta^3\text{-}\overline{CH\cdots CH\cdots CH(CH_2)}_3)(NCMe)_2]$

(1.0 g, 2.5×10^{-3} mol) and diphos (1.0 g, 2.5×10^{-3} mol) in MeOH (20 cm^3) was heated under reflux for 0.75 h. The solution was allowed to cool to room temperature whereupon an orange crystalline solid precipitated. The product was collected by filtration, washed with MeOH and dried *in vacuo*. Yield 1.34 g (75%). Found for $[MoBr(CO)_2(\eta^3\text{-}\overline{CH\cdots CH\cdots CH(CH_2)}_3)(diphos)]$: C, 57.6; H, 4.81%. Calc. for $C_{34}H_{33}P_2O_2BrMo$: C, 57.4; H, 4.64%. ν(CO) (Nujol) 1925 and 1830 cm^{-1}.

Preparation of

$[Mo(CO)_2(\eta^3\text{-}\overline{CH\cdots CH\cdots CH(CH_2)}_3)(pda)py]$

A mixture of Napda (0.104 g, 8.53×10^{-4} mol), $[MoBr(CO)_2(\eta^3\text{-}\overline{CH\cdots CH\cdots CH(CH_2)}_3)(bipy)]$ and pyridine (1.5 cm^3) was heated with acetone (5 cm^3) for 15 h during which time the deep red colour of the solution lightened to a pale orange. After cooling, solid NaBr was removed by filtration and the filtrate treated with deaerated water (10 cm^3). Most of the acetone present in the solution was removed with a stream of N_2 gas and the product allowed to crystallize overnight at 0°C. After filtering, the solid was washed with water and dried *in vacuo*. Yield *ca* 50%. Found: C, 52.1; H, 5.20; N, 3.81%. Calc. for $C_{18}H_{21}NO_4Mo$: C, 52.6; H, 5.10; N, 3.41%. ν(CO) (Nujol) 1820 and 1910 cm^{-1}.

Molybdenum-mediated coupling reactions of

$(\overline{CH_2)_nCH{=}CHCH}Br$

(*where* $n = 3$–5)

The general procedure used is illustrated by reference to 3-bromocyclohexene in the presence of Napda and $Mo(CO)_4$bipy. Other reactions were carried out in an analogous manner.

3-Bromocyclohexene (10.1 g, 0.063 mol) was added dropwise to a stirred suspension of $Mo(CO)_4$bipy (5.05 g, 0.014 mol) and Napda (7.66 g, 0.063 mol) in dried oxygen-free toluene. The resulting mixture was stirred and heated under reflux for 0.5 h in an atmosphere of N_2 gas. After cooling, the reaction mixture was filtered and the solvent removed under reduced pressure. The resulting brown oil was chromatographed on 100–200-mesh florisil using hexane as eluant. The product, 3,3′-bicyclohexenyl,[12] was isolated as a colourless oil. Yield 3.22 g (63%). ^{13}C NMR data, mixture of diastereoisomers: 22.4 (t, 49, both C-4s), 25.5 (t, 63, both C-5s), 26.1 (t, 39, both C-6s), 40.3 (d, 45, both C-3s), 127.7 and 128.0 (d, 36, C-1s), and 130.5 and 130.7 (d, 28 and 38, C-2s).

3,3′-Bicycloheptenyl[13] was isolated as a mixture of diastereoisomers in a total yield of 61%. ^{13}C NMR data: 27.0 (t, 97, both C-6s), 28.9, 30.6, 31.2, 31.4 and 31.5 (t, 61, 55, 43, 48 and 61, C-4s, C-5s and C-7s, *not* respectively and with one coincidence), 45.6 and 46.0 (d, 42 and 39, C-3s), 131.4 and 131.7 (d, 37, C-1s), and 136.2 and 136.5 (d, 42 and 45, C-2s).

(*Z*)-(*Z*)-3,3′-bicyclooctenyl was prepared similarly in a 90% yield. ^{13}C NMR data* on the mixture of diastereoisomers. Diastereoisomer **A**: 26.1 (t, 54, C-

* For each diastereoisomer, the C′ set of carbons is identical to the unprimed set and so is included in the data given.

5), 27.4 (t, 75, C-8 and C-7), 29.7 (t, 46, C-6), 34.4 (t, 48, C-4), 40.9 (d, 38, C-3), 129.4 (d, 49, C-1) and 134.4 (d, 47, C-2). Diastereoisomer **B**: 26.0 (t, 43, C-5), 27.0 (t, 69, C-8 and C-7), 30.0 (t, 40, C-6), 34.6 (t, 31, C-4), 41.3 (d, 30, C-3), 129.3 (d, 31, C-1) and 133.2 (d, 37, C-2).

Preparation of 3-*(cyclohex-2-enyl)pentan-2,4-dione*

3-Bromocyclohexene (0.49 g, 2.5×10^{-3} mol) was added dropwise to a stirred suspension of Napda (0.30 g, 2.5×10^{-3} mol) in toluene (5 cm^3). The resulting mixture was heated under reflux for 15 h and then cooled to room temperature and filtered. Toluene was evaporated from the filtrate under reduced pressure to yield the product as a light brown oil (*ca* 40%). The same product was formed more readily (4 h) using MeOH as solvent, and was purified by column chromatography. Found: C, 73.3; H, 8.90%. Calc. for $C_{11}H_{16}O_2$: C, 73.3; H, 8.90%. ^{13}C NMR data: 20.8 (t, 64, C-5'), 25.0 (t, 50, C-4'), 26.8 (t, 53, C-6'), 29.6 and 30.0 (q, 40 and 36, C-1 or C-5), 35.6 (d, 49, C-3'), 74.8 (d, 64, C-3), 127.3 (d, 46, C-1'), 129.9 (d, 61, C-2'), and 203.4 and 203.6 (s, 10 and 9, C-2 or C-4).

Preparation of $[MoX(CO)_2(\eta^3\text{-}C_5H_7O_2)(bipy)]$ (*where* X = Cl *or* Br)

Propargyl halide ($8{,}45 \times 10^{-3}$ mol) was added dropwise to a stirred suspension of $PPh_4[MoX(CO)_3(bipy)]$ (8.45×10^{-3} mol) in dried oxygen-free MeOH at −17°C. The reaction mixture was stirred for 0.5 h at −17°C and then allowed to warm to room temperature and stirred for a further 0.5 h. The brown product was filtered, washed with cold MeOH and dried *in vacuo*. Yield 40% for X = Cl or Br. Found: C, 45.7; H, 3.50; N, 6.49%. ν(CO) (Nujol) 1995, 1930 and 1665 cm^{-1}. Calc. for $C_{17}H_{15}N_2O_4ClMo$: C, 46.1; H, 3.39; N, 6.33%. Found: C, 41.8; H, 3.09; N, 5.76%. Calc. for $C_{17}H_{15}N_2O_4BrMo$: C, 41.9; H, 3.08; N, 5.75%. ν(CO) (Nujol) 1995, 1930 and 1665 cm^{-1}. Both products decomposed on standing and were only sparingly soluble in CH_2Cl_2 or CH_3NO_2. The ^1H NMR spectrum of the chloro-complex was recorded in CD_2Cl_2: δ (ppm) 2.54 (q, J = 2 Hz, 1, CH), 3.08 (s, 3, OMe), 3.15 (d, J = 2 Hz, 3, CMe) and 7.5–8.7 (m, 8, aromatics).

Reaction of $[MoBr(CO)_2(\eta^3\text{-}C_5H_7O_2)(bipy)]$ *with* $NaBH_4$

Solid $NaBH_4$ (1.07 g, 0.028 mol) was stirred for 1 h with a suspension of $[MoBr(CO)_2(\eta^3\text{-}C_5H_7O_2)(bipy)]$ (6.90 g, 0.014 mol) in MeOH (250 cm^3) held at −78°C. The mixture was then allowed to warm to room temperature and stirring was continued for a further 0.3 h. Methanol was removed at reduced pressure to leave a gum which was extracted with Et_2O. After filtration and evaporation of the solvent, the crude oil was chromatographed on 63–200-mesh silica using 6:1 petroleum/ether–ethyl acetate as eluant. Careful fractionation yielded 0.16 g of pure dimethylmethylsuccinate.[14]

Acknowledgement—We thank the University of Bath for a studentship for C.R.W.

REFERENCES

1. B. M. Trost and M. Lautens, *J. Am. Chem. Soc.* 1982, **104**, 5543; 1983, **105**, 3343.
2. C. G. Hull and M. H. B. Stiddard, *J. Organomet. Chem.* 1967, **9**, 519.
3. B. J. Brisdon and G. F. Griffin, *J. Chem. Soc., Dalton Trans.* 1975, 1999.
4. B. J. Brisdon and A. A. Woolf, *J. Chem. Soc., Dalton Trans.* 1978, 291.
5. J. W. Faller, H. H. Murray, D. L. White and K. H. Chao, *Organometallics* 1983, **2**, 400.
6. P. W. Jolly, In *Comprehensive Organometallic Chemistry* (Edited by G. Wilkinson, F. G. A. Stone and E. W. Abel), Vol. 8, Chap. 56.5, p. 713. Pergamon Press, Oxford (1982).
7. P. Helquist, *Tetrahedron Lett.* 1978, 1913; N. A. Cortese and R. F. Heck, *J. Org. Chem.* 1977, **42**, 3491.
8. C. Charrier, J. Collin, J. Y. Merour and J. L. Roustan, *J. Organomet. Chem.* 1978, **162**, 57.
9. J. Chatt, G. J. Leigh and N. Thankarajan, *J. Organomet. Chem.* 1971, **29**, 105.
10. B. J. Brisdon, D. A. Edwards and J. White, *J. Organomet. Chem.* 1978, **156**, 427.
11. A. I. Vogel, *Textbook of Practical Organic Chemistry*, 4th edition, p. 401. Longman, London (1978).
12. P. de Mayo, J. B. Stothers and W. Templeton, *Can. J. Chem.* 1961, **39**, 488.
13. J. Muzart and J. P. Pete, *J. Chem. Soc., Chem. Commun.* 1980, 257.
14. W. Bremser, L. Ernst, B. Franke, R. Gerharts and A. Hardt, *Carbon-13 NMR Spectral Data*, spectrum No. 7217. Verlag Chemie, Weinheim, F.R.G. (1981).

Polyhedron Vol. 5, No. 1/2, pp. 445–449, 1986
Printed in Great Britain

0277-5387/86 $3.00 + .00
© 1986 Pergamon Press Ltd

MONO- AND BINUCLEAR MOLYBDENUM CARBONYL COMPLEXES WITH CHARGE-TRANSFER ABSORPTIONS IN THE NEAR IR

WOLFGANG KAIM,* SYLVIA ERNST and STEPHAN KOHLMANN

Institut für Anorganische Chemie der Universität, Niederurseler Hang, D-6000 Frankfurt am Main 50, F.R.G.

(*Received* 18 *June* 1985)

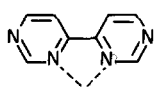
Abstract—Molybdenum(0) carbonyl complexes with very long wavelength charge-transfer absorptions (λ = 700–1000 nm) have been obtained via lowering of the complex lowest unoccupied molecular orbital, viz. by using strongly π-accepting α-diimine ligands, and via raising of the metal highest occupied molecular orbital, viz. by employing the electron-rich metal fragment $Mo(P^nBu_3)_2(CO)_2$. The electronic structures of these compounds were studied by electron and IR spectroscopy, by cyclic voltammetry and by ESR of the anion radicals.

Intense absorptions in the visible region have long been observed for molybdenum carbonyl complexes of α-diimines such as 1,10-phenanthroline,[1] 2,2′-bipyridine,[2] diazabutadienes,[3] pyridine-carbaldimines,[4] 2,2′-bipyrimidine,[5] 2,2′-bipyrazine,[6] 4,4′-bipyrimidine (bpm) (**1**)[7] and 3,3′-bipyridazine.[8] Although binuclear tetracarbonylmolybdenum complexes of 2,2′-bipyrimidine[5] and dicarbonylbis (phosphane)molybdenum complexes of 2,2′-bipyridine[9,10] exhibit long-wavelength absorption maxima up to 675[5] and 810 nm[9], respectively, we set out to push this limit further into the near-IR region of the spectrum in order to understand the interactions between metal fragments and highly π-electron-deficient ligands. Furthermore, there is a need for photocatalyzing absorbers in that spectral region since most photosensitizers used so far have absorption maxima at far smaller wavelengths.[11]

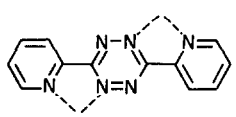
Two approaches to obtain molybdenum carbonyl complexes with metal-to-ligand charge-transfer (MLCT) absorptions in the near IR are described here, employing specially designed α-diimine ligands which have rather positive reduction potentials and are not yet commercially available.

(i) The $Mo(P^nBu_3)_2(CO)_2$ fragment with a rather high lying metal-centered HOMO (highest occupied molecular orbital)[12] was coordinated to the ligand **1** which was recently established to be the best π-acceptor among the bidiazines with α-diimine structure.[7]

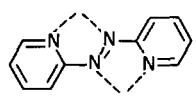
(ii) Mono- and binuclear tetracarbonylmolybdenum complexes of the ligands 3,6-di-2-pyridyl-1,2,4,5-tetrazine [**2** (dptz)] and azo-2,2′-bipyridine [**3** (abpy)] were studied: both these potentially binucleating bis(chelate) ligands contain the azo function —N=N— and are, therefore, highly π-electron-deficient.[13]



1 (BPM)



2 (DPTZ)



3 (ABPY)

Electron and IR spectroscopy as well as cyclic voltammetry allow an assessment of the energy levels relevant to the CT transitions; in addition, ESR studies of the anion radicals help to establish the character of the half-occupied molecular orbital, i.e. the LUMO (lowest unoccupied molecular orbital) of the neutral complex.

* Author to whom correspondence should be addressed.

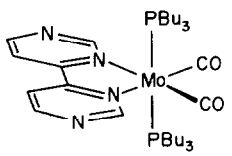
Table 1. Spectral data of molybdenum carbonyl complexes with π-electron-deficient α-diimine ligands

	ν(CO)[a] (cm^{-1})				λ_{max} (nm)			E (V vs SCE)[b]	
					Hexane	Toluene	THF	Oxidation	Reduction
$Mo(CO)_4(bpm)$[7]	2010	1910	1900sh	1855	[c]	630 380	580 365	+0.74[d]	−0.87 −1.48
$Mo(P^nBu_3)_2(CO)_2(bpm)$		1865	1785		862 507	865 505	870 510	−0.14	−1.21
$Mo(CO)_4(dptz)$	2005	1928(br)		1877	[c]	688	637	[d]	−0.30[e]
$Mo_2(CO)_8(dptz)$	1995	1940(br)		1875	[c]	909	849	[d]	−0.18
$Mo(CO)_4(abpy)$	2008	1942(br)		1878	630	627	620	[d]	−0.69
$Mo_2(CO)_8(abpy)$	1990	1953	1935sh	1880	952[f]	918	901	[d]	−0.06

[a] THF solution.
[b] Cyclic voltammetry (100 mV s^{-1}) in CH_3CN–0.1 M $Bu_4N^+ClO_4^-$.
[c] Insufficient solubility.
[d] Irreversible oxidation wave.[14]
[e] DMF–0.1 M $Bu_4N^+ClO_4^-$.
[f] Isooctane solution.

RESULTS AND DISCUSSION

Table 1 summarizes the spectroscopic data which are relevant to the electronic structures of the complexes. The data from this table and the absorption spectrum shown in Fig. 1 illustrate that the first approach, i.e. raising the metal-centered HOMO via PR_3 introduction in the *cis*-position



leads indeed to compounds with very low-energy charge-transfer absorptions. Compared to corresponding 2,2′-bipyridine complexes (λ_{max} = 810 and 524 nm in benzene[9]) the bpm complex $Mo(bpm)(P^nBu_3)_2(CO)_2$ exhibits a bathochromically shifted first and a hypsochromically shifted second allowed CT absorption: the latter is assigned to a transition from the metal orbitals to the second lowest unoccupied molecular orbital (SLUMO) of ligand **1**.[10]

The shifts relative to the corresponding tetracarbonylmolybdenum complex[7] are mainly due to a strongly raised HOMO level, as indicated by the considerably lowered oxidation potential (Table 1), while the reduction potential of the complex has been shifted to a much lesser extent. In agreement with previous results on such α-diimine complexes[9,10] we observe a very small positive solvatochromism[15] for the near-IR (NIR) band: however, we do not attribute this phenomenon to a reversal of the transition character (MLCT → LMCT[10]); it rather seems that phosphine substitution in such complexes leaves the ground state less polarized and/or the excited state more polarized, and eventually this may turn the negative into a positive solvatochromism. Support for this explanation comes from an

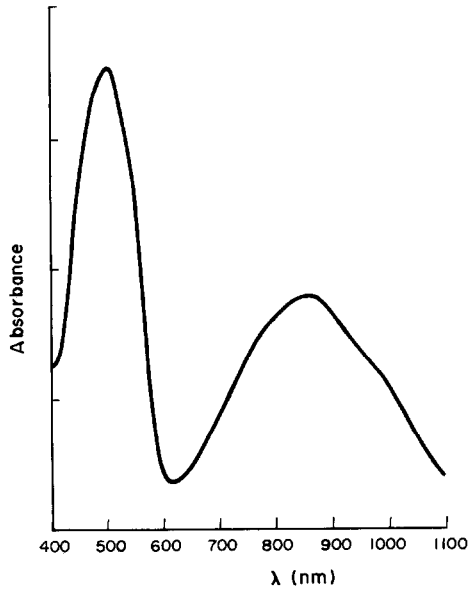


Fig. 1. VIS–NIR absorption spectrum of *cis*-$Mo(P^nBu_3)_2(CO)_2(bpm)$ in hexane.

ESR study of the anion radical complex $Mo(P^nBu_3)_2(CO)_2(bpm^{\cdot-})$ which clearly shows (Fig. 2) a similarity to the tetracarbonylmolybdenum complex radical,[7,8] except for a large ^{31}P coupling[9] originating from hyperconjugative (π^*/σ^*_{Mo-P}) spin transfer to the ^{31}P nuclei in the *cis*-position.[16,17] These results indicate that the MO which has taken up an electron still has a predominantly π^* (bpm) character.

Finally, a comparison of CO stretching frequencies between bpm (Table 1) and 2,2'-bipyridine dicarbonyl complexes [ν(CO) = 1818 and 1745 cm^{-1} in CS_2[9]] also illustrates the better back-bonding behaviour of the former ligand; the favourable combination of good π-acceptor *and* σ-donor properties of bpm[7] becomes manifest through relatively high values of ν(CO).

In the second approach, mono- and binuclear tetracarbonylmolybdenum(0) complexes of the very π-electron-deficient ligands **2** and **3** were prepared.[13] Whereas the mononuclear species have CT absorptions still in the visible region, the binuclear complexes absorb between 810 and 950 nm, exhibiting high extinction coefficients (ε) of $\sim 10^4$–10^5 $M^{-1}\,cm^{-1}$ and negative solvatochromism (Table 1). These extremely low-energy transitions are primarily the result of an additional lowering of the π^*-acceptor levels by double $Mo(CO)_4$ coordination: electrochemical data (Table 1) show that the binuclear complexes are reduced at potentials similar to that of the saturated calomel reference electrode (SCE)!

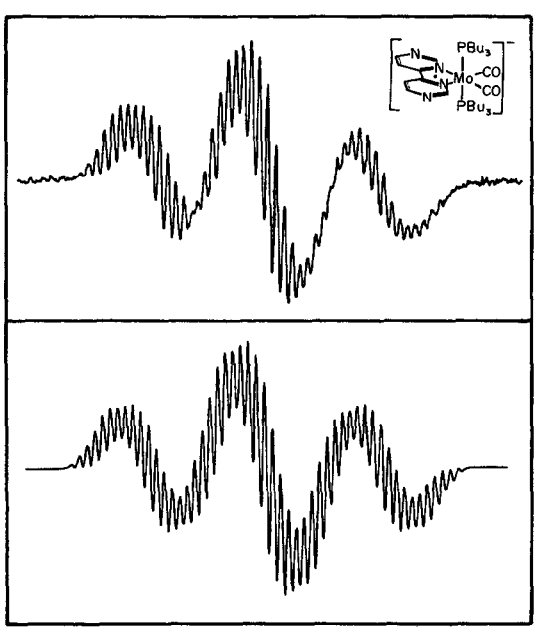


Fig. 2. Experimental (top) and computer-simulated (bottom) ESR spectrum of the anion radical complex *cis*-$Mo(P^nBu_3)_2(CO)_2(bpm^{\cdot-})$, generated with potassium in THF. The high-field component of the ^{31}P triplet is severely affected by anisotropic line broadening. Computer simulation parameters: $a_{^{31}P} = 1.974$ mT (2P), $a_N = 0.283$ mT (2N), $a_N = 0.24$ mT (2N), $a_H = 0.14$ mT (4H), line width 0.06 mT, $g = 2.0024$.

Reversible reduction occurring at such positive potentials has allowed us to obtain persistent anion radical complexes by chemical reductants such as potassium metal in THF. These radical products were readily prepared from the binuclear tetracarbonylmolybdenum species: however, the anion radical complex $Mo_2(CO)_8(abpy)^{\cdot-}$) displayed a very complex ESR hyperfine pattern, indicating extensive spin delocalization on to the pyridine rings. On the other hand, the spectrum of the complex $Mo_2(CO)_8(dptz^{\cdot-})$ is comparatively simple (Fig. 3), showing interaction of the unpaired electron only with the two pairs of ^{14}N nuclei in the central tetrazine ring and with the magnetically active ($I = \frac{5}{2}$) molybdenum isotopes $^{95,97}Mo$. The larger of the two ^{14}N coupling constants is assigned to the two metal-coordinated nitrogen centers of the tetrazine ring because of Hückel MO calculation results[18] and because of the general increase of $a_{^{14}N}$ upon molybdenum carbonyl coordination.[17,19–21] Since both isotopes ^{95}Mo (15.8% natural abundance) and ^{97}Mo (9.6% natural abundance) have similar magnetic moments and identical nuclear spins ($I = \frac{5}{2}$), they have not been treated separately. According to statistics,[17,18] the probabilities of the three possible isotope combinations are 0.557 for the species with no $^{95,97}Mo$ isotopes, 0.379 for the complex with one magnetically active isotope $^{95,97}Mo$, and 0.064 for the species where both molybdenum centers have a nuclear spin of $\frac{5}{2}$. The combination with one isotope $^{95,97}Mo$ gives rise to observable satellites (Fig. 3) due to further splitting of the main spectrum into a sextet ($I = \frac{5}{2}$).

Thus, the paramagnetic compound $Mo_2(CO)_8(dptz^{\cdot-})$ represents another example of binuclear molybdenum carbonyl complexes with bridging anion radical ligands: previously studied complexes have included pyrazine and 4,4'-bipyridine,[19,20] quinoxaline, phenazine and 1,2-bis(pyridyl)ethene,[20] 2,1,3-benzochalcogenadiazole[21] and 2,2'-bipyrimidine[17] anion radicals. Some apparently related radical complexes reported recently[22] have not been analyzed in detail. In all analyzed cases, the results for the ligand-centered singly occupied molecular orbital (SOMO), the LUMO of the neutral complex, confirm the assignment of the intense low-energy absorption as a metal-to-ligand ($\pi^* \leftarrow d$) CT transition.

The very unusual electronic situation in the binuclear tetracarbonylmolybdenum complexes with the dptz and abpy ligands is also reflected by

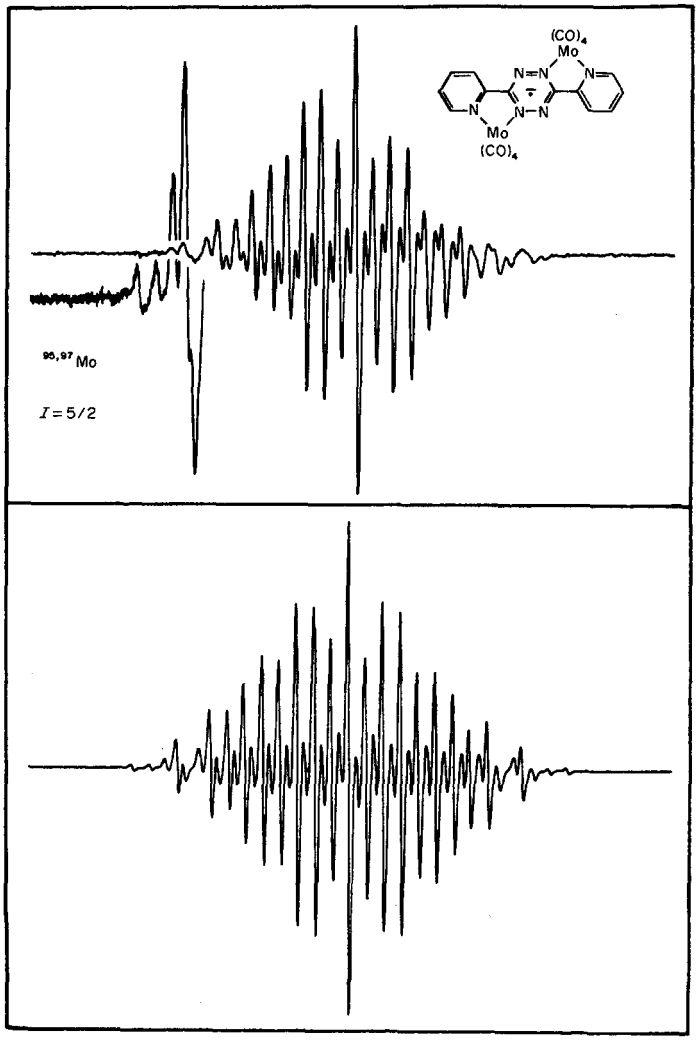


Fig. 3. Experimental (top) and computer-simulated (bottom) ESR spectrum of the anion radical complex $Mo_2(CO)_8(dptz^{\cdot-})$ in THF, counterion K^+. The amplified wing section (top) reveals $^{95,97}Mo$ isotope coupling. Computer simulation parameters: $a_N = 0.640$ mT (2N), $a_N = 0.418$ mT (2N), $a_{^{95,97}Mo} = 0.220$ mT (2 Mo, 25.4% natural abundance), line width 0.05 mT, $g = 2.0045$.

their carbonyl stretching frequencies; the four IR-active vibrational transitions are compressed into a frequency range of only 110 cm^{-1} (Table 1). Force constant calculations according to the Cotton–Kraihanzel method[23] yield values of $k_1 = 14.43$, $k_2 = 15.70$ and $k_i = 0.16$ mdyn $Å^{-1}$, and indicate unusually[6,24] strong back-bonding with these highly π-electron-deficient α-diimine ligands.

EXPERIMENTAL

The molybdenum complexes were prepared and studied taking the usual precautions, excluding air, moisture and intense light. Spectra were recorded on the following instruments: Pye Unicam SP 1800 (VIS absorption spectra), Perkin–Elmer Lambda 9 (NIR absorption spectra), Perkin–Elmer 283 B (IR spectra), Varian E9 (ESR spectra), Bruker WH 270 (^1H NMR spectra), and PAR 173/175 (cyclic voltammetry). Anion radical complexes were generated by potassium reduction of the neutral complexes in THF *in vacuo*: computer simulations of the spectra were performed on an HP 72220 S plotter using the VAX 750/11 and the available program.[25] Microanalyses were carried out by Prof. W. Ried and his staff at this Department.

Ligands **1–3** were prepared according to known procedures.[7,13] The complex $Mo(P^nBu_3)_2(CO)_2(bpm)$ was obtained from **1**[7] and $Mo(P^nBu_3)_3(CO)_2(CH_3CN)$ by the method of tom Dieck *et al.*[9] and was purified by recrystallization from toluene–acetonitrile. Dark-blue crystals. Yield 87%. ^1H NMR (C_6D_6): δ 0.79 (m, 18H), 1.09 (m,

24H), 1.32 (m, 12H), 7.05 (d, 2H), 7.94 (d, 2H), 10.40 (s, 2H). Found: C, 57.07; H, 8.40; N, 7.70%. Calc. for $C_{34}H_{60}MoN_4P_2O_2$: C, 57.13; H, 8.46; N, 7.83%. Tetracarbonylmolybdenum complexes of ligands **2** and **3** were synthesized from tetracarbonyl(η^2,η^2-bicyclo[2.2.1]hepta-2,4-diene)molybdenum and the ligands in toluene.[13]

Acknowledgements—This work has been supported by the Deutsche Forschungsgemeinschaft, Fonds der Chemischen Industrie, Flughafen Frankfurt/Main AG, BASF AG and by the Karl Winnacker Foundation. We thank Mr. D. Ventur and Prof. K. Wieghardt (Ruhr-Universität Bochum) for absorption measurements in the NIR region.

REFERENCES

1. W. Hieber and F. Mühlbauer, *Z. Anorg. Allg. Chem.* 1935, **221**, 337.
2. E. W. Abel, M. A. Bennett and G. Wilkinson, *J. Chem. Soc.* 1959, 2323.
3. H. Bock and H. tom Dieck, *Angew. Chem.* 1966, **78**, 549; *Angew. Chem., Int. Ed. Engl.* 1966, **5**, 520; *Chem. Ber.* 1967, **100**, 228.
4. H. Brunner and W. A. Herrmann, *Chem. Ber.* 1972, **105**, 770.
5. C. Overton and J. A. Connor, *Polyhedron* 1982, **1**, 53.
6. R. J. Crutchley and A. B. P. Lever, *Inorg. Chem.* 1982, **21**, 2276.
7. S. Ernst and W. Kaim, *Angew. Chem.* 1985, **97**, 431; *Angew. Chem., Int. Ed. Engl.* 1985, **24**, 430.
8. S. Ernst and W. Kaim, *Inorg. Chim. Acta* (in press).
9. H. tom Dieck, K.-D. Franz and F. Hohmann, *Chem. Ber.* 1975, **108**, 163.
10. R. W. Balk, D. J. Stufkens and A. Oskam, *Inorg. Chim. Acta* 1978, **28**, 133.
11. J. R. Bolton, *Science* 1978, **202**, 705; In *Inorganic Chemistry: Toward the 21st Century* (Edited by M. H. Chisholm), p. 3. ACS Symposium Series 211, American Chemical Society (1983).
12. Cf. C. J. Pickett and D. Pletcher, *J. Organomet. Chem.* 1975, **102**, 327.
13. S. Kohlmann, S. Ernst and W. Kaim, *Angew. Chem.* 1985, **97**, 698; *Angew. Chem., Int. Ed. Engl.* 1985, **24**, 684.
14. Cf. H. tom Dieck and E. Kühl, *Z. Naturforsch.* 1982, **37B**, 324.
15. C. Reichardt, *Solvent Effects in Organic Chemistry*, p. 196. Verlag Chemie, Weinheim (1979). Cf. also I. W. Renk and H. tom Dieck, *Chem. Ber.* 1972, **105**, 1403.
16. W. Kaim, *J. Organomet. Chem.* 1984, **262**, 171.
17. W. Kaim, *Inorg. Chem.* 1984, **23**, 3365.
18. W. Kaim, S. Ernst, S. Kohlmann and P. Welkerling, *Chem. Phys. Lett.* 1985, **118**, 431.
19. W. Kaim, *Inorg. Chim. Acta* 1981, **53**, L151.
20. W. Kaim, *Chem. Ber.* 1982, **115**, 910.
21. W. Kaim, *J. Organomet. Chem.* 1984, **264**, 317.
22. J. A. Connor, E. J. James and C. Overton, *Polyhedron* 1985, **4**, 69; cf. also ref. 5.
23. F. A. Cotton and C. S. Kraihanzel, *J. Am. Chem. Soc.* 1962, **84**, 4432.
24. W. Kaim, S. Ernst and S. Kohlmann, manuscript in preparation.
25. W. Kaim and H. Bock, *J. Organomet. Chem.* 1979, **164**, 281.

Polyhedron Vol. 5, No. 1/2, pp. 451–459, 1986
Printed in Great Britain

0277–5387/86 $3.00 + .00
© 1986 Pergamon Press Ltd

ACETALDEHYDE COMPLEXES OF MOLYBDENUM

J. TREVOR GAUNTLETT and MARK J. WINTER*

Department of Chemistry, The University, Sheffield S3 7HF, U.K.

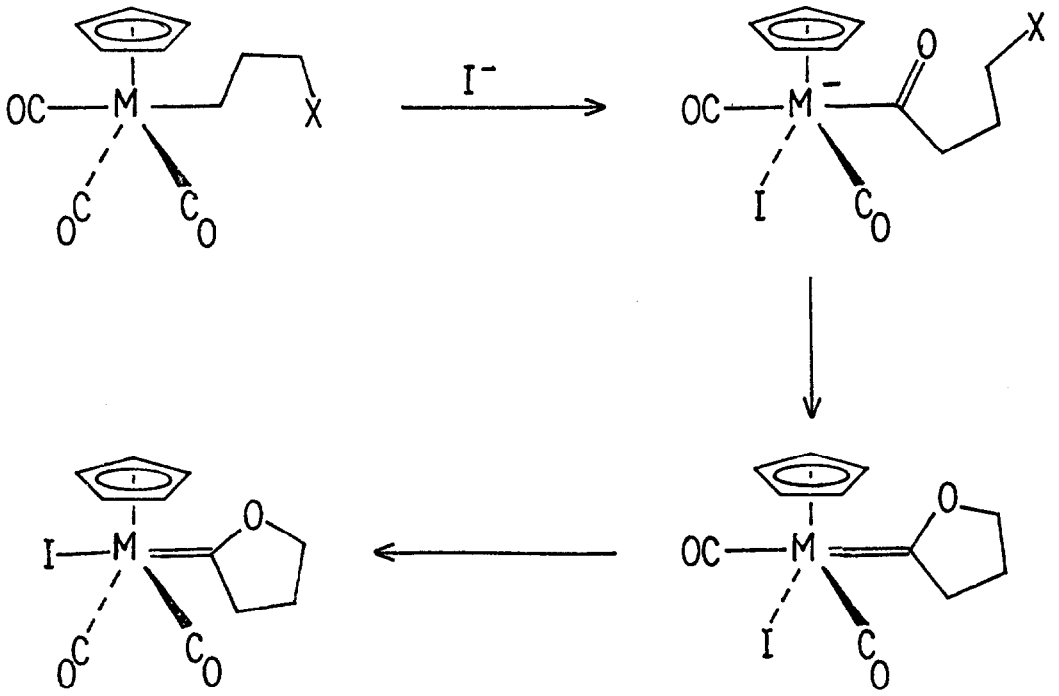
(*Received* 17 *June* 1985)

Abstract—Addition of $LiEt_3BH$ to a solution of $MoMe(CO)_3(\eta\text{-}C_5H_5)$ allows the successive observation of the formyl alkyl $[Mo(CHO)Me(CO)_2(\eta\text{-}C_5H_5)]^-$, the hydrido acyl $[Mo(COMe)H(CO)_2(\eta\text{-}C_5H_5)]^-$, and the ultimate product, a species formulated as a complex of coordinated acetaldehyde, $[Mo(CO)_2(\eta^2\text{-}MeCHO)(\eta\text{-}C_5H_5)]^-$. All three anions are spectroscopically characterized. Addition of MeI to the acetaldehyde complex in the presence of PPh_3 or CO results in smooth formation of *trans*-$MoMe(CO)_2(PPh_3)(\eta\text{-}C_5H_5)$ or $MoMe(CO)_3(\eta\text{-}C_5H_5)$ together with the evolution of acetaldehyde; the latter case is therefore a stoicheiometric synthesis of acetaldehyde. The reaction of $PhCH_2Br$ with $[Mo(CO)_2(\eta^2\text{-}MeCHO)(\eta\text{-}C_5H_5)]^-$ provides a high-yield synthesis of $Mo(CO)_2(\eta^3\text{-}CH_2C_6H_5)(\eta\text{-}C_5H_5)$ while the η^3-allyl complex $Mo(CO)_2(\eta^3\text{-}C_3H_5)(\eta\text{-}C_5H_5)$ is formed in the corresponding reaction of allyl bromide. The position of alkylation is different using $[Me_3O][BF_4]$ and the primary product $Mo(\eta^2\text{-}CHMeOMe)(CO)_2(\eta\text{-}C_5H_5)$ arises from alkylation of the aldehyde oxygen atom. This species reacts with PPh_3 with O → Mo bond cleavage and formation of $Mo(CHMeOMe)(CO)_2(PPh_3)(\eta\text{-}C_5H_5)$. According to the conditions of workup the cationic ylide complex $[Mo(CHMePPh_3)(CO)_2(PPh_3)(\eta\text{-}C_5H_5)][BF_4]$ can also be formed. Reaction of $[Mo(\eta^2\text{-}MeCHO)(CO)_2(\eta\text{-}C_5H_5)]^-$ with several oxidizing agents, such as Fe(III), $[Fe(\eta\text{-}C_5H_5)_2]^+$, $[C_7H_7]^+$ or $[Mo(CO)_3(\eta\text{-}C_7H_7)]^+$, leads to the η^2-acetaldehyde complex $Mo_2(CO)_4(\mu\text{-}\eta^2\text{-}MeCHO)(\eta\text{-}C_5H_5)_2$ in which the carbon atom of the aldehyde is bound to a single metal but the oxygen atom bridges both metal atoms. Formally the aldehyde is a four-electron donor to the dimolybdenum system. The same product arises in the reaction of both $[M(CO)_3(\eta\text{-}C_5H_5)][BF_4]$ (M = Mo or W) with $[Mo(CO)_2(\eta^2\text{-}MeCHO)(\eta\text{-}C_5H_5)]^-$, no heterobimetallic aldehyde compounds are formed suggesting that $Mo_2(CO)_4(\mu\text{-}\eta^2\text{-}MeCHO)(\eta\text{-}C_5H_5)_2$ is formed after an initial electron-transfer process.

A short time ago we reported syntheses of cyclic carbene complexes **1** and **2** through the iodide-induced cyclization of $M([CH_2]_3X)(CO)_3(\eta\text{-}C_5H_5)$ (**3**) (Scheme 1).[1,2] Other nucleophiles such as CN^-, SPh^- or $[W(CO)_3(\eta\text{-}C_5H_5)]^-$ are suitable for this cyclization[2–4] and a related reaction leading to a cationic species is also known.[5,6] Perhaps naively we thought that a nucleophilic hydride source might induce a similar such cyclization so forming a hydride carbene of type **4**. It occurred to us that such a species might react with nucleophiles and that it would be possible to observe hydride to carbene migrations. This is important since, although such processes are often invoked to explain aspects of carbene chemistry, well-defined examples are rare.

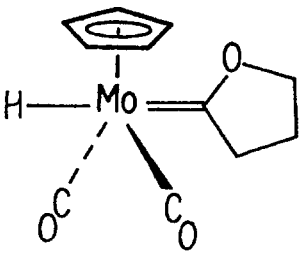
One such hydride source is $LiEt_3BH$. In fact, the major isolated product from the reaction of $LiEt_3BH$ and **3** is compound **5** rather than **4**.[7] It is possible to view formation of **5** as proceeding by an analogous cyclization step forming the hydrido carbene **4** which subsequently undergoes a hydride to carbene migratory insertion reaction in which the ring oxygen atom functions as an intramolecular source of nucleophile (Scheme 2, path A). Compound **5** is also obtained from the reaction of carbene **1** with $LiEt_3BH$, although probably by a different mechanism.[8] These processes are quite complex and one of the ways we attempted to understand these results was to initiate a study on the interactions of hydride-donor reagents with molybdenum complexes containing simpler alkyl functions. A suitable reaction is that of $MoMe(CO)_3(\eta\text{-}C_5H_5)$ (**6**) with

* Author to whom correspondence should be addressed.

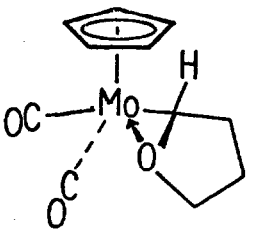


1 M=Mo
2 M=W

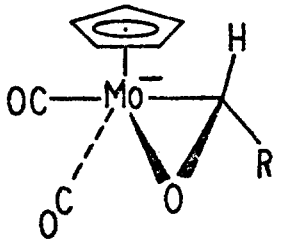
Scheme 1. Nucleophile-induced cyclization of $Mo[(CH_2)_3X](CO)_3(\eta\text{-}C_5H_5)$.



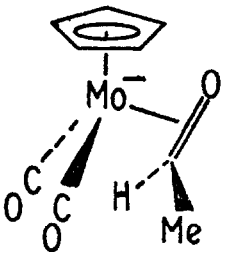
4



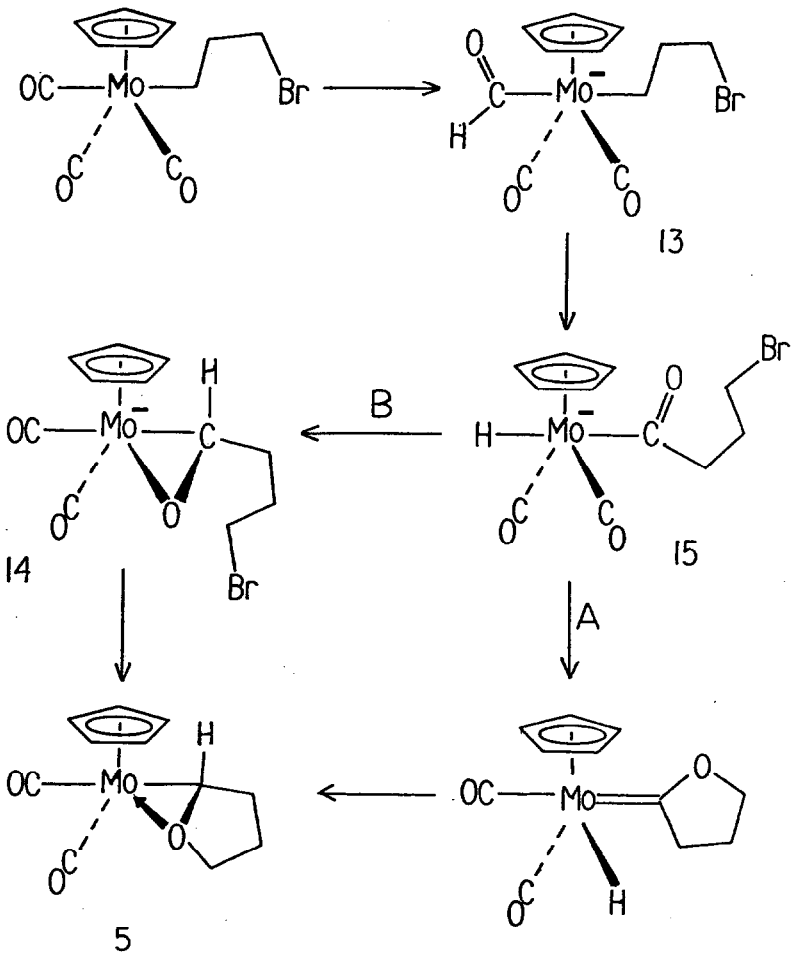
5



7 R=Me
11 R=Et
12 R=CH_2Ph



8

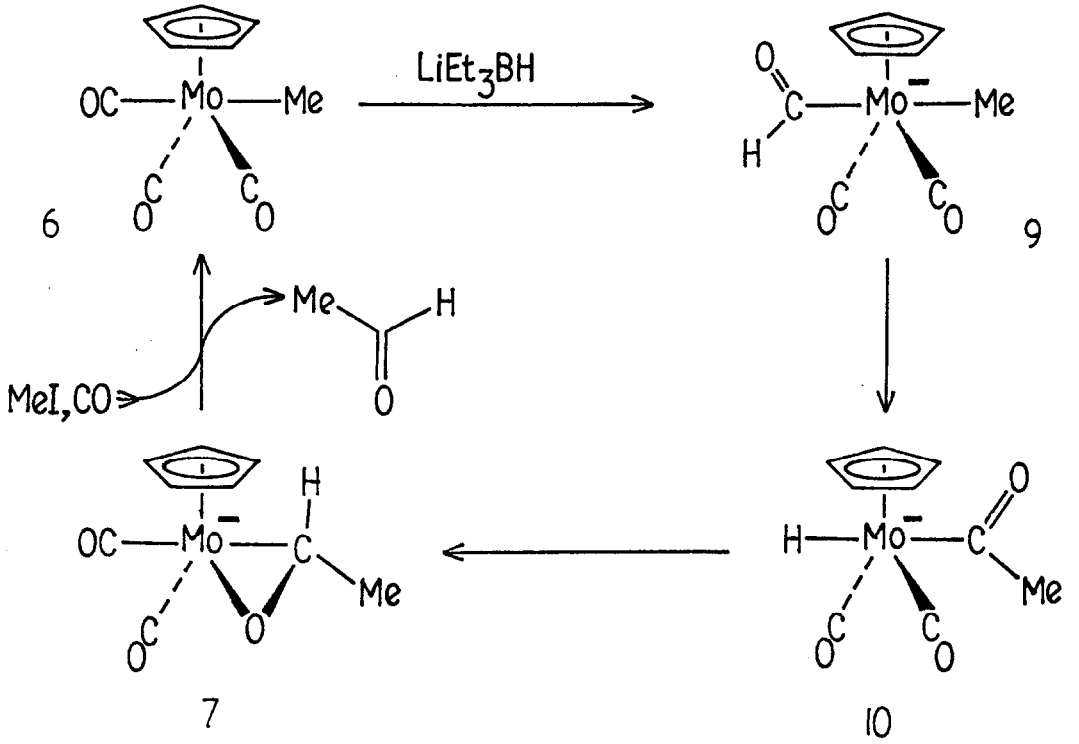


Scheme 2. Two possible pathways for the formation of $\overline{Mo[\eta^2\text{-}CH(CH_2)_3O]}(CO)_2(\eta\text{-}C_5H_5)$ from the reaction of $Mo[(CH_2)_3Br](CO)_3(\eta\text{-}C_5H_5)$ with $LiEt_3BH$.

$LiEt_3BH$, the initial aim being to identify the position of hydride attack at the metal complex.

This reaction proceeds readily at room temperature and the ultimate product is a spectroscopically characterized anion formulated as $[Mo(CO)_2(\eta^2\text{-}MeCHO)(\eta\text{-}C_5H_5)]^-$ (7).[9,10] We have succeeded in isolating **7** with a 12-crown-4 lithium complex as counter ion as a solid but have yet to obtain suitable crystals for X-ray analysis. Until we have a crystal structure of this molecule we choose to depict this molecule with the representation **7**, a metalla-oxirane, in common with representations of other aldehyde or ketone complexes that have been crystallographically characterized.[11–14] However, the alternative representation as **8** also seems reasonable. It is noteworthy that the IR spectrum of the crown complex is identical to that of the parent species in THF solution, suggesting that **7** exists as solvent-separated ion pairs in solution rather than contact ion pairs. It is also possible to write dimeric structures for this species: such a possibility is currently being examined but the chemistry of **7** delineated thus far can be rationalized satisfactorily using **7** as a representation.

The anion **7** is not the primary product: by initiating the reaction at −78°C and allowing the reaction to warm slowly to room temperature it is possible to identify two intermediates, the formyl alkyl **9** and the hydrido acyl **10** (Scheme 3) by monitoring the ^1H and ^{13}C NMR and the IR spectra at low temperatures.[9,10] Formyl complexes arising from hydride additions to carbonyls are now well-known, although there are comparatively few molybdenum examples.[15–18] They are characterized by high-frequency signals in the ^1H NMR spectrum,[19] in this case a signal is observed at δ 14.3. The relative intensities of the bands in the carbonyl IR spectrum[20] and the presence of only a single carbonyl signal in the ^{13}C NMR spectrum are in accord with the *trans* geometry depicted. The



Scheme 3. Stoicheiometric synthetic cycle for acetaldehyde based on $MoMe(CO)_3(\eta\text{-}C_5H_5)$.

rearrangement to the hydrido acyl is unusual although there are some examples of complexes containing both hydride and acyl ligands.[21–24] Compound **10** is characterized by a low-frequency signal (δ −5.15), indicative of a metal hydride. We presume that the driving force converting **9** to **10** is the higher bond energy associated with an Mo—H bond relative to an Mo—alkyl bond. Compound **10** undergoes a formal migration of the hydride to the acyl carbon (one could also view this as a hydride to carbenoid atom migration). We do not yet know whether this step is inter- or intramolecular. The important feature of this last step is that a hydride ligand and an acyl ligand combine at a metal to produce a ligated aldehyde.

The closely related complexes $[Mo(CO)_2(\eta^2\text{-}RCHO)(\eta\text{-}C_5H_5)]^-$ (**11**, R = Et; and **12**, R = CH_2Ph) are formed in the reactions of $MoR(CO)_3(\eta\text{-}C_5H_5)$ with $LiEt_3BH$. Although not fully spectroscopically characterized the IR spectra in the carbonyl region, at least, are identical to that of **7** in THF.

Formation of **7** in this reaction allows us to comment on the formation of **5** in the reaction of **1** with $LiEt_3BH$. There are two items of information relevant here. The results of monitoring by low-temperature NMR spectroscopy suggest that the initial product is a formyl complex (**13**) [δ(THF) 14.2]. The results of IR monitoring clearly shows that the ultimate product, **5**, is produced at the expense of an intermediate whose IR spectrum in the carbonyl region is identical to that of **7**. This species is almost certainly **14**. Although we have not unambiguously identified a hydride resonance in the NMR spectrum of this reaction upon warming it does seem likely that **15** is an intermediate by analogy to the formation of **7**. Therefore, compound **5** is formed through ring closure from an anionic aldehyde complex **14** (Scheme 2, path B) rather than migration of hydride to a carbene ligand (Scheme 2, path A).

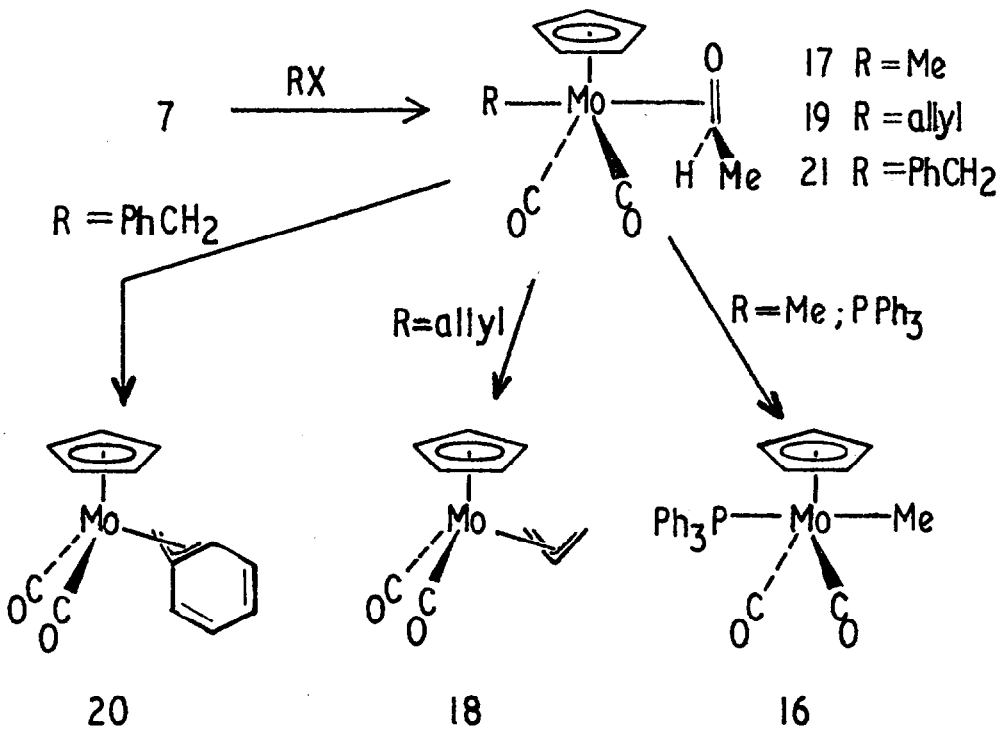
Having established a working model for the mechanism of formation of **5** an investigation of the chemistry of **7** was clearly required, with views to contrasting its reactivity with that of $[Mo(CO)_3(\eta\text{-}C_5H_5)]^-$, to see if the aldehyde could be liberated, and to determine whether a modified system could catalytically generate aldehydes.

Addition of MeI to a THF solution containing **7** results in a very slow reaction whose only identified ultimate product is a low yield of **6**, some of which at least arises from reaction of the very small quantities of $[Mo(CO)_3(\eta\text{-}C_5H_5)]^-$ generally present in solutions of **7** with MeI. Even a prolonged reaction time does not result in any observed products in the reaction of **7** with PPh_3: in particular, there is no tendency for the PPh_3 to exchange with the MeCHO

ligand in the anion **7**.[10] However, when **7** is treated with MeI in the presence of PPh_3 the phosphine complex *trans*-$MoMe(CO)_2(PPh_3)(\eta\text{-}C_5H_5)$ (**16**) is formed smoothly. We regard this as proceeding by nucleophilic replacement of the I^- of MeI by anion **7**, giving an undetected intermediate $MoMe(CO)_2(MeCHO)(\eta\text{-}C_5H_5)$ (**17**) (Scheme 4) from which MeCHO is evolved through substitution of the labile MeCHO by the two-electron ligand PPh_3. An alternative two-electron ligand is provided by CO itself. Addition of MeI to a solution of **7** maintained under a CO atmosphere (1 atm) provides the alkyl **6** in very good yield, together with MeCHO, which may be analysed by GLC and GC–mass spectrometry.[10] These two reactions probably share the same intermediate (**17**). The last result is particularly interesting in that it closes a stoicheiometric cycle for the synthesis of acetaldehyde (Scheme 3).

Both these two reactions employ an external or intermolecular source of a two-electron ligand. It is also possible to arrange matters so that the new two-electron ligand is provided by an intramolecular source. Addition of allyl bromide to a solution of **7** swiftly results in formation of the known η^3-allyl derivative, $Mo(CO)_2(\eta^3\text{-}C_3H_5)(\eta\text{-}C_5H_5)$ (**18**), isolated in moderate yield after chromatography and crystallization.[25] The probable intermediate is **19**, a labile complex from which MeCHO is displaced by intramolecular attack of the pendant ene group at the metal. An interesting related phenomenon is observed in the reaction of **7** with benzyl bromide. Here the major product is the η^3-benzyl $Mo(CO)_2(\eta^3\text{-}CH_2Ph)(\eta\text{-}C_5H_5)$ (**20**), isolated in 64% yield after chromatography and crystallization. This is a known compound,[26] but the previous synthesis is of low yield and relatively arduous. The η^1-benzyl $Mo(\eta^1\text{-}CH_2Ph)(CO)_3(\eta\text{-}C_5H_5)$ is isolated in very low yield as a byproduct, probably arising from reaction of the small quantities of $[Mo(CO)_3(\eta\text{-}C_5H_5)]^-$ present in the solution of **7** with $PhCH_2Br$. Compound **20** will be formed from the intermediate **21**: in this case the aromatic ring itself is the intramolecular source of nucleophile.

These reactions rely upon the nucleophilic replacement of halide from an organic halide: effectively this is the formal addition of an R^+ group to the metal. Another source of R^+ is provided by the reagent $[Me_3O][BF_4]$, but it is quite common for it to display a different reactivity with organotransition-metal substrate when compared to RX. This is the case here. Addition of solid $[Me_3O][BF_4]$ to a THF solution of **7** at −78°C followed by warming towards ambient temperature provides a solution whose IR spectrum in the carbonyl region is superimposable upon that of **5**, suggesting that methylation occurs at the oxygen

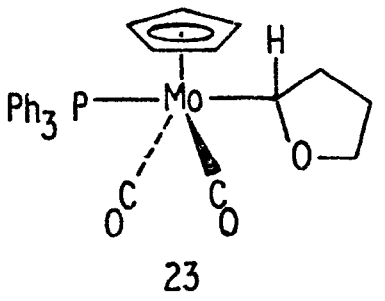


Scheme 4. Reactions of $[Mo(\eta^2\text{-}MeCHO)(CO)_2(\eta\text{-}C_5H_5)]^-$ with C_3H_5Br, $PhCH_2Br$ and MeI–PPh_3.

atom and that the product is **22**. Regrettably the product is extremely sensitive to air and decomposes upon attempted chromatography, so it remains unisolated as a pure material.

Compound **5** reacts with PPh_3 to give **23**, in which the Mo ← O bond is cleaved by the two-electron PPh_3 ligand. This is entirely reasonable, since one can regard the oxygen–molybdenum interaction in **5** as an ether coordinated to a metal and therefore expected to be very labile. Analogus behaviour is observed for **22**, supporting the structural assignment.

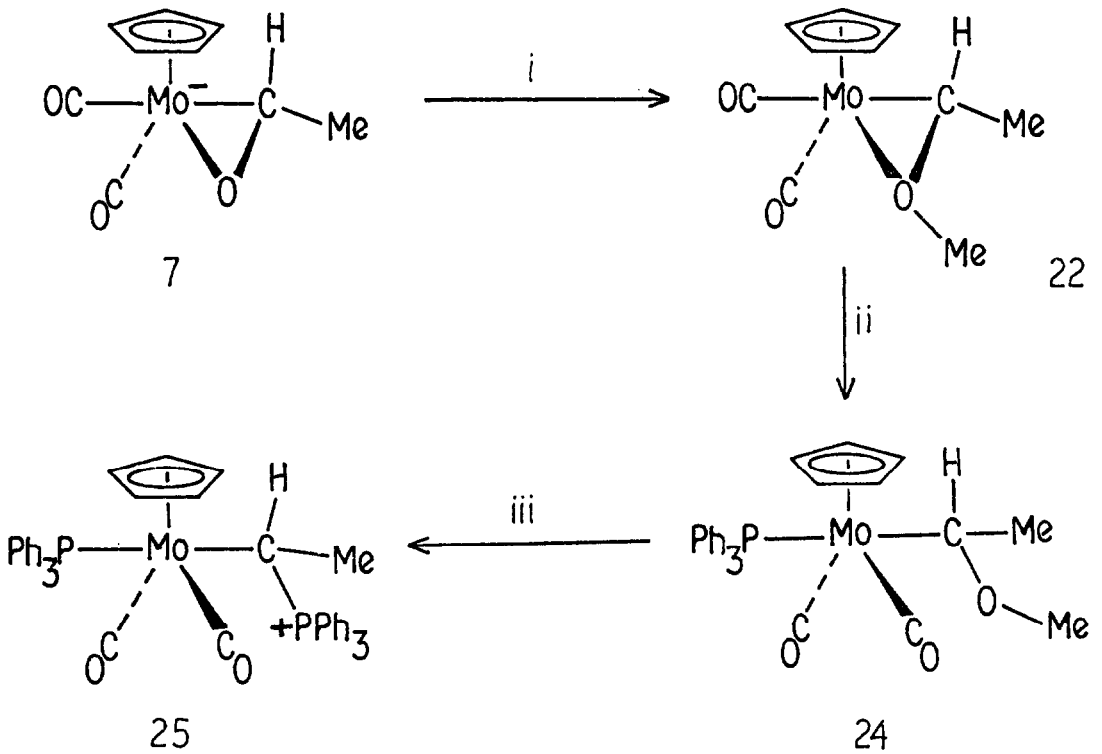
This reaction is conveniently carried out by allowing a solution of **7** in THF to warm up from −78°C to ambient temperature in the presence of solid PPh_3 and solid $[Me_3O][BF_4]$. Neither reagent is particularly soluble under these conditions, but during the time taken to warm up the IR spectrum of the reaction mixture changes first to one indicating formation of **22** (that is, identical to the IR spectrum of the reaction involving $[Me_3O][BF_4]$ alone) but whose bands in turn are replaced by two new bands typical of a *trans*-$MoR(CO)_2(PPh_3)(\eta\text{-}C_5H_5)$ molecule and which overlap with those of the cyclic alkyl **23**. Provided the reaction mixture is filtered through alumina to remove excess $[Me_3O][BF_4]$



23

before removal of solvent the expected *trans*-$Mo(CHMeOMe)(CO)_2(PPh_3)(\eta\text{-}C_5H_5)$ (**24**) is isolable, although somewhat reactive. The ^1H NMR spectrum of **24** is informative and, in particular, a signal {$\delta(CDCl_3)$: 5.15 [d of q, 1 H, J(HH) 6.5, J(HP) 3 Hz]} is as expected for the CH proton coupled to the protons of the methyl group and the *trans* P atom.

If the reaction is not filtered prior to solvent removal a further reaction proceeds (during workup) with excess $[Me_3O][BF_4]$ and a cationic ylide (**25**) is isolable along with lesser quantities of other minor neutral products. We believe that attack of excess $[Me_3O][BF_4]$ upon **24** removes the OMe^- function (Scheme 5) and the resulting transient cationic



Scheme 5. Reactions of $[Mo(\eta^2\text{-}MeCHO)(CO)_2(\eta\text{-}C_5H_5)]^-$ with $[Me_3O][BF_4]$–PPh_3. (i) $[Me_3O][BF_4]$ alone, (ii) $[Me_3O][BF_4]$ and PPh_3 (filtration before solvent removal), and (iii) $[Me_3O][BF_4]$ and PPh_3 without filtration before solvent removal.

alkylidene is stabilized by a second molecule of PPh_3.

Clearly $[Me_3O][BF_4]$ alkylates **7** preferentially at the oxygen of coordinated acetaldehyde rather than at the metal as is the case for MeI although there is evidence for alkylation at the metal to a very minor degree, small quantities of the known methyl complex $MoMe(CO)_2(PPh_3)(\eta\text{-}C_5H_5)$ (**16**) are also isolable from the reaction.[27,28]

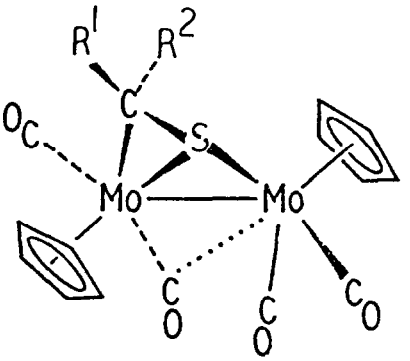
The product obtained by oxidation of **7** with any one of several oxidizing agents was unexpected to us. Addition of, for instance, $[Fe(\eta\text{-}C_5H_5)_2]^+$ to a THF solution of **7** results in the formation of **26** in 11% yield. The structure of **26** is the subject of an X-ray crystallographic study[29] and shows the MeCHO ligand to bridge the dimolybdenum centre in an asymmetric fashion. There is also a semi-bridging carbonyl of the type known for many related molecules of Mo_2 and W_2.[30–34] The Mo–Mo bond length is consistent with a single Mo–Mo bond.[34,35] One can view the bonding as coordination of the C=O bond to one molybdenum atom and donation of an oxygen lone pair to the second. Acetaldehyde therefore functions as a four-electron ligand in this molecule. The analogous complex $Mo_2(CO)_4(\mu\text{-}\eta^2\text{-}PhCH_2CHO)(\eta\text{-}C_5H_5)_2$ is also available by oxidation of the benzyl species (**12**).

In a formal sense, this molecule is an addition product of MeCHO across the Mo–Mo triple bond of $[Mo(CO)_2(\eta\text{-}C_5H_5)]_2$. However, we have, as yet, been unable to synthesize the molecule by this route either by photochemical or thermal means. There is literature precedent for some sulphur-containing analogues. Addition of $R^1R^2C{=}S$ takes place smoothly across dimolybdenum of $[Mo(CO)_2(\eta\text{-}C_5H_5)]_2$ for a wide range of R^1 and R^2 to give species **27** with a Mo_2CS core whose structure is completely analogous to the Mo_2CO core of **26**.[36] These molecules are fluxional on the NMR time scale upon warming but analogous behaviour is not observed for **26** since decomposition occurs upon warming to 60°C in C_6D_6.

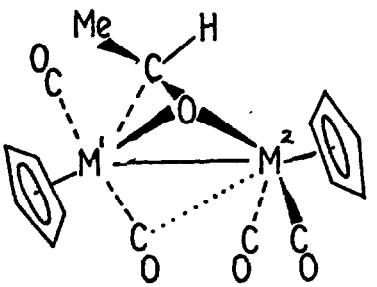
One possibility for the reaction mechanism is for the oxidizing agent to accept an electron from the anion **7**, giving a 17-electron species (Scheme 6) which dimerizes with loss of MeCHO to give **26**. In support of this acetaldehyde is detected in the reaction mixture by GC–mass spectrometry.

Other one-electron acceptors such as Fe(III), $[C_7H_7]^+$ or $[Mo(CO)_3(\eta\text{-}C_7H_7)]^+$ provide the same product but in each case there are byproducts whose nature depends upon the actual oxidizing agent employed.

Reaction of $[Mo(CO)_3(\eta\text{-}C_5H_5)][BF_4]$[37] with **7** in THF similarly results in the formation of **26** (21%), together with quantities of $[Mo(CO)_3(\eta\text{-}C_5H_5)]_2$ (**28**) (13%), but in this case there is the question as to whether both Mo atoms of **26** originate from the anionic species or one from each reagent. This question is probably answered by the result of employing $[W(CO)_3(\eta\text{-}C_5H_5)][BF_4]$[37] in place of the Mo cation. The only product containing an aldehyde ligand isolated is **26**, containing two Mo atoms. There is no sign of either of the two possible heterobimetallic species **31** or **32**. The other products isolated from chromatography are all three complexes, $(\eta\text{-}C_5H_5)(OC)_3M^1\text{-}M^2(CO)_3(\eta\text{-}C_5H_5)$ (**28–30**). This implies that **26** is formed by an electron-transfer process as for the other oxidizing agents. The formation of all these three possible hexacarbonyl compounds can be rationalized similarly and by making the assumption that when the 17-electron



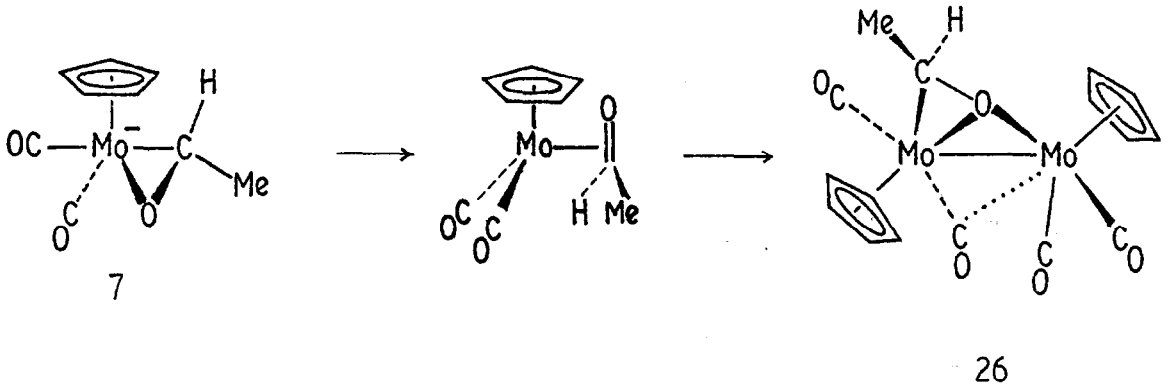
27



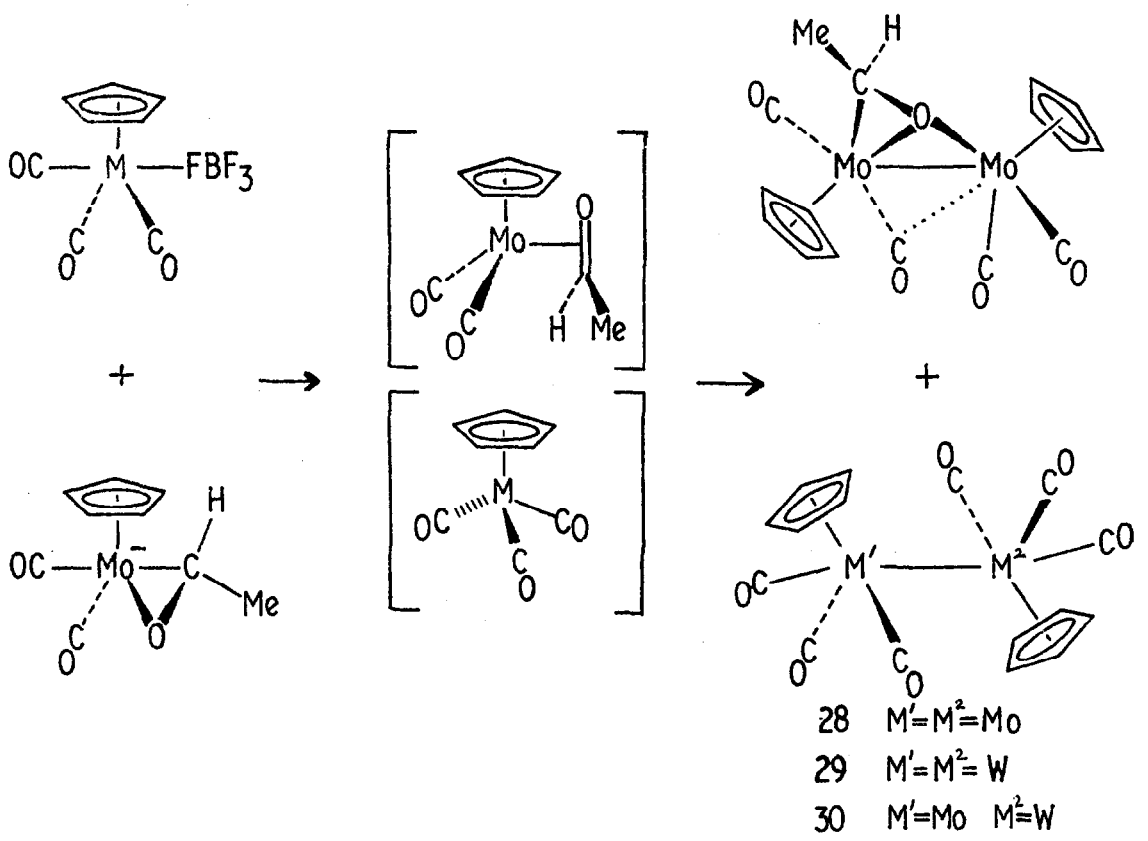
31 M^1=Mo, M^2=W

32 M^1=W, M^2=Mo

species combine in all possible permutations to form metal–metal bonds (Scheme 7) one or two moles of acetaldehyde are then lost and disproportionation reactions give the isolated hexacarbonyls. In no case is it necessary to invoke a direct metal–metal bond formation between **7** and $[W(CO)_3(\eta\text{-}C_5H_5)][BF_4]$ as the initial step, but this does not dismiss this possibility as accounting for at least some of the heterobimetallic product.



Scheme 6. Reaction of $[Mo(\eta^2\text{-MeCHO})(CO)_2(\eta\text{-}C_5H_5)]^-$ with $[Mo(CO)_3(\eta\text{-}C_5H_5)][BF_4]$.



Scheme 7. Reaction of $[Mo(\eta^2\text{-MeCHO})(CO)_2(\eta\text{-}C_5H_5)]^-$ with $[W(CO)_3(\eta\text{-}C_5H_5)][BF_4]$.

Acknowledgements—We should like to acknowledge generous support from the S.E.R.C. and The Royal Society, and the S.E.R.C. for a research studentship (to J.T.G).

REFERENCES

1. N. A. Bailey, P. L. Chell, A. Mukhopadhyay, H. E. Tabbron and M. J. Winter, *J. Chem. Soc., Chem. Commun.* 1982, 215.
2. N. A. Bailey, P. L. Chell, C. P. Manuel, A. Mukhopadhay, D. Rogers, H. E. Tabbron and M. J. Winter, *J. Chem. Soc., Dalton Trans.* 1983, 2397.
3. T. Kruck and L. Liebig, *Chem. Ber.* 1973, **106**, 1055.
4. H. Adams, N. A. Bailey and M. J. Winter, *J. Chem. Soc., Dalton Trans.* 1984, 273.
5. F. A. Cotton and C. M. Lukehart, *J. Am. Chem. Soc.* 1971, **93**, 2672.
6. F. A. Cotton and C. M. Lukehart, *J. Am. Chem. Soc.* 1973, **95**, 3552.
7. H. Adams, N. A. Bailey, P. Cahill, D. Rogers and M. J. Winter, *J. Chem. Soc., Chem. Commun.* 1983, 831.

8. M. J. Winter, unpublished results.
9. J. T. Gauntlett, B. F. Taylor and M. J. Winter, *J. Chem. Soc., Chem. Commun.* 1984, 420.
10. J. T. Gauntlett, B. F. Taylor and M. J. Winter, *J. Chem. Soc., Dalton Trans.* 1985, 1815.
11. M. W. Creswick and I. Bernal, *Inorg. Chim. Acta* 1983, **71**, 41.
12. S. Gambarotta, G. Floriani, A. Chiesi-Villa and C. Guastini, *J. Am. Chem. Soc.* 1982, **104**, 2019.
13. K. L. Brown, G. R. Clark, C. E. L. Headford, K. Marsden and W. R. Roper, *J. Am. Chem. Soc.* 1979, **101**, 503.
14. H. Berke, G. Huttner, G. Weiler and L. Zsolnai, *J. Organomet. Chem.* 1981, **219**, 353.
15. J. A. Gladysz and J. C. Selover, *Tetrahedron Lett.* 1978, 319.
16. J. C. Selover, M. Marsi, D. W. Parker and J. A. Gladysz, *J. Organomet. Chem.* 1981, **206**, 317.
17. W. Tam, W.-K. Wong and J. A. Gladysz, *J. Am. Chem. Soc.* 1979, **101**, 1589.
18. W. Tam, G.-Y. Lin and J. A. Gladysz, *Organometallics* 1982, **1**, 525.
19. J. A. Gladysz, *Adv. Organomet. Chem.* 1982, **20**, 1.
20. A. R. Manning, *J. Chem. Soc. A* 1967, 1824.
21. C. A. Tolman, S. D. Ittel, A. D. English and J. P. Jesson, *J. Am. Chem. Soc.* 1979, **101**, 1742.
22. J. W. Suggs, *J. Am. Chem. Soc.* 1978, **100**, 640.
23. T. B. Rauchfuss, *J. Am. Chem. Soc.* 1979, **101**, 1045.
24. M. J. Breen, G. L. Geoffroy, A. L. Rheingold and W. C. Fultz, *J. Am. Chem. Soc.* 1983, **105**, 1069.
25. M. Cousins and M. L. H. Green, *J. Chem. Soc.* 1963, 889.
26. R. B. King and A. Fronzaglia, *J. Am. Chem. Soc.* 1966, **88**, 709.
27. K. W. Barnett and P. M. Treichel, *Inorg. Chem.* 1967, **6**, 294.
28. I. S. Butler, F. Basolo and R. G. Pearson, *Inorg. Chem.* 1967, **6**, 2074.
29. H. Adams, N. A. Bailey, J. T. Gauntlett and M. J. Winter, *J. Chem. Soc., Chem. Commun.* 1984, 1361.
30. M. D. Curtis and W. M. Butler, *J. Organomet. Chem.* 1978, **155**, 131.
31. W. I. Bailey, Jr, F. A. Cotton, J. D. Jameson and J. R. Kolb, *J. Organomet. Chem.* 1976, **121**, C23.
32. J. A. Beck, S. A. R. Knox, R. F. D. Stansfield, F. G. A. Stone, M. J. Winter and P. Woodward, *J. Chem. Soc., Dalton Trans.* 1982, 195.
33. W. I. Bailey, Jr, M. H. Chisholm, F. A. Cotton and L. A. Rankel, *J. Am. Chem. Soc.* 1978, **100**, 5674.
34. W. I. Bailey, Jr, D. M. Collins and F. A. Cotton, *J. Organomet. Chem.* 1977, **135**, C53.
35. R. D. Adams, D. M. Collins and F. A. Cotton, *Inorg. Chem.* 1974, **13**, 1086.
36. H. Alper, N. D. Silavwe, G. I. Birnbaum and F. R. Ahmed, *J. Am. Chem. Soc.* 1979, **101**, 6582.
37. W. Beck and K. Schloter, *Z. Naturforsch.* 1978, **33B**, 1214.

Polyhedron Vol. 5, No. 1/2, pp. 461–471, 1986
Printed in Great Britain

0277–5387/86 $3.00 + .00
© 1986 Pergamon Press Ltd

η^3-ALLYL COMPLEXES OF MOLYBDENUM: REACTIONS OF $[MoCl(\eta^3\text{-}C_3H_5)_3]_2$ AND THE CRYSTAL STRUCTURE OF $[MoOAc(\eta^3\text{-}C_3H_5)_3]$

R. BENN, S. HOLLE, P. W. JOLLY,* C. KRÜGER, C. C. ROMÃO, M. J. ROMÃO, A. RUFIŃSKA and G. SCHROTH

Max-Planck-Institut für Kohlenforschung, D-4330 Mülheim a. d. Ruhr, F.R.G.

(*Received* 11 *June* 1985)

Abstract—$[MoCl(\eta^3\text{-}C_3H_5)_3]_2$ reacts with donor ligands (L) with cleavage of the chloride bridges to give $[MoCl(L)(\eta^3\text{-}C_3H_5)_3]$ complexes from which the halide may be substituted by an alkyl group through reaction with Grignard reagents. Metathetical replacement is observed upon treatment with silver acetate or thallium acetylacetonate. The ^1H NMR spectra of these tris(η^3-allyl)molybdenum complexes indicate that the three allyl groups are magnetically inequivalent and asymmetrically bonded to the metal atom. This is borne out by a crystal-structure determination of $[MoOAc(\eta^3\text{-}C_3H_5)_3]$. Treatment of the chloride with bidentate chelating ligands leads to ionic species of the type $[Mo(L\text{–}L)(\eta^3\text{-}C_3H_5)_3]^+X^-$, while the product of the reaction with lithium in the presence of trimethylphosphite is $[Mo\{P(OMe)_3\}_3(\eta^3\text{-}C_3H_5)_2]$.

The remarkable growth of organomolybdenum chemistry in the last 15 years has taken place with the practical exclusion of tetra(η^3-allyl)molybdenum as a starting material—even though this complex was first reported in 1963.[1] This is particularly surprising since it was clearly realized at the start of the renaissance of modern organo-transition-metal chemistry that a very profitable approach is to study those complexes in which the metal interacts solely with labile organic ligands as opposed to more conventional systems stabilized by the less labile η-cyclopentadienyl and CO groups.[2] The reason for this neglect is probably two-fold: firstly, tetra(η^3-allyl)molybdenum is not as easy to prepare as some of the other homoleptic η^3-allyl-transition-metal complexes, e.g. bis(η^3-allyl)nickel, and secondly having a filled metal valence shell it might be expected to be relatively inert.

We have developed an improved synthesis of tetra(η^3-allyl)molybdenum while the isolation of $[MoCl(\eta^3\text{-}C_3H_5)_3]_2$ from the reaction with HCl has provided a new entry into the chemistry of the η^3-allyl-molybdenum system. Some initial results have been mentioned in a preliminary communication.[3]

RESULTS AND DISCUSSION

The original preparation of $[Mo(\eta^3\text{-}C_3H_5)_4]$ (**1**) from $MoCl_5$ and allylMgCl suffers from irreproducibility, low yield (0–20%) and contamination with an equal amount of the dark green dimer $[Mo_2(\eta^3\text{-}C_3H_5)_4]$.[1,2,4,5] These disadvantages can be largely compensated by reacting $MoCl_4 \cdot 2THF$[6] with a slight excess of allylMgCl at room temperature in ether: **1** is obtained in a reproducible 40% yield as a yellow crystalline solid practically uncontaminated by the dimer [eqn (1)]. **1** is stable for short periods in

$$MoCl_4 \cdot 2THF + 4C_3H_5MgCl \xrightarrow[-\ 2THF]{-\ 4MgCl_2} \underset{\mathbf{1}}{[Mo(\eta^3\text{-}C_3H_5)_4]} \quad (1)$$

air and may be sublimed in a high vacuum at 60–70°C. It is soluble in all common solvents and may be recrystallized from pentane or ethanol.

Tetra(η^3-allyl)molybdenum is chemically rather inert towards nucleophiles and could be recovered

* Author to whom correspondence should be addressed.

unchanged from reactions with ethylene [50 atm, room temperature (rt), 24 h], butadiene (rt, 24 h), C_5H_5Na (Na : Mo = 2 : 1, rt, 70 h), toluene (85°C, 5 h), $P(OMe)_3$ (neat, 65°C, 5 h) and LiMe (rt). In addition no reaction was observed with cyclopentadiene (20 h, 50°C), H_2 (1 atm, rt) or MeI (4 days, rt) while treatment with CBr_4 or H_2SO_4 led to decomposition. A slight reaction was observed with CO : after 24 h at rt under 100 atm of CO a trace of $Mo(CO)_6$ was formed with liberation of 1,5-hexadiene.

Reaction with gaseous HCl in pentane at −70°C, however, led to the quantitative formation of a pink solid which decomposes above −30°C and which analyses as the chloride **2** [eqn (2)]. A related iodide

$$2[Mo(\eta^3\text{-}C_3H_5)_4] + 2HCl \xrightarrow{-2C_3H_6} \langle(\text{—Mo(Cl)(Cl)—Mo—})\rangle_3 \quad (2)$$

2

complex could be isolated from the reaction with iodine in ether at −40°C. **2** is practically insoluble in the common organic solvents and could not be characterized by NMR spectroscopy. Its formulation as a dimer with bridging chloride atoms follows from the chemistry described below and established organometallic practice.

2 dissolves in methanol at −30°C to give a yellow solution from which, however, the starting material could be isolated by cooling to −78°C. Similar behaviour is observed if a few drops of water are added to a THF suspension of **2**, implying the equilibrium shown as eqn (3) in which reaction with

$$\mathbf{2} + 2L \rightleftharpoons \langle(\text{—Mo(Cl)(L)})\rangle_3 \quad (3)$$

3

the methanol or water causes rupture of the chloride bridges. The bond formed by *P*- or *N*-donor ligands is apparently stronger than that formed by *O*-donor ligands and in the case of the reactions of **2** with NCMe, pyridine, $P(OMe)_3$ and PMe_3 it proved possible to isolate the adducts **3** as yellow solids which decompose above −30°C. The structure of these adducts follows from the ^1H NMR spectra which are discussed in the following section : the 3-allyl groups are magnetically inequivalent and asymmetrically bonded to the metal. The reaction with *P*-donor ligands is not general and steric factors apparently determine whether reaction occurs. That with PMe_3 [cone angle (θ) = 118 ± 4°][7] is slower than that with $P(OMe)_3$ (θ = 107 ± 2°) while larger ligands such as $P(OPh)_3$ (θ = 121 ± 10°), PPh_3 (θ = 145 ± 2°) and PCy_3 (θ = 179 ± 10°) fail to react.

The chloride bridges in **2** can also be cleaved by reaction of a toluene suspension with $AlCl_3$: a violet solution results whose ^1H NMR spectrum suggests the formation of **4** [eqn (4)] : Addition of ether to this

$$\mathbf{2} + AlCl_3 \longrightarrow 2\langle(\text{—Mo(Cl)(Cl)})\rangle_3\text{—}AlCl_2 \quad (4)$$

4

solution leads to precipitation of the starting material. Similar behaviour has been previously reported upon reaction of $[MoCl(\eta^3\text{-}C_3H_5)(\eta^6\text{-}C_6H_6)]$ with $AlEt_2Cl$ and $AlEtCl_2$.[8,9]

Addition of excess acetonitrile to **2** followed by $TlBF_4$ leads to formation of an ionic tris(η^3-allyl) molybdenum-bis-ligand complex [eqn (5)]. Related

$$\mathbf{2} + 4MeCN \xrightarrow[-2TlCl]{2TlBF_4} 2\langle(\text{—Mo(NCMe)(NCMe)})\rangle_3^{+}\,BF_4^- \quad (5)$$

complexes have been isolated from reactions involving ethylenediamine and bis(dimethylphosphino)ethane, but not with the sterically more demanding tetramethylethylenediamine or bis(dicyclohexylphosphino)ethane.

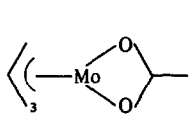
A series of molybdenum–alkyl complexes (**5**) have been isolated by reacting the PMe_3 and $P(OMe)_3$ adduct **3** with Grignard reagents [eqn (6)]. Here

$$\langle(\text{—Mo(Cl)(PR}_3)\text{—})\rangle_3 + R'MgX \xrightarrow{-MgXCl} \langle(\text{—Mo(R')(PR}_3)\text{—})\rangle_3 \quad (6)$$

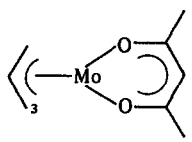
3 **5**

again steric requirements make themselves apparent in that, although methyl, ethyl and allyl complexes stabilized by PMe_3 could be isolated, no reaction was observed with Pr^{i}MgCl.

Metathetical replacement of the chloride occurs if **2** is treated with silver acetate and thallium acetylacetonate to give **6** and **7**. The crystal structure of **6** is described in a following section. Treatment of

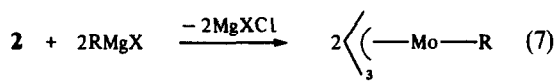


6



7

the chloride **2** with Grignard reagents, in the absence of donor ligands, results in the formation of molybdenum–alkyl systems containing bridging (or agostic)[10] β-hydrogen atoms [eqn (7)]. The



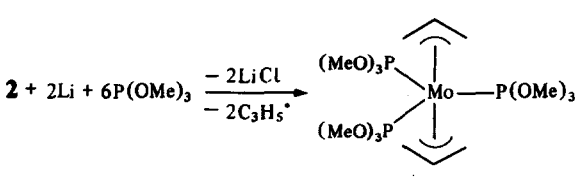
(7)

ramifications of this reaction will be the subject of a subsequent publication.[11] The reaction of **2** with sodium or thallium cyclopentadienide which results in the formation of the paramagnetic complex $[Mo(\eta^3\text{-}C_3H_5)_2(\eta^5\text{-}C_5H_5)]$ has already been reported.[3]

In an attempt to prepare a $[MoL(\eta^3\text{-}C_3H_5)_3]$ complex, the chloride **2** was reduced with lithium powder in the presence of trimethylphosphite. However, reduction to Mo(II) occurred and the isolated product has the composition

$$[Mo\{P(OMe)_3\}_3(\eta^3\text{-}C_3H_5)_2].$$

The ^{31}P NMR spectrum of this molecule consists of the characteristic signals for an A_2B spin system while the ^1H NMR spectrum shows that both allyl groups are magnetically equivalent and asymmetrically bonded to the metal atom suggesting the structure **8** [eqn (8)], in which the metal occupies a trigonal bipyramidal environment.



8 (8)

NMR SPECTROSCOPIC INVESTIGATIONS

The following qualitative description of the structures of the complexes **3**–**7** is based on their low-temperature, 400-MHz ^1H NMR spectra. In all of these complexes the three allyl groups are unique and bonded as η^3-ligands to the Mo atom. The terminal C atoms of each group are inequivalent and as a result the six *syn*- and six *anti*-protons are magnetically inequivalent and can be readily distinguished by their characteristic coupling constants. The results have been brought together in Table 1. Coupling between the P atom and the allylic protons are observed for **3** [L = PMe_3 or $P(OMe)_3$] and **5**, indicating that, under the measurement conditions, ligand dissociation is not occurring. In the case of the pyridine adduct **3** (L = py), the ^1H chemical shifts of the ligand molecule do not exclude unambiguously that dissociation is occurring. The protons of the Mo σ-bonded C atom in **5** (L = PMe_3) (34 and 35, see Table 1) are diastereotopic: however, since the three allyl groups are also inequivalent, a distinction between a quasi-tetrahedral and a square planar arrangement of the ligands around the metal atom cannot be made. That the structures of **3**–**7** in solution are similar to that observed in the crystal for the acetate **6** (see following section) is, however, underlined by detailed ^1H NMR studies using magnetization transfer difference spectroscopy[12] carried out for the $AlCl_3$ adducts **4** and **6** and the acetylacetonate complex **7** (Fig. 1).

Spectrum B in Fig. 1 suggests that the *meso*-C atoms of the η^3-allyl groups containing protons 21–25 and 1–5 are directed at each other. This is supported by the NOE interaction of the *syn*-proton 23 with the *syn*-proton 3 (spectrum C). This experiment also establishes the mutual arrangement of the protons in both of these allyl groups. The arrangement of the third allyl group (having protons 11–15) relative to these follows from spectrum D which establishes that the *syn*-proton 13 is in close proximity to the *anti*-proton 25 of the neighbouring allyl group. The proximity of the *syn*-proton 12 to the *anti*-proton 4 follows from spectrum E which also establishes the arrangement of the methyl groups in the acetylacetonate ligand, while the close proximity of the *meso*-proton 11 to this group follows from spectrum F.

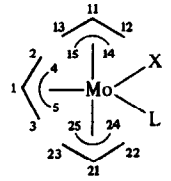
The η^1-allyl complex **5** (L = PMe_3), in contrast to $[Pd(PMe_3)(\eta^1,\eta^3\text{-allyl})_2]$,[13] exhibits no exchange between the η^1- and η^3-allyl groups (up to 273 K at 200 MHz). However, in the case of the complexes $[MoClAlCl_3(\eta^3\text{-}C_3H_5)_3]$ (**4**) and **7** magnetization transfer difference spectroscopy at 243 and 263 K, respectively, show the existence of slow exchange processes which in both cases lead to an equilibration of two of the allyl groups. This exchange, which involves all three proton types (*meso*, *syn* and *anti*), will be discussed in detail for **7**. The spectra of this complex at 263 K show that, in the third allyl group (having protons 21–25, see Fig. 1), the *syn*- and *anti*-protons 23 and 25 exchange. This, which is presumably the result of the familiar η^1–η^3-allyl rearrangement, generates a free coordination site at the molybdenum and is followed by rearrangement of the acetylacetonate group and

Table 1. ^{1}H NMR data of the [MoX(L)(η^3-C_3H_5)$_3$] complexes[a]

Complex	Conditions (solvent, T, Hz)	δ_{meso} (Hn, m)	δ_{anti} (Hn, m)	δ_{syn} (Hn, m)	J (Hz)	Miscellaneous
[MoOAc(η^3-C_3H_5)$_3$]	CD_2Cl_2, 193 K, 400 MHz	4.56 (H1, m)	3.62 (H4, d)	3.03 (H2, d)	8.5 ($J_{1,2}$); 8.3 ($J_{11,12}$); 8.3 ($J_{21,22}$)	δ 1.70 (OMe, s)
		4.53 (H11, m)	1.67 (H14, d)	3.56 (H12, d)	8.5 ($J_{1,3}$); 8.0 ($J_{11,13}$); 8.5 ($J_{21,23}$)	
	$\delta_{solv.}$ = 5.32	4.98 (H21, m)	0.90 (H24, d)	3.29 (H22, d)	12.0 ($J_{1,4}$); 12.5 ($J_{11,14}$); 11.8 ($J_{21,24}$)	
			0.29 (H5, d)	1.33 (H3, d)	11.0 ($J_{1,5}$); 11.9 ($J_{11,15}$); 13.9 ($J_{21,25}$)	
			3.19 (H15, d)	3.56 (H13, d)	~2.6 ($J_{2,4}$); 2.5 ($J_{12,14}$); 2.7 ($J_{22,24}$)	
			1.19 (H25, d)	3.04 (H23, d)	~1.8 ($J_{3,5}$); 2.3 ($J_{13,15}$); 2.5 ($J_{23,25}$)	
[Moacac(η^3-C_3H_5)$_3$]	d_8-THF, 193 K, 400 MHz	4.89 (H1, m)	4.00 (H4, d)	2.97 (H2, d)	8.6 ($J_{1,2}$); 8.5 ($J_{11,12}$); 8.9 ($J_{21,22}$)	δ 5.29 (CH, s)
		4.51 (H11, m)	1.79 (H14, d)	3.28 (H12, d)	8.3 ($J_{1,3}$); 7.4 ($J_{11,13}$); 8.9 ($J_{21,23}$)	δ 1.89 (Me, s)
	$\delta_{solv.}$ = 3.58	5.43 (H21, m)	1.21 (H24, d)	2.98 (H22, d)	12.5 ($J_{1,4}$); 12.7 ($J_{11,14}$); 12.6 ($J_{21,24}$)	δ 1.71 (Me, s)
			0.25 (H5, d)	1.44 (H3, d)	11.0 ($J_{1,5}$); 11.1 ($J_{11,15}$); 13.4 ($J_{21,25}$)	
			3.05 (H15, d)	3.19 (H13, d)	2.7 ($J_{2,4}$); 2.5 ($J_{12,14}$); 2.7 ($J_{22,24}$)	
			2.10 (H25, d)	2.84 (H23, d)	2.3 ($J_{3,5}$); 1.5 ($J_{13,15}$); 1.2 ($J_{23,25}$)	
[MoClAlCl$_3$(η^3-C_3H_5)$_3$]	d_8-Toluene, 233 K, 400 MHz	3.10 (H1, m)	3.10 (H4, m)	2.32 (H2, d)	$-(J_{1,2})$;[b] 8.6 ($J_{11,12}$); 8.7 ($J_{21,22}$)	[b]
		4.15 (H11, m)	2.23 (H14, d)	2.73 (H12, d)	$-(J_{1,3})$;[b] 8.4 ($J_{11,13}$); 8.1 ($J_{21,23}$)	
	$\delta_{solv.}$ = 2.09	5.77 (H21, m)	2.94 (H24, d)	3.41 (H22, d)	$-(J_{1,4})$;[b] 12.5 ($J_{11,14}$); 12.1 ($J_{21,24}$)	
			−0.38 (H5, m)	0.58 (H3, d)	$-(J_{1,5})$;[b] 13.7 ($J_{11,15}$); 13.5 ($J_{21,25}$)	
			1.60 (H15, d)	2.26 (H13, d)		
			1.07 (H25, d)	3.62 (H23, d)		
[MoCl(py)(η^3-C_3H_5)$_3$] (L = py)	CD_2Cl_2, 193 K, 400 MHz	4.78 (H1, m)	3.74 (H4, d)	2.82 (H2, d)	8.0 ($J_{1,2}$); 9.0 ($J_{11,12}$); 7.7 ($J_{21,22}$)	δ 8.85 (d, *o*-H)
		5.07 (H11, m)	2.46 (H14, d)	3.10 (H12, d)	8.6 ($J_{1,3}$); 8.9 ($J_{11,13}$); 8.2 ($J_{21,23}$)	7.31 (t, *n*-H)
	$\delta_{solv.}$ = 5.32	5.58 (H21, m)	3.29 (H24, d)	3.68 (H22, d)	12.8 ($J_{1,4}$); 12.4 ($J_{11,14}$); 10.4 ($J_{21,24}$)	7.74 (t, *p*-H)
			0.29 (H5, d)	1.54 (H3, d)	10.7 ($J_{1,5}$); 13.7 ($J_{11,15}$); 13.0 ($J_{21,25}$)	
			2.94 (H15, d)	2.88 (H13, d)		
			1.41 (H25, d)	3.23 (H23, d)		
[MoCl{P(OMe)$_3$}(η^3-C_3H_5)$_3$] [L = P(OMe)$_3$]	CD_2Cl_2, 233 K, 400 MHz	3.71 (H1, m)	2.21 (H4, dd)	2.90 (H2, dd)	8.3 ($J_{1,2}$); 9.6 ($J_{11,12}$); 8.2 ($J_{21,22}$)	δ 3.76 (d, Me)
		4.50 (H11, m)	2.51 (H14, dd)	3.53 (H12, dd)	8.5 ($J_{1,3}$); 8.8 ($J_{11,13}$); 8.2 ($J_{21,23}$)	1.7 ($J_{11,P}$); 3.0 ($J_{21,P}$)
	$\delta_{solv.}$ = 5.32	5.20 (H21, m)	3.55 (H24, d)	3.60 (H22, d)	12.5 ($J_{1,4}$); 14.0 ($J_{11,14}$); 11.7 ($J_{21,24}$)	12.9 ($J_{2,P}$); 1.6 ($J_{3,P}$)
			−0.14 (H5, d)	1.90 (H3, d)	11.0 ($J_{1,5}$); 12.2 ($J_{11,15}$); 12.5 ($J_{21,25}$)	8.4 ($J_{13,P}$); 11 ($J_{23,P}$)
			1.52 (H15, dd)	2.92 (H13, d)	~2.4 ($J_{2,4}$)	5.1 ($J_{4,P}$); 4.0 ($J_{15,P}$)
			0.54 (H25, dd)	3.58 (H23, dd)		4.3 ($J_{25,P}$)

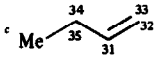
$[MoCl(PMe_3)(\eta^3\text{-}C_3H_5)_3]$ (L = PMe_3)	d_8-THF, 233 K, 400 MHz $\delta_{solv.}$ = 3.58	3.95 (H1, m) 4.67 (H11, m) 5.07 (H21, m)	2.05 (H4, dd) 2.79 (H14, d) 3.43 (H24, d) −0.13 (H5, d) 1.39 (H15, dd) 0.49 (H25, dd)	2.68 (H2, dd) 3.42 (H12, d) 3.48 (H22, dd) 1.98 (H3, d) 2.63 (H13, d) 3.09 (H23, dd)	8.4 ($J_{1,2}$); 9.3 ($J_{11,12}$); 8.1 ($J_{21,22}$) 8.6 ($J_{1,3}$); 8.9 ($J_{11,13}$); 8.4 ($J_{21,23}$) 12.0 ($J_{1,4}$); 13.7 ($J_{11,14}$); 11.3 ($J_{21,24}$) 11.0 ($J_{1,5}$); 12.0 ($J_{11,15}$); 12.5 ($J_{21,25}$) 2.5 ($J_{2,4}$); ~1.2 ($J_{12,14}$); 2.4 ($J_{22,24}$)	δ 1.53 (d, Me) 9.0 ($J_{P,Me}$); 1.0 ($J_{11,P}$) 2.7 ($J_{21,P}$); 12.6 ($J_{2,P}$) 7.0 ($J_{13,P}$); 13.4 ($J_{23,P}$) 5.2 ($J_{4,P}$); 2.8 ($J_{15,P}$) 5.7 ($J_{25,P}$)
$[MoMe\{P(OMe)_3\}(\eta^3\text{-}C_3H_5)_3]$ (R = OMe, R′ = Me)	d_6-acetone, 233 K, 400 MHz $\delta_{solv.}$ = 2.04	4.24 (H1, m) 4.35 (H11, m) 4.39 (H21, m)	2.24 (H4, dd) 1.31 (H14, d) 2.97 (H24, d) −0.21 (H5, d) 0.81 (H15, dd) −0.11 (H25, dd)	2.60 (H2, dd) 3.14 (H12, d) 2.66 (H22, dd) 1.87 (H3, d) 2.57 (H13, d) 2.97 (H23, dd)	8.6 ($J_{1,2}$); 9.5 ($J_{11,12}$); 7.6 ($J_{21,22}$) 8.8 ($J_{1,3}$); 8.9 ($J_{11,13}$); 7.8 ($J_{21,23}$) 12.6 ($J_{1,4}$); 13.1 ($J_{11,14}$); 11.2 ($J_{21,24}$) 11.7 ($J_{1,5}$); 11.7 ($J_{11,15}$); 11.1 ($J_{21,25}$)	3.72 (OMe, d, $J_{H,P}$ 9.6) −1.29 (Me, d, $J_{H,P}$ 10.5) 1.5 ($J_{11,P}$); 3.6 ($J_{21,P}$) 10.0 ($J_{2,P}$); 1.0 ($J_{3,P}$) 7.4 ($J_{13,P}$); 14.0 ($J_{23,P}$) 4.6 ($J_{4,P}$); 4.2 ($J_{15,P}$) 5.1 ($J_{25,P}$)
$[Mo\text{-}\eta^1\text{-}C_3H_5(PMe_3)(\eta^3\text{-}C_3H_5)_3]$ (R = Me, R′ = C_3H_5)	d_6-acetone, 213 K, 400 MHz $\delta_{solv.}$ = 2.04	4.07 (H1, m) 4.28 (H11, m) 4.45 (H21, m)	2.67 (H4, d) 2.07 (H14, d) 1.83 (H24, d) −0.04 (H5, dd) −0.20 (H15, d) 0.52 (H25, d)	2.65 (H2, d) 2.60 (H12, d) 2.85 (H22, d) 2.41 (H3, dd) 1.87 (H13, d) 2.34 (H23, dd)	7.6 ($J_{1,2}$); 8.4 ($J_{11,12}$); 9.6 ($J_{21,22}$) 7.7 ($J_{1,3}$); 8.5 ($J_{11,13}$); 9.1 ($J_{21,23}$) 10.7 ($J_{1,4}$); ~12.1 ($J_{11,14}$); 13.2 ($J_{21,24}$) 11.1 ($J_{1,5}$); 11.4 ($J_{11,15}$); 11.4 ($J_{21,25}$) 2.7 ($J_{2,4}$); 2.3 ($J_{12,14}$); 0 ($J_{22,24}$) ~1.7 ($J_{3,5}$); ~1.5 ($J_{13,15}$); 0 ($J_{23,25}$) 3.6 ($J_{1,P}$); 0 ($J_{11,P}$); ~0.7 ($J_{21,P}$) 0 ($J_{2,P}$); 11.0 ($J_{12,P}$); 0 ($J_{22,P}$) 14.5 ($J_{3,P}$); 0 ($J_{13,P}$); 5.7 ($J_{23,P}$) 7.0 ($J_{5,P}$); 0 ($J_{15,P}$); ~2.0 ($J_{25,P}$)	5.63 (H31, m);[c] 4.40 (H32, d) 4.37 (H33, d); −1.17 (H34, dd) 0.63 (H35, dd); 1.36 (Me, d, $J_{7,9}$) 9.9 ($J_{31,32}$); 16.4 ($J_{31,33}$) 8.2 ($J_{31,34}$); 9.0 ($J_{31,35}$) 2.8 ($J_{32,35}$); −9.6 ($J_{34,35}$) 5.3 ($J_{34,P}$); 20.9 ($J_{35,P}$) 7.9 ($J_{6,P}$)

[a] Proton-numbering scheme:



[b] Degenerate spin system.

[c]



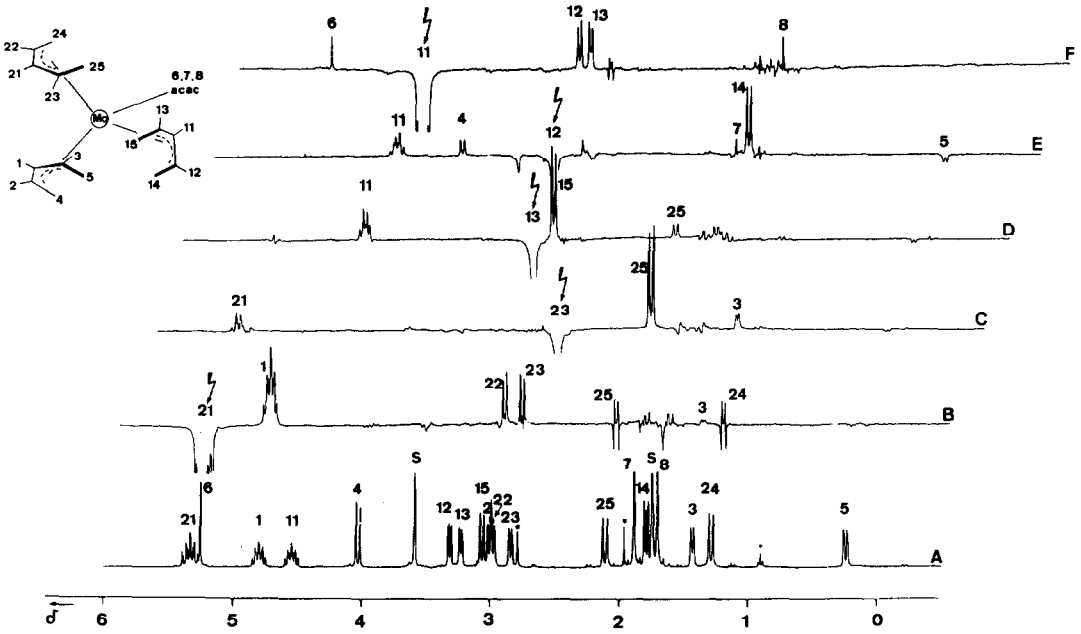
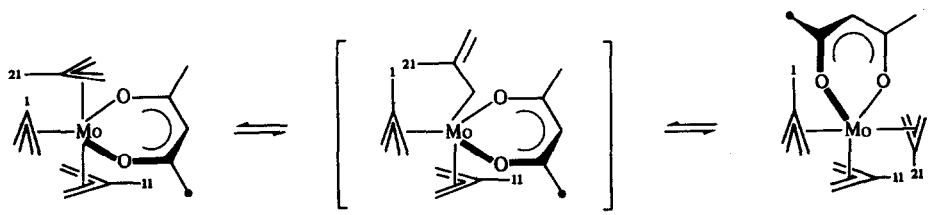


Fig. 1. 400-MHz ^{1}H NMR spectra of 7 at 233 K. (A) Normal spectrum. B–F nuclear-Overhauser difference spectra (the saturated signal is indicated by an arrow); signals for neighbouring protons appear in the difference spectra as positive signals (spectrum E shows a negative NOE for proton 5). S, solvent; *, impurity.



(9)

recomplexation of the allyl group [eqn (9)]. As a result the protons 11–15 now occupy the environment originally held by protons 1–5. In addition, an exchange of the methyl groups of the acetylacetonate group has occurred which is experimentally observed. A similar effect is found for the $AlCl_3$ adduct **4** but, in this case, the most plausible explanation involves rotation of the third allyl group about the Mo–allyl coordination axis which would lead to the observed pair-wise equilibration in this group of the *syn*- and *anti*-protons.

THE MOLECULAR STRUCTURE OF 6

The molecular structure of **6**, was determined by a single-crystal X-ray structural investigation and is shown in Fig. 2 with the atomic labelling scheme. Table 2 contains bond lengths and angles, and the positional parameters of all the atoms are given as supplementary data.

The coordination geometry about the molybdenum atom is defined by the mid-points (D1, D2 and D3) of the three allyl groups as well as by the mid-point (D4) of the acetate ligand (see footnote in Table 2 for the definition of the mid-points). The resulting six bond angles involving the metal atom may be divided into two groups: whereas two angles are significantly larger than the tetrahedral value [D1–Mo–D3 (140.0°) and D2–Mo–D4 (141.6°)], the remaining four angles have an average value of *ca* 96° (see Table 2). The molecular geometry can thus be best described as a distorted tetrahedron.

The three allyl groups are bonded unsymmetrically to the metal atom as indicated by non-equivalent C—C and Mo—C bond distances (see Table 2). The allyl group C6–C7–C8 opposite to the acetate group is least distorted with Mo—C6 and Mo—C8 differing only by 0.01 Å (±3 ESD). For the

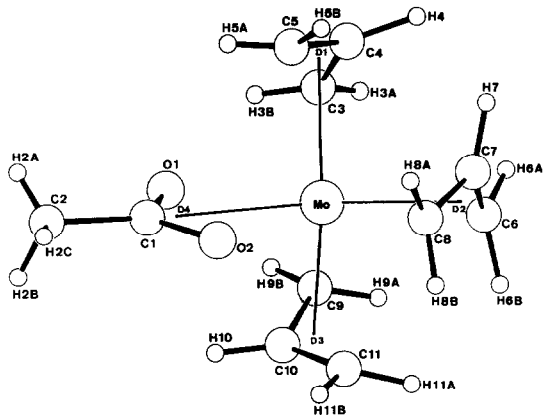


Fig. 2. Molecular structure of $[MoOAc(\eta^3\text{-}C_3H_5)_3]$.

Table 3. Intramolecular nonbonding contacts (Å)

C1...H5A	2.66(2)	H3A...H6A	2.61(3)
C1...H1O	2.67(2)	H31...H9A	2.88(3)
O1...H3B	2.41(2)	H3A...H9B	2.76(3)
O1...H5A	2.40(2)	H3B...H9B	2.50(3)
O1...H9B	2.90(2)	H4...H6A	2.57(3)
O1...H1O	2.42(2)	H4...H7	1.95(3)
O2...H5A	2.88(2)	H5B...H7	2.61(3)
O2...H1O	2.83(2)	H5B...H8A	2.68(3)
O2...H11B	2.67(2)	H6A...H9A	2.78(3)
		H6B...H9A	2.42(3)
		H6B...H11A	1.97(3)
		H8B...H11A	2.45(3)
		H8B...H11B	2.48(4)

remaining allyl groups, this distortion is more pronounced, being 0.05 Å for Mo—C9 vs Mo—C11 and 0.02Å for Mo—C3 vs Mo—C5. All C—C distances lie, however, within the normal range for η^3-allyl systems. The observed asymmetry is a result of the different electronic and steric environment of each ligand. The relative positioning of the allyl groups can be described by the dihedral angles between their planes: 32.2° between C3–C4–C5 and C6–C7–C8, 46.6° between C3–C4–C5 and C9–C10–C11 and 64.3° between C6–C7–C8 and C9–C10–C11. The planar acetate group is also non-symmetric in its bonding to the molybdenum, with O2 being 0.016 Å closer to the metal than atom O1. The plane defined by C1–C2–O1–O2 (±0.002 Å) forms an angle of 76.5° with that of the allyl group C6–C7–C8 and angles of 48.8 and 23.5° with the allyl groups C3–C4–C5 and C9–C10–C11, respectively.

Intramolecular contacts smaller than 3.0 Å are shown in Table 3. Severe crowding of the four ligands

Table 2. Bond lengths (Å) and angles (°) with ESDs in parentheses[a]

Mo—O1	2.230(1)	C1—O1	1.269(2)
Mo—O2	2.214(1)	C1—O2	1.271(2)
Mo—C3	2.319(2)	C1—C2	1.496(3)
Mo—C4	2.307(2)	C3—C4	1.398(3)
Mo—C5	2.296(2)	C4—C5	1.410(3)
Mo—C6	2.327(6)	C6—C7	1.408(3)
Mo—C7	2.296(2)	C7—C8	1.399(3)
Mo—C8	2.336(2)	C9—C10	1.427(3)
Mo—C9	2.305(2)	C10—C11	1.395(3)
Mo—C10	2.252(2)		
Mo—C11	2.354(2)		
Mo—D1	2.054		
Mo—D2	2.068		
Mo—D3	2.049		
Mo—D4	2.160		
D1—Mo—D3	140.0	O1—C1—O2	117.2(1)
D2—Mo—D3	102.2	C2—C1—O1	121.5(2)
D1—Mo—D2	95.5	C2—C1—O2	121.3(2)
D2—Mo—D4	141.6	C3—C4—C5	121.6(2)
D3—Mo—D4	90.2	C6—C7—C8	121.9(2)
D1—Mo—D4	97.9	C9—C10—C11	120.6(2)

[a] D1 = mid-point of allyl group C3–C4–C5, D2 = mid-point of allyl group C6–C7–C8, D3 = mid-point of allyl group C9–C10–C11, and D4 = mid-point of acetate O1–C1–O2.

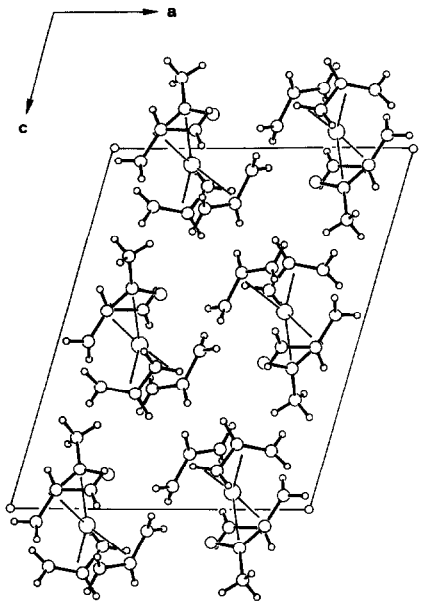


Fig. 3. View of the unit cell as projected onto the plane *ac*.

around the metal is indicated by short contacts between the hydrogen atoms of all three allyl groups and of the acetate group. The two shortest contacts, H4...H7 1.95(3) and H6B...H11A 1.97(3) Å, are much smaller than the sum of the van der Waal's radii for hydrogen atoms (2.4 Å).

No unusually short intermolecular contacts (< 3.0 Å) between non-hydrogen atoms are observed within the unit cell (see Fig. 3).

EXPERIMENTAL

All experiments were carried out under an argon atmosphere. Solvents (ether, THF, toluene and pentane) were dried and freed from dissolved oxygen by distillation form $Na[AlEt_4]$. CH_2Cl_2 and acetonitrile were dried over CaH_2, and acetone over P_2O_5.

^1H NMR spectra were measured with Bruker WP 80 (80-MHz) and WH 400 (400-MHz) instruments. ^{31}P NMR spectra were measured with a Bruker WP 80 (32.4-MHz) instrument. Mass spectra were measured with a Varian CH 5 instrument.

Microanalysis was carried out by Dornis and Kolbe, Microanalytical Laboratory, Mülheim a. d. Ruhr.

$[Mo(\eta^3\text{-}C_3H_5)_4]$ (1)

$MoCl_4 \cdot 2THF$[6] (20 g, 52.37 mmol) was added in three batches to a stirred solution of allylMgCl in diethyl ether (660 cm^3, 0.38 M) at room temperature. The reaction mixture was cooled to 0°C and stirred overnight. The solvent was evaporated and the residue extracted with pentane at room temperature. Air was bubbled through the resulting green solution for *ca* 2 min in order to decompose traces of $[Mo_2(\eta^3\text{-}C_3H_5)_4]$ and then filtered through an Avicell bed. The yellow solution was concentrated *in vacuo* and cooled under argon. Lemon-yellow crystals were deposited which were collected, dried *in vacuo* and stored at −30°C. Yield 5.72 g (42% of theoretical value). Found: C, 55.2; H, 8.0; Mo, 36.7%. Calc. for $C_{12}H_{20}Mo$: C, 55.4; H, 7.8; Mo, 36.9%.

$[MoCl(\eta^3\text{-}C_3H_5)_3]_2$ (2)

Dry gaseous HCl was bubbled slowly through a pentane solution of **1** (0.72 g, 2.76 mmol) and stirred at −70°C. A bright pink precipitate was formed and treatment was continued until the mother liquor became colourless. The solid was collected at −70°C, washed with pentane and ether and dried in a high vacuum at −50°C. Yield 0.7 g (quantitative). Found: C, 42.6; H, 5.6; Cl, 13.9; Mo, 37.8%. Calc. for $C_9H_{15}ClMo$: C, 42.5; H, 5.9; Cl, 13.9; Mo, 37.7%.

$[MoI(\eta^3\text{-}C_3H_5)_3]$

Iodine (3.17 g, 12.5 mmol) in ether was added slowly to a solution of **1** (3.25 g, 12.5 mmol) in 100 cm^3 of ether stirred at −60°C. The reaction mixture was allowed to reach −40°C for 1 h and the resulting brown precipitate was isolated at −60°C, washed with ether, dried in a high vacuum and stored at −78°C. Yield 3.89 g (90% of theoretical value). Found: C, 31.5; H, 4.5; Mo, 27.8; I, 36.2 (rest)%. Calc. for $C_9H_{15}IMo$: C, 31.2; H, 4.4; Mo, 27.7; I, 36.7%.

$[MoOAc(\eta^3\text{-}C_3H_5)_3]$ (6)

2 (2.30 g, 9.04 mmol) was dissolved in CH_2Cl_2 and treated with a 50% excess of silver acetate (2.2 g) at −20°C. The solution was stirred for a further 20 h. The solvent was removed *in vacuo* and the residue extracted with pentane at −10°C. The concentrated pentane solution was cooled to −78°C and the resulting yellow crystalline precipitate isolated, dried in a high vacuum and stored at −30°C. Yield 1.51 g (60% of theoretical value). The compound decomposes slowly at room temperature and rapidly at 57°C. Found: C, 48.4; H, 6.6; Mo, 35.2%. Calc. for $C_{11}H_{18}O_2Mo$: C, 48.5; H, 6.7; Mo, 35.3%. MS: *m/z* 280 [M^+], 238, 195. ^1H NMR spectrum: see Table 1.

$[Moacac(\eta^3\text{-}C_3H_5)_3]$ (7)

2 (1.04 g, 4.09 mmol) was suspended in 30 cm^3 THF at −78°C and Tlacac (1.55 g, 5.11 mmol) in

THF was added. A yellow-brown suspension was formed which was stirred overnight at −78°C. The reaction mixture was filtered through Avicel and the solvent removed in a high vacuum. The residue was taken up in pentane at −40°C and the solution cooled to −78°C. A yellow solid precipitated which was isolated and dried in a high vacuum at −78°C. Yield 0.60 g (46.2% of theoretical value). Found: C, 52.9; H, 6.7; Mo, 30.4%. Calc. for $C_{14}H_{22}O_2Mo$: C, 52.8; H, 6.9; Mo, 30.2%. ^{1}H NMR spectrum: see Table 1.

[MoCl(NCMe)(η^3-C_3H_5)$_3$] (**3**, L = MeCN)

2 (0.40 g, 1.54 mmol) was added to MeCN (10 cm^3) at −30°C to give a yellow suspension. The solution was concentrated to *ca* 3 cm^3 and CH_2Cl_2 added. The resulting solution was concentrated at −30°C to give yellow crystals which were washed with MeCN at −30°C, dried in a high vacuum and stored at −30°C. Yield 0.36 g (80% of theoretical value). Found: C, 44.6; H, 6.1; Cl, 11.9; N, 4.8; Mo, 32.6%. Calc. for $C_{11}H_{18}ClNMo$: C, 44.7; H, 6.1; Cl, 12.0; N, 4.7; Mo, 32.6%. The ^{1}H NMR spectrum showed the presence of isomers and was not analysed in detail.

[MoCl(py)(η^3-C_3H_5)$_3$] (**3**, L = py)

This was prepared similarly, in 80% yield, as orange crystals soluble in CH_2Cl_2 and which decompose above −30°C. Found: C, 50.4; H, 6.0; Cl, 10.6; N, 4.3; Mo, 28.6%. Calc. for $MoC_{14}H_{20}NCl$: C, 50.4; H, 6.0; Cl, 10.6; N, 4.2; Mo, 28.8%. ^{1}H NMR spectrum: see Table 1.

[MoCl(PMe_3)(η^3-C_3H_5)$_3$] (**3**, L = PMe_3)

This was prepared similarly, in 59% yield, as a yellow solid. Found: Cl, 11.1; P, 9.8; Mo, 30.5%. Calc for $C_{12}H_{24}ClPMo$: Cl, 10.7; P, 9.4; Mo, 29.0%. ^{1}H NMR spectrum: see Table 1. ^{31}P NMR (32.4 MHz, d_8-THF, rt): δ −5.5.

[MoCl{P(OMe)$_3$}(η^3-C_3H_5)$_3$] [**3**, L = P(OMe)$_3$]

This was prepared similarly, in 60% yield, as a yellow solid from ether. Found: C, 38.2; H, 5.9; Cl, 9.3; P, 8.3; Mo, 25.4%. Calc. for $C_{12}H_{24}O_3ClPMo$: C, 38.1; H, 6.4; Cl, 9.4; P, 8.2; Mo, 25.3%. ^{1}H NMR: see Table 1. ^{31}P NMR (32.4 MHz, CD_2Cl_2, −30°C): δ 146.4.

[MoMe{P(OMe)$_3$}(η^3-C_3H_5)$_3$] (**5**; R = OMe, R′ = Me)

2 (0.16 g, 0.63 mmol) was suspended in ether (30 cm^3) at −30°C and treated successively with P(OMe)$_3$ (1 cm^3, 8.48 mmol) and MeMgI (0.29 cm^3 in ether, 0.63 mmol) to give a yellow suspension. The solvent was removed *in vacuo* and pentane (80 cm^3) added. The solution was filtered, concentrated, cooled to −78°C and the yellow precipitate was isolated and dried in a high vacuum at −78°C. Yield 0.10 g (44% of theoretical value). Found: Mo, 27.2; P, 8.9%. Calc. for $C_{13}H_{27}OPMo$: Mo, 26.8; P, 8.7%. ^{1}H NMR: see Table 1. ^{31}P NMR (32.4 MHz, d_6-acetone, −30°C): δ 159.4.

[MoMe(PMe_3)(η^3-C_3H_5)$_3$] (**5**; R = Me, R′ = Me)

This was prepared similarly, in 34% yield, by reacting [MoCl(PMe_3)(η^3-C_3H_5)$_3$] with MeMgI in ether. Found: Mo, 30.3; P, 10.1%. Calc. for $C_{13}H_{27}PMo$: Mo, 31.0; P, 10.0%. ^{31}P NMR (32.4 MHz, d_8-THF, −80°C): δ 3.8.

[MoEt(PMe_3)(η^3-C_3H_5)$_3$] (**5**; R = Me, R′ = Et)

This was prepared similarly, in 63% yield, as a yellow solid by reacting [MoCl(PMe_3)(η^3-C_3H_5)$_3$] with EtMgI in ether. Found: Mo, 29.1; P, 9.2%. Calc. for $C_{20}H_{29}PMo$: Mo, 29.6; P, 9.6%. ^{31}P NMR (32.4 MHz, d_6-acetone, −30°C): δ 2.3.

[Mo-η^1-C_3H_5(PMe_3)(η^3-C_3H_5)$_3$] (**5**; R = Me, R′ = C_3H_5)

This was prepared similarly as a yellow solid by reacting **2** successively with PMe_3 and allylMgCl in ether at −78°C. Found: Mo, 28.9; P, 9.3%. Calc. for $C_{15}H_{29}PMo$: Mo, 28.6; P, 9.2%. ^{1}H NMR spectrum: see Table 1. ^{31}P NMR (32.4 MHz, d_6-acetone, −30°C): δ 1.6.

[Mo-η^1-C_3H_5{P(OMe)$_3$}(η^3-C_3H_5)$_3$] (**5**; R = OMe, R′ = C_3H_5)

This was prepared similarly in 83% purity (NMR) by reacting [MoCl{P(OMe)$_3$}(η^3-C_3H_5)$_3$] with allylMgCl in ether at −78°C. ^{31}P NMR (32.4 MHz, d_6-acetone, −60°C): δ 159.6.

[Mo(NCMe)$_2$(η^3-C_3H_5)$_3$]$^+$$BF_4^-$

MeCN (2 cm^3) was added to **2** (0.65 g, 2.56 mmol) at −30°C. CH_2Cl_2 (30 cm^3) was added to the yellow suspension followed by $TlBF_4$ (0.74 g, 2.56 mmol). The reaction was stirred overnight at −30°C, filtered and the resulting orange solution concentrated, treated with cold ether and cooled to −78°C. A yellow precipitate was formed which was isolated and dried in a high vacuum. Yield 0.64 g (64% of theoretical value). Found: Mo, 24.6; N, 7.1; F,

19.7%. Calc. for $C_{13}H_{21}BF_4N_2Mo$: Mo, 24.7; N, 7.2; F, 19.6%.

A related PF_6 complex was prepared, as yellow crystals, by reacting $[MoI(\eta^3\text{-}C_3H_5)_3]_2$ with MeCN and $AgPF_6$ in ether–CH_2Cl_2 at −30°C. Yield 60%. Found: C, 35.1; H, 5.3; N, 6.2; Mo, 20.5%. Calc. for $C_{13}H_{21}PF_6N_2Mo$: C, 35.0; H, 4.7; N, 6.3; Mo, 21.5%.

$[Mo(H_2NC_2H_4NH_2)(\eta^3\text{-}C_3H_5)_3]^+PF_6^-$

This was prepared similarly as a yellow compound in low yield by reacting **2** with ethylendiamine and NH_4PF_6 in CH_2Cl_2. Found: Mo, 22.8; N, 6.7; P, 7.2; F, 27.3%. Calc. for $C_{11}H_{23}F_6PN_2Mo$: Mo, 22.6; N, 6.6; P, 7.3; F, 26.9%.

$[Mo(Me_2PC_2H_4PMe_2)(\eta^3\text{-}C_3H_5)_3]^+BF_4^-$

This was prepared similarly, in 51% yield, by reacting **2** with $Me_2PC_2H_4PMe_2$ and $TlBF_4$ in CH_2Cl_2. Found: Mo, 20.7; P, 13.5; F, 16.3%. Calc. for $C_{15}H_{31}BF_4P_2Mo$: Mo, 21.1; P, 13.6; F, 16.7%. ^{31}P NMR (32.4 MHz, d_6-acetone, −80°C): δ 48.0/44.7 ($J_{P,P}$ 45.2 Hz).

$[Mo\{P(OMe)_3\}_3(\eta^3\text{-}C_3H_5)_2]$ (**8**)

2 (0.36 g, 0.71 mmol) was treated at −30°C with $P(OMe)_3$ (3 cm^3) and the resulting yellow precipitate dissolved in THF (30 cm^3). Excess Li powder (0.5 g) was added and the mixture stirred at −30°C for 4 h. The reaction mixture was filtered and the solution evaporated to dryness and the residue washed with pentane (5 × 10 cm^3) at −78°C. Extraction with ether at −30°C gave a yellow solution from which yellow crystals were obtained after concentration and cooling. These were dried in a high vacuum at −30°C. Yield 0.67 g (70% of theoretical value). The complex decomposes slowly at rt and rapidly at 70–75°C. Found: C, 32.9; H, 7.1; P, 16.9; Mo, 17.4% Calc. for $C_{15}H_{37}O_9P_3Mo$: C, 32.7; H, 6.8; P, 16.9; Mo, 17.4%. MS: *m/z* 552 [M^+], 428 [$M^+ - P(OMe)_3$], 302 [$M^+ - 2P(OMe)_3/2H$]. ^{31}P NMR (32.4 MHz, *d*-toluene, −30°C): AB_2 spin system [δ_A 193.6, δ_{B_2} 176.4 ($J_{P,P}$ 58.1 Hz)]. ^1H NMR (0°C, d_8-toluene, 233 K):* δ 5.61 (H1, m), 2.58 (H2, m), 2.72

* ^1H numbering scheme:

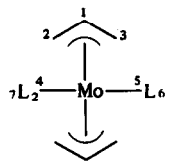


Table 4. Experimental data for the crystal structure of $[MoOAc(\eta^3\text{-}C_3H_5)_3]$

Formula	$C_{11}H_{18}O_2Mo$
Molecular weight	278.2
Colour	Yellow
Crystal size (mm)	0.25 × 0.17 × 0.50
Space group	$P2_1/c$
a (Å)	11.153(2)
b (Å)	7.603(1)
c (Å)	14.078(1)
β (°)	105.920(5)
Z	4
V (Å^3)	1147.97
d_c (g cm^{-3})	1.61
μ(Mo-K_α) (cm^{-1})	10.90 (no correction for absorption)
Enraf–Nonius CAD-4 diffractometer	
Radiation	Mo-K_α, graphite monochromator
Temperature (K)	100
Reflections measured	11,555 ($\pm h, \pm k, l$)
θ limits	$1.5 \leqslant \theta \leqslant 35.9°$
R_{av}	0.019
Unique observed reflections	4894 ($\pm h, k, l$) [$I > 2\sigma(I)$]
Hydrogen atom positions	Found 15, calculated 3 (bonded to carbon C2)
Refined parameters	199
R	0.025
R_w	0.037
Residual electron density (around Mo atom) (*e* Å^{-3})	0.9

(H3, m), 1.91 (H4, m), 1.53 (H5, m), 3.49 (H6, d), 3.33 (H7, t); $J_{1,2}$ 6.5 Hz, $J_{1,3}$ 6.3 Hz, $J_{1,4}$ 9.3 Hz, $J_{1,5}$ 8.9 Hz, $J_{2,3}$ 3.5 Hz, $J_{2,4}$ 0 Hz, $J_{3,5}$ 0 Hz, $J_{2,P}$ 0 Hz, $J_{3,P}$ 15.8 Hz, $\sum J_{4,P}$ 13.5 Hz, $\sum J_{5,P}$ 11.7 Hz, $J_{6,P}$ 9.8 Hz, $\sum J_{7,P}$ 9.1 Hz).

The same complex (^{31}P NMR) was formed on treating **2** with $LiAlH_4$ followed by extraction with pentane at $-10°C$ as well as in the reaction of $[MoCl\{P(OMe)_3\}(\eta^3\text{-}C_3H_5)_3]$ with allylMgCl. The product of the reaction of **2** with PMe_3 and Li in THF at $-30°C$ could not be isolated analytically pure but presumably has an analogous structure. ^{31}P NMR (32.4 MHz, d_6-acetone $-30°C$): A_2B spin system [δ_{A_2} 9.1, δ_B 5.0 ($J_{P,P}$ 34.1 Hz)].

Experimental details of the X-ray structural determination are summarized in Table 4. A single crystal of **6**, recrystallized from methanol, was mounted in a glass capillary under argon and maintained at low temperature (100 K) for all subsequent measurements. Two independent data sets were collected (see Table 4) and equivalent reflections were averaged ($R_{av} = 0.019$) to give 4894 unique observed data. These were assigned sigmas from counting statistics and used in the subsequent solution and refinement of the structure.

The Mo atom position was deduced from a Patterson map, and a phased Fourier synthesis revealed all non-hydrogen atoms. In a difference Fourier synthesis following the anisotropic refinement of the heavier atoms, the allylic hydrogen atoms could be located. Three hydrogen atoms bonded to C2 were placed at calculated positions. All the hydrogen atoms were included in the final stages of the refinement, convergence being obtained at $R = 0.025$ ($R_w = 0.037$). In addition to several locally written programs, the following programs were used: TRACER by Lawton and Jacobson for cell reduction; Sheldrick's SHELX-76 for Fourier calculations and initial least-squares refinement; GFMLS, a highly modified version of ORFLSD, by Hirshfeld, Coppens, Leiserowiz and Rabinovich for subsequent full-matrix least-squares refinement; Davis' DAESD for bond distance and angle calculations, XANADU by Roberts and Sheldrick for best-plane and torsion angle calculations; and Johnson's ORTEP for the molecular drawings.

Acknowledgements—C. C. R. thanks the Alexander von Humboldt Stiftung for the award of a stipendium. M. J. R. thanks the INIC, Lisboa and the Max-Planck-Gesellschaft for financial support. Both thank the Instituto Superior Tecnico, Lisboa, Portugal, for leave of absence. R. B., A. R. and G. S. were responsible for the ^{1}H NMR spectral investigations, and C. K. and M. J. R. for the X-ray diffraction determination.

REFERENCES

1. W. Oberkirch, Dissertation, Techn. Hochschule Aachen (1963).
2. G. Wilke, B. Bogdanović, P. Heimbach, W. Keim, M. Kröner, W. Oberkirch, K. Tanaka, E. Steinrücke, D. Walter and H. Zimmermann, *Angew. Chem.* 1966, **78**, 157.
3. P. W. Jolly, C. Krüger, C. C. Romão and M. J. Romão, *Organometallics* 1984, **3**, 936.
4. J. P. Candlin and H. Thomas, *Adv. Chem. Ser.* 1974, **132**, 212.
5. F. A. Cotton and J. R. Pipal, *J. Am. Chem. Soc.* 1971, **93**, 5441.
6. J. R. Dilworth and R. L. Richards, *Inorg. Synth.* 1980, **20**, 120.
7. C. A. Tolman, *J. Am. Chem. Soc.* 1970, **92**, 2956.
8. M. L. H. Green and W. E. Silverthorn, *J. Chem. Soc., Dalton Trans.* 1973, 301.
9. M. L. H. Green, L. C. Mitchard and W. E. Silverthorn, *J. Chem. Soc., Dalton Trans.* 1973, 1403, 2177.
10. M. Brookhart and M. L. H. Green, *J. Organomet. Chem.* 1983, **250**, 395.
11. S. Holle, P. W. Jolly and C. C. Romão, manuscript in preparation.
12. R. Benn, A. Rufińska and G. Schroth, *J. Organomet. Chem.* 1981, **217**, 91.
13. B. Henc, P. W. Jolly, R. Salz, S. Stobbe, G. Wilke, R. Benn, R. Mynottt, K. Seevogel, R. Goddard and C. Krüger, *J. Organomet. Chem.* 1980, **191**, 449.

Polyhedron Vol. 5, No. 1/2, pp. 473–485, 1986
Printed in Great Britain

0277–5387/86 $3.00 + .00
Pergamon Press Ltd

ACTIVATION OF H_2 AND SO_2 BY Mo AND W COMPLEXES: FIRST EXAMPLES OF MOLECULAR-H_2 COMPLEXES, SO_2 INSERTION INTO METAL–HYDRIDE BONDS, AND HOMOGENEOUS HYDROGENATION OF SO_2

G. J. KUBAS† and R. R. RYAN

Los Alamos National Laboratory, University of California, Los Alamos. NM 87545, U.S.A.

(*Received* 3 *July* 1985)

Abstract—Our recent work on small-molecule activation by low-valent organometallic Mo and W complexes is summarized. Stereochemical control of Mo–SO_2 coordination geometry has been achieved since the SO_2 in $Mo(CO)_2(PPh_3)_2(SO_2)(L)$ can bind as a σ-base (η^1), as a π-acid (η^2), or as an isomeric mixture of *both forms* merely by fine-tuning the donor–acceptor nature of the single *cis* ligand, L. Modification towards bulky phosphines led to a synthetic pathway to the formally 16-electron complexes, $M(CO)_3(PR_3)_2$ (R = Cy or Pr^i), the structures of which show agostic M···H—C interaction. This weak interaction can readily be supplanted by others, including the first example of coordination of molecular H_2. Neutron diffraction studies of $W(CO)_3(PPr^i_3)_2(\eta^2\text{-}H_2)$ show that W—H = 1.89(1) Å and H—H = 0.82(1) Å. ^1H NMR of the HD complex provides a useful spectroscopic diagnostic for molecular coordination (J_{HD} = 33.5 Hz). Complete H–D isotopic exchange occurs for $D_2 + H_2$ complex, even in the solid state. Reductions of SO_2 by hydrides and H_2 have been studied. Addition of SO_2 to solutions of $(\eta^5\text{-}C_5R_5)M(CO)_3H$ [R = H (= Cp) or Me (= Cp*)] produced $(\eta^5\text{-}C_5R_5)M(CO)_3(SO_2H)$, the first example of SO_2 insertion into an M—H bond. The —S(O)(OH) complexes are thermally unstable, decomposing at 25–75°C to SO_2 reduction products, including water and sulfido–oxo cluster complexes. A dithionite-bridged complex, $[Cp^*Mo(CO)_3]_2(\mu\text{-}S_2O_4)$, has also been obtained from the hydride–SO_2 reaction. Homogeneous catalysis of SO_2 reduction by H_2 has been effected using $[Cp^*Mo(\mu\text{-}S)(\mu\text{-}SH)]_2$ catalyst. Clean conversion to sulfur and water occurs in chlorobenzene–butanol at 1–3 atm and 25–100°C at a rate of up to 350 catalyst turnovers h^{-1}. Weak bases such as Et_3N and ROH greatly increase the rate.

Our recent findings and those of others indicate that low-valent group 6 organometallic complexes are well-suited for studies of the activation of SO_2, molecular H_2,[1] C—H,[2] and O—H[3] bonds, and also of the stereochemical control of metal–ligand (e.g. Mo–SO_2) coordination geometry.[4] Indeed, $Cr(CO)_5$ has been well recognized as a prototype mononuclear transition-metal fragment,[5] forming complexes with weak ligands such as methane in low-temperature matrices.[6] Formally 16-electron complexes, of which $M(CO)_3(PCy_3)_2$ is an example,[2,7] have been found that offer a similar type of chemistry with the advantage of room-temperature adduct stability conferred by the bulky phosphines. Because of this stability, the first examples of molecular-H_2 complexes have been characterized as isolable, crystalline solids.[1]

In this paper we summarize much of our recent work on small-molecule activation by Mo and W complexes. In general, both metals give similar chemistry, but, since the W complexes possess greater thermal and air stability, they often were more readily characterized. Our research has emphasized SO_2–transition-metal chemistry, with recent work directed towards SO_2 reduction. The pursuit of this goal led to the recent serendipitous

† Author to whom correspondence should be addressed.

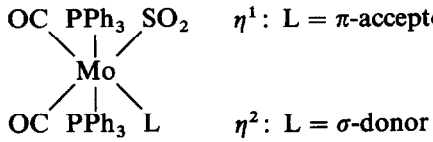
discovery of the W and Mo dihydrogen complexes. Little is known about the elementary steps of SO_2 reduction, and we have found that Mo complexes offer an excellent opportunity for studying stepwise reactions of SO_2 with hydrogen and hydride ligands. The overall goal of our efforts, in addition to understanding the mechanistic processes which occur during SO_2 reduction on heterogeneous catalysts, has been to develop a *homogeneous* catalytic SO_2 reduction cycle.

COORDINATION OF SO_2 TO Mo(0) AND W(0) COMPLEXES

The primary focus of our research has been the synthesis, structure, bonding and reaction chemistry of transition-metal–SO_2 complexes.[4(b)] The diversity of bonding modes exhibited by SO_2–metal complex interactions is unequalled by any other ligand, making SO_2 a remarkably versatile bonding probe for transition-metal complexes. Studies of octahedral d^6 complexes of the group 6 metals have contributed much to our understanding of SO_2 coordination. In particular, the ability of SO_2 to coordinate in an η^1-planar or η^2 (S,O-bonded) fashion to Mo(0) and W(0) has been advantageous in regard to our understanding of the π-acceptor ability of SO_2. Insight into the reactivity of coordinated SO_2, for example the basicity of the uncoordinated oxygen atom in η^2-SO_2, has also been obtained.

Interestingly, $Mo(CO)_3(phen)(SO_2)$ and $Mo(CO)_2(bipy)(SO_2)_2$ contain η^2-SO_2 ligands,[8] whereas η^1-planar SO_2 was found in all previously structurally characterized SO_2 complexes of d^6-metals.[4(b)] A large variety of d^6 Mo– and W–SO_2 complexes has since been systematically synthesized and characterized to determine the extent and nature of stereochemical control of the metal–SO_2 bonding geometry.[4,9] For d^6-complexes in general, and Mo(0) and W(0) in particular, the η^1-planar and η^2 geometries have been observed whereas the η^1-pyramidal has not and is not expected on the basis of simple orbital participation schemes, i.e.

η^2 fashion, depending upon the nature of L:[4]



η^1: L = π-acceptor

η^2: L = σ-donor

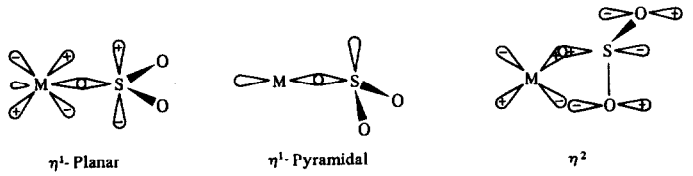
The bonding mode is remarkably sensitive to fine-tuning just *one* ligand and for the complex containing L = alkylisocyanide the coexistence of both an η^1-planar SO_2 isomer and an η^2-SO_2 isomer in apparent equimixture was observed. This is the first direct observation of spontaneous linkage isomerism of coordinated SO_2, although it has been implicated in reactions of coordinated SO_2. From these and related studies the following conclusions may be drawn:

(a) The η^2-geometry involves more M → SO_2 π-donation and less SO_2 → M σ-donation than does the η^1-planar case. The η^2-geometry is, therefore, generally discouraged by strongly π-accepting ligands and encouraged by strongly σ-donating ligands.

(b) The existence of a D–M–A (D = donor or weak π-acceptor, A = acceptor) conformation *cis* to SO_2 promotes η^2-bonding and dictates the orientation of the S—O_m bond: in all cases, the sulfur atom lies closest to the acceptor ligand (e.g. CO).

The latter can be attributed to a polarization of π-electron density toward the better π-accepting ligands in the plane *cis* to the SO_2. The unsymmetrical η^2-SO_2 ligand is oriented to best compete for the π-electron density with the sulfur atom nearer the carbonyls since the $2b_1$ acceptor orbital is largely sulfur *p* in character with a smaller oxygen *p* contribution.

The coordinated SO_2 in the Mo complexes is neither reversibly bound nor reactive with oxygen to form sulfato complexes. For those complexes containing η^1-planar SO_2, this behavior is consistent with the majority of known η^1-planar SO_2 complexes of all metal coordination types. The behavior of the η^2-complexes, however, is in contrast



η^1- Planar η^1- Pyramidal η^2

Control of the SO_2 bonding mode has been achieved by the proper choice of the σ-donating vs π-accepting ancillary ligands as well as their geometric disposition with respect to the SO_2. For example, the SO_2 ligand in *cis,trans*-$Mo(CO)_2(PPh_3)_2(SO_2)(L)$ has been found to coordinate in either η^1-planar or to that of η^2-SO_2 in four- and five-coordinate complexes.[4(b)] One important difference between the octahedral η^2-SO_2 complexes and the lower-coordinate systems is the inaccessibility of the η^1-pyramidal SO_2 bonding mode in the octahedral complexes. In general, the η^1-pyramidal SO_2

geometry is not far removed energetically from that of the η^2-geometry for the four- and five-coordinate η^2-SO_2 complexes. The great majority of η^1-pyramidal SO_2 complexes contain reversibly bound SO_2 and react with oxygen to give sulfato complexes.[4(b)] Thus, an intermediate species containing an η^1-pyramidal SO_2 might be involved in the reversible coordination of SO_2 and sulfato reaction of the four- and five-coordinate η^2-SO_2 complexes. For the octahedral η^2-SO_2 systems, such a reaction pathway would be blocked by the very high energy of the η^1-pyramidal species and, in general, d^6 η^2-complexes do not react with O_2 to form sulfates.

Since the discovery of η^2-SO_2 bonding in transition-metal complexes,[10] there has been considerable interest in this bonding mode and in the extent to which S—O bond activation actually occurs and whether it can be exploited in reaction chemistry studies. This form of coordinated SO_2 has shown some intriguing examples of reactivity quite different from that presently known for the η^1-planar, η^1-pyramidal or bridging SO_2 coordination modes. The bonding of η^2-SO_2 has been suggested to primarily involve π-donation from the metal to the LUMO of SO_2, which is antibonding with respect to the S—O bond and bonding with respect to the O–O interaction.[4(b)] This type of interaction would be expected to lengthen S—O distances, increase the terminal oxygen basicity, and enhance coordination by Lewis acids. The complex

$$Ru(CO)_2(PPh_3)_2(\eta^2\text{-}SO_2 \cdot SO_2) \text{ (I)}$$

was found to contain a second SO_2 coordinated as a Lewis acid to the terminal oxygen of the η^2-SO_2 (Fig. 1).[11] It exhibits the longest coordinated S—O bond and the lowest ν(SO) value of any of the reported η^2-SO_2 complexes.[4(b)] An unusual reactivity was observed: the complex slowly reacted with excess SO_2 in the absence of oxygen to generate the bidentate sulfate complex[12] $Ru(SO_4)(CO)_2(PPh_3)_2$ (the same complex that was obtained on reaction of **I** with molecular oxygen[13]) plus PPh_3S and an unidentified ruthenium species which appeared to contain bridging carbonyls. The only products obtained in the presence of excess PPh_3 are $Ru(SO_4)(CO)_2(PPh_3)_2$ and PPh_3S. In an attempt to explore the effect of enhanced basicity of the ancillary ligand, a variety of complexes of the type $Ru(CO)_2(SO_2)(PR_3)_2$ were prepared where PR_3 = (A) triphenylphosphine, (B) *p*-tolyldiphenylphosphine, (C) tribenzylphosphine, and (D) tricyclohexylphosphine. For A–C the reactivity is essentially identical with $\sim$10% of the corresponding SO_4 complexes formed in 2 days in SO_2-saturated benzene solutions. For D, a different complex was isolated after 1 day which analyzes for $Ru(CO)_2(S_2O_4)(PCy_3)_2$ and is monomeric by solution molecular weight studies. Since this species continues to react and generate the sulfato complex, $Ru(CO)_2(SO_4)(PCy_3)_2$, it appears likely that this is an intermediate in the reaction and that the reaction should be depicted as $M^0(SO_2 \cdot SO_2) \rightarrow M^{2+}(S_2O_4)^{2-} \rightarrow M^{2+}(SO_4)^{2-} + \frac{1}{8}S_8$ (the S_8 reacts with PR_3 to form SPR_3). At this point there appears to be no clear trend in the reactivity that can be related to the phosphine basicity, but other factors such as steric effects could dominate.

Other studies of Mo–SO_2 complexes have produced well-defined illustrations of the basicity of

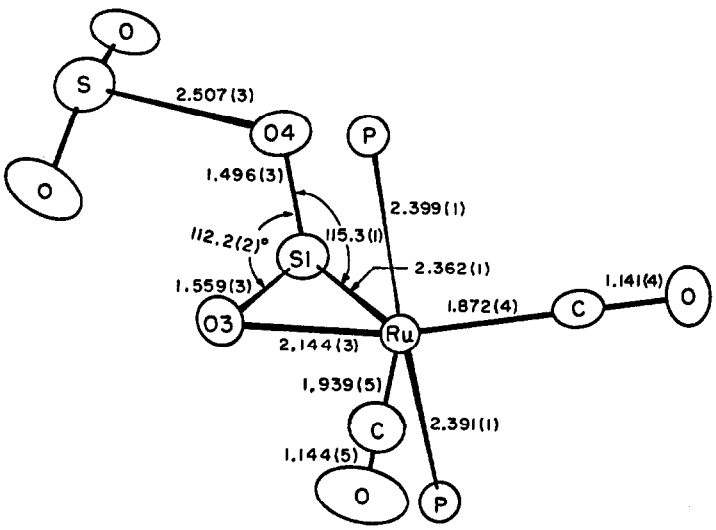


Fig. 1. Structure of $Ru(CO)_2(PPh_3)_2(\eta^2\text{-}SO_2 \cdot SO_2)$.

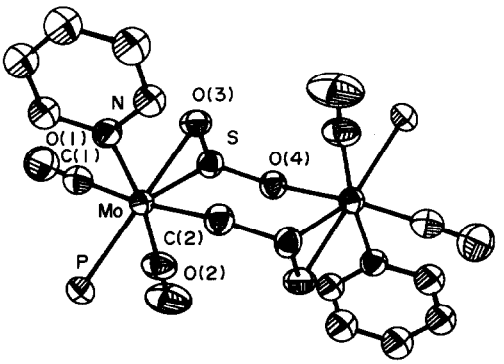


Fig. 2. Structure of $[Mo(CO)_2(PPh_3)(py)(SO_2)]_2$.

the terminal oxygen of η^2-SO_2. The structure of $[Mo(CO)_2(PPh_3)(py)(SO_2)]_2$ showed the first example of SO_2 coordinated to metals by way of all three of its atoms (Fig. 2).[4(a),14] This complex was spontaneously formed in solution from $Mo(CO)_2(PPh_3)_2(pyridine)(\eta^2\text{-}SO_2)$ by loss of PPh_3. Thus, the terminal oxygen of the η^2-SO_2 ligand in this complex apparently possesses sufficient basicity to displace PPh_3, a surprising result since PPh_3 is an excellent ligand. Even more striking is the finding that the dimer will precipitate in the presence of a large excess of pyridine, a strong competing ligand, and is not readily cleaved by pyridine and other strongly basic ligands. The low solubility of $[Mo(CO)_2(pyridine)(PPh_3)(\mu\text{-}SO_2)]_2$ may provide some driving force for its formation, but nonetheless the Mo–O bond [Mo—O(4)] must be relatively strong (bond length = 2.24 Å) and indeed is only 0.05 Å longer than that for Mo—O(3). Further indication of the oxygen basicity in Mo–SO_2 complexes was given by Schenk and Baumann,[9] who reported O-silylation of both η^1- and η^2-complexes.

An interesting series of complexes of the type $Mo(CO)_2L_3(SO_2)$ (L = $PMePh_2$ or $CyNH_2$) has been synthesized and found to contain η^1-planar SO_2. The geometry was unexpected because the presence of three σ-donating ancillary ligands would appear to favor η^2-bonding. The X-ray crystal structure of $Mo(CO)_2(CyNH_2)_3(SO_2)$ revealed that the cyclohexylamine ligands coordinate in *facial* fashion.

The most intriguing feature of this complex was found to be its novel reactivity with oxygen:

$$Mo(CO)_2(CyNH_2)_3(SO_2) + O_2 \xrightarrow[(H_2O)]{DMSO} [CyNH_3]_2[SO_4] + 2CO + [CyNH_3][Mo_xO_y].$$

The production of *uncoordinated* sulfate from SO_2 complexes has not been observed and a catalytic method for SO_2 oxidation to sulfate would be of considerable interest. However, the mechanism may involve reaction of dissociated ligands since SO_2 and $CyNH_2$ were found to give $[CyNH_3][HSO_3]$ in DMSO, and air-oxidation of the bisulfite to sulfate was catalyzed by the molybdate coproduct of the reaction. Thus, it is probable that oxidation of the metal with concomitant ligand loss occurs initially, followed by reaction of SO_2, $CyNH_2$ and H_2O to give bisulfite and eventually sulfate.

ACTIVATION OF H—H AND C—H BONDS: MOLECULAR-H_2 COMPLEXES

The discovery[2,7] of a facile synthetic pathway to stable 16-electron complexes, $M(CO)_3(PCy_3)_2$ (M = Mo or W), has provided an unparalleled opportunity to study small-molecule activation, in particular the first examples of molecular-H_2 complexes.[1] The complexes are the only ones of which we are aware that activate *both* H—H and C—H bonds. The synthesis evolved serendipitously from our work on Mo–SO_2 complexes, specifically *mer,trans*-$Mo(CO)_3(PR_3)_2(SO_2)$.[4(a)] During attempts to optimize their preparation from *fac*-tricarbonyl complexes containing labile ligands, $M(CO)_3$(cycloheptatriene) was found to be a viable precursor to formally coordinatively unsaturated species:

$$M(CO)_3(cycloheptatriene) + 2PCy_3 \xrightarrow[argon]{ether} M(CO)_3(PCy_3)_2 + C_7H_8.$$

The observation of the striking deep blue-purple color of the 16-electron complexes was a key factor in their identification.

The stability of the complexes is largely a result of the well-known steric demands imposed by bulky phosphine ligands. The labile cycloheptatriene in the starting complex, $M(CO)_3$(cycloheptatriene), occupies *three* coordination sites but is effectively displaced by only *two* phosphine ligands, thereby opening up the sixth coordination site. Because of the phosphine bulk, the cycloheptatriene is squeezed out of the coordination sphere of the metal. The phosphine size must, of course, be large enough such that three cannot easily fit around the metal in an octahedral array, but curiously the synthesis succeeds for PCy_3, PPr^i_3 and PCy_2Pr^i, but not for other phosphines with similar cone angles. The use of smaller phosphines results in the formation of $Mo(CO)_3(PR_3)_3$.

The structure of $W(CO)_3(PCy_3)_2$ shows the addition of a distal phosphine hydrogen to the metal coordination sphere (Fig. 3). This agostic interaction

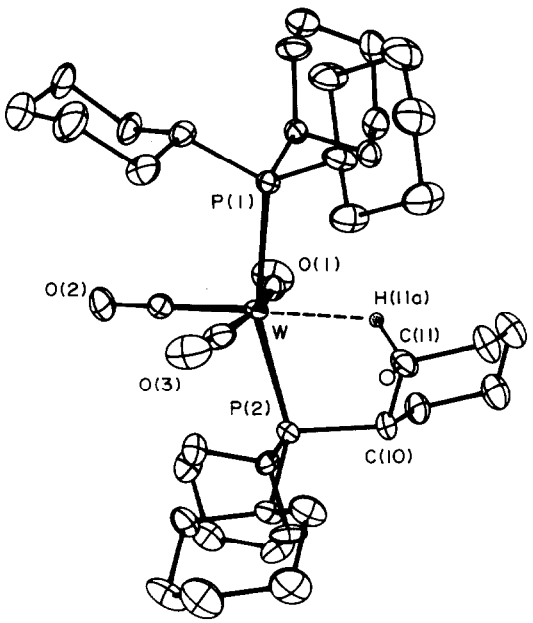


Fig. 3. Structure of $W(CO)_3(PCy_3)_2$.

[ν(CH) = 2552 cm^{-1}] is the first well-defined example of its type for an alkylphosphine. Importantly the highly distorted geometry about P(2)

$$[W—P(2)—C(9) = 122.0(2)°,$$

and

$$W—P(2)—C(10) = 99.0(2)°]$$

is evidence that the tungsten atom exerts a strong *attractive* force upon the (11a) atom. Note that this is in distinct contrast with several other coordinatively unsaturated complexes in which hydrogen atoms from coordinated phosphine groups are located near the open site about the metal. For example, the triphenylphosphine ligands in both $RhHCl(SiCl_3)(PPh_3)_2$[15] and $RuCl_2(PPh_3)_3$[16] have normal, undistorted geometries. LaPlaca and Ibers[16] attribute the particular location of ring hydrogen atoms near the metal in these complexes to "geometric" effects, rather than any true metal–hydrogen bonding interactions. The same is apparently true in the case of the Mo(CO)(diphos)$_2$ (diphos = diphenylphosphinoethane) molecule,[17] another example of a formally five-coordinate complex with a group 6 metal.

Although refinement of the hydrogen atom positions was unsuccessful, the idealized position of the activated hydrogen atom is *ca* 2.17 Å from the metal [W—C(11) = 2.943(6) Å]. The overall structure of the PPr^i_3 analogue is basically similar, although disorder hampers precise description of the crucial distorted portion of the molecule.

$M(CO)_3(PR_3)_2$ readily "add" donor ligands, which displace the C—H group from the metal center. The resultant *mer,trans*-$M(CO)_3(PR_3)_2L$ can contain reversibly bound donors (e.g. H_2, N_2, C_2H_4 and H_2O) or irreversibly bound groups (e.g. CO, SO_2 and pyridine).

As with other unsaturated complexes, the ability to bind additional ligands is strongly influenced by steric factors. For example, as also found for Mo(CO)(diphos)$_2$,[17] the complexes coordinate primary but not secondary or tertiary amines. Other ligands which fail to form isolable adducts include propylene, cyclohexene, butadiene, C_2F_4 and furan. Nevertheless, certain strong ligands, such as phosphines (e.g. PPh_3) and phosphites, will form adducts despite their relative bulkiness. Also, in spite of the strong Lewis acidity of the metal atom in $M(CO)_3(PR_3)_2$, it has been shown that CO_2 does not add, even in liquid CO_2.[3] A hydrido-bicarbonate complex, $W(CO)_3(PCy_3)_2(H)(HCO_3)$, has been suggested as the result of reaction with "wet" CO_2.[3] The same authors propose that the H_2O complex is a precursor to the bicarbonate and contains hydrido–hydroxo ligands resulting from oxidative addition. This activation of O—H bonds by Mo and W is a promising area for exploration also.

Molecular-H_2 *coordination*

The activation of hydrogen by transition-metal complexes, i.e. oxidative addition to form hydride complexes, has been well studied because of its importance in catalysis. The geometry of approach of the H_2 molecule to the metal ("end-on" or "side-on") has long been the subject of discussion,[18] and recent theoretical studies favored sideways addition to a 16-electron ML_5 center.[5] The existence of transient side-on molecular-H_2 coordination has been proposed, particularly in "direct hydrogen transfer" reaction processes,[19] but until our work a well-characterized molecular-H_2 complex had not been isolated. Spectroscopic evidence for $Cr(CO)_5(H_2)$ (stable at low temperature but short-lived at 25°C) has recently been observed,[20] and, several years prior to this, we reported novel complexes, $M(CO)_3(PCy_3)_2(H_2)$ (M = Mo or W), with unusual IR features.[7] These room-temperature stable complexes, along with $W(CO)_3(PPr^i_3)_2(H_2)$, were then shown to contain the η^2-H_2 ligand,[1] one of the last "holdouts" in the realm of small-molecule coordination. More importantly, the H_2 complexes (including newly reported examples[21]) represent incipient oxidative addition of a diatomic molecule, giving an unprecedented opportunity for study.

The complexes are readily synthesized in excellent yields from the 16-electron precursors,

$M(CO)_3(PR_3)_2$, or directly from $M(CO)_3$ (cycloheptatriene) and PR_3 under H_2. As for $M(CO)_3(PR_3)_2$, the complexes could be formed only for $R_3 = Cy_3$, Pr^i_3 or Cy_2Pr^i. The H_2 ligand readily dissociates reversibly in solution although crystals of the complexes can be handled even in air for short periods. X-ray structural studies revealed an octahedral geometry for $W(CO)_3(PPr^i_3)_2(H_2)$ and the H_2 molecular ligand was first observed by room-temperature neutron diffraction studies at the Los Alamos Pulsed Neutron Source. Subsequent low-temperature neutron studies[21(d)] at both the Brookhaven National Laboratory and Los Alamos were necessary in order to properly model a disorder in one of the phosphino ligands and resulted in the determination, with resonable precision, of H—H and W—H distances of 0.82(1) and 1.89(1) Å (Fig. 4). The H_2 is symmetrically bonded parallel to the P—W—P axis, and the overall coordination geometry is nearly octahedral. Similarly X-ray structural studies of $M(CO)_3(PCy_3)_2(H_2)$ demonstrated an octahedral geometry. Refinement of preliminary neutron diffraction data, despite a disorder of H_2 and CO due to centrosymmetry at the metal, show the H_2 to be bound in a similar fashion to that in the PPr^i_3 analog. It should be noted that the structures of a series of group 6 *hydride* complexes, including $MoH_2(PMe_3)_5$, all showed non-octahedral phosphine positions.[22]

Spectroscopic studies confirmed the structural data, and a useful NMR diagnostic for molecular-H_2 coordination, was found to be the value of J_{HD} for the monodeuterated species, e.g. $W(CO)_3(PPr^i_3)_2(HD)$. The ^1H spectrum (90 MHz) of the H_2 complex showed only a single broad major* resonance at *ca* −4 ppm from 70 to −80°C, but the HD complex gave a 1:1:1 triplet with $J_{HD} = 33.5$ Hz (Fig. 5). This value is an order of magnitude larger than that for, say, hydride and deuteride compounds and is 77% of that for HD gas (43.2 Hz).[23] Solid-state ^2H NMR studies shows that, for $W(CO)_3(PPr^i_3)_2(D_2)$, the D_2 undergoes rotational motion about the metal–D_2 axis at a rate greater than 130 kHz at ambient temperature.

IR spectroscopy provided the first hint of molecular-H_2 coordination, and subsequent thorough IR and Raman examinations of the H_2, HD and D_2 complexes located four of the six

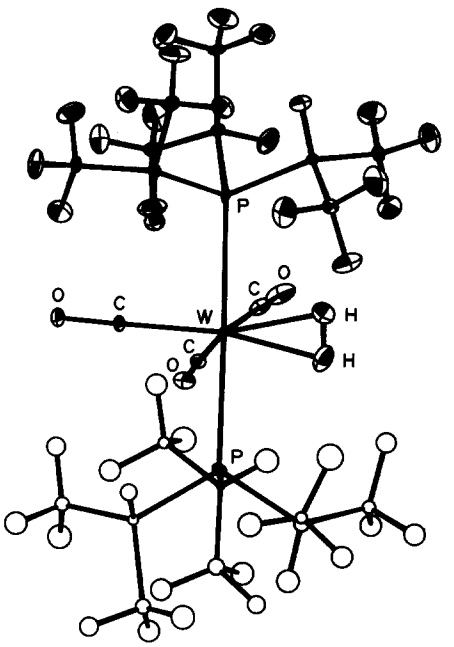


Fig. 4. Structure of $W(CO)_3(PPr^i_3)_2(H_2)$.

fundamental modes expected for η^2-H_2 (Table 1). The use of fully deuterated PCy_3 enabled location of ν(HH) as a weak, broad band at 2690 cm^{-1} in the Nujol mull IR spectrum of

$$W(CO)_3[P(C_6D_{11})_3]_2(H_2)$$

(Fig. 6). This value is some 1500 cm^{-1} lower than that of free H_2. Failure to observe ν(HH) in the Raman experiments may have been due to sample decomposition (even at 77 K). The electronic spectrum of $W(CO)_3(PPr^i_3)_2(H_2)$ shows a band at 364 nm.

In regard to the chemistry of the coordinated H_2, isotopic exchange has been found to occur between $W(CO)_3(PR_3)_2(H_2)$ and D_2 gas in both solution and

Table 1. Vibrational frequencies [ν (cm^{-1})] for solid $W(CO)_3(PCy_3)_2(H_2)$ and isotopically substituted species[a]

	HH	HD	DD
ν(HH)	2690 (IR)[b]	2360 (IR)	~1900 (R)
$\nu_a(WH_2)$	1570 (IR)	~1350 (IR)[b]	~1132 (IR)[b]
$\nu_s(WH_2)$	953 (IR, R)	791 (IR, R)	703 (IR, R)
$\delta(WH_2)$	~450 (IR)[b]		319 (IR)

* A minor (*ca* 15–20%) resonance appears on cooling or on changing to higher field (200 MHz). This resonance, which coalesces with the major peak at or above room temperature, is a triplet ($J = 38$ Hz) in certain temperature ranges, suggesting P–H coupling and the possibility of a hydride form in equilibrium with the H_2 form.[21(c)]

[a] IR samples were Nujol mulls; Raman samples were enclosed in capillaries and excited by the 5682-Å line of a Kr laser. Similar results were obtained for the P-*i*-Pr_3 analogues.

[b] Partially obscured. ν(HH) was relatively clear in the $P(C_6D_{11})_3$ analogue.

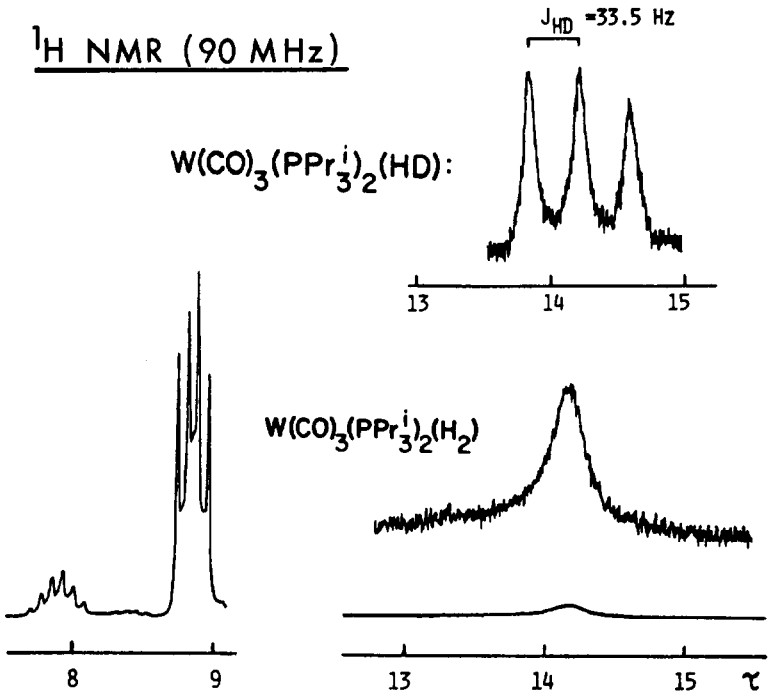


Fig. 5. ^{1}H NMR spectra in C_6D_6 at 35°C.

solid states at 20°C, giving within days a statistical mixture of H_2, HD and D_2 species. Neither the phosphine nor solvent hydrogen atoms exchange. At this point the mechanism for this process is unknown. The solid–gas scrambling is particularly interesting since transient phosphine dissociation cannot be providing vacancies for coordination of a second H_2 and D_2 molecule. The H_2 complexes do not catalyze hydrogenation of ethylene under mild conditions (toluene, 1 atm, 20°C), presumably because of limited available coordination sites (i.e. steric crowding by the phosphines).

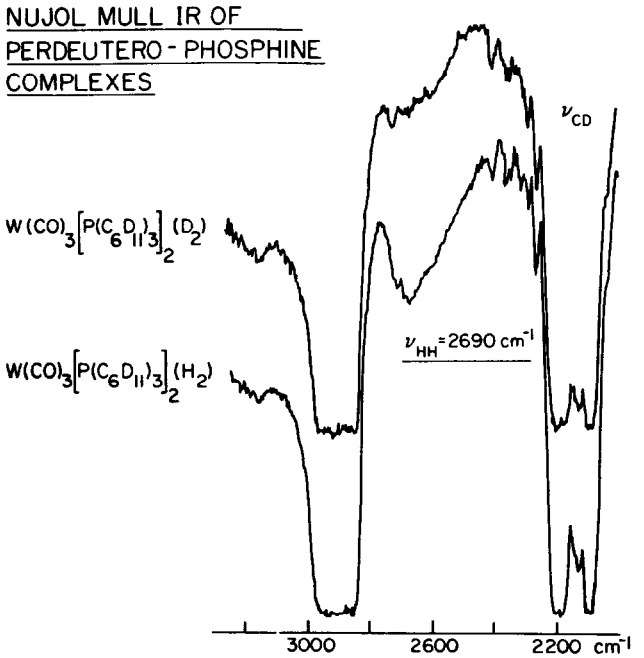


Fig. 6. IR spectra of $W(CO)_3[P(C_6D_{11})_3]_2(H_2)$ and D_2 species.

Theoretical calculations of H_2 binding in the model complex, $W(CO)_3(PH_3)_2(H_2)$, indicate that the observed conformation of the complex is stable by 16.8 kcal mol^{-1} relative to $W(CO)_3(PH_3)_2 + H_2$.[24] The conformation with the H—H rotated by 90° was only 0.3 kcal mol^{-1} less stable, in agreement with the NMR results, indicating only a small barrier to rotation. The studies also indicated that the bonding of H_2 to the metal involves primarily σ-donation to the metal, with very little backbonding into the σ^*-orbital of H_2. For the minimum-energy structure the H—H distance was 0.79 Å, close to that observed (0.82 Å) although the W—H distances were longer than those determined (2.15 vs 1.89 Å).

Two obvious questions arise: do more H_2 complexes exist and why do $M(CO)_3(PR_3)_2(H_2)$ coordinate dihydrogen while $MoH_2(PMe_3)_5$[22(a)] and related complexes[22] proceed to the hydride? We now have evidence that the known 16-electron complex $Mo(diphos)_2(CO)$,[17] which contains a weak M···H—C interaction, gives very similar H_2 complexes.[21(c)] Thus complexes which weakly coordinate a distal hydrogen atom are clearly excellent candidates for H_2 coordination. While the bulkiness of the phosphine ligands is no doubt important in determining whether the H_2 is arrested rather than cleaved by the metal, other factors are also involved. The electronic influence of the ligand *trans* to H_2 may be crucial, judging by the fact that the H_2 complexes [including $Cr(CO)_5(H_2)$] contain *trans*-CO while none of the structurally-characterized group 6 polyhydrides[22] contain any CO ligands at all. These principles may not apply to other metal systems,[21(b)] and only the discovery of further examples of H_2 coordination will provide understanding.

REDUCTION OF SO_2 BY GROUP 6 METAL HYDRIDES AND HYDROGEN

Hydride reduction: insertion of SO_2 into a metal–hydride bond

The reduction of SO_2 with H_2 or other agents such as CO to give sulfur and H_2O is an attractive method for SO_2 conversion. In the objectives of our studies of transition-metal–SO_2 complexes, we include metal systems that will act as catalysts for the reduction of SO_2 or will provide models for the elementary steps in a catalytic cycle. Transition-metal–hydride complexes have been shown to be important intermediates in catalytic cycles involving hydrogenation of organic substrates. Thus, in seeking homogeneous systems to catalytically or stoichiometrically hydrogenate SO_2, we are examining the reactions of metal–hydride complexes with SO_2. Much of our work has focused upon molybdenum and tungsten complexes as these metals are abundant, nonstrategic, and contained in proven catalysts in industrial processes.

A wide variety of reaction types have been found depending on the nature of steric and electronic factors. The system Cp_2MH_2 (M = Mo or W) cleanly and rapidly reduced SO_2 to $Cp_2M(S_2O_3)$ and H_2O, representing partial reduction of the SO_2.[25] Strong acids such as HCl convert $Cp_2M(S_2O_3)$ to H_2O, SO_2 and new types of cationic metal–sulfur complexes[25] in a manner similar to the conversion of ionic thiosulfate to H_2O, SO_2 and S_8. We speculate that a well-defined color change upon the addition of SO_2 to Cp_2MoH_2 may be due to adduct formation which is then followed by SO_2 insertion into the Mo—H bond. SO_2 inserts into the metal–hydride bond in $C_5H_5M(CO)_3H$ (R = H or Me; M = Mo or W) to form $(C_5R_5)M(CO)_3(SO_2H)$.[26] The reaction occurs readily at room temperature, and the insertion product precipitates upon addition of SO_2 to a concentrated solution of $(C_5R_5)M(CO)_3H$ in organic solvents. X-ray crystallography of $CpMo(CO)_3(SO_2H)$ confirmed that an S-bound insertion occurred (Fig. 7). Although both S–O distances are significantly longer than that normally found in SO_2 complexes (*ca* 1.45 Å)[4(b)] the difference in the two distances [S–O(1) = 1.637(6), S–O(2) = 1.515(6)] is sufficient to indicate that the H atom is bound to O(1). A peak appeared in the difference maps near O(1) and refined to a chemically reasonable position for an H-atom if the thermal parameter was fixed. *Sulfinate* ligands bound to transition metals have been

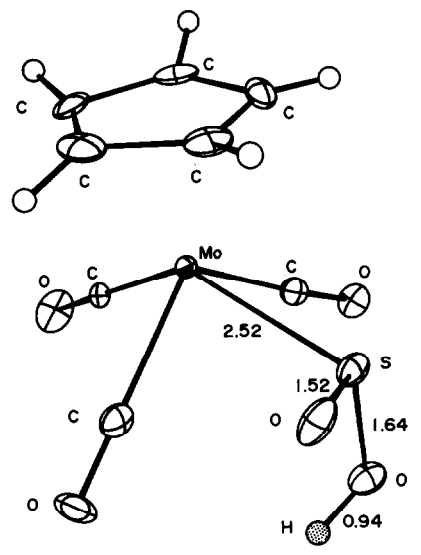
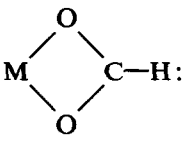


Fig. 7. Structure of $CpMo(CO)_3(SO_2H)$.

structurally characterized for *S*-sulfinates or *O*-sulfinates[27,28] with an alkyl or aryl bound to the sulfur and spectroscopic evidence exists for *O,O*-sulfinate and those of the type M—S(O)—OR.[29] The present study affords the first structural characterization of the latter type as well as the first direct evidence for insertion into a M—H bond.

The complexes $(C_5R_5)M(CO)_3(SO_2H)$ can be considered to be metallo analogues of organic sulfinic acids. RSO_2H.[30] A metallo *sulfonic* acid, $CpFe(CO)_2[S(O)_2OH]$, is known,[31] but is not a result of an insertion reaction. There appears to be no well-characterized precedent for the SO_2H^- ligand (or free anion) although a sulfinate structure, $Ru(SO_2H)_2(PPh_2Me)_3$, was tentatively formulated for the product of the $RuH_2(PPh_2Me)_4$–SO_2 reaction.[32] In contrast with SO_2, insertion of CO_2 into metal–hydride bonds is well known and results in metal–oxygen coordination,

M—O—C(O)H or 

definitive identification of a metallocarboxylic acid, M—C(O)—OH, derived by CO_2 insertion is lacking.[33]

For the reaction:

$$(C_5R_5)Mo(CO)_3H + SO_2 \xrightarrow{\text{solvent}} (C_5R_5)Mo(CO)_3(SO_2H)$$

the solution equilibrium lies far to the left; NMR shows that SO_2 readily extrudes on dissolution, unless excess SO_2 is present. $Cp^*Mo(CO)_3(SO_2H)$ ($Cp^* = C_5Me_5$) in liquid SO_2 at −40°C shows a broad resonance for the OH proton at δ 3.89, which shifts on addition of H_2O, reflecting proton exchange. A weak, broad IR stretch near 2550 cm^{-1} is assigned to ν(OH), on the basis of ^2H and ^{18}O substitution.

The mechanism of the SO_2 insertion may be a *concerted* process, involving attack on the coordinated hydride, analogous to the attack on α-carbon proposed for the alkyl analogues, $CpM(CO)_3S(O)_2R$.[34] It is reasonable that SO_2 initially coordinates to the hydride much as it does to metal-bound halides and pseudohalides.[4(b)]

A significant finding in terms of SO_2 reduction is the thermal instability of the solid complexes, which undergo auto-redox within 1 day [25°C for $CpMo(CO)_3(SO_2H)$, and 55–75°C for the W and Cp* analogues] to products indicative to S(IV) → S(II−) reduction and metal oxidation:

$$(C_5R_5)M(CO)_3(SO_2H) \xrightarrow{\Delta} [(C_5R_5)M(CO)_3]_2 + [(C_5R_5)MS_xO_y]_n + H_2O + CO.$$

A complex mixture of sulfido and oxo–sulfido complexes generally resulted, although for R = Me and M = Mo, the reaction was cleaner, yielding $[(C_5Me_5)MoO(\mu\text{-}S)]_2$[35] and a species analyzing as "$(C_5Me_5)_3Mo_3S_2O_4$" (see Fig. 8). Prolonged reactions of solutions of $(C_5R_5)M(CO)_3H$ with SO_2 in 4 : 1 stoichiometry also gave reduction of SO_2, and for R = Me and M = Mo the products were nearly identical to those for thermolysis of the SO_2 complex. Thus it would appear that the insertion complexes are logical intermediates in the SO_2 reduction. A possible further (or alternate) intermediate has also been isolated and structurally characterized. A solution-unstable dithionite-bridged complex, $[(C_5Me_5)Mo(CO)_3]_2(\mu\text{-}S_2O_4)$

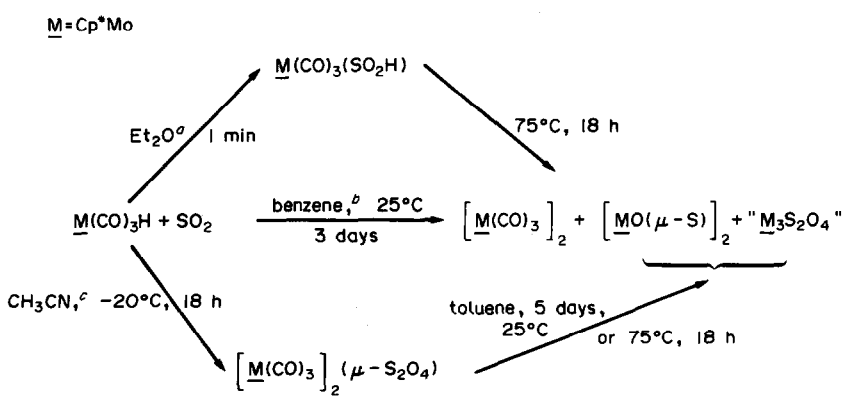


Fig. 8. Reactions of $Cp^*Mo(CO)_3H$ with SO_2.

(Fig. 9), crystallized slowly at −20°C from dilute CH_3CN solutions of $Cp^*Mo(CO)_3H$ containing excess SO_2. No H_2 was produced in this or any other of the hydride–SO_2 reactions; the hydride protons transfer to an oxygen atom to form H_2O. Conceivably, the dithionite species is produced by S—S coupling of two deprotonated $Cp^*Mo(CO)_3(SO_2H)$ fragments (an oxidation step is also required). The dithionite decomposes in solution, converting within minutes to a series of products. After several days, only two major products formed (plus CO and CO_2): the same two oxo–sulfido complexes produced from thermolysis of the insertion product or prolonged solution reaction of $(C_5Me_5)Mo(CO)_3H$ and SO_2. Thermolysis of the solid dithionite at 75° C for 18 h gave the same complexes, along with CO and CO_2 (from transfer of oxygen to CO).

The S-bound dithionite represents the first structurally characterized example of its type although this geometry had been proposed for $[CpFe(CO)_2]_2(S_2O_4)$ and $[M(CO)_5]_2(S_2O_4)$ (M = Mn or Re).[36] The S—S bond distance of 2.266(1) Å for the C_{2h} S_2O_4 is shorter than that found in $Na_2S_2O_4$ and other structures with C_{2v} $S_2O_4^{2-}$ ion (2.35–2.39 Å).[37] These unexpectedly long distances have generally eluded attempts at theoretical description. The S—S distance in the Mo complex is significantly longer than that in diphenyl disulfone [2.193(1) Å],[38] the only other structure we know of for which the S_2O_4 moiety is found in approximate C_{2h}-symmetry.

As previously mentioned, the prolonged solution reactions of SO_2 and $(C_5R_5)M(CO)_3H$ in all cases eventually yield a mixture of sulfido and/or oxo metal complexes and water as a result of SO_2 reduction. The nature of the final products depends on the metal, R group, solvent, temperature and hydride:SO_2 ratio. For example, whereas $[CpW(CO)_3]_2(\mu\text{-S})$[39] is found to be both the major as well as the initially observed sulfur-containing product for M = W, the Mo analogue is unstable and rapidly decomposes in solution with CO loss to a *mixture* of sulfide products. Complexes of the type $[Cp^*M(CO)_3]_2S$ are *not* observed for the Cp* systems, but rather *oxo-containing* products such as $[Cp^*MO(\mu\text{-S})]_2$ are prevalent in hydride–SO_2 reactions. However, for M = W, a *double* sulfide-bridged complex, $[Cp^*W(CO)_2(\mu\text{-S}\cdot SO_2)]_2$, with a strong sulfide–$SO_2$ interaction can also be isolated (Fig. 10).[39] The different products isolated in these reactions may thus merely reflect different stabilities rather than major differences in mechanisms.

Summarizing, the SO_2H unit appears to be inherently unstable, certainly when coordinated to transition metals [reduction of SO_2 by $(\mu\text{-}H_2)Os_3(CO)_{10}$ is also believed to proceed via an SO_2H complex][40] and also in sulfinic acids, RSO_2H,

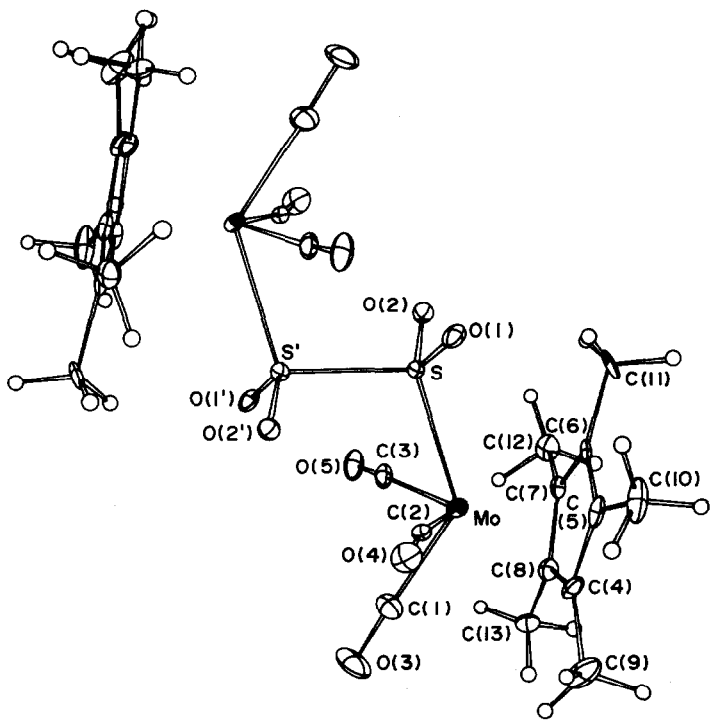


Fig. 9. Structure of $[Cp^*Mo(CO)_3]_2(S_2O_4)$.

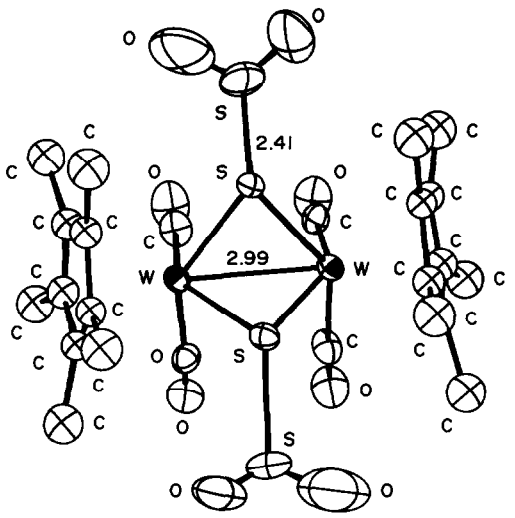
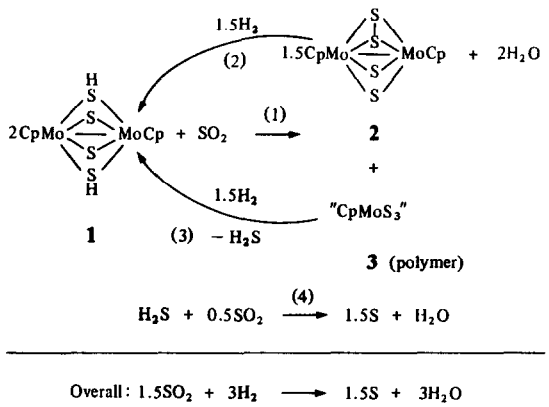


Fig. 10. Structure of $[Cp^*W(CO)_2(\mu\text{-}S \cdot SO_2)]_2$.

which readily disproportionate at 25–75°C.[30] One can conclude that the SO_2H ligand is even more reactive in solution since it could not be observed spectroscopically except at low temperature, where its reactivity was suppressed. Thus, the SO_2H species would appear to be a key intermediate in the reduction of SO_2 by hydrogen-containing complexes.

Hydrogen reduction of SO_2: the first example of a catalytic homogeneous system

Reduction of SO_2 by H_2 over heterogeneous catalysts is known. An effective heterogeneous catalyst has been found to be Ru–Al_2O_3 which readily and cleanly promoted hydrogenation to sulfur and H_2O under mild conditions (150°C, 1 atm), without catalyst poisoning.[41] Catalysis of SO_2 reduction by transition-metal species is a difficult problem in homogeneous systems because of catalyst poisoning by sulfur. As seen in the previous section, metal sulfides and oxysulfides readily form and no well-defined homogeneous systems catalyzed by transition-metal complexes have been reported. However, a possible means to circumvent the sulfiding problem was suggested by a reaction of SO_2 with a metallothiol complex, $[W(CO)_5(SH)]^-$, in which elemental sulfur was found to be produced. Instead of using metal-bound hydrogen to reduce SO_2, one could conceivably use the active hydrogen contained in *SH groups* ligated to a sulfur-saturated metal center. Furthermore, a remarkable addition of hydrogen to a dinuclear sulfur-bridged molybdenum complex to form a metallothiol $[(Me_nCp)MoS(SH)]_2$ (**1**) has been described in the literature.[42] This SH complex has been found[42] to homogeneously catalyze the reaction of sulfur with H_2 in $CHCl_3$ solution to form H_2S, and one could easily envision extension to SO_2 reduction. Experiments have indeed confirmed room-temperature reaction of $SO_2 + H_2$, in a closed flask, to give elemental sulfur and H_2O under mild conditions (25–75°C, 1–3 atm of H_2). The *stoichiometric* reaction of SO_2 with **1** (no H_2) produces $(Me_nCp)_2Mo_2(\mu\text{-}S)_2(\mu\text{-}S_2)$ (**2**), an insoluble sulfur-rich species $(Me_nCpMoS_3)_x$ (**3**), and H_2O. Both **2** and **3** readily react with H_2 to regenerate **1**, and H_2S is also generated from the excess sulfur in **3**. In the catalytic system, H_2S is produced but rapidly reacts with unconsumed SO_2 via the Claus reaction to give the observed products, sulfur and H_2O. The mechanism of the catalysis conceivably involves the above reactions (see Scheme 1) but is obviously quite complex in nature.



Scheme 1.

If the catalysis is terminated at or before complete SO_2 consumption, sulfur is the product. If the reaction is allowed to continue (assuming excess H_2 is present), the S_8 is hydrogenated to H_2S as the final product. Actually, a parallel catalytic cycle based on SO_2 reduction by H_2S produced from the S_8–H_2 reaction undoubtedly occurs in addition to the cycle shown in the Scheme 1. Importantly, the catalyst is stable to oxygenation by SO_2, although the presence of atmospheric oxygen results in $(Me_5Cp)_2Mo_2(O)S_3$[43] being formed.

Both reaction (1) and the overall catalysis have been carefully studied in regard to variations in reaction conditions (Table 2). In both instances, SO_2 reduction proceeds at a slow rate if $CHCl_3$ is used as solvent. However, the rate of catalysis increases several hundred fold (e.g. from 0.4 to 355 turnovers h^{-1}) if weakly basic solvents such as alcohols and/or catalytic amounts of Bronsted bases such as amines are present in the catalyst solution. For example, using only 0.04 mmol of **1**, 6.1 mmol of SO_2 is cleanly reduced by H_2 (27 mmol, ~3 atm) in 34 min at 75°C in 1:1 butanol–chlorobenzene (25 cm^3) containing

Table 2. Summary of catalytic reactions of SO_2 (3–8 mmol) and H_2 (12–17 mmol) to give sulfur and H_2O[a]

Solvent	Catalyst $[Me_nCpMoS(SH)]_2$	Temperature (°C)	P_{H_2} (atm)	Reaction time (h)	Catalyst turnovers h^{-1} (average)[b]
Toluene	$n = 0$	60	1.2	64	0.3
$CHCl_3$	$n = 1$	65	1.2	240	0.2
$CHCl_3$	$n = 5$	75	2.8	144	0.4
PhCl	$n = 5$	100	2.8	5.8	18.4
4:1 PhCl–BzOH	$n = 5$	20	1.2	15.5	1.8
4:1 PhCl–BzOH	$n = 5$	100	1.2	1.0	34.0
4:1 PhCl–BuOH	$n = 5$	75	2.8	1.4	110
1:1 PhCl–BuOH	$n = 5$	75	2.8	1.0	203
PhCl + Bu_3N[c]	$n = 5$	75	2.8	1.2	121
1:1 PhCl–BuOH + Bu_3N[d]	$n = 5$	75	2.8	0.6	355

[a] Magnetically-stirred in a closed 250- or 500-cm^3 flask, using 0.04–0.1 mmol catalyst in 25–50 cm^3 of solvent.
[b] Based on SO_2 consumption (assuming 2 mmol of catalyst converts 1.5 mmol SO_2).
[c] 0.1 cm^3 (0.42 mmol).
[d] 0.025 cm^3 (0.105 mmol).

0.1 mmol of Bu_3N. Similar rate enhancements by weak bases occur for reaction (1) and the Claus reaction [(4)], which also is very slow in $CHCl_3$ but is known[44] to be promoted by donor solvents (e.g. H_2O and alcohols) and weak bases. If $CHCl_3$ is the solvent for the catalysis, the Claus reaction occurs inefficiently mainly along the upper flask walls (sulfur deposition is observed) where H_2O (from SO_2 reduction) condenses and acts to promote it. If alcohols or small amounts of amines are present in the catalyst solution, the H_2S–SO_2 reaction [(4)] occurs rapidly and completely in the solution phase. In this context, the reactivities of $(\mu\text{-}SH)_2Fe_2(CO)_6$ and $Cp_2Ti(SH)_2Mo(CO)_4$ have been found to be also promoted by bases such as amines.[45] The mechanism for base promotion of reaction (1) may be proton abstraction followed by electrophilic attack of SO_2 on S^-. In this regard, the complex μ-$SH[W(CO)_5]_2^-$ was found to be much more reactive to heterocumulenes (e.g. MeN=C=O) in its deprotonated form,[46] and SO_2 is a type of heterocumulene. Alternatively, initial coordination of SO_2 to the sulfur atom of the SH ligand, similar to Lewis acid coordination of SO_2 to SR ligands in L_nCuSR,[47] could occur. In both cases, base-assisted proton transfer to an oxygen atom could result in formation of an $MSSO_2H$ group, giving what amounts to insertion of SO_2 into the S—H bond. Since, as discussed above, the SO_2H unit is unstable in both RSO_2H and the MSO_2H complexes, the proposed $MSSO_2H$ group would likewise be expected to decompose with eventual formation of H_2O and polysulfide (S_n^{2-}). This is precisely what is observed [reaction (1) of Scheme 1)], since the sulfur-rich product, **3**, almost certainly contains polysulfide. The implications of the above chemistry, which has recently been reported,[48] could extend to hetereogeneous sulfide catalysts such as hydrodesulfurization catalysts. Thus, we plan to investigate such catalysts for SO_2 reduction and to determine whether bases promote reaction.

Acknowledgements—This work was performed under the auspices of the Department of Energy, Division of Chemical Sciences, Office of Basic Energy Sciences. We thank Drs P. J. Vergamini and H. J. Wasserman for structural data on the H_2 complexes.

REFERENCES

1. G. J. Kubas, R. R. Ryan, B. I. Swanson, P. J. Vergamini and H. J. Wasserman, *J. Am. Chem. Soc.* 1984, **106**, 451.
2. H. J. Wasserman, G. J. Kubas and R. R. Ryan, submitted to *J. Am. Chem. Soc.*
3. M. G. Mason and J. A. Ibers, *J. Am. Chem. Soc.* 1982, **104**, 5153.
4. (a) G. J. Kubas, G. D. Jarvinen and R. R. Ryan, *J. Am. Chem. Soc.* 1983, **105**, 1883; (b) R. R. Ryan, G. J. Kubas, D. C. Moody and P. G. Eller, *Struct. Bonding* 1981, **46**, 47.
5. J. Saillard and R. Hoffmann, *J. Am. Chem. Soc.* 1984, **106**, 2006.
6. M. A. Graham, R. N. Perutz, M. Poliakoff and J. J. Turner, *J. Organomet. Chem.* 1982, **34**, C34; J. A. Welch, K. A. Peters and V. Vaida, *J. Phys. Chem.* 1982, **86**, 1941.
7. G. J. Kubas, *J. Chem. Soc., Chem. Commun.* 1980, 61.

8. G. J. Kubas, R. R. Ryan and V. McCarty, *Inorg. Chem.* 1980, **19**, 3003.
9. W. A. Schenk and F. Baumann, *Chem. Ber.* 1982, **115**, 2615; *J. Organomet. Chem.* 1983, **256**, 261; 1984, **260**, C6.
10. D. C. Moody and R. R. Ryan, *J. Chem. Soc., Chem. Commun.* 1976, 503; D. C. Moody and R. R. Ryan, *Inorg. Chem.* 1977, **16**, 2473.
11. D. C. Moody and R. R. Ryan, *J. Chem. Soc., Chem. Commun.* 1980, 1230.
12. D. C. Moody and R. R. Ryan, *Cryst. Struct. Commun.* 1976, **5**, 145.
13. J. Valentine, D. Valentine, Jr and J. P. Collman, *Inorg. Chem.* 1971, **10**, 219.
14. G. D. Jarvinen, G. J. Kubas and R. R. Ryan, *J. Chem. Soc., Chem. Commun.* 1981, 305.
15. K. W. Muir and J. A. Ibers, *Inorg. Chem.* 1970, **9**, 440.
16. S. J. LaPlaca and J. A. Ibers, *Inorg. Chem.* 1965, **4**, 778.
17. M. Sato, T. Tatsumi, T. Kodama, M. Hidai, T. Uchida and Y. Uchida, *J. Am. Chem. Soc.* 1978, **100**, 4447; T. Tatsumi, H. Tominaga, M. Hidai and Y. Uchida, *J. Organomet. Chem.* 1980, **199**, 63.
18. P. J. Brothers, *Prog. Inorg. Chem.* 1981, **28**, 1.
19. H. H. Brintzinger, *J. Organomet. Chem.* 1979, **171**, 337.
20. (a) R. Sweany, *J. Am. Chem. Soc.* 1985, **107**, 2374; (b) R. K. Upmacis, G. E. Gadd, M. Poliakoff, M. B. Simpson, J. J. Turner, R. Whyman and A. F. Simpson, *J. Chem. Soc., Chem. Commun.* 1985, 27; (c) S. P. Church, F.-W. Grevels, H. Hermann and K. Shaffner, *ibid.* 1985, 30.
21. (a) R. H. Crabtree and M. Lavin, *J. Chem. Soc., Chem. Commun.* 1985, 794; (b) R. H. Morris, J. F. Sawyer, M. Shirahiarn and J. D. Zubkowski, *J. Am. Chem. Soc.* 1985, **107**, 5581; (c) G. J. Kubas, R. R. Ryan and D. A. Wrobleski, submitted to *J. Am. Chem. Soc.*; (d) P. J. Vergamini, H. J. Wasserman and T. Keotzle, manuscript in preparation.
22. (a) M. B. Hursthouse, D. Lyons, M. Thornton-Pett and G. Wilkinson, *J. Chem. Soc., Chem. Commun.* 1983, 476; (b) P. Meakin, L. J. Guggenberger, W. G. Peet, E. L. Muetterties and J. P. Jesson, *J. Am. Chem. Soc.* 1973, **95**, 1467; (c) E. B. Lobkovskii, V. D. Makhaev, A. P. Borisov and K. N. Semenko, *Zh. Strukt. Khim.* 1979, **20**, 944; (d) D. Gregson, J. A. K. Howard, J. N. Nicholls, J. L. Spencer and D. G. Turner, *J. Chem. Soc., Chem. Commun.* 1980, 572; (e) L. F. Rhodes, J. D. Zubkowski, K. Folting, J. C. Huffman and K. G. Caulton, *Inorg. Chem.* 1982, **21**, 4185.
23. B. D. Nageswara Rao and L. R. Anders, *Phys. Rev.* 1965, **140**, A112.
24. P. J. Hay, *Chem. Phys. Lett.* 1984, **103**, 466.
25. G. J. Kubas and R. R. Ryan, *Inorg. Chem.* 1984, **23**, 3181.
26. G. J. Kubas, H. J. Wasserman and R. R. Ryan, *Organometallics* 1985, **4**, 2012.
27. D. A. Langs and C. R. Hare, *J. Chem. Soc., Chem. Commun.* 1967, 853.
28. M. R. Churchill and J. Wormald, *Inorg. Chem.* 1971, **10**, 572.
29. T. A. George and D. D. Watkins, Jr, *Inorg. Chem.* 1973, **12**, 398.
30. (a) S. Oae, *Organic Chemistry of Sulfur*, Chap. 11, Plenum Press, New York (1977). (b) S. Detoni and D. Hadzi, *J. Chem. Soc.* 1955, 3163.
31. C. A. Poffenberger and A. Wojcicki, *Inorg. Chem.* 1980, **19**, 3795.
32. S. Komiya and A. Yamamoto, *Bull. Chem. Soc. Jpn* 1976, **49**, 784.
33. D. J. Darensbourg and R. A. Kudaroski, *Adv. Organomet. Chem.* 1983, **22**, 129.
34. (a) J. O. Kroll and A. Wojcicki, *J. Organomet. Chem.* 1974, **66**, 95; (b) M. Graziani, J. P. Bibler, R. M. Montesano and A. Wojcicki, *ibid.* 1969, **16**, 507.
35. M. Rakowski DuBois, M. C. VanDerveer and R. C. Haltiwanger, *Inorg. Chem.* 1981, **20**, 3064.
36. N. H. Tennent, S. R. Su, C. A. Poffenberger and A. Wojcicki, *J. Organomet. Chem.* 1975, **102**, C46; (b) C. A. Poffenberger, N. H. Tennent and A. Wojcicki, *ibid.* 1980, **191**, 107; (c) P. Reich-Rohrwig, A. C. Clark, R. L. Downs and A. Wojcicki, *ibid.* 1978, **145**, 57.
37. (a) J. D. Dunitz, *Acta Cryst.* 1956, **9**, 579; (b) C. Th. Kiers and A. Vos, *ibid.* 1978, **B34**, 1499; (c) A. Magnusson and L. Johnasson, *Acta Chem. Scand.* 1982, **A36**, 429.
38. C. Th. Keirs and A. Vos, *Recl Trav. Chim. Pays-Bas* 1972, **91**, 127.
39. G. J. Kubas, H. J. Wasserman and R. R. Ryan, *Organometallics* 1985, **4**, 419.
40. G. D. Jarvinen and R. R. Ryan, *Organometallics* 1984, **3**, 1434.
41. D. C. Moody, R. R. Ryan and K. V. Salazar, *J. Catal.* 1981, **70**, 221.
42. M. Rakowski DuBois, M. C. VanDerveer, D. L. DuBois, R. C. Haltiwanger and W. K. Miller, *J. Am. Chem. Soc.* 1980, **102**, 7456.
43. H. Brunner, W. Meier, J. Wachter, F. Guggolz, T. Zahn and L. Ziegler, *Organometallics* 1982, **1**, 1107.
44. N. F. Albertson and J. P. McReynolds, *J. Am. Chem. Soc.* 1943, **65**, 1690.
45. (a) D. Seyferth and R. S. Henderson, *J. Organomet. Chem.* 1981, **218**, C34; (b) D. Seyferth and G. B. Womack, *J. Am. Chem. Soc.* 1982, **104**, 6839; (c) D. Seyferth, G. B. Womack, L.-C. Song, M. Cowie and B. W. Hames, *Organometallics* 1983, **2**, 928; (d) C. J. Ruffing and T. B. Rauchfuss, *ibid.* 1985, **4**, 524.
46. R. J. Angelici and R. G. W. Gingerich, *Organometallics* 1983, **2**, 89.
47. P. G. Eller and G. J. Kubas, *J. Am. Chem. Soc.* 1977, **99**, 4346.
48. G. J. Kubas and R. R. Ryan, *J. Am. Chem. Soc.* 1985, **107**, 6138.

Polyhedron Vol. 5, No. 1/2, pp. 487–495, 1986
Printed in Great Britain

0277–5387/86 $3.00 + .00
Pergamon Press Ltd

ISOTOPIC ^{18}O EXCHANGE BETWEEN SOLVENT WATER AND AQUO MOLYBDENUM IONS

GARRY D. HINCH, DONALD E. WYCOFF and R. KENT MURMANN*

Department of Chemistry, University of Missouri, Columbia, MO 65203, U.S.A.

(*Received* 17 *June* 1985)

Abstract—Recent applications of ^{18}O transfer and kinetic exchange experiments coupled with X-ray crystal structures has led to the establishment or confirmation of aqueous structures of some aqueous molybdenum ions. The mechanisms by which molybdenum-coordinated OH_2, OH^- and O^{2-} are exchanged with solvent are not well-understood. Now there are several ions which have been carefully studied and some suggestions as to mechanism can be made. A summary of oxygen transfer and kinetic exchange studies is made for the aquo ions MoO_4^{2-}, $Mo_2O_4^{2+}$, $Mo_3O_4(OH_2)_9^{4+}$ and several of their complexes. Interpretation of oxygen transfer accompanying reduction to lower oxidation states gives some structural and kinetic information about the reduced ion. Some new data are presented on complexes of these oxidation states which allow an estimate of the rate behavior of oxo and bridged-hydroxo groups in the neutral and basic region not accessible with the uncomplexed aquo ion.

Studies on the isotopic ^{18}O exchange between solvent water and aquo, hydroxo or oxo groups coordinated to metal ions can give information about the number of oxygens of a particular type surrounding the metal ion, the number of different types of bound oxygens, the kinetic properties of these oxygens and the mechanism by which exchange occurs. A knowledge of the oxygen exchange reaction kinetics for an aquo ion:

$$n(H_2O^*) + [M(OH_2)_n]^{z+} \underset{k_{-1}}{\overset{k_1}{\rightleftharpoons}} n(H_2O) + [M(^*OH_2)_n]^{z+}$$

is necessary for an understanding of substitution reactions of the ion. Likewise, for an oxo ion or hydroxy-bridged species, the rate of isotopic exchange may be closely related to the rates of substitution reactions on it.

Isotopic ^{18}O methods utilizing mass spectrometry are very precise and accurate even by today's standards but are not suitable for rapid exchanges. In a few cases reactions with $t_{1/2}$s of less than 2 s have been kinetically studied but under usual experimental conditions half-times of greater than 1 min are needed for accurate results. Thus other methods such as NMR, IR, sound absorption, laser Raman and mass spectra of the parent molecule or fragment are used when applicable for the more rapid exchanges.

The forerunners in this field were Cohn and Urey (1938)[1] and Hall and Alexander (1940).[2] The area was significantly advanced by the innovative studies of Taube *et al.* (1950–)[3] and since that time a slow stream of results has been published by a few small groups throughout the world. A review[4] appeared in 1982 covering all metals and some generalizations were suggested for predicting rate laws along with mechanistic interpretations. Since that time, new results have been obtained on molybdenum aquo species and complexes and offer an insight into the structural and kinetic variety obtainable with this metal. Thus we will describe the results of the application of ^{18}O tracer and exchange techniques to the aqueous ions of molybdenum.

EXPERIMENTAL

In most cases, two types of measurements are made: (a) determination of the number of oxygens coordinated to a metal which are slow to exchange, and (b) measurement of the rate of exchange of those oxygen atoms. For both types the basic experiment is the same. A solution of the ion to be studied at

* Author to whom correspondence should be addressed.

equilibrium is treated with a small quantity of highly enriched ^{18}O water to change the overall ^{18}O content of the solvent. At times very close to that of mixing (experiment a) or at later times (experiment b) either the solvent or the complex ion is sampled. Generally the complex ion is sampled and its total ^{18}O content measured. For this purpose it is necessary to be able to quickly remove the ion from solution, as a well-defined solid, at low temperature without losing or catalyzing the exchange of the oxygens under investigation. The precipitate should be non-hydrated, form very quickly and once formed not exchange its oxygen with the solvent during the period of collection, purification and drying. Its exact composition has to be known either from analysis or better from a single-crystal X-ray determination.

For isotopic analysis, the oxygen in the solid salt has to be converted to a pure simple gas. CO_2 is generally used and the conversion to it done in a non-quantitative manner by heating the sample with $Hg(CN)_2$ and $HgCl_2$ in a sealed glass tube for an hour at 425°C.[5] During this time all oxygens become isotopically equivalent and the CO_2 is separated from the other products by preparative gas chromatography. After further purification in a vacuum line the 46/(44 + 45) ratio is measured with a mass spectrometer. Generally the enrichments are low [less than 3× normal (0.6%)] and ratio measurements can be made to 0.1% of enriched minus normal. Usually it is necessary to know the enrichment of the solvent which is accomplished by the equilibration of a portion of it (3 days, 25°C) with a small amount of CO_2 in a sealed tube, separating and measuring the ^{18}O content of the purified CO_2. From the amounts of water and CO_2 and the isotopic fractionation factor the solvent enrichment is calculated.[6]

The rate of exchange for a single exchange is first-order (McKay plot),[7] i.e. ln $(1-F)$ vs time is linear, slope = k_{obs} and:

$$R = k_{obs}\left(\frac{ab}{a+b}\right) = k[\,]^n[\,]^m\ldots,$$

where a and b are the concentrations of exchanging oxygen atoms and solvent oxygen atoms, respectively. Nonlinear behavior of McKay plots is indicative of a chemical reaction occurring or more than one type of oxygen in the ion under study.

RESULTS AND DISCUSSION

Mo(VI)

The first aqueous molybdenum ion to be kinetically studied by ^{18}O techniques was MoO_4^{2-}, a tetrahedral ion which appears to be monomeric in the moderately alkaline region.[8,9] The latter study,[9] which included WO_4^{2-} was restricted to the alkaline region so as not to involve protonated species or oligomers derived from them. Von Felton *et al.*[9] precipitated the ion with Ba^{2+} as anhydrous $BaMoO_4$ and the zero-time exchange was essentially zero, suggesting that the only important ion in solution has four oxygens surrounding it and that the precipitate has all of the characteristics, which were given earlier, necessary for a quantitative study. The isotopic measurement was carried out on highly purified CO obtained by inductively heating the salt with graphite in a vacuum system.

The half-time for exchange was short, in the region of 5–20 s at 5°C and followed the rate equation:

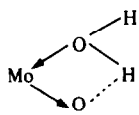
$$R/[MoO_4^{2-}] = k_0 + k_1[OH^-]$$

rather well over the range

$$[OH^-] = 3\text{–}150 \times 10^{-3}\ \text{M}.$$

The activation parameters were $\Delta H^* = 62.8(2.5)$ and 70.3(5.0) kJ M^{-1} and $\Delta S^* = -43.5(9)$ and $-2.5(13)$ J K^{-1} M^{-1} for k_0 and k_1, respectively.

The k_0 term for MoO_4^{2-} and WO_4^{2-} are nearly the same, about 0.4 s^{-1} in the region of 25°C but much larger than that for CrO_4^{2-}, which is about 3×10^{-7} s^{-1}. The main difference is attributed to the larger values for the enthalpy of activation with CrO_4^{2-}, reflecting the "tighter" Cr—O bonds compared to those of Mo(VI) or W(VI). The similarity of the molybdenum and tungsten rates is fortuitive due to an unusually large negative ΔS^* for tungsten which compensates for its small value for ΔH^*. The kinetic solvent H/D isotope effect for k_0 is 3.6 and for k_1 is 2.3, about the same as for the tungsten analogue, suggesting proton transfer in the rate-determining steps. An isokinetic graph, ΔH^* vs ΔS^*, for k_0 for three tetrahedral ions, WO_4^{2-}, MoO_4^{2-} and ReO_4^{-},[10] is linear, suggesting a common rate-determining step. It is suggested that the mechanism for the k_0 term is of the solvent-assisted dissociative



type, while for the k_1 term the metal ion expands its coordination sphere as the yl-oxygen leaves. Since it has not been possible to determine the order with respect to water, a more precise suggestion as to the mechanism cannot be made. A wide and important region of study for this ion is left open, that of the neutral and faintly acid areas. Here $HMoO_4^-$ would be expected to dominate the kinetic expression and the rate should be accelerated dramatically as we

approach acidic conditions similar to that seen for other oxy-anions. Interpretation of ^{18}O results would be highly dependent on knowing the exact species and their concentration as a function of pH and total [Mo].

Mo(V)

The next study described is for the ion $MoOCl_5^{2-}$, at the other extreme of the acid–base scale.[11] The ion exists only at high [acid] and $[Cl^-]$ according to spectral studies. Structural information about the ion in solution comes from analysis, X-ray crystal structures and spectral evidence, mostly in the solid state. The ^{18}O exchange studies could be conducted without interference from other forms of Mo(V) in 9.2 M HCl down to 2.6 M HCl + 8.9 M LiCl. Cs_2MoOCl_5 was used as the precipitating agent and CO_2 as the analyzed gas. The zero-time exchange showed about 5% induced exchange which could not be reduced by experimental variations. Since the structure of the anhydrous precipitated salt is known from X-ray diffraction and analysis and essentially no exchange takes place after short times of contact with enriched solvent, the ion cannot expand its coordination number with solvent water in solution. For instance $[Cl_5Mo(OH)_2]^{2-}$ cannot form reversibly. The experiment also proved that there is 1.0 ± 0.1 slowly exchanging oxygen in the aqueous ion.

The rate of isotopic oxygen exchange is slow, $t_{1/2}$ = 1–2 h, and is dependent on [acid], $[Cl^-]$ and $[MoOCl_5^{2-}]$. At constant ionic strength (LiCl) (12.1 M), k_{obs} was nearly constant from 2 to 10 M HCl but increased significantly between 10 and 13 M. Increased $[Cl^-]$ decreased k_{obs} if the acidity was below 10 M but not if above. A plot of k_{obs} vs $[MoOCl_5^{2-}]$ at constant [HCl] (12.1 M) showed a linear relationship with the intercept zero at $[MoOCl_5^{2-}] = 0$. The best fit to all of the data was given by the expression:

$$R = k_1[MoOCl_5^{2-}]/[Cl^-] + k_2[MoOCl_5^{2-}]^2[HCl].$$

In these very concentrated solutions one cannot confidently conclude mechanistic paths from the form of the rate equation. However the first term, k_1, is consistent with an aquation equilibrium step followed by the rate-determining isotopic exchange. The intermediate aquo ion has been isolated and its solid structure determined (Fig. 1).[14] The rate-determining step would be of the internal electronic rearrangement (IER) type which requires a labile water or OH^- group *cis* or *trans* to the yl-oxygen. The second term, k_2, requires two complex ions and a

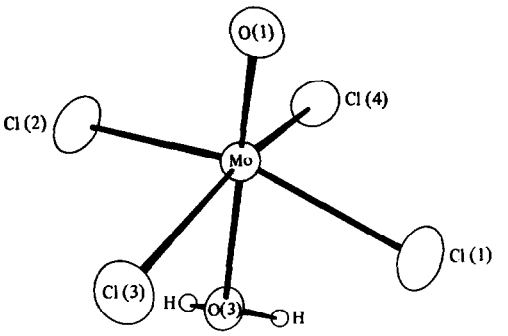


Fig. 1. ORTEP drawing of $[MoOCl_4(OH_2)]^-$.

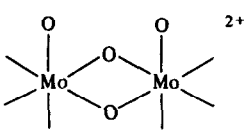
positive acid effect in the activated state. A reasonable explanation of this data lies in first protonating a complex ion forming a hydroxo complex and then a slowly reversible reaction would produce a bridged oxo complex and cause isotopic exchange:

$$[Cl_5MoO]^{2-} + H^+_{aq.} \overset{K}{\rightleftharpoons} [Cl^5MoOH]^-,$$

$$H^+ + [Cl_5MoOH]^- + [Cl_5MoO]^{2-} \overset{k_2}{\rightleftharpoons} [Cl_5Mo{-}O{-}MoCl_5]^{2-} + H_2O.$$

There is ample evidence for the protonation of dioxo complexes in $[Re(en)_2O_2]^+$, $[Mo(CN)_4O_2]^{4-}$, and more recently even with $VO^{2+}(aq)$.[12] Dimerization in hydrolyzed Mo(V) solutions has been postulated even in strongly acid solutions[13,14] (HCl) and it dominates the chemistry in dilute acid or neutral solution.[15] $[MoOBr_5]^{2-}$ follows essentially the same behavior but is slightly faster. This more rapid rate probably reflects the greater tendency toward hydrolysis. This suggests that stronger ligands, i.e. SCN^- or chelating ligands ($EDTA^{4-}$) would lower the rate of yl-oxygen exchange.

Over a wide range of mildly acidic solutions, Mo(V) exists almost exclusively as a dimer, aquated $Mo_2O_4^{2+}$. The evidence behind this formulation is its diamagnetism, ion exchange properties, spectral properties and X-ray solid structures of complexes. The present evidence supports a dimeric *cis*-structure with three distinguishable oxygen types.



Measurement of the rate of oxygen exchange with this ion was complicated by the fact that no precipitating agents were known with reasonably suitable properties. It was found[16] that during the conversion to the $EDTA^{4-}$ complex (whose X-ray

structure is known), no isotopically different solvent oxygen was introduced and the resulting ion could be quantitatively and quickly removed from solution with $[Pt(en)_3]^{4+}$. Thus one could "follow" the yl and bridging oxygens, but not the coordinated water since it was replaced by $EDTA^{4-}$. Also, once formed, all oxygens of $[Mo_2O_4(EDTA)]^{2-}$, including those of the organic ligand, are very slow to exchange even in solution. For this conversion the time-zero induced exchange average was 2.9(1.5)%.[16] This established that the 4.0(0.1) oxygens attached to Mo in $[Mo_2O_4(EDTA)]^{2-}$ came from the first-coordination sphere of Mo(V)(aq) and not from the solvent. The two types of oxygen proved to have quite different exchange rates over a wide range of conditions. At 0°C in 0.5 M H^+, 2.04(6) oxygens exchange rapidly with a half-time of about 4 m. The slowly exchanging oxygens were also counted and found to number 1.98(3) and the exchange half-time at 40°C was about 70 h in 0.5 M acid. The McKay plots were highly linear for the fast oxygens but the rate appeared to increase with time for the slow oxygen exchange. The non-linear behavior could easily be removed by having Hg(1) present which reduces Mo(VI). It was thought that either disproportionation or oxidation with traces of oxygen generated Mo(VI), which catalyzed the exchange. The slow oxygens were shown to increase their exchange rates with increasing $[MoO_4^{2-}]$ in the 1–3 mM range and so the exchange is very sensitive to it.

The fast oxygens were shown to be the yl-oxygens by laser-Raman IR spectroscopy where the spectrum was taken in 90% ^{18}O water before and after the fast oxygens exchanged. Assignment of the 950-cm^{-1} region to the yl-oxygen and the 760-cm^{-1} region to the bridging oxygen was done on the basis of the spectra of solid complexes. Only the yl-oxygen, 950 cm^{-1}, changed in a short time.

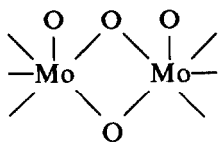
The yl-oxygen exchange showed an invariance to $[Mo_2O_4^{2+}]$ and [acid] in the ranges 0.002–0.039 and 0.01–3.1 M, respectively, and increasing $[Cl^-]$ lowered the rate constant by only a small amount. The latter effect could not be separated from that due to ionic strength changes.

On the other hand the bridging oxygens followed the rate law:

$$R/[Mo_2O_4^{2+}] = k[H^+]^2,$$

with the rate decreasing as the ionic strength or $[Cl^-]$ increased.

The yl-oxygen exchange was thought to occur through a solvent-assisted dissociative path or an IER mechanism utilizing the waters in the other coordinating positions. The bridging oxygen exchange was thought to occur through the H^+-assisted reversible opening of the



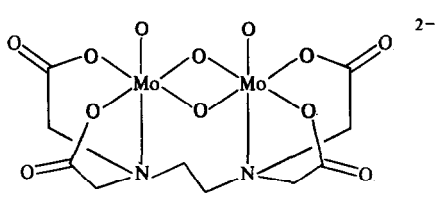
ring, breaking either one or both of the bridging bonds. The activation parameters for the bridging oxygens are $\Delta H^* = 108.1(6.7)$ kJ M^{-1}, $\Delta S^* = 1.7(0.8)$ J M^{-1} K^{-1}. At 0°C the calculated $t_{1/2}$ for the bridging oxygens is about 3 years in 1.0 M acid.

With respect to the $[monomer]^2/[dimer]$ equilibrium value, it can be shown from the ^{18}O data that K for the dissociation to the monomer cannot be greater than 4×10^{-6} at 40°C. This is in agreement with the essentially complete diamagnetic properties of Mo(V) solutions in dilute acid media.

Nothing firm is known about the exchange rate of the coordinated waters. Substitution for them with NCS^-,[17] EDTA[18] or ox^{-2} is quite fast but, as we note with Mo(IV), this does not necessarily mean that the water exchange is equally rapid. However, at the present time all available evidence points to a relative high lability for the coordinated waters.

Complexes of $Mo_2O_4^{2+}$

The EDTA complex of Mo(V), $[Mo_2O_4(EDTA)]^{2-}$ is a well-studied, well-behaved ion. In water solution, 0.07 M, pH 4.67, at 80°C the maximum exchange on any oxygen in yl- or bridging positions after 4.25 days was 1%. In acetic acid–acetate ion buffer at pH = 4.00 (other conditions the same) 83% of the yl-oxygen enrichment remains and essentially no bridging oxygen exchange occurs in the same time. In these experiments the yl-oxygens had 96% of the enrichment of the bridging oxygens as determined experimentally.



In strongly basic media only one type of oxygen exchanges, presumably the yl-oxygen.[19] At 25°C, $k = 4 \times 10^{-4}$ s^{-1} at a pH of 12.96 and the only major term in the rate equation is first order in $[OH^-]$. Considerable decomposition occurs during the kinetic experiments in basic media. Of all the complexes of $Mo_2O_4^{2+}$, that of $EDTA^{4-}$ is by far the most stable to exchanging either type of oxygen.

In order to ascertain the effect of the organic bridge

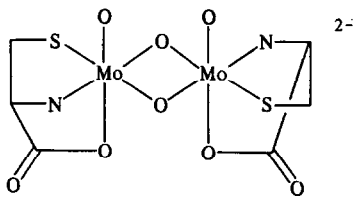


Fig. 2. $[Mo_2O_4(cysteine)_2]^{2-}$.

between the two metal ions in $Mo_2O_4^{2+}$ the complex $[Mo_2O_4(l+\text{ cysteine})_2]^{2-}$ was studied (Fig. 2). This ion showed a relatively rapidly exchanging pair of oxygens which follow first-order behavior well and a much slower pair which seemed to be somewhat erratic (Fig. 3). The velocity of both reactions were mildly affected by pH changes. At 25°C and a pH of 6.0, k_1 was 5.5×10^{-4} s^{-1}, while at pH 7.5 it equalled 4.0×10^{-4} s^{-1} (see Table 1). k_2 was 3.6×10^{-6} and 1.6×10^{-5} s^{-1}. In a stronger base, pH > 9 the rate of exchange had a positive $[OH^-]$ dependency.[19]

The sulfur-bridged analogue $[Mo_2O_2S_2(l+\text{ cysteine})_2]^{2-}$ gave values for the yl-rate constant of about half that of the oxygen-bridged complex under comparable, nearly neutral, conditions (Table 2).

However, this is highly misleading since the oxygen- and sulfur-bridged complexes behave differently in other ways. For instance the pH dependence shows a maximum k at a pH of about 6.5 for the oxygen-bridged complex, while the sulfur-bridged complex follows the rate equation (Fig. 4):

$$R/[\text{complex}] = k_0 + k_1[OH^-].$$

At 25.0° C, $\mu = 0.30$ with $LiClO_4$, $k_0 = 1.0(3) \times 10^{-4}$ s^{-1} and $k_1 = 5.1(3) \times 10^3$ m^{-1} s^{-1}. Another rather startling difference is the salt effect. From Table 1 one sees only a small ionic strength effect while Table 2 shows a very large effect. For instance for the sulfur analogue at 25°C the half-time changes from 1.0 to 120 min on increasing the ionic strength from 0.033 to 0.50 with NaCl. While the direction of this effect is the same for the oxygen- and sulfur-bridged complexes, the magnitude is not.

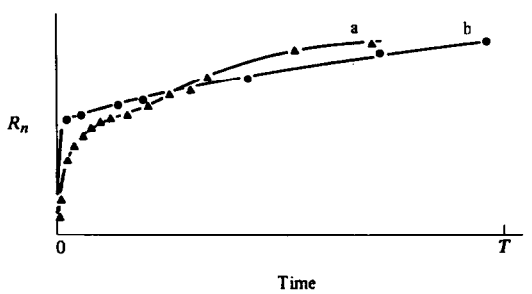


Fig. 3. Change in ^{18}O content of $[Mo_2O_4(cysteine)_2]^{2-}$ with time: pH = 7.75 (a) or 6.05 (b) (buffered). Point T = 3000 min for a, or 6000 min for b.

Table 1. pH Dependence of the fast and slow exchange for $[Mo_2O_4(cysteine)_2]^{2-}$ [a]

pH	k_1 (s^{-1})	k_2 (s^{-1})
6.05	5.5×10^{-4}	3.6×10^{-6}
6.27	7.0×10^{-4}	7.6×10^{-6}
7.09	5.8×10^{-4}	1.2×10^{-5}
7.75	2.8×10^{-4}	2.2×10^{-5}
6.35	6.3×10^{-4}	8.3×10^{-6} [b]

[a] [complex] = 0.040 M, I = 0.50 M NaCl, buffer = 2,6-lutidine–HCl except at pH 7.75 (2,4,6-trimethylpyridine–HCl), pH ± 0.10, temperature 25.00 ± 0.03°C.
[b] I = 0.68 M NaCl.

The abnormal behavior of the bridging oxygen exchange for $[Mo_2O_4(cysteine)_2]^{2-}$ as shown in Fig. 3 is not understood. The increase in the rate of isotopic exchange shortly after the first type of oxygen has been exchanged suggested a chemical change which is autocatalytic and which also results in oxygen exchange. We have been trying to see if this effect is related to the catalytic effect of these solutions toward olefin hydrogenation.

A study of the ion $[Mo_2O_4(ox)_2(OH_2)_2]^{2-}$ was undertaken because it does not contain the additional bridge between the metal ions and also has a water in an equatorial position (Fig. 5). ^{18}O

Table 2. pH effects on the oxygen exchange of $[Mo_2O_2S_2(cysteine)_2]^{2-}$ [a]

Complex	pH	Salt	I	k (s^{-1})
.016	6.05	NaCl	0.50	6.4×10^{-5} [b]
.011	—	—	0.033	2.4×10^{-3} [b]
.011	—	—	0.033	1.1×10^{-2}
.012	—	CsCl	0.51	9×10^{-5}
.012	—	NaCl	0.50	9.4×10^{-5}
.013	—	$LiClO_4$	0.55	1.5×10^{-4}
.017	—	$N(propyl)_4I$	0.50	1.7×10^{-4}
.016	—	$NaNO_3$	0.50	1.9×10^{-4}
.018	—	$N(propyl)_4NO_3$	0.51	3.0×10^{-4}
.0155	5.91	$LiClO_4$	0.300	1.5×10^{-4}
.0155	6.19	$LiClO_4$	0.301	1.9×10^{-4}
.0155	6.75	$LiClO_4$	0.301	3.6×10^{-4}
.0155	7.18	$LiClO_4$	0.301	9.4×10^{-4}
.0155	7.46	$LiClO_4$	0.302	1.5×10^{-3}

[a] 25.0°C, unbuffered unless pH given, when 2,6-lutidine buffer (0.15 M).
[b] 0°C.

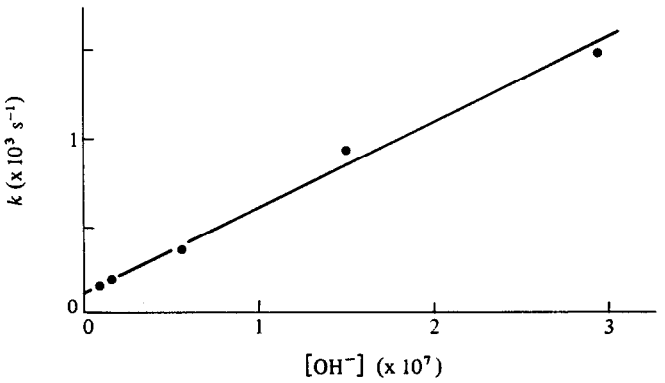


Fig. 4. Rate constants for O-exchange with $[Mo_2O_2S_2(cysteine)_2]^{2-}$ at 25°C.

exchange with this ion shows a single first-order plot corresponding to 4.0(1) oxygens and the other two oxygens exchange at least 1000 times slower. It was shown that the exchanging oxygens are yl-type *and* the coordinated waters and they cannot be distinguished from one another. In the pH region 3.8–5.1 the observed rate constant increased by about 50%. At a pH of 5.0 and 25°C the value of k was about 7×10^{-6} s^{-1}. The activation parameters at pH = 5.05, [ox^{2-} buffer] = 0.01 M, [complex] = 0.08 M, are $\Delta H^* = 88.3(1.2)$ kJ M^{-1} and $\Delta S^* = -46.9(1.0)$ J M^{-1} K^{-1}.

At this point it may be useful to try to generalize the features which appear to determine the rate of yl- and bridge oxygen exchange when they are coordinated to Mo(V). The latter appear in general to exchange very slowly. In either high acid or base the reaction proceeds more rapidly but even here the half-time is still in the many minutes to an hour range. Complexation of the positions normally occupied by water in the aquo ion by negative ions does not affect the bridging oxygen exchange rate strongly. However there is a suggestion that the coordination of a sulfur atom in a equatorial position does increase the bridging oxygen exchange rate probably due to a *trans*-effect. The yl-oxygens exchange more rapidly and are more affected by the other coordinated ligands and by solution conditions. While the rate of exchange is generally independent of acidity it is often sensitive to basic conditions. However this base sensitivity and the magnitude of the k_0 term seems to be related to water molecule(s) coordinated in one or more of the other octahedral positions. In the $EDTA^{4-}$ complex, such a water is not available and so the rate is quite slow while with cysteine the carboxyl oxygen *trans* to the yl-oxygen is reversibly exchanged for water at a fairly rapid rate. For the oxalato complex neither the water nor the yl-oxygen are very rapid or very slow to exchange but their rates appear to be related in some way. We suggest that the application of the IER mechanisms gives a reasonable explanation of their experimental behavior. In it a proton transfer from a water to yl-oxygen followed by metal ion electronic rearrangement effectively exchanges the OH_2 to $=O$ positions. If the (coordinated water)-isotopic exchange with solvent is rate-determining and the IER rate is roughly of the same order of magnitude or faster then the two types of oxygen atoms would appear to exchange at the same rate as is found. This approach also would suggest that any ligand which replaces water in either the equatorial or apical positions would lower the rate of yl-oxygen exchange, which is generally found.

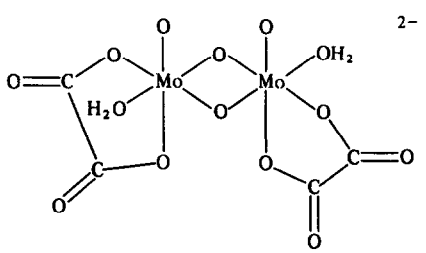


Fig. 5. $[Mo_2O_4(ox)_2(OH_2)_3]^{2-}$.

Mo(IV)

The first conclusive evidence that the +4 oxidation state of molybdenum in aqueous solution was a trimer (Fig. 6) came from ^{18}O studies directed toward measuring the rates of oxygen exchange.[20,21] Again the main problem was finding a method of precipitating the anhydrous ion quickly from aqueous solution at low temperatures. While not ideal, tetramethyl ammonium thiocyanate gave a solid complex which served this purpose. The NCS^- complexed very rapidly (and at the same time slowed down the exchange) and the $(CH_3)_4N^+$ salt of $[Mo_3O_4(NCS)_9]^{5-}$ precipitated. Within 2 min at

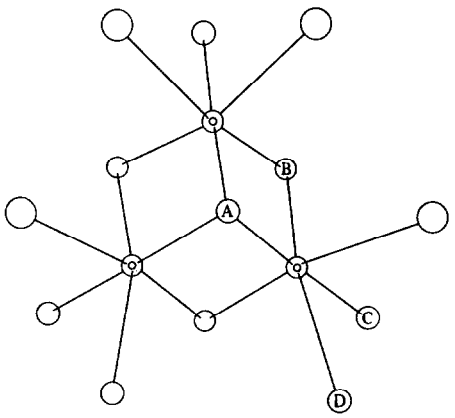


Fig. 6. $Mo_3O_4^{4+}$(aq).

0°C the majority of the precipitation took place, too short at time for rearrangement to occur. With ^{18}O enrichment in the solvent, at minimal contact times, the portion of enrichment transferred to the solid was less than 5% of that possible. Since the crystal structure of the precipitated solid[22] contained the Mo_3O_4 core all of the oxygens (four) in that core had to exchange slowly in solution. That Mo environment, shown in Fig. 6, contains two types of oxygen: one capping, and three bridging in addition to solvent water. Furthermore, it was possible to convert $Mo_3O_4^{4+}$(aq) through this sequence:

$$\rightarrow [Mo_3O_4(NCS)_9]^{5-} \rightarrow Mo_3O_4^{4+} \rightarrow [Mo_3O_4(ox)_3(OH_2)_3]^{2-} \rightarrow Mo_3O_4^{4+} \rightarrow [Mo_3O_4(SCN)_9]^{5-},$$

with less than 4% core oxygen exchange with the solvent. Even more remarkable, and a fact of considerable importance, is the transfer of $Mo_3O_4^{4+}$ core oxygens through the sequence $Mo_3O_4^{4+}$(aq) → Mo(hydroxide)↓ → $Mo_3O_4^{4+}$(aq), where at least 96% oxygen retention occurred. One usually expects extreme base catalysis of oxygen exchange but apparently that only occurs for the waters not the core oxygens.

Type A oxygen (Fig. 6) exchanges at a rate significantly faster than type B. At 30°C the half-life is about 4 days in 1.0 M acid and the number of oxygens exchanged at this rate was 1.1(1). The rate was not affected significantly by small acidity (0.8–1.2 M) or $[Mo_3O_4^{4+}]$ (0.08–0.14 M) changes.

Type B oxygen exchange (bridging) is very slow in 1.1 M CH_3SO_3H. Only a fraction of the total exchange occurred in 534 days at 25°C. During this period, appreciable oxidation occurred to Mo(V) but its presence did not cause rapid exchange. The half-life was estimated to be 5 ± 2 years and is not highly sensitive to acidity.

Type C water exchange was investigated by following the loss in enrichment in

$$[Mo_3O_4(*OH_2)_6(*OH_2)_3]^{4+}.$$

The ion was converted rapidly to

$$[Mo_3O_4(ox)_3(*OH_2)_3]^{2-},$$

whose crystal structure was determined as the easily precipitated $[Pt(en)_2]^{2+}$ salt. A count of the number of waters exchanging gave 3.0(2), suggesting that the exchanging waters were correctly identified. Of course, since the other six waters (type D) are replaced upon forming the complex no information about them can be obtained. The half-time for C type water exchange is about 1 h at 25°C in 1.0 M CH_3SO_3H. The reaction rate was not sensitive to light or $[Mo_3O_4]^{4+}$, increased slightly with ionic strength and was not affected by 10^{-4} M $Mo_2O_4^{2+}$ or MoO_4^{2-}. The rate constant was sensitive to pH and followed the rate law:

$$k_{obs} = k_0 + k_{oh}/[H^+].$$

The k_{oh} term most likely occurs through hydrolysis of one of the D-type waters leading to a lowered charge on the ion and an increased rate constant. The activation parameters were nearly the same for both terms, being $\Delta H^* = 100$ kJ M^{-1} and $\Delta S^* = 30$ J M^{-1} K^{-1} (averaged). The high value for ΔS^* suggests appreciable dissociative character leading to the activated state.

The effect of other complexing agents in the D-positions on the exchange rates of the C waters was estimated for Cl^-, NCS^- and ox^{2-}. With Cl^- the effect is a small decrease as Cl^- increases while NCS^- is much more effective in lowering the rate. This is probably due to its large association constants and the larger number of positions occupied for a particular concentration. The *tris*-oxalato complex had to be studied in less acidic media to retain the coordinated oxalate ion and to prevent oxygen exchange on the carboxylic acid groups. Actually there was a slight increase in rate constant with the oxalate complex but this is probably due in large part to the large change in acidity. Thus D water replacement by another ligand appears to cause a lowering of $k_{exch.}$, at least in the acid region.

Efforts to measure the exchange rate for type D waters utilized $[Mo(CN)_8]^{4-}$ as a precipitating agent. This reaction is not clean and neither the reaction nor the product are ideal for this type of experiment. Nevertheless, several runs gave half-times of about 25(5) min at 0°C in 1.2 M acid. This is remarkably slower than anticipated, especially since the NCS^-,[23] ox^{2-} and $EDTA^{4-}$[24] complexes form much more rapidly. Ion pairing must be extremely important in H_2O replacement by anions.

Table 3.

Oxygen type	Protons	Mo—O(av.) (Å)	Approximate $t_{1/2}$[a] [temperature (°C)]
A	0	2.020(3)	1×10^5 (0)
B	0	2.916(7)	2×10^8 (22)
C	2	2.163(3)	2×10^5 (0)
D	2	2.26(2)[b]	1×10^3 (0)

[a] 1 MH^+.
[b] This value comes from the SCN^- complex structure.

The exchange rates under nominal conditions are compared with metal–oxygen distances in the solid state in Table 3.

Oxygen transfer upon reduction of $Mo_3O_4^{4+}$(aq)

It has been conclusively demonstrated[24–26] that $Mo_3O_4^{4+}$(aq) can be reduced to two, well-defined, ions, $Mo(IV)(III)_2$ and $Mo(III)_3$, which all evidence show to be trimeric. It is of interest to know if the $Mo_3O_4^{4+}$ core remains intact in these ions. Toward this purpose the following sequence of reactions were carried out[21] utilizing ^{18}O enrichment in the core oxygens of $Mo_3O_4^{4+}$(aq):

$$Mo_3O_4^{4+} \rightarrow Mo(IV)(III)_2 \text{ or } Mo(III)_3$$
$$\rightarrow Mo_3O_4^{4+} \rightarrow [Mo_3O_4(ox)_3(OH_2)_3]^{2-}.$$

Reduction was accomplished either electrolytically or with zinc metal at 20(1)°C with identical results. In all cases, greater than 93% and as high as 97% retention of all four oxygens was found. Furthermore in one experiment a solution of $Mo(III)_3$ was allowed to exchange with solvent at room temperature for *2 months* and no (±3%) exchange was detected. Clearly the trimeric structure including the core oxygens exists in these reduced ions and solvent oxygen does not replace or become equivalent to them over a long time even though protonation no doubt takes place.

Oxygen transfer upon reduction of $[Mo_2O_4(EDTA)]^{2-}$

A similar study was made on the electrolytic and Zn(Hg) reduction products of $[Mo_2O_4(EDTA)]^{2-}$. It has been shown[27,28] that this produces $[Mo_2O_2(OH)_2(EDTA)]^{4-}$ and, when using Zn(Hg) as the reductant, an intermediate tetramer $[Mo(III)(IV)]_2$ was observed. Oxidation back to the original complex was accomplished with O_2. Using an acetate buffer at a pH of 4.95 and electrolytic reduction times of 3–24 h the core oxygen retention was 70–79(2)%. When carried out in enriched solvent with reduction times of 3–24 h, 75(2)% of the core oxygen was retained. This corresponds to 0.98(5) of four oxygens reaching isotopic equilibrium with the solvent.

When using Zn(Hg) (for reduction), the isotopic oxygen transfer was constant with time for at least 29 h. Thus the reduced ion does not exchange (±3%) in that time. A significantly higher transfer of solvent oxygen did occur which corresponds to 1.68(5) oxygens, out of four, becoming equivalent to that in the solvent. The interpretation of these results is still tentative and relates to the intermediates (tetramers) formed in the oxidation back to the starting material and the tetrameric $[Mo(III)(IV)_2]_2$ formed in the Zn(Hg) reduction.

Acknowledgements—We wish to express our appreciation to Guo Wei and the University Research Council.

REFERENCES

1. M. Cohn and H. C. Urey, *J. Am. Chem. Soc.* 1938, **60**, 679.
2. N. F. Hall and O. R. Alexander, *J. Am. Chem. Soc.* 1940, **62**, 3455.
3. J. P. Hunt and H. J. Taube, *Chem. Phys.* 1950, **18**, 757; H. L. Friedman, H. Taube and J. P. Hunt, *J. Chem. Phys.* 1950, **18**, 759; R. A. Plane and H. Taube, *J. Phys. Chem.* 1952, **56**, 33.
4. J. Gamsjäger and R. K. Murmann, In *Advances in Inorganic and Bioinorganic Mechanisms* (Edited by A. G. Sykes), Vol. 2, p. 318. Academic Press, New York (1983).
5. M. Anbar and S. Guttmann, *Int. J. Appl. Radiat. Isot.* 1959, **4**, 233.
6. L. A. Webster, M. H. Wahl and H. C. Urey, *J. Chem. Phys.* 1935, **3**, 129.
7. H. A. C. McKay, *Nature (London)* 1938, **142**, 997; H. A. C. McKay, *J. Am. Chem. Soc.* 1943, **65**, 702.
8. Ref. 2; G. Grier and C. H. Brubaker, *Inorg. Chem.* 1966, **5**, 321.
9. H. Von Felton, B. Wernli, H. Gamsjäger and P. Baertschi, *J. Chem. Soc., Dalton Trans.* 1978, 496.
10. R. K. Murmann, *J. Phys. Chem.* 1967, **71**, 974; *ibid.* 1971, **93**, 4184.
11. Chang-Su Kim and R. K. Murmann, *Inorg. Chem.* 1984, **23**, 263; for $K_{10}(MoCl_6)_3[MoO(OH)Cl_4]\cdot H_2O$, see E. O. Schlemper and R. K. Murmann, unpublished structure.
12. I. Nagypal, I. Fabian and R. E. Connick, *Acta Chim. Acad. Sci. Hung.* 1982, **110**, 447.
13. G. P. Haight, Jr, *J. Inorg. Nucl. Chem.* 1962, **24**, 663.
14. Chang-Su Kim, R. K. Murmann and E. O. Schlemper, *Transition Met. Chem.* 1984, **9**, 260.

15. F. A. Cotton and G. Wilkinson, *Advanced Inorganic Chemistry*, 4th Edn, p. 868. John Wiley, New York (1980).
16. R. K. Murmann, *Inorg. Chem.* 1980, **19**, 1765.
17. Y. Sasaki, R. S. Taylor and A. G. Sykes, *J. Chem. Soc., Dalton Trans.* 1975, 396.
18. Y. Sasaki and A. G. Sykes, *J. Chem. Soc., Dalton Trans.* 1984, 1468.
19. C. R. Landis, P. R. Robinson, R. K. Murmann and G. P. Haight, Jr, In *Proceedings of the Third International Conference on the Chemistry and Uses of Molybdenum* (Edited by H. F. Barry and P. C. H. Mitchell), p. 245. Climax Molybdenum Co., An Arbor, MI (1979).
20. R. K. Murmann and M. E. Shelton, *J. Am. Chem. Soc.* 1980, **102**, 3984.
21. K. R. Rodgers, R. K. Murmann, E. O. Schlemper and M. E. Shelton, *Inorg. Chem.* 1985, **24**, 1313.
22. E. O. Schlemper, M. S. Hussein and R. K. Murmann, *Cryst. Struct. Commun.* 1982, **11**, 89.
23. S. F. Ojo, Y. Sasaki, R. S. Taylor and A. G. Sykes, *Inorg. Chem.* 1976, **15**, 1006; P. Kathirgamanathan, A. B. Soares, D. T. Richens and A. G. Sykes, *Inorg. Chem.* 1985, **24**, 2950.
24. D. T. Richens and A. G. Sykes, *Inorg. Chim. Acta* 1981, **54**, 13.
25. D. T. Richens and A. G. Sykes, *Inorg. Chem.* 1982, **21**, 418.
26. M. T. Paffett and F. C. Anson, *Inorg. Chem.* 1983, **22**, 1347.
27. G. G. Kneale, A. J. Geddes, Y. Sasaki, T. Shibahara and A. G. Sykes, *J. Chem. Soc., Chem. Commun.* 1975, 356.
28. T. Shibahara and A. G. Sykes, *J. Chem. Soc., Dalton Trans.* 1978, 95.

Polyhedron Vol. 5, No. 1/2, pp. 497–503, 1986
Printed in Great Britain

0277-5387/86 $3.00 + .00
© 1986 Pergamon Press Ltd

STRUCTURE, BONDING AND ACID–BASE PROPERTIES OF PROTONATED MONOMETALATE IONS AND POLYMETALATE IONS FORMING CHAINS OR RINGS OF CORNER-SHARING MO_4 TETRAHEDRA OF TRANSITION METALS OF GROUPS V AND VI—A THEORETICAL APPROACH

KARL-HEINZ TYTKO

Institut für Anorganische Chemie, Universität Göttingen, 3400 Göttingen, F.R.G.

(*Received* 17 *June* 1985)

Abstract—It is shown that statements in the literature on the state of the mono- and diprotonated monomolybdate (and monotungstate) species in aqueous solution based on the pK_a values of the species disagree with the rules on the acid strength of oxoacids of Pauling and Ricci. A new approach to explain the protonation behaviour of the monochromate, monovanadate, monomolybdate and monotungstate species and to account for the enhanced basicity and stability of the polymetalate ions formed by corner-sharing MO_4 tetrahedra is given. The decisive feature is seen in the resonance structures of the tetrahedral and octahedral monomers and tetrahedral polymeric species in which positive and negative charges are separated, the negative charges being located on terminal oxygen atoms, thus enhancing the basicity of the species. The resonance structures in question are favoured by the size of the oxoanions (large distances between the charges) and by coordinated H_2O molecules (in the case of the octahedrally coordinated monomers) which facilitate separation of the charges by acceptance of the positive charge. Double bonds inside the chain are decisive for the enhanced stability of the polymeric species.

The state of the protonated monomolybdate and monotungstate species in aqueous solution is a matter of controversial discussions. The "real" formulae of $HMoO_4^-$ and H_2MoO_4 have been proposed to be

$[MoO(OH)_5]^-$,[1–10] $[MoO_2(OH)_3(H_2O)]^-$,[11,12]

$[MoO_3(OH)(H_2O)_2]^-$,[13] $[MoO_3(OH)]^-$ [14,15]*

and

$Mo(OH)_6$,[1–7,9,14,15]* $[MoO_2(OH)_2(H_2O)_2]$,[12,13]

and analogously the formulae

$[Mo(OH)_5(H_2O)]^+$,[3,4,7,16–19]

$[MoO_2(OH)(H_2O)_3]^+$ [12]

and

$[Mo(OH)_4(H_2O)_2]^{2+}$ [17]

have been suggested for the products of further protonation. Similar propositions have been made for corresponding tungstate species (cf. Refs 13 and 20). These propositions have been made to explain abnormal values of pK_a,[1–10] ΔG^o and ΔS^o,[14,15] ^{95}Mo and ^{97}Mo magnetic resonance observations,[11] or to account for the prevalence of a *cis*-MoO_2 unit[11,12] or the rapid aggregation processes in oxomolybdenum(VI) solutions.[13] For protonated monochromate and monovanadate species, however, only the tetrahedral structure is proven (cf. Refs 21 and 22).

The difficulties in establishing the state of the protonated monomolybdate and monotungstate ions in solution arise from the very low concentrations in which these species appear so that the usual methods of investigation cannot be applied.

In the present paper it will be shown that all statements in the literature on the coordination number of the mono- and diprotonated monomolybdate and monotungstate ions based on the pK_a values are incorrect and a new interpretation

* A tetrahedral monoprotonated monomolybdate ion $[MoO_3(OH)]^-$ and an octahedral diprotonated monomolybdate ion $Mo(OH)_6$ have also been proposed on the basis of computed Coulomb interaction energies.[41]

of the observed pK_a values and the enhanced basicity and stability of the polymetalate ions formed by corner-sharing MO_4 tetrahedra will be given.

INCOMPATIBILITY OF THE STATEMENTS IN THE LITERATURE FOR THE FIRST PROTONATION STEPS OF THE MONOMOLYBDATE ION WITH THE RULES ABOUT THE ACID STRENGTH OF THE ACIDS $MO_m(OH)_n$

The scheme mostly preferred for the first two protonation steps of the monomolybdate ion is, according to the literature:[1-10]

$$MoO_4^{2-} \overset{+H^+ \; +2H_2O}{\rightleftharpoons} [MoO(OH)_5]^- \overset{+H^+}{\rightleftharpoons} Mo(OH)_6. \quad (1)$$

Although this scheme has been postulated to explain the experimentally observed acid constants of the mono- ($pK_a \approx 3.7$, cf. Ref. 13) and diprotonated ($pK_a \approx 3.8$, cf. Ref. 13) monomers according to Pauling's and Ricci's rules[23,24] about the acid strength of the acids $MO_m(OH)_n$, it clearly contradicts these rules. As Table 1(a) shows, the observed pK_a of ≈ 3.8 for the diprotonated monomer differs strongly from that expected for the formulations in eqn (1), namely ≈ 9.0. On the other hand the observed pK_a of ≈ 3.7 for the monoprotonated monomer is similar to that expected for the tetrahedral acids HMO_4^- (considering the difference between non-metal and transition-metal oxoacids) [see Table 1(d)]. Therefore the formulation of the monoprotonated monomer in eqn (1) is incorrect and should be written $[MoO_3(OH)]^-$. The experimentally determined ΔG^o and ΔS^o values for the two reaction steps have also been interpreted to show the presence of the species $[MoO_3(OH)]^-$.[14,15] The diprotonated monomer, however, cannot be the species $[MoO_2(OH)_2]$. The expected pK_a of ≈ -3 [Table 1(c)] differs considerably from that observed, namely ≈ 3.8. Therefore the formulation $Mo(OH)_6$ might be correct from this point of view. This formulation, however, contradicts a rule according to which isopolymetalate ions built up by MO_6 octahedra cannot be centrosymmetric with the inversion centre on an M atom as a consequence of the great tendency for *cis*-location of π-interactions and a *trans*-effect in each of the MO_6 octahedra.[25,26] This rule should also apply to the octahedrally coordinated monomeric species. A similar view has also been

Table 1. Acid constants of some relevant oxoacids, $MO_m(OH)_n$, according to the literature (transition-metal oxoacids in parentheses)

Acid–base	pK_a
(a) $M(OH)_n$–$MO(OH)_{n-1}^-$	
$Te(OH)_6$–$TeO(OH)_5^-$	8.80,[31] 8.8[33]
$Si(OH)_4$–$SiO(OH)_3^-$	9.5,[32] 10.0[33]
$Ge(OH)_4$–$GeO(OH)_3^-$	8.59[31]
$B(OH)_3$–$BO(OH)_2^-$	9.24,[32] 9.22,[31] 9.2[33]
$As(OH)_3$–$AsO(OH)_2^-$	9.22[31]
$Cl(OH)$–ClO^-	7.25,[32,33] 7.50[31]
$Br(OH)$–BrO^-	8.68,[31] 8.7[33]
$I(OH)$–IO^-	10.0[33]
Average	8.95
(b) $MO(OH)_{n-1}^-$–$MO_2(OH)_{n-2}^{2-}$	
$TeO(OH)_5^-$–$TeO_2(OH)_4^{2-}$	10.33,[34] 11.04[35]
$GeO(OH)_3^-$–$GeO_2(OH)_2^{2-}$	13[31]
Average	11.5
(c) $MO_2(OH)_2$–$MO_3(OH)^-$	
$SO_2(OH)_2$–$SO_3(OH)^-$	−3,[32,33] large negative value[31]
$SeO_2(OH)_2$–$SeO_3(OH)^-$	−3,[33] large negative value[31]
$[CrO_2(OH)_2$–$CrO_3(OH)^-$	1,[1] −1[30]]
(d) $MO_3(OH)^-$–MO_4^{2-}	
$SO_3(OH)^-$–SO_4^{2-}	1.92[31-33]
$SeO_3(OH)^-$–SeO_4^{2-}	1.90,[36] 1.79,[37] 2.05[31]
$[CrO_3(OH)^-$–CrO_4^{2-}	6.04,[1] 6.52[38]]

expressed by other authors.[11,12] The formula $[MoO_2(OH)_2(H_2O)_2]$ has been proposed to account for the rapid aggregation processes in molybdate solutions.[13]

FUNDAMENTAL STATEMENTS TO EXPLAIN STRUCTURE, BONDING AND ACID–BASE PROPERTIES OF THE SPECIES UNDER DISCUSSION

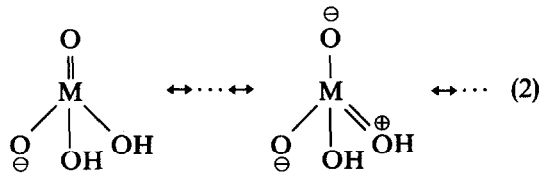
The following considerations are fundamentally based on four statements:

(1) The validity of the well-known relations between the acid constants and the formulae $MO_m(OH)_n$ of the acids detected by Pauling and Ricci[23,24] is assumed as a general principle. That means the basicity of a species depends mainly on the average number of terminal O atoms which are available for each negative charge.

(2) Each O atom forms, summed over the various bonds, two covalent bonds unless its charge is compensated ionically by cations. The group VI elements form, summed over the various bonds, six covalent bonds, and the group V elements five covalent bonds, as is the case with the polymetalate ions (cf. Refs 27–29).

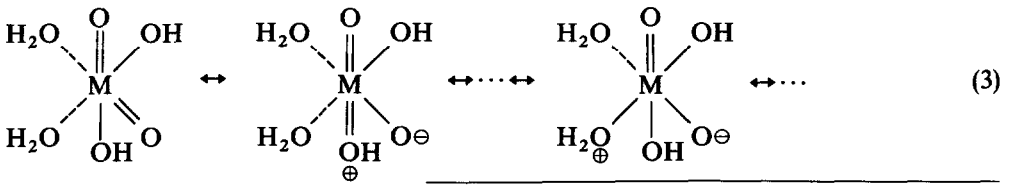
(3) The coordination number of the central metal cation of the metalate ion depends upon the radius of the metal cation (space requirements of the O-containing ligands) and upon the protonation state of the metalate ion (organization of more space for additional ligands).

(4) The resonance of type:



(2)

in the case of the tetrahedrally coordinated M atoms and:



(3)

in the case of the octahedrally coordinated M atoms enhances the basicity of the species by charge separation and offers an excellent possibility for charge delocalization being a stabilizing factor. It is favoured by the size of the monomeric species, since in this case charge separation is favoured (larger distances between the charges), which is also favoured by coordinated H_2O molecules.

RESULTS FOR THE PROTONATED MONOMETALATE IONS

The monomeric species of main-group and subgroup elements of groups VI and V and their experimentally determined protonation constants considered in this paper are listed in Table 2 together with the ionic radii of the central atoms of the oxoanions.

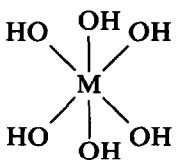
The enhanced basicity of the transition-metal oxometalate ions in general

The oxometalate ions of the transition metals are larger (also, the *d*-orbitals are more accessible[30]) and therefore show a greater tendency to undergo a charge separation than the non-metal oxoanions according to the schemes shown in Figs 1 and 2(a) by which the basicity of the species is enhanced. In this way the two to four orders of magnitude larger protonation constants of the unprotonated and protonated monometalate ions (compared with those of the corresponding main-group elements) can be explained.

The further enhanced basicity of the octahedrally coordinated oxometalate ions

Octahedrally coordinated monomers have been discussed in the literature for the mono- and diprotonated molybdate[1–10] and tungstate ions.[1,13,20] However, as has been shown above, the pK_a values of the monopronated monomers are in accordance with a tetrahedral coordination while those of the diprotonated monomers are in disaccord with a tetrahedral coordination. Extension of the coordination sphere of the metal atom can occur by coordination of two H_2O molecules, in this case opening up the possibility for an enhanced stabilization and enhanced basicity by resonance according to the schemes shown in Fig. 2(b).

The structure



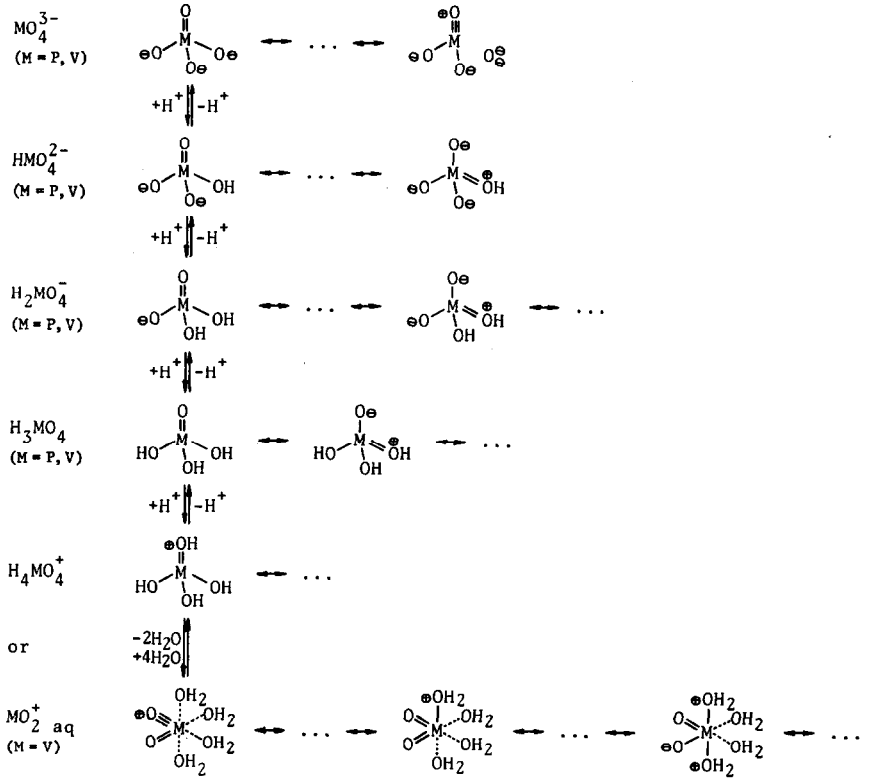


Fig. 1. Resonance formulae for unprotonated and protonated monomeric oxoanions of group V elements showing the enhanced basicity and stability of most of the species.

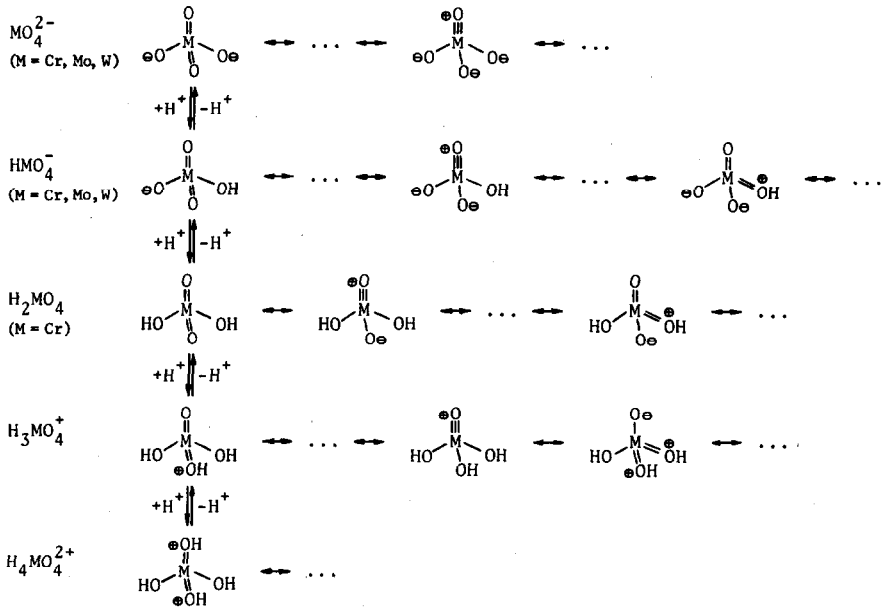


Fig. 2(a). Resonance formulae for unprotonated and protonated tetrahedral monomeric oxoanions of group VI elements showing the enhanced basicity and stability of most of the species.

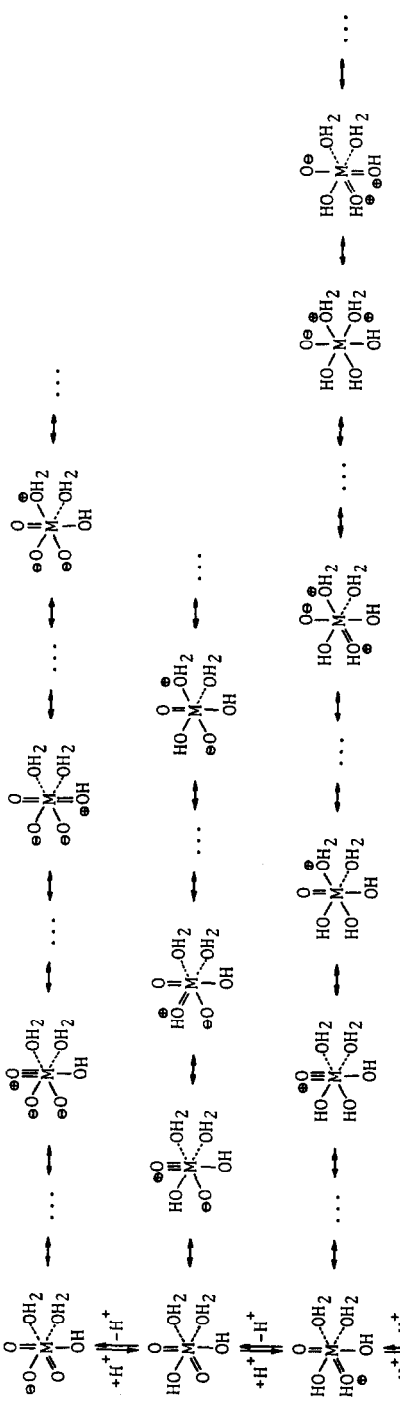


Fig. 2(b). Resonance formulae for protonated octahedral monomeric oxoanions of group VI elements showing the enhanced basicity of the first protonation products and their excellent stabilization by charge delocalization.

Table 2. Protonation constants of the monomeric oxo species of main group and subgroup elements of groups VI and V to be explained in this paper and ionic radii of the elements

	S	Cr	Mo	W	P	V
Ion	S^{6+}	Cr^{6+}	Mo^{6+}	W^{6+}	P^{5+}	V^{5+}
Radius (Å)[39]	0.29	0.52	0.62	0.68	0.34	0.59
Species	SO_4^{2-}	CrO_4^{2-}	MoO_4^{2-}	WO_4^{2-}	PO_4^{3-}	VO_4^{3-}
log K_p	1.9[a]	6.3[a]	3.7[13]	3.8[13]	11.3[40]	13.2[40]
Species	HSO_4^-	$HCrO_4^-$	$HMoO_4^-$	HWO_4^-	HPO_4^{2-}	HVO_4^{2-}
log K_p	−3[a]	0[a]	3.8[13]	4.3[13]	6.4[40]	7.7[40]
Species			"H_2MoO_4"		$H_2PO_4^-$	$H_2VO_4^-$
log K_p			0.9[17]		1.7[40]	3.7[40]
Species						H_3VO_4
log K_p						3.2[40]

[a] See Table 1.

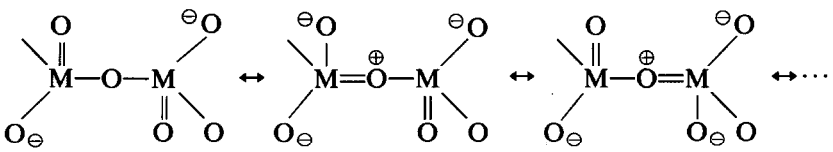
often proposed in the literature,[1–7,9,14,15] cannot be stabilized by resonance nor is its basicity enhanced. We therefore propose the protonation scheme:

$$MoO_4^{2-} \overset{+H^+}{\rightleftharpoons} [MoO_3(OH)]^- \overset{+H^+ \; +2H_2O}{\rightleftharpoons} [MoO_2(OH)_2(H_2O)_2]$$

$$\overset{+H^+}{\rightleftharpoons} [MoO(OH)_3(H_2O)_2]^+ \overset{+H^+}{\rightleftharpoons} [Mo(OH)_4(H_2O)_2]^{2+}, \qquad (4)$$

in which, in each case, the most basic O atoms (those bearing a negative charge, namely the terminal ones) become protonated [see Fig. 2(b)].*

explains the enhanced basicity and stability of the polymetalate ions (polychromate and polyvanadate ions) forming chains or rings of corner-sharing MO_4 tetrahedra, compared with the analogous non-metal polyanions (polysulphate and polyphosphate ions):



(5)

RESULTS FOR THE POLYMETALATE IONS FORMING CHAINS OR RINGS OF CORNER-SHARING MO_4 TETRAHEDRA

The above-mentioned resonance enhancing the basicity of the tetrahedral oxoanions [eqn (2)] also

These polymeric metalate ions are stabilized by the double bonds *inside* the chain. Due to the smaller size of the corresponding non-metal ions and, consequently, a higher repulsion energy the higher charged resonance formulae, and hence these polymeric species, are less favoured.

* The contribution of the coordinated H_2O molecules to the stabilization of the diprotonated monomer with respect to the basicity of the monoprotonated monomer would correspond to ≈ 3.8 pK_a units, as the difference between the experimentally observed pK_a of ≈ 3.8 and the average pK_a of the main-group oxoacids $MO_2(OH)_2$ [≈ -3, see Table 1(c)], corrected by ≈ 3 pK_a units (2–4, see above) for the change from a non-metal to a transition-metal oxoacid.

REFERENCES

1. G. Schwarzenbach and J. Meier, *J. Inorg. Nucl. Chem.* 1958, **8**, 302.
2. E. F. C. H. Rohwer and J. J. Cruywagen, *J. S. Afr. Chem. Inst.* 1963, **16**, 26.
3. E. F. C. H. Rohwer and J. J. Cruywagen, *J. S. Afr. Chem. Inst.* 1964, **17**, 145.

4. E. F. C. H. Rohwer and J. J. Cruywagen, *J. S. Afr. Chem. Inst.* 1969, **22**, 198.
5. J. Chojnacka, *Rocz. Chem.* 1963, **37**, 259.
6. D. V. S. Jain, *Indian J. Chem.* 1970, **8**, 945.
7. J. J. Cruywagen and H. A. C. McKay, *J. Inorg. Nucl. Chem.* 1970, **32**, 255.
8. D. S. Honig and K. Kustin, *J. Phys. Chem.* 1972, **76**, 1575.
9. D. S. Honig and K. Kustin, *Inorg. Chem.* 1972, **11**, 65.
10. G. Wiese and D. Böse, *Z. Naturforsch.* 1972, **27B**, 897.
11. R. R. Vold and R. L. Vold, *J. Magn. Reson.* 1975, **19**, 365.
12. M. T. Pope, *Heteropoly and Isopoly Oxometalates*, p. 43. Springer, Berlin (1983).
13. K. H. Tytko and O. Glemser, *Adv. Inorg. Chem. Radiochem.* 1976, **19**, 239.
14. J. J. Cruywagen and E. F. C. H. Rohwer, *Inorg. Chem.* 1975, **14**, 3136.
15. J. J. Cruywagen and E. F. C. H. Rohwer, *J. S. Afr. Chem. Inst.* 1976, **29**, 30.
16. E. F. C. H. Rohwer and J. J. Cruywagen, *J. S. Afr. Chem. Inst.* 1966, **19**, 11.
17. J. J. Cruywagen, J. B. B. Heyns and E. F. C. H. Rohwer, *J. Inorg. Nucl. Chem.* 1976, **38**, 2033.
18. J. J. Cruywagen, J. B. B. Heyns and E. F. C. H. Rohwer, *J. Inorg. Nucl. Chem.* 1978, **40**, 53.
19. E. F. C. H. Rohwer, J. J. Cruywagen and H. G. Raubenheimer, *J. S. Afr. Chem. Inst.* 1972, **25**, 338.
20. Ref. 12, p. 49.
21. Ref. 12, pp. 35, 128, 129.
22. D. L. Kepert, *The Early Transition Metals*, pp. 181, 288. Academic Press, London (1972).
23. L. Pauling, *General Chemistry*. Edward, Ann Arbor, MI (1944).
24. J. E. Ricci, *J. Am. Chem. Soc.* 1948, **70**, 109.
25. M. A. Porai-Koshits and L. O. Atovmyan, *Sov. J. Coord. Chem.* 1975, **1**, 1065.
26. M. A. Porai-Koshits and L. O. Atovmyan, *Russ. J. Inorg. Chem.* 1981, **26**, 3171.
27. I. Böschen, B. Buss and B. Krebs, *Acta Cryst.* 1974, **B30**, 48.
28. B. Krebs and I. Paulat-Böschen, *Acta Cryst.* 1982, **B38**, 1710.
29. H. Vivier, J. Bernard and H. Djomaa, *Rev. Chim. Miner.* 1977, **14**, 584.
30. N. Bailey, A. Carrington, K. A. K. Lott and M. C. R. Symons, *J. Chem. Soc.* 1960, 290.
31. F. A. Cotton and G. Wilkinson, *Anorganische Chemie*, 4th Edn, p. 238. Verlag Chemie, Weinheim (1982).
32. Autorenkollektiv, *Anorganikum*, 3rd Edn, p. 426. VEB Deutscher Verlag der Wissenschaften, Berlin (1970).
33. H. R. Christen, *Grundlagen der allgemeinen und anorganischen Chemie*, pp. 260, 264. Sauerländer & Salle, Aarau (1968).
34. F. Fouasson, *Ann. Chim.* 1948, **3**, 594.
35. J. E. Earley, D. Fortnum, A. Wojcicki and J. O. Edwards, *J. Am. Chem. Soc.* 1959, **81**, 1295.
36. A. V. Pamfilov and A. L. Agafonova, *Zh. Fiz. Khim.* 1950, **24**, 1147; *Chem. Abstr.* 1951, **45**, 2293.
37. A. L. Agafonova, *J. Gen. Chem. USSR* 1947, **17**, 1055; *Chem. Abstr.* 1948, **42**, 1788.
38. J. R. Howard, V. S. K. Nair and G. H. Nancollas, *Trans. Faraday Soc.* 1958, **54**, 1034.
39. *Table of Periodic Properties of the Elements*. Sargent–Welch, Skokie, IL (1968).
40. C. F. Baes and R. E. Mesmer, *The Hydrolysis of Cations*, pp. 206, 207. John Wiley, New York (1976).
41. J. Chojnacki, *Bull. Acad. Pol. Sci., Ser. Sci. Chim.* 1963, **11**, 365.

Polyhedron Vol. 5, No. 1/2, pp. 505–506, 1986
Printed in Great Britain

0277–5387/86 $3.00 + .00
© 1986 Pergamon Press Ltd

PREPARATION OF TRIANGULAR AND CUBIC MOLYBDENUM CLUSTERS AS AQUA IONS

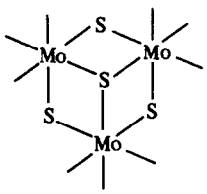
P. KATHIRGAMANATHAN, M. MARTINEZ and A. G. SYKES*

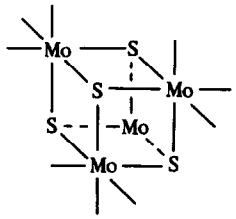
Department of Inorganic Chemistry, The University, Newcastle upon Tyne NE1 7RU, U.K.

(*Received* 8 *July* 1985)

Abstract—Further use of an electrochemical procedure for the formation of triangular and cubic molybdenum cluster complexes as aqua ions is reported.

Details of the preparation of green coloured aqua ions, $[Mo_3S_4(H_2O)_9]^{4+}$ and $[Mo_4S_4(H_2O)_9]^{5+}$, in high yields (60 and 30% of Mo) in a single electrochemical experiment have recently been reported.[1] The method involves reduction of the





Mo(V) complex di-μ-sulphidobis-[1-cysteinato-molybdate(V)], $Na_2[Mo_2S_2O_2(cys)_2]\cdot 3H_2O$,[2] in 2 M HCl under N_2 (or Ar) at a Hg pool electrode (−0.85 V vs NHE) for 12 h. The dark brown product is then diluted to $[H^+] = 0.30$ M and 2 l of 0.5 M *p*-toluenesulphonic acid (HPTS) added. After leaving to stand in air for 24 h the solution is loaded onto a Dowex column and the 4+ and 5+ products eluted with 2 and 3 M HPTS, respectively.[1] It is now evident that there is some sort of interaction of Hg with $Mo_3S_4^{4+}$, and the spectrum obtained is more like that of $[Mo_3OS_3(H_2O)_9]^{4+}$. The crystal structure of $[Mo_4S_4(edta)_2]^{3-}$ and other Mo_4S_4 complexes have been determined.[3] A similar procedure with $Na_2[Mo_2O_4(cys)_2]\cdot 5H_2O$ gives the red product $[Mo_3O_4(H_2O)_9]^{4+}$ (~20% of Mo), which is now well-characterized,[4] and $[Mo_4O_4(H_2O)_{12}]^{5+}$ (~3% of Mo). The triangular complexes are known to have apical μ_3-ligands.[5]

With some modification the above procedure has now been extended to the preparation of selenido and tellurido analogue complexes. Those with Se were prepared by electrolytic reduction (−0.85 V) of $[Mo_2O_4(cys)_2]^{2+}$ (4×10^{-2} M, 70 ml) in the presence of Se powder (2 g), first in H_2O (12 h), and then for a further period with HCl adjusted to 0.5 M (36 h). The brown solution obtained is again left in air for 24 h. Dowex 50W X2 column chromatography gives yellow-green products, which can be eluted with 2 M HPTS (37% of Mo) and 3 M HPTS (8%), respectively. Thiocyanato complexes have been prepared and analysed. The aqua ions have absorption peaks for $Mo_3Se_4^{4+}$ (375 and 625 nm) and $Mo_4Se_4^{5+}$ (380 sh and 500 sh). There is also a substantial yield of the μ_3-selenido complex $Mo_3O_3Se^{4+}$. A similar procedure with tellurium (3 g) has been used to prepare tellurido complexes. Assuming these to be analogue complexes, the absorption peaks are for $Mo_3Te_4^{4+}$ (390 and 632 nm) and $Mo_4Te_4^{5+}$ (380 and 636 nm).

From the electrolysis of pairs of $Mo(V)_2$ complexes from $[Mo_2O_4(cys)_2]^{2-}$, $[Mo_2O_3S(cys)_2]^{2-}$ and $[Mo_2O_2S_2(cys)_2]^{2-}$ in equimolar amounts, triangular and cubic complexes with mixed μ(O) and μ(S) ligands are obtained as aqua ions. The range of triangular complexes general formula $[Mo_3O_xS_{4-x}(H_2O)_9]^{4+}$, including three prepared by Shibahara *et al.*,[6] is now complete, and includes symmetrical complexes $Mo_3O_4^{4+}$, $Mo_3SO_3^{4+}$, $Mo_3OS_3^{4+}$ and $Mo_3S_4^{4+}$, and unsymmetrical complexes $Mo_3SO_3^{4+}$, $Mo_3S_2O_2^{4+}$ (two forms) and $Mo_3S_3O^{4+}$.[7] All are in oxidation state Mo(IV)$_3$.† Selected UV–visible spectra (Fig. 1) indicate a gradual shift in peak positions to higher wavelengths with increasing sulphide content. Cyclic voltammograms (Fig. 2) give reversibility for each of the triangular complexes. Constant-potential coulometry done at potentials slightly more negative than the respective reduction peak potential shown in the cyclic voltammogram gives three electron reductions per cluster.

* Author to whom correspondence should be addressed.

† The complex $Mo_3S_4^{4+}$ has also been prepared by Cotton and his colleagues from $M(CO)_6$.

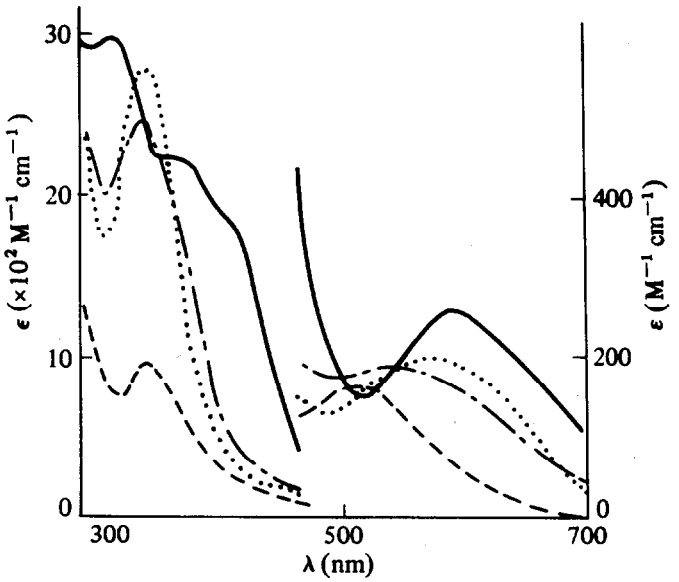


Fig. 1. UV spectra of the unsymmetrical triangular $Mo(IV)_3$ aqua ions $Mo_3O_3S^{4+}$ (– – –), $Mo_3O_2S_2^{4+}$ (two μ_2-sulphido ligands) (– · – · –), $Mo_3O_2S_2^{4+}$ (μ_2-S and μ_3-S ligands) (· · · · ·) and $Mo_3OS_3^{4+}$ (——) in 2 M HPTS.

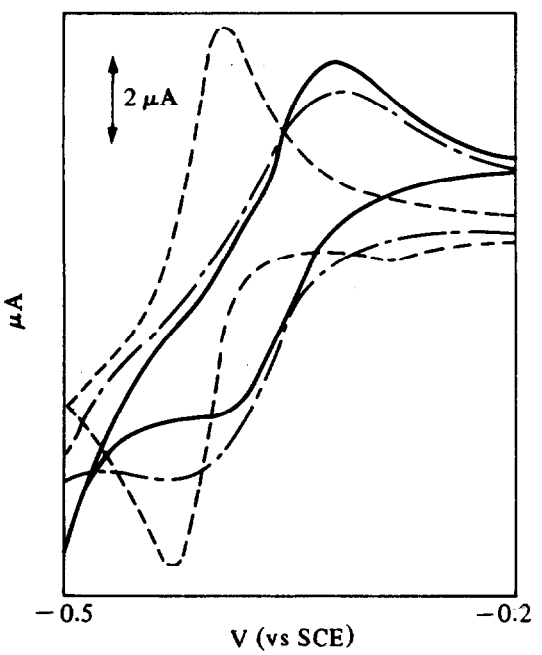


Fig. 2. Cyclic voltammograms of the $Mo(IV)_3$ aqua ions $Mo_3O_3S^{4+}$ (μ_3-sulphido) (– – –), $Mo_3OS_3^{4+}$ (μ_3-sulphido) (– · – · –) and $Mo_3S_4^{4+}$ (——) in 2 M HPTS at a hanging mercury electrode.

Similar electrochemical preparative procedures are currently under investigation to obtain W and Nb aqua ions. A range of aqua ions including $W_2O_4^{2+}$ (yellow),[8] $W_3O_4^{4+}$ (orange),[9] $W_4O_5^{5+}$ (brown-red) and a W(III) containing (green) ion have been identified in varying amounts depending on conditions employed which are at present being more carefully defined. In other related work there is evidence for formation of an aqua ion of niobium in oxidation state less then V, and preliminary results indicate a mixed-valence trimeric structure.

Acknowledgement—M.M. thanks the CIRIT from Generalitat de Catalunya for financial support.

REFERENCES

1. P. Kathirgamanathan, M. Martinez and A. G. Sykes, *J. Chem. Soc., Chem. Commun.* 1985, 953.
2. A. Kay and P. C. H. Mitchell, *J. Chem. Soc. A* 1970, 2421; F. A. Armstrong, T. Shibahara and A. G. Sykes, *Inorg. Chem.* 1978, **17**, 189.
3. For example T. Shibahara, H. Kuraya, K. Matsumoto and S. Ooi, *J. Am. Chem. Soc.* 1984, **106**, 789; A. Müller, W. Eltzner, H. Bogge and R. Jostos, *Angew. Chem., Int. Ed.* Engl. 1982, **21**, 795.
4. K. R. Rodgers, R. K. Murmann, E. O. Schlemper and M. E. Shelton, *Inorg. Chem.* 1985, **24**, 1313.
5. A. Bino, F. A. Cotton and Z. Dori, *J. Am. Chem. Soc.* 1978, **100**, 5252.
6. T. Shibahara, H. Hattori and H. Kuroya, *J. Am. Chem. Soc.* 1984, **106**, 2710; T. Shibahara, personal communication.
7. P. Kathirgamanathan, M. Martinez and A. G. Sykes, *J. Chem. Soc., Chem. Commun.* 1985, 1437.
8. A. B. Soares, R. C. Taylor and A. G. Sykes, *J. Chem. Soc., Dalton Trans.* 1980, 1101.
9. M. Segawa and Y. Sasaki, *J. Am. Chem. Soc.* 1985, **107**, 5565.

Polyhedron Vol. 5, No. 1/2, pp. 507–509, 1986
Printed in Great Britain

0277–5387/86 $3.00+.00
© 1986 Pergamon Press Ltd

AQUEOUS Mo(IV): FORMATION, DISPROPORTIONATION AND PROPERTIES

G. P. HAIGHT* and K. M. RAHMOELLER†

University of Illinois, Urbana, IL 61801, U.S.A.

(*Received* 28 *June* 1985)

Abstract—A number of reactions relating to the solution chemistry of Mo(IV) are discussed.

Aqueous Mo(IV) has been the subject of many conflicting reports and speculations since 1940.[1] For example: (1) Mo(IV) has been deduced to be the active catalyst in reductions of inert oxoanions present in low, steady-state concentrations arising from its disappearance by a second-order disproportionation reaction.[2] Recently, *stable* $MO_3O_4^{4+}$ has been found to be inert to such catalysis.[3] (2) $Mo^{3+}(aq)$ is reported[4] to be oxidized to 90% $Mo_2O_4^{2+}$ and 10% $Mo_3O_4^{4+}$ with O_2, whereas we find a potential break for 100% formation of $Mo_2O_4^{2+}$ when the reaction is done rapidly. (3) Up to 70% $Mo_3O_4^{4+}$ can be formed when $Mo_2O_4^{2+}$ is reduced by Cr^{2+},[4] while earlier reports and our potentiometric titrations yield only Mo(III) as $Mo_2(OH)_2^{4+}$ with the same reducing agent.

In this paper we present evidence for the rapid disproportionation in H_2O of Mo(IV) monomers, dimers and polymeric chlorides without direct formation of stable, inert $Mo_3O_4^{4+}$, which forms only by slow conproportionation of Mo(V) or Mo(VI) with Mo(III), and by oxidation of $Mo_2(OH)_2^{4+}$ via the formation of mixed-valence oligomers from which $Mo_2O_4^{2+}$ and $Mo_3O_4^{4+}$ both form. Slow conproportionation of $Mo_2O_4^{2+}$ and $Mo_2(OH)_2^{4+}$ appears to account for varying amounts of $Mo_3O_4^{4+}$ being observed in systems reacting over long periods.[1,3] It is too slow to be a factor in potentiometric titrations used in this study.

DISPROPORTIONATION OF Mo(IV)

$MoCl_4$, $(Et_4N)_2MoCl_6$ and

$$(NH_4)_2[MoCl_4(SnCl_3)_2]$$

each catalyze the reduction of NO_3^- or ClO_4^- by Sn(II) giving kinetics similar to reactions initiated by Mo(VI).[1] Addition of each of these compounds to water or aqueous acid results in rapid disproportionation of Mo(IV):

$$12MoCl_4 + 12H_2O \rightarrow 3Mo_2O_4^{2+} + 2Mo_3Cl_{12}^{3-} + 24H^+ + 24Cl^-, \quad (1)$$

$$2MoCl_6^{2-} + 2H_2O \overset{\text{(seconds)}}{\rightleftharpoons} 2MoCl_5(OH_2)^{-1} + 2Cl^- \rightleftarrows MoOCl_5^{2-} + Mo(OH_2)Cl_5^{2-} + 2H^+, \quad (2)$$

$$2MoCl_4(SnCl_3)_2^{2-} + 2H_2O \leftrightarrows 2SnCl_3^- + \tfrac{1}{3}Mo_3Cl_{12}^{3-} + \tfrac{1}{2}Mo_2O_4^{2-}. \quad (3)$$

The driving force appears to be the formation of Mo(V)≡O multiple bonds. $MoOCl_5^{2-}$ is the Mo(V) product in ≥9 M HCl, but hydrolyzes to $Mo_2O_4^{2+}$ in dilute acid. $Mo_3Cl_{12}^{3-}$ has been identified by its UV–visible spectrum‡ and the kinetics of its dissociation (to be reported elsewhere):

$$Mo_3Cl_{12}^{3-} + 6H_2O \xrightarrow{k_1} 3[MoCl_4(H_2O)_2^-] \text{(minutes)} \xrightarrow{H_2O} Mo(OH_2)_6^{3+} \text{(hours)}, \quad (4)$$

$$3Mo_2O_4^{2+} + 6Mo^{3+} \xrightarrow{H_2O} 4Mo_3O_4^{4+} \quad \text{(hours)}. \quad (5)$$

* Author to whom correspondence should be addressed.

† Present address: Physical Chemistry Department, General Motors, Detroit, MI 48089, U.S.A.

‡ The Mo(III) product could not be isolated from solution due to its rapid dissociation. $Mo_2Cl_9^{3-}$ and $Mo_3Cl_{12}^{3-}$ both exhibit similar visible spectra and dissociation kinetics, although $Mo_3Cl_{12}^{3-}$ appeared a better match. A partially aquated form of $Mo_2Cl_9^{3-}$ could be the initial product of $MoCl_4$ disproportionation or of $Mo_3Cl_{12}^{3-}$ dissociation: however, stoichiometry and spectra dictate a preference for $Mo_3Cl_{12}^{3-}$.[5]

Hydrolysis of dinuclear[6] and trinuclear Mo(IV) alkoxides[7] led to disproportionation only for the dimeric species, which apparently dissociates on hydrolysis:

$$2[Mo(OEt)_4] \xrightarrow{H_3O^+} Mo_2O_4^{2+} + 2Mo^{3+}_{(aq)}, \quad (6)$$

$$3H_3O^+ + Mo_3O(OEt)_9^+ \rightarrow Mo_3O_4^{4+} + 9EtOH. \quad (7)$$

It appears unlikely that oxidation or reduction of monomeric Mo(III) or Mo(V) will result in direct formation of $Mo_3O_4^{4+}$.

OXIDATION OF Mo(III)

$Mo(H_2O)_6^{3+}$, $Mo_2(OH)_2^{4+}$ and various complexes of the latter have been titrated to potentiometric endpoints using oxidants Ce^{4+}, $Cr_2O_7^{2-}$, NO_3^-, VO^{2+}, ClO_3^-, ClO_4^-, $Co(C_2O_4)_3^{3-}$ and O_2 (bubbled rapidly until a potential change occurs) to discover pathways to and around $Mo_3O_4^{4+}$. Product analyses of species present at endpoints have made delineation of likely pathways possible.

Oxidation of $Mo^{3+}(aq)$ *(monomeric)*

The half reaction:

$$2Mo^{3+} + 4H_2O \rightarrow Mo_2O_4^{2+} + 8H^+ + 4e^- \quad (8)$$

describes the overall result of all oxidations of monomeric Mo^{3+} at the first potential break. Ce^{4+} and $Cr_2O_7^{2-}$ could effect further oxidation and a second potential break for:

$$Mo_2O_4^{2+} \rightarrow 2MoO_2^{2+}(aq) + 2e^-. \quad (9)$$

ClO_4^- is initially inert,[8] exhibiting autoacceleration as Mo(V) is formed. Since Mo^{3+}, a d^3 ion, must lose electrons from two different t_{2g}-orbitals, and Mo(IV) is known to disproportionate fast, the following mechanism leading to 100% formation of Mo(V) is compelling:

$$Mo^{3+} + [Ox] \rightarrow Mo(IV), \quad (I)$$

$$2Mo(IV) \rightarrow Mo^{3+} + Mo{\equiv}O^{3+}, \quad (II)$$

$$2Mo{\equiv}O^{3+} + 2H_2O \rightarrow Mo_2O_4^{2+} + 4H^+. \quad (III)$$

Scheme 1.

Mo(IV) could be oxidized directly with the same overall result:

$$Mo(IV) + Ox \rightarrow O{\equiv}Mo(V). \quad (IIa)$$

If oxidation (with O_2) is done *slowly*, $Mo_2O_4^{2+}$ may react with Mo^{3+} to give variable amounts of $Mo_3O_4^{4+}$ by reaction (5).[3]

OXIDATION OF $Mo_2(OH)_2^{4+}$

Using all the above oxidants as titrants and conproportionation with Mo(VI) give a surprising potential break at average oxidation state for Mo of +4.5. At the endpoint it is possible to separate and identify $Mo_2O_4^{2+}$ and $Mo_3O_4^{4+}$, with half of the molybdenum in each species:[1,9]

$$6Mo_2(OH)_2^{4+} \xrightarrow{[Ox]} 2Mo_3O_4^{4+} + 3Mo_2O_4^{2+} + 12H^+ + 18e^-, \quad (10)$$

$$2H_2O + 3Mo_2(OH)_2^{4+} + 6Mo(VI) \rightarrow 2Mo_3O_4^{4+} + 3Mo_2O_4^{2+} + 10H^+. \quad (11)$$

Using ^{95}Mo NMR for isotopic labelling it is found that half of the molybdenum in each product of reaction (11) originates in each reactant. Complete scrambling of Mo, the stoichiometry and the need to use dimeric Mo_2(III) all suggest a build up of mixed-valence oligomers, from which the two very stable products may form.

STERIC HINDRANCE TO OLIGOMERIZATION

If this mechanism is correct, complexation of the $Mo_2(OH)_2^{4+}$ should prevent formation of these intermediates by removal of coordination sites necessary for oligomerization, and new stoichiometries could result. In the cases of the oxidation of the EDTA and TACN (1,4,7-triazacyclononane) complexes of $Mo_2(OH)_2^{4+}$, $Mo_2O_4^{2+}$ complexes become the dominant, if not the only, product of potentiometric titration. The $[Mo_2(OH)_2EDTA]$ complex can be partially oxidized (no potential break) to $Mo_4O_6(EDTA)_2^{4-}$. The latter may be titrated to $[Mo_2O_4EDTA]^{2-}$ as the only product. If

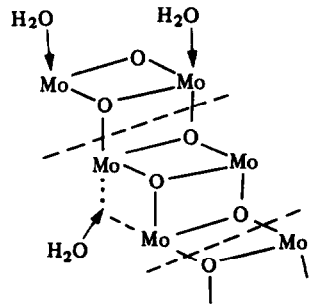
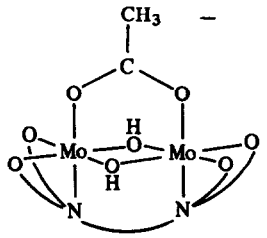


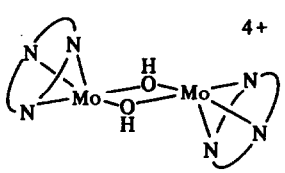
Fig. 1. Oligomer fragment showing how water-assisted cleavage of an $(Mo_2O_2)_n$ oligomer could produce both $Mo_2O_4^{2+}$ and $Mo_3O_4^{4+}$. If $n = 12$ the observed stoichiometry is realized. The dashed lines indicate how trimers and dimers may be obtained from a simply constructed intermediate.

placed in acid, EDTA dissociates and the undetermined aquation product(s) are oxidized to $Mo_3O_4^{4+}$ and $Mo_2O_4^{2+}$ in the usual 2:3 ratio. In the special case of oxidation by Mo(VI), deviations from the $3Mo_2O_4^{2+} + 2Mo_3O_4^{4+}$ stoichiometry also occur. With EDTA as ligand (I), only the $Mo_3O_4^{4+}$

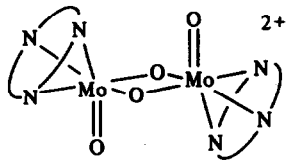


I

core forms. That direct formation of $Mo_3O_4^{4+}$ is permitted only in this case suggests that addition of more than one Mo(VI) to $Mo_2(OH)_2^{4+}$ to form oligomers is preferred to trimer formation in the absence of steric hindrance from ligands. With TACN as ligand, oxidation of *anti*-$Mo_2(OH)_2(TACN)_2^{4+}$ (II) with Mo(VI) gives *anti*-$Mo_2O_4(TACN)_2^{2+}$ (III) which slowly isomerizes[10] to



II



III

the more common *syn*-$Mo_2O_4(TACN)_2^{2+}$. No $Mo_3O_4^{4+}$ forms. Apparently the steric hindrance prevents formation of even the Mo(IV) trimer, allowing Mo(VI) no other role than as a simple oxidant.

REDUCTION OF Mo(VI) AND Mo(V)

Potentiometric titrations of Mo(VI) in 1 M methylsulfonic acid using Cr^{2+} and V^{2+} gave two breaks for the reactions:

$$2Mo(VI) + 2e^- \xrightarrow{H_2O} Mo_2O_4^{2+}, \quad (12)$$

$$6H^+ + Mo_2O_4^{2+} + 4e^- \rightarrow Mo_2(OH)_2^{4+} + 2H_2O. \quad (13)$$

Quick product separation and analysis showed no formation of $Mo_3O_4^{4+}$ at intermediate stages of the titration. Investigation of conditions and time of contact between Mo(III) products and Mo(V) reactants may yet reveal favorable conditions for forming $Mo_3O_4^{4+}$ by reduction of $Mo_2O_4^{2+}$ and/or Mo(VI).

CONCLUSIONS

Most Mo(IV) aquo or oxo species disproportionate in water making assembly of stable, inert $Mo_3O_4^{4+}$ cores difficult. However, special pathways and slow conproportionations do lead to $Mo_3O_4^{4+}$, making it very likely that minor differences in experimental procedure will give different stoichiometries for appearently similar redox processes.

REFERENCES

1. G. P. Haight, M. D. Johnson and K. M. Rahmoeller, *Isr. J. Chem.* 1985, **25**, 177.
2. G. P. Haight, Jr and W. F. Sager, *J. Am. Chem. Soc.* 1952, **74**, 6056.
3. I. W. Boyd, G. P. Haight, Jr and N. C. Howlader, *Inorg. Chem.* 1981, **20**, 3115.
4. Referee's comment on this paper.
5. W. H. Delphin, R. A. D. Wentworth and M. S. Matson, *Inorg. Chem.* 1974, **13**, 2552.
6. M. H. Chisholm, W. W. Reichert and P. Thornton, *J. Am. Chem. Soc.* 1978, **100**, 2744.
7. M. H. Chisholm, K. Folting, J. C. Huffman and C. C. Kirkpatrick, *Inorg. Chem.* 1984, **23**, 1021.
8. E. F. Hills and A. G. Sykes, *Polyhedron* 1986, **5**, 511.
9. K. M. Rahmoeller, Thesis, University of Illinois, Urbana, IL (1985).
10. K. Wieghardt, M. Hahn, W. Swiridoff and J. Weiss, *Inorg. Chem.* 1984, **23**, 94.

Polyhedron Vol. 5, No. 1/2, pp. 511–512, 1986
Printed in Great Britain

0277–5387/86 $3.00+.00
© 1986 Pergamon Press Ltd

KINETIC STUDIES ON THE REACTIONS OF AQUA Mo^{3+} WITH O_2 AND ClO_4^-

ELAINE F. HILLS and A. G. SYKES*

Department of Inorganic Chemistry, The University, Newcastle upon Tyne NE1 7RU, U.K.

(*Received* 1 *July* 1985)

Abstract—Kinetic studies are reported for two fundamental reactions of the hexaaquamolybdenum(III) ion with O_2 and ClO_4^-.

Previously the reaction of O_2 with aqua metal ions Cr^{2+},[1] V^{2+},[2] Fe^{2+} [3] and U(IV),[4] have been studied, and there are extensive investigations of the reactions of O_2 with a range of Co(II),[5] Cu(I)[6] and Ru(II)[7] complexes. In the case of Mo^{3+}, the oxidation state of the metal ion changes by $2e^-$ to give Mo(V), a feature which is relevant also to the V^{2+}, Cr^{2+} (possibly) and U(IV) studies. However, with V^{2+} and Cr^{2+} in excess the final product is the III state ion, and the oxidation of U(IV) is believed to proceed with intermediate formation of U(V).

The reaction of Mo^{3+} with O_2 in *p*-toluenesulphonic acid (HPTS) solutions, $I = 2.0$ M (LiPTS), is summarized by eqn (1):

$$2Mo^{3+} + O_2 + 2H_2O \rightarrow Mo_2O_4^{2+} + 4H^+, \quad (1)$$

where $Mo_2O_4^{2+}$ is the di-μ-oxo Mo(V) ion, $[Mo_2O_4(H_2O)_6]^{2+}$.[8] Even when there is a deficiency of Mo^{3+}, the reaction conforms to this equation. Use of isotopically labelled O_2, followed by IR spectroscopy of the isolated $Mo_2O_4^{2+}$ product, has demonstrated that some and possibly all of the ^{18}O is taken up in the di-μ-oxo positions.[9] At 25°C, with Mo^{3+} in large excess, three stages are observed by stopped-flow spectrophotometry, and an intense yellow coloured intermediate is formed which we choose to write as MoO_2Mo^{6+}, consistent with minimal-composition requirements. The oxidation state of the Mo in this intermediate is uncertain, and is presumably in the III–V range. There is no evidence for formation of aqua $Mo(IV)_3$ [or any as yet unidentified monomeric or dimeric Mo(IV) aqua ion] as an intermediate, except on bubbling O_2 through a solution of Mo^{3+} (2.3×10^{-2} M), when ~10% of red $Mo(IV)_3$ is obtained.

The kinetics of the decay of the intermediate at the 395-nm peak ($\varepsilon = 2300$ M^{-1} cm^{-1} per dimer), give rate constants, k_{3obs}, which can be expressed as in eqn (2):

$$k_{3obs} = \frac{K_1K_2k_3[Mo^{3+}]^2}{1 + K_1[Mo^{3+}] + K_1K_2[Mo^{3+}]^2}. \quad (2)$$

The various constants (in 2 M HPTS) are as defined in eqns (3)–(5):

$$Mo^{3+} + O_2 \rightleftharpoons MoO_2^{3+} \quad (K_1 = 360\ M^{-1}), \quad (3)$$

$$MoO_2^{3+} + Mo^{3+} \rightleftharpoons MoO_2O^{6+} \quad (K_2 = 535\ M^{-1}), \quad (4)$$

$$MoO_2Mo^{6+} \rightarrow \text{products} \quad (k_3 = 0.23\ s^{-1}). \quad (5)$$

Applications of a non-rigorous consecutive treatment to the last two, and then the first two stages has provided estimates of the rate constants for eqns (3) and (4). Refinement has been carried out using KINSIM for consecutive equilibria.[10] Rate constants k_1 (180 M^{-1} s^{-1}) and k_2 (42 M^{-1} s^{-1}) are in excess of previous substitution rate constants for Mo^{3+}. With O_2 in excess of Mo^{3+} an alternative route for conversion of MoO_2^{3+} to $Mo_2O_4^{2+}$ has been identified.

Taube[11] has recently reviewed the reactivity of reducing metal ions (Ti^{3+}, V^{2+}, V^{3+} and Ru^{2+}) with ClO_4^-. Notable examples in which no reaction occurs are with Cr^{2+}, Eu^{2+} and Sn^{2+}. In all cases in which reaction takes place, it appears that an oxo product, the VO^{2+} aqua ion in the case of V^{2+} and V^{3+}, is formed. With Mo^{3+} there are no stable mononuclear oxo products, since Mo(IV) exists as the trimeric $Mo_3O_4^{3+}$ ion[12] and Mo(V) as dimeric $Mo_2O_4^{2+}$. Transient monomeric aqua ions having the required structure cannot however be ruled out.

* Author to whom correspondence should be addressed.

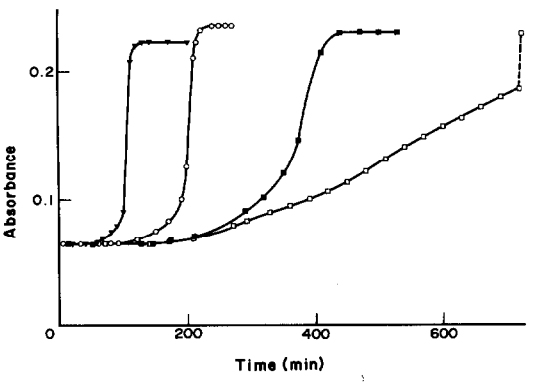


Fig. 1. Absorbance changes at 385 nm for the reaction (25°C) of Mo^{3+} (4.3×10^{-3} M) with ClO_4^- at $[H^+] = 0.30$ M, $I = 1.0$ M (LiPTS). Concentrations of perchlorate (introduced as $LiClO_4$) were: 0.20 (□), 0.30 (■), 0.50 (○) and 0.70 (▼).

This situation results in more complicated kinetics as indicated below.

The kinetics with ClO_4^- (≥ 0.2 M) in excess monitored by $Mo(V)_2$ formation is characterized by slow initiation, rapid propagation and termination (Fig. 1). No evidence was obtained for formation of either $Mo(III)_2$ or $Mo(IV)_3$ as intermediates. At 25°C solutions of Mo^{3+}, $(2.2–8.6) \times 10^{-3}$ M, have been found to exhibit no apparent reactivity with ClO_4^- (0.2–0.7 M) over a period of at least 0.5 h (and as long as 3 h for $[HClO_4] = 0.2$ M), after which a complete reaction can be observed in as little as 1 h, e.g. with $[ClO_4^-] = 0.7$ M, $[H^+] = 0.3$ M, $I = 2.0$ M (LiPTS). For the procedure used and in the absence of ClO_4^-, there was no detectable reaction of Mo^{3+} over 4 h.

Overall, the reaction is faster at higher $[ClO_4^-]$, higher $[Mo^{3+}]$, and at the higher $[H^+]$ in the range investigated. The length of the initiation period is dependent on whether the source of ClO_4^- is $LiClO_4$ or $HClO_4$ (slower rates) at constant $[H^+]$. Details of the precise mechanism remain uncertain. The features displayed are quite different to all previous studies.

REFERENCES

1. R. M. Sellers and M. G. Simič, *J. Am. Chem. Soc.* 1974, **98**, 6145.
2. J. Swinehart, *Inorg. Chem.* 1965, **4**, 1069.
3. P. George, *J. Chem. Soc.* 1954, 4349.
4. G. Gordon and H. Taube, *Inorg. Chem.* 1962, **1**, 69.
5. J. Simplicio and R. G. Wilkins, *J. Am. Chem. Soc.* 1969, **91**, 1325.
6. J. S. Thompson, *J. Am. Chem. Soc.* 1984, **106**, 4657.
7. D. M. Stanbury, O. Haas and H. Taube, *Inorg. Chem.* 1980, **19**, 518.
8. M. Ardon and A. Pernick, *Inorg. Chem.* 1973, **12**, 2482.
9. R. K. Murmann, *Inorg. Chem.* 1980, **19**, 1765.
10. B. A. Barshop, R. F. Wrenn and C. Frieden, *Anal. Biochem.* 1983, **130**, 134.
11. H. Taube, In *Mechanistic Aspects of Inorganic Reactions* (Edited by D. B. Rorabacher and J. Endicott), p. 151. ACS Symposium Series 198.
12. R. K. Murmann and M. E. Shelton, *J. Am. Chem. Soc.* 1980, **102**, 1984.

Polyhedron Vol. 5, No. 1/2, pp. 513–520, 1986
Printed in Great Britain

0277–5387/86 $3.00 + .00
© 1986 Pergamon Press Ltd

THE ELECTROCHEMISTRY OF A DIMERIC AND TWO MONOMERIC *CIS*-TRIOXOMOLYBDENUM(VI) COMPLEXES CONTAINING CYCLIC TRIAMINE LIGANDS IN PROTIC AND APROTIC MEDIA: MODEL COMPOUNDS FOR THE ACTIVE SITE IN FORMATE DEHYDROGENASE

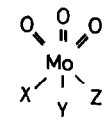
WILLY HERRMANN and KARL WIEGHARDT*

Lehrstuhl für Anorganische Chemie I der Ruhr-Universität, D-4630 Bochum, F.R.G.

(*Received* 7 *June* 1985)

Abstract—The electrochemistry of two monomeric *cis*-trioxomolybdenum(VI) complexes containing cyclic triamine ligands *N,N',N''*-trimetyl-1,4,7-triazacyclononane (L) (**1**) or 1,4,7-triazacyclononane (L') (**2**) has been studied in protic (CH_3SO_3H) and aprotic media (DMF) by cyclic voltammetry at an HMD electrode. **1** and **2** are quasi-reversibly reduced by a $2e^-, 4H^+$ step in acidic solutions to give monomeric $[LMo(IV)O(OH_2)_2]^{2+}$ and $[L'MoO(OH_2)_2]^{2+}$, which in the case of **1** is further reduced to a monomeric Mo(III) species which then undergoes a reversible chemical reaction (dimerization?). In contrast, reduced **2** undergoes chemical reactions (dimerization or trimerization of $[L'MoO(OH_2)_2]^{2+}$ or comproportionation reactions) due to the fact that the unmethylated cyclic amine in **2** is sterically less demanding. **1** and **2** are redox-inactive in DMF (+1.0 to −1.7 V vs Ag–AgCl at a Pt or a glassy-carbon electrode). Dimeric $[L_2Mo_2O_5](PF_6)_2$, **3**, is reversibly reduced to a $Mo(V)_2$ dimer ($2e^-, 2H^+$ process) and, finally, to a $Mo(III)_2$ dimer ($4e^-, 4H^+$) in 0.1 M CH_3SO_3H at an HMD electrode, contrasting with the behavior in aprotic medium (DMF, Pt electrode), where two reversible one-electron transfer processes generating the blue, mixed-valence species Mo(VI)/(V) and an $Mo(V)_2$ dimer have been observed.

A number of enzymes containing monomeric Mo(VI), Mo(V) or Mo(IV) have been characterized and the structures of their first coordination spheres have been elucidated with an encouraging degree of certainty by EXAFS and EPR-spectroscopy.[1–3] While the oxidized forms of the enzymes sulfite oxidase, xanthine oxidase and nitrate reductase appear to have a *cis*-dioxomolybdenum(VI) or a *cis*-oxosulfidomolybdenum(VI) moiety in common, there is evidence for a *cis*-trioxomolybdenum(VI) entity in the enzyme formate dehydrogenase (CO_2 reductase) isolated from *Clostridium pasteurianum*.[4,5] Interestingly, and in contrast to the afore-mentioned enzymes, there is no evidence for coordination by sulfur ligands. Instead, additional oxygen or nitrogen ligands were found and a plausible structure of the active site has been proposed. These observations have lead to increasing efforts to synthesize simple low molecular weight model complexes of molybdenum which mimic spectroscopic and reactivity patterns of these enzymes.[1,2,6] Extremely useful information concerning the catalytic activity of enzymes and their



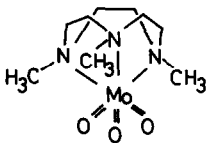
X,Y,Z = O, N

model compounds have been obtained from electrochemical studies, which have focussed to a great extent on *cis*-dioxomolybdenum complexes.[7–17] To date no such study has been carried out on simple monomeric *cis*-trioxomolybdenum(VI) complexes with the exception of the aqua-ion $MoO_3(OH_2)_3$.[18] This is due to the fact that, until very recently, stable monomeric complexes with this entity were not available. Thus

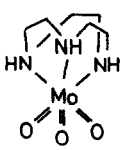
* Author to whom correspondence should be addressed.

(dien)MoO_3[19] (dien = diethylenetriamine) is known to undergo ligand dissociation in aqueous solution,[20] and $[(nta)MoO_3]^{3-}$ (nta = nitrilotriacetate) dimerizes in acidic solution.[21]

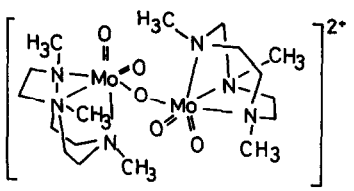
We have prepared two *cis*-trioxomolybdenum(VI) complexes **1** and **2** using the small tridentate cyclic macrocycles *N,N',N''*-trimethyl-1,4,7-triazacyclononane and 1,4,7-triazacyclononane.[22] **1** and **2** are stable in acidic aqueous solution and no ligand dissociation has been observed even in 2 M $HClO_4$.



1



2



3

We report here a cyclic voltammetric study of **1** and **2** in an aprotic medium and in acidic (CH_3SO_3H) solution. In addition, we have further investigated the electrochemistry of the dimer **3**[23] in a protic medium.

RESULTS

Electrochemistry of 1, 2 *and* 3 *in aprotic media*

The monomeric complexes **1** and **2** were found to be redox-inactive in acetonitrile (0.1 M TBA-PF_6 supporting electrolyte) at a Pt-button or glassy-carbon electrode in the potential range +1.0 to −1.7 V vs Ag–AgCl. Even in aqueous 0.1 M KNO_3 no reaction has been observed.

In contrast, binuclear $\mathbf{3}(PF_6)_2$ in acetonitrile has been shown previously to be reduced in two reversible one-electron reactions yielding an intensely blue mixed-valence species Mo(VI)/Mo(V) and, finally, a yellow dimer of Mo(V), which is a strong reductant:[23]

$$\begin{aligned}&[L_2Mo_2O_5]^{2+} + e^- \rightleftharpoons [L_2Mo_2O_5]^+ \\ &+ e^- \rightleftharpoons [L_2Mo_2O_5], \\ &E_1 = -0.77\ \text{V}, \\ &E_2 = -1.88\ \text{V vs } Fc^+\text{–Fc}.\end{aligned} \qquad (1)$$

Electrochemistry of 1 *in acidic solution* (*pH* 0.3–1.3)

The cyclic voltammogram (CV) of **1** in 0.1 M CH_3SO_3H, at a hanging mercury drop electrode (HMDE) (Fig. 1) consists of two reduction and one oxidation wave in the potential range +0.3 to −0.8 V vs normal hydrogen electrode (NHE). The second reduction wave (peak c) is less intense than the first (a) and it reduces the height of oxidation peak b. In a reduced range (+0.3 to −0.30 V) only one reduction and one oxidation wave are observed (peaks a and b).

In Table 1 the diagnostic criteria of the CV in the potential range +0.3 to −0.3 V for peaks a and b are summarized and they are commented on as follows:

(1) The reduction potential, E_p^a, and the oxidation potential, E_p^b, are shifted to more cathodic and anodic potentials, respectively, with increasing scan rates: it is a symmetrical shift of *ca* 38 mV in going from 50 mV s^{-1} to 1.0 V s^{-1}.

(2) For the peak half-width potential, $E_{p/2}^a$, a small cathodic shift (maximum 25 mV) with increasing scan rates (0.5–1.0 V s^{-1}) is observed, whereas $E_{p/2}^b$ appears to be independent of the scan rate.

(3) The peak potential difference, ΔE_p^{ab}, increases with increasing scan rates (ΔE_p = 100 mV s^{-1} and 176 mV at 1.0 V s^{-1}), indicating a substantial kinetic inhibition of the electron-transfer process.

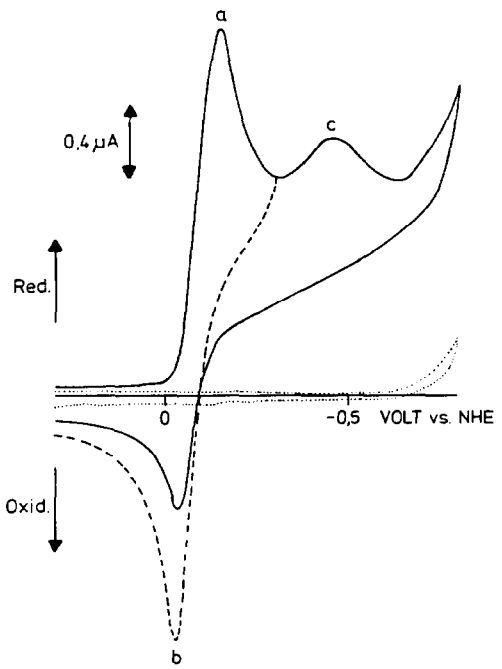


Fig. 1. CV of **1** in 0.1 M CH_3SO_3H (HMDE 25°C, scan rate 100 mV s^{-1}) in the potential range +0.3 to −0.3 V (broken line) and +0.3 to −0.8 V vs NHE (solid line).

Table 1. Diagnostic criteria derived from CVs of **1** in CH_3SO_3H at an HMDE [25°C, $\mu = 0.5$ M (KNO_3)]

pH	Scan rate ($V\ s^{-1}$)	$\lvert E_p^a - E_{p/2}^a\rvert$[d] (V)	$\lvert E_p^b - E_{p/2}^b\rvert$[d] (V)	ΔE_p^{ab}[e] (mV)	CF^a ($\mu A\ V^{-1/2}\ s^{1/2}\ mmol^{-1}\ l$)	CF^b ($\mu A\ V^{-1/2}\ s^{1/2}\ mmol^{-1}\ l$)	I_p^b/I_p^a
(A) Potential range +0.3 to −0.3 vs NHE							
1.0	0.05	0.059	0.048	100	12.5	13.5	1.08
1.0	0.10	0.065	0.049	114	12.2	13.5	1.11
1.0	0.20	0.067	0.053	125	12.0	13.3	1.11
1.0	0.50	0.068	0.065	150	11.5	13.2	1.15
1.0	1.00	0.073	0.080	176	11.2	12.8	1.14
(B) Potential range +0.3 to −0.8 V vs NHE							
					E^{fg} (V vs NHE)	E_p^{ch} (V vs NHE)	
0.3	0.05	0.038	0.030	52	+0.020	−0.405	
0.3	0.20	0.040	0.038	63	+0.019	−0.445	
0.72	0.05	0.043	0.038	55	−0.020	−0.385	
0.72	0.20	0.045	0.039	66	−0.020	−0.425	
0.96	0.05	0.047	0.037	74	−0.051	−0.375	
0.96	0.20	0.054	0.042	81	−0.056	−0.42	
1.28	0.05	0.057	0.045	86	−0.090	−0.45	
1.28	0.20	0.065	0.044	100	−0.092	−0.455	

[d] Peak half-width of peaks a and b (Fig. 1).
[e] Peak potential difference between peak a and peak b.
[g] Formal redox potential $(E_p^a - E_p^b)/2$.
[h] Reduction potential of peak c.

(4) The formal redox potential $E_{1/2}$ $[(E_p^a - E_p^b)/2]$ (−0.075 V vs NHE) is *independent* of the scan rate.

These diagnostic criteria are indicative of a quasi-reversible redox wave. Although the rather large peak potential difference ($|E_p^a - E_p^b| = \Delta E_p^{ab}$) seems to point to a one-electron transfer; the peak half-width potential differences, $|E_p^a - E_{p/2}^a|$ and $|E_p^b - E_{p/2}^b|$ (especially the latter), indicate a two-electron transfer process which is kinetically inhibited ($|E_p^b - E_{p/2}^b|$ is 0.048 V at a scan rate of 50 mV s^{-1}).

The current functions, CF^a and CF^b, are nearly identical indicating that the same number of electrons is transferred. In addition, the current ratio, I_p^b/I_p^a, and $E_{1/2}$ are independent of the scan rate. Therefore, a quasi-reversible reduction of **1** by two electrons yielding a monomeric Mo(IV) species is proposed. Coulometric measurements would settle this point unambiguously but have not been possible due to adsorption effects of **1** at the mercury pool electrode. Similar effects have been reported for $MoO_3(OH_2)_3$ in 2.0 M CF_3SO_3H at a mercury electrode.[18]

In the extended potential range to −0.8 V (Fig. 1) the second reduction peak c observed shifts to more cathodic potentials with increasing scan rates (E_p^c = −0.435 to −0.52 V vs NHE at scan rates of 0.05–1.0 V s^{-1}). Peak c has no influence on $|E_p^a - E_{p/2}^a|$, $|E_p^b - E_{p/2}^b|$ and ΔE_p^{ab} but a marked reduction of the current of the oxidation peak b is evident. Whereas in the potential range 0.3 to −0.3 V the peak current function of peak b, CF^b, is independent of the scan rate a *decrease* is observed in the extended range with *increasing* scan rate. This is paralleled by a decreasing I_p^b/I_p^a in the extended and a constant ratio (1.1) in the reduced range (Fig. 2). This behavior is typical for an E_rC_r mechanism for reduction peak a and a C_rE_r mechanism for oxidation peak b.[26]

The nature of this equilibrium reaction has been investigated in the following manner: if the potential is kept constant for 15, 30, 45 and 60 s at a potential of the returning point of −0.3 V during a normal cyclic voltammetry experiment in the *reduced* potential range (+0.3 to −0.3 V), I_p^b/I_p^a remains constant (1.1) independent of the delay times chosen. In contrast, during the same experiment but with a potential at the returning point of −0.65 V I_p^b/I_p^a decreases to 0.56 at a scan rate of 50 mV s^{-1} (0.39 at 200 mV s^{-1}) (Fig. 2). These values are also independent of the delay times at the returning point and are identical to those in continuously scanned CV experiments.

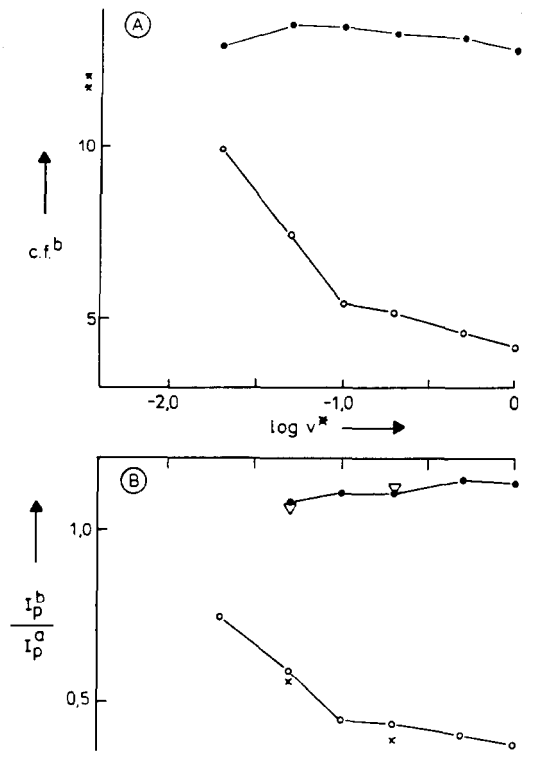


Fig. 2. Plots of CF^b (A) and I_p^b/I_p^a (B) vs the logarithm of the scan rate of **1** in 0.1 M CH_3SO_3H: (●——●) potential range +0.3 to −0.3 V vs NHE, and (○——○) potential range +0.3 to −0.8 V vs NHE.

These observations allow the following conclusions to be made.

(1) The equilibrium reaction occurs after the second reduction.

(2) The reaction is reversible (CF decreases with increasing scan rates).

(3) The equilibration reaction is fast on the time scale of a cyclic voltammetric experiment.

It has not been possible to evaluate the number of electrons transferred at the second reduction step, c, from a coulometry experiment nor from values of $|E_p^c - E_{p/2}^c|$, but the peak current function, CF^c, does indicate a one-electron transfer reaction (3.3–5.4 $\mu A\ V^{-1/2}\ s^{1/2}\ mmol^{-1}\ l$).

Thus the redox scheme of **1** may be summarized at this point by eqn (2):

$$\mathbf{1} \underset{-2e^-}{\overset{+2e^-}{\rightleftharpoons}} \text{Mo(IV)} \overset{+e^-}{\rightleftharpoons} \text{Mo(III)} \rightleftarrows \text{Mo(III)}_2(?). \quad (2)$$

In the following section the pH dependence of this scheme will be investigated. The CVs of four solutions were recorded and diagnostic criteria were evaluated ($[H^+]$: 0.5, 0.2 or 0.1; 0.05 M CH_3SO_3H: the ionic strength was adjusted to 0.5 M with KNO_3). The data are summarized in Table 1. CVs were again recorded in the reduced (0.3 to −0.3 V) and extended (0.3 to −0.8 V) potential range. The behaviour of the diagnostic criteria E_p^a, $E_p^b = f(v)$, $\Delta E_p = f(v)$ and $E^f = f(v)$ is identical in all four solutions and confirms the results presented above: the reduction peak a and the oxidation peak b correspond to a quasi-reversible two-electron transfer process. Both peaks shift with increasing pH to more cathodic potentials. The formal redox potential E_{exp}^f as a function of pH is expressed as in eqn (3):

$$E_{exp}^f(\text{V vs NHE}) = +0.055 - 0.110\text{pH}. \quad (3)$$

According to eqn (4) the number of protons involved in this step is calculated to be four if the number of electrons transferred is two:

$$E_{exp}^f = E_{1/2} - 0.059\frac{m}{n}\text{pH}, \quad (4)$$

where m = number of protons, and n = number of electrons.

The quasi-reversible first reduction of **1** may be written as:

$$\text{LMo(VI)O}_3 + 4H^+ + 2e^- \rightleftarrows [\text{LMo(IV)O(OH}_2)_2]^{2+}. \quad (5)$$

Both monomeric species are stable—at least on the time scale of a cyclic voltammetry experiment. It is noted that the nature of the supporting electrolyte does not change this picture: CVs in 0.5 M HCl are identical to those measured in CH_3SO_3H. Thus no rapid substitution reactions of the Mo(IV) species are observed. The data available for the second irreversible reduction peak c do not allow a clear-cut interpretation, although the diagnostic criteria do indicate a rapid equilibration reaction to occur after this reduction step. Also the pH dependence of reduction peak c is not conclusive and has not been investigated further. Thus the following redox scheme has been established for **1**:

$$\text{LMo(VI)O}_3 \underset{-4H^+,2e^-}{\overset{+4H^-,2e^-}{\rightleftharpoons}} [\text{LMoO(OH}_2)_2]^{2+} \overset{+1e^-}{\rightleftharpoons} \text{Mo(III)} \rightleftarrows \text{Mo}_2\text{(III)}\ (?). \quad (6)$$

Electrochemistry of **2** *in acidic solution*

The CV of **2** (Fig. 3) measured in 1.0 M CH_3SO_3H exhibits features resembling those of **1** in 0.1 M CH_3SO_3H, but also significant differences are detected. Apart from the reduction peaks (a′ and c′) and the oxidation peak (b′) two additional irreversible waves (e′ and f′) are observed. The small reduction peak e′ has no detectable chemical influence on the form and intensity of all other peaks,

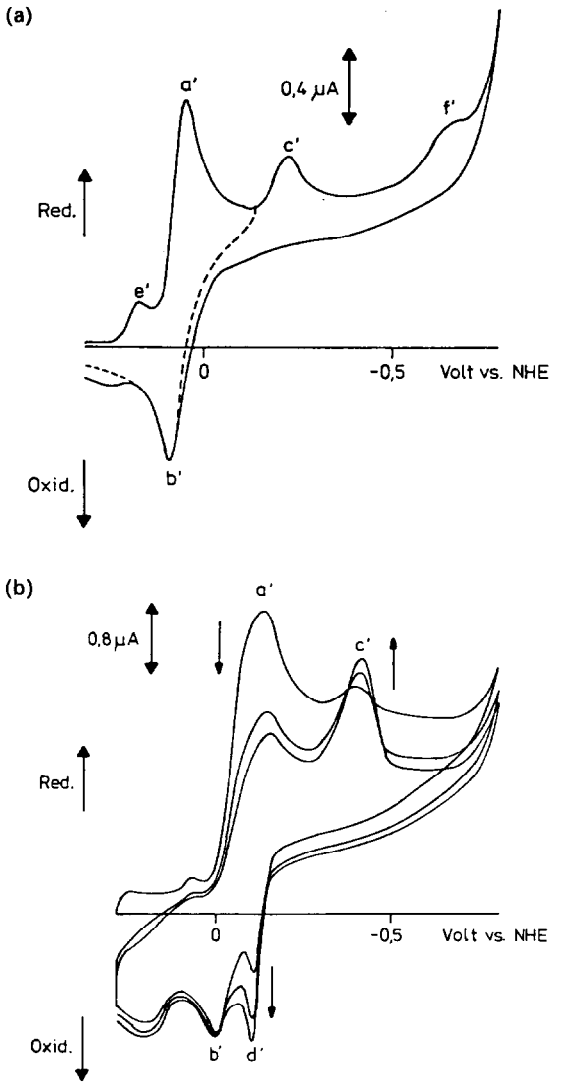


Fig. 3. (A) CV of **2** in 1.0 M CH_3SO_3H (HMD E, 25°C, $v = 50$ mV s^{-1}) in the potential range +0.3 to −0.8 V (solid line) and +0.3 to −0.15 V (broken line). (B) CV of **2** in 0.1 M CH_3SO_3H ($v = 50$ mV s^{-1}, 25°C, HMDE): three consecutive scans.

its potential is independent of pH and its intensity is so small that a diffusion-controlled charge transfer of the actual sample can be ruled out. It is either due to a small impurity of **2** or—more likely—an adsorption effect at the surface of the stationary mercury electrode. Diagnostic criteria for the reduction peak a' indicate a quasi-reversible two-electron transfer: the peak half-width potential $|E_p^{a'} - E_{p/2}^{a'}|$ is 0.034 V at a scan rate of 20 mV s^{-1} and 0.046 V at 500 mV s^{-1}: the peak current function in this range of scan rates is 10.3–8.4 μA $V^{-1/2}$ $s^{1/2}$ $mmol^{-1}$ l. The same results are obtained for the oxidation peak b', but there is a significant difference in the voltammetric behaviour of **1** and **2** concerning peaks a and b and a' and b'. The current function of peak b' is a function of the sweep rate both in the extended potential range (+0.3 to −0.80 V) *and* in the reduced range (+0.3 to −0.15 V), contrasting with the behaviour of peak b of **1**. The oxidation current of b' increases with increasing sweep rate and, consequently, the peak current ratio, $I_p^{b'}/I_p^{a'}$, increases. *This indicates that a chemical reaction occurs after the first reduction of* **2** *in contrast to* **1** *where a chemical reaction has been observed only after the second reduction step.* The half-wave potential, $(E_p^{a'} + E_p^{b'})/2$, varies linearly with pH over the range 0.3–1.5 and it is deduced that the first two-electron redox process involves four protons.

Therefore, we propose that again a monomeric Mo(IV) aqua complex is generated according to eqn (7), which irreversibly undergoes subsequent chemical reactions:

$$L'MoO_3 + 4H^+ + 2e^- \rightleftarrows [L'MoO(OH_2)_2]^{2+}. \quad (7)$$

In contrast to **1** the voltammetric behaviour of **2** in 0.1 M CH_3SO_3H is less ideal especially if the sweep rate is decreased. Therefore, it was not possible to study the nature of the subsequent chemical reaction in detail and to establish the exact nature of the products involved. Nevertheless, Fig. 3 nicely shows that upon repetitive scanning (50 mV s^{-1}) in the potential range +0.3 to −0.8 V the heights of the reduction peak c' and the oxidation peak d' increase, whereas peaks a' and b' decrease.

In keeping in line with the known chemistry of Mo(VI)–Mo(V)– and Mo(IV)–oxo complexes containing sterically non-demanding ligands it appears to be likely that $[L'MoO(OH_2)_2]^{2+}$ either comproportionates with **2** to yield a dimeric Mo(V)–oxo species [eqn (8)]:

$$[L'Mo(IV)O(OH_2)_2]^{2+} + L'Mo(VI)O_3 \rightarrow [L'_2Mo(V)_2O_5] + H_2O + 2H^+, \quad (8)$$

or, alternatively, simply dimerizes or trimerizes $\{[L'_3Mo(IV)_3O_4]^{4+}$ (?)$\}$ [eqn (9)]:

$$x[L'Mo(IV)O(OH_2)_2]^{2+} \xrightarrow{x=2} [L'_2Mo_2O_2(OH)_2]^{2+} + 2H_2O + 2H^+$$
$$\xrightarrow{x=3} [L'_3Mo_3O_4]^{4+} + 5H_2O + 2H^+. \quad (9)$$

The formation of *syn*- or *anti*-$[L'_2Mo(V)_2O_4]^{2+}$ species can be ruled out since their electrochemistry does not resemble any aspect of the present investigation.[27] It is noted that the trimer $[L'_3Mo_3O_4]^{4+}$ and its tungsten analogue have been synthesized and isolated as $ZnBr_4^{2-}$ salts.[28]

Electrochemistry of **3** *in acidic solution*

The CV of **3** in 0.1 M CH_3SO_3H at an HMD E in the potential range +0.4 to −0.8 V vs NHE is shown in Fig. 4. Two reduction peaks, a and c, and two oxidation peaks, b and d, are observed. Peaks e and f are due to a small impurity of **1** which is generated during the synthesis of **3**. The redox potential and pH dependence of the latter are identical with those of **1**. **1** is *not* produced via conceivable oxo-bridge cleavage process of **3** (or any other chemical reaction during the cyclic voltammetry experiment) as is readily deduced from multiple-scanning CVs. In fact, we have no evidence for a monomer–dimer equilibrium of **1** and **3** in acidic aqueous solution.

The potentials of peaks a and b are independent of the scan rate: the peak half-widths of 43 and 37 mV as well as the peak potential difference, $|E_p^a - E_p^b|$, of 47 mV are indicative of a reversible two-electron transfer reaction. The corresponding diagnostic criteria for peaks c and d are slightly dependent on the sweep rate ($E_{cd}^f = -0.216$ to -0.224 V at scan rates of 20–200 mV s^{-1}). The peak half-width and the peak potential difference would agree with a quasi-reversible two-electron transfer but the peak current function, CF^c, is twice as large as the corresponding value for CF^a (as is CF^d compared with CF^b). Therefore, we conclude that the second reduction step involves a quasi-reversible four-electron transfer reaction. The current peak ratios I_p^b/I_p^a and I_p^d/I_p^c are independent of the scan rate but deviate from the expected value of 1.0 due to experimental difficulties in defining proper basis lines in the CV.

These results are supported by coulometric measurements. At a controlled potential of −0.05 V vs NHE 2.05±0.1 electrons per dimeric **3** are transferred. During the electrolysis the colour of the solution changes to yellow. Reoxidation yields again a colourless solution of **3** (via electrolysis or oxygen). Electrolyses at more negative potentials (−0.60 V vs NHE) yielded 5.5±0.5 transferred electrons per dimer.

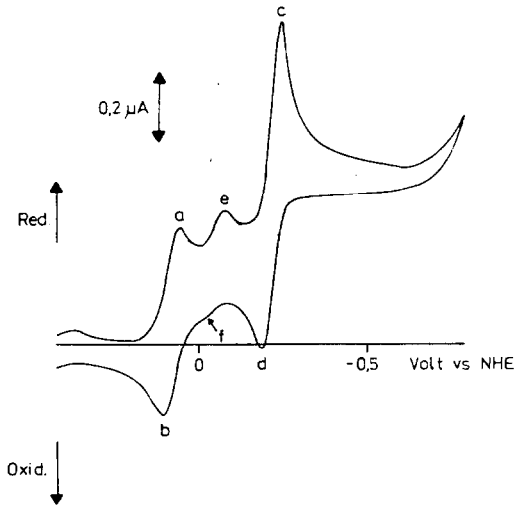


Fig. 4. CV of $3(PF_6)_2$ in 0.1 M CH_3SO_3H (HMDE, 25°C, $v = 20$ mV s^{-1}).

The dependences of the formal redox potentials E_{ab}^f and E_{cd}^f as a function of pH have been investigated ($I = 0.1$ M, $LiClO_4$–$HClO_4$; HMDE; 20°C). In the pH range 1.1–3.1 linear dependences have been observed according to eqns (10) and (11):

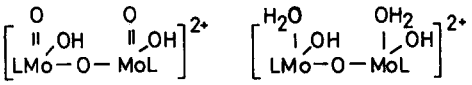
$$E_{ab}^f(\text{V vs NHE}) = +0.12 - 0.056\text{pH}, \quad (10)$$

$$E_{cd}^f(\text{V vs NHE}) = -0.185 - 0.054\text{pH}. \quad (11)$$

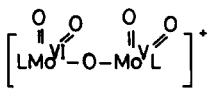
Thus the first reduction wave involves $2e^-$ and $2H^+$ and the second wave involves $4e^-$ and $4H^+$. This leads to the following reaction scheme [eqn (12)]:

$$Mo(VI)_2 \underset{-2e^-,2H^+}{\overset{+2e^-,2H^+}{\rightleftharpoons}} Mo(V)_2 \underset{-4e^-,4H^+}{\overset{+4e^-,4H^+}{\rightleftharpoons}} Mo(III)_2. \quad (12)$$

We propose structures **A** and **B** for the dimeric $Mo(V)_2$ and $Mo(III)_2$ species generated in acidic solution. Interestingly, **3** is reduced in alkaline



aqueous solutions (pH > 7) via a one-electron transfer to produce the blue, paramagnetic mixed-valence species Mo(VI)Mo(V) (**C**). The same species is formed in aprotic media (DMF and CH_3CN).[23]



This species is also generated chemically by reduction of **3** with $NaBH_4$ in oxygen-free aqueous solution. Figure 5 shows the EPR spectrum of such a solution at 20°C. The spectrum clearly shows that the unpaired electron is delocalized over both molybdenum atoms.

Concluding remarks

The electrochemistry of various monomeric *cis*-dioxomolybdenum(VI) complexes has in the past been studied in aprotic media.[7–17] In virtually all these cases one-electron reductions yielding Mo(V) complexes have been established with subsequent complications due to dimerization reactions affording diamagnetic $Mo(V)_2$ dimers. Since the molybdenum-containing enzymes react *in vivo* in

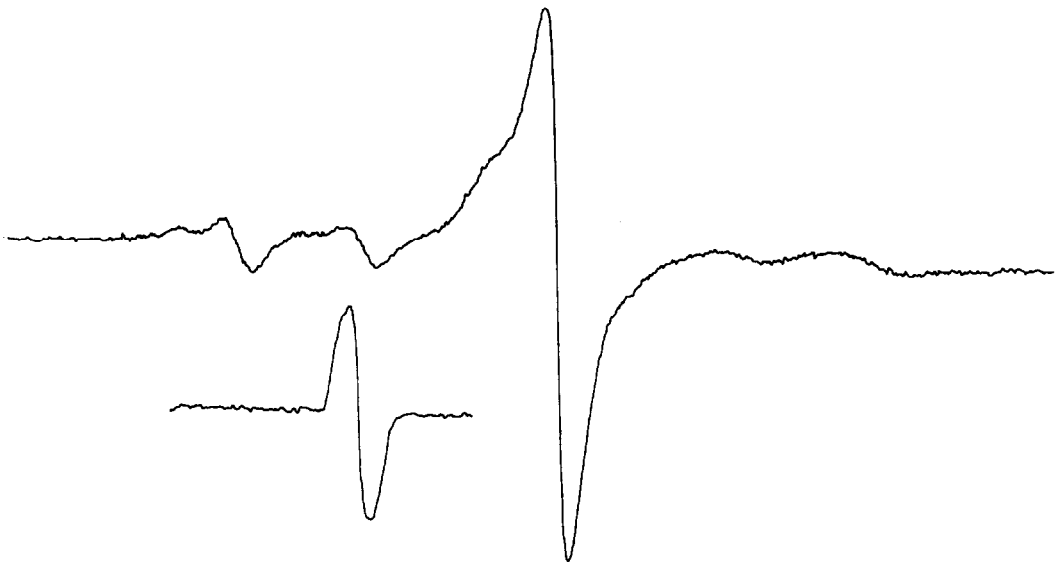


Fig. 5. EPR spectrum of $[L_2Mo_2O_5]^+$ in aqueous solution at 20°C ($g = 1.958$).

aqueous solution where protons and electrons are available, electrochemical studies of model compounds in aqueous solution over a wide range of pH should complement the above studies.

To the best of our knowledge **1** represents the first example where a stable monomeric Mo(IV) species, $[LMoO(OH_2)_2]^{2+}$ is generated by a reversible $2e^-$, $4H^+$ step. Paggett and Anson[18] have shown previously that the protonated form of $MoO_3(OH_2)_3$ in strongly acidic solution is reduced by a $1e^-$, $2H^+$ step generating a monomeric Mo(V) aqua-ion which rapidly dimerizes to the well-known, diamagnetic $Mo(V)_2$ aqua ion. Schultz *et al.*[9,24] have shown that *cis*-dioxo-bis(catecholato)molybdenum(VI) is reduced in acidic solution to monomeric Mo(V) ($1e^-$, $2H^+$) and Mo(III) species ($2e^-$, $2H^+$). No evidence for Mo(IV) intermediates has been found.

EXPERIMENTAL

The preparations of complexes **2** and **3** have been described previously.[22,23]

cis - *Trioxo*(N,N',N'' - *trimethyl* - 1,4,7 - *triazacyclononane*)*molybdenum*(*VI*) (**1**)

To a slurry of MoO_3 (0.75 g, 5 mmol) in water (25 cm^3) *N,N',N''* - trimethyl - 1,4,7 - triazacyclononane[24] (1.7 g, 10 mmol) was added with stirring and gently warmed until a clear colourless solution was obtained. This solution was rapidly poured into an ethanol–ether mixture (1 : 1, 100 cm^3) at room temperature. The colourless precipitate was filtered off, washed with ethanol and air dried (yield 1.1 g). The crude product was recrystallized from hot CH_2Cl_2 to give colourless plates of **1**. Calc. for $(C_9H_{21}N_3)MoO_3 \cdot 0.5H_2O$: C, 34.3; H, 6.71; N, 13.3; Mo, 30.4%. Found: C, 34.1; H, 6.7; N, 13.2; Mo, 30.3%.

Apparatus

CVs were recorded with Princeton Applied Research equipment, which included the model 264 A potentiostat–galvanostat/programmer, the electrochemical cell SM 303 A and an X–Y recorder (Kipp & Zonen). As a working electrode a stationary mercury drop (HMDE, 0.010 cm^2) was employed: a Pt-wire auxiliary electrode and the reference electrode (Ag–AgCl in saturated NaCl) completed the standard three-electrode system. Potentials were measured at 25 ± 0.5°C under an argon atmosphere. Solutions were $\sim 10^{-3}$ M in sample and 0.1 M in supporting electrolyte. Potentials were corrected to the NHE by adding 0.200 V to the measured potential.

Coulometric measurements were made in a Metrohm electrolysis cell at a mercury pool electrode, with an Ag wire as a counter electrode and the reference electrode (Ag–AgCl in saturated NaCl). The Ag wire was in a 0.1 M $LiClO_4$ solution which was separated from the working solution by a diaphragm. The potential was controlled during electrolysis by a potentiostat Model 173 equipped with the coulometry modul M 179 (PAR).

Acknowledgements—We thank Doz. Dr. W. Kaim (Universität Frankfurt/Main) for measuring the EPR spectrum and the Fonds der Chemischen Industrie for financial support.

REFERENCES

1. W. E. Newton and S. Otsuka (Eds), *Molybdenum Chemistry of Biological Significance.* Plenum Press, London (1980).
2. M. Coughlan (Ed.), *Molybdenum and Molybdenum-containing Enzymes.* Pergamon Press, New York (1980).
3. S. P. Cramer, In *Advances in Inorganic and Bioinorganic Mechanisms* (Edited by A. G. Sykes), Vol. 2, p. 259. Academic Press, London (1983).
4. P. A. Scherer and R. K. Thauer, *Eur. J. Biochem.* 1978, **85**, 125.
5. (a) S. P. Cramer, In *Advances in Inorganic and Bioinorganic Mechanisms* (Edited by A. G. Sykes), Vol. 2, p. 303. Academic Press, London (1983). (b) S. P. Cramer, C. L. Liu, L. E. Mortenson, J. T. Spence, S. M. Liu, I. Yamamoto and L. G. Ljungdahl, *J. Inorg. Biochem.* 1985, **23**, 119.
6. J. T. Spence, *Coord. Chem. Rev.* 1983, **48**, 59.
7. A. F. Isbell and D. T. Sawyer, *Inorg. Chem.* 1971, **10**, 2449.
8. L. J. de Hayes, H. C. Faulkner, W. H. Doub and D. T. Sawyer, *Inorg. Chem.* 1975, **14**, 2110.
9. L. M. Charney and F. A. Schultz, *Inorg. Chem.* 1980, **19**, 1527.
10. R. D. Taylor, J. P. Street, M. Minelli and J. T. Spence, *Inorg. Chem.* 1978, **17**, 3207.
11. J. T. Spence, M. Minelli and P. Kroneck, *J. Am. Chem. Soc.* 1980, **102**, 4538.
12. O. A. Rajan and A. Chakravorty, *Inorg. Chem.* 1981, **20**, 660.
13. I. W. Boyd and J. T. Spence, *Inorg. Chem.* 1982, **21**, 1602.
14. C. Pickett, S. Kumar, P. A. Vella and J. Zubieta, *Inorg. Chem.* 1982, **21**, 908.
15. T. Malinski, H. Ledon and K. M. Kadish, *J. Chem. Soc., Chem. Commun.* 1983, 1077.
16. H. Ledon, F. Varescou, T. Malinski and K. M. Kadish, *Inorg. Chem.* 1984, **23**, 263.
17. J. Topich and J. T. Lyon III, *Inorg. Chem.* 1984, **23**, 3202; *Polyhedron* 1984, **3**, 55.
18. M. I. Paffett and F. C. Anson, *Inorg. Chem.* 1981, **20**, 3967.
19. W. F. Marzluff, *Inorg. Chem.* 1964, **3**, 395; F. A. Cotton and R. C. Elder, *Inorg. Chem.* 1964, **3**, 397.
20. R. S. Taylor, P. Gans, P. F. Knowles and A. G. Sykes, *J. Chem. Soc., Dalton Trans.* 1972, 24.
21. R. J. Butcher, H. Kipton, J. Powell, C. J. Wilkins and S. H. Yong, *J. Chem. Soc., Dalton Trans.* 1976, 356; R. J. Butcher and B. R. Penfold, *J. Cryst. Mol. Struct.* 1976, **6**, 13.
22. K. Wieghardt, M. Hahn, W. Swiridoff and J. Weiss, *Inorg. Chem.* 1984, **23**, 94.
23. K. Wieghardt, G. Backes-Dahmann, W. Herrmann and J. Weiss, *Angew. Chem.* 1984, **96**, 890; *Angew. Chem., Int. Ed. Engl.* 1984, **23**, 899.
24. L. M. Charney, H. O. Finklea and F. A. Schultz, *Inorg. Chem.* 1982, **21**, 549.
25. K. Wieghardt, P. Chaudhuri, B. Nuber and J. Weiss, *Inorg. Chem.* 1982, **21**, 3086.
26. R. S. Nicholson and I. Shain, *Anal. Chem.* 1964, **36**, 706.
27. K. Wieghardt and W. Herrmann, to be published.
28. P. Chaudhuri, K. Wieghardt, W. Gebert, I. Jibril and G. Huttner, *Z. Anorg. Allg. Chem.* 1985, **521**, 23.

Polyhedron Vol. 5, No. 1/2, pp. 521–526, 1986
Printed in Great Britain

0277-5387/86 $3.00 + .00
© 1986 Pergamon Press Ltd

COMPLEXATION BETWEEN MOLYBDENUM(VI) AND CITRATE: A POTENTIOMETRIC AND CALORIMETRIC INVESTIGATION

J. J. CRUYWAGEN* and R. F. VAN DE WATER

Department of Chemistry, University of Stellenbosch, Stellenbosch, 7600 South Africa

(*Received* 11 *June* 1985)

Abstract—The molybdenum(VI)–citrate system has been investigated in the pH_c range 7.5–2.0 by potentiometric and enthalpimetric titrations at 25°C in 1 M NaCl. The potentiometric data were treated with the computer program MINIQUAD taking into account side reactions of molybdate and citrate with hydrogen ions. A reaction model comprising the complexes $(1,1,1)^{4-}$, $(1,1,2)^{3-}$, $(1,1,3)^{2-}$, $(2,1,4)^{3-}$ and $(2,1,5)^{2-}$ gave a satisfactory description of the data; the numbers refer to the values of p, q and r in the general formula $(MoO_4^{2-})_p(Cit^{3-})_q(H^+)_r$. The enthalpy and entropy changes for the formation of these complexes were calculated from the enthalpimetric data using the values of the now known formation constants. Equilibrium constants as well as enthalpy and entropy changes for the successive protonations of citrate have also been determined.

Although complex formation between molybdenum(VI) and citrate in acid solution has been reported by many workers[1–9] very little is known about the composition and stability of the complexes. Several authors[1,3–6] have suggested the existence of complexes with a molybdenum : citrate ratio of 1 : 1 but there is disagreement about the number of protons involved. Complexes with molybdenum : citrate ratios of 1 : 2 and 2 : 1 have also been proposed.[4,7,8] A number of 1 : 1 complexes with charge 2− have been isolated[8] by crystallization with cations such as Ba^{2+}, Pb^{2+} and Ag^+. Recently a bridged dinuclear complex of composition $M_2[Mo_2O_5OH(H_2O)(C_6H_5O_7)]\cdot 0.5H_2O$ where M is K^+ or NH_4^+, was synthesized and its photochemical decomposition studied.[9]

To determine the exact stoichiometry of the complexes in solution in this ternary multi-equilibrium system is difficult. In addition to complexation both citrate and molybdate are protonated upon acidification, while molybdate can also form several isopoly ions.[10] All these simultaneous equilibria have to be taken into account in the interpretation of experimental results if the complexes are to be correctly identified. This can best be done by equilibrium analysis through computer treatment of suitable data. A comprehensive potentiometric investigation was therefore carried out and the equilibrium data analyzed with the program MINIQUAD[11] to establish the compositions and stability constants of the molybdenum(VI)–citrate complexes. This paper also reports the results of a calorimetric investigation of the complexation equilibria in which the enthalpy and entropy changes for the formation of the various complexes have been determined.

EXPERIMENTAL

Reagents and solutions

All reagents were of analytical grade (Merck p.a.) and solutions were prepared with water obtained from a Milli-Q system. Sodium molybdate and sodium chloride solutions were prepared from the recrystallized salts. These solutions and sodium citrate solution were standardized gravimetrically by evaporating known volumes to dryness and heating at 160°C to constant weight. Potassium hydrogen phthalate was used to standardize a sodium hydroxide solution. Hydrochloric acid and citric acid solutions were standardized by titration with the sodium hydroxide solution.

* Author to whom correspondence should be addressed.

Potentiometric measurements

Potentiometric titrations were carried out at 25°C in 1 M (Na)Cl medium by either adding hydrochloric acid to molybdate–citrate mixtures or adding sodium hydroxide to molybdate–citric acid–hydrochloric acid mixtures. A stream of purified nitrogen was passed through 1.0 M sodium chloride and then bubbled slowly through the reaction vessel to stir the solution and to exclude carbon dioxide from the system. The molybdate : citrate ratios were 4:1, 1:1 and 1:4 for molybdenum(VI) concentrations of 0.01, 0.04 and 0.05 M. A total of 389 data points obtained from 12 titrations, some in duplicate, were used in the computations. The free hydrogen ion concentration, h, was determined by measuring the potential to ± 0.2 mV with a Radiometer PHM64 research pH-meter using a Ross electrode. The following equation was applied for the calculation of the hydrogen ion concentration from the measured potential, E:

$$E = E^o + 59.16 \log h. \quad (1)$$

A value for E^o was determined before each experiment by titration of 1 M sodium chloride with a (0.1 M hydrochloric acid + 0.90 M sodium chloride) solution, and checked afterwards by a single e.m.f. measurement of the solution used to determine E^o. The titration data were considered acceptable only if the difference between the E^o values was $\leqslant 0.3$ mV. The Ross electrode proved to be very stable and the difference was usually $\leqslant 0.2$ mV.

The first three dissociation constants of citric acid were also determined by potentiometric titration at 25°C in 1 M (Na)Cl medium as described previously.[12]

Calorimetric measurements

An isothermal titration calorimeter, Tronac Model 550, described elsewhere[13,14] was used for the measurements. The titrant, either sodium hydroxide or hydrochloric acid was added with a 2.5-cm^3 Gilmont precision microburet at constant speed to 20 cm^3 (or in some experiments 25 cm^3) solution in the reaction vessel. The number of heat pulses supplied by the control heater (displayed in digital form and printed) was obtained during fixed time intervals, typically 100 s. The speed of titrant delivery was dictated by the concentrations of the reagents and amount of heat involved. In a typical run 30 readings were taken during the addition of 2.5 cm^3 titrant at a speed of 0.05 cm^3 min^{-1}.

The following experiments were carried out:

(a) titration of 0.1 M citrate with 1 M hydrochloric acid;

(b) titration of 0.05 M molybdate and 0.05 M citrate with 1 M hydrochloric acid; and

(c) titration of 0.01 M molybdate, 0.01 M citric acid and 0.02 M hydrochloric acid with 0.5 M sodium hydroxide.

The control heater of the calorimeter is calibrated electrically. The system was checked by determining the enthalpy change for the neutralization of 0.01 M sodium hydroxide with 0.1 M hydrochloric acid. After correction for the heat of dilution a value of 55.9 kJ mol^{-1} was obtained, in good agreement with 56.0 kJ mol^{-1} reported by Hale *et al.*[15] for ionic strength 0.01 M.

All the solutions used in the titrations were made 1.0 M with respect to chloride by addition of sodium chloride. To correct for heat of dilution of the titrant, blank titrations were carried out in each case.

RESULTS AND DISCUSSION

Complexes and formation constants

The results of a number of representative potentiometric titrations are shown as normalized curves in Fig. 1 where P is plotted against pH_c. The

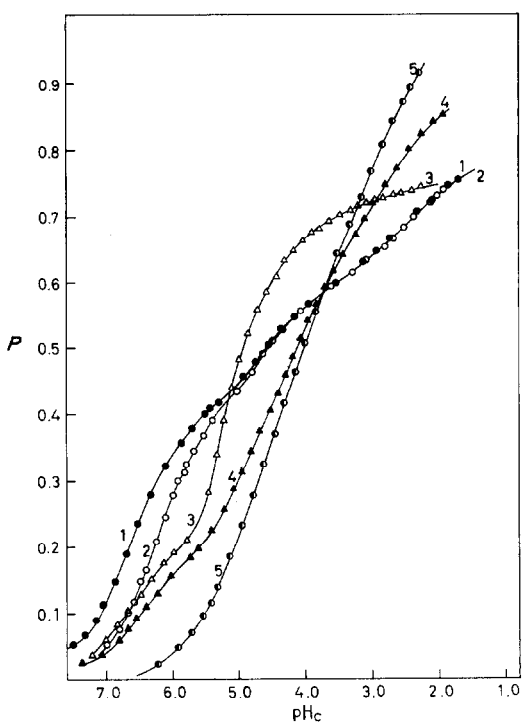


Fig. 1. P as a function of pH_c ($-\log h$) for some representative potentiometric titrations: (1) $B = C = 0.05$ M; (2) $B = C = 0.01$ M; (3) $B = 0.04$ M, $C = 0.01$ M; (4) $B = 0.01$ M, $C = 0.04$ M; and (5) $C = 0.02$ M.

function P, which represents the fraction of the total negative charge neutralized by protonation, is given by:

$$P = \frac{H-h}{2B+3C}, \quad (2)$$

where H, B and C are the total analytical concentrations of hydrogen ions, molybdate and citrate respectively. These normalized curves give some useful preliminary information about the system. For example, complexation at high pH_c is indicated by higher P values than that caused by protonation of citrate or molybdate alone. In the pH_c range 2–3, on the other hand, citrate and molybdate are more easily protonated than the complex species. Furthermore, the inflections shown by the curves at pH values of 6, 5 and 3.5 indicate the presence of at least three relatively stable complexes with charges corresponding to P values of about 0.2, 0.4 and 0.6.

The equilibria for the various possible complex formation reactions can be represented by the general equation:

$$p\mathrm{MoO_4^{2-}} + q\mathrm{Cit^{3-}} + r\mathrm{H^+} \rightleftharpoons (\mathrm{MoO_4^{2-}})_p(\mathrm{Cit^{3-}})_q(\mathrm{H^+})_r. \quad (3)$$

For brevity a complex with overall formation constant β_{pqr} is denoted by the stoiciometric coefficients p, q and r which define its composition, i.e. $(p,q,r)^{(2p+3q-r)}$. The computer program MINIQUAD[11] was used to examine various reaction models, taking the well-known R factor (derived from the error square sum) as a measure of the agreement between experimental and calculated data. The program also calculates χ^2 which should have a value of less than 12.6 at the 95% confidence level. In practice, however, χ^2 is often greater than 12.6.[16] Protonation and condensation equilibria of uncomplexed molybdate were taken into account using known equilibrium constants for 1 M sodium chloride medium.[17] The following six species were included in the computations: $HMoO_4^-$, $Mo(OH)_6$, $Mo_7O_{24}^{6-}$, $HMo_7O_{24}^{5-}$, $H_2Mo_7O_{24}^{4-}$ and $Mo_8O_{26}^{4-}$.

Equilibrium constants pertaining to 1 M sodium chloride, needed to provide for the protonation of the three carboxylate groups of citrate, were determined in separate titrations. Using MINIQUAD to treat the data, the following values for the constants were obtained (error limits 3σ):

$\log \beta_{011} = 5.12 \pm 0.01$, $\log \beta_{012} = 9.17 \pm 0.01$,

$\log \beta_{013} = 11.94 \pm 0.01$ ($R = 0.0021$, $\chi^2 = 11.32$).

These values can be compared with the extrapolated values for the constants in 1 M sodium perchlorate medium,[18] namely 5.22, 9.36 and 12.2.

In the case of a three-component system, a great number of species derived from various possible combinations of p, q and r values must be considered in the computer treatment of equilibrium data before a reaction model can be proposed with confidence. For the present system the most logical starting point was to test a model comprising only mononuclear complexes. Since P varies from ~0.05 to 0.75 for the pH_c range investigated, the following four complexes, $(1,1,1)^{4-}$, $(1,1,2)^{3-}$, $(1,1,3)^{2-}$ and $(1,1,4)^-$, corresponding to P values of 0.2, 0.4, 0.6 and 0.8, respectively, were included in the model. With these complexes a reasonable fit was obtained ($R = 0.0090$ and $\chi^2 = 349.5$). However, in addition to the rather large value of χ^2, the agreement between the experimental and calculated data for titrations where molybdate was in excess was unsatisfactory. This finding suggested that some polynuclear complexes might also be present.

Dinuclear molybdo-oxalate complexes, $(2,2,5)^{3-}$ and $(2,2,6)^{2-}$, have been shown to exist in solution[19,20] whereas the potassium salt of the $(2,2,6)^{2-}$ complex has been isolated previously.[21] In view of this and the recent synthesis of the potassium and ammonium salts[9] of the molybdo-citrate complex, $(2,1,5)^{2-}$, the next step was to introduce species with $p = 2$ and values of either 1 or 2 for q, while r was varied with the restriction that species with a negative charge greater than 6− were neglected. Inclusion of the two dinuclear complexes $(2,1,4)^{3-}$ and $(2,1,5)^{2-}$ in the model resulted in a considerable decrease in the sum of squares and a very good fit ($R = 0.0045$ and $\chi^2 = 10.1$). These species were accepted at the expense of the $(1,1,4)^-$. Most of the other complexes tried, were rejected by the program (β-negative) or occurred in such low concentrations that their inclusion in the model was not justified. The $(2,1,3)^{4-}$ complex, for example, was accepted and resulted in a slightly lower sum of squares but also caused a small increase in χ^2 ($R = 0.0043$ and $\chi^2 = 12.7$). The standard deviation of its formation constant, however, was rather high ($\log \beta_{213} = 22.0 \pm 0.1$) and the maximum concentration only 5.7% of the total molybdenum concentration. This complex is, therefore, not included in the reaction model.

Complexes with $p = 3$ or 4 and $2 \leqslant q \leqslant p$ were also tested in an attempt to further improve the above model; species with p values of up to at least 4 merited inclusion in the model in view of the tetranuclear complex of molybdenum(VI) with malic acid, i.e. $(4,2,10)^{4-}$, which has been isolated recently as a caesium salt.[22] Again complexes with a negative charge greater than 6− were not considered and r values were chosen accordingly. A few complexes with $p = 5$ or 6 were tried, e.g. $(5,2,12)^{4-}$,

Table 1. Formation constants and thermodynamic quantities for the various molybdenum(VI)–citrate complexes in 1 M (Na)Cl ($T = 298$ K)

Complex	($\log \beta_{pqr} \pm 3\sigma$)	ΔG (kJ mol^{-1})	ΔH^o (kJ mol^{-1})	$T\Delta S^o$ (kJ mol^{-1})
$(1,1,1)^{4-}$	8.25 ± 0.02	-47.1	-49.4 ± 0.4 $(49 \pm 1)^a$	-2.3
$(1,1,2)^{3-}$	15.08 ± 0.01	-86.1	-60.2 ± 0.2 (60 ± 1)	25.9
$(1,1,3)^{2-}$	19.66 ± 0.02	-112.2	-67.4 ± 0.2 (65 ± 2)	44.8
$(2,1,4)^{3-}$	27.27 ± 0.18	-155.6	-124 ± 6	31.6
$(2,1,5)^{2-}$	31.86 ± 0.05	-181.9	-125.9 ± 0.3 (128 ± 2)	56.0

[a] Figures in parentheses refer to reverse titration (see text).

$(6,2,13)^{5-}$ and $(6,3,15)^{6-}$, which have P values of 0.75, 0.72 and 0.71, respectively. None of these complexes, however, could help to improve the model; some were rejected by the program while others caused a failure in linear minimization[11] or an increase in the error square sum.

The reaction model, therefore, accepted as giving the best description of the data consists of the following five species: $(1,1,1)^{4-}$, $(1,1,2)^{3-}$, $(1,1,3)^{2-}$, $(2,1,4)^{3-}$ and $(2,1,5)^{2-}$. The formation constants are listed in Table 1. The value of 8.25 for $\log \beta_{111}$ can be compared with a value of 8.4 estimated from polarographic measurements at 2°C.[6] No values for any of the other equilibrium constants are available from the literature. However, the agreement between the protonation constants of the $(1,1,2)^{3-}$ and $(2,1,4)^{3-}$ complexes, $10^{4.58}$ and $10^{4.59}$, is noteworthy and these values also tally with those of the first two protonation constants of citrate, namely $10^{5.12}$ and $10^{4.05}$. The distribution of the various species as a function of pH_c for an equimolar (0.05 M) solution of molybdate and citrate is shown in Fig. 2. Under these conditions the $(2,1,4)^{3-}$ complex is present at relatively low concentrations, but with molybdate in excess as in the case of a 4:1 ratio of molybdate to citrate, the maximum relative concentration attained by this complex is 17.4% (in terms of molybdate). It is seen that the $(1,1,2)^{3-}$ and $(1,1,3)^{2-}$ complexes are major components in the system and are the species responsible for the inflections at $P = 0.4$ and 0.6 in the titration curves (Fig. 1).

Thermodynamic quantities

The amount of heat measured during the isothermal titration of molybdate and citrate with hydrochloric acid, Q (corrected for heats of dilution),

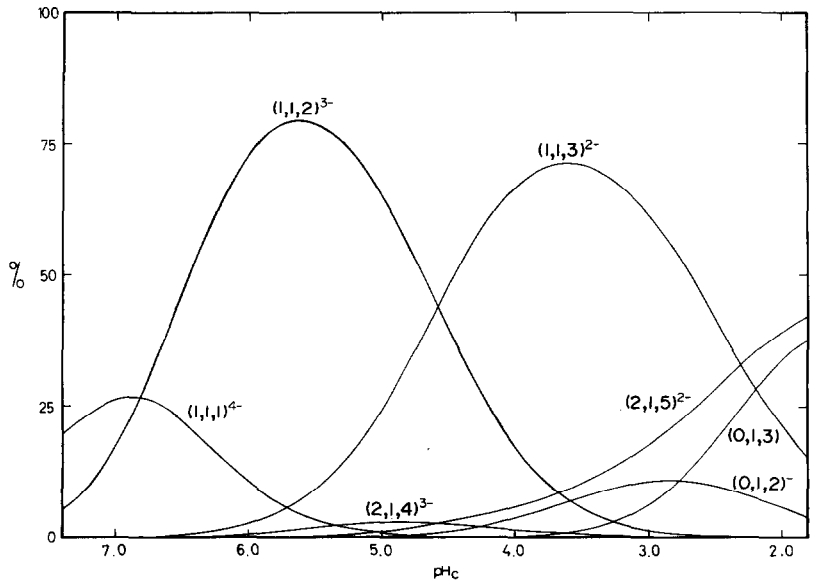


Fig. 2. Concentration of various species expressed as a percentage of the total concentration of molybdate [or citrate for $(0,1,2)^-$ and (0,1,3) species] as a function of pH_c for the enthalpimetric titration of an equimolar solution of molybdate and citrate (0.05 M) with 1 M hydrochloric acid.

Table 2. Thermodynamic quantities for the protonation of citrate in 1 M (Na)Cl ($T = 298$ K)

	ΔG^o (kJ mol^{-1})	ΔH^o (kJ mol^{-1})	$T\Delta S^o$ (kJ mol^{-1})
First protonation	−29.2	−1.32	27.9
Second protonation	−23.1	−4.45	18.6
Third protonation	−15.8	−4.29	11.5

is given by

$$Q = \sum n_{pqr}\Delta H^o_{pqr}, \quad (4)$$

where n_{pqr} is the number of moles formed and ΔH^o_{pqr} is the molar enthalpy change for a given species (p,q,r) at 25°C in 1 M sodium chloride medium. Values for n_{pqr} at each titration point were calculated from the concentrations of the species obtained by simultaneous solution (using Newton's method)[23] of the three mass balance equations:

$$B = b + \sum p\beta_{pqr}b^p c^q h^r, \quad (5)$$

$$C = c + \sum q\beta_{pqr}b^p c^q h^r, \quad (6)$$

$$H = h + \sum r\beta_{pqr}b^p c^q h^r, \quad (7)$$

where b, c and h are the free concentrations of MoO_4^{2-}, Cit^{3-} and H^+, respectively. The set of linear equations thus obtained from corresponding Q and n values were solved for the unknown ΔH^o_{pqr} parameters following a least-squares procedure.[24]

Under the conditions chosen for the enthalpimetric titrations (molybdate : citrate ratio 1 : 1) the protonation and condensation equilibria of molybdate could be neglected. The heat involved in the protonation of citrate, however, had to be taken into account in the calculations since the maximum concentration of the protonated species was, respectively, 3.6, 11 and 34% of the total citrate concentration. Since ΔH^o values for these species have been reported only for ionic strengths $\leqslant 0.15$ and furthermore show a clear dependence on ionic strength,[18,25] especially ΔH^o_{011}, values pertaining to 1 M sodium chloride were evaluated from data collected in separate titrations. These values and the other thermodynamic parameters for the protonation of citrate are given in Table 2. When the ΔH^o values of this investigation are compared with those reported[25] for ionic strength 0.15, namely 1.7, −3.3 and −4.7 kJ mol^{-1} for the three successive protonation steps, it is seen that ΔH^o_{011} is the most affected by the increase in ionic strength. Both enthalpy and entropy values are quite normal for this type of protonation reaction.[26] A characteristic feature is the decreasing trend in $T\Delta S^o$ values with successive protonation.

The thermodynamic parameters for complex formation are listed in Table 1. Because of the low concentration of the $(2,1,4)^{3-}$ complex under the conditions of the enthalpimetric titration [$\leqslant 5.8\%$ (Fig. 2)] ΔH^o_{214} could not be determined with the same accuracy as the other enthalpy values. To obtain a higher concentration of this complex relative to the mononuclear complexes, molybdate must be in excess of citrate. Under such conditions, however, reactions of the MoO_4^{2-}–H^+ subsystem can no longer be neglected and corrections will have to be applied for the enthalpies concerned. Although ΔH^o values for some of these reactions have been determined[27–30] a complete and reliable set of values for 1 M sodium chloride required to provide for heat effects of all these equilibria are not as yet* available.

To verify the reliability of the ΔH^o_{pqr} values, a reverse titration (in duplicate) was done in which a mixture of molybdate, citric acid and hydrochloric acid was titrated with sodium hydroxide. For this experiment the total amount of heat measured (corrected for heats of dilution) is given by:

$$Q = n_a\Delta H^o_w + \sum n_{pqr}(\Delta H^o_{pqr} + r\Delta H^o_w),$$

where n_a is the number of moles of free acid neutralized and ΔH^o_w is the enthalpy change for the formation of water. A value of 56.1 kJ mol^{-1} for ΔH^o_w pertaining to 1 M sodium chloride was determined in a separate titration. The ΔH^o_{pqr} values were computed according to the procedure described above except that ΔH^o_{214} was fixed at the value determined in the forward titration; the lower concentrations of molybdate and citrate used as well as the fact that fewer data points were collected during the reverse titration (28 instead of 77) precluded its inclusion as an unknown parameter. These ΔH^o_{pqr} values (shown in parentheses in Table 1) agreed well, within the 3σ error limits, with those obtained from the results of the forward titration.

The themodynamic parameters for the $(1,1,2)^{3-}$ complex are comparable to those determined[20] for the molybdenum(VI)–oxalate complex $(1,1,2)^{2-}$,

* A calorimetric study of molybdenum(VI) equilibria in this laboratory is nearing completion.

i.e. $\Delta G^o = -77.7$, $\Delta H^o = -59.5$ and $T\Delta S^o = 18.2$ kJ mol^{-1}.

The relatively large negative enthalpy change for complex formation can be ascribed to additional bond energy arising from an increase in coordination number of molybdate from four to six. The value -49.4 kJ mol^{-1} for the enthalpy of formation for the $(1,1,1)^{4-}$ complex, for instance, is nearly the same as the enthalpy change (-46.5 kJ mol^{-1}) for the second protonation of molybdate where an expansion of coordination number was indicated by the observed thermodynamic quantities.[28] The small negative value for $T\Delta S^o_{111}$ may be rationalized as follows: a loss of entropy should accompany complex formation, but this loss will be opposed by a gain in entropy caused by the weaker hydration of the complex than that of the smaller reacting species, especially that of the hydrogen ions. The ΔH^o values for the stepwise protonation of the complexes are negative and comparable to that of citrate itself, while the positive $T\Delta S^o$ values are typical for a reaction of hydrogen ions with anions.[26]

In the structure proposed[9] for the potassium salt of the $(2,1,5)^{2-}$ complex, the hydroxyl oxygen and the β-carboxylate of citrate is coordinated to one molybdenum atom while an α-carboxylate is coordinated to the other molybdenum of the dimeric unit. It is most likely that citrate also coordinates tridentate via the same groups in the formation of the mononuclear complexes.

Acknowledgements—Financial support by the South African C.S.I.R. is gratefully acknowledged. We thank Misses J. Huisamen and R. B. van Zyl for assistance with some of the experimental work.

REFERENCES

1. E. R. Clark, *J. Inorg. Nucl. Chem.* 1962, **24**, 1381.
2. R. A. Chalmers and A. G. Sinclair, *J. Inorg. Nucl. Chem.* 1967, **29**, 2065.
3. V. M. Tarayan, Z. Z. Termendzhyan and D. S. Gaibakyan, *Arm. Khim. Zh.* 1970, **23**, 901.
4. A. A. Fedorov and A. V. Pavlinova, *Zh. Anal. Khim.* 1974, **27**, 202.
5. K. Ogura and Y. Enaka, *Electrochim. Acta* 1977, **22**, 833.
6. S. E. Creager, D. A. Aikens and H. M. Clark, *Electrochim. Acta* 1982, **27**, 1307.
7. A. A. Fedorov and A. V. Pavlinova, *Zh. Obshch. Khim.* 1972, **42**, 238.
8. S. Prasad and L. P. Pandey, *J. Proc. Inst. Chem.* 1965, **37**, 207.
9. J. D. Pedrosa de Jesus, M. de D. Farropas, P. O'Brien, R. D. Gillard and P. A. Williams, *Transition Met. Chem.* 1983, **8**, 193.
10. F. A. Cotton and G. Wilkinson, *Advanced Inorganic Chemistry*, 4th Edn, p. 852. Interscience, New York (1980).
11. A. Sabatini, A. Vacca and P. Gans, *Talanta* 1974, **21**, 53.
12. J. J. Cruywagen and J. B. B. Heyns, *Talanta* 1983, **30**, 197.
13. J. J. Christensen, H. D. Johnston and R. M. Izatt, *Rev. Sci. Instrum.* 1968, **39**, 1356.
14. J. J. Christensen, J. W. Gardner, D. J. Eatough, P. J. Watts and R. M. Hart, *Rev. Sci. Instrum.* 1973, **44**, 481.
15. J. D. Hale, R. M. Izatt and J. D. Christensen, *J. Phys. Chem.* 1963, **67**, 2605.
16. A. Vacca, A. Sabatini and M. A. Gristina, *Coord. Chem. Rev.* 1975, **16**, 161.
17. J. J. Cruywagen, *Inorg. Chem.* 1980, **19**, 552.
18. G. Arena, R. Cali, M. Grasso, S. Musumeci, S. Sammartano and C. Rigano, *Thermochim. Acta* 1980, **36**, 329.
19. A. Beltrán, F. Caturla, A. Cervilla and J. Beltrán, *J. Inorg. Nucl. Chem.* 1981, **43**, 3277.
20. J. J. Cruywagen and R. F. van de Water, 28th S.A. Chemical Institute Convention, Poster P29, Stellenbosch (1984).
21. F. A. Cotton, S. Morehouse and J. S. Wood, *Inorg. Chem.* 1964, **3**, 1603.
22. C. B. Knobler, A. J. Wilson, R. N. Hider, I. W. Jensen, B. R. Penfold, W. T. Robinson and C. T. Wilkins, *J. Chem. Soc., Dalton Trans.* 1983, 1299.
23. D. M. Hirst, *Mathematics for Chemists*, p. 242. MacMillan, London (1976).
24. W. J. Dixon (Ed.) *BMDP Statistical Software*, p. 237. University of California Press, Berkeley, CA (1981).
25. R. G. Bates and G. D. Pinching, *J. Am. Chem. Soc.* 1949, **71**, 1274.
26. J. J. Christensen, L. D. Hansen and R. M. Izatt, *Handbook of Proton Ionization Heats.* Wiley Interscience, New York (1976).
27. R. Arnek, *Ark. Kemi* 1970, **32**, 55.
28. J. J. Cruywagen and E. F. C. H. Rohwer, *Inorg. Chem.* 1975, **14**, 3136.
29. N. D. Jesperson, *J. Inorg. Nucl. Chem.* 1973, **35**, 3873.
30. N. Kiba and T. Takeuchi, *J. Inorg. Nucl. Chem.* 1974, **36**, 842.

Polyhedron Vol. 5, No. 1/2, pp. 527–534, 1986
Printed in Great Britain

0277–5387/86 $3.00 + .00
© 1986 Pergamon Press Ltd

COMPLEXATION AND REDOX REACTIONS OF MOLYBDENUM IONS WITH A QUINONIC REDUCIBLE LIGAND IN AQUEOUS SOLUTION

J. F. VERCHERE*

Laboratoire de Chimie Physique Organique, Faculté des Sciences, BP 67, 76130 Mont-Saint-Aignan, France

and

J. M. POIRIER

Laboratoire de Chimie Analytique, Université de Paris V, 4, avenue de l'Observatoire, 75005 Paris, France

(*Received* 14 *June* 1985)

Abstract—Aqueous acidic solutions of Mo(VI), Mo(V) and Mo(IV) form 1 : 1 complexes with bromanilic acid [H_2B (2,5-dibromo-3,6-dihydroxy-1,4-benzoquinone)], which is a quinonic ligand, easily reducible to 1,4-dibromo-2,3,5,6-tetrahydroxybenzene (H_4B). The electrolysis of the H_2B–Mo(VI) complex yielded first the H_2B–Mo(V) complex, and second a mixture of Mo(V) and H_4B. The Mo(V) was finally reduced to Mo(III). In contrast, only two polarographic waves were observed, the second one corresponding to the reduction of Mo(V) to Mo(III). The first wave (3 F mol^{-1}) was attributed to the simultaneous reduction of H_2B and Mo(VI) by the two-step catalytic process:

$$H_2B + 2H^+ + 2e \rightarrow H_4B, \quad (1)$$

$$2Mo(VI) + H_4B \rightarrow 2Mo(V) + H_2B. \quad (2)$$

The stoichiometry of step (2) was demonstrated in an independent experiment. The electronic spectra of the three complexes showed that the ligand had a fully deprotonated structure. A charge-transfer band was observed at about 400 nm in the Mo(V) and Mo(IV) complexes. It agreed with the hypothesis of increasing electron transfer to the ligand from the molybdenum atom as the oxidation number decreased. It resulted eventually in an effective redox reaction with Mo(III) according to eqn (3):

$$H_2B + Mo(III) \rightarrow H_4B + Mo(V). \quad (3)$$

Molybdenum in its various oxidation states is implicated in many redox reactions, which sometimes are of great biological importance. This prompted early research on its electrochemistry in aqueous medium, which is now quite well understood.[1–4] However, this element reacts in most cases in the form of complex species rather than as the more simple aqua ions. Recent studies have been devoted to the influence of ligands like catechol[5] or aminopolycarboxylic acids[6] on the redox behaviour of molybdenum couples.

In such cases, the complexation modified the respective stabilities of the oxidized and reduced forms, but did not play any part in the electron transfer itself, since the ligands were not reducible.

The aim of this work was to investigate the possibility of effective ligand assistance to the electron transfer. We chose a quinonic ligand, since the electrochemical reversibility of many quinone–hydroquinone couples is known to be excellent. The

* Author to whom correspondence should be addressed.

synthesis and stability of the Mo(VI) complexes of bromanilic acid (H_2B) (2,5-dibromo-3,6-dihydroxy-1,4-benzoquinone) have been described earlier.[7] This paper presents the preparation and electrochemistry of the related complexes of Mo(V) and Mo(IV).

EXPERIMENTAL

Chemicals

Sodium molybdate (Prolabo) and H_2B (Eastman) were used as obtained. All other products were of reagent grade.

Mo(VI) solutions were prepared by dissolving weighted sodium molybdate in distilled water. They were standardized against standard Fe(II) solutions by redox titration in phosphoric acid, according to the method of Rao and Sagi.[8]

Mo(V) solutions were prepared by electrolysis of Mo(VI) solutions in 3 M HCl {$C = 0.2$ M, potential (E) $= -0.4$ V [saturated calomel electrode (SCE)]}.

They were standardized by UV analysis ($\lambda = 295$ nm, $\varepsilon = 1750$ l mol^{-1} cm^{-1}).

Mo(III) solutions were prepared by electrolysis of Mo(V) solutions in 3 M HCl [$C = 0.2$ M, $E = -1.0$ V(SCE)].

Their purity was checked by polarography. Since the green solutions obtained initially became red after some days because of the formation of chloro complexes, only fresh solutions were used in this work.

Mo(IV) solutions were prepared following the method of Souchay *et al.*,[9] as slightly modified:

$$\text{Mo(V)} + \text{Mo(III)} \xrightarrow[2\text{ h, }80°\text{C}]{1\text{ M HCl}} 2\text{Mo(IV)} \quad (C = 0.05\text{ M}).$$

They were standardized by redox titration.

Purified dinitrogen was bubbled through the solutions in order to avoid aerial oxidation.

Apparatus

Polarographic measurements were made in a water-jacketed cell kept at 298 K. A Tacussel PRG-3 three-electrode polarograph was used, with a platinum wire counter electrode and an SCE as reference electrode. The height of the mercury column was 50 cm.

Electrolysis were performed in a water-jacketed two-compartment cell kept at 298 K. The compartments were separated by a medium-porosity glass frit. The cathode was a mercury pool (40 cm^2). The anode was a platinum sheet of similar surface. The current source was a Tacussel PRT 20/2 potentiostat. The quantity of electricity was measured by a Tacussel IG-4 integrator. After each electrolysis, an aliquot of the solution was withdrawn and examined spectrophotometrically.

UV spectra were recorded on a Unicam SP 800 B spectrophotometer, using quartz cells of 0.1 cm width. A Metrohm E 353 B pH-meter was used for pH measurements, with Metrohm EA 120 X glass electrodes.

RESULTS AND DISCUSSION

Electrochemical behaviour of the ligand

H_2B behaves like a typical quinone at the mercury electrode. It forms with its reduction product H_4B (1,4-dibromo-2,3,5,6-tetrahydroxybenzene) a reversible redox couple: $H_4B \rightleftharpoons H_2B + 2H^+ + 2e$.

The variation in the half-wave E ($E_{1/2}$) when the pH increases is shown on Fig. 1. The normal redox E of the H_4B–H_2B couple = 210 mV(SCE). Two breaks occur on the diagram at the pK_a values of H_2B (p$K_1 = 0.22$ and p$K_2 = 2.70$) determined by UV spectroscopy.[7] Other breaks are found at the pK_a values of H_4B.

Because of the fast oxidation of H_4B at high pH, these values could not be precisely measured spectroscopically. The spectrum of molecular H_4B was nevertheless obtained. This species is colorless and absorbs only in the UV ($\lambda = 295$ nm, $\varepsilon = 300$ l mol^{-1} cm^{-1}).

Electroreduction of the Mo(VI)–bromanilate complex

The electrochemical behaviour of the complexes of H_2B with Mo(VI), Mo(V) and Mo(IV) was studied in acidic medium (pH $\leqslant$ 2.5) in which they were particularly stable. In consequence, the reduction product of the ligand was always present as the molecular species H_4B and the free ligand was

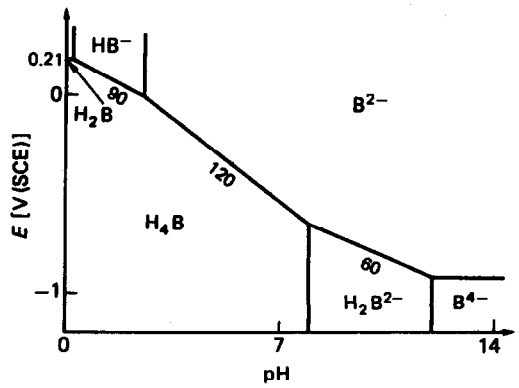


Fig. 1. Electrochemical diagram of H_2B and its reduced form H_4B ($t = 25$°C). Slopes of lines in mV.

mainly the HB^- ion. On the other hand, the structure of the ligand in all three complexes was very close to that of the B^{2-} ion, as proved by comparison of their UV spectra (Fig. 5).

In chloroacetate buffer (pH = 2.50, I = 1 M), we prepared a 10^{-3} M solution of the 1 : 1 bromanilate–Mo(VI) complex which is almost undissociated at this pH.[7] A typical polarogram of the complex was composed of two waves, A and B (Table 1). The three-electron wave, A, was somewhat ill-defined. The two-electron wave, B, was very similar to the reduction wave of uncomplexed Mo(V) under the same conditions: 2 F mol^{-1} and $E_{1/2} = -0.61$ V(SCE).

The electrolysis of the solution was performed on the plateau of wave A [$E = -0.5$ V(SCE)]. The colour of the solution shifted from purple to brown. When 1 F mol^{-1} had been absorbed, wave B remained unchanged, while wave A had decreased by 33%. It was verified that the brown solution contained the bromanilate–Mo(V) complex described hereafter, identical to a sample prepared by mixing the ligand and Mo(V) at the same pH.

The electrolysis was continued until the complete disappearance of wave A occurred, which needed the absorption of another 2 F mol^{-1}. Wave B was thus slightly shifted to $E_{1/2} = -0.56$ V(SCE) and the anodic wave of H_4B appeared. A UV spectrum of the reduced solution confirmed the complete reduction of H_2B to H_4B. A second electrolysis was then made on the plateau of wave B [$E = -0.9$ V(SCE)]. Another 2 F mol^{-1} were needed for this wave to disappear, and the observation of a new anodic wave [$E_{1/2} = -0.20$ V(SCE)] characteristic of uncomplexed Mo(III) in the same conditions.

Reaction between Mo(VI) and H_4B

The results of the electrolysis on the plateau of wave A disagreed with those of the polarographic study, in which wave A indicated a reduction of the complex by three electrons. It should have yielded a mixture of Mo(V) and H_4B, and H_2B was indeed reducible at the $E_{1/2}$ of wave A. On the contrary, the electrolysis showed a two-step reduction:

$$Mo(VI) + e \rightarrow Mo(V),$$

$$H_2B + 2e + 2H^+ \rightarrow H_4B.$$

In order to reconcile the two experiments, we assumed that the first reduction product was H_4B, which rapidly reduced Mo(VI) to Mo(V) in a subsequent step. This hypothesis was verified by reducing the ligand H_2B alone to H_4B under the same conditions as previously, and then introducing known amounts of a standard Mo(VI) solution in the colorless solution. A brown colour rapidly appeared, indicating the formation of the bromanilate–Mo(V) complex.

The stoichiometry of this reaction was determined by a polarographic study, with complete exclusion of aerial dioxygen in order to avoid the oxidation of either H_4B or Mo(V).

Figure 2 represents the variations in the intensities of the polarographic waves vs the ratio q ([Mo(VI)]/[H_4B]) in chloroacetate buffer (pH 2.50). The wave heights refer to 1 mole of H_4B. When q increased, the anodic wave of H_4B decreased and two cathodic waves appeared. They were identified as the waves A and B found previously in the case of the H_2B–Mo(V) complex. Wave B had an intensity of 4 F mol^{-1} H_4B because free Mo(V) is reduced at the same E as complexed Mo(V). It can be seen that the reaction was complete for $q = 2$, when the anodic wave of H_4B disappeared. The reaction could thus be written:

$$2Mo(VI) + H_4B \rightarrow H_2B + 2Mo(V) + 2H^+.$$

Table 1. Polarographic waves of the ligand and of the complexes of Mo(VI), Mo(V) and Mo(IV)[a]

Species	Wave	Intensity (F mol^{-1})	$E_{1/2}$ [V(SCE)]	pH
H_2B	Cathodic	2	−0.02	2.5
H_4B	Anodic	2	−0.02	2.5
Mo(VI) complex	A	3	−0.10	2.5
	B	2	−0.63	
Mo(V) complex	A	2	−0.10	2.5
	B	2	−0.63	
Mo(IV) complex	A	2	0.03	2.0
	B	1	−0.47	

[a] Conditions: t = 25°C, and I = 1.0 M (chloroacetate buffer).

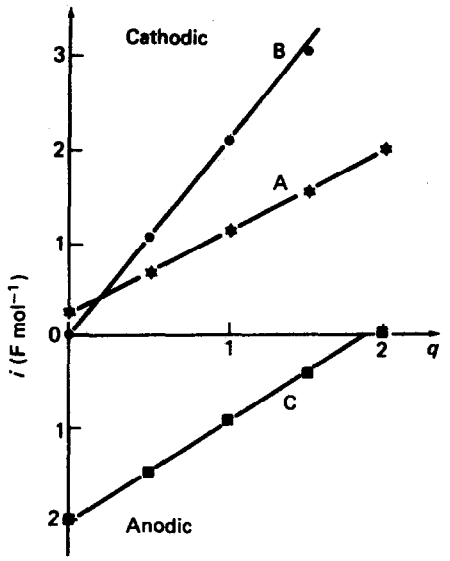


Fig. 2. Stoichiometry of the reduction of Mo(VI) by H_4B. Intensity (i) of the polarographic waves at $t = 25°C$, pH = 2.50, and $q = [Mo(VI)]/[H_4B]$. (A) Wave A ($E_{1/2} = -0.10$ V), (B) Wave B ($E_{1/2} = -0.63$ V), and (C) anodic wave of H_4B ($E_{1/2} = -0.02$ V).

Interpretation of the electrochemical behaviour of complexes

Wave A of the H_2B–Mo(V) complex is easy to account for: it corresponds to the reduction of the ligand released near the electrode by the dissociation of the complex. This is why its $E_{1/2}$ is lower than that for the free ligand [$E_{1/2} = -0.10$ instead of -0.02 V(SCE) at pH 2.5].

Wave B corresponds to the reduction of Mo(V) released at the E of wave A, when the reduced ligand loses its complexing ability. In consequence, it is almost identical to that of free Mo(V). The same interpretation can be applied to wave B of the H_2B–Mo(VI) complex. On the other hand, the existence of the three-electron wave A of the Mo(VI) complex is more difficult to explain, since free Mo(VI) is not reducible at its $E_{1/2}$. We cannot exclude the possibility of a dissociation of the complex near the electrode, releasing a monomeric species of Mo(VI) which would be more reducible than the free polymeric Mo(VI). However, the more probable explanation involves a catalytic reduction of Mo(VI) by the reduced form of the ligand H_4B, following the scheme:

$$H_2B + 2e + 2H^+ \rightarrow H_4B,$$

$$H_4B + 2Mo(VI) \rightarrow 2Mo(V) + H_2B + 2H^+,$$

which results in the following overall reduction of Mo(VI):

$$2Mo(VI) + 2e \rightarrow 2Mo(V).$$

Finally, wave A of the Mo(VI)–H_2B complex would be due to the simultaneous reduction of H_2B (2 F.mol^{-1}) and Mo(VI) (1 F mol^{-1}) in a 1 : 1 ratio.

A detailed study of the parameters of wave A could not be done in order to demonstrate its catalytic character, since the plateau was not horizontal and its height could not be measured with sufficient accuracy. Final evidence for the catalytic nature of wave A was found in the identity of the $E_{1/2}$ of waves A in the Mo(VI) and Mo(V) complexes. Since wave A of the Mo(V) complex is ascribed to the reduction of the dissociated ligand, and because the two complexes are of almost identical stability (as shown below), one can expect wave A of the Mo(VI) complex to be found at the same E as the Mo(V) complex.

Stability of the Mo(V)–bromanilate complex

The composition of this species was determined by spectrophotometry. The mole ratio method showed the formation of a 1 : 1 complex. A typical plot of the absorbance variation vs addition of Mo(V) to H_2B is given in Fig. 3, showing that the complex is very stable at pH 2.00.

In the presence of a two-fold excess of Mo(V), we verified that the complex was almost undissociated between pH 1 and 4. However, its spectrum changed with acidity and an isosbestic point was observed ($\lambda = 357$ nm, $\varepsilon = 10{,}000$ 1 mol^{-1} cm^{-1}). This was related to an acid–base equilibrium between two species only, identified as C_1 (present at pH < 2) and C_2 (present at pH > 4.3). Knowing the molar absorbances of pure C_1 and C_2, we obtained the proportions of C_1 and C_2 as a function of pH, and calculated the pK_a value for the equilibrium:

$$C_1 \rightleftharpoons C_2 + H^+,$$

$$pK_a = 3.00 \pm 0.05 \quad (t = 25°C,\ I = 1.0\ M).$$

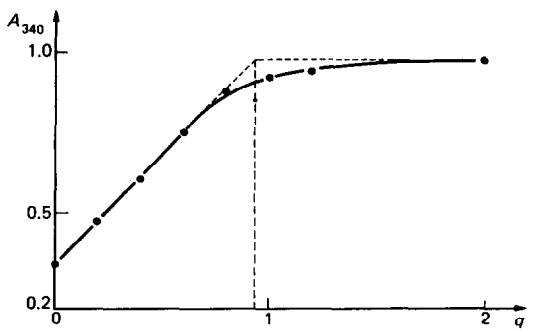


Fig. 3. Composition of the bromanilate–Mo(V) complex at pH 2.00: $[H_2B] = 5 \times 10^{-4}$ mol 1^{-1}, $t = 25°C$, $I =$ 1 M ($HCOO^-$), $\lambda = 340$ nm, cell length = 1 mm and $q = [Mo(V)]/[H_2B]$.

Since only *one* proton was exchanged per mol of complex, we were led to assume a monomeric formula for both C_1 and C_2, as for the related Mo(VI) species.[7] It is shown below that this hypothesis gave satisfactory results for the stability constant of the Mo(V) "acidic" complex. However, free aqua Mo(V) is generally thought to be dimeric[10] in acidic medium.

The nature of the "basic" complex C_2 could not be investigated directly because of the precipitation of Mo(V) hydroxide at pH > 4.5. This is why we studied the formation of the C_1 complex in perchloric acid medium. We found that an invariant equilibrium constant could be calculated only if the complexation was assumed to involve monomeric Mo(V):

$$\mathrm{Mo(V)} + \mathrm{H_2B} \rightleftharpoons \mathrm{C_1} + n\mathrm{H^+},$$

with a formation constant, K:

$$K = \frac{[\mathrm{C_1}][\mathrm{H^+}]^n}{[\mathrm{Mo(V)}][\mathrm{H_2B}]},$$

and a conditional constant,[11] K':

$$K' = \frac{[\mathrm{C_1}]}{[\mathrm{Mo(V)}][\mathrm{H_2B}]} = \frac{K}{[\mathrm{H^+}]^n}.$$

The analytical concentrations of the complex C_1 and the free ligand H_2B were measured spectrophotometrically. Free Mo(V) was obtained by difference from total Mo(V). The results in several acidic media are given in Table 2. It can be seen that $n = 2$.

Assuming that the monomeric Mo(V) is present as the cation MoO_2^+, the formation of C_1 could be written:

$$\mathrm{MoO_2^+} + \mathrm{H_2B} \rightleftharpoons [\mathrm{MoO_2B}]^- + 2\mathrm{H^+}$$

(water molecules are omitted).

The formula of C_2, the conjugate base of C_1, could thus be written as $[MoO_2(OH)B]^{2-}$.

The equilibrium constants for the complexation of Mo(VI) and Mo(V) in aqueous perchloric acid:

$$\mathrm{Mo(VI)}: \mathrm{HMoO_3^+} + \mathrm{H_2B} \rightleftharpoons [\mathrm{MoO_3HB}]^- + 2\mathrm{H^+},$$

$$\mathrm{Mo(V)}: \mathrm{MoO_2^+} + \mathrm{H_2B} \rightleftharpoons [\mathrm{MoO_2B}]^- + 2\mathrm{H^+},$$

can be compared in Table 2. As expected from Pearson's[12] considerations on increasing "hard" character of metal ion with increasing oxidation number, the Mo(VI) complex is more stable than the Mo(V) complex.

The Mo(III)–bromanilate reaction

The electroreduction of the Mo(V)–bromanilate complex could not result in the formation of a Mo(III) complex because the ligand was reduced before Mo(V) at the mercury drop electrode. In fact, the examination of redox potentials of the couples of molybdenum and the H_4B–H_2B couple revealed that the ligand H_2B was thermodynamically reducible by Mo(III). Owing to the irreversibility of the redox steps involving molybdenum, it was not possible to predict whether Mo(V) or Mo(IV) would be the oxidation product.

We investigated the reaction in the same conditions as above (chloroacetate buffer, pH 2.00), by titrating a 10^{-3} M solution of H_2B by a standard solution of Mo(III) present in its dimeric form.[13] The reaction was very fast and measurements were made 2 min after the addition of Mo(III).

Figure 4 represents the variations of the intensities of the polarographic waves vs the ratio $q([\mathrm{Mo(III)}]/[\mathrm{H_2B}])$ in chloroacetate buffer of pH 2.00.

When q increased, the cathodic wave of the ligand (species HB^-) decreased while the anodic wave of H_4B appeared. The reduction ratio was exactly equal to q and was complete for $q = 1$.

Thus, each molybdenum atom was oxidized by one ligand molecule, which indicated a two-electron

Table 2. Complexes of H_2B with Mo(VI) and Mo(V): variation in the conditional stability constants with acidity[a]

Complex	$[HClO_4]$ (mol l^{-1})	$[NaClO_4]$ (mol l^{-1})	K' (l mol^{-1})	K ($K' \cdot [H^+]^2$) (mol l^{-1})
Mo(V)	0.50	1.50	15,200 + 450	3800 ± 100
	1.00	1.00	3800 ± 120	3800 ± 120
	2.00	0.00	1080 ± 80	4300 ± 300
Mo(VI)	1.00	1.00	7000 ± 300	7000 ± 300
	2.00	0.00	1875 ± 100	7500 ± 400

[a] Condition: $t = 25°C$. K' is the conditional stability constant (see text).

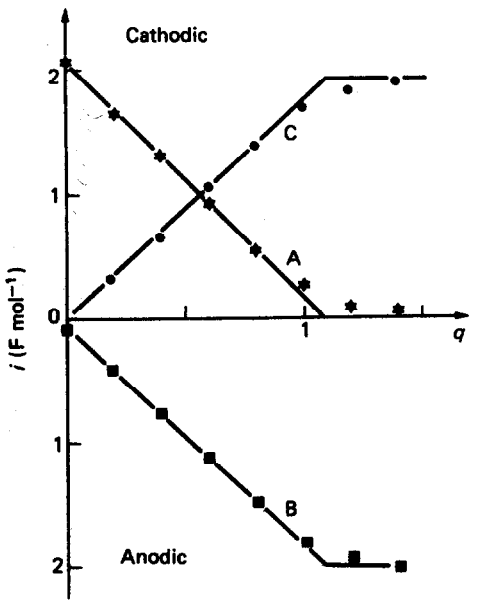


Fig. 4. Stoichiometry of the reduction of H_2B by Mo(III). Intensity (i) of the polarographic waves at $t = 25°C$, pH = 2.00, and $q = [Mo(III)]/[H_2B]$. (A) cathodic wave of H_2B ($E_{1/2} = 0.03$ V), (B) anodic wave of H_4B ($E_{1/2} = 0.03$ V), and (C) sum of waves at $E_{1/2} = -0.45$ and -0.65 V.

transfer:

$$Mo(III) + H_2B + 2H^+ \rightarrow H_4B + Mo(V).$$

Further evidence for the formation of Mo(V) was given by the simultaneous appearance of two cathodic waves ($E_{1/2} = -0.45$ and -0.65 V, sum of intensities = 2 F mol^{-1}). The unexpected transient wave at $E_{1/2} = -0.45$ V could be due either to some formation of intermediate Mo(IV) from the mixture of Mo(III) and Mo(V) or to the preliminary oxidation of Mo(III) to a species of Mo(V) which rapidly turned into "classical" Mo(V). The resulting Mo(V) rapidly complexed the remaining H_2B to give the already described Mo(V)–H_2B complex. Accordingly, we observed in the solution spectrum a transient band ($\lambda = 330$ nm) which had a maximum intensity for $q = 0.5$ and which disappeared at $q = 1$. This finding was in agreement with the formation of a 1:1 complex between H_2B and Mo(V).

Discussion of the redox reduction of Mo(III)

Like most oxidizing agents, H_2B oxidized Mo(III) to Mo(V) and the Mo(IV) state could not be detected. On the other hand, reduction of organic substrates by Mo(III) is not common. The literature gives scanty examples in the cases of nitro and nitroso compounds[14] and methylene blue.[15]

We could not find any spectral evidence of complex formation preceding the redox reaction between Mo(III) and H_2B. Such complex formation was expected to be slow, since d^3 ions like Mo(III) have high crystal-field stabilization energies which slow down their substitution rates.[16] Accordingly, complexes of Mo(III) with oxygenated ligands have been shown to be stable in the case of acetylacetone[17] and EDTA,[18] and the complexation of monomeric Mo(III) by thiocyanate ions has been reported to be slow.[19]

Because the reduction of H_2B by Mo(III) was very fast, it could lead to the conclusion that the electron transfer occurred without preliminary complexation of the metal ion. In other words, the mechanism would belong to the "outer-sphere" type.

The Mo(IV)–bromanilate complex

Neither the electroreduction of the Mo(VI) and Mo(V) complexes of the bromanilate ion nor the oxidation of Mo(III)–ligand mixtures allowed us to obtain the corresponding Mo(IV) complex. Thus we investigated the direct reaction between H_2B and Mo(IV) prepared independently.

In contrast with the fast reactions of the ligand with Mo(VI) and Mo(V), the spectral evolution of mixtures of H_2B and Mo(IV) was found to be surprisingly slow. It indicated a probable two-step process, since the absorbance increased rapidly at $\lambda = 340$ nm, and then more slowly. The second evolution defined an isosbestic point ($\lambda = 320$ nm) which did not belong to the spectrum of the initial mixture of the reactants. It could be due to the use of a slight excess of Mo(IV), but, when the concentration of Mo(IV) was lower than that of ligand, the reaction became extremely slow and was obscured by a slow oxidation of the complex.

As expected if the final spectrum was characteristic of the Mo(IV) complex, its absorbance increased with the pH and the initial concentration of Mo(IV).

At pH 2, the mole ratio method indicated that the complex was likely to have a 1:1 composition. Its formation was almost complete when a two-fold excess of Mo(IV) was used. A polarogram recorded in the same conditions as before (pH 2, chloroacetate buffer, $C = 10^{-3}$ mol l^{-1}) presented two cathodic waves (Table 1):

(1) wave A, corresponding to the bielectronic reduction of the ligand released near the electrode by the complex dissociation; and

(2) wave B, very close to that of free Mo(IV),[9,20] corresponding to the reduction of Mo(IV) to Mo(III).

The intensity of wave B gave clear evidence that we were actually dealing with a Mo(IV) species. We did

not attempt to calculate its stability constant, because its slow formation made it difficult to know if the equilibrium was reached (without aerial oxidation of the complex) and because its structure was probably polynuclear. Indeed, a dimeric[21] structure had long been accepted for the free aquo ion and this species was recently shown to be trimeric.[22,23]

The corresponding cluster, $[Mo_3O_4]^{4+}$, was also observed[24] in the related oxalate[25] and EDTA complexes.[26] However, another series of complexes containing a $[Mo_3O_2]^{8+}$ central group has recently been described.[27] Owing to these results, the sluggishness of the complexation of Mo(IV) could be due to some sort of structural reorganization of the molybdenum coordinating centre. Other examples can be found in the slow reactions of Mo(IV) with tartrate[28] and thiocyanate[29] ions. More surprisingly, in the latter case, the kinetic data could only be rationalized by assuming that free and complexed Mo(IV) species were monomeric.[29]

Charge-transfer spectra of the complexes

The electronic spectra of the complexes of Mo(VI), Mo(V) and Mo(IV) are compared in Fig. 5. The main bands, situated near $\lambda = 335$ nm, are quite similar in wavelength and intensity to that of the uncomplexed bromanilate ion B^{2-} ($\lambda = 334$ nm, $\varepsilon = 26{,}500$ l mol^{-1} cm^{-1}). They can be attributed to electronic transitions occurring inside the ligand cycle, which possess an important aromatic character.[7] Thus the ligand is fully deprotonated in all three complexes.

A remarkable phenomenon is the occurrence of a charge-transfer band at about $\lambda = 400$ nm, which increases in intensity as the oxidation state of molybdenum decreases. It can be attributed to a transition of an electron from an excited metal orbital to an antibonding π-orbital of the ligand. As pointed out by Orgel[30] such an electronic transition is redox in type, the metal being oxidized and the ligand reduced. This was demonstrated in the present case since a more reducing metal ion, like Mo(III), indeed reduced the ligand H_2B to H_4B. This sort of process is much less common than the inverse phenomenon in which the ligand reduces the metal ion. Its observation in the present study gives much support to the invoked participation of the ligand to the redox reactions of the molybdenum atom.

In this respect, our results contrast strongly with those reported on the electrochemistry of Mo(VI) complexes formed with non-reducible ligands.[5,6] They exemplify a peculiar type of redox process in molybdenum chemistry, in which the ligand functions as a redox catalyst.

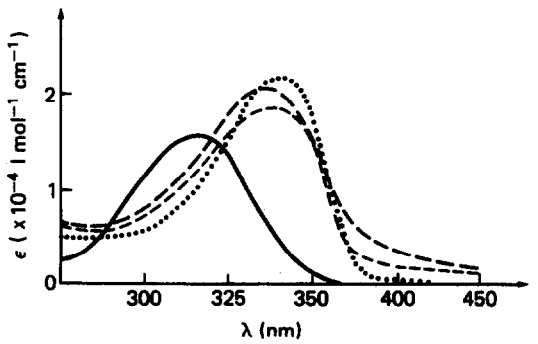


Fig. 5. Spectra of H_2B and its complexes with Mo(VI), Mo(V) and Mo(IV) at pH 2.00: (———) HB^- ion, uncomplexed; (····) Mo(VI) complex; (– – –) Mo(V) complex; and (— — —) Mo(IV) complex.

REFERENCES

1. M. Lamache and P. Souchay, *J. Chim. Phys.* 1973, **70**, 384.
2. M. N. Hull, *Electroanal. Chem.* 1974, **51**, 57.
3. P. Chalilpoyil and F. C. Anson, *Inorg. Chem.* 1978, **17**, 2418.
4. M. T. Paffett and F. C. Anson, *Inorg. Chem.* 1984, **23**, 1996.
5. L. M. Charney and F. L. Schultz, *Inorg. Chem.* 1980, **19**, 1527.
6. K. Ogura and Y. Enaka, *Electrochim. Acta* 1978, **23**, 767.
7. J. M. Poirier and J. F. Verchere, *Talanta* 1979, **26**, 341, 349.
8. G. G. Rao and S. R. Sagi, *Talanta* 1963, **10**, 169.
9. P. Souchay, M. Cadiot and M. Duhameaux, *C. R. Acad. Sci.* 1966, **262**, 1524; M. Lamache-Duhameaux, *Rev. Chim. Minér.* 1968, **5**, 459.
10. M. Ardon and A. Pernick, *Inorg. Chem.* 1973, **12**, 2484.
11. A. Ringbom, *Complexation in Analytical Chemistry* (French translation), p. 32. Dunod, Paris (1967).
12. R. G. Pearson, *Hard and Soft Acids and Bases*, p. 53. Dowden, Hutchinson & Ross, Stroudsburg, PA (1973).
13. M. Ardon and A. Pernick, *Inorg. Chem.* 1974, **13**, 2275.
14. M. V. Gapchenko, *Zavod. Lab.* 1941, **10**, 245.
15. S. R. Sagi and T. Bosebabu, *Talanta* 1976, **23**, 465.
16. L. E. Orgel, *An Introduction to Transition Metal Chemistry. Ligand-field Theory* (French translation), p. 113. Dunod, Paris (1964).
17. M. L. Larson and F. W. Moore, *Inorg. Chem.* 1962, **1**, 856.
18. J. Kloubek and J. Podlaha, *J. Inorg. Nucl. Chem.* 1971, **33**, 2981.
19. Y. Sasaki and A. G. Sykes, *J. Chem. Soc., Dalton Trans.* 1975, 1048.
20. M. T. Paffett and F. C. Anson, *Inorg. Chem.* 1983, **22**, 1347.
21. M. Ardon and A. Pernick, *J. Am. Chem. Soc.* 1973, **95**, 6871.

22. R. K. Murmann and M. E. Shelton, *J. Am. Chem. Soc.* 1980, **102**, 3984.
23. S. P. Cramer, P. K. Eidem, M. T. Paffett, J. R. Winkler, Z. Dori and H. B. Gray, *J. Am. Chem. Soc.* 1983, **105**, 799.
24. A. Bino, F. A. Cotton and Z. Dori, *J. Am. Chem. Soc.* 1978, **100**, 5252.
25. E. Wendling and R. Rohmer, *Bull. Soc. Chim. Fr.* 1964, 360.
26. A. Bino, F. A. Cotton and Z. Dori, *J. Am. Chem. Soc.* 1979, **101**, 3842.
27. F. A. Cotton, Z. Dori, D. O. Marler and W. Schwotzler, *Inorg. Chem.* 1983, **22**, 3104.
28. B. Viossat, *Rev. Chim. Minér.* 1972, **9**, 737.
29. J. F. Ojo, Y. Sasaki, R. S. Taylor and A. G. Sykes, *Inorg. Chem.* 1976, **15**, 1006.
30. Ref. 16, p. 109.

Polyhedron Vol. 5, No. 1/2, pp. 535–537, 1986
Printed in Great Britain

0277–5387/86 $3.00 + .00
© 1986 Pergamon Press Ltd

ELECTROCHEMICAL STUDIES OF MOLYBDATE AND THIOMOLYBDATES

JINGFENG YOU, DAXU WU and HANQIN LIU*

Fujian Institute of Research on the Structure of Matter, Chinese Academy of Sciences, Fuzhou, Fujian, China

(*Received* 2 *July* 1985)

Abstract—The cyclic voltammogram of sodium molybdate in weak acid solution exhibits two main reduction waves, one at −0.8 V (SCE) from the $[Mo_7O_{24}]^{6-}$ anion and the other at −1.3 V (SCE) from $[MoO_4]^{2-}$. The former is quasi-reversible and relates to three oxidation waves. The thiomolybdates give only one irreversible reduction wave at about −1.1 V (SCE). The reduction mechanism has also been discussed.

The molybdate anion in weak acid solution polymerizes to form different species, e.g. $[MoO_4]^{2-}$, $[Mo_2O_7]^{2-}$, $[Mo_7O_{24}]^{6-}$ etc., depending on the pH values. The thiomolybdate anions, $[MoO_xS_{4-x}]^{2-}$ ($x = 0$–3), prepared from molybdate are important reactants in synthesizing molybdenum complexes. During the investigation of iron–molybdenum–sulfur compounds it is found that the redox behavior of molybdate and thiomolybdate anions is complicated and should be studied in detail in various reaction mediums, including aqueous solution at various pH values and different organic solvents.

EXPERIMENTAL

^{95}Mo NMR spectra were recorded at 310 K on a Varian FT-80A NMR. ESR signals were determined by a Brüker ER-420 spectrometer.

The cyclic voltammeter used is composed of a DHE-1 electrochemical multipurpose instrument and an X–Y recorder or a Gould OS 4200 memorized oscilloscope. The cyclic voltammogram was performed with the three-electrode system: a platinum auxiliary electrode, an SCE reference electrode, and a working electrode. In aqueous solution, a hanging mercury drop electrode was used as a working electrode and its surface area was about 0.04 cm^2. With the organic solvent, a platinum electrode with 0.12 cm^2 area was adopted. The experiments were carried out under a dinitrogen atmosphere.

Analytical grade $Na_2[MoO_4]$ and $(NH_4)_6[Mo_7O_{24}]$ were used without further purification. $[NH_4]_2[MoS_4]$, $Cs_2[MoOS_3]$, $[NH_4]_2[MoO_2S_2]$ and $K_2[MoO_3S]$ were prepared according to the method indicated in the literature.[1,2] All samples were checked by ^{95}Mo NMR, UV–Vis and IR spectrometry to ensure their purity.

RESULTS AND DISCUSSION

Cyclic voltammogram of $Na_2[MoO_4]$, with $Na_2[SO_4]$ (1.0 M) as its supporting electrolyte, exhibits four reduction and three oxidation waves in aqueous buffer solution in a pH range of 7.0–3.0. The reduction waves pc1, pc2, pc3 and pc4 are at −0.2, −0.4, −0.8 and −1.3. V (SCE), respectively. The three oxidation waves, pa1, pa2 and pa3, are located at −0.6, −0.4 and 0.0 V (SCE), respectively. Figure 1 shows a typical example. HAc–NaAc, $(CH_2COOH)_2$ or $Na_2[B_4O_7]$, are used as buffer solutions. Cyclic voltammograms are very similar no matter what type of buffer solution is used, but the pH value must be kept between 7 and 4.

Molybdate anions, $[MoO_4]^{2-}$ and $[Mo_7O_{24}]^{6-}$, are in equilibrium in aqueous solution:

$$7[MoO_4]^{2-} + 8H^+ \rightleftharpoons [Mo_7O_{24}]^{6-} + 4H_2O. \quad (1)$$

* Author to whom correspondence should be addressed.

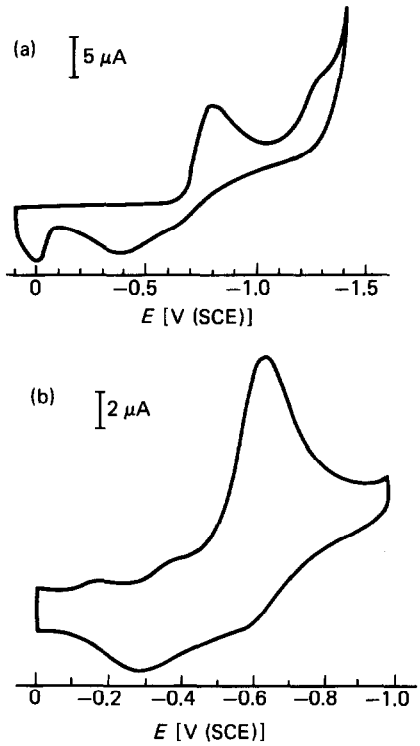


Fig. 1. Cyclic voltammogram of $Na_2[MoO_4]$ with $Na_2[SO_4]$ (1.0 M), in NaAc–HAc (0.1 N) in aqueous solution. (a) $C = 2.24\,mM\,l^{-1}$, pH = 5.77, $v = 0.14\,V\,s^{-1}$. (b) $C = 2.25\,mM\,l^{-1}$, pH = 4.87, $v = 0.055\,V\,s^{-1}$.

In weak acid solution, however, the equilibrium is shifted to the right as indicated by ^{95}Mo NMR spectroscopy. The sharp ^{95}Mo NMR peak of $[MoO_4]^{2-}$ begins to broaden at pH = 7.0 and a second broad peak appears at 45 ppm downfield of the first peak. This second peak is assigned to the anion of $[Mo_7O_{24}]^{6-}$, which dominates in solutions at pH $\leqslant$ 5.7.

The ratio of peak currents, i_{pc3}/i_{pc4}, depends on the pH value and scan rate as shown in Fig. 2. This ratio increases with the concentration of $Na_2[MoO_4]$. Therefore, it can be seen that pc3 and pc4 do not come from the same species, nor do they come from the consequent reduction products. The fact that the peak current function, I_{pc3} ($\equiv i_{pc3} \cdot v^{-1/2} \cdot ([MoO_4]^{2-})^{-1}$), increases with the decrease of pH value suggests that the reduction wave of pc3 is associated with the species $[Mo_7O_{24}]^{6-}$ and that of pc4 with the species $[MoO_4]^{2-}$. As indicated in eqn (1), a decrease in pH value will result in more $[Mo_7O_{24}]^{6-}$ species, or tend to increase the molar ratio of $[Mo_7O_{24}]^{6-}/[MoO_4]^{2-}$. Further evidence for the above assignment is that thiomolybdate anions, which exist in a monomolybdenum form at pH

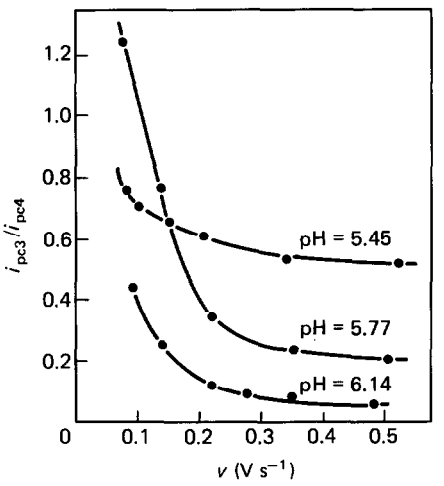


Fig. 2. i_{pc3}/i_{pc4} vs scan rate v at various pH values.

= 6.0, exhibit only one irreversible reduction wave at about −1.1 V (SCE). In a solution of NaAc–HAc (pH = 6.0) with $Na_2[SO_4]$ (1.0 N) as its supporting electrolyte, the irreverisble reduction waves, E_{pc}, are at −1.33, −1.12, −1.06, −1.07 and −1.08 V (SCE) for $Na_2[MoO_4]$, $K_2[MoO_3S]$, $[NH_4]_2[MoO_2S_2]$, $Cs_2[MoOS_3]$ and $[NH_4]_2[MoS_4]$, respectively. The assignment of pc3 and pc4 to different species in equilibrium state can also be indicated by the fact that $I_{pc3} + I_{pc4}$ is constant at each pH value as shown in Fig. 4.

With controlled-potential coulometry at −0.900 V(SCE), it is found that the reduction wave of pc3 is a two-electron process. In this process, some diamagnetic precipitates are found, which have been

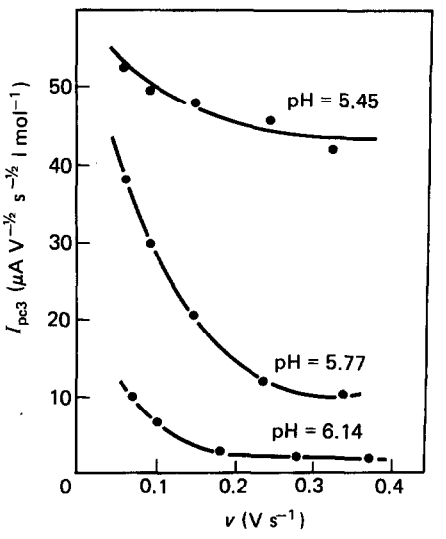


Fig. 3. I_{pc3} vs scan rate v at various pH values.

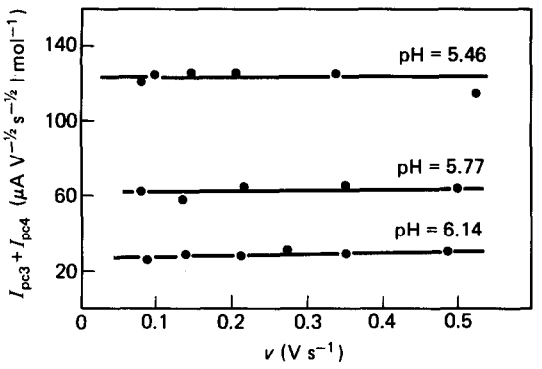


Fig. 4. $I_{pc3}+I_{pc4}$ vs scan rate v at various pH values. $[Na_2MoO_4] = 2.21$ mmol l^{-1}.

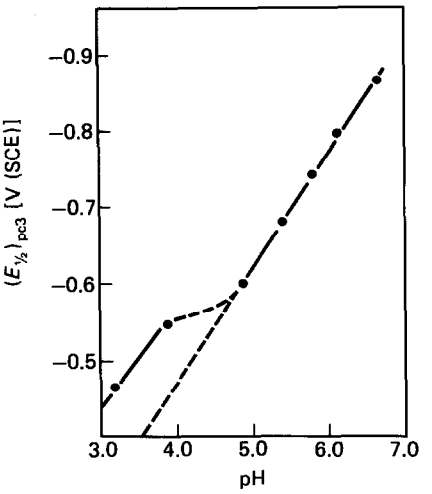


Fig. 5. Plot of $E_{1/2}$ vs pH.

confirmed by our magnetic susceptibility measurement. The two-electron process has also been confirmed by the slope method:[3]

$$\alpha \cdot n = \frac{RT}{F} \cdot \frac{1}{K},$$

where K is the slope of the plot E_{pc3} vs ln $\sqrt{v}$. The average $\alpha \cdot n$ determined by this method is 0.93 $\pm$0.19. If $n = 2$, then $\alpha = 0.465$, which is a reasonable value.[3]

By limiting the scan range, all oxidation waves, pa1, pa2 and pa3, are quasi-reversible vs the reduction wave pc3. The sum of the peak area of the three oxidation waves is equal to that of pc3 in the cyclic voltammogram.

As indicated by eqn (1), since pc4 is associated with $[MoO_4]^{2-}$, I_{pc4} should have decreased as the pH value dropped. In fact, however, as pc4 is a catalytic wave to evolve hydrogen gas, I_{pc4} actually increases as the pH value is lowered. The cross-over of the two curves at lower pH values can thus be explained.

As shown in Fig. 4, $I_{pc3}+I_{pc4}$ increases as the pH is lowered. This is an indication that proton transfer might be involved in the reduction process. By extrapolation of E_{pc3} to $v = 0$ and subtracting 15 mV, the half-wave potential $(E_{1/2})_{pc3}$ can be established for each pH value. A straight line has been obtained by plotting $E_{1/2}$ vs pH as shown in Fig. 5. The line can be expressed as:

$$(E_{1/2})_{pc3} = 0.130 - 0.150 \text{ pH}, \quad 4.8 < \text{pH} < 6.7.$$

The number of protons involved in the reduction process is $(150/60) \times 2 = 5$.

In conclusion, molybdate and thiomolybdates can be reduced more easily if they first polymerize to form molecules composed of two or more molybdenum atoms before the reduction takes place. This fact also agrees with the result of Pan *et al.*[4] Mo(VI) in molybdate and thiomolybdates is generally reduced to Mo(IV) in weak acid solution involving protonation. In general, polymerization, protonation or ligation change the coordination number of molybdenum in the compounds, thereby making the reduction easier.

REFERENCES

1. M. A. Harmer and A. G. Sykes, *Inorg. Chem.* 1980, **19**, 2881.
2. A. Müller, H. Dornfeld, H. Schulze and R. C. Sharma, *Z. Anorg. Allg. Chem.* 1980, **468**, 193.
3. R. S. Nicholson and I. Shain, *Anal. Chem.* 1964, **36**, 706.
4. W. Pan, M. E. Leonowicz and E. I. Stiefel, *Inorg. Chem.* 1983, **22**, 672.

Polyhedron Vol. 5, No. 1/2, pp. 539–545, 1986
Printed in Great Britain

0277–5387/86 $3.00 + .00
© 1986 Pergamon Press Ltd

REDOX REACTIONS BETWEEN COMPLEXES OF MOLYBDENUM AND IRON

H. DIEBLER* and C. MILLAN†

Max-Planck-Institut für Biophysikalische Chemie, 34 Göttingen-Nikolausberg, F.R.G.

(*Received* 30 *June* 1985)

Abstract—Several redox reactions between complexes of molybdenum (oxidation states III–VI) and iron in aqueous solution have been investigated with respect to their stoichiometry, kinetics and mechanism. The reactions include the oxidation of Mo^{3+} and $Mo_2O_4^{2+}$ by Fe^{3+}, and of $Mo_2O_4^{2+}$, $Mo_2O_2S_2^{2+}$ and $Mo_3O_4^{4+}$ by $Fe(phen)_3^{3+}$ (phen = 1,10-phenanthroline). The reduction of Mo(VI) by Fe(II) in 8 M HCl and of $Mo(CN)_8^{3-}$ by Fe^{2+} have also been investigated. Three separate reaction steps were detected in the oxidation of Mo^{3+} to Mo(VI) and in the reduction of $Mo(CN)_8^{3-}$ by Fe^{2+}. In the oxidation of $Mo_2O_4^{2+}$ by Fe^{3+}, and of $Mo_2O_4^{2+}$ and $Mo_3O_4^{4+}$ by $Fe(phen)_3^{3+}$, however, only one reaction effect was observed. The rate equations reveal that, in these reactions, the transfer of the first electron represents the rate-determining step. The rate constants of individual electron-transfer steps are discussed in terms of mechanisms, thermodynamic effects and the nature of the coordinating ligands.

All of the Mo enzymes also contain Fe, and it has been suggested that direct electron transfer occurs between the Mo and Fe centers in some of these enzymes during the catalytic action.[1] In order to learn more about the general features of redox processes between Mo and Fe compounds, we have studied the kinetics of a series of redox reactions between simple complexes of these two metal ions. The reactions include the oxidation of Mo^{3+} and $Mo_2O_4^{2+}$ by Fe^{3+}, of $Mo_2O_4^{2+}$, $Mo_2O_2S_2^{2+}$ and $Mo_3O_4^{4+}$ by $Fe(phen)_3^{3+}$ (phen = 1,10-phenanthroline), and the reduction of Mo(VI) by Fe(II) and of $Mo(CN)_8^{3-}$ by Fe^{2+}.

EXPERIMENTAL

Solutions of the metal complexes used have been prepared and standardized according to procedures described in the literature.[2] All solutions were kept and handled under an atmosphere of N_2. Absorption measurements were carried out by means of a Cary 118C spectrophotometer. The kinetics of the redox processes were followed spectrophotometrically using a Cary 118C spectrophotometer, a stopped-flow apparatus or a temperature-jump apparatus. The latter two instruments had been built at our institute. The reaction signals of the stopped-flow and relaxation measurements were stored in a transient recorder (Datalab DL 905 or DL 920) and evaluated either by means of an electronic simulator (developed by Dr C. R. Rabl) or by computer fitting procedures. At least three individual measurements were made with each solution studied.

RESULTS

Mo(VI) + Fe(II)

In accordance with reported redox potentials[3] Mo(VI) is reduced to Mo(V) by Fe(II) in strong HCl solution, e.g. 8 M HCl. Under these conditions Mo(VI) is present in the form of MoO_2Cl_2[4] and Mo(V) as $MoOCl_5^{2-}$ (or H_2MoOCl_5).[5] The Mo(V) complex is of a green colour and its solution shows absorption maxima near 450 and 710 nm. Spectrophotometric titrations of Mo(VI) with Fe(II) in 8 M HCl confirmed the 1 : 1 stoichiometry and revealed that the equilibrium is far to the side of the products.

The kinetics of the fast redox reaction were studied

* Author to whom correspondence should be addressed.

† Permanent address: Instituto Central de Quimica, Universidad de Concepcion, Concepcion, Chile.

by means of the stopped-flow technique with a large excess of Fe(II) (0.01–0.1 M) over Mo(VI) (0.001–0.005 M). The reaction was monitored at 710 nm, following the formation of Mo(V). In all experiments a single exponential reaction curve was observed (half-lifes 2.5–18 ms). The dependence of the apparent first-order rate constant on the concentration of Fe(II) is shown in Fig. 1. The straight line passes through the origin (i.e. the back reaction is negligible) and yields a second-order rate constant:

$$k = 3.6 \times 10^3\ M^{-1}\ s^{-1}\ (20°C, 8\ M\ HCl).$$

$Mo_2O_4^{2+} + Fe^{3+}$

In dilute $HClO_4$ Mo(V) exists in form of a dimer of structure $(H_2O)_3MoO(\mu\text{-}O)_2OMo(H_2O)_3^{2+}$,[6] usually abbreviated by $Mo_2O_4^{2+}$. Spectrophotometric titrations of $Mo_2O_4^{2+}$ with Fe^{3+} at 384 nm (an absorption maximum of $Mo_2O_4^{2+}$) indicated a stoichiometry according to:

$$Mo_2O_4^{2+} + 2Fe^{3+} \rightleftharpoons 2Mo(VI) + 2Fe^{2+}, \quad (1)$$

with the equilibrium far to the side of the products [the predominant form of Mo(VI) under the conditions of this study is a monomeric cationic species,[7] $HMoO_3^+$].

The kinetics of this reaction have been investigated with a large excess of Fe^{3+} (0.01–0.04 M) over $Mo_2O_4^{2+}$ (0.001 M) and at H^+ concentrations of 0.4–1.5 M ($HClO_4$), and ionic strength (I) of 2.0 M ($NaClO_4$). The reaction was monitored at 450 nm, observing the decrease in $[Mo_2O_4^{2+}]$. Only one reaction effect was detected (half-lifes 8–90 s). Plots of $\log(A_t - A_\infty)$ vs t were linear for more than 90% of the reaction. The dependence of the pseudo first-order rate constant on $[Fe^{3+}]$ is shown in Fig. 2 for various H^+ concentrations. The apparent second-order constant (slopes of Fig. 2) depends on $[H^+]$ as shown in Fig. 3. The data reveal that the rate equation is of the form:

$$-d[Mo_2O_4^{2+}]/dt = (k_a + k_b/[H^+]) \times [Mo_2O_4^{2+}][Fe^{3+}], \quad (2)$$

with $k_a \leqslant 0.2\ M^{-1}\ s^{-1}$ and $k_b = 1.27\ s^{-1}$ (25°C, $I = 2.0$ M).

The overall reaction [eqn (1)] is assumed to proceed by a step-wise transfer of two electrons from

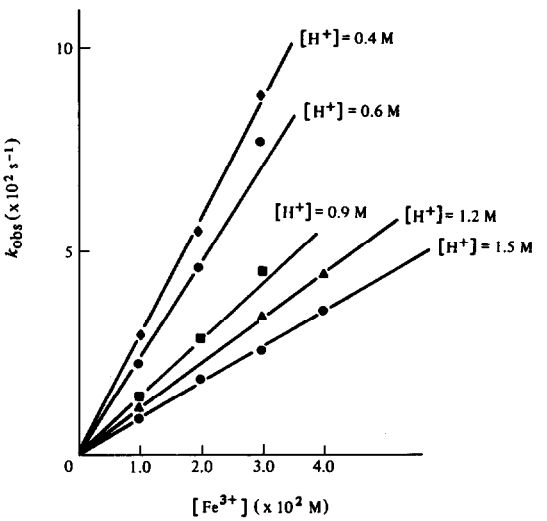


Fig. 2. Oxidation of $Mo_2O_4^{2+}$ by Fe^{3+}. Dependence of the pseudo first-order rate constant on $[Fe^{3+}]$ and $[H^+]$ [25°C, $I = 2.0$ M ($NaClO_4$)].

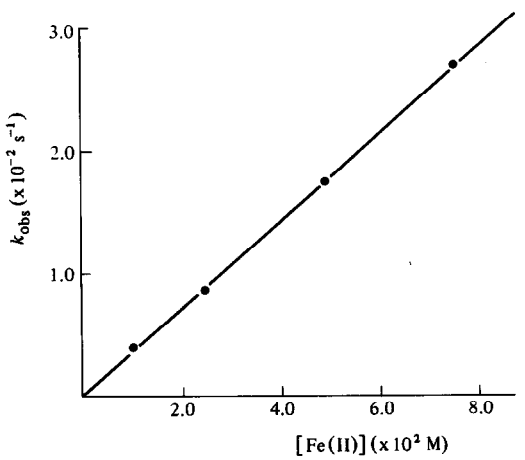


Fig. 1. Reduction of Mo(VI) by Fe(II). Dependence of the apparent first-order rate constant on [Fe(II)] (20°C, 8 M HCl).

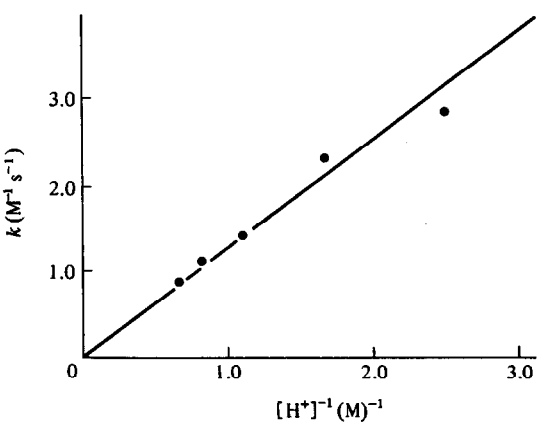


Fig. 3. Oxidation of $Mo_2O_4^{2+}$ by Fe^{3+}. Dependence of the apparent second-order rate constant on $[H^+]^{-1}$ [25°C, $I = 2.0$ M ($NaClO_4$)].

the Mo(V) dimer to two Fe(III), with Mo(V)Mo(VI) as a steady-state intermediate. The form of eqn (2) clearly demonstrates that the first electron-transfer step is rate-determining in the overall reaction. Assuming that the term with $k_b/[H^+]$ [eqn (2)] indicates a reaction path in which $Mo_2O_4^{2+}$ is oxidized by $FeOH^{2+}$, this interpretation yields, with a K_H ($[FeOH^{2+}][H^+]/[Fe^{3+}]$) of 1×10^{-3} M^{-1} (25°C, $I = 2$ M),[8] a second-order rate constant (k) of 1.3×10^3 $M^{-1}\,s^{-1}$ for the oxidation by $FeOH^{2+}$.

$Mo_2O_4^{2+} + Fe(phen)_3^{3+}$

Measurements of the kinetics of the oxidation of $Mo_2O_4^{2+}$ by the phen complex of Fe(III) have been carried out either with the Mo(V) dimer in excess (1.1×10^{-4}–1.1×10^{-3} M) over Fe(III) (5.6×10^{-5} M) or with Fe(III) in excess (5×10^{-5}–2.6×10^{-4} M) over $Mo_2O_4^{2+}$ (5×10^{-6}–1×10^{-5} M): $[H^+] = 0.5$–1.5 M ($HClO_4$), $I = 2.0$ M ($NaClO_4$). The strong absorption of the Fe(II) product at 510 nm was used in order to follow the reaction. Both series of measurements conform to the rate law:

$$d[Fe(II)]/dt = 2k_1[Fe(III)][Mo_2O_4^{2+}], \quad (3)$$

with $k_1 = k_a + k_b/[H^+]$.

The form of the rate law demonstrates that the first electron-transfer step (rate constant k_1) is again the rate-determining process. The studies with excess of $Mo_2O_4^{2+}$ yielded $k_a = 13.5\,M^{-1}s^{-1}$, and $k_b = 9\,s^{-1}$, and those with excess of $Fe(phen)_3^{3+}$ gave $k_a = 11.5$ $M^{-1}s^{-1}$, and $k_b = 4\,s^{-1}$. The two values of k_a are in fair agreement but those of k_b differ appreciably. In case of excess of Fe(III) the low reactant concentrations slow down the redox process (half-lifes 170–740 s) and some spontaneous decomposition of the Fe(phen) complexes occurs during the time of the reaction.[9] Therefore, the results of this series may be considered as less reliable. The moderate variation of the rate with $[H^+]$ can be assigned to a contribution of the reaction path $Mo_2O_4(H_2O)_5OH^+ + Fe(phen)_3^{3+}$. Similar results had been reported by Cayley *et al.*[10] for this system under conditions somewhat different from ours: $k_a = 31\,M^{-1}s^{-1}$, $k_b = 6.0\,s^{-1}$ [$I = 1.0$ M ($LiClO_4$)].

$Mo_2O_2S_2^{2+} + Fe(phen)_3^{3+}$

The structure of this Mo(V) species is analogous to that of the oxo complex, $(H_2O)_3MoO(\mu\text{-}S)_2OMo(H_2O)_2^{2+}$.[11] The rate of its oxidation by $Fe(phen)_3^{3+}$ is rather low and some spontaneous decomposition of the Fe(phen) complexes occurs during the time of the reaction. High concentrations of $Mo_2O_2S_2^{2+}$ were used (1.8×10^{-3}–8.1×10^{-3} M) in order to enhance the rate of reaction. A reaction curve (510 nm) is shown in Fig. 4. The final value of the absorbance corresponds to practically complete reduction of the Fe(III) complex. Contrary to all other systems described so far, the reaction curves are not exponential. This behaviour can be accounted for either by a change in the rate-determining step during the reaction or by the formation of a non-steady-state intermediate. Important information can be evaluated very conveniently from the initial rate of reaction. The initial slopes of the reaction curves are given by:

$$(dA/dt)_o = k[Mo_2O_2S_2^{2+}] \times [Fe(III)]_o\varepsilon_{Fe(III)}. \quad (4)$$

The dependence of $(dA/dt)_o$ on $[Mo_2O_2S_2^{2+}]$ yields $k = 0.8$ $M^{-1}s^{-1}$ (25°C, 1 M $HClO_4$). If k_1 denotes the rate constant of the first electron-transfer step, then $k = k_1$ in the non-steady-state model (formation of a true intermediate) and $k = 2k_1$ if steady-state conditions are maintained and a change in the rate-determining step occurs.

$Mo_3O_4^{4+} + Fe(phen)_3^{3+}$

In aqueous solution Mo(IV) exists in the form of trimeric species characterized by a $Mo_3O_4^{4+}$ core.[12] Spectrophotometric measurements of $Mo_3O_4^{4+}$–$Fe(phen)_3^{3+}$ mixtures (510 nm, 1 M HCl indicated a stoichiometry of the redox reaction according to:

$$6Fe(phen)_3^{3+} + Mo_3O_4^{4+} \rightleftharpoons 6Fe(phen)_3^{2+} + 3Mo(VI). \quad (5)$$

The reaction curves observed in the kinetic studies {$[Mo_3O_4^{4+}] = 4 \times 10^{-5}$–$2.2 \times 10^{-4}$ M, $[Fe(phen)_3^{3+}] = 4 \times 10^{-5}$ M, 25°C, 1.0 M HCl, $I = 2.0$ M (NaCl), 510 nm} were always single

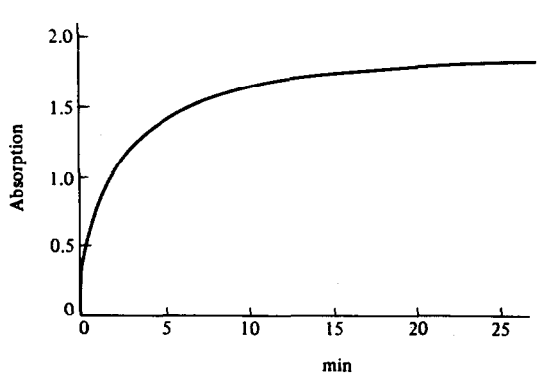


Fig. 4. Oxidation of $Mo_2O_2S_2^{2+}$ by $Fe(phen)_3^{3+}$. Reaction curve with $[Mo_2O_2S_2^{2+}] = 8.1 \times 10^{-3}$ M and $[Fe(phen)_3^{3+}] = 1.8 \times 10^{-4}$ M (25°C, 1.0 M $HClO_4$, $I = 1.0$ M, $\lambda = 510$ nm).

exponentials and the apparent first-order rate constant depends on $[Mo_3O_4^{4+}]$ as shown in Fig. 5. The results reveal a rate law of the form:

$$d[Fe(II)]/dt = 6k_1[Mo_3O_4^{4+}][Fe(III)], \quad (6)$$

which indicates that the first electron-transfer process is rate-determining. For this step a rate constant (k_1) of 51 $M^{-1} s^{-1}$ [25°C, 1 M HCl, I = 2.0 M (NaCl)] is obtained.

$$Mo(H_2O)_6^{3+} + Fe(H_2O)_6^{3+}$$

The monomeric aquo ion $Mo(H_2O)_6^{3+}$ is stable only in strongly acidic non-complexing solutions.[13] The results of a spectrophotometric titration of Mo^{3+} with Fe^{3+} in 1 M *p*-toluenesulfonic acid (HPTS) at 450 nm (at this wavelength the absorption of the Fe species is very small) is shown in Fig. 6. Obviously the Mo(III) is first oxidized to Mo(V) and then to Mo(VI). The spectrum at the position of the first break is that of the Mo(V) dimer, $Mo_2O_4^{2+}$.

In the kinetic studies of the oxidation of Mo^{3+} by Fe^{3+} (stopped-flow techniques, λ = 450 nm), three reaction effects were observed with Fe^{3+} in excess: a fast one in the millisecond range, and two slower ones with half-lifes of seconds. The fast effect describes the disappearance of Mo^{3+}. The rate law of this process was found to be:

$$-d[Mo^{3+}]/dt = k_f[Mo^{3+}][Fe^{3+}], \quad (7)$$

with $k_f = 1.3 \times 10^3$ $M^{-1} s^{-1}$ (25°C, 1 M HPTS).

The nature of the first true intermediate (between Mo^{3+} and $Mo_2O_4^{2+}$) is unknown. Equation (7) demonstrates, however, that the rate-determining step on the way to this intermediate is given by:

$$Mo^{3+} + Fe^{3+} \xrightarrow{k_f} Mo(IV) + Fe^{2+}. \quad (8)$$

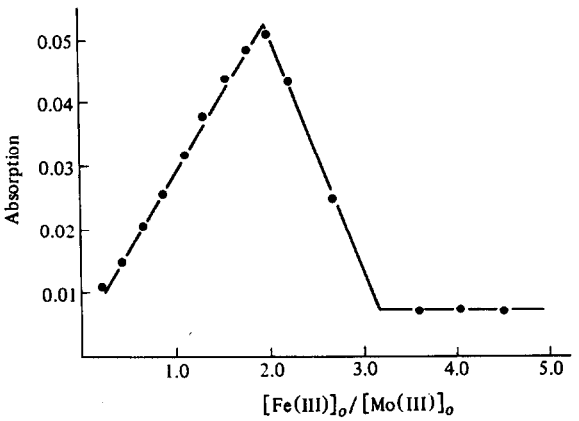


Fig. 6. Spectrophotometric titration of 2.3×10^{-3} M Mo^{3+} with 0.6 M Fe^{3+} (25°C, 1.0 M HPTS, I = 1.0 M, λ = 450 nm).

An experimental curve of the two slower processes is shown in Fig. 7. The decrease in and recovery of the signal intensity reflect the formation and disappearance of $Mo_2O_4^{2+}$. The final part of the curve is described by a single exponential function and a rate constant (k) of 0.5 $M^{-1} s^{-1}$ (1 M HPTS, I = 1.0 M) has been evaluated for the oxidation of the intermediate $Mo_2O_4^{2+}$ by Fe^{3+} in these experiments. This value is consistent with the one which was determined directly [see above, k = 1.27 $M^{-1} s^{-1}$ (1 M $HClO_4$, I = 2.0 M)], since like-charged reactants are expected to react with a higher rate at the higher ionic strength.

Attempts were made to fit the total experimental curve (Fig. 7) with the help of a computer program based on a four-step mechanism of the type Mo(III) → Mo(IV) → Mo(V) → $Mo(V)_2$ → Mo(V)Mo(VI)

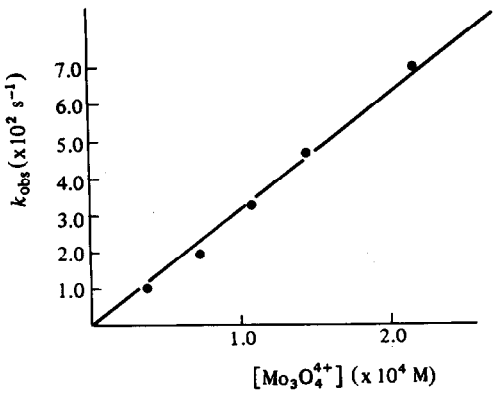


Fig. 5. Oxidation of $Mo_3O_4^{4+}$ by $Fe(phen)_3^{3+}$. Dependence of the apparent first-order rate constant on $[Mo_3O_4^{4+}]$ [25°C, 1.0 M HCl, I = 2.0 M (NaCl)].

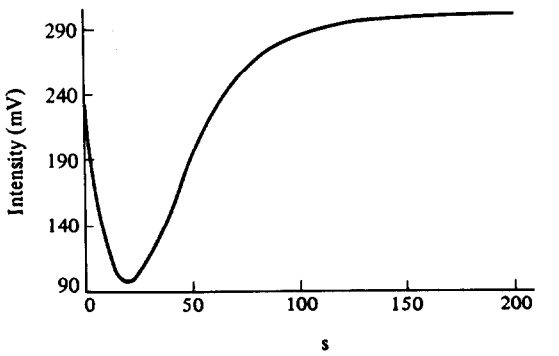


Fig. 7. Oxidation of Mo^{3+} by Fe^{3+}. Reaction curve with $[Mo^{3+}] = 1.2 \times 10^{-3}$ M and $[Fe^{3+}]$ = 0.045 M (25°C, 1.0 M HPTS, I = 1.0 M, λ = 450 nm).

and assuming that: (a) either monomeric Mo(IV), or (b) monomeric Mo(V) is the first true intermediate. Neither assumption gave a very good fit [although (a) was better than (b)], deviations occurring in particular near the intensity minimum. Possibly the neglect of all back reactions is not justified, or the assumed mechanism is incorrect.

$Mo(CN)_8^{3-} + Fe^{2+}$

The product of the reduction of $Mo(CN)_8^{3-}$ by Fe^{2+} was identified by its spectrum to be $Mo(CN)_8^{4-}$. A spectrophotometric titration in 0.1 M $HClO_4$ confirmed the expected 1:1 stoichiometry. Thus:

$$Fe^{2+} + Mo(CN)_8^{3-} \overset{K_r}{\rightleftharpoons} Fe^{3+} + Mo(CN)_8^{4-}. \quad (9)$$

A quantiative evaluation of the spectrophotometric data yielded a value for K_r of 11.7 [25°C, 0.1 M $HClO_4$, I = 1.0 M ($NaClO_4$), 387 nm].

In studies of the kinetics of reaction (9) by stopped-flow techniques ($[Mo(CN)_8^{3-}] = 2 \times 10^{-5}$ M, $[Fe^{2+}] = 1 \times 10^{-4}$–$6 \times 10^{-4}$ M), one reaction effect in the millisecond range was detected. The absorbance at the starting point of this reaction (λ = 387 nm) is not that calculated from the initial concentration of $Mo(CN)_8^{3-}$ and it is concluded that other reaction steps precede the one observed by the stopped-flow method. This was confirmed by studies with the temperature-jump relaxation technique which showed that there are two more reaction effects, one in the microsecond range (τ = 100–400 μs) and one with a time constant <0.2 μs (cable T-jump). The results demonstrate that the reaction does not proceed by an outer-sphere path, and the following three-step inner-sphere mechanism is considered:

$$\text{(a)} \quad Mo(V) + Fe(II) \underset{k_{-1}}{\overset{k_1}{\rightleftharpoons}} Mo(V)Fe(II),$$

$$\text{(b)} \quad Mo(V)Fe(II) \underset{k_{-2}}{\overset{k_2}{\rightleftharpoons}} Mo(IV)Fe(III), \quad (10)$$

$$\text{(c)} \quad Mo(IV)Fe(III) \underset{k_{-2}}{\overset{k_3}{\rightleftharpoons}} Mo(IV) + Fe(III).$$

Steps (a) and (c) involve inner-sphere substitution processes, the time constants of which should be measurable by the techniques used. Therefore, the extremely rapid process was assigned to step (b), yielding $1/\tau_b = k_2 + k_{-2} > 5 \times 10^6$ s^{-1}. This very fast effect is not observed in the absence of Fe(II) and Fe(III), i.e. it is not due to a protonation reaction of the $Mo(CN)_8$ species.

The relaxation time of the microsecond effect depends on the concentration of Fe(II) but is independent of [Fe(III)]. This effect is assigned to step (a), to which the rapid equilibrium (b) is coupled. Then, with [Fe(II)] $\gg$ [Mo(V)]:

$$1/\tau_a = k_{-1}/(1 + K_2) + k_1[Fe(II)], \quad (11)$$

where $K_2 = k_2/k_{-2}$. A plot of $1/\tau_a$ vs [Fe(II)] gave $k_1 = 1.15 \times 10^6$ M^{-1} s^{-1} [3.0°C, 0.1 M $HClO_4$, I = 1 M ($NaClO_4$)]. (In order to reduce cavitation effects, the T-jump experiments were carried out at low temperature.)

The slow effect is assigned to step (c) with (a) and (b) as preequilibria. It is evaluated more conveniently from the stopped-flow rather than from the T-jump measurements. The apparent first-order rate constant is given by:

$$\frac{1}{k_{obs}} = \frac{1 + K_2}{k_3 K_2} + \frac{1}{k_3 K_1 K_2 [Fe(II)]}. \quad (12)$$

A plot of $1/k_{obs}$ vs $1/$[Fe(II)] yielded $k_3 K_1 K_2 = 3.2 \times 10^5$ M^{-1} s^{-1}. $K_1 K_2$ was determined from K_r and K_3 ([Mo(IV)Fe(III)]/[Mo(IV)][Fe(III)]) = 172 M^{-1} (obtained during this study by spectrophotometric measurements), leading finally to $k_3 = 160$ s^{-1}, and $k_{-3} = 2.75 \times 10^4$ M^{-1} s^{-1}.

DISCUSSION

The rates of individual reaction steps which have been determined during this study are summarized in Table 1. The mechanism of the reduction of Mo(IV) by Fe(II) in 8 M HCl is uncertain, but Cl^- is known to be a good bridging ligand and an inner-sphere mechanism may tentatively be assumed. It can safely be excluded that the formation of the precursor complex (inner- or outer-sphere) is rate-limiting, since both the diffusion-controlled encounter of the reactants and substitution at an Fe(II) center are very rapid processes. Thus, either the electron-transfer step or (in the case of an inner-sphere mechanism) the dissociation of the successor complex must be rate-limiting. An additional complication arises from the fact that the overall reaction includes ligand exchange processes ($MoO_2Cl_2 \rightarrow MoOCl_5^{2-}$).

The interesting point in the oxidation of $Mo_2O_4^{2+}$ by Fe^{3+} is the origin of the term showing a $1/[H^+]$ dependence. Three possible mechanisms may be considered: (a) $FeOH^{2+}$ reacts with the Mo(V) dimer via an efficient inner-sphere path with OH^- bridging;[14] (b) $Mo_2O_4(H_2O)_5OH^+$ reacts with $Fe(H_2O)_6^{3+}$ by an OH^--bridged inner-sphere path; and (c) reaction via inner-sphere structures which result from rate-determining substitution of a terminal oxygen of $Mo_2O_4^{2+}$ at $Fe(H_2O)_5OH^+$ and $Fe(H_2O)_6^{3+}$, respectively. A comparison with other Fe^{3+} and $FeOH^{2+}$ reactions[15] disfavours (b) and (c).

Table 1.

Reaction	Rate constant ($M^{-1} s^{-1}$)	Conditions
$MoO_2Cl_2 + Fe(II) \rightarrow MoOCl_5^{2-} + Fe(III)$	3.6×10^3	20°C, 8 M HCl
$Mo_2O_4^{2+} + Fe^{3+} \rightarrow Mo(V)Mo(VI) + Fe^{2+}$	$\leqslant 0.2$	25°C, I = 2 M ($NaClO_4$)
$Mo_2O_4^{2+} + FeOH^{2+} \rightarrow Mo(V)Mo(VI) + Fe^{2+}$	1.3×10^3	25°C, I = 2 M ($NaClO_4$)
$Mo_2O_4^{2+} + Fe(phen)_3^{3+} \rightarrow Mo(V)Mo(VI) + Fe(phen)_3^{2+}$	13	25°C, I = 2 M ($NaClO_4$)
$Mo_2O_2S_2^{2+} + Fe(phen)_3^{3+} \rightarrow Mo(V)Mo(VI) + Fe(phen)_3^{2+}$	0.8 or 0.4	25°C, 1 M $HClO_4$
$Mo_3O_4^{4+} + Fe(phen)_3^{3+} \rightarrow Mo(IV)_2Mo(V) + Fe(phen)_3^{2+}$	51	25°C, 1 M HCl, I = 2 M (NaCl)
$Mo^{3+} + Fe^{3+} \rightarrow Mo(IV) + Fe^{2+}$	1.3×10^3	25°C, 1 M HPTS
$Mo(CN)_8^{3-} + Fe^{2+} \rightarrow [(CN)_7Mo(V)CNFe(II)]^-$	1.1×10^6	3°C, 0.1 M $HClO_4$, I = 1 M ($NaClO_4$)
$[(CN)_7Mo(V)CNFe(II)]^- \underset{k_{-2}}{\overset{k_2}{\rightleftharpoons}} [(CN)_7Mo(IV)CNFe(III)]^-$	$k_2 + k_{-2} > 5 \times 10^6 s^{-1}$	
		3°C, 0.1 M $HClO_4$, I = 1 M ($NaClO_4$)
$[(CN)_7Mo(IV)CNFe(III)]^- \underset{k_{-3}}{\overset{k_3}{\rightleftharpoons}} Mo(CN)_8^{4-} + Fe^{3+}$	$k_3 = 160 s^{-1}$	25°C, 0.1 M $HClO_4$, I = 1 M ($NaClO_4$)
	$k_{-3} = 2.7 \times 10^4$	25°C, 0.1 M $HClO_4$, I = 1 M ($NaClO_4$)

Thus interpretation (a) is considered to be the most likely. The results of Sasaki *et al.*[16] on substitution at $Mo_2O_4(H_2O)_6^{2+}$ indicate that the replacement of water at the Mo(V) dimer may well be the rate-determining step in mechanism (a).

The oxidation processes involving $Fe(phen)_3^{3+}$ must proceed, of course, by outer-sphere pathways. The higher rate of the oxidation of $Mo_2O_4^{2+}$ by $Fe(phen)_3^{3+}$ (13 $M^{-1} s^{-1}$), compared to the oxidation by $Fe(H_2O)_6^{3+}$ ($\leqslant 0.2 M^{-1} s^{-1}$, probably also outer-sphere), is easily rationalized in terms of Marcus' theory: $Fe(phen)_3^{3+}$ is the stronger oxidizing agent (higher ΔG^o), and the Fe–phen complexes have a much higher self-exchange rate than the Fe–aquo complexes.[17]

The rate of oxidation of $Mo_2O_2S_2^{2+}$ by $Fe(phen)_3^{3+}$ is more than one order of magnitude lower than that of $Mo_2O_4^{2+}$. The low reductive power of $Mo_2O_2S_2^{2+}$ is observed also in other cases: $Mo_2O_2S_2^{2+}$ is not noticeably oxidized by air, and, after the addition of Fe^{3+}, no oxidation was found to occur within 24 h. Obviously the μ-thio ligands stabilize the Mo(V) state relative to Mo(VI) more than the μ-oxo ligands.

The rate of the first electron-transfer step in the oxidation of $Mo_3O_4^{4+}$ by $Fe(phen)_3^{3+}$ was found to be 51 $M^{-1} s^{-1}$ in 2 M chloride solution. While these studies were in progress, a paper by Harmer *et al.* appeared[18] which reported on the kinetics of this reaction in perchlorate solution (they had managed to keep $Mo_3O_4^{4+}$ stable in the presence of ClO_4^-) and gave a rate constant of only 0.47 $M^{-1} s^{-1}$. Since spectrophotometric studies had provided evidence for the coordination of Cl^- to the trimeric Mo(IV) ion[19] in chloride solution

$$[Mo_3O_4(H_2O)_{9-n}Cl_n^{+(4-n)}],$$

it is probably the strong reduction of the electrostatic repulsion which provides most of the rate enhancement in the chloride medium.

The reaction between Mo^{3+} and Fe^{3+} in non-complexing media is also strongly retarded by electrostatic repulsion. Using an (educated) estimate of 4×10^{-2} M^{-1} for the outer-sphere association constant under our conditions, the first-order rate constant of the outer-sphere precursor complex $[k_1 (k/K_0)]$ is $\approx 1.3 \times 10^3/0.04 = 3 \times 10^4 s^{-1}$. This value is by orders of magnitude too high for substitution at Fe^{3+}[15] or Mo^{3+}.[13] It has to be concluded, therefore, that this redox reaction proceeds by an outer-sphere path.

Finally, the rate constants for the formation of the inner-sphere complexes Mo(V)CNFe(II) from $Mo(CN)_8^{3-} + Fe^{2+}$ ($k_1 = 1.1 \times 10^6$ $M^{-1} s^{-1}$) and Mo(IV)CNFe(III) from $Mo(CN)_8^{4-} + Fe^{3+}$ ($k_{-3} = 2.7 \times 10^4$ $M^{-1} s^{-1}$) appear reasonable for substitution at $Fe(H_2O)_6^{2+}$ and $Fe(H_2O)_6^{3+}$, respectively, if the charge effects are taken into account. The electron transfer within the inner-sphere complex is fast, $k_2 + k_{-2} > 5 \times 10^6 s^{-1}$. This might have been expected, since cyano ligands are known to be very good electron-transferring groups. For instance, the outer-sphere reduction of $Mo(CN)_8^{3-}$ by $Fe(CN)_6^{4-}$ occurs with a second-order rate constant of 3×10^4 $M^{-1} s^{-1}$ and that of $Mo(CN)_8^{3-}$ by $W(CN)_8^{4-}$ with one of 5×10^6 $M^{-1} s^{-1}$.[20] Considering the charge type of these reactions (-3 and -4), the first-order electron-transfer rates within the encounter com-

plexes (i.e. through two layers of CN^- ligands) are estimated to be near 1×10^7 s^{-1} and 1×10^9 s^{-1}, respectively.

Acknowledgement—Thanks are due to the DAAD (Deutscher Akademischer Austauschdienst) for a fellowship to C.M., to the Universidad de Concepcion for partial support to C.M., and to Prof. A. G. Sykes for private communications.

REFERENCES

1. E. I. Stiefel, *Prog. Inorg. Chem.* 1977, **22**, 1.
2. References are given in the dissertation of C. Millan, Göttingen (1982).
3. G. Charlot, *Oxidation–Reduction Potentials*, Tables of Constants and Numerical Data, Vol. 8. Pergamon Press, Oxford (1958).
4. (a) F. A. Cotton and G. Wilkinson, *Advanced Inorganic Chemistry*, 3rd Edn, p. 951. Wiley Interscience, New York (1972). (b) J. Aveston, E. W. Anacker and J. S. Johnson, *Inorg. Chem.* 1964, **3**, 735.
5. (a) Ref. 4(a), p. 966; (b) S. Himeno, A. Saito and M. Hasegawa, *Inorg. Chim. Acta* 1984, **88**, 93.
6. M. Ardon and A. Pernick, *Inorg. Chem.* 1973, **12**, 2484.
7. J. J. Cruywagen, J. B. B. Heyns and E. F. C. H. Rohwer, *J. Inorg. Nucl. Chem.* 1978, **40**, 53; J. F. Ojo, R. S. Taylor and A. G. Sykes, *J. Chem. Soc., Dalton Trans.* 1975, 500.
8. C. F. Baes and R. E. Mesmer, *The Hydrolysis of Cations*, p. 230. John Wiley, New York (1976).
9. J. E. Dickens, F. Basolo and N. M. Neumann, *J. Am. Chem. Soc.* 1957, **79**, 1286; T. S. Lee, I. M. Kolthoff and D. L. Leussing, *J. Am. Chem. Soc.* 1948, **70**, 3596.
10. G. R. Cayley, R. S. Taylor, R. K. Wharton and A. G. Sykes, *Inorg. Chem.* 1977, **16**, 1377.
11. B. Spivack and Z. Dori, *J. Chem. Soc., Chem. Commun.* 1977, 909.
12. A. Bino, F. A. Cotton and Z. Dori, *J. Am. Chem. Soc.* 1978, **100**, 5252; R. K. Murman and M. E. Shelton, *J. Am. Chem. Soc.* 1980, **102**, 3984.
13. Y. Sasaki and A. G. Sykes, *J. Chem. Soc., Dalton Trans.* 1975, 1048.
14. N. Sutin, *Acc. Chem. Res.* 1968, **1**, 225.
15. M. Grant and R. B. Jordan, *Inorg. Chem.* 1981, **20**, 55; B. Perlmutter-Hayman and E. Tapuhi, *J. Coord. Chem.* 1976, **6**, 31.
16. Y. Sasaki, R. S. Taylor and A. G. Sykes, *J. Chem. Soc., Dalton Trans.* 1975, 396.
17. B. S. Brunschwig, C. Creutz, D. H. Macartney, T.-K. Sham and N. Sutin, *Faraday Discuss. Chem. Soc.* 1982, **74**, 113.
18. M. A. Harmer, D. T. Richens, A. B. Soares, A. T. Thornton and A. G. Sykes, *Inorg. Chem.* 1981. **20**, 4155.
19. P. Souchay, M. Cadiot and B. Viossat, *Bull. Soc. Chim. Fr.* 1970, 892.
20. R. J. Campion, N. Purdie and N. Sutin, *Inorg. Chem.* 1964, **3**, 1091.

Polyhedron Vol. 5, No. 1/2, pp. 547–550, 1986
Printed in Great Britain

0277–5387/86 $3.00 + .00
© 1986 Pergamon Press Ltd

MOLYBDATES IN AQUEOUS CORROSION INHIBITION—III. EFFECTS OF MOLYBDATE IN THE ANODIC FILMING OF STEEL

A. J. BENTLEY,* L. G. EARWAKER,* J. P. G. FARR,† M. SAREMI and A. M. SEENEY

Department of Metallurgy and Materials and *Department of Physics, University of Birmingham, Birmingham B15 2TT, U.K.

Abstract—Molybdates inhibit the aqueous corrosion of steel. We show that molybdate can promote film formation, extend the anodic passive range, and lower the residual passive current. By *in situ* analysis for molybdenum on electrode surfaces we find that MoO_4^{2-} is adsorbed weakly but copiously in some films. The mechanism of corrosion inhibition by molybdates is discussed.

The literature on the effects of molybdate in the protection of steel from aqueous corrosion grows slowly. An overall view is obscured by the variety of experimental conditions adopted by different workers, and early fundamental work does not directly relate to probable situations in the field.[1] In Fig. 1 a brief comparison is presented of the anodic behaviours of mild steel prepared by: (i) etching (E), and (ii) metallographic polishing (A), and (iii) by cleansing without removing its native oxide (NO). Simulated cooling water (SCW) is used, containing realistic amounts of Cl^- and SO_4^{2-} in the aerated state.[2] In Fig. 2 it is shown that MoO_4^{2-} is an anodic passivator, effective even when the steel is in its more active condition. However, although promising, these effects are too mild to be of immediate use to the corrosion engineer; their significance is mechanistic.

In practice a wide range of corrosion inhibitors is applied to the protection of steel. Many inhibitors are filming agents, protecting the anodically polarised surface under specific conditions for film formation and maintenance, so that formulations for water treatment are rarely, if ever, simple. Nevertheless, examples can be presented of significant improvements in the passivation of steel by well-known and new film-formers, in conjunction with molybdate. Once the respective appropriate conditions for the formation and maintenance of the primary films are provided, the additional presence of molybdate has several general effects and therefore some common mechanisms can be sought. A summary of filming agents tested previously has been given elsewhere.[1] Further examples are given in Fig. 3.

Experiments have involved: (i) the measurement of test electrode potentials, (ii) linear sweep voltammetry,[3] (iii) a.c. electrode impedance measurements,[4] and (iv) surface analysis. Results show that molybdate can promote film formation, extends the anodic passive range and lowers the residual passive current; furthermore it reduces the trans-passive current and can induce the repassivation of pits when corrosive potentials are relaxed. However in *ex situ* analytical experiments only small amounts of Mo are found on electrode surfaces, especially those that have not undergone an active–passive transition.[3] It has now been possible to make *in situ* elemental analyses on test electrodes in a thin-layer cell, using proton-induced characteristic X-ray emission.[5] The technique is shown in Figs 4 and 5 and some results are presented in Fig. 6. It is found that MoO_4^{2-} is adsorbed weakly but copiously in some films, depending on the electrochemical conditions.

Some conclusions can be drawn regarding mechanisms of corrosion inhibition. First, the protectiveness of the composite passivating films in which MoO_4^{2-} is adsorbed is consistent with the effect of molybdate on the ion-selectivity of hydrous ferric oxide films in chloride solutions, demonstrated by Sakashita and Sato[6] (although adsorption probably involves the outer filming agent which is itself adsorbed on residual underlying metal oxide). The net effect is that a barrier is presented, under fairly specific conditions of pH, the presence of accompanying cations, and temperature, to aggress-

† Author to whom correspondence should be addressed.

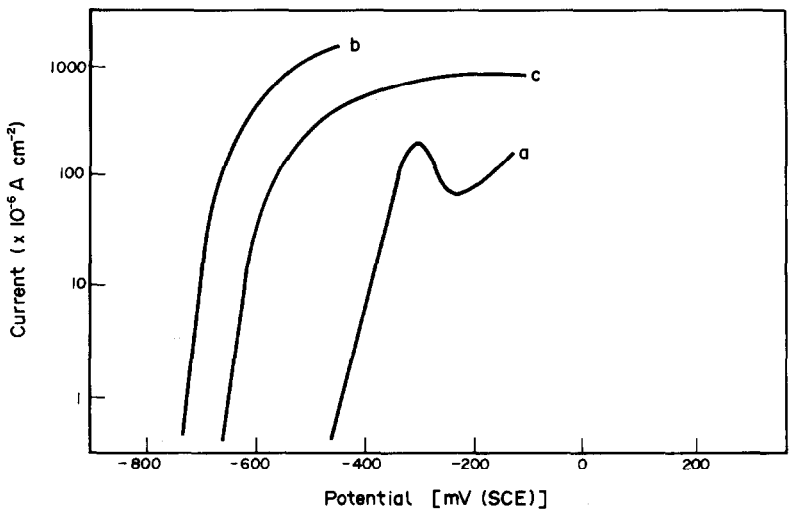


Fig. 1. The effect of static mild steel electrode surface pretreatments in SCW, pH 8.5, on the anodic polarization response after 1-h immersion.

Pretreatment	E_{corr} (mV)
(a) NO	−450
(b) E	−750
(c) A	−640

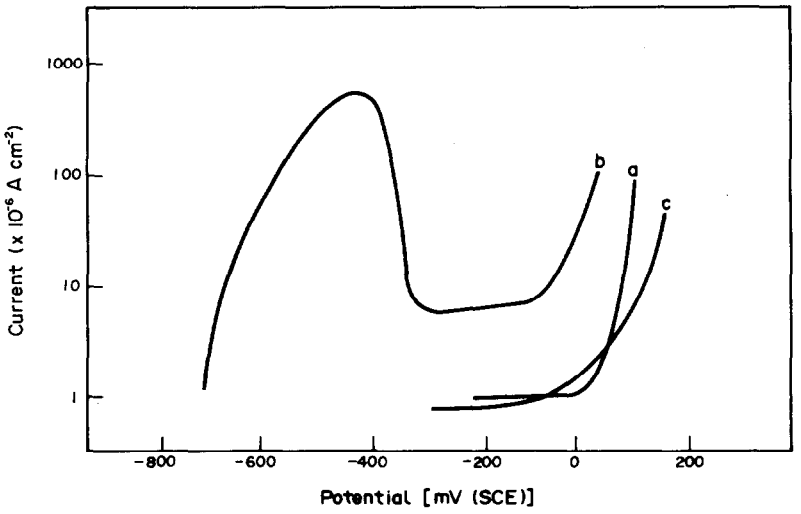


Fig. 2. The effect of static mild steel electrode surface pretreatment in SCW + 500 ppm MoO_4^{2-}, pH 8.5, on the anodic polarization response after 1-h immersion.

Pretreatment	E_{corr} (mV)
(a) NO	−210
(b) E	−680
(c) A	−245

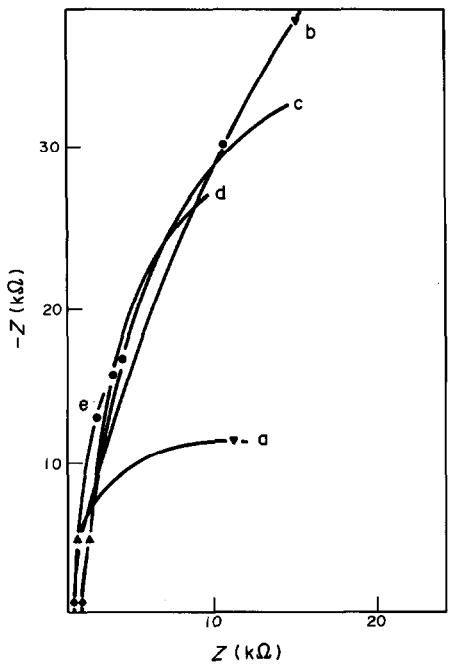


Fig. 3. Impedance analysis comparing the filming and complexing agents effects in SCW + 500 ppm MoO_4^{2-} + 500 ppm agent, pH 8.5. Samples rotated at 1000 rpm for 15 min. NO surface.

Symbol	Agent	E_{corr} (mV)
a	Base solution, no agent	−318
b	Cinnamate	−269
c	Polyethyleneimine	−275
d	Citrate	−265
e	Hexamine	−304

Code	Frequency (Hz)
▼	0.65
●	6.5
▲	65
◆	650

ive anions such as Cl^- and SO_4^{2-}. When pitting does occur the MoO_4^{2-} concentrated on the surface from considerable dilution in the bulk water is released by the establishment of cathodic potentials around the localized anodes. It concentrates within pits as do other anions and in a locally acidic environment[7] neutralizes Cl^- by the formation of oxysalts[4] or by stabilizing a chloride salt film.[8]

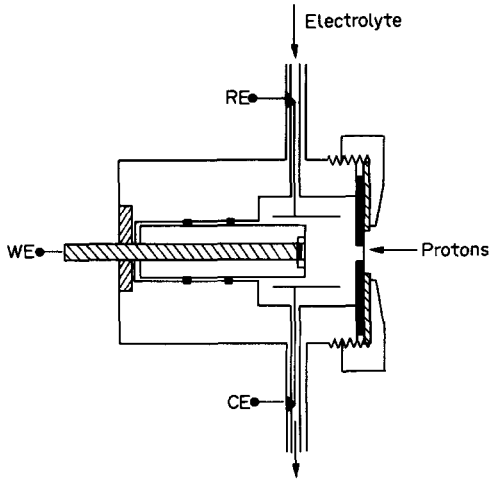


Fig. 4. Thin-layer cell for *in situ* analysis of electrochemically controlled surfaces (CESA). The working electrode (WE) is withdrawn to permit free circulation of dilute electrolyte. For analysis it is moved forward so that a thin (5-μm) electrolyte layer remains between it and the window. A titanium window functioned satisfactorily as a counter electrode (CE). RE = reference electrode.

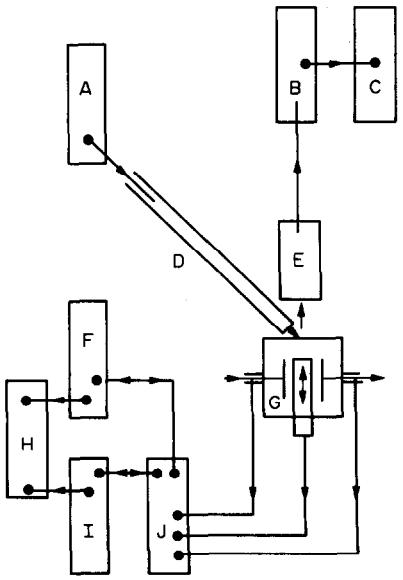


Fig. 5. Experimental arrangement for CESA. A = accelerator, B = signal manipulation, C = data handling, D = beam line, E = SiLi detector, F = microcomputer, G = CESA cell, H = plotter, I = FRA, and J = potentiostat.

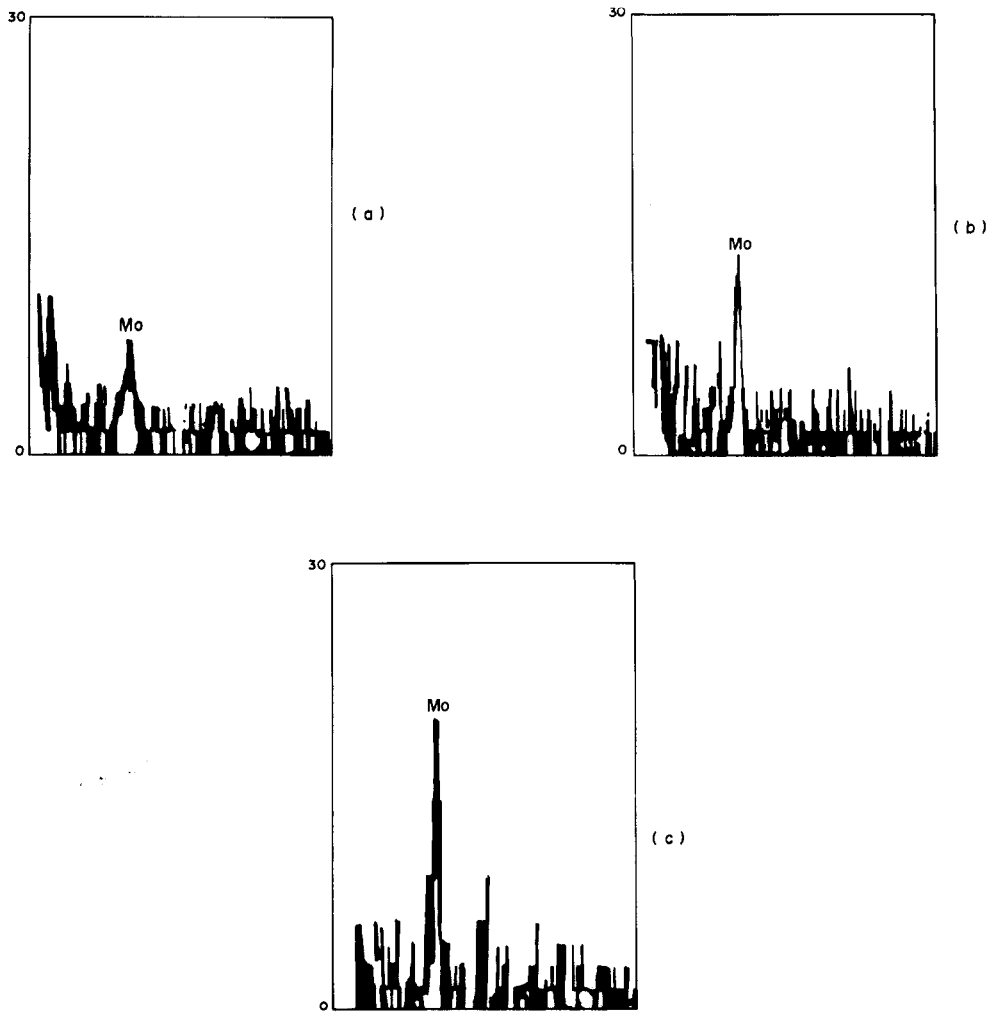


Fig. 6. Experimental CESA results (PIXE: Mo counts vs channel number). (a) Solution = SCW + 500 ppm MoO_4^{2-}, pH 8.5, sample 50 μm from window, NO soak for 10 min, potential = 195 mV (SCE), no Mo adsorption (signal due to Mo in solution). (b) (a) + 1-h soak, potential = 185 mV (SCE), increased Mo adsorption. (c) (b) + 1-h soak, potential = 183 mV (SCE), further increased Mo adsorption.

REFERENCES

1. J. P. G. Farr and M. Saremi, *Proceedings of the International Conference on Chemistry and Uses of* Cr, Mo, W (Edited by J. R. Dilworth and M. F. Lappert), Paper L15. Royal Society of Chemistry, Dalton Division London (1983).
2. E. A. Lizlovs, *Corrosion* 1976, **32**, 263.
3. J. P. G. Farr and M. Saremi, *Surf. Technol.* 1983, **19**, 137.
4. J. P. G. Farr and M. Saremi, *J. Electrochem. Soc.* 1984, **131**, 302C.
5. A. J. Bentley, L. G. Earwaker, J. P. G. Farr and A. M. Seeney, *Surf. Technol.* 1984, **23**, 99.
6. M. Sakashita and N. Sato, *Corros. Sci.* 1977, **17**, 473.
7. A. M. Smith, M. H. Peterson and B. F. Brown, *Corrosion* 1970, **26**, 539.
8. J. R. Ambrose, In *Passivity of Metals* (Edited by R. P. Frankenthal and J. Kruger), p. 740. The Electrochemical Society, Pennington, NJ (1978).

Polyhedron Vol. 5, No. 1/2, pp. 551–559, 1986
Printed in Great Britain

0277–5387/86 $3.00+ .00
Pergamon Press Ltd

MOLYBDATE IN CORROSION INHIBITION—A REVIEW

M. S. VUKASOVICH

AMAX Materials Research Center, P.O. Box 1568, Ann Arbor, MI 48106, U.S.A.

and

J. P. G. FARR*

Department of Metallurgy and Materials, University of Birmingham, Birmingham B15 2TT, U.K.

(*Received* 1 *July* 1985)

Abstract—It has been nearly 50 years since molybdate compounds were first identified and used practically as corrosion inhibitors. They are now recognized as amongst the most broadly applicable of inhibitors chiefly because of their efficacy to protect both ferrous and nonferrous metals and their very low toxicity. This review summarizes fundamental and applied studies dealing with molybdate inhibition and includes descriptions of their practical applications. It also summarizes certain of their physical and chemical properties and emphasizes those environmental aspects relevant to their use in corrosion inhibition.

Corrosion-inhibiting[1] behaviour was first attributed to the molybdate anion in 1939. That year, two patents were issued which described the utilization of soluble molybdates in alcohol–water antifreezes to protect automobile cooling systems from corrosion.[2,3] While still used in antifreezes, molybdate corrosion inhibition has been extended to a diverse variety of other practical applications. Though many specific reports have been published on molybdate corrosion inhibition, the subject has received but a single brief review.[4] The present review is the first of a series that will cover both fundamental and applied aspects of molybdate inhibition, it includes a section on the environmental and regulatory factors which favour its commercial application.

PROPERTIES OF MOLYBDATES

Simple molybdates have the general formula M_2MoO_4, and contain the discrete tetrahedral ion MoO_4^{2-} in both their solid form and in aqueous solution. The chemistry and properties of Mo(VI) aquo ions are described elsewhere.[5–10] The simple alkali metal and ammonium salts, which are readily water-soluble, are most commonly used in corrosion inhibition. The calcium, zinc and strontium molybdates have only slight water solubility, but this property makes them attractive as corrosion-inhibiting paint pigments. In contrast to its congener Cr(VI), the simple Mo(VI) oxyanion is a very weak oxidant, a property rendering the simple molybdates compatible in most systems containing easily oxidized functional organic substances.

The tetrahedral simple molybdate species which is stable in neutral and alkaline solutions condenses and polymerizes upon acid hydrolysis to octahedral Mo_7 and Mo_8 species. The condensation occurs in definite steps and begins at approximately pH 6 to form the heptamolybdate ($Mo_7O_{24}^{6-}$) ion, which reaction is complete by pH 4.5. Between pH 2.9 and 1.5, condensation to $Mo_8O_{28}^{4-}$ is complete. At pH 0.9, the isoelectric point, molybdic acid ($MoO_3 \cdot H_2O$) precipitates, and at still lower pH the cationic dioxomolybdenum(VI) species (MoO_2^{2+}) forms. The type of molybdate species present in solution will vary with pH as indicated and also with concentration.[11]

Pourbaix[12] has used established equilibrium relations to develop potential–pH equilibrium diagrams for many metal–water systems at 25°C and

* Author to whom correspondence should be addressed.

included those for Mo and Fe. Kodama and Ambrose[13] superimposed these diagrams to show that simple molybdate is not an oxidizer of the ferrous ion, a conclusion arrived at experimentally in early studies by Robertson[14] and Pryor and Cohen.[15]

ENVIRONMENTAL ASPECTS OF MOLYBDATE USE IN CORROSION INHIBITION

Commercial acceptance of any inhibitor for a given application is dependent on a variety of techno-economic factors, and also on its environmental acceptability or safety. Molybdates are one of relatively few inorganic inhibitors not considered to be toxic pollutants. Because of this, and their efficacy, molybdates are increasingly being substituted for inhibitors such as chromate, nitrite, phosphate and borate.

Biochemical role

Molybdenum has long been identified as a micronutrient essential to plant life,[16,17] and as playing a major biochemical role in animal health as a constituent of several important enzyme systems.[18,19] Several studies have indicated that molybdenum-deficient diets may be associated with the incidence of various forms of cancer.[20–24]

Molybdenum toxicity

Unlike many other transition metals, molybdenum has been described as having an extremely low or even negligible toxicity.[25] Sax[26] reviewed molybdenum and states that "Molybdenum and its compounds are said to be somewhat toxic, but in spite of their considerable use in industry, industrial poisoning by molybdenum has yet to be reported." In a recent listing of the potential carcinogenicity of metal ions,[27] molybdenum compounds are shown in the lowest potentially carcinogenic category.

Molybdenosis in ruminants was identified in the early 1930s, and has since been explored extensively.[28] It was found that molybdenum was not causing a direct toxic effect in ruminants, but that high dietary molybdenum resulted in depleted body copper levels. The resulting malady was manifested as that of copper deficiency. Today, the molybdenosis risk in ruminants is routinely avoided by copper supplementation.[29] It has been shown that aquatic species, in general, are relatively insensitive to molybdenum from sodium molybdate. Bluegill, rainbow trout, channel catfish, fathead minnow, water flea and scud exposed to varying concentrations showed no effect at levels ranging from 1800 $mg\,l^{-1}$ for the water flea and scud to 7500 $mg\,l^{-1}$ for the channel catfish.[30]

The U.S. Occupational Safety and Health Administration[31] and the Mining Safety Health Administration[32] have adopted threshold limit values (TLV) for worker exposure to various airborne chemicals. The most recent TLV published by the American Conference of Government Industrial Hygienists 1984–1985[33] show the time-weighted average TLV for soluble molybdenum particulates as 5 $mg\ m^{-3}$ and for insoluble particulates as 10 $mg\,m^{-3}$. For comparison, the TLV for total particulates in the nuisance dust category is also shown as 10 $mg\ m^{-3}$.

Impact of federal regulations on molybdenum use

From an environmental perspective, five statutes, and their associated regulations, govern the use and disposal of chemicals within the United States. These are the Safe Drinking Water Act,[34] the Resource Conservation and Recovery Act (RCRA),[35] the Clean Water Act (CWA),[36] the Comprehensive Environmental Response Liability Act,[37] and the Toxic Substances Control Act (TSCA).[38] Molybdenum is not a regulated parameter under any of these statutes. The TSCA requires all existing chemical substances be registered. Sodium molybdate has been assigned a Chemical Abstract Service number of 7631-95-0 but has not been selected for toxicity testing. Under the RCRA, molybdenum is neither a listed hazardous waste nor a hazardous constituent. Section 311 of the CWA lists 299 substances as hazardous if spilled in waterways. No molybdenum compound is included.

In summary, sodium molybdate and other molybdates free of accompanying toxic elements or compounds, exhibit an environmental compatibility within the framework of their commercial utilization as a corrosion inhibitor.

APPLICATION OF MOLYBDATES IN CORROSION INHIBITION

The application of molybdates in corrosion inhibition is increasing rapidly. The purpose of this section is to indicate some significant fields; full reviews will be published elsewhere.

Engine coolants

Important early references are 2, 3 and 39. For the application to aluminium and its alloys see Refs 40–47. Antifreezes are covered in patents,[40,48–50] papers[43,47,51,52] and company specifications (e.g. Ref. 53).

Paints

The earliest relevant reference is to zinc tungstate;[54] molybdenum compounds were first used as pigments,[55] and much later for their corrosion inhibition.[56–67] Molybdates can also be usefully incorporated in to an anodized aluminium surface.[67–70] More recently inhibiting combinations of molybdate with other pigments have been developed.[71–82] There is an extensive literature on paint formulation.[61,67,83–117]

Cooling waters

Quite small quantities of molybdate have been reported to be effective in reducing the corrosiveness of cooling waters[56,118,119] and even brine.[56] To match the efficiency of chromate[120] a variety of synergistic systems have been tried.[121–166] This is a developing field with considerable challenges from the unhappy juxtaposition of incompatible alloys and metals and from the variable quality of cooling waters.

Metal-working fluids

Nitrite has been the established inhibitor of the rusting of machinery tooling and workpieces, often used with alkanolamines. It is now being replaced because of the risk of carcinogenic nitrosamine formation.[167] Molybdate allows the partial[168–170] or, in complex formulations, the complete replacement of nitrite[171–173] and it can be cost-effective.[174]

SYNERGISTS OF MOLYBDATE INHIBITION

In commercial practice combinations are used to take advantage of synergisms between inhibitors and to cope with multi-metal systems.

The molybdate–nitrite synergistic combination has been applied to engine antifreeze,[2] to open or fully aerated[127] and closed or partially de-aerated[151,163] recirculating cooling water, primer paints,[109] metal-working fluids[169,170,173] and coal-water slurries.[175] It was shown that the effect of molybdate in this combination was to reduce the critical current density and of nitrite to reduce passive current density during the inhibition of mild steel.[176] The pitting potential was also increased. Another study dealing with this combination showed oxygen is needed for the synergism to be operative, at a minimum concentration between 1 and 2.5 mg l^{-1}.[163]

Cathodic inhibitors are synergists of molybdate inhibition.[177] In neutral or alkaline solutions, these cations can stifle the cathodic reaction of the corrosion process, usually through the formation of an adherent, insoluble oxide, hydroxide or carbonate film. Ni^{2+}, Mn^{2+} and, most efficiently, Zn^{2+} synergize molybdate inhibition of steel in aerated, neutral and alkaline cooling tower water.[135] Ca^{2+}, another cathodic inhibitor usually present as hardness in cooling water, significantly increased the corrosion protection of steel already synergistically inhibited with MoO_4^{2-}–Zn^{2+}.[128] Anodic–cathodic polarization curves for steel in a neutral, low-hardness cooling water are shown in Refs 157 and 176, Zn^{2+} produces an increase in the slope of the cathodic curve, but the synergism is evident from a noble shift in the critical potential for passivation even though the passive region remains unaffected. It was proposed that Zn^{2+} adsorbs and blocks the cathodic sites as proposed previously[178] for Zn^{2+} in dilute acid solution.

Numerous other substances have been identified as synergists of molybdate inhibition. Among these are the copper alloy inhibitors benzotriazole and tolyltriazole. The corrosion inhibition of steel and aluminium in cooling water were found to be synergized with either triazole used with molybdate at weight ratios of between 1:2.5 and 1:5, respectively.[130] The molybdate–triazole combination has also been used to protect ferrous and nonferrous metals in automotive antifreezes.[39] Chromate strongly synergizes the molybdate inhibition of both ferrous and nonferrous metals[118] and this combination is still used in some cooling-water treatments in locales where a low level of chromate is tolerable. Another widely used synergistic combination is molybdate–organic phosphonate.[127,128,134,138,142,164,179–181] A further benefit was found to be derived when inorganic phosphate and benzotriazole were added to the molybdate–organic phosphonate.[182] Inorganic phosphates themselves are also synergistic with molybdate.[156] Equal weight parts of either sodium tripolyphosphate ($Na_5P_3O_{10}$) or hexametaphosphate [$(NaPO_3)_6$] and sodium molybdate were reported to be more protective of steel than these phosphates with chromate.[183] Finally, many examples are reported of organic inhibitors that are synergistic with molybdate for the protection of ferrous and nonferrous metals.[155,169,170,173,174]

THE MECHANISM OF THE INHIBITION OF CORROSION OF STEEL BY MOLYBDATE

An understanding of the effects of molybdate in promoting or providing inhibition in the field

depends on the establishment of a laboratory phenomenology to match the industrial experience that has been reviewed in previous sections. Extensive laboratory work is necessary to identify the controlling factors in particular situations of corrosion or protection, to form a basis for a diagnostic approach to "real" situations. Progress has been slow; at present, model experiments and existing theory permit useful discussion of corrosion inhibition by molybdates, *inter alia*, on steel in neutral and alkaline aqueous systems containing mild oxidants.

Phenomenology

Surface. The steel surface that is merely degreased and thoroughly washed retains its "native" oxide. This is not an ideal start-point for a purely electrochemical experiment but it is realistic and therefore it is considered here. On mild steel the native oxide may be up to 0.1 μm thick and its composition and structure is still a matter for research. Earlier work was oriented towards the identification of Fe_2O_3 and Fe_3O_4 crystalline phases in aged oxide layers.[184] Recently there has been a growing interest in the non-crystalline or "gel-like" parts of the surface film. Thus X-ray absorption fine structure experiments[185,186] suggest a marked difference between *in situ* formed films and *ex situ* structures. There is agreement with results from the use of other techniques,[187–190] notably Mössbauer spectroscopy, that films formed in moist air contain hydrogen or hydroxyl and that desiccation and increasing crystallinity are features of ageing.[186] The product of an electrolytic active–passive transition is a gel-like structure approaching FeO·OH molecular composition.[191] There is some agreement on the absence of Fe(II) in such films. The difference between such electrochemically passivated films and the "native" oxide seems largely in the degree of crystallinity; the native oxide undoubtedly contains variable proportions of crystalline to uncrystalline FeO·OH and some hydration; furthermore it may have a variable porosity due to its history of ageing and desiccation.

There are, therefore, three distinguishable experimental situations:

(i) The active–passive transition, which involves the filming of an initially oxide-free surface at a critical potential or current. Molybdate and any co-reagents may interact with the anodic steel surface (which is likely to be hydroxylated in both acid and alkali[192–195] or they may effect the solubility of the initially formed Fe(II) species.

(ii) Where the passivation is by formation of a gel-like FeO·OH film, molybdate and co-reagent may be incorporated from its initiation, or in a subsequent process.

(iii) The modification of an existing native oxide, as must often occur in "real" situations.

Electrochemistry. The cathodic effect of Mo(VI) appears to be insignificant in corrosion or its prevention. Its behaviour as an anodic inhibitor, especially in conjunction with other "primary" film formers, is manifest[196,197] in:

(i) measurements of corrosion potentials;

(ii) potentiostated current–voltage measurements, including linear sweep voltammetry; and

(iii) a.c. impedance measurements.

With some reservations, it is concluded[196,197] from laboratory experiments that:

(i) Mo(VI) promotes the passivation of active steel, by more effective film formers than itself;

(ii) it reduces the passivation current, i.e. the leakage current through the passivating film;

(iii) it extends the anodic passive range, i.e. it shifts the pitting potential to more anodic values; and

(iv) it promotes the repassivation of the pits produced during anodic excursions in to transpassivity.

Presence of Mo *on the surface.* The detection and estimation of molybdenum in surface films on metals, including steel, has proved difficult. XPS, Auger Spectroscopy, SIMS and Rutherford backscattering of α-particles have been applied successfully *ex situ*.[152,156,198,199]

It seems generally true that, from whatever inhibitor formulation, most Mo is found on steel surfaces that have undergone active–passive or passive–active transitions. Mo yields on previously passivated surfaces soaked in Mo(VI)-bearing water have been low, regardless of the *ex situ* analytical techniques applied. Recent *in situ* analyses,[200] have shown that this is because Mo(VI) is weakly, if copiously, adsorbed; there are considerable handling losses *in ex situ* analyses.

Mechanism

Molybdate. There is no evidence at present that Mo(VI) modifies the kinetics or dissolution mechanism of active, film-free iron. It seems likely that the promotion of active–passive transition is due to the early formation of insoluble Fe(III) molybdate which contributes to the necessary electrode polarization.[12]

Impedance measurements, in particular, show that Mo(VI) stabilizes the native oxide on unetched

steel. This oxide is slowly dissolved by aggressive cooling waters; but the electrode impedance actually increases in the presence of molybdate. Various theories have been proposed to account for this.[201–204] Currently there is acceptance that molybdate is adsorbed on the porous oxide surface, probably by processes of ion exchange. This adsorption produces a layer impermeable to other anions, particularly to Cl^- and SO_4^{2-}. The theory, whilst plausible, has limited experimental support.[191,205] However, it is consistent with much that is known about the adsorption of anions and cations on FeO·OH mineral species.[206,207] The nature of the oxide surface is subject to on-going research. There is dispute concerning the extent to which associated water is structured, the significance of porosity, the identification of adsorption sites and the nature of the adsorption bond.[208–213] For the present purpose, agreement that the isoelectric point for FeO·OH is about or above pH 8 suggests that moderate alkalinity is necessary to optimize MoO_4^{2-} ion exchange. It may also be concluded that the usefulness of Mo(VI) in the absence of co-passivators should not be underrated. That Mo(VI) is not a strong passivator does not exclude it from being effective in improving the barrier properties of oxide or, indeed, other films.

Molybdate with other film formers: synergism. The behaviour of molybdate in conjunction with other film-forming agents is more difficult to discuss because the surface chemistries of these substances are specific and there may also be complexing between Mo(VI) and other electrolyte species. Often, usefully synergistic compounds provide a primary passivating film more readily than does Mo(VI) on its own, or even in the presence of oxidant. Given the correct chemical conditions, the addition of molybdate promotes primary film formation, reduces the passive current (i.e. increases the impedance of the passivated surface) and extends the anodic range of passivation. Very much better barrier films than the Mo(VI)-bearing native oxide are obtained on mild steel. Usually the chemistry of filming involves the deposition of the filming agent on to native oxide. However with some surface-active chelating agents, the native oxide seems to be displaced and thinner passive films result.[214] The behaviours of citrate and phosphate, each in the presence of Mo(VI), contrast interestingly.[157] Very protective but thin films are obtained with citrate; good protection with Mo(IV)–orthophosphate involves much thicker layers.[120,122,157] It appears impossible to generalize about the interaction of Mo(VI) and the primary film formers; nevertheless, in many cases it seems that the improvement in passivation does come from such interactions rather than from exchange on the surface of underlying oxide as previously described. Again the Mo(VI) is held weakly and is readily released by perturbations in the electrode conditions.

Molybdate in anodic pits. It is common to all the Mo(VI)-passivated systems explored in the transpassive condition (with or without synergists) that Mo is readily found in pits, by *ex situ* analytical techniques. Such observations have been made in corrosion experiments conducted up to 250°C.[215] The molybdenum species in pits are agreed to be inhibiting, slowing down pit growth and presumably ensuring that some incipient pits do not reach a critical condition for continued growth. A general mechanism of inhibition is not agreed. Adsorption of molybdate on the pit wall is supported in Sugimoto and Sawada[216] and Kodama and Ambrose.[217] However conditions in an active pit are conducive to the accumulation of molybdate with, for example, Cl^-, and to low pH. A pH of 3.5 within a pit has been reported[218] for an external, bulk pH from 2 to 10. In more concentrated neutral NaCl solutions the pit pH has been reported[219] to be below 1.0, and the Cl^- concentration rose to 6.2 M. These conditions are consistent with the formation of molybdochloride that may hydrolyse to a molybdate-stabilized oxide film when the anodic pitting condition relaxes.[215,220]

Thus the repassivation of steel in the presence of molybdate involves transfer of the anion from its accumulation in surface films, to the pit. One may speculate that release from the composite film is due to the establishment of cathodic conditions around the pit.[221]

REFERENCES

1. "NACE Glossary of Corrosion Terms", *Mater. Perform.* 1968, **7**(10), 68.
2. A. L. Bayes, U.S. Patent 2,147,395 (1939).
3. H. Lamprey, U.S. Patent 2,147,409 (1939).
4. A. Cepero, Yu. I. Kudelin and V. A. Timonir, *Rev. Cienc. Quim.* 1982, **13**(1), 93.
5. P. C. H. Mitchell, *Q. Rev.* 1966, **20**, 103.
6. F. A. Cotton and G. Wilkinson, *Advanced Inorganic Chemistry*, 3rd Edn, p. 944. Interscience, New York (1972).
7. G. A. Tsigdinos and C. H. Hallada, Isopoly compounds of molybdenum, tungsten and vanadium, Bulletin Cdb-114. AMAX, Inc., Greenwich, CT (1969).
8. G. A. Tsigdinos, Heteropoly compounds of molybdenum and tungsten, Bulletin Cdb-12a (Revised). AMAX, Inc., Greenwich, CT (1969).
9. G. A. Tsigdinos and F. W. Moore, Simple molybdates of the elements, Bulletin C-110. AMAX, Inc., Greenwich, CT (1981).

10. D. T. Richens and A. G. Sykes, *Comments Inorg. Chem.* 1981, **1**, 141.
11. D. F. Baes and R. E. Mesmer, *The Hydrolysis of Cations*, p. 256. John Wiley, New York (1976).
12. M. Pourbaix, *Atlas of Electrochemical Equilibria in Aqueous Solutions*, 2nd Edn, p. 275. National Association of Corrosion Engineers, Houston, TX (1974).
13. T. Kodama and J. R. Ambrose, *Corrosion* 1977, **33**, 155.
14. W. D. Robertson, *J. Electrochem. Soc.* 1951, **98**, 94.
15. M. J. Pryor and M. Cohen, *J. Electrochem. Soc.* 1953, **100**, 203.
16. A. J. Anderson, *J. Aust. Inst. Agric. Sci.* 1942, 873.
17. M. Neenan, *Proc. Soil Sci. Soc. Fla* 1953, **13**, 178.
18. E. C. DeRenzo, E. Kaleita, P. G. Heytler, J. J. Oleson, B. L. Hutchings and J. H. Williams, *Arch. Biochem. Biophys.* 1953, **45**, 247.
19. D. A. Richert and W. W. Westerfield, *J. Biol. Chem.* 1953, **203**, 915.
20. R. J. Burrell, W. A. Roach and A. Shadwell, *J. Nat. Cancer Inst.* 1966, **35**, 201.
21. B. A. Nemenko, M. M. Moldakulova and S. N. Borina, *Vopr. Onkol.* 1976, **22**, 75.
22. Department of Chemical Etiology and Carcinogenesis, Cancer Institute, Chinese Academy of Medical Sciences, Henan Hydrogeological Team, Laboratory of Henan Geological Bureau, Health Bureau of Anyang District and Linxian Office of Esophageal Cancer Prevention and Treatment, *Chin. J. Oncol.* 1980, **2**, 29.
23. X. M. Luo, S. M. Lu and Y. Y. Liu, *Chin. J. Epidemiol.* 1982, **3**, 91.
24. X. M. Luo, *Trace Substances in Environmental Health*—XVI, p. 357. University of Missouri (1983).
25. H. J. Ashmead, *J. Appl. Nutr.* 1972, **24**, 8.
26. N. I. Sax, *Dangerous Properties of Industrial Materials*, 5th Edn, p. 836. Reinhold, New York (1979).
27. H. Sigel (Ed.), *Metal Ions in Biological Systems, Vol. 10: Carcinogenicity and Metal Ions.* Marcel Dekker, New York (1980).
28. E. J. Underwood, In *Molybdenum in the Environment* (Edited by W. R. Chappell and K. K. Peterson), Vol. 1, p. 9. Marcel Dekker, New York (1976).
29. M. Phillippo, W. R. Humphries, I. Bremner, T. G. Atkinson and G. Henderson, *Molybdenum Induced Infertility in Cattle.* Rowett Research Institute, Bucksburn, Aberdeen (1984).
30. Bionomics, Inc., Wareham, MA, Bioassay Report, conducted for Climax Molybdenum Company of Michigan, Ann Arbor, MI (1973).
31. Occupational Safety and Health Act, Public Law 91-596, December 29 (1970), 84 Stat. 1593; 29 U.S.C. 655 *et seq.*, as amended.
32. Federal Mine Safety Health Act of 1977; 86 U.S.C. 801 *et seq.*, as amended.
33. 1. SBN 0-936712-54-6, American Conference of Governmental Industrial Hygienists, 6500 Glenway Avenue, Building D-5, Cincinnati, OH 45211.
34. Safe Water Drinking Act, Public Law 93-523, December 16 (1974), 88 Stat. 1660; 42 U.S.C. 300 *et seq.*, as amended.
35. Resource Conservation and Recovery Act, Public Law 94-580, October 21 (1976), 90 Stat. 95; 42 U.S.C. 3251 *et seq.*, as amended.
36. Federal Water Pollution Control Act, as amended by the Clean Water Act, Public Law 92-500, October 18 (1972), 86 Stat. 816, 33 U.S.C. 1251 *et seq.*, as amended.
37. Comprehensive Environmental Response Compensation and Liability Act of (1980), Public Law 96-510, December 11 (1980), 94 Stat. 2767; 42 U.S.C. 9601 *et seq.*, as amended.
38. Toxic Substances Control Act, Public Law 94-469, October 11 (1976), 90 Stat. 2003; 15 U.S.C. 2601 *et seq.*, as amended.
39. A. D. Meighan, U.S. Patent 2,803,604 (1957).
40. G. W. Lewis, Jr, Research Project No 37, Climax Molybdenum Company of Michigan, Ann Arbor, MI (1961).
41. R. R. Wiggle, V. Hospadaruk and E. A. Styloglu, *Mater. Perform.* 1981, **20**(6), 13.
42. L. C. Rowe, In *Corrosion Inhibitors* (Edited by C. C. Nathan), p. 173. National Association of Corrosion Engineers, Houston, TX (1973).
43. M. S. Vukasovich and F. J. Sullivan, *Mater. Perform.* 1983, **22**(8), 25.
44. J. C. Wilson, S. T. Hirozawa and J. J. Conville, U.S. Patent 4,440,721 (1984).
45. P. Veerabhadra Rao, K. Seetharamaiah and T. L. Rama Char, *J. Electrochem. Soc. India* 1974, **23**(1), 7.
46. R. R. Wiggle, V. Hospadaruk and F. M. Tibaudo, Paper No. 810038, Society of Automotive Engineers, Detroit, MI (1981).
47. M. S. Vukasovich and F. J. Sullivan (Eds), *Inhibitors and Coolant Corrosivity.* 2nd International Symposium on Engine Coolants and Their Testing, American Society for Testing and Materials, Philedelphia, PA (1984).
48. S. T. Hirozawa, European Patent Application 0,042,937A1 (1982).
49. T. Yoshioka, Japanese Patent 8217472 (1982).
50. P. R. Engelhardt and E. M. Ventura, British Patent Application 8409522 (1984).
51. L. C. Rowe, R. L. Chance and M. S. Walker, *Mater. Perform.* 1983, **22**(6), 17.
52. N. M. Potter, R. B. Loranger and H. E. Vergosen III, American Laboratory (1984), p. 104.
53. Automotive engine coolant, concentrate–ethylene glycol type. General Motors Engineering Standard GM 6043-M. General Motors Corp., Warren, MI (1983).
54. G. Rigg, U.S. Patent 1,031,377 (1912).
55. D. H. Killefer and A. Linz, *Molybdenum Compounds: Their Chemistry and Technology*, p. 163. Interscience, New York (1952).
56. W. D. Robertson, *Chem. Eng.* 1950, **57**, 290.
57. D. H. Killefer, *Paint, Oil Chem. Rev.* 1954, **117**, 24.
58. W. D. Robertson, *J. Electrochem. Soc.* 1951, **98**, 94.
59. A. K. Choudhury and S. C. Shome, *J. Sci. Ind. Res.* 1958, **17A**, 30.

60. A. K. Choudhury and S. C. Shome, *J. Sci. Ind. Res.* 1959, **18A**, 568.
61. H. O. Shoen and B. G. Brand, *Off. Dig. Fed. Soc. Paint Technol.* 1960, **32**, 1522.
62. H. E. Weisbergy, *Paint Varn. Prod.* 1968, **58**(3), 32.
63. M. Kronstein, W. A. Von Burgsdorff, N. Hanan and D. L. Weir, *Aust. Finish. Rev.* 1966, **12**, 13.
64. M. Kronstein, U.S. Patent 3,272,663 (1966).
65. S. L. Chisolm, U.S. Patent 3,311,529 (1967).
66. M. Kronstein, U.S. Patent 3,528,860 (1970).
67. P. Schnake, D. P. Jensen and R. H. Albrecht, NASA Contract NAS 8-11788, Final Report (1964).
68. R. C. Spooner, U.S. Patent 2,899, 368 (1959).
69. E. F. Barkman, U.S. Patent 3,257,244 (1966).
70. H. B. Romans, U.S. Patent 3,272,665 (1966).
71. J. V. Hunn, U.S. Patent 3,353,979 (1967).
72. T. Kirkpatrick and J. J. Nilles, U.S. Patent 3,677,783 (1972).
73. F. W. Moore, D. R. Robitaille and H. F. Barry, U.S. Patent 3,726,694 (1973).
74. D. R. Robitaille, M. S. Vukasovich and H. F. Barry, U.S. Patent 3,874,883 (1975).
75. D. R. Robitaille, M. S. Vukasovich and H. F. Barry, U.S. Patent 3,969,127 (1976).
76. M. S. Vukasovich and F. J. Sullivan, U.S. Patent 4,017,315 (1977).
77. H. Shibasaki, H. Tsuchiya and T. Michikawa, Japanese Patent 75119833 (1975).
78. D. G. E. Kerfoot, U.S. Patent 4,132,667 (1979).
79. Kansai Paint Co. Ltd, British Patent 1,415,488 (1975).
80. K. Nakajo, K. Kanezawa and S. Sato, Japanese Patent 7509596 (1975).
81. Dai Nippon Toryo Co. Ltd, British Patent 1,459,069 (1976).
82. G. L. Roberts, Jr and R. G. Fessler, U.S. Patent 3,346,604 (1967).
83. J. Ruf, In *Proceedings of the 8th Congress of the International Union Electrodeposition and Surface Finishes*, p. 280 (1972).
84. J. Ruf, *Ferbe & Lack* 1973, **79**(1), 22.
85. R. Pantzer, *Pigm. Resin. Technol.* 1975, **4**(4), 13.
86. R. Pantzer, *Pigm. Resin. Technol.* 1975, **4**(5), 5.
87. H. Goldschmiedt, *Paint Manuf.* 1975, **45**, 22.
88. R. Lapesin, V. Longo and G. Torriano, *J. Oil. Colour Chem. Assoc.* 1975, **58**, 286.
89. W. M. Tomc, Corrosion/76, Paper No. 132. National Association of Corrosion Engineers, Houston, TX (1976).
90. A. Marchese, A. Papo and G. Torriano, *Anti-Corros. Methods Mater.* 1976, **23**(9), 4.
91. Dai-Nippon Toryo Co. Ltd, Japanese Patent 79020215 (1979).
92. J. C. Laout, *Surfaces* 1979, **18**(127), 68.
93. H. Makishima, M. Hosoda, E. Kasiwagi and T. Hayashi, German Patent 2,518,275 (1976).
94. Nippon Muki Kagaku Co., Japanese Patent 78031495 (1978).
95. D. E. A. Williams-Wynn, In *6th National Symposium on Non-Conventional Coatings, OCCA (South Africa), Port Elizabeth* (1976), p. 22.
96. Chugoku Marine Paints, Japanese Patent 77032966 (1977).
97. A. Papo, G. Torriano and R. Lapasin, *Br. Corros. J.* 1977, **12**(2), 92.
98. J. Boxall and J. A. Von Fraunhofer, *Polym. Paint Colour J.* 1977, **167**(3958), 738.
99. Dai-Nippon Toryo Co. Ltd, Japanese Patent 77003818 (1977).
100. Dai-Nippon Toryo Co. Ltd, Japanese Patent 77000767 (1977).
101. Dai-Nippon Toryo Co. Ltd, Japanese Patent 76048769 (1976).
102. J. Anisfeld, *Farbe & Lack* 1975, **81**(11), 1024.
103. Anon., *Ind. Finish. Surf. Coat.* 1975, **27**(326), 28.
104. R. J. Cole, *Rep. Prog. Appl. Chem.* 1975, **58**, 207.
105. L. R. Horn, *Paint Varn. Prod.* 1973, **63**(2), 29.
106. D. G. E. Kerfoot, German Patent 2,814,454 (1978).
107. M. A. Abou-Khalil, *Paint Manuf.* 1978, **48**(1), 36.
108. W. J. Banke, *Mod. Paint Coat.* 1980, **70**(2), 45.
109. F. J. Sullivan and M. S. Vukasovich, *Mod. Paint Coat.* 1981, **71**(3), 41.
110. R. W. Flynn and M. J. Grourke, U.S. Patent 4,243,416 (1981).
111. R. W. Flynn and M. J. Grourke, U.S. Patent 4,243,417 (1981).
112. M. T. Orillion, U.S. Patent 4,298,657 (1981).
113. C. R. Hegedus, U.S. Patent Application 6,437,086 (1982).
114. M. H. L. Garnaud, *Polym. Paint Colour J.* 1984, **174**(4117), 268.
115. Bulletins 331 and 342. Sherwin Williams Chemicals, Cleveland, OH.
116. Bulletins C-385, 81B10 and 81B14. Rohm and Haas Co., Philadelphia, PA.
117. Bulletin "Heucophos: new anticorrosive pigments chromate- and leadfree". Dr Hans Heubach GmbH, Langelsheim, F.R.G.
118. J. I. Bregman, U.S. Patent 3,024,301 (1962).
119. G. B. Hatch, *Corrosion* 1965, **21**, 129.
120. D. A. Carter and C. C. Nathan, *Mater. Prot.* 1969, **8**(9), 61.
121. D. M. Brasher and J. E. Rhoades-Brown, *Br. Corros. J.* 1969, **4**, 74.
122. A. Weisstuch and C. E. Schell, *Corrosion* 1972, **28**, 299.
123. D. M. Brasher and J. E. Rhoades-Brown, *Br. Corros. J.* 1973, **8**, 50.
124. A. Von Koeppen, G. A. Emerle, K. Nishio and B. A. Metz, *Mater. Prot. Perform.* 1973, **12**(7), 23.
125. R. Mitchell, U.S. Patent 3,723,347 (1973).
126. K. M. Verona, M. P. Gupta, S. Bhaskaron and B. B. Sinka, *Fert. Technol.* 1975, **12**(4), 337.
127. D. R. Robitaille, *Mater. Perform.* 1976, **15**(11), 40.
128. D. R. Robitaille and J. G. Bilek, *Chem. Eng.* 1976, **83**(12), 79.
129. R. D. Hogue, T. M. King and R. S. Mitchell, U.S. Patent 3,989,637 (1976).
130. C. O'Neal, Jr and R. N. Borger, *Mater. Perform.* 1976, **15**(2), 9.
131. T. Kodama and J. R. Ambrose, *Corrosion* 1977, **33**, 155.

132. J. Pelikan, J. Vosta and V. Cozl, *Sb. Vys. Sk. Chem.-Technol. Praze, Technol. Paliv.* 1977, **D35**, 77.
133. N. K. Rezental, Yu. I. Kuznetsov and N. M. Kashurnikov, *Tr. Nauchno-Issled. Inst. Betona Zhelezobetona* 1977, **24**, 77.
134. T. C. Breske, *Mater. Perform.* 1977, **16**(2), 17.
135. M. S. Vukasovich and D. R. Robitaille, *J. Less-Common Met.* 1977, **54**, 437.
136. R. Oppenheim, *Brew. Dig.* 1977, **52**(9), 48.
137. K. M. Verma and M. P. Gupta, *Fert. Technol.* 1978, **15**(2), 121.
138. R. J. Lipinski and R. F. Weidner, *Heat./Piping/Air Cond.* 1978, **50**(1), 103.
139. F. Suzuki, U.S. Patent 4,176,059 (1979).
140. D. R. Robitaille and M. S. Vukasovich, U.S. Patent 4,149,969 (1979).
141. R. J. Lipinski, U.S. Patent 4,138,353 (1979).
142. K. M. Verma, M. P. Gupta, N. R. Ghosh and B. B. Sinka, *Fert. Technol.* 1979, **16**(2), 135.
143. R. J. Lipinski, *Proc. Int. Water Conf., Eng. Soc. West. PA* 1979, **40**, 99.
144. D. R. Robitaille, *Ind. Water Eng.* 1979, **16**(16), 14.
145. R. J. Lipinski, U.S. Patent 4,217,216 (1980).
146. P. Cieslinski, *Chlodnictwo* 1980, **15**(7), 11.
147. R. D. Hogue, T. M. King and R. S. Mitchell, U.S. Patent 4,209,487 (1980).
148. W. J. Ward, *Proc. Int. Water Conf., Eng. Soc. West. PA* 1980, **41**, 177.
149. R. J. Lipinski, U.S. Patent 4,246,030 (1981).
150. J. Lu, S. C. Chen, Y. C. Ju and P. S. Chen, In *Proceedings of the 8th International Congress on Metal corrosion*, Vol. 2, p. 1182 (1981).
151. F. C. Sessa and R. M. Post, *The Betz Indicator* 1981, **52**(3), 9.
152. J. Zucker, *Proc. Tech. Assoc. Pulp Paper Ind.* 1982, **2**, 457.
153. J. P. G. Farr and M. Saremi, *Surf. Technol.* 1982, **17**(1), 19.
154. D. R. Robitaille, *Chem. Eng.* 1982, **89**(20), 139.
155. I. L. Rozenfeld, S. Ch. Verdiev, A. M. Kyazimov and A. Kh. Bairamov, *Zashch. Met.* 1982, **18**, 866.
156. D. M. Drazic and C. S. Hao, *Corros. Sci.* 1983, **23**, 683.
157. J. P. G. Farr and M. Saremi, *Surf. Technol.* 1983, **19**(2), 137.
158. M. Khobaib, L. Quakenbush and C. T. Lynch, *Corrosion* 1983, **39**, 253.
159. E. J. Latos and J. C. Payne, U.S. Patent 4,409,121 (1983).
160. T. F. Colturi and K. J. Kozelski, *Mater. Perform.* 1984, **23**(8), 43.
161. C. A. Jones, *J. Cooling Tower Inst.* 1985, **6**(1), 9.
162. R. J. Franco, N. Dinielli and R. J. Nowicki, Corrosion/85, Paper No. 133. National Association of Corrosion Engineers, Houston, TX (1985).
163. T. R. Weber, M. A. Stranick and M. S. Vukasovich, Corrosion/85, Paper No. 122. National Association of Corrosion Engineeers, Houston, TX (1985).
164. P. G. Bird and K. Nishio, U.S. Patent 3,891,568 (1975).
165. A. Marshall and N. Richardson, U.S. Patent 4,239,648 (1980).
166. A. E. Bischof and P. Goldstein, *Mater. Prot. Perform.* 1971, **10**(12), 26.
167. E. O. Bennett and D. L. Bennett, *Tribol. Int.* 1984, **17**, 341.
168. M. Noda, H. Nakai, M. Sasaki and Z. Kanno, Japanese Patent 79116338 (1979).
169. M. S. Vukasovich, *Lubr. Eng.* 1980, **36**, 708.
170. M. S. Vukasovich and D. R. Robitaille, U.S. Patent 4,313,837 (1982).
171. K. W. Koh, U.S. Patent 4,218,329 (1980).
172. C. J. Fette, *Lubr. Eng.* 1979, **35**, 625.
173. M. S. Vukasovich, In *Proceedings of the 3rd International Colloquium on Lubrication in Metal Working, Machining and Metal Forming Processes.* Technishe Akademie Esslingen, Nellingen (1982).
174. M. S. Vukasovich, *Lubr. Eng.* 1984, **40**, 456.
175. V. S. Sastri, R. Beauprie and M. Desgagne, Report ERP/PMRL 81-71 (OP). CANMET, Department of Energy, Mines and Resources, Ottawa, Canada; presented at the 7th International Conference on Slurry Transportation (1982).
176. M. A. Stranick, In *Proceedings of the Fourth International Conference on the Chemistry and Uses of Molybdenum* (Edited by H. F. Barry and P. C. H. Mitchell), p. 123. Climax Molybdenum Co., Ann Arbor, MI (1982).
177. H. Leidheiser, Jr, *Corrosion* 1980, **36**, 339.
178. D. M. Drazic and L. Z. Vorkapic, *Corros. Sci.* 1978, **18**, 907.
179. K. Nishio, U.S. Patent 3,891,568 (1972).
180. P. Labine, T. Wells, J. Minalga, S. Roberts and B. Ritts, Corrosion/82, Paper No. 227. National Association of Corrosion Engineers, Houston, TX (1982).
181. J. P. G. Farr and M. Saremi, In *Proceedings of the Fourth International Conference on the Chemistry and Uses of Molybdenum* (Edited by H. F. Barry and P. C. H. Mitchell), p. 128. Climax Molybdenum Co., Ann Arbor, MI (1982).
182. S. K. Saksenberg, Corrosion/81, Paper No. 189. National Association of Corrosion Engineers, Houston, TX (1981).
183. M. Shigehiro and T. Suzuka, Japanese Patent 4218210 (1967).
184. E.g. M. Cohen, In *Passivity of Metals* (Edited by R. P. Frankenthal and J. Kruger), p. 160. The Electrochemical Society, New York (1978).
185. J. Kruger, G. G. Long, M. Kuriyama, A. I. Goldman, in *Passivity of Metals and Semi-Conductors* (Edited by M. Froment), p. 163. Elsevier, Amsterdam (1983).
186. R. W. Hoffman, In *Passivity of Metals and Semi-Conductors* (Edited by M. Froment), p. 147. Elsevier, Amsterdam (1983).
187. H. T. Yolken, J. Kruger and J. P. Calvert, *Corros. Sci.* 1968, **8**, 103.
188. T. Noda, K. Kudo and N. Sato, *Z. Phys. Chem. N.F.* 1975, **98**, 271.
189. W. F. O'Grady, *J. Electrochem. Soc.* 1980, **127**, 555.
190. O. J. Murphy, J. O'M. Bockris, T. E. Pou, D. L. Cocke and G. Sparrow, *J. Electrochem. Soc.* 1982, **129**, 2149.

191. T. E. Pou, O. J. Murphy, V. Young and J. O'M. Bockris, *J. Electrochem. Soc.* 1984, **131**, 1243.
192. K. F. Bonhoffer and K. E. Heusler, *Z. Electrochem.* 1957, **61**, 122; K. E. Heusler, *ibid.* 1958, **62**, 582.
193. J. O'M. Bockris, D. Drazic and A. R. Despic, *Electrochim. Acta* 1961, **4**, 325.
194. E. J. Kelly, *J. Electrochem. Soc.* 1965, **112**, 124.
195. W. J. Lorenz, Y. Yamaoka and H. Fischer, *Ber. Bunsenges.* 1963, **67**, 932.
196. J. P. G. Farr and M. Saremi, In *Proceedings of the Conference on Recent Developments in the Chemistry of* Cr, Mo *and* W (Edited by J. R. Dilworth and M. F. Lappert), Paper L15. Royal Society of Chemistry, Dalton Division, London (1983).
197. J. P. G. Farr and M. Saremi, Electrochemical Society, 166th Meeting, New Orleans (1984), Extended Abstracts, Vol. 84-2, No. 264, p. 371.
198. R. C. McCune, R. L. Shilts and S. M. Ferguson, *Corros. Sci.* 1982, **22**, 1049.
199. J. R. Ambrose, In *Passivity of Metals* (Edited by R. P. Frankenthal and J. Kruger), p. 740. The Electrochemical Society, New York (1978).
200. A. J. Bentley, L. G. Earwaker, J. P. G. Farr and A. M. Seeney, *Surf. Technol.* 1984, **23**, 99.
201. M. J. Pryor and M. Cohen, *J. Electrochem. Soc.* 1953, **100**, 203.
202. M. Stern, *J. Electrochem. Soc.* 1958, **105**, 638.
203. G. H. Cartledge, *Corrosion* 1962, **18**, 3166.
204. M. Keddman and C. Pallotta, *J. Electrochem. Soc.* 1985, **132**, 781.
205. M. Sakashita and N. Sato, *Corros. Sci.* 1977, **17**, 473.
206. J. B. Harrison and V. E. Berkheiser, *Clays Clay Miner.* 1982, **30**, 97.
207. O. K. Borggaard, *Clays Clay Miner.* 1983, **31**, 230.
208. G. A. Parks and P. L. de Bruyn, *J. Phys. Chem.* 1962, **66**, 967.
209. G. Y. Ouada and P. L. de Bruyn, *Surf. Sci.* 1966, **4**, 48.
210. R. J. Atkinson, A. M. Posner and J. P. Quirk, *J. Phys. Chem.* 1967, **71**, 550.
211. D. E. Yates, S. Levine and T. W. Healey, *J. Chem. Soc., Faraday Trans.* 1 1974, **10**, 1807.
212. A. Breeuwsma and J. Lyklema, *Discuss. Faraday Soc.* 1971, **52**, 324.
213. Y. G. Berubé, G. Y. Ouada and P. L. de Bruyn, *Surf. Sci.* 1967, **8**, 448.
214. N. Hackerman and K. Ogura, In *Proceedings of the VI International Congress on Metallic Corrosion, Sydney*, p. 129. Australasian Corrosion Society (1975).
215. P. Vanslembrouk, W. Bogaerts and A. Von Haute, In *Passivity of Metals and Semi-Conductors* (Edited by M. Froment), p. 393. Elsevier, Amsterdam (1983).
216. K. Sugimoto and Y. Sawada, *Corrosion* 1976, **32**, 347.
217. T. Kodama and J. R. Ambrose, *Corrosion* 1977, **33**, 155.
218. A. J. Smith, M. H. Peterson and B. F. Brown, *Corrosion* 1970, **26**, 539.
219. T. Suzuki and Y. Kitamura, *Corrosion* 1973, **29**, 18.
220. J. R. Ambrose, In *Passivity of Metals* (Edited by R. P. Frankenthal and J. Kruger), p. 740. The Electrochemical Society, New York (1978).
221. A. J. Bentley, L. G. Earwaker, J. P. G. Farr, M. Saremi and A. M. Seeney, *Polyhedron* 1986, **5**, 547.

Polyhedron Vol. 5, No. 1/2, pp. 561–565, 1986
Printed in Great Britain

0277–5387/86 $3.00 + .00
© 1986 Pergamon Press Ltd

THE NATURE OF AMIDE LIGATION TO THE METAL SITES OF FeMoco

M. ANTON WALTERS, STEPHEN K. CHAPMAN and WILLIAM H. ORME-JOHNSON*

Department of Chemistry, Massachusetts Institute of Technology, Cambridge, MA 02139, U.S.A.

(*Received* 18 *June* 1985)

Abstract—The nature of the ligation of *N*-methylformamide (NMF) to the metal sites of FeMoco has been investigated. The IR spectrum of FeMoco in NMF shows an intense band at 1600 cm^{-1} which we assign to the ν(C=O) stretch of ligated NMF. This frequency is characteristic of *N*-deprotonated amide ligands, indicating that NMF ligation to FeMoco is predominantly through nitrogen. Hence NMF behaves as an anionic ligand. The importance of the amide functionality for FeMoco extraction has been further examined and a new extracting agent, 2-pyrrolidinone, has been employed. We hypothesize that, in the MoFe-protein, the primary coordination of the cofactor is via deprotonated backbone amide ligands.

Nitrogenase catalyses the reduction of dinitrogen to ammonia. The enzyme system consists of two separately purifiable proteins; the MoFe-protein and the Fe-protein.[1] The MoFe-protein (which has a molecular weight of about 240,000 and an $\alpha_2\beta_2$ subunit pattern[2]) contains two iron–molybdenum cofactors known as FeMoco.[2] The composition of FeMoco has been reported to be $MoFe_6S_{8-9}$.[3] FeMoco was first isolated by Shah and Brill[4] by extraction from acid-denatured MoFe-protein into *N*-methylformamide, NMF. Until now NMF and formamide have been the only extracting agents which reliably separate FeMoco from the MoFe-protein. We have investigated why NMF is so successful in the extraction of FeMoco, and report here on vibrational studies designed to elucidate the manner in which NMF ligates the metal sites of FeMoco. Based on our results we have developed a hypothesis as to the properties essential for extraction of the cofactor from the MoFe-protein.

The amide I [ν(C=O)] band of secondary amides is estimated to have a potential-energy distribution of 70–80% pure C=O stretch.[5,6] It is, however, coupled to the central C—N stretch and the N—H stretch, and can be affected, via electron delocalization, by hydrogen bonding[5–7] or deprotonation[8–10] of the amide nitrogen. The ν(C=O) band is observed in the range 1680–1630 cm^{-1} in the solid and liquid states of the pure secondary amide, and 1700–1650 cm^{-1} in dilute non-hydrogen bonding solution. These ranges are characteristic of both the *cis* and *trans* forms of secondary amides.[5] Vibrational studies of metal–amide complexes have shown that the ν(C=O) frequency is sensitive to the type of ligation of amides, which sometimes exhibit linkage isomerism. Using the carbonyl stretching frequency as a marker band in Fourier-transform IR (FT-IR) experiments, we reported here on the nature of the amide–metal bond in the NMF-extracted FeMoco where NMF acts as a solvent and as a ligand[11] for the cofactor metal centers.

MATERIALS AND METHODS

Anaerobicity

Manipulations of FeMoco were carried out either in a Vacuum/Atmosphers model M040-1 glove box (helium atmosphere) or by Schlenck line techniques. Unless otherwise specified, solutions of FeMoco were 1 mM in sodium dithionite. Stock 1 M sodium dithionite solutions were 0.25 M in potassium hydroxide.

* Author to whom correspondence should be addressed.

Cell growth and protein purification

In this work, the conditions for growth and derepression of nitrogenase synthesis in *Azotobacter vinelandii* were as previously described.[1] A *nif B* mutant of *Klebsiella pneumoniae* (used to provide *nif B*$^-$ MoFe-protein for FeMoco assays) was grown using medium (b) described by Hawkes and Smith.[12] Nitrogenase proteins were purified (with minor modifications) and assayed by previously published procedures.[1]

FeMoco extraction, concentration and characterisation

FeMoco was isolated using modifications of methods already described.[3,4] All solutions were 2 mM in sodium dithionite, and maintained at 4°C where possible. Solutions were thoroughly vortexed at each step to ensure complete mixing. Purified MoFe-protein [40–50 mg in 0.5 cm^3 of 0.025 M Tris–HCl (pH 7.4), 0.25 M NaCl] was diluted six-fold in doubly distilled water. To this solution was added 0.1 cm^3 of 1.0 M citric acid, whereupon the solution turned green. After 3 min the solution was neutralized by the addition of 0.4 cm^3 of 0.5 M Na_2HPO_4, causing the protein to precipitate. After ~30 min the protein was separated by centrifugation at ~120 *g* for 10 min. The (colourless) supernatant was removed and the pellet resuspended in 0.5 cm^3 of dimethylformamide (DMF) (Aldrich) by vortexing for ~5 s. The protein was again separated by centrifugation (~600 *g* for 10 min) and the DMF wash repeated. After DMF washing, 0.5 cm^3 of NMF (Aldrich) was added and the sample vigorously vortexed for ~5 min and chilled in an ice bath for 5–10 min. The protein was removed by centrifugation (~1400 *g* for 10 min) and the clear green coloured FeMoco solution collected. The NMF extraction step was repeated twice after which no further colour was observed in the extract. The extracted FeMoco was concentrated to 0.2–0.3 cm^3 using a vacuum distillation procedure already described,[1] and then filtered to remove solid impurities. Extractions using 2-pyrrolidinone (Aldrich) were carried out as above but at room temperature because of the higher melting point of this amide (20°C). 2-Pyrrolidinone was recrystallized before use.

For FT-IR experiments, NMF-extracted FeMoco samples were concentrated either to dryness or almost to dryness on zinc selenide plates using vacuum distillation. Typical solutions were ~0.3 mM in FeMoco, 2.0 mM in sodium dithionite, and 0.5 mM in potassium hydroxide, before concentration. Fully desalted samples (no dithionite or potassium hydroxide present) were prepared by passage of the concentrated FeMoco solution down a Sephadex G-10 (Pharmacia) column equilibrated with degassed NMF.

Specific activities of FeMoco were determined by enzymatic assays of reconstituted *nif B*$^-$ Kp1 (crude extract). Activities of FeMoco used for FT-IR experiments were in the range 180–220 nmol C_2H_2 reduced min^{-1} (nmol Mo)$^{-1}$. Samples used for FT-IR studies displayed the characteristic FeMoco EPR spectrum. Fe/Mo ratios for FeMoco were determined by atomic absorption spectroscopy as previously described,[3] and were found to be in the region of 7–8 for most samples.

Preparation of sodium NMF (NaNMF) and N-deuterated NMF

NaNMF, $NaHC(O)NCH_3$, was prepared by the method of Fones:[13] 1 g (17 mmol) of NMF was added to sodium dried xylene under nitrogen. To this 0.4 g (17 mmol) sodium hydride was added and the mixture refluxed overnight under nitrogen. The product was washed with ethyl ether, vacuum dried and stored in a dry box. Yield 89%. Calc.: C, 29.6; H, 5.0; N, 17.3; Na, 28.3%. Found: C, 29.3; H, 4.7; N, 17.0; Na, 28.1%.

N-deuterated NMF, $HC(O)NDCH_3$, was produced by the addition of 3.0 ml D_2O to 6.6 g NMF followed by distillation to remove H_2O and HOD. This was repeated three times yielding a product for which >95% H–D exchange was determined by ^1H NMR (methyl group singlet at 2.8 ppm) and IR [ν(N—D) 2471 cm^{-1}].

FT-IR studies: instrumentation and procedures

IR spectra were recorded at 2-cm^{-1} resolution using Nicolet 7199 and 60SX FT-IR spectrometers, with KBr optics and MCT detectors. During data collection, sample cells were maintained at room temperature in a dry-air or nitrogen-purged atmosphere. For studies involving NMF-extracted FeMoco, anaerobic cells with zinc selenide windows (Harrick Scientific) were used. All other data were obtained using demountable cells with sodium chloride windows.

RESULTS AND DISCUSSION

The spectrum of the FeMoco–NMF complex prepared as a dry film in an IR cell is shown in Fig. 1. The vibrational bands above 2000 cm^{-1} are assigned to predominantly N—H and C—H stretching vibrations based on a simple group frequency analysis. The broad band at 3246 cm^{-1} appears in the region where ν(N—H) of amides and ν (O—H) of hydroxyl generally occur.[14] When NMF is replaced by exchange with N-deuterated NMF, or when the

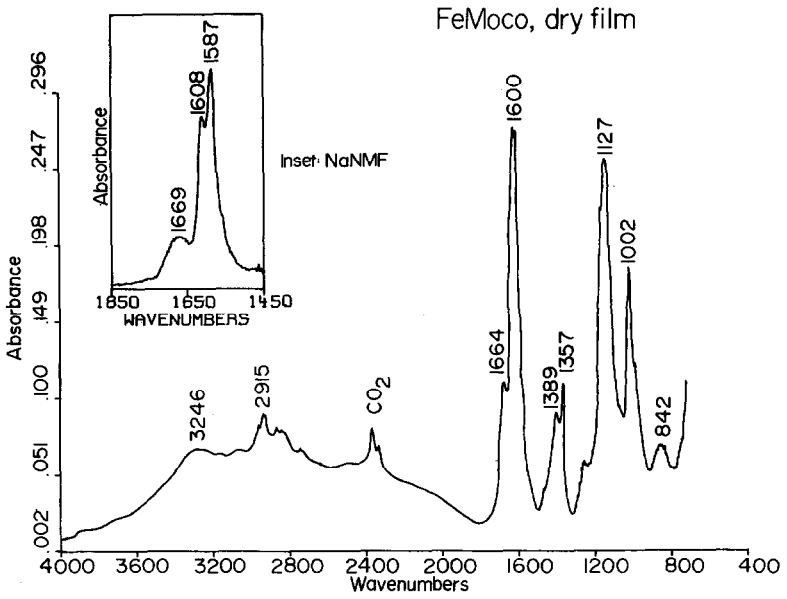


Fig. 1. FT-IR spectrum of FeMoco–NMF complex, 2-cm^{-1} resolution. The sample was prepared as a dry film on the inner face of one of the zinc selenide windows of an anaerobic sample cell. Inset: FT-IR spectrum of NaNMF as a Nujol mull.

FeMoco solution is desalted chromatographically on a Sephadex G-10 column, the positions of the bands above 2000 cm^{-1} are unaffected. Similarly, these bands appear in the spectra of FeMoco solutions isolated from MoFe-protein in either D_2O or H_2O buffer. Accordingly, the 3246-cm^{-1} band is tentatively assigned to a ν(N—H) stretch, possibly from an amino acid, which may be present in preparations of FeMoco obtained by the methods employed in this study. The weak, sharp peaks in the 3000-cm^{-1} region are due primarily to the formyl and methyl C—H stretching vibrations of NMF.[6]

The FeMoco–NMF complex exhibits a prominent vibrational band at 1600 cm^{-1} in its IR spectrum indicative of NMF bonding as an *N*-deprotonated, *N*-bound ligand to certain of the metal centers of FeMoco. Support for this assignment is provided by numerous spectroscopic investigations of transition-metal–amide complexes. In a study of a series of cobalt(III) pentaamine–amide complexes which included two linkage isomers of formamide (Table 1), Balahura and Jordan[10] reported a large ν(C=O) frequency decrease of 65 cm^{-1} (relative to free hydrogen bonding NMF) for one complex with formamide as an *N*-bound, *N*-deprotonated anionic ligand. For other complexes incorporating neutral DMF or formamide, ν(C=O) differed little from the carbonyl frequencies of the free ligands. The large frequency decrease in the *N*-bound anionic ligand was attributed to an enhanced contribution from the resonance structure incorporating an N=C—O^- linkage. A similar explanation for the lowering of a carbonyl stretching frequency was presented by Rosenberg[15] and Kieft and Nakamoto[9] in their studies of bis(glycinamido)copper(II) monohydrate. The occurrence of NMF as a deprotonated anionic ligand in the FeMoco–NMF complex is consistent with the suggestion by Yang *et al.*[11] that NMF in alkaline media is more effective than acidic NMF in extracting FeMoco from its protein matrix. The weak band at 1665 cm^{-1} is likely due to excess NMF solvate judging from its frequency and the decrease in its intensity with extensive sample drying. It may however arise from a normal mode of anionic NMF since the intensity pattern of the carbonyl region

Table 1. Amide carbonyl frequencies

Sample	Frequency (cm^{-1})	Reference
FeMoco	1600	This work
NMF, no hydrogen bonding	1724	5, 7
NMF, hydrogen bonding	1667	5, 7
NaNMF	1608, 1587	This work
Copper(II) bisglycinamide	1570	9
Cobalt(III)$(NH_3)_5$-L		10
L = DMF, O-bound	1655	
L = formamide, *O*-bound	1675	
L = formamide, *N*-Bound	1675	
L = formamide anion, *N*-bound	1600	

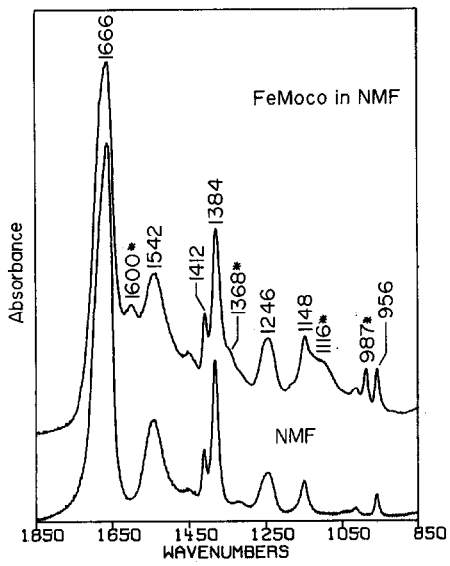


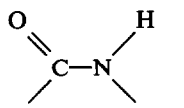
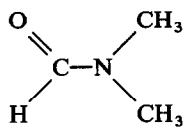
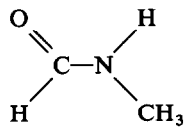
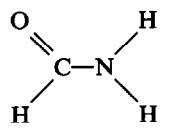
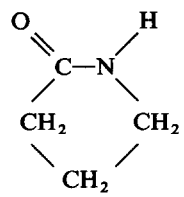
Fig. 2. Top: FT-IR spectrum of FeMoco in NMF, 2-cm^{-1} resolution. The sample was prepared as a liquid film and placed as in Fig. 1. Asterisks denote vibrational bands unique to the FeMoco–NMF complex. Bottom: FT-IR spectrum of NMF solution used for the preparation of FeMoco sample.

bands appearing in the spectrum of the FeMoco–NMF complex bear a resemblance to those of NaNMF (Fig. 1).

Bands occurring in the region below 1600 cm^{-1} cannot be assigned in detail without recourse to a normal-mode analysis. Further isotopic labeling studies currently underway should aid in this effort. However, we assign the intense band at 1127 cm^{-1} to dithionite or one of its reaction products. This follows from the observation that the 1127-cm^{-1} band is not seen in desalted samples in which dithionite has been removed.

Significantly, after anaerobic NMF extraction of FeMoco, the nature of NMF bonding was found to be independent of the physical state of FeMoco. The carbonyl stretching frequency was identical for FeMoco prepared as a dry film either under fully anaerobic conditions or after prolonged exposure to oxygen prior to drying, despite the fact that rapid and complete activity loss occurs upon exposure of FeMoco to air. Typically, we found that samples of the cofactor could not be resuspended in NMF after they had been taken to dryness. In a somewhat more demanding experiment, an NMF solution of FeMoco was concentrated on a zinc selenide IR plate resulting in a liquid thin film which could be rediluted for cofactor specific activity measurements following IR data acquisition. The data obtained in this manner are shown in Fig. 2 along with a solvent reference spectrum. The bands unique to the FeMoco solution spectrum are the same as those observed in the dry film spectrum, indicative of *N*-bound anionic NMF ligation to FeMoco in the

Table 2. Extractants for FeMoco

		Required for extraction
DMF		Does *not* extract
NMF		Extracts well
Formamide		Extracts poorly
Pyrrolidinone		Extracts well

solution state. A 30% decrease in FeMoco specific activity was recorded following IR measurements, most likely the result of oxygen damage. This, however, does not alter the conclusions about the mode of NMF bonding to FeMoco.

The results of our vibrational studies on NMF-extracted FeMoco suggested that other primary and secondary amides should be suitable for the extraction and stabilization of FeMoco. Support for this has been provided by the successful extraction of FeMoco using the cyclic amide 2-pyrrolidinone. The extraction of FeMoco from acid-denatured protein using 2-pyrrolidinone (at 25°C) works equally as well as NMF. In parallel experiments the yields of recovered FeMoco were almost the same (varying between 50 and 70% in both cases) for NMF and 2-pyrrolidinone extracts. Using 2-pyrrolidinone, an average Fe/Mo ratio of 7 ± 1 was obtained for FeMoco extracts. The average specific activity of these samples was 190 ± 30 nmol C_2H_2 reduced min^{-1} (nmol of Mo)$^{-1}$. Both the Fe/Mo ratio and average activity of FeMoco in 2-pyrrolidinone are identical to the values found for FeMoco in NMF (see Materials and Methods for Fe/Mo ratio and activity of NMF-extracted FeMoco samples). Cofactor extracted using 2-pyrrolidinone also exhibits an EPR spectrum identical to that obtained by NMF extraction.

The fact that the cyclic amide 2-pyrrolidinone is able to extract FeMoco indicates that other amides should also be suitable. Presumably the pK_a of the neutral amide is important in this context, and may help to explain why formamide extracts less well than NMF and 2-pyrrolidinone. A summary of the amides used in FeMoco extractions is shown in Table 2.

In conclusion, it would appear from our vibrational studies that NMF is ligated to FeMoco via deprotonated nitrogen, thus contributing significantly to the overall negative charge of the FeMoco–NMF complex. An earlier report[11] suggesting that NMF is the predominant ligand of isolated FeMoco is consistent with the results of this work, but we cannot rule out the occurrence of additional ligands. Further, it has been shown that, in addition to NMF, other secondary amides, e.g. 2-pyrrolidinone, are readily able to extract FeMoco. The results of FT-IR and extraction experiments have implications for the nature of FeMoco binding in the protein. We suggest that FeMoco resides in a protein site where it is bound by deprotonated backbone peptide nitrogens. Work is in progress on this topic. The suggestion of deprotonated amide coordination by the protein is of course very different to the type of binding of 4Fe–4S clusters, for example, which are typically held in the protein by thiolate linkages. Rawlings *et al.*[16] reported that, based on EPR measurements, benzenethiol binds to cofactor, and Burgess *et al.*[17] have quantiated this at one thiolate per Mo atom. The occurrence of FeMoco coordination to the protein via deprotonated peptide nitrogens, a novel feature in proteins, as well-precedented in the coordination chemistry of transition-metal ions.[18]

Acknowledgements—This work was supported by the NSF (8205764-pcm). We thank the S.E.R.C. for postdoctoral support for SKC.

REFERENCES

1. B. K. Burgess, D. B. Jacobs and E. I. Steifel, *Biochim. Biophys. Acta* 1980, **614**, 196.
2. See, for example: (a) M. J. Nelson, P. A. Lindahl and W. H. Orme-Johnson, In *Advances in Inorganic Biochemistry* (Edited by G. L. Eichhorn and L. G. Marzilli), Vol. 4, p. 1 (1982). (b) W. H. Orme-Johnson, *Annu. Rev. Biophys. Chem.* 1985, **14**, 419.
3. M. J. Nelson, M. A. Levy and W. H. Orme-Johnson, *Proc. Natl Acad. Sci. U.S.A.* 1983, **80**, 147.
4. V. K. Shah and W. J. Brill, *Proc. Natl Acad. Sci. U.S.A.* 1977, **74**, 3249.
5. F. R. Dollish, W. G. Fateley and F. F. Bentley, *Characteristic Raman Frequencies of Organic Compounds*, p. 121. Wiley, New York (1974).
6. I. Suzuki, *Bull. Chem. Soc. Jpn* 1962, **35**, 540.
7. E. A. Cutmore and H. E. Hallam, *Spectrochim. Acta* 1969, **25A**, 1767.
8. W. Kutzelnigg and R. Mecke, *Spectrochim. Acta* 1962, **18**, 549.
9. J. A. Kieft and K. Nakamoto, *Inorg. Chim. Acta* 1968, **2**, 225.
10. R. J. Balahura and R. B. Jordan, *J. Am. Chem. Soc.* 1970, **92**, 1533.
11. S.-S. Yang, W. H. Pan, G. D. Friesen, B. K. Burgess, J. L. Corbin, E. I. Stiefel and W. E. Newton, *J. Biol. Chem.* 1982, **257**, 8042.
12. T. R. Hawkes and B. E. Smith, *Biochem. J.* 1983, **209**, 43.
13. W. S. Fones, *J. Org. Chem.* 1949, **14**, 1099.
14. L. J. Bellamy, *The Infra-red Spectra of Complex Molecules*. Chapman & Hall, London (1975).
15. A. Rosenberg, *Acta Chem. Scand.* 1957, **11**, 1390.
16. J. Rawlings, V. K. Shah, J. R. Chisnell, W. J. Brill, R. Zimmerman, E. Munck and W. H. Orme-Johnson, *J. Biol. Chem.* 1978, **253**, 1001.
17. B. K. Burgess, E. I. Steifel and W. E. Newton, *J. Biol. Chem.* 1980, **255**, 353.
18. See, for example: L. L. Diaddario, W. R. Robinson and D. W. Margerum, *Inorg. Chem.* 1983, **22**, 1021 (and references therein).

Polyhedron Vol. 5, No. 1/2, pp. 567–572, 1986
Printed in Great Britain

0277–5387/86 $3.00 + .00
© 1986 Pergamon Press Ltd

IRON–MOLYBDENUM COFACTOR OF *AZOTOBACTER VINELANDII* NITROGENASE: OXIDATION–REDUCTION PROPERTIES AND STRUCTURAL INSIGHTS

W. E. NEWTON*
Western Regional Research Center, USDA–ARS, Berkeley, CA 94710, U.S.A.

F. A. SCHULTZ
Department of Chemistry, Florida Atlantic University, Boca Raton, FL 33432, U.S.A.

S. F. GHELLER, S. LOUGH and J. W. McDONALD
Battelle–Kettering Research Laboratory, Yellow Springs, OH 45387, U.S.A.

and

S. D. CONRADSON, B. HEDMAN and K. O. HODGSON
Department of Chemistry, Stanford University, Stanford, CA 94305, U.S.A.

(*Received* 4 *July* 1985)

Abstract—Structural, oxidation–reduction and compositional probes of the iron–molybdenum cofactor (FeMoco) from the MoFe protein of *Azotobacter vinelandii* nitrogenase have been undertaken, via a variety of physicochemical techniques, to gain insight into the nature of this entity. Using highly concentrated (> 1 mM) solutions of extruded FeMoco in *N*-methylformamide (NMF), details of its oxidation–reduction behavior have been garnered for the first time. A combination of cyclic voltammetry, potentiometry and electron paramagnetic resonance (EPR) spectroscopy has shown that, of the two "quasi-reversible", couples observed, the more-positive couple (at *ca* −0.3 V vs NHE) corresponds to the "oxidized"-to-"semi-reduced" change as demonstrated by the production of the unique $S = \frac{3}{2}$ EPR signal of FeMoco on titration through this couple with aliquots of aqueous dithionite. Plots of EPR intensity vs added electrons and Nernst plots of these data are consistent with the involvement of a single electron in this process. The more negative couple at *ca* −1.0 V may well involve the substrate-reducing state of FeMoco. No synthetic Mo–Fe–S–O compound has yet been found which duplicates these electrochemical properties. X-ray absorption spectroscopy studies at the Mo *K*-edge of similar highly concentrated FeMoco solutions have produced high-quality data in terms of the near-edge (XANES) spectra. Comparisons with similar data sets from FeMoco bound within the protein matrix indicate some (but not radical) structural flexibility or variability around the Mo site. The XANES of a variety of synthetic Mo compounds, which fall into three major categories: (i) Mo in an approximately tetrahedral environment, e.g. $[Fe(MoS_4)_2]^{3-}$, which exhibits two inflection points on the Mo absorption edge at *ca* 20,004 and 20,010 eV; (ii) Mo in all-sulfur, pseudo-octahedral environment, e.g. the dicubane $[Mo_2Fe_6S_8(SEt)_9]^{3-}$, which has a single inflection point at *ca* 20,010 eV; and (iii) Mo in a mixed sulfur–oxygen, pseudo-octahedral environment, e.g. $[Mo_2Fe_6S_8(SEt)_6(OMe)_3]^{3-}$, which has two inflection points at *ca* 20,012 and 20,020 eV, have also been obtained. The XANES of FeMoco, both within and outside the protein, show a marked similarity to those of compounds of the third category, indicating Mo nearest neighbors of 3O (or N) and 3S from anionic ligands. These results are consistent with the structural data derived from the deconvolution of the EXAFS of similar extruded and protein-bound FeMoco samples. Oxidative decomposition studies of isolated FeMoco are also consistent with a coordination environment of only three S atoms around Mo.

* Author to whom correspondence should be addressed.

The iron–molybdenum cofactor (FeMoco) is the extruded, putative N_2-reducing site of the enzyme nitrogenase.[1] The MoFe protein component of nitrogenase contains two such cofactors, each of which accounts for one Mo, *ca* 50% (six–eight atoms) of the Fe and probably eight or nine S atoms[2–4] arranged in a cluster, so far unrecognized elsewhere in biology.[3–10] Structural, oxidation–reduction and compositional probes of the FeMoco from the MoFe protein of *Azotobacter vinelandii* nitrogenase have been undertaken, via a variety of physical and chemical techniques, to gain insight into the nature of this entity. These probes include a combination of cyclic voltammetry, potentiometry and electron paramagnetic resonance (EPR) spectroscopy, X-ray absorption spectroscopy (XAS) and the oxidative elicitation and trapping of thiomolybdates.

Inasmuch as a major function of FeMoco is to transfer electrons to the substrate, experiments designed to characterize its electrochemical behavior have been undertaken both to determine the extent to which the redox properties of extruded FeMoco correlate with those of FeMoco bound within the intact MoFe protein and to establish correspondence between oxidation levels and spectroscopic properties. Herein, the redox properties of isolated FeMoco, as characterized by both cyclic voltammetry (CV) and chemical redox titrations with voltammetric, potentiometric and EPR spectroscopic monitoring, are discussed.[11] As part of our continuing XAS studies of the Mo environments in nitrogenase,[6,12] good quality Mo *K*-edge X-ray data have been collected for both the dithionite-reduced state of the MoFe protein and free FeMoco and a variety of Mo compounds, including bimetallic clusters of several structural types. These XANES of FeMoco and the synthetic clusters are compared and, together with the EXAFS data, provide a more detailed insight into the structure at the Mo site of the native cluster. These compositional insights are in line with the results of the oxidative decomposition of FeMoco, in the presence and absence of trapping agents, when trithiomolybdate is elicited.

EXPERIMENTAL

Materials

The synthetic Mo compounds were prepared by methods in the indicated literature references.

The MoFe protein of *A. vinelandii* was purified to homogeneity as described previously.[13] The specific activity of the protein samples used was always >2000 nmol C_2H_2 reduced min^{-1} (mg protein)$^{-1}$.

FeMoco was prepared from such protein by the large-scale HCl–NaOH modification[3] of the original isolation method.[2] *N*-methylformamide (NMF) extracts were concentrated either by vacuum distillation[13] followed by centrifugation to separate solid material or by column chromatography on DE-52 DEAE cellulose (Whatman) in NMF.[11] Sample solutions had [Mo] = 0.6–1.7 mM, Fe/Mo = 6.05–7.10, and activities in the UW45 reconstitution assay[2] of 224–276 nmol C_2H_2 reduced min^{-1} (ng-atom Mo)$^{-1}$. All sample solutions were 1–2 mM in $Na_2S_2O_4$. Sample integrity was monitored by activity determinations, which revealed $<10\%$ decrease after XAS and electrochemical measurements. Similarly, the before and after EPR spectra (at 10 K) were virtually identical and corresponded to those of previous preparations.[3,9]

XAS measurements

All data were acquired at the Stanford Synchrotron Radiation Laboratory under dedicated synchroton radiation production conditions. Spectra were calibrated with Mo foil, with the first inflection point in the edge absorption spectrum taken as 20,003.9 eV. Synthetic compounds were measured as solids at ambient temperature. Spectra of MoFe protein and FeMoco samples were obtained in aqueous buffer at 2–4°C and NMF solutions at -15 to -25°C, respectively. All measurements were performed under anaerobic conditions. Second derivatives of the absorbance vs energy were obtained by differentiation of a third-order polynomial fit to the data over an interval of ± 3.5 eV on each side of a data point.

Electrochemistry and chemical redox titrations

CV and chemical redox titrations were conducted in a small-volume (100 cm^3) cell that consisted of a Teflon collar threaded onto the shaft of an inverted glassy carbon (working) electrode (Bioanalytical Systems, West Lafayette, IN). A Pt wire auxiliary electrode was inserted through the Teflon collar. The reference electrode, a miniature Ag–AgCl (1M KCl) electrode (MI-401, Microelectrodes Inc., Londonderry, NH), was immersed directly in the sample solution at the time of measurement. The Teflon cell was evacuated for 12–24 h in the antechamber of the glove box before use. About 50–75 cm^3 of FeMoco solution was transfered to the cell for electrochemical measurements. For chemical titrations, appropriate quantities of aqueous 0.02 M $Na_2S_2O_4$ were mixed with aliquots (350-cm^3) of FeMoco solution. Sixty microliters were then transferred to the electrochemical cell and the

remainder to a matched quartz EPR tube and frozen 10 min after dithionite addition. The equilibrium potential was determined by measuring the potential difference between the glassy carbon and Ag–AgCl electrodes. Cyclic voltammograms were generated with a Bioanalytical Systems CV-1B potentiostat. All electrochemical and recording equipment was connected to the cell by shielded cable passing through an air-tight seal in the glove box. Except as noted, all potentials have been corrected to NHE.

Oxidative decompositions

Two experimental protocols were used. In a typical dioxygen-titration experiment, FeMoco (4 cm^3 of an NMF solution of 50–60 μM in Mo) in a suitable spectroscopic cell was treated with successive measured aliquots (100–350 cm^3) of air. The visible spectrum (350–800 nm) was monitored until invariant after each addition and then recorded. The final treatment of all samples was bubbling with dioxygen for 2 min. Again, a final spectrum was recorded, when stable. In all cases, visible absorption bands at 465 and 395 nm were observed, consistent with the formation of $[MoOS_3]^{2-}$.

The second procedure involved mixing aliquots of chromatographically purified FeMoco (300–500 cm^3 of a >1 mM in Mo anaerobic NMF solution) with an excess of $(Ph_3P)_2CuNO_3$ (10 mg) in acetonitrile in air. Red, but poorly formed, crystals developed after several days at 5°C to leave a colorless solution. Visible (λ_{max} 380 nm in $CHCl_3$) and IR [ν(Mo=O) 910 cm^{-1}, ν(Mo—S—Cu), 445, 452 cm^{-1}] spectroscopy are consistent with the cubane[14] formulation $[OMo(CuPPh_3)_3S_3Br]$.

RESULTS AND DISCUSSION

Oxidation–reduction properties

The FeMoco within the protein exhibits three oxidation states: (i) FeMoco(s-r), the EPR-active, $S = \frac{3}{2}$ semi-reduced form that is produced and maintained in the presence of excess $Na_2S_2O_4$; (ii) FeMoco(ox), with $S = 0$ and EPR-silent, prepared by dye oxidation of FeMoco(s-r); and (iii) FeMoco(red), the integer spin, EPR-silent, substrate-reducing state, achieved only in the full nitrogenase system.[15–17] The MoFe protein does not exchange electrons directly with an electrode, but requires redox mediators, such as the viologens.[17] Even then, its redox couples exhibit considerable hysteresis. The average potentials for the two couples in the *A. vinelandii* MoFe protein are -0.17 and -0.465 V vs NHE,[17] although the latter, being the substrate turnover potential, may be too positive because it neglects any contribution from the energy-yielding ATP hydrolysis that is mandatory for catalysis.

Because shifts[18] of *ca* -0.4 V in redox potential are experienced by [4Fe–4S] clusters upon transfer from an aqueous protein matrix into an organic solvent (as a synthetic analogue), by analogy, waves at *ca* -0.57 and -0.87 V vs NHE, respectively, were sought in cyclic voltamograms of isolated FeMoco. In fact, cyclic voltammetry of oxidized, EPR-silent FeMoco does show two reduction processes, one beginning at *ca* -0.4 V vs NHE and a second at *ca* -1.1 V with the related oxidation waves occurring at -0.21 and -0.85 V, respectively, in reasonable agreement with the predictions. Thus, oxidized cofactor appears to be interconverted with its semi-reduced form by reduction at *ca* -0.4 V and oxidation at *ca* -0.2 V to give a formal potential of -0.3 V. The second quasi-reversible redox process has a formal potential of -1.00 V. If these processes correspond directly to those of protein-bound FeMoco, this second wave represents reduction to the substrate-reducing state. Because the separation of the oxidation and reduction waves is in the range of 120–240 mV (at $v = 0.1$ V s^{-1}), some charge-transfer irreversibility accompanying the cofactor reductions is indicated in line with the hysteresis associated with the protein-bound FeMoco redox processes. The mean values of the current parameter for reduction of FeMoco(s-r), following electrochemical reduction of FeMoco(ox), and for oxidation of FeMoco(s-r), produced by the one-electron chemical reduction of FeMoco(ox), are 331 and 284 $\mu A\ s^{1/2}\ V^{-1/2}\ cm^{-2}\ mM^{-1}$, respectively, when the Mo concentration is corrected for the 78% EPR activity exhibited by the samples. These two values are not unreasonable for one-electron transfers in NMF (cf. 375 $\mu A\ s^{1/2}\ V^{-1/2}\ cm^{-2}\ mM^{-1}$ for methyl viologen in NMF) and support a one-electron stoichiometry for both redox processes.

To confirm the one-electron stoichiometry, a sample of EPR-silent FeMoco was titrated with sodium dithionite while monitoring the CV, potentiometric and EPR spectroscopic responses. The initial rest potential was -0.23 V. As dithionite was added: (i) the solution rest potential shifted from values more positive than -0.3 V to more negative values, (ii) the primary reduction current decreased and the primary oxidation current increased, and (iii) the $S = \frac{3}{2}$ EPR signal developed to maximum intensity after addition of 0.78 electrons (g-atom Mo)$^{-1}$. A Nernst plot of these data had a potential at half-intensity of -0.30 V and a reciprocal slope of 65 mV ($n = 0.91$ at 25°C).

The foregoing results demonstrate that FeMoco is converted from its oxidized to semi-reduced state by

a chemically reversible, one-electron transfer. Based on the similarity in potentials and our ability to monitor oxidized and reduced species during the course of these titrations, this chemical process is the same as that observed by direct CV measurements.

Attempts to determine the electrochemical behavior in 0.1 M $[Et_4N]Br$–NMF of $[Fe_4S_4(SPh)_4]^{2-}$,[18] $[Fe(MoS_4)_2]^{3-}$,[19] $[Fe(WS_4)_2]^{3-}$,[19] and $[Mo_2Fe_6S_8(SPh)_9]^{3-}$[20] were made, but each of these molecules either decomposes in NMF or exhibits behavior so different from its reported electrochemistry in other solvents that a significant chemical change must have taken place. Thus, these compounds cannot be closely correlated models for FeMoco. A model with two quasi-reversible redox couples separated by 0.7 V at *ca* −0.3 and −1.0 V vs NHE in a polar aprotic solvent or at *ca* +0.1 and −0.6 V vs NHE in aqueous solution could indicate close correlation with FeMoco. Perusal of electrochemical data reported for Mo–Fe–S–O cluster complexes, however, shows that none fully satisfy this criterion, although of course, no data set was collected in NMF.

Structural insights

The most incisive structural information on FeMoco has come from XAS.[6,12,21,22] XAS is the general term used to describe both the edge, near (or above) edge (XANES) and extended fine structure (EXAFS) regions of the X-ray absorption spectrum. The edge and XANES regions, collectively referred to as XANES herein, provide insights into the geometric and electronic state of the absorbing atoms, while the EXAFS region provides metrical details of the coordination sphere around the absorber. Comparisons of the XANES of a variety of Mo compounds with those from FeMoco, both within and free of the MoFe protein, show a distinct correlation between the shapes of the absorption edge features and the environment of nearest-neighbor atoms around the Mo atom. The Mo compounds investigated constitute an extensive set of mononuclear compounds and both linear and cubane cluster types, in which two–four sulfide and one–three Fe atoms are within bonding distances of the Mo atom. Certain examples contain thiolates and alkoxides coordinated to the Mo atom also. The XANES of these synthetic compounds fall into three distinct subsets, which correlate with certain attributes of their structures.

Members of the first subset contain $[MoS_4]^{2-}$ as the common unit. Compounds examined were $[NH_4]_2[MoS_4]$,[23,24] $[X_2FeMoS_4]^{2-}$ (X = PhS[25] or Cl[26]), $[(Cl_2Fe)_2MoS_4]^{2-}$[27] and $[Fe(MoS_4)_2]^{3-}$.[19,28] Spectral features are identical, within the experimental limitations, for all compounds up to 20,020 eV. Inflection points occur near 20,004 and 20,011 eV, corresponding to a lower energy shoulder and the principal absorption edge discontinuity, respectively. Corresponding low-energy features have been observed in the XANES of all compounds containing terminal Mo=O or Mo=S groups.[21,22]

The second subset consists of the double cubanes

$$[Mo_2Fe_6S_8(SEt)_9]^{3-}\ ^{29,30}$$

and

$$[Mo_2Fe_7S_8(SEt)_{12}]^{3-/4-}\ ^{29,31}$$

plus $Mo(S_2C_6H_4)_3$.[32] The common feature of this category is the $Mo–S_6$ coordination unit. The spectra reveal a single inflection point at *ca* 20,011 eV for all compounds corresponding to the principal absorption discontinuity.

The third group consists of the single cubane

$$[MoFe_3S_4(SEt)_3Fe(cat)_3]^{3-}\ ^{33}$$

and the methoxy-bridged dicubane

$$[Mo_2Fe_6S_8(SEt)_6(OMe)_3]^{3-},^{30,34}$$

both with MoS_3O_3 coordination units of effective C_{3v}-symmetry. The inflection point of the principal absorption discontinuity occurs at 20,012–20,013 eV, which is slightly, but consistently, higher than those for the second subset and may result from the lower polarizability of the O ligands relative to S. In contrast to the previous subsets, these curves also exhibit a shoulder at higher energies.

Because of this observed association between the XANES of the Mo compounds and the structures of the first shell of the Mo atom's nearest neighbors, information about the Mo site of nitrogenase may be obtained by a comparison of XANES spectra. The XANES appears to be more sensitive to the atoms and chemical nature of the bonds between the Mo and its neighbors than to metrical and symmetry variations. Thus, close correspondence of the XANES from the sample of interest to that from a standard implies structural and chemical similarity more than identity, while a difference in the XANES is an unequivocal indication of a structural difference. The XANES of the FeMoco samples are very similar to one another and have their inflection points, the principal absorption discontinuity, at 20,012–20,013 eV with a shoulder at 20,018–20,020 eV. On the basis of the comparisons of XANES of the synthetic compounds and the nitrogenase samples in the region 20,000–20,020 eV, the following unambiguous conclusions can be drawn concerning the Mo site structure in the enzyme and cofactor. It is most closely approached by those compounds

possessing MoS_3O_3 coordination units with Mo–O bond lengths in the 2.1–2.2-Å range. This similarity indicates that the nearest neighbors of Mo in nitrogenase consist of a significant number of both singly bound hard and soft ligands. Any changes in the structure resulting from the extraction of FeMoco from the protein must be sufficiently small so that the basic structure is conserved. These conclusions based on XANES studies are completely consistent with and complementary to results from Mo EXAFS studies.[6,12]

Support for these conclusions was sought through the controlled oxidative degradation of FeMoco. These efforts were based on a previous report that thiomolybdates were released from the intact MoFe protein by the appropriate acid–base treatment[35] and our observation that FeMoco is decomposed with respect to its iron atoms by dioxygen.[3] Thus, when FeMoco was subjected to controlled dioxygenation in a spectral cell with monitoring over 350–800 nm, the initial, virtually featureless FeMoco spectrum showed some striking changes. First, a feature at 500–600 nm appeared, possibly due to a species containing an Mo–S–Fe unit,[10,19] followed by a general absorbance decrease over the whole range. The final spectrum had, as its only major absorption bands, absorbances at 465 and 395 nm, which are characteristic of $[MoOS_3]^{2-}$.[23] A steeply rising background starting at *ca* 400 nm, however, made quantitative spectral simulation difficult, but at least 75% (and maybe all) of the released thiomolybdates must be $[MoOS_3]^{2-}$. Confirmation of this conclusion was obtained when a $(PPh_3)_2Cu$ trap was employed for the released thiomolybdate. The red crystals, which formed when FeMoco was mixed with an aerobic $(PPh_3)_2CuNO_3$ solution, were shown to be $[OMo(CuPPh_3)_3S_3Br]$ by a combination of visible, IR and Raman spectroscopies, plus X-ray data from the poorly diffracting crystals. Even though these last data were severely limited by the poor crystal quality, they clearly showed the basic cubane structure of the molecule and the presence of bromide.

A reasonable interpretation of these data is that FeMoco contains an MoS_3 core, consistent with our EXAFS results.[6,12] In fact, these data constitute a refinement in that they firm up the number of S neighbors to Mo in extruded FeMoco, the softest parameter from the EXAFS investigation, by clearly distinguishing between the two possibilities of 3 and 4. A comparison of these data with the mixture of tetra- and tri-thiomolybdates observed on treatment of the intact MoFe protein[35] suggests that, again in line with the EXAFS results, a real difference exists in the first coordination sphere of Mo within and outside the protein matrix.

Acknowledgements—We thank B. Bolton and S. Kint for obtaining the Raman and IR spectra, respectively. We gratefully acknowledge support through grants No. PCM-81-10355 (to WEN), PCM-82-08115 (to KOH) and CHE-82-11694 (to FAS) from the National Science Foundation and 5-RO1-AM-30812 (to WEN) from the Department of Health and Human Resources, Public Health Service. Stanford Synchroton Radiation Laboratory is supported by the Department of Energy, Office of Basic Energy Sciences, the National Institutes of Health, Biotechnology Resource Program and the National Science Foundation, Division of Materials Research.

REFERENCES

1. T. R. Hawkes, P. A. McLean and B. E. Smith, *Biochem. J.* 1984, **217**, 317.
2. V. K. Shah and W. J. Brill, *Proc. Natl Acad. Sci. U.S.A.* 1977, **74**, 3249.
3. S.-S. Yang, W.-H. Pan, G. D. Friesen, B. K. Burgess, J. L. Corbin, E. I. Stiefel and W. E. Newton, *J. Biol. Chem.* 1982, **257**, 8042.
4. M. J. Nelson, M. A. Levy and W. H. Orme-Johnson, *Proc. Natl Acad. Sci. U.S.A.* 1983, **80**, 147.
5. B. K. Burgess and W. E. Newton, In *Nitrogen Fixation, The Chemical–Biological–Genetic Interface* (Edited by A. Müller and W. E. Newton), p. 83. Plenum Press, New York (1983).
6. W. E. Newton, B. K. Burgess, S. C. Cummings, S. Lough, J. W. McDonald, J. F. Rubinson, S. D. Conradson and K. O. Hodgson, In *Advances in Nitrogen Fixation Research* (Edited by C. Veeger and W. E. Newton), p. 160. Martinus Nijhoff, The Hague (1984).
7. M. R. Antonio, B.-K. Teo, W. H. Orme-Johnson, M. J. Nelson, S. E. Groh, P. A. Lindahl, S. M. Kauzlarich and B. A. Averill, *J. Am. Chem. Soc.* 1982, **104**, 4703.
8. J. Rawlings, V. K. Shah, J. R. Chisnell, W. J. Brill, R. Zimmerman, E. Munck and W. H. Orme-Johnson, *J. Biol. Chem.* 1978, **253**, 1001.
9. B. K. Burgess, E. I. Stiefel and W. E. Newton, *J. Biol. Chem.* 1980, **255**, 353.
10. (a) R. H. Holm, *Chem. Soc. Rev.* 1981, **10**, 455; (b) D. Coucouvanis, *Acc. Chem. Res.* 1981, **14**, 201; (c) B. A. Averill, *Struct. Bonding (Berlin)* 1983, **53**, 59.
11. F. A. Schultz, S. F. Gheller, B. K. Burgess, S. Lough and W. E. Newton, *J. Am. Chem. Soc.* 1985, **107**, 5364.
12. B. K. Burgess, S.-S. Yang, C.-B. You, J.-G. Li, G. B. Friesen, W.-H. Pan, E. I. Stiefel, W. E. Newton, S. D. Conradson and K. O. Hodgson, In *Current Perspectives in Nitrogen Fixation* (Edited by A. H. Gibson and W. E. Newton), p. 71. Elsevier–North-Holland, Amsterdam (1981).
13. B. K. Burgess, D. B. Jacobs and E. I. Stiefel, *Biochim. Biophys. Acta* 1980, **614**, 196.
14. A. Müller, H. Bogge and U. Schimanski, *Inorg. Chim. Acta* 1983, **69**, 5.
15. (a) E. Munck, H. Rhodes, W. H. Orme-Johnson, L. C. Davis, W. J. Brill and V. K. Shah, *Biochim. Biophys. Acta* 1975, **400**, 32; (b) R. Zimmerman, E. Munck, W. J. Brill, V. K. Shah, M. T. Henzl, J. Rawlings and W. H.

Orme-Johnson, *Biochim. Biophys. Acta* 1978, **537**, 185; (c) B. H. Hunyh, E. Munck and W. H. Orme-Johnson, *Biochim. Biophys. Acta* 1979, **576**, 192; (d) J. P. Smith, M. H. Emptage and W. H. Orme-Johnson, *J. Biol. Chem.* 1982, **257**, 2310.

16. M. J. O'Donnell and B. E. Smith, *Biochem. J.* 1978, **173**, 831.
17. (a) G. D. Watt, A. Burns and S. Lough, *Biochemistry* 1980, **19**, 4926; (b) G. D. Watt, A. Burns and D. L. Tennent, *Biochemistry* 1981, **20**, 7277; (c) S. Lough, A. Burns and G. D. Watt, *Biochemistry* 1983, **22**, 4062.
18. (a) C. L. Hill, J. Renaud, R. H. Holm and L. E. Mortenson, *J. Am. Chem. Soc.* 1977, **99**, 2549; (b) B. V. DePamphilis, B. A. Averill, T. Herskovitz, L. Que, Jr and R. H. Holm, *J. Am. Chem. Soc.* 1974, **96**, 4159.
19. G. D. Friesen, J. W. McDonald, W. E. Newton, W. B. Euler and B. M. Hoffman, *Inorg. Chem.* 1983, **22**, 2202.
20. G. Christou and C. D. Garner, *J. Chem. Soc., Dalton Trans.* 1980, 2354.
21. S. P. Cramer, K. O. Hodgson, W. O. Gillum and L. E. Mortenson, *J. Am. Chem. Soc.* 1978, **100**, 3398.
22. (a) F. W. Kutzler, C. R. Natoli, D. K. Misemer, S. Doniach and K. O. Hodgson, *J. Chem. Phys.* 1980, **73**, 3274; (b) F. W. Kutzler, R. A. Scott, J. M. Berg, K. O. Hodgson, S. Doniach, S. P. Cramer and C. H. Chang, *J. Am. Chem. Soc.* 1981, **103**, 6083.
23. J. W. McDonald, G. D. Friesen, L. D. Rosenhein and W. E. Newton, *Inorg. Chim. Acta* 1983, **72**, 205.
24. (a) M. G. Kanatzidis and D. Coucouvanis, *Acta Cryst.* 1983, **C39**, 835; (b) P. J. Lapasset, N. Chezeau and P. Belounge, *ibid.* 1976, **B32**, 3087.
25. D. Coucouvanis, P. Stremple, E. D. Simhon, D. Swenson, N. C. Baenziger, M. Draganjac, L. T. Chan, A. Simopoulos, V. Papaefthymiou, A. Kostikas and V. Petrouleas, *Inorg. Chem.* 1983, **22**, 293.
26. (a) R. H. Tieckelmann, H. C. Silvis, T. A. Kent, B. H. Huynh, J. V. Waszczak, B.-K. Teo and B. A. Averill, *J. Am. Chem. Soc.* 1980, **102**, 5550; (b) B.-K. Teo, M. R. Antonio and B. A. Averill, *ibid.* 1983, **105**, 3751.
27. D. Coucouvanis, E. D. Simhon, P. Stremple, M. Ryan, D. Swenson, N. C. Baenziger, A. Simopoulos, V. Papaefthymiou, A. Kostikas and V. Petrouleas, *Inorg. Chem.* 1984, **23**, 741.
28. D. Coucouvanis, E. D. Simhon amd N. C. Baenziger, *J. Am. Chem. Soc.* 1980, **102**, 6644.
29. T. E. Wolff, J. M. Berg, K. O. Hodgson, R. B. Frankel and R. H. Holm, *J. Am. Chem. Soc.* 1979, **101**, 4140.
30. S. R. Acott, G. Christou, C. D. Garner, T. J. King, F. E. Mabbs and R. M. Miller, *Inorg. Chim. Acta* 1979, **35**, L337.
31. (a) T. E. Wolff, P. P. Power, R. B. Frankel and R. H. Holm, *J. Am. Chem. Soc.* 1980, **102**, 4694; (b) T. E. Wolff, J. M. Berg, P. P. Power, K. O. Hodgson and R. H. Holm, *Inorg. Chem.* 1980, **19**, 430.
32. E. I. Stiefel, R. Eisenberg, R. C. Rosenberg and H. B. Gray, *J. Am. Chem. Soc.* 1966, **88**, 2956; (b) M. Cowie and M. J. Bennett, *Inorg. Chem.* 1976, **15**, 1584.
33. T. E. Wolff, J. M. Berg and R. H. Holm, *Inorg. Chem.* 1981, **20**, 174.
34. L. Huang and S. Lin, *Jiegou Huaxue* (*J. Struct. Chem.*) 1984, **3**, 25.
35. W. G. Zumft, *Eur. J. Biochem.* 1978, **91**, 345.

Polyhedron Vol. 5, No. 1/2, pp. 573–576, 1986
Printed in Great Britain

0277-5387/86 $3.00 + .00
© 1986 Pergamon Press Ltd

STUDIES ON THE OXIDATION STATE OF MOLYBDOPTERIN

K. V. RAJAGOPALAN,* STEVEN KRAMER and SUSAN GARDLIK

Department of Biochemistry, Duke University Medical Center, Durham, NC 27710, U.S.A.

(*Received* 26 *June* 1985)

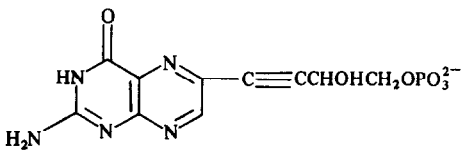
Abstract—Molybdopterin, the organic component of the molybdenum cofactor common to all molybdenum-containing enzymes except nitrogenase, is proposed to contain two vicinal thiols capable of complexing Mo. The pterin ring is in an unknown state of reduction in the active cofactor. We have used subtractive difference spectroscopy for examining the reduction state of the pterin in sulfite oxidase and xanthine oxidase under rigorously anaerobic conditions in 6 M guanidinium chloride. It is concluded that the molybdopterin is in the tetrahydro form in both enzymes. Alkylation of molybdopterin with iodoacetamide in denatured samples of sulfite oxidase yields a derivative which contains two alkyl groups per phosphate and is in the tetrahydro form. These findings are in accord with the proposed presence of two thiols in the cofactor, and provide additional evidence for the state of reduction in the pterin.

The Mo cofactor common to all hydroxylase-type molybdoenzymes is functionally identified as a substance which can be released from purified Mo-containing proteins by any of a variety of denaturation techniques and is then capable of reconstituting the apoprotein of nitrate reductase in extracts of *Neurospora crassa nit-1* cells.[1] Studies on degradation products of the cofactor in our laboratory have shown that the organic component of Mo cofactor is a novel pterin with a phosphorylated 4-carbon side chain, postulated to contain a pair of vicinal sulfhydryl groups.[2] The extreme instability of the Mo cofactor, especially under oxidizing conditions, has been interpreted to be due to the oxidation of a reduced form of pterin, termed molybdopterin, present in the active cofactor. The structures of two major oxidized derivatives of molybdopterin, termed form A and form B, and of urothione, a urinary metabolite of Mo cofactor,[2] are shown in Fig. 1 along with the proposed structure of the Mo cofactor.

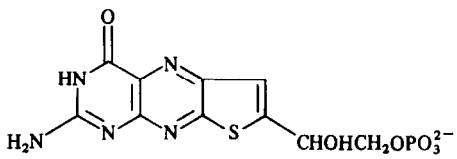
Studies on sulfite oxidase have shown that molybdopterin is bound tightly but non-covalently to the protein, is present in a stoichiometry of 1 : 1 : 1 with respect to protein subunit and Mo, and does not contain the thiophene ring present in form B and urothione.[3] Examination of the phosphate content and yield of form A from several molybdoenzymes has shown that all of the enzymes studied contain one molybdopterin per subunit.[4] The fact that molybdopterin can be isolated in a form which retains most of its activity and is virtually devoid of amino acids rules out the presence of a peptide in the Mo cofactor.[5] To date there is no evidence for the presence of any organic constituent other than molybdopterin in the cofactor.

As shown in Fig. 1D, we have proposed that Mo is complexed to molybdopterin via the vicinal sulfhydryl groups.[2] Evidence for the existence of a complex has been derived from our demonstration that the Mo cofactor released from denatured sulfite oxidase at pH 7 is fully active in the *nit-1* reconstitution assay in the absence of extraneous Mo for a short duration whereas cofactor released at pH 8 is devoid of activity in the absence of molybdate.[6] The Mo cofactor relased at pH 7.0 is rendered molybdate-dependent by treatment with Hg^{2+} and other sulfhydryl reagents, indicating thiolate ligation of the Mo in the cofactor.[6] The marked protection afforded by arsenite against inactivation by sulfhydryl reagents presumably reflects the strong binding of arsenite to the vicinal SH groups in the cofactor.[7]

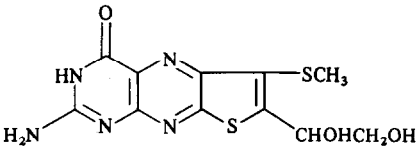
* Author to whom correspondence should be addressed.



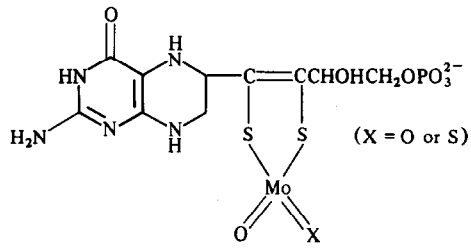
1A



1B



1C



1D

Fig. 1. Structures of molybdopterin and derivatives.

More recently, we have initiated investigations on the oxidation state of molybdopterin in several enzymes. The electronic spectra of pterins are well documented, and can be used to differentiate oxidized, dihydro and tetrahydro forms. In the case of molybdoenzymes the spectral intensities of the protein and of the other prosthetic groups are so much greater than those of pterins that direct observations of the spectral features of molybdopterin is not possible.

The simplest catalytically active Mo protein, the Mo domain of rat liver sulfite oxidase, displays an absorption spectrum[8] which is largely due to the weak chromophore resulting from the binding of Mo(VI) to thiolate ligands, and does not provide information about the state of reduction of the pterin ring in the active cofactor. It is therefore necessary to disrupt the structure of the chromophore before assessing the spectral properties of the pterin.

The extreme instability of Mo cofactor after separation from Mo proteins, leading to loss of activity and generation of multiple species, has made it impossible as yet to isolate the active material in a homogenous state for structural and spectroscopic studies. We have therefore devised procedures for examining the spectral properties of uncomplexed molybdopterin in sulfite oxidase and xanthine oxidase under denaturing conditions. We have also characterized an alkylated inactive derivative prepared from sulfite oxidase and the results are presented here.

METHODS

Alkylation of molybdopterin

Chicken liver sulfite oxidase (10–20 mg/ml) in 0.05 M phosphate buffer, pH 7.8, was mixed with 10 volumes of dimethyl sulfoxide containing 1 mM sodium EDTA and 10 mM sodium ascorbate. The solutions were made anaerobic prior to mixing by repeated evacuation and flushing with oxygen-free nitrogen. After 5 min at room temperature an aliquot was removed for assay of molybdopterin activity by the *nit-1* reconstitution system. At this time, a 100-fold molar excess of an anaerobic solution of iodoacetamide was added to the mixture. After 2 h at room temperature the sample was applied to an *aerobic* QAE-Sephadex column. The column was washed with 0.01 N acetic acid and the carboxamidemethylated molybdopterin (cam-MPT) could then be eluted, together with the ascorbate, with 0.01 N HCl. This material was rapidly frozen in a dry ice–ethanol bath and lyophilized overnight.

The lyophilized material was redissolved in 4 cm^3 of 50 mM ammonium acetate and the cam-MPT was purified by reverse-phase HPLC using an Alltech C18 column and a Spectra-Physics SP8700 solvent delivery system. All HPLC solvents were continuously sparged with helium (ultra high purity grade). Two peaks of cam-MPT were obtained by this procedure. The material in the second peak was rapidly converted to the material in the first peak if precautions to exclude oxygen were not taken dur-

ing fraction collection. Further purification of this, more oxidized, cam-MPT derivative was then accomplished by reverse-phase HPLC using 5% MeOH–95% 100 mM triethylamine with 100 mM acetic acid, pH 6.8, as the mobile phase.

The material in the second peak was pure after reverse-phase HPLC in ammonium acetate and was collected in anaerobic serum vials or cuvettes. Absorption spectra were obtained on a Shimadzu UV-240 spectrophotometer.

For proof of alkylation, as well as the determination of the stoichiometry of the reaction, 0.01 mCi of [1-^{14}C]iodoacetamide (New England Nuclear) was included in the initial iodoacetamide solution. Phosphate analysis of cam-MPT was done by the method of Ames.[9]

Preparation of apo-xanthine oxidase

Apo-xanthine oxidase was made by dialyzing the enzyme against deaerated 6 M guanidine–HCl and 10 mM DTT, pH 7.0, for 24 h, then against 6 M guanidine HCl, pH 7.0, for 48 h.

Difference spectra

To obtain the difference spectrum of the pterin, a solution of apo-xanthine oxidase in 6 M guanidine–HCl (pH 7.0), 1 mM EDTA, and an appropriate amount of FAD was used as the reference against an anaerobic solution of fully active xanthine oxidase in 6 M guanidine–HCl and 1 mM EDTA, pH 7.0. The active enzyme solution was made anaerobic by flushing with nitrogen for 20 min.

Absorption and difference spectra were obtained using a Shimadzu UV240 spectrophotometer. Fluorescence spectra were obtained with an Aminco–Bowman spectrofluorometer.

RESULTS

The UV–visible absorption spectrum of xanthine oxidase is largely composed of the contributions of the Fe/S centers and flavin, and of the protein itself. The spectral properties of the active Mo center of the enzyme are not known, but may be similar to that of the Mo domain of sulfite oxidase.[8] In the presence of 6 M guanidine–HCl, the Fe/S centers and the Mo—S bonds are destroyed, and the resulting spectrum should be the sum of those of the protein, free FAD and free molybdopterin. By using a reference sample containing matching concentrations of molybdopterin-free apoprotein and FAD it should be possible to isolate the absorption spectrum of the pterin in the sample cuvette. Such a difference spectrum of molybdopterin in xanthine oxidase is shown in Fig. 2, along with that of tetrahydrobiopterin in guanidine–HCl. The difference spectrum is clearly that of a tetrahydropterin, with an extinction coefficient appropriate for a stoichiometry of one molybdopterin per subunit. Under the conditions of this experiment the FAD remained fully oxidized, suggesting that the tetrahydro form is the native oxidation state of molybdopterin in xanthine oxidase. Similar results were also obtained in the case of sulfite oxidase. Thus we conclude that in both xanthine oxidase and sulfite oxidase the pterin ring of molybdopterin is in the fully reduced state, as shown in Fig. 1D.

Alkylated molybdopterin

When sulfite oxidase was denatured by addition of 10 volumes of dimethyl sulfoxide and then treated with iodoacetamide, the Mo cofactor activity of the preparation was abolished in about 2 h. No loss of activity occurred in the absence of iodoacetamide. The inactivated molybdopterin was isolated from the mixture by procedures described in Methods. Figure 3 shows the HPLC elution pattern of the sample eluted from the QAE-Sephadex with 0.01 N HCl. The large peak representing unabsorbed material was mainly ascorbate. The peaks labeled A and B both contained radioactivity from the [^{14}C]iodoacetamide. When the two fractions were collected in anaerobic containers and re-examined by HPLC, their elution properties were unaltered. However, if the fractions were collected in air, material from peak B was wholly converted to the

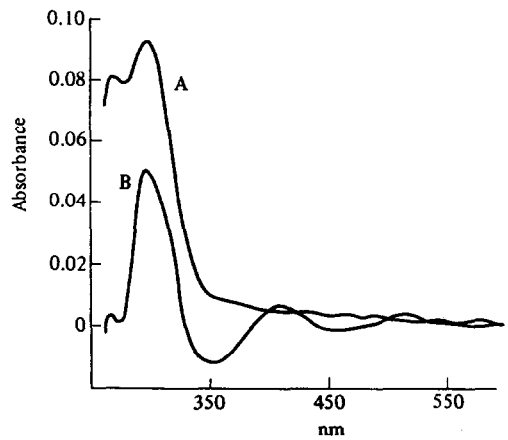


Fig. 2. Difference spectrum (B) of molybdopterin of bovine milk xanthine oxidase in 6 M guanidine–HCl. The sample cuvette contained 1.4 mg/ml of xanthine oxidase, while the reference cuvette contained equivalent concentrations of apoprotein and FAD. Spectrum A is that of tetrahydrobiopterin under the same conditions.

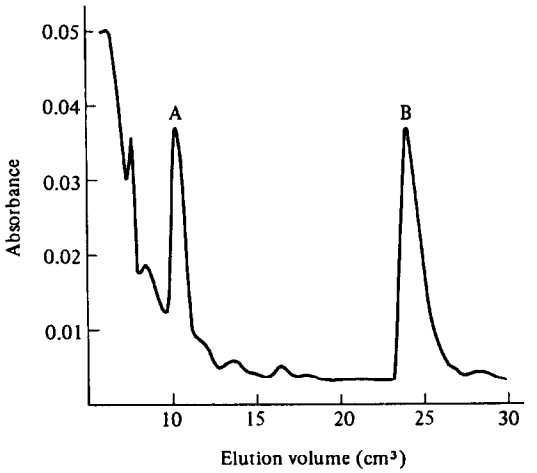


Fig. 3. HPLC analysis of alkylated molybdopterin. Conditions for HPLC are described in Methods. The elution profile was monitored at 280 nm using a Spectra-Physics 8440 detector.

earlier eluting form. These results showed that peak A represents the oxidized form of peak B.

The absorption spectrum of anaerobically collected peak B material is shown in Fig. 4, and corresponds to that of a tetrahydropterin. Air oxidation in the cuvette resulted in an altered absorption spectrum identical to that of the peak A sample, presumably a fully oxidized form.

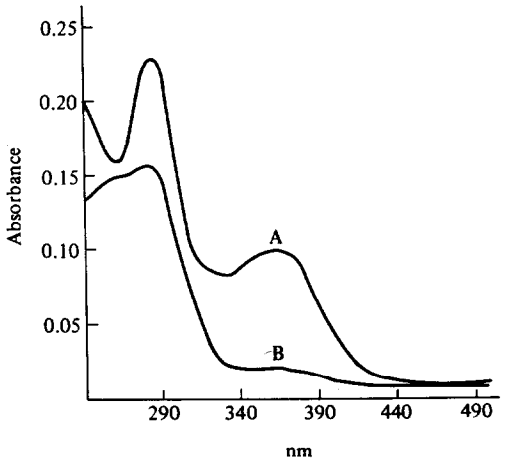


Fig. 4. Absorption spectrum of cam-MPT in 100 mM triethylamine–acetic acid, pH 6.8, containing 5% methanol. Spectrum B is that of the anaerobic sample corresponding to peak B in Fig. 3. Spectrum A was recorded after complete oxidation in air, and is identical to that displayed by material from peak A in Fig. 3.

DISCUSSION

The data presented here indicate that the Mo cofactor present in xanthine oxidase as well as in sulfite oxidase contains the metal complexed to the tetrahydro form of molybdopterin. The procedure used for difference spectroscopy was designed to eliminate steps which could lead to oxidative modification of the pterin. Artifactual reduction of an oxidized form to a tetrahydro form is considered unlikely because of the absence of exogenous reductants and the observation that the FAD of the xanthine oxidase sample remained fully oxidized during the time of the experiment. In the case of sulfite oxidase, further support for this is derived from the isolation of the alkylated pterin in the tetrahydro state.

The reaction of two molecules of iodoacetamide with each molecule of molybdopterin supports the proposed presence of two vicinal SH groups in active molybdopterin. We are currently carrying out mass spectroscopic studies on cam-MPT and hope to obtain unequivocal evidence for the proposed structure of molybdopterin.

Acknowledgement—Funds for the studies reported here were provided by research grant GM00091 from the National Institutes of Health.

REFERENCES

1. J. L. Johnson, In *Molybdenum and Molybdenum-containing Enzymes* (Edited by M. Coughlan), p. 347. Pergamon Press, Oxford (1980).
2. J. L. Johnson and K. V. Rajagopalan, *Proc. Natl Acad. Sci. U.S.A.* 1982, **79**, 6856.
3. J. L. Johnson, B. E. Hainline, K. V. Rajagopalan and B. H. Arison, *J. Biol. Chem.* 1984, **259**, 5414.
4. O. Meyer and K. V. Rajagopalan, *J. Bacteriol.* 1984, **157**, 643.
5. S. Kramer, R. V. Hageman and K. V. Rajagopalan, *Arch. Biochem. Biophys.* 1984, **233**, 821.
6. R. C. Wahl, R. V. Hageman and K. V. Rajagopalan, *Arch. Biochem. Biophys.* 1984, **230**, 264.
7. R. V. Hageman and K. V. Rajagopalan, In *Nitrogen Fixation and* CO_2 *Metabolism* (Edited by P. W. Ludden and J. H. Burris), p. 133. Elsevier–North-Holland, New York (1984).
8. J. L. Johnson and K. V. Rajagopalan, *J. Biol. Chem.* 1977, **252**, 2017.
9. B. N. Ames, *Methods Enzymol.* 1966, **8**, 115.

Polyhedron Vol. 5, No. 1/2, pp. 577–580, 1986
Printed in Great Britain

0277-5387/86 $3.00 + .00
© 1986 Pergamon Press Ltd

PROPERTIES OF THE MOLYBDENUM DOMAIN OF NITRATE REDUCTASE

MICHAEL J. BARBER* and LARRY P. SOLOMONSON

Department of Biochemistry, University of South Florida, College of Medicine, Tampa, FL 33612, U.S.A.

(*Received* 17 *June* 1985)

Abstract—Partial reduction of the complex metalloflavoprotein nitrate reductase resulted in the appearance of a triad of Mo(V) EPR signals with a g_{av} of approximately 1.97. The precise g values and lineshapes were dependent upon the pH of the medium and the presence of anions. Potentiometric titrations revealed that midpoint potentials for both the Mo(VI)–Mo(V) and Mo(V)–Mo(IV) redox couples were pH-dependent. Treatment of the native enzyme with a specific inactivating protease from corn yielded two fragments of M_r 280,000 and 28,000. The large fragment contained Mo and heme whereas the small fragment contained FAD.

Nitrate reductase (NR) catalyses the rate-limiting step, the two-electron reduction of NO_3^- to NO_2^-, in the pathway of nitrate assimilation.[1] The enzyme from *Chlorella vulgaris* has been purified to homogeneity and found to contain Mo, in combination with a substituted pterin cofactor,[2] FAD and a b_5-type cytochrome prosthetic group in a 1:1:1 stoichiometry per subunit (M_r = 96,000) of the homotetrameric native enzyme.[3] Reducing equivalents from the physiological donor, NADH, enter the enzyme at the FAD domain and are transferred to the acceptor, NO_3^-, via the Mo center.

The initial spectroscopic studies of the enzyme have demonstrated that a variety of Mo(V) EPR signals can be elicited following partial reduction of the enzyme with either NADH or dithionite, some of which show superhyperfine coupling to an exchangeable proton.[3]

EXPERIMENTAL

NR was purified to homogeneity from *C. vulgaris* as previously described[4] using standard growth media or medium enriched in ^{95}Mo. Enzyme activities were monitored as previously described,[4] purified NR exhibiting a specific activity of >80 units mg^{-1} (NADH:NR) and an A_{280}/A_{413} ratio of <1.8. NR was extensively dialysed into zwitterionic buffers and stored at 77 K. NR was cleaved into its domain fragments by treatment with purified corn inactivator protease[5] [3.3 μg protease (mg enzyme)$^{-1}$] at 25°C until >95% inactivation of NADH:NR activity was achieved. Protein fragments were separated by chromatography on Sephacryl S-300. EPR samples, prepared using controlled reduction techniques and potentiometric titrations were performed as previously described.[3,6] EPR spectra were recorded using a Varian E109 spectrometer equipped with a variable-temperature accessory and operating at 9 GHz. g values were determined with reference to Mn–DPPH and xanthine oxidase "resting I" standards. Double integrations of EPR spectra were performed as described by Barber and Siegel[6] using CuEDTA as standard.

RESULTS AND DISCUSSION

Low-temperature EPR spectra of oxidized, native NR showed no signals due to Mo(V). However, partial reduction of the enzyme with dithionite yielded the spectra shown in Fig. 1. While the form of the Mo(V) spectrum was complex and was observed to vary between samples, particularly those containing anions such as chloride or phosphate, in zwitterionic buffers two major species were detected, the proportions of each dependent upon the pH. At low pH (7.0), a rhombic spectrum was identified that

* Author to whom correspondence should be addressed.

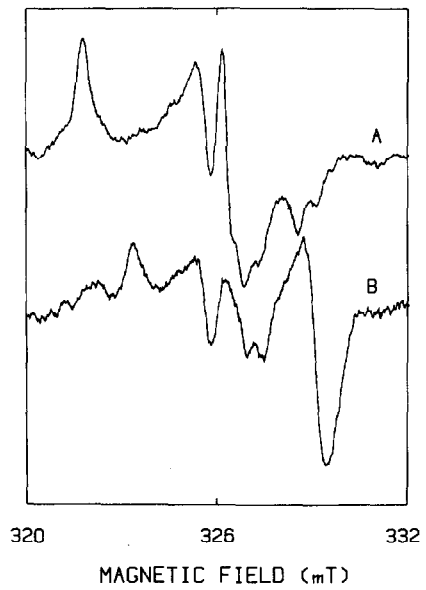


Fig. 1. EPR spectra of the Mo center in NR. (A) NR (11.5 μM heme) in 50 mM MOPS buffer containing 0.1 mM EDTA (pH 7.0) was poised at -57 mV in the presence of mediator dyes (14 μM) using dithionite as reductant. (B) NR (8.3 μM heme) in 50 mM CHES buffer containing 0.1 mM EDTA (pH 9.0) was poised at -132 mV in the presence of mediator dyes (20 μM). Spectra were recorded at 173 K using 10-mW microwave power and a modulation amplitude of 0.25 mT. The field scale corresponds to a microwave frequency of 8.985 GHz.

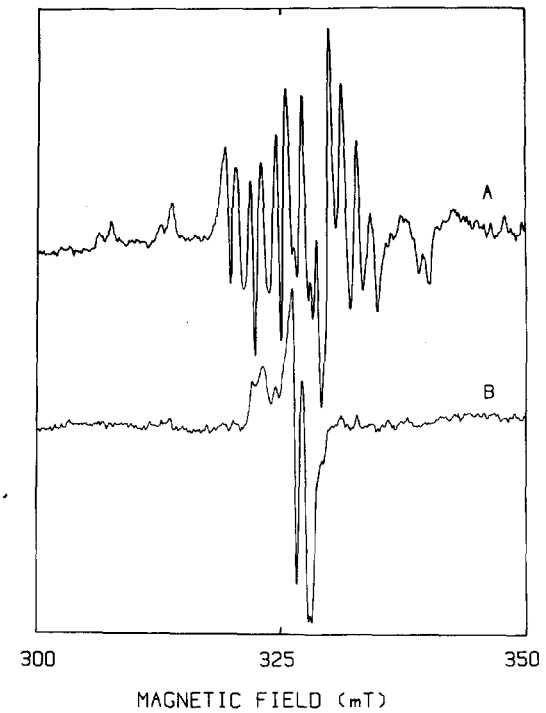


Fig. 2. EPR spectra of ^{95}Mo-containing NR. (A) NR (23 μM heme), purified from *C. vulgaris* grown on a medium enriched in $^{95}MoO_4^{2-}$, in 50 mM MOPS buffer containing 0.1 mM EDTA and 200 mM KCl (pH 7.0) was poised at -49 mV in the presence of mediator dyes (100 μM). (B) NR (9 μM heme) was poised at -37 mV under identical conditions as for spectrum A. EPR spectra were recorded under conditions described in Fig. 1, except that for spectrum A, the microwave power and modulation amplitude were increased to 30 mW and 0.4 mT, respectively. The field scale corresponds to a frequency of 8.984 GHz.

showed no evidence for superhyperfine coupling to protons and exhibited g values of $g_1 = 1.995$, $g_2 = 1.967$ and $g_3 = 1.954$ ("low pH"). At alkaline pH (9.0), a second rhombic species was detected, again showing no superhyperfine coupling, with g values of $g_1 = 1.985$, $g_2 = 1.952$ and $g_3 = 1.949$ ("high pH"). At low pH and in the presence of anions such as chloride, a third Mo(V) species was observed with g values of $g_1 = 1.995$, $g_2 = 1.968$ and $g_3 = 1.966$. In contrast to the "low pH" and "high pH" species, the "anion" signal showed superhyperfine coupling to a single, exchangeable, proton with coupling constants of $A_1 = 1.2$ mT, $A_2 = 1.1$ mT and $A_3 = 1.5$ mT. Similar signals were obtained in the presence of phosphate and fluoride. Confirmation that this signal was due to Mo(V) was achieved by purifying NR from *Chlorella* grown on a medium enriched with $^{95}MoO_4^{2-}$. Partial reduction of the enzyme yielded a broad, complex EPR signal centered around $g = 1.98$ that showed multiple lines with those occurring at extreme low and high field resolved into doublets (Fig. 2). ^{1}H and ^{95}Mo hyperfine coupling constants were estimated to be of the order of 1.2–1.3 and 5.5–6.0 mT, respectively. In addition to perturbing the EPR parameters of the Mo center, anions were also observed to stimulate the NADH : NR activity of the enzyme without affecting the NADH : CR activity. Whilst phosphate exhibited the greatest stimulation of activity, corresponding to nearly a four-fold increase at pH 7 (50 mM phosphate), both chloride and fluoride caused similar effects, though of lower magnitude. At pH 9, stimulation of NADH : NR activity was also observed.

The behavior of the Mo(V) EPR signals during potentiometric titrations of the native enzyme at pH 7 and 9 are shown in Fig. 3. At high potential, Mo(V) was undetectable: however, as the potential was decreased the Mo(V) signals were observed to appear, to reach maximum intensity at -40 (pH 7) and -130 mV (pH 9), corresponding to approximately 38% conversion of Mo to the quinquivalent state, and to decrease at more negative potentials. No change in the lineshape of

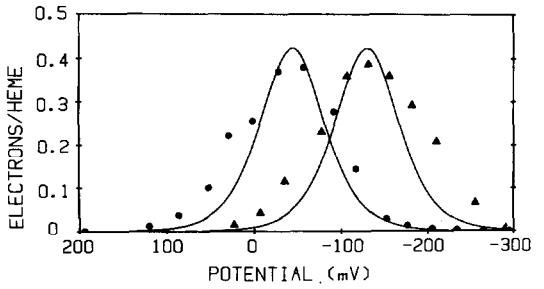


Fig. 3. Behavior of the Mo(V) EPR signal during potentiometric titrations. (●) NR (11.5 μM heme) in 50 mM MOPS buffer containing 0.1 mM EDTA (pH 7.0) was poised at various potentials using dithionite as reductant in the presence of mediator dyes (14 μM). (▲) NR (8.3 μM heme) in 50 mM CHES buffer containing 0.1 mM EDTA (pH 9.0). The curves fitted to the data points correspond to redox processes involving two, consecutive, one-electron redox steps with potentials, pH 7: Mo(VI)–Mo(V) = −34 mV and Mo(V)–Mo(IV) = −54 mV; pH 9: Mo(VI)–Mo(V) = −120 mV and Mo(V)–Mo(IV) = −140 mV.

either the "low pH" or "high pH" signals was observed throughout the course of either titration. Behavior of this type is typical of a reduction process involving two, consecutive, one-electron redox steps corresponding to the reactions:[7]

$$\text{Mo(VI)} \overset{E_1}{\longleftrightarrow} \text{Mo(V)} \overset{E_2}{\longleftrightarrow} \text{Mo(IV)},$$

with E_1 and E_2 corresponding to the midpoint potentials of the Mo(VI)–Mo(V) and Mo(V)–Mo(IV) couples. Values obtained for these couples at pH 7 and 9 were $E_1 = -34$ and -120 mV and $E_2 = -54$ and -140 mV, respectively. The shift in the position of the titration curve to lower potential with increasing pH and the corresponding decrease in both Mo redox couples indicates the involvement of protons in both redox steps. Values of ΔE/pH of -43 mV for both couples would indicate that reduction of Mo(VI) to Mo(V) and Mo(V) to Mo(IV) involve the addition of one electron and one proton in each reaction.

Incubation of native NR at room temperature in the presence of an isolated corn inactivator protease was observed to result in the time-dependent abolition of both NADH:NR and NADH:CR activity, whereas, in contrast, $MV^{\cdot+}$:NR activity remained unchanged. Chromatographic separation of the fragments produced following proteolysis yielded two fragments. The first, eluting just behind the column void volume, exhibited $MV^{\cdot+}$:NR activity, corresponded to an M_r of 280,000, comprised four identical polypeptide chains and was referred to as the "large fragment". Comparison of the visible spectra of this fragment (Fig. 4B) with that of the native enzyme (Fig. 4A) showed the characteristic bands corresponding to the presence of a cytochrome component. Addition of NADH failed to reduce the heme center but reduction could be ahieved using dithionite. In addition, controlled reduction of the fragment with dithionite yielded an EPR signal identical to that of the native enzyme, due to the formation of Mo(V) and indicating that the "large fragment" contained both the Mo and cytochrome components. In contrast, the "small fragment" (Fig. 4C) showed visible maxima at 390, 413 and 455 nm (the peak at 413 nm indicating contamination with a small amount of residual

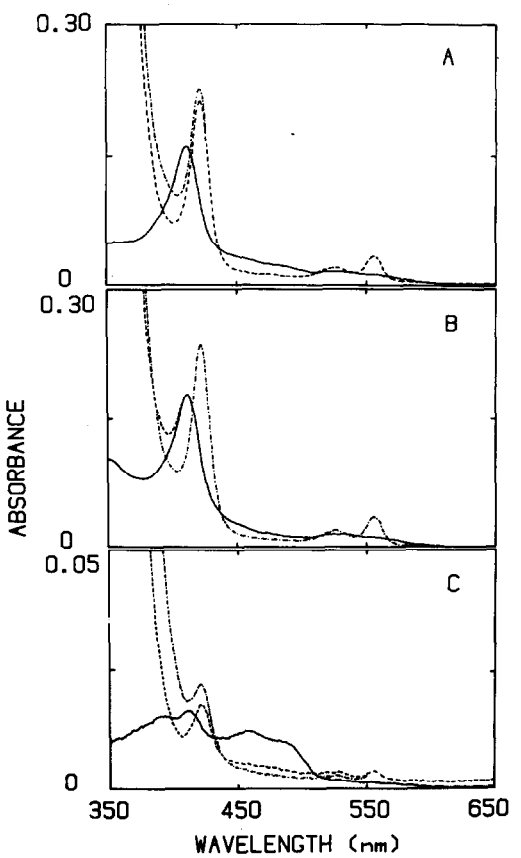


Fig. 4. Visible spectra of NR and the fragments obtained following treatment with corn inactivator protease. (A) (——) NR (0.88 μM heme) in 80 mM potassium phosphate buffer containing 0.15 mM EDTA, 0.5 M KCl and 0.15 mM DTE (pH 7.8); (– – –) enzyme reduced with NADH (1 mM); and (–·–·–) enzyme reduced with dithionite (1 mM). (B) (——) Large fragment (1 μM heme) in the same buffer as A, (– – –) large fragment reduced with NADH (1 mM), and (–·–·–) large fragment reduced with dithionite (1 mM). (C) (——) Small fragment in same buffer as A, (– – –) small fragment reduced with NADH (1 mM), and (–·–·–) small fragment reduced with dithionite (1 mM).

heme), was reduced by NADH, exhibited an M_r of 28,000 and showed no quaternary structure. These results indicate that the "small fragment" contained both a functional NADH-binding site and the FAD prosthetic group and represented a small flavin domain that could be readily cleaved from the main protein structure without destroying its functionality with respect to nitrate reduction. In addition, an intact flavin domain is essential for the transfer of reducing equivalents from NADH to heme and Mo.

Acknowledgements—We would like to thank Alison Robbins for skilled technical assistance. This work was supported by grants from the U.S.D.A., N.I.H. and N.S.F.

REFERENCES

1. E. J. Hewitt, *Annu. Rev. Plant Physiol.* 1975, **26**, 73.
2. L. P. Solomonson, M. J. Barber, W. D. Howard, J. L. Johnson and K. V. Rajagopalan, *J. Biol. Chem.* 1984, **259**, 849.
3. W. D. Howard and L. P. Solomonson, *J. Biol. Chem.* 1982, **257**, 10243.
4. W. D. Howard and L. P. Solomonson, *J. Biol. Chem.* 1981, **256**, 12725.
5. L. P. Solomonson, W. D. Howard, T. Yamaya and A. Oaks, *Arch. Biochem. Biophys.* 1984, **233**, 469.
6. M. J. Barber and L. M. Siegel, *Biochemistry* 1982, **21**, 1638.
7. W. M. Clark, *Oxidation–Reduction Potentials of Organic Systems*. Williams & Wilkins, Baltimore, MD (1960).

Polyhedron Vol. 5, No. 1/2, pp. 581–585, 1986
Printed in Great Britain

0277–5387/86 $3.00 + .00
© 1986 Pergamon Press Ltd

PURIFICATION OF THE MOLYBDOENZYME NITRATE REDUCTASE: PRODUCTION AND CHARACTERIZATION OF MONOCLONAL ANTIBODIES

B. A. NOTTON* and R. J. FIDO

Long Ashton Research Station, University of Bristol, Long Ashton, Bristol BS18 9AF, U.K.

and

G. GALFRE

Monoclonal Antibody Centre, Institute of Animal Physiology, Babraham, Cambridge CB2 4AT, U.K.

(*Received* 17 *June* 1985)

Abstract—The molybdoenzyme NADH–nitrate reductase (NADH–NR) (EC 1.6.6.1) has been purified 3400-fold, by a multi-stage procedure, to homogeneity from spinach (*Spinacea oleracea* L.). The enzyme had a specific activity of 102 μmol NO_2^- produced min^{-1} mg^{-1}. Denaturing electrophoresis revealed two subunits of molecular weight 110,000 and 120,000 and was substantially free of proteolytic degradation products. Extinction coefficients of the functional haem were 127 mM at 412 nm (oxidized) and 172 mM at 423 nm (NADH-reduced). A set of monoclonal antibodies was raised to the pure NR. Six selected for further cloning were all γG type and bound to five distinct and one overlapping site on the enzyme. The various activities of the NR (NADH-oxidizing and nitrate-reducing) were differentially inhibited by the monoclonal antibodies. NADH–NR activities of extracts of roots and leaves of a variety of species were inhibited to different extents.

Nitrate reductase (NR) (EC 1.6.6.1) from higher plants is the rate-limiting enzyme in the assimilation of inorganic nitrogen.[1–3] In most of the species examined, NR has a preference for NADH† as the electron donor to reduce nitrate to nitrite and also displays two partial activities: (1) a dehydrogenase function, reducing one-electron donors such as cytochrome *c* with NADH; and (2) nitrate reduction with $FMNH_2$ and $MV^{\cdot}$ as donors. The dehydrogenase function is independent of the molybdenum prosthetic group (molybdo-pterin) and the nitrate-reducing function is independent of the NADH donation site. From the few species examined, NR has been shown to have a molecular weight of 200,000–250,000, made up of two subunits of approximately 100,000 plus the molybdo-pterin complex. It has prosthetic groups of FAD, cytochrome b_{557} and molybdenum and electron flow occurs via these three components (see Fig. 1). The enzyme is unstable both *in vivo* and *in vitro* and has been purified from relatively few species.[4–8] Native electrophoresis (PAGE) of purified NR often results in a single protein band which is enzymically active: however, denaturing electrophoresis (SDS–PAGE) reveals multiple bands.[1,9,10] These are due to the presence of proteolytically nicked subunits which remain associated with the enzyme during its purification and the occurrence of these fragments can be decreased by using protectants against

* Author to whom correspondence should be addressed.

† Abbreviations: ELISA, enzyme-linked immunosorbent assay; FAD, flavin–adenine dinucleotide; $FMNH_2$, flavin nucleotide (reduced form); McAb, monoclonal antibody; $MV^{\cdot}$, methyl viologen (reduced form); NADH, nicotinamide–adenine dinucleotide (reduced form); PAGE, polyacrylamide gel electrophoresis; SDS, sodium dodecyl sulphate.

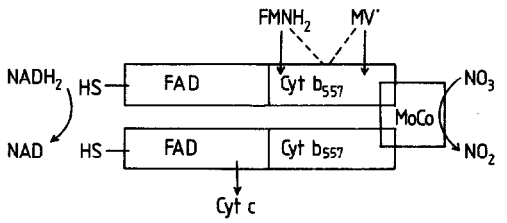


Fig. 1. Schematic representation of spinach NR showing prosthetic groups, subunit structure and various enzymic activities.

proteolysis.[11] The stability of NR means that purifications result in small yields, the 200 μg kg^{-1} reported here being one of the best. A study of the structure and function of the enzyme is therefore restricted. Our ability to purify NR,[12] and the knowledge that NR is a good antigen,[13] led us to attempt the preparation of a set of McAbs which would have potentially a four-fold use: (1) large-scale purification by affinity chromatography, (2) probes for the molecular structure, (3) quantification of the enzyme in the presence of impurities, and (4) intracellular localization. We report here further characterization of the six McAbs previously obtained.[21]

MATERIALS AND METHODS

Spinach plants (*Spinacea oleracea* L., cv. Noorman) were grown under greenhouse conditions using a nutrient flow technique and Long Ashton nitrate nutrient.[14] Leaves were taken from plants 6–8 weeks old and frozen at −20°C before use. Enzyme activities of NR, NADH–NR, NADH–cytochrome *c* reductase (NADH–cyt *c* Rase) and $FMNH_2$–NR used standard methods.[15] MV–NR used 0.2 mM MV instead of FMN.

Electrophoresis was done in vertical gel slabs using the standard formulations for a 3.75% stacking gel (pH 6.8), 7.5% resolving gel (pH 8.8) and reservoir buffer (pH 8.3) as described for native PAGE[16] and SDS–PAGE.[17] Protein samples (10–50 μg) were made either 10% with glycerol (native PAGE) or heated for 3 min at 90°C with an equal volume of 2% SDS, 5% mercaptoethanol, 10% glycerol in 62.5 mM Tris buffer (pH 6.8) (SDS–PAGE). Bromophenol blue was used as the marker dye. Molecular weights were estimated from the mobility of standard proteins. Gels were stained with 1% Coomassie brilliant blue R250. Vertical gel strips were cut from the gel slabs for scanning spectrophotometrically.

Enzyme extraction and purification used modifications of our earlier method.[4] All operations were done at 4°C and buffers contained 1 mM EDTA. Frozen spinach leaves were macerated with 1 volume of 5 mM phosphate buffer (pH 7.5) containing 10 μM leupeptin.[11] The macerate was filtered through muslin and centrifuged to remove debris. Nucleic acids were precipitated by the addition of streptomycin sulphate [5 mg (g leaf)$^{-1}$] and removed by centrifuging. The supernatant was made 50% saturated with $(NH_4)_2SO_4$ and the precipitate collected, redissolved in 5 mM phosphate buffer (pH 7.5) and desalted on Sephadex G 25 for chromatography on hydroxapatite. The column was washed with 5 mM phosphate buffer and the NR-containing fraction eluted with 100 mM phosphate buffer (pH 7.5) containing 10 μM FAD and 5% $(NH_4)_2SO_4$. The NR fraction was concentrated by precipitation with 50% saturated $(NH_4)_2SO_4$, the precipitate redissolved in 100 mM phosphate buffer (pH 7.5) containing 10 μM FAD and 50 mM KCl, and submitted to molecular sieve chromatography (Biogel A 1.5 m). Active fractions were precipitated as before, redissolved in 5 mM phosphate buffer (pH 7.5) containing 10 μM FAD and applied slowly to a column of blue–Sepharose. After removal of unbound material the column was inverted and bound NR eluted using 100 mM phosphate buffer (pH 7.5) containing 10 μM FAD and 150 μM NADH. The NR was concentrated by precipitation and the chromatography repeated, including the inversion technique, using 5′-AMP–Sepharose.[12] Active fractions were retained separately.

Female rats were injected with 200 μg of pure NR followed by booster injections after 37 and 62 days. Response to the antigen was measured by the ability of the antiserum to inhibit the NADH–NR of a suitably diluted NR preparation.[13] Hybrid myelomas were derived from spleen cells of rats showing a strong positive response to NR, by fusion[18] with either rat myeloma lines Y3Agl 2.3[19] or YB 2/3.0 Ag20.[20] Supernatants from confluent cultures were tested for McAb activity by an ELISA. Selected positive cell lines were either frozen or cloned.[21] Cell lines giving positive ELISA supernatants were also tested for their ability to inhibit activities of NR after a 1-h incubation at 4°C.

Antibodies were labelled with [^{3}H]lysine by incubating cell lines in labelled culture media and secreted immunoglobulins were analysed by SDS–PAGE after reduction with 2-mercaptoethanol.[22]

Competition between McAbs for the same site on the NR protein used ^{3}H-labelled McAbs diluted with each of the unlabelled McAbs. The mixtures were incubated overnight with NR attached to PVC plates. Counts obtained were plotted against volume of unlabelled McAb.

RESULTS AND DISCUSSION

The purification of NR from 2 kg of spinach leaves is summarized in Table 1. The final product was 400 μg of a 3400-fold purified enzyme having a nominal specific activity of 102 units of activity (mg protein)$^{-1}$. This figure was obtained with the commonly used protein standard, bovine serum albumin (BSA). However, BSA is known to behave in an abnormal manner with the assay reagent used[23] and the resultant specific activity has been shown to be 30% too high compared with using NR as its standard,[24] i.e. a corrected figure of 71.4. Based on the purification data, the initial enzyme activity and the final recovery (5.6%), spinach leaves contained approximately 3.5 mg NR (kg fresh weight)$^{-1}$. Although the recovery figure is low, this is a substantial improvement on most other attempted large-scale purifications. The destruction of NR during all chromatography stages[25] has been considerably decreased by the inclusion of FAD in the buffers and particularly by inverting the columns in the last two affinity chromatography stages.[12]

The light absorption spectrum of the pure NR (Fig. 2) shows a Soret band at 412 nm typical of NRs so far isolated from eukaryotic sources.[1–3] The 280:412 nm ratio is now approximately 2:1. The functional nature of the haem was confirmed by reducing the NR with NADH, resulting in a shift of the Soret to 423 nm and the appearance of α and β bands at 557 and 523 nm. Reoxidation with nitrate led to the production of nitrite and a reversion of the spectrum back to the native oxidized form. Extinction coefficients (mM) of the haem, based on a molecular weight of 200,000 were 127 (412 nm) (oxidized) and 172 (423 nm), 17.5 (525 nm) and 29 (557 nm) (NAHD-reduced). These coefficients are similar to those reported for NR from *Chlorella*.[26] Native PAGE of purified NR typically resulted in only one protein band[1,9,10] after both blue- and 5'-AMP–Sepharose. In both cases this band also displayed NADH–NR activity. However, SDS–PAGE resulted in multiple banding of the post blue–Sepharose-purified NR (Fig. 3A) similar to previous reports,[4,9–11] but the post 5'-AMP–Sepharose NR revealed only a doublet (Fig. 3B) corresponding to molecular weights of 110,000 and 120,000 with trace amounts (< 10%) of smaller proteins. This result has been recently confirmed by other workers[27] who regarded spinach NR as consisting of two equal sized subunits of molecular weight 120,000 and the doublet resulting from the loss of a small peptide by proteolysis. Identity of both bands as being related to NR was confirmed by cross-reaction with McAbs to the enzyme. It seems, therefore, that 5'AMP–Sepharose is capable of removing associated proteolytically nicked peptides from the NR.

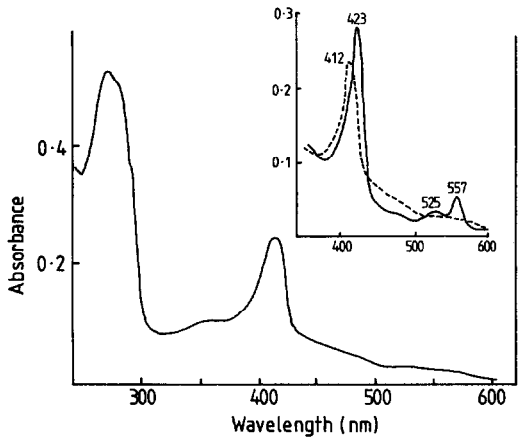


Fig. 2. Absorption spectrum of purified NR.[12] Sample contained 400 μg ml^{-1} in 5 mM phosphate buffer at pH 7.5 and was measured at room temperature. Insert shows the effect of reduction with NADH (——) and reoxidation with nitrate (– – –) on the haem.

Table 1. Purification of NR from spinach leaves (crude extract obtained from 2 kg of frozen leaves)

Stage	Total activity (mol NO_2^- produced min^{-1})	Specific activity	Purification factor
Crude extract	367	0.03	1.0
Streptomycin	272	0.02	0.8
$(NH_4)_2SO_4$	243	0.02	0.8
Hydroxyapatite	139	0.20	6.7
Biogel A 1.5 m	82	0.22	7.1
Blue–Sepharose	42	7.14	224.5
5'-AMP–Sepharose	30	65.68	2189.1
Best fraction	21	102.96	3431.9

Antisera were obtained from rats injected with pure NR inhibited NADH–NR activity, the dilution required for 50% inhibition varied six-fold. Non-immune serum had no inhibitory properties.

Cells obtained as a result of fusion of rat spleen cells with myeloma cells[18] were cultured and exudates tested by ELISA for the presence of McAbs. Those giving a positive were subcultured and samples stored in liquid N_2. Negative ELISA cultures were stopped. From the celll cultures 24 were ELISA-positive, 16 from Y3Agl 2.3 and eight from YB3/3.0 rat myelomas. Of these, six, designated AFRC MAC 74–79, were selected for cloning in soft agar and further growth.[21]

Analysis by SDS–PAGE of [^{3}H]lysine-labelled

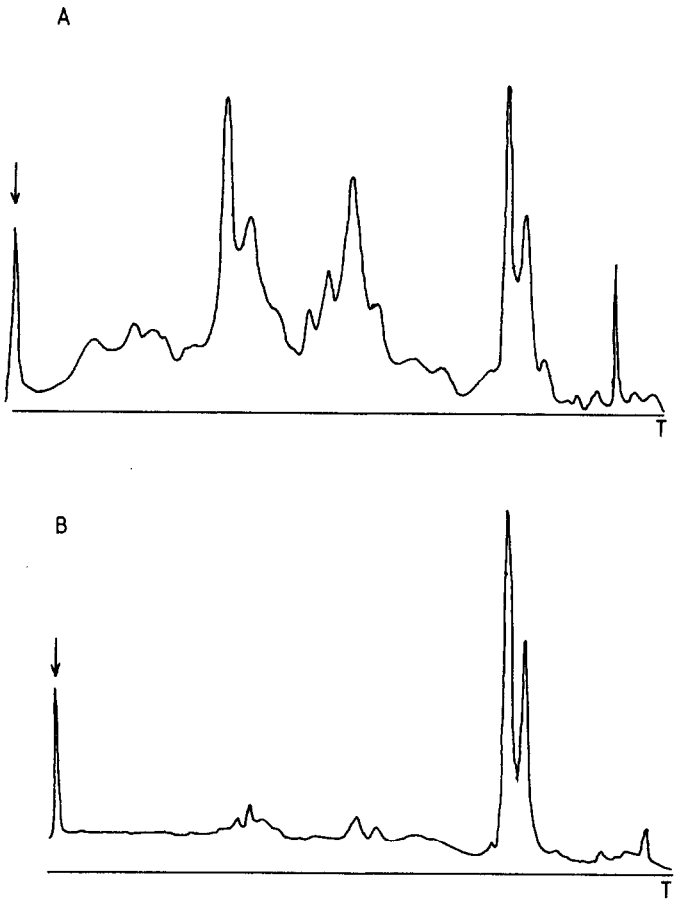


Fig. 3. Gel scan of subunit of 20 μg of purified NR separated by SDS–PAGE and stained with Coomassie brilliant blue R250.[12] (A) Post blue–Sepharose and (B) best fraction of post 5′-AMP–Sepharose. T = top of gel. ↓ bromophenol blue marker.

McAbs showed that MAC 77–79 were all heavy-chain class γ. However, attempts to purify the McAb using protein A–Sepharose were not successful, presumably because the IgGs were of a subclass not recognized by protein A.[28]

Competition of one McAb with the others, for a particular antigenic site on NR, over a limited dilution range of 10 : 1–1 : 20, showed that MAC 76 and 77 were mutually competitive and therefore bound at the same or overlapping sites. They also had the same enzyme inhibitory properties (see below). MAC 74, 75, 78 and 79 were non-competitive and, therefore, bound at unique sites on the NR.

Antibodies were concentrated either by pressure filtration, using a 20,000 cut-off ultrafiltration membrane, or by precipitation with $(NH_4)_2SO_4$ at 50% saturation followed by resolution and dialysis to remove salt. Equal volumes of the McAbs and a suitably diluted semi-purified NR were incubated at 4°C for 1 h before determining residual activities. The results (Table 2) show that MAC 74, 76 and 77 strongly and MAC 75 weakly inhibit all nitrate-reducing (terminal) activities of NR (NADH–NR, $FMNH_2$–NR and MV–NR) while MAC 78 and 79 inhibit NADH acceptor activities (NADH–NR and NADH–cyt *c* Rase) (see Fig. 1). Preliminary tests using pure NR indicate that MAC 78 binds close to the NADH site, inhibiting both acceptor activities equally, while MAC 79 binds closer to the cyt *c* site and preferentially inhibits the NADH–cyt *c* Rase activity.

Inhibition of terminal activities resulted in a stimulation of acceptor activities and vice versa, possibly as a result of binding of the McAbs affecting the changes in tertiary structure of the enzyme on reduction.

Crude extracts of roots and leaves of both spinach and a variety of other species (barley, wheat, oats, marrow, pea, oilseed rape and cucumber) were tested against McAbs for inhibition of their NADH–NR activity. While all the McAbs which inhibited the terminal activities of spinach (MAC 74–77) were effective to varying degree with the other species, indicating a partial recognition, only MAC 74 was

Table 2. Inhibition of NR activities by McAbs (effect of McAbs MAC 74–79 on the various activities of a semi-purified NR from spinach leaves)

	Residual activity[a]			
McAb	NADH–NR	NADH–Cyt *c* Rase	$FMNH_2$–NR	MV–NR
74	9	120	15	20
75	75	115	55	45
76	16	120	17	26
77	17	100	28	26
78	55	59	150	105
79	73	73	124	86

[a] Results are expressed as % of control activities obtained after equal volumes of supernatant and a suitably diluted NR preparation were incubated for 1 h at 4°C.

inhibitory in every case and was obviously directed against an invariant site on the NR. MAC 78 and 79 was only effective against spinach and marrow NR (to some extent), which may be due to a greater variation in structure at this end of the molecule.

Although McAbs have been raised to a number of plant proteins this is one of the few cases reported of McAbs against a higher-plant enzyme. We feel that McAbs are particularly useful as probes of protein structure and although MAC 74–79 gave negative ELISAs against xanthine dehydrogenase, the isolation of an McAb against the molybdo-pterin complex which is common to a number of molybdoenzymes (NR, xanthine dehydrogenase and sulphite oxidase)[29] would be particularly useful. It may be present amongst the remaining 18 cell lines yet to be cloned.

REFERENCES

1. B. A. Notton and E. J. Hewitt, In *Nitrogen Assimilation of Plants* (Edited by E. J. Hewitt and C. V. Cutting), p. 227. Academic Press, London (1979).
2. E. J. Hewitt and B. A. Notton, In *Molybdenum and Molybdenum-containing Enzymes* (Edited by M. Coughlan), p. 273. Pergamon Press, Oxford (1980).
3. M. G. Guerrero, J. M. Vega and M. Losada, *Annu. Rev. Plant Physiol.* 1981, **32**, 169.
4. B. A. Notton, R. J. Fido and E. J. Hewitt, *Plant Sci. Lett.* 1977, **8**, 165.
5. W. H. Campbell and J. Smarelli, *Plant Physiol.* 1978, **61**, 611.
6. J. H. Sherrard and M. J. Dalling, *Plant Physiol.* 1979, **63**, 346.
7. T. Kuo, A. Kleinhofs and R. L. Warner, *Plant Sci. Lett.* 1980, **17**, 371.
8. M. G. Redinbough and W. H. Campbell, *Plant Physiol.* 1983, **71**, 205.
9. J. L. Wray and D. W. Kirk, *Plant Sci. Lett.* 1981, **23**, 207.
10. W. H. Campbell, *Nitrate Assimilation: Molecular and Genetic Aspects*, p. 7. Gatersleben, G.D.R. (1982).
11. McA. Campbell and J. L. Wray, *Phytochemistry* 1983, **22**, 2375.
12. R. J. Fido and B. A. Notton, *Plant Sci. Lett.* 1984, **37**, 87.
13. B. A. Notton, L. Graf, R. C. Povey and E. J. Hewitt, *Biochim. Biophys. Acta* 1974, **364**, 45.
14. E. J. Hewitt, Sand and water culture methods used in the study of plant nutrition, Commonwealth Bureau of Horticulture, Technical Communication 22, Farnham Royal (1966).
15. J. L. Wray and P. Filner, *Biochem. J.* 1970, **119**, 715.
16. B. D. Hames, In *Gel Electrophoresis of Proteins* (Edited by B. D. Hames and R. Rickwood), p. 1. IRL Press, Oxford (1981).
17. U. K. Laemmli, *Nature (London)* 1970, **277**, 680.
18. G. Galfre and C. Milstein, *Methods Enzymol.* 1981, **73**, 3.
19. G. Galfre, C. Milstein and B. Wright, *Nature (London)*, 1979, **277**, 131.
20. J. V. Kilmartin, B. Wright and C. Milstein, *J. Cell Biol.* 1982, **93**, 576.
21. B. A. Notton, R. J. Fido and G. Galfre, *Planta* 1985, **165**, 114.
22. U. K. Laemmli and M. Favre, *J. Mol. Biol.* 1973, **80**, 575.
23. M. M. Bradford, *Anal. Biochem.* 1976, **72**, 248.
24. M. G. Redinbough and W. H. Campbell, *Anal. Biochem.* 1985, **147**, 144.
25. B. A. Notton, In *Metals and Micronutrients, Uptake and Utilisation by Plants* (Edited by D. A. Robb and W. S. Pierpoint), p. 219. Academic Press, London (1983).
26. L. P. Solomonson, G. H. Lorimer, R. L. G. Hall, R. Bochers and J. L. Bailey, *J. Biol. Chem.* 1975, **250**, 4120.
27. H. Nakagawa, Y. Yonemura, H. Yamamoto, T. Sato, N. Ogura and R. Sato, *Plant Physiol.* 1985, **77**, 124.
28. J. Rousseaux, M. T. Picque and H. Bazin, *Mol. Immunol.* 1981, **18**, 639.
29. J. L. Johnson, In *Molybdenum and Molybdenum-containing Enzymes* (Edited by M. Coughlan), p. 347. Pergamon Press, Oxford (1980).

Polyhedron Vol. 5, No. 1/2, pp. 587–589, 1986
Printed in Great Britain

0277-5387/86 $3.00 + .00
© 1986 Pergamon Press Ltd

THE LIGAND ENVIRONMENT OF MOLYBDENUM IN THE MOLYBDENUM COFACTOR, INVESTIGATED BY EPR

G. N. GEORGE, T. R. HAWKES, G. D. JONES and R. C. BRAY*

School of Chemistry and Molecular Sciences, University of Sussex, Brighton BN1 9QJ, U.K.

(*Received* 1 *July* 1985)

Abstract—Frozen-solution EPR studies of Mo(V) in the active molybdenum cofactor, in the form of a complex with thiophenol, have been carried out in extension of the work of Hawkes and Bray (*Biochem. J.* 1984, **222**, 587). Isotopic substitution with ^{95}Mo, ^{17}O and ^{2}H, and computer simulations of the spectra were employed. C_s-symmetry and weak coupling to exchangeable ^{17}O and ^{2}H nuclei are indicated. A local structure for the molybdenum environment in the cofactor is suggested.

The structures of molybdoenzymes[1] such as xanthine oxidase,[2] nitrate reductase[3] and sulphite oxidase,[3] have been extensively investigated by EPR of Mo(V). Molybdenum in all molybdoenzymes other than nitrogenase is present as the molybdenum cofactor, but work on this essential constituent of the enzymes has lagged behind that on the enzymes because of its instability. Degradation studies[4] of the cofactor indicate it to be a reduced pteridine derivative, with molybdenum attached to a side chain via sulphur ligands. In earlier work we have shown that under rigorously anaerobic conditions the active cofactor may be extracted[5] from xanthine oxidadase in the presence of dithionite and converted[6] as a thiophenol complex to the Mo(V) state in 80–100% yield. In this procedure, thiophenol presumably displaces cysteinyl ligands from the protein. Frozen-solution EPR spectra indicated a well-defined species, whose parameters were reported as $g_{\|} = 2.0258$ and $g_{\perp} = 1.9793$. We now report additional EPR studies[7] on this species, involving isotopic substitution experiments, which permit important structural conclusions to be derived.

EXPERIMENTAL

Molybdenum cofactor activity was measured[5] by complementation of apo-nitrate reductase of the *nit-1* mutant of *Neurospora crassa*. The cofactor was extracted[5] in the presence of dithionite from purified xanthine oxidase into dimethylsulphoxide containing approximately 5% H_2O and converted,[6] in the presence of 0.1 M thiophenol, to the Mo(V) state by controlled oxidation. EPR spectra of frozen samples were recorded and simulated.[2] Enrichment[2] with stable isotopes involved starting from xanthine oxidase incubated in ^{2}H- or ^{17}O-enriched water, or from enzyme prepared following *in vivo* enrichment with ^{95}Mo.

RESULTS

The EPR spectra of the thiophenol complex of the molybdenum cofactor are illustrated in Fig. 1. Spectra were recorded both at 9 [Fig. 1(a)] and 35 [Fig. 1(b)] GHz. The spectra, plotted on a g value scale, are indistinguishable from one another and indicate an accurately axial g-tensor.

Experiments carried out using ^{17}O-enriched water showed definite broadening of the spectrum. This was particularly apparent in the $g_{\perp}$-region of the spectrum. Broadening corresponded (for one oxygen ligand) to $A(^{17}O)_{\perp} = 0.4$ mT. Similar experiments employing ^{2}H-enriched water gave smaller, though almost certainly definite, broadening, corresponding in this case (again assuming a single ligand) to $A(^{2}H)_{\perp} = 0.3$ mT.

Figure 2 illustrates the spectrum of the ^{95}Mo cofactor at 9 GHz. The experimental spectrum is shown in Fig. 2(a). The signal-to-noise ratio is considerably better than that achieved in our earlier

* Author to whom correspondence should be addressed.

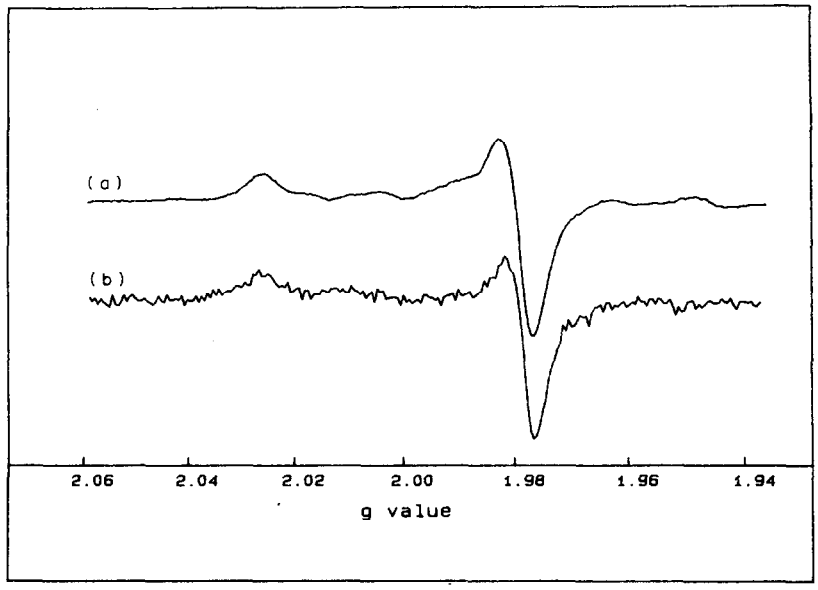


Fig. 1. EPR spectra of the thiophenol complex of the molybdenum cofactor at 9 (a) and 35 (b) GHz. The spectra are plotted on a g-value scale. Spectra were recorded at about 120 K.

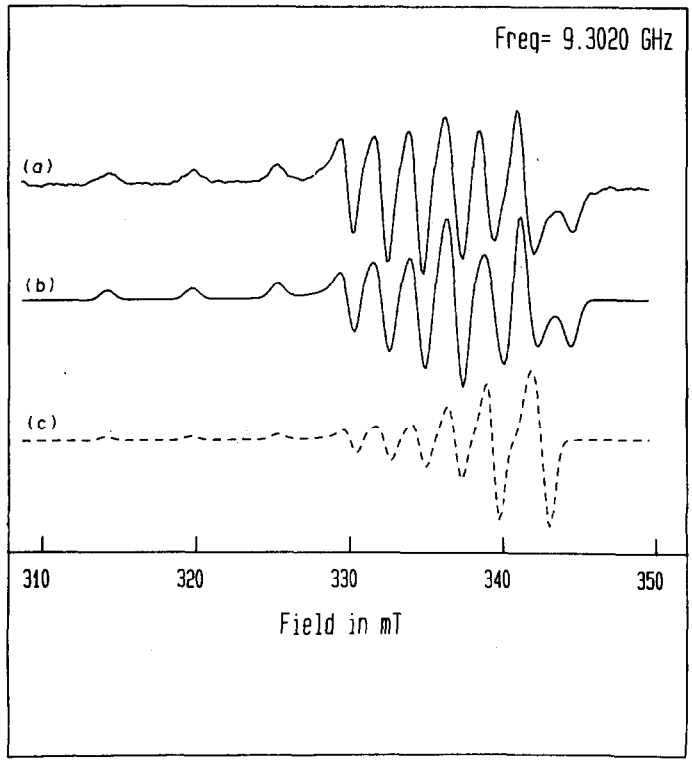


Fig. 2. EPR spectrum of the ^{95}Mo cofactor–thiophenol complex. (a) Experimental spectrum, corresponding to 100% enrichment with the isotope, obtained by subtracting a small amount of the spectrum of unenriched cofactor from that of the enriched sample. The computer simulation (b) was obtained by using the following parameters: $g_{xx} = 1.9779$, $g_{yy} = 1.9779$, $g_{zz} = 2.0260$, $A_{xx} = 64$, $A_{yy} = 64$, $A_{zz} = 159$ (hyperfine couplings in MHz); $\alpha_{xz} = 12°$ (angle of non-coincidence of the axes of g and A, convention of Rose). The unsatisfactory simulation (c) was based on the same parameters, except that $\alpha_{xz} = 0°$ was assumed.

work.[6] We were able to produce an accurate simulation [Fig. 2(b)] of the spectrum by using the parameters as listed in the caption. It was necessary to introduce a single angle of non-coincidence of the axes of g and A. If coincident axes were assumed, a totally inadequate simulation [Fig. 2(c)] was obtained. Conversely, if additional angles of non-coincidence of the axes, greater than about 5°, were introduced, then the fit became significantly worse.

DISCUSSION

The finding that the thiophenol complex of the molybdenum cofactor shows an axial g-tensor and one rather than two angles of non-coincidence of the axes of g and A, is in contrast to the situation[8] for various EPR-active species from molybdoenzymes. Current data are most readily interpreted[7] (cf. Refs 9–11) in terms of local C_s-symmetry at the molybdenum centre. Most of the enzyme species showing[3,12,13] coupling to ^{17}O and ^{2}H are presumed to contain a hydroxyl ligand of molybdenum, and we therefore assume that this is the case for the cofactor–thiophenol complex. Furthermore, the EPR parameters are comparable to those expected for an oxo complex of molybdenum having sulphur ligands. Combining these facts, we suggest the structure shown in Fig. 3 as a likely one for the cofactor–thiophenol complex.

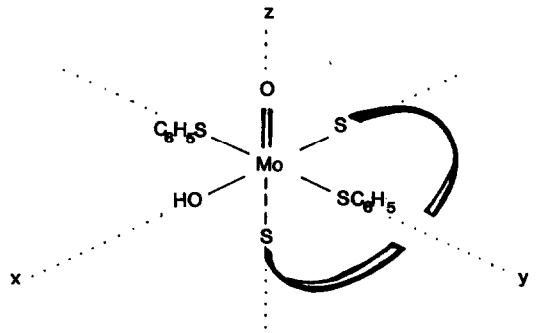


Fig. 3. Suggested co-ordination of molybdenum in the thiophenol complex of the molybdenum cofactor. The axes of A are approximately along the bond directions, as indicated, with the xz plane as the mirror plane. The curved line represents the organic part of the cofactor, co-ordinated to the metal via axial and equatorial sulphur atoms. In the enzyme the thiophenol ligands would presumably be replaced by cysteinyl residues from the protein.

Acknowledgements—This work was supported by grants from the SERC, the MRC, the AFRC and the Wellcome Trust.

REFERENCES

1. R. C. Bray, *Adv. Enzymol. Relat. Areas Mol. Biol.* 1980, **51**, 107.
2. R. C. Bray and G. N. George, *Biochem. Soc. Trans.* 1985, **13**, 560.
3. R. C. Bray, *Polyhedron* 1986, **5**, 591.
4. J. L. Johnson, B. E. Hainline, K. V. Rajagopalan and B. H. Arison, *J. Biol. Chem.* 1984, **259**, 5414.
5. T. R. Hawkes and R. C. Bray, *Biochem. J.* 1984, **219**, 481.
6. T. R. Hawkes and R. C. Bray, *Biochem. J.* 1984, **222**, 587.
7. G. N. George and G. D. Jones, unpublished work.
8. G. N. George, D.Phil. Thesis, University of Sussex (1983); G. N. George and R. C. Bray, unpublished work.
9. C. D. Garner, P. Lambert, F. E. Mabbs and T. J. King, *J. Chem. Soc., Dalton Trans.* 1977, 1191.
10. M. I. Scullane, R. D. Taylor, M. Minelli, J. T. Spence, K. Yamanouchi, J. H. Enemark and N. D. Chasteen, *Inorg. Chem.* 1979, **18**, 3213.
11. M. A. Hitchman, C. D. Olson and R. L. Belford, *J. Chem. Phys.* 1969, **50**, 1195.
12. R. C. Bray and S. Gutteridge, *Biochemistry* 1982, **21**, 5992.
13. F. F. Morpeth, G. N. George and R. C. Bray, *Biochem. J.* 1984, **220**, 235.

Polyhedron Vol. 5, No. 1/2, pp. 591–595, 1986
Printed in Great Britain

0277–5387/86 $3.00 + .00
© 1986 Pergamon Press Ltd

THE NATURE OF THE HIGH-pH–LOW-pH TRANSITION IN SULPHITE OXIDASE AND NITRATE REDUCTASE

R. C. BRAY

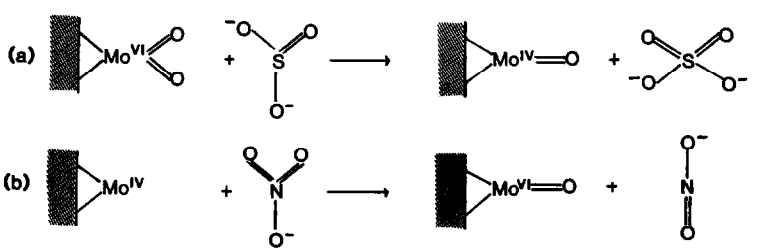
School of Chemistry and Molecular Sciences, University of Sussex, Brighton BN1 9QJ, U.K.

(*Received* 1 *July* 1985)

Abstract—The structures of the molybdenum centres in nitrate reductase and sulphite oxidase, and their reactions with substrates, are discussed in the light of work in the literature on model compounds and of work on the enzymes by EXAFS and EPR spectroscopy. EXAFS indicates that the metal in Mo(VI) states of the enzymes bears more oxo ligands than it does in Mo(IV) states. This is consistent with the enzymes functioning by oxo transfer mechanisms, shuttling between Mo(VI) and Mo(IV) states. The relevance of EPR work on the structures of Mo(V) states of the enzymes is discussed. EPR provides information complementary to that from EXAFS. At the same time, because of the complexities in the enzymes that it reveals, EPR indicates that caution needs to be exercised in interpreting EXAFS data. EPR shows that, for both enzymes, two different forms of the Mo(V) state are in pH- and anion-dependent equilibrium. In the low-pH forms the metal bears hydroxyl and anion ligands. The structure of the high-pH form is less certain but recent work indicates that it, too, may contain a hydroxyl ligand.

This paper summarizes recent work relating to the catalytic reactions occurring at the molybdenum centres of the enzymes sulphite oxidase and nitrate reductase. Particular emphasis is placed on sulphite oxidase from chicken liver and on nitrate reductase from anaerobically grown *Escherichia coli*, and on studies of these enzymes in the author's laboratory by EPR spectroscopy of Mo(V). The enzymes are involved respectively in catabolism of sulphur-containing amino acids prior to excretion as sulphate, and in the reduction of nitrate utilized under anaerobic conditions as an energy source. Oxidation–reduction centres, present in the enzymes in addition to molybdenum and involved in reaction with the second substrates and in electron transfer to or from molybdenum, are haem in sulphite oxidase, and haem and iron–sulphur in nitrate reductase. The very closely related nitrate reductase from *Pseudomonas aeruginosa* will not be discussed here, nor will the quite similar assimilatory nitrate reductases from spinach and *Chlorella vulgaris*, though some EPR studies have been reported[1–3] on each of these enzymes.

EXAFS data[4,5] on the enzymes under consideration and oxo-transfer studies on model compounds[6–8] indicate reactions to be overall as illustrated in Scheme 1. The numbers of oxo groups shown in the oxidized and reduced forms of the enzymes are those indicated by EXAFS. The reactions as formulated are consistent with



Scheme 1.

theoretical studies,[9] which indicate particular stability for molybdenum species having a single oxo group. (Note that EXAFS indicates an extra oxo ligand in *Chlorella* nitrate reductase in comparison with the *E. coli* enzyme. There may, however, be uncertainties relating to interpretation of published EXAFS data, because effects of anions on the enzymes, as discussed below, were not taken into account. It must be remembered that EXAFS does not distinguish, for example, S from Cl or P.)

EPR has been more successful[10] than EXAFS in identifying ligands of molybdenum in molybdoenzymes. However, the question arises as to what EPR can tell us about sulphite oxidase and nitrate reductase, since the catalytic reactions as formulated in Scheme 1 indicate involvement of Mo(IV) and Mo(VI), whereas EPR studies provide information only on Mo(V). Accepting that EPR might give information only indirectly relevant to the catalytic reactions, we note, nevertheless, the method's utility for unambiguous identification of ligands through studies of hyperfine couplings, and its considerable potential for yielding additional structural information (e.g. Ref. 11).

Molybdenum in enzymes may be titrated reversibly from the Mo(VI) state, through Mo(V), to Mo(IV) and the two redox potentials controlling these processes may be evaluated (e.g. Ref. 12). The enzymes generally show a maximum of about 40% conversion of molybdenum to the Mo(V) state. Oxidized sulphite oxidase gives rise[13] to Mo(V) signals within a few tens of milliseconds or less, on adding the substrate, sulphite. This no doubt results from reduction to Mo(IV), followed by rapid partial transfer of electrons to other centres. Nitrate reductase shows Mo(V) signals when isolated, these probably corresponding to enzyme molecules locked in a "dead-end" state, with the rest of the molecule oxidized, and unable to donate the single electron to nitrate. Signals from the enzyme may be increased[14] by addition of dithionite. The above facts indicate both that EPR is highly relevant to mechanistic studies of the enzymes and that their Mo(V) states may well be in rapid equilibrium with Mo(IV) or Mo(VI) states, or perhaps with both of these.

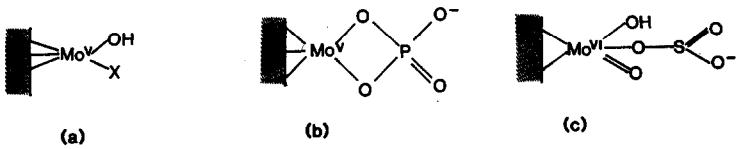
EPR data relating to the structures of chicken liver sulphite oxidase and *E. coli* nitrate reductase will be considered together. It has been known[15] for some years that the molybdenum centres of the enzymes, when in the Mo(V) oxidation state, exist in high- and low-pH forms, distinguished by different EPR spectra. The low-pH signals show well-resolved hyperfine coupling from a single proton (A_{av} about 1 mT) exchangeable with the solvent, whereas the high-pH spectra show no such coupling and have slightly different g values, with lower values of g_{av}. pK values for interconversion between the species were given[16,17] as 8.2 and 8.3, respectively, for sulphite oxidase and nitrate reductase.

All currently available data are consistent with the low-pH species having the structure shown in Scheme 2(a), with the molybdenum atom bearing a hydroxyl ligand and an anion ligand. Evidence for this is as follows.

Interconversion between the species has been found to depend on the anion concentration as well as on the pH. Particularly for sulphite oxidase, it was shown[13] that a 10-fold increase in chloride concentration had the effect of increasing the apparent pK value for the interconversion by 1 pH unit. Variation in the nature of the anion ligand causes (particularly for nitrate reductase[14]) small changes in the form of the low-pH EPR spectrum, with different ligands each giving slightly different g and A values. With fluoride as a ligand, hyperfine coupling to ^{19}F ($A_{av} = 0.71$ mT for nitrate reductase[14] and about 0.5 mT for sulphite oxidase[13]) is observed.

The characteristic large and predominantly isotropic hyperfine coupling from a proton in the low-pH spectrum disappears on dissolving the enzymes in ^2H_2O. Coupling for this proton, for example[14] in the nitrate complex of nitrate reductase [$A(^1H) = 1.46, 1.11, 1.09$ mT], is comparable in magnitude and in extent of anisotropy with coupling of the proton from a hydroxyl ligand of molybdenum in irradiated molybdate crystals[18] [$A(^1H)$ 0.96, 0.71, 1.32 mT]. The latter seems a good model for the enzymes and appears to be the only authenticated report in the literature of EPR work on a Mo(V)—OH compound.

Evidence for oxygen as a ligand has been provided[19,20] by substitution studies with ^{17}O,



Scheme 2.

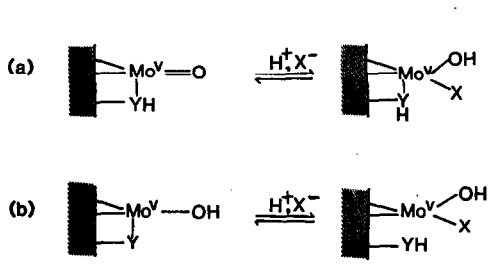
carried out by dissolving the enzymes in enriched water. Spectra have not so far been evaluated in detail, in contrast to those for similar species from xanthine oxidase, for which ^{17}O couplings and angular relationships have been evaluated.[21] Nevertheless coupling is clearly detectable in the low-pH species from sulphite oxidase. Though so far no ^{17}O substitution has been reported for nitrate reductase, there seems no reason to doubt that for both enzymes, the structure of the low-pH species is that of Scheme 2(a).

Still further support for the structure of Scheme 2(a) has been obtained from studies of the phosphate complex of sulphite oxidase. This is believed to have the structure given in Scheme 2(b). When the pH of samples of sulphite oxidase is decreased in the presence of a mixture of phosphate and chloride ions, then the high-pH species is replaced progressively, as the pH value decreases, by a mixture of the low-pH chloride species and the phosphate species, with the relative proportions of these depending on the ratio of the concentrations of the two ions.[13] The spectrum of the phosphate complex is unlike that of other anion complexes in that it shows[22] no coupling to protons. Furthermore, on dissolving in ^{17}O-enriched water there is no change in the spectrum. However, if ^{17}O-enriched phosphate is employed, using ordinary water as solvent, then coupling to this nucleus is clearly seen[23] in the spectrum. The data are thus fully consistent with the structure of Scheme 2(b), in which phosphate acts as a bidentate ligand, in contrast to the monodentate ligand, X^-, in Scheme (2a). Phosphate is an inhibitor of sulphite oxidase and the structure of Scheme 2(b) seems particularly significant since it is analogous to a plausible intermediate in the enzyme's action on sulphite.

We now turn to the structure of the high-pH species. The signal from this is not affected by anions but is affected[19,20] (for sulphite oxidase) by ^{17}O-enriched water. Until quite recently it was assumed that in the signal-giving species the hydroxyl and anion ligands of the low-pH species had been replaced by an oxo group. However, recent work casts some doubt on this. For nitrate reductase, although this was overlooked in the original work,[17] use of ^2H_2O as solvent results[14] in a significant sharpening of the high-pH spectrum. This means that there must be a coupled proton in the signal-giving species, though the coupling is not sufficient to result in resolved splittings. The data are explicable[14] in terms of a single coupled proton with $A(^1H)$ 0.38, 0.32, 0.33 mT.

A comparably coupled proton also exists in the high-pH species from sulphite oxidase, though here its effects on the spectrum are of a more subtle nature. This proton manifests[24] itself by producing features in the spectrum due to "spin flip" transitions, in which the spin of the coupled proton flips simultaneously with that of the unpaired electron. Such transitions[25] (not previously observed in a biological system) result in shoulders which are not easily saturated on raising the microwave power, and which appear on either side of EPR lines, separated from one another by twice the proton NMR frequency, i.e. by 1.0 mT at the fields in question (9 GHz). These spectral features, disappearing in ^2H_2O are observable[13] in the high-pH spectrum of sulphite oxidase, being particularly apparent at the g_1 feature. Detailed interpretation by George[24] reveals that the proton is coupled quite reasonably strongly to molybdenum [$A(^1H)$ 0.4, 0.4, 0.7 mT]. However, splittings or broadening effects of the proton on the spectrum are effectively lost, due to magic angle effects in relation to non-coincidence of the axes of g and A.

In the light of the above data were not able to elucidate unambiguously the structure of the high-pH species. Possible alternative schemes for the high-pH–low-pH transition are given in Scheme 3(a) and (b). Scheme 3(a) is an adaptation of an earlier scheme,[13] with the high-pH species bearing an oxo ligand replaced by a hydroxyl in the low-pH species. The hydroxyl proton "seen" in the low-pH species is the one whose dissociation controls the pK. An additional ligand, Y, bears the more weakly coupled proton of the high-pH species. In the low-pH species, although this second proton is still present, its coupling is supposed to have become undetectably small due to the change of structure. In the alternative, Scheme 3(b), molybdenum bears a hydroxyl ligand in both high- and low-pH species, whose proton is strongly coupled in the low-pH and less so in the high-pH species. In this scheme[24] the ligand Y, present in the high-pH species, dissociates from the metal in formation of the low-pH species, being replaced by the anion X^-, with Y becoming protonated. It is dissociation of this proton, which is not detectably coupled to molybdenum, that controls the pK. In partial analogy with Scheme 3(b), work[26] with model compounds has shown that a ligand of molybdenum (in this case a nitrogen atom)



Scheme 3.

may be reversibly protonated and deprotonated, between species having quite distinct EPR parameters, with the proton apparently not showing coupling to molybdenum in either. Bearing in mind the substantial magnitude of the proton coupling [$A(^1H)_{av} = 0.5$ mT] in the high-pH species from sulphite oxidase, Scheme 3(b) tends to be favoured in the author's laboratory. Though further variations of schemes for the high-pH–low-pH transition could be suggested, it is important to note that in principle, a combination of careful EPR studies with ^{17}O and EXAFS should certainly be capable of distinguishing between the alternatives of Scheme 3(a) and (b).

In attempting to relate the EPR data to the enzyme mechanisms (Scheme 1), we need to bear a number of points in mind. It is perhaps surprising that there seems to have been a lack of detailed steady-state kinetic studies on these enzymes, particularly of studies taking proper account of the two-substrate nature of the reactions. Such work could in principle establish basic points such as whether pK values in the enzymes, or in the substrates, or both, control the profiles (cf. Refs 13 and 17) of enzyme activity against pH. At the present time we have no more than hints as to whether activity of the enzymes shows anion-dependent pK values analogous to the ones detected by EPR. Nor do we know, for instance, whether the true substrate of sulphite oxidase is SO_3^{2-} or HSO_3^-. Steady-state kinetic studies might also provide information as to whether anion inhibitors bind to oxidized or reduced forms of the enzymes. Perhaps more definitively, pre-steady-state kinetic studies could establish whether the oxidation or the reduction step of the turnover is rate-limiting for the enzymes. Only if reaction of substrates with molybdenum is rate-limiting are subtle changes to the structure of the molybdenum centre likely to be crucial to turnover rates.

Mo(V) complexes such as those of the low-pH forms of Scheme 3 might arise by replacement of oxo groups of Mo(VI) species by anions, as in electrochemical reactions[6,7] of model compounds. It is attractive to think of EPR-detectable anion-bearing species from the enzymes as being analogous in structure to complexes of the enzymes with substrate molecules, formed before reaction takes place. Binding of substrate to molybdenum might occur via an increase in co-ordination number. On the other hand, in the case of sulphite oxidase, should it be that the true substrate is HSO_3^-, this could react by addition across a Mo(VI)—oxo bond to give the species of Scheme 2(c). For nitrate reductase, an anion ligand in the Mo(IV) form might simply be exchanged for nitrate. Starting from such species, plausible oxo transfer mechanisms can readily be written.

Complexities revealed by EPR work, particularly in relation to anion effects, make it clear that caution needs to be used in interpreting most published EXAFS work on molybdoenzymes, since this seems not to have been taken into account. It should be added that EPR has provided no support for the suggestions[5] that *E. coli* nitrate reductase carries a relatively heavy atom, "X", 2.8 Å from Mo. If this atom were paramagnetic, as are most of the possible candidates such as iron, it would be coupled to Mo, and there are no indications whatever of this in the EPR data. The enzyme shows Mo(V) EPR spectra quite typical of the metal in all other molybdoenzymes (other than nitrogenase). Whether additional EXAFS studies will substantiate the existence of "X" remains to be seen.

Thus it is particularly desirable that further work by EXAFS should take account of effects of pH and anions on the enzymes. Additional studies, by both EPR and EXAFS, should also seek more carefully than hitherto to relate the species being studied to kinetic data on the enzymes. The way seems open for work leading to considerably deeper understanding than at present exists of these enzymes.

Acknowledgements—I thank my co-workers, as listed in the references, for their part in the published work described. I also thank Dr G. N. George for discussions and Dr S. Cramer for drawing my attention to Ref. 9. The work was supported by grants from the MRC and the SERC.

REFERENCES

1. C. Godfrey, C. Greenwood, A. J. Thomson, R. C. Bray and G. N. George, *Biochem. J.* 1984, **224**, 601.
2. S. Gutteridge, R. C. Bray, B. A. Notton, R. J. Fido and E. J. Hewitt, *Biochem. J.* 1983, **213**, 137.
3. L. P. Solomonson, M. J. Barber, D. W. Howard, J. L. Johnson and K. V. Rajagopalan, *J. Biol. Chem.* 1984, **259**, 849.
4. S. P. Cramer, R. Wahl and K. V. Rajagopalan, *J. Am. Chem. Soc.* 1981, **103**, 7721.
5. S. P. Cramer, L. P. Solomonson, M. W. W. Adams and L. E. Mortenson, *J. Am. Chem. Soc.* 1984, **106**, 1471.
6. J. M. Berg and R. H. Holm, *J. Am. Chem. Soc.* 1985, **107**, 917.
7. B. B. Kaul, J. H. Enemark, S. L. Merbs and J. T. Spence, *J. Am. Chem. Soc.* 1985, **107**, 2885.
8. J. M. Berg and R. H. Holm, *J. Am. Chem. Soc.* 1985, **107**, 925.
9. A. K. Rappé and W. A. Goddard, *J. Am. Chem. Soc.* 1982, **104**, 3287.
10. R. C. Bray, In *Flavins and Flavoproteins* (Edited by R. C. Bray, P. C. Engel and S. G. Mayhew), p. 707. de Gruyter, Berlin (1984).

11. G. N. George, T. R. Hawkes, G. D. Jones and R. C. Bray, *Polyhedron* 1986, **5**, 587.
12. S. P. Vincent, *Biochem. J.* 1979, **177**, 757.
13. R. C. Bray, S. Gutteridge, M. T. Lamy and T. Wilkinson, *Biochem. J.* 1983, **211**, 227.
14. G. N. George, R. C. Bray, F. F. Morpeth and D. H. Boxer, *Biochem. J.* 1985, **227**, 925.
15. R. C. Bray, *Adv. Enzymol. Relat. Areas Mol. Biol.* 1980, **51**, 107.
16. H. J. Cohen, I. Fridovich and K. V. Rajagopalan, *J. Biol. Chem.* 1971, **246**, 374.
17. S. P. Vincent and R. C. Bray, *Biochem. J.* 1978, **171**, 639.
18. T. Yamase, R. Sasaki and T. Ikawa, *J. Chem. Soc., Dalton Trans.* 1981, 628.
19. S. P. Cramer, J. L. Johnson, K. V. Rajagopalan and T. H. Sorrell, *Biochem. Biophys. Res. Commun.* 1979, **91**, 434.
20. R. C. Bray and S. Gutteridge, *Biochemistry* 1982, **21**, 5992.
21. F. F. Morpeth, G. N. George and R. C. Bray, *Biochem. J.* 1984, **220**, 235.
22. M. T. Lamy, S. Gutteridge and R. C. Bray, *Biochem. J.* 1980, **185**, 397.
23. S. Gutteridge, M. T. Lamy and R. C. Bray, *Biochem. J.* 1980, **191**, 285.
24. G. N. George, *J. Magn. Reson.* 1985, **64**, 384.
25. H. Zeldes and R. Livingstone, *Phys. Rev.* 1954, **96**, 1702.
26. P. Subramanian, J. T. Spence, R. Ortego and J. H. Enemark, *Inorg. Chem.* 1984, **23**, 2564.

Polyhedron Vol. 5, No. 1/2, pp. 597–606, 1986
Printed in Great Britain

0277–5387/86 $3.00 + .00
© 1986 Pergamon Press Ltd

BIOLOGICAL CONTRIBUTIONS TO MINERAL CYCLING IN NATURE WITH REFERENCE TO MOLYBDENUM

BRUCE C. KELLEY

Biotechnology Australia Pty Ltd, P.O. Box 20, Roseville, NSW 2069, Australia

(*Received* 10 *June* 1985)

Abstract—While the biological functions of molybdenum have been well studied, the mobilization of this element from its mineral hosts is poorly understood. This in part results from the low solubility product of molybdenum disulphide, its peculiar electronic structure which resists chemical and biological attack, and its toxicity to the growth of metal sulphide leaching bacteria. However, considering the low concentrations of molybdenum in many natural systems, chemoautotrophic and thermophilic acidophiles may make significant contributions to the molybdenum cycle in nature. The physiology and metabolism of these organisms is discussed in relation to metal sulphide dissolution, with special reference to molybdenum disulphide.

A variety of naturally occurring elements, including iron, sulphur and molybdenum, bear similarities in their ability to form a variety of chemical compounds and to participate in electron-transfer reactions through valence-state transitions. These attributes contribute to the important biological functions of these elements in living organisms, and, in turn, provide the basis for the microbial cycling of a large number of mineral elements in nature. The present discussion is not centred on the structure and function of the metalloproteins involved in such oxidation–reduction reactions, but rather on the contribution of specialized microorganisms in oxidizing large amounts of inorganic compounds and therefore their involvement in mineral transformations. There have been many excellent reviews on this subject,[1–7] to which the reader is directed.

Unlike the major mineral elements, molybdenum transformations have received little attention despite the importance of molybdenum in a diversity of living systems. As stated above, the chemolithotrophic bacteria represent important biological mediators of mineral ore solubilization. Although these bacteria exhibit a low tolerance to soluble molybdenum,[8] they may still make considerable contributions to molybdenum transformation on a global scale, particularly when the low concentration of molybdenum in natural systems is considered. In addition, the recently recognized tolerance of thermoacidophilic microorganisms to relatively high levels of molybdenum[9,10] and their contribution to the increased mobilization of this element is important from both the biological and industrial viewpoint. This paper aims to provide a simplified overview of the metabolism of the chemolithotrophic bacteria, and their contribution to the mobilization of biologically and industrially important elements, with specific reference to molybdenum.

SULPHIDE MINERAL DEGRADATION

The microbially-assisted degradation of sulphide-based minerals is a biochemical process which involves a complex interaction between organisms, medium and mineral surfaces. Since the initial demonstrations of the contribution of iron-oxidizing bacteria[11,12] to mineral sulphide dissolution, the majority of studies on the biodegradation of minerals have centred on the activities of the acidophilic chemolithotrophic bacterium *Thiobacillus ferrooxidans*. However, in a natural leaching environment it is likely that a diverse group of organisms are involved in a series of complex interactions, as discussed by Lundgren and Malouf.[7] The extent to which sulphide mineral degrades depends on the development of a microbial pH succession,[13] which in turn is influenced by factors

Table 1. Examples of iron- and sulphur-oxidizing bacteria associated with mineral sulphide ores

Temperature profile	Microorganism	Growth mode
Mesophile	*T. ferrooxidans*	Oxidizes reduced iron and sulphur compounds, autotrophic
	T. thiooxidans	Oxidizes sulphur and reduced sulphur compounds, e.g. $S_2O_3^{2-}$ and S^{2-}; autotrophic
	Leptospirillum ferrooxidans	Oxidizes reduced iron only; autotrophic
Moderate thermophile	Unnamed	Oxidizes iron, sulphur and mineral sulphides at 50°C; organic compound requirement
Extreme thermophile	*Sulfolobus*	Oxidizes iron, sulphur and mineral sulphides at 55–85°C; can use CO_2, simple organic compounds or is heterotrophic

including the physical and chemical characteristics of the mineral, climatic conditions and the availability at reaction sites of water, oxygen and carbon dioxide. The complex microbial associations which develop on the minerals are dominated by the organisms with sulphur and iron-oxidizing abilities which possess tolerance to high levels of acidity and high concentrations of heavy metals. Some examples of important microorganisms involved in leaching metals from mineral sulphide ores are listed in Table 1. These types of organisms exhibit diversity with respect to the nature of their energy sources for growth, their carbon requirements, temperature and pH optima for growth. An important ubiquitous and well-studied member of the natural consortium is *T. ferrooxidans* and aspects of this organism's physiology and metabolism are briefly discussed below.

PHYSIOLOGY OF *T. FERROOXIDANS*

T. ferrooxidans is a Gram-negative rod and displays optimum growth at pH 2.0–2.5 and at temperatures of 25–35°C. Energy for growth is derived from the oxidation of reduced valence state iron and sulphur compounds. Carbon dioxide is the sole source of carbon for growth and the organism prefers the ammonium ion as the nitrogen source, although the ability to fix dinitrogen has been reported.[14]

CARBON METABOLISM

T. ferrooxidans is obligatorily dependent on carbon dioxide as a source of cellular carbon. Indeed, the growth of this organism is sensitive to many organic acids. This probably relates to the large transmembrane pH gradient operating in organisms with an internal pH near neutrality and growing in a highly acidic environment. Such a pH gradient may permit the accumulation of weak acids into the cell cytosol,[15,16] resulting in cytosolic acidification and death.

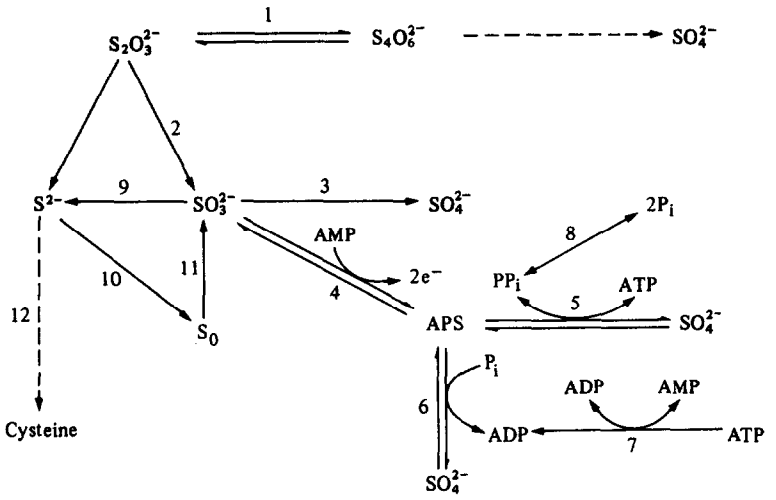
The carbon metabolism of *T. ferrooxidans* is characteristic of a chemolithotroph. Carbon dioxide assimilation is via the Calvin–Benson cycle, catalysed by the enzyme ribulose bisphosphate carboxylase.[17–19] The metabolism of carbon by this organism has recently been reviewed in brief by Ingledew.[16] A more detailed review on this subject is provided by Matin.[15] The Krebs cycle in *T. ferrooxidans* is incomplete and therefore cannot assume its generally recognized catabolic role in generating energy and reducing power. Instead, the Krebs cycle performs a biosynthetic role, providing carbon skeletons for the synthesis of amino acids. Poly(β-hydroxybutyrate) represents the major storage product in this organism.[16]

SULPHUR METABOLISM

The biochemical pathways of sulphur oxidation are quite complex. The oxidation of inorganic sulphide to sulphate can be simply represented as follows:[1]

$$S^{2-} \rightarrow S^{6+} + 8e^{-}. \quad (1)$$

As discussed by Torma,[1] a series of intermediate products are formed during this oxidative process, although intermediate-product identification may not be possible due to chemical instability. A simplified scheme of sulphur metabolism in *T. ferrooxidans* is presented in Fig. 1. The oxidative metabolism of inorganic sulphur compounds has been discussed at length by Tuovinen.[20] Thiosulphate may be oxidized directly to tetrathionite by the thiosulphate-oxidizing enzyme. Alternatively, thiosulphate is oxidized by initial



Reaction	Enzyme
1	Thiosulphate - oxidizing enzyme
2	Rhodanese
3	AMP - independent sulphite oxidase
4	APS - reductase
5	ATP - sulphurylase
6	ADP - sulphurylase
7	Adenylate kinase
8	Pyrophosphatase
9	Sulphite reductase
10	Sulphide oxidase
11	Sulphur - oxidizing enzyne
12	*O*-acetylserine sulphydrase

Fig. 1. Simplified scheme of inorganic sulphur compound metabolism in *T. ferrooxidans*.

rhodanese-catalysed cleavage to sulphide and sulphite (Fig. 1). The latter chemical species probably represents a key metabolite in this rather complex sequence of reactions.[1] Sulphite in turn may be oxidized to sulphate by the enzyme AMP-independent sulphite oxidase[20] in an energy-linked process. An alternative pathway would involve the production of adenosine-5′-sulphatophosphate (APS) by the enzyme APS-reductase. APS in turn would be coupled to substrate-level phosphorylation by ADP-sulphurylase and adenylate kinase activities[20] (Fig. 1). Thus sulphate and ATP would result.

The reductive assimilation of sulphur into cellular protein in this organism has also been discussed by Tuovinen.[20] During growth on ferrous iron, sulphate is actively assimilated into APS[21] prior to its reduction via sulphite and sulphide into cellular protein.[20] During growth on thiosulphate, however, the cleavage of this compound provides a continual source of sulphide which can be incorporated into cellular protein.[20,22] Under these conditions, the major pathway of thiosulphate utilization would probably proceed in the oxidative direction[20] via APS-reductase to ultimately produce sulphate and ATP (Fig. 1).

The structure–function relationships and oxidative mechanisms of the sulphur pathway are discussed in detail elsewhere.[23,24]

IRON METABOLISM

Under optimum conditions, *T. ferrooxidans* grows aerobically at pH 2.0 with an electron-transport chain operating between the two half-reactions as follows:

$$2Fe^{2+} \rightarrow 2Fe^{3+} + 2e^- \quad (2)$$

$$2e^- + \tfrac{1}{2}O_2 + 2H^+ \rightarrow H_2O \quad (3)$$

$$\text{Sum: } 2Fe^{2+} + \tfrac{1}{2}O_2 + 2H^+ \rightarrow 2Fe^{3+} + H_2O \quad (4)$$

The steady-state E_h during growth of the Fe^{2+}–Fe^{3+} couple is about +770 mV and that of the $\frac{1}{2}O_2$–H_2O couple at the cytosolic pH (pH 5.5–6.0) is +890 mV.[16,25] There is, therefore, little energy available to the cell from this oxidative reaction. Chemolithotrophic bacteria that use high redox

potential substrates which are energetically unfavourable typically rely on a high throughput of electrons along the electron-transport chain. High oxidase rates, up to 10 times those reported for beef heart mitochondria,[16] are achieved since the cells develop high concentrations of some electron-transport components. As pointed out by Ingledew,[16] the copper protein rusticyanin, which is the proposed primary electron acceptor of the respiratory chain, accounts for approximately 5% of the total cell protein, while for cytochrome *c* the figure more closely approximates 10%. The components of the electron-transport chain have received considerable study.[16,26,27]

Since the Fe^{2+}–Fe^{3+} couple is so electropositive (+770 mV), it is not possible to directly reduce NADP ($NADP^+$–NADPH, $E_o = -320$ mV). Reduced pyridine nucleotides are essential for cellular processes such as carbon dioxide fixation. The mechanism of NADPH production is assumed to be via an energy-dependent reversal of electron flow. Such a process, while generally documented in chemolithotrophs,[16] has only been observed on two occasions in *T. ferrooxidans*.[28,29] Ingledew[16] provides an excellent discussion on the thermodynamics and possible mechanism of reversed electron transport in this organism.

The nature of the electron-transport chain operating during iron oxidation can now be considered. Most of the electron flux occurs between Fe^{2+} and O_2 while less than 10% of the electrons flow "uphill" from Fe^{2+} to NADP.[16] The electron-transport chain has been modelled[16,25] and can be summarized as follows. Fe^{2+} is oxidized outside of the cell membrane. Cytosolic oxidation of Fe^{2+} would not be expected to occur since the cytosolic pH (5.5–6.0) would favour rapid autooxidation of the Fe^{2+} substrate and chemical precipitation of the Fe^{3+} product. Both rusticyanin and cytochrome *c* are considered as soluble components of the periplasmic space.[25] Ingledew *et al.*[25] consider that one of the multiple forms of cytochrome *c* present may be bound to the cell membrane as is the terminal oxidase, cytochrome a_1, where O_2 reduction occurs at the inner or cytosolic surface of the cell membrane.

Although the components involved in reversed electron transport have yet to be fully identified or purified, the respiratory studies of DiSpirito and Tuovinen[30] provide some insight into the comprehensive pathways of electron transport accompanying Fe^{2+} oxidation.

ENERGY GENERATION

The relationship between electron flow and ATP generation in *T. ferrooxidans* has been discussed in terms of the chemi-osmotic theory.[16,25,31] The chemi-osmotic hypothesis broadly proposes that electron transfer along an H^+-impermeable membrane results in a translocation of H^+ out of the cell. This occurs as a function of the spatial distribution of respiratory chain components which can therefore be considered as redox-coupled H^+ pumps. The energy from the oxidative reaction (substrate oxidation) is thus translocated and conserved as an electrochemical gradient. This proton motive force is made up of a chemical and an electrical component and is responsible for driving H^+ back into the cell via a reversible ATPase which in turn drives the phosphorylation of ADP.[16,25,31] In *T. ferrooxidans*, the chemi-osmotic theory is also invoked,[16,25,31] although the component contributions to the proton motive force are different. The acidity of external medium coupled with the neutrality of the cytosol provides a large and favourable chemical potential of H^+ into the cell. The organism thus uses the acidic environment to its advantage, generating a transmembrane pH gradient by internal proton consumption (reduction of oxygen at the cytosol–cell membrane interface) and using this gradient for the synthesis of ATP via the reversible ATPase system. This therefore represents a simple chemi-osmotic model that does not postulate redox-coupled proton pumps, and is consistent with the environment in which the organism lives.

MICROBIAL LEACHING

The dissolution of a large number of metal sulphides has been shown to be bacterially assisted. Examples of some of the more common sulphides have been considered by Manchee[4] and Ehrlich[5] and include arsenopyrite (AsFeS), orpiment (As_2S_3), bismuthite (Bi_2S_3), enargite [$Cu_3(As,Sb)S_4$], chalcopyrite ($CuFeS_2$), bornite (Cu_5FeS_4), covellite (CuS), chalcocite (Cu_2S), tetrahedrite ($Cu_8Sb_2S_7$), marcasite (FeS), pyrite (FeS_2), molybdenite (MoS_2), pentlandite [$(NiFe)_9S_8$], millerite (NiS), galena (PbS), uraninite (UO_2) and sphalerite (ZnS). The metal sulphides resist bacterial attack to varying degrees[2] and it is of interest that molybdenite is quite recalcitrant.[2] For discussions on the leaching of various metal sulphides together with appraisals of commercial leaching methods, the reader is directed to a large number of excellent reviews.[1–4,7,32]

MECHANISMS OF MICROBIAL DEGRADATION OF SULPHIDE MINERALS

Iron plays a key role in mineral sulphide degradation. Thus, attempts to demonstrate "direct"

bacterial oxidation of mineral sulphides must necessarily exclude iron.

In an iron-free environment, Torma and Bosecker[6] found that the rate of metal dissolution was proportional to the solubility product of the respective metal sulphide. Thus metal sulphide dissolution at the mineral surface provides the sulphide moiety as the oxidizable substrate for the bacterial metabolic system:[6]

$$MS \rightleftharpoons M^{2+} + S^{2-}, \quad (5)$$

where M = bivalent metal.

Torma and Bosecker[6] further suggested that substrate dissociation from the mineral surface, rather than bacterial attachment, is the prerequisite for bacterial oxidation of the insoluble metal sulphides.

In an elegant series of experiments, Tributsch and Bennett[33,34] also demonstrated that metal sulphides with high solubility products are good substrates for bacterial leaching. However, other conditions also apply, such as an excess of holes in the valence band or electron extraction by Fe^{3+} (see later). Thus, in the absence of iron, protons (H^+) were shown to play a central catalytic role in the mechanism of bacterial oxidation of metal sulphides.[33,34] Proton-catalysed reactions chemically break surface bonds, including electronic-state transitions into the forbidden energy gap. This leads to the formation of weakly bonded $SH^{\delta-}$ groups which are, in turn, removed from the sulphide surface through complex formation with an unidentified molecular carrier used by the bacterium.[33,34]

As indicated above, iron is often associated with the leaching system. Indeed, one of the most important naturally occurring growth substrates for *T. ferrooxidans* is the iron sulphide mineral, iron pyrites (FeS_2), which is often associated with other more valuable minerals. Iron is brought into solution by the aqueous oxidation of pyrite by molecular oxygen. In an excellent review, Lowson[35] identifies three reaction paths for pyrite oxidation, namely bacterial, chemical and electrochemical, restricting discussion to the latter two. The chemical oxidation path is a three-step process:

(i) the oxidation of pyrite by molecular oxygen:

$$2FeS_2 + 7O_2 + 2H_2O \rightarrow 2FeSO_4 + 2H_2SO_4; \quad (6)$$

(ii) the oxidation of ferrous iron to ferric iron by molecular oxygen, which is thought to be the rate-limiting step;

(iii) the oxidation of pyrite by ferric iron.

Thermodynamic data predicts sulphate formation[35,36] as shown in eqn (7):

$$FeS_2 + 7Fe_2(SO_4)_3 + 8H_2O \rightarrow 15FeSO_4 + 8H_2SO_4. \quad (7)$$

However, in acid ferric medium, elemental sulphur is often produced[4,36] [see eqn (8)]:

$$FeS_2 + Fe_2(SO_4)_3 \rightarrow 3FeSO_4 + S_0. \quad (8)$$

The electrochemical pathway is the summation of two half-cell reactions:[35]

(i) the cathode:

$$O_2 + 4H^+ + 4e^- \rightarrow 2H_2O, \quad (9)$$

(ii) the anode:

$$FeS_2 + 8H_2O \rightarrow Fe^{3+} + 2SO_4^{2-} + 16H^+ + 15e^-. \quad (10)$$

Both the chemical and electrochemical reactions make important contributions to localized iron environments in nature.[35] In the natural environment, the large number of physical–chemical parameters involved would greatly influence the kinetics and direction of pyrite dissolution.

Thus, the bacterium is presented with reduced iron and sulphur compounds as energy sources for growth:

$$4FeSO_4 + O_2 + 2H_2SO_4 \rightarrow 2Fe_2(SO_4)_3 + 2H_2O, \quad (11)$$

$$2S_0 + 3O_2 + 2H_2O \rightarrow 2H_2SO_4. \quad (12)$$

The products of these reactions, ferric sulphate and sulphuric acid, provide an excellent means of dissolving a variety of mineral sulphides by what is sometimes termed the "indirect" mechanism of bacterial attack:

$$MS + Fe_2(SO_4)_3 \rightarrow MSO_4 + 2FeSO_4 + S_0, \quad (13)$$

where M = bivalent metal.

The ferrous sulphate produced can be recycled as a bacterial-growth substrate [see eqn (11)].

When ferric iron is present, there is less need to break chemical bonds in the mineral sulphide surface by proton interaction,[33,34] although proton concentration is critical to maintain ferric iron solubility. Ferric iron may directly break chemical bonds by extracting electrons from the valence band of the sulphide provided that energetic constraints are met.[33,34] This may provide an efficient means of sulphide oxidation.

In the natural leaching system, it is likely that all of these parameters, including the solid state, chemical and electrochemical properties of the mineral sulphide, the presence or absence of iron,

particularly trivalent iron, and the proton concentration are important in the relationship between *T. ferrooxidans* and the mineral sulphide.

MOLYBDENUM MINERALS

Molybdenum does not occur in the free state in nature. There are two recognized ores of molybdenum, namely molybdenite (MoS_2) and wulfenite ($PbMoO_4$). Molybdenite is the chief ore of molybdenum and is relatively widely distributed, frequently occurring in small veins or scattered as small flakes, and often associated with granites and pegmatities. The chief source is the U.S., with smaller but significant producers including the U.S.S.R., Chile, China, Canada, Japan and Norway.

Geologically, molybdenum exhibits two important valence states, +4 and +6. The lower valence state is largely limited to molybdenite, while the higher valence state is characteristic of molybdates formed in surface environments. The weathering of molybdenum minerals yields molybdate ion in solution, chiefly as MoO_4^{2-} at pH values above 5 or 6, and $HMoO_4^-$ at lower pH values. Thus molybdenum is probably present in soils chiefly as absorbed molybdate (MoO_4^{2-}). The successful use of soil molybdenum content analysis as a geological prospecting tool for molybdenum would indicate that molybdenum in soils is largely dependent on parent mineral content.

The complex area of molybdenum mineral weathering, speciation, chemistry, soil solution transport, interaction with other materials and adsorption in relation to physico-chemical parameters will not be considered here.

APPLICATIONS OF MOLYBDENUM

Industrial

The industrial uses of molybdenum are largely confined to metallurgical applications (90%), of which the iron and steel industry accounts for some 70% of the total usage. Steels (carbon, stainless, alloys and specialized), cast irons, superalloys and other welding alloys are important end products of molybdenum. The use of molybdenum lies in its enhancement of strength, toughness, wear and corrosion resistance. Non-metallurgical applications include lubricants, catalysts in petroleum refining processes, paint and dye pigments, and chemical usage in flame retardants and smoke suppressants. When considering major end use product areas, molybdenum applications extend to machinery (35%), transportation (20%), oil and gas (15%), chemicals (11%), electrical (9%) and miscellaneous (10%).

Biological

The biological significance of molybdenum is extremely well-documented and will only be briefly mentioned here. Molybdenum represents an important metal component of a variety of enzymes that are found in micro-organisms, plants and animals. Examples of the reactions catalysed by molydoproteins are shown in Table 2. The suitability of molybdenum as a participant in electron-transfer reactions is attributable to its complex chemical properties. Molybdenum can undergo two-electron transfers and possesses some four oxidation states which appear biologically relevant, namely +6, +5, +4 and +3. Molybdenum transitions between +6 and +4 oxidation states have been reported but it is likely that a variety of electron-transfer reactions operate between the various oxidation states. The molybdenum-containing cofactor, which is common to the different molybdo-enzymes, will be covered in detail by other participants at this Symposium.

BIOLOGICAL LEACHING OF MOLYBDENITE

The microbiological leaching of molybdenite (MoS_2) by chemolithotrophic bacteria has been generally reported as follows:[1]

$$2MoS_2 + 9O_2 + 6H_2O \rightarrow 2H_2MoO_4 + 4H_2SO_4. \quad (14)$$

Recently, Lyalikova and Lebedeva[37] implied that different microorganisms may oxidize different moieties of the molybdenite molecule. The chemolithotrophic bacteria would oxidize the sulphur moiety[1] [see eqn (14)]. However, molybdenum chemistry could predict the following reaction:[37]

$$2MoS_2 + 9O_2 + 2H_2O \rightarrow 2(MoO_2 \cdot SO_4) + 2H_2SO_4. \quad (15)$$

Their calculations[37] showed that the oxidation of molybdenum dioxide would provide sufficient energy for growth of an autotrophic organism. Such a culture of molybdenum-oxidizing bacteria was obtained, growing on molybdenum dioxide as substrate:

$$MoO_2 + O_2 \rightarrow MoO_3. \quad (16)$$

Indeed, their evidence suggested that molybdenite was oxidized by two microorganisms, one that oxidized molybdenite and the other molybdenum dioxide.[37] This interesting observation, together

Table 2. Reactions catalysed by molybdoproteins

Enzyme	Conversion catalysed
Nitrogenase	Nitrogen → two ammonia
Nitrate reductase	Nitrate → nitrate
Chlorate reductase	Chlorate → chlorite
Tetrathionate reductase	Tetrathionate → two thiosulphate
Thiosulphate reductase	Thiosulphate → sulphite + sulphide
Sulphite oxidase	Sulphite → sulphate
Xanthine oxidase	Xanthine → uric acid
Formate dehydrogenase	Formate → bicarbonate
Carbon monoxide oxidoreductase	Carbon monoxide → carbon dioxide
Acetaldehyde oxidase	Acetaldehyde → acetate

with identification and characterization of the organisms involved, awaits further examination.

Historically, Bryner and Anderson[38] first provided conclusive evidence that molybdenite can be oxidized by autotrophic bacteria or by their reaction products. In the presence of undefined bacterial cultures, a seven-fold increase in molybdenite dissolution was observed over sterile controls. Soluble molybdenum was present in a 1:4 ratio of penta- and hexavalent forms. In the presence of pyrite, a significant increase in molybdenum sulphide oxidation was observed, indicating the importance of indirect mechanisms of molybdenite solubilization. Such mechanisms have been discussed above. Indeed, the contribution of direct (Fe^{3+}-independent) bacterial attack cannot be determined from these early studies[38] as no efforts were made to totally exclude iron from the system.[38]

The use of mesophilic chemolithotrophic microorganisms in leaching molybdenite is largely restricted due to the toxicity to growth of such organisms by soluble molybdenum.[8,38,39] In a comprehensive study,[8] molybdenum was shown to be lethal to *T. ferrooxidans* at concentrations above 5 mg l^{-1}. Variations in tolerance to different metals were coupled to the type of oxidizable substrate.[8] While oxidizing thiosulphate, the organism was more sensitive to heavy metals than when oxidizing iron. It has recently been shown[40] that the presence and oxidation of ferrous iron may afford a protective effect on *T. ferrooxidans* from a range of heavy metals, particularly cobalt. The alleviation of inhibition by toxic metals of iron oxidation by non-inhibitory concentrations of disodium ethylenediamine tetraacetic acid (EDTA) has also been recently evaluated.[41] The picture for molybdenum, however, remains unclear and further studies aimed at elucidating the lethal effects and mechanism of action of this metal have not been forthcoming.

In commercial leaching operations involving toxic metal species such as molybdenum, the use of protective agents such as EDTA would be unlikely to be practical from economic considerations. A remote or two-stage operation physically separating the bacterial generation of ferric iron from the chemical or indirect interaction with the mineral sulphide ore in question may provide the basis for a leaching process.[3,32] However, the relative ease with which other base metals, particularly copper-, zinc- and nickel-based minerals, are leached has tended to limit research input into molybdenum solubilization and recovery.

Attempts to enhance molybdenite oxidation have been recently successful through the use of high-temperature sulphur-oxidizing bacteria of the genus *Sulfolobus*. As early as 1966, Brierley[42] first reported the isolation of an organism resembling *Sulfolobus* from an acid thermal spring drainage in Yellowstone National Park. Detailed characterization of these acidophilic thermophiles was later presented by Brock *et al.*,[43] who demonstrated that *Sulfolobus* represents a new genus of bacterium characterized as a facultative autotroph with distinctive morphology and growing on sulphur or a variety of sulphur compounds. Growth was further characterized by a low pH optimum (2–3) and temperatures ranging from 55 to 85°C. The organism originally isolated by Brierley[42] was examined in greater detail[44] and found to closely resemble *Sulfolobus* as described by Brock *et al.*[43] Unlike *Sulfolobus* however, the isolate oxidized ferrous iron in addition to sulphur and was unable to use yeast extract as an energy source.[44] Nevertheless, growth on iron and sulphur substrates was enhanced by the provision of yeast extract (0.02%).[44]

In applying this *Sulfolobus*-like organism to mineral sulphide substrates, Brierley and Murr[9] first demonstrated the ability of acido-thermophilic bacteria to leach molybdenite. In a preliminary report,[9] molybdenite concentrates could be oxidized

in the presence of the thermophilic isolate in shake flask experiments. Maximum yields (13.3% yield after 30 days) were observed in the presence of yeast extract (0.02%) and ferrous sulphate (1%). Over similar times, uninoculated controls reported only 0.1% molybdenum recovery. The organism therefore exhibited a unique tolerance to relatively high levels of molybdenum, far in excess of that previously reported for mesophilic chemoautotrophic bacteria.[8] In addition, scanning electron micrograph analysis showed isolate attachment to molybdenite fines.[9] The use of scanning electron microscopy as a tool in bioextractive research was further highlighted by the demonstration of microcolony formation on molybdenite fines,[45] although attachment was not clearly indicated. In a more specific study,[46] attempts were made to correlate mineral properties of molybdenite with the attachment of *Sulfolobus* to find out whether attachment was random or specifically related to mineral surface characteristics. No correlation could be found between bacterial attachment and dislocation lines or structural abnormalities on the mineral surface, thus leading the authors to conclude that crystal dislocations probably do not play an important role.[46] Brierley,[2] however, has questioned the validity of this conclusion based on insufficient mineralogical and chemical definition of the material used, the possibility of a contribution to dislocation lines through the inclusion of gangue mineral, and artificial defect introduction resulting from thin-section preparation. Brierley[2] clearly indicates that dislocations represent active sites of crystal changes which may provide obvious benefits for effective biological or chemical exploitation and that further work is required before bacterial attachment to molybdenite fines is more clearly understood. Indeed, the whole area of a bacterial attachment mechanism relating to a large number of mineral ores awaits resolution.

In any commercial operation where molybdenum may be present as a major or minor component of the mineral being extracted or its associated gangue, the use of chemoautotrophic bacteria may be in doubt, due to the low tolerance to molybdenum of these organisms.[8] The improved leaching of molybdenite by *Sulfolobus*[9] therefore provided the stimulus for further demonstrations of biologically catalysed molybdenum solubilization. In a detailed study, Brierley[10] reported on the tolerance of *Sulfolobus* to high concentrations of soluble molybdenum. Initial studies[9] showed that tolerance to hexavalent molybdenum at 60°C was high, although the tolerance varied according to whether the cells were actively growing or not. Oxygen uptake studies[10] revealed that cell respiration was only slightly impaired at 2.0 g l^{-1} (21 mM) Mo(VI). The organism was still capable of active growth at a soluble molybdenum concentration of 0.75 g l^{-1} (7.8 mM). As reported above, the maximum tolerance of chemoautotrophic *Thiobacilli* is approximately 0.005–0.09 g l^{-1}.[8]

The high-temperature organism was further evaluated in batch reactor studies designed to evaluate the leaching of a variety of molybdenite-containing materials.[10] Molybdenite waste and tailings could not be leached due to the acid-consuming nature of the associated gangue minerals which displaced the pH above physiologically favoured conditions. No attempts were made to maintain the pH (2–3) by pH control. High grade (7.3% molybdenum) run-of-mine ore could be successfully leached.[10] Molybdenite concentrate was also biologically leached in a batch reactor system at 60°C. The maximum dissolution observed over a 30-day period was 26.5 mg Mo l^{-1} day^{-1} (13.3% yield) and required the addition of yeast extract (0.02%) and ferrous sulphate (1%). In batch reactors, a biphasic kinetic leaching pattern was established with a gradual cessation of molybdenite leaching.[10] This effect, ascribed to the build-up of inhibitory products in the liquor, could be overcome by the operation of a semi-continuous process, replacing the medium periodically with fresh leaching solution. Brierley[10] argues that industrial processes, reliant on continuous liquor flows, would eliminate this problem of toxic product build up. A variety of organic compounds were tested for their ability to stimulate leaching.[10] The highest rates were obtained with either yeast extract or sucrose, provided ferrous iron was present. Indeed, the presence of ferrous sulphate was most important in molybdenite oxidation, whereas sulphur was inhibitory.[10] When ferrous iron was replaced by pyrite, soluble molybdenum levels were reduced if the pyrite concentration exceeded 50% of total solid substrate. This was considered to be due to preferential pyrite oxidation or precipitation of ferrimolybdite.[10] The latter possibility might also be expected to occur when soluble ferrous iron is included.

During the course of these experiments, Brierley[10] made the interesting observation that the organism reduced soluble oxidized hexavalent molybdenum to molybdenum blue, the pentavalent state, while oxidizing sulphur. In a recent publication,[47] the anaerobic reduction of molybdenum by *Sulfolobus* species was investigated. Both *Sulfolobus brierleyi* and *S. acidocaldarius* oxidized sulphur aerobically and anaerobically, simultaneously inducing a blue colouration in the medium attributable to a reduced form of molybdenum.[48] The results[47] indicated that

Sulfolobus may be using Mo(VI) as an electron acceptor, as previously discussed by Brierley.[2] The generation of pentavalent molybdenum even under aerobic conditions was considered likely due to the poor solubility of oxygen at 60°C. The complexity of the structures of Mo(VI) and Mo(V) in solution under these conditions, coupled with the enhancing effect of aluminium on Mo(VI) reduction,[47] has not as yet permitted elucidation of this proposed redox couple. Appropriate controls excluded the possibility of chemical effects and it would therefore appear that the reduction requires the intervention of these unique bacteria or their reaction intermediates or products.

The ability of these high-temperature bacteria to enhance molybdenum dissolution, coupled with apparent molybdenum reduction under microaerophilic or anaerobic conditions, enhances the metabolic versatility of these unique organisms. In addition, these findings further implicate the importance of the biological molybdenum cycle in nature.

CONCLUSIONS

Although molybdenum is regarded as a rare metal, it is distributed widely in nature and occurs as independent mineral deposits. While molybdenum has many practical uses and is commercially a valuable commodity, the real significance of this element lies in its biological functions which are common across a diversity of life forms. Indeed, it represents an essential functional component in a large number of biochemical systems.

While much is now known of the complex chemistry and biochemistry of molybdenum, the mobilization of this element from its mineral hosts through natural weathering and biodegradative processes remains poorly understood. There may be several reasons for this. Molybdenite is considered to be quite recalcitrant or resistant to biological attack.[2] This in turn probably relates to the low solubility product of molybdenum disulphide.[34] This compound is a layer-type transition metal sulphide with a peculiar electronic structure which does not favour a chemical reaction with protons, and is therefore extremely resistant against bacterial attack and chemical oxidation.[34] Mesophilic chemolithotrophs are generally most implicated in the biologically assisted dissolution of metal sulphides, yet these organisms show low tolerance to soluble molybdenum.[8,38,39] The extreme thermophiles show greater tolerance[9,10] and have been shown to enhance molybdenite solubilization and to mediate valence-state transitions between soluble molybdenum species through as yet unknown mechanisms. However, the difficulties associated with working with such mesophilic and thermophilic bacteria, coupled with the problems outlined above and the complex solution chemistry of molybdenum, may have tended to restrict progress in this area of research.

The gradual depletion of natural high-grade resources of some specific elements may necessitate the development of alternative extractive technologies. Thus biological mining is likely to find applications in the extraction of high-value metals from low-grade zones of mineralization. Conventional approaches may be more severely limited by economic constraints related to mineral deposit size and value. Future research may well be directed by industrial demands towards the mobilization and recovery of more exotic mineral elements, including molybdenum. This can only help to contribute to our increased understanding of the biological significance and cycling of molybdenum in nature.

REFERENCES

1. A. E. Torma, *Adv. Biochem. Eng.* 1977, **6**, 1.
2. C. L. Brierley, *CRC Crit. Rev. Microbiol.* 1978, **6**, 207.
3. D. P. Kelly, P. R. Norris and C. L. Brierley, In *Microbial Technology: Current State, Future Prospects* (Edited by A. T. Bull, D. C. Ellwood and R. C. Rutledge), p. 263. Cambridge University Press, Cambridge (1979).
4. R. Manchee, *Trends Biochem. Sci.* 1979, **4**, 77.
5. H. L. Ehrlich, *Geomicrobiology*. Marcel Dekker, New York (1981).
6. A. E. Torma and K. Bosecker, In *Progress in Industrial Microbiology* (Edited by M. J. Bull), Vol. 16, p. 77. Elsevier, Amsterdam (1982).
7. D. G. Lundgren and E. E. Malouf, In *Advances in Biotechnological Processes*, Vol. 1, p. 223. Alan R. Liss, New York (1983).
8. O. H. Tuovinen, S. I. Niemela and H. G. Gyllenberg, *Antonie van Leeuwenhoek* 1971, 489.
9. C. L. Brierley and L. E. Murr, *Science* 1973, **179**, 488.
10. C. L. Brierley, *J. Less-Common. Met.* 1974, **36**, 237.
11. A. R. Colmer and M. E. Hinkle, *Science* 1947, **106**, 253.
12. K. L. Temple and A. R. Colmer, *J. Bacteriol.* 1951, **62**, 605.
13. B. J. Ralph, In *Biogeochemical Cycling of Mineral forming Elements* (Edited by P. Trudinger and D. J. Swaine), p. 369. Elsevier, New York (1979).
14. M. E. Mackintosh, *J. Gen. Microbiol.* 1978, **105**, 215.
15. A. Matin, *Annu. Rev. Microbiol.* 1978, **32**, 433.
16. W. J. Ingledew, *Biochim. Biophys. Acta* 1982, **683**, 89.
17. J. W. Maciag and D. Lundgren, *Can. J. Eng.* 1964, **48**, 669.
18. G. A. Din, I. Suzuki and H. Lees, *Can. J. Microbiol.* 1967, **13**, 1, 413.

19. N. L. Gale and J. V. Beck, *J. Bacteriol.* 1967, **94**, 1052.
20. O. H. Tuovinen, In *Conference Bacterial Leaching* (Edited by W. Schwartz), p. 9. Verlag Chemie, Weinheim (1977).
21. O. H. Tuovinen, B. C. Kelley and D. J. D. Nicholas, *Arch. Microbiol.* 1975, **105**, 123.
22. B. C. Kelley, O. H. Tuovinen and D. J. D. Nicholas, *Arch. Microbiol.* 1976, **109**, 205.
23. G. I. Karavaiko and T. A. Pivovarova, In *Conference Bacterial Leaching* (Edited by W. Schwartz), p. 37. Verlag Chemie, Weinheim (1977).
24. D. Lundgren and T. Tano, In *Metallurgical Application of Bacterial Leaching and Related Microbiological Phenomena* (Edited by L. E. Murr, A. E. Torma and J. A. Brierley), p. 151. Academic Press, New York (1978).
25. W. J. Ingledew, J. C. Cox and P. J. Halling, *FEMS Microbiol. Lett.* 1977, **2**, 193.
26. J. G. Cobley and B. A. Haddock, *FEBS Lett.* 1975, **60**, 29.
27. W. J. Ingledew and J. G. Cobley, *Biochim. Biophys. Acta* 1980, **590**, 141.
28. M. I. H. Aleem, H. Lees and D. J. D. Nicholas, *Nature (London)* 1963, **200**, 759.
29. G. V. Tikhonova, L. L. Lisenkova, N. G. Doman and V. P. Skulachev, *Biokhimiya* 1967, **32**, 725.
30. A. A. DiSpirito and O. H. Tuovinen, *Arch. Microbiol.* 1982, **133**, 28.
31. J. G. Cobley and J. C. Cox, *Microbiol. Rev.* 1983, **47**, 579.
32. O. H. Tuovinen and D. P. Kelly, *Int. Metall. Rev.* 1974, **19**, 21.
33. H. Tributsch and J. C. Bennett, *J. Chem. Tech. Biotechnol.* 1981, **31**, 565.
34. H. Tributsch and J. C. Bennett, *J. Chem. Tech. Biotechnol.* 1981, **31**, 627.
35. R. T. Lowson, *Chem. Rev.* 1982, **82**, 461.
36. J. E. Dutrizac and R. J. C. MacDonald, *Miner. Sci. Eng.* 1974, **6**, 59.
37. N. N. Lyalikova and E. V. Lebedeva, *Geomicrobiol. J.* 1984, **3**, 307.
38. L. C. Bryner and R. Anderson, *Ind. Eng. Chem.* 1957, **49**, 1721.
39. L. C. Bryner and A. K. Jameson, *Appl. Microbiol.* 1958, **6**, 281.
40. T. Sugio, C. Domatsu, T. Tano and K. Imai, *Appl. Environ. Microbiol.* 1984, **48**, 461.
41. S. S. Roy Mahaptra and A. K. Mishra, *Curr. Microbiol.* 1984, **11**, 1.
42. J. A. Brierley, Ph.D. Thesis, Montana State University (1966).
43. T. D. Brock, K. M. Brock, R. T. Belly and R. L. Weiss, *Arch. Mikrobiol.* 1972, **84**, 54.
44. C. L. Brierley and J. A. Brierley, *Can. J. Microbiol.* 1973, **19**, 183.
45. C. L. Brierley, J. A. Brierley and L. E. Murr, *Res./Dev.* 1973, **24**, 24.
46. V. K. Berry and L. E. Murr, *Metall. Trans.* 1975, **6B**, 488.
47. C. L. Brierley and J. A. Brierley, *Zentralbl. Bakteriol. Hyg., I. Abt. Orig.* 1982, **C3**, 289.
48. F. A. Cotton and G. Wilkinson, *Advanced Inorganic Chemistry, A Comprehensive Text.* John Wiley, New York (1980).

Polyhedron Vol. 5, No. 3, pp. 743–752, 1986
Printed in Great Britain

0277-5387/86 $3.00+.00
Pergamon Press Ltd

OXIDATIVE BREAKDOWN OF POLYMERIC PLUTONIUM(IV) HYDROXIDE BY CERIUM(IV)

D. J. SAVAGE* and T. W. KYFFIN

Dounreay Nuclear Power Development Establishment, Caithness KW14 7TZ, U.K.

(*Received* 4 *February* 1985; *accepted after revision* 27 *July* 1985)

Abstract—The breakdown of polymeric plutonium(IV) hydroxide (plutonium colloid) by cerium(IV) has been studied spectrophotometrically by monitoring the formation of plutonium(VI). Reaction rate variations were studied with changes in cerium(IV), acid and plutonium colloid concentrations. A reaction mechanism involving the formation of $[Ce_2O(OH)_2]^{4+}$ and its reaction with the polymer surface to produce two plutonium(V) ions is postulated to explain the observed kinetic data, in particular the maximum in the reaction rate at around 0.3 M nitric acid.

Plutonium(IV) cations hydrolyse under conditions of low acidity to form either a hydrous oxide precipitate or more frequently a colloidal "solution" of polymeric hydroxide. The conditions for colloid formation have been studied by several authors.[1–5] The process can be represented by eqns (1) and (2):

$$Pu^{4+} + 4H_2O \rightleftharpoons Pu(OH)_4 + 4H^+, \quad (1)$$

$$nPu(OH)_4 \rightarrow (PuO_2)_n + 2nH_2O. \quad (2)$$

Reactions (1) and (2) must be incomplete to provide the charge necessary to stabilize the colloid.

Reversal of the hydrolysis and polymerization occurs at increased acidity. Normally the breakdown of plutonium colloid is very slow[1,5] because of the difficulty in reversing the polymerization reaction (2). It has been shown that the rate of reconversion into ionic forms, in nitric acid solution, increases with nitric acid strength and decreases with colloid age.[1] The depolymerization rate is significantly increased by anions which complex plutonium(IV) strongly.[5] The fluoride ion is outstandingly effective in this respect; for example, aged colloid is completely reconverted to ionic plutonium species in less than 5 min at 20°C using 0.4 M nitric acid containing 0.05 M fluoride. Consequently, fluoride is often employed in the analysis of solutions which may contain colloidal plutonium hydroxide.[6]

The exceptional effectiveness of fluoride ions is believed to arise from their small size and high charge density, permitting them to penetrate the colloid molecules by replacing hydroxyl groups. Their ability to complex with plutonium(IV) then results in removal of a plutonium atom from the colloid molecule with the lower polarizability of fluoride inhibiting bridging-bond formation between plutonium atoms.

A common analytical technique for plutonium measurement is to oxidize the plutonium to plutonium(VI) with cerium(IV) and to measure the plutonium(VI) spectrophotometrically at 831 nm.[6–8] During attempts to extend this technique to the estimation of plutonium(IV) colloid concentrations by performing the measurements with and without a fluoride pretreatment, it was obvious that cerium(IV) was itself capable of converting polymeric plutonium(IV) hydroxide into simple plutonium(IV) cations. The mechanism for this reaction is obviously different from that postulated for fluoride. This paper studies the conversion of colloidal plutonium(IV) hydroxide to ionic species by reaction with cerium(IV). An examination of the relationship between the cerium(IV) concentration, the plutonium concentration and the acidity dependence of the reaction has been used in an attempt to elucidate a probable reaction mechanism.

EXPERIMENTAL

Plutonium(VI) *measurement*

Cerium(IV) is a strong oxidant ($E^\ominus = 1.6$ V in dilute nitric acid)[9] and will oxidize ionic plutonium species to plutonium(VI). This reaction has been used in a titrimetric analytical procedure[10] and as

* Author to whom correspondence should be addressed.

the basis of a spectrophotometric technique.[6–8] The latter technique was used in this study to follow the breakdown of plutonium colloid by monitoring the formation of the plutonium(VI) peak at 831 nm, using a Perkin–Elmer Hitachi 200 spectrophotometer.

Preparation of plutonium colloid

The polymeric plutonium hydroxide solutions were prepared by heating a plutonium nitrate solution (of known plutonium concentration and free acidity) with a little hydrogen peroxide to form plutonium(IV), neutralizing most of the free acid with sodium hydroxide and diluting to known volume to give about 2.5 mg plutonium cm^{-3} and about 0.02 M calculated free acidity. The stock solutions were apple green.

The ionic plutonium content of these colloid solutions was checked by measuring the visible spectrum at 477, 567, 603 and 831 nm, corresponding to the absorption maxima of plutonium(IV), plutonium(V), plutonium(III) and plutonium(VI), respectively. The only ionic plutonium found was plutonium(VI), which ranged from 1 to 12% of the total plutonium present, depending upon the batch.

Depolymerization rate measurement

The breakdown of plutonium colloid was examined by adding ceric ammonium nitrate in dilute nitric acid of the desired strength. Aliquots of plutonium colloid stock were added and the mixture was then diluted to volume and transferred to the spectrophotometer. The reaction time was the elapsed time from adding the plutonium colloid aliquot.

Initial reaction rates were calculated from the first measurement of ionic plutonium(VI), which was normally obtained 3 min after initiating the reaction, corrections being made for the ionic plutonium present in the original colloid sample.

RESULTS

Cerium(IV) *oxidation of plutonium*(IV)

The oxidation of plutonium(IV) by cerium(IV) can be expressed as follows:

$$Pu^{4+} + 2H_2O + 2Ce^{4+} \rightleftharpoons PuO_2^{2+} + 4H^+ + 2Ce^{3+}. \quad (3)$$

It follows from this equation that the kinetics of the reaction may be slow and that both the equilibrium and rate should vary with acidity. The acid dependence of the reaction has been observed in other applications[10] although the redox potential is nearly independent of the acidity between 0.5 and 2 M nitric acid.[9]

Some preliminary measurements of the rate of this reaction were made in order to assess the minimum acceptable concentrations of cerium(IV) in the depolymerization rate measurements. Oxidation of any ionic plutonium must be more rapid than the breakdown of plutonium colloid.

The time required for oxidation of plutonium(IV) with cerium(IV) was estimated at a range of acidities. The results for the oxidation of a 0.00059 M plutonium(IV) solution at 16 ± 1°C are shown in Table 1. These show that, with decreasing acidity, progressively lower cerium(IV) concentrations are required to oxidize 99% of the plutonium present within 5 min.

Reaction of cerium(IV) *with colloidal plutonium*(IV)

Some typical plots of the proportion of colloid converted to plutonium(VI) vs reaction time are shown in Figs 1 and 2. These show that the time for

Table 1. Time required for the oxidation of plutonium(IV) by cerium(IV)

Acidity (M)	Cerium(IV) concentration (M)	% of plutonium converted to plutonium(VI) within		
		3 min	5 min	10 min
3	0.05	95.2	98.9	100.0
	0.03	79.2	89.1	98.3
2	0.02	94.6	99.0	100.0
1	0.01	99.6	99.8	100.0
0.5	0.005	100.4	100.0	100.0
	0.002	75.0	79.7	86.9
0.2	0.005	100.2	99.8	100.0
0.05	0.002	100.0	—	100.0

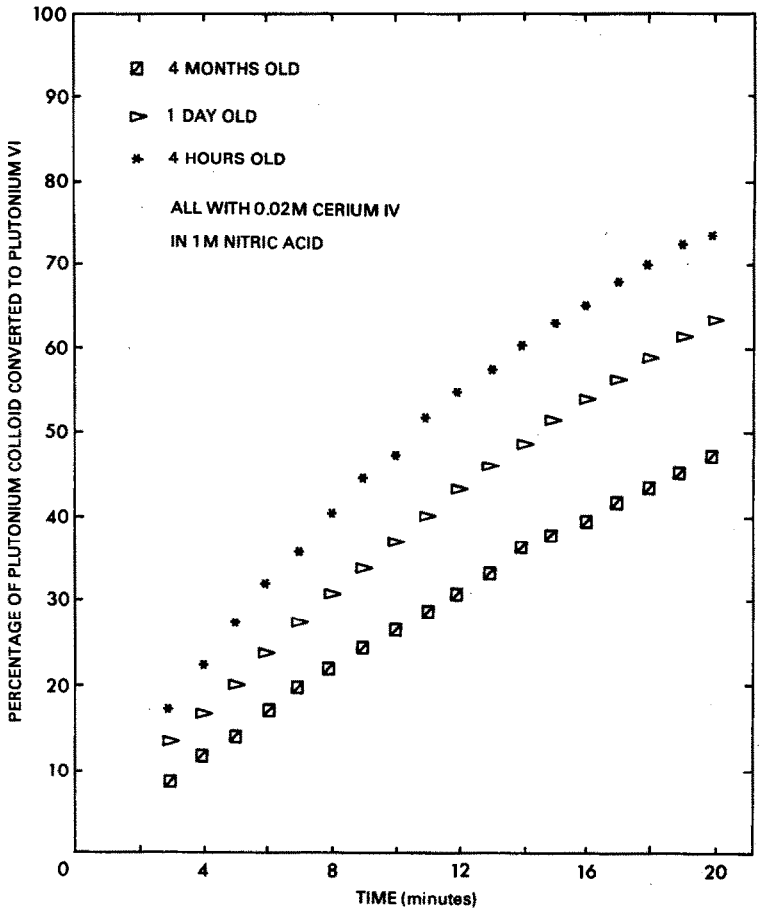


Fig. 1. Conversion of plutonium colloid to plutonium(VI) by cerium(IV).

the reaction to reach 50% pf completion is in the region 5–30 min. The data in Fig 1 show that the reaction rate varies with the colloid batch or age, under identical experimental conditions. Figure 2 shows that, for one batch of colloid, the breakdown rate varies with both cerium(IV) concentration and solution acidity.

Cerium(IV) does not form complexes with plutonium(IV) but it does produce plutonium(VI) from polymeric plutonium(IV) hydroxide. If it is assumed that reversal of the hydrolysis–polymerization reaction by acid is still involved, a reaction of the type:

$$(PuO_2)_n \xrightarrow{H^+} nPu^{4+} \xrightarrow{Ce^{4+}} nPuO_2^{2+} \qquad (4)$$

is probable. In this case the initial rate of breakdown is expected to be given by an expression of the type:

$$-\frac{dPu_c}{(dt)_{init}} = k[Ce(IV)]^x[H^+]^y[Pu_c]^z, \qquad (5)$$

where [ ] represents the concentrations (or, more strictly, activities) of the reacting species, Pu_c represents colloidal plutonium(IV), and x, y and z are simple exponents. Thus, a plot of log

$$-\frac{dPu_c}{(dt)_{init}} \text{ vs log } [Ce(IV)]$$

at constant cerium(IV) and plutonium colloid concentrations should be a straight line of slope x. Similar plots vs log $[H^+]$ and $[Pu_c]$ should give y and z, respectively.

Initial reaction rates were calculated for the first 3 min of the reaction at $16 \pm 1°C$. Colloid of the same batch and age was used for all measurements of any one variable so that it was valid to express $[Pu_c]$ by the actual plutonium concentration.

The maximum acceptable measured initial rate is limited by the requirement of an approximately constant plutonium colloid concentration during the period of measurement, and by the experimentally imposed limit of about 3 min between reaction initiation and measurement. Rates up to about 1×10^{-6} mol l^{-1} s^{-1} have been used to this work.

The minimum rate is limited by the requirement that the plutonium(VI) produced by colloid breakdown can be measured in the presence of the

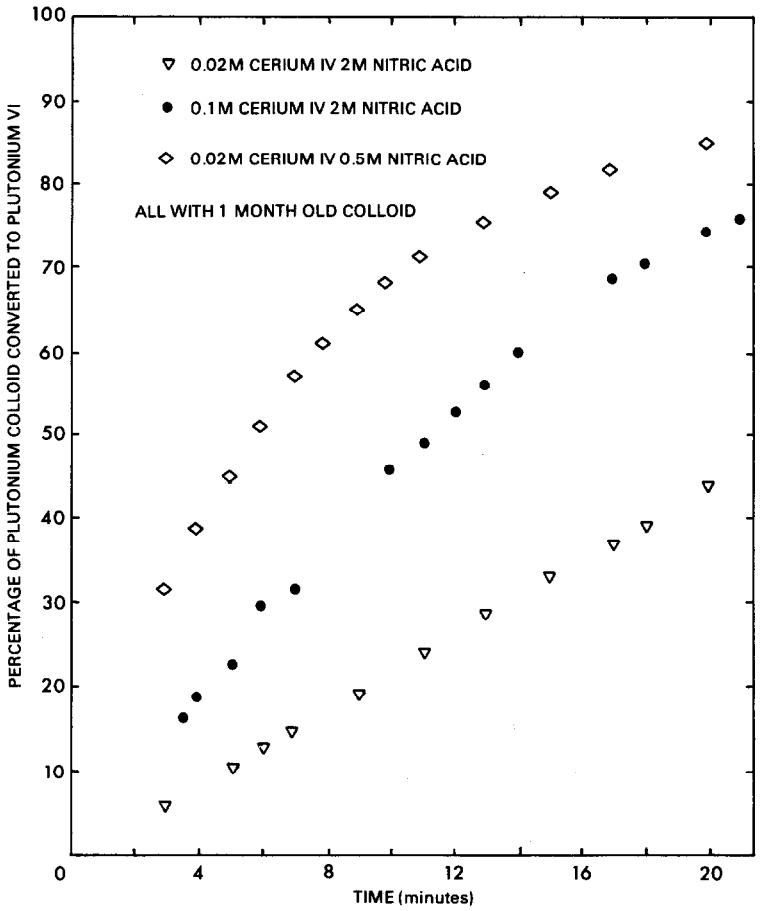


Fig. 2. Conversion of plutonium colloid to plutonium(VI) by cerium(IV).

plutonium(VI) present initially. This limitation becomes critical when the rate falls below about 1.5×10^{-7} mol of plutonium l^{-1} s^{-1}.

The minimum cerium(IV) concentration is limited by the requirement that any plutonium(IV) present is almost completely oxidized during the reaction period. This is particularly important at acidities above 1 M. The data in Table 1 have been used to assess the minimum acceptable concentration. At low acidities the cerium(IV) concentration is limited by the stoichiometric requirement of 2 mol of cerium(IV) per mol of plutonium.[1]

The results for the variation of the initial rate with cerium(IV) concentration (Fig. 3), at various fixed acidities between 0.05 and 3 M, lie on a series of approximately parallel lines with a slope of about 0.5. More detailed examination of the calculated slopes, listed in Table 2, shows that the value alters systematically with acidity.

The results for the variation of the initial rate with acidity, at various fixed cerium(IV) concentrations (Fig. 4), lie on a series of approximately parallel curves. Although the practical limitations discussed above mean that some curves are incomplete, it is obvious that they pass through a definite maximum at about 0.3 M acid. At acidity levels above 0.5 M, the plots become straight lines with a negative slope close to unity. The results are listed in Table 2.

The variation of initial rate with plutonium colloid concentration, at various fixed acidities and constant cerium(IV) concentration, gives parallel straight lines, with a slope of unity, as shown in Fig. 5 and Table 2.

Thus, for acidities between 0.5 and 3 M, the breakdown rate can be expressed approximately by the equation:

$$-\frac{dPu_c}{(dt)_{init}} = k[H^+]^{-1}[Ce(IV)]^{0.5}[Pu_c].$$

Reversal of the hydrolysis reaction by acid, as initially postulated, is not a rate-limiting reaction. The dependence of colloid breakdown on both cerium(IV) concentration and the hydroxyl concentration of the acid solution suggests that a cerium(IV) hydroxide species may be involved and the rate maximum at 0.3 M acid suggests that

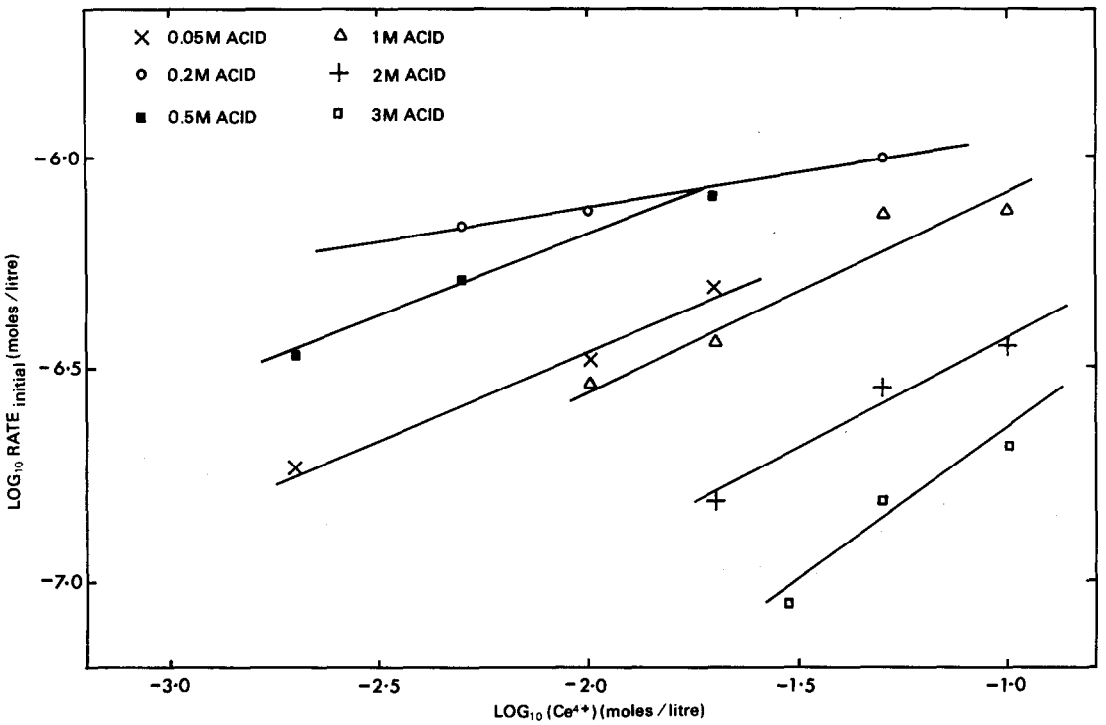


Fig. 3. Variation of plutonium colloid breakdown rate with cerium(IV) concentration at various acidities.

a rate-limiting species reaches its maximum concentration under such conditions.

DISCUSSION

It is first necessary to consider the probable cerium(IV) species present in low nitric acid media, when nitrate complexing and hydrolysis can take place simultaneously.

Although anionic nitrate complexes are formed in 6 M nitric acid, the nitrate complexing is weak, with equilibrium constant values of about 1 (0.6,[11] 2[12] and 0.2[13]) reported for the first nitrate complex.

Using a mean value for

$$K_1 \{[Ce(IV)NO_3]/Ce(IV)][NO_3]\}$$

of 1, the ratio of cerium(IV) nitrate complex to uncomplexed cerium(IV) is 0.3 in 0.3 M nitrate

Table 2. Vatiation of initial reaction rate with reactant concentration

Acidity (M)	Cerium(IV) concentration (M)	Plutonium colloid concentration	Slope	
3.0			0.68	
2.0			0.54	Cerium(IV) concentration
1.0	Varied	Constant	0.46	dependence
0.5			0.37	(see Fig. 3)
0.2			0.25	
0.05			0.42	
	0.1		−1.1	Acid dependence
Varied	0.05	Constant	−1.4	(see Fig. 4)
	0.02		−1.2	
0.5	Constant	Varied	1.03	Plutonium colloid
2.0			1.01	dependence
				(see Fig. 5)

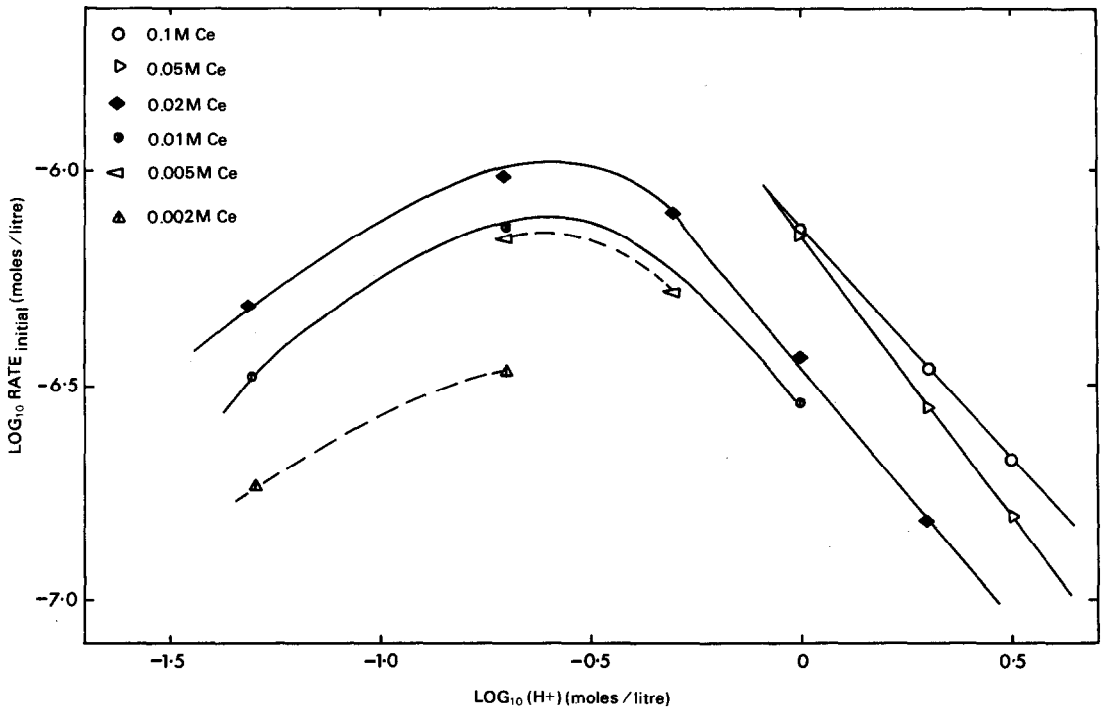


Fig. 4. Variation of plutonium colloid breakdown rate with acidity at various cerium(IV) concentrations.

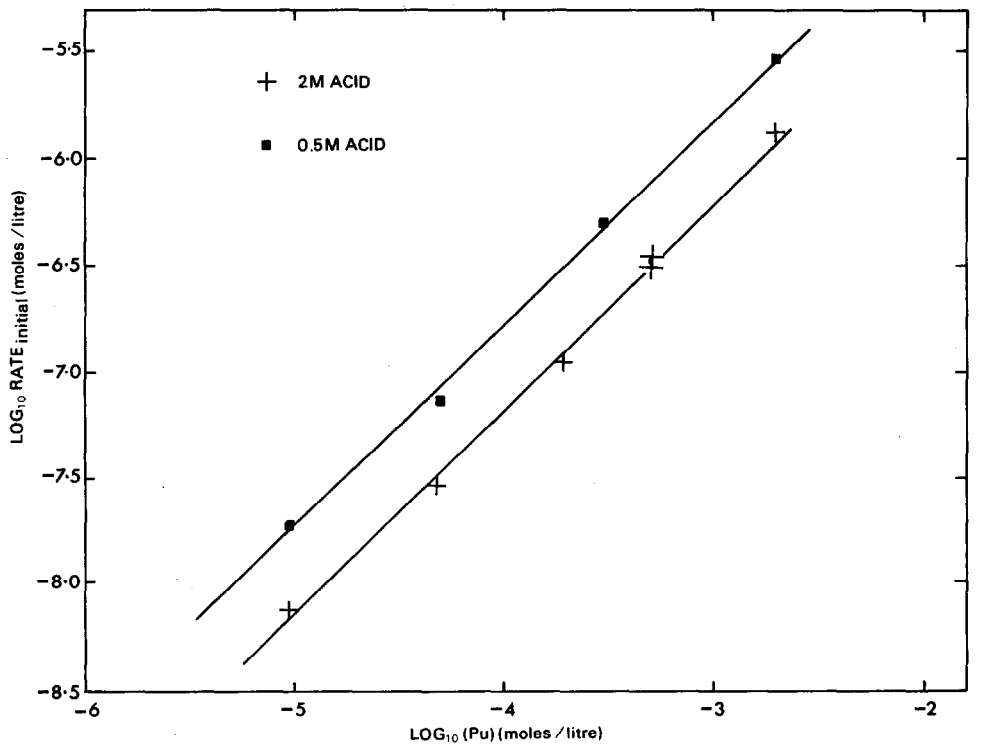


Fig. 5. Variation of plutonium colloid breakdown rate with plutonium colloid concentration at various acidities.

solution. Thus, about 80% of cerium(IV) is uncomplexed by nitrate in 0.3 M nitrate solution, and nitrate complexing can be largely ignored.

Hardwick and Robertson[14] deduce that cerium(IV) exists as a mixture of Ce^{4+}, $[Ce(OH)]^{3+}$ and a dimer, probably $(Ce–O–Ce)^{6+}$, with equilibrium constants of:

$$K = \frac{[Ce(OH)^{3+}][H^+]}{[Ce^{4+}]} = 5.2$$

and

$$K_1 = \frac{[(Ce–O–Ce)^{6+}]}{[Ce(OH)^{3+}]^2} = 16.5.$$

These data apply at 25°C and in ionic strength of 2, although they show that the equilibria are not greatly affected by either temperature or ionic strength. The data are consistent with measurements of the cerium(III)–cerium(IV) redox potential.[9]

Other works[15,16] have assumed that hydrolysis does not involve the formation of dimers. They have shown that, in 2 M perchloric acid, formation of the first hydrolysis complex $[Ce(OH)]^{3+}$ is almost complete, and that the equilibrium constant for the second hydrolysis step:

$$K_2 = \frac{[\{Ce(OH)_2\}^{2+}][H^+]}{[Ce(OH)^{3+}]}$$

has a value of 0.6[15] or 0.2.[16] Thus at about 0.3 M acid the second hydrolysis species has become more important than the first. Further hydrolysis can occur. The extent of this will obviously increase at low acidities, and therefore the second hydrolysis species will pass through a concentration maximum.

Cerium(IV) has been shown to exist as oxo- or hydroxo-bridged dimers even in 6 M nitric acid, with equilibrium constant values for

$$2Ce(IV) \rightleftharpoons [Ce(IV)]_2$$

reported as 17[17,18] and 20.[19]

It follows that both the first and second hydrolysis species are unlikely to exist in significant quantities as monomers.

The dimerization of the first hydrolysis species can be represented by:

$$2[Ce(OH)]^{3+} \rightleftharpoons [Ce(IV)–O–Ce(IV)]^{6+}.$$

If a similar reaction is envisaged for the second hydrolysis species then:

$$2[Ce(OH)_2]^{2+} \rightleftharpoons [HO–Ce(IV)–O–Ce(IV)–OH]^{4+} + H_2O.$$

Since the dimer $(Ce_2O)^{6+}$ will predominate over the monomer, this suggests that the actual course of the hydrolysis may involve:

$$(Ce_2O)^{6+} \overset{OH^-}{\rightleftharpoons} [Ce_2O(OH)]^{5+} \overset{OH^-}{\rightleftharpoons} [Ce_2O(OH)_2]^{4+}$$

rather than formation of $[Ce(OH)_2]^{2+}$.

Danesi[20] studied the hydrolysis of cerium(IV) in a 3 M sodium nitrate medium, assuming that in 1 M acid unhydrolysed species only are present. The data discussed above suggest that a significant proportion (about 25%) will be present as monomeric or dimeric hydrolysis species under these conditions. Danesi[20] calculated that the hydrolysis proceded via two dimeric species and finally formed a polymeric species, and he gave stability constant data for this formation. He also stated that the work would not distinguish between unhydrolysed cerium(IV) and the first hydrolysis product in 1 M acid. In the latter case, the hydroxide content of the hydrolysis species would be increased. Calculation of the variation of these species with acidity shows that the intermediate species passes through a concentration maximum (see Fig. 6) at about 0.1 M acid in a 3 M nitrate solution. Reduction of the total nitrate concentration to the levels used in this work will reduce the extent of nitrate complexing, and so shift the hydrolysis to higher acidities.

Thus, the literature data suggest that, in 0.3 M nitric acid, cerium(IV) exists predominantly as the dimer of the second hydrolysis stage, i.e. as $[Ce_2O(OH)_2]^{4+}$ or a closely related species, and that this species will pass through a concentration maximum close to this acidity. As 0.3 M is the acidity at which the rate of the oxidative breakdown of plutonium colloid reaches a maximum, if follows that $[Ce_2O(OH)_2]^{4+}$ is probably the active cerium species.

The structural similarities of cerium(IV) and plutonium hydroxides suggests that the cerium(IV) hydroxide can combine with hydroxyl sites on the surface of the plutonium hydroxide polymer to form plutonium–oxygen–cerium groups similar to the normal metal–oxygen–metal bonding of the polymer. The redox reaction can then proceed by transfer of an electron from the plutonium oxygen bond to the cerium oxygen bond on the other side of the same oxygen atom with simultaneous oxygen–metal cleavage. Two routes are possible. With the involvement of one electron transfer per plutonium atom, the hydroxide polymer is converted into ionic plutonium(V):

$$(PuO_2)_n + nCe^{4+} \rightarrow n(PuO_2)^+ + nCe^{3+},$$

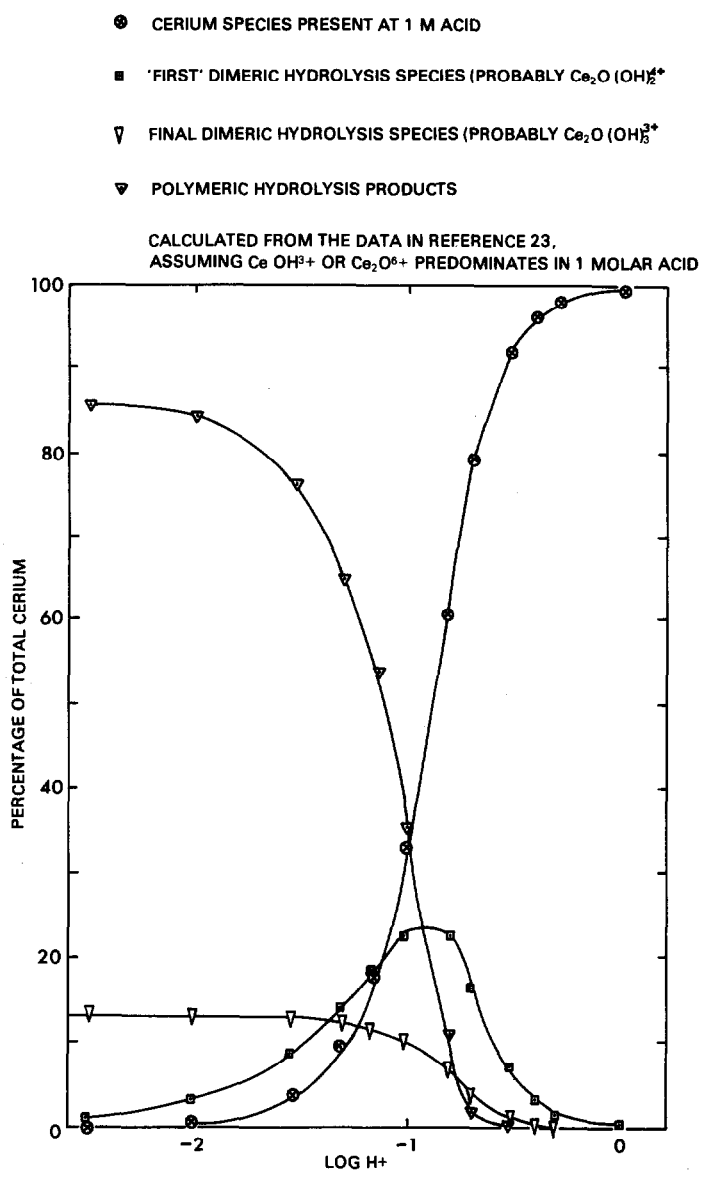


Fig. 6. Variations of cerium species with acidity.

which will be rapidly oxidized[21] to plutonium(VI) in solution, while the transfer of two electrons per plutonium atom will produce ionic plutonium(VI) $(PuO_2)^{2+}$ directly.

If one dimeric cerium(IV) molecule reacts with two hydroxyl groups and two plutonium sites on the colloid surface (probably in two stages), to form a transition complex which breaks to form two free plutonium(V) ions in solution which are themselves rapidly oxidized, the limiting reaction in 0.5–3 N HNO_3 becomes:

$$2\,\text{Pu sites} + (Ce_2O)^{6+} + 2OH^- \rightarrow 2(PuO_2)^{2+} + [Ce_2O(OH)_2]^{2+},$$

and the measured rate will be:

$$\frac{dPu_5}{dt} = -\frac{dPu_c}{dt} = k[(Ce_2O)^{6+}]^{0.5}[OH^-][Pu_c].$$

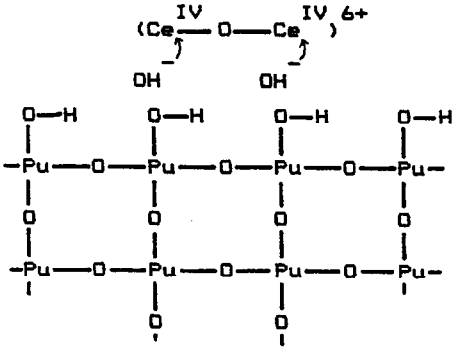
Therefore, as the oxidation of plutonium(V) to plutonium(VI) is rapid, the observed rate will be:

$$\frac{dPu_6}{dt} = k[Ce(IV)]^{0.5}[H^+]^{-1}[Pu_c],$$

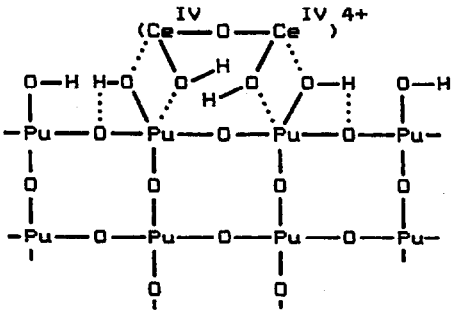
which is identical with the expression which fits the observed data for a colloid batch. The reaction of one dimeric cerium(IV) molecule with the plutonium colloid to produce two free plutonium(V) ions in

solution is therefore the probable reaction route, with $[Ce_2O(OH)_2]^{4+}$ as the reacting species.

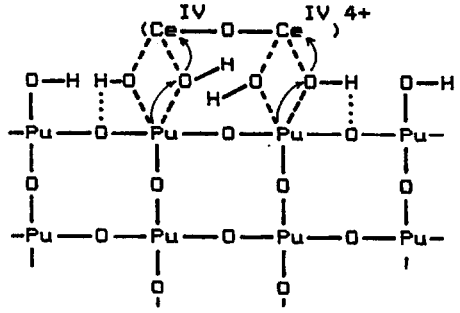
A probable reaction pathway for the depolymerization is:



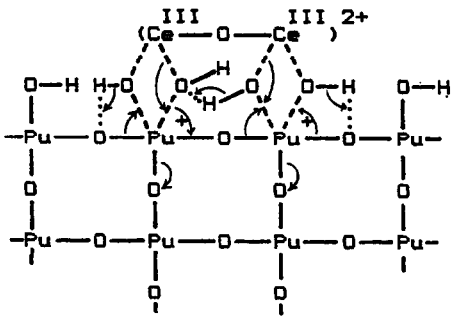
REACTANTS



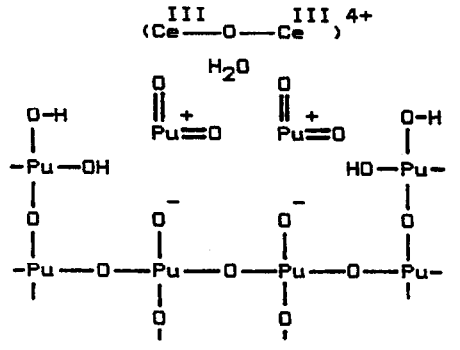
REACTIVE INTERMEDIATE



CHARGE TRANSFER



BREAKDOWN OF COMPLEX



PRODUCTS

$$PuO_2^{+} + Ce^{4+} \longrightarrow PuO_2^{2+} + Ce^{3+}$$

OXIDATION OF Pu^{V} (RAPID)

This involves the formation of an intermediate activation complex.

The proposed mechanism is consistent with the steady change in cerium(IV) concentration dependence with acidity (see Table 2). In 3 N nitric acid solution the proportion of monomeric cerium(IV) species will be higher (because of nitrate complexing and reduced hydrolysis) and reactions of the type $2Ce(IV) \rightleftharpoons [Ce(IV)]_2$ may contribute to the overall rate. At lower acidities, this type of reaction will be less important, and some of the plutonium colloid may even be oxidized by a polymeric rather than by a dimeric species.

CONCLUSIONS

Cerium(IV) reacts with polymeric plutonium hydroxides to simultaneously breakdown the polymer and oxidize the plutonium to plutonium(VI). The rate of breakdown increases with cerium(IV) concentration, but decreases with increasing acidity above 0.5 M nitric acid. The experimental data between 0.5 M and 3 M nitric acid

will fit a rate expression:

$$\text{Rate} = k[\text{Pu}][\text{Ce(IV)}]^{0.5}[\text{H}^+]^{-1}.$$

The rate of breakdown passes through a maximum at about 0.3 M nitric acid. Literature data suggests that, in 0.3 M nitric acid, cerium(IV) exists largely as a dimeric hydrolysis species, probably $[\text{HO–Ce(IV)–O–Ce(IV)–OH}]^{4+}$. A reaction mechanism is postulated which will fit both the observed maximum in the reaction rate, and the observed rate equation at higher acidities. $Ce_2O(OH)_2$ combines with the polymer surface through hydroxyl bridges to two plutonium atoms. Simple electron transfer in these bridges simultaneously reduces two cerium atoms to cerium(III), oxidizes two plutonium atoms to plutonium(V), and breaks the oxygen–metal bonds holding the plutonium atoms to the polymer. At acidities higher than 0.5 M nitric acid, cerium(IV) probably exists as $(Ce_2O)^{6+}$. Before the oxidative breakdown can proceed, reactions such as $(Ce_2O)^{6+} + 2OH^- \rightleftharpoons [Ce_2O(OH)_2]^{4+}$ are necessary to form the reactive species and contribute to the rate-controlling step in the 0.5–3 M nitric acid range, to explain the inverse acidity dependence.

REFERENCES

1. D. W. Okenden and G. A. Welch, *J. Chem. Soc.* 1956, 3358.
2. D. A. Costanzo, R. E. Biggers and J. T. Bell, *J. Inorg. Nucl. Chem.* 1973, **35**, 609.
3. V. L. Schuelein, ARH-SA-233. Atlantic Richfield Handford, Washington (1975).
4. J. H. Miles, AERE-R-8830. United Kingdom Atomic Energy Authority, Harwell (1977).
5. D. A. Costanzo and R. E. Biggers, ORNL-TM-585. Oak Ridge National Laboratory, TN (1963).
6. D. J. Savage and N. D. Cook, ND-R-309(D). United Kingdom Atomic Energy Authority, Risley (1979).
7. P. Cauchetier, *Anal. Chim. Acta* 1981, **124**, 449.
8. W. Dams, *Quantitative Spectrochemical Plutonium Determination.* In KfK 3578, p. 98. Kernforschungszentrum Karlsruhe, Karlsruhe (1983).
9. E. Wadsworth, F. R. Duke and C. A. Goetz, *Anal. Chem.* 1957, **29**, 1824.
10. A. Macdonald and D. J. Savage, Plutonium accountancy in reprocessing plants by ceric oxidation, ferrous reduction and dichromate titration. A novel method. In *Proceedings of the IAEA Conference on Nuclear Safeguards Technology, Vienna, 2–6 October* 1978, Vol. 1, p. 651. IAEA, Vienna.
11. V. I. Levin, G. P. Korpusov, N. M. Mariko, E. N. Patrusheva, N. P. Prokhorova and G. F. Platnov, *Sov. At. Energy (Engl. Transl.)* 1964, **15**, 828.
12. D. Peschanski and J. M. Fruchart, *C. R. Acad. Sci.* 1965, **260**, 3073.
13. I. A. Lebedev, B. F. Myasoedov and V. Ya. Frenkel, *Zh. Neorg. Khim.* 1973, **18**, 3224.
14. T. J. Hardwick and E. Robertson, *Can. J. Chem.* 1951, **29**, 818.
15. M. S. Sherrill, C. B. King and R. C. Spooner, *J. Am. Chem. Soc.* 1943, **65**, 170.
16. F. B. Baker, T. W. Newton and M. Kahn, *J. Phys. Chem.* 1960, **64**, 109.
17. B. D. Blaustein and T. W. Gryder, *J. Am. Chem. Soc.* 1957, **79**, 540.
18. H. L. Conley, UCRL-9332. California University, Livermore, CA (1960).
19. M. K. Dorfman and J. W. Gryder, *Inorg. Chem.* 1962, **1**, 799.
20. P. R. Danesi, RT/CHI(66)39. Comitato Nazionale Energia Nucleare, Roma (1966).
21. C. Keller, *The Chemistry of the Transuranium Elements.* Verlag Chemie, Weinheim (1971).

Polyhedron Vol. 5, No. 3, pp. 753–760, 1986
Printed in Great Britain

0277–5387/86 $3.00+.00
© 1986 Pergamon Press Ltd

THEORETICAL STUDY OF THE STATIC JAHN–TELLER EFFECT—II* THREE-MODE VIBRONIC COUPLING IN OCTAHEDRAL HALOCOMPLEXES WITH TRIPLY DEGENERATE ELECTRONIC STATES

PETER PELIKÁN, MARTIN BREZA and ROMAN BOČA†

Departments of Physical Chemistry and Inorganic Chemistry, Slovak Technical University, CS-812 37 Bratislava, Czechoslovakia

(*Received* 10 *July* 1985; *accepted* 27 *July* 1985)

Abstract—A new analytic formula for the adiabatic potential surface of the three-mode vibronic coupling T_{2g}–$(a_{1g}+e_g+t_{2g})$ in octahedral systems with triply degenerate electronic states was obtained. This formula includes linear and quadratic vibronic terms as well as the harmonic and anharmonic part of normal vibrations. The necessary potential constants (seven vibronic and nine force constants) were evaluated from the numerical maps of adiabatic potential surfaces (APS) by applying a non-linear regression analysis. Numerical calculations of APS were obtained for nine hexahalo complexes using the CNDO–UHF method.

The theory of vibronic coupling is able to predict an analytic form of the adiabatic potential surface (APS) in the presence of electron degeneracy. Considerations resulting in an analytic form of the APS for triply degenerate electronic states in the reference octahedral configuration have been published by many authors.[2–15] They were used in interpreting the physical and chemical properties of various materials where the Jahn–Teller effect occurs. The electric and magnetic polarization, the spectroscopic characteristics in the ESR, NMR, electron and ionization spectroscopy, problems of stereochemistry, crystallochemistry and chemical reactivity belong to them. Nevertheless, those considerations were based only on the two-mode vibronic coupling scheme T–$(e+t_2)$ or they were limited only to linear vibronic and quadratic force constants.

In this paper the analytic form of the APS has been derived for a more complete three-mode coupling scheme T–(a_1+e+t_2). Moreover, the vibronic coupling constants as well as the quadratic and cubic force constants have been calculated for some hexahalo complexes of the first-row transition metals by a purely theoretical, non-empirical way. They resulted from a non-linear regression analysis applied to a numerical map of the APS calculated by the CNDO–UHF version of the MO–LCAO–SCF method.

METHOD

The approach used below closely resembles the method outlined for the doubly degenerate electronic terms.[16,17] It may be summarized by the following points.

(i) For the three-state strong coupling case the unperturbed (zero-order) wave function stands:

$$\Psi^0 = \theta_u(r,[Q^0])\chi_u(Q)+\theta_v(r,[Q^0])\chi_v(Q) + \theta_w(r,[Q^0])\chi_w(Q) = \theta_u^0\chi_u + \theta_v^0\chi_v+\theta_w^0\chi_w, \quad (1)$$

where $\theta_u(r,[Q^0])$ are the electronic wave functions and $\chi_u(Q)$ are the vibration functions, r and Q being the electron and nuclear coordinates, respectively. The reference configuration of nuclei is denoted by $[Q^0]$.

(ii) The APS $W(Q)$ is obtained as a root of the secular equation:

$$\det\begin{pmatrix} U_{uu}-W; & U_{uv}; & U_{uw} \\ U_{vu}; & U_{vv}-W; & U_{vw} \\ U_{wu}; & U_{wv}; & U_{ww}-W \end{pmatrix} = 0. \quad (2)$$

The matrix elements U_{uv} contain a Taylor expansion

* For Part I, see Ref. 1.

† Author to whom correspondence should be addressed.

of the Hamiltonian $H_{uv} = \langle\theta_u^0|\hat{H}(r,Q)|\theta_v^0\rangle$:

$$U_{uv} = E_u^0\delta_{uv} + H_{uv}^{(1)} + H_{uv}^{(2)} + \cdots + E_{uv}^{(2)} + \cdots \quad (3)$$

as well as the energy correction originating from the higher orders of the perturbation theory, where a weak vibronic coupling with excited states is considered.[18] The latter term is neglected.

(iii) The Hamiltonian in the frozen-nuclei approximation contains the electronic kinetic energy ($\hat{T}_e$), the interelectronic repulsion ($\hat{V}_{ee}$), the electron–nuclear attraction ($\hat{V}_{eN}$) and the internuclear repulsion ($\hat{F}_{NN}$):

$$\hat{H}(r,Q) = \hat{T}_e(r) + \hat{V}_{ee}(r) + \hat{V}_{eN}(r,Q) + \hat{F}_{NN}(Q). \quad (4)$$

Therefore, its Taylor terms $[H_{uv}^{(n)}]$ may be split into the electron–nuclear part, $V_{uv}^{(n)}$, and the purely nuclear (scalar) part, $F_{uv}^{(n)}$:

$$H_{uv}^{(n)} = V_{uv}^{(n)} + F_{uv}^{(n)}\delta_{uv}. \quad (5)$$

They are:

$$V_{uv}^{(n)} = \frac{1}{n!}\sum_{k_1\ldots k_n}^{m}\left\langle\theta_u^0\left|\left[\frac{\partial^n\hat{V}_{eN}(r,Q)}{\partial Q_{k_1}\ldots\partial Q_{k_n}}\right]_0\right|\theta_v^0\right\rangle \Delta Q_{k_1}\ldots\Delta Q_{k_n}, \quad (6)$$

$$F_{uv}^{(n)} = \frac{1}{n!}\sum_{k_1\ldots k_n}^{m}\left[\frac{\partial^n\hat{F}_{NN}(Q)}{\partial Q_{k_1}\ldots\partial Q_{k_n}}\right]_0\Delta Q_{k_1}\ldots\Delta Q_{k_n}\delta_{uv}. \quad (7)$$

(iv) The symmetrized normal vibration coordinates may be chosen as the internal displacement coordinates, $\Delta Q = Q - Q^0$, each of them belonging to a γ class of the Γ representation of the molecular symmetry group in the reference configuration. The matrix elements $V_{uv}^{(n)}$ are expressible via the reduced matrix elements $X(\Gamma_u,\Gamma_v;\Gamma_{k_1},\ldots,\Gamma_{k_n})$ and the Clebsch–Gordan (Wigner) coefficients which have been tabulated.* Consequently, the APS becomes a function of a limited number of vibronic constants.

(v) Having derived an analytic form of the APS, the problem of the evaluation of the potential constants appears. First, a numerical map, $W(Q_1,\ldots,Q_m)$, of the APS is to be obtained by a quantum-chemical calculation of the total molecular energy for fixed nuclear coordinates. Then the regression of calculated points of the APS $W^c(Q_i)$ on its analytic form will proceed. The fitting is realized by the least-squares method with weighing:

$$\mathscr{F} = \sum_i [W^c(Q_i) - W^a(Q_i)]^2 w_i^2 = \min, \quad (8)$$

where $W^a(Q_i)$ are the approximate energies calculated for a trial set of potential constants from the analytic form of the APS. The statistical weights (w_i) were chosen in accordance with the metric weighing concept:

$$w_i = \left(\sum_k Q_k^2\right)^{-1/2}, \quad (9)$$

* The linear term is reduced according to the Wigner–Eckart theorem as:

$$V_{uv}^k = \langle\theta_u^0|[\partial\hat{V}(r,Q)/\partial Q_k]_0|\theta_v^0\rangle = X(\Gamma_u,\Gamma_v;\Gamma_k)C^{\Gamma_u\Gamma_k\Gamma_v}_{\gamma_u\gamma_k\gamma_v}.$$

The reduction of a quadratic term, V_{uv}^{kl}, needs a successive decomposition of the operator part, $[\partial^2\hat{V}(r,Q)/\partial Q_k\partial Q_l]_0$, according to the Wigner formula.[19]

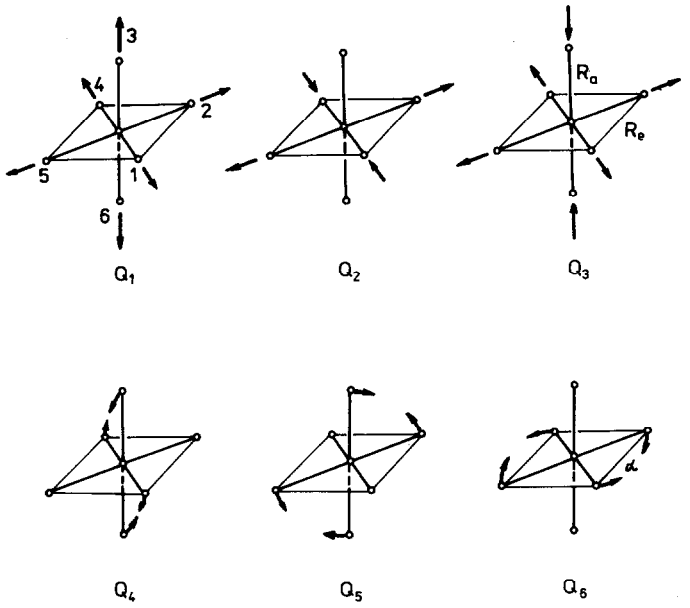


Fig. 1. Some internal and normal vibration coordinates of octahedral systems.

where Q_k is a set of displacement coordinates for a given point of the APS (Fig. 1).

VIBRONIC COUPLING $T_{2g}(a_{1g}+e_g+t_{2g})$

The octahedral system ML_6 has 15 normal modes of vibration belonging to the a_{1g} (coordinate Q_1), e_g (Q_2 and Q_3), t_{2g} (Q_4, Q_5 and Q_6), t_{2u}, t'_{1u} and t''_{1u} irreducible representations. Notice, the relation:

$$[\Gamma_t \times \Gamma_t] = A_{1g}+E_g+T_{2g} \tag{10}$$

holds for a symmetrized direct product of t-type irreducible representations ($t = t_{1g}$, t_{2g}, t_{1u} or t_{2u}). Therefore, the linear vibronic term $V^k_{uv} = \langle\theta^0_u|[\partial\hat{V}(r,Q)/\partial Q_k]_0|\theta^0_v\rangle$ is reduced to a non-zero element only if the representation of Q_k is contained in the reducible representation of $[\Gamma_{t_{2g}} \times \Gamma_{t_{2g}}]$. Consequently, only the coordinates Q_1-Q_6 are vibronic active in the linear coupling. The reduction of quadratic terms V^{kl}_{uv} according to the Wigner formula[19] gave one of the principal results of this paper:

$$\begin{aligned}
\mathbf{V}^{(1)}+\mathbf{V}^{(2)} = \mathbf{C}_1\Big[& X_a Q_1 + \frac{1}{2}X_{aa}Q_1^2 \\
& + \frac{1}{2\sqrt{2}}X_{ee}(Q_2^2+Q_3^2) \\
& + \frac{1}{2\sqrt{3}}X_{tt}(Q_4^2+Q_5^2+Q_6^2)\Big] \\
& + \mathbf{C}_2\Big[X_e Q_2 + X_{ae}Q_1Q_2 + \frac{1}{2\sqrt{2}}X_{ee}(Q_2^2-Q_3^2) \\
& + \frac{1}{2\sqrt{2}}X_{tt}(Q_5^2-Q_4^2)\Big] \\
& + \mathbf{C}_3\Big[X_e Q_3 + X_{ae}Q_1Q_3 + \frac{1}{2\sqrt{2}}X_{ee}2Q_2Q_3 \\
& + \frac{1}{2\sqrt{2}}X_{tt}(Q_4^2+Q_5^2-2Q_6^2)\Big] \\
& + \mathbf{C}_4\Big[X_t Q_4 + X_{at}Q_1Q_4 \\
& + \frac{1}{2}X_{et}Q_4(\sqrt{3}Q_2-Q_3) - \frac{1}{\sqrt{2}}X_{tt}Q_5Q_6\Big] \\
& + \mathbf{C}_5\Big[X_t Q_5 + X_{at}Q_1Q_5 \\
& - \frac{1}{2}X_{et}Q_5(\sqrt{3}Q_2+Q_3) - \frac{1}{\sqrt{2}}X_{tt}Q_4Q_6\Big] \\
& + \mathbf{C}_6\Big[X_t Q_6 + X_{at}Q_1Q_6 \\
& + \frac{1}{2}X_{et}2Q_3Q_6 - \frac{1}{\sqrt{2}}X_{tt}Q_4Q_5\Big].
\end{aligned} \tag{11}$$

Here X_e, X_t, X_{aa}, X_{ee}, X_{tt}, X_{ae}, X_{at} and X_{et} are the reduced matrix elements of a given symmetry ($a = a_{1g}$, $e = e_g$, $t = t_{2g}$). The matrices $\mathbf{C}_1$–$\mathbf{C}_6$ are formed by the Wigner coefficients in the space of the original triplet of electronic functions:

$$\mathbf{C}_1 = \begin{pmatrix} 1 & 0 & 0 \\ 0 & 1 & 0 \\ 0 & 0 & 1 \end{pmatrix}, \quad \mathbf{C}_2 = \frac{\sqrt{3}}{2}\begin{pmatrix} 1 & 0 & 0 \\ 0 & -1 & 0 \\ 0 & 0 & 0 \end{pmatrix},$$

$$\mathbf{C}_3 = \frac{1}{2}\begin{pmatrix} -1 & 0 & 0 \\ 0 & -1 & 0 \\ 0 & 0 & 2 \end{pmatrix},$$

$$\mathbf{C}_4 = \frac{-1}{\sqrt{2}}\begin{pmatrix} 0 & 0 & 0 \\ 0 & 0 & 1 \\ 0 & 1 & 0 \end{pmatrix}, \quad \mathbf{C}_5 = \frac{-1}{\sqrt{2}}\begin{pmatrix} 0 & 0 & 1 \\ 0 & 0 & 0 \\ 1 & 0 & 0 \end{pmatrix},$$

$$\mathbf{C}_6 = \frac{-1}{\sqrt{2}}\begin{pmatrix} 0 & 1 & 0 \\ 1 & 0 & 0 \\ 0 & 0 & 0 \end{pmatrix}.$$

The expansion of the internuclear repulsion up to the cubic terms for the six vibronic active coordinates is:

$$\begin{aligned}
\mathbf{F}^{(1)}+\mathbf{F}^{(2)}+\mathbf{F}^{(3)} = \mathbf{C}_1\Big\{ & F_a Q_1 \\
& + \frac{1}{2}F_{aa}Q_1^2 + \frac{1}{2\sqrt{2}}F_{ee}(Q_2^2+Q_3^2) \\
& + \frac{1}{2\sqrt{3}}F_{tt}(Q_4^2+Q_5^2+Q_6^2) + \frac{1}{6}F_{aaa}Q_1^3 \\
& + \frac{1}{12}F_{eee}(3Q_2^2Q_3-Q_3^3) \\
& + \frac{1}{3\sqrt{2}}F_{aee}Q_1(Q_2^2+Q_3^2) \\
& + \frac{1}{3\sqrt{3}}F_{att}Q_1(Q_4^2+Q_5^2+Q_6^2) \\
& - \frac{1}{2\sqrt{6}}F_{ttt}Q_4Q_5Q_6 \\
& - \frac{1}{6\sqrt{3}}F_{ett}[Q_4^2(Q_3-\sqrt{3}Q_2) \\
& + Q_5^2(Q_3+\sqrt{3}Q_2) - 2Q_6^2Q_3]\Big\}.
\end{aligned} \tag{12}$$

The vibronic Hamiltonian considered here has the form:

$$\mathbf{U} = E^0\mathbf{1} + \mathbf{V}^{(1)} + \mathbf{V}^{(2)} + \mathbf{F}^{(1)} + \mathbf{F}^{(2)} + \mathbf{F}^{(3)}. \quad (13)$$

Since it contains a scalar part, i.e. terms standing by the Wigner matrix $\mathbf{C}_1 = \mathbf{1}$, the APS becomes:

$$\begin{aligned} W(Q_1, Q_2, Q_3, Q_4, Q_5, Q_6) &= \varepsilon_i + E^0 \\ &+ \frac{1}{2}K_{aa}Q_1^2 + \frac{1}{2}K_{ee}(Q_2^2 + Q_3^2) \\ &+ \frac{1}{2}K_{tt}(Q_4^2 + Q_5^2 + Q_6^2) + T_{aaa}Q_1^3 \\ &+ T_{aee}Q_1(Q_2^2 + Q_3^2) \\ &+ T_{att}Q_1(Q_4^2 + Q_5^2 + Q_6^2) \\ &+ T_{eee}Q_3(3Q_2^2 - Q_3^2) \\ &+ T_{ttt}Q_4Q_5Q_6 + T_{ett}[Q_4^2(Q_3 - \sqrt{3}Q_2) \\ &+ Q_5^2(Q_3 + \sqrt{3}Q_2) - 2Q_6^2Q_3]. \end{aligned} \quad (14)$$

The vibronic correction term (ε_i) is obtained as the lowest eigenvalue of the symmetric matrix V defined by the elements:

$$\begin{aligned} V_{11} &= \frac{1}{2}A_e(Q_3 - \sqrt{3}Q_2) \\ &+ \frac{1}{2}B_{ee}(Q_2^2 - Q_3^2 - 2\sqrt{3}Q_2Q_3) \\ &+ \frac{1}{2}Z_{ae}Q_1(Q_3 - \sqrt{3}Q_2) \\ &+ \frac{1}{\sqrt{6}}B_{tt}(-2Q_4^2 + Q_5^2 + Q_6^2), \\ V_{12} &= A_tQ_6 - Z_{et}Q_3Q_6 \\ &+ Z_{at}Q_1Q_6 + B_{tt}Q_4Q_5, \\ V_{13} &= A_tQ_5 + \frac{1}{2}Z_{et}Q_5(Q_3 + \sqrt{3}Q_2) \\ &+ Z_{at}Q_1Q_5 + B_{tt}Q_4Q_6, \\ V_{22} &= \frac{1}{2}A_e(Q_3 + \sqrt{3}Q_2) \\ &+ \frac{1}{2}B_{ee}(Q_2^2 - Q_3^2 + 2\sqrt{3}Q_2Q_3) \\ &+ \frac{1}{2}Z_{ae}Q_1(Q_3 + \sqrt{3}Q_2) \\ &+ \frac{1}{\sqrt{6}}B_{tt}(Q_4^2 - 2Q_5^2 + Q_6^2), \\ V_{23} &= A_tQ_4 + \frac{1}{2}Z_{et}Q_4(Q_3 - \sqrt{3}Q_2) \\ &+ Z_{at}Q_1Q_4 + B_{tt}Q_5Q_6, \\ V_{33} &= -A_eQ_3 - B_{ee}(Q_2^2 - Q_3^2) \\ &+ \frac{1}{\sqrt{6}}B_{tt}(Q_4^2 + Q_5^2 - 2Q_6^2) \\ &- Z_{ae}Q_1Q_3. \end{aligned} \quad (15)$$

In the final formulas, eqns (14) and (15), $A_e = -X_e$ and $A_t = -X_t/\sqrt{2}$ are the linear vibronic constants; $B_{ee} = -X_{ee}/2\sqrt{2}$, $B_{tt} = X_{tt}/2$, $Z_{et} = -X_{et}/\sqrt{2}$, $Z_{ae} = -X_{ae}$ and $Z_{at} = -X_{at}/\sqrt{2}$ are the quadratic vibronic constants; $K_{aa} = F_{aa} + X_{aa}$, $K_{ee} = (F_{ee} + X_{ee})/\sqrt{2}$ and $K_{tt} = (F_{tt} + X_{tt})/\sqrt{3}$ are the harmonic force constants; and $T_{aaa} = F_{aaa}/6$, $T_{eee} = F_{eee}/12$, $T_{ttt} = -F_{ttt}/2\sqrt{6}$, $T_{aee} = F_{aee}/3\sqrt{2}$, $T_{att} = F_{att}/3\sqrt{3}$ and $T_{ett} = -F_{ett}/6\sqrt{3}$ are the anharmonicity constants.* Moreover, the relation:

$$K_a = X_a + F_a = \langle\theta_u^0|[\partial\hat{H}(r, Q)/\partial Q_1]_0|\theta_u^0\rangle = 0 \quad (16)$$

holds for the optimum octahedral geometry where this gradient component vanishes.

NUMERICAL APPLICATION

The semiempirical CNDO–UHF method was used[20–22] for the total-energy calculation of systems systematically displaced from the octahedral geometry. The numerical map of the APS $W^c(Q_1, Q_2, Q_3, Q_4, Q_5, Q_6)$ obtained in this way contains *ca* 80 points for each system under study. The energy cut-off for the total molecular energy was 10^{-4}–10^{-5} eV.

Calculations were performed for nine hexahalo complexes having a triply degenerate electronic state in the reference octahedral configuration: MnX_6^{4-} in $^2T_{2g}$ state, CoX_6^{3-} in $^5T_{2g}$ state and CoX_6^{4-} in $^4T_{1g}$ state with X = F, Cl or Br.

The evaluation of potential constants—nine force constants and seven vibronic constants—occurring in the analytic form of the APS [eqns (14) and (15)] is not a trivial problem. The minimization procedure [eqn (8)] represents a non-linear optimization of 16 parameters. A rapid convergence was obtained by splitting the whole process into the linear and the non-linear part. The procedure was accelerated by successive optimizations of selected potential constants for some cuts of the APS.

The results of the regression are listed in Table 1. Each quantity is presented to a significant number of digits (the order of the last number being higher

* The cubic terms T_{ijk} in reality partly include the third-order vibronic coupling terms V^{ijk}, i.e. those terms which are reduced by the Wigner matrix $\mathbf{C}_1$. Therefore, both the F_{ijk} and K_{ijk} notations are left and the T_{ijk} notation is used in this sense.

Table 1. The calculated constants of the APS for MX_6^q complexes

Quantity	X =	MnX_6^{4-}, $^2T_{2g}$ state			CoX_6^{3-}, $^5T_{2g}$ state			CoX_6^{4-}, $^4T_{1g}$ state		
		F	Cl	Br	F	Cl	Br	F	Cl	Br
A_e (10^{10} eV m^{-1})		−0.0546	−0.039	−0.0743	−0.127	−0.255	0.078	−0.08101	−0.0610	−0.0597
A_t (eV rad^{-1})		−0.001	0.107	−0.062	0.178	0.33	0.003	0.057492	0.004	−0.045
B_{ee} (10^{20} eV m^{-2})		−1.736	−2.00	−1.55	−12.8	−15.49	−11.60	0.344304	−0.032	1.576
B_{tt} (eV rad^{-2})		0.01	0.04	0.23	6.5	−7.6	6.3	5.72368	1.3	−0.04
Z_{ae} (10^{20} eV m^{-2})		−5.081	−0.07	0.12	−2.1	3.89	8.12	1.75734	−0.50	0.43
Z_{at} (10^{10} eV m^{-1} rad^{-1})		0.02	−0.1	12.6	7.4	−76.8	19.2	2.89708	1.2	−0.2
Z_{et} (10^{10} eV m^{-1} rad^{-1})		−0.10	−0.1	7.12	5.2	16.0	9.5	2.05031	2.4	0.2
K_{aa} (10^{20} eV m^{-2})		17.910	21.064	25.766	44.06	35.89	41.07	33.453	30.605	34.626
K_{ee} (10^{20} eV m^{-2})		13.182	14.190	8.45	30.73	18.10	15.88	9.818	16.507	18.529
K_{tt} (eV rad^{-2})		5.0	15.28	5.49	39.15	0.6	12.20	2.28	7.25	6.83
T_{aaa} (10^{30} eV m^{-3})		39.52	−4.17	−1.36	9.1	4.1	10.1	−4.76	−5.62	0.05
T_{aee} (10^{30} eV m^{-3})		20.5	−18.5	−2.05	−108.8	7.5	−17.3	149.2	−19.5	−24.9
T_{att} (10^{10} eV m^{-1} rad^{-2})		−329.0	−116.0	−166.0	480.0	−580.0	−314.0	−216.0	−287.0	−260.0
T_{eee} (10^{30} eV m^{-3})		−17.81	−5.8	56.7	−20.0	30.7	29.4	−104.0	−18.5	6.6
T_{ett} (10^{10} eV m^{-1} rad^{-2})		188.0	135.0	−114.5	829.0	74.0	212.0	−159.0	−12.0	−92.0
T_{ttt} (eV rad^{-3})		1092.0	1006.0	−164.0	3207.0	−540.0	311.0	−163.0	41.0	−212.0
ρ		0.99772	0.99989	0.99991	0.99951	0.99816	0.99957	0.99994	0.99991	0.99978
R-factor		0.059	0.019	0.013	0.030	0.071	0.029	0.010	0.013	0.021

Table 2. The calculated characteristics of extremum points on the APS

Type	Quantity[a]	X =	MnX_6^{4-}, $^2T_{2g}$ state			CoX_6^{3-}, $^5T_{2g}$ state			CoX_6^{4-}, $^4T_{1g}$ state		
			F	Cl	Br	F	Cl	Br	F	Cl	Br
O_h	R^0 (pm)		219.643	249.40	262.472	199.352	230.80	247.505	207.37	237.759	253.484
D_{4h}	Q_1^0 (pm)		0.185	0.003	−0.004	0.004	0.18	−0.27	−0.048	0.007	−0.003
	Q_3^0 (pm)		−0.679	−0.39	−1.04	0.15	1.7	−1.3	−0.67	−0.38	−0.27
	E_{JT} (meV)		0.18	0.08	0.42	0.05	3.5	0.52	0.26	0.11	0.08
	R_a^0 (pm)		220.11	249.62	263.07	199.27	229.9	248.17	207.74	237.98	253.64
	R_e^0 (pm)		219.52	249.29	262.17	199.40	231.4	247.01	207.15	237.65	253.40
D_{3d}	Q_1^0 (pm)		0.086	0.040	1.1	0.47		0.000		0.002	0.086
	$Q_5^0 = Q_4^0 = Q_6^0$ (rad)		−0.004	0.009	−0.033	−0.008		−0.0003		−0.0003	−0.006
	E_{JT} (meV)		0.04	0.45	2.1	0.40		0.00		0.00	0.23
	R^0 (pm)		219.68	249.41	262.01	199.54		247.50		237.76	253.52
	$\alpha_{12}^0 = \alpha_{13}^0 = \alpha_{23}^0$ (°)		90.12	89.74	90.95	90.23		90.01		90.01	90.17
D_{2h}	Q_1^0 (pm)		0.23	0.029	0.012	0.11		0.24			
	Q_3^0 (pm)		0.45	0.22	−1.11	0.18		−0.29			
	Q_6^0 (rad)		0.010	−0.008	−0.005	−0.005		0.004			
	E_{JT} (meV)		0.05	0.41	0.42	0.44		0.07			
	R_a^0 (pm)		219.48	249.28	263.12	199.29		247.77			
	R_e^0 (pm)		219.87	249.47	262.16	199.45		247.52			
	α_{12}^0 (°)		89.72	90.22	90.14	90.13		89.88			

[a] E_{JT} is the Jahn–Teller stabilization energy. Coordinates are illustrated in Fig. 1.

than the standard deviation). Some statistical characteristics, namely the correlation coefficient ρ (> 0.997) and the discrepancy factor R (< 0.07), imply that the form of the functional dependence for the total energy used is correct.

To open the discussion of numerical applications it must be mentioned that the CNDO/2 version of the MO–LCAO–SCF method used has its quantitative limitations. For example, the stretching force constants are overestimated by a factor of two and the vibronic constants are probably underestimated. The latter originates in the approximation of the $\hat{V}(r, Q)$ operator through an average of coulomb integrals in the CNDO/2 method. Consequently, the Jahn–Teller distortions and stabilization energies may be understimated. Nevertheless, valuable conclusions from data listed in Table 1 can be drawn. They will be discussed together with calculated characteristics of the extremum points of the APS as they appear in Table 2.

(i) The quadratic vibronic coupling constants Z_{ae}, Z_{at} and Z_{et} adopt significant values; they are of the same order as the vibronic constants B_{ee} and B_{tt}. Thus, the importance of these terms is clearly demonstrated.

(ii) The neglect of the a_{1g} admixture in the vibronic coupling ($Z_{ae} = Z_{at} = 0$) makes the regression considerably worse: ρ becomes lower and the R-factor higher. Analogically, the neglect of anharmonicities of normal vibrations ($T_{ijk} = 0$) leads to dramatic changes in the quality of the regression. Notice, these terms used to be omitted in the majority of papers where only $T\text{–}(e + t_2)$ coupling is considered.

(iii) The harmonic force constants fulfil the relation $K_{aa} > K_{ee}$. Thus, the e_g-mode (tetragonal distortion) is a softer mode relative to the a_{1g}-mode (symmetric stretching), so that the distortion is easier.

(iv) Three types of energy minima exist on the APS: the tetragonal minima along the e_g-mode (D_{4h}-symmetry), the trigonal minima along the t_{2g}-mode (D_{3d}-symmetry) and the mixed-type, orthorhombic minima (D_{2h}-symmetry).[23]

(v) The coordinates of extremum points are determined by the vibronic and force constants. If only the tetragonal distortions are considered, the corresponding cut of the APS adopts an explicit form:

$$W(Q_1, Q_3) = \mathbf{C}_1\left(W^0 + \frac{1}{2}K_{aa}Q_1^2 + \frac{1}{2}K_{ee}Q_3^2\right) - \mathbf{C}_2\frac{1}{2\sqrt{2}}X_{ee}Q_3^2 + \mathbf{C}_3(X_eQ_3 + X_{ae}Q_1Q_3), \quad (17)$$

where the anharmonicity terms were omitted. The coordinates of the stationary points are evaluated from the vanishing-gradient condition: $(\partial W/\partial Q_1)_0 = (\partial W/\partial Q_3)_0 = 0$. They are:

$$Q_3^0 = (C_3)_{ii}\frac{A_e}{K_{ee}}\left[1 - \frac{(C_3)_{ii}^2Z_{ae}^2}{K_{aa}K_{ee}} - \frac{2(C_2)_{ii}B_{ee}}{K_{ee}}\right], \quad (18)$$

$$Q_1^0 = (C_3)_{ii}Q_3^0Z_{ae}/K_{aa}. \quad (19)$$

Now, some trends in Tables 1 and 2 become more clear. It is seen that the coordinate Q_3^0 is proportional to A_e and the coordinate Q_1^0 to Z_{ae}. The a_{1g} admixture in the vibronic coupling manifests itself in the nonzero value of Z_{ae} and, consequently, in the shift of the coordinate Q_1^0. This effect was never discussed before.

(vi) The calculated degree of tetragonal distortion of Q_3 (~ 0.001–0.013) (in units of 10^{-10} m) for T_{1g} and T_{2g} reference states is much lower in comparison with analogous complexes having the E_g electronic state where a Q_3 of ~ 0.017–0.076 is predicted by the same method.[17] The trigonal distortions ($\Delta\alpha$) are 0.1–1.0°.

(vii) Although the absolute values of the degree of distortion are underestimated by the simple CNDO method used, the trends in the calculated force constants, vibronic constants, coordinates of stationary points and the Jahn–Teller stabilization energies seem correct. The solid state, however, contributes to these quantities as well and it probably manifests itself in an amplification of the degree of distortion.

REFERENCES

1. P. Pelikán, M. Breza and R. Boča, *Polyhedron* 1985, **4**, 1543.
2. A. D. Liehr, *J. Phys. Chem.* 1963, **67**, 389; 471.
3. U. Öpik and M. H. L. Pryce, *Proc. R. Soc.* 1957, **238A**, 425.
4. W. Moffit and W. Thorson, *Phys. Rev.* 1957, **108**, 1251.
5. I. B. Bersuker and V. Z. Polinger, *Zh. Eksp. Teor. Fiz.* 1974, **66**, 2078.
6. M. C. M. O'Brien, *Proc. Phys. Soc.* 1965, **86**, 847.
7. M. D. Sturge, *Phys. Rev.* 1965, **140A**, 880.
8. M. D. Sturge, in *Solid State Physics* (Edited by F. Seitz, D. Turnbull and H. Ehrenreich), Vol. 20. Academic Press, New York (1967).
9. T. Toyozawa and M. Inone, *J. Phys. Soc. Jpn* 1966, **21**, 1663.
10. M. C. M. O'Brien, *J. Phys.* 1971, **C4**, 2524.
11. I. B. Bersuker and V. Z. Polinger, *Phys. Lett.* 1973, **44A**, 495.
12. I. B. Bersuker and V. Z. Polinger, *Phys. Status Solidi* 1973, **B60**, 85.
13. I. B. Bersuker and B. G. Vekhter, *Fiz. Tverd. Tela* 1963, **5**, 2432.
14. A. Ranfagni, D. Mugnai, N. Bacci, M. Montagne, O. Pille and G. Vilhani, *Phys. Rev.* 1979, **B20**, 5358.

15. A. E. Nikiforov, S. Yu. Shashkin and A. I. Krotkii, *Phys. Status Solidi* 1980, **B98**, 289.
16. P. Pelikán, M. Breza and M. Liška, *Inorg. Chim. Acta* 1980, **45**, L1.
17. R. Boča, P. Pelikán, M. Breza and J. Gažo, *Polyhedron* 1983, **2**, 921.
18. I. Özkan and L. Goodman, *Chem. Rev.* 1979, **79**, 275.
19. J. S. Griffith, *The Theory of Transition Metal Ions.* Dickens, Northampton (1964).
20. J. A. Pople and D. L. Beveridge, *Approximate Molecular Orbital Theory.* McGraw-Hill, New York (1970).
21. D. W. Clack, N. S. Hush and J. R. Yandle, *J. Chem. Phys.* 1972, **57**, 3503.
22. R. Boča, Program MOSEM2. Slovak Technical University, Bratislava (1980).
23. P. Pelikán and M. Breza, *Chem. Papers* 1984, **39**, 255.

Polyhedron Vol. 5, No. 3, pp. 761–763, 1986
Printed in Great Britain

0277-5387/86 $3.00 + .00
Pergamon Press Ltd

ROLE OF CYANIDE IN REACTION WITH *CIS*-DICHLOROBIS(2,2'-BIPYRIDINE)Co(III) CHLORIDE IN WATER

G. SCHIAVON* and F. MARCHETTI

Istituto Chimico "G. Ciamician", Bologna University, Italy

(*Received* 11 *October* 1984; *accepted* 27 *July* 1985)

Abstract—Although cyanide does not substitute chloride in the *cis*-dichlorobis (ethylenediamine)Co(III) cation in water, it does so in the analogous 2,2'-bipyridine-containing complex.

Many years ago, Chan and Tobe[1] reported that, according to experimental conditions, the reaction between *trans*-$[Co(en)_2Cl_2]Cl$ (en = ethylenediamine) and KCN in aqueous solution led to the formation of *trans*-$[Co(en)_2(OH)Cl]^+$ or products resulting from the disproportionation or redox-catalyzed reactions. In no case was the substitution of one or both chlorine atoms in the substrate by cyanide verified.

However the substitution of one atom of labile chlorine, by cyanide was realized by Chan and Tobe[1] with the reaction between *trans*-$[Co(en)_2(SO_3)Cl]$ and KCN in aqueous solution. This result together with that of Ray and Sarma,[2] who obtained the *cis*-$[Co(en)_2(CN)_2]^+$ by means of the reaction in water between KCN and $[Co(en_2(S_2O_3)_2]^-$, led Chan and Tobe[1] to the conclusion that the presence of SO_3^{2-} and $S_2O_3^{2-}$ groups assists the entry of cyanide (for unknown reasons at the time) into the Co(III) coordination sphere.

The *trans*-$[Co(en)_2(SO_3)CN]$ obtained by Chan and Tobe,[1] after being treated with concentrated HCl, gave the *trans*-$[Co(en)_2(CN)Cl]^+$ cation.[1]

Ohkawa *et al.*[3] prepared afterwards the form *cis*-$[Co(en)_2(CN)X]^+$ ($X = Cl^-$, Br^- or I^-), starting from *cis*-$[Co(en)_2(SO_3)CN]$ and the suitable halogen acid.

In 1969 Maki and Sakuraba[4] reported the preparation of mixed cyano-Co(III) complexes and, among others, that of *cis*-$[Co(bpy)_2(CN)_2]^+$ (bpy = 2,2'-bipyridine), *cis*-$[Co(phen)_2(CN)_2]^+$ (phen = 1,10-phenanthroline) and

$$cis\text{-}[Co(en)_2X(CN)]^{n+},$$

where $X = NO_2^-$, SO_3^{2-}, H_2O or CN^-. In the first two cases, the substrate was the corresponding dichloro-complex, while, for ethylenediamine-containing complexes, the substrate was the corresponding $[Co(en)_2XCl]^{n+}$ complex. In every case the cyano-group was supplied by an AgCN saturated solution. According to the AA the substitution of labile chloride by cyanide was made possible by the low concentration, thus realized, of the entering ligand.

On the other hand Palade *et al.*[5] prepared and characterized the *cis*-$[Co(phen)_2(CN)_2]^+$ cation by heating an aqueous solution of the corresponding dichloro-complex mixed with a 3% aqueous solution of KCN.

We have prepared and characterized

$$cis\text{-}[Co(bpy)_2(CN)Cl]^+$$

by the reaction between *cis*-$[Co(bpy)_2Cl_2]^+$ and KCN in aqueous solution and with a molar ratio between the reagents of 1 : 1.† When the molar ratio between the dichloro-complex and KCN was 1 : 2, the nucleophilic substitution product was the *cis*-$[Co(bpy)_2(CN)_2]^+$ cation.

From the chlorocyano-complex we have obtained, always in aqueous solution, the *cis*-$[Co(bpy)_2(CN)OH]^+$ cation with LiOH (1 : 1), and the *cis*-$[Co(bpy)_2(CN)_2]^+$ cation with KCN (1 : 1).

We have also performed molar conductance measurements on 5×10^{-4} M aqueous solutions of

$$cis\text{-}[Co(bpy)_2(CN)Cl]ClO_4,$$

$$cis\text{-}[Co(bpy)_2(CN)OH]ClO_4$$

* Author to whom correspondence should be addressed.

† We have already quoted the *cis*-$[Co(bpy)_2(CN)Cl]^+$ cation in Ref. 6 as an intermediate product in the preparation of the *cis*-$Co(bpy)_2(SO_3)CN$ compound.

and

$$cis\text{-}[Co(bpy)_2(CN)_2]ClO_4.$$

In all cases, the value for the molar conductance was 92 Ω^{-1} cm^2, which is peculiar to a uni-univalent electrolyte. However, while the specific conductivity was constant with time in the last two cases, the specific conductivity of solution of *cis*-$[Co(bpy)_2(CN)Cl]ClO_4$ slowly increased at 25°C. This fact indicates that the aquation reaction is taking place.

It seems evident that the cyano-group entering the coordination sphere of the dichloro-complex containing 2,2'-bipyridine, to substitute one or two chlorine atoms in aqueous solution, is due to the presence of the two aromatic α-diimine molecules. In fact it is known that, in octahedral complexes containing ammonia or amines having a hydrogenated (therefore protonatable) nitrogen atom, the reaction is always "base-catalyzed" when the entering ligand is, as in the case of CN^-, a relatively strong base. The process is of S_N1cb type and the product of the nucleophilic substitution reaction is the corresponding hydroxo-complex as verified by Chan and Tobe.[1]

With the aromatic α-diimines coordinating by two pyridine-like nitrogen atoms, the catalysis fails and the competition: hydroxide ion-entering ligand is overcome by the cyano-group, because of its higher nucleophilicity.

We must also consider the fact that 2,2'-bipyridine, unlike ethylenediamine, is a potential π-acceptor[7] and belongs to the class of "soft" bases as does the cyano-group. Therefore, between the latter and the two molecules of aromatic α-diimines a mutual stabilizing effect takes place, which Jørgensen called "symbiosis".[8] To this symbiosis phenomenon could also be referred the function developed by the SO_3^{2-} and $S_2O_3^{2-}$ groups in favouring the substitution of the labile Cl^- by CN^- in the Co(III) octahedral coordination sphere.[1]

Finally, even though 2,2'-bipyridine is a weaker σ-donor than ethylenediamine, the stabilities of its coordination complexes are greater.[9]

EXPERIMENTAL

Conductivity measurements were carried out on an Analytical Control model 101 conductivity meter. IR spectra of Nujol mulls were recorded on a Perkin–Elmer 397 spectrophotometer.

cis-*Dichlorobis*(2,2'-*bipyridine*)Co(III) *chloride*

This was prepared and purified according to Palade's method.[10]

cis - *Chlorocyanobis*(2,2' - *bipyridine*)Co(III) *per - chlorate*

To an aqueous solution of *cis*-dichlorobis(2,2'-bipyridine)Co(III) chloride dihydrate (1.5 g, 2.9 mmol in 130 cm^3 of water) an aqueous solution of KCN (0.189 g, 2.9 mmol in 2 cm^3 of water) was dropwise added with stirring at room temperature. The red-brown colour of the solution turned to orange. By adding solid $LiClO_4$ a pink precipitate was obtained, which was filtered, washed with ethyl alcohol and ether, and recrystallized from hot water [yield 1.1 g (70%)]. (Found: C, 47.3; H, 3.0; N, 13.5%. $CoC_{21}H_{16}N_4Cl_2O_4$ requires: C, 47.35; H, 3.00; N, 13.15%.) Its IR spectrum shows a band at ν = 2140 cm^{-1} attributed to the cyano-group coordinated to the metal.

cis - *Hydroxycyanobis*(2,2' - *bipyridine*)Co(III) *perchlorate*

To an aqueous solution of *cis*-chlorocyanobis(2,2'-bipyridine)Co(III) perchlorate (0.6 g, 1.13 mmol in 350 cm^3 of hot water) an aqueous solution of LiOH (0.027 g, 1.13 mmol in 10 cm^3 of water) was added. To the warm solution a saturated solution of $LiClO_4$ was added. On cooling the concentrated solution a brownish-yellow precipitate was obtained, which was filtered, washed with water, ethanol and ether, and recrystallized from hot water [yield 0.38 g (65%)]. (Found: C, 49.4; H, 3.1; N, 13.3%. $CoC_{21}H_{17}N_5ClO_5$ requires: C, 49.05; H, 3.31; N, 13.62%.) Its IR spectrum shows the band of cyanide coordinated at ν = 2140 cm^{-1} and two bands at ν = 1670 and 1630 cm^{-1}, which can be attributed to the hydroxide ion coordinated to the metal, since these two bands do not appear in the IR spectra of the other compounds examined.

cis-*Dicyanobis*(2,2'-*bipyridine*)Co(III) *perchlorate*

(a) To an aqueous solution of *cis*-chlorocyanobis(2,2'-bipyridine)Co(III) perchlorate (0.5 g, 0.94 mmol in 330 cm^3 of hot water) was added the equivalent amount of KCN dissolved in a minimum amount of water. By adding solid $LiClO_4$, and cooling, a yellow precipitate followed which was filtered, washed with water, ethanol and ether, and recrystallized from hot water [yield 0.42 g (86%)]. (Found: C, 50.4; H, 3.0; N, 16.3%. $CoC_{22}H_{16}N_6ClO_4$ requires: C, 50.50; H, 3.06; N, 16.07%.) Its IR spectrum shows a cyano-group band at ν = 2140 cm^{-1}.

(b) To an aqueous solution of *cis*-dichlorobis(2,2'-bipyridine)Co(III) chloride dihydrate (0.5 g, 0.97 mmol in 50 cm^3 of water) was added a solution of KCN in a minimum amount of water (0.126 g,

1.94 mmol). Proceeding as in (a), we obtain the same compound, characterized by elemental analysis, IR spectrophotometrical and conductivity measurements.

REFERENCES

1. S. C. Chan and M. L. Tobe, *J. Chem. Soc.* 1963, 966.
2. P. Ray and B. Sarma, *J. Indian Chem. Soc.* 1951, **28**, 59.
3. K. Ohkawa, J. Hidaka and Y. Shimura, *Bull. Chem. Soc. Jpn* 1966, **39**, 1715; 1967, **40**, 2830.
4. N. Maki and S. Sakuraba, *Bull. Chem. Soc. Jpn* 1969, **42**, 1908; N. Maki, *ibid.* 1969, **42**, 2275.
5. D. M. Palade, M. K. Boreiko and T. N. Volokh, *Chem. Abstr.* 1972, **76**, 30275e.
6. G. Schiavon, F. Marchetti and C. Paradisi, *Inorg. Chim. Acta* 1979, **33**, L101.
7. J. Reinhold, R. Benedix, B. Birner and H. Henning, *Inorg. Chim. Acta* 1979, **33**, 209.
8. C. K. Jørgensen, *Inorg. Chem.* 1964, **3**, 1201.
9. E. C. Niedehoffer, A. E. Martell, P. Rudolf and A. Clearfield, *Inorg. Chem.* 1982, **21**, 3734.
10. D. M. Palade, A. V. Ablov and V. N. Zubarev, *Russ. J. Inorg. Chem.* 1969, **14**, 227.

Polyhedron Vol. 5, No. 3, pp. 765–766, 1986
Printed in Great Britain

0277–5387/86 $3.00 + .00
© 1986 Pergamon Press Ltd

ROLE OF CYANIDE AS A BRIDGING LIGAND IN *CIS*-AQUOCYANOCo(III) COMPLEXES CONTAINING 2,2′-BIPYRIDINE AND 1,10-PHENANTHROLINE

G. SCHIAVON,* F. MARCHETTI and M. PATRIKAKI

Istituto Chimico "G. Ciamician", Universita' di Bologna, Bologna, Italy

(*Received* 27 *June* 1985; *accepted* 16 *September* 1985)

Abstract—*Cis*-aquocyanobis(2,2′-bipyridine)Co(III) and *cis*-aquocyanobis(1,10-phenanthroline)Co(III) cations present in their IR spectra a cyano-group band in a Nujol mull at $\nu = 2200\ cm^{-1}$. To justify the shift in the frequency from 2140 to 2200 cm^{-1} of cyanide in these compounds, we have hypothesized that the cyano group is a bridge between the metal atom and one hydrogen atom of the water molecule in the *cis* position on the Co(III) coordination sphere.

We have previously reported[1] the kinetics of the aquation reactions of *cis*-$[Co(bpy)_2(CN)Cl]^+$ (**1**) (bpy = 2,2′-bipyridine) and

cis-$[Co(phen)_2(CN)Cl]^+$ (**2**)

(phen = 1,10-phenanthroline), and the preparation of compound **1**.[2]

We now report the preparation of compound **2** and the aquocyano derivatives of **1** and **2**.

Just as for **1**, the *cis*-$[Co(phen)_2(CN)Cl]^+$ complex can be prepared by the reaction in water between *cis*-$[Co(phen)_2Cl_2]^+$ and KCN. As in the case of the bpy-containing complex (**1**), so in the present case the aromatic α-diimine (phen) is the ligand which assists, since with it no "base-catalysed" process of the type S_N1cb is possible, the cyanide's entry into the coordination sphere of Co(III), by virtue of the analogy between phen and cyanide, both soft bases and π-acceptor ligands (Jørgensen "symbiosis"[3]).

Both of the chlorocyano complexes (**1** and **2**) have very low values for the aquation rate constant at 25°C,[1] compared to the corresponding *cis*-dichloro and *cis*-chloronitro complexes.

Furthermore, neither Ag^+ nor Hg^{2+} is able to cause a fast hydrolysis. However, addition of minute amounts of $[Co(N–N)_2(CN)Cl]$ (N–N = bpy or phen) results in immediate hydrolysis of the *cis*-chlorocyano in the *cis*-aquocyano complex.

This faster aquation reaction is manifested by the fact that, on treating the reaction mixture with solid $LiClO_4$, a precipitate was obtained which has an IR spectrum with two cyano-group bands at $\nu = 2200$ and 2140 cm^{-1}, indicating the presence of two compounds. By ion exchange chromatography of the reaction mixture we obtained two fractions. The first one gave the *cis*-$[Co(N–N)_2(CN)Cl]^+$ cation characterized by elemental analysis, which has an IR spectrum with the cyano-group band at $\nu = 2140\ cm^{-1}$. The second fraction gave the *cis*-$[Co(N–N)_2(CN)OH_2]^{2+}$ cation, characterized by elemental analysis, which has an IR spectrum with the cyano-group band at $\nu = 2200\ cm^{-1}$, and two new bands at $\nu = 465$ and $450\ cm^{-1}$, which we have attributed to the water molecule coordinated to the metal.

We have justified the frequency $\nu(CN) = 2200\ cm^{-1}$ in the IR spectra of the aquocyano cation derivatives from **1** and **2**, admitting that, since the cyano group and the water molecule are *cis* to each other, with no possibility of *cis–trans* isomerization at all for the complexes, a hydrogen bond was formed between the free nitrogen end of the coordinated cyanide and the oxygen atom of the water molecule. In this way the cyanide bridged, intermolecularly, the cobalt atom and the proton. From there the stretching frequency of the coordinated cyano-group shifted to higher values.

It is known, in fact, that a nitrogen atom at the free end of coordinated cyanide can be engaged in the formation of a bond with: (a) a metal atom, as in the case of binuclear or bridged cyano complexes;[4] (b) a proton;[5] and (c) a Lewis acid, as in the case of BF_3 (acid–base adducts).[6] In every case the stretching

* Author to whom correspondence should be addressed.

frequency of the coordinated cyanide is shifted to a higher value.

EXPERIMENTAL

cis-Dichlorobis (1,10-phenanthroline) Co(III) chloride

This was prepared according to Ref. 7.

cis - Chlorocyanobis(1,10 - phenanthroline)Co(III) chloride

To an aqueous solution of *cis*-dichlorobis(1,10-phenanthroline)Co(III) chloride (2 g, 3.8 mmol in 10 cm^3 of water) an aqueous solution of KCN (0.25 g, 3.8 mmol in 2 cm^3 of water) was added dropwise, with stirring at room temperature. The purple solution turned to a yellow-orange color. Solid LiCl was added to the reaction mixture, which was then concentrated to a small volume. By adding ethanol and ether (1 : 1) a pale pink precipitate followed, which was recrystallized from water (yield 1.29 g, 65%). Found: C, 58.3; H, 3.0; N, 13.4. $CoC_{25}H_{16}N_5Cl_2$ requires: C, 58.1; H, 3.1; N, 13.6%. Its IR spectrum shows a cyano-group band at $\nu = 2140\ cm^{-1}$.

cis - Aquocyanobis(1,10 - phenanthroline)Co(III) perchlorate

Minute amounts of *cis*-chlorocyanobis(1,10-phenanthroline)Co(II), opportunely prepared, were added to a solution of *cis*-chlorocyanobis(1,10-phenanthroline)Co(III) chloride (1.96 g, 3.8 mmol in 20 cm^3 of water). The cationic species were absorbed at the top of a column of Amberlite 15 (H) (30 × 1 cm) and eluted, first with 0.1 M HCl and then with 4 M $HClO_4$. The first eluate gave, on adding solid $LiClO_4$, a pale hazel colored precipitate of *cis*-$[Co(phen)_2(CN)Cl]ClO_4$. Found: C, 52.1; H, 2.9; N, 11.9. $CoC_{25}H_{16}N_5Cl_2O_4$ requires: C, 51.7; H, 2.8; N, 12.1%. Its IR spectrum shows a cyano-group band at $\nu = 2140\ cm^{-1}$.

The second eluate, yellow-orange in color, gave, on adding solid $LiClO_4$, a pale-pink precipitate of *cis*-$[Co(phen)_2(CN)OH_2](ClO_4)_2$. Found: C, 45.2; H, 2.8; N, 10.7. $CoC_{25}H_{18}N_5Cl_2O_9$ requires: C, 45.3; H, 2.7; N, 10.6%. Its IR spectrum shows a cyano-group band at $\nu = 2200\ cm^{-1}$ and two bands at $\nu = 465$ and $450\ cm^{-1}$, which we have attributed to the water molecule coordinated in the *cis* position with respect to the cyanide in the octahedral coordination sphere of Co(III).

cis - Chlorocyanobis(2,2' - bipyridine)Co(III) perchlorate

This was prepared according to Ref. 2.

cis-Aquocyanobis(2,2'-bipyridine)Co(III) perchlorate

Minute amounts to *cis*-$[Co(bpy)_2(CN)Cl]$, opportunely prepared, were added to a solution of *cis*-$[Co(bpy)_2(CN)Cl]ClO_4$ (0.66 g, 1.24 mmol in 250 cm^3 of water). The red-orange color of the solution immediately turned to orange-yellow. After 30 min the solution was filtered. From the pale-orange filtrate an orange precipitate was obtained by adding solid $LiClO_4$. The precipitate was redissolved in hot water and the cationic species were absorbed at the top of a column of Amberlite 15 (H). The eluate with 0.1 M $HClO_4$, which was nearly colorless, was discarded. The eluate with 4 M $HClO_4$, orange-yellow in color, after concentration in a water bath, and on adding solid $LiClO_4$, gave a pale-yellow precipitate, which was washed with water, ethanol and diethyl ether, and recrystallized from hot water. Found: C, 41.7; H, 3.0; N, 11.2. $CoC_{21}H_{18}N_5Cl_2O_9$ requires: C, 41.0; H, 2.1; N, 11.4%. Its IR spectrum shows the cyano-group band at $\nu = 2200\ cm^{-1}$ and two bands at $\nu = 465$ and $450\ cm^{-1}$, attributed to the water molecule coordinated to the metal.

REFERENCES

1. G. Schiavon and F. Marchetti, *Polyhedron* 1985, **4**, 1143.
2. G. Schiavon and F. Marchetti, *Polyhedron* 1986, **5**, 761.
3. C. K. Jørgensen, *Inorg. Chem.* 1964, **3**, 1201.
4. D. F. Shriver, S. A. Shriver and S. E. Anderson, *Inorg. Chem.* 1965, **4**, 725.
5. M. F. A. Dove and J. G. Hallet, *J. Chem. Soc. (A)* 1969, 1204.
6. D. F. Shriver, *J. Am. Chem. Soc.* 1963, **85**, 1405.
7. M. P. Hancock, J. Josephsen and C. E. Schaffer, *Acta Chem. Scand.* 1976, **30**, 79.

Polyhedron Vol. 5, No. 3, pp. 767–770, 1986
Printed in Great Britain

0277–5387/86 $3.00+.00
© 1986 Pergamon Press Ltd

{RuNO}^{6} AND {RhNO}^{6} COMPLEXES WITH 2,2′-BIPYRIDINE AND 1,10-PHENANTHROLINE

K. K. PANDEY* and S. R. AHUJA

Department of Chemistry, Devi Ahilya Vishwavidyalaya, Indore 452001, India

and

V. VIJAYVERGIYA

Department of Chemistry, Indian Institute of Technology, New Delhi, India

(*Received* 15 *March* 1985; *accepted after revision* 27 *July* 1985)

Abstract—The reactions of nitrosyl halides NOX (X = Cl, Br or Br_3) and N_2O_3 with $RuCl_3(H_2O)_3$ and $RhCl_3(H_2O)_3$ in the presence of 2,2′-bipyridine and 1,10-phenanthroline results in the formation of neutral nitrosyl complexes of types $Ru(NO)X_3(L–L)$ and $Rh(NO)X_2(L–L)$ (L–L = 2,2′-bipyridine or 1,10-phenanthroline).

Nitrosyl halides NOX (X = Cl or Br) besides nitric oxide have been used as nitrosylating agents in the synthesis of transition-metal nitrosyl complexes.[1–15] In this paper the reactions of nitrosyl chloride, nitrosyl bromide, nitrosyl tribromide and N_2O_3 with $RuCl_3(H_2O)_3$ and $RhCl_3(H_2O)_3$ in the presence of 2,2′-bipyridine and 1,10-phenanthroline are described. The structure of the resulting nitrosyl complexes are proposed on the basis of IR, UV, visible and magnetic measurements, and elemental analysis.

EXPERIMENTAL

All the chemicals used were of chemically pure or AnalaR grade. All solvents were dried by standard procedures and distilled just prior to use.

NOX (X = Cl, Br or Br_3) and N_2O_3 were prepared by the literature methods.[16–19]

Reaction of NOX (X = Cl, Br *or* Br_3) *with* $RuCl_3(H_2O)_3$ *in the presence of L–L* (*L–L = 2,2′-bipyridine or 1,10-phenanthroline*)

A saturated solution of NOCl in dichloromethane (50 cm^3) was added to an ethanolic solution of $RuCl_3(H_2O)_3$ (0.2 g) and the resulting mixture was refluxed for 30 min. A solution of L–L (0.8 g) in 20 cm^3 ethanol was added to the above solution and the reaction mixture was again refluxed for 15 min. Brown shining crystals of $[Ru(NO)Cl_3(L–L)]$ were separated out, which were washed with ethanol and diethylether, and dried in air.

By a similar procedure, the reaction of NOBr and $NOBr_3$ in dichloromethane (10 cm^3, *ca* 2 M) with $RuCl_3(H_2O)_3$ in the presence of L–L gave brown shining crystals of $[Ru(NO)Br_3(L–L)]$. These were filtered and washed with ethanol and diethylether, and dried in air.

Reaction of N_2O_3 *with* $RuCl_3(H_2O)_3$ *in the presence of L–L* (*L–L = 2,2′-bipyridine or 1,10-phenanthroline*)

A saturated green solution of N_2O_3 in dichloromethane (20 cm^3) was added with stirring to 20 cm^3 of an alcoholic solution of $RuCl_3(H_2O)_3$ (0.2 g) and the resulting mixture was refluxed for 30 min. A solution of L–L (0.8 g) in 20 cm^3 ethanol was added. It was refluxed for 15 min. Brown crystals of $[Ru(NO)Cl_3(L–L)]$ were separated out which were centrifuged, washed with ethanol and diethylether, and dried in air.

Reaction of NOX (X = Cl, Br *or* Br_3) *with* $RhCl_3(H_2O)_3$ *in the presence of L–L* (*L–L = 2,2′-bipyridine or 1,10-phenanthroline*)

A saturated solution of NOCl in dichloromethane (50 cm^3) was added dropwise to a stirred ethanolic

* Author to whom correspondence should be addressed.

solution of $RhCl_3(H_2O)_3$ (0.25 g) and the resulting mixture was refluxed for 40 min. A solution of L–L (1.0 g) in 20 cm^3 ethanol was added to the above solution and the reaction mixture was again refluxed for 15 min. Red-brown shining crystals of $[Rh(NO)Cl_2(L–L)]$ were separated out which were washed with ethanol and diethylether, and dried in air.

By a similar procedure, the reaction of NOBr and $NOBr_3$ in dichloromethane (10 cm^3, *ca* 2 M) with $RhCl_3(H_2O)_3$ in the presence of L–L gave red-brown shining crystals of $[Rh(NO)Br_2(L–L)]$. These were centrifuged, washed with ethanol and diethylether, and dried in air.

Reaction of N_2O_3 *with* $RhCl_3(H_2O)_3$ *in the presence of L–L (L–L = 2,2′-bipyridine or 1,10-phenanthroline)*

A saturated green solution of N_2O_3 in dichloromethane (20 cm^3) was added with stirring to 20 cm^3 of an ethanolic solution of $RhCl_3(H_2O)_3$ (0.2 g) and the resulting solution was refluxed for 1 h. A solution of L–L (1.0 g) in 20 cm^3 ethanol was added. It was again refluxed for 15 min. Red-brown crystals of $[Rh(NO)Cl_2(L–L)]$ were separated out which were centrifuged, washed with ethanol and diethylether, and dried in air.

Carbon, hydrogen and nitrogen analyses of the complexes were performed by the Microanalytical Section of the Indian Institute of Technology, New Delhi, India. The halogen estimations were carried out by standard methods.[20] For estimation of phosphorus, samples were decomposed with Na_2O_2, sugar and $NaNO_3$ in a Parr bomb crucible, extracted with water and, after adding conc. H_2SO_4, heated till the evolution of SO_3 fumes ceased. Extraction with H_2O and filtration, if necessary, were carried out. Phosphorus was estimated gravimetrically as ammonium phosphomolybdate. The IR spectra of the samples were recorded with a Perkin–Elmer Model 580 spectrophotometer in the range 4000–250 cm^{-1}. Samples were prepared as KBr pellets. The electronic spectra (ruthenium complexes in dichloromethane and rhodium complexes in nitrobenzene solution) were recorded on a Varian 634 S spectrophotometer. The magnetic measurements were made on a Gouy balance. Conductivity measurements of the compounds were made on a Remi Conductivity Meter type 2LH with milimolar solutions in nitrobenzene. All the compounds are found to be non-conducting.

RESULTS AND DISCUSSION

The reactions of NOX with $MCl_3(H_2O)_3$ (M = Ru or Rh) in the presence of ligands L–L (L–L = 2,2′-bipyridine or 1,10-phenanthroline) resulted in the formation of $\{MNO\}^6$ complexes of types $[Ru(NO)X_3(L–L)]$ and $[Rh(NO)X_2(L–L)]$ in about 60% yield, respectively, as:

$$RuCl_3(H_2O)_3 + NOX + L–L \rightarrow [Ru(NO)X_3(L–L)] + \cdots$$

$$RhCl_3(H_2O)_3 + NOX + L–L \rightarrow [Rh(NO)X_2(L–L)] + \cdots$$

Ruthenium nitrosyl complexes

All the complexes are air-stable, diamagnetic and sparingly soluble in dichloromethane, nitrobenzene and pyridine. The IR spectra of the complexes show a sharp band in the region 1830–1840 cm^{-1} due to ν(NO), at 335 cm^{-1} due to ν(Ru—Cl), and bands due to 2,2′-bipyridine or 1,10-phenanthroline. Complexes with a similar composition, $[Ru(NO)Cl_3(L–L)]$, but with a higher nitrosyl stretching frequency [ν(NO) = 1880 cm^{-1}], have been reported previously.[21] The corrected nitrosyl stretching frequencies [ν'(NO)] according to Ibers' rules[22] fall above 1620 cm^{-1}, which indicates a linear bonding of the nitrosyl group. The diamagnetic behaviour and linear bonding mode of the nitrosyl group suggest that the oxidation state of the metal ion is 2^+ and these complexes are regarded as complexes between Ru(II) and NO^+. The ruthenium ion thus has a d^6 electronic configuration.

The visible spectra of the complexes show three bands around 18,000, 20,700 and 26,000 cm^{-1}. However, the extinction coefficients of these bands are much higher compared to the ones found normally for octahedral complexes. These may be charge-transfer bands[23] [$d\pi \rightarrow \pi^*$ (NO), halogen $\rightarrow d\pi$ or $d\pi \rightarrow \pi^*$ (L–L)]. However, the bands at 18,000 and 20,700 cm^{-1} may be *d–d* singlet $\rightarrow$ singlet transitions, in which case the intensity of the bands may arise due to: (i) the covalent nature of the complex, and (ii) the lowering of the symmetry of the molecule whereby the centre of symmetry is lost.

Rhodium nitrosyl complexes

All the complexes are air-stable, diamagnetic, red-brown solids, insoluble in benzene and dichloromethane, and soluble in nitrobenzene and pyridine. The IR spectra of the complexes exhibit absorption bands at 1625 cm^{-1} due to ν(NO), at 350 cm^{-1} due to ν(Rh—Cl) and bands due to 2,2′-bipyridine and 1,10-phenanthroline. The diamagnetic behaviour suggests that the rhodium in the complexes is present either in a 1^+ [Rh(I)–NO^+] or a 3^+ [Rh(III)–NO^-] oxidation state. The determi-

Table 1.

Complex[a]	Colour	M.p.[b] (°C)	Elemental analysis [found (calc.)] (%) C	H	N	Cl/Br
$Ru(NO)Cl_3(Bipy)$	Brown	> 350	30.8 (30.50)	2.1 (2.03)	10.5 (10.67)	26.8 (27.07)
$Ru(NO)Br_3(Bipy)$	Brown	> 350	22.8 (22.77)	1.4 (1.52)	8.1 (7.97)	45.1 (45.54)
$Ru(NO)Cl_3(Phen)$	Brown	> 350	34.8 (34.50)	2.0 (1.92)	10.2 (10.06)	25.2 (25.50)
$Ru(NO)Br_3(Phen)$	Brown	> 350	25.9 (26.13)	1.3 (1.45)	7.6 (7.62)	43.1 (43.55)
$Rh(NO)Cl_2(Bipy)$	Red-brown	> 350	33.5 (33.33)	2.1 (2.22)	11.5 (11.66)	19.9 (19.72)
$Rh(NO)Br_2(Bipy)$	Red-brown	> 350	26.9 (26.72)	1.9 (1.78)	9.0 (9.35)	35.4 (35.63)
$Rh(NO)Cl_2(Phen)$	Red-brown	> 350	37.2 (37.50)	2.0 (2.08)	10.7 (10.94)	18.6 (18.49)
$Rh(NO)Br_2(Phen)$	Red-brown	> 350	30.4 (30.44)	1.8 (1.69)	8.8 (8.88)	34.1 (33.82)

[a] Bipy, 2,2′-bipyridine; Phen, 1,10-phenanthroline.
[b] All complexes decompose without melting.

nation of the ν(NO) according to Ibers' rules showed this band at *ca* 1600 cm^{-1}, i.e. below 1620 cm^{-1}. This is evidence of the presence of a bent nitrosyl group. Thus, the formal oxidation state of rhodium in these complexes is 3^+, [Rh(III)–NO^-] and not 1^+, [Rh(I)–NO^+]. For penta-coordinated mononitrosyl complexes of group VIII transition metals, square-pyramidal and trigonal bipyramidal geometries with bent apical and linear equatorial nitrosyl bonding, respectively, have been found from X-ray structural determination[24] and theoretical calculations.[25] Thus, the structures of $Rh(NO)X_2(L–L)$ (X = Cl or Br, L–L = 2,2′-bipyridine or 1,10-phenanthroline) are probably square-pyramidal with bent apical nitrosyl bonding. The visible spectra of the complexes show two bands around 20,400 and 23,500 cm^{-1}. The extinction coefficients are high and these bands may be charge-transfer bands.

Acknowledgment—One of us (SRA) is grateful to the C.S.I.R., New Delhi, India, for the award of a Senior Research Fellowship.

Table 2.

Complex[a]	Important IR bands (cm^{-1}) ν(M—Cl)	ν(NO)	ν'(NO)[b]	Electronic absorption bands (cm^{-1})
$Ru(NO)Cl_3(Bipy)$	355	1832	1802	18,000, 20,800, 25,900, 36,300, 44,400
$Ru(NO)Br_3(Bipy)$	—	1835	1805	18,000, 21,000, 25,000, 37,000, 43,400
$Ru(NO)Cl_3(Phen)$	355	1840	1810	18,000, 21,000, 26,300, 36,300, 43,400
$Ru(NO)Br_3(Phen)$	—	1830	1800	18,000, 21,500, 25,600, 37,000, 43,400
$Rh(NO)Cl_2(Bipy)$	350	1630	1600	20,400, 23,400
$Rh(NO)Br_2(Bipy)$	—	1625	1595	20,400, 23,500
$Rh(NO)Cl_2(Phen)$	350	1620	1590	20,400, 23,500
$Rh(NO)Br_2(Phen)$	—	1630	1600	20,800, 23,200

[a] For Bypy and Phen, see Table 1.
[b] Corrected nitrosyl stretching frequencies [ν'(NO)] have been calculated by Ibers' empirical rules (22).

REFERENCES

1. W. P. Griffith, J. Lewis and G. Wilkinson, *J. Chem. Soc.* 1961, 775.
2. G. R. Crooks and B. F. G. Johnson, *J. Chem. Soc. A* 1968, 1236.
3. G. R. Crooks and B. F. G. Johnson, *J. Chem. Soc. A* 1970, 1662.
4. J. R. Fowler and J. Kleinberg, *Inorg. Chem.* 1970, **9**, 1005.
5. B. F. G. Johnson and R. Davis, *J. Chem. Soc., Dalton Trans.* 1972, 508.
6. K. D. Hodge and J. V. Rund, *Inorg. Chem.* 1975, **14**, 525.
7. W. L. Waters and P. G. Marsh, *J. Org. Chem.* 1975, **40**, 3344.
8. P. Legzdins and J. T. Malito, *Inorg. Chem.* 1975, **14**, 1875.
9. K. E. Voss, S. D. Hudman and J. Kleinberg, *Inorg. Chim. Acta* 1976, **20**, 78.
10. N. G. Connelly and C. Gardner, *J. Chem. Soc., Dalton Trans.* 1976, 1525.
11. K. K. Pandey, S. Datta and U. C. Agarwala, *Transition Met. Chem.* 1979, **4**, 337.
12. K. K. Pandey and U. C. Agarwala, *J. Inorg. Nucl. Chem.* 1980, **42**, 293.
13. K. K. Pandey, S. R. Ahuja, N. S. Poonia and S. Bharti, *J. Chem. Soc., Chem. Commun.* 1982, 1268.
14. H. W. Roesky, K. K. Pandey, W. Clegg, M. Noltemayer and G. M. Sheldrick, *J. Chem. Soc., Dalton Trans.* 1984, 719.
15. K. K. Pandey and S. R. Ahuja, *Inorg. Chem.* 1985, **24**, 2855.
16. Shell, International Research Maatschappij, N.U., Neth Appl 61512661 (Cl.CO.1b) 1967, **31**, 3; *Chem. Abstr.* 1967, **67**, 66184C.
17. W. G. Burns and H. J. Bernstein, *J. Chem. Phys.* 1950, **18**, 1669.
18. R. L. Datta and N. R. Chatterjee, *J. Am. Chem. Soc.* 1923, **45**, 481.
19. G. Brauer, *Handbook of Preparative Inorganic Chemistry*, 2nd Edn, Vol. 1. Academic Press, New York (1963).
20. A. I. Vogel, *A Text Book of Quantitative Inorganic Analysis*, 3rd Edn, p. 433. Longmans Green, London (1961).
21. M. B. Fairy and R. J. Irving, *J. Chem. Soc. A* 1966, 475.
22. B. L. Haymore and J. A. Ibers, *Inorg. Chem.* 1975, **14**, 3060.
23. W. R. McWhinnie and J. D. Miller, *Adv. Inorg. Chem. Radiochem.* 1969, **12**, 135.
24. B. L. Haymore and J. A. Ibers, *Inorg. Chem.* 1975, **14**, 2610.
25. R. Hoffman, M. M. L. Chen, M. Elean, A. R. Rossi and D. M. P. Mingos, *Inorg. Chem.* 1974, **13**, 2666.

Polyhedron Vol. 5, No. 3, pp. 771–777, 1986
Printed in Great Britain

0277–5387/86 $3.00 + .00
© 1986 Pergamon Press Ltd

ATOMIC ARRANGEMENT OF A ZINC–TELLURITE GLASS

VLADIMIR KOZHUKHAROV*
Institute of Chemical Technology, Sofia-1156, Bulgaria

HERBERT BÜRGER
Friedrich-Schiller-Universität, Otto-Schott Institut, Jena 6900, G.D.R.

and

STOIKO NEOV* and BOZHKO SIDZHIMOV
Institute of Nuclear Research and Nuclear Energy, Bulgarian Academy of Sciences, Sofia-1184, Bulgaria

(*Received* 14 *December* 1984; *accepted after revision* 27 *July* 1985)

Abstract—By means of the neutron diffraction method the atomic arrangement of a zinc–tellurite glass with composition 80% TeO_2 + 20 mol % ZnO has been studied. Analysis of the radial distribution functions (RDF_{exp} and RDF_{model}) shows the presence of some changes in the basic structural units at the glass transition. Approximately 35% of the Te atoms conserve the same coordination state as in the α-TeO_2 crystal structure. The remaining Te atoms are of lower coordination. The Gaussian distribution of the O—O distances of the first coordination sphere ($\bar{R}$ = 2.95 Å) indicates an increasing assymmetry of TeO_4, TeO_{3+1}, TeO_3 and ZnO_{4+1+1} polyhedra. The observed variations of the Te—Te, Te—second O and O—second O distances greater than 3.0 Å have an essential contribution to tellurite melt amorphization. An attempt is made to give a stereochemical representation of the glass structure on the basis of the obtained RDF_{exp}.

Tellurium(IV) oxide in combination with ZnO forms stable glasses. Data on glass properties are reported in the literature.[1,2] Because of the wide glass-formation range which is close to the extremum for binary tellurite glasses, the ZnO–TeO_2 system is used as a basis for multicomponent optical glass synthesis.[3,4] For example the influence of $ZnCl_2$ and ZnO on the refractive indices and the dispersion coefficients of the glasses in the TeO_2–WO_3, TeO_2–BaO and TeO_2–Na_2O systems have been discussed.[5–7] The above-mentioned indicate undoubtedly the existence of a practical interest in the zinc-tellurium-containing systems as a choice of compositions for superheavy optical flint glasses.[8–11] Apart from their applications there is a lack of data on structural investigations of these glasses in the literature.

In the present work we have investigated the short range order of a tellurite glass with composition 80% TeO_2 + 20 mol % ZnO.† The presence of atoms of significantly different atomic numbers in the investigated sample, $_8$O, $_{30}$Zn and $_{52}$Te, necessitated the use of the neutron diffraction method. The nuclei of O, Te and Zn have similar scattering amplitudes ($b_O = 0.580 \times 10^{-14}$ m, $b_{Zn} = 0.570 \times 10^{-14}$ m, $b_{Te} = 0.580 \times 10^{-14}$ m) and therefore the measured diffuse scattering intensity will be sensitive to the light oxygen nuclei distribution. Hence the experimental radial distribution function (RDF_{exp}) will contain information about the O—O distances.

EXPERIMENTAL

Phase diagram

The phase diagram of the TeO_2–ZnO system is well known.[12] Phase analysis confirms the existence

* Authors to whom correspondence should be addressed.

† All compositions are given in mol %.

of two compounds, namely $Zn_2Te_3O_8$ (monoclinic) and $ZnTeO_3$ (orthorhombic), in accordance with Hanke's data.[13,14] The eutectic point is located in the TeO_2-rich region at 21% ZnO and a temperature of 590°C. The electron microscopic investigations of the glasses do not establish phase separation in the system.[12]

Materials and glass synthesis

Materials used (TeO_2 and ZnO) were of Analar grade. The X-ray diffraction study of the initial TeO_2 material shows that there was only a paratellurite (α-TeO_2) polymorphous phase. A batch of 50 g of the material placed in a Pt crucible was directly melted in an electric furnace. Melting was achieved in a dry-air atmosphere at a temperature of 750°C for 40 min. The glass melt was quenched to room temperature by pouring on to a copper mold. The bulk glass sample had not been additionally tempered or thermally treated. After glass density measurements (5.283 g cm^{-3}) the sample was crushed and directly investigated by the neutron diffraction method.

Methods

Neutron diffraction patterns were obtained by a diffractometer installed at the WWR-M reactor (LINPH, U.S.S.R.). The experimental spectrum was taken at a constant step of $2\theta = 0.1°$ in the angular range $2\theta \in [4.125°]$. The wavelength of the monochromatic neutron beam was $\lambda = 1.113$ Å. The points required for Fourier transformation distributed at a constant $\Delta Q = 0.05$ Å^{-1} ($Q = 4\pi \sin\theta/\lambda$) were calculated by a parabolic interpolation of the experimental data. The obtained curve, presented in Fig. 1, shows the characteristic behaviour of glassy substances with broad diffusion maxima located in the range 0.4–10 Å^{-1}. For establishing the normalized diffraction intensity [$i(Q)$]:

$$i(Q) = [I(Q) - I_\infty]/(I_\infty - I_0) \qquad (1)$$

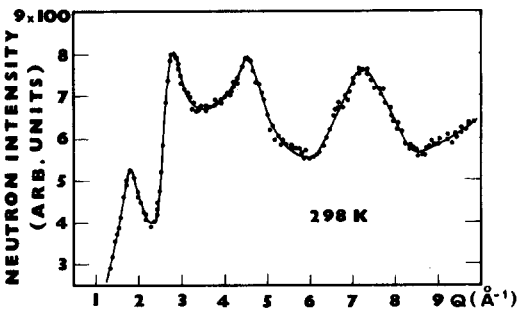


Fig. 1. Intensity of diffracted neutrons as a function of Q at room temperature.

the values of the structurally independent coherent scattering (I_∞) and the multiple and incoherent scattering (I_0) should be evaluated. As shown in Ref. 15, I_∞ is found from the constant integral intensity theorem:

$$\int_0^\infty Q^2 I(Q)\, dQ = \int_0^\infty Q^2 I_\infty\, dQ. \qquad (2)$$

I_0 is defined from the formulae in Ref. 16, while μR is experimentally measured by passing a thin neutron beam along the diameter of the cylindrical powder sample. For elimination of the influence of the upper limit of the Fourier integral on the RDF curve the modifying function:

$$M(Q) = \sin\frac{Q\Delta}{2}\Big/\frac{Q\Delta}{2} \qquad (3)$$

proposed by Lorch,[17] where $\Delta = 2\pi/Q_{max}$ has been used. The RDF is a sum of $m(m+1)/2$ interatomic distributions, where m is the number of different kinds of atoms. It is necessary to note that the neutron diffraction experiment by itself does not permit a unique interpretation of the RDF_{exp}. This problem may partially be solved by a model approach consisting in the selection of such an initial structure, whose RDF is comparable with the experimentally obtained RDF curve for a glass sample. This approach has been used in the present work.

RESULTS

The measured diffraction spectrum is shown on Fig. 1. Four well-expressed diffraction maxima are observed at Q values of 1.8, 2.8, 4.5 and 7.2 Å^{-1}, respectively. The last maximum is symmetrically broadened. Performing the Fourier transformation we obtain the $F(R)$ function presented in Fig. 2 (curve 1). The calculated, up to $R = 10$ Å, $F(R)$ curve has nine peaks, two of which (P3 and P5) are not well resolved (see Fig. 2). The $F(R)$ function maxima are due to maxima in the atomic density at: P1 (1.95 Å), P2 (2.90 Å), P3 (3.90 Å) (diffuse), P4 (4.65 Å), P5 (5.20 Å) (unresolved), P6 (5.80 Å), P7 (7.15 Å), P8 (8.0 Å) and P9 (9.0 Å). The accuracy of determination of the position of the P1–P4 peaks is $\Delta R \leqslant 0.03$ Å and for peaks P5–P9 it is 0.10 Å. From our former structural investigations on tellurite glasses[18,19] it is known that peaks P1–P6 are sensitive to the influence of the second component in the glass and are shifted towards lower R values. This kind of R value lowering is especially evident in cases when the second component possesses a stable cation–anion coordination and has a high bond strength. The peak shift is illustrated in Fig. 2.

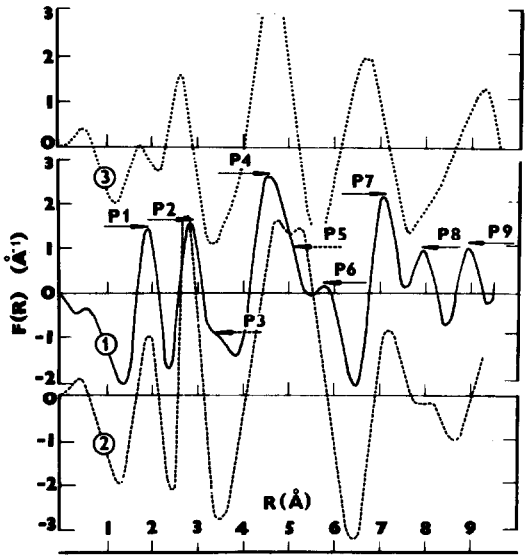


Fig. 2. Comparison between Fourier transform curves of the normalized intensity [$i(Q)$] glasses with compositions: 80% TeO_2 + 20% ZnO (curve 1), 80% TeO_2 + 20% Li_2O (curve 2)[19] and 80% TeO_2 + 20% P_2O_5 (curve 3).[18]

Figure 3 represents a comparison of the RDF_{model} curves for ZnO and α-TeO_2. There is an essential difference in the O—O distance distributions; curve 1, peak P2 at 3.35 Å, curve 2, peak P2 at 2.85 Å.

DISCUSSION

The RDF_{exp} is shown in Fig. 4 (curve 1). For a comparison and a more reliable interpretation of the results, RDF_{model} curves for an 80% TeO_2 + 20% ZnO glass (curve 2), and for $Zn_2Te_3O_8$ (curve 3), are also shown in Fig. 4.

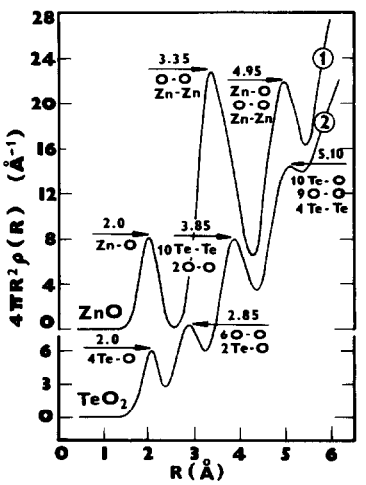


Fig. 3. Model RDF curves of ZnO (curve 1) and α-TeO_2 (curve 2).

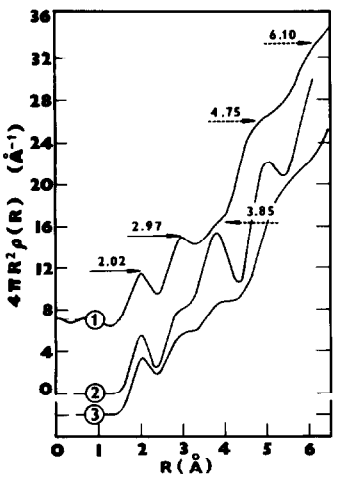


Fig. 4. A comparison of the RDF_{exp} (curve 1) of the glass investigated with the RDF_{model} (curve 2) of a glass with composition 80% TeO_2 + 20% ZnO and the RDF_{model} (curve 3) of $Zn_2Te_3O_8$ atomic density.

The RDF_{exp} curve

$$\left[4\pi R^2 \sum_i^m \sum_j^m n_i \bar{b}_i \bar{b}_j Z_{ij}(R)\right]$$

[Fig. 4 (curve 1)], where

$$\bar{b}_i = \frac{b_i}{\sum_i^m n_i b_i^2}$$

and $Z_{ij}(R)$ is the partial distribution of j-atoms around i-atoms, exhibits well-expressed coordination maxima located at R_1 = 2.02 Å (peak P1), R_2 = 2.97 Å (peak P2) and two unresolved maxima at 3.85 (peak P3) and 4.75 Å (peak P4), respectively. The interpretation of the peaks at ~5.8–6.1, 7.2, 8.0 Å etc. in Fig. 2 (curve 1) includes large uncertainties. That is why our discussion will be confined to the first four maxima, since these peaks carry the most essential information about the short-range order in the glasses.

On the basis of Te(IV), O(II) and Zn(II) ion radii of 0.83, 1.36 and 0.83 Å, respectively, we may claim that the P1 maximum is due to the contribution of the Te–O and Zn–O interatomic distances. This conclusion is supported by the fact that the main building units of the initial crystal structures persist to a great extent in the vitreous state too. This tendency exists even for metal–metalloid glasses which have been considered until recently as entirely disordered.[20] According to Lindqvist[21] the basic structural unit in α-TeO_2 is derived from a TeO_4 trigonal bipyramid with two equal Te—O_{eq} distances of 1.90 Å and two equal Te—O_{ax} distances of 2.08 Å. For the ZnO polyhedron the Zn—O distance ($\bar{R}_{Zn-O}$) in the ZnO_4 tetrahedron is 1.98 Å.

In general, the RDF_{model} curves are of the type:

$$4\pi R^2\rho_{ij}(R) = \sum_k \frac{Z_{ij}(R_k)}{\sqrt{2\pi\sigma(R_k)}} \times \left(\frac{R}{R_k}\right)^2 \exp\left[-\frac{R-R_k}{2\sigma(R_k)}\right]^2, \quad (4)$$

where it is supposed that $\sigma(R) \sim \sqrt{R}$, i.e. the structural diffusion model[22] is valid. The coordination numbers of the kth coordination spheres of radius R_k were calculated on the basis of the α-TeO_2, ZnO and $Zn_2Te_3O_8$ crystal structures. Summing the RDF_{model} for α-TeO_2 and ZnO (presented in Fig. 3) in accordance with their molar ratio (80 : 20) we have obtained the additive RDF (curve 2) given in Fig. 4. Figure 4 also shows the RDF_{model} for $Zn_2Te_3O_8$ (curve 3). Since peak P1 is a result of the distribution of the Te—O and Zn—O distances of the first coordination sphere we could define the type and degree of deformation of the building units in the glass. Taking into account the location of the composition in the phase diagram,* according to the "level rule" it follows that, in the sub solidus region at temperatures below the eutectic temperature (596°C), there should coexist two solid phases, TeO_2 and $Zn_2Te_3O_8$. By summing the RDF_{model} of α-TeO_2 [Fig. 3 (curve 2)] and $Zn_2Te_3O_8$ [Fig. 4 (curve 3)] in a 5 : 1 ratio we have obtained the resultant RDF_{model} curve for the 80% TeO_2 + 20% ZnO glass given in Fig. 5.

The comparison of the RDF_{exp} with the RDF_{model} curves for the 80% TeO_2 + 20% ZnO glass, calculated in two ways, and with the model curve for $Zn_2Te_3O_8$, for R smaller than 3 Å, shows that the main structural units in the glass are similar to those in paratellurite plus zinc–tellurite and they are predominantly those of $Zn_2Te_3O_8$. The experimentally obtained coordination number value of Te atoms in the investigated glass is 3.35.

From the average values of the interatomic distances $\bar{R}_{Te-O}$ (1.99 Å) for α-TeO_2[21] and $\bar{R}_{Te(1)-O}$ = 1.97 Å, $\bar{R}_{Te(2)-O}$ = 2.05 Å and $\bar{R}_{Zn-O}$ = 2.19 Å in $Zn_2Te_3O_8$[23] we obtained for the theoretical position of P1 a value of 2.03 Å. This value is in good correlation with that experimentally obtained by us (2.02 Å for P1 from curve 1 in Fig. 4). This coincidence shows that the shortest interatomic distances are conserved and the glass network is built on the basis of paratellurite and zinc–tellurite cation–oxygen networks. This is a good confirmation of our previous results for TeO_2-rich compositions (located in the initial crystallization field for TeO_2) or located in the eutectic point region.[18,19,24,25] It was established that TeO_4 polyhedra in tellurite glasses exhibit a clear tendency towards deformation and mobility of one of the Te—O_{ax} bonds. Due to the lack of a center of symmetry in the polyhedron this axial bond can easily undergo an elongation to a value greater than 2.2 Å. In this case we assume that there is a 3+1 coordination state for the Te atom. An analogous stereochemical surrounding of the Te atom has also been reported for glasses in the TeO_2–B_2O_3 system.[26] Zemann[27] stated that the axial bond in the crystalline tellurites is not strictly defined and can vary from 2.08 to 2.98 Å. According to the literature[28,29] however, it can exceed the upper limit of 2.9 Å. For example, for $BaTeO_3$(II) Te(1) the fourth Te—O distance is 3.25 Å, while for $BaTeO_3$(II) Te(3) it is 3.40 Å. An extreme case of elongation of the fourth Te—O bond was reported for $K_2TeO_3 \cdot 3H_2O$,[30] possessing three Te—O distances of 1.85 Å and a fourth one of 3.87 Å. It is obvious that in this case we cannot speak about four-coordination of the Te atom, but rather should consider typical TeO_3 groups. It has been established[27] that the three shortest Te–O distances vary from 1.78 to 2.15 Å,[27,29] which shows a relatively unstable configuration. From this review, it is clear that there is no strongly defined cation–anion structure, the oxygen atoms lie at different distances, influenced by both internal and external factors.

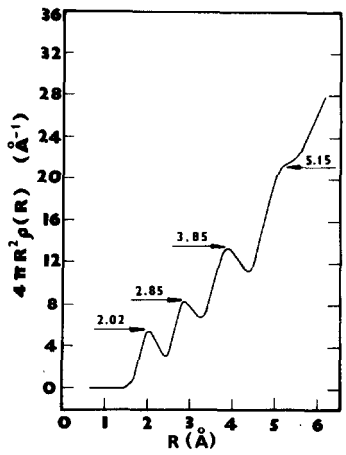


Fig. 5. RDF_{model} curve of a glass, obtained by summing up in 5 : 1 ratio curve 2 from Fig. 3 and curve 3 from Fig. 4.

On the basis of the discussion above and the data obtained for the coordination number of Te atoms, we may accept that there are approximately 35% of the Te atoms in the glass in the form of a TeO_4 configuration and 65% of the Te atoms in the form of

* Our composition choice is based on two concepts: (1) a correlation with the eutectic composition, where stable glasses of important practical use are synthesized; and (2) a comparison with glass structural data of other systems at the same molar ratio.

a TeO_{3+1} and/or a TeO_3 stereochemical surrounding. With the aid of this method a sharp boundary between these two states cannot be drawn.

While the position of the first coordination maximum in the RDF_{model} shows a good coincidence with the observed position in the glass, the RDF_{model} in the 2.5–4.5 Å region is essentially different from the experimental one. In particular, there is considerable disagreement in the interval 3.5–4.5 Å, in which the Te–Te, Te—second O, Zn—Zn and Zn—second O distances are located. Peak P2 is mainly due to the contribution of the O—O distances. While, for α-TeO_2, it is located at 2.83 Å, for the ZnO RDF_{model} P2 is observed at 3.35 Å. This great difference in the O—O distances of both basic polyhedra building the glass network leads to a broadening of the P2 maximum. This is established by the RDF_{exp} as well as by the RDF_{model} curves (see Fig. 4). The P2 in RDF_{exp} is observed at 2.9 Å. This elongation of distances is greater than 2.85 Å and the increase in the minimum between P2 and P3 (unresolved) is predominantly due to the O—O distances in the ZnO polyhedra (see Fig. 3). At the position of the expected minimum, the ZnO RDF curve has its maximum contribution. Due to these oppposite tendencies in the resultant RDF_{model} and RDF_{exp} curves, the minimum is smoothed over and even disappears; only a fluctuation in the region around 3.25 ± 0.4 Å remains in the RDF curves in Fig. 4.

In agreement with our previous results[18,19,24,25] there is also an unresolved peak, P3, which is mainly due to the Te—Te distribution. RDF_{exp} shows that the distances of approximately 3.9 Å are considerably changed. Te—Te, Te—Zn, O—second O and Te—second O are bonds with such distances. The broadening of peak P3 shows that it is one of the main structural characteristics of the glass transition.

What are the basic structural changes taking place at distances greater than 3.0 Å? Greater than this value there are many differences in number and specific influence on the RDF interatomic distances. It was established that the Te—Te distances are the most sensitive to the transition to the glassy state. This may be explained by the fact that the shortest Te—Te distance in α-TeO_2 is 3.76 Å. This long distance between the two heavy metal cations leads to an assumption that some weak metal bonds are present. A comparison[11,31,32] carried out of the bond energy (D_{R-R}) in some glass formers shows that it decreases in the sequence:

B_2O_3	P_2O_5	SiO_2	GeO_2	As_2O_3	TeO_2
R_k (Å)					
0.20	0.35	0.41	0.53	0.43	0.56
$\bar{R}_{R-O}$ (Å)					
1.26	1.52	1.55	1.63	1.80	1.99
D_{R-R} (kcal mol^{-1})					
—	51.3	42.2	37.6	32.1	33.0

It is established that the Te atoms have the greatest ion radius and the biggest mass, the highest value of average Te–O distance and the lowest Te—Te bond energy, near to that of As—As in As_2O_3. We should like to note here that, during the glass transition, the $\bar{R}_{Te-Te}$ of 3.80 Å between two tellurite–oxygen chains (see Fig. 6) is not preserved. This is due to the fact, that along the *c*-axis in paratellurite there are channels which are able to incorporate even the second-component polyhedra.*

Therefore the atomic arrangement in a zinc–tellurite glass can most accurately be described taking into account the preceding discussion, the analysis of the RDF_{exp} and RDF_{model} curves, as well as the structural building of paratellurite chains (Fig. 6) and the $Zn_2Te_3O_8$ crystal structure.† For a Te–Zn–O glass having an eutectic composition, we consider that the stereochemical structural model given in Fig. 7 is close to reality. It may be described as follows.

The experimentally established elongation of one $Te—O_{ax}$ bond in TeO_4 building units as well as the absence of a contribution to the RDF_{exp} of Te–Te, Te–Zn and O–second O pairs shows, that the connection between the two chains is weakened markedly. The RDF_{exp} [Fig. 4 (curve 1)] and the RDF_{model} [Fig. 4 (curve 3)] lead to the conclusion that both structures are similar. On the other hand, it is well known that in the $Zn_2Te_3O_8$ structure[13] $^1_\infty[Te(4)Te_2(3+1)O_8]$ chains are formed where, for one TeO_4 polyhedron, there are two TeO_3 trigonal pyramids. For the investigated glass, and on the basis of our calculations, only 35% of the Te atoms have TeO_4 surroundings. The connection between chains is accomplished by Zn atoms conventionally

* The existence of channels in tellurite minerals is well known. For example Mätzat[23] reports that for $\{(Zn,Fe)_2[TeO_3]_3\}Na_xH_{2-x} \cdot yH_2O$ there are channels 8.28 Å in diameter, while for Denningit mineral, according to Refs 33 and 34, a channel of diameter 4.97 Å is formed.

† According to Hanke,[13] in the compound $Zn_2Te_3O_8$ there are infinite chains formed, with two trigonal pyramids TeO_3 for one TeO_4E trigonal bipyramid. The central Te atom has a coordination number of 3+1 or 3 since the fourth oxygen atom is shared by the next TeO_3 pyramid at a distance of 2.41 Å. Chains are isolated from each other (R_{min} = 2.72 Å). The bond between them is formed by Zn atoms of 4+1+1 oxygen coordination: the greatest Zn—O distance is equal to 2.47 Å.

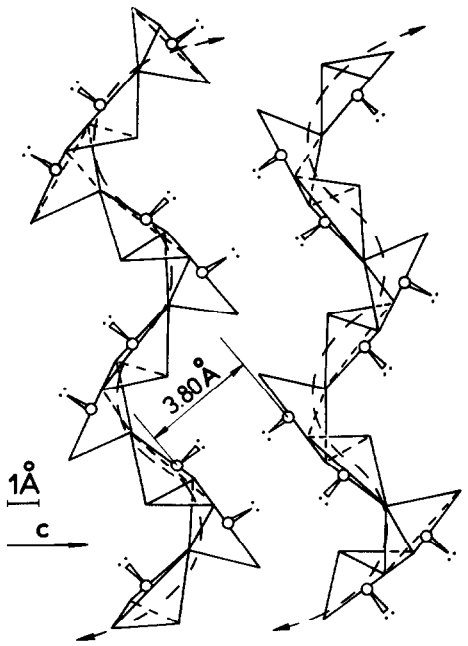


Fig. 6. Illustration of two Te–O chains in paratellurite (*c*-axis).

coordinated 4 + 1 + 1. Figure 7 illustrates the atomic arrangement nature of a zinc–tellurite glass with an eutectic composition. Parts of ZnO_{4+1+1} polyhedra are incorporated into and between the $^{1}_{\infty}[TeO_4 \cdot TeO_3]$ chains. In the bridging area, chains

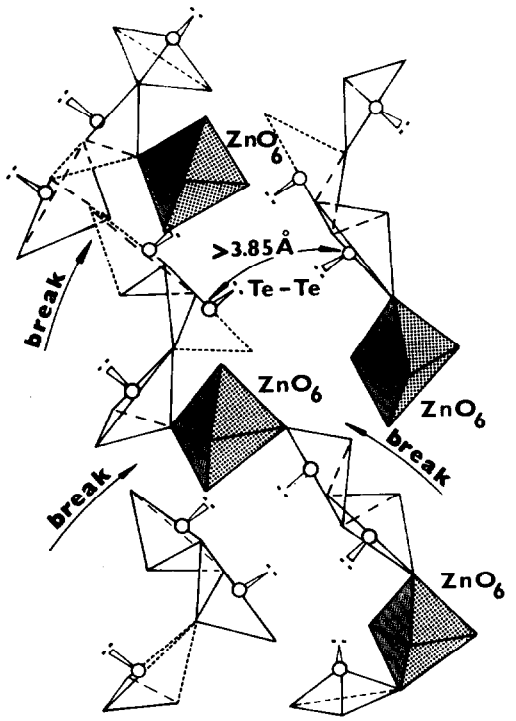
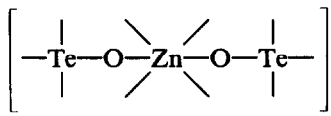


Fig. 7. Model illustrating the nature of the atomic arrangement in the investigated glass.

are weakly connected by



chains. Such a connection shows that it is probable that a number of ZnO_{4+1+1} polyhedra take site positions.

CONCLUSIONS

(1) It has been proved that there are no essential changes in TeO_4, TeO_3 and ZnO_6 polyhedra in the glass because the average value of the interatomic Te—O and Zn—O distances is preserved. It has been established that the O–O pairs in the glass at different distances greater than 2.2 Å are fixed. This causes an increase in the asymmetry of the TeO_4, TeO_{3+1} and ZnO_{4+1+1} polyhedra.

(2) The oxygen network of the glass is built of atoms at a mean distance, $\bar{R}_{O-O}$ of 2.95 Å. This value is close to the $\bar{R}_{O-O}$ of 2.85 Å for α-TeO_2. Such a small difference in the average values is probably due to the strong influence of the O—O distances in ZnO_{4+1+1} polyhedra.

(3) It has been experimentally proved that the average coordination number of the Te atoms is 3.35. Therefore it follows that approximately 35% of the Te atoms are in a TeO_4E trigonal bipyramidal surrounding and 65% of the Te atoms have a lower coordination number.

(4) It has been confirmed that the Te–Te, Te–second O and O–second O pairs in the region of 3.9 Å do not contribute significantly to the RDF_{exp}. Distances in this region are greatly changed in the glassy state and it can be accepted that they have a definitive contribution in the amorphization of tellurite melts. It is assumed that there are weak cation bonds of the Te—Te and Te—Zn type (via oxygen atoms) in the glass, connecting the different chains.

(5) The proposed model attempts to present stereochemically the atomic arrangement of the studied zinc–tellurite glass and to explain it in terms of short-range order.

Acknowlegement—We are heartily thankful to Dr V. Plahtii from the Institute of Nuclear Physics, Leningrad, for enabling us to carry out the neutron diffraction measurements.

REFERENCES

1. M. Redman and J. Chen, *J. Am. Ceram. Soc.* 1967, **50**, 523.
2. W. Vogel, H. Bürger, F. Foiger, R. Ochrling, G. Winterstein, H. Rateenberger and Ch. Ludwig, *Silikattechnik* 1974, **25**, 206.

3. H. Bürger, K. Fink, W. Vogel, V. Kozhukharov and M. Marinov, *Glastechn. Ber.* 1985, **58**, 211.
4. M. Marinov, V. Kozhukharov and I. Gugov, *Glastechn. Ber. Sonderband L* 1983, **56**, 839.
5. A. Yakhkind and S. Chebotarev, *Fiz.-Khim. Stekla* 1980, **6**, 485.
6. *Ibid.* 1980, **6**, 164.
7. *Ibid.* 1984, **10**, 311.
8. W. Vogel, *Glas-chemie.* VEB Deutscher Verlag für Grundstoffindustrie, Leipzig (1979).
9. A. Yakhkind, *J. Am. Ceram. Soc.* 1966, **49**, 670.
10. M. Imaoka and T. Yamazaky, *J. Ceram. Assoc. Jpn* 1968, **76**, 160.
11. H. Bürger, W. Vogel and V. Kozhukharov, *Infrared Phys.* 1985, **25**, 395.
12. M. Marinov and V. Kozhukharov, *C. R. Acad. Bulg. Sci.* 1972, **25**, 329.
13. K. Hanke, *Naturwissenschaften* 1966, **53**, 273.
14. *Ibid.* 1967, **54**, 199.
15. A. Skrishevkii, *Struktornoi Analiz Zhidkostei (Vishaya Shkola)* 1971, 107.
16. A. Blech and B. Averbach, *Phys. Rev.* 1965, **137**, A1113.
17. E. Lorch, *J. Phys. C* 1969, **9**, 229.
18. S. Neov, I. Gerasimova, V. Kozhukharov and M. Marinov, *J. Mater. Sci.* 1980, **15**, 1153.
19. S. Neov, V. Kozhukharov, I. Gerasimova, K. Krezhov and B. Sidzhimov, *J. Phys. C* 1979, **12**, 2475.
20. A. Wright, C. Cornell and J. Allen, *J. Non-Cryst. Sol.* 1980, **42**, 69.
21. O. Lindqvist, *Acta Chem. Scand.* 1961, **21**, 1473.
22. G. Prins, *Naturwissenschaften* 1931, **19**, 435.
23. E. Mätzat, *Tschermaks Mineral Petrogr. Mitt. Sonderdruk Bd.XII, H-1*, 1967, 108.
24. S. Neov, I. Gerasimova, K. Krezhov, B. Sidzhimov and V. Kozhukharov, *Phys. Status Solidi A* 1978, **47**, 743.
25. V. Kozhukharov, S. Neov, I. Gerasimova and P. Mikula, *J. Mater. Sci.* (in press),
26. H. Bürger, W. Vogel, V. Kozhukharov and M. Marinov, *J. Mater. Sci.* 1984, **19**, 403.
27. J. Zemann, *Monatsh. Chem.* 1971, **102**, 1209.
28. M. Kocak, C. Platte and M. Trömel, *Z. Anorg. Allg. Chem.* 1979, **453**, 93.
29. M. Trömel, private communication (1978).
30. G. Johansson and O. Lindgvist, *Acta Cryst.* 1978, **B34**, 2959.
31. L. Pauling, *The Nature of the Chemical Bond*, 3rd Edition, pp. 82, 505, 514 and 532. Cornell University Press, Ithaca, NY (1960).
32. D. Beeman, R. Lyndson and M. Anderson, *J. Non-Cryst. Sol.* 1980, **42**, 61.
33. E. Walitzi, *Naturwissenschaften* 1964, **51**, 334.
34. E. Walitzi, *Tschermaks Mineral. Petrogr. Mitt.* 1965, **10**, 16.

Polyhedron Vol. 5, No. 3, pp. 779–785, 1986
Printed in Great Britain

0277–5387/86 $3.00 + .00
© 1986 Pergamon Press Ltd

SOLID-STATE ^{27}Al NMR STUDIES ON POLYCRYSTALLINE ALUMINATES OF THE SYSTEM CaO–Al_2O_3

D. MÜLLER* and W. GESSNER

Central Institute of Inorganic Chemistry, Academy of Sciences of the G.D.R., DDR-1199 Berlin-Adlershof, G.D.R.

A. SAMOSON and E. LIPPMAA

Institute of Chemical Physics and Biophysics of the Estonian Academy of Sciences, Tallinn 200001, U.S.S.R.

and

G. SCHELER

Department of Physics of the Friedrich Schiller University, DDR-6900 Jena, G.D.R.

(*Received* 19 *June* 1985; *accepted* 31 *July* 1985)

Abstract—^{27}Al NMR isotropic chemical-shift and quadrupole-coupling data have been determined for a series of polycrystalline calcium aluminates with varying CaO/Al_2O_3 ratios. The data were derived from static and magic-angle spinning NMR spectra recorded at different magnetic field strengths up to 11.7 T. The chemical-shift and quadrupole-coupling data are discussed with regard to the crystal structure of the compounds studied. It is shown that structural effects are reflected more sensitively in the quadrupole-coupling data than in the chemical shifts. In favourable cases crystallographically different Al sites could be resolved in the NMR spectra.

^{27}Al NMR can provide structural information about the environment of the Al nuclei in polycrystalline and amorphous samples using either quadrupole-coupling data or chemical shifts. In the first case, the quadrupole moment of the Al nucleus is used as a sensitive probe for the electric field gradient (EFG) at the nuclear site. In the second case, the magnetic shielding of the aluminium by its electronic environment is investigated. Recent studies[1–3] have shown that, by employing magic-angle spinning (MAS) techniques at high magnetic fields, the second method proved to be a powerful tool for the determination of the coordination state of Al–O polyhedra. Subsequently this new method has been applied to structural studies of numerous inorganic materials including zeolites (see Ref. 4 and references cited therein), glasses,[5–7] cements,[8] clay minerals and layer silicates.[9–11]

The spread of chemical-shift values for AlO_4 tetrahedra reflects, beyond the Al coordination with oxygen atoms, more subtle influences on the Al shielding. Such influences are, for example, effects of neighbouring atoms in the second coordination sphere, cation effects and influences of the lattice geometry such as bond angles and distances.[12] For the detection of these subtle structural influences on the Al shielding a very precise determination of the chemical-shift values is necessary. Al as a quadrupolar nucleus, however, gives rise to particular experimental difficulties with regard to a determination of the actual chemical-shift values. In evaluating MAS NMR spectra of quadrupolar nuclei with non-integral spin, quadrupole-induced shift effects[13] have to be eliminated. This has been performed by means of combined high- and low-field ^{27}Al NMR measurements in the case of $LiAlO_2$ polymorphs.[14]

In the present work we extended our systematic studies of ^{27}Al chemical shifts and EFGs at the Al

* Author to whom correspondence should be addressed.

sites to a series of calcium aluminates with varying CaO/Al_2O_3 ratios. For them MAS NMR spectra and spectra of the static samples were recorded at different magnetic fields (up to the highest commercially available magnetic field strength of 11.7 T). The $CaO–Al_2O_3$ system has been extensively characterized crystallographically as well as thermodynamically.[15] De Jong *et al.*[16] have recently discussed the connectivity of the AlO_4 tetrahedra in this system. In some of these structures Al occurs at different Al sites. The present study also aims to show to what extent those different Al sites can be resolved in the ^{27}Al NMR spectra.

EXPERIMENTAL

^{27}Al NMR spectra were recorded at 1.4, 6.4, 8.45 and 11.7 T. The measurements were carried out on a Bruker-Physik CXP-200 equipped with a 8.45-T magnet (^{27}Al frequency 93.8 MHz) and on a Bruker-Physik AM 500 (11.7 T, 130.3 MHz) high-resolution NMR spectrometer (Tallinn). The measurements at 6.4 T (^{27}Al frequency 70.4 MHz) were made on a FKS 176 solid-state high-resolution NMR spectrometer (Jena). All high-field ^{27}Al NMR spectra were recorded both with static samples and with rapid MAS techniques (spinning rates 3–7 kHz). Whereas for the MAS NMR spectra usually between 100 and 1000 free induction decays (FIDs) with 1-s time intervals were accumulated, for the static spectra at lower frequencies up to 10,000 FIDs with 0.1-s time intervals were accumulated. Radio-frequency pulses of 1–2 μs duration were applied. In addition, in some cases, conventional low-field ^{27}Al NMR measurements were carried out on a wide-line NMR spectrometer at 16 MHz, recording the first derivative of the spectra. Quadrupole-coupling constants (e^2qQ/h) and asymmetry parameters (η) of the EFG at the Al sites were determined from computer simulation of the static spectra and/or the MAS NMR spectra using least-squares fitting procedures.

Chemical shifts [δ (ppm)] measured relative to an external standard of aqueous $AlCl_3$ solution are denoted by a positive sign for low-field shifts. The actual chemical-shift values (considering quadrupole-induced shift effects[13]) were obtained by different methods:

(i) directly from the fitted MAS spectra;
(ii) from the spinning sidebands of the satellite transitions;[17]
(iii) by adding a correction term which considers quadrupole-induced shifts to the experimental, field-dependent, apparent chemical-shift value of the MAS spectrum;[12,14]
(iv) from the fitted static spectrum; and
(v) from the extrapolation of the field-dependent apparent chemical shift.

In most cases satisfactory agreement was achieved with the different methods. It is clear that, for a determination of e^2qQ/h and η static low-field spectra are to be preferred, whereas most accurate chemical shifts are obtained from the MAS NMR spectra at highest fields. The resulting errors of the derived values are included in Table 1.

The samples under investigation were prepared by standard procedures and checked by X-ray powder diffraction.

RESULTS AND DISCUSSION

Table 1 contains the derived ^{27}Al chemical-shift values and quadrupole-coupling data for compounds of the $CaO–Al_2O_3$ system. The compounds in Table 1 are arranged in order of increasing CaO/Al_2O_3 ratio. The NMR data were obtained from the static and MAS NMR spectra recorded at magnetic field strengths of between 1.4 and 11.7 T. Table 1 also includes some structural data of the crystallographically different Al sites (coordination number and Al—O bond lengths).

The $CaO–Al_2O_3$ system starts with the compound $CaO \cdot 6Al_2O_3$ (CA_6).* According to Kato and Saalfeld[18] the structure of CA_6 contains five crystallographically different Al sites, namely three types of octahedral Al, a tetrahedral Al and a pentacoordinated Al. In the highfield ^{27}Al MAS NMR spectra of CA_6 three of the five types of Al sites can be detected separately. Figure 1 shows the static and the MAS NMR spectrum of CA_6 at 130.3 MHz. In addition to the signal of tetrahedral Al at 65 ppm, the spectrum exhibits two resolved signals due to octahedral Al at 9 and 16 ppm. Whereas the position of the signal at 16 ppm is nearly field-independent, the former, more intense signal is shifted to 7.5 ppm at 70.4 MHz, which is due to the above-mentioned quadrupole-induced shifts. Therefore this signal must be attributed to the more strongly distorted AlO_6 octahedra. Accordingly the signal at 9 ppm is assigned to the 12 AlO_6 octahedra per unit cell with noticeably varying Al—O distances of between 1.818 and 1.995 Å.[18] Correspondingly the signal at 16 ppm is assigned to the remaining six octahedral Al(3) and Al(4) atoms with identical and nearly identical Al—O distances, respectively. Comparison of the observed intensities of the NMR signals (about 2 : 1) confirms the assignment.

* $CaO \triangleq C$; $Al_2O_3 \triangleq A$; $H_2O \triangleq H$.

Table 1. ^{27}Al NMR chemical-shift and quadrupole-coupling data of the different Al–O polyhedra in the $CaO–Al_2O_3$ system

Compound	Al site[a]	Al—O distance (Å)	Reference	e^2qQ/h (MHz)	η	Chemical shift (ppm)
CA_6	$12\times Al(1)^{oct}$	1.995 1.818 1.970 1.860	18	$\sim 1.5\pm0.3$[b]	(0)	9 ± 0.3[b]
	$4\times Al(2)^{oct}$	1.865 1.896		<1[b]	(0)	16 ± 0.3[b]
	$2\times Al(3)^{oct}$	1.883				
	$4\times Al(4)$	1.801 1.828		2.0 ± 0.3[b]	(0)	65 ± 0.3[b]
	$2\times Al(5)^{pent}$	2.187 1.839			Not detected	
CA_2	Al(1)	1.751 1.751 1.813[c] 1.799[c]	21	6.7 ± 0.2[de]	0.8 ± 0.1[de]	78 ± 1[ef]
	Al(2)	1.745 1.761 1.714 1.768[c]		13 ± 1[d]	0.1 ± 0.1[d]	60 ± 20[d]
CA	Al(1)	1.763 1.769 1.731 1.752	23	2.7 ± 0.2[d]	0.85 ± 0.05[d]	80.5 ± 0.5[ef]
	⋮	⋮				83.3 ± 0.5[ef]
	Al(6)	1.753 1.759 1.756 1.751				
C_4A_3	Al(1)	1.75	25	2.4 ± 0.1[d]	0.95 ± 0.05[d]	80.3 ± 1[f]
C_5A_3	Al(1)	1.766 1.727 1.810 1.747	26		Not measured	
	⋮	⋮				
	Al(4)	1.778 1.764 1.786 1.735				
$C_{12}A_7$	$4\times Al(1)$	3×1.73 1×1.75	27	11 ± 1[d]	0.2 ± 0.1[d]	85 ± 8[d]
	$3\times Al(2)$	4×1.73		3.7 ± 0.2[d]	0.9 ± 0.1[d]	79 ± 1[f]
C_3A	Al(1)	1.741 1.768 1.766 1.729	28	9.7 ± 0.3[de]	0.3 ± 0.1[de]	85 ± 3[e]
	Al(2)	1.749 1.764 1.748 1.757				

[a] Tetrahedral Al sites if not denoted otherwise.
[b] Value estimated from the field-dependent quadrupole-induced shift in the MAS spectra.
[c] Al—O distance to tri-coordinated oxygen atom.
[d] Value determined from the fitted static spectrum.
[e] Value determined from the fitted MAS spectrum.
[f] Value derived from the spinning sidebands of the satellite transition.[17]

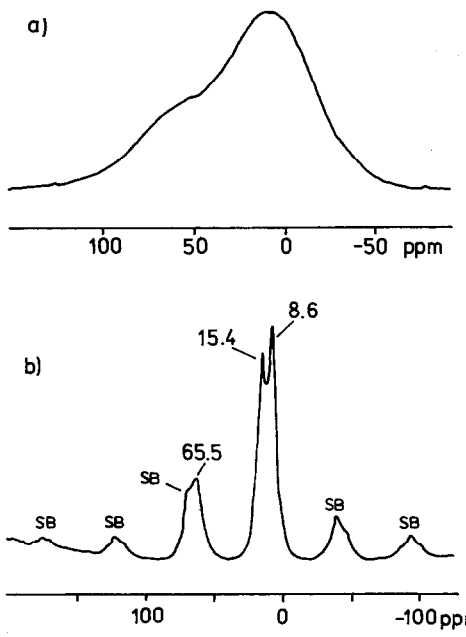


Fig. 1. ^{27}Al NMR spectra at 130.3 MHz of CA_6. (a) Static spectrum and (b) MAS spectrum; spinning sidebands (SB) are marked.

Because of the superposition of the NMR signals it was not possible to derive the e^2qQ/h and η values for the individual structural units directly from the static spectrum. Estimations of e^2qQ/h were made from the field-dependent quadrupole-induced shifts of the signals in the MAS NMR spectra (assuming $\eta = 0$).

A separate signal of the Al atoms at pentahedral sites, which should amount for 8% of the total intensity, could not be detected by NMR spectroscopy. This is obviously due to a strong quadrupolar broadening. Likewise, in the NMR spectrum of the corresponding barium aluminate, BA_6,[19] signals occur only for tetrahedral Al (at 71 ppm) and octahedral Al (at 9 ppm). A splitting of the latter signal is not observed in the NMR spectrum of BA_6.

It should be noted that the relatively low chemical-shift value for the tetrahedral Al in CA_6 correlates with the lengthened Al—O distance. We confirmed[19] this relationship in a series of compounds with related structural units.

Interpretation of recent Al-K_α measurements[20] of CA_6 which are discussed in terms of dominant penta-coordinated Al and hexa-coordinated Al (no tetrahedral Al), contrasts with the above-mentioned structure of CA_6 and with our NMR results. Apparently, this method is less favourable for the determination of the coordination state of Al in materials with mixed AlO_n polyhedra.

On increasing the CaO/Al_2O_3 ratio the next representative of the CaO–Al_2O_3 system is $CaO \cdot 2Al_2O_3$ (CA_2). The structure of CA_2 contains two types of fully condensed AlO_4 tetrahedra which share one or two, respectively, of the bridging oxygen atoms with two other tetrahedra forming so-called "triclusters".[21] It is plausible that this peculiarity of the connection of the tetrahedra, i.e. the existence of such tri-coordinated oxygen atoms adjacent to the usual bridging oxygen atoms, leads to anisotropic charge distributions at the Al sites and should produce large EFGs. Indeed, the NMR spectrum of the static sample at 70.4 MHz shows two broad, superimposed signals [see Fig. 2(a)]. The corresponding NMR spectra recorded at 93.83 and 130.3 MHz show the theoretical field dependence expected for quadrupolar lines in second-order perturbation theory. Large e^2qQ/h of 6.7 MHz with $\eta = 0.8$ and of 13 MHz with $\eta = 0$, respectively, were obtained from the computer fit of the superimposed static spectrum. According to the zero η which corresponds to axial symmetry of the EFG, we assign the latter broad signal to such AlO_4 tetrahedra having only one tri-coordinated oxygen atom. Subsequently the narrower signal is assigned to the other type of AlO_4 tetrahedra having two oxygen atoms of this type (non-axial symmetry). It should be noted that the intensity of the broad signal only amounts for about 50% of the expected value. This is probably

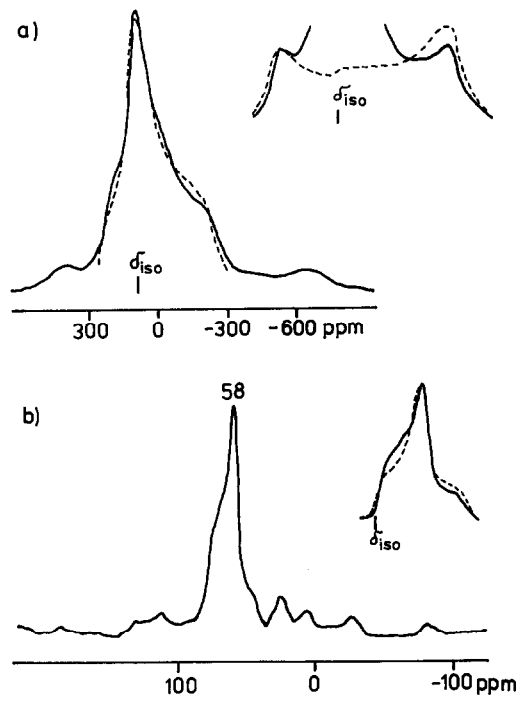


Fig. 2. ^{27}Al NMR spectra of CA_2. (a) Static spectrum at 70.4 MHz. On the right the broad component of the spectrum is shown vertically expanded. (b) MAS spectrum at 130.3 MHz [(– – –) fitted lineshape; the resulting locations of δ_{iso} are marked].

due to the fundamental difficulties in the detection of very broad lines by pulsed NMR techniques. In this connection the size of the e^2qQ/h derived for the AlO_4 tetrahedra in CA_2 is interesting since the values give an idea of the quadrupole line broadening of such "triclusters" which are also discussed as possible structural units in glasses.[7,22] The ^{27}Al MAS NMR spectrum at 130.3 MHz of CA_2 [see Fig. 2(b)] only shows the narrowed line of the AlO_4 tetrahedra with nonaxial symmetry together with spinning sidebands of the satellite transitions. The computer simulation of the MAS NMR spectrum confirms the quadrupole-coupling data derived from the static spectrum and provides a chemical-shift value of 78 ppm for this type of AlO_4 tetrahedra. For the other AlO_4 tetrahedra only a rough value of 60 ± 20 ppm can be estimated from the simulation of the broad component of the static spectrum.

At a CaO/Al_2O_3 ratio of 1.0 the compound $CaO \cdot Al_2O_3$ (CA) occurs. According to Hörkner and Müller-Buschbaum[23] the structure of CA consists of six-rings of AlO_4 tetrahedra forming two-dimensional infinite sheets. There are six different AlO_4 tetrahedra which differ only slightly in their Al—O distances.

The derivative ^{27}Al NMR spectrum at 16 MHz of the static CA sample could satisfactorily be simulated by assuming only one set of e^2qQ/h and η values.[24] This is not surprising with regard to the similarity of the geometry of the six AlO_4 tetrahedra. At higher measuring frequencies, however, shoulders appear in the MAS NMR spectra which indicate the existence of more than one signal with different chemical shifts. The MAS NMR spectrum at 130.3 MHz is shown in Fig. 3. From analysis of the spinning sidebands of the satellite transitions which are distinctly split into two peaks, chemical-shift values of 80.5 and 83.3 ppm are determined. Using these chemical-shift values and the common quadrupole-coupling data derived at low field, the MAS NMR spectrum was simulated by a superposition of two lines. As shown in Fig. 3(b), a satisfactory agreement with the experimental spectrum was achieved. As a possible reason for the two different chemical shifts the variation of the mean Al—O—Al angles (between 121 and 124°) can be discussed. However, an assignment of the two signals to distinct Al sites in the structure is not accomplished.

In the compound $4CaO \cdot 3Al_2O_3$ (C_4A_3), a sodalith-like phase, there is only one type of AlO_4 tetrahedra which form a cubooctahedron.[25] As expected the MAS NMR spectrum of C_4A_3 (not shown) exhibits only one sharp signal at 79 ppm. Compared to C_4A_3, the corresponding hydrate phase $C_4A_3H_3$ contains two kinds of AlO_4

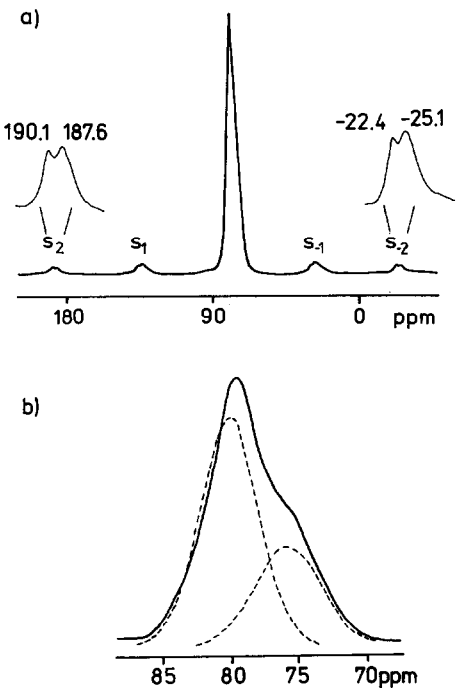


Fig. 3. ^{27}Al MAS NMR spectrum at 130.3 MHz of CA. (a) Total MAS spectrum; the second spinning sidebands of the neighboured satellite transition are shown expanded. (b) Central line of the MAS spectrum; the two signals resulting from the line separation (see text) are indicated by hatched lines.

tetrahedra, regular and distorted. Because of their different quadrupole-coupling constants the two Al sites can be resolved in the MAS NMR spectrum.[19]

At a CaO/Al_2O_3 ratio of 1.67 the compound $5CaO \cdot 3Al_2O_3$ (C_5A_3) with a structure of twisted sheets of distorted AlO_4 tetrahedra is known.[26] Unfortunately, all the samples available to us contained considerable amounts of CA. Therefore we must exclude this phase from our considerations.

The next compound to be discussed is $12CaO \cdot 7Al_2O_3$ ($C_{12}A_7$) at a CaO/Al_2O_3 ratio of 1.7. According to Bartl and Scheller[27] this compound can be formulated as

$$Ca_{12}[AlO_2]_6[AlO_{2.5}]_8.$$

In addition to the tetrahedral Al in completely connected $[AlO_2]^-$ groups, $C_{12}A_7$ also contains AlO_4 tetrahedra with one non-bridging oxygen atom (usually denoted as Q^3 groups). Correspondingly the static NMR spectra at 70.4, 93.8 and 130.3 MHz show in each case a superposition of a sharp and an extremely broad line. (Both lines show the theoretical dependence on the magnetic field.) For example, the MAS NMR spectrum at 70.4 MHz is shown in Fig. 4. From the simulation of the superimposed spectra a large

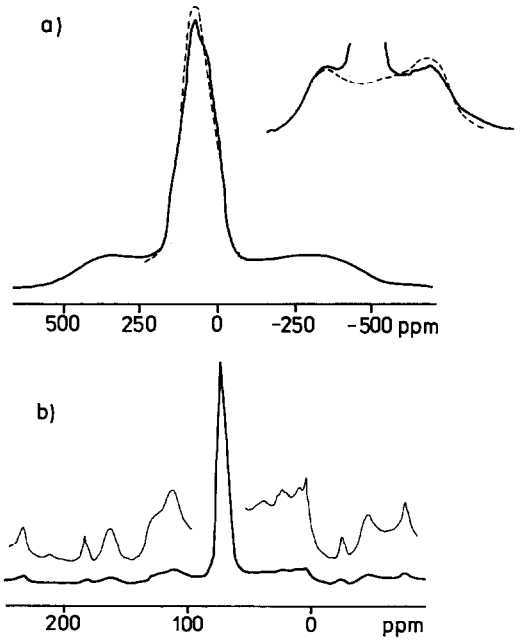


Fig. 4. ^{27}Al NMR spectra of $C_{12}A_7$. (a) Static spectrum at 70.4 MHz. On the right the vertical expansion of the broad component of the spectrum is shown [(– – –) fitted lineshape]. (b) MAS spectrum at 130.3 MHz. In addition the amplified spinning sidebands are shown.

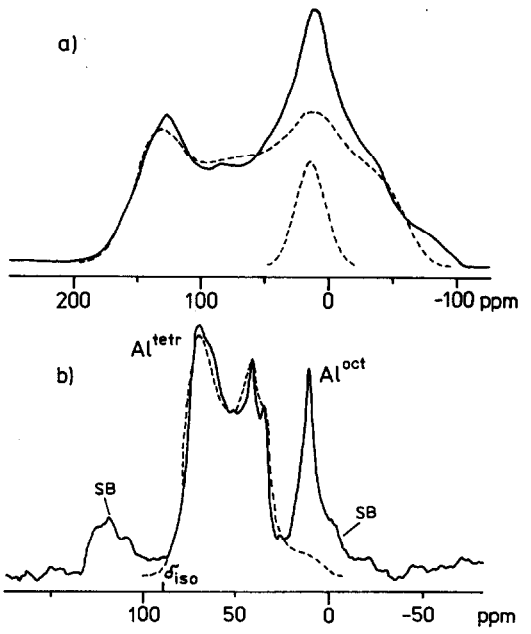


Fig. 5. ^{27}Al NMR spectra at 130.3 MHz of C_3A. (a) Static spectrum, and (b) MAS spectrum [(– – –) fitted lineshape]. The signal near 10 ppm is due to octahedral Al and indicates a partial hydration of the sample.

e^2qQ/h value of 11 MHz and a zero η (axial symmetry of the EFG tensor) results for the broad signal which is therefore assigned to the Q^3 group.

In this connection the size of the large EFG of these AlO_4 branching groups has to be emphasized. The distortion of these tetrahedra are also reflected in the shorter Al—O distance of the single terminal oxygen atom compared with the other Al—O distances of 1.78 Å.[27]

For the undistorted AlO_4 tetrahedra of $C_{12}A_7$ a chemical shift value of 79 ppm was determined from the MAS NMR spectrum at 130.3 MHz. Unfortunately, under our experimental conditions no separate line due to the Q^3 groups was observed in the MAS NMR spectrum. Therefore for the latter groups only a rough value of 85 ± 8 ppm could be estimated from the computer simulation of the corresponding static spectrum.

The last compound of the $CaO–Al_2O_3$ system is $3CaO \cdot Al_2O_3$ (C_3A) at a CaO/Al_2O_3 ratio of 3.0. In the structure of C_3A[28] there are two types of Al atoms which are arranged in six-membered rings of AlO_4 tetrahedra (Q^2 group). The NMR spectrum of the static C_3A sample is shown in Fig. 5(a). An e^2qQ/h of 9.6 MHz and an η of 0.3 result from the computer simulation of the spectrum. The derived data represent mean values for both types of AlO_4 tetrahedra which do not markedly differ in their interatomic distance bond angles.[28]

The deviation of the simulated spectrum at its peak near 10 ppm suggests a partial hydration of the C_3A sample. This suggestion is confirmed by the MAS NMR spectrum which shows, in addition to the signal of the AlO_4 groups, a sharp peak at 10 ppm obviously due to regular AlO_6 groups. The spectrum of another well-dried sample at 70.4 MHz did not show any additional signal of octahedral Al. From the simulation of the MAS NMR spectrum of C_3A at 130.3 MHz [Fig. 5(b)] a chemical-shift value of 85 ppm can be derived for the groups of the six-membered rings of AlO_4 tetrahedra. This value is in good agreement with the value determined from the simulation of the static spectrum.

CONCLUSIONS

Apart from the known influence of the coordination state of aluminium, other structural factors such as interatomic distances and bond angles cause only weak changes in the ^{27}Al chemical-shift values in the calcium aluminates studied. So, for example, only slight variations in the chemical-shift values are observed between the various AlO_4 tetrahedra with different numbers of bridging oxygen atoms. A systematic study of such condensation effects of the AlO_4 tetrahedra, which also includes the measurement of other selected

aluminates and aluminate hydrates, is given elsewhere.[19]

Compared to the chemical shift structural effects are reflected more sensitively in the e^2qQ/h and η. Therefore resolved NMR spectra were only obtained in such cases where the crystallographically different Al sites also have clearly differing EFGs.

REFERENCES

1. D. Müller, W. Gessner, H.-J. Behrens and G. Scheler, *Chem. Phys. Lett.* 1981, **79**, 59.
2. V. M. Mastikhin, O. P. Krivoruchko, B. P. Zolotovskii and R. A. Buyanov, *React. Kinet. Catal. Lett.* 1981, **18**, 117.
3. D. Freude and H.-J. Behrens, *Cryst. Res. Technol.* 1981, **16**, K36.
4. J. Klinowski, *Prog. Nucl. Magn. Reson. Spectrosc.* 1984, **16**, 237.
5. E. Hallas, U. Haubenreisser, M. Hähnert and D. Müller, *Glastech. Ber.* 1983, **56**, 63.
6. D. Müller, G. Berger, I. Grunze, G. Ladwig, E. Hallas and U. Haubenreisser, *Phys. Chem. Glasses* 1983, **24**, 37.
7. G. Engelhardt, M. Nofz, K. Forkel, F.-G. Wihsmann, M. Mägi and E. Lippmaa, *Phys. Chem. Glasses* 1985, **26**, 157.
8. D. Müller, A. Rettel, W. Gessner and G. Scheler, *J. Magn. Reson.* 1984, **57**, 152.
9. N. C. M. Alma, R. G. Hays, A. Samoson and E. Lippmaa, *Anal. Chem.* 1984, **56**, 729.
10. J. Sanz and J. M. Serratosa, *J. Am. Chem. Soc.* 1984, **106**, 4790.
11. J. G. Thompson, *Clay Miner.* 1984, **19**, 229.
12. D. Müller, E. Jahn, G. Ladwig and U. Haubenreisser, *Chem. Phys. Lett.* 1984, **109**, 332.
13. E. Kundla, A. Samoson and E. Lippmaa, *Chem. Phys. Lett.* 1981, **83**, 229; S. Ganapathy, S. Schramm and E. Oldfield, *J. Chem. Phys.* 1982, **77**, 4360; H.-J. Behrens and B. Schnabel, *Physica* 1982, **114B**, 185; D. Müller, *Ann. Phys. (Leipzig)* 1983, **39**, 451.
14. D. Müller, W. Gessner and G. Scheler, *Polyhedron* 1983, **2**, 1195.
15. M. Allibert, C. Chantillou, K. T. Jacob and R. Lourtou, *J. Am. Chem. Soc.* 1981, **64**, 307; I. Eliezer, N. Eliezer, R. E. Howard and P. Viswanadham, *J. Phys. Chem.* 1981, **85**, 2835.
16. B. H. W. S. De Jong, C. M. Schramm and V. E. Parziale, *Geochim. Cosmochim. Acta* 1983, **47**, 1223.
17. A. Samoson, Thesis, Estonian Academy of Sciences, Tallinn (1984).
18. K. Kato and H. Saalfeld, *Neues Jahrb. Mineral. Abh.* 1968, **109**, 192.
19. D. Müller, W. Gessner, A. Samoson, E. Lippmaa and G. Scheler, submitted to *J. Chem. Soc., Dalton Trans.*
20. Y. Z. Bai, S. Fukushima and Y. Gohshi, *Yogyo Kyokai-Shi* 1984, **92**, 475.
21. V. I. Ponomarev, D. M. Kheiker and N. V. Belov, *Kristallografiya (USSR)* 1970, **15**, 1140.
22. E. D. Lacy, *Phys. Chem. Glasses* 1963, **4**, 234.
23. W. Hörkner and Hk. Müller-Buschbaum, *J. Inorg. Nucl. Chem.* 1976, **38**, 983.
24. D. Müller, W. Gessner and A.-R. Grimmer, *Z. Chem.* 1977, **17**, 453.
25. V. I. Ponomarev, D. M. Kheiker and N. V. Belov, *Kristallografiya* 1970, **15**, 918.
26. M. G. Vincent and J. W. Jeffery, *Acta Cryst.* 1978, **B34**, 1422.
27. H. Bartl and T. Scheller, *Neues Jahrb. Mineral. Monatsh.* 1970, 547.
28. P. Mondal and J. W. Jeffery, *Acta Cryst.* 1975, **B31**, 689.

Polyhedron Vol. 5, No. 3, pp. 787–789, 1986
Printed in Great Britain

0277–5387/86 $3.00 + .00
© 1986 Pergamon Press Ltd

PREPARATION AND CRYSTAL DATA OF THE SPINEL SERIES $Co_{1+2s}Cr_{2-3s}Sb_sO_4$ $(0 \leqslant s \leqslant \frac{2}{3})$

P. GARCÍA CASADO

Facultad de Farmacia, Universidad de Navarra, E-31080 Pamplona, Spain

and

I. RASINES*

Instituto Elhúyar, Serrano 113, E-28006 Madrid, Spain

(*Received* 15 *April* 1985; *accepted after revision* 31 *July* 1985)

Abstract—Eight polycrystalline materials of the new spinel series $Co_{1+2s}Cr_{2-3s}Sb_sO_4$ ($s = 0$, 0.10 ... 0.60 or 0.67) have been prepared and studied by X-ray powder diffraction. The series goes from $CoCr_2O_4$ ($s = 0$) to $Co_{7/3}Sb_{2/3}O_4$ ($s = \frac{2}{3}$), with a gradually increasing from 8,3346(3) ($s = 0$) to 8.5330(6) Å ($s = \frac{2}{3}$), and u slightly decreasing from 0.261 ($s = 0$) to 0.258 ($s = \frac{2}{3}$). Interatomic distances are given. The series may be thought as the result of progressive substitution of Cr^{3+} by $\frac{2}{3}Co^{2+} + \frac{1}{3}Sb^{5+}$ in the normal spinel $CoCr_2O_4$. This substitution can be total, so that $CoCr_2O_4$ *becomes* $Co_{7/3}Sb_{2/3}O_4$.

Recently the authors have suggested[1,2] that an oxide spinel constituted by three equal or different metals, M, M′ and M″, in oxidation states m, m' and m'', can be a member of the series $M_sM'_dM''_cO_4$, where $d = (8-3m''-ms+m''s)/(m'-m'')$ and $e = (3m'-8+ms-m's)/(m'-m'')$, s, d and e being positive. This suggestion has been confirmed for the series $Co_{3-s}Al_sO_4$ ($0 \leqslant s \leqslant 2$),[1] and $Mn_{1+s}Cr_{2-3s}Sb_sO_4$ ($0.05 \leqslant s \leqslant 0.30$).[2] This second series may be conceived of as the result of partial substitution of Cr^{3+} by $\frac{2}{3}Mn^{2+} + \frac{1}{3}Sb^{5+}$ in the normal spinel $MnCr_2O_4$. At first sight the mentioned substitution could be performed for s values up to $\frac{2}{3}$, but in fact it could not be accomplished for $s > \frac{1}{3}$, because in these cases a mixture of phases was found.[2]

The hypothetical series $M(II)_{1+2s}Cr_{2-3s}Sb_sO_4$ is limited by two compounds: for $s = 0$, the *chromite* MCr_2O_4; for $s = \frac{2}{3}$, the oxide $M_{7/3}Sb_{2/3}O_4$. Whereas all the *chromites* are spinels, only two $M_{7/3}Sb_{2/3}O_4$ compounds with spinel structure are known,[3] those of Co and Zn. Thus, in these two cases it seems feasible to prepare the complete series $M_{1+2s}Cr_{2-3s}Sb_sO_4$, i.e. for s values from zero up to $\frac{2}{3}$. In fact, the oxide for which M = Co and $s = 0.50$ has been described[4] as a spinel with $a = 8.499$ Å.

This paper aims to report how the series $Co_{1+2s}Cr_{2-3s}Sb_sO_4$ was prepared and the X-ray diffraction data for eight samples ($s = 0, 0.10 \ldots 0.60$ or 0.67) of the series. These data are relevant especially for the first and last members, because dark green $CoCr_2O_4$ has been known since 1927, but it has not been completely studied: according to the last investigation[5] its lattice constant a was 8.332 ± 0.005 Å, but the oxygen positional parameter (u) was not determined. On the other hand, for black $Co_{7/3}Sb_{2/3}O_4$, $a = 9.523$ Å; and $u = 0.255 \pm 0.005$, origin at center, ($\bar{3}m$), was determined[6] from the intensity ratios of some reflections.

EXPERIMENTAL

The samples were prepared from mixtures of analytical grade Co_3O_4, Cr_2O_3 and Sb_2O_3, of molar ratios Co : Cr : Sb = $(1+2s):(2-3s):s$ ($s = 0, 0.10 \ldots 0.60$ or 0.67), which were heated in air at 953, 1173, 1273, 1473 and 1500 K during 1 day. After each thermal treatment the materials were quenched and ground. Additional experimental details were as indicated elsewhere.[7] The unit-cell parameters, a,

* Author to whom correspondence should be addressed.

were refined from the 2θ values of at least eight of the last 12 reflections using the program PARAM.[8] The intensities were calculated with the program LAZY-PULVERIX,[9] using scattering factors for neutral atoms, Debye–Waller, Lorentz and polarization factors, and correction for anomalous dispersion. The arbitrarily chosen Debye–Waller factors, B_j, for the calculation of the intensities were 0.30 and 0.80 Å^2 for Sb and oxygen atoms respectively; the values 0.60 and 0.63 Å^2 for Co and Cr, respectively, were obtained from these two by interpolation of the respective atomic masses between those of oxygen and Sb. Intensities were calculated for u equal to 0.255, 0.256 ... 0.263, origin at centre, $(\bar{3}m)$, and assuming tetrahedral (a) sites occupied by Co atoms for all the samples. The disrepancy factor between observed and calculated intensities:

$$R = (\sum |I_o^{1/2} - I_c^{1/2}|)/\sum I_o^{1/2}$$

was computed after making $\sum I_o$ equal to $\sum I_c$, and taking into account all the reflections with $I_o > 5$. For each member of the series, the u value taken as observed was that leading to the smallest R.

RESULTS AND DISCUSSION

The eight samples of composition $Co_{1+2s}Cr_{2-3s}Sb_sO_4$ ($0 \leqslant s \leqslant \frac{2}{3}$) were obtained as powders coloured from dark grey blue ($s = 0$), blackish blue ($s = 0.10$ and 0.20) to black ($s = 0.30$, 0.40 ... 0.67), which gave good X-ray diffraction patterns* characteristic of spinels. The a values showed a gradual variation, confirming the existence of the series. Thus, $Co_{1+2s}Cr_{2-3s}Sb_sO_4$ ($0 \leqslant s \leqslant \frac{2}{3}$) is a series of cubic spinels, space group $Fd\bar{3}m$ (No. 227), $Z = 8$, with the a and observed u_o values which are shown in Table 1. For $CoCr_2O_4$, $Co_2Cr_{0.5}Sb_{0.5}O_4$, and $Co_{7/3}Sb_{2/3}O_4$, the observed unit-cell parameters compare with those previously determined.[4–6] Calculated intensities,* I_c, were obtained for the distribution of cations and u_o values of Table 1, where the best R factors are also shown.

Observed u_o values can be compared with those calculated, u_c, using the expression $u_c = 3r^2 + (33r^2 - 8)^{1/2} - 8/24(r^2 - 1)$, where r is the ratio of the octahedral, d_o, to the tetrahedral, d_t, M—O distances. This expression is deduced taking into account that $d_o = a(3u^2 - 2u + 3/8)^{1/2}$, and $d_t = a3^{1/2}(u - 1/8)$. Assuming the distribution of cations indicated in the supplementary material,* and the corresponding ionic radii[10] (Å), values for d_o, d_t, r and u_c are obtained.* The u_c agree acceptably with the u_o.

Table 1. Crystal data for the spinels $Co_{1+2s}Cr_{2-3s}Sb_sO_4$, with ESDs in parentheses

s	a (Å)	u_o	u_c	R
0.00	8.3346(3)	0.261	0.261	0.042
0.10	8.3461(4)	0.260	0.260	0.030
0.20	8.3783(3)	0.260	0.260	0.029
0.30	8.4187(5)	0.260	0.259	0.025
0.40	8.4577(3)	0.260	0.259	0.027
0.50	8.4909(4)	0.259	0.258	0.031
0.60	8.5185(4)	0.259	0.258	0.031
0.67	8.5330(6)	0.258	0.257	0.043

Table 2 shows the observed M—O and O—O distances at tetrahedral (a) and octahedral (d) sites. The O—O distances have been calculated from the following expressions: at tetrahedral sites, O—O = $a2^{1/2}(2u - \frac{1}{4})$; for octahedral positions, O—O = $a2^{1/2}(\frac{3}{4} - 2u)$; O—O′ = $a(4u^2 - 2u + \frac{3}{8})^{1/2}$. As can be deduced from Table 2, the distances M—O and O—O for tetrahedral positions remain unaltered along the series, equal 1.967(9) and 3.212(14) Å, respectively. The ESD obtained for these distances illustrate the precision of the method, which consists in establishing u_o and, as a function of a and u_o, the M—O and O—O distances. The mentioned ESD are those calculated for a u_o absolute error of 0.0006 units. Assuming this u_o error, from the expressions which give the distances M—O, O—O and O—O′ for octahedral sites as a function of a and u_o the following ESDs are deduced for these distances: 0.005, 0.014 and 0.0006 Å respectively.

Table 2. Observed interatomic distances (Å) in the spinels $Co_{1+2s}Cr_{2-3s}Sb_sO_4$ ($0 \leqslant s \leqslant \frac{2}{3}$).

	Tetrahedral (a) sites		Octahedral (d) sites		
s	M—O	O—O	M—O	O—O	O—O′
0.00	1.963	3.206	1.996	2.687	2.952
0.10	1.952	3.187	2.007	2.715	2.956
0.20	1.959	3.199	2.014	2.725	2.967
0.30	1.969	3.215	2.024	2.738	2.981
0.40	1.978	3.320	2.033	2.751	2.995
0.50	1.971	3.218	2.049	2.786	3.006
0.60	1.977	3.229	2.056	2.795	3.016
0.67	1.966	3.210	2.067	2.824	3.020

* The data have been deposited with the Editor and are available on request.

Table 2 shows how the tetrahedral M—O bond lengths are constant along the series, whereas the octahedral M—O distances increase with s. These results could be anticipated, because the series $Co_{1+2s}Cr_{2-3s}Sb_sO_4$ ($0 \leqslant s \leqslant \frac{2}{3}$) can be thought of as derived from the normal spinel $CoCr_2O_4$ through progressive substitution of two Cr^{3+} by two of the more voluminous cations, $\frac{2}{3}Mn^{2+} + \frac{1}{3}Sb^{5+}$. This substitution takes place at the octahedral sublattice, whereas the tetrahedral sites remain unaltered, occupied by Co^{2+} ions. Hence, the mentioned substitution has to be accomplished keeping unchanged the tetrahedral M—O distances and progressively increasing the octahedral ones.

From these results and those of the previous paper,[2] it is concluded that in the series $M_{1+2s}Cr_{2-3s}Sb_sO_4$, limited by the oxides MCr_2O_4 ($s = 0$) and $M_{7/3}Sb_{2/3}O_4$ ($s = \frac{2}{3}$), when both of these oxides are spinels, s can adopt all the values from zero to $\frac{2}{3}$, i.e. all the $\lambda+$ chromium of MCr_2O_4 can be substituted by $\frac{2}{3}M\frac{1}{3}Sb$. On the other hand, when the oxide $M_{7/3}Sb_{2/3}O_4$ is not a spinel, only half the chromium in MCr_2O_4 can be substituted, and s can vary only up to $\frac{1}{3}$.

Acknowledgements—We express our gratitude to Miss B. Galar for technical assistance. One of us, I.R., acknowledges the financial aid of the Comisión Asesora de Investigación Científica y Técnica.

REFERENCES

1. P. García Casado and I. Rasines, *J. Solid State Chem.* 1984, **52**, 187.
2. P. García Casado and I. Rasines, *Polyhedron* 1985, **4**, 517.
3. R. J. Hill, J. R. Craig and G. V. Gibbs, *Phys. Chem. Miner.* 1979, **4**, 317.
4. P. Tarte and J. Preudhomme, *J. Solid State Chem.* 1979, **29**, 273.
5. E. Whipple and A. Wold, *J. Inorg. Nucl. Chem.* 1962, **24**, 23.
6. J. Dulac and A. Durif, *C. R. Acad. Sci.* 1960, **251**, 747.
7. P. García Casado and I. Rasines, *Z. Krist.* 1982, **160**, 34.
8. M. Martínez Ripoll, PARAM. Refinamiento por mínimos cuadrados de parámetros. Instituto Rocasolano, C.S.I.C., Madrid.
9. R. Yvon, W. Jeitschko and E. Parthé, *J. Appl. Cryst.* 1977, **10**, 73.
10. R. D. Shannon, *Acta Cryst.* 1976, **A32**, 751.

Polyhedron Vol. 5, No. 3, pp. 791–798, 1986
Printed in Great Britain

0277–5387/86 $3.00+.00
© 1986 Pergamon Press Ltd

COPPER–TUNGSTEN COMPLEXES WITH BRIDGING TOLYLMETHYLIDYNE LIGANDS: CRYSTAL STRUCTURE OF THE COMPOUND $[CuW_2(\mu_3\text{-}CC_6H_4Me\text{-}4)(CO)_4(PPh_3)(\eta\text{-}C_5H_5)_2]\cdot CH_2Cl_2$

MATHIAS MÜLLER-GLIEMANN, SIMON V. HOSKINS, A. GUY ORPEN, ANDREW L. RATERMANN and F. GORDON A. STONE

Department of Inorganic Chemistry, The University of Bristol, Bristol BS8 1TS, U.K.

(*Received* 8 *July* 1985; *accepted* 31 *July* 1985)

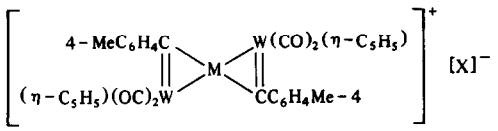
Abstract—The complexes $[W(\equiv CC_6H_4Me\text{-}4)(CO)_2(\eta\text{-}C_5H_5)]$ and $[Cu(NCMe)_4][PF_6]$ in dichloromethane combine to form the salt $[Cu\{W(\equiv CC_6H_4Me\text{-}4)(CO)_2(\eta\text{-}C_5H_5)\}_2][PF_6]$, but the latter very readily dissociates in solution releasing the tolylmethylidynetungsten compound. The more stable salt $[CuW(\mu\text{-}CC_6H_4Me\text{-}4)(CO)_2(NCMe)(PPh_3)(\eta\text{-}C_5H_5)][PF_6]$ is obtained by addition of $[W(\equiv CC_6H_4Me\text{-}4)(CO)_2(\eta\text{-}C_5H_5)]$ to a dichloromethane solution of $[Cu(NCMe)_4][PF_6]$ previously treated with 1 mol equivalent of PPh_3. In the presence of additional PPh_3, however, no copper–tungsten complex is formed. Several reactions of $[CuW(\mu\text{-}CC_6H_4Me\text{-}4)(CO)_2(NCMe)(PPh_3)(\eta\text{-}C_5H_5)][PF_6]$ have been studied, but these led only to release of $[W(\equiv CC_6H_4Me\text{-}4)(CO)_2(\eta\text{-}C_5H_5)]$. The compounds $[\{CuH(PPh_3)\}_6]$ and $[W(\equiv CC_6H_4Me\text{-}4)(CO)_2(\eta\text{-}C_5H_5)]$ react in toluene at room temperature to give $[W(CO)_2(\eta^3\text{-}CH_2C_6H_4Me\text{-}4)(\eta\text{-}C_5H_5)]$ and the new cluster compound $[CuW_2(\mu_3\text{-}CC_6H_4Me\text{-}4)(CO)_4(PPh_3)(\eta\text{-}C_5H_5)_2]$. The structure of the latter species has been established by X-ray diffraction. A CuW_2 metal triangle [Cu—W 2.640(2) and 2.610(2), and W—W 3.064(1) Å] is asymmetrically capped by a CC_6H_4Me-4 group [μ_3-C—Cu 2.130(9), μ_3-C—W 2.035(9) and 2.122(9) Å]. The copper atom is ligated by a PPh_3 molecule, and each tungsten by an η^5-cyclopentadienyl and two carbonyl groups. The copper atom is weakly co-ordinated in a semi-bridging manner by two of the CO ligands, one on each tungsten, and is also very weakly bound to a third. The molecule undergoes dynamic behaviour in solution.

The alkylidyne–tungsten compound $[W(\equiv CC_6H_4Me\text{-}4)(CO)_2(\eta\text{-}C_5H_5)]$ reacts with a variety of low-valent metal–ligand fragments to afford complexes with metal–metal bonds bridged by the CC_6H_4Me-4 group.[1,2] Most of the *d*-block elements are represented among the products of these reactions, and complexes of this class are also known with bonds between tungsten and copper, silver or gold. For example, the dicopper–tungsten species $[Cu_2W(\mu_3\text{-}CC_6H_4Me\text{-}4)(CO)_2(\eta\text{-}C_5H_5)(\eta\text{-}C_5Me_5)_2]$ is obtained by treating $[W(\equiv CC_6H_4Me\text{-}4)(CO)_2(\eta\text{-}C_5H_5)]$ with $[Cu(thf)(\eta\text{-}C_5Me_5)]$ (thf = tetrahydrofuran).[3] Moreover, the latter reagent is sufficiently reactive to add to the unsaturated C=W bonds in $[PtW(\mu\text{-}CC_6H_4Me\text{-}4)(CO)_2(PMe_3)_2(\eta\text{-}C_5H_5)]$ and $[Pt\{W(\equiv CC_6H_4Me\text{-}4)(CO)_2(\eta\text{-}C_5H_5)\}_2]$ to give, respectively, the trimetal compound $[CuPtW(\mu_3\text{-}CC_6H_4Me\text{-}4)(CO)_2(PMe_3)_2(\eta\text{-}C_5H_5)(\eta\text{-}C_5Me_5)]$ and the pentanuclear metal compound $[Cu_2PtW_2(\mu_3\text{-}CC_6H_4Me\text{-}4)_2(CO)_4(\eta\text{-}C_5H_5)_2(\eta\text{-}C_5Me_5)_2]$. In this paper we report some further studies directed towards the synthesis of complexes containing copper–tungsten bonds and bridging to tolylmethylidyne groups.

RESULTS AND DISCUSSION

In earlier work,[4] the gold- and silver–ditungsten salts **1** and **2** were prepared from $[W(\equiv CC_6H_4Me\text{-}4)(CO)_2(\eta\text{-}C_5H_5)]$ by treating the latter with either $[AuCl\{S\cdot(CH_2)_3\cdot CH_2\}]$, in the presence of $TlPF_6$, or $[Ag(NCMe)_4][BF_4]$, respectively. Whereas **1** is stable in thf solution, under similar conditions the silver cation readily dissociates the "carbyne–tungsten" ligands. We were interested in

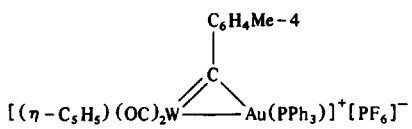
establishing whether the copper–ditungsten salt (**3**) could be obtained, and if so to compare its stability in solution with those of **1** and **2**.



	M	X
1	Au	PF_6
2	Ag	BF_4
3	Cu	PF_6

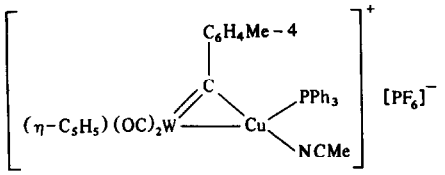
Reaction between $[Cu(NCMe)_4][PF_6]$ and $[W(\equiv CC_6H_4Me\text{-}4)(CO)_2(\eta\text{-}C_5H_5)]$ in CH_2Cl_2 at room temperature afforded, after addition of light petroleum, orange crystals of **3**. The IR spectrum of this product in the carbonyl region, measured in CH_2Cl_2, showed two bands (2021 and 1942 cm^{-1}) very similar to those seen in the spectra of **1** (2024 and 1969 cm^{-1}) and **2** (2020 and 1956 cm^{-1}). Not unexpectedly, in view of the salt-like nature of **1**–**3**, the carbonyl stretching bands occur at higher frequencies than the corresponding bands in the spectrum of $[W(\equiv CC_6H_4Me\text{-}4)(CO)_2(\eta\text{-}C_5H_5)]$ (1984 and 1906 cm^{-1}, measured in CH_2Cl_2).

Attempts to obtain NMR data for **3** led only to the observation of peaks due to free $[W(\equiv CC_6H_4Me\text{-}4)(CO)_2(\eta\text{-}C_5H_5)]$. Moreover, when the IR spectrum of **3** was measured in thf solution, the only CO stretching bands observed were those due to the tolylmethylidynetungsten compounds It is thus apparent that **3** is even more labile than **2**, and that, overall, the ligating properties of the carbyne–tungsten compound decreases in the order Au(I) > Ag(I) > Cu(I).



4

Earlier we reported[5] the synthesis of the gold–tungsten salt (**4**) by treating $[W(\equiv CC_6H_4Me\text{-}4)(CO)_2(\eta\text{-}C_5H_5)]$ with $[AuCl(PPh_3)]$ in CH_2Cl_2 in the presence of $TlPF_6$. With the object of obtaining a copper analogue of **4**, reactions between $[W(\equiv CC_6H_4Me\text{-}4)(CO)_2(\eta\text{-}C_5H_5)]$ and $[Cu(NCMe)_4][PF_6]$ in the presence of PPh_3 were investigated, using CH_2Cl_2 as solvent. It was found that whether an isolable copper–tungsten complex was formed depended on the amount of PPh_3 added to the copper salt prior to addition of this reagent to a CH_2Cl_2 solution of the tolylmethylidynetungsten compound. Using one equivalent of PPh_3, the orange salt **5** could be isolated.



5

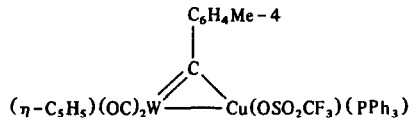
However, when two equivalents of PPh_3 were added to the copper–acetonitrile cation, or if the latter was treated with a mol equivalent of $Ph_2PCH_2PPh_2$, no reaction subsequently occurred with the tungsten compound. Not surprisingly, in view of these observations, treatment of **5** with PPh_3 regenerates $[W(\equiv CC_6H_4Me\text{-}4)(CO)_2(\eta\text{-}C_5H_5)]$. Evidently, the $[Cu(NCMe)(PPh_3)]^+$ fragment is able to bond a molecule of $[W(\equiv CC_6H_4Me\text{-}4)(CO)_2(\eta\text{-}C_5H_5)]$ to produce **5**, whereas $[Cu(PPh_3)_2]^+$ cannot form a stable adduct with the alkylidyne–tungsten compound.

It is interesting to contrast **4** with **5**. In these species the gold and copper centres are co-ordinated by two and three ligands, respectively, assuming that the C≡W system, being akin to an alkyne,[1] occupies one co-ordination site.

Earlier it was observed that, in solution, **4** readily dissociates, affording a mixture of complexes, including the species $[Au(PPh_3)_2]^+$ and the cation of **1**.[5] Although **5** appeared to be reasonably stable in solution, allowing definitive NMR data to be obtained (see below), reactions of the copper–tungsten salt with Cl^-, I^- or CN^-, in CH_2Cl_2, led to the release of $[W(\equiv CC_6H_4Me\text{-}4)(CO)_2(\eta\text{-}C_5H_5)]$. A similar decomposition of **5** occurred on treatment with SR^-, BH_4^- or H^-, or with sodium naphthalenide in the presence of CO.

Compound **5** was fully characterised spectroscopically. The IR spectrum had the expected two CO stretching bands (2014 and 1946 cm^{-1}). The ^1H NMR spectrum showed resonances due to the MeCN, Me-4 and C_5H_5 groups, and these signals had the expected relative peak intensities. The ^{31}P–$\{^1H\}$ NMR spectrum consisted of a singlet signal at δ 0.2 ppm, due to the PPh_3 ligand, and a resonance at δ −144.2 [heptet, J(PF) 713 Hz] characteristic of the anion PF_6^-. The ^{13}C–$\{^1H\}$ NMR spectrum was especially informative, with a diagnostic resonance for the μ-C nucleus at 294.9 ppm. The corresponding peak in the spectrum of **4** is observed at 292.6 ppm, and occurs as a doublet due to ^{31}P–^{13}C coupling.[5] The absence of such coupling on the bridging carbyne resonance of **5** suggests that, in the latter, the acetonitrile ligand is *transoid* to the μ-C group, with the PPh_3 ligand *cisoid*.

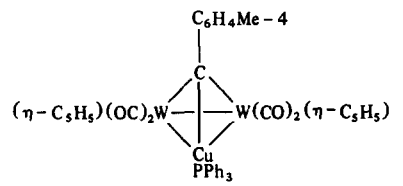
Treatment of the trifluoromethanesulfonate (benzene)copper complex [$Cu(SO_3CF_3)(0.5\ C_6H_6)$] with 1 mol equivalent of PPh_3 in CH_2Cl_2, followed by addition of this mixture to [$W(\equiv CC_6H_4Me\text{-}4)(CO)_2(\eta\text{-}C_5H_5)$] afforded the salt **6** in which the SO_3CF_3 anion is co-ordinated to copper. The $^{13}C\text{-}\{^1H\}$ NMR spectrum showed the characteristic resonance for the bridging carbyne–carbon nucleus at δ 292.3 ppm, while the CF_3 group gave a quartet signal [J(FC) 319 Hz] at 120.2 ppm.



6

During the course of our studies we also investigated the reaction between [$W(\equiv CC_6H_4Me\text{-}4)(CO)_2(\eta\text{-}C_5H_5)$] and the hexanuclear copper complex [$\{CuH(PPh_3)\}_6$].[6] It was anticipated that the product of this reaction might have been a copper–tungsten complex containing both bridging hydrido and tolylmethylidyne ligands, or alternatively, a species having a μ-CH(C_6H_4Me-4) group, if Cu–H addition across the C≡W bond occurred. In practice the reaction proceeded in an unexpected manner.

Treatment of [$W(\equiv CC_6H_4Me\text{-}4)(CO)_2(\eta\text{-}C_5H_5)$] with [$\{CuH(PPh_3)\}_6$] in toluene at room temperature afforded a mixture of two products separated by column chromatography on alumina. The first eluate contained the known[7] *p*-methylbenzyltungsten complex [$W(\eta^3\text{-}CH_2C_6H_4Me\text{-}4)(CO)_2(\eta\text{-}C_5H_5)$], which we have observed previously[8] as a product of reactions involving [$W(\equiv CC_6H_4Me\text{-}4)(CO)_2(\eta\text{-}C_5H_5)$]. The second product was a purple crystalline compound. Examination of the ^1H NMR spectrum of this species (**7**) failed to reveal any



7

resonance attributable to the presence of a hydrido ligand in the molecule. The $^{13}C\text{-}\{^1H\}$ NMR spectrum had a resonance at δ 339.6 ppm, appearing as a doublet [J(PC) 7 Hz] with ^{183}W satellite peaks [J(WC) 94 Hz]. This signal seemed almost certainly to be due to a bridging carbon nucleus of a tolylmethylidyne group, rather than that arising from the ligated carbon of a μ-CH(C_6H_4Me-4) fragment. In confirmation of this, a fully coupled ^{13}C NMR spectrum established that no proton was attached to the carbon nucleus responsible for the resonance at δ 339.6 ppm. It was thus evident that the structure of **7** could not be resolved without a single-crystal X-ray diffraction study.

The crystals studied were grown from CH_2Cl_2, and the crystal structure consists of isolated molecules of **7** and CH_2Cl_2, in equimolar amounts, separated by normal van der Waals' contact distances. The molecular structure is illustrated in Fig. 1, and selected bond lengths and angles are given in Table 1. Molecules of **7** contain two tungsten and one copper atom forming an approximately isosceles triangle [Cu—W(1) 2.610(2), Cu—W(2) 2.640(2), and W(1)—W(2) 3.064(1) Å]. The CuW_2 triangle is asymmetrically capped by the μ_3-CC_6H_4Me-4 ligand [Cu—C(120) 2.130(9), W(1)—C(120) 2.035(9), and W(2)—C(120) 2.122(9) Å]. Each tungsten is further ligated by a η^5-cyclopentadienyl and two carbonyl ligands. The copper atom is bound to a triphenylphosphine ligand [Cu—P 2.217(3) Å]. The copper is also weakly co-ordinated by two of the carbonyl ligands [C(2)O(2) and C(10)O(10)] in a semi-bridging manner, and very weakly attached to a third [C(20)O(20)], a feature discussed further below.

The copper–tungsten bond lengths are very

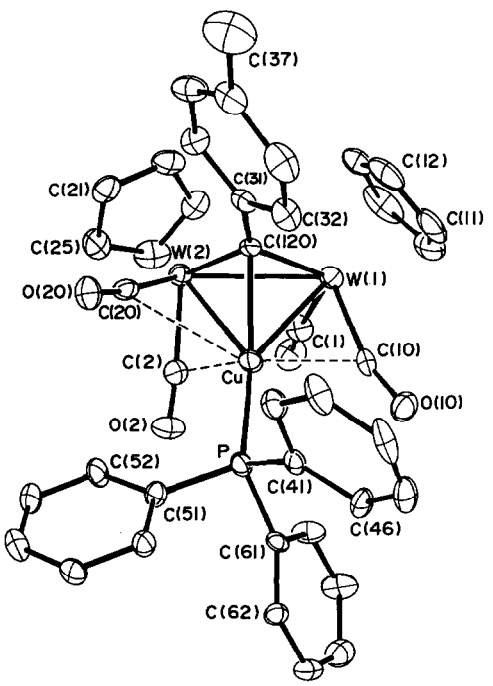


Fig. 1. The molecular geometry of [$CuW_2(\mu_3\text{-}CC_6H_4Me\text{-}4)(CO)_4(PPh_3)(\eta\text{-}C_5H_5)_2$], showing the atomic labelling scheme. All hydrogen atoms and the CH_2Cl_2 molecule have been omitted for clarity.

Table 1. Bond distances (Å) and angles (°) for the complex $[CuW_2(\mu_3\text{-}CC_6H_4Me\text{-}4)(CO)_4(PPh_3)(\eta\text{-}C_5H_5)_2]\cdot CH_2Cl_2$

W(1)—W(2)	3.064(1)	W(1)—Cu	2.610(2)	W(2)—C(23)	2.371(12)	W(2)—C(24)	2.323(13)
W(1)—C(1)	1.971(12)	W(1)—C(10)	1.973(10)	W(2)—C(25)	2.326(11)	Cu—P	2.217(3)
W(1)—C(120)	2.035(9)	W(1)—C(11)	2.309(16)	Cu—C(10)	2.307(10)	Cu—C(2)	2.514(10)
W(1)—C(12)	2.349(18)	W(1)—C(13)	2.355(15)	Cu—C(120)	2.130(9)	Cl(1)—C(999)	1.714(20)
W(1)—C(14)	2.347(13)	W(1)—C(15)	2.273(18)	Cl(2)—C(999)	1.665(23)	P—C(41)	1.825(9)
W(2)—Cu	2.640(2)	W(2)—C(20)	1.951(10)	P—C(51)	1.830(9)	P—C(61)	1.816(9)
W(2)—C(2)	1.948(10)	W(2)—C(120)	2.122(9)	O(1)—C(1)	1.171(15)	O(10)—C(10)	1.177(13)
W(2)—C(21)	2.306(13)	W(2)—C(22)	2.373(13)	O(20)—C(20)	1.161(12)	O(2)—C(2)	1.164(13)
				C(120)—C(31)	1.450(13)		
W(2)—W(1)—Cu	54.8(1)	W(2)—W(1)—C(1)	66.4(3)				
Cu—W(1)—C(1)	82.4(3)	W(2)—W(1)—C(10)	111.8(3)	W(1)—Cu—C(120)	49.6(2)	W(2)—Cu—C(120)	51.5(2)
Cu—W(1)—C(10)	58.5(3)	C(1)—W(1)—C(10)	93.5(5)	P—Cu—C(120)	149.0(3)	C(10)—Cu—C(120)	88.9(2)
W(2)—W(1)—C(120)	43.6(2)	Cu—W(1)—C(120)	52.8(3)	C(2)—Cu—C(120)	95.5(3)	Cu—P—C(41)	108.6(3)
C(1)—W(1)—C(120)	109.2(4)	C(10)—W(1)—C(120)	101.8(4)	Cu—P—C(51)	120.0(3)	C(41)—P—C(51)	103.8(4)
W(1)—W(2)—C(20)	115.6(3)	W(1)—W(2)—Cu	53.8(1)	Cu—P—C(61)	114.5(3)	C(41)—P—C(61)	104.5(4)
W(1)—W(2)—C(2)	96.1(3)	Cu—W(2)—C(20)	71.9(3)	C(51)—P—C(61)	103.9(4)	Cl(1)—C(999)—Cl(2)	109.6(1)
C(20)—W(2)—C(2)	88.2(4)	Cu—W(2)—C(2)	64.4(3)	W(1)—C(1)—O(1)	170.3(10)	W(1)—C(10)—Cu	74.7(3)
Cu—W(2)—C(120)	51.8(2)	W(1)—W(2)—C(120)	41.4(2)	W(1)—C(10)—O(10)	163.4(9)	Cu—C(10)—O(10)	121.3(7)
C(2)—W(2)—C(120)	115.8(4)	C(20)—W(2)—C(120)	79.4(4)	W(2)—C(20)—O(20)	174.1(8)	W(2)—C(2)—Cu	71.3(3)
W(1)—Cu—W(2)	71.4(1)	W(1)—Cu—P	146.2(1)	W(2)—C(2)—O(2)	172.6(8)	Cu—C(2)—O(2)	116.0(7)
W(2)—Cu—P	141.0(1)	W(1)—Cu—C(10)	46.8(2)	W(1)—C(120)—W(2)	94.9(4)	W(1)—C(120)—Cu	77.6(3)
W(2)—Cu—C(10)	116.7(2)	P—Cu—C(10)	99.4(3)	W(2)—C(120)—Cu	76.8(3)	W(1)—C(120)—C(31)	131.7(7)
W(1)—Cu—C(2)	95.7(2)	W(2)—Cu—C(2)	44.3(2)	W(2)—C(120)—C(31)	131.2(7)	Cu—C(120)—C(31)	121.1(6)
P—Cu—C(2)	105.3(2)	C(10)—Cu—C(2)	120.8(3)				

similar to the Cu–W separation in [CuPtW(μ_3-CC_6H_4Me - 4)$(Co)_2(PMe_3)_2(\eta$ - $C_5H_5)(\eta$ - $C_5Me_5)$] [Cu—W = 2.648(3) Å].[3] The capping carbyne atom [C(120)] in **7** is, however, less strongly bound to copper [C(120)—Cu 2.130(9) Å] than the μ_3-C atom in [CuPtW(μ_3-CC_6H_4Me-4)$(CO)_2(PMe_3)_2$ $(\eta$-$C_5H_5)(\eta$-$C_5Me_5)$] [μ_3-C—Cu 1.96(2) Å]. The C(120)—W distances in **7** [2.035(9) and 2.122(9) Å] are similar to those found [2.035(14) and 2.050(11) Å] in the compound [$ReW_2(\mu$-Br)(μ-CC_6H_4Me-4) (μ_3-CC_6H_4Me-4)(μ-CO)$(CO)_3(\eta$-$C_5H_5)_2$].[9] The asymmetry of the C(120)—W distances in **7** is not paralled by any asymmetry in the W—μ_3-C—C_{ipso} angles [W(1)—C(120)—C(31) 131.7(7), and W(2)—C(120)—C(31) 131.2(7)°]. The Cu—C(120)—C(31) angle [121.1(6)°] in **7** is less obtuse than the W—C(120)—C(31) angles, indicating that the C_6H_4Me-4 substituent on C(120) "leans" towards the copper. A similar feature is found[3] in the structure of [CuPtW(μ_3-CC_6H_4Me-4)$(CO)_2$ $(PMe_3)_2(\eta$-$C_5H_5)(\eta$-$C_5Me_5)$], [Cu—μ_3-C—C(tolyl) 121.3(12), Pt—C—C(tolyl) 131.4(13), and W—C—C(tolyl) 128.8(13)°].

The carbonyl ligands all show non-linear geometries to a greater or lesser extent; the degree of non-linearity correlating with the interaction of the carbon atoms with the copper [W(1)—C(1)—O(1) 170.3(10), W(1)—C(10)—O(10) 163.4(9), W(2)—C(2)—O(2) 172.6(8), and W(2)—C(20)—O(20) 174.1(8)°; C(1)...W(2) 2.905(12), C(10)—Cu 2.307(10), C(2)—Cu 2.514(10), and C(20)...Cu 2.752(10) Å]. The weak Cu...C(O) interactions are presumably to allow delocalisation of electron density from the filled copper d_π-orbitals. It is noticeable that while the P–Cu vector points to the middle of the μ_3-CW_2 triangle [W(1)—Cu—P 146.2(1), W(2)—Cu—P 141.0(1), and C(120)—Cu—P 149.0(3)°] the Cu...C(O) interactions lie in a belt around the extension of this vector [P—Cu—C(10) 99.4(3), P—Cu—C(2) 105.3(2), and P—Cu...C(20) 107.1(3)°].

The binding of $AuPR_3$, $AgPR_3$ or $CuPR_3$ fragments in transition-metal clusters has been explained by the isolobal analogy between such fragments and CH_3 or H. Recently Evans and Mingos[10] have pointed out that, for $CuPR_3$ (unlike $AuPR_3$), the empty 4*p* orbitals may play a part in the bonding in addition to the *sp* hybrid orbital. This leads to the isolobal mapping:



each fragment having one valence electron and three valence orbitals (one σ and two π). The $W(CO)_2$ $(\eta$-$C_5H_5)$ fragment is isolobal with CH and hence a $(\eta$-$C_5H_5)(OC)_2W(\mu$-CC_6H_4Me-4)$W(CO)_2(\eta$-$C_5H_5)$ group would be expected to have frontier orbitals related to those of the cyclopropenyl radical (C_3H_3) albeit with lowered symmetry (C_s at most, rather than D_{3h} or C_{3v}). This argument therefore likens **7** to $C_4H_4^{2+}$, the dication of tetrahedrane. Clearly a more quantitative description of the bonding in **7** is required for understanding its stability. It is likely that the lowered symmetry of **7** due to replacement of CH by $W(CO)_2(\eta$-$C_5H_5)$, and the Cu...CO interactions, lift the degeneracy of orbitals (e.g. the HOMO of "cyclopropenyl"). Seemingly the copper 4*p* orbitals are of secondary importance, interacting with one of the "*e*" set of the μ-CW_2 "cyclopropenyl" ring π-orbitals to assist in Cu...CO bonding. Interestingly the strongest Cu—CO interaction [Cu—C(10) 2.307(10) Å] is orthogonal to the Cu—C(120) bond, and lies close to the trimetal plane.

The ^{13}C-{^1H} and ^1H NMR spectra of **7** show one cyclopentadienyl environment and two carbonyl sites present in solution. In view of the X-ray diffraction results this implies that **7** is fluxional in solution undergoing a rearrangement which brings about time-averaged C_s-symmetry on the NMR timescale. This process amounts to racemisation of the chiral structure adopted by **7** in the solid state, with the environments of C(10) and C(20), and C(1) and C(2) rendered equivalent, as shown in Scheme 1. A similar process, involving "wagging" of $Mo(CO)_2(\eta$-$C_5H_5)$ groups is responsible for related fluxionality in $[Mo_2(CO)_4(\mu$-HCCH)$(\eta$-$C_5H_5)_2]$.[11]

The formation of **7** and [W(η^3-$CH_2C_6H_4Me$-4) $(CO)_2(\eta$-$C_5H_5)$] from the reaction between [W(≡CC_6H_4Me-4)$(CO)_2(\eta$-$C_5H_5)$] and [{CuH $(PPh_3)\}_6$] evidently involves a complicated pathway, leading to an unexpected stoichiometry. Isolation of [W(η^3-$CH_2C_6H_4Me$-4)$(CO)_2$ $(\eta$-$C_5H_5)$] indicates that hydrogenation and cleavage of a C≡W tungsten bond has occurred, presumably involving hydrogen transfer from the copper reagent. The latter obviously functions as the source of the $CuPPh_3$ fragment found in **7**.

EXPERIMENTAL

The complexes [W(≡CC_6H_4Me-4)$(CO)_2(\eta$-$C_5H_5)$],[12] [{CuH$(PPh_3)\}_6$][13] and [Cu$(NCMe)_4$] $[PF_6]$[14] were prepared by published methods. The reagent [Cu(0.5 $C_6H_6)SO_3CF_3$] was obtained from Fluka. Solvents were rigorously dried before use, and all reactions were carried out in Schlenk tubes under oxygen-free nitrogen. Light petroleum refers to the fraction with b.p. 40–60°C. Alumina used in chromatography was BDH aluminium oxide (Brockman activity II).

The IR spectra were recorded with a Nicolet 10-MX FT spectrophotometer and the NMR measurements were made with a JNM-FX 90Q instrument. ^{31}P chemical shifts (ppm) are positive to high frequency of 85% H_3PO_4 (external).

Reactions involving the complex $[Cu(NCMe)_4][PF_6]$

The compounds $[Cu(NCMe)_4][PF_6]$ (0.18 g, 0.33 mmol) and $[W(\equiv CC_6H_4Me\text{-}4)(CO)_2(\eta\text{-}C_5H_5)]$ (0.28 g, 0.65 mmol) were stirred in CH_2Cl_2 (20 cm^3) for 30 min. The solvent was reduced *in vacuo* to *ca* 5 cm^3, and light petroleum (15 cm^3) was layered upon the CH_2Cl_2 solution. After diffusion (24 h) between the two layers, orange crystals formed. The solvent was removed with a syringe, and the crystals of $[Cu\{W(\equiv CC_6H_4Me\text{-}4)(CO)_2(\eta\text{-}C_5H_5)\}_2][PF_6]$ (**3**) (0.55 g, 82%) were dried *in vacuo*; ν_{max}(CO) at 2021s and 1942m cm^{-1} (in CH_2Cl_2). When the IR spectrum was measured in thf only bands in the CO region (1983 and 1910 cm^{-1}) due to free $[W(\equiv CC_6H_4Me\text{-}4)(CO)_2(\eta\text{-}C_5H_5)]$ were observed.

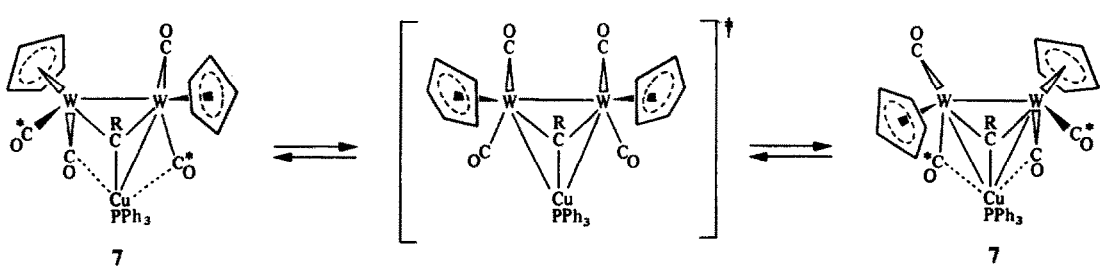
A suspension of $[Cu(NCMe)_4][PF_6]$ (0.28 g, 0.70 mmol) in CH_2Cl_2 (10 cm^3) was treated with PPh_3 (0.19 g, 0.70 mmol) in CH_2Cl_2 (5 cm^3). The mixture was then added to $[W(\equiv CC_6H_4Me\text{-}4)(CO)_2(\eta\text{-}C_5H_5)]$ (0.30 g, 0.70 mmol) in the same solvent (10 cm^3), and the reactants stirred for 10 min. The solvent was removed *in vacuo* and the resulting oil treated with diethyl ether (*ca* 100 cm^3). After a few hours crystals appeared. The supernatant liquid was removed with a syringe, and the orange product washed with diethyl ether (2×10 cm^3) and dried *in vacuo*, affording orange *microcrystals* of $[CuW(\mu\text{-}CC_6H_4Me\text{-}4)(CO)_2(NCMe)(PPh_3)(\eta\text{-}C_5H_5)][PF_6]$ (**5**) (0.56 g, 83%) (Found: C, 45.3; H, 2.9%. $C_{35}H_{30}CuNO_2PW$ requires C, 45.7; H, 3.3%), m.p. 100–102°C, ν_{max}(CO) at 2014s and 1946m cm^{-1} (in CH_2Cl_2). NMR (in $CDCl_3$): ^1H, δ 2.11 (s, 3H, MeCN), 2.28 (s, 3H, Me-4), 5.71 (s, 5H, C_5H_5) and 7.17–7.49 (m, 19H, C_6H_4 and Ph); ^{13}C–$\{^1H\}$, δ 294.9 (μ-CC_6H_4Me-4), 213.6 (CO), 149.8–129.1 (C_6H_4 and Ph), 119.8 (Me*C*N), 92.7 (C_5H_5), 22.1 (Me-4) and 2.2 ppm (*Me*CN); ^{31}P–$\{^1H\}$, δ 0.2 (PPh_3) and −144.2 ppm [heptet, PF_6, J(PF) 713 Hz].

Reaction between $[W(\equiv CC_6H_4Me\text{-}4)(CO)_2(\eta\text{-}C_5H_5)]$ *and* $[Cu(SO_3CF_3)(0.5\ C_6H_6)]$

The reagent $[Cu(SO_3CF_3)(0.5\ C_6H_6)]$ (0.19 g, 0.70 mmol) in CH_2Cl_2 (10 cm^3) was added to a solution of PPh_3 (0.19 g, 0.70 mmol) in the same solvent (5 cm^3). The resulting mixture was then added to a CH_2Cl_2 (10 cm^3) solution of $[W(\equiv CC_6H_4Me\text{-}4)(CO)_2(\eta\text{-}C_5H_5)]$ (0.30 g, 0.70 mmol) with stirring for 10 min. The solvent was removed *in vacuo*, and the oily residue was treated with diethyl ether–light petroleum (1 : 1, 100 cm^3). After a few hours orange crystals appeared. The supernatant liquid was removed with a syringe and the product washed with 2×10 cm^3 portions of diethyl ether–light petroleum (1 : 1), and dried *in vacuo* to afford orange *microcrystals* of $[CuW(\mu\text{-}CC_6H_4Me\text{-}4)(OSO_2CF_3)(CO)_2(PPh_3)(\eta\text{-}C_5H_5)]$ (**6**) (0.45 g, 73%) (Found: C, 45.8; H, 3.2%. $C_{34}H_{27}CuF_3O_5PSW$ requires C, 46.3; H, 3.1%), m.p. 113–115°C, ν_{max}(CO) at 2016s and 1941m cm^{-1} (in CH_2Cl_2). NMR (in $CDCl_3$): ^1H, δ 2.21 (s, 3H, Me-4), 5.77 (s, 5H, C_5H_5) and 7.00–7.43 (m, 19H, C_6H_4 and Ph); ^{13}C–$\{^1H\}$, δ 292.3 (μ-CC_6H_4Me-4), 215.5 (CO), 149.8–128.9 (C_6H_4 and Ph), 120.2 [q, CF_3, J(FC) 319 Hz], 93.0 (C_5H_5) and 22.0 ppm (Me-4).

Reaction between $[W(\equiv CC_6H_4Me\text{-}4)(CO)_2(\eta\text{-}C_5H_5)]$ *and* $[\{CuH(PPh_3)\}_6]$

The compound $[W(\equiv CC_6H_4Me\text{-}4)(CO)_2(\eta\text{-}C_5H_5)]$ (0.18 g, 0.45 mmol) in toluene (10 cm^3) was treated with $[\{CuH(PPh_3)\}_6]$ (0.18 g, 0.09 mmol) in the same solvent (10 cm^3). The mixture was stirred for 2 h, the solvent was removed *in vacuo*, and the residue dissolved in diethyl ether–light petroleum (1 : 5, 5 cm^3) and chromatographed on



Scheme 1.

an alumina column (2 × 10 cm). Elution with diethyl ether–light petroleum (1:5) gave a red eluate which afforded the known compound $[W(CO)_2(\eta^3\text{-}CH_2C_6H_4Me\text{-}4)(\eta\text{-}C_5H_5)]$ (0.05 g, 27%), identified spectroscopically.[8] Elution of the column with diethyl ether–light petroleum (1:1) produced a purple solution. Reduction in the volume of the solvent to *ca* 5 cm^3 gave purple crystals of $[CuW_2(\mu_3\text{-}CC_6H_4Me\text{-}4)(CO)_4(PPh_3)(\eta\text{-}C_5H_5)_2]\cdot CH_2Cl_2$ (7) (0.18 g, 55%) (Found: C, 43.7; H, 2.9; Cl, 6.5; P, 2.8%. $C_{40}H_{32}CuO_4PW_2\cdot CH_2Cl_2$ requires C, 43.8; H, 3.1; Cl, 6.3; P, 2.8%), ν_{max}(CO) at 1921m, 1863s, 1908w and 1776m cm^{-1} (in toluene). NMR (in CD_2Cl_2): ^1H, δ 2.12 (s, 3H, Me-4), 5.23 (s, 10H, C_5H_5), 6.80 (m, 4H, C_6H_4) and 7.29 (m, 15H, Ph); $^{13}C\text{-}\{^1H\}$, δ 339.6 [d, μ_3-C, J(PC) 7, J(WC) 94 Hz], 235.9 [CO, J(WC) 181 Hz], 222.1 [CO, J(WC) 171 Hz], 168.4 [$C^1(C_6H_4)$], 135.8–123.2 (C_6H_4 and Ph), 90.7 (C_5H_5) and 22.1 ppm (Me-4); $^{31}P\text{-}\{^1H\}$, δ 23.3 ppm (PPh_3).

Crystal structure determination for $7\cdot CH_2Cl_2$

Crystal data for $7\cdot CH_2Cl_2$. $C_{40}H_{32}CuO_4PW_2\cdot CH_2Cl_2$, M = 1123.8, monoclinic, space group, $P2_1/c$ (No. 14), a = 10.034(4), b = 21.514(8), c = 17.964(6) Å, β = 91.73(3)°, U = 3876(2) Å^3, Z = 4, D_c = 1.93 g cm^{-3}, D_m = 1.94 g cm^{-3}, $F(000)$ = 2152 electrons, Mo-K_α X-radiation (graphite monochromator), $\bar{\lambda}$ = 0.71069 Å, μ(Mo-K_α) = 68.2 cm^{-1}. A small single-crystal (*ca* 0.45 × 0.23 × 0.25 mm) of $7\cdot CH_2Cl_2$ was glued under N_2 in a thin-walled glass capillary for diffraction study on a Nicolet *P3m* diffractometer. Intensity data were collected for a unique quadrant of reciprocal space by $\theta/2\theta$ scans of width 2.4° + $\Delta_{\alpha_1\alpha_2}$ for $4 < 2\theta < 50°$. For $2\theta > 40°$ only those reflections with 2*s* prescan counts > 25 s^{-1} were recorded. Of the 6454 data measured, 5512 remained after averaging of duplicate and symmetry related measurements, of these 4630 with $I \geqslant 1.5\sigma(I)$ were used in structure solution and refinement. An absorption correction was applied by a six-parameter fit, minimising discrepancies between 119 pairs of reflection intensities (0*kl*) and (0*kl̄*); transmission coefficients varied between 0.055 and 0.093. The structure was solved by conventional heavy-atom (Patterson and difference Fourier) methods and refined by blocked cascade full-matrix least squares. All non-hydrogen atoms were refined with anisotropic vibrational parameters, and all hydrogen atoms with fixed U_{iso} = *ca* 1.2 times U_{iso} for the bonded carbon atom. Hydrogen atoms were held in idealised geometries with C—H = 0.96 Å. Final residual indices at convergence were R = 0.044, R' = 0.052 and S = 1.09.* Weights (w) were set equal to $[\sigma_c^2(F_o)+gF_o^2]$, where g = 0.001 was chosen to minimise the variation of S with $|F_o|$.† Final electron density difference syntheses showed no features of magnitude > 1.4 *e* Å^{-3}; the largest being < 1 Å from tungsten atoms. All calculations were made on a Nicolet R3m/E structure determination system using the SHELXTL program package,[15] with complex neutral atom scattering factors taken from Ref. 16.

Acknowledgements—We thank the S.E.R.C. for support, the Deutscher Akademischer Austanschdienst for a Scholarship (to M.M-G.), and Dr J. C. Jeffery for helpful discussion.

REFERENCES

1. F. G. A. Stone, In *Inorganic Chemistry: Toward the 21st Century* (Edited by M. H. Chisholm). ACS Symposium Series 1983, **211**, 383; *Angew. Chem., Int. Ed. Engl.* 1984, **23**, 89.
2. J. A. Abad, L. W. Bateman, J. C. Jeffery, K. A. Mead, H. Razay, F. G. A. Stone and P. Woodward, *J. Chem. Soc., Dalton Trans.* 1983, 2073; U. Behrens and F. G. A. Stone, *J. Chem. Soc., Dalton Trans.* 1984, 1605.
3. G. A. Carriedo, J. A. K. Howard and F. G. A. Stone, *J. Chem. Soc., Dalton Trans.* 1984, 1555.
4. G. A. Carriedo, J. A. K. Howard, K. Marsden, F. G. A. Stone and P. Woodward, *J. Chem. Soc., Dalton Trans.* 1984, 1589.
5. G. A. Carriedo, J. A. K. Howard, F. G. A. Stone and M. J. Went, *J. Chem. Soc., Dalton Trans.* 1984, 2545.
6. M. R. Churchill, S. A. Begman, J. A. Osborne and J. Wormald, *Inorg. Chem.* 1972, **11**, 1818.
7. F. A. Cotton and T. J. Marks, *J. Am. Chem. Soc.* 1969, **91**, 1339.
8. J. A. K. Howard, J. C. Jeffery, J. C. V. Laurie, I. Moore, F. G. A. Stone and A. Stringer, *Inorg. Chim. Acta* 1985, **100**, 23; J. C. Jeffery, A. L. Ratermann and F. G. A. Stone, *J. Organomet. Chem.* 1985, **289**, 367.
9. G. A. Carriedo, J. C. Jeffery and F. G. A. Stone, *J. Chem. Soc., Dalton Trans.* 1984, 1597.
10. D. G. Evans and D. M. P. Mingos, *J. Organomet. Chem.* 1982, **232**, 171.
11. W. I. Bailey, M. H. Chisholm, F. A. Cotton and L. A. Rankel, *J. Am. Chem. Soc.* 1978, **100**, 5764.

* $R = \sum||F_o|-|F_c||/\sum|F_o|$; $R' = [\sum w(|F_o|-|F_c|)^2/\sum wF_o^2]^{\frac{1}{2}}$; $S = [\sum w(|F_o|-|F_c|)^2/(N_o-N_v)]^{\frac{1}{2}}$.

† The atomic positional and thermal parameters, together with lists of F_o/F_c values have been deposited as supplementary material with the Editor, from whom copies are available on request. Atomic co-ordinates have also been deposited with the Cambridge Crystallographic Data Centre.

12. E. O. Fischer, T. Selmayr, F. R. Kreissl and U. Schubert, *Chem. Ber.* 1977, **110**, 2574; E. O. Fischer, T. L. Lindner, G. Huttner, P. Friedrich, F. R. Kreissl and J. O. Besenhard, *Chem. Ber.* 1977, **110**, 3397.
13. R. D. Stephens, *Inorg. Synth.* 1979, **19**, 87.
14. G. J. Kubas, *Inorg. Synth.* 1979, **19**, 90.
15. G. M. Sheldrick, SHELXTL system of crystallographic programs for use with the Nicolet *P3m* system, Cambridge (1976), updated Göttingen (1982).
16. *International Tables for X-ray Crystallography*, Vol. 4. Kynoch Press, Birmingham (1974).

Polyhedron Vol. 5, No. 3, pp. 799–803, 1986
Printed in Great Britain

0277–5387/86 $3.00 + .00
© 1986 Pergamon Press Ltd

X-RAY CRYSTAL STRUCTURE OF MANGANESE(II) BIS(ETHYLENEDIPHOSPHINETETRAACETATO)NICKELATE(II) HEXADECAHYDRATE

J. PODLAHOVÁ,* B. KRATOCHVÍL, V. LANGER† and J. PODLAHA

Department of Inorganic Chemistry, Charles University, 128 40 Prague, Czechoslovakia

(*Received* 1 *July* 1985; *accepted* 31 *July* 1985)

Abstract—X-ray structure analysis of the title compound (diffractometer data, $R = 0.061$ for 2805 reflections) confirmed the structure proposed on the basis of spectral evidence for the series of isostructural complexes, $M_3[NiL_2](H_2O)_{16}$, where

$$H_4L = (HO_2CCH_2)_2PCH_2CH_2P(CH_2CO_2H)_2$$

and M = Mn, Fe, Co, Ni, Zn or Cd. The compound studied is monoclinic, $P2_1/c$, $a = 9.990(3)$, $b = 28.51(2)$, $c = 14.828(9)$ Å, $\beta = 94.50(5)°$, $Z = 4$. Nickel(II) is coordinated by two P,P-chelating ligand anions in a rather distorted square planar environment. The carboxyl groups of the ligand are not coordinated to nickel; three of them remain free and five are bonded, together with 10 of the total of 16 water molecules, to the manganese(II) ions. The environments of three manganese ions thus formed are all nearly octahedral but differ in the number and bonding mode of the carboxyls (monodentate and/or bridging bidentate). The carboxyl-to-manganese bonds produce a three-dimensional structure of the compound which is further stabilized by hydrogen bonding.

Ethylenediphosphinetetraacetic acid[1,2] is the formal phosphorus analogue of the familiar EDTA but, in contrast to it, coordinates metal ions in a variety of ways, depending mainly on the degree of soft character of the metal ion. For example, nickel(II) can be bonded either to phosphorus or to the carboxyl groups of the ligand (but apparently not to both types of donors simultaneously) with the formation of square planar, square pyramidal and octahedral complexes.[3] The obvious candidate for confirming this variety of structural types by X-ray structure determination is the $Ni_2L(H_2O)_8$ complex, in which two modes of nickel(II) coordination seem to be present simultaneously. It follows from spectral, magnetic and powder pattern evidence[3] that this complex belongs to the isostructural series, $M_3[NiL_2](H_2O)_{16}$, where M = Mn, Fe, Co, Ni, Zn or Cd. Since we did not succeed in preparing single crystals of $Ni_2L(H_2O)_8$ we decided to carry out the structure determination of the well-crystallized, isostructural manganese derivative.

EXPERIMENTAL

The synthesis of the complex has been described.[3]

Crystal data

$C_{20}H_{56}Mn_3NiO_{32}P_4$, $M = 1156.1$; prismatic, $0.15 \times 0.10 \times 0.30$ mm; monoclinic, $P2_1/c$, $a = 9.990(3)$, $b = 28.51(2)$, $c = 14.828(9)$ Å, $\beta = 94.50(5)°$, $V = 4210(4)$ Å^3, $D_m = 1.787(2)$ (flotation in bromoform–benzene), $D_c = 1.823$ g cm^{-3}, $Z = 4$; Syntex $P2_1$ diffractometer, Mo-K_α radiation, $\lambda = 0.71069$ Å, $\mu = 15.0$ cm^{-1}. The cell dimensions were obtained by least-squares refinement of 11 precisely centered reflections in the range $6 < \theta < 17°$. The techniques used for data collection and reduction and for solution and refinement of the structure using a SHELX76 program were the same as described previously.[4] During the early stages in the structure solution it was impossible to distinguish nickel from manganese on the basis of electron density values. Spectral and magnetic

* Author to whom correspondence should be addressed.
† Present address: Institute of Macromolecular Chemistry, Czechoslovak Academy of Sciences, 162 06 Prague, Czechoslovakia.

properties,[3] however, clearly indicated that nickel is the atom that is coordinated by four phosphorus donors. This assignment was finally confirmed during anisotropic refinement which led to unreliable temperature factors if nickel was changed for manganese or vice versa. Although the positions of methylene hydrogens were obvious in the difference map, they were not included in the refinement because of limitations in the computer memory; their calculated coordinates are therefore given. All water hydrogens except four were located in the difference map and their positions were refined isotropically using one, overall value of $U_{iso} = 0.106$ Å^2. The final R values were

$$R = \sum|\Delta F|/\sum|F_o| = 0.061$$

and

$$R_w = (\sum|w\Delta F|^2/\sum w|F_o|)^{1/2} = 0.057,$$

with $w = [\sigma^2(F_o)]^{-1}$. Final atomic coordinates, thermal parameters and a list of bond lengths and angles have been deposited with the Cambridge Crystallographic Data Centre.

RESULTS AND DISCUSSION

A perspective drawing of the formula unit including intermolecular carboxylate bonds is given in Fig. 1 together with the atom numbering. Table 1 summarizes distances and angles within the metal ion environments. The structure consists of

Table 1. Distances (Å) and angles (°) within the coordination polyhedrons of the metal ions (ESDs in parentheses)

Distance		Angle			
		Ni environment			
Ni—P(1)	2.212(4)	P(1)—Ni—P(2)	85.4(1)	P(1)—Ni—P(3)	159.4(1)
Ni—P(2)	2.223(4)	P(2)—Ni—P(3)	98.0(1)	P(2)—Ni—P(4)	160.8(1)
Ni—P(3)	2.215(4)	P(3)—Ni—P(4)	84.9(1)		
Ni—P(4)	2.211(4)	P(4)—Ni—P(1)	98.7(1)		
		Mn(1) environment			
Mn(1)—W(1)	2.282(11)	O(13)[a]—Mn(1)—O(43)	94.4(4)	W(4)—Mn(1)—W(2)	88.6(4)
Mn(1)—W(4)	2.220(11)	O(13)[a]—Mn(1)—W(4)	87.4(4)	W(2)—Mn(1)—W(3)	86.6(4)
Mn(1)—W(2)	2.142(11)	O(13)[a]—Mn(1)—W(3)	89.4(4)	W(2)—Mn(1)—W(1)	89.3(4)
Mn(1)—W(3)	2.205(11)	O(13)[a]—Mn(1)—W(1)	94.7(4)	W(3)—Mn(1)—W(1)	89.1(4)
Mn(1)—O(43)	2.186(9)	O(43)—Mn(1)—W(4)	92.0(4)	O(13)[a]—Mn(1)—W(2)	174.3(4)
Mn(1)—O(13)[a]	2.119(9)	O(43)—Mn(1)—W(3)	175.2(4)	O(43)—Mn(1)—W(2)	89.8(4)
		O(43)—Mn(1)—W(1)	87.6(4)	W(4)—Mn(1)—W(1)	177.9(4)
		W(4)—Mn(1)—W(3)	91.1(4)	Mn(1)—W(1)—Mn(2)	111.0(4)
		Mn(2) environment			
Mn(2)—W(1)	2.263(12)	O(44)—Mn(2)—O(14)[a]	94.3(4)	W(1)—Mn(2)—O(11)[b]	88.0(3)
Mn(2)—W(5)	2.168(11)	O(44)—Mn(2)—W(1)	93.0(3)	O(11)[b]—Mn(2)—W(6)	88.2(4)
Mn(2)—W(6)	2.167(11)	O(44)—Mn(2)—W(6)	89.3(4)	O(11)[b]—Mn(2)—W(5)	88.1(4)
Mn(2)—O(11)[b]	2.206(9)	O(44)—Mn(2)—W(5)	91.1(4)	W(6)—Mn(2)—W(5)	95.9(4)
Mn(2)—O(44)	2.209(9)	O(14)[a]—Mn(2)—W(1)	91.9(4)	O(44)—Mn(2)—O(11)[b]	177.3(3)
Mn(2)—O(14)[a]	2.143(9)	O(14)[a]—Mn(2)—W(6)	176.4(4)	O(14)[a]—Mn(2)—O(11)[b]	88.2(4)
		O(14)[a]—Mn(2)—W(5)	83.9(4)	W(1)—Mn(2)—W(5)	174.4(4)
		W(1)—Mn(2)—W(6)	88.0(4)		
		Mn(3) environment			
Mn(3)—W(7)	2.274(10)	W(7)—Mn(3)—W(10)	90.9(4)	O(31)—Mn(3)—W(8)	88.2(5)
Mn(3)—W(8)	2.125(12)	W(7)—Mn(3)—O(31)	89.9(4)	W(9)—Mn(3)—W(8)	92.0(4)
Mn(3)—W(9)	2.239(10)	W(7)—Mn(3)—W(8)	86.9(4)	W(9)—Mn(3)—O(21)[c]	87.4(4)
Mn(3)—W(10)	2.184(11)	W(7)—Mn(3)—O(21)[c]	94.0(4)	W(8)—Mn(3)—O(21)[c]	91.5(5)
Mn(3)—O(21)[c]	2.230(10)	W(10)—Mn(3)—O(31)	90.4(4)	W(7)—Mn(3)—W(9)	178.3(4)
Mn(3)—O(31)	2.165(10)	W(10)—Mn(3)—W(9)	90.2(4)	W(10)—Mn(3)—W(8)	177.3(4)
		W(10)—Mn(3)—O(21)[c]	90.0(4)	O(31)—Mn(3)—O(21)[c]	176.1(3)
		O(31)—Mn(3)—W(9)	88.8(4)		

Symmetry code for Tables 1 and 2: [a] $1-x, 1-y, -z$; [b] $x+1, y, z$; [c] $x+1, \frac{1}{2}-y, \frac{1}{2}+z$; [d] $1-x, \frac{1}{2}+y, \frac{1}{2}-z$; [e] $x, \frac{1}{2}-y, \frac{1}{2}+z$; [f] $1-x, 1-y, 1-z$; [g] $1-x, y-\frac{1}{2}, \frac{1}{2}+z$; [h] $x-1, \frac{1}{2}-y, z-\frac{1}{2}$

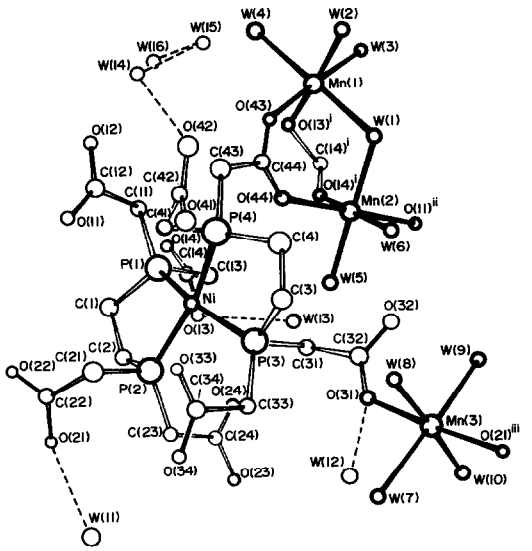


Fig. 1. Perspective view of the formula unit of the complex. W denotes an oxygen atom of a water molecule. Hydrogen atoms (omitted for clarity) are given the numbers of their bonding partners. Symmetry codes i, ii and iii correspond to [a], [b] and [c] in Table 1.

coordination polyhedra of the metal ions linked by intra- and intermolecular acetate groups, resulting in a three-dimensional network. Water molecules are of both the coordinated and lattice types and take part in extensive water-to-water and water-to-carboxylate hydrogen bonding which contributes to the stabilization of the structure.

The environment of nickel(II) is considerably distorted and can be considered as originating from a square by closing the P(1)—Ni—P(2) and P(3)—Ni—P(4) angles and twisting the appropriate PNiP planes to a dihedral angle of 29.6°, which corresponds to alternating the phosphorus atoms 0.383(3) Å below and above the mean NiP_4 plane. As the distortion of the two PNiP moieties is nearly identical and the nickel atom lies very closely within the mean plane, the effective symmetry of the coordination polyhedron approximates to D_2. Analogous but less serious distortions of this type, common in nickel(II) complexes of chelating bis(tertiary phosphines),[5] have usually been ascribed to the sterical bulk of the ligands. As can be seen from idealized geometry calculations, the unusually large distortion of the NiP_4 core found here is probably related to bonding of the acetate groups to manganese, especially through the bridging bidentate carboxyls involving C(14) and C(44). This explanation is supported by the comparison to a closely related nickel(II) complex with a little more sterically bulky phosphineacetate ligand,[4]

$HO_2CCH_2(C_6H_5)PCH_2CH_2P(C_6H_5)CH_2CO_2H$:

the P_4 core in this complex is considerably closer to the ideal square, obviously because the protonized acetate groups do not take part in any significant interaction except hydrogen bonding.

Because of its pronounced hard character, manganese(II) cannot compete with nickel(II) for the phosphorus donors; instead, it acts as the counterion to the NiL_2^{6-} anion. The three manganese ions are coordinated altogether by five carboxyl groups and 10 water molecules, forming three slightly distorted MnO_6 octahedra with an average Mn—O distance of 2.19(5) Å, average O—Mn—O angles of 90(3) and 179(4)° and a mean distance of the atoms from the octahedral equatorial planes of 0.00(3) Å. The Mn(1) and Mn(2) atoms are a part of a cluster of two octahedra sharing one axial water molecule and two *cis*-equatorial bridging bidentate carboxyl groups from two different formula units. A further monodentate carboxyl group belonging to a third formula unit is bonded to Mn(2) in the *trans*-equatorial position. The remaining coordination sites are occupied by water molecules. This arrangement strongly resembles a fragment of the structure of manganese(II) acetate tetrahydrate.[6] The Mn(3) atom belongs to a separate octahedron consisting of two axial monodentate carboxyl groups (one intramolecular and one from a fourth formula unit), completed by four equatorial water molecules. This system of carboxyl-to-manganese bonding constitutes the three-dimensional structure of the complex.

The distances and angles in the ligands are unexceptional and, compared to the free ligand,[2] reflect the coordination to the metal ions. Notably, the angles at the phosphorus atoms vary between 98.8 and 130.7° according to the distortion of the NiP_4 moiety. Both chelate rings adopt a λ-skew conformation with PCCP torsional angles of 44°. The CCOO fragments of the acetate groups are all remarkably planar and are of three different types with respect to the manganese ions: uncoordinated [involving C(24), C(34) and C(42)], monodentate to Mn(2) or Mn(3) [C(12), C(22) and C(32)] and bridging bidentate to the Mn(1), Mn(2) cluster [C(14) and C(44)]. The various environments of the carboxyl groups hardly influence, however, their geometry in any systematic and significant manner; this effect is common for many similar, extensively hydrogen-bonded carboxylate structures (see, for example, Ref. 7 for a recent review). In the present case, the C—O distances range from 1.212 to 1.279 Å [mean 1.25(2)], the O—C—O angles from 123.1 to 127.8° [mean 125(2)] and the C—C—O angles from 112.9 to 122.1° [mean 118(3)]. Undoubtedly, hydrogen bonding is the main averaging factor in the carboxylate geometry.

Table 2. Geometry of hydrogen bonds: distances (Å) and angles (°) with ESDs in parentheses

Oxygen atoms		Hydrogen atom	X—Y	X—H	Y—H	X—H—Y
X	Y					
W(1)	O(12)[b]	(W1)A	2.62(1)	1.0(2)	1.6(2)	160(10)
	O(41)[f]	(W1)B	2.63(2)	0.9(1)	1.7(1)	171(14)
W(2)	O(23)[d]	(W2)A	2.65(2)	0.8(2)	1.9(2)	155(15)
	O(41)[f]	(W2)B	2.79(2)	0.8(2)	2.1(2)	162(15)
W(3)	O(34)[d]	(W3)A	2.68(2)	1.4(2)	1.3(2)	152(12)
	W(11)[d]	(W3)B	2.72(2)	1.2(2)	1.7(2)	137(10)
W4)	W(7)[d]	(W4)A	2.89(2)	0.8(2)	2.3(2)	128(14)
	W(12)[d]	(W4)B[i]	2.59(3)			
W(5)	O(22)[b]	(W5)A	2.61(2)	0.8(2)	2.3(2)	104(14)
	W(13)	(W5)B	2.67(2)	1.0(2)	1.9(2)	130(11)
W(6)	O(32)	(W6)A	2.66(2)	1.0(2)	2.0(2)	121(12)
	O(42)[f]	(W6)B	2.69(2)	0.7(2)	2.1(2)	152(17)
W(7)	O(24)[e]	(W7)A	2.70(1)	1.0(2)	1.7(2)	168(11)
	O(22)[c]	(W7)B	2.72(2)	1.0(2)	1.8(2)	151(12)
W(8)	O(23)[e]	(W8)A	2.66(1)	1.0(2)	2.2(2)	109(12)
	W(15)[f]	(W8)B	2.66(2)	0.6(3)	2.1(2)	164(23)
W(9)	O(32)	(W9)A	2.70(1)	1.0(2)	1.9(2)	130(12)
	O(33)[b]	(W9)B	2.69(1)	0.9(2)	1.9(2)	149(12)
W(10)	O(34)[b]	(W10)A	2.70(1)	1.1(2)	1.6(2)	162(10)
	W(16)[g]	(W10)B[i]	2.73(2)			
W(11)	W(9)[h]	(W11)A	2.89(2)	1.3(2)	1.8(2)	138(11)
	O(21)	(W11)B	2.90(2)	1.0(2)	2.5(2)	104(10)
W(12)	O(31)	(W12)A[i]	2.57(3)			
		(W12)B[i]				
W(13)	O(13)	(W13)A	2.81(1)	1.2(2)	1.7(2)	144(10)
	W(16)[a]	(W13)B	2.78(2)	0.8(2)	2.1(2)	141(12)
W(14)	O(42)	(W14)A	2.67(2)	1.3(2)	1.4(2)	172(11)
		(W14)B		1.3(2)		
W(15)	O(43)	(W15)A	2.79(2)	0.8(2)	2.0(2)	170(12)
	W(14)	(W15)B	2.62(3)	1.3(2)	1.5(2)	139(10)
W(16)	O(12)	(W16)A	2.72(1)	1.2(2)	2.1(2)	106(10)
	W(15)	(W16)B	2.98(2)	0.9(2)	2.4(2)	128(12)

[i] Not found.

The O—H...O contacts which satisfy the criteria for hydrogen bonding[8] are summarized in Table 2. In general, each carboxylate oxygen except O(11), O(14) and O(44) acts as either a one- or a two-proton acceptor from water molecules. The environments of the water oxygen atoms approximate to trigonal or tetrahedral geometry and involve manganese ions as electron acceptors and carboxylate and/or water oxygen atoms as proton acceptors.

The present structure applies also for the other members of the isostructural series with Fe, Co, Ni, Zn and even Cd in place of Mn. Hence, the behaviour of the ligand towards nickel(II) is totally different from that of its nitrogen analogue, the formally similar complex of which, $Ni_2EDTA(H_2O)_6$, is composed[9] of the aquanickel(II) cations and the $Ni(EDTA)^{2-}$ anions with a hexadentate chelating ligand. Most probably, the remarkable tendency of nickel(II) to form the low-spin NiP_4 core is the factor that is mainly responsible for the difference.

REFERENCES

1. J. Podlahová and J. Podlaha, *Collect. Czech. Commun.* 1980, **45**, 2049.
2. J. Podlahová, B. Kratochvíl, V. Langer, J. Šilha and J. Podlaha, *Collect. Czech. Chem. Commun.* 1981, **46**, 3063.
3. J. Podlahová, L. Kavan, J. Šilha and J. Podlaha, *Polyhedron* 1984, **3**, 963.
4. J. Podlahová, B. Kratochvíl and V. Langer, *Inorg. Chem.* 1981, **20**, 2160.

5. T. S. Cameron and C. K. Prout, *Acta Cryst.* 1972, **28B**, 2021; B. L. Barnett, C. Krueger, Y.-H. Tsay, R. H. Summerville and R. Hofman, *Chem. Ber.* 1977, **110**, 3900; D. J. Brauer and C. Krueger, *J. Organomet. Chem.* 1979, **165**, C39; D. L. Allen, V. C. Gibson, M. L. H. Green, J. F. Skinner, J. Bashkin and P. D. Grebenik, *J. Chem. Soc., Chem. Commun.* 1983, 895; P. Dapporto, M. Ciampolini, N. N. Nardi and F. Zanobini, *Inorg. Chim. Acta* 1983, **76**, L153; H. M. Buch, P. Binger, R. Goddard and C. Krueger, *J. Chem. Soc., Chem. Commun.* 1983, 648; M. Basato, B. Corain, G. Favero and G. Valle, *Z. Krist.* 1984, **167**, 153.
6. E. F. Bertaut, T. Q. Duc, P. Burlet, P. Burlet, M. Thomas and J. M. Moreau, *Acta Cryst.* 1974, **30B**, 2234.
7. M. A. Porai-Koshits and T. N. Polynova, *Koord. Khim.* 1984, **10**, 725.
8. M. Falk and O. Knop, In *Water—A Comprehensive Treatise* (Edited by F. Franks), Vol. 2, p. 70. Plenum Press, New York (1973). R. Taylor and O. Kennard, *J. Am. Chem. Soc.* 1982, **104**, 5063.
9. A. I. Pozhidayev, N. N. Neronova, T. N. Polynova, M. A. Porai-Koshits and N. A. Ezerskaya, *Zh. Neorg. Khim.* 1981, **26**, 1418.

Polyhedron Vol. 5, No. 3, pp. 805–810, 1986
Printed in Great Britain

0277–5387/86 $3.00 + .00
Pergamon Press Ltd

POLAROGRAPHIC STUDY OF MIXED-LIGAND COMPLEX STABILITY CONSTANTS AND KINETIC PARAMETERS OF REDUCTION OF Cr(III)–ETHYLENEDIAMINE–SUCCINATE SYSTEM

JYOTI SHARMA and ARVIND KUMAR

Department of Chemistry, Delhi University, Delhi 110007, India

B. K. PURI*

Department of Chemistry, Indian Institute of Technology, Hauz Khas, New Delhi 110016, India

and

M. SATAKE

Faculty of Engineering, Fukui University, Fukui 910, Japan

(*Received* 22 *July* 1985; *accepted* 1 *August* 1985)

Abstract—Stability constants of the binary species Cr(III)–ethylenediamine, Cr(III)–succinate and mixed-ligand complex Cr(III)–ethylenediamine–succinate have been determined polarographically by the method of Sundaresan and Sundaram at 30 ± 0.2°C at a constant ionic strength [$\mu = 0.6$ M (NH_4ClO_4)]. The values of the stability constants obtained by this method are compared with those reported in the literature. The positive values of the mixing constants for the mixed-ligand complexes indicate that the mixed-ligand complexes are more stable than simple binary complexes. The reduction of the simple and mixed complexes is irreversible at a dropping mercury electrode: therefore, kinetic parameters like the standard rate constant, transfer coefficient and activation energy have also been calculated.

Mixed complexes of chromium have been studied extensively by various techniques.[1–4] After the development of Schaap and McMaster's method[5] for the determination of composition and stability constants of the mixed-ligand complexes, the polarographic technique has also received considerable attention in this field. Recently mixed-ligand complexes of certain transition metals have been studied polarographically.[6] Although, the polarographic behaviour of chromium in the presence of different electrolytes[7] and complexing agents[8,9] has been studied, a survey of the literature reveals that the mixed-ligand complex Cr(III)–ethylenediamine (en)–succinate has not been studied polarographically so far. In the present paper, the polarographic investigation of the binary and ternary complexes formed by Cr(III) with en and succinate ligands is reported using the method of Sundaresan and Sundaram.[10] Various kinetic parameters, i.e. the reaction rate constant, transfer coefficient (α) and activation energy (Q), have also been calculated in each case.

EXPERIMENTAL

Materials

All the chemicals used were of analytical grade and their solutions were prepared in conductivity water. The ionic strength (μ) was maintained constant [0.6 M (NH_4ClO_4)]. En and sodium succinate were used as

* Author to whom correspondence should be addressed.

Table 1. Cr(III)–en system[a]

[En] (M)	$\Delta E_{1/2}$ (V vs SCE)	$F'_0(X)$ ($\times 10^{-4}$)	$F'_1(X)$ ($\times 10^{-6}$)	$F'_2(X)$ ($\times 10^{-7}$)	$F'_3(X)$ ($\times 10^{-8}$)
0.01	0.282	4.92	4.67	—	—
0.02	0.300	9.81	4.78	1.40	6.00
0.03	0.312	15.54	5.09	1.96	5.88
0.04	0.322	22.80	5.63	2.82	5.36
0.05	0.330	30.98	6.14	3.28	6.16
0.06	0.338	42.10	6.97	4.11	6.52
0.07	0.345	55.93	7.94	4.91	6.73

[a] Cr(III) = 0.5 mM, μ = 0.6 M (NH_4ClO_4), temperature = 30 ± 0.2°C, t = 3.6 s, $D = 2.0 \times 10^{-6}$ cm^2 s^{-1}, $\alpha = 0.308$.

$1/C = 2.5 \times 10^3$, $\beta_{10}/C = 4.5 \times 10^6$, $\beta_{20}/C = 2.0 \times 10^6$, $\beta_{30}/C = 6.1 \times 10^8$, $K_s = 7.56 \times 10^{-5}$ cm s^{-1}.

$\beta_{10} = 1.8 \times 10^3$, $\beta_{20} = 8.0 \times 10^2$, $\beta_{30} = 2.44 \times 10^5$, $Q = 54.10$ kcal mol^{-1}.

$\log \beta_{10} = 3.25$, $\log \beta_{20} = 2.903$, $\log \beta_{30} = 5.397$.

ligands. Triton X-100 (0.002%) was used as the maximum suppressor.

Apparatus and procedure

Polarograms in all instances were recorded at 30 ± 0.2°C with a manual polarograph (Toshniwal CLO2) in conjunction with a polyflex galvanometer (Toshniwal PL 50). A sturated calomel electrode (SCE) was used as the reference electrode. It was connected to the polarographic cell through a potassium chloride agar–agar bridge. The dropping mercury electrode (DME) had the following characteristics: $m^{2/3}t^{1/6} = 2.120$ mg$^{2/3}$ s$^{-1/2}$, and $h_{corr} = 30$ cm in 0.1 M NH_4ClO_4 with open circuit. Oxygen was expelled by passing a slow stream of purified nitrogen into the test solution.

RESULTS AND DISCUSSION

Cr(III) gives two well-defined reversible diffusion-controlled waves in NH_4ClO_4 with $E_{1/2} = -0.9$ V and -1.46 V vs SCE. However, in the presence of en and succinate separately it only gives a single well-defined wave. The slopes of linear plots of $\log i/(i_d - i)$ vs $E_{d.e}$ are of the order of 80 ± 1 mV in both the cases, indicating an irreversible reduction. $E_{3/4} - E_{1/4}$ values also confirm irreversible reduction of the metal complexes. The number of electrons (n) involved in the reduction process was determined by the millicoulometric method of DeVries and Kroon.[11] This gave $n = 3$ in all cases. The value of $n\alpha$ was obtained by equating the slope of the log plot to $-0.0542/n\alpha$. The values of α are given in Tables 1 and 2 for Cr(III)–en and Cr(III)–succinate systems.

Table 2. Cr(III)–succinate system[a]

[Succinate] (M)	$\Delta E_{1/2}$ (V vs SCE)	$F'_0(Y)$ ($\times 10^{-2}$)	$F'_1(Y)$ ($\times 10^{-3}$)	$F'_2(Y)$ ($\times 10^{-3}$)	$F'_3(Y)$ ($\times 10^{-4}$)
0.04	0.140	2.14	3.85	—	—
0.08	0.155	3.80	4.01	5.12	3.40
0.12	0.166	5.80	4.33	6.15	3.12
0.16	0.175	8.19	4.74	9.40	2.95
0.20	0.184	11.57	5.48	9.40	3.50
0.24	0.192	15.66	6.27	11.15	3.64

[a] Cr(III) = 0.5 mM, μ = 0.6 M (NH_4ClO_4), temperature = 30 ± 0.2°C, t = 3.6 s, $D = 2.2 \times 10^{-6}$ cm^2 s^{-1}, $\alpha = 0.508$.

$1/C = 6 \times 10^1$, $\beta_{01}/C = 3.6 \times 10^3$, $\beta_{02}/C = 2.4 \times 10^3$, $\beta_{03}/C = 3.31 \times 10^4$, $K_s = 1.00 \times 10^{-4}$ cm s^{-1}, $Q = 52.37$ kcal mol^{-1}.

$\beta_{01} = 60$, $\beta_{02} = 40$, $\beta_{03} = 5.5 \times 10^2$.

$\log \beta_{01} = 1.7781$, $\log \beta_{02} = 1.602$, $\log \beta_{03} = 2.741$.

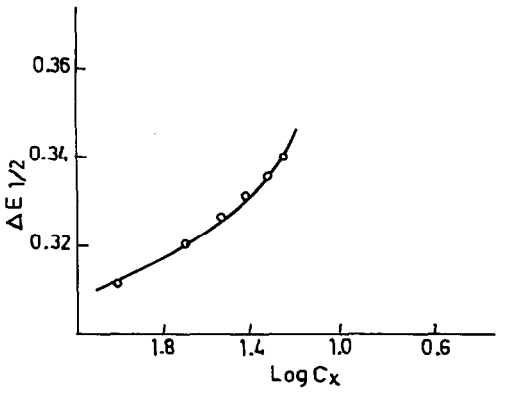


Fig. 1. Cr(III)–en system. Plot of log C_x vs $\Delta E_{1/2}$. Cr(III) = 0.5 mM, μ = 0.6 M (NH_4ClO_4), $m^{2/3}t^{1/6}$ = 2.120 $mg^{2/3}$ $s^{-1/2}$, h_{corr} = 30.0 cm, temperature = 30±0.2°C.

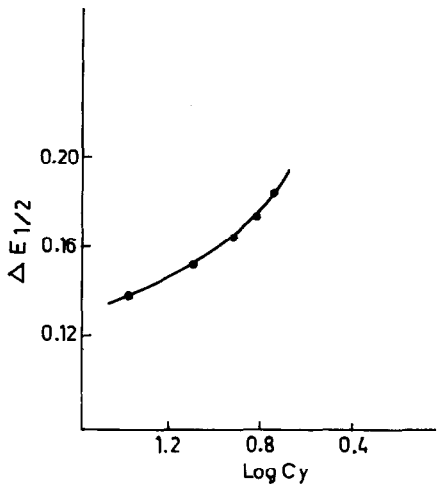


Fig. 2. Cr(III)–succinate system. Plot of log C_y vs $\Delta E_{1/2}$. Conditions as in Fig. 1.

Since these complexes are reduced irreversibly at the DME, the composition, stability constants and reaction rate constants were calculated by the method of Sundresan and Sundaram.[10] The Q of the electrode reaction was calculated by the usual relationship:[12] $Q = 577.8(5.097 - \log K_s)$ (K_s = standard rate constant). The values are summarized in Tables 1 and 2.

Cr(III)–*en and* Cr(III)–*succinate systems*

The formation of the complex is evident in both cases as the $E_{1/2}$ gets shifted to a more negative potential with increasing concentration of the ligand, en or succinate. A plot of $\Delta E_{1/2}$ vs log [X] (where X is en or succinate) was a smooth curve (Figs 1 and 2), indicating the formation of successive complexes. The function $F'(X)$ has been calculated at different concentrations of ligands and is represented in Figs 3 and 4. The analysis shows that Cr(III) reacts with these ligands in ratios of 1 : 1, 1 : 2 and 1 : 3. The values of the stability constants and K_s are given in Tables 1 and 2.

Cr(III)–*en–succinate system*

After studying simple complexes of Cr(III) with en and succinate separately, attempts have been made to study the mixed complexes of Cr(III) with en and succinate present together. The present study of these mixed complexes was carried out at two different concentrations of succinate ions. The concentration of en was varied from 0.01 to 0.07 M

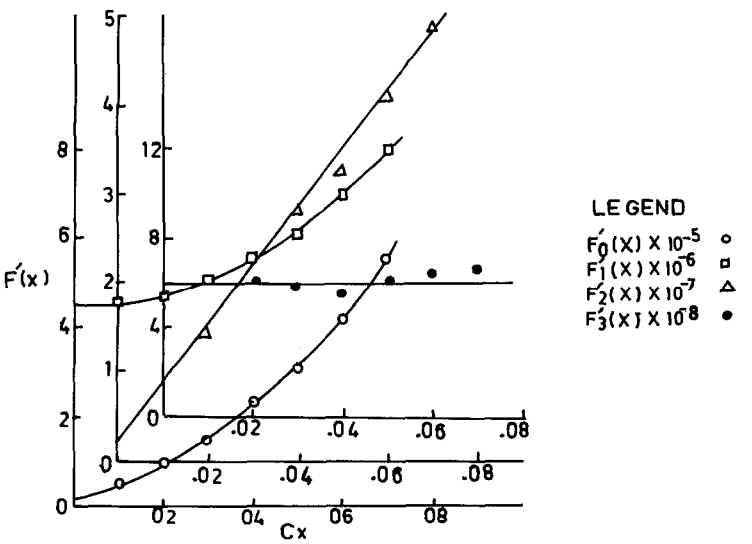


Fig. 3. Cr(III)–en system. Plot of $F'(X)$ vs C_x. Conditions as in Fig. 1.

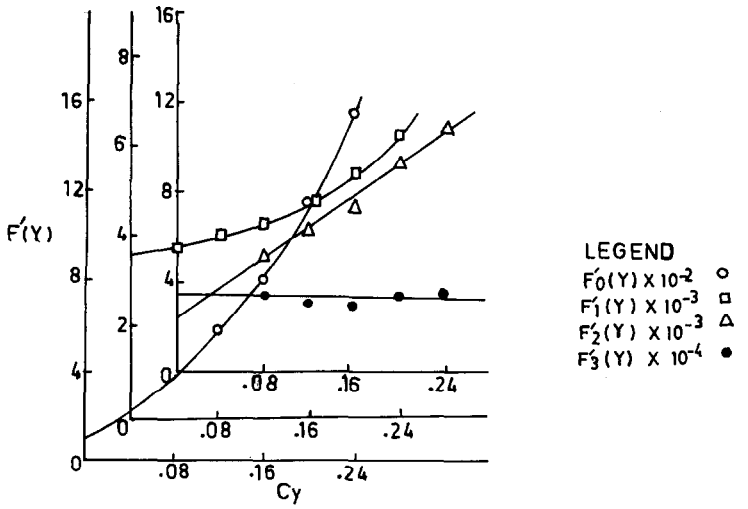


Fig. 4. Cr(III)–succinate system. Plot of $F'(X)$ vs C_y. Conditions as in Fig. 1.

(Table 3) while that of succinate was kept constant at 0.08 M in one set, series 1, and 0.16 M in the second set, series 2. The ionic strength and metal ions concentration were the same as for the binary systems. The $E_{1/2}$ values were more negative than those obtained in the absence of succinate, indicating the formation of mixed complexes. The slopes of a conventional log plot and also from $E_{3/4}-E_{1/4}$ indicate irreversible reduction: therefore, the method of Schaap and McMaster[5] cannot be applied for the determination of stability constants of this system. Hence, the method of Sundaresan and Sundaram[10] has been applied to estimate the stability constants of the mixed-ligand complexes and kinetic parameters. It is inferred that Cr(III) forms two mixed complexes $[Cr(en)(succinate)_2]^-$ (1:1:2) and $[Cr(en)_2(succinate)]^+$ (1:2:1) with the ligands.

Table 3. Cr(III)–en–succinate system[a]

[En] (M)	$\Delta E_{1/2}$ (V vs SCE)	$F'(X,Y)$ ($\times 10^{-5}$)	$F'(X,Y)$ ($\times 10^{-6}$)	$F'(X,Y)$ ($\times 10^{-7}$)	$F'(X,Y)$ ($\times 10^{-9}$)
		[Succinate] = 0.08 M (fixed)			
0.01	0.296	0.85	3.50	—	—
0.02	0.308	1.35	4.25	6.20	—
0.03	0.318	1.98	4.93	6.40	1.60
0.04	0.328	2.91	6.02	7.50	1.47
0.05	0.338	4.27	7.54	9.08	1.49
0.06	0.348	6.27	9.62	11.04	1.57
0.07	0.356	8.53	11.47	12.10	1.50
		[Succinate] = 0.16 M (fixed)			
0.01	0.302	1.07	3.70	—	—
0.02	0.313	1.63	4.60	5.50	1.75
0.03	0.324	2.49	5.90	8.00	2.00
0.04	0.334	3.66	7.40	9.75	1.92
0.05	0.346	5.81	10.20	13.40	2.28
0.06	0.354	7.90	12.00	14.16	2.02
0.07	0.362	10.73	14.33	15.48	1.92

[a] Cr(III) = 0.5 M, μ = 0.6 M (NH_4ClO_4), temperature = 30 ± 0.2°C, t = 13.6 s, $D = 2.6 \times 10^{-6}$ cm^2 s^{-1}, α = 0.308.
Series 1: $K/C = 5 \times 10^4$, $L/C = 3 \times 10^8$, $M/C = 1.6 \times 10^7$, $N/C = 1.52 \times 10^9$.
Series 2: $K/C = 7 \times 10^4$, $L/C = 3.5 \times 10^6$, $M/C = 2 \times 10^7$, $N/C = 1.98 \times 10^9$.

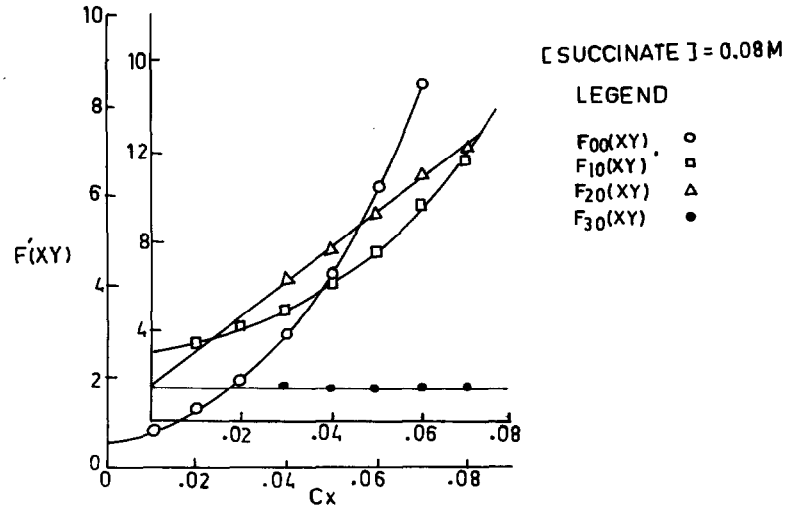


Fig. 5. Cr(III)–en–succinate system. [Succinate] = 0.08 M. Rest of the conditions as in Fig. 1.

From the plots of $F'(X,Y)$ vs C_x (concentration of en) (Figs 5 and 6, and Table 3) the following intercept values are obtained.

Series 1—[succinate] = 0.08 M:

$$K/C = 5 \times 10^4, \quad L/C = 3 \times 10^6,$$

$$M/C = 1.6 \times 10^6, \quad N/C = 1.52 \times 10^9.$$

Series 2—[succinate] = 0.16 M:

$$K/C = 7 \times 10^4, \quad L/C = 3.5 \times 10^6,$$

$$M/C = 2 \times 10^7, \quad N/C = 1.98 \times 10^9.$$

The constants K/C, L/C, M/C and N/C were evaluated graphically from the functions calculated at different concentrations of the ligand. The parameter C was obtained from the stability constants of the Cr(III)–succinate system. Hence, the parameters C, L, M and N were calculated and solved algebraically for stability constants of mixed complexes. The stability constants evaluated for the mixed-ligand complexes from intercept data are: log β_{11} = negative, log $\beta_{12} = 4.277$, and log $\beta_{21} = 5.225$. The negative value of β_{11} indicates the absence of $[Cr(en)(succinate)]^+$ in the aqueous solution. Stability constants of mixed complexes have also been calculated from the statistical consideration according to the relationship given by Tedesco and Martinez.[13] Log $\beta_{12} = 4.09$ and log $\beta_{21} = 4.96$ indicate that they are quite close to the present study.

The K_s for the reduction of mixed-ligand complexes is as calculated from the parameters C, t =

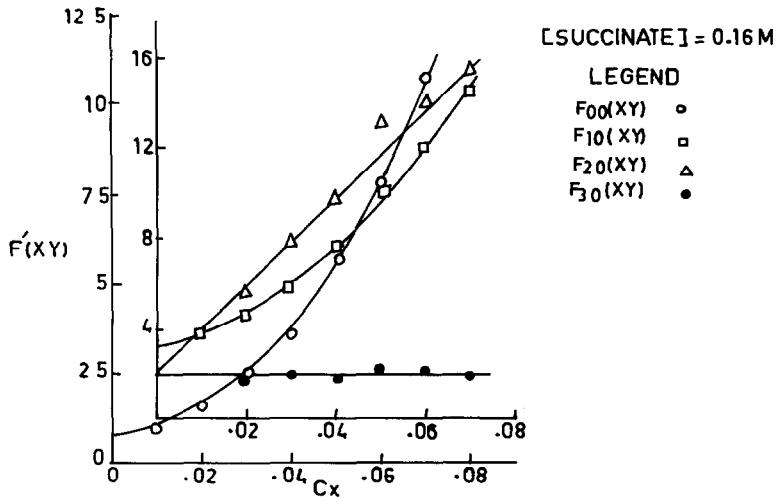


Fig. 6. Cr(III)–en–succinate system. [Succinate] = 0.16 M. Rest of the conditions as in Fig. 1.

Equilibrium	log K
1. $Cr^{3+} + en + 2(succinate)^{2-} \rightleftharpoons [Cr(en)_2(succinate)_2]^-$	4.277
2. $Cr^{3+} + 2en + succinate^{2-} \rightleftharpoons [Cr(en)_2(succinate)]^+$	5.225
3. $[Cr(succinate)_2]^- + en \rightleftharpoons [Cr(en)(succinate)_2]^-$	2.675
4. $[Cr(en)]^{3+} + 2(succinate)^{2-} \rightleftharpoons [Cr(en)(succinate)_2]^-$	1.374
5. $[Cr(en)_2]^{3+} + succinate^{2-} \rightleftharpoons [Cr(en)_2(succinate)]^+$	2.322
6. $[Cr(succinate)_3]^{3-} + en \rightleftharpoons [Cr(en)(succinate)_2]^- + succinate^{2-}$	1.536
7. $[Cr(succinate)_3]^{3-} + 2en \rightleftharpoons [Cr(en)_2(succinate)]^+ + 2(succinate)^{2-}$	3.625
8. $[Cr(en)_2]^{3+} + 2(succinate)^{2-} \rightleftharpoons [Cr(en)_2(succinate)]^+ + succinate^{2-}$	2.322
9. $[Cr(en)(succinate)_2]^- + en \rightleftharpoons [Cr(en)_2(succinate)]^+ + succinate^{2-}$	0.948

3.6 s, $D = 2.6 \times 10^{-6}$ cm^2 s^{-1} and $\alpha = 0.308$ (from log plot), and was found to be 5.97×10^{-5} cm s^{-1}. Q for the complex was found to be 53 kcal mol^{-1}.

The mixing constants[14] (K_m) for the reactions are given below:

$$[Cr(en)]^{3+} + [Cr(succinate)_2]^- \rightleftharpoons [Cr(en)(succinate)_2]^- + Cr^{3+}, \quad (1)$$

$$\tfrac{1}{2}[Cr(en)_2]^{3+} + [Cr(succinate)_2]^- \rightleftharpoons [Cr(en)(succinate)_2]^- + \tfrac{1}{2}Cr^{3+}, \quad (2)$$

$$[Cr(en)_2]^{3+} + [Cr(succinate)]^+ \rightleftharpoons [Cr(en)_2(succinate)]^+ + Cr^{3+}, \quad (3)$$

$$K_m(1) = \beta_{12}/(\beta_{10})(\beta_{02}),$$

$$K_m(2) = \beta_{12}/(\beta_{20})^{1/2}(\beta_{02}),$$

$$K_m(3) = \beta_{21}/(\beta_{20})(\beta_{01}),$$

which indicate the relative stability of mixed complexes in solution as compared to parent binary complexes. A positive value of K_m shows that the mixed complexes are more stable than simple complexes.

The results of the present study are summarized above. The numerical values show the logs of the equilibrium constants of the reactions indicated.

From these equilibrium constant values, it is evident that en can replace succinate from the mixed complex $[Cr(en)(succinate)_2]^-$ and thus the complexing tendency of en is higher than that of succinate.

Acknowledgements—Our sincere thanks are due to U.G.C. for providing financial assistance and also to Dr N. K. Kaushik for a valuable discussion.

REFERENCES

1. E. G. Sare and D. V. Jahangirdar, *J. Inorg. Nucl. Chem.* 1975, **37**, 985.
2. S. P. Tripathi, R. C. Sharma and G. K. Chaturvedi, *J. Inst. Chem. (Indian)*, 1980, **52**, 211.
3. M. Tanaka, *J. Inorg. Nucl. Chem.* 1974, **36**, 151.
4. H. Irving and D. N. Edigton, *J. Inorg. Nucl. Chem.* 1961, **21**, 169.
5. W. B. Schaap and D. L. McMaster, *J. Am. Chem. Soc.* 1961, **83**, 4699.
6. D. G. Dhuley and V. G. Dongre, *Indian J. Chem.* 1981, **20A**, 208.
7. L. Meites, *Polarographic Techniques*. Interscience, New York (1965).
8. J. J. Lingane and H. Kerlinger, *Ind. Eng. Chem. Anal.* 1941, **13**, 79.
9. Fischeroms, *Collect. Czech. Chem. Commun.*, 1965, **30**, 1771.
10. R. Sundaresan and A. K. Sundaram, *Indian J. Chem.* 1974, **12**, 868.
11. T. DeVries and J. L. Kroon, *J. Am. Chem. Soc.* 1953, **75**, 2484.
12. K. B. Yatsimuskii and V. P. Vasiler, *Instability Constants of Complex Compounds*. Pergamon Press, New York (1960).
13. P. H. Tedesco and J. Martinez, *J. Inorg. Nucl. Chem.* 1980, **42**, 95.
14. S. L. Jain, J. Kishan and R. C. Kapoor, *Indian J. Chem.* 1979, **18A**, 133.

Polyhedron Vol. 5, No. 3, pp. 811–813, 1986
Printed in Great Britain

0277-5387/86 $3.00 + .00
© 1986 Pergamon Press Ltd

PREPARATION AND SPECTROCHEMICAL PROPERTIES OF SOLUBLE VANADOPHOSPHATE POLYANIONS WITH BICAPPED-KEGGIN STRUCTURE

KENJI NOMIYA, KATSUHIKO KATO and MAKOTO MIWA*

Department of Industrial Chemistry, Faculty of Engineering, Seikei University, Musashino, Tokyo 180, Japan

(*Received* 8 *July* 1985; *accepted* 2 *September* 1985)

Abstract—Some soluble forms in aqueous and nonaqueous media of vanadophosphate with a bicapped-Keggin structure have been prepared. Some isopoly decavanadates derived during such preparations have also been reported. Their spectrochemical data (IR, UV–vis and MCD) are presented.

Vanadium is an element which can form hetero- and isopolyanions. Such vanadopolyanions are structurally distinct from the polyanions formed by elements such as molybdenum and tungsten, although the coexistence of vanadium with molybdenum, or tungsten, sometimes leads to mixed polyanions structurally related to the molybdo- or the tungstopolyanion.[1] In 1980, Sasaki *et al.*[2,3] determined the structure of the vanadophosphate polyanion by X-ray analysis, showing it to be a Keggin framework capped by two VO_5 trigonal bipyramids. The two caps occupy the *trans*-position of six pits on the surface of the Keggin framework. Confirmation of this conclusion has been obtained in the form of an insoluble guanidinium salt,

$$(CN_3H_6)_8H[PV_{14}O_{42}]\cdot 7H_2O,$$

isolated from aqueous solutions of phosphate and vanadate (P : V = 1 : 4) at pH 2.7. This salt, which is easily obtained by sodium salt metathesis, is the most suitable one for the X-ray study. However, other salts, which are soluble in aqueous and nonaqueous media, and suitable for spectrochemical studies, have been poorly characterized. In this paper, we report the preparation of a soluble vanadophosphate with counterions and show their spectrochemical data (IR, UV–vis and MCD). Furthermore, we also report briefly on the isopoly decavanadate, $[V_{10}O_{28}]^{6-}$, derived during such preparations.

EXPERIMENTAL

Preparations

$(CN_3H_6)_8H[PV_{14}O_{42}]\cdot H_2O$ (1).[3] $NaNO_3$ [4.5 g (37 mmol)] was dissolved in 25 cm^3 hot water, to which 6.2 cm^3 of 1.5 mol dm^{-3} phosphoric acid was added. The pH of the deep red solution is adjusted to 2–3 by 3 mol dm^{-3} nitric acid. Then, an aqueous solution containing 5.0 g (52.3 mmol) guanidine hydrochloride was added with stirring. Brown precipitates were immediately formed, which were insoluble in almost all solvents and could not be recrystallized. They were washed several times with ethanol and then thoroughly with water. Found: C, 5.0; H, 3.1; N, 17.8. Calc. for $(CN_3H_6)_8H[PV_{14}O_{42}]\cdot H_2O$: C, 5.0; H, 2.7; N, 17.5%.

From the coloured aqueous washings, orange needle crystals of isopoly decavanadate are obtained. Found: C, 5.0; H, 3.3; N, 17.6. Calc. for $(CN_3H_6)_6[V_{10}O_{28}]\cdot 6H_2O$: C, 5.0; H, 3.4; N, 17.7%

In the preparation of vanadophosphate, other precipitating agents could not be used in place of guanidine hydrochloride. For instance, when an aqueous solution containing tetrabutylammonium bromide was added, the tetrabutylammonium salt of decavanadate was mainly obtained. It could be recrystallized from acetonitrile. Found: C, 33.9; H, 6.7; N, 2.5. Calc. for $[(C_4H_9)_4N]_3H_3[V_{10}O_{28}]$: C, 34.2; H, 6.6; N, 2.5%.

* Author to whom correspondence should be addressed.

(K, H)$_9$[$PV_{14}O_{42}$]·nH_2O (**2**). The deep red aqueous solution obtained in the preparation of **1**, the pH of which had been adjusted to 2–3 by nitric acid, was kept at 50°C in a steam bath, to which an aqueous solution at 50°C containing 10 g KCl was slowly added. After stirring, the solution was left standing overnight at room temperature. Fine black crystals were obtained with a yield of 4.8 g. They were very soluble in water, slightly soluble in methanol and ethanol, and almost insoluble in ether, acetone and acetonitrile. In this preparation, the reaction temperature of 50°C was important: if it was lower, compound **2** was contaminated by an orange compound, potassium decavanadate, and, at room temperature, the latter became the main product.

[$(C_4H_9)_4N$]$_4H_5$[$PV_{14}O_{42}$]·$4H_2O$ (**3**). Compound **2** (3.5 g) was dissolved in water (below 50°C) and then an aqueous solution containing excess tetrabutylammonium bromide was added. After stirring at 50–60°C for a few minutes, dark brown precipitates were collected on a filter which could be recrystallized from acetonitrile. They were very soluble in acetonitrile, slightly soluble in acetone, and insoluble in water, methanol, ethanol and ether. Found: C, 31.3; H, 6.2; N, 2.3. Calc. for [$(C_4H_9)_4N$]$_4H_5$[$PV_{14}O_{42}$]·$4H_2O$: C, 31.2; H, 6.4; N, 2.3%. From the red aqueous filtrate in this preparation, the same precipitates could not be obtained again even by further addition of the aqueous solution of tetrabutylammonium bromide. The filtrate contained salts with different compositions of counterions because the evaporated solids showed the characteristic IR of vanadophosphate.

The tetrabutylammonium salt (**3**) was also obtained by another method. The red aqueous solution containing compound **2** (5 g) was passed through an H^+-ion exchange resin column (Dowex-50W) and eluted with water. The vanadophosphate was converted to the free-acid form without decomposition. The eluted aqueous solution was evaporated to a small volume and then an aqueous solution containing excess tetrabutylammonium bromide was added. After stirring at 50–60°C for a few minutes, dark brown precipitates were filtered and recrystallized from acetonitrile. Found: C, 31.2; H, 6.3; N, 2.3. Calc. for [$(C_4H_9)_4N$]$_4H_5$[$PV_{14}O_{42}$]·$4H_2O$: C, 31.2; H, 6.4; N, 2.3%.

In order to compare IR spectra, sodium decavanadate $Na_6[V_{10}O_{28}]\cdot nH_2O$ was prepared from $NaVO_3$ and glacial acetic acid by a modification described in the literature.[4]

UV–vis absorption spectra were measured on an Hitachi 340-spectrophotometer with a computer keyboard attached. The MCD spectra were recorded by a JASCO J-40AS spectropolarimeter with a 1-T electromagnet mounted on it. IR spectra were recorded by a JASCO IR-G spectrophotometer. Measurements were made at room temperature.

RESULTS AND DISCUSSION

Some salts of vanadophosphate obtained here, except the guanidinium salt, are soluble in appropriate solvents. The potassium salt (**2**) especially is very soluble in water and can be used for preparing other salts.

The acidity of the free acid of vanadophosphate obtained as a powder from the eluted solution of a cation-exchange resin column was not as strong as that of the Keggin molybdo- and tungsto-heteropolyacids. In fact, acid catalysis of the polymerization of benzyl alcohol to polybenzyl could not be observed.[5]

Generally, the maximum number of bulky tetrabutylammoniums in the counterions is significantly related to the size, rather than to the charge, of the polyanion. For instance, the maximum number is four for the Keggin heteropolyanion and six for the Dawson one. Thus, it should be noted that it is four in the bicapped-Keggin vanadophosphate.

IR spectra of vanadophosphate (D_{2d}-symmetry) with some counterions are shown in Fig. 1. The vibrational structure of the polyanion moiety is

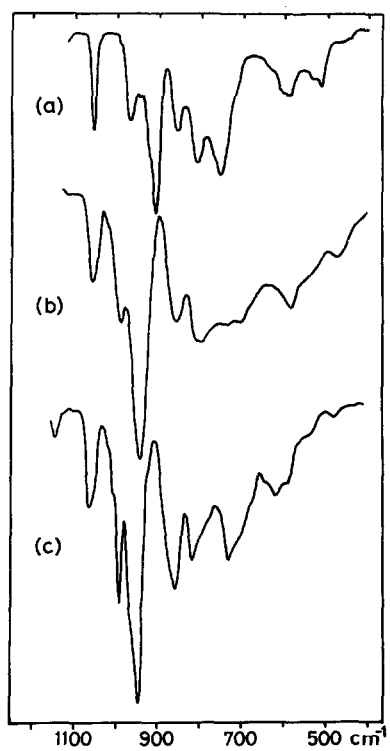


Fig. 1. IR spectra measured in KBr disk of vanadophosphates with counterions: (a) $(CN_3H_6)_8H[PV_{14}O_{42}]\cdot H_2O$, (b) (K, H)$_9$[$PV_{14}O_{42}$]·$nH_2O$, and (c) [$(C_4H_9)_4N$]$_4H_5$[$PV_{14}O_{42}$]·$4H_2O$.

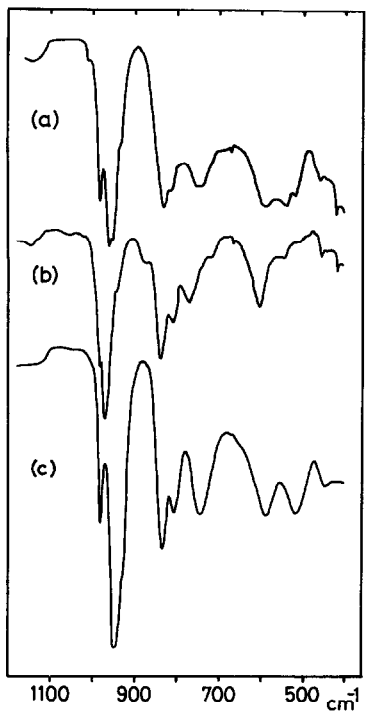


Fig. 2. IR spectra measured in KBr disk of decavanadates with counterions: (a) $(CN_3H_6)_6[V_{10}O_{28}]\cdot 6H_2O$, (b) $[(C_4H_9)_4N]_3H_3[V_{10}O_{28}]$, and (c) $Na_6[V_{10}O_{28}]\cdot nH_2O$.

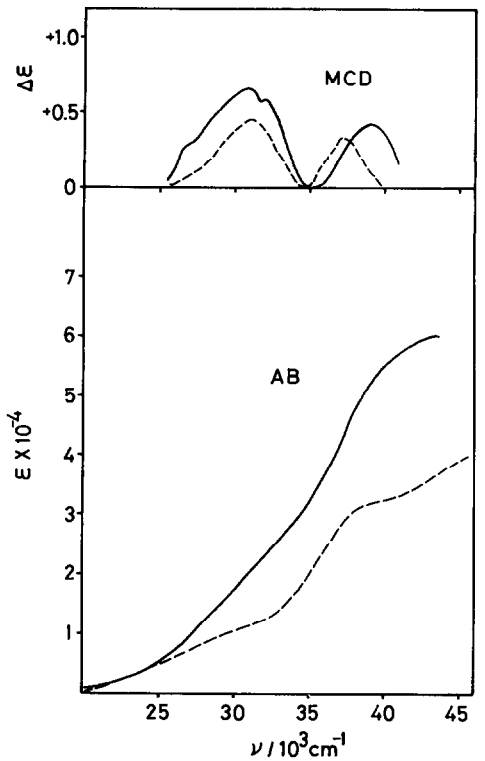


Fig. 3. Electronic absorption and MCD spectra in acetonitrile solution of $[(C_4H_9)_4N]_4H_5[PV_{14}O_{42}]\cdot 4H_2O$ (full line) and $[(C_4H_9)_4N]_3H_3[V_{10}O_{28}]$ (dashed line).

subtly changed by counterions, especially in the low-frequency region. The characteristic band at 1050–1060 cm^{-1} is due to P—O stretching and many bands in the region of 1000–500 cm^{-1} are due to the various V—O vibrations. These patterns are more complicated than those of a Keggin heteropolyanion with T_d-symmetry. The IR spectra of decavanadate are also changed by counterions, depending upon whether the proton is contained or not (Fig. 2). IR patterns of $(CN_3H_6)_6[V_{10}O_{28}]$ and $Na_6[V_{10}O_{28}]$ are very close to each other; however, they are different from that of $[(C_4H_9)_4N]_3H_3[V_{10}O_{28}]$ in the region of 850–600 cm^{-1}. These are presumably caused by either or both of two possibilities, the existence of an anion–anion interaction in the case of a small-size counterion[6] and the protonation of the surface oxygens of the polyanion.[7]

Electronic absorption and MCD spectra in acetonitrile solution are shown in Fig. 3 as full lines for $[(C_4H_9)_4N]_4H_5[PV_{14}O_{42}]\cdot 4H_2O$ and as dashed lines for $[(C_4H_9)_4N]_3H_3[V_{10}O_{28}]$. All of these absorptions and MCD are due to the V ← O charge-transfer (CT) transitions. In the absorption spectra, there is a very broad shoulder (ε *ca* 20,000) around 30,000 cm^{-1} and a strong broad band (ε *ca* 60,000) around 43,000 cm^{-1} for the vanadophosphate, and a shoulder (ε *ca* 10,000) around 30,000 cm^{-1} and a broad band (ε *ca* 32,000) around 40,000 cm^{-1} for the decavanadate. The intensities of the absorptions of vanadophosphate are larger than those of decavanadate. The absorption position of the lowest-energy CT is almost unchanged in the two vanadopolyanions; however, that of the second CT of vanadophosphate is shifted more to the high-frequency region than that of decavanadate. These tendencies are also observed in the MCD spectra, which consist of two positive components. No negative MCD component appears in this region. The MCD in the first CT region of vanadophosphate contains further components.

REFERENCES

1. M. T. Pope, *Heterpoly and Isopoly Oxometalates.* Springer, New York (1983).
2. R. Kato, A. Kobayashi and Y. Sasaki, *J. Am. Chem. Soc.* 1980, **102**, 6572.
3. R. Kato, A. Kobayashi and Y. Sasaki, *Inorg. Chem.* 1982, **21**, 240.
4. G. K. Johnson and R. K. Murmann, *Inorg. Synth.* 1979, **19**, 140.
5. K. Nomiya, T. Ueno and M. Miwa, *Bull. Chem. Soc. Jpn* 1980, **53**, 827.
6. C. Rocchiccioli-Deltcheff, M. Fournier and R. Franck, *Inorg. Chem.* 1983, **22**, 207.
7. H. T. Evans, Jr and M. T. Pope, *Inorg. Chem.* 1984, **23**, 501.

Polyhedron Vol. 5, No. 3, pp. 815–819, 1986
Printed in Great Britain

0277–5387/86 $3.00 + .00
© 1986 Pergamon Press Ltd

STEREOSELECTIVE ASSOCIATION BETWEEN OPTICALLY ACTIVE TRIS(1,10-PHENANTHROLINE)RUTHENIUM(II) AND TRIS(ACETYLACETONATO)COBALT(III) IN WATER

ETSURO IWAMOTO,* HITOKO SAITO and YUROKU YAMAMOTO

Department of Chemistry, Faculty of Science, Hiroshima University, Hiroshima 730, Japan

(*Received* 29 *April* 1985; *accepted after revision* 2 *September* 1985)

Abstract—Stereoselective interactions between tris(acetylacetonato)cobalt(III) [$Co(acac)_3$] and optically active Λ-$(+)_{546}$-tris(1,10-phenanthroline)ruthenium(II) chloride [Λ-$[Ru(phen)_3]Cl_2$] were investigated by measuring the distribution coefficients of racemic $Co(acac)_3$ between carbon tetrachloride and water containing Λ-$[Ru(phen)_3]^{2+}$ or pure water, and the optical rotations of the aqueous phase was measured over the temperature range 10–40° C. The Λ-isomer of $Co(acac)_3$ is "salted-in" more strongly by Λ-$[Ru(phen)_3]^{2+}$ than the Δ-isomer. The association constants between Λ-$[Ru(phen)]^{2+}$ and Λ- or Δ-$Co(acac)_3$ were calculated by using the optical rotation to give $K(\Lambda\text{–}\Lambda) = 3.86$ and $K(\Lambda\text{–}\Delta) = 3.80$ at 25°C, respectively. The temperature dependence of the association constants showed that the enthalpy and entropy changes for the Λ–Λ association is slightly more positive than those for the Λ–Δ association. This was discussed from the viewpoint of hydrophobic interactions.

The optical resolution of neutral tris(β-diketonato)metal chelates has been effectively carried out by liquid column chromatography.[1–6] Recently a facile large-scale optical resolution of the neutral chelates through selective complex formation with (2*R*,3*R*)-(−)dibenzoyltartaric acid was also reported.[7] However, the enantioselective interactions in solution have not been investigated quantiatively, probably because the weak interactions make it difficult to study batchwise equilibria, although, from a theoretical point of view, chiral discrimination energies for a complex analogous to the acetylacetone complex have been discussed.[8]

Recently, we showed that the tris(1,10-phenanthroline)–iron(II) chelate cation $[Fe(phen)_3]^{2+}$ "salts-in" more tris(acetylacetonato)cobalt(III) [$Co(acac)_3$] with large positive transfer enthalpy and entropy changes than do aliphatic ions such as tetraalkylammonium ions.[9] Such large aromatic ions strongly interact with non-electrolytes in aqueous solution due to the sigificantly coupled action of the structural effects of water and a van der Waals' interaction. We also found that this interaction leads to a stereoselective interaction between the optically active Δ-$[Ni(phen)_3]^{2+}$ ion and the Δ- or Λ-isomer of $Co(acac)_3$,[10] applied to the "salting-in" chromatography to optically resolve the octahedral neutral metal chelates.[5]

In the present paper, as an extention of the above findings, we investigated the stereoselective association thermodynamically. The optical active ruthenium(II) metal chelate electrolyte Λ-$[Ru(phen)_3]Cl_2$, which does not racemize, was used in place of optically active Δ-$[Ni(phen)_3]Cl_2$, which racemizes with a rate constant of 3.35×10^{-4} min^{-1} at 25°C. The partition method with solvent extraction was used for this salting-effect study. CCl_4 was selected as a solvent because $Co(acac)_3$ is distributed in water in such a way that the concentration in water can be determined spectrophotometrically.

EXPERIMENTAL

The tris(1,10-phenanthroline)ruthenium(II) salt was prepared by refluxing an aqueous solution of ruthenium(III) chloride (0.2 mol) with sodium tartrate (0.06 mol) until a greenish brown solution resulted, and then adding 1,10-phenanthroline (0.6 mol). The heating was continued until the colour changed to a deep orange red, when the mixture was filtered. The optically active complex Λ-$(+)_{546}$-$[Ru(phen)_3](ClO_4)_2 \cdot 2H_2O$ was resolved, in a

* Author to whom correspondence should be addressed.

similar manner to the iron complex, by the method of Dwyer and Gyarfas,[11] using the above solution and antimony (+)-tartrate. The perchlorate was transformed to the more soluble chloride with a Dowex 21K anion exchange resin in the Cl^- form with as little distilled water as possible. This solution gave a molecular rotation ($[M]_{546}$) of $-20{,}300$. The concentration of $[Ru(phen)_3]^{2+}$ determined spectrophotometrically.[12] $Co(acac)_3$ was prepared by a well-established procedure.[13] CCl_4 of reagent grade was used as received. The density of solutions was measured using a digital densimeter (Anton Paar Model DMA 02D).

Partition experiments

An aqueous solution (50 cm^3) of $[Ru(phen)_3Cl_2$ was agitated with CCl_4 solution (20 cm^3) containing *ca* 0.3 g of $Co(acac)_3$ for 1 h in a thermostatted water bath (± 0.05°C). After standing for 30 min, the aqueous solution (40 cm^3) was pipetted out and shaken with CCl_4 (10 cm^3) to extract $Co(acac)_3$. After separation, the CCl_4 extract was washed with water (1 cm^3) to prevent optical contamination by $[Ru(phen)_3]Cl_2$. The CCl_4 extraction was repeated 3 times, leading to a percentage extraction of $Co(acac)_3$ of more than 99%. The absorbance at 590 nm, molecular rotation at 546 nm, and circular dichroism of each CCl_4 solution were measured at ambient temperature using an Hitachi Model 139 spectrophotometer, a Perkin–Elmer Model 141 polarimeter, and a Jasco model J-40CS polarimeter, respectively.

RESULTS AND DISCUSSION

The distribution coefficient (K_d) is defined as the ratio of the concentration (mol kg^{-1}) of $Co(acac)_3$ in the aqueous phase to that in the organic phase. The K_d value for pure water is independent of the concentration (Table 1). Thus, the variation in activity coefficients of $Co(acac)_3$ in both phases is negligible. The CCl_4 solution containing an amount (*ca* 0.3 g) of $Co(acac)_3$ was used throughout the following experiments. The temperature dependence of K_d for Λ-$[Ru(phen)_3]Cl_2$ concentrations (mol kg^{-1}) of 0, 0.0976 and 0.144 is shown in Fig. 1. Increasing the temperature results in a decrease in K_d and increasing the concentration of the ruthenium chelate cation increases K_d. Furthermore, the temperature dependence of K_d in the presence of the ruthenium chelate cation is slightly less than that in pure water. These results are compatible with the view that the non-electrolyte $Co(acac)_3$ is a hydrophobic solute which is exothermically distributed in water and is endothermically salted in by the large aromatic cation $[Ru(phen)_3]^{2+}$, as observed for the salting effect of $[Fe(phen)_3]^{2+}$.[9]

Table 1. Dependence of the K_d^o of $Co(acac)_3$ on its concentration at 25°C[a]

$Co(acac)_3$[b] (g)	$-\log K_d^o$
0.1	1.336
0.2	1.339
0.3	1.338
0.4	1.339
0.5	1.331
	1.337[c]

[a] Aqueous : organic volume ratio is 20 : 50.
[b] Initial amounts in 20 cm^3 of CCl_4.
[c] Obtained using the solubility ratio from Ref. 18.

The optical rotations and concentrations of $Co(acac)_3$ partitioned in the aqueous phase containing the optically active Λ-ruthenium chelate cation were measured in the CCl_4 extracts without the ruthenium cation. The $Co(acac)_3$ is back-extracted into CCl_4 by four successive extractions but no appreciable absorbance was observed in the fourth extract within experimental error. Molecular rotations of each of the three extracts are shown in Fig. 2, and, as expected, it is clearly demonstrated that the later extract gives the higher molecular rotation. Figure 3 shows a typical CD spectrum of $Co(acac)_3$ distributed in the Λ-ruthenium chelate aqueous solution which is assigned to the Λ-isomer of $Co(acac)_3$.[4] Thus, the aqueous phase with the ruthenium chelate cation contained the Λ-isomer of

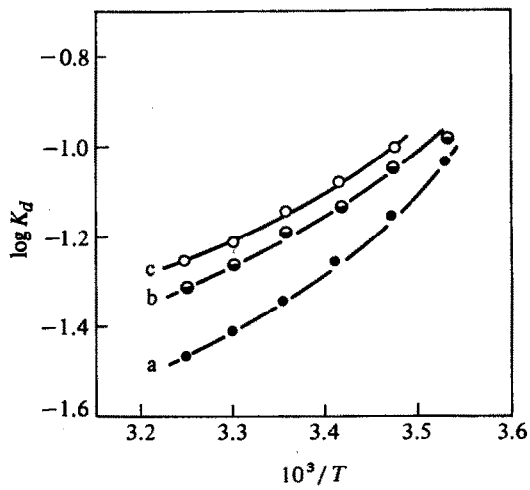


Fig. 1. Temperature (T) dependence of the distribution coefficient (K_d) of $Co(acac)_3$ between aqueous and CCl_4 phases. Concentration of $[Ru(phen)_3]^{2+}$ in water (mol kg^{-1}): (a) 0, (b) 0.0976, and (c) 0.144.

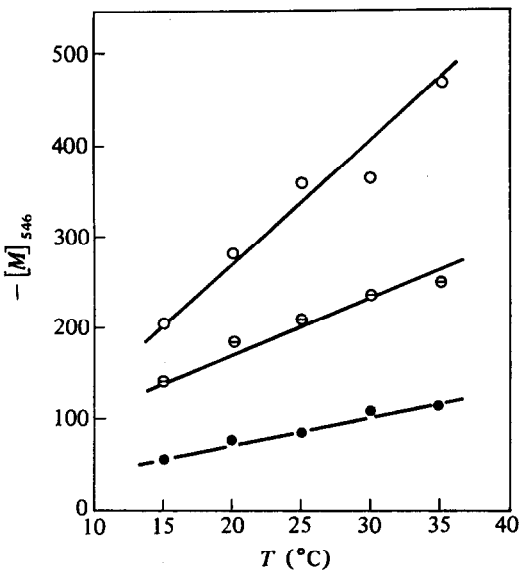


Fig. 2. Temperature (T) dependence of the molecular rotation ($[M]_{546}$) of $Co(acac)_3$ in CCl_4 extracts from the Λ-$[Ru(phen)_3]Cl_2$ solution (0.144 mol kg^{-1}). Extracts: (a) first, (b) second, and (c) third.

$Co(acac)_3$ as the excessive enantiomer, showing that the Λ–Λ pair interaction is stronger than the Λ–Δ pair interaction.

This observation is very similar to one made by Dwyer and Gyarfas.[14] Their performance was based on the view that the peripheral atoms in the tris-acetylacetone cobalt(III) complex probably carry a slight negative charge, and hence negative or anionic asymmetrical fields are associated with the antipodal form: therefore tris(ethylenediamine)cobalt(III) was selected as a multiply-charged optically active cation with which the maximum differential interaction in solution would be expected. However, our observation[9] concerning salting effects on the solubility of $Co(acac)_3$ showed that tris(ethylenediamine)cobalt(III) bromide "salts-out" it with a Setschnow coefficient (k_s) of 0.45 at 25°C but tris(1,10-phenanthroline)iron(II) bromide "salts-in" with a k_s of −2.7. These results caused us to expect that the phenanthroline complex could interact stereoselectively with $Co(acac)_3$ while the ethylenediamine complex could not. In practice we failed to observe the optical resolution of $Co(acac)_3$ by tris(ethylenediamine)cobalt(III) with the same procedure as for tris(1,10-phenanthroline)ruthenium(II). As stated later, the hydrophobic property of the optically active cation seems the most important. If the complex cation is triply-charged, even the phenanthroline complex "salts-out" $Co(acac)_3$: the k_s for tris(1,10-phenanthroline)cobalt(III) bromide is 0.21.

Table 2 summarizes the concentrations of $Co(acac)_3$ distributed in each phase for concentrations of 0.144 and 0.0976 mol kg^{-1} of the ruthenium chelate electrolyte, and the molecular rotation ($[M]_{546}$), and percentage resolution (R) in the aqueous phase, which was estimated by using an $[M]_{546}$ value of −28,920 for the complete resolution.[15]

Now we consider the association equilibria between $[Ru(phen)_3]^{2+}$ and $Co(acac)_3$ in aqueous solutions, assuming that $[Ru(phen)_3]Cl_2$ is completely dissociated and the $Co(acac)_3$ salted in by the ruthenium chelate cations is ascribed only to the association between them. The equilibria are:

$$\Lambda_{Ru}+\Lambda \rightleftharpoons \Lambda_{Ru}\Lambda, \qquad \Lambda_{Ru}+\Delta \rightleftharpoons \Lambda_{Ru}\Delta, \tag{1}$$

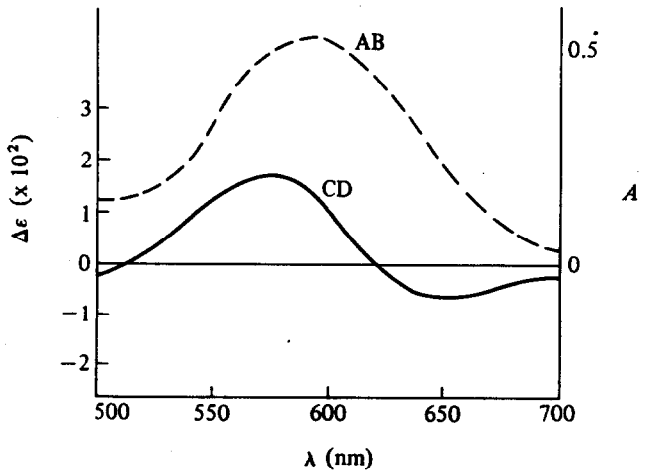


Fig. 3. Absorption (AB) and CD spectra for Λ-$Co(acac)_3$ (3.42×10^{-3} mol dm^{-3}) with $[M]_{546} = 50$ in the CCl_4 extract.

Table 2. Distribution results and Λ–Λ and Λ–Δ pair association constants for Λ-$[Ru(phen)_3]^{2+}$ and $Co(acac)_3$ at various temperatures[a]

t (°C)	K_d^o ($\times 10^2$)	$[Co(acac)_3]_w$[b] ($\times 10^3$ mol kg^{-1})	$[Co(acac)_3]_o$[c] ($\times 10^2$ mol kg^{-1})	$-[M]_{546}$	R (%)	$K(\Lambda\text{–}\Lambda)$	$K(\Lambda\text{–}\Delta)$
		(a) $[\Lambda\text{-}Ru(phen)_3^{2+}] = 0.0976$ mol kg^{-1}					
10	8.23	2.41	2.31	33.8	0.12	2.77	2.73
15	7.07	2.11	2.34	47.6	0.16	2.88	2.84
20	5.70	1.79	2.39	53.7	0.19	3.26	3.22
25	4.59	1.52	2.42	59.4	0.21	3.69	3.63
30	3.90	1.35	2.48	94.4	0.33	4.08	3.97
35	3.46	1.26	2.49	102	0.35	4.80	4.71
		(b) $[\Lambda\text{-}Ru(phen)_3^{2+}] = 0.144$ mol kg^{-1}					
15		2.30	2.32	75.9	0.26	2.82	2.77
20		2.00	2.37	103	0.36	3.38	3.31
25		1.71	2.41	114	0.39	3.86	3.80
30		1.50	2.44	133	0.46	4.06	3.96
35		1.39	2.46	142	0.49	4.46	4.34

[a] Amount of $Co(acac)_3$ in CCl_4 is *ca* 0.3 g.
[b] In aqueous phase.
[c] In organic phase.

with corresponding association constants $K(\Lambda\text{–}\Lambda)$ and $K(\Lambda-\Delta)$, respectively, where Λ_{Ru} is Λ-$[Ru(phen)_3]^{2+}$, and Λ and Δ are the Λ- and Δ-isomers of $Co(acac)_3$. The total concentration of $Co(acac)_3$, C_t, is written as:

$$C_t = [\Lambda_{Ru}\Lambda] + [\Lambda_{Ru}\Delta] + C_o, \qquad (2)$$

where C_o is the concentration of $Co(acac)_3$ when the ruthenium cation is absent, and is estimated using K_d and the concentration of $Co(acac)_3$ in CCl_4, C_{CCl_4}:

$$C_o = K_d C_{CCl_4}. \qquad (3)$$

For free $Co(acac)_3$:

$$[\Lambda] = [\Delta] = C_o/2. \qquad (4)$$

The excess Λ-isomer concentration, C, is given as:

$$C = [\Lambda_{Ru}\Lambda] - [\Lambda_{Ru}\Delta] = C_t R. \qquad (5)$$

The concentration of the ruthenium complex used is larger than that of $Co(acac)_3$:

$$[\Lambda_{Ru}] \gg [\Lambda_{Ru}\Lambda] \quad \text{and} \quad [\Lambda_{Ru}\Delta]. \qquad (6)$$

Using eqns (2)–(6) and K_d values, the association constants $K(\Lambda\text{–}\Lambda)$ and $K(\Lambda\text{–}\Delta)$ were calculated and are given in the last two columns in Table 2. The thermodynamic quantities of the Λ–Λ and Λ–Δ associations at a ruthenium complex concentration of 0.144 mol kg^{-1}, at which R is greater than at 0.0976 mol kg^{-1}, were calculated from the temperature dependence of the association constants in Table 2 and tabulated in Table 3.

The association constants of around 4 is comparable with the ionic association constant for

Table 3. Theremodynamic quantities of the Λ–Λ and Λ–Δ associations for Λ-$[Ru(phen)_3]^{2+}$–$Co(acac)_3$ at 25°C[a]

	ΔG^o (kJ mol^{-1})	ΔH^o (kJ mol^{-1})	ΔS^o (J mol^{-1} K^{-1})
Λ–Λ	−3.35	16.3	66
Λ–Δ	−3.31	15.9	64
Difference	−0.04	0.4	2

[a] Concentration of the ruthenium chelate cation is 0.144 mol kg^{-1}. Errors in the parameters are around 10%.

$[Fe(phen)_3]^{2+}Br^-$.[16] Considering that $Co(acac)_3$ is a non-polar non-electrolyte without the possibility of hydrogen bonding, the value seems rather large. The hydrophobic property of the tris(1,10-phenanthroline)metal(II) chelate cations[9,17] is mainly responsible for the marked association. As shown in Table 3, this association process has positive enthalpy and entropy changes and may be attributed to the resultant effect of the overlapping of their hydrophobic co-spheres: Strengthened hydrogen-bonded networks of water in the co-sphere of $Co(acac)_3$ are released by overlapping with the co-sphere of $[Ru(phen)]^{2+}$ and thereby the water molecules return to ordinary water with positive enthalpy and entropy changes.[9] The slight preference for the Λ-isomer compared to the Δ-isomer by the Λ-ruthenium chelate cation is accompanied by more positive enthalpy and entropy changes. Unfortunately, there are errors of around 10% in the free-energy and enthalpy changes and their differences between the two pairs seem unclear. However, the temperature trend for the Λ–Λ pair preference is reliable since it is based on direct measurements of the degree of chiral discrimination. These increases in enthalpy and entropy are explained by the view that the stronger van der Waals' interaction for the analogous like-chirality pair, where the three-bladed ligand planes of both of the solutes are parallel to each other if they approach along their three-fold axis, affects more favorably the co-sphere overlapping.

Acknowledgement—The work has been partially supported by a Grant-in-Aid for Scientific Research No. 58540363 from the Ministry of Education, Science and Culture.

REFERENCES

1. T. Moeller and E. Gulyas, *J. Inorg. Nucl. Chem.* 1958, **5**, 245.
2. J. P. Collman, R. P. Blair, R. L. Marshal and L. Slade, *Inorg. Chem.* 1963, **2**, 576.
3. R. C. Fay, A. Y. Girgis and U. Klabunde, *J. Am. Chem. Soc.* 1970, **92**, 7056.
4. B. Norden and I. Jonas, *Inorg. Nucl. Chem. Lett.* 1976, **12**, 33, 43.
5. M. Yamamoto, E. Iwamoto, A. Kozasa, K. Takemoto, Y. Yamamoto and A. Tatehata, *Inorg. Nucl. Chem. Lett.* 1980, **16**, 71.
6. A. Yamagishi, R. Ohnishi and M. Soma, *Chem. Lett.* 1982, 85.
7. A. F. Drake, J. M. Gould, S. F. Mason, C. Roshini and F. J. Woodley, *Polyhedron* 1983, **2**, 537.
8. R. Kuroda, S. Mason, C. Rodger and R. H. Seal, *Chem. Phys. Lett.* 1978, **57**, 1.
9. E. Iwamoto, Y. Tanaka, H. Kimura and Y. Yamamoto, *J. Solution Chem.* 1980, **9**, 841.
10. E. Iwamoto, M. Yamamoto and Y. Yamamoto, *Inorg. Nucl. Chem. Lett.* 1977, **13**, 399.
11. F. P. Dwyer and E. C. J. Gyarfas, *Proc. R. Soc. N.S.W.* 1949, **83**, 174.
12. C. V. Banks and J. W. O'Laughlin, *Anal. Chem.* 1957, **29**, 1412.
13. B. E. Bryant and W. C. Fernelius, *Inorg. Synth.* 1957, **5**, 188.
14. F. P. D. Dwyer and E. C. Gyarfas, *Nature (London)* 1951, **168**, 29.
15. R. C. Fay, A. Girgis and U. Klabunde, *J. Am. Chem. Soc.* 1970, **92**, 7056 (and references therein).
16. Y. Yamamoto, E. Sumimura, K. Miyoshi and T. Tominaga, *Anal. Chim. Acta* 1973, **64**, 225.
17. Y. Yamamoto, T. Tominaga and S. Tagashira, *Inorg. Nucl. Chem. Lett.* 1975, **11**, 825.
18. P. D. Hopkins and B. E. Douglas, *Inorg. Chem.* 1964, **3**, 357.

Polyhedron Vol. 5, No. 3, pp. 821–832, 1986
Printed in Great Britain

0277-5387/86 $3.00 + .00
© 1986 Pergamon Press Ltd

VIBRATIONAL SPECTRA AND STRUCTURE OF $AlCl_3NH_3$ AND MOLTEN MIXTURES WITH MCl–$AlCl_3$ (M = Li, Na, K OR Cs)

T. ØSTVOLD and E. RYTTER*

Institute of Inorganic Chemistry, University of Trondheim, N-7034 Trondheim-NTH, Norway

and

G. N. PAPATHEODOROU

Institute of Chemical Engineering and High Temperature Chemical Processes, University of Patras, GR-26110 Patras, Greece

(*Received* 20 *June* 1985; *accepted* 2 *September* 1985)

Abstract—Raman and IR spectra were obtained of molten $AlCl_3NH_3$, $AlCl_3ND_3$ and $AlBr_3NH_3$ in addition to chloroaluminate mixtures of the $AlCl_3NH_3$. The main spectral features of the gaseous $AlCl_3NH_3$ molecules having a C_{3v}-symmetry are retained in the molten and glassy states. Some additional bands were observed both in the pure liquid and in mixtures with chloroaluminate melts. The spectra indicated that the dissociation reaction $2AlCl_3NH_3 = AlCl_4^- + [AlCl_2(NH_3)_2]^+$ occurs with $K \simeq 3 \times 10^{-3}$ (mole fraction basis). Frequency shifts found on liquefaction demonstrate that extensive hydrogen bonding takes place between $AlCl_3NH_3$ molecules. This observation is supported by the glass-forming nature of $AlCl_3NH_3$. The molecule $Al_2Cl_6NH_3$ seems to exist in binary $AlCl_3$–$AlCl_3NH_3$ melts.

The production of aluminium by electrolysis in chloroaluminate melts (Alcoa process)[1] requires high-purity $AlCl_3$ which at present is obtained by chlorination of Al_2O_3. Undesirable chlorination of hydrocarbons, however, makes this process difficult to commercialize, despite the efficient electrolysis stage. A direct dehydration of $AlCl_3 \cdot 6H_2O$ would be advantageous for the production of $AlCl_3$, and a method in analogy with the NH_3 route for the dehydration of $MgCl_2 \cdot 6H_2O$ has been suggested.[2,3] The thermal stability of $AlCl_3NH_3$ has for this reason been studied in chloride melts.[3,4]

The present paper deals with the structure of this compound in the pure state and in some neutral and acidic chloroaluminate melts, as determined by IR and Raman spectroscopy. The interpretation of the spectra benefitted from comparison with the corresponding pure bromide and deuterated compound.

An ethane-like structure has been established for $AlCl_3NH_3$ and $AlBr_3NH_3$ by mass spectroscopy and electron diffraction[5–7] in the gas phase, as well as by a single-crystal X-ray investigation.[8] It has generally been assumed that the structure is staggered, thus adopting C_{3v}-symmetry. Recent *ab initio* MO calculations verifies the increased stability of this conformation.[9,10] The IR[9] and Raman spectra[10] of the chloride vapour have been reported, and most of the spectral assignments seem to be well-established.

The spectra of the solid[9,11] glass and liquid [12,13] show features distinctly different from those of the vapour. A description of the condensed phases in terms of dissociation, association and hydrogen bonding will be discussed. To our knowledge, no structural study of molten mixtures between $AlCl_3NH_3$ and $AlCl_3$ or alkali chlorides has been presented previously.

EXPERIMENTAL

All handling of salts was done in a glove box (< 5 ppm H_2O), or *in vacuo* ($< 10^{-5}$ torr). The alkali

* Author to whom correspondence should be addressed.

chlorides (p.a., Merck), except LiCl, were purified by recrystallization from the melt. Before melting the salts were dried at 400°C *in vacuo* for 2–3 h. The purification of LiCl (p.a., Merck) and $AlCl_3$ (p.a., Fluka) and the synthesis of $AlCl_3NH_3$ from $AlCl_3$ and NH_4Cl (p.a., Merck) are described elsewhere.[4,14]

$AlCl_3ND_3$ was synthesized in the same way as $AlCl_3NH_3$ using ND_4Cl (99% D, Stohler Isotope Chemicals) and $AlCl_3$ as starting materials. $AlBr_3NH_3$ was prepared from $AlBr_3$, obtained from a reaction between Al and HBr, and NH_4Br (99.5%, Hopkin & Williams). Both $AlBr_3$ and NH_4Br were purified by 5-times distillation–sublimation. The NH_4AlBr_4 salt formed by melting together $AlBr_3$ and NH_4Br in an evacuated silica tube was distilled twice, collecting HBr in a liquid N_2 cold trap.

The properly cleaned and baked-out Raman cells were filled with pure $AlCl_3NH_3$ or the different haloaluminate melts. The cells were sealed *in vacuo* and placed in a resistance-heated furnace. The Raman spectra were recorded with two different units. The data on pure $AlCl_3NH_3$ and on the $AlCl_3NH_3$–$CsAlCl_4$ melts were recorded using an Ar^+ laser from Control Laser Corporation (15 W). The scattered light was analyzed with a double monochromator (Jobin–Yvon) and detected with an RCA-C31034 photomultiplier and PAR photon-counting electronics. The Raman spectra of the other salts were excited with a Coherent CR-8 Ar^+ laser (8 W). The laser was passed through a Claisenfilter and the scattered light was analyzed with a double monochromator (Spex Ramalog 6) and detected with an RCA-C31034 photomultiplier and photon-counting electronics. The IR emission and specular reflection spectra were recorded using a method developed by Rytter *et al.*[15–17] using a thin film between a diamond window and a gold-plated nickel backplate.

RESULTS

The Raman spectra of $AlCl_3NH_3$ (g, l and glass) are shown in Fig. 1. The gas spectrum is from Papatheodorou *et al.*[10] and is given for comparison. The $AlCl_3NH_3$ glass was obtained by quenching the Raman cell in water after the salt had been melted. If the salt was properly synthesized, the glass was stable for several weeks. The IR emission spectra of $AlCl_3NH_3$ (g, l and s) are shown in Fig. 2 together with the reflectance spectrum of $AlCl_3ND_3$(l). The Raman spectrum of $AlBr_3NH_3$(l) is given in Fig. 3. The vibrational frequencies of all the neat compounds are collected in Table 1.

To study the possible decomposition reaction:

$$2AlCl_3NH_3(l) = AlCl_4^- + [AlCl_2(NH_3)_2]^+ \quad (1)$$

mixtures of $AlCl_3NH_3$ with $MAlCl_4$ ($M^+ = Li^+$, Na^+, K^+ or Cs^+), were examined. Figures 4–6 show the intensity variations with composition for the Raman frequencies around 400 cm^{-1}.

Vapour pressure and mass spectrometric studies of KCl–$AlCl_3$–$AlCl_3NH_3$ melts[4] show that the molecules $Al_2Cl_6NH_3$ and $AlCl_3NH_3$ are stable above this melt. To verify if $Al_2Cl_6NH_3$ also exists in the melt, Raman spectra of $AlCl_3$–$AlCl_3NH_3$ molten mixtures were recorded. The results are given in Fig. 7 and Table 2.

DISCUSSION

Condensed $AlCl_3NH_3$

It is evident from Figs 1 and 2 that the main spectral features of gaseous $AlCl_3NH_3$ are preserved upon condensation. However, distinct frequency shifts takes place and some new bands appear (see Table 1). These differences are interpreted in terms of H...Cl hydrogen bonding and dissociation in the liquid. Some oligomerization or polymerization, involving aluminium with higher coordination numbers, cannot be ruled out, but seem to contribute less to the structure.

The polarized Raman bands at 418 and 349 cm^{-1} are neither seen in the gas nor in the solid.[8–11] They are attributed to the symmetric AlCl stretching vibrations of $[AlCl_2(NH_3)_2]^+$ and $AlCl_4^-$, respectively. The latter value corresponds well to data for tetrachloroaluminate melts.[19] In this context it is interesting that electrical-conductivity measurements suggest some dissociation into ionic species.[20] Further substantiation of the formation of ions is given below in a quantiative approach.

Hydrogen bonding is expected to reduce the NH stretching frequencies and give rise to broader bands.[21] In Table 1 and Fig. 1 it is seen that the antisymmetric stretch (ν_7) is reduced from 3387 to 3295 cm^{-1} and the symmetric stretch (ν_1) from 3300 to 3243 cm^{-1} upon liquefaction. These Raman shifts are accompanied by the band broadenings (FWHH) (*ca* 38 → 66 cm^{-1} and 16 → 27 cm^{-1}). The ν_1 shift is influenced by Fermi resonance with $2\nu_8$ (NH_3 antisymmetric deformation). As ν_8 is unchanged, the resonance will be stronger in the liquid. This fact accounts for the enhanced intensity of the overtone and the frequency reduction from 3195 to 3178 cm^{-1}. In contrast, hydrogen bonding strengthens the force constants involved in the symmetric NH_3 deformation and NH_3 rocking.[21] Consequently, ν_2 increases from 1263 (1261) to 1332 cm^{-1} and ν_9 from 702 (697) to 731 cm^{-1}. As shown in Table 3, these effects are larger for the glass and the solid. It is also noteworthy that the influence of hydrogen bonding

on the NH stretching frequencies is roughly twice that of complexation of ammonia.

Little is known about torsional modes of ammines, and for $AlCl_3NH_3$ with ideal C_{3v}-symmetry this vibration (ν_6) is inactive in Raman as well as in the IR. A band at 1024 cm^{-1} in the IR melt spectrum, however, can be assigned to the combination $\nu_6 + \nu_9$, thus establishing the torsion at *ca* 293 cm^{-1}. The corresponding difference band is seen as a shoulder at *ca* 440 cm^{-1}. A similar interpretation of the gas-phase spectrum yields a torsional frequency of 276 cm^{-1}.[9] The 17 cm^{-1} higher value in the liquid is a further manifestation of hydrogen bonding. Additional verification comes from the deuterated sample which gives the sum at 820 cm^{-1} and the difference at 405 cm^{-1}, implying $\nu_6 = 208$ cm^{-1} and $\nu_9 = 612$ cm^{-1}. The latter mode is seen as a broad band in the IR spectrum, whereas the shift factor for the torsion of 1.41 matches exactly the value predicted by the Teller–Redlich product rule.

Gas–liquid–glass transformation does not alter the symmetric AlCl stretch at 378 cm^{-1}, but the antisymmetric counterpart is shifted from 536 to 502 cm^{-1} (Table 3). In the $AlCl_3$ deformation and rocking region below 300 cm^{-1}, the spectral appearance changes distinctly. We will think that that originates in the H...Cl interactions. The upward shift in the symmetric deformation from 200 to 251 cm^{-1} is particularly large. The explanation may partly be that there are differences in the purity of the mode.

A related problem is detected for the AlN mode assigned[9,10] at *ca* 480 cm^{-1} in the free molecule. No likely candidates in the neighbourhood of this value are found in any of the spectra of condensed materials. Our suggestion is that this vibration is

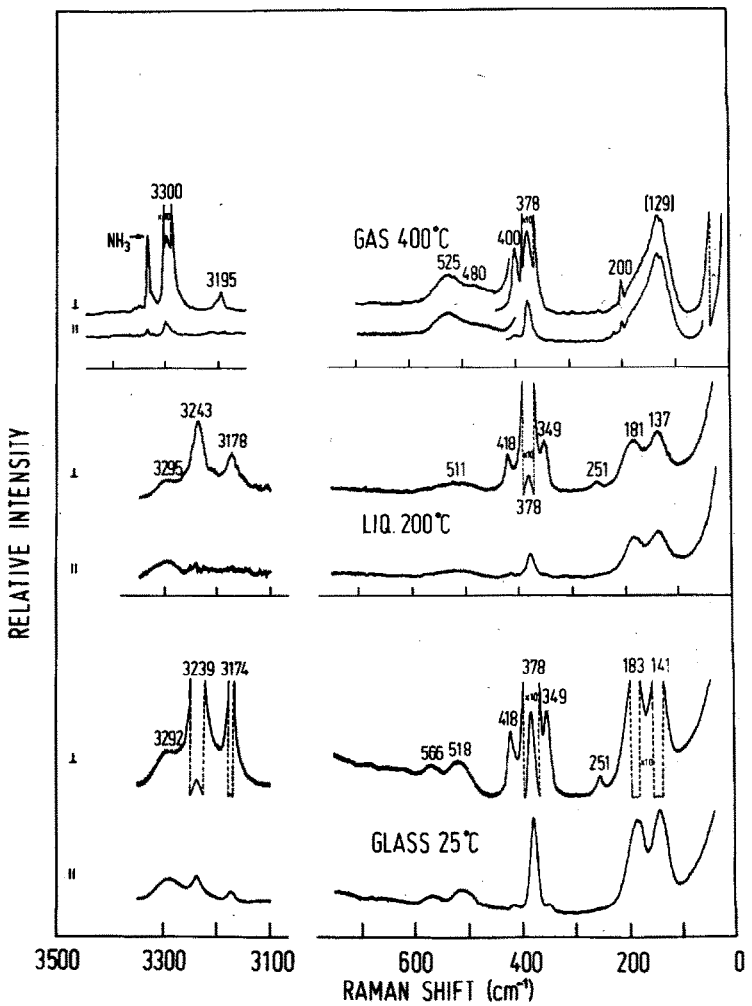


Fig. 1. Raman spectra of $AlCl_3NH_3$. The gas spectrum is from Papatheodorou *et al.*[10] For the liquid and glass spectra $\lambda_0 = 457.9$ nm, power = 400 mW, time constant (τ) = 0.06 s (except for higher frequencies of lower spectrum where $\tau = 0.3$ s), spectral slit width = 5 cm^{-1}, scan rate = 50 cm min^{-1}, chart speed = 5 cm min^{-1}.

Table 1. Raman and IR frequencies (cm^{-1}) for $AlCl_3NH_3$, $AlCl_3ND_3$ and $AlBr_3NH_3$[a]

$AlCl_3NH_3$				$AlCl_3ND_3$		$AlBr_3NH_3$		Interpretation	
Liquid		Vapour		Liquid	Vapour[b]				
Raman (200°C)	IR emission (145°C)	Raman (400°C)	IR transmission (350°C)[b]	IR reflection (155°C)	IR transmission (345°C)	Liquid[c] Raman (173°C)	Vapour[d] Raman (400°C)	(numbering based on C_{3v}-symmetry)	
3295 vw	—[e]	3387 w, br	3395 m	2459 s	2532 m		3390 w, br	$\nu_7(E)$	NH antisymmetric stretch
3243 m, p	—	3300 s, p	3302 m	2357 m	2399 w	3228 m, p	3295 s, p	$\nu_1(A_1)$	NH symmetric stretch
3178 w, p	—	3195 w, p	3193 vw			3163 m, p	3189 w, p	$2\nu_8(A_1+E)$	
1605 vw	1612 w		1614 w	1165 vw	1184 w		(1595)	$\nu_8(E)$	NH_3 antisymmetric deformation
	1512 vw				1125 vw			$\nu_2+\nu_{11}(E)$	
	1419 w							$2\nu_9(A_1+E)$	
1340 vw	1332 vs		1263 vs	1028 s	976 vs			$\nu_2(A_1)$	NH_3 symmetric deformation
	1024 w		978 w	820 w	795 vw			$\nu_6+\nu_9(E)$	"Torsion"
	731 s		702 vs	≃600 vs	594 vs			$\nu_9(E)$	NH_3 rock
	613 vw							$\nu_4+\nu_5(A_1)$	

566[f] vw	565 sh 520 sh	≃480 w, p	474 s		450 s, br	525 w		$\nu_3(A_1)$ $\nu_4+\nu_{12}(E)$	AlN stretch
511 vw	502 vs	525 m, br	536 vs	≃500 vs	≃500 s	430 w	440 w	$\nu_{10}(E)$	AlX antisymmetric stretch
	440 sh		427 vw	405 vw	392 w			$\nu_9-\nu_6(E)$	
418 m, p						286 w, p		$AlX_2(NH_3)_2^+$	AlX symmetric stretch
		400 m, p						$2\nu_5(A_1)$	Fermi resonance
378 vs, p	380 m	378 vs, p	378 w	374 m	372 m	255 vs, p	255 s, p	$\nu_4(A_1)$	AlX symmetric stretch
349 m, p						208 s, p		AlX_4^-	AlX symmetric stretch
251 w, p		200 m, p	200 s	241 vw	196 s	173 w, p	149 s, p	$\nu_5(A_1)$	AlX_3 symmetric deformation
181 m	193 m	≃175 sh	186 s	186 m	187 s	160 w 137 s, p		$\nu_{11}(E)$	AlX_3 rock
137 m	146 w	129 s	123 m	140 w	120 s	89 s	85 s	$\nu_{12}(E)$	AlX_3 antisymmetric deformation

[a] Raman frequencies for the glass at 25°C are found in Fig. 1 and IR emission frequencies for the gas and solid are given in Fig. 2. Abbreviations: v, very; br, broad; sh, shoulder; s, strong; m, medium; w, weak; p, polarized; X = Cl or Br.

[b] Reference 9. Only the main frequencies are included here.

[c] Additional weak, polarized bands at 329 and 312 cm^{-1}.

[d] Reference 10.

[e] Not investigated.

[f] Glass value (see Fig. 1).

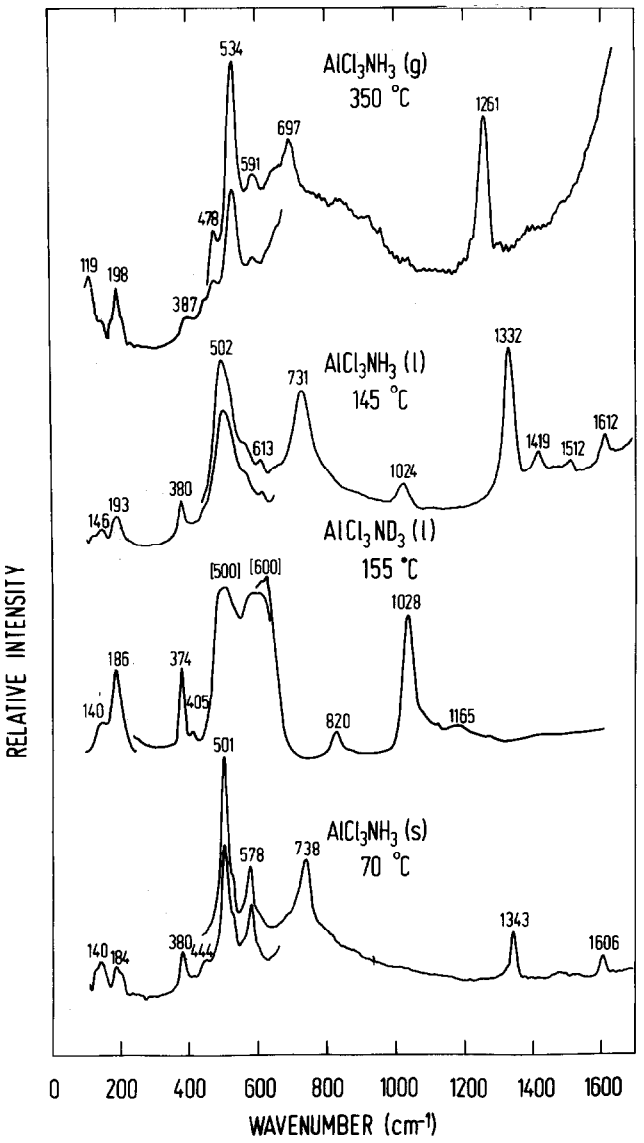


Fig. 2. IR emission spectra of $AlCl_3NH_3$ (g, l and s) and IR reflection spectrum of $AlCl_3ND_3$(l). Thick melts are used as reference.[17]

found at a higher frequency, possibly at 566 cm^{-1} (or 518 cm^{-1}) as observed in the Raman spectrum of the glass (Fig. 1); compare the shoulder at 565 cm^{-1} in the IR spectrum of the liquid and 578 cm^{-1} for the solid (Fig. 2). Presumably a synergetic effect operates. As hydrogen bonding weakens the N—H bonds, Al—N is strengthened. In turn, Al—Cl becomes weaker (chlorine will act as a better donor), the hydrogen bond stronger and N—H even weaker, cf. Gutmann's rules.[24] The result is an additional contribution to the Al—N bond strength. Alternatively, it may be observed that hydrogen bonding is expected to increase the lengths of both types of bonds adjacent to Al—N. In fact, the Al—Cl gas-phase and solid values are 2.102(5) and 2.111 Å, respectively, whereas Al—N contracts from 1.998(19) to 1.921 Å.[6,8]

Liquid $AlBr_3NH_3$

Due to insufficient distillation of the starting material, the Raman spectrum of $AlBr_3NH_3$(l) shows an appreciable amount of $AlBr_4^-$. The molten salt fundamentals of the tetrabromoaluminate ion in NH_4AlBr_4 are situated at 397 (w; ν_3, F_2), 209 (vs, p; ν_1, A_1), 113 (m; ν_4, F_2) and 74 cm^{-1} (m; ν_2, E), all of which are recognized in Fig. 3.

The interpretation of all other bands in the figure follows closely the assignments for $AlCl_3NH_3$ (g and l) and $AlBr_3NH_3$(g). As in the case for the chlor-

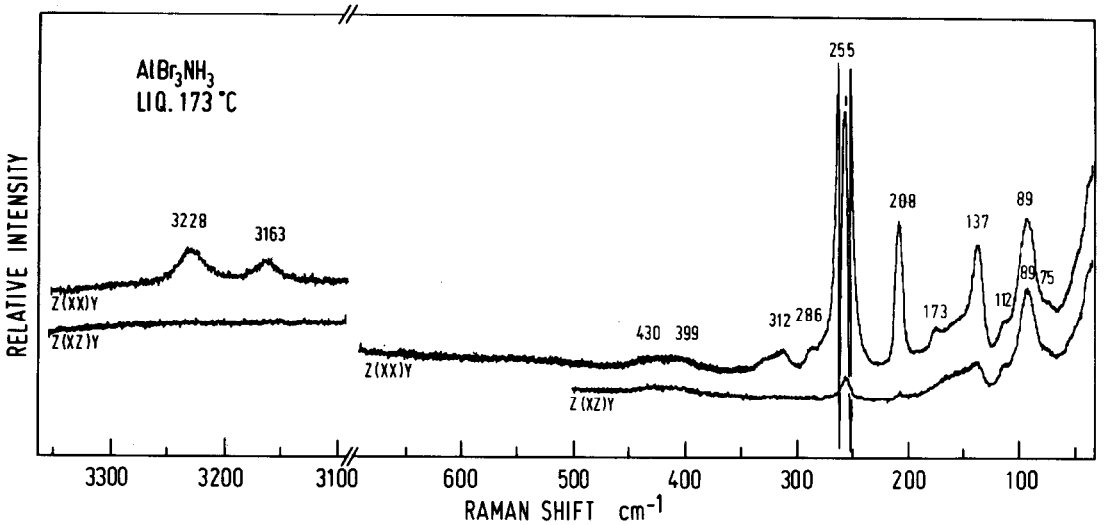


Fig. 3. Raman spectra of $AlBr_3NH_3$(l). λ_0 = 514.5 nm, power = 125 mW, τ = 1 s, scan rate = 0.2 cm s^{-1}, chart speed = 1 cm min^{-1}, spectral slit width = 8 cm^{-1}.

ide molecule, on going from liquid to gaseous $AlBr_3NH_3$ the NH symmetric stretch (ν_1) increases from 3228 to 3294 cm^{-1}, whereas the $AlBr_3$ symmetric deformation (ν_5) decreases from 173 to 149 cm^{-1}. A comparison between the $AlBr_3NH_3$(l) and $AlCl_3NH_3$(l) spectra shows that the ammonia frequencies are practically unchanged whereas the aluminium halide modes follow the mass difference. Some additional features between 310 and 350 cm^{-1} are ascribed to combinations or overtones. The AlN stretch expected in the range 450 to 550 cm^{-1} is apparently extremely weak in the Raman spectrum, although a band barely observable at *ca* 525 cm^{-1} has been attributed to this fundamental. The low intensity may be correlated with the high ionicity

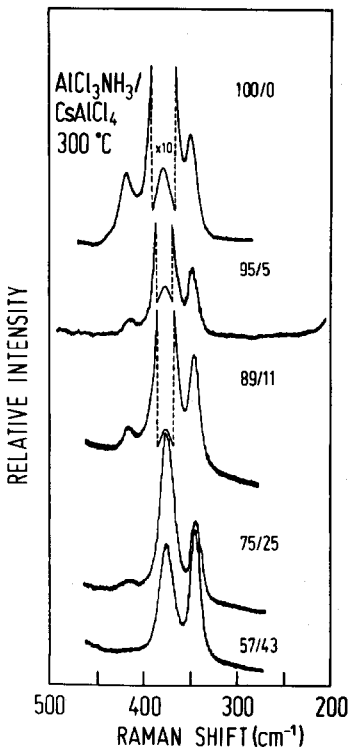


Fig. 4. Raman spectra of $AlCl_3NH_3$–$CsAlCl_4$ melts. λ_0 = 457.9 nm, power = 300 mW, τ = 0.02 s, spectral slit width = 3.5 cm^{-1}, scan rate = 50 cm min^{-1}, chart speed = 5 cm min^{-1}.

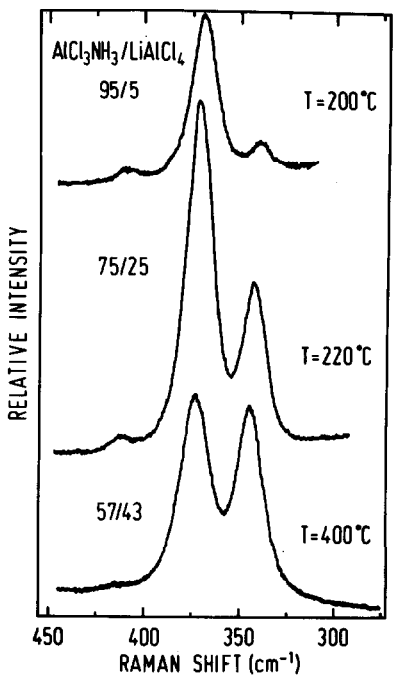


Fig. 5. Raman spectra of $AlCl_3NH_3$–LiCl melts. λ_0 = 488 nm, power = 75 mW, τ = 1 s, scan rate = 0.02 cm s^{-1}, chart speed = 0.2 cm min^{-1}, spectral slit width = 8 cm^{-1}.

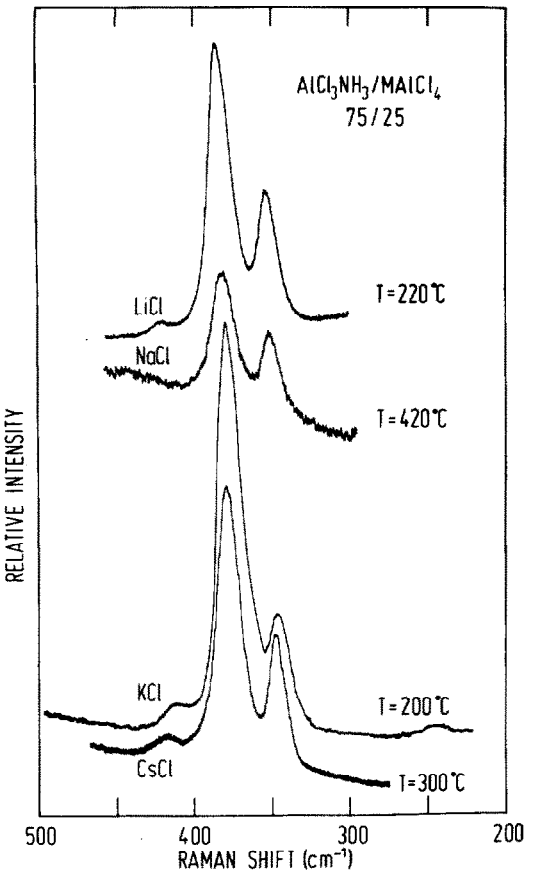


Fig. 6. Raman spectra of $AlCl_3NH_3$–$MAlCl_4$ melts (M = Li, Na, K or Cs). The polarized spectra of the LiCl- and CsCl-containing systems are run under the conditions specified in Figs 5 and 4, respectively. The spectra of the NaCl- and KCl systems are obtained with $\lambda_0 = 488$ nm, power = 30 mW, $\tau = 1$ s, scan rate = 0.5 cm s^{-1}, chart speed = 1 cm min^{-1}, spectral slit width = 8 cm^{-1}.

of the Al—N bond as found by *ab initio* MO calculations.[9] Complexation gives rise to a net flux in charge from the hydrogen to the chlorine atoms in $AlCl_3NH_3$.

Assignments for the $AlBr_3$ deformation and rocking modes must be regarded as tentative. In Table 3 it is demonstrated that the former type does not follow the same smooth trend as the corresponding NH_3 vibrations, as might be expected from differences in kinematic coupling, vibrational mixing and structural change. Note that the AlX_3 entities are transformed from planar to pyramidal during complexation. Additional support to the assignment of the AlX_3 symmetric deformation hence comes from the weak Raman intensity as this mode is inactive for free AlX_3. A special feature only for the bromide is the splitting of the $AlBr_3$ rock into one polarized and one depolarized component. This observation indicates breakdown of the ideal C_{3v}-symmetry. The explanation favoured is the 10–20% content of NH_4AlBr_4. The presence of the ammonium ion may cause a prevalence of asymmetrical hydrogen bonding.

The approximately equal melting points of $AlCl_3NH_3$ and $AlBr_3NH_3$, the higher vapour pressure of the bromide and the reduced tendency to form glass are consistent with the general belief that chlorine is a more efficient hydrogen bond donor atom than bromine. It therefore is intriguing that the spectroscopic results (Table 3) indicate that the N—H bond strength is approximately the same for both liquids. Note, however,the uncertainty due to the ν_1–$2\nu_8$ Fermi resonance that influences the position of the NH symmetric stretch.

Dissociation of $AlCl_3NH_3$

The dissociation equilibrium in eqn (1) was investigated by adding $AlCl_4^-$ in the form of $MAlCl_4$

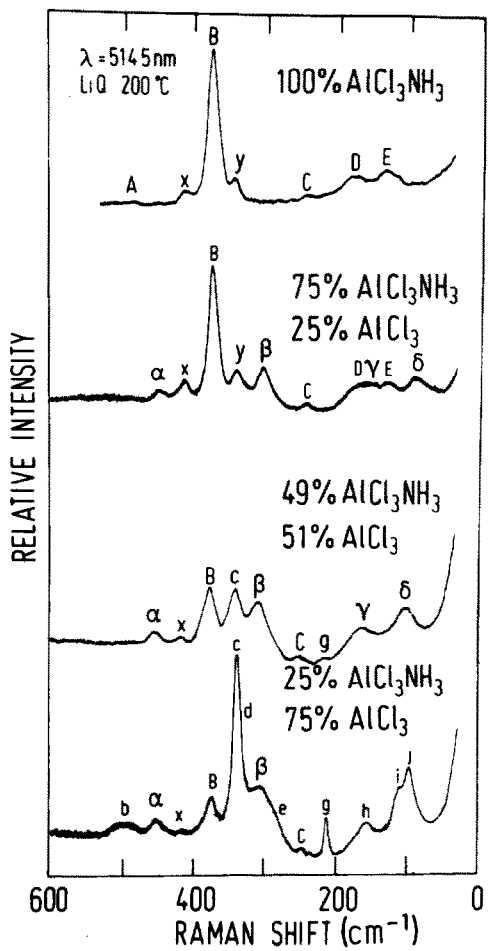


Fig. 7. Raman spectra of $AlCl_3NH_3$-$AlCl_3$ liquid mixtures at 200°C. $\lambda_0 = 514.5$ nm, power = 700 mW, $\tau = 1$ s, scan rate = 0.2 cm s^{-1}, chart speed = 1 cm min^{-1}, spectral slit width 8 cm^{-1}. Frequency assignments: $AlCl_3NH_3$: A–E; $[AlCl_2(NH_3)_2]^+$: x; $AlCl_4^-$: y; $Al_2Cl_6NH_3$: α–δ; Al_2Cl_6: b–j.

Table 2. Raman frequencies (cm^{-1}) for $AlCl_3$–$AlCl_3NH_3$ molten mixtures at 200°C[a]

100% $AlCl_3NH_3$	75% $AlCl_3NH_3$	49% $AlCl_3NH_3$	25% $AlCl_3NH_3$	100%[b] $AlCl_3$	Interpretation[c]
	98 m	97 m			$Al_2Cl_6NH_3$ (δ)
			102 s	102 s	Al_2Cl_6 (j)
			118 sh	118 s	Al_2Cl_6 (i)
137 m	135 m				$AlCl_3NH_3$ (E)
	157 m	160 m			$Al_2Cl_6NH_3$ (γ)
			163 m	166 w	Al_2Cl_6 (h)
181 m	180 m				$AlCl_3NH_3$ (D)
		216 w	217 m	218 m	Al_2Cl_6 (g)
251 vw	250 w	251 w	252 vw		$AlCl_3NH_3$ (C)?
			280 sh	290 w	Al_2Cl_6 (e)
	307 s	306 s	311 s		$Al_2Cl_6NH_3$ (β)
		340 s	341 vs	341 vs	Al_2Cl_6 (c)
349 m	344 m				$AlCl_4^-$ (y)
378 vs	377 vs	377 s	377 m		$AlCl_3NH_3$ (B)
418 m	416 m	415 w	417 vw		$[AlCl_2(NH_3)_2]^+$ (x)
	451 w	453 m	454 w		$Al_2Cl_6NH_3$ (α)
511 vw					$AlCl_3NH_3$ (A)
			500 w	512 w	Al_2Cl_6 (b)

[a] See footnote to Table 1. All bands between 200 and 500 cm^{-1} were found to be polarized.
[b] Ref. 18.
[c] The symbols refer to Fig. 7. The complete set of bands a–j for molten Al_2Cl_6 is found in Ref. 19.

(M = Li, Na, K or Cs). As expected, such an addition increases the Raman intensity of the 349 cm^{-1} band (y, $AlCl_4^-$) relative to the 378 cm^{-1} band (B, $AlCl_3NH_3$) at the expense of the 418 cm^{-1} band {x, $[AlCl_2(NH_3)_2]^+$} but without any significant change in band positions.

By resolving the spectrum from 300 to 450 cm^{-1} into three bands, the peak intensities in Table 4 were obtained. Employing a procedure similar to the one used for dissociation of $Al_2Cl_7^-$,[25] it was thus possible to calculate the equilibrium constant of eqn (1). It is assumed that the intensities of the totally symmetric AlCl stretching vibration of the three species are proportional to the concentrations. Thus, a stoichiometric equilibrium constant is obtained. This constant approaches the thermodynamic value if the activity coefficients cancel, as very well may be the case. It follows that:

$$n^o_{MCl} = n_{AlCl_4^-} - n_{[AlCl_2(NH_3)_2]^+}, \quad (2)$$

$$n^o_{AlCl_3NH_3} = n_{AlCl_3NH_3} + 2n_{[AlCl_2(NH_3)_2]^+}, \quad (3)$$

$$K = \frac{n_{[AlCl_2(NH_3)_2]^+} n_{AlCl_4^-}}{n^2_{AlCl_3NH_3}} \quad (4)$$

and

$$I_B/I_y = k n_{AlCl_3NH_3}/n_{AlCl_4^-}. \quad (5)$$

Employing intensity data from two different compositions one obtains eight equations to match the six unknown concentrations, k and K. In this way, several equilibrium constants were calculated for each $MAlCl_4$–$AlCl_3NH_3$ system. The results were improved by including the intensity I_x through the relationship:

$$K = k' \frac{I_x I_y}{I_B^2}, \quad (6)$$

evaluating an average k' and recalculating K from eqn (6) for each composition.

The results given in Table 4 show an average equilibrium constant of 3.2×10^{-3}, or *ca* 5% dissociation. The deviation from the *ca* 1% value inferred from conductivity measurement[20] probably is due to reduced ionic mobilities as a result of hydrogen bonding. The calculated equilibrium constant seems to increase with tetrachloroaluminate addition. A more ionic melt enhances the dissociation of the neutral ammine into ionic species. Thus, the spectroscopic data give information on variations in the activity coefficient term. Another effect is that larger alkali ions give more ionic liquids.

The alternative dissociation reaction:

$$2AlCl_3NH_3 = AlCl_2NH_2 + NH_4^+ + AlCl_4^- \quad (7)$$

can be regarded as a mutual autoionization of $AlCl_3$ and NH_3. This possibility cannot be rejected from the spectral data or equilibrium constant calcula-

Table 3. Frequency shifts (cm^{-1}) of NH_3, $AlCl_3$ and $AlBr_3$ upon complexation and condensation[a]

Compound	AX antisymmetric stretch	AX symmetric stretch	AX_3 antisymmetric deformation	AX_3 symmetric deformation
		NH_3 in $AlCl_3NH_3$		
$NH_3(g)$[b]	3444 ↑	3337 ↑	1627 ↑	950 ↓
	2555	*2419*	*1191*	*749*
$AlCl_3NH_3(g)$	3395	3300	1614	1263
	2532	*2399*	*1184*	*976*
$AlCl_3NH_3(l)$	3295	3243	1612	1332
	2459	*2357*	*1165*	*1028*
$AlCl_3NH_3(s)$	3287 ↓	3234 ↓	1606 ↓	1343 ↓
		$AlCl_3$ in $AlCl_3NH_3$		
$AlCl_3(g)$[c]	616 ↑	375	148 ↑	214 ↑
$AlCl_3NH_3(g)$	536	378	129	200
	≃500	*372*	*120*	*196*
$AlCl_3NH_3(l)$	502	378	137	251
	≃500	*374*	*140*	*241*
$AlCl_3NH_3$(glass)	(518)	378	141 ↓	251 ↓
$AlCl_3NH_3(s)$	501	380	140	—
		NH_3 in $AlBr_3NH_3$		
$NH_3(g)$[b]	3444 ↑	3337 ↑	1627 ↑	950
$AlBr_3NH_3(g)$[d]	3390	3294	(1595)	—
$AlBr_3NH_3(l)$	—	3228 ↓	—	—
		$AlBr_3$ in $AlBr_3NH_3$		
$AlBr_3(g)$[e]	503 ↑	230 ↓	94 ↑	176 ↑
$AlBr_3NH_3(g)$[d]	440	255	85	149
$AlBr_3NH_3(l)$	430 ↓	255 ↓	89 ↓	173 ↓

[a] Values for deuterated compounds are given in italics.
[b] See Ref. 22 for NH_3 values. Deuterated frequencies from Ref. 2.
[c] Reference 18.
[d] Reference 10.
[e] References 10 and 23.

tion. Formation of a three-coordinated highly acidic aluminium atom is, however, improbable.

$AlCl_3NH_3$ *in* $AlCl_3$

The successive addition of the Lewis base NH_3 to the Lewis acid Al_2Cl_6 may be formulated as:

$$Al_2Cl_6 + NH_3 = Al_2Cl_6NH_3, \quad (8)$$

$$Al_2Cl_6NH_3 + NH_3 = 2AlCl_3NH_3. \quad (9)$$

From this it follows that the associative redistribution reaction:

$$2AlCl_3NH_3 + Al_2Cl_6 = 2Al_2Cl_6NH_3 \quad (10)$$

may play an important part when $AlCl_3NH_3$ is added to pure $AlCl_3$. In addition, formation of ionic species cannot be excluded:

$$Al_2Cl_6 + Al_2Cl_6NH_3 = [Al_2Cl_5NH_3]^+ + Al_2Cl_7^-, \quad (11)$$

$$2Al_2Cl_6NH_3 = [Al_2Cl_5(NH_3)_2]^+ + Al_2Cl_7^- \quad (12)$$

$$Al_2Cl_6NH_3 + AlCl_3NH_3 = [Al_2Cl_5(NH_3)_2]^+ + AlCl_4^-, \quad (13)$$

$$2AlCl_3NH_3 = [AlCl_2(NH_3)_2]^+ + AlCl_4^-. \quad (14)$$

In Fig. 7 and Table 2, the Raman bands have been attributed to neutral and ionic entities in the melt according to these reaction schemes. The interpretation is based on systematic intensity variations of individual or groups of bands, overall stoichiometry, the well-characterized spectra[19] of Al_2Cl_6, $Al_2Cl_7^-$,

Table 4. Intensities and stoichiometric equilibrium constants for dissociation of $AlCl_3NH_3$ in molten mixtures with $MAlCl_4$ (M = Li, K or Cs)

mol % ($MAlCl_4$)	I_x $\{[AlCl_2(NH_3)_2]^+\}$	I_B ($AlCl_3NH_3$)	I_y ($AlCl_4^-$)	K ($\times 10^{-3}$)
0	5.98	66.72	6.3	1.2
$LiAlCl_4$				
5.3	1.95	28.7	4.5	2.1
25	2.6	62.7	27.75	3.5
42.9	0.65	35.45	32.78	3.3
$KAlCl_4$				
4.8	2.57	38.9	7.07	2.3
11.1	3.85	64.8	17.9	3.2
25	1.55	41.7	22.8	3.9
$CsAlCl_4$				
5.4	1.55	36.9	9.3	2.0
11.1	2.4	37.15	10.18	3.4
25.6	1.16	18.51	8.32	5.4
43.1	0.35	14.59	14.12	4.5

$AlCl_4^-$ and $AlCl_3NH_3$ as well as of $[AlCl_2(NH_3)_2]^+$ and assumptions regarding frequency shifts.

In particular, it is evident that the spectrum of $AlCl_3NH_3$ (bands A–E) and its dissociation products $AlCl_4^-$ (y) and $[AlCl_2(NH_3)_2]^+$ (x) gradually disappears as Al_2Cl_6 (bands b–j) is added. That a simple mixture of the two compounds is far from the whole story, is most clearly seen by the presence of the α- and β-bands at intermediate compositions. The most straightforward interpretation of the data is in terms of eqn (10), i.e. $Al_2Cl_6NH_3$ is formed at intermediate compositions.

The striking similarities, both in frequencies and intensities, between the β-, γ- and δ-bands in Fig. 7 and the corresponding bands for $Al_2Cl_7^-$ deserve a comment. In $AlCl_3$–CsCl mixtures, the frequencies found[19] were 306, 161 and 96 cm^{-1}, which may be compared to the present values of 306, 160 and 97 cm^{-1} (Table 2). However, the symmetric AlCl terminal stretch expected for $Al_2Cl_7^-$ at 431 cm^{-1} is apparently shifted to 453 cm^{-1} (α). Besides, it seems impossible to incoporate a positive species to the required extent, although the main band of $[Al_2Cl_5(NH_3)_2]^+$ may be hidden in the y–c envelope in Fig. 7, cf. the width of the c-band for the 49–51% composition.

We conclude that $Al_2Cl_6NH_3$ is formed in the molten $AlCl_3$–$AlCl_3NH_3$ system, possibly with some dissociation into ionic species. As for the pure ammine, hydrogen bonding is of course expected to be important in these mixtures. Another result that may be inferred from Fig. 7 is that the relative concentration of $Al_2Cl_6NH_3$ is less than the concentration of $Al_2Cl_7^-$ in the alkali chloride–$AlCl_3$ melts. This difference may be caused by factors like hydrogen bonding, counterion influence and the basicity of Cl^- vs NH_3.

Acknowledgements—We thank O. Lier, L. Ø. Ekornrød and M.-A. Einarsrud for participation in the experimental work.

REFERENCES

1. K. Grjotheim, C. Krohn and H. A. Øye, *Aluminium* 1975, **51**, 697.
2. G. H. Bøe and T. Østvold, Norwegian patent No. 150 846 (1985).
3. T. Foosnæs, B. Knapstad and T. Østvold, *Acta Chem. Scand.* (in press).
4. K. Nakamura, T. Østvold and H. A. Øye, *Yoyuen* 1984, **27**, 7.
5. M. Hargittai, J. Tamas, M. Bihari and I. Hargittai, *Acta Chim. Acad. Sci. Hung.* 1979, **99**, 127.
6. M. Hargittai, I. Hargittai, V. P. Spiridonov, M. Pelissier and J. F. Labarre, *J. Mol. Struct.* 1975, **24**, 27.
7. M. Hargittai, I. Hargittai, V. P. Spiridonov and A. A. Ivanov, *J. Mol. Struct.* 1977, **39**, 225.
8. K. N. Semenenko, E. B. Lobkovskii, V. B. Polyakova, I. I. Korobow and O. V. Kravchenko, *Koord. Khim.* 1978, **4**, 1649.
9. C. E. Sjøgren and E. Rytter, *Spectrochim. Acta* 1985, **41A**, 1277.
10. G. N. Papatheodorou, L. A. Curtiss and V. A. Maroni, *J. Chem. Phys.* 1983, **78**, 3303.
11. W. Sawodny and J. Goubeau, *Z. Phys. Chem.* (*Neue Folge*) 1965, **44**, 227.

12. J. Goubeau and H. Siebert, *Z. Anorg. Allg. Chem.* 1947, **254**, 126; 1950, **261**, 63.
13. H. Gerding and H. Houtgraaf, *Recl Trav. Chim. Pays-Bas* 1955, **74**, 15.
14. K. Grjotheim, R. Nicolic and H. A. Øye, *Acta Chem. Scand.* 1970, **24**, 489.
15. E. Rytter, J. Hvistendahl and T. Tomita, *J. Mol. Struct.* 1982, **79**, 323.
16. E. Rytter, Extended Abstract, 163rd Meeting, The Electrochemical Society, San Francisco (1983).
17. J. Hvistendahl, E. Rytter and H. A. Øye, *Appl. Spectrosc.* 1983, **37**, 182.
18. T. Tomita, C. E. Sjøgren, P. Klæboe, G. N. Papatheodorou and E. Rytter, *J. Raman Spectrosc.* 1983, **14**, 415.
19. E. Rytter, H. A. Øye, S. J. Cyvin, B. N. Cyvin and P. Klæboe, *J. Inorg. Nucl. Chem.* 1973, **35**, 1185.
20. W. Klemm and E. Tanke, *Z. Anorg. Chem.* 1931, **200**, 354.
21. K. Nakamoto, *Infrared and Raman Spectra of Inorganic and Coordination Compounds.* Wiley, New York (1978).
22. S. J. Cyvin, B. N. Cyvin and I. Hargittai, *J. Mol. Struct.* 1974, **23**, 385.
23. C. E. Sjøgren, P. Klæboe and E. Rytter, *Spectrochim. Acta* 1984, **40A**, 457.
24. V. Gutmann, *Coord. Chem. Rev.* 1975, **15**, 207; 1976, **18**, 225.
25. H. A. Øye, E. Rytter, P. Klæboe and S. J. Cyvin, *Acta Chem. Scand.* 1971, **25**, 559.

Polyhedron Vol. 5, No. 3, pp. 833–838, 1986
Printed in Great Britain

0277-5387/86 $3.00 + .00
© 1986 Pergamon Press Ltd

RADIATION-CHEMICAL PROCESSES AS DISCLOSURE OF ELECTRONIC STATES IN A BIS(DINITROGEN) MOLYBDENUM COMPLEX

J. O. DZIĘGIELEWSKI,* B. JEŻOWSKA-TRZEBIATOWSKA,†
R. GIL-BORTNOWSKA and R. GRZYBEK

Department of Inorganic and Radiation Chemistry, Institute of Chemistry,
Silesian University, 40006 Katowice, Szkolna 9 Street, Poland

(*Received* 1 *July* 1985; *accepted* 2 *September* 1985)

Abstract—On the basis of experimental data the energy levels of the central-atom orbitals in the complex $[Mo(N_2)_2(dppe)_2]$ [dppe = 1,2-bis(diphenylphosphine)ethane] were calculated. Using the diagram thus obtained the electronic configuration of the irradiation-generated ion, $[Mo(N_2)_2(dppe)_2]^-$, was determined to be as follows: $(b_{2g})^2 (e_g)^4 (b_{1g})^1$ or $(b_{2g})^2 (e_g)^4 (e_u)$. The yields from the decomposition of $[Mo(N_2)_2(dppe)_2]$ in the solid phase in a hydrogen atmosphere were determined on the basis of the decrease in band intensities at 306 and 377 nm: $G(-Mo—N_2)_{306nm} = 0.01$, and $G(-Mo—P)_{377nm} = 0.1$ (molecules per 100 eV). In toluene solution it was found that $G(-Mo—N_2) > G(-Mo—P)$. The yields observed were in accordance with the calculated levels. Using a mass spectrometer the volatile products of $[Mo(N_2)_2(dppe)_2]$ radiolysis in H_2 and O_2 atmospheres were identified as H_3N, H_4N_2, NO and N_2O. In the light of the results mentioned above (as well as the IR results) a mechanism for the radiolysis of $[Mo(N_2)_2(dppe)_2]$ in the solid phase was proposed.

Compounds of transition metals in low oxidation states with 1,2-bis(diphenylphosphine)ethane (dppe) are used in the fixation and reduction of molecular nitrogen (N_2), and the $[Mo(N_2)_2(dppe)_2]$ molecule is the subject of great interest.[1–19] Introduction of N_2 into the coordination sphere of Mo(0) may be carried out without any problem.[3] The chemical reduction of coordinated nitrogen, e.g. by using either acids or alkyl halides, is not efficient enough and is connected with the oxidation of the central atom.[20,21] Thus, the recycling of his complex in the fixation of N_2 becomes impossible without previous reduction of the central ion. The irradiation of $[Mo(N_2)_2(dppe)_2]$ by means of UV light leads to N_2 elimination.[11,22,23] N_2 may be liberated from the complex with no π-acceptor ligands (except N_2) with the help of ionizing radiation.[24]

Taking into account the low reactivity of dppe towards e_s^- [25] {which is supported by the invariability of this ligand in the irradiated $[MoOCl(dppe)_2]Cl$ complex,[26] as well as assuming, that—as in the case of the other complex—the lower-energy molecule orbitals would be filled by e_s^-} one should expect that, as a result of the irradiation of $[Mo(N_2)_2(dppe)_2]$, N_2 will not be immediately eliminated from this compound. Although the energy level sequence of the molecular orbitals in $[Mo(N_2)_2(dppe)_2]$ is not established so far, it is assumed that the a_{2u}-level [π(Mo—N_2)] is undoubtedly higher than the other potentially acceptor orbitals: e_u [π(Mo—P)], a_{1g} and b_{1g}.[22] Thus, the Mo—N_2 σ-bond is attenuated by the formation of the $[Mo(N_2)_2(dppe)_2]^-$ ion (this ion is formed through the filling of the a_{1g}-orbital), whereas attenuation of the Mo—P σ-bond is caused by the filling of the b_{1g}-orbital. Hence the determination of the yields from the destruction of both the Mo—N_2 and the Mo—P bond as a result of the irradiation as well as the suggestion of the $[Mo(N_2)_2(dppe)_2]^-$ ion electronic state should contribute to the explanation of the electron configuration either at the ground or the excited state of the $[Mo(N_2)_2(dppe)_2]$ molecule. Moreover, the determination of the gaseous pro-

* Author to whom correspondence should be addressed.
† Institute of Chemistry, Wrocław University, Joliot-Curie 14 Street, 50383 Wrocław, Poland.

ducts of radiolysis as well as the finding that the changes in the $[Mo(N_2)_2(dppe)_2]$ molecule caused by irradiation (by means of IR spectroscopy) are the purpose of this work.

EXPERIMENTAL

$[Mo(N_2)_2(dppe)_2]$ was prepared as previously described.[3] Samples (0.2 g) of $[Mo(N_2)_2(dppe)_2]$ were placed into glass tubes provided with suitable taps. The air was pumped out and the sample washed out with hydrogen, nitrogen or oxygen, then pumping out was done, and the sample filled with hydrogen, nitrogen or oxygen. Air-tight tubes with $[Mo(N_2)_2(dppe)_2]$ were irradiated in the cobalt source "Issliedowatiel" at dose rate of 6×10^{16} eV min^{-1} g^{-1} or 3.8×10^{17} eV min^{-1} ml^{-1} in toluene solution. The solutions of $[Mo(N_2)_2(dppe)_2]$ in toluene (1.2×10^{-4} mol dm^{-3}) were saturated with argon, then irradiated. The absorption bands of the unstable products of radiolysis were determined at 77 K in a frozen solution of $[Mo(N_2)_2(dppe)_2]$ in tributylphosphate (TBP) (freshly purified), saturated with argon. The non-irradiated frozen solution of $[Mo(N_2)_2(dppe)_2]$ in TBP was used as a reference. The absorption bands were measured on a Beckman 5240 spectrophotometer: the weighed portions of $[Mo(N_2)_2(dppe)_2]$ after irradiation were dissolved in tetrahydrofuran. IR spectra were taken in KBr discs on a Specord 75 spectrophotometer. The gaseous products were pumped out from the irradiation samples, and examined by means of an WSM-2 mass spectrometer using an ionization energy of 100 eV.

RESULTS AND DISCUSSION

In the frozen solution of $[Mo(N_2)_2(dppe)_2]$ in TBP, as a result of the irradiation, a low-intensity band appears at 580 nm (OD = 0.03, optical path = 1 cm), which disappears rapidly. This band may be attributed to the $(b_{1g})^1 \rightarrow (a_{1g})^1$ transition in the $[Mo(N_2)_2(dppe)_2]^-$ ion formed as a result of the interaction of e_s^- with the Mo(0) complex. The assignment of the band at 580 nm was made on the basis of Fig. 1. In the dose range up to 60 kGy no change was observed in the absorption band as well as in the frequency modes when the sample was irradiated in an N_2 atmosphere. A linear decrease in absorbance at 306 ($\varepsilon = 2.3 \times 10^4$) and 377 nm ($\varepsilon = 1.37 \times 10^4$) was observed in an H_2 atmosphere up to 60 kGy. The calculated yields from bond decomposition are as follows: $G(-Mo—N_2) =$ 0.01/100 eV [on the basis of the decrease in the band intensity at 306 nm corresponding to the charge transfer from Mo to N_2 (MLCT)] and $G(-Mo—P) = 0.1/100$ eV [on the basis of the decrease in the band at 377 nm—the charge transfer from Mo to P (MLCT)]. The vibrations in $[Mo(N_2)_2(dppe)_2]$ together with some assignments are presented in Fig. 2. The assignment was based on papers [19,27–29] as well as compared with free ligand and complex IR spectra. There were no changes observed in the frequency modes of $[Mo(N_2)_2(dppe)_2]$ irradiated in an H_2 atmosphere in comparison with those of the non-irradiated sample (the small decrease in the amount of N_2 in the complex does not reach the sensitivity limit of the IR method and so no changes in the intensity of the N_2 and Mo—N_2 vibrations were detected). Mo—P IR vibrations appear at about 350–520 cm^{-1}.[28] Assuming a D_{4h}-symmetry for the MoP_4 unit E_u [ν(Mo—P)] and A_{2u} and B_{2u} [δ(Mo—P)] IR vibrations are expected. In the 350–520-cm^{-1} region a strong variation also appears [δ(CCC) in the plane of the phenyl ring]. As follows from the above the Mo—P symmetrical vibrations appear in the Raman region, e.g. A_{1g} at 170 cm^{-1},[19] but we could not observe any Mo—P bond cleavage in the IR absorption. The lowering of the vibration frequency of N_2 (at 1970 cm^{-1}) is observed when higher doses are used. The lowering of some vibration frequencies and the appearance of new vibrations can be seen when $[Mo(N_2)_2(dppe)_2]$ is irradiated in an O_2 atmosphere (Table 1). Data in Table 1 show that the irradiation of

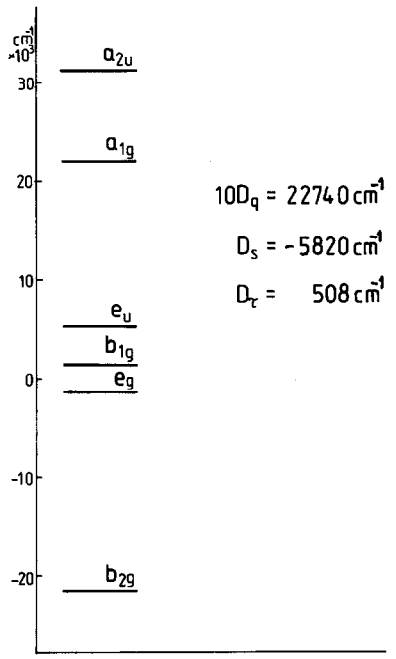


Fig. 1. Parameters of the ligand field and the energy level diagram of the central-atom orbitals for complex $[Mo(N_2)_2(dppe)_2]$, calculated on the basis of the absorption bands.

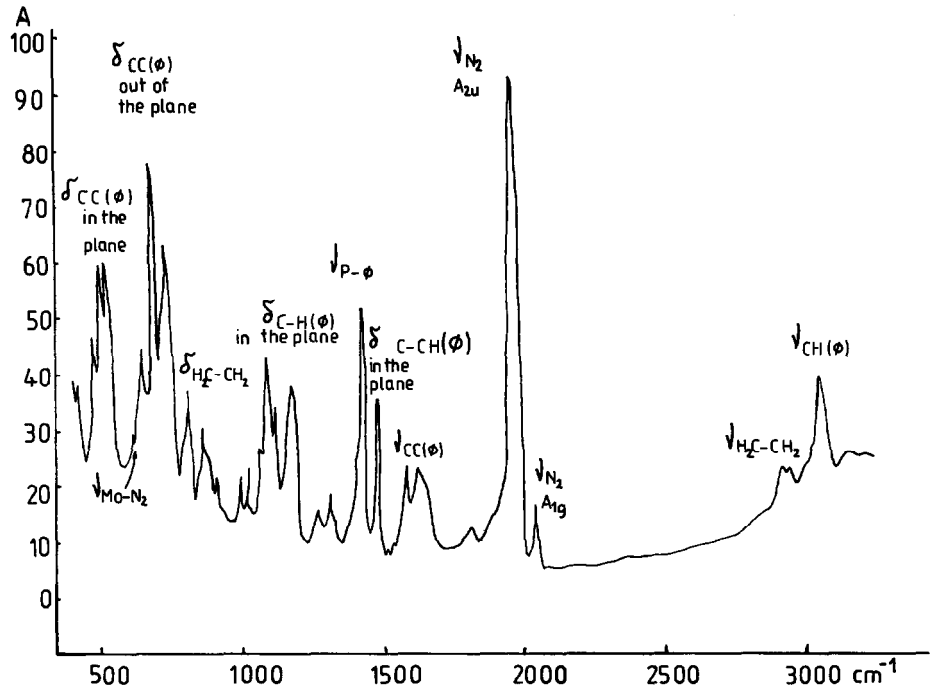


Fig. 2. IR spectrum of $[Mo(N_2)_2(dppe)_2]$ in KBr tablet.

$[Mo(N_2)_2(dppe)_2]$ in an O_2 atmosphere leads: (a) to the destruction of this compound, (b) to the addition of oxygen to the ligand fragment, and (c) to the oxidation of Mo. The relative intensities of the mass spectral peaks of both the gaseous ions and the volatile products forming as a result of the irradiation of $[Mo(N_2)_2(dppe)_2]$ in an H_2 or an O_2 atmosphere are presented in Tables 2 and 3. It follows from Tables 2 and 3 that, as a result of the irradiation of $[Mo(N_2)_2(dppe)_2]$ in an H_2 atmosphere, the nitrogen is converted partly into H_4N_2 and H_3N, and about 40% of the nitrogen liberated from the coordination sphere remains unchanged. In an O_2 atmosphere the coordinated nitrogen is converted into NO and N_2O, but about 10% of the liberated nitrogen remains unchanged. The behaviour of $[Mo(N_2)_2(dppe)_2]$ towards the ionizing radiation is different from towards UV or VIS light as shown by our results.

Table 1. Changes in the vibration frequency as a result of the irradiation (60-kGy) of $[Mo(N_2)_2(dppe)_2]$ in an O_2 atmosphere

Vibration frequency (cm^{-1})	Intensity[a]	Assignment	
		Disappearing	Appearing
2030	w	$\nu(N_2)$	—
1970	vs	$\nu(N_2)$	—
1430	s	$\nu(p\text{-}C_6H_5)$	—
1165	s	—	$\nu(P{=}O)$
1120	s	—	$\nu(P{=}O)$
940	m	—	$\nu(M{=}O)$
850	m	$\delta(CH_2{-}CH_2)$	—

[a] w, weak; m, medium; s, strong; vs, very strong.

In the solid phase, the Mo—N_2 bond is ruptured by γ-radiation, with a lower efficiency. In the case of the Mo—P bond a higher decomposition yield is observed. γ-Irradiation of the toluene solution of $[Mo(N_2)_2(dppe)_2]$ (1.2×10^{-4} mol dm^{-3}) saturated with argon results in the following yields: $G(-Mo{-}N_2) = 0.012$ and $G(-Mo{-}P) = 0.007$ bonds/100 eV. In toluene solutions, the ionizing radiation has a similar effect to UV or VIS light, i.e. it breaks the Mo—N_2 bond. It should be noted, however, that in toluene as well as in benzene solutions the excited states of the solvent molecules (i.e. $^1B_{2u}$ and $^3B_{1u}$) are produced as a result of the irradiation. The triplet state is especially important, in which 430-nm radiation is absorbed by the solvent[30] {this region is almost covered by the ligand field transition for $[Mo(N_2)_2(dppe)_2]$}. Thus the result of the transfer of excitation energy from the solvent to the complex is the same as that of light absorption, i.e. the rupture of the Mo—N_2 bond.[11,22]

The absorption bands of $[Mo(N_2)_2(dppe)_2]$ with respect to the character of the electron transitions are

Table 2. Comparative intensities of mass spectrum peaks of the gaseous ions as well as the volatile products formed as a result of the irradiation of $[Mo(N_2)_2(dppe)_2]$ in an H_2 atmosphere

	Dose							
	1 kGy		7 kGy		10 kGy		50 kGy	
M^+/e	Relative intensity	Assignment	Relative intensity	Assignment	Relative intensity	Assignment	Relative intensity	Assignment
14	5.8	N	4.5	N	3.9	N	11.0	N
15	1.1	NH	0.7	NH	7.7	NH	8.0	NH
16	2.4	NH_2	2.2	NH_2	10.0	NH_2	13.0	NH_2
17	1.1	NH_3	1.6	NH_3	7.7	NH_3	32.0	NH_3
18	7.2	NH_4	8.1	NH_4	66.7	NH_4		
28	100.0	N_2	100.0	N_2	100.0	N_2	190.0	N_2
29	48.3	N_2H	46.1	N_2H			6.0	N_2H
30	0.9	N_2H_2	1.6	N_2H_2	2.6	N_2H_2	8.0	N_2H_2
31	0.9	N_2H_3	1.6	N_2H_3	9.0	N_2H_3	11.0	N_2H_3
32	35.1	N_2H_4	32.6	N_2H_4	73.1	N_2H_4	200.0	N_2H_4
33	4.4	N_2H_5	3.6	N_2H_5	23.1	N_2H_5		

well known. The bands at 306 and 377 nm were attributed to a charge transfer from the central atom to the ligand (MLCT): Mo → P(3*d*) and Mo → $N_2(\pi^*)$.[11,31,32] The band at 440 nm was that one of LFT.[33–36] In spite of this, there is some controversy about the order of the electron levels in the *trans*-$[Mo(N_2)_2(dppe)_2]$ complex. Dubois and Hoffman,[37] on the basis of the semiempirical MO scheme suggested, that the b_{2g}-level is the highest filled level in the ground state. The configuration $(e_g)^4$ $(b_{2g})^2$ was also accepted by other authors.[33–35] The e_g-level was suggested by Chatt *et al.*[38] to be the highest filled level and this suggestion was supported by *ab initio* SCF molecular-orbital calculations.[39]

Table 3. Comparative intensities of mass spectrum peaks of the gaseous ions formed as a result of the irradiation of $[Mo(N_2)_2(dppe)_2]$ at 48 kGy, and different $O_2:N_2$ (coordinated) volume ratios, under standard conditions

	$V_{O_2}:V_{N_2}$ 5:1		$V_{O_2}:V_{N_2}$ 2:1	
M^+/e	Relative intensity	Assignment	Relative intensity	Assignment
14	4	N	7	N
16	19	O	8	O
28	10	N_2	12	N_2
30	75	NO	200	NO
32	200	O_2	72	O_2
44	8	N_2O	16	N_2O

The experimental results of our work[26,40] are partially in accordance with the MO diagram calculated by Murrell *et al.*[39] The radiation-induced reduction of $[MoOCl(dppe)_2]Cl$ [diamagnetic complex with $(b_2)^2$ configuration[26]] gave $[MoOCl(dppe)_2]$ with the configuration $(b_2)^2$ $(e)^1$.[40] The disproportionation of Mo(III) leads to $[MoCl_2(dppe)_2]$[26,40] with $(b_{2g})^2$ $(e_g)^2$ configuration (μ_{eff} = 2.98 BM).[26]

It is expected that the $(b_{2g})^2$ $(e_g)^4$ configuration in the diamagnetic *trans*-$[Mo(N_2)_2(dppe)_2]$ is caused by the reduction of Mo(II) to Mo(0). These experimental conclusions are in accordance with the calculations of Murrell *et al.*[39] as well as with the fact that the Mo—N_2 bond is shorter than the Mo—P bond.[9,10] The $(b_{2g})^2$ $(e_g)^4$ configuration does not contradict the fact of photodissociation of N_2 without $[Mo(N_2)_2(dppe)_2]$, because the absorption of radiation connected with the transition $^1A_1 \rightarrow {}^3E\,(b_{2g})^2\,(e_g)^4 \rightarrow (b_{2g})^2\,(e_g)^3\,(a_{1g})^1$ is the reason for the simultaneous weakness of the Mo—N_2 π-bond (decrease in the number of e_g-level electrons) as well as for the cleavage of the Mo—N_2 σ-bond (filling of the a_{1g}-level). The absorption of 440-nm radiation may also lead to the excitation $^1A_1 \rightarrow {}^3A_2\,(b_{2g})^2\,(e_g)^4$ $\rightarrow (b_{2g})^1\,(e_g)^4\,(b_{1g})^1$. Thus, the accepted first state of excitation, b_{1g}, is in accordance with the yields from $[Mo(N_2)_2(dppe)_2]$ decomposition found in toluene solution. In considering the population, the transition $^1A_1 \rightarrow {}^3E$ is more probable than $^1A_1$ $\rightarrow {}^3A_2$, so the decomposition yield of Mo—N_2 is higher than that of Mo—P. This fact is also influenced by the higher donor capacity of dppe in

comparison with that of N_2. The first excited state, b_{1g}, is in agreement with the decomposition yields of $[Mo(N_2)_2(dppe)_2]$ in the solid phase in an H_2 atmosphere. The energy level diagram of the central atom for the $[Mo(N_2)_2(dppe)_2]$ complex calculated on the basis of the experimental data {the absorption bands of $[Mo(N_2)_2(dppe)_2]$} is shown in Fig. 1. From Fig. 2 it is evident that b_{1g} is the first unfilled state. Thus, the interaction of $[Mo(N_2)_2(dppe)_2]$ with e^- leads to the configuration $(b_{2g})^2 (e_g)^4 (b_{1g})^1$ or $(b_{2g})^2 (e_g)^4 (e_u)^1$ (because of the small energy interval between the e_u- and b_{1g}-orbitals). The filling of the b_{1g} or $3d$(P) state results in the rupture of the Mo—P bond in the solid phase. The anion, $[Mo(N_2)_2(dppe)_2]^-$, formed in the solution may disappear on reaction with the cation. A reaction of this type takes place in the case of $(dppe)^-$ in CH_3OH.[25] If the a_{1g}-level is lower than b_{1g}, as assumed by Murrell *et al.*,[39] the decomposition yield of Mo—N_2 is higher than that of Mo—P in the solid phase. The band occurring in frozen TBP solution at 480 nm is well interpreted by the diagram in Fig. 1. The $(b_{1g})^1 \rightarrow (a_{1g})^1$ transition which is expected on the basis of this diagram should have an energy of 20,000 cm^{-1} (in a non-polar solvent). The experimental frequency (in a polar solvent) equals 20,800 cm^{-1}, in good agreement with the diagram. The band for the $[Mo(N_2)_2(dppe)_2]^-$ ion, in accordance with Murrell *et al*'s[39] diagram, i.e. $(a_{1g})^1 \rightarrow (b_{1g})^1$ should be at 37,100 cm^{-1}. Therefore the MO sequence calculated by Murrell *et al.*,[39] i.e.

$$3b_{2g} < 4e_g < 16a_{1g} < e_u < 4b_{1g},$$

may be changed to the following one:

$$3b_{2g} < 4e_g < 4b_{1g} < 8e_u < 16a_{1g}.$$

Taking into account the results described above, it can be noted that the radiation investigations may be applied as an essential complementary method for the determination of the electronic states of complex compounds.

In the light of the results presented the following mechanism is proposed for $[Mo(N_2)_2(dppe)_2]$ radiolysis in the solid phase in an H_2 atmosphere:

$$[Mo(N_2)_2(dppe)_2] \rightarrow M^+ + e^-, \tag{1}$$

$$[Mo(N_2)_2(dppe)_2] + e^- \rightarrow [Mo(N_2)_2(dppe)_2]^- \tag{2}$$

$$[Mo(N_2)_2(dppe)_2]^- \rightarrow [Mo(N_2)_2(dppe)] + (dppe)^-, \tag{3}$$

$$[Mo(N_2)_2(dppe)_2] + H \rightarrow \left[\begin{matrix} & N_2 & \\ Mo & & (dppe)_2 \\ & N_2H & \end{matrix} \right], \tag{4}$$

$$\left[\begin{matrix} & N_2 & \\ Mo & & (dppe)_2 \\ & N_2H & \end{matrix} \right] + H_2 \rightarrow \left[\begin{matrix} & N{-}NH_3 & \\ Mo & & (dppe)_2 \\ & N_2 & \end{matrix} \right] \text{ and } \left[\begin{matrix} & N_2 & \\ Mo & & (dppe)_2 \\ & NH{-}NH_2 & \end{matrix} \right] \tag{5}$$

$$\left[\begin{matrix} & N{-}NH_3 & \\ Mo & & (dppe)_2 \\ & N_2 & \end{matrix} \right] \rightarrow H_3N + [Mo(N_2)(dppe)_2] + N, \tag{6}$$

$$\left[\begin{matrix} & NH{-}NH_2 & \\ Mo & & (dppe)_2 \\ & N_2 & \end{matrix} \right] + H_2 \rightarrow H_4N_2 + [Mo(N_2H)(dppe)_2], \tag{7}$$

$$N + N \rightarrow N_2. \tag{8}$$

REFERENCES

1. M. Hidai, K. Tominari and Y. Uchida, *J. Chem. Soc., Chem. Commun.* 1969, 814.
2. T. A. George and C. D. Seibold, *J. Chem. Soc., Chem. Commun.* 1973, 2544.
3. T. A. George and M. E. Noble, *Inorg. Chem.* 1978, **17**, 1678.
4. T. A. George and C. D. Seibold, *J. Organomet. Chem.* 1971, **27**, C13.
5. C. Miniscloux, G. Martino and L. Sajus, *Bull. Soc. Chim. Fr.* 1973, **7–8**, 2183.
6. M. Hidai, K. Tominari and Y. Uchida, *J. Am. Chem. Soc.* 1972, **94**, 110.
7. A. P. Borisov, W. D. Machaiev and K. N. Semenenco, *Coord. Chim.* 1979, **5**, 948.
8. L. K. A. Atkinson, A. M. Mawby and D. C. Smith, *J. Chem. Soc., Chem. Commun.* 1971, 151.
9. T. Uchida, Y. Uchida, M. Hidai and T. Kodoma, *Bull. Chem. Soc. Jpn* 1971, **44**, 2883.
10. T. Uchida, Y. Uchida, M. Hidai and T. Kodoma, *Acta Cryst.* 1975, **B31**, 1179.
11. R. J. Thomas, W. Laurence and A. Diamantis, *Inorg. Chim. Acta Lett.* 1978, **30**, L353.
12. J. Connor and R. Riley, *J. Chem. Soc., Dalton Trans.* 1979, 1318.
13. T. Tatsumi, M. Hidai and Y. Uchida, *Inorg. Chem.* 1975, **14**, 2530.
14. D. C. Busby and T. A. George, *J. Organomet. Chem.* 1976, **118**, C16.
15. J. Chatt, A. J. Pearman and R. L. Richards, *J. Chem. Soc., Dalton Trans.* 1977, 1852.
16. D. C. Beran, J. Chatt, G. J. Leigh and E. G. Leelamani, *J. Organomet. Chem.* 1977, **139**, C59.
17. M. Nardelli, C. Pelizzi and G. Predien, *J. Organomet. Chem.* 1981, **204**, 75.
18. H. M. Colguhoun, *Transition Met. Chem.* 1981, **6**, 57.
19. H. M. Colguhoun and R. A. Head, *Inorg. Chim. Acta* 1980, **45**, L123.
20. J. Chatt, G. A. Heath and G. J. Leigh, *J. Chem. Soc., Chem. Commun.* 1972, 444.
21. T. Takahashi, Y. Mirobe, M. Sato, Y. Uchida and M. Hidai, *J. Am. Chem. Soc.* 1980, **102**, 7461.
22. A. Cannana, H. Herman and H. Kisch, *J. Organomet. Chem.* 1980, **187**, 349.
23. L. J. Archer and T. A. George, *Inorg. Chim. Acta Lett.* 1980, **44**, L129.
24. M. Wenturi, A. Breccia, Q. G. Mulazzani and M. D. Ward, *Atti Accad. naz. Lincei, Rend. U. Sci. Fis., Mat. nat.* 1974, **56**, 366.
25. J. O. Dzięgielewski, *Tetrahedron* 1986, **42**, 109.
26. H. Czarnik-Matusewicz, J. O. Dzięgielewski, *Radiochem. Radioanal. Lett.* 1982, **51**, 355.
27. J. O. Dzięgielewski, J. Hanuza, B. Jeżowska-Trzebiatowska and J. Z. Siemion, *J. Prikładnoj Spektroscopii* 1973, **19**, 275.
28. W. B. Poliakova, A. N. Borisov, W. D. Machaiev and K. J. Siemienienko, *Koord. Chim.* 1980, **6**, 743.
29. J. H. S. Green and W. Kynastan, *Spectrochim. Acta* 1969, **25A**, 1677.
30. J. H. Baxendale and M. Fiti, *J. Chem. Soc., Faraday Trans. 2* 1972, **68**, 218.
31. A. Caruana and H. Kisch, *Angew. Chem., Int. Ed. Engl.* 1979, **18**, 328.
32. T. A. George, D. C. Busby and S. D. A. Iske, Jr, *Adv. Chem. Ser.* 1978, **168**, 147.
33. M. Wrighton, *Inorg. Chem.* 1974, **13**, 905.
34. M. Wrighton, G. S. Hammond and H. B. Gray, *J. Am. Chem. Soc.* 1971, **93**, 4336.
35. M. Wrighton, G. S. Hammond and H. B. Gray, *Mol. Photochem.* 1973, **5**, 179.
36. M. Wrighton, *Chem. Rev.* 1974, **74**, 401.
37. D. L. Dubois and R. Hoffman, *Nouv. J. Chim.* 1973, **1**, 479.
38. J. Chatt, G. J. Leigh, C. J. Pickett, R. L. Richards and A. J. L. Pombeiro, *Nouv. J. Chim.* 1978, **2**, 541.
39. J. N. Murrell, A. Al-Derzi, G. F. Leigh and M. F. Guest, *J. Chem. Soc., Dalton Trans.* 1980, 1425.
40. J. O. Dzięgielewski, *Polyhedron* 1984, **3**, 1131.
41. A. J. L. Pombeiro, *Rev. Port. Quim.* 1979, **21**, 90.

Polyhedron Vol. 5, No. 3, pp. 839–843, 1986
Printed in Great Britain

0277-5387/86 $3.00 + .00
© 1986 Pergamon Press Ltd

EXTRACTION OF 1:1 ELECTROLYTES FROM AQUEOUS SOLUTIONS BY RESINS CONTAINING DIBENZO-18-CROWN-6 AS ANCHOR GROUPS

ANGELA F. DANIL DE NAMOR* and ELIZABETH SIGSTAD†

Department of Chemistry, University of Surrey, Guildford, Surrey GU2 5XH, U.K.

(*Received* 1 *July* 1985; *accepted* 2 *September* 1985)

Abstract—The electrolyte concentration dependence of the distribution ratio of 1 : 1 electrolytes between resins containing dibenzo-18-crown-6 and water at 298 K was studied. The apparent equilibrium constants for the process taking place when the resin is equilibrated with aqueous solutions of different electrolytes are reported. The results obtained clearly reflect the influence of the anion on the extraction of cations by the resin containing the macrocyclic ligand.

The extraction of 1 : 1 electrolytes from water to non-aqueous solvents by the use of macrocyclic ligands is an area of considerable interest. Extraction studies of 1 : 1 electrolytes using naturally occurring antibiotics were reported by Eisenman *et al.*[1] in 1967. The discovery of synthetic macrocyclic ligands such as crown ethers[2] and cryptands[3] and their specific ion-bonding properties encouraged their use for the extraction of metal ions from aqueous to non-aqueous media.[4–27] Among the factors that should be taken into consideration in solvent extraction processes involving liquid–liquid systems and chelating agents are those concerned with the recovery of the solvent as well as the extracting material. The latter factor seems to be more relevant in the case of crown ethers and cryptands because of the relatively high cost of these ligands. Hence, the use of solid materials containing macrocyclic ligands, easily recycled, is greatly advantageous. Among these materials are those prepared by Blasius and coworkers[28–36] using crown ethers and cryptands as anchor groups. Distribution data as reported by these authors[31,36] for several 1:1 electrolytes in a water–resin system are referred to a given electrolyte concentration.

This work is concerned with measurements of distribution data at several electrolyte concentrations for a number of alkali metal salts in the water–ϕDB18C6‡ system at 25°C in order to derive an expression for the equilibrium constant for the extraction process.

EXPERIMENTAL

Resin preparation

ϕDB18C6 was prepared according to the technique suggested by Blasius *et al.*,[28] using DB18C6 (Sigma Chemical Co.), formic acid (BDH) [98% (w/v)] and formaldehyde (BDH) [37.40% (w/v)]. The product obtained was extracted with methanol (May & Baker Ltd) for 48 h, dried in a vacuum oven at 100°C for 1 day and finally milled in a mortar. It was kept in a desiccator with P_4O_{10} for a period of at least 2 weeks before use in order to ensure the minimal amount of water in the sample. The water content of the resin determined by a thermogravimetric method, using a Stanton Redcroft TG 750 thermobalance, was never greater than 2%. The percentages of C and H determined by microanalysis carried out at the University of Surrey were 68.39 and 5.95%, respectively.

Reagents used

Potassium thiocyanate (KSCN), potassium iodide (KI), potassium bromide (KBr), potassium chloride (KCl), sodium thiocyanate ($NaSCN \cdot H_2O$),

* Author to whom correspondence should be addressed.
† Present address: Universidad Nacional de Santiago del Estero, Avda Belgrano 1912(S), Santiago del Estero, Argentina.

‡ Throughout this paper we use the notation given by Blasius to indicate the resin containing dibenzo-18-crown-6 (DB18C6) as anchor group.

sodium iodide (NaI), rubidium iodide (RbI) and caesium iodide (CsI) (all BDH Analar grade) were dried at 105°C for several days before use. Potassium and sodium picrate (KPi and NaPi) were prepared by neutralizing a solution of picric acid with the corresponding hydroxide solution [5% (w/v)]. The yellow precipitate formed was then filtered off and the product obtained was twice recrystallized from water and dried for several days in a vacuum oven at 60°C.

Capacity measurements of ϕDB18C6 and 1:1 electrolytes in aqueous solution at 25°C

The resin was accurately weighed (±0.00001 g) in a plastic container. A volume (50 cm^3) of an accurately analysed aqueous solution of the electrolyte was added. The contents left in a thermostat (25 ± 0.05°C) under continuous stirring. After an overnight equilibration period an aliquot of the solution was taken and analysed. A further volume (25 cm^3) of solution was added to the resin and the container was left in a thermostat for a further period of 12 h. The procedure was followed subsequently until no further uptake of electrolyte by the resin was observed. This was done in duplicate.

Distribution experiments

To weighed samples of resin (±0.00001 g) were added known volumes of accurately analysed solutions of different electrolye concentration. The mixture was left in a water bath at 25 ± 0.05°C until equilibration was attained. Aliquot samples of the equilibrium solutions were removed and analysed by the methods described below. Blank experiments were carried out by equilibrating weighed samples of resin with water. No presence of distribuends were detected.

Methods of analysis

Halides and thiocyanates were determined by the volumetric method suggested by Vogel[37] based on the precipitation of the halide and thiocyanate by the addition of silver nitrate in the presence of an adsorption indicator like dichlorofluoroscein in the case of chlorides and thiocyanates, and eosin in the case of bromides and iodides. The results were checked by potentiometric titrations.

Picrates were analysed spectrophotometrically at 350 nm using a Pye–Unicam SP 8100 visible–UV spectrophotometer. The extinction coefficient as calculated by regression analysis of the data was 14.473 $cm^{-1}\ M^{-1}$.

RESULTS AND DISCUSSION

Distribution ratio

The value obtained in this work for the capacity of ϕDB18C6 from microanalysis (2.59×10^{-3} mol g^{-1} dry resin) is in excellent agreement with that reported by Blasius *et al.*[35] The effective capacities of ϕDB18C6 at 25°C, defined as the maximum amount of electrolyte taken up by the resin for the different 1:1 electrolytes when water is the reaction media, are reported in Table 1. Taking into account the number of crown ether units in the polymer framework as given by microanalysis data, it is quite clear from the results that, for all 1:1 electrolytes, the value of 2.59×10^{-3} mol g^{-1} of dry resin is not obtained when water is used as the solvent. This observation is again in line with results previously reported by Blasius.

The variation of the distribution coefficients at 25°C with the initial molar concentration of the alkali-metal salts is shown in Fig. 1 for KSCN, KI, KBr, KCl, NaSCN and NaI, and in Fig. 2 for KPi and NaPi. It was not possible to measure the distribution ratio for KPi at higher concentrations than 2×10^{-2} mol cm^{-3}. The solubility of this salt in water is 2.36×10^{-3}.[39] Figure 3 shows the distribution data obtained for RbI and CsI. For all the electrolytes considered distribution values generally decrease with increasing solution concentration, this effect being more pronounced for electrolytes containing large anions such as iodide, thiocyanate and picrates. The clear dependence of the distribution ratio with the initial concentration of the electrolyte in the solution phase could be attributed to an increase in interaction in the resin phase as the number of sites available for extraction decreases. The distribution data shows the influence of the anion on the extraction of the alkali-metal cations from the

Table 1. Effective capacities of ϕDB18C6 with alkali-metal salts in water at 298 K

Electrolyte	Capacity (mol g^{-1})
KSCN	1.47×10^{-3}
KI	1.40×10^{-3}
KBr	1.13×10^{-3}
KCl	9.50×10^{-4}
KPi	1.15×10^{-3}
NaSCN	1.29×10^{-3}
NaI	1.15×10^{-3}
NaPi	1.08×10^{-3}
RbI	1.18×10^{-3}
CsI	9.50×10^{-4}

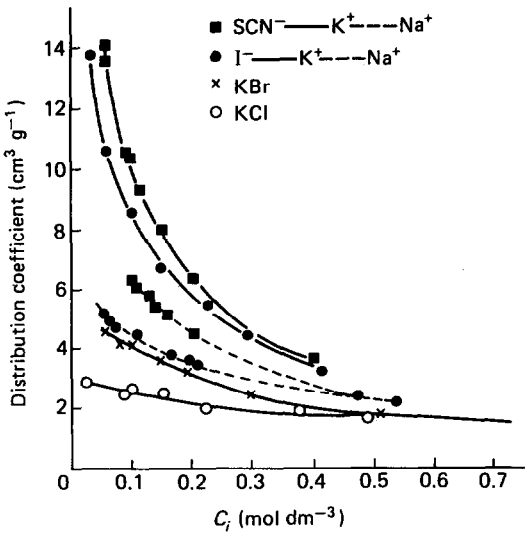


Fig. 1. Distribution of sodium and potassium salts between ϕDB18C6 and water at different electrolyte concentrations at 298 K.

aqueous solution by ϕDB18C6. Considering the potassium salts, values for the distribution coefficients are in the order $Pi^- > SCN^- > I^- > Br^- > Cl^-$. Comparison of partition data for a given cation and different anions in a water–non-aqueous media system clearly show that the transfer of the anion plays an important role in the distribution of the cation. The results obtained from distribution studies for the 1 : 1 electrolytes in the ϕDB18C6–water system shows that the distribution coefficients obtained follow the same trend as that generally observed from the free energy of transfer

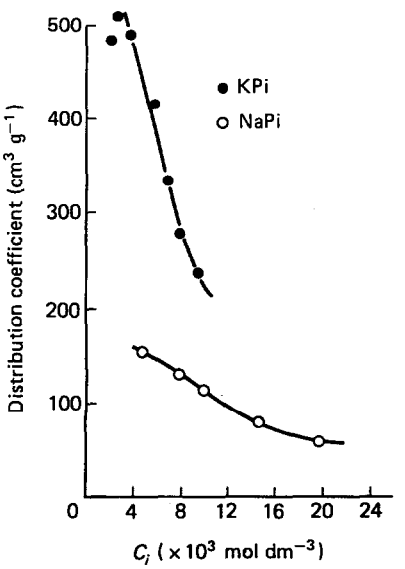


Fig. 2. Distribution of NaPi and KPi between ϕDB18C6 and water at different electrolyte concentrations at 298 K.

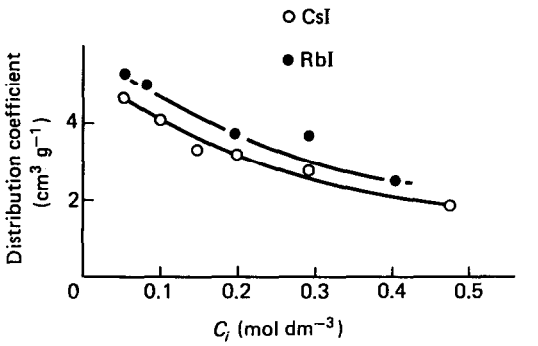


Fig. 3. Distribution of RbI and CsI between ϕDB18C6 and water at different electrolyte concentrations at 298 K.

data of anions (Ph_4AsPh_4B convention) from water to non-aqueous solvents.[38,39]

Extraction equilibrium constant

The resin used in this work is characterized by an anchor group (DB18C6) containing donor atoms capable of forming strong co-ordinative bonds with metal ions. Since electroneutrality must be maintained, cations and anions from the solution enter the resin phase. Provided that the electrolytes are fully dissociated in the solvent, the process taking place when a solution of 1 : 1 electrolyte ($M^+ + A^-$) is equilibrated with a resin containing an anchor group (L) may be described by:

$$M^+(aq.) + A^-(aq.) + \overline{nL} \rightarrow \overline{M^+L_nA^-}, \qquad (1)$$

where barred formulae are used to indicate the species in the resin phase. In eqn (1) n is defined as the average number of moles of crown ether units that take up 1 mol of the electrolyte from the solution phase. The n value is obtained from the ratio between the total capacity (C_T^-) as obtained from microanalysis and the effective capacity of the resin as shown in Table 1. If the molar fraction scale is chosen for the resin phase and the molar scale for the solution phase, the rational equilibrium constant (K_{ext}) for eqn (1) may be represented by:

$$K_{ext} = \frac{\bar{x}_{(M^+L_nA^-)}}{[M^+]_{aq.}[A^-]_{aq.}[1 - n\bar{x}_{(M^+L_nX^-)}]^n}, \qquad (2)$$

where $\bar{x}_{(M^+L_nA^-)}$ and $[1 - n\bar{x}_{(M^+L_nA^-)}]$ are the notations used to indicate the mole fraction of the electrolyte and ligand in the resin phase, respectively, and $[M^+]_{aq.}$ and $[A^-]_{aq.}$ are the equilibrium molar concentrations of the cation and anion in the solution phase. The rational distribution coefficient (D_R) may be defined by:

$$D_R = \frac{\bar{x}_{(M^+L_nA^-)}}{[M^+]_{aq.}}. \qquad (3)$$

Replacing eqn (3) in eqn (2) gives:

$$K_{ext} = \frac{D_R}{[A^-]_{aq.}[1 - n\bar{x}_{(M^+L_nA^-)}]^n} \quad (4)$$

Equation (5) is simply a rearranged form of eqn (2):

$$K_{ext}[1 - n\bar{x}_{(M^+L_nA^-)}]^n = \frac{D_R}{[A^-]_{aq.}}. \quad (5)$$

Taking logarithms on both sides of eqn (5), eqn (6) is obtained:

$$\log \frac{D_R}{[A^-]_{aq.}} = \log K_{ext} + \log [1 - n\bar{x}_{(M^+L_nA^-)}]^n. \quad (6)$$

According to eqn (6) a plot of log $D_R/[A^-]_{aq.}$ against log $[1 - n\bar{x}_{(M^+L_nA^-)}]^n$ should give a straight line. The intercept of this line will give log K_{ext} and the slope should be equal to unity. Figure 4 shows the plots obtained for the electrolytes KSCN, KI, KBr, KCl, KPi, NaSCN, NaI, NaPi, RbI and CsI. In all cases a linear relationship was obtained with slope values about unity which indicates that the assumptions made to derive eqn (6) seem to be reasonable. The apparent equilibrium constants (log K_{ext}) as obtained by eqn (6) for 1:1 electrolytes are presented in Table 2.

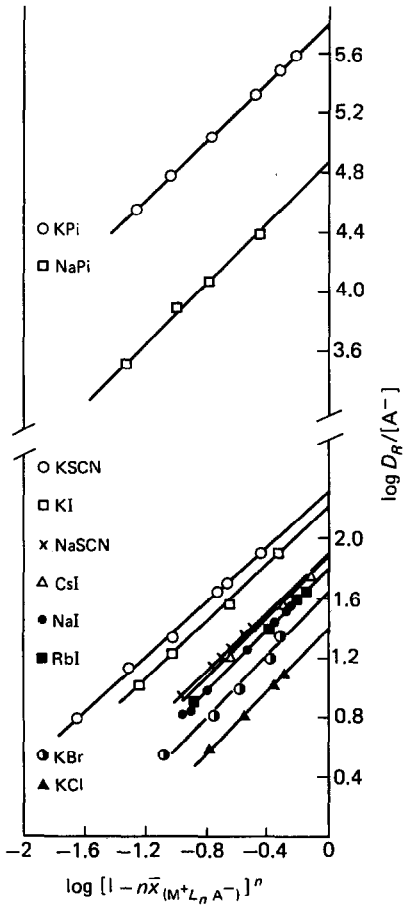


Fig. 4. Plot of log $D_R/[A^-]$ against log $[1 - n\bar{x}_{(M^+L_nA^-)}]^n$ in water at 298 K.

Table 2. Rational equilibrium constants for the extraction of 1:1 electrolytes from aqueous solutions at 298 K using eqn (6) in text

Electrolyte	log K_{ext}
KSCN	2.33
KI	2.23
KBr	1.64
KCl	1.40
KPi	5.81
NaSCN	1.91
NaI	1.84
NaPi	4.85
RbI	1.79
CsI	1.90

The equilibrium constants (log K_{ext}) reflect the selectivity of ϕDB18C6 towards the different 1:1 electrolytes. Quite remarkable is the effect of the anion on the extraction constants, particularly the picrates. An approximate evaluation can be made by taking the ratio between K_{ext} values for the electrolytes containing the same cation and different anions. It is shown that the extraction of a given cation, in this case potassium, is increased by factors of about 1.5×10^4, 8.9×10^3, 2.1×10^3 and 1.5×10^3 when picrate is the anion with respect to chloride, bromide, iodide and thiocycnate, respectively. Although the values for the extraction constants (log K_{ext}) are only apparent, the results obtained are still undoubtedly of considerable practical importance.

REFERENCES

1. G. Eisenman, S. M. Ciani and G. Szabo, *J. Membr. Biol.* 1967, **1**, 294.
2. C. J. Pedersen, *J. Am. Chem. Soc.* 1967, **89**, 2495.
3. J. M. Lehn, *Struct. Bonding* 1973, **1**, 16.
4. C. J. Pedersen and H. K. Frendsdorff, *Angew. Chem., Int. Ed. Engl.* 1972, **11**, 16.
5. G. Eisenman, S. M. Ciani and G. Szabo, *Fed. Proc.* 1968, **27**, 1289.
6. H. K. Frendsdorff, *J. Am. Chem. Soc.* 1971, **93**, 4684.
7. A. Sadakane, T. Iwachido and K. Töei, *Bull. Chem. Soc. Jpn* 1975, **48**, 60.
8. C. J. Pedersen, *Fed. Proc.* 1968, **27**, 1305.
9. K. Kina, K. Shiraishi and N. Ishibashi, *Bunseki Kayaku* 1978, **27**, 291.
10. J. Rais and P. Selucky, *Radiochem. Radioanal. Lett.* 1971, **6**, 257.

11. P. R. Danesi, H. Meider-Gorican, R. Chiarizia and G. Scibona, *J. Inorg. Nucl. Chem.* 1975, **37**, 1479.
12. J. W. Mitchell and D. L. Shanks, *Anal. Chem.* 1975, **47**, 642.
13. T. Sekine, H. Wakabayashi and Y. Hasegawa, *Bull. Chem. Soc. Jpn* 1978, **51**, 645.
14. A. M. T. Jaber, G. J. Moody and J. D. R. Thomas, *J. Inorg. Nucl. Chem.* 1971, **39**, 1689.
15. Y. Marcus and L. E. Asher, *J. Phys. Chem.* 1978, **82**, 1246.
16. T. Kimura, I. Washima and T. Tshimoro, *Chem. Lett. Jpn* 1977, 563.
17. Y. Takeda and H. Kato, *Bull. Chem. Soc. Jpn* 1979, **52**, 1027.
18. Y. Takeda, *Bull. Chem. Soc. Jpn* 1980, **52**, 2501.
19. T. Takeda, Y. Wada and S. Fujiwara, *Bull. Chem. Soc. Jpn* 1981, **54**, 3727.
20. H. Noguchi, H. Nakamura, M. Nagamatsu and M. Yoshio, *Bull. Chem. Soc. Jpn* 1982, **55**, 156.
21. Y. Takeda, *Bull. Chem. Soc. Jpn* 1983, **56**, 2589.
22. S. Kopolow, T. E. Hogen-Esch and J. Smid, *Macromolecules* 1971, **4**, 359.
23. S. Kopolow, T. E. Hogen-Esch and J. Smid, *Macromolecules* 1973, **6**, 133.
24. P. Gramain and Y. Frere, *Macromolecules* 1979, **12**, 1038.
25. P. Gramain and Y. Frere, *Polymer* 1980, **21**, 921.
26. P. Gramain, M. Kleiber and Y. Frere, *Polymer* 1980, **21**, 915.
27. A. Warshawsky and N. Kahana, *J. Am. Chem. Soc.* 1982, **104**, 2663.
28. E. Blasius, W. Adrian, K. P. Jansen and G. Klautske, *J. Chromatogr.* 1974, **96**, 89.
29. E. Blasius and K. P. Jansen, *Chem.-Ing.-Tech.* 1975, **47**, 594.
30. E. Blasius and D. G. Maurer, *J. Chromatogr.* 1976, **125**, 511.
31. E. Blasius, K. P. Jansen, W. Adrian, G. Klautske, R. Lorscheider, P. G. Maurer, V. B. Nguyen, T. Nguyen-Tien, G. Scholten and J. Stockemer, *Z. Anal. Chem.* 1977, **284**, 337.
32. E. Blasius, K. P. Jansen and W. Neuman, *Microchim. Acta* 1977, **11**, 279.
33. E. Blasius, K. P. Jansen, H. Luxenburger, V. B. Nguyen, H. Klotz and J. Stockemer, *J. Chromatogr.* 1978, **167**, 307.
34. E. Blasius, K. P. Jansen, M. Keller, H. Lander, T. Nguyen-Tien and G. Scholten, *Talanata* 1980, **27**, 107.
35. E. Blasius, K. P. Jansen, W. Adrian, W. Klein, H. Klotz, H. Luxenburger, E. Mernke, V. B. Nguyen, T. Nguyen-Tien, R. Rausch, J. Stockemer and Q. Toussaint, *Talanta* 1980, **27**, 127.
36. E. Blasius and H. Sander, *Z. Anal. Chem.* 1980, **303**, 177.
37. A. I. Vogel, *Quantitative Inorganic Analysis*, 3rd Edn. Longmans, London (1961).
38. A. F. Danil de Namor, T. Hill and E. Sigstad, *J. Chem. Soc., Faraday Trans.* 1 1983, **79**, 2713.
39. A. F. Danil de Namor and L. Ghousseini, *J. Chem. Soc., Faraday Trans.* 1 1984, **80**, 2893.

Polyhedron Vol. 5, No. 3, pp. 845–858, 1986
Printed in Great Britain

0277–5387/86 $3.00 + .00
© 1986 Pergamon Press Ltd

MIXED ISOCYANIDE–1,4-DIAZA-1,3-BUTADIENE COMPLEXES OF MOLYBDENUM AND TUNGSTEN—II.* SPECIES OF THE TYPE $[M(CO)_3(CNR)(R'\text{-DAB})]^{1+,0,1-}$

ANDREW BELL and RICHARD A. WALTON†

Department of Chemistry, Purdue University, West Lafayette, IN 47907, U.S.A.

(*Received* 8 *May* 1985; *accepted* 5 *September* 1985)

Abstract—The complexes $M(CO)_4(R'\text{-DAB})$ (M = Mo or W; R'-DAB = R'—N=CH—CH=N—R'; R' = *i*-Pr, *t*-Bu, Cy or *p*-tol) undergo substitution of a single CO ligand by isocyanide ligands RNC (R = Me, $CHMe_2$, CMe_3, C_6H_{11} or xylyl), in refluxing toluene to give *fac*-$M(CO)_3(CNR)(R'\text{-DAB})$. Synthesis of the latter complexes can also be achieved, at ambient temperature, through the use of the nitrile complexes, $Mo(CO)_3(NCMe)_3$ and $W(CO)_3(NCEt)_3$: the method involves substitution of the nitrile ligands first by R'-DAB, then by RNC. The intermediate compounds $Mo(CO)_3(NCMe)(R'\text{-DAB})$ and $W(CO)_3(NCEt)(R'\text{-DAB})$ have also been isolated and characterized. Oxidation of dark blue-purple $Mo(CO)_3(NCMe)(t\text{-Bu-DAB})$ and $Mo(CO)_3(CNR)(t\text{-Bu-DAB})$ (R = Me or CMe_3) with $[Cp_2Fe]PF_6$ in dichloromethane solution produces the paramagnetic (17-electron), orange complexes $[Mo(CO)_3(NCMe)(t\text{-Bu-DAB})]PF_6$ and $[Mo(CO)_3(CNR)(t\text{-Bu-DAB})]PF_6$, respectively. The molybdenum cations, $[Mo(CO)_3(NCMe)(t\text{-Bu-DAB})]PF_6$ and $[Mo(CO)_3(CNCMe_3)(t\text{-Bu-DAB})]PF_6$, react with two and one equivalent of *tert*-butyl isocyanide, respectively, to yield dark red *cis, trans*-$[Mo(CO)_2(CNCMe_3)_2(t\text{-Bu-DAB})]PF_6$. Reduction of *cis, trans*-$[Mo(CO)_2(CNCMe_3)_2(t\text{-Bu-DAB})]PF_6$ with cobaltocene in acetone yields the analogous dark blue zerovalent species *cis, trans*-$Mo(CO)_2(CNCMe_3)_2(t\text{-Bu-DAB})$. The compounds $[Mo(CO)(CNR)_4(t\text{-Bu-DAB})](PF_6)_2$ and $Mo(CO)_3(CNR)(t\text{-Bu-DAB})$ are produced, via a disproportionation reaction, when solutions of the cations $[Mo(CO)_3(CNR)(t\text{-Bu-DAB})]^+$ (R = Me or CMe_3) are reacted with ~three equivalents of RNC. On the other hand, the reaction between *tert*-butyl isocyanide and $[Mo(CO)_3(CNCMe_3)(i\text{-Pr-DAB})]^+$ gives seven-coordinate $[Mo(CNCMe_3)_5(i\text{-Pr-DAB})](PF_6)_2$ and $Mo(CO)_3(CNCMe_3)(i\text{-Pr-DAB})$. The ligand-based reduction of the complexes $M(CO)_3(CNR)(R'\text{-DAB})$ (M = Mo or W) is readily accessible in THF upon addition of one molar equivalent of THF-soluble $LiEt_3BH$ to yield solutions that contain the radical anions $[M(CO)_3(CNR)(R'\text{-DAB})]^{-\cdot}$. The complexes synthesized in this work have been characterized on the basis of their spectroscopic and electrochemical properties, including ESR spectral studies on the paramagnetic 17- and 19-electron complexes.

We have shown[1] that the reactions of the molybdenum(II) complexes $Mo(CO)_3(R'\text{-DAB})(SnCl_3)Cl$, where R'-DAB represents R'—N=CH—CH=N—R', with an excess of alkyl isocyanide (CNR) in the presence of KPF_6 lead to the seven-coordinate mixed isocyanide–R'-DAB species

$$[Mo(CNR)_4(R'\text{-DAB})Cl]PF_6$$

and

$$[Mo(CNR)_5(R'\text{-DAB})](PF_6)_2$$

in the case of R' = *i*-Pr or Cy. However, when the *tert*-butyl-DAB (*t*-Bu-DAB) ligand is used, such reactions proceed with the reductive elimination of the elements of $SnCl_4$ and the formation of $Mo(CO)_3(CNR)(t\text{-Bu-DAB})$. A similar reaction was used[1] to give the analogous tungsten(0) complex $W(CO)_3(CNR)(t\text{-Bu-DAB})$ in the case of R = CMe_3. We have now developed some general procedures for the synthesis of a broad range of complexes of the

* For Part I see Ref. 1.

† Author to whom correspondence should be addressed.

type $M(CO)_3(CNR)(R'\text{-DAB})$. In this report we give an account of these syntheses and a full characterization of these complexes, including an examination of their redox chemistry. The generation and isolation of the 17-, 18- and 19-electron species $[M(CO)_3(CNR)(R'\text{-DAB})]^{1+,0,1-}$ are described.

EXPERIMENTAL

Starting materials

The following compounds were prepared by standard literature procedures: methyl isocyanide,[2] *iso*propyl isocyanide,[3] *tert*-butyl isocyanide,[3] cyclohexyl isocyanide,[3] *N,N'*-di-*iso*-propylethylenediimine [*iso*propyl-DAB (*i*-Pr-DAB)],[4] *N,N'*-di-*tert*-butylethylenediimine (*t*-Bu-DAB),[4] *N,N'*-dicyclohexylethylenediimine [cyclohexyl-DAB (Cy-DAB)][4,5] $Mo(CO)_4(R'\text{-DAB})$ (R' = *i*-Pr, *t*-Bu or Cy).[6] The complex $W(CO)_4$(t-Bu-DAB) was prepared by heating a mixture of $W(CO)_6$ and *t*-Bu-DAB in xylene at reflux for 24 h. The work up was then identical to that described by tom Dieck.[6] Lithium triethylborohydride [1.0 M $LiEt_3BH$ in THF ("Super-Hydride"), Aldrich Chemical Co.], ferrocene, cobaltocene and 2,6-dimethylphenyl isocyanide (xylylNC, Fluka AG) were obtained from commercial sources as were all reagents and solvents. The solvents dichloromethane, acetonitrile and THF were distilled under N_2 from P_4O_{10}, CaH_2 and sodium benzophenone ketyl, respectively, before use.

The hexacarbonyls $Mo(CO)_6$ and $W(CO)_6$ were obtained from Pressure Chemical Co. and were converted into the nitrile derivatives $Mo(CO)_3(NCMe)_3$ and $W(CO)_3(NCEt)_3$ using established procedures.[7,8] For convenience in handling, these nitrile complexes were usually generated *in situ* and then reacted further with RNC or R'-DAB ligands.

Samples of the oxidizing agent ferricinium hexafluorophosphate ($[Cp_2Fe]PF_6$) were prepared as described in the literature.[9]

Reaction procedures

All reactions were carried out under a dry nitrogen atmosphere, and all reaction solvents were dried and deoxygenated prior to use by purging with N_2 gas for 15 min. In those cases where compounds were prepared by very similar procedures (see Sections A–D) details of representative preparations only will be given. In those instances where microanalytical data are not given, identification of products is based upon their spectroscopic and electrochemical properties.

A. Preparation of $Mo(CO)_3(NCMe)(R'\text{-DAB})$ (R' = *t*-Bu or Cy). (i) $Mo(CO)_3(NCMe)$(*t*-Bu-DAB). A quantity of $Mo(CO)_3(NCMe)_3$ was generated *in situ* by heating $Mo(CO)_6$ (5.0 g, 18.94 mmol) in 50 cm^3 of freshly distilled acetonitrile for 36 h. Without isolating the tris(acetonitrile) product, solid *t*-Bu-DAB (3.20 g, 18.94 mmol) was added to the pale yellow solution. The reaction mixture was stirred at room temperature for 30 min, whereupon the solution turned dark purple and a dark blue-purple microcrystalline material separated. The solid was collected by filtration and washed with diethyl ether and hexane and dried *in vacuo*. A further quantity of the product was obtained by evaporating the filtrate to dryness. Recrystallization was effected from an acetonitrile–petroleum ether mixture to give dark purple crystals having a metallic luster; yield 7.07 g (96%). Found: C, 46.5; H, 6.0. Calc. for $C_{15}H_{23}MoN_3O_3$: C, 46.3; H, 5.9%.

(ii) $Mo(CO)_3(NCMe)$(Cy-DAB). This product was prepared by a procedure analogous to that described in Section A(i): yield 92%.

B. Preparation of $W(CO)_3(NCEt)(R'\text{-DAB})$ (R' = *i*-Pr, *t*-Bu *or* Cy). (i) $W(CO)_3(NCEt)$(*i*-Pr-DAB). A 100-cm three-necked flask was charged with $W(CO)_3(NCEt)_3$ (2.0 g, 4.62 mmol) and *i*-Pr-DAB (0.711 g, 5.08 mmol). Addition of 25 cm^3 of dichloromethane by syringe and stirring the mixture under a nitrogen atmosphere resulted in the formation of a royal blue solution. The mixture was then stirred vigorously for 2 h at ambient temperature. After this period, the reaction solution was filtered to remove a small amount of a beige insoluble material, which was subsequently discarded, and the dark blue filtrate was taken to dryness under a stream of nitrogen. The purple-blue product was recrystallized from propionitrile–petroleum ether mixtures to give shiny dark purple platelets: yield 1.77 g (83%). Found: C, 36.6; H, 4.7. Calc. for $C_{14}H_{21}N_3O_3W$: C, 36.3; H, 4.5%.

(ii) $W(CO)_3(NCEt)$(*t*-Bu-DAB). Yield 74%. Found: C, 39.6; H, 5.7%. Calc. for $C_{16}H_{26}N_3O_3W$: C, 39.1; H, 5.1%.

(iii) $W(CO)_3(NCEt)$(Cy-DAB). Yield 86%. Found: C, 43.1; H, 5.3. Calc. for $C_{20}H_{29}N_3O_3W$: C, 44.2; H, 5.3%.

C. Reactions of $M(CO)_4(R'\text{-DAB})$ (M = Mo *or* W) *with isocyanides*. (i) $Mo(CO)_3(CNCMe_3)$(*t*-Bu-DAB). A mixture of $Mo(CO)_4$(*t*-Bu-DAB) (1.00 g, 2.66 mmol) and 1.2 equivalents of *tert*-butyl isocyanide (0.34 cm^3, 3.20 mmol) in 30 cm^3 of toluene was stirred for 1 h at reflux. During the reaction period, the solution turned from a dark red to a royal blue. Upon cooling the reaction solution to 0°C,

dark purple-blue crystals precipitated. The product was collected by filtration and washed with copious amounts of diethyl ether and petroleum ether prior to being dried *in vacuo*. An additional quantity of the product was obtained by taking the blue toluene filtrate to dryness and recrystallizing the product from acetone–diethyl ether: yield 0.92 g (80%). Found: C, 50.5; H, 7.1; N, 9.7. Calc. for $C_{18}H_{29}MoN_3O_3$: C, 50.1; H, 6.8; N, 9.7%.

(ii) $Mo(CO)_3(CNMe)(t\text{-Bu-DAB})$. Yield 54%. Found: C, 47.1; H, 6.0. Calc. for $C_{15}H_{23}MoN_3O_3$: C, 46.3; H, 5.9%.

(iii) $Mo(CO)_3(CNCHMe_2)(t\text{-Bu-DAB})$. Yield 63%. Found: C, 49.0; H, 7.3. Calc. for $C_{17}H_{27}MoN_3O_3$: C, 48.9; H, 6.5%.

(iv) $Mo(CO)_3(CNC_6H_{11})(t\text{-Bu-DAB})$. Yield 67%. Found: C, 52.5; H, 7.2. Calc. for $C_{20}H_{31}MoN_3O_3$: C, 52.5; H, 6.8%.

(v) $Mo(CO)_3(CNxylyl)(t\text{-Bu-DAB})$. Yield 74%. Found: C, 54.9; H, 5.7. Calc. for $C_{22}H_{29}MoN_3O_3$: C, 55.1; H, 6.1%.

(vi) $Mo(CO)_3(CNCMe_3)(i\text{-Pr-DAB})$. Yield 58%. Found: C, 47.5; H, 6.1. Calc. for $C_{16}H_{25}MoN_3O_3$: C, 47.6; H, 6.2%.

(vii) $W(CO)_3(CNMe)(t\text{-Bu-DAB})$. Yield 73%. Found: C, 45.9; H, 5.6. Calc. for $C_{15}H_{23}MoN_3O_3$: C, 46.3; H, 5.9%.

(viii) $W(CO)_3(CNCMe_3)(t\text{-Bu-DAB})$. Yield 68%. Found: C, 41.4; H, 5.8. Calc. for $C_{18}H_{29}N_3O_3W$: C, 41.6; H, 5.6%.

(ix) $W(CO)_3(CNxylyl)(t\text{-Bu-DAB})$. Yield 75%. Found: C, 46.9; H, 5.3. Calc. for $C_{22}H_{29}N_3O_3W$: C, 46.6; H, 5.2%.

D. Preparation of $M(CO)_3(CNR)(R'\text{-DAB})$ *from* $M(CO)_3(CNR)_3$ (M = M *or* W). (i) $Mo(CO)_3(CNCMe_3)(Cy\text{-DAB})$. A quantity of $Mo(CO)_3(NCMe)_3$ was prepared by heating a mixture of $Mo(CO)_6$ (3.0 g, 11.4 mmol) and 50 cm^3 of freshly distilled acetonitrile at reflux for 24 h. The reaction mixture was then allowed to cool to room temperature and Cy-DAB (2.53 g, 11.5 mmol) was added to the solution. The mixture was stirred for 15 min at ambient temperature by which time the solution had turned a royal blue color. Addition of *tert*-butyl isocyanide (1.25 cm^3, 11.8 mmol) yielded a dark purple-blue solution upon further stirring of the mixture for 15 min. Filtration of the reaction mixture afforded an olive green insoluble material, and the filtrate was taken to dryness under reduced pressure. The purple-blue crystals which resulted were recrystallized from acetone–petroleum ether and dichloromethane–hexane mixtures: yield 4.29 g (78%). Found: C, 54.0; H, 6.7. Calc. for $C_{22}H_{33}MoN_3O_3$: C, 54.7; H, 6.8%.

(ii) $Mo(CO)_3(CNCMe_3)(t\text{-Bu-DAB})$. Yield 96%. The identity of the product was confirmed by its spectroscopic and electrochemical properties which were identical to those of an authentic sample as prepared in Section C(i).

(iii) $Mo(CO)_3(CNCMe_3)(i\text{-Pr-DAB})$. Yield 84%.

(iv) $Mo(CO)_3(CNMe)(t\text{-Bu-DAB})$. Yield 75%.

(v) $Mo(CO)_3(CNCHMe_2)(Cy\text{-DAB})$. Yield 78%.

(vi) $Mo(CO)_3(CNxylyl)(i\text{-Pr-DAB})$. Yield 92%.

(vii) $Mo(CO)_3(CNxylyl)(Cy\text{-DAB})$. Yield 94%.

(viii) $Mo(CO)_3(CNCMe_3)(p\text{-tol-DAB})$. Yield 32%.

An alternative to the preceding procedure involved the reaction of the isolated mononitrile complexes $M(CO)_3(NCR)(R'\text{-DAB})$ (see Sections A and B) with one equivalent of RNC (R = Me, $CHMe_2$, CMe_3, C_6H_{11} or xylyl) at room temperature in deoxygenated dichloromethane. Representative experimental details for this synthetic method are described for the preparation of $W(CO)_3(CNCMe_3)(i\text{-Pr-DAB})$ from $W(CO)_3(NCEt)(i\text{-Pr-DAB})$.

(ix) $W(CO)_3(CNCMe_3)(i\text{-Pr-DAB})$. Typically, a quantity of $W(CO)_3(NCEt)(i\text{-Pr-DAB})$ (0.5 g, 1.08 mmol) was stirred in 15 cm^3 of dry, deoxygenated dichloromethane at room temperature. The addition of *tert*-butyl isocyanide (0.114 cm^3, 1.08 mmol) to the royal blue solution changed the reaction medium to a dark purple color. The mixture was stirred at room temperature for 6 h, and then taken to dryness under reduced pressure to yield small dark purple crystals. The product was washed with copious amounts of petroleum ether, and the solid then recrystallized from acetone–diethyl ether: yield 0.45 g (85%). Found: C, 39.5; H, 5.5. Calc. for $C_{16}H_{25}N_3O_3W$: C, 39.2; H, 5.1%.

(x) $W(CO)_3(CNxylyl)(i\text{-Pr-DAB})$. Yield 86%.

(xi) $W(CO)_3(CNCMe_3)(Cy\text{-DAB})$. Yield 91%.

(xii) $W(CO)_3(CNxylyl)(Cy\text{-DAB})$. Yield 94%.

(xiii) $W(CO)_3(CNC_6H_{11})(t\text{-Bu-DAB})$. Yield 85%.

E. Oxidation of $Mo(CO)_3(NCMe)(t\text{-Bu-DAB})$ *to* $[Mo(CO)_3(NCMe)(t\text{-Bu-DAB})]PF_6$. A 25-$cm^3$ three-necked flask was charged with $Mo(CO)_3(NCMe)(t\text{-Bu-DAB})$ (0.5 g, 1.285 mmol) and $[Cp_2Fe]PF_6$ (0.425 g, 1.285 mmol). The addition of 10 cm^3 of dry acetonitrile with stirring resulted in an immediate reaction to form a dark orange-red solution. The reaction mixture was then filtered under nitrogen to remove any insoluble materials, which were discarded, and 80 cm^3 of anhydrous diethyl ether were added to the filtrate. The bright orange crystals that precipitated after about 10 min were collected by filtration and washed with copious amounts of diethyl ether before being dried *in vacuo*: yield 0.49 g (71%). Found: C, 34.0; H, 4.9. Calc. for $C_{15}H_{23}F_6MoN_3O_3P$: C, 33.7; H, 4.3%.

The air-sensitive orange solid could be recrystallized from acetonitrile–diethyl ether and dichloromethane–diethyl ether mixtures. Orange-

red colored solutions of the complex turned colorless almost immediately upon exposure to air.

F. Oxidations of $Mo(CO)_3(CNR)(R'\text{-DAB})$. (i) $[Mo(CO)_3(CNMe)(t\text{-Bu-DAB})]PF_6$. A 15-$cm^3$ aliquot of freshly distilled dichloromethane was syringed into a flask containing $Mo(CO)_3(CNMe)(t\text{-Bu-DAB})$ (0.25 g, 0.643 mmol) and $[Cp_2Fe]PF_6$ (0.215 g, 0.650 mmol), whereupon the solution immediately changed from royal blue to dark red-orange in color. The reaction mixture was filtered under nitrogen, and addition of 50 cm^3 of anhydrous diethyl ether to the filtrate precipitated an orange solid. The product was collected by filtration, washed with diethyl ether, and dried *in vacuo*. Recrystallization from dichloromethane–diethyl ether afforded bright orange crystals of the above formulation: yield 0.254 g (74%). Found: C, 33.7; H, 4.5. Calc. for $C_{15}H_{23}F_6MoN_3O_3P$: C, 33.7; H, 4.3%.

The solid is extremely air- and moisture-sensitive in the solid state, and solutions of the complex decompose very rapidly when exposed to the air.

(ii) $[Mo(CO)_3(CNCMe_3)(t\text{-Bu-DAB})]PF_6$. Yield 82%.

Although the compounds $[Mo(CO)_3(CNR)(R'\text{-DAB})]PF_6$ (R = Me or CMe_3, R' = *t*-Bu) could be isolated as solids, their use as starting complexes in this way was inconvenient because of their extreme air sensitivity. Accordingly, when solutions of the monocations were required they were normally generated *in situ* through the reaction of $Mo(CO)_3(CNR)(R'\text{-DAB})$ with $[Cp_2Fe]PF_6$ in dichloromethane solution. These solutions were then used for reactions involving isocyanide and/or R'-DAB.

G. Preparation of cis, trans-$[Mo(CO)_2(CNCMe_3)_2(t\text{-Bu-DAB})]PF_6$. (i) *From* $[Mo(CO)_3(CNCMe_3)(t\text{-Bu-DAB})]PF_6$. A dark orange-red solution of the cation $[Mo(CO)_3(CNCMe_3)(t\text{-Bu-DAB})]PF_6$ was prepared by stirring a mixture of $Mo(CO)_3(CNCMe_3)(t\text{-Bu-DAB})$ (0.60 g, 1.39 mmol) and $[Cp_2Fe]PF_6$ (0.465 g, 1.41 mmol) in 15 cm^3 of freshly distilled dichloromethane at room temperature for 15 min. A mixture of *tert*-butyl isocyanide (0.15 cm^3, 1.42 mmol) and *t*-Bu-DAB (0.234 g, 1.39 mmol) dissolved in 15 cm^3 of dry dichloromethane was then added dropwise to the resulting solution. The orange-red solution changed to a dark red color during the addition of the reagents and CO gas evolution occurred. The reaction mixture was stirred at room temperature for 30 min, filtered, and the filtrate taken to dryness under reduced pressure. The bright red solid so obtained was washed with copious amounts of diethyl ether until the washes were colorless in order to ensure that all traces of ferrocene and unreacted $Mo(CO)_3(CNCMe_3)(t\text{-Bu-DAB})$ had been removed. The product was then recrystallized from dichloromethane–diethyl ether and acetone–diethyl ether mixtures: yield 0.77 g (88%). Found: C, 41.6; H, 6.6. Calc. for $C_{22}H_{38}F_6MoN_4O_2P$: C, 41.8; H, 6.1%.

(ii) *From* $[Mo(CO)_3(NCMe)(t\text{-Bu-DAB})]PF_6$. A sample of the complex $[Mo(CO)_3(NCMe)(t\text{-Bu-DAB})]PF_6$ (0.305 g, 0.571 mmol) was dissolved in 15 cm^3 of freshly distilled dichloromethane, and a mixture of *tert*-butyl isocyanide (0.121 cm^3, 1.15 mmol) and *t*-Bu-DAB (0.1 g, 0.595 mmol) dissolved in 15 cm^3 of dichloromethane was then added dropwise with rapid stirring. Reaction for 30 min and a work-up and purification procedure as described in Section G(i) gave crystals of *cis, trans-*$[Mo(CO)_2(CNCMe_3)_2(t\text{-Bu-DAB})]PF_6$; yield 0.31 g (85%).

H. Reduction of cis, trans-$[Mo(CO)_2(CNCMe_3)_2(t\text{-Bu-DAB})]PF_6$ *to form cis, trans-*$Mo(CO)_2(CNCMe_3)_2(t\text{-Bu-DAB})$. Dry deoxygenated acetone (15 cm^3) was syringed into a flask containing *cis, trans-*$[Mo(CO)_2(CNCMe_3)_2(t\text{-Bu-DAB})]PF_6$ (0.418 g, 0.662 mmol) and Cp_2Co (0.125 g, 0.662 mmol). The mixture was stirred at room temperature for 30 min during which time the color of the solution became turquoise blue. The solution was filtered under nitrogen to remove an olive green solid ($[Cp_2Co]PF_6$) and the clear, blue filtrate was evaporated to dryness under reduced pressure. The blue solid was recrystallized from diethyl ether–petroleum ether and dichloromethane–petroleum ether mixtures: yield 0.21 g (65%). Found: C, 53.8; H, 8.6. Calc. for $C_{22}H_{38}MoN_4O_2$: C, 54.3; H, 7.8%.

I. Reactions of $[Mo(CO)_3(CNR)(R'\text{-DAB})]PF_6$ *with isocyanides.* (i) $[Mo(CO)(CNCMe_3)_4(t\text{-Bu-DAB})](PF_6)_2$. A solution of $[Mo(CO)_3(CNCMe_3)(t\text{-Bu-DAB})]PF_6$ was generated by stirring a mixture of $Mo(CO)_3(CNCMe_3)(t\text{-Bu-DAB})$ (0.40 g, 0.928 mmol) and $[Cp_2Fe]PF_6$ (0.31 g, 0.937 mmol) in 25 cm^3 of dichloromethane at room temperature for 15 min. The dark red-orange solution was filtered under nitrogen, and three equivalents of *tert*-butyl isocyanide (0.295 cm^3, 2.784 mmol) were added dropwise to the filtrate. The reaction mixture immediately turned a dark red-purple color and CO gas was evolved. It was stirred for 1 h and then taken to dryness under reduced pressure. The purple residue was extracted with diethyl ether to yield a red solid and a royal blue ethereal solution. The red solid was collected by filtration and recrystallized from dichloromethane–diethyl ether, and finally from methanol–diethyl ether to give red-orange crystals of $[Mo(CO)(CNCMe_3)_4(t\text{-Bu-DAB})](PF_6)_2$: yield 0.38 g (45%). Found: C, 40.4; H, 6.3; N, 9.1. Calc. for $C_{31}H_{56}F_{12}MoN_6OP_2$: C, 40.7; H, 6.1; N, 9.2%.

The blue diethyl ether filtrate was evaporated to dryness under a stream of nitrogen gas and the solid recrystallized from dichloromethane–petroleum ether to give purple-blue microcrystals: yield 0.16 g (40%). This solid was identified as $Mo(CO)_3(CNCMe_3)$(*t*-Bu-DAB) on the basis of its spectroscopic and electrochemical properties which were identical to those of an authentic sample [see Section C(i)].

(ii) $[Mo(CNCMe_3)_7](PF_6)_2$. The dropwise addition of four equivalents of *tert*-butyl isocyanide (0.98 cm^3, 9.285 mmol) to a mixture of $[Mo(CO)_3(CNCMe_3)$(*t*-Bu-DAB)$]PF_6$ (1.336 g, 2.320 mmol) {formed from $Mo(CO)_3(CNCMe_3)$(*t*-Bu-DAB) (1.0 g, 2.320 mmol) and $[Cp_2Fe]PF_6$ (0.768 g, 2.320 mmol)} in 25 cm^3 of dichloromethane caused the red-orange solution to change color immediately to a dark purple-blue and evolution of CO to occur. The reaction mixture was stirred at room temperature for 6 h, and the solution then taken to dryness under reduced pressure. The residue was washed with copious amounts of diethyl ether to give a yellow powder and a royal blue ether solution. The yellow product was recrystallized from dichloromethane–diethyl ether and methanol–diethyl ether before drying it *in vacuo*: yield 1.0 g (45%). The identity of this yellow complex as $[Mo(CNCMe_3)_7](PF_6)_2$ was confirmed by comparison of its spectroscopic and electrochemical properties with those exhibited by an authentic sample.[10,11]

The ether extract was evaporated to dryness to yield a quantity of $Mo(CO)_3(CNCMe_3)$(*t*-Bu-DAB) (0.40 g), whose identity was confirmed by its spectroscopic and electrochemical properties.

(iii) $[Mo(CNCMe_3)_5$(*i*-Pr-DAB)$](PF_6)_2$. Dark red-purple crystals of this complex were obtained by a procedure analogous to that described in Section I(i) through the reaction between $Mo(CO)_3(CNCMe_3)$(*i*-Pr-DAB) (0.5 g, 1.266 mmol), $[Cp_2Fe]PF_6$ (0.42 g, 1.269 mmol), and three equivalents of *tert*-butyl isocyanide (0.40 cm^3, 3.79 mmol) in 15 cm^3 of freshly distilled dichloromethane: yield 0.65 g (50%). Found: C, 41.9; H, 6.8. Calc. for $C_{33}H_{61}F_{12}MoN_7P_2$: C, 42.1; H, 6.5%.

The work up of the blue filtrate followed by recrystallization of the product from dichloromethane–petroleum ether gave a small quantity of $Mo(CO)_3(CNCMe_3)$(*i*-Pr-DAB): yield 0.08 g (16%).

(iv) $[Mo(CO)(CNMe)_4$(*t*-Bu-DAB)$](PF_6)_2$. A brick red powder with this stoichiometry was obtained by the use of a procedure similar to that described in Section I(i) with $Mo(CO)_3(CNMe)$(*t*-Bu-DAB) (0.109 g, 0.281 mmol), $[Cp_2Fe]PF_6$ (0.093 g, 0.281 mmol) and three equivalents of methyl isocyanide (0.50 cm^3, 0.625 mmol) in 20 cm^3 of dichloromethane: yield 0.10 g (48%). Characterization was based on its IR spectral and cyclic voltammetric properties which were very similar to those of its *tert*-butyl isocyanide analogue.

J. Reaction of $[Mo(CO)_3(NCMe)$(*t*-Bu-DAB)$]PF_6$ *with* tert-*butyl isocyanide.* $[Mo(CO)(CNCMe_3)_4$(*t*-Bu-DAB)$](PF_6)_2$. A quantity of $[Mo(CO)_3(NCMe)$(*t*-Bu-DAB)$]PF_6$ (0.823 g, 1.542 mmol) was prepared from $Mo(CO)_3(NCMe)$(*t*-Bu-DAB) (0.6 g, 1.542 mmol) and $[Cp_2Fe]PF_6$ (0.51 g, 1.542 mmol) in 35 cm^3 of dichloromethane. Dropwise addition of five equivalents of *tert*-butyl isocyanide (0.81 cm^3, 7.710 mmol) to the resulting solution resulted in an immediate color change from dark red-orange to a dark purple-blue and the evolution of CO. A work up procedure identical to the one described in Section I(i) gave $[Mo(CO)(CNCMe_3)_4$(*t*-Bu-DAB)$](PF_6)_2$ (0.54 g, 38%) and $Mo(CO)_3(CNCMe_3)$(*t*-Bu-DAB) (0.37 g, 56%). These two products were identified on the basis of their spectroscopic and electrochemical properties which were identical to those exhibited by authentic samples of the compounds [see Sections C(i) and I(i)].

K. Attempted preparation of $[Mo(CNCMe_3)_5$(*t*-Bu-DAB)$](PF_6)_2$ *from* $[Mo(CO)(CNCMe_3)_4$(*t*-Bu-DAB)$](PF_6)_2$. A quantity of *tert*-butyl isocyanide (0.029 cm^3, 0.274 mmol) was syringed into a stirred red-orange solution of $[Mo(CO)(CNCMe_3)_4$(*t*-Bu-DAB)$](PF_6)_2$ (0.20 g, 0.219 mmol) in 25 cm^3 of dichloromethane. The reaction mixture was heated at reflux for 12 h, cooled to 0°C, and then taken to dryness under a stream of nitrogen. The yellow solid was collected, washed with water, diethyl ether and hexane, and recrystallized from acetone–diethyl ether: yield 0.13 g (61%). This product was deduced, on the basis of IR spectral and cyclic voltammetric data, to be $[Mo(CNCMe_3)_7](PF_6)_2$.[10,11]

L. Preparation of $Li[Mo(CO)_3(CNMe)$(*t*-Bu-DAB)$]$. Solutions that contained the molybdenum and tungsten radical anions $[M(CO)_3(CNR)(R'$-DAB)$]^{-\cdot}$ were prepared by the following general procedure. The tetrahydrofuran-soluble reducing agent $LiEt_3BH$ (1.0 M in THF; 0.15 cm^3, 0.150 mmol) was added dropwise to a solution of $Mo(CO)_3(CNMe)$(*t*-Bu-DAB) (0.060 g, 0.154 mmol) in 5 cm^3 of freshly distilled THF. The color of the solution changed almost immediately to a pale orange-yellow and gas evolution (BEt_3 and H_2) occurred as the monoanion was formed. Solutions containing the resulting molybdenum (and tungsten) radicals could be handled quite easily using conventional techniques.

Physical measurements

IR spectra were recorded as Nujol mulls between KBr plates or as dichloromethane solutions using an IBM Instruments IR/32 Fourier Transform (4800–400 cm^{-1}) spectrometer. Electronic absorption spectra were recorded on an IBM Instruments 9420 UV–Visible spectrophotometer. ^1H NMR spectra were recorded at 90 MHz on a Perkin–Elmer R-32 spectrometer. The residual protons of acetone-d_6 ($\delta = 2.05$ ppm vs TMS) were used as reference. Electrochemical measurements were made in dichloromethane solvents that contained 0.2 M tetra-*n*-butylammonium hexafluorophosphate (TBAH) as supporting electrolyte. $E_{1/2}$ values were determined as $(E_{p,a}+E_{p,c})/2$ and are referenced to the Ag–AgCl electrode at room temperature. Voltammetric experiments were performed using a Bioanalytical Systems Inc. Model CV-1A instrument in conjunction with a Hewlett–Packard Model 7035B x–y recorder. X-band ESR spectra were recorded using a Varian E-109 spectrometer.

Analytical procedures

Elemental microanalyses were performed by Dr H. D. Lee of the Purdue University Microanalytical Laboratory.

RESULTS AND DISCUSSION

Synthetic procedures and spectroscopic characterization of $M(CO)_3(CNR)(R'\text{-DAB})$

Two, high-yield, synthetic methods have been devised for the synthesis of the complexes $M(CO)_3(CNR)(R'\text{-DAB})$ (M = Mo or W; R = Me, $CHMe_2$, CMe_3, C_6H_{11} or xylyl; R′ = *i*-Pr, *t*-Bu, Cy or *p*-tol) as outlined by the sequence of reactions shown in eqns (1) and (2):

$$M(CO)_6 \rightarrow M(CO)_4(R'\text{-DAB}) \rightarrow M(CO)_3(CNR)(R'\text{-DAB}), \quad (1)$$

$$M(CO)_6 \rightarrow M(CO)_3(NCR)_3 \rightarrow M(CO)_3(NCR)(R'\text{-DAB}) \rightarrow M(CO)_3(CNR)(R'\text{-DAB}). \quad (2)$$

Representative examples, which are given in Experimental, show the generality of both procedures. Both methods are superior to that involving the reaction of $M(CO)_3(R'\text{-DAB})(SnCl_3)Cl$ (M = Mo or W) with RNC,[1] since these latter reactions proceed (via the reductive elimination of $SnCl_4$) only in the cases where R′ = *t*-Bu. As indicated in eqn (2), it is possible to isolate the blue-purple nitrile precursors $M(CO)_3(NCR)(R'\text{-DAB})$, and this has been done for a few such derivatives (M = Mo, R = Me, R′ = *t*-Bu or Cy; M = W, R = Et, R′ = *i*-Pr, *t*-Bu or Cy).

The new complexes prepared are dark blue or purple solids. They are generally stable to atmospheric oxygen in the solid state, and dissolve in organic solvents, especially the more polar ones, imparting an intense blue to purple coloration to the solution. It should be noted that the isocyanide complexes are very stable in solution, while solutions of the nitrile complexes decompose quite rapidly (even in deoxygenated solvents), thereby complicating the measurement of their solution spectral properties.

Microanalytical data, together with ^1H NMR spectral data (recorded in acetone-d_6),* confirmed the stoichiometries of these complexes. The chemical shifts of the azomethine protons indicate that the R′-DAB ligands are in the σ,σ-bidentate coordination mode.[12,13] Their IR spectra [ν(CN) and ν(CO) modes] are presented in Table 1, together with representative electronic absorption spectral data. As is often the case, the ν(CN) modes for the coordinated nitrile ligand are extremely weak in some instances not seen.[14] The IR spectra of the octahedral, diamagnetic complexes $M(CO)_3(CNR)(R'\text{-DAB})$, show a single isocyanide stretching mode at $\sim 2100\ cm^{-1}$ and three intense carbonyl stretching absorptions, both in the solid state and in solution, in the region 1940–1780 cm^{-1}. This implies that in the isocyanide complexes the three carbonyl ligands are in a *facial* arrangement and that the solid-state structure of the complexes persists in solution. Likewise, the nitrile complexes exhibit similar spectral properties and hence, most likely, possess the same rigid stereochemistry. This is also the structure of the 2,2′-bipyridine complex $Mo(CO)_3(NCEt)(bpy)$.[15]

The most noteworthy feature in the electronic absorption spectra of $M(CO)_3(CNR)(R'\text{-DAB})$ (M = Mo or W) is the intense absorption in the visible region ($\lambda_{max} \sim 580$ nm) assignable to a metal-to-ligand (R′-DAB) charge transfer. We find that the location and ε_{max} value of this band depends on the polarity of the solvent (solvatochromism) and the solvent shifts are comparable to those observed for the parent species $M(CO)_4(R'\text{-DAB})$.[16,17] An analogous metal-to-ligand charge-transfer band is found at 529 nm in the electronic absorption spectrum of $Mo(CO)_3(NCEt)(bipy)$.[15]

* Resonances due to the isocyanide and R′-DAB ligands had the correct integrated intensities [see A. Bell, Ph.D. Thesis, Purdue University (1985)].

Table 1. Spectroscopic data for mixed isocyanide–1,4-diaza-1,3-butadiene complexes of molybdenum and tungsten

Complex	IR absorption (cm^{-1})				Electronic absorption spectra[a] (nm)
	ν(CO)		ν(CN)		
	Nujol mull	Dichloromethane	Nujol mull	Dichloromethane	
$Mo(CO)_3(NCMe)(t\text{-Bu-DAB})$	1896s, 1790s, 1771s	1914s, 1802s, 1793s	[b]	[b]	[c]
$Mo(CO)_3(NCMe)$(Cy-DAB)	1891s, 1792s, 1770s	1912s, 1801s, 1790s	[b]	[b]	[c]
$Mo(CO)_3(CNMe)(t\text{-Bu-DAB})$	1910s, 1819s, 1790s	1923s, 1827s, 1798s	2168s	2159m	575 (7000), 354 (2700), 305 (sh)
$Mo(CO)_3(CNCHMe_2)$(Cy-DAB)	1900s, 1819s, 1794s	1921s, 1846s, 1808s	2143s	2139m	574 (3800), 393 (2600), 319 (7100)
$Mo(CO)_3(CNCHMe_2)(t\text{-Bu-DAB})$	1902s, 1827s, 1792s	1921s, 1835s, 1798s	2141s	2139m	578 (7200), 350 (1400), 316 (sh)
$Mo(CO)_3(CNCMe_3)(i\text{-Pr-DAB})$	1904s, 1810sh, 1802s	1925s, 1844s, 1810s	2151s	2130m	[c]
$Mo(CO)_3(CNCMe_3)(t\text{-Bu-DAB})$	1900s, 1813s, 1798s	1921s, 1835s, 1798s	2141s	2132m	579 (6900), 351 (2600), 305 (sh)
$Mo(CO)_3(CNCMe_3)$(Cy-DAB)	1900s, 1815sh, 1806s	1923s, 1840s, 1806s	2147s	2132m	581 (7100), 355 (2100), 312 (sh)
$Mo(CO)_3(CNCMe_3)(p\text{-tol-DAB})$	1927s, 1858s, 1806s	1941s, 1864s, 1838s	2134s	2134m	580 (8300), 351 (2800), 305 (sh)
$Mo(CO)_3(CNC_6H_{11})(t\text{-Bu-DAB})$	1900s, 1817s, 1794s	1921s, 1824s, 1798s	2137s	2134m	578 (3500), 392 (2400), 319 (6800)
$Mo(CO)_3$(CNxylyl)(*i*-Pr-DAB)	1906s, 1842s, 1806s	1927s, 1856s, 1817s	2087s	2089m	574 (2800), 393 (2600), 319 (7100)
$Mo(CO)_3$(CNxylyl)(*t*-Bu-DAB)	1900s, 1819s, 1794s	1921s, 1846s, 1808s	2097s	2087m	576 (2600), 392 (2200), 320 (6700)
$Mo(CO)_3$(CNxylyl)(Cy-DAB)	1908s, 1842s, 1810s	1925s, 1854s, 1815s	2091s	2089m	[c]
$W(CO)_3(NCEt)(t\text{-Pr-DAB})$	1894s, 1798s	[c]	2276vw	[c]	[c]
$W(CO)_3(NCEt)(t\text{-Bu-DAB})$	1887s, 1785s, 1763s	[c]	2270vw	[c]	[c]
$W(CO)_3(NCEt)$(Cy-DAB)	1898s, 1798s, 1784s	[c]	[b]	[c]	[c]
$W(CO)_3(CNMe)(t\text{-Bu-DAB})$	1902s, 1817s, 1788s	1919s, 1837s, 1800s	2163s	2153m	582 (11,200), 350 (2400), 300 (sh)
$W(CO)_3(CNCMe_3)(i\text{-Pr-DAB})$	1900s, 1815s, 1801s	1925s, 1844s, 1813s	2149s	2128m	570 (12,800), 354 (2400)
$W(CO)_3(CNCMe_3)(t\text{-Bu-DAB})$	1892s, 1810s, 1792s	1918s, 1835s, 1800s	2137s	2126m	585 (10,800), 350 (2500), 310 (sh)
$W(CO)_3(CNCMe_3)$(Cy-DAB)	1896s, 1813s, 1796s	1923s, 1842s, 1806s	2140s	2127m	[c]
$W(CO)_3(CNC_6H_{11})(t\text{-Bu-DAB})$	1894s, 1815s, 1796s	1918s, 1825s, 1800s	2134s	2130m	[c]
$W(CO)_3$(CNxylyl)(*i*-Pr-DAB)	1902s, 1844s, 1806s	1927s, 1858s, 1821s	2095s	2085m	570 (10,400), 389 (4700), 335 (sh)
$W(CO)_3$(CNxylyl)(*t*-Bu-DAB)	1892s, 1817s, 1792s	1918s, 1846s, 1810s	2091s	2085m	581 (11,100), 443 (sh), 386 (4500), 313 (sh)
$W(CO)_3$(CNxylyl)(Cy-DAB)	1904s, 1844s, 1810s	1925s, 1856s, 1819s	2085s	2084m	570 (11,500), 389 (4900), 322 (sh)

[a] Data recorded from 800 to 300 nm in dichloromethane; ε_{max} values ($\times 10^{-3}$ M^{-1} cm^{-1}) are given in parentheses.
[b] Not observed.
[c] Not measured.

Table 2. Cyclic voltammetric data for mixed isocyanide–1,4-diaza-1,3-butadiene complexes of molybdenum and tungsten[a]

Complex	$E_{p,a}$	$E_{1/2}$(ox)	$E_{p,c}$(1)	$E_{p,c}$(2)
$Mo(CO)_4$(*i*-Pr-DAB)	+1.69	+0.69	−1.50	—
$Mo(CO)_4$(*t*-Bu-DAB)	+1.76	+0.70	−1.47	—
$Mo(CO)_4$(Cy-DAB)	+1.72	+0.67	−1.51	—
$Mo(CO)_3$(NCMe)(*t*-Bu-DAB)	+1.33	+0.21	−1.43	−1.81
$Mo(CO)_3$(NCMe)(Cy-DAB)	+1.43	+0.21	−1.55	−1.92
$Mo(CO)_3$(CNMe)(*t*-Bu-DAB)	+1.34	+0.31	−1.60	—
$Mo(CO)_3(CNCHMe_2)$(*t*-Bu-DAB)	+1.37	+0.29	−1.64	—
$Mo(CO)_3(CNCHMe_2)$(Cy-DAB)	+1.34	+0.31	−1.61	—
$Mo(CO)_3(CNCMe_3)$(*i*-Pr-DAB)	+1.25	+0.28	−1.66	—
$Mo(CO)_3(CNCMe_3)$(*t*-Bu-DAB)	+1.37	+0.30	−1.63	—
$Mo(CO)_3(CNCMe_3)$(Cy-DAB)	+1.38	+0.30	−1.65	—
$Mo(CO)_3(CNC_6H_{11})$(*t*-Bu-DAB)	+1.60	+0.34	−1.59	—
$Mo(CO)_3$(CNxylyl)(*i*-Pr-DAB)	+1.29	+0.35	−1.61	—
$Mo(CO)_3$(CNxylyl)(*t*-Bu-DAB)	+1.44	+0.38	−1.61	—
$Mo(CO)_3$(CNxylyl)(Cy-DAB)	+1.33	+0.35	−1.51	—
$W(CO)_4$(*t*-Bu-DAB)	+1.82	+0.70	−1.38	—
$W(CO)_3$(NCEt)(*i*-Pr-DAB)	+1.19	+0.18	−1.39	−1.79
$W(CO)_3$(NCEt)(*t*-Bu-DAB)	+1.22	+0.15	−1.39	−1.84
$W(CO)_3$(NCEt)(Cy-DAB)	+1.36	+0.18	−1.37	−1.79
$W(CO)_3$(CNMe)(*t*-Bu-DAB)	+1.37	+0.32	−1.29	—
$W(CO)_3(CNCMe_3)$(*i*-Pr-DAB)	+1.46	+0.37	−1.62	—
$W(CO)_3(CNCMe_3)$(*t*-Bu-DAB)	+1.37	+0.28	−1.57	—
$W(CO)_3(CNC_6H_{11})$(*t*-Bu-DAB)	+1.45	+0.26	−1.61	—
$W(CO)_3$(CNxylyl)(*i*-Pr-DAB)	+1.42	+0.42	−1.49	—
$W(CO)_3$(CNxylyl)(*t*-Bu-DAB)	+1.35	+0.36	−1.52	—
$W(CO)_3$(CNxylyl)(Cy-DAB)	+1.47	+0.35	−1.57	—

[a] In V vs Ag–AgCl with a Pt-bead electrode and 0.2 M tetra-*n*-butylammonium hexafluorophosphate (TBAH) as supporting electrolyte. Recorded at a scan rate of 200 mV s^{-1}.

Redox properties of $M(CO)_3$(L)(R'-DAB) (M = Mo *or* W; L = RCN *or* RNC)

The electrochemical properties of these nitrile and isocyanide complexes are given in Table 2 along with some related data for the $M(CO)_4$(R'-DAB) complexes taken from Ref. 1. These results are in good agreement with those expected on the basis of existing data for $M(CO)_4$(R'-DAB) and $M(CO_3$(L)(R'-DAB) (L = PR_3, MeCN or THF).* The half-wave or peak potentials vs Ag–AgCl for 0.2 M TBAH–dichloromethane solutions were measured by the cyclic voltammetric technique, and the voltammograms of $Mo(CO)_3$(NCMe)(*t*-Bu-DAB) and $Mo(CO)_3(CNCMe_3)$(*t*-Bu-DAB) are shown in Fig. 1. In all instances the octahedral complexes exhibit a couple [$E_{1/2}$(ox)] corresponding to a one-electron oxidation (as determined by coulometry). For sweep rates 50 to 400 mV s^{-1}, these couples are characterized by $i_{p,a}/i_{p,c} \simeq 1$ and the ratio $i_p/v^{1/2}$ was constant, in accordance with diffusion control. The potential separation between the coupled anodic and cathodic peaks, ΔE_p, is close to 75 mV for a sweep rate of 200 mV s^{-1} and increases slightly with increase in scan rate. These properties are (with our cell configuration[19]) consistent with electron-transfer processes which are reversible or approach reversibility.

The tricarbonyl complexes $M(CO)_3$(NCR)(R'-DAB)(M = Mo, R = Me, R' = *t*-Bu or Cy; M = W, R = Et, R' = *i*-Pr, *t*-Bu or Cy) possess a reversible oxidation at *ca* +0.20 V (M = Mo or W) vs Ag–AgCl, and a second (irreversible) oxidation between +1.1 and +1.5 V. Two irreversible reductions at $E_{p,c} \sim -1.5$ and −1.9 V for M = Mo, and $E_{p,c} \sim -1.4$ and −1.8 V for M = W, are also found (Fig. 1). Similarly, the monoisocyanide complexes $M(CO)_3$(CNR)(R'-DAB) (M = Mo or W; R = Me,

* These electrochemical measurements[18] were made at a platinum bead electrode in 0.1 M tetraethylammonium perchlorate–acetonitrile solutions at ambient temperatures and a scan rate of 100 mV s^{-1}. Potentials were referenced to an Ag–AgCl electrode.

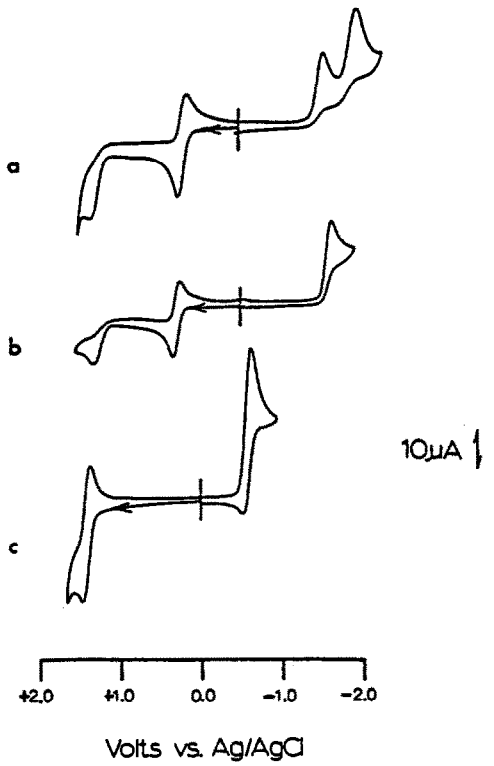


Fig. 1. Cyclic voltammograms (recorded at $v = 200$ mV s^{-1} using a Pt-bead electrode) for 0.2 M TBAH–dichloromethane solutions of: (a) $Mo(CO)_3(NCMe)(t\text{-Bu-DAB})$, (b) $M(CO)_3(CNCMe_3)(t\text{-Bu-DAB})$, and (c) $[Mo(CO)(CNCMe_3)_4(t\text{-Bu-DAB})](PF_6)_2$.

$CHMe_2$, CMe_3, C_6H_{11} or xylyl; R′ = *i*-Pr, *t*-Bu or Cy) exhibit a reversible couple at *ca* +0.30 V vs Ag–AgCl, and a second (irreversible) oxidation between +1.2 and +1.6 V is further observed. The existence of only one irreversible reduction process in the cyclic voltammogram of these complexes (at $E_{p,c} \sim -1.4$ to −1.6 V) distinguishes them from the analogous nitrile species.

In comparing the $E_{1/2}$ values of the tetracarbonyl complexes $M(CO)_4$(R′-DAB) with those of their nitrile or isocyanide derivatives (Table 2), we see that the $E_{1/2}$ values for the latter species are shifted to more negative potentials. This reflects the superior σ-donor ability of nitriles or isocyanides and/or their poorer π-accepting ability compared to CO when bound to the group 6 metals. Thus, the nitriles and isocyanides are better able to stabilize the metal(I) oxidation state relative to the CO ligand. Indeed, the bulk electrolyses of dichloromethane solutions of several $Mo(CO)_3$(L)(R′-DAB) complexes (L = MeCN or RNC) afforded solutions that contain 17-electron oxidized species. Furthermore, oxidation of the complexes $Mo(CO)_3(NCMe)(t\text{-Bu-DAB})$ and $Mo(CO)_3(CNR)$(R′-DAB) to the corresponding monocations has been achieved chemically by use of the rather mild oxidizing agent ferricinium hexafluorophosphate ($[Cp_2Fe]PF_6$). This procedure produced samples of the orange-red, crystalline, 17-electron compounds $[Mo(CO)_3(NCMe)(t\text{-Bu-DAB})]PF_6$ and $[Mo(CO)_3(CNR)(t\text{-Bu-DAB})]PF_6$ (R = Me or CMe_3) with the accompanying formation of ferrocene. The generation of the analogous tungsten monocations was not possible either by use of controlled potential electrolysis or by chemical means under the conditions we employed. This presumably attests to their reactivity and/or instability in comparison to their molybdenum congeners. While the molybdenum monocations decompose very rapidly upon exposure to oxygen, their solutions can be manipulated quite easily under nitrogen.

Relative to their neutral precursors, the monocations have IR spectra in which the ν(CO) modes shift to higher energy by 100–140 cm^{-1} (Table 3). This shift, and a similar one in the case of the ν(CN) modes of the RNC ligands, is expected because of the decrease in backbonding to the π^*-levels of the CO and RNC ligands.

The X-band ESR spectra of the paramagnetic 17-electron species were recorded at −160°C on frozen dichloromethane solutions; the measured g values are presented in Table 3, and a spectral trace of $[Mo(CO)_3(CNMe)(t\text{-Bu-DAB})]PF_6$ is shown in Fig. 2. Although some structure is apparent in the very broad signals, no semblance of hyperfine structure attributable to interaction with the coordinated nitrogens of the R′-DAB molecules is discernible.

Although the reduction processes [$E_{p,c}(1)$ and $E_{p,c}(2)$ in Table 2] which are seen in the cyclic voltammograms of 0.2 M TBAH–dichloromethane solutions of the $M(CO)_3$(L)(R′-DAB) complexes are irreversible electrochemically (Table 2 and Fig. 1), the 19-electron radical complexes $Li[M(CO)_3(CNR)(R'\text{-DAB})]$ (M = Mo or W; R = Me, CMe_3 or xylyl; R′ = *i*-Pr, *t*-Bu or Cy) have been generated chemically by utilizing the commercially available triethylborohydride reagent, viz. $LiEt_3BH$.[20] The attractiveness of this procedure is that only volatile by-products (H_2 and BEt_3) are formed, and the reducing agent is THF-soluble.

The resulting paramagnetic complexes have been characterized by X-band ESR spectroscopy (Fig. 2), and Table 4 summarizes the pertinent ESR data for the complexes. The ESR parameters indicate that the unpaired electron is centered mainly in the ligand π-system for all the radical anion complexes investigated; the coordination of the $M(CO)_3(CNR)$ moiety to the radical ligand is, however, evident from the metal isotope splittings in the ESR spectra (Fig. 2 and Table 4). Further, the ESR spectral data for

Table 3. Spectroscopic properties of some $[Mo(CO)_3(L)(t\text{-Bu-DAB})]PF_6$ complexes

Complex	IR absorption (cm^{-1})[a]		X-band ESR[b]
	ν(CO)	ν(CN)	g_{av}
$[Mo(CO)_3(NCMe)(t\text{-Bu-DAB})]PF_6$	2024s, 1929s, 1880s 2027s, 1927s, 1894s[c]	2323w, 2290w 2284w[c]	2.207
$[Mo(CO)_3(CNMe)(t\text{-Bu-DAB})]PF_6$	2029s, 1936s, 1896s 2033s, 1948s, 1911s[c]	2230s 2222m[c]	2.152
$[Mo(CO)_3(CNCMe_3)(t\text{-Bu-DAB})]PF_6$	[d]	[d]	2.209

[a] IR spectra recorded as Nujol mulls.
[b] Recorded at −160°C in dichloromethane.
[c] IR spectra recorded in dichloromethane solutions.
[d] Not measured.

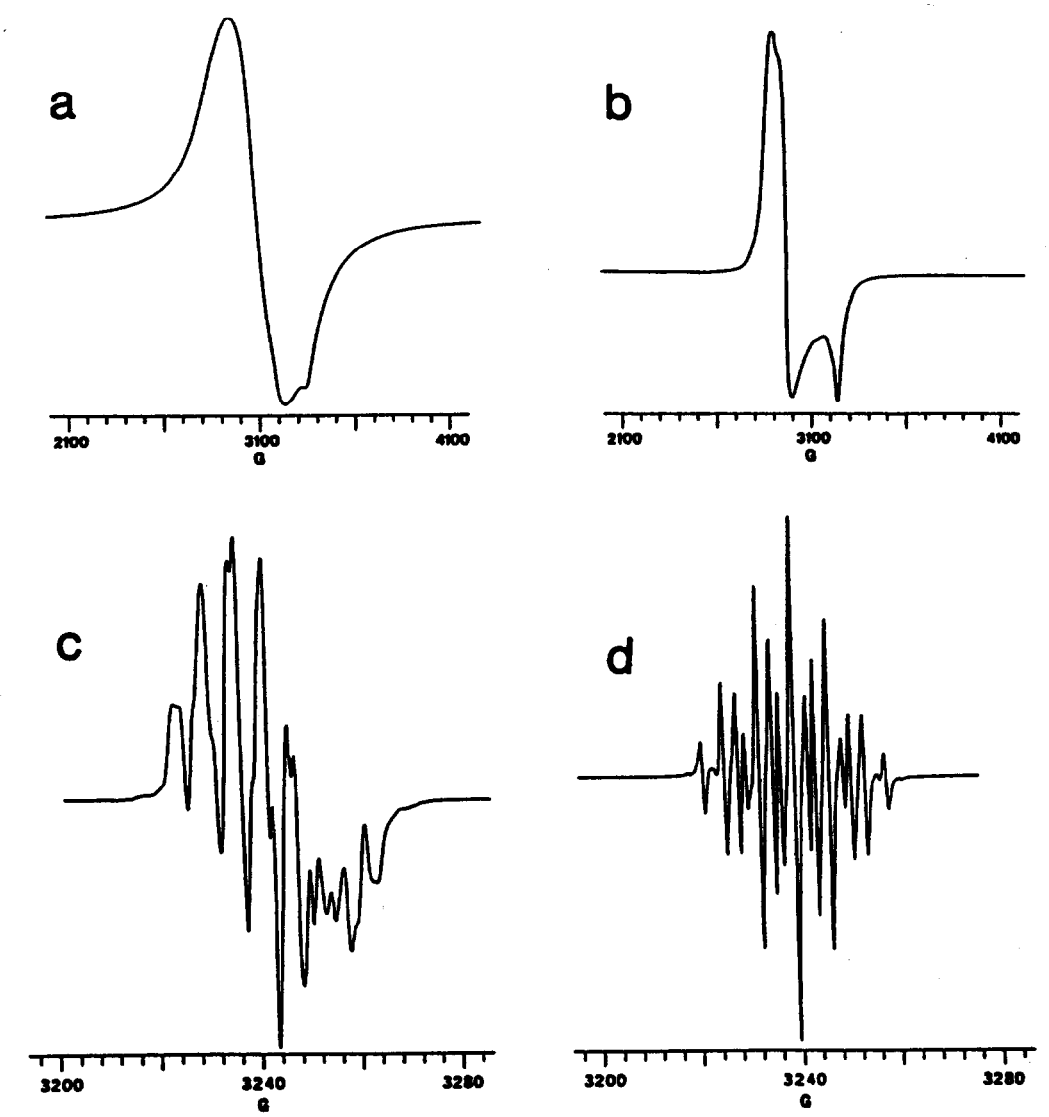


Fig. 2. X-band ESR spectra of: (a) $[Mo(CO)_3(CNMe)(t\text{-Bu-DAB})]PF_6$, (b) $[Mo(CO)_2(CNCMe_3)_2(t\text{-Bu-DAB})]PF_6$, (c) $Li[Mo(CO)_3(CNCMe_3)(Cy\text{-DAB})]$, and (d) $Li[W(CO)_3(CNMe)(t\text{-Bu-DAB})]$. Spectra a and b were recorded as frozen dichloromethane solutions (−160°C), while spectra c and d were recorded as THF solutions at room temperature.

the complexes clearly distinguishes them from the previously characterized ligand radicals, and the radical anionic complxes K[M(CO)$_4$(R′-DAB)] (M = Mo or W).[18,21,22] The most prominent features of the ESR spectra can be interpreted in terms of coupling to the diazabutadiene nitrogens, azomethine protons, and protons on the alkyl substituents (i.e. R′ = *i*-Pr or Cy).

Reactivity studies

While the 18-electron neutral complexes Mo(CO)$_3$(CNR)(R′-DAB) are unreactive toward an excess of RNC or R′-DAB, activation of these complexes by a one-electron oxidation to the monocationic 17-electron species enables further substitution chemistry to be developed. Thus, the addition of dichloromethane solutions containing one equivalent and two equivalents of *tert*-butyl isocyanide, respectively, to solutions of the red-orange complexes [Mo(CO)$_3$(CNCMe$_3$)(*t*-Bu-DAB)]PF$_6$ (prepared *in situ*) and [Mo(CO)$_3$(NCMe)(*t*-Bu-DAB)]PF$_6$, gave *cis, trans*-[Mo(CO)$_2$(CNCMe$_3$)$_2$(*t*-Bu-DAB)]$^+$ with concomitant CO evolution. The dark blue neutral dicarbonyl *cis, trans*-Mo(CO)$_2$(CNCMe$_3$)$_2$(*t*-Bu-DAB) is easily prepared by the chemical reduction of the cation using cobaltocene in acetone solution. The related 2,2′-bipyridyl complex Mo(CO)$_2$(CNEt)$_2$(bpy) has been assigned a *cis, cis*-structure on the basis of its IR spectral properties.[15]

The ν(CO) and ν(CN) modes in the IR spectra of [Mo(CO)$_2$(CNCMe$_3$)$_2$(*t*-Bu-DAB)]$^{1+,0}$ complexes again proved to be useful as a means of distinguishing between the 17- and 18-electron congeners (see Table 5). The ν(CO) bands shift by between +100 and +120 cm^{-1} upon changing from the zerovalent complex to the monocation and, in addition, the ν(CN) absorption increases by *ca* 110 cm^{-1} as the formal charge on the metal complex increases; both of these shifts reflect a decrease in the π-back donation to the CO and RNC π^* molecular orbitals. The same IR spectral pattern exists for the 18-electron complex, *cis, trans*-Mo(CO)$_2$(CNCMe$_3$)$_2$(*t*-Bu-DAB) and for the oxidized species, thereby indicating that no major geometrical change is associated with the redox process (Table 5). The ^{1}H NMR spectral properties of the neutral complex support the proposed geometry and integration of 1,4-diaza-1,3-butadiene and isocyanide resonances,† together with the elemental microanalyses, showed excellent agreement with the proposed stoichiometry.

The above chemical and spectral observations are in agreement with the results of electrochemical studies which were carried out on *cis, trans*-[Mo(CO)$_2$(CNCMe$_3$)$_2$(*t*-Bu-DAB)]$^{1+,0}$ in 0.2 M TBAH–dichloromethane solution (Table 5). The substitution of one carbonyl ligand by an iso-

† For an acetone-d_6 solution, δ +1.39 (s, CMe$_3$), +1.62 (s, *t*-Bu) and +8.46 (s, C—H).

Table 4. Coupling constants (A_X) (G) and g values of the radical anions Li[M(CO)$_3$(CNR)(R′-DAB)][a]

		R′-DAB(H,H)[b]						
M	CNR	R′	R″	A_N	$A_{H(R'')}$	$A_{H(R')}$	A_M[c]	g
Mo	CNMe	*t*-Bu	H	6.10	4.7	[d]	2.6	1.9991
Mo	CNCMe$_3$	*i*-Pr	H	7.05	4.25	1.50	3.1	1.9967
Mo	CNCMe$_3$	Cy	H	6.70	[e]	[e]	[e]	1.9967
Mo	CNxylyl	*i*-Pr	H	7.05	4.25	1.50	3.0	1.9999
Mo	CNxylyl	*t*-Bu	H	7.00	4.20	[d]	3.7	1.9986
Mo	CNxylyl	Cy	H	6.80	[e]	[e]	[e]	1.9980
W	CNMe	*t*-Bu	H	6.90	4.30	[d]	6.2	1.9998
W	CNCMe$_3$	*i*-Pr	H	6.90	4.10	1.40	6.5	2.0036
W	CNxylyl	*t*-Bu	H	7.00	4.20	[d]	6.1	2.0014
W	CNxylyl	Cy	H	6.80	[e]	[e]	[e]	2.0037

[a] Measured in THF solutions at ambient temperatures.

[b] The 1,4-diaza-1,3-butadienes, R′—N=CR″—CR″=N—R′, have the general formula R′-DAB(H,H), where R″ = H.

[c] ^{95,97}Mo, 25.4% natural abundance, $I = \frac{5}{2}$; ^{183}W = 14.2%; $I = \frac{1}{2}$.

[d] Not observed.

[e] Spectra were not analyzed in detail.

Table 5. IR spectra, and cyclic voltammetric and conductivity data for isocyanide complexes derived from reactions of the monocations $[Mo(CO)_3(CNR)(t\text{-Bu-DAB})]^+$

Complex	IR absorptions (cm^{-1})[a]		$E_{p,a}$(ox)[b]	$E_{1/2}$(ox)[b]	$E_{p,c}$(red)[b]	Λ_m[c]
	ν(CN)	ν(CO)				
$Mo(CO)_2(CNCMe_3)_2(t\text{-Bu-DAB})$	2026s[d]	1838s, 1773s	+1.06	−0.26	−1.83	—
$[Mo(CO)_2(CNCMe_3)_2(t\text{-Bu-DAB})]PF_6$	2141s[d] 2141m[d,f]	1939s, 1850s 1948s, 1842s[f]	+1.06	−0.26[e]	−1.83	137
$[Mo(CO)(CNMe)_4(t\text{-Bu-DAB})](PF_6)_2$	2211s, 2179sh	1905s	—	+1.39	−0.71	—
$[Mo(CO)(CNCMe_3)_4(t\text{-Bu-DAB})](PF_6)_2$	2186s, 2168s 2176s, 2157s[f]	1927sh, 1896s 1919s[f]	—	+1.40	−0.67	230

[a] IR spectra recorded as Nujol mulls unless otherwise stated.
[b] Cyclic voltammetric data recorded in 0.2 M TBAH–dichloromethane: values in V vs Ag–AgCl, with a Pt-bead electrode and a sweep rate of 200 mV s^{-1}.
[c] Values in Ω^{-1} cm^2 mol^{-1}; measured on 10^{-3} M solutions in acetonitrile at room temperature.
[d] This ν(CN) mode has a shoulder at ~40 cm^{-1} to higher energy that reflects some departure from non-linearity of the *trans*-$Mo(C{\equiv}N{-}C)_2$ unit.
[e] Value for $E_{1/2}$(red) reported.
[f] IR spectra recorded in dichloromethane solutions.

cyanide in $Mo(CO)_3(CNR)(R'\text{-DAB})$ to produce $Mo(CO)_2(CNR)_2(R'\text{-DAB})$ causes a change in the electrochemistry. The oxidation of $Mo(CO)_2(CNR)_2(R'\text{-DAB})$ to its monocation occurs at a lower potential [compared to that of $Mo(CO)_3(CNR)(R'\text{-DAB})$], as is expected when a carbonyl ligand is replaced by a less effective π-acceptor RNC ligand. Several electrochemical investigations have examined the *cis* ⇄ *trans* isomerizations that occur in carbonyl derivatives of the types $Mo(CO)_4(PR_3)_2$,[23] $Mo(CO)_2(P\text{–}P)_2$ [where $P\text{–}P = Ph_2P(CH_2)_nPPh_2$; $n = 1\text{–}3$[24–26] and $Mo(CO)_4(carbene)_2$[27] following their oxidation. Particularly relevant to the present case is the conversion of *cis*, *cis*-$Mo(CO)_2(CNR)_2(PR_3)_2$ to the *all trans*-isomer upon oxidation.[28] We find that no such isomerization occurs when the 18-electron complex *cis*, *trans*-$Mo(CO)_2(CNCMe_3)_2$(*t*-Bu-DAB) is oxidized. The bonding constraints and electronic properties imposed by the chelating R'-DAB ligand do not favor such a stereochemical change.

The X-band ESR spectrum of the paramagnetic species, *cis*, *trans*-$[Mo(CO)_2(CNCMe_3)_2(t\text{-Bu-DAB})]^+$, was recorded at −160°C on a frozen dichloromethane solution (Fig. 2) and the measured g values found to be as follows: $g_1 = 2.199$, $g_2 = 2.166$, and $g_3 = 1.981$.

Three equivalents of alkyl isocyanide RNC (R = Me or CMe_3) react very rapidly with the activated complexes $[Mo(CO)_3(CNR)(t\text{-Bu-DAB})]^+$ at room temperature to give the seven-coordinate molybdenum(II) complex $[Mo(CO)(CNR)_4(t\text{-Bu-DAB})](PF_6)_2$ (Fig. 1 and Table 5),* as well as the reduced starting complex $Mo(CO)_3(CNR)(t\text{-Bu-DAB})$. Disproportionation of the molybdenum(I) complex, in the presence of RNC, apparently occurs to give an intermediate, reactive, dicationic molybdenum(II) complex and the reduced product $Mo(CO)_3(CNR)(t\text{-Bu-DAB})$: the dicationic species then reacts further with RNC to yield the final product, $[Mo(CO)(CNR)_4(t\text{-Bu-DAB})]^{2+}$. The same products, $Mo(CO)_3(CNR)(t\text{-Bu-DAB})$ and $[Mo(CO)(CNR)_4(t\text{-Bu-DAB})]^{2+}$, are isolated if four equivalents of isocyanide are added to $[Mo(CO)_3(NCMe)(t\text{-Bu-DAB})]PF_6$. Upon addition of four equivalents of isocyanide to the $[Mo(CO)_3(CNCMe_3)(t\text{-Bu-DAB})]^+$ complex, the reaction proceeds to the homoleptic seven-coordinate isocyanide complex $[Mo(CNCMe_3)_7]^{2+}$ rather than to $[Mo(CNCMe_3)_5(t\text{-Bu-DAB})](PF_6)_2$. In accord with this result, when $[Mo(CO)(CNCMe_3)_4(t\text{-Bu-DAB})](PF_6)_2$ is reacted with *tert*-butyl isocyanide (one equivalent) loss of CO and *t*-Bu-DAB occurred to give the homoleptic isocyanide complex $[Mo(CNCMe_3)_7](PF_6)_2$ as a major product.

If a different 1,4-diaza-1,3-butadiene ligand is employed, namely *i*-Pr-DAB, a similar disproportionation reaction takes place, but the final molybdenum(II) product is the dication $[Mo(CNCMe_3)_5(i\text{-Pr-DAB})]^{2+}$, a species we have isolated previously[1] in a different study. Accordingly, the exact course of these reactions is dependent on the R'-DAB ligand used and this is supported by other work. Specifically, we have shown that complexes of the type $[Mo(CNR)_5(R'\text{-DAB})]^{2+}$ (R' = *i*-Pr or Cy) can be prepared by the action of RNC (R = $CHMe_2$ or CMe_3) on the seven-coordinate molybdenum(II) complexes $Mo(CO)_3(R'\text{-DAB})(SnCl_3)Cl$.[1] However, under similar conditions, the *t*-Bu-DAB derivative $Mo(CO)_3(t\text{-Bu-DAB})(SnCl_3)Cl$ undergoes reductive elimination to form the octahedral complexes $Mo(CO)_3(CNR)(t\text{-Bu-DAB})$.

Acknowledgement—We thank the National Science Foundation (Grant No. CHE82-06117) for support.

REFERENCES

1. A. Bell and R. A. Walton, *J. Organomet. Chem.* 1985, **290**, 341.
2. J. Casanova, Jr, R. E. Schuster and N. D. Werner, *J. Chem. Soc.* 1963, 4280.
3. (a) W. D. Weber, G. W. Gokel and I. K. Ugi, *Angew. Chem., Int. Ed. Engl.* 1972, **11**, 530; (b) R. E. Schuster, J. E. Scott and J. C. Casanova, Jr, *Organic Synthesis.* Collect. Vol. 3, p. 772. Wiley, New York (1973).
4. J. M. Kliegman and R. K. Barnes, *Tetrahedron* 1970, **26**, 2555.
5. A. T. T. Hsieh and B. O. West, *J. Organomet. Chem.* 1976, **112**, 285.
6. (a) H. tom Dieck and I. W. Renk, *Chem. Ber.* 1971, **104**, 92; (b) H. Bock and H. tom Dieck, *Angew. Chem., Int. Ed. Engl.* 1966, **5**, 520.
7. D. P. Tate, J. M. Augl and W. R. Knipple, *Inorg. Chem.* 1961, **1**, 433.
8. G. J. Kubas, *Inorg. Chem.* 1983, **22**, 692.
9. D. N. Hendrickson, Y. S. Sohn and H. B. Gray, *Inorg. Chem.* 1971, **10**, 1559.
10. C. M. Giandomenico, L. H. Hanau and S. J. Lippard, *Organometallics* 1982, **1**, 142.
11. W. S. Mialki, R. E. Wild and R. A. Walton, *Inorg. Chem.* 1981, **20**, 1380.
12. L. H. Staal, D. J. Stufkens and A. Oskam, *Inorg. Chim. Acta* 1978, **26**, 255.
13. H. tom Dieck, I. W. Renk and K. D. Franz, *J. Organomet. Chem.* 1975, **94**, 417.

*The ^1H NMR spectrum of $[Mo(CO)(CNCMe_3)_4(t\text{-Bu-DAB})](PF_6)_2$ in acetone-d_6 is as follows: δ +1.60 (s, *t*-Bu), +1.70 (s, CMe_3) and +8.71 (s, C—*H*).

14. See, for example, M. G. B. Drew, D. G. Tisley and R. A. Walton, *J. Chem. Soc., Chem. Commun.* 1970, 600.
15. J. A. Connor and C. Overton, *J. Chem. Soc., Dalton Trans.* 1982, 2397.
16. H. tom Dieck and I. W. Renk, *Angew. Chem., Int. Ed. Engl.* 1970, **9**, 793.
17. H. Bock and H. tom Dieck, *Chem. Ber.* 1967, **100**, 228.
18. H. tom Dieck and E. Kühl, *Z. Naturforsch.* 1982, **37B**, 324.
19. T. C. Zietlow, D. D. Klendworth, T. Nimry, D. J. Salmon and R. A. Walton, *Inorg. Chem.* 1981, **20**, 947.
20. See, for example, J. A. Gladysz, G. M. Williams, W. Tam and D. L. Johnson, *J. Organomet. Chem.* 1977, **140**, C1; D. Seyferth, R. S. Henderson and L.-C. Song, *Organometallics* 1982, **1**, 125.
21. K. D. Franz, H. tom Dieck, U. Krynitz and I. W. Renk, *J. Organomet. Chem.* 1974, **60**, 361.
22. K. D. Franz, H. tom Dieck, K. A. Ostoja Starzewski and F. Hohmann, *Tetrahedron* 1975, **31**, 1465.
23. A. M. Bond, D. J. Darensbourg, E. Mocellin and B. J. Stewart, *J. Am. Chem. Soc.* 1981, **103**, 6827.
24. F. L. Wimmer, M. R. Snow and A. M. Bond, *Inorg. Chem.* 1974, **13**, 1617.
25. A. M. Bond, R. Colton and J. J. Jackowski, *Inorg. Chem.* 1975, **14**, 2526.
26. A. M. Bond, B. S. Grabaric and J. J. Jackowski, *Inorg. Chem.* 1978, **17**, 2153.
27. R. D. Riecke, H. Kojima and K. Öfele, *J. Am. Chem. Soc.* 1976, **98**, 6735.
28. K. A. Conner and R. A. Walton, *Organometallics* 1984, **2**, 169.

Polyhedron Vol. 5, No. 3, pp. 859–862, 1986
Printed in Great Britain

0277-5387/86 $3.00 + .00
© 1986 Pergamon Press Ltd

SOME NEW OBSERVATIONS ON TELLURIUM DITHIOCARBAMATE CHEMISTRY

MOHAMMED A. K. AHMED and WILLIAM R. McWHINNIE*

Department of Molecular Sciences, University of Aston, Birmingham B4 7ET, U.K.

and

PIERRE GRANGER

Université de Rouen, Institut Universitaire de Technologie de Rouen,
76130 Mont-Saint-Aignan, France

(*Received* 11 *July* 1985; *accepted* 9 *September* 1985)

Abstract—New examples of $[Te(IV)(S_2C \cdot NR_2)_4]$ compounds have been synthesized (where R = Bu^i, Ph or CH_2Ph). Evidence is found from ^{125}Te NMR spectroscopy of a ligand exchange reaction involving $[Te(IV)(S_2C \cdot NR_2)_4]$ (R = Et or CH_2Ph) which has a rate comparable with the time scale of the NMR experiment. $[Te(IV)(S_2C \cdot NR_2)_4]$ undergoes a UV-promoted stoichiometric reaction with dioxygen to give TeO_2 and disulphide.

Tellurium(IV) dithiocarbamates[1,2] continue to find application as accelerators in rubber vulcanization,[3] and have also attracted the interest of crystallographers[4] who have shown the tellurium atom to be eight-co-ordinate in dodecahedral (D_{2d}) co-ordination. We have recently established that the compounds show great promise as stabilizers of polypropene[5] and report in this paper the synthesis of some new compounds which were required to assist those investigations, together with some observations of previously unreported chemical behaviour.

EXPERIMENTAL AND RESULTS

Synthesis

Quantitative yields of the following compounds were obtained via the indicated literature methods: $[Te(IV)(S_2C \cdot NMe_2)_4]$, m.p. 165°C (lit.[6] 165°C); $[Te(IV)(S_2C \cdot NEt_2)_4]$, m.p. 123–124°C (lit.[6] 124°C); $[Te(II)(S_2C \cdot NMe_2)_2]$, m.p. 265°C (lit.[7] > 250°C); $[Te(II)(S_2C \cdot NEt_2)_2]$, m.p. 162–163°C (lit.[8] 164°C).

Tetrakis(dibenzyldithiocarbamato)tellurium(IV). This compound was prepared by an adaptation of Murrill's method.[1] Sodium hydroxide (1.6 g, 0.04 mol) in water (8 cm^3) was added to TeO_2 (3.19 g, 0.02 mol) and heated to dissolve the oxide. The solution was set aside. A solution of dibenzylamine (17.8 g, 0.08 mol) in ethanol (70 cm^3) was treated with sodium hydroxide (3.2 g, 0.08 mol) in water (10 cm^3) whilst cooling and stirring. Carbon disulphide (6.08 g, 0.08 mol) was then added gradually with continued cooling over 30 min to maintain the temperature below 10°C. Water (60 cm^3) was added to dissolve the heavy precipitate, the resulting solution being added to that of sodium tellurite which had been set aside. The reaction mixture was cooled by the addition of ice. The solution was treated with HCl (5%) with continued cooling; the total volume was increased to 300 cm^3. The yellow precipitate was filtered washed and recrystallized from benzene [m.p. 160°C (dec.)]. The yield was quantitative.

Tetrakis(di-isobutyldithiocarbamato)tellurium(IV) and tetrakis(diphenyldithiocarbamato)tellurium(IV). These were prepared by a similar method.

Bis(dibenzyldithiocarbamato)tellurium(II). This was prepared by an adaptation of Foss's method.[7]

Analytical data are given in Table 1.

Reactions

Solutions of tellurium dithiocarbamates (equimolar proportions) in xylene were prepared as

* Author to whom correspondence should be addressed.

follows:

$[Te(IV)(S_2C\cdot NEt_2)_4]$
$+[Te(IV)(S_2C\cdot N(CH_2Ph)_2)_4]$,

$[Te(IV)(S_2C\cdot NEt_2)_4]+[Te(IV)(S_2C\cdot Ph_2)_4]$,

$[Te(IV)(S_2C\cdot NEt_2)_4]+[Te(IV)(S_2C\cdot Me_2)_4]$.

The solutions were refluxed for periods between 2 and 10 h and examined by thin-layer chromatography (TLC). In all cases the following species were positively identified: $[Te(IV)(S_2C\cdot NR_2)_4]$, $[Te(II)(S_2C\cdot NR_2)_2]$ and $(S_2C\cdot NR_2)_2$. There were also other spots which did not correlate to known species.

An equimolar mixture of $[Te(IV)(S_2C\cdot NMe_2)_4]$ and $[Te(IV)(S_2C\cdot NEt_2)_4]$ was heated in a sealed quartz tube for periods ranging from 10 min to 1 h. TLC examination of chloroform solutions of the cooled mixtures showed the presence of $[Te(IV)(S_2C\cdot NR_2)_4]$, $[Te(II)(S_2C\cdot NR_2)_2]$ and $(S_2C\cdot NR_2)_2$, and other unidentified species (10 min heating). The solution heated for 1 h contained no tellurium(IV) compounds.

^1H *NMR spectroscopy.* Equimolar mixtures of the following pairs of tellurium(IV) dithiocarbamates were prepared in $CDCl_3$:

$[Te(IV)(S_2C\cdot NEt_2)_4]+[Te(IV)(S_2N(CH_2Ph)_2)_4]$,

$[Te(IV)(S_2C\cdot NEt_2)_4]+[Te(IV)(S_2N\cdot Ph_2)]$.

No change in spectra was discernible with time, the observed trace being the sum of the two components.

^{125}Te *NMR spectroscopy.* Only one mixture was sufficiently soluble in $CDCl_3$ for study:

$[Te(IV)(S_2C\cdot NEt_2)_4]+[Te\{S_2C\cdot N(CH_2Ph)_2\}_4]$.

An equimolar mixture of the maximum attainable concentration was examined in a 10-mm sample tube. A broad resonance was observed with a chemical shift the average of those obtained from the single sharp resonances of the pure components. Unfortunately, cooling the mixture resulted in crystallization of the solution, rendering it unsuitable for further NMR investigation.

Photochemical reaction of $[Te(IV)(dtc)_4]$ *and* $[Te(II)(dtc)_2]$ *with dioxygen* (*dtc = dithiocarbamate*). $[Te(IV)(S_2C\cdot NEt_2)_4]$ shows an absorption maximum at 420 nm ($\varepsilon = 3.38\times10^3$) and 255 nm ($\varepsilon = 1.5\times10^5$). Irradiation of chloroform or benzene solutions of the compound in the presence of air over 14 days gave a white precipitate of TeO_2 (quantitative). Chromatography of the solution showed the presence of $(S_2C\cdot NEt_2)_2$. When concentrations were very low ($\sim10^{-6}$ M), the reaction was complete after only a few minutes. The reaction appears to be general for soluble *tetrakis*(dithiocarbamato)tellurium(IV) species and also proceeds for soluble *bis*(dithiocarbamato) tellurium(II) compounds. The reaction does not proceed in the dark nor in the absence of dioxygen.

The stoichiometry is accurately:

$$\{Te(dtc)_n\}+O_2\rightarrow TeO_2 + \frac{n}{2}(S_2C\cdot NR_2)_2 \quad (n = 2 \text{ or } 4).$$

Table 1. Analytical data for tellurium dithiocarbamates

Compound	M.p. (°C)	Colour	% C (calc.)	% H (calc.)	% N (calc.)	% S (calc.)
$Te(S_2CNEt_2)_2$	162–163	Red	28.4 (28.3)	5.0 (4.7)	6.5 (6.6)	30.0 (30.2)
$Te(S_2CNEt_2)_4$	123–124	Yellow	33.4 (33.4)	5.7 (5.6)	8.2 (7.8)	34.0 (35.6)
$Te(S_2CNMe_2)_2$	265	Orange-red	19.9 (19.6)	3.4 (3.3)	7.8 (7.6)	33.8 (34.8)
$Te(S_2CNMe_2)_4$	165	Yellow	24.3 (23.7)	3.9 (3.9)	9.3 (9.2)	42.1 (42.5)
$Te[S_2CN(CH_2C_6H_5)_2]_2$	175	Flesh	53.0 (53.6)	4.1 (4.2)	4.0 (4.2)	19.1 (19.9)
$Te[S_2CN(CH_2C_6H_5)_2]_4$	160	Orange	59.8 (59.2)	5.1 (4.6)	4.7 (4.6)	21.2 (21.1)
$Te[S_2CN(C_4H_9)_2]_4$	124	Yellow	45.3 (45.8)	6.7 (7.6)	5.4 (5.9)	26.3 (27.1)
$Te[S_2CN(C_6H_5)_2]_4$	209–210	Orange	55.9 (56.5)	3.6 (3.6)	5.0 (5.1)	23.2 (24.1)

Table 2. IR and ^{1}H NMR data

Compound	ν(CN) (cm^{-1})	ν(CS) (cm^{-1})	ν(TeS) (cm^{-1}) Asymmetric	ν(TeS) (cm^{-1}) Symmetric	^{1}H NMR (σ ppm vs TMS) J (Hz) ($CDCl_3$)
$Te(S_2CNMe_2)_4$	1510 s	970 s	350 s	310 w	
$Te(S_2CNMe_2)_2$	1510 s	970 s, 980 sh	350 s	310 w	
$Te(S_2CNEt_2)_4$	1490 s	990 m, 1005 sh	360 s	320 s	1.08–1.62 (CH_3, triplet, 24H) 3.61–4.02 (CH_2, quartet, 16H)
$Te(S_2CNEt_2)_2$	1490 s	990 m, 1005 sh	365 s	305 s	1.12–1.53 (CH_3, triplet, 12H) 3.53–4.04 (CH_2, quartet, 8H)
$Te[S_2CN(C_4H_9)_2]_4$	1480 s	975 s, 968 sh	350 s	285 s	
$Te(S_2CNPh_2)_4$	1495 s	1010 s	320 m	280 s	
$Te[S_2CN(CH_2Ph)_2]_4$	1500 s	1000 s, 1010 sh	270 s	230 m	5.15 (CH_2, singlet, 16H) 7.35 (aromatic, singlet, 40H)
$Te[S_2CN(CH_2Ph)_2]_2$	1500 s	1000 s, 1010 sh	330 w	285 m	

Physical measurements

IR spectra were measured for KBr discs with a Perkin–Elmer 599B spectrophotometer. ^{1}H NMR spectra were taken with a Perkin–Elmer R12B instrument (60 MHz) and ^{125}Te NMR spectra were obtained with a Bruker WH 90C spectrometer as previously described.[9] TLC was carried out on silica gel plates.

Pertinent spectroscopic data are given in Table 2.

DISCUSSION

The limited solubility of the well-known *tetrakis*(dimethyldithiocarbamato)tellurium(IV) in common solvents at ambient temperature led us to synthesize new, more soluble, examples (Table 1). Three aspects of the work merit brief discussion.

IR spectra

Table 2 lists characteristic frequencies for the dithiocarbamato complexes [ν(CN), ν(CS) and ν(TeS)]. In all the complexes ν(CN) is a strong band in the range 1490–1510 cm^{-1}. ν(CS) was a strong to medium band in the range 970–1010 cm^{-1}. These observations agree with previous reports.[10,11] Some workers have attempted to use solution IR data to differentiate mono- and bidentate dithiocarbamato groups:[6,12] however, since all crystallographic data to date[4,13–16] show unsymmetrically bidentate dithiocarbamato groups to be co-ordinated to tellurium it is clearly unwise to infer more from our IR data than the fact that the similarity of major spectral features of our new compounds to those of known structure implies that the new compounds belong to the same structural class.

Exchange and dissociative reactions

Simple experiments were carried out in which equimolar mixtures of *tetrakis*(dithiocarbamato) tellurium(IV) compounds were refluxed in xylene. TLC examination of the solution after periods of reflux between 2 and 10 h revealed evidence for the following decomposition:

$$[Te(IV)(S_2C\cdot NR_2)_4] \rightarrow [Te(II)(S_2C\cdot NR_2)] + R_2N\cdot C(S)S{-}S(S)C\cdot NR_2,$$

but, in addition, several spots were seen which did not correlate to known species. More rigorous conditions (sealed tube) led to total decomposition of the tellurium(IV) compound.

^{1}H NMR spectroscopy was uninformative since the spectra of equimolar mixtures of tellurium(IV) dithiocarbamates were indistinguishable from the sum of the component spectra: however, ^{125}Te NMR spectra were much more informative. The chemical shift for $[Te\{(S_2C\cdot N(CH_2Ph)_2\}_4]$ was 867.5 ppm (vs Me_2Te) in $CDCl_3$ solution and that for $[Te(S_2C\cdot NEt_2)_4]$ in the same solvent was 841.2 ppm: both resonances were sharp. An equimolar mixture of the compounds gave a *broad* band centred on 852 ppm, i.e. approximately the mean of the values for the single compounds. Unfortunately, cooling produced precipitation, but the results even as they stand clearly concur with an exchange process and hint that the unidentified spots in the TLC analysis may well correspond to mixed-ligand species.

Undue speculation as to the mechanism of exchange would not be justified, but the other data we possess suggest that a redox mechanism involving reductive elimination of disulphide from tellurium(IV) and oxidative addition of disulphide to tellurium(II) is probable.

Reaction with oxygen

During the course of this work we observed that, under the influence of UV light, the tellurium(IV) and tellurium(II) dithiocarbamates reacted with dioxygen in a clean stoichiometric reaction. This reaction could be of significance in the UV stabilization of polypropene by $[Te(IV)(S_2C \cdot NR_2)_4]$ since, not only does it help to remove oxygen, but in doing so it releases disulphide, itself a powerful antioxidant.

Acknowledgement—One of us (MAKA) thanks the Iraqi Government for study leave.

REFERENCES

1. P. I. Murrill, U.S. Patent 1,921,091 (1930).
2. P. I. Murrill, U.K. Patent 359,328 (1931).
3. W. R. McWhinnie and J. E. Stuckey, *The Use of Selenium and Tellurium in Rubber Technology*. Selenium and Tellurium Development Corporation Inc. (1983).
4. S. Husebye, In *Proceedings of the Fourth International Conference on the Organic Chemistry of Selenium and Tellurium* (Edited by F. J. Berry and W. R. McWhinnie), pp. 298–369. University of Aston in Birmingham (1983).
5. M. A. K. Ahmed, S. Abed Ali, W. R. McWhinnie and G. Scott, accepted for publication in *J. Appl. Polym. Sci.*
6. G. St. Nikolou, N. Jordanov and I. Havezou, *J. Inorg. Nucl. Chem.* 1971, **33**, 1055.
7. O. Foss, *Inorg. Synth.* 1953, **4**, 91.
8. O. Foss, *Acta Chem. Scand.* 1949, **3**, 708.
9. P. Granger, S. Chapelle, W. R. McWhinnie and A. Z. Al-Rubaie, *J. Organomet. Chem.* 1981, **220**, 149.
10. G. Aravamudan, C. Janakiram and B. G. Sejekan, *Phosphorus Sulphur* 1978, **5**, 185.
11. B. G. Sejekan, C. Janakiram and G. Aravamudan, *J. Inorg. Nucl. Chem.* 1978, **40**, 211.
12. J. Wu, P. F. Lott and H. A. Droll, *Inorg. Chem.* 1970, **9**, 193.
13. S. Husebye and S. E. Svaeren, *Acta Chem. Scand.* 1973, **27**, 763.
14. G. C. Rout, M. Seshasayee, K. Radha and G. Aravamudan, *Acta Cryst.* 1983, **C39**, 1021.
15. C. Fabiani, R. Spagna, A. Vaciago and L. Zambonelli, *Acta Cryst.* 1971, **B27**, 1499.
16. S. Husebye, *Acta Chem. Scand.* 1970, **24**, 2198.

Polyhedron Vol. 5, No. 3, pp. 863–870, 1986
Printed in Great Britain

0277–5387/86 $3.00 + .00
© 1986 Pergamon Press Ltd

β-ALKOXYCARBONYL ALKYL TIN CHELATES—I. OXINATES AND SUBSTITUTED OXINATES: PREPARATION AND SPECTROSCOPIC STUDIES

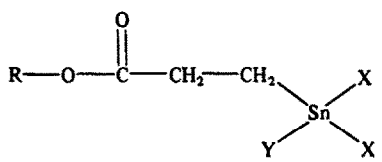
BARUN KANTI DEB and AMIYA KANTI GHOSH*

Department of Chemistry, University of North Bengal, Darjeeling 734430, India

(*Received* 11 *March* 1985; *accepted after revision* 18 *September* 1985)

Abstract—β-Alkoxycarbonyl ethyl tin chlorides, the so-called "estertins" (a unique class of PVC stabilizer) form stable coordination complexes with bidentate ligands like oxine and substituted oxines. A number of complexes of the types R_2SnL_2, R_2SnLX, $RSnL_2X$ and $RSnL_3$, where R = $CH_3CO_2CH_2CH_2$, $C_4H_9CO_2CH_2CH_2$, $CH_3CO_2CH(CH_3)CH_2$ or $CH_3COCH_2C(CH_3)_2$, X = Cl or SCN, and L = oxine, 5,7-dichloro oxine or 5,7-dibromo oxine, have been prepared and characterized by elemental analysis, electronic, IR and PMR spectral data. Possible structural features of the isolated complexes are discussed.

Hutton *et al.*[1–3] developed a simple, relatively inexpensive and non-hazardous preparation for "estertins" having the general formula I:



R = alkyl or aryl group, Y = $ROCOCH_2CH_2$ or halogen, X = halogen

I

Subsequent work[4] has established their application as excellent PVC stabilizers with relatively low mammalian toxicities. Poller,[5] after consideration of relevant facts, suggested that reduction of Lewis acidity of the resulting organotin chloride will improve the efficiency of a stabilizer and prepared di-(4-ketopentyl)tindi(isooctyl thioglycolate), in which it was expected that the keto groups would be free in the stabilizer while co-ordinated to tin in the corresponding dichloride. They showed that the ketopentyl tin compounds are more than twice as effective in stabilization as the corresponding dialkyl tin derivatives. Lewis acidity of the β-alkoxycarbonyl alkyl tin compounds (i.e. estertins) has not been investigated extensively so far, particularly with bidentate ligands. Attempts were therefore being made to prepare such complexes. In this paper we would like to report the preparation of different types of β-alkoxycarbonyl alkyl tin complexes with oxine and substituted oxines and also their characterization by elemental analysis and electronic, IR and PMR spectral data.

EXPERIMENTAL

Synthesis

Analytical-grade reagents and dry and distilled solvents were used.

Preparation of β-alkoxycarbonyl ethyl tin chlorides and related compounds. The compounds used are of the types R_2SnCl_2 and $RSnCl_3$, where R = $CH_3CO_2CH_2CH_2$, $C_4H_9CO_2CH_2CH_2$, $CH_3CO_2CH(CH_3)CH_2$ and $CH_3COCH_2C(CH_3)_2$. All these compounds were prepared by reported methods.[1–3]

General method of preparation of complexes. Except for β-alkoxycarbonyl ethyl tin thiocyanato complexes, others were prepared by reacting stoichiometric quantities of β-alkoxycarbonyl alkyl tin chlorides and the ligands in appropriate molar ratios. The hydrochloric acid liberated was neutralized with ammonia solution (17 N) and the resulting ammonium chloride was removed by filtration. The filtrate was refluxed, concentrated and

* Author to whom correspondence should be addressed.

the complexes were isolated and purified by fractional crystallization.[6]

β-Alkoxycarbonyl thiocyanato oxinates were prepared by treating β-alkoxycarbonyl ethyl tin chloro oxinates with a suspension of potassium thiocyanate in hot ethanol.[6] Potassium chloride produced in the reaction was removed by filtration and the filtrate was concentrated. The product crystallized out was then purified.

Some typical preparations of complexes

$(CH_3CH_2CH_2CH_2)_2Sn$(5,7-dichloro oxine)$_2$

A hot benzene solution (100 cm^3) of 5,7-dichloro oxine (1.28 g, 5.98 mmol) was added to a 50 cm^3 solution of $(CH_3CO_2CH_2CH_2)_2SnCl_2$ (1.09 g, 2.99 mmol) in benzene and heated in a water bath. A few drops of ammonia solution were added and the precipitate filtered. The filtrate was refluxed for 2 h, concentrated and treated with an equal volume of methanol. The solution was refrigerated for several hours and a heavy yellow layer was produced. The layer, gummy in nature, was extracted with hot methanol, concentrated and kept overnight. Yellow crystals which appeared were purified from the same solvent.

$CH_3CO_2CH_2CH_2Sn(oxine)_2Cl$

A chloroform solution of

$CH_3CO_2CH_2CH_2SnCl_3$

(0.94 g, 3.01 mmol) and oxine (0.87 g, 6.00 mmol) was mixed and heated in a water bath for 10 min. The colour changed to deep yellow when a few drops of ammonia were added to it. After filtration the filtrate was refluxed for 2 h, concentrated to minimum volume, methanol was added, followed by refrigeration overnight. Yellow crystals separated when the solution was scratched with a spatula. The product was crystallized from the chloroform–methanol mixture.

$C_4H_9CO_2CH_2CH_2Sn(oxine)_2(SCN)$

A suspension of potassium thiocyanate (0.20 g, 2.06 mmol) in hot ethanol was added to a hot solution of $C_4H_9CO_2CH_2Sn(oxine)_2Cl$ (1.14 g, 1.99 mmol) while stirring with a magnetic stirrer for an hour. Potassium chloride produced in the reaction was filtered off and the filtrate was evaporated to dryness and then extracted with chloroform. The chloroform extract was concentrated and refrigerated for a few hours. The yellow solid formed was purified by several crystallizations from ethanol.

Spectroscopic data

The electronic spectra were recorded on a Backman DU-2 spectrophotometer and/or a Pye–Unicam SP 8-300 using methanol (Uvasol, E. Merck) as the solvent. The IR spectra were recorded as Nujol mulls using a Backman IR-20 spectrophotomer equipped with KBr windows. The PMR spectra in $CDCl_3$ against internal standard TMS were recorded on a Varian EM-390 and/or Zeol, Japan, FT NMR and/or a Varian A-60 spectrophotometer.

RESULTS AND DISCUSSION

The complexes isolated in the present investigation are listed in Table 1, together with their analytical, electronic and IR spectral data. All the complexes are yellow in colour.

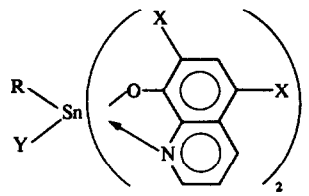
Electronic spectra

The electronic spectra of β-alkoxycarbonyl ethyl tin oxinates correspond to those of other chelated metal oxinates.[7–10] Meinema *et al.*[8] reported that the shift to a longer wavelength of the 320-nm absorption of oxine in an organometallic complex is generally considered to be a reliable indication of the presence of a chelating oxine ligand. All the spectra of oxinate complexes are characterized by a strong band in the region 370–375 nm. The 310-nm band of oxine, a π–π^* transition, suffers a bathochromic shift to 370–375 nm in all β-alkoxycarbonyl ethyl tin oxinates. The considerable shift observed in these cases and near constancy of the oxinates absorption at ~375 nm indicate strongly that a chelate formation of similar stability has taken place.[8,9] The inflexion observed in the region 310–375 nm in most oxinate complexes may be due to the presence of some free ligand produced from the rupture of the Sn—N bond in methanol.[9,11]

In substituted oxine complexes two well-separated bands are observed at ~338–340 and ~385–390 nm. From its position and intensity, the band at ~385–390 nm is supposed to be the ligand band shifted from its original position (at 324 nm), which suggests that in solution these organotin compounds contain a chelated substituted oxinate ligand.[8,13] The other band at ~338–340 nm in β-alkoxycarbonyl ethyl tin (substituted oxinates) is in the same position as the usual ^1L_b band, insensitive to changes in solvent or substituent.[13] This band may also be due to the presence of some free ligand produced in methanol[9,11] and is observed in the spectra of other metal oxinates.[8]

The large bathochromic shift of the π–π^* transition in β-alkoxycarbonyl ethyl tin oxinate and

substituted oxinate complexes is consistent with the presence of Sn ← N coordination. The complexes are, thus, structurally quite similar to other organotin oxinates[10] and may be formulated as **II**:

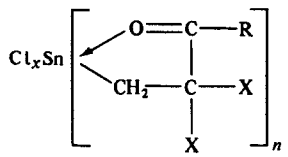


R = $CH_3CO_2CH_2CH_2$, $C_4H_9CO_2CH_2CH_2$ or $CH_3CO_2CH(CH_3)CH_2$, X = H, Cl or Br; Y = R, Cl or SCN

II

IR spectra

From the spectroscopic data (IR and PMR) and also from the fact that the carbonyl stretching frequency remains unaffected by dilution in toluene or ethereal solvents, Hutton *et al.*[1] suggested the following structure for β-alkoxycarbonyl ethyl tin chloride (**III**):



R = OCH_3, OC_4H_9 or CH_3; X = H or CH_3; x = 2 or 3; n = 1 or 2

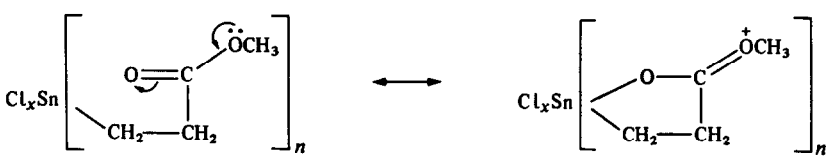
III

They also proposed that the methoxy oxygen lone-pair electrons are also involved in the delocalization of the ester carbonyl electron density on tin and reported the intramolecular coordination as follows (**IV**):

IR spectra of all the β-alkoxycarbonyl ethyl tin oxinates and substituted oxinates (Table 1) show that the carbonyl stretching frequency of these compounds appeared at higher wavenumbers than the carbonyl frequencies in the parent Lewis acids (i.e. in β-alkoxycarbonyl ethyl tin chlorides). This indicates the nonchelating nature of the ester carbonyl group. The intramolecular carbonyl coordination of the β-alkoxycarbonyl ethyl tin chlorides is cleaved (**V**), which is indicated by the shift in the ν(C=O) frequency appearing in the region 1720–1730 cm^{-1} in all cases.

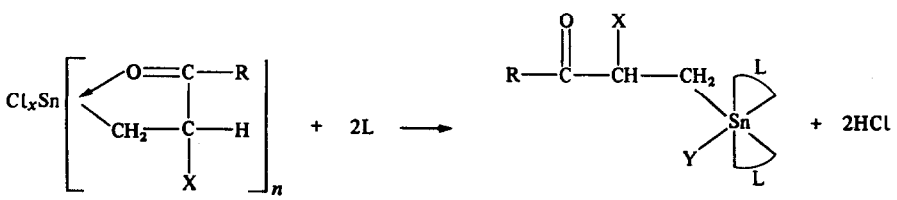
The cleavage of intramolecular carbonyl coordination is expected due to increased electron density on tin via the ligands and, also, possibly due to steric reasons.

The IR spectra of oxine and β-alkoxycarbonyl ethyl tin oxinates are very complex due to the presence of a large number of vibrational modes due to ring-stretching deformation, inplane and out-of-plane ring and CH deformation etc. In all the β-alkoxycarbonyl ethyl tin oxinates the carbonyl stretching frequency is assigned at ~1720–1730 cm^{-1}. As expected the OH stretching mode of oxine at ~3200 cm^{-1} disappeared in these complexes, confirming bonding through the oxygen atom of the ligand. Both ν(Sn—C) and ν(Sn—O) peaks appeared between 400 and 600 cm^{-1}.[12,14,15] All the spectra of the oxine complexes show, in addition to the Sn—C stretching modes, one other strong absorption band at ~520–540 cm^{-1}, which is absent in spectrum of the ligand and, therefore, may be assigned to Sn—O vibration (oxygen of the 8-OH group).[12] The presence of a number of ligand bands in the region expected for Sn—C stretching has



x = 2 or 3, n = 1 or 2

IV



R = OCH_3, OC_4H_9 or CH_3; X = H or CH_3; Y = $ROCH(X)CH_2$ or Cl; L = ligand; x = 2 or 3; n = 1 or 2

V

Table 1. Analytical data, electronic (in methanol) and IR [Nujol mulls (cm^{-1})] spectral data of β-alkoxycarbonyl ethyl tin complexes

Compound [m.p. (°C), yield (%), reflux period (h)]	Analyses (%)[k]				Electronic spectra	IR spectra			
	C	H	N	Sn	λ_{max} (nm) [log ε_{max}]	ν(C=O)	ν(C=O) for >C—O—Sn site		ν(Sn—O) and others
1 $R^{I}_{2}SnL_{2}$[ad] (152, 75, 1)	53.8 (53.7)	4.3 (4.5)	4.8 (4.8)	20.4 (20.5)	370 (315) [3.48]	1729	1102	522	
2 $R^{I}_{2}SnL(SCN)$[be] (105, 68, 2)	44.1 (43.6)	4.1 (4.0)	5.4 (5.7)	24.0 (24.0)	370 (315) [3.21]	1715	1120	545 2050	 [ν(C≡N)]
3 $R^{I}SnL_{2}Cl$[d] (172, 65, 2)	49.7 (49.9)	3.3 (3.6)	5.0 (5.3)	22.3 (22.5)	375 (315) [3.76]	1730	1110	530	
4 $R^{I}SnL_{2}(SCN)$[bd] (82, 60, 2[i])	49.8 (50.0)	3.5 (3.4)	7.8 (7.6)	21.5 (21.6)	372 (310) [3.43]	1720	1105	540 2020	 [ν(C≡N)]
5 $R^{I}SnL_{3}$[ad] (200,[j] 55, 4)	57.9 (58.3)	4.0 (4.0)	6.7 (6.6)	18.5 (18.6)	—	1720	1100	519	
6 $R^{II}SnL_{2}Cl$[ad] (168, 68, 2)	51.6 (52.5)	3.6 (4.4)	4.9 (4.9)	20.7 (20.8)	375 (315) [3.72]	1730	1102	535	
7 $R^{II}SnL_{2}(SCN)$[be] (78, 70, 1[i])	52.4 (52.5)	4.4 (4.2)	7.1 (7.1)	20.0 (20.0)	374 (315) [3.65]	1720	1100	525 2020	 [ν(C≡N)]
8 $R^{II}SnL_{3}$[ad] (181, 4, 58)	59.8 (60.0)	4.7 (4.6)	6.1 (6.2)	17.4 (17.5)	—	1728	1100	535	
9 $R^{III}SnL_{2}Cl$[ad] (165, 72, ½)	50.5 (50.8)	3.7 (3.9)	5.2 (5.2)	21.8 (21.9)	375 [4.03]	1722	1100	520	
10 $R^{IV}SnL_{2}Cl$[ad] (220, 52, 2)	53.0 (53.2)	4.5 (4.3)	6.0 (5.2)	21.8 (22.0)	369 (310)	—	—	1630 3320	[ν(>C=CH—)] [ν(OH)]
11 $R^{I}_{2}SnL^{1}_{2}$[ch] (155, 69, 2)	44.0 (43.4)	3.1 (3.1)	3.8 (3.9)	16.4 (16.5)	338 [3.83] 385 [3.86]	1730	1100		

12	$R^{I}SnL^{I}_{2}Cl^{cf}$	40.1	2.3	3.9	17.8	340 [3.48]	1732	1110
	(200, 68, 2)	(39.6)	(2.3)	(4.2)	(17.8)	390 [3.64]		
13	$R^{II}SnL^{I}_{2}Cl^{cg}$	41.8	2.9	4.1	16.7	340 [3.48]	1720	1110
	(180, 65, 2)	(42.3)	(3.0)	(4.0)	(16.8)	390 [3.64]		
14	$R^{III}SnL^{I}_{2}Cl^{cf}$	41.7	2.4	4.9	17.4	340 [3.69]	1720	1105
	(190, 74, 2)	(40.5)	(2.5)	(4.1)	(17.5)	385 [3.69]		
15	$R^{I}_{2}SnL^{II}_{2}{}^{ad}$	35.1	2.3	3.2	13.2	340 [3.70]	1730	1100
	(167, 68, 1)	(34.8)	(2.5)	(3.1)	(13.3)	388 [3.69]		
16	$R^{I}SnL^{II}_{2}Cl^{ad}$	31.1	1.6	3.0	14.0	340 [3.63]	1722	1100
	(160, 71, 1)	(31.2)	(1.8)	(3.3)	(14.1)	390 [3.76]		
17	$R^{II}SnL^{II}_{3}{}^{ad}$	35.0	2.4	4.0	10.3	340 [4.80]	1725	1102
	(155, 72, 1)	(35.4)	(2.2)	(4.6)	(10.3)	390 [4.84]		
18	$R^{III}SnL^{II}_{2}Cl^{ad}$	32.4	2.2	3.4	13.8	340 [3.96]	1730	1105
	(152, 76, 1)	(32.1)	(2.0)	(3.3)	(13.9)	390 [4.04]		

L = oxine, L^{I} = 5,7-dichloro oxine, L^{II} = 5,7-dibromo oxine, $R^{I} = CH_3CO_2CH_2CH_2$, $R^{II} = C_4H_9CO_2CH_2CH_2$, $R^{III} = CH_3CO_2CH(CH_3)CH_2$, $R^{IV} = CH_3COCH_2C(CH_3)_2$; [a,b] and [c] refer to reaction medium (chloroform, ethanol and benzene, respectively). [d,e,f,g] and [h] refer to solvent for crystallization (chloroform–methanol mixture, ethanol, benzene–methanol mixture, chloroform–benzene mixture and methanol, respectively). [i]Stirred instead of refluxing. [j]Decomposition point. [k]Calculated value in parentheses. λ_{max} in parentheses are influxions. λ_{max} in methanol of L, L^{I} and L^{II} is at 370, 324 and 325 nm, respectively.

ν(C=O) of $R^{I}_{2}SnCl_2$ at 1677 cm^{-1}, of $R^{I}SnCl_3$ at 1660 cm^{-1}, of $R^{II}_{2}SnCl_2$ at 1675 cm^{-1}, of $R^{II}SnCl_3$ at 1640 cm^{-1}, of $R^{III}SnCl_3$ at 1640 cm^{-1}, and of $R^{IV}SnCl_3$ at 1662 cm^{-1}.

created some confusion in assigning the Sn—C band of complexes in a conclusive manner. As the spectra were recorded using KBr windows, the region below 400 cm^{-1}, where the Sn ← N stretching frequency is expected,[7,12,14] could not be explored. The C=N stretching frequency somewhat coupled with pyridine ring vibration appears as a strong band in oxine at 1580 cm^{-1}, whereas, however, in all the complexes this band shifts to ~1560–1570 cm^{-1}.[16] In all the complexes the presence of a quinoline ring can easily be identified from the appearance of characteristic absorptions such as: (i) a number of bands (more than six) due to ring-breathing vibrations between 1360 and 1625 cm^{-1}, (ii) a sharp band due to the C—O stretching frequency at the >C—O—Sn site (1100 cm^{-1}),[17] and (iii) a number of sharp and strong bands due to the CH deformation modes in the region between 900 and 700 cm^{-1}.[18]

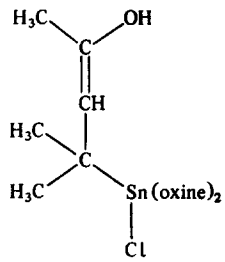
The spectra of the thiocyanate complexes show a very strong band at ~2000–2050 cm^{-1}, in addition to other bands, like the corresponding halide complexes. The ambidentate ligand SCN can coordinate to metal either through the sulphur or the nitrogen, or it can act as a bridge. Though the C—S stretching frequency is more useful in distinguishing these two isomers[19] oxine has many absorptions in this region that they may obscure the C—S stretching band. Hence, on the basis of the C≡N stretching frequency alone, the thiocyanate group may be thought to be linked to tin through the nitrogen as is suggested by Sabatini and Bertini.[19] Hence, a penta-coordinated trigonal bipyramidal structure for the

$$(CH_3CO_2CH_2CH_2)_2Sn(oxine)(SCN)$$

complex[12,20,21] and a hexa-coordinated distorted octahedral geometry (where the *cis*- and *trans*-configurations are less significant) for R_2SnL_2 ($R = CH_3CO_2CH_2CH_2$; L = oxine, 5,7-dichloro oxine or 5,7-dibromo oxine) and $RSnXL_2$ ($R = CH_3CO_2CH_2CH_2$, $C_4H_9CO_2CH_2CH_2$ or $CH_3CO_2CH(CH_3)CH_2$; X = Cl or SCN; L = oxine, 5,7-dichloro oxine or 5,7-dibromo oxine) type of complexes[22–24] may be suggested.

In the IR spectra of all the 5,7-disubstituted oxine complexes, the complete absence of any ν(OH) frequency at the region around 3200 cm^{-1}, the shift of the carbonyl stretching frequency to higher wavenumbers between 1720 and 1735 cm^{-1} and also the presence of some other characteristic bands show the existence of substituted oxines in the complexes. The C=N stretching frequency somewhat coupled with pyridine ring vibration of the substituted oxines at 1580 cm^{-1} shifts to ~1550–1560 cm^{-1} in the complexes.[16] The bands at ~1280, 1190 and 1150 cm^{-1} in the most of these complexes may be attributed to the substituted pyridine ring vibrations.[23] Like oxine complexes these also show a sharp band of C—O stretching frequency (at the >C—O—Sn site) at ~1100 cm^{-1}.[17]

The IR spectrum of the compound $CH_3COCH_2C(CH_3)_2Sn(oxine)_2Cl$ is quite different from all of the other oxinate complexes. The compound showed a strong absorption at 3320 cm^{-1} and the total absence of the ν(C=O) band at ~1720 cm^{-1}. It also showed a new peak at 1630 cm^{-1}, which may possibly be due to the >C=CH group. All these bands may point to an unusual structure of type[3] **VI**:



VI

Without the absence of such an enol form it is rather difficult to explain the IR spectrum of this compound, because it strongly suggests the formation of an oxinate complex in all other aspects.

PMR spectra

From the integration of the curves in PMR spectra, the ratio of different protons have been found to be consistent with the composition of the complexes. In general, on complex formation all types of protons in β-alkoxycarbonyl ethyl groups should exhibit shielding and thereby resonate at a higher magnetic field, which is in agreement with an increased electron density on the tin via ligand donation. In addition, the normal inductive effect of the corresponding ligand and the magnetic influence of the tin atom also combine to govern the alkyl resonance positions. Depending upon the basicity of the donor, the α-methylene protons should be shielded most. Methyl propionate in $CDCl_3$ furnished methoxy signal at 3.66 (ppm) while in β-alkoxycarbonyl ethyl tin chlorides this signal is shifted to downfield due to deshielding of the methyl protons by the lone pair of electrons of methoxy oxygen delocalized because of the coordinated tin.

Due to complex formation, the alkyl protons (H_α, H_β and H_c)* attached to tin in all of the β-alkoxycarbonyl ethyl tin oxinates are shielded compared to the parent organotin chlorides. In β-alkoxycarbonyl ethyl thiocyanato oxinates the amount of shielding is less than the corresponding chloro oxinate complexes due to the less electronegative character of the thiocyanate group. The α-methylene protons in all of the oxinate complexes are mostly shielded, except in

$$CH_3CH(CH_3)CH_2CO_2Sn(oxine)_2Cl,$$

where the methoxy proton is shielded most. When the chlorine atoms are replaced by the ligands, the ester coordination is disrupted, as seen from the IR spectra. Further evidence for the non-chelating nature of the ester carbonyl group in these complexes is obtained from the chemical shift values of β-methylinic and methyl protons. Both the protons in the complexes also suffer shielding and revert to positions characteristic of the free ester group.

The chemical shifts observed for the ring protons in β-alkoxycarbonyl ethyl tin oxinates show that the proton at 2-position of quinoline ring is most affected while the other protons remain practically unaltered or slightly altered. Electron donation to tin has produced a deshielding of the 2-H proton of oxine in

$$(CH_3CO_2CH_2CH_2)_2Sn(oxine)_2(SCN),$$

$$CH_3CO_2CH_2CH_2Sn(oxine)_3$$

and

$$C_4H_9CO_2CH_2CO_2Sn(oxine)_3,$$

and is observed at a lower magnetic field compared to the resonance positions in the free ligand. Shielding of the 2-H proton is observed in all other oxinates, which indicates that

$$(CH_3CO_2CH_2CH_2)_2Sn(oxine)(SCN),$$

$$CH_3CO_2CH_2CH_2Sn(oxine)_3$$

and

$$C_4H_9CO_2CH_2CH_2Sn(oxine)_3$$

possibly appear to involve a greater extent of chelation in solution compared to the other complexes. It is expected that the 2-H proton of oxine will appreciably be affected due to donation of electrons from the neighbouring nitrogen atom and consequently this proton would suffer a considerable downfield shift. But the actual position of such protons may also be influenced by other factors.[25] In certain cases, it may be possible that a ring current effect and other factors can compensate such a downfield shift, and as a result these protons may resonate at a higher magnetic field also. Moreover the presence of the Sn—Cl bond may influence the position of the aromatic proton resonances. Hence, it may not be possible to conclude in a definite manner about the extent of chelation from such a downfield shift of the 2-H proton only. In chloro oxinate complexes H_α, H_β and H_c protons are less shielded compared to bis- or trisoxinate complexes which may be due to Sn—Cl bond and other steric factors.

In $(CH_3CO_2CH_2CH_2)_2Sn$(5,7-dichloro oxine)$_2$ shielding of H_α, H_β and H_c protons is observed and the shielding of the α-methylene proton is maximum. The ring protons at the 3- and 6-positions appear as two separate signals at 7.52 and 7.70 ppm, respectively, while the protons at the 2- and 4-positions are shielded by 9.10 and 8.54 ppm as expected.

In β-alkoxycarbonyl 5,7-dibromo oxinates H_α, H_β and H_c protons are also shielded. Like oxinates, the α-methylene proton is shielded most, except in $CH_3CO_2CH(CH_3)CH_2Sn$ (5,7-dibromo oxine)$_2$Cl, where the methoxy proton is shielded most. In $CH_3CO_2CH_2CH_2Sn$(5,7-dibromo oxine)$_2$Cl and $CH_3CO_2CH(CH_3)CH_2Sn$(5,7-dibromo oxine)$_2$Cl the greater shielding of the H_α, H_β and H_c protons than that of similar oxine complexes may possibly be due to the higher donor capacity of 5,7-dibromo oxine compared to oxine.

The chemical shifts observed for the aromatic ring protons in substituted oxine complexes are consistent with the shifts reported earlier.[26–28] The electron donation to tin on coordination has produced a deshielding of the ligand protons at the 2-position and, in some cases, at the 4-position also, the magnitude of which appears to be influenced by the inductive effect of the alkyl groups. The downfield shift of these protons may be attributed to a strong interaction between tin and nitrogen. The behaviour of the 2-H proton can be explained by the paramagnetic anisotropic effect of the Sn—N bond of substituted oxine ligands and to an intramolecular electric field, and that of the 4-H proton by the latter effect.[29] The deshielding of the 6-H proton of substituted oxine complexes possibly indicates a reduced electron density at C-6. This can arise from electron movement towards the metal through a $d\pi$–

---

* $\underset{H_c\,H_\beta\,H_\alpha}{CH_3OCOCH_2CH_2}$, $\underset{H_c\,H_\beta\,H_\alpha}{CH_3CH_2CH_2CH_2OCOCH_2CH_2}$, $\underset{H_c\,H_\beta\,H_\alpha}{CH_3OCOCH(CH_3)CH_2}$.

$p\pi$ overlap between the metal and the oxygen atom.[30]

The PMR spectra of the complexes

$CH_3CO_2CH_2CH_2Sn(oxine)_2(SCN)$,

$CH_3CO_2CH_2CH_2Sn(oxine)_3$,

$C_4H_9CO_2CH_2CH_2Sn(oxine)_3$,

$CH_3CO_2CH_2CH_2Sn(5,7\text{-dibromo oxine})_2Cl$,

$CH_3CO_2CH(CH_3)CH_2Sn(5,7\text{-dibromo oxine})_2Cl$

and

$C_4H_9CO_2CH_2CH_2Sn(5,7\text{-dibromo oxine})_3$

possibly indicate the presence of geometrical isomers which require further careful investigation for confirmation.

Acknowledgements—One of us (B.K.D.) thanks the University of North Bengal for the award of a J.R.F. We gratefully acknowledge Dr R. E. Hutton (AKZO Chemie, U.K., Ltd) for the gift of a few estertin chlorides and reprints of papers. We are grateful to the Central Drug Research Institute, Lucknow, for recording some PMR and electronic spectra.

REFERENCES

1. R. E. Hutton, J. W. Burley and V. Oakes, *J. Organomet. Chem.* 1978, **156**, 369.
2. J. W. Burley, P. Hope, R. E. Hutton and C. J. Groenenboom, *J. Organomet. Chem.* 1979, **170**, 21.
3. R. E. Hutton and V. Oakes, In *Organotin Compounds: New Chemistry and Applications* (Edited by J. J. Zuckerman), Advances in Chemistry, Series 157, Chap. 8. American Chemical Society, Washington, D.C. (1976).
4. D. Lanigan and E. L. Weinberg, In *Organotin Compounds: New Chemistry and Applications* (Edited by J. J. Zuckerman), Advances in Chemistry, Series 157, Chap. 9. American Chemical Society, Washington, D. C. (1976).
5. R. C. Poller, In *Organotin Compounds: New Chemistry and Applications* (Edited by J. J. Zuckerman), Advances in Chemistry, Series 157, Chap. 12. American Chemical Society, Washington, D.C. (1976).
6. B. K. Deb, Ph.D. Thesis, University of North Bengal, India (1983).
7. K. Kawakami and R. Okawara, *J. Organomet. Chem.* 1966, **6**, 249.
8. H. A. Meinema, E. R. Rivarota and J. G. Noltes, *J. Organomet. Chem.* 1969, **17**, 71.
9. L. Roncucci, G. Faraglia and R. Barbieri, *J. Organomet. Chem.* 1966, **6**, 278.
10. K. Kawakami, Y. Kawasaki and R. Okawara, *Bull. Chem. Soc. Jpn* 1967, **40**, 2693.
11. D. Dutta, B. Majee and A. K. Ghosh, *J. Organomet. Chem.* 1975, **84**, 231.
12. V. G. Kumar Das, N. S. Weng and P. J. Smith, *Inorg. Chim. Acta* 1981, **49**, 149.
13. C. D. Barsode, P. Umapathy and D. N. Sen, *J. Indian Chem. Soc.* 1977, **54**, 1172.
14. R. C. Poller, *The Chemistry of Organotin Compounds*, Chaps 11 and 13. Logos, New York (1970). *J. Organomet. Chem.* 1970, **24**, 341.
15. R. Okawara and M. Ohara, In *Organotin Compounds* (Edited by A. K. Sawyer), Vol. 2, p. 253. Marcel Dekker, New York (1973).
16. R. J. Magee and L. Gordon, *Talanta* 1963, **10**, 851.
17. R. G. Charles, H. Freiser, R. Friedel, L. E. Hilliard and W. D. Johnston, *Spectrochim. Acta* 1956, **8**, 1.
18. L. J. Bellamy, *The Infrared Spectra of Complex Molecules*. Chapman & Hall, London (1975).
19. A. Sabatini and I. Bertini, *Inorg. Chem.* 1965, **4**, 959.
20. M. A. Mullins and C. Curran, *Inorg. Chem.* 1968, **7**, 2584.
21. R. C. Poller and J. N. R. Ruddick, *J. Chem. Soc. (A)* 1969, 2273.
22. E. O. Schlemper, *Inorg. Chem.* 1967, **6**, 2012.
23. H. Shindo, *Pharm. Bull.* 1957, **5**, 472.
24. P. G. Harrison and T. J. King, *J. Chem. Soc., Dalton Trans.* 1974, 2298.
25. B. C. Baker and D. T. Sawyer, *Inorg. Chem.* 1969, **8**, 1160.
26. C. D. Barsode, P. Umapathy and D. N. Sen, *J. Indian Chem. Soc.* 1976, **LIII**, 761.
27. H. Diaz and J. P. Nathan, *Spectrochim. Acta* 1969, **25A**, 1547.
28. H. Gershon and M. W. McNeil, *J. Heterocycl. Chem.* 1971, **8**, 129, 821.
29. K. Yoshikane, *Org. Magn. Reson.* 1970, **2**, 165 (*Chem. Abstr.* 1970, **73**, 719039).
30. B. Sen, G. L. White and J. D. Wander, *J. Chem. Soc., Dalton Trans.* 1972, 447.

Polyhedron Vol. 5, No. 3, pp. 871–875, 1986
Printed in Great Britain

0277–5387/86 $3.00 + .00
© 1986 Pergamon Press Ltd

SYNTHESIS AND SPECTROSCOPIC CHARACTERIZATION OF ARSENIC(III), ANTIMONY(III), BISMUTH(III), TIN(II) AND LEAD(II) DITHIOCARBAMATE ADDUCTS

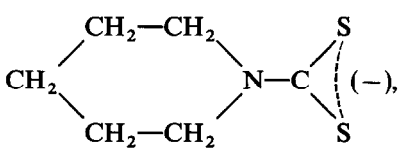
ANTONIO COSTANTINO FABRETTI, ALEARDO GIUSTI, CARLO PRETI, GIUSEPPE TOSI and PAOLO ZANNINI*

Department of Chemistry, University of Modena, Via G. Campi, 183, 41100 Modena, Italy

(*Received* 27 *June* 1985; *accepted* 18 *September* 1985)

Abstract—The complexes of arsenic(III), antimony(III), bismuth(III), tin(II) and lead(II) with monomethylsubstituted piperidinodithiocarbamates of general formula $M(Rdtc)_3$ and $M(Rdtc)_2$ have been prepared and characterized by spectroscopic methods. The results of the spectroscopic studies indicate that the dithiocarbamate ligands are always bidentate, in both the 1 : 3 and the 1 : 2 complexes. All the complexes are nonconducting in DMF solution. The thermal behaviour of the complexes has been investigated by TG and DTG techniques. The molecular weight determinations indicate that the trisdithiocarbamates of arsenic and antimony are monomeric, while the bismuth trisderivatives tend to dimerize: polymeric structures can be suggested for the tin(II) and lead(II) compounds.

As a contribution to the problem of the coordinating behaviour of the heterocycle-containing dithiocarbamate ligands and on the reactivity of their coordination compounds, we report in this study the preparation and characterization of new complexes of arsenic(III), antimony(III), bismuth(III), tin(II) and lead(II) with monomethylsubstituted piperidine dithiocarbamates:



i.e. 2-, 3- or 4-methylpiperidine dithiocarbamate, hereafter abbreviated as 2-Me-, 3-Me- or 4-MePipdtc.

We have previously described complexes of cyclic dithiocarbamates with many *d*- and *p*-block metals:[1–4] furthermore, the reactivity of the complexes obtained towards bidentate nitrogen donor ligands, the mass spectral investigations and the structural characterization by XPS techniques have been investigated and some preliminary results have already been reported.[5–8]

This paper is an extension of our previous research studies on the dithiocarbamates in which dialkyl groups are replaced by heterocycles and, as a further extension, the heterocycle bears aryl or alkyl groups in different positions on the ring.

RESULTS AND DISCUSSION

The complexes obtained, with their analytical data and other physical properties, are reported in Table 1, Table 2 lists the most important IR bands with their assignments, and Table 3 shows the electronic spectral data.

The complexes are micro-crystalline, soluble in benzene, nitrobenzene, *N*,*N*′-dimethylformamide (DMF), carbon tetrachloride and chloroform. Conductance measurements in DMF solution indicate the absence of ionic species in solution and hence the covalent nature of the complexes.

IR spectra

The most important IR peaks of the free ligand sodium salts and of the complexes are reported in Table 2: the spectra of the complexes show the vibrational modes characteristic of the methyl group at the same wavenumbers as in the free ligands.[3]

The band in the 1442–1420-cm^{-1} range is indicative of a considerable double-bond character

* Author to whom correspondence should be addressed.

Table 1. Analytical data

Compound	Colour	% N found (calc.)	% C found (calc.)	% H found (calc.)	% S found (calc.)
As(2-MePipdtc)$_3$	White	7.0 (7.0)	42.1 (42.2)	5.9 (6.1)	32.2 (32.2)
As(3-MePipdtc)$_3$	White	7.0 (7.0)	41.8 (42.2)	6.0 (6.1)	32.2 (32.2)
As(4-MePipdtc)$_3$	White	7.0 (7.0)	42.2 (42.2)	6.1 (6.1)	32.1 (32.2)
Sb(2-MePipdtc)$_3$	Yellow	6.6 (6.5)	39.0 (39.1)	5.6 (5.6)	30.2 (29.8)
Sb(3-MePipdtc)$_3$	Pale yellow	6.5 (6.5)	38.8 (39.1)	5.6 (5.6)	29.7 (29.8)
Sb(4-MePipdtc)$_3$	White	6.5 (6.5)	39.0 (39.1)	5.7 (5.6)	29.8 (29.8)
Bi(2-MePipdtc)$_3$	Yellow	5.7 (5.7)	34.0 (34.5)	4.8 (5.0)	26.0 (26.3)
Bi(3-MePipdtc)$_3$	Yellow	5.6 (5.7)	34.2 (34.5)	4.8 (5.0)	25.9 (26.3)
Bi(4-MePipdtc)$_3$	Pale yellow	5.8 (5.7)	34.3 (34.5)	5.0 (5.0)	26.3 (26.3)
Sn(2-MePipdtc)$_2 \cdot 2H_2O$	Dark yellow	5.7 (5.6)	33.6 (33.4)	5.6 (5.6)	25.3 (25.5)
Sn(3-MePipdtc)$_2 \cdot 2H_2O$	Orange-yellow	5.6 (5.6)	33.4 (33.4)	5.7 (5.6)	24.9 (25.5)
Sn(4-MePipdtc)$_2 \cdot 2H_2O$	Pink-yellow	5.6 (5.6)	33.4 (33.4)	5.7 (5.6)	25.2 (25.5)
Pb(2-MePipdtc)$_2$	Light yellow	4.9 (5.0)	30.2 (30.2)	4.3 (4.4)	22.9 (23.1)
Pb(3-MePipdtc)$_2$	White	4.9 (5.0)	30.0 (30.2)	4.2 (4.4)	22.9 (23.1)
Pb(4-MePipdtc)$_2$	White	5.0 (5.0)	29.8 (30.2)	4.3 (4.4)	23.0 (23.1)

in the carbon–nitrogen bond: this fact could be explained by taking into account the electron-releasing ability of the heterocyclic group bearing a methyl substituent, which forces the electron density towards the sulphur atoms, thus producing a greater double-bond character in the CN bond, which, as a consequence, is shifted to higher energies. In the metal dithiocarbamates here reported the bands assigned to ν(C$\overset{+}{-}$N) in the above reported range lie between the stretching frequencies of ν(CN) and ν(C=N), in the ranges 1350–1250 and 1690–1640 cm^{-1}, respectively. The blue shift of the ν(C$\overset{+}{-}$N) depends on the nature of the central atom and moves to higher frequencies in the orders Sn > Pb and As > Sb > Bi, respectively, for the 1:2 and 1:3 complexes. As regards the influence of the position of the methyl group on the piperidine ring, the ν(C$\overset{+}{-}$N) values increases in the order 2-MePipdtc < 3-MePipdtc < 4-MePipdtc.

The band observed at 950–933 cm^{-1} has been

Table 2. Most important IR bands (cm^{-1})

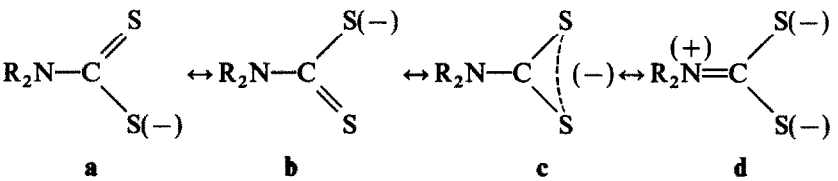
Compound	ν(CN)	ν(CS)	ν(CS) + δ(NCS)	ν(M—S)
2-MePipdtcNa $\cdot$ 2.5H_2O	1407vs	943s	532ms	—
3-MePipdtcNa $\cdot$ 2.5H_2O	1418vs	951s	530ms	—
4-MePipdtcNa $\cdot$ 2.5H_2O	1424vs	950s	522ms	—
As(2-MePipdtc)$_3$	1430vs	933m	538m	348s, 309m, 233m
As(3-MePipdtc)$_3$	1432vs	948ms	537m	361s, 286m, 239m
As(4-MePipdtc)$_3$	1442vs	950m	526m	350s, 296m, 216ms
Sb(2-MePipdtc)$_3$	1428vs	934m	536ms	338m, 305m, 234m
Sb(3-MePipdtc)$_3$	1432vs	945ms	540m	344vs, 283s, 233m
Sb(4-MePipdtc)$_3$	1440vs	948s	530s	318vs, 277s, 220m
Bi(2-MePipdtc)$_3$	1423vs	934m	536m	326m, 302m, 239m
Bi(3-MePipdtc)$_3$	1433vs	947s	537m	335s, 286s, 231m
Bi(4-MePipdtc)$_3$	1440vs	948s	528s	332s, 281m, 208m
Sn(2-MePipdtc)$_2 \cdot 2H_2O$	1436vs	938m	535ms	339m
Sn(3-MePipdtc)$_2 \cdot 2H_2O$	1442vs	945ms	546m	342m
Sn(4-MePipdtc)$_2 \cdot 2H_2O$	1445vs	947ms	529m	331vs
Pb(2-MePipdtc)$_2$	1420vs	934ms	536ms	320s
Pb(3-MePipdtc)$_2$	1428vs	947s	536m	334vs
Pb(4-MePipdtc)$_2$	1436vs	949s	526m	318vs

Table 3. Solid-state electronic spectra (cm^{-1})

Compound	Band I	Band II	Band III
As(2-MePipdtc)$_3$	38,460	32,260sh	28,170
As(3-MePipdtc)$_3$	38,460	32,785sh	28,570
As(4-MePipdtc)$_3$	38,460	32,785sh	28,570
Sb(2-MePipdtc)$_3$	38,460	31,745sh	27,400
Sb(3-MePipdtc)$_3$	37,740	31,250sh	27,400
Sb(4-MePipdtc)$_3$	38,760	32,260sh	28,570
Bi(2-MePipdtc)$_3$	38,150	30,300sh	27,030
Bi(3-MePipdtc)$_3$	37,735	30,300sh	27,400
Bi(4-MePipdtc)$_3$	36,760	30,300sh	27,400
Sn(2-MePipdtc)$_2 \cdot 2H_2O$	38,460	34,480sh	28,980
Sn(3-MePipdtc)$_2 \cdot 2H_2O$	38,460	33,330sh	28,980
Sn(4-MePipdtc)$_2 \cdot 2H_2O$	38,460	33,330sh	29,410
Pb(2-MePipdtc)$_2$	37,450	32,260sh	28,170
Pb(3-MePipdtc)$_2$	36,765	31,250sh	28,570
Pb(4-MePipdtc)$_2$	37,040	31,545sh	28,985

associated with the stretching vibration of the carbon–sulphur bond and indicates that the dithioligands act in a bidentate way: in fact, only one strong or medium-strong band is present, whereas a doublet is expected in the 1000 ± 70 cm^{-1} region in the case of monodentate coordination.[9–11] The analysis of the position of the $\nu(C{=}N)$ mode gives further confirmation of such behaviour: this band, in fact, undergoes blue shifts in all the complexes, while for unidentate coordination the frequency of this stretching would undergo downward shifts or remain unchanged at the same value as for the free sodium dithiocarbamate salt.[12]

By comparing the stretching values of the carbon–nitrogen bond with those of the previously reported complexes with piperidine dithiocarbamate, we observe that the upward shift of $\nu(C{=}N)$ on passing from the sodium salts to their metal complexes is higher in the case of dithiocarbamate ligands bearing a methyl group on the piperidine ring. This behaviour may be explained by taking into account the inductive effect of the methyl group which causes an increase in the carbon–nitrogen bond order. In fact the structure of the dithioligands can be represented by the formalism:

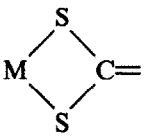


a **b** **c** **d**

and the dithiocarbamate group can behave as a monodentate ligand in the resonance forms **a** and **b**, and as a bidentate S,S′-donor ligand in forms **c** and **d**, giving rise to complexes in which both the sulphur atoms behave as electron donors to the metal ion, thus forming a four-membered chelate ring.

From the above mentioned IR data we can conclude that structure **d** contributes more in the case of the methyl derivatives than in the case of the non-substituted piperidine dithiocarbamates.

The vibrational modes present between 546 and 526 cm^{-1} can be ascribed to the contribution of $\nu(CS) + \delta(SCS)$ and to



ring deformation as previously shown by a detailed IR isotopic study on nickel(II) and copper(II) dithiocarbamates.[2]

In all the hydrated complexes (Table 1) medium-strong bands are present at 3450 cm^{-1} and in the 1640–1630-cm^{-1} range, which are clearly due to $\nu(OH)$ and $\delta(HOH)$, respectively: the absence of the vibrational modes activated by the coordination to the metal (wagging, twisting and rocking) suggests that coordinated water is not present and these results are confirmed by thermogravimetric studies (see below).

In the far-IR region the bands of the ligands are unchanged in the spectra of the complexes: in

addition, new bands, absent in the spectra of the starting materials, are observed in the 361–216-cm^{-1} range. For the 1:3 derivatives the band between 361 and 318 cm^{-1} is due largely to M—S bond stretching, while the two further absorptions in the 309–216-cm^{-1} range could be due to complex normal modes involving both metal–sulphur bond stretching and ring deformation modes. In the 1:2 derivatives the ν(M—S) vibrations are located at 342–331 and 334–318 cm^{-1} for tin(II) and lead(II) complexes, respectively.[13,14]

Electronic spectral studies

The solid-state electronic spectra are given in Table 3: all the complexes show three absorption bands due to the chromophore group NCS_2[15] (these absorptions are indicated as band I, band II and band III).

Band I is assigned to an intramolecular charge transfer in the ligand, i.e. a $\pi^* \leftarrow \pi$ transition located mainly in the N⇢C⇢S group.[16,17] The position of this band is slightly affected by the nature of the central atom, the sequence following the orders As > Sb > Bi and Sn > Pb, in agreement with the electronegativities of the elements.

Band II is also attributed to a $\pi^* \leftarrow \pi$ transition of the S⇢C⇢S group:[18] this band is present as a shoulder and this fact clearly indicates the equivalence of the C⇢S bonds in the complexes. As regards the different metals, the same trend as for the band I is observed.

Band III is a low-intensity band and may be assigned either to a $\pi^* \leftarrow n$ electronic transition located on the sulphur atom or to a charge transfer from ligand to metal.[19–21] The frequency of band III decreases, as already observed for bands I and II, from arsenic to bismuth.

Molecular-weight determinations

The molecular-weight determinations of the complexes show that the arsenic(III) and antimony(III) derivatives are monomeric in nitrobenzene solution, the bismuth complexes show a tendency to dimerize, while polymeric structures could be suggested for the tin(II) and lead(II) dithiocarbamates. By comparing the results obtained for the piperidine dithiocarbamate bismuth complex previously reported, which was monomeric, this tendency of bismuth to dimerize could be explained taking into account the more pronounced π-back donation associated with the lower electron density on the bismuth atom and with the decreased basicity of the amine.

Thermogravimetric studies

The thermogravimetric studies were performed by means of TG and DTG techniques.

The arsenic(III) derivatives were stable up to 200°C, then undergo decomposition and very likely are transformed into As_2O_3 around 350°C. The crucible is completely empty by the time that the temperature reaches 600°C.

The antimony(III) complexes decompose very rapidly in the 200–275°C range: a small loss is observed between 275 and 550°C and the resulting compound, Sb_2O_3 (calc. 23.8%, found 24.1%), is stable up to 950°C. No transformation into Sb_2O_4 is observed.

The bismuth(III) derivatives rapidly decompose in the 200–250°C range, then continuous weight loss is detected up to 950°C: at this temperature yellow Bi_2O_3 is formed (calc. 31.8%, found 31.9%).

As for the tin(II) derivatives, after the loss of two water molecules in the 35–150°C range, the dithiocarbamates are transformed into a polysulphide of type Sn_xS_y, which, above 950°C, gives SnO_2 as the end product.

The lead dithiocarbamates decompose at 300°C rapidly, then slowly up to 440°C. From this temperature gain in weight is observed up to 750°C, probably due to a formation of mixed oxides. Above this temperature a weight loss occurs leading to PbO (calc. 40.2%, found 40.5%).

EXPERIMENTAL

Preparation of the ligands

The sodium salts of the ligands were prepared by reaction of 2-methyl-, 3-methyl- or 4-methylpiperidine (reagent grade) in dry ethyl ether with carbon disulphide and adding NaOH under vigorous stirring over a 5-h period. The molar ratio amine:CS_2:NaOH = 1:1:1: the crude products were recrystallized from isopropyl alcohol.

Analyses. Found for 2-MePipdtcNa·$2.5H_2O$: C, 34.4; H, 7.0; N, 5.8; S, 26.2%; 3-MePipdtcNa·$2.5H_2O$: C, 34.1; H, 7.1; N, 5.7; S, 26.0%; 4-MePipdtcNa·$2.5H_2O$: C, 34.9; H, 7.0; N, 5.9; S, 26.3%. Calc. for $C_7H_{12}NS_2Na \cdot 2.5H_2O$: C, 34.7; H, 7.1; N, 5.8; S, 26.5%.

Preparation of the complexes

Commercial arsenic, antimony and bismuth trichloride, tin dichloride and lead nitrate of high-purity grade were used. For the preparation of the 1:3 derivatives the metal halide in acetone or

dichloromethane and methanol solution was treated with the ligands dissolved in acetone in a 1:3 stoichiometrical ratio. The lead compounds were obtained by reaction of the corresponding dithiocarbamates in the 1:2 molar ratio in aqueous or ethanol solution. The tin(II) derivatives have been prepared by adding dropwise a solution of $SnCl_2$ in absolute ethanol to an ethanolic solution of the dithiocarbamates with continued stirring. The precipitates were filtered, washed with acetone, dry ethyl ether and dried *in vacuo* over P_4O_{10}. Repeated syntheses and elemental analyses gave reproducible results.

IR measurements

The IR spectra were recorded in the 4000–50-cm^{-1} region with a Perkin–Elmer 180 spectrophotometer of the Instruments Centre of Modena University. The spectra in the 4000–400-cm^{-1} region were measured as KBr discs or Nujol mulls. Far-IR spectra were measured on Nujol mulls supported between polyethylene sheets. Atmospheric water was removed from the spectrophotometer housing by flushing with dry nitrogen.

Electronic spectra

The electronic spectra have been recorded with a Shimadzu MPS-50L spectrophotometer in the solid state in the 5000–45,000-cm^{-1} range, the method of Dyer *et al.*[22] being used.

Molecular-weight determinations

The molecular weights were determined in nitrobenzene RP, treated with magnesium sulphate, by the cryoscopic method.

Thermal analyses

Thermogravimetric analyses (TG and DTG) were performed in air on a Mettler TG50 thermobalance equipped with a Mettler TC10TA processor. A scan rate of 10°C min^{-1} was used.

Conductivity measurements

These measurements were carried out with a WTW LBR type conductivity bridge for freshly prepared 10^{-3} M solutions in DMF at 25±0.1°C.

Analyses

Carbon, nitrogen, hydrogen and sulphur were determined using a Carlo Erba 1106 elemental analyzer.

Acknowledgements—We thank Mr G. Pistoni for elemental analyses, the Instruments Centre of Modena University for the availability of the use of the Perkin–Elmer 180 spectrometer and the Consiglio Nazionale delle Ricerche of Italy for financial support.

REFERENCES

1. A. C. Fabretti, F. Forghieri, A. Giusti, C. Preti and G. Tosi, *Inorg. Chim. Acta* 1984, **86**, 127 (and references therein).
2. H. O. Desseyn, A. C. Fabretti, F. Forghieri and C. Preti, *Spectrochim. Acta* 1985, **41A**, 1105.
3. G. C. Franchini, A. Giusti, C. Preti, L. Tassi and P. Zannini, *Polyhedron* 1985, **4**, 1553.
4. A. C. Fabretti, G. C. Franchini, C. Preti, G. Tosi and P. Zannini, *Transition Met. Chem.* 1985, **10**, 284.
5. A. Benedetti, C. Preti and G. Tosi, *J. Mol. Struct.* 1983, **98**, 155.
6. A. Benedetti, C. Preti, L. Tassi, G. Tosi and P. Zannini, *J. Mol. Struct.* 1985, **129**, 107.
7. C. Furlani, G. Polzonetti, C. Preti and G. Tosi, *Inorg. Chim. Acta* 1983, **73**, 105.
8. C. Furlani, G. Polzonetti, C. Preti and G. Tosi, *Gazz. Chim. It.* 1983, **113**, 609.
9. F. Bonati and R. Ugo, *J. Organomet. Chem.* 1967, **10**, 257.
10. T. N. Srivastava and V. Kumar, *J. Organomet. Chem.* 1976, **107**, 55.
11. G. St. Nikolov, N. Jordanov and K. Daskalova, *Inorg. Nucl. Chem. Lett.* 1970, **6**, 723.
12. C. O'Connor, J. D. Gilbert and G. Wilkinson, *J. Chem. Soc. (A)* 1969, 84.
13. C. Preti, G. Tosi and P. Zannini, *J. Mol. Struct.* 1979, **53**, 35.
14. C. Preti, G. Tosi and P. Zannini, *J. Mol. Struct.* 1980, **65**, 283 (and references therein).
15. C. K. Jorgensen, *Inorganic Complexes.* Academic Press, London (1963).
16. C. K. Jorgensen, *J. Inorg. Nucl. Chem.* 1962, **24**, 1571.
17. F. Takami, S. Wakahara and T. Maeda, *Tetrahedron Lett.* 1971, 2645.
18. M. J. Janssen, *Recl Trav. Chim. Pays-Bas* 1960, **79**, 1066.
19. D. C. Bradley and M. H. Gitlitz, *J. Chem. Soc. (A)* 1969, 1152.
20. M. J. Janssen, *Recl Trav. Chim. Pays-Bas* 1960, **79**, 454.
21. M. L. Shankaranarayana and C. C. Patel, *Acta Chem. Scand.* 1965, **19**, 1113.
22. G. Dyer, J. C. Hartley and L. M. Venanzi, *J. Chem. Soc. (A)* 1965, 1293.

Polyhedron Vol. 5, No. 3, pp. 877–882, 1986
Printed in Great Britain

0277-5387/86 $3.00 + .00
© 1986 Pergamon Press Ltd

COMPLEXES OF DIBENZO-24-CROWN-8 WITH SOME SODIUM MONOALKYL BENZENEAZOPHOSPHONATES

LJ. TUŠEK-BOŽIĆ* and D. SEVDIĆ

Department of Physical Chemistry, Institute Rudjer Bošković, Zagreb, Yugoslavia

(*Received* 8 *August* 1985; *accepted* 20 *September* 1985)

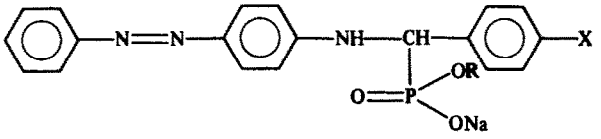
Abstract—Syntheses and properties of complexes of dibenzo-24-crown-8 with the sodium monoethyl ester and the sodium monobutyl ester of [α-(4-benzeneazoanilino)-*N*-benzyl]phosphonic acid, [α-(4-benzeneazoanilino)-*N*-4-hydroxybenzyl]phosphonic acid and [α-(4-benzeneazoanilino)-*N*-4-methoxybenzyl]phosphonic acid have been studied. The crystalline complexes formed were found to depend not only on the size of the cation and the crown ether cavity but also on the choice of anion and the reaction solvent. It was shown that the molecular structure and electronic configuration of the anion are important factors in a salt–ligand system which influence the ease of solubilization and charge separation in solution. The complexes obtained were characterized on the basis of conductance measurements and UV, IR and ^{1}H NMR spectra.

Crown ethers are of considerable importance because of their ability to form complexes with alkali and other metal cations. This complexation process permits solvation of the ionic salts in non-aqueous solvents, a phenomenon frequently utilized in phase-transfer catalytic systems.[1,2] In addition, crown ethers can also serve as good model systems for biochemical and biological membrane transport agents, such as the macrocyclic antibiotics.[3] The mechanism of these species in complexing ions is similar to that of the crown ethers.[4] The effectiveness of crown ethers as potential phase-transfer reagents and catalysts is determined by the degree of lipophilicity they possess and by the stability of the complexes they form.

The widespread use of crown ethers requires that the details of crown ether complexation be investigated. While a good deal of effort has been directed towards complexes with simple alkali metal salts (i.e. halide, thiocyanate and perchlorate), less attention has been directed towards complexes with the salts of chelating organic anions. The chelating anions mostly used were those derived from 8-hydroxyquinoline, 1-nitroso-2-naphtol, nitrophenols and amino-, hydroxy- or nitrobenzoic acids.[5–9] Salts of organic anions have often been investigated because of their relevance to natural systems.

In our earlier papers we studied some alkali picrate and tetraphenylborate complexes with various crown ethers.[8,10–12] The synthesis and characterization of the crystalline complexes,[8] the association equilibria between the alkali cations and the crown ethers,[10] as well as the ion-pair formation between the crown ether–cation complexes and different anions in nonaqueous media,[11,12] were reported. As an extension of these investigations, the complexes of some sodium monoalkyl benzeneazophosphonates have recently been studied.[13] In this paper we describe the preparation and properties of new complexes between the crown ether dibenzo-24-crown-8 (DB24C8) and sodium salts of monoalkyl esters of some benzeneazophosphonic acids (NaA_1–NaA_6). The influences of the size

* Author to whom correspondence should be addressed.



Salt	R	X
NaA_1	Et	H
NaA_2	*n*-Bu	H
NaA_3	Et	OH
NaA_4	*n*-Bu	OH
NaA_5	Et	OMe
NaA_6	*n*-Bu	OMe

of the hole in the crown ether and the diameter of the metal cation, the size and charge density of the anion, as well as the solvent used, on the formation of salt complexes have been investigated and discussed.

EXPERIMENTAL

Starting materials

DB24C8 (systematic name 6,7,9,10,12,13,20,21,23,24,26,27-dodecahydrodibenzo[b,n][1,4,7,10,13,16,19,22]octaoxacyclotetracosin), prepared as previously described,[14] was purified by repeated recrystallization from methanol. Sodium salts of the monoethyl and monobutyl esters of [α-(4-benzeneazoanilino)-*N*-benzyl]phosphonic acid (NaA_1 and NaA_2), [α-(4-benzeneazoanilino)-*N*-4-hydroxybenzyl]phosphonic acid (NaA_3 and NaA_4) and [α-(4-benzeneazoanilino)-*N*-4-methoxybenzyl]phosphonic acid (NaA_5 and NaA_6) were prepared by the methods reported earlier,[15,16] recrystallized twice from absolute ethanol and dried *in vacuo* at approximately 60°C for several hours.

Analytical-grade solvents were used throughout the preparation of the salt complexes. For conductivity measurements, methanol was purified by the method published in Ref. 17.

Preparation of complexes

General procedure. An equimolar amount of crown ether and sodium salt of monoalkyl esters of benzeneazophosphonic acids (NaA_1–NaA_6) was refluxed together in ethanol or acetonitrile to give a clear solution, which was filtered hot and set aside to crystallize at room temperature. Complexes of sodium monoethyl benzeneazophosphonates were gradually formed by removal of solvent. The precipitate was filtered off, washed with a small amount of cold reaction solvent, and dried. The filtrate was again subjected to crystallization or evaporation to dryness to ascertain the presence of any second new product. Complexes of sodium monobutyl benzeneazophosphonates were obtained as syrups after the whole of the solvent was driven off, which solidified slowly on standing. The homogeneity of the crystals was ascertained under the microscope. All complexes obtained were dried under high vacuum at ambient temperature without decomposition, giving stable anhydrous complexes.

We attempted the synthesis of all complexes in methanol, ethanol and acetonitrile solutions. Complexes of sodium salts NaA_1–NaA_4 were isolated from ethanol, while those of sodium salts NaA_5 and NaA_6 precipitated only from acetonitrile solutions. From methanol solutions free crown ether was gradually precipitated, and no complex could be isolated.

Physical measurements and analysis

IR spectra were recorded on KBr pellets and Nujol mulls in the region 4000–200 cm^{-1} using a Perkin–Elmer 580 B spectrophotometer. ^1H NMR spectra were determined on a JEOL FX90Q Fourier Transform NMR spectrometer in $CDCl_3$ solutions with TMS as the internal standard. UV spectra were obtained in methanolic solutions with a Perkin–Elmer 124 model spectrophotometer. Thermogravimetric measurements were performed with a Cahn RG electromicro balance applying a heating rate of 2° min^{-1} in an atmosphere of static air. Melting points were recorded using a hot-stage microscopy and are uncorrected. Conductivity measurements were performed in methanol using a CD 7A Tacussel conductivity bridge. The solutions were thermostated at 25 ± 0.02°C by a double water bath and stirred by means of a magnetic stirrer. The procedure of measuring and calculation of equivalent limiting conductivity and ion-pair association constants of the sodium salt complexes was the same as described elsewhere.[12] The conductance data were analyzed by the Fuoss–Onsager theory in the usual form,[18] through an iterative machine calculation procedure using the expanded form of Fuoss–Hsia conductance equation.

Chemical analyses were performed in the Microanalytical Laboratory of the Rudjer Bošković Institute.

RESULTS AND DISCUSSION

The physical properties and the results of the elemental analysis of the novel complexes, as well as the conductance data, are given in Table 1. The well-defined 1 : 1 (metal : crown) salt complexes are yellow or orange solids. Some of them are hygroscopic compounds, as well as are the free sodium salts, but after drying *in vacuo* they were obtained in an anhydrous form, as was confirmed by elemental and thermogravimetric analyses, and spectral data.

The dimensions of the crown ether hole and the metal ion basically control the stoichiometry of the complex and the lattice position of the metal ion with respect to the crown ether hole. This relationship holds best for the smaller, relatively rigid ligand

Table 1. Analytical results and some physical properties of the novel complexes

Complex	Reaction solvent	M.p. (°C)	Analytical data (%)[a] C	H	N	P	Na	Limiting conductance[bc] (Ω^{-1} cm^2 mol^{-1})
Na(DB24C8)A_1	Ethanol	94–96	62.2 (62.4)	6.2 (6.2)	5.0 (4.9)	3.7 (3.6)	2.6 (2.7)	72.4 (97.7)
Na(DB24C8)A_2	Ethanol	90–91	63.3 (63.1)	6.3 (6.4)	4.6 (4.7)	3.2 (3.5)	2.4 (2.6)	69.9 (91.6)
Na(DB24C8)A_3	Ethanol	97–98	61.1 (61.3)	6.1 (6.1)	4.6 (4.8)	3.7 (3.5)	2.5 (2.6)	70.2 (96.4)
Na(DB24C8)A_4	Ethanol	94–95	61.7 (62.0)	6.5 (6.3)	4.5 (4.6)	3.6 (3.4)	2.5 (2.5)	68.9 (90.8)
Na(DB24C8)A_5	Acetonitrile	91–93	61.5 (61.6)	6.2 (6.2)	4.7 (4.7)	3.3 (3.5)	2.4 (2.6)	68.8 (95.6)
Na(DB24C8)A_6	Acetonitrile	89–90	62.1 (62.4)	6.5 (6.4)	4.7 (4.5)	3.5 (3.3)	2.6 (2.5)	67.6 (89.9)

[a] Required values are given in parentheses.
[b] In methanol at 25°C.
[c] Data for the free salts NaA_1–NaA_6 are given in parentheses.

molecules. A larger and more flexible crown ether can fold to produce smaller cavities and then bind smaller cations. The formation of complexes between DB24C8 (hole diameter about 4.7 Å) and sodium salts (cationic diameter 1.94 Å) is a good example of this property. A stable complex may be formed if a change in conformation can occur to give one in which the spatial distribution of the oxygen atoms can establish interactions with the cation. Whether this can occur depends largely on the balance between the increase in the free energy on forming ion–dipole bonds with the cation and the energy required by the ligand to achieve an ideal conformation for complexation. Previous studies with DB24C8 have shown that sodium salts may react to give 1:1 and 2:1 complexes, respectively, regardless of the nature of the anion.[5,8,19,20] For example, while the complex with sodium thiocyanate is a bimetallic complex, where the nitrogen atoms of the anions bridge two sodium ions,[5] in sodium picrate and tetraphenylborate complexes it is unlikely that the related anions can take part in this type of bonding, and only 1:1 complexes were obtained.[8,19]

Sodium salts of monoalkyl benzeneazophosphonates produce 1:1 complexes with DB24C8 from a 1:1 as well as a 2:1 reaction mixture, regardless of the anion used. The stoichiometry of the complexes was also conductometrically confirmed. The very low melting points of the complexes obtained, as against the high melting points of the free sodium salts (above 220°C), indicate that the charge of the sodium ion in the complexes is extensively delocalized. Some degree of charge transfer between the sodium ion and anion can take place, increasing the stability of the complex. Although conductance data and some spectral evidences (see later) confirmed that all sodium salts form complexes in alcoholic solutions, they cannot always be isolated in the solid state. Generally, it was shown that the failure to isolate the metal salt complexes can be attributed either to the strong M^+A^- ion association as a consequence of which M^+ fails to cause the necessary polarization of the crown ether molecule (acetonitrile solutions), or to the strong hydrogen bonding between the anion or cation and the media of synthesis (alcoholic solutions). The isolation possibility of a complex is not necessarily related to its solution stability. Differences which were observed in the preparation of complexes of sodium monoalkyl benzeneazophosphonates can be attributed to the different solubilities of sodium salts in the solvent of reaction. The very low solubility of sodium salts NaA_1–NaA_4 in acetonitrile may contribute to our failure to isolate their complexes from acetonitrile solutions.

For a better understanding of the interaction forces which act in solution between the cation–crown complexes formed and the surrounding solvent molecules, a systematic conductometric study of crown ether complexes has been undertaken in methanol at 25°C. The equivalent conductance dependence on the concentration of complexes with sodium salts of monoethyl esters is shown in Fig. 1. which plots equivalent conductance as a function of (concentration)$^{1/2}$. The values of the equivalent conductance at infinite dilution (Λ_o) of the complexes are compared with those obtained for the free sodium

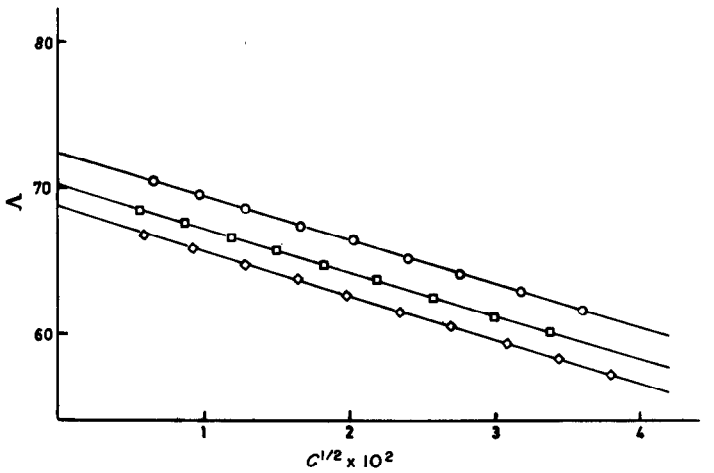


Fig. 1. Equivalent conductance [Λ (Ω^{-1} cm^2 mol^{-1})] vs (concentration)$^{1/2}$ {$C^{1/2}$ [(mol l^{-1})$^{1/2}$]} plots of complexes: (○) Na(DB24C8)A_1, (□) Na(DB24C8)A_3 and (◇) Na(DB24C8)A_5.

salts,[13] and the results obtained are summarized in Table 1. The great differences between the Λ_o values of the free sodium salts and their sodium salt complexes can be explained by assuming that the crown ether complexation considerably increases the size of the cation and that the structure of the complex is such that a few solvent molecules can remain associated with the cation. Undoubtedly, the sodium ion is less strongly bonded to the solvent dipoles than to the negatively charged oxygen of the crown ether, with the consequence that the solvodynamic unit of the sodium cation in pure methanol has a smaller size than the complex cation in the presence of the crown compound. With completely dissociated ion-pairs, where the sodium ion is more exposed to the solvent, some additional interaction of the sodium complex with the solvent molecules causes a further decrease in the complex mobility. The gradation in Λ_o values of the complexes reflects the different final size of the solvodynamic ion–crown units.

The conductivity data obtained show no association with ion-pairs for crown ether complexes in pure methanol. Ion-pair separation is favored when more oxygen atoms are available for co-ordinating with the alkali ion and when the polyether ring is large enough to accommodate the cation. In this case the positive charge of the cation is strongly shifted and there is no appreciable formation of ion-pairs with the anion. This assumption corroborates the results obtained for the conductance of sodium picrate complexes of DB24C8 and some crown ethers with an 18-membered polyether ring.[11,13,21]

Spectral studies

UV spectra. The UV spectra of the complexes dissolved in methanol indicate metal–crown ether interaction. DB24C8 has, in methanol, a characteristic absorption at 276 nm. Upon complex formation distinctive changes in this peak may be noticed if alkali salts themselves do not absorb too strongly in the region of 270–290 nm.[22] In the spectra of complexes of sodium monoalkyl benzeneazophosphonates a slight hypsochromic shift, and the appearance of a new peak in some cases not clearly separated from the main one at about 280 nm, can be attributed to complex formation (see Table 2). It is evident that interactions between crown ether and sodium salts can take place in solution even when it is not possible to isolate the complex in crystalline form.

Sodium salts give an absorption maximum at 397 nm (log ε = 4.45) which corresponds to conjugation of the azo group with aromatic rings (π–π^* transition). It remains unchanged upon complex formation, suggesting that there is no co-ordinated ionic benzeneazophosphonato group.[13]

IR spectra. IR spectra of the crown ether complexes with sodium monoalkyl benzeneazophosphonates are too complex to allow a complete assignment of the absorption bands. However, in every case the spectrum of the solid complex distinctively differed from that of the physical mixture of the constituents. Generally, the greatest changes may be noticed in the region 1260–900 cm^{-1}, where bands arising from various modes of vibration of ether and methylene groups are present. Since all sodium salts alone give a series of complex bands between 1165 and 1240 cm^{-1}, characteristic of asymmetric PO_2^- stretching, and very strong and broad bands between 1070 and 1110 cm^{-1}, characteristic of the symmetric stretching of the ionized PO_2^- group, as well as medium or strong absorption bands around 1150 cm^{-1} due to the C—O—(P) part of the P—O—C bond,[16,23,24] it is

Table 2. Selected UV, IR and ^{1}H NMR data for DB24C8[a] and its sodium salt complexes

Compound	UV (nm)[b] λ_{max} (log ε)	IR (cm^{-1})[c] ω, $\tau(CH_2)$	^{1}H NMR [δ (ppm)][d] H_1	H_2	H_3	$H_{arom.}$
DB24C8	276 (3.64)	960s, 938m, 922s	4.16	3.89	3.83	6.88
Na(DB24C8)A_1	270 (4.07), 280sh (3.96)	945s, 925m	4.13	3.80	3.71	6.87
Na(DB24C8)A_2	271 (4.10), 281sh (3.95)	939m, 923m	4.12	3.82	3.72	6.88
Na(DB24C8)A_3	271 (4.12), 281 (4.02)	939m, 918sh	4.02	3.61	3.49	6.84
Na(DB24C8)A_4	271 (4.15), 280sh (4.01)	940m, 924m	4.04	3.59	3.49	6.85
Na(DB24C8)A_5	270 (4.21), 280 (3.99)	940m, 920sh	4.13	3.80	3.71	6.87
Na(DB24C8)A_6	271 (4.18), 280sh (4.01)	938m, 915w	4.12	3.81	3.70	6.88

[a] Results included for the sake of comparison.
[b] In methanol—270–290-nm region.
[c] KBr pellets. Abbreviations: s, strong; m, medium; w, weak; br, broad.
[d] In $CDCl_3$ relative to TMS. Protons are designated by the number of the carbon to which they are attached (see Fig. 2).

impossible to determine the exact position of the bands assigned to the ether groups. Considerable changes may, however, be noticed in the 1000–900-cm^{-1} region, which contains bands attributed to wagging, twisting and rocking modes of vibration of the methylene groups. While free DB24C8 has two strong bands at 958 and 920 cm^{-1}, and a medium one at 936 cm^{-1} associated with these vibrations, the complexes are characterized by a strong or medium band around 940 cm^{-1} and a medium or weak band around 920 cm^{-1} (Table 2). Less restriction on the coupling of these vibrational modes in the salt complexes is probably due to some bonding between the oxygen atoms of the crown ether ring and the sodium ion.

^{1}H NMR spectra. The proton chemical shifts of DB24C8 and its sodium salt complexes are summarized in Table 2. The resonances of the anion protons are omitted.[13] Free crown ether has three sets of resonant signals at about $\delta = 4.16$ ppm for methylene protons of the polyether ring.[14] The complex spectrum in the ether region can be attributed to the chemically nonequivalent ether fragments (Fig. 2), and the main reason for the separation of the ether resonances is the chemical-shift anisotropy of the benzo groups. Comparison with the spectra of complexes shows chemical-shift differences for all ether protons between complexed and noncomplexed crown ethers. The shift for the aromatic protons remains essentially unchanged on complexation. In the spectra of complexes with sodium salts of nonsubstituted and 4-methoxy-substituted benzeneazophosphonates the so-called "inner" CH_2—O—CH_2 polyether ring protons (H_2 and H_3) are shifted upfield by 7–12 Hz, while the so-called "outer" Ar—O—CH_2 protons (H_1) are shifted upfield only by 3–4 Hz. For the complexes with 4-hydroxy-substituted benzenazophosphonates these chemical shift differences are more visible, so the inner protons are shifted upfield by 26–31 Hz and outer protons by 10–12 Hz, respectively. The close proximity of the crown ether molecule to the aromatic rings of the anion causes a stronger upfield shift of the inner protons and a somewhat lesser one

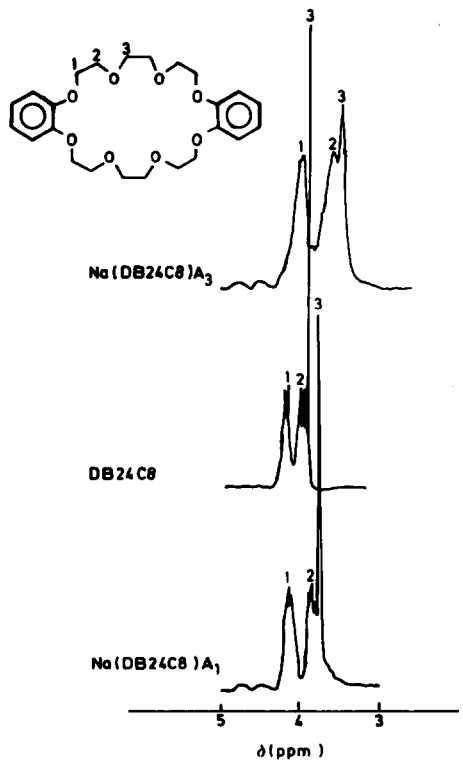


Fig. 2. ^{1}H NMR spectra of the ether region of DB24C8 and two of its complexes in $CDCl_3$. Shifts are relative to TMS.

of the outer protons in spite of the complexation with the sodium cation, which, in itself, would induce a downfield shift due to the increased electronegativity of the oxygen atoms. A similar situation was observed in the spectrum of the sodium tetraphenylborate complex, while the sodium perchlorate and picrate complexes with DB24C8 show a slight upfield shift for the inner protons and a slight downfield shift for the outer protons.[8] Obviously, the anion has an important role in the resulting chemical shift of the polyether ring protons.

In a salt–ligand system the choice of anion is important, as well as the choice of ligand, for the ease of solubilization and the resulting charge separation in solution.

Acknowledgement—We thank the Foundation for Scientific Research of SR Croatia, Zagreb, for financial support.

REFERENCES

1. W. P. Weber and G. W. Gokel, *Phase Transfer Catalysis in Organic Synthesis*. Springer, Berlin (1977). *Compendium of Phase Transfer Reactions and Ion-Pair Extractions*. Fluka, Buchs, Switzerland (1978).
2. R. M. Izatt and J. J. Christensen, *Process In Macrocyclic Chemistry*, Wiley Interscience, New York, Vol. 1 (1981); Vol. 2 (1982).
3. G. Eisenman, S. M. Ciani and G. Szabo, *J. Membr. Biol.* 1968, **1**, 294.
4. F. Vögtle and E. Weber, *Angew. Chem.* 1979, **91**, 813.
5. N. S. Poonia and M. R. Truter, *J. Chem. Soc., Dalton Trans.* 1973, 2062; N. S. Poonia, B. P. Yaday and V. W. Bhaywart, *Inorg. Nucl. Chem. Lett.* 1977, **13**, 119.
6. N. S. Poonia, *J. Am. Chem. Soc.* 1974, **94**, 1012.
7. M. Bourgoin, K. H. Wong, J. Y. Hui and J. Smid, *J. Am. Chem. Soc.* 1975, **97**, 3462; R. Sinta, P. S. Rose and J. Smid, *J. Am. Chem. Soc.* 1983, **105**, 4337.
8. Lj. Tušek, H. Meider-Goričan and P. R. Danesi, *Z. Naturforsch.* 1976, **31B**, 330.
9. E. Buncel, H. S. Shin, R. A. Bannard, J. C. Purdon and B. G. Cox, *Talanta* 1984, **31**, 585.
10. Lj. Tušek-Božić and P. R. Danesi, *J. Inorg. Nucl. Chem.* 1979, **41**, 833.
11. Lj. Tušek-Božić and B. Božić, *Croat. Chem. Acta* 1984, **57**, 119.
12. Lj. Tušek-Božić and B. Božić, *Electrochim. Acta* 1985, **30**, 789.
13. Lj. Tušek-Božić and D. Sevdić, *Polyhedron* 1985, **4**, 1959.
14. C. J. Pedersen, *J. Am. Chem. Soc.* 1967, **89**, 7017.
15. V. Jagodić and Lj. Tušek, *J. Org. Chem.* 1972, **37**, 1222.
16. Lj. Tušek and V. Jagodić, *Croat. Chem. Acta* 1977, **49**, 829.
17. E. E. Kay, Z. Zawoyyski and D. F. Evans, *J. Phys. Chem.* 1965, **69**, 4208.
18. R. M. Fuoss and F. Accascina, *Electrolytic Conductance*. Interscience, New York (1959).
19. D. G. Parsons, M. R. Truter and J. N. Wingfield, *Inorg. Chim. Acta* 1975, **14**, 45.
20. D. L. Hughes, *J. Chem. Soc., Dalton Trans.* 1976, 2374.
21. D. F. Evans, S. L. Wellington, J. A. Nadis and E. L. Cussler, *J. Solution Chem.* 1972, **1**, 499.
22. C. J. Pedersen and H. K. Frensdorf, *Angew. Chem., Int. Ed. Engl* 1972, **11**, 16.
23. V. Jagodić and Lj. Tušek, *Croat. Chem. Acta* 1972, **44**, 445; V. Jagodić, *Croat. Chem. Acta* 1977, **49**, 127.
24. L. C. Thomas, *Interpretation of the Infrared Spectra of Organophosphorus Compounds*. Heyden, London (1974).

Polyhedron Vol. 5, No. 3, pp. 883–886, 1986
Printed in Grueat Britain

0277–5387/86 $3.00 + .00
© 1986 Pergamon Press Ltd

BINUCLEAR SCHIFF BASE COMPLEX OF COBALT(II) LINKED BY *m*-PHTHALOYL AS A BRIDGING GROUP

K. KASUGA,* T. OISHI and Y. YAMAMOTO

Department of Chemistry, Faculty of Science, Shimane University, Matsue 690, Japan

(*Received* 8 *May* 1985; *accepted* 2 *October* 1985)

Abstract—A binuclear cobalt(II) complex with an unsymmetrical quadridentate Schiff base linked by *m*-phthaloyl was prepared and characterized. The complex formed both 1 : 1- and 2 : 1-type oxygenated species in a benzene solution containing 1% of pyridine at room temperature. Although the mononuclear cobalt(II) complex did not significantly catalyze the auto-oxidation of *N*,*N*,*N*′,*N*′-tetramethyl-*p*-phenylenediamine, the reaction was catalyzed by the binuclear cobalt(II) complex.

Binuclear metal complexes have been widely investigated in view of their magnetism and catalytic activities.[1–5] For instance, flexible copper(II) complexes have received considerable attention for their resemblance to Type-III copper proteins.[6–8] Previously, we prepared Schiff base copper(II) complexes linked by dithiol or phthaloyl, and investigated their catalytic activities.[9,10] Binuclear cobalt(II) complexes have also been studied as catalysts for various redox reactions, e.g. tetrakis(bipyridyl)(μ - peroxo)(μ - hydroxo)dicobalt(III) catalyzed the auto-oxidation of 2,5-di-*tert*-butylphenol.[11] Collman *et al.* also studied the catalytic potency of binuclear cobalt(II) cofacial porphyrin complexes for the electroreduction of oxygen to water.[12,13] In this paper, we report the preparation of the binuclear cobalt(II) complex with a Schiff base linked by *m*-phthaloyl (Fig. 1) and its oxygenation, as well as a catalytic activity for the auto-oxidation of *N*,*N*,*N*′,*N*′-tetramethyl-*p*-phenylenediamine (TMPD).

EXPERIMENTAL

Preparation of the mononuclear cobalt(II) complex

A free mononuclear ligand, *N*-(1-methyl-3-oxobutylidene) - *N*′ - salicylideneethylenediamine, was prepared by elimination of copper(II) ion from its complex with hydrogen sulfide.[10] In the present experiment, the ligand was prepared as follows: to 600 cm^3 of a benzene solution containing 50 cm^3 (0.5 mol) of acetylacetone and 56 cm^3 (0.5 mol) of salicylaldehyde, 33 cm^3 (0.5 mol) of ethylenediamine was added dropwise, and the mixture was refluxed for *ca* 3 h. After evaporation of the solvent under a reduced pressure, 300 cm^3 of ethanol was added to the residue, which was stirred for a few minutes. On standing the solution at −7 to −10° C for *ca* 30 min, large amounts of *N*,*N*′-disalicylideneethylenediamine (Salen) were precipitated and were filtered off. After adding adequate amounts of *n*-hexane to the filtrate, the solution was left overnight at 2–4°C. Yellow needles of the ligand then precipitated were washed by *n*-hexane and were dried under a reduced pressure at room temperature. Found: C, 68.3; H, 7.2; N, 11.4%. Calc. for $C_{14}H_{18}N_2O_2$: C, 68.3; H, 7.4; N, 11.4%. ^1H NMR (dimethylsulfoxide-d_6): δ 2.05 (3H, s, CH_3), 2.18 (3H, s, CH_3), 3.96–4.29 (4H, m, CH_2CH_2), 5.54 (H,

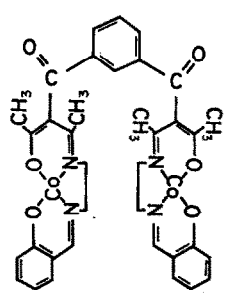


Fig. 1. Binuclear Schiff base complex of cobalt(II) linked by *m*-phthaloyl.

* Author to whom correspondence should be addressed.

s, CH), 7.69–8.45 (4H, m, benzene), and 9.67 (H, s, azomethine). Cobalt(II) acetate tetrahydrate (0.52 g, 2.1 mmol) was added to 20 cm^3 of an acetone solution of the free ligand (0.50 g, 2.0 mmol), and the solution was stirred at room temperature for 20–30 min under a nitrogen atmosphere. Orange precipitates were then obtained and were recrystallized from acetone (yield 62%). Found: C, 54.0; H, 5.3; N, 9.0%. Calc. for $C_{14}H_{16}N_2O_2Co \cdot 0.5H_2O$: C, 53.9; H, 5.5; N, 9.0%.

Preparation of the binuclear cobalt(II) complex

A free binuclear ligand was obtained by elimination of copper(II) ion from its complex which was prepared by the method described before:[10] gaseous hydrogen sulfide was bubbled through a chloroform solution of the copper(II) complex at room temperature for 10–20 min. After filtering off copper(II) sulfide, active charcoal was added to the filtrate, and the mixture solution was stirred for several minutes. After filtering off the charcoal, crude precipitates of the free ligand were obtained by concentrating the filtrate to adequate amounts under a reduced pressure. The pale yellow ligand was then obtained by column chromatography on silica gel using dichloromethane as an eluent. Found: C, 66.4; H, 5.5; N, 8.5%. Calc. for $C_{36}H_{38}N_4O_6 \cdot 0.5CH_2Cl_2$: C, 65.9; H, 5.9; N, 8.4%. ^{1}H NMR (dimethylsulfoxide-d_6): 1.88 (6H, s, CH_3), 2.05 (6H, s, CH_3), 4.13–4.22 (8H, m, CH_2CH_2), 7.81–8.56 (8H, m, benzene), and 9.54 (2H, s, azomethine). To 20 cm^3 of the acetone solution containing 0.50 g (0.80 mmol) of the free ligand, 0.42 g (1.7 mmol) cobalt(II) acetate tetrahydrate was added under a nitrogen atmosphere. After stirring the solution at room temperature for 10–20 min, dark brown precipitates were obtained and were recrystallized from acetone under a nitrogen atmosphere (yield 7%). Found: C, 55.0; H, 4.7; N, 6.8%. Calc. for $C_{36}H_{34}N_4O_6Co_2 \cdot 3H_2O$: C, 54.7; H, 5.1; N, 7.1%.

Measurements

The electronic and ^{1}H NMR spectra were obtained by the method described before.[10] The measurements of oxygen affinities of the complexes were also carried out by the method described before.[14]

RESULTS AND DISCUSSION

The free binuclear ligand was obtained by elimination of copper(II) ion from its complex with hydrogen sulfide, and was identified by elemental analysis, ^{1}H NMR and electronic spectra. In the ^{1}H NMR spectrum of the binuclear ligand, the signal for the methine proton of the mononuclear ligand disappeared, and new signals for benzene protons of the phthaloyl group were observed, indicating that the Schiff base ligands are linked by the bridging group. The signals for the methyl groups of the binuclear ligand are somewhat shifted to higher magnetic fields, compared to those of the mononuclear ligand, due to an anisotropic effect of a carbonyl group in the bridging group. The electronic spectrum of the binuclear ligand shows a π–π^* absorption band at 320 nm, and that of the mononuclear species is at 310 nm. Acetone is a suitable solvent for preparation of the mono- and binuclear cobalt(II) complexes. With other solvents such as water, methanol and ethanol, as well as a solvent mixture of acetone and water, the pure complexes could not be obtained. The mono- and binuclear cobalt(II) complexes show *d–d* absorption bands at 490 and 485 nm in a benzene solution, respectively. Both complexes also show charge-transfer bands around 400 nm.

Oxygenation

Spectral changes were recorded for benzene solutions of the mono- and binuclear cobalt(II) complexes containing 1% of pyridine at different partial pressures of oxygen at 20°C. When the mononuclear complex was oxygenated, a new band was observed at 530 nm, as was seen in the oxygenation of other mononuclear cobalt(II) complexes.[15–17] With increasing partial pressure of oxygen, the intensity of the band was monotonously increased. If the mononuclear cobalt(II) complex forms only a 1:1-type oxygenated species, the equilibrium constant for oxygenation (K) is given by the following relation:

$$P(O_2) = -1/K + (\varepsilon_2 - \varepsilon_1)[\text{Co(II) complex}]_t[P(O_2)]/(A - A_o), \quad (1)$$

where A_o and A are the absorbances at 550 nm in the absence of oxygen and at the proper partial pressure of oxygen, ε_1 and ε_2 are the molar absorption coefficients of the cobalt(II) complex and the oxygenated species, $P(O_2)$ is the partial pressure of oxygen, and $[\text{Co(II) complex}]_t$ is the total concentration of the complex. The plot of $P(O_2)$ against $[P(O_2)]/(A - A_o)$ gave a straight line with a slope nearly equal to 1. This implies that the 1:1-type oxygenated species is predominantly formed in the solution, and the value of log K is -2.95 $torr^{-1}$ (1 torr = 133.322 Pa). This value is in the range of those which were previously reported for the cobalt(II) complexes with *N,N'*-bis(1-methyl-3-oxobutylidene)ethylenediamine, *N,N'*-bis(1-methyl-

3-oxo-3-phenylpropyridene)ethylenediamine and their derivatives.[18,19] It is interesting that the cobalt(II) complex with the unsymmetrical quadridentate Schiff base forms the 1:1-type species, because the cobalt(II) complex with Salen forms a 2:1-type peroxo-bridged species at room temperature.[20]

In the case of the binuclear cobalt(II) complex, the intensity of the band around 500 nm also increased on oxygenation. However, it reached a maximum when the $P(O_2)$ was *ca* 230 torr, and then gradually decreased with an increase in oxygen pressure (Fig. 2).

The same tendency has also been reported for the mononuclear cobalt(II) complexes with a Jäger-type ligand: the species formed under a high partial pressure is the 1:1-type species, and the species under a low oxygen pressure is the 2:1-type peroxo-bridged species.[15] Therefore, the following scheme might represent the oxygenation reaction of the binuclear cobalt(II) complex:

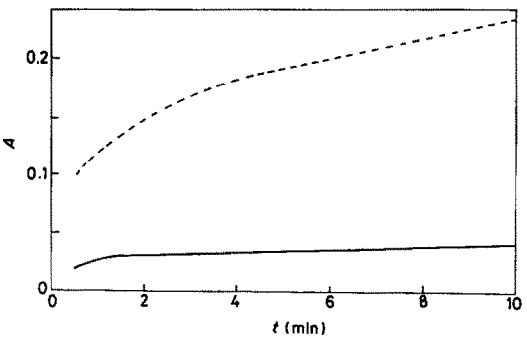
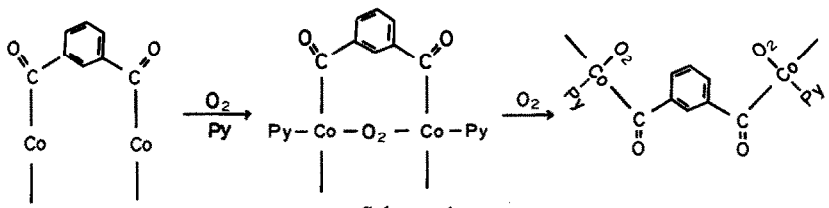


Fig. 3. Time course of the absorbance at 560 nm for the auto-oxidation of TMPD by oxygen in the presence of the cobalt(II) complexes at 20°C; a solvent mixture of methanol and *N*,*N*-dimethylformamide [1:1 (v/v)] was employed: $[TMPD]_t = 5.00 \times 10^{-4}$ mol dm^{-3}: (——) the mononuclear cobalt(II) complex, $[complex]_t = 2.50 \times 10^{-4}$ mol dm^{-3}; (– – –) the binuclear cobalt(II) complex, $[complex]_t = 1.25 \times 10^{-4}$ mol dm^{-3}.



Scheme 1.

At present, both oxygenated species of the mono- and binuclear complexes have not been isolated as a solid.

Catalytic activities

The catalytic activities of the cobalt(II) complexes for the auto-oxidation of TMPD are shown in Fig. 3.

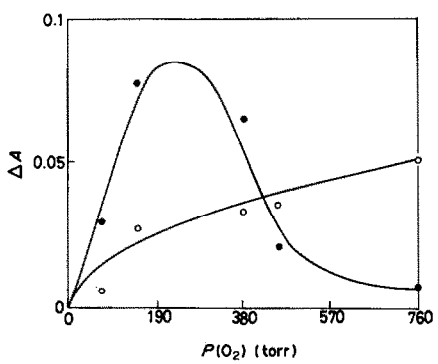
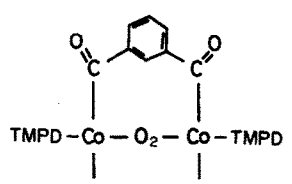


Fig. 2. Plots of absorbance vs partial pressure of oxygen in the benzene solution containing 1% of pyridine at 20°C: (○) the mononuclear cobalt(II) complex, $[complex]_t = 2.00 \times 10^{-4}$ mol dm^{-3}, wavelength used for the measurement = 560 nm; (●) the binuclear cobalt(II) complex, $[complex]_t = 1.00 \times 10^{-4}$ mol dm^{-3}, wavelength = 500 nm. The absorances are shown as differences from that of the nonoxygenated species.

Although the mononuclear cobalt(II) complex did not show an effective catalytic activity, the binuclear complex greatly catalyzed the reaction. It has been reported that the catalytic activity of the binuclear copper(II) complexes for the auto-oxidation of TMPD is closely related to the presence of two adjacent copper(II) ions with the optimum copper(II)–copper(II) distance: e.g. oxygen simultaneously accepts two electrons from the TMPD molecules through the copper(II) ions, resulting in peroxide.[8] The binuclear cobalt(II) complex may form the following intermediate which catalyzes the auto-oxidation of TMPD in a similar manner to the binuclear copper(II) complexes reported by Nishida *et al.*:[5–8]



Scheme 2.

The reaction was not catalyzed by the binuclear copper(II) complex with the ligand used for the present experiment,[10] presumably due to the fact

that the ligand is not flexible enough to form the intermediate. However, the binuclear cobalt(II) complex can form the 2 : 1-type oxygenated species, which indicates that the intermediate must be formed easily, showing the catalytic activity.

REFERENCES

1. J. A. Fee, *Struct. Bonding* 1975, **23**, 1.
2. I. M. Klotz and D. M. Kurtz, Jr, *Acc. Chem. Res.* 1984, **17**, 16.
3. A. E. Martell and K. Nag, *J. Chem. Soc., Dalton Trans.* 1983, 2429.
4. B. C. Whitmore and R. Eisenberg, *Inorg. Chem.* 1983, **22**, 1.
5. T. Izumitani, M. Nakamura, H. Okawa and S. Kida, *Bull. Chem. Soc. Jpn* 1982, **55**, 2122.
6. Y. Nishida, M. Oishi and S. Kida, *Inorg. Chim. Acta* 1980, **46**, L69.
7. N. Oishi, Y. Nishida and S. Kida, *Chem. Lett.* 1981, 1031.
8. Y. Nishida, M. Takeuchi, N. Oishi and S. Kida, *Inorg. Chim. Acta* 1983, **75**, 113.
9. K. Kasuga, T. Nagahara, M. Miyasato and Y. Yamamoto, *Inorg. Chim. Acta* 1984, **93**, 141.
10. K. Kasuga, T. Nagahara and Y. Yamamoto, *Polyhedron* 1985, **4**, 415.
11. S. A. Bedell and A. E. Martell, *Inorg. Chem.* 1983, **22**, 364.
12. J. P. Collman, P. Deniserich, Y. Konai, M. Marrocco, C. Koval and F. A. Anson, *J. Am. Chem. Soc.* 1980, **102**, 6027.
13. R. D. Richard, Jr, C. S. Bencosme, J. P. Collman and F. C. Anson, *J. Am. Chem. Soc.* 1983, **105**, 2710.
14. K. Kasuga, T. Nagahara, A. Tsuge, K. Sokabe and Y. Yamamoto, *Bull. Chem. Soc. Jpn* 1983, **56**, 95.
15. K. Kubokura, H. Okawa and S. Kida, *Bull. Chem. Soc. Jpn* 1978, **51**, 2036.
16. V. M. Mishowski, J. L. Robbins, I. M. Teitel and H. B. Gray, *Inorg. Chem.* 1975, **14**, 2318.
17. G. McLendon, S. R. Pickens and A. E. Martell, *Inorg. Chem.* 1977, **16**, 1551.
18. A. L. Crumbliss and F. Basolo, *J. Am. Chem. Soc.* 1970, **92**, 55.
19. K. Kasuga, Y. Iida, Y. Yamamoto, M. Aihara and M. Kudo, *Inorg. Chim. Acta* 1984, **84**, 113.
20. R. D. Jones, D. A. Summerville and F. Basolo, *Chem. Rev.* 1979, **79**, 139.

Polyhedron Vol. 5, No. 3, pp. 887–893, 1986
Printed in Great Britain

0277-5387/86 $3.00 + .00
© 1986 Pergamon Press Ltd

ELECTROCHEMISTRY AND OXYGENATION KINETICS OF TETRADENTATE SCHIFF BASE MANGANESE(II) COMPLEXES

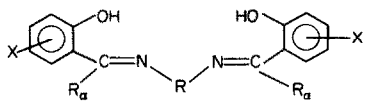
F. C. FREDERICK and L. T. TAYLOR*

Department of Chemistry, Virginia Polytechnic Institute and State University, Blacksburg, VA 24061, U.S.A.

(*Received* 21 *June* 1985; *accepted after revision* 4 *October* 1985)

Abstract—The electrochemistry and oxygenation kinetics of a series of Mn(II) complexes containing ligands derived from substituted salicylaldehyde and linear diamines have been studied. Complexes prepared from ethylenediamine produce cyclic voltammograms with a quasi-reversible Mn(II)–Mn(III) couple and oxygenation reactions which are first-order in both complex and O_2, indicating formation of an Mn(III)–O_2^- species as the slow step in the reaction. The ease of oxidation/oxygenation increases with increasing electron-donating ability of substituents on the salicyladehyde rings. Complexes with from six to 10 methylene groups in the diamine precursor produce highly irreversible voltammograms and oxygenation data which can not be interpreted in terms of a simple mechanism. Polymerization of the complexes is advanced as an explanation for these effects.

Mn(II) complexes containing polydentate ligands are often found to be oxidizable, either by electrochemical anodization or exposure to molecular oxygen.[1,2] We have previously described the electrochemical and oxygenation properties of a series of Mn(II) and Mn(III) complexes containing polydentate Schiff base ligands,[3–8] among them the tetradentate species shown in structure **I**. Redox



I: X = NO_2, CH_3O, Cl, H, or CH_3; R_α = H, Ph; R = *o*-Ph or $(CH_2)_n$

potentials and oxygenation products were found to be dependent on the aryl (X) and imine carbon (R_α) substituents as well as the nature of the bridging (R) group. Oxygen sensitivity was also dependent on the physical state of the complex and, if in solution, the solvent choice in a number of instances. Cationic complexes such as those prepared from pyridine-2-carboxaldehyde instead of salicylaldehyde were oxygen-insensitive and electrochemically inactive.

This paper describes the oxygenation kinetics of some of these Mn(II) complexes [X = 3-CH_3O, 5-Cl or H; R = $(CH_2)_n$ (n = 2, 4, 6, 7, 8 or 10); R_α = H].

The oxygenation products of these complexes have been well characterized, but no firm data on the reaction mechanisms had previously been acquired. Also, comparison of results obtained with the tetradentate chelates with those previously reported for tridentate complexes[3] adds support to a number of theories earlier advanced to explain the tridentate results.

EXPERIMENTAL

Syntheses

The following complexes were prepared according to previously reported literature procedures:[4] Mn($SALC_2$), Mn(3-MeO$SALC_2$), Mn(5-Cl$SALC_2$), Mn($SALC_4$), Mn($SALC_6$), Mn($SALC_7$), Mn($SALC_8$) and Mn($SALC_{10}$).

Electrochemical studies

Voltammetric studies were performed using a combination 551 Potentiostat–Galvanostat and 567 Function Generator from ECO Instruments. The electrodes used were a Beckman platinum disc (working), Fisher saturated calomel (reference) and platinum coil (counter). Solutions were $\sim 10^{-3}$ M complex in degassed dimethylsulfoxide (DMSO) or

* Author to whom correspondence should be addressed.

pyridine, with 0.1 M tetraethylammonium perchlorate as supporting electrolyte.

Kinetic studies

The reaction of complexes with O_2 was studied by following the change in the concentration of either the complex or O_2 as a function of time in an excess ($>10:1$) of the other reactant. The concentration of complex was followed by repetitively scanning the UV spectrum of the solution with an Aminco DW-2 Spectrophotometer. The concentration of O_2 was followed using a 731 Clark-type oxygen electrode from Transidyne General Corp. The order of the reaction with respect to the reactants, specific rate constants, and activation parameters were determined by standard methods.[9]

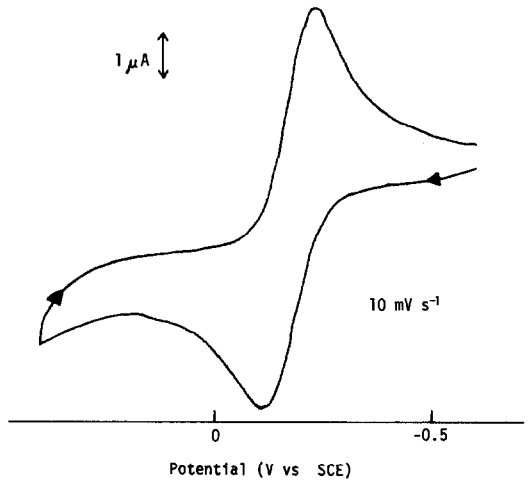


Fig. 1. Cyclic voltammogram of Mn(3-MeOSALC$_2$) in pyridine.

RESULTS AND DISCUSSION

Electrochemical studies

The voltammetric properties of the complexes are a function of the polymethylene chain length. The complexes thus divide themselves into two groups, the substituted Mn(XSALC$_2$) type and the longer chain Mn(SALC$_n$) type. Mn(SALC$_4$) falls into a group by itself, as it was insufficiently soluble in either DMSO or pyridine to give measureable voltammetric signals.

The voltammograms of the Mn(XSALC$_2$) complexes are similar to those previously reported for Mn(SALOPHEN) tetradentate complexes.[5] In both DMSO and pyridine, the complexes exhibit a single pair of coupled peaks, with approximately equal oxidation and reduction currents (Fig. 1), and a constant value for $i_{ox}/n^{1/2}$. The peak separation (Table 1) is greater than 59 mV, and generally increases with increasing scan rate. Comparison of these results with other systems leads to an assignment of the peaks to a quasi-reversible Mn(III)–Mn(II) couple. The solution geometry of both oxidation states is undoubtedly octahedral, with a planar tetradentate ligand and *trans*-coordinated solvent molecules. A cathodic shift in peak potentials is observed on going from pyridine to DMSO. Since the *relative* stabilization of the two manganese oxidation states determines the redox potential, Mn(II) is apparently more favored when coordinated to pyridine than when coordinated to DMSO (Fig. 2).

Voltammograms of the longer-chain complexes could only be obtained in pyridine because of their low solubility in DMSO. A typical voltammogram

Table 1. Peak potentials for XSALEN complexes (V vs SCE)

Complex	Scan rate (mV s^{-1})	$E_{ox}{}^a$	$E_{red}{}^a$	$E_{ox}{}^b$	$E_{red}{}^b$
Mn(3-MeOSALC$_2$)	1	−0.18	−0.29	−0.13	−0.22
	10	−0.20	−0.27	−0.12	−0.22
	100	−0.19	−0.28	−0.05	−0.24
Mn(SALC$_2$)	1	−0.22	−0.36	−0.10	−0.28
	10	−0.25	−0.33	−0.06	−0.23
	100	−0.24	−0.33	+0.06	−0.31
Mn(5-ClSALC$_2$)	1	−0.15	−0.21	0.00	−0.12
	10	−0.14	−0.21	+0.04	−0.13
	100	−0.13	−0.23	+0.15	−0.18

[a] In DMSO.
[b] In pyridine.

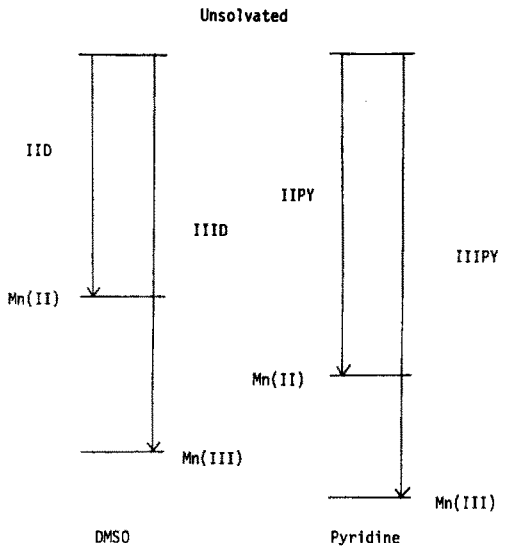


Fig. 2. Coordinated solvent effect on macrocyclic complex redox potentials.

(Fig. 3) contains a large "hump" on or near the solvent oxidation wave on the initial anodic scan, and a smaller, normally shaped cathodic peak on the reverse sweep. The peaks are quasi-reversible in that their separation increases with increasing scan rate, but, unlike the $Mn(XSALC_2)$ complexes, the separation is much greater than 59 mV even at very low scan rates (1 mV s^{-1}). The earlier report of an irreversible reduction for $Mn(SALC_7)(NCS)$[9] is in agreement with this work. A plausible explanation was advanced in this case wherein the monomeric Mn(III) species was suggested to be reduced to a polymeric Mn(II) species. The $Mn(SALC_n)$ species were previously postulated to be polymeric with bridging ligands in the solid state, based on their low solubilities and ESR spectra,[4] and a carry over of this property to a solution phase seems possible. The data therefore imply that the redox scheme is: (1) oxidation of a Mn(II) polymer, (2) slow depolymerization to give an electroactive Mn(III) monomer, and (3) reduction of the monomer with immediate reformation of the Mn(II) polymer.

Voltammograms of $Mn(SALC_{10})$ exhibit further irregularities. At relatively high scan rates, its voltammograms resemble those of the other $Mn(SALC_n)$ complexes. However, as the scan rate is decreased, a second reduction peak grows in at a potential cathodic to the first reduction peak. Such a change is usually indicative of reaction of the initial oxidation product [monomeric Mn(III)] to produce a second electroactive species which is oxidized at a slightly different potential. In this case, the new species has a more negative reduction potential [i.e. it has a more stable Mn(III) center]. Since one way to stabilize Mn(III) is by adding more ligands, one explanation for these time-dependent voltammograms may arise from a slow solvent attack on initially tetrahedral Mn(III) monomers to produce octahedral Mn(III) monomers with two-coordinated solvent molecules. We have found that bi-[10] and tridentate[3] Schiff base complexes of Mn produce time-dependent voltammograms explainable by solvent attack and/or loss. Assignment of tetrahedral geometry to the initial oxidation product seems feasible since it should resemble the Mn(II) starting material, which has been shown to have "pseudo-tetrahedral" geometry in the solid state.[4] A second irregularity occurs when a second anodic scan is performed immediately after a slow cathodic scan. A second oxidation peak is now found anodic to the "hump". Since it is found only after a slow cathodic scan where reduction of a large amount of octahedral Mn(III) is occurring, we

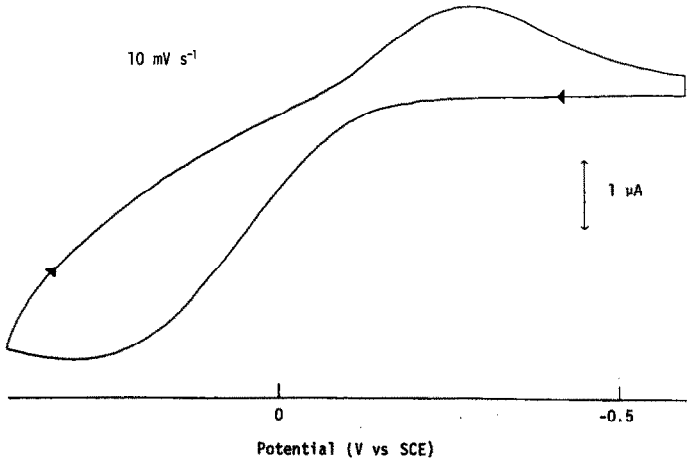


Fig. 3. Cyclic voltammogram of $Mn(SALC_8)$ in pyridine.

believe this peak is due to oxidation of accummulated octahedral Mn(III) which slowly loses solvent before quick collapse to the Mn(II) polymer.

Oxygenation kinetics

Oxygen uptake studies have shown that all of these complexes oxygenate in two distinct steps, first to a μ-oxo-Mn(III) dimer, and second, to a di-μ-oxo-Mn(IV) dimer. However, as in the electrochemical study, the complexes are again separable into short- and long-chain groups. Also, no information could be gained on Mn(SALC$_4$) because its reaction with O_2 was too slow to be conveniently followed via repetitive scanning spectrophotometry. This was also true for Mn(5-ClSALC$_2$), an effect directly attributable to the strong electron-withdrawing effect of the Cl substituent.

A typical repetitive spectrophotometric scan for the oxygenation of Mn(SALC$_2$) in DMSO at low temperature is shown in Fig. 4. Only the first step in the overall reaction (formation of the μ-oxo-dimer) is seen. There is a significant difference between these changes and those of bi-[10] and tridentate[3] complexes in that the tetradentates exhibit a monotonic increase across the spectral range while the other complexes have isobestic points in their spectra. This may be attributed to differences in the changes in ligand geometry and coordination number during oxygenation, and also the fact that the oxidized tetradentate complexes are oxo-bridged dimers, while bi- and tridentate Mn(III) complexes are believed to be monomers with no incorporated reduced form of O_2.

The second step can be observed if the temperature is raised, if the MeO complex is used, or if pyridine is used as the solvent (Fig. 5). Two points should be noted on Fig. 5. First, an isosbestic point occurs at 355 nm. This is fortunate because separation of the spectral changes due to the discrete steps would be difficult without this feature. A different type of spectral change is to be expected for this step since formation of *cis* metal–oxygen bonds requires folding of the ligand from a planar structure. Second, there is no incubation period in the reaction as opposed to that found in the earlier manometric studies.

Numerical analysis of both the UV spectral changes and Clark electrode data for the first oxygenation step show that it is first-order in both complex and O_2. No attempt was made to study the kinetics of the second step. The first step is therefore believed to be:

$$\text{Mn(II)L} + O_2 \rightarrow \text{LMn(III)}\text{–}O_2^-$$

Table 2, however, which gives activation parameters for the first step, shows that there is some complexity in the system. The greater rate constants and lower activation energies for oxygenation of the MeO complex were predictable because of the activating MeO group. Also, if the previously advanced theory of solvent replacement by O_2 in the RDS is correct,[3] then the lower E_a values in DMSO relative to pyridine are no surprise since pyridine is apparently a better ligand for the Mn(II) complexes than DMSO. The difference in E_a values is larger here than observed for the tridentate complexes, however, because there is no competition between a potentially tridentate ligand donor oxygen and solvent for the axial coordination position.

Solvent and substituent effects on activation entropies are not quite as straightforward. The

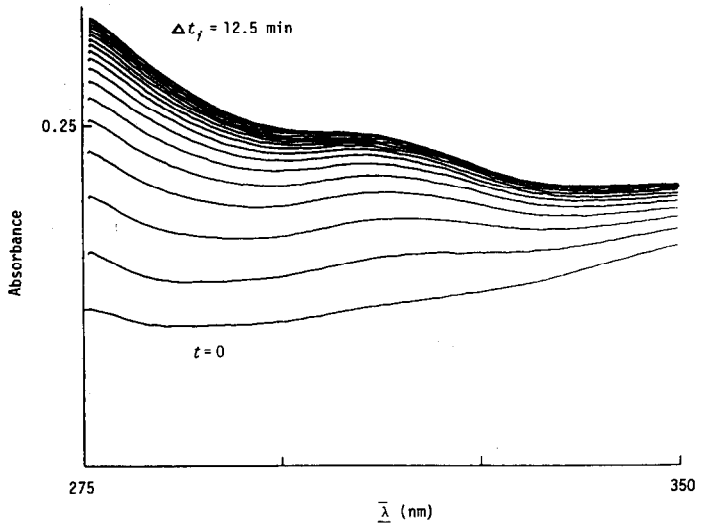


Fig. 4. Repetitive scan of oxygenation of Mn(SALC$_2$) in DMSO.

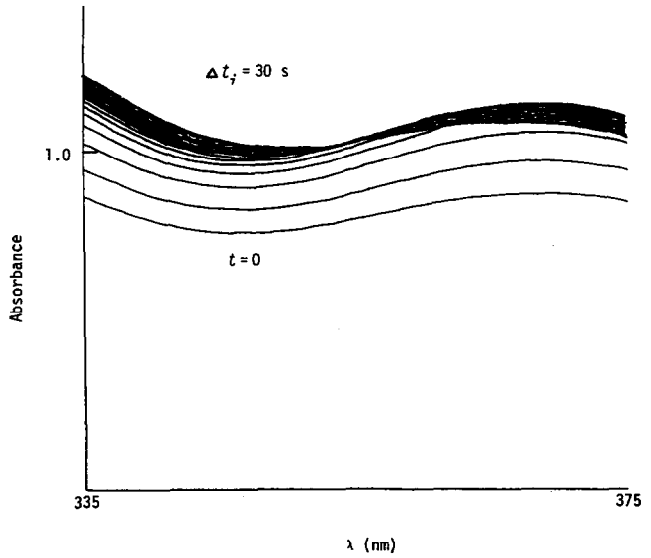


Fig. 5. Repetitive scan of oxygenation of $Mn(SALC_2)$ in pyridine.

addition of the MeO group lowers ΔS by ~ 10 eu in both solvents, and changing from DMSO to pyridine increases ΔS by ~ 40 eu for both $Mn(SALC_2)$ and $Mn(3\text{-}MeOSALC_2)$. Better electron donation by the tetradentate ligand, due to the attached MeO group, should both lessen the degree of solvent coordination in the Mn(II) complex via more complete neutralization of the metal charge, and increase the degree of O_2 coordination in the transition state by increasing the available electron density to transfer and produce $O_2^{\delta-}$. Both of these factors tend to decrease the value of ΔS by decreasing the randomness of the transition state with respect to the ground state. The solvent effect on ΔS may be due to two factors. First, expulsion of a more tightly held pyridine will produce a greater change in randomness than a relatively loosely held DMSO. Second, electrorestriction of DMSO by the transition state will be greater than for pyridine due to its greater dipole moment, further lowering ΔS in DMSO. The remaining steps in the reaction are not accessible via kinetic studies but a reasonable possibility is the Ochiai sequence:[11]

$$\text{LMn(III)–}O_2^- + \text{Mn(II)L} \rightarrow \text{Mn(III)–}O_2^{2-}\text{–Mn(III)L},$$

$$\text{LMn(III)–}O_2^{2-}\text{–Mn(III)L} \rightarrow 2\text{LMn(III)–}O^-,$$

$$\text{LMn(III)–}O^- + \text{Mn(II)L} \rightarrow \text{LMn(III)–}O^{2-}\text{– Mn(III)L}.$$

Table 2. Kinetic parameters for tetradentate oxygenations

Complex	Solvent	T (°C)	k^a ($M^{-1}\,min^{-1}$)	E_a (kcal mol^{-1})	$\Delta S^{\neq}$ (eu)
$Mn(SALC_2)$	DMSO	21.8	12.4 (0.6)		
		35.1	29 (2)	11.4	−25
		47.9	58 (4)		
	Pyridine	22.3	19.7 (1.3)		
		35.8	123 (10)	22	10
		47.9	320 (40)		
$Mn(3\text{-}MeOSALC_2)$	DMSO	23.3	320 (20)		
		33.8	470 (20)	5.6	−38
		39.7	510 (30)		
	Pyridine	6.6	47 (5)		
		16.0	110 (10)	17.2	0
		23.7	300 (20)		

[a] Averages with errors in parentheses.

The longer-chain complexes exhibit spectral changes in pyridine similar to those of the $Mn(XSALC_2)$ complexes (i.e. a monotonic increase in absorption across the spectrum). In DMSO, however, the absorbance decreases to a flat line above zero absorbance, typical of a suspension rather than a solution. The Mn(II) complexes are much more soluble in pyridine than in DMSO, and the differences carries over to their μ-oxo-Mn(III) products. $Mn(SALC_{10})$ differs from the other three long-chain complexes in that its Mn(III) product is soluble, possibly due to the longer alkyl chain imparting more "organic" character to the complex, and thus greater compatibility with the solvent. Continuing the scans for a longer period results in a further change to a relatively featureless spectrum similar to that of the Mn(II) complex. This is due to the second step of the reaction, formation of di-μ-oxo-Mn(IV).

Clark electrode data showed that the oxygenation reaction with the long-chain chelates was first order in O_2, but difficulties were encountered when the order of the reaction with respect to the complex was being determined. First-order plots showed marked curvature, as did second- and half-order plots. This immediately eliminates the following reactions from being the RDS:

$$Mn(II)L + O_2 \rightarrow LMn(III)\text{–}O_2^- \quad \text{(first-order)}, \quad (1)$$

$$2Mn(II)L \rightleftharpoons [Mn(II)L]_2,$$

$$[Mn(II)L_2]_2 + O_2 \rightarrow L_2Mn(II)Mn(III)\text{–}O_2^- \quad \text{(second-order)}, \quad (2)$$

$$[Mn(II)L]_2 \rightleftharpoons 2Mn(II)L,$$

$$Mn(II)L + O_2 \rightarrow LMn(III)\text{–}O_2^- \quad \text{(half-order)}. \quad (3)$$

A second-order reaction which could not be immediately eliminated is:

$$Mn(II)L + O_2 \rightleftharpoons LMn(III)\text{–}O_2^-,$$

$$LMn(III)\text{–}O_2^- + Mn(II) \xrightarrow{RDS} LMn(III)\text{–}O_2^{2-}\text{–}Mn(III)L.$$

Steric hindrance by the relatively bulky C_n chains could slow down formation of the μ-peroxo dimer until it was the RDS. However, with a 10:1 excess of O_2, the first step would use up essentially all of the complex, and further reaction would proceed only as Mn(II) was removed by the second step and was replaced by the reverse reaction in the initial equilibrium. This would, of course, not be seen as a second-order reaction. Such a quick reaction with O_2, however, has not previously been seen for any Mn Schiff base complexes, even with electron-donating substituents. Furthermore, since O_2 and Mn(II) are only consumed in the first step, the manometric studies should have shown a virtually instantaneous uptake of O_2, and the spectral studies very quick absorbance changes, if this were the mechanism. They did not, therefore this mechanism may be tentatively ruled out.

Two mechanisms with mixed orders were also investigated. One involved reactive monomeric and dimeric species:

$$Mn(II)L + O_2 \overset{k_1}{\rightarrow} LMn(III)\text{–}O_2^-,$$

$$[Mn(II)L]_2 + O_2 \overset{k_2}{\leftarrow} L_2Mn(II)Mn(III)\text{–}O_2^-.$$

Numerical fits[12] to the data with this assumed mechanism, however, gave very poor results. One assumption in the fit was a dynamic equilibrium between the two complex species, and failure to follow this may explain the bad fit, and, therefore, this mechanism cannot be discarded. A final possibility is the mechanism:

$$Mn(II)L + O_2 \overset{k_1}{\rightarrow} LMn(III)\text{–}O_2^-,$$

$$LMn(III)\text{–}O_2^- + Mn(II)L \overset{k_2}{\rightarrow} LMn(III)\text{–}O_2^{2-}\text{–}Mn(III)L,$$

where the rates are approximately equal. Unfortunately, no general graphical or numerical solution can be derived for this mechanism:[13] therefore, its existence must remain speculation.

In conclusion, we have studied the electrochemistry and oxygenation kinetics of a series of Mn(II) complexes with tetradentate Schiff base ligands. Ligand modifications causing either electronic or steric changes in the ligands have been shown to have a substantial effect on these properties.

Acknowledgements—This research was supported by NIH Research Grant No. 21844-01. We would like to thank Dr John Mason for valuable conversations on the potential oxygenation mechanisms.

REFERENCES

1. W. M. Coleman and L. T. Taylor, *Coord. Chem. Rev.* 1980, **32**, 1.
2. H. Connors, C. A. McAuliffe and J. James, *Rev. Inorg. Chem.* 1981, **3**, 199.
3. F. C. Frederick, W. M. Coleman and L. T. Taylor, *Inorg. Chem.* 1983, **22**, 792.
4. S. J. E. Titus, W. M. Barr and L. T. Taylor, *Inorg. Chim. Acta* 1979, **32**, 103.
5. R. K. Boggess, J. W. Hughes, W. M. Coleman and L. T. Taylor, *Inorg. Chim. Acta* 1980, **38**, 183.

6. W. M. Coleman and L. T. Taylor, *Inorg. Chem.* 1977, **16**, 1114.
7. W. M. Coleman and L. T. Taylor, *J. Inorg. Nucl. Chem.* 1980, **42**, 683.
8. W. M. Coleman, R. K. Boggess, J. W. Hughes and L. T. Taylor, *Inorg. Chem.* 1981, **20**, 1253.
9. R. G. Wilkins, *The Study of Kinetics and Mechanism of Reactions of Transition Metal Complexes.* Allyn & Bacon, Boston, MA (1974).
10. F. C. Frederick and L. T. Taylor, unpublished results.
11. E. I. Ochiai, *Inorg. Nucl. Chem. Lett.* 1974, **10**, 453.
12. P. B. Kelter and J. D. Carr, *Anal. Chem.* 1979, **51**, 1828.
13. C. Capellos and B. H. J. Bielski, *Kinetic Systems.* Wiley Interscience, New York (1973).

Polyhedron Vol. 5, No. 3, pp. 895–898, 1986
Printed in Great Britain

0277–5387/86 $3.00
© 1986 Pergamon Press Ltd

THE PREPARATION OF $Ta_2Cl_6(PhN)_2(Me_2S)_2$ BY REACTION OF $Ta_2Cl_6(Me_2S)_3$ WITH PhNNPh: CRYSTAL STRUCTURE OF THE PRODUCT

JO ANN M. CANICH, F. ALBERT COTTON,* STAN A. DURAJ and WIESLAW J. ROTH

Department of Chemistry and Laboratory for Molecular Structure and Bonding, Texas A&M University, College Station, TX 77843, U.S.A.

(*Received* 24 *July* 1985; *accepted* 5 *September* 1985)

Abstract—The d^0–d^0 ditantalum complex, $(PhN)(Me_2S)Cl_2Ta(\mu\text{-}Cl)_2TaCl_2(Me_2S)(PhN)$, has been prepared from the reaction of $Ta_2Cl_6(Me_2S)_3$ and azobenzene in a benzene–toluene solution. Single-crystal X-ray data show that the dinuclear compound adopts a distorted edge-sharing bioctahedral structure with a Ta–Ta′ distance of 4.096(1) Å. Other crystallographic data are: monoclinic space group $C2/c$, $a = 20.621(4)$ Å, $b = 7.653(2)$ Å, $c = 16.812(5)$ Å, $\beta = 96.66(2)°$, $V = 2635(2)$ Å^3, $Z = 4$. The principal structural dimensions are as follows: Ta=NPh distance of 1.747(8) Å; Ta—SMe_2 distance of 2.627(3) Å; Ta—Cl distances of 2.344(3) and 2.316(3) Å for Ta—$Cl(2)_t$ and Ta—$Cl(3)_t$, and 2.751(3) and 2.454(2) Å for Ta—$Cl(1)_b$ and Ta—$Cl(1)'_b$, respectively. The title compound is isostructural with the previously reported niobium complex, $Nb_2Cl_6(PhN)_2(Me_2S)_2$.

In our earlier report we showed that the N=N bond in PhNNPh reacts with the Nb=Nb bond in $Nb_2Cl_6(Me_2S)_3$ to give a product in which there are two Nb=N bonds, namely,

$$Nb_2Cl_6(PhN)_2(Me_2S)_2.^1$$

It has since been reported that the same product can be obtained from $Nb_2Cl_6(Me_2S)_3$ by reacting it with PhN_3, whereby the required PhN moieties are generated by loss of N_2.[2] We should like to report here that the PhNNPh reagent also reacts smoothly with $Ta_2Cl_6(Me_2S)_3$ to generate the title compound, which is the exact analogue of the previously reported niobium compound and forms isomorphous crystals.

EXPERIMENTAL

All manipulations were carried out under an atmosphere of argon. Standard Schlenk and vacuum line techniques were used. Toluene, benzene and hexane were freshly distilled from benzophenone ketyl prior to use. Solutions were transferred via stainless steel cannulae and/or syringes. Azobenzene was deaerated *in vacuo* at 25°C. $Ta_2Cl_6(Me_2S)_3$[3] was prepared according to the published procedure. The IR spectrum was recorded on a Perkin–Elmer 783 spectrophotometer.

$[TaCl_2(Me_2S)(PhN)]_2(\mu\text{-}Cl)_2$

A solution of $Ta_2Cl_6(Me_2S)_3$ (0.50 g, 0.66 mmol) in 15 cm^3 of benzene–toluene 2:1 (v/v) was filtered and to the filtrate azobenzene (0.40 g, 2.2 mmol) was added. The reaction mixture was stirred for 48 h during which time the color of the solution changed gradually from yellow-brown to red-brown, and in the same time a precipitate was formed. Hexane (20 cm^3) was added to this solution and the solid was filtered off. It was washed 3 times with 10-cm^3 aliquots of freshly distilled hexane, and dried *in vacuo* [yield 55% (0.32 g)]. IR (Nujol) (cm^{-1}): 1320(sh), 1295(w), 1280(sh), 1255(m), 1190(w), 1150(w), 1035(sh), 1025(m), 1000(w), 860(s), 810(w), 740(m), 720(m) and 685(m).

Crystallographic quality single crystals were prepared by a slightly different procedure. The solution of $Ta_2Cl_6(Me_2S)_3$ in benzene–toluene (20 cm^3) [1:1 (v/v)] was carefully covered with a layer of azobenzene in hexane (20 cm^3) in a Schlenk tube, and the reaction mixture was allowed to stand undisturbed for 2–3 weeks. Large, blocklike, red

* Author to whom correspondence should be addressed.

Table 1. Crystal data

Formula	$Ta_2C_{16}H_{22}Cl_6N_2S_2$
Formula weight	881.11
Space group	*C2/c*
Systematic absences	*hkl*, $h+k \neq 2n$
	h0l, $l \neq 2n$
a (Å)	20.621(4)
b (Å)	7.653(2)
c (Å)	16.812(5)
β (°)	96.66(2)
V (Å^3)	2635(2)
Z	4
d_{calc} (g cm^{-3})	2.220
Crystal size (mm)	$0.25 \times 0.3 \times 0.4$
μ(Mo-K_α) (cm^{-1})	90.07
Data collection instrument	CAD-4
Radiation (monochromated in incident beam)	Mo-K_α (λ = 71073 Å)
Orientation reflections, number, range (2θ)	25, $18.92 \leqslant 2\theta \leqslant 36.24$
Temperature (°C)	22
Scan method	ω–2θ
Data collection range (2θ) (°)	$5 \leqslant 2\theta \leqslant 50$
Number of unique data, total with $F_o^2 > 3\sigma(F_o^2)$	2307, 1794
Number of parameters refined	127
Transmission factors (max, min)	0.9979, 0.8503
R^a	0.0396
R_w^b	0.0476
Quality-of-fit indicator[c]	1.155
Largest shift/esd, final cycle	0.00
Largest peak (*e* Å^{-3})	0.756

[a] $R = \sum ||F_o| - |F_c|| / \sum |F_o|$.
[b] $R_w = [\sum w(|F_o| - |F_c|)^2 / \sum w|F_o|^2]^{1/2}$; $w = 1/\sigma^2(|F_o|)$.
[c] Quality-of-fit = $[\sum w(|F_o| - |F_c|)^2 / (N_{obs} - N_{parameters})]^{1/2}$.

crystals of $[TaCl_2(Me_2S)(PhN)]_2(\mu\text{-}Cl)_2$ were formed upon mixing of the two solutions [yield 48% (0.28 g)]. The IR spectrum of these crystals is identical with the IR spectrum obtained above.

X-ray crystallography

General procedures have already been described elsewhere.[4] Information about data collection and structure refinement for

$$[TaCl_2(Me_2S)(PhN)]_2(\mu\text{-}Cl)_2$$

is given in Table 1. The intensity data were corrected for Lorentz and polarization effects. The tantalum atoms were found by employing a Patterson function. Full-matrix least-squares refinement and difference Fourier calculations were applied to find the other non-hydrogen atoms. All 14 atoms were refined anisotropically.*

RESULTS AND DISCUSSION

Synthesis

The reaction of

$$(Me_2S)Cl_2Ta(\mu\text{-}Me_2S)(\mu\text{-}Cl)_2TaCl_2(Me_2S)$$

with $C_6H_5NNC_5H_5$ in a benzene–toluene solution yields red crystals, proven by X-ray crystallography to contain

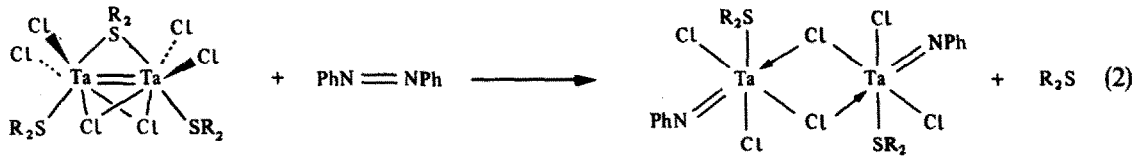
$$(Me_2S)(PhN)Cl_2Ta(\mu\text{-}Cl)_2TaCl_2(PhN)(Me_2S)$$

molecules. This reaction is identical to the reaction previously reported by us of $Nb_2Cl_6(Me_2S)_3$ and

* *Supplementary material available*—Tables of structure factors and anisotropic thermal parameters (11 pages) have been deposited with the Editor at Queen Mary College. Positional parameters and isotropic thermal parameters have been forwarded to the Director, Cambridge Crystallographic Data Centre.

azobenzene. We emphasize this analogy since the chemistry of particular niobium complexes is not always identical to that of their tantalum analogues. As in the case of the niobium compound, $Nb_2Cl_6(Me_2S)_2(PhN)_2$, the new tantalum complex, $Ta_2Cl_6(Me_2S)_2(PhN)_2$, can be regarded as the product of an inorganic double bond metathesis reaction in which Ta=Ta and N=N bonds react to furnish two Ta=N bonds, as represented schematically in eqn (1) and in detail in eqn (2):

$$Ta{=}Ta + N{=}N \longrightarrow 2Ta{=}N, \qquad (1)$$



(2)

This type of reaction has general similarities to some other previously reported cases where starting materials containing metal–metal multiple bonds react with non-metallic reagents that also contain multiple bonds, thereby generating products containing metal to non-metal bonds in a manner that is synthetically useful. Two pertinent examples are provided by reactions (3)[5] and (4):[6]

$$Mo_2(OPr^i)_8 + O_2 \rightarrow 2MoO(OPr^i)_4, \qquad (3)$$

$$W_2(OCMe_3)_6 + RCCR \rightarrow 2W(CR)(OCMe_3)_3. \qquad (4)$$

Molecular structure

The crystal structure of

$$[TaCl_2(Me_2S)(PhN)]_2(\mu\text{-}Cl)_2$$

is comprised of discrete binuclear molecules, which reside on centers of inversion. A view of the molecular structure is shown in Fig. 1, which also defines the numbering scheme. Tables 2 and 3 list interatomic distances and angles.

The molecular structure of

$$[TaCl_2(Me_2S)(PhN)]_2(\mu\text{-}Cl)_2$$

is essentially identical with that previously reported for its isostructual niobium analogue, as is to be expected. It is a dimer consisting of two octahedra sharing a common edge. The octahedra are distorted, however, from that idealization due primarily to a strong *trans*-weakening effect of the Ta=N bonds on two of the tantalum-bridging chlorine bonds. The dimensions of the two octahedral $TaCl_4(Me_2S)(PhN)$ units are very similar to those found in the niobium analogue. Thus, the Ta–Ta′ separation is 4.096(1) Å [cf. 4.096(2) Å in the niobium analogue], which suggests that there is no direct interaction between the two tantalum ions as is to be expected for two such d^0 centers. The Ta—Cl distances in

$$[TaCl_2(Me_2S)(PhN)]_2(\mu\text{-}Cl)_2$$

are as predicted: shorter for the terminal chlorine atoms, Ta—Cl(2) = 2.344(3) Å and Ta—Cl(3) = 2.316(3) Å, and longer for the bridging chlorine

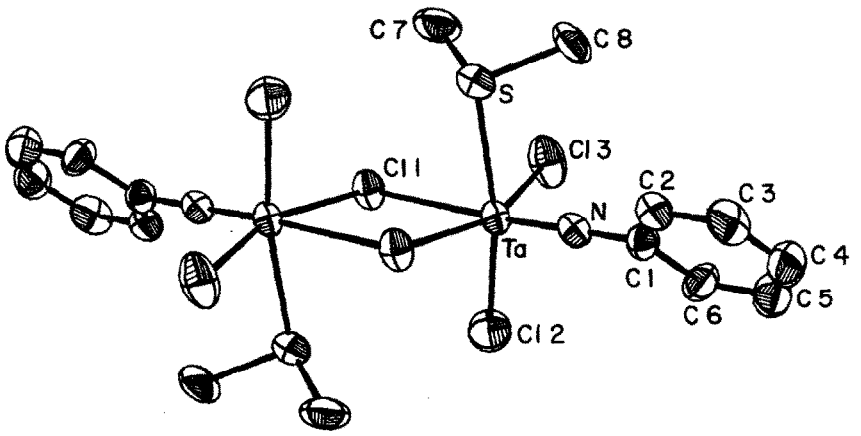


Fig. 1. ORTEP drawing of the $[TaCl_2(SMe_2)(NC_6H_5)]_2(\mu\text{-}Cl)_2$ complex, which also defines the labeling scheme. The thermal ellipsoids enclose 50% of electron density.

Table 2. Bond lengths (Å) for $[TaCl_2(SMe_2)(NC_6H_5)]_2(\mu\text{-}Cl)_2$[a]

Ta—Ta′	4.096(1)[b]
Ta—Cl(1)	2.751(3)
Ta—Cl(1)′	2.454(2)
Ta—Cl(2)	2.344(3)
Ta—Cl(3)	2.316(3)
Ta—S	2.627(3)
Ta—N	1.747(8)
S—C(7)	1.818(14)
S—C(8)	1.834(12)
N—C(1)	1.397(12)
C(1)—C(2)	1.407(15)
C(1)—C(6)	1.405(14)
C(2)—C(3)	1.387(15)
C(3)—C(4)	1.38(2)
C(4)—C(5)	1.41(2)
C(5)—C(6)	1.40(2)

[a] Numbers in parentheses are estimated standard deviations of the least significant digits.

[b] Non-bonding contact.

Table 3. Bond angles (°) for $[TaCl_2(SMe_2)(NC_6H_5)]_2(\mu\text{-}Cl)_2$[a]

Cl(1)—Ta—Cl(1)′	76.37(9)
Cl(1)—Ta—Cl(2)	86.1(1)
Cl(1)—Ta—Cl(3)	84.7(1)
Cl(1)—Ta—S	84.06(9)
Cl(1)—Ta—N	171.4(3)
Cl(1)′—Ta—Cl(2)	92.4(1)
Cl(1)′—Ta—Cl(3)	158.6(1)
Cl(1)′—Ta—S	82.11(9)
Cl(1)′—Ta—N	97.2(3)
Cl(2)—Ta—Cl(3)	96.3(1)
Cl(2)—Ta—S	169.7(1)
Cl(2)—Ta—N	99.9(3)
Cl(3)—Ta—S	86.1(1)
Cl(3)—Ta—N	100.5(3)
S—Ta—N	89.5(3)
Ta—Cl(1)—Ta′	103.63(9)
Ta—S—C(7)	110.3(5)
Ta—S—C(8)	104.4(5)
C(7)—S—C(8)	100.0(7)
Ta—N—C(1)	176.4(8)
N—C(1)—C(2)	120.7(9)
N—C(1)—C(6)	118(1)
C(2)—C(1)—C(6)	121(1)
C(1)—C(2)—C(3)	120(1)
C(2)—C(3)—C(4)	119(1)
C(3)—C(4)—C(5)	123(1)
C(4)—C(5)—C(6)	119(1)
C(1)—C(6)—C(5)	118(1)

[a] Numbers in parentheses are estimated standard deviations of the least singificant digits.

atoms, Ta—Cl(1) = 2.751(3) Å and Ta—Cl(1)′ = 2.454(2) Å.

As in the isostructural niobium complex, the $Ta{=}NC_6H_5$ bonding is of special interest. The Ta=N—C(1) fragment is essentially linear with an angle of 176.4(8)°. The Ta=N bond length of 1.747(8) Å is very short, like that in the niobium analogue, 1.733(7) Å, but this is not unusual since the Ta=N bond lengths in other structurally characterized imido-tantalum complexes are similarly short. For example, in $(THF)_2Cl_3Ta{=}N{-}(CH_3)C{=}C(CH_3){-}N{=}TaCl_3(THF)_2$[7] and $[(CH_3)_2N]_3Ta{=}NC(CH_3)_3$[8] the Ta=N bond lengths are 1.75(1) and 1.77(2) Å, respectively.

Acknowledgement—We thank the Robert A. Welch Foundation, Grant A-494, for support.

REFERENCES

1. F. A. Cotton, S. A. Duraj and W. J. Roth, *J. Am. Chem. Soc.* 1984, **106**, 4749.
2. L. G. Hubert-Pfalzgraf and G. Aharonian, *Inorg. Chim. Acta* 1985, **100**, L21.
3. F. A. Cotton and R. C. Najjar, *Inorg. Chem.* 1981, **20**, 2716.
4. See, for example, A. Bino, F. A. Cotton and P. E. Fanwick, *Inorg. Chem.* 1979, **18**, 3558.
5. M. H. Chisholm, K. Folting, J. C. Huffman and C. C. Kirkpatrick, *Inorg. Chem.* 1984, **23**, 1021.
6. M. L. Listemann and R. R. Schrock, *Organometallics* 1985, **4**, 74.
7. F. A. Cotton and W. T. Hall, *Inorg. Chem.* 1978, **17**, 3525.
8. W. A. Nugent and R. L. Harlow, *J. Chem. Soc., Chem. Commun.* 1978, 579.

Polyhedron Vol. 5, No. 3, pp. 899–900, 1986
Printed in Great Britain

0277-5387/86 $3.00 + .00
© 1986 Pergamon Press Ltd

COMMUNICATION

DIAMAGNETIC ANISOTROPY OF THE Mo≡Mo BOND IN $Mo_2(O_2CR)_4$ TYPE COMPLEXES

PRADYOT A. AGASKAR and F. ALBERT COTTON*

Department of Chemistry and Laboratory for Molecular Structure and Bonding, Texas A&M University, College Station, TX 77843, U.S.A.

(*Received* 29 *May* 1985; *accepted* 5 *September* 1985)

Abstract—By using newer structural and NMR data for $Mo_2(O_2CR)_4$ compounds with R = PhCH(OH) and CH_3 the diamagnetic anisotropy of the Mo–Mo quadruple bonds has been estimated as $-(210 \pm 30) \times 10^{-36}$ m^3 per molecule.

The fact that M–M multiple bonds, like those in organic compounds, should be magnetically anisotropic to an extent that should give rise to measurable effects in NMR spectra was first pointed out by San Filippo[1] in 1972. Qualitative use of this concept was made a few years later[2,3] in interpreting the NMR spectra of $M_2(NR_2)_6$ molecules.

More recently McGlinchey[4] pointed out that these anisotropies of M–M multiple bonds should be calculable, at least approximately, by combining quantitative structural data obtained from X-ray crystallography with chemical-shift differences measured in solution NMR spectra. The contribution to the chemical shift of protons in the R groups of complexes of the type $Mo_2(O_2CR)_4$ can be calculated from NMR data by using the general equation derived by McConnell[5] [eqn (1)]:

$$\Delta\sigma_d = \chi \frac{(1 - 3\cos^2\theta)}{3\bar{r}^3} \qquad (1)$$

where $\chi = (\chi_{\parallel} - \chi_{\perp})$, r is the distance from the center of the Mo≡Mo bond and θ is the angle between $\bar{r}$ and the Mo≡Mo bond axis. McGlinchey[4] made such calculations using data obtained by San Filippo.[1,6] For the compound

$$Mo_2Br_2(n\text{-}Bu_3P)_2(O_2CC_6H_5)_2,$$

he compared the chemical shifts of the *ortho*- and *meta*-hydrogen atoms of the benzoate ligands, and his result for χ was in the range -600 to -1000×10^{-36} m^3 per molecule. We believe this is an overestimate.

We have recalculated the value of χ using the crystal structure data[7,8] for the two compounds $Mo_2(O_2CCH(OH)C_6H_5)_4$ (**1**) and $Mo_2(O_2CCH_3)_4$ (**2**) to calculate the geometric factors [i.e. the coefficient of χ in eqn (1)] for the —CH protons in **1** and the —CH_3 protons in two orientations in **2**. The latter were averaged and the two values then are 2.95×10^{27} m^{-3} in **1** and 2.93×10^{27} m^{-3} in **2**.

The NMR spectra of compounds **1** and **2** were measured in DMSO-d_6 solutions at 200 MHz on a Varian XL-200 spectrometer. The choice of reference points for estimating what these shifts would be in the absence of the Mo≡Mo bond but with all other factors the same poses a practical problem. No ideal model compounds are available and we have made the practical choice of using the chemical shift values for the free ligands as standards. This leads to $\Delta\sigma_d$ values of 0.52 for **1** and 0.70 for **2**.

The values of χ calculated by us using the above values of the geometric factors and the appropriate values of $\Delta\sigma_d$ in eqn (1) are then -176×10^{-36} m^3 per molecule for **1** and -239×10^{-36} m^3 per molecule for **2**.

The discrepancy between these values is somewhat larger than we would have liked and presumably shows that the approximations and assumptions made in calculating them are imperfect. Nonetheless, the average value of about $-210 \times$

* Author to whom correspondence should be addressed.

10^{-36} m^3 per molecule seems very reasonable in comparison with the value of -142×10^{-36} m^3 calculated by McGlinchey[4] for the Mo–Mo triple bond in $Mo_2(NMe_2)_6$. The results we have obtained should be more reliable than the higher estimate made earlier by McGlinchey for the Mo≡Mo bond since it is derived from rather large measured values and makes no assumptions other than that specified above concerning the reference points.

Acknowledgements—We thank the National Science Foundation for support and Professor M. J. McGlinchey for correspondence.

REFERENCES

1. J. San Filippo, *Inorg. Chem.* 1972, **11**, 3140.
2. M. H. Chisholm, F. A. Cotton, B. A. Frenz, W. W. Reichert, L. W. Shive and B. R. Stults, *J. Am. Chem. Soc.* 1976, **98**, 4469.
3. M. H. Chisholm, F. A. Cotton, M. W. Extine and B. R. Stults, *J. Am. Chem. Soc.* 1976, **98**, 4477.
4. M. J. McGlinchey, *Inorg. Chem.* 1980, **19**, 1392.
5. H. M. McConnell, *J. Chem. Phys.* 1957, **27**, 226.
6. J. A. Potenza, R. J. Johnson and J. San Filippo, *Inorg. Chem.* 1976, **15**, 2215.
7. F. A. Cotton, L. R. Falvello and C. A. Murillo, *Inorg. Chem.* 1983, **22**, 382.
8. F. A. Cotton, Z. C. Mester and T. R. Webb, *Acta Cryst.* 1974, **B30**, 2788.

Polyhedron Vol. 5, No. 3, pp. 901–902, 1986
Printed in Great Britain

0277-5387/86 $3.00 + .00
© 1986 Pergamon Press Ltd

COMMUNICATION

SYNTHESIS AND MOLECULAR STRUCTURE OF $(NBu_4)_x[Pt(C_6Cl_5)_2(\mu\text{-}Cl)_2Ag]_x$: A NOVEL CHAIN POLYMERIC COMPOUND

R. USON,* J. FORNIES, M. TOMAS and J. M. CASAS

Department of Inorganic Chemistry, University of Zaragoza, 50009 Zaragoza, Spain

and

F. ALBERT COTTON* and LARRY R. FALVELLO

Department of Chemistry and Laboratory for Molecular Structure and Bonding, Texas A&M University, College Station, TX 77843, U.S.A.

(*Received* 27 *August* 1985; *accepted* 30 *September* 1985)

Abstract—The reaction of the NBu_4^+ salt of *trans*-$[PtCl_2(C_6Cl_5)_2]^{2-}$ with AgNO in acetone–methanol affords polymeric $[Pt(C_6Cl_5)_2(\mu\text{-}Cl)_2Ag]_x^{x-}$, as the NBu_4^+ salt. The chain anion consists of planar $Pt(C_6Cl_5)_2Cl_2$ units linked by Ag atoms, in which there are Ag—Cl bonds of two types: those which result in $Pt(\mu\text{-}Cl)Ag$ links and those in which *ortho*-Cl atoms of C_6Cl_5 units make close approaches (3.01 and 3.09 Å) to Ag atoms.

We recently have described[1,2] several unusual compounds containing Pt–Ag bonds and C_6F_5 groups attached to the Pt atoms. An unusual feature in these compounds was the interaction of *ortho*-F atoms in the C_6F_5 groups with the Ag atoms in a way that seemed important in the stabilization of the clusters. The first of these novel compounds, the tetrameric $(NBu_4)_2[Pt_2Ag_2Cl_4R_4]$ ($R = C_6F_5$), was prepared[1] by reacting $(NBu_4)_2[trans\text{-}PtCl_2R_2]$ with $AgClO_4$ or $AgNO_3$. We now report that an analogous reaction, starting from the C_6Cl_5 derivative, leads to the polymeric heteronuclear compound $\{(NBu_4)[Pt(C_6Cl_5)_2(\mu\text{-}Cl)_2]Ag\}_x$ (I).

Compound I can easily be prepared (88% yield) from $(NBu_4)_2[trans\text{-}PtCl_2(C_6Cl_5)_2]$[3] in acetone–methanol according to eqn (1):

$$(NBu_4)_2[trans\text{-}PtCl_2(C_6Cl_5)_2] + AgNO_3 \rightarrow NBu_4NO_3 + \frac{1}{x}\{(NBu_4)[Pt(C_6Cl_5)_2(\mu\text{-}Cl)_2Ag]\}_x \quad (1)$$

It is a yellow solid† which is very insoluble in all common solvents, although stable when in contact with them. Crystals suitable for X-ray diffraction studies‡ were obtained by very slow diffusion (*ca* −25°C) of an acetone solution of $AgClO_4$ into a dichloromethane solution of

$$(NBu_4)_2[trans\text{-}PtCl_2(C_6Cl_5)_2]$$

(molar ratio 1 : 1) both separated by an inert layer of 1,2-dichlororoethane.§

---

*Authors to whom correspondence should be addressed.

†Calc. for $C_{28}H_{36}NCl_{12}PtAg$: C, 30.13; H, 3.22; N, 1.25%. Found: C, 29.80; H, 3.02; N, 1.12%.

‡Space group $C2/c$, $a = 19.300(3)$ Å, $b = 26.523(4)$ Å, $c = 8.450(2)$ Å, $\beta = 103.53(2)°$, $Z = 4$. By using 1487 reflections with $F_o^2 > 3\sigma(F_o^2)$ and 156 parameters, refinement converged at $R = 0.061$.

§Some relevant IR data (in cm^{-1}): (a) for $(NBu_4)_2[trans\text{-}PtCl_2(C_6Cl_5)_2]$, ν(Pt—Cl) = 310(s), X-sensitive mode of the C_6Cl_5 group[3] = 820(m), and ν(Pt—Cl) = 600(m); (b) for $\{(NBu_4)[Pt(C_6Cl_5)_2Cl_2Ag]\}_x$, ν(Pt—Cl) = 310(m), X-sensitive mode = 825(m), and ν(Pt—C) = 598(m).

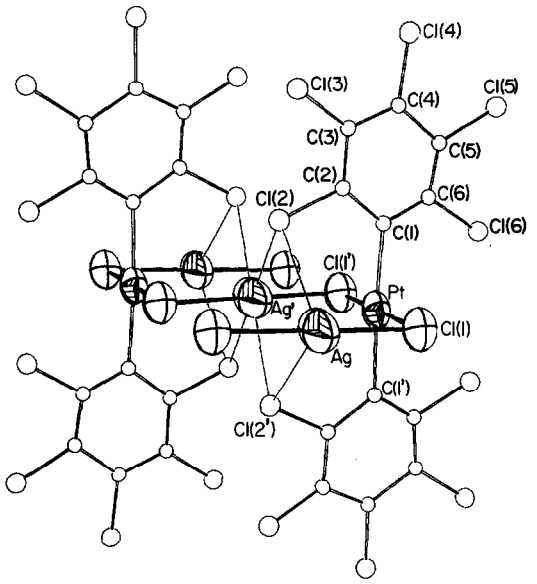


Fig. 1. A portion of the polymeric $[Pt(C_6Cl_5)_2(\mu\text{-}Cl)_2Ag]_x^{x-}$ anion. Some important distances are: Pt—C(1) = 2.08(2) Å, Pt—Cl(1) = 2.324(5) Å, Ag—Cl(1) = 2.477(5) Å, Ag—Cl(2) = 3.010(8) Å or 3.092(8) Å, Ag–Pt = 3.203(1) Å.

The structure consists of $[NBu_4]^+$ cations and polymeric anions. A representative segment of the latter is shown in Fig. 1. The Pt atoms are located on crystallographic two-fold axes and the Ag atoms on inversion centers. Each Pt atom is in a planar *trans*-$PtCl_2(C_6Cl_5)_2$ unit with normal Pt—Cl distances, and each Ag atom is in a linear Cl—Ag—Cl unit, with Ag—Cl distances short enough to imply considerable bonding there as well. There is unlikely to be any significant Pt–Ag or Ag–Ag bonding, in view of the long distances.

An important additional stabilizing factor for this structure is a set of interactions between the Ag atoms and the Cl(2) atoms. The latter are positioned so as to bridge (not quite symmetrically) adjacent Ag atoms, thus completing about each Ag atom a rhombically distorted octahedron of Cl atoms.

The role of the *ortho*-Cl atoms of the C_6Cl_5 groups in this structure is reminiscent of that played by *ortho*-F atoms in previously reported compounds, e.g. $(NBu_4)_2[Pt_2Ag_2Cl_4(C_6F_5)_4]$, but differs in important ways. It seems likely that the greater size of the Cl atom militates against coplanarity of an entire Ag···Pt—C—C—Cl unit, which would be analogous to what occurs with the C_6F_5 groups. The arrangement that has been found is an acceptable alternative. The fact that the Ag atoms receive electron density from six Cl atoms makes Pt → Ag bonding unnecessary as well as sterically infeasible.

Studies in progress on the chemical reactivity of this novel polymeric compound have shown that it is possible to cleave the polymeric anion and at least two different fragments,

$$(NBu_4)[PtAgCl_2(C_6Cl_5)_2L]$$

or $[Pt(C_6Cl_5)_2Cl_2Ag_2L_2]$, can be isolated.

Acknowledgements—We thank the CAICYT (Spain) and the Robert A. Welch Foundation for support.

REFERENCES

1. R. Uson, J. Fornies, M. Tomas, F. A. Cotton and L. R. Falvello, *J. Am. Chem. Soc.* 1984, **106**, 2482; R. Uson, J. Fornies, B. Menjon, F. A. Cotton, L. R. Falvello and M. Tomas, *Inorg. Chem.* 1985, **24**, 4651.
2. R. Uson, J. Fornies, M. Tomas, J. M. Casas, F. A. Cotton and L. R. Falvello, *J. Am. Chem. Soc.* 1985, **107**, 2556.
3. R. Uson, J. Fornies, F. Martinez, M. Tomas and I. Reoyo, *Organometallics* 1983, **2**, 1386.

Polyhedron Vol. 5, No. 3, pp. 903–905, 1986
Printed in Great Britain

0277-5387/86 $3.00 + .00
© 1986 Pergamon Press Ltd

COMMUNICATION

PREPARATION AND STRUCTURAL CHARACTERIZATION OF $Os_2Cl_4(Ph_2Ppy)_2(O_2CCH_3)$: A MIXED-LIGAND COMPOUND WITH AN Os_2^{5+} CORE AND A BOND ORDER OF 2.5

F. ALBERT COTTON,* KIM R. DUNBAR and MAREK MATUSZ

Department of Chemistry and Laboratory for Molecular Structure and Bonding, Texas A&M University, College Station, TX 77843, U.S.A.

(*Received* 2 *August* 1985; *accepted* 14 *October* 1985)

Abstract—Dichlorotetraacetatodiosmium(III) reacts with 2-(diphenylphosphino)pyridine (abbreviated Ph_2Ppy) in the presence of trimethylsilyl chloride to yield the title compound (**1**) as determined by X-ray crystallography. The molecule contains a cisoid arrangement of two Ph_2Ppy ligands which are distorted from the ideal eclipsed conformation by 30°. A single bridging acetate is also present, and it is twisted about the dimetal unit by 34°. The Os—Os distance of 2.395(1) Å, representing a formal bond order of 2.5, is the longest distance reported for a diosmium multiple bond. An investigation of the electrochemistry of **1** by cyclic voltammetry reveals two processes: a reversible oxidation at $E_{1/2} = +0.95$ V and a quasi-reversible reduction at $E_{1/2} = -0.34$ V vs Ag–AgCl.

Recent work in this laboratory has expanded the chemistry of multiply-bonded diruthenium complexes to include a wide range of Ru(II, III) species, a few of them being mixed-ligand compounds.[1–4] The methods used to prepare many of these new complexes involved either the trimethylsilyl chloride induced substitution of bidentate oxygen donor ligands, or the direct reaction of a ligand with the diruthenium starting material at high temperatures. The syntheses of several interesting diosmium complexes were effected by employing similar conditions, but, in general, the chemistry of the triply-bonded diosmium compounds has been little explored.[5–7]

Presently, we are investigating the substitution chemistry of diosmium tetraacetate. Our preliminary studies indicate that it exhibits an interesting and diverse reactivity. The molecule $Os_2Cl(chp)_4$ (chp = 6-chloro-2-hydroxypyridinato) was prepared from the melt reaction between $Os_2Cl_2(O_2CCH_3)_4$ and Hchp, and the structure was shown to be comprised of four chp ligands in a completely polar arrangement (also called the 4:0 arrangement) and a lone axial chloride.[8] This compound and the present example (**1**) are derivatives of the Os_2^{5+} dinuclear oxidation state. The formation of these neutral Os(II, III) compounds via spontaneous reduction of the triply-bonded Os_2^{6+} parent complex during the course of the substitution, attests to the stability of the Os_2^{5+} core. Furthermore, both $Os_2Cl(chp)_4$ and $Os_2Cl_4(Ph_2Ppy)_2(O_2CCH_3)$ are air-stable in the solid state and in solutuion. The tendency for Os_2^{6+} compounds to undergo a one-electron electrochemical reduction has been documented, and this result was exploited by Walton and co-workers to prepare Os(II, III) complexes by chemical reduction.[7]

Compound **1** was prepared by the reaction of $Os_2Cl_2(O_2CCH_3)_4$ (0.10 g) with 2-(diphenylphosphino)pyridine (0.30 g) in the presence of excess Me_3SiCl in refluxing toluene for 24 h. The red-brown product precipitated from the reaction solution and was separated from the unreacted tetraacetate by extraction with dichloromethane [yield 21 mg (26%)]. About 50 mg of $Os_2Cl_2(O_2CCH_3)_4$ was recovered. Crystals of a quality suitable for an X-ray diffraction study were grown by layering hexane over a solution of **1** in dichloromethane. The compound crystallized as the solvate $Os_2Cl_4(Ph_2Ppy)_2(O_2CCH_3)\cdot CH_2Cl_2$.

The structural identity of **1** has been proven by

* Author to whom correspondence should be addressed.

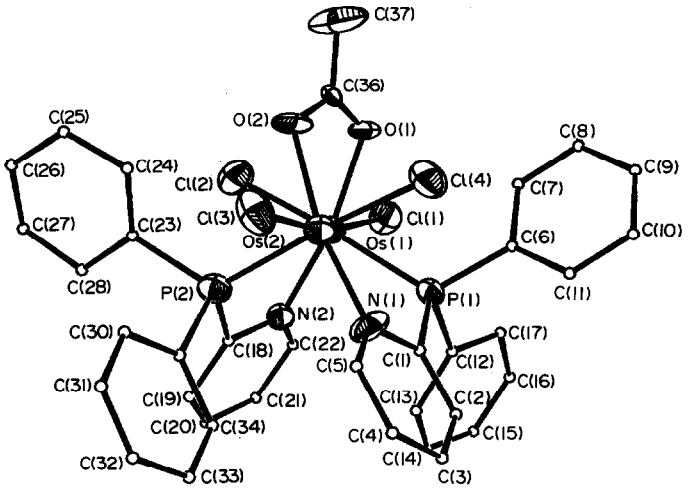


Fig. 1. Molecular structure of **1**. Some important distances (Å) and angles (°) are: Os(1)—Os(2) = 2.395(1), Os(1)—Cl(1) = 2.428(5), Os(1)—Cl(2) = 2.377(5), Os(1)—P(1) = 2.329(5), Os(1)—N(2) = 2.09(2), Os(1)—O(1) = 2.101(13), Os(2)—Cl(3) = 2.421(6), Os(2)—Cl(4) = 2.365(5), Os(2)—P(2) = 2.331(6), Os(2)—N(1) = 2.06(2), Os(2)—O(2) = 2.104(13), Cl(1)—Os(1)—Os(2) = 156.9(1), Cl(3)—Os(2)—Os(1) = 156.3(2), N(2)—Os(1)—Cl(2) = 83.6(4), Cl(2)—Os(1)—O(1) = 83.7(4), O(1)—Os(1)—P(1) = 101.7(4), P(1)—Os(1)—N(2) = 90.8(4), Cl(4)—Os(2)—N(1) = 84.1(5), N(1)—Os(2)—P(2) = 90.2(5), P(2)—Os(2)—O(2) = 102.8(4), O(2)—Os(2)—Cl(4) = 82.9(4).

a single-crystal X-ray study.* An IR spectrum of the complex revealed the presence of both acetate and Ph_2Ppy groups. In addition, electrochemical measurements support the formulation of the complex as a mixed-valence Os(II)Os(III) species. Cyclic voltammetric measurements of $Os_2Cl_4(Ph_2Ppy)_2(O_2CCH_3)$ in dichloromethane revealed an oxidation couple located at $E_{1/2} = +0.95$ V and a reduction at $E_{1/2} = -0.34$ V vs Ag–AgCl. The latter process represents the formation of an Os_2^{4+} species at a reasonably accessible potential. This suggests that it may be feasible to reduce compound **1** chemically. However, it must be noted that the process is "quasi-reversible", i.e. $i_{p,c}/i_{p,a} \neq 1$.

A side view of **1** along the Os—Os bond axis is presented in Fig. 1. This ORTEP diagram depicts clearly the twisting exhibited by the bridging groups to minimize repulsive interactions. The *cis*-Ph_2Ppy ligands are bonded in a "head-to-tail" arrangement (each Os center is bonded to one P and one N atom). The chloride ligands in **1** are of two types: those of one set occupy axial sites [Cl(1) and Cl(3)] and those of a second set [Cl(2) and Cl(4)] are in terminal positions, which are located on opposite sides of the molecule. The axial Os—Cl bonds are not colinear with the Os—Os bond [average Os—Os—Cl(axial) = 156.6]. The existence of such a deviation for dirhodium and diosmium carboxylates which contain axial chloride ligands has been noted in some earlier studies.[6,10] The terminal chlorides are so disposed that the planes defined by atoms Cl(2)—Os(1)—Os(2) and Os(1)—Os(2)—Cl(4) form a dihedral angle of 127°. This is a considerable deviation from the ideal 180° expected for equatorially arranged ligands.

A notable structural feature is the Os—Os distance which is 2.395(1) Å in **1**. As mentioned earlier, this corresponds to a bond order of 2.5, formulated as such because the compound is of the

* Crystal data for

$Os_2Cl_4(Ph_2Ppy)_2(O_2CCH_3)\cdot CH_2Cl_2$:

$Os_2Cl_6P_2O_2N_2C_{37}H_{33}$, $M = 1192.75$, monoclinic, space group $P2_1/n$, $a = 10.496(3)$ Å, $b = 20.688(5)$ Å, $c = 18.440(5)$, $\beta = 91.62(2)°$, $V = 4003(3)$, $Z = 4$, $d_{calc} = 1.826$ g cm^{-3}. A total of 5889 reflections were collected in the range $4 < 2\theta < 45°$ using graphite-monochromated Mo-K_α radiation ($\lambda = 0.71073$ Å). The positions of the two Os atoms were obtained from a Patterson map, and the remaining non-hydrogen atoms were located from alternating least-squares refinements and difference Fourier maps. The structure was refined using 2902 reflections having $F_o^2 > 3\sigma(F_o)^2$ to give residuals of $R(F) = 0.0515$ and $R_w = 0.0566$. All non-hydrogen atoms were refined anisotropically with the exception of N(2), C(11), C(18) and C(27). An empirical absorption correction based on psi scans was applied during data reduction, and after the location of all the atoms, the program DIFABS[9] was applied to further eliminate the absorption problems that are common to thin acicular crystals.

d^5–d^6 type with a total of 11 electrons to place in the molecular-orbital scheme. The ground state of these Os_2^{5+} complexes as defined by recent preliminary magnetic measurements consists of contributions from spin states derived from both $\sigma^2\pi^4\delta^2\delta^{*1}\pi^{*2}$ and $\sigma^2\pi^4\delta^2\delta^{*2}\pi^{*1}$ (or $\sigma^2\pi^4\delta^2\pi^{*3}$) configurations.[7,8] The Os—Os distance in the present compound is one of the longest reported Os—Os multiple bonds,† and it is appreciably longer by (0.047 Å) than that found in $Os_2Cl(chp)_4$.[8] This significant difference may perhaps be attributed to the more highly distorted nature of the bridging groups in $Os_2Cl_4(Ph_2Ppy)_2(O_2CCH_3)$, a situation which probably results in less orbital overlap and hence an increase in the Os—Os bond length.

Acknowledgement—We thank the National Science Foundation for financial support.

† The unusual asymmetric complex $Os_2Cl_3(PhNpy)_3$ has an Os—Os distance of 2.392(1) Å which is not statistically different from 2.395(1) Å.

REFERENCES

1. A. R. Chakravarty, F. A. Cotton and D. A. Tocher, *Inorg. Chem.* 1984, **23**, 4030.
2. A. R. Chakravarty, F. A. Cotton and D. A. Tocher, *J. Am. Chem. Soc.* 1984, **106**, 6409.
3. A. R. Chakravarty, F. A. Cotton and D. A. Tocher, *Inorg. Chem.* 1985, **24**, 172.
4. A. R. Chakravarty, F. A. Cotton and D. A. Tocher, *Inorg. Chem.* 1985, **24**, 1263.
5. A. R. Chakravarty, F. A. Cotton and D. A. Tocher, *J. Chem. Soc., Chem. Commun.* 1984, 501; A. R. Chakravarty, F. A. Cotton and D. A. Tocher, *Inorg. Chem.* 1984, **23**, 4697.
6. A. R. Chakravarty, F. A. Cotton and D. A. Tocher, *Inorg. Chim. Acta* 1984, **89**, L15; A. R. Chakravarty, F. A. Cotton and D. A. Tocher, *Inorg. Chem.* 1985, **24**, 1334.
7. S. M. Tetrick, V. T. Coombe, G. A. Heath, T. A. Stephenson and R. A. Walton, *Inorg. Chem.* 1984, **23**, 4567.
8. F. A. Cotton, K. R. Dunbar and M. Matusz, submitted for publication.
9. N. Walker and D. Stuart, *Acta Cryst.* 1983, **A39**, 158.
10. A. R. Chakravarty, F. A. Cotton and D. A. Tocher, *Organometallics* 1985, **4**, 8.

Polyhedron Vol. 5, No. 3, pp. 907–909, 1986
Printed in Great Britain

0277–5387/86 $3.00 + .00
© 1986 Pergamon Press Ltd

COMMUNICATION

A MIXED OXO–THIO-BRIDGED TRITUNGSTEN TRIANGULAR CLUSTER COMPLEX

ZVI DORI*

Department of Chemistry, Technion—Israel Institute of Technology, Haifa, Israel

and

F. ALBERT COTTON,* ROSA LLUSAR and WILLI SCHWOTZER

Department of Chemistry and Laboratory for Molecular Structure and Bonding, Texas A&M University, College Station, TX 77843, U.S.A.

(*Received* 10 *September* 1985; *accepted* 31 *October* 1985)

Abstract—The preparation and structural definition and UV–visible spectrum of the $[W_3(\mu_2\text{-}O)_3(\mu_3\text{-}S)(NCS)_9]^{5-}$ ion are reported. The W—W distances, averaged according to C_{3v} virtual symmetry, are 2.612[6] Å.

There has recently been intense activity in the study of the cuboidal $[Mo_4S_4]^{n+}$ species[1–7] as well as of their important fragment, the $[Mo_3S_4]^{4+}$ unit,[8–12] and the entire series[5,13,14] of mixed oxo–thio species, $[Mo_3S_nO_{4-n}]^{4+}$ of which there are eight, counting isomers and end members. Synthetic routes have been diverse, but it is notable that Sykes and coworkers have demonstrated the existence of a completely general route in which appropriate dinuclear species, with selected O- and S-contents, e.g. $Mo_2O_2(\mu\text{-}S)_2L_n$, are used as building blocks. Similar successful activity is not as yet in evidence for the potential tungsten analogs of these molybdenum compounds. It may also be noted that the Sykes-type synthetic route will in any case not be available because the corresponding tungsten starting materials are unavailable.

Our own routes to Mo_3S_4 and Mo_4S_4 species,[7,11,12] which are different from those of other workers, have the advantage that they should be readily applicable to tungsten analogs as well. An exploration of this possibility has been underway for some time and reports on perthio species will be forthcoming. We wish to report here a more surprising and interesting result, namely, the isolation and structure proof of the first mixed oxo–thio tritungsten species,

$$[W_3(\mu_2\text{-}O)_3(\mu_3\text{-}S)(NCS)_9]^{5-}.$$

Tungsten hexacarbonyl (1 g) and 0.8 g of anhydrous Na_2S were refluxed, under N_2, in 100 cm^3 of acetic anhydride for 12 h. A red precipitate which formed upon cooling of the reaction mixture, was separated by filtration and dissolved in 0.2 M HCl. This solution was passed through a Dowex 50W-X2 cation exchange column, washed with 0.5 M HCl and then eluted with 4 M HCl. This eluate was diluted 10 times and passed again through a cation exchanger. After washing with H_2O the column was soaked with 0.5 M NH_4SCN and left under N_2 for 24 h before it was eluted. To this purple eluate propylenediamine dihydrochloride was added and after 10 days standing in air well-formed purple crystals were obtained. Because of spectral changes that occurred during this period, accompanied by the distinctive smell of H_2S, we are certain that partial hydrolysis of a perthio precursor was occurring during this 10-day period.

The spectrum given by a solution of these purple crystals is shown in Fig. 1. The crystallographic

*Authors to whom correspondence should be addressed.

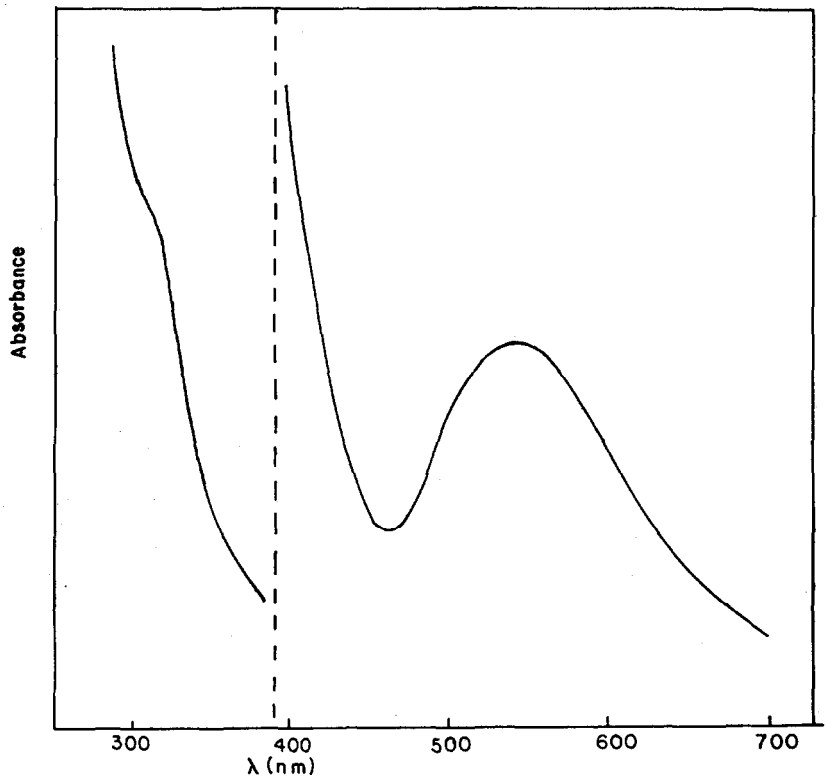


Fig. 1. Electronic absorption spectrum of $[W_3(\mu_3\text{-}S)(\mu_2\text{-}O)_3(NCS)_9]^{5-}$. The absorbance is given on an arbitrary scale.

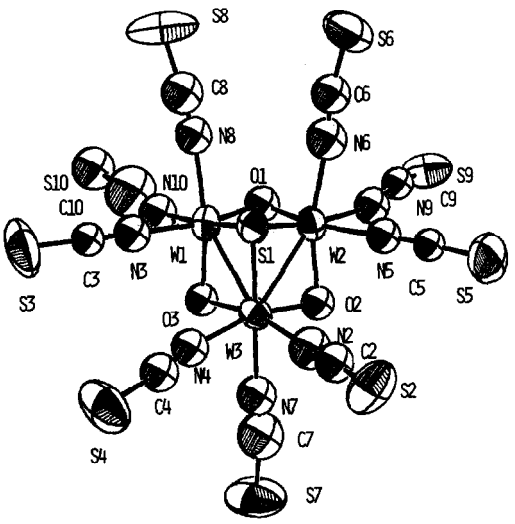


Fig. 2. ORTEP representation of the cluster anion. Thermal ellipsoids are drawn at 50% probability.

* Monoclinic crystals, $P2_1/c$, with $a = 16.616(5)$ Å, $b = 11.744(3)$ Å, $c = 23.780(10)$ Å, $\beta = 109.20(2)°$, $Z = 4$. Refinement is continuing. Current residuals are: $R = 0.051$, and $R_w = 0.066$ for a fit of 253 variables to 1713 data with $F_o^2 > 3\sigma(F_o^2)$. A table of positional parameters has been deposited with the Editor at Queen Mary College and copies are available on request.

work* was not straightforward because the crystals have a pronounced tendency to twinning and scattered X-rays relatively poorly despite their attractive visual appearance.

The $[W_3(\mu_2\text{-}O)_3(\mu_3\text{-}S)(NCS)_9]^{5-}$ anion is shown in Fig. 2. It has effectively C_{3v}-symmetry and the following principal dimensions (averaged accordingly): W—W, 2.612[6] Å; W—S, 2.34[2] Å; W—O, 1.98[2] Å. These may be compared with those previously reported[13] for

$$[Mo_3(\mu_2\text{-}O)_3(\mu_3\text{-}S)(HNTA)_3]^{2-},$$

viz. 2.589, 2.360 and 1.917 Å.

Acknowledgement—We thank the National Science Foundation for support.

REFERENCES

1. A. Müller, W. Eltzner, H. Bögge and R. Jostes, *Angew. Chem., Int. Ed. Engl.* 1982, **21**, 795.
2. A. Müller, W. Eltzner, W. Clegg and G. M. Sheldrick, *Angew Chem., Int. Ed. Engl.* 1982, **21**, 536.
3. T. Shibahara, H. Kuroya, K. Matsumoto and S. Ooi, *J. Am. Chem. Soc.* 1984, **106**, 789.
4. T. C. W. Mak, K. S. Jasim and C. Chieh, *Inorg. Chem.* 1985, **24**, 1587.
5. P. Kathirgamanathan, M. Martinez and A. G. Sykes,

In *Abstracts of Fifth Climax International Conference on the Chemistry and Uses of Molybdenum, July* 1985, p. 133.
6. P. Kathirgamanathan, M. Martinez and A. G. Sykes, *J. Chem. Soc., Chem. Commun.* 1985, 953.
7. F. A. Cotton, M. P. Diebold, Z. Dori, R. Llusar and W. Schwotzer, *J. Am. Chem. Soc.* 1985, **107**, 6735.
8. T. R. Halbert, K. McGauley, W.-H. Pan, R. S. Czernuszewicz and E. I. Stiefel, *J. Am. Chem. Soc.* 1984, **106**, 1849.
9. A. Müller and U. Reinsch, *Angew. Chem., Int. Ed. Engl.* 1980, **19**, 72.
10. N. C. Howlader, G. P. Haight, Jr, T. W. Hambley, G. A. Lawrance, K. M. Rahmoeller and M. R. Snow, *Aust. J. Chem.* 1983, **36**, 377.
11. F. A. Cotton, Z. Dori, R. Llusar, D. O. Marler and W. Schwotzer, *Inorg. Chim. Acta* 1985, **102**, L25.
12. F. A. Cotton, Z. Dori, R. Llusar and W. Schwotzer, *J. Am. Chem. Soc.* 1985, **107**, 6734.
13. T. Shibahara, H. Hattori and H. Kuroya, *J. Am. Chem. Soc.* 1984, **106**, 2710.
14. P. Kathirgamanathan, M. Martinez and A. G. Sykes, *J. Chem. Soc., Chem. Commun.* 1985, 1437.

Polyhedron Vol. 5, No. 3, pp. 911–912, 1986
Printed in Great Britain

0277–5387/86 $3.00 + .00
© 1986 Pergamon Press Ltd

COMMUNICATION

DICHLOROBIS(1,2,5-TRIPHENYLPHOSPHOLE)PALLADIUM(II) IN CARBONYLATION REACTIONS

B. M. CHOUDARY,* N. PRABHAKAR REDDY and M. ZAFAR JAMIL

Regional Research Laboratory, Hyderabad 500007, India

(*Received* 30 *July* 1985; *accepted* 2 *September* 1985)

Abstract—*trans*-Dichlorobis(1,2,5-triphenylphosphole)palladium(II) was synthesised and found to carbonylate organic halides at near atmospheric pressures and gave better yields than its triphenylphosphine analogue.

Stable complexes of 1-substituted-3,4-dimethylphospholes with palladium,[1] platinum[2] and ruthenium[3] have been reported. $Ru(RDMP)Cl_2$ (RDMP = 1-alkyl-3,4-dimethylphosphole) exhibited the ability to catalyse the hydrogenation of 1-heptene to heptane at rates comparable with its phosphine analogue. The complex $RhH(PDBP)_4$ (PDBP = 1-phenyldibenzophosphole) is 7 times more active as a hydrogenation catalyst than the well-known Wilkinson catalyst, $RhCl(PPh_3)_3$.[4] We were interested in comparing the reactivity of palladium complexes of phospholes with that of triphenylphosphine and chose the carbonylation reactions of some organic halides because of their industrial importance.

The present work deals for the first time with the preparation of a new complex of palladium with 1,2,5-triphenylphosphole (TPP) and demonstrates its utility in the carbonylation of some organic halides. The choice of TPP as a ligand is expected to simulate the conditions prevailing in the palladium–triphenylphosphine complex, but with a difference in the free movement of two of the three phenyl groups in the electronic environment around the palladium.

EXPERIMENTAL

Measurements and materials

Spectra were recorded on Perkin–Elmer (IR), V.G. Micromass Ltd (mass) and JEOL FX 90Q (NMR) spectrometers. Standard procedures were used for determining the elements. Carbonylation reactions were carried in a Berghof autoclave (Teflon lined). All solvents were dried by standard procedures. TPP was synthesised from 1,4-diphenyl-1,3-butadiene and phenylphosphonous dichloride.[5]

Preparation of $PdCl_2(TPP)_2$

A solution of TPP (1.97 mmol) in benzene (6 cm^3) was added to a solution of $PdCl_2(PhCH_2CN)_2$ (0.973 mmol) in benzene (8 cm^3) with stirring. The stirring was continued for 5 min and the mixture was allowed to stand at room temperature. The orange crystals formed were filtered off, washed with benzene and dried *in vacuo* at 60°C. Yield 0.748 g (98%).

Carbonylation of aryl, benzyl and phenacyl halides

A mixture of substrate (15 mmol), sodium acetate (20 mmol), and palladium catalyst (0.15 mmol) in 25 cm^3 ethanol was heated in an autoclave pressurized with carbon monoxide (20 psi). After 24 h the reaction mixture was filtered gravimetrically and washed with 50 cm^3 ethanol. The solution was concentrated under reduced pressure and diluted with 100 cm^3 water and extracted with small portions of pentane or dichloromethane. The combined extracts were washed successively with 2 N HCl, saturated aqueous sodium carbonate solution and saturated aqueous sodium chloride solution. The solution was dried over anhydrous sodium sulphate, concentrated and distilled under reduced pressure. The products (Table 1) thus obtained were identified by IR NMR and mass spectra.

* Author to whom correspondence should be addressed.

Table 1. Carbonylation of aryl, benzyl and phenacyl halides

S. No.	Halide	Temperature (°C)	Product	Yield (%) $PdCl_2(TPP)_2$	Yield (%) $PdCl_2(PPh_3)_2$
1	C_6H_5I	60	$C_6H_5CO_2C_2H_5$	90	70
2	$C_6H_5CH_2Cl$	80	$C_6H_5CH_2CO_2H_5$	65	55
3	$C_6H_5COCH_2Cl$	70	$C_6H_5COCH_2CO_2C_2H_5$	40	25

RESULTS AND DISCUSSION

trans-Dichlorobis(TPP)palladium(II) was obtained in good yield (98%). It is an orange tetracoordinated complex and elemental analysis gave the molecular formula $PdCl_2(TPP)_2$. Found: Pd, 13.3; C, 66.1; H, 4.3; P, 7.2; Cl, 8.8%. Calc. for $PdCl_2(TPP)_2$: Pd, 13.2; C, 65.8; H, 4.3; P, 7.7; Cl, 8.9%.

The IR spectrum shows a single stretching frequency at 360 cm^{-1} for the Pd—Cl bond and 450 cm^{-1} for the Pd—P bond, which indicates a *trans*-configuration for the complex due to its D_{2h}-symmetry.[6] The resultant *trans*-orientation of the complex unlike 1-substituted 3,4-dimethylphosphole which has a *cis*-configuration may be ascribed to the expected larger van der Waals' repulsive forces due to the phenyl moiety. The complex is very stable and gave better yields in carbonylation reactions than the phosphine analogue under identical conditions as reported in Table 1. The results obtained with the phosphole complex at near atmospheric pressures were comparable with those of its phosphine analogue even at 200 psi carbon monoxide pressure.[7] No palladium deposition was observed after completion of the carbonylation reaction. The used catalyst gave almost same yields of carbonylated products.

Acknowledgement—We thank the C.S.I.R., India, for providing financial support to N. Prabhakar Reddy.

REFERENCES

1. J. J. MacDougall, E. M. Holt, P. De Meester, N. W. Alcock, F. Mathey and J. H. Nelson, *Inorg. Chem.* 1980, **19**, 1439; J. J. MacDougall, J. H. Nelson, F. Mathey and J. J. Mayerle, *Inorg. Chem.* 1980, **19**, 709.
2. J. J. MacDougall, J. H. Nelson and F. Mathey, *Inorg. Chem.* 1982, **21**, 2145.
3. L. M. Wilkes, J. H. Nelson, L. B. McCusker, K. Seff and F. Mathey, *Inorg. Chem.* 1983, **22**, 2476.
4. D. E. Dudd, D. G. Holah, A. N. Hughes and B. C. Hui, *Can. J. Chem.* 1974, **52**, 775.
5. I. G. M. Campbell, R. C. Cookson, M. B. Hocking and A. N. Hughes, *J. Chem. Soc.* 1965, 2184.
6. D. M. Adams, *Metal–Ligand and Related Vibrations*. St Martin's Press, New York (1968).
7. J. K. Stille and P. K. Wong, *J. Org. Chem.* 1975, **40**, 532.

Polyhedron Vol. 5, No. 3, pp. 913–915, 1986
Printed in Great Britain

0277–5387/86 $3.00 + .00
© 1986 Pergamon Press Ltd

COMMUNICATION

EFFECTS OF AXIAL LIGAND ON THE OXIDATION OF TRIPHENYLPHOSPHINE CATALYZED BY NITRO(TETRAPHENYLPORPHYRINATO)COBALT COMPLEXES

KENICHI YAMAMOTO

Faculty of Pharmaceutical Sciences, University of Tokyo, Hongo, Bunkyo-ku, Tokyo 113, Japan

(*Received* 23 *August* 1985; *accepted* 4 *October* 1985)

Abstract—Nitro(tetraphenylporphyrinato)cobalt complexes catalyze the oxidation of triphenylphosphine to triphenylphosphine oxide by molecular oxygen. The effects of axial ligands in the nitro cobalt complexes on this oxidation reaction were studied. 4-Cyanopyridine gave the best yield. This result suggests that the more unstable is nitro(tetraphenylporphyrinato)cobalt complex the better the yield obtained.

5,10,15,20 - Tetraphenylporphyrinatocobalt(II) ([Co(tpp)]) reacts with nitrogen monoxide and produces five-coordinate nitrosyl(tetraphenylporphyrinato)cobalt(II) ([Co(tpp)(NO)]).[1] In the presence of an axial ligand (L), this nitrosyl cobalt complex reacts with molecular oxygen to give a nitro(tetraphenylporphyrinato)cobalt complex ([Co(tpp)(NO_2)(L)]).[2] This [Co(tpp)(NO_2)(L)] reacts with triphenylphosphine, resulting in triphenylphosphine oxide. So, under an atmosphere of oxygen, [Co(tpp)(NO_2)(L)] catalyzes the oxidation of triphenylphosphine by molecular oxygen [eqns (1) and (2)]:[3]

$$[Co(tpp)(NO)] + L + \tfrac{1}{2}O_2 \rightarrow [Co(tpp)(NO_2)(L)], \quad (1)$$

$$[Co(tpp)(NO_2)(L)] + PPh_3 \rightarrow [Co(tpp)(NO)] + Ph_3PO + L. \quad (2)$$

In this communication we present the effects of axial ligands such as 1-Meim,* 4-Mepy, py and 4-CNpy, which were used in the previous work,[4] on the yield in this oxidation reaction.

5,10,15,20-Tetraphenylporphyrin (H_2tpp) and [Co(tpp)] were synthesized by the literature methods, respectively.[5,6] Nitrosyl(tetraphenylporphyrinato)cobalt(II) was prepared from NO gas and [Co(tpp)] according to the literature method.[1] Nitro cobalt complexes were prepared from [Co(tpp)(NO)] and O_2 gas at a pressure of 1 atm in 1,2-dichloroethane (DCE) solution containing 5% (v/v) axial ligand in a reactor before the oxidation was started. A 5-cm^3 three-necked round bottom flask equipped with a thermometer, a condenser, and a long syringe needle, by which O_2 was passed through the solution during the oxidation reaction, was used as a reactor. After the formation of the nitro cobalt complex, confirmed by monitoring the visible spectrum in the 350–700-nm range—([Co(tpp)(NO)]: λ_{max} (DCE) 413 nm ($\varepsilon = 1.40 \times 10^5$ mol^{-1} dm^3 cm^{-1}), 538 nm (1.68×10^4), 584 nm (sh, 2.81×10^3); [Co(tpp)(NO_2)(py)]: λ_{max} (DCE) 433 nm ($\varepsilon = 3.35 \times 10^5$ mol^{-1} dm^3 cm^{-1}), 512 nm (sh, 5.58×10^3), 549 nm (1.51×10^4), 588 nm (sh, 5.98×10^3)—triphenylphosphine was added to the solution. The oxidation was carried out at 60°C for 16 h with the solution being stirred magnetically on an oil bath. After 16 h, aliquots of the solution were taken by a micro syringe and analyzed by a liquid chromatography {column, 4.3 mm × 15 cm, packed with Partisil-5, ODS-3, Whatman Inc., U.S.A.; eluant CH_3OH and H_2O mixture [75:25 (v/v)]}. As the internal standard, the base involved in the reacted solution was used.

*Abbreviations: py, pyridine; 4-Mepy, 4-methylpyridine; 1-Meim, 1-methylimidazole; pip, piperidine; 4-CNpy, 4-cyanopyridine.

Table 1. Oxidation of triphenylphosphine to triphenylphosphine oxide catalyzed by [Co(tpp)(NO$_2$)(L)]

Experiment	Complex	[Co]^a (mol dm^{-3})	[PPh$_3$]/[Co]^a	Solvent	Ph$_3$PO yield^b (%)
1	[Co(tpp)(NO$_2$)(4-CNpy)]	6.74×10^{-3}	10	DCE + 5% 4-CNpy	537
2	[Co(tpp)(NO$_2$)(py)]	6.74×10^{-3}	10	DCE + 5% py	500
3	[Co(tpp)(NO$_2$)(4-Mepy)]	6.74×10^{-3}	10	DCE + 5% 4-Mepy	404
4	[Co(tpp)(NO$_2$)(1-Meim)]	6.74×10^{-3}	10	DCE + 5% 1-Meim	300
5	[Co(tpp)(NO$_2$)(PPh$_3$)]	6.74×10^{-3}	10	DCE + 5% PPh$_3$	157
6	CoCl$_2$	6.74×10^{-3}	10	DCE	40

^{a} [Co] and [PPh$_3$] represent the initial concentrations of [Co(tpp)(NO$_2$)(L)] and PPh$_3$, respectively: temperature (60°C), reaction time (16 h), and dioxygen pressure (1 atm) were the same as in Ref. 3.
^{b} Based on catalyst.

Table 2. IR data of NO$_2$ group in [Co(tpp)(NO$_2$)(L)] complexes

Complex	ν_{as} (cm^{-1})	ν_s (cm^{-1})	δ (cm^{-1})	Reference
NO$_2$ gas	1618	1320	750	8
[Co(tpp)(NO$_2$)(py)]^a	1306	1210(m)^b	812	Present work
[Co(tpp)(NO$_2$)(4-Mepy)]^a	1307	1205 (m)	810	Present work
[Co(tpp)(NO$_2$)(1-Meim)]^a	1310	1200 (m)	810	Present work
[Co(tpp)(NO$_2$)(pip)]^a	1304	1200 (m)	807	Present work
[Co(tpp)(NO$_2$)(im)]^c	1310	1260	820	9
CH$_3$NO$_2$	1582	1384	647	10
NO$_2^-$ ion	1335	1250	830	11

^{a} KBr disk.
^{b} m stands for "masked" by the ligand absorptions, and the precise absorption frequencies were not clear.
^{c} Solvent is benzene.

Table 1 shows the yields of triphenylphosphine oxide based on the catalyst. The yield depended apparently on the axial ligand (L) and decreased in order as follows:

4-CNpy > py > 4-Mepy > 1-Meim.

In this oxidation reaction, the following factors seem to be responsible for the yield: (a) the ease of formation of the nitro cobalt complex, (b) the ease of reproduction of the nitrosyl cobalt complex, and (c) the coordination geometry or the charge distribution of the nitro group in [Co(tpp)(NO$_2$)(L)]. As is shown by eqns (1) and (2), the stronger the coordination of the axial ligand to the cobalt ion the more stable the nitro cobalt complex formed and reproduction of the nitrosyl cobalt complex becomes more difficult. As the measure of the coordinating ability of the ligand, the values of the equilibrium constants (K^L) (mol^{-1} dm^3) for the reaction shown in eqn (3):[4(c)]

$$[\text{Co(tpp)}] + \text{L} \overset{K^L}{\rightleftharpoons} [\text{Co(tpp)(L)}] \qquad (3)$$

were used. Though the log K^L values were obtained in DCE at room temperature (23°C), the sequence of the values may not be different at 60°C. The coordinating abilities of axial ligand decreased in the following order, 1-Meim (log K^L = 3.22) > 4-Mepy (2.99) > py (2.92) > 4-Cpy (2.57). This sequence is in the reverse order to the yields of triphenylphosphine oxide shown above.

The IR spectra of the isolated nitro cobalt complexes were measured to study the IR spectra of the nitro groups in [Co(tpp)(NO$_2$)(L)].* The frequencies of the asymmetric [ν_{as} (cm^{-1})], symmetric [ν_s (cm^{-1})] and deformation vibrations [δ (cm^{-1})][2,7] are shown in Table 2. It indicates that

* Solid [Co(tpp)(NO$_2$)(L)] complexes were isolated by a modification of the literature method[2] for the IR spectra sample (KBr tablets): L = 1-Meim, 4-Mepy, py and pip. The 4-CNpy complex could not be isolated, though it was formed in the solution.

the nitro groups seem to be nearly nitro anion forms in all the nitro cobalt complexes. The NO_2 group of the analogous

[Co(tpp)(NO_2)(3,5-dimethylpyridine)]

was already shown as the NO_2^- form in the X-ray analysis data.[12] The differences in absorption frequencies among the different axial base complexes are small probably because all the Co–NO_2 bonds are nearly ionic. From the fact that the sequence of the yield is opposite to that of the coordinating ability of axial ligand, factor (b) seems to be the most effective on the yield of this oxidation reaction.

REFERENCES

1. W. R. Scheidt and J. L. Hoard, *J. Am. Chem. Soc.* 1973, **95**, 8281.
2. S. J. Clarkson and F. Basolo, *Inorg. Chem.* 1973, **12**, 1528.
3. B. S. Tovrog, S. E. Diamond and F. A. Mares, *J. Am. Chem. Soc.* 1979, **101**, 270.
4. (a) K. Yamamoto and T. Kwan, *J. Catal.* 1970, **18**, 354; (b) T. Takayanagi, H. Yamamoto and T. Kwan, *Bull. Chem. Soc. Jpn* 1975, **48**, 2618; (c) K. Yamamoto, to be published.
5. A. D. Adler, F. R. Longo, J. D. Finarelli, J. Goldmacher, J. Assour and L. Korsakoff, *J. Org. Chem.* 1967, **32**, 476.
6. P. Rothemund and A. R. Menotti, *J. Am. Chem. Soc.* 1948, **70**, 1808.
7. K. Nakamoto, J. Fujita and H. Murata, *J. Am. Chem. Soc.* 1958, **80**, 4817.
8. J. C. D. Brand, J. L. Hardwick, R. J. Pirkle and J. Seliskar, *Can. J. Phys.* 1973, **51**, 2184.
9. K. Tsuji, M. Imaizumi, A. Oyoshi, I. Mochida, H. Fujitsu and K. Takeshita, *Inorg. Chem.* 1982, **21**, 721.
10. J. P. Wilson, *J. Chem. Phys.* 1943, **11**, 361.
11. F. A. Miller and C. H. Wilkins, *Anal. Chem.* 1952, **24**, 1253.
12. W. R. Scheidt and J. A. Ramanuja, *Inorg. Chem.* 1975, **14**, 2643.

Polyhedron Vol. 5, No. 3, pp. 917–920, 1986
Printed in Great Britain

0277–5387/86 $3.00 + .00
© 1986 Pergamon Press Ltd

COMMUNICATION

A NOVEL ACCESS TO THE ANIONIC PERMETHYLATED *FAC*-TRIPOD LIGAND $[C_5Me_5Co\{P(O)(OEt)_2\}_3]^-$, AND ITS DERIVED TRINUCLEAR AND BINUCLEAR COMPLEXES

ENRIQUE ROMÁN E.,* FERNANDO TAPIA C. and SERGIO HERNÁNDEZ M.

Facultad de Química, Pontificia Universidad Católica de Chile, Casilla 6177, Santiago, Chile

(*Received* 18 *November* 1985; *accepted* 20 *November* 1985)

Abstract—$[C_5Me_5Co\{P(O)(OEt)_2\}_3]Co(II)$ was obtained in high yield from the reaction of C_5Me_5Li with $Co(acac)_3$ and diethylphosphite in a one-step synthesis. This provides high-yield synthetic routes to several decamethylated triple-decker sandwiches $[C_5Me_5Co\{P(O)(OEt)_2\}_3]M$ [M = Co(III) or Ti(IV)], and pentamethylated binuclear complexes $[C_5Me_5Co\{P(O)(OEt)_2\}_3]M'L_n$, $\{M'L_n = [Re(CO)_3]^+, [VO(acac)]^+$ or $[Ru(\eta\text{-}C_6Me_6)]^{2+}\}$.

We are interested in triple-decker sandwiches in connection with electrochemical studies,[1,2] in particular in their application to multi-step electron transfer reactions that do not imply changes in the molecular configuration of such complexes. Moreover, binuclear compounds having a VO^{2+} active center coordinated with the *fac*-tripod ligand $[C_5H_5Co\{P(O)(OEt)_2\}_3]^-$ have proved to be active in cathecol regio-specific catalysis.[3]

We now report the easy and efficient synthesis of the Co(III) decamethylated triple-decker sandwich **1**, which is the precursor for the preparation of the anionic *fac*-tridentate ligand **2**, isolated as the sodium salt. The addition of C_5Me_5Li in THF to the air-stable complex $Co(acac)_3$ yields an intermediate complex that might correspond to the 16-electron complex $[C_5Me_5Co(acac)]^+$. The latter complex reacts with diethylphosphite at high temperature, affording the trinuclear complex **1** in 90% yield [reaction (2)]. In this reaction no formation of the decamethylated cobalticinium ion was detected unlike what is observed in Wilkinson's reaction[4] [reaction (1)]:

$$2Co(aca)_3 + 4CpMgBr \xrightarrow[\text{benzene}]{} 2[Cp_2Co]Br + MgBr_2 + 3Mg(acac)_2 \quad (1)$$

$$Cp = C_5H_5^- \qquad 65\%$$

$$Co(acac)_3 + Cp^*Li \xrightarrow[\text{(ii) HOP(OEt)}_2]{\text{(i) THF, 273 K}} [Cp^*Co\{P(O)(OEt)_2\}_3]_2Co \quad (2)$$

$$Cp^* = C_5Me_5^- \qquad \mathbf{1}\ (90\%)$$

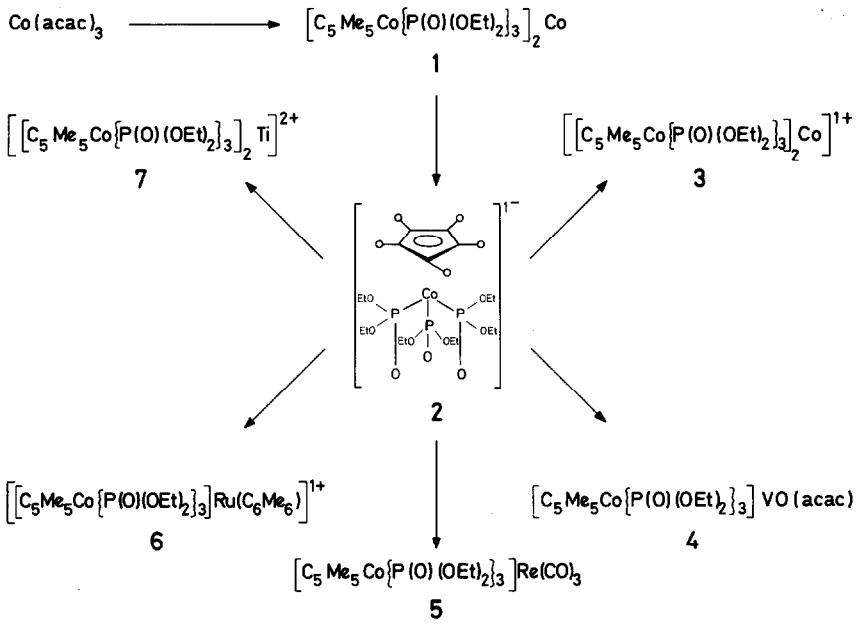
Oxidative cyanidation of **1** in methanol affords the pentamethylated *fac*-tridentate ligand **2** in high yield (90%). The latter is readily *fac*-coordinated with several acid metallic centers such as Co(III), Ti(IV), $[Re(CO)_3]^+$, $[VO(acac)]^+$ and $[Ru(\eta\text{-}C_6Me_6]^{2+}$, thus leading to new triple-decker sandwich compounds **3** and **7** as well as to new binuclear compounds **4**, **5** and **6** (see Scheme 1). All these were characterized by ^1H NMR, IR spectra, magnetic measurements, and microanalysis (see Table 1).

To conclude, reaction (2) provides a simple and convenient route to the preparation of decamethylated triple-decker sandwich compounds as well as binuclear pentamethylated compounds containing the *fac*-tridentate pentamethylated ligand **2**. This facilitates the comparison of their various physicochemical properties with the series of complexes having non-permethylated Cp rings.[5]

EXPERIMENTAL

All solvents were of reagent grade, dried by standard procedures, and all reactions were conducted using Schlenk standard techniques.

* Author to whom correspondence should be addressed.



Scheme 1.

Table 1. Spectroscopic and magnetic characterization of the complexes[a]

Compound	^{1}H NMR[b]	IR spectra [ν (cm^{-1})][c]	Magnetic data[d]
1	—	ν_s(C—O—P) 1115(s), ν_{as}(PO_2) 1030(s) ν(C—C) 920(s), δ(P=O) 580(s)	μ (BM) 5.23
2	3.98 (m, 12H, CH_2) 1.70 [q, 15H, Cp*: $J_{H(Cp^*)-P}$ 0.90 Hz] 1.20 [t, 18H, CH_3: $^3J_{(HCCH)}$ 7.0 Hz]	ν_s(C—O—P) 1155(s), δ(P=O) 575(s)	—
3	4.22 (m, 12H, CH_2) 1.78 [q, 15H, Cp*: $J_{H(Cp^*)-P}$ 1.3 Hz] 1.38 [t, 18H, CH_3: $^3J_{(HCCH)}$ 7.0 Hz]	ν_s(C—O—P) 1185(s), ν_{as}(PO_2) 1040(s) δ(P=O) 560(s), δ(PF_6) 830(s)	—
4	—	ν_s(V=O) 935(s), δ(P=O) 585(s) ν(C=O)acac 1580(m), ν(C—O—P) 1135(s)	μ (BM) 1.65 g_{iso} 1.965 A_o (G) 110.4
5	4.08 (m, 12H, CH_2) 1.64 [q, 15H, Cp*: $J_{H(Cp^*)-P}$ 0.92 Hz] 1.30 (t, 18H, CH_3: $^3J_{(HCCH)}$ 7.0 Hz]	ν(C≡O) 2.000(s), 1.865(s) δ(P=O) 595 (s), ν_s(C—O—P) 1105(s)	—
6	4.08 (m, 12H, CH_2) 2.06 (s, 18H, C_6Me_6) 1.53 [q, 15H, Cp*: $J_{H(Cp^*)-P}$ 0.95 Hz] 1.32 [t, 18H,CH_3: $^3J_{(HCCH)}$ 7.0 Hz]	ν_s(C—O—P) 1105(m), δ(P=O) 600(m) δ(PF_6) 840(s)	—
7	4.14 (m, 12H, CH_2) 1.70 [q, 15H, Cp*: $J_{H(Cp^*)-P}$ 0.90 Hz] 1.34 [t, 18H, CH_3: $^3J_{(HCCH)}$ 7.0 Hz]	ν_s(C—O—P) 1100(m), δ(P=O) 635(m) δ(PF_6) 840(s)	—

[a] Cp*, π-C_5Me_5; Me, CH_3; acac, acetylacetonate.
[b] $CDCl_3$ solvent, δ ppm (TMS internal reference).
[c] KBr disc.
[d] Magnetic susceptibility measured at 295 K in a Faraday balance or calculated by Evans' method. ESR parameters (isotropic g and hyperfine constant A_o) measured at 295 K.

Instruments

IR: Perkin–Elmer 567 grating spectrophotometer; ESR: Brucker ER-420 with ER-400 X-RL cavity; Faraday balance and ^1H NMR: Varian-XL-100 spectrometer (using Evans's method for the determination of magnetic susceptibility). Satisfactory analyses were obtained for all new compounds at the Service Central d'Analyse (CNRS), Vernaison, France. $Co(acac)_3$,[6(a)] $Vo(aca)_2$,[6(b)] $K_2[Re(CO)_3Br_3]$[6(c)] and the dimer $[(C_6Me_6)RuCl_2]_2$[6(d)] were prepared by methods reported in the literature.

Synthesis of $[C_5Me_5Co\{P(O)(OEt)_2\}_3]Co$ (1)

2.58 g (18.192 mmol) of C_5Me_5Li in 20 cm^3 THF were added to a $Co(acac)_3$ suspension [3.24 g (9.096 mmol)], in an equal amount of THF at 273 K with constant stirring for 1 h. To the filtered and vacuum-dried brown solution, 30 cm^3 of diethylphosphite were added. The solution was then heated at 403 K for 24 h. Concentration and cooling of the solution yields **1** (90% yellow crystals recrystallized from MeOH–CH_2Cl_2). Found: C, 41.0; H, 7.0; P, 14.2. Calc. C, 41.5; H, 7.1; P, 14.6%.

Synthesis of $[C_5Me_5Co\{P(O)(OEt)_2\}_3]Na$ (2)

2.89 g (2.28 mmol) of **1** and 1.037 g (15.96 mmol) of NaCN were suspended in methanol, and a homogeneous solution was obtained by bubbling air through it. After solvent elimination in a vacuum system the resulting solid was extracted with diethyl ether, and crystallized by cooling (253 K). Yellow crystals were separated (yield 70%). Found: C, 41.5; H, 7.5; P, 14.4. Calc. C, 42.0; H, 7.2; P, 14.8%.

Synthesis of $[C_5Me_5Co\{P(O)(OEt)_2\}_3]Co(PF_6)$ (3)

1.50 g (2.3087 mmol) of **2** and 0.425 g (1.1945 mmol) of $Co(acac)_3$ were dissolved in 30 cm^3 of CH_2Cl_2. After HPF_6(aq) addition a yellow dichloromethane solution was obtained, which was washed with water, then concentrated, and the complex was precipitated with ether. Recrystallization from an ether–CH_2Cl_2 mixture gives yellow crystals (yield 70%). Found: C, 37.2; H, 6.5; P, 15.2. Calc. C, 37.3; H, 6.4; P, 15.3%.

Synthesis of $[C_5Me_5Co\{P(O)(OEt)_2\}_3]VO(acac)$ (4)

0.50 g (0.796 mmol) of $VO(acac)_2$ and 0.212 g (0.796 mmol) of **2** in 20 cm^3 CH_2Cl_2 were mixed under magnetic stirring at room temperature for 1 h; then, after filtration and crystallization from methanol, green crystals (60% yield) were obtained. Found: C, 41.7; H, 6.9; P, 12.0. Calc. C, 42.0; H, 6.7; P. 12.1%.

Synthesis of $[C_5Me_5Co\{P(O)(OEt)_2\}_3]Re(CO)_3$ (5)

0.253 g (0.430 mmol) of $K_2[Re(CO)_3Br_3]$ and 0.2704 g (0.430 mmol) of **2** in 50 cm^3 THF with a catalytical amount of the *n*-But_4NBr phase transfer agent (0.015 g) were heated at reflux temperature for 12 h. After solvent evaporation the solid was chromatographed on an alumina column. Crystallization from CH_2Cl_2 yields 60% of yellow crystals (**5**). Found: C, 33.8; H, 5.1; P, 10.5. Calc. C, 34.3; H, 5.1; P, 10.6%.

Synthesis of $[C_5Me_5Co\{P(O)(OEt)_2\}_3Ru(\eta\text{-}C_6Me_6)](PF_6)$ (6)

0.1278 g (0.191 mmol) of the dimer $[(C_6Me_6)RuCl_2]_2$ and 0.240 g (0.382 mmol) of **2** in 50 cm^3 of water were heated at reflux temperature for 2 h. Then, 0.0623 g (0.382 mmol) of NH_4PF_6 was added and the solution extracted with CH_2Cl_2 and chromatographed in an alumina column. Crystallization from CH_2Cl_2 yields 65% of orange crystals (**6**). Found: C, 40.0; H, 6.4; P, 12.0. Calc. C, 40.2; H, 6.2; P, 12.2%.

Synthesis of $[C_5Me_5Co\{P(O)(OEt)_2\}_3]_2Ti(PF_6)_2$ (7)

0.0991 g (0.398 mmol) of Cp_2TiCl_2 and 0.50 g (0.796 mmol) of **2** in water were mixed under magnetic stirring for 2 h at room temperature. Then, 0.1298 g (0.796 mmol) of NH_4PF_6 were added. The solid was extracted with CH_2Cl_2 and chromatographed on a silica column (CH_2Cl_2–ether eluant). Recrystallization from CH_2Cl_2–ether yields 75% of yellow crystals (**7**). Found: C, 33.9; H, 6.1; P, 16.1. Calc. C, 34.1; H, 5.8; P, 16.1%.

Acknowledgement—This work was supported by Dirección de Investigación Pontificia Universidad Católica de Chile through Grant No. 32/84.

REFERENCES

1. N. El Murr, A. Chaloyard and W. Klaüi, *Inorg. Chem.* 1979, **18**, 2629.
2. E. Román E., F. Tapia C., A. Schön and E. Samuel, manuscript in preparation.
3. E. Román E., F. Tapia C., M.-T. Garland, J.-Y. Le Marouille and Ch. Giannotti, *J. Organomet. Chem.* 1985, **297**, C8.
4. G. Wilkinson, *J. Am. Chem. Soc.* 1952, **74**, 6148.

5. (a) E. J. Miller, S. J. Landon and T. B. Brill, *Organometallics* 1985, **4**, 533; (b) W. Klaüi, W. Ebespoch and R. Schwarz, *J. Organomet. Chem.* 1983, **252**, 347 (and references therein).
6. (a) E. Bryant and W. C. Fernelius, In *Inorganic Syntheses* (Edited by T. Moeller), Vol. 5, p. 188. McGraw-Hill, New York (1957). (b) R. A. Rowe and M. M. Jones, *ibid.*, Vol. 5, p. 114 (1957); (c) R. Colton and J. E. Knapp, *Aust. J. Chem.* 1972, **25**, 9; (d) M. A. Bennett, T. N. Huang, T. W. Matheson and A. K. Smith, In *Inorganic Syntheses* (Edited by J. P. Falckler), Vol. 21, p. 75. J. Wiley, New York (1980).

Polyhedron Vol. 5, No. 3, pp. 921–923, 1986
Printed in Great Britain

0277–5387/86 $3.00 + .00
© 1986 Pergamon Press Ltd

COMMUNICATION

REPLACEMENT OF TERMINAL AND BRIDGING OXO GROUPS BY PHENYLIMIDO GROUPS IN (η-C_5H_5)OMo(μ-O)$_2$OMo(η-C_5H_5) GIVING (η-C_5H_5)(NPh)Mo(μ-NPh)$_2$Mo(NPh)(η-C_5H_5)

MALCOLM L. H. GREEN* and KELLY J. MOYNIHAN

Inorganic Chemistry Laboratory, South Parks Road, Oxford OX1 3QR, U.K.

(*Received* 22 *November* 1985; *accepted* 27 *November* 1985)

Abstract—The treatment of (η-C_5H_5)OMo(μ-O)$_2$MoO(η-C_5H_5) with excess phenylisocyanate at reflux in tetrahydrofuran yields the arylimido-substituted complex (η-C_5H_5)(NPh)Mo(μ-NPh)$_2$Mo(NPh)(η-C_5H_5), which has been characterized by elemental analysis, and mass, IR and ^{1}H NMR spectra.

Transition-metal–imido complexes have been proposed to be intermediates in industrial processes[1,2] and enzymatic transformations.[3,4] An attractive route to metal–imido complexes proceeds *via* reaction between a metal–oxo group and an organoisocyanate,[5] viz.:

$$[M]{=}O + RNCO \rightarrow [M]{=}NR + CO_2.$$

The versatility of this route is relatively unexplored. Here we describe replacement of the oxygen atoms in the units Mo=O and of Mo—O—Mo, giving M=NPh and Mo—NPh—Mo moieties, respectively.

EXPERIMENTAL

All manipulations were carried out under dry nitrogen or *in vacuo* using standard Schlenk techniques. Solvents were dried, distilled and degassed prior to use. IR spectra were recorded on mulls between CsI plates using a Pye–Unicam SP 2000 spectrophotometer. ^{1}H NMR spectra (300 MHz) were recorded at probe temperature using a Bruker WH300 instrument. Chemical shifts, in ppm relative to Me_4Si, were calibrated using protio impurity peaks of the deuterated solvents as internal standards. C, H and N analyses were performed by the analytical service of this laboratory.

The compound (η-C_5H_5)OMo(μ-O)$_2$MoO(η-C_5H_5) was prepared by the method of Cousins and Green.[6] Phenylisocyanate (PhNCO) (Aldrich Co. Ltd) was used as received.

Synthesis of (η-C_5H_5)(NPh)Mo(μ-NPh)$_2$Mo(NPh)(η-C_5H_5) (1)

A Rotoflo ampoule was charged with (η-C_5H_5)OMo(μ-O)$_2$MoO(η-C_5H_5), tetrahydrofuran (thf) (30 cm^3), (0.34 g, 0.88 mmol) and phenylisocyanate (*ca* 1 cm^3). The mixture was stirred at 70°C for 4 days. On cooling to room temperature a bright orange microcrystalline powder separated. This was collected, washed with ice-cold thf (2 × 3 cm^3) and dried *in vacuo* for 3 h at 60°C. Recrystallization was from dichloromethane–petroleum ether (b.p. 40–60°C). Yield 0.25 g (41%).

Analysis. Found (calc.): C, 59.7 (59.5); H, 4.4 (4.4); N, 8.2 (8.2)%. The mass spectrum (FAB) shows an envelope corresponding to the parent ion, for $^{96}Mo_2$ at $m/z = 686$.

IR data (mull, cm^{-1}): 1577m, 1322ms, 1288m, 1263s, 1164mw (1159sh), 1065mw (1055sh), 1020mw, 1005mw, 994w, 989w, 964m, 907m, 894w, 820w, 809ms, 790ms, 751s (720sh), 695m (660sh), 516vw, 501w, 391w, 360vw, 320w and 273vw. ^{1}H NMR data will be presented and discussed in the text.

* Author to whom correspondence should be addressed.

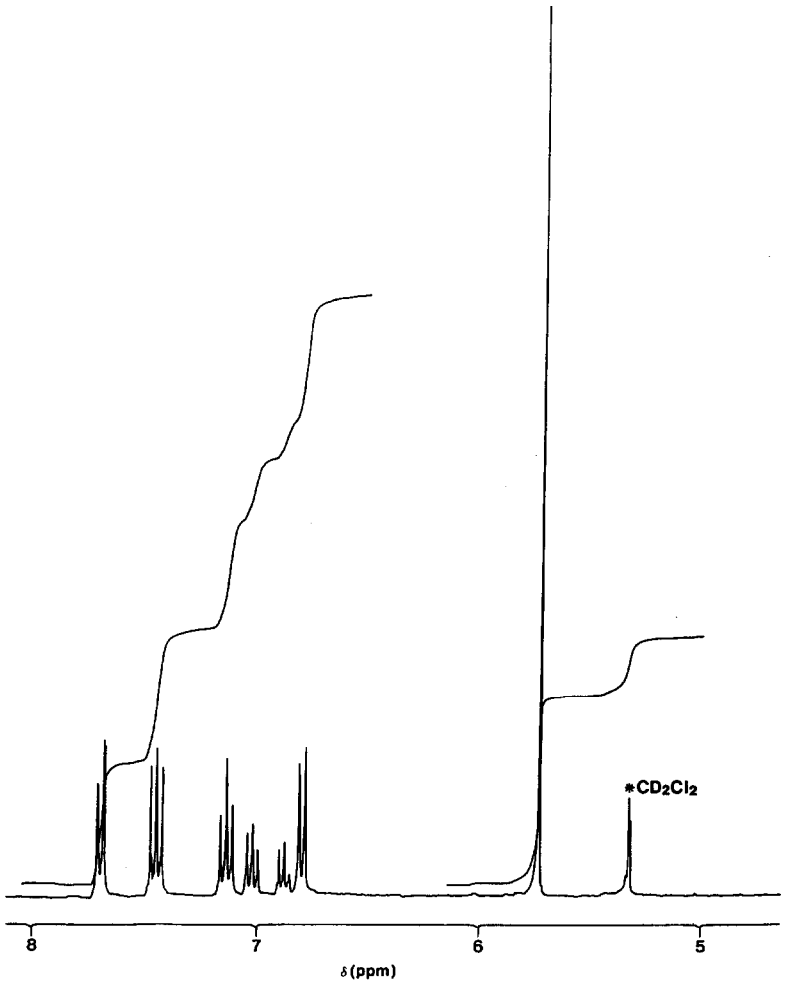


Fig. 1. 300-MHz ^{1}H NMR spectrum of (η-C_5H_5)(NPh)Mo(μ-NPh)$_2$Mo(NPh)(η-C_5H_5) (in CD_2Cl_2).

RESULTS AND DISCUSSION

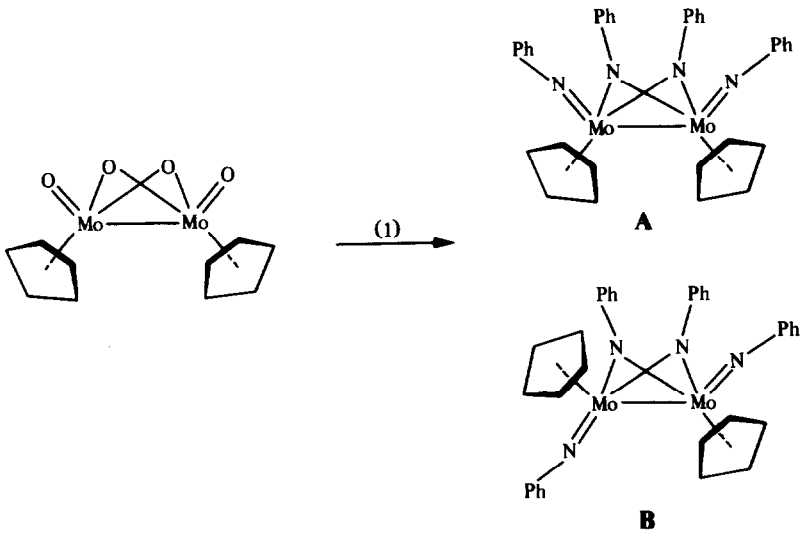
Treatment of [η-$C_5H_5MoO(\mu$-O)]$_2$ with PhNCO gives diamagnetic orange-red crystals of [η-C_5H_5Mo(NPh)(μ-NPh)]$_2$ (**1**) in high yield.

The formulation of **1** is supported by analytical and IR spectroscopic data and especially by its ^{1}H NMR spectrum. The ^{1}H-NMR spectrum of **1** (Fig. 1) shows a sharp singlet at δ 5.73 assignable to magnetically equivalent cyclopentadienyl groups and the pattern of resonances in the aromatic region indicates that two different types of phenylimido groups are associated with each molybdenum centre. The two equally intense pseudo doublets in the spectrum, corresponding to *ortho* protons of NPh moieties, are especially suggestive that both bridging and terminal imido ligands are present in the complex. The more intense pseudo triplets and the less intense pseudo triplets in the spectrum are representative of the *meta* and *para* protons, respectively, belonging to the two distinct types of phenylimido groups in **1**. The data are compatible with two structures for **1** (Scheme 1).

A is the most likely since most dinuclear species of this type exhibit a *cis* geometry.[7,8] Further, the complex (η-C_5H_5)(NR)Cr(μ-NR)Cr(NR)(η-C_5H_5) (R = $SiMe_3$) has structure **A** in the solid state.[9]

The solid complex (**1**) is stable in air, but the orange solutions in (thf or CH_2Cl_2) undergo slow decomposition in air. Compound **1** is unreactive towards ethylene, butadiene, CO_2, H_2 H_2O and pyridine but reacts with HCl gas, giving intractable material.

Acknowledgements—We would like to thank the S.E.R.C. for financial support and the N.S.E.R.C. (Canada) for a postdoctoral fellowship to K.J.M.



Scheme 1. (1) PhNCO at 70°C for 4 days.

REFERENCES

1. J. D. Burrington and R. K. Grasselli, *J. Catal.* 1979, **59**, 79.
2. M. A. Andrews and H. D. Kaesz, *J. Am. Chem. Soc.* 1979, **101**, 7255.
3. J. Chatt, J. R. Dilworth and R. L. Richards, *Chem. Rev.* 1978, **78**, 589.
4. D. Mansuy, P. Battioni and J. P. Mahr, *J. Am. Chem. Soc.* 1982, **104**, 4487.
5. W. A. Nugent and B. L. Haymore, *Coord. Chem. Rev.* 1980, **31**, 123.
6. M. Cousins and M. L. H. Green, *J. Chem. Soc.* 1 1969, 16.
7. E. I. Stiefel, *Prog. Inorg. Chem.* 1977, **22**, 1.
8. B. Spivak and Z. Dori, *Coord. Chem. Rev.* 1975, **17**, 99.
9. N. Wiberg, H. W. Haring and U. Schubert, *Z. Naturforsch.* 1978, **33B**, 1365.

Polyhedron Vol. 5, No. 3, pp. 925–926, 1986
Printed in Great Britain

0277-5387/86 $3.00 + .00
Pergamon Press Ltd

NEWSLETTER 1985: IUPAC COMMISSION ON NOMENCLATURE OF INORGANIC CHEMISTRY

INTRODUCTION

The objective of this Newsletter is to inform the readers of this journal about ongoing activities of this commission* and to draw attention to its recently published nomenclature documents. Chemists are invited to write about inorganic chemistry nomenclature problems to the present vice chairman: Professor Daryle H. Busch, Department of Chemistry, The Ohio State University, 140 West 18th Avenue, Columbus, OH 43210, U.S.A., or to any of its members.*

RECENTLY PUBLISHED DOCUMENTS

In addition to the book of nomenclature,[1] the commission has published several documents about topics that have evolved since 1970. The recommendations that have been published from 1982 on deal with isotopically labeled and isotopically substituted compounds,[2] inorganic and coordination polymers[3] (joint activity with the Nomenclature Commission of the Macromolecular Division), and nitrogen hydrides.[4] Short summaries of these recommendations are given below.

ISOTOPICALLY LABELED AND ISOTOPICALLY SUBSTITUTED COMPOUNDS[2]

These rules provide a general system of nomenclature for inorganic compounds whose isotopic nuclide composition deviates from that which occurs in nature. They are also suitable for designating individual isotopic molecular species. An isotopically modified organic residue occurring in an inorganic compound, such as an organic ligand in a coordinated entity, is named according to the rules of the Nomenclature of Organic Chemistry.

There is one other general system in use for describing isotopically modified compounds. It is based on an extension of the principles proposed by Boughton for designating compounds containing hydrogen isotopes, and, although mainly used in the index nomenclature of The Chemical Abstracts Service, it is found in the literature and in some chemical catalogs.

The system of nomenclature for isotopically modified inorganic compounds codified in these rules provides for recognition of various types of isotopic modification, and thus was chosen over the system based on the Boughton principles.

INORGANIC AND COORDINATION POLYMERS[3]

The fundamental principles of polymer nomenclature, which were developed to provide a framework for the unambiguous systematic naming of single-strand organic polymers, are extended to embrace inorganic and coordination polymers. The structures treated are regular single-strand polymers, that is polymers comprising repeating units linked exclusively through single atoms, and regular quasi-single-strand polymers, in which each repeating unit terminates at a single atom on one side but at a plurality of atoms on the other.

The name of the polymer is the name of the constitutional repeating unit (CRU) prefixed by the terms "poly", "catena", or other appropriate structural indicator, the CRU in turn being named by the citing, in order of appearance along the chain, of its constituent subunits, which are the largest structural fragments of the CRU that can be named according to established principles of inorganic and/or coordination nomenclature.

The document contains rules for the identification and orientation of the CRU, and it contains many examples of inorganic/coordination polymer structures together with the recommended names.

NITROGEN HYDRIDES[4]

These rules apply mainly to nitrogen hydrides containing one or two nitrogen atoms. The hydrides are considered as inorganic, although many of their derivatives are organic: the rules compromise between the relevant systems of nomenclature.

The benefit of a systematic nomenclature based on the name "azane" for NH_3 and the atom name "nitrogen" is outlined. However, due to common practice, names from "ammonia" (NH_3), "hydrazine" (N_2H_4), "diazene" (N_2H_2) and "nitrogen" (N) are retained for present use. The cations derived from the nitrogen hydrides by the addition of one or two hydrogen ions are named using the "ium" ending, and the anions derived by the loss of one or more hydrogen ions by the use of the "ide" ending in the established manner. The anions resulting from the loss of all hydrogen as ions from the nitrogen hydrides are named from the atom, e.g. nitride (N^{3-}). The problem of naming ligands N_nH_m attached to transition-metal ions where the actual valence bond structure of the ligand is indeterminate has been explored. The rules recommend that H_nH_m ligands should be named as neutral molecular species where possible, otherwise as anions, zwitterions or cationic ligands in that order of priority, but not as radicals. A table of ligand names is appended.

* Present Titular Members of the Committee are: Y. Jeannin (chairman), D. H. Busch, E. Fluck, P. Fodor-Csanyi, G. J. Leigh, J. Reedijk and E. Samuel.

ONGOING ACTIVITIES

Due to many new fields and to the discovery of many new types of compounds since the publication of the Red Book (1970), it was felt necessary to completely revise the Rules for Nomenclature in Inorganic Chemistry. The commission has agreed to publish a basic manual with the following contents:

(1) Aims, function and methods.
(2) Grammar.
(3) Elements and symbols.
(4) Formulae.
(5) Stoichiometric names.
(6) Solid-state chemistry.
(7) Neutral molecular compounds.
(8) Ions, radicals and salts.
(9) Oxoacids.
(10) Coordination compounds.
(11) Boron compounds.

In addition to this basic material, the commission intends to publish a part II, made up of chapters dealing with more advanced and detailed recommendations covering more specialized fields such as those mentioned above,[2-4] heteropolyanions[5] (almost completed, publication expected in 1985), organometallic compounds, inorganic rings and chains (all in preparation).

Individual chemists are encouraged to write to the commission if they would have ideas or suggestions about these topics or to include other subjects, or if they feel that a particular field is lacking accepted rules of nomenclature.

CORRESPONDENCE, SMALL MATTERS THAT MATTER ETC.

CNIC is a unit of an international public service organization, IUPAC, and we are volunteer chemists from about the world. Since nomenclature is our responsibility, we invite your inquiries and suggestions. We can serve you best if we know your needs and opinions. At worst, we should know someone who can name your cluster—or your ligand! Of course, some people already bring us their questions.

CNIC was formed to eliminate the Tower of Chemical Babel and almost every chemist has both appreciated and despised the tedium of the systematic and proper chemical nomenclature that CNIC is obliged to generate. In this second era of the computer evolution, names, formulae and the like are constrained by the inevitable super-literal reaction of the computer. With sympathy, but because precision and uniformity are increasingly important, we will just point out a few conventions that deserve to be observed.

(1) Representatives from all over the world agreed years ago (1970) to name the coordinated water molecule "aqua". Please do not call it aquo!!

(2) When numerical prefixes are used in naming a *coordination entity*, all vowels remain in the name. In technicalese: "there is no elision of vowels". For example, $[Al(H_2O)_6]^{3+}$ is the hexaaquaaluminium(3+) ion.

(3) This should not seem odd but it seems to cause some problems. The formulae of the common oxoanions are not considered to be *coordination formulae*. Consequently, they are not enclosed in square brackets, but rather in parentheses: $[Ni(H_2O)_6](ClO_4)_2$.

REFERENCES

1. International Union of Pure and Applied Chemistry, *Nomenclature of Inorganic Chemistry* (1970), 2nd Edition. Butterworths, London (1971).
2. Nomenclature of isotopically modified compounds, *Pure Appl. Chem.* 1981, **53**, 1887.
3. Nomenclature for regular single-strand and quasi-single-strand inorganic and coordination polymers, *Pure Appl. Chem.* 1985, **57**, 149.
4. The nomenclature of hydrides of nitrogen and derived cations, anions, and ligands. *Pure Appl. Chem.* 1982, **54**, 2545.
5. Nomenclature of heteropolyanions, in preparation (1985).

Polyhedron Vol. 5, No. 3, p. 927, 1986
Pergamon Press Ltd. Printed in Great Britain

BOOK REVIEWS

Structure and Bonding, Vol. 59/60, Actinides—Chemistry and Physical Properties. Edited by L. Manes, Springer, Berlin, 1985, ix+305 pp., DM164.

The 60 volumes of *Structure and Bonding* have become an indispensable feature of the modern science library. In my experience it is difficult to write too highly of them. The reviews have authority, they are up-to-date, and beautifully produced. The authors, editors and publishers deserve our gratitude.

The title of Vol. 59/60 belies its contents for it is an overview of actinide solid-state physics. As such it is perhaps of greater interest to the physicist, theoretical chemist or chemical physicist than to the person I perceive as the average reader of *Polyhedron*, for the coordination and organometallic chemistries of the actinide elements are not covered. The literature is covered through 1983–1984 and there are some 1985 references.

The book is organized in six chapters and a conclusion on probable developments in the field. The first by Fournier and Manes illustrates the importance of the 5*f* wavefunctions in determining the physical properties of actinide solids, particularly the metals. There is a summary of the main experimental evidence which justifies the theoretical descriptions. In Chapter B (Muller and Spirlet) the preparation of high-purity actinide metals and compounds is described. Compounds in this context refer to the binary halides, oxides, nitrides etc. Chapter C (Manes and Benedict) deals with relationships between structural and thermodynamic properties and Chapter D (Fournier) with the magnetic properties. Chapter E (Naegele, Ghijsen and Manes) is an important review of the photoelectron spectroscopy of actinide metals and oxides in relation to bonding. The results are correlated with the itinerant/localized character of the unsaturated electron shells. The final chapter (Brooks) is a discussion of the most advanced theory of 5*f* bonding in actinide solids.

As is usual in *Structure and Bonding*, the whole is exceptionally well-produced.

Department of Chemistry **J. I. BULLOCK**
University of Surrey
Guildford

Structure and Bonding, Vol. 61, Cation Ordering and Electron Transfer. By C. Gleitzer, J. B. Goodenough, B. G. Hyde, M. O'Keeffe and U. Weser. Springer, Berlin, x+167 pp., DM98.

The present volume of this well-established series is concerned broadly with cation ordering and electron transfer. The first chapter (Gleitzer and Goodenough) considers mixed valency with reference to three model systems: Fe_3O_4 (magnetite), as a representative of the ferrospinels and iron oxides with spinel-related structures; $Fe_{1-\delta}O$ (wüstite), as illustrative of a system with random defects and clustering; and $CaFeO_3$ (a perovskite), as illustrative of a system with strong Fe^4–O–Fe^4 interactions. The second chapter (Keefe and Hyde) concentrates on an alternative approach to non-molecular crystal structures, viz. one of laying emphasis on the arrangements of cations, rather than anions, in determining the packing, and on the attendant advantages of this approach. These two chapters on different aspects of oxide structures comprise the bulk (144 pp.) of Vol. 61: they are erudite, well-written and well-illustrated and important reading for solid-state chemists. The final, short chapter by Weser is on the rather different subject of redox-reactions of sulphur-containing amino-acid residues in proteins and metalloproteins—an XPS study. The link, such as it is, with the earlier chapters is via electron transport reactions. The volume is well-produced and a fitting complement to earlier ones in this series.

Department of Chemistry **R. J. H. CLARK**
University College
20 Gordon Street
London WC1H 0AJ

Polyhedron Vol. 5, No. 3, p. 927, 1986
Pergamon Press Ltd. Printed in Great Britain

BOOK REVIEWS

Structure and Bonding, Vol. 59/60, Actinides—Chemistry and Physical Properties. Edited by L. Manes, Springer, Berlin, 1985, ix+305 pp., DM164.

The 60 volumes of *Structure and Bonding* have become an indispensable feature of the modern science library. In my experience it is difficult to write too highly of them. The reviews have authority, they are up-to-date, and beautifully produced. The authors, editors and publishers deserve our gratitude.

The title of Vol. 59/60 belies its contents for it is an overview of actinide solid-state physics. As such it is perhaps of greater interest to the physicist, theoretical chemist or chemical physicist than to the person I perceive as the average reader of *Polyhedron*, for the coordination and organometallic chemistries of the actinide elements are not covered. The literature is covered through 1983–1984 and there are some 1985 references.

The book is organized in six chapters and a conclusion on probable developments in the field. The first by Fournier and Manes illustrates the importance of the 5*f* wavefunctions in determining the physical properties of actinide solids, particularly the metals. There is a summary of the main experimental evidence which justifies the theoretical descriptions. In Chapter B (Muller and Spirlet) the preparation of high-purity actinide metals and compounds is described. Compounds in this context refer to the binary halides, oxides, nitrides etc. Chapter C (Manes and Benedict) deals with relationships between structural and thermodynamic properties and Chapter D (Fournier) with the magnetic properties. Chapter E (Naegele, Ghijsen and Manes) is an important review of the photoelectron spectroscopy of actinide metals and oxides in relation to bonding. The results are correlated with the itinerant/localized character of the unsaturated electron shells. The final chapter (Brooks) is a discussion of the most advanced theory of 5*f* bonding in actinide solids.

As is usual in *Structure and Bonding*, the whole is exceptionally well-produced.

Department of Chemistry **J. I. BULLOCK**
University of Surrey
Guildford

Structure and Bonding, Vol. 61, Cation Ordering and Electron Transfer. By C. Gleitzer, J. B. Goodenough, B. G. Hyde, M. O'Keeffe and U. Weser. Springer, Berlin, x+167 pp., DM98.

The present volume of this well-established series is concerned broadly with cation ordering and electron transfer. The first chapter (Gleitzer and Goodenough) considers mixed valency with reference to three model systems: Fe_3O_4 (magnetite), as a representative of the ferrospinels and iron oxides with spinel-related structures; $Fe_{1-\delta}O$ (wüstite), as illustrative of a system with random defects and clustering; and $CaFeO_3$ (a perovskite), as illustrative of a system with strong Fe^4–O–Fe^4 interactions. The second chapter (Keefe and Hyde) concentrates on an alternative approach to non-molecular crystal structures, viz. one of laying emphasis on the arrangements of cations, rather than anions, in determining the packing, and on the attendant advantages of this approach. These two chapters on different aspects of oxide structures comprise the bulk (144 pp.) of Vol. 61: they are erudite, well-written and well-illustrated and important reading for solid-state chemists. The final, short chapter by Weser is on the rather different subject of redox-reactions of sulphur-containing amino-acid residues in proteins and metalloproteins—an XPS study. The link, such as it is, with the earlier chapters is via electron transport reactions. The volume is well-produced and a fitting complement to earlier ones in this series.

Department of Chemistry **R. J. H. CLARK**
University College
20 Gordon Street
London WC1H 0AJ

Polyhedron Vol. 5, No. 4, pp. 929–931, 1986
Printed in Great Britain

0277–5387/86 $3.00+.00
Pergamon Journals Ltd

NORMAL-COORDINATE ANALYSIS OF THE TiO_5^{6-} ION

E. M. NOUR* and M. ZAKY

Faculty of Science, Zagazig University, Zagazig, Egypt

and

Sh. SALLAM

Faculty of Science, Suez Canal University, Ismalia, Egypt

Abstract—Normal-coordinate analysis for the TiO_5^{6-} ion in M_2TiO_5 (M = rare earths) has been made on the basis of C_{4v}-symmetry and using the Wilson's GF matrix method. The observed frequencies have been quantitatively assigned according to the obtained values of the potential-energy distributions. Force constants for the different bonds and angles have been calculated. The Ti—O′ (axial) and Ti—O (equatorial) stretching force constants were calculated to be 4.15 and 2.48 mdyn $Å^{-1}$, respectively.

The IR and Raman spectra for M_2TiO_5 (M = rare earths) have been reported.[1] Some of the observed frequencies were tentatively assigned on the basis of qualitative analysis and others were left unassigned. Therefore, further detailed investigations seem necessary.

The TiO_5^{6-} ion is of interest because of the way that titanium in this compound is five coordinated, whereas six coordination is more frequently observed. X-ray studies indicate[1] that the isolated ion has C_{4v}-symmetry with a short axial Ti—O′ bond.

In the present study we have made a normal-coordinate analysis for the TiO_5^{6-} ion and have obtained potential-energy distributions in order to assign the observed frequencies. Force constants are reported for the different bonds and angles.

NORMAL-COORDINATE ANALYSIS

An XY_5 molecule[2] may be trigonal bipyramid (D_{3h}) or tetragonal pyramid (C_{4v}). X-ray structural studies indicate[1] that the isolated $TiO'O_4^{6-}$ ion has a square pyramidal structure with C_{4v}-symmetry as shown in Fig. 1. The short Ti—O′ bond occupies the axial position with a bond distance of 1.77 Å, while the equatorial Ti—O has a bond distance of 1.92 Å. All angles are approximately equal to 90°. Group theoretical analysis shows that the $TiO'O_4^{6-}$ ion should display nine fundamental vibrations, three of which are doubly degenerate. These modes of vibration are distributed as follows:

$$\Gamma_{vib.} = 3A_1\,(\text{IR and R}) + 2B_1\,(\text{R}) + B_2\,(\text{R}) + 3E\,(\text{IR and R}),$$

where IR and R refer to IR and Raman activities. From these fundamentals, one, A_1, is related to the axial Ti—O′ bond stretch, while the equatorial Ti—O bond stretch shows three modes, belonging to A_1+B_1+E. The axial angle, bends are related to A_1+B_1+E, while the remaining two modes, B_2+E, are associated with the equatorial angle bends.

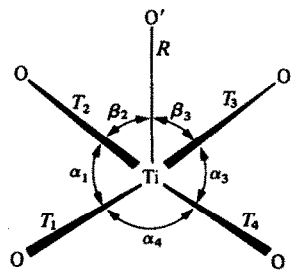


Fig. 1. Definition of the internal coordinates in the TiO_5^{6-} ion.

* Present address: Department of Chemistry, Faculty of Science, Qatar University, Doha, P.O. Box 2713, Qatar. Author to whom correspondence should be addressed.

The internal coordinates for the $TiO'O_4^{6-}$ ion are defined as given in Fig. 1. The symmetry coordinates used in the calculations for the C_{4v}-symmetry are constructed as follows:

A_1: $S_1 = R$, Ti—O′ stretch;
$S_2 = \frac{1}{2}(T_1 + T_2 + T_3 + T_4)$, Ti—O stretch;
$S_3 = \frac{1}{2}(\alpha_1 + \alpha_2 + \alpha_3 + \alpha_4)$, redundant;
$S_4 = \frac{1}{2}(\beta_1 + \beta_2 + \beta_3 + \beta_4)$, O′—Ti—O bend.

B_1: $S_5 = \frac{1}{2}(T_1 + T_3 - T_2 - T_4)$, Ti—O stretch;
$S_6 = \frac{1}{2}(\beta_1 + \beta_3 - \beta_2 - \beta_4)$, O′—Ti—O bend.

B_2: $S_7 = \frac{1}{2}(\alpha_1 + \alpha_3 - \alpha_2 - \alpha_4)$, O—Ti—O bend.

E: $\left.\begin{aligned} S_8 &= \tfrac{1}{2}(T_1 - T_2 - T_3 + T_4) \\ S_9 &= \tfrac{1}{2}(T_1 + T_2 - T_3 - T_4) \end{aligned}\right\}$, Ti—O stretch;

$\left.\begin{aligned} S_{10} &= \tfrac{1}{2}(\beta_1 - \beta_2 - \beta_3 + \beta_4) \\ S_{11} &= \tfrac{1}{2}(\beta_1 + \beta_2 - \beta_3 - \beta_4) \end{aligned}\right\}$, O′—Ti—O bend.

$$\left.\begin{aligned} S_{12} &= \frac{1}{\sqrt{2}}(\alpha_1 - \alpha_3) \\ S_{13} &= \frac{1}{\sqrt{2}}(\alpha_4 - \alpha_2) \end{aligned}\right\}, \text{ O—Ti—O bend.}$$

The normal-coordinate analysis was carried out on the basis of Wilson's GF matrix method.[3] A general quadratic potential-energy function has been used where the potential energy is expressed in terms of harmonic force constants associated with the coordinates of the molecule, i.e. bonded distances and the angle between them. However, the normal vibration can be calculated[3] from the secular equation:

$$(GF - \lambda E) = 0,$$

where E is the diagonal unit matrix and $\lambda = 4\pi^2 C^2 \nu^2$. A version of the Snyder–Schachtschneider programs[4] was used in the computation process.

Table 1. Force constants for $TiO'O_4$ ion

Symbol	Description[a]	Value[b]
F_R	Ti—O′ str.	4.15
F_T	Ti—O str.	2.48
F_α	O—Ti—O bend	0.99
F_β	O′—Ti—O bend	1.28
F_{RT}	Ti—O′, Ti—O	0.32
F_{TT}	Ti—O, Ti—O	0.22
$F_{\alpha\alpha}$	O—Ti—O, O—Ti—O	0.20
$F_{\beta\beta}$	O′—Ti—O, O′—Ti—O	0.31
$F_{R\beta}$	Ti—O′, O′—Ti—O	0.15

[a] str. = stretch.
[b] The units are mdyn Å^{-1} for $F_{str.}$ and $F_{str.str.}$; mdyn rad^{-1} for $F_{str.bend}$; mdyn Å rad^{-2} for F_{bend} and $F_{bend.bend}$.

In the frequency calculations the force constants were introduced and systematically adjusted so as to give the best agreement between the practically observed frequencies reported by Paques-Ledent[1] and the calculated values. The force constants and their values are given in Table 1.

The vibrations of a molecule may be described[5] in terms of normal coordinates, Q_e, which are related to the symmetry coordinates, S_k, by the linear transformation:

$$S_k = \sum_e L_{ke} Q_e,$$

where L_k are the normalized amplitudes of vibration. For a vibration of frequency ν_a associated with the normal coordinate Q_a, the potential energy of the molecule is given by:

$$2V = Q_a \sum_{ij} F_{ij} L_{ia} L_{ja}.$$

Table 2. Observed and calculated frequencies amd assignments for $TiO'O_4^{6-}$ ion

Wavenumber (cm^{-1}) Observed	Calculated	Assignment[a]
787	784	A_1: ν_1, sym. Ti—O′ str.
555	560	ν_2, sym. Ti—O str.
360	356	δ_3, sym. O′—Ti—O bend
486	490	B_1: ν_4, antisym. Ti—O str.
150	161	δ_5, antisym. O′—Ti—O bend
295	297	B_2: δ_6, antisym. O—Ti—O bend
648	652	E: ν_7, antisym. Ti—O str.
324	330	δ_8, antisym. O′—Ti—O bend
235	237	δ_9, antisym. O—Ti—O bend

[a] sym. = symmetric, antisym. = antisymmetric, and str. = stretch.

Table 3. Potential-energy distributions[a] for $TiO'O_4^{6-}$ ion

	F_R	F_T	F_α	F_β
ν_1	97	3	0	0
ν_2	12	88	0	0
ν_3	3	0	0	97
ν_4	0	100	0	0
ν_5	0	0	0	100
ν_6	0	0	100	0
ν_7	0	90	5	5
ν_8	0	4	8	88
ν_9	0	3	89	8

[a] Normalized to total 100 for the diagonal force constant distributions.

Table 4. XY force constants for XY_5 compounds

		F_{XY} (mdyn Å^{-1})		
Compound	Geometry	Axial	Equatorial	Reference
IF_5	C_{4v}	4.68	3.64	6
BrF_5	C_{4v}	4.02	3.19	6
ClF_5	C_{4v}	3.01	2.57	6
TiO_5^{6-}	C_{4v}	4.15	2.48	Present work
PF_5	D_{3h}	3.93	5.47	8
AsF_5	D_{3h}	4.21	5.20	8
VF_5	D_{3h}	3.64	4.28	8

Such terms are large only when $i = j$, where the diagonal force constants, F_{ii}, are much greater than the off-diagonal ones, F_{ij}. Accordingly, the term $\frac{1}{2}F_{ii}L_{ia}^2$ represents the distribution of the potential energy among symmetry coordinates. Therefore, a concrete assignments of the observed frequencies given in Table 2 for the $TiO'O_4^{6-}$ ion may be achieved on the basis of the calculated values of the potential-energy distributions for the different modes as given in Table 3. Descriptions of all the vibrational modes are shown in Fig. 2.

It is of interest to see that the axial Ti—O' stretching force constant is of much higher value than that of the equatorial Ti—O bond. Their values are 4.15 and 2.48 mdyn Å^{-1}, respectively. Using the bond-stretching force constant as an approximate measure of the equilibrum bond strength, it appears that the axial Ti—O' bond is 1.67 times stronger than the equatorial Ti—O bond. This result is in good agreement with the reported force constants for other XY_5 molecules. In the majority of the XY_5 molecules with C_{4v}-symmetry[6,7] (as in TiO_5^{6-}), the

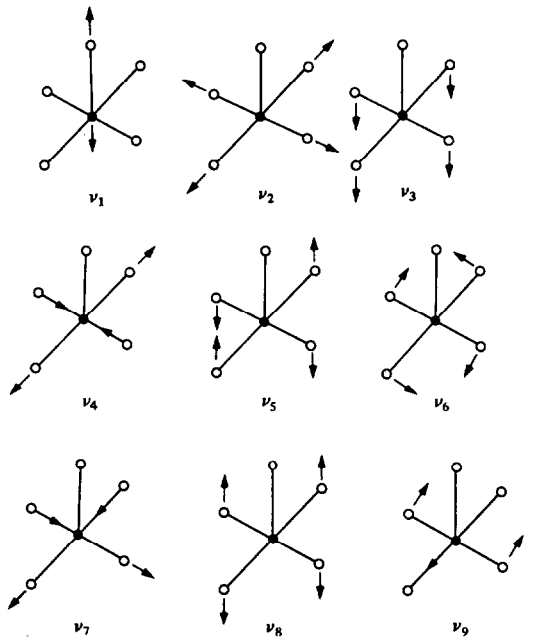


Fig. 2. Vibrational modes for TiO_5^{6-} ion.

axial stretching force constant is higher than the equatorial force constant. This is opposite to the trend found for XY_5 molecules with D_{3h}-symmetry[8] as given in Table 4 for the fluoride compounds. Rossi and Hoffmann[2] have reviewed and discussed the strength of both the axial and equatorial bonds in compounds with a square pyramidal structure with C_{4v}-symmetry. They concluded that the axial bond is the strongest with weaker equatorial bonds in metal complexes with electronic structures d^0 (as in TiO_5^{6-}), d^6 and d^{10}. The situation is reversed, with stronger equatorial and weaker axial bonds, in complexes with d^4- and d^8-configurations.

REFERENCES

1. M. Th. Paques-Ledent, *Spectrochim. Acta* 1976, **32**, 1339.
2. A. R. Rossi and R. Hoffmann, *Inorg. Chem.* 1975, **14**, 365.
3. E. B. Wilson, J. C. Decius and P. C. Cross, *Molecular Vibrations*. McGraw-Hill, New York (1955).
4. J. H. Schachtschneider, *Vibrational Analysis of Polyatomic Molecules, V and VI*. Technical Report, Shell Development Co., Emeryville, CA (1964).
5. S. Califano, *Vibrational States*. John Wiley, New York (1976).
6. G. M. Begun, W. H. Fletcher and D. F. Smith, *J. Chem. Phys.* 1965, **42**, 2236.
7. K. O. Christe, E. C. Curtis, C. J. Schack and D. Pilipovich, *Inorg. Chem.* 1972, **11**, 1679.
8. H. Selig, J. H. Holloway, J. Tyson and H. H. Claassen, *J. Chem. Phys.* 1970, **53**, 2559.

Polyhedron Vol. 5, No. 4, pp. 933–935, 1986
Printed in Great Britain

0277–5387/86 $3.00+.00
Pergamon Journals Ltd

POLAROGRAPHIC STUDY OF THE COORDINATED Cd(II)–LEUCINATE SYSTEM

G. RUIZ-CABRERA, C. QUINTANA-PERERA, J. C. RODRIGUEZ-PLACERES and A. AREVALO*

Department of Physical Chemistry, University of La Laguna, Tenerife, Canary Islands, Spain

(*Received* 8 *July* 1985; *accepted* 18 *September* 1985)

Abstract—The coordinated Cd(II)–leucinate system has been studied polarographically in an aqueous medium and at constant ionic strength ($\mu = 1.0$) (adjusted with $NaClO_4$). The stabilization of the coordinated species $[CdL_2]$ and $[CdL_3]^-$ has been established, with stability constants $\beta_2 = 3.0 \times 10^7$ l^2 mol^{-2} and $\beta_3 = 8.2 \times 10^{10}$ l^3 mol^{-3}, respectively.

The importance of a knowledge of systems with simple molecules in the study of complex biological macromolecules[1–6] has prompted us to undertake a series of works on metallic ion–amino acid coordination.[7–9]

The polarographic analysis of the coordinated Cd(II)–leucinate system in an aqueous medium is reported here. To the best of our knowledge, this system has only been studied on one previous occasion[10] by the potentiometric method. The mean values obtained under the two conditions assayed were: $\beta_1 = 1 \times 10^4$ l mol^{-1} and $\beta_2 = 2.9 \times 10^7$ l^2 mol^{-2}, and no trace was detected of the presence in the medium of complexes with a greater number of ligands.

EXPERIMENTAL

Each of the i–E curves was plotted with a Metrohm E506 polarograph with an E505 polarographic stand. Pt (EA285) and Ag–AgCl–NaCl, sat. Metrohm EA427 electrodes were used as counter and reference electrodes, respectively, and the working one was a DME. The temperature in the cell was 25 ± 0.05°C. The ionic strength was adjusted to $\mu = 1.0$ with $NaClO_4$. Measurements of pH were carried out with a pHM84 digital potentiometer with a GK2401C radiometer combined electrode. The concentration of metal ion was maintained constant at 2×10^{-5} M in all recordings. Drop-time was controlled at 3.0 s.

The sodium perchlorate and cadmium sulfate were Merck products of p.a. quality, the L-leucine was from Sigma and the sodium hydroxide used for adjusting the pH was also of p.a. quality from May & Baker. The values of pK_1 (2.37) and pK_2 (9.62) were taken from Perrin.[11]

RESULTS

Leucine in aqueous solution gives rise to an equilibrium between its protonated forms, neutral and leucinate ion, governed by the acidity constants. At a sufficiently high pH, the complexes with leucinate will predominate, since its concentration will be significant and the corresponding stability constants are much higher than those of the possible species coordinated with the neutral leucine.

The two studies were carried out, varying the pH of an initial solution, and, therefore the concentrations of the different forms of leucine, between the limits indicated in Table 1.

From plots of log $[(\bar{i}_d - \bar{i})/\bar{i}]$ vs E the reduction was shown to have taken place through a reversible bielectronic process. The half-wave potentials were also obtained from these plots (Table 1).

The analysis of the equilibria was carried out following the method of De Ford and Hume,[12] accepting as the value of β_1 that proposed by Datta *et al.*[10] The good linear dependence found for F_2 vs [leucinate] (Fig. 1) points to the existence in the medium of complexes with two and three leucinate ligands. This is the first experimental evidence of the formation of the species $[CdL_3]^-$.

* Author to whom correspondence should be addressed.

Table 1. Analysis of the Cd(II)–leucinate–$NaClO_4$ system in an aqueous medium[a]

$[L_T]$ ($\times 10^2$ M)	pH	$[L^-]$ ($\times 10^3$ M)	$\bar{i}_d$ (mm)	$-E'_{1/2}$ (mV)	F_0 ($\times 10^{-2}$)	F_1 ($\times 10^{-5}$)	F_2 ($\times 10^{-8}$)
10.34	7.57	0.9136	63.8	582.4	1.023	1.109	1.104
				582.8	1.055	1.144	1.143
10.33	7.72	1.284	60.6	592.6	2.383	1.848	1.361
				592.8	2.420	1.877	1.384
10.32	7.83	1.647	57.6	600.4	4.601	2.787	1.631
				600.2	4.530	2.744	1.605
10.31	7.93	2.064	57.9	608.8	8.802	4.260	2.015
				609.0	8.940	4.327	2.048
10.30	8.02	2.525	57.3	616.2	15.82	6.261	2.440
				615.6	15.10	5.976	2.327
10.29	8.12	3.154	57.6	623.8	28.44	9.014	2.826
				624.4	29.80	9.445	2.963
10.28	8.22	3.935	57.7	632.2	54.60	13.87	3.499
				631.6	52.11	13.24	3.339
10.27	8.32	4.902	57.3	640.8	107.4	21.91	4.449
				640.6	105.7	21.56	4.378
10.27	8.41	5.963	58.1	648.2	188.4	31.59	5.281
				648.6	194.4	32.60	5.450
10.25	8.51	7.384	58.6	657.1	373.5	50.58	6.836
				656.8	364.9	49.42	6.679
10.23	8.61	9.111	58.6	664.8	680.1	74.64	8.181
				665.0	690.8	75.82	8.311
10.21	8.71	11.19	57.9	672.0	1191	106.4	9.500
				672.2	1210	108.1	9.651

[a] De Ford and Hume method. Characteristics of the reduction of Cd(II) in 1 M $NaClO_4$: $-E'_{1/2} = 526.8$ mV, $\bar{i}_d = 86.1$ mm.

The values for the stability constants were obtained by the square minima method and are given in Table 2.

Their acceptable general agreement allows us to propose the following constants of the coordinated species $[CdL_2]$ and $[CdL_3]^-$: $\beta_2 = 3 \times 10^7$ l^2 mol^{-2}, and $\beta_3 = 8.2 \times 10^{10}$ l^3 mol^{-3}. The value of β_2 is in perfect agreement with that reported in the literature:[10] $\beta_2 = 2.9 \times 10^7$ l^2 mol^{-2}.

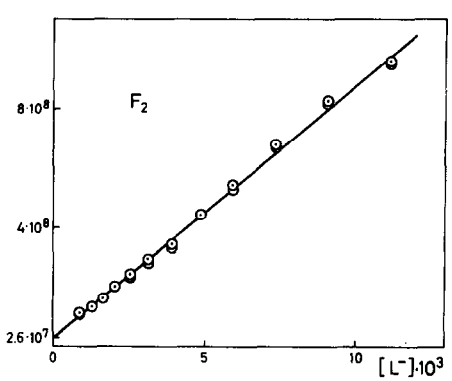


Fig. 1. Plot of function F_2 vs [leucinate].

Table 2. Stability constants of the simple system of Cd(II) with leucinate ligand

Study	β_2 (l^2 mol^{-2})	β_3 (l^3 mol^{-3})
1	3.5×10^7	7.9×10^{10}
2	2.6×10^7	8.5×10^{10}

REFERENCES

1. H. C. Freeman, In *Inorganic Biochemistry* (Edited by G. E. Eichhorns), pp. 121–126. Elsevier, Amsterdam (1973).
2. R. S. Giordano and R. D. Bereman, *J. Am. Chem. Soc.* 1974, **96**, 1015.
3. A. Levitzki, I. Pecht and M. Anbar, *Nature (London)* 1965, **207**, 1386.
4. V. S. Sharma and J. Schubert, *J. Am. Chem. Soc.* 1969, **91**, 6291.
5. V. S. Sharma, J. Schubert, H. B. Brooks and F. Sicilio, *J. Am. Chem. Soc.* 1970, **92**, 822.
6. H. Siegel, *Angew. Chem.* 1969, **81**, 161.

7. J. C. Rodriguez-Placeres, G. Pastor, J. A. Sanchez and A. Arevalo, *Quim. Anal.* 1985, **4**, 191.
8. J. C. Rodriguez-Placeres, F. Ramos-Steffens, G. Pastor and A. Arevalo, *An. Quim.* (in press).
9. J. C. Rodriguez-Placeres, M. T. Sanz-Alaejos and F. Garcia-Montelongo, *An. Quim.* (in press).
10. S. P. Datta, R. Leberman and B. R. Rabin, *Trans. Faraday Soc.* 1959, **55**, 1982.
11. D. D. Perrin, *J. Chem. Soc.* 1958, 3125.
12. D. D. de Ford and D. N. Hume, *J. Am. Chem. Soc.* 1951, **73**, 5321.

Polyhedron Vol. 5, No. 4, pp. 937–944, 1986
Printed in Great Britain

0277–5387/86 $3.00+.00
Pergamon Journals Ltd

COMPLEXES OF Ag(I) WITH LIGANDS CONTAINING SULPHUR DONOR ATOMS

S. KRZEWSKA* and H. PODSIADŁY

Institute of Chemistry, Wrocław University, Wrocław, Poland

(*Received* 17 *July* 1985; *accepted* 18 *September* 1985)

Abstract—Potentiometric studies of silver complexes with thiourea, thiohydantoin, cysteine and thiobarbituric acid in a perchloric medium are reported. Thiohydantoin, cysteine and thiobarbituric acid form sparingly soluble precipitates with silver ions. Only thiourea forms soluble, colourless complexes with coordination numbers 1–4 and a dinuclear complex $[Ag_2tu_6]^{2+}$. Solubility products and stability constants of those complexes were determined.

Ligands containing sulphur atoms in the −2 oxidation state coordinate easily with many metals, especially with those showing the properties of soft acids, as, for example, Cu(I), Ag(I), Au(I), Hg(II) etc. Those ligands also show reducing properties and often the complexing reaction is accompanied by a redox reaction. An example of such a reaction is the reaction of Cu(II) with thiourea[1–3] or Fe(III) with thiourea.[4–6]

Silver ions, which usually form linear complexes with coordination number 2 with sulphur donors in aqueous solution, form complexes with maximum coordination number $n = 4$. Silver and thiourea complexes were studied both as solids[7–9] and in solution.[10–17]

In solution mononuclear silver–thiourea complexes with coordination number = 1–4[10–16] prevail. Shulman and Saveleva[17] have proved that in solution a stable dinuclear complex, $[Ag_2tu_3]^{2+}$, is also present. Formation of a complex with the same chemical composition was observed by Berthon and Berg[18] for the silver–thiosemicarbazide system.

In this paper we present potentiometric studies of silver complexes with thiourea, thiohydantoin, cysteine and thiobarbituric acid in a perchloric acid medium. For the silver–thiourea system, besides mononuclear complexes, the dinuclear complex $[Ag_2tu_6]^{2+}$ was obtained and its stability determined.

EXPERIMENTAL

Potentiometric measurements were carried out by means of pHM 4 "Radiometer" and OP 208 "Radelkis" pH meters. Indicator electrodes were silver and platinum electrodes in a redox formamidine disulfide–thiourea system. The reference electrode was a silver–silver chloride electrode immersed in a solution of 0.01 M $AgClO_4$ and 0.99 M $HClO_4$. The electrode was joined to the examined solution by a salt bridge of the "Wilhelm" type, filled with a solution of 1.00 M $HClO_4$. Measurements were carried out at a constant temperature (25 ± 0.1°C) and in a constant ionic medium (1 M ClO_4^-).

Silver perchlorate solution was obtained from silver carbonate and perchloric acid. The solution was kept in darkness in order to prevent silver ion reduction. The silver ion concentration was determined by potentiometric titration against sodium chloride using a silver electrode as the indicator electrode.

Thiourea concentration was determined potentiometrically by titrating it with a Ce^{4+} solution using a platinum indicator electrode. Thiobarbituric acid and thiohydantoin concentrations were determined by pH metric titration with sodium hydroxide solution. All solutions were prepared using double distilled water.

RESULTS

Thiohydantoin, cysteine and thiobarbituric acid form sparingly soluble precipitates with silver ions. Solubility products of those complexes were determined potentiometrically. The indicator electrode was a silver electrode, linear over a wide range of concentrations, whose slope was in agreement with the Nernst equation. Figure 1 shows an $AgClO_4$ solution titration with thiohydantoin solution

* Author to whom correspondence should be addressed.

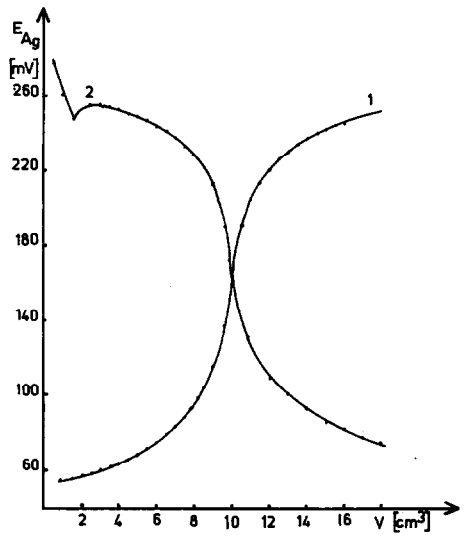


Fig. 1. Dependence of silver–silver chloride electrode potential on Ag^+ : th molar ratio. Curve 1: $V_o = 50$ cm^3, $[Ag^+] = 1.92$ mM, $V = 0$–18 cm^3, [th] = 9.75 mM, $[HClO_4] = 0.5$ M = constant. Curve 2: $V_o = 50$ cm^3, [th] = 1.96 mM, $V = 0$–18 cm^3, $[Ag^+] = 9.65$ mM, $[HClO_4]$ = 0.5 mM = constant.

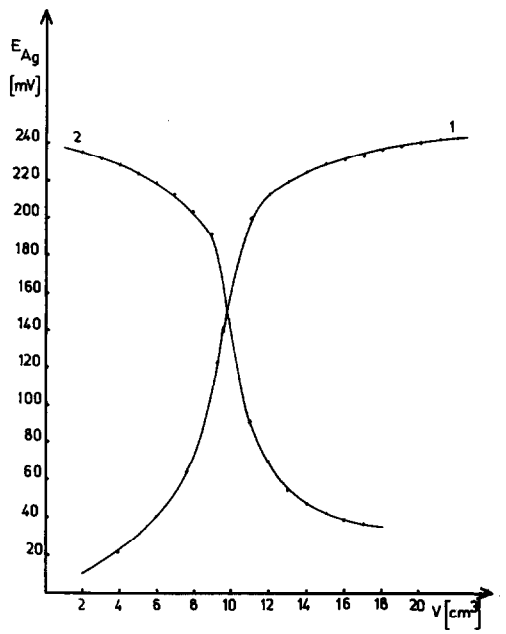


Fig. 2. Silver–silver chloride electrode potential dependence on Ag^+ : cys molar ratio. Curve 1: $V_0 = 50$ cm^3, $[Ag^+] = 1.92$ mM, $V = 0$–18 cm^3, [cys] = 9.84 mM, $[HClO_4] = 0.5$ M = constant. Curve 2: $V_o = 50$ cm^3, [cys] = 1.97 mM, $V = 0$–18 cm^3, $[Ag^+] = 9.65$ mM, $[HClO_4] = 0.5$ M = constant.

(curve 1) and a thiohydantoin solution titration with $AgClO_4$ solution (curve 2) in a 0.5 M $HClO_4$ medium. During titration a sparingly soluble compound of molar ratio Ag : th = 1 : 1 is formed. The solubility product of that compound is 1.78×10^{-9} (m dm^{-3})^2.

Cysteine reacts in a similar way with silver ions. In a 0.5 M $HClO_4$ medium a sparingly soluble complex of molar ratio Ag : cys = 1 : 1 was found. The solubility product of this compound was determined from the equivalence point of the curve of the silver perchlorate solution titration with the cysteine solution (Fig. 2, curve 1) and from the curve of the cysteine solution titration with the silver perchlorate solution (Fig. 2, curve 2). As Fig. 2 shows, those curves are not completely symmetrical and solubility products determined from the equivalence points differ slightly. Thus, the silver cysteinate solubility product determined from the equivalence point of curve 2 (152 mV) is 5.6×10^{-9} (m dm^{-3})^2. The values of the solubility products of silver cysteinate and silver thiohydantoinate are given in Table 1. These values were calculated from potentiometric measurements performed in the presence of cysteine or thiohydantoin excess. Then:

$$[th]_f = [th]_t - [Ag^+]_t \quad (1)$$

and

$$[Ag^+]_f = \frac{E - E^o}{58}. \quad (2)$$

In the system with thiobarbituric acid, formation of sparingly soluble compounds with the following compositions occurred: Ag_2(tba), Ag(tba) and $Ag(tba)_2$. Figure 3 shows the $AgClO_4$ solution titration with the thiobarbituric acid solution in a 0.5 M $HClO_4$ medium. Figure 3 shows clearly that two equivalence points appear on the titration curve: one at a molar ratio (Ag : tba) of 2 : 1, the

Table 1. Solubility product values of silver thiohydantionate (Agth) and silver cysteinate (Agcys)[a]

	pK_{so}Agth		pK_{so}Agcys	
	1	2	3	4
(a)	8.76 (3)	8.78 (4)	8.50 (2)	8.31 (7)
	8.75 (10)	8.77 (3)	8.45 (8)	8.30 (4)
	8.74 (2)	8.75 (7)	8.44 (4)	
		8.74 (2)	8.43 (3)	
(b)	pK_{so}Agth		pK_{so}Agcys	
	8.75		8.40	

[a] Columns 1 and 3: silver ion solutions were titrated with thiohydantoin (1) and cysteine (3) solutions. Columns 2 and 4: thiohydantoin (2) and cysteine (4) solutions were titrated with silver ion solution. Number in parentheses shows how many times the value occurs.

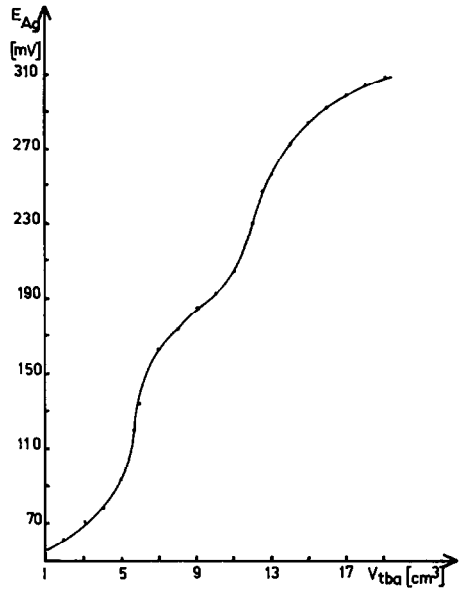


Fig. 3. Potentiometric titration of the solution containing 10 cm^3 9.65 mM $AgClO_4$ in 0.5 M $HClO_4$ with thiobarbituric acid solution (8.61 mM in 0.5 M $HClO_4$).

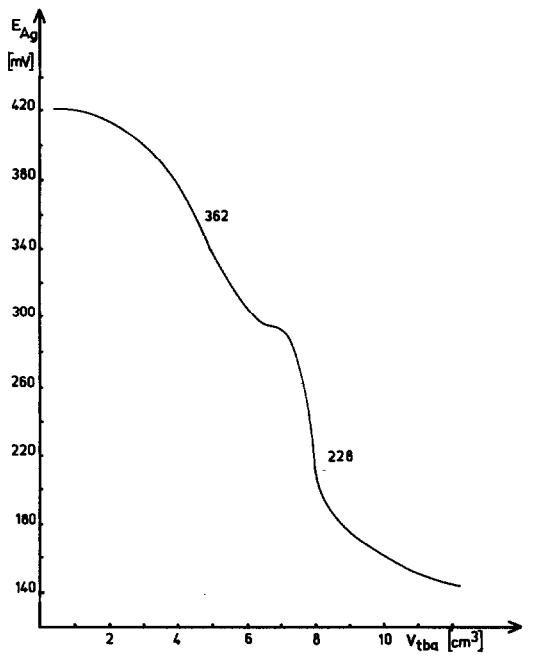


Fig. 4. Potentiometric tiration of the solution containing 5 cm^3 17.2 mM of thiobarbituric acid in 0.5 M $HClO_4$ with silver perchlorate solution (9.65 mM in 0.5 M $HClO_4$).

other at an Ag : tba ratio of 1 : 1. From the titration curve equivalence points free silver ion concentrations were determined and the solubility products of those compounds were calculated. Thus, the solubility product determined for Ag_2(tba) is 1.24×10^{-11} (m dm^{-3})^3 while the K_{so} for the compound with Ag : tba = 1 : 1 is 9.61×10^{-12} (m dm^{-3})^2. Five series of silver ion titrations with thiobarbituric acid were made. Table 2 shows solubility product values calculated from the equivalence points of each titration curve.

Figure 4 shows a thiobarbituric acid solution titration with $AgClO_4$ solution. As can be seen in Fig. 4 two equivalence points appear on the titration curve, which correspond to the formation of $Ag(tba)_2$ and Ag(tba) compounds. The solubility product value for $Ag(tba)_2$ complex is 1.52×10^{-23} (m dm^{-3})^3, while that for Ag(tba) is 12.2×10^{-12} (m dm^{-3})^2. The latter value is in agreement with the values of the corresponding solubility products determined from the silver perchlorate solution titration with thiobarbituric acid solution (Table 2).

In the perchloric acid medium thiourea and silver ions form soluble complexes. Besides mononuclear complexes which are are well known and described in the literature,[10–16] studies were carried out in order to find silver–thiourea polynuclear complexes. Potentiometric measurements were carried out with a large, constant ligand excess. Under such conditions it can be assumed that the free thiourea concentration is the same as the total thiourea concentration. The silver ion reaction with thiourea can be presented by the following equation:

$$qAg^+ + ptu = [Ag_q tu_p]^{q+}. \quad (3)$$

Since, in solution, there is a large ligand excess, the

Table 2. Solubility product values of silver–thiobarbituric acid (tba) complexes[a]

	E_{ep} (mV)	tba : Ag^+	pK_{so}
(a)	125	1:2	10.91
	231	1:1	11.02
	129	1:2	10.55
	229	1:1	10.95
	130	1:2	10.61
	230	1:1	10.99
	127	1:2	10.44
	230	1:1	10.99
	136	1:2	11.00
	229	1:1	10.95
(b)	362	2:1	22.82
	228	1:1	10.91
	363	2:1	22.86
	229	1:1	10.95
(c)		1:1	10.98
		1:2	10.67
		2:1	22.84

[a] (a) $AgClO_4$ solution titration with tba solution, (b) tba solution titration with $AgClO_4$ solution, and (c) mean values of silver–tba complexes.

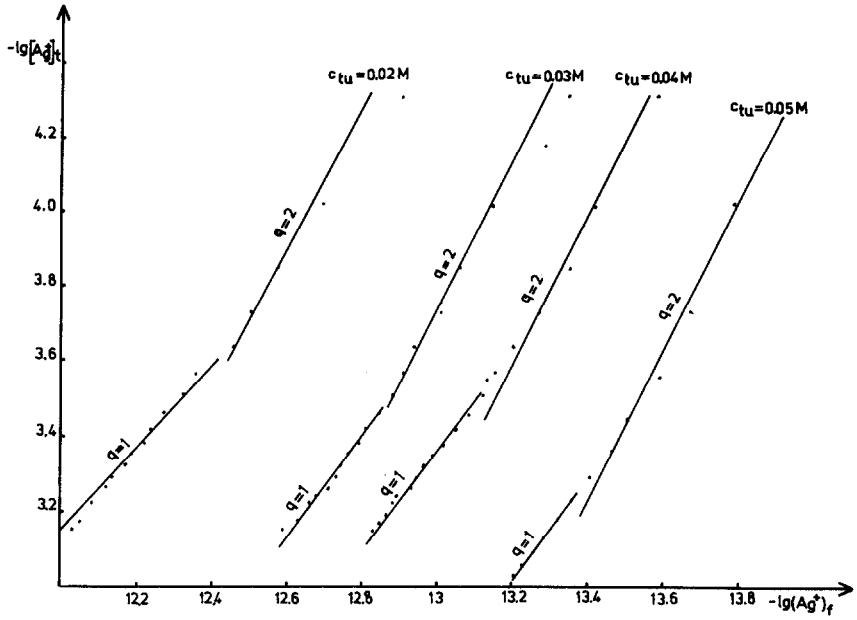


Fig. 5. Determination of the number of nuclei ($\bar{q}$) in a silver–thiourea complex at a constant ligand concentration.

total silver ion concentration is:

$$[Ag^+]_t = \sum_0^q \sum_0^p q[Ag_q tu_p] = \sum_0^q \sum_0^p q\beta_{qp}[Ag^+]^q[tu]^p. \tag{4}$$

Hence:

$$\left(\frac{\partial \log [Ag^+]_t}{\partial \log [Ag^+]}\right)_{[tu]} = \bar{q}. \tag{5}$$

Dependence diagrams of $\log [Ag^+]_t$ on $\log [Ag^+]$ for some thiourea concentrations are presented in Fig. 5. As can be seen, over quite a large concentration range dinuclear silver–thiourea complexes exist in solution.

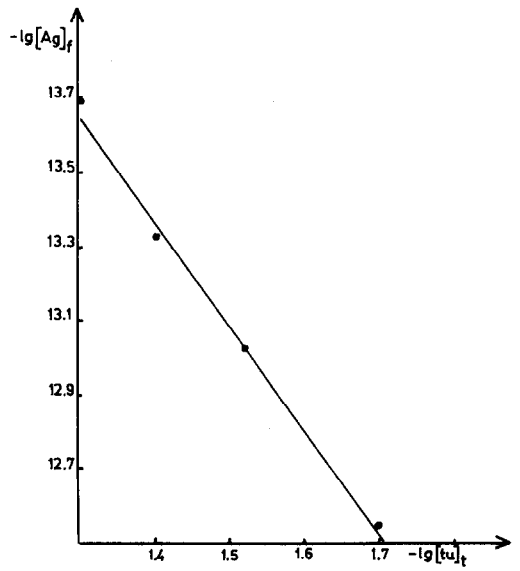


Fig. 6. Determination of the silver–thiourea complex composition at a constant total silver ion concentration.

The number of coordinated thiourea molecules can be determined from the following equation:

$$\left(\frac{\partial \log [Ag^+]}{\partial \log [tu]_t}\right)_{[Ag^+]_t} = \frac{\bar{p}}{q}. \tag{6}$$

A graphical presentation of the $\bar{p}/q$ determination is shown in Fig. 6. Taking into account the determined values of p and q, the reaction for silver–thiourea dinuclear complex formation can be presented as follows:

$$2Ag^+ + 6tu = [Ag_2tu_6]^{2+}.$$

The stability constant of this complex is:

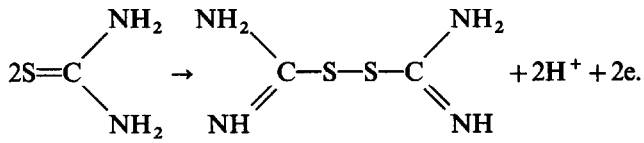
$$\beta_{26} = \frac{[Ag_2tu_6^{2+}]}{[Ag^+]^2[tu]^6}. \tag{7}$$

The calculated stability constant values are presented in Table 3.

Table 3. Stability constant values of dinuclear silver–thiourea (tu) complexes in 0.5 M $HClO_4$ medium

$[tu]_t$ (M dm^{-3})	$\log \beta_{26}$
0.02	31.10
0.03	30.95
0.04	31.10
0.05	31.20
Mean value	31.09

For the examination of the stability of mononuclear silver–thiourea complexes the measurements of ligand oxidized and reduced form redox potentials were applied. The result of monoelectronic thiourea oxidation is formamidine disulfide which forms with thiourea a reversible redox system:[19]



The redox potential of formamidine disulfide–thiourea in 1 M perchloric acid solution is:

$$E = E^{o\prime}_{fds} + (RT/F) \ln \frac{[fds]^{1/2}}{[tu]}, \qquad (8)$$

where $E^{o\prime}_{fds}$ = formal redox potential of formamidine disulfide–thiourea system in 1 M $HClO_4$.

Initial measurements have proved that in the concentration range studied formamidine disulfide does not form complexes with silver ions. Silver perchlorate solution titration with formamidine disulfide solution was carried out at a constant silver ion concentration. The silver electrode potential has a constant value during titration, which proves that formamidine disulfide does not react with the silver ions.

Formamidine disulfide was obtained by thiourea coulometric oxidation in 1 M $HClO_4$ solution on the platinum electrode at a potential of 1400 mV vs SCE.

Potentiometric studies of mononuclear silver–thiourea complexes were carried out in the following way: in each series silver ion and formamidine disulfide concentrations were constant. In such a system the redox potential depends only on the thiourea concentration:

$$E = E'_f - (RT/F) \ln [tu],$$
$$E'_f = E^{o\prime}_{fds} + (RT/F) \ln [fds^{2+}]^{1/2} = \text{constant}. \qquad (9)$$

The dependence of the platinum electrode redox potential on the logarithm of the thiourea concentration at a constant concentration of formamidine disulfide is linear over a large concentration range and its slope corresponds to the Nernst equation.

From redox potential measurements the free thiourea concentration can be determined. Knowing the free thiourea concentration, the average ligand number was calculated:

$$\bar{n} = \frac{[tu]_t - [tu]}{[Ag^+]_t}.$$

Figure 7 shows the average ligand number dependence on the logarithm of the free thiourea concentration for various total silver ion concentrations. As can be seen from the formation curve, over the concentration range studied, mononuclear complexes are present.

Stability constants of silver–thiourea complexes were determined graphically by means of Olerup's method[20] (Fig. 8). Table 4 shows stability constant values for each silver ion concentration value.

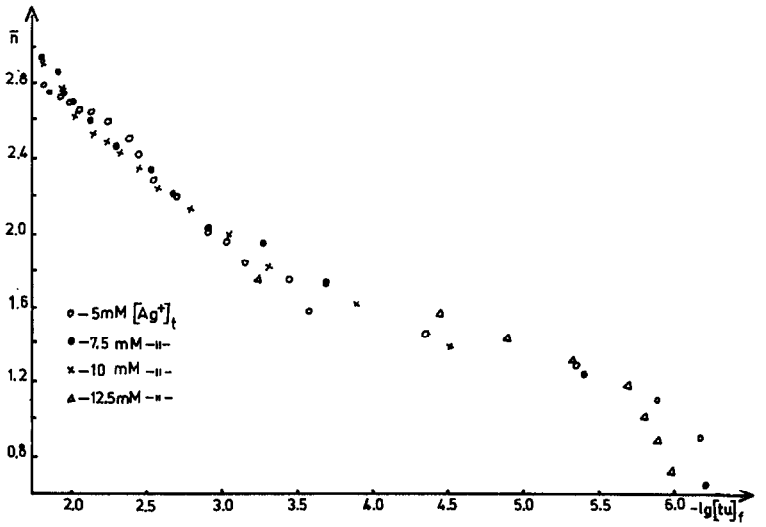


Fig. 7. Average ligand number dependence on log free thiourea concentration.

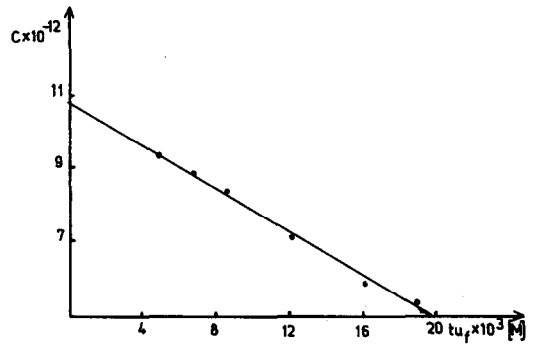


Fig. 8. Graphical determination of the silver–thiourea complex stability constants.

Table 4. Stability constant values of mononuclear silver–thiourea complexes in 1 M $HClO_4$ medium

$[Ag^+]_t$ ($M\ dm^{-3}$)	$\log \beta_1$	$\log \beta_2$	$\log \beta_3$	$\log \beta_4$
5.0×10^{-3}	6.27	10.40	12.58	14.04
7.5×10^{-3}			12.56	13.84
10.0×10^{-3}	5.79	10.96	12.54	13.95
12.5×10^{-3}	5.87	10.80		

DISCUSSION

Silver complexes with sulphur-containing ligands studied in this work are sparingly soluble compounds. Only thiourea molecules, which may not form anions, form soluble, colourless complexes with coordination numbers 1–4 and a dinuclear complex, $[Ag_2tu_6]^{2+}$. Thiohydantoin and cysteine form 1:1 complexes, while in the case of

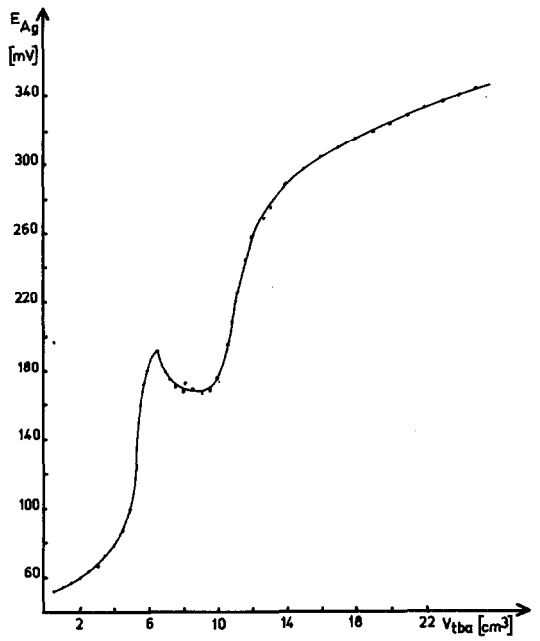


Fig. 10. Silver electrode potential dependence on the thiobarbituric acid volume after full stabilization of the potential value at each titration point.

thiobarbituric acid, sparingly soluble compounds [Ag_2tba, Ag(tba) and $Ag(tba)_2$] were found. Reactions forming scarcely soluble silver compounds with cysteine and thiobarbituric acid are slow reactions. Following the addition of an appropriate ligand amount, the silver–silver chloride electrode potential does not stabilize at once but after a time which depends on the molar ratio of metal to ligand. Figure 9 shows silver electrode potential dependence on the duration of the silver–thiobarbituric acid reaction at different molar ratios of metal ion and ligand.

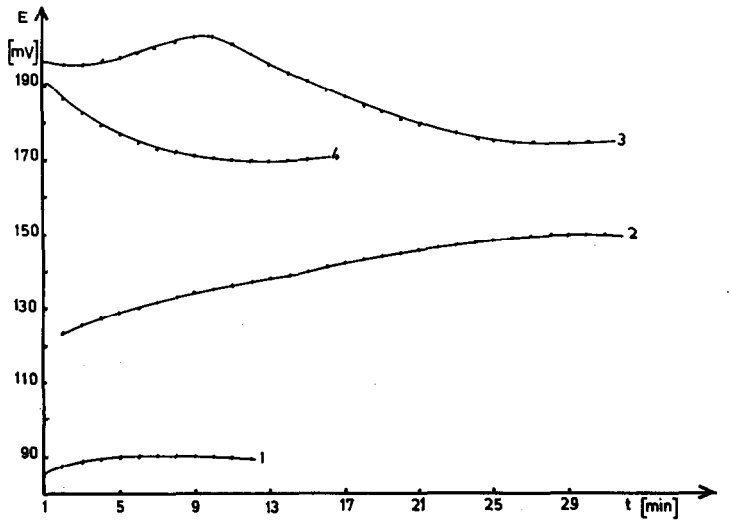


Fig. 9. Silver electrode potential dependence on the reaction time of Ag(I) and thiobarbituric acid for different proportions of metal and ligand.

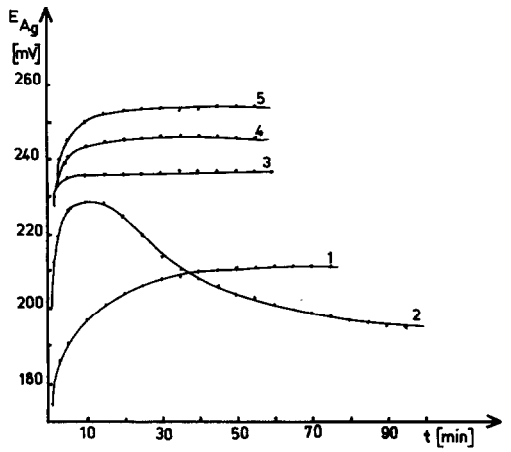


Fig. 11. Silver electrode potential dependence on the reaction time of Ag(I) and cysteine.

Figure 10 shows the $AgClO_4$ solution titration with thiobarbituric acid after a full silver electrode potential stabilization at each titration point. A long time of equilibrium stabilization, as well as a characteristic potential maximum, seen in Fig. 10, are probably connected with the change in the complex structure and transformation of the Ag_2(tba) into the Ag(tba) complex. A similar silver electrode potential dependence on the reaction time was obtained for the silver ion–cysteine reaction

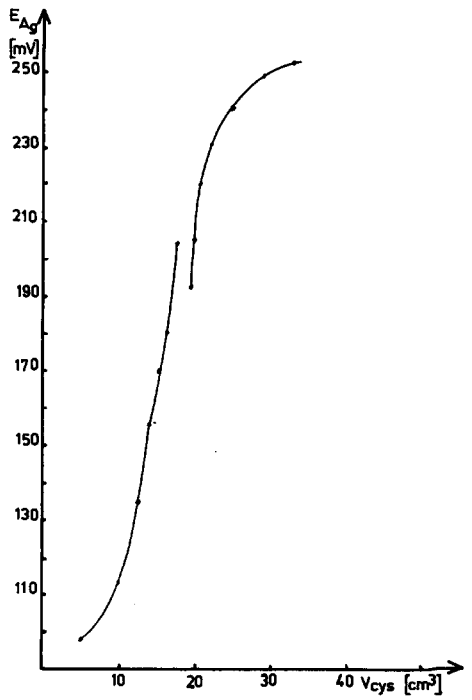


Fig. 12. Silver electrode potential dependence on the cysteine concentration after full stabilization of the silver electrode potential value.

Table 5. Experimental and literature stability constant values of mononuclear silver–thiourea complexes

	This work	Reference 10	Reference 15
$\log \beta_1$	6.05	7.3	7.04
$\log \beta_2$	10.71	10.6	10.61
$\log \beta_3$	12.56	12.68	12.84
$\log \beta_4$	13.95	13.78	13.62

(Fig. 11). At a 1 : 1 molar silver : cysteine ratio there appears to be a maximum on the curve of $E_{Ag} = f(t)$. This result shows that the reaction character is complex. Probably, besides the 1 : 1 complex, a certain amount of another complex is formed, but this could not be proved unequivocally by means of potentiometric measurements. The diagram of silver ion potentiometric titration with cysteine solution after full stabilization of the potential value at each titration point (Fig. 12) shows only a discontinuity at a molar ratio of 1 : 1. We did not manage to find the other equivalence point.

The determined values of silver complex solubility products with the ligands studied are shown in Tables 1 and 2. The silver–thiourea dinuclear complex was isolated in a crystalline state by Udupa and Krebs.[8] The authors presented the structure of this complex on the basis of X-ray measurements.

Stability constant values of mononuclear silver–thiourea complexes were determined using the redox potential measurements of a thiourea–formamidine disulfide system. The stability constants values determined by us are in a good agreement with the stability constants values determined from the silver electrode potential measurements which are presented in Table 5.

REFERENCES

1. S. Krzewska and H. Podsiadły, *J. Inorg. Nucl. Chem.* 1980, **42**, 83.
2. S. Krzewska, L. Pajdowski and H. Podsiadły, *J. Inorg. Nucl. Chem.* 1980, **42**, 87.
3. S. Krzewska, H. Podsiadły and L. Pajdowski, *J. Inorg Nucl. Chem.* 1980, **42**, 89.
4. N. Pustelnik and R. Sołoniewicz, *Monatsh. Chem.* 1975, **106**, 673.
5. N. Pustelnik and R. Sołoniewicz, *Monatsh. Chem.* 1978, **109**, 33.
6. P. J. McCarthy and J. M. Walker, *Can. J. Chem.* 1978, **56**, 9.
7. E. A. Vizzini and E. L. Amma, *J. Am. Chem. Soc.* 1966, **88**, 2872.
8. M. R. Udupa and B. Krebs, *Inorg. Chim. Acta* 1973, **7**, 271.

9. S. Ahrland, J. Chatt, N. R. Davies and A. A. Williams, *J. Chem. Soc.* 1958, 264.
10. A. Bellomo, D. D. Marco and A. D. Robertis, *Talanta* 1973, **20**, 1255.
11. G. N. Shivrin and E. M. Shivrina, *Tsvetn. Met.* 1977, **6**, 22.
12. G. N. Shivrin and E. M. Shivrina, *Tsvetn. Met.* 1971, **1**, 47.
13. G. N. Shivrin and E. M. Shivrina, *Tsvetn. Met.* 1976, **5**, 43.
14. L. Pajdowski and S. Krzewska, *Pr. Nauk Inst. Chem. Nieorg. Metal. Pierwiastkow Rzadkich Politech. Wrocław* 1973, **17**, 155.
15. G. Berthon and C. Luca, *Bull. Soc. Chim. Fr.* 1969, **2**, 432.
16. E. Baibarieva, V. V. Movchan, O. G. Dzyuba and T. M. Tulupa, *Zh. Neorg. Khim.* 1978, **23**, 1546.
17. V. M. Shulman and Z. A. Saveleva, *Izv. Sib. Otd. Akad. Nauk SSSR, Ser. Khim. Nauk* 1970, **2**, 124.
18. G. Berthon and T. Berg, *J. Chem. Thermodyn.* 1976, **8**, 1145.
19. P. W. Preisler and L. Berger, *J. Am. Chem. Soc.* 1974, **69**, 322.
20. F. J. C. Rossotti and H. S. Rossotti, *The Determination of Stability Constants*. New York (1961).

Polyhedron Vol. 5, No. 4, pp. 945–950, 1986
Printed in Great Britain

0277–5387/86 $3.00+.00
Pergamon Journals Ltd

REACTIVITY OF ARSENIC SELENIDES AND TELLURIDE: COBALT COMPLEXES CONTAINING THE SELENA- OR TELLURA-DIARSIRENE CYCLIC UNITS *TRIHAPTO*-BONDED TO THE METAL ATOM—CRYSTAL AND MOLECULAR STRUCTURES OF [(TRIPHOS)Co(As_2Se)](BF_4)(C_2H_5OH) AND [(TRIPHOS)Co(As_2Te)](BF_4)(C_6H_6)$_{0.5}$

MASSIMO DI VAIRA, MAURIZIO PERUZZINI and PIERO STOPPIONI*

Dipartimento di Chimica, Università di Firenze and Istituto I.S.S.E.C.C., Via Maragliano, 77, 50144 Firenze, Italy

(*Received* 8 *July* 1985; *accepted* 2 *October* 1985)

Abstract—The reaction of $Co(BF_4)_2(H_2O)_6$ with arsenic selenides and telluride, As_4Se_3, As_2Se_3 and As_2Te_3 in the presence of 1,1,1-tris(diphenylphosphinomethyl)ethane (triphos), yielded the complexes

[(triphos)Co(As_2Se)](BF_4)(C_2H_5OH) (**1**)

and

[(triphos)Co(As_2Te)](BF_4)(C_6H_6)$_{0.5}$ (**2**).

The molecular structures of the complexes have been determined by single-crystal X-ray diffraction methods. The isomorphous compounds crystallize in the monoclinic space group $P2_1/n$ with $Z = 4$ and unit-cell dimensions: (**1**) $a = 17.034(8)$ Å, $b = 20.640(9)$ Å, $c = 13.116(6)$ Å, $\beta = 105.37(6)°$; (**2**) $a = 17.076(7)$ Å, $b = 20.419(9)$ Å, $c = 13.215(7)$ Å, $\beta = 105.15(7)°$. The metal atom in both compounds is in a six-coordinate environment formed by the triphos P atoms and by the atoms of the heterocyclic As_2Se or As_2Te unit.

The E_4X_3 (E = P, X = S or Se; E = As, X = S) cage molecules react with transition-metal–ligand systems to give different products depending on the nature of the metal atom and its oxidation state.[1] In particular, a substantial cleavage of the cage molecules occurs in the reactions with cobalt(II) and nickel(II) tetrafluoroborate in the presence of triphos [triphos = 1,1,1-tris(diphenylphosphinomethyl)ethane], affording stable complexes which contain the heterocyclic E_2X (E = P, X = S or Se;[2] E = As, X = S[3]) or the homocyclic E_3 (E = P[4] or As[5]) units η^3-bonded to the metal atom. Other small molecules formed by atoms of groups V and VI react with transition-metal complexes, affording compounds which contain either "bare" pnicogen[6] or chalcogen[7] atoms, or small groups of such atoms, like S_2,[8] P_2,[9] P_3,[10] As_3[11] or S_5[12] bound to the metal atom. Among such compounds, those containing S or P are much more numerous than the Se, Te or As derivatives. This is probably due to the markedly different chemical behaviour of the latter elements with respect to that of the lighter ones of the same groups.

Here we report the synthesis and characterization of the compounds

[(triphos)Co(As_2Se)](BF_4)(C_2H_5OH) (**1**)

and

[(triphos)Co(As_2Te)](BF_4)(C_6H_6)$_{0.5}$ (**2**)

which contain the new As_2Se and As_2Te cyclic units η^3-bonded to the metal. The comparison between the structures of the present compounds and those of the isomorphous [(triphos)Co(E_2X)](BF_4)(C_6H_6) (E = P, X = S or Se;[2] E = As, X = S[3]) complexes reveals the effects due to the presence of the heavier and larger atoms of groups V and VI in the As_2Se and As_2Te rings.

* Author to whom correspondence should be addressed.

EXPERIMENTAL

All solvents were reagent grade and were dried by distillation from suitable agents.[13] All reactions and manipulations were carried out under dry nitrogen. Electronic spectra, conductivity and magnetic susceptibilities were measured by procedures already described.[14] ^{31}P NMR spectra were collected (at 32.19 MHz) on a Varian CFT20 spectrometer. ^{31}P positive chemical shifts are downfield relative to H_3PO_4 at 0.0 ppm.

The compound As_2Te_3 was purchased from Ventron GMBH and used without any purification; the ligand triphos[15] and As_4Se_3[16] were prepared according to published procedures. As_2Se_3 was synthesized by reacting in a sealed tube under nitrogen gray As and black Se in a 2:3 ratio for 3 days at 410°C. The solid obtained was finely powdered and stored in an inert atmosphere.

Synthetic procedures

Preparation of **1**. *Procedure A.* Finely powdered As_4Se_3 (3 mmol) was added to a solution of $Co(BF_4)_2(H_2O)_6$ (1 mmol) in ethanol (10 cm^3) and triphos (1 mmol) in tetrahydrofuran–benzene (1:1) (50 cm^3). The resulting mixture was refluxed for 5 days with magnetic stirring and then filtered. The solid was washed with warm dichloromethane (20 cm^3). The combined filtrate and washing solutions were concentrated to dryness *in vacuo*. The solid was extracted with hot dichloromethane (40 cm^3) and ethanol–benzene (2:1) (40 cm^3) was added. Red crystals of the compound were obtained by concentrating the solution. The complex was collected on a sintered-glass frit, in a closed system, and washed with ethanol and then light petroleum (b.p. 40–70°C) before being dried (yield 50–55%). The compound, which crystallizes with one molecule of ethanol, was recrystallized from dichloromethane and ethanol–benzene (1:1).

Procedure B. As_2Se_3 (2 mmol) was added to a solution of $Co(BF_4)_2(H_2O)_6$ (1 mmol) in ethanol (10 cm^3) and triphos (1 mmol) in tetrahydrofuran–benzene (1:1) (50 cm^3). The resulting mixture was refluxed for 4 days with magnetic stirring and then filtered. The compound $[(triphos)Co(As_2Se)](BF_4)$ was isolated as described for procedure A.

Preparation of **2**. As_2Te_3 (2 mmol) was added to a solution of $Co(BF_4)_2(H_2O)_6$ (1 mmol) in ethanol (10 cm^3) and triphos (1 mmol) in tetrahydrofuran–benzene (1:1) (40 cm^3). The mixture was refluxed for 8 days, then filtered while hot and ethanol–benzene (1:1) (30 cm^3) was added. Dark-red crystals of the compound were obtained by concentrating the solution. The complex was collected by the procedure described above for the As_2Se derivative (yield 15–20%). The compound could not be recrystallized due to its tendency to decompose in solution, releasing tellurium.

X-ray crystal structures

Diffraction data for compounds **1** *and* **2**. These were collected at room temperature from crystals of dimensions $0.20 \times 0.20 \times 0.25$ mm (**1**) and $0.15 \times 0.10 \times 0.20$ mm (**2**) using a Philips PW 1100 four-circle diffractometer and graphite-monochromated Mo-K_α radiation ($\lambda = 0.71069$ Å). Lattice constants were determined by least-squares refinement of the angular settings of 24 reflections with $22 < 2\theta < 40°$ (**1**) and $18 < 2\theta < 22°$ (**2**).

Crystal data. (**1**) $C_{43}H_{45}As_2BCoF_4OP_3Se$, $M_r = 1045.3$, monoclinic, $a = 17.034(8)$ Å, $b = 20.640(9)$ Å, $c = 13.116(6)$ Å, $\beta = 105.37(6)°$, $U = 4446.4$ Å^3, $Z = 4$, $D_c = 1.56$ g cm^{-3}, $F(000) = 2096$, μ(Mo-K_α) = 28.2 cm^{-1}, space group $P2_1/n$.

(**2**) $C_{44}H_{42}As_2BCoF_4P_3Te$, $M_r = 1086.9$, monoclinic, $a = 17.076(7)$ Å, $b = 20.419(9)$ Å, $c = 13.215(7)$ Å, $\beta = 105.15(7)°$, $U = 4447.6$ Å^3, $Z = 4$, $D_f = 1.66$ g cm^{-3}, $D_c = 1.62$ g cm^{-3}, $F(000) = 2148$, μ(Mo-K_α) = 26.5 cm^{-1}, space group $P2_1/n$.

Crystals of **2** did not provide good material for X-ray diffraction, probably due to larger effects of disorder (see below) in the structure of **2** than in that of **1**. The intensities of all reflections with $k > 0$ and $l > 0$ were measured in the ranges $5 < 2\theta < 44°$ (**1**) and $5 < 2\theta < 40°$ (**2**) in the θ–2θ scan mode with a scan width of $(1.10 + 0.30 \tan\theta)°$ and scan speed of 6° min^{-1}. No crystal decay was observed. Of the total 5912 (**1**) and 4529 (**2**) reflections recorded 2432 (**1**) and 1450 (**2**) having $I > 3\sigma(I)$ were used for structure determination after correction for Lorentz, polarization and X-ray absorption effects. Crystallographic calculations were carried out using SHELX 76.[17]

The structures of the two compounds, which are isomorphous to each other as well as to the $[(triphos)Co(E_2X)](BF_4)(C_6H_6)$ (E = P, X = S or Se;[2] E = As, X = S[3]) complexes previously investigated, were refined assuming as initial values for the atomic coordinates those from the latter structures. All atoms heavier than carbon were assigned anisotropic thermal parameters, whereas the other atoms were refined isotropically. The solvent molecule in each structure was assigned an overall temperature factor. Phenyl groups of the triphos ligand were refined as rigid bodies with idealized geometry. Hydrogen atoms of the triphos ligand were introduced in calculated positions (C—H = 1.00 Å) with an overall temperature factor. The BF_4^- anion was imposed a tetrahedral geometry, the value of the B—F distance being refined. The

scattering factors for the neutral atoms and the anomalous dispersion corrections for Co, Se, As and Te were taken from Ref. 18. It was impossible to identify the As and Se atoms in the triatomic ring of **1**. Therefore, in analogy with the model used for the P_2S derivative,[2] each site of the ring was assigned 0.67 As and 0.33 Se occupancy factors. This led to comparable U_{iso} values for the three sites. The ratio of the C—C and C—O bond lengths in the solvate ethanol molecule of **1** was constrained to an idealized value:[19] the O atom, identified on the basis of peak heights and contact distances, was found from ΔF maps to be distributed with essentially an equal probability between two positions. For **1** no peaks >0.7 *e* Å^{-3} were observed in the final electron-density difference map, and refinement with the weighting scheme $w = [\sigma^2(F_o)+0.0001|F_o|^2]^{-1}$ led to $R = 0.056$ ($R' = 0.062$). For **2** it was evident from the peak heights in ΔF Fourier maps that the Te atom was distributed over at least two sites of the As_2Te ring with different occupancy factors. Refinement of the population parameters of the three sites was performed by the procedure already described for the P_2Se[2] and As_2S[3] isomorphs, i.e. imposing that the U_{iso} values for the three sites should be close to each other. The occupancy factors so obtained [essentially 1.00 As for the site labelled As(1), whereas sites As(2) and Te had 0.80 and, respectively, 0.20 As occupancy factors with complementary Te population parameters] were in reasonable agreement with those previously determined for the P_2Se isomorph,[2] allowing for replacement of As for P and of Te for Se. The solvate benzene molecule was highly disordered, with peak heights <1 *e* Å^{-3} in ΔF Fourier maps. The compromise 0.5 value of its population parameter, lower than indicated by the D_f value, was assigned on the basis of the *R* criterion and in order to avoid an exceedingly high value of the overall temperature factor. Such a benzene ring, without H atoms, was imposed an idealized geometry: the C—C distance was refined to 1.38 Å and the overall *U* value to 0.195(2) Å^2. For **2** no peaks >0.8 *e* Å^{-3} were observed in the final electron-density difference map and refinement with the weighting scheme $w = [\sigma^2(F_o)+0.0005|F_o|^2]^{-1}$ led to $R = 0.068$ ($R' = 0.076$). Final atomic positional and thermal parameters, bond lengths and angles and F_o/F_c values have been deposited as supplementary material with the Editor, from whom copies are available on request. Atomic coordinates have also been submitted to the Cambridge Crystallographic Data Centre.

RESULTS AND DISCUSSION

The reaction of cobalt(II) tetrafluoroborate in the presence of the tripod ligand triphos with As_4Se_3, As_2Se_3 or As_2Te_3 affords complexes of formula [(triphos)Co(As_2X)](BF_4) [X = Se(**1**) or Te(**2**)]. The analytical data (Table 1) for the complexes, which crystallize with solvent molecules in the lattice, are in good agreement with the proposed formula. The complexes behave as 1:1 electrolytes in nitroethane[20] (Table 1). The diamagnetic compounds are moderately air-stable in the solid state. They are slightly soluble in acetone and dichloromethane, whereupon the compound containing the selenadiarsirene unit is stable under nitrogen, whereas the As_2Te derivative decomposes in a short time even in an inert atmosphere by releasing tellurium. A similar behaviour has been found for telluradiphosphirane,[21] which is the only compound containing a Te atom in a three-membered ring so far reported. The low solubility of both compounds here described prevented us from obtaining ^{77}Se and ^{125}Te NMR spectra. The ^{31}P–{^{1}H} NMR spectra of the compounds (Table 2) exhibit a broad resonance at low field (32.56 and 32.39 ppm for compounds **1** and **2**, respectively) affected by the cobalt quadrupole moment, that is assigned to the three atoms of the ligand. The triphos $\delta(^{31}P)$ values are practically identical for complexes **1** and **2** and for all the isostructural [(triphos)Co(E_2X)](BF_4) complexes

Table 1. Analytical and conductivity data for the complexes

	Compound	Λ_M[a] (Ω^{-1} cm^2 M^{-1})	Analysis (%): found (calc.) C	H	Co	P	As	Other
1	[(triphos)Co(As_2Se)](BF_4)(C_2H_5OH)	84	49.5 (49.4)	4.6 (4.3)	5.5 (5.6)	8.9 (8.9)	14.3 (14.3)	Se: 7.4 (7.5)
2	[(triphos)Co(As_2Te)](BF_4)(C_6H_6)$_{0.5}$	91	48.5 (48.6)	4.0 (3.9)	5.3 (5.4)	8.4 (8.5)	13.6 (13.8)	Te: 11.9 (11.7)

[a] Molar conductance of *ca* 10^{-3} M nitroethane solution at 20°C.

Table 2. $^{31}P-\{^1H\}$ NMR and electronic spectral data for the complexes

	Compound	δ^a (ppm)	ΔP^b	λ_{max} (nm) [ε ($dm^3\ mol^{-1}\ cm^{-1}$)]^c
1	[(triphos)Co(As_2Se)](BF_4)(C_2H_5OH)	32.56 (br)	58.11	470 (sh) (~760), 380 (sh) (~2850)
2	[(triphos)Co(As_2Te)](BF_4)(C_6H_6)$_{0.5}$	32.39 (br)	57.94	500 (sh) (~700), 390 (2760)

[a] Chemical shifts are relative to 85% H_3PO_4. Positive chemical shifts are downfield : br = broad ; sh = shoulder. The complexes were dissolved in $(CD_3)_2CO$.

[b] $\Delta P = \delta P$ (coord.) $- \delta P$ (free ligand).

[c] Absorption maxima for CH_2Cl_2 solution at 20°C.

(E = P, X = S or Se[2]; E = As, X = S[3]) having the P_2S, P_2Se or As_2S cyclic unit *trihapto* bonded to the metal. The scarce sensitivity of the triphos chemical shift to replacement of the chalcogen or pnicogen atoms in the triatomic ring might be due to involvement of the triphos P atoms in lower-energy molecular orbitals than the atoms of the cyclic unit. The absorption spectra of the compounds in dichloromethane solution (Table 2) exhibit a shoulder and a band at *ca* 470–500 and 380–390 nm, respectively. In the spectrum of the [(triphos)Co(As_2S)](BF_4) derivative the same transitions occur at 450 and 380 nm, their frequencies decreasing slightly with increasing atomic number of the heteroatom in the As_2X ring. The same trend had been noticed for the P_2X (X = S or Se) derivatives[2] and may be related in part to the accompanying increase, in the mean, of the metal to As_2X or P_2X ring distances, proved by the results of previous [2,3] structural analyses combined with those reported here. The crystal structures of the isomorphous compounds **1** and **2** consist of [(triphos)Co(As_2X)]$^+$ cations (X = Se or Te), BF_4^- anions, and interposed ethanol or benzene molecules from the solvent. Figure 1 shows a perspective view of the cation in compound **1**, the geometry of the cation in **2** being closely similar. Selected values of bond distances and angles in the two structures are listed in Table 3. The metal atom in each cation is in a six-coordinate environment formed by the triphos P atoms and the atoms of the As_2X unit in a staggered arrangement similar to that previously found for the compounds containing the P_3 homocyclic[10] or the E_2X (E = P, X = S or Se;[2] E = As, X = S[3]) heterocyclic inorganic rings. The distances from the metal atom to the P atoms of the triphos ligand in either compound [2.205(4)–2.227(9) Å] are in the range of values already found for the isomorphous derivatives.[2,3] A detailed analysis of the dimensions of the $CoAs_2X$ moieties in the two compounds is prevented

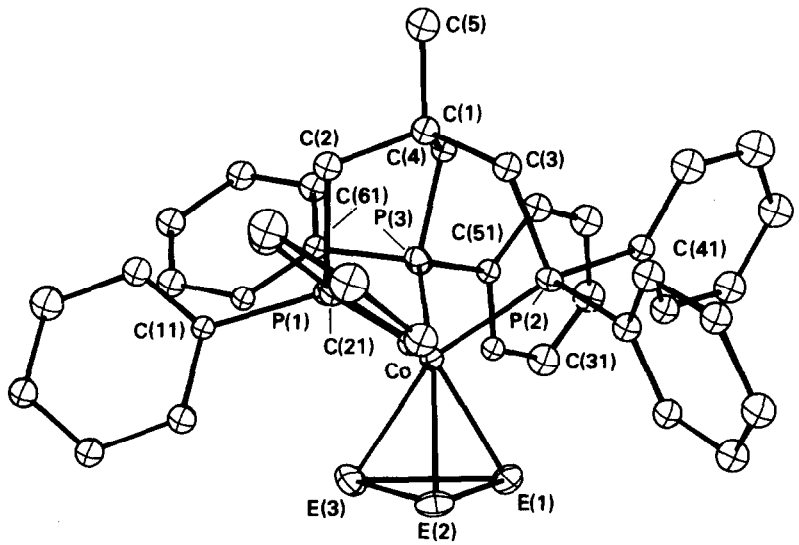


Fig. 1. Perspective view of the [(triphos)Co(As_2Se)]$^+$ cation with 20% probability ellipsoids. The E(1)–E(3) sites have 0.67 As and 0.33 Se occupancy. Only the first carbon atom of each phenyl group is labelled. The [(triphos)Co(As_2Te)]$^+$ cation has substantially the same structure with As_2Te ring site occupancies as specified in Experimental and in footnote [b] to Table 3.

Table 3. Selected bond distances (Å) and angles (°) for the compounds [(triphos)Co(As_2Se)](BF_4)(C_2H_5OH) (**1**)[a] and [(triphos)Co(As_2Te)](BF_4)(C_6H_6)$_{0.5}$ (**2**)[b]

1		**2**	
Co—E(1)	2.393(2)	Co—As(1)	2.413(5)
Co—E(2)	2.413(2)	Co—As(2)	2.476(5)
Co—E(3)	2.410(2)	Co—Te	2.582(4)
Co—P(1)	2.218(4)	Co—P(1)	2.227(9)
Co—P(2)	2.205(4)	Co—P(2)	2.206(8)
Co—P(3)	2.212(4)	Co—P(3)	2.218(9)
E(1)—E(2)	2.363(2)	As(1)—As(2)	2.408(5)
E(1)—E(3)	2.353(2)	As(1)—Te	2.497(5)
E(2)—E(3)	2.365(2)	As(2)—Te	2.539(4)
E(1)—Co—E(2)	58.9(1)	As(1)—Co—As(2)	59.0(2)
E(1)—Co—E(3)	58.7(1)	As(1)—Co—Te	59.9(1)
E(1)—Co—P(1)	153.7(1)	As(1)—Co—P(1)	154.9(3)
E(1)—Co—P(2)	101.0(1)	As(1)—Co—P(2)	98.7(3)
E(1)—Co—P(3)	106.7(1)	As(1)—Co—P(3)	107.1(3)
E(2)—Co—E(3)	58.7(1)	As(2)—Co—Te	60.2(1)
E(2)—Co—P(1)	96.6(1)	As(2)—Co—P(1)	97.1(3)
E(2)—Co—P(2)	106.0(1)	As(2)—Co—P(2)	105.1(3)
E(2)—Co—P(3)	160.2(1)	As(2)—Co—P(3)	160.9(3)
E(3)—Co—P(1)	101.9(1)	Te—Co—P(1)	103.1(2)
E(3)—Co—P(2)	158.4(1)	Te—Co—P(2)	157.7(3)
E(3)—Co—P(3)	102.8(1)	Te—Co—P(3)	102.1(2)
P(1)—Co—P(2)	94.6(2)	P(1)—Co—P(2)	94.9(3)
P(1)—Co—P(3)	94.3(2)	P(1)—Co—P(3)	94.1(3)
P(2)—Co—P(3)	89.5(1)	P(2)—Co—P(3)	89.3(3)
Co—E(1)—E(2)	61.0(1)	Co—As(1)—As(2)	61.8(2)
Co—E(1)—E(3)	61.0(1)	Co—As(1)—Te	63.4(1)
E(2)—E(1)—E(3)	60.2(1)	As(2)—As(1)—Te	62.3(1)
Co—E(2)—E(1)	60.1(1)	Co—As(2)—As(1)	59.2(2)
Co—E(2)—E(3)	60.6(1)	Co—As(2)—Te	61.9(1)
E(1)—E(2)—E(3)	59.7(1)	As(1)—As(2)—Te	60.5(1)
Co—E(3)—E(1)	60.3(1)	Co—Te—As(1)	56.7(1)
Co—E(3)—E(2)	60.7(1)	Co—Te—As(2)	57.8(1)
E(1)—E(3)—E(2)	60.1(1)	As(1)—Te—As(2)	57.1(1)

[a] Each of the E(1)–E(3) sites has been assigned 0.67 As and 0.33 Se occupancy factors (see Experimental).

[b] The As(2) and Te sites have the following fractional As/Te occupancies: As(2) (0.80 As, 0.20 Te), Te (0.20 As, 0.80 Te).

by the disorder affecting the triatomic rings. It should however be noted that the overall geometry of the $CoAs_2Se$ fragment in **1** is approximately tetrahedral (Table 3), with metal to ring-site and intraring distances definitely longer [by *ca* 0.14 and 0.24 Å, respectively] than the corresponding distances in the CoP_2S part of the thiadiphosphirene derivative.[2] The geometry of the $CoAs_2Te$ moiety in **2** is less regular, due to the presence of the large Te atom. The site with the highest Te population is indeed involved in rather long bond distances; in particular, its distance from the metal site, of 2.582(4) Å, is definitely longer than any of the corresponding bond lengths found for compounds of this series.

Although the assignment of the oxidation number of the metal atom in these compounds is not unambiguous, the compounds may be considered to contain cobalt(I), assuming that the As_2X moiety behaves as a neutral four-electron donor, consistently with the electron-counting procedure already used for triphosphirene complexes.[10] Therefore, reduction of the metal atom should occur in the formation of the present or previous[2,3] compounds with the [(triphos)Co(E_2X)](BF_4) stoichiometry as it has been considered[10] to occur in the formation of the [(triphos)M(P_3)]$^{n+}$ complexes [M = Co,[22] Rh[23] or Ir[23]; $n = 0$: M = Ni,[4] Pd[24] or Pt[24]; $n = 1$) or of the triple-decker com-

pounds with P_3 or As_3 internal slices.[10] In such processes, at variance with those where no reduction of the metal atom occurs,[1(a),1(c),1(d)] substantial cleavage of the reacting cage molecule (P_4, As_4, or a molecule of the E_4X_3 class) is invariably involved. An unprecedented feature of the present results is however due to the fact that compounds with the [(triphos)Co(As_2X)](BF_4) stoichiometry have now been obtained not only by reaction of a cobalt(II) salt with the molecular As_4Se_3 compound, but also with polymeric species, such as As_2Se_3[25] or As_2Te_3.[26] While these results are compatible with the view that the disruptive attack of the chalcogenide by the metal–ligand system involves a redox process, they point to the efficiency of the (triphos)Co system in directing the course of the reaction toward the formation of compounds with suitable electron counts, irrespective of the structure of the chalcogenide used as a reactant.

Acknowledgements—Thanks are expressed to Mr F. Nuzzi for microanalyses. Financial support for this work from Italian C.N.R. under the "Progetto Finalizzato Chimica Fine e Secondaria" is gratefully acknowledged.

REFERENCES

1. (a) M. Di Vaira, M. Peruzzini and P. Stoppioni, *Inorg. Chem.* 1983, **22**, 2196; (b) M. Di Vaira, M. Peruzzini and P. Stoppioni, *J. Chem. Soc., Chem. Commun.* 1983, 903; (c) M. Di Vaira, M. Peruzzini and P. Stoppioni, *J. Chem. Soc., Dalton Trans.* 1985, 291; (d) C. A. Ghilardi, S. Midollini and A. Orlandini, *Angew. Chem., Int. Ed. Engl.* 1983, **22**, 790.
2. M. Di Vaira, M. Peruzzini and P. Stoppioni, *J. Chem. Soc., Dalton Trans.* 1984, 359.
3. M. Di Vaira, P. Innocenti, S. Moneti, M. Peruzzini and P. Stoppioni, *Inorg. Chim. Acta* 1984, **83**, 161.
4. M. Di Vaira, L. Sacconi and P. Stoppioni, *J. Organomet. Chem.* 1983, **250**, 183.
5. P. Stoppioni and M. Peruzzini, *J. Organomet. Chem.* 1983, **262**, C5.
6. A. Vizi-Orosz, V. Galamb, G. Pàlyi, L. Markò, G. Bor and G. Natile, *J. Organomet. Chem.* 1976, **107**, 235; D. Seyferth, J. S. Merola and R. S. Henderson, *Organometallics* 1982, **1**, 859.
7. L. Y. Goh, T. W. Hambley and G. B. Robertson, *J. Chem. Soc., Chem. Commun.* 1983, 1458; L. Y. Goh, C. Wei and E. Sinn, *J. Chem. Soc., Chem. Commun.* 1985, 462; W. A. Herrmann, C. Hecht, M. L. Ziegler and B. Balbach, *J. Chem. Soc., Chem. Commun.* 1984, 686.
8. H. Brunner, J. Wachter, E. Guggolz and M. L. Ziegler, *J. Am. Chem. Soc.* 1982, **104**, 1765.
9. O. J. Scherer, H. Sitzmann and G. Wolmershäuser, *J. Organomet. Chem.* 1984, **268**, C9.
10. M. Di Vaira and L. Sacconi, *Angew. Chem., Int. Ed. Engl.* 1982, **21**, 330 (and references listed therein).
11. I. Bernal, H. Brunner, W. Meier, H. Pfisterer, J. Wachter and M. L. Ziegler, *Angew. Chem., Int. Ed. Engl.* 1984, **23**, 438.
12. D. Coucouvannis, P. R. Patil, N. G. Kanatzidis, B. Detering and N. C. Baenziger, *Inorg. Chem.* 1985, **24**, 24.
13. O. O. Perrin, W. L. F. Armarego and D. R. Perrin, *Purification of Laboratory Chemicals.* Pergamon Press, Oxford (1966).
14. L. Sacconi and R. Morassi, *J. Chem. Soc. A* 1968, 2997; L. Sacconi, I. Bertini and F. Mani, *Inorg. Chem.* 1968, **7**, 1417.
15. W. Hewertson and H. R. Watson, *J. Chem. Soc.* 1962, 1490.
16. B. H. Christian, R. J. Gillespie and J. F. Sawyer, *Inorg. Chem.* 1981, **20**, 3410.
17. G. M. Sheldrick, "SHELX 76" System of Computing Programs, University of Cambridge (1976).
18. *International Tables for X-ray Crystallography*, Vol. 4. Kynoch Press, Birmingham (1974).
19. "Interatomic Distances", Chemical Society, Special Publication No. 18 (1965).
20. W. J. Geary, *Coord. Chem. Rev.* 1971, **7**, 81.
21. W.-W. du Mont, T. Severengiz and B. Meyer, *Angew. Chem., Int. Ed. Engl.* 1983, **22**, 983.
22. C. A. Ghilardi, S. Midollini, A. Orlandini and L. Sacconi, *Inorg. Chem.* 1980, **19**, 301.
23. C. Bianchini, C. Mealli, A. Meli and L. Sacconi, *Inorg. Chim. Acta* 1979, **37**, L543.
24. P. Dapporto, L. Sacconi, P. Stoppioni and F. Zanobini, *Inorg. Chem.* 1981, **20**, 3834.
25. N. Morimoto, *Mineral. J.* 1954, **1**, 160.
26. G. J. Carron, *Acta Cryst.* 1963, **16**, 338.

Polyhedron Vol. 5, No. 4, pp. 951–958, 1986
Printed in Great Britain

0277–5387/86 $3.00+.00
Pergamon Journals Ltd

MIXED ALKYL ISOCYANIDE–1,4-DIAZA-1,3-BUTADIENE COMPLEXES OF CHROMIUM: A SERIES OF 17-, 18- AND 19-ELECTRON SPECIES OF THE TYPE $[Cr(CO)_3(CNR)(R'\text{-DAB})]^{1+,0,1-}$

ANDREW BELL and RICHARD A. WALTON*

Department of Chemistry, Purdue University, West Lafayette, IN 47907, U.S.A.

(*Received* 16 *August* 1985; *accepted* 30 *September* 1985)

Abstract—The chromium(0) complexes $Cr(CO)_3(CNR)(R'\text{-DAB})$ (R = Me, $CHMe_2$, CMe_3 or xylyl; R′ = *i*-Pr, *t*-Bu, Cy or *p*-tol) can be prepared by the reaction of $Cr(CO)_3(NCMe)_3$ with equimolar quantities of R′-DAB and RNC. These complexes are oxidized to the paramagnetic 17-electron salts $[Cr(CO)_3(CNR)(R'\text{-DAB})]PF_6$ by $[(\eta^5\text{-}C_5H_5)_2Fe]PF_6$ in ethanol, and can be reduced to the paramagnetic 19-electron radical anions $[Cr(CO)_3(CNR)(R'\text{-DAB})]^-$ using Na–Hg in tetrahydrofuran. The spectroscopic (IR, ^1H NMR, electronic absorption and ESR) and electrochemical properties of the $[Cr(CO)_3(CNR)(R'\text{-DAB})]^{1+,0,1-}$ species (where appropriate) have been recorded. The dark red monocationic species $[Cr(CO)_3(CNR)(R'\text{-DAB})]PF_6$ are subject to disproportionation in solution to give separable mixtures of dark blue $Cr(CO)_3(CNR)(R'\text{-DAB})$ and green $[Cr(CNR)_4(R'\text{-DAB})](PF_6)_2$.

Our discovery of the pairs of six- and seven-coordinate homoleptic chromium(II) isocyanide complexes $[Cr(CNR)_6]^{2+}$ and $[Cr(CNR)_7]^{2+}$ (R = alkyl),[1–3] and subsequent studies of their redox behavior[1,2] and substitution chemistry with nitric oxide[4] and phosphine ligands,[2] have in turn led us to explore other strategies for the synthesis of complexes that contain Cr—CNR bonds. At the outset, our objective had been to prepare mixed isocyanide–1,4-diaza-1,3-butadiene complexes of chromium of the type $[Cr(CNR)_5(R'\text{-DAB})](PF_6)_2$,† in order to compare their chemistry to the molybdenum(II) analogues $[Mo(CNR)_5(R'\text{-DAB})](PF_6)_2$ (R = *i*-Pr or *t*-Bu, R′ = *i*-Pr or C_6H_{11}).[5] While we have not yet been able to prepare these seven-coordinate chromium(II) species and, indeed, have evidence that they might not be stable, we have isolated the chromium(0) complexes $Cr(CO)_3(CNR)(R'\text{-DAB})$. An examination of their redox properties shows that the sets of 17-, 18- and 19-electron species $[Cr(CO)_3(CNR)(R'\text{-DAB})]^{1+,0,1-}$ can be isolated. Details of their chemistry are reported herein.

EXPERIMENTAL

Starting materials

The isocyanides RNC (R = Me, $CHMe_2$ or CMe_3)[6,7] and the 1,4-diaza-1,3-butadiene ligands R′-DAB[8,9] were prepared by standard literature procedures. Ferrocene (Strem Chemicals Inc.) and $Cr(CO)_6$ (Pressure Chemical Co.) were obtained from commercial sources, as were all reagents and solvents. CH_2Cl_2, acetonitrile and tetrahydrofuran (THF) were distilled under N_2 from P_2O_5, CaH_2 and sodium benzophenone ketyl, respectively, before use.

Samples of the oxidizing agent ferricinium hexafluorophosphate ($[(\eta^5\text{-}C_5H_5)_2Fe]PF_6$) were prepared as described in the literature.[10] Chromium hexacarbonyl was converted into the air-sensitive acetonitrile complex $Cr(CO)_3(NCMe)_3$ by heating small quantities of $Cr(CO)_6$ (~10 mmol) with a large excess of acetonitrile (50–75 cm^3).[11] The reaction mixture was cooled and the excess solvent removed at 25°C under reduced pressure. For convenience in handling, this nitrile complex was usually generated *in*

* Author to whom correspondence should be addressed.

† R′-DAB is the abbreviation used for the group of 1,4-diaza-1,3-butadienes of general formula

$$R'N{=}CH{-}CH{=}NR',$$

where R′ = *i*-Pr, *t*-Bu, Cy or *p*-tol.

situ and then reacted further with the R'-DAB and RNC ligands.

Reactions procedures

All reactions were carried out under a dry nitrogen atmosphere, and all reaction solvents were dried and deoxygenated prior to use by purging with N_2 gas for 15 min. In those cases where compounds were prepared by very similar procedures (see Sections A–E), details of representative recipes only will be given. In those instances where microanalytical data are not given, identification of products is based upon their spectroscopic and electrochemical properties.

A. Preparation of $Cr(CO)_3(CNR)(R'\text{-DAB})$ (R = Me, $CHMe_2$, CMe_3 or xylyl; R' = *i*-Pr, *t*-Bu, Cy or *p*-tol). (i) $Cr(CO)_3(CNMe)$(*t*-Bu-DAB). The metal hexacarbonyl, $Cr(CO)_6$ (5.0 g, 22.7 mmol), was heated at reflux for 6 days in 100 cm^3 of freshly distilled acetonitrile. After this time, the murky yellow solution was cooled to ambient temperature. The solution of $Cr(CO)_3(NCMe)_3$, so generated, was treated with *tert*-butyl-DAB (3.82 g, 22.7 mmol) whereupon the reaction mixture quickly changed color to an intense royal blue. The solution was stirred for approximately 11 h. The addition of an equivalent of CH_3NC (1.27 cm^3, 22.7 mmol) at this time turned the mixture a darker blue. After stirring the resulting mixture for a further 15 min, it was filtered to remove a crop of purple-blue crystals. The filtrate was reduced in volume and petroleum ether was added to precipitate a further quantity of purple crystals. The combined crops of crystals was recrystallized from CH_2Cl_2–hexane and acetone–diethyl ether: yield 7.13 g (91%). Found: C, 51.4; H, 6.9; N, 11.9%. Calc. for $C_{15}H_{23}CrN_3O_3$: C, 52.2; H, 6.7; N, 12.2%.

(ii) $Cr(CO)_3(CNCHMe_2)$(*i*-Pr-DAB). Purple-blue crystals of this compound were isolated in 75% yield by an analogous procedure to that described in Section A(i). This complex was identified by its spectroscopic and electrochemical properties which were fully in accord with this formulation.

(iii) $Cr(CO)_3(CNCMe_3)$(*i*-Pr-DAB)·$0.5(CH_3)_2CO$. Yield 88%. Found: C, 54.1; H, 7.6% Calc. for $C_{17.5}H_{28}CrN_3O_{3.5}$: C, 54.1; H, 7.2%. The presence of one half of a mole of acetone as a solvent of crystallization was confirmed by ^1H NMR spectroscopy.

(iv) $Cr(CO)_3(CNCMe_3)$(*t*-Bu-DAB). Yield 81%. Found: C, 56.6; H, 8.2%. Calc. for $C_{18}H_{29}CrN_3O_3$: C, 55.8; H, 7.5%. An alternative method for preparing this compound involved the reaction of $Cr(CO)_4$(*t*-Bu-DAB)[12] with slightly more than one equivalent of *tert*-butyl isocyanide in refluxing toluene for 1 h: yield 32%. This product was identified on the basis of its spectroscopic and electrochemical properties.

(v) $Cr(CO)_3(CNCMe_3)$(Cy-DAB)·H_2O. Yield 90%. Found: C, 57.7; H, 7.6; N, 9.1%. Calc. for $C_{22}H_{35}CrN_3O_4$: C, 57.7; H, 7.6; N, 9.2%. The presence of a molecule of water of crystallization was established by ^1H NMR spectroscopy.

(vi) $Cr(CO)_3$(CNxylyl)(*i*-Pr-DAB). Yield 88%. Found: C, 58.8; H, 6.1%. Calc. for $C_{20}H_{25}CrN_3O_3$: C, 59.0; H, 6.1%.

(vii) $Cr(CO)_3(CNCMe_3)$(*p*-tol-DAB). Yield 54%. This complex was identified on the basis of its spectroscopic properties.

B. Oxidations of $Cr(CO)_3(CNR)(R'\text{-DAB})$. (i) $[Cr(CO)_3(CNCMe_3)$(*t*-Bu-DAB)$]PF_6$. The complex $Cr(CO)_3(CNCMe_3)$(*t*-Bu-DAB) (1.0 g, 2.58 mmol) was dissolved in 10 cm^3 of dry ethanol and a quantity of $[(\eta^5\text{-}C_5H_5)_2Fe]PF_6$ (0.855 g, 2.58 mmol) was added to the solution which was stirred at ambient temperature for 20 min. After this time, the initial blue solutions had turned dark red in color, and the dark red crystals which precipitated were collected by filtration, washed with ethanol and diethyl ether, and dried *in vacuo*: yield 1.17 g (85%). The compound may be recrystallized from acetone–ethanol or CH_2Cl_2–diethyl ether mixtures. Found: C, 41.5; H, 6.0%. Calc. for $C_{18}H_{29}CrF_6N_3O_3P$: C, 40.6; H, 5.4%.

The red crystals are very stable with respect to air oxidation and hydrolysis, but solutions of the product disproportionate at temperatures above −10°C to yield the chromium(0) and chromium(II) species,

$$Cr(CO)_3(CNCMe_3)(t\text{-Bu-DAB})$$

and

$$[Cr(CNCMe_3)_4(t\text{-Bu-DAB})](PF_6)_2,$$

respectively [see Section C(i)].

(ii) $[Cr(CO)_3$(CNMe)(*t*-Bu-DAB)$]PF_6$. Yield 85%. Found: C, 36.4; H, 4.7; N, 8.4%. Calc. for $C_{15}H_{23}N_3CrF_6O_3P$: C, 36.7; H, 4.8; N, 8.6%.

(iii) $[Cr(CO)_3$(CNxylyl)(*i*-Pr-DAB)$]PF_6$ Yield 90%. Found: C, 44.3; H, 5.4%. Calc. for $C_{20}H_{25}CrF_6N_3O_3P$: C, 43.5; H, 5.4%.

(iv) $[Cr(CO)_3(CNCHMe_2)$(*i*-Pr-DAB)$]PF_6$. Yield 57%.

(v) $[Cr(CO)_3(CNCMe_3)$(*i*-Pr-DAB)$]PF_6$. Yield 74%.

C. Disproportionation reactions of $[Cr(CO)_3(CNR)(R'\text{-DAB})]PF_6$. (i) *Thermal disproportionation of* $[Cr(CO)_3(CNCMe_3)$(*t*-Bu-DAB)$]PF_6$. A solution of $[Cr(CO)_3(CNCMe_3)$(*t*-Bu-DAB)$]PF_6$ (0.52 g, 0.97 mmol) in 20 cm^3 of freshly distilled CH_2Cl_2 was stirred at ambient temperature for 24 h. By the end of

this period, the original dark red solution had turned a blue-green in color. The addition of 40 cm^3 of diethyl ether to the reaction mixture precipitated a kelly green solid which was separated from the royal blue solution by filtration, washed with diethyl ether, and vacuum dried. The product, $[Cr(CNCMe_3)_4(t\text{-Bu-DAB})](PF_6)_2$, was recrystallized from CH_2Cl_2–diethyl ether mixtures: yield 0.13 g (16%). Found: C, 42.4; H, 6.4%. Calc. for $C_{30}H_{56}CrF_{12}N_6P_2$: C, 42.7; H, 6.6%. The dark blue filtrate was evaporated to dryness under reduced pressure to yield a blue-purple microcrystalline solid (0.11 g, 20%). This was identified as $Cr(CO)_3(CNCMe_3)(t\text{-Bu-DAB})$ on the basis of its spectroscopic and electrochemical properties [see Section A(iv)].

(ii) *Reaction of* $[Cr(CO)_3(CNCMe_3)(t\text{-Bu-DAB})]PF_6$ *with tert-butyl isocyanide.* A mixture of $[Cr(CO)_3(CNCMe_3)(t\text{-Bu-DAB})]PF_6$ (0.44 g, 0.83 mmol) and six equivalents of *tert*-butyl isocyanide (0.525 cm^3, 4.97 mmol) in 20 cm^3 of CH_2Cl_2 was stirred at room temperature for 24 h. The complexes $[Cr(CNCMe_3)_4(t\text{-Bu-DAB})](PF_6)_2$ (0.29 g, 51%) and $Cr(CO)_3(CNCMe_3)(t\text{-Bu-DAB})$ (0.13 g, 49%) were isolated by using a procedure similar to that described in Section C(i). The spectroscopic and electrochemical properties of these products confirmed their identities.

(iii) *Reaction of* $[Cr(CO)_3(CNCMe_3)(i\text{-Pr-DAB})]PF_6$ *with tert-butyl isocyanide.* The complex, $[Cr(CNCMe_3)_4(i\text{-Pr-DAB})](PF_6)_2$, was prepared in 50% yield using a procedure analogous to that described in Section C(ii). A comparable quantity of the blue-purple complex $Cr(CO)_3(CNCMe_3)(i\text{-Pr-DAB})$ was also isolated. Both complexes were identified on the basis of their spectroscopic and electrochemical properties.

D. Attempted conversion of $[Cr(CNCMe_3)_4(t\text{-Bu-DAB})](PF_6)_2$ *to* $[Cr(CNCMe_3)_5(t\text{-Bu-DAB})](PF_6)_2$. A quantity of the six-coordinate complex $[Cr(CNCMe_3)_4(t\text{-Bu-DAB})](PF_6)_2$ (0.2 g, 0.24 mmol) was placed in a test tube and to it was added sufficient *tert*-butyl isocyanide (~1 cm^3) to form a slurry. This mixture was stirred rapidly at room temperature for 1 h. After this time, the green solid was filtered off and washed with diethyl ether. The green powder so obtained was shown by cyclic voltammetry and its spectroscopic properties to be unreacted starting material.

E. Generation of the reduced complex $Na[Cr(CO)_3(CNCMe_3)(i\text{-Pr-DAB})]$. The title complex, and other chromium-containing radical anions of this type, were generated by the following general procedure. Typically, a solution of $Cr(CO)_3(CNCMe_3)(i\text{-Pr-DAB})$ (0.05 g, 0.14 mmol) in 4 cm^3 of freshly distilled THF was syringed into a flask containing a 1% Na–Hg amalgam (prepared by adding 0.1 g of sodium metal to 10 g of elemental mercury). The reaction mixture was stirred at room temperature for 15 min, after which time the mixture was set aside. The pale yellow supernatant reaction solution which contained the monoanion was carefully transferred (via a syringe) to a nitrogen-flushed EPR tube. Solutions of the paramagnetic complexes were found to be stable for at least several days at room temperature under anerobic conditions.

Physical measurements

IR spectra were recorded as Nujol mulls between KBr plates or as dichloromethane solutions using an IBM Instruments IR/32 Fourier transform (4800–400 cm^{-1}) spectrometer. Electronic absorption spectra were recorded on an IBM Instruments 9420 UV–Visible spectrophotometer. ^1H NMR spectra were recorded at 90 MHz on a Perkin–Elmer R-32 spectrometer. The residual protons of acetone-d_6 ($\delta = 2.05$ ppm vs TMS) were used as reference. Electrochemical measurements were made in CH_2Cl_2 solvent that contained 0.2 M tetra-*n*-butyl ammonium hexafluorophosphate (TBAH) as supporting electrolyte. $E_{1/2}$ values were determined as $(E_{p,a}+E_{p,c})/2$ and are referenced to the Ag–AgCl electrode at room temperature. Voltammetric experiments were performed using a Bioanalytical Systems, Inc., Model CV-1A instrument in conjunction with a Hewlett–Packard Model 7035B x–y recorder. X-band ESR spectra were recorded using a Varian E-109 spectrometer.

Analytical procedures

Elemental microanalyses were performed by Dr H. D. Lee of the Purdue University microanalytical laboratory.

RESULTS AND DISCUSSION

A simple high-yield one-pot synthesis of the blue-purple chromium(0) complexes $Cr(CO)_3(CNR)(R'\text{-DAB})$ (R = Me, $CHMe_2$, CMe_3 or xylyl; R′ = *i*-Pr, *t*-Bu, Cy or *p*-tol) has been developed involving the sequence of reactions shown in eqn (1):

$$Cr(CO)_6 \xrightarrow{MeCN} Cr(CO)_3(NCMe)_3 \xrightarrow{R'\text{-DAB}} Cr(CO)_3(NCMe)(R'\text{-DAB}) \xrightarrow{RNC} Cr(CO)_3(CNR)(R'\text{-DAB}). \quad (1)$$

The IR spectra of these complexes [ν(CN) and ν(CO)

modes] and electronic absorption spectra [λ_{max} *ca* 610 nm, Cr(*d*) → R′-DAB(π^*) charge-transfer band] (see Table 1) resemble the properties of the related derivatives *fac*-M(CO)$_3$(CNR)(R′-DAB) (M = Mo or W).[13]* ^{1}H NMR spectroscopy confirms the stoichiometry of these complexes based upon integration of the RNC and R′-DAB ligand resonances (Table 1).

The electrochemical properties of these isocyanide complexes, as measured by the cyclic voltammetric technique, are given in Table 2 along with related data for the Cr(CO)$_4$(R′-DAB) complexes measured under the same conditions.† The two sets of complexes display qualitatively similar behavior, which is in turn similar to that exhibited by the molybdenum complexes Mo(CO)$_3$(CNR)(R′-DAB),[13] although for the latter species all potentials are shifted by *ca* +0.2 V relative to Cr(CO)$_3$(CNR)(R′-DAB). In the case of Cr(CO)$_3$(CNR)(R′-DAB), a reversible one-electron process occurs at $E_{1/2} \simeq +0.05$ V vs Ag–AgCl and this has been shown by coulometry to correspond to a one-electron oxidation. For sweep rates of 50 to 400 mV s^{-1} this couple is characterized by $i_{p,a}/i_{p,c} \simeq 1$ and the ratio $i_p/v^{1/2}$ was constant in accord with diffusion control. The potential separation between the anodic and cathodic peaks, ΔE_p, is close to 75 mV for a sweep rate of 200 mV s^{-1} and increases slightly with an increase in scan rate. With our cell configuration these properties are consistent with electron transfer processes which are reversible or approach reversibility.[16]‡ The chemical reversibility of the redox process at *ca* +0.05 V is demonstrated by the ease of preparing the crystalline, dark orange-red, 17-electron compounds [Cr(CO)$_3$(CNR)(R′-DAB)]PF$_6$ using ferricinium hexafluorophosphate as the oxidant. The best solvent for these reactions is ethanol since the PF_6^- salts are rather insoluble in this medium and precipitate quite quickly as the oxidation proceeds. The chromium(I) monocations are very stable in the solid state but solutions of these complexes decompose via a disproportionation reaction (*vide infra*).

The electrochemical properties of these complexes (measured in 0.2 M TBAH–CH_2Cl_2) are similar to those of the parent neutral species except that the process at $E_{1/2}$ *ca* +0.05 V now corresponds to a one-electron reduction of the bulk species. The formation of the monocations leads to a sizeable increase in the energies of the C≡N and C≡O stretching modes (Table 1). The shift of ν(CN) and ν(CO) to higher energies is in accord with the expected decrease in metal-to-ligand π-back bonding as the positive charge at the metal center increases. The X-band ESR spectra of dichloromethane solutions of [Cr(CO)$_3$(CNR)(R′-DAB)]PF$_6$ (recorded at −160°C) give broad signals ($g \sim 2.03$–2.10) which display no resolvable hyperfine structure attributable to interaction with the coordinated nitrogen of the R′-DAB ligands [Table 1 and Fig. 1(a)].

Although the reduction process ($E_{p,c}$ in Table 2) which is observed in the cyclic voltammograms of 0.2

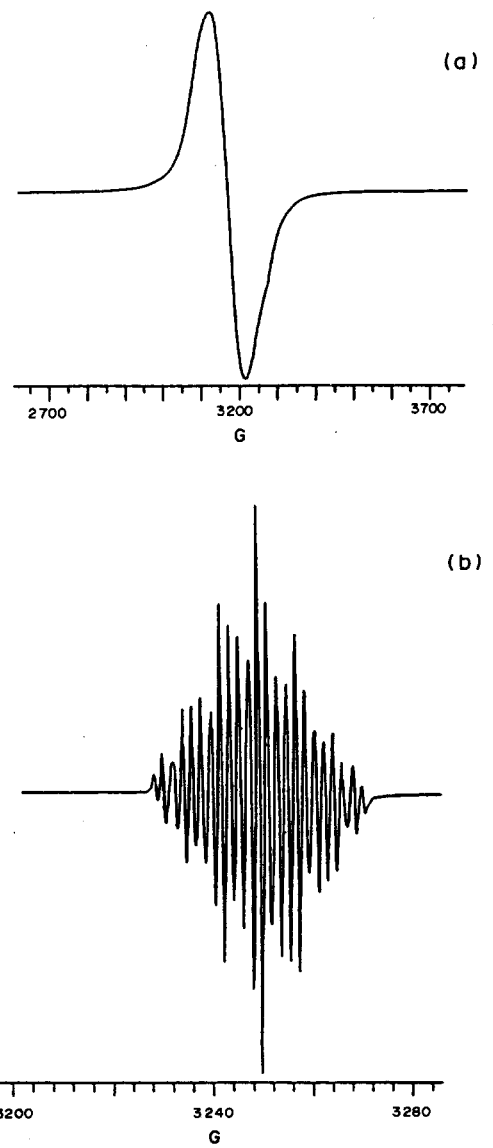


Fig. 1. X-band ESR spectra: (a) [Cr(CO)$_3$(CNCMe$_3$)(*i*-Pr-DAB)]PF$_6$ in CH_2Cl_2 at −160°C and (b) Na[Cr(CO)$_3$(CNCMe$_3$)(*i*-Pr-DAB)] in THF at room temperature.

* The 2,2′-bipyridine (bpy) complexes *fac*-Cr(CO)$_3$(CNR)(bpy) (R = Et or *p*-tol) are also known.[14]

† Our data for the Cr(CO)$_4$(R′-DAB) complexes are in good agreement with results from an earlier study.[15]

‡ Under these same experimental conditions we find that the ferricinium–ferrocene couple has an $E_{1/2}$ value of +0.47 V vs Ag–AgCl.

Table 1. Spectroscopic properties of $Cr(CO)_3(CNR)(R'\text{-DAB})$ and their monocations

Complex	IR spectra (cm^{-1})[a]		Electronic absorption spectra[b] (nm)	^1H NMR (δ)[c]		g_{av}[d]
	ν(CN)	ν(CO)		RNC	R'-DAB	
$Cr(CO)_3(CNMe)(t\text{-Bu-DAB})$	2156m	1918s, 1835s, 1794s	610 (6.5), 382 (2.6)	3.33s	1.51s, 8.40s	
$Cr(CO)_3(CNCHMe_2)(i\text{-Pr-DAB})$	2137m, 2123sh	1923s, 1848s, 1808s	607 (7.7), 380 (2.2)	1.28d, 3.89spt	1.51d, 4.27spt, 8.39s	
$Cr(CO)_3(CNCMe_3)(i\text{-Pr-DAB})$	2128m	1923s, 1848s, 1808s	608 (10.9), 379 (3.2)	1.32s	1.49d, 4.29spt, 8.19s	
$Cr(CO)_3(CNCMe_3)(t\text{-Bu-DAB})$	2128m	1916s, 1835s, 1796s	616 (7.1), 380 (2.8)	1.37s	1.65s, 8.42s	
$Cr(CO)_3(CNCMe_3)(Cy\text{-DAB})$	2128m	1921s, 1844s, 1806s	608 (8.3), 381 (2.3)			
$Cr(CO)_3(CNCMe_3)(p\text{-tol-DAB})$	2133m	1945s, 1875s, 1844s		1.39s	3.40s, 7.34s, 8.46s	
$Cr(CO)_3(CNxylyl)(i\text{-Pr-DAB})$	2085m	1923s, 1862s, 1817s	603 (9.5), 410 (7.1)	2.33s, 7.14s	1.58d, 4.52spt, 8.48s	
$[Cr(CO)_3(CNMe)(t\text{-Bu-DAB})]PF_6$	2224m	2041s, 1936sh, 1902s	[e]			2.100
$[Cr(CO)_3(CNCHMe_2)(i\text{-Pr-DAB})]PF_6$	2205s[f]	2041s, 1946sh, 1885s[f]				
$[Cr(CO)_3(CNCMe_3)(i\text{-Pr-DAB})]PF_6$	2166m	2058m, 2042m, 1960s, 1910sh				2.076
$[Cr(CO)_3(CNCMe_3)(t\text{-Bu-DAB})]PF_6$	2188m	2043s, 1940sh, 1904s	[e]			2.063[g]
$[Cr(CO)_3(CNxylyl)(i\text{-Pr-DAB})]PF_6$	2110m	2054s, 1962s, ~1930sh	[e]			2.034[h]

[a] IR spectra recorded on CH_2Cl_2 solutions unless otherwise stated.

[b] Spectra recorded in CH_2Cl_2: ε_{max} values ($M^{-1}\,cm^{-1} \times 10^{-3}$) are given in parentheses.

[c] All spectra were recorded on acetone-d_6 solutions at room temperature. Abbreviations: d, doublet; m, multiplet; s, singlet; spt, septet.

[d] Recorded at $-160°C$ on frozen CH_2Cl_2 solutions.

[e] The lowest-energy electronic transition is at *ca* 540 nm: viz. λ_{max} 524 (2.3) for R = Me, R' = *t*-Bu; λ_{max} 538 (2.0) for R = CMe_3, R' = *t*-Bu; λ_{max} 550 (3.3) for R = xylyl, R' = *i*-Pr.

[f] Recorded as Nujol mull.

[g] Magnetic moment (Evans method, CH_2Cl_2) = 1.87 BM.

[h] Magnetic moment (Evans method, CH_2Cl_2) = 1.78 BM.

Table 2. Cyclic voltammetric data for solutions of $Cr(CO)_3(CNR)(R'\text{-DAB})$ in 0.2 M TBAH–CH_2Cl_2[a]

Complex	$E_{p,a}$	$E_{1/2}$(ox)	$E_{p,c}$
$Cr(CO)_4$(*i*-Pr-DAB)	+1.49	+0.42	−1.48
$Cr(CO)_4$(*t*-Bu-DAB)	+1.47	+0.41	−1.50
$Cr(CO)_4$(Cy-DAB)	+1.45	+0.40	−1.48
$Cr(CO)_3(CNMe)$(*t*-Bu-DAB)	+1.06	−0.02	−1.80
$Cr(CO)_3(CNCHMe_2)$(*i*-Pr-DAB)	+1.04	+0.01	−1.75
$Cr(CO)_3(CNCMe_3)$(*i*-Pr-DAB)	+1.30	+0.05	−1.99
$Cr(CO)_3(CNCMe_3)$(*t*-Bu-DAB)	+1.20	+0.01	−1.78
$Cr(CO)_3(CNCMe_3)$(Cy-DAB)	+1.21	+0.01	−1.86
$Cr(CO)_3$(CNxylyl)(*i*-Pr-DAB)	+1.11	+0.08	−1.77

[a] Potentials are in V vs Ag–AgCl with a Pt-bead electrode. Data recorded at a scan rate of 200 mV s^{-1}.

M TBAH–CH_2Cl_2 solutions of $Cr(CO)_3(CNR)(R'\text{-DAB})$ is irreversible electrochemically, THF solutions that contain the 19-electron radical anions can be generated using sodium amalgam as the reducing agent. The resulting paramagnetic complexes have been characterized by X-band ESR spectroscopy and a typical spectrum is shown in Fig. 1(b). The data distinguish these systems from the previously characterized ligand radicals although the ESR parameters indicate that the unpaired electron is centered mainly on the R'-DAB ligand π-system. In the specific case of the chromium complex $[Cr(CO)_3(CNCMe_3)(i\text{-Pr-DAB})]^-$ [Fig. 1(b)], for which $g = 1.9991$, the hyperfine coupling arises from the interactions with two ^{14}N nuclei ($A_N = 7.05$ G), two protons (C—H; $A_H = 3.60$ G), two *iso*-propyl protons ($CHCMe_2$; $A_{H'} = 1.80$ G) and a single chromium nucleus (^{53}Cr, 9.5%, $I = 3/2$, $A_{Cr} = 3.8$ G).

The dark red monocationic species $[Cr(CO)_3(CNR)(R'\text{-DAB})]PF_6$ (R' = *i*-Pr or *t*-Bu) are unstable in solution and decompose above −10°C to give a mixture of the dark blue chromium(0) complex $Cr(CO)_3(CNR)(R'\text{-DAB})$ and the kelly green chromium(II) complex $[Cr(CNR)_4(R'\text{-DAB})](PF_6)_2$ (*vide infra*). This particular reaction requires that a significant proportion of the chromium complex be "sacrificed" in order to provide the requisite number of RNC ligands to form stable $[Cr(CNR)_4(R'\text{-DAB})](PF_6)_2$. In accord with this, we find that the yields of the isolated chromium(0) and chromium(II) species is no more than *ca* 20% each. However, when an excess of free RNC (six equivalents) is added to the initial solution an essentially quantitative conversion to an equimolar mixture of $Cr(CO)_3(CNR)(R'\text{-DAB})$ and $[Cr(CNR)_4(R'\text{-DAB})](PF_6)_2$ ensues. This disproportionation reaction, which is represented in eqn (2):

$$2[Cr(CO)_3(CNR)(R'\text{-DAB})]PF_6 + 3RNC \rightarrow Cr(CO)_3(CNR)(R'\text{-DAB}) + [Cr(CNR)_4(R'\text{-DAB})](PF_6)_2 + 3CO, \quad (2)$$

was studied in the case of R = CMe_3 and R' = *i*-Pr or *t*-Bu.

The properties of the chromium(II) complexes $[Cr(CNCMe_3)_4(R'\text{-DAB})](PF_6)_2$ (R' = *i*-Pr or *t*-Bu), as prepared in the aforementioned fashion, accord with those of complexes of this type that have been prepared by the reaction of R'-DAB ligands with $[Cr(CNR)_6](PF_6)_2$ in CH_2Cl_2.*† The appropriate data are presented in Table 3, and closely resemble the properties exhibited by other complexes of the type $[Cr(CNR)_4L_2](PF_6)_2$ as has been described elsewhere.[2] As an aside, we note that when the reactions between $[Cr(CNR)_6](PF_6)_2$ (R = CMe_3 or C_6H_{11}) and 2,2'-bipyridine (bpy) were carried out in dichloromethane solution at room temperature (stoichiometric ratios of 1 : 1–1 : 4), they led in all instances to the generation of the tris-bpy

* For further details of the preparation of $[Cr(CNR)_4(R'\text{-DAB})](PF_6)_2$ by this route see A. Bell, Ph.D. Thesis, Purdue University (1985).

† The IR spectra of the mixed ligand complexes $[Cr(CNR)_4(R'\text{-DAB})](PF_6)_2$ exhibit two ν(CN) modes, an observation which is in accord with their possessing a *cis* geometry. The electrochemical properties of the six-coordinate complexes were investigated by the cyclic voltammetric technique. In all instances, the complexes exhibit a one-electron oxidation at *ca* +0.7 V and two one-electron reductions at *ca* −0.5 and *ca* −1.3 V. These data are consistent with values obtained for the species $[Cr(CNR)_6]^{2+}$, $[Cr(CNR)_4(PR_3)_2]^{2+}$ and $[Cr(CNR)_4(dppe)]^{2+}$.[2]

Table 3. Properties of $[Cr(CNR)_4(R'\text{-DAB})](PF_6)_2$ complexes

Complex	IR spectra (cm^{-1})[a]	Half-wave potential[b]				
	ν(CN)	$E_{1/2}$(ox)	$E_{1/2}$(red)(1)	$E_{1/2}$(red)(2)	μ_{obs}[c]	Λ_M[d]
$[Cr(CNCMe_3)_4(i\text{-Pr-DAB})](PF_6)_2$[e]	2203s, 2193s; 2200sh,[f] 2191s[f]	+0.72 (80)	−0.54 (120)	−1.35 (150)	—	234
$[Cr(CNCMe_3)_4(t\text{-Bu-DAB})](PF_6)_2$[e]	2197s, 2188s; 2193s,[f] 2182s[f]	+0.71 (80)	−0.57 (120)	−1.41 (130)	2.92	221
$[Cr(CNC_6H_{11})_4(p\text{-tol-DAB})](PF_6)_2$[g]	2215s, 2223sh	+0.80 (90)	−0.37 (190)	−1.25 (190)	—	265

[a] IR spectra recorded as Nujol mull unless otherwise stated.

[b] In V vs Ag–AgCl: recorded on CH_2Cl_2 solutions with a Pt-bead electrode and 0.2 M TBAH as supporting electrolyte; values of $E_{p,a} - E_{p,c}$ (in mV) at a sweep rate of 200 mV s^{-1} are given in parentheses.

[c] Value in BM: measured by the Evans method on a CH_2Cl_2 solution at room temperature.

[d] Values in Ω^{-1} cm^2 mol^{-1}: measured on acetonitrile solutions (*ca* 10^{-3} M) at room temperature.

[e] Complex prepared from reaction of $[Cr(CO)_3(CNCMe_3)(R'\text{-DAB})]PF_6$.

[f] Recorded on CH_2Cl_2 solution.

[g] Complex prepared from reaction of $[Cr(CNC_6H_{11})_6](PF_6)_2$.

chromium(III) complex $[Cr(bpy)_3](PF_6)_3$. This reactivity is quite different from that previously observed between the homoleptic seven-coordinate molybdenum(II) complexes $[Mo(CNR)_7]^{2+}$ and bpy. In the latter instances, non-redox substitution of only two isocyanide ligands occurs.[17]

Acknowledgement—We thank the National Science Foundation (Grant CHE82-06117) for support of this work.

REFERENCES

1. W. S. Mialki, T. E. Wood and R. A. Walton, *J. Am. Chem. Soc.* 1980, **102**, 7105.
2. W. S. Mialki, D. E. Wigley, T. E. Wood and R. A. Walton, *Inorg. Chem.* 1982, **21**, 480.
3. J. C. Dewan, W. S. Mialki, R. A. Walton and S. J. Lippard, *J. Am. Chem. Soc.* 1982, **104**, 133.
4. D. E. Wigley and R. A. Walton, *Organometallics* 1982, **1**, 1322.
5. A. Bell and R. A. Walton, *J. Organomet. Chem.* 1985, **290**, 341.
6. J. Casanova, Jr, R. E. Schuster and N. D. Werner, *J. Chem. Soc.* 1963, 4280.
7. W. D. Weber, G. W. Gokel and I. K. Ugi, *Angew. Chem., Int. Ed. Engl.* 1972, **11**, 530.
8. J. M. Kliegman and R. K. Barnes, *Tetrahedron* 1970, **26**, 2555.
9. A. T. T. Hsieh and B. O. West, *J. Organomet. Chem.* 1976, **112**, 285.
10. D. N. Hendrickson, Y. S. Sohn and H. B. Gray, *Inorg. Chem.* 1971, **10**, 1559.
11. D. P. Tate, J. M. Augl and W. R. Knipple, *Inorg. Chem.* 1961, **1**, 433.
12. (a) H. tom Dieck and I. W. Renk, *Chem. Ber.* 1971, **104**, 92; (b) H. Bock and H. tom Dieck, *Angew. Chem., Int. Ed. Engl.* 1966, **5**, 520.
13. A. Bell and R. A. Walton, *Polyhedron* 1986, **5**, 845.
14. J. A. Connor and C. Overton, *J. Chem. Soc., Dalton Trans.* 1982, 2397.
15. H. tom Dieck and E. Kühl, *Z. Naturforsch.* 1982, **37B**, 324.
16. T. C. Zietlow, D. D. Klendworth, T. Nimry, D. J. Salmon and R. A. Walton, *Inorg. Chem.* 1981, **20**, 947.
17. A. Bell, S. J. Lippard, M. Roberts and R. A. Walton, *Organometallics* 1983, **2**, 1562.

Polyhedron Vol. 5, No. 4, pp. 959–965, 1986
Printed in Great Britain

0277–5387/86 $3.00 + .00
Pergamon Journals Ltd

TRIPHENYLTIN SUBSTITUTED BENZOATES: A SPECTROSCOPIC STUDY OF STRUCTURE IN SOLUTION AND SOLID PHASES

K. C. MOLLOY and K. QUILL

School of Chemical Sciences, National Institute for Higher Education, Glasnevin, Dublin 9, Ireland

and

S. J. BLUNDEN and R. HILL*

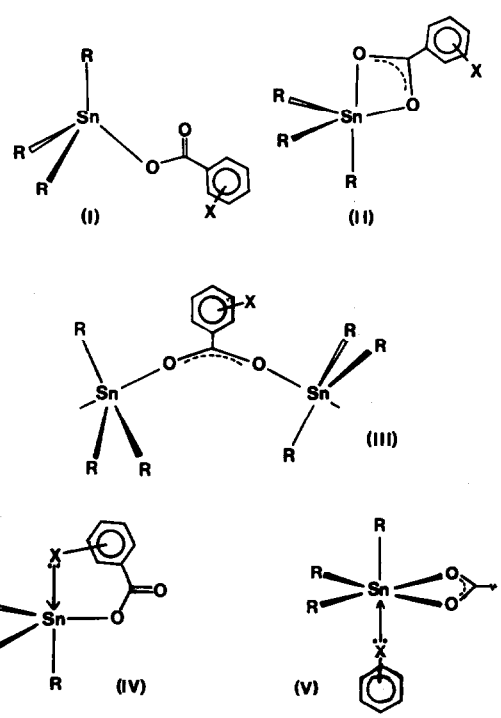
International Tin Research Institute, Greenford, Middlesex UB6 7AQ, U.K.

(*Received* 20 *August* 1985; *accepted* 4 *October* 1985)

Abstract—^{119}Sn NMR and Mössbauer spectroscopic data have been recorded for 12 compounds of formula $Ph_3SnO_2CC_6H_4X$ (X = H, Me-2, NH_2-2, NMe_2-2, Cl-2, Cl-3, Cl-4, OH-2, OH-4, SMe-4 or OMe-2) and $Ph_3SnO_2CC_{10}H_7$-1. On the basis of these measurements all the compounds are assigned a coordination number of four at tin in solution, and, with the exception of the Cl-2 and OH-2 derivatives, retain this structure in the solid. Both of these latter compounds exhibit enhanced Mössbauer quadrupole splittings (3.71 and 2.97 mm s^{-1}), which are attributed to carboxylate- and hydroxyl-bridged structures, respectively. The variable-temperature Mössbauer spectra of two compounds (X = OMe-2 or OH-2) are discussed.

In recent years, triphenyltin compounds (Ph_3SnX) have achieved commercialization as toxicants in marine anti-fouling paints.[1–3] Fouling arises from the settlement, attachment and growth of marine animals and plants on submerged structures, and in general, plants are more resistant to this class of organotin biocide than other fouling species.[4–6] As part of an investigation intended to overcome this drawback and hence widen the spectrum of biocidal activity, we have synthesized a series of triphenyltin arylcarboxylates for raft testing.[7] In this report we consider the spectroscopic evidence for the structures of these compounds, determined in the solid state primarily by ^{119}Sn Mössbauer spectroscopy, in non-aqueous solutions by ^{119}Sn NMR, and linked by IR data in both phases.

Triorganotin derivatives of ring-substituted benzoic acids are rich with structural possibilities, centred around the triad of structures **I–III**. In addition to a tetrahedral geometry at tin arising from a monodentate carboxylate ligand, a bidentate ligand can either chelate (**II**) or bridge (**III**) tin atoms to result in variations on a trigonal bipyramidal geometry at the metal. In instances where the ring



* Author to whom correspondence should be addressed.

substituent is non-passive in a coordination sense due to the presence of lone electron pairs or hydrogen bonding possibilities (e.g. X = OCH_3, NH_2 etc.), coordination between X and tin can occur at the expense of (IV), or in addition to (V), the bond from the acyl oxygen. In the solid state available examples are dominated by III,[8] with only one crystallographically authenticated claim being made for structure I, namely tricyclohexylstannyl 3-indolylacetate,[9] while data for $Ph_3SnO_2CC_6H_4X$ (X = NH_2-2, NH_2-4, NMe_2-2, OH-2, OMe-2 or SMe-4) have all been interpreted in terms of the five-coordinate structure II.[10,11] Distinctions between these architectures are important, since chelated structures, e.g. II, have been shown in some cases to lead to a significant decrease in biocidal activity.[12] Moreover, conflicting structural data have recently appeared in the literature relating to these systems,[10,11,13–15] which we now assess in the light of our own studies.

EXPERIMENTAL

Spectroscopic studies

^{119}Sn NMR spectra were recorded under nuclear Overhauser suppressed conditions, in 10-mm tubes on a JEOL FX60Q spectrometer, with field frequency lock to external D_2O. ^{119}Sn chemical shifts (δ ^{119}Sn) are relative to Me_4Sn and are accurate to ± 0.1 ppm.

IR spectra were recorded in the region 4000–200 cm^{-1} on a Perkin–Elmer 1330 spectrometer, either in CCl_4 or toluene solutions [0.2 g (3.0 cm)$^{-3}$], or as KBr discs.

^{119}Sn Mössbauer spectra were obtained using a constant acceleration, microprocessor controlled spectrometer (Cryophysics Ltd, Oxford, U.K.), with a 512 channel data store. A barium stannate source was used at room temperature and samples were packed in perspex discs and cooled to 80 K using a liquid nitrogen cryostat. Isomer shift data are relative to SnO_2 as reference; spectral data obtained at both collaborating institutions were identical within experimental error. Details of the variable-temperature experiment, including the method of data acquisition and manipulation are described elsewhere.[8] Samples containing 1 mg ^{119}Sn cm^{-2} were used to minimize saturation effects and to comply as fully as possible with the criteria of a "thin sample", while maintaining the viability of the experiment, i.e. good-quality spectra accumulated in

Table 1. Analytical data[a] for Ph_3SnX

	X	M.p. (lit.) (°C)	C	H	N	Sn	Cl
1	$O_2CC_6H_5$	85–87 (84–85.5[b])[c]	63.6 (63.7)	4.4 (4.3)		25.1 (25.3)	
2	$O_2CC_6H_4NH_2$-2	110–112 (108–109[d])[e]	61.4 (61.7)	4.5 (4.3)	2.9 (2.9)	23.9 (24.5)	
3	$O_2CC_6H_4NMe_2$-2	80–82 (79–80[f])[g]	62.8 (63.0)	5.2 (4.9)	2.7 (2.7)	23.2 (23.2)	
4	$O_2CC_6H_4Cl$-3	88–90[g]	59.4 (59.4)	3.9 (3.8)		23.7 (23.5)	7.0 (7.0)
5	$O_2CC_6H_4Cl$-4	128–134 (131–135[h])[c]	59.0 (59.4)	3.7 (3.8)		23.5 (23.5)	7.1 (7.0)
6	$O_2CC_6H_4OH$-2	122–124 (123–124[i])[c]	60.8 (61.6)	4.0 (4.1)		24.4 (24.4)	
7	$O_2CC_6H_4OH$-4	141–143 (117[j])[k]	62.3 (61.6)	4.2 (4.1)		24.5 (24.4)	
8	$O_2CC_6H_4OMe$-2	110–112 (107–108[i])[l]	62.3 (62.3)	4.5 (4.4)		23.6 (23.7)	
9	$O_2CC_6H_4Me$-2	68–70[e]	63.9 (64.3)	4.5 (4.5)		24.4 (24.5)	
10	$O_2CC_{10}H_7$-1	127–129[c]	66.5 (66.8)	4.3 (4.2)		22.4 (22.8)	
11	$O_2CC_6H_4SMe$-4[m]	143–145 (141–143[i])[g]	60.6 (60.4)	4.4 (4.3)		23.4 (23.0)	
12	$O_2CC_6H_4Cl$-2	58–60[c]	58.7 (59.4)	3.8 (3.8)		23.5 (23.5)	6.9 (7.0)
13	OC(Ph)CHCO(Ph)	146–148 (135–136[n])[g]	68.9 (69.0)	4.6 (4.7)		20.6 (20.8)	

[a] Calculated values in parentheses.
[b] R. C. Poller, *J. Inorg. Nucl. Chem.* 1962, **24**, 593.
[c] Recrystallized from petroleum ether.
[d] Reference 15.
[e] Recrystallized from ether–petroleum ether.
[f] Reference 10.
[g] Obtained analytically pure after reaction solvent removal.
[h] Reference 14.
[i] Reference 11.
[j] Reference 24.
[k] Recrystallized from benzene.
[l] Recrystallized from toluene–petroleum ether.
[m] Sulphur found: 6.1; calc.: 6.2%.
[n] Reference 17.

ca 12 h. For temperatures above 110 K, samples containing 1.5 mg ^{119}Sn cm^{-2} were required to maintain this condition. However, data from the two parts of each experiment coalesced into a single line which exhibited no systematic curvature, suggesting that vibrational anharmonicity within the lattice is also absent.

Synthesis

Compounds **2**, **3**, **8**, **11** and **13** (Table 1) were prepared by an azeotropic dehydration reaction between stoichiometric amounts of triphenyltin hydroxide and either the appropriate arylcarboxylic acid or 1,3-diphenylpropane-1,3-dione, in refluxing toluene and using a Dean and Stark trap. Reflux times were typically 2 h. The remaining compounds in Table 1 were prepared by refluxing together reagents using acetone as the reaction solvent. Recrystallization solvents, m.ps and analytical data for all the compounds studied are given in Table 1.

DISCUSSION

Solution-state structure

^{119}Sn NMR data for a range of triphenylstannyl esters of substituted benzoic acids (**1–12**) are given in Table 2. The data are measured in non-coordinating solvents, and show no concentration dependence for the chemical shift. This shift is a sensitive indicator of coordination number at tin, shifts moving to low frequency with increasing number of bonds to the metal. The relevant reference data for this discussion are $(Ph_3Sn)_2O$ (−83.6 ppm) and

$Ph_3SnOC(Ph)CHCO(Ph)$ (−221.2 ppm)

which are unambiguously four-[16] and five-coordinate (**II**),[17] respectively, in the solid state and it is unlikely in either case that this situation will alter upon dissolution. The chemical shifts for **1–12** lie in the range −96.2 to −124.5 ppm and can confidently be assigned to a four-coordinate metal atom (**I**). Our data corroborate previous work, which has associated a chemical-shift range of −40 to −120 ppm for Ph_3SnX compounds of coordination number four.[13,14]

These structural inferences can be extrapolated to the solid state, by consideration of $\nu_{asym}(C{=}O)$, as measured in KBr discs or CCl_4 solutions (Table 2). Assignment of these bands cannot however be made with total confidence due to the presence of absorptions associated with stretching vibrations of the benzene ring, which occur in the same region of the spectrum. For **1–11**, the data are essentially independent of phase, and hence imply that the carboxylate moiety is unidentate in the solid state

Table 2. ^{119}Sn NMR (ppm)[a] and IR (cm^{-1})[b] spectroscopic data for Ph_3SnX

			$\nu_{asym}(C{=}O)$	
	X	δ ^{119}Sn[c]	Solid	Solution[c]
1	$O_2CC_6H_5$	−114.3	1622	1618
2	$O_2CC_6H_4NH_2$-2	−119.5	1615	1622
3	$O_2CC_6H_4NMe_2$-2	−124.5	1613	1613
4	$O_2CC_6H_4Cl$-3	−105.9	1627	1638
5	$O_2CC_6H_4Cl$-4	−108.2	1638	1638
6	$O_2CC_6H_4OH$-2	−96.2	1629	1630
7	$O_2CC_6H_4OH$-4	−114.5[d]	1605	1605[d]
8	$O_2CC_6H_4OMe$-2	−121.9	1629	1628
9	$O_2CC_6H_4Me$-2	−119.9	1625	1628
10	$O_2CC_{10}H_7$-1	−116.2	1622	1628
11	$O_2CC_6H_4SMe$-4	−115.6	1628	1636
12	$O_2CC_6H_4Cl$-2	−106.3	1540	1640
13	OC(Ph)CHCO(Ph)	−221.2[e]		
14	OH	−83.3		
15	$OSnPh_3$	−83.6		

[a] Relative to Me_4Sn.

[b] ±3 cm^{-1}.

[c] CCl_4 solution unless indicated otherwise.

[d] Toluene solution.

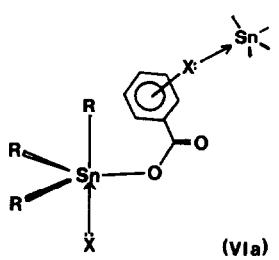
[e] The previously reported value of −82.2 ppm (S. J. Blunden and P. J. Smith, *J. Organomet. Chem.* 1982, **226**, 157) is incorrect and is believed to have been due to either Ph_3SnOH or $(Ph_3Sn)_2O$.

also. This rules out **II**, **III** and **V** as viable structures in this latter phase, and calls into question the interpretation of the X-ray crystallographic data for $Ph_3SnO_2CC_6H_4X$ (X = NH_2-2, NMe_2-2, OH-2, OMe-2 or SMe-4)[10,11] which the authors discuss in terms of a five-coordinate structure (**II**). Structures involving additional coordination via X: → Sn cannot be entirely eliminated. Structures of type **IV** can be discounted since chelation should persist in solution, but an alternative five-coordinate species incorporating intermolecular X: → Sn coordination (**VI**) is still possible.

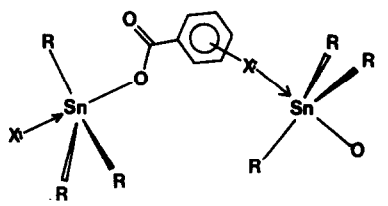
In contrast, IR data for the Cl-2 derivative (**12**) varies markedly between solution and the solid state, and follows the established pattern for a carboxylate-bridged structure (**III**) in the solid, with breaking of the intermolecular bond upon dissolution. The ^{119}Sn NMR data under the conditions of dilution employed in the study indicate that the tin is, as expected from the IR data, four-coordinate in solution (δ ^{119}Sn −106.3 ppm). In principle, the ^{119}Sn chemical shift of compounds with this structure should show a concentration dependence, with shifts moving to low frequency (more negative values) as concentration (and hence the degree of association) increases. This was not observed in this study, and at the concentration levels used [0.2–0.8 g 3.0 cm)$^{-3}$] the variation in shift was negligible (−106.3 to −107.1 ppm). We conclude that at these concentrations complete dissociation of the polymer into discrete molecules had always occurred.

Solid-state structure

Indirect evidence for the solid-state structure of organotin compounds can be derived from Mössbauer spectroscopy. In this context, the most useful parameter is the quadrupole splitting (QS), for which parameter a given range is associated with a particular coordination number and geometry at tin: 1.00–2.40 mm s^{-1} (**I**), 1.70–2.40 mm s^{-1} (**II**) and 3.00–4.00 mm s^{-1} (**III**).[18] From the foregoing discussion of ^{119}Sn NMR and IR data, two structures are possible for **1**–**11** in the solid state, namely **I** and **VI**. While this latter variation could give rise to a *cis*-$OXSnR_3$ geometry (**VIa**), intermolecular bonding invariably results in the



(VIa)



(VI b)

trans-$OXSnR_3$ structure (**VIb**)[19,20] and should show Mössbauer parameters similar to structure **III**, i.e. QS ~ 3.00–4.00 mm s^{-1}. Mössbauer data for the triphenyltin carboxylates studied are given in Table 3. Compounds **1**–**5** and **7**–**10** all have QS in the range 2.30–2.55 mm s^{-1}, and of the two alternative structures indicated are only consistent with **I**. However, it should be noted that these QS data could also be interpreted in terms of chelated structures **II** and **IV**, *and only with the help of ancillary spectroscopic data (IR and ^{119}Sn NMR) can a valid distinction between these alternatives be made.* Indeed, QS data for five-coordinated **13** (2.25 mm s^{-1}) overlap with the above, and cannot be differentiated on the basis of Mössbauer data alone.

QS data for **6** (2.97 mm s^{-1}) and **12** (3.71 mm s^{-1}) must be considered separately from those above. The solid-state structure for **6** reveals an intramolecular C=O···Sn separation of 3.071(2) Å, and an intermolecular HO···Sn interaction at 3.035(2) Å.[11] Since intermolecular interactions such as the latter will be absent in dilute solutions, ^{119}Sn NMR data indicate that the C=O···Sn intramolecular distance of 3.071(2) Å is fortuitous, and does not represent a bonding interaction (*vide supra*). The enhanced QS value in the solid state relative to other four-coordinated analogues can thus be attributed to the intermolecular HO···Sn bond, which results in coordination expansion at tin to five, and formation of a *trans*-O_2SnR_3 geometry (**VIb**). A parallel bonding situation is evident in the two analogous arylazobenzoates (**16** and **17**).[21] The structure of **16** shows (at best) weak intramolecular C=O···Sn coordination to produce a type **II** structure (QS = 2.36 mm s^{-1}) in which the 2-OH group is involved in intramolecular hydrogen bonding. Intramolecular bonding of this latter type is precluded on steric grounds in the 4-OH derivative (**17**) (QS = 3.06 mm s^{-1}) and thus the hydroxyl group in all likelihood assumes an intermolecular, bridging role akin to **6**.

The 2-chloro derivative (**12**), whose ^{119}Sn NMR and IR data collectively point toward a carboxylate-bridged structure (**III**), shows the highest QS recorded in this study (3.71 mm s^{-1}), and is totally consistent with such a *trans*-O_2SnR_3 environment

Table 3. ^{119}Sn Mössbauer data for Ph_3SnX

	X	IS[a]	QS[a]	Γ_1[b]	Γ_2[b]
1	$O_2CC_6H_5$	1.24	2.55	0.97	0.93
4	$O_2CC_6H_4Cl$-3	1.27	2.42	0.95	0.96
5	$O_2CC_6H_4Cl$-4	1.24	2.36	0.96	0.93
6	$O_2CC_6H_4OH$-2	1.34	2.97	1.01	1.01
7	$O_2CC_6H_4OH$-4	1.31	2.55	1.02	1.02
8	$O_2CC_6H_4OMe$-2	1.25	2.30	1.03	1.03
9	$O_2CC_6H_4Me$-2	1.25	2.42	0.92	0.92
10	$O_2CC_{10}H_7$-1	1.23	2.33	0.98	0.95
11	$O_2CC_6H_4SMe$-4	1.27	2.42	1.02	1.01
12	$O_2CC_6H_4Cl$-2	1.34	3.71	1.07	0.93
13	OC(Ph)CHCO(Ph)	1.13	2.25		
16	$O_2CC_6H_4(N_2C_6H_3OH$-2, Me-5)-2[c]	1.28	2.36		
17	$O_2CC_6H_4(N_2C_{10}H_6$-1, OH-4)-2[c]	1.35	3.06		

[a] ± 0.04 mm s^{-1}.
[b] Full width at half height.
[c] Reference 21.

about tin in the solid. From the relative magnitudes of the QS for **6** and **12**, we also conclude that the intermolecular C=O···Sn bond is shorter than 3.0 Å.

Finally, we have attempted to distinguish coordination polymers such as **6** from discrete monomers, e.g. **8**, using variable-temperature ^{119}Sn Mössbauer spectroscopy. Data recorded over the temperature (T) range 78–145 K for compounds **6** and **8** are shown in Fig. 1. We have previously correlated the lattice structure of phenyltin compounds with the temperature coefficient of the natural logarithm of the recoil-free-fraction (a):

$$a = -\frac{\mathrm{d}[\ln f(T)]}{\mathrm{d}T} = -\frac{\mathrm{d}[\ln A(T)]}{\mathrm{d}T},$$

$$a = -\frac{\mathrm{d}[-6E_R T/k\theta M^2]}{\mathrm{d}T},$$

where A is the area under the Mössbauer resonance, E_R the Mössbauer recoil energy and θ_M a characteristic temperature for the lattice, equivalent to the Debye temperature.[22] Under these systematics, in plots of ln A vs T the shallowest slopes are exhibited by linear or zig-zag polymers (10^2a = 0.9–1.5 K^{-1}) while monomeric lattices have 10^2a in excess of 1.20 K^{-1}, except in cases of extremely efficient packing where a more rigid lattice, akin to that of a polymer, results.[23] On the other hand, flexible polymers of an "S" or helical construction afford the tin a vibrational freedom enjoyed in non-associated lattices and steeper slopes ($10^2a \sim 1.70$ K^{-1}) are observed in ln A vs T plots.

The values of 10^2a for compounds **6** (1.36 K^{-1}) and **8** (1.46 K^{-1}) are very similar and consistent with discrete molecules within the lattice. Furthermore, this similarity in behaviour is also in accord with an approximately equal effective vibrating mass for the two cases, in consonance with the near equality in their molecular weights. Comparison can be drawn with Ph_4Sn (10^2a = 1.37 K^{-1})[22] and a series of chelated triphenyltin carboxylates, $Ph_3SnO_2CC_6H_4(N_2R$-$o)$ (10^2a = 1.53–1.71 K^{-1}).[21]

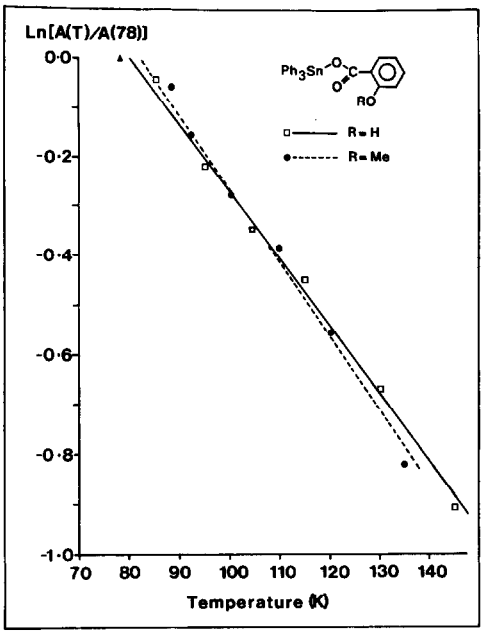


Fig. 1. Plot of $\log_e$ (normalized area) vs temperature for **8** and **6**. The slopes of the lines are 1.46×10^{-2} K^{-1} (r = 0.993, seven points) and 1.36×10^{-2} K^{-1} (r = 0.997, eight points), respectively. The point ▲ (78, 0.00) is common to both plots.

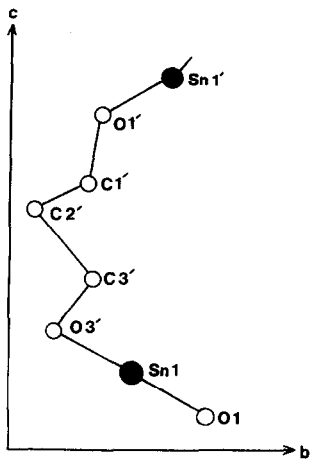


Fig. 2. Polymer propagation in **6**, shown as a projection of part of the cell contents onto the *bc* plane. Only atoms linking metal centres are included for clarity. Data taken from Ref. 11.

In contrast, carboxylate-bridged triorganotins adopt polymers of "stretched-S" construction and are typified by $Ph_3SnO_2CCH_3$ ($10^2a = 1.91\ K^{-1}$).[8]

The variable-temperature Mössbauer experiment is clearly insensitive to the intermolecular Sn···OH interaction in **6**, which weakly associates adjacent molecules. This is, perhaps, not surprising. The Sn···O bond is long (3.035 Å)[11] and hence weak. In addition, and equally importantly, the spatial arrangement of the bridging unit —OC·C_6H_4O— (Fig. 2) lies off the Sn–Sn′ vector, producing a polymer which, like $Ph_3SnO_2CCH_3$, is of flattened helix or "S"-form, and hence plays no role in inhibiting the vibrational motion of the Mössbauer atom. The nature of the Sn···OH interaction in **6** thus manifests itself more clearly in perturbations of the electric field gradient about tin, and hence in the QS, rather than in the lattice dynamics of the metal atom.

CONCLUSIONS

Of the triphenyltin arylcarboxylic acid derivatives studied, most (**1–5** and **7–11**) form four-coordinated structures about tin in both the solid and in solution. Derivatives of 2-OH and 2-Cl benzoic acids are also four-coordinate at tin in dilute solutions, but expand the coordination number to five in the solid, via intermolecular OH···Sn and C=O···Sn linkages, respectively.

These results are in general agreement with other spectroscopic studies on these and related systems[13,14,24] but in the cases of NH_2-2, NMe_2-2, OH-2 and OMe-2 benzoic acid derivatives conflict with the interpretation of X-ray crystallographic data[10,11] in which emphasis is placed upon a weakly bidentate carboxylate group and a five-coordinate geometry about tin. While cases such as these, which are at the interface of two coordination geometries, will always be subjective in their analysis, our work highlights the importance of spectroscopic methods in making these assessments. Moreover, the crystallographic data must be reviewed in terms of both distances and angles about tin *in toto* and not selectively, and our appraisal of the data under these terms reveals a far less clear-cut picture than that presented by the original authors. For example, in the case of $Ph_3SnO_2CC_6H_4NMe_2$-2, while the intramolecular Sn—O bond lengths (2.115 and 2.564 Å) suggest chelation by the carboxylate group, the angular changes are not totally in accord, viz. angles within the "equatorial" plane (which should change from 109°28′ towards 120°) are 122.1, 112.6 and 104.9°, while between the "axial" α-carbon of the phenyl ring and ligating atoms in the "equatorial" girdle about tin (which should change from 109°28′ towards 90°) the angles are 92.9, 108.4, and 114.8°. Many (but in fairness not all!) of these angular variations are simply in accord with the expected rehybridization within a tetrahedral framework, which concentrates *p*-character in the bond to the more electronegative oxygen, hence naturally closing from 109°28′ angles involving oxygen while opening those which only involve carbon. In short, interpretation of this data in terms of a coordination number of five at tin is tenuous, and underlines our recommendations for the need of ancillary spectroscopic data in such circumstances.

We are currently trying to identify those factors which influence the choice of chelated vs bridged structures in systems of this type and will report our findings in a subsequent paper.

Acknowledgements—We thank the National Board for Science and Technology (Ireland) for financial support (to K.C.M.) and the International Tin Research Council (London) for permission to publish these results.

REFERENCES

1. S. J. Blunden, P. A. Cusack and R. Hill, *The Industrial Uses of Tin Chemicals*. Royal Society of Chemistry, London (1985).
2. C. J. Evans and P. J. Smith, *J. Oil Colour Chem. Assoc.* 1975, **58**, 160.
3. C. J. Evans and R. Hill, *Rev. Si, Ge, Sn and Pb Compounds* 1983, **7**, 57.
4. A. T. Phillip, *Prog. Org. Coat.* 1973/4, **2**, 159.
5. A. T. Phillip, *Aust. OCCA Proc. News* 1973, July, 17.
6. G. Bocksteiner, presented at the 3rd Royal Australian Naval Underwater Paints Symposium, 1973.

7. A. J. Crowe, J. T. Gisborne, R. Hill and P. Robinson, unpublished work.
8. K. C. Molloy, T. G. Purcell, K. Quill and I. W. Nowell, *J. Organomet. Chem.* 1984, **267**, 237 (and references therein).
9. K. C. Molloy, T. G. Purcell, E. Hahn, H. Schumann and J. J. Zuckerman, *Organometallics* 1986, **5**, 85.
10. R. G. Swischer, J. F. Vollano, V. Chandrasekhar, R. O. Day and R. H. Holmes, *Inorg. Chem.* 1984, **23**, 3147.
11. J. F. Vollano, R. O. Day, D. N. Rau, V. Chandrasekhar and R. H. Holmes, *Inorg. Chem.* 1984, **23**, 3153.
12. S. J. Blunden, P. J. Smith and B. Sugavanam, *Pest. Sci.* 1984, **15**, 253.
13. J. Holecek, M. Nadvornik, K. Handlir and A. Lycka, *J. Organomet. Chem.* 1983, **241**, 177.
14. J. Holecek, K. Handlir, M. Nadvornik and A. Lycka, *J. Organomet. Chem.* 1983, **258**, 147.
15. L. E. Khoo and F. E. Smith, *Inorg. Chim. Acta* 1981, **53**, L83.
16. C. Glidewell and D. C. Liles, *Acta Cryst.* 1978, **B34**, 1693.
17. G. M. Bancroft, B. W. Davies, N. C. Payne and T. K. Sham, *J. Chem. Soc., Dalton Trans.* 1975, 973.
18. A. G. Davies and P. J. Smith, *Comprehensive Organometallic Chemistry*, p. 525. Pergamon Press, Oxford (1982).
19. P. A. Cusack, P. J. Smith, J. D. Donaldson and S. M. Grimes, *A Bibliography of X-ray Crystal Structures of Tin Compounds.* Publication No. 533, International Tin Research Institute (1981); P. J. Smith, *J. Organomet. Chem. Libr.* 1981, **12**, 97.
20. J. A. Zubieta and J. J. Zuckerman, *Prog. Inorg. Chem.* 1978, **24**, 251.
21. P. G. Harrison, K. Lambert, T. J. King and B. Magee, *J. Chem. Soc., Dalton Trans.* 1983, 363.
22. K. C. Molloy and K. Quill, *J. Chem. Soc., Dalton Trans* 1985, 1417.
23. J. L. Lefferts, K. C. Molloy, J. J. Zuckerman, I. Haiduc, M. Curtui, C. Guta and D. Ruse, *Inorg. Chem.* 1980, **19**, 2861.
24. M. A. Mesubi, *Spectrochim. Acta* 1976, **32A**, 1327.

Polyhedron Vol. 5, No. 4, pp. 967–971, 1986
Printed in Great Britain

0277–5387/86 $3.00+.00
Pergamon Journals Ltd

O,O-DIALKYL/ALKYLENE DITHIOPHOSPHATE COMPLEXES OF ORGANO-RHODIUM(I)

YASH PAL SINGH and R. C. MEHROTRA*

Chemical Laboratories, University of Rajasthan, Jaipur 302004, India

(*Received* 30 *July* 1985; *accepted* 4 *October* 1985)

Abstract—Reactions of $[(COD)RhCl]_2$ with $MS_2P(OR)_2$ and $H_4NS_2\overline{POGO}$ yield neutral four-coordinate complexes with the general formulae $(COD)Rh[S_2P(OR)_2]$ and $(COD)Rh[S_2\overline{POGO}]$, respectively [where COD = η-cycloocta-1,5-diene; M = Na or NH_4; R = C_2H_5, *i*-C_3H_7 or *n*-C_3H_7; G = $(CH_3)_2C\text{-}C(CH_3)_2$, $CH_2C(CH_3)_2CH_2$ or $(CH_3)CHCH_2C(CH_3)_2$]. These complexes are monomeric in nature and have been characterized by IR, ^1H and ^{31}P NMR spectroscopy, the last technique being specially useful in revealing the bidentate nature of the ligand.

O,O-dialkyl dithiophosphoric acids occupy a unique position amongst the sulphur- and phosphorus-containing ligands due to their various possible (mono- and bidentate, chelating/bridging) modes of bonding.[1–5] In addition, they are receiving extensive potential biocidal,[6] agricultural[7] and industrial applications, (e.g. as pesticides, antioxidants, oil additives and colouring agents for plastics and analytical reagents). Recently, *O,O*-alkylene dithiophosphoric acids and their metal complexes have been reported from these laboratories.[8–11]

An extensive survey of literature revealed that no systematic study of dithiophosphate complexes of organo-platinum metals[12,13] in general and organo-rhodium in particular has been reported. In the present communication, we present the synthesis and characterization of *O,O*-dialkyl/alkylene dithiophosphate derivatives of organo-rhodium(I).

EXPERIMENTAL

The *O,O*-dialkyl dithiophosphoric acids[14] and *O,O*-alkylene dithiophosphoric acids[8] and their sodium/ammonium salts were prepared by the literature methods. bis[*n*-Cycloocta-1,5-diene rhodium(I) chloride] was prepared by the method of Chatt and Venanzi.[15]

Molecular weights of representative compounds were determined cryoscopically. IR spectra (4000–200 cm^{-1}) were recorded as CsI pallets or Nujol mull. ^1H NMR spectra were recorded in $CDCl_3$ solution using TMS as internal reference. ^{31}P NMR spectra were recorded in benzene–$CDCl_3$ solution using TMP (trimethyl phosphate) as external reference with a JEOL FX-100 spectrometer.

Reaction of bis[η-cycloocta-1,5-diene chloride] with ammonium O,O-diisopropyl dithiophosphate in 1:2 molar ratio

A benzene solution of $[(COD)RhCl]_2$ (0.25 g, 0.51 mmol) was added to the benzene suspension of ammonium salt of *O,O*-diisopropyl dithiophosphoric acid (0.27 g, 1.02 mmol). The reaction mixture was stirred for about 2 h, during which the colour of the solution changed from yellow to wine red. The NH_4Cl was filtered. The excess solvent was distilled from the filtrate. A yellow microcrystalline compound obtained was dried under reduced pressure at the room temperature and recrystallized from benzene–hexane mixture.

Details of similar syntheses along with analytical data of the products are summarized in Table 1.

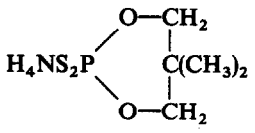
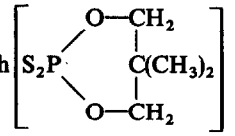
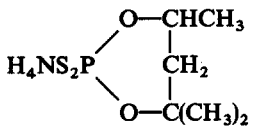
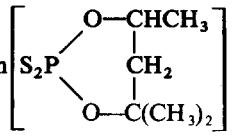
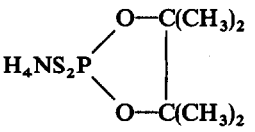
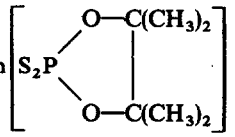
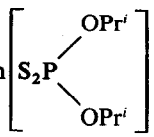
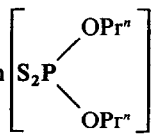
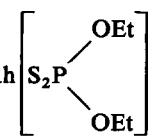
RESULTS AND DISCUSSION

The reactions of cyclooctadiene rhodium chloride dimer with the sodium or ammonium salts of dialkyl/alkylene dithiophosphoric acid were carried out in 1:2 molar ratio in benzene:

$$[(COD)RhCl]_2 + 2MS_2P(OR)_2 \rightarrow 2(COD)Rh[S_2P(OR)_2] + 2MCl, \quad (1)$$

* Author to whom correspondence should be addressed.

Table 1. Synthetic and analytical data for dialkyl/alkylene dithiophosphates of organo-rhodium(I)

Reactants		Product Physical state % yield	% Analysis: found (calc.)			Molecular weight: found (calc.)
$[(COD)RhCl]_2$	$(RO)_2PS_2M/\overline{OGOPS_2}M$		C	H	S	
(1) $[(COD)RhCl]_2$			38.4 (38.2)	5.2 (5.4)	15.5 (15.7)	—
0.34	0.28	Brown crystals 90				
(2) $[(COD)RhCl]_2$			39.7 (39.8)	6.1 (6.2)	15.1 (15.2)	—
0.21	0.19	Brown crystals 88				
(3) $[(COD)RhCl]_2$			39.9 (39.8)	6.1 (6.1)	15.1 (15.2)	435 (422)
0.30	0.28	Yellow crystals 85				
(4) $[(COD)RhCl]_2$	$H_4NS_2P(OPr^i)_2$		40.2 (40.1)	6.3 (6.2)	15.2 (15.1)	432 (424)
0.25	0.27	Yellow crystals 85				
(5) $[(COD)RhCl]_2$	$NaS_2P(OPr^n)_2$		40.0 (40.1)	6.3 (6.2)	15.2 (15.1)	—
0.30	0.30	Yellow sticky liquid 95				
(6) $[(COD)RhCl]_2$	$NaS_2P(OEt)_2$		35.6 (35.5)	5.6 (5.6)	16.0 (16.2)	—
0.28	0.26	Yellow crystals 85				

$$[(COD)RhCl]_2 + 2H_4NS_2\overline{POGO} \rightarrow 2(COD)Rh[S_2\overline{POGO}] + 2NH_4Cl, \quad (2)$$

where COD = η-cyclooctadiene; M = Na or NH_4; R = C_2H_5, i-C_3H_7 or n-C_3H_7; G = $(CH_3)_2CC(CH_3)_2$, $CH_2C(CH_3)_2CH_2$ or $(CH_3)_2CCH_2CH(CH_3)$.

Reaction (1) occurs readily and is completed with 2–3 h of stirring at room temperature, whereas the reaction (2) required 12–18 h of stirring for completion under similar conditions. The compounds are micro-crystalline solids (Table 1) {except for $(COD)Rh[S_2P(OPr^n)_2]$ which is a yellow liquid}, soluble in common organic solvents. The molecular

Table 2. Selected IR frequencies (cm^{-1}) of dialkyl/alkylene dithiophosphates of organo-rhodium(I)

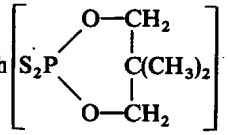
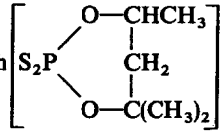
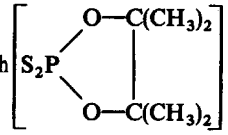
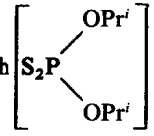
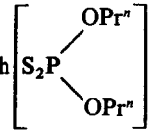
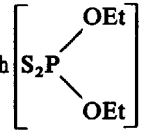
Compound	ν(COD) vibrations	ν[(P)—O—C]	Ring vibrations	ν[P—O—(C)]	ν(P—S)	ν(P—S)
(1) (COD)Rh 	1420–1450	1030	960	800	660	540
(2) (COD)Rh 	1420–1450	1030	940	860	650	600
(3) (COD)Rh 	1430–1460	1000	940	840	640	560
(4) (COD)Rh 	1420–1450	1000	940	860	620	540
(5) (COD)Rh 	1430–1455	1000	940	850	640	560
(6) (COD)Rh 	1420–1450	1020	950	840	640	560

Table 3. NMR spectral data for dithiophosphates of organo-rhodium(I)

Compound	Chemical shift [δ (ppm)][a] ^{1}H NMR (in $CDCl_3$)		^{31}P NMR (in benzene)
(1) (COD)Rh[S_2P(O—C(CH$_3$)$_2$)(O—C(CH$_3$)$_2$)]	1.6–2.6, m, 8H 4.5, bs, 4H	(COD-Rh)	112.16
	1.5, s, 12H	(CH_3)	
(2) (COD)Rh[S_2P(O—CHCH$_3$)(CH$_2$)(O—C(CH$_3$)$_2$)]	1.6–2.6, m, 8H 4.6, bs, 4H	(COD-Rh)	94.26
	4.5–5.0, m, 1H	(OCH)	
	1.0–2.0, 11H	(CH_3, CH_2)	
(3) (COD)Rh[S_2P(O—CH$_2$)(C(CH$_3$)$_2$)(O—CH$_2$)]	1.6–2.6, m, 8H 4.5, bs, 4H	(COD-Rh)	—
	1.10, s, 6H	(CH_3)	
	4.0, d, 4H	(OCH_2)	
	J = 15 Hz		
(4) (COD)Rh[S_2P(OEt)(OEt)]	1.6–2.6, m, 8H 4.5, bs, 4H	(COD-Rh)	95.59
	1.4, t, 6H	(CH_3)	
	4.20, g, 4H	(CH_2)	
(5) (COD)Rh[S_2P(OPr^i)(OPr^i)]	1.6–2.6, m, 8H 4.5, bs, 4H	(COD-Rh)	96.25
	1.4, s, 12H	(CH_3)	
	5.1, m, 2H	(CHO)	
(6) (COD)Rh[S_2P(OPr^n)(OPr^n)]	1.6–2.6, m, 12H 4.55, bs, 4H	(COD-Rh + CH_2)	
	3.3, t, 4H	(OCH_2)	—
	2.1, s, 6H	(CH_3)	
	0.9, t, 6H	(CH_3)	

[a] s = singlet; d = doublet; t = triplet; q = quartet; m = multiplet; bs = broad signal.

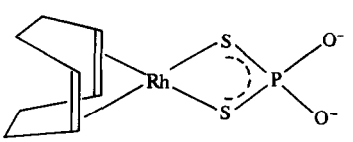
weight determinations of two representative compounds reveal their monomeric nature.

In the IR spectra of these derivatives (Table 2) the bands present in the regions 1000–1050 cm and 800–860 cm^{-1} are assigned to ν(P)—O—C and P—O—(C) vibrations respectively. Two strong bands in the region ~650 and ~540 cm^{-1} which may be assigned to ν(P···S) and ν(P—S) modes, respectively,[16] have also been observed. The bands due to ν(P···S) vibrations show a shift on 20 cm^{-1} as compared to their positions in the spectra of corresponding ligands which is suggestive of their bidentate nature in these complexes. The band present in the region 900–950 cm^{-1} may be due to ring vibrations.[17,18] A sharp band at ~1450 cm^{-1} in the spectra of all these derivatives is due to the cyclooctadiene moiety.[19]

The ^{1}H NMR spectra (Table 3) show the proton resonances characteristic of all the corresponding alkyl/alkylene[8,9] and cyclooctadiene groups.[17] A sharp singlet in the range δ 3.1–3.7 ppm, characteristic of the S—H proton in the free dithiophosphoric acids[8] is absent from the ^{1}H NMR spectra of the organo-rhodium(I) compounds.

^{31}P NMR spectra (proton-decoupled) have been recorded (Table 3) and the high chemical-shift values compared to the parent ligands further confirm the bidentate mode (suggested by their IR spectra) of bonding of these ligand moieties[5] in our rhodium complexes.

On the basis of the evidences discussed so far, the following structure with a four-coordinate rhodium metal atom may be proposed for these dialkyl/alkylene dithiophosphates of organorhodium(I).



Acknowledgement—We thank the Department of Science and Technology for financial assistance.

REFERENCES

1. J. R. Wasson, G. M. Woltermann and H. J. Stoklosa, *Top. Curr. Chem.* 1973, **35**, 65.
2. B. P. Singh, G. Srivastava and R. C. Mehrotra, *Coord. Chem. Rev.* 1984, **55**, 207.
3. B. P. Singh, G. Srivastava and R. C. Mehrotra, *J. Organomet. Chem.* 1979, **171**, 35.
4. J. L. Lefferts, K. C. Molloy, J. J. Zuckerman, I. Haiduc, C. Guta and D. Ruse, *Inorg. Chem.* 1980, **19**, 286.
5. C. Glidewell, *Inorg. Chim. Acta* 1977, **25**, 159.
6. D. R. Baker, U.S. Patent 4012421 (1977); *Chem. Abstr.* 1977, **87**, 6201.
7. H. Kubo, *Agric. Biol. Chem.* 1965, **29**, 43.
8. H. P. S. Chauhan, C. P. Bhasin, G. Srivastava and R. C. Mehrotra, *Phosphorus Sulphur* 1983, **15**, 49.
9. R. J. Rao, G. Srivastava and R. C. Mehrotra, *J. Organomet. Chem.* 1983, **258**, 155.
10. R. J. Rao, G. Srivastava, R. C. Mehrotra, B. S. Saraswat and J. Masson, *Polyhedron* 1984, **3**, 485.
11. R. J. Rao, G. Srivastava and R. C. Mehrotra, *Phosphorus Sulfur* (in press).
12. F. Faraone, *J. Chem. Soc., Dalton Trans.* 1975, 541.
13. F. Faraone and P. Piraino, *Inorg. Chim. Acta* 1976, **16**, 80.
14. D. E. C. Corbridge, *Top. Phosphorus Chem.* 1969, **6**, 235.
15. J. Chatt and L. M. Venanzi, *Nature* (*London*) 1956, **177**, 852.
16. L. J. Bellamy, *Infrared Spectra of Complex Molecules*, p. 311. Methuen, London (1966).
17. J. Cason, W. N. Baxter and W. De Acetes, *J. Org. Chem.* 1959, 247.
18. R. Jones and A. R. Katritzky, *J. Chem. Soc.* 1960, 4376.
19. S. D. Robinson and B. L. Shaw, *J. Chem. Soc.* 1965, 4997.

Polyhedron Vol. 5, No. 4, pp. 973–981, 1986
Printed in Great Britain

0277–5387/86 $3.00 + .00
Pergamon Journals Ltd

COMPLEXES OF HYDROXAMATES—II. MECHANISTIC STUDIES INVOLVED IN THE NICKEL–GLYCINEHYDROXAMATE–PYRIDOXAL SYSTEM

MOHAMED S. EL-EZABY,* HAYAT M. MARAFIE and HUSAM M. ABU-SOUD

Department of Chemistry, Faculty of Science, University of Kuwait, Kuwait

(*Received* 27 *June* 1985; *accepted* 4 *October* 1985)

Abstract—The formation constants of the binary complexes of Ni(II) with glycinehydroxamic acid (GX) were determined by pH-metric titration at 25°C and $I = 0.15$ M NaCl. In addition, the mechanism of complex formation was studied under the same experimental conditions as the equilibrium study using the stopped-flow technique. It has been concluded that Ni^{2+} and $NiOH^{+}$ were the active species in the complex formation reactions. The interaction of GX with pyridoxal (PL) in the absence of metal ions was proved to occur at pH $\geqslant$ 5 by polarographic and spectrophotometric techniques, and was found to be fast enough not to be followed by the stopped-flow technique. The formation constants were also determined by pH-metric titration. However, the reaction of PL with Ni(II)–GX was investigated at pH > 7.0. Ternary-complex formation was proved to exist prior to the possible formation of the Schiff base metal complex. Furthermore, deprotonation of the hydroxamic NH group was found compatible with the proposed reaction mechanism.

Hydroxamic acids exist in nature as trihydroxamic and dihydroxamic acids. They are found to be constituents of antibiotics, growth factors, tumour inhibitors, cell-division factors and pigments. In addition, they also show antituberculous, antifungal and antileukaemic activities.[1–5] Monohydroxamic acids, on the other hand, were used as colorimetric and gravimetric reagents. They have been used recently in attempts to design metal chelates, specially for Fe(III), as suitable oral sources of metals for mammals[6–8] and as a suitable reagent for the treatment of metal-overload and related diseases.[9,10] Glycinehydroxamic acid (GX) (a monohydroxamic acid) forms stable complexes with Ni(II) and Fe(III).[7,11] The complexes of Fe(III) have been proved to react with apotransferrin.[7]

Pyridoxal (PL), a vitamin B_6 compound, forms less stable metal complexes[12,13] than GX. PL and its phosphorylated form are able to undergo trans-amination with amino acids and to serve as catalysts for a variety of other reactions of amino acids in the absence of enzymes.[14] The present work describes the equilibria and reaction kinetics involved in the Ni(II)–GX system. Moreover, the interaction of pyridoxal with GX in the presence and absence of Ni(II) was also investigated.

EXPERIMENTAL

Materials

PL hydrochloride (PL · HCl) (Merck, >99%) and GX (Sigma, >98%) were analytically pure and were used without purification. Stock solutions of PL and GX were 0.10 and 0.05 M, respectively. The GX solution was also ~0.05 M in HCl. They were kept in the dark at 4°C. A stock solution of $NiCl_2$ (~0.1 M) was prepared. The concentration was checked by EDTA complexometric titration as previously described.[15] The ionic strength was kept constant by adding the appropriate amount of an NaCl (2 M) solution at 0.15 M.

Measurements

The pH titration was performed as previously reported,[15] utilizing an Orion Research Ionalyzer type 901 in the pH mode, equipped with a Ross combination pH electrode model 81-02. Kinetic measurements were done using a Durrum stopped-flow apparatus. The optical path length was 20 mm.

* Author to whom correspondence should be addressed.

The mixing syringes and cuvette were thermostatted at 25°C. The kinetic data were acquired and processed by an on-line micro-processor-based system.[16] The observed rate constants were calculated for kinetic data for up to an 85% completed reaction. The absorption spectra were carried out on a Schimadzu model 240 spectrophotometer in the wavelength range 600–200 nm.

Determination of the protonation constants of GX and PL and the formation constants of the binary species in the Ni(II)–GX–PL system were done using the MINIQUAD-75 program.[17] The procedures used to select the correct equilibrium model were similar to those reported previously.[15] In potentiometric measurements, the range of the total Ni(II) concentration (T_{Ni}) was $1.0–2.0 \times 10^{-3}$ M that of GX (T_{GX}) was $1.0–3.0 \times 10^{-3}$ M, and that of PL (T_{PL}) was $1.0–4.0 \times 10^{-3}$ M. In kinetic measurements, T_{Ni} was $0.5–1.0 \times 10^{-4}$ M, T_{GX} was $0.5–5.0 \times 10^{-3}$ M and T_{PL} was $1.0–3.0 \times 10^{-2}$ M.

Polarographic measurements were taken by a Polarocord E506 for solutions of 0.5 M in NaCl, the height of the mercury column was 80 cm, and the drop time was 2.0 s. Deoxygenation of the solution to be polarographed was achieved by passing purified nitrogen through it.

RESULTS AND DISCUSSION

Equilibrium study

Binary complexes of the Ni(II)–GX *system.* The titration of GX (0.002 M) with NaOH (0.1 M) in the presence or absence of Ni(II) did not show signs of precipitation when the concentration of the ligand was twice or more than twice that of the metal ions in the pH range ~5.0–10.0. However, the precipitation of a red crystalline product occurred in the pH range ~7.5–8.5 upon standing overnight. This product was reported previously as $Ni(GX)_2$.[11] The titration data were assessed by the MINIQUAD program where four equilibrium models were found to

Table 1. Formation constants involved in Ni(II)–GX–PL–H system at 25°C and $I = 0.15$ M: n = No. of titration points, Xi^2 = chi square, R = reliability factor, S = sum of squared residuals, σ = standard deviation; l, p, q, s are the stoichiometric coefficients for GX, PL, Ni(II) and H^+

System		l	p	q	s	log β ($\pm\sigma$)	pH range	n	Xi^2	R	S ($\times 10^6$)	Reported log β
GX–H		1	0	0	1	9.549 (0.004)	7.0–10					
		1	0	0	2	17.147 (0.004)						
PL–H		0	1	0	1	8.477 (0.001)	3.0–9.0	114	14	0.009	0.11	
		0	1	0	2	12.573 (0.001)						
PL–GX–H		1	1	0	0	4.335 (0.002)	6.7–10.0	144	119	0.024	2.65	
		1	1	0	1	13.035 (0.003)						
		1	1	0	2	21.041 (0.003)						
Ni–GX–H	(a)	1	0	1	0	7.043 (0.005)	5.6–9.3	262	24	0.019	1.36	6.8[a]
		1	0	1	−1	−0.232 (0.013)						
		1	0	1	−2	−8.692 (0.017)						
		2	0	1	0	13.651 (0.003)						13.5[a]
	(b)	1	0	1	0	6.702 (0.007)	5.6–9.3	262	51	0.018	1.20	
		1	0	1	−1	0.059 (0.004)[b]						
		1	0	1	−2	−8.970 (0.012)[b]						
		2	0	1	1	20.389 (0.003)						
		2	0	1	0	13.201 (0.003)						
	(c)	1	0	1	0	6.711 (0.005)	5.6–9.3	262	51	0.018	1.2	
		1	0	1	−1	0.052 (0.003)						
		2	0	1	1	20.376 (0.003)						
		2	0	1	0	13.251 (0.002)						
		2	0	1	−1	3.847 (0.008)[b]						
	(d)	1	0	1	0	7.045 (0.002)	5.6–9.3	262	19	0.019	1.30	
		1	0	1	−1	−0.216 (0.004)						
		2	0	1	0	13.643 (0.001)						
		2	0	1	−1	3.968 (0.006)						

[a] Reference 11.

[b] The true values should be corrected by the addition of pK_w (13.76) to 13.82, 18.55 and 17.6 for NiGXOH, $NiGX(OH)_2$ and $Ni(GX)_2OH$, respectively.

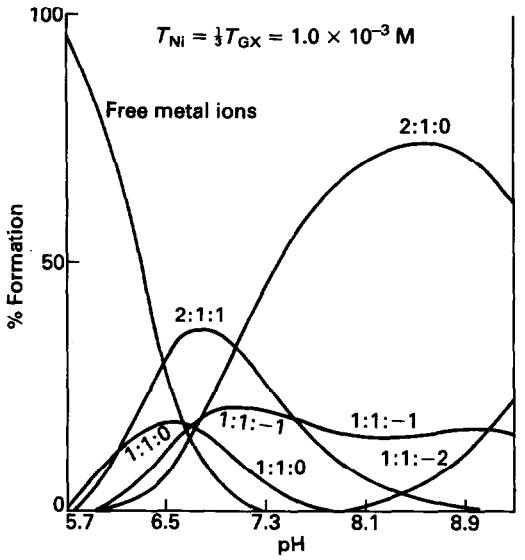


Fig. 1. Distribution diagram of the binary Ni(II)–GX complex system.

describe the Ni(II)–GX system. They are not very different and are depicted in Table 1. The structure of $Ni(GX)_2$ has been elucidated previously and the coordination about the Ni(II) atom is square planar with four nitrogen atoms of the two glycinohydroxamato ligands occupying the four coordination sites.[11] The dihydroxy species may be also similar in geometry to that of the bis(glycinohydroxamato) nickel(II), and it occurs at pH >8.5. Formation constants of the complexes of Ni(II) with glycine are smaller in magnitude than with GX which is attributed to the involvement of the NOH group rather than the —C=O group in the metal ligation.

The presence of 2:1:1 (2GX:Ni:H) species may also describe bis(glycinohydroxamato) nickel(II) species in which the NOH group of one of the ligands is not deprotonated.

The distribution diagram of the percent formation of the complexes as a function of pH is shown in Fig. 1 for one of the successful equilibrium models. It is noticeable that the 2:1:0 species exists predominantly at pH $\geqslant$7.5.

Interaction of GX *with* PL. GX reacted with PL in the pH range 5.0–10.0, as evidenced from the changes in the PL spectra in the wavelength range 220–450 nm upon addition of a 1:1 mole ratio of GX (GX has no spectra at wavelengths greater than 240 nm) (Fig. 2). At lower pH (<7.0), an increase in absorbance was observed in the wavelength range 200–350 nm. At higher pH (>7.0) there was a decrease in absorbance in the wavelength range 340–450 nm, a red shift in the PL wavelength band with the maximum at 300 nm (at pH ~ 10.0), and a blue shift as well as an increase in absorbance of the spectral band of PL in the wavelength range 200–270 nm. After mixing overnight spectra were identical in the presence and absence of a few drops of EDTA solution (to complex any trace metal ions if it happens to exist as impurities). Polarographic evidence of the interaction of PL with GX has been obtained at pH = 7.0 for the equilibrated mixture. The irreversible wave so obtained for PL at $E_{1/2} \approx -1.0$ V, has been replaced by two overlapping irreversible waves at $E_{1/2} = 1.02$ and 1.13 V in the PL–GX system (Fig. 3).

A variation in pH was observed as a function of time when a mixture of GX and PL was titrated with 0.10 M NaOH. The potentiometric data were

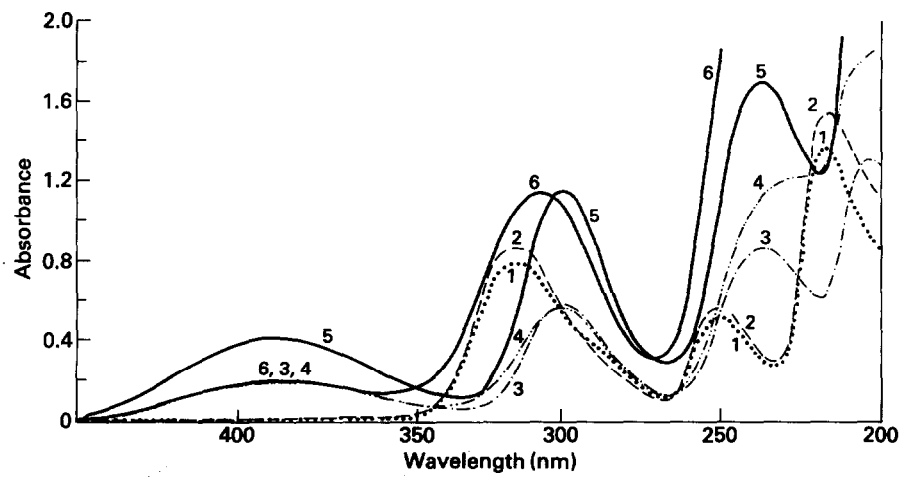


Fig. 2. Absorption spectra of PL, GX and a mixture of PL and GX: (1) PL, pH = 5.18, $T_{PL} = 1 \times 10^{-4}$ M; (2) PL + GX, pH = 5.14, $T_{PL} = T_{GX} = 1 \times 10^{-4}$ M; (3) PL, pH = 10.15, $T_{PL} = 1 \times 10^{-4}$ M; (4) PL + GX, pH = 10.16, $T_{PL} = T_{GX} = 1 \times 10^{-4}$ M; (5) PL, pH = 10.01, $T_{PL} = 2 \times 10^{-4}$ M; and (6) PL + GX, pH = 10.01, $T_{PL} = 2 \times 10^{-4}$ M, $T_{GX} = 1 \times 10^{-3}$ M.

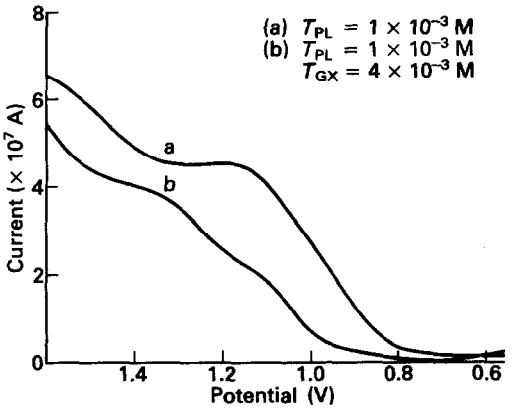


Fig. 3. Polarograms of PL and a mixture of PL and GX.

obtained after equilibration (after 10 min of a small addition of the titrant). Assessment of the data in the pH range 6.7–10.0 for mixtures of GX and PL at different mole ratios (using the MINIQUAD program) indicated the presence of three species. Their stoichiometries, together with their formation constants, are depicted in Table 1. Figure 4 shows the distribution diagram of the condensed species of PL with GX. The fully unprotonated species is predominant at pH > 7.0, while the protonated species are predominant at lower pH values.

Kinetic study

Complexes of Ni(II) *with* GX. An aqueous solution of $Ni(ClO_4)_2$ has been reported to exhibit three main spectral bands at 1149 ($\varepsilon = 2.0$), 690 (shoulder) and 395 ($\varepsilon = 4.6$) nm, which were ascribed to $^3T_{2g}(F) \leftarrow {}^3A_{2g}(F)$, $^3T_{1g}(F) \leftarrow {}^3A_{2g}(F)$ and $^3T_{1g} \leftarrow {}^3A_{2g}(F)$, respectively.[18] Similarly, an aqueous $NiCl_2$ solution showed the same bands, except that they are shifted slightly to shorter wavelengths. However, in the presence of GX, Ni(II) exhibited only one band in the visible region which is similar in pattern to that at ~ 690 nm with the exception that it appears at ~ 446 nm with greater intensity. The band at 395 nm is probably shifted to a shorter wavelength (250 nm). The intensities of these bands are pH-dependent, which indicated that complex formation is enhanced by loss of H^+ from GX. The variation in intensity served as the basis for the evaluation of the formation constants of the existing complexes.[19]

The addition of an Ni(II) solution to GX resulted in the formation of an orange colour at pH ≈ 7.0, which changed to red as the pH increased. Precipitation of red crystals occurred on standing at pH > 7.5. The kinetic data were obtained at wavelength of 250 nm, where the absorbance was mainly due to the complex. Figure 5 shows the observed rate constant (k_{obs}) (under pseudo-first-order conditions) as a function of pH and the analytic concentration of GX ($T_{GX} \gg T_{Ni}$). Figure 6 shows the k_{obs} values as a function of T_{GX} at interpolated values of pH obtained from Fig. 5. The dependence is not linear, with the intercept greater than zero, and it is more or less quadratic. Since the intercept values are usually the result of experimental points which suffer

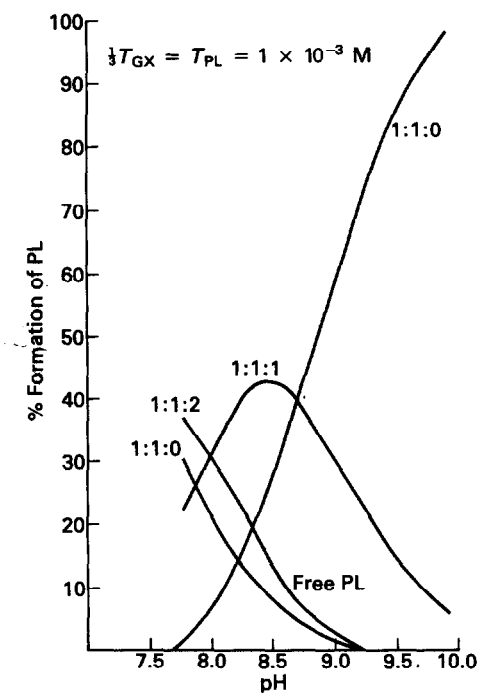


Fig. 4. Distribution diagram of the GX–PL compounds.

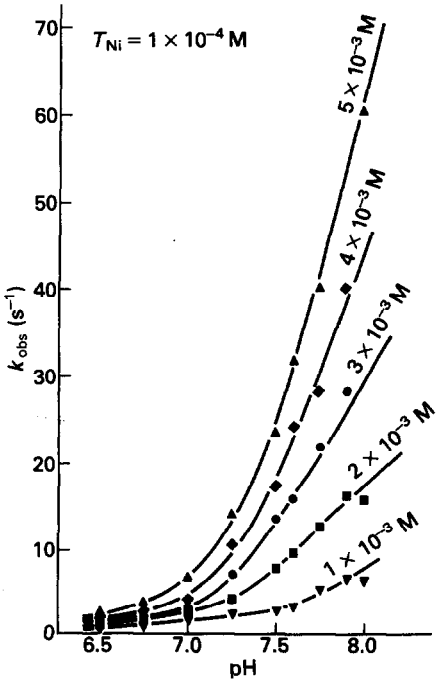


Fig. 5. Dependence of k_{obs} on pH at various T_{GX} and constant T_{Ni}.

from inherited uncertainties, one cannot rely on them for the interpretation of their dependence on pH. If $(k_{obs}-a)/T_{GX}$ (a represents the value of the adjusted intercept at a given pH) is plotted vs T_{GX} linear relationships were obtained (Fig. 7), i.e.:

$$(k_{obs}-a)/T_{GX} = b+cT_{GX}. \quad (1)$$

The ligand and metal species encountered in the pH range used (~6.7–8) are numerous. They are GXH_2^+, GXH and GX^- for the ligand, and Ni^{2+} and $NiOH^+$ for Ni(II). Several reactions may be considered to take place between these species. In order to simplify the mechanism a few reactions are going to be considered in which it has been assumed that the products are mainly $NiGX^+$ and $Ni(GX)_2$. This assumption is reasonable since excess ligand with respect to metal was used throughout the kinetic work. Scheme 1 describes the reactions which probably take place in solution.

$$\begin{array}{ll}
Ni^{2+}+GXH_2^+ \rightleftarrows NiGX^+ + 2H^+; & k_1, k_{-1};\\
\quad\downarrow\uparrow & \\
Ni^{2+}+GXH \rightleftarrows NiGX^+ + H^+; & k_2, k_{-2};\\
\quad\downarrow\uparrow & \\
Ni^{2+}+GX^- \rightleftarrows NiGX^+; & k_3, k_{-3};\\
 & \\
NiOH^+ + GXH_2^+ \rightleftarrows NiGX^+ + H^+ + H_2O; & k_4, k_{-4};\\
\quad\downarrow\uparrow & \\
NiOH^+ + GXH \rightleftarrows NiGX^+ + H_2O; & k_5, k_{-5};\\
\quad\downarrow\uparrow & \\
NiOH^+ + GX^- \rightleftarrows NiGX^+ + OH-; & k_6, k_{-6};\\
\quad\downarrow\uparrow +GX^- & \\
Ni^{2+}+2GXH_2^+ \rightleftarrows NiGX_2 + 4H^+; & k_7, k_{-7};\\
\quad\downarrow\uparrow & \\
Ni^{2+}+2GXH \rightleftarrows Ni(GX)_2 + 2H^+; & k_8, k_{-8};\\
\quad\downarrow\uparrow & \\
Ni^{2+}+2GX^- \rightleftarrows Ni(GX)_2; & k_9, k_{-9};\\
 & \\
NiOH^+ + 2GXH_2^+ \rightleftarrows Ni(GX)_2 + H_2O + 3H^+; & k_{10}, k_{-10};\\
\quad\downarrow\uparrow & \\
NiOH^+ + 2GXH \rightleftarrows Ni(GX)_2 + H_2O + H^+; & k_{11}, k_{-11};\\
\quad\downarrow\uparrow & \\
NiOH^+ + 2GX^- \rightleftarrows Ni(GX)_2 + OH^-; & k_{12}, k_{-12}.
\end{array}$$

Scheme 1.

k_is and k_{-i}s are the forward and backward rate constants.

The above mechanism can be described by the following differential equation:

$$\begin{aligned}
Q_2\frac{dC_2}{dt} = &\left(\frac{T_{Ni}-C_2Q_2}{Q_1}\right)(T_{GX}Q_3+T_{GX}^2Q_4)\\
&+K_{OH}[OH^-]\left(\frac{T_{Ni}-C_2Q_2}{Q_1}\right)\\
&\times(T_{GX}Q_5+T_{GX}^2Q_6)-C_2\\
&\times[(Q_7/K_{1C}\alpha_2T_{GX})+Q_8], \quad (2)
\end{aligned}$$

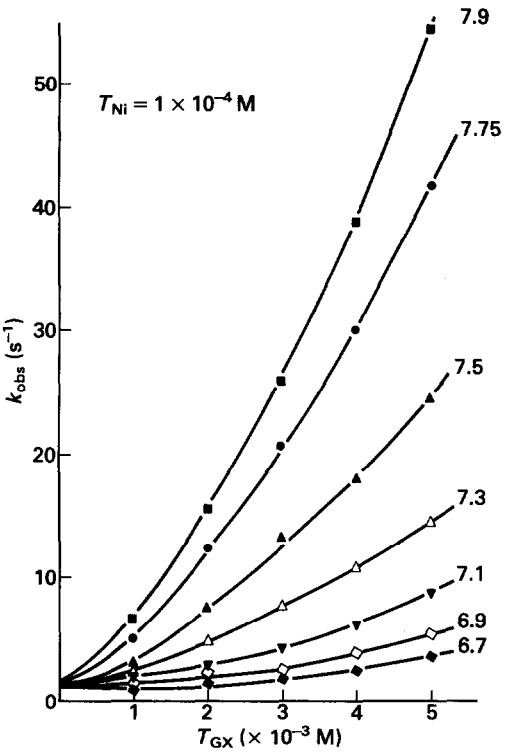


Fig. 6. Dependence of k_{obs} on T_{GX} at various values of pH taken from Fig. 5.

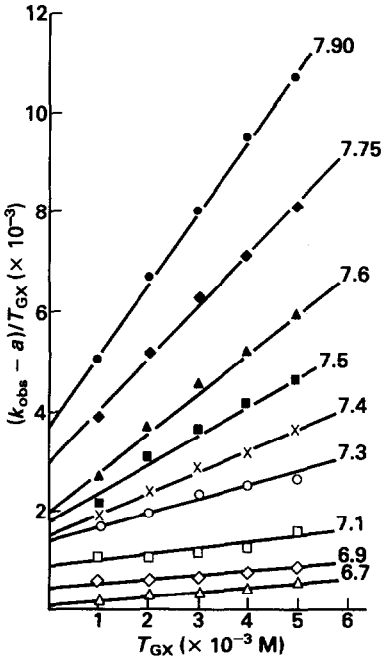


Fig. 7. Plot of $(k_{obs}-a)/T_{GX}$ as a function of T_{GX} at various values of pH.

where:

$$Q_1 = 1 + K_{OH}[OH^-],$$

$$Q_2 = 1 + (K_{1C}\alpha_2 T_{GX})^{-1},$$

$$K_{OH} = [NiOH^+]/[Ni^{2+}][OH^-],$$

$$K_{1C} = C_2/C_1\alpha_2 T_{GX},$$

$$C_1 = [NiGX^+],$$

$$C_2 = [Ni(GX)_2],$$

$$\alpha_0 = [GXH_2^+]T_{GX}^{-1} = [H^+]^2/[H^+]^2 + K_{1h}[H^+] + K_{1h}K_{2h},$$

$$\alpha_1 = [GXH]T_{GX}^{-1} = [H^+]K_{1h}/[H^+]^2 + K_{1h}[H^+] + K_{1h}K_{2h},$$

$$\alpha_2 = [GX^-]T_{GX}^{-1} = K_{1h}K_{2h}/[H^+]^2 + K_{1h}[H^+] + K_{1h}K_{2h},$$

K_{1h} and K_{2h} are the first and second dissociation constants of GXH_2^+,

$$Q_3 = k_1\alpha_0 + k_2\alpha_1 + k_3\alpha_2,$$

$$Q_4 = k_7\alpha_0^2 + k_8\alpha_1^2 + k_9\alpha_2^2,$$

$$Q_5 = k_4\alpha_0 + k_5\alpha_1 + k_6\alpha_2,$$

$$Q_6 = k_{10}\alpha_0^2 + k_{11}\alpha_1^2 + k_{12}\alpha_2^2,$$

$$Q_7 = k_{-1}[H^+]^2 + (k_{-2} + k_{-4})[H^+] + (k_{-3} + k_{-5}) + k_{-6}[OH^-]$$

and

$$Q_8 = k_{-7}[H^+]^4 + k_{-10}[H^+]^3 + k_{-8}[H^+]^2 + k_{-11}[H^+] + k_{-9} + k_{-12}[OH^-].$$

The integrated form of eqn (2) is expressed as follows:

$$\ln \frac{C_\infty}{C_{2,t} - C_{2,\infty}} = k'(GX)t, \quad (3)$$

where $C_{2,\infty}$ and $C_{2,t}$ are the concentration of C_2 at infinity and time t, and k' is the overall rate constant which may be correlated with $k_{obs}(GX)$, i.e.:

$$k_{obs}(GX) = \frac{Q_8}{Q_2} + \left(\frac{Q_3 + Q_5K_{OH}[OH^-]}{Q_1}\right)T_{GX} + \left(\frac{Q_4 + Q_6K_{OH}[OH^-]}{Q_1}\right)T_{GX}^2, \quad (4)$$

where:

$$a = Q_8/Q_2 \approx Q_8, \quad (5)$$

$$b = (Q_3 + Q_5K_{OH}[OH^-])/Q_1 \approx Q_3 + Q_5K_{OH}[OH^-] \quad (6)$$

and

$$c = (Q_4 + Q_6K_{OH}[OH^-])/Q_1 \approx Q_4 + Q_6K_{OH}[OH^-], \quad (7)$$

where $Q_1 \approx Q_8 = 1$ (under the experimental conditions of this work).

It has been found that $a(=Q_8)$ is a linear function of the reciprocal of $[H^+]$ [Fig. 8(a)], with intercept $(=k_{-9})$ and slope $(=k_{-12})$ equal to 0.74 and 1.6×10^{-8}, respectively. If b is multiplied by $([H^+] + K_{1h}[H^+] + K_{1h}K_{2h})$ and plotted vs $[H^+]$ a straight line is obtained [Fig. 8(b)] with intercept $(=k_5K_{OH}K_wK_{1h} + K_{1h}K_{2h}k_3)$ equal to 1.0×10^{-12} and slope $(=k_4K_{OH}K_w + k_2K_{1h})$ equal to 6.4×10^{-5}. The parameter c, if multiplied by

$$\frac{[H^+]^2 + K_{1h}[H^+] + K_{1h}K_{2h})^2}{[H^+]^2},$$

is partly dependent on $[H^+]$ and partly dependent on $[H^+]^{-1}$. Figure 8(c) shows such a dependence: in the case of the reciprocal dependence on $[H^+]$ the intercept $(=k_8K_{1h}^2)$ and slope $(=k_{11}K_{1h}^2K_{OH})$ are equal to 1.6×10^{-9} and 8.8×10^{-18}, respectively, while in the case of the linear dependence on $[H^+]$ the intercept $(=k_8K_{1h}^2)$ and slope $(=k_{10}K_{OH})$ are equal to 1.1×10^{-9} and 7.3×10^{-3}, respectively. With the knowledge of the values of the constants K_w, K_{1h}, K_{2h} and K_{OH} the possible values of the microrate constants k_2, k_3, k_4, k_5, k_8, k_{10}, k_{11}, k_{-9} and k_{-12} may be determined. The values are 2.6×10^2, 1.6×10^5, 3.2×10^5, 2×10^6, 2.5×10^6, $\ll 1$, $\ll 1$, 0.74 and 1.6×10^6, respectively. It seems from these results that the active Ni(II) species in NiGX formation are the Ni^{2+} and $Ni(OH)^{2+}$, but only Ni^{2+} in the case of the formation of the $Ni(GX)_2$ complex.

Complexes of the Schiff base of PL *and* GX *with* Ni(II). Addition of PL in excess to a solution of Ni(II) GX did not show signs of precipitation in the pH range 7.5–10.0. The reaction was slower than that of GX with Ni(II). It was pH-dependent at constant T_{PL} (initial concentration of PL) (Fig. 9). If k_{obs} is plotted as a function of T_{PL} at various interpolated pH values straight lines of significant positive slopes and negative intercepts are obtained. The lines intersected at a fixed concentration of T_{PL} (Fig. 10), i.e.:

$$k'_{obs}(Sch) = d + eT_{PL}. \quad (8)$$

(at constant T_{Ni}, T_{GX} and pH), where $k'_{obs}(Sch)$ is the observed rate constant for the Ni(II)–Schiff base complexation reaction. In the case of $T_{GX} = 5T_{Ni} = 5 \times 10^{-3}$ M, this concentration is equal to 4×10^{-3} M (Fig. 10). Although the negative intercept has no physical meaning, yet it may indicate that Schiff base–Ni(II) complexes are not likely formed when the concentration of PL is less than or equal to $4 \times$

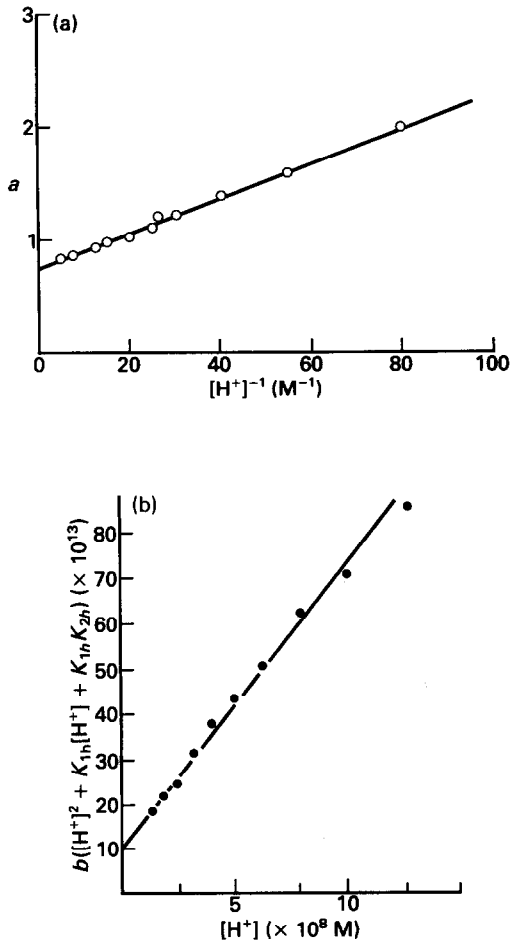


Fig. 8. (a) Plot of a as a function of $[H^+]^{-1}$. (b) Plot of $b([H^+]^2+[H^+]K_{1h}+K_{1h}K_{2h})$ as a function of $[H^+]$. (c) Plot of $c([H^+]^3+[H^+]K_{1h}+K_{1h}K_{2h})^2/[H^+]^{-2}$ as a function of $[H^+]^{-1}$.

10^{-3} M. This type of reaction has been encountered in Schiff base complex formation with Cu(II).[20] It was explained as due to the prior formation of a ternary complex. Similarly, a ternary complex of Ni(II) may also be formed with PL and GX $[Ni(PL)_f(GX)_j(H)_k]$ prior to the Schiff base complex formation. In such a case, eqn (8) can be rewritten as follows:

$$k'_{obs}(Sch) = e(T_{PL} - T'_{PL}), \qquad (9)$$

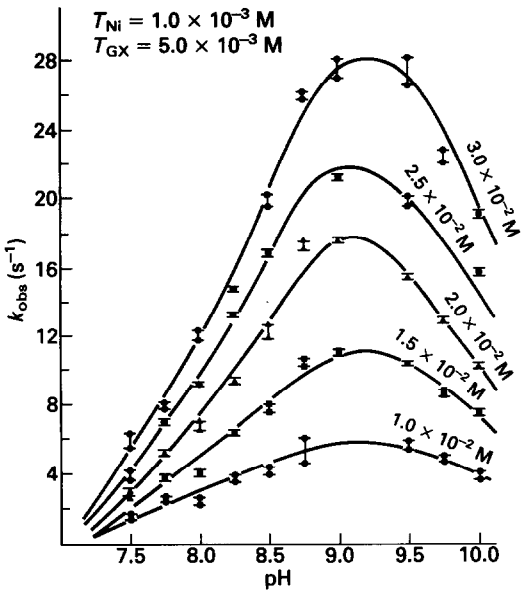


Fig. 9. Dependence of k_{obs} on pH at various T_{PL} and constant T_{Ni} and T_{GX}.

where T'_{PL} is the initial concentration of PL not involved in the Schiff base complex formation with GX ($\leqslant 4\times10^{-3}$ M in this case).

The interacting species of PL and Ni(II)–GX in the pH range of the study are considered to be HPL, PL^-, GX^-, GXH, $NiGX^+$ and $Ni(GX)_2$. Other complex species have been neglected for simplicity. The reaction mechanism which may describe the kinetic data shown in Figs 9 and 10 is visualized in Scheme 2.

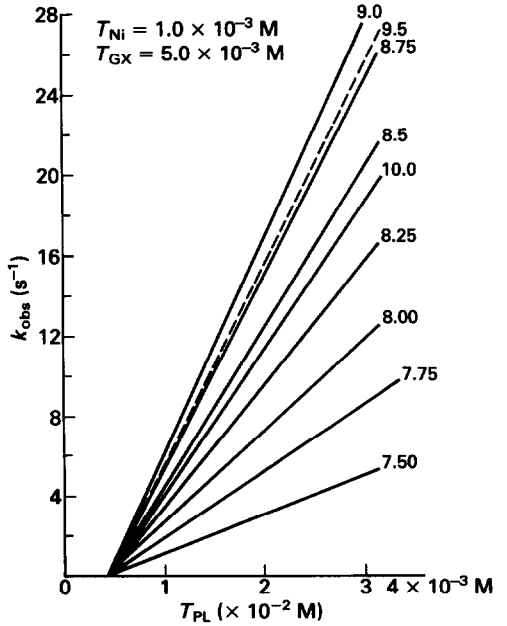


Fig. 10. Dependence of k_{obs} on T_{PL} at various values of pH.

(a) $NiGX^+ + HPL \rightarrow Ni\ Sch\ H^+$, k_{13};

$\downarrow\uparrow$

(b) $NiGX^+ + PL^- \rightarrow Ni\ Sch$, k_{14};

$\downarrow\uparrow$

(c) $NiGX^+ + PL^+ + OH^- \rightarrow Ni\ Sch\ H_{-1}$, k_{15};

$\downarrow\uparrow$

(d) $Ni(GX)_2 + HPL \rightarrow NiGX\ Sch\ H$, k_{16};

(e) $Ni(GX)_2 + PL- \rightarrow NiGX\ Sch$, k_{17};

(f) $Ni(GX)_2 + PL^- + OH^- \rightarrow NiGX\ Sch\ H_{-1}$, k_{18};

(g) $HPL + GXH \rightarrow Sch\ H_2$, k_{19};

(h) $HPL + GX^- \rightarrow Sch\ H^-$ } k_{20};
or $PL^- + GXH \rightarrow Sch\ H^-$ }

(i) $PL^- + GX^- \rightarrow Sch^{-2}$, k_{21}.

Scheme 2.

Sch is the condensation product (Schiff base) of GX and PL (its formation is a fast process and beyond the ability of the stopped-flow kinetic technique to measure), and Ni Sch H, Ni Sch, Ni Sch H_{-1}, NiGX Sch H, NiGX Sch and NiGX Sch H_{-1} are the various Ni(II) complexes with the condensed product. Here, the reactions were assumed to be irreversible since the intercepts (describing the backward rate constants) of the linear relation described by eqn (9) have been assumed to be equal to zero. The rate equation describing the mechanism shown in Scheme 2 is as follows:

$$-\frac{d[Ni(GX)_2]}{Q_2\,dt} = Ni(GX)_2 Q_{12}, \qquad (10)$$

where:

$$Q_{12} = \frac{k_{13}\alpha'_1 T_{PL}}{K_{1C}\alpha_2 T_{GX}} + \frac{k_{14}\alpha'_2 T_{PL}}{K_{1C}\alpha_2 T_{GX}} + \frac{k_{15}\alpha'_2 T_{PL} K_w}{[H^+]K_{1C}\alpha_2 T_{GX}} + k_{16}\alpha'_1 T_{PL} + k_{17}\alpha'_2 T_{PL} + k_{18}\alpha'_2 T_{PL} K_w/[H^+].$$

Upon integration of eqn (10), and correlating the result with eqn (9), the following relation is obtained:

$$k_{obs}(Sch) = Q_{12}/Q_2. \qquad (11)$$

Now the slope e in eqn (9) is as follows (if $Q_2 \approx 1$):

$$e = \frac{k_{13}\alpha'_1}{K_{1C}\alpha_2 T_{GX}} + \frac{k_{14}\alpha'_2}{K_{1C}\alpha_2 T_{GX}} + \frac{k_{15}\alpha'_2 K_w}{[H^+]K_{1C}\alpha_2 T_{GX}} + k_{16}\alpha'_1 + k_{17}\alpha'_2 + k_{18}\alpha'_2 K_w/[H^+]. \qquad (12)$$

Equation (12) is non-linear with respect to $[H^+]$ since α_2, α'_1, and α'_2 are also pH-dependent and an approximation should be considered if the curve shown in Fig. 11 could be interpreted. Plotting

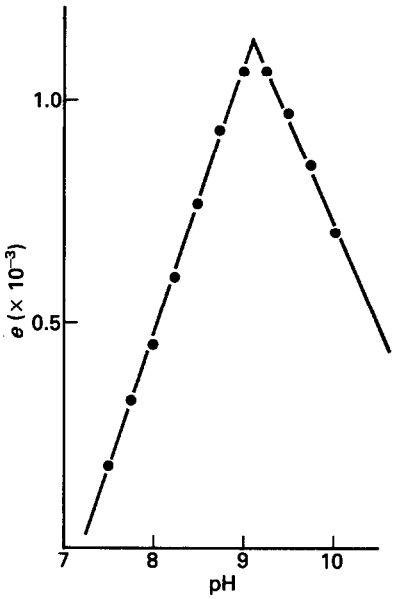
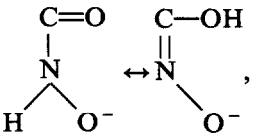


Fig. 11. Dependence of e on pH.

$e[H^+]/\alpha'_2$ vs α_2^{-1} resulted in a linear relationship in the pH range 7.75–10.00 with a very small intercept and a significant slope [Fig. 12(a)]. In such a case, the terms containing k_{13}, k_{14}, k_{16} and k_{17} are ignored in this pH range and $k_{15}K_w/K_{1C}T_{GX} = 3.53 \times 10^{-7}$ and $k_{15} = 5.6 \times 10^{11}$. Since the intercept is very small it should be expected that $k_{18} \leqslant 10^{12}$. On the other hand, the plot of $e[H^+]/\alpha'_2$ vs $[H^+]/\alpha_2$ is only linear in the pH range 9.25–10.00 if all terms in eqn (12) are ignored except for $([H^+]k_{14})/K_{10}\alpha_2 T_{GX}$ and $k_{18}K_w$ [Fig. 12(b)]. In such a case k_{14} is equal to 6.5×10^6 and $k_{18} \approx 2.5 \times 10^6$. If these approximations are correct, the most important reactions in Scheme 2 should be (b), (c) and (f) in which (c) and (f) show a kind of deprotonation of the Ni(II)–Schiff base complex. This may occur through the deprotonation of the tautomeric form of GX coordinating with Ni(II) and PL:



a situation which may account for the presence of the binary species $NiGXH_{-1}$ in aqueous solution at pH > 5.5 (Fig. 1).

In Scheme 2, a substitution reaction between the already fast Schiff base formation and the binary species of Ni(II) with GX was ignored since the rate of the reaction found was not compatible with the general rates of Ni(II) substitution reactions.

Acknowledgements—We would like to thank the University of Kuwait for the provision of Research Grant SCO21.

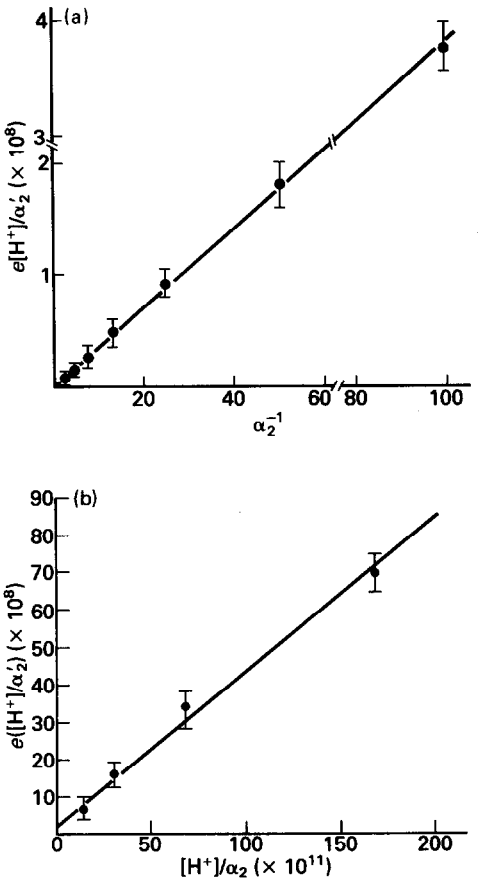


Fig. 12. (a) Plot of $e[H^+]/\alpha_2'$ as a function of α_2^{-1}. (b) Plot of $e[H^+]/\alpha_2'$ as a function of $[H^+]/\alpha_2$.

REFERENCES

1. H. Maehr, *Pure Appl. Chem.* 1971, **28**, 603.
2. J. B. Neilands, *Science* 1967, **156**, 1443.
3. O. Mikes and T. Turkova, *Chem. Listy* 1964, **58**, 65.
4. R. T. Coutts, *Can. J. Pharm. Sci.* 1967, **2**, 27.
5. J. H. Weisburger and E. K. Weisburger, *Pharm. Rev.* 1973, **25**, 1.
6. D. A. Brown, M. V. Chidambaram, J. J. Clarks and D. M. McAleese, *Bioinorg. Chem.* 1978, **9**, 3.
7. D. A. Brown, M. V. Chidambaram and J. D. Glennon, *Inorg. Chem.* 1980, **19**, 3260.
8. D. A. Brown and M. V. Chidambaram, In *Metal Ions in Biological Systems* (Edited by H. Sigel), Vol. 14, p. 125. Marcel Dekker, New York (1982).
9. W. F. Anderson and M. C. Hiller, *Symposium of Development of Iron Chelators for Clinical Use.* DHEA Publication, NIH.
10. K. N. Raymond, W. R. Harris, C. J. Carrano and F. L. Weith, In *Inorganic Chemistry in Biology and Medicine* (Edited by A. E. Martell), p. 313. A.C.S. Symposium Series No. 140 (1980).
11. D. A. Brown, A. L. Roche, T. A. Pakkanen, T. T. Pakkanen and K. Smolander, *J. Chem. Soc., Chem. Commun.* 1982, 676.
12. M. S. El-Ezaby and F. R. El-Eziri, *J. Inorg. Nucl. Chem.* 1976, **38**, 8, 1901.
13. D. L. Leussing and N. Huq, *Anal. Chem.* 1966, **38**, 1388.
14. D. E. Metzler, *Biochemistry.* Academic Press, New York (1977).
15. M. S. El-Ezaby, M. Rashad and N. M. Moussa, *Polyhedron* 1983, **2**, 245.
16. T. S. Hassan, A. H. G. El-Dhaher, H. Marafie, H. Abu Soûd and M. S. El-Ezaby, *Comput. Chem.* 1984, **8**, 309.
17. P. Gaus, A. Sabastini and A. Vacca, *Inorg. Chim. Acta* 1976, **18**, 237.
18. B. N. Figgis, *Introduction to Ligand Fields.* Interscience, New York (1966).
19. M. S. El-Ezaby, M. M. Hassan and S. Fareed, to be published.
20. N. Al-Awadi, M. S. El-Ezaby and H. M. Abu Soûd, *Inorg. Chim. Acta* 1982, **67**, 131.

Polyhedron Vol. 5, No. 4, pp. 983–990, 1986
Printed in Great Britain

0277–5387/86 $3.00+.00
Pergamon Journals Ltd

COMPLEXES OF IRON(III) WITH BENZOYLACETONE 1-NAPHTHOYLHYDRAZONE

VUKADIN M. LEOVAC,* LUKA J. BJELICA, LJILJANA S. JOVANOVIĆ and STEPAN YU. CHUNDAK†

Institute of Chemistry, Faculty of Sciences, V. Vlahovića 2, 21000 Novi Sad, Yugoslavia

(*Received* 17 *July* 1985; *accepted* 4 *October* 1985)

Abstract—One mono(ligand) and three bis(ligand) octahedral complexes (cationic, anionic and non-electrolyte type) of iron(III) and benzoylacetone 1-naphthoylhydrazone have been prepared and characterized by elemental analysis, conductivity measurements, IR and electronic spectra, as well as by linear sweep and cyclic voltammetry. It has been found that formation of these complexes can be explained by the nature of this tridentate (ONO) ligand, taking part in coordination as both a mono- and a dianion.

Due to the diverse properties of carboxylic acid hydrazides and hydrazones and their wide application in many fields (medicine, analytical chemistry etc.), we have witnessed an increased interest in the study of their complexing affinities toward different transition metals.[1–4] There have been described[5,6] the complexes of both 1-naphthoic acid hydrazide and salicylidenehydrazone with some 3*d* elements, showing that coordination had been accomplished via NO and ONO sets of donor atoms, respectively.

Since we could not find in the literature information on iron(III) complexes with benzoylacetone 1-naphthoylhydrazone (H_2L), we have undertaken the task of their preparation and characterization by some physico-chemical methods.

EXPERIMENTAL

Chemicals and methods

Chemicals and some of the methods employed have been already described.[7]

The iron content was determined by a complexometric method[8] after complex decomposition with concentrated nitric and sulphuric acid.

Melting points were determined by Kofler apparatus with no corrections.

Thermogravimetric measurements were carried out on a Paulik–Paulik–Erdey derivatograph in the air atmosphere, employing MgO as a standard. The mass of the sample was 100 mg and the heating rate was 10°C min^{-1}.

Preparation of the ligand and complexes

Ligand. H_2L was synthesized according to the general procedure[9] in the following way. An equimolar mixture of methanolic solutions of 1-naphthoic acid and benzoylacetone was heated with reflux for about 1 h. After cooling to room temperature the white microcrystalline hydrazone precipitate was filtered off and washed with MeOH and Et_2O. Yield 80%. The results of elemental analysis of the ligand recrystallized from MeOH, together with those for the complexes, have been presented in Table 1.

Complexes

$Fe(HL)Cl_2$. To the hot solution of 0.66 g of H_2L in 5 cm^3 of EtOH, a concentrated ethanolic solution of $FeCl_3 \cdot 6H_2O$ (0.54 g) was added (mole ratio 1:1). The solution was left at room temperature for about 12 h. The black crystals (formed in the dark green solution) were filtered off and washed with EtOH and Et_2O. Yield 0.72 g.

$[Fe(HL)_2]Cl$. The mixture of 0.54 g (2 mmol) of

* Author to whom correspondence should be addressed.
† Permanent address: Faculty of Chemistry, Uzhgorod State University, Uzhgorod, U.S.S.R.

Table 1. Analytical data for Fe(III) complexes[a]

Compound	Fe	C	H	N
H_2L		76.6 (76.3)	5.4 (5.5)	8.5 (8.5)
$Fe(HL)Cl_2$	12.0 (12.2)	56.5 (55.3)	5.4 (3.8)	6.4 (6.1)
$[Fe(HL)_2]Cl$	7.4 (7.4)	65.9 (67.2)	4.4 (4.6)	7.4 (7.5)
Fe(HL)L	7.7 (7.8)	68.6 (70.7)	4.6 (4.7)	8.0 (7.8)
$Li[FeL_2]\cdot 2.5CH_3OH$[b]	7.0 (7.0)	66.7 (66.8)	4.5 (5.3)	7.2 (7.0)

[a] Calculated values in parentheses.
[b] MeOH 10.5 (10.0).

$FeCl_3\cdot 6H_2O$ and 0.40 g (3 mmol) of sodium acetate was dissolved by heating in 5 cm^3 of EtOH. The precipitated NaCl was filtered off and 1.3 g of H_2L (4 mmol), dissolved in 5 cm^3 of EtOH, added to the filtrate. The dark green crystals formed during 48 h of keeping the reaction mixture at room temperature were filtered off and washed with EtOH and Et_2O. Yield 1.20 g.

Fe(HL)L. 0.75 g (1 mmol) of $[Fe(HL)_2]Cl$ was dissolved by heating in 10 cm^3 of MeOH and the obtained solution filtrated out. Then 0.20 g of lithium acetate was added to the filtrate and the mixture heated for 2–3 min. The solution colour changes from dark green into the dark one. After cooling to room temperature, about 2 h later, the dark brown crystals were filtered off and washed with MeOH. Yield 0.54 g.

$Li[FeL_2]\cdot 2.5CH_3OH$. 0.70 g (1 mmol) of Fe(HL)L was dissolved at room temperature in 20 cm^3 of Et_2O (dissolution is not complete). Then 0.080 g (2 mmol) of $LiOH\cdot H_2O$ dissolved in 5 cm^3 of MeOH was added. The obtained solution after stirring was left for about 5 h. The black needle-like crystals were filtered off and washed with EtOH. Yield 0.50 g.

RESULTS AND DISCUSSION

General physico-chemical characteristics of complexes

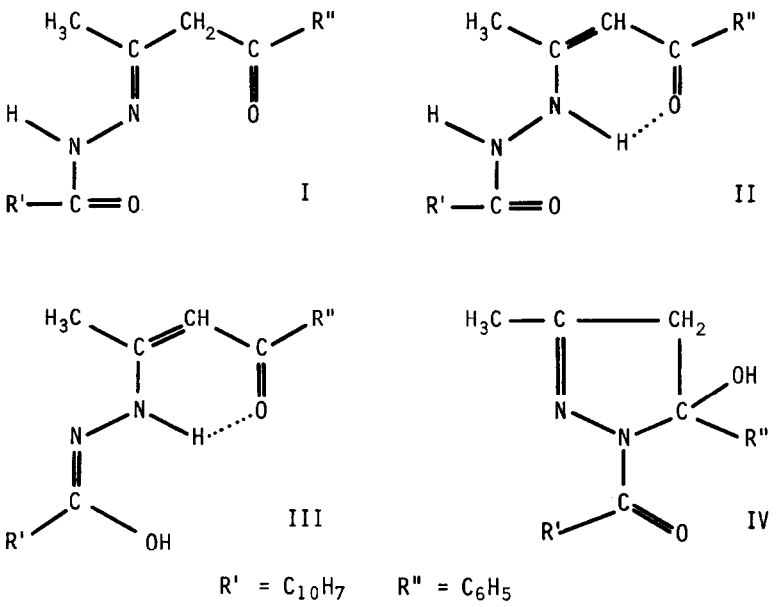
As seen from Table 1, H_2L forms with Fe(III) one mono(ligand) and three bis(ligand) complexes of cationic, anionic and non-electrolyte type. The complexes are black or dark green crystalline substances, stable in air. They melt (without decomposition) at temperatures considerably higher than the melting point of the ligand itself (Table 2). From the only crystallosolvate, $Li[FeL_2]\cdot 2.5CH_3OH$, the methanol loss is observed at relatively high temperature (120°C). The complexes are insoluble in water, while they are dissolved in MeOH, EtOH, Me_2CO and DMF. Besides, the neutral and anionic complexes are soluble in Et_2O and $CHCl_3$.

Formation of three different types of bis(ligand) complexes can be explained by the fact that the ligand can take part in coordination as both the mono- (HL^-) and the dianion (L^{2-}). It has been shown[9] that the reaction of benzoylacetone with a number of aromatic acids hydrazides yields the

Table 2. Some physico-chemical characteristics of the Fe(III) complexes

Complex	M.p.[a] (°C)	Molar conductivity ($S\ mol^{-1}\ cm^2$) MeOH	Molar conductivity ($S\ mol^{-1}\ cm^2$) DMF	μ_{eff} (BM)
$Fe(HL)Cl_2$	232	100.7	31.1	5.84
$[Fe(HL)_2]Cl$	173	65.2	15.8	5.93
Fe(HL)L	182	4.3	3.7	6.03
$Li[FeL_2]\cdot 2.5CH_3OH$	203	59.2	38.3	5.89

[a] Melting point of the ligand 106°C.



Scheme 1.

products which can exist in different tautomeric forms. In the case of H_2L four different structures are possible, viz. hydrazonic (I), enhydrazonic (II), enhydrazone-α-oxyazinic (III) and 5-oxypyrazolinic (IV) (Scheme 1).

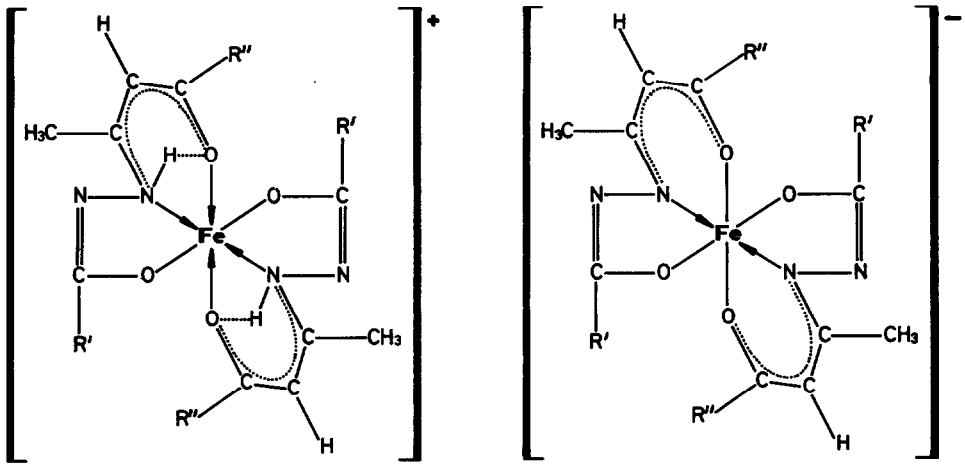
It has been demonstrated[9,10] that a tautomeric rearrangement can take place in the complexing process of some similar ligands with metal ions. In view of the composition of the synthesized complexes, it can be concluded that our ligand behaves as a tridentate one, and, as mentioned above, is deprotonated in two stages. Because of that it cannot be engaged in the complex in its cyclic form (IV), since in that case it could not behave either as a tridentate ligand (for the stereochemistry reasons), or as a diprotic acid. The hydrazone form (I) is potentially tridentate, but it has only one mobile proton located at the amide nitrogen. On the other hand, enhydrazine form (II) can behave as a tridentate ONO type ligand, having two protons which can be replaced by metal ion. However, it has been recently established that chelate compounds of many ions of transition metals with the aldehyde[11] or ketone[12] hydrazones are formed via an α-oxyazine tautomeric form of the ligand (Scheme 2).

Since form II has an acylhydrazine fragment —NH—NH-COR it can be assumed that the complex formation process is preceded by formation of the enhydrazone-α-oxyazine isomer (III), which satisfies both conditions: it can act as a tridentate ligand and, depending on the reaction conditions, give one or two protons. This supposition is supported by the IR spectral data. An analysis of the IR spectra shows that these are similar for all the complexes, but differ from that of the ligand. Thus, in the region of valence vibrations of multiple bonds the spectrum of free ligand contains a band at 1700 cm^{-1} which can be attributed to the valence C=O group vibration. Also, the bands appearing at 1605 and 1590 cm^{-1} are characteristic of nitrogen derivatives of β-diketones, having a ketoenamine (enhydrazine) structure.[13] In the region of NH valence vibrations, the absorption band at 3290 cm^{-1} can be assigned to the NH bonds taking part in both inter- and intramolecular hydrogen bonds. On the other hand, in the spectra for the complexes ν(C=O) is missing, which indicates that the tautomeric form of the ligand engaged has been changed. In addition, the distinct ν(NH) band is not also observed. Finally, the spectra of both the ligand and complexes contain a band at 1265–1270 cm^{-1} which can be assigned to the C—O group.

Molar conductivity

As seen from Table 2, all complexes, with the exception of Fe(HL)L, behave in MeOH solutions as 1:1 electrolytes (molar conductivity 80–115).[14] In contrast to this, the molar conductivities measured in DMF are significantly lower than the expected ones (65–90).[14] However, these observations are in agreement with those for Fe(III) complexes with the semicarbazone-based ligands,[7] and a similar explanation can be given.

Lower conductivities of $[Fe(HL)_2]Cl$ and $Li[FeL_2]$ in DMF can be attributed to the formation of ion pairs between the weakly solvated Cl^- and the complex cation, and Li^+ with the complex anion,



$[Fe(HL)_2]^+$ $[FeL_2]^-$

R′ = $C_{10}H_7$, R″ = C_6H_5

Scheme 2.

respectively. On the other hand, the conductivity of $Fe(HL)Cl_2$ (monomer) should imply its dissociation into $Fe(HL)Cl^+$ and Cl^-. Since the probability for a tetra- or penta-coordinated Fe(III) with such a planar ligand is low, it seems plausible to assume the existence of a dimer $[Fe(HL)_2][FeCl_4]$ in the solution. However, in contrast to the analogous complexes previously described,[7] the presence of a dimeric structure for Fe(HL)L cannot be proved (apparently, it is only formed under the voltammetric conditions, i.e. in the presence of a supporting electrolyte). Conductivities of $[Fe(HL)_2]Cl$ and $Fe(HL)Cl_2$ show an increase with ageing of the solution (about 20% during 24 h), which suggests that some structural changes take place in their solutions.

Magnetic susceptibility

It is evident from Table 2 that all the complexes have the values for effective magnetic moments characteristic for the high-spin Fe(III) state (d^5-system). Therefore, it can be concluded that H_2L behaves towards Fe(III) as a ligand with a relatively weak ligand field.

Electronic spectra

Similar to some analogous compounds,[15] H_2L and some of its complexes undergo, in solution, certain structural transformations, which is reflected in the appearance of the electronic spectra (Table 3).

The absorption maximum at 30,210 cm^{-1} in the spectrum for a freshly prepared solution of H_2L shows a rapid decrease with time, as illustrated in Fig. 1 (insets). The absorbance after 6 h falls to about one-third of the starting value, remaining approximately the same afterwards. At the same time, two new maxima emerge at 34,250 and 35,460 cm^{-1}, respectively, and they do not exhibit a time effect. The same maxima have been also observed in the spectrum of 1-naphthoic acid hydrazide. Therefore, H_2L in the solution undergoes significant structural changes which can be explained by (a gradual) formation of the cyclic 5-oxypyrazoline form (IV).[9]

Similar changes, though less pronounced, are also observed in the spectra of $Fe(HL)Cl_2$ and $[Fe(HL)_2]Cl$. The emergence of maxima at about 34,000 and 35,000 cm^{-1} might suggest that one ligand from the $[Fe(HL)_2]^+$ entity is replaced by Cl^-; the further process being the same as for free H_2L. Besides, in view of the similarity of the spectra for the two complexes, it should be supposed that the absorption is mainly due to their common constituent, i.e. $[Fe(HL)_2]^+$, which implies a dimeric structure ($[Fe(HL)_2][FeCl_4]$) for $Fe(HL)Cl_2$ in solution.

In contrast to the above, the spectra for Fe(HL)L and $Li[FeL_2]$ exhibit no time effect.

The electronic spectra for all complexes, except for $Li[FeL_2]$, recorded in the presence of an electrolyte (especially of LiCl), employed in voltammetric measurements, differ significantly from those obtained for the pure solutions. The difference is most pronounced in the case of Fe(HL)L; the spectrum in the presence of LiCl appearing as if composed of those for the cationic and anionic complex, which suggests formation of the dimeric $[Fe(HL)_2][FeL_2]$ structure.

On the basis of common characteristics of the

Table 3. Electronic spectral data in DMF

Compound		$\lambda_{max}{}^{a}$ (ε^{b})
H_2L	$t = 0$	30,210 (1.81), ~ 35,200 (0.73 sh)[c]
	$t = 24$ h	~ 31,600 (0.72 b.p.),[d] 34,250 (0.92), 35,460 (0.96)
$Fe(HL)Cl_2$[e]	$t = 0$	~ 18,900 (0.13 sh), ~ 27,800 (1.63 b.p.), 31,550 (1.90)
	$t = 24$ h	~ 18,900 (0.15 sh), ~ 27,500 (1.54 b.p.), 31,850 (1.78), 33,900 (1.66), 35,340 (1.54)
$[Fe(HL)_2]Cl$	$t = 0$	~ 18,900 (0.23 sh), 27,900 (2.61 b.p.), 31,350 (2.90), ~ 32,200 (2.90)
	$t = 24$ h	~ 18,900 (0.19 sh), 27,320 (2.29), 32,150 (2.51 sh), 34,010 (2.60), 35,340 (2.43)
$Li[FeL_2] \cdot 2.5CH_3OH$		~ 19,500 (0.63), 25,840 (2.95), ~ 34,200 (2.81 sh), 35,710 (3.06)
$Fe(HL)L$[e]		~ 19,000 (0.33 sh), 26,880 (3.04), 33,560 (2.90), ~ 36,700 (2.20 sh)

[a] In cm^{-1}.
[b] In $dm^3\ mol^{-1}\ cm^{-1} \times 10^{-4}$.
[c] Shoulder.
[d] Broad peak.
[e] Taken as monomer.

spectra for all complexes and the corresponding values for the absorbance coefficients, it can be concluded that the maxima observed below 30,000 are probably due to the d–π^* interactions and those at higher wavelength are characteristic of the intraligand π–π^* transitions. The absence of maxima belonging to the d–d transitions is not unusual for Fe(III) complexes,[16] especially if it is taken into

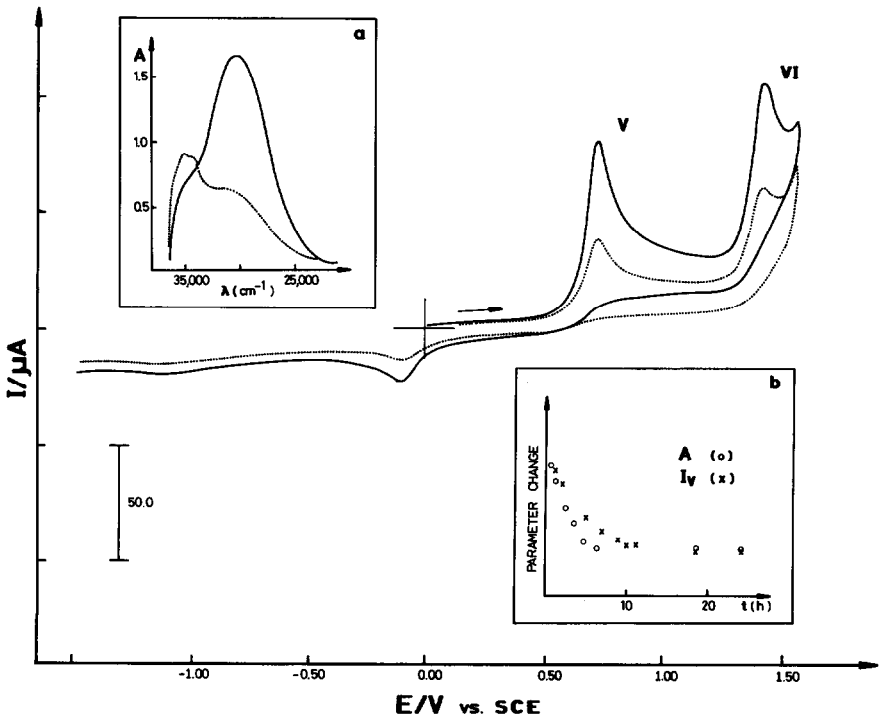


Fig. 1. Cyclic voltammograms for H_2L in 0.1 M $LiClO_4$ recorded at glassy carbon electrode (0.200 V s^{-1}) 1 (——) and 11 h (···) after preparing the solution. Inset a: UV spectra recorded after 15 min (——) and 24 h (···). Inset b: change of absorbance at 30,210 cm^{-1} (○) and current at peak V (×) (0.200 V s^{-1}) with time.

account their possible overlapping with the charge-transfer absorptions. Besides, the presence of a number of broad maxima, especially in the region of 27,000–30,000 cm^{-1}, indicate that the levels of electronic transitions in the complexes are not well defined.

Voltammetric studies

Ligand. The above structural changes of the ligand molecule in a DMF solution with time are reflected on the appearance of its cyclic voltammograms (Fig. 1). In the presence of $LiClO_4$ as supporting electrolyte, the oxidation occurs in two steps having the characteristics of the apparently two-electron irreversible process (peaks V and VI); the peak heights falling gradually to about one third of the starting value in about 6 h. Analogously, in the rotating disc experiment for a freshly-made solution the resulting two-electron waves are gradually transformed into those corresponding to the one-electron processes. The controlled potential electrolysis at the potential of peak V results in $n_{app} = 1.0$ and the dimeric product is reduced at -1.17 V ($n_{app} = 0.9$). On the other hand, the electrolysis at peak VI is not possible because of the close potential span limit.

On the cyclic voltammograms for H_2L, as well as for the complexes, recorded in the presence of Cl^-, a cathodic shift of peak V takes place with the slope of about 60 mV for a 10-fold increase in its concentration. This suggests occurrence of ion pairing of the reaction product with one Cl^- ion. It is accompanied by disappearance of the reduction peak at about 0.0 V, while the peak at about -1.30 V becomes more pronounced. The presence of Cl^- causes a significant cathodic shift of the anodic potential limit, so that the second oxidation peak (VI) cannot be recorded.

As for reduction of H_2L, it occurs in three steps at the potentials more cathodic from -2.0 V. The processes are coupled to irreversible chemical reactions whose mechanisms need further investigations.

Complexes. It has been found that the investigated complexes have the voltammetric characteristics similar to those of Fe(III) complexes with semicarbazone-based ligands.[7]

Cyclic voltammograms recorded for the anionic complex (Fig. 2) in the presence of $LiClO_4$ exhibit one reduction peak (II) (anodic counterpart III) corresponding to one-electron quasi-reversible process and three main oxidation peaks (IV–VI). The potentials of peaks II and III depend on the Li^+ concentration which might be attributed to the ion-pair formation. The slope of $+70$ mV indicates the association of one Li^+ with one reduced species ($[FeL_2]^{2-}$); the corresponding K_{ass} being about 6×10^3 mol^{-1} l.

The oxidations at peaks IV and V are followed by irreversible chemical reactions. By controlled-potential electrolysis at the plateau of peak IV ($n_{app} = 1.1$) the anionic bis(ligand) complex is transformed into the mono(ligand) one and the ligand in its oxidized form. A further oxidation at peak V with $n_{app} = 1.7$ results in decomposition of the complex, giving rise to the peaks representing reduction of Fe^{3+} and the oxidized ligand at about $+0.30$ and -1.25 V, respectively.

Cyclic voltammograms for the complexes having $[Fe(HL)_2]^+$ cation recorded in perchlorate medium are less defined. Three peaks (at -0.04, -0.45 and

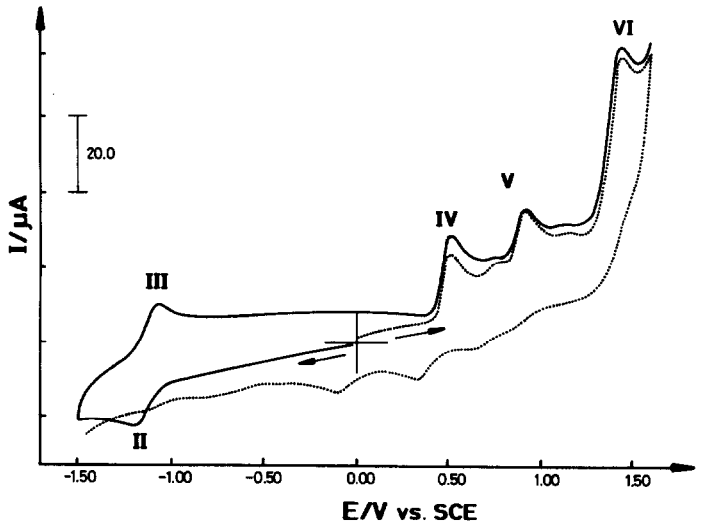


Fig. 2. Cyclic voltammograms of $Li[FeL_2]$ in 0.1 M $LiClO_4$, at glassy carbon electrode (0.200 V s^{-1}).

−1.16 V) representing one-electron reduction of different complex species, together with the more or less pronounced anodic counterparts, are observed. Besides, there appear the ligand oxidation peaks V and VI; the former one being of interest since it is observed in the potential region available in the presence of all supporting electrolytes.

Addition of Cl^- (as LiCl) causes an unequal cathodic potential shift of the two more anodic reduction peaks for the cationic complex and finally they merge into one peak. The slope of $\Delta E/\Delta \log [Cl^-]$ of about −160 mV for the peak at −0.45 V corresponds to the interaction with three Cl^- species. This means that one ligand entity in the bis(ligand) complex had been replaced with three Cl^-, giving thus $[Fe(HL)Cl_3]^-$.

Cyclic voltammograms recorded for cationic and anionic complexes in the presence of LiCl have been presented in Fig. 3. From the voltammetric data collected in Table 4 it is evident that potentials of all peaks depend on the sweep rate, indicating thus the presence of certain kinetic/chemical complications.

An attempt has been made to characterize better the electron transfer occurring at the potential of peak I. The constant potential electrolysis resulted in 0.4 mol of electrons per mole of reactant, giving rise to peak II, which is characteristic of reduction of $[FeL_2]^-$ anion. At the same time, the anodic peak at about 0.0 V, identified as oxidation of $FeCl_2$, showed a proportional enhancement. Therefore, the following reaction scheme (ECC mechanism), confirmed also by the rotating-disc experiment, might be assumed:

$$E \quad [Fe(HL)Cl_3]^- + e \rightarrow [Fe(HL)Cl_3]^{2-},$$

$$C \quad [Fe(HL)Cl_3]^{2-} + [Fe(HL)Cl_3]^- \rightarrow [Fe(HL)_2]^+ + FeCl_2 + 4Cl^-,$$

$$C \quad [Fe(HL)_2]^+ + 2HL^- \rightarrow [FeL_2]^- + 2H_2L.$$

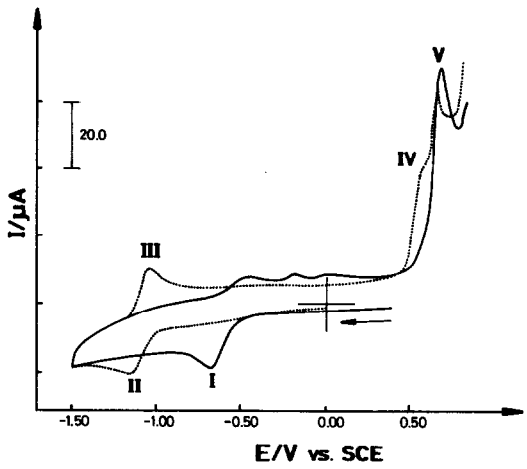


Fig. 3. Cyclic voltammograms of $[Fe(HL)_2]Cl$ (——) and $Li[FeL_2]$ (···) in 0.1 M LiCl at glassy carbon electrode (0.200 V s^{-1}).

Reoxidation of the starting complex (either after reduction at peak I or subsequently at peak II) can be achieved at the potential of $FeCl_2$ oxidation. However, if an oxidation is carried out at the potential of peak V, a complete decomposition of the complex (resulting in $FeCl_4^-$ and the ligand in its oxidized form) is attained. Its regeneration by reduction at cathodic potentials cannot be accomplished.

Cyclic voltammograms for other two complexes, $Fe(HL)Cl_2$ and Fe(HL)L (i.e. $[Fe(HL)_2][FeCl_4]$ and $[Fe(HL)_2][FeL_2]$) reflect their dimeric structure in the solution. They contain peaks representing reduction of the corresponding constituents taken separately with the current functions being approximately the same for each peak. This means that the species involved in the dimers are present in equimolar ratios.

All the complexes can be easily protonated and

Table 4. Peak potentials of complexes in DMF solutions (0.1 M LiCl)[a]

Complex	v[b]	$E_{(I)}$[c]	$E_{(II)}$	$E_{(III)}$	$E_{(IV)}$	$E_{(V)}$
$Li[FeL_2]\cdot 2.5CH_3OH$	0.02		−1.14	−1.06	+0.53	+0.64
	0.20		−1.17	−1.05	+0.56	+0.68
	2.00		−1.31[d]	−1.02	+0.58	+0.71
$[Fe(HL)_2]Cl$	0.02	−0.64				+0.64
	0.20	−0.69				+0.68
	2.00	−0.76				+0.72

[a] Glassy carbon working electrode.
[b] Sweep rate in V s^{-1}.
[c] Electrode potentials in V vs SCE. Letters in parentheses denote the corresponding peak.
[d] Peak II disappears, and a new one arises.

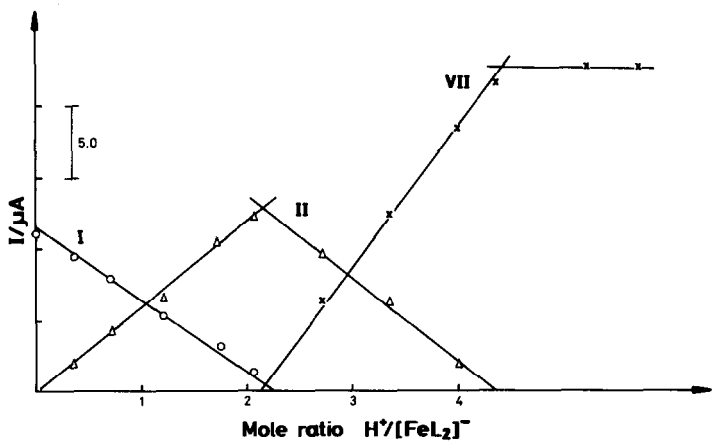


Fig. 4. Peak current changes (obtained at 0.200 V s^{-1}) for particular peaks during titration of $Li[FeL_2]$ with H^+.

thus quantitatively transformed into the corresponding more acidic forms. The course of such a titration of $Li[FeL_2]$ by H^+ ions generated from a Pd–H electrode,[17] monitored via recording the cyclic voltammograms, has been illustrated in Fig. 4. As the final result, the voltammogram is obtained having only the peaks for reduction of $FeCl_4^-$ (VII) and oxidation of the ligand (peak V). This means that a complete decomposition of the complex has been achieved. The same can be concluded on the basis of the corresponding UV spectra.

REFERENCES

1. A. P. Grekov, *Organicheskaya khimiya gidrazina.* Tekhnika, Kiev (1966).
2. Yu. P. Kitaev and B. I. Buzykin, *Gidrazony.* Nauka, Moscow (1974).
3. M. Katyal and G. Dutt, *Talanta* 1975, **22**, 151.
4. T. V. Troepol'skaya and E. N. Munin, *Gidrazony v koordinatsionoi khimii*, In *Khimiya gidrazonov* (Edited by Yu. P. Kitaev). Nauka, Moscow (1977).
5. S. Yu. Chundak, S. F. Manole, S. S. Butsko and N. V. Gerbeleu, *Koord. Khim.* 1975, **1**, 840.
6. S. Yu. Chundak, N. V. Gerbeleu and S. S. Butsko, *Zh. Neorg. Khim.* 1984, **29**, 1481.
7. V. M. Leovac, L. Bjelica and Lj. Jovanović, *Polyhedron* 1985, **4**, 233.
8. G. Schwarzenbach and H. Flaschka, *Die komplexometrische Titration.* Ferdinand Enke, Stuttgart (1965).
9. S. I. Yakimovich, V. N. Nikolaev and E. Yu. Kutsenko, *Zh. Org. Khim.* 1982, **18**, 762.
10. V. G. Yusupov, S. D. Nasirdinov and N. A. Parpiev, *Koord. Khim.* 1981, **7**, 921.
11. L. El-Sayed and M. F. Iskander, *J. Inorg. Nucl. Chem.* 1971, **33**, 435.
12. J. F. Alcock, R. J. Baker and A. A. Diamantis, *Aust. J. Chem.* 1972, **25**, 289.
13. Ya. F. Freimanis, *Khimiya enaminoketonov, enaminoiminov, enaminitionov.* Zinatne, Riga (1974).
14. W. J. Geary, *Coord. Chem. Rev.* 1971, **7**, 81.
15. E. N. Munin, T. V. Troepol'skaya, A. P. Stolyarov and Yu. P. Kitaev, *Koord. Khim.* 1981, **7**, 345.
16. F. A. Cotton and G. Wilkinson, *Advanced Inorganic Chemistry*, p. 761. Wiley Interscience, New York (1980).
17. Lj. Jovanović, L. Bjelica and F. F. Gaál, *Monatsh. Chem.* 1985, **116**, 443.

Polyhedron Vol. 5, No. 4, pp. 991–994, 1986
Printed in Great Britain

0277–5387/86 $3.00+.00
Pergamon Journals Ltd

4-AMINOANTIPYRINE SCHIFF-BASE COMPLEXES OF LANTHANIDE AND URANYL IONS

G. SHANKAR, R. R. PREMKUMAR and S. K. RAMALINGAM*

Department of Inorganic Chemistry, School of Chemistry, Madurai Kamaraj University, Madurai 625021, India

(*Received* 28 *August* 1985; *accepted* 7 *October* 1985)

Abstract—Using a new tridentate ligand, acetylacetone-4-aminoantipyrine (AAP) complexes of lanthanide nitrates having the general formula $[Ln(AAP)_2](NO_3)_3$ (where Ln = Pr, Nd, Sm, Gd, Dy or Y) have been prepared. Uranyl complexes of salicylaldehyde-4-aminoantipyrine (SAAP) of general formulae $[UO_2(SAAP)_2](X)_2$ (where X = NO_3 or I) and $[UO_2(SAAP)_2(OAc)_2]$ have also been prepared. The complexes have been characterized by IR, electronic, NMR, conductivity and analytical techniques. While SAAP acts as bidentate ligand without using its hydroxyl group, AAP acts as tridentate ligand involving hydroxyl coordination. The covalency parameter δ has been calculated for the Pr and Nd complexes.

We have synthesized some new Schiff-base metal complexes of heterocyclic amines which are physiologically active and structurally interesting. Previously we reported[1] that in some uranyl Schiff-base complexes the NMR evidence pointed to the —OH group coordinating to the metal in a protonated form. This paper reports the isolation and structure elucidation of the complexes of the Schiff-base ligands salicylaldehyde-4-aminoantipyrine (SAAP) [Fig. 1(a)] and acetylacetone-4-aminoantipyrine (AAP) [Fig. 1(b)] with UO_2^{2+} and Ln^{3+} ions, respectively. The point of interest here is that both AAP and SAAP are capable of acting as bi- or tridentate ligands depending on whether or not the functional group —OH is involved in coordination.[2,3]

EXPERIMENTAL

Uranyl nitrate, uranyl acetate (BDH) and 4-aminoantipyrine (Fluka) were high-purity grade and used as such. An acetone solution of uranyl iodide was prepared metathetically from the nitrate. The lanthanide nitrates were prepared from their respective oxides. SAAP was prepared as reported earlier.[2]

Preparation of AAP

Ethanolic solutions of 4-aminoantipyrine (20.3 g, 0.1 mol) and acetylacetone (10 g, 0.1 mol) were refluxed together for 4 h over a steam bath. The excess solvent was removed by evaporation and the concentrated solution was cooled in an ice bath with stirring. The Schiff base (AAP) which separated out as a cream coloured powder was collected and dried in air (m.p. 136°C).

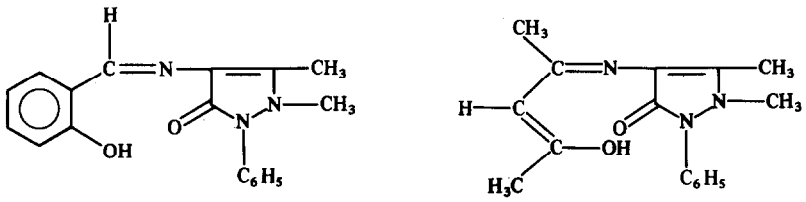
Preparation of uranyl complexes of SAAP

The uranyl salt (1 mmol and SAAP (2 mmol) were refluxed together in acetone over a steam bath for 1 h. The solution was cooled and the complex obtained was washed with acetone and dried over P_4O_{10} *in vacuo*.

Preparation of lanthanide complexes of AAP

An acetone solution of lanthanide nitrate (2 mmol) was added to an acetone solution of AAP (4 mmol), keeping the mixture stirred. The complex that separated out was allowed to stand for half an hour, filtered, washed with acetone and dried over P_4O_{10} *in vacuo*.

* Author to whom correspondence should be addressed.



(a) SAAP (b) AAP

Fig. 1. Ligands used in the preparation of complexes.

Physical methods

Conductivity studies were carried out using a Toshniwal conductivity bridge, type CLO102A using DMF as solvent. The IR spectra of the ligands and complexes were recorded in the range 200–4000 cm^{-1} on a Perkin–Elmer 577 spectrophotometer using KBr disc technique. Electronic spectra of the complexes were recorded on a Bausch & Lomb spectronic 2000 instrument in the range 300–850 nm using DMF as solvent. PMR spectra were recorded on a Perkin–Elmer R32 spectrophotometer operating at 90 MHz using TMS as internal standard and DMSO-d_6 as solvent. C, H, N and metal analyses were performed by the usual methods. The elemental analyses data for the complexes along with molar-conductance values are given in Table 1.

RESULTS AND DISCUSSION

Uranyl complexes

The complexes are stable, non-hygroscopic, orange-yellow coloured solids. They are insoluble in acetone, ethanol, chloroform, benzene etc.; but are soluble in DMF and DMSO.

The IR spectral band assignments for SAAP and its complexes are shown in Table 2. The ligand has bands around 3000 cm^{-1} [ν(OH)], at 1650 cm^{-1} [ν(C=O)] and at 1585 cm^{-1} [ν(C=N)]. In the complexes, the hydroxyl frequency appears at the same region as in the ligand. The carbonyl frequency occurs around 1610 cm^{-1} and the azomethine frequency around 1560 cm^{-1}, indicating that these two groups are involved in bonding. In the acetate

Table 1. Analytical and conductance data of the complexes

Compound	Found (calc.) C	H	N	M	Molar conductance (Ω^{-1} cm^{-2} mol^{-1})
$[UO_2(SAAP)_2(NO_3)_2$	42.7	3.3	11.0	23.4	190
	(42.8)	(3.4)	(11.1)	(23.6)	
$[UO_2(SAAP)_2]I_2$	37.7	2.9	7.3	20.4	200
	(38.0)	(3.0)	(7.4)	(20.9)	
$[UO_2(SAAP)_2(OAc)_2]$	47.8	3.9	8.3	23.7	15.31
	(47.9)	(4.0)	(8.4)	(23.7)	
$[Pr(AAP)_2](NO_3)_3$	42.2	4.2	14.0	15.5	210
	(42.8)	(4.2)	(14.1)	(15.6)	
$[Nd(AAP)_2](NO_3)_3$	42.0	4.1	13.6	15.8	215
	(42.7)	(4.2)	(14.0)	(16.0)	
$[Sm(AAP)_2](NO_3)_3$	42.3	4.2	13.8	16.5	215
	(42.4)	(4.2)	(13.9)	(16.5)	
$[Gd(AAP)_2](NO_3)_3$	41.9	4.0	13.6	17.0	220
	(42.0)	(4.2)	(13.8)	(17.2)	
$[Dy(AAP)_2](NO_3)_3$	41.2	4.0	13.6	17.1	215
	(41.8)	(4.1)	(13.7)	(17.6)	
$[Y(AAP)_2](NO_3)_3$	45.4	4.5	14.9	14.4	210
	(45.5)	(4.5)	(14.9)	(10.4)	

Table 2. Important IR bands (cm^{-1}) of uranyl complexes[a]

Compound	ν(OH) w	ν(C=O) s	ν(C=N) s	ν_{anion} s
SAAP	2920–3040	1650	1580	—
$[UO_2(SAAP)_2](NO_3)_2$	2920–3040	1610	1560	1380, 1040, 835
$[UO_2(SAAP)_2]I_2$	2920–3040	1600	1560	—
$[UO_2(SAAP)_2(OAc)_2]$	2920–3040	1600	1560	1650

[a] w = weak, s = strong.

complex, a sharp band at 1650 cm^{-1}, which is absent in the nitrate complex, confirms the ν(C=O) of acetate, indicating thereby the unidentate coordination of acetate ion.[4] For the nitrate complex, bands at 1380, 1040 and 835 cm^{-1} correspond to ν_3, ν_1 and ν_2 frequencies of the free nitrate ion.[5]

The conductivity data of the nitrate and iodide complexes show them to be 1:2 electrolytes,[6] while the acetate complex behaves as a non-electrolyte. The elemental analyses are in agreement with a 1:2 stoichiometry between metal and ligand. Judging on these lines, SAAP can be considered to act as a neutral bidentate ligand.

The IR bands due to the uranyl group appear at 920 cm^{-1} [ν_{as}(U—O)], 810 cm^{-1} [ν_s(U—O)] and 250 cm^{-1} (O—U—O bend). These observations indicate that the UO_2 moiety is virtually linear.[7]

The electronic spectra of the nitrate and iodide complexes show absorption bands at 302, 313, 328 (sh) and 433 nm (sh), while that of the acetate complex show bands at 302 and 313 nm, attributable to charge-transfer transitions.[1]

From the foregoing discussion the complexes can be formulated as $[UO_2(SAAP)_2](NO_3)_2$, $[UO_2(SAAP)_2]I_2$ and $[UO_2(SAAP)_2(OAc)_2]$, indicating a probable coordination number of 6, 6 and 8, respectively, for the U(VI) ion in the complexes.

Thus, in contrast to many earlier reports on hydroxyl coordination in Schiff-base complexes of the uranyl ion, the present one appears unique in that the hydroxyl group is not involved in coordination.

Lanthanide complexes

The complexes are stable and non-hygroscopic solids, insoluble in acetone, alcohol, benzene, chloroform etc.; but soluble in DMF and DMSO.

The IR spectral band assignments for the ligand and complexes are shown in Table 3. The ligand exhibits bands at 3180 cm^{-1} [ν(OH)], 1680 cm^{-1} [ν(C=O)] and 1620 cm^{-1} [ν(C=N)]. In the spectra of the complexes, these appear at 3200, 1615–1625 and 1570–1580 cm^{-1}, respectively, indicating thereby that the ligand functions as a neutral tridentate ligand. This is corroborated by PMR spectra wherein the —OH peak appears at 13.45 δ for the ligand and at 13.50 δ for the Y complex.

In the IR spectra of the Pr and Nd complexes, the band at 1710 cm^{-1} is difficult to account for. The slight increase in —OH frequency in the complexes may be due to an increase in the C—O bond order.[8,9] The complexes exhibit bands at 1375–1380 and 805–810 cm^{-1} which are assigned to ν_3 and ν_2 vibrations of ionic nitrate. The conductivity data of the

Table 3. Important IR bands (cm^{-1}) of lanthanide complexes[a]

Compound	ν(OH) m	ν(C=O) m	ν(C=N) m	$\nu_3(NO_3)$ s	$\nu_2(NO_3)$ s
AAP	3180	1680	1620	—	—
$[Pr(AAP)_2](NO_3)_3$	3200	1580	1580	1380	815
$[Nd(AAP)_2](NO_3)_3$	3220	1580	1580	1380	815
$[Sm(AAP)_2](NO_3)_3$	3200	1570	1570	1375	805
$[Gd(AAP)_2](NO_3)_3$	3220	1580	1580	1380	810
$[Dy(AAP)_2](NO_3)_3$	3220	1580	1580	1380	810
$[Y(AAP)_2](NO_3)_3$	3200	1580	1580	1375	805

[a] m = medium, s = strong.

complexes show them to be 1:3 electrolytes. The complexes can be formulated as $[Ln(AAP)_2](NO_3)_3$.

The electronic absorption spectra of the Pr and Nd complexes show characteristic sharp bands. The assignments are as follows:

Pr complex [wavelength (nm)]:
$3H_4 \rightarrow 3P_2$ (443); $3P_1$ (471), $3P_0$ (482); $^1D_2$ (591).

Nd complex [wavelength (nm)]:
$^4I_{9/2} \rightarrow {}^2G_{9/2}$ (512); $^4G_{7/2}$ (526); $^4G_{5/2}$, $^2G_{7/2}$ (582); $^4S_{3/2}$ (738); $^4F_{7/2}$ (747); $^4F_{5/2}$ (800).

Sinha's[10] covalency parameter (δ) values calculated for these two complexes are +0.30 for the Pr complex, and −0.39 for the Nd complex. This leads to the inference that the Pr complex exhibits a certain degree of covalency.

The analytical data of the complexes are in good agreement for 1:2 stoichiometry. The data also indicate water molecules to be absent, which is also evident from PMR spectrum where no peak attributable to water proton is found. Thus the lanthanide ion can be said to have a coordination number of 6 in these complexes.

REFERENCES

1. V. Rajaram, K. Paulraj and S. K. Ramalingam, *Transition Met. Chem.* 1983, **8**, 335.
2. T. Radhakrishnan, P. T. Joseph and C. P. Prabhakaran, *J. Inorg. Nucl. Chem.* 1976, **38**, 2217.
3. P. K. Radhakrishnan, P. Indrasenan and C. G. R. Nair, *Polyhedron* 1984, **3**, 67.
4. F. A. Cotton and G. Wilkinson, *Advanced Inorganic Chemistry* 3rd Edn, p. 641. Wiley Eastern (1972).
5. C. C. Addison and B. M. Gatehouse, *J. Chem. Soc.* 1960, 613.
6. J. V. Quagliano, J. Fujita, G. Franz, D. S. Phillips, J. Walmsby and S. Y. Tyree, *J. Am. Chem. Soc.* 1961, **83**, 3770.
7. H. Mahanta and K. C. Dash, *J. Inorg. Nucl. Chem.* 1977, **39**, 1345.
8. R. G. Vijay and J. P. Tandon, *J. Inorg. Nucl. Chem.* 1977, **39**, 1242.
9. D. H. Busch and J. C. Bailar Jr., *J. Am. Chem. Soc.* 1956, **78**, 113.
10. S. P. Sinha, *Spectrochim. Acta* 1966, **22**, 57.

Polyhedron Vol. 5, No. 4, pp. 995–998, 1986
Printed in Great Britain

0277–5387/86 $3.00+.00
Pergamon Journals Ltd

COMPLEXES OF LANTHANIDE PERCHLORATES WITH 4-*N*-(2′-HYDROXY-1′-NAPHTHYLIDENE)AMINOANTIPYRINE

P. K. RADHAKRISHNAN

Department of Chemistry, University College, Trivandrum 695034, India

(*Received* 18 *July* 1985; *accepted* 7 *October* 1985)

Abstract—Lanthanide perchlorate complexes with 4-*N*-(2′-hydroxy-1′-naphthylidene) aminoantipyrine [HNAAP(HL)] of types $[Ln(L)_2ClO_4]$ (where Ln = La, Pr, Nd or Sm) and $[Ln(HL)_4](ClO_4)_3$ (where Ln = Gd, Tb, Dy, Ho or Y) have been synthesized and characterized. HNAAP acts as a monovalent terdentate ligand in the complexes of the lighter lanthanides and as a neutral bidentate ligand in the complexes of the heavier lanthanides. The perchlorate group is coordinated only in the complexes of the lighter lanthanides.

As part of our studies on lanthanide complexes of pyrazol-5-one type ligands,[1–5] some complexes of lanthanide perchlorates with 4-*N*-(2′-hydroxy-1′-naphthylidene)aminoantipyrine [HNAAP(HL)] were synthesized and characterized. The present complexes include those of La(III), Pr(III), Nd(III), Sm(III), Gd(III), Tb(III), Dy(III), Ho(III) and Y(III). Of these, the perchlorate group and the phenolic oxygen of the ligand are coordinated to the lighter lanthanides, viz. La(III), Pr(III), Nd(III) and Sm(III).

EXPERIMENTAL

Reagents

The perchlorates of La, Pr, Nd, Sm, Gd, Tb, Dy, Ho and Y were prepared from the respective oxides (99.9% pure) as reported earlier.[1] The ligand, HNAAP, was prepared from 4-aminoantipyrine and 2-hydroxy-1-naphthaldehyde by the method reported earlier.[6]

Preparation and analysis of the complexes

La, Pr, Nd *and* Sm *complexes.* Solutions of the perchlorate of La, Pr, Nd or Sm (0.2 mol) and HNAAP (0.4 mol) in hot dry acetone were mixed and the resulting solution was refluxed on a water bath for 1 h. The precipitated complex was filtered, washed several times with hot acetone and dried *in vacuo* over P_4O_{10}.

Gd, Tb, Dy, Ho *and* Y *complexes.* Solutions of the perchlorate of Gd, Tb, Dy, Ho or Y (0.2 mol) and HNAAP (1.2 mol) in hot dry acetone were mixed and the resulting solution was kept under reflux for about 1 h. The black viscous mass obtained on concentrating the solution was washed several times with hot benzene to remove the excess ligand. The separated complex was recrystallized by dissolving it in the minimum amount of dry acetone and stirring vigorously with dry diethylether. It was dried *in vacuo* over P_4O_{10}.

The complexes were analysed for their metal and perchlorate contents by the conventional methods.[7,8]

Physical methods

The physical methods used in the present investigation were the same as described earlier.[2] The solid state electronic spectra of the complexes were recorded in the range 350–850 nm on a Shimadzu UV-200S spectrophotometer by reflectance technique using MgO as the reference material.

RESULTS AND DISCUSSION

All the complexes are non-hygroscopic solids. The complexes of La, Pr, Nd and Sm are insoluble in almost all the common solvents. However, the complexes of Gd, Tb, Dy, Ho and Y are soluble in acetone, acetonitrile, methanol, ethanol and nitrobenzene, and insoluble in benzene, carbon tetrachloride and chloroform. The molar-conductance

values of the complexes of Gd, Tb, Dy, Ho and Y in nitrobenzene (Table 1) indicate 1:3 electrolytic behaviour.[9] Thus the complexes may be formulated (Table 1) as $[Ln(L)_2ClO_4]$ (where Ln = La, Pr, Nd or Sm) and $[Ln(HL)_4](ClO_4)_3$ (where Ln = Gd, Tb, Dy, Ho or Y).

The IR spectra (Table 2) of the complexes of La, Pr, Nd and Sm indicate that HNAAP bind the metal through carbonyl oxygen, azomethine nitrogen and phenolic oxygen (deprotonated): the ν(C=O) and ν(C=N) bands of the complexes are considerably lower than the corresponding ones (around 1635 and 1590 cm^{-1}, respectively) of the free ligand, and the ν(O—H) band of HNAAP (around 3440 cm^{-1}) is absent and the ν_a(C—O) band of HNAAP (around 1310 cm^{-1}) is shifted to higher frequency in the complexes.[10,11] However, in the complexes of Gd, Tb, Dy, Ho and Y, HNAAP is coordinated through the carbonyl oxygen and azomethine nitrogen: the ν(C=O) and ν(C=N) bands are shifted to lower frequency and the ν(O—H) and ν_a(C—O) bands are not appreciably shifted.[10,11] The IR spectra (Table 2) also show the presence of a unidentate perchlorate group in the complexes of La, Pr, Nd and Sm, and an ionic perchlorate group in the complexes of Gd, Tb, Dy, Ho and Y in accordance with the literature.[12]

The electronic spectra of the complexes show that most of the *f–f* bands of the lanthanide ions are obscured in these complexes by the very strong ligand to metal charge-transfer band. However, in the Pr and Nd complexes the following *f–f* bands are observed, the tentative assignments of which are given in brackets:

Pr complex:
16.84 kK ($^3H_4 \rightarrow {}^1D_2$);

Nd complex:
18.94 kK ($^4I_{9/2} \rightarrow {}^4G_{7/2}$); 17.07 kK ($^4I_{9/2} \rightarrow {}^4G_{5/2}, {}^2G_{7/2}$); 14.66 kK ($^4I_{9/2} \rightarrow {}^4F_{9/2}$); 13.41 kK ($^4I_{9/2} \rightarrow {}^4F_{7/2}$); 12.47 kK ($^4I_{9/2} \rightarrow {}^2H_{9/2}$).

An appreciable red shift is observed in these *f–f* bands compared to the position in the aquo ion.[13,14] The Sinha covalency parameters[14] calculated for these two complexes ($\delta = 1.194$ for the Pr complex and 1.133 for the Nd complex) indicate a reasonable covalency for the lanthanide–ligand bond. Further, from the shape of the hypersensitive $^4I_{9/2} \rightarrow {}^4G_{5/2}, {}^2G_{7/2}$ transition of Nd(III), a coordination number of 7[15,16] may be assigned to the complex $[Nd(L)_2ClO_4]$.

The magnetic data (Table 1) indicate that all the complexes, except those of La and Y, are paramagnetic as expected. The observed magnetic moments agree closely with the Van Vleck values[17] in all these complexes which shows that the 4*f* electrons do not participate in bonding.

The thermogravimetric (TG) analysis of the complexes (Table 1) shows that the complexes of La, Pr, Nd and Sm are more stable (up to ~300°C) than the complexes of Gd, Tb, Dy, Ho and Y (up to ~240°C). The La and Pr complexes undergo decomposition in two stages as denoted by the DTG peaks around 350 and 460°C. The Nd and Sm complexes undergo a three-stage decomposition as shown by the DTG peaks around 350, 400 and 480°C. The complexes of Gd, Tb, Dy, Ho and Y undergo decomposition in three stages as represented by the DTG peaks around 295–320, 415–445 and 490–505°C. The decomposition of all the complexes is complete in the range 520–580°C and the respective stable rare-earth oxides are formed.

Table 1. Analytical, conductance and magnetic moment data of lanthanide perchlorate complexes of HNAAP

Complex	Decomposition temperature from TG (°C)	Metal (%)		Perchlorate (%)		Molar conductance[a] (Ω^{-1} cm^2 mol^{-1})	μ_{eff} (BM)
		Found	Calc.	Found	Calc.		
(1) $[La(L)_2ClO_4]$	320	14.7	14.6	10.5	10.5	Insoluble	—
(2) $[Pr(L)_2ClO_4]$	300	14.6	14.8	10.1	10.4	Insoluble	3.58
(3) $[Nd(L)_2ClO_4]$	300	15.2	15.1	10.8	10.4	Insoluble	3.64
(4) $[Sm(L)_2ClO_4]$	300	15.3	15.6	10.3	10.3	Insoluble	1.68
(5) $[Gd(HL)_4](ClO_4)_3$	240	8.2	8.3	16.0	15.8	62.32	7.72
(6) $[Tb(HL)_4](ClO_4)_3$	240	8.3	8.4	15.7	15.8	63.15	9.45
(7) $[Dy(HL)_4](ClO_4)_3$	240	8.4	8.6	15.6	15.8	62.95	10.40
(8) $[Ho(HL)_4](ClO_4)_3$	220	8.7	8.7	15.6	15.8	62.43	10.34
(9) $[Y(HL)_4](ClO_4)_3$	240	5.0	4.9	16.7	16.4	66.09	—

[a] 10^{-3} M solution in nitrobenzene used. HL = HNAAP.

Table 2. Important IR absorptions (cm^{-1}) of lanthanide perchlorate complexes of HNAAP[a]

Compound	ν(O—H)	ν(C=O)	ν(C=N)	ν_a(C—O)	$\nu_4+\nu_1(ClO_4)$ coordinated / $\nu_3(ClO_4)$ ionic	$\nu_2(ClO_4)$ coordinated / $\nu_1(ClO_4)$ ionic	$\nu_5+\nu_3(ClO_4)$ coordinated / $\nu_4(ClO_4)$ ionic
(1) $[La(L)_2ClO_4]$	—	1615 vs	1545 vs	1325 s	1095 vs 1075 vs	915 w	630 m 620 m
(2) $[Pr(L)_2ClO_4]$	—	1615 vs	1545 vs	1325 s	1095 vs 1080 vs	915 w	630 m 620 m
(3) $[Nd(L)_2ClO_4]$	—	1615 vs	1545 vs	1325 s	1095 vs 1080 vs	915 w	630 m 620 m
(4) $[Sm(L)_4ClO_4]$	—	1615 vs	1545 vs	1325 s	1090 vs 1070 vs	915 w	630 m 620 m
(5) $[Gd(HL)_4](ClO_4)_3$	3450 m, br	1605 vs	1575 vs	1315 s	1090 vs	925 w	620 m
(6) $[Tb(HL)_4](ClO_4)_3$	3440 m, br	1610 vs	1575 vs	1315 s	1090 vs	925 w	620 m
(7) $[Dy(HL)_4](ClO_4)_3$	3440 m, br	1610 vs	1575 vs	1315 s	1090 vs	930 w	620 m
(8) $[Ho(HL)_4](ClO_4)_3$	3440 m, br	1610 vs	1570 vs	1315 s	1090 vs	925 w	620 m
(9) $[Y(HL)_4](ClO_4)_3$	3440 m, br	1615 vs	1575 vs	1315 s	1090 vs	930 w	620 m

[a] HL = HNAAP; br = broad; m = medium; w = weak; s = strong; vs = very strong.

Acknowledgements—I wish to express my sincere thanks to Prof. C. G. R. Nair, Prof. C. P. Prabhakaran and Dr P. Indrasenan for helpful discussions, and to Prof. C. P. Joshua for providing facilities in the Department of Chemistry, University of Kerala, Trivandrum.

REFERENCES

1. C. G. R. Nair and P. K. Radhakrishnan, *Proc. Indian Acad. Sci. (Chem. Sci.)* 1981, **90**, 541.
2. P. K. Radhakrishnan, P. Indrasenan and C. G. R. Nair, *Polyhedron* 1984, **3**, 67.
3. P. K. Radhakrishnan and C. G. R. Nair, *Indian J. Chem.* 1984, **23A**, 569.
4. P. K. Radhakrishnan, *J. Indian Chem. Soc.* 1984, **61**, 838.
5. P. K. Radhakrishnan, *J. Less Common Met.* 1985, **107**, 45.
6. T. Radhakrishnan, P. T. Joseph and C. P. Prabhakaran, *J. Inorg. Nucl. Chem.* 1976, **38**, 2217.
7. I. M. Kolthoff and P. J. Elving (Eds), *Treatise on Analytical Chemistry*, Vol. 8, Part II. Interscience, New York (1963).
8. E. Kurz, G. Kober and M. Berl, *Anal. Chem.* 1958, **30**, 1983.
9. W. J. Geary, *Coord. Chem. Rev.* 1971, **7**, 81.
10. L. Doretti, S. Sitran, F. Madalosso, G. Bandoli and G. Paolucci, *J. Inorg. Nucl. Chem.* 1980, **42**, 1060.
11. J. Chacko, C. P. Prabhakaran and C. G. R. Nair, *Indian J. Chem.* 1975, **13**, 411.
12. B. J. Hathaway and A. E. Underhill, *J. Chem. Soc.* 1961, 3091.
13. S. P. Sinha, *J. Inorg. Nucl. Chem.* 1965, **27**, 115.
14. S. P. Sinha, *Spectrochim. Acta* 1966, **22**, 57.
15. D. G. Karraker, *Inorg. Chem.* 1967, **6**, 1863.
16. D. G. Karraker, *Inorg. Chem.* 1968, **7**, 473.
17. J. H. Van Vleck and N. Frank, *Phys. Rev.* 1929, **34**, 1494.

Polyhedron Vol. 5, No. 4, pp. 999–1005, 1986
Printed in Great Britain

0277–5387/86 $3.00+.00
Pergamon Journals Ltd

SYNTHESIS AND STRUCTURAL INVESTIGATIONS OF SOME ALKYLAMINE PENTACYANOFERRATE(II) COMPLEXES

D. V. PARWATE and A. N. GARG*

Department of Chemistry, Nagpur University, Nagpur 440 010, India

(*Received* 25 *April* 1985; *accepted after revision* 9 *October* 1985)

Abstract—A series of alkylamine pentacyanoferrate(II) complexes, $Na_3[Fe(CN)_5L]\cdot(H_2O)_x$, where L = $(CH_3)_2NH$, $(C_2H_5)_2NH$, $(C_3H_7)_2NH$, $(C_4H_9)_2NH$, $(C_6H_5)_2NH$, $(C_2H_5)_3N$, $(C_4H_9)_3N$ or $C_6H_{11}NH_2$, were synthesized and characterized by analysis, magnetic, IR and Mössbauer spectroscopic studies. Characteristic C≡N and Fe—C≡N vibrational frequencies were found to be affected by the nature of the substituent. Mössbauer spectra exhibited a two-line quadrupole doublet with isomer shifts (δ) −0.04 to 0.49 mm s^{-1} (relative to sodium nitroprusside) and quadrupole splitting (ΔE_Q) of 0.73–1.92 mm s^{-1}. A correlation of δ vs ΔE_Q has been attempted and the sign of the electric field gradient predicted. Bonding characteristics seem to change from simple mono- and dialkylamines to bulky di- and trialkylamines in pentacyanoferrate(II) complexes.

Pentacyanoferrate(II) complexes, $[Fe(CN)_5L]^{3-}$, have long been known.[1,2] Recently, several workers have reported the synthesis and structural investigations of such complexes with various substituents (L), such as H_2O, NH_3, CO, NO_2^-, SO_3^{2-}, Py, NO^+, $P(C_6H_5)_3$, POX_3, DMSO, pyrazine, $N_2H_5^+$, N_2, enH^+, RNH_2 etc.[3–18] In most of these complexes, bonding characteristics were investigated with regard to the σ-donor and π-acceptor nature of the ligands.[4–18] The Mössbauer spectrum of $Na_3[Fe(CN)_5NH_3]\cdot H_2O$ was first reported in 1963 by Fluck *et al.*[4] NMR studies have also been carried out on the nature and bonding in pentacyanoferrate(II) complexes.[19,20] Recently, some unusual pentacyanoferrate complexes were reported and metal–ligand charge transfer band positions were correlated with isomer shift (δ) and quadrupole splitting (ΔE_Q) values.[21,22] Rasmussen and Meyers[23] have studied pyrazine-substituted complexes and shown the sensitivity of ΔE_Q to lowered symmetry to be similar to the case of pyrrolidine-substituted complexes.[24] We have synthesized some new pentacyanoferrates(II), $Na_3[Fe(CN)_5L]\cdot(H_2O)_x$, where L = $(CH_3)_2NH$, $(C_2H_5)_2NH$, $(C_3H_7)_2NH$, $(C_4H_9)_2NH$, $(C_6H_5)_2NH$, $(C_2H_5)_3N$, $(C_4H_9)_3N$ or $C_6H_{11}NH_2$, and studied their magnetic, and IR and Mössbauer spectroscopic behaviour. An attempt has also been made to correlate the spectroscopic data with the bonding characteristics of the ligand L *vis-à-vis* CN ligands. The sign of the electric field gradient (EFG) is also predicted from the δ vs ΔE_Q correlation plot.

EXPERIMENTAL

All reagents used were AnalaR (BDH), GR (S. Merck) or of high-purity grade (Koch-Light, U.K., and Fluka, Switzerland) except for the 40% solution of dimethylamine. Solvents were distilled and dried before use. The complexes were prepared following the procedures described in the literature.[2,3,25]

Preparation of the complexes

A solution containing 3 g sodium nitroprusside (SNP) (1 mol) and 2 g sodium acetate was cooled and mixed with an ice-cold solution of the respective amine (20–25 cm^3) in ethanol. The solution was continuously stirred and additional amounts of amine were added until a negative test for nitroprusside was obtained. The mixture was kept in a freezing mixture for varying times (a few hours to a day) during which the complex separated out:

$$Na_2[Fe(CN)_5NO] + CH_3COONa + \text{amine (L)} \rightarrow Na_3[Fe(CN)_5L] + CH_3COOH.$$

* Author to whom correspondence should be addressed.

Complete precipitation of the compound was effected by the addition of cold absolute ethanol. The complexes were filtered and dried *in vacuo* over fused $CaCl_2$. Since the complexes are unstable on prolonged standing, all the measurements were carried out within a week.

The complexes were characterized by C, H and N analysis using a Coleman Analyzer at USIC, Nagpur. The Fe content was estimated by first decomposing the complex and then measuring spectrophotometrically using 1,10-phenanthroline reagent.[26]

Physical measurements

The Mössbauer spectra were recorded at room temperature on a transducer-driven Mössbauer spectrometer (ECIL, Hyderabad) in constant-velocity mode. An ~5 mCi $^{57}Co(Rh)$ source (Amersham International, U.K.) was used. The spectrometer was calibrated using natural iron foil (25 μm).[27] SNP was used as a standard and all the δ values are reported with respect to (wrt) SNP. Spectral lines were assumed to have a Lorentzian line shape.

IR spectra were recorded on a SPECORD 75 IR spectrophotometer in the range 4000–400 cm^{-1} using a Nujol medium. Magnetic moments were calculated using the Gouy balance method and $Hg[Co(SCN)_4]$ as a standard at room temperature.

RESULTS

The complexes are coloured and obtained in low yields. The analytical data of C, H, N and Fe for all the complexes (Table 1) agree well with the proposed molecular formula. Table 2 gives the characteristic IR frequencies. These assignments were made on the basis of the literature where similar types of complexes have been studied.[11,14,28] All of the complexes exhibit a well-resolved quadrupole doublet. Typical Mössbauer spectra of diethyl and dibutylamine substituted complexes are shown in Fig. 1. The Mössbauer parameters δ and ΔE_Q along with linewidths are given in Table 3. Partial isomer shift (pis) and partial quadrupole splitting (pqs) values for the new ligands were calculated on the basis of the point charge formalism, assuming an additivity concept[29] and substituting pis = 0.01 and pqs = −0.84 mm s^{-1} for the CN^- ligands.[8] These are also given in Table 3, along with magnetic moments calculated from magnetic susceptibility measurements.

DISCUSSION

If one of the CN^- ligands in hexacyanoferrate(II), $[Fe(CN)_6]^{4-}$, is substituted by a neutral ligand L to give $[Fe(CN)_5L]^{3-}$, the octahedral geometry remains unaffected but the symmetry is lowered from O_h to approximately C_{4v}. MO calculations of the

Table 1. Analytical characterization of some alkylamine-substituted pentacyanoferrate(II) complexes, $Na_3[Fe(CN)_5L]\cdot(H_2O)_x$

Complex	Colour	Solubility in water (alcohol)[a]	% C (calc.)	% H (calc.)	% N (calc.)	% Fe (calc.)
$Na_3[Fe(CN)_5\{(CH_3)_2NH\}]\cdot(H_2O)_2$	Greenish yellow	Sol. (Sp. sol.)	24.6 (25.0)	3.7 (3.3)	24.7 (25.0)	16.2 (16.6)
$Na_3[Fe(CN)_5\{(C_2H_5)_2NH\}]\cdot(H_2O)_2$	Steel gray	Sol. (Insol.)	28.5 (29.6)	4.3 (4.1)	24.4 (23.1)	14.9 (15.3)
$Na_3[Fe(CN)_5\{(C_2H_5)_3N\}]\cdot(H_2O)_2$	Middle buff	Sol. (Sp. sol.)	34.9 (33.7)	4.6 (4.8)	20.9 (21.4)	14.1 (14.2)
$Na_3[Fe(CN)_5\{(C_3H_7)_2NH\}]\cdot(H_2O)_3$	Pale cream	Sol. (Sp. sol.)	31.6 (32.1)	4.9 (5.6)	19.0 (20.4)	13.8 (13.9)
$Na_3[Fe(CN)_5\{(C_4H_9)_2NH\}]\cdot H_2O$	Portland gray	Sol. (Sp. sol.)	39.5 (38.8)	5.1 (5.2)	20.8 (20.9)	13.7 (13.9)
$Na_3[Fe(CN)_5\{(C_4H_9)_3N\}]\cdot(H_2O)_2$	Pale rose	Sol. (Insol.)	43.6 (42.9)	6.2 (6.5)	16.3 (17.6)	11.2 (11.7)
$Na_3[Fe(CN)_5\{(C_6H_5)_2NH\}]\cdot H_2O$	Pale rose	Sol. (Insol.)	47.1 (46.5)	2.8 (2.9)	18.9 (19.0)	12.7 (12.6)
$Na_3[Fe(CN)_5\{(C_6H_{11}NH_2\}]$	Yellow	Sp. sol. (Insol.)	34.0 (33.9)	4.2 (4.4)	19.8 (21.5)	13.8 (14.3)

[a] Sol., soluble; Sp. sol., sparingly soluble; Insol., insoluble.

Table 2. Characteristic IR frequencies for some alkylamine-substituted pentacyanoferrate(II) complexes[a]

Substituent (L)	ν(CN) (cm^{-1})	ν(Fe—C) (cm^{-1})	ν(O—H) (cm^{-1})	δ(H—O—H) (cm^{-1})	δ(Fe—C≡N) (cm^{-1})
$(CH_3)_2NH$	2180w 2050b 2020m	490sh	3450b	1600m,b	550w
$(C_2H_5)_2NH$	2180w 2150w 2130m 2030s	480vw	3520b	1600m	550b
$(C_2H_5)_3N$	2180w 2150w 2140s 2050w	490vw	3550b	1600m	640m
$(C_3H_7)_2NH$	2070m 2050m 2010s	460vw	3400b	1610s	570m
$(C_4H_9)_2NH$	2180w 2155w 2140m	480vw	3450b	1600m	640w
$(C_4H_9)_2N$	2180w 2160w 2140s	490w	3500b	1600s	650m
$(C_6H_5)_2NH$	2170w 2150w 2130m	490w	3420b	1600m	640w
$C_6H_{11}NH_2$	2130w 2050w 2010m	480sh	3400b	1590m,b	550b

[a] s, strong; m, medium; w, weak; vw, very weak; sh, shoulder; b, broad.

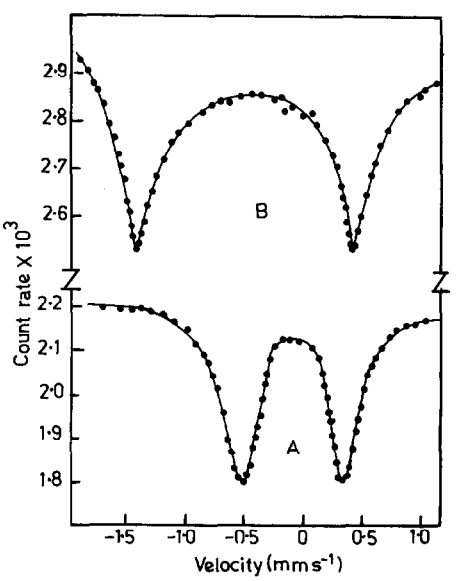


Fig. 1. Mössbauer spectra of diethylamine (A) and dibutylamine (B) pentacyanoferrate(II) complexes.

nitroprusside anion, $[Fe(CN)_5NO]^{2-}$, have shown that a tetragonal distortion along the axial ligand causes further splitting of t_{2g}-obitals into d_{yz}, d_{zx} and d_{xy} (also called e and b_2).[30] The X-ray crystal structure[31] of sodium nitroprusside shows that the ligands NO and *trans* CN^- are approximately collinear with the central Fe atom slightly displaced in the direction of the NO group from the plane of four pseudo-equivalent CN groups. Braga *et al.*[15] have performed multiple scattering calculations for the isoelectronic iron(II) pentacyanides $[Fe(CN)_5NO]^{2-}$, $[Fe(CN)_5CO]^{3-}$ and $[Fe(CN)_5N_2]^{3-}$, and calculated covalency effects due to 3*d* and 4*p* populations (π-back donation and σ-donation, respectively), electron densities and the EFG at the iron nucleus, which were experimentally verified. In the present study the $[Fe(CN)_5L]^{3-}$ complexes are assumed to be similar to the nitroprusside except that L is a σ-bonding ligand without any possibility of $d_\pi \rightarrow p_\pi$ back donation.

Table 3. Mössbauer parameters and magnetic-moment data for some alkylamine-substituted pentacyanoferrate(II) complexes, $Na_3[Fe(CN)_5L]\cdot(H_2O)_x$

L	δ^a (mm s^{-1})	ΔE_Q (mm s^{-1})	Linewidths (Γ_1, Γ_2) (mm s^{-1})	pis (mm s^{-1})	pqs (mm s^{-1})	Sign of EFG	Magnetic moment (BM)
$(CH_3)_2NH$	0.49±0.03	0.73±0.03	0.22, 0.28	0.28	−0.48	−ve	1.30
$(C_2H_5)_2NH$	0.40±0.03	0.86±0.02	0.32, 0.27	0.19	−0.41	−ve	1.15
$(C_2H_5)_3N$	0.03±0.04	1.77±0.03	0.27, 0.29	−0.18	0.05	+ve	1.01
$(C_3H_7)_2NH$	0.35±0.03	0.85±0.04	0.35, 0.31	0.14	−0.42	−ve	0.96
$(C_4H_9)_2NH$	−0.04±0.04	1.82±0.03	0.35, 0.31	−0.25	0.07	+ve	1.25
$(C_4H_9)_3N$	0.05±0.03	1.92±0.04	0.28, 0.34	−0.16	0.12	+ve	0.85
$(C_6H_5)_2NH$	0.02±0.03	1.75±0.03	0.33, 0.27	−0.19	0.04	+ve	1.28
$C_6H_{11}NH_2$	0.48±0.03	0.82±0.04	0.38, 0.36	0.27	−0.43	−ve	1.06

[a] Wrt SNP.

There seems to be a minor change, depending on the nature of the sixth ligand L. Therefore, an asymmetry (or EFG at the Fe nucleus) is generated in all the complexes, primarily due to the ligand contribution with the possibility of a small contribution from asymmetric expansion of the e and b_2 electrons. We have observed small magnetic moments, 0.85–1.30 BM, which may be due to a contribution from the orbital motion of electrons or ligands.

IR spectra

Various vibrational modes were assigned by comparison with those of other monosubstituted pentacyanoferrate(II) complexes[11,14,18] and other literature references.[28,32] At least three ν(CN) stretching modes were observed in the range 2180–2010 cm^{-1} in accordance with the group theoretical prediction (i.e. A_1+E) assuming a C_{4v} point group for the $[Fe(CN)_5L]^{3-}$ moiety. Another very important characteristic mode is due to Fe—C≡N bending, δ(Fe—CN) being observed in the range 550–650 cm^{-1}. A very weak band, observed at ~480 cm^{-1}, has been assigned to ν(Fe—C) stretching vibrations in accordance with the assignments of Fluck *et al.*[14] The stretching mode of Fe—N could not be assigned as this is expected to be observed at ~250 cm^{-1}.

Intense broad peaks in the region 3600–3400 cm^{-1} arose mainly due to weakly bonded water molecules in the lattice. The exact assignments of various bands in this region is not possible, due to several overtones and combinations of bending vibrations. Similarly a sharp to medium intensity band at ~1600 cm^{-1} has been assigned to a bending mode of H_2O molecules occupying interstitial positions.

An interesting feature of the characteristic ν(CN) and δ(Fe—CN) vibrational frequencies is that these could be divided into two well-defined groups, one observed at ~2020 and 550 cm^{-1} for $(CH_3)_2NH$-, $(C_2H_5)_2NH$-, $(C_3H_7)_2NH$- and $C_6H_{11}NH_2$-substituted complexes, and another at ~2140 and 650 cm^{-1} for $(C_2H_5)_3N$-, $(C_4H_9)_2NH$-, $(C_4H_9)_3N$- and $(C_6H_5)_2NH$-substituted complexes. This shifting by ~100 cm^{-1} in both cases may be indicative of a difference in the bonding of the alkylamine group with $[Fe(CN)_5]^{3-}$, dividing them into two groups, group 1 and group 2, respectively. It may be noted that the Fe—C stretching frequencies remain totally unaffected by the substitution. Perhaps the Fe—N stretching frequencies could have correlated well and given some insight about any possible change in bonding characteristics but were not available to us. Earlier, also, several workers[17,18] have correlated the variation in the CN stretching frequency with the nature of the sixth ligand and the change in its bonding characteristics.

Mössbauer parameters

The EFG (V_{zz}) may be represented by:

$$V_{zz} = (1-\gamma_\infty)(V_{zz})_L + (1-R)[(V_{zz})_{CF} + (V_{zz})_{MO}],$$

where $(V_{zz})_{CF}$, the contribution of the aspherical population of the d-orbitals due to crystal field splitting, will be zero for the Fe(II) low-spin (t_{2g}^6) configuration. Thus, any observed ΔE_Q in such compounds is due to $(V_{zz})_L$ and the aspherical electron distribution in the valence molecular orbitals $(V_{zz})_{MO}$. The latter may arise due to anisotropic bond properties,[33] as in the case of $[Fe(CN)_5L]^{3-}$. Here the metal-to-ligand bond is influenced by both a σ- and a π-interaction, and their

relative strengths compared with CN^-. If L is a stronger σ-donor than CN^-, $N(d_{z^2}) > N(d_{x^2-y^2})$ (where N represents the electron population in respective d-orbitals) and a negative contribution to $(V_{zz})_{MO}$ may result along M—L. However, if L is a more effective π-acceptor than CN^-, $N(d_{xy}) > [N(d_{xz}) + N(d_{yz})]/2$, because of a more pronounced charge delocalization from M → L (i.e. $d_\pi \rightarrow p_\pi$) and a positive contribution to $(V_{zz})_{MO}$ is expected. The net effect is to make $(V_{zz})_{MO}$ more negative with increasing $(\sigma - \pi)$.

All the complexes exhibit a well-resolved quadrupole doublet with $\delta = -0.04$ to 0.44 mm s^{-1} (wrt SNP) and $\Delta E_Q = 0.73$–1.92 mm s^{-1}. The δ values are characteristic of low-spin Fe(II) in an octahedral geometry[8,32] and a decrease in the order

$$(CH_3)_2NH > (C_2H_5)_2NH > (C_3H_7)_2NH > (C_6H_5)_2NH > (C_4H_9)_2NH$$

for the dialkylamine-substituted complexes. For the two trialkylamine-substituted complexes studied here, δ values are very low, and for the cyclohexylamine-substituted complex it is almost equal to that for the dialkylamine-substituted complexes. It is known that, on further substitution with bulky alkyl groups in NH_3, its basic character changes (due to hyperconjugation as in trialkylamine), resulting in an increase in electron density and hence decreasing δ values. For mono-, di- and tributylamine-substituted complexes, δ values were found to be 0.28, −0.04 and 0.05 mm s^{-1} (wrt SNP), which supports the assumption that the basic character of amines may affect the σ-donor property of the amine ligands. A cursory look at the δ values in Table 3 also divides the ligands into two groups. Group 1, consisting of $(CH_3)_2NH$-, $(C_2H_5)_2NH$-, $(C_3H_7)_2NH$- and $C_6H_{11}NH_2$-substituted complexes, has higher δ values; and group 2, consisting of $(C_2H_5)_3N$-, $(C_4H_9)_2NH$-, $(C_4H_9)_3N$- and $(C_6H_5)_2NH$-substituted complexes, has lower δ values.

As already described, a strong asymmetry is generated due to the presence of the odd ligand L, resulting in an observable ΔE_Q. Earlier it had been observed in a study of several amine- and monoalkylamine-substituted complexes that ΔE_Q was ~0.80 mm s^{-1}, which is insignificantly affected by alkyl group substitution.[10–17] For the cyclohexylamine-substituted complex, $\Delta E_Q = 0.82 \pm 0.04$ mm s^{-1}. It was expected that, with a flip-flop process (i.e. chair–boat) in the C_6H_{11} group, the distortion would be larger, but that did not seem to happen. It seems that with monalkylamines, irrespective of the nature of the alkyl group, the observed $\Delta E_Q \leqslant 1.0$ mm s^{-1}. In the present study of several di- and trialkylamine (with bulky alkyl groups) substituted complexes, a wide range of ΔE_Q values (0.73–1.92 mm s^{-1}) has been observed. For dialkylamine-substituted complexes, ΔE_Q values increase in the order

$$(CH_3)_2NH < (C_2H_5)_2NH \sim (C_3H_7)_2NH < (C_6H_5)_2NH < (C_4H_9)_2NH.$$

For the dimethylamine-substituted complex, our ΔE_Q value is comparable to that observed by Monaghan and Fanning.[10] The increase in ΔE_Q values, though not very regular, suggests increasing distortion in geometry with substitution of heavier alkyl groups. The two trialkylamine [viz. $(C_2H_5)_3N$ and $(C_4H_9)_3N$] substituted complexes exhibited ΔE_Q values of 1.77 and 1.92 mm s^{-1}, respectively, indicating the largest distortions. Again, the observed ΔE_Q values clearly divide the ligands into two well-defined groups. For group 1 ligands, ΔE_Q is ~0.80 mm s^{-1}, and for group 2 ligands it is ~1.80 mm s^{-1}, which is even higher than that observed for SNP, where strong π-bonding has been suggested. It is further noticed that group 1 ligand complexes exhibit higher δ and low ΔE_Q values while group 2 complexes yield lower δ and high ΔE_Q values.[34] Therefore, it may be quite possible that some sort of change in bonding characteristics may take place from group 1 to group 2 ligands, which may be responsible for more than doubling the ΔE_Q values. It is observed that the distinct ranges of δ and ΔE_Q values for groups 1 and 2, correlating well with C≡N stretching and Fe—C≡N bending vibrational frequencies, may be due to distinct differences between the bonding characteristics of groups 1 and 2. A plausible way of looking at this is that the bonding characteristics of the CN ligands *trans* to alkylamine L may be affected by substitution with heavier alkyl groups. According to Ballhausen and Gray,[35] in all tetragonally distorted complexes of MX_5L type almost all the π-bonding is axially directed and planar π-orbitals remain non-bonded. It is quite possible that d_π-orbitals (d_{yz} and d_{zx}) may be pushed by the bulky alkyl groups, as a result of which the Fe atom may become slightly displaced away from the plane containing the four CN^- towards the axial CN^-, *trans* to L, and the π-bonding character may increase. If π-back donation in *trans* CN is increased with the substitution of a heavier alkyl group then either ν(CN) or δ(Fe—CN) is likely to increase in accordance with our observation. This is similar to increased π-bonding character towards the NO ligand in SNP, where lifting of Fe by 0.183 Å has been confirmed.[31] This slight push of the Fe atom out of the plane can explain the large ΔE_Q values for group 2 ligands quite well.

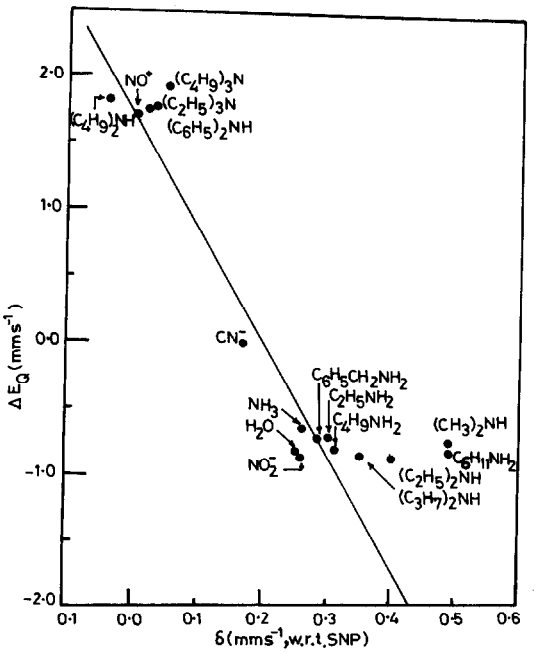


Fig. 2. Correlation of isomer shift (δ) vs quadrupole splitting (ΔE_Q) values in some monosubstituted pentacyanoferrate(II) complexes,

$$Na^+[Fe(CN)_5L^{n-}]^{-3\pm n}\cdot(H_2O)_x.$$

Correlation of δ and ΔE_Q

Such correlations have been extensively used for elucidating structure and bonding characteristics,[8] the sign of the EFG[36,37] and qualitatively separating σ-donor and π-acceptor characteristics.[38] According to this correlation, the sign of the EFG for some isostructural compounds could be predicted provided we know it for some other similar compounds by independent experimental methods.[39] A plot of δ vs ΔE_Q for

$$Na^+[Fe(II)(CN)_5L^n]^{-3+n}\cdot(H_2O)_x,$$

where L = NO^+-, CO-, H_2O-, NH_3-, NO_2^-- or SO_3^{2-}-substituted mono-, di- and trialkylamines, is shown in Fig. 2. It is observed that a linear correlation is obtained only if a positive sign for the EFG is assumed for $(C_2H_5)_3N$-, $(C_4H_9)_2NH$-, $(C_4H_9)_3N$- and $(C_6H_5)_2NH$-, and a negative sign for $(CH_3)_2NH$-, $(C_2H_5)_2NH$-, $(C_3H_7)_2NH$- and $C_6H_{11}NH_2$-substituted complexes. Also, these predictions are in agreement with those obtained from pis and pqs values, which are also indicative of the relative importance of σ- and π-bonding characteristics.[8,34] However, the sign of the EFG needs to be experimentally verified by a crystal orientation or a magnetic perturbation method.

Acknowledgements—Financial assistance from the CSIR, New Delhi, is gratefully acknowledged. We thank Prof. K. N. Munshi, Head of the Chemistry Department for encouragement.

REFERENCES

1. W. Manchot and P. Woringer, *Ber. Dtsch. Chem. Ges.* 1913, **46**, 3514.
2. H. F. Williams, *Cyanogen Compounds: Their Chemistry, Detection and Estimation*, 2nd Edn, p. 254. Edward Arnold, New York (1948).
3. G. Brauer (Ed.), *Handbook of Preparative Inorganic Chemistry*, Vol. 2, p. 1513. Academic Press, New York (1965).
4. E. Fluck, W. Kerler and W. Neuwirth, *Angew. Chem., Int. Ed. Engl.* 1963, **2**, 277; *Z. Phys.* 1963, **175**, 200.
5. E. Fluck, *Adv. Inorg. Chem. Radiochem.* 1964, **6**, 433.
6. E. Fluck and P. Kuhn, *Z. Anorg. Allg. Chem.* 1967, **350**, 263.
7. B. M. Chadwick and A. G. Sharpe, *Adv. Inorg. Chem. Radiochem.* 1966, **8**, 84.
8. G. M. Bancroft, *Mössbauer Spectroscopy: An Introduction for Inorganic Chemists and Geochemists*, p. 94. McGraw-Hill, London (1973).
9. H. E. Toma, E. Giesbrecht, J. M. Malin and E. Fluck, *Inorg. Chim. Acta* 1975, **14**, 11.
10. C. P. Monaghan and J. C. Fanning, *J. Phys. Chem.* 1978, **82**, 1045.
11. J. A. Olabe and P. J. Aymonino, *J. Inorg. Nucl. Chem.* 1974, **36**, 1221; *ibid.* 1976, **38**, 225.
12. P. J. Aymonino, M. A. Blessa, J. A. Olabe and E. Frank, *Z. Naturforsch.* 1976, **31B**, 1532.
13. S. Alonso, C. O. Dell Vedova, N. E. Katz, M. A. Martinez and P. J. Aymonino, *J. Inorg. Nucl. Chem.* 1978, **40**, 2074.
14. E. Fluck, H. Inoue, M. Nagao and S. Yanagisawa, *J. Inorg. Nucl. Chem.* 1979, **41**, 287.
15. M. Braga, A. C. Pavao and J. R. Leite, *Phys. Rev. B* 1981, **23**, 4328.
16. A. N. Garg and P. N. Shukla, *Z. Naturforsch.* 1981, **36B**, 59.
17. A. S. Brar and S. K. Mazumdar, *Radiochem. Radioanal. Lett.* 1981, **48**, 329; *Solid State Commun.* 1983, **45**, 981.
18. H. Inoue, M. Sasagawa, E. Fluck and T. Shirai, *Bull. Chem. Soc. Jpn* 1983, **56**, 3434.
19. H. E. Toma and J. A. Vanin, *Inorg. Chim. Acta* 1979, **33**, L157.
20. B. N. Narayanan and P. T. Manoharan, *J. Inorg. Nucl. Chem.* 1978, **40**, 1993.
21. C. R. Johnson and R. E. Shepherd, *Inorg. Chem.* 1983, **22**, 3503.
22. K. J. Moore, L. Lee and J. D. Patterson, *Inorg. Chem.* 1983, **22**, 1244.
23. P. G. Rasmussen and E. A. Meyers, *Polyhedron* 1984, **3**, 183.
24. V. Weihofen, *Z. Naturforsch.* 1972, **27B**, 565.
25. D. J. Kenney, T. P. Flymn and J. B. Gallini, *J. Inorg. Nucl. Chem.* 1961, **20**, 75.
26. A. I. Vogel, *A Text Book of Quantitative Inorganic Analysis*, p. 742. Longman, London (1978).

27. D. V. Parwate, Ph.D. Thesis, *Mössbauer Spectroscopic Studies of Iron Complexes*. Nagpur University, Nagpur, India (1984).
28. K. Nakamoto, *Infrared Spectra of Inorganic and Coordination Compounds*, p. 180. Wiley Interscience, New York (1963).
29. G. M. Bancroft, M. J. Mays and B. E. Prater, *Chem. Commun.* 1968, 1374; *J. Chem. Soc. A* 1970, 956.
30. P. T. Manoharan and H. B. Gray, *J. Am. Chem. Soc.* 1965, **87**, 3340.
31. P. T. Manoharan and W. C. Hamilton, *Inorg. Chem.* 1963, **2**, 1043; F. Bottomlay and P. S. White, *Acta Cryst.* 1975, **B35**, 2193.
32. C. N. R. Rao, *Chemical Applications of Infrared Spectroscopy*, p. 360. Academic Press, New York (1963).
33. P. Gutlich, In *Mössbauer Spectroscopy* (Edited by U. Gonser), p. 53. Springer, Heidelberg (1975).
34. D. V. Parwate and A. N. Garg, *Z. Naturforsch.* 1985, **40B**, 1495.
35. C. J. Ballhausen and H. B. Gray, *Inorg. Chem.* 1963, **2**, 426.
36. A. N. Garg, *Radiochem. Radioanal. Lett.* 1975, **22**, 157.
37. D. V. Parwate and A. N. Garg, *J. Radioanal. Nucl. Chem. Lett.* 1984, **87**, 379.
38. T. K. Sham, R. E. Watson and M. L. Perlman, *Mössbauer Spectroscopy and Its Chemical Applications* (Edited by J. G. Stevens and G. K. Shenoy), Advances in Chemistry Series No. 194, p. 39. American Chemical Society, Washington, DC (1981).
39. R. W. Grant, *Mössbauer Effect Methodology* 1966, **2**, 23.

Polyhedron Vol. 5, No. 4, pp. 1007–1011, 1986
Printed in Great Britain

0277–5387/86 $3.00+.00
Pergamon Journals Ltd

DETERMINATION OF THE SOLUBILITY PRODUCT CONSTANTS OF Ni(II) AND Cu(II) COMPLEXES WITH *N*-SUBSTITUTED HYDRAZINEDITHIOCARBOXYLIC ACIDS

A. IZQUIERDO*

Department of Analytical Chemistry, Faculty of Chemistry, University of Barcelona, Diagonal 647, Barcelona, Spain

and

J. GUASCH, M. FERRE and F. X. RIUS

Department of Analytical Chemistry, Faculty of Chemistry of Tarragona, University of Barcelona, Tarragona, Spain

(*Received* 12 *September* 1985; *accepted* 23 *October* 1985)

Abstract—A rigorous procedure to evaluate the solubility product constants of very slightly soluble hydrazinedithiocarboxylate complexes is reported, using the competitive effect of EDTA to dissolve the insoluble chelates. A previous knowledge of the stability constants of the soluble complexes involved as well as an accurate control of the pH and concentration of the competitive ligand is required. The solubility products of 2-methylhydrazinedithiocarboxylate and 3,3-dimethylhydrazinedithiocarboxylate complexes with Ni(II), and 3-methyl-3-phenylhydrazinedithiocarboxylate complexes with Ni(II) and Cu(II), have been determined at 25°C and $I = 0.01$ M from solubility data obtained by atomic absorption measurements. The values determined when the method is applied to the Ni–dimethylglyoxime system are in accordance with those found in the literature, giving confidence on the reliability of the procedure proposed.

An increasing number of papers dealing with methods of synthesis and studies on the structural properties of hydrazinedithiocarboxylates (dithiocarbazates) are coming to light.[1] However, only a few works giving information on the equilibrium of these compounds with hydronium or metal ions are reported. Apart from Izquierdo *et al.* who have recently published the stability constants of several *N*-substituted dithiocarbazate complexes with hydronium ions,[2] and Cu(II) and Ni(II) in aqueous solution,[3] only Byr'ko *et al.*[4] have reported values on the protonation constants of the hydrazinium dithiocarbazate. No information concerning the solubility equilibria of dithiocarbazate complexes has been found.

In previous work[2] it was shown that dithiocarbazates react with many transition-metal ions to give very sparingly soluble complexes. Several methods to determine the solubility product constants could be applied.[5] One of the most important takes advantage of the competition established between the metal ion and the proton to be bound to the ligand: however, it cannot be employed in the present study because of the instability of the dithiocarbazates at low pH values and the small influence of the acidity on the complex formation. The simpler evaluation of ion concentrations in solution coming from the solubilization of the pure solid chelates in a given volume of water is not recommended owing to the small solubility of the dithiocarbazate complexes under study, which would give rise to extremely low concentrations of both free ligand and metal ion in solution.

In the present paper, the determination of the

* Author to whom correspondence should be addressed.

solubility product constants of 2-methyldithiocarbazate and 3,3-dimethyldithiocarbazate complexes with Ni(II), and 3-methyl-3-phenyldithiocarbazate complexes with Ni(II) and Cu(II), is described. The method is based on the competitive effect between EDTA and the ligand under study to bind the metal ion which forms the insoluble chelate initially. In this way, a sufficient amount of the complexes is dissolved and the solubility can be evaluated by measuring the overall concentration of metal ion in solution by atomic absorption spectroscopy (AAS).

The reliability of the method has been assessed by applying it to the Ni–dimethylglyoxime complex, whose solubility product constant has long been reported.[6,7]

EXPERIMENTAL

Reagents

To 50 cm^3 of an 0.1 M aqueous nitrate solution of each metal ion were added, dropwise and with constant stirring, 120 cm^3 of 0.1 M aqueous solutions of the dithiocarbazates. The precipitates were collected in a No. 4 porosity sintered-glass crucible, washed with water and ethanol and dried at 110°C until constant weight. Elemental analyses showed a complete agreement between required and found values, corresponding to a formula $M(DTC)_2$, where DTC stands for the neutral ligand. A standard procedure for the precipitation of the Ni–dimethylglyoxime complex was followed.[8]

Measurements

A Beckman 4260 IR spectrophotometer (KBr disks) was used to record the IR spectra and a Cahn RG Electrobalance TGS-1 (Perkin–Elmer) was used to obtain the thermogravimetric curve. The complexes are stable up to 255°C.

All pH measurements of the filtered solutions were carried out in a water-jacketed vessel maintained at 25 ± 0.1°C with a Radiometer PHM 64 Research pH-meter along with a G-202B glass electrode and a K-401 saturated calomel Radiometer electrode, standardized with buffer solutions of pH 6.865 and 9.180 (25°C) according to the NBS.[9]

The analytical metal ion concentrations in aqueous solution were determined by AAS with an Instrumentation Laboratory Inc. IL 551 spectrophotometer.

Determination of solubility product constants

To similar amounts of the slightly soluble complexes contained in five series (five members each) of 50-cm^3 volumetric flasks were added different known amounts of the standardized EDTA (disodium salt) solutions and the same volume of phosphate buffer solution ($I = 0.01$ M, pH = 7.70) in each series. In another five series (five members each) of 50-cm^3 flasks containing solid complexes were added the same known amount of standardized EDTA (disodium salt) solution and different buffer solutions ($I = 0.01$ M, pH = 6.40–8.90) in each series. Therefore the two available experimental parameters (pH and free competitive ligand concentration) were varied. The flasks were filled with millipore distilled water, placed in a thermostatic bath at 25 ± 0.1°C and smoothly shaken. Once the equilibrium for each complex had been reached (after at least 76 h), the suspensions were filtered off, the pH measured exactly and the total concentration of metal ion determined in the clear solutions by AAS.

Buffer solutions ($I = 0.01$ M) have been prepared as described by Perrin and Dempsey.[10] The pH range was set between 6.40 and 8.90 in order to avoid reagent decomposition in highly acidic media and the appreciable formation of metallic hydroxo-complexes in basic media. Phosphate and Tris were employed to prepare buffer solutions due to the formation of very weak complexes with Ni(II) and Cu(II).[11]

RESULTS AND DISCUSSION

Polyaminocarboxylic acids constitute one of the best groups of complexing agents. Moreover, it has been reported that they do not form mixed complexes with dithiocarbamate ligands:[12] hence, EDTA has been chosen as a competing ligand because, in addition to the previous advantages, its equilibria with both hydronium and metal ions has been extensively studied.

In the presence of an adequate concentration of EDTA, the slightly soluble dithiocarbazate complexes can be partially dissolved, giving rise to a certain amount of soluble EDTA complexes and free ligands in accordance with the equilibrium:

$$M(DTC)_2 + HY^{3-} \leftrightarrows MY^{2-} + 2DTC^- + H_3O^+, \quad (1)$$

where $M(DTC)_2$ stands for the insoluble metal ion dithiocarbazato complexes, DTC^- represents the deprotonated ligand and HY^{3-} the predominant form of EDTA at the working pH. The amount of dissolved complex depends on the free EDTA concentration and the pH: consequently, the careful control of both parameters is compulsory.

The following competing equilibria may exist in solution too:

Protonation of dithiocarbazate:

$$nH_3O^+ + DTC^- \leftrightarrows H_nDTC^{n-1},$$
$$\beta_n^{DTC} = [H_nDTC]/[H_3O^+]^n[DTC]. \quad (2)$$

Protonation of EDTA:

$$nH_3O^+ + Y^{4-} \leftrightarrows H_nY^{n-4},$$
$$\beta_n^Y = [H_nY]/[Y][H_3O^+]^n. \quad (3)$$

Formation of dithiocarbazate soluble complexes:

$$M^{2+} + nDTC \leftrightarrows M(DTC)_n^{n-2},$$
$$\beta_n = [M(DTC)_n]/[M][DTC]^n. \quad (4)$$

Formation of mixed EDTA–DTC–metal ion complexes:

$$M(DTC)_n + qHY^{3-} \leftrightarrows M(DTC)_pY_q + (n-p)DTC^-. \quad (5)$$

Formation of mixed dithiocarbazato-metal ion complexes with hydronium and/or hydroxyl ions and polynuclear complexes.

Prior to the determination of the solubility product constants, the presence of mixed EDTA–DTC–metal ion complexes has been tested spectrophotometrically, with no evidence for significant concentrations of these species. Assuming that the concentration of buffer component–metal ion complexes is expected to be negligible due to the small value of their formation constants and the pH range chosen, and the unlikely existence of polynuclear complexes in this study because of the reduced free metal ion to free dithiocarbazate concentration ratio, it can be assumed that the following equations will hold:

$$S = C_M = \sum_0^2 [M(DTC)_n] + [MY] + [M]\left(\sum_0^2 \beta_n[DTC]^n + K_{MY}[Y]\right), \quad (6)$$

$$2S = C_{DTC} = \sum_0^2 n[M(DTC)_n] + \sum_0^1 [H_nDTC] = [M]\sum_0^2 n\beta_n[DTC]^n + [DTC]\alpha_{DTC(H)}, \quad (7)$$

$$C_Y = \sum_0^4 [H_nY] + [MY] = [Y]\{\alpha_{Y(H)} + K_{MY}[M]\}, \quad (8)$$

where S denotes the molar solubility of metal dithiocarbazato complexes,

$$K_{MY} = [MY]/[M][Y], \quad (9)$$

$$\alpha_{DTC(H)} = \sum_0^1 \beta_n^{DTC}[H]^n \quad (10)$$

and

$$\alpha_{Y(H)} = \sum_0^4 \beta_n^Y[H]^n, \quad (11)$$

since one and four protons could be involved in the acid–base equilibria of dithiocarbazates[2] and EDTA,[13] respectively, in the pH range used. From all parameters involved in the equilibria, the molar solubility S can be known from experimental AAS measurements, pH and C_Y are rigorously checked for each series, and the stability constants have been reported elsewhere.[2,3,13] Hence, the unknowns consist of the free ion concentrations of the dithiocarbazate ([DTC]), metal ion ([M]) and competing ligand ([Y]). From eqn (7):

$$[M] = \frac{2S - [DTC]\alpha_{DTC(H)}}{\beta_1[DTC] + 2\beta_2[DTC]^2}. \quad (12)$$

Substituting eqn (12) into eqn (8) and rearranging gives:

$$[Y] = \frac{C_Y}{\alpha_{Y(H)} + K_{MY}\left\{\dfrac{2S - [DTC]\alpha_{DTC(H)}}{\beta_1[DTC] + 2\beta_2[DTC]^2}\right\}}. \quad (13)$$

Introducing eqns (12) and (10) into eqn (6) results in a single polynomial equation with [DTC] as the sole unknown. The fifth-degree polynomial has been solved rigorously with a desk-computer aid. Only one root is of clear chemical significance. Once [DTC] has been determined for each particular series, [M] can be easily found by solving the equation:

$$(\beta_2[DTC]^2 + \beta_1[DTC] + 1)K_{MY}[M]^2 + \{\beta_2[DTC]^2\alpha_{Y(H)} + K_{MY}C_Y + \beta_1[DTC]\alpha_{Y(H)} + \alpha_{Y(H)} - K_{MY}S\}[M] - \alpha_{Y(H)}S = 0, \quad (14)$$

derived from combining eqns (8) and (6). The solubility product (K_{sp}) is then calculated by means of the expression:

$$K_{sp} = [M][DTC]^2. \quad (15)$$

The EDTA protonation constants (β_n^Y) have a role in the K_{sp} calculation through the auxiliary function $\alpha_{Y(H)}$:

$$\alpha_{Y(H)} = \sum_0^4 \beta_n^Y[H]^n = 1 + K_1^Y[H] + K_1^YK_2^Y[H]^2 + K_1^YK_2^YK_3^Y[H]^3 + K_1^YK_2^YK_3^YK_4^Y[H]^4. \quad (16)$$

The terms including the K_3^Y and K_4^Y protonation constants are negligible with respect to all other terms on the right side of eqn (16) in the pH range

Table 1. Evaluation of the solubility product constants at 25°C

Ligand	Equilibrium	I (M)	$\log [K_{sp} \pm s(K_{sp})]$	$\log K_{sp}$ (lit. value)
2-Methyldithiocarbazate $[NH_2N(CH_3)CS_2]^-$	$Ni + 2L \leftrightarrows NiL_2$	0.01	-19.79 ± 0.17	
3,3-Dimethyldithiocarbazate $[(CH_3)_2NNHCS_2]^-$	$Ni + 2L \leftrightarrows NiL_2$	0.01	-15.88 ± 0.02	
3-Methyl-3-phenyldithiocarbazate $[(C_6H_5)(CH_3)NNHCS_2]^-$	$Ni + 2L \leftrightarrows NiL_2$ $Cu + 2L \leftrightarrows CuL_2$	0.01 0.01	-23.88 ± 0.08 -25.62 ± 0.12	
2,3-Butanedionedioxime (dimethylglyoxime)	$Ni + 2L \leftrightarrows NiL_2$	0.1 Dilute 0.05 (NaCl) 0	-23.06 ± 0.07	-23.66 (6) -23.37 (7) -23.89 (16)

used: therefore, the values given by Carini and Martell[14] (log $K_1^Y = 10.71$ and log $K_2^Y = 6.14$ at 25°C and $I = 0.01$ M) are adequate to calculate K_{sp} under the present conditions.

The values of the formation constants of the Ni(II) and Cu(II) complexes with EDTA [log $K_{NiY} = 19.6$ and log $K_{CuY} = 19.9$ ($I = 0.01$ M and 25°C)] have been calculated from those reported as selected values by Anderegg[13] at $I = 0.1$ M and 25°C and the Davies extension of the Debye–Hückel equation:[15]

$$\log Y_{\pm} = -\frac{0.5 Z_A Z_B I^{1/2}}{1 + I^{1/2}} + 0.1 Z_A Z_B I.$$

The uncertainty associated with the new values found (mean deviation $= \pm 0.25$) do not appreciably influence the precision of the solubility product constants since the error introduced by the experimental solubility values is comparatively much greater. The values of the solubility product obtained are given in Table 1.

The method has been tested by determining the solubility product of the Ni–dimethylglyoxime system at $I = 0.1$ M and 25°C. The following constants have been applied—protonation constant of dimethylglyoxime:[17] log $K_1 = 10.55$; protonation constants of EDTA:[13] log $K_1 = 10.26$, log $K_2 = 6.18$, log $K_3 = 2.78$ and log $K_4 = 2.1$; formation constants of Ni(II) complexes with dimethylglyoxime:[18] log $\beta_1 = 9.0$, log $\beta_2 = 17.62$; and formation constant of Ni(II) complex with EDTA:[13] log $\beta_1 = 18.52$. The value of the solubility product constant found is given in Table 1. The result obtained is in reasonable agreement with those reported in the literature for different ionic strengths: therefore, confidence has been given on the reliability of the procedure used.

The method proposed thus offers a rigorous way to determine solubility product constants of very insoluble complexes. Taking into account the detection limit by flame AAS[19] for Ni (0.005 mg l^{-1}) and Cu (0.003 mg l^{-1}), it can be concluded that the smallest K_{sp}s attainable by this method are *ca* $10^{-33.4}$ and $10^{-33.3}$, respectively. If flameless AAS or even more sensitive techniques (viz. inductively coupled plasma or anodic stripping voltammetry) are employed, the limit of K_{sp} can be lowered down to *ca* $10^{-38.5}$, values that can not be attained by gravimetric, conductimetric or spectrophotometric methods.

REFERENCES

1. R. A. Haines and W. J. Louch, *Inorg. Chim. Acta* 1983, **71**, 1 (and references therein).
2. A. Izquierdo, J. Guasch and F. X. Rius, *Talanta* 1985, **32**, 73.
3. A. Izquierdo, J. Guasch and F. X. Rius, *Polyhedron* 1985, **4**, 897.
4. V. M. Byr'ko, A. I. Brusev, T. I. Tikhonova, N. V. Baibakova and L. J. Shepel, *Zh. Anal. Khim.* 1975, **30**, 1885.
5. E. S. Amis, In *Treatise on Analytical Chemistry* (Edited by I. M. Kolthoff and P. S. Elving), 2nd edition, Part I, Vol. 3. John Wiley, New York (1983).
6. C. V. Banks and D. W. Barnum, *J. Am. Chem. Soc.* 1958, **80**, 3579.
7. H. Christopherson and E. B. Sandell, *Anal. Chim. Acta* 1954, **10**, 1.
8. I. M. Kolthoff, E. B. Sandell, E. J. Meehan, S. Bruckenstein, *Quantitative Chemical Analysis*, 4th edition. Macmillan, New York (1968).
9. R. G. Bates, *J. Res. Nat. Bur. Stand.* 1962, **A66**, 179.
10. D. D. Perrin and B. Dempsey, *Buffers for pH and Metal Ion Control*, 4th edition, Table 3.8. Chapman & Hall, London (1974).

11. L. G. Sillén and A. E. Martell, *Stability Constants of Metal Ion Complexes*, 2nd edition. Special Publication No. 17, The Chemical Society, London (1964).
12. M. J. Janssen, *J. Inorg. Nucl. Chem.* 1958, **8**, 340.
13. G. Anderegg, *Critical Survey of Stability Constants of EDTA Complexes*. IUPAC Chemical Data Series No. 14, Pergamon Press, Oxford (1977).
14. F. F. Carini and A. E. Martell, *J. Am. Chem. Soc.* 1953, **75**, 4810.
15. T. S. Lee and O. Popovych, In *Treatise on Analytical Chemistry* (Edited by I. M. Kolthoff and P. J. Elving), 2nd edition, Part I, Vol. 1. John Wiley, New York (1978).
16. D. Rosales and J. M. Cano-Pavon, *Anal. Chem.* 1982, **54**, 123.
17. V. M. Savostina, E. K. Astakhova and V. M. Peshkova, *Vestn. Mosk. Univ., Khim.* 1962, 2.
18. V. M. Savostina, E. K. Astakhova and V. M. Peshkova, *Russ. J. Inorg. Chem.* 1964, **9**, 42.
19. J. D. Winefordner and R. C. Elser, *Anal. Chem.* 1971, **43**, 24A.

Polyhedron Vol. 5, No. 4, pp. 1013–1015, 1986
Printed in Great Britain

0277–5387/86 $3.00+.00
Pergamon Journals Ltd

IMMOBILIZED LIGANDS ON SILICA: UPTAKE OF COBALT AND OTHER METALS BY 1-NITROSO-2-NAPHTHOL

M. C. GENNARO,* E. MENTASTI and C. SARZANINI

Dipartimento di Chimica Analitica, Università di Torino, Via P. Giuria, 5-10125 Torino, Italy

(*Received* 18 *June* 1985; *accepted* 23 *October* 1985)

Abstract—This paper deals with the preparation and properties of a material formed by 1-nitroso-2-naphthol chemically bound on silica. Its uptake ability towards Co(II), Hg(II), Cu(II), Pb(II), Cd(II), Zn(II) and Al(III) was investigated, as well as the conditions for the release of metals previously fixed.

In metal trace analysis, it is often necessary to determine concentration levels below or near to the detection limits of the available instrumentation. In these conditions, suitable preconcentration methods have to be performed. Among the proposed techniques, in recent years the use of chelating materials able to fix metal traces from great volumes of their diluted solutions was shown to be very effective.

A literature survey shows that ligands of very different structure and properties, as well as substrates of different composition, were throughly employed.[1–6] Although different ligand structures and affinities towards metals are possible, selectivity is hard to achieve. A chelating agent which shows good selectivity is 1-nitroso-2-naphthol.

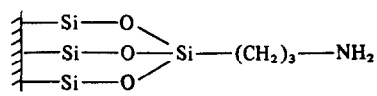
It was employed after chemical immobilization on a polystyrene–divinylbenzene copolymer,[7] or after support on silica gel.[8] Its use allowed the separation of Pb(II) and Co(II), respectively, from other metal ions.

It seemed, therefore, of interest to study the behaviour of this ligand with respect to preconcentration studies. For this purpose, a material was prepared in which 1-nitroso-2-naphthol was chemically bound on silica gel.

EXPERIMENTAL

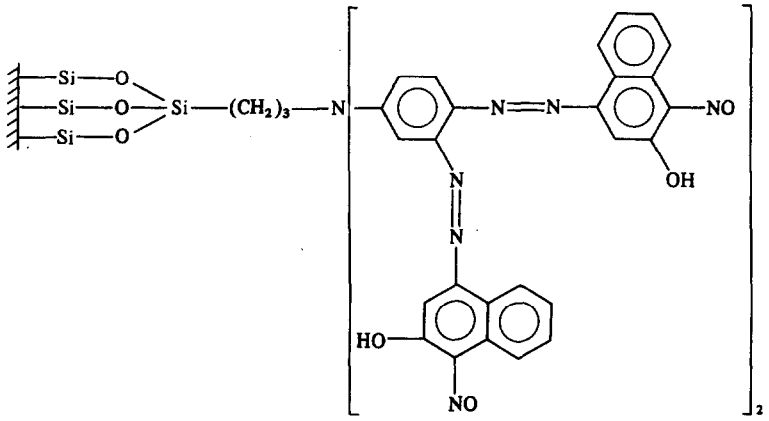
The silica–1-nitroso-2-naphthol material was prepared according to procedures described previously.[9,10]

Silica gel BDH 60–120 mesh was activated at 450°C overnight. Twenty grams were then refluxed in the presence of 200 g of toluene and 60 cm^3 of 3-amine-propyl-triethoxy-silane for about 2 h. After cooling, the partially functionalized silica was filtered and repeatedly rinsed with diethyl ether.



The yield of the reaction was evaluated by a back alkalimetric titration. Fifteen grams of product (about 1.2 mmol —NH_2) were mixed with 2.4 mmol of 2,4-dinitrochlorobenzene, dimethylformamide (200 cm^3) and water (50 cm^3) as solvent, in the presence of sodium acetate (10 g). The mixture was refluxed at about 70°C for about 12 h with continuous stirring. After cooling, the nitro-compound was filtered, rinsed with doubly distilled water (DDW) and ethanol [1:1 (v/v)] by using a Soxhlet extractor to ensure complete removal of reagents. In order to reduce the nitro to amino groups, the subsequent reaction was carried on in the presence of 50 cm^3 of 37% HCl, $SnCl_2$ in excess and 300 cm^3 of water. The reaction was continued for about 24 h, by adding diluted HCl, $SnCl_2$ and Zn powder. The product was filtered and repeatedly rinsed. After desiccation (P_4O_{10}) the intermediate product was then diazotized with excess HNO_2 in an acidic medium (HCl) and was treated, through a coupling reaction, with 1-nitroso-2-naphthol (1.7 g in 50 cm^3 of water, pH around 8 with NaOH). The final product was repeatedly washed with DDW and dimethylketone in order to remove unreacted ligand and dried *in vacuo*.

* Author to whom correspondence should be addressed.



0.8 x 4 cm Econo-Column Bio-Rad columns were used in order to support the prepared material.

All reagents were analytical-grade chemicals. DDW from quartz was employed.

A plasma emission spectrograph ("Spectraspan IV", SMI, Andover, MA) was employed for the metal measurement for both solutions, containing, respectively, the metal fraction unretained by the material and the metal fraction fixed and afterwards eluted, when possible, with a proper reagent.

A two-point calibration was used. The most appropriate wavelength for the emission measurement of each metal was chosen. At this wavelength, the accuracy and precision of the measurement were evaluated, as listed in Table 1.

An Orion pH-meter model 811, equipped with a combined glass–calomel electrode, was used for the pH measurement and adjustment.

RESULTS AND DISCUSSION

0.50 g of the functionalized material were packed in a polypropylene Bio-Rad column. After swelling, the chelating ability was tested towards solutions of the following metal ions: Co(II), Hg(II), Cu(II), Pb(II), Cd(II), Zn(II) and Al(III). In order to avoid metal-hydrolyzed insoluble species formation, all the solutions were adjusted to pH 3.0.

Table 1. Spectral and statistical data for plasma emission spectroscopic measurements

Cation	Accuracy	Precision (%)
Co(II)	345.3	100.1 ± 0.9
Hg(II)	253.6	98.5 ± 0.9
Cu(II)	324.7	99.6 ± 0.3
Pb(II)	405.8	99.2 ± 1.0
Cd(II)	214.4	99.6 ± 1.0
Zn(II)	213.8	100.1 ± 1.2
Al(III)	396.1	99.9 ± 0.5

Co(II) was always quantitatively retained from solutions (100.00 cm^3) with a concentration ranging between 1.00 and 25.00 ppm. This result is confirmed by the spectroscopic emission measurement performed on the filtered solutions, which gave no detectable Co(II). To release the fixed Co(II) the following reagents in the indicated amounts were tested: 1.00 N HCl (10.00 cm^3), 1.00 N HCl (20.00 cm^3), 5.00 N HCl (10.00 cm^3), 5.00 N HCl (20.00 cm^3), 1.00 N $HClO_4$ (20.00 cm^3), 1.00 N HNO_3 (20.00 cm^3), and 5.00 N CH_3COOH (20.00 cm^3). None of the indicated reagents was more effective than others; in each experiment the release of about 5% of the residual fixed metal was achieved. This observation agrees with the very low solubility reported for the complex formed by Co(II) with 1-nitroso-2-naphthol, whose exact composition is not known; it is also suggested that a partial oxidation of Co(II) may take place, due to the reagent itself; coprecipitation of the products of reaction may also occur. Literature data furthermore show the formation of a complex species with a ligand: metal molar ratio equal to 3, which shows a very high stability constant (log β around 46), so that the low solubility of the precipitate as well as the high stability of the complex may explain the behaviour of Co(II) in material studied, as observed by other authors for similar materials.[8]

Solutions of high Co(II) concentration were prepared and fluxed. From a solution (100.00 cm^3) at a concentration of 200.00 ppm, a capacity of 0.492 mmol of Co(II) (g of material)$^{-1}$ was obtained.

The uptake on the material of some cations which do not give rise to a precipitate with the ligand was also investigated. Solutions (100.00 cm^3) were prepared at pH = 3.0, containing, respectively,

Cu(II), Pb(II), Hg(II), Cd(II), Zn(II) and Al(III) at 25.00 ppm each.

The solutions were fluxed through the modified silica (0.50 g) in the column and the unretained fraction of the metal in the filtered solution was measured. Differently from Co(II), for the above-mentioned metals the recovery of metal previously fixed on the functionalized material was possible.

For Cd(II), Zn(II), Al(III) and Pb(II), the release was quantitatively gained by employing 10.00 cm^3 of 1.0 N HCl. For the release of Cu(II), 20.00 cm^3 of 1.00 N HCl were necessary, whilst Hg(II) was released by using 1.00 N HNO_3 (10.00 cm^3).

The results obtained are listed in Table 2. It may be noticed that about 90% Cu(II) is retained; this situation agrees with the high stability of the complex which Cu(II) forms with the investigated ligand.

Table 2. Uptake of a series of metals by the investigated material (0.50 g)

	mg			Retained
Metal	Total	Unretained	Released	(%)
Co(II)	0.10	0.0	0.0	100.0
Co(II)	0.50	0.0	0.0	100.0
Co(II)	1.00	0.0	0.0	100.0
Co(II)	2.50	0.0	0.0	100.0
Hg(II)	2.50	0.0	2.40±0.03	100.0
Cu(II)	2.50	0.24±0.01	2.14±0.02	90.4
Pb(II)	2.50	2.17±0.01	0.33±0.01	13.2
Cd(II)	2.50	2.36±0.02	0.13±0.01	5.6
Zn(II)	2.50	2.33±0.01	0.14±0.01	6.8
Al(III)	2.50	2.36±0.02	0.14±0.01	5.6
Co(II)	20.00	5.52±0.01	0.00	72.4

Hg(II), however, shows an unexpected behaviour; although its complex with the ligand is not so stable, it is quantitatively fixed on the functionalized material.

These results indicate the poor selectivity of the prepared material in fixing metals. On the other hand, it offers the advantage of a very high capacity, towards Co(II), of the order of 500 $\mu mol\ g^{-1}$. The impossibility of releasing Co(II) previously fixed, which makes impossible the application to the preconcentration of Co(II), may offer a series of advantages: the separation which is not achieved in the uptake step may be gained, within an error of about 5%, by performing the elution with HCl and HNO_3 in the proper amounts; the release of all metals other than Co(II) is thus achieved.

The material might also be usefully employed when the removal of a great amount of Co(II) from a liquid sample (such as an industrial waste) is desired.

REFERENCES

1. M. C. Gennaro, C. Baiocchi, E. Campi, E. Mentasti and R. Aruga, *Anal. Chim. Acta* 1983, **151**, 339.
2. R. E. Sturgeon, S. S. Berman, S. N. Willie and J. A. H. Desaulniers, *Anal. Chem.* 1981, **53**, 2337.
3. A. Miyazaki and R. M. Barnes, *Anal. Chem.* 1981, **53**, 299.
4. C. Sarzanini, E. Mentasti, M. C. Gennaro and C. Baiocchi, *Ann. Chim. (Rome)* 1983, **73**, 385.
5. C. Sarzanini, E. Mentasti, M. C. Gennaro and E. Marengo, *Anal. Chem.* 1985, **57**, 1960.
6. M. B. Colella, S. Siggia and R. M. Barnes, *Anal. Chem.* 1980, **52**, 967.
7. J. P. Ghosh and H. R. Das, *Talanta* 1981, **28**, 274.
8. K. Terada and K. Nakamura, *Talanta* 1981, **28**, 123.
9. J. M. Hill, *J. Chromat.* 1973, **76**, 455.
10. J. P. Ghosh, J. Pramanick and H. R. Das, *Talanta* 1981, **28**, 957.

Polyhedron Vol. 5, No. 4, pp. 1017–1021, 1986
Printed in Great Britain

0277–5387/86 $3.00+.00
Pergamon Journals Ltd

SYNTHESIS AND SPECTRAL STUDIES OF β-DIKETONE AND β-KETOESTER DERIVATIVES OF ALUMINIUM ZIRCONIUM ISOPROPOXIDE

RAMA JAIN, A. K. RAI and R. C. MEHROTRA*

Department of Chemistry, University of Rajasthan, Jaipur 302004, India

(*Received* 5 *August* 1985; *accepted* 10 *October* 1985)

Abstract—The reactions of aluminium zirconium heptaisopropoxide [$AlZr(OPr^i)_7$] with some β-diketones and β-ketoesters, resulting in the formation of derivatives of type $ZrAl(OPr^i)_{(7-x)}L_x$ (where L = acetylacetone, benzoylacetone, methylacetoacetate or ethylacetoacetate; $x = 1$ or 2) have been carried out. These newly synthesized compounds have been characterized by elemental analyses, and IR and NMR (^{27}Al, ^1H and ^{13}C) spectral studies.

The coordination chemistry of β-diketone and β-ketoester derivatives of metals are of particular interest as, in these derivatives, metals have been shown to increase their coordination number up to 8.[1–3] These derivatives also exhibit some interesting structural properties.[4,5] Although some of this class of compounds have been synthesized, characterized and their structural studies investigated,[6] the corresponding derivatives of bimetallic alkoxides have received scanty attention. In the present paper, the synthesis, characterization and structural features of some β-diketone and β-ketoester derivatives of aluminium zirconium heptaisopropoxide [$ZrAl(OPr^i)_7$] are described.

EXPERIMENTAL

Special precautions were taken to prevent hydrolysis.

Benzene (BDH) was dried over a sodium wire. Acetylacetone, methylacetoacetate and ethylacetoacetate were dried by refluxing over aluminium isopropoxide and distillation (b.ps 135–137, 168–170 and 180°C, respectively). Benzoyl acetone was used after distillation under reduced pressure.

Aluminium isopropoxide,[7] zirconium isopropoxide[8] and $ZrAl(OPr^i)_7$,[9] were prepared using literature methods. Zirconium and aluminium were estimated as ZrO_2 and $(C_9H_6NO)_3Al$, respectively.[10] IR spectra were recorded in the range 4000–200 cm^{-1} as Nujol mulls on a Perkin–Elmer 577 grating spectrophotometer. NMR (^1H and ^{13}C) were recorded in $CDCl_3$ on a multinuclear JEOL FX90Q NMR spectrometer using TMS as the internal standard. ^{27}Al NMR spectra were also recorded in $CDCl_3$ and benzene using aluminium isopropoxide as the reference.

Reaction of $ZrAl(OPr^i)_7$ *with acetylacetone in* 1:1 *molar ratio*

Acetylacetone (0.44 g, 4.40 mmol) was added to $ZrAl(OPr^i)_7$ (2.13 g, 4.01 mmol) in benzene (~40 cm^3) and an exothermic reaction occurred. The reaction mixture was refluxed for ~2 h with azeotropic fractionation of isopropanol with benzene. The progress of the reaction was checked by estimating the amount of isopropanol in the azeotrope. After completion of the reaction, the solvent was stripped off, and the product distilled at 110–115°C/0.3 mmHg to give a yellow viscous liquid (72% yield). The azeotrope collected between 72 and 80°C was found to contain 0.23 g isopropanol (calc. for 1 mol 0.24 g).

Found: Zr, 16.1; Al, 4.7%. Calc. for $[ZrAl(OPr^i)_6(acac)]$: Zr, 16.0; Al, 4.7%.

The other β-diketone derivatives were also synthesized similarly. The synthetic and analytical data for these reactions are shown in Table 1.

Reaction of $ZrAl(OPr^i)_7$ *with methylacetoacetate in* 1:1 *molar ratio*

A mixture of $ZrAl(OPr^i)_7$ (1.34 g, 2.52 mmol) and methylacetoacetate (0.30 g, 2.58 mmol) was refluxed in benzene (~40 cm^3) for ~2 h, and, after azeotropic

* Author to whom correspondence should be addressed.

Table 1. Synthetic and analytical data for β-diketone and β-ketoester derivatives of $ZrAl(OPr^i)_7$

S. No.	Reactants (mmol)	Molar ratio	Product yield (%) (distilled)	Physical state + volatility (°C/mmHg)	Analysis: % found (calc.) Zr	Al
1	$ZrAl(OPr^i)_7$ + $CH_3COCH_2COCH_3$ 4.01 4.40	1:1	$[ZrAl(OPr^i)_6(CH_3COCHCOCH_3)]$ 72	Yellow viscous liquid 110.15/0.3	16.1 (16.0)	4.7 (4.7)
2	$ZrAl(OPr^i)_7$ + $CH_3COCH_2COCH_3$ 5.14 10.50	1:2	$[ZrAl(OPr^i)_5(CH_3COCHCOCH_3)_2]$ 65	Yellow viscous liquid 126.0/0.2	15.1 (14.9)	4.4 (4.4)
3	$ZrAl(OPr^i)_7$ + $C_6H_5COCH_2COCH_3$ 2.22 2.22	1:1	$[ZrAl(OPr^i)_6(C_6H_5COCHCOCH_3)]$ 43	Dark yellow viscous liquid 168–170/0.2	14.5 (14.4)	4.3 (4.3)
4	$ZrAl(OPr^i)_7$ + $C_6H_5COCH_2COCH_3$ 2.11 4.25	1:2	$[ZrAl(OPr^i)_5(C_6H_5COCHCOCH_3)_2]$ 98[a]	White crystalline solid	12.6 (12.4)	3.5 (3.7)
5	$ZrAl(OPr^i)_7$ + $CH_3COCH_2COOCH_3$ 2.52 2.58	1:1	$[ZrAl(OPr^i)_6(CH_3COCHCOOCH_3)]$ 87	Colourless viscous liquid 122–125/0.05	15.7 (15.5)	4.4 (4.6)
6	$ZrAl(OPr^i)_7$ + $CH_3COCH_2COOCH_3$ 2.84 5.77	1:2	$[ZrAl(OPr^i)_5(CH_3COCHCOOCH_3)_2]$ 82	White solid 132–135/0.05	14.3 (14.2)	4.1 (4.2)
7	$ZrAl(OPr^i)_7$ + $CH_3COCH_2COOC_2H_5$ 3.14 3.15	1:1	$[ZrAl(OPr^i)_6(CH_3COCHCOOC_2H_5)]$ 85	Colourless viscous liquid	15.3 (15.2)	4.5 (4.5)
8	$ZrAl(OPr^i)_7$ + $CH_3COCH_2COOC_2H_5$ 1.71 3.61	1:2	$[ZrAl(OPr^i)_5(CH_3COCHCOOC_2H_5)_2]$ 70	White solid 145–150/0.2	13.6 (13.6)	4.0 (4.0)

[a] Crude yield.

removal of isopropanol and solvent, gave a highly viscous colourless liquid which was distilled at 122–125°C/0.05 mmHg (87% yield).

Found: Zr, 15.7; Al, 4.4%. Calc. for $[ZrAl(OPr^i)_6(CH_3COCHCOOCH_3)]$: Zr, 15.5; Al, 4.6%.

The other β-ketoester derivatives were also prepared similarly, and the analytical data for the products are summarized in Table 1.

RESULTS AND DISCUSSION

The reactions of $ZrAl(OPr^i)_7$ with β-diketones and β-ketoesters in different molar ratios in refluxing benzene have been carried out. These reactions can be represented by the following general equation:

$$ZrAl(OPr^i)_7 + xL \rightarrow ZrAl(OPr^i)_{7-x}L_x + xPr^iOH\uparrow,$$

where $x = 1$ or 2; L = acetylacetone, benzoylacetone, methylacetoacetate or ethylacetoacetate.

The products obtained were found to be light yellow or colourless viscous liquids or solids, soluble in common organic solvents. Some of the β-diketonate derivatives, like $[ZrAl(OPr^i)_6(acac)]$,

$$[ZrAl(OPr^i)_5(acac)_2]$$

and

$$[ZrAl(OPr^i)_6(C_6H_5COCHCOCH_3)],$$

were found to be distillable under reduced pressure, whereas $[ZrAl(OPr^i)_5(C_6H_5COCHCOCH_3)_2]$ underwent decomposition.

The corresponding β-ketoester derivatives were distilled in quantitative yield without any decomposition.

IR spectra

The characteristic absorption bands observed in the IR spectra of these derivatives in the range 4000–200 cm^{-1} are summarized in Table 2, and tentatively assigned.[12,13] Three sets of stretching vibrations for ν(Al—O) at 710±20, 675±20 and 615±15 cm^{-1}, and two sets of ν(Zr—O) at 570±20 and 470±10 cm^{-1} have been identified. The two bands at 1600±30 and 1530±10 cm^{-1} are assigned to ν(C···O) and ν(C···C) vibrations, respectively. The presence of a ν(C···O) band in these derivatives at a lower frequency in comparison with the corresponding ligands indicates the coordination of the keto group of the ligand moiety to the metal atom.[14] Bands for terminal as well as bridging isopropoxy groups have been identified.

NMR (^1H *and* ^{27}Al)

$ZrAl(OPr^i)_7$. The ^1H NMR spectrum of $ZrAl(OPr^i)_7$ shows three types of methyl proton doublets, indicating the presence of three types of isopropoxy groups: these may be assigned to the bridging groups (δ 1.36–1.44 ppm) and the terminal

Table 2. Some relevant IR frequencies (cm^{-1})[a] for β-diketone and β-ketoester derivatives of $ZrAl(OPr^i)_7$

S. No.	Compound	ν(Zr—O)	ν(Al—O)	Terminal ν(C—O)	ν(C···C)	ν(C···O)
1	$[ZrAl(OPr^i)_6(CH_3COCHCOCH_3)]$	570s 470m	680s 655w 605w	1030vs	1530vs	1600vs
2	$[ZrAl(OPr^i)_5(CH_3COCHCOCH_3)_2]$	590m 440w	700m 675m 610w	1035vs	1540vs	1610vs
3	$[ZrAl(OPr^i)_6(C_6H_5COCHCOCH_3)]$	580s 480w	725m 690w	1025s	1530vs 1605vs	1575s
4	$[ZrAl(OPr^i)_5(C_6H_5COCHCOCH_3)_2]$	560m 470w	710s 675w	1010vs	1520vs 1590vs	1560vs
5	$[ZrAl(OPr^i)_6(CH_3COCHCOOCH_3)]$	580s 480brs	700s 630m	1025vs	1535vs	1620vs 1575m
6	$[ZrAl(OPr^i)_5(CH_3COCHCOOCH_3)_2]$	580s 480m	730m 695m	1020vs	1535vs	1620vs 1585m
7	$[ZrAl(OPr^i)_6(CH_3COCHCOOC_2H_5)]$	580s 480s	740m 690brm 630w	1025vs	1535vs	1630vs 1570m
8	$[ZrAl(OPr^i)_5(CH_3COCHCOOC_2H_5)_2]$	580s 460m	730s 630m	1025vs	1525vs	1630vs 1575m

[a] vs, very strong; s, strong; m, medium; br, broad.

groups [δ 1.22–1.29 ppm (bonded to zirconium) and δ 1.10–1.16 ppm (bonded to aluminium)].

The ^{27}Al chemical shift observed at δ 65.14 ppm confirms the tetrahedral nature[15,16] of the aluminium in $ZrAl(OPr^i)_7$.

$[ZrAl(OPr^i)_6(acac)]$. The ^{1}H NMR spectrum of $[ZrAl(OPr^i)_6(acac)]$ also exhibits three types of isopropoxy group, indicating the presence of four terminal (on both zirconium and aluminium) and two bridging isopropoxy groups. A new doublet observed in the δ 1.93–1.99 ppm region may be assigned to the methyl protons of the acetylacetone moiety.[17] The presence of a doublet may be attributed to a *cis* arrangement of the ligand moiety attached to the metal atom.[18–21] (The *cis* form exhibits two resonances due to the non-equivalent environment of the terminal group.)

In $[ZrAl(OPr^i)_6(acac)]$, the acetylacetone moiety may attach either to the zirconium or the aluminium atom of the molecule. In the case of $ZrAl(OPr^i)_7$, the zirconium atom has a coordination number of 5 and it has a greater tendency to attain a coordination number of 6, as indicated by its dimeric nature in refluxing benzene and its monomeric nature in isopropanol, with the formation of $[ZrAl(OPr^i)_7 \cdot Pr^iOH]$.[9] Thus, the incoming acetylacetone moiety, which acts as a bidentate ligand, must replace one of the terminal isopropoxy groups at the zirconium atom in order to acquire a stable coordination number of 6.

In contrast to this prediction, the ^{27}Al chemical shift (δ −0.732 ppm) suggests a penta-coordination for aluminium which is only possible when the incoming group replaces the isopropoxy group on aluminium instead of zirconium.

$[ZrAl(OPr^i)_6(C_6H_5COCHCOCH_3)]$,

$[ZrAl(OPr^i)_6(CH_3COCHCOOCH_3)]$

and $[ZrAl(OPr^i)_6(CH_3COCHCOOC_2H_5)]$. The proton spectra of these compounds also show the types of isopropoxy groups observed in the previous case. Beside the above, signals corresponding to $-CCH_3$ (singlet), $O-CH_3$ (singlet), $O-CH_2$ (quartet), $-C_6H_5$ (multiplet) and O—CH (multiplet) have also been observed and the results are summarized in Table 3.

$[ZrAl(OPr^i)_5(acac)_2]$,

$[ZrAl(OPr^i)_5(CH_3COCHCOOCH_3)_2]$

and $[ZrAl(OPr^i)_5(CH_3COCHCOOC_2H_5)_2]$. The PMR spectra exhibit a multiplet for the methyl protons of the isopropoxy groups. The presence of a doublet for methyl protons (δ 1.88–1.99 ppm) of the ligand moieties indicates that the ligand moieties are attached to zirconium as well as to aluminium, appearing separately but not assignable with certainty on the basis of ^{1}H NMR alone.

However, ^{27}Al NMR shows a single signal at δ 4.557 ppm suggesting hexa-coordination for aluminium.[22,23] Thus, both of the ligand moieties are on the aluminium atom. The presence of both the ligand moieties on aluminium may give rise to different geometrical isomers which may be the reason for the splitting observed in $-CH_3$, $O-CH_3$ and =CH protons in ^{1}H NMR spectra.[24]

Table 3. ^{1}H NMR spectral data for β-diketone and β-ketoester derivatives of $ZrAl(OPr^i)_7$[a]

S. No.	Compound	δ (ppm)[a]
1	$ZrAl(OPr^i)_7$	1.10–1.43td, 42H, $-C(CH_3)_2$; 4.13–4.58m, 7H, —OCH
2	$[ZrAl(OPr^i)_6(CH_3COCHCOCH_3)]$	1.08–1.40td, 36H, $-C(CH_3)_2$; 1.93–1.99d, 6H, $-CH_3$; 4.06–4.50m, 6H, —OCH; 5.36–5.56m, 1H, =CH
3	$[ZrAl(OPr^i)_5(CH_3COCHCOCH_3)_2]$	0.96–1.40m, 30H, $-C(CH_3)_2$; 1.92d, 1.99s, 12H, $-CH_3$; 4.04–4.44m, 5H, —OCH; 5.36–5.59m, 2H, =CH
4	$[ZrAl(OPr^i)_6(C_6H_5COCHCOCH_3)]$	1.08–1.40td, 36H, $-C(CH_3)_2$; 2.08s, 3H, CH_3; 4.04–4.55m, 6H, OCH; 6.27s, 1H, =CH; 7.16–7.45m, 5H, $-C_6H_5$
5	$[ZrAl(OPr^i)_6(CH_3COCHCOOCH_3)]$	1.08–1.40td, 36H, $-C(CH_3)_2$; 1.86s, 3H, CH_3; 3.64s, 3H, $-OCH_3$; 4.06–4.58m, 6H, —OCH; 4.82–5.02m, 1H, =CH
6	$[ZrAl(OPr^i)_5(CH_3COCHCOOCH_3)_2]$	1.12–1.36m, 30H, $-C(CH_3)_2$; 1.99–2.07d, 6H, CH_3; 3.76–3.79d, 6H, OCH_3; 3.92–4.44m, 5H, OCH; 4.99–5.10, 2H, =CH
7	$[ZrAl(OPr^i)_6(CH_3COCHCOOCH_2CH_3)]$	1.08–1.38td, 39H, $-C(CH_3)_2$; 1.86s, 3H, CH_3; 3.62–3.76q, 2H, OCH_2; 4.06–4.54m, 6H, OCH; 4.82–5.02m, 1H, =CH
8	$[ZrAl(OPr^i)_5(CH_3COCHCOOCH_2CH_3)_2]$	1.07–1.37m, 36H, $-C(CH_3)$; 1.81–1.93dd, 6H, CH_3; 3.64–3.67q, 4H, OCH_2; 4.05–4.41m, 5H, OCH; 4.81–4.95m, 2H, =CH

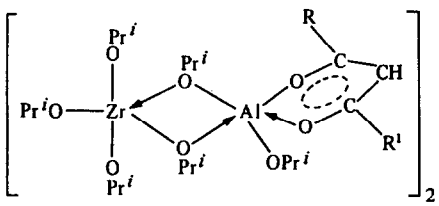
[a] In $CDCl_3$, δ relative to TMS.

^{13}C NMR spectra

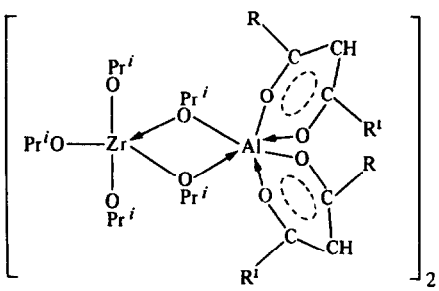
^{13}C NMR spectra are recorded only for two compounds in $CDCl_3$.

$[ZrAl(OPr^i)_6(CH_3COCHCOOCH_3)]$ and $[ZrAl(OPr^i)_5(CH_3COCHCOOCH_3)_2]$. ^{13}C NMR spectra of these compounds show the signals due to methyl carbons of isopropoxy groups as well as that of the ligand moieties in the δ 24.18–27.99 ppm region as a complex multiplet. The multiplicity of the signals may be due to different intramolecular stereochemical changes in the molecule due to its complexation. The signals due to $-OCH_3$, $-OCH$ and $=CH$ are $\delta \sim 51.51$, 69.10 and 87.70 ppm, respectively. Two types of signals were observed for C···O and O—C···O at $\delta \sim 185.59$ and 173.64 ppm, respectively, which may be due to the weak chelation of the C=O group to the metal atom.

On the basis of the above studies, the following plausible structures have been suggested for these derivatives.



1 : 1 molar product



1 : 2 molar product

R = CH_3 or C_6H_5, R' = CH_3, OCH_3 or C_2H_5

Acknowledgement—One of us (R.J.) is grateful to the University Grants Commission, New Delhi, for providing financial assistance.

REFERENCES

1. R. E. Sievers, B. W. Ponder, M. L. Morris and R. S. Moshier, *Inorg. Chem.* 1963, **2**, 693.
2. R. N. Kapoor, S. Prakash and P. N. Kapoor, *Bull. Chem. Soc. Jpn* 1967, **40**, 1384.
3. U. B. Saxena, A. K. Rai, V. K. Mathur and R. C. Mehrotra, *J. Chem. Soc. A* 1970, 904.
4. G. Doyle and P. Stuart Tobias, *Inorg. Chem.* 1968, **7**, 2484.
5. J. J. Howe and T. J. Pinnavaia, *J. Am. Chem. Soc.* 1969, **91**, 5378.
6. R. C. Mehrotra, R. Bohra and D. P. Gaur, *Metal β-Diketonates and Allied Derivatives*. Academic Press, London (1978).
7. H. Adkins, *J. Am. Chem. Soc.* 1922, **44**, 2178.
8. D. C. Bradley, R. C. Mehrotra and W. Wardlaw, *J. Chem. Soc.* 1952, 2027.
9. D. C. Bradley, R. C. Mehrotra and D. P. Gaur, *Metal Alkoxides*. Academic Press, London (1978).
10. A. I. Vogel, *A Text Book of Quantitative Inorganic Analyses*. ELBS and Longmans, London (1973).
11. R. C. Mehrotra, *J. Indian Chem. Soc.* 1953, **30**, 585.
12. D. C. Bradley and A. H. Westlake, In *Proceedings of the Symposium on Coordination Chemistry, Tihany, Hungary*. Hungarian Academy of Science, Budapest (1965).
13. C. G. Barraclough, D. C. Bradley, J. Lewis and I. M. Thomas, *J. Chem. Soc.* 1961, 2601.
14. J. Lewis, R. F. Long and C. Oldham, *J. Chem. Soc.* 1965, 6740.
15. J. W. Akitt and Alan Farthing, *J. Chem. Soc., Dalton Trans.* 1981, 1624.
16. J. W. Akitt, *J. Chem. Soc., Dalton Trans.* 1984, 147.
17. J. A. S. Smith and E. J. Wilkins, *J. Chem. Soc.* 1966, 1749.
18. R. W. Jones and R. C. Fay, *Inorg. Chem.* 1973, **12**, 2599.
19. R. C. Fay and R. N. Lowry, *Inorg. Chem.* 1967, **6**, 1512.
20. J. W. Faller and A. Davison, *Inorg. Chem.* 1967, **6**, 182.
21. N. Serpone and R. C. Fay, *Inorg. Chem.* 1967, **6**, 1835.
22. J. W. Akitt and Alan Farthing, *J. Chem. Soc., Dalton Trans.* 1981, 1615.
23. S. J. Kartik, E. Tarien, G. A. Elgavish and G. L. Eichhorn, *Inorg. Chem.* 1983, **22**, 525.
24. T. J. Pinnavaia, L. J. Matienzo and Y. A. Peters, *Inorg. Chem.* 1970, **9**, 993.

Polyhedron Vol. 5, No. 4, pp. 1023–1025, 1986
Printed in Great Britain

0277–5387/86 $3.00+.00
Pergamon Journals Ltd

INHIBITORY ACTIVITY OF BIVALENT TRANSITION-METAL COMPLEXES WITH DIAMINES TOWARD A DIAMINE OXIDASE

G. DEVOTO, M. MASSACESI and G. PONTICELLI

Istituto di Chimica Generale, Inorganica ed Analitica, Università di Cagliari, Cagliari, Italy

and

R. MEDDA and G. FLORIS*

Istituto di Chimica Biologica, Università di Cagliari, Cagliari, Italy

(*Received* 15 *July* 1985; *accepted* 23 *October* 1985)

Abstract—Various complexes of bivalent transition metals with diamines have been synthesized and studied "*in vitro*" with a diamine oxidase. The inhibition type and K_i value of these compounds have been determined. For the linear-chain diamine complexes the inhibition was competitive and the highest inhibition was for the 1,3-diaminopropane–copper complexes.

Diamine oxidases [amine:oxygen oxidoreductase deaminating (EC 1.4.3.6)] are enzymes evenly distributed among living organisms.[1] They catalyse the oxidation of one primary amino group of a substrate according to the following reaction:

$$R{-}CH_2{-}NH_2 + O_2 + H_2O \rightarrow R{-}CHO + NH_3 + H_2O_2.$$

Despite their broad distribution their physiological role is not fully understood. In plants they are found mainly in seedlings,[2] where cell proliferation requires a fast metabolism of polyamines.[3,4]

An important tool in studying the function of an enzyme is to find specific inhibitors and to follow their effects. Several papers have been published concerning the inhibition of amine oxidase (AO). AO isolated from different sources showed a large variability in specificity toward substrates and sensitivity to inhibitors.[4] Bardsley and Ashford[5] reported the inhibition of pig kidney AO (PKAO) by substrate analogues as a useful tool in probing the structure–function relationship of the enzyme action. Crabbe and Bardsley[6,7] used substrate analogues on the human placental AO to determine if drugs used in pregnancy could modify the activity of the enzyme. Inhibition of PKAO by antihistaminic agents and related drugs on the basis of the chemical relationship of the enzyme substrates has been reported by Finazzi Agró *et al.*[8] and Lorenz *et al.*[9] Joshi and Prakash[10] reported that, during the germination of *Sorghum vulgaris*, two seed inhibitors of pea AO (PSAO) appeared, one, heat-labile, inhibited the enzyme *in vitro*, while the other, heat-stable, inhibited the enzyme synthesis. Macholán and Minář reported the depression of the synthesis of PSAO in growth processes using competitive inhibitors.[11]

Recently AO from lentil seedlings (LSAO) has been purified to homogeneity.[12] This enzyme is similar to other plant AOs. LSAO is inhibited *in vitro* by complexes between bivalent transition metals and some diamines with different metal–ligand ratios: these inhibitors are very similar to the natural substrates of the enzyme. Therefore, it seems of interest to study the influence of the number and nature of the ligands on the inhibitory activity of the complex.

* Author to whom correspondence should be addressed.

EXPERIMENTAL

Ethylenediamine (en), 1,3-diaminopropane (tn), 1,4-diaminobutane (put) and 1,5-diaminopentane (cad), Fluka purum, were commercially available.

$CuCl_2 \cdot 2H_2O$, $Cu(NO_3)_2 \cdot 3H_2O$, $CuSO_4 \cdot 5H_2O$, $NiCl_2 \cdot 6H_2O$, $CoCl_2 \cdot 6H_2O$, $ZnCl_2$, ZnI_2, $CdCl_2 \cdot 2.5H_2O$, $HgCl_2$, K_2PdCl_4 and K_2PtCl_4 were commercially available, while $CuBr_2$ was prepared by literature methods.

Preparation of the complexes

The complexes were prepared by dissolving appropriate amounts of metal salts and ligands in hot MeOH. After cooling the solution, the precipitated complexes were washed in petroleum ether and dried over P_4O_{10}. The cobalt complexes were prepared in acetone solution. The palladium and platinum complexes were precipitated by a hot aqueous alcoholic solution.

Complexes of general formula $M(L)_nX_2$ (where M = Cu, Ni, Co, Zn, Cd, Hg, Pd or Pt; L = en or tn; n = 1 or 2; X = Cl, Br, I or NO_3), and $Cu_3(put)_2Cl_6$ and $Cu_3(cad)_2Cl_6$ have been obtained.

All the complexes have been characterized by elemental analyses (C, H and N), conductance measurements, IR and diffuse reflectance electronic spectra.

Purification of LSAO

LSAO was purified from *Lens esculenta* seedlings by Floris *et al.*[12] The enzyme activity was measured polarographically with a Gilson GME Oxygraph at 37°C using 10 mM putrescine as substrate. The incubation mixture (1 cm^3) contained 4 μg purified LSAO in 0.1 M K-phosphate buffer (pH 7) or 0.1 M Tris–HCl buffer (pH 8).

The effect of the inhibitors was tested by adding these compounds to the incubation mixture in the presence and in the absence of 100 μg crystalline beef liver catalase (Sigma, St. Louis, MO).

The inhibition constants were determined by Dixon plots.[13]

RESULTS AND DISCUSSION

The structures of the complexes in the solid state are reported in Table 1. The X-ray determinations of some compounds are known: $Cu(en)_2X_2$ (X = Cl, Br or I), square planar pseudooctahedral;[14] $Ni(en)_2Cl_2$, square pyramidal;[15] $M(en)Cl_2$ (M = Pd or Pt), square planar;[16] $Hg(en)Cl_2$, polymeric transoctahedral;[17] and $Cu(tn)_2(NO_3)_2$, octahedral.[18] The $Zn(en)Cl_2$ and $Cd(en)Cl_2$ structures seem equal to that of $Hg(en)Cl_2$ by an IR study.[19] The structure of the other complexes is assigned on the basis of electronic and IR data (Ponticelli *et al.*, unpublished results).

Table 1. Competitive inhibitors of LSAO

Complex	Structure in the solid state	K_i (mM)	Inhibitory activity (%) $C = 3.5 \times 10^{-5}$ M
$Cu(en)_2Cl_2$	Square planar, pseudooctahedral[14]	0.035	50.0
$Cu(en)_2Br_2$	Square planar, pseudooctahedral[14]	0.035	50.0
$Cu(en)_2I_2$	Square planar, pseudooctahedral[14]	0.035	50.0
$Cu(tn)_2Br_2$	Square planar, pseudooctahedral[14]	0.009	100.0
$Cu(tn)_2(NO_3)_2$	Octahedral[18]	0.080	20.0
$Cu_3(put)_2Cl_6$	Polymeric square pyramidal	0.050	27.0
$Cu_3(cad)_2Cl_6$	Polymeric square pyramidal	0.010	94.0
$Co(en)_2Cl_2$	Square planar	0.180	10.0
$Ni(en)_2Cl_2$	Distorted octahedral	0.035	50.0
$Zn(en)_2I_2$	Square pyramidal	0.030	69.0
$Cd(en)_2Cl_2$	Distorted octahedral	0.105	15.0
$Co(en)Cl_2$	Tetrahedral	0.140	12.5
$Ni(en)Cl_2$	Polymeric octahedral	0.052	25.0
$Zn(en)Cl_2$	Polymeric octahedral[19]	0.020	71.0
$Pd(en)Cl_2$	Square planar[16]	0.105	15.0
$Cd(en)Cl_2$	Polymeric octahedral[19]	0.860	3.1
$Pt(en)Cl_2$	Square planar[16]	0.100	15.8
$Hg(en)Cl_2$	Polymeric octahedral[17]	—	—

Table 1 also reports the inihibition types with the K_i values determined by Lineweaver–Burk and Dixon plots.

It is well known that LSAO catalyzes the oxidation of the diamines put to 1,10-diaminodecane.[12] This is the reason why the inhibition caused by $Cu_3(put)_2Cl_6$ and $Cu_3(cad)_2Cl_6$ was expected.

No activity is found with 1,2-diaminoethane and 1,3-tn free ligands.[12] A matter of interest is therefore the competitive inhibition of LSAO by the above-mentioned $M(L)_nX_2$ complexes.

Since in aqueous solution the compounds may show solvolysis in the apical position or in the bridging halides,[20] and a variety of species containing the metal ion may be present and cannot be separated from each other in the experiments described, the inhibitory activity is also expressed in % using a 3.5×10^{-5} M solution of the complexes (Table 1). The same inhibitory activity is found when using 0.1 M K-phosphate (pH 7) or 0.1 M Tris–HCl (pH 8) as the buffer.

The inhibitory activity of the $M(en)_2X_2$ complexes toward the enzyme generally does not change with the anion and decreases in the order Zn, Ni, Cu, Cd and Co. The inhibitory effect of the $M(en)Cl_2$ derivatives decreases in the order Zn, Ni, Pd, Co, Pt, Cd and drops to zero with Hg.

No inhibitory activity is found when the free ligands or the metal salts are used by themselves at the same concentration as in the complexes.

With regard to the inhibitory mechanism it is most probable that the interaction of the complexes occurs with the active site of the enzyme and that the enzyme–inhibitor interaction is very stable.

REFERENCES

1. B. Mondovi and A. Finazzi Agró, In *Structure and Function Relationships in Biochemical Systems* (Edited by F. Bossa, E. Chiancone, A. Finazzi Agró and R. Strom), p. 141. Plenum Press, New York (1982).
2. E. Werle and E. Pechman, *Liebigs Ann.* 1949, **562**, 44.
3. A. Raina and J. Janne, *Med. Biol.* 1975, **53**, 121.
4. F. Buffoni, *Pharmacol. Rev.* 1966, **18**, 1163.
5. W. G. Bardsley and J. S. Ashford, *Biochem. J.* 1972, **128**, 153.
6. M. J. C. Crabbe and W. G. Bardsley, *Biochem. Pharmacol.* 1974, **23**, 2983.
7. M. J. C. Crabbe and W. G. Bardsley, *Biochem. J.* 1974, **139**, 183.
8. A. Finazzi Agró, G. Floris, M. B. Fadda and C. Crifó, *Agents Actions* 1979, **9**, 244.
9. W. Lorenz, H. Therman, H. Hamelmann, A. Schmal, D. Maroske, H. J. Reimann, J. Kusche, F. Schingale, P. Dormann and P. Keck, In *International Symposium on Histamine H_2-Receptor Antagonists* (Edited by C. J. Wood and M. H. Simkins), p. 151. Smith, Kline & French, London (1973).
10. B. H. Joshi and V. Prakash, *Experientia* 1982, **38**, 315.
11. L. Macholán and J. Minář, *Biol. Plant.* 1974, **16**, 86.
12. G. Floris, A. Giartosio and A. Rinaldi, *Phytochemistry* 1983, **22**, 1871.
13. M. Dixon, *Biochem. J.* 1953, **55**, 170.
14. I. M. Procter, B. J. Hathaway and P. Nicholls, *J. Chem. Soc. (A)* 1968, 16781
15. A. S. Antsyshkina and M. A. Porai-Koshits, *Dokl. Akad. Nauk S.S.S.R.* 1962, **143**, 105.
16. J. Iball, M. MacDougall and S. Scrimgeour, *Acta Cryst.* 1975, **B31**, 1672.
17. V. K. Brodersen, *Z. Anorg. Allg. Chem.* 1959, **142**, 298.
18. A. Pajunen, *Suom. Kemistil.* 1969, **B42**, 15.
19. G. Newman and D. B. Powell, *J. Chem. Soc.* 1961, 477.
20. K. Sone and S. Utsuno, *Bull. Chem. Soc. Jpn* 1966, 1813.

Polyhedron Vol. 5, No. 4, pp. 1027–1029, 1986
Printed in Great Britain

0277–5387/86 $3.00+.00
Pergamon Journals Ltd

COMMUNICATION

THE GEOMETRIES AND ELECTRONIC STRUCTURES OF TWO TERMINAL-PHOSPHINIDENE COMPLEXES

JUNG-GOO LEE, JAMES E. BOGGS and ALAN H. COWLEY*

Department of Chemistry, The University of Texas at Austin, Austin, TX 78712, U.S.A.

(*Received* 15 *August* 1985; *accepted* 14 *October* 1985)

Abstract—*Ab initio* MO calculations have been carried out on the terminal-phosphinidene complexes $HPCr(CO)_5$ and $HPNi(CO)_3$.

Terminal-phosphinidene complexes of the type $RPML_n$ (R = Ph or Me; M = Cr, Mo, W)[1] and $RPFe(CO)_4$ [R = 2,4,6-(*t*-Bu)$_3$C$_6$H$_2$][2] have been implicated as short-lived species. However, so far such compounds have eluded isolation. We have therefore undertaken a theoretical study of the prototypical terminal-phosphinidene complexes $HPCr(CO)_5$ (**1**) and $HPNi(CO)_3$ (**2**).

Since the molecules are rather large, it was necessary to employ idealized octahedral and tetrahedral geometries for **1** and **2**, respectively (Fig. 1). The M—C and C—O bond lengths for **1** and **2** are based on those of $H(HO)CCr(CO)_5$[3] and $Ni(CO)_4$,[4] respectively. The P—H bond length was assumed to be 1.42 Å in both complexes. All calculations were carried out with the GUGA program[5] which employs the restricted Hartree–Fock method for both closed- and open-shell systems. The basis sets for Cr (^7S) and Ni (^3F) were of the MINI-2 type[6] supplemented with 4*p* orbitals. Orbital exponents of 0.077 and 0.111 were used for Cr and Ni, respectively. A 3G CGTO minimal basis set was utilized for the C, O, H and P atoms.[7]

Geometry optimization afforded the values R = 2.33 Å, $\alpha = 110°$, and $\theta = 45°$ for **1**, and R = 2.19 Å, $\alpha = 102°$, and $\theta = 30°$ for **2**. For both complexes, the computed metal–phosphorus bond lengths are close to the sums of the respective metal–phosphorus covalent radii. The fact that, in contrast to, for example,

$H(HO)CCr(CO)_5$[3]

and

$H(OH)SiCr(CO)_5$,[8]

both **1** and **2** adopt staggered conformations is presumably a consequence of the phosphorus lone pair. However, the computed rotational barriers for **1** (0.29 kcal mol^{-1}) and **2** (0.25 kcal mol^{-1}) are extremely small. The computed metal–phosphorus bond dissociation energies are 38.1 and 74.9 kcal mol^{-1} for **1** and **2**, respectively. Comparison with $H(HO)SiCr(CO)_5$ (29.6 kcal mol^{-1}), which was investigated with a similar method and basis set,[8] suggests that terminal phosphinidenes are bound to Cr more strongly than terminal silylenes. The computed force constant and frequency for the Cr—P bond of **1** (staggered conformation) are 1.60 mdyn Å^{-1} and 370 cm^{-1}, respectively.

For both **1** and **2**, the metal–phosphorus σ-bond is formed by electron transfer from the HOMO of the phosphinidene [primarily P($3p_z$)] to the LUMO of the $Cr(CO)_5$ or $Ni(CO)_3$ fragment. Back-transfer of electrons stems from interaction of the HOMO of the metal carbonyl fragment to the LUMO ($3p_y$) of the HP moiety. The net result is that, for both **1** and **2**, the HOMO and HOMO-1 are of the π- and σ-symmetry, respectively (Fig. 2). The gap between the π- and σ-MOs is 0.6 and 0.3 eV for **1** and **2**, respectively.

The LUMO of $HPCr(CO)_5$ is very low lying (0.008 eV). Moreover, the LUMO features a large AO coefficient at the phosphorus center [0.82 at P($3p_y$)]. As a consequence, the chromium–phosphinidene complex is anticipated to undergo facile nucleophilic attack at phosphorus. Both the LUMO [0.71 at P($3p_y$)] and the HOMO [0.66 at P($3p_y$)] of **2** feature

* Author to whom correspondence should be addressed.

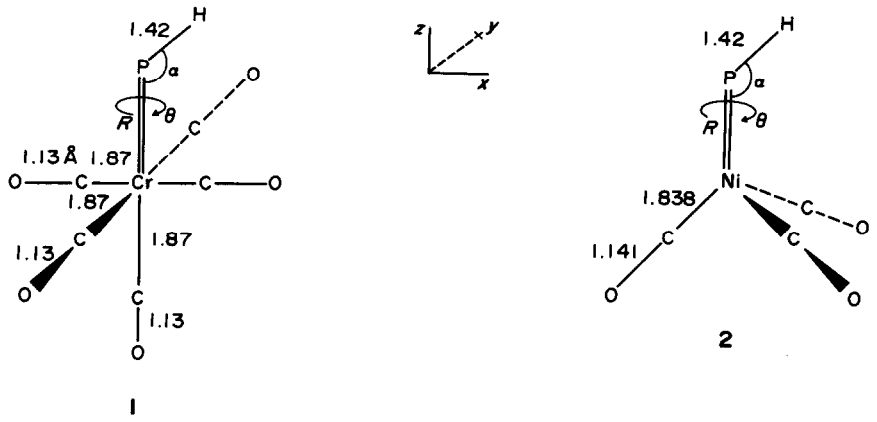


Fig. 1. Geometries of metal–phosphinidene complexes. Both complexes are shown with a rotational angle (θ) of 0°.

large phosphorus AO coefficients: moreover, the LUMO is relatively low-lying (1.3 eV). The nickel–phosphinidene complex is therefore predicted to be reactive toward both nucleophilic and electrophilic reagents.

We have made a preliminary investigation of the triplet state of $HPCr(CO)_5$. For the PH fragment, we compute that the triplet state is more stable than the singlet state by 45 kcal mol^{-1}. Clearly, the method used here overemphasizes the stability of the triplet state, since this figure exceeds the experimental value[9] by 23 kcal mol^{-1}. Like Nakatsuji *et al.*,[3] we calculate that, for the $Cr(CO)_5$ fragment, the singlet state is more stable than the triplet state by 7 kcal mol^{-1}. When the HP and $Cr(CO)_5$ fragments are bonded, the triplet state ($R = 2.67$ Å, $\alpha = 102°$, and $\theta = 45°$) is favored over the singlet state by 27.4 kcal mol^{-1} (at the staggered geometry). However, we anticipate that this gap will be decreased when correlation effects are included. Consequently, we

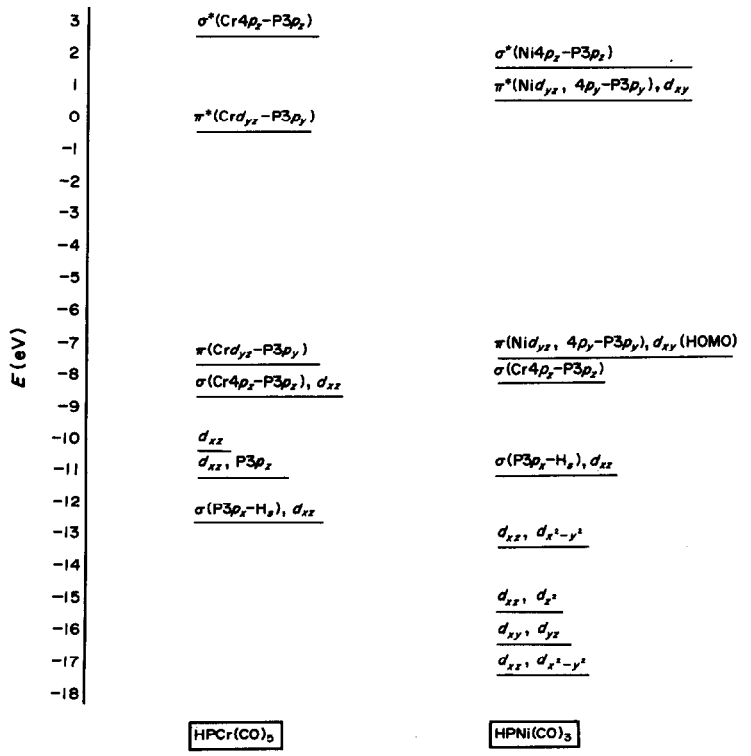


Fig. 2. MOs for $HPCr(CO)_5$ (**1**) and $HPNi(CO)_3$ (**2**) in eclipsed conformations.

predict that the singlet and triplet states of **1** are very close in energy. Further calculations are in progress on **1** and **2** and the related complexes $HPCr(CO)_4$ and $HPNi(CO)_2$.

Acknowledgements—We thank the National Science Foundation and the Robert A. Welch Foundation for financial support. Dr Pfister-Guillouzo and co-workers have performed PSONDO calculations on $HPCr(CO)_5$. We thank Dr Pfister-Guillouzo for her courtesy in sending a preprint of this manuscript.

REFERENCES

1. A. Marinetti, F. Mathey, J. Fischer and A. Mitschler, *J. Am. Chem. Soc.* 1982, **104**, 4484; A. Marinetti and F. Mathey, *Organometallics* 1982, **1**, 1488; 1984, **3**, 456; 1984, **3**, 1492.
2. D. H. Champion and A. H. Cowley, *Polyhedron* 1985, **4**, 1791.
3. H. Nakatsuji, J. Ushio, S. Han and T. Yanezawa, *J. Am. Chem. Soc.* 1983, **105**, 426.
4. L. Hedberg, T. Iijima and K. Hedberg, *J. Chem. Phys.* 1979, **70**, 3224.
5. B. R. Brooks, W. D. Ladig, P. Saxe, J. D. Goddard and H. F. Schaefer, In *Unitary Group for the Evaluation of Electronic Matrix Elements* (Edited by J. Hinze), p. 158. Springer, Berlin (1981).
6. H. Tatewaki and S. Huzinaga, *J. Chem. Phys.* 1979, **71**, 4339.
7. A. N. Tavouktsoglou and S. Huzinaga, *J. Chem. Phys.* 1980, **72**, 1385 for C and O; H. Tatewaki and S. Huzinaga, *J. Comput. Chem.* 1980, **1**, 205 for H; Y. Sakai, H. Tatewaki and S. Huzinga, *J. Comput. Chem.* 1981, **2**, 100 for P.
8. H. Nakatsuji, J. Ushio and T. Yanezawa, *J. Organomet. Chem.* 1983, **258**, Cl.
9. P. F. Zittel and W. C. Lineberger, *J. Chem. Phys.* 1976, **65**, 1236.

Polyhedron Vol. 5, No. 4, pp. 1031–1033, 1986
Printed in Great Britain

0277–5387/86 $3.00+.00
Pergamon Journals Ltd

COMMUNICATION

CATALYSIS BY HETEROPOLYACIDS—VIII. IMMOBILIZATION OF KEGGIN-TYPE HETEROPOLYACIDS ON POLY(4-VINYLPYRIDINE)

KENJI NOMIYA, HIROYUKI MURASAKI and MAKOTO MIWA*

Department of Industrial Chemistry, Faculty of Engineering, Seikei University, Musashino, Tokyo 180, Japan

(*Received* 28 *August* 1985; *accepted* 18 *November* 1985)

Abstract—Anchoring of a Keggin-type heteropolyacid (HPA) to a polymeric support and the effect of heterogenization on the HPA catalysis of the oxidation of a primary diol have been studied. A coloured HPA such as $H_6[Co(II)W_{12}O_{40}]$ (blue green), $H_4[SiMo_{12}O_{40}]$ (yellow) or $H_3[PMo_{12}O_{40}]$ (yellow), as the Keggin-type HPA and poly(4-vinylpyridine) as a polymeric support have been used. The anchoring of $H_6[Co(II)W_{12}O_{40}]$ has led to a markedly increased stability of the oxidation catalyst.

Generally, Keggin-type heterpolyacids (HPAs) $\{H_n[XM_{12}O_{40}]$ (X = heteroatom, M = Mo or W)$\}$ have both a strong Brønsted acidity and are oxidizable.[1] Previously we have reported the polycondensation of benzyl alcohols and the Friedel–Crafts-type reaction of aromatics on the basis of their acid catalysis,[2,3] and the oxidation of cyclohexanol to cyclohexanone and further to adipic acid on the basis of their oxidation catalysis.[4] Recently we have also described the oxidation reactions of primary diols such as 1,4-butane- and 1,5-pentanediols to the corresponding dicarboxylic acids via hydroxy-carbonic acids as intermediates. Such intermediates detected were γ-butyro- and δ-valero lactones resulting from an intramolecular condensation.[5] In the oxidation reactions, the tetrabutylammonium (Y) salt of the HPA as the main catalyst and H_2O_2 as a reoxidizing reagent have been used. In this work, we have tried immobilizing, by anchoring the HPA catalyst to a polymer, in order to further facilitate the recovery of it from the system and recycling in comparison with the case of the Y salt. Since a pyridine is attached to the HPA in the form of the pyridinium counterion, as in Y, we chose poly(4-vinylpyridine) [abbreviated hereinafter to poly(4-VP)] as a polymeric support. Adsorption of the HPA on poly(4-VP) was readily confirmed by using a coloured HPA, such as $H_6[Co(II)W_{12}O_4]$, $H_4[SiMo_{12}O_{40}]$ or $H_3[PMo_{12}O_{40}]$. The immobilized HPA was characterized by analyses and IR spectra, and was used as a catalyst for the reaction of 1,4-butanediol to γ-butyrolactone.

* Author to whom correspondence should be addressed.

EXPERIMENTAL

Preparation

Free HPAs, $H_6[Co(II)W_{12}O_{40}]$ (blue green), $H_4[SiMo_{12}O_{40}]$ (yellow) and $H_3[PMo_{12}O_{40}]$ (yellow), were prepared by the usual methods,[6,7] and are hydrated. They were also converted to the Y salts, $Y_4H_2[CoW_{12}O_{40}]$, $Y_4[SiMo_{12}O_{40}]$ and $Y_3[PMo_{12}O_{40}]$, which contain no solvated molecules. Poly(4-VP), the degree of polymerization of which was *ca* 3000, was obtained by the radical polymerization of 4-vinylpyridine initiated by benzoyl peroxide at 47–50°C under nitrogen.[8]

Immobilization of HPAs

To a methanol solution containing 0.1 g of poly(4-VP), which was slightly acidified with nitric acid, the methanol solution containing appropriate amounts of the HPA (X = Co, 3.00 g; X = Si, 1.99 g; and X = P, 1.99 g) was added and stirred for about 30 min

at 30–35°C. The coloured precipitates were filtered, washed thoroughly with methanol and dried *in vacuo*. If the filtrate was still coloured, the methanol solution containing 0.1 g of poly(4-VP) was again added and the coloured precipitates were isolated. This procedure was repeated until the filtrate became colourless. Coloured precipitates were produced by adsorption of the HPA on the polymer, which was characterized by analyses and IR spectra. The stoichiometry of the adsorption of the HPA on the polymer was calculated from the total amounts of poly(4-VP) consumed and the weight of precipitates obtained in each run. The acid catalysis of these immobilized HPAs was tested for polycondensation of benzyl alcohol.[2]

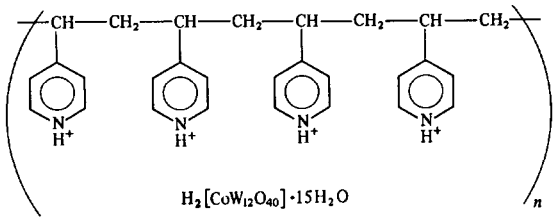
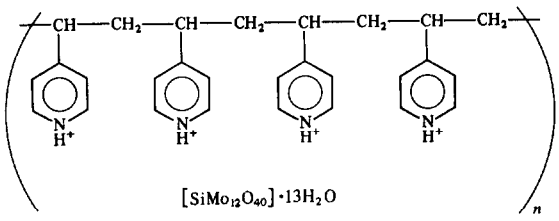
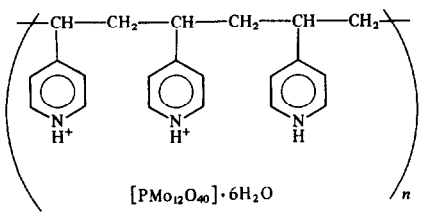
Oxidation of 1,4-*butanediol*

This reaction was performed by refluxing a mixture of the substrate (8 g), the immobilized HPA (170 mg) and 30% aqueous H_2O_2 (15 g) for an appropriate time. After the reaction, the HPA was filtered off, water in the filtrate was evaporated and the residue was extracted with benzene. One of the products, γ-butyrolactone, was obtained by distillation of the extracts under reduced pressure (bp_{22} *ca* 93°C), and identified by ^1H NMR, IR and TCD gas chromatography.

RESULTS AND DISCUSSION

The IR spectra of each immobilized HPA in the 1100–700-cm^{-1} region showed four stretching vibrations [M—terminal oxygen, M—O—M octahedral edge- and corner-sharings, and heteroatom (X)—triply bridged oxygen], characteristic of the Keggin structure.[7] These bands were shifted in the direction observed for the cation exchange from proton to Y, and the magnitudes of the shifts caused by immobilizing were less than half that observed in the Y exchange. The stoichiometry of the adsorption of the HPA on poly(4-VP) indicated that one molecule of HPA interacted with some pyridine groups in the polymer. Since the amount of HPA adsorbed on 0.1 g of the polymer was *ca* 0.51 g for X = Co, *ca* 0.44 g for X = Si, and *ca* 0.46 g for X = P, the number of interacting pyridines was formally estimated to be 5.6, 4 and 3.8, respectively. In these calculations, the contribution from the solvated waters in each HPA was ignored. The

Table 1. Analytical data of immobilized HPAs

Immobilized HPA	C (%)	H (%)	N (%)
			
For $(C_{28}H_{34}N_4[CoW_{12}O_{40}]\cdot 15H_2O)_n$			
Calc.	9.3	1.8	1.6
Found	9.3	1.6	1.6
			
For $(C_{28}H_{32}N_4[SiMo_{12}O_{40}]\cdot 13H_2O)_n$			
Calc.	13.6	2.4	2.3
Found	13.5	2.0	2.3
			
For $(C_{21}H_{24}N_3[PMo_{12}O_{40}]\cdot 6H_2O)_n$			
Calc.	11.2	1.6	1.9
Found	11.2	1.4	1.8

number of interacting pyridines was further explicitly determined by elemental analyses of the immobilized HPA. The analytical data (Table 1) suggest that adjacent pyridines in the polymer are attached to the HPA in the form of the pyridinium counterion, and constitute the new polymeric units, and, moreover, the number of interacting pyridines corresponds to the number of Y groups in the Y salt of the HPA, i.e. $Y_4H_2[Co(II)W_{12}O_{40}]$, $Y_4[SiMo_{12}O_{40}]$ and $Y_3[PMo_{12}O_{40}]$. Since some of the protons of the starting HPA are consumed by protonation to the pyridines in the polymeric unit, acid catalysis of the immobilized HPA could not be expected. In fact, they showed no catalytic activity for the polycondensation of benzyl alcohol to polybenzyl. From this viewpoint, the immobilized HPA is also very close to the Y salts. However, significant differences in the catalysis were observed in the oxidation of 1,4-butanediol.

When the immobilized form of the X = Co HPA was used as the main catalyst, γ-butyrolactone was obtained with a 16% yield after an 18-h refluxing. The number of moles of lactone produced per mole of catalyst per hour was 16.5. In this reaction, the catalyst was very stable and the Keggin structure of the HPA in it was retained after the reaction. The recovery of the catalyst from the system was easy and its reuse was possible several times without a decrease in its activity. On the contrary, the Y salt of the X = Co HPA decomposed after several hours refluxing, and neither recovery nor reuse was possible. In the cases of X = Si and P, both the immobilized forms and the Y salts functioned as good catalysts for the oxidation of the 1,4-diol. However, the reaction time of the immobilized catalyst was markedly shortened. For instance, the time until the H_2O_2 initially used was completely consumed was 3 h for X = Si and 4 h for X = P in the immobilized HPA, whereas it was 11 h for X = Si and 16 h for X = P in the Y salt. For these reaction times, the yields of γ-butyrolactone by both the immobilized catalyst and the Y salt were comparable, 22% for X = Si and 26% for X = P. However, concerning the stability of the catalyst, the Y salt was more excellent than the immobilized catalyst. This is in contrast to the case of X = Co.

REFERENCES

1. M. T. Pope, *Heteropoly and Isopoly Oxometalates*, p. 30. Springer, New York (1983).
2. K. Nomiya, T. Ueno and M. Miwa, *Bull. Chem. Soc. Jpn* 1980, **53**, 827.
3. K. Nomiya, Y. Sugaya, S. Sasa and M. Miwa, *Bull. Chem. Soc. Jpn* 1980, **53**, 2089.
4. K. Nomiya, M. Miwa and Y. Sugaya, *Polyhedron* 1984, **3**, 607.
5. K. Nomiya, M. Miwa and Y. Shoda, 45th Annual Meeting of the Chemical Society of Japan (1982), Abstract No. 1H42.
6. E. O. North and W. Haney, *Inorg. Synth.* 1939, **1**, 127.
7. K. Nomiya, R. Kobayashi and M. Miwa, *Bull. Chem. Soc. Jpn* 1983, **56**, 2272.
8. T. Okubo and N. Ise, *J. Am. Chem. Soc.* 1973, **95**, 2293.

Polyhedron Vol. 5, No. 4, pp. 1035–1036, 1986
Printed in Great Britain

0277–5387/86 $3.00+.00
Pergamon Journals Ltd

COMMUNICATION

THE REACTION OF *o*-XYLYLENE COMPLEXES OF RUTHENIUM WITH ALKYNES UNDER OXIDATIVE CONDITIONS

CHRISTINE L. SKERRATT, S. DAVID CHAPPELL, RICHARD D. BOWEN, RICHARD C. STORR and DAVID J. COLE-HAMILTON*†

School of Chemistry, University of Liverpool, P.O. Box 147, Liverpool L69 3BX, U.K.

(*Received* 23 *September* 1985; *accepted* 25 *November* 1985)

Abstract—Oxidation of *o*-xylylene complexes of ruthenium in the presence of dimethyl(acetylenedicarboxylate) produces the dimethylesters of 1,4-dihydronaphthalene-2,3-dicarboxylic acid and naphthalene-2,3-dicarboxylic acid.

o-Quinodimethanes are important intermediates in a large number of organic transformations, including the synthesis of pharmacologically active compounds such as steroids.[1,2] Although a number of efficient routes to these reactive species has been developed, the precursors tend not to be readily accessible and a new, direct route from a cheap starting material is therefore highly desirable.

In recent years, *o*-quinodimethane (xylylene) complexes of a number of different metals have been synthesized by a variety of routes.[3–9] However, no successful attempts to liberate *o*-quinodimethane from the metal under mild conditions have been reported. Thus, *o*-quinodimethane was not removed from $[C_8H_8Fe(CO)_3]$ by oxidation,[3] although, on thermolysis, benzocyclobutane was formed and reaction with $AlCl_3$ gave benzocyclopentanone.[10]

The only trapping of an *o*-quinodimethane liberated from a metal complex involves the binuclear $[\{CpCo(CO)\}_2C_8H_8]$, from which the bridging xylylidene ligand was displaced with phosphines and intercepted by dienophiles or else dimerized.[11]

We now report the first indication that *o*-quinodimethanes can be liberated from ruthenium complexes $\{[C_8H_8RuP_3]$ ($P = PMe_2Ph$ or $PMePh_2$)$\}$ by oxidation.

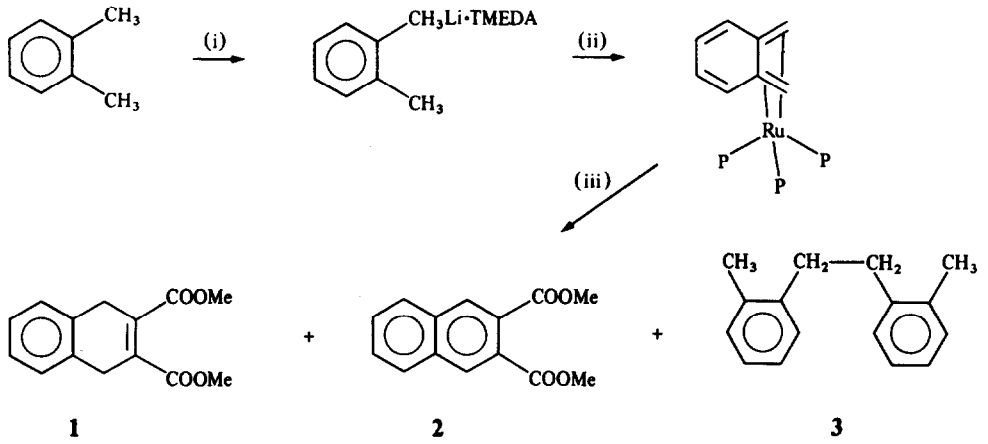
Treatment of these complexes in CH_2Cl_2 in the presence of dimethyl(acetylenedicarboxylate) (DMAD) with an excess of aqueous cerium(IV) ammonium nitrate affords the dihydronaphthalene (**1**) and naphthalene (**2**) in yields of 14 and 2%, respectively ($P = PMePh_2$).‡ The other major products are the phosphine oxide and the bibenzyl (**3**). With the less reactive dienophile $Me—C{\equiv}C—CO_2Me$, no adduct was detected and the amount of **3** increased. No reaction occurred between the complex and acetylene in the absence of oxidant and the simplest explanation is therefore that free *o*-quinodimethane is produced.

The yields of **1** and **2** have yet to be optimized by choice of oxidant and reaction conditions. However, the fact that $[C_8H_8RuP_3]$ can be prepared directly from *o*-xylene[5] (Scheme 1) gives the procedure great potential as a route to *o*-quinodimethane-derived products.

* Author to whom correspondence should be addressed.

† Present address: Department of Chemistry, University of St. Andrews, St. Andrews, Fife KY16 9ST, U.K.

‡ The compounds were characterized by comparison of GLC, GLC–mass spectrometry and ^1H NMR spectra, the last on a mixture of the two compounds obtained by column chromatography, with authentic **1** and the literature **1** and **2**.[12]



1 2 3

Scheme 1. Synthesis of naphthalene derivatives from *o*-xylene: (i) BuLi, TMEDA, hexane, 25°C; (ii) $RuCl_2P_4$ or $[Ru_2Cl_3P_6]^+Cl^-$, diethylether, 25°C; (iii) excess Ce^{4+}, MeOOCC≡CCOOMe, CH_2Cl_2–H_2O, 25°C.

Acknowledgements—We thank the SERC for support (S.D.C.) and for a grant to purchase a high-field NMR spectrometer, and Johnson Matthey Ltd for loans of ruthenium salts. D.J.C.-H. is the Sir Edward Frankland Fellow of the Royal Society of Chemistry, 1984–1985.

REFERENCES

1. W. Oppoltzer, *Synthesis* 1978, 793.
2. T. Kametani, *Pure Appl. Chem.* 1979, **51**, 747.
3. W. R. Roth and J. D. Meir, *Tetrahedron Lett.* 1967, 2053.
4. J. D. Oliver, Ph.D. thesis, Austin, Texas (1971) (*Chem. Abstr.* 1972, 106413).
5. S. D. Chappell, D. J. Cole-Hamilton, A. M. R. Galas and M. B. Hursthouse, *J. Chem. Soc., Dalton Trans.* 1982, 1867.
6. M. A. Bennett, I. J. McMahon and T. W. Turney, *Angew. Chem., Int. Ed. Engl.* 1982, **21**, 379.
7. W. H. Hersh, F. J. Hollander and R. G. Bergman, *J. Am. Chem. Soc.* 1983, **105**, 5834.
8. J. W. Hull and W. L. Gladfelter, *Organometallics* 1983, 1, 1716.
9. M. F. Lappert, C. L. Raston, G. L. Rowbottom, B. W. Skelton and A. H. White, *J. Chem. Soc., Dalton Trans.* 1984, 399.
10. B. F. G. Johnson, J. Lewis and D. J. Thompson, *Tetrehedron Lett.* 1974, 3789.
11. W. H. Hersh and R. G. Bergman, *J. Am. Chem. Soc.* 1983, **105**, 5846.
12. D. N. Butler and R. A. Snow, *Can. J. Chem.* 1975, **53**, 256.

Polyhedron Vol. 5, No. 5, pp. 1037–1104, 1986
Printed in Great Britain

0277–5387/86 $3.00+.00
Pergamon Journals Ltd

POLYHEDRON REPORT NUMBER 15

THE STRUCTURAL CHEMISTRY OF METAL THIOLATE COMPLEXES

IAN G. DANCE
School of Chemistry, University of New South Wales, Kensington, N.S.W. 2033, Australia

CONTENTS

1. INTRODUCTION 1038
1.1. Scope and restrictions 1038
1.2. Background 1038
1.3. General characteristics and organization of this Report. 1039
1.4. Incorporation of sulfide and polysulfide ions 1039
1.5. Biological metal thiolate coordination 1040

2. DESCRIPTION OF MOLECULAR STRUCTURE TYPES 1040
2.1. Monometallic structures 1040
2.2. Bimetallic structures 1045
2.3. Trimetallic structures 1048
2.4. Tetrametallic structures 1053
2.5. Pentametallic structures 1057
2.6. Hexametallic structures 1059
2.7. Heptametallic structures 1065
2.8. Octametallic structures 1065
2.9. Nonametallic structures 1069
2.10. Decametallic structures 1070
2.11. M_{12} structures 1072
2.12. M_{14} structures 1073

3. DESCRIPTION OF NON-MOLECULAR STRUCTURES 1073
3.1. One-dimensionally non-molecular structures 1074
3.2. Two-dimensionally non-molecular structures 1076

4. RELATED COMPOUNDS WITH COORDINATED DISULFIDE OR COORDINATED THIOL. 1079
4.1. Coordinated RSH 1080
4.2. Coordinated REER (E = S, Se or Te). 1080

5. STRUCTURAL PATTERNS AND PROPERTIES 1081
5.1. General characteristics. 1081
5.2. Metal oxidation states and coordination numbers 1081
5.3. Structural units 1081
5.4. Molecular symmetry and molecular distortions 1083
5.5. Topological relationships: families and progressions of polyhedra 1083
5.6. Thiolate bridges and bridging stereochemistry 1087
5.7. Packing of thiolate substituents over aggregate surfaces 1091
5.8. Dimensions 1092
5.9. Metal–metal interactions 1093
5.10. Structural influences of heteroligands 1094

6. STRUCTURAL PRINCIPLES FOR METAL THIOLATE COMPOUNDS 1094

7. CONCLUSIONS 1095
7.1. Thiolate as a pseudohalide ligand 1095
7.2. Comparison with alcoxides 1096

8. SPECULATION AND OUTLOOK 1096

1. INTRODUCTION

The organothiolate anion (RS^-) is a fundamental ligand type.* Together with the homologous organoselenolate (RSe^-) and organotellurolate (RTe^-), and alcoxide (RO^-) and aryloxide (ArO^-) anions, the thiolate anion may be classified as a pseudohalide, comparable as a ligand with Cl^-, Br^- and I^-. In metal complexes RS^- can be compared with HS^- and S^{2-}. This comparison highlights the appeal of RS^- to coordination chemists, part of which is that the organothiolate ligand can be regarded as sulfide with a handle, and a further part is that the substituent R can be manipulated powerfully and adjusted delicately to effect steric and electronic control of ligation ability. Consequently, the coordination chemistry of organochalcogenide ligands is potentially more variable than that of the "naked" chalcogenide ions, or of "naked" halide ions.

The categorization of RS^- as a pseudohalide rests in part on the one-electron oxidation [eqn 1]:

$$RS^- \rightleftharpoons \tfrac{1}{2}RSSR + e^-, \tag{1}$$

quantification of which is complicated by chemical irreversibility, and in part on the Bronsted basicity [eqn (2)]:

$$RS^- + H^+ \rightleftharpoons RSH. \tag{2}$$

Thiolates are stronger Bronsted bases than the halides, pK_a^{RSH} values in water ranging from 11.1 (Bu^tSH) through 9.4 ($PhCH_2SH$) to 6.6 (PhSH).[1,2] A third pseudohalide attribute of RS^- is metal complex formation comparable with that of the halides: the better known structural aspect of this characteristic is the subject of this Report.

1.1. *Scope and restrictions*

In order to concentrate on the fundamental chemistry of the thiolate ligand function, this Report emphasizes complexes of monofunctional thiolate ligands. Numerous chelating ligands incorporating a thiolate donor have been concocted and deployed for various purposes,[3,4] but in these cases the intrinsic metal thiolate chemistry is obscured by the geometrical, thermodynamic and electronic influences of the remainder of the ligand. Therefore complexes of the amino acid cysteine functioning as a chelate ligand are excluded, but complexes involving the cysteinate side chains of a polypeptide are included. For the same purpose of focusing on innate ligating characteristics of thiolates, this Report will emphasize complexes which contain only thiolate ligands (homothiolate complexes) or at least a large proportion of thiolate ligands. Comparative descriptions of alcoxide metal complexes (for which there is an extensive secondary literature[5,6]) and selenolate and tellurolate complexes will be included where pertinent.

1.2. *Background*

In this Report the principal emphasis is on the geometrical structures of metal thiolate complexes. Synthetic methods, chemical reactivities and physical properties will be treated in a separate article. The purpose here is to describe and analyse the menagerie of structure types confirmed or probable for metal thiolate compounds, and to elucidate structural principles. Thiolate ligands have a reputation for bridging metal atoms, a reputation engendered by the insolubility and presumed polymeric structures of the familiar metal thiolates $\{[M(SR)_n]_p\}$, frequently formed when thiolate ions and metal ions are

* R represents any non-coordinating function. Other abbreviations used generally in this Report are: Ar, arene substituent; E, chalcogen; X, halogen; t, terminal; b, bridging; ax or a, axial; eq or e, equatorial; i, inner; o, outer.

mixed in protic media. However, the paradigm of bridging thiolate, initiated by Jensen[7] who proposed the structure type **1D-D** below for $[Ni(SR)_2]_\infty$, has been confirmed only in recent years. The first crystal structure of a homothiolate compound [molecular $Hg(SMe)_2$] was reported in 1964,[8] and prior to 1974 there was only one report of the crystal structure of a homothiolate compound with a *non-molecular* structure, namely $[Hg(SBu^t)_2]$.[9]

The structural novelties to be found with other metals were presaged by the report[10] in 1965 of the hexagonal "tiara" structure of $Ni_6(SEt)_{12}$, and the 1969 report[11] of $[Cd_{10}(SCH_2CH_2OH)_{16}]^{4+}$, which is related to the sphalerite structure. Since 1973 there has been sustained effort on the designed syntheses of metal thiolate complexes, supported by structural characterization by diffraction methods, and now almost 70 structure types are known. Almost all of these results have appeared since the early reviews[12,13] which covered the structures of metal thiolates. A limited collection of metal thiolate structures was published in 1984.[14]

1.3. *General characteristics and organization of this Report*

This Report contains descriptive, analytical, evaluative and speculative sections. The descriptive section is subdivided in terms of the structural molecularity of the compounds. Structurally molecular compounds, that is those totally enclosed by non-bonding (van der Waals') boundaries, are treated before one-dimensionally non-molecular (chain) structures, which are followed by two-dimensionally non-molecular (layer) structures. No instances of three-dimensionally non-molecular metal thiolate structures are known (or expected, in view of the spatial requirements of the thiolate substituents). *Structural* molecularity carries no connotations of size or charge.

Molecular structures are subdivided primarily according to increasing number of metal atoms, then according to increasing metal oxidation state, while the finest subdivision is according to metal coordination number. In all cases the first description is of *observed* geometrical structure, followed by more speculative discussion of bonding and electronic structure.

A significant characteristic of most of the structures to be described is actual low symmetry combined with an approach to high symmetry. It is convenient and instructive to symmetrize and idealize the observed structures, and to rationalize deviations from these idealizations. By this means geometrical relationships between apparently diverse structures can be extracted and evaluated. The highest symmetry occurs in the core of M and S atoms, and the structure descriptions are presented with this symmetrization imposed. The substituents R are responsible for the lowered actual symmetry in several different ways: one source of dissymmetry is the pyramidal stereochemistry at the S atom of the doubly-bridging thiolate causing the S—R bonds to be non-radial and allowing *configurational* isomers which cannot adhere to the symmetry of the M, S core. A second originates in repulsions between a small proportion of contiguous substituents, a third is due to various *conformations* of terminal SR ligands, and a fourth is the asymmetry of R alone.

The initial descriptions of the structures in Sections 2 and 3 are made in relatively coarse focus, with a tendency towards idealization, in order to achieve an overview and systematization of the field. Subsequently details of the thiolate substituents and their effects are described in Sections 5.4 and 5.7, and a more finely focussed view of structural dimensions follows in Section 5.8.

In some crystal structures there occurs a disparity of M—S distances and S—M—S angles, referenced to normal symmetrizations. These structures are analysed in terms of primary and secondary metal thiolate coordination, or in terms of weak (secondary) association of molecular units.

1.4. *Incorporation of sulfide and polysulfide ions*

Descriptions of metal thiolates benefit by comparison with compounds containing S^{2-} (the unsubstituted thiolate) and polysulfide ions S_x^{2-} (the "inorganic thiolate").* Mixed sulfide–thiolate–metal complexes $\{[S_wM_x(SR)_y]^z\}$ have been studied in detail since 1973 for M = Fe, and more recently for other metals. Structural relationships exist between binary M–SR compounds, binary M–S compounds (both molecular and non-molecular), and ternary M–S–SR compounds. An emerging theme concerns the structural congruence of different compounds from this set, and in particular the

* Complexes of organopolysulfides (RS_x^-) have not yet been characterized.

occurrence of molecular cages, mainly with thiolate ligands, as fragments of non-molecular structures, mainly metal sulfides.

Redox relationships involving thiolate and sulfide ions as ligands are also pertinent.[15] The oxidation products of sulfide, S_x^{2-} (x = 2, 4, 5, 6, 8 or 9), have now been found as ligands in a variety of bonding modes,[16-19] while the immediate oxidation product of thiolate, RSSR, is a distinctly uncompetitive ligand type. Polysulfide ions (S_x^{2-}) function similarly to chelating dithiolate ligands ($^-SRS^-$) in many complexes.

1.5. *Biological metal thiolate coordination*

Metal thiolate coordination occurs naturally, primarily through the thiolate side chain of the amino acid cysteine.[20] Crystal X-ray diffraction analyses[20,21] have clearly defined the metal cysteinate coordination in the following metalloprotein sites: (i) tetrahedral Zn coordination by four cysteinates in alcohol dehydrogenase and aspartate carbamoyl transferase,[22] (ii) tetrahedral Zn coordination by two cysteinates, one histidine and one water or substrate ligand in alcohol dehydrogenase; (iii) Fe with four cysteinates and tetrahedral stereochemistry in rubredoxin; (iv) pseudotetrahedral Cu with one cysteinate, one methionine and two histidine ligands in plastocyanin; (v) $Fe_2S_2(S\text{-cys})_4$ ferredoxins,[21] (vi) $Fe_3S_3(S\text{-cys})_5$ ferredoxins,[21,23] and (vii) $Fe_4S_4(S\text{-cys})_4$ ferredoxins.[20,21] In addition, physicochemical data imply metal cysteinate coordination in: (viii) cytochrome *P*-450 (cysteinate axial to heme Fe), (ix) cytochrome *c* oxidase (cysteinate bridging two Cu atoms[24]), (x) Mn(III) phosphatases,[25,26] (xi) Fe_3 ferredoxins from *Desulfovibrio gigas* and aconitase,[20] and (xii) various Mo-containing oxidoreductase enzymes.[20]

The metallothioneins constitute a unique class of metalloproteins which are polymetallic with *exclusive* coordination by the cysteine thiolate function.[27,28] The best characterized metallothioneins contain seven M atoms (Zn and/or Cd), a singularly high proportion, 20/61, of cysteinate side chains, and are devoid of aromatic amino acids. A determination of crystal structure is expected.[29] All cysteinate groups are metal-bound, some as bridging ligands probably in aggregates with three and four M atoms[30-34] as described in Sections 2.3.6 and 2.4.4. The metals Zn, Cd, Hg, Cu, Ag and Pb induce the formation of metallothioneins, and can be involved in their probable functions of metal storage and metal detoxification by sequestration.

It has been partial knowledge of the structures, properties and functions of metallocysteine proteins which has stimulated much of the recent development of metal thiolate chemistry, particularly the pioneering research by Holm.[35]

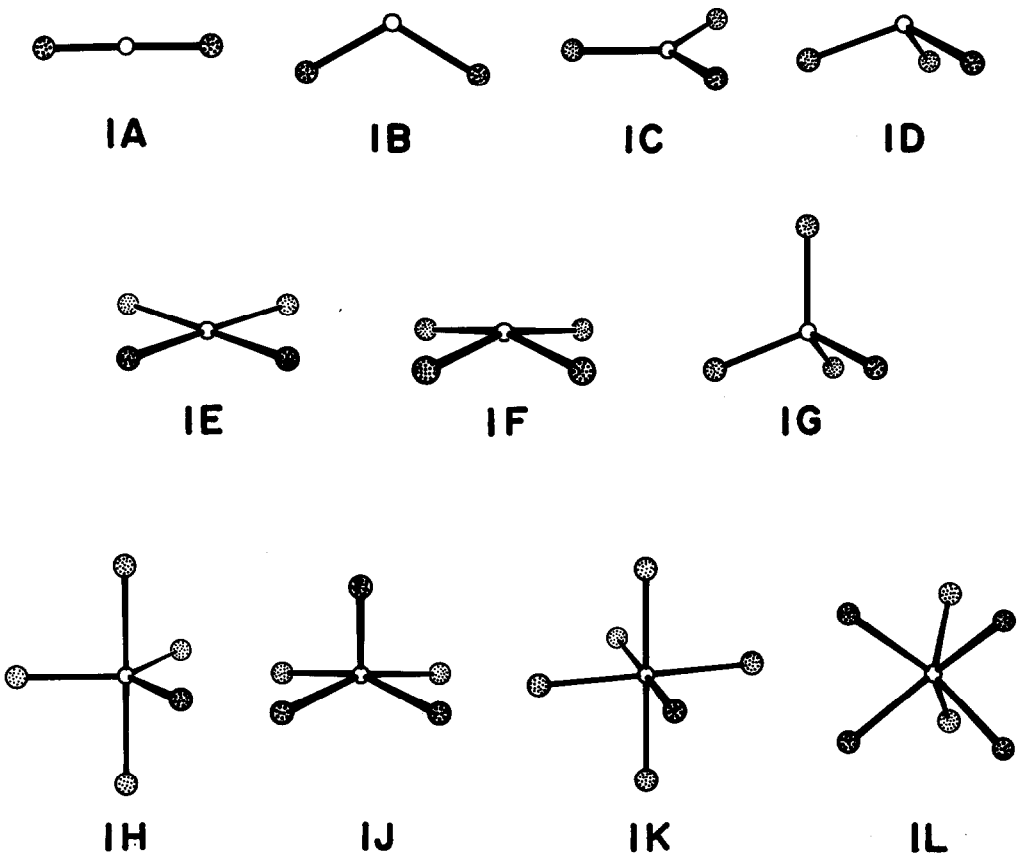
2. DESCRIPTION OF MOLECULAR STRUCTURE TYPES

Not all of the following structure types have been confirmed by diffraction methods. Structures indicated by other physical data, and structures which can reasonably be postulated to exist, at least in solution, have been included to maintain completeness. Also included are some structure types which occur in related metal halide/pseudohalide/alkyl systems, and which are discussed as possible structures for metal thiolates.

The diagrams of idealized structure types show M atoms as small open circles, while the SR ligands are usually presented as larger dotted circles at the S positions only, since the substituent configurations and conformations are variable. Where substituents are included the small filled circles represent α-carbon atoms. Stipled circles denote heteroatoms.

2.1. *Monometallic structures*

2.1.1. *Linear* $M(SR)_2$ (**1A**). This structure is established in the mercury thiolates $[Hg(SR)_2]$ {where R = Me,[8] Et,[36] $CH_2CH_2CONHMe$,[37] $[CH_2CH_2NMe_3]^+$,[38] or $[C_5H_9NHMe]^+$ (4-thiolato-*N*-methylpiperidinium)[39]}, in $[HOOCCH(NH_3)CH_2SHgSCH_2CH(NH_3)COO^-]^+$,[40] and in $[Cu(SC_6HMe_4\text{-}2,3,5,6)_2]^-$.[41] It is probable that structure **1A** also occurs in the anions $[M(SC_6F_5)_2]^-$ (M = Cu, Ag or Au[42,43]) and $[ClAuSC_6F_5]^-$.[43] Molecular weight data on $[Cu(SPh)_2]^-$ (Ph_4P^+), and the vibrational spectra of $[Au(SR)_2]^-$ (Ph_4P^+, PPN^+ or Bu_4N^+) (R = Me, Bu^t or Ph),[44] point to the occurrence of the same structure. Related compounds in which the structure is confirmed are $[AuS_9]^-$ (Ph_4As^+)[45] {and possibly $[AgS_9]^-$ (Ph_4P^+)[46]}, in which a linear S–Au–S segment is



contained in a 10-membered ring, Et_3PAuSR (SR = 2,3,4,6-tetra-*O*-acetyl-1-thio-β-D-glucopyranose),[47] $[O_3SSAuSSO_3]^{3-}$,[48] and $PhHgSC_6H_3Me_2$-2,6.[49]

Linear coordination by two bridging alkyl or aryl thiolates is confirmed in other structures (e.g. **5A** and **5B**) for Cu(I) and Ag(I). Therefore, since two bridging ligands, and therefore two terminal thiolate ligands, can provide an electron density sufficient to coordinatively saturate these metals, it can be expected that $[M(SR)_2]^-$ complexes with structure **1A** will occur in solution in equilibria involving these metals and thiolates. These labile equilibria are not readily characterized, and the compositions and structures of crystals from the solutions need not reflect compositions and structures of complexes in solution. For instance, $[Cu(SPh)_3]^{2-}$ with Ph_4P^+ in CH_3CN crystallizes as $[Cu(SPh)_2]^-$, but with Et_4N^+ in CH_3CN–OPr^i_2 it crystallizes as $[Cu(SPh)_3]^{2-}$.[50,51] The properties of many $Hg(SR)_2$ are consistent with digonal coordination.[52,53] In this structure type the M and S atoms are exposed, and the occurrence of secondary M---S interactions is common. These secondary connections usually approach the estimated van der Waals' contact distance of *ca* 3.6 Å. Solid-state aggregation patterns are sometimes regular, with pseudo-octahedral stereochemistry around Hg, while in $[Hg(SCH_2CH_2NMe_3)_2]^{2+}$ (ClO_4^-)[38] there are discrete aggregates of three and six Hg atoms, as in Fig. 1. The alternative one-dimensionally non-molecular structure (**1D-C**) with tetrahedral primary coordination occurs in $Hg(SBu^t)_2$,[9] $Hg(SeMe)_2$[53] and related compounds (see Section 3.1.3).

2.1.2. *Bent* $M(SR)_2$ (**1B**). This structure is known in $Sn(SAr)_2$,[54] where Ar is the hindered substituent 2,4,6-tri-*t*-butylphenyl. The S—Sn—S angle of 85.4° is remarkably small, but not much smaller than the corresponding angles of 88.8° in $Sn(OAr')_2$ (Ar' = 2,6-di-*t*-butyl-4-methylphenyl)[55] or of 104.7° in $Sn[N(SiMe_3)_2]_2$.[56] Structure **1B** could be expected in species $[Tl(SR)_2]^-$.

2.1.3. *Trigonal planar* $M(SR)_3$ (**1C**). This structure is confirmed in $[Cu(SPh)_3]^{2-}$ crystallized with Ph_4P^+,[50] or Et_4N^+,[51] and in $[Hg(TePh)_3]^-$ (Ph_4P^+),[57] each of which is closely planar. There are substantial differences between the CuS_3 cores of the $[Cu(SPh)_3]^{2-}$ ions, that with Et_4N^+ being essentially D_{3h} while that with Ph_4P^+ is distorted towards C_{2v}. The Cu—S distance and S—Cu—S angle disparities, 2.335 vs 2.274 Å and 135.4 vs 111.7 and 113.0°, respectively, are correlated as described in Section 5.8. This distortion towards linear two-coordination in the crystal phase of

$(Ph_4P^+)_2[Cu(SPh)_3]$ can be coupled with the observation of its dissociation [eqn (3)]:

$$[Cu(SPh)_3]^{2-} \rightleftharpoons [Cu(SPh)_2]^- + PhS^- \quad (3)$$

which occurs even in aprotic solvents,[50]* and with the fact that, relative to the Et_4N^+ salt, the Ph_4P^+ salt has a lower-energy electronic absorption in both solid and solution phases.[51] In the presence of Et_4N^+, $[Cu(SPh)_3]^{2-}$ does not dissociate in aprotic solvents. Evidently Ph_4P^+--$[Cu(SPh)_3]^{2-}$ associations (Ph--Ph) influence both the geometrical structure and the dissociative equilibria of $[Cu(SPh)_3]^{2-}$.

Crystalline $(Ph_4P)[Hg(EPh)_3]$ (E = S or Se) are not isomorphous with the Te homolog.[57] The vibrational spectra of $(Ph_4P)[Hg(SPh)_3]$ have been interpreted in terms of trigonal pyramidal HgS_3 coordination:[58(a)] in fact $(Bu_4N)[Hg(SPh)_3]$ has trigonal planar coordination,[58(b)] while the same anion, when crystallized with Me_4N^+, adopts the dimeric structure $[(PhS)_2Hg(\mu\text{-}SPh)_2Hg(SPh)_2]^{2-}$ (**2E**).[58(c)] The IR and Raman spectra of complexes (cat)$[Hg(SR)_3]$ (R = Me in ethanol solution and R = Bu^t)[59] indicate that they are trigonal planar.

A possible member of this structural class is the recently reported tris(isopropylthio)silylenium ion $\{[(Pr^iS)_3Si]^+\}$.[60]

2.1.4. *Pyramidal* $M(SR)_3$ (**1D**). There is IR and Raman spectroscopic evidence[42] that $M(SC_6F_5)_3$ (M = Sb or Bi) are pyramidal in ethanol solution. These two compounds, which are crystallographically isomorphous and monomeric in nitromethane, are soluble in a wide range of organic solvents.[42] The primary coordination in tris(2-pyridinethiolato)antimony(III) is pyramidal SbS_3 (symmetry C_3, Sb—S 2.47 Å, S—Sb—S 90.0° : Sb--N 2.83 Å).[61] Structure **1D**, rather than **1C**, is indicated by the low-frequency vibrational spectra of $[Hg(SPh)_3]^-$ (Ph_4P^+),[58] and may occur also in the monometallic anions $[M(SC_6F_5)_3]^-$ (M = Sn or Pb).[42] Diffraction analysis has confirmed structure **1D** in $[Pb(EPh)_3]^-$ (E = S or Se) (Ph_4As^+),[62] while multinuclear NMR studies reveal the existence of a series of species $[M(SPh)_x(SePh)_{3-x}]^-$ (x = 0–3, M = Sn or Pb) in methanol solution and for which the same structure is presumed.[63] It is probable that structure **1D** also occurs in compounds $M(SPh)_x(SePh)_{3-x}$ (M = As, Sb or Bi, x = 0–3).

2.1.5. *Square planar* $M(SR)_4$ (**1E**). Surprisingly no instance of this simple structure type with monodentate thiolate ligands has been confirmed by diffraction methods, but it probably occurs in the ions $[M(SC_6F_5)_4]^{2-}$ (M = Ni,[64] Pd or Pt[43,65]), $[Pt(SC_6Cl_5)_4]^{2-}$[66] and $[Au(SC_6F_5)_4]^-$. It is significant that $[Ni(SC_6F_5)_4]^{2-}$ (Ph_3MeAs^+) is diamagnetic and presumed to be square planar,[64] while $[Ni(SPh)_4]^{2-}$ (Ph_4P^+) is known[67,68] to be tetrahedral (structure **1G**). Tetrahedral coordination of Ni or Pt (M) by thiolate ligands also occurs in $[(\eta^5\text{-}C_5H_5)_2M'(\mu\text{-}SMe)_2M(\mu\text{-}SMe)_2M'(\eta^5\text{-}C_5H_5]^{2+}$ (PF_6^-) (M′ = Nb or Ta),[69,70] but in these compounds there may be M--M′ bonding, and the electron

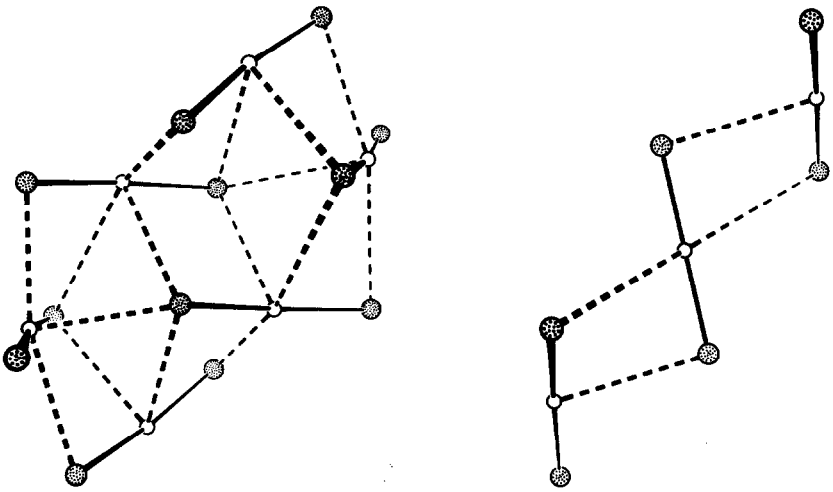


Fig. 1. Aggregates of six and three RSHgSR units in crystalline $[Hg(SCH_2CH_2NMe_3)_3]^{2+}$ $(ClO_4^-)_2$. The broken lines are the elongated secondary bonds.

* In aprotic solvents the thermodynamic activity of the PhS^- product of dissociation (3), relative to the activity of the associated complex, is greater than in protic solvents, and therefore dissociation is least favoured in aprotic solvents.

distribution may be such that the M population is closer to d^{10}, for which tetrahedral stereochemistry is normal.[71] As $(Ph_4P)_2[Ni(SPh)_4]$ is one of a series of isostructural crystals $\{(Ph_4P)_2[M(SPh)_4]\}$ with tetrahedral stereochemistry,[68] it is to be suspected that the coordination stereochemistry is a consequence of a lattice energy dominated by the cation. Chelate complexes with square planar stereochemistry are $[M(SCH_2CH_2S)_2]^{2-}$ [M = Cr[72(a)] or Ni[72(b)]] and the remarkable spin-triplet Co(III) complex $[Co(SCH_2CH_2S)_2]^-$,[72(a)] while $[M(S_4)_2]^{2-}$ (M = Ni or Pd)[18] are square planar, the latter with a slight tetrahedral distortion.

2.1.6. *Pyramidal* $M(SR)_4$ (**1F**). This structure may occur in $[Sb(SC_6F_5)_4]^-$ (and metal-substituted chloro derivatives) and $[Bi(SC_6F_5)_4]^-$.[42]

2.1.7. *Tetrahedral* $M(SR)_4$ (**1G**). This homothiolate structure occurs widely, and has been established crystallographically for the following complexes:

(a) the ions $[M(SPh)_4]^{2-}$ (M = Mn, Fe, Co, Ni, Zn or Cd), which form a series of isomorphous crystals with Ph_4P^+,[68,73–75] and the ions $[M(SPh)_4]^{2-}$ (M = Co, Zn or Cd) in crystals with Me_4N^+;[76]

(b) the ions $[M(SC_6H_4Cl\text{-}4)_4]^{2-}$ (M = Fe, Zn, Cd or Hg) in crystals with Me_4N^+;[76,77]

(c) $[Fe(SEt)_4]^{2-}$ (Et_4N^+);[78]

(d) the Fe(III) species $[Fe(SC_6HMe_4\text{-}2,3,5,6)_4]^-$ (Et_4N^+),[79] $[Fe(SC_6H_2Pr^i_3\text{-}2,4,6)_4]^-$ (Ph_4P^+),[80] $[Fe(SPh)_4]^-$ (Et_4N^+)[81] and $[Fe(SEt)_4]^-$ (Pr_4N^+);[81]

(e) $Mo(SBu^t)_4$;[82]

(f) $Sn(SePh)_4$;[83]

(g) $[Ga(SEt)_4]^-$ (Pr_4N^+);[81,84]

(h) $[M(SCH_2CH_2S)_2]^{2-}$ [M = Mn[85] or Co[72(a)]];

(i) the Fe(II) and Fe(III) complexes $[Fe(S_2\text{-}o\text{-}xyl)_2]^{2-,-}$ of the large-bite chelating dithiolate ligand $1,2\text{-}C_6H_3(CH_2S)_2$;[86]

(j) $[Hg(S_6)_2]^{2-}$ (Et_4N^+),[87] with a slightly distorted tetrahedral HgS_4 coordination from two 1,6-chelating S_6^{2-} ions.

Additional homothiolate compounds for which the tetrahedral monometallic structure is very probable include the ions $[M(SC_6F_5)_4]^{2-}$ (M = Co,[43,64,88,89] Zn,[43,89] Cd[43,89] or Hg[43,89]) and numerous uncharged compounds $[M(SR)_4]$ (M = Ge[90] or Sn[91]) which are monomeric in solution.

Tetrahedral monometallic structures have been established for the following complexes containing heteroligands: $[MeN(CH_2CH_2)_3NZn(SPh)_3]$,[92] $[CH_3CNCo(SC_6HMe_4\text{-}2,3,5,6)_3]^-$ (Pr_4N^+),[93] $[SSi(SPh)_3]^-$ $(HNC_5H_5^+)$,[94] $(piperidine)_2Zn(SPh)_2$,[95] $(1,10\text{-phen})Zn(SC_6H_4Me\text{-}4)_2$,[96] $Cl_2Co(SC_5H_4NHMe)_2$,[97] $(Ph_3P)_3AgSPh$[98] and $HB(3,5\text{-}Me_2Pz)_3CoSC_6F_5$.[99–101] Crystal structures have been determined for many compounds of the type Ar_3MSR (M = Ge, Sn or Pb).[102]

2.1.8. *Proteins containing* $M(S\text{-}cys)_4$ *coordination.* Tetrahedral $M(SR)_4$ coordination by cysteine is known from diffraction studies to occur in three enzymes:[22] (i) rubredoxin (Rd) (M = Fe),[103,104] which has two oxidation states, Rd_{ox} and Rd_{red}; (ii) liver alcohol dehydrogenase (LADH) (M = Zn);[105] and (iii) aspartate carbamoyl transferase (M = Zn[Fe]).[23] The cysteinyl locations in the polypeptide sequences are 3, 6, 39 and 42 for Rd_{ox} from *Clostridium pasteurianum*[104] and *Desulfovibrio vulgaris*,[103] 97, 100, 103 and 111 for horse LADH, and 109, 114, 137 and 140 for aspartate carbamoyl transferase from *E. coli*.[23] A common pattern in these sequences is separation by two residues of cysteinyl residues directly chelating a single M atom.

In LADH the $Zn(S\text{-}cys)_4$ section of the protein appears to have a purely structural function, the active site being another Zn atom coordinated by two cysteines and one histidine, and by water or substrate. Aspartate carbamoyl transferase contains different catalytic (Cat) and regulatory (Reg) subunits. The $Zn(S\text{-}cys)_4$ section is in the Reg chain, establishing an ordered domain which provides for well-defined tight interactions between Reg and Cat. All of the substructures (e.g. loops ending at cysteine residues) determined by the coordination of Zn^{2+} to the four cysteines of the Reg chain participate in the interactions between Reg and Cat chains.

In Rd the $Fe(S\text{-}cys)_4$ region is the site of enzymatic activity, which is electron transfer. Despite early reports to the contrary, the available structural results reveal relatively small variations from tetrahedral stereochemistry. In Rd *ex C. pasteurianum* the Fe—S distances are 2.24(1), 2.29(1), 2.30(1) and 2.33(1) Å, and the S—Fe—S angles range from 103.7(4) to 114.3(5)°.[104]

2.1.9. *Trigonal bipyramidal* $M(SR)_5$ (**1H**). Only one five-coordinate $M(SR)_5$ structure is confirmed,

that of $[Sn(SPh)_5]^-$ (Me_4N^+).[106] The stereochemistry is distorted trigonal bipyramidal, in which the Sn—S^{ax} distances are 2.499(2) and 2.574(2) Å, and the Sn—S^{eq} distances 2.477(1), 2.483(1) and 2.483(1) Å. The S^{ax}—Sn—S^{ax} angle is 172.7°, and the S^{eq}—Sn—S^{eq} angles 111.5, 121.5 and 125.0°. The distortion occurs mostly in the S^{ax}—Sn—S^{eq} angles, which range from 75.8 to 97.9° without evident correlation with the benzenethiolate ligand orientations.

A set of remarkable trigonal bipyramidal complexes $[(CH_3CN)M(SAr)_4]$[107] and $[(CO)M(SAr)_4]$[108] (M = Ru or Os), is formed by the hindered ligands SAr (2,3,5,6-tetramethylbenzenethiolate and 2,4,6-triisopropylbenzenethiolate). An isostructural compound is $[(CH_3CN)Ru(SeAr)_4]$.[109] The heteroligand is in the axial position. Both ruthenium thiolate compounds with acetonitrile have elongated axial bonds in a fairly regular trigonal bipyramid: average dimensions are Ru—S^{eq} 2.108 Å, Ru—S^{ax} 2.378 Å, Ru—N^{ax} 2.102 Å, S^{ax}—Ru—N^{ax} 178.2°, S^{eq}—Ru—S^{eq} range 114–124°. The absence of stereochemical distortion by the bulky 2,6-substituents of the arenethiolate ligands is significant. All four acetonitrile compounds are known to be susceptible to one-electron oxidation and one-electron reduction: it appears[107] that both oxidation and reduction are chemically reversible.

A class of trigonal bibyramidal complexes $[MXY(SR)_3]^z$, with X and Y axial, is emerging. Instances are $[Re(NCCH_3)(PPh_3)(SPh)_3]$ {and probably $[Re(CO)(PPh_3)(SPh)_3]$ by replacement of the CH_3CN},[110] $[Mo(NO)(SAr)_4]^-$,[111] $[W(NO)Cl(SPh)_3]^-$[111] and $[Mo(NO)Cl(SBu^t)_3]^-$.[111] A pattern in the molecular structures is orientation of the aryl substituents of the equatorial thiolate ligands towards (and the S non-bonding electrons away from) the more strongly bound pi-acceptor ligand $NCCH_3$ or NO, and elongation of the other axial bond.

Structural information is not yet available on the monometallic anions $[Sn(SC_6F_5)_5]^-$, $[ClSn(SC_6F_5)_4]^-$ and $[Cl_2Sn(SC_6F_5)_3]^-$,[42] or on the compounds $Nb(\overline{SPh})_5$ and $Ta(\overline{SPh})_5$.[112]

2.1.10. *Square pyramidal* $XM(SR)_4$ (**1J**). This structure type is now established for V, Mo, W, Tc and Re. Crystallographic data are available for: $[OM(SPh)_4]^-$ (Ph_4As^+) (M = Mo[113] or Re[114]), $[OM(SC_6HMe_4\text{-}2,3,5,6)_4]^-$ [M = Mo (Et_4N^+) or W (Pr_4N^+)],[115] $[ORe(SC_6H_2Me_3\text{-}2,4,6)_4]^-$ (Et_3NH^+),[116] $[ORe(SC_6H_3Pr^i_2\text{-}2,6)_4]^-$,[116] $[OV(SCH_2CH_2S)_2]^{2-}$ (Me_4N^+,Na^+),[117] (Na^+),[118] $[(Ph_3PN)Re(SPh)_4]$,[110] $[OTc(SCH_2CH_2S)_2]^-$ (Ph_4As^+),[119] $[SRe(SCH_2CH_2S)_2]^-$ (Me_4N^+),[120] $[SV(SCH_2CH_2S)_2]^{2-}$ (Ph_4P^+),[118] $[OTc(SCH_2CH_2O)_2]^-$ (Ph_4As^+)[121] and $[OTc(SCH_2C(O)S)_2]^-$ (Bu_4N^+).[122] According to similarities of physical properties it is proposed that the following related complexes possess the same molecular structure: $[OM(EPh)_4]^-$ (M = Mo or W, E = S or Se),[123,124] $[ORe(SePh)_4]^-$[114] and $[ORe(SCH_2CH_2S)_2]^-$.[120]

In all cases the stereochemistry is very close to square pyramidal. Basal angles at the metal range from 81 to 87°, and the displacement of the metal from the basal plane ranges from 0.72 to 0.82 Å {in $[OTc(SCH_2CH_2O)_2]^-$ and $[OMo(SPh)_4]^-$, respectively}, except in the complex $[SRe(SCH_2CH_2S)_2]^-$, where the Re atom is 0.4 Å above the basal plane.[120] A comparative compilation of stereochemical data for OMS_4 cores is available.[114] In both $[OMo(SPh)_4]^-$ and $[ORe(SPh)_4]^-$ the benzenethiolate ligands are arrayed approximately as a turbine with C_4-symmetry about the axial bond.

2.1.11. $M(SR)_6$ [*octahedral* (**1K**) *and trigonal prismatic* (**1L**)]. No instances of these structures with monodentate thiolate ligands are known. Re(V) coordinated by six alkyl thiolate functions occurs in the complex $[(CH_3C(CH_2S)_3)_2Re]^-$ (Ph_4P^+).[125] The regular stereochemistry is twisted trigonally by only 6° from a trigonal prism, and, consequently, the eclipsed inter-ligand S—S distances are relatively short (2.80, 2.80 and 2.85 Å), appreciably less than the non-bonded van der Waals' contact distance of 3.6 Å. In the absence of any steric influence on coordination stereochemistry in this complex, it is suggested that direct attractive interactions occur between these S donor atoms, and contribute electronically to the stabilization of the trigonal prismatic stereochemistry.* In $[Ti(SCH_2CH_2S)_3]^{2-}$ with projected twist angles (ϕ) of 35–42°, the stereochemistry is between octahedral (ϕ = 60°) and trigonal prismatic (ϕ = 0°).[72(a)]

Six-coordinate monometallic thiolate complexes with heteroligands have been characterized structurally: examples are (bipy)$Sn(SPh)_4$[127] and *cis*-$(Bu^tNC)_4Mo(SBu^t)_2$.[128,129]

* Note that these are not the same attractive interactions as those proposed for the triangular edges of trigonal prismatic tris-dithiolene complexes.[126]

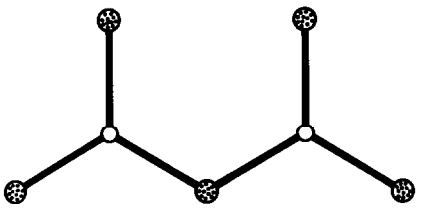
2.2. *Bimetallic structures*

Bridging thiolate ligands are now introduced. Although relatively few dimetallic homothiolate structures are confirmed, a large number of closely related heteroligand structures are known and leave little doubt about the feasibility of structures proposed below.

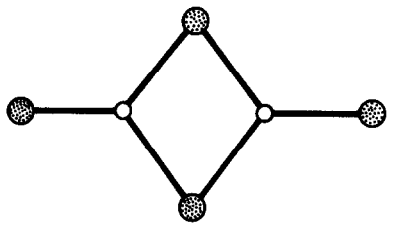
2.2.1. *Two-coordinate* RMS(μ-SR)MSR (**2A**). This structure type has been proposed for Cu(I) species with stoichiometry $[Cu_2(SR)_3]$ (R = $[CH_2CH_2NMe_3]^+$ or $[CH_2CH_2SO_3]^-$) in solution.[130] The same stoichiometry occurs in the confirmed tetrametallic structure type **4C**.



2A



2B



2C



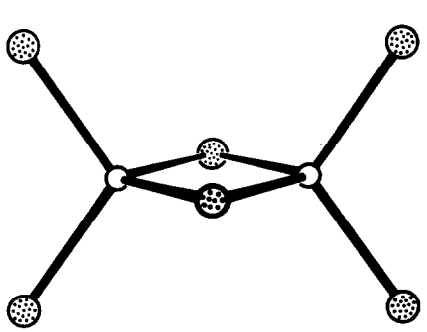
2D

2.2.2. *Three-coordinate metal* (**2B** *and* **2C**). Neither of these structures has been confirmed for thiolate ligands, although precedents exist in comparable chloride complexes such as $[Cl_2Ag(\mu\text{-}Cl)AgCl_2]^{3-}$[131] and $[ClCu(\mu\text{-}Cl)_2CuCl]^{2-}$,[132] and in the polysulfide $[Ag_2(S_6)_2]^{2-}$ (Ph_4P^+)[46] which has structure **2C** with cyclic 1,6-S_6 linkages of the bridging and terminal positions.

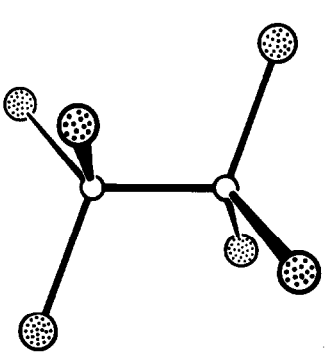
2.2.3. $(RS)_2M(\mu\text{-}SR)_2M(SR)_2$ (*planar four-coordinate metal*) (**2D**). No instance of this structure is confirmed. It probably occurs in the diamagnetic anion $[Ni_2(S_2\text{-}o\text{-}xyl)_3]^{2-}$.[86] Structure **2D** is proposed[42] for the organge-red dianion $[Au_2(SC_6F_5)_6]^{2-}$ which is formally Au(II) and in which alternative structures with an Au—Au bond or mixed oxidation states have been discounted:[42] crystallographic confirmation of the structure is essential for this anion.

Structure **2D** has been established for closely related compounds with heteroligands in terminal positions. Coplanar metal coordination squares occur in $(Ph_3P)(C_6F_5S)Pd(\mu\text{-}SC_6F_5)_2Pd(SC_6F_5)(PPh_3)$, which is centrosymmetric.[133,134] Non-coplanar metal coordination planes occur in $(\mu\text{-}SCH_2Ph)_2[NiS_2CSCH_2Ph]_2$ (dihedral angle 114°),[135] $(\mu\text{-}SBu^t)_2[PdS_2CSBu^t]^2$ (dihedral angle 132°),[135] $(\mu\text{-}SEt)_2[PtCl(PPr_3)]_2$ (dihedral angle 130°),[136] $(\mu\text{-}SEt)_2(AuMe_2)_2$ (dihedral angle 141°),[137] $(\mu\text{-}SPh)_2[Rh(CO)PMe_3]_2$ (dihedral angle 113°),[138] $(\mu\text{-}SBu^t)_2[Ir(CO)P(OMe)_3]_2$ (dihedral angle 123°)[139] and (cyclo-octadiene)$Rh(\mu\text{-}SPh)_2Rh(CO)_2$ (dihedral angle 135°).[140]

2.2.4. $(RS)_2M(\mu\text{-}SR)_2M(SR)_2$ (*tetrahedral metal coordination*) (**2E**). This structure is confirmed for

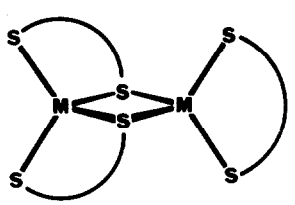


2E

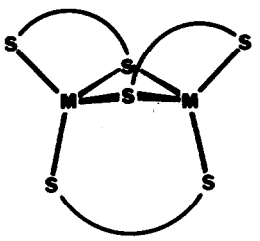


2F

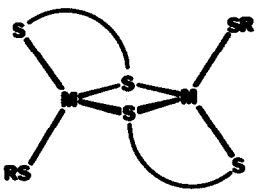
$[Hg_2(SMe)_6]^{2-}$,[59] $[Hg_2(SPh)_6]^{2-}$ (Me_4N^+),[58(c)] $[Fe_2(SEt)_6]^{2-}$ and $[Co_2(SEt)_6]^{2-}$,[141] and is intimated for $[M_2(SEt)_6]^{2-}$ (M = Mn, Zn or Cd).[141] These all occur in a centrosymmetric (or pseudo-centrosymmetric) configuration with *anti* substituents on the bridging ligands, while $[Co_2(SEt)_6]^{2-}$ also crystallizes in the *syn* configuration [**B4** (see Section 5.6.2.3)] (non-planar M_2S_2). NMR data show that these configurational isomers interconvert rapidly in acetone at 200 K, with a slower exchange of terminal and bridging thiolate ligands.[141] Structure **2E** occurs with chelating ligands in $[M_2(S_2\text{-}o\text{-xyl})_3]^{2-}$ (M = Mn, Fe or Co). The Fe compound when crystallized with Et_4N^+ from MeCN has the connectivity **2Ea**, and the Fe and Co compounds when crystallized with Me_4N^+ from MeOH have the connectivity **2Eb**.[141–144] The related complex $[Fe_2(S_2\text{-}o\text{-xyl})_2(SPh)_2]^{2-}$ (Me_4N^+) has a different connectivity (**2Ec**).[142]



2Ea



2Eb

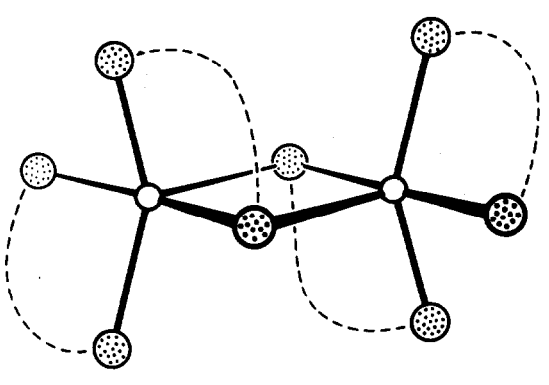


2Ec

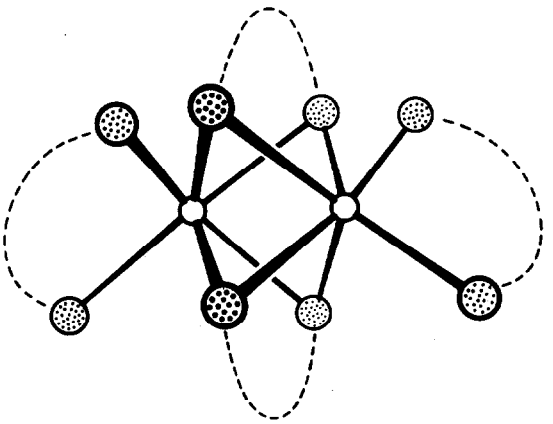
Heteroligand complexes with structure **2E** are known in the series $[(RS)_2FeE_2Fe(SR)_2]^z$ (RS = SPh, SC_6H_4Me or half S_2-*o*-xyl; E = S or Se)[145,146] and $[(E_5)FeE_2Fe(E_5)]^{2-}$ (E = S[147] or Se[148]). Thiolate ligands occur in bridging positions only in $[(Ph_3P)_2Cu(\mu\text{-SPh})_2Cu(PPh_3)_2]$,[149] $(NO)_2Fe(\mu\text{-SEt})_2Fe(NO)_2$[150] and $[Cl_2Zn(\mu\text{-SR})_2ZnCl_2]$ (SR = 4-thiolato-*N*-methylpiperidinium),[151] and in $Me_2Tl(\mu\text{-SPh})_2TlMe_2$,[152] which is distorted severely from a tetrahedral stereochemistry at Tl with C—Tl—C = 164°. $[Mo_2(S_2)_6]^{2-}$ (NH_4^+) also has structure **2E**, but with η^2-S_2 ligands in bridging and terminal positions.[153]

2.2.5. *Metal–metal-bonded* $(RS)_3MM(SR)_3$ (**2F**). This exceptional structure occurs in the centrosymmetric molecule $[Si_2(SPh)_6]$[94] and contravenes the generalization that thiolate bridging prevails over metal–metal bonding in maintaining polymetallic thiolate aggregates. Attempts to prepare compounds $(RS)_3Mo{=}Mo(SR)_3$ by reaction of sterically hindered thiols (unlikely to form bridges) with the analogous compounds $Y_3Mo{=}MoY_3$ (Y = hindered or elimination-stabilized alkyl, NR_2 or OR), have led to $[(Me_2N)_2(Bu^tS)MoMo(SBu^t)(NMe_2)_2]$[154] and compounds $[Y(ArS)_2MoMo(SAr)_2Y]$ (Y = NMe_2 or OR, ArS = 2,4,6-trimethylbenzenethiolate).[155]

2.2.6. *Dimetallic structures with metal coordination numbers greater than* 4. There are to date few structurally confirmed instances of homothiolate complexes in this class, but there are data on numerous related structures which contain and define the pertinent structural units. By construction from these data it is possible to postulate structures of types $(RS)_nM(\mu\text{-SR})_2M(SR)_n$ (n = 3 or 4),



2G



2K

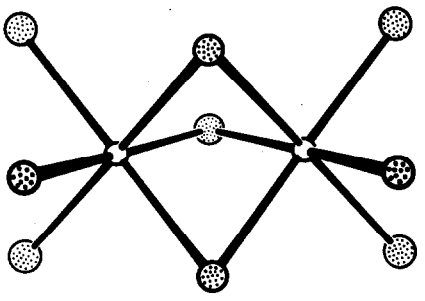
$(RS)_3M(\mu\text{-SR})_3M(SR)_3$ and $(RS)_2M(\mu\text{-SR})_4M(SR)_2$ with two, three or four doubly-bridging thiolates, and it is reasonable to predict that they will be confirmed in crystals after further synthetic enterprise.

2.2.7. $(RS)_3M(\mu\text{-}SR)_2M(SR)_3$ (**2G**). Although not known with monodentate thiolates, this type occurs in the complexes $[M_2(SCH_2CH_2S)_4]^{2-}$, which are essentially isostructural for M = Mn(III)[85,156] and Fe(III).[157] The non-chelated M—S bond in the centrosymmetric ion is 0.27 Å (Fe) or 0.30 Å (Mn) longer than the mean of the other four, and is axial in the distorted trigonal bipyramidal stereochemistry at the metal. Known structures **2G** but with oxide or sulfide heteroligands in the bridging positions, are $[(\mu\text{-}E)_2\{EMo(SPh)_2\}_2]^{2-}$ (E = O[158] or S[159]) $[(\mu\text{-}S)_2\{M(SBu^t)_2(PMe_2Ph)\}_2]$ (M = Mo[128] or W[160]) and $[(\mu\text{-}S)_2\{Mo(SBu^t)_2(NHMe_2)\}_2]$.[161] In the last three instances the bridge is exactly planar. The metal stereochemistry is approximately square pyramidal in the first two structures, while in the last three it is approximately trigonal bipyramidal with a bridging sulfide and a terminal heteroligand in axial positions. Therefore, these last three are presented as two trigonal bipyramids linked along an axial–equatorial edge.

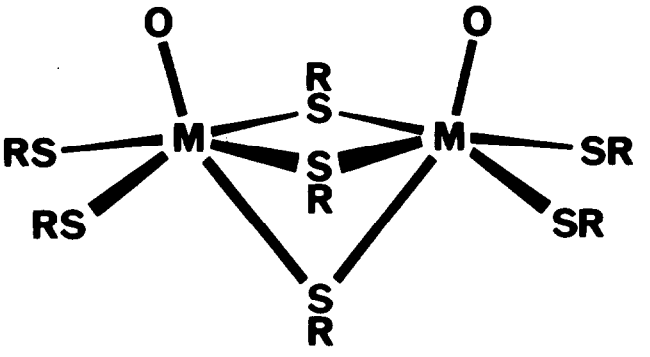
Many complexes possess $L_3M(\mu\text{-}SR)_2ML_3$ structures, with organo, hydride, carbonyl or phosphine ligands (L) in terminal positions. Except as discussed in Section 5.6 for the information they provide about the geometry and stereodynamics of thiolate bridges, these compounds are beyond the scope of this Report.

2.2.8. $(RS)_4M(\mu\text{-}SR)_2M(SR)_4$. Octahedra linked by two bridging thiolate ligands occur in the Mo(III) complexes $[(L\text{–}L)Cl_2Mo(\mu\text{-}SEt)_2MoCl_2(L\text{–}L)]$.[162] The Ti(IV) phenoxide complex $[(PhOH)(PhO)_3Ti(\mu\text{-}OPh)_2Ti(OPh)_3(PhOH)]$ has the same centrosymmetric structure,[163] with three notable stereochemical features: (i) an almost planar stereochemistry occurs at the oxygen atoms of the bridging ligands, (ii) the two terminal phenoxide ligands approximately *trans* to the bridging ligands have Ti—O—C angles of 169 and 175°, and (iii) phenol is coordinated with Ti—O = 2.20 Å (although the H atom was not located crystallographically).

2.2.9. $(RS)_3M(\mu\text{-}SR)_3M(SR)_3$ (**2H**). Although the well-known confacial bioctahedron is not yet



2H



2J

established for a homothiolate molecule, the $M(\mu\text{-}SR)_3M$ bridging section has been characterized in $[Cl_2(Me_2S)W(\mu\text{-}SEt)_3WCl_2(SMe_2)]$,[164] in $[(CO)_3Fe(\mu\text{-}SMe)_3Fe(CO)_3]^+$,[165] and in the thoroughly characterized double-cubane structures (**8G** and **9A**), where triply-bridging sulfide ions take the place of the terminal thiolate ligands on M. Analogous tris double-bridging occurs in $[(\mu\text{-}SH)_3\{Fe(ppp)\}_2]^+$ [ppp = $Ph_2PCH_2CH_2P(Ph)CH_2CH_2PPh_2$].[166] The complex $[L_3Mo(\mu\text{-}SMe)_3MoL_3]^{3+}$ (L = 1-methylimidazole)[167] is relevant, although not crystallographically confirmed.

The complex $[Mo_2O_2(SCH_2Ph)_7]^-$[168] almost certainly has the tri-bridged $[(\mu\text{-}SCH_2Ph)_3\{OMo(SCH_2Ph)_2\}_2]$ structure (**2J**). It is a member of the set $[(\mu\text{-}SR)_2(\mu\text{-}Z)\{OMo(SR)_2\}_2]^-$ [R = Ph, C_6H_4Me-4, $\frac{1}{2}(CH_2CH_2)$ or $\frac{1}{2}(CH_2CH_2CH_2)$], in which alcoxide or amide ligands can occur as the third bridging ligand Z. Structural details for this type are established by the diffraction analyses[168,169] of the four compounds $[Mo_2O_3(SCH_2CH_2O)_3]^{2-}$, $[Mo_2O_2(SCH_2CH_2O)_3(SCH_2OH)]^-$, $[Mo_2O_2(SCH_2CH_2O)_3Cl]^-$ and $[Mo_2O_2(SCH_2CH_2O)_2Cl_3]^-$, and of $[Mo_2O_2(OMe)(SC_6H_4Me)_6]^-$.[170] In all cases the bridging bonds *trans* to both OMo(V) groups are elongated. A compilation of geometrical data for $\{OMo(\mu\text{-}X)_3MoO\}$ bridges involving thiolate is available.[170] Analogous thiolate coordination, but with diazene functions in place of the oxo ligands, occurs in $[Mo_2(NNHPh)(NNPh)(SCH_2CH_2S)_3(SCH_2CH_2SH)]^{2-}$.[171]

2.2.10. $(RS)_2M(\mu\text{-}SR)_4M(SR)_2$. This type of structure is found in the ion $[V_2(SCH_2CH_2S)_4]^{2-}$

(Ph_4P^+),[117] (Et_4N^+),[172] (Ph_4P^+)[173] with connectivity **2K**, which is distinctly different from the connectivity **2G** for the same formulation. Significant characteristics of **2K** are: (i) the ion has exact[172] or virtual[173] D_2-symmetry; (ii) the bridging V—S distances are in two sets (*ca* 2.39 and *ca* 2.53 Å); (iii) the metal coordination stereochemistry (C_{2v}) is unusual, and can be visualized as a cube without two positions connected by a face diagonal; (iv) the structure can be regarded as two VS_4 square planes, staggered about the V- -V axis, intersecting in the bridging region; (v) the V—V distance is short (*ca* 2.61 Å), indicative of a single bond; and (vi) the complex is diamagnetic, suggesting (but not confirming) electronic coupling through the thiolate bridges.

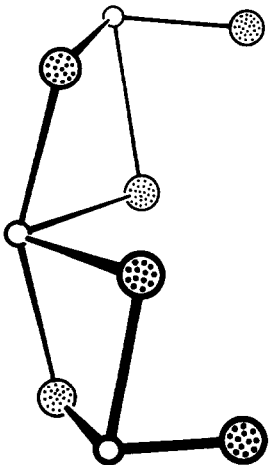
The tetra double-bridged section of **2K** has been characterized by structure determination for three complexes with pi-arene terminal ligands, namely $[(\mu\text{-SMe})_4\{Mo(\eta^5\text{-}C_5H_5)\}_2]^{0,+}$,[174] in two oxidation states, and $[(\mu\text{-SMe})_4\{Mo(\eta^6\text{-}C_6H_5Me)\}_2]^{2+}$.[167] The M—S—M bridge angles are acute (64–65°).

2.2.11. *Miscellaneous structures.* The polysulfide complexes $[(S_6)M(S_8)M(S_6)]^{4-}$ (M = Cu[175] or Ag[176]) each contain two three-coordinate M atoms chelated by the S_6 rings and connected by an elongated central polysulfide (S_8^{2-}).

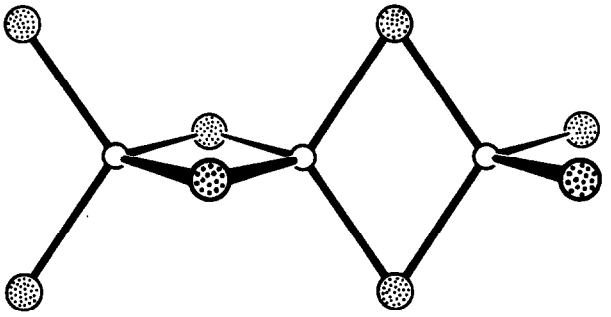
2.3. *Trimetallic structures*

Cyclic and linear trimetallic structures have proliferated since 1980, with recognition of the $Fe_3S_3(S\text{-cys})_5$ ferredoxins, the preparation of diverse complexes with hetereoligands, and the consolidation of knowledge of the $(\mu\text{-}S\text{-cys})_3M_3(S\text{-cys})_6$ aggregate (M = Zn or Cd) in metallothioneins. Although no homothiolate structure has yet been reported, the data on various heteroligand complexes allow the development of principles and the definition of structure types. In view of the report[29] of the crystallization of metallothionein from rat liver it is not unreasonable to expect that diffraction results from a metalloprotein may define a cyclic trimetallic homothiolate aggregate prior to results form any simple coordination complex or synthetic analogue.

2.3.1. $RSM(\mu\text{-}SR)_2M(\mu\text{-}SR)_2MSR$ (**3A**). This structure (symmetry C_2) occurs with R = 2,6-diisopropylphenyl (M = Sn or Pb).[54] The central metal is four-coordinate in a pseudo trigonal bipyramidal stereochemistry $[M(S^{ax})_2(S^{eq})_2$, $M—S^{ax}$ elongated by 0.2 Å, $S^{eq}—M—S^{eq} = 87°$, $S^{ax}—M—S^{ax} = 146°]$ and the terminal metal atoms are three-coordinate pyramidal (S—M—S = 74, 90 and 94°). $[PhSCu(\mu\text{-}S)_2Mo(\mu\text{-}S)_2CuSPh]^{2-}$ (Pr_4N^+, symmetry C_2) contains trigonal planar Cu atoms linked through tetrahedral tetrathiomolybdate.[177]



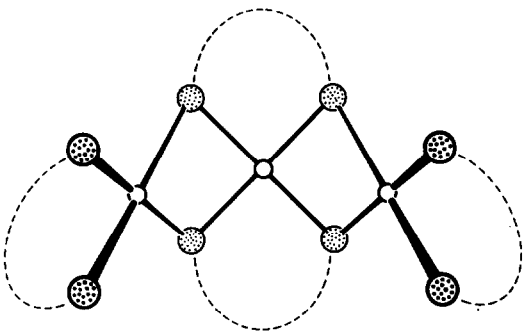
3A



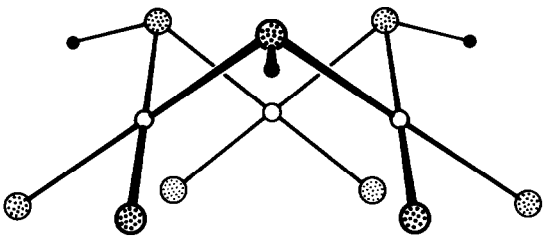
3B

2.3.2. *Linear* $(RS)_2M(\mu\text{-}SR)_2M(\mu\text{-}SR)_2M(SR)_2$ (*tetrahedral coordination*) (**3B**). This type but with bridging sulfide occurs in the complexes $[(RS)_2Fe(\mu\text{-}S)_2Fe(\mu\text{-}S)_2Fe(SR)_2]^{3-}$ (R = Et or Ph).[78,178] The $Fe(III)_3S_8$ core of the complex with R = Ph[78] approaches D_{2d}-symmetry: the Fe—Fe—Fe angle is 172.9°: the two Fe_2S_2 rhombs are planar to within 0.06 Å, and mutually perpendicular to within 0.5°: the internal angles are 102.8° at the central Fe atom, 105.6° at the terminal iron atom, and 75.6° at the sulfide ion. The same structure probably occurs in $[(PhS)_2Fe(\mu\text{-}S)_2V(\mu\text{-}S)_2Fe(SPh)_2]^{3-}$,[179] and is confirmed for $[Cl_2Fe(\mu\text{-}S)_2M(\mu\text{-}S)_2FeCl_2]^{z-}$ (M, $z-$ = Mo; 2–;[180,181] W, 2–;[181] or V, 3–[179]).

2.3.3. $(RS)_2M(\mu\text{-}SR)_2M(\mu\text{-}SR)_2M(SR)_2$ *with planar metal coordination.* The one instance of three edge-linked square planes is $[Ni_3(S_2\text{-}o\text{-}xyl)_4]^{2-}$ (Et_4N^+)[144] which has the chelate connectivity shown as **3C**. The dihedral angle between coordination planes is *ca* 130°. The conformation with coplanar coordination planes has not yet been reported.

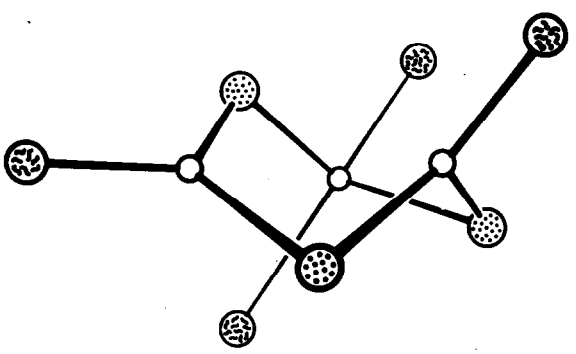


3C

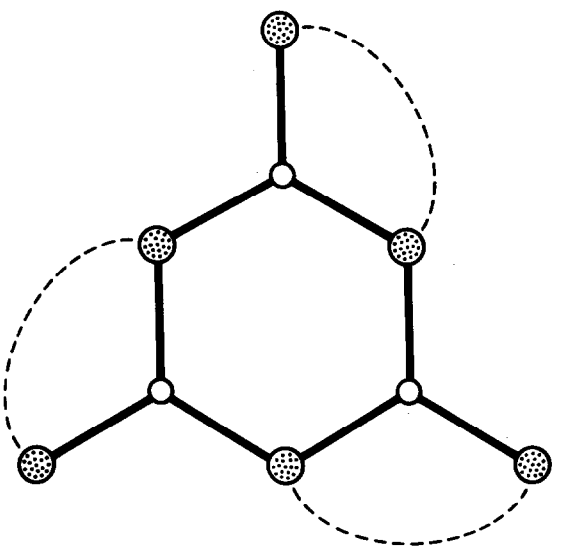


3H

2.3.4. *Linear* $(RS)_3M(\mu\text{-}SR)_3M(\mu\text{-}SR)_3M(SR)_3$ (*octahedral coordination*). Although without confirmed independent existence, this structure constitutes the central region of the centrosymmetric double-cubane structure **9A**.



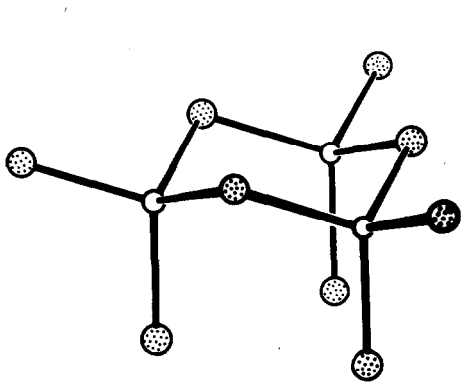
3D



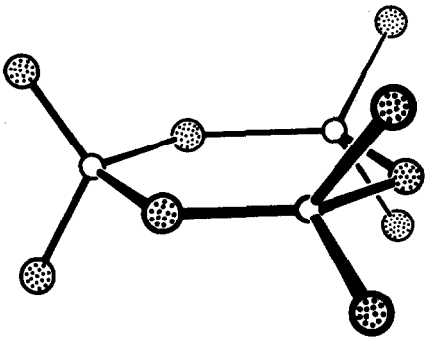
3E

2.3.5. *Cyclic* $(\mu\text{-}SR)_3(MSR)_3$ (*three-coordinate metal*). The closest approach to this structure type is found in $(\mu\text{-}SAr)_3(CuPPh_3)_2Cu(PPh_3)_2$ (Ar = Ph or C_6H_4Cl-4)[182] where two of the M atoms in the cycle have one terminal phosphine ligand and the third is coordinated by two terminal phosphine ligands (**3D**). The salient stereochemical property of this and other cyclic structures is the ring conformation. Here the conformation is a slightly twisted boat, in which the unique diagonal is not that which posseses the two-fold symmetry of the $S_3Cu_3P_4$ connectivity, but another which permits isoclinical rather than pseudo-axial directions for the two bulky phosphine ligands coordinated to one copper atom. Bond lengths in the cycle are unexceptional, but Cu—S—Cu angles range widely from 87 through 105 to 124°, and are correlated with the inclinations of the S–C vectors at the pyramidal S atoms.[182]

The ions $[Cu_3(S_6)_3]^{3-}$ (Et_4N^+)[19] and $[Cu_3(S_4)_3]^{3-}$ $(NH_4^+$ or $Ph_4P^+)$,[175] prepared from copper(II) acetate and ethanolic polysulfide solution, contain a puckered cyclic core with chelating 1,6-hexasulfide or 1,4-tetrasulfide ions connecting bridging and terminal positions as shown in **3E**.



3F



3G

2.3.6. *Cyclic* $(\mu\text{-SR})_3(M(SR)_2)_3$ (*tetrahedral metal coordination*). It is proposed that an $[M_3(S\text{-cys})_9]^{3-}$ aggregate in zinc and cadmium metallothioneins has structure **3F**, which is a fragment of the established adamantanoid $M_4(SR)_{10}$ cage structure **4F**. The removal of one MSR moiety from **4F** to form **3F** in chair conformation generates three parallel, axial, terminal M—S bonds, and therefore it is expected that some conformational modification of the $(\mu\text{-SR})_3M_3$ ring will occur. In this context the planar structure **3G** of the complex $[(\mu\text{-SPh})_3(FeCl_2)_3]^{3-}$ (Et_4N^+) is significant, particularly as it is reported that the three phenyl rings are coplanar with the cycle.[178] Only the six terminal Cl atoms which complete the pseudo-tetrahedral coordination at the Fe atoms deviate from the molecular plane. The Fe—S—Fe angles of 139, 139 and 142° are unusually large.

In this and many other structures with doubly-bridging thiolate (particularly **3D**, **4E** and **4F**) there exists good correlation between the M—S—M angle (θ) and the angle of inclination (ϕ) of the corresponding S–C vector to the M—S—M plane. This relationship extends over a wide range (50° for θ, 60° for ϕ) of stereochemistry at the S atom.[182,183] It may be postulated that, for isolated $(\mu\text{-SR})_3M_3$ cycles, the M—S—M angles, and therefore to some extent the cycle conformation, are quite variable and strongly dependent on the directions of approach of the C—S bonds to the cycle. These latter may be determined by crystal packing effects in small molecules, and by a polypeptide secondary structure in metallocysteine proteins. The cause of the total planarity of the $(\mu\text{-SPh})_3Fe_3$ cycle is not yet revealed.

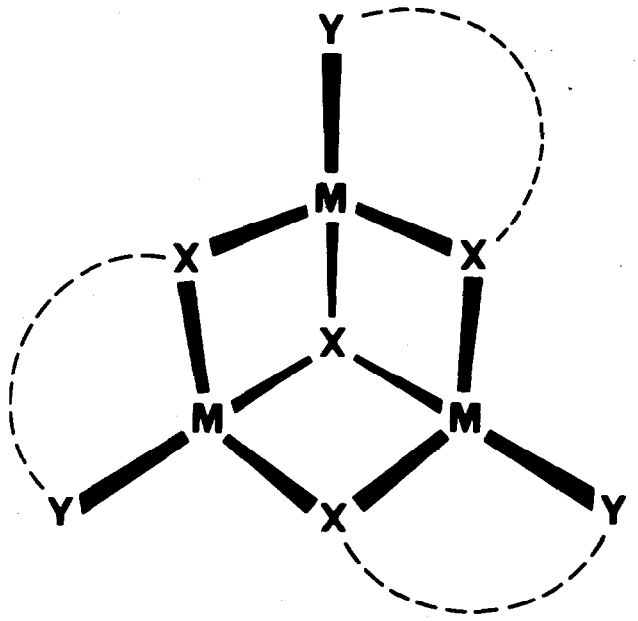
The compounds $(\mu\text{-SMe})_3(BX_2)_3$ (X = Cl or Br)[184] occur in regular chair conformation with one axial and two equatorial S—C bonds: the S stereochemistry is consistent with the above correlation.

2.3.7. *Cyclic* $(\mu\text{-SR})_3M(SR)_2)_3$ (*planar metal coordination*) (**3H**). In this uncommon structure type three metal coordination planes [*cis*-$(\mu\text{-SR})_2M(SR)_2$] share vertices such that the $(\mu\text{-SR})_3M_3$ cycle has a chair conformation. Close approaches to **3H** occur in the ethyltrithiocarbonate derivative $(\mu\text{-SEt})_3Pd_3(S_2CSEt)_3$[135] and in $Pd_3(SCH_2CH_2SCH_2CH_2S)_3$:[185] in both compounds the bridging thiolate substituents are all equatorial.

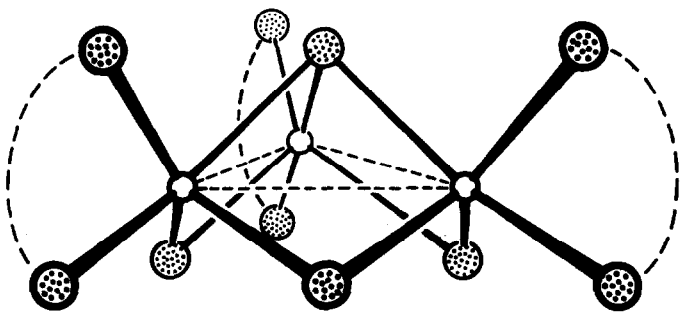
2.3.8. *Cyclic* $(\mu_3\text{-S})(\mu\text{-SR})_3(MSR)_3$ (**3J**). In this centred version of **3E**, an apical triply-bridging sulfide ion completes tetrahedral coordination for each of the three M atoms in a triangle. The structure is known only for the flexible, large-bite, chelating *o*-xylyl dithiolates of Fe, Co and Ni.[186–189]

2.3.9. 3-Fe *ferredoxins*. A cyclic structure with bridging sulfide and terminal thiolate ligands occurs in 3-Fe ferredoxins: it has been confirmed in crystals of ferredoxin I from *Azotobacter vinelandii*.[21,23] In *A. vinelandii* one terminal ligand is an O atom which is not part of the polypeptide chain, probably OH or OH_2. The irregular $(\mu\text{-S})_3Fe_3(S\text{-cys})_5O$ structure (at 0.2 Å/5° precision) is shown diagrammatically in Fig. 2. The six-membered Fe_3S_3 ring has a flattened twist conformation in which there is an approximate two-fold axis through Fe3–S1. In the ideal twist structure S2 and S3 would be displaced ±1.4 Å from coplanar Fe3–S1–Fe1–Fe2: in fact that the displacements of the bridging S atoms from the Fe_3 plane are S1 −0.2 Å, S2 −0.5 Å, and S3 +0.5 Å. The four-coordinate stereochemistry around the Fe atoms is quite irregular, with angles at Fe in the ranges 85–153, 78–149 and 74–151° for Fe1, Fe2 and Fe3, respectively. As shown in Fig. 2, four Fe—S(cys) bonds are approximately perpendicular to the ring plane, while the other Fe—S(cys) and the Fe—O bonds are almost parallel to the plane. Angles at bridging sulfide are relatively large, range 113–131°, with the degree of puckering of the $(\mu\text{-S})_3M_3$ cycle intermediate between those of $(\mu\text{-SPh})_3Cu_3(PPh_3)_4$ and $[(\mu\text{-SPh})_3Fe_3Cl_6]^{3-}$.

Ferredoxin II from *D. gigas*[190] and inactive beef heart aconitase[191] contain 3-Fe aggregates with



3J



3L

2.7-Å separations (from EXAFS measurements) between Fe atoms, distinctly different from the 4.1-Å separation in *A. vinelandii*. Models proposed for the cores of these two proteins include **3B**, **3J** and **3K**.

2.3.10. *Cyclic* $(\mu_3\text{-S})(\mu\text{-S})_3M_3(SR)_6$ (**3L**). The compound $[Mo_3S_4(SCH_2CH_2S)_3]^{2-}$, obtained by reaction of $[Mo_3S(S_2)_6]^{2-}$ with excess $^-SCH_2CH_2S^-$,[192] has this three-fold structure in which each Mo(IV) atom is five-coordinate (trigonal bipyramidal, μ_3-S axial). The Mo atoms occur sandwiched

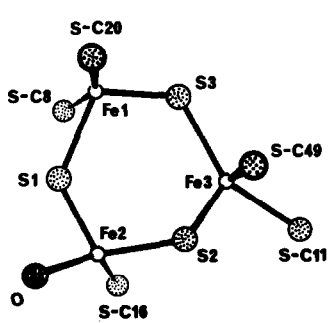
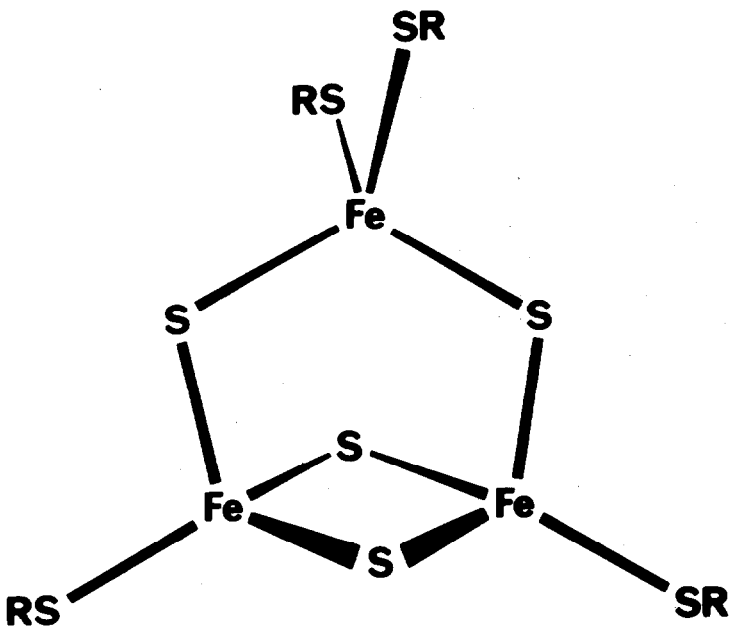
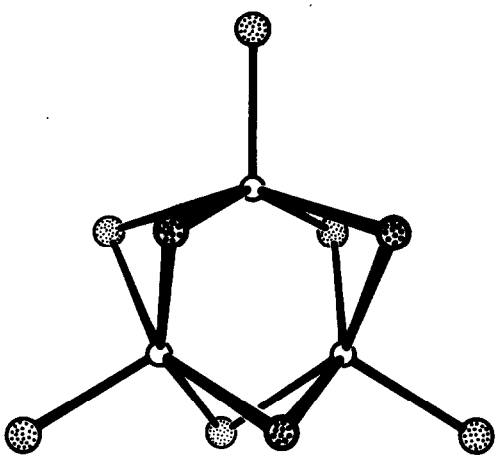


Fig. 2. Coordination structure (at 0.2-Å resolution) of the $(\mu\text{-S})_3Fe_3$(*S*-cysteine)$_3$O core of ferredoxin I from *A. vinelandii*, with the cysteine residues numbered.



3K



3M

between two triangular layers of S atoms, and in this sense (but not in terms of local metal coordination) there is some resemblance of **3L** with the two-dimensionally non-molecular MoS_2 structure type.

2.3.11. *Cyclic* $(\mu\text{-SR})_6(ML)_3$ (**3M**). Two compounds are derivatives of this D_{3d} structure, in which the triangle of metal atoms is spanned by two doubly-bridging thiolate ligands on each edge. The S atoms constitute a trigonal prism with the M atoms outside the rectangular faces, and the terminal ligands (L) complete the square pyramidal $(\mu\text{-SR})_4ML$ coordination. The structures established are $(\mu\text{-SEt})_5(\mu\text{-CO})(CoCO)_3$[193] and $(S\text{–}S)_3(NiPPh_3)_3$[194] in which (S–S) is the rigid chelating dithiolate ligand hexachloronaphthalene-1,8-dithiolate.

In structure **3M** the configurations of the thiolate substituents may be axial or equatorial relative to the principal axis of the S_6 trigonal prism, but the substituents are subject to steric restrictions due to the relatively short (2.9–3.4 Å) edges of the prism when M is a metal of the first transition series. These S—S distances are much less than half the sum of the van der Waals' radii of even the smallest substituents on contiguous thiolate ligands, and, therefore, it is not possible for substituents connected by an edge normal to the trigonal axis to be both axial, or for substituents connected by an edge parallel to the

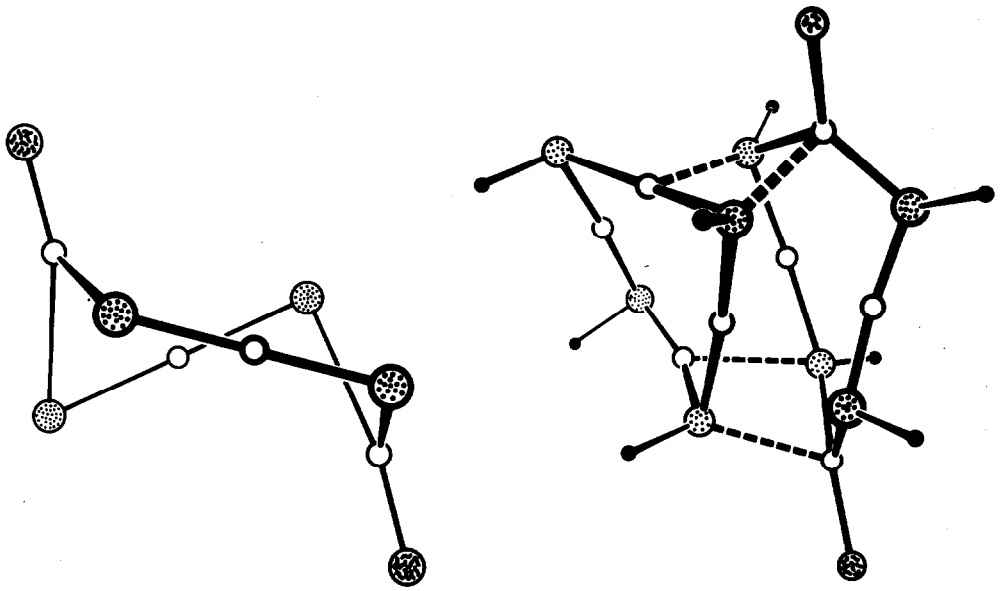
trigonal axis to be both equatorial. Neither is it possible to arrange axial–equatorial alternation of substituents around trigonal prismatic $(\mu\text{-SR})_6M_3$, but five bridging thiolates can occur without interference. This argument was used to rationalize the composition of $(\mu\text{-SEt})_5(\mu\text{-CO})Co_3(CO)_3$.[193] The chelate rings of the Ni compound require all S—C bonds to be equatorial.

2.4. *Tetrametallic structures*

No acyclic structures are known. With four bridged M atoms, mono-, bi- and tricyclic structures are possible, and are established.

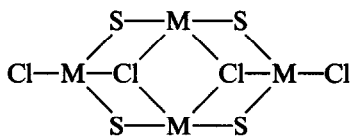
2.4.1. *Monocyclic* $(\mu\text{-SR})_4M_4$. This monocycle occurs 3 times in two guises in the compounds $(Et_2MeCSAg)_8(PPh_3)_2$[195] and $(Bu^tSCu)_4(PPh_3)_2$.[196] The 1,3-diligated cycle **4A** occurs with the *anti* conformation shown in the Cu compound (S—Cu—S angles 176, 173, 119 and 117°), while the Ag aggregate, shown as **4B**, consists of a slightly buckled $(\mu\text{-SR})_4Ag_4$ cycle and a $(\mu\text{-SR})_4Ag_2(AgPPh_3)_2$ cycle, confacially linked by secondary Ag···S interactions, all 0.5 Å longer than the primary Ag–S bonding. Angles at the two-coordinate Ag atoms in the cycle are in the range 166–174°, a consequence of the secondary connections.

Unsubstituted **4A** occurs in the analogous compound $(CuOBu^t)_4$,[197] which is smaller, more tightly bound and symmetrical than the thiolate analogs.



4A **4B**

2.4.2. *Heteroligated* $(\mu\text{-SBu}^t)_4M_4$ *structures.* Attention should be drawn to structural relationships between some derivatives $[M(SR)Cl]_4$ of Zn, Cd and Hg with tertiary thiolates. The compounds are $M_4[SC(CH_3)_2CH_2NH_2]_4Cl_4\cdot 2H_2O$ [M = Zn[198] or Cd[199]] and $Hg_4(SBu^t)_4Cl_4(py)_2$,[200] with structures all based on the framework



(which has the composition and five of the six rhomboidal M_2X_2 structural units of the cubane structure **4H**). The relationships between the structures are expressed in terms of Fig. 3: (i) when M = Zn or Cd the additional heteroligand coordination occurs only at M_B, via R = CH_2NH_2 (L is absent), whereas when M = Hg and R = CH_3 additional heteroligand coordination occurs only via L = pyridine; (ii) as M changes Zn → Cd → Hg the M_A—Cl distance changes from primary bonding (Zn—Cl = 2.27 Å, Cd—Cl = 2.41 Å) to non-bonding (Hg), while the M_B—Cl distance decreases from

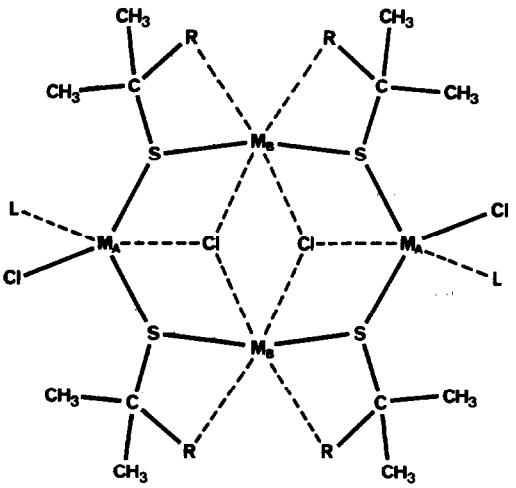
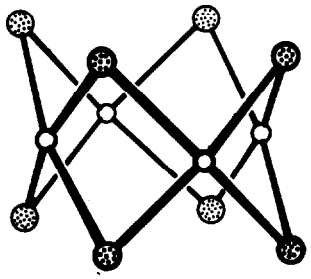


Fig. 3. Framework of variable primary and secondary bonding connections in $[M(SR)Cl]_4$ and derivatives (M = Zn, Cd or Hg).

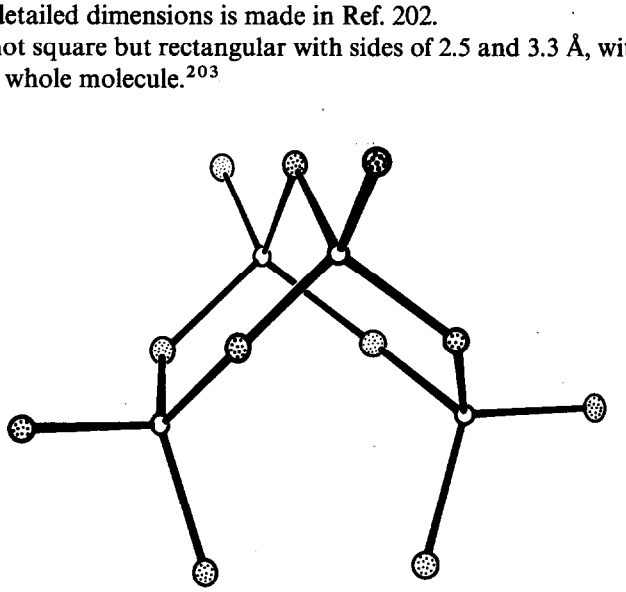
non-bonding (Zn--Cl = 3.4 and 3.5 Å) through weak secondary bonding (Cd--Cl = 2.95 Å) to intermediate bonding (Hg—Cl = 2.70 and 2.81 Å).

2.4.3. *cyclo*-$(\mu\text{-SR})_8M_4$ (**4C**). The Ni complex of 4-mercapto-*N*-methylpiperidine has this square array of Ni atoms, with two double thiolate bridges outside each edge of the square to provide approximately square planar coordination at each Ni atom.[201] The Ni atoms are displaced 0.2 Å outside their coordination planes. The substituents alternate axial and equatorial to the primary axis of the virtual D_{2d} molecule. Analysis of the detailed dimensions is made in Ref. 202.

In $(\mu\text{-SEt})_8(CoCO)_4$ the Co_4 array is not square but rectangular with sides of 2.5 and 3.3 Å, with pseudo-D_{2h}-symmetry maintained for the whole molecule.[203]



4C



4D

2.4.4. *Bicyclic* $(\mu\text{-SR})_5M_4(SR)_6$ (**4D**). This structure, postulated for the $Cd_4(S\text{-cys})_{11}$ aggregate of metallothioneins (Section 1.5), is derived from the well-known adamantanoid $(\mu\text{-SR})_6(MSR)_4$ structure (**4F**) by replacement of a bridging thiolate with additional terminal thiolate ligands on each of the separated M atoms. However this introduces substantial crowding in the vicinity of the inserted ligands, which must be relieved by flattening of the two fused $(\mu\text{-SR})_3M_3$ cycles, or by their adoption of the double-twist conformation. No instance or derivative of this structure has yet been confirmed crystallographically. The homonuclear decoupled ^{113}Cd NMR of metallothioneins supports the metal connectivity of this structure, with ^{113}Cd–^{113}Cd coupling between the two Cd atoms bridged directly across the pseudo two-fold axis being larger than for the other four Cd–Cd couplings.[30]

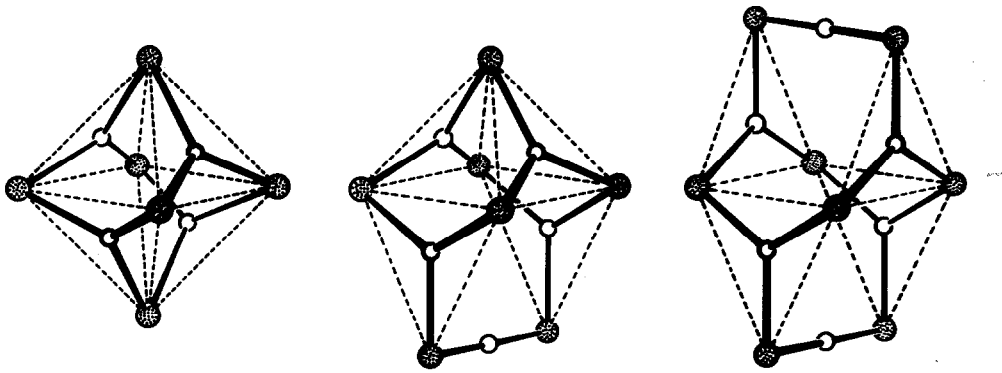


Fig. 4. Structures **4E**, **5A** and **6A**, showing the polyhedral expansion mechanism which relates the three cages.

2.4.5. (μ-SR)$_6$M$_4$ (**4E**). This molecular cage (see Fig. 4) contains a doubly-bridging thiolate ligand across each of the six edges of the M_4 tetrahedron such that each metal has a trigonal planar coordination. The M_4S_6 core can be described as an octahedron of S atoms with M atoms at the midpoints of four faces: in terms of the component polyhedra the structure is *tetrahedro*-M_4-*octahedro*-S_6. The T_d-symmetry of this core is necessarily thwarted by the thiolate substituents, as discussed below. An alternative description[204] of the core recognizes four fused M_3S_3 cycles, each in a severely distorted chair conformation.

This structure is established, but only for Cu(I), in $[Cu_4(SMe)_6]^{2-}$ and $[Cu_4(SPh)_6]^{2-}$[50,204,205]* In all cases (four independent crystal structure determinations of $[Cu_4(SPh)_6]^{2-}$) the Cu atoms lie slightly outside their S_3 coordination planes: the mean displacement is 0.07 Å. This observation, together with the Cu- -Cu distances (range 2.64–2.85 Å, mean 2.74 Å), indicates little direct bonding between the three-coordinate Cu atoms. The aggregate is maintained primarily by the bridging thiolate ligands.

Configurational isomerism of the molecule including the thiolate substituents is due to the pyramidal stereochemistry at the S atoms. Inversion of the doubly-bridging thiolates allows three configurational isomers (each chiral) described in terms of the axial (a)–equatorial (e) distribution of the three S–C vectors in each of the four fused M_3S_3 cycles in the structure.[204] The three isomers are **I** [aaa,aae,aee,eee], **II** [aae,aae,aae,eee] and **III** [aae,aae,aee,aee], **I** and **III** being asymmetric while **II** is C_3. All five instances of $[Cu_4(SR)_6]^{2-}$ occur as isomer **III**, which has the least number (two) of contiguous axial–axial substituents. The asymmetry of the substituent array correlates well with geometrical distortions of the Cu_4S_6 core from its potentially high (T_d) symmetry. Due to intramolecular repulsions between substituents the axial–axial pairs of ligands subtend enlarged S—Cu—S angles, and in all four $[Cu_4(SPh)_6]^{2-}$ cages the following correlation exists between pairwise substituent orientation and S—Cu—S angle:

ax—ax substituents, mean S—Cu—S 138.0 (s† 4.1)°,

ax—eq substituents, mean S—Cu—S 118.3 (s 6.2)°,

eq—eq substituents, mean S—Cu—S 108.1 (s 2.1)°.

Corresponding S—Cu—S values for $[Cu_4(SMe)_6]^{2-}$ with the smaller substituent, 128.0 (0.4†), 118.0 (5.4) and 119.6 (1.1), respectively, deviate less from the 120° ideal. While the susceptibility of the cage to substituent repulsions is more in variation of bond angle than in bond distance, there is a secondary influence on Cu—S distances which are coupled electronically to opposite S—Cu—S angles within each CuS_3 coordination plane (see Section 5.8).

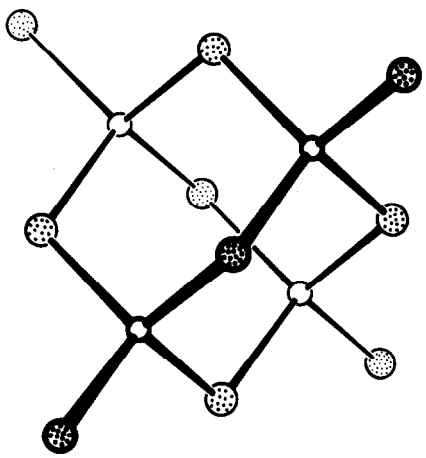
---

* A comparable cage with halide ligands is $[Cu_4I_6]^{2-}$.[206]

† The standard deviation (s) quoted in statistical analyses is that of the sample of n values: $s = [\Sigma(x-\bar{x})^2/(n-1)]^{1/2}$.

The vertices of the S_6 octahedron in **4E** are linked by three α,ω-chelating polysulfide ligands in the cages $[Cu_4(S_4)(S_5)_2]^{2-}$ and $[Cu_4(S_4)_2(S_5)]^{2-}$ which crystallize together.[207]

2.4.6. $(\mu\text{-SR})_6(MSR)_4$ (**4F**). The framework of this molecular cage structure is widely known amongst compounds organic (adamantane), organometallic [e.g. $S_6(SnMe)_4$] and inorganic (e.g. P_4S_{10}),[94] and is ubiquitous amongst the thiolates of metals adopting tetrahedral coordination. Four M atoms, each with one terminal thiolate ligand, are arrayed as a tetrahedron outside the faces of an octahedron formed by the S atoms of the six doubly-bridging thiolate ligands. The metal coordination is $(\mu\text{-SR})_3MSR$. T_d-symmetry is possible for the M_4S_{10} core of this *octahedro*-$(\mu\text{-SR})_6$-*tetrahedro*-M_4-*tetrahedro*-$(SR)_4$ cage, commonly known as the "adamantanoid" cage structure, but the thiolate substituents necessarily break almost all of this high symmetry.



4F

Structure **4F** was first described[208,209] for $[Co_4(SPh)_{10}]^{2-}$ with Me_4N^+. The corresponding isomorphous crystals of $[Mn_4(SPh)_{10}]^{2-}$,[85] $[Fe_4(SPh)_{10}]^{2-}$[210] and $[Zn_4(SPh)_{10}]^{2-}$,[211] have since been subjected to detailed diffraction analysis. Crystal structures have been determined also for $(Et_4N^+)(Et_3NH^+)[Cd_4(SPh)_{10}]^{2-}$[212] and $(Et_3NH^+)_2[Zn_4(SPh)_{10}]^{2-}$,[213] and $(Me_4N)_2[Fe_4(SEt)_{10}]^{2-}$.[141] In addition, structural details are available for related complexes with hetero-ligands in terminal positions, namely $[Zn_4(SPh)_8Cl_2]^{2-}$ {with which $[Co_4(SPh)_8Cl_2]^{2-}$ as the Me_4N^+ salt is isostructural}[214] and $[Fe_4(SPh)_6Cl_4]^{2-}$ (Ph_4P^+).[215] The adamantanoid cage structure is found also in the repeat unit of the one-dimensionally non-molecular crystal structure of *catena*-$(\mu\text{-SPh})[(\mu\text{-SPh})_6Zn_4(CH_3OH)(SPh)]$ where one methanol, one terminal thiolate and two doubly-bridging thiolate ligands complete the coordination of the four Zn atoms (see Section 3.1.6).

An important NMR study has characterized the ligand and metal exchange reactions of $[M_4(SPh)_{10}]^{2-}$ (M = Fe, Co, Zn or Cd), in acetonitrile,[210] while solution equilibria involving $[Co_4(SPh)_{10}]^{2-}$ have been characterized by electronic spectra.[209]

The four fused $(\mu\text{-SR})_3M_3$ cycles approach the ideal chair conformation. Molecular configurational isomerism, arising through inversion at the pyramidal S atoms of the six doubly-bridging thiolates, is analogous to that in **4E** with the same three isomers possible. All of the above-listed instances of the adamantanoid cage structure **4F** occur as the asymmetric isomer **III** [aae,aae,aee,aee] with only two ax–ax ligand pairs, except for the Fe complexes $[Fe_4(SPh)_{10}]^{2-}$, $[Fe_4(SEt)_{10}]^{2-}$ and $[Fe_4(SPh)_6Cl_4]^{2-}$, which are the asymmetric isomer **I** [aaa,aae,aee,eee] with four ax–ax ligand pairs.

The $(\mu\text{-SPh})_6M_4$ core of these structures is angularly floppy, and in all cases the S_6 polyhedron is distorted from a regular octahedron in the manner that increases the S– –S distances between pairs of parallel axial SPh substituents. Thus, in $[Fe_4(SPh)_6Cl_4]^{2-}$ the S_{ax}—Fe—S_{ax} angles average 116.4(2)° while the S_{ax}—Fe—S_{eq} and S_{eq}—Fe—S_{eq} angles average 102.4(3)°. Corresponding average S_{ax}– –S_{ax} and S_{ax}– –S_{eq} plus S_{eq}– –S_{eq} distances are 4.01(4) and 3.68(9) Å, respectively. Similar angular distortions, without significant variation in M—S distances, occur in the other structures.

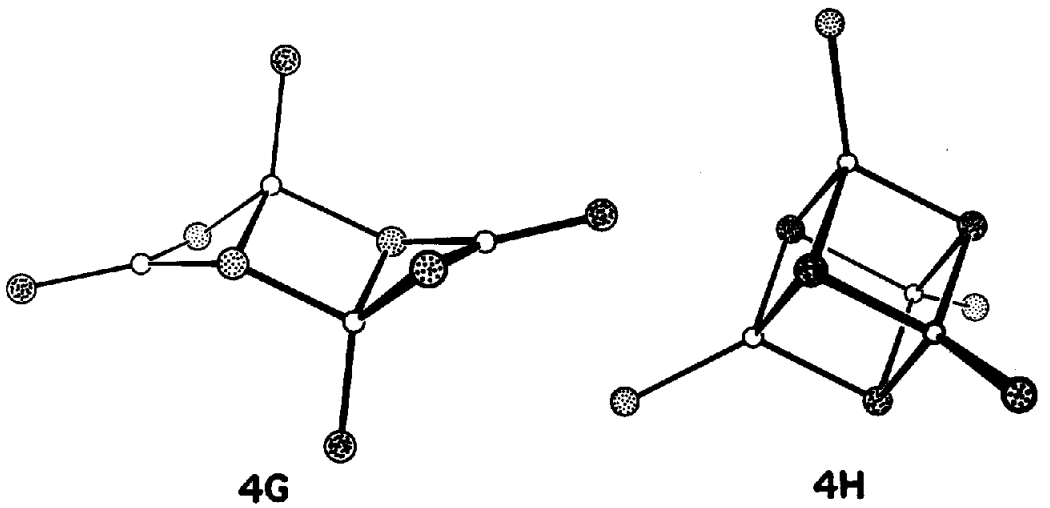
In all examples of this structure type the metal atoms are displaced slightly outward along the pseudo-three-fold axes such that the mean M—S_b—M and S_b—M—S_t angles are several degrees larger, and the mean S_b—M—S_b angles several degrees smaller than 109.5°. This effect, which need not

break the idealized T_d-symmetry, can be expressed also by the ratio of mean M– –M to mean S_b– –S_b distances, values of which are 1.064, 1.034, 1.035 and 1.051 for $[M_4(SPh)_{10}]^{2-}$ (M = Mn, Fe, Co or Cd), respectively, and 1.040, 1.024 and 1.003 for $[Fe_4(SPh)_6Cl_4]^{2-}$, $[Zn_4(SPh)_8Cl_2]^{2-}$ and $Zn_4(SPh)_8(MeOH)$, respectively. Further comparisons of metrical details of the adamantanoid cage structures are made in Refs 215 and 85.

Antiferromagnetic interaction between M atoms is reported for $[Co_4(SPh)_{10}]^{2-}$[209] and $[Mn_4(SPh)_{10}]^{2-}$.[85] The total interaction energy, $9J \approx 150\,cm^{-1}$ for $[Co_4(SPh)_{10}]^{2-}$, is negligible as a chemical bonding influence, and is consistent with the absence of direct M–M bonding in this structure type. Scalar coupling between Cd nuclei through μ-SPh has been observed in the ^{113}Cd NMR spectra of $[Cd_4(SPh)_{10}]^{2-}$.[216,217]

Although thiourea (tu) is not a thiolate ligand, it supports structure **4F** in $[Cu_4(tu)_{10}]^{4+}$.[218] A heteroligand occurrence of **4F** is $(\mu\text{-SMe})_4(\mu\text{-S})_2(GaI)_4$.[219]

2.4.7. *Tricyclic* $(\mu_3\text{-SR})_2(\mu\text{-SR})_2(ML)_4$ (**4G**). This structure is known only for $Cu_4(SPh)_4(PPh_3)_4$.[220] It is a slightly flattened and twisted version of the "step" structure known for halide-bridged analogues with bulky phosphine ligands.



4G **4H**

2.4.8. *Derivatives of the* $(\mu_3\text{-SR})_4M_4$ *cubane core.* The homothiolate cubane structure $(\mu_3\text{-SR})_4(MSR)_4$ (**4H**), with triply-bridging and terminal thiolate ligands, has not yet been realized, although it has been proposed, without evidence, for copper metallothionein.[221] Compounds with heteroligands in either the terminal or bridging positions of **4H** are known. The series $[(\mu_3\text{-E})_4Fe_4(SR)_4]^{z-}$ (E = S or Se, z = 2 or 3) has been thoroughly investigated as analogues of the 4-Fe ferredoxins, and structural details, including those of the proteins, have been reviewed.[21,35] These structures are composed of concentric tetrahedra (slightly compressed) of E_4 and Fe_4, with congruent S_4 axes, but the E_4 tetrahedra are substantially larger so that E—Fe—E angles average 104° while Fe—E—Fe angles average 74°.

More recently metal-substituted cubanes, $[(RS)_3Fe_3(\mu_3\text{-S})_4M(cat)L]^{z-}$ (M = Mo or W; cat = substituted catecholate; L = RS^-, CN^-, OPh^-, PR_3 or solvent), with six-coordinate heterometals, have been prepared and fully characterized.[222–226] The cluster core is known in two oxidation states $[MFeS_4]^{2+,3+}$ in which the variability of the electron population is accommodated principally at the Fe atoms.[225]

The compound $(\mu_3\text{-SMe})_4[Re(CO)_3]_4$ maintains triply-bridging thiolate ligands in the cubane core,[227] as most probably do the complexes $(\mu_3\text{-SR})_4(PtMe_3)_4$.[228,229]

2.5. *Pentametallic structures*

2.5.1. $(\mu\text{-SR})_7M_5$ (**5A**). This cage occurs in $[M_5(SPh)_7]^{2-}$ (M = Cu or Ag)[205,230] (see Fig. 5). All thiolate ligands are doubly-bridging, providing a trigonal planar coordination for four M atoms and an almost linear digonal coordination for the fifth. Although the overall molecule is asymmetric, the M_5S_7 core is approximately C_{2v}. The polyhedra constituted by the M_5, S_7 or M_5S_7 sets are not regular, and

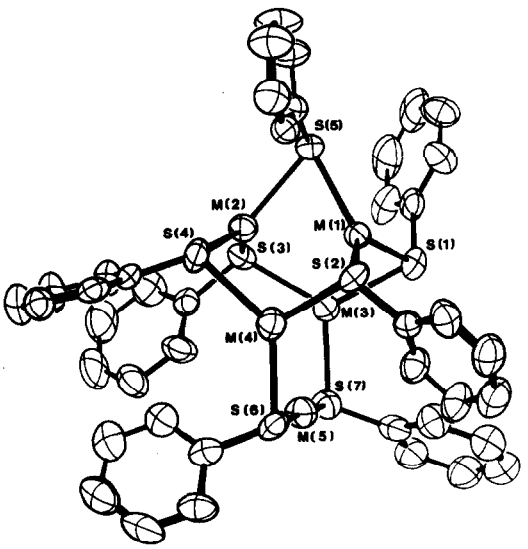
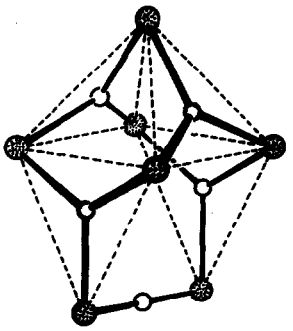


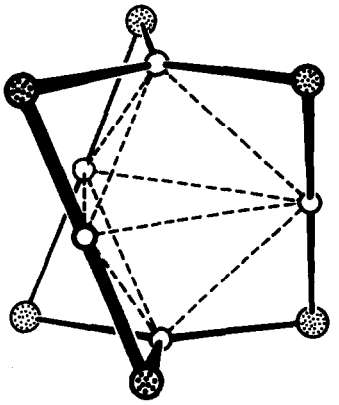
Fig. 5. Structure (**5A**) of $[M_5(SPh)_7]^{2-}$ (M = Cu or Ag).

this cage structure is best visualized as an expansion of the $M_4(SR)_6$ cage (**4E**) by an opening of one of the (μ-SR) vertices of the latter and insertion of the digonal (μ-SR)–M–(μ-SR) moiety (see Fig. 4). There is no structural evidence for energetically significant direct bonding between M atoms, and, as a consequence of the relatively low connectivities at the M and S atoms, substantial angular distortions are observed for the cage **5A**.

2.5.2. (μ-SR)$_6$M$_5$ (**5B**). Complexes $[Ag_5(SBu^t)_6]^-$ (Et_4N^+) and $[Cu_5(SBu^t)_6]^-$ (Et_4N^+ or Et_3NH^+) contain this cage.[205,231,232] The six doubly-bridging thiolate ligands provide trigonal planar coordination for two M atoms (M^{trig}) and digonal (almost linear) coordination for three M^{dig} atoms. The M_5 polyhedron is a trigonal bipyramid, and the S_6 polyhedron approximates to a trigonal antiprism. D_3-symmetry is the ideal for the M_5S_6 core, and need not be broken by the substituent array R_6. In the crystals with Et_4N^+ the Bu^t groups maintain a close approximation to D_3 for the whole cage (angle of antiprismatic twist is *ca* 50°), but in the Et_3NH^+ crystal one SBu^t ligand is inverted and as a consequence of increased steric interaction between Bu^t groups the Cu_5S_6 core suffers symmetry reduction, mainly as angular distortions.



5A

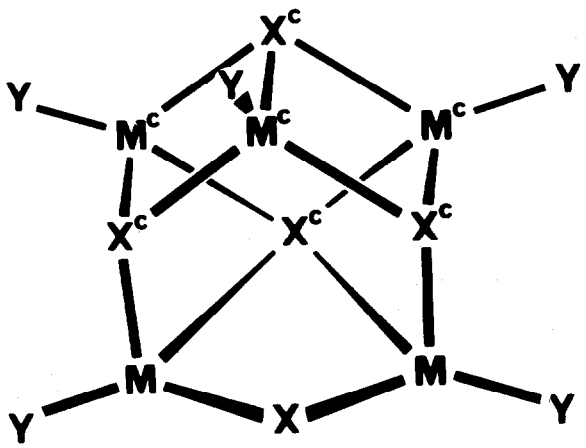


5B

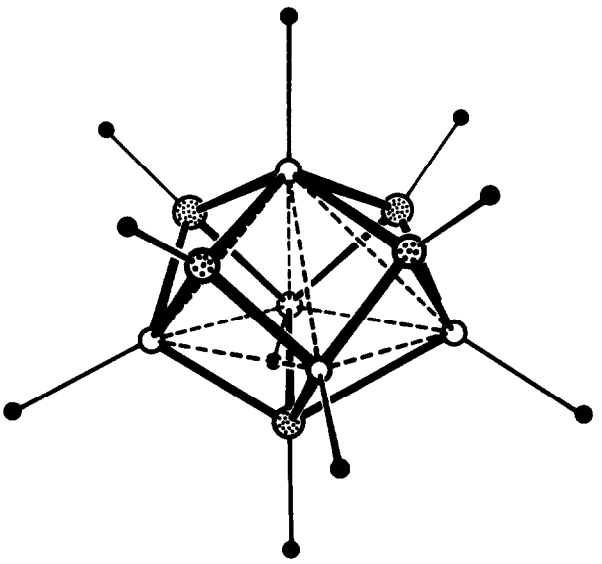
In symmetrical $[Cu_5(SBu^t)_6]^-$ the coordination of each Cu^{trig} atom is effectively planar, but the three Cu^{dig} atoms are each displaced *ca* 0.19 Å from the edges of the S_6 antiprism towards the centroid of the cage: the mean S—Cu^{dig}—S is 170°. This implies attractive Cu···Cu interactions, but the mean

dimensions Cu^{dig}--Cu^{dig} = 3.23 Å and Cu^{dig}--Cu^{trig} = 2.72 Å are not consistent with substantial Cu–Cu bonding. The cage is held together essentially by the bridging thiolate ligands.* In **5B** an increased trigonal twist moves the substituents R away from the equatorial region of the molecule and decreases the separations of the M^{dig} atoms.

Topological relationships between **5A**, **5B** and other thiolate cages are discussed in Sections 5.5.1, 5.5.2 and 5.5.3.



5C



5D

2.5.3. $(R'MSR)_5$. Compounds $RZnSBu^t$ (R = Me or Et), formed by reaction of ZnR_2 with Bu^tSH, are pentameric in benzene solution,[234] and crystals of the methyl derivative contain a pentametallic cage.[235] This partly irregular cage can be conceptualized in two ways: it can be regarded as an expanded cubane where the atoms marked M^c and X^c in diagram **5C** correspond to the seven vertices of the cube, but in place of the last M triconnected to the $(X^c)_3$ tripod there is an M–X–M moiety connected to two pairs of X^c, with the connections to the quadruply-bridging X elongated by 0.2–0.5 Å. An idealization of this structure is **5D** with one five-coordinate Zn atom and one quadruply-bridging thiolate ligand: in fact **5D** is comprised of an M_5 square pyramid and an inverted S_5 square pyramid, which intersect in a staggered conformation.

2.6. *Hexametallic structures*

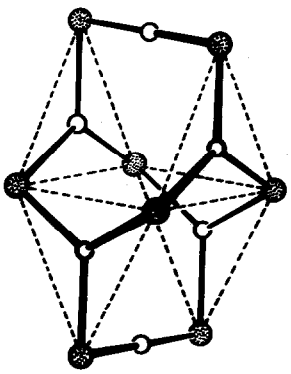
Variety prevails among actual and potential hexametallic thiolate aggregates. Two structures, **6A** and **6B**, are known for homothiolate complexes: structure **6C** has terminal phosphine ligands: two quite different structures, **6D** and **6E**, involve sulfides in bridging positions: and new sulfide and polysulfide aggregates, **6F** and **6G**, suggest potential arrangements for thiolate structures. One of the two *octahedro*-M_6 structures well known with halide ligands is plausible and one is implausible for metal thiolates.

2.6.1. $(\mu\text{-SR})_8M_6$ (**6A**). The **6A** ideal contains four trigonal and two digonal metal atoms, and can be produced by continuation of the polyhedral expansion that converted **4E** to **5A** (see Fig. 4). Each M^{trig} is linked to two other M^{trig} and one M^{dig} by doubly-bridging thiolate ligands. This ideal has not been observed, and, in view of its anticipated non-rigidity due to a low connectivity at both the M and the S atoms, is not expected. The crystalline compound $(Me_4N)_2[Ag_6(SPh)_8]$[236] has a low-symmetry structure which has been interpreted in terms of distorted **6A**, twisted in order to create two extra intra-cage connections between Ag and S and provide mechanical stability. There are also inter-cage

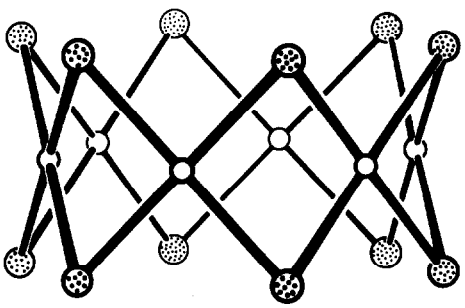
* The unique cluster $[Cu_5Ph_6]^-$ has the same framework as **5B**, but with less twist on the C_6 trigonal prism and shorter Cu^{dig}--Cu^{dig} distances (2.45 Å), indicative of Cu–Cu bonding.[233]

connections at the digonal ends. Consequently, two of the M atoms are four-coordinate, and four of the thiolate ligands become triply-bridging.

2.6.2. *Hexagono*-$(\mu\text{-SR})_{12}M_6$ (**6B**). This macrocyclic molecule contains a regular hexagon of M atoms, bridged over the edges by pairs of doubly-bridging thiolate ligands such that each metal has a planar coordination (approximately square). The S atoms constitute a larger hexagonal prism, with M atoms at the centres of its rectangular faces. The S–C vectors of the substituents alternate axial and equatorial (relative to the hexagonal axis) around the S_6 hexagons to allow D_{3d} molecular symmetry. The structure is confirmed in $Ni_6(SEt)_{12}$,[10] $Pd_6(SPr^i)_{12}$,[237,238] $M_6(SCH_2CH_2OH)_{12}$ (M = Ni or Pd),[239] $[Ni_6(SCH_2CH_2CH_2NHMe_2)_{12}]^{6+}$ [240] and $Ni_6[SCH_2CH(Me)OH]_{12}$.[241]



6A



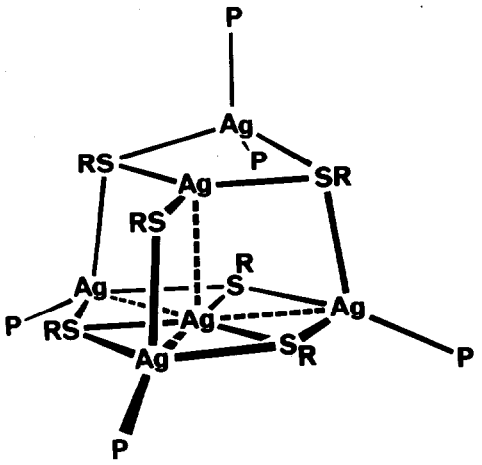
6B

These compounds with branched alkyl substituents are appreciably soluble in indifferent solvents, consistent with their molecular structure, and the solution molecular weights of related homologous compounds also indicate the hexameric structure **6B**.[237,242–244] There are, however, appreciable solubility variations with the identity of R,[237,244] and in some preparations it is found that the one compound can be obtained in soluble and insoluble forms[242,243] with the soluble form less stable. It therefore appears that molecules **6B** can convert to non-molecular solid-state structures, possibly **1D-E**. Investigations by pH titration[241] led to the conclusion that $Ni(SR)_2$ [R = CH_2CH_2OH or $CH_2CH(Me)OH$] are predominantly hexameric in aqueous solution at 25° C. Other species in solution have a lesser degree of oligomerization. At 75°C the solution compositions change, and the titration data have been interpreted in terms of open-chain species $[Ni(Ni(SR)_2)_n]^{2+}$ with a statistical distribution of *n*.

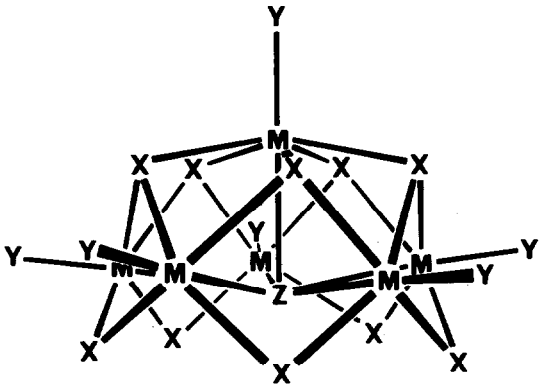
Although topologically different, **6B** has the same composition, metal coordination stereochemistry, and doubly-bridging ligands, as the *cuboctahedro*-$(\mu\text{-X})_{12}$-*octahedro*-M_6 structure (**6L**) adopted by the comparable compounds Pd_6Cl_{12}[245,246] and Pt_6Cl_{12}.[247,248]

2.6.3. $Ag_6(SAr)_6(PPh_3)_5$ (**6C**). This molecular aggregate, reported for Ar = C_6H_4Cl-4,[249] is shown in full in Fig. 6. When simplified as in **6C** it can be described in terms of an $Ag_5(SAr)_6$ central cage, with PPh_3 ligands terminal at three of the Ag atoms, and an $Ag(PPh_3)_2$ appendage inserted between two bridging thiolates. The $Ag_5(SR)_6$ core, when symmetrized, contains a basal unit comprised of an irregular hexagon of alternating Ag and S atoms (Ag_b^{per} and S_b) centered by an Ag_b^{cen} atom with trigonal $(S_b)_3$ coordination. A trigonal planar podal unit, $Ag_{pod}(S_{pod})_3$, is parallel to the basal plane and attached to it by three S_{pod}—Ag_b^{per} bonds. Tetrahedral coordination of each Ag_b^{per} atom is completed by a terminal PPh_3 ligand. The $Ag(PPh_3)_2$ addendum bridges two S_{pod} atoms, and the complete molecule is enclosed within 21 aryl substituents. The connectivity of this aggregate is unique, but it is possible to propose a structural relationship between the $Ag_5(SR)_6$ core of **6C** and the structure **5B** (see Section 5.5.3).

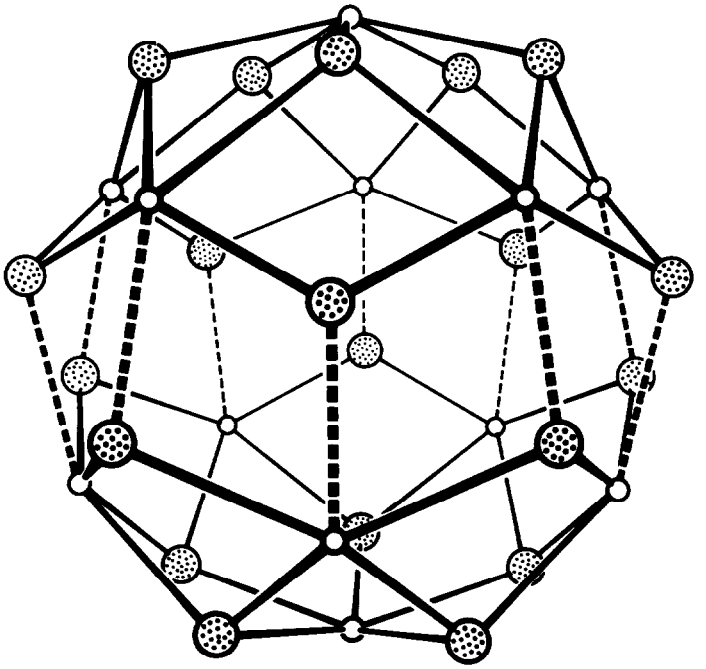
2.6.4. *Pentagonal pyramido*-$[M_6S_{17}]^{4-}$ (**6D**). The sulfide clusters $[M_6S_{17}]^{4-}$ (M = Nb or Ta) [prepared from $M(OEt)_5 + (Me_3Si)_2S$] possess structure **6D** (X = Y = S) which contains a pentagonal pyramid of M atoms, one triply-bridging sulfide over each triangular face, one doubly-bridging sulfide below each edge of the M_5 pentagon, one terminal sulfide (Y) on each metal, and one inner hextuply-bridging sulfide ion (Z) *trans* to each terminal sulfide.[250] The M and bridging sulfide atoms in this cage can be visualized alternatively as half of the array *icosahedro*-M_{12}-*pentagonal dodecahedro*-$(\mu\text{-S})_{20}$, as shown in **6E**, with the intersecting M_{12} and S_{20} polyhedra occurring as reciprocal Platonic polyhedra



6C



6D



6E

(i.e. they sustain a vertex–face interchange). It is conceivable that the frameworks **6D** and **6E** will be found to occur with thiolate ligands replacing sulfide ligands in terminal positions, and possibly doubly-bridging positions in **6D**, as, for instance, in $(\mu_6\text{-S})(\mu_3\text{-S})_5(\mu\text{-SR})_5(\text{MSR})_6$.

2.6.5. $(\mu_4\text{-S})(\mu_3\text{-S})_2(\mu\text{-S})_6\text{Fe}_6(\text{SR})_2$ (**6F**). Aggregates $[\text{Fe}_6\text{S}_9(\text{SR})_2]^{4-}$ (R = Me,[253] Et,[78] Bu^t,[251,252] CH_2Ph[253,254] or Ph[251,252]) possess structure **6F** (virtually C_{2v}) in which the metal array is a square of four Fe atoms with two (*trans*) coplanar (within 0.2 Å) equilateral triangles. Sulfide ions bridge the six edges of the Fe_6 polygon and cap the M_4 square and the two M_3 triangles. Thiolate ligands occur only at the two terminal positions of **6F**. Each metal has tetrahedral coordination. These complexes are formed in diverse reactions, $\text{Fe(SR)}_3 + \text{Na}_2\text{S}_2$,[253,254] $\text{FeCl}_3 + \text{Li}_2\text{S} + \text{LiSR} + \text{LiOMe}$,[251,252] $[\text{Fe(SR)}_4]^{2-} + \text{S}_8$,[78] and $[\text{Fe}_3\text{S}_4(\text{SEt})_4]^{3-}$ heated,[78] and undergo reversible one-electron oxidation and terminal ligand substitution.

The complex with R = Me has been crystallized as $[\text{Na}_2\{\text{Fe}_6\text{S}_9(\text{SMe})_2\}_2]^{6-}$ (Et_4N^+) in which two clusters (**6F**) are linked by two Na^+ ions, each with an S_6 coordination as shown in **6G**. This larger aggregate contains four fused $\{\text{NaFe}_3\text{S}_4\}$ cubanoid units.[253]

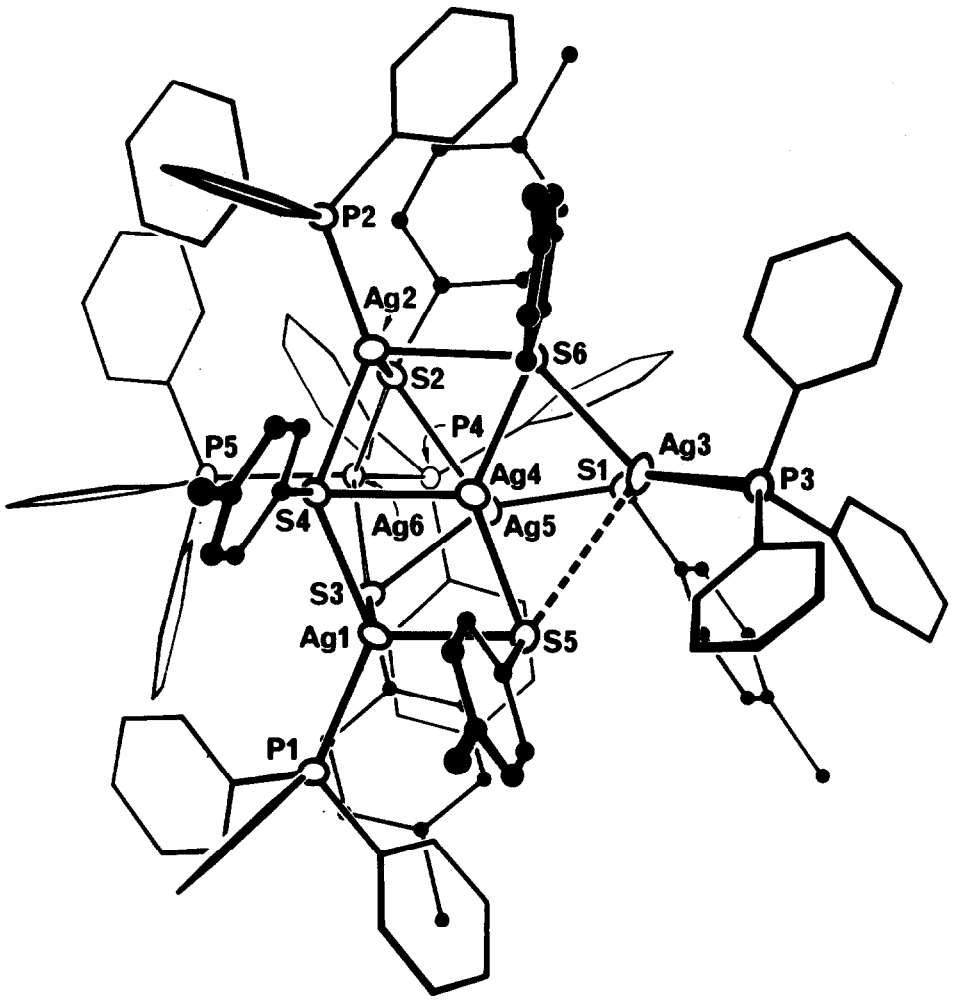
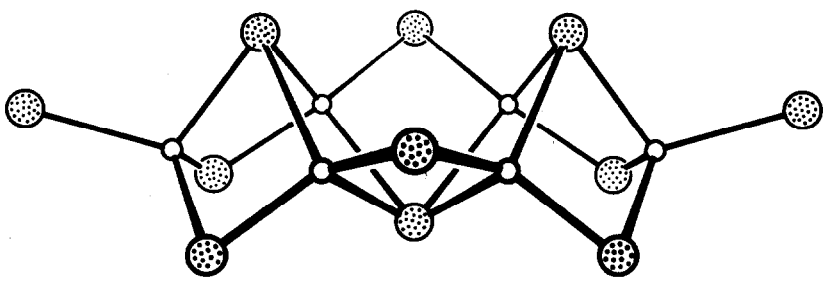
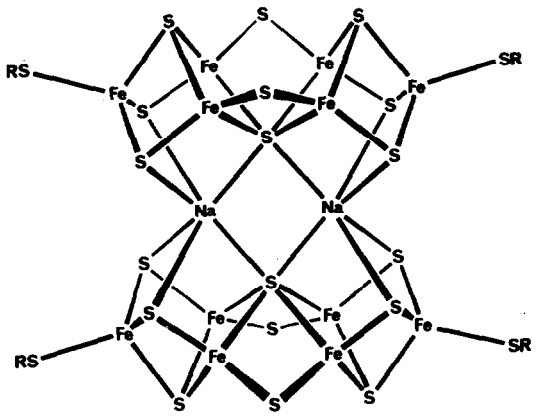


Fig. 6. Structure (**6C**) of $Ag_6(SC_6H_4Cl)_6(PPh_3)_5$, with the thiolate substituent atoms marked as closed circles. The broken line is an elongated bond.

2.6.6. $[(\mu_3\text{-}S)_6M_6X_6]^{z-}$ (**6H**). Structure **6H** has been confirmed in three non-thiolate complexes at two different oxidation levels: $[Fe_6S_6Cl_6]^{3-}$ (prepared from $6FeCl_2+9NaSPh+3Et_4NCl+6S$ in MeCN),[255,257] $[Fe_6S_6Cl_6]^{2-}$ (prepared from $3[Fe_4S_4Cl_4]^{2-}+2[FeCp_2]^+ \rightarrow 2[Fe_6S_6Cl_6]^{2-}+2FeCp_2$)[258] and $[Fe_6S_6I_6]^{2-}$ (prepared from $Fe+S_8+I_2+I^-$).[256] The thiolate complex $[Fe_6S_6(SC_6H_4Me)_6]^{3-}$ can be prepared by substitution of $[Fe_6S_6Cl_6]^{3-}$, and probably has structure **6H**, but is unstable in favour of $[Fe_4S_4(SAr)_4]^{2-}$.[257] Structure **6H** is a logical extension of the cubanoid $S_4M_4X_4$ structure type, with the same coordination stereochemistry at the M and S atoms.

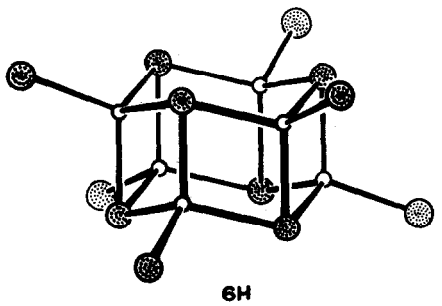


6F

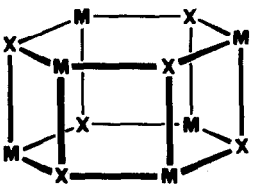


6G

2.6.7. *Hexagono-prismo*-$(\mu_3\text{-SR})_6M_6L_6$ (**6J**). Structure **6J** (X = SR), a variant of the **6H** ion in which only the bond angles at the M and S are affected, has been proposed but not confirmed for the hexamers



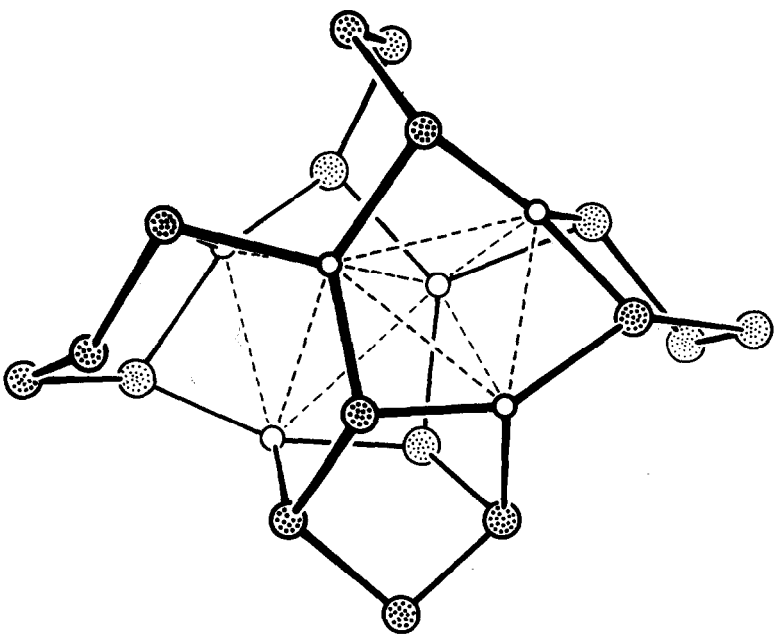
6H



6J

$(MeMSPr^i)_6$ (M = Zn or Cd) which occur in freezing benzene solutions.[259] The Zn compound is octameric, structure **8E**, in crystals.[260]

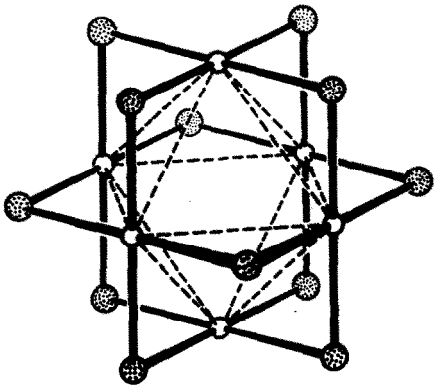
2.6.8. $[M_6(S_5)(S_4)_3]^{2-}$ (**6K**). The intriguing polysulfide aggregate $[Cu_6(S_5)(S_4)_3]^{2-}$ (Ph_4P^+) has



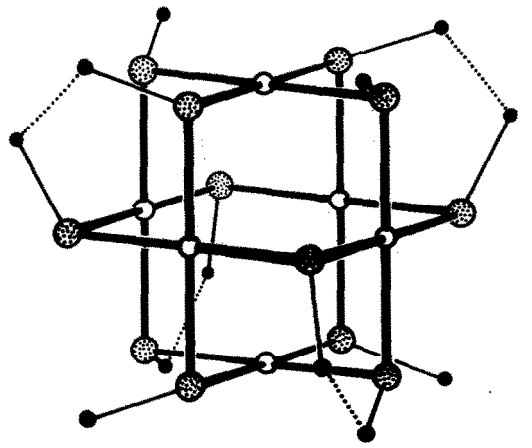
6K

been prepared from the reactions $S_8 + [Cu_4(SPh)_6]^{2-}$,[261] or methanolic S_x^{2-} solution + $Cu(acac)_2$.[262] The structure with symmetry C_2 has the M atoms arranged essentially as an edge-sharing pair of tetrahedra, with terminal S atoms of the S_x^{2-} ligands bridging all but two of the external edges of the tetrahedra, and M–S–S–M bridges on the other two edges. The polysulfide ligands provide eight terminal-S donor atoms in **6K**, and these S atoms could be conceived as thiolate ligands, in which case structure **6K** would be analogous to $[M_6(SR)_8]^{2-}$ (**6A**) with four M atoms trigonal and two digonal. In **6K** it is the non-terminal-S atoms in the S_5^{2-} ligands which complete the trigonal coordination of the last two Cu atoms.

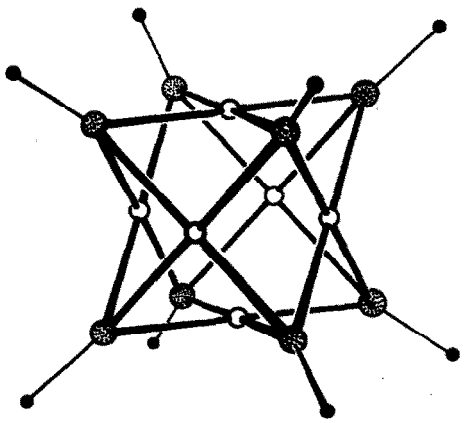
2.6.9. *Cuboctahedro*-(μ-SR)$_{12}$-*octahedro*-M_6 (**6L**). This structure type is well-known in clusters with monatomic ligands, but as shown by diagram **6M** it is not possible to accommodate the substituents of pyramidal doubly-bridging thiolate ligands. The minimum number of conflicts between substituents axial to the rectangular chair $M_3(SR)_3$ cycles is four: these conflicts (C_α–C_α separation *ca* 2 Å) could be removed by chelation with dithiolate ligands, or through some substitution by monatomic (sulfide) ligands. No complexes of this type have been reported.



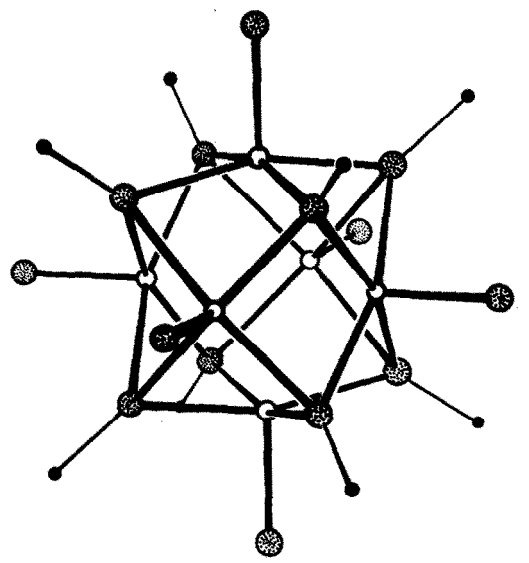
6L



6M



6N

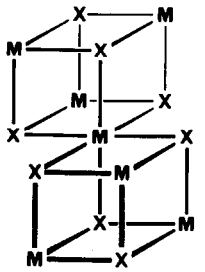


6P

2.6.10. *Hexahedro*-(μ_3-SR)$_8$-*octahedro*-M$_6$ (**6N**). Difficulties due to conflict between ligand substituents do not occur in the **6N** core. No thiolate examples of this otherwise well-known cluster structure type have yet been reported, but a methoxide analogue with terminal methoxide ligands, [(μ_3-OMe)$_8$(MoOMe)$_6$]$^{2-}$ (**6P**), has been fully characterized.[263] Structure **6N** with triply-bridging sulfide and terminal phosphine ligands to create metal five-coordination occurs in the set of clusters [S$_8$M$_6$(PPh$_3$)$_6$]^z (M = Fe or Co; z = 0, + or 2+),[264–267] and in S$_8$Co$_6$(CO)$_6$.[268]

2.7. *Heptametallic structures*

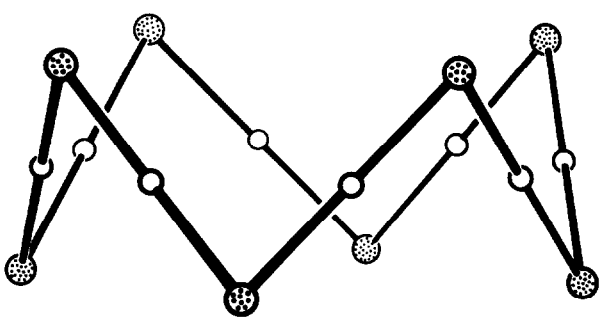
The first heptametallic thiolate complex [Cu$_7$(SCH$_2$CH$_2$S)$_4$(SEt)]$^{2-}$ has been intimated without structural details.[269] A structural precedent is set by the alcoxide-bridged compounds R$_6$Zn$_7$(μ_3-OMe)$_8$ (R = Me[270] or Et[271]), in which a pair of cubanoid cages share a vertex (**7A**).



7A

2.8. *Octametallic structures*

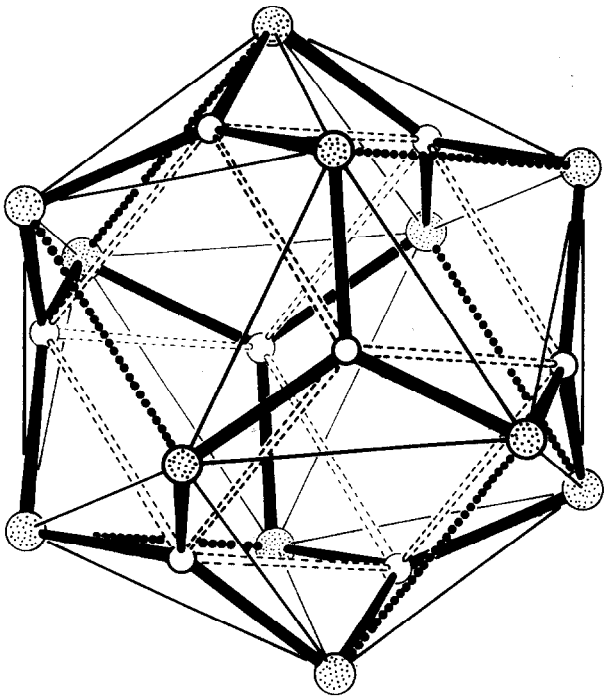
2.8.1. *Cyclo*-(MSR)$_8$ (**8A**). Molecular weight measurements[272,273] indicate that silver tertiary-alkane thiolates are octameric [(AgSR^t)$_8$] in solution. A possible structure is the puckered cycle of zig-zag digonal segments (**8A**): this is consistent with the cyclic and zig-zag patterns of other AgSR structures (see Section 3.1.1). **8A** is conceivable as a derivative of the crown S$_8$ structure, with Ag atoms inserted in all S–S bonds.



8A

2.8.2. *Centro*-(μ_8-Z)-*hexahedro*-M$_8$-*icosahedro*-(μ-SR)$_{12}$ (**8B**). Here a cube of M atoms contains a monatomic ligand (Z) at the body centre, with doubly-bridging thiolate ligands over its 12 edges such that the S$_{12}$ array is an icosahedron containing metal atoms in the centres of 8 of its 20 triangular faces. Diagram **8B** shows the structure without the central ligand. T_h-symmetry (T_h is a sub-group of I_h, O_h) is possible for the core, excluding the substituents R. The Z–M bond is abnormally long, and a lesser part of the metal coordination, which is essentially trigonal unless there are additional terminal ligands. The **8B** structural core occurs in [ICd$_8$(SCH$_2$CH$_2$OH)$_{12}$]$^{3+}$, crystallized with 3I$^-$ which provide (with some I bridging) terminal coordination at five of the Cd atoms as shown in Fig. 7.[274] Two other Cd atoms complete similar trigonal bipyramidal coordination through chelating ligand OH functions, while the eighth Cd has three terminal OH donors.

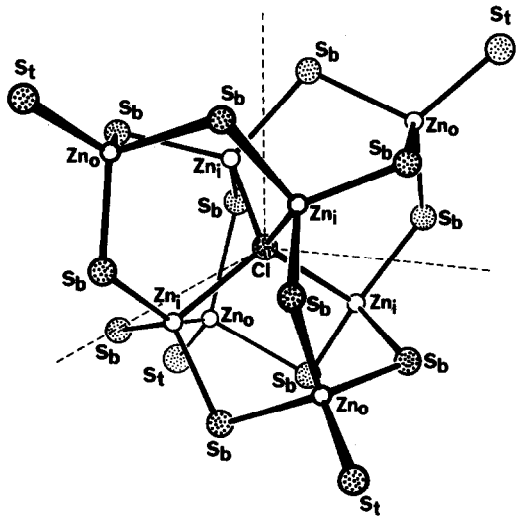
The **8B** core occurs also in the chelated cages [ClM(I)$_8$(SCMe$_2$CQ)$_{12}$M(II)$_6$] [M(I) = Cu or Ag,



8B

M(II) = Cu or Ni], and Q contains a donor function.[275-278] The vertices of the S_{12} icosahedron are linked in pairs (without breaking the T_h-symmetry) by the outer chelate units, as shown by the dotted connections in **8B**, each chelate spanning a face of the inner $M(I)_8$ cube.

2.8.3. *Centro-Z-tetrahedro-*M_4*-icosahedro-*(μ-$SR)_{12}$*-tetrahedro-*$(MSR)_4$ (**8C**). Structure **8C** can be regarded as a derivative of **8B**, in which the metal atoms are displaced alternatively inside and outside the faces of the $(SR)_{12}$ icosahedron: the M_8 polyhedron is a tetracapped tetrahedron, i.e. the concentric bitetrahedron. The inner M atoms (M^i) complete their tetrahedral coordination at the central monatomic ligand, while the outer M atoms (M^o) each have one terminal thiolate ligand for this purpose. One occurrence of **8C** is known, in $[ClZn_8(SPh)_{16}]^-$,[279,280] although reproduceable preparation has not yet been secured. The normal tetrahedral stereochemistry at all atoms in this structure suggests that it should occur with other metals and central monatomic ligands: the preparative difficulty is largely one of solubility.



8C

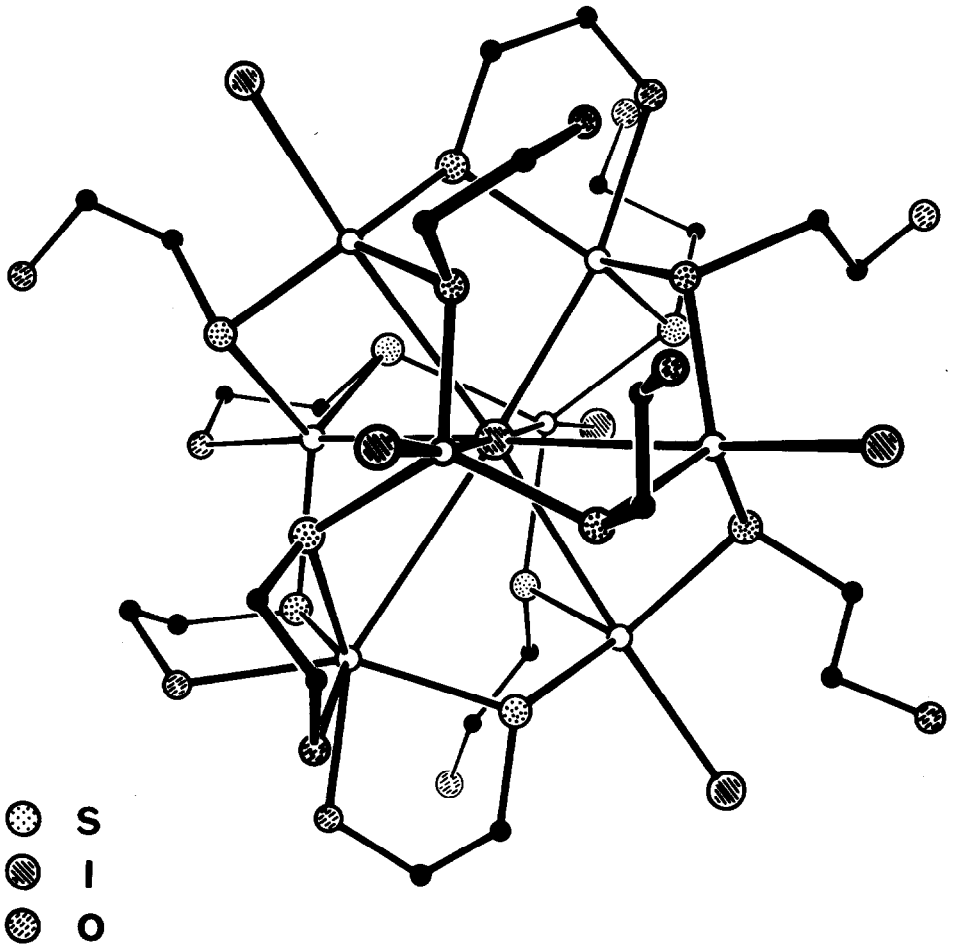
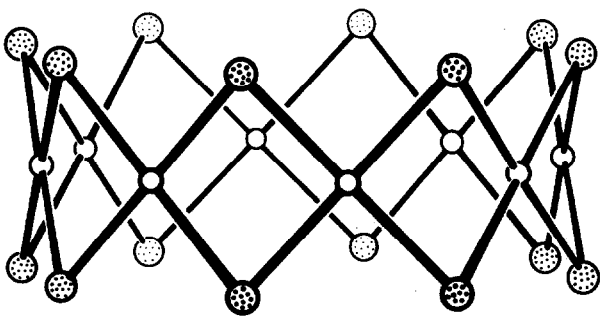


Fig. 7. Structure of $[(\mu_8\text{-I})Cd_8(SCH_2CH_2OH)_{12}]I_3$.

Aggregate **8C** is unique, being composed of expanding, concentric, regular polyhedra, alternating between M and donor atoms as specified in the heading to this section. The structure is distinctive also because the array of bridging substituents also has a high virtual symmetry, that of the rare point group T (the mirror elements of T_h being necessarily broken at the pyramidal S atoms). This occurs because the 12 phenyl substituents, inclined obliquely to the surface of the globular molecule, are packed regularly over its surface.

Structures **8B** and **8C** belong to a set of four, in which an icosahedron or cuboctahedron of doubly-bridging thiolate ligands is associated with a cube or bitetrahedron of M atoms, as described in Section 5.5.5.

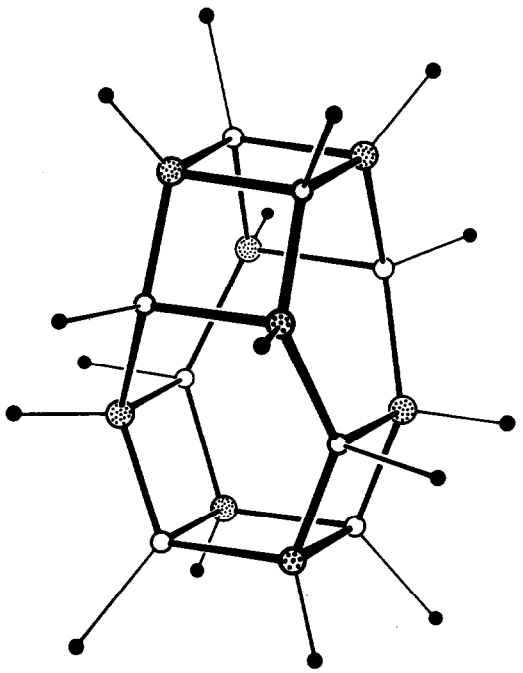
2.8.4. *Octagono*-$(\mu\text{-SR})_{16}M_8$ (**8D**). The octagonal toroid **8D** continues the series **4C** (square) and **6B**



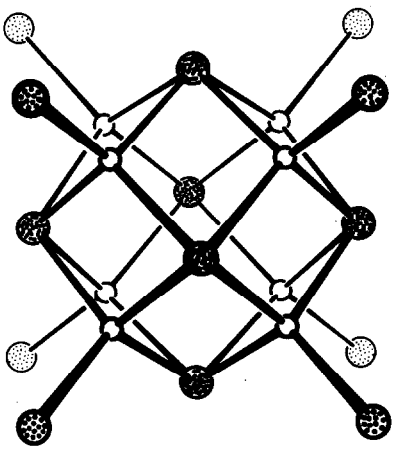
8D

(hexagonal) of toroidal molecules $[M_n(SR)_{2n}]$ which have virtual D_{nd}-symmetry. It is known for the very soluble compound $Ni_8(SCH_2COOEt)_{16}$[202] in which all except one of the ligand substituents are externally pendant. The unique substituent, with axial departure from its bridging S atom, bends around to re-enter the centre of the molecule along the toroid axis, such that the ester oxygen atom is distantly (3.0 Å) located in the axial coordination positions of two Ni atoms. The re-entrant EtO moiety largely fills the van der Waals' cavity of the toroid, and it is this reception by the toroid of its own ligand tail which probably accounts for the abnormal size of **8D** relative to the frequently occurring **6B**. All other geometrical properties of **8D** are normal.

2.8.5. $(R'MSR)_8$ (**8E**). Structure **8E**, comprised of six M_2S_2 cycles and four slightly non-planar M_3S_3 cycles, with symmetry S_4, occurs in crystalline $(MeZnSPr^i)_8$.[260] Tetrahedral stereochemistry exists at all Zn and S atoms, which are subject to positional disorder in the crystal. This compound, like its Cd homolog, is hexameric in cold benzene solution.[234,259]



8E

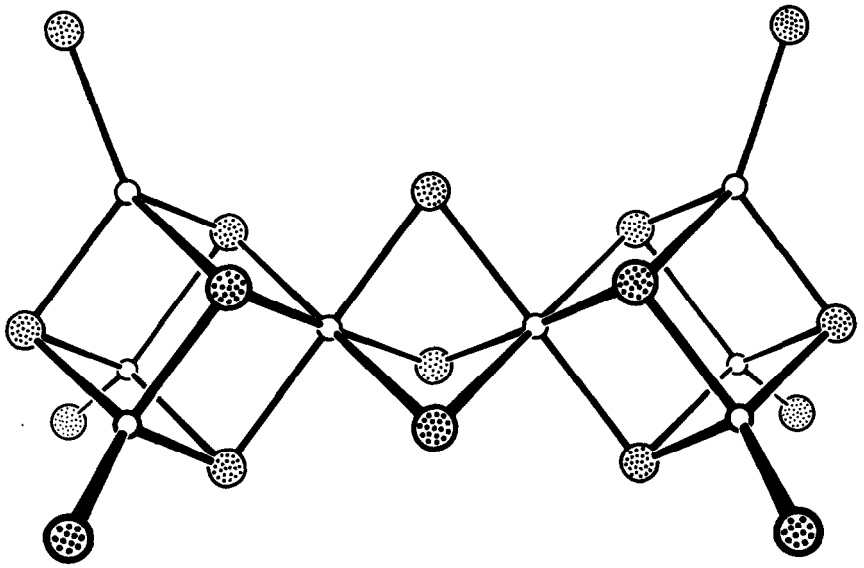


8F

2.8.6. *Octahedro-*$(\mu_4\text{-SR})_6$*-hexahedro-*$(MSR)_8$ (**8F**). Here, in symmetry O_h, a cube of M atoms intersects an octahedron of quadruply-bridging ligands (S^{2-}) to form a rhombic dodecahedron. Terminal thiolate ligands complete tetrahedral coordination at the M atoms. The structure is known so far only for Co (but is expected for other metals such as Mn, Fe, Zn and Cd), with S^{2-} as the quadruply-bridging ligand, and in two cluster oxidation states. $[S_6(CoSPh)_8]^{4-}$ is prepared by the reaction $[Co_4(SPh)_{10}]^{2-} + 3HS^-$,[281] and can be reduced by sodium acenaphthylenide to $[S_6(CoSPh)_8]^{5-}$.[281,282] The structural consequence of reduction is only a very small increase in the length of the terminal Co—SPh bonds. The molecular structure **8F** is part of the non-molecular structure of the mineral pentlandite (M_9S_8), in which the M_8S_{14} units share sulfide vertices and are linked by additional octahedrally coordinated M atoms. However the $[S_6(CoSPh)_8]^{4-,5-}$ cages are not electronically equivalent to the pentlandite aggregate, and have a significantly larger (by *ca* 20%) core volume.

2.8.7. *Bis-cubanoid cages* $[(\mu\text{-Y})_3\{M'(\mu_3\text{-X})_4(ML)_3\}_2]^{z-}$ (**8G**). A series of compounds is known in which three doubly-bridging thiolate or alcoxide ligands (Y) link two cubane clusters (**4H**) such that one M atom (M') in each acquires an octahedral coordination. The identities (M, M', X, Y, L and *z*, respectively) of the compounds characterized are: Fe, Mo, S, SAr, SAr, 3,[283,284] Fe, Mo (or W), S, SEt, SEt, 3,[285,286] Fe, Mo (or W), S, OMe, SPh, 3,[284,287] and Fe, Mo, SPh (or SEt), Cl (or Br), 3.[288]

2.8.8. *Bis-adamantanoid cages* $[M_8(SR)_{19}]$. Here two adamantanoid cages are connected through a shared terminal ligand. Although not yet reported for thiolate ligands, the structure is known for

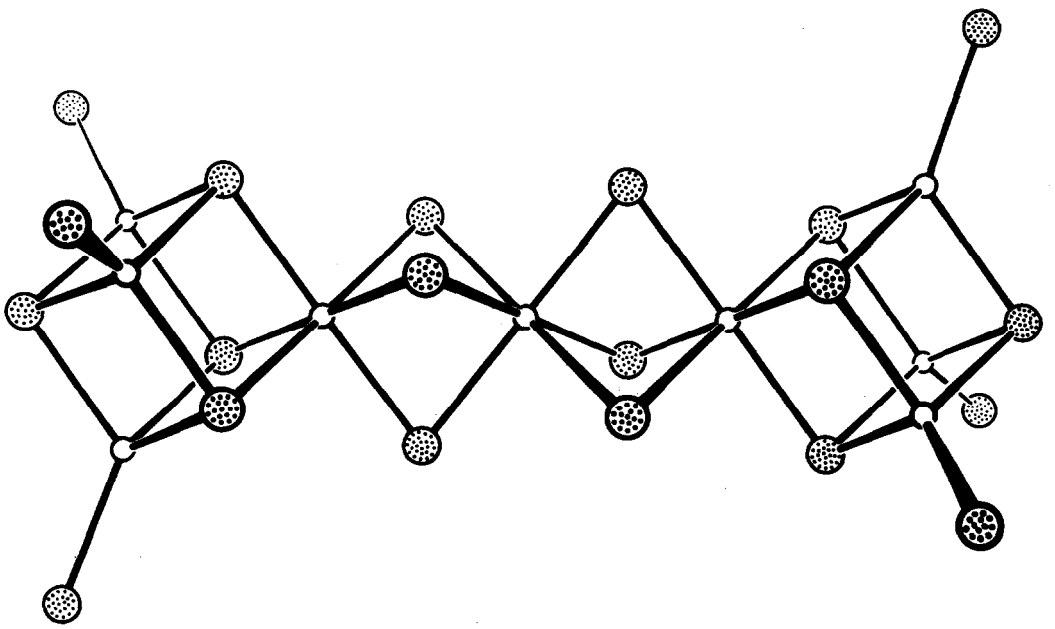


8G

sulfides in $[Ge_8S_{19}]^{6-}$ (Cs^+).[94] Thiolate bridging between adamantanoid cages is established in the *catena*-polyadamantanoid structure **1D-G** of $Zn_4(SPh)_8(MeOH)$.

2.9. *Nonametallic structures*

2.9.1. *Metal-linked bis-cubanoid cages* $[M''\{(\mu\text{-}SR)_3M'(\mu_3\text{-}S)_4(MSR)_3\}_2]^{z-}$ (**9A**). These elongated bis-cubanes connected by an extra M atom (M″) are obtained in reactions very similar to those yielding the directly linked bis-cubanes (**8G**). All characterized complexes have four-coordinate Fe(M) and six-coordinate Mo or W (M′) in the cubane clusters, Fe as the connecting metal (M″), thiolate as the doubly-bridging and terminal ligands, and overall charge 3− or 4−: $[Mo_2Fe_7S_8(SEt)_{12}]^{3-}$, $[W_2Fe_7S_8(SEt)_{12}]^{4-}$ and $[Mo_2Fe_7S_8(SEt)_{12}]^{4-}$.[289–291] The central Fe atom has slightly twisted trigonal antiprismatic stereochemistry, and undergoes localized electron transfer at a potential less negative than reduction of the cubanoid cage, and therefore the two different oxidation states of the isolated complexes correspond to Fe(II) (high spin) and Fe(III) (low spin) at the central atom.



9A

2.10. *Decametallic structures*

Two closely related M_{10} aggregate structures are known, both based on a tetracapped octahedron of M atoms. The fundamental $M_{10}S_{20}$ framework is conceivable as the fusion of four adamantanoid units (**4F**) creating a super-tetrahedron with symmetry T_d. This array is a 30-atom macro-tetrahedral fragment of the cubic sphalerite lattice.

2.10.1. *Tetrahedro*-(μ_3-X)$_4$-*octahedro*-M$_6$-*truncated tetrahedro*-(μ-SR)$_{12}$-*tetrahedro*-(MSR)$_4$ (**10A**). This structure occurs for four complexes $[X_4M_{10}(SPh)_{16}]^{4-}$ (X = S or Se, M = Zn or Cd), prepared by reaction of $[M_4(SPh)_{10}]^{2-}$ with the chalcogen.[292,293] The chalcogenide ions are located at the triply-bridging positions above four faces of the octahedron of inner M atoms, while the other four faces are capped by tripodal (μ-SR)$_3$MSR units. The X_4 set is therefore a tetrahedron, and the 12 doubly-bridging thiolate ligands constitute the tetratruncated tetrahedron shown as **10Ab**. The structure of the cadmium sulfide compound is shown in Fig. 8. As in the adamantanoid structure this framework can have high symmetry (T_d) without requiring local tetrahedral coordination stereochemistry, but in fact each of the 30 metal or chalcogenide atoms has virtual tetrahedral or part-tetrahedral stereochemistry. Direct M–M bonding is absent. Inclusion of the substituents of the 12 doubly-bridging thiolate ligands lowers the maximum symmetry to T, and inversion at these pyramidal S atoms allows 186 molecular configurational isomers. Two different crystal structures with two different configurational isomers, both with molecular symmetry S_4, have been observed to date. At least one of these crystal structures will accommodate cations Me_4N^+ or Et_3NH^+ without change, and the crystalline compounds appear to possess high thermodynamic stability, being formed under a variety of preparative conditions.

The surface of the super-tetrahedron **10A** is formed by four equivalent hexagonal faces **10Aa**, each equivalent to three fused M_3S_3 rings in chair conformation, with six peripheral substituents R either axial or equatorial to the face. At the face-centre there is one three-coordinate chalcogenide atom, and thus this face represents the smallest portion of the surface of the non-molecular metal chalcogenide, with one accessible reaction site.

^{113}Cd NMR confirms that structure **10A** is maintained in solution, the spectrum revealing isotope ^{113}Cd–E–^{111}Cd coupling within the inner Cd_6 octahedron, and coupling between the inner and outer Cd atoms.[217]

2.10.2. $[Cd_{10}(SCH_2CH_2OH)_{16}]^{4+}$ (**10B**). In this ion (with ClO_4^-[294] or SO_4^{2-}[11,295]) triply-bridging thiolate ligands occur in place of the triply-bridging chalcogenide ions at the centres of the faces of **10A**. The tetrahedral coordination of the outer M atoms by terminal thiolate ligands in **10A** is replaced by *fac*-CdS_3O_3 octahedral coordination using three OH donors from the three doubly-bridging thiolate ligands which now chelate the caps: for reasons of clarity only two of these are shown on diagram **10B**. In addition, the OH groups of the triply-bridging SCH_2CH_2OH ligands coordinate by chelation to four of the six inner Cd atoms, making them pseudo trigonal bipyramidal, as shown in **10B**. With this

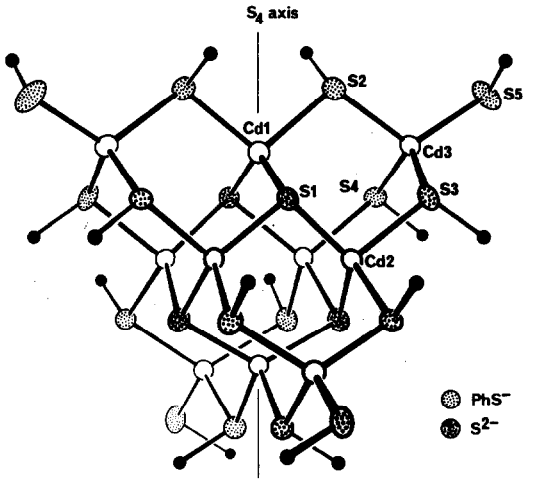
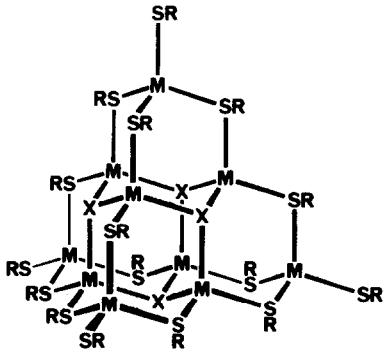
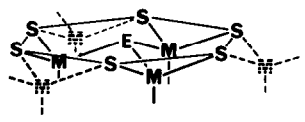


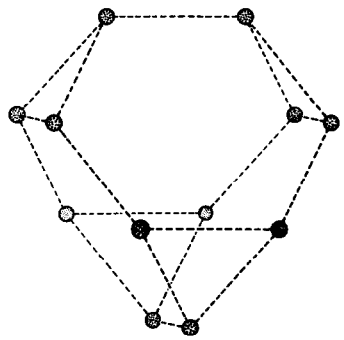
Fig. 8. Structure (**10A**) of $[S_4Cd_{10}(SPh)_{16}]^{4-}$ with S_4 crystallographic symmetry. Phenyl substituents are represented by C_α atoms only.



IOA

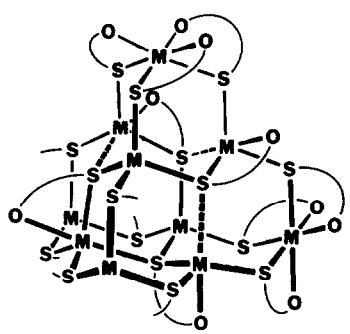


IOAa



IOAb

connectivity, and with the Cd coordination of three types [tetrahedral CdS_4 ($\times 2$), trigonal bipyramidal CdS_4O ($\times 4$) and octahedral CdS_3O_3 ($\times 4$)], the maximum symmetry of **10B** is only S_4, and there is in fact considerable distortion in the crystal structure. At the five-coordinate Cd atoms an axial Cd—(μ_3-S) bond is elongated by *ca* 0.3 Å relative to the equatorial bonds which are two Cd—(μ-S) and one Cd—(μ_3-S).



IOB

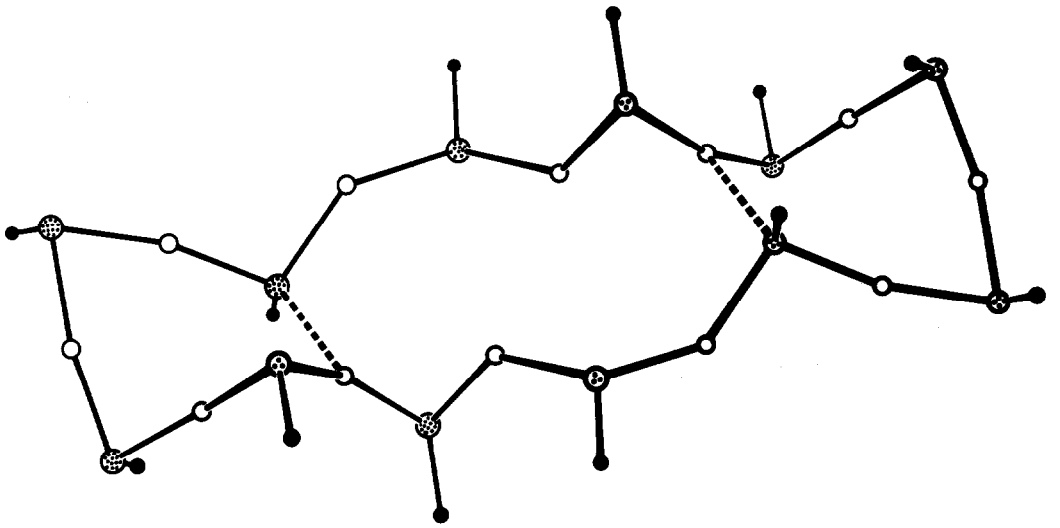
The ^{113}Cd NMR of **10B** has been examined in solution and crystal phases.[294,296,297] In solution the CdS_4 and CdS_4O sites exchange rapidly (*ca* 10^4 s^{-1}[294,297]), probably by a mechanism indicated by the crystal structure in which the triply-bridging ligands rotate, in concert, their chelating OH functions around the three inner Cd atoms of the hexagonal faces (**10Aa**). The solid-state NMR reveals, in addition to the large chemical-shift differences of the three coordination types, appreciable chemical-shift differences of up to 82 ppm due to variations in the crystal environment and hydrogen bonding of the aggregate.[294]

2.10.3. *Molecular* $M_{10}(SR)_{20}$. Geometrical analysis reveals that there is limited steric crowding on the hexagonal faces (**10Aa**) of **10A**, which means that a substituent could radiate from a triply-bridging thiolate (or selenolate) ligand in place of the chalcogenide bridge, yielding uncharged molecules $M_{10}(SR)_{20}$ or $M_{10}(SeR)_4(SR)_{16}$ with the same framework of M and donor atoms as **10A**. It is known

that $[Cd_{10}(SCH_2CH_2OH)_{16}]^{4+}$ (which does have thiolate coordinated at the centre of the face **10Aa**) in solution reacts with excess thiolate,[295] which could generate $Cd_{10}(SCH_2CH_2OH)_{20}$ with structure **10C**.

2.11. M_{12} *structures*

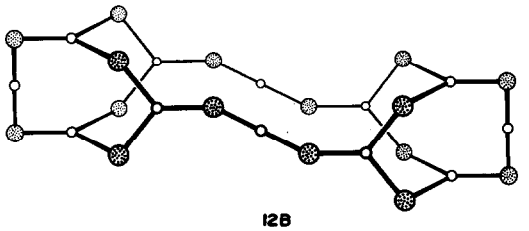
2.11.1. *cyclo*-$(\mu$-$SR)_{12}M_{12}$ (**12A**). This 24-membered ring of alternating Ag and S atoms occurs in crystalline silver cyclohexanethiolate.[298,299] The crystal structure contains these cyclic molecules overlapped, with longer, weaker, secondary Ag--S interactions between molecules. The centrosymmetric cycle **12A**, which also contains two transannular secondary bonds (marked as broken lines), is in an elongated "chaise longue" conformation in the crystal. (Alternatively, it is a complete lounge room, with 12 cyclohexyl "chairs" around the periphery!)



12A

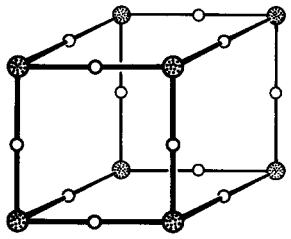
The molecular weights of silver *sec*-alkanethiolates in solution indicate the general formulation $(AgSR^{sec})_{12}$,[272,273] suggesting that structure **12A** occurs generally. Association of these molecules may occur.[299]

2.11.2. $[M_6(SR)_8]_2$ (**12B**). In $(Me_4N)_2[Ag_6(SPh)_8]$ the cages idealized as **6A** are butt-jointed to form hour-glass-shaped aggregates (**12B**). The ideal **12B** is large and open, with an average of only 32/28 Ag—S bonds per Ag, S atom, and thus is subject to crystal and solution forces which produce angular distortions and secondary Ag--S interactions *ca* 0.3 Å longer than the remainder of the Ag—S bonds.[236]



12B

2.11.3. *Cuboctahedro*-M_{12}-*hexahedro*-$(\mu_3$-$SR)_8$ (**12C**). The non-thiolate cage $[(\mu_3\text{-}S)_8Cu_{12}]^{4-}$ (Ph_4P^+), isolated from the reaction of $CuCl_2$, EtS^- and Li_2S in methanol, has structure **12C** in which triply-bridging sulfide ions cap the triangular faces of a cuboctahedron of Cu atoms (edges 2.77–2.95 Å). Each Cu atom is displaced slightly from digonal coordination towards the centre of the cuboctahedron such that S—Cu—S = 167–171°.[300] $[Au_{12}S_8]^{4-}$ (Ph_4As^+), isolated from solutions of gold sulfides in concentrated aqueous sodium sulfide, has the same framework but with almost linear (178–179°) S–Au–S segments.[301] The structural precedent is therefore established for $[(\mu_3\text{-}SR)_8M_{12}]^{4+}$ (M = Cu, Ag or Au), in which thiolate substituent interference is unlikely: a requirement of very strongly electron-releasing thiolate ligands is expected.



12C

2.12. M_{14} *structures*

A set of M_{14} complexes with an inner cube of metal atoms bridged by thiolate chelate ligands which include also an outer octahedron of M atoms has been mentioned in Section 2.8.2.

2.12.1. *cyclo*-$(\mu\text{-SR})_{14}M_{14}(PPh_3)_4$. The compactly folded monocyclic structure shown in Fig. 9 occurs in crystalline $(\mu\text{-SBu}^t)_{14}Ag_{14}(PPh_3)_4$.[195] The 28-membered centrosymmetric monocycle of alternating Ag and S atoms contains 10 linear S–Ag–S segments, and four bent segments in which PPh_3 ligands are attached to trigonal planar Ag atoms. There is a pseudo-two-fold axis along the length of this molecule, which contains opposed "zig-zag" segments along the central sides, connected by four "crossover" segments to four trigonal "bending" segments, which are linked by two linear "end-connecting" segments. It is significant that there are no secondary Ag–S interactions: the opposing directions of S–Ag–S segments related by the pseudo-two-fold axis allow the closest approach of segments across the molecule to be between Ag atoms at non-bonding distances of *ca* 3.1 Å.

3. DESCRIPTION OF NON-MOLECULAR STRUCTURES

A very large number of metal thiolates, particularly the uncharged $\{M(SR)_n\}_p$ compounds where R is not bulky, are insoluble or sparingly soluble in inert solvents and are therefore presumed to be structurally non-molecular. However confirmation of structural non-molecularity has been achieved in a very small proportion of these compounds because the insolubility makes it difficult to obtain crystals with a quality sufficient for diffraction analysis. Techniques that have been applied successfully to the problem of crystal growth are: (i) addition of non-coordinating solubilizing functions to the

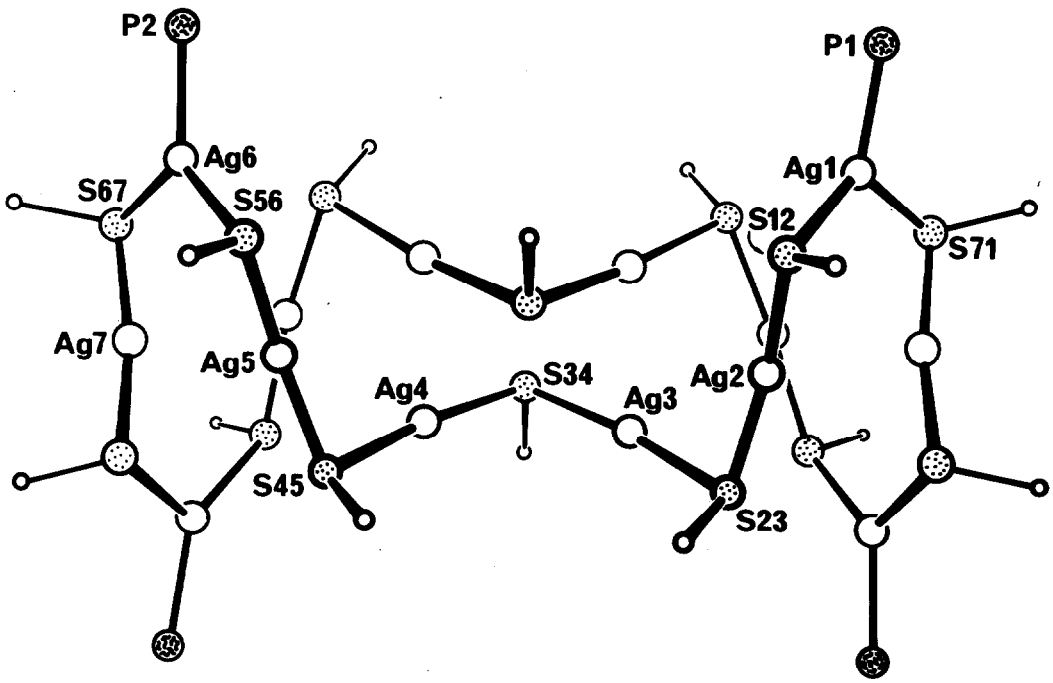
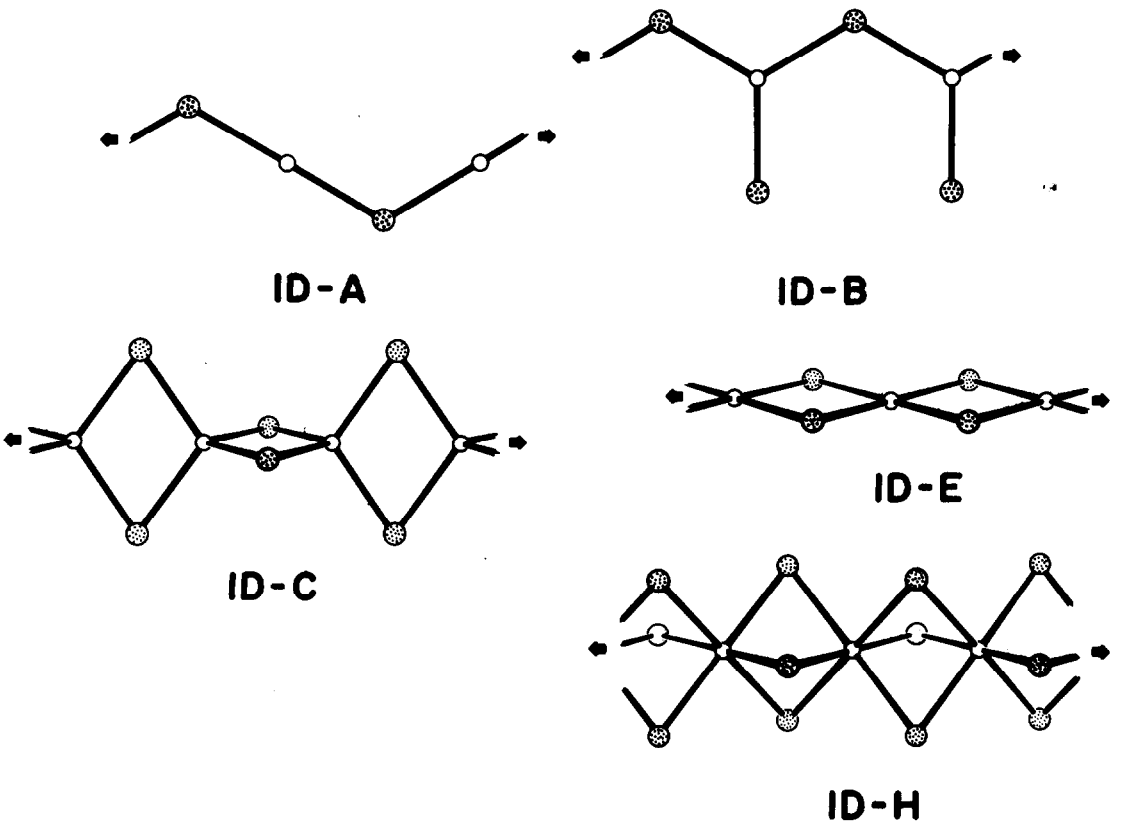


Fig. 9. Centrosymmetric coordination structure of $(\mu\text{-SBu}^t)_{14}Ag_{14}(PPh_3)_4$, with thiolate substituents marked as C_α atoms only.

thiolate substituents R,[302] (ii) a controlled slow shift of an equilibrium connecting the insoluble compound and a soluble (further ligated) species in solution, and (iii) a controlled thermal polymerization.[303]

3.1. *One-dimensionally non-molecular structures*



3.1.1. *catena*-$[(\mu\text{-SR})M]_\infty$ (**1D-A**). Crystalline $AgSCMeEt_2$ contains well-separated infinite chains, each *chain* being composed of two intertwined but unconnected *strands* with alternating Ag atoms and doubly-bridging thiolate ligands.[304] Each strand contains approximately planar zig-zag S–Ag–S–Ag–S–Ag–S segments of type **1D-A**, which are connected at their ends by single Ag atoms (also linearly coordinated) linking segments on one side of the chain to parallel segments on the opposite side of the chain. The two strands of the chain thereby wind around each other at every fourth Ag atom without interstrand bonding, as shown in Fig. 10. The shortest distances between the strands are not secondary Ag–S contacts, but non-bonding Ag···Ag at 2.89 Å.

This compound, like other $AgSR^{tert}$ compounds, is octametallic $[(AgSR)_8]$ in benzene solution.[272] The crystal structure allows postulation of a cyclic zig-zag structure **8A** for the molecule (see Section 2.8.1), and of a straightforward mechanism for interconversion of the non-molecular crystal structure and the molecule $(AgSR)_8$ in solution.[304]

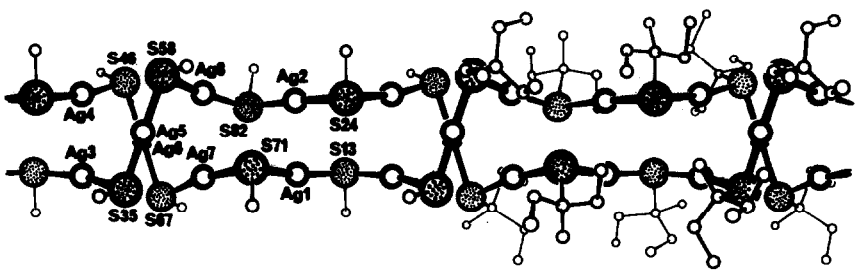


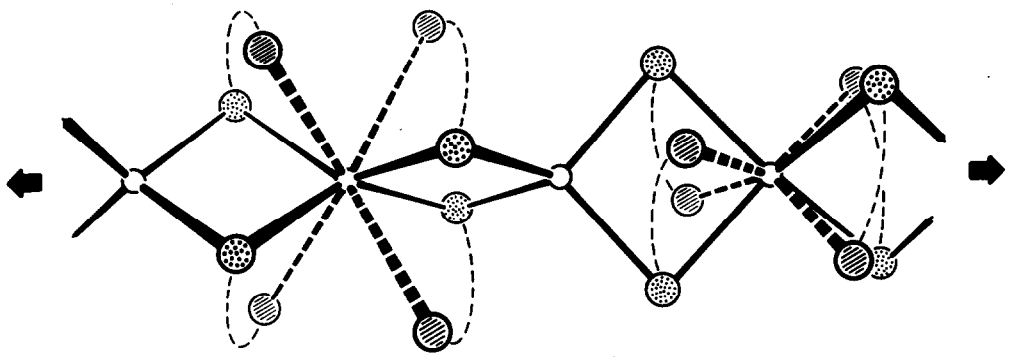
Fig. 10. Crystal structure of *catena*-$AgSCMeEt_2$ showing the two intertwined strands of one chain, viewed almost parallel to the planes which contain the zig-zag segments. Strand crossover occurs at Ag5, Ag6. Two repeat units are shown, with the ligand substituents abbreviated to C_α on the left.

It has been mentioned[298] that $AgSCMe_2Et$ is one dimensionally non-molecular in crystals, but details have not been reported.

3.1.2. *catena*-$[(\mu\text{-SR})MSR]_\infty$ (**1D-B**). This structure with a three-coordinate metal is not known as such (and could be unfavourable relative to a double-bridged structure), but derivatives with heteroligands in the non-bridging positions are known. Several compounds [MeSHgX and their derivatives[200,305]] contain $[(\mu\text{-SMe})Hg]_\infty$ spines, in which the Hg—S bonds (2.41–2.47 Å) are short relative to the remainder of the Hg coordination, and the S—Hg—S angles range from 135 to 163°. A similar interpretation has been given for $Pb[SCH_2CH_2N(CH_2CH_2)_2O](NO_3)$.[306]

3.1.3. *catena*-$[(\mu\text{-SR})_2M]_\infty$ (*tetrahedral metal coordination*) (**1D-C**). This well-known non-molecular structure type is represented by thiolates and selenolates of Zn, Cd and Hg in the solid state: $Hg(SBu^t)_2$,[9] $Hg(SeBu^t)_2$,[307] $Hg(SeMe)_2$,[308] $[Cd\{SCH(CH_2CH_2)_2NHCH_3\}_2]^{2+}$,[309,310] and $Cd(SCH_2COOEt)_2$.[311] In addition, structure **1D-C** probably occurs in $M(SBu^t)_2$ (M = Zn or Cd), because their low-frequency IR spectra are very similar to that of $Hg(SBu^t)_2$ and different from molecular $Hg(SR)_2$ species.[312] In most instances the M_2E_2 bridge straddles a centre of symmetry (requiring the *anti*-planar configuration), with M—S—M *ca* 82°: an exception is $Hg(SeMe)_2$, where two different bridge cycle geometries alternate along the chain. One cycle is folded, with an *endo–syn*-$(SeR)_2$ configuration, and Hg—Se—Hg = 101°, while the other is centrosymmetric, Hg—Se—Hg = 82°, but with one pair of Hg—Se bonds 0.15 Å longer.

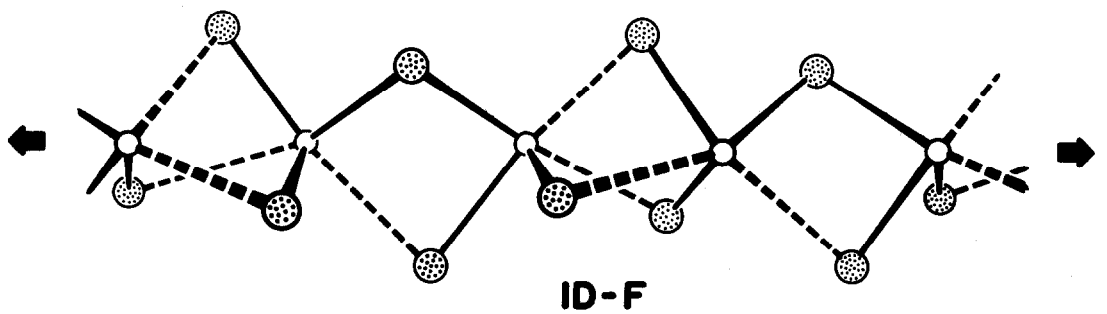
A variation on this type occurs in *catena*-$[Cd(\mu\text{-}SCH_2COOEt)_2]$[311] where there is additional secondary Cd coordination by carbonyl O atoms, to create two coordination stereochemistries: (i) pseudo-dodecahedral CdS_4+O_4, and (ii) tetra-*O*-capped tetrahedral CdS_4, which alternate along the chain as shown in **1D-D**.



1D-D

3.1.4. *catena*-$[(\mu\text{-SR})_2M]_\infty$ (*square planar metal coordination*) (**1D-E**). This structure, proposed[7] for insoluble compounds with M = Ni, Pd or Pt, has not yet been confirmed.

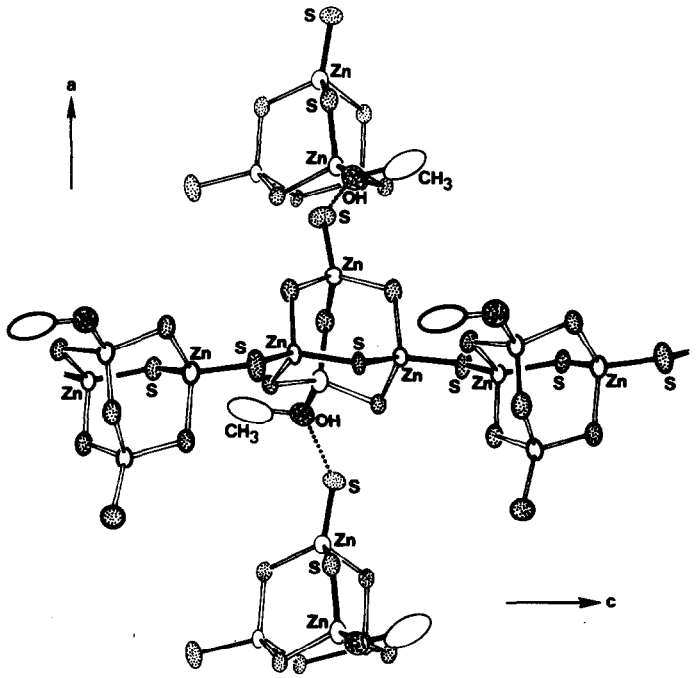
3.1.5. *catena*-$[(\mu\text{-SR})_3M(\mu\text{-SR})_2M]$ (**1D-F**). Here five-coordinate M atoms are connected alternately by two and three double bridges. The structure occurs for M = Pb, and the gross stereochemistry at the M is pseudo-octahedral with one position vacant. In $[Pb_2(SCH_2CH_2NMe_3)_5]^{4+}$ (PF_6^-) there are two crystallographically independent chains of this form in the crystal.[302] In fact the Pb—S distances are in two sets: at each Pb atom there are three mutually orthogonal primary bonds <3.0 Å (in most cases 2.5–2.8 Å) and two secondary interactions of 3.1–3.4 Å which are also *cis*. According to this separation of primary and secondary coordination, the chain consists of secondarily associated $[Pb_2(SR)_5]$ units.



1D-F

3.1.6. *catena*-(μ-SR)-[(μ-SR)$_6$M$_4$(SR)L] (**1D-G**). This structure, confirmed for the homologous series $Zn_4(SPh)_8(ROH)$ (R = Me, Et, Pr or Bu),[303] consists of adamantanoid cages linked in one dimension by bridging thiolate ligands, with one thiolate and one heteroligand ROH in the two remaining terminal positions. The crystals can be grown by slow thermal polymerization of a solution of $Zn(SPh)_2$ in ROH : depolymerization and repolymerization reactions occur, and it is possible that a similar structure occurs with MeCN as the heteroligand. Two features of the structure are notable, one being the wide (140°) angle at the inter-adamantanoid-bridging thiolate, the other the hydrogen bonding between the alcohol and the terminal thiolate ligand of a different chain. Hydrogen bonding involving a coordinated thiolate is rarely observed in crystal structures.

3.1.7. *catena*-[(μ-SR)$_3$M]$_\infty$ (**1D-H**). This one-dimensional extension of the bridging unit in **9A** may



1D-G

well occur in insoluble M(SR)$_3$ compounds such as Ln(SAr)$_3$[313] and M(SPh)$_3$ (M = Cr or Mo),[314] but has not yet been confirmed crystallographically.

3.2. *Two-dimensionally non-molecular structures*

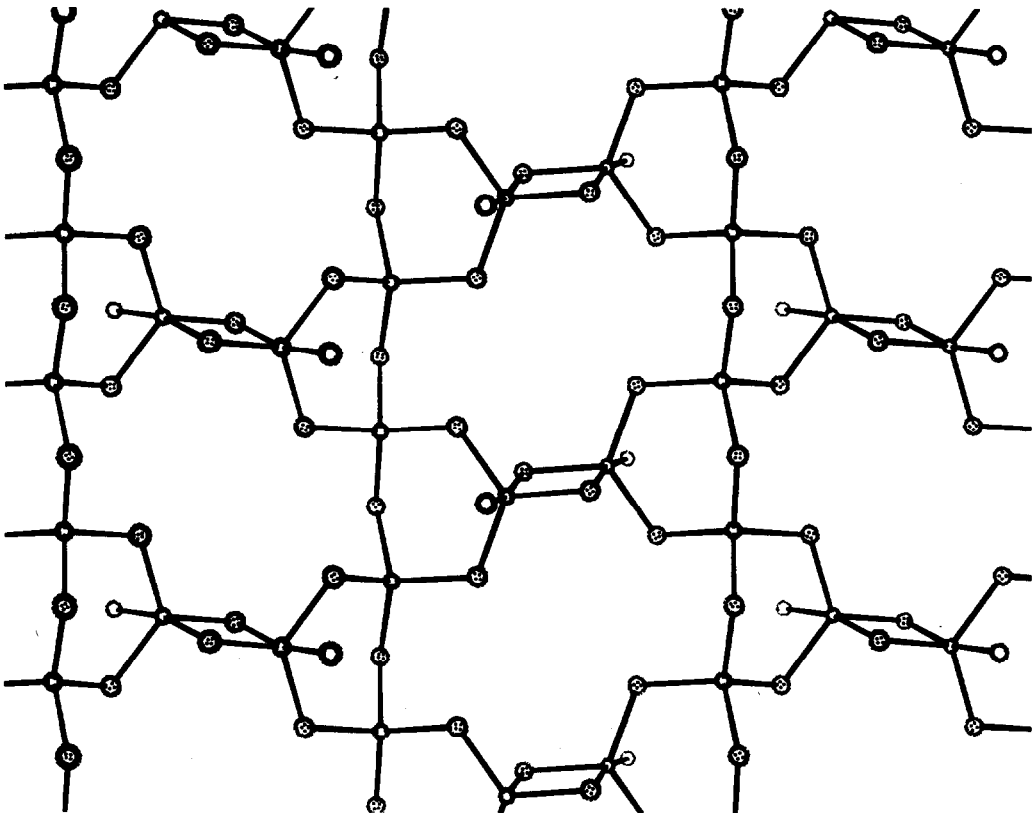
A two-dimensionally non-molecular (layer) structure has been confirmed by single-crystal diffraction for only one compound, [Cd(SCH$_2$CH$_2$OH)$_2$].[315] There is good evidence from powder diffraction for a layer structure in some (AgSAr)$_\infty$ compounds (Section 3.2.2).

Structural constraints arising from the volume required by the thiolate substituent become more pronounced in two-dimensionally non-molecular structures. Substituents now extend from an approximately planar surface, and consequently the packing density of substituents is greater (for the same surface density of S atoms) than in a more molecular type with a necessarily curved molecular surface.

For steric reasons it is not feasible that many two-dimensionally non-molecular metal sulfide or metal halide structures are adopted by metal thiolates. The lamellar MS_2 structure types cannot be modified by addition of substituents at the S atoms to create six-coordination of M with triply-bridging thiolates because the S atoms are separated by less than double the van der Waals' radius of even the smallest substituent, CH_3.

3.2.1. [Cd(SCH$_2$CH$_2$OH)$_2$]$_\infty$ (**2D-A**). Crystals of this compound, grown by a slow neutralization technique, contain buckled layers in which the Cd coordination is primarily Cd(μ-SR)$_4$, with secondary coordination by an alcohol function at one of the two crystallographically distinct Cd atoms.[315] The Cd–S network is shown diagrammatically in **2D-A**, as the Cd primary coordination tetrahedra linked

through vertices and edges, with the secondary coordination at the Cd which shares two vertices and one edge. $Cd_3(\mu\text{-}SR)_3$ and $Cd_2(\mu\text{-}SR)_2$ cycles are present. The structure is open, with hydrogen bonding between OH groups within and between the layers.



2D-A

3.2.2. $[AgSAr]_\infty$ (**2D-B**). The polycrystalline diffraction patterns of $[AgSC_6H_4X\text{-}4]_\infty$ (X = H or Cl) show well-developed progressions of intense axial (00*l*) reflections up to $l = 7$, indicative of a structure containing layers of Ag and S atoms. Other weak non-axial reflections are present, consistent with the occurrence of at least some crystallographic registry of layers. The interlayer spacings are 14.14 and 16.37 Å for X = H and Cl, respectively. The homologous Cu(I) compounds manifest different diffraction patterns, without evidence of layering.[316]

The postulated structure contains a central slab of connected Ag and S atoms, from which the aryl substituents extend, on either side, at a steep inclination (ϕ). This model is supported by its agreement with the observed interlayer spacings. Referring to the cross-sectional parameters of the layer (Fig. 11),

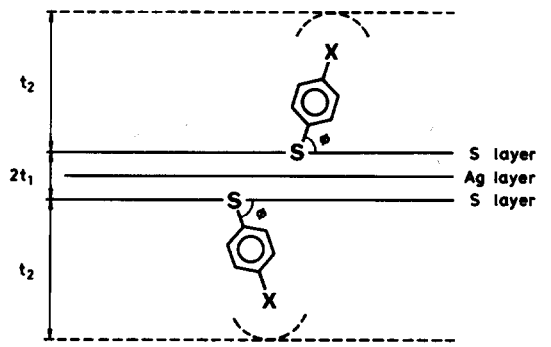
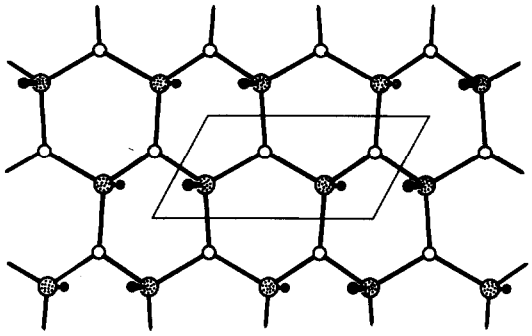


Fig. 11. Postulated layer structure for $[AgSAr]_\infty$ (**2D-B**) with definitions of the thickness of the central Ag–S slab and the thickness of the van der Waals' boundaries (broken lines) formed by aryl substituents inclined to the slab at angle ϕ.

the thickness $(2t_1 + 2t_2)$ of the layer between the planes formed by the van der Waals' boundaries of opposite substituents is calculated as 13.9 and 16.0 Å (X = H and Cl): if $\phi = 90°$, $t_1 = 0$. Assuming that there is no interlayer penetration of substituents, the thickness of the layer represents the axial repeat distance of the crystal structure, and it is clear that excellent agreement between calculated and observed interlayer distances can be achieved for X = both H and Cl with $t_1 = ca$ 0.1 Å ($\phi = 90°$).

A possible hexagonal network for the central Ag–S slab, shown in **2D-B**, requires a triply-bridging thiolate and allows a normal trigonal planar three-coordinate Ag. With representative dimensions, the thickness $2t_1$ of this slab is *ca* 1 Å, requiring $\phi = ca$ 70° for agreement with the measured layer separations. In this layer structure the smallest separation between S---X axes of parallel aryl substituents is *ca* 4.4 Å, sufficient for the aryl substituents to pack over both surfaces of the slab, but insufficient for mutual penetration of substituents in adjacent layers.

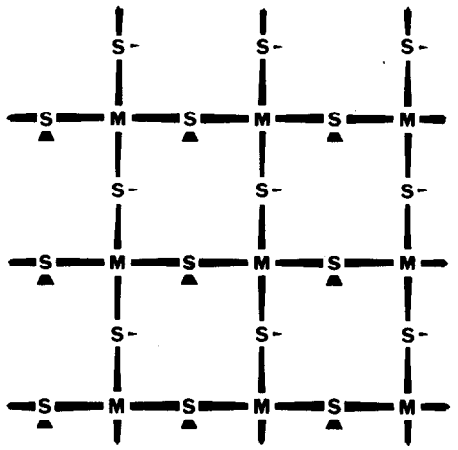


2D-B

Reasonable two-dimensionally non-molecular structures ($[AgSR]_\infty$) with only two-coordinate Ag (and therefore doubly-bridging thiolate) are difficult to postulate, as they would involve a fabric woven with threads like those in structure **1D-A** above.

3.2.3. *Postulated structures with linked* $M(\mu\text{-}SR)_4$ *tetrahedra.* It is unlikely that metal thiolates could occur with layer structures in which coordination tetrahedra share four *edges*, as this would require quadruply-bridging thiolate, $[MSR]_\infty$ stoichiometry, and limit the substituent volume by requiring parallel substituent axes to adhere to a *ca* 4 Å square network. *Vertex* linkage of tetrahedra in two dimensions allows doubly-bridging thiolate with more space for thiolate substituents, and the formulation $[M(SR)_2]_\infty$. The simplest structure type is shown diagrammatically in **2D-C**, which shows a straightforward unhindered pattern for ligand substituent orientations.

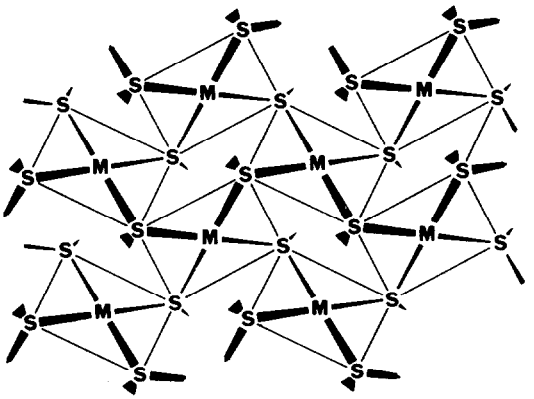
A larger structure type for $[M(SR)_2]_\infty$, with tetrahedral $M(\mu\text{-}SR)_4$ coordination throughout, contains vertex-linked adamantanoid units, $[M_4(\mu\text{-}SR)_6(\mu\text{-}SR)_{4/2}]_\infty$, in the same pattern as **2D-C**.



2D-C

3.2.4. *Postulated structure with linked* $M(\mu\text{-}SR)_4$ *square planes.* A layer structure possible for compounds $M(SR)_2$ (M = Ni, Pd or Pt), with square planar coordination, is shown in **2D-D**. Each

square plane is linked to four others through vertices only, in analogy to the network of **2D-C**. In order to form appropriate angles at the doubly-bridging thiolates the coordination planes are tilted with respect to the plane of the extended layer. By further twisting as shown about axes normal to the layer plane the substituents leaving the pyramidal S atoms can be inclined steeply to the layer plane.



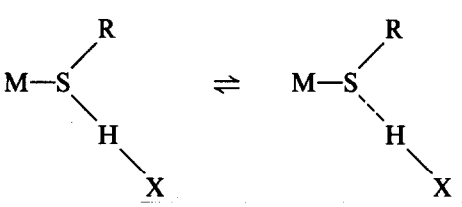
2D-D

3.2.5. *Miscellaneous and heteroligand compounds.* The crystal structure of $Pb(SCH_2CH_2S)$ is pseudo two-dimensionally non-molecular in sandwich form, with Pb atoms between layers of S atoms, and peripheral CH_2 groups.[317] The six Pb–S connections vary in length (2.66, 2.66, 3.03, 3.06, 3.38 and 3.58 Å). MeSHgBr has a two-dimensionally non-molecular structure in which chains resulting from the primary Hg coordination by doubly-bridging SMe (Hg—S = 2.44 Å, S—Hg—S = 163°) are linked secondarily by triply-bridging Br.[305]

Crystalline $\{Pb(SCH_2CH_2OH)(NO_3)\}_\infty$ contains the two-dimensional Pb–S layer network of **2D-B**, with the cycles distorted from hexagonal towards quadrilateral, and with additional out-of-plane coordination of Pb atoms by OH and NO_3 ligands.[318]

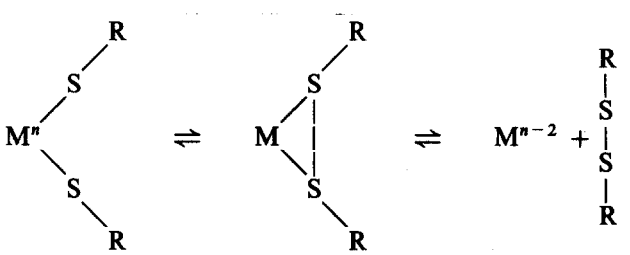
4. RELATED COMPOUNDS WITH COORDINATED DISULFIDE OR COORDINATED THIOL

Protonated (RSH) and oxidized (RSSR) thiolate, being uncharged, are uncompetitive ligands. They occur, usually singly, in a small number of compounds. Coordinated RSH may function as a hydrogen bond donor in the Bronsted conjugate of coordinated RS^-, functioning as a hydrogen acceptor [eqn (4)]:



(4)

Coordinated RSSR is one component of the redox addition–elimination process [eqn (5)]:



(5)

A precedent exists for the formation of bridging coordinated RSSR by dimerization of coordinated

thiolate in the reversible system:[319]

$$2[(\eta^5\text{-Cp})(CO)(PR_3)FeSPh]^+ \rightleftharpoons [(\eta^5\text{-Cp})(CO)(PR_3)Fe(\mu\text{-}SPh)_2Fe(PR_3)(CO)(\eta^5\text{-Cp})]^{2+}. \quad (6)$$

4.1. *Coordinated* RSH

Acid and redox properties of EtSH (and H_2S) coordinated to $(NH_3)_5Ru$(II,III) have been measured.[320]

$Rh_2(OAc)_4$ combines readily with $PhCH_2SH$ to form centrosymmetric $(PhCH_2SH)Rh(\mu\text{-}O_2CCH_3)_4Rh(HSCH_2Ph)$ with an Rh—S distance of 2.55 Å.[321] The presence of the thiol H atom was confirmed by the S—H stretching frequency (2550 cm^{-1}) in the IR, and its position [S—H = 1.21(3) Å] was refined with the X-ray diffraction data.

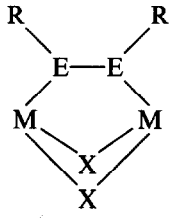
The compound (PhSH)Fe(TPP)(SPh) (TPP is tetraphenylporphyrin)[322] in its low-spin structure appears to have octahedral Fe(III) coordinated at 2.27 Å to PhS^- and at 2.43 Å to PhSH, but the thiol H atom could not be detected in the diffraction studies. $[IrH(SCH_2CH_2PPh_2)(HSCH_2CH_2PPh_2)CO]^+(Cl^-)$ contains a chelated coordinated thiol, confirmed by diffraction detection and indirect NMR detection of the thiol H atom, which is hydrogen bonded to the lattice Cl^-.[323]

Hydrogen bonding from coordinated MeOH to terminally coordinated PhS^- (S--O = 3.03 Å) occurs in $Zn_4(SPh)_8(MeOH)$ [see **1D-G** (Section 3.1.6)].

4.2. *Coordinated* REER (E = S, Se *or* Te)

Despite many recent reports of investigations of reaction mixtures containing RSSR, particularly with Mo, Fe and Cu, the uncharged disulfide ligands are generally uncompetitive with anionic ligands also present, and complexes containing coordinated RSSR are still relatively rare. Non-molecular compounds of copper(I) halides with dialkyldisulfides have been characterized.[324] The molecules $[Ph_2E_2Ag(\mu\text{-}E_2Ph_2)_2AgE_2Ph_2]^{2+}$ (AsF_6^-) (E = S or Se isostructural[325]) contain terminal monodentate and 1,2-bridging PhEEPh ligands.

A series of carbonyl compounds with REER coordinated symmetrically to two M atoms, with the support of two halide bridges as shown in diagram **A**, have been well characterized for nine compounds with M = Mn or Re, X = Br or I, and E = S, Se or Te.[326–329] The weakness of REER binding in these compounds (S < Se < Te) is revealed by facile displacement of REER by THF and CO, and by REER exchange reactions.[329] The compound $Me_3Pt(\mu\text{-}Br)_2(\mu\text{-}Se_2Me_2)PtMe_3$[330] also has structure **A**.



A

Geometrical results consistent with a bonding interaction between the S atoms of adjacent thiolate ligands, i.e. the first stage of the reductive elimination [eqn (5)], appear in $[(PhS)_2MoO(\mu\text{-}O)_2OMo(SPh)_2]^{2-}$[158] and $[(ArS)_2MoO(\mu\text{-}SAr)_2(\mu\text{-}OMe)MoO(SAr)_2]^-$.[170] The phenyl conformational isomer which allows orbital overlap between the pair of terminal PhS ligands has an S--S distance contracted by 0.25 Å, to 2.94 Å (S—Mo—S 74°). A similar geometrical effect occurs for the terminal ligands of $[(\eta^5\text{-}C_5H_5)_2Mo(SBu^t)_2]$[331] and for two of the doubly-bridging ligands of $[Cl_2(Me_2S)W(\mu\text{-}SEt)_3W(SMe_2)Cl_2]$[164] where the pair of ligands with the *exo–syn* configuration allowing bent overlap of S orbitals are separated by 3.05 Å, 0.55 Å less than the van der Waals'

contact, and the W—S bonds involved are slightly elongated by 0.04 Å. Further diminution of the S---S distance to 2.77 Å (S—Mo—S 70°) occurs in $MoO_2(SCMe_2CH_2NHMe)_2$.[332,333]

Complexes with disulfide coordination enforced by chelation are listed in Ref. 334.

5. STRUCTURAL PATTERNS AND PROPERTIES

5.1. *General characteristics*

The propensity of the thiolate ligand to occur as pyramidal double bridges M—(μ-SR)—M and thereby to form aggregated metal complexes is evident. Thiolate groups also function readily as terminal ligands, less frequently as triple bridges, and rarely in quadruply-bridging positions. It is noted also that there are no instances of aggregates with both triply-bridging and terminal thiolate ligands: for instance the cubane derivative *tetrahedro*-(μ_3-SR)$_4$-*tetrahedro*-(MSR)$_4$ is not known. The polymetallic aggregates are maintained by the thiolate bridges, with direct bonding between M atoms usually negligible or absent.

Amongst the compounds characterized by crystallographic diffraction analysis there is a preponderance of structurally molecular polymetallic complexes. This statistic does not necessarily mean that cages and clusters are more numerous or more stable than monometalic complexes, or that non-molecular compounds are in a minority, but is a practical consequence of the greater solubility of monometallic complexes in equilibria with polymetallic complexes, and of the insolubility and poor crystallinity of non-molecular compounds.

5.2. *Metal oxidation states and coordination numbers*

In thiolate complexes metal oxidation states and coordination numbers tend to occur at the low ends of the ranges for complexes of non-π-acid ligands, as illustrated by the collection of data in Table 1.

It has been pointed out[253] that for the five distinct Fe–S–SR clusters $[Fe_2S_2(SR)_4]^{2-}$ (**2E**), $[Fe_3S(SR)_6]^{2-}$ (**3J**), $[Fe_3S_4(SR)_4]^{3-}$ (**3B**), $[Fe_4S_4(SR)_4]^{2-}$ (**4H**) and $[Fe_6S_9(SR)_2]^{4-}$ (**6F**) there is an approximate correlation between the average Fe oxidation state and the proportions of S^{2-} and RS^- ligands per Fe atom. This proposed stability condition is:

$$\text{mean oxidation state} = 0.54[N_{RS}/N_{Fe} + 2.5(N_S/N_{Fe})] + 0.51, \quad (7)$$

where N_{RS}, N_S and N_{Fe} are the numbers of RS^-, S^{2-} and Fe per cluster. The 2.5 times larger influence of the proportion of sulfide ligands (N_S/N_{Fe}) is considered a reflection of stronger stabilization by S^{2-} (compared to RS^-) of higher oxidation states. Equation (7) can be legitimately extended to postulated clusters *triangulo*-$[Fe(III)_3(\mu\text{-}S)_3(SR)_6]^{3-}$ (**3F** or **3G**) and *hexahedro*-$[Fe(II)_8(\mu_4\text{-}S)_6(SR)_8]^{4-}$ (**8F**). It should be appreciated that M–S–SR clusters undergo change in total oxidation state without change in composition, and that the doubly-, triply- and quadruply-bridging S^{2-} ligands probably have different influences.

5.3. *Structural units*

Structural moieties which can be recognized in many of the polymetallic aggregates described above are cyclic-(μ-SR)$_2$M$_2$, cyclic-(μ-SR)$_3$M$_3$ and cyclic-(μ-SR)$_4$M$_4$. Of these cyclic-(μ-SR)$_3$M$_3$ is most prevalent, and its favourability is emphasized by the ubiquity of the adamantanoid cage **4F** which is composed of four fused (μ-SR)$_3$M$_3$ cycles each in chair conformation.

The smaller cyclic unit (μ-SR)$_2$M$_2$ occurs mainly in *bi*metallic molecules: most *poly*metallic structure types with two or more (μ-SR)$_2$M$_2$ cycles have them connected through the metal atoms ("spiro"-linkage at M) which is necessary to avoid triply-bridging thiolates (**3A, 3B, 3C, 3M, 4C, 6B, 8D, 9A, 1D-C, 1D-D** and **2D-A**). The few instances of polymetallic compounds with (SR)$_2$M$_2$ cycles fused through thiolate are less general: (μ_3-SMe)$_4$Re$_4$(CO)$_{12}$, (μ_3-SR)$_4$Pt$_4$(R′)$_{12}$ (Section 2.4.8), $(SPh)_4Cu_4(PPh_3)_4$ (**4G**), $(SBu^t)_5(ZnMe)_5$ (**5C**), $(SPh)_6Ag_6(PPh_3)_5$ (**6C**) and $(SPr^i)_8(ZnMe)_8$ (**8E**). In this regard the (μ-SR)$_2$M$_2$ structural unit is different from the (μ-SR)$_3$M$_3$ and (μ-SR)$_4$M$_4$ structural units, which can be and are fused without thiolate triple-bridging. All of the many other polymetallic molecules with fused S$_2$M$_2$ cycles involve sulfide or polysulfide as the triply-bridging ligand, with thiolate ligands in terminal positions.

Table 1. Metal oxidation states and coordination numbers in representative metal thiolate complexes[a]

Oxidation No.	Coordination No.	Terminal thiolate ligand only	Bridging thiolate ligand only	Mixed ligand
I	2	$[Cu(SAr)_2]^-$	$[(\mu\text{-}SCMeEt_2)Ag]$ $[M_5(SBu^t)_6]^-$ $[M_5(SPh)_7]^{2-}$ (M = Cu or Ag)	
	3		$[Cu_4(SR)_6]^{2-}$	$(AgSBu^t)_8(PPh_3)_2$
	3		$[M_5(SBu^t)_6]^-$ $[M_5(SPh)_7]^{2-}$	$(CuSBu^t)_4(PPh_3)_2$
II	2	$Hg(SR)_2$		ArHgSr
	3	$[Pb(EPh)_3]^-$ (E = S or Se) $[Hg(TePh)_3]^-$		
	4	$[M(SR)_4]^{2-}$ (M = Mn, Fe, Co, Ni, Zn, Cd or Hg)		$[(RS)_2M(\mu\text{-}SR)_2M(SR)_2]^{2-}$ (M = Fe, Co or Hg)
	6		$[Fe(\mu\text{-}SR)_6\{MoS_4(FeSR)_3\}_2]^{4-}$	
III	4	$[M(SR)_4]^-$ (M = Fe or Ga)		
	6		$[Fe(\mu\text{-}SR)_6\{MoS_4(FeSR)_3\}_2]^{4-}$	
IV	4	$Sn(SePh)_4$		
	5	$[Sn(SPh)_5]^-$		$LM(SAr)_4$ (L = MeCN or CO, M = Ru or Os)
V	5			$[EM(SPh)_4]^-$ (E = O or S, M = Mo or W)
	6	$[Re(SR)_6]^-$ [b]		

[a] R and M indicate series of complexes.
[b] See Section 2.1.11.

The cyclic $(\mu\text{-SR})_4M_4$ moiety occurs in **4A**, **4B**, **4C**, **5A**, **5B**, **6A**, **8B**, **8C** and **12C**.

Smaller structures can be recognized as fragmentary units of larger structures. For instance, **3F** is part **4D**, of **4F**, and of **6H**.

5.4. *Molecular symmetry and molecular distortions*

High symmetry is a characteristic of molecular $[M_x(SR)_y]$ aggregates. In most instances the combined array M_xS_y is less symmetrical as a polyhedron than the separate M_x and S_y polyhedra, which are frequently regular (all vertices identical, and all faces identical) or semi-regular (all vertices identical) and concentric. These M_x and S_y polyhedra may intersect, or be radially distinct in an "onion shell" arrangement of alternating metal and ligand polyhedra. The order of the idealized molecular point group is usually equal to or higher than the number of S atoms. Almost invariably the array R_y of $[M_x(SR)_y]$ cannot maintain the higher symmetry of the M_xS_y array: mirror elements in particular are incommensurate with thiolate bridges. Thus the actual molecular symmetries of these cages, and the observed crystallographic site symmetries are generally very much lower than the potential symmetries of the M_xS_y cores.

The M_xS_y cores of $[M_x(SR)_y]$ aggregates tend to have low connectivities, that is a small number of framework bonds per M, S atom. One consequence of this is a structural non-rigidity which is manifest in distortions of the core polyhedra from idealized symmetry. The distortions are primarily angular (see Section 5.8). The degree of mechanical flexibility and distortion is inversely related to the connectivity, and increases with the size of the $M_n(SR)_n$ cycles which constitute the aggregate, while the direction of distortion can usually be traced to the intramolecular interactions between thiolate substituents.

The smallest deformations which can be clearly defined and which can be unambiguously attributed to intramolecular substituent repulsions occur in structures **4E** and **4F** with the $(\mu\text{-SR})_6M_4$ core [12 bonds per 10 atoms, $M_3(SR)_3$ cycles], and have already been described in Sections 2.4.5 and 2.4.6. The angular floppiness is trapped in the crystal as a flap of the M–(μ-SR)–M plane about the M--M line.

Structure $[M_5(SBu^t)_6]^-$ (**5B**), with 12 bonds between 11 core atoms and $M_4(SR)_4$ cycles only, is also inherently floppy. In the one configurational isomer where the substituents maintain the D_3-symmetry of the core, the angular distortions of the core are minimal, and are opposed by substituent repulsions. Inversion of one doubly-bridging thiolate, as occurs in another crystallographically observed isomer, causes the affected $S—M^{trig}—S$ angles to deviate by up to 27° from the 120° ideal, compared with the $<5°$ deviations in the D_3-isomer.[232]

Drastic deformation occurs in structure **6A** $\{[Ag_6(SR)_8]^{2-}\}$, where the idealized arrangement contains only 16 bonds between 14 polyhedral atoms, with $M_4(SR)_4$ cycles only: this connectivity is unable to support the idealized structure, which is found partially contorted and collapsed, with stabilization provided by intramolecular secondary M–S connections. Similar secondary connections occur in some cyclic $(AgSR)_p$ molecules which would otherwise have only $2p$ cyclic bonds per molecule (see Section 5.6.1).

Another mechanism for provision of mechanical stabilization to low-connected floppy aggregates is incorporation of a central monatomic ligand with normal bonds to M^i atoms (**8C**) or long connections to a larger number of M atoms [**6D**(**6E**) and **8B**].

The molecular cage $(\mu_3\text{-S})_8M_{12}$ (**12C**) is remarkable in this context because it is large and empty, contains only M_4S_4 cycles, and has 24 bonds for 20 atoms. Apparently the S^{2-} ligands engage more rigid triple-bridges than RS^- ligands.

5.5. *Topological relationships: families and progressions of polyhedra*

A considerable number of topological relationships between *idealized* structures of metal thiolates have been recognized, and are outlined here. These relationships involve polyhedral expansion operations and polyhedral capping. Also, some complete structures are fragments of larger complete structures. The following descriptions which are couched in terms of conversion processes are not meant to imply mechanisms: it is very likely that most of these systems are involved in very mobile equilibria, and that factors such as solubility have determined the identity of species isolated.

5.5.1. *Polyhedral expansion* $[M_4(SR)_6$, $M_5(SR)_7$ *and* $M_6(SR)_8]$. The *octahedro*-$(\mu\text{-SR})_6$-*tetrahedro*-M_4 structure **4E** undergoes two stages of polyhedral expansion to form $(\mu\text{-SR})_7M_5$ (**5A**) and then (μ-

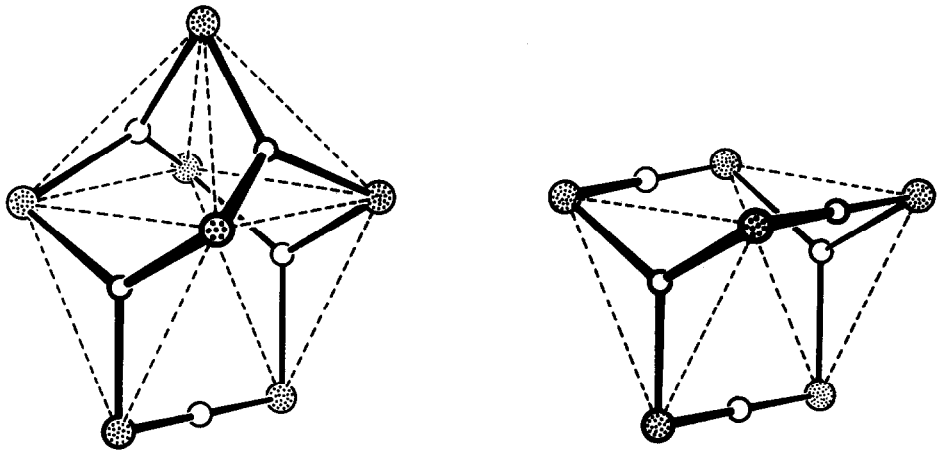


Fig. 12. Relationship between the idealized cage polyhedra of structures **5A** and (trigonal prismatic) **5B**.

$SR)_8M_6$ (**6A**) as shown in Fig. 4. Each stage of the expansion involves replacement of a doubly-bridging thiolate which links two trigonal planar coordination units by a digonal and linear (μ-SR)–M–(μ-SR) function, requiring a separation of the trigonal planes. The second stage occurs at the vertex most distant from that of the first stage. The addition of two-coordinate M atoms decreases cage rigidity, as already mentioned, and hence continued polyhedral expansion by this mechanism is limited by the collapse of the resulting structures.

5.5.2. *Polyhedral contraction* [$M_5(SR)_7$ *and* $M_5(SR)_6$]. Structure **5A** contains a trigonal prism of doubly-bridging thiolate ligands, the basis of **5B**, as shown in Fig. 12. Conversion of **5A** to **5B** is readily envisaged as removal of the unique doubly-bridging thiolate at the vertex opposite the digonal M atom, concomitant with shift of the two-coordinate M atoms so created into digonal stereochemistry, and followed by a trigonal twist about the axis through the two trigonal M atoms.

Monocyclic **4A** (either diligated or unsubstituted) is a component of bicyclic **5A**.

5.5.3. $M_5(SR)_6$ *polyhedra.* The compound $Ag_6(SAr)_6(PPh_3)_5$ (**6C**) contains an $Ag_5(SR)_6$ core which is ideally comprised of a basal unit *centro*-Ag-*hexagono*-$(SR)_3Ag_3$ straddled by a trigonal $Ag(SR)_3$ podal unit (see Section 2.6.3). This idealization contains *octahedro*-$(SR)_6$, which signifies the relationship with other $M_5(SR)_6$ structures shown in Fig. 13.[249] The *trigonal bipyramido*-M_5-*trigonal prismo*-$(SR)_6$ structure [Fig. 13(a)] is partially twisted about the three-fold axis to generate **5B**, and then this twisting is continued by the three digonal M atoms which drop into the lower trigonal plane as shown by the arrows in Fig. 13(b), thereby creating the base-centred hexagonal unit of **6C**. The upper trigonal plane of **5B** becomes the podal trigonal unit of **6C**.

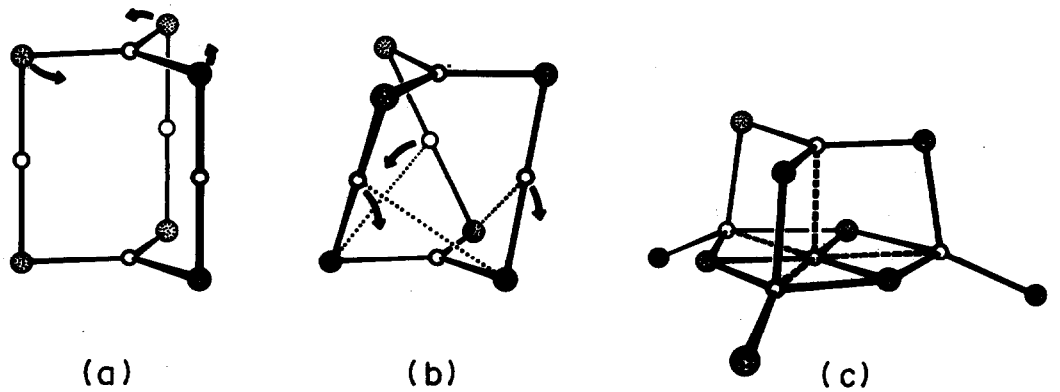


Fig. 13. Relationships between $M_5(SR)_6$ cage polyhedra. (a) *Trigonal-bipyramido*-M_5-*trigonal prismo*-S_6, twisting towards (b) *octahedro*-S_6 (**5B**), collapsing to (c) *base-centred-trigonal-pyramido*-M_5-*octahedro*-S_6 (part of **6C**), with added terminal phosphine ligands.

Structure **5B** which has thiolate ligands bridging the edges of an M_5 trigonal bipyramid is not very different from the face-bridged *trigonal bipyramido*-M_5 structure $(\mu_3\text{-SR})_6M_5$. This alternative has thiolate bridges over all six faces of the M_5 trigonal bipyramid, and can be described also as a trigonal prism of thiolate S atoms with M atoms in the centres of all five faces. Three metals are four-coordinate and two are three-coordinate. This structure is not known for metal thiolates, although it is known with oxide as the triply-bridging ligands in $Cp_5V_5O_6$.[335] The thiolate structure **3M** is a relative without two M atoms.

5.5.4. *Toroidal molecules* $[(\mu\text{-SR})_{2n}M_n]$. Monocyclic structures **3M, 4C, 6B** and **8D** are based on the M_n regular polygon, with two doubly-bridging thiolate ligands between each metal pair, such that there are two slightly larger $(SR)_n$ polygons which sandwich the M_n polygon. Except in the triangular molecule which involves chelating thiolates, the thiolate substituents alternate axial/equatorial around each $(SR)_n$ polygon, and on this basis the odd membered toroids ($n = 5$ or 7) are not expected (see also Section 2.3.11). Toroid size does not appear to be influenced by the M—S—M angles at the folded $(\mu\text{-SR})_2M_2$ bridges, while toroids with $n > 8$ are sufficiently empty to probably require included guest molecules for existence.[202]

Structure **3C**, which also contains chelating ligands, is a semi-circular half of the hexagonal toroid **6B**.

5.5.5. *The ensemble of high-symmetry* $(\mu\text{-SR})_{12}M_8$ *structures.* **8B** and **8C** belong to a set of four structures in which an icosahedron or cuboctahedron of doubly-bridging thiolate ligands is associated with a cube or bitetrahedron of metal atoms.[280] Figures 14 and 15 provide comparative views of the

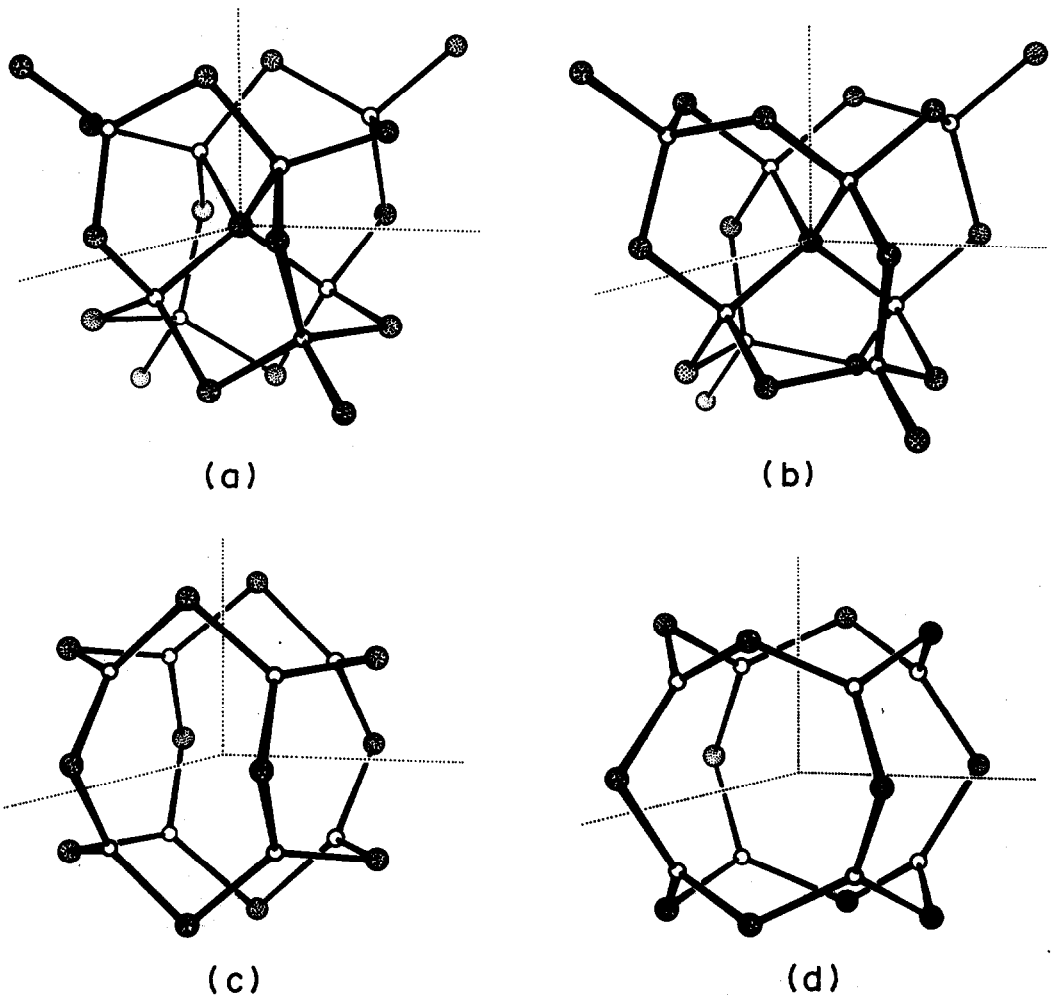


Fig. 14. Comparative views of: (a) *centro-Z-bitetrahedro*-M_8-*icosahedro*-$(SR)_{12}$, (b) *centro-Z-bitetrahedro*-M_8-*cuboctahedro*-$(SR)_{12}$, (c) *hexahedro*-M_8-*icosahedro*-$(SR)_{12}$, and (d) *hexahedro*-M_8-*cuboctahedro*-$(SR)_{12}$.

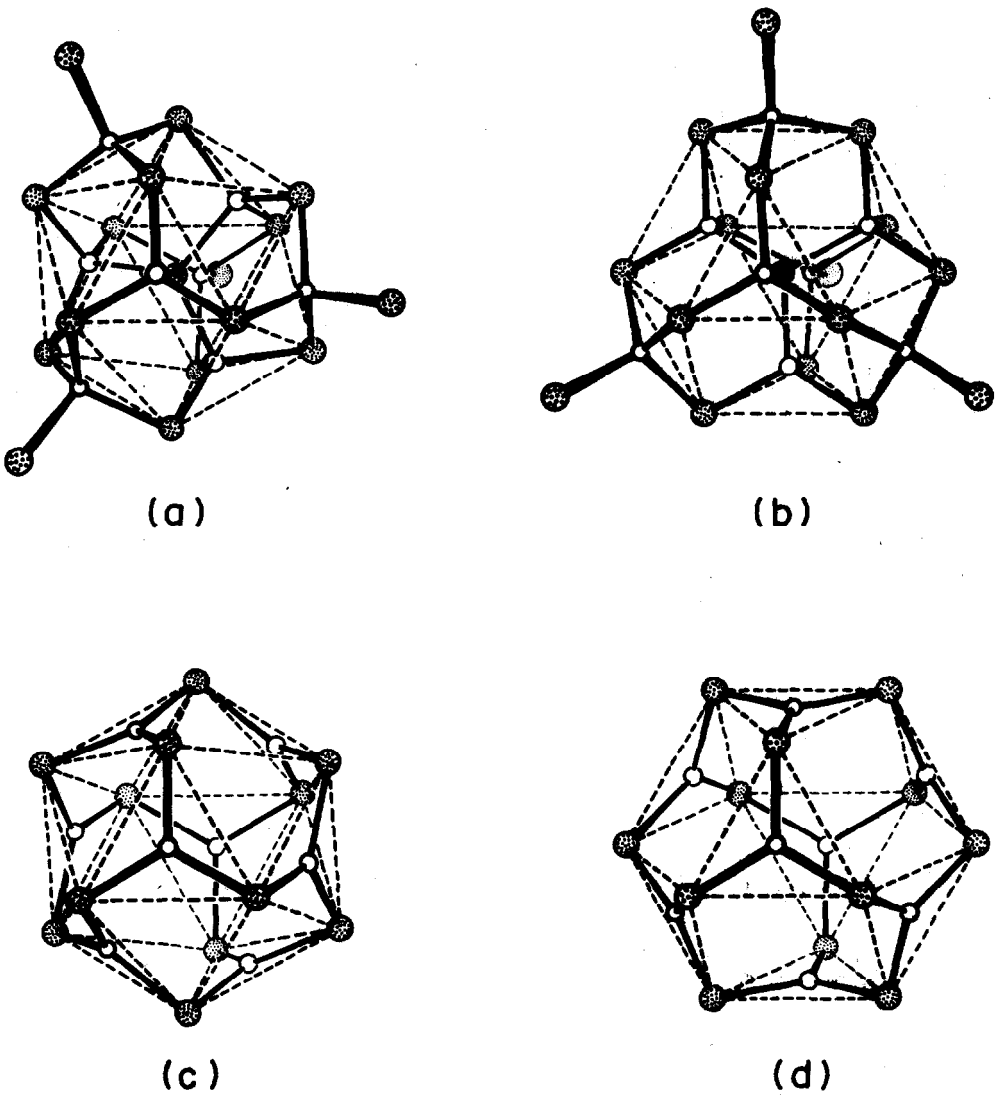


Fig. 15. Comparative views of: (a) *centro-Z-bitetrahedro*-M_8-*icosahedro*-$(SR)_{12}$, (b) *centro-Z-bitetrahedro*-M_8-*cuboctahedro*-$(SR)_{12}$, (c) *hexahedro*-M_8-*icosahedro*-$(SR)_{12}$, and (d) *hexahedro*-M_8-*cuboctahedro*-$(SR)_{12}$.

structures in this set. A central ligand and terminal ligands are required for the *bitetrahedro*-M_8 arrays, and may be present for *hexahedro*-M_8. These four structures are interconvertible without bond-breaking. In each of the four the array of substituents belonging to the bridging thiolate ligands can and probably will have a high symmetry (T or T_h): the array of α-carbon atoms $[(C_\alpha)_{12}]$ is close to a cuboctahedron when S_{12} is an icosahedron, and close to an icosahedron when S_{12} is a cuboctahedron.[280]

5.5.6. *Structural congruence of molecular and non-molecular structures.* The adamantanoid cage **4F** is a fragment of the cubic (sphalerite or zinc blende) MX structure, corresponding to the unit cell of the latter as shown in Fig. 16. Thus there is structural congruence between a *molecular* cage with thiolate ligands and the *non-molecular* structure adopted by metal sulfides (and other chalcogenides). This structural congruence extends to poly-adamantanoid cages, and in particular to the tetra-adamantanoid supertetrahedral cage of **10A** which involves both chalcogenide and thiolate ligands.* The size of these poly-adamantanoid molecules can increase indefinitely without disrupting this

* The hypothetical thiolate cage $M_{10}(SR)_{20}$ described in Section 2.10.3 also adheres to this congruence.

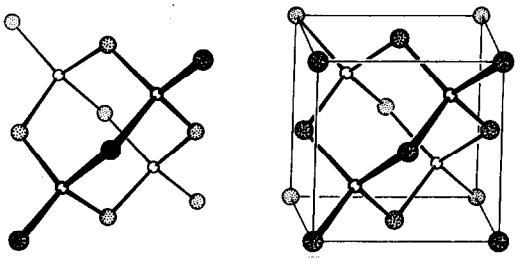


Fig. 16. Correspondence between the adamantanoid molecular structure (**4F**) and the cubic unit cell of sphalerite.

congruence, a fact which leads to speculation about larger molecular structures (Section 8). Analogous molecular fragments of the hexagonal (wurtzite) MX structure, terminated with thiolate ligands, are not as readily conceivable because the unprecedented $(\mu_3\text{-SR})_2M(SR)_2$ units would be required.[293]

The cubic cage $[S_6(CoSR)_8]^{4-}$ (**8F**) is a fragment of the non-molecular structure of the mineral pentlandite (M_9S_8) in which the cages are linked through octahedrally coordinated M atoms.[281] Here it is less feasible to build larger molecules as more extensive fragments of the non-molecular structure.

Structures **10A** and **4F** are both portions of the cubic MX lattice, but their central core polyhedra have an inverse relationship. The core of **4F** (or **4E**) is *tetrahedro*-M_4-*octahedro*-S_6 while the core of **10A** is *octahedro*-M_6-*tetrahedro*-S_4 as shown in Fig. 17. This can occur because the M and X sites in MX are equivalent.

5.5.7. The cubic structure **8F**, known only with sulfide ligands in the quadruply-bridging roles, can be constructed from the adamantanoid cage **4D** by addition of four M–SR caps as shown in Fig. 18. This converts a cage constructed from $M_3(SR)_3$ cycles only to one constructed from $M_2(SR)_2$ cycles only. **8F** can be conceived of also as **6H** plus two M–SR caps, as shown in Fig. 19.

5.5.8. $X_4M_{10}(SR)_{16}$ (**10A**) and $XM_8(SR)_{16}$ (**8C**) both have idealized T_d-symmetry (ignoring substituents) and an outer $(MSR)_4$ tetrahedron connected by four tris-sets of doubly-bridging thiolates to an inner polyhedron of M atoms. The inner section is either an M_6 octahedron with four faces capped by chalcogenide (**10A**) or an M_4 tetrahedron centred with a single atom (**8C**). As a consequence of these differing inner metal polyhedra, the 12 connecting thiolates constitute either a truncated tetrahedron or an icosahedron.

5.6. *Thiolate bridges and bridging stereochemistry*

Classifications of thiolate bridges first separate primary and secondary thiolate bridging. Primary bridges involve M—S bonds of similar (normal) length, while secondary connections to thiolate S are elongated, and provide metal coordination additional to the normal minimum coordination number.

5.6.1. *Secondary* M–S *bridging*. Secondary bridging and variations in bridge bond lengths are most pronounced with the heavier late- and post-transition metals Ag, Hg, Cd and Pb, where the coordination sphere is loose and flexible. Molecules with low-coordinate M atoms and, therefore, a low connectivity are often supported by intramolecular secondary bridges, and where such M atoms are exposed on the surface of the molecule intermolecular secondary bridges are evident in crystal

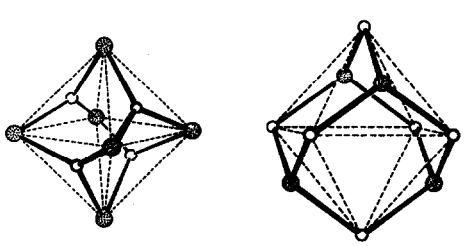


Fig. 17. M–S interchange relationship between the cores of adamantanoid **4F** (or **4E**) and tetra-adamantanoid **10A**.

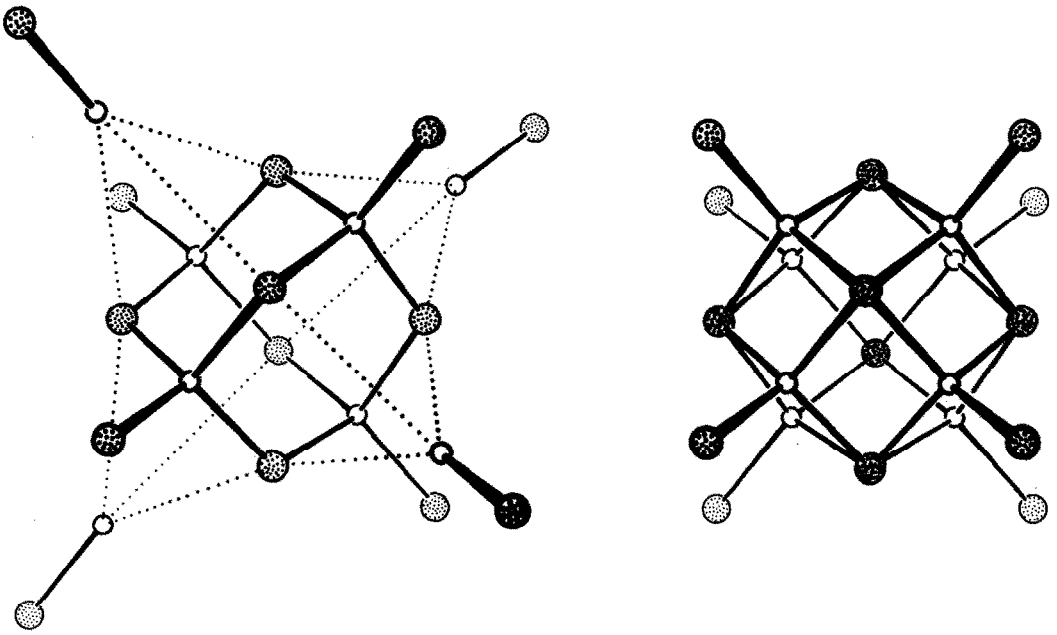


Fig. 18. **8F** as tetra-capped **4F**.

structures. Examples are the molecules $(AgSC_6H_{11})_{12}$ and $[Ag_6(SPh)_8]^{2-}$ which possess both intra- and intermolecular secondary Ag---S bridges, both *ca* 0.3 Å longer than the primary Ag–(SR)–Ag bridges. Two $(\mu\text{-SR})_4Ag_4$ molecular cycles are associated confacially by four secondary Ag---Sr bridges elongated by 0.5 Å relative to the primary bridges in **4B**. Despite the prevalence of intermolecular secondary bridging amongst two-coordinate silver thiolate structures, there is one silver thiolate structure, one-dimensionally non-molecular $\{(\mu\text{-SCMe}_2\text{Et})Ag\}_\infty$, where association of strands occurs with a conspicuous absence of Ag---S secondary bridging (see Section 3.1.1). $Hg(SR)_2$ molecules in the crystal phase associate with Hg---SR secondary bridging ranging in length up to the van der Waals' limit: for example, when R = Et the extra connections are at 3.54 Å (1 Å longer than the primary bonds), and when R = $[CH_2CH_2NMe_3]^+$ they range from 2.95 to 3.80 Å.[38]

5.6.2. *Primary thiolate bridging.* Primary bridges are classified in two stages: first according to the number and arrangement of M–S connections, and secondly in terms of the stereochemistry at S. The M–S connectivity types are organized by the number of M atoms per bridge, the number of bridges per metal pair, and whether the bridge is part of a cyclic (supported) or acyclic (unsupported) structure.

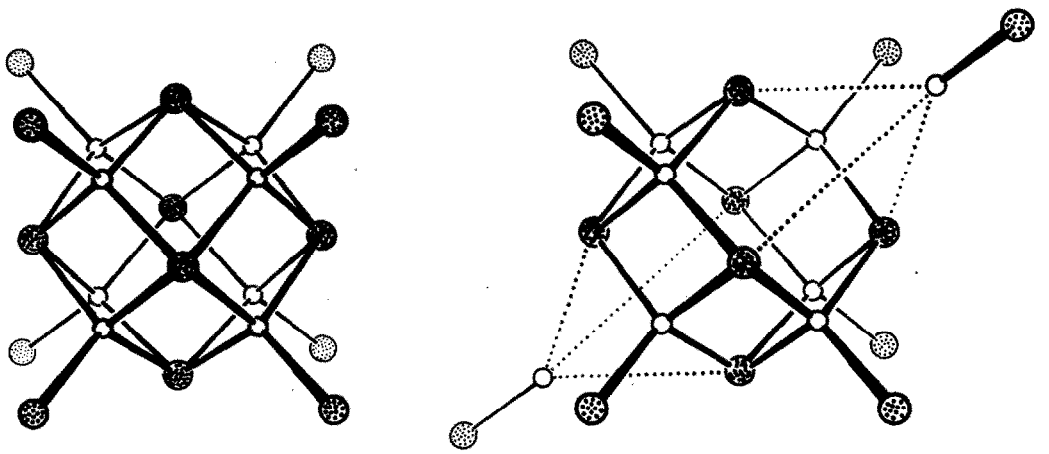


Fig. 19. **8F** as bi-capped **6H**.

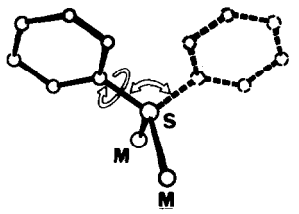
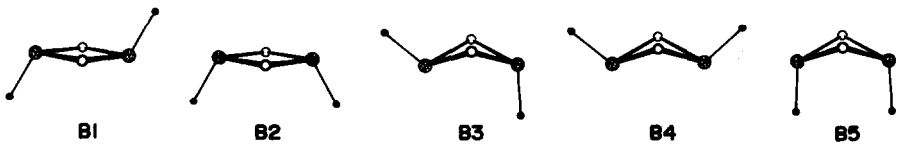


Fig. 20. The configurational (inversion) and conformational (rotation) degrees of freedom at doubly-bridging thiolate.

Stereochemical questions of configuration at the bridging S atom and conformation of the substituent, illustrated in Fig. 20, are discussed in Section 5.6.3 below.

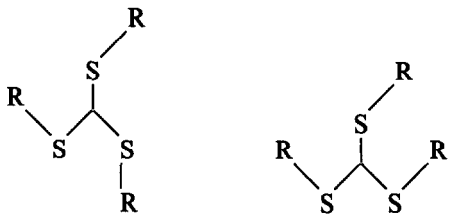
5.6.2.1. One unsupported double-bridge (M—S—M) has a rare occurrence in $(CO)_5W(\mu\text{-}SC_6Cl_5)W(CO)_5$ with a W—S—W angle of 132°.[336]

5.6.2.2. One double-bridge (M—S—M), supported only by its occurrence in a larger cyclic structure which indirectly connects the M atoms, appears in the structure types **3D, 3E, 3F, 3G, 3H, 4A, 4B, 4E, 4F, 5A, 5B, 6A, 8A, 8B, 8C, 10A** and **12A**, and also in **1D-A, 1D-G** and **2D-A**. It is evident even from the smallest trimetallic cycles (**3D** and **3G**) that the M—S—M angles can vary widely.



5.6.2.3. The bis double-bridge $[M(\mu\text{-}SR)_2M]$ occurs in modes unsupported (**2C, 2D, 2E, 2G, 3A, 3B, 3C, 4G, 1D-C, 1D-D** and **2D-A**) and supported (**3M, 4C, 6B** and **8D**) by additional cyclic connections. The M_2S_2 quadrilateral may be planar or folded about the S—S diagonal, and the M—S—M angle is variable, ranging from 67 to 100°. With planar M_2S_2 the configurations of R_2 are *anti* (**B1**) and *syn* (**B2**), while with non-planar M_2S_2 the configurations of the two R groups are *anti* (**B3**), *exo–syn* (**B4**) and *endo–syn* (**B5**). Bridge stereochemistry and stereodynamics are discussed further in Section 5.6.3.

5.6.2.4. The tris double-bridge $[M(\mu\text{-}SR)_3M]$ occurs unsupported in **2H, 2J, 8G** and **9A**. Two $(SR)_3$ configurational isomers are possible, *symmetric* (**B6**) {e.g. $[(CO)_3Fe(\mu\text{-}SMe)_3Fe(CO)_3]^{+}$[165]} and *asymmetric* (**B7**) {e.g. $(\eta\text{-}C_7H_7)Mo(\mu\text{-}SBu^t)_3Mo(CO)_2[P(OMe)_3]$[337]}:



5.6.2.5. The tetrakis double-bridge $[M(\mu\text{-}SR)_4M]$ occurs in $[V_2(SCH_2CH_2S)_4]^{2-}$ (**2K**) and $[(\eta\text{-}Cp)Mo(\mu\text{-}SMe)_4Mo(\eta\text{-}Cp)]^{0,+}$ (Section 2.2.10).

5.6.2.6. The unsupported triple-bridge $[(\mu_3\text{-}SR)M_3]$ is unknown.

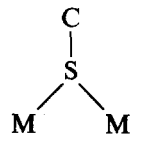
5.6.2.7. The supported triple-bridge $[(\mu_3\text{-}SR)M_3]$ is relatively rare. Primary bridges where the three M—S bond lengths differ by less than 0.1 Å occur in $(Bu^tS)_5(ZnMe)_5$ (Section 2.5.3, three instances), $Ag_6(SC_6H_4Cl)_6(PPh_3)_5$ (**6C**, three instances), and $(\mu_3\text{-}SMe)_4Re_4(CO)_{12}$[227] (four instances). Geometrical details are unavailable for the eight instances in $(MeZnSPr^i)_8$ (**8E**). $Ag_6(SAr)_6(PPh_3)_5$, $[Cd_{10}(SCH_2CH_2OH)_{16}]^{4+}$ (ClO_4^-) (**10B**) and $[Ag_6(SPh)_8]^{2-}$ contain triple-bridges in which one M—S bond is 0.2–0.4 Å longer than the other two and which, because it increases metal coordination numbers beyond the minima of 2 for Ag and 4 for Cd, can be regarded as secondary bridging.

5.6.2.8. A supported quadruple-bridge $[(\mu_4\text{-}SR)M_4]$ can be claimed for one Bu^tS^- ligand in

$(Bu^tS)_5(ZnMe)_5$ (Section 2.5.3): the Zn—S distances are disparate (2.51, 2.51, 2.71 and 2.98 Å), but are not secondary bridges because the Zn atoms depend on them to maintain four coordination.

5.6.3. *Stereochemistry at bridging* S.

5.6.3.1. Double-bridges. In all except five of more than 300 instances of doubly-bridging thiolate



in the crystalline state the stereochemistry of the three bonds to the S is pyramidal or pseudo-pyramidal.[183] The exceptional alternative stereochemistry is planar M_2SC.

In the normal pyramidal stereochemistry the M—S—M angles range from 65 to 120°, and the inclination ϕ of the S–C vector to the MSM plane ranges from 45 to 79°, with some evidence of correlation of these two angles.[183] An electronic distinction between alkyl and aryl thiolate is clearly apparent in complexes $[Cu_4(SR)_6]^{2-}$ (Section 2.4.5), where ϕ is 74.9° (s = 3.5°) for R = Me and 63.0° (s = 3.1°) for R = Ph, at an unchanged Cu—S—Cu angle of 73.6° (s = 1.7°) and independent of substituent steric repulsions.[204]

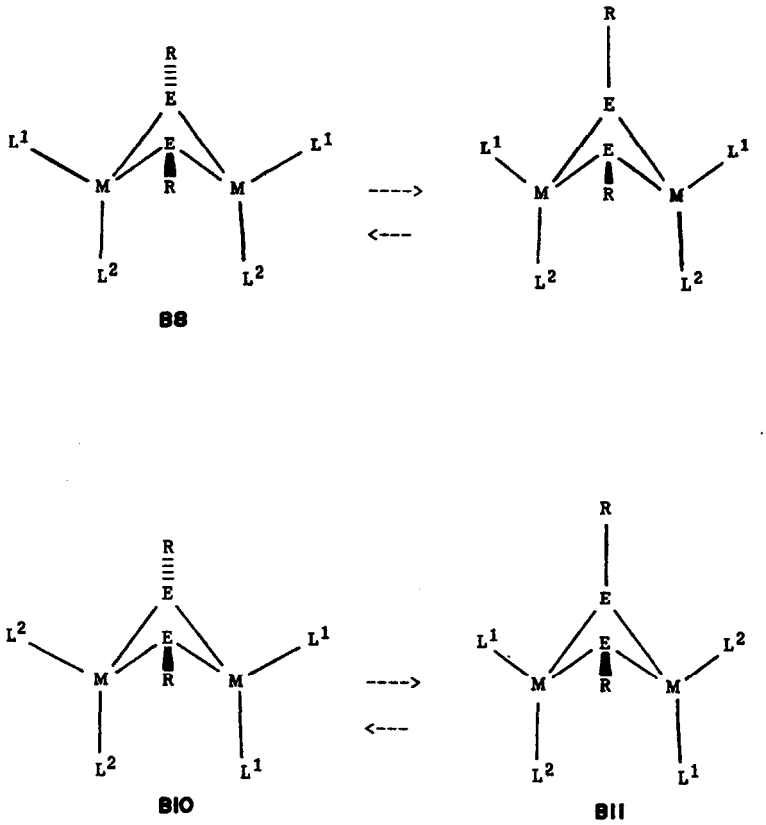
The exceptional planar stereochemistry for a doubly-bridging thiolate occurs at the two bridges of $(Ph_3P)_2Cu(\mu\text{-}SAr)_2Cu(PPh_3)_2$[149] and the three bridges of $[(\mu\text{-}SPh)_3Fe_3Cl_6]^{3-}$.[178] The planarity in the Cu compound can be attributed to crowding of Ph substituents, but the cause in the Fe compound is not yet apparent. Unlike doubly-bridging aryl thiolate, doubly-bridging phenolate adopts a planar or near planar stereochemistry in a large proportion of the complexes with confirmed structures: examples are $(\mu\text{-}OPh)_2Ti_2(OPh)_2Cl_4$,[338] $(\mu\text{-}OPh)_2Ti_2(OPh)_6(PhOH)_2$[163] and $(\mu\text{-}OPh)_2Mo_2(OPh)_4Cl_4$.[339]

The NMR spectra of complexes with doubly-bridging thiolates in solution reveal that the inversion of the configuration at the pyramidal S is in general a relatively rapid (*ca* 10^2 s^{-1}) process. Most information is available for complexes with the unsupported bis double-bridge and terminal heteroligands. Examples of the established processes and their inversion barriers are: (i) **B8** ↔ **B9** (*cis* heteroligands) [L^1L^2M = (η-Cp)(CO)Ru, ER = SePh, ΔG^* = 70 kJ mol^{-1}]; and (ii) **B10** ↔ **B11** (*trans* heteroligands) [L^1L^2M = (η-Cp)(CO)Ru, ER = SePh, ΔG^* = 66 kJ mol^{-1}, and L^1L^2M = (η-Cp)(CO)Ru, ER = SCH_2Ph, ΔG^* = 59 kJ mol^{-1}].[340]

In $[Cl_2OW(\mu\text{-}SBu^t)_2(\mu\text{-}Cl)WOCl_2]^-$, where a bis double-bridge is butressed by an additional (weaker) heterobridge, ΔG^* = 75 kJ mol^{-1} for thiolate inversion.[341] Where the $(\mu\text{-}ER)_2M_2$ cycle of the bis double-bridge is non-planar it may also undergo inversion through a planar E_2M_2 transition state, a process which does *not* require inversion at the S. Such a ring inversion appears to be facile [ΔG^* *ca* 40 kJ mol^{-1} in $(\mu\text{-}SBu^t)_2\{Rh(C_8H_8)\}_2$[140]] only when M–M bonding is clearly absent. At tris double-bridges the free energies of activation for S inversion (**B6** ↔ **B7**) range from 46 to 59 kJ mol^{-1} in $(\eta^7\text{-}C_7H_7)Mo(\mu\text{-}SR)_3Mo(CO)_2(PR_3)$.[342] Abel's review[343] of extensive studies of the stereodynamics of metal complexes of chalcogenide ligands (mainly R_2E) contains data compilations. General patterns extracted from these data are that inversion barriers are decreased substantially by metal coordination, and: (i) decrease with decreased metal electronegativity, (ii) decrease with increased ligand π conjugation, and (iii) increase as E expands from S to Se.

Stereodynamic information for *homo*thiolate complexes is virtually non-existent, largely because systems of interest are subject to rapid exchange by dissociative processes as well as intramolecular configurational isomerism. Paramagnetic shifted ^1H NMR spectra reveal that the inversion of the pyramidal bridging thiolate in $[M_4(SPh)_{10}]^{2-}$ (**4F**) (M = Fe or Co) is fast even at 240 K, whereas SPh ligand exchange is slow (NMR time scale).[210]

5.6.3.2. Triple-bridges. The orthodox stereochemistry for a triply-bridging thiolate has one C and three M atoms subtending pseudo tetrahedral angles at the S atom. However, this stereochemistry is *not* adopted by any of the five triply-bridging thiolates in $Ag_6(SC_6H_4Cl)_6(PPh_3)_5$ (see Fig. 6). At each of two such ligands two S—Ag bonds and the S—C bond are virtually coplanar, while the third S—Ag bond is inclined to this plane at 63 or 67°. At the other three ligands there occurs an unusual stereochemistry, related to the regular tetrahedron by the reflection of two M atoms (M′) as shown in Fig. 21. The S atom lies well outside its coordination polyhedron, and yet all angles at the S are approximately tetrahedral (105–130°), except for the two M—S—M′ (57 and 70°). The unorthodox stereochemistry for triply-bridging thiolate ligands in this compound is possibly dictated by the



crowding of 21 aryl substituents over its surface, and is further evidence of the flatness of the potential surface around the S atoms.

5.7. *Packing of thiolate substituents over aggregate surfaces*

The structures available to metal thiolate aggregates $[M_x(SR)_y]$ {like those with other comparable, bent, non-chelating ligands [XR (where X = O, NH, NH_2, PH, PH_2 or CH_2)]} can be restricted by the requirement that the substituents R be arranged without mutual interference over the surface of the aggregate. This substituent influence arises because the S—C bonds of doubly-bridging thiolate ligands (and sometimes triply-bridging SR) are inclined to the surface of the molecule. Configurational isomerism is due to inversion at pyramidal doubly-bridging S atoms, and where a M–(μ-S)–M plane does not pass through the cluster centroid the two configurational isomers will have different inclinations of the S—C bonds to the molecular surface. These isomers are labelled *radial* and *tangential*[280] (although they will rarely be inclined at angles of 90 or 0°, respectively, to the molecular surface). The *tangential* isomer is the more susceptible to substituent interference. In general terms, the

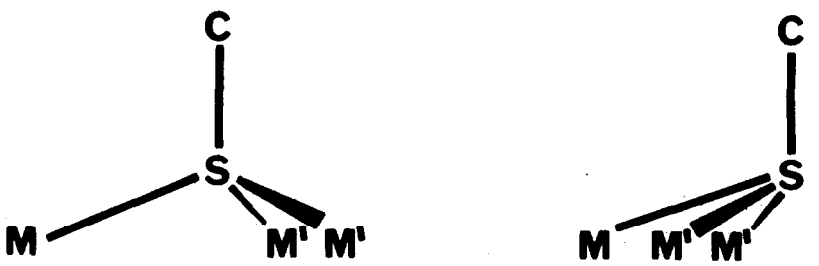


Fig. 21. Orthodox and unorthodox stereochemistry at triply-bridging thiolate, related by reflection of two M′ atoms through the plane containing S—C perpendicular to M—S—C.

separations of substituents on the aggregate surface are decreased by decreased centroid—S—C angles and by increased centroid—S distances (i.e. decreased surface curvature). In many cases the R_y array must possess less symmetry than the S_y array: for instance the R_6 set of *octahedro*-(μ-SR)$_6$-*tetrahedro*-M_4 (in **4E** and **4F**) can have a maximum symmetry of C_3, much less than the O_h for the S_6M_4 core.

Two levels of influence by the substituents can be recognized. At the lower level, and especially where the R_y-symmetry is necessarily less than the S_y-symmetry, a configurational isomer with a relatively high R_y-symmetry is observed in the crystal and the R--R interactions which remain are relieved by angular displacement of the M–(μ-SR)–M bridges involved. Consequently the S_y polyhedron is distorted according to the R_y-symmetry, and there are angular distortions of metal coordination polyhedra. This effect is evident in structures **4E**, **4F**, **5A**, **5B** and **10A**, and can be expected for structures **3F** and **4D**. The higher level of influence occurs when the substituents can be accommodated only when they are packed in a high-symmetry array. This occurs in structure **8C**.

A structural feature which increases the packing density of substituents over the molecular surface is apparent in some silver thiolates where two-coordinate M atoms are linked in strands {—(μ-SR)—M—(μ-SR)—M—}$_n$. In both a cyclic molecule (Fig. 9) and a one-dimensionally non-molecular structure [**1D-A** (Fig. 10)] two strands are entwined at the shortest non-bonding separation, such that the surface area per strand is effectively halved and the substituents (tertiary alkyl in both cases) can more fully encompass the double-stranded chain.

Metal complexes and aggregates with thiolate (or alcoxide) ligands are distinguished from clusters with tertiary phosphine (amine) ligands, another large class with bulky ligands, by the different inclinations of the ligand volume elements. In the phosphine class the substituent "cones" are usually perpendicular to the molecular surface, while in the thiolate class the ligand "cones" are usually inclined to the surface. Clusters with primary phosphide ligands (RHP^- or RP^{2-}) are relevant sterically to thiolate aggregates.

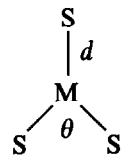
5.8. *Dimensions*

Disregarding the quite pronounced variations in distance associated with secondary M–SR interactions, primary M—S bond distances in metal thiolates are close to the values of the analogous metal chlorides. In compounds such as $[S_4Fe_4Cl_2(SPh)_2]^{2-}$[215] and $[(\mu\text{-SPh})_6(ZnCl)_2(ZnSPh)_2]^{2-}$,[214] where internal comparisons are possible, and in compound pairs such as $[(\mu\text{-SPh})_6(FeSPh)_4]^{2-}$ and $[(\mu\text{-SPh})_6(FeCl)_4]^{2-}$, the M—SPh bond is 0.02–0.06 Å longer than the M—Cl bond. Differences due to alkyl vs aryl thiolate substituents are negligible: in the "ferromantane" (**4F**) cages $\{[Fe_4(SR)_{10}]^{2-}$ (R = Et[141] or Ph[210])$\}$ the terminal Fe—S distance is 0.013 Å longer for R = Et, but, in contrast, the bridging Fe—S distance is 0.014 Å shorter for R = Et.

Variations in bond length due to a change in the coordination number of the thiolate S atom or the metal are prominent. In general the M–(μ-SR) distance for doubly-bridging thiolate is 0.05–0.1 Å longer than the comparable terminal M–SR distance. Unimpeded evaluations of the extension due to thiolate bridging are available from species such as: $[(\mu\text{-SEt})_2\{M(SEt)_2\}_2]^{2-}$ (**2E**) 0.070 Å for M = Fe and 0.090 Å for M = Co;[141] $[(\mu\text{-SPh})_6(MSPh)_4]^{2-}$ (**4F**) 0.076 Å for M = Fe,[210] and 0.064 Å for Co[209]. The effect of metal coordination number appears in the complexes $[M_5(\mu\text{-SPh})_7]^{2-}$ (**5A**), where the M atoms are all coordinated by doubly-bridging SPh ligands but with coordination numbers of 2 and 3: there are elongations of M—S of 0.11 (Cu) and 0.14 Å (Ag) when the coordination number is increased from 2 to 3.[230] More variety occurs in $(\mu_3\text{-SPh})_2(\mu\text{-SPh})_2Cu_4(PPh_3)_4$ (**4G**), where the dependence is $\{Cu^{tet}\text{–}(\mu_3\text{-SPh})$, 2.417 and 2.484$\}$ > $\{Cu^{tet}\text{–}(\mu\text{-SPh})$, 2.328$\}$ ≈ $\{Cu^{trig}\text{–}(\mu_3\text{-SPh})$, 2.313$\}$ > $\{Cu^{trig}\text{–}(\mu\text{-SPh})$, 2.278 Å$\}$.[220] In $[S_4M_{10}(SPh)_{16}]^{4-}$ (**10A**) there are four distinct M—S bond types which are differentiated only slightly. With reference to the shortest bond length, $\{(\mu\text{-SPh})_3M\}$–SPh, the increases are (for Zn and Cd, respectively) 0.02 and 0.01 Å in $\{(\mu\text{-SPh})_2(\mu_3\text{-S})M\}$—($\mu_3$-S), 0.09 and 0.09 Å in $\{(\mu\text{-SPh})_2(SPh)M\}$—($\mu$-SPh), and 0.12 and 0.13 Å in $\{(\mu\text{-SPh})(\mu_3\text{-S})_2M\}$—($\mu$-SPh).[293]

In metal coordination environments which are symmetrical according to the above criteria, variations are still observed in metal thiolate bond lengths. For instance, differences of up to 0.1 Å occur in M—S distances around one trigonal M–(μ-SR)$_3$ site. A rationale for this variability can be proposed. There is a correlation of the M—S distances with opposite S—M—S bond angles, and the angles are influenced by the interferences between thiolate substituents described in Section 2.4.5. The influence of S—M—S angle on M—S distance is most apparent in trigonal planar stereochemistry,

i.e. d (range 0.1 Å) is correlated with θ (range 40°):



For 36 instances of Cu(μ-SPh)$_3$ coordination in complexes $[Cu_4(SPh)_6]^{2-}$ (**4E**) the correlation is linear, $d = a\theta + b$ [$a = 2.05 \times 10^{-3}$ Å deg^{-1}, $b = 2.044$ Å, correlation coefficient (r) 0.75]. For M(μ-SPh)$_3$ coordination in $[M_5(SPh)_7]^{2-}$ (**5A**), a, b and r are 1.98×10^{-3} Å deg^{-1}, 2.033 Å and 0.79 for M = Cu and 2.74×10^{-3} Å deg^{-1}, 2.176 Å and 0.84 for M = Ag. For 12 instances of Cu(μ-SMe)$_3$ coordination in $[Cu_4(SMe)_6]^{2-}$ $r = 0.84$. These correlations permit extraction of ideal trigonal Cu(μ-SR)$_3$ bond lengths, 2.278 Å for R = Ph and 2.290 Å for R = Me. For the six Cu—SPh bonds in two crystals of $[Cu(SPh)_3]^{2-}$ a, b and r are 2.65×10^{-3} Å deg^{-1}, 1.954 Å and 0.67. The intensity of correlation is less ($a = 1.48 \times 10^{-3}$ Å deg^{-1}) in $[Hg(TePh)_3]^-$.

The linearity of the d–θ correlation is not expected to extend into the secondary bonding domain.

It has been argued[155] that the Mo—S distance of 2.32 Å in $(ArS)_2(Pr^iO)MoMo(OPr^i)(SAr)_2$ (**2F**) (Ar = 2,4,6-trimethylphenyl) with Mo–Mo triple bonding is shortened by *ca* 0.1 Å due to ArS–Mo π-bonding.

In complexes with tetrahedral M(SAr)$_4$ coordination (Section 2.1.7) the S—M—S angles have been observed to deviate from 109.5° by up to 11°, an effect which has been attributed[74] to ligand steric congestion. This interpretation is partly refuted by the absence of stereochemical distortion in more highly coordinated homologues (see Section 2.1.9).

5.9. *Metal–metal interactions*

A large proportion of the known polymetallic aggregates with non-thiolate ligands contain M—M bonds, often as the dominant cohesive force, and it is pertinent to enquire whether M–M interactions, attractive or repulsive, exist in polymetallic thiolate complexes. This assessment is based primarily on M—M distances and stereochemistry: observed antiferromagnetic coupling of paramagnetic sites merely allows characterization of bonding interactions less energetic than 4 kJ mol^{-1}, which is insignificant as an M—M bond.

Evaluation of M—M distances as indicators of M–M bonding must be made with reference to the remainder of the metal coordination and particularly the coordination number: M–M separations in the elemental metals where the coordination number is often 12 are unsuitable as reference distances for isolated M—M single bonds between low-coordinate metal atoms. Illustration of the variability of M—M bond distance with metal coordination capacity, and of the approach to be adopted with polymetallic thiolate complexes, can be made with the structure $\{AgSCMeEt_2\}_\infty$ (**1D-A**).[304] The closest contact between Ag atoms (in different strands of the chain) is 2.89 Å, which is equal to the interatomic separation in Ag metal. These Ag atoms have near linear (μ-SR)–Ag–(μ-SR) coordination, and there are no secondary Ag– –S interactions, indicative of excess bonding capacity at Ag. In fact the slight bending of S—Ag—S is in the sense that the Ag– –Ag distance increases, and therefore the interpretation of this geometry is that it represents the onset of a weak repulsion between coordinatively saturated Ag atoms. The important conclusion is that 12-coordinate Ag with no ligands is *bonding* with Ag at 2.88 Å, while two-coordinate Ag with anionic thiolate ligands is *non-bonding* with Ag at the same distance.

Thus distorted metal stereochemistry is an indicator, with M—M distance, of M–M bonding. Application of these criteria to polymetallic thiolates leads to the conclusion that M–M bonding is uncompetitive with thiolate bridge bonding, and is negligible in all except the compounds described in Section 2.2.5. In some thiolate cages M atoms are displaced slightly from the centroid of their thiolate coordination sphere, towards each other, and it is probable that the reason for this is weak attractive interaction between the M atoms.* This occurs in $[Cu_5(SBu^t)_6]^-$ (**5B**) where the digonal Cu atoms are

* The alternative explanation that the bonding at the S atom of the bridge causes contraction of M—S—M angles is discounted by the wide variability of such angles and the many larger values of M—S—M.

displaced inwards by 0.2 Å, and in $[M_5(SPh)_7]^{2-}$ (**5A**) (M = Cu or Ag) two of the M atoms are located 0.2–0.3 Å from their trigonal coordination planes towards each other.

5.10. *Structural influences of heteroligands*

Metal thiolate complexes with only a minor proportion of heteroligands are evaluated here. These complexes can be divided into two structural classes, depending on the coordination propensities of the heteroligand *relative to thiolate* as reference ligand. Where the heteroligand is monatomic with bridging abilities, as occurs frequently with sulfide, and occasionally with halide, the heteroligand usually plays a structure-expanding role as a central or near-central bridge. At the other extreme are heteroligands which, relative to thiolate, are non-bridging. This class contains oxide, carbonyl, acetonitrile, alkyl, halides, amines and phosphines, which play a structure-terminating role.

Polysulfide ligands (S_x^{2-}) are able to bridge and terminate in polymetallic complexes, and it appears that they have similarities with chelating thiolate ligands. Therefore, when polysulfides are present as heteroligands in metal thiolate complexes it is expected that they could function in either or both of the above structural roles.

The monatomic structure-expanding heteroligands have variable and metal-dependent structural influences. For example, with thiolate ligands only the metals Fe(II), Co(II), Zn(II) and Cd(II) form comparable complexes, $[M(SR)_4]^{2-}$ (**1G**), $[M_2(SR)_6]^{2-}$ (**2E**) and $[M_4(SR)_{10}]^{2-}$ (**4F**), all with a typical tetrahedral coordination. However, in the presence of sulfide or halide ligands these metals form aggregates with distinctly different structures, such as $[S_4Fe_4(SR)_4]^{2-}$ (**4H**), $[S_9Fe_6(SR)_2]^{4-}$ (**6F**), $[S_6Co_8(SR)_8]^{4-}$ (**8F**), $[ClZn_8(SR)_{16}]^{-}$ (**8C**), $[ICd_8(SR)_{12}]^{3+}$ (**8B**) and $[S_4Cd_{10}(SR)_{16}]^{4-}$ (**10A**).

Structure-terminating heteroligands lead to a reduction in the size of metal thiolate aggregates, according to their proportional presence. For instance, in the series of copper and silver thiolates with phosphines, $[(MSR)_x(PR'_3)_y]$, the number of M atoms in the aggregate, x, is inversely related to the proportion y/x of phosphine ligands:

x	y/x	Complex	Structure
1	3	$(Ph_3P)_3AgSPh$	**1G**
2	2	$(Ph_3P)_4(CuSPh)_2$	**2E**
3	1.3	$(Ph_3P)_4(CuSPh)_3$	**3D**
4	1	$(Ph_3P)_4(CuSPh)_4$	**4G**
4	0.5	$(Ph_3P)_2(CuSBu^t)_4$	**4A**
6	0.83	$(Ph_3P)_5(AgSC_6H_4Cl)_6$	**6C**
14	0.28	$(Ph_3P)_4(AgSBu^t)_{14}$	Fig. 9

The structural attributes of the structure-expanding and the structure-terminating types of heteroligands both provoke correlations with non-molecular structure types. The structure-expanding ligands lead to the possibility of molecular structures which are fragments of the non-molecular structures of corresponding binary compounds such as metal sulfides (see Sections 5.5.6 and 8). On the other hand, small proportions of structure-terminating heteroligands in metal thiolates can be conceived of as enclosing fragments of non-molecular metal thiolate structures. This is pertinent in cases such as the copper and silver arenethiolates listed above, where the structures of the parent compounds ($[MSAr]_n$) are unknown, presumed to be non-molecular, and difficult to obtain due to crystallization problems.

6. STRUCTURAL PRINCIPLES FOR METAL THIOLATE COMPOUNDS

From the foregoing data and generalizations a set of principles governing the structures of metal thiolate compounds can be developed, and proposed for evaluation in future research.

(1) Metal coordination numbers are at the low ends of normal ranges. This is attributed to the strongly electron-releasing characteristic and polarizability of thiolate ligands.* M(I) is usually two-

* Corroboration of this view is found in the ν(NO) data: 1675 cm^{-1} for $[Mo(NO)(SPh)_4]^-$ and 1694 cm^{-1} for $[Mo(NO)Cl_4]^-$.[111]

coordinate, M(II) is usually four-coordinate, and M(III) and M(IV) are usually five- and six-coordinate.

(2) Thiolate ligands do not have any prominent influence on metal coordination stereochemistry for the coordination numbers (4–6) where dual stereochemistry can occur.

(3) Thiolate ligands are usually doubly-bridging or terminal. Triple-bridging can be achieved by conventional thiolate ligands, sometimes with a dissymmetry which is similar to a double primary bridging plus a secondary bridging connection. Thiolate bridging can be prevented by incorporation of steric bulk.

(4) Polymetallic cages are maintained by thiolate bridges, not metal–metal bonds, and are normally comprised of fused $M_2(SR)_2$, $M_3(SR)_3$ or $M_4(SR)_4$ cyclic moieties.

(5) Polymetallic cages constructed with two-connected thiolate and two-, three- or four-connected M atoms have insufficient bonds for framework rigidity and are subject to angular distortions from idealized high-symmetry structures. Non-rigidity and distortions increase with cage size and with size (n) of the $M_n(SR)_n$ cycles which comprise the cage.

(6) Polymetal thiolate aggregates can frequently be idealized in terms of highly symmetric cyclic or globular structures containing regular polygons or polyhedra (deltahedra) of M atoms. These idealized structures are related in series by polyhedral expansion or polyhedron-capping operations.

(7) Low connectivities at M and thiolate S atoms, and the consequent cage non-rigidity, allow additional secondary (elongated) M--S connections which increase rigidity: secondary bridging may be intra- or intermolecular.

(8) Cage expansion is limited by the reduction in rigidity which it incurs. A mechanism for mechanical stabilization of globular cages with more than 10–14 M and S atoms is incorporation of an internal (spherical) heteroligand.

(9) Compounds with two-coordinate M atoms and doubly-bridging thiolate ligands are comprised of zig-zag strands of {–(μ-SR)–M–(μ-SR)–M–} segments linear at the M and bent at the S. Although coordinatively saturated these strands can associate in opposed pairs, presumably in order to maximize the coverage by substituents of the remaining molecular surface and to maximize crystal density. A skein-type folding of the strand occurs in cyclic molecules, while two strands are intertwined to form the chain of one-dimensionally non-molecular structures. Recognizable structural functions that: (i) extend a strand (zig-zag segments), (ii) intertwine double strands (crossover segments), and (iii) terminate a chain (bend and end segments) may be combined in the construction of molecules.

(10) Doubly-bridging thiolate normally adopts pyramidal stereochemistry at the S atom, but inversion is fast in solution and in the crystalline phase the inversion barrier (*ca* 40–70 kJ mol^{-1}) can be overcome by steric forces.

(11) In (μ-SR)$_3$M$_3$ cycles in a chair conformation the three R substituents are usually mixed equatorial and axial in configuration, but three axial substituents are possible, although with some expansion of S—M—S angles as a consequence.

(12) Substituent conflict can occur in folded (μ-SR)$_4$M$_4$ cycles, limiting the configurations available to the cycles and the structures of cages which contain fused cycles of this type.

7. CONCLUSIONS

7.1. *Thiolate as a pseudohalide ligand*

The structural component of the pseudohalide attributes for thiolates, introduced at the outset, can now be assessed. There is no extended similarity between the structures currently known for metal thiolates and for metal halides. Most of the metal thiolate structures reported here, including the paradigmatic thiolate structures which are the polygonal toroids, the adamantanoid structures, and the monocyclic chains, do not have metal halide counterparts. Similarly, there are widespread metal halide structure types that are not yet represented amongst metal thiolate structures: instances are square planar MX_4, octahedral MX_6, planar M_2X_6, *octahedro*-M_6X_{12} and *octahedro*-M_6X_8. On the other hand, structural correspondence between thiolate and halide complexes occurs for the simpler types **1A**, **1C**, **1D**, **1F**, **1G**, **1H**, **1J**, **2D**, **2E**, **2H**, **4E**[206] and **4G**.

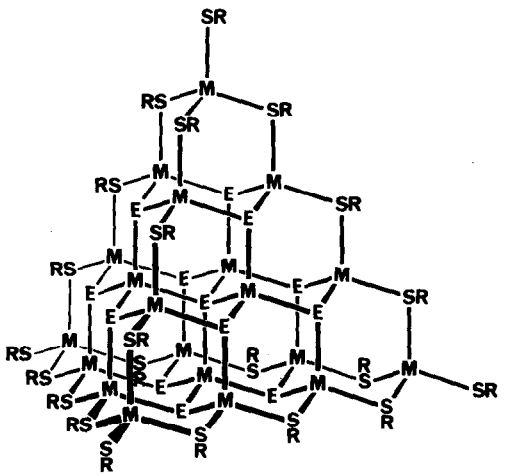
The thiolate substituent is the obvious structural differentiator from halide. Halide can and does play a central spherically coordinated role in aggregation, as for instance in structures **8B** and **8C** (see also Section 2.4.2).

7.2. Comparison with alcoxides

Apart from the results of fruitful recent investigations of the alcoxide chemistry of molybdenum and tungsten in low oxidation states,[344] knowledge of the structures of metal alcoxides and metal phenoxides[345] is still somewhat fragmentary. Nevertheless, there are instances of corresponding or related alcoxide/thiolate structures, some of which have been cited above in Sections 2.1.10, 2.2.9 and 2.8.7. Small alcoxide ligands have a greater propensity to triple-bridging than thiolates.

8. SPECULATION AND OUTLOOK

It is possible to conceive of larger homologues of some established metal thiolate structures. The paradigmatic adamantanoid cage (**4F**) is the basis for an unlimited series of polyadamantanoid aggregates, of which the first member, the supertetrahedral tetra-adamantanoid cage structure (**10A**), is established. Members of this series are molecular fragments of the non-molecular sphalerite lattice. The thiolate ligands in **10A** function as termini at the edges and vertices of the supertetrahedron, without disruption of the molecular lattice structure or modification of the metal coordination stereochemistry, and the thiolate ligands do not affect the faces. Therefore, larger supertetrahedral fragments of sphalerite can also be vertex- and edge-terminated in the same fashion to form hypothetical but legitimate macromolecules.[293] The next member of this series of supertetrahedra would be $[E_{13}M_{20}(SR)_{22}]^{8-}$ (**20**), in which there is only one structural element not present in **10A**, namely the tetrahedrally coordinated central chalcogenide ion, which is the predominant component of the bulk metal chalcogenide. It is also possible that surface (μ_3-E) groups on **20** or larger homologues could be replaced by triply-bridging thiolate ligands, as justified in Section 2.10.3.



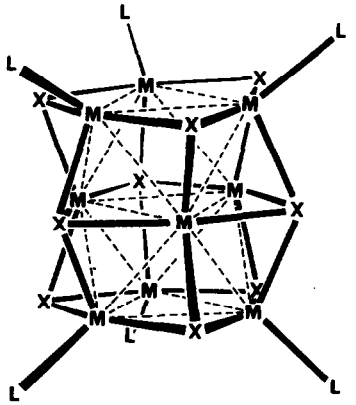
20

It has been suggested[253,281] that the structure of the cluster centre of the iron–molybdenum cofactor of nitrogenase could be based on the *octahedro*-$(\mu_4\text{-S})_6$-*hexahedro*-M_8 aggregate of **8F**, specifically $[(\mu_4\text{-S})_6(FeSR)_7MoL_n]$.

In the past few years there has been a spate of discoveries of unprecedented metal thiolates with unpredicted structures, together with unprecedented metal polysulfide complexes. Monosulfide ions have occurred in some of these compounds. In view of the structural relationships between these ligand types, and, in particular, the close correspondence between chelating polysulfide ligands and thiolate ligands, it is not unreasonable to expect that metal thiolate complexes with some similarity to the beautiful (**6D** and **12C**) and the bizarre (**6K**) sulfide and polysulfide species will appear after suitable synthetic enterprise.

Predictions of new thiolate complexes can be made on this basis from structures described in Sections 2.3.2, 2.4.8, 2.6.4, 2.6.6, 2.6.10, 2.7, 2.8.6, 2.8.9, 2.10.3 and 2.11.3. In addition, the ion $[(\mu_4\text{-S})_3(\mu_3\text{-S})_6Ni_9(PEt_3)_6]^{2+}$ (**9B**)[346] provides a precedent for thiolate structures. The metal framework is a confacial bioctahedron, with three quadruply-bridging sulfide ligands (X) in the equatorial plane, and six triply-bridging sulfide ligands (X) located in the upper and lower planes of Ni atoms which carry the six terminal ligands. The S_9 array is also a confacial bioctahedron,

compressed along the three-fold axis and rotated about it by 60° from the Ni_9 bioctahedron. The terminal and triply-bridging ligand positions could be occupied by thiolate ligands, allowing the postulation of analogous structures such as $[(\mu_4\text{-S})_3(\mu_3\text{-S})_6M_9(SR)_6]$ and $[(\mu_4\text{-S})_3(\mu_3\text{-SR})_6M_9(SR)_6]$, with charges 4− and 2+, respectively, if the core electron population is unchanged.



98

The variety of the structural relationships in Section 5.5 supports the expectation that many more varied polymetallic thiolate complexes will be discovered, but it is also expected that they will not contravene the principles proposed in Section 6.

Acknowledgements—Dr Marcia Scudder provided valuable assistance in the preparation of this Report, and Martin Dudman drew the diagrams. The financial support of the author's research by the Australian Research Grants Scheme is gratefully acknowledged.

REFERENCES

1. J. P. Danehy and K. N. Parameswaran, *J. Chem. Eng. Data* 1968, **13**, 386.
2. M. R. Crampton, In *The Chemistry of the Thiol Group* (Edited by S. Patai), Part 1. 1974, **1**, 379.
3. M. Akbar Ali and S. E. Livingstone, *Coord. Chem. Rev.* 1974, **13**, 101.
4. J. L. Corbin, K. F. Miller, N. Pariyadath, J. Heinecke, A. E. Bruce, S. Wherland and E. I. Stiefel, *Inorg. Chem.* 1984, **23**, 3404.
5. D. C. Bradley, R. C. Mehrohtra and D. P. Gaur, *Metal Alcoxides*. Academic Press, London (1978).
6. R. C. Mehrohtra, *Adv. Inorg. Chem. Radiochem.* 1983, **26**, 269.
7. K. A. Jensen, *Z. Anorg. Allg. Chem.* 1944, **252**, 227.
8. D. C. Bradley and N. R. Kunchur, *J. Chem. Phys.* 1964, **40**, 2258.
9. N. R. Kunchur, *Nature (London)* 1964, **204**, 468.
10. P. Woodward, L. F. Dahl, E. W. Abel and B. C. Crosse, *J. Am. Chem. Soc.* 1965, **87**, 5251.
11. P. Strickler, *J. Chem. Soc., Chem. Commun.* 1969, 655.
12. R. C. Mehrotra, V. D. Gupta and S. Sukhani, *Inorg. Chim. Acta Rev.* 1968, **2**, 111.
13. D. C. Bradley and K. J. Fisher, In *M.T.P. International Review of Science, Inorganic Chemistry, Series* 1 (Edited by D. W. A. Sharp), Vol. 5, p. 65. Butterworths, London (1972).
14. J. R. Dilworth, In *Sulfur, Its Significance for Chemistry, for the Geo-, Bio-, and Cosmosphere and Technology* (Edited by A. Muller and B. Krebs), Studies in Inorganic Chemistry, Vol. 5, p. 141. Elsevier, Amsterdam (1984).
15. W.-H. Pan, M. A. Harmer, T. R. Halbert and E. I. Stiefel, *J. Am. Chem. Soc.* 1984, **106**, 459.
16. A. Muller, M. Romer, H. Bogge, E. Krickemeyer and D. Bergmann, *J. Chem. Soc., Chem. Commun.* 1984, 348.
17. G. Henkel, P. Betz and B. Krebs, *J. Chem. Soc., Chem. Commun.* 1984, 314.
18. A. Muller, E. Krickemeyer, H. Bogge, W. Clegg and G. M. Sheldrick, *Angew. Chem., Int. Ed. Engl.* 1983, **22**, 1006.
19. A. Muller and U. Schimanski, *Inorg. Chim. Acta* 1983, **77**, L187.
20. W. E. Newton, In *Sulfur, Its Significance for Chemistry, for the Geo-, Bio-, and Cosmosphere and Technology* (Edited by A. Muller and B. Krebs), Studies in Inorganic Chemistry, Vol. 5, p. 409. Elsevier, Amsterdam (1984).
21. C. D. Stout, In *Iron–Sulfur Proteins* (Edited by T. G. Spiro), Chap. 3. John Wiley, New York (1982).
22. H. L. Monaco, J. L. Crawford and W. N. Lipscomb, *Proc. Natl Acad. Sci. U.S.A.* 1978, **75**, 5276.

23. D. Ghosh, S. O'Donnell, W. Furey, Jr, A. H. Robbins and C. D. Stout, *J. Mol. Biol.* 1982, **158**, 73.
24. L. Powers, B. Chance, Y. Ching and P. Angiolillo, *Biophys. J.* 1981, **33**, 95a.
25. Y. Sugiura, H. Kawabe, H. Tanaka, S. Fujimoto and A. Ohara, *J. Am. Chem. Soc.* 1981, **103**, 963; *J. Biol. Chem.* 1981, **256**, 10664.
26. H. Kawabe, Y. Sugiura and H. Tanaka, *Inorg. Chim. Acta* 1983, **79**, 112.
27. J. H. R. Kagi and M. Nordberg (Eds), *Metallothionein.* Birkhauser, Basel (1979).
28. M. Vasak and J. H. R. Kagi, In *Metal Ions in Biological Systems* (Edited by H. Sigel), Vol. 15, p. 213. Marcel Dekker, New York (1983).
29. K. A. Melis, D. C. Carter, C. D. Stout and D. R. Winge, *J. Biol. Chem.*, 1983, **258**, 6255.
30. J. D. Otvos and I. M. Armitage, In *Biochemical Structure Determination by NMR* (Edited by B. D. Sykes, J. Glickson and A. A. Bothner-By), Chap. 4. Marcel Dekker, New York (1981).
31. J. D. Otvos and I. M. Armitage, *Proc. Natl Acad. Sci. U.S.A.* 1980, **77**, 7094.
32. J. D. Otvos, R. W. Olafson and I. M. Armitage, *J. Biol. Chem.* 1982, **257**, 2427.
33. Y. Boulanger, I. M. Armitage, K. A. Miklossy and D. R. Whinge, *J. Biol. Chem.* 1982, **257**, 13717.
34. J. K. Nicholson, P. J. Sadler, K. Cain, D. E. Holt, M. Webb and G. E. Hawkes, *Biochem. J.* 1983, **211**, 251.
35. J. M. Berg and R. H. Holm, in *Iron–Sulfur Proteins* (Edited by T. G. Spiro), Chap. 1. John Wiley, New York (1982).
36. D. C. Bradley and N. R. Kunchur, *Can. J. Chem.* 1965, **43**, 2786.
37. C. Perchard, G. Zuppiroli, P. Gouzerh, Y. Jeannin and F. Roberts, *J. Mol. Struct.* 1981, **72**, 119.
38. I. G. Dance, P. J. Guerney and M. L. Scudder, unpublished results.
39. H. Barrera, J. C. Bayon, P. Gonzales-Duarte, J. Sola, J. M. Vinas, J. L. Brianso, M. C. Brianso and X. Solans, *Polyhedron* 1982, **1**, 647.
40. N. J. Taylor and A. J. Carty, *J. Am. Chem. Soc.* 1977, **99**, 6143.
41. S. A. Koch, R. Fikar, M. Millar and T. O'Sullivan, *Inorg. Chem.* 1984, **23**, 121.
42. M. Muller, R. J. H. Clark and R. S. Nyholm, *Transition Met. Chem.* 1978, **3**, 369.
43. W. Beck, K. H. Stetter, S. Tadros and K. E. Schwarzhans, *Chem. Ber.* 1967, **100**, 3944.
44. G. A. Bowmaker and B. C. Dobson, *J. Chem. Soc., Dalton Trans.* 1981, 267.
45. G. Marbach and J. Strahle, *Angew. Chem., Int. Ed. Engl.* 1984, **23**, 246.
46. A. Muller, E. Krickemeyer, M. Zimmermann, M. Romer, H. Bogge, M. Penk and K. Schmitz, *Inorg. Chim. Acta* 1984, **90**, L69.
47. D. T. Hill and B. M. Sutton, *Cryst. Struct. Commun.* 1980, **9**, 679.
48. H. Ruben, A. Zalkin, M. O. Faltens and D. H. Templeton, *Inorg. Chem.* 1974, **13**, 1836.
49. L. G. Kuz'mina, N. G. Bokii, Yu. T. Struchkov, D. N. Kravtsov and E. M. Rokhlina, *Zh. Strukt. Khim.* 1974, **15**, 491.
50. D. Coucouvanis, C. N. Murphy and S. K. Kanodia, *Inorg. Chem.* 1980, **19**, 2993.
51. C. D. Garner, J. R. Nicholson and W. Clegg, *Inorg. Chem.* 1984, **23**, 2148.
52. A. J. Canty, R. Kishimoto, G. B. Deacon and G. J. Farquharson, *Inorg. Chim. Acta* 1976, **20**, 161.
53. A. P. Arnold, A. J. Canty, B. W. Skelton and A. H. White, *J. Chem. Soc., Dalton Trans.* 1982, 607.
54. P. B. Hitchcock, M. F. Lappert, B. J. Samways and E. L. Weinberg, *J. Chem. Soc., Chem. Commun.* 1983, 1492.
55. B. Cetinkaya, I. Gumrukcu, M. F. Lappert, J. L. Atwood, R. D. Rogers and M. J. Zaworotko, *J. Am. Chem. Soc.* 1980, **102**, 2088.
56. T. Fjeldberg, H. Hope, M. F. Lappert, P. P. Power and A. J. Thorne, *J. Chem. Soc., Chem. Commun.* 1983, 639.
57. U. Behrens, K. Hoffmann and G. Klar, *Chem. Ber.* 1977, **110**, 3672.
58. (a) J. Liesk and G. Klar, *Z. Anorg. Allg. Chem.* 1977, **435**, 103; (b) G. Christou, K. Folting and J. C. Huffmann, *Polyhedron* 1984, **3**, 1247; (c) G. A. Bowmaker, I. G. Dance and M. L. Scudder, unpublished results.
59. G. A. Bowmaker, I. G. Dance, B. C. Dobson and D. A. Rogers, *Aust. J. Chem.* 1984, **37**, 1607.
60. J. B. Lambert and W. J. Schulz, Jr, *J. Am. Chem. Soc.* 1983, **105**, 1671.
61. A. P. Bozopoulos, S. C. Kokkou, P. J. Rentzeperis and P. Karagiannidis, *Acta Cryst.* 1984, **C40**, 944.
62. P. A. W. Dean, J. J. Vittal and N. C. Payne, *Inorg. Chem.* 1984, **23**, 4232.
63. J. J. I. Arsenault and P. A. W. Dean, *Can. J. Chem.* 1983, **61**, 1516.
64. B. R. Hollebone and R. S. Nyholm, *J. Chem. Soc.* (*A*) 1971, 332.
65. R. S. Nyholm, J. F. Skinner and M. H. B. Stiddard, *J. Chem. Soc.* (*A*) 1968, 38.
66. C. R. Lucas and M. E. Peach, *Inorg. Nucl. Chem. Lett.* 1969, **5**, 73.
67. D. G. Holah and D. Coucouvanis, *J. Am. Chem. Soc.* 1975, **97**, 6917.
68. D. Swenson, N. C. Baenziger and D. Coucouvanis, *J. Am. Chem. Soc.* 1978, **100**, 1932.
69. K. Prout, S. R. Critchley and G. V. Rees, *Acta Cryst.* 1974, **B30**, 2305.
70. J.-C. Caran, B. Meunier and K. Prout, *Acta Cryst.* 1979, **B35**, 1709.
71. M. L. H. Green, *Pure Appl. Chem.* 1972, **30**, 373.
72. (a) J. R. Dorfman, Ch. Pulla Rao and R. H. Holm, *Inorg. Chem.* 1985, **24**, 453; (b) J. R. Dorfman, T. Costa and R. H. Holm, cited in Ref. 85.

73. D. Coucouvanis, D. Swenson, N. C. Baenziger, D. G. Holah, A. Kostikas, A. Simopoulos and V. Petrouleas, *J. Am. Chem. Soc.* 1976, **98**, 5721.
74. D. Coucouvanis, D. Swenson, N. C. Baenziger, C. Murphy, D. G. Holah, N. Sfarnas, A. Simopoulos and A. Kostikas, *J. Am. Chem. Soc.* 1981, **103**, 3350.
75. D. Coucouvanis, C. N. Murphy, E. Simhon, P. Stremple and M. Draganjac, *Inorg. Synth.* 1982, **21**, 23.
76. I. G. Dance, A. D. Rae and M. L. Scudder, unpublished results.
77. S. Choudhury, I. G. Dance, P. J. Guerney and A. D. Rae, *Inorg. Chim. Acta* 1983, **70**, 227.
78. K. S. Hagen, A. D. Watson and R. H. Holm, *J. Am. Chem. Soc.* 1983, **105**, 3905.
79. M. Millar, J. F. Lee, S. A. Koch and R. Fikar, *Inorg. Chem.* 1982, **21**, 4105.
80. M. Millar, S. A. Koch and R. Fikar, *Inorg. Chim. Acta* 1984, **88**, L15.
81. S. A. Koch, L. E. Maelia and M. Millar, *J. Am. Chem. Soc.* 1983, **105**, 5944.
82. S. Otsuka, M. Kamata, K. Hirotsu and T. Higuchi, *J. Am. Chem. Soc.* 1981, **103**, 3011.
83. D. H. R. Barton, H. Dadoun and A. Gourdon, *Nouv. J. Chim.* 1982, **6**, 53.
84. L. E. Maelia and S. A. Koch, Abstract INOR 156, 188th American Chemical Society Meeting, Philadelphia, August 1984.
85. T. Costa, J. R. Dorfman, K. S. Hagen and R. H. Holm, *Inorg. Chem.* 1983, **22**, 4091.
86. R. W. Lane, J. A. Ibers, R. B. Frankel, G. C. Papaefthymiou and R. H. Holm, *J. Am. Chem. Soc.* 1977, **99**, 84.
87. A. Muller, J. Schimanski and U. Schimanski, *Angew. Chem., Int. Ed. Engl.* 1984, **23**, 159.
88. B. R. Hollebone, *J. Chem. Soc.* (*A*) 1971, 481.
89. W. Beck, W. P. Fehlhammer, K. H. Stetter and S. Tadros, *Chem. Ber.* 1967, **100**, 3955.
90. R. C. Mehrotra, V. D. Gupta and D. Sukhani, *J. Inorg. Nucl. Chem.* 1967, **29**, 83.
91. R. C. Mehrotra, V. D. Gupta and D. Sukhani, *J. Inorg. Nucl. Chem.* 1967, **29**, 1577.
92. J. de Courcy, I. G. Dance, P. J. Guerney and M. L. Scudder, unpublished results.
93. S. A. Koch, R. Fikar, M. Millar and T. O'Sullivan, *Inorg. Chem.* 1984, **23**, 121.
94. B. Krebs, *Angew. Chem., Int. Ed. Engl.* 1983, **22**, 113.
95. G. Hillier and I. G. Dance, unpublished results.
96. T. L. Cremers, D. R. Bloomquist, R. D. Willett and G. A. Crosby, *Acta Cryst.* 1980, **B36**, 3097.
97. E. Binamira-Soriaga, M. Lundeen and K. Seff, *Acta Cryst.* 1979, **B35**, 2875.
98. I. G. Dance, L. J. Fitzpatrick and M. L. Scudder, unpublished results.
99. J. S. Thompson, J. L. Zitzmann, T. J. Marks and J. A. Ibers, *Inorg. Chim. Acta* 1980, **46**, L101.
100. J. S. Thompson, T. Sorrell, T. J. Marks and J. A. Ibers, *J. Am. Chem. Soc.* 1979, **101**, 4193.
101. J. S. Thompson, T. J. Marks and J. A. Ibers, *Proc. Natl Acad. Sci. U.S.A.* 1977, **74**, 3114.
102. E. W. Abel and D. A. Armitage, *Adv. Organomet. Chem.* 1967, **5**, 1.
103. E. T. Adman, L. C. Sieker, L. H. Jensen, M. Bruschi and J. LeGall, *J. Mol. Biol.* 1977, **112**, 113.
104. K. D. Watenpaugh, L. C. Sieker and L. H. Jensen, *J. Mol. Biol.* 1979, **131**, 509.
105. H. Eklund, B. Nordstrom, E. Zeppezauer, G. Soderlund, I. Ohlsson, T. Boiwe, B.-O. Soderberg, O. Tapia, C.-I. Branden and A. Akeson, *J. Mol. Biol.* 1976, **102**, 27.
106. I. G. Dance, S. Katende and J. C. Calabrese, unpublished results.
107. S. A. Koch and M. Millar, *J. Am. Chem. Soc.* 1983, **105**, 3362.
108. M. Millar and S. A. Koch, Abstract INOR 97, 188th American Chemical Society Meeting, Philadelphia, August 1984.
109. T. O'Sullivan, N. de Vries and M. Millar, Abstract INOR 173, 188th American Chemical Society Meeting, Philadelphia, August 1984.
110. J. R. Dilworth, B. D. Neaves, J. P. Hutchinson and J. A. Zubieta, *Inorg. Chim. Acta* 1982, **65**, L223.
111. P. T. Bishop, J. R. Dilworth, J. Hutchinson and J. A. Zubieta, *Inorg. Chim. Acta* 1984, **84**, L15.
112. H. Funk and M. Hesselbarth, *Z. Chem.* 1966, **6**, 227.
113. J. R. Bradbury, M. F. Mackay and A. G. Wedd, *Aust. J. Chem.* 1978, **31**, 2423.
114. A. C. McDonell, T. W. Hambley, M. R. Snow and A. G. Wedd, *Aust. J. Chem.* 1983, **36**, 253.
115. T. O'Sullivan, M. Millar, V. Chebolu, S. Soong and S. A. Koch, Abstract INOR 172, 186th American Chemical Society Meeting, August 1983.
116. P. J. Blower, J. R. Dilworth, J. Hutchinson, T. Nicholson and J. Zubieta, *Inorg. Chim. Acta* 1984, **90**, L27.
117. R. W. Wiggins, J. C. Huffman and G. Christou, *J. Chem. Soc., Chem. Commun.* 1983, 1313; J. K. Money, J. C. Huffman and G. Christou, *Inorg. Chem.* 1985, **24**, 3297.
118. D. Szeymies, B. Krebs and G. Henkel, *Angew. Chem., Int. Ed. Engl.* 1984, **23**, 804.
119. J. E. Smith, E. F. Byrne, F. A. Cotton and J. C. Sekutowski, *J. Am. Chem. Soc.* 1978, **100**, 5571.
120. P. J. Blower, J. R. Dilworth, J. P. Hutchinson and J. A. Zubieta, *Inorg. Chim. Acta* 1982, **65**, L225.
121. A. G. Jones, B. V. DePamphilis and A. Davison, *Inorg. Chem.* 1981, **20**, 1617.
122. B. V. DePamphilis, A. G. Jones, M. A. Davis and A. Davison, *J. Am. Chem. Soc.* 1978, **100**, 5570.
123. G. R. Hanson, A. A. Brunette, A. C. McDonell, K. S. Murray and A. G. Wedd, *J. Am. Chem. Soc.* 1981, **103**, 1953.

124. J. R. Bradbury, A. F. Masters, A. C. McDonell, A. A. Brunette, A. M. Bond and A. G. Wedd, *J. Am. Chem. Soc.* 1981, **103**, 1959.
125. P. J. Blower, J. R. Dilworth, J. P. Hutchinson and J. Zubieta, *Transition Met. Chem.* 1982, **7**, 353.
126. R. Eisenberg, *Prog. Inorg. Chem.* 1970, **12**, 295.
127. J. L. Hencher, M. Khan, F. F. Said, R. Sieler and D. G. Tuck, *Inorg. Chem.* 1982, **21**, 2787.
128. M. Kamata, T. Yoshida, S. Otsuka, K. Hirotsu and T. Higuchi, *J. Am. Chem. Soc.* 1981, **103**, 3572.
129. M. Kamata, K. Hirotsu, T. Higuchi, K. Tatsumi, R. Hoffmann, T. Yoshida and S. Otsuka, *J. Am. Chem. Soc.* 1981, **103**, 5772.
130. V. Vortisch, P. Kroneck and P. Hemmerich, *J. Am. Chem. Soc.* 1976, **98**, 2821.
131. J. C. Bowles and D. Hall, *Acta Cryst.* 1975, **B31**, 2149.
132. L. Banci, A. Bencini, A. Dei and D. Gatteschi, *Inorg. Chim. Acta* 1984, **84**, L11.
133. R. H. Fenn and G. R. Segrott, *J. Chem. Soc., Dalton Trans.* 1972, 330.
134. R. H. Fenn and G. R. Segrott, *J. Chem. Soc. (A)* 1970, 3197.
135. J. P. Fackler and W. J. Zegarski, *J. Am. Chem. Soc.* 1973, **95**, 8566.
136. M. C. Hall, J. A. J. Jarvis, B. T. Kilbourn and P. G. Owston, *J. Chem. Soc., Dalton Trans.* 1972, 1544.
137. H. W. Chen, C. Paparizos and J. P. Fackler, Jr, *Inorg. Chim. Acta* 1985, **96**, 137.
138. J.-J. Bonnett, P. Kalck and R. Poilblanc, *Inorg. Chem.* 1977, **16**, 1514.
139. J.-J. Bonnett, A. Thorez, A. Maisonnat, J. Galy and R. Poilblanc, *J. Am. Chem. Soc.* 1979, **101**, 5940.
140. R. Hill, B. A. Kelly, F. G. Kennedy, S. A. R. Knox and P. Woodward, *J. Chem. Soc., Chem. Commun.* 1977, 434.
141. K. S. Hagen and R. H. Holm, *Inorg. Chem.* 1984, **23**, 418.
142. G. Henkel, W. Tremel and B. Krebs, *Angew. Chem.* Suppl. 1983, 323.
143. G. Henkel, W. Tremel and B. Krebs, *Angew. Chem., Int. Ed. Engl.* 1983, **22**, 319.
144. W. Tremel, B. Krebs and G. Henkel, *Angew. Chem., Int. Ed. Engl.* 1984, **23**, 634.
145. J. G. Reynolds and R. H. Holm, *Inorg. Chem.* 1980, **19**, 3257.
146. J. J. Mayerle, S. E. Denmark, B. V. DePamphilis, J. A. Ibers and R. H. Holm, *J. Am. Chem. Soc.* 1975, **97**, 1032.
147. D. Coucouvanis, D. Swenson, P. Stremple and N. C. Baenziger, *J. Am. Chem. Soc.* 1979, **101**, 3392.
148. H. Strasdeit, B. Krebs and G. Henkel, *Inorg. Chim. Acta* 1984, **89**, L11.
149. I. G. Dance, P. J. Guerney, A. D. Rae and M. L. Scudder, *Inorg. Chem.* 1983, **22**, 2883.
150. J. T. Thomas, J. H. Robertson and E. G. Cox, *Acta Cryst.* 1958, **11**, 599.
151. M. C. Brianso, J. L. Brianso, W. Gaete, J. Ros and C. Suner, *J. Chem. Soc., Dalton Trans.* 1981, 852.
152. P. J. Burke, L. A. Gray, P. J. C. Hayward, R. W. Matthews, M. McPartlin and D. G. Gillies, *J. Organomet. Chem.* 1977, **136**, C7.
153. A. Muller, W. O. Nolte and B. Krebs, *Inorg. Chem.* 1980, **19**, 2835.
154. M. H. Chisholm, J. F. Corning and J. C. Huffman, *Inorg. Chem.* 1983, **22**, 38.
155. M. H. Chisholm, J. F. Corning and J. C. Huffman, *Inorg. Chem.* 1984, **23**, 754.
156. G. Christou and J. C. Huffman, *J. Chem. Soc., Chem. Commun.* 1983, 558.
157. M. R. Snow and J. A. Ibers, *Inorg. Chem.* 1973, **12**, 249.
158. I. G. Dance, A. G. Wedd and I. W. Boyd, *Aust. J. Chem.* 1978, **31**, 519.
159. K. F. Miller, A. E. Bruce, J. L. Corbin, S. Wherland and E. I. Stiefel, *J. Am. Chem. Soc.* 1980, **102**, 5102.
160. J. R. Dilworth and R. L. Richards, *J. Chem. Soc., Dalton Trans.* 1983, 1489.
161. M. H. Chisholm, J. F. Corning and J. C. Huffman, *Inorg. Chem.* 1982, **21**, 286.
162. F. A. Cotton and G. L. Powell, *J. Am. Chem. Soc.* 1984, **106**, 3371.
163. G. W. Svetich and A. A. Voge, *Acta Cryst.* 1972, **B28**, 1760.
164. P. M. Boorman, V. D. Patel, K. A. Kerr, P. W. Codding and P. van Roey, *Inorg. Chem.* 1980, **19**, 3508.
165. A. J. Schultz and R. Eisenberg, *Inorg. Chem.* 1973, **12**, 518.
166. M. di Vaira, S. Midollini and L. Sacconi, *Inorg. Chem.* 1979, **18**, 3466.
167. W. E. Silverthorn, C. Couldwell and K. Prout, *J. Chem. Soc., Chem. Commun.* 1978, 1009.
168. I. W. Boyd, I. G. Dance, A. E. Landers and A. G. Wedd, *Inorg. Chem.* 1979, **18**, 1875.
169. I. G. Dance and A. E. Landers, *Inorg. Chem.* 1979, **18**, 3487.
170. I. Buchanan, W. Clegg, C. D. Garner and G. M. Sheldrick, *Inorg. Chem.* 1983, **22**, 3657.
171. T.-C. Hsieh, K. Gebreyes and J. Zubieta, *J. Chem. Soc., Chem. Commun.* 1984, 1172.
172. J. R. Dorfman and R. H. Holm, *Inorg. Chem.* 1983, **22**, 3179.
173. D. Szeymies, B. Krebs and G. Henkel, *Angew. Chem., Int. Ed. Engl.* 1983, **22**, 885.
174. N. G. Connelly and L. F. Dahl, *J. Am. Chem. Soc.* 1970, **92**, 7470.
175. A. Muller, F.-W. Baumann, H. Bogg M. Romer, E. Krickemeyer and K. Schmitz, *Angew. Chem., Int. Ed. Engl.* 1984, **23**, 632.
176. A. Muller, M. Romer, H. Bogge, E. Krickemeyer, F.-W. Baumann and K. Schmitz, *Inorg. Chim. Acta* 1984, **89**, L7.
177. S. R. Acott, C. D. Garner, J. R. Nicholson and W. Clegg, *J. Chem. Soc., Dalton Trans.* 1983, 713.
178. K. S. Hagen and R. H. Holm, *J. Am. Chem. Soc.* 1982, **104**, 5496.
179. Y. Do, E. D. Simhon and R. H. Holm, *J. Am. Chem. Soc.* 1983, **105**, 6731.

180. D. Coucouvanis, N. C. Baenziger, E. D. Simhon, P. Stremple, D. Swenson, A. Simopoulos, A. Kostikas, V. Petrouleas and V. Papaefthymiou, *J. Am. Chem. Soc.* 1980, **102**, 1732.
181. D. Coucouvanis, E. D. Simhon, P. Stremple, M. Ryan, D. Swenson, N. C. Baenziger, A. Simopulos, V. Papaefthymiou, A. Kostikas and V. Petrouleas, *Inorg. Chem.* 1984, **23**, 741.
182. I. G. Dance, L. J. Fitzpatrick and M. L. Scudder, *J. Chem. Soc., Chem. Commun.* 1983, 546.
183. I. G. Dance and M. L. Scudder, to be published.
184. S. Pollitz, F. Zettler, D. Forst and H. Hess, *Z. Naturforsch.* 1976, **31B**, 897.
185. E. M. McPartlin and N. C. Stephenson, *Acta Cryst.* 1969, **B25**, 1659.
186. G. Henkel, W. Tremel and B. Krebs, *Angew. Chem., Int. Ed. Engl.* 1981, **20**, 1033.
187. K. S. Hagen, G. Christoú and R. H. Holm, *Inorg. Chem.* 1983, **22**, 309.
188. G. Henkel, W. Tremel and B. Krebs, *Angew. Chem., Int. Ed. Engl.* 1983, **22**, 318.
189. W. Tremel, B. Krebs and G. Henkel, *Inorg. Chim. Acta* 1983, **80**, L31.
190. M. R. Antonio, B. A. Averill, I. Moura, J. J. G. Moura, W. H. Orme-Johnson, B.-K. Teo and A. V. Xavier, *J. Biol. Chem.* 1982, **257**, 6646.
191. H. Beinert, M. H. Emptage, J.-L. Dreyer, R. A. Scott, J. E. Hahn, K. O. Hodgson and A. J. Thomson, *Proc. Natl Acad. Sci. U.S.A.* 1983, **80**, 393.
192. T. R. Halbert, K. McGauley, W.-H. Pan, R. S. Czernuszewicz and E. I. Stiefel, *J. Am. Chem. Soc.* 1984, **106**, 1849.
193. C. H. Wei and L. F. Dahl, *J. Am. Chem. Soc.* 1968, **90**, 3960.
194. W. P. Bosman and H. G. M. van der Linden, *J. Chem. Soc., Chem. Commun.* 1977, 714.
195. I. G. Dance, L. J. Fitzpatrick, M. L. Scudder and D. Craig, *J. Chem. Soc., Chem. Commun.* 1984, 17.
196. I. G. Dance, L. J. Fitzpatrick and M. L. Scudder, unpublished results.
197. T. Greiser and E. Weiss, *Chem. Ber.* 1976, **109**, 3142.
198. W. J. Hu, D. Barton and S. J. Lippard, *J. Am. Chem. Soc.* 1973, **95**, 1170.
199. T. G. Fawcett, C.-C. Ou, J. A. Potenza and H. J. Schugar, *J. Am. Chem. Soc.* 1978, **100**, 2058.
200. A. J. Canty, C. L. Raston and A. H. White, *Aust. J. Chem.* 1978, **31**, 677.
201. W. Gaete, J. Ros, X. Solans, M. Font-Altaba and J. L. Brianso, *Inorg. Chem.* 1984, **23**, 39.
202. I. G. Dance, M. L. Scudder and R. Secomb, *Inorg. Chem.* 1985, **24**, 1201.
203. C. H. Wei, L. Marko, G. Bor and L. F. Dahl, *J. Am. Chem. Soc.*, 1973, **95**, 4840.
204. I. G. Dance, G. A. Bowmaker, G. R. Clark and J. K. Seadon, *Polyhedron* 1983, **2**, 1031; I. G. Dance and J. C. Calabrese, *Inorg. Chim. Acta* 1976, **19**, L41.
205. G. A. Bowmaker and L.-C. Tan, *Aust. J. Chem.* 1979, **32**, 1443.
206. G. A. Bowmaker, G. R. Clark and D. K. P. Yuen, *J. Chem. Soc., Dalton Trans.* 1976, 2329.
207. A. Muller, M. Romer, E. Krickemeyer and H. Bogge, *Naturwissenschaften* 1984, **71**, 43.
208. I. G. Dance and J. C. Calabrese, *J. Chem. Soc., Chem. Commun.* 1975, 762.
209. I. G. Dance, *J. Am. Chem. Soc.* 1979, **101**, 6264.
210. K. S. Hagen, D. W. Stephan and R. H. Holm, *Inorg. Chem.* 1982, **21**, 3928.
211. I. G. Dance and M. L. Scudder, unpublished results.
212. K. S. Hagen and R. H. Holm, *Inorg. Chem.* 1983, **22**, 3171.
213. J. L. Hencher, M. Khan, F. F. Said and D. G. Tuck, *Inorg. Nucl. Chem. Lett.* 1981, **17**, 287.
214. I. G. Dance, *Inorg. Chem.* 1981, **20**, 2155.
215. D. Coucouvanis, M. Kanatzidis, E. Simhon and N. C. Baenziger, *J. Am. Chem. Soc.* 1982, **104**, 1874.
216. P. A. W. Dean and J. J. Vittal, *J. Am. Chem. Soc.* 1984, **106**, 6436.
217. I. G. Dance and J. K. Saunders, *Inorg. Chim. Acta* 1985, **96**, L71.
218. I. G. Dance, A. E. Landers and M. L. Scudder, to be published.
219. A. Boardman, S. E. Jeffs, R. W. Small and I. J. Worrall, *Inorg. Chim. Acta* 1984, **83**, L39.
220. I. G. Dance, L. J. Fitzpatrick and M. L. Scudder, *Inorg. Chem.* 1985, **24**, 2547.
221. J. Bordas, M. H. J. Koch, H.-J. Hartmann and U. Weser, *FEBS Lett.* 1982, **140**, 19.
222. W. H. Armstrong and R. H. Holm, *J. Am. Chem. Soc.* 1981, **103**, 6246.
223. W. H. Armstrong, P. K. Mascharak and R. H. Holm, *Inorg. Chem.* 1982, **21**, 1699.
224. P. K. Mascharak, W. H. Armstrong, Y. Mizobe and R. H. Holm, *J. Am. Chem. Soc.* 1983, **105**, 475.
225. P. K. Mascharak, G. C. Papaefthymiou, W. H. Armstrong, S. Foner, R. B. Frankel and R. H. Holm, *Inorg. Chem.* 1983, **22**, 2851.
226. R. E. Palermo and R. H. Holm, *J. Am. Chem. Soc.* 1983, **105**, 4310.
227. W. Harrison, W. C. Marsh and J. Trotter, *J. Chem. Soc., Dalton Trans.* 1972, 1009.
228. J. R. Hall, D. A. Hirons and G. A. Swile, *J. Organomet. Chem.* 1979, **174**, 355.
229. T. G. Appleton and J. R. Hall, *Aust. J. Chem.* 1980, **33**, 2387.
230. I. G. Dance, *Aust. J. Chem.* 1978, **31**, 2195.
231. I. G. Dance, *J. Chem. Soc., Chem. Commun.* 1976, 68.
232. G. A. Bowmaker, G. R. Clark, J. K. Seadon and I. G. Dance, *Polyhedron* 1984, **3**, 535.
233. P. G. Edwards, R. W. Gellert, M. W. Marks and R. Bau, *J. Am. Chem. Soc.* 1982, **104**, 2072.

234. G. E. Coates and D. R. Ridley, *J. Chem. Soc.* 1965, 1870.
235. G. W. Adamson, N. A. Bell and H. M. M. Shearer, *Acta Cryst.* 1982, **B38**, 462.
236. I. G. Dance, *Inorg. Chem.* 1981, **20**, 1487.
237. R. G. Hayter and F. S. Humiec, *J. Inorg. Nucl. Chem.* 1964, **26**, 807.
238. N. Kunchur, *Acta Cryst.* 1968, **B24**, 1623.
239. R. O. Gould and M. M. Harding, *J. Chem. Soc.* (*A*) 1970, 875.
240. J. Suades, unpublished results cited in Ref. 201.
241. R. M. Taylor, PhD thesis, University of Edinburgh (1967).
242. E. W. Abel and B. C. Crosse, *J. Chem. Soc.* (*A*) 1966, 1377.
243. E. W. Abel and C. R. Jenkins, *J. Organomet. Chem.* 1968, **14**, 285.
244. F. G. Mann and D. Purdie, *J. Chem. Soc.* 1935, 1549.
245. H. Schafer, U. Wiese, K. Rinke and K. Brendel, *Angew. Chem., Int. Ed. Engl.* 1967, **2**, 253.
246. A. Yatsimirski and R. Ugo, *Inorg. Chem.* 1983, **22**, 1395.
247. K. Brodersen, G. Theile and H. G. Schnering, *Z. Anorg. Allg. Chem.* 1965, **337**, 120.
248. M. F. Pilbrow, *J. Chem. Soc., Dalton Trans.* 1975, 2432.
249. I. G. Dance, L. J. Fitzpatrick and M. L. Scudder, *Inorg. Chem.* 1984, **23**, 2276.
250. J. Sola, Y. Do, J. M. Berg and R. H. Holm, *J. Am. Chem. Soc.* 1983, **105**, 7784.
251. G. Christou, R. H. Holm, M. Sabat and J. A. Ibers, *J. Am. Chem. Soc.* 1981, **103**, 6269.
252. G. Christou, M. Sabat, J. A. Ibers and R. H. Holm, *Inorg. Chem.* 1982, **21**, 3518.
253. H. Strasdeit, B. Krebs and G. Henkel, *Inorg. Chem.* 1984, **23**, 1816.
254. G. Henkel, H. Strasdeit and B. Krebs, *Angew. Chem., Int. Ed. Engl.* 1982, **21**, 201.
255. M. G. Kanatzidis, W. R. Dunham, W. R. Hagen and D. Coucouvanis, *J. Chem. Soc., Chem. Commun.* 1984, 356.
256. W. Saak, G. Henkel and S. Pohl, *Angew. Chem., Int. Ed. Engl.* 1984, **23**, 150.
257. M. G. Kanatzidis, W. R. Hagen, W. R. Dunham, R. K. Lester and D. Coucouvanis, *J. Am. Chem. Soc.* 1985, **107**, 953.
258. D. Coucouvanis, M. Kanatzides, W. R. Dunham and W. R. Hagen, *J. Am. Chem. Soc.* 1984, **106**, 7998.
259. G. E. Coates and A. Lauder, *J. Chem. Soc.* (*A*) 1966, 264.
260. G. W. Adamson and H. M. M. Shearer, *J. Chem. Soc., Chem. Commun.* 1969, 897.
261. G. Henkel, P. Betz and B. Krebs, *J. Chem. Soc., Chem. Commun.* 1984, 314.
262. A. Muller, M. Romer, H. Bogge, E. Krickemeyer and D. Bergmann, *J. Chem. Soc., Chem. Commun.* 1984, 348.
263. M. H. Chisholm, J. A. Heppert and J. C. Huffman, *Polyhedron* 1984, **3**, 475.
264. (a) F. Cecconi, C. A. Ghilardi and S. Midollini, *J. Chem. Soc., Chem. Commun.* 1981, 640; (b) A. Agresti, M. Bacci, F. Cecconi, C. A. Ghilardi and S. Midollini, *Inorg. Chem.* 1985, **24**, 689.
265. C. Cecconi, C. A. Ghilardi and S. Midollini, *Inorg. Chim. Acta* 1982, **64**, L47.
266. F. Cecconi, C. A. Ghilardi, S. Midollini and A. Orlandini, *Inorg. Chim. Acta* 1983, **76**, L183.
267. F. Bottomley and F. Grein, *Inorg. Chem.* 1982, **21**, 4170.
268. G. Gervasio, R. Rossetti, P. L. Stanghellini and G. Bor, *Inorg. Chim. Acta* 1984, **83**, L9.
269. Footnote 10 in P. Betz, B. Krebs and G. Henkel, *Angew. Chem., Int. Ed. Engl.* 1984, **23**, 311.
270. M. L. Ziegler and J. Weiss, *Angew. Chem., Int. Ed. Engl.* 1970, **9**, 905.
271. M. Ishimori, T. Hagiwara, T. Tsuruta, Y. Kai, N. Yasuoka and N. Kasai, *Bull. Chem. Soc. Jpn* 1976, **49**, 1165.
272. S. Åkerstrom, *Acta Chem. Scand.* 1964, **18**, 1308.
273. S. Åkerstrom, *Ark. Kemi.* 1965, **24**, 505.
274. H. B. Burgi, H. Gehrer, P. Strickler and F. K. Winkler, *Helv. Chim. Acta* 1976, **59**, 2558.
275. P. J. M. W. L. Birker and H. C. Freeman, *J. Am. Chem. Soc.* 1977, **99**, 6890.
276. H. J. Schugar, C. Ou, J. A. Thich, J. A. Potenza, R. A. Lalancette and W. J. Furey, *J. Am. Chem. Soc.* 1976, **98**, 3047.
277. P. J. M. W. L. Birker, *Inorg. Chem.* 1979, **18**, 3502.
278. P. J. M. W. L. Birker, J. Reedijk and G. C. Verschoor, *Inorg. Chem.* 1981, **20**, 2877.
279. I. G. Dance, *J. Chem. Soc., Chem. Commun.* 1980, 818.
280. I. G. Dance, *Aust. J. Chem.* 1985, **38**, 1391.
281. G. Christou, K. S. Hagen and R. H. Holm, *J. Am. Chem. Soc.* 1982, **104**, 1744.
282. G. Christou, K. S. Hagen, J. K. Bashkin and R. H. Holm, *Inorg. Chem.* 1985, **24**, 1010.
283. G. Christou, C. D. Garner and F. E. Mabbs, *J. Chem. Soc., Chem. Commun.* 1978, 740.
284. G. Christou and C. D. Garner, *J. Chem. Soc., Dalton Trans.* 1980, 2354.
285. T. E. Wolff, J. M. Berg, K. O. Hodgson, R. B. Frankel and R. H. Holm, *J. Am. Chem. Soc.* 1979, **101**, 4140.
286. G. Christou, C. D. Garner, R. M. Miller and T. J. King, *J. Inorg. Biochem.* 1979, **11**, 349.
287. G. Christou, C. D. Garner, T. J. King, C. E. Johnson and J. D. Rush, *J. Chem. Soc., Chem. Commun.* 1979, 503.
288. G. Christou and C. D. Garner, *J. Chem. Soc., Chem. Commun.* 1980, 613.
289. T. E. Wolff, J. M. Berg, P. P. Power, K. O. Hodgson, R. H. Holm and R. B. Frankel, *J. Am. Chem. Soc.* 1979, **101**, 5454.

290. T. E. Wolff, P. P. Power, R. B. Frankel and R. H. Holm, *J. Am. Chem. Soc.* 1980, **102**, 4694.
291. T. E. Wolff, J. M. Berg, P. P. Power, K. O. Hodgson and R. H. Holm, *Inorg. Chem.* 1980, **19**, 430.
292. A. Choy, D. Craig, I. G. Dance and M. L. Scudder, *J. Chem. Soc., Chem. Commun.* 1982, 1246.
293. I. G. Dance, A. Choy and M. L. Scudder, *J. Am. Chem. Soc.* 1984, **106**, 6285.
294. S. Lacelle, W. C. Stevens, D. M. Kurtz, Jr, J. W. Richardson, Jr and R. A. Jacobson, *Inorg. Chem.* 1984, **23**, 930.
295. G. Schwartzenbach, K. Gautschi, J. Peter and K. Tunaboylu, *Trans. R. Inst. Technol., Stockholm* 1972, **271**, 295.
296. P. M. Dubois, W. C. Stevens, T. T. P. Heung, S. Lacelle, B. C. Gerstein and D. M. Kurtz, Jr *J. Am. Chem. Soc.* 1981, **103**, 4400.
297. R. A. Haberkorn, L. Que, Jr, W. O. Gillum, R. H. Holm, C. S. Liu and R. C. Lord, *Inorg. Chem.* 1976, **15**, 2408.
298. S. Hong, A. Olin and R. Hesse, *Acta Chem. Scand.* 1975, **A29**, 583.
299. I. G. Dance, *Inorg. Chim. Acta* 1977, **25**, L17.
300. P. Betz, B. Krebs and G. Henkel, *Angew. Chem., Int. Ed. Engl.* 1984, **23**, 311.
301. G. Marbach and J. Straehle, *Angew. Chem., Int. Ed. Engl.* 1984, **23**, 715.
302. I. G. Dance, P. J. Guerney, A. T. Baker, A. D. Rae and M. L. Scudder, *Aust. J. Chem.* (in press).
303. I. G. Dance, *J. Am. Chem. Soc.* 1980, **102**, 3445.
304. I. G. Dance, L. J. Fitzpatrick, A. D. Rae and M. L. Scudder, *Inorg. Chem.* 1983, **22**, 3785.
305. A. J. Canty, C. L. Raston and A. H. White, *Aust. J. Chem.* 1979, **32**, 311.
306. I. G. Dance and P. J. Guerney, *Aust. J. Chem.* 1981, **34**, 57.
307. A. P. Arnold and A. J. Canty, *Inorg. Chim. Acta* 1981, **55**, 171.
308. A. P. Arnold, A. J. Canty, B. W. Skelton and A. H. White, *J. Chem. Soc., Dalton Trans.* 1982, 607.
309. J. C. Bayon, M. C. Brianso, J. L. Brianso and P. Gonzalez Duarte, *Inorg. Chem.* 1979, **18**, 3478.
310. R. E. Marsh and V. Schomaker, *Inorg. Chem.* 1981, **20**, 299.
311. I. G. Dance, M. L. Scudder and R. Secomb, *Inorg. Chem.* 1983, **22**, 1794.
312. A. J. Canty, R. Kishimoto, G. B. Deacon and G. J. Farquharson, *Inorg. Chim. Acta* 1976, **20**, 161.
313. Ln = lanthanide: K. S. Gharia, M. Singh, S. Mathur, R. Roy and B. S. Sankhla, *Synth. React. Inorg. Met–Org. Chem.* 1982, **12**, 337.
314. D. A. Brown, W. K. Glass and B. Kumar, *J. Chem. Soc.* (*A*) 1969, 1510.
315. H. B. Burgi, *Helv. Chim. Acta* 1974, **57**, 513.
316. I. G. Dance and H. R. M. Banda, unpublished results.
317. P. A. W. Dean, J. J. Vittal and N. C. Payne, *Inorg. Chem.* 1985, **24**, 3594.
318. W. Clegg, I. L. Abrahams and C. D. Garner, *Acta Cryst.* 1984, **C40**, 1367.
319. P. M. Treichel, L. D. Rosenhein and M. S. Schmidt, *Inorg. Chem.* 1983, **22**, 3960.
320. C. G. Kuehn and H. Taube, *J. Am. Chem. Soc.* 1976, **98**, 689.
321. G. C. Christoph and M. Tolbert, Abstract P6, American Crystallographic Association Meeting, March 1980.
322. J. P. Collman, T. N. Sorrell, K. O. Hodgson, A. K. Kulsrestha and C. E. Strouse, *J. Am. Chem. Soc.* 1977, **99**, 5180.
323. D. W. Stephan, *Inorg. Chem.* 1984, **23**, 2207.
324. P. M. Boorman, K. A. Kerr, R. A. Kydd, K. J. Moynihan and K. A. Valentine, *J. Chem. Soc., Dalton Trans.* 1982, 1401.
325. H. W. Roesky, T. Gries, P. G. Jones, K.-L. Weber and G. M. Scheldrick, *J. Chem. Soc., Dalton Trans.* 1984, 1781.
326. I. Bernal, J. L. Atwood, F. Calderazzo and D. Vitali, *Isr. J. Chem.* 1977, **15**, 153.
327. J. Korp, I. Bernal, J. L. Atwood, F. Calderazzo and D. Vitali, *J. Chem. Soc., Dalton Trans.* 1979, 1492.
328. F. Calderazzo, D. Vitali, R. Poli, J. L. Atwood, R. D. Rogers, I. M. Cummings and I. Bernal, *J. Chem. Soc., Dalton Trans.* 1981, 1004.
329. J. L. Atwood, I. Bernal, F. Calderazzo, L. G. Canada, R. Poli, R. D. Rogers, C. A. Veracini and D. Vitali, *Inorg. Chem.* 1983, **22**, 1797.
330. E. W. Abel, A. R. Khan, K. Kite, K. G. Orrell, V. Sik, T. S. Cameron and R. W. Cordes, *J. Chem. Soc., Chem. Commun.* 1979, 713.
331. M. A. A. F. de C. T. Carrondo, P. M. Matias and G. A. Jeffrey, *Acta Cryst.* 1984, **C40**, 932.
332. E. I. Stiefel, K. F. Miller, A. E. Bruce, J. L. Corbin, J. M. Berg and K. O. Hodgson, *J. Am. Chem. Soc.* 1980, **102**, 3624.
333. J. M. Berg, D. J. Spira, K. O. Hodgson, A. E. Bruce, K. F. Miller, J. L. Corbin and E. I. Stiefel, *Inorg. Chem.* 1984, **23**, 3412.
334. M. M. Kadooka, L. G. Warner and K. Seff, *Inorg. Chem.* 1976, **15**, 812.
335. F. Bottomley, D. E. Paez and P. S. White, *J. Am. Chem. Soc.* 1982, **104**, 5651.
336. M. K. Cooper, P. A. Duckworth, M. Saporta and M. McPartlin, *J. Chem. Soc., Dalton Trans.* 1980, 570.
337. I. B. Benson, S. A. R. Knox, P. J. Naish and A. J. Welch, *J. Chem. Soc., Chem. Commun.* 1978, 878.
338. K. Watenpaugh and C. N. Caughlan, *Inorg. Chem.* 1966, **5**, 1782.
339. B. Kamenar and M. Penavic, *J. Chem. Soc., Dalton Trans.* 1977, 356.

340. S. D. Killops and S. A. R. Knox, *J. Chem. Soc., Dalton Trans.* 1978, 1260.
341. V. D. Patel, P. M. Boorman, K. A. Kerr and K. J. Moynihan, *Inorg. Chem.* 1982, **21**, 1383.
342. I. A. Benson, S. A. R. Knox, P. J. Naish and A. J. Welch, *J. Chem. Soc., Dalton Trans.* 1981, 2235.
343. E. W. Abel, S. K. Bhargava and K. G. Orrell, *Prog. Inorg. Chem.* 1984, **32**, 1.
344. M. H. Chisholm, *Polyhedron* 1983, **2**, 681.
345. K. C. Malhrotra and R. L. Martin, *J. Organomet. Chem.* 1982, **239**, 159.
346. F. Cecconi, C. A. Ghilardi and S. Middolini, *Inorg. Chem.* 1983, **22**, 3802.

Polyhedron Vol. 5, No. 5, pp. 1105–1108, 1986
Printed in Great Britain

0277–5387/86 $3.00+.00
Pergamon Journals Ltd

DIOXOURANIUM(VI) COMPLEXES OF 3-BENZAMIDORHODANINE AND ITS SUBSTITUTED DERIVATIVES

KAMAL M. IBRAHIM, ABD EL-HAMMID M. SHALLABY, ASHRAF A. EL-BINDARY and MOHSEN M. MOSTAFA*

Chemistry Department, Faculty of Science, Mansoura University, Egypt

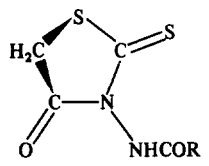
(*Received* 20 *August* 1985; *accepted* 7 *October* 1985)

Abstract—The synthesis and characterization of some dioxouranyl(VI) complexes containing 3-benzamidorhodanine and its substituted derivatives as ligands are reported. The structure of complexes is discussed on the basis of spectral (UV, IR and NMR), elemental analyses, conductivities, molecular weights and thermal analysis (DSC, DTA, TGA and TG) results. IR spectra show that the ligands are bidentate coordinating via the amide nitrogen (NH) and the carbonyl oxygen of rhodanine in the *enol* form with displacement of a proton from the latter group. Also, NMR studies suggest that the enolization and coordination occurs via the carbonyl oxygen of rhodanine and not through the carbonyl of the amide moiety. Finally, the thermal studies suggest the existence of a *cis*-form for the isolated uranyl complexes.

Although the coordination chemistry of the dioxouranyl(VI) ion has been studied extensively, no work including 3-benzamidorhodanine and its substituted derivatives as ligands has been reported. Also, in continuation of our earlier work[1–3] on the uranyl complexes and in view of the importance of these ligands in the inhibition of mycobacterium tuberculosis,[4] we report herein the preparation and characterization of some uranyl(VI) complexes by conventional physical and chemical methods. The possible mode of the complexes is discussed on the basis of IR, UV and NMR spectral data. Both *cis*- and *trans*-structures have been proposed for the isolated solid complexes but all the results are in favour of the former.

EXPERIMENTAL

The ligands (**1**) were synthesized as reported earlier.[4,5]



1

R = C_6H_5 (BR, m.p. 182°C), *o*-OH·C_6H_4 (OHBR, m.p. 96°C), *p*-Cl·C_6H_4 (PCBR, m.p. 176°C), *p*-CH_3O·C_6H_4 (PMEBR, m.p. 162°C), *o*-Cl·C_6H_4 (OCBR, m.p. 173°C), *p*-CH_3-C_6H_4 (PMBR, m.p. 162°C), or C_5H_4N (INR, m.p. 196°C).

Preparation and analysis of the complexes

A methanolic solution of uranyl acetate dihydrate (1 mmol) was added to a solution of the ligands under investigation (2 mmol) in MeOH. The reaction mixture was heated under reflux for 30 min. On cooling and scratching a red and/or orange precipitate (yield 70–85%) was formed. The precipitate was filtered off and washed with cold MeOH followed by Et_2O. The complexes separated from INR and OHBR were brown in colour. The

* Author to whom correspondence should be addressed.

elemental analyses were carried out in our laboratory (uranium was determined gravimetrically as U_3O_8).

Physical measurements

All measurements were carried out as reported earlier.[1–3] Thermogravimetric analysis was carried out using a GDTD 16 thermoanalyzer, Setaram, France.

RESULTS AND DISCUSSION

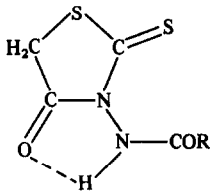
This study indicates that 3-benzamidorhodanine and its substituted derivatives form stable complexes with the formula $[UO_2(HL)_2(MeOH)_2]$ (where H_2L = bidentate monoanionic ligand). The complexes are insoluble in common organic solvents, partially soluble in MeOH and easily soluble in dimethylformamide (DMF) and dimethylsulphoxide (DMSO). The molar conductivities in DMSO at 25°C are in the 16–30 ohm^{-1} cm^2 mol^{-1} range, indicating a non-electrolytic nature.[6] The relatively high value (30 ohm^{-1} cm^2 mol^{-1}) for the complex $[UO_2(OCBR\text{-}H)_2(MeOH)_2]$ may suggest a partial dissociation in DMSO. The magnetic susceptibility measurements at room temperature indicate that the complexes are diamagnetic as expected. Molecular weight determinations suggest a monomeric structure for all complexes (Table 1).

The IR spectra of the free ligands show a broad band centred in the 3330–3220-cm^{-1} region assigned to ν(NH). The strong band in the 1765–1740-cm^{-1} and a shoulder in the 1770–1755-cm^{-1} region are both assigned to the free and hydrogen-bonded carbonyl oxygens of the rhodanine moiety. The strong band in the 1710–1660-cm^{-1} region is attributed to the carbonyl oxygen of the amide moiety. The broadness of the NH band as well as the existence of a shoulder which is characteristic for the carbonyl oxygen of the rhodanine moiety may suggest hydrogen bonding. Moers and coworkers[7] investigated the NMR spectra of rhodanine and its alkyl derivatives with Cu(I) salts and found two signals in the 13.18–13.04- and 4.45–4.32-ppm regions assigned to δ(NH) and $\delta(CH_2)$, respectively. Our ^1H NMR studies for the free ligands under investigation in d_6-DMSO also show two signals at δ 13.2–11.3 and 4.6–4.35 ppm which are similar to those observed by Moers.[7] Those signals are also assigned to the protons of NH and CH_2, respectively, in the spectra of the free ligands under investigation. The existence of the NH signal at high values downfield of TMS suggests strong hydrogen bonding. This bond occurs between NH and the

Table 1. Analytical and physical data

Compound	Colour	M.p. (°C)	Yield (%)	% Calc. (found) C	H	U	Molecular weight	Λ_m in DMSO (ohm^{-1} cm^2 mol^{-1})
$[UO_2(INR\text{-}H)_2(MeOH)_2]$	Brown	215	85	28.6 (28.9)	2.4 (2.9)	28.4 (28.2)	839 (805)	17.0
$[UO_2(BR\text{-}H)_2(MeOH)_2]$	Red	176	85	31.6 (31.3)	2.6 (2.7)	28.4 (28.7)	—	17.0
$[UO_2(OHBR\text{-}H)_2(MeOH)_2]$	Reddish-brown	223	85	30.4 (29.5)	2.6 (3.2)	27.4 (27.5)	869 (863)	13.0
$[UO_2(PCBR\text{-}H)_2(MeOH)_2]$	Red	192	70	29.2 (29.0)	2.2 (2.8)	26.3 (26.2)	906 (854)	18.0
$[UO_2(PMEBR\text{-}H)_2(MeOH)_2]$	Red	188	80	32.1 (32.2)	2.9 (3.2)	26.5 (26.5)	897 (909)	16.0
$[UO_2(OCBR\text{-}H)_2(MeOH)_2]$	Orange	199	75	29.2 (28.7)	2.2 (2.3)	26.3 (26.4)	906 (840)	30.0
$[UO_2(PMBR\text{-}H)_2(MeOH)_2]$	Red	202	70	33.3 (33.0)	3.0 (3.7)	27.6 (27.5)	—	—

carbonyl oxygen of rhodanine as in **2**.



2

The ligands are more likely coordinated in a bidentate fashion via NH and the enolized carbonyl oxygen of rhodanine with displacement of a proton from the latter group. This is supported by the following evidence.

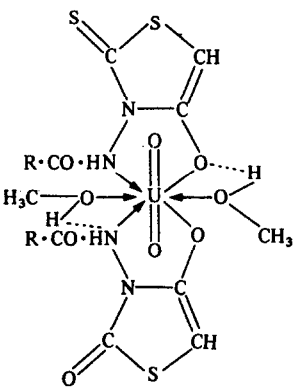
There is no ν(CO) of rhodanine and new bands at 1590 and 1190 cm^{-1}, assigned to ν(C=C) and ν(C—O),[8] appear. ν(NH) moves to a lower wavenumber. The thioketo-group bands remain more or less at the same positions. New bands in the 580–540- and 460–440-cm^{-1} regions are assigned to ν(UO)[9] and ν(UN),[10] respectively. The spectra of the uranyl(VI) complexes exhibit a strong band at 910 cm^{-1} characteristic of the asymmetric stretching frequency (ν_3) of the dioxouranium ion. The position of this band as well as the colour of the complexes (yellow or orange) indicates the participation of both N and O atoms in the coordination while the S atom is inert toward chelation.

The mode of coordination is also confirmed from the NMR data in which the NH signal is shifted to lower values (8.9–8.15 ppm) upfield of TMS. This indicates the destruction of the hydrogen bond as well as the coordination through the NH group. The disappearance of the CH_2 signal with the simultaneous appearance of a new signal in the 7.5–7.3-ppm region is attributed to the proton of the CH=C group. This signal is too close to the multiplet signals of the phenyl ring but is well-defined.

It is worth mentioning that the carbonyl oxygen of amide moiety is shifted, in the spectra of the ligand, to a higher wavenumber on complexation.[7] Although all the previous studies by others[11] for rhodanine and its related compounds with some divalent metal ions had shown that the carbonyl oxygen of rhodanine is inert in complexation, we are quite confident from the above discussion that this group is the backbone of chelation.

The UV spectra of the free ligands in Nujol mull show bands at 230, 250, 290, 315 and 380 nm assigned, respectively, to Ph → Ph*, $\pi \rightarrow \pi^*$ (phenyl), $n \rightarrow \pi^*$ (CO amide), $n \rightarrow \pi^*$ (CO rhodanine) and $n \rightarrow \pi^*$ (CS). The absence of the band due to $n \rightarrow \pi^*$ (CO rhodanine) on complexation with the simultaneous appearance of a new band in the 410–390-nm region is attributed to $\pi \rightarrow \pi^*$ (CH=C) as a sequence of enolization. Also, it can be taken as evidence for the participation of the carbonyl oxygen of rhodanine in chelation. Moreover, the bands due to $n \rightarrow \pi^*$ (CO amide) and $n \rightarrow \pi^*$ (CS) remain more or less at the same positions. Finally, the band in the 20,200–18,900-cm^{-1} range is assigned to a $^1E_g \rightarrow {}^3\pi_u$ transition.[12]

Differential scanning calorimetry as well as the thermal gravimetric analysis show two exothermic peaks before the melting points for all uranyl(VI) complexes. One peak is in the 80–77°C range and probably corresponds to the loss of one methanol molecule which is attached to NH(O—H...N) group (structure **3**). The second peak is in the 125–117°C range and represents the removal of the second methanol molecule which is linked to the C—O group (O—H...O). This observation indicates that the two coordinated methanol molecules are not identical and their positions within the complex are different. Also, the existence of two different protons for the methyl and hydroxyl resonances in the NMR spectra of the uranyl complexes coincides with the data obtained from the thermal analyses. Moreover, the observation of two signals due to the protons of the free and hydrogen-bonded NH, in the NMR spectra of the complexes, in the 8.85–8.15- and 8.9–8.25-ppm regions, respectively. All these may suggest the existence of the *cis*-form rather than the *trans*-form as shown in **3**.



3

All the results are in favour of our previous studies.[1–3] The pale-colour uranyl(VI) complexes (yellow or orange) contain N and O as donor atoms while those dark in colour (brown and black) must contain an S atom as a potential site in addition to both N and/or O atoms. Also, thermogravimetric

analyses show that the mass loss of the uranyl complexes is in accordance with the *cis*-form and the existence of two different coordinated methanol molecules.

REFERENCES

1. A. M. Shallaby, M. M. Mostafa, K. M. Ibrahim and M. N. H. Moussa, *Spectrochim. Acta* 1984, **40A**, 999.
2. A. M. Shallaby, K. M. Ibrahim, A. A. El-Bindary and M. M. Mostafa, *Transition Met. Chem.* 1985, **10**, 328.
3. K. M. Ibrahim, A. M. Shallaby, A. A. El-Bindary and M. M. Mostafa, unpublished results.
4. S. Tadashi and O. Masaki, *J. Pharm. Soc. (Jpn)* 1955, **75**, 1535.
5. F. C. Brown, C. K. Bradsher, E. C. Morgan, M. Tetenbaum and P. Wilder, *J. Am. Chem. Soc.* 1956, **78**, 384.
6. W. J. Geary, *Coord. Chem. Rev.* 1971, **7**, 81.
7. F. G. Moers and J. J. Steggerda, *J. Inorg. Nucl. Chem.* 1981, **30**, 3217.
8. N. S. Biradar, B. R. Patil and V. H. Kulkarni, *J. Inorg. Nucl. Chem.* 1975, **37**, 1901.
9. K. Nakamoto, *Infrared Spectra of Inorganic and Coordination Compounds.* Wiley, New York (1970).
10. J. R. Ferraro, *Low Frequency Vibrations of Inorganic and Coordination Compounds.* Plenum, New York (1971).
11. F. G. Moers, J. W. M. Goossens and J. P. M. Langhout, *J. Inorg. Nucl. Chem.* 1973, **35**, 855.
12. P. McGlynn, J. K. Smith and W. C. Neely, *J. Mol. Spect.* 1961, **6**, 164.

Polyhedron Vol. 5, No. 5, pp. 1109–1110, 1986
Printed in Great Britain

0277–5387/86 $3.00+.00
Pergamon Journals Ltd

LATTICE ENERGIES OF THE ALKALI METAL BIFLUORIDES: A CORRECTION

JOHN EMSLEY

Department of Chemistry, King's College, Strand, London WC2R 2LS, U.K.

and

DAVID A. JOHNSON*

Department of Chemistry, The Open University, Milton Keynes MK7 6AA, U.K.

(*Received* 5 *August* 1985; *accepted* 9 *October* 1985)

Abstract—Revised auxiliary thermodynamic data allow an improvement in the lattice energies of the alkali metal and ammonium bifluorides which were calculated in a previous paper (*Polyhedron* 1985, **4**, 489). The lattice energies of the bifluorides now exceed those calculated by classical ionic models, but the difference between the lattice energies of the fluorides and bifluorides decreases steadily with increasing cation size.

The results of Ref. 1 have been recalculated with the following modifications:

(i) Apart from $\Delta H_f^\circ(F^-)(g) = -255.1 \pm 2$ kJ mol^{-1} calculated from the electron affinity[2,3] and dissociation energy[4] of fluorine, and the ion cyclotron resonance measurement,[5] all auxiliary data were taken from Ref. 6.

(ii) The lattice energies of MHF_2 and MF, written as $\Delta H_L^\circ(MX)(s)$ and expressed as enthalpies at 298.15 K, were calculated from equations of the type:

$$\Delta H_L^\circ(MX)(s) = \Delta H_f^\circ(M^+)(g) + \Delta H_f^\circ(X^-)(g) - \Delta H_f^\circ(MX)(s). \quad (1)$$

(iii) Values of the thermochemical radius of HF_2^- were calculated from the two-term rather than the one-term Kapustinskii equation.[7(a)]

The results are given in Table 1, together with some of the auxiliary data, and ΔU, the difference between the lattice enthalpies of the fluorides and bifluorides.

The important differences from the figures calculated in Ref. 1 are as follows: firstly, the cycle values of $\Delta H_L^\circ(MHF_2)(s)$ are higher by amounts varying from 28 to 53 kJ mol^{-1}. They now exceed the highest theoretically calculated sums of the coulombic, repulsive and dispersion energies[8] by some 40 kJ mol^{-1}.

Secondly, ΔU now decreases regularly with cation radius in accordance with very crude ionic models.[7(b)] Nevertheless, the decrease is not so severe as to invalidate a major conclusion of Ref. 1: there is no sound basis for the assignment of equal lattice energies to $[N(CH_3)_4]F$ and $[N(CH_3)_4]HF_2$. Consequently the fairly good agreement between the value of ΔH_m° for the process:

$$HF(g) + F^-(g) = HF_2^-(g),$$

which was obtained by making this assumption,[9] and the ion cyclotron resonance value,[5] is probably due to an inaccurate determination of the value of ΔH_m° for the reaction:

$$[N(CH_3)_4]F(s) + HF(g) = [N(CH_3)_4]HF_2(s).$$

Thirdly, the values of $r(HF_2^-)$ in Table 1 span only 5 pm and average 145 pm. If this is combined with $r(NH_4^+) = 146$ pm,[10] and substituted in the two-term Kapustinskii equation, we find $\Delta H_L^\circ(NH_4HF_2)(s) = 735$ kJ mol^{-1}. To obtain a cycle value for comparison, we derive $\Delta H_f^\circ(NH_4^+)(g) = 638 \pm 6$ kJ mol^{-1} from the photo-ionization proton affinity of Ceyer *et al.*[11] This choice lies comfortably within the range spanned by other experimental values,[12,13] and, with the help of eqn (1),

* Author to whom correspondence should be addressed.

Table 1. Thermodynamic properties of the alkali metal bifluorides and fluorides

	Li	Na	K	Rb	Cs
$-\Delta H_f^\circ(MHF_2)(s)$ (kJ mol^{-1})	942.3	920.3	927.7	922.6	923.8
$\Delta H_f^\circ(M^+)(g)$ (kJ mol^{-1})	685.8	609.4	514.3	490.1	458.0
$\Delta H_L^\circ(MHF_2)(s)$ (kJ mol^{-1})	939	841	753	724	693
$r(M^+)$ (pm)	74	102	138	149	170
$r(HF_2^-)$ (pm)	144	147	145	147	142
$-\Delta H_f^\circ(MF)(s)$ (kJ mol^{-1})	616.0	573.6	567.3	557.7	553.5
$\Delta H_L^\circ(MF)(s)$ (kJ mol^{-1})	1047	928	827	793	756
ΔU (kJ mol^{-1})	108	87	74	69	64

it yields $\Delta H_L^\circ(NH_4HF_2)(s) = 752 \pm 9$ kJ mol^{-1}. This exceeds the value estimated from the Kapustinskii equation by nearly 20 kJ mol^{-1}, a discrepancy which is reinforced by noting that, although the ionic radius of NH_4^+ is significantly larger than that of K^+, the cycle lattice energies of KHF_2 and NH_4HF_2 are virtually identical. However, the discrepancy is readily explained as a stabilization of NH_4HF_2 by cation–anion hydrogen-bonding, a phenomenon whose structural consequences have been noted by Pauling.[14]

REFERENCES

1. J. Emsley, *Polyhedron* 1985, **4**, 489.
2. H. P. Popp, *Z. Naturforsch.* 1967, **A22**, 254.
3. R. M. Milstein and S. R. Berry, *J. Chem. Phys.* 1971, **55**, 4146.
4. CODATA Task Group, *J. Chem. Thermodyn.* 1978, **10**, 903.
5. J. W. Larson and T. B. McMahon, *J. Am. Chem. Soc.* 1982, **104**, 5848.
6. D. D. Wagman, W. H. Evans, V. B. Parker, R. H. Schumm, I. Halow, S. M. Bailey, K. L. Churney and R. L. Nuttall, *The NBS Tables of Chemical Thermodynamic Properties.* American Chemical Society (1982).
7. D. A. Johnson, *Some Thermodynamic Aspects of Inorganic Chemistry*, 2nd Edn: (a) p. 48; (b) Chap. 3. Cambridge University Press, Cambridge (1982).
8. H. D. B. Jenkins and K. F. Pratt, *J. Chem. Soc., Faraday Trans. 2* 1977, **73**, 812.
9. S. A. Harrel and D. H. McDaniel, *J. Am. Chem. Soc.* 1964, **86**, 4497.
10. R. D. Shannon and C. T. Prewitt, *Acta Cryst.* 1970, **B26**, 1046.
11. S. T. Ceyer, P. W. Tiedemann, B. H. Mahan and Y. T. Lee, *J. Chem. Phys.* 1979, **70**, 14.
12. S. G. Lias, D. M. Shold and P. Ausloos, *J. Am. Chem. Soc.* 1980, **102**, 2540.
13. H. M. Rosenstock, R. Buff, M. A. A. Ferriera, S. G. Lias, A. C. Parr, R. L. Stockbauer and J. L. Holmes, *J. Am. Chem. Soc.* 1982, **104**, 2337.
14. L. Pauling, *The Nature of the Chemical Bond*, 3rd Edn, p. 462. Cornell University Press, Ithaca, NY (1960).

Polyhedron Vol. 5, No. 5, pp. 1111–1118, 1986
Printed in Great Britain

0277–5387/86 $3.00+.00
Pergamon Journals Ltd

SPATIAL NOTATION FOR TRANSITION-METAL CLUSTERS

TIEN-YAU LUH* and HENRY N. C. WONG

Department of Chemistry, The Chinese University of Hong Kong, Shatin, N.T., Hong Kong

and

BRIAN F. G. JOHNSON

University Chemical Laboratory, Lensfield Road, Cambridge CB2 1EW, U.K.

(*Received* 2 *September* 1985; *accepted* 14 *October* 1985)

Abstract—By the use of a modified Föppl notation and replacement methods, the spatial distribution for metal nuclei and ligands of metal clusters can unequivocally be assigned. For example, the notation for $H_2Os_3(CO)_{10}$ can be written as σ^1_1,σ^1_5-H-[3]-[(2):2:(4):2:(2)].

Metal clusters demonstrate an enormous variety of nuclearity with fascinating structural complexity.[1] Ingenious and practical approaches have been made by several research groups in connection with the systematic classification of clusters concerning their electron numbers and bonding properties.[2–17] These methods are useful in discerning the arrangement of the metal nuclei. However, there is no simple method by which the relative positions of metal nuclei and ligands may be described. Indeed, the description of the spatial distribution of these species in metal clusters is a nontrivial problem.[18] Here, it is our intention to put forth a relatively simple notation system which permits a useful method of describing clusters.[19]

Numerous examples in the literature demonstrates that the ligands in clusters occupy positions that define the vertices of regular and semiregular polyhedra.[1] The Föppl notation[20] has been employed for illustrating the structure and fluxional behaviour of binary metal carbonyls.[21] The basic idea of this approach is to consider a metal polyhedron sitting inside a ligand polyhedron envelope. We felt that this could be applied to the systematic description of cluster structures.

The following rules are hence proposed:

Rule 1

The structures of metal and ligand polyhedra are described by an appropriately modified Föppl notation (*Table* 1) *written in sequence in square brackets with a hyphen between the brackets. The notation therefore has the general form* $[m_1:\ldots:m_p:\ldots:m_n]$-$[l_1:\ldots:l_i:\ldots:l_z]$.

In this paper, the metallic part of a cluster may be constituted by one or more metal atoms. Thus, the term "metal polyhedron" will also designate not only polyhedra in the geometrical sense but also an isolated atom or groups of two or three atoms which, in the geometrical sense, do not constitute polyhedra.

By the use of this rule, the mononuclear metal carbonyls $Ni(CO)_4$ (1), $Fe(CO)_5$ (2) and $Mo(CO)_6$ (3) can be expressed as [1]-[1:3], [1]-[1:3:1], and [1]-[1:4:1], respectively (Fig. 1).

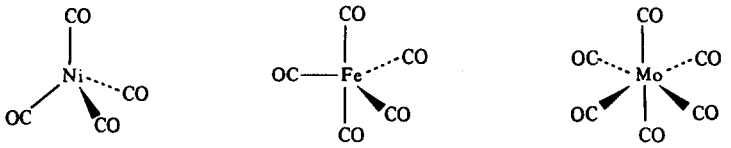
Table 1. Modified Föppl notation[1(d),20]

n	Designates planar polygon with *n* vertices
(*n*)	Designates planar polygon with *n* vertices which is in an anti-prismatic configuration to a previously assigned *n*-vertex polygon.[a]
n'	Designates a polygon of *n* vertices which is not strictly planar.[b]

[a] Cf. Rule 3 and Fig. 2.

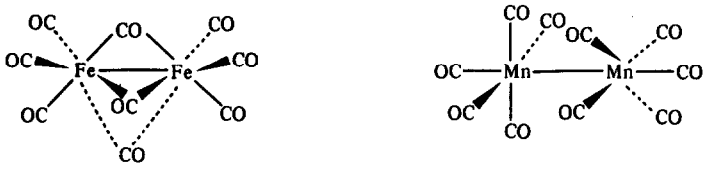
[b] *n'* must be even. Therefore, an *n'* polygon can also be described as two anti-prismatic *n'*/2 polygons. Hence, for example, the chair-form of a hexagon which constitutes two anti-prismatic triangles is named as 6' rather than 3:(3). Cf. Fig. 1.

* Author to whom correspondence should be addressed.

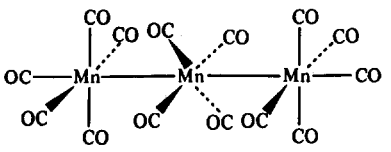


1 2 3

Fig. 1. Structures of $Ni(CO)_4$(1), $Fe(CO)_5$ (2) and $Mo(CO)_6$ (3).



4 5



6

Fig. 2. Structures of $Fe_2(CO)_9$ (4), $Mn_2(CO)_{10}$ (5) and $[Mn_3(CO)_{14}]^{2-}$ (6).

Rule 2

All metal polyhedra are numbered along the principal rotation axis.[22]

Thus, the notation [1 : 1] rather than [2] is used to define the metal polyhedron in the dinuclear metal complexes $Fe_2(CO)_9$ (4) and $Mn_2(CO)_{10}$ (5). Similarly, [1 : 1 : 1] is employed to demonstrate a linear three metal nuclei, $[Mn_3(CO)_{14}]^{2-}$ (6) (Fig. 2). In a similar manner, tetrahedron, butterfly skeleton and puckered four-membered ring skeletons are distinguished by the notations [1 : 3], [2 : (2)] and [4′], respectively (Fig. 3).

Rule 3

Viewing along the principal rotation axis two eclipsed lines, or one polygon having at least one edge which is parallel to a line, or two polygons having at least one pair of eclipsed edges are considered as prismatic. Otherwise, they are denoted as antiprismatic (*see Table* 1). Some graphic representations of various arrangements are presented in Fig. 4.

Polygons need not necessarily be regular. They can also be puckered, and in this case the projection on the plane perpendicular to the principal rotation axis will be considered.

The use of this rule is particularly useful to identify whether there exist bridging ligands or not. To illustrate, considering a metal triangle inside a ligand hexagon, two commonly seen orientation patterns in metal clusters are shown in Fig. 5. In the first case [Fig. 5(a)], the two polygons are prismatic and can be denoted as [3]-[6]. When clusters have such spatial arrangement, all of these six ligands are terminal. On the other hand, when three of these six ligands are bridging ligands, the two polygons are then antiprismatic as shown in Fig. 5(b), and are represented by the notation [3]-[(6)].

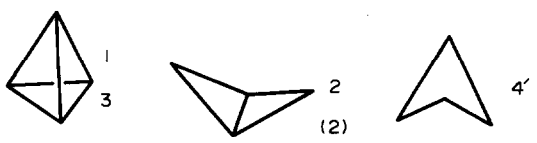


Fig. 3. Föppl notations for tetrahedron, butterfly and puckered four-membered ring skeletons.

Rule 4

A metal polyhedron is considered as a basic set. The orientation of the planes defined by the polygons in the ligand polyhedron is related to this basic set.

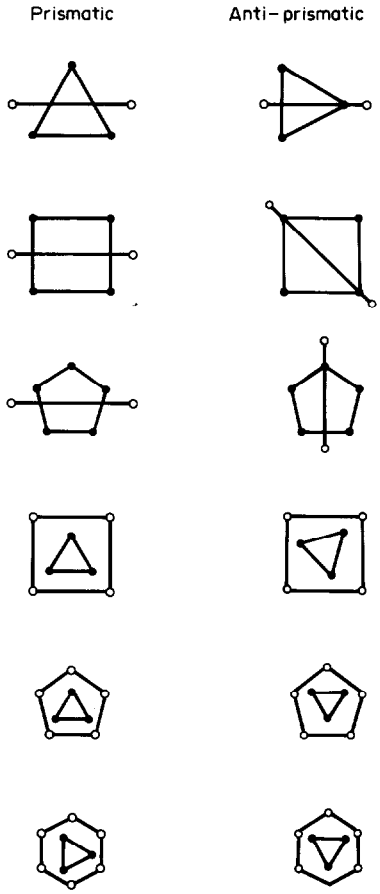


Fig. 4. Graphic representations of prismatic (a) and anti-prismatic (b) arrangements.

Rule 5

The plane of the polygon (or the line) defined by the very first number, l_i, *which is larger than or equal to 2 in the modified Föppl notation of the ligand polyhedron should be parallel to the plane of the polygon (or the line) defined by the first number,* m_i, *which is larger than or equal to 2, of the metal polyhedron. Hence, the polygon* m_i *defines the orientation of the polygon* l_i, *which, in turn, defines the orientation of the rest of the polygons in the ligand polyhedron.*

Considering **4**, the triangle formed by the three bridging COs is anti-prismatic to those defined by other two sets of three terminal CO ligands.

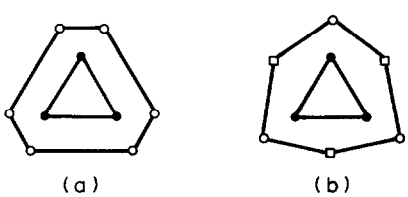


Fig. 5. Two orientation patterns of a triangle inside a hexagon.

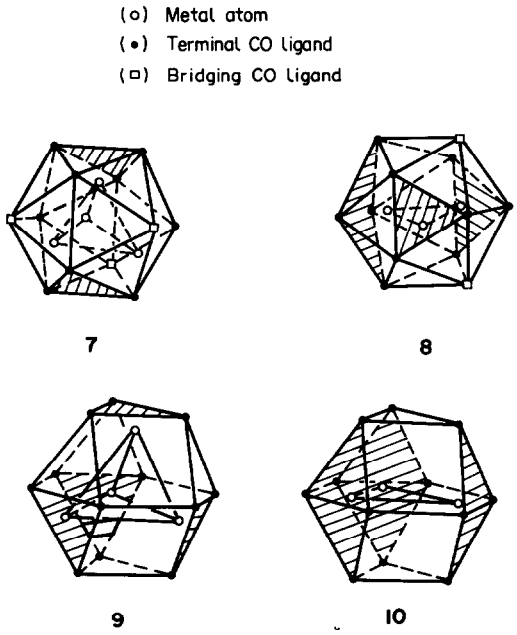


Fig. 6. Structures of $Co_4(CO)_{12}$ (**7**), $Fe_3(CO)_{12}$ (**8**), $Ir_4(CO)_{12}$ (**9**) and $Os_3(CO)_{12}$ (**10**).

Consequently, the ligand polyhedron in **4** is denoted as [3:(3):3] and the notation for **4** is [1:1]-[3:(3):3]. In a similar manner, the notations for **5** and **6** can be written as [1:1]-[1:4:(4):1] and [1:1:1]-[1:4:(4):4:1], respectively.

The CO ligands in either $Co_4(CO)_{12}$ (**7**) or $Fe_3(CO)_{12}$ (**8**) form an eicosahedron (Fig. 6). On the other hand, the 12 COs in $Ir_4(CO)_{12}$ (**9**) or $Os_3(CO)_{12}$ (**10**) occupy the vertices of an anticuboctahedron (Fig. 6). Therefore, $m_i = 3$. The ligand polyhedron is represented by [3:(6′):(3)], where $l_i = 3$ and the triangle defined by the last number, which is (3), is anti-prismatic to that defined by l_i. Moreover, the two triangles formed by m_i and l_i are also anti-prismatic. Consequently, the notation for **7** should be [1:3]-[(3):6′:3]. It is noteworthy that the 6′-polygon in the ligand envelop is also anti-prismatic to the 3-polygon, or triangle, in the metal polyhedron. In other words, three out of six vertices of the ligand 6′-polygon are anti-prismatic to the three vertices of the metal 3-polygon. Therefore, three COs are sitting as bridging ligands. The ligand eicosahedron in **8** can be represented by [2:(2):4:(2):2] and l_i is anti-prismatic to the triangle defined by three metal atoms. Thus, the notation for **8** should be [3]-[(2):2:(4):2:(2)].

Similarly, the notations for **9** and **10** can be expressed by [1:3]-[(3):(6):3] and [3]-[3:6:3], respectively.

The application of these rules to symbolize various binary clusters is given in Table 2.

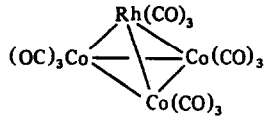
Table 2. Some notations for binary metal clusters

Formula	Notation	Reference
$Ni(CO)_4$	[1]-[1:3]	24
$Fe(CO)_5$	[1]-[1:3:1]	25
$Mo(CO)_6$	[1]-[1:4:1]	26
$Fe_2(CO)_9$	[1:1]-[3:(3):3]	27
$Mn_2(CO)_{10}$	[1:1]-[1:4:(4):1]	28
$[Mn_3(CO)_{14}]^{2-}$	[1:1:1]-[1:4:(4):4:1]	29
$Fe_3(CO)_{12}$	[3]-[(2):2:(4):2:(2)]	30
$Os_3(CO)_{12}$	[3]-[3:6:3]	31
$Re_3Cl_{12}^{3-}$	[3]-[3:(6):3]	32
$[Ni_3(CO)_6]^{2-}$	[3]-[(6')]	33
$Co_4(CO)_{12}$	[1:3]-[(3):6':3]	34
$Ir_4(CO)_{12}$	[1:3]-[(3):(6):3]	35
$[Fe_4(CO)_{13}]^{2-}$	[1:3]-[(3):3:6:1]	36
$Re_4(CO)_{16}$	[4]-[4:8:4]	37
$[Ni_5(CO)_{12}]^{2-}$	[1:3:1]-[(3):6:(3)]	38
$Os_5(CO)_{16}$	[1:3:1]-[(3):3:4:3:(3)]	39
$Mo_5Cl_{13}^{2-}$	[1:4]-[1:(4):(8')]	40
$Ni_6(CO)_{12}$	[3:3]-[(6'):(6')]	33
$Pt_6(CO)_{12}$	[3:3]-[(6):(6)]	41
$[Co_6(CO)_{14}]^{4-}$	[1:4:1]-[1:(4):4:(4):1]	42
$Rh_6(CO)_{16}$	[1:4:1]-[2:(2):4:4:2:(2)]	43
$[Os_6(CO)_{18}]^{2-}$	[1:4:1]-[3:6':(6'):3]	44
$[(Nb_6Cl_{12})Cl_6]^{2-}$	[1:4:1]-[1:4:(8):4:1]	45

Rule 6

Clusters containing more than one kind of metal nuclei or ligands are first considered as binary system. When the majority of vertices of a polyhedron is occupied by one kind of metal nuclei (or ligands), this polyhedron is first treated as if all vertices were occupied by these single metal nuclei (or ligands). A replacement method[18] *is employed to treat the other metal nuclei (or ligands), which are henceforth named as heteronuclei (or heteroligands).*

For example, the C_2H_4 ligand in $Fe(CO)_4(C_2H_4)$ is considered to be a replacement of a CO ligand in $Fe(CO)_5$. The rhodium nucleus in $Co_3Rh(CO)_{12}$ (**11**) is similarly regarded as a replacement (Fig. 7).



11

Fig. 7. Structure of $Co_3Rh(CO)_{12}$ (**11**).

* Bidentate and polydentate ligands will be treated in the future.

Rule 7

When clusters contain an equal number of N *nuclei, the one with the highest atomic number is chosen as the basic element for the metal polyhedron. The other metal nuclei are considered as replacement(s) of the metal polyhedron. Monodentate ligands are treated similarly according to the Cahn–Ingold–Prelog sequence rule.*[23]*

To illustrate, the basic element for the metal polyhedron of $Os_2Co_2(CO)_{12}H_2$ is osmium. This polyhedron is hence considered to constitute four osmium atoms and two of which are replaced by cobalt nuclei.

In a similar manner, the basic element for the ligand polyhedron of $Ni(CO)_2(PPh_3)_2$ is PPh_3.

Rule 8

When there are more than one equivalent principal rotation axes in the metal polyhedron containing heteronuclei, the axis is chosen such that the numbering (see Rules 11–13) *for the heteronuclei is minimum. For homonuclear clusters containing heteroligands, the principal rotation axis is similarly selected such that the numbering (see Rules* 11–13) *for the heteroligand becomes the smallest possible number.*

The use of this rule is illustrated in Fig. 8. The

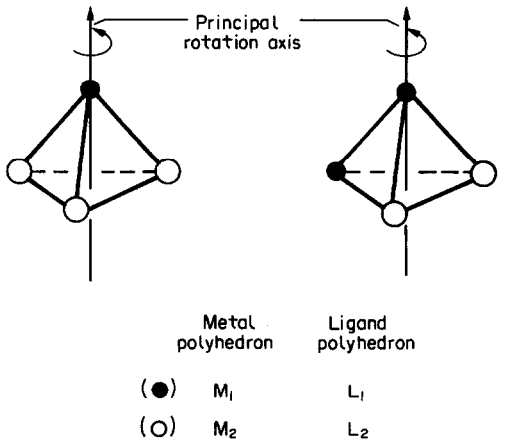


Fig. 8. Diagrammatic expression of the principal rotation axis for heteronucleus- or heteroligand-replaced tetrahedron. M_2s or L_2s in both cases are treated as basic elements.

principal rotation axis is chosen such that the numbering for the heteronuclei M_1 is smallest.

Taking $Ni(CO)_2(PPh_3)_2$ as an example, the principal rotation axis is shown in Fig. 8 where L_1 is CO.

Rule 9

The positions of heteronuclei and heteroligands are represented by $\Delta^{p}_{m_i}$ *and* $\sigma^{q}_{l_i}$,* *respectively.* Δ_{m_i}*s denote the layers defined by the polygons* $m_1, m_2, \ldots m_n$ *occupied by heteronuclei and* σ_l*s denote the layers defined by the polygons* $l_1, l_2, \ldots l_z$ *occupied by the heteroligands. The superscripts* p *and* q *are numerals representing the relative positions of heteronuclei or heteroligands belonging to each layer.*

The definition of Δ_{m_i} or σ_{l_i} can best be represented by the illustration shown in Fig. 9. The four layers of the eicosahedron are defined.

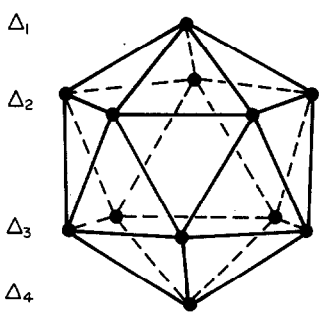


Fig. 9. Spatial notation for layers of eicosahedron.

* The symbol Δ is used because most metal polyhedra in metal clusters are *deltahedra*. The letter σ is employed for ligands from Greek συν- which means together, and from συμπερτλαμβανω which means to include.



12 **13**

Fig. 10. Structures of two isomers of $Fe(CO)_4(PPh_3)$ (**12** and **13**).

Rule 10

The clusters can thus be represented by the general notation $\Delta^{1}_{m_1}\cdots$-M_a-$\Delta^{p}_{m_m}\cdots$-$M_b \ldots \sigma^{q}_{l_i}\cdots$-$L_a$-$\sigma^{z}_{l_j}\cdots$-$L_b \ldots$-$[m_1 : \ldots : m_l : \ldots : m_n]$-$[l_1 : \ldots : l_i : \ldots : l_z]$, *where* M_a, $M_b, \ldots$ *are atomic symbols of heteronuclei, and* L_a *and* L_b *are formulae of heteroligands.*

Rule 11

For clusters having more than one kind of heteronuclei in a polygon layer m_l, *the positions of these heteronuclei are designated as* $\Delta^{1}_{m_1}$-M_a-$\Delta^{p}_{m_1}$-M_b- ... *if* $M_a \neq M_b \ldots$ *or* $\Delta^{1,p\cdots}_{m_1}$-M_a *if* $M_a = M_b \ldots$. *Smallest possible numbers* p ..., *which are counted clockwise, are used. For a polygon layer occupied by only one kind of heteronuclei, superscripts* 1, p, ... *can be omitted. A similar treatment is used for a ligand polyhedron.*

For example, the assignments of the position(s) of heteroligands for the two isomeric structures of $Fe(CO)_4(PPh_3)$ (**12** and **13**) can be denoted as σ_1- and σ^{1}_{2}-PPh_3-[1]-[1 : 3 : 1], respectively (Fig. 10).

Similarly, the notation for **11** is Δ_1-Rh-[1 : 3]-[(3) : 6′ : 3] (Fig. 7).

Rule 12

For clusters having more than one kind of heteronuclei belonging to different polygon layers Δ_{m_1}, $\Delta_{m_m} \ldots$ *with the numbering in the* Δ_{m_1} *layer defined (Rule* 11), *the numbering in* $\Delta_{m_m} \ldots$ *layers is related to that in the* Δ_{m_1} *layer. The vertex of the polygon* m_1 *which is closest to the project point of the* $\Delta^{1}_{m_1}$ *to* Δ_{m_m} *layer, when counting clockwise, is assigned as* $\Delta^{1}_{m_m}$, *and the numbering of the remaining vertices of the polygon in the* Δ_{m_m} *layer is thus defined. The position(s) of heteroligands can be located in a similar manner by using a metal polyhedron as the basis.*

The use of these rules for numbering polyhedra is illustrated in Fig. 11. The positions of the two triangles in the triprism [Fig. 11(a)] can be denoted in a straightforward manner. Nevertheless, for the trigonal antiprism [Fig. 11(b)], Δ^{1}_{2} is thus located by the use of Rule 12. Figure 12 shows that a tetrahedron is sitting inside an anticuboctahedron.

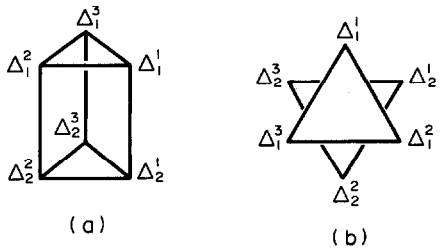
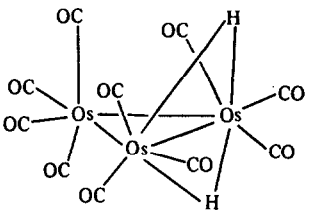


Fig. 11. Numbering for two triangles in prismatic (a) and anti-prismatic (b) orientation.



17

Fig. 14. Structure of $H_2Os_3(CO)_{10}$ (**17**).

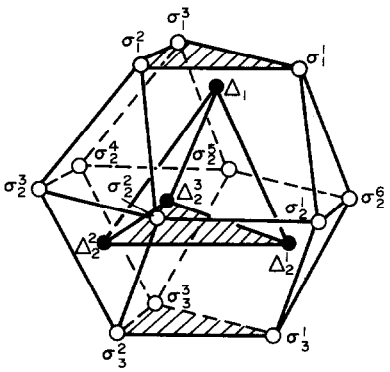


Fig. 12. Numbering for a tetrahedron inside an anti-cuboctahedron.

The notation for the binary system having such structure can be written as [1:3]-[3:6:3]. The numberings for the central tetrahedron is trivial. The planes of σ_1 and σ_3 triangles are in a prismatic relation to the plane of the Δ_2 triangle. Accordingly the numbering for these triangles can easily be assigned. The hexagon layer (σ_2), on the other hand, is anti-prismatic to these three-membered rings. Hence, the σ_2^1 position is first designated according to Rules 11 and 12, and the numberings for the remaining vertices of the hexagon can easily be ascribed.

Rule 13

For two or more than two layers, Δ_{m_1,m_m}, . . . , *occupied by only one kind of heteronuclei, the symbol(s) can be simplified and written as* Δ_{m_1,m_m}... . *Heteroligands are treated similarly.*

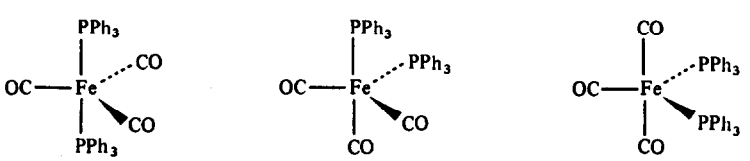
Considering three isomeric structures of $Fe(CO)_3(PPh_3)_2$ (**14–16**), they can be denoted at $\sigma_{1,3}$-, σ_1,σ_2^1- and $\sigma_2^{1,2}$-PPh_3-[1]-[1:3:1], respectively (Fig. 13).

A bridged hydride is also regarded as a replacement. To illustrate this, the 10 COs and two Hs in $H_2Os_3(CO)_{10}$ (**17**) form an eicosahedron (Fig. 14). Thus, the two Hs can be treated as substituents, and the spatial arrangement for $H_2Os_3(CO)_{12}$ is similar to that for $Fe_3(CO)_{12}$ (**8**). Hence the notation for **17** should be σ_1^1,σ_5^1-H-[3]-[(2):2:(4):2:(2)].

Examples of the use of these rules for denoting metal clusters containing heteronuclear or heteroligands are shown in Table 3.

In order to specify the structure of a metal cluster, we propose to combine its formula with its notation. For example, triiron dodecacarbonyl (**8**) can be written as $Fe_3(CO)_{12}$:[3]-[(2):2:(4):2:(2)]. More precisely, when a formal nomenclature is required, $Fe_3(CO)_{12}$ can also be called triiron[3]-dodecacarbonyl[(2):2:(4):2:(2)]. For a heteronuclear cluster, for instance, $H_3CoRu_3(CO)_{12}$ can be denoted as $H_3CoRu_3(CO)_{12}$: Δ_1-Co-σ_3-H-[1:3]-[3:6:(3):3] or Δ_1-Co-cobalttriruthenium[1:3]-σ_3-H-trihydridododecacarbonyl-[3:6:(3):3].

In summary, we have depicted rules for naming transition-metal clusters. At the present stage, clusters with some kind of symmetry can easily and unequivocally be described. We are currently extending this system in the hope of naming "unsymmetrical" clusters.



14 **15** **16**

Fig. 13. Structures of three isomers of $Fe(CO)_3(PPh_3)_2$ (**14–16**).

Table 3. Some notations for metal clusters containing heteronuclei and/or heteroligands

Formula	Notation	Reference
trans-$Fe(CO)_3(PPh_3)_2$	$\sigma_{1,3}$-PPh_3-[1]-[1:3:1]	—
fac-$Fe(CO)_3(PPh_3)_2$	σ_1,σ_2^1-PPh_3-[1]-[1:3:1]	—
mer-$Fe(CO)_3(PPh_3)_2$	$\sigma_2^{1,2}$-PPh_3-[1]-[1:3:1]	—
$Co_2(CO)_6(PhC{\equiv}CPh)$	σ_2-PhC≡CPh-[1:1]-[3:1:3]	46
$CpFe_2(CO)_3$(*i*-BuNC)	σ_1^1,σ_3^1-Cp-σ_1^2-*i*-BuNC-[1:1]-[2:(2):2]	47
$[CpFeNO]_2$	$\sigma_{1,3}$-Cp-[1:1]-[1:2:1]	48
$CpMo(CO)_2W(CO)_5(CH_3S)$	Δ_1-Mo-σ_1^1-Cp-σ_2-SMe-[1:1]-[3:1:2:3]	49
$Mn_2Fe(CO)_{14}$	Δ_2-Fe-[1:1:1]-[1:4:(4):4:1]	50
$Ru_3(CO)_{10}(NPh)(NCO)$	σ_4^1-NCO-σ_4^3-NPh-[1:2]-[2:(2):4:(4′)]	51
$[Me_3C_6H_2)_3Nb_3Cl_6]^{n+}$	σ_2-$Me_3C_6H_2$-[3]-[(3):3:(3)]	52
$Re_3Cl_3Br_7H_2O$	$\sigma_2^{1,3,5}$-Cl-$\sigma_2^{2,4}$-H_2O-[3]-[3:(6):3]	53
$[Pd_3Cl(PPh_2)_2(Et_3P)_3]^+$	$\sigma^{1,3}$-PPh_2-σ^5-Cl-[3]-[(6′)]	54
$H_2Os_3(CO)_{10}$	σ_1^1,σ_5^1-H-[3]-[(2):2:(4):2:(2)]	55
$HOs_3(CO)_9(SMe)(C_2H_4)$	σ_1^1-SMe-σ_3^2-C_2H_4-σ_5^1-H-[3]-[(2):2:(4):2:(2)]	56
$Cp_3Mo_3S_4$	σ_2-Cp-[3]-[1:3:(3)]	57
$Cp_4Cr_4O_4$	$\sigma_{1,3}$-Cp-[1:3]-[1:(3):3:1]	58
$H_3CoRu_3(CO)_{12}$	Δ_1-Co-σ_3-H-[1:3]-[3:6:(3):3]	59
$Co_4(CO)_{10}(PPh)_2$	$\sigma_{1,5}$-PPh-[4]-[1:4:2:4:1]	60
$Ru_4(CO)_{12}(PhC{\equiv}CPh)$	σ_5-PhC≡CPh-[2:(2)]-[2:4:4:(2):1]	61
$[Mo_2Ni_3(CO)_{16}]^{2-}$	$\Delta_{1,3}$-Mo-[1:3:1]-[1:4:(6):4:1]	62
$Cp_6Ti_6O_8$	$\sigma_{1,3,1}$-Cp-[1:4:1]-[1:(4):4:(4):1]	63
$[(Ph_3P)_{12}Au_{13}Ag_{12}Cl_6]^{m+}$	$\Delta_{1,4,6,9}$-Ag-σ_3-Cl-[1:5:1:(5):1:5:1:(5):1]-[1:5:6:5:1]	64

REFERENCES

1. (a) P. Chini, *J. Organomet. Chem.* 1980, **200**, 37; (b) P. Chini, G. Longoni and V. G. Albano, *Adv. Organomet. Chem.* 1976, **14**, 285; (c) B. F. G. Johnson (Ed.), *Transition Metal Clusters.* Wiley Interscience, Chichester (1980); (d) R. E. Benfield and B. F. G. Johnson, *Top. Stereochem.* 1981, **12**, 253; (e) R. E. Benfield and B. F. G. Johnson, *Transition Met. Chem.* 1981, **6**, 131; (f) W. C. Trogler and M. C. Manning, *Coord. Chem. Rev.* 1981, **38**, 89.
2. (a) B. K. Teo, M. B. Hall, R. F. Fenske and L. F. Dahl, *J. Organomet. Chem.* 1974, **70**, 413; (b) B. K. Teo, M. B. Hall, R. F. Fenske and L. F. Dahl, *Inorg. Chem.* 1975, **14**, 3103.
3. (a) K. Wade, *J. Chem. Soc., Chem. Commun.* 1971, 792; (b) K. Wade, *Inorg. Nucl. Chem. Lett.* 1972, **8**, 559, 563; (c) K. Wade, *Electron Deficient Compounds.* Nelson, London (1971); (d) K. Wade, *Adv. Inorg. Chem. Radiochem.* 1976, **18**, 1; (e) D. M. P. Mingos, *Acc. Chem. Res.* 1984, **17**, 311.
4. R. B. King and D. H. Rouvray, *J. Am. Chem. Soc.* 1977, **99**, 7834.
5. A. J. Stone, *Inorg. Chem.* 1981, **20**, 563.
6. (a) J. Halpern, *Discuss. Faraday Soc.* 1968, **46**, 7; (b) F. G. A. Stone, *Acc. Chem. Res.* 1981, **14**, 318; (c) D. M. P. Mingos, *Trans. Am. Crystal. Assoc.* 1980, **16**, 17; (d) T. A. Albright, *ibid.* 1980, **16**, 35.
7. (a) J. W. Lauher, *J. Am. Chem. Soc.* 1978, **100**, 5305; (b) J. W. Lauher, *ibid.* 1979, **101**, 2604; (c) J. W. Lauher, *J. Organomet. Chem.* 1981, **213**, 25.
8. G. Ciani and A. Sironi, *J. Organomet. Chem.* 1980, **197**, 233.
9. D. M. P. Mingos, *Nature (London), Phys. Sci.* 1972, **236**, 99; (b) R. Mason, K. M. Thomas and D. M. P. Mingos, *J. Am. Chem. Soc.* 1973, **95**, 3802; (c) R. Mason and D. M. P. Mingos, *MTP Int. Rev. Sci.: Phys. Chem., Ser. Two* 1975, **11**, 121; (d) R. E. Williams, *Inorg. Chem.* 1971, **10**, 210.
10. (a) M. Elian, M. M. L. Chen, D. M. P. Mingos and R. Hoffmann, *Inorg. Chem.* 1976, **15**, 1148; (b) B. E. R. Schilling and R. Hoffmann, *J. Am. Chem. Soc.* 1979, **101**, 3456; (c) R. Hoffmann, B. E. R. Schilling, R. Bau, H. D. Kaesz and D. M. P. Mingos, *ibid.* 1978, **100**, 6088.
11. (a) D. M. P. Mingos, *J. Chem. Soc., Dalton Trans.* 1974, 133; (b) D. M. P. Mingos, *ibid.* 1976, 1163; (c) D. M. P. Mingos and M. I. Forsyth, *ibid.* 1977, 610; (d) D. G. Evans and D. M. P. Mingos, *Organometallics* 1983, **2**, 435.
12. (a) M. B. Hall and R. F. Fenske, *Inorg. Chem.* 1972, **11**, 768; (b) N. M. Kostic and R. F. Fenske, *ibid.* 1983, **22**, 666; (c) A. B. Rives, X.-Z. You and R. F. Fenske, *ibid.* 1982, **21**, 2286.
13. (a) D. E. Sherwood, Jr and M. B. Hall, *Inorg. Chem.* 1982, **21**, 3458; (b) D. E. Sherwood, Jr and M. B. Hall, *Organometallics* 1982, **1**, 1519; (c) P. T. Chesky and M. B. Hall, *Inorg. Chem.* 1981, **20**, 4419.
14. (a) F. A. Cotton and G. G. Stanley, *Chem. Phys. Lett.* 1978, **58**, 450; (b) B. E. Bursten, F. A. Cotton and G. G. Stanley, *Isr. J. Chem.* 1980, **19**, 132.
15. (a) A. Q. Tang, *Org. Chem. (Shanghai)* 1984, 227; (b) G. X. Xu, In *New Frontiers in Organometallic Chemistry* (Edited by Y. Z. Huang, A. Yamamoto and B. K. Teo), p. 73. Science Press, Beijing (1984).
16. (a) B. K. Teo, *Inorg. Chem.* 1984, **23**, 1251; (b) B. K. Teo,

G. Longoni and F. R. K. Chung, *Inorg. Chem.* 1984, **23**, 1257.
17. B. F. G. Johnson (Ed.) *Polyhedron Symposia-in-Print Number 1, Polyhedron* 1984, **3**, 1277.
18. IUPAC, *Nomenclature of Organic Chemistry, Sections A, B, C, D, E, F and H.* Pergamon Press, Oxford (1979).
19. For a preliminary communication, see T.-Y. Luh, H. N. C. Wong and B. F. G. Johnson, *Angew. Chem., Int. Ed. Engl.* 1985, **24**, 45.
20. L. Föppl. *J. Reine Angew. Math.* 1912, **141**, 251.
21. B. F. G. Johnson, *J. Chem. Soc., Chem. Commun.* 1976, 211.
22. F. A. Cotton, *Chemical Applications of Group Theory.* Wiley, New York (1971).
23. R. S. Cahn, C. K. Ingold and V. Prelog, *Angew. Chem.* 1966, **78**, 413; *Angew. Chem., Int. Ed. Engl.* 1966, **5**, 385; R. S. Cahn and O. C. Dermer, *Introduction to Chemical Nomenclature*, 5th Edn, p. 131. Butterworths, London (1979); V. Prelog and G. Helmchen, *Angew. Chem.* 1982, **94**, 614; *Angew. Chem., Int. Ed. Engl.* 1982, **21**, 567.
24. J. Ladell, B. Post and I. Fankuchen, *Acta Cryst.* 1952, **5**, 795.
25. J. Donohue and A. Caron, *Acta Cryst.* 1964, **17**, 663.
26. W. Rüdorff and U. Hofmann, *Z. Phys. Chem. B* 1935, **28**, 351.
27. H. M. Powell and R. V. G. Ewens, *J. Chem. Soc.* 1939, 286.
28. L. F. Dahl and R. E. Rundle, *Acta Cryst.* 1963, **16**, 419.
29. R. Bau, S. W. Kirtley, T. N. Sorrell and S. Winarko, *J. Am. Chem. Soc.* 1974, **96**, 998.
30. F. A. Cotton and J. M. Froup, *J. Am. Chem. Soc.* 1974, **96**, 4155.
31. M. R. Churchill and B. G. DeBoer, *Inorg. Chem.* 1977, **16**, 878.
32. J. A. Bertrand, F. A. Cotton and W. A. Dallase, *Inorg. Chem.* 1968, **2**, 1166.
33. J. C. Calabrese, L. F. Dahl, A. Cavalieri, P. Chini, G. Longoni and S. Martinengo, *J. Am. Chem. Soc.* 1974, **96**, 2616.
34. F. H. Carve, F. A. Cotton and B. A. Frenz, *Inorg. Chem.* 1976, **15**, 380.
35. M. R. Churchill and J. P. Hutchinson, *Inorg. Chem.* 1978, **17**, 3528.
36. R. J. Doedens and L. F. Dahl, *J. Am. Chem. Soc.* 1966, **88**, 4847.
37. M. R. Churchill and R. Bau, *Inorg. Chem.* 1968, **7**, 2606.
38. G. Longoni, P. Chini, L. D. Lower and L. F. Dahl, *J. Am. Chem. Soc.* 1975, **97**, 5034.
39. B. E. Reichert and G. M. Sheldrick, *Acta Cryst.* 1977, **B33**, 175.
40. K. Jodden, H. G. V. Schnering and H. Schafer, *Angew. Chem., Int. Ed. Engl.* 1975, **14**, 570.
41. J. C. Calabrese, L. F. Dahl, P. Chini, G. Longoni and S. Martinengo, *J. Am. Chem. Soc.* 1974, **96**, 2614.
42. V. G. Albano, P. L. Bellon, P. Chini and V. Scatturin, *J. Organomet. Chem.* 1969, **16**, 461.
43. E. R. Corey, L. F. Dahl and W. Beck, *J. Am. Chem. Soc.* 1963, **85**, 1202.
44. M. McPartlin, C. R. Eady, B. F. G. Johnson and J. Lewis, *J. Chem. Soc., Chem. Commun.* 1976, 883.
45. R. A. Field, D. L. Kepert, B. W. Robinson and A. H. White, *J. Chem. Soc., Dalton Trans.* 1973, 1858.
46. W. G. Sly, *J. Am. Chem. Soc.* 1959, **81**, 18.
47. I. L. C. Campbell and F. S. Stephens, *J. Chem. Soc., Dalton Trans.* 1975, 982.
48. J. L. Calderon, S. Fontana, E. Frauendorfer, V. W. Day and S. D. A. Iske, *J. Organomet. Chem.* 1974, **64**, C16.
49. J. E. Guerchais, J. L. LeQuere, F. Y. Petillon, L. Manojlovic-Muir, K. W. Muir and D. W. A. Sharp, *J. Chem. Soc., Dalton Trans.* 1982, 283.
50. P. A. Agron, R. D. Ellison and H. A. Levy, *Acta Cryst.* 1967, **23**, 1079.
51. P. Mastropasqua, A. Riemer, H. Kirsch and C. Krüger, *J. Organomet. Chem.* 1978, **148**, C40.
52. M. R. Churchill and S. W. Y. Chang, *J. Chem. Soc., Chem. Commun.* 1974, 248.
53. M. Elder, G. J. Gainsford, M. D. Papps and B. R. Penfold, *J. Chem. Soc., Chem. Commun.* 1969, 731.
54. G. W. Bushnell, K. R. Dixon, P. M. Moroney, A. D. Rattray and C. Wan, *J. Chem. Soc., Chem. Commun.* 1977, 709.
55. A. J. Orpen, A. V. Rivera, E. G. Bryan, D. Pippard, G. M. Sheldrick and K. D. Rouse, *J. Chem. Soc., Chem. Commun.* 1978, 723.
56. B. F. G. Johnson, J. Lewis, D. Pippard and P. R. Riathby, *J. Chem. Soc., Chem. Commun.* 1978, 551.
57. P. J. Vergamini, H. Vahrenkamp and L. F. Dahl, *J. Am. Chem. Soc.* 1971, **93**, 6327.
58. F. Bottomley, D. E. Paez and P. S. White, *J. Am. Chem. Soc.* 1981, **103**, 5581.
59. W. L. Gladfelter and G. L. Geoffroy, *Adv. Organomet. Chem.* 1980, **18**, 207; G. L. Geoffroy, *Acc. Chem. Res.* 1980, **13**, 469.
60. R. C. Ryan and L. F. Dahl, *J. Am. Chem. Soc.* 1975, **97**, 6904.
61. R. Mason and K. M. Thomas, *J. Organomet. Chem.* 1972, **3**, C39.
62. J. K. Ruff, R. P. White and L. F. Dahl, *J. Am. Chem. Soc.* 1971, **93**, 2159.
63. J. C. Huffman, J. G. Stone, W. C. Krusell and K. G. Caulton, *J. Am. Chem. Soc.* 1977, **99**, 5830.
64. B. K. Teo and K. Keating, *J. Am. Chem. Soc.* 1984, **106**, 2224.

Polyhedron Vol. 5, No. 5, pp. 1119–1124, 1986
Printed in Great Britain

0277–5387/86 $3.00+.00
Pergamon Journals Ltd

SYNTHESIS AND CHARACTERIZATION OF DIOXOOSMIUM(VI) COMPLEXES OF HYDROXYCARBOXYLIC ACIDS

C. C. HINCKLEY* and PIOTR A. KIBALA

Department of Chemistry and Biochemistry, Southern Illinois University, Carbondale, IL 62901, U.S.A.

(*Received* 12 *July* 1985; *accepted after revision* 17 *October* 1985)

Abstract—The synthesis and characterization of stable well-defined osmium(VI)–hydroxycarboxylic acid complexes is reported for the first time. The reaction of dipotassium tetramethylosmate(VI) with hydroxycarboxylic acids [glycolic, 2-hydroxyisobutyric, (*S*)-(+)-mandelic and *o*-salicylic] in the presence of pyridine led to the formation of *trans*-dioxo(oxoacidato)dipyridineosmium(VI) complexes. Elemental analysis, and IR, ^{1}H NMR, ^{13}C NMR and mass spectrometer were used to characterize the new complexes. A structure in which O=Os=O group is perpendicular to the plane produced by the two nitrogen atoms of the pyridine ligands and the two oxygen atoms of the oxoacidato group is proposed for the complexes. In the structure, oxoacidato groups form five- or six-membered rings with the osmium atom.

In this paper, we report the preparation of stable osmyl complexes with hydroxycarboxylic acids. The compounds have been characterized using elemental analyses, and NMR and IR spectroscopy. Mass spectrometry and cyclic voltammetry were used in supporting studies. The structure proposed for the compounds incorporates binding of a carboxylic group to the osmyl similar to that found in osmyl amino acid complexes.[1] In one of the compounds prepared salicylic acid is the ligand. This complex exhibits an unusual six-membered ring structure including the osmium atom.

RESULTS AND DISCUSSION

Preparation

Several α-hydroxycarboxylic acids [glycolic, 2-hydroxyisobutyric and (*S*)-(+)-mandelic] have been reacted with an Os(VI) complex in the presence of pyridine. After several days at −20°C, methano–pyridine solutions of dipotassium tetramethylosmate(VI) (DTMO) with α-hydroxycarboxylic acids yield brown, crystalline materials that can be easily separated via filtration. Magnetic measurements show all of them to be diamagnetic. The results of elemental analysis for the compounds listed in Table 1 are consistent with a formulation in which two pyridine ligands and one α-hydroxycarboxylic acid group are bound to one OsO_2 moiety.

IR spectra

Selected vibrational frequencies for these complexes are listed in Table 2. All complexes display a strong band in the 840–850-cm^{-1} region. This band is assigned to an O=Os=O asymmetric stretch and is characteristic of the osmyl moiety. A strong C=O band around 1700 cm^{-1} in each of the compounds is slightly lower in frequency than the one in the respective free hydroxycarboxylic acid. Only the glycolic acid complex contains an additional carbonyl frequency at 1667 cm^{-1} that is not present in the parent glycolic acid. In the 590–610-cm^{-1} region a medium strength band in each complex is assigned to the CO_2 wagging mode. A strong band at 1610 cm^{-1}, characteristic of C—C stretching vibrations in aromatic rings, is also found for all of these complexes.

* Author to whom correspondence should be addressed.

Table 1. Elemental analyses of *trans*-dioxo(oxoacidato)dipyridineosmium(VI)

Compound	Formula		C	H	N	O	Cl
$OsO_2[CH_2(O)COO](py)_2$	$OsO_5N_2C_{12}H_{12}$	c	31.7	2.7	6.2	17.6	
		f	31.8	2.8	6.2		
$OsO_2](CH_3)_2C(O)COO](py)_2$	$OsO_5N_2C_{14}H_{16}$	c	34.8	3.3	5.8	16.6	
		f	35.0	3.3	5.9		
$OsO_2[d\text{-}C_6H_5CH(O)COO](py)_2$	$OsO_5N_2C_{18}H_{16}$	c	40.7	3.0	5.3	15.1	
		f	41.0	3.1	5.4		
$OsO_2[o\text{-}OC_6H_4COO](py)_2$	$OsO_5N_2C_{17}H_{14}$	c	39.5	2.7	5.4	15.5	0.0
		f	39.7	2.8	5.3	14.7	2.1

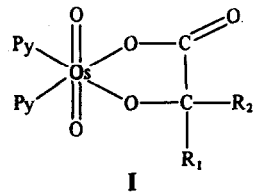
NMR spectra

Proton NMR spectra are consistent with the formulation in which bonding of α-hydroxycarboxylic acids to osmium takes place through both carboxylic and hydroxyl groups. Table 3 lists the spectral line positions, along with their multiplicity and the number of protons they represent, of all the complexes. Spectra of the glycolic and 2-hydroxyisobutyric acid complexes are almost identical. Only the positions of the aliphatic protons are different. The 5.17-ppm singlet of the oxoacetato complex is produced by the CH_2 group of the ring, while the 1.64-ppm singlet in the spectrum of the oxoisobutyrato complex is assigned to $C(CH_3)_2$ protons.

The remaining lines are produced by the protons of the two pyridine ligands. With the help of the ^1H NMR spectrum of free pyridine, the necessary line assignments have been made. The ^1H NMR spectrum of pyridine shows three groups of spectral lines: one downfield doublet at 8.60 ppm produced by two *ortho* protons, and two multiplets at 7.00 and 7.60 ppm produced by *meta* and *para* protons, respectively. Based on that information the two downfield doublets in the ^1H NMR of oxoacidato complexes of Os(VI) can be viewed as *ortho* protons of the two pyridine ligands. The two remaining multiplets are produced by the overlap of the spectral lines of *meta* and *para* protons of both pyridines. The downfield multiplet can be associated with the *meta* protons. The other multiplet represents the *para* protons. The respective spectral lines of pyridine protons in the oxoacidato Os(VI) complexes are downfield from those found in free pyridine.

The presence of two doublets for *ortho* protons indicates that both pyridines, though chemically equivalent, are not equivalent magnetically. The molecule is asymmetric.

The proposed structure for the new complexes is:



I

In this structure the O=Os=O group is perpendicular to the plane produced by two nitrogen atoms of the pyridine ligands and two oxygen atoms

Table 2. Selected vibrational frequencies of several *trans*-dioxo(oxoacidato)dipyridineosmium(VI) complexes

Compound	C=O	C=C	O=Os=O	CO_2 (wag)
$OsO_2[CH_2(O)COO](py)_2$	1702.1 (s) 1666.9 (s)	1608.6 (s)	848.5 (s)	606.7 (w)
$OsO_2[(CH_3)_2C(O)COO](py)_2$	1692.6 (s)	1609.8 (s)	842.0 (s)	593.2 (w)
$OsO_2[d\text{-}C_6H_5CH(O)COO](py)_2$	1686.3 (s)	1610.3 (s)	844.0 (s)	592.8 (w)
$OsO_2[o\text{-}OC_6H_4COO](py)_2$	1643.9 (s)	1610.0 (s) 1598.6 (s)	852.8 (s)	593.6 (w)

Table 3. ^{1}H NMR spectral line positions of several *trans*-dioxo(oxoacidato)dipyridineosmium(VI) complexes

Compound					
$OsO_2[CH_2(O)COO](py)_2$	5.20(s)2		7.58(m)4 7.99(q)2		8.78(d)2 8.97(d)2
$OsO_2[(CH_3)_2C(O)COO](py)_2$	1.64(s)6		7.57(m)4 7.95(q)2		8.77(d)2 8.96(d)2
$OsO_2[d\text{-}C_6H_5CH(O)COO](py)_2$	5.88(s)1	7.36(q)3	7.57(m)6 7.98(m)2		8.83(d)2 9.00(d)2
$OsO_2[o\text{-}OC_6H_4COO](py)_2$	6.96(m)2	7.38(t)1	7.62(q)4 8.05(m)2	8.35(d)1	8.85(d)2 8.94(d)2

of the oxoacidato group. The ^{1}H NMR spectrum of the (*S*)-(+)-mandelic acid complex, *trans*-dioxo[(*S*)-(+)-oxo(phenyl)acetato]dipyridineosmium(VI), is also in good agreement with the proposed structure. However, its interpretation is not straightforward due to the overlap of the spectral lines of pyridine protons with the spectral lines of the protons from the phenyl group.

Mass spectrometry was used to determine whether the new class of osmyl compounds were monomeric or dimeric species. The mass spectrum of *trans*-dioxo(oxoacidato)dipyridineosmium(VI) was recorded. The interpretation of this spectrum is not simple since osmium has several isotopes with natural abundance higher than 10%. Despite the complexity of the spectrum, the molecular ion can be easily identified. Its molecular weight is 456 as expected for the monomeric species.

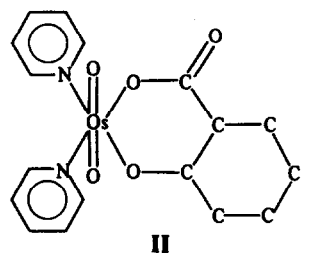
The question of the existence of a larger ring size involving the osmium atom has been explored through a synthesis of an *o*-salicylic acid complex.

The preparation devised for the synthesis of oxoacidato complexes of α-hydroxycarboxylic acids did not produce crystalline materials in this case. However, when the reaction mixture was evaporated to dryness, a brown osmium-containing compound could be extracted with CH_2Cl_2. This solid was recrystallized from CH_2Cl_2 through *n*-heptane layering. The brown crystals that were isolated were diamagnetic.

The elemental analysis results for the crystalline material are listed in Table 1. The presence of some chlorine has been detected. This probably comes from CH_2Cl_2 in the crystalline lattice. If one makes the assumption that the salicylate complex is in fact *trans*-dioxo(*o*-oxobenzoato)dipyridineosmium(VI), then the ratio of CH_2Cl_2 to $OsO_2[o\text{-}OC_6H_4COO](py)_2$ can be calculated. It was found to be 2:13. The elemental analysis results are in excellent agreement with the calculated composition based on this ratio. Furthermore, the molecular weight of the crystalline material was determined osmometrically in CH_2Cl_2 and found to be 440. This compares favorably with the value of 459 calculated for the 2:13 ratio of CH_2Cl_2 to *trans*-dioxo(*o*-oxobenzoato)dipyridineosmium(VI). The molecular weight determined for the salicylate complex indicates a monomeric structure for the material.

The structural features of this complex were inferred from its IR spectrum. Selected vibrational frequencies of this complex are listed in Table 2. The IR spectrum of the salicylato complex is similar to those found for other oxoacidato compounds of Os(VI). The strong band at 852.8 cm^{-1} is assigned to an O=Os=O asymmetric stretch. The band at 1643.9 cm^{-1} is probably due to C=O vibrations and is less than the C=O vibration in salicylic acid. Two bands are present at 1610.0 and 1598.6 cm^{-1}. The former is assigned to an aromatic C—C stretching vibration of the pyridine ring. All other oxoacidato complexes have this frequency within ± 2 cm^{-1}. The latter are interpreted as stretching vibrations of aromatic carbon atoms in the phenyl ring of salicylic acid.

Table 3 lists the spectral line positions along with their multiplicity and relative band areas for the ^{1}H NMR spectrum of this compound. The assignments of the spectral lines are consistent with the structure:



II

The assignment of the proton NMR absorptions of the salicylate ring has been made to be consistent with the spectrum of neat salicylic acid.

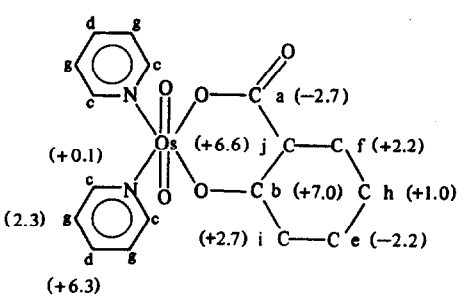
The positions of ^{13}C spectral lines along with their intensities are listed in Table 4. Assignments are based on the line assignments of the pure starting materials and are presented in the figure accompanying Table 1. The numbers in parentheses represent spectral line shifts of pure starting materials. Two downfield lines have been assigned to the carboxylic carbon of the salicylic group and the carbon atom to which the hydroxyl group is attached. Six spectral lines that can be viewed as three doublets at 126, 141 and 150 ppm are assigned to pyridine carbons: *meta*, *para* and *ortho*, respectively. Three upfield lines are due to the ring carbon bound to the carboxylate group and the two atoms that are at *meta* positions to it. The remaining two atoms of the salicylate ring give rise to the 132.9- and 133.7-ppm lines. The ^{13}C NMR spectrum fully supports the presence of a six-membered ring that includes the osmium atom. This is the first osmyl compound to have this feature.[2]

Cyclic voltammetry

The electrochemical properties of OsO_2(oxoacidato)$(py)_2$ have been explored with the help of cyclic voltammetry. The details of that study are summarized in Table 5. The electrochemical behavior of all of the compounds is very similar. They display one oxidation and two reduction waves. All waves are irreversible. The anodic wave represents oxidation of Os(VI) complexes to OsO_4. Of the two cathodic waves the first one could be interpreted as reduction of OsO_4 to an Os(VI) product, while the second one represents the reduction of that product to an Os(IV) species. This behavior is consistent with the electrochemical properties expected for osmium +6 compounds.

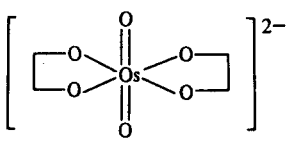
Table 4. ^{13}C NMR spectral line positions of *trans*-dioxo(*o*-oxobenzoato)dipyridineosmium(VI)

Line No.	Intensity	Frequency (Hz)	ppm
1 (a)	402.16	8549.74	169.938
2 (b)	243.88	8504.76	169.044
3 (c)	1419.63	7576.39	150.592
4 (c)	1488.51	7547.00	150.007
5 (d)	687.06	7137.49	141.868
6 (d)	678.43	7121.69	141.554
7 (e)	751.91	6727.92	133.727
8 (f)	833.34	6686.75	132.909
9 (g)	1150.97	6347.65	126.169
10 (g)	1180.01	6338.64	125.990
11 (h)	443.74	6049.72	120.247
12 (i)	653.31	6044.15	120.136
13 (j)	413.74	6028.02	119.816

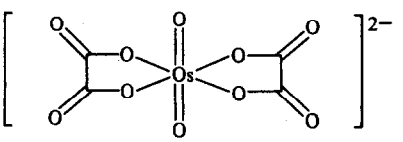


All of these new complexes display a ring structure that involves a central osmium atom. These rings have five or six atoms. Compounds of similar type are represented by Os(VI) monoesters.[3] However, in those complexes oxygen atoms are bound to sp^3 carbons, while in our compounds one of the oxygen atoms forms a bond with an sp^2 carbon atom.

There are several examples of dioxoosmium(IV) complexes with two five-membered rings that include a common osmium center:

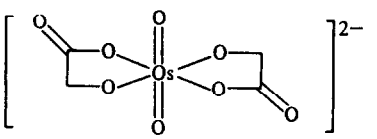


III



IV

They are made from other dioxoosmium(VI) materials through exchange of ligands.[4,5] However, we were unable to synthesize an Os(VI) complex that includes two oxoacidato rings:



V

Exchange of $K_2[OsO_2(MeO)_4]$ with glycolic acid leads to a polymeric osmium glycolate with mixed oxidation states of +3 and +4, while the other hydroxacarboxylic acids produce mixtures of oily polymeric materials that are impossible to separate.[6]

Table 5. Electrochemical properties of several *trans*-dioxo(oxoacidato)dipyridineosmium(VI) complexes

Compound	E_a	E_{c1}	E_{c2}
$OsO_2[CH_2(O)COO](py)_2$	2.00	−0.95	−1.68
$OsO_2[(CH_3)_2C(O)COO](py)_2$	2.02	−1.22	−1.88
$OsO_2[d\text{-}C_6H_5CH(O)COO](py)_2$	2.02	−0.93	−1.67
$OsO_2[o\text{-}OC_6H_4COO](py)_2$	1.58	−0.88	−1.54

EXPERIMENTAL

Materials

OsO_4 was purchased from Stevens Metallurgical Co. and was used as received. Hydroxycarboxylic acids were purchased from Aldrich Chemical Co. All other reagents were purchased from different commercial sources and used without additional purification.

Elemental analysis

Determination of all the elements except for osmium was carried out by either Galbraith or MicAnal Laboratories.

Spectroscopy

IR spectra were recorded as KBr pellets containing 1–3 mg of sample per 400 mg of KBr. KBr was dried under high vacuum at 130°C for 24 h and stored in a desiccator filled with nitrogen or divided into 400-mg portions and sealed in vials. A Perkin–Elmer Model 297 or Nicolet Model 20DX FTIR spectrometer was employed.

The ^1H NMR spectra were recorded on a Perkin–Elmer R32 90-MHz spectrometer. ^{13}C FT NMR and ^1H FT NMR spectra were recorded on a Nicolet 200-MHz instrument. The NMR data are reported in the following manner: chemical shift (ppm) with respect to tetramethylsilane as the internal standard, followed by the multiplicity (m = multiplet, q = quartet, t = triplet, d = doublet, s = singlet) and the number of protons represented by the peak(s).

The mass spectrum of *trans*-dioxo(oxoacetato)dipyridineosmium(VI) as recorded at the Midwest Center for Mass Spectrometry at the University of Nebraska-Lincoln. Fast-atom bombardment was used as the ionization method.

Magnetic measurements

Magnetic susceptibilities were determined at ambient temperature using a Faraday balance. $HgCo(CNS)_4$ which has a high magnetic susceptibility of 16.44×10^{-6} cgs units was used as a standard for the calibration of a balance. The Faraday balance was constructed by Cahn Instruments Inc. Five fifteen-milligram samples were used for each determination. Magnetic susceptibilities were corrected for diamagnetism.

Cyclic voltammetry

Electrochemical properties of osmium compounds were investigated by means of cyclic voltammetry. The measurements were done on a locally constructed instrument. A three-electrode system was used to avoid problems associated with solution resistance. Voltammograms were recorded on an X–Y recorder. Electrochemical studies were performed in CH_2Cl_2. $(n\text{-}Bu_4N)PF_6$ was used as a supporting electrolyte, usually as a 0.2 M solution. The concentration of the osmium complex was 10^{-3}–5×10^{-3}. A platinum bead served as a working electrode, platinum wire as a counter electrode and an Ag–0.1 M $AgNO_3$ in CH_3CN electrode was used as a reference. The reference electrode made contact with a solution through a Vycor tip. The typical scan rate was 300 mV s^{-1}. Anodic and cathodic currents were calculated from voltammograms. For comparison with literature data, the potentials measured vs a silver–silver nitrate electrode were converted to an SCE reference electrode. The correction was +0.337 V.

Synthesis of trans-*dioxo(oxoacetato)dipyridineosmium(VI)*

In a typical preparation 0.5 g (2 mmol) of OsO_4 was dissolved in 10 cm^3 of methanol. To this solution 4 cm^3 of 1 N KOH in methanol were added. The initial red color of the solution changed to green in about 5 min. The green solution of DTMO was treated with 40 cm^3 of ethyl ether. The resulting precipitate was removed by centrifugation. The supernatant was discarded and the remaining solid was washed with an additional 40 cm^3 of ethyl ether

and centrifuged again. The sediment was mixed with 20 cm^3 of pyridine to form a very fine suspension. To this suspension 0.9129 g (12 mmol) of glycolic acid in 10 cm^3 of ethanol was added and the reaction mixture was placed in a freezer (−20°C) for a week. After that time the resulting white-brown solid was filtered and washed with water, yielding brown crystals. They were, in turn, washed with ethyl ether and vacuum dried. The yield was 0.56 g (63% with respect to osmium).

Synthesis of trans-*dioxo(oxoisobutyrato)dipyridine-osmium(VI)*

A 0.5-g (2-mmol) sample of OsO_4 was dissolved in 10 cm^3 of methanol. To this solution 4 cm^3 of 1 N KOH methanol were added. The initial red color of the solution changed to green in about 5 min. The green solution of DTMO was treated with 40 cm^3 of ethyl ether. The brown-gray solid that resulted was centrifuged out, washed with 40 cm^3 of ethyl ether and centrifuged again. The sediment was mixed with 20 cm^2 of pyridine to form a very fine suspension to which 1.2547 g (12 mmol) of 2-hydroxy isobutyric acid in 10 cm^3 of ethanol was added. The reaction mixture was placed in a freezer (−20°C) for a week. After that time the resulting brown crystals were filtered, washed with water, ethyl alcohol and ethyl ether, and vacuum dried. Yield 0.58 g (61% with respect to osmium).

Synthesis of trans-*dioxo*[(S)-(+)-*oxo(phenyl)acetato*] *dipyridineosmium(VI)*

A 0.5-g (2-mmol) sample of OsO_4 is dissolved in 10 cm^3 of methanol. To this solution 4 cm^3 of 1 N KOH in methanol were added. The initially red solution changed to green in about 5 min. The green DTMO solution was treated with 40 cm^3 of ethyl ether to produce a brown-gray solid that was centrifuged out, washed with an additional 40 cm^3 of ethyl ether and centrifuged again. The sediment was mixed with 20 cm^3 of pyridine and 1.8305 g (12 mmol) of (*S*)-(+)-mandelic acid in 10 cm^3 of ethyl alcohol to form a very fine suspension that was placed in a freezer (−20°C) for a week. After that time the brown crystalline product was filtered, washed with water, ethanol and ethyl ether, and vacuum dried. Yield 0.47 g (45% with respect to osmium).

Synthesis of trans-*dioxo*(o-*oxobenzoato)dipyridine-osmium(VI)*

A 0.5-g (12-mmol) sample of OsO_4 was dissolved in 10 cm^3 of methanol. To this solution 4 cm^3 of 1 N KOH in methanol were added. The initially red solution turned green in about 5 min. The green DTMO solution was treated with 40 cm^3 of ethyl ether to produce a brown-gray precipitate that was centrifuged, washed with an additional 40 cm^3 of ethyl ether and centrifuged again. The sediment was mixed with 20 cm^3 of pyridine, 1.6766 g (12 mmol) of salicylic acid in 10 cm^3 of ethanol and placed in a freezer for a week. After that time the reaction mixture was evaporated to dryness on a rotavap. The brown solid that resulted was dissolved in CH_2Cl_2 and washed several times with 20-cm^3 portions of water, 5% HCl and 5% NaOH. The organic layer was dried with $MgSO_4$ and evaporated to dryness. The brown product was redissolved in acetone and filtered through a silica gel. The acetone solution was evaporated to dryness and the product was crystallized from CH_2Cl_2 through layering with *n*-heptane. The yield was 0.26 g (25% with respect to osmium).

REFERENCES

1. W. J. Roth and C. C. Hinckley, *Inorg. Chem.* 1981, **20**, 2023.
2. W. P. Griffith and C. J. Raub, *Osmium, Gmelin Handbuch der Anorganischen Chemie*, Suppl. Vol. 1. Springer, Berlin (1980).
3. P. N. Rylander, *Engelhard Ind., Tech. Bull.* 1968, **9**, 90.
4. Ref. 2, p. 186.
5. Gmelin Handbuch, *Osmium*, pp. 66, 78, 81, 89, 92–93, 97 (1939).
6. P. A. Kibala, dissertation, Southern Illinois University (1984).

Polyhedron Vol. 5, No. 5, pp. 1125–1130, 1986
Printed in Great Britain

0277–5387/86 $3.00+.00
Pergamon Journals Ltd

SOME NEW DERIVATIVES OF Cr(III) WITH URACIL, URIDINE AND 5′-UMP

JUAN J. FIOL and ANGEL TERRÓN

Departamento de Química Inorgánica, Facultad de Ciencias, Universidad de Palma de Mallorca, 07071 Palma de Mallorca, Spain

and

VIRTUDES MORENO*

Departamento de Química Inorgánica, Facultad de Química, Universidad de Barcelona, 43005 Tarragona, Spain

(*Received* 27 *June* 1985; *accepted* 23 *October* 1985)

Abstract—Some new Cr(III) compounds with uracil, uridine and 5′-UMP were obtained by reaction of the starting complexes *cis*-$[Cr(en)_2Cl_2]Cl$ and $[Cr(NH_3)_5Cl]Cl_2$ with the base, nucleoside and nucleotide. The complexes were characterized by their elemental analysis, conductivity, reflectance and IR data. In the case of uracil and uridine compounds, indirect bonding of Cr(III) to the pyrimidine ring seems to occur through the C_4=O and $-NH_3(-NH_2)$ groups of the starting complexes. In the 5′-UMP complex direct bonding is inferred through the phosphate group with additional interactions by hydrogen bonds involving the C_4=O group.

The presence of Cr(III) in biological processes such as glucose metabolism (glucose tolerance factor)[1,2] is well known, as well as its role in the kinetic mechanisms of DNA and RNA polymerases, which catalyse the replication and transcription of DNA.[3] Taking this into account, the study of kinetically inert Cr(III) complexes with nucleotides and their constituents is of interest. This paper is a follow-up of previous studies of the interaction of Cr(III) with nucleotides, nucleosides and bases.[4,5] Until now very few studies of Cr(III) with uracil (URA), uridine (URD) and 5′-UMP in the solid state have been performed.[5,6]

In comparison with other bases and nucleotides the formation of URA and URD complexes proved more difficult because the heterocyclic nitrogens were protonated in a wide range of pH, making coordination by nitrogen possible only under basic conditions different from those found in biological systems.[7,8] By using a suitable dissolving agent, coordination by carbonyl oxygen is possible.[9,10] Recently, the preparation of divalent 3*d* metallic ion complexes of uracil with a bidentate bond through the N(3), C_2=O sites were reported.[11]

In the complexes of 5′-UMP, the phosphate oxygens are the main point for coordination with the metal ion.[12,13]

EXPERIMENTAL

The analyses of carbon, hydrogen and nitrogen were carried out in a Carlo Erba model 1106 microanalyzer in the Institute of Bio-Organic Chemistry in Barcelona and in a Perkin–Elmer 240.B in the Faculty of Chemistry, Tarragona.

The chlorine analysis was determined by the Schoniger method using a 638 Metrohm Titro Processor, by burning the sample in O_2 over sodium bisulphite. Dissolutions were assessed by Volhard.

The sodium content was determined by flame photometry in a Perkin–Elmer 703 spectrophotometer. The working conditions were: λ = 590 nm and 0.2-nm slit with an acetylene–air flame oxidant.

The phosphorus content was determined by using the colorimetric method for phosphomolybdovanadate.[14] The measurements were carried out in a

* Author to whom correspondence should be addressed.

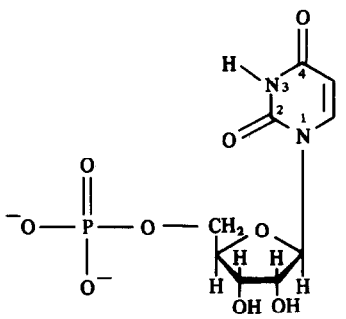


Fig. 1. 5′-UMP.

Perkin–Elmer 552 UV–visible spectrophotometer at 390 nm and 2-nm slit.

Chromium was determined by using the colorimetric method for chromate.[15] The measurements were performed in a Perkin–Elmer 552 UV–visible spectrophotometer at 375 nm and 2-nm slit.

The conductivities were measured with a Crison 525 conductimeter. The cell constant was determined by using a water solution of 10^{-2} N KCl ($k = 1.04\ cm^{-1}$).

The IR spectra were registered in the solid state (KBr pellets) in a Perkin–Elmer 683 IR spectrophotometer with an IR data station.

The reflectance spectra were recorded in the solid state in a Perkin–Elmer 552 UV–visible spectrophotometer with an integrating sphere attachment.

The complexes were prepared using URA (Merck), URD and $Na_2$5′-UMP (Serva) without further purification. The starting complexes *cis*-$[Cr(en)_2Cl_2]Cl$ and $[Cr(NH_3)_5Cl]Cl_2$ were prepared by the methods described in the literature.[16,17]

Synthesis of cis-$[Cr(en)_2Cl_2]Cl \cdot (URA)_2 \cdot \frac{1}{2}AcOEt$, cis-$[Cr(en)_2Cl_2]Cl \cdot (URD)_2$, $[Cr(NH_3)_5Cl]Cl_2$ (URA) *and* $[Cr(NH_3)_5Cl]Cl_2$(URD)

These four complexes were obtained in an ethyl acetate medium in a similar way to that described by Goodgame.[10,18] 0.5 mmol of the *cis*-$[Cr(en)_2Cl_2]Cl \cdot H_2O$ complex {1 mmol of $[Cr(NH_3)_5Cl]Cl_2$} and 1 mmol of finely powdered URA or URD were mixed and about 15 cm^3 ethyl acetate were added. The mixture was then reflux heated by constant stirring for between 5 and 16 h, depending on the case, until the reaction was complete. The product was filtered, washed with ethyl acetate (2.5 cm^3), and dried over P_4O_{10}.

Synthesis of $Na_2[Cr(en)_2(5'\text{-}UMP)_2(5'\text{-}UMPH)] \cdot 7H_2O$

Finely powdered dry samples {0.5 mmol of *cis*-$[Cr(en)_2Cl_2]Cl \cdot H_2O$ and 1 mmol of $Na_2$5′-UMP} were mixed and about 15 cm^3 ethyl acetate were added. The mixture was then reflux heated by constant stirring for 10 h until the reaction was complete. The product was filtered off, washed with ethyl acetate (2.5 cm^3), and dried over P_4O_{10}. Subsequently, this compound was dissolved in 11 cm^3 of water (pH = 6.9) and heated to 55°C for 10 min in a temperature-controlled bath. The complex was precipitated by addition of ethanol, then filtered, washed with ethanol and dried over P_4O_{10}.

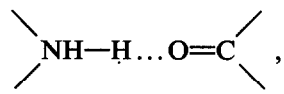
The composition of the complexes and the analytical results are shown in Table 1.

RESULTS AND DISCUSSION

Table 2 records the IR data for the compounds obtained with URA and URD. The assignment has been carried out according to the literature.[19–21]

In general, the IR spectra present no noticeable variations in comparison with those of URA, URD and the starting compounds so that one expects the initial environment of the metallic ion to be almost unchanged by the presence of URA or URD.

For the URA compounds, splitting of the bands is observed in the ν(C=O) region. The band corresponding to $\nu(C_4{=}O)$ (1671 cm^{-1}) shifts to lower frequencies (1665 and 1645 cm^{-1}) for the ethylenediamine compound, and to 1669 and 1646 cm^{-1} for the ammonia compound, indicating charge donation by this group probably as a result of a hydrogen bond



direct interaction with Cr(III) being ruled out by the presence of bands in the lower region of the spectrum assignable at δ(NMN) + ν(M—X) with no important shifts or changes in their relative intensity.[22,23]

In the case of the URD compounds, there is no shift in the ν(C=O) region and variations are minimal. The bands belonging to the starting complexes still appear in the lower region, probably coupled to the 357-, 310- and 287-cm^{-1} bands due to ν(ribose),[18] inferring an interaction through hydrogen bonds between URD and the initial system with possible participation of the ribose ring OH.

The remaining bands belonging to the vibrations of the starting complexes remain at approximately the same frequency, except for the 1583–1570-cm^{-1} [$\delta(NH_2)$] and 1608-cm^{-1} [$\delta(NH_3$deg.)] bands which overlap as a shoulder appearing at higher frequencies, which might indicate participation of these groups in the bond.

Table 3 records the IR data for the 5′-UMP complex. For this compound there are changes in

Table 1. Analytical data and some physico-chemical properties of the compounds

Compound	Found (calc.) (%) C	H	N	Cl	Cr	P	Na	Colour	M.p. (°C)	Λ_M (Ω^{-1} cm^2 mol^{-1}) 10^{-3} M at 20°C
cis-$[Cr(en)_2Cl_2]Cl \cdot (URA)_2 \cdot \frac{1}{2}AcOEt$	30.0 (30.7)	4.9 (5.1)	20.7 (20.5)	17.9 (19.4)	8.6 (9.5)			Brown	250(d)	105 in MeOH
cis-$[Cr(en)_2Cl_2]Cl \cdot (URD)_2$	34.7 (34.4)	5.2 (5.2)	14.5 (14.6)	13.0 (13.9)	6.1 (6.8)			Brown	140(d)	110 in MeOH
$[Cr(NH_3)_5Cl]Cl_2(URA)$	13.5 (13.5)	5.4 (5.3)	27.7 (27.6)	29.8 (29.9)	13.8 (14.6)			Pink	260(d)	245 in water
$[Cr(NH_3)_5Cl]Cl_2(URD)$	22.4 (22.1)	5.5 (5.5)	20.0 (21.0)	22.0 (21.8)	10.5 (10.7)			Pink	205(d)	243 in water
$Na_2[Cr(en)_2(5'\text{-}UMP)_2 \cdot (5'\text{-}UMPH)] \cdot 7H_2O$	28.0 (28.4)	5.1 (4.9)	10.2 (10.7)	— —	4.6 4.0	7.0 7.1	3.6 3.5	Brown	260(d)	192 in water

Table 2. IR data for the URA and URD compounds (cm^{-1})[a]

Tentative assignment	URA	*cis*-$[Cr(en)_2Cl_2] \cdot Cl(URA)_2 \cdot \frac{1}{2}AcOEt$	$[Cr(NH_3)_5Cl] \cdot Cl_2(URA)$	URD	*cis*-$[Cr(en)_2Cl_2] \cdot Cl(URD)_2$	$[Cr(NH_3)_5Cl] \cdot Cl_2(URD)$
$\nu(C_2{=}O)$	1715s,b	1716s	1720s	1694s,b		1695sh
$\nu(C_4{=}O) + \nu(C{=}C)$	1671s,b	1665–1661s,b	1669s	1681s,b	1680s,b	1680s
		1645s	1646s	1670s,b	1668s,b	1667s
				1615m	1615m	1612m[b]
$\delta(NH_2)$ [$\delta(NH_3$asymm.)]		1590s,sh[c]	1615sh[b]		1591m[c]	
$\delta(N{-}H) + \nu$(ring)	1508m	1508m	1508w			
	1452s	1454s	1454m	1470s	1470s	1470m
	1417s	1418s	1419m	1421s	1422s	1421m
	1389s	1392m	1391w	1396s	1397s	1397m
$\nu(C{-}N) + \nu$(ring)	1237s	1236s	1238s	1271s	1271s	1271m
$\nu(N{-}H)$	855s	859m	855m	854w	854w	850w
$\nu(M{-}N)$, $\delta(NMN) + \delta(NMX) + \nu(MX)$		479, 352, 321w[d]	462w, 300m[e]		474w, 352, 312m[d]	458w, 306m[e]

[a] s = strong, m = medium, b = broad, sh = shoulder, w = weak, ν = stretching, δ = bending.
[b] $\delta(NH_3$asymm.) of $[Cr(NH_3)_5Cl]Cl_2$ at 1608 cm^{-1}.
[c] $\delta(NH_2)$ of *cis*-$[Cr(en)_2Cl_2]Cl \cdot H_2O$ at 1583–1570 cm^{-1}.
[d] For the *cis*-$[Cr(en)_2Cl_2]Cl \cdot H_2O$ complex bands at 479w, 433w, 350w, 320w and 276w cm^{-1}.
[e] For the $[Cr(NH_3)_5Cl]Cl_2$ complex bands at 460m, 433w and 300m cm^{-1}.

Table 3. IR data for the 5′-UMP complex (cm^{-1})

Tentative assignment	$Na_2$5′-UMP	$Na_2[Cr(en)_2(5'\text{-UMP})_2(5'\text{-UMPH})]\cdot 7H_2O$
$\nu(C_2{=}O)$	1704–1689b	1695s
$\nu(C_4{=}O)$	1679b	
$\delta(NH)+\nu(C{=}C)$	1630w	1632sh
	1478m	1467m
	1429m	1431m
ν(ring)	1394m	1395, 1386m
	1284m	1275m
	1267m	
$\nu(PO_3$asymm.$)+$	1125s,b	
ν[C—O(sugar)]	1092s–1081b	1114s
		1066s
$\nu(PO_3$symm.$)$	981s	984s
ν[C—O(sugar)]$+\nu$(ring)	939s	
$\delta(NH)+\nu(P{-}O)+$	874w	
PO_3symm. def. + deg. def.	818s	816m
	763m	769m
	565m	551m
	534m	540m

frequency and intensity in the bands appearing mainly in the $\nu(C{=}O)$, ν(ring) and $\nu(PO_3^{2-})$ areas. The 1679-cm^{-1} peak, corresponding to $\nu(C_4{=}O)+\nu(C{=}C)$ shifts at 1632 cm^{-1}, appears as a shoulder, which seems to indicate some kind of interaction through the carbonyl group. The ring-stretching bands also vary in frequency as a consequence of restructuring the ring charge. In the region between 1200 and 900 cm^{-1}, bands appear due to the stretching vibrations of the phosphate group which are also altered. The bands due to $\nu(PO_3$assym.$)+\nu$[C—O(sugar)] settle at two peaks (1114 and 1066 cm^{-1}), and are considerably shifted in frequency, while the band corresponding to $\nu(PO_3$symm.$)$ is shifted slightly at higher frequencies. The 939-cm^{-1} band disappeared. All this infers that the phosphate group of a nucleotide is involved in the metal bond, with additional interaction with the pyrimidine ring, probably through the $C_4{=}O$ group. In this case, it is expected that the other nucleotides not coordinated to the Cr(III) will remain associated with the one coordinated by stacking phenomena or by interaction between the bases through hydrogen bonds.[24] The bands due to "ethylenediamine" and ν(M—N) which overlap with the 5′-UMP bands lose their definition and cannot be observed. The M—Cl bands are not observed either, which is in agreement with the results of the elemental analysis.

The diffuse reflectance spectra of the compounds obtained are consistent with approximately octahedral geometries of Cr(III). The values of $10Dq$ and B' parameters were found using Tanabe and Sugano's diagram[25] (Table 4).

Bands appear on these spectra due to transitions of the URA ring in the 300–240-nm region, which appear modified as a consequence of donation via $C_4{=}O$ and subsequent restructuring of the ring charge. Bands also appear corresponding to ν_1 and ν_2 transitions with practically no change in frequency compared to those of the starting complexes, confirming the permanence of the initial environment of the metallic ion in the case of the URA and URD compounds. The derivative of 5′-UMP presents a considerably lower $10Dq$ value, indicating coordination with —O donor. Probably, the Cl^- has been substituted by the oxygen of the phosphate or $C_4{=}O$ group. The low B' value is consistent with interaction through the $C_4{=}O$ group, permitting back bonding of the electronic density of the chromium to the URA ring carbonyl group. This interpretation is consistent with the reduction in frequency of the $C_4{=}O$ bond, as has been indicated when studying the IR spectrum.

For the "ethylenediamine" derivatives, various peaks are observed in the 465–605-nm area as a result of splitting through loss of symmetry at the $^4T_{2g}$ level, whose average value corresponds to a ν_1 transition. This splitting of the first transition into three peaks is consistent with a C_{2v}-geometry for the geometric environment of Cr(III) for which reason the configuration of the *cis*-$Cr(en)_2Cl_2$ starting

Table 4. Diffuse reflectance spectra of the complexes (bands in nm)

Compound	$\pi \rightarrow \pi^*$		$\nu_2[^4T_{1g}(F) \rightarrow {}^4A_{2g}]$	$\nu_1 (^4T_{2g} \rightarrow {}^4A_{2g})$	$10Dq$ (cm^{-1})	B' (cm^{-1})
URA	244s, 290sh					
cis-$[Cr(en)_2Cl_2)Cl \cdot (URA)_2 \cdot \frac{1}{2}AcOEt$[a]	249s, 294s	325s	362vs, 430vs } Average 396	465s, 495s, 605s } Average 521	18,600	600
$[Cr(NH_3)_5Cl]Cl_2(URA)$[b]	241s, 284s		367s	520s	18,952	824
URD	247s, 290sh					
cis-$[Cr(en)_2Cl_2]Cl \cdot (URD)_2$[a]	256s, 290s	325s	363vs, 431vs } Average 396	465s, 495s, 608s } Average 522	18,694	584
$[Cr(NH_3)_5Cl]Cl_2(URD)$[b]	247s, 280sh		370s	520s	18,684	786
$Na_2$5'-UMP	250s, 292s					
$Na_2[Cr(en)_2(5'\text{-UMP})_2 \cdot (5'\text{-UMPH})] \cdot 7H_2O$	255s, 300sh	325s	363vs, 431vs } Average 397	470s, 495s, 560s, 606s } Average 532	18,207	638

[a] For the *cis*-$[Cr(en)_2Cl_2]Cl \cdot H_2O$ complex bands at 325s, 363s, 431s, 465s, 495s and 605s cm^{-1}.
[b] For the $[Cr(NH_3)_5Cl]Cl_2$ complex bands at 368s, 433 sh and 520s cm^{-1}.

complex has been retained. In the derivative of 5'-UMP four bands appear, some of which must be spin-forbidden.

Λ_M values were obtained for the complexes of URA and URD, confirming the results of the IR and reflectance spectra, as they indicated the presence of types of electrolytes coinciding with those of the starting complexes[26] (Table 1).

The Λ_M value for the 5'-UMP complex indicates a situation corresponding to a 1:2 electrolyte, implying the existence of nucleotides associated by stacking phenomena or hydrogen bonds to the coordination sphere of Cr(III). Taking into account steric hindrance considerations and the IR and UV data, the structure of this compound can be interpreted as a pseudo-octahedral geometry with a C_{2v}-symmetry environment and bonding of Cr(III) to a nucleotide through the C_4=O group or the phosphate group, the other two being joined to the coordinated one. Rearrangement of the complex system in solution with release of the associated nucleotides is a possibility which cannot be ruled out.

Acknowledgement—This work was supported in part by "Vicerrectorat d'Investigació de la Universidad de Palma de Mallorca" with an "Ajut a la Investigació" and by CAICYT.

REFERENCES

1. E. W. Toepfer, W. Mertz, M. M. Polansky, E. E. Roginski and W. R. Wolf, *J. Agric. Food Chem.* 1977, **25**, 163.
2. S. Langard (Ed.), *Biological and Environmental Aspects of Chromium.* Elsevier Biomedical Press, Amsterdam (1982).
3. W. W. Cleland and A. S. Mildvan, *Adv. Inorg. Biochem.* 1979, **1**, 163.
4. J. J. Fiol, A. Terrón and V. Moreno, *Inorg. Chim. Acta* 1984, **83**, 69.
5. J. Campomar, submitted for publication in *Inorg. Chim. Acta.*
6. J. Campomar, A. Terrón, J. J. Fiol and V. Moreno, *XX Reunión Bienal de la Real Sociedad Española de Química, Castellón*, Comunicación 4-2°.
7. I. Mutikainen and P. Lumme, *Acta Cryst.* 1980, **B36**, 2237.
8. R. Weiss, H. Venner, *Hoppe-Seyler's Z. Physiol. Chem.* 1969, **350**, 396.
9. A. R. Sarkar and P. Ghosh, *Inorg. Chim. Acta* 1983, **78**, L-39.
10. M. Goodgame and K. W. Johns, *J. Chem. Soc., Dalton Trans.* 1977, 1680.
11. P. Ghosh, T. K. Mukhopadhyay and A. R. Sarkar, *Transition Met. Chem.* 1984, **9**, 46.
12. B. E. Fischer and R. Bau, *J. Chem. Soc., Chem. Commun.* 1977, 272.
13. B. A. Cartwright, D. M. L. Goodgame, I. Jeeves and A. C. Skapski, *Biochim. Biophys. Acta* 1977, **477**, 195.
14. F. D. Snell, *Encyclopedia of Industrial Analysis*, Vol. 17, p. 67. Wiley, New York (1973).
15. E. B. Sandell, *Colorimetric Metal Analysis.* Wiley, New York (1959).
16. W. C. Fernelius (Ed.), *Inorganic Syntheses*, Vol. 2, p. 200 (1978).
17. G. Brauer, *Química Inorgánica Preparativa.* Reverté, Barcelona (1968).
18. M. Goodgame and K. W. Johns, *J. Chem. Soc., Dalton Trans.* 1978, 1294.
19. M. Tsuboi, *Basic Principles in Nucleic Acid Chemistry*, Vol. 1, p. 400. P.O.P. Ts'o, Academic Press (1974).
20. R. C. Lord and G. J. Thomas, *Spectrochim. Acta* 1967, **23A**, 2251.
21. H. Susi and R. Ard, *Spectrochim. Acta* 1971, **A27**, 1549.
22. K. Nakamoto, *Infrared and Raman Spectra of Inorganic and Coordination Compounds.* Wiley, New York (1978).
23. I. Nakagawa and T. Shimanouchi, *Spectrochim. Acta* 1966, **22**, 759.
24. D. Voet and A. Rich, *Prog. Nucleic Acid Res. Mol. Biol.* 1970, **10**, 183.
25. A. B. Lever, *Inorganic Electronic Spectroscopy*, 2nd Edn. Elsevier, Amsterdam (1984).
26. W. J. Geary, *Coord. Chem. Rev.* 1971, **7**, 81.

Polyhedron Vol. 5, No. 5, pp. 1131–1134, 1986
Printed in Great Britain

0277–5387/86 $3.00+.00
Pergamon Journals Ltd

POTENTIOMETRIC STUDIES ON COMPLEXES IN Cr(III)–L-ASPARTIC ACID–DL-METHIONINE OR DL-ETHIONINE SYSTEMS

JOANNA MASŁOWSKA* and LONGIN CHRUŚCIŃSKI

Institute of General Food Chemistry, Technical University, 90-924 Łódź, B. Stefanowskiego 4/10, Poland

(*Received* 11 *December* 1984; *accepted after revision* 23 *October* 1985)

Abstract—Simple and mixed-ligand complexes of Cr(III) with L-aspartic acid and DL-methionine or DL-ethionine have been investigated by potentiometric measurements at 25°C and 0.1 M ($NaClO_4$) ionic strength. The stability constants of the complexes and tendency toward mixed-ligand complex formation have been determined.

Cr(III) is an essential metal ion for living organisms. Mertz first described a chromium dependence in rats and later showed that chromium is an essential co-factor for insulin and is required for normal glucose tolerance in rats.[1–3] Studies on the isolation and characterization of biological chromium complexes have shown that various amino acids and nicotinic acid serve as structural components of the active complex.[4–8]

Investigations of the stability of mixed-ligand complexes will help toward understanding the driving forces that lead to the formation of such complexes in biological systems. Stability constants of the binary complexes of Cr(III) with several amino acids were obtained by Tsuchiya *et al.*[9,10] and Khan and Malik,[11] but only one paper[12] was concerned with the determination of stability constants of mixed-ligand complexes of Cr(III) with amino acids.

In previous papers[13–15] we described studies of complexes of Ni(II) and Cr(III) with sulphur-containing amino acids. We now report potentiometric investigation of simple and mixed-ligand complexes in Cr(III)–L-aspartic acid (L-asp)–DL-methionine (DL-met) or DL-ethionine (DL-eth) systems.

EXPERIMENTAL

Materials

L-asp acid (Merck), DL-met (Fluka) and DL-eth (Fluka) were purified by recrystallization from water–ethanol solutions. Their purity was tested by chromatographic and potentiometric methods.

Chromium perchlorate was prepared from chromium hydroxide, perchlorate acid and hydrogen peroxide.[16] The stock solution of chromium perchlorate was standardized by a redoxymetric method.[17] For the pH-metric titration an approximately 1 M NaOH solution, carbonate-free, was used.

Apparatus

All measurements were carried out under nitrogen (freed from oxygen) in a special vessel described previously.[18] A digital OP-208 pH-meter (Radelkis) with OP-0718P glass and OP-0830P calomel reference electrodes was used for the measurements. The pH standards were 0.05 M potassium hydrogen phthalate (pH = 4.008) and 0.025 M KH_2PO_4 and 0.025 M Na_2HPO_4 phosphate buffer (pH = 6.865) at 25°C. To calibrate the glass electrode within the acid range of pH, a standard $HClO_4$ solution with an ionic strength (μ) of 0.1 ($NaClO_4$) was used. An NaOH solution was added from an ABU-11 burette (Radiometer).

Measurement methods

Potentiometric investigations of the simple Cr(III) complexes with amino acids were carried out at metal : ligand ratios of 1 : 1, 1 : 3 and 1 : 6, and those of mixed-ligand complexes at metal : ligand A : ligand B ratios of 1 : 1 : 1, 1 : 3 : 3 and 1 : 6 : 6. The concentration

* Author to whom correspondence should be addressed.

of Cr(III) was 3×10^{-3} or 5×10^{-3} M. The μ of the solutions was maintained constant at 0.1 ($NaClO_4$).

Because of the slow achievement of an equilibrium between Cr(III) ions and ligands we used special techniques, similar to those described in other papers.[9,10,12]

For each measurement series, tens of solution samples were prepared, containing Cr(III) ions, and one or two amino acids of concentration and μ as above: volume = 70 cm^3. Various amounts of NaOH were added to each sample. The samples were heated for 2 h at 80°C, and then they were stored for 1.5 months at a constant temperature of 25 ± 0.1°C.

The equilibrium process was monitored by periodically measuring the pH value of the solution. It was found that equilibrium was achieved within 1 month. Turbid samples with precipitated chromium hydroxide were rejected. The volume of added NaOH was plotted vs pH to obtain a simulated titration curve. The protonation constants of the amino acids were determined on the basis of classical titration curves.[19] Values for dissociation constants and stability constants of Cr(III) complexes were calculated with the aid of the MINIQUAD computer program,[20] using an ODRA 1305 computer.

RESULTS AND DISCUSSION

Based on the potentiometric data obtained for binary systems, values of $\bar{n}$ (average ligand number) and the concentration of free uncomplexed ligand ([L]) were determined. Plots of formation curves are shown in Fig. 1. The formation curves reach a maximum at $\bar{n} = 1.8$ for L-asp, $\bar{n} = 1.2$ for DL-met and $\bar{n} = 1.6$ for DL-eth. The formation curves for various Cr:L ratios do not overlap, which shows that the formation curve depends on the Cr(III) concentration. This indicates the formation of complexes different from mononuclear 1:1 and 1:2 complexes. The pH range (1.8–4.3) and the protonated forms of ligands occurring within this pH range suggest the possibility of the formation of protonated species. The appearance of such complexes meant that it was impossible to use graphic methods for the determination of stability constants. Among several possible models for complexes appearing in the binary systems, the best fit to the experimental data was obtained for the Cr(III)–L-asp system with ML, ML_2 and MHL complexes, and for the Cr(III)–DL-met and Cr(III)–DL-eth systems with ML, ML_2 and MHL complexes.

The values of the stability constants for binary Cr(III) complexes are given in Table 1. Table 1 also contains the protonation constants of the ligands investigated.

The formation of mixed-ligand complexes in the Cr(III)–L-asp (A)–DL-met (B) or DL-eth (B) systems was confirmed by the composition curve which was found using the assumption that mixed-ligand complexes were not formed. The composition and titration curves for the systems containing the Cr(III) ion and two ligands do not overlap. The possibility of the formation of the following complexes was considered: MAB, MHAB, MH_2AB, MA_2B and

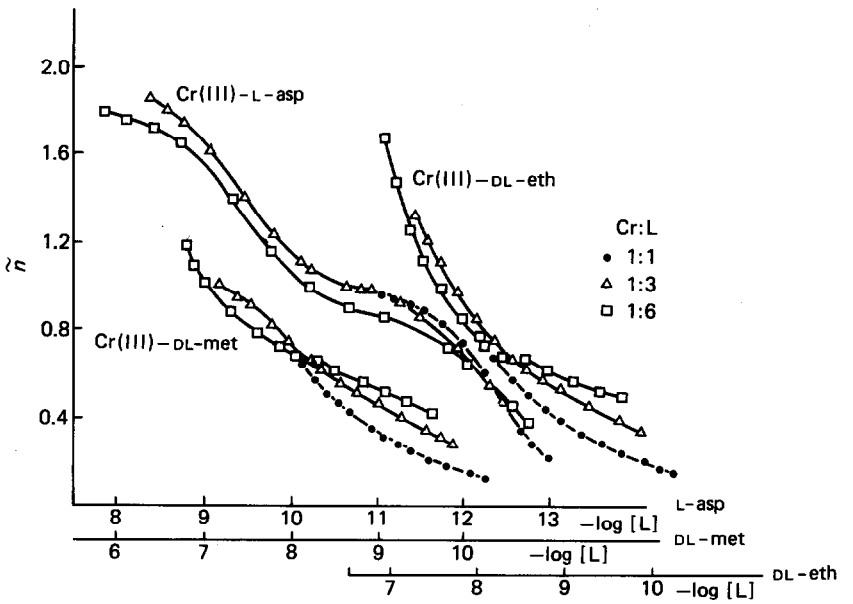


Fig. 1. Formation curves, $\bar{n} = f(-\log [L])$, for the Cr(III)–L–H_2O systems, where L = L-asp, DL-met or DL-eth.

Table 1. Stability constants (log β_{pqr}) of $M_pH_qL_r$ complexes formed in the Cr(III)–L–H_2O systems and protonation constants (log β_n) of H_nL ligand, where L = L-asp, DL-met or DL-eth: 25°C, μ = 0.1 ($NaClO_4$)[a]

	L-asp	DL-met	DL-eth
log β_1	9.918(3)	9.150(3)	9.190(4)
log β_2	13.882(5)	11.471(4)	11.400(4)
log β_3	15.814(5)		
log β_{101}	12.46(7)	8.35(6)	8.46(4)
log β_{111}		11.41(8)	11.50(6)
log β_{102}	21.86(5)	15.52(7)	15.67(7)
log β_{112}	24.30(10)		

[a] Standard deviation values in parentheses.

MAB_2. The best fit to the experimental data was obtained for the MAB and MHAB complexes. The stability constants for the mixed-ligand complexes are given in Table 2. The values are also given for the parameters determining the tendency toward mixed-ligand complex formation: Δ log K_{MAB}, showing the difference between the stability of the binary and ternary complexes, the disproportionation constant (log χ_{MAB}) and Δ_{MAB} [the stabilization constant (difference between the measured and statistically calculated stability constants) for the MAB complex].

It is clear from a comparison of the stability constants that L-asp forms considerably more stable complexes with Cr(III) than does DL-met or DL-eth. This results from the possible formation of five- and six-member chelate rings for L-asp complexes. The values of the stability constants for the binary complexes determined by us are consistent with the literature data. Tsuchiya *et al.*[10] obtained log β_{101} = 10.1 and log β_{102} = 19.6 at 25°C and μ = 0.1 for L-asp, and Santappa *et al.*[12] for the same ligand obtained log β_{101} = 12.15, log β_{102} = 21.13 and log β_{112} = 24.07 at 50°C. Khan and Malik[11] reported values for log β_{101}, log β_{102} and log β_{103} of 8.3, 14.5 and 19.8, respectively, for methionine. There is no value for ethionine in the literature.

The values of the stability constants for mixed Cr(III) complexes (Table 2) show that DL-met and DL-eth as well as L-asp from complexes with similar stabilities, the somewhat higher stability of DL-eth complexes resulting from the higher basicity of this amino acid. For statistical reasons,[21] if Δ log K_{MAB} > −0.4, log χ_{MAB} > 0.6 and Δ_{MAB} is positive then there is an increase in the stability of mixed complexes compared to the binary ones. Negative values of log K_{MAB} for DL-met and DL-eth suggest a shift in the equilibrium of eqn (1) (Table 2) to the left. The values of log χ_{MAB} in Table 2 are higher than 0.6, which suggests stabilization of the mixed complexes compared to the binary ones, and the positive value of Δ_{MAB} points to an increase in the stability of mixed-ligand complexes compared to the statistical case.

The concentration distribution of particular forms of complexes (Figs 2 and 3) shows that the binary MA and MA_2 complexes and the mixed-ligand MHAB complex are predominant within the given pH range and that the mixed-ligand MAB complex is insignificant, which is confirmed by the negative value of Δ log K_{MAB}.

Table 2. Stability constant (log β_{pqrs}) of $M_pH_qA_rB_s$ complexes formed in the Cr(III)–A–B–H_2O systems where A = L-asp, and B = DL-met or DL-eth: 25°C, μ = 0.1 ($NaClO_4$)[a]

	System	
	Cr(III)–L-asp–DL-met	Cr(III)–L-asp–DL-eth
log β_{1011}	19.75(6)	19.84(12)
log β_{1111}	23.90(12)	24.08(7)
log K_{MAB}[b]	−1.06	−1.08
log χ_{MAB}[c]	2.12	2.15
Δ_{MAB}[d]	0.76	0.77

[a] Standard deviation values in parentheses.

[b] $MA + MB \rightleftarrows MAB + M$, log K_{MAB} = log β_{MAB} − (log β_{MA} + log β_{MB}).

[c] $MA_2 + MB_2 \rightleftarrows 2MAB$, log χ_{MAB} = 2 log β_{MAB} − (log β_{MA_2} + log β_{MB_2}).

[d] Δ_{MAB} = log $\beta_{calc.}$ − log $\beta_{stat.}$

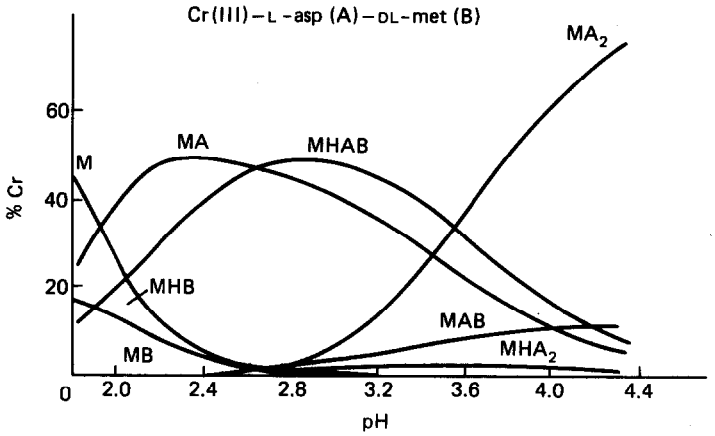


Fig. 2. Concentration distribution of complexes in the Cr(III)–L-asp–DL-met system.

4

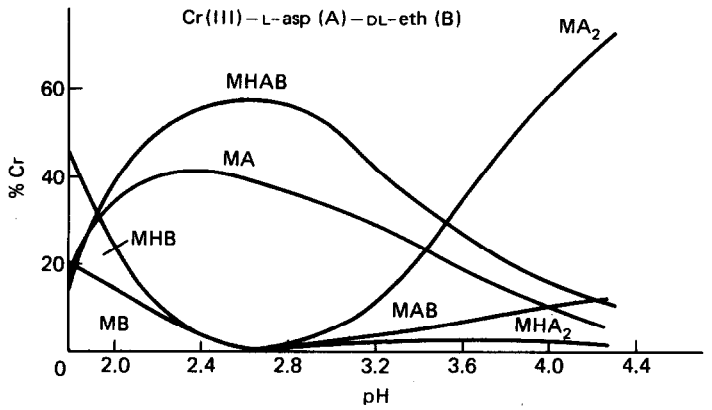


Fig. 3. Concentration distribution of complexes in the Cr(III)–L-asp–DL-eth system.

REFERENCES

1. W. Mertz and K. Schwartz, *Am. J. Physiol.* 1959, **196**, 614.
2. W. Mertz, *Physiol. Rev.* 1969, **49**, 163.
3. W. Mertz, *Science* 1981, **213**, 1332.
4. W. Mertz, E. W. Toepfer, E. E. Roginski and M. M. Polansky, *Fed. Proc.* 1974, **33**, 2275.
5. E. W. Toepfer, W. Mertz, M. M. Polansky, E. E. Roginski and W. R. Wolf, *J. Agric. Food Chem.* 1977, **25**, 1962.
6. N. Mirsky, A. Weiss and Z. Dori, *J. Inorg. Biochem.* 1978, **8**, 419.
7. J. V. Ardle, E. Lanbenfels, A. L. Shorter and H. L. Ammon, *Polyhedron* 1982, **1**, 471.
8. J. C. Chang, L. E. Gerdom, N. C. Baenziger and H. M. Goff, *Inorg. Chem.* 1983, **22**, 1739.
9. H. Matsukawa, M. Ohta, S. Takata and R. Tsuchiya, *Bull. Chem. Soc. Jpn* 1965, **38**, 1235.
10. H. Mizuochi, S. Shirakata, E. Kyuno and R. Tsuchiya, *Bull. Chem. Soc. Jpn* 1970, **43**, 397.
11. A. A. Khan and W. U. Malik, *J. Indian Chem. Soc.* 1963, **40**, 564.
12. K. Venkatachalpathi, M. S. Nair, D. Ramaswamy and M. Santappa, *J. Chem. Soc., Dalton Trans.* 1982, 291.
13. J. Masłowska and L. Chruściński, *J. Inorg. Nucl. Chem.* 1981, **43**, 1981.
14. J. Masłowska and L. Chruściński, *Polyhedron* 1984, **3**, 523.
15. J. Masłowska and L. Chruściński, *Polyhedron* 1984, **3**, 1329.
16. J. Rasko and Z. Saymosi, In *Thermal Analysis*, Vol. 1, p. 506. Proceeding Fourth, ICTA Budapest. Akademiai Kiado, Budapest (1975).
17. J. Minczewski and Z. Marczenko, In *Chemia Analityczna*, Vol. 2, p. 271. PWN, Warsaw (1973).
18. D. D. Perrin and I. G. Sayce, *Chem. Ind.* 1966, 661.
19. H. Rossotti, *The Study of Ionic Equilibria. An Introduction.* Longman, London (1978).
20. A. Sabatini, A. Vacca and T. P. Gans, *Talanta* 1974, **21**, 53.
21. H. Sigel, *Metal Ions in Biological Systems*, Vol. 2, Chap. 2, p. 63. Marcel Dekker, New York (1973).

Polyhedron Vol. 5, No. 5, pp. 1135–1139, 1986
Printed in Great Britain

0277–5387/86 $3.00+.00
Pergamon Journals Ltd

POTENTIOMETRIC STUDIES ON MIXED-LIGAND COMPLEXES OF Cr(III) WITH DL-METHIONINE, DL-ETHIONINE AND OTHER AMINO ACIDS

JOANNA MASŁOWSKA* and LONGIN CHRUŚCIŃSKI

Institute of General Food Chemistry, Technical University, 90-924 Łódź, B. Stefanowskiego 4/10, Poland

(*Received* 4 *September* 1985; *accepted* 4 *October* 1985)

Abstract—Binary and ternary complexes of Cr(III) with amino acids have been investigated by the potentiometric method using a glass electrode in the Cr(III)–A–B–H_2O systems, where A = DL-methionine or DL-ethionine, and B = L-glutamic acid, DL-α-amino-*n*-butyric acid, L-serine or L-threonine. The stability constants of the complexes and a tendency toward mixed-ligand complex formation have been determined.

The biological significance and function of the Cr(III) ion as an essential microelement have been described in papers by Mertz[1–5] and other authors,[6–8] as partly summarized in our previous paper.[9]

Doubtless the participation of mixed Cr(III) complexes with amino acids in the formation of biologically active forms in living organisms has encouraged us to start our studies on the interactions between Cr(III) ion and amino acids in aqueous solutions. As mentioned previously,[9] the literature concerning the determination of stability constants of Cr(III) complexes with amino acids by the potentiometric method, particularly of mixed complexes, is extremely scarce.[10–13]

Carrying on our investigations of the thermodynamic equilibrium between Ni(II) and Cr(III) ions with amino acids,[9,14–17] in the present paper we report the results of examinations of simple and mixed Cr(III) complexes formed in Cr(III)–amino acid (A)–amino acid (B) systems where A = DL-methionine (DL-met) or DL-ethionine (DL-eth), and B = L-glutamic acid (L-glu), DL-α-amino-*n*-butyric acid (DL-ambut), L-serine (L-ser) or L-threonine (L-tre).

EXPERIMENTAL

Reagents

The following were used as ligands after being additionally purified by crystallization from water–ethanol solutions: DL-met (Reanal), DL-eth (Fluka), L-glu (Merck), DL-ambut (Reanal), L-ser (Merck) and L-tre (Merck). Their purity was tested by a chromatographic method. Chromium perchlorate was prepared and standardized as described previously.[9] For the pH-metric titration, a 1.0415 M solution, carbonate-free, was used.

Apparatus

Potentiometric measurements were carried out by means of a digital OP-208 pH-meter (Radelkis) with OP-0718P glass and OP-0830P calomel electrodes.

The measurement vessel and calibration procedure were as described previously.[9] The NaOH solution used for titration was added from an ABU-11 burette (Radiometer). The ionic strength (μ) of the solutions was 0.1 ($NaClO_4$) at 25°C.

Measurement methods

To determine the composition and stability constants of the complexes, samples of their solutions with variable initial composition were titrated with NaOH solution.

Because of the very slow achievement of an equilibrium between Cr(III) ions and amino acid molecules we used a titration technique typical for Cr(III) complexes, as described elsewhere.[9,11,13] Titration curves were prepared from pH-measurements of tens of samples with constant ratios of the concentrations of Cr(III) ions and amino acids within the given measurement series, and with various amounts of added NaOH. Before measure-

* Author to whom correspondence should be addressed.

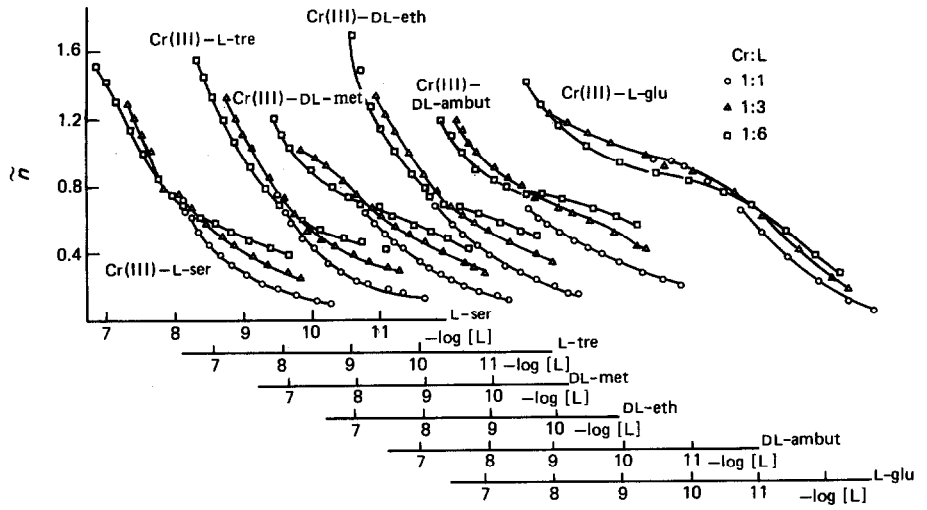


Fig. 1. Formation curves, $n = f(-\log [L])$, for the Cr(III)–L–H_2O systems, where L = DL-met, DL-eth, DL-ambut, L-ser, L-tre or L-glu.

ments, the samples were maintained at 25°C for a period to reach equilibrium. For binary systems the initial metal:ligand ratios were 1:1, 1:3 and 1:6, while for the ternary systems the metal:ligand A:ligand B initial ratios were 1:1:1, 1:3:3 and 1:6:6. The concentration of Cr(III) ions was 3×10^{-3} or 5×10^{-3} M. The stability constants of the complexes were found by means of the MINIQUAD program,[18] using an ODRA 1305 computer.

RESULTS AND DISCUSSION

Analysis of the Bjerrum formation curves, $n = f(-\log [L])$ (Fig. 1), determined from potentiometric measurements shows that, in the systems under investigation, besides mononuclear complexes of compositions 1:1 and 1:2, other complexes may also appear. The formation curves found for various initial Cr(III):L ratios do not overlap. The low pH range (1.8–4.3) and the existence of protonated ligand forms within this range suggest the possible formation of complexes with a protonated ligand. The formation curves for systems containing DL-ambut, L-ser and L-tre (Fig. 1), and DL-met and DL-eth (see also Ref. 9), show similar courses, which suggests the same model for the formation and appearance of the complexes. The course of the formation curve for L-glu is different. Calculations made for the binary systems showed that the best fit to the experimental data was obtained when the formation of the following types of complexes was taken into consideration: ML, ML_2 and MHL for DL-met, DL-eth, DL-ambut, L-ser and L-tre, and ML, ML_2, MHL and MHL_2 for L-glu.

The values of the stability constants of the Cr(III) complexes formed in the systems investigated are given in Table 1, which also includes the protonation constants of the ligands.

Table 1. Stability constants (log β_{pqr}) of $M_pH_qL_r$ complexes formed in the Cr(III)–L–H_2O system and protonation constants (log β_n) of H_nL ligand, where L = L-glu, DL-met, DL-eth, DL-ambut, L-ser or L-tre: 25°C, $\mu = 0.1$ ($NaClO_4$)[a]

	L-glu	DL-ambut	DL-met	DL-eth	L-ser	L-tre
$\log \beta_1$	9.974(4)	9.622(3)	9.150(3)	9.190(4)	9.171(6)	9.103(7)
$\log \beta_2$	14.500(6)	12.156(2)	11.471(4)	11.400(4)	11.382(8)	11.265(7)
$\log \beta_3$	16.801(8)					
$\log \beta_{101}$	11.79(8)	8.84(6)	8.35(10)	8.46(4)	8.31(6)	8.17(8)
$\log \beta_{111}$	14.58(7)	12.25(7)	11.41(8)	11.50(6)	11.27(4)	11.04(10)
$\log \beta_{102}$	19.46(10)	16.09(3)	15.52(11)	15.67(7)	15.44(9)	15.30(9)
$\log \beta_{112}$	24.19(11)					

[a] Standard deviation values in parentheses.

The titration curves for the mixed systems did not agree with the composition curves theoretically calculated using the assumption that mixed complexes are not formed in the given systems. This would suggest that mixed complexes can appear in the ternary systems investigated. As in Ref. 9, the possibility exists of the formation of mixed complexes of various types as simple, protonated and polynuclear complexes. The best fit to the experimental data was obtained when it was assumed that complexes are formed of types MAB and MHAB. This is supported by the fact that the stability constants for these complexes (Table 2) have small standard deviations. Table 2 also includes values of other parameters describing the stability and tendency to form mixed complexes in the given systems. Below Table 2 are the equations used to calculate the values of these parameters.

The values of the stability constants shown in Table 1 prove that Cr(III) forms complexes of high stability with the amino acids investigated. A characteristic increase in the stability constant $\log \beta_{101}$ is seen with increasing ligand basicity, expressed by the pK of the amino group of the amino acid. The increasing order of $\log \beta_{101}$ is as follows: L-tre < L-ser < DL-met < DL-eth < DL-ambut < L-glu. The values of the stability constants of Cr(III) with L-tre and L-ser show that it is doubtful that the hydroxyl group of these amino acids takes part in the coordination. Similarly, participation of the thioether group of DL-met and DL-eth in the coordination can be excluded since the values of the stability constants of all the complexes are much the same, which suggests a classical type of coordination of amino acids through amino and carboxyl groups. Only the higher values of the stability constants of the L-glu complexes [similar to L-aspartic acid (L-asp[9,13])] point to a tridentate coordination of this amino acid and the possibility of the atom of five- and seven-member chelate rings. The values of the stability constants of simple Cr(III) complexes with the amino acids investigated are similar to those found potentiometrically by other authors. Khan and Malik[10] found that the stability constants of Cr(III) complexes with methionine and serine were: $\log K_1 = 8.3$, $\log K_2 = 6.2$ and $\log K_3 = 5.3$; and $\log K_1 = 8.0$ and $\log K_2 = 5.2$, respectively, at 25°C and $\mu = 0.1$.

Venkatachalapathi *et al.*[13] found the following values of the constants: $\log \beta_{101} = 11.39$, $\log \beta_{111} = 14.04$, $\log \beta_{102} = 18.96$, and $\log \beta_{112} = 23.91$ for L-glu at 50°C and $\mu = 0.1$.

There are no data for ethionine, threonine and α-aminobutyric acid in the literature.

Based on the stability constants of the mixed complexes, it can be stated that, in the ternary systems investigated, mixed complexes of comparable stabilities are formed; somewhat higher values were obtained for complexes containing DL-eth compared to DL-met complexes.

According to Sigel,[19] if $\Delta \log K_{MAB} > -0.4$ and $\log \chi_{MAB}$ is > 0.6, at positive values of Δ_{MAB} there is an increase in the stability of mixed-ligand complexes compared to the simple ones. From the analysis of these parameters for the systems investigated it follows that the values of $\Delta \log K_{MAB}$ decrease in the following order for ligand B (also using data from our previous paper[9]): DL-ambut ≈ L-ser > L-tre > L-

Table 2. Stability constants ($\log \beta_{pqrs}$) of $M_pH_qA_rB_s$ complexes formed in the Cr(III)–A–B–H_2O systems, where A = DL-met or DL-eth; B = L-glu, DL-ambut, L-ser or L-tre: 25°C, $\mu = 0.1$ ($NaClO_4$)[a]

A	B	$\log \beta_{1011}$	$\log \beta_{1111}$	$\Delta \log K_{MAB}$[b]	$\log \chi_{MAB}$[c]	Δ_{MAB}[d]
DL-met	L-glu	18.75(12)	22.68(8)	−1.39	2.52	0.95
DL-met	DL-ambut	16.25(10)	20.06(11)	−0.94	0.89	0.14
DL-met	L-ser	15.72(11)	19.64(12)	−0.94	0.48	−0.06
DL-met	L-tre	15.52(10)	19.35(18)	−0.97	0.28	−0.16
DL-eth	L-glu	18.82(11)	22.75(9)	−1.43	2.51	0.95
DL-eth	DL-ambut	16.31(10)	20.21(14)	−0.99	0.86	0.13
DL-eth	L-ser	15.80(14)	19.82(11)	−0.97	0.49	−0.06
DL-eth	L-tre	15.62(16)	19.53(21)	−1.01	0.23	−0.17

[a] Standard deviation values in parentheses.
[b] $MA + MB \rightleftharpoons MAB + M$, $\Delta \log K_{MAB} = \log \beta_{MAB} - (\log \beta_{MA} + \log \beta_{MB})$.
[c] $MA_2 + MB_2 \rightleftharpoons 2MAB$, $\log \chi_{MAB} = 2 \log \beta_{MAB} - (\log \beta_{MA_2} + \log \beta_{MB_2})$.
[d] $\Delta_{MAB} = \log \beta_{calc.} - \log \beta_{stat.}$.

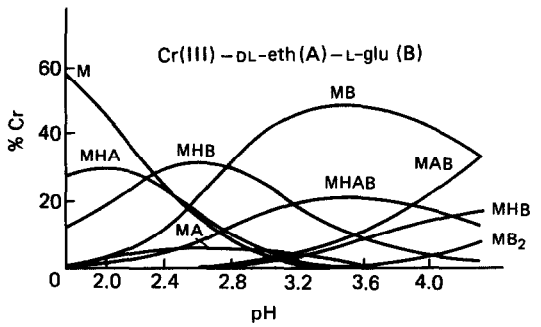


Fig. 2. Concentration distribution of complexes in the Cr(III)–DL-eth (A)–L-glu (B) system.

asp > L-glu. The tendency to form mixed complexes also decreases in the same order. Values of log $\chi_{MAB} > 0.6$ and $\Delta_{MAB} > 0$ are for all the mixed complexes except for those containing L-ser and L-tre. The values of log χ_{MAB} show that there is a greater tendency to form 1 : 2 mixed complexes from the simple complex than 1 : 1 ones. Thus, it can be stated that the tendency to form mixed complexes is a moderate one in all the systems except those which contain L-ser and L-tre. As is also seen from Table 2, the tendency to form mixed protonated complexes is greater than that to form mixed non-protonated complexes.

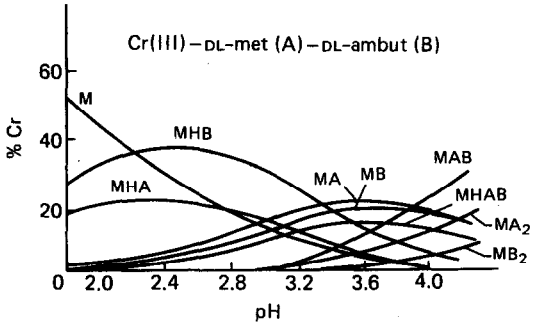


Fig. 3. Concentration distribution of complexes in the Cr(III)–DL-met (A)–DL-ambut (B) system.

These conclusions are supported by the curves of percent share of particular complex vs pH. The plots shown in Figs 2–4 are typical for the systems investigated. In the Cr(III)–DL-met or DL-eth–L-glu systems (Fig. 2), the highest shares are for MHA and MHB complexes at pH 1.8–2.8. Within the pH range 2.8–4.3 there is about 50% of MB (at pH 3.6) and about 20% of MHAB (at pH 3.3). At pH 4.3 the share of MAB was about 30%.

In the Cr(III)–DL-met or DL-eth–DL-ambut system (Fig. 3), MHA and MHB complexes prevail up to pH 3.3. The share of MHAB (about 17% at pH 3.6) is lower than that of MA and MB, and, above pH 3.9, the MAB complex predominates.

In the Cr(III)–DL-met or DL-eth–L-ser or L-tre system the highest shares are for MHA and MHB for pH 1.8–2.9, while for pH 2.9–4.2 MA, MB and MHAB complexes are predominant. At pH 4.2, the share of the MAB complex is about 25%.

REFERENCES

1. W. Mertz and K. Schwartz, *Am. J. Physiol.* 1959, **196**, 614.
2. W. Mertz, *Physiol. Rev.* 1969, **163**, 49.
3. W. Mertz, *Science* 1981, **213**, 1332.
4. W. Mertz, E. W. Toepfer, E. E. Roginski and M. M. Polansky, *Fed. Proc.* 1974, **33**, 2275.
5. E. W. Toepfer, W. Mertz, M. M. Polansky, E. E. Roginski and W. R. Wolf, *J. Agric. Food Chem.* 1977, **25**, 1962.
6. N. Mirsky, A. Weiss and Z. Dori, *J. Inorg. Biochem.* 1979, **8**, 419.
7. J. V. McArdle, E. Lanbefels, A. L. Shorter and H. L. Ammon, *Polyhedron* 1982, **1**, 471.
8. J. C. Chang, L. E. Gerdom, N. C. Baenziger and H. M. Goff, *Inorg. Chem.* 1983, **22**, 1739.
9. J. Masłowska and L. Chruściński, *Polyhedron* 1986, **5**, 1131.
10. A. A. Khan and W. U. Malik, *J. Indian Chem. Soc.* 1963, **40**, 564.
11. H. Matsukawa, M. Ohta, S. Takata and R. Tsuchiya, *Bull. Chem. Soc. Jpn* 1965, **38**, 1235.

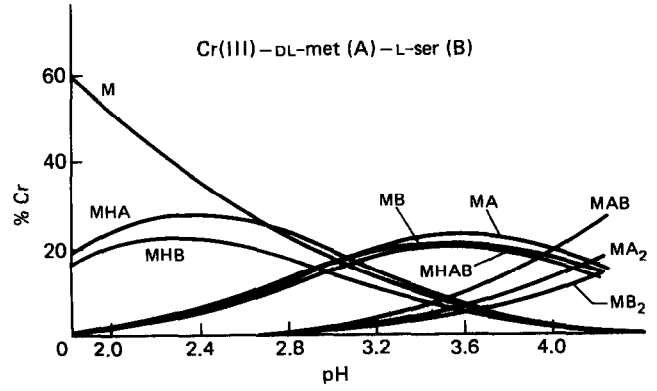


Fig. 4. Concentration distribution of complexes in the Cr(III)–DL-met (A)–L-ser (B) system.

12. H. Mizouchi, S. Shirakata, E. Kyuno and R. Tsuchiya, *Bull. Chem. Soc. Jpn* 1970, **43**, 397.
13. K. Venkatachalapathi, M. S. Nair, D. Ramaswamy and M. Santappa, *J. Chem. Soc., Dalton Trans.* 1982, 291.
14. J. Masłowska and L. Chruściński, *J. Inorg. Nucl. Chem.* 1981, **43**, 3398.
15. J. Masłowska and L. Chruściński, *Polyhedron* 1984, **3**, 523.
16. J. Masłowska and L. Chruściński, *Polyhedron* 1984, **3**, 1329.
17. J. Masłowska and L. Chruściński, *Acta Univ. Lodz., Folia Chim.* 1984, **3**, 23.
18. A. Sabatini, A. Vacca and T. P. Gans, *Talanta* 1974, **21**, 53.
19. H. Sigel, *Metal Ions in Biological Systems*, Vol. 2, Chap. 2. Marcel Dekker, New York (1973).

Polyhedron Vol. 5, No. 5, p. 1141, 1986
Pergamon Journals Ltd. Printed in Great Britain

ANNOUNCEMENT

THIRTEENTH INTERNATIONAL CONFERENCE ON ORGANOMETALLIC CHEMISTRY

The Thirteenth International Conference on Organometallic Chemistry will be held in Turin, Italy (4–9 September 1988). For further information contact: Professor Luciano Milone, Istituto di Chimica Generale ed Inorganica, Facoltà di Farmacia, Via P. Giuria 9, I-10125, Turin, Italy.

Polyhedron Vol. 5, No. 6, pp. 1143–1147, 1986
Printed in Great Britain

0277–5387/86 $3.00+.00
Pergamon Journals Ltd

AZIDE LIGAND SUBSTITUTION REACTION IN ZINC BIS(DIETHYLDITHIOCARBAMATE)

M. T. KOSTANSKI*† and W. MENDYK

Department of Chemistry, Poznan Technical University, 60-965 Poznan, Poland

(*Received* 27 *June* 1985; *accepted* 7 *October* 1985)

Abstract—The azide ligand substitution reaction in tetrahedral zinc bis(diethyldithiocarbamate) has been studied by extraction. The reaction has been shown to proceed by both solvent and azide ion interactions, with $k_0 = 5.0 \times 10^{-4}$ s^{-1} and $k_1 = 1.9 \times 10^{-3}$ M^{-1} s^{-1}. A general discussion of the reaction mechanism is provided.

The reaction of sodium azide with iodine is induced by organic compounds of sulphur-containing thiolic or thionic groups. Among other compounds several dithiocarbamates were analyzed with very favourable detection limits.[1–6] The so-called "iodo-azide" reaction was also applied to the determination of traces of several metals. This method is based on the assumption of the inertness of some of chelate complexes formed with the sulphur-containing ligands. Diethyldithiocarbamate (dedtc) was also successfully applied in this analytical method.[7,8]

Our investigations of the ligand exchange reactions in the diethyldithiocarbamato complexes using the radio tracer method indicated the inertness of Co(III) and Cr(III) chelates.[9,10] Complexes of Ni(II), Cu(II), Zn(II) and Fe(III) were labile. It was found that both $Cr(dedtc)_3$ and $Co(dedtc)_3$ undergo in DMF a very slow ligand exchange via a dissociative mechanism, with an activation energy of 15.9 and 21.1 kcal mol^{-1}, respectively. These results are in agreement with those obtained by Palazzotto *et al.*,[11] Moriyasu and Hashimoto,[12] Duffy,[13] Duffy *et al.*,[14] Beinrohr and Garaj,[15] and Liska *et al.*[16] However, all the above mentioned studies were performed in non-aqueous solutions. Due to the specific experimental conditions in the iodo-azide reaction (i.e. aqueous solution and very high azide ion concentration) it was interesting to investigate the ligand substitution in detc complexes in these conditions. In this work we examine the reaction of $Zn(dedtc)_2$ with the azide ion in aqueous medium. It has been demonstrated that the solvent extraction is a very useful technique for the examination of the ligand substitution reactions of water-insoluble chelates. This technique was therefore applied throughout the experimental part of this work.

EXPERIMENTAL

Reagents

$Zn(dedtc)_2$ labelled with ^{65}Zn was prepared similarly to a method described in Ref. 17 using radioactive $^{65}ZnSO_4$ (OPiDI, Swierk, Poland). All other reagents were of analytical grade. Chloroform was purified by shaking with sodium bicarbonate, washing with water and finally distilling. A stock solution of 1×10^{-3} M $Zn(dedtc)_2$ in $CHCl_3$ was prepared by weighing: working solutions were obtained by appropriate dilution of the stock solution. Investigations were conducted in the pH range 5.8–6.9: the pH of the aqueous phase was adjusted with $HClO_4$ and did not change during the kinetic run due to the formation of the N_3^-–HN_3 buffer. Because of the very high concentration of azide ion applied (1.5–4.0 M), the ionic strength was not kept constant and varied with the NaN_3 concentration. The concentration of $Zn(dedtc)_2$ in the $CHCl_3$ phase varied from 1×10^{-5} to 1×10^{-4} M.

Extraction procedure

Experiments were performed in a specially designed glass extraction vessel which allowed the measurements of the radioactivity of both phases

* Author to whom correspondence should be addressed.
† Present address: Department of Chemistry, University of Arizona, Tucson, AZ 85721, U.S.A.

without having to withdraw aliquots of either phase. The vessel was agitated with a magnetic stirrer, whose stirring speed was adjusted by an autotransformer. In order to assure that the mass transport across the phase boundary was not the rate-determining process preliminary experiments on the influence of the stirring speed on the reaction's kinctics were undertaken. Further experiments were carried out in the "plateau" region where there was no influence of the stirring conditions and the whole process was controlled by the rate of reaction. Thirty cubic centimetres of the organic phase containing $Zn(dedtc)_2$ was introduced into the extraction vessel and its radioactivity was measured with an NaI well-type scintillation counter. The aqueous phase containing azide ions was then carefully added and the phases stirred for determined time intervals. After phase separation the radioactivities of both phases were measured and their sum agreed within 1% with the initial activity of the organic phase. Finally, the pH of the aqueous phase was measured with a pH-meter. Experiments which were duplicated agreed within 10%.

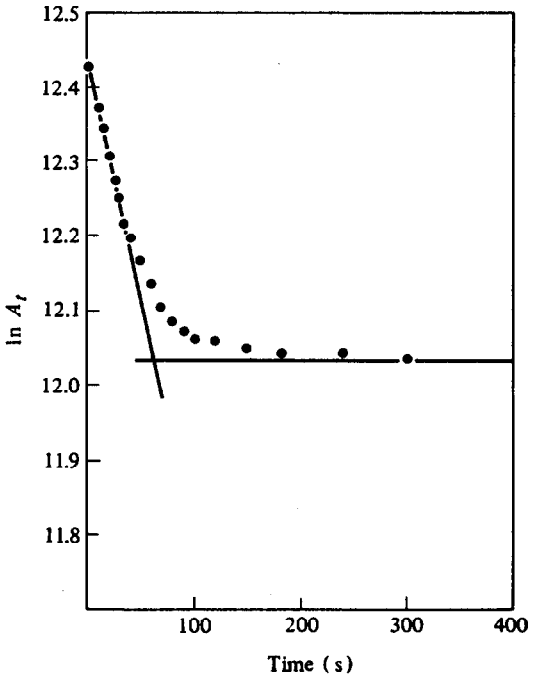


Fig. 1. Plot of $\ln A_t = f(t)$ for the experimental conditions: $[N_3^-] = 3$ M, $[Zn(dedtc)_2] = 3 \times 10^{-5}$ M, pH = 6.12.

Kinetic experiments

Kinetic runs were carried out under pseudo-first-order conditions with azide ions in the aqueous phase being in large excess over $Zn(dedtc)_2$ in the organic phase. All experiments were made at ambient temperature (21 ± 1°C). The pseudo-first-order rate constants (k_{absd}) were determined from the equation:

$$\ln \frac{[Zn]_t - [Zn]_\infty}{[Zn]_0 - [Zn]_\infty} = \ln \frac{A_t - A_\infty}{A_0 - A_\infty} = kt,$$

where $[Zn]_0$, $[Zn]_t$, $[Zn]_\infty$, A_0, A_t and A_∞ are total concentrations of Zn in the aqueous phase and their respective radioactivities at reaction times zero, t, and after completion of the reaction. Since the value of A_0 was zero and A_∞ was constant, plots of $\ln A_t = f(t)$ were used to calculate the rate constants.

RESULTS AND DISCUSSION

A typical plot of $\ln A_t$ against time (t) is presented in Fig. 1. None of these plots was linear, which indicates complex reaction kinetics. Moreover, the value of $A_{aq,t=\infty}/A_{o,t=\infty}$ depends on the concentrations of $Zn(dedtc)_2$ and the azide ion.

Both facts suggest that reversible, consecutive reactions operate in the system and that one of the reaction's products accumulates in the aqueous phase. This, in turn, influences the position of the attained equilibrium. The concentration of Zn in the aqueous phase in the equilibrium can be calculated from the following equations:

$$\beta_{Zn(dedtc)_2} = \frac{[Zn(dedtc)_2]}{[Zn] \cdot [dedtc)]^2}, \quad (1)$$

$$P = \frac{[Zn(dedtc)_2]_o}{[Zn(dedtc)_2]}, \quad (2)$$

$$[Zn]_t = [Zn](1 + \beta_1[N_3] + \beta_2[N_3]^2 + \beta_3[N_3]^3 + \beta_4[N_3]^4), \quad (3)$$

$$[Zn]_t = 2[dedtc^-], \quad (4)$$

where P is the distribution constant of $Zn(dedtc)_2$, β_1–β_4 are consecutive stability constants for the zinc azide complexes, $\beta_{Zn(dedtc)_2}$ is the stability constant of the zinc dedtc complex and $[Zn]_t$ is the total concentration of zinc in the aqueous phase. For the pH applied in this study (5.8–6.9) the protonation of the $dedtc^-$ ion and further extraction of the Hdedtc formed ($K_{HA} = 4.17 \times 10^{-4}$ [18]) as well as the protonation of the azide ion ($K_{HA} = 3.61 \times 10^{-5}$ [19]) can be neglected. Since the high azide ion concentrations were applied, the first two terms in the parentheses in eqn (3) can also be omitted. Solving eqns (1)–(4) with $P = 1.9 \times 10^5$,[20] $\beta_{Zn(dedtc)_2}$

$= 3.98 \times 10^{10}$,[20,21] $\beta_2 = 22$, $\beta_3 = 220$ and $\beta_4 = 780$,[22] and known initial concentration of $Zn(dedtc)_2$ and the azide ion, the position of the equilibrium was calculated. These values along with the experimental data are presented in Table 1. It is seen from Table 1 that there is a fairly good agreement between calculated and experimental values describing the position of the equilibrium. Small differences are probably caused by the change in the ionic strength.

The values of k_{obsd} in Table 1 were calculated from the linear part of the plot of $\ln A_t = f(t)$. The dependence of k_{obsd} on the azide ion concentration is presented in Fig. 2. From the plot of $k_{obsd} = f([N_3])$ a value for k_1 of 1.9×10^{-3} M^{-1} s^{-1} was obtained. The Y-intercept gave a value for k_0 of 5×10^{-4} s^{-1}. Assuming that the distribution of $Zn(dedtc)_2$ between both phases is very fast, the rate constants obtained can be replaced by $k'_1 = k_1 P = 3.6 \times 10^2$ and $k'_0 = k_0 P = 9.5 \times 10^1$.

No influence of pH on the reaction rate was found in the pH region 5.8–6.9. The value for k_0 of 5.0×10^{-4} obtained agrees with that reported by Wyttenbach[23] for metal isotopic exchange in $Zn(dedtc)_2$ ($k_0 = 4.6 \times 10^{-4}$). It is apparent from the above data that the value of k_0 reported by Wyttenbach[23] is in fact the rate constant for the solvent path. Since the azide ion is not a very good nucleophile and water is always in much higher concentration than the azide ion, the value of k_1 obtained being only moderately higher than k_0 seems reasonable. The probable reaction mechanism for the substitution reaction with the azide ion is shown in Scheme 1.

Applying the steady-state approximation for **B**, **C** and **D**, and assuming that $k_{-1} \gg k_2[N_3]$, $k_{-2} \gg k_3$ and $k_{-3} \gg k_3$, eqn (5) is obtained:

$$k_{obsd} = k_a \frac{[N_3]^2}{k_{-3}[S{-}S] + k_4[N_3]}, \qquad (5)$$

where:

$$k_a = \frac{k_1 k_2 k_3}{k_{-1} k_{-2}} = K_1 K_2 k_3.$$

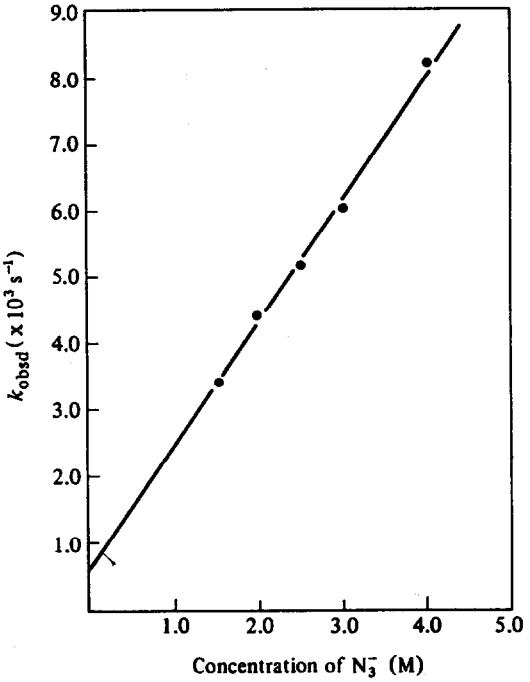
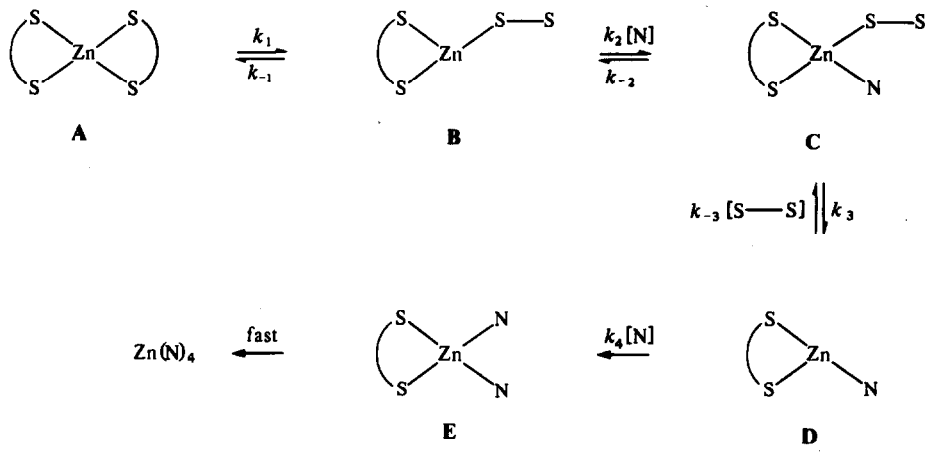


Fig. 2. Dependence of k_{obsd} on the azide ion concentration. Experimental conditions: $[Zn(dedtc)_2] = 3 \times 10^{-5}$ M, pH = 6.12.

Table 1. Calculated and experimental data for azide ligand substitution in $Zn(dedtc)_2$ at pH = 6.12

Initial concentration		Calculated value		Experimental data	
$[N_3^-]$ (M)	$[Zn(dedtc)_2]$ (M)	$[Zn]_t$ ($\times 10^6$M)	$\frac{[Zn]_t}{[Zn(dedtc)_2]_i}$	$\frac{A_t}{A_i}$	k_{obsd} ($\times 10^3$ M^{-1} s^{-1})
2.5	1×10^{-4}	11.7	0.117	0.13	5.34
2.5	5×10^{-5}	9.1	0.181	0.19	4.87
2.5	3×10^{-5}	7.4	0.248	0.25	5.18
2.5	1×10^{-5}	4.6	0.461	0.48	5.23
4.0	3×10^{-5}	12.6	0.420	0.47	8.24
3.0	3×10^{-5}	9.2	0.306	0.34	6.05
2.0	3×10^{-5}	5.7	0.190	0.19	4.41
1.5	3×10^{-5}	4.2	0.138	0.15	3.40



Scheme 1.

It is apparent from eqn (5) that, depending on the relative magnitudes of k_{-3}[S—S] and $k_4[N_3]$, the k_{obsd} may have various values and show different dependences on the azide ion concentration. For the initial period of the reaction the dedtc$^-$ concentration is very low and we can assume that $k_4[N_3] \gg k_{-3}$[S—S], which leads to eqn (6):

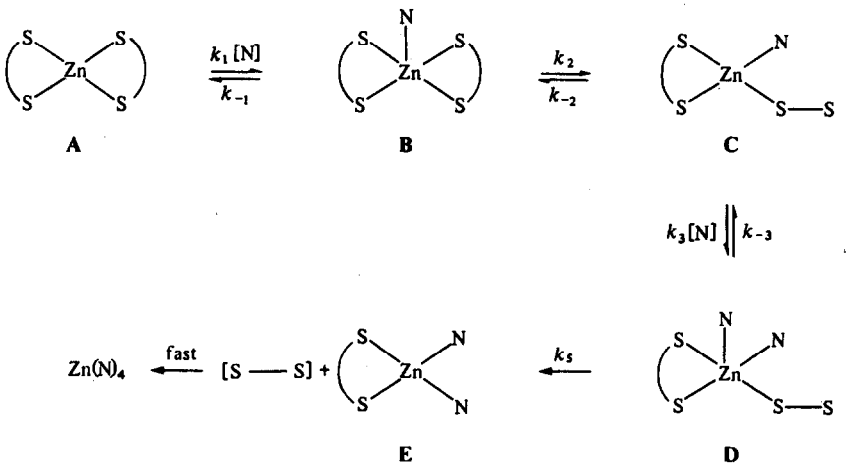
$$k_{obsd} = k_b[N_3], \tag{6}$$

where $k_b = K_1K_2k_3/k_4$. With the progress of the reaction the concentration of the dedtc$^-$ ion increases and can no longer by neglected. This is visualized in the deviation from linearity in the ln $A_t = f(t)$ plot shown in Fig. 1. Addition of a small (0.1 cm^3) volume of Nadedtc solution to the aqueous phase to a final concentration of 1×10^{-5} M greatly influenced the reaction and totally deviated the plot of ln $A_t = f(t)$ from linearity. Zn(dedtc)$_2$ in the solid state is a dimer with Zn atoms having a coordination number of 5.[24] Similar properties were found for zinc bis(dimethyldithiocarbamate).[25] Both complexes are monomeric in benzene and chloroform solutions.[25,26] These facts indicate the relative ease of the formation of five-coordinate Zn complexes. It was therefore interesting to check the possibility of the associative mechanism for the azide ligand substitution in tetrahedral Zn(dedtc)$_2$ with the five-coordinate intermediate. The alternative mechanism is presented in Scheme 2.

Applying the steady-state approximation for **C** and **D**, and assuming that $1 \gg (k_5/k_{-2})[N_3]$, eqn (7) is obtained:

$$k_{obsd} = \frac{k_aK_1[N_3]^2}{1+K_1[N_3]}, \tag{7}$$

where $K_1 = k_1/k_{-1}$ and $k_a = k_1k_5/k_{-2}$.



Scheme 2.

From eqn (7) it is seen that the overall reaction order may be second-, intermediate second–first- or first-order. Assuming reversibility of the reaction between **D** and **E** the concentration of the dedtc$^-$ ion will also influence the kinetics, decreasing the rate with progress of the reaction. Although the relative ease of formation of pentacoordinated Zn complexes[27] may suggest that an associative mechanism operates, on the basis of the data presented it is difficult to make definite conclusions. Since the value of k_0 obtained may be regarded as the rate constant for the solvent path, the associative mechanism seems more plausible. Such an associative mechanism was also proposed for the substitution reactions in planar dithiolato complexes of Ni, Pd and Pt with such a strong nucleophile as the CN^- ion.[28–31]

Acknowledgements—One of us (M.T.K.) express his appreciation to the U.S. Department of State for the award of a Fulbright Fellowship, and to the University of Arizona for providing the research facilities during the final stages of the present investigation.

REFERENCES

1. Z. Kurzawa and E. Kubaszewski, *Chem. Anal.* (*Warsaw*) 1974, **19**, 263.
2. Z. Kurzawa and A. Krzyminska, *Chem. Anal.* (*Warsaw*) 1977, **22**, 671.
3. Z. Kurzawa and A. Krzyminska, *Chem. Anal.* (*Warsaw*) 1978, **23**, 177.
4. Z. Kurzawa and J. Puacz, *Chem. Anal.* (*Warsaw*) 1978, **23**, 417.
5. Z. Kurzawa and B. Karska, *Chem. Anal.* (*Warsaw*) 1980, **25**, 465.
6. Z. Kurzawa and J. Puacz, *Fresenius' Z. Anal. Chem.* 1979, **296**, 160.
7. Z. Kurzawa and E. Kubaszewski, *Chem. Anal.* (*Warsaw*) 1974, **19**, 483.
8. Z. Kurzawa and E. Kubaszewski, *Chem. Anal.* (*Warsaw*) 1976, **21**, 565.
9. M. Kostanski and S. Magas, *Radiochim. Acta* 1980, **27**, 27.
10. M. Kostanski and S. Magas, *Bull. Acad. Pol. Sci., Ser. Sci. Chim.* 1980, **28**, 423.
11. M. C. Palazzotto, D. J. Duffy, B. L. Edgar, L. Que, Jr and L. H. Pignolet, *J. Am. Chem. Soc.* 1973, **95**, 4537.
12. M. Moriyasu and H. Hashimoto, *Chem. Lett.* 1980, 117.
13. N. V. Duffy, *Inorg. Chim. Acta* 1981, **47**, 31.
14. N. V. Duffy, W. G. Movius and D. L. Ulrich, *Inorg. Chim. Acta* 1982, **64**, L91.
15. E. Beinrohr and J. Garaj, *Collect. Czech. Chem. Commun.* 1980, **45**, 1785.
16. O. Liska, G. Guichon and H. Collin, *J. Chromatogr.* 1979, **171**, 145.
17. A. Wyttenbach and S. Bajo, *Anal. Chem.* 1975, **47**, 1813.
18. K. I. Aspila, C. L. Chakrabarti and V. S. Sastri, *Anal. Chem.* 1973, **45**, 363.
19. S. Ahrland and E. Avsar, *Acta Chem. Scand. A* 1975, **29**, 881.
20. Yu. I. Usatenko, V. S. Barkalov and F. M. Tulyupa, *J. Anal. Chem. U.S.S.R.* 1970, **25**, 363.
21. R. R. Scharfe, V. S. Sastri and C. L. Chakrabarti, *Anal. Chem.* 1973, **45**, 413.
22. E. F. A. Neves and L. Sant'Agostino, *Anal. Chim. Acta* 1970, **49**, 591.
23. A. Wyttenbach, *J. Inorg. Nucl. Chem.* 1981, **43**, 1937.
24. M. Bonamico, G. Mazzone, A. Vaciago and L. Zambonelli, *Acta Cryst.* 1965, **19**, 898.
25. H. P. Klug, *Acta Cryst.* 1966, **21**, 536.
26. L. Malatesta, private communication cited in Refs 23 and 24.
27. F. A. Cotton and G. Wilkinson, *Advanced Inorganic Chemistry*, pp. 590–591. John Wiley, New York (1980).
28. R. G. Pearson and D. A. Sweigert, *Inorg. Chem.* 1970, **9**, 1167.
29. R. G. Pearson and M. J. Hynes, *J. Coord. Chem.* 1971, **1**, 245.
30. M. J. Hynes and A. J. Moran, *J. Chem. Soc., Dalton Trans.* 1973, 2280.
31. M. J. Hynes and P. F. Brannick, *J. Chem. Soc., Dalton Trans* 1977, 2281.

Polyhedron Vol. 5, No. 6, pp. 1149–1156, 1986
Printed in Great Britain

0277–5387/86 $3.00+.00
Pergamon Journals Ltd

PROTONATION AND COMPLEX FORMATION OF THE *CIS* AND *TRANS* ISOMERS OF ALICYCLIC β-AMINO ACIDS

F. GAIZER*

Department of Inorganic and Analytical Chemistry, A. József University, Szeged, P.O. Box 440, Hungary

and

G. GÖNDÖS and L. GERA

Department of Organic Chemistry, A. József University, Szeged, Dóm tér 8, Hungary

(*Received* 8 *August* 1985; *accepted* 7 *October* 1985)

Abstract—The protonation constants of β-alanine and the *cis* and *trans* isomers of aliphatic 2-amino-1-carboxylic acids containing a cyclohexane, cyclopentane or cyclohexene(4) ring were determined pH-metrically, as were the formation constants of their complexes with Ni^{2+}, Cu^{2+}, Hg^{2+} and Cd^{2+} ions. The analysis of about 70 formation constants revealed significant differences between the behaviours of the different ligands, each of which has a fixed β-alanine conformation. It is concluded that complex formation is primarily determined by the nature of the fixed β-alanine conformation and in some cases by the type of aliphatic ring.

In its protonation and complex formation processes, β-alanine is presumed to take part in a number of conformeric forms, to each of which micro constants can be assigned. The measured protonation and complex stability constants[1–3] are actually average values, therefore. To substantiate this assumption and to elucidate the differences in behaviour between the individual conformers, we have determined the protonation and complex stability constants of compounds with a fixed β-alanine conformation.

Some alicyclic 2-amino-1-carboxylic acids were chosen as model compounds. In cyclohexane and cyclopentane compounds of this type, the substituents can occupy axial or equatorial positions. We have also investigated the analogous cyclohexene(4)-β-amino acid in which, as a consequence of the double bond, the ring is more planar, whereby the valence directions are slightly modified and the substituents occupy quasi-axial or quasi-equatorial positions. In all three ring systems the carboxylic group can only be situated equatorially. Thus, depending on the position of the amino group, two isomers can be formed: in the *cis* isomers the positions of the two groups are opposite (e.g. equatorial–axial), while in the *trans* isomers they are identical (e.g. diequatorial).

The pH-metric studies reported in this paper were made not only on the above six amino-carboxylic acids but also on β-alanine.

EXPERIMENTAL

Chemicals

The amino-carboxylic acids were prepared as previously described.[4,5] All other chemicals used were of analytical grade.

The pH-metric measurements were performed in sodium perchlorate solution of 0.5 mol dm^{-3} ionic strength at 25±0.1°C by using an ORION digital potentiometer (with an accuracy of 0.1 mV). The measuring electrode was a RADELKIS OP 718 P glass electrode, and the reference electrode was a RADELKIS OP 820 Ag–AgCl electrode. In the electrode the separating electrolyte solution was 0.5 mol dm^{-3} sodium perchlorate. During the experiments 50.0 cm^3 0.01 mol dm^{-3} solutions of the compounds, containing 0.01 mol dm^{-3} perchloric acid, were titrated under a nitrogen atmosphere with

* Author to whom correspondence should be addressed.

0.1 mol dm^{-3} sodium hydroxide also containing 0.4 mol dm^{-3} sodium perchlorate. For the compounds available in larger amount the pH-metric measurements in the presence of metal ions were carried out at two metal : ligand ratios.

The results were evaluated by the least-squares computer program described earlier.[6] The refinements were carried out for the sum of the squares of the residuals of the electromotive forces $[\sum(\Delta E^2)]$. As a characterization of the extent of the fit, the standard deviations (σ) of the electromotive forces are given in the tables: σ (mV) = $\sqrt{\sum(\Delta E^2)/\mathrm{NMP}-\mathrm{NP}-1}$, where NMP denotes the number of measured points and NP the number of parameters to be refined.

For calculation of the protonation and stability constants, the values of $E^{\ominus}$, j_H, j_{OH} and K_W obtained from the blank titration curves were used.[6] Optimization of only the $E^{\ominus}$ values was considered necessary. The parallel measurements and those made at two metal : ligand ratios were evaluated simultaneously by using the individual $E^{\ominus}$ values.

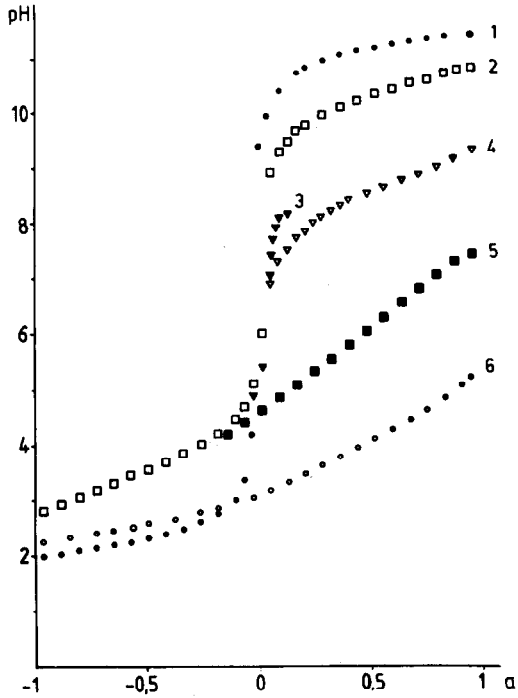


Fig. 1. pH-metric titration of 0.02 mol dm^{-3} *cis*-cyclohexane-β-amino acid in the absence of metal (2), and in the presence of 0.01 mol dm^{-3} Cd^{2+} (3), Ni^{2+} (4), Cu^{2+} (5) and Hg^{2+} (6). 1 is the blank curve.

RESULTS

As typical pH-metric measurements, the titration curves of the cyclohexane *cis* derivative are shown in Fig. 1. The protonation constants of the compounds studied are listed in Table 1. It can be seen that, in some cases, the differences, for both the amino and the carboxyl groups, exceed the experimental errors. The protonation constants of the amino groups (and also the experimental errors) are almost the same as or larger than that for β-alanine (cyclopentane derivatives). With one exception, the protonation constants of the carboxyl groups are lower than that for β-alanine.

The stability constants of the *nickel(II) complexes* are shown in Table 2. In the saturated derivatives, only the formation of two complexes could be

Table 1. Protonation constants of some alicyclic β-amino acids

Cyclo-aliphatic ring	Configuration	log K_1	log β_2	log K_2	No. of measured points	σ (mV)
Cyclohexane	*cis*	10.54_5	14.03_6	3.49_{10}	48	0.83
		10.44	13.91	3.47	Nikolasev *et al.*[7] I = 0.1 M (KNO_3), 25°C	
	trans	10.01_5	13.48_6	3.47_{10}	49	1.44
Cyclohexene(4)	*cis*	10.19_6	13.48_7	3.29_{12}	48	2.26
	trans	10.28_5	13.61_7	3.33_{10}	48	2.93
Cyclopentane	*trans*	9.90_5	13.65_{10}	3.75_{12}	48	2.96
	cis	10.10_4	13.63_6	3.53_8	48	0.87
β-Alanine	This work	10.08_4	13.78_6	3.70_6	49	0.93
		10.23	13.78	3.55	May and Felsing[8] I = 0, 25°C	
		10.10	13.76	3.66	Nagypál *et al.*[9] I = 1 M (KCl), 25°C	

Table 2. Stability constants of some alicyclic β-amino acids and β-alanine with Ni^{2+}

Cyclo-aliphatic ring	Configuration	T_L/T_M	Measured pH range	log β values of ML	ML_2	MLH_{-1}	ML_2H_{-1}	log K_1	log β_2	log K_2	log $K_{ML}^{ML_2}$	log $K_{MLH_{-1}}^{ML_2H_{-1}}$	No. of measured points	σ (mV)
Cyclohexane	*cis*	2.07 4.14	2.7–8.7 2.7–10.5	4.50_4	—	-4.50_6	—	10.46_3	13.38_4	3.42_6	—	—	39 38	1.84
	trans	3.1	2.4–9.6	3.56_{11}	—	-5.34_6	—	9.97_4	13.43_5	3.46_8	—	—	40	1.65
Cyclohexene(4)	*cis*	1.9 3.8	2.6–9.6 2.6–10.5	4.67_4	7.81_{20}	-4.5_{10}	—	10.20_2	13.48_4	3.28_5	3.04	—	49 49	2.47
	trans	2.2	3.2–10.5	4.67_6	7.81_{20}	-4.48_{12}	—	10.25_4	13.55_8	3.30_6	3.04	—	49	2.25
Cyclopentane	*cis*	2.3 4.6	2.9–9.1 2.8–9.9	3.94_6	—	-4.88_8	—	10.05_3	13.56_4	3.51_4	—	—	46 48	2.73
β-Alanine	This work	2.0 3.9	2.9–9.5 2.9–10.2	4.54_4	7.66_{34}	-4.70_{23}	-2.31_{23}	10.10_2	13.76_3	3.66_3	3.12	2.39	49 50	1.79
	Irving *et al.*[10]			4.63	8.03						3.4		$I = 0.1$ M (KCl), 20°C	
	Sharma *et al.*[11]			4.71	8.25						3.54		$I = 0.2$ M (KCl), 25°C	
	Leussing and Hanna[12]			4.46	7.84	$\log \beta_3 = 9.55$					3.38		$I = 0.5$ M (KCl), 25°C	

substantiated. Inclusion of a third species definitely made the fit worse. The two unsaturated ligands appear to be slightly better complex-forming agents than β-alanine. Formation of the NiL_2 species can be substantiated unambiguously in these systems, as in the case of β-alanine (Fig. 2B).

The *cis*-cyclohexane derivative and the two unsaturated ligands are evidently better complex-forming agents than β-alanine with the *copper(II)* ion (Table 3). Formation of the CuL_2 species with these ligands and with β-alanine is particularly intensive (Fig. 3). Occasionally, in other systems too, but without exception in the case of copper(II), the distribution curves reveal that the HL species displays two, more or less sharp, maxima[13,14] as a function of pH.

Of the investigated metal ions, *mercury(II)* forms the most stable complexes (Table 4). Except for the *cis*-cyclopentane derivative, all four types of complexes could be substantiated. The distribution curves in Fig. 4 show that hydroxo complex formation is also very important in these systems.

For the *cadmium(II) complexes*, only the stability

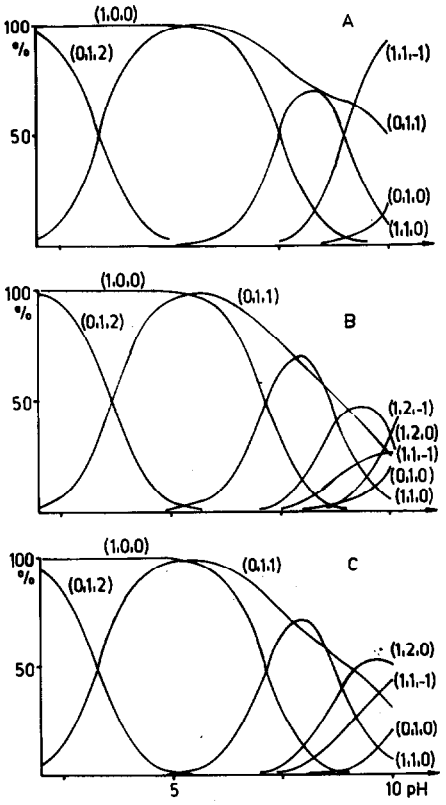


Fig. 2. Percentage distributions of total nickel(II) in its different complexes, and of total ligand in the nickel-free species. $T_{Ni^{2+}} = 0.01$ and $T_L = 0.03$ mol dm^{-3}. Ligands: (A) *cis*-, and (C) *trans*-cyclohexane-β-amino acid; and (B) β-alanine.

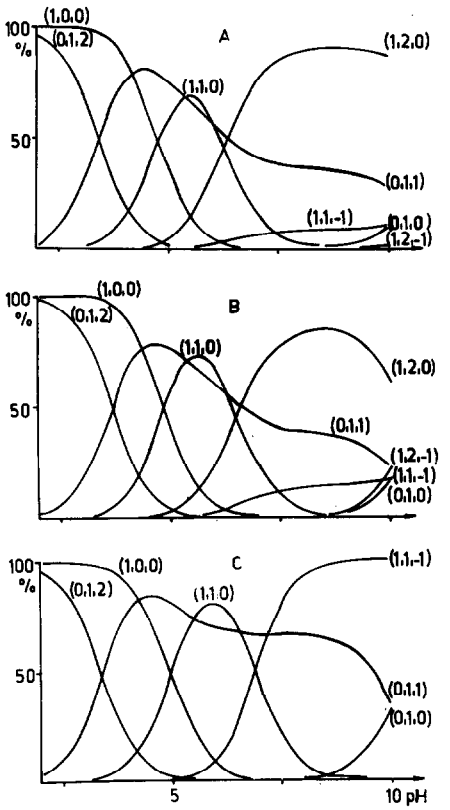


Fig. 3. Same as Fig. 2, but for copper(II).

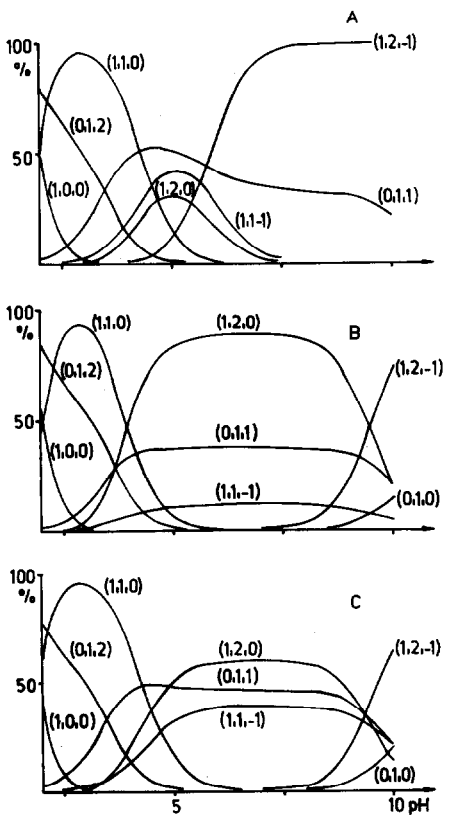


Fig. 4. Same as Fig. 2, but for mercury(II).

Table 3. Stability constants of some alicyclic β-amino acids and β-alanine with Cu^{2+}

Cyclo-aliphatic ring	Configuration	T_L/T_M	Measured pH range	log β values of ML	ML_2	MLH_{-1}	ML_2H_{-1}	log K_1	log β_2	log K_2	log $K_{ML}^{ML_2}$	log $K_{MLH_{-1}}^{ML_2H_{-1}}$	No. of measured points	σ (mV)
Cyclohexane	*cis*	1.9 3.8	2.7–6.9 2.7–10.6	7.32_2	13.31_8	-0.14_{22}	1.56_{99}	10.56_2	14.05_2	3.41_2	5.99	1.7	45 47	1.8
	trans	2.0 3.05	2.5–6.9 2.5–7.3	6.65_5	—	-0.27_7	—	10.02_4	13.42_4	3.4_4	—	—	36 40	2.49
Cyclohexene(4)	*cis*	1.9 3.7	2.6–7.7 2.6–10.7	7.31_4	13.29_8	-0.56_{20}	—	10.20_3	13.44_3	3.24_3	5.98	—	48 46	2.67
	trans	4.0	2.5–10.6	7.40_2	13.34_{14}	-0.04_{45}	—	10.25_4	13.46_4	3.21_4	5.94	—	41	2.63
Cyclopentane	*cis*	2.1 4.2	2.8–7.5 2.8–10.1	6.94_4	12.67_{11}	-0.37_{27}	2.52_{38}	10.09_2	13.52_5	3.43_5	5.73	2.89	50 47	1.97
	trans	2.0 4.0	2.8–7.4 2.8–10.5	6.86_6	12.40_6	—	—	9.95_3	13.61_{10}	3.68_8	5.54	—	47 47	3.24
β-Alanine	This work	2.0 4.0	2.9–8.15 2.9–10	6.90_2	12.31_7	-0.52_{10}	1.88_{47}	10.11_2	13.79_2	3.68_2	5.41	2.4	42 48	1.12
	Irving *et al.*[10]			7.13	12.6	ML(OH)							I = 0.1 M (KCl), 20°C	
	Nagypál *et al.*[9]			6.65	11.85	13.07	—	10.10	13.76	3.66	5.2		I = 1 M (KCl), 25°C	

Table 4. Stability constants of some alicyclic β-amino acids and β-alanine with Hg^{2+}

Cyclo-aliphatic ring	Configuration	T_L/T_M	Measured pH range	log β values of ML	ML_2	MLH_{-1}	ML_2H_{-1}	log K_1	log β_2	log K_2	log $K_{ML}^{ML_2}$	log $K_{MLH_{-1}}^{ML_2H_{-1}}$	No. of measured points	σ (mV)
Cyclohexane	*cis*	2.0	2.3–5.3	11.45_7	18.9_{34}	6.88_8	13.44_7	10.35_5	13.83_4	3.48_5	7.45	6.56	50	0.99
		4.0	2.4–5.3										38	
	trans	3.2	2.26–10.2	11.29_{14}	18.65_{61}	6.61_{34}	9.30_{27}	10.00_3	13.46_3	3.46_3	7.36	2.69	47	2.67
		4.7	2.48–9.96										49	
Cyclohexene(4)	*cis*	1.9	2.0–7	15.90_{15}	22.34_{22}	9.67_{21}	13.39_{16}	10.18_6	13.27_6	3.09_6	6.42	3.72	43	3.32
		3.8	2.2–10.1										48	
	trans	1.9	2.17–6.8	25.18_{42}	31.62_{50}	18.92_{82}	22.64_{70}	10.23_6	13.42_8	3.19_8	6.44	3.72	25	7.03
		4.0	2.16–9.87										23	
Cyclopentane	*cis*	2.2	2.3–4.8	11.16_6	17.90_{66}	6.87_8	—	9.97_3	13.53_3	3.56_3	6.74	—	46	1.36
		4.3	2.4–10										49	
β-Alanine	This work	2.0	2.3–4.8	11.30_6	19.48_{10}	6.51_{23}	10.02_{10}	10.13_4	13.83_2	3.70_4	8.18	3.51	47	1.65
		4.0	2.4–10										48	

Table 5. Stability constants of some alicyclic β-amino acids and β-alanine with Cd^{2+}

Cyclo-aliphatic ring	Configuration	T_L/T_M	pH range of complex formation	No. of measured points	log β values of ML	ML_2	MLH_{-1}	ML_2H_{-1}	log K_1	log β	σ (mV)
Cyclohexane	*cis*	1.95	8–9	31	3.63_8	6.92_{16}			10.46_3	13.83_3	1.83
		3.91		30	3.64_7		-5.76_{17}		10.46_3	13.83_4	1.86
	trans	3.15	8–9	30	3.03_{26}		-6.29_{19}		10.0_6	13.46_7	1.97
				30	2.95_{35}	6.09_{12}			10.0_4	13.46_6	1.94
Cyclopentane	*cis*	2.17	8–9	33	3.26_7		-5.88_{15}		10.08_2	13.57_3	1.52
		4.33		31	3.21_9	6.43_{17}			10.07_2	13.57_2	1.54
Cyclohexene(4)	*cis*	3.83	8–9.7	38	3.42_8		-6.28_{10}		10.19_4	13.50_5	1.90
				38	3.33_{13}	6.30_{18}			10.18_4	13.50_4	2.44
β-Alanine		2	8–9.9	45	3.41_6	6.05_{52}	-6.69_{81}	-3.30_{29}	10.1_4	13.81_4	1.82
		4		36							

constant of the CdL species can be determined. The data in Table 5 reveal that these equilibrium studies do not provide reliable information about he compositions and stability constants of other species formed. Complex formation with *cobalt(II)* and *zinc(II)* ions is very weak too.

DISCUSSION

Protonation constants

Amino group protonation constants larger than that for β-alanine can probably be explained by the fact that, in these compounds, those β-alanine conformations are fixed which favour protonation of the amino nitrogen. The protonation constants of the *cis* derivative of cyclohexane is significantly larger than those of all the other compounds in Table 1. This is certainly a consequence of the repulsive effect of the 4,6-diaxial hydrogens of the ring, which leads to fixing of the amino group in a position such that the non-bonding electron pair on the nitrogen is directed away from the ring, which makes proton bonding much easier. However, the possibility can not be excluded that a hydrogen bond in another position is formed between the protonated amino group and the carboxyl group, resulting in an increase in the protonation constant. The protonation constant of the amino group of the *trans*-cyclohexane derivative, however, is considerably smaller than that of the *cis* isomer, which can be attributed to the screening effect of the neighbouring carboxyl group.

In the cyclopentane and cyclohexene derivatives, the protonation constants of the amino groups are not significantly influenced by whether the functional groups are in the *cis* or the *trans* position. In the cyclohexene derivatives, the slightly larger protonation constants may be due to the molecules being sterically less crowded.

With regard to the protonation constants of the carboxyl groups, that of the *trans*-cyclopentane derivative is the largest, in accordance with expectations. This compound corresponds to the staggered conformation of β-alanine. Due to the free rotation about the C—C bonds, β-alanine exists in many other conformations which are less favourable for proton uptake; the protonation constant of this ligand is almost the average for these processes. The explanation why the stability constants for the other compounds are lower than that of the carboxyl group of β-alanine may be that, in these derivatives, the skew conformation of β-alanine is fixed, which is less favourable for protonation. The equally more inhibited uptake of protons in the cyclohexene derivatives can certainly be attributed to the fact that, due to the flattening of the ring, the difference between the positions of axial and equatorial groups decreases and the configuration formed is even less optimum.

Nickel(II), copper(II) and mercury(II) complexes

Of the examined metal ions, only nickel(II), copper(II) and mercury(II) undergo complex formation to such an extent that the compositions and stability constants of the resulting species can be determined sufficiently accurately to allow reliable conclusions on the complex-forming characteristics of the different β-alanine conformers.

As concerns the stability constants of these metal complexes, primarily coordination of the amino groups occurs; if the position of the carboxyl group and the directions of its non-bonding electron pairs are favourable, stable chelate formation can be assumed. However, the compositions and stabilities of the complexes differ from metal to metal: the complexes of nickel(II) are octahedral, those of copper(II) are square planar, and those of mercury(II) are, in all probability, octahedral.

The σ and the errors in the stability constants presented in Tables 2–4 suggest that there is no need to suppose the formation of more than four complexes to describe any of the examined systems. For β-alanine, with the exception of CuL(OH),[9] only the stability constants of the (1,1,0)* and (1,2,0) complexes have so far been determined.[1–3] Our experiments indicate that, for all three metal ions, the formation of both (1,1,−1) and (1,2,−1) species can be assumed. The tris-β-alanino complexes, however, could not be substantiated in any of the systems.

In general, it is true for the complexes of the investigated ligands [except for the mercury(II) complexes of the two unsaturated ligands] that the *cis*-cyclohexane derivative forms the most stable complexes. This seems somewhat surprising. However, models reveal that the free rotation of the carboxyl group and the positions of the neighbouring hydrogens of the functional groups bring about conditions favourable for chelate formation. In the *trans*-cyclopentane derivative, the substituents are somewhat farther from each other, which results in weaker chelate formation.

Among the examined ligands, the *trans*-cyclohexane derivative appears to be the weakest complex-forming agent. We assume that the reason for this is that the two functional groups are too close,

* The complexes $M_qL_pH_r$ are denoted by (q,p,r).

which is unfavourable for chelate formation. For similar reasons, the analogous cyclopentane derivative also seems a weaker complex-forming agent.

With the two unsaturated ligands, there is no substantial or inexplicable difference between either the two nickel(II) complexes or the two copper(II) complexes. This seems reasonable on the basis of models for, as a consequence of the respective quasi-axial–quasi-equatorial and quasi-diequatorial directions of the valences of the carbon atoms containing functional groups and of the free rotation of the carboxyl group, the ligands can assume configurations in which the distances between the donor atoms are practically the same. Naturally, the orientation of the planes of the cyclohexene rings and those formed by the coordination sphere differ considerably. The difference between the stabilities of the two $(1,1,-1)$ complexes of copper(II) can probably be explained by this. In the *cis*-cyclohexene derivative, one of the ring hydrogens is situated above the z-axis, thereby impeding the formation of the hydroxo complex. The same explanation may be given for the fact that no hydroxo complex formation could be detected for the *trans*-cyclopentane derivative.

The mercury(II) complexes of the two unsaturated ligands differ significantly in behaviour from the other compounds. The fairly large stability constants suggest practically quantitative complex formation, but, since ligand deprotonation during complex formation is also practically quantitative, the difference in stability of the two derivatives can be attributed to the uncertainty in the experimental errors of the pH-metric measurements. The present equilibrium studies do not allow reliable conclusions, but the formation of polynuclear complexes is not considered improbable.

Our equilibrium data alone, of course, are not enough to substantiate all the factors and the extents of their effects in the protonation and complex formation of the examined compounds. The present experiments, however, unambiguously demonstrate that there are well-detectable differences between the protonation constants of the individual β-alanine conformers. It seems that, in the determination of the compositions and stabilities of the nickel(II), copper(II) and mercury(II) complexes, the principal factor is what kind of β-alanine conformer is fixed in each ligand and thus how distant the donor atoms are from each other. The influence of the rings on complex formation seems somewhat less appreciable.

Acknowledgement—We wish to express our gratitude to Mrs Mária Palotai for her valuable help in carrying out the experiments.

REFERENCES

1. L. G. Sillén and A. E. Martell, *Stability Constants of Metal-ion Complexes.* Special Publication No. 17, Chemical Society, London (1964).
2. L. G. Sillén and A. E. Martell, *Stability Constants of Metal-ion Complexes.* Suppl No. 1. Special Publication No 25, Chemical Society, London (1971).
3. D. D. Perrin, *Stability Constants of Metal-ion Complexes, Part B, Organic Ligands.* IUPAC Chemical Data Series No. 22. Pergamon Press, Oxford (1979).
4. H. Plieninger and K. Schneider, *Chem. Ber.* 1959, **92**, 1594.
5. G. Bernáth, K. L. Láng, G. Göndös, P. Márai and K. Kovács, *Acta Chim. Acad. Sci. Hung.* 1972, **74**, 479.
6. F. Gaizer, *Acta Chim. Acad. Sci. Hung.* 1980, **103**, 397.
7. V. Nikolasev, G. Göndös and G. Bernáth, *Acta Phys. Chem. Szeged* 1969, **15**, 147.
8. M. May and W. A. Felsing, *J. Am. Chem. Soc.* 1951, **73**, 406.
9. I. Nagypál, F. Debreczeni and F. Erdődi, *Inorg. Chim. Acta* 1982, **57**, 125.
10. H. Irving, R. J. P. Williams, D. J. Ferrett and A. E. Williams, *J. Chem. Soc.* 1954, 3494.
11. V. S. Sharma, H. B. Mathur and P. S. Kilkarni, *Indian J. Chem.* 1965, **3**, 146, 475.
12. D. L. Leussing and E. M. Hanna, *J. Am. Chem. Soc.* 1966, **88**, 693.
13. I. Nagypál and M. T. Beck, *Coord. Chem. Rev.* 1982, **43**, 233.
14. I. Nagypál, M. T. Beck and A. D. Zuberbühler, *Talanta* 1983, **30**, 593.

Polyhedron Vol. 5, No. 6, pp. 1157–1164, 1986
Printed in Great Britain

0277–5387/86 $3.00+.00
Pergamon Journals Ltd

GALLIUM(III) PORPHYRINS: SYNTHESIS AND PHYSICOCHEMICAL CHARACTERISTICS OF HALOGENO GALLIUM(III) PORPHYRINS—X-RAY CRYSTAL STRUCTURE OF CHLORO-(5,10,15,20-TETRAPHENYLPORPHYRINATO) GALLIUM(III)

ATHANASSIOS COUTSOLELOS and ROGER GUILARD*

Laboratoire de Synthèse et d'Electrosynthèse Organométallique associé au C.N.R.S. (UA 33), Faculté des Sciences "Gabriel", 6, Boulevard Gabriel, 21100 Dijon, France

and

DANIEL BAYEUL and CLAUDE LECOMTE

Laboratoire de Minéralogie et Cristallographie (UA 809), Faculté des Sciences, Centre de 2ème Cycle, B.P. No. 239, 54506, Vandoeuvre-les-Nancy, France

(*Received* 8 *August* 1985; *accepted* 14 *October* 1985)

Abstract—Chlorogallium(III) porphyrins [Ga(Por)Cl] were obtained in good yield by treating the corresponding free bases with gallium trichloride. The action of the hydrogen halides HX (X = F or I) on chloro derivatives Ga(Por)Cl led to the corresponding halogeno complexes Ga(Por)X. These derivatives were characterized on the basis of mass spectrometry, ^{1}H NMR, and UV–visible data. The crystal structure of the title compound has been determined by X-ray diffraction methods. $C_{44}N_4H_{28}GaCl$ [Ga(TPP)Cl], F_w = 717.9 g, tetragonal, *I*4/*m*, a = 13.508(2) Å, c = 9.846(2) Å, V = 1797(3) Å^3, Z = 2, D_x = 1.326, μ = 11.1 cm^{-1}, $F(000)$ = 736 $\bar{e}$, room temperature, $R(F)$ = 0.044, $R_w(F)$ = 0.049 for 1237 unique reflections. Ga(TPP)Cl is isomorphic to Fe(TPP)Cl: both gallium and chloride atoms are statistically averaged by the crystallographic mirror plane. The gallium–chlorine distance is 2.196(2) Å, whereas the gallium atom lies 0.317(1) Å from the perfect porphyrin plane.

Recently, Wynne[1,2] and Marks[3–6] described the synthesis and characterization of inorganic–organic polymers in which a metallic or pseudometallic element alternates in a linear chain with an atom such as oxygen or dicoordinate fluorine. The metallic or pseudometallic element is always the central atom of a phthalocyanine system and the bridge-stacked polymeric structure is rigid. These derivatives are electrical conductors after iodine oxidation.[7–13] In a preliminary paper,[14] we pointed out a series of similar systems, the large phthalocyanine ring being replaced by a porphyrin ligand. Difference Fourier analysis of EXAFS spectra of the hydroxo and fluorogallium(III)-2,3,7,8,12,13,17,18-octamethylporphyrins [Ga(OMP)OH† and Ga(OMP)F] afforded some evidence for the polymeric structure of the latter complex.[14]

In this paper we report the synthesis and complete description of the Ga(Por)F complexes, and the detailed preparation of the Ga(Por)Cl precursors. The effort below focuses also on the characterization of the Ga(Por)I complexes and on the description of the crystal structure of Ga(TPP)Cl which is, as far as we know, the first X-ray study of a gallium(III) porphyrin.

EXPERIMENTAL

Preparation of complexes

The chloro, fluoro, and iodo complexes were synthesized following a general procedure described below.

* Author to whom correspondence should be addressed.

‡ Abbreviations: Por, unspecified porphyrinate(2−); OEP, 2,3,7,8,12,13,17,18-octaethylporphyrinate(2−); TPP, 5,10,15,20-tetraphenylporphyrinate(2−); OMP, 2,3,7,8,12,13,17,18-octamethylporphyrinate(2−).

Chloro-(porphyrinato) gallium(III). To a solution of porphyrin (9.35 mmol) and $GaCl_3$ (13.7 mmol) in acetic acid (400 cm^3) sodium acetate (61 mmol) was added in acetic acid (25 cm^3). The mixture was refluxed for 12 h, then the resulting solution was cooled down to 0°C and the precipitate obtained was recrystallized. The reaction mixture also contains small amounts of acetato-(porphyrinato) gallium(III).

Fluoro-(porphyrinato) gallium(III). Chloro-(porphyrinato) gallium(III) (80 mmol) was dissolved in 200 cm^3 of methanol. After the addition of 10 cm^3 of an aqueous solution of hydrofluoric acid (40%) the mixture was stirred for 16 h. The excess hydrofluoric acid was removed by vacuum distillation (at 240°C and 2.5×10^{-3} mmHg). The residual precipitate was washed with heptane and cooled methanol, and recrystallized.

Iodo-(porphyrinato) gallium(III). Chloro-(porphyrinato) gallium(III) (80 mmol) was dissolved in 200 cm^3 of toluene and a gentle stream of hydroiodic acid was bubbled through the toluene solution (4 h). After reaction, the solvent was removed under reduced pressure and the residual precipitate was dried at 80°C under 15 mmHg, and recrystallized.

The reaction conditions, yields and elemental analyses for all the complexes are summarized in Table 1.

Table 1. Experimental data and yields

Complex	Recrystallization solvent[a]	Yield (%)	Molecular formula	Analysis (%)[b] C	H	N	X[c]	Ga
$\mathbf{1}_1$ Ga(OMP)Cl	C	86	$C_{28}H_{28}N_4ClGa$	63.8 (63.97)	5.4 (5.37)	10.0 (10.66)	6.5 (6.74)	13.2 (13.26)
$\mathbf{1}_2$ Ga(OEP)Cl	B	75[d]	$C_{36}H_{44}N_4ClGa$	67.9 (67.78)	7.0 (6.95)	9.0 (8.78)	5.5 (5.56)	10.8 (10.93)
$\mathbf{1}_3$ Ga(TPP)Cl	B	71[d]	$C_{44}H_{28}N_4ClGa$	73.0 (73.62)	3.9 (3.93)	7.5 (7.81)	4.8 (4.93)	9.3 (9.71)
$\mathbf{2}_1$ Ga(OMP)F	A	67	$C_{28}H_{28}N_4FGa$	65.5 (66.04)	5.4 (5.54)	10.8 (11.00)	3.7 (3.73)	12.8 (13.69)
$\mathbf{2}_2$ Ga(OEP)F	B	75	$C_{36}H_{44}N_4FGa$	69.4 (69.57)	7.2 (7.14)	8.9 (9.02)	3.0 (3.05)	11.0 (11.22)
$\mathbf{2}_3$ Ga(TPP)F	B	80	$C_{44}H_{28}N_4FGa$	75.3 (75.35)	3.9 (4.02)	7.6 (7.98)	2.8 (2.71)	9.6 (9.94)
$\mathbf{3}_1$ Ga(OMP)I	B	57	$C_{28}H_{38}N_4IGa$	55.4 (55.47)	4.5 (4.65)	9.0 (9.24)	20.5 (19.14)	11.7 (11.50)
$\mathbf{3}_2$ Ga(OEP)I	B	72	$C_{36}H_{44}N_4IGa$	59.3 (59.36)	6.0 (6.09)	7.6 (7.69)	17.2 (17.29)	8.5 (9.57)
$\mathbf{3}_3$ Ga(TPP)I	B	62	$C_{44}H_{28}N_4IGa$	65.3 (65.38)	3.4 (3.49)	6.9 (6.93)	15.6 (15.58)	7.9 (8.62)

[a] A = methanol, B = toluene, C = chloroform, D = heptane.
[b] Calculated values are given in parentheses.
[c] X = F, Cl or I.
[d] About 3.5% of the free base is transformed to the corresponding acetato derivative Ga(Por)AcO.

Physical measurements

Elemental analyses were performed by the "Service de Microanalyses du C.N.R.S.". Mass spectra were obtained in the electron-impact mode with a Finnigan 3300 spectrometer; ionizing energy 30–70 eV, ionizing current 0.4 mA, source temperature 250–400°C. ^1H NMR spectra were recorded on a JEOL FX 100 or Bruker WM 400 of the CEREMA ("Centre de Résonance Magnétique" of University of Dijon). Spectra were measured for complex (5 mg) solutions in 0.6 cm^3 of DMSO or $CDCl_3$ with tetramethylsilane as internal reference. IR spectra were recorded on a Perkin–Elmer 580 B apparatus. Samples were prepared as 1% dispersions in CsI pellets or Nujol mulls. Electronic absorption spectra were recorded on a Perkin–Elmer spectrophotometer using 5×10^{-3} mol l^{-1} methanolic solutions.

Crystal and molecular structure determination

A suitable crystal of Ga(TPP)Cl was obtained from recrystallization of the complex in a solution of toluene. Preliminary Weissenberg photographs along the $\vec{c}$ axis revealed a four-fold symmetry and systematic extinction of the type $h+k+l = 2n+1$,

Table 2. Experimental conditions

Formula	$C_{44}N_4H_{28}ClGa$
Formula weight	717.9
Space group	Tetragonal $I4/m$
Extinctions	$h+k+l=2n+1$
Crystal dimensions (mm^3)	$0.1\times0.15\times0.3$
Crystal habit	Tetragonal octahedron
Crystal color	Dark blue
Lattice parameters	See Abstract
Diffractometer	Enraf–Nonius CAD4F
Radiation	Cu-K_α
Scan	$\omega-2\theta$
$\theta_{min}-\theta_{max}$ (°)	1–70
Scan speed (° min^{-1})	$0.5<v<3.0$
Scan range	$0.8+0.15\tan\theta$
Take-off angle (°)	3
Aperture (mm)	$3+3\tan\theta$
h, k, l limits	$-16<h<16, 0<k<16, -10<l<0$
Number of reflections measured	2223
Number of unique reflections	1480
Agreement factor $R_i(F)$ between symmetry-related reflections	0.028
Number of reflections used $[I>3\sigma(I)]$ (N)	1237
Number of parameters (N_p)	79
N/N_p	15
Programs	SHELX 76[16] and ORTEP
$R(F)$, $R_w(F)$	0.044, 0.049
Goodness of fit	1.10
w	$2.4/[\sigma^2(F)+0.0006F^2]$
$\left(\frac{\Delta}{\sigma}\right)_{max}$	4×10^{-2} for U_{33} (Ga)

leading to the centrosymmetric space group $I4/m$ and to the non-centrosymmetric $I4$ or $I\bar{4}$ space groups. Experimental conditions and details of the calculations are given in Table 2. The crystal structure was solved by the heavy-atom method, assuming the space group $I4/m$. As observed for Fe(TPP)Cl,[15] the gallium and chlorine atoms are statistically disordered up and below the mirror plane m. The good convergence of the least-squares process confirmed the choice of the space group; furthermore refinements in the $I4$ and $I\bar{4}$ space groups did not improve the convergence results. All the hydrogen atoms were found in difference Fourier maps and added as fixed contributors to the least-squares calculations. The scattering factors were taken from Refs 16 and 17; all non-hydrogen atoms were refined anisotropically. A summary of the least-squares results is given in Table 2. Fractional atomic coordinates, anisotropic thermal parameters and a list of structure factors has been deposited as supplementary data with the Editor, from whom copies are available on request.*

RESULTS AND DISCUSSION

During the last decade gallium(III) porphyrin complexes possessing the axial ligands Cl^-,[18,19] RO^-[20,21] and RCO_2^-[22] have been reported. Two general methods have been used to synthesize the gallium(III) porphyrins: the first one used $Ga(Acac)_2$ for metallation in phenol,[20] and the second $NH_4Ga(SO_4)_2\cdot12H_2O$ in acetic acid.[19] We have prepared the chloro-gallium(III) porphyrins (**1**) by the action of $GaCl_3$ on porphyrins in acetic acid. The complexes **1** were obtained with very satisfactory yields varying from 70 to 90%. Treatment of Ga(Por)Cl (**1**) with HF in methanol and HI in toluene led, respectively, to the fluoro-Ga(Por)F (**2**) and iodo-Ga(Por)I (**3**) derivatives. The yield of the reaction depends on the nature of the axial and equatorial ligands (57–80%).

In most of the mass spectra of complexes **1** and **2**, the molecular peak appears.† Its intensity is very

*Atomic coordinates have also been deposited with the Cambridge Crystallographic Data Centre.

† The relative intensity of the peaks $M^{+\cdot}$, $[M+1]^+$ and $[M+2]^+$ is attributable to the abundance of the natural isotopes ^{69}Ga and ^{71}Ga (see Table 3).

high for the chloro and fluoro derivatives and corresponds in a few cases to the parent peak. However for Ga(OMP)F the fragment ion $[M-F+1]^+$ is higher. The same ion $[M-X]^+$ is the most abundant for the iodo complexes **3** while the intensity of the molecular peak is very low (0.32–2.50%) and does not appear for Ga(TPP)I. These data are in good agreement with the more labile character of the metal–iodine bond compared to the metal–fluorine or metal–chlorine bonds. Moreover the typical morphology of the mass spectrum of Ga(OMP)F may be due to a particular coordination scheme when the gallium atom is bound to a planar macrocycle.

Ga(Por)X exhibit electronic absorption spectra belonging to "normal" class[23] (Table 4). They show an intense band in the 395–415-nm region and two bands between 500 and 600 nm (α- and β-bands). One

Table 3. Characteristic mass spectral and IR data

		Mass spectra			
	Complex	*m/z*	Relative intensity	Fragmentation pattern	IR (cm^{-1}) ν(Ga—X)[a]
1$_1$	Ga(OMP)Cl	524	83.75	$M^{+\cdot}$	370
		525	63.38	$[M+1]^+$	
		526	100.00	$[M+2]^+$	
		489	68.09	$[M-X]^+$	
		490	74.29	$[M-X+1]^+$	
1$_2$	Ga(OEP)Cl	636	35.48	$M^{+\cdot}$	332
		637	37.32	$[M+1]^+$	
		638	100.00	$[M+2]^+$	
		601	3.22	$[M-X]^+$	
1$_3$	Ga(TPP)Cl	716	90.23	$M^{+\cdot}$	352
		717	100.00	$[M+1]^+$	
		718	78.80	$[M+2]^+$	
		681	1.87	$[M-X]^+$	
		682	1.50	$[M-X+1]^+$	
2$_1$	Ga(OMP)F	508	4.28	$M^{+\cdot}$	562
		509	67.14	$[M+1]^+$	
		510	24.28	$[M+2]^+$	
		489	71.42	$[M-X]^+$	
		490	100.00	$[M-X+1]^+$	
2$_2$	Ga(OEP)F	620	100.00	$M^{+\cdot}$	550
		621	91.07	$[M+1]^+$	
		622	81.25	$[M+2]^+$	
		601	11.60	$[M-X]^+$	
		602	7.14	$[M-X+1]^+$	
2$_3$	Ga(TPP)F	700	10.63	$M^{+\cdot}$	588
		701	31.91	$[M-1]^+$	
		702	100.00	$[M+2]^+$	
		681	23.40	$[M-X]^+$	
		682	29.78	$[M-X+1]^+$	
3$_1$	Ga(OMP)I	616	0.32	$[M+1]^+$	210
		489	100.00	$[M-X]^+$	
		490	18.95	$[M-X+1]^+$	
3$_2$	Ga(OEP)I	728	2.50	$[M+1]^+$	235
		601	100.00	$[M-X]^+$	
		602	80.00	$[M-X+1]^+$	
3$_3$	Ga(TPP)I	681	19.48	$[M-X]^+$	261
		682	100.00	$[M-X+1]^+$	

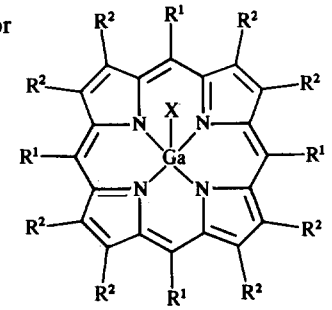
[a] X = Cl, F or I.

Table 4. UV–visible spectroscopic data

Compound	UV–visible [λ (nm)][a]				
	$B(1,0)$	$B(0,0)$	$Q(2,0)$	$Q(1,0)$ (or α)	$Q(0,0)$ (or β)
1_1 Ga(OMP)Cl	375 (15.9)	395 (117.7)	489 (1.2)	529 (4.4)	567 (5.6)
1_2 Ga(OEP)Cl	377 (14.6)	397 (99.0)	489 (0.3)	531 (3.3)	568 (4.6)
1_3 Ga(TPP)Cl	395 (4.5)	414 (63.3)	509 (0.5)	548 (2.3)	587 (0.8)
2_1 Ga(OMP)F	376 (80.1)	395 (560.2)	488 (3.9)	529 (20.2)	567 (27.2)
2_2 Ga(OEP)F	377 (15.9)	397 (139.4)	491 (0.7)	529 (4.4)	567 (5.9)
2_3 Ga(TPP)F	394 (10.2)	414 (141.3)	509 (1.1)	548 (4.9)	587 (1.7)
3_1 Ga(OMP)I	375 (7.6)	395 (110.1)	491 (0.9)	530 (4.2)	568 (5.4)
3_2 Ga(OEP)I	377 (9.4)	397 (81.1)	489 (0.4)	529 (2.6)	567 (3.4)
3_3 Ga(TPP)I	395 (6.4)	414 (48.6)		548 (2.6)	587 (1.1)

[a] 10^{-3} ε ($dm^3\ mol^{-1}\ cm^{-1}$) given in parentheses.

Table 5. ^1H NMR data for



Compound	R^1	R^2	Protons of R^1			Protons of R^2	
				Multiplicity/ intensity	δ	Multiplicity/ intensity	δ
1_1 Ga(OMP)Cl[a]	H	CH_3		s/4	10.43	s/24	3.66
1_2 Ga(OEP)Cl[b]	H	C_2H_5		s/4	10.34	t/24 m/16	1.96
1_3 Ga(TPP)Cl[b]	C_6H_5	H	*o*-H *m,p*-H	m/8 m/12	8.20 7.75	s/8	9.07
2_1 Ga(OMP)F[a]	H	CH_3		s/4	10.43	s/24	3.66
2_2 Ga(OEP)F[b]	H	C_2H_5		s/4	10.35	t/24 m/16	1.96 4.16
2_3 Ga(TPP)F[b]	C_6H_5	H	*o*-H *o'*-H *m,p*-H	m/4 m/4 m/12	8.29 8.14 7.78	s/8	9.08
3_1 Ga(OMP)I[a]	H	CH_3		s/4	10.44	s/24	3.66
3_2 Ga(OEP)I[b]	H	C_2H_5		s/4	10.36	t/24 m/16	1.95 4.17
3_3 Ga(TPP)I[b]	C_6H_5	H	*o*-H *m,p*-H	m/8 m/12	8.21 7.75	s/8	9.07

Solvent: [a] DMSO, [b] $CDCl_3$.

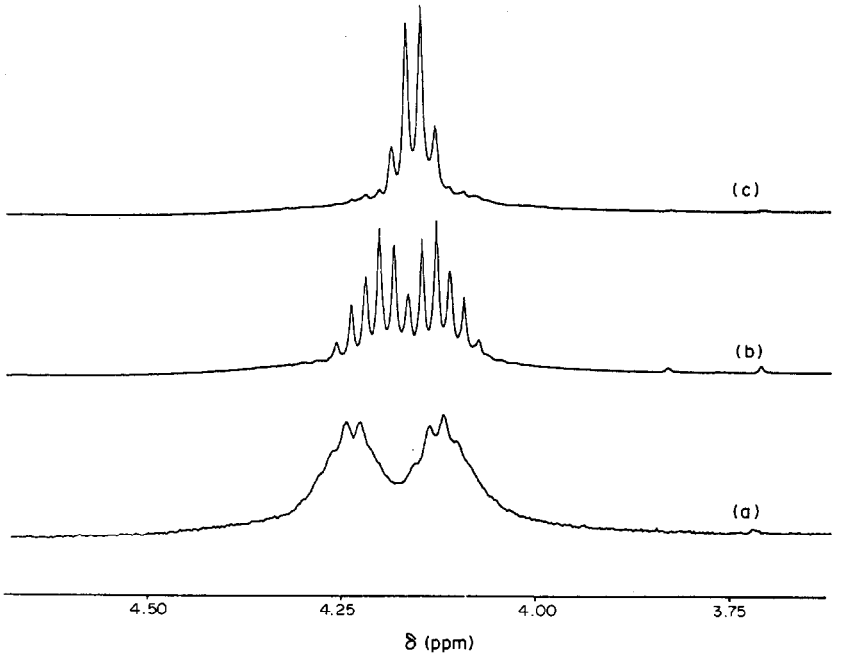


Fig. 1. Resonance signal of A and B methylenic protons of: (a) Ga(OEP)I, (b) Ga(OEP)Cl, and (c) Ga(OEP)F.

extra band [$Q(2, 0)$] is observed in the visible region and another one appears blue shifted compared to the Soret band. As previously reported by Gouterman *et al.*[24,25] in tin octaethylporphyrin dihalides (with halide = F, Cl, Br or I), the shifts in the transition energies and relative intensities of the α- and β-bands depend on the charge and polarizability of the axial ligand and correlate with changes in the electron density in the porphyrin ring.

The IR spectra of the whole isolated chloro complexes show one band in the region 330–370 cm^{-1}, assigned to the Ga—Cl stretching (Table 3). This characteristic band is found between 550 and 590 cm^{-1} for the fluoro derivatives, and between 210 and 261 cm^{-1} for the iodo compounds.

^1H NMR characteristics of the Ga(Por)X complexes at ambient temperatures are listed in Table 5. The spectra of Ga(OMP)X give poor structural information since the resonance lines corresponding to the *meso* and methylic protons are two singlets which appear in the same region whatever the nature of X. The bridge-stacked polymeric structure of Ga(OMP)F being demonstrated on the basis of EXAFS spectroscopy,[14] the same arrangement could be postulated for Ga(OMP)Cl and Ga(OMP)I in the solid state. We have also studied NMR characteristics of the gallio-octaethylporphyrin systems. At the same concentration we observe an ABR_3 multiplet for the ethyl groups of Ga(OEP)Cl and Ga(OEP)I which can be explained only by the presence of a non-octahedral monomeric structure.[26,27] In contrast the resonance signal of the methylenic protons of Ga(OEP)F is a quadruplet and these protons have very similar chemical shifts (see Fig. 1). These observations may be consistent with a polymeric structure for Ga(OEP)F similar to that of Ga(OMP)F, the two other complexes 'being pentacoordinate.

At room temperature the resonances of the *ortho* phenyl protons are broad for Ga(TPP)Cl and Ga(TPP)I, and split in a doublet for Ga(TPP)F. This reflects the well-known phenomenon of the restricted rotation of phenyl rings.[18,19,28–31] If the effect of axial ligands on the rate of phenyl ring rotation is not very well established, it is clear that the

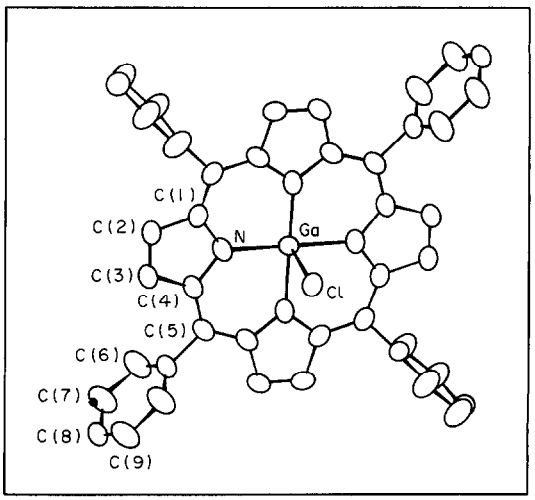


Fig. 2. ORTEP view of Ga(TPP)Cl.

Table 6. Bond distances (Å) and angles (°)

Ga—N(1)	2.021(2)	Ga—Cl	2.196(2)
N(1)—C(1)	1.385(4)	N(1)—C(4)	1.381(4)
C(1)—C(2)	1.434(4)	C(3)—C(4)	1.432(5)
C(4)—C(5)	1.390(4)	C(1)—C(5)	1.390(5)
C(2)—C(3)	1.340(5)	C(5)—C(6)	1.498(4)
C(6)—C(7)	1.364(3)	C(7)—C(8)	1.398(5)
C(8)—C(9)	1.358(4)	Cl(1)—N(1)	3.210(2)
N(1)—Ga—Cl(1)	99.06(3)	N(1)—Ga—N(1)^{i}	88.58(9)
N(1)—Ga—N(1)^{ii}	161.89(5)	C(1)—N(1)—C(4)	105.5(3)
C(1)—C(2)—C(3)	107.3(3)	C(2)—C(1)—N(1)	109.8(3)
C(2)—C(3)—C(4)	107.7(3)	C(3)—C(4)—C(5)	124.3(3)
N(1)—C(4)—C(5)	125.9(3)	N(1)—C(1)—C(5)	125.9(3)
C(5)—C(6)—C(7)	120.5(2)	C(3)—C(4)—N(1)	109.8(3)
C(7)—C(8)—C(9)	119.9(2)	C(6)—C(7)—C(8)	120.5(2)

chemical-shift difference is higher when the axial ligand is the more electronegative halide (X = F). It thus appears that the coordination polyhedron of the metal does not possess planar symmetry with respect to the porphyrinic plane and the metal should be out of this plane. The above assumptions are confirmed by the X-ray crystal structure of Ga(TPP)Cl.

Figure 2 is an ORTEP view of the molecule and Table 6 gives the bond lengths and angles. The crystal structure is isomorphic to that of Fe(TPP)Cl[15] and Ti(TPP)Br_2.[32] The statistically averaged molecule of *I4/m* symmetry is centered at the origin and at every other lattice point of the unit cell. Hence the coordination polyhedron of the metallic atom is a square pyramid [Ga—N = 2.021(1) Å, Ga—Cl = 2.196(2) Å]. Eaton *et al.*[19] postulated an in-plane position of the gallium atom and a highly distorted macrocycle for the chloro substituted tetraphenylporphyrinate gallium(III). In contrast for Ga(TPP)Cl the metal atom lies 0.317(1) Å from the crystallographically required perfect porphyrin plane. The bond distances and angles in the porphyrinic group are statistically equal to those usually found.

REFERENCES

1. R. S. Nohr and K. J. Wynne, *J. Chem. Soc., Chem. Commun.* 1981, 1210.
2. P. Brant, D. C. Weber, S. G. Haupt, R. S. Nohr and K. J. Wynne, *J. Chem. Soc., Dalton Trans.* 1985, 269.
3. T. J. Marks, *J. Coatings Technol.* 1976, **48**, 53.
4. T. J. Marks and D. W. Kalina, In *Extended Linear Chain Compounds* (Edited by J. S. Miller), Vol. 1, Chap. 6, p. 197. Plenum Press, New York (1982).
5. C. W. Dirk and T. J. Marks, *Inorg. Chem.* 1984, **23**, 4325.
6. E. Ciliberto, K. A. Doris, W. J. Pietro, G. M. Reisner, D. E. Ellis, I. Fragalà, F. H. Herbstein, M. A. Ratner and T. J. Marks, *J. Am. Chem. Soc.* 1984, **106**, 7748.
7. T. E. Phillips and B. M. Hoffman, *J. Am. Chem. Soc.* 1977, **99**, 7734.
8. C. J. Schramm, D. R. Stojakovic, B. M. Hoffman and T. J. Marks, *Science* 1978, **200**, 47.
9. M. Cowie, A. Gleizes, G. W. Grynkewich, D. W. Kalina, M. S. McClure, R. P. Scaringe, R. C. Teitelbaum, S. L. Ruby, J. A. Ibers, C. R. Kannewurf and T. J. Marks, *J. Am. Chem. Soc.* 1979, **101**, 2921.
10. K. F. Schoch, Jr., B. R. Kundalkar and T. J. Marks, *J. Am. Chem. Soc.* 1979, **101**, 7071.
11. P. M. Kuznesof, K. J. Wynne, R. S. Nohr and M. E. Kenney, *J. Chem. Soc., Chem. Commun.* 1980, 121.
12. B. M. Hoffman, T. E. Phillips, C. J. Schramm and S. K. Wright, In *Molecular Metals* (Edited by W. E. Hatfield), p. 393. Plenum Press, New York (1979).
13. R. S. Nohr, P. M. Kuznesof, K. J. Wynne, M. E. Kenney and P. G. Siebenman, *J. Am. Chem. Soc.* 1981, **103**, 4371.
14. J. Goulon, P. Friant, C. Goulon-Ginet, A. Coutsolelos and R. Guilard, *Chem. Phys.* 1984, **83**, 367.
15. J. L. Hoard, G. H. Cohen and M. D. Glick, *J. Am. Chem. Soc.* 1967, **89**, 1992.
16. G. M. Sheldrick, *Programm for Crystal Structure Determination*. University of Cambridge, U.K. (1976).
17. *International Tables of X-ray Crystallography*, Vol. 4. Kynoch Press, Birmingham, U.K. (1974).
18. A. Laurie, W. Shroyer, C. Lorbereau, S. S. Eaton and G. R. Eaton, *J. Org. Chem.* 1980, **45**, 4296.
19. S. S. Eaton, D. M. Fishwild and G. R. Eaton, *Inorg. Chem.* 1978, **17**, 1542.
20. J. W. Buchler, L. Puppe, K. Rohbock and H. H. Schneehage, *Chem. Ber.* 1973, **106**, 2710.
21. J. W. Buchler and L. Puppe, *Liebigs Ann. Chem.* 1974, 1046.
22. A. Coutsolelos and R. Guilard, unpublished results.
23. M. Gouterman, In *The Porphyrins* (Edited by D. Dolphin), Vol. 3, p. 1. Academic Press, New York (1978).
24. M. Gouterman, F. P. Schwarz and P. D. Smith, *J. Chem. Phys.* 1973, **59**, 676.

25. M. Gouterman, F. P. Schwarz and P. D. Smith, *J. Chem. Phys.* 1974, **61**, 3491.
26. C. A. Busby and D. Dolphin, *J. Mag. Reson.* 1976, **23**, 211.
27. R. J. Abraham and K. M. Smith, *Tetrahedron Lett.* 1971, **36**, 3335.
28. S. S. Eaton and G. R. Eaton, *J. Am. Chem. Soc.* 1977, **99**, 6594.
29. S. S. Eaton and G. R. Eaton, *J. Chem. Soc.* 1975, **97**, 3660.
30. D. V. Behere, R. Birdy and S. Mitra, *Inorg. Chem.* 1982, **21**, 386.
31. J. Huet, A. Gaudemer, C. Boucly-Goester and P. Boucly, *Inorg. Chem.* 1982, **21**, 3413.
32. C. Lecomte, J. Protas, J. C. Marchon and M. Nakajima, *Acta Cryst.* 1978, **B34**, 2856.

Polyhedron Vol. 5, No. 6, pp. 1165–1170, 1986
Printed in Great Britain

0277–5387/86 $3.00+.00
Pergamon Journals Ltd

RELATIVE STABILITIES OF METAL COMPLEXES OF 4-(2-PYRIDYLAZO)RESORCINOL AND 4-(2-THIAZOLYLAZO)RESORCINOL

EMIKO OHYOSHI

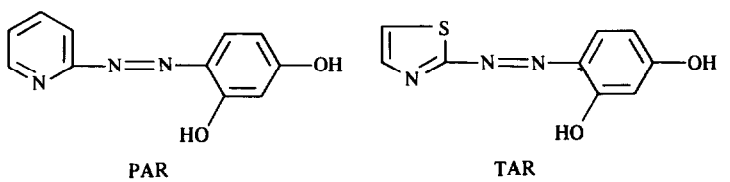
Yatsushiro National College of Technology, Hirayamashinmachi 2627, Yatsushiro, Kumamoto 866, Japan

(*Received* 10 *September* 1985; *accepted* 23 *October* 1985)

Abstract—The stability constants of 1 : 1 complexes of 4-(2-pyridylazo)resorcinol (PAR) and 4-(2-thiazolylazo)resorcinol (TAR) with Mn(II), Ni(II), Cu(II) and Zn(II) have been determined spectrophotometrically at $\mu = 0.1$ and 25°C. The method is based on indirect estimation of the protonated and normal complexes by measuring the ligand absorption peak. Both protonated and normal complexes of these metals with PAR are more stable than those with TAR. The reverse order was previously observed for the pronated complexes of the lanthanides(III). The different behaviour of the 3*d* transition metals(II) compared to the lanthanides(III) is discussed. The proton dissociation constants of the protonated complexes of PAR or TAR with various metals are also discussed.

The two reagents 4-(2-pyridylazo)resorcinol (PAR) and 4-(2-thiazolylazo)resorcinol (TAR) have the same reactive group (a heterocyclic nitrogen, azo group, and *o*-hydroxyl group as shown in Fig. 1) available for possible coordination to metal ions, and appear to be very similar in character. According to Irving and Rossotti,[1] a linear relation should be obtained between the logarithms of the stability constants for complexes of such a pair of ligands with a series of metal ions. However, no attempt has been made to correlate the stability constants for complexes of PAR with TAR. Both reagents are a dibasic acid and simultaneously form the protonated and the normal type of complexes with most metal ions. Therefore, it is necessary to study such a correlation for complexes of the same type. In general, TAR forms less stable complexes with metal ions than PAR because of the lower basicity of the thiazole rings. From the results previously obtained for the lanthanide complexes of PAR[2] and TAR,[3] this was valid for the normal complexes but the reverse order was observed for the protonated complexes. It is of interest to study the relative stabilities of these complexes with some 3*d* transition-metal ions whose coordination properties are different from those of lanthanide ions. Also of interest is the effect of the complexed metal ions on the acidity of the protonated complexes of PAR or TAR. Corsini *et al.*,[4] who studied the 1 : 2 PAR complexes of some 3*d* transition metals by potentiometry, reported that the order of acidity follows the stability order of the protonated complexes. However, the acidity should be proportional to the relative stability of the normal and the protonated complexes.

In this study, we made a comparison of the



PAR TAR

Fig. 1. Structures of PAR and TAR.

stability of complexes, first of the same type (the normal or the protonated type), formed by PAR and TAR, and, second, of different types, formed by PAR or TAR with some 3*d* transition metals(II) and lanthanides(III).

EXPERIMENTAL

Materials

All chemicals used were of reagent grade. PAR and TAR were obtained from Dojindo Chemical Co., and their purities were checked by using thin-layer chromatography.[5] A weight quantity of PAR or TAR was dissolved in a small volume of 1.0 M NaOH and the solutions were diluted with distilled water to prepare the stock solutions of 2.0×10^{-3} M. Standard metal salt solutions with concentrations of about 0.02 M [Cu(II), Ni(II) or Zn(II)] and 0.1 M [Mn(II)] were prepared from nitrates. The metal solutions were standardized by EDTA titrations using TAR (Cu and Ni), xylenol orange + methylthymol blue (Mn), and xylenol orange (Zn) as indicators. The solutions of various pH values used were mixtures of 0.1 M HNO_3 and 0.1 M $NaNO_3$ at various ratios (pH < 1.5), and 0.1 M $NaNO_3$ buffered with chloroacetate (pH 1.5–3), acetate (pH 4–5), and hexamine (pH 5–7). Complexation between the metal and the buffer ions was neglected under the conditions used.

Procedure

The metal solution was added in small steps, 20–50×10^{-3} cm^3 each, using a microliter pipet, to 10 cm^3 of PAR or TAR solution ($1.5–3.0 \times 10^{-5}$ M) of constant pH, to give concentrations of 10^{-4}–10^{-2} M. Before and after addition of the metal for each $20–50 \times 10^{-3}$ cm^3, the absorbance around the peak of the ligand, which depends on the pH (385–413 nm for PAR and 420–440 nm for TAR), was measured by using a Shimadzu UV 200s spectrophotometer. Each spectrum had a well-defined isosbestic point which varied according to the metal ions used and the pH. No precipitation occurred under these experimental conditions.

RESULTS AND DISCUSSION

Determination of the stability constants

When the ligand, H_2L, such as PAR or TAR, itself has an intense absorption peak, the stability constants of the metal complexes, MHL and ML, can indirectly be estimated by utilizing the ligand absorption peak.[6] The absorbance at the free ligand peak measured in the absence (A_o) and the presence (A) of the metal under conditions where $C_M \gg C_L$ (C_M and C_L are the total concentrations of the metal and the ligand), i.e. formation of the 1 : 1 complexes, MHL and ML, is assumed, can be related to their stability constants, K_{MHL} and K_{ML}, as follows (the charges are omitted for simplicity):

$$C_L = [MHL] + [ML] + [L'], \quad (1)$$

$$A = \varepsilon_{MHL}[MHL] + \varepsilon_{ML}[ML] + \varepsilon_{L'}[L'], \quad (2)$$

where L′ is the free ligand not combined with metal, and ε_{MHL}, ε_{ML} and $\varepsilon_{L'}$ are the molar extinction coefficients of MHL, ML and L′, respectively, at the free ligand peak. With the stability constants, $K_{MHL} = [MHL]/([M][HL])$ and $K_{ML} = [ML]/([M][L])$, the acid dissociation constants of H_2L, $K_1 = [H][HL]/[H_2L]$ and $K_2 = [H][L']/[HL]$, and α-coefficient,[7] $\alpha_L = [L']/[L]$, eqns (1) and (2) can be transformed into the following expressions:

$$[M](K_{MHL}K_1[H] + K_{ML}K_1K_2)/(\alpha_L K_1 K_2) = C_L/[L'] - 1, \quad (3)$$

$$A/\varepsilon_{L'} = [L']\{1 + (\varepsilon_{MHL}K_{MHL}K_1[H] + \varepsilon_{ML}K_{ML}K_1K_2)[M]/(\varepsilon_{L'}\alpha_L K_1 K_2)\}. \quad (4)$$

Combining eqns (3) and (4), and substituting C_M for [M] (since $C_M \gg C_L$) and A_o for $C_L\varepsilon_{L'}$, we obtain:

$$\frac{K_{MHL}K_1[H] + K_{ML}K_1K_2}{\alpha_L K_1 K_2} - \frac{\varepsilon_{MHL}K_{MHL}K_1[H] + \varepsilon_{ML}K_{ML}K_1K_2}{\varepsilon_{L'}\alpha_L K_1 K_2} \times \frac{A_o}{A} = (A_o/A - 1)/C_M. \quad (5)$$

From eqn (5), a linear relation between $(A_o/A - 1)/C_M$ and A_o/A should be obtained at a constant pH where $\varepsilon_{L'}$ remains constant. The product of the intercept of the *y*-axis [$y = (A_o/A - 1)/C_M$], y_o, at a fixed pH and $\alpha_L K_1 K_2$ is given as a function of [H]:

$$y_o \times \alpha_L K_1 K_2 = K_{MHL}K_1[H] + K_{ML}K_1K_2. \quad (6)$$

If a protonated ligand species, H_3L, is formed at low pH values, eqn (6) can be written as:

$$\alpha_L K_o K_1 K_2 y_o = K_{MHL}K_o K_1[H] + K_{ML}K_o K_1 K_2, \quad (7)$$

where $K_o = [H][H_2L]/[H_3L]$. According to eqn (6) or (7), a linear plot of the left-hand side of eqn (6) or (7) vs [H] should be obtained in a pH range where no hydrolysis of the metal ion occurs. From the slope and the intercept of the line, both

K_{MHL} and K_{ML} values can be determined. In this experiment, we used PAR (H_2P) or TAR (H_2T) as the ligand, H_2L, and Mn(II), Ni(II), Cu(II) or Zn(II) as the metal.

Under conditions where $C_M \gg C_L$, the pH ranges had to be greatly varied from metal to metal to give an observable decrease in the absorbance of the ligand peak with increasing C_M. The pH values were 5.5–6.4 (Mn), 4.2–5.5 (Zn),[6] 2.1–2.5 (Ni) and 1.2–1.7 (Cu) for the PAR complexes, and 6.5–7.1 (Mn), 5.3–6.0 (Zn), 4.2–4.7 (Ni) and 1.5–2.2 (Cu) for the TAR complexes. The results of the plots according to eqn (5) for the Cu(II)–TAR and the Mn(II)–PAR system are shown in Fig. 2. Similar linear plots with a negative slope were obtained for all the other systems studied. To confirm the value of the intercept (y_o) we tried to plot the data at another wavelength around the ligand peak and obtained a line having the same intercept (the slope is different).

To determine the stability constants of MHL and ML complexes we plotted the relationship expressed by eqn (6) or (7). The values, $pK_o = 2.69$, $pK_1 = 5.50$ and $pK_2 = 12.30$[8] for PAR, and $pK_o = 0.98$, $pK_1 = 6.23$ and $pK_2 = 9.44$[9] for TAR, were used for calculation of $\alpha_L K_o K_1 K_2$ or $\alpha_L K_1 K_2$. All the plots exhibited straight lines, some of which had intercepts but others passed through the origin. This indicates that both MHL and ML complexes exist in the former group, including the Mn–PAR, the Mn–TAR and the Zn–TAR system, but there is only the MHL complex in the latter, including the Ni–PAR, the Ni–TAR, the Cu–PAR and the Cu–TAR system. By use of the least-squares method, the stability constants, both K_{MHL} (slope) and K_{ML} (intercept) for the former group, but only K_{MHL} (slope) for the latter group, were determined.

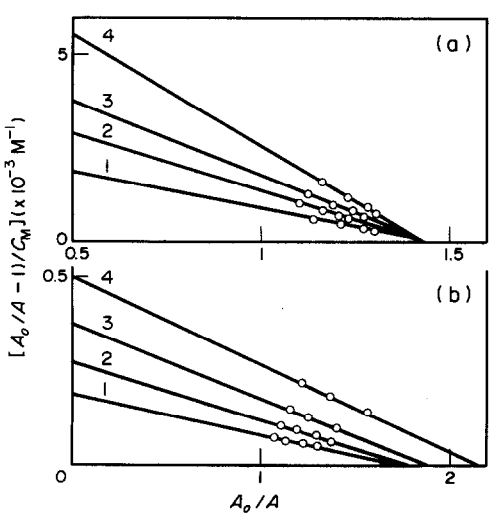


Fig. 2. Plots according to eqn (5) at different pH values for the Cu–TAR (a) and Mn–PAR (b) systems: (a) pH 1.56 (1), 1.70 (2), 1.83 (3), and 1.94 (4); (b) pH 5.73 (1), 5.89 (2), 6.16 (3), and 6.37 (4).

To obtain K_{ML} for the latter group, we studied the acid–base equilibrium: MHL = ML+H. The solution involving only the MHL complex was used for this study. The spectral changes of the solution with increasing pH showed a well-defined isosbestic point in each system. The analysis of the data gave the proton dissociation constant of MHL, K^H_{MHL}, from which K_{ML} could be calculated by eqn (8):

$$K_{ML} = K_{MHL} K^H_{MHL} / K_2. \quad (8)$$

This equation is also used to obtain K^H_{MHL} for the former group. The values of K_{MHL}, K_{ML} and K^H_{MHL} are listed together with those previously obtained for the PAR–Zn complexes,[6] and the PAR[2,6]– and TAR[3]–lanthanide complexes in Table 1. The values for the PAR–Cu complexes and the TAR–Cu and TAR–Ni complexes obtained here are in good agreement with those reported in the literature.[9–11]

Relationship between stabilities of PAR (H_2P) and TAR (H_2T) complexes

The stabilities of complexes of the same type (ML or MHL), formed by a similar pair of ligands, H_2P and H_2T, with two different series of metal ions are compared by plotting log K_{MP} vs log K_{MT} or log K_{MHP} vs log K_{MHT} (Figs 3 and 4). For both types of complexes, the plots yield two separate lines, respectively, one for the transition metals and the other for the lanthanides. This suggests that there would be a clear difference in the coordination mode of these ligands toward the two series of metal complexes.

Irving and Rossotti[1] derived the theoretical relationship between the logarithms of the stability constants for metal complexes of a similar pair of ligands, A and B, as follows:

$$\log K_{MA} = \log K_{MB} + (\log K_{HA} - \log K_{HB}). \quad (9)$$

This equation is based on the assumption that the term including the partial molar free energy of each species S, denoted $\bar{G}^o_S$, $1/RT\{(\bar{G}^o_{MB} - \bar{G}^o_{MA}) - (\bar{G}^o_{HB} - \bar{G}^o_{HA})\}$, and the term including the activity coefficient can be neglected when ligands A and B are similar in character. For PAR and TAR in this study, there are two possible forms of the proton ligand complexes, H_3L^+ and H_2L. Thus, the following equations corresponding to eqn (9) will be given for the normal [eqn (10) or (11)] and the protonated [eqn (12) or (13)] complexes:

$$\log K_{MP} = \log K_{MT} + (\log K_{H_3P} K_{H_2P} K_{HP} - \log K_{H_3T} K_{H_2T} K_{HT}), \quad (10)$$

Table 1. Stability constants, K_{MHL} and K_{ML}, and proton dissociation constants of MHL, K^{H}_{MHL}, for metal complexes of 4-(2-pyridylazo)resorcinol (PAR) and 4-(2-thiazolylazo) resorcinol (TAR) ($\mu = 0.1$, 25°C)[a]

	PAR			TAR		
	log K_{MHL}	log K_{ML}	pK^{H}_{MHL}	log K_{MHL}	log K_{ML}	pK^{H}_{MHL}
Mn	2.40	8.48	6.22	2.02	5.52	5.94
Ni	7.70	14.05	5.95	6.12	10.21	5.35
					10.0[b]	5.4[b]
Cu	9.93	17.31	4.92	8.25	13.59	4.10
	9.90[c]	17.22[c]	5.00[c]		13.55[d]	4.24[d]
Zn	5.05[e]	11.2[e]	6.15[e]	4.28	7.80	5.92
Lanthanide[f]						
La	3.18	8.91	6.57	3.61	6.93	6.12
Ce	3.78	9.61	6.47	4.08	7.44	6.08
Pr	3.95	9.78	6.47	4.27	7.65	6.06
Nd	4.07	10.02	6.35	4.40	7.79	6.05
Sm–Tb	4.28	10.25	6.33	4.71	8.10	6.05
Dy	4.29	10.36	6.23	4.71	8.10	6.05
Ho	4.29	10.47	6.12	4.71	8.10	6.05
Er	4.31	10.52	6.09	4.71	8.10	6.05
Tm	4.34	10.57	6.07	4.74	8.34	5.84
Yb, Lu	4.39	10.70	5.99	4.77	8.78	5.43

[a] Relative errors of K_{MHL} and K_{ML} are 5–10 and 8–15%, respectively.
[b] Reference 9.
[c] Reference 10.
[d] Reference 11.
[e] Reference 6.
[f] References 2, 3 and 6.

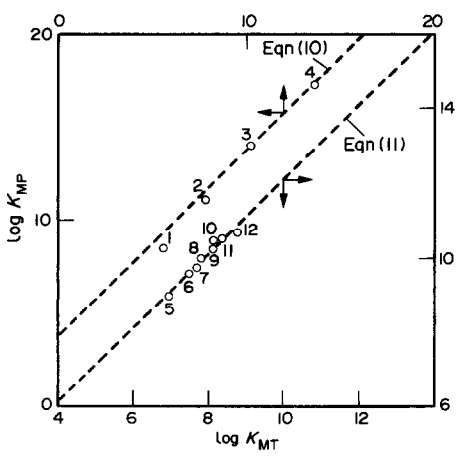


Fig. 3. Relationship between the stability constants for the normal type of metal complexes with PAR (K_{MP}) and TAR (K_{MT}). (1) Mn, (2) Zn, (3) Ni, (4) Cu, (5) La, (6) Ce, (7) Pr, (8) Nd, (9) Sm–Ho, (10) Er, (11) Tm, and (12) Yb, Lu.

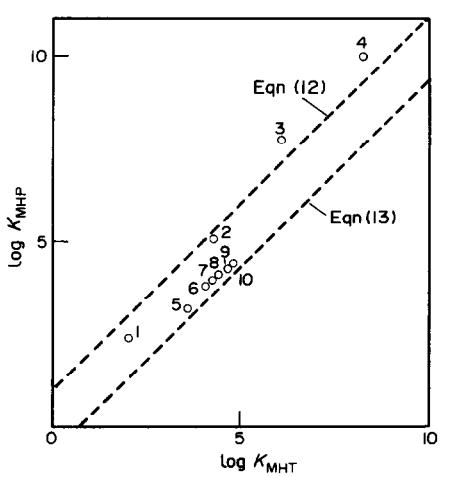


Fig. 4. Relationship between the stability constants for the protonated type of metal complexes with PAR (K_{MHP}) and TAR (K_{MHT}). (1) Mn, (2) Zn, (3) Ni, (4) Cu, (5) La, (6) Ce, (7) Pr, (8) Nd, (9) Sm–Tm, and (10) Yb, Lu.

$$\log K_{MP} = \log K_{MT} + (\log K_{H_2P}K_{HP} - \log K_{H_2T}K_{HT}), \quad (11)$$

and

$$\log K_{MHP} = \log K_{MHT} + (\log K_{H_3P}K_{H_2P} - \log K_{H_3T}K_{H_2T}), \quad (12)$$

$$\log K_{MHP} = \log K_{MHT} + (\log K_{H_2P} - \log K_{H_2T}), \quad (13)$$

where K_{H_3P}, K_{H_2P} and K_{HP} are the protonation constants of H_2P, HP and P, and K_{H_3T}, K_{H_2T} and K_{HT} are those of H_2T, HT and T. These equations are based on the following assumptions:

$$1/RT\{\bar{G}^o_{MT} - \bar{G}^o_{MP} - (\bar{G}^o_{H_3T} - \bar{G}^o_{H_3P})\} \simeq 0 \text{ [eqn (10)]},$$

$$1/RT\{\bar{G}^o_{MT} - \bar{G}^o_{MP} - (\bar{G}^o_{H_2T} - \bar{G}^o_{H_2P})\} \simeq 0 \text{ [eqn (11)]},$$

$$1/RT\{\bar{G}^o_{MHT} - \bar{G}^o_{MHP} - (\bar{G}^o_{H_3T} - \bar{G}^o_{H_3P})\} \simeq 0 \text{ [eqn (12)]},$$

$$1/RT\{\bar{G}^o_{MHT} - \bar{G}^o_{MHP} - (\bar{G}^o_{H_2T} - \bar{G}^o_{H_2P})\} \simeq 0 \text{ [eqn (13)]},$$

and the term including the activity coefficients $\simeq 0$. The theoretical relationships between log K_{MP} and log K_{MT} given by eqn (10) or (11), and those between log K_{MHP} and log K_{MHT} given by eqn (12) or (13) are shown by dotted lines in Figs 3 and 4, respectively.

For the normal complexes, as is seen in Fig. 3, the experimental points for the transition metals and the lanthanides fall closely on the theoretical lines of eqns (10) and (11), respectively. Although the data points somewhat deviated from the theoretical lines (Fig. 4), eqns (12) and (13) can be applied to the protonated complexes of the transition metals and lanthanides, respectively. From these facts, the stabilities of the two series of metal complexes are found to be related to the stabilities of each of the two forms of proton–ligand complexes (H_3L^+ and H_2L), i.e. the heterocyclic nitrogens of the ligands are coordinated to the transition metals but not to the lanthanides. Thus, both PAR and TAR act as a tridentate ligand (a heterocyclic nitrogen, azo nitrogen, and *o*-hydroxyl oxygen) for the transitions metals as indicated by Geary *et al.*,[8] but as a bidentate ligand for the lanthanides.

Relationship between stabilities of normal and protonated complexes of PAR (H_2P) or TAR (H_2T)

A comparison was made of complexes of a pair of ligands, P and HP, or T and HT, with various metal ions. Although the individual complexes of both pairs of ligands differ in stability from metal to metal the values of K_{MP}/K_{MHP} or K_{MT}/K_{MHT} are relatively close together. This indicates a linear relationship between log K_{MP} and log K_{MHP}, or log K_{MT} and log K_{MHT}. If we can assume that:

$$1/RT\{\bar{G}^o_{MHP} - \bar{G}^o_{MP} - (\bar{G}^o_{H_2P} - \bar{G}^o_{HP})\} \simeq 0,$$

$$1/RT\{\bar{G}^o_{MHT} - \bar{G}^o_{MT} - (\bar{G}^o_{H_2T} - \bar{G}^o_{HT})\} \simeq 0,$$

and the term including the activity coefficients $\simeq 0$, the theoretical relationships for both systems are given by eqns (14) and (15):

$$\log K_{MP} = \log K_{MHP} + \log K_{HP} - \log K_{H_2P}, \quad (14)$$

$$\log K_{MT} = \log K_{MHT} + \log K_{HT} - \log K_{H_2T}. \quad (15)$$

Plots of log K_{MP} vs log K_{MHP} or of log K_{MT} vs log K_{MHT} are shown in Fig. 5 together with the theoretical (dotted) lines. The experimental points, with the exception of the Cu(II)–TAR system, lie near the theoretical lines, although most of them for the PAR complexes are in positions somewhat lower than the lines. There is a small but significant effect of the complexed metal ion on the acidity of the protonated complexes (the K^H_{MHL} value in Table 1 which is proportional to the K_{ML}/K_{MHL} value), i.e. the effect increases with increasing the π-bonding tendencies for the transition metals or increasing the charge densities for the lanthanides. The largest effect is observed for Cu(II) which is able to form a stable π-bond with an aromatic nitrogen.[12,13]

In conclusion, the theoretical relationship between the stabilities for complexes of a similar pair of ligands, PAR and TAR, can generally be applied to understand the coordination mode of the ligands toward different series of metal ions.

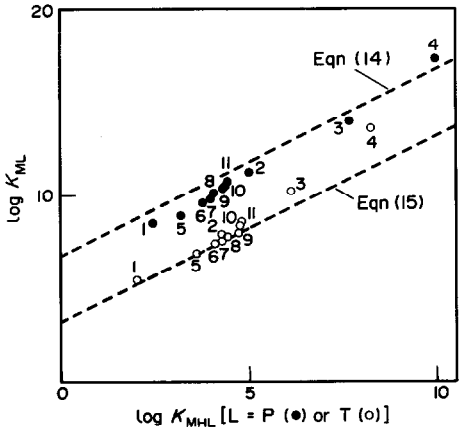


Fig. 5. Relationship between the stability constants for the normal and the protonated types of metal complexes, formed by PAR (●) or TAR (○). (1) Mn, (2) Zn, (3) Ni, (4) Cu, (5) La, (6) Ce, (7) Pr, (8) Nd, (9) Sm–Er, (10) Tm, and (11) Yb, Lu.

Acknowledgement—I acknowledge the financial support of this work by a Grant-in-Aid for Scientific Research from the Ministry of Education (No. 60540383).

REFERENCES

1. H. Irving and H. Rossotti, *Acta Chem. Scand.* 1956, **10**, 72.
2. E. Ohyoshi, *Talanta* 1984, **31**, 1129.
3. E. Ohyoshi, *Bull. Chem. Soc. Jpn* 1985, **58**, 405.
4. A. Corsini, Q. Fernando and H. Freiser, *Inorg. Chem.* 1963, **2**, 224.
5. F. H. Pollard, G. Nickless, T. J. Samuelson and R. G. Anderson, *J. Chromatogr.* 1964, **16**, 231.
6. E. Ohyoshi, *Anal. Chem.* 1983, **55**, 2404.
7. A. Ringbom, *Complexation in Analytical Chemistry*. Interscience, New York (1963).
8. W. J. Geary, G. Nickless and F. H. Pollard, *Anal. Chim. Acta* 1962, **27**, 71.
9. S. P. Mushran and L. Sommer, *Collect. Czech. Chem. Commun.* 1969, **34**, 3693.
10. S. Funahashi, S. Yamada and M. Tanaka, *Inorg. Chem.* 1971, **10**, 257.
11. M. Hnilickova and L. Sommer, *Talanta* 1966, **13**, 667.
12. R. Griesser and H. Sigel, *Inorg. Chem.* 1970, **9**, 1238.
13. P. R. Huber, R. Griesser and H. Sigel, *Inorg. Chem.* 1971, **10**, 945.

Polyhedron Vol. 5, No. 6, pp. 1171–1181, 1986
Printed in Great Britain

0277–5387/86 $3.00+.00
Pergamon Journals Ltd

SEMI-EMPIRICAL EVALUATION OF MOLECULAR-ORBITAL PARAMETERS, AND SPIN–ORBIT, DIPOLAR AND FERMI-CONTACT TERMS OF VO^{2+} ION IN LATTICES

M. SALAGRAM,*† N. SATYANARAYANA and S. RADHAKRISHNA

Department of Physics, Indian Institute of Technology, Madras 6000036, India

(*Received* 13 *May* 1985; *accepted* 31 *October* 1985)

Abstract—The ESR spectra of the VO^{2+} ion doped in oxalate, tartrate and cadmium crystals taken in the polycrystalline form are analysed. The transition energies ΔE_1 and ΔE_2 obtained from the electronic absorption spectra of the VO^{2+}-doped single crystals in conjunction with the spin-Hamiltonian parameters obtained from ESR data are used to evaluate the spin–orbit coupling constant, the dipolar term and the Fermi-contact term. The bonding coefficient β_2^2 is evaluated from the available molecular-orbital theories and the experimental data. The various terms evaluated are correlated and the general behaviour of the VO^{2+} ion in various ligand fields of different symmetries is discussed.

When paramagnetic radicals or ions are fixed but randomly oriented in a powder sample, the ESR spectrum will consist of an envelope of the absorptions at all possible orientations of the species.[1] Thus, ESR studies on polycrystalline samples are expected to provide valuable information, such as the nature of the g- and A-tensors of the paramagnetic ion in a given environment. The quantitative data obtainable from the ESR spectra of polycrystalline samples together with the electronic absorption data is generally sufficient to calculate important molecular-orbital (MO) parameters which, besides the single-crystal data, throw further light on the ligand environment and its effect on the electronic structure of the paramagnetic ion embedded in a crystal.

The method of evaluation of the spin–orbit coupling constant (λ), the Fermi-contact term (K), the bonding (β_1^2 and β_2^2) and other parameters for the vanadyl (VO^{2+}) ion using a semi-empirical MO approach is reported in the present paper. The approach itself is based on the crystal field[2,3] and MO theories[4,5] proposed so far to explain the electronic structure of the VO^{2+} ion.

The lattices chosen for the study were: potassium oxalate monohydrate (POMH), $K_2C_2O_4 \cdot H_2O$; ammonium oxalate monohydrate (AOMH), $(NH_4)_2C_2O_4 \cdot H_2O$; potassium hydrogen oxalate (PHO), KHC_2O_4; $3CdSO_4 \cdot 8H_2O$; cadmium ammonium sulphate hexahydrate (CdASH), $Cd(NH_4)_2(SO_4)_2 \cdot 6H_2O$; cadmium potassium sulphate hexahydrate (CdKSH), $CdK_2(SO_4)_2 \cdot 6H_2O$; and strontium tartrate tetrahydrate (SrTrTH), $SrC_4H_4O_6 \cdot 4H_2O$. The electronic (optical) absorption and ESR studies on the VO^{2+} ion doped in all the above single crystals were carried out by the authors and either have already been published[6–8] or are in the process [9–12] of publication.

The discussion of the parameters for the VO^{2+} ion calculated from such a variety of crystalline matrices is not only expected to correlate the optical absorption and ESR data on single crystals but also expected to lead to many important conclusions about covalency effects, hydrogen bonding effects and ligand field effects on the VO^{2+} ion. The magnitudes of the parameters and the corresponding conclusions reported in this paper would serve as a cross-check on the consistency of single-crystal data while establishing the general characteristic pattern of the electronic and paramagnetic behaviour of the VO^{2+} ion in various host environments.

EXPERIMENTAL

Crystals of POMH, AOMH, $3CdSO_4 \cdot 8H_2O$, CdASH and CdKSH doped with VO^{2+} were grown

* Author to whom correspondence should be addressed.

† Present address: Department of Physics, P. G. College of Science, Saifabad, Osmania University, Hyderabad 500004 (A.P.), India.

by a slow-evaporation method from their respective saturated solutions consisting of 1–2% by weight of $VOSO_4 \cdot 5H_2O$. PHO crystals were grown similarly from a solution containing equivalent amounts of potassium oxalate and oxalic acid and 1% by weight of $VOSO_4 \cdot 5H_2O$. SrTrTH crystals doped with VO^{2+} ions (2% by weight) were grown by a "gel" method.[12]

The crystals were crushed and ground into fine powder and separately taken in thin quartz tubes. The ESR spectra of each of the above polycrystalline samples were recorded at 300 or 77 K on a Varian E-4 X-band spectrometer. The optical absorption spectra were recorded using a Cary-14 spectrophotometer.

RESULTS AND DISCUSSION

ESR spectra

The ESR spectra of VO^{2+}-doped AOMH, PHO, CdASH, CdKSH and SrTrTH polycrystalline samples exhibit the expected 16 lines corresponding to the usual parallel and perpendicular components of g- and hyperfine (hf) A-tensors. As a typical representative, the ESR spectra of VO^{2+}-doped CdASH polycrystalline samples is shown in Fig. 1. It can be seen that the parallel and perpendicular components are well-resolved.

All these spectra suggest the characteristic behaviour of the VO^{2+} ion. The ion exhibits only one 16-line pattern in any polycrystalline sample irrespective of the number of substitutional or interstitial[6–12] sites that it actually occupies in the single crystal, provided all the sites are chemically equivalent. The pattern suggests that g and A are axially symmetric in nature. Despite the general resemblance in the ESR spectra, the small variations in the magnitudes of the principal components of g and A (Table 1) are indicative of a sensitive behaviour of VO^{2+} in different ligand field environments. In Table 1, VO^{2+} data for $Zn(NH_4)_2(SO_4)_2 \cdot 6H_2O$ (ZASH)[13] and $NH_4Al(SO_4)_2 \cdot 12H_2O$ (alum)[14] crystals are included as typical examples for comparison[15] with the present data.

Figure 2 shows the first derivative ESR spectrum of VO^{2+}-doped POMH polycrystalline samples recorded at 77 K. In contrast to the typical spectra observed in other lattices, the spectrum does not give a simple picture of $g_\parallel$ and $g_\perp$, and $A_\parallel$ and $A_\perp$, but exhibits the rhombic nature of g- and A-tensors in conformity with the results obtained from single-crystal studies.[6]

Similarly, the ESR spectrum of VO^{2+}-doped

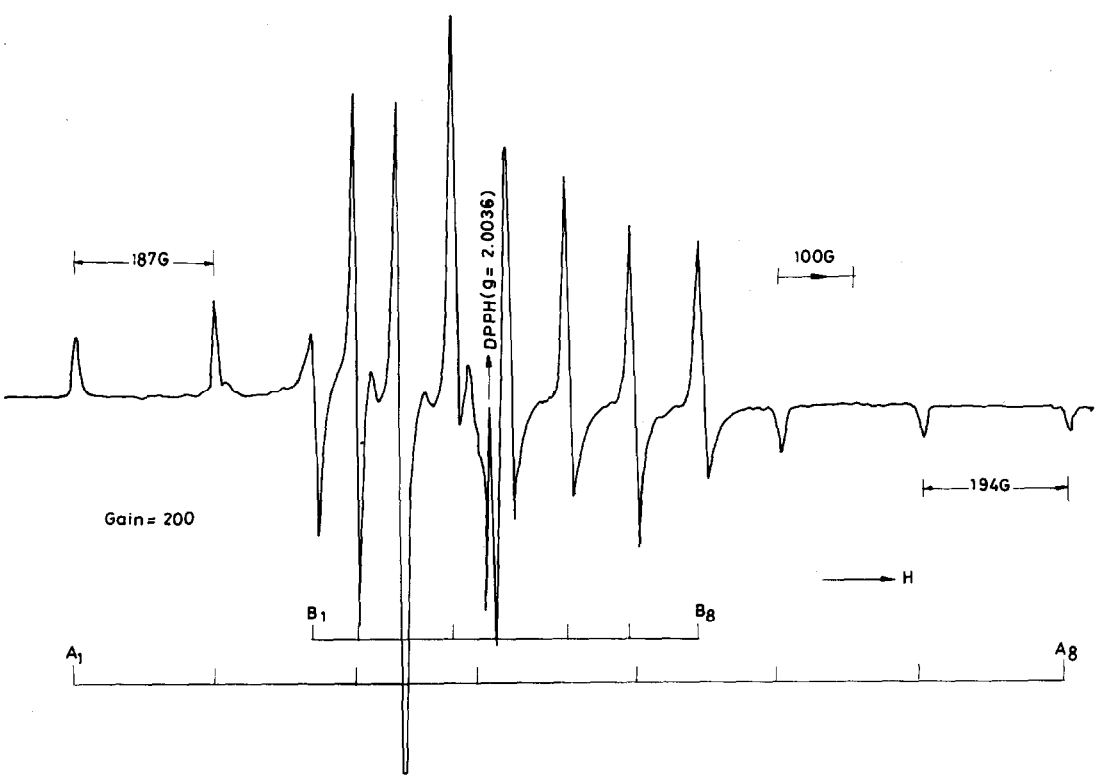


Fig. 1. Typical EPR spectrum of VO^{2+}-doped $Cd(NH_4)_2SO_4 \cdot 6H_2O$ polycrystalline sample recorded at 300 K.

Table 1. Spin-Hamiltonian parameters of VO^{2+} in various lattices: hyperfine parameters are given in G

Host lattice	g_{zz} ($g_\parallel$)	$\frac{g_{xx}+g_{yy}}{2}$ ($g_\perp$)	g_o	A_{zz} ($A_\parallel$)	$\frac{A_{xx}+A_{yy}}{2}$ ($A_\perp$)	A_o	Reference
$K_2C_2O_4 \cdot H_2O$	1.940	1.993	1.976	−177.5	−58.5	−98.2	Present work
$(NH_4)_2C_2O_4 \cdot H_2O$	1.930	1.981	1.964	−196	−73	−114	Present work
KHC_2O_4	1.936	1.992	1.973	−190.5	−81	−117.5	Present work
$3CdSO_4 \cdot 8H_2O$	1.923	1.987	1.969	−199	−78	−117	Present work
$Cd(NH_4)_2(SO_4)_2 \cdot 6H_2O$	1.946	1.994	1.979	−190	−74	−112	Present work
$CdK_2(SO_4)_2 \cdot 6H_2O$	1.930	1.986	1.972	−196	−74	−113	Present work
$SrC_4H_4O_6 \cdot 4H_2O$	1.943	1.990	1.974	−185.4	68.5	−107.5	Present work
$Zn(NH_4)_2(SO_4)_2 \cdot 6H_2O$	1.932	1.980	1.964	−203	−78	−118	13
$NH_4Al(SO_4)_2 \cdot 12H_2O$	1.940	1.978	1.965	−187.2	−70.9	−110	14

$3CdSO_4 \cdot 8H_2O$ polycrystalline samples shown in Fig. 3 is again different not only from the typical spectra but also from that of POMH : VO^{2+} shown in Fig. 2. Although, the usual 16-line pattern is obvious, the distinct resolution in the extreme lines (Fig. 3) shows that two chemically inequivalent sites for VO^{2+} are present in the lattice and each of them exhibit axially symmetric g- and A-tensors in conformity with single-crystal data. The spin-Hamiltonian parameters derived from all the spectra are given in Table 1. A further justification of the observed $\tilde{g}$ and $\tilde{A}$ can be given in terms of bonding coefficients and other MO parameters computed from these experimental data.

Electronic absorption spectra

The electronic absorption spectra of VO^{2+} in all the present lattices have been reported.[6–12] They reveal a variety of behaviour for the VO^{2+} ion in the lattices. A typical representative spectrum observed in PHO : VO^{2+} is shown in Fig. 4. The spectra in the cases of AOMH, PHO, CdASH,

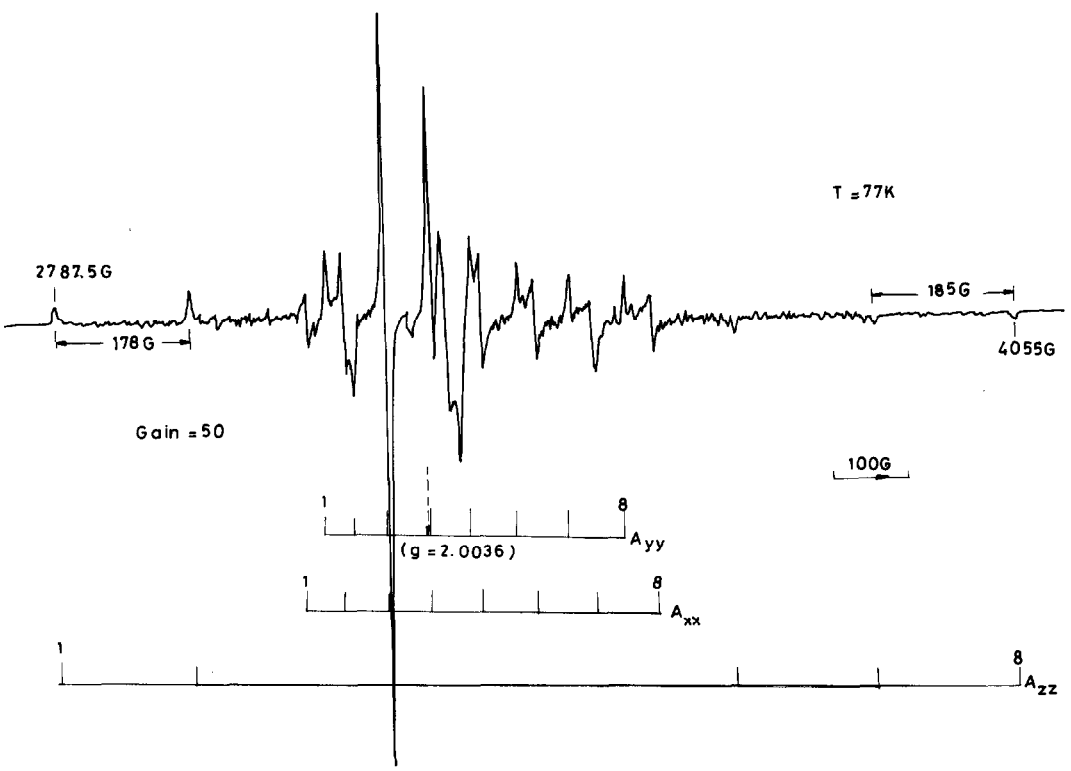


Fig. 2. EPR spectrum of VO^{2+}-doped $K_2C_2O_4 \cdot H_2O$ polycrystalline sample recorded at 77 K.

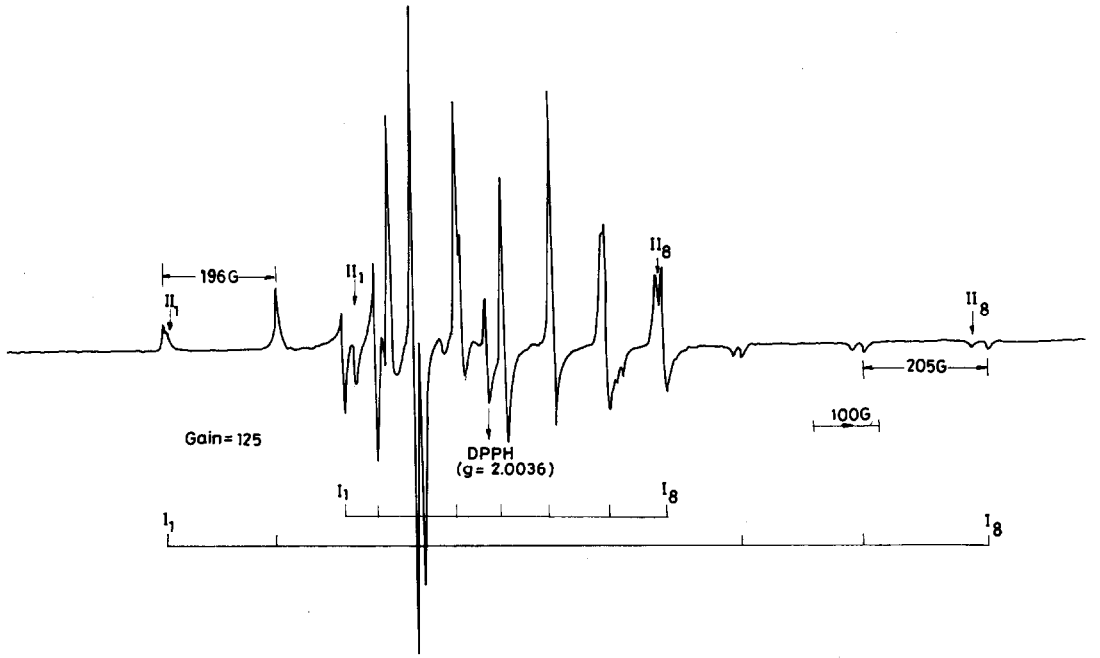


Fig. 3. EPR spectrum of VO^{2+}-doped $3CdSO_4 \cdot 8H_2O$ polycrystalline sample recorded at 300 K.

CdKSH and SrTrTH are generally similar, however, with individual variations in the band positions and their intensities. The variations cause differences in the magnitudes of the transition energies (given in Table 2) which, in turn, affect the bonding and MO parameters computed from these data.

Interestingly, the optical absorption spectrum[6] of POMH : VO^{2+} is entirely different from the spectra of the above samples and suggests a low-symmetry (C_2) site for VO^{2+}. Similarly, the site symmetry of VO^{2+} in $3CdSO_4 \cdot 8H_2O$ as determined by polarization studies[9] is also C_2, although the actual band positions are different.

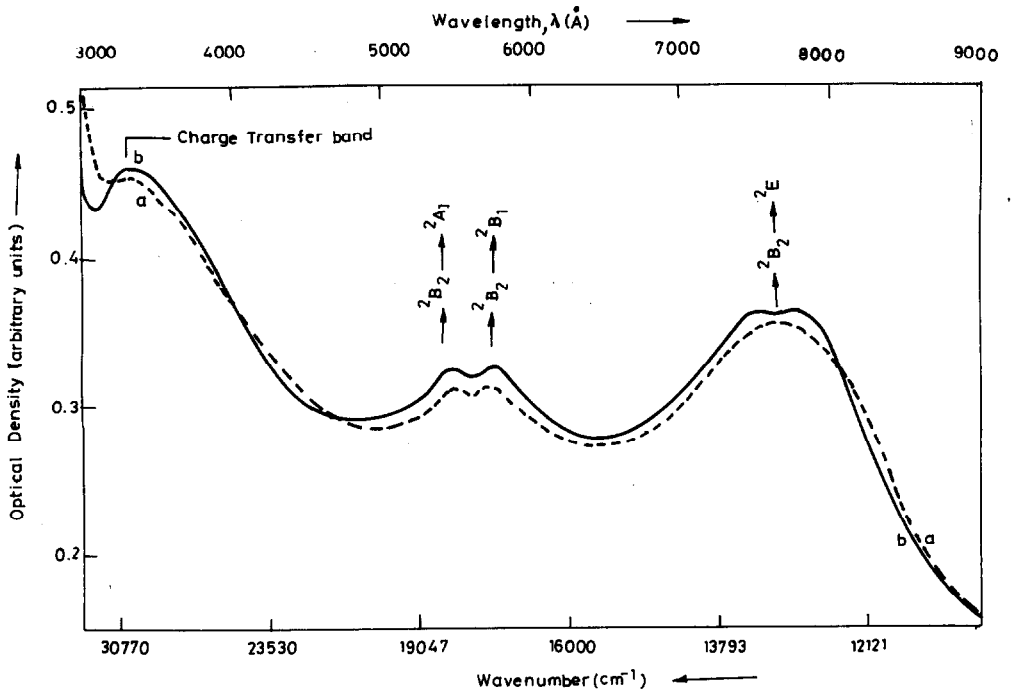


Fig. 4. Typical electronic absorption spectrum of $KHC_2O_4 : VO^{2+}$ recorded at 300 (a) and 80 K (b).

Table 2. Electronic absorption spectral data pertaining to transition energies in the VO^{2+} ion in different matrices and calculated values of the spin–orbit coupling constant (λ) and isotropic hf parameter (A_o) with its sign (in G)

Host lattice	Ligands	Approximate site symmetry	ΔE_2 ($b_2 \rightarrow e_\pi^*$) (cm^{-1})	ΔE_1 ($b_2 \rightarrow b_1$) (cm^{-1})	λ (cm^{-1})	A_o (G)	Reference
$K_2C_2O_4 \cdot H_2O$	O^{2-}, H_2O	C_2	11,530	15,384	86.3	−98.2	Present work
$(NH_4)_2C_2O_4 \cdot H_2O$	O^{2-}, H_2O	C_{4v}	12,780	16,260	102	−114	Present work
KHC_2O_4	O^{2-}	C_{4v}	12,990	16,800	142	−117.5	Present work
$3CdSO_4 \cdot 8H_2O$	O^{2-}, H_2O	C_2	12,500	14,760	121	−117	Present work
$Cd(NH_4)_2(SO_4)_2 \cdot 6H_2O$	H_2O	C_{4v}	14,035	16,000	85	−112	Present work
$CdK_2(SO_4)_2 \cdot 6H_2O$	H_2O	C_{4v}	12,038	13,698	113	−113	Present work
$SrC_4H_4O_6 \cdot 4H_2O$	O^{2-}, H_2O	C_{4v}	12,500	13,200	86	−107.5	Present work
$Zn(NH_4)_2(SO_4)_2 \cdot 6H_2O$	H_2O	C_{4v}	13,000	16,000	142.7	−118	13
$NH_4Al(SO_4)_2 \cdot 12H_2O$	H_2O	C_{4v}	13,000	15,700	140.1	−110	14

Calculation of λ

The VO^{2+} ion consists of a single unpaired electron (d^1-system) in a non-degenerate ground state d_{xy}, and it is expected[16] for the ion that $g_\parallel < g_\perp$. The principal parameters evaluated from single-crystal and polycrystal (ESR) spectra of all the present lattices show (Table 1) that $(g_{zz})g_\parallel < g_\perp(g_{xx}, g_{yy})$. Assuming pure d-orbitals and using first- and second-order perturbation theory, the spin-Hamiltonian parameters can be related to the transition energies:

$$\Delta E_1(d_{xy} \rightarrow d_{x^2-y^2} \quad \text{or} \quad b_2 \rightarrow b_1^*)$$

and

$$\Delta E_2(d_{xy} \rightarrow d_{xz}, d_{yz} \quad \text{or} \quad b_2 \rightarrow e_\pi^*)$$

by the expressions:

$$g_\parallel = g_e - \frac{8\lambda}{\Delta E_1} \quad \text{and} \quad g_\perp = g_e - \frac{2\lambda}{\Delta E_2}, \qquad (1)$$

where g_e is the free-electron "g" value, i.e. 2.0023. Using the values of ΔE_1 and ΔE_2 (Table 2) derived from the optical absorption spectra, and g parameters from Table 1, λ values have been evaluated and are included in Table 2.

A value for λ of 250 cm^{-1} is reported[17] for the free V^{4+} ion. The reduction in the magnitude of λ for the double bonded oxovanadium (molecular) complex $(V{=}O)^{2+}$ is attributed to substantial π-bonding. Kivelson and Lee[18] have theoretically predicted a value of 170 cm^{-1} for λ for C_{4v}-symmetry. While the λ values in most lattices of the present work (Table 2) are within reasonable limits of predicted value, the reduction in λ for the VO^{2+} ion in some lattices has to be accounted for in terms of the individual structural natures of the compounds.

In POMH, where $\lambda = 86.3$ cm^{-1}, the VO^{2+} ion is at a very low symmetry site. In CdASH, where $\lambda = 85$ cm^{-1}, the VO^{2+} ion replaces a large-size Cd^{2+} ion relative to the Zn^{2+} ion in ZASH and the ligand oxygens of water molecules about the Cd^{2+} ion are in a different arrangement from those of other tutton salts.[19] In SrTrTH, where $\lambda = 86$ cm^{-1}, the oxygen ligands forming a distorted octahedron are bonded to either water hydrogens or carbon atoms.[20] In all such cases of low-symmetry ligand fields and covalency effects arising from hydrogen bonding, eqn (1) cannot be applied rigorously, hence the reduction in the λ value. These effects are also reflected in the magnitudes of the g- and A-parameters with a bearing on the MO coefficients and bonding parameters which are calculated in the following sections.

Sign of hf coupling constant and calculation of P

The expressions for the hf interaction constant are given[21] by:

$$A_\parallel = -P\left(\frac{4}{7} + K + \frac{3}{7}\frac{\lambda}{\Delta E_1}\right), \qquad (2a)$$

$$A_\perp = P\left(\frac{2}{7} - K - \frac{3}{14}\frac{\lambda}{\Delta E_1}\right), \qquad (2b)$$

where $P = 2\gamma\beta\beta_N\langle r^{-3}\rangle$.

In eqn (2), P is the direct dipolar term which takes into account the dipole–dipole interaction of the electron moment with the nuclear moment, and K is the Fermi-contact term representing the unpaired electron density at the vanadium nucleus. Watson[22] has calculated the $\langle r^{-3}\rangle$ value to be 3.67 Å U for the d^1-electron in V^{4+} and this gives a value for P of 171.2 G.

Solving eqn (2a) and (2b), the expression for P is

given by:

$$P = \frac{7(A_\parallel - A_\perp)}{2 + \frac{3}{2}\frac{\lambda}{\Delta E_1}}. \quad (3)$$

Neglecting the second-order effects and taking negative values for $A_\parallel$ (or A_{zz}) and $A_\perp$ [or $(A_{xx}+A_{yy})/2$], the P values are calculated from eqn (3) for the data in the present work and are given in Table 3. If $A_\parallel$ is taken to be negative and $A_\perp$ positive, the P value will be more than 270 G, which is far from the expected value. Thus, the signs of both $A_\parallel$ and $A_\perp$ are taken as negative and are indicated in Table 2 in the form of the isotropic hf constant (A_o) (*vide infra*). The value of P was theoretically calculated to be +136 G by McGarvey for vanadyl complexes.[23] The calculated P values (Table 3) do not deviate much from this expected value and the values for ΔE_1 seem to be justifiable in this case.

Calculation of MO coefficients and bonding parameters

ΔE_1 is dependent on the σ- and π-donor strength of the in-plane ligands while ΔE_2 reflects the difference between the in-plane and the axial ligand π-bonding to vanadium in a vanadyl complex.[24] The deviations in ΔE_1 and ΔE_2 values are accountable in terms of MO bonding coefficients for the VO^{2+} ion and such an analysis was made by Ballhausen and Gray[4] (BG) using the LCAO–MO method. The method of description of the magnetic properties of the complexes such as $VO(H_2O)_5^{2+}$ involves the evaluation of the matrix elements between the ground state of symmetry $^2B_2$ and antibonding orbitals of symmetry $^2B_1$ and ^2E. The LCAO–MO wave functions for these orbitals are:[4,25]

$$|^2B_2\rangle = \beta_2|d_{xy}\rangle - \beta_2'\langle\theta_{b_2}\rangle, \quad \text{ground state}$$

$$|^2B_1\rangle = \beta_1|d_{x^2-y^2}\rangle - \beta_1'\langle\theta_{b_1}\rangle, \quad (4)$$

$$|^2E\rangle = e_\pi|d_{xz}\rangle - e_\pi'\langle\theta_x\rangle \quad \text{and} \quad e_\pi|d_{yz}\rangle - e_\pi'\langle\theta_y\rangle,$$

where d-functions represent the metal orbitals and the group orbitals are given by ligand θ-functions of appropriate symmetry.

The g values observed so far for most vanadyl complexes are generally lower than 2.0023 and the ESR data in the present work (Table 1) also support this observation. This lowering is related to the spin–orbit interaction of the ground-state d_{xy}-level with low-lying excited states. The interaction is given by[26] the following first-order expressions:

$$g_e - g_\parallel = 8\beta_1^2\beta_2^2\lambda/\Delta E_1, \quad (5a)$$

$$g_e - g_\perp = 2\beta_2^2 e_\pi^2\lambda/\Delta E_2. \quad (5b)$$

The isotropic and anisotropic g and A parameters are related by the equations:

$$A_o = (A_\parallel + 2A_\perp)/3 \quad \text{or} \quad (A_{zz}+A_{xx}+A_{yy})/3, \quad (6)$$

$$g_o = (g_\parallel + 2g_\perp)/3 \quad \text{or} \quad (g_{zz}+g_{xx}+g_{yy})/3. \quad (7)$$

The hf coupling constants are related to P and to an indirect dipolar interaction caused by the anisotropy in g values. Neglecting small corrections, the expressions are:

$$A_\parallel = -PK - \frac{4}{7}\beta_2^2 P - (g_e - g_\parallel)P - \frac{3}{7}(g_e - g_\perp)P, \quad (8)$$

$$A_\perp = -PK + \frac{2}{7}\beta_2^2 P - \frac{11}{14}(g_e - g_\perp)P. \quad (9)$$

Combining eqns (8) and (9) with (6) and (7) gives

Table 3. Calculated values of the dipolar term (P), Fermi-contact term (K) and molecular-orbital coefficient (β_2^2) for the VO^{2+} ion in various lattices

Host lattice	Ligands	P (G)	K	β_2^2	Reference
$K_2C_2O_4 \cdot H_2O$	O^{2-}, H_2O	138.8	0.68	0.932	Present work
$(NH_4)_2C_2O_4 \cdot H_2O$	O^{2-}, H_2O	143.5	0.77	0.925	Present work
KHC_2O_4	O^{2-}	127.8	0.89	0.927	Present work
$3CdSO_4 \cdot 8H_2O$	O^{2-}, H_2O	141.1	0.80	0.914	Present work
$Cd(NH_4)_2(SO_4)_2 \cdot 6H_2O$	H_2O	135.3	0.81	0.938	Present work
$CdK_2(SO_4)_2 \cdot 6H_2O$	H_2O	140.0	0.78	0.939	Present work
$SrC_4H_4O_6 \cdot 4H_2O$	O^{2-}, H_2O	136.4	0.76	0.936	Present work
$Zn(NH_4)_2(SO_4)_2 \cdot 6H_2O$	H_2O	145	0.78	0.933	13
$NH_4Al(SO_4)_2 \cdot 12H_2O$	H_2O	135.7	0.77	0.945	14

the expression:

$$A_o = -PK-(g_e-g_o)P. \quad (10)$$

Because of the various approximations made in all these equations, highly accurate values for bonding coefficients are not expected. Only the relative values and the order of the molecular parameters are important and the results reported here are more qualitative than quantitative in nature. Combining eqns (8) and (9), and eliminating K, one arrives at the following expression for β_2^2:

$$\beta_2^2 = (A_\perp - A_\parallel)\frac{7}{6P} - \frac{3}{4}g_e + \frac{7}{6}g_\parallel - \frac{5}{12}g_\perp. \quad (11)$$

Thus, β_2^2 can be computed in terms of the empirical data, taking $A_\parallel$ and $A_\perp$ to be negative (from Table 1). The expression for K, from eqn (10), is:

$$K = -\frac{A_o}{P} - (g_e - g_o), \quad (12)$$

and thus K can be evaluated from the data given in Tables 1 and 4. The calculated values of β_2^2 and K for the present data are given in Table 3 along with the ligands of the VO^{2+} ion.

McGarvey[23] also evaluated the β_2^2 using slightly different spin-Hamiltonian parameters for vanadyl-doped crystals and the values are close to the values obtained in the present work. The β_2^2 value is nearly constant and close to unity. This suggests that the ground-state b_2-orbital is non-bonding, as predicted by BG theory.[4]

Correlation between the evaluated parameters

Since the ligands in all the matrices chosen for the present work are only oxygens either non-bonded or bonded to water-hydrogen or carbon atoms, the properties like electronegativity, π-bonding ability, crystal field strength etc. are nearly the same for all the ligands. Precisely for this reason the variation in the g-parameter in various lattices (Table 1) is really insignificant. However, the variation in the hf parameter. A is significant establishing that the electron–nuclear hf interaction is influenced much more by any slight change in the ligand environment (like in the POMH:VO^{2+} system[6]) than the electron–Zeeman or fine-structure interaction.

Relation between K *and hf interaction term* A_o. The isotropic contact term K is a parameter representing the isotropic Fermi-type interaction between electronic and nuclear spins. K is an independent property of the central ion and it serves as a check on the experimental results.[26]

From eqn (12) we find that K is proportional to A_o. Consistent with this fact, it is found that K is lowest for POMH, for which A_o is also the lowest (Tables 1 and 3). For other lattices, A_o and K are proportionately higher. Figure 5 gives a plot of K vs A_o which is a straight line in agreement with eqn (12).

The relation between K and hf interactions of paramagnetic ions has been the subject of many studies.[15,26] If the unpaired electron is not confined to the vanadium nucleus, contact with the metal nucleus is reduced and this causes a smaller hf interaction. Then, the origin of K should be an indirect process. It was first postulated by Abragam *et al.*[27] and later by others[23,26] that the unpaired electrons in the d-orbitals polarize the inner s-shell electrons. McGarvey[23] has shown that the single electron in the d_{xy}-orbital of the d^1 (VO^{2+}) system polarizes the electrons in the filled $2s$ and $3s$ orbitals, thereby creating a finite spin-density at the vanadium nucleus.

Relation between K *and* β_2^2. The value of K is directly proportional to the d-orbital population for

Table 4. ESR data indicating the deviations of g from the free-electron value (g_e) (2.0023) and anisotropy in g and A for VO^{2+} in different lattices

Host lattice	g_o	g_e-g_o ($\times 10^{-3}$)	$\Delta g(g_\perp-g_\parallel)$ ($\times 10^{-3}$)	$g_e-g_\parallel$ ($\times 10^{-3}$)	$\Delta A(A_\parallel-A_\perp)$ (G)	Reference
$K_2C_2O_4\cdot H_2O$	1.976	26.3	52.5	62.5	−119	Present work
$(NH_4)_2C_2O_4\cdot H_2O$	1.964	38.3	51.0	72.3	−123	Present work
KHC_2O_4	1.973	29.3	55.5	65.8	−109.5	Present work
$3CdSO_4\cdot 8H_2O$	1.969	33.3	64.0	79.3	−121	Present work
$Cd(NH_4)_2(SO_4)_2\cdot 6H_2O$	1.979	23.3	48.0	56.3	−116	Present work
$CdK_2(SO_4)_2\cdot 6H_2O$	1.972	30.3	56.0	72.3	−122	Present work
$SrC_4H_4O_6\cdot 4H_2O$	1.974	28.3	47	59.3	−116.9	Present work
$Zn(NH_4)_2(SO_4)\cdot 6H_2O$	1.964	38.3	48	70.3	−125	13
$NH_4Al(SO_4)_2\cdot 12H_2O$	1.965	37.3	38	62.3	−116.3	14

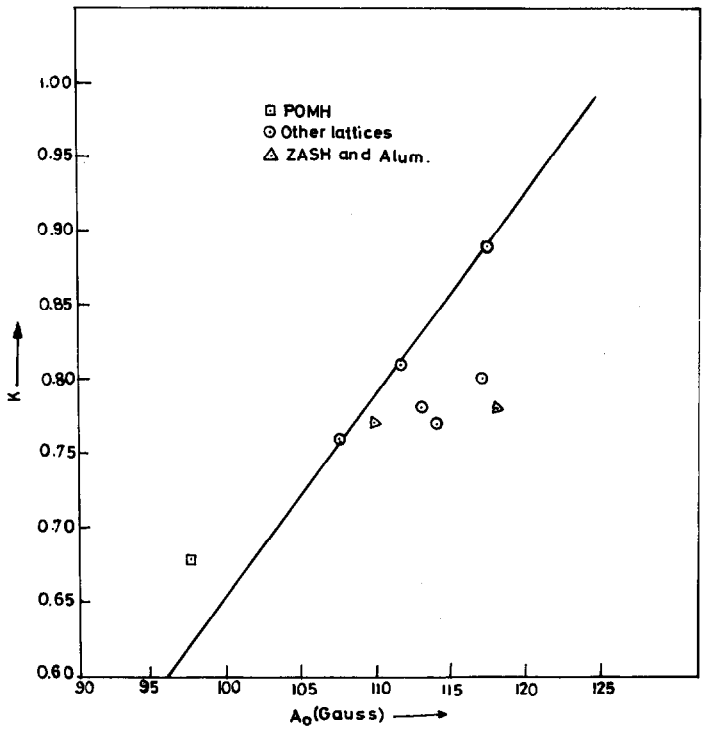


Fig. 5. Plot of the Fermi-contact term (K) as a function of the isotropic hyperfine coupling constant (A_o) (assumed to be negative).

the unpaired electron according to the equation:

$$K = (\beta_2^2)K_o, \tag{13}$$

where K_o is the free-ion polarization. A plot of β_2^2 vs K is shown in Fig. 6, and is almost a straight line passing through the origin, conforming to eqn (13). Some of the points do not lie exactly on the line and the scatter indicates the possible deviations due to

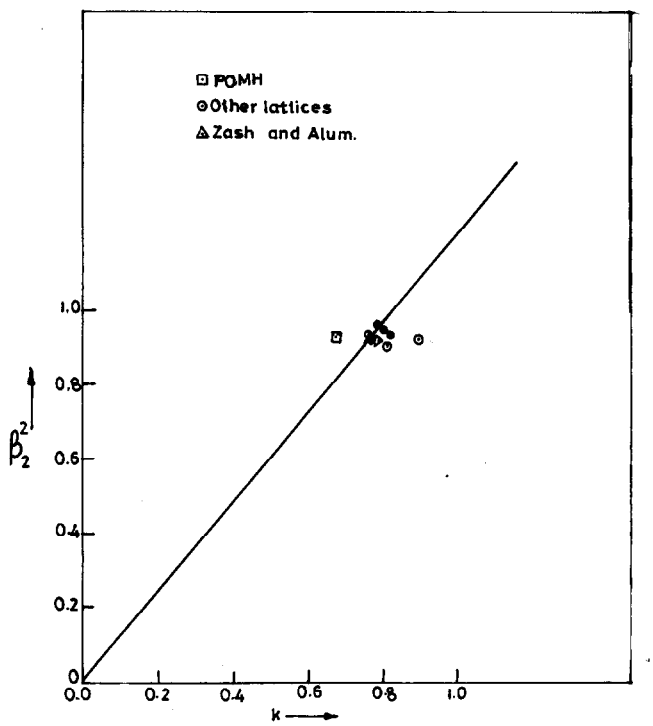


Fig. 6. Plot of bonding coefficient (β_2^2) vs Fermi-contact term (K).

the second-order contributions to K together with probable inadequacies in the existing theories (*vide infra*).

While K is lowest for POMH, the β_2^2 values are nearly the same for all the lattices (Table 3) and close to unity, indicating that the delocalization of electrons is not great and, hence, the π-bonding ability of the oxygen ligands is poor. Thus VO^{2+} in POMH is less covalently bonded than the overestimated covalency predicted by the BG theory.[4] In that case, the major change in K must be due to either the $4s$ σ-bonding effect or d_{xy}, $4s$ mixing. In low-symmetry vanadyl complexes, it is believed[23] that the d_{xy}, $4s$ mixing mechanism is responsible for the observed low value of A_o (and also K). In POMH, and to some extent in SrTrTH also, this mechanism must be operative. Since this should lead to a higher ΔE_1 value than 15,384 cm^{-1}, it is probable that inversion of the levels occurs,[28] in which case[6] $\Delta E_1 = 17{,}543$ cm^{-1} as required. Accordingly, P will be highest (Table 3), leading to the lowest β_2^2 in proportion to the lowest K.

Further, in POMH only the sixth ligand is O_W (water oxygen) which, though weak, increases the ligand field along the z-axis alone. As a result ΔE_2 is lowered in energy by the decrease in V=O π-bonding. This explains why ΔE_2 is lowered in POMH (11,530 cm^{-1}) and is smaller than in many other vanadyl complexes.[28] Besides the low-symmetry ligand field effects, hydrogen-bonding effects also give the same results.[24,29] Such hydrogen-bonding effects may be offered as the reason for the reduction in ΔE_2 and K for the VO^{2+} ion not only in POMH but also in SrTrTH and ammonium alum.

Relation between K, β_1^2 *and* e_π^2. The order of other evaluated bonding coefficients, β_1^2 and e_π^2, in relation to K does not seem to be in reasonable agreement with that expected from eqn (5) together with eqn (12). Since none of the available theories[2-5] for electronic absorption spectra of the VO^{2+} ion observed in the various lattices of the present work is uniquely applicable,[7] there is an element of uncertainty in the transitions assigned and, hence, in the values of ΔE_1 and ΔE_2. Even the optical-polarization technique does not yield accurate transition energies because in any of the lattices chosen VO^{2+} does not have a single unique orientation. As mentioned earlier, the discrepancies in the relation between K and bonding coefficients clearly bring out the inadequacy of crystal field and MO theories for the VO^{2+} ion.

Relation between g *anisotropy and ligand field strength.* The anisotropy in g is measured by the difference (Δg) in the $g_\perp$ and $g_\parallel$ components, i.e. $\Delta g = g_\perp - g_\parallel$, and it is related to the ligand field strength. Assuming that the axial field experienced by the VO^{2+} ion in a lattice is due to the double

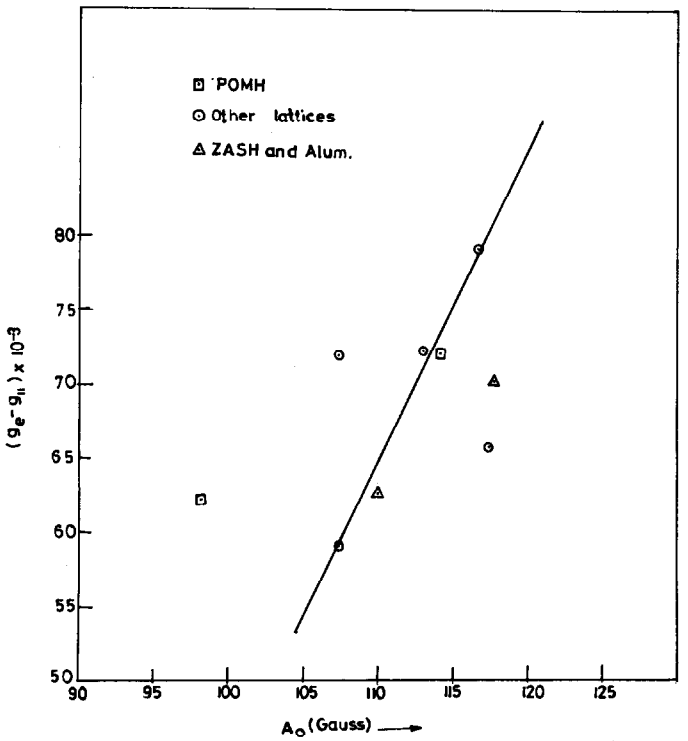


Fig. 7. Graph giving the linear relationship between $g_e - g_\parallel$ and the isotropic hyperfine coupling constant (A_o) (assumed to be negative).

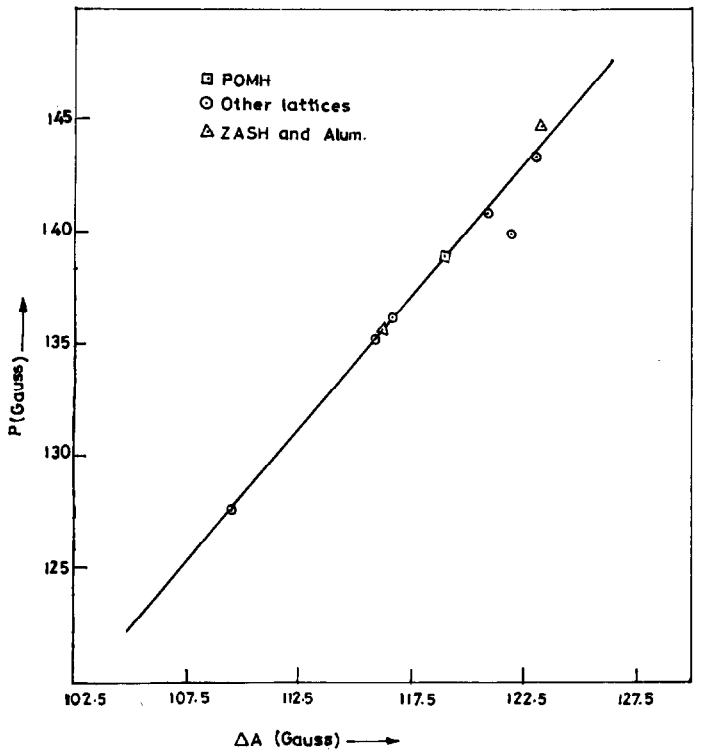


Fig. 8. Plot giving the linear increase in the dipolar term (P) with increase in anisotropy (ΔA) of the hyperfine coupling constant.

bonded oxygen and the in-plane field is due to the ligands, Δg is smaller for strong field ligands. From the Δg values given in Table 4, we find that Δg is smallest for alums and highest for $3CdSO_4 \cdot 8H_2O$. Thus, oxygens directly bonded to hydrogen are probably stronger than pure or indirectly-hydrogen-bonded oxygen ligands. Interestingly, a low-symmetry field such as seen in POMH need not be due to strong ligands.

Relation between $g_e - g_\parallel$ *and* A_o. It has been shown from eqns (5), (11) and (12) that K is proportional to β_2^2, β_1^2 and $1/\Delta E_1$. Since K and A_o are directly related, A_o is proportional to the quantity $\beta_1^2\beta_2^2/\Delta E_1$. Combining eqn (5a) with this, we infer that the relation between $g_e - g_\parallel$ and A_o must be linear. The plot of $g_e - g_\parallel$ against A_o (from Tables 1 and 4) is shown in Fig. 7 and the general behaviour seems to be in agreement with the theoretical predictions.

Relation between hf anisotropy (ΔA) *and* P. The anisotropy in A is measured by the difference (ΔA) in $A_\parallel$ and $A_\perp$, i.e. $\Delta A = A_\parallel - A_\perp$. The ΔA values are given in Table 4.

The anisotropy arises because of a direction-dependent interaction of electron-spin with nuclear spin. However, the direct dipolar term P accounts for the dipole interaction of the electron magnetic moment with the nuclear magnetic moment [see eqn (2)]. Thus, P and ΔA are related by eqn (3), which shows that, as the anisotropy in the hf coupling constant increases, P should increase provided ΔE_1 is nearly constant. A plot of P vs ΔA is given in Fig. 8. The graph is almost a straight line with little scatter.

Thus, the relationship between various parameters of the VO^{2+} ion discussed so far is exact and unambiguous when ESR theory is predominantly involved. An inexact, ambiguous relationship arises mostly due to uncertainties in the theories of electronic absorption spectra.

REFERENCES

1. K. D. J. Root and M. T. Rogers, In *Spectroscopy in Inorganic Chemistry* (Edited by C. N. R. Rao and J. R. Ferraro), Vol. 2, p. 127. Academic Press, New York (1971).
2. C. K. Jorgensen, *Acta Chem. Scand.* 1957, **11**, 73.
3. T. R. Ortolano, J. Selbin and S. P. McGlynn, *J. Chem. Phys.* 1964, **41**, 262.
4. C. J. Ballhausen and H. B. Gray, *Inorg. Chem.* 1962, **1**, 111.
5. L. G. Vanquickenborne and S. P. McGlynn, *Theor. Chim. Acta* 1968, **9**, 390.
6. (a) S. Radhakrishna, B. V. R. Chowdary and M. Salagram, *J. Chem. Phys.* 1980, **72**, 1908; (b) M. Salagram, *Physica B+C* (1985) (communicated).

7. (a) S. Radhakrishna and M. Salagram, *Phys. Status Solidi A* 1980, **62**, 441; (b) M. Salagram, Ph.D. thesis, I.I.T., Madras (1980).
8. S. Radhakrishna and M. Salagram, *Solid State Commun.* 1983, **47**, 77.
9. N. Satyanarayana, *Spectrochim. Acta* 1985, **41A**, 1185.
10. N. Satyanarayana and S. Radhakrishna, *J. Chem. Phys.* (in press).
11. N. Satyanarayana and S. Radhakrishna, *Cryst. Latice Defects Amorph. Mater.* (in press).
12. N. Satyanarayana, K. Hariharan and S. Radhakrishna, *J. Mater. Sci.* (in press).
13. R. H. Borcherts and C. Kikuchi, *J. Chem. Phys.* 1964, **40**, 2270.
14. K. V. S. Rao, M. D. Sastry and P. Venkateswarlu, *J. Chem. Phys.* 1968, **49**, 4984.
15. A. Kasi Viswanath, *J. Chem. Phys.* 1977, **67**, 3744.
16. E. Banks, M. Greenblatt and B. R. McGarvey, *J. Solid State Chem.* 1971, **3**, 308.
17. T. M. Dunn, *Trans. Faraday Soc.* 1961, **57**, 1441.
18. D. Kivelson and S. K. Lee, *J. Chem. Phys.* 1964, **41**, 1896.
19. H. Montgomery and E. C. Lingafetter, *Acta Cryst.* 1966, **20**, 728.
20. G. K. Ambady, *Acta Cryst.* 1968, **B24**, 1548.
21. R. M. Golding, *Mol. Phys.* 1962, **5**, 369.
22. R. E. Watson, Iron Series Hartree Fock Calculations. Technical report No. 12, Solid State and Molecular Theory Group, Massachusetts Institute of Technology (1959).
23. B. R. McGarvey, *J. Phys. Chem.* 1967, **71**, 51.
24. L. J. Boucher, Edmund C. Tynan and T. F. Yen, In *Electron Spin Resonance of Metal Complexes* (Edited by T. F. Yen), p. 111. Plenum Press, New York (1969).
25. K. De Armond, B. B. Garrett and H. S. Gutowsky, *J. Chem. Phys.* 1965, **42**, 1019.
26. A. H. Maki and B. R. McGarvey, *J. Chem. Phys.* 1958, **29**, 31, 35.
27. (a) A. Abragam and M. H. L. Pryce, *Proc. Roy. Soc.* 1951, **A205**, 135; **A206**, 164; (b) A. Abragam, J. Horwitz and M. H. L. Pryce, *ibid.* 1955, **A230**, 169.
28. J. Selbin, *Coord. Chem. Rev.* 1966, **1**, 293.
29. M. Narayana, S. G. Satyanarayana and G. Siva Ramasastry, *Mol. Phys.* 1976, **31**, 203.

Polyhedron Vol. 5, No. 6, pp. 1183–1190, 1986
Printed in Great Britain

0277–5387/86 $3.00+.00
Pergamon Journals Ltd

DINUCLEAR Pd(II) AND Rh(I) COMPLEXES OF TETRA-ACETYLETHANE: LINKAGE ISOMERIZATION OF TETRA-ACETYLETHANE DIANION IN Pd(II) COMPLEXES

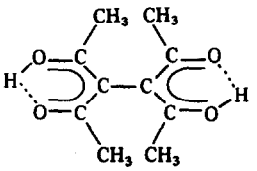
SHINSAKU YAMAZAKI

Chemistry Laboratory, Gakuen College Kochi, 292 Asahi Tenjin-cho, Kochi 780, Japan

(*Received* 6 *December* 1984; *accepted after revision* 31 *October* 1985)

Abstract—The Pd(II) and Rh(I) complexes of tetra-acetylethane [H_2dahd (3,4-diacetyl-2,4-hexadiene-2,5-diol)] with O,O'-bonded chelates, represented as $[M_2(O_2,O'_2\text{-dahd})(L_2)_2][X]_m$ {M = Pd, $L_2 = (PPh_3)_2$ or bdpe [1,2-bis(diphenylphosphino)ethane], X = BF_4 or PF_6, $m = 2$; M = Rh, L = Co, $m = 0$}, have recently been prepared. $[Pd_2(O_2,O'_2\text{-dahd})(PPh_3)_4][PF_6]_2$ reacts with the potentially bidentate 1,10-phenanthroline (phen) to give the five-coordinate complex $[Pd(PPh_3)(phen)_2][PF_6]_2$ and $[Pd(O_1,O'_1\text{-dahd})(phen)]_n$, the latter of which is rather insoluble in organic solvents. $[Pd(O_1, O'_1\text{-dahd})(phen)]_n$ in CH_2Cl_2 readily transforms to a monomer complex $[Pd(C^3,O'\text{-dahd})phen)]$. These anomalous Pd(II) and Rh(I) complexes of the tetra-acetylethane dianion have been characterized from elemental analyses, conductance, IR, ^1H and ^{13}C NMR spectroscopy, magnetic susceptibility and ESR spectroscopy.

Despite a number of studies being directed to β-diketonate Pd(II) and Pt(II) complexes with a variety of coordination modes,[1–9] tetra-acetylethane [H_2dahd (3,4-diacetyl-2,4-hexadiene-2,5-diol)] complexes with second- or third-row transition metals



have been strangely elusive. It is well known that the first-row transition metals easily form insoluble coordination polymers of dahd,[10,11] whose characterization has thus been restricted. However, the ligand is attractive because it may form bifunctional O_2-chelates with a metal. The crystal structure of H_2dahd has been established by X-ray and neutron diffraction studies to have the di-enolic form of γ,γ′-bis(acetylacetone),[12] in which the position of the enolic hydrogen is asymmetric.[13] This solid structure of H_2dahd is also consistent with that in solution (experimental), while acetylacetone is well known to undergo keto–enol tautomerization. This gives rise to a preliminary question concerning chelate coordination of the dahd anion to the metal as to which is stabilized more, the six- or the seven-membered ring. The latter case, in which each 2,5-diketonate group might be in the conjugated form by coordination through oxygen atoms, seems improbable from a first glance at a molecular model: for electronic reasons the dahd ligand may be expected to form one ligand plane which would inappropriately mean two oxygen atoms of the 2,5-diketonate group approaching so close as to be at an unlikely bond distance.

With these in mind, a dahd–Pd(II) complex, $[Pd(dahd)_{1/2}(PPh_3)_2][PF_6]$, has been prepared by an analogous procedure to that of [Pd(*o*-acac)$(PPh_3)_2][PF_6]$.[14] A corresponding bdpe [1,2-bis(diphenylphosphino)ethane] complex $[Pd(dahd)_{1/2}$(bdpe)$][BF_4]$ has been obtained, by treating $PdCl_2$(bdpe) with $AgBF_4$ and H_2dahd, in a moderate yield. Some physical properties of these new complexes resemble those of the acac complex, as expected. No spectral evidence to confirm that these complexes have the dahd ligand chelating with a seven-membered ring has been obtained, and firm evidence should solely depend on X-ray diffraction studies. The data suggest that the γ,γ′-bis(diketonate) groups of the dahd are highly conjugated.

Accordingly, these complexes may be denoted as $[Pd_2(O_2,O'_2\text{-dahd})(L_2)_2][X_2]$ [$L_2 = (PPh_3)_2$ or bdpe, $X = BF_4$ or PF_6].

$Rh_2(O_2,O'_2\text{-dahd})(CO)_4$ has also been prepared by reacting $Rh_2Cl_2(CO)_4$ with Na_2dahd.

By reacting $[Pd_2(O_2,O'_2\text{-dahd})(PPh_3)_4][PF_6]_2$ with the potentially bidentate 1,10-phenanthroline (phen), a polymeric $[Pd(dahd)(phen)]_n$, always concomitant with a trace amount of the paramagnetic species, and a monomeric $Pd(C^3,O'\text{-dahd})(phen)$ have successively been isolated. From IR, ^1H and ^{13}C NMR, and ESR spectroscopy, these unusual complexes have been characterized, in which polymeric $[Pd(dahd)(phen)]_n$ is rather insoluble in organic solvents and is supposed to contain six-membered chelates of dahd with Pd(II) and dahd is newly bound to the Pd(II) as an *O_1-uni,O'_1-unidentate* bridging ligand. Small amounts of paramagnetic species included in this complex are also discussed in the light of the novel linkage isomerization of dahd bound to Pd(II).

EXPERIMENTAL

The solvents acetone and CH_2Cl_2 were distilled over $CaCl_2$, and diethylether over Na before use. Elemental analyses were performed by the Microanalytical Centre, Department of Pharmaceutical Sciences, Kyoto University. IR spectra were recorded on an Hitachi 260-10 IR spectrometer. Spectrometers used for NMR studies were: ^1H NMR, JEOL 100; ^{13}C NMR, JEOL FX-90Q (22.49 MHz) operating in the Fourier transform mode with a flip angle of 30° and a pulse repetition time of 3 s to observe the relative integral ratio. Mass spectral measurement was carried out using a Hitachi RMU-6 by a direct-beam method at under 90°C and 50 eV. Molecular weights were obtained by using a Corona Molecular Weight Apparatus M-117 (vapor pressure osmometer) at 30°C in CH_2Cl_2 based on its calibration by benzil. Electroconductivity was measured using a DKK AO-6 instrument in a dried acetone solution (*ca* 3.3×10^{-4} M). ESR spectra of the solid were recorded on a Varian E line Century Series EPR spectrometer using a quartz tube with a field of 3400 ± 400 G, microwave frequency of 9.483–9.488 GHz, and the cavity with the empty sample tube was checked *in situ*. Magnetic susceptibility was obtained by the Faraday method using a Cho-Keiryo Magnetic Balance MSB-10 at 300 K.

H_2dahd

H_2dahd was prepared by the literature procedure.[15] *m/z*: [M^+], 198; [$M-H_2O$], 180, ^1H NMR ($CDCl_3$): δ(Me) 2.00 (6-H), δ(OH), 16.65 (1-H) ppm. IR (Nujol mull): ν(C—C) + ν(C—O) + δ(O—H), 1600 (vs, br) cm^{-1}.

Na_2dahd–$(CH_3OH)_x$

H_2dahd (2 g) was suspended in CH_3OH and a CH_3OH solution of NaOH (~0.9 g) was added to the former solution, when the suspension became a homogeneous solution. The solution was then reduced to ~5 cm^3 and addition of diethylether to the residual solution gave a pale brown solid, which was recrystallized from CH_3OH–diethyl ether (3 g, 100%). ^1H NMR [$CDCl_3$–$(CD_3)_2CO$]: δ(Me)(dahd), 1.87 (s, br) ppm: δ(Me) (CH_3OH of solvation), 3.18 ppm.

$[Pd_2(dahd)(PPh_3)_4][PF_6]_2$

$[Pd(PPh_3)_4][PF_6]_2$[14] (1.7 g) was suspended in acetone (50 cm^3), and an acetone solution containing H_2dahd (0.23 g) was added to the solution. The suspension gradually became a canary yellow homogeneous solution. After 24 h, the solution was reduced in volume to 15 cm^3 under reduced pressure and addition of diethylether to the solution gave canary yellow crystals, which were recrystallized from acetone–CH_2Cl_2 and ethylether to give yellow needles (1.1 g, 100%). Found: C, 56.7; H, 4.3; P, 10.0%. Calc. for the molecular formula with two acetones of solvation: C, 56.7; H, 4.5; P, 10.0%. IR (Nujol mull); ν(CO) (acetone of solvation), 1704 (vs) cm^{-1}. Conductance (acetone): Λ_M, 258 $\Omega^{-1} \cdot cm^2 \cdot mol^{-1}$.

$[Pd_2(dahd)(bdpe)_2][BF_4]_2$

$PdCl_2$(bdpe) (2.2 g), prepared *in situ* by reacting $PdCl_2(PhCN)_2$ with an equimolar quantity of bdpe, was suspended in acetone containing H_2dahd (0.8 g). An acetone solution of $AgBF_4$ (1.6 g) was added to the solution. The suspension gradually became a transparent yellow solution, while white AgCl was precipitated. After 2 h, the precipitate of AgCl was filtered (1 g. 200% per Pd atom). The solution was reduced in volume to 10 cm^3 and addition of diethylether to the residual solution gave yellow crystals, which were recrystallized from CH_2Cl_2–diethylether (2 g, 66%). Found: C, 52.3; H, 4.3%. Calc. for the molecular formulae with $(CH_2Cl_2)_{2/3}$ of solvation: C, 52.4; H, 4.3%. ^1H NMR [$(CD_3)_2CO$–$(CD_3)_2SO$]: $\delta(CH_2)$ (CH_2Cl_2 of solvation) 5.60 ppm.

Rh_2(dahd)$(CO)_4$

$Rh_2Cl_2(CO)_4$ (0.6 g) was dissolved in CH_2Cl_2 and Na_2dahd–$(CH_3OH)_x$ (0.4 g) was added to the solution. The solution gradually gave a yellow solid. After 2 h, the solid product was filtered and washed with water, CH_3OH and diethylether (0.6 g, 63%). Found: C, 32.4; H, 2.2%, $M = 475$. Calc. for the molecular formulae: C, 32.7; H, 2.3%, $M = 514$.

Catena-[Ph(dahd)(phen)]$_n$

$[Pd_2$(dahd)$(PPh_3)_4][PF_6]_2$–$[(CH_3)_2CO]_2$ (0.5 g) was dissolved in acetone (25 cm^3), and the solution was charged with dried nitrogen for 1 h. Then, an acetone solution containing phen monohydrate (0.2 g) was added to the former solution. The yellow solution gradually turned orange while a yellow crystalline solid precipitated. After 3 h, the yellow solid was filtered and washed with a few cm^3 of acetone, then instantly dried *in vacuo* and preserved (for its EPR spectrum *vide infra*). The product relatively sensitive in air was washed furthermore with diethylether (the diethylether phase was coloured yellow, but species included in it were uncharacterized) to yield 0.08 g (34%). Found: C, 54.0; H, 4.1; N, 5.8%. Calc. for the molecular formulae: C, 54.7; H, 4.1; N, 5.8%. Magnetic susceptibility: $\chi_g = -0.50 \times 10^{-6}$ cgs emu.

The filtrate separated from [Pd(dahd)(phen)]$_n$ (acetone phase) was reduced in volume to $\sim$10 cm^3 and addition of diethylether to the residual solution gave orange crystals of $[Pd(PPh_3)(phen)_2][PF_6]_2$–$(CH_3)_2CO$[14] (0.24 g, 48%).

Pd(C^3,O′-dahd)(phen)

Catena-[Ph(dahd)(phen)]$_n$ ($\sim$0.5 g) was dissolved in CH_2Cl_2 ($\sim$20 cm^3), and the solvent was removed by natural vaporization at room temperature to give pale orange crystals. Found: C, 54.7; H, 4.2; N, 5.8%. M (osmometry in CH_2Cl_2) = 469. Calc. for the molecular formulae: C, 54.7; H, 4.2; N, 5.80%, $M = 483$. Magnetic susceptibility: $\chi_g = -0.66 \times 10^{-6}$ cgs emu.

Rh_2(dahd)$(CO)_2(PPh_3)_2$

Rh_2(dahd)$(CO)_4$ (0.27 g) was suspended in CH_2Cl_2, and PPh_3 (0.29 g) was added to the solution, when the solution turned yellow and was homogeneous, and CO was evolved. Then the solution was reduced in volume under reduced pressure by warming to $\sim$10 cm^3, when the yellow solution turned orange. Addition of diethylether to the residual solution gave a mixture of yellow and orange solids. To the suspension solution, more CH_2Cl_2 was added. By warming the solution for a few minutes, a homogeneous canary yellow solid, which is insoluble in organic solvents, could be obtained. Found: C, 58.2; H, 4.3%. Calc. for the molecular formulae: C, 58.7; H, 4.3%.

RESULTS AND DISCUSSION

IR, and ^{1}H and ^{13}C NMR, data of $[Pd_2$(dahd)$(PPh_3)_4][PF_6]_2$, $[Pd_2$(dahd)$(bdpe)_2][BF_4]_2$ and Rh_2(dahd)$(CO)_4$, as given in Tables 1 and 2, show that dahd coordinates to the metal with symmetrical *O*-bonding bi-functional chelation.

These spectral data are quite comparable with those of $[Pd(acac)(PPh_3)_2][PF_6]$[14] and $Rh(acac)(CO)_2$.[16] The IR spectra of all the dahd complexes also show a single and strong absorption band due to $\nu(C{=}O)+\nu(C{=}C)$, which may indicate that the diketonates of dahd are highly conjugated by its chelation with metal compared to the acac complexes [two bands for the Pd(II) complex and three bands for the Rh(I) complex]. One should notice that *O*,*O*′-bonding dahd improbably chelates with metal forming a seven-membered ring. Accordingly, it is concluded that in these Pd(II) and Rh(I) complexes the dahd dianion bridges two metal nuclei with *O*,*O*′-bonded six-membered chelates.

Some carbonyls in Rh_2(dahd)$(CO)_4$ are readily displaced by PPh_3, forming $[Rh_2$(dahd)$(CO)_2(PPh_3)_2]_n$, which is rather insoluble in organic solvents. For both complexes, IR absorption bands for the carbonyl stretching vibration are also comparable with those of the corresponding acac complexes, $Rh(acac)(CO)_2$ and $Rh(acac)(CO)(PPh_3)$ (Table 1).[16]

Unexpectedly, $[Pd_2$(dahd)$(PPh_3)_4][PF_6]_2$ reacts with phen in acetone to give a rather insoluble complex {[Pd(dahd)(phen)]$_n$} and the five-coordinate complex $[Pd(PPh_3)(phen)_2][PF_6]_2$.[14] [Pd(dahd)(phen)]$_n$ in CH_2Cl_2 transforms to a monomer complex [Pd(C^3,*O*′-dahd)(phen)].

^{1}H NMR of the monomer complex Pd(dahd)(phen) and its ^{13}C–{^{1}H} NMR (carried out with a flip angle of 30° to observe the relative integral ratio of four carbonyl and Me carbons on the dahd ligand) show dahd with two equivalent Me groups, while the other two are non-equivalent. They also exhibit a non-equivalency of the two nitrogen atoms of the phen. A ^{1}H NMR resonance at 2.33 due to two equivalent acetyl groups and that at 2.51 due to another group of dahd are both in a comparatively lower field region close to those of γ-carbon-bonded β-diketonate complexes of Pd(II) and Pt(II),[6] while the third resonance at 2.07 cor-

Table 1. IR and ^{1}H NMR data

Compound	ν(CO)	ν(C=O)	ν(C=C)	ν(C—O)[a]	δ(Me)	δ(CH)	δ(OH)	δ(CH$_2$)[b]
H_2dahd				1600 (vs, br)[c]	2.00(6)		16.65(1)	
[Pd(acac)(PPh$_3$)$_2$][PF$_6$]			1561 (vs)	1523 (vs)[c]	1.50(6)	5.38(1)		
[Pd$_2$(dahd)(PPh$_3$)$_4$][PF$_6$]$_2$				1547 (vs)	1.43[d]			
[Pd$_2$(dahd)(bdpe)$_2$][BF$_4$]$_2$				1555 (vs)	1.93(6)			3.14(4)[e]
Rh(acac)(CO)$_2$[f]	2086 (vs)[g] 2015 (vs)		1582 (s)	1565 (s), 1524 (s)				
Rh$_2$(dahd)(CO)$_4$	2085 (vs) 2002 (vs)			1558(vs)	1.94			
Rh$_2$(dahd)(CO)$_2$(PPh$_3$)$_2$	1984 (vs)			1565 (vs)				
Rh(acac)(CO)(PPh$_3$)[f]	1983 (vs)		1589 (s)	1570 (s) 1515(s)	1.56(3) 2.05(3)	5.40(1)		
Pd(dahd)(phen)		1740 (vw)			2.51(3)			
		1680 (vs)	1605 (s)	1545 (vs)	2.33(6)			
		1628 (m)	1600 (s)		2.07(3)			
[Pd(dahd)(phen)]$_n$		1667 (vs)	1627 (m) 1611 (m)	1508 (vs)				

[a] In cm^{-1}; measured in Nujol mulls unless otherwise indicated.
[b] In $CDCl_3$ unless otherwise indicated. Chemical shifts are relative to Me_4Si at 0.00.
[c] These absorption bands are due to ν(C···O)+ν(C···C) and in H_2dahd this band is overlapped with δ(O—H).
[d] In $(CD_3)_2CO$.
[e] In $(CD_3)_2CO$–$(CD_3)_2SO$ mixed solutions; doublet with J_{PH} = 22.0 Hz: CH_2Cl_2 of solvate appeared at 5.60 ppm.
[f] Ref. 16.
[g] In CH_2Cl_2.

Table 2. $^{13}C-\{^1H\}$ NMR data[a]

Compound	Carbonyl carbon	3,4-Carbon	Me carbon	Phen ring carbon
H_2dahd	192.4	108.0	23.5	
phen				150.2 ($C^{2,9}$), 123.5 ($C^{3,8}$) 136.4 ($C^{4,7}$), 126.8 ($C^{5,6}$) 128.7 ($C^{13,14}$), 145.8 ($C^{11,12}$)
Rh_2(dahd)$(CO)_4$[b]	188.1 183.7 (CO)	112.9	26.8	
$[Pd(dahd)(PPh_3)_4][PF_6]_2$	188.1	126.0	26.6	153.1, 148.2 (C^2, C^9); 127.7, 124.9 (C^3, C^8)
Pd(dahd)(phen)[c]	202.9 (2, $C^{2,7}$)	118.3 (C^4)	30.7 (2, $C^{1,8}$)	
	195.0 (1, C^9)	[d]	28.1 (1, C^6, C^{10})	
	190.3 (1, C^5)		25.0 (1, C^6, C^{10})	138.5, 137.9 (C^4, C^7); 126.4 (C^5, C^6) 129.6, 129.5 (C^{13}, C^{14}); 145.4, 145.1 (C^{11}, C^{12})[e]

[a] Measured in $CDCl_3$.

[b] $|J_{RhC}|$ (CO) = 73.24, $|J_{RhC^{3,4}}|$ (dahd) = 3.06, $|J_{RhC}|$ (Me of dahd) = 1.22 Hz.

[c] Measured with flip angle of 30° to observe the relative intensities of the groups which are given in parentheses.

[d] Any signal due to C^3 could not be discerned.

[e] The signals due to $C^{11,12}$ were observed with very weak intensities.

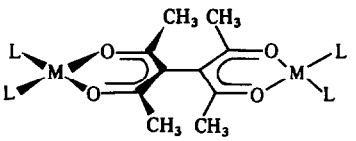


Fig. 1. Proposed structure of $[M_2(dahd)(L_2)_2][X]_n$ (M = Pd, L = PPh_3, X = PF_6^-, $n = 2$; M = Pd, L_2 = bdpe, X = BF_4^-, $n = 2$; M = Rh, L = CO, $n = 0$).

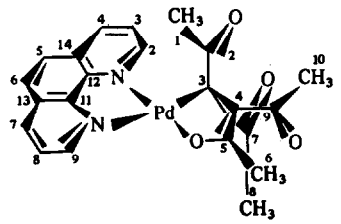


Fig. 2. Proposed structure of monomeric Pd(dahd)(phen).

responding to the fourth Me group of dahd is close to the free H_2dahd ligand. These indicate that the complex has a low symmetry with one carbonyl of dahd bound to the metal through its enolic oxygen, while the other three, in the keto form, are liberated from the metal. Characteristic IR absorption bands of the complex evidently show those in which two absorption bands in the region 1600–1700 cm^{-1} are due to ν(C═O), 1535 cm^{-1} to ν(C—O), and 1595 cm^{-1} due to ν(C═C), respectively, of the dianionic dahd ligand. Another coordination site of the dianionic dahd ligand to Pd(II) would be shown by the ^{13}C NMR spectrum, particularly for its 3-carbon nucleus. However, the ^{13}C NMR signal due to the 3-carbon of the dahd could not, unfortunately, de discerned owing to broad resonances that might be caused from an interaction with its *trans* ^{14}N quadrupole nucleus.[8,17]

Other conceivable structures for this complex are also depicted in Fig. 3. Structure **B** is improbable because the presumed dienol 2,5-diketonate group with a seven-membered chelate ring with Pd(II) may mean dahd forming a ligand plane that may improbably cause its two oxygen atoms to approach so close as to be at an unlikely bond distance. Another extreme structure (**C**) with allylic formation through carbonyl oxygen and 3-carbon atoms has also been excluded because the NMR spectra for the structure should show four unequivalent Me and carbonyl groups for the dahd. Any dynamic structure of **C** averaging two carbonyl or Me groups, in total equivalent to four groups, is still unlikely. For electronic reasons, the assumed allylic formation through the 2(5)-carbonyl and 3(4)-carbon of the dianionic dahd should require atoms lying on the same plane as one occupied by the 5(2)-carbonyl and 4(3)-carbon, while the stereochemistry of an assumed configuration would impose enough distortion to prevent allylic formation. In addition, even in the β-diketonate Pd(II) complexes, such an example has not been found except in the case of allylic formation through a terminal carbon.

Structure **D** for a protonated species, as found in $K[Pt(acac)_2Cl]$,[18] has been precluded because no ^1H NMR resonance due to O—H has been observed.

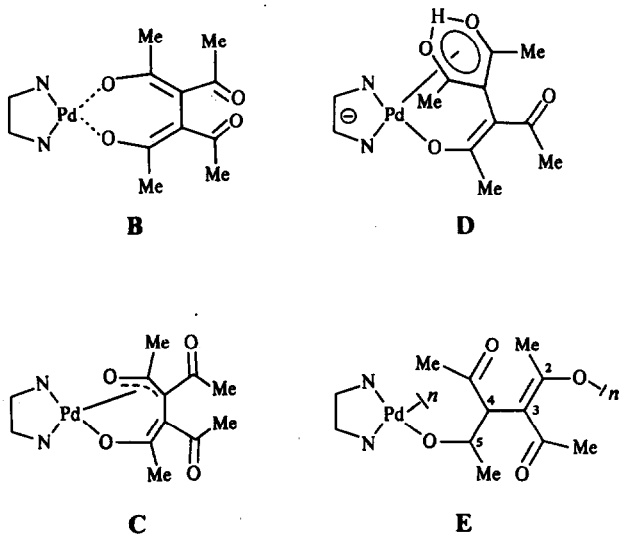


Fig. 3. Four conceivable structures of monomeric Pd(dahd)(phen) which are unlikely.

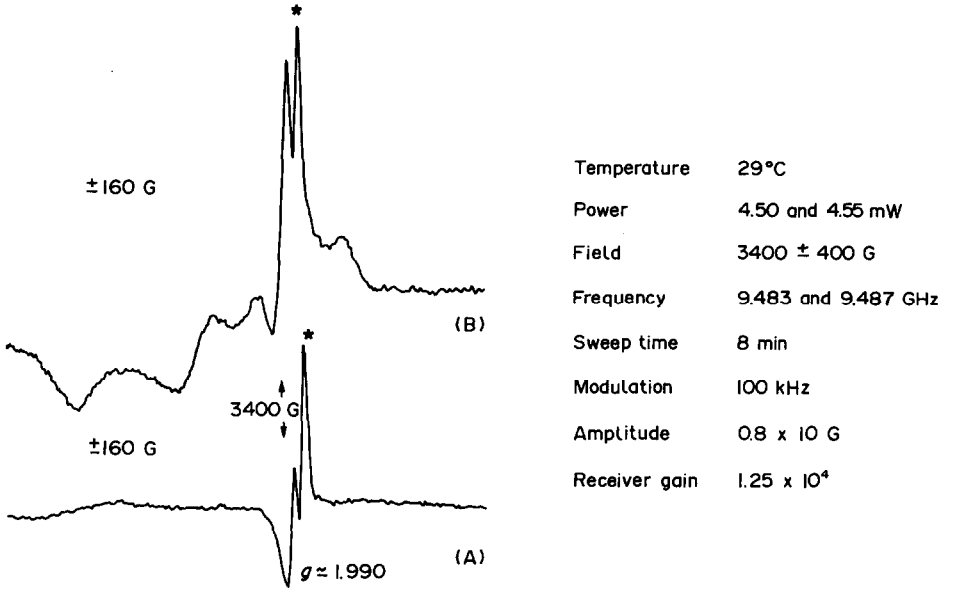


Fig. 4. ESR spectra of [Pd(dahd)(phen)]$_n$, showing paramagnetic species included: (A) after washing with diethylether, and (B) before washing with diethylether. The g values are directly estimated from the field resonances without using any references. * Due to impure quartz tube.

These conditions only fit **A** of Pd(C^3,O'-dahd)(phen), consistent with the spectral data.

The other complex Pd(dahd)(phen) was rather insoluble in organic solvents, except in CH_2Cl_2 or $CHCl_3$ (transformation to the monomer complex with an M—C bond), and its spectral evidences have been restricted. This complex may be a polymeric [Pd(dahd)(phen)]$_n$. Characteristic IR absorption bands of this complex (Table 1) show that the 2,5- or 2,7-diketonate group of dahd no longer chelates the metal in such a conjugated form as observed in [Pd(O_2,O'_2-dahd)(PPh_3)$_4$][PF_6]$_2$. Three strong absorptions in the region 1600–1700 cm^{-1} apparently correspond to ν(C═O) and ν(C═C), and at 1508 cm^{-1} to ν(C—O) of the dahd. In this case also, any corresponding absorptions due to ν(O—H)[18] or ν(C∴O) have not been observed at greater than 3100 or in the region 1510–1600 cm^{-1}.

A probable configuration of this complex is accordingly one in which the coordination of the dahd to Pd(II) is as an O_1-uni,O_1-unidentate bridging ligand, that is [Pd(μ-O_1,O'_1-dahd)(phen)]$_n$. The

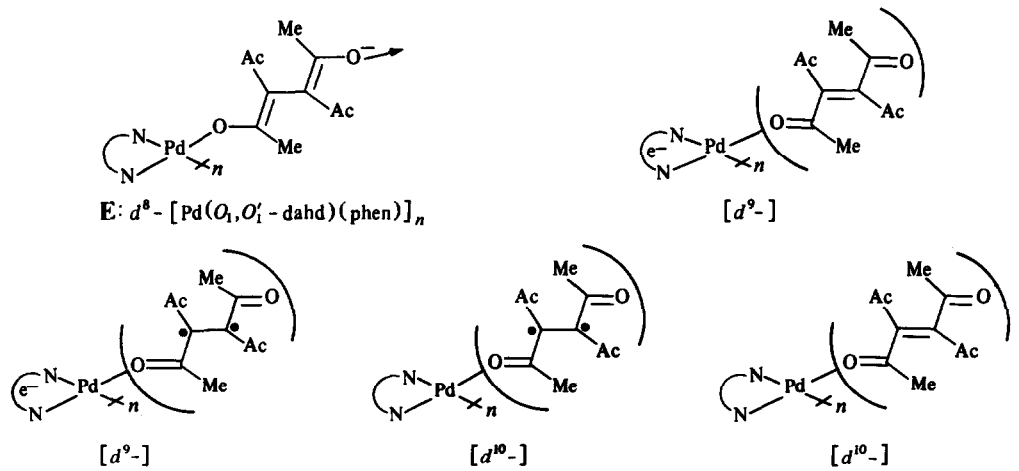


Fig. 5. Assumed paramagnetic intermediates of Pd(C^3,O'_2-dahd)(phen), given by two-electron transfer from d^8-[Pd(O_1,O'_1-dahd)(phen)]$_n$.

result of magnetic-susceptibility measurements was diamagnetism, corresponding to a Pd(II) complex. However, unexpectedly, this complex was always contaminated with a paramagnetic species in only a trace amount. Its ESR spectrum (Fig. 4) show these and two other resonances could be obtained, one of which is in the background with a very wide resonance. Nevertheless, the diamagnetism of the species can conceivably be enough to be caused by compensation of the relatively large diamagnetic contribution from the predominant d^8-complex $[Pd(O_1,O'_1\text{-dahd})(phen)]_n$. Noticeably, $[Pd(O_1,O'_2\text{-dahd})(phen)]_n$ precipitated from the reaction solution was contaminated with species soluble in diethylether and its ESR spectrum shows six resonances with no hyperfine structures. No definite evidence for these concomitant species has been obtained. However, it may be tempting to speculate that these paramagnetic species, despite only minute amounts, because $[Pd(O_1,O'_1\text{-dahd})(phen)]_n$ is an isomer of $Pd(C^3,O'\text{-dahd})(phen)$ whose transformation may proceed via any species of dahd with its 3- or 4-carbon atom activated as a methylene structure or a carbocation radical. The configuration of the dahd linkage mode as an O_1-uni-O'_1-unidentate bridging ligand to Pd(II) may allow a likely conjugated system through its two–five carbon atoms which may presumably facilitate electron transfer from dahd to the metal or the phen ligand.[19] Such an assumption may give four idealized species in which the dahd is oxidized to form a tetra-acetylethylene (Fig. 5). Nevertheless, any details of the concomitant species with $[Pd(O_1,O'_1\text{-dahd})(phen)]_n$ are uncertain at present.

Acknowledgements—I am grateful to Dr K. Hata (JEOL Ltd) for obtaining ^{13}C–$\{^1H\}$ FT-NMR spectral data, and to Dr W. Mori (Osaka University) for obtaining magnetic-susceptibility data.

REFERENCES

1. S. Baba, T. Ogura and S. Kawaguchi, *Inorg. Nucl. Chem. Lett.* 1971, **7**, 1195; D. Gibson, J. Lewis and C. Oldham, *J. Chem. Soc. A* 1970, 72.
2. Y. Nakamura, K. Isobe, H. Morita, S. Yamazaki and S. Kawaguchi, *Inorg. Chem.* 1972, **11**, 1573.
3. Z. Kanda, Y. Nakamura and S. Kawaguchi, *Inorg. Chem.* 1978, **17**, 910.
4. S. Okeya, N. Yanase, Y. Nakamura and S. Kawaguchi, *Chem. Lett.* 1978, 699.
5. N. Yanase, Y. Nakamura and S. Kawaguchi, *Inorg. Chem.* 1980, **19**, 1575.
6. S. Matsumoto and S. Kawaguchi, *Bull. Chem. Soc. Jpn* 1981, **54**, 1704.
7. S. Okeya, Y. Nakamura, S. Kawaguchi and T. Hinomoto, *Bull. Chem. Soc. Jpn* 1982, **55**, 477.
8. S. Okeya, Y. Kawakita, S. Matsumoto, Y. Nakamura, S. Kawaguchi, N. Kaneshita, K. Miki and N. Kasai, *Bull. Chem. Soc. Jpn* 1984, **57**, 1850.
9. H. Tanaka, K. Isobe, S. Kawaguchi and S. Okeya, *Bull. Chem. Soc. Jpn* 1984, **57**, 1850.
10. J. P. Schaffer and P. J. Wheatley, *J. Chem. Soc. A* 1966, 528.
11. L. F. Power, K. E. Turner and F. H. Moore, *Inorg. Nucl. Chem. Lett.* 1972, **8**, 313.
12. J. S. Oh and J. C. Bailar, *J. Inorg. Nucl. Chem.* 1962, **24**, 1225.
13. R. G. Charles, *J. Phys. Chem.* 1960, **64**, 1747.
14. S. Yamazaki, *Inorg. Chem.* 1982, **21**, 1638 : S. Yamazaki, *Polyhedron* 1985, **4**, 1915.
15. R. G. Charles, *Org. Synth.* 1959, **39**, 61.
16. S. Yamazaki, *28th Coordination Chemistry Symposium, Chemical Society of Japan*, 1978 (*Ehime University*), p. 179.
17. G. C. Levy and G. L. Nelson, *"Carbon-13 Nuclear Magnetic Resonance for Organic Chemists"*, Chap. 2. John Wiley, New York (1972).
18. See Ref. 1; G. Allen, J. Lewis, R. Long and C. Oldham, *Nature* (*London*) 1964, **202**, 589.
19. Y. Kaizu, T. Yazaki, Y. Torii and H. Kobayashi, *Bull. Chem. Soc. Jpn* 1970, **43**, 2068.

Polyhedron Vol. 5, No. 6, pp. 1191–1195, 1986
Printed in Great Britain

0277–5387/86 $3.00+.00
Pergamon Journals Ltd

SYNTHESIS AND STRUCTURE OF HEXABENZYL-DIMOLYBDENUM (Mo≡Mo)

SHARON M. BESHOURI and IAN P. ROTHWELL*

Department of Chemistry, Purdue University, West Lafayette, IN 47907, U.S.A.

and

KIRSTEN FOLTING, JOHN C. HUFFMAN and WILLIAM E. STREIB

Molecular Structure Center, Indiana University, Bloomington, IN 47405, U.S.A.

(*Received* 9 *September* 1985; *accepted* 31 *October* 1985)

Abstract—The homoleptic benzyl $Mo_2(CH_2Ph)_6$ has been obtained by reaction of either $MoCl_4(thf)_2$ or $Mo_2(OPr^i)_6$ with $Mg(CH_2Ph)_2$. The dark-red, sparingly soluble complex has been characterized by ^1H and ^{13}C NMR as well as by a solid-state structure analysis. Pertinent bond distances (Å) and angles (°) for the unbridged, ethane-like molecule which contains crystallographic S_6-symmetry are: Mo—Mo = 2.175(1), Mo—C = 2.162(2), Mo—Mo—C = 97.61(6), and Mo—C—C(Ph) = 98.9(1).

Following our recent studies on the structure and reactivity of benzyl complexes of Gp 4 metals (Ti and Zr)[1,2] we have begun an investigation into the analogous compounds of the heavier Gp 6 elements Mo and W. During attempts to prepare the tetrabenzyl $Mo(CH_2Ph)_4$ for comparison with the known Ti, Zr and Hf analogues[3] we have isolated crystals of the dinuclear benzyl compound $Mo_2(CH_2Ph)_6$. Although briefly referred to in the literature,[4,5] details concerning the spectroscopic and structural characteristics of this molecule have not been reported. We wish to report here both a fortuitous as well as rational synthesis of this complex together with details of its molecular structure.

RESULTS AND DISCUSSION

Synthesis

Attempts to obtain tetrabenzyl-molybdenum by reaction of $MoCl_4(thf)_2$ with $Mg(CH_2Ph)_2$ (>2 equivalents) in thf to a brown-red solution from which deep-red crystals of a compound identified as $Mo_2(CH_2Ph)_6$ could be isolated on suitable workup. The compound is only very sparingly soluble in hydrocarbon solvents (hexane, benzene or toluene) and is stable in air for a number of hours in the solid state. The molecular structure of the complex was confirmed by a single crystal X-ray diffraction study (*vide infra*). Higher yields of the compound can be achieved by alkylation of the dimolybdenum alkoxide $Mo_2(OPr^i)_6$ as shown in eqn (1):

$$Mo_2(OPr^i)_6 + 3Mg(CH_2Ph)_2 \rightarrow Mo_2(CH_2Ph)_6 + 3Mg(OPr^i)_2. \quad (1)$$

It has previously been shown that the analogous alkyl, $Mo_2(CH_2SiMe_3)_6$, can also be obtained via this dinuclear alkoxide.[6]

The product is obtained as a deep-red crystalline precipitate from toluene. Although only sparingly soluble, both ^1H and ^{13}C NMR spectra were obtained in toluene-d_8. The methylene resonance, δ 3.70 ppm, is significantly downfield of the position normally found for diamagnetic benzyl complexes such as $M(CH_2Ph)_4$ (M = Zr or Hf)[1,3] and we ascribe this low-field shift to the deshielding caused by the diamagnetic anisotropy associated with the Mo–Mo triple bond. The Mo—$\underline{C}H_2Ph$ carbon resonates at δ 64.6 ppm. Attempts to obtain a more soluble derivative by use of the alkylating agent $Mg(CH_2Ph\text{-}p\text{-}Me)_2$ (CH_2Ph-*p*-Me = *p*-tolyl) allowed the isolation of $Mo_2(CH_2Ph\text{-}p\text{-}Me)_6$ as red

*Author to whom correspondence should be addressed.

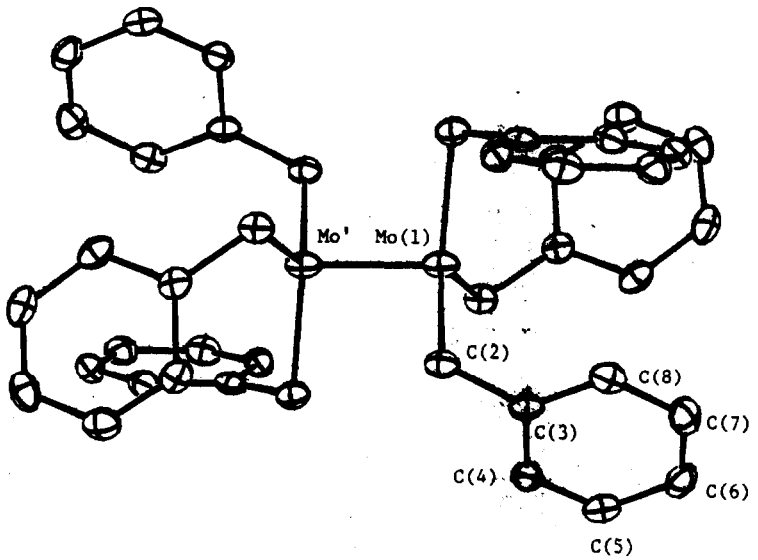


Fig. 1. ORTEP view of $Mo_2(CH_2Ph)_6$ (hydrogen atoms omitted) along with numbering scheme. Because of the crystallographic S_6-symmetry of the molecules, all benzyl groups are equivalent.

cubes, but again the complex was only sparingly soluble.

Solid-state molecular structure of $Mo_2(CH_2Ph)_6$

An ORTEP view of the $Mo_2(CH_2Ph)_6$ molecule is shown in Fig. 1 along with the numbering scheme. Selected bond distances and angles are given in Table 1 while Table 2 contains the crystallographic data. The complex can be seen to adopt the unbridged, staggered, ethane-like geometry typical of M_2X_6 (M = Mo or W) type complexes[5,7] with the molecule containing crystallographic S_6-symmetry making all benzyl ligands equivalent (Fig. 2). The Mo—Mo distance of 2.175(1) Å is comparable to that of the only other reported Mo_2R_6 complex, $Mo_2(CH_2SiMe_3)_6$, 2.167(?) Å.[4] Both of these distances are considerably shorter than found in the molecules $Mo_2(NMe_2)_6$, 2.211(2) and 2.217(2) Å,[8] and $Mo_2(OCH_2CMe_3)_6$, 2.222(2) Å,[9] and possible electronic reasons for the shorter Mo≡Mo distance in the alkyl complexes have been discussed.[5]

Table 1. Selected bond distances (Å) and angles (°) for $Mo_2(CH_2Ph)_6$

Mo(1)—Mo(1)′	2.175(1)
Mo(1)—C(2)	2.162(2)
C(2)—C(3)	1.482(3)
C(3)—C(4)	1.400(3)
C(3)—C(8)	1.401(3)
C(4)—C(5)	1.381(3)
C(5)—C(6)	1.382(3)
C(6)—C(7)	1.381(4)
C(7)—C(8)	1.390(3)
Mo(1)—Mo(1)′—C(2)	97.61(6)
C(2)—Mo(1)—C(2)′	118.28(3)
Mo(1)—C(2)—C(3)	98.9(1)

The size of the Mo—C—Ph angle is worthy of note. An important characteristic of high-valent early-transition-metal and actinide benzyl compounds is the interaction of the π-cloud of the aromatic ring with the electron-deficient metal center.[1] This is indicated in structural studies by small M—C—Ph angles as well as short M—C (*ortho* and *ipso*) distances. An η^3 bonding mode somewhat analogous to that found in 18-electron systems is sometimes used to describe the situation, but in the actinide case a more extensive multisite bonding mode has been proposed.[10,11] Although the Lewis acidity of the Mo_2^{6+} core in Mo_2X_6 compounds has been well documented,[12] the Mo—C—Ph angle of 98.9(1)° found in $Mo_2(CH_2Ph)_6$ is too large to indicate any significant electron donation from the aryl ring to the metal. However, this angle is significantly smaller than that reported for $Mo_2(CH_2SiMe_3)_6$, 121.1(?)°,[4] although steric effects clearly cannot be ignored. The Mo—C distance of 2.162(2) Å in $Mo_2(CH_2Ph)_6$ is only slightly shorter than the corresponding bond distances in $Mo_2(CH_2Ph)_2(NMe_2)_4$,[13] 2.182(5) and 2.0201(5) Å, and $Mo_2(OPr^i)_4(CH_2Ph)_2(PMe_3)$,[14] 2.22(1) Å.

EXPERIMENTAL

All reactions were carried out under an atmosphere of dry, oxygen-free nitrogen using standard

Table 2. Crystallographic data for $Mo_2(CH_2Ph)_6$

Formula	$Mo_2C_{42}H_{42}$
Formula weight	738.67
Space group	$R\bar{3}$
a (Å)	14.682(6)
b (Å)	14.682(6)
c (Å)	13.182(5)
γ (°)	120.00(2)
Z	3
V (Å^3)	2461.94
Density (calc.) (g cm^{-3})	1.495
Crystal size (mm)	$0.20 \times 0.20 \times 0.20$
Crystal color	Red
Radiation	Mo-K_α ($\lambda = 0.71069$ Å)
Linear absorption coefficient (cm^{-1})	7.741
Temperature (°C)	−154
Detector aperture	3.0 mm wide × 4.0 mm high 22.5 cm from crystal
Sample-to-source distance	23.5
Takeoff angle (°)	2.0
Scan speed (°) (min^{-1})	4.0
Scan width (°)	$2.0 + 0.692 \tan\theta$
Background counts (S)	8
2θ range (°)	6–50
Data collected	5907
Unique data	971
Unique data with $F_o > 3.00\sigma(F)$	862
$R(F)$	0.0188
$R_w(F)$	0.0205
Goodness of fit	0.513
Largest δ/σ	0.006

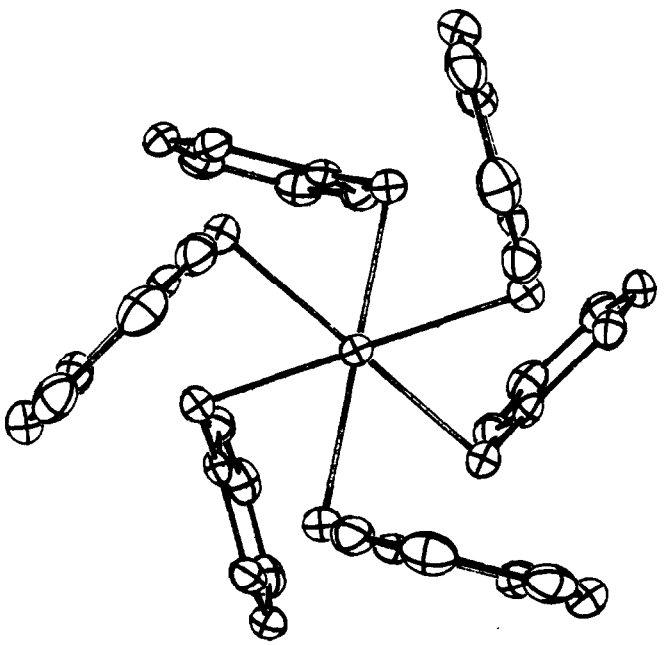


Fig. 2. ORTEP view of $Mo_2(CH_2Ph)_6$ looking down the Mo–Mo triple bond (S_6-axis).

Schlenck and glove box techniques. Solvents were distilled under nitrogen from sodium benzophenone and stored under nitrogen. $MoCl_4(thf)_2$,[15] $Mo_2(OPr^i)_6$[9] and $Mg(CH_2Ph)_2$[16] were obtained by literature methods. ^1H NMR and ^{13}C spectra were recorded on a Varian Associates XL-200 spectrometer.

Preparations

$Mo_2(CH_2Ph)_6$. (a) *From* $MoCl_4(thf)_2$: to a suspension of $MoCl_4(thf)_2$ (2.7 g, 7.0 mmol) in thf (50 cm^3) cooled to 0°C was slowly added solid $Mg(CH_2Ph)_2$ (3.2 g, 15 mmol) through a solid addition funnel. The reaction mixture was allowed to warm up to room temperature and stirred overnight. Filtration followed by cooling the resulting red filtrate gave large, deep-red cubes of product. Yield ~50 mg. ^1H NMR (toluene-d_8): δ 3.70 (s, CH_2Ph), 6.8–7.3 (m, C_6H_5). $\{^1H\}$–^{13}C NMR (toluene-d_8): 64.6 ($\underline{C}H_2Ph$).

(b) *From* $Mo_2(OPr^i)_6$: to a solution of $Mo_2(OPr^i)_6$ (0.5 g, 0.92 mmol) in toluene (25 cm^3) was added $Mg(CH_2Ph)_2$ (0.63 g, 3.0 mmol). The resulting deep-red mixture was stirred overnight. Filtration afforded a powdery sample of $Mo_2(CH_2Ph)_6$ while cooling the filtrate yielded large red cubes of product. Yield = ~200 mg.

$Mo_2(CH_2Ph\text{-}p\text{-}Me)_6$. Using a similar procedure to that in (b) above, $Mo_2(CH_2Ph\text{-}p\text{-}Me)_6$ was obtained as deep-red crystals. Found: C, 70.1; H, 6.9%. Calc. for $Mo_2C_{48}H_{54}$: C, 70.1; H, 6.6%. ^1H NMR (toluene-d_8): δ 3.72 (s, $\underline{CH_2}Ph$), 2.15 (s, $CH_2Ph\text{-}\underline{CH_3}$), 6.8–7.2 (m, $CH_2C_6\underline{H_4}CH_3$).

Crystallographic studies

General operating procedures and a listing of programs have been published previously.[17] Crystal data are summarized in Table 2.

A small well-formed crystal was selected and transferred to the goniostat using standard inert-atmosphere handling techniques. The crystal was cooled to −154°C for characterization and data collection. A search of a limited hemisphere of reciprocal space yielded a set of reflections which exhibited three-fold symmetry and could be indexed using a rhombohedrally centered hexagonal lattice. The diffraction symmetry was determined to be $\bar{3}$, requiring the space group to be either $R\bar{3}$ or $R\bar{3}$. The structure was solved and refined in the space group $R3$.

The only sensible calculated density required six $Mo(CH_2C_6H_5)_3$ units in the unit cell. A trial structure based on three dimers placed at $R3$ sites in the unit cell proved to be correct. Initially the Mo atoms were placed with a separation of 2.3 Å. A difference map phased on the Mo atom revealed the atoms in the benzyl group. The structure was refined using full-matrix least squares. All hydrogen atoms were located in a subsequent difference map and were included in the refinement with isotropic thermal parameters. All non-hydrogen atoms were refined using anisotropic thermal parameters. The final R was 0.019, using 862 reflections with $F > 3.0\sigma(F)$.

A final difference Fourier was essentially featureless, the largest peak being 0.27 e Å^{-1}.*

Acknowledgements—We thank the National Science Foundation (Grant CHE-8219206 to I.P.R.) for support of this research. S.M.B. thanks the Purdue Research Fund for a David Ross Fellowship.

REFERENCES

1. S. L. Latesky, A. K. McMullen, G. P. Niccolai, I. P. Rothwell and J. C. Huffman, *Organometallics* 1985, **4**, 902.
2. S. L. Latesky, A. K. McMullen, I. P. Rothwell and J. C. Huffman, *J. Am. Chem. Soc.* 1985, **107**, 5981.
3. (a) G. R. Davis, J. A. Jarvis, B. T. Kilbourn and A. J. Pids, *J. Chem. Soc., Chem. Commun.* 1971, 677; (b) G. R. Davis, J. A. Jarvis and B. T. Kilbourn, *J. Chem. Soc., Chem. Commun.* 1971, 1511.
4. F. Hug, W. Mowant, A. Shortland, A. C. Skapski and G. Wilkinson, *J. Chem. Soc., Chem. Commun.* 1971, 1079.
5. F. A. Cotton and R. A. Walton, *Multiple Bonds between Metal Atoms*. John Wiley, New York (1982).
6. L. Chamberlain, J. Keddington and I. P. Rothwell, *Organometallics* 1982, **1**, 1098.
7. M. H. Chisholm, *Polyhedron* 1983, **2**, 681.
8. M. H. Chisholm, F. A. Cotton, B. A. Frenz, W. W. Reichert, L. W. Shive and B. R. Stults, *J. Am. Chem. Soc.* 1976, **98**, 4469.
9. M. H. Chisholm, F. A. Cotton, C. A. Murillo and W. W. Reichert, *Inorg. Chem.* 1977, **16**, 1801.
10. E. A. Mintz, K. G. Moloy, T. J. Marks and V. W. Day, *J. Am. Chem. Soc.* 1982, **104**, 4692.
11. P. G. Edwards, R. A. Andersen and A. Zalkin, *Organometallics* 1984, **3**, 293.
12. M. H. Chisholm and I. P. Rothwell, *Prog. Inorg. Chem.* 1982, **29**, 1.

* Atomic coordinates, thermal parameters, and F_o/F_c data have been deposited with the Editor as supplementary data; atomic coordinates have also been deposited with the Cambridge Crystallographic Data Centre.

13. M. J. Chetcuti, M. H. Chisholm, K. Folting, D. A. Haitko, J. C. Huffman and J. Janos, *J. Am. Chem. Soc.* 1983, **105**, 1163.
14. M. H. Chisholm, J. C. Huffman and R. J. Tatz, *J. Am. Chem. Soc.* 1984, **106**, 5385.
15. J. R. Dillworth and R. L. Richards, *Inorg. Synth.* 1980, **20**, 119.
16. R. R. Schrock, *J. Organomet. Chem.* 1976, **122**, 209.
17. M. H. Chisholm, K. Folting, J. C. Huffman and C. C. Kirkpatrick, *Inorg. Chem.* 1984, **23**, 1021.

Polyhedron Vol. 5, No. 6, pp. 1197–1199, 1986
Printed in Great Britain

0277–5387/86 $3.00+.00
Pergamon Journals Ltd

PREPARATION AND ^{31}P NMR SPECTRA OF *N*-THIOCYANATO DERIVATIVES OF SOME ORGANOPHOSPHORUS(III) HALIDES

RUSMIDAH ALI and KEITH B. DILLON*

Chemistry Department, University of Durham, South Road, Durham DH1 3LE, U.K.

(*Received* 27 *September* 1985; *accepted* 6 *November* 1985)

Abstract—The compounds $RP(NCS)_2$ (R = Ph, Me, Et or C_6F_5) have been prepared, and ^{31}P NMR data have been recorded both for them and for their precursors RPX(NCS) (X = Cl or Br). They are all thermally unstable, particularly the alkylphosphorus compounds, thus accounting for some discrepancies with literature NMR data. The NCS group has been shown to be *N*-bonded in each instance by means of IR spectroscopy.

Various methods have been described in the literature for preparing thiocyanato derivatives of organophosphorus(III) halides, usually involving either reaction of RPX_2 (X = Cl or Br) with a metal thiocyanate such as AgSCN,[1–4] $Hg(SCN)_2$,[2] $Pb(SCN)_2$[2] or NH_4NCS,[2] or exchange with a thiocyanato compound of silicon[5,6] or germanium.[5] ^{31}P NMR shifts of 37.9 ppm for $MeP(NCS)_2$,[2] 33.0 ppm for $PhP(NCS)_2$[6] and 62.2 ppm for $C_6F_5P(NCS)_2$[4] have also been reported, but these values do not appear to be self-consistent when compared with the shifts of the starting materials (Table 2). Furthermore the preparative procedures required heating in each case, usually under reflux in a suitable solvent,[1–6] and thiocyanato compounds of phosphorus are often thermally unstable.[4,7,8] Fild[4] found that further heating of freshly-distilled $C_6F_5P(NCS)_2$ led to complete transformation to a mixture of two substances, which could not be separated by distillation. From NMR and other evidence he deduced that these were pentavalent phosphorus thiocyanato and cyano compounds[4] [eqn (1)]:

$$2C_6F_5P(NCS)_2 \rightarrow C_6F_5P(S)(NCS)_2 + C_6F_5P(S)(CN)_2. \quad (1)$$

No NMR data have been reported for the intermediate halogenothiocyanato compounds RPX(NCS) (X = Cl or Br). We have therefore prepared the compounds $RP(NCS)_2$ (R = Ph, Me, Et or C_6F_5) under mild conditions from $RPCl_2$, and monitored the NMR spectra during the reactions, enabling shift values to be derived for RPCl(NCS) and $RP(NCS)_2$. The pentafluorophenyl compound has been similarly prepared from $C_6F_5PBr_2$. The compounds have been isolated and further characterized by elemental analysis, carried out as soon as possible to minimize the risk of decomposition. The thiocyanato group has been shown to be *N*-bonded in each case by means of IR spectroscopy.

EXPERIMENTAL

All manipulations including NMR sample preparation were carried out either under an inert atmosphere of dry nitrogen or *in vacuo*. Chemicals of the best available commercial grade were used, in general without further purification. $C_6F_5PBr_2$ was prepared by reaction of the Grignard reagent C_6F_5MgBr with PBr_3,[9] and $C_6F_5PCl_2$ was either prepared similarly from C_6F_5MgCl and PCl_3,[9] or by reaction of $C_6F_5PBr_2$ with Et_4NCl (2 equivalents) in CH_2Cl_2. The ^{31}P NMR spectrum showed when reaction was complete. The CH_2Cl_2 was removed *in vacuo*, the product was extracted into low-boiling (303–313 K) petroleum ether, the Et_4NBr was filtered off, and the solvent was removed *in vacuo* to leave $C_6F_5PCl_2$.

Dithiocyanatophenylphosphine [$PhP(NCS)_2$]

Dichlorophenylphospine (0.99 g, 5.53 mmol) was dissolved in CH_2Cl_2 and an excess of AgSCN (2.40 g, 14.46 mmol) was added, with constant stirring. The reaction mixture was allowed to stir for 1–2 h,

* Author to whom correspondence should be addressed.

Table 1. Elemental analyses for dithiocyanato-organophosphines

	Analysis (%)									
	Found					Calculated				
Compound	C	H	N	P	S	C	H	N	P	S
$PhP(NCS)_2$	41.2	2.2	8.1	13.8	27.5	42.9	2.2	12.5	13.8	28.6
$MeP(NCS)_2$	23.2	1.7	15.9	19.3	40.0	22.2	1.9	17.3	19.1	39.5
$EtP(NCS)_2$	28.5	3.0	15.3	16.9	35.7	27.3	2.9	15.9	17.6	36.4
$C_6F_5P(NCS)_2$	30.6	—	7.2	10.5	19.4	30.6	—	8.9	9.9	20.4

and the excess AgSCN and AgCl were then removed by filtration. The solvent was removed *in vacuo* to yield a yellow liquid.[1] Elemental analyses for this and the other compounds prepared are given in Table 1. In each case analysis was carried out as quickly as possible after preparation of the compound, in view of their thermal instability (Results and Discussion).

Dithiocyanatomethylphosphine [$MeP(NCS)_2$]

The above reaction was repeated using $MePCl_2$ (0.73 g, 6.24 mmol) and AgSCN (2.32 g, 13.98 mmol), with stirring for 1 h. A yellow liquid was isolated, and was analysed immediately.

Dithiocyanatoethylphosphine [$EtP(NCS)_2$]

This compound had not been previously reported in the literature, but was similarly prepared from $EtPCl_2$ (0.66 g, 5.04 mmol) and AgSCN (1.87 g, 11.27 mmol). It was isolated as a yellow liquid.

Dithiocyanatopentafluorophenylphosphine [$C_6F_5P(NCS)_2$]

A similar reaction between $C_6F_5PBr_2$ (4.50 g, 12.58 mmol) and AgSCN (5.02 g, 30.25 mmol), with stirring for 2–3 h, led to isolation of the compound as a yellow liquid.[4]

^{31}P NMR spectra were recorded at 307.2 K as described previously;[7] chemical shifts were measured relative to external 85% H_3PO_4, and are quoted with the downfield (higher frequency) direction taken as positive. IR spectra were also recorded as indicated in earlier papers, as were microanalyses for C, H, N and P.[7,10] Sulphur was determined by titration with $Ba(ClO_4)_2$ following an oxygen flask combustion, with sulphonazo III as the indicator.

RESULTS AND DISCUSSION

The reactions were initially monitored by adding a smaller amount of AgSCN than required for complete substitution to a solution of RPX_2 in CH_2Cl_2, with stirring, and recording the ^{31}P NMR spectrum of the mixture. Two signals upfield from that of the starting material were observed in each instance (Table 2), assigned to RPX(NCS) and $RP(NCS)_2$. The value of 61.2 ppm for $C_6F_5P(NCS)_2$ is in good agreement with the result of Fild[4] for the freshly-distilled compound. The shift separation between $RPCl_2$ and $RP(NCS)_2$ is slightly larger for aliphatic than for aromatic R groups, but is quite similar for R = Me or Et, and for R = Ph or C_6F_5. There is a striking discrepancy, however, between our results and literature data for $PhP(NCS)_2$ (δ 33.0 ppm[6]) and $MeP(NCS)_2$ (δ 37.9 ppm[2]). This is discussed below.

The compounds were isolated as yellow liquids

Table 2. $\delta(^{31}P)$ (ppm) for *N*-thiocyanato derivatives of RPX_2

		$\delta(^{31}P)$ (ppm) for		
R	X	RPX_2	RPX(NCS)	$RP(NCS)_2$
CH_3	Cl	192.6	141.8	103.3
C_2H_5	Cl	199.8	150.0	112.9
C_6H_5	Cl	161.3	117.7	88.7
C_6F_5	Cl	135.6	90.4	61.2
C_6F_5	Br	111.3	79.1	61.2

(Experimental), and all proved to be thermally unstable at room temperature, so analyses were carried out as soon as possible after preparation. $PhP(NCS)_2$ readily turned to a dark brown viscous liquid giving low C, N and S analyses, while the methyl and ethyl compounds were even more unstable, quickly becoming reddish-brown and viscous even within the entry port of the inert atmosphere box. The most stable material was $C_6F_5P(NCS)_2$; this compound had been isolated by Fild[4] by distillation, but further heating led to a mixture of two substances which could not be separated by distillation, and gave higher-field ^{31}P signals at 7 and −40 ppm. These were deduced to arise from $C_6F_5P(S)(NCS)_2$ and $C_6F_5P(S)(CN)_2$, respectively. In support of this hypothesis a chemical shift of 6.8 ppm was measured for $C_6F_5P(S)(NCS)_2$, but the cyano compound could not be isolated pure.[4] It therefore seems probable that the signals reported previously for $MeP(NCS)_2$[2] and $PhP(NCS)_2$[6] may be due to one of the corresponding decomposition products, possibly $RP(S)(NCS)_2$ (R = Me or Ph), although it is not then apparent why two signals were not detected in the earlier work.

The IR spectra of the phenyl, methyl and ethyl compounds all showed strong, broad absorptions between 2150 and 1850 cm^{-1} for the asymmetric stretch of the NCS moiety, as expected for thiocyanato groups bonded to phosphorus via the nitrogen atom.[11,12] The same mode of coordination has been deduced from vibrational spectroscopic studies of $C_6F_5P(NCS)_2$[3] and $P(NCS)_3$,[11,12] as well as in the phosphorus(V) compounds $PO(NCS)_3$,[11,12] $PhPO(NCS)_2$,[11] $PS(NCS)_3$[11] and $PhPS(NCS)_2$.[11]

We therefore conclude that thiocyanato derivatives of organophosphorus(III) halides may be prepared and isolated, but that their thermal stability is low, particularly for alkyl-substituted compounds. The NCS groups are coordinated through nitrogen in all of the compounds prepared, and reliable ^{31}P shift data have now been obtained for RPCl(NCS), $RP(NCS)_2$ (R = Ph, Me, Et or C_6F_5) and $C_6F_5PBr(NCS)$.

Acknowledgement—We thank the Universiti Teknologi Malaysia for the award of a research studentship (to R.A.).

REFERENCES

1. A. Michaelis, *Ann. Chem.* 1896, **293**, 193.
2. L. Maier, *Helv. Chim. Acta* 1963, **46**, 2667.
3. M. Fild, O. Glemser and I. Hollenberg, *Naturwissenschaften* 1966, **53**, 130.
4. M. Fild, *Z. Naturforsch.* 1968, **23B**, 604.
5. H. H. Anderson, *J. Am. Chem. Soc.* 1953, **75**, 1576.
6. A. N. Pudovik, G. V. Romanov and T. Ya. Stepanova, *J. Gen. Chem. U.S.S.R.* 1979, **49**, 1248.
7. K. B. Dillon and A. W. G. Platt, *J. Chem. Soc., Dalton Trans.* 1982, 1199.
8. K. B. Dillon and A. W. G. Platt, *J. Chem. Soc., Dalton Trans.* 1983, 1159.
9. K. B. Dillon and J. Lincoln, *Polyhedron* 1985, **4**, 1333.
10. K. B. Dillon, R. N. Reeve and T. C. Waddington, *J. Chem. Soc., Dalton Trans.* 1977, 1410.
11. D. B. Sowerby, *J. Inorg. Nucl. Chem.* 1961, **22**, 205.
12. K. Oba, F. Watari and K. Aida, *Spectrochim. Acta* 1967, **23A**, 1515.

Polyhedron Vol. 5, No. 6, pp. 1201–1206, 1986
Printed in Great Britain

0277–5387/86 $3.00+.00
Pergamon Journals Ltd

REACTIONS OF π-ALLYLTRICARBONYLIRON HALIDES AND THE SYNTHESIS OF NEW ORGANOIRON COMPOUNDS

KAMALENDU DEY,* DHANANJOY KONER, PRABIR KUMAR BHATTACHARYYA and AMITAVA GANGOPADHYAY

Department of Chemistry, University of Kalyani, Kalyani 741235, India

and

KULDIP K. BHASIN and RAVINDRA D. VERMA

Department of Chemistry, Punjab University, Chandigarh 160014, India

(*Received* 15 *May* 1985; *accepted after revision* 25 *November* 1985)

Abstract—The reactions of $[\pi\text{-}C_3H_5Fe(CO)_3X]$ [where X = Cl (**1**), Br (**2**) or I (**3**)] with different chemical species are described. Thus, **2** and **3** react with $Ph_2C{=}NLi$ in Et_2O to yield $[(\pi\text{-}C_3H_5)(CO)_3Fe(N{=}CPh_2)]$, while the reaction of **1** with PhC(=S)N(Me)Li in THF yielded a novel σ-allylironcarbonyl compound. Ethynyl magnesium bromide, $HC{\equiv}CMgBr$, reacts with **3** in THF to give a π-allyltricarbonyl ethynyliron complex, which undergoes a dipolar cycloaddition reaction with $PhC{\equiv}N{-}O$ in Et_2O, yielding a novel organoiron complex, [(μ-CO)bis{5(σ-allyltricarbonyliron)(3-phenylisoxazole)}]. The reaction of $[\pi\text{-}C_3H_5(CO)_3FeNa]$ with $ClCH_2CH_2NMe_2$ is also described. Data on molar conductances, molecular weights, and IR and ^1H NMR spectra, were used to assign structures.

The study of the reactivity of π- and σ-allyl transition metal complexes is significant for various reasons, one being their involvement in many catalytic processes. In many such reactions formation of cationic allyl metal complexes as intermediates have been proposed. As not much work is available on the synthesis and reactivity of cationic allyliron carbonyl complexes,[1,2] we have synthesized and studied the reactivity of such cationic iron complexes. Very recently we have described[3] the reactions of $[\pi\text{-}C_3H_5(CO_3)X]$ [where X = Br (**2**) or I (**3**)] leading to the successful isolation of cationic and neutral π- and σ-allyliron carbonyl complexes. We have further studied the reactions of $\pi\text{-}C_3H_5(CO_3)Cl$ (**1**), **2** and **3** leading to the novel synthesis of organoiron compounds, and the present paper describes these results.

EXPERIMENTAL

Elemental analyses, spectroscopic measurements and measurement of conductances were done as described previously.[4–6] All manipulations were carried out under nitrogen and solvents were dried and purified by usual procedures.

Preparation of the starting materials

$Ph_2C{=}NLi$[7] (**4**), PhC(=S)N(Me)Li[8] (**5**) and $HC{\equiv}CMgBr$[9] (**6**) were synthesized as described in the literature. The π-allyltricarbonyliron halide complexes were prepared by a previously published method.[1] The compound $ClCH_2CH_2NMe_2$ (Sigma Chemical Co.) was used as obtained without further purification, while $PhC{\equiv}N{-}O$ (**7**) was synthesized by the literature methods[10] and used immediately. Molecular weights were determined osmometrically in benzene, cyclohexane or chloroform.

Physical methods

IR spectra (KBr discs and Nujol mulls) were recorded on a Perkin–Elmer 781 spectrophotometer; ^1H (60-MHz) NMR spectra for the complexes in d_6-acetone or $CDCl_3$ solutions, with TMS as internal reference, were recorded at room

* Author to whom correspondence should be addressed.

temperature in a Varian T 60 instrument. Molecular weights were determined osmometrically in benzene, cyclohexane or chloroform solution using a vapour pressure Macrolab Osmometer (Model 301A).

Reactions of **1**, **2** *and* **3**

Reactions of **2** *and* **3** *with* **4**. Ether solution (25 cm^3) of **4** (0.9 g, 0.005 mol) was added dropwise to a magnetically stirred ether solution (30 cm^3) of **2** (1.3 g, 0.005 mol) or **3** (1.53 g, 0.005 mol) at 0°C. After about 1 h the mixture was filtered and the coloured filtrate, on concentration and cooling to −20°C, yielded a brown mass, which on fractional crystallization from a pentane–ether mixture [50 : 50 (v/v)] at −10°C gave [(π-C_3H_5)$(CO)_3$Fe(N=CPh_2)] (**8**) in 60% yield, m.p. 63–65°C (d).

Reaction of **1** *with* **5**. To a magnetically stirred solution of **5** (0.78 g, 0.005 mol) in THF (25 cm^3) was added a solution of **1** (1.1 g, 0.005 mol) in THF (25 cm^3) at about −40°C and the stirring was continued for 1 h and then raised to room temperature and filtered. The filtrate was chromatographed through SiO_2 and the major brown band was eluted with a benzene–ether [50 : 50 (v/v)] mixture, which yielded orange–red crystals of **9** in 52% yield, m.p. 88–91°C (d). From the other two minor bands (dark red and red) no definite compounds could be isolated in the pure state.

Reaction of **3** *with* **6**. A solution of **6** (1.26 g, 0.01 mol) in THF (150 cm^3) was added slowly to a stirred solution of **3** (3.0 g, 0.01 mol) in THF (50 cm^3) at −10°C and stirred for 30 min more, followed by work up (hydrolysis with saturated aqueous NH_4Cl solution) and extraction with a pentane–hexane [50 : 50 (v/v)] mixture, dried with anhydrous Na_2SO_4 and concentrated and cooled to −20°C to yield a red powder, [(π-C_3H_5)$(CO)_3$Fe(C≡CH)] (**10**) in 55% yield.

Reaction of **10** *with benzonitrile oxide* (**7**). A solution of **10** (1.0 g, 0.005 mol) in an ether–THF mixture (50 cm^3) [50 : 50 (v/v)] was added to a solution of **7** (0.6 g, 0.005 mol) in a benzene–THF mixture (100 cm^3) [50 : 50 (v/v)] at −10°C and stirred at that temperature for 2 h to yield a coloured solution, which on concentration and cooling gave reddish-brown [(μ-CO)bis{5(σ-allyltricarbonyliron)3-phenylisoxazole}] (**11**) in about 50% yield, m.p. 110–112°C (d). The brown filtrate on evaporation and titration with Et_2O gave a light brown powder, which has not been identified yet.

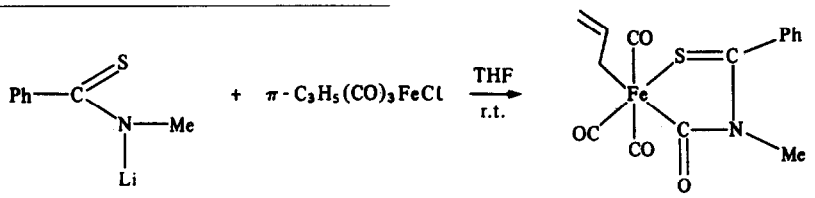
Reaction of [(π-C_3H_5)$(CO)_3$FeNa] (**12**) *with* 2-*chloroethyldimethylamine* ($ClCH_2CH_2NMe_2$) (**13**). Complex **3** (0.6 g, 0.002 mol) in 50 cm^3 of THF was treated with elemental sodium (0.095 g, 0.004 g atom) and stirred for 2 h and then filtered directly into a solution of **13** (0.3 g, 0.002 mol) in THF (50 cm^3) at about 35°C. The mixture was stirred for 3 h and filtered. The filtrate was evaporated to dryness and then extracted with a benzene–hexane [50 : 50 (v/v)] mixture, which gave an orange-red π-allyliron complex, [(π-C_3H_5)$(CO)_2$Fe(C=O)$CH_2CH_2NMe_2$] (**14**), in 42% yield, m.p. 79–82°C (d). No pure compound was isolated from the benzene–hexane-insoluble dark solid.

RESULTS AND DISCUSSION

The reaction [eqn (1)] of **2** or **3** with **4** (1 : 1 molar ratio) in Et_2O, subsequent removal of the precipitated LiX, and vacuum concentration of the filtrate yielded brown **8**. The complex was stable under an inert atmosphere, but unstable in air and sensitive to light. Irradiation with UV light gave an unidentified deep red powder:

$$\underset{\textbf{2 or 3}}{\pi\text{-}C_3H_5(CO)_3FeX} + \underset{\textbf{4}}{Ph_2C{=}NLi} \xrightarrow{Et_2O,\,0^\circ C} \underset{\textbf{8}}{\pi\text{-}C_3H_5(CO)_3Fe\cdot N{=}CPh_2}. \quad (1)$$

The reaction of **1** with a stoichiometric amount of **5** in THF leads, according to eqn (2), to the novel σ-allyl complex **9** in about 52% yield. This was also stable only under an inert atmosphere and sensitive to light. Treatment of solutions of **3** with **6** in THF

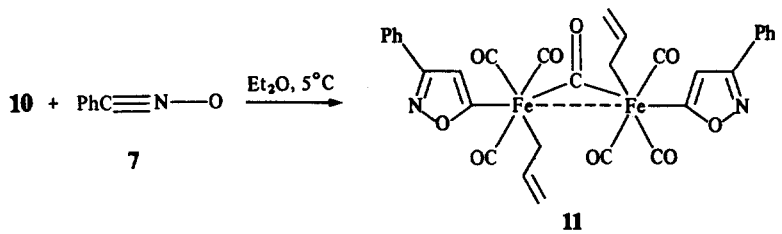


5 **1** **9** (2)

at −10°C yielded the π-allyltricarbonylethynyliron(II) complex (**10**) [eqn (3)]:

$$\underset{\textbf{6}}{3 + HC{\equiv}CMgBr} \xrightarrow{THF,\,-10^\circ C} \underset{\textbf{10}}{\pi\text{-}C_3H_5(CO)_3Fe\cdot C{\equiv}CH}. \quad (3)$$

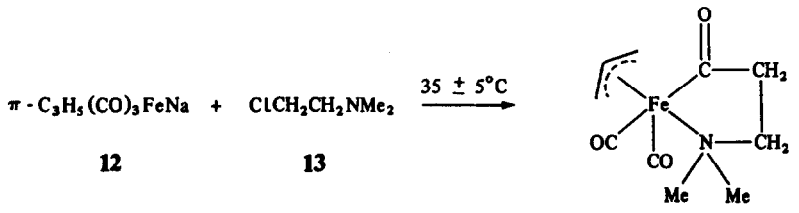
Complex **10** was found to be a good 1,3-dipolarophile. Reaction of **10** with **7** in Et_2O at 5°C proceeded to give **11**, in the form of a carbonyl-bridged dimer, possibly with a linkage between two iron centres, as shown in eqn (4):



(4)

In the absence of X-ray crystal structural data, the present proposed structure for complex **11** must be considered as tentative.

Treatment of **3** with Na in THF produced the sodium salt (**12**), which, in turn, reacted with **13** to give **14** [eqn (5)]:



(5)

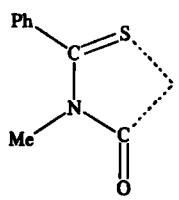
All of these complexes are coloured, stable in an inert atmosphere, unstable in air and soluble in suitable organic solvents, and the solutions are stable for 1–3 h. Complexes **8–11** and **14** are non-conducting in nitromethane. Elemental analyses (Table 1) support their formulations. Molecular weights are also in agreement with these formulae.

In the IR spectra of **8**, **10** and **14** the expected π-

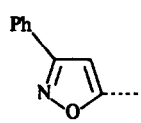
Table 1. Elemental analysis and molecular weights of some organoiron complexes

Serial No.	Complex	% Found (calc.) C	H	N	Fe	Molecular weight (calc.)
8	$(\pi\text{-}C_3H_5)(CO)_3Fe(N{=}CPh_2)$	63.6 (63.2)	4.7 (4.1)	4.0 (3.9)	15.4 (15.5)	332 (360.85)
9	$(\sigma\text{-}C_3H_5)(CO)_3Fe(L\text{–}L)^a$	49.3 (48.4)	4.0 (3.7)	4.2 (4.0)	16.6 (16.1)	345 (358.85)
10	$(\pi\text{-}C_3H_5)(CO)_3Fe(C{\equiv}C\text{—}H)$	47.0 (46.6)	2.8 (2.9)	—	27.3 (27.2)	—
11	$[(\sigma\text{-}C_3H_5)(CO)_3FeL^b]_2CO$	55.0 (54.9)	3.7 (3.2)	4.9 (4.1)	16.8 (16.5)	656 (679.7)
14	$(\pi\text{-}C_3H_5)(CO)_2Fe(L_1\text{–}L_1)^c$	47.0 (47.5)	6.2 (5.9)	5.6 (5.5)	22.8 (22.1)	245 (252.85)

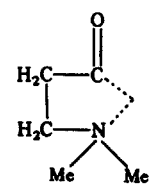
[a] L–L stands for



[b] L stands for

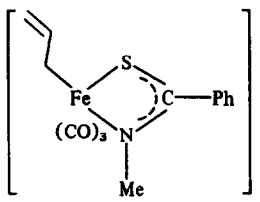


[c] $L_1\text{–}L_1$ stands for

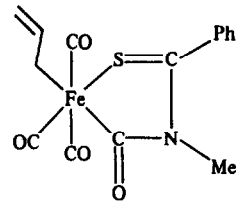


Broken lines show the bonding sites

allylic, C---C---C, bands are observed around 1515–1525 cm^{-1}. Two or three very strong bands were observed around 1930–2080 cm^{-1} in complexes **8–11** and **14**, which may be assigned to ν(C≡O) absorption.[11,12] In addition a medium intense band was observed around 1858 cm^{-1} in complex **11** supporting the presence of a bridging CO group. The same compound (**11**) also showed three IR absorption bands around 1610, 1475 and 1385 cm^{-1}, supporting thereby the presence of a substituted isoxazole moiety in that complex.[13] The absorption at 1610 cm^{-1} appears as a very strong band with a shoulder at ~1600 cm^{-1}. This shoulder may be considered as a ring ν(C=N) absorption.[14] However, the presence of a σ-allylic group in this complex complicates this interpretation (see later discussion). The ν(C≡C) for **10** also absorbs in the ν(C≡O) region. Complexes, **9** and **14** show additional bands [for ν(C=O)] around 1631 and 1625 cm^{-1}, respectively. These relatively low energy absorptions suggest the presence of a carbamoyl function in these complexes,[15–19] which is formed by the insertion of a CO group between iron and nitrogen in complex **9a**, the possible intermediate species that might be formed in the synthesis of complex **9** [see eqn (2) above]. The tricarbonyl nature of the complex is retained, the additional CO being derived from the decomposed carbonyl complex. This may account for the low yield of complex **9**. The low yield of the carbonyl-bridged dimeric complex **11** may be accounted for similarly. The nucleophilic attack of metal-bound N to the C of CO may give rise to complex **9** with a five-membered ring:[20]



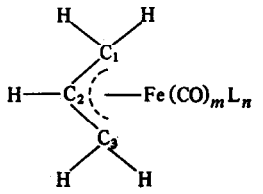
9a



9

The presence of the σ-allylic group in complexes **9** and **11** is demonstrated by the appearance of IR bands for ν(C=C) (allylic) in the 1610–1600 cm^{-1} region.[21] Two strong bands, one at about 685 cm^{-1} and another at about 500 cm^{-1} (slightly broad), were observed in complex **14** and may tentatively be assigned to the Fe—N stretching mode, which might be coupled with the N—CH_3 stretching mode.[20–22] Other important chromophoric groups (e.g. C=S, C=N, C=O etc.) present in these complexes could easily be identified from the IR spectral bands.[22]

These structural features of the present iron complexes have also been substantiated by the ^1H NMR spectral data (Table 2):



8 $m = 3$, $L_n = N{=}CPh_2$
10 $m = 3$, $L_n = C{\equiv}CH$
14 $m = 2$, $L_n = Me_2NCH_2CH_2C{=}O$

In complexes **8**, **10** and **14** (see Fig. 1) absorption of the proton at C_2 appears as complex bands around δ 4.7–5.1 ppm. A pair of doublets (broad) centred at around δ 2.7 and 1.8 ppm, which may be *syn* and *anti* protons at the C_1 and C_3 carbon atoms, respectively, are also observed for these complexes. These bands cannot be further resolved at room temperature. However, the integration is approximately correct for these formulations. These proton NMR data support the presence of π-allyl ligands[21,23–26] in complexes **8**, **10** and **14**. Complex **10** shows an additional band at δ 3.25 (singlet) ppm, showing the presence of acetylinic proton.

The synthesis, proton NMR spectral studies and X-ray crystal structure determination of σ-allyl-palladium(II) and σ-allyl-platinum(II) complexes have received much attention in the last few years,[26–31] in view of the role of these species as intermediates in the catalytic reactions of π-allyl metal complexes. Surprisingly, very few σ-allyliron complexes are known,[1,19] and in this sense the present complexes **9** and **11** are significant in representing some stable types of σ-allyliron complexes in solutions. The chelated (S, C and N, C) bonded ligands in complexes **9** and **14**, formed *in situ*, by the insertion of a CO molecule between Fe—N and Fe—C bonds, respectively, appear to be very strongly bound to iron so that the proton NMR spectra of complexes **9** and **14** at room temperature can be satisfactorily

Table 2. ^{1}H NMR spectroscopic data[a] for the η^1- and η^3-allylic complexes[b]

Serial No.	Complex[c]	Allyl protons[d]
8	$(\pi\text{-}C_3H_5)(CO)_3Fe(N{=}CPh_2)$	4.72 (m, 1H, CH), 2.80 (d, br, 2H, *syn*-CH_2), 1.90 (d, br, 2H, *anti*-$3H_2$)
9	$(\sigma\text{-}C_3H_5)(CO)_3Fe(L\text{–}L)$	2.80 (d, br, 2H, —CH_2), 6.00 (m, 1H, —CH=), 4.60 (m, 2H, =CH_2)
10	$(\pi\text{-}C_3H_5)(CO)_3Fe(C{\equiv}C\text{—}H)$	4.85 (m, 1H, CH), 2.82 (d, br, 2H, *syn*- —CH_2), 1.92 (d, br, 2H, *anti*- —CH_2)
11	$[(\sigma\text{-}C_3H_5)(CO)_3FeL]_2CO$	2.68 (d, br, 2H, —CH_2), 5.98 (m, 1H, —CH=), 4.50 (m, 2H, =CH_2),
14	$(\pi\text{-}C_3H_5)(CO)_2Fe(L_1\text{–}L_1)$	5.10 (m, 1H, CH), 2.80 (d, br, 2H, *syn*- —CH_2), 1.90 (d, br, 2H, *anti*-—CH_2)

[a] Chemical shifts (δ) ppm in d_6-acetone or $CDCl_3$ with TMS as internal reference.

[b] For **8**: 7.4–7.9 (m, 10H, Ph); **9**: 6.77–7.5 (m, 5H, Ph), 2.5 (S, 3H, N—CH_3); **10**: 3.25 (S, 1H, C≡CH); **11**: 7.5–7.8 (m, 5H, Ph), 7.01 (br, 1H, isoxazole); **14**: 2.86 (br, 6H, N—Me_2); 2.23 ppm for N—Me_2 in the free ligand.

[c] For abbreviations of the ligands see Table 1.

[d] η^1-Allyl ligand for complexes **9** and **11**; η^3-allyl ligand for complexes **8**, **10** and **14**.

interpreted in terms of rigid σ-allyliron bonding. In complex **9** the absorption of N—CH_3 and C_6H_5 protons appear as singlet and multiplets at δ 2.5 and 6.77 ppm, respectively. On the other hand, the presence of a σ-allylic ligand is demonstrated by the appearance of bands[1] at δ 2.80 ppm (broad, doublets) for Fe—CH_2, at δ 4.60 ppm (complex) for =CH_2 and at δ 6.00 ppm (complex) for —CH= species. Integrations of these bands are correct for these formulations. Similarly, the presence of the π-allyl ligand has been confirmed for complex **14**. The most interesting feature of the ^{1}H NMR spectrum of compound **14** is the low-field shift of the N—Me absorption in the complex (N—Me, δ 2.86 ppm) compared to the free-ligand absorption (N—Me, δ 2.23 ppm), the reason for which may be ascribed to the donation of electrons from N to Fe.

Acknowledgements–The financial supports received from the DST, Government of India, and CSIR, New Delhi, are acknowledged. Spectroscopic measurements were done in the CDRI, Lucknow, and in the laboratory of Prof. T. P. Dasgupta, Department of Chemistry, University of Jamaica, West Indies, which are gratefully acknowledged.

REFERENCES

1. R. S. Bayoud, E. R. Biehl and P. C. Reeves, *J. Organomet. Chem.* 1979, **174**, 297.
2. P. Lewnon, A. M. Rosan and M. Rosenblum, *J. Am. Chem. Soc.* 1977, **99**, 8426.
3. K. Dey, D. Koner and S. B. Ray, *J. Chem. Soc., Dalton Trans.* 1982, 2385.
4. K. Dey, A. K. Biswas and A. K. Sinha Ray, *Indian J. Chem.* 1981, **20A**, 848.
5. K. Dey, R. K. Maiti and J. K. Bhar, *Indian J. Chem.* 1981, **20A**, 810.
6. K. Dey and H. Werner, *Chem. Ber.* 1979, **112**, 823; *J. Organomet. Chem.* 1977, **137**, C28.
7. I. Pattison, K. Wade and B. K. Wyatt, *J. Chem. Soc. A* 1969, 837.
8. (a) B. J. Wakefield, *The Chemistry of Organolithium Compounds*, p. 33. Pergamon Press, Oxford (1974). (b) H. Brunner and J. Wachter, *J. Organomet. Chem.* 1977, **142**, 133.
9. H. O. Berger, H. Nöth, G. Rub and B. Wrackmeyer, *Chem. Ber.* 1980, **113**, 1235.
10. A. Werner, *Ber.* 1894, **27**, 2199; *Organic Synthesis—Collective Volume—5* (Chief Editor H. E. Baumgarten), p. 504. John Wiley, New York (1973).
11. R. Uson, V. Riera, J. Gimeno, M. Laguna and M. P. Gamasa, *J. Chem. Soc., Dalton Trans.* 1979, 996.
12. J. W. Connoliy and C. D. Hoff, *J. Organomet. Chem.* 1978, **160**, 467.
13. A. R. Katritzky, *Q. Rev.* 1959, **13**, 353.
14. A. I. Meyers, *J. Org. Chem.* 1959, **24**, 1233.
15. R. B. King, *J. Am. Chem. Soc.* 1963, **85**, 1918.
16. R. J. Angelici and D. L. Denton, *Inorg. Chim. Acta* 1968, **2**, 3.
17. R. J. Angelici, *Acc. Chem. Res.* 1972, **5**, 335.
18. W. Danzer, W. Beck and M. Keubler, *Z. Naturforsch.* 1976, **31B**, 1360.
19. H. Brunner and J. Wachter, *J. Organomet. Chem.* 1977, **142**, 133.
20. T. Inglis, M. Kilner, T. Reynoldson and E. E. Rovertson, *J. Chem. Soc., Dalton Trans.* 1975, 924.
21. H. Kurosawa, *J. Chem. Soc., Dalton Trans.* 1979, 939.
22. K. Nakamoto, *Infrared Spectra of Inorganic and Coordination Compounds*, p. 193. John Wiley, New York (1963).
23. D. H. Gibson and D. K. Erwin, *J. Organomet. Chem.* 1975, **86**, C31.
24. J. A. Kaduk and J. A. Ibers, *J. Organomet. Chem.* 1977, **139**, 199.
25. A. N. Nesmeyanov, Yu. A. Ustynyuk, I. I. Kritskaya and G. A. Shchembelov, *J. Organomet. Chem.* 1968, **14**, 395.

26. S. Numta, R. Okawara and H. Kurosawa, *Inorg. Chem.* 1977, **16**, 1737.
27. G. Carturan, A. Scrivanti, U. Belluco and F. Morandini, *Inorg. Chim. Acta* 1978, **27**, 37.
28. J. C. Hoffman, M. P. Laurant and J. K. Kochi, *Inorg. Chem.* 1977, **16**, 2639.
29. N. M. Boag, M. Green, J. L. Spencer and F. G. A. Stone, *J. Organomet. Chem.* 1977, **127**, C51.
30. H. C. Clark and C. R. Jablonski, *Inorg. Chem.* 1975, **14**, 1518.
31. H. Kurosawa and G. Yoshida, *J. Organomet. Chem.* 1976, **120**, 297.

Polyhedron Vol. 5, No. 6, pp. 1207–1212, 1986
Printed in Great Britain

0277–5387/86 $3.00+.00
Pergamon Journals Ltd

BOND LENGTH BASED BOND ORDERS FOR BORANE CLUSTER COMPOUNDS

NOEL W. THOMAS

H. H. Wills Physics Laboratory, University of Bristol, Royal Fort, Tyndall Avenue, Bristol BS8 1TL, U.K.*

(*Received* 5 *September* 1985; *accepted* 25 *November* 1985)

Abstract—The known molecular structures of several *closo* borane cluster compounds, together with established electron-counting rules, are used to derive a relationship between bond length and bond order for boron–boron two-centre bonds. This relationship is useful in deducing the distribution of electronic charge, and the approach can be extended to other homonuclear clusters.

The relationship between the structures of *closo* boron hydrides and their total enthalpies of atomization has been studied by two sets of workers. Wade *et al.*[1,2] have used a simple power law to relate the enthalpy of a boron–boron bond to its length. The total enthalpies of atomization of the clusters are then regarded as the sum of the enthalpies of all the bonds in the polyhedral cage. By contrast, Fuller and Kepert[3] have considered the total enthalpy of atomization of a cluster as made up of all boron–boron interactions, both bonded and non-bonded. To this end they use a bireciprocal relationship between the enthalpy of interaction of two boron atoms and their internuclear separation.

In this paper, a procedure analogous to that of Wade *et al.* is carried out, to relate the number of electrons in a given B—B bond to its corresponding length. The relationship is expressed as a polynomial, and the resulting order–length curve has a form similar to that for carbon–carbon bonds derived in the 1950s.[4] The method assumes, as a starting point, that the total number of skeletal electrons in a borane or carborane cluster, $(CH)_a(BH)_pH_q^{c-}$, is given by $3a+2p+q+c$, according to the electron-counting rules developed by Wade.[5] These rules have been proved to be very effective in rationalizing the chemistry of these compounds.

EXPERIMENTAL

Derivation of the order–length relationship for B—B *bonds*

The crystal structures of five *closo* boron hydrides, $B_nH_n^{2-}$, have been determined, where $n = 6$, 8, 9, 10 or 12[6–10] (Fig. 1). Knowledge of five independent structures allows us to express the number of electrons in a B—B bond as a polynomial of order four with respect to the bond length, i.e.:

$$p_i = A_{BB}+B_{BB}d+C_{BB}d_i^3+D_{BB}d_i^3+E_{BB}d_i^4. \quad (1)$$

In this equation, p_i is the number of electrons in the bond i, and d_i is its length. A_{BB}, B_{BB}, C_{BB}, D_{BB} and E_{BB} are variable parameters to be determined. For a given compound, $B_nH_n^{2-}$, the total number of skeletal electrons in the cluster is given by $\Sigma_{i=1,N}p_i$, where N is the total number of bonds in the cluster. By considering electron-counting rules,[5] it is known that the n atoms in the cluster are held together by $2(n+1)$ skeletal electrons, distributed over the B—B bonds. So, for each compound:

$$\sum_{i=1,N} p_i = 2(n+1). \quad (2)$$

Substituting for p from eqn (1):

$$2(n+1) = A_{BB}N+B_{BB}\sum_{i=1,N} d_i+C_{BB}\sum_{i=1,N} d_i^2 + D_{BB}\sum_{i=1,N} d_i^3+E_{BB}\sum_{i=1,N} d_i^4. \quad (3)$$

n is the number of atoms in the cluster, N the number of bonds in the cluster, and d_i is the length

* Present address: Department of Ceramics, Houldsworth School of Applied Science, The University of Leeds, Leeds LS2 9JT, U.K.

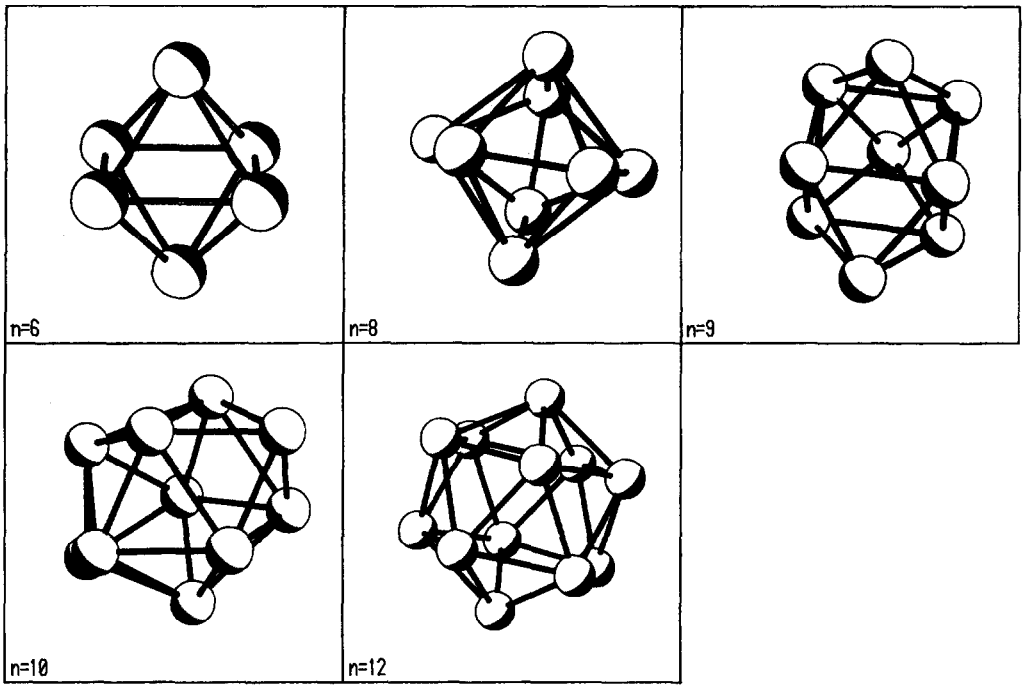


Fig. 1. Shapes of the polyhedral skeletons for *closo* clusters $B_nH_n^{2-}$: $n = 6$, 8, 9, 10 or 12.

of the ith bond. The summations in eqn (3) are evaluated for each cluster (Table 1), so that eqn (3) reduces to five simultaneous linear equations in the unknowns A_{BB}, B_{BB}, C_{BB}, D_{BB} and E_{BB}. For example, the equation for the $B_6H_6^{2-}$ cluster is:

$$14 = 12A_{BB} + 20.23B_{BB} + 34.12C_{BB} + 57.53D_{BB} + 97.00E_{BB}. \quad (4)$$

The simultaneous equations were solved numerically,[11] to yield the following parameters for boron–boron bonds:

$$A_{BB} = 0.92905 \times 10^3 \text{ electrons},$$

$$B_{BB} = -0.22361 \times 10^4 \text{ electrons Å}^{-1},$$

$$C_{BB} = 0.20238 \times 10^4 \text{ electrons Å}^{-2},$$

$$D_{BB} = -0.81409 \times 10^3 \text{ electrons Å}^{-3},$$

$$E_{BB} = 0.12263 \times 10^3 \text{ electrons Å}^{-4}.$$

The order of a given B—B bond is simply the number of electron pairs it contains, and the curve of bond order vs bond length obtained with these parameters is plotted in Fig. 2(a). This curve is reasonable apart from a minimum at a bond length of 1.87 Å. There is no physical basis for such a minimum, however. Assuming that this method is sound, its presence is a result of incorrect electron counts in some of the compounds and/or unreliable structural data. To establish which of the five clusters is causing this minimum, the above procedure was applied to sets of four structures and sets of three structures at a time. The most satisfactory curve was obtained from the structures of $B_6H_6^{2-}$, $B_{10}H_{10}^{2-}$ and $B_{12}H_{12}^{2-}$, as shown in Fig. 2(b). As only three structures are being considered, coefficients D_{BB} and E_{BB} in eqn (1) are set to zero. The values obtained for the other coefficients are as follows:

$$A_{BB} = 0.21781 \times 10^2 \text{ electrons},$$

$$B_{BB} = -0.20620 \times 10^2 \text{ electrons Å}^{-1},$$

$$C_{BB} = 0.49785 \times 10^1 \text{ electrons Å}^{-2}.$$

Note that these coefficients define the order–length relationship only within the range of bond lengths from 1.56 to 1.94 Å; bonds with lengths outside this range are not found in these *closo* clusters.

In deriving the order–length curve shown in Fig. 2(b), the structural data of compounds $B_8H_8^{2-}$ and $B_9H_9^{2-}$ have been omitted from the analysis. The above coefficients can be used, however, to calculate the total number of electrons involved in boron–boron bonding in these two clusters. The $B_8H_8^{2-}$ cluster is found to have 17.16 bonding electrons, and the $B_9H_9^{2-}$ cluster has 18.58; electron-counting rules, by comparison, ascribe 18 electrons to the former compound, and 20 electrons to the latter.

Table 1. Structural data for the five *closo* boron hydrides, with summations over bond lengths (Å) quoted to four significant figures

Cluster	N	Point symmetry	B—B bond lengths (d_i)	$\sum d_i$	$\sum d_i^2$	$\sum d_i^3$	$\sum d_i^4$	Reference
$B_6H_6^{2-}$	12	O_h	1.686×12	0.2023×10^2	0.3412×10^2	0.5753×10^2	0.9700×10^2	6
$B_8H_8^{2-}$	18	D_{2d}	1.560×2, 1.717×4, 1.757×8, 1.928×4	0.3175×10^2	0.5622×10^2	0.9988×10^2	0.1781×10^3	7
$B_9H_9^{2-}$	21	C_{2v}	1.682×4, 1.712×4, 1.731×4, 1.810×1, 1.851×4, 1.933×4	0.3745×10^2	0.6696×10^2	0.1201×10^3	0.2159×10^3	8
$B_{10}H_{10}^{2-}$	24	C_1	1.640×1, 1.655×1, 1.663×1, 1.674×1, 1.685×1, 1.691×1, 1.701×1, 1.715×1, 1.771×2, 1.778×1, 1.785×1, 1.786×1, 1.801×1, 1.803×1, 1.809×2, 1.811×1, 1.823×1, 1.828×1, 1.830×1, 1.832×1, 1.843×1, 1.886×1	0.4237×10^2	0.7490×10^2	0.1326×10^3	0.2351×10^3	9
$B_{12}H_{12}^{2-}$	30	T_h	1.755×6, 1.780×24	0.5324×10^2	0.9450×10^2	0.1677×10^3	0.2977×10^3	10

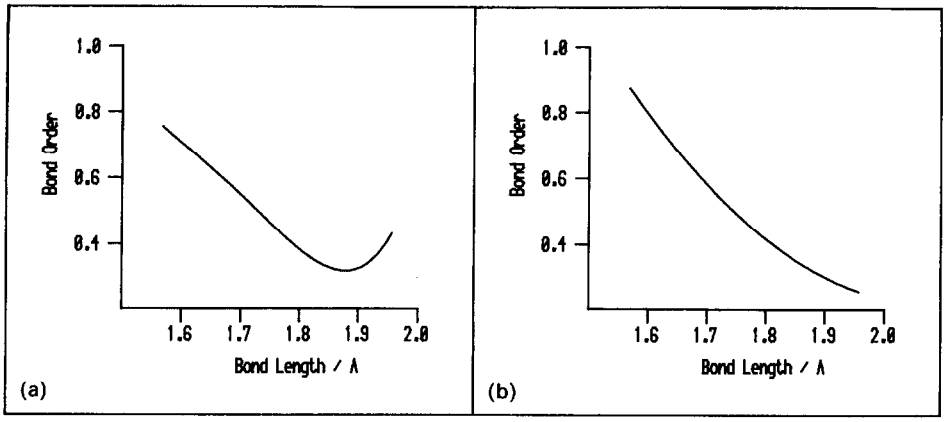


Fig. 2. (a) Curve of bond order vs bond length obtained from all five *closo* compounds. (b) Curve of bond order vs bond length obtained from compounds $B_6H_6^{2-}$, $B_{10}H_{10}^{2-}$ and $B_{12}H_{12}^{2-}$ only.

Several points can be made about this apparent discrepancy. First, the total number of bonding electrons contained in the skeletal cages may be less than $2(n+1)$ because of incomplete charge transfer from the relevant cations. Secondly, this method calculates the number of electrons involved in bonding: it is possible that the overlap of boron atoms in the $B_8H_8^{2-}$ and $B_9H_9^{2-}$ polyhedral cages is inadequate for use of all the $2(n+1)$ valence electrons in bonding. There is also experimental evidence that $B_8H_8^{2-}$ and $B_9H_9^{2-}$ species use their skeletal electrons less effectively than the $B_6H_6^{2-}$, $B_{10}H_{10}^{2-}$ and $B_{12}H_{12}^{2-}$ compounds.[2,12-14] It appears, therefore, that the order–length curve derived above is applicable to all *closo* borane clusters, to a good approximation.

Application to nido *and* arachno *boranes*

The validity of this approach may be assessed by calculating distributions of electronic charge in *nido* and *arachno* boranes. These systems can be regarded as clusters made up of B—B two-centre bonds and B—H—B bridge bonds. Table 2 summarizes the results obtained for three *nido* and two *arachno* boranes whose structures are known. The total number of bonding electrons in a *nido* cluster, B_nH_{n+4}, is $2n+4$; and the total number in an *arachno* cluster, B_nH_{n+6}, is $2n+6$, according to electron-counting rules.[5] Coefficients A_{BB}, B_{BB} and C_{BB} are used to calculate the total electronic charge distributed over boron–boron two-centre bonds in these compounds. The remaining charge is assumed to be distributed over the B—H—B bonds, of which there are four in *nido* clusters. The six *endo* hydrogen atoms in *arachno* boranes may be either bridging or terminal in character. In the case of B_4H_{10}, there are four bridging and two extra terminal hydrogen atoms; and in B_5H_{11} there are three bridging and three terminal atoms among its *endo* hydrogen atoms. It is seen in Table 2 that the average charge per B—H—B bridge bond varies between 1.34 and 1.64 electrons for the three *nido* compounds, B_5H_9, B_6H_{10} and $B_{10}H_{14}$; these values are of the correct order of magnitude: the hydrogen atoms can be considered to contribute one electron to the bridge bonds; and the contributions of the boron atoms will vary according to the different geometries adopted by the B—H—B bonds.

For the *arachno* clusters, however, the average charge per B—H—B bond is 2.58 electrons for the B_4H_{10} species, and 3.20 electrons for the B_5H_{11} compound. These values are erroneously large: either the method is inappropriate for *arachno* clusters, or the assumed role of the terminal *endo* hydrogen atoms must be brought into question. If it happens that these *endo* atoms do not *donate* an electron to the framework, but, rather, behave similarly to the *exo* hydrogen atoms in withdrawing charge from the boron atoms in forming B—H bonds, then the total number of electrons in the cage will be significantly less than $2n+6$. There is structural evidence that similar bonds do link both *endo* and *exo* terminal hydrogen atoms in both these *arachno* clusters. In B_4H_{10}, there are four *exo* B—H terminal bonds of length 1.190 Å, and two *endo* B—H terminal bonds of length 1.191 Å, and in B_5H_{11}, both *exo* and *endo* terminal bonds have lengths within the narrow range from 1.190 to 1.213 Å. The $2n+6$ electron-counting rule assumes that *endo* hydrogen atoms donate an electron to the cage-bonding. However, it is instructive to examine the different distributions of charge that would result if this rule were violated; Table 3 summarizes the alternative distributions.

It is seen that reasonable results are obtained for

Table 2. *Nido* and *arachno* boranes: distributions of bonding electrons over B—B two-centre and B—H—B three-centre bonds calculated with the use of electron-counting rules

Compound	Total charge[5] (electrons)	Charge distributed over B—B bonds (electrons)	Charge distributed over B—H—B bridge bonds (electrons)	Number of B—H—B bridge bonds	Average charge per B—H—B bridge bonds (electrons)
B_5H_9[15]	14	8.63	5.37	4	1.34
B_6H_{10}[16]	16	9.44	6.56	4	1.64
$B_{10}H_{14}$[17]	24	18.18	5.82	4	1.46
B_4H_{10}[15]	14	3.68	10.32	4	2.58
B_5H_{11}[15]	16	6.39	9.61	3	3.20

the charge distributed over the B—H—B bonds in these two compounds, provided that the $2n+6$ electron-counting rule is not applied.

DISCUSSION

This order–length relationship is a useful method of rationalizing the known structures of borane clusters, and in particular the variations in B—B bond lengths. It could be used to test the feasibility of alternative polyhedral arrangements which are consistent with known total electronic charges. And it has applications also in understanding patterns of reactivity, which are known to be dependent upon electronic charge distributions. Its self-consistency implies that the electron density in these compounds is, indeed, concentrated within the polyhedral surfaces.

A notable weakness of the approach is that it fails to take account of the partitioning of charge between atomic centres and interatomic bonds; so a formal calculation of residual atomic charges cannot be made. This is not a serious defect for the homonuclear clusters considered in this paper, but

Table 3. *Arachno* boranes B_4H_{10} and B_5H_{11}: variation of charge distributions with behaviour of *exo* terminal hydrogen atoms

	Compound					
	B_4H_{10}			B_5H_{11}		
Type of behaviour of *endo* terminal hydrogen atoms[a]	A	B	C	A	B	C
Total charge in cage (electrons)	14	12	10	16	13	10
Charge distributed over B—B bonds	3.68	3.68	3.68	6.39	6.39	6.39
Charge distributed over B—H—B bridge bonds	10.32	8.32	6.32	9.61	6.61	3.61
Number of B—H—B bridge bonds	4	4	4	3	3	3
Average charge per B—H—B bridge bond	2.58	2.08	1.58	3.20	2.20	1.20

[a] The total charge in the cage varies according to the behaviour of the *endo* terminal hydrogen atoms: for type A behaviour, *endo* H atoms donate an electron to the cage, giving rise to total charge of $(2n+6)$ electrons; for type B behaviour, *endo* H atoms do not add or remove any electrons from the cage; for type C behaviour, *endo* H atoms withdraw an electron from the cage. These three types of behaviour are limiting cases which indicate how the average charge per B—H—B bridge bond is affected.

problems are likely to arise for heteronuclear clusters, e.g. carboranes. In these compounds, the electronic charge distribution is influenced strongly by differences in electronegativity between atoms in the clusters. There is no reason, however, why a similar treatment should not be applied to other homonuclear *closo* clusters, such as metal carbonyl compounds.

This method does show, however, that the electron-counting rules for *closo* and *nido* boranes, coupled merely with an analysis of geometrical structures, provide a sensible and applicable picture of boron hydride chemistry.

All calculations have been carried out on a DEC VAX 11/750 computer, using software written by the author.

Acknowledgement—I thank Professor K. Wade for stimulating my interest in this field during my sojourn at the Department of Chemistry, University of Durham.

REFERENCES

1. C. E. Housecroft and K. Wade, *Inorg. Nucl. Chem. Lett.* 1979, **15**, 339.
2. C. E. Housecroft, R. Snaith and K. Wade, *Inorg. Nucl. Chem. Lett.* 1979, **15**, 342.
3. D. J. Fuller and D. L. Kepert, *Inorg. Chem.* 1982, **21**, 163.
4. C. A. Coulson, *Proc. R. Soc.* 1951, **A207**, 91.
5. K. Wade, *Adv. Inorg. Chem. Radiochem.* 1976, **18**, 1.
6. R. Schaefer, Q. Johnson and G. S. Smith, *Inorg. Chem.* 1965, **4**, 917.
7. L. J. Guggenberger, *Inorg. Chem.* 1969, **8**, 2771.
8. L. J. Guggenberger, *Inorg. Chem.* 1968, **7**, 2260.
9. J. T. Gill and S. J. Lippard, *Inorg. Chem.* 1975, **14**, 751.
10. J. A. Wunderlich and W. N. Lipscomb, *J. Am. Chem. Soc.* 1960, **82**, 4427.
11. NAG Subroutine Library, Numerical Algorithms Group, Oxford, U.K.
12. C. E. Housecroft and K. Wade, *Inorg. Chem.* 1983, **22**, 1391.
13. E. L. Muetterties and W. H. Knoth, *Polyhedral Boranes*. Marcel Dekker, New York (1968).
14. R. L. Middaugh, *Boron Hydride Chemistry* (Edited by E. L. Muetterties), Chap. 8. Academic Press, New York (1975).
15. E. Switkes, I. R. Epstein, J. A. Tossell, R. M. Stevens and W. N. Lipscomb, *J. Am. Chem. Soc.* 1970, **92**, 3837.
16. I. R. Epstein, J. A. Tossell, E. Switkes, R. M. Stevens and W. N. Lipscomb, *Inorg. Chem.* 1971, **10**, 171.
17. A. Tippe and W. C. Hamilton, *Inorg. Chem.* 1969, **8**, 464.

Polyhedron Vol. 5, No. 6, pp. 1213–1216, 1986
Printed in Great Britain

0277–5387/86 $3.00+.00
Pergamon Journals Ltd

COMPLEXES OF PALLADIUM(II) AND PLATINUM(II) WITH 2-HYDRAZINOPYRIDINE AND 8-HYDRAZINOQUINOLINE

D. A. EDWARDS* and S. J. LARTER

School of Chemistry, University of Bath, Bath BA2 7AY, U.K.

(*Received* 23 *August* 1985: *accepted* 25 *November* 1985)

Abstract—The square planar complexes *cis*-$[MCl_2(hypy)]$, *cis*-$[MCl_2(hyqu)]$, $[Pt(hypy)_2][PtCl_4]$, $[Pd(hypy)_2][ClO_4]_2$ and $[Pd(hyqu)_2][ClO_4]_2$ (M = Pd or Pt, hypy = 2-hydrazinopyridine, hyqu = 8-hydrazinoquinoline), in which hypy and hyqu act as bidentate chelating ligands, have been prepared and characterized. Complexes containing hyqu do not appear to have been isolated previously.

Schiff bases have been used as multidentate ligands in coordination chemistry for many years. Many have been prepared simply by reacting 2-hydrazinopyridine (hypy) with suitable aldehydes and ketones. Typical examples are the terdentate ligand paphy[1] produced by condensation of hypy with pyridine-2-aldehyde and the quadridentate ligand arising from the reaction of two equivalents of hypy with one of diacetyl.[2] However, it is surprising to find that hypy itself has been neglected as a potential ligand. It would be expected to act in a bidentate manner, bonding via the pyridyl-nitrogen and the terminal hydrazino-nitrogen donor atoms. The only known complexes are $[Fe(hypy)_3]Cl_n$ ($n = 2$ or 3), reported[3] as early as 1933, and $[M(hypy)_3][ClO_4]_2$ (M = Fe, Co or Ni) and $[Co(hypy)_3][ClO_4]_3$ briefly documented[4] in 1969 without preparative, spectroscopic or magnetic data. In view of this sketchy knowledge of hypy as a ligand, we report here the isolation and characterization of some palladium(II) and platinum(II) complexes.

This study has also been extended to include the related ligand 8-hydrazinoquinoline (hyqu) which would also be expected to act as a chelating ligand but with the formation of six-membered, rather than five-membered, rings. As far as we have been able to ascertain, the only previous mention[5] of the use of hyqu as a ligand is a brief indication that it has been tested for complex formation with nickel chloride, the stability of the resulting, uncharacterized, complex being less than that of a related 8-aminoquinoline (amqu) complex. Amqu has found more use as a ligand, the complexes *cis*-$[MCl_2(amqu)]$ (M = Pd or Pt)[6] being most closely related to those reported here.

* Author to whom correspondence should be addressed.

EXPERIMENTAL

Hypy[7] [yield 70%, m.p. 48°C (lit. 46–48°C)] and hyqu[8] [yield 65%, m.p. 65°C (lit. 64°C)] were prepared according to literature procedures. Apart from the ^1H NMR spectrum of hypy,[9] no other NMR data have been reported for these compounds. The ^1H and ^{13}C NMR spectra of the free ligands were therefore recorded using $CDCl_3$ solutions (hypy: ^{13}C: 107.1, d, C^3; 114.3, d, C^5; 137.4, d, C^4; 147.6, d, C^6; 161.4, s, C^2; hyqu: ^1H: 8.7, d, 1, H^2; 8.0, d, 1, H^4; 6.8–7.6, m, 4, H^3, H^5, H^6 and H^7; 3.0–4.2, br, 3, $NHNH_2$; ^{13}C: 105.8, d, C^7; 115.9, d, C^5; 121.5, d, C^3; 127.5, d, C^6; 128.5, s, C^{10}; 135.9, d, C^4; 137.6, s, C^9; 147.2, s, C^8; 147.3, d, C^2). A 70 eV EI mass spectrum of hyqu showed major ions (*m/z*, relative intensity, assignment) at: 159, 100, $[hyqu]^+$; 142, 67, $[hyqu-NH_3]^+$; 129, 57, $[hyqu-N_2H_2]^+$, i.e. $[quinoline]^+$; 102, 17, $[quinoline-HCN]^+$.

Preparations

Dichloro(2-hydrazinopyridine)palladium(II). A concentrated aqueous solution of K_2PdCl_4 (0.50 g, 1.53 mmol) was added to an ethanolic solution of hypy (0.18 g, 1.65 mmol). A precipitate immediately appeared. The reaction mixture was thoroughly stirred, allowed to stand for a few minutes and then filtered. The pale brown product was washed with ethanol and ether, and dried in air. Yield 0.28 g

(64%). Found: C, 21.2; H, 2.52; N, 14.7%. Calc. for $C_5H_7Cl_2N_3Pd$: C, 21.0; H, 2.46; N, 14.7%.

Bis(2-hydrazinopyridine)platinum(II) tetrachloroplatinate(II). The addition of a concentrated aqueous solution of K_2PtCl_4 (0.50 g, 1.20 mmol) to an ethanolic solution of hypy (0.14 g, 1.28 mmol) gave a green solution which slowly deposited a dark green precipitate on standing at room temperature. After 1 h this product was filtered off, washed with ethanol and ether, and dried in air. It slowly turned brown on prolonged exposure to moist air. Yield 0.14 g (31%). Found: C, 16.2; H, 1.91; N, 11.5%. Calc. for $C_5H_7Cl_2N_3Pt$: C, 16.0; H, 1.88; N, 11.2%.

Dichloro(2-hydrazinopyridine)platinum(II). Aqueous solutions of K_2PtCl_4 (0.50 g, 1.20 mmol) and hypy (0.14 g, 1.28 mmol) were mixed to give a green solution which was heated to boiling. As the temperature increased the green colour was replaced by a brown colour and, just before the solution reached its boiling point, a pale brown precipitate appeared. After cooling, this product was filtered off, washed with water and ethanol, and dried in air. Yield 0.28 g (60%). Found: C, 16.2; H, 1.82; N, 11.2%. Calc. for $C_5H_7Cl_2N_3Pt$: C, 16.0; H, 1.88; N, 11.2%.

Bis(2-hydrazinopyridine)palladium(II) perchlorate. An aqueous solution of K_2PdCl_4 (0.50 g, 1.53 mmol) was added to a mixed aqueous solution of hypy (0.35 g, 3.30 mmol) and $NaClO_4 \cdot H_2O$ (3.30 g, 23.5 mmol). A sandy-yellow precipitate formed immediately. The reaction mixture was heated to boiling, allowed to cool and the product filtered off, washed with water, then ethanol, and dried in air. Yield 0.51 g (63%). Found: C, 23.0; H, 2.69; N, 16.6%. Calc. for $C_{10}H_{14}Cl_2N_6O_8Pd$: C, 22.9; H, 2.69; N, 16.1%.

Dichloro(8 - hydrazinoquinoline)palladium(II). A concentrated aqueous solution of K_2PdCl_4 (0.56 g, 1.71 mmol) was added to an ethanolic solution of hyqu (0.30 g, 1.89 mmol). A brown precipitate formed immediately. The reaction mixture was heated to boiling, allowed to cool and the product filtered off, washed with ethanol, then ether, and dried in air. Yield 0.39 g (68%). Found: C, 31.6; H, 2.50; N, 12.6%. Calc. for $C_9H_9Cl_2N_3Pd$: C, 32.1; H, 2.70; N, 12.5%.

Dichloro(8 - hydrazinoquinoline)platinum(II). A concentrated aqueous solution of K_2PtCl_4 (0.50 g, 1.20 mmol) was added to an ethanolic solution of hyqu (0.21 g, 1.32 mmol). On boiling the reaction mixture the colour darkened and a brown precipitate formed. After cooling this was filtered off, washed with ethanol, then ether, and dried in air. Yield 0.22 g (42%). Found: C, 25.3; H, 2.10; N, 9.90%. Calc. for $C_9H_9Cl_2N_3Pt$: C, 25.4; H, 2.13; N, 9.88%.

Bis(8-hydrazinoquinoline)palladium(II) perchlorate. Mixing an aqueous solution of K_2PdCl_4 (0.50 g, 1.53 mmol) and an ethanolic solution of hyqu (0.52 g, 3.26 mmol) and $NaClO_4 \cdot H_2O$ (1.80 g, 12.8 mmol) gave an immediate sandy-brown precipitate. The reaction mixture was boiled, allowed to cool and the product filtered off, washed with ethanol, then ether, and dried in air. Yield 0.49 g (51%). Found: C, 34.1; H, 3.03; N, 13.6%. Calc. for $C_{18}H_{18}Cl_2N_6O_8Pd$: C, 34.7; H, 2.91; N, 13.5%.

Physical measurements

IR spectra of Nujol and hexachlorobutadiene mulls were recorded using a Perkin–Elmer 599B spectrometer. Conductivity measurements were carried out at 25°C on 10^{-3} M acetonitrile solutions using a Wayne–Kerr Autobalance bridge and a dip-type cell with platinum electrodes. Magnetic measurements were carried out at room temperature by the Gouy method. Electronic spectra were recorded using a Cecil Instruments CE 595 spectrophotometer. Proton and ^{13}C NMR spectra were recorded using JEOL PS 100 and FX-90Q spectrometers, respectively. Mass spectra were obtained using a VG 7070E spectrometer.

RESULTS AND DISCUSSION

The ^{13}C NMR spectrum of hypy, and the ^1H and ^{13}C NMR spectra of hyqu, do not appear to have been reported previously, so chemical-shift values, multiplicities and assignments are given in Experimental. The hydrazino protons appear as a broad singlet in the ^1H NMR spectra. The assignment of the ^{13}C NMR spectrum of hypy follows simply from that suggested for 2-aminopyridine.[10] In the decoupled ^{13}C NMR spectrum of hyqu the weak quaternary C^8 signal is virtually coincident with that associated with C^2, so only six intense and two weak resonances are observed as well-separated signals. In an off-resonance spectrum the C^8 signal is easily detected almost exactly midway between the two components of the C^2 doublet. The assignments proposed then follow those suggested[11] for 8-aminoquinoline.

The bidentate chelating behaviour of hypy and hyqu has been demonstrated by the preparation of the four *cis*-$[MCl_2(ligand)]$ (M = Pd or Pt, ligand = hypy or hyqu) complexes from K_2MCl_4. The reactions employing K_2PdCl_4 may be carried out at room temperature, but boiling solutions are required for the preparation of the platinum analogues, room-temperature reactions leading to alternative dark green products, discussed below.

Table 1. IR bands (cm^{-1})

Complex	ν(MCl)	ν(M–pyridyl nitrogen)	ν(ClO)	δ(OClO)
$PdCl_2$(hypy)	330s, 323s	255w		
$PtCl_2$(hypy)	325s, 315s	240w		
$PdCl_2$(hyqu)	325s, 315s	255w		
$PtCl_2$(hyqu)	320s, 310s	240w		
$[Pd(hypy)_2][ClO_4]_2$		255w	~1100vs,vbr	620vs
$[Pd(hyqu)_2][ClO_4]_2$		260w	~1100vs,vbr	620vs

The *cis*-[MCl_2(ligand)] complexes are, as expected, diamagnetic and are sufficiently soluble in acetonitrile to produce 10^{-3} M solutions which are essentially non-conducting at 25°C (Λ_M below 10 Ω^{-1} cm^2 mol^{-1}) (1:1 electrolytes have Λ_M in the range 120—160 Ω^{-1} cm^2 mol^{-1}). Thus the complexes are formulated as *cis*-square planar monomers with hypy and hyqu bonding through the pyridyl-nitrogen and hydrazino-NH_2 lone pairs. IR spectral evidence (Table 1) supports this proposal, two ν(MCl) bands being detected for each complex at similar frequencies to those of the related *cis*-[MCl_2(amqu)] (M = Pd or Pt) complexes.[6] A further band at *ca* 250 cm^{-1} can be assigned to a mode containing considerable metal–pyridyl-nitrogen stretching character, such a band being found at 227 cm^{-1} for *cis*-[$PtCl_2L$] (L = 2-aminomethylpyridine).[12] We are unable to suggest assignments for metal–hydrazino-nitrogen stretching frequencies, because both the free ligands and the complexes have a multiplicity of bands in the 400–500-cm^{-1} region of the IR spectra. As expected, the ν(NH) frequencies are lowered on coordination, e.g. uncoordinated hypy has ν(NH) at 3295, 3230 and 3150 cm^{-1}, whereas *cis*-[$PtCl_2$(hypy)] has ν(NH) at 3220, 3120 and 3040 cm^{-1}.

When aqueous K_2PtCl_4 and ethanolic hypy solutions are mixed at room temperature and the reaction mixture not warmed, a dark green, rather than a pale brown, product can be isolated which also has an analysis in agreement with the formulation $PtCl_2$(hypy). The intense green colour is reminiscent of a group of complexes that possess columnar structures with alternating, and strongly interacting, planar $[PtL_4]^{2+}$ and $[PtCl_4]^{2-}$ ions.[13] The prototype is Magnus' green salt $[Pr(NH_3)_4][PtCl_4]$ and several $[Pt(L_2)_2][PtCl_4]$ examples are known (L_2 = bidentate nitrogen donor chelating ligand, e.g. 2,2′-bipyrimidine[14]). The colour should not, however, be regarded as necessarily indicative of this structural type. Thus, for example, *cis*-$[PtCl_2(ampy)_2]\cdot H_2O$ (ampy = 2-aminopyridine bonded via the pyridyl-nitrogen only) is also green but suggested to be a square-planar monomer.[15] Nevertheless, we formulate our product as [Pt hypy)$_2$][$PtCl_4$] since: (i) only one IR band, at 315 cm^{-1}, is clearly assignable to υ(PtCl) as predicted for $[PtCl_4]^{2-}$, (ii) the complex has an absorption band with a maximum at 670 nm, a similar wavelength to the absorption peak maximum (690 nm) of $[Pt(bipym)_2][PtCl_4]$, (bipym = 2,2′-bipyrimidine),[14] and (iii) a 10^{-3} M solution in acetonitrile has a Λ_M of 154 Ω^{-1} cm^2 mol^{-1} per empirical formula unit. No attempts were made to find conditions which may have led to the hyqu analogue.

Reactions of K_2PdCl_4 with an excess of either hypy or hyqu in the presence of sodium perchlorate lead to the immediate formation of diamagnetic $[Pd(hypy)_2][ClO_4]_2$ and $[Pt(hyqu)_2][ClO_4]_2$ products. These complexes show the expected bi-univalent electrolyte behaviour as 10^{-3} M solutions in acetonitrile with Λ_M values of 280 and 286 Ω^{-1} cm^2 mol^{-1}, respectively. The normal Λ_M range for 10^{-3} M solutions of bi-univalent electrolytes in this solvent is 220–300 Ω^{-1} cm^2 mol^{-1}. The IR spectra of these two complexes show very strong bands (Table 1) associated with the ν(ClO) and δ(OClO) vibrations of the tetrahedral anions, a single band at *ca* 250 cm^{-1} assigned to ν(Pd–pyridyl nitrogen) but no bands in the ν(PdCl) region. These complexes are similar in type to $[Pd(phen)_2][ClO_4]_2$, which is known to contain square planar cations,[16] but in the hypy and hyqu complexes the bidentate ligands are unsymmetrical. As a result, the pyridyl-nitrogen donor atoms (and, of course, the hydrazino-nitrogen donor atoms) can be disposed in either *cis* or *trans* positions. The observation of only one ν(Pd–pyridyl nitrogen) band for each complex suggests that the *trans* isomers are favoured.

REFERENCES

1. C. F. Bell, *Rev. Inorg. Chem.* 1979, **1**, 133.
2. F. Lions and K. V. Martin, *J. Am. Chem. Soc.* 1958, **89**, 3858.
3. B. Emmert and O. Schneider, *Chem. Ber.* 1933, **66**, 1875.

4. B. Chiswell and F. Lions, *Aust. J. Chem.* 1969, **22**, 71.
5. P. H. Neilsen and O. Dahl, *Acta Chem. Scand.* 1966, **20**, 1113.
6. H. A. Hudali, J. V. Kingston and H. A. Tayim, *Inorg. Chem.* 1979, **18**, 1391.
7. H. Gregory and L. F. Wiggins, *J. Chem. Soc.* 1949, 2546.
8. S. Hünig and H. Werner, *Annalen* 1959, **628**, 46.
9. *The Aldrich Library of NMR Spectra*, 2nd edn. Aldrich Chemical Co. Inc., Milwaukee, WI (1984).
10. *Carbon*-13 *NMR Spectral Data*, 3rd edn. Verlag Chemie, Weinheim (1981).
11. A. M. Kook, S. L. Smith and E. V. Brown, *Org. Magn. Reson.* 1984, **22**, 730.
12. M. L. Niven, G. C. Percy and D. A. Thornton, *J. Mol. Struct.* 1980, **68**, 73.
13. H. J. Keller, in *Extended Linear Chain Compounds* (Edited by J. S. Miller), Vol. 1, Ch. 8. Plenum Press, New York (1982).
14. P. M. Kiernan and A. Ludi, *J. Chem. Soc., Dalton Trans.* 1978, 1127.
15. S. Haghighi, C. A. McAuliffe, W. E. Hill, H. H. Kohl and M. E. Friedman, *Inorg. Chim. Acta* 1980, **43**, 113.
16. J. V. Rund, *Inorg. Chem.* 1968, **7**, 24.

Polyhedron Vol. 5, No. 6, pp. 1217–1221, 1986
Printed in Great Britain

0277–5387/86 $3.00+.00
Pergamon Journals Ltd

PREPARATIVE CHEMISTRY WITH $[Ru(\eta^6\text{-ARENE})(H_2O)_3]^{2+}$: BIS-ARENE AND MONOBENZENE COMPLEXES WITH O, N AND S DONORS

MONIKA STEBLER-RÖTHLISBERGER and ANDREAS LUDI*

Institut für Anorganische Chemie, Universität Bern, CH-3000 Bern 9, Switzerland

(*Received* 14 *November* 1985; *accepted* 18 *November* 1985)

Abstract—The preparation, and electronic, ^1H and ^{13}C NMR spectra of the complex ions $[Ru(\eta^6\text{-}C_6H_6)L_3]^{2+}$ (L = acetonitrile, dimethylsulphoxide, dimethylsulphide or tetrahydrothiophene) from $[Ru(\eta^6\text{-}C_6H_6)(H_2O)_3]^{2+}$ are reported. The NMR data of coordinated benzene are discussed in terms of the π-backbonding capacity of the monodentate ligand.

Half-sandwich complexes of general stoichiometry $[Ru(\eta^6\text{-arene})L_1L_2L_3]^{2+}$ have been conventionally prepared using $[Ru(\eta^6\text{-arene})Cl_2]_2$ as the starting reagent, affording monomeric species still retaining one or two chloro ligands.[1] The chloro-bridged dimeric precursor itself is obtained by the reaction of "$RuCl_3 \cdot xH_2O$" with cyclohexadiene.[2] Hydrolysis of the dimer produces the ion $[Ru(\eta^6\text{-arene})(H_2O)_3]^{2+}$, which shows a very high tendency to dimerize and tetramerize.[3] We became interested in the monomeric ruthenium–arene–triaqua cation because it is a remarkable link between the classical hexaaqua ions and the organometallic $Ru(\eta^6\text{-arene})_2^{2+}$ sandwich compounds. A solution study of a variety of $Os(benzene)^{2+}$ complexes and some of their ruthenium analogs led to the conclusion that these Os(II)– and Ru(II)–arene moieties are perfectly stable in an aqueous environment, at least in the dark.[4] Our investigation of the $Ru(H_2O)_6^{2+/3+}$ couple[5] and of the formation, the molecular structure, and the substitution kinetics of $[Ru(\eta^6\text{-}C_6H_6)(H_2O)_3]^{2+}$[6] initiated a more general study of these "piano-stool" complexes, including the variation of the arene ligand and, more importantly, of the three monodentate ligands. Owing to its rather high substitution lability the ion $[Ru(\eta^6\text{-}C_6H_6)(H_2O)_3]^{2+}$ is a very convenient precursor in preparative ruthenium chemistry, as in a recent report dealing with the specific case of phosphine ligands.[7]

*Author to whom correspondence should be addressed.

EXPERIMENTAL

Two different procedures have been used for the synthesis of the $[Ru(\eta^6\text{-arene})(H_2O)_3]^{2+}$ complex ion:

(A) An aqueous acidic (0.1 M) solution of the dimeric $[Ru(\eta^6\text{-arene})Cl_2]_2$[2] (2 mmol) is stirred for 3 h with the stoichiometric amount of an appropriate silver salt [SO_4^{2-}, tos^- (*p*-toluenesulphonate) or $tmms^-$ (2,4,6-trimethylbenzenesulphonate)]. Solid AgCl is removed by filtration.

(B) $Ru(H_2O)_6^{2+}$ salts[5] smoothly react under argon in tetrahydrofuran or ethanol with cyclohexadiene to produce $[Ru(\eta^6\text{-}C_6H_6)(H_2O)_3]^{2+}$ in very good yield.[6] 1,3- as well as 1,4-cyclohexadiene may be used as the reagent. ^1H NMR monitoring of the reaction reveals the conversion of the 1,4- into the 1,3-isomer prior to substitution and further rearrangement. The complex disproportionation reaction produces the arene complex together with cyclohexene and cyclohexane.[6]

Subsequent concentration of the solutions obtained by procedures A or B under reduced pressure at 40°C and cooling to 5°C affords crystalline salts of the $[Ru(\eta^6\text{-arene})(H_2O)_3]^{2+}$ ion.

Substitution of the three water molecules by other monodentate ligands (L) is carried out under quite mild conditions:

L	Solvent	*T* (°C)	Yield (%)	Color
Acetonitrile (AN)	AN	40	63	Yellow-white
Dimethylsulphoxide (DMSO)	H_2O	50	50	Orange
Dimethylsulphide (DMS)	MeOH	25	85	Yellow
Tetrahydrothiophene (THTP)	MeOH	50	90	Yellow

Microcrystalline solids of the resulting $[Ru(\eta^6\text{-}C_6H_6)L_3]^{2+}$ ions are isolated as PF_6^- salts.

$[Ru(\eta^6\text{-}C_6H_6)(H_2O)_3]^{2+}$ is also a convenient precursor for simple and efficient syntheses of the known mixed bis-arene complexes $[Ru(\eta^6\text{-}C_6H_6)(\eta^6\text{-arene})]^{2+}$ (arene = benzene, mesitylene, hexamethylbenzene, *p*-cymene or anisole), originally prepared from $[Ru(\eta^6\text{-arene})Cl_2]_2$.[8] $Ru(\eta^6\text{-}C_6H_6)(H_2O)_3(tos)_2$ (0.87 mmol) dissolved in trifluoroacetic acid (20 cm^3) is heated for 1 h under reflux with 20 cm^3 of the appropriate arene. The resulting reaction mixture is evaporated to dryness under reduced pressure and the residue is dissolved in MeOH. Colorless solids are precipitated as tos^- or BF_4^- salts with yields in the 80–98% range.

Ruthenium was determined spectrophotochemically;[9] elemental analyses were carried out by Ciba-Geigy, Basel. Analytical results are collected in Table 1. ^1H NMR spectra were measured with a Bruker WP 80 or a Varian EM 360 instrument, and ^{13}C NMR spectra with a Varian XL 100. UV–VIS spectra were recorded on a Cary 17 DX.

RESULTS

Whereas complete removal of the chloro ligands is rather difficult for the conversion of $[Ru(\eta^6\text{-arene})Cl_2]_2$ into monomeric $[Ru(\eta^6\text{-arene})L_3]^{2+}$ species,[2,4] the precursor $[Ru(\eta^6\text{-arene})(H_2O)_3]^{2+}$ offers a very facile and efficient route for the synthesis of these half-sandwich complexes for a variety of monodentate ligands (L). As a byproduct of this study $[Ru(\eta^6\text{-arene})(H_2O)_3]^{2+}$ is also shown to be a very good starting reagent for high-yield preparations of mixed bis-arene compounds, $[Ru(\eta^6\text{-arene})(\eta^6\text{-arene})]^{2+}$.

The isolated solid salts of $[Ru(\eta^6\text{-arene})L_3]^{2+}$ are perfectly stable in air. Their solutions in aqueous and non-aqueous solvents do not show any feature in the cyclic voltammetry that could be assigned to a reversible redox process. In other words, the compounds described in this study are neither oxidized nor reduced in the potential interval −0.25 to +1 V (vs NHE). This considerably enhanced stability of the oxidation state II of ruthenium is generally attributed to the π-backbonding behavior of the arene ligands (cf. next section).

Solution spectra of the various half-sandwich complex ions exhibit absorption bands in the short visible and the UV region (Table 2). The lowest-energy band generally is observed around 400 nm. Considering the intensity of these absorptions we assign them to charge-transfer transitions which are significantly red-shifted with respect to the corresponding bis-arene compounds.[1,2] The very similar spectra for $[Ru(\eta^6\text{-}C_6H_6)(H_2O)_3]^{2+}$ and $[Ru(\eta^6\text{-}C_6H_6)(DMSO)_3]^{2+}$ are accepted as supporting evidence for oxygen-coordinated DMSO in line with the NMR data.

^1H and ^{13}C NMR spectroscopic results of the various complex ions are collected in Tables 3 and 4. We observe an overall upfield shift for the signals

Table 1. Analytical data[a]

	Ru	C	H	S	H_2O	N	F
$[Ru(\eta^6\text{-}C_6H_6)(H_2O)_3](tos)_2$	17.6	41.7	4.6	11.1	9.4		
	17.3	41.6	4.6	11.0	9.7		
$[Ru(\eta^6\text{-}C_{10}H_{14})(H_2O)_3](tos)_2$[b]	16.0	45.6	5.4	10.2	8.6		
	15.3	45.3	5.4	10.9	9.4		
$[Ru(\eta^6\text{-}C_6(CH_3)_6)(H_2O)_3]SO_4 \cdot 2H_2O$	21.6	30.8	6.0	6.9	19.3		
	22.6	32.5	6.2	7.1	19.4		
$[Ru(\eta^6\text{-mes})(H_2O)_3]SO_4 \cdot H_2O$[c]	26.0	27.8	5.2	8.2	18.5		
	25.0	27.1	5.3	8.0	20.8		
$[Ru(\eta^6\text{-}C_6H_6)(AN)_3](PF_6)_2$	17.1	24.3	2.5			7.1	38.5
	16.9	24.3	2.7			7.1	38.3
$[Ru(\eta^6\text{-}C_6H_6)(DMSO)_3](PF_6)_2$	14.4	20.5	3.4	13.7			32.4
	14.0	21.0	3.4	13.7			31.3
$[Ru(\eta^6\text{-}C_6H_6)(THTP)_3](PF_6)_2$	13.8	29.5	4.1	13.1			31.1
	13.5	29.7	4.2	13.1			31.2
$[Ru(\eta^6\text{-}C_6H_6)(DMS)_3](PF_6)_2$	15.4	22.0	3.7	14.7			34.8
	15.2	22.2	3.7	14.8			34.3

[a] Upper line: calculated; lower line: found.
[b] $C_{10}H_{14}$ = *p*-cymene.
[c] mes = mesitylene.

Table 2. UV–VIS spectra of $[Ru(arene)L_3]^{2+}$ ions

	λ (nm)	ε ($M^{-1}\,cm^{-1}$)
$[Ru(\eta^6\text{-}C_6H_6)(H_2O)_3]^{2+}$ [a]	400	550
	314	750
	248 sh	
$[Ru(\eta^6\text{-}C_6(CH_3)_3H_3)(H_2O)_3]^{2+}$ [a]	402	610
	315	660
	250 sh	
$[Ru(\eta^6\text{-}C_6(CH_3)_6)(H_2O)_3]^{2+}$ [a]	415	700
	326	680
	240 sh	
$[Ru(\eta^6\text{-cymene})(H_2O)_3]^{2+}$ [a]	404	670
	316	750
	268	820
$[Ru(\eta^6\text{-}H_6C_6)(AN)_3]^{2+}$ [b]	368	570
$[Ru(\eta^6\text{-}C_6H_6)(DMSO)_3]^{2+}$ [b]	400	1500
$[Ru(\eta^6\text{-}C_6H_6)(DMS)_3]^{2+}$ [b]	387	2290
$[Ru(\eta^6\text{-}C_6H_6)(THTP)_3]^{2+}$ [b]	390	1410

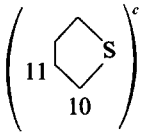
[a] 0.5 M H_2SO_4.
[b] Acetone, PF_6^- salts.

Table 3. ^1H and ^{13}C NMR spectra of $[Ru(\eta^6\text{-arene})(H_2O)_3]^{2+}$ complex ions[a]

Arene	Atom	^1H	^{13}C
Benzene	1	6.1, s (6)	81.9
p-Cymene (1-isopropyl-4-methylbenzene)	1	—	93.3
	2, 6	5.7, d (2)	94.1
	3, 5	5.5, d (2)	93.0
	4	—	93.3
	7	2.1, s (3)	23.5
	8	2.6, s (1)	32.2
	9, 9′	1.2, d (6)	22.6
Mesitylene (1,3,5-trimethylbenzene)	1	—	74.2
	2	5.1, s (3)	102.5
	7	2.2, s (9)	24.6
Hexamethylbenzene	1	—	90.8
	7	2.1, s (18)	17.3

[a] Chemical shifts (δ) in ppm; numbering scheme: ring atoms, 1–6; methyl, 7; isopropyl, 8, 9, 9′: s, singlet; d, doublet; number of protons in parantheses: ^1H: WP-80, D_2O, TMSP; ^{13}C: XL-100, D_2O, TMSP.

Table 4. ^1H and ^{13}C NMR spectra of $[Ru(\eta^6\text{-}C_6H_6)L_3]^{2+}$ complex ions[a]

L	Atom	^1H	^{13}C
H_2O[b]	1	6.1, s (6)	81.9
DMSO $[(C_{(10)}H_3)_2SO]$[c]	1	6.2, s (6)	81.0
	10	3.0, m (18)	38.5
AN $[C_{(10)}H_3\text{-}C_{(11)}N]$[c]	1	6.5, s (6)	89.0
	10	2.6, s (9)	3.6
	11	—	86.2
DMS $[(C_{(10)}H_3)_2S]$[d]	1	6.6, s (6)	92.9
	10	2.7, s (18)	26.5
THTP 	1	6.7, s (6)	93.6
	10	3.5, m (12)	43.7
	11	2.3, m (12)	31.1

[a] Cf. footnote of Table 3.
[b] ^1H: WP-80, D_2O, TMSP; ^{13}C: XL-100, D_2O, TMSP.
[c] ^1H: EM-360, $(CD_3)_2CO$, TMS; ^{13}C: XL-100, $(CD_3)_2CO$, TMS.
[d] ^1H: EM-360, $(CD_3)_2SO$, TMSP; ^{13}C: XL-100, $(CD_3)_2SO$, TMSP.

Table 5. Chemical-shift differences for $[Ru(\eta^6\text{-}C_6H_6)L_3]^{2+}$[a]

L	Δ [$^1H(C_6H_6)$]	Δ [$^{13}C(C_6H_6)$]
N_2H_4[b]	1.7	—
H_2O	1.2	46.5
DMSO	1.0	47.4
AN	0.8	39.4
DMS	0.7	35.5
THTP	0.6	34.8

[a] Free benzene: 7.27 and 128.4 ppm for ^1H and ^{13}C NMR, respectively; $\Delta = \delta$(complex ion) $- \delta$(free C_6H_6).
[b] R. H. Crabtree and A. L. Pearman, *J. Organomet. Chem.* 1977, **141**, 325.

of the carbon and hydrogen atoms within the ring of the arene ligands compared to the free aromatic molecule. The uncoordinated hydrocarbons show ^1H signals for the ring protons between 6.73 ppm (mesithylene) and 7.27 ppm (benzene) and ^{13}C resonances between 126 and 136 ppm. Significantly smaller shifts, upfield as well as downfield, are recorded for the C and H atoms of the ring substituents.

DISCUSSION

The most important general feature of the NMR data for the arene ligands, the high-field shift of the ring carbon and hydrogen signals (Table 3), is attributed to π-backbonding within the ruthenium–arene moiety.[10] Accordingly, electron density is removed from the metal atom to the arene molecule, thus leading to an enhanced shielding of the ring atoms. This effect is opposed by the positive charge of the metal center. We do not attempt, however, to assess a closer or quantitative relation between these or other effects on the chemical shifts.

A somewhat more informative picture is presented by the NMR data for $[Ru(\eta^6\text{-}C_6H_6)L_3]^{2+}$ (Table 4). ^1H and ^{13}C NMR signals of coordinated benzene show a strong dependence on the bonding properties of the ligand L, in particular, whether L itself is a π-acceptor or not. Spectroscopic data of η^6-benzene can thus be used to probe selected properties of the remaining monodentate ligands. The ordering of ligands according to measured ^1H and ^{13}C shift differences (Table 5) matches a ligand series of π-acidity observed for ruthenium(II) pentaammine complexes.[11] The selection of ligands employed in our study ranges from virtually pure σ-donors, such as H_2O, to the typical π-acceptors AN and dialkyl sulfide. The observed NMR behavior is thus qualitatively attributed to the influence of the monodentate ligand competing in the bonding scheme of the $[Ru(\eta^6\text{-arene})L_3]^{2+}$ ions with the aromatic molecule. π-Acidity is also strongly reflected in thermodynamic and kinetic properties of related hexacoordinated complex ions such as $[Ru(H_2O)_6]^{2+}$ and $Ru(AN)_6^{2+}$. The reduction potential of the $[Ru(H_2O)_6]^{3+/2+}$ couple is 0.21 V, whereas $Ru(AN)_6^{2+}$ cannot be oxidized up to 1.9 V.[12] Similarly, the rates for ligand exchange are $2 \times 10^{-2}\,s^{-1}$ for water[13] and $10^{-9}\,s^{-1}$ for AN.[14] Current studies in our laboratory dealing with a variety of ligands within the series $[Ru(\eta^6\text{-arene})_2]^{2+} \rightarrow [Ru(\eta^6\text{-arene})L_3]^{2+} \rightarrow RuL_6^{2+}$ are expected to provide further insight into this relationship between electronic structure and chemical reactivity.

Acknowledgements—We thank Ciba-Geigy, Basel, for performing the microanalyses and the Swiss National Science Foundation for financial support (Grant No. 2.430-9.84).

REFERENCES

1. M. A. Bennett, M. I. Bruce and T. W. Matheson, In *Comprehensive Organometallic Chemistry* (Edited by G. Wilkinson, F. G. A. Stone and E. W. Abel), Vol. 4, p. 691. Pergamon Press, Oxford (1982). E. A. Seddon and K. R. Seddon, *The Chemistry of Ruthenium*. Elsevier, Amsterdam (1984).

2. M. A. Bennett and A. K. Smith, *J. Chem. Soc., Dalton Trans.* 1974, 233.
3. R. O. Gould, C. L. Jones, D. F. Robertson and T. A. Stephenson, *J. Chem. Soc., Chem. Commun.* 1977, 222.
4. Y. Hung, W. J. Kung and H. Taube, *Inorg. Chem.* 1981, **20**, 457.
5. P. Bernhard, H. B. Bürgi, J. Hauser, H. Lehmann and A. Ludi, *Inorg. Chem.* 1982, **21**, 3936.
6. M. Stebler, H. B. Bürgi and A. Ludi, *Proceedings of the XIIth International Conference on Organometallic Chemistry, Vienna* (1985). M. Stebler, W. Hummel, P. A. Pittet, H. B. Bürgi, A. E. Merbach and A. Ludi, to be published.
7. O. H. Bailey and A. Ludi, *Inorg. Chem.* 1985, **24**, 2582.
8. M. A. Bennett and T. W. Matheson, *J. Organomet. Chem.* 1979, **175**, 87.
9. E. D. Marshall and R. R. Rickard, *Anal. Chem.* 1950, **22**, 795; J. L. Woodhead and J. M. Fletcher, *J. Chem. Soc.* 1961, 5039.
10. D. M. P. Mingos, In *Comprehensive Organometallic Chemistry* (Edited by G. Wilkinson, F. G. A. Stone and E. W. Abel), Vol. 3, p. 1. Pergamon Press, Oxford (1982).
11. H. Lehmann, K. J. Schenk, G. Chapuis and A. Ludi, *J. Am. Chem. Soc.* 1979, **101**, 6197.
12. P. Bernhard, Ph.D. Thesis, University of Bern (1984).
13. P. Bernhard, L. Helm, I. Rapaport, A. Ludi and A. E. Merbach, *J. Chem. Soc., Chem. Commun.* 1984, 302.
14. A. E. Merbach, personal communication.

Polyhedron Vol. 5, No. 6, pp. 1223–1226, 1986
Printed in Great Britain

0277–5387/86 $3.00+.00
Pergamon Journals Ltd

ON THE *E–Z* ISOMERIZATION IN PHOSPHAALKENE METAL COMPLEXES

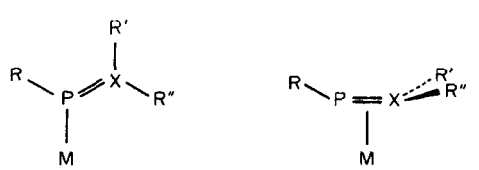
MINH THO NGUYEN, M. A. McGINN and A. F. HEGARTY*

Department of Chemistry, University College, Belfield, Dublin 4, Ireland

(*Received* 8 *October* 1985; *accepted* 9 *December* 1985)

Abstract—Extended Hückel calculations of the model $(MeP{=}CMe_2)Cr(CO)_5$ showed that η^1-complexation of phosphaethene with the transition-metal fragment reduces the rotation barrier about the P=C bond. This is due to stabilization of the non-planar transition state by an additional π-interaction. Because the P—M bond in the planar complex is of σ character, the angle of rotation around this bond is determined by the non-bonding repulsions between the substituents on the phosphaalkene and $M(CO)_5$ groups.

The ability of phosphaalkenes RRC=PR [and also diphosphenes (RP=PR′) and iminophosphanes (RP=NR′)] to form transition-metal complexes has been recognized for several years, and a number of such compounds have now been characterized both structurally and spectroscopically.[1–12] These have shown that the phosphaethene system has a choice of two co-ordination modes—η^1 via the phosphorus lone pair (**I**) or η^2 via the P=C double bond (**II**). The majority of known compounds adopt the η^1-mode, but a few examples of η^2-co-ordination have been characterized recently—$(\eta^2$-(mesityl)P=C$(Ph)_2)Pt(PPh_3)_2$,[2] $(\eta^2$-(xylyl)P=C$(Ph)_2)Ni(bipy)$[4] and $(\eta^2$-$((Me_3Si)_2CH)$P=C$(SiMe_3)_2)Ni(PMe_3)_2$.[6]



I **II**

Preference for the η^2-mode over η^1 seems to depend on the nature of the metal atom (for example, no η^2-bonded chromium complex has yet been observed). However, a recent HFS-LCAO-X_α study of η^1- and η^2-binding in $(\eta^2$-(mesityl)P=C$(Ph)_2)Pt(PPh_3)_2$[2] revealed only a small energy difference between the two structures, suggesting that the incorporation of very bulky groups into the phosphaethene might be sufficient to tip the balance in favour of the η^1-geometry.

An interesting feature of these molecules has recently been noted by Yoshifuji and co-workers, who have reported the structure and properties of the η^1-pentacarbonylchromium complexes of *cis*-(mesityl - 2,4,6 - tri - *tert* - butylphenyldiphosphene)[1] and *cis*-(P-2,4,6-tri-*tert*-butylphenyl)phenylphosphaethene.[11] They found that *trans* → *cis* isomerization can occur easily in the complex, but not in the isolated species, and inferred that the energy barrier to rotation about the P=P or P=C bond is lowered by co-ordination.

A preliminary self-consistent charge and configuration extended Hückel[13] study of a model pentacarbonylchromium η^1-phosphaethene complex was carried out (the η^2-bonding mode was not considered because no such structure has been experimentally observed). The objectives were to: (a) establish the main conformational features of the structures, (b) assess the relative importance of the σ and π contributions to the M—P bond, and (c) explain the decrease in the energy barrier to rotation about the P=C bond.

The geometries of the model complexes (η^1-$MeP{=}CMe_2)Cr(CO)_5$ (**III**), based on available structural data[10] are shown in Fig. 1. Methyl groups were used as substituents on the phosphaethene ligands to simulate as far as possible the bulky groups which are a common feature of all the experimentally known molecules. These were disposed so as to minimize non-bonded repulsions between the hydrogen atoms.

* Author to whom correspondence should be addressed.

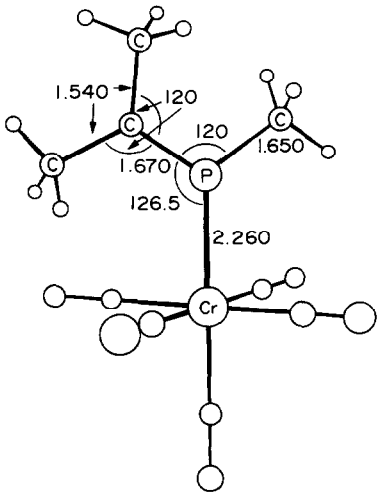
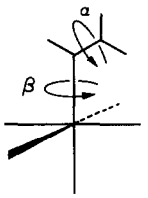


Fig. 1. Model geometries for (η^1-$H_3CP{=}C(CH_3)_2$)Cr$(CO)_5$ (**III**).

Calculations on the isolated ligands [Fig. 2(a)] show that for $MeP{=}CMe_2$, where there are no *cis* and *trans* isomers for the model, the barrier to internal rotation is 2.12 eV (compared to a value of 3.2 eV calculated for $HP{=}CH_2$ with the same method and basis).

Optimization of the P=C and P—Cr rotation angles, α and β (**IV**), of the complex, shows that the lowest-energy pathway for isomerization by rotation occurs at $\beta = 45°$ (i.e. when the Cr—P—C plane bisects an edge of the octahedron). The energy profiles for the variation in α at this angle are shown in Fig. 2(b).



IV

The barrier to P=C rotation in **III** is 1.1 eV, approximately half of that calculated for unco-ordinated phosphaethene, and also comparable with the experimental findings.[11] The origin of the decrease in barrier height was examined in detail for **III**, because in this case only "planar" and "non-planar" (rotation transition state) geometries must be considered. An energy level diagram showing the isolated and complexed planar and non-planar geometries is depicted in Fig. 3. The fragment orbitals of $M(CO)_5$ have been analysed by several groups.[14] The LUMO is a σ-symmetry hybrid consisting of d_{z^2} contributions, related to the e_g-set of

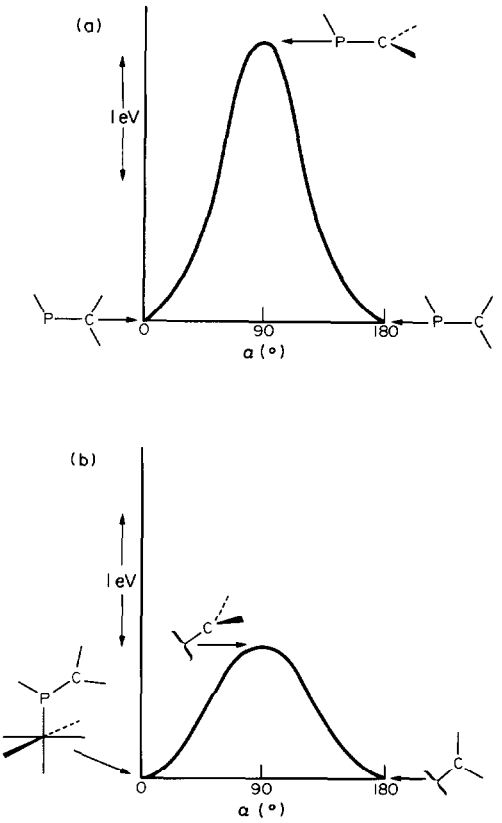


Fig. 2. Energy barriers to rotation in isolated (a) and co-ordinated (b) $H_3CP{=}C(CH_3)_2$.

an octahedron. Similarly, the HOMOs are derived from the t_{2g} octahedral set and comprise a d_{xz} and d_{yz} π-symmetry degenerate pair and a lower-lying δ-symmetry d_{xy}-orbital.

In the case of the "planar" co-ordinate phosphaethene complex, the major bonding interaction is of σ-type between the d_{z^2} LUMO of $M(CO)_5$ and the phosphorus-lone-pair-character HOMO of phosphaethene. The π-character $M(CO)_5$ HOMOs are destabilized slightly by interaction with the low-lying π phosphaethene-bonding MO, but interaction is weak. The π^*-orbital lies too high in energy to interact. Hence the Cr—P bond is almost purely σ in nature and its strength should not be affected by rotation. The presence for the $\beta = 45°$ geometry thus arises solely from steric repulsion between the $M(CO)_5$ and methyl groups. This is confirmed by calculations on the $HP{=}CH_2$ complex which indicate an almost zero rotational barrier.

For the complexed non-planar (rotation transition state) phosphaethene, the picture is quite different. The destabilization of the HOMOs of the unco-ordinated ligand relative to the planar structure accounts almost entirely for the energy barrier to P=C rotation in the isolated ligand. The LUMO

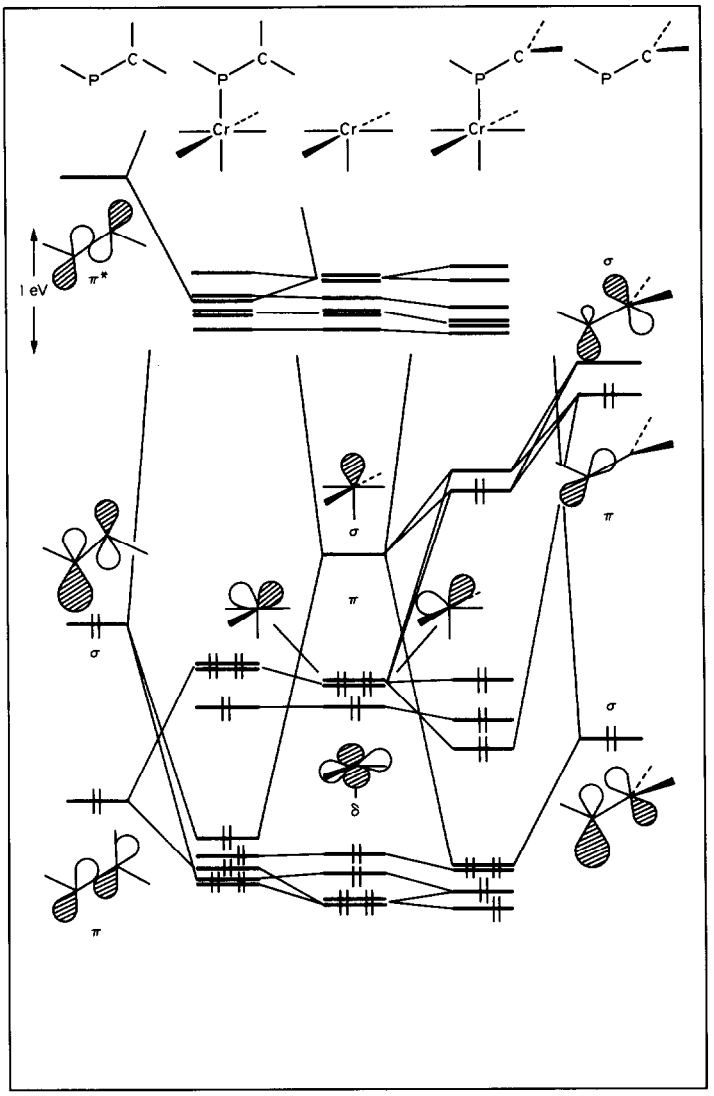


Fig. 3. Energy level diagram for (η^1-$H_3CP{=}C(CH_3)_2$)$Cr(CO)_5$ in "planar" (left) and "non-planar" (right) conformations.

lies much lower than that in the planar conformer, resulting in a very small HOMO–LUMO separation. The σ-interaction is smaller in this case than in the "planar" complex, because the energy separation between orbitals of suitable symmetry is bigger. This, combined with the destabilization of the HOMO levels largely accounts for the rotational barrier in the complex. The reason that this barrier is lower is an additional stabilizing interaction which occurs between the π $M(CO)_5$ HOMOs and the HOMO of phosphaethene. (The latter orbital is almost exclusively phosphorus p_π.) The antibonding interaction between these orbitals gives rise to the HOMO of the complex.

In summary, the SCCC calculations on the model ($MeP{=}CMe_2$)$Cr(CO)_5$ complex show that η^1-complexation of phosphaethene with the transition-metal fragment reduces the energy barrier to isomerization via rotation about the P=C bond. This is due to stabilization of the non-planar transition structure by an additional π-interaction. In the planar complex, the P—M bond is almost exclusively of σ character, and thus the angle of rotation around the P—M bond is determined by the non-bonding repulsions between the substituents on the phosphaethene and $M(CO)_5$ group.

REFERENCES

1. M. Yoshifuji, T. Hashida, N. Inamoto, K. Hirotsu, T. Horiuchu, T. Higuchi, K. Ito and S. Nagase, *Angew. Chem., Int. Ed. Engl.* 1985, **24**, 211.
2. Th. A. Van der Knaap, F. Bickelhaupt, J. G. Kraay-

kamp, G. Van Koten, J. P. C. Bernards, H. T. Edzes, W. S. Veeman, E. de Boer and E. J. Baerends, *Organometallics* 1984, **3**, 1804.
3. Th. A. Van der Knaap, L. W. Jenneskens, H. J. Meenwissen, F. Bickelhaupt, D. Walther, E. Dinjus, E. Uhlig and A. L. Spek, *J. Organomet. Chem.* 1983, **254**, C33.
4. H. W. Kroto, J. F. Nixon, M. J. Taylor, A. A. Frew and K. W. Muir, *Polyhedron* 1982, **1**, 89.
5. T. C. Klebach, R. Lourens, F. Bickelhaupt, H. Van der Poel, G. Van Koten and C. H. Stam, *J. Am. Chem. Soc.* 1982, **104**, 1756.
6. A. H. Cowley, R. A. Jones, C. A. Stewart, A. L. Stuart, J. L. Atwood, W. E. Hunter and H. M. Zhang, *J. Am. Chem. Soc.* 1984, **106**, 7015.
7. S. I. Al-Resayes, S. I. Klein, H. W. Kroto, M. F. Meidene and J. F. Nixon, *J. Chem. Soc., Chem. Commun.* 1983, 930.
8. R. H. Nielson, R. J. Thoma, I. Vickovic and W. H. Watson, *Organometallics* 1984, **3**, 1132.
9. H. W. Kroto, S. I. Klein, M. F. Meidene, J. F. Nixon, R. K. Harris, K. J. Packer and P. Reams, *J. Organomet. Chem.* 1985, **280**, 281.
10. R. Appel, C. Casser, M. Immenkeppel and F. Knoch, *Angew. Chem., Int. Ed. Engl.* 1984, **23**, 895.
11. M. Yoshifuji, K. Toyota and N. Inamoto, *Tetrahedron Lett.* 1985, **26**, 1727.
12. S. Pohl, *J. Organomet. Chem.* 1977, **142**, 185, 195.
13. (a) R. Hoffmann and W. N. Lipscomb, *J. Chem. Phys.* 1962, **32**, 2872; 1962, **32**, 3179, 3489; (b) R. Hoffmann, *J. Chem. Phys.* 1963, **39**, 1397; (c) J. Howell, A. Rossi, D. Wallace, K. Haraki and R. Hoffmann, *FORTICON* 8: *a Computer Program for Self-consistent Charge and Configuration Calculations* (QCPE 344).
14. (a) S. Shaik, R. Hoffmann, C. R. Fisel and R. H. Summerville, *J. Am. Chem. Soc.* 1980, **102**, 4555; (b) M. Elian and R. Hoffmann, *Inorg. Chem.* 1975, **14**, 1058.

Polyhedron Vol. 5, No. 6, pp. 1227–1231, 1986
Printed in Great Britain

0277–5387/86 $3.00+.00
Pergamon Press Ltd

SYNTHESIS AND SPECTROSCOPIC INVESTIGATION OF ADDUCTS OF DIORGANO TIN(IV) DICHLORIDE

J. C. TREHAN, R. K. SHARMA and C. P. SHARMA*

National Physical Laboratory, Hillside Road, New Delhi 110012, India

(*Received* 12 *July* 1985; *accepted after revision* 12 *December* 1985)

Abstract—Adducts of bis-*p*-biphenyl tin(IV) dichloride of types $(p\text{-}C_6H_5\text{-}C_6H_4)_2SnCl_2 \cdot 2L$ and $(p\text{-}C_6H_5\text{-}C_6H_4)_2SnCl_2 \cdot L_1$ (where 2L = pyridine, piperidine, α-, β- or γ-picolines, isoquinoline or morpholine and L_1 = 2,2′-bipyridine or 1,10 phenanthroline) have been prepared by the reaction of bis-*p*-biphenyl tin(IV) dichloride with the corresponding ligand in 1:2 and 1:1 molar ratios in acetone. IR, ^1H NMR and Mössbauer studies indicate that the biphenyl group occupies the *trans* position, except in morpholine, where it is in the *cis* position.

Organotin halides, like the tetrahalides of tin, react with certain electron pair donors to form addition compounds.[1–6] From a review on organotin compounds[1] it is clear that the majority of adducts are of type $R_xSnX_{4-x} \cdot 2L$ (where R = organic radical, X = halogen, and L = electron pair donor). Studies have been done on both types of adducts, i.e. adducts with symmetric diorgano tin dichlorides as well as adducts with asymmetric diorgano tin dichloride.[1–10] Jaura *et al.*[3,7,9,10] have carried out stereochemical investigations on asymmetric diorgano tin dichloride adducts and with the help of IR and Mössbauer spectroscopy have concluded that organic R groups occupy positions *trans* and *cis* to the halogens. Similar types of arrangement of the organo and halogen groups have also been supported by different workers[1–19] on the basis of spectral studies, e.g. IR, NMR and Mössbauer, and also by crystal structures.

The present paper describes the synthesis and spectroscopic investigation of some new adducts of bis-*p*-biphenyl tin dichloride of type $(p\text{-}C_6H_5\text{-}C_6H_4)_2SnCl_2 \cdot 2L$ (where L = pyridine, α-, β- or γ-picoline, morpholine, piperidine or isoquinoline) and $(p\text{-}C_6H_5\text{-}C_6H_4)_2SnCl_2 \cdot L_1$ where (L_1 = 2,2′-bipyridyl or 1,10-phenanthroline.

* Author to whom correspondence should be addressed.

EXPERIMENTAL

(a) All the required organic solvents, e.g. benzene, petroleum, ether (60–80°C), acetone, dichloromethane etc., were purified and dried before use by standard methods.

(b) Nitrobenzene for conductance measurements was purified as described by Fay and Lowry.[20]

(c) Pyridine, α-, β- and γ-picoline, piperidine, morpholine, isoquinoline, 2,2′-bipyridyl and 1,10-phenanthroline (A.R.B.D.H.) were used.

(d) Bis-*p*-biphenyl tin dichloride was prepared as described in the literature.[21]

Bis-p-*biphenyl tin(IV) dichloride* · 2*pyridine*

A solution of dichloro bis-*p*-biphenyl tin (0.4957 g, 1 mmol) in acetone (50 cm^3) was added dropwise to a solution of pyridine (0.1582 g, 2 mmol) in acetone (50 cm^3). The solvent was concentrated to 10 cm^3 under reduced pressure and then precipitated by adding petroleum ether dropwise with constant shaking. The complex was filtered and dried *in vacuo*. Recrystallization from benzene gave a white solid (70% yield).

Complexes with α-, β- and γ-picoline, morpholine, piperidine and isoquinoline were prepared by the same method. Bis-*p*-biphenyl tin(IV) dichloro 2,2′-bipyridyl and 1,10-phenanthroline were also

Table 1. Analytical data for addition compounds of bis-*p*-(biphenyl) tin(IV) dichloride with nitrogen donors

	Complex	Physical state and m.p. (°C)	% C Found (calc.)	% H Found (calc.)	% Sn Found (calc.)	% Cl Found (calc.)
1	$(C_6H_5\text{-}C_6H_4)_2SnCl_2 \cdot 2$pyridine	White solid 148	62.6 (62.4)	4.4 (4.3)	18.3 (18.2)	10.6 (10.9)
2	$(C_6H_5\text{-}C_6H_4)_2SnCl_2 \cdot 2\alpha$-picoline	White solid 102	63.0 (63.1)	4.8 (4.7)	17.8 (17.4)	10.1 (10.4)
3	$(C_6H_5\text{-}C_6H_4)_2SnCl_2 \cdot 2\beta$-picoline	White solid 162–164	63.3 (63.1)	4.4 (4.7)	17.5 (17.4)	10.1 (10.4)
4	$(C_6H_5\text{-}C_6H_4)_2SnCl_2 \cdot 2\gamma$-picoline	White solid 175–177	63.5 (63.1)	4.6 (4.7)	17.1 (17.4)	10.0 (10.4)
5	$(C_6H_5\text{-}C_6H_4)_2SnCl_2 \cdot 2$morpholine	White solid 165	57.2 (57.3)	5.3 (5.4)	17.6 (17.7)	10.1 (10.6)
6	$(C_6H_5\text{-}C_6H_4)_2SnCl_2 \cdot 2$piperidine	White solid 160	61.1 (61.3)	5.8 (6.0)	17.2 (17.8)	10.2 (10.7)
7	$(C_6H_5\text{-}C_6H_4)_2SnCl_2 \cdot 2,2'$-bipyridyl	White solid 210–214	63.0 (62.6)	4.8 (5.0)	18.5 (18.2)	11.0 (10.9)
8	$(C_6H_5\text{-}C_6H_4)_2SnCl_2 \cdot 2$isoquinoline	White solid 187	67.0 (66.9)	4.4 (4.2)	15.3 (15.8)	9.6 (9.4)
9	$(C_6H_5\text{-}C_6H_4)_2SnCl_2 \cdot 1,10$-phenanthroline	White solid 198	62.9 (63.0)	5.4 (5.3)	17.9 (17.3)	10.6 (10.3)

prepared by the same method using (p-C_6H_5-$C_6H_4)_2SnCl_2$ (0.495 g, 1 mmol) and 2,2′-bipyridyl (0.1562 g, 1 mmol).

Analytical data of these complexes are reported in Table 1.

IR spectra

IR spectra were recorded with a Perkin–Elmer 621 grating spectrometer, with the main emphasis in the 600–250-cm^{-1} region.

^{1}H *NMR*

Proton magnetic resonance spectra were recorded at ambient temperature (28°C) at a sweep width of 900 Hz with a Perkin–Elmer R-32 spectrometer. Spectra were recorded in triplicate. The magnetic field sweep was calibrated with a standard sample of chloroform and tetramethyl silane (1%) in deuterated chloroform.

Mössbauer spectroscopy

Mössbauer spectra were recorded as reported earlier.[22]

RESULTS AND DISCUSSION

The new bis-p-biphenyl tin(IV) dichloride adducts of types (p-C_6H_5-$C_6H_4)_2SnCl_2 \cdot 2L$ (where L = pyridine, α-, β- or γ-picoline, morpholine, isoquinoline or piperidine) and (p-C_6H_5-$C_6H_4)_2SnCl_2 \cdot L_1$ (where L_1 = 2,2′-bipyridine or 1,10-phenanthroline) have been prepared from bis-p-biphenyl tin(IV) dichloride and the corresponding ligand in acetone in 1:2 and 1:1 molar ratios according to the following equations:

$$(p\text{-}C_6H_5\text{-}C_6H_4)_2SnCl_2 + 2L \rightarrow (p\text{-}C_6H_5\text{-}C_6H_4)_2SnCl_2 \cdot 2L,$$

$$(p\text{-}C_6H_5\text{-}C_6H_4)_2SnCl_2 + L_1 \rightarrow (p\text{-}C_6H_5\text{-}C_6H_4)_2SnCl_2 \cdot L.$$

The isolated products were of high purity as indicated by their satisfactory elemental analysis and ^{1}H NMR spectroscopy. The complexes are white crystalline solids, fairly stable in a dry and inert atmosphere, and are soluble in most of the common organic solvents like acetone, chloroform and benzene, but insoluble in petroleum ether.

IR spectra

In the IR studies reported in Table 2 the main emphasis is on the 650–200-cm^{-1} region where there are Sn—C and Sn—Cl stretching frequencies.

In all the adducts of bis-p-biphenyl tin(IV) dichloride reported here we get one strong band (~550–600 cm^{-1}) which may be assigned to a

Table 2. Important IR data of bis-*p*-biphenyl tin(IV) dichloride with nitrogen donors[a]

	Compound	ν(Sn—C)	ν_{asym}(Sn—Cl)	ν_{sym}(Sn—Cl)
1	$(p\text{-}C_6H_5\text{-}C_6H_4)_2SnCl_2 \cdot 2$pyridine	555 (s)	275 (m)	245 (w)
2	$(p\text{-}C_6H_5\text{-}C_6H_4)_2SnCl_2 \cdot 2\alpha$-picoline	560 (m)	290 (m)	270 (w)
3	$(p\text{-}C_6H_5\text{-}C_6H_4)_2SnCl_2 \cdot 2\beta$-picoline	550 (s)	275 (m)	245 (m)
4	$(p\text{-}C_6H_5\text{-}C_6H_4)_2SnCl_2 \cdot 2\gamma$-picoline	545 (m)	290 (m)	280 (m)
5	$(p\text{-}C_6H_5\text{-}C_6H_4)_2SnCl_2 \cdot 2$morpholine	570 (s)	—	230 (m)
6	$(p\text{-}C_6H_5\text{-}C_6H_4)_2SnCl_2 \cdot 2$piperidine	565 (s)	285 (m)	235 (w)
7	$(p\text{-}C_6H_5\text{-}C_6H_4)_2SnCl_2 \cdot 2,2'$-bipyridyl	550 (m)	290 (m)	270 (w)
8	$(p\text{-}C_6H_5\text{-}C_6H_4)_2SnCl_2 \cdot 2$isoquinoline	585 (m)	270 (m)	235 (m)
9	$(p\text{-}C_6H_5\text{-}C_6H_4)_2SnCl_2 \cdot 1,10$-phenanthroline	582 (m)	285 (m)	240 (m)

N—H stretching frequencies (cm^{-1}) of the bases and adducts

Piperidine	3292
$(p\text{-}C_6H_5\text{-}C_6H_4)_2SnCl_2 \cdot 2$piperidine	3170
Morpholine	3345
$(p\text{-}C_6H_5\text{-}C_6H_4)_2SnCl_2 \cdot 2$morpholine	2292

[a] s, strong; vs, very strong; m, medium; w, weak.

Sn—C stretching vibration, which suggests that the phenyl group occupies the *trans* position.[11,23,24]

Each complex reported here, except for the morpholine complex, shows two bands corresponding to symmetric and asymmetric Sn—Cl stretching (~245 and 290 cm^{-1}, respectively). This suggests that chlorine atoms occupy the *cis* position. In the case of the morpholine adducts, only one Sn—Cl stretching frequency appears to be IR-active. The chlorines are thus likely to occupy a linear position.[19] N—H stretching frequencies in the cases of the piperidine and morpholine complexes decrease, as is evident from Table 2. This is also due to the donation of electrons by nitrogen on coordination.[25]

^{1}H *NMR spectra*

The ^{1}H NMR spectra of the bis-*p*-biphenyl tin(IV) dichloride adducts are given in Table 3 and correlations of the resonance signals with various groups present in the molecules have been made.

Table 3. Proton chemical shifts (τ values in ppm) in $CdCl_3$ for addition compounds of bis-*p*-biphenyl tin dichloride with nitrogen donors[a]

	Complex	Resonance signals due to biphenyl protons	Resonance signals due to NR protons		
			CH_3	CH_2	CH
1	$(p\text{-}C_6H_5\text{-}C_6H_4)_2SnCl_2 \cdot 2$pyridine	2–3 (m)			
2	$(p\text{-}C_6H_5\text{-}C_6H_4)_2SnCl_2 \cdot 2\alpha$-picoline	2–3 (m)	7.4 (s)		
3	$(p\text{-}C_6H_5\text{-}C_6H_4)_2SnCl_2 \cdot 2\beta$-picoline	2–3 (m)	7.75 (s)		
4	$(p\text{-}C_6H_5\text{-}C_6H_4)_2SnCl_2 \cdot 2\gamma$-picoline	2–3 (m)	7.70 (s)		
5	$(p\text{-}C_6H_5\text{-}C_6H_4)_2SnCl_2 \cdot 2$morpholine	2–3 (m)	—	6.15 (NH—CH_2) 7.85 (O—CH_2)	
6	$(p\text{-}C_6H_5\text{-}C_6H_4)_2SnCl_2 \cdot 2$piperidine	2–3 (m)	—	6.1 (NH—CH_2) 8.40 (C—CH_2)	
7	$(p\text{-}C_6H_5\text{-}C_6H_4)_2SnCl_2 \cdot 2,2'$-bipyridyl	2–3 (m)	—	—	
8	$(p\text{-}C_6H_5\text{-}C_6H_4)_2SnCl_2 \cdot 1,10$-phenanthroline	2–3 (m)	—	—	
9	$(p\text{-}C_6H_5\text{-}C_6H_4)_2SnCl_2 \cdot 2$isoquinoline	2–3 (m)	—	—	

[a] m, multiplet; s, singlet.

Table 4. Mössbauer data of bis-*p*-biphenyl tin(IV) dichloride adducts

	Compound	IS[a] (mm s^{-1})	QS[b] (mm s^{-1})
1	$(p\text{-}C_6H_5\text{-}C_6H_4)_2SnCl_2 \cdot 2$pyridine	1.30	4.01
2	$(p\text{-}C_6H_5\text{-}C_6H_4)_2SnCl_2 \cdot 2$piperidine	1.33	3.72
3	$(p\text{-}C_6H_5\text{-}C_6H_4)_2SnCl_2 \cdot 2\alpha$-picoline	1.27	3.91
4	$(p\text{-}C_6H_5\text{-}C_6H_4)_2SnCl_2 \cdot 2\beta$-picoline	1.29	3.63
5	$(p\text{-}C_6H_5\text{-}C_6H_4)_2SnCl_2 \cdot 2\gamma$-picoline	1.35	3.85
6	$(p\text{-}C_6H_5\text{-}C_6H_4)_2SnCl_2 \cdot 2$isoquinoline	1.31	3.70
7	$(p\text{-}C_6H_5\text{-}C_6H_4)_2SnCl_2 \cdot 2,2'$-bipyridyl	1.28	3.82
8	$(p\text{-}C_6H_5\text{-}C_6H_4)_2SnCl_2 \cdot 2$morpholine	1.15	2.32

[a] Mössbauer measurements were carried out at 88 K. All the IS values are with respect to $BaSnO_3$ absorbent at room temperature.
[b] Values are correct within ± 0.05 mm s^{-1}.

Mössbauer spectra

The Mössbauer data, including the isomer shift (IS) and quadrupole splitting (QS), of bip-*p*-biphenyl tin dichloride adducts are summarized in Table 4. The IS values are well within the range characteristic of Sn(IV) species.

It is evident from Table 4 that the IS values of the picoline adducts lie in the range 1.25–1.30 mm s^{-1}, which shows that the values are almost constant within experimental error. This reveals that the *s*-electron density on the tin atom remains almost unchanged even on co-ordination with picolines. In the case of the isoquinoline adduct the IS is $\sim$1.31 mm s^{-1}, which is higher than in the case of the picoline adducts. This indicates an increased *s*-electron density on the tin nucleus on complexation with isoquinoline in contrast to the picoline adducts. This is probably due to the greater p_π–d_π bonding effect of isoquinoline than of picolines.

In the case of the adduct with morpholine, there is a variation in the IS, which is $\sim$1.15 mm s^{-1}, which indicates a decrease in the *s*-electron density around the tin atom. This is probably due to the hydrogen bonding between morpholine and the chlorine atom of the organo tin chloride which is expected to reduce the electron density on the central tin atom. This suggests that the chlorine atom and the morpholine adduct lie close to each other.

QS values for all the adducts reported here, except for the morpholine adduct, are in the range 3.7–4.0 mm s^{-1}. This value of about 4 mm s^{-1} suggests a *trans* arrangement of the organic groups in these adducts.[15,26–28] However, for the morpholine adduct the situation is different. The QS value is 2.32 mm s^{-1}, not far away from 2 mm s^{-1}, suggesting that the organic groups around the tin atom occupy *cis* positions. Earlier Hendrichar[8] reported a *trans* alkyl configuration on the basis of NMR data for the symmetrical dialkyl tin dichloride γ-picoline adduct.

Thus, on the basis of elemental analysis, and IR, ^{1}H NMR and Mössbauer studies, all the adducts reported here, except for the morpholine adduct, can be assigned the structure in Fig. 1(a). The morpholine adduct can be assigned the structure in Fig. 1(b).

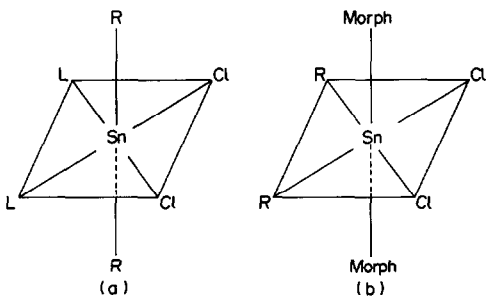


Fig. 1.

REFERENCES

1. R. K. Ingham, S. D. Rosenberg and H. Gilman, *Chem. Rev.* 1960, **60**, 459.
2. T. Tanaka, Y. Matsumura and R. Okawara, *Bull. Chem. Soc. Jpn* 1968, **41**, 1497.
3. K. L. Jaura and K. Lal, *J. Less Common Met.* 1977, **55**, 93.
4. J. S. Morrison and H. M. Heandler, *J. Inorg. Nucl. Chem.* 1967, **29**, 393.
5. J. D. Donaldson and D. G. Nicholson, *J. Chem. Soc.* 1970, 145.
6. K. Issleib and H. Reinhold, *Z. Anorg. Allg. Chem.* 1962, **314**, 113.

7. K. L. Jaura, K. K. Dhingra, R. K. Mahajan and K. Lal, *Z. Anorg. Allg. Chem.* 1978, **445**, 242.
8. D. G. Hendrichar, *J. Inorg. Nucl. Chem. Lett.* 1969, **5**, 115.
9. K. L. Jaura, R. K. Mahajan, R. K. Bhanot, K. K. Sharma and K. Lal, *Z. Anorg. Allg. Chem.* 1980, **468**, 231.
10. K. L. Jaura and V. K. Verma, *Indian J. Chem.* 1978, **16A**, 618.
11. R. J. H. Clark, A. G. Davies and R. J. Puddephat, *J. Chem. Soc. A* 1968, 1828.
12. N. N. Greenwood and J. N. R. Ruddick, *J. Chem. Soc. A* 1967, 1679.
13. M. A. Mullins and C. Curran, *Inorg. Chem.* 1967, **6**, 2017.
14. J. Philip, M. A. Mullins and C. Curran, *Inorg. Chem.* 1968, **7**, 1895.
15. B. W. Fitzsimmons, N. J. Seeley and A. W. Smith, *Chem. Commun.* 1968, 390; *J. Chem. Soc. A* 1969, 143.
16. N. W. G. Debye, E. Rosenberg and J. J. Zuckerman, *J. Am. Chem. Soc.* 1968, **90**, 3234.
17. N. W. Isaacs, C. H. L. Kennard and W. Kitching, *J. Chem. Soc., Chem. Commun.* 1961, 820.
18. F. W. Einstein and B. R. Penfold, *J. Chem. Soc. A* 1968, 3019.
19. R. C. Poller, J. N. R. Ruddick and M. Thevarasa, *J. Chem. Soc. A* 1969, 2327.
20. R. C. Fay and R. N. Lowry, *Inorg. Chem.* 1967, **6**, 1512.
21. T. V. Talalaeva, M. A. Zaitseva and K. A. Kocheshkov, *J. Gen. Chem. U.S.S.R.* 1946, **16**, 901; *Chem. Abstr.* 1947, **41**, 2014.
22. C. P. Sharma, N. Kumar, M. C. Khandpal, S. Chandra and V. G. Bhide, *J. Inorg. Nucl. Chem.* 1981, **43**, 923.
23. R. C. Poller, *The Chemistry of Organotin Compounds.* Lagos Press, London (1970).
24. J. P. Clark and C. J. Wilkins, *J. Chem. Soc. A* 1966, 871.
25. N. N. Greenwood and K. Wade, *J. Chem. Soc.* 1960, 1130.
26. R. V. Parish and R. H. Platt, *J. Chem. Soc. A* 1969, 2145.
27. B. F. E. Ford and J. R. Sams, *J. Organomet. Chem.* 1971, **31**, 47.
28. J. G. A. Luizten and G. J. M. Vander Kark, *J. Appl. Chem.* 1961, **11**, 35.

Polyhedron Vol. 5, No. 6, pp. 1233–1235, 1986
Printed in Great Britain

0277–5387/86 $3.00+.00
Pergamon Journals Ltd

COMMUNICATION

SYNTHESIS, SPECTRAL PROPERTIES AND REACTIONS OF THE NOVEL DINUCLEAR ALKYNE COMPLEXES $[M(\mu\text{-}I)I(CO)(NCMe)(\eta^2\text{-}PhC_2R)]_2$ (M = Mo OR W, R = Ph OR Me)

PAUL K. BAKER* and ELAINE M. KEYS

Department of Chemistry, University College of North Wales, Bangor, Gwynedd LL57 2UW, U.K.

(*Received* 6 *December* 1985; *accepted* 19 *December* 1985)

Abstract—$[MI_2(CO)_3(NCMe)_2]$ (M = Mo or W) and PhC_2R (R = Ph or Me) react in CH_2Cl_2 to initially afford the "four-electron" alkyne complexes $[MI_2(CO)(NCMe)_2(\eta^2\text{-}PhC_2R)]$, which subsequently dimerize to the novel iodide-bridged compounds $[M(\mu\text{-}I)I(CO)(NCMe)(\eta^2\text{-}PhC_2R)]_2$, with loss of acetonitrile. These complexes react *via* symmetrical cleavage of the iodide bridges.

Alkynes are becoming increasingly important as ligands in organometallic chemistry, mainly due to their unique ability to utilize the filled alkyne perpendicular π-bonding orbitals, which permits the possibility of variable electron donor interactions which can formally be two, three or four electrons. This depends on the electronic configuration of the metal and the bonding properties of the other ligands in the coordination sphere.[1] Although a large number of six-coordinate d^4 mononuclear alkyne complexes have been reported for molybdenum(II) and tungsten(II)—$[MX(CO)(\eta^2\text{-}PhC_2Ph)(\eta^5\text{-}C_5H_5)]$ (M = Mo or W; X = Cl, Br or I);[2] $[Mo(CO)(S_2CNR_2)_2(\eta^2\text{-}RC_2R)]$ (R = alkyl or aryl);[3] $[M(SR)(CO)(\eta^2\text{-}R^1C_2R^1)(\eta^5\text{-}C_5H_5)]$ (R = CF_3 or C_6F_5; R^1 = Me, CF_3 or Ph);[4] $[WMe(CO)(\eta^2\text{-}RC_2R)(\eta^5\text{-}C_5H_5)]$ (R = alkyl or aryl);[5] $[MoLL^1(\eta^2\text{-}RC_2R^1)(\eta^5\text{-}C_5H_5)][BF_4]$ {L,L^1 = CO or PR_3; L = L^1 = $P(OMe_3)$; R, R^1 = Me, Ph etc.};[6] $[Mo(^tBuS)_2(^tBuNC)_2(RC_2R^1)]$ (R,R^1 = H or Ph);[7] $[MoX_2(CO)L_2(\eta^2\text{-}PhC_2R)]$ (X = Cl or Br, L = phosphine, R = H or Ph);[8] $[Mo(SR)\{P(OMe)_3\}(\eta^2\text{-}MeC_2Me)(\eta^5\text{-}C_5H_5)]$ (R = Me, *p*-$NH_2C_6H_4$, *p*-$MeOC_6H_4$, *p*-MeC_6H_4, C_6H_5 or *p*-$NO_2C_6H_4$)[9]—hitherto very few dinuclear compounds of this type have been reported. In this communication we describe the synthesis of the novel iodide-bridged dimers $[M(\mu\text{-}I)I(CO)(NCMe)(\eta^2\text{-}PhC_2R)]_2$ (M = Mo or W, R = Ph or Me), and preliminary studies of their reactivity.

Equimolar quantities of PhC_2R (R = Ph or Me) and $[MI_2(CO)_3(NCMe)_2]$[10] react in CH_2Cl_2 to give the crystalline complexes $[M(\mu\text{-}I)I(CO)(NCMe)(\eta^2\text{-}PhC_2R)]_2$. These complexes are stable in the solid state when stored under argon at 0°C, and have been fully characterized by elemental analysis (C, H and N) and by IR and ^1H NMR spectroscopy (Table 1). The complexes are thermally unstable, i.e. similar to the well-known halide-bridged dimers[11] $[M(\mu\text{-}X)X(CO)_4]_2$ (M = Mo or W; X = Cl, Br and I), and their thermal instability is reflected by their high reactivity. They react via symmetrical cleavage of the iodide bridges (Scheme 1). The ^{13}C NMR spectrum of **4** shows resonances at δ (ppm) = 207.7 and 206.9 (s, CO), 199.7 (s, PhC≡), 196.9 (s, MeC≡), 136.7 (s, ≡C—C), 130.6 (s, *o*-Ph), 129.2 (s, *m*-Ph), 128.7 (s, *p*-Ph), 117.48 (s, N≡CMe), 23.52 (s, ≡CMe) and 4.55 (s, NCMe). The low-field resonances due to the "acetylenic" carbon atoms are typical of terminally bonded "four-electron" alkynes coordinated to molybdenum(II) or tungsten(II).[6-9]

It is proposed that these reactions proceed via the mononuclear intermediates $[MI_2(CO)(NCMe)_2(\eta^2\text{-}PhC_2R)]$. For example, reaction of $[MoI_2(CO)_3$

* Author to whom correspondence should be addressed.

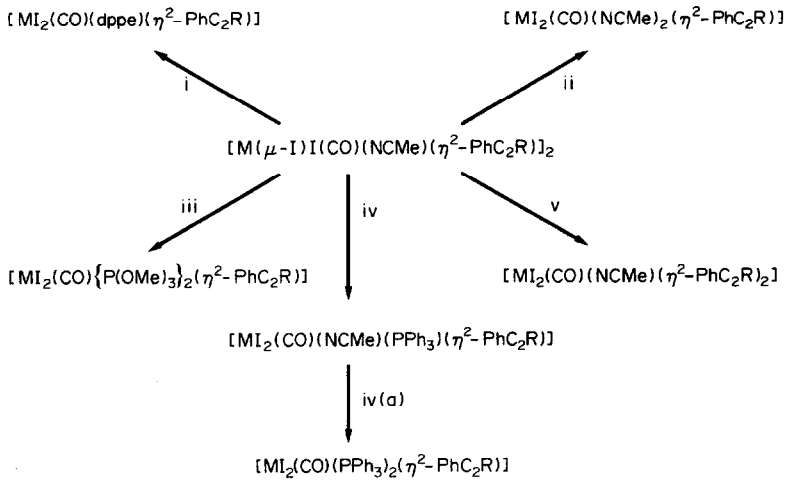
Table 1. IR and ^{1}H NMR data for $[M(\mu\text{-}I)I(CO)(NCMe)(\eta^2\text{-}PhC_2R)]_2$

	M	R	ν(CO)[a] (cm^{-1})	ν(CN)[a] (cm^{-1})	ν(C≡C)[a] (cm^{-1})	^{1}H NMR[b] data (δ)
1	Mo	Ph	2050(s), 2005(s)	2315(w), 2290(w)	1690(w)	2.40 (s, 6H, NCMe) 7.49 (m, 20H, Ph)
2	Mo	Me	2045(s), 1990(s)	2315(w), 2240(w)	1620(w)	2.48 (s, 6H, NCMe) 3.54 (s, 6H, ≡CMe) 7.59 (m, 10H, ≡CPh)
3	W	Ph	2065(s), 2000(s)	2310(w), 2290 (w)	1675(w)	2.65 (s, 6H, NCMe) 7.61 (s, 20H, ≡CPh)
4	W	Me	2050(s), 1990(s)	2315(w), 2285(w)	1610(w)	2.72 (s, 6H, NCMe) 3.21 (s, 6H, ≡CMe) 7.62 (m, 10H, ≡CPh)

[a] Spectra recorded in $CHCl_3$: s, strong; w, weak.
[b] Spectra recorded in $CDCl_3$ (+25°C) and referenced to $SiMe_4$.

$(NCMe)_2]$ with PhC_2Ph in CH_2Cl_2 at room temperature proceeds rapidly with effervescence of CO which ceases after 15 min. An IR spectrum of this solution shows not only carbonyl bands due to the dimer at ν = 2050 and 2005 cm^{-1}, but also a very intense carbonyl band at 1978 cm^{-1}. This band is due to $[MoI_2(CO)(NCMe)_2(\eta^2\text{-}PhC_2Ph)]$ (**5**) and decreases with time until after 12 h only the bands due to the dimer **1** are observed. **5** can be prepared by reacting $[MoI_2(CO)_3(NCMe)_2]$ with PhC_2Ph in acetonitrile at 40°C for 2 h, when removal of solvent affords very air-sensitive red crystals of **5** which has been fully characterized by elemental analysis (C, H and N), and IR and ^{1}H NMR spectroscopy. The room-temperature ^{1}H NMR spectrum of **5** in $CDCl_3$ showed a methyl resonance at δ = 2.45 ppm which after 12 h shows two MeCN resonances at δ = 2.40 (dimer **1**) and 2.12 ppm (uncoordinated MeCN). Hence the proposed mechanism for the formation of the dimer is given in Scheme 2.

The preparation of a wide variety of these dinuclear complexes of molybdenum(II) and tungsten(II) with different alkynes, RC_2R^1 (R, R^1 = Me and Me, CH_2Cl and CH_2Cl, Me and SPh, Me and *p*-tolS etc.) has been carried out and a wide range of different rates of dimerization has been observed. It appears that the larger and more electron-deficient alkynes dimerize more slowly (probably due to there being less electron density on the metal,



Scheme 1. M = Mo or W; R = Me and Ph. Reagents: (1) dppe in CH_2Cl_2; (ii) NCMe, warm to 40°C; (iii) $P(OMe)_3$ in CH_2Cl_2; [iv and iv(a)] PPh_3 in CH_2Cl_2; and (v) PhC_2R in CH_2Cl_2.

(a) $[MoI_2(CO)_3(NCMe)_2] \longrightarrow [MoI_2(CO)_2(NCMe)_2] + CO$

(b) $[MoI_2(CO)_2(NCMe)_2] \xrightarrow{PhC_2Ph} [MoI_2(CO)_2(NCMe)_2(\eta^2\text{-}PhC_2Ph)]$

(c) $[MoI_2(CO)_2(NCMe)_2(\eta^2\text{-}PhC_2Ph)] \longrightarrow [MoI_2(CO)(NCMe)_2(\eta^2\text{-}PhC_2Ph)] + CO$

(d) $2[MoI_2(CO)(NCMe)_2(\eta^2\text{-}PhC_2Ph)] \longrightarrow [Mo(\mu\text{-}I)I(CO)(NCMe)(\eta^2\text{-}PhC_2Ph)]_2 + 2NCMe$

Scheme 2.

and hence a stronger M—N bond). The chemistry of these complexes is currently being investigated in this laboratory and is extremely diverse (Scheme 1).

Acknowledgement—E.M.K. thanks the S.E.R.C. for a studentship.

REFERENCES

1. J. L. Templeton and B. C. Ward, *J. Am. Chem. Soc.* 1980, **102**, 3288.
2. J. L. Davidson and D. W. A. Sharp, *J. Chem. Soc., Dalton Trans.* 1975, 2531.
3. J. W. McDonald, W. E. Newton, C. T. C. Creedy and J. Coubin, *J. Organomet. Chem.* 1975, **92**, C25.
4. P. S. Braterman, J. L. Davidson and D. W. A. Sharp, *J. Chem. Soc., Dalton Trans.* 1976, 241.
5. H. G. Alt, *J. Organomet. Chem.* 1977, **11**, 340.
6. S. R. Allen, P. K. Baker, S. G. Barnes, M. Green, L. Trollope, L. M. Muir and K. W. Muir, *J. Chem. Soc., Dalton Trans.* 1981, 873.
7. M. Kamata, T. Yoshida, S. Otsuka, K. Hirotsu, T. Higuchi, M. Kido, K. Tatsumi and R. Hoffmann, *Organometallics* 1982, **1**, 227.
8. P. B. Winston, S. J. N. Burgmayer and J. L. Templeton, *Organometallics* 1983, **2**, 167.
9. S. R. Allen, T. H. Glauert, M. Green, K. A. Mead, N. C. Norman, A. G. Orpen, C. J. Shraverien and P. Woodward, *J. Chem. Soc., Dalton Trans.* 1984, 2747.
10. P. K. Baker, S. G. Fraser and E. M. Keys, *J. Organomet. Chem.* (in press).
11. R. Colton, *Coord. Chem. Rev.* 1971, **6**, 269.

Polyhedron Vol. 5, No. 6, p. 1237, 1986
Pergamon Journals Ltd. Printed in Great Britain

BOOK REVIEW

Gmelin Handbook of Inorganic Chemistry. Sn—Organotin Compounds, Part 12, Tripropyltin– and Tributyltin–Oxygen Compounds. H. Schumann and I. Schumann, Springer, Berlin, 1985. ISBN 3-540-93521-5, x+266 pp., DM997.

This is the twelfth Gmelin volume on organotin compounds, and covers only tripropyltin– and tributyltin–oxygen compounds, but it is a key volume as the tri-*n*-butyltin derivatives are the most familiar in both the laboratory and industry.

The unstable hydroxides are included but surprisingly not the much more familiar bistrialkyltin oxides; perhaps they are to appear in a future volume. The alkoxides, ketonates and acylates follow, then the derivatives of the carbonic and carbamic acids, the peroxides, and the derivatives of the oxyacids of the halogens, nitrogen, phosphorus etc., and there is a separate section on free radicals containing R_3SnO groups.

For example, 18 pp. are devoted to tributyltin methoxide. Its preparations and physical properties are critically presented, and then its reactions with 168 reagents are tabulated, with footnotes on particular reactions. This section contains 125 references.

The many applications of the compounds in industry and agriculture are included, and there is a formula index.

The presentation, now wholly in English, is of the familiar very high standard of these volumes, and the errors are very few. The literature is covered up to the end of 1982.

Again, all chemists handling organotin compounds are indebted to Herbert and Ingeborg Schumann for presenting this important section of organotin chemistry in such a convenient and lucid format.

Department of Chemistry
University College London
20 *Gordon Street*
London WC1H 0AJ, U.K.

A. G. DAVIES

Polyhedron Vol. 5, No. 7, pp. 1239–1246, 1986
Printed in Great Britain

0277-5387/86 $3.00+.00
Pergamon Journals Ltd

WHOLE EQUILIBRIUM ANALYSIS OF THE INNER- AND OUTER-SPHERE CHROMIUM(III)–PHOSPHINATE COMPLEX SYSTEM

HIROHIKO WAKI,* QI FENG, KAZUHISA TSURUTA and SHIGERU OHASHI

Department of Chemistry, Faculty of Science, Kyushu University, Hakozaki, Fukuoka, Japan

(*Received* 18 *September* 1985; *accepted* 6 *November* 1985)

Abstract—The stability constants of the inner- and outer-sphere chromium(III)–phosphinate complexes have been evaluated by two ion-exchange methods: one is the Donnan exclusion chromatography and the other is the cation-exchange equilibrium method: $\log K_{1,0} = 2.7$, $\log K_{2,0} = 1.8$, $\log K_{3,0} = 1.3$, $\log K_{4,0} = 1.6$, $\log K_{5,0} = 0.71$, and $\log K_{6,0} = 0.079$ for inner-sphere complexes; $\log K_{0,1} = 0.90$, and $\log K_{0,2} = 0.079$ for outer-sphere complexes; and $\log K_{1,1} = 0.56$ for the inner–outer mixed-sphere complex—all these being values at 50°C (20°C for $K_{1,1}$) and ionic strength of 0.2. Donnan exclusion chromatography has been proved as an effective method for such a system involving inert species. A total scheme has been clarified for this complex system under the conditions studied and the characteristic absorption spectrum of each chromium–phosphinate complex has also been established.

Although a large number of studies on inert chromium(III) complexes have been made,[1,2] there have only been a few reports with qualitative work[3,4] concerning the complexation between chromium(III) and phosphinate. A complete analysis on a whole chromium(III)–phosphinate complex system has not yet been made.

When chromium(III) reacts with phosphinate under appropriate conditions, it may be expected that inert inner-sphere complexes $\{[Cr(PH_2O_2)_m(H_2O)_n)]^{(m-3)-}\}$ [ligand number $(n+m) = 6$], outer-sphere complexes $\{[Cr(H_2O)_6 \cdot (PH_2O_2)_m]^{(3-m)+}\}$ $(m = 0–3)$ and mixed inner–outer-sphere complexes such as $[Cr(PH_2O_2)(H_2O)_5 \cdot (PH_2O_2)]^+$ or $[Cr(PH_2O_2)(H_2O)_5 \cdot (PH_2O_2)_2]$ are formed simultaneously. Inner-sphere complexes may be distinguished and separated from outer-sphere complexes by different reaction rates for complexation. Since the mutual separation of labile outer-sphere complexes is impossible, the analyses can only be done by means of the equilibrium technique.

In this work the analysis of a whole inner- and outer-sphere equilibrium system was attempted by combining the recently developed Donnan exclusion chromatography[5–7] and the cation-exchange equilibrium method.

EXPERIMENTAL

Reagents and ion-exchangers

Chromium(III) perchlorate, sodium phosphinate, sodium perchlorate and tetramethylammonium chloride were of commercially available reagent grade. Chromium(III) phosphinate solution was prepared by passing chromium(III) perchlorate solution through a column of the phosphinate form Dowex 1-X4 (100–200-mesh). A cross-linked dextran gel-type cation exchanger, SP-Sephadex C-25 (Pharmacia Fine Chemicals), was used for the chromatographic separations and well-conditioned Dowex 50W-X4 (100–200-mesh) of sodium form for batch equilibrium analyses.

Time dependence measurement of the absorption spectrum of the chromium(III)–phosphinate complexes

The chromium(III) perchlorate solution was mixed with sodium phosphinate solution resulting

* Author to whom correspondence should be addressed.

in a 0.00509 M chromium(III) perchlorate–0.305 M sodium phosphinate solution. Absorption spectrum of this solution was measured at appropriate time intervals with a Hitachi Recording Spectrophotometer EPS-3T and a 5-cm cell at $20 \pm 1°C$. The absorption spectrum of a 0.00509 M chromium(III) perchlorate solution was used as the spectrum at zero time.

Preparation of the equilibrium mixture of the chromium(III)–phosphinate complexes

Since it is impossible to prepare an equilibrium mixture containing all chromium(III)–phosphinate complex species in balanced abundance in just a single solution, three solutions were separately prepared by mixing chromium(III) phosphinate or chromium(III) perchlorate with sodium phosphinate at different ratios. The ionic strengths of the solution mixtures were adjusted to about 0.2 with sodium perchlorate and perchloric acid, if necessary. The chromium(III) and phosphinate concentrations, and the pH of the resulting solutions, are shown in Table 1. The solutions were kept at 50°C for about 2 weeks to reach equilibrium.

Separation of the inner-sphere complexes by Donnan exclusion chromatography

A gradient elution technique was employed. A mixing chamber initially containing 200 cm^3 of water and a reservoir containing a 3 M tetramethylammonium chloride solution were connected to a column packed with SP-Sephadex C-25 of tetramethylammonium form swollen with water to make a bed of 1.5 cm $\phi \times 90$ cm. After passing 65 cm^3 of eluant through the column (at that moment the concentration of the eluant flowing into the column top was about 1 M) 1 cm^3 of the sample solution of chromium–phosphinate complexes prepared as described in the foregoing section was added to the ion-exchanger bed. The gradient elution continued at a flow rate of 70 $cm^3 h^{-1}$ until all the components were eluted. The chromium complex species in the effluent were automatically detected at 420 nm with an Atto variable-wavelength spectrophotometer LDC Model Spectromonitor III, which was connected to the end of the separating column, to make an elution curve. For the determination of the inner-sphere stability constants, a quantitative analysis of chromium was made spectrophotometrically by a diphenylcarbazide method for each part of the effluent. When necessary phosphinate ions combined with chromium were spectrophotometrically determined with a molybdenum(V)–molybdenum(VI) reagent after liberation from the complexes using EDTA.

Cation-exchange equilibrium anlyses for the outer-sphere complex formation

Stability constants of the outer-sphere complexes were determined by a cation-exchange equilibrium

Table 1. Sample solution compositions and conditions for Donnan exclusion chromatography

Sample solution		I	II	III
Composition of the sample mixture (M)	$Cr(ClO_4)_3$			0.0203
	$Cr(PH_2O_2)_3$	0.0193	0.0193	
	$NaPH_2O_2$	0.140	0.0200	0.0200
pH of the sample solution		3.6	3.0	0.91
Sample volume injected (ml)		1.00	1.00	2.00
Amount of chromium species found after chromatography (mmol)	$[Cr(PH_2O_2)_6]^{3-}$	8.47×10^{-4}		
	$[Cr(PH_2O_2)_5(H_2O)]^{2-}$	5.54×10^{-3}	8.07×10^{-4}	
	$[Cr(PH_2O_2)_4(H_2O)_2]^{-}$	9.52×10^{-3}	4.65×10^{-3}	
	$[Cr(PH_2O_2)_3(H_2O)_3]$		3.63×10^{-3}	
	$[Cr(PH_2O_2)_2(H_2O)_4]^{+}$		5.85×10^{-3}	2.74×10^{-3}
	$[Cr(PH_2O_2)(H_2O)_5]^{2+}$			1.89×10^{-2}
	$[Cr(H_2O)_6]^{3+}$			1.82×10^{-2}
Calculated free $PH_2O_2^-$ ion concentration in the original sample solution (M)		0.121	2.97×10^{-2}	7.80×10^{-3}

analysis proposed by Schubert.[8] A series of solutions containing chromium perchlorate and excess sodium phosphinate of different concentrations were prepared. Sodium perchlorate was added to each solution to maintain the sodium ion concentration and the ionic strength constant. 50 cm³ of this solution was equilibrated with 0.5 g of Dowex 50W-X4, sodium form for 10 min at 50°C. The distribution ratio of chromium was calculated from the absorbance measurement of the equilibrated supernatant by the following equation:

$$D = \frac{A^o - A}{A} \cdot \frac{V}{m},$$

where A^o and A are the absorbances at the same wavelength (preferably at the absorption maximum) of the initial solution and the solution at equilibrium, respectively, V is the volume of the solution in cm³ and m is the gravity of the ion-exchanger in g. The amounts of chromium taken were adjusted so that its sorbed amount was maintained approximately constant in all batches, because a constant loading of chromium should fulfil the requirement of a constant sodium concentration and an unvaried activity coefficient in using equations for the ion-exchange method. It was confirmed that equilibration for 10 min does not give any inner-sphere complex formation. The same batch equilibration was made on the solution without phosphinate ligand to obtain the D^o value.

The stability constant of the mixed inner–outer-sphere complex was determined by a similar cation-exchange equilibrium analysis. The sample solution of $[Cr(PH_2O_2)(H_2O)_5]^{2+}$ was obtained from the effluent (containing 1 M sodium perchlorate as eluant) in the Donnan exclusion chromatography. This species was mixed with excess sodium phosphinate and sodium perchlorate of different concentrations and the 50 cm³ solution was shaken with 2 g of the same resin at 20°C for 20 min. The chromium sorbed on the resin was analysed using a diphenylcarbazide method after stripping and the distribution ratio was calculated as:

$$D = \frac{\bar{m}_{Cr}}{m^o_{Cr} - \bar{m}_{Cr}} \cdot \frac{V}{m},$$

where m^o_{Cr} and $\bar{m}_{Cr}$ are the total amount of chromium initially given and in the resin at equilibrium, respectively.

Construction of characteristic absorption spectra on individual inner-sphere complexes

The absorption spectrum of the effluent containing the individual chromium–phosphinate complex species isolated by Donnan exclusion chromatography was measured with a Hitachi Recording Spectrophotometer EPS-3T and a 5-cm cell. In combination with the elemental analysis of chromium, each characteristic absorption spectrum was obtained.

RESULTS AND DISCUSSION

A general behavior of absorption spectra of chromium(III)–phosphinate complexes with time

The time dependence of the absorption spectra of the solution containing chromium(III) perchlorate and sodium phosphinate at 20°C is shown in Fig. 1. The chromium(III) aqua ions have two characteristic peaks at wavelengths 410 and 580 nm in the visible-light region. The absorption peak at 410 nm first shifted instantaneously after the addition of

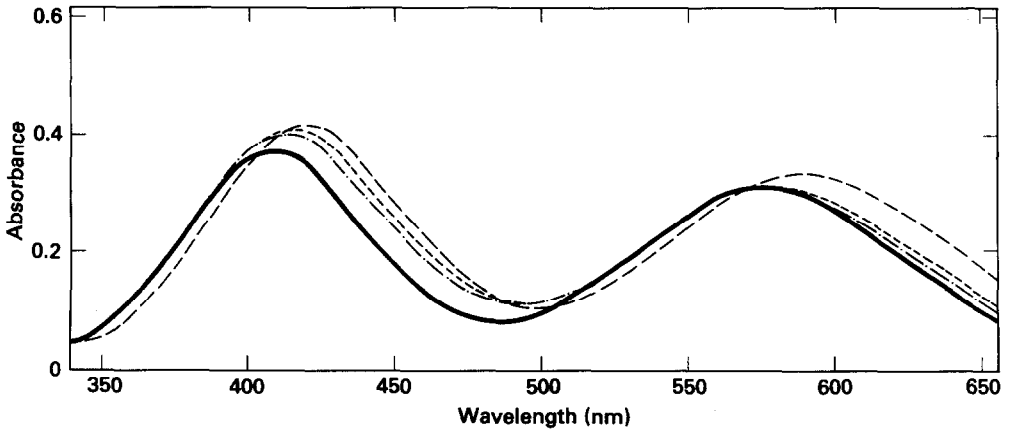


Fig. 1. Time dependence of absorption spectra of chromium(III) complexes: (———) 5.09×10^{-3} M $Cr(ClO_4)_3$ solution; and (– – –) 2.5 min, (– – –) 2.3 h, and (———) 30 h after mixing of 5.09×10^{-3} M $Cr(ClO_4)_3$ and 0.305 M $NaPH_2O_2$.

phosphinate and thereafter both peaks changed only very slowly with time, always shifting to longer wavelengths. Clearly the former phenomenon reflects the outer-sphere complex and the latter the inner-sphere complex formation with phosphinate ions. This fact indicates that the presence of both types of complex should be taken into account when a considerable time has elapsed after mixing. Consequently, the equilibrium analysis for outer-sphere complexes or the separation of inner-sphere complexes must be carried out as rapidly as possible, while the equilibrium analyses for inner-sphere types have to be made after the establishment of equilibrium with a very long time even at an elevated temperature.

Donnan exclusion chromatogram for chromium(III)–phosphinate complexes with a cation-exchanger column

In order to know the whole formation equilibrium on inner and outer complexes, the mutual separation of inner-sphere complexes is crucial since its chromatogram can give some of the stability constants directly and shows a general picture of species distribution. The Donnan exclusion chromatography[5,6] seems to be the most convenient for such a separation, because all successive anionic and cationic inner-sphere complexes $[Cr(PH_2O_2)_m(H_2O)_{6-m}]^{(m-3)-}$ could be separated from each other rapidly with a single cation-exchanger column. A typical elution curve for a synthesized sample, a mixture of solutions prepared separately, on an SP-Sephadex column is shown in Fig. 2, from which it is seen that each component could be almost quantitatively isolated in a rather short time.

According to the theory of Donnan exclusion chromatography, the elution position (retention time) for an excluded component depends only on its ionic charge, and the higher the anionic charge the earlier the ion elutes. Thus the elution peaks within one column volume revealed in the chromatogram of Fig. 2 could be assigned to $[Cr(PH_2O_2)_6]^{3-}$, $[Cr(PH_2O_2)_5(H_2O)]^{2-}$, $[Cr(PH_2O_2)_4(H_2O)_2]^{-}$ and $[Cr(PH_2O_2)_3(H_2O)_3]$ in that order. The unreacted phosphinate ions come out together with $[Cr(PH_2O_2)_4(H_2O)_2]^{-}$. The succeeding peaks are $[Cr(PH_2O_2)_2(H_2O)_4]^{+}$, $[Cr(PH_2O_2)(H_2O)_5]^{2+}$ and $[Cr(H_2O)_6]^{3+}$ (the last), respectively, which were confirmed by a direct analysis of the effluent for chromium and phosphorus.

For the sample solution with a real equilibrium, the analysis of chromium in the first four peaks of the chromatogram and the free phosphinate ion concentration may directly give the stepwise stability constants of the inner-sphere complexes, $K_{4,0}$, $K_{5,0}$ and $K_{6,0}$. On the other hand, the same analyses for subsequent peaks do not always give the stability constants $K_{1,0}$, $K_{2,0}$ and $K_{3,0}$, since these peaks correspond not only to pure inner-sphere complexes but also to outer-sphere or mixed inner–outer-sphere complexes which were present, if any, in the original solution. For example, $[Cr(H_2O)_6 \cdot (PH_2O_2)]^{2+}$ or $[Cr(H_2O)_6 \cdot (PH_2O_2)_2]^{+}$ should be eluted only as $[Cr(H_2O)_6]^{3+}$ by the release of phosphinate ions which were bound in the outer coordination sphere during the elution with an eluant containing no phosphinate ions. The true distribution among all species could be determined only by combining the chromatographic results with batch equilibrium data obtained separately.

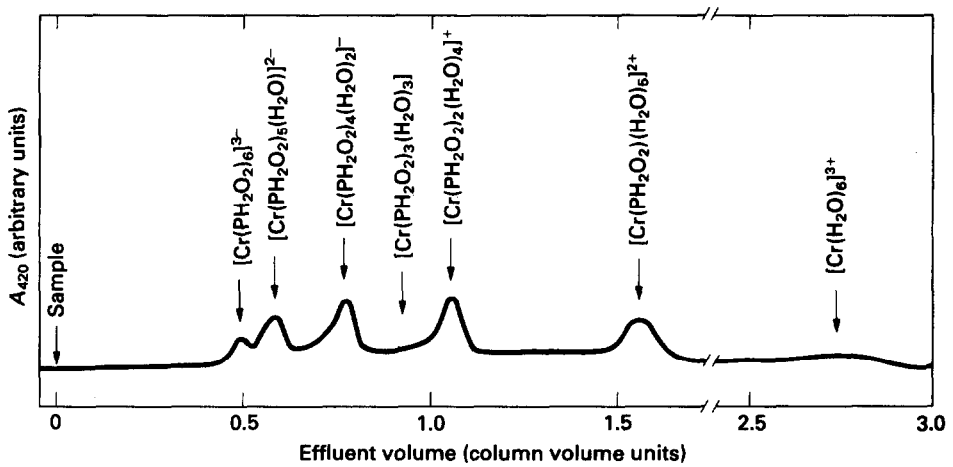


Fig. 2. A typical Donnan exclusion chromatogram for inner-sphere complexes of chromium(III) and phosphinate. Column: SP-Sephadex C-25, $N(CH_3)_4^+$ form, 1.5 cm $\phi \times 90$ cm; sample: mixture of $Cr(PH_2O_2)_3$ and $NaPH_2O_2$ not in equilibrium; eluant: 1–3 M $N(CH_3)_4Cl$ gradient; flow rate: 70 $cm^3 h^{-1}$.

These treatments are described in the following section.

General equations for stability constants in a chromium(III)–phosphinate complex system

A general equation for the overall stability constant of a chromium(III)–phosphinate complex is given by:

$$\beta_{n,m} \equiv \frac{[Cr(PH_2O_2)_n(H_2O)_{6-n}\cdot(PH_2O_2)_m^{(3-n-m)+,(n+m-3)-}]}{[Cr(H_2O)_6^{3+}][PH_2O_2^-]^{n+m}}, \quad (1)$$

where n and m are the ligand numbers bound in the inner and outer sphere, respectively.

The corresponding stepwise stability constant is defined as:

$$K_{n,m}^{in} \equiv \frac{[Cr(PH_2O_2)_n(H_2O)_{6-n}\cdot(PH_2O_2)_m^{(3-n-m)+,(n+m-3)-}]}{[Cr(PH_2O_2)_{n-1}(H_2O)_{7-n}\cdot(PH_2O_2)_m^{(4-n-m)+,(n+m-4)-}][PH_2O_2^-]} \quad (2)$$

for inner-sphere coordination of the ligand, or:

$$K_{n,m}^{out} \equiv \frac{[Cr(PH_2O_2)_n(H_2O)_{6-n}\cdot(PH_2O_2)_m^{(3-n-m)+,(n+m-3)-}]}{[Cr(PH_2O_2)_n(H_2O)_{6-n}\cdot(PH_2O_2)_{m-1}^{(4-n-m)+,(n+m-4)-}][PH_2O_2^-]} \quad (3)$$

for outer-sphere binding. Here the assumption $1 \leqslant n \leqslant 6$ [eqn (2)] or $0 \leqslant n \leqslant 6$ [eqn (3)], and $0 \leqslant m \leqslant 3-n$ may be reasonable, since chromium(III) has a coordination number of 6 and outer-sphere binding takes place only by a weak electrostatic attraction between the hydrated cation (complex) and phosphinate anion.

Determination of the outer-sphere stability constants $K_{0,1}$ *and* $K_{0,2}$

$K_{0,1}$ and $K_{0,2}$ were determined by Schubert's cation-exchange equilibrium analysis[8] at 50°C using the following relation:

$$\frac{D_{Cr}^o}{D_{Cr}} = 1 + K_{0,1}[PH_2O_2^-] + K_{0,1}K_{0,2}[PH_2O_2^-]^2 + \cdots, \quad (4)$$

where D_{Cr} and D_{Cr}^o are the distribution ratios of chromium when the phosphinate ligand is present and absent, respectively. The D_{Cr}^o/D_{Cr} vs $[PH_2O_2^-]$ plot showed a parabola, indicating only the presence of the first and second outer-sphere complexes $[Cr(H_2O)_6\cdot(PH_2O_2)]^{2+}$ and $[Cr(H_2O)_6\cdot(PH_2O_2)_2]^+$ (Fig. 3). The best fit of the experimental data to a parabola with a least-squares treatment resulted in $\log K_{0,1} = 0.90$ and $\log K_{0,2} = 0.0079$, and the negligible presence of the third outer-sphere complex $[Cr(H_2O)_6\cdot(PH_2O_2)_3]$.

Determination of the outer-sphere stability constant $K_{1,1}$

$K_{1,1}$ was determined by the same method as described above:

$$\frac{D_{Cr}^o}{D_{Cr}} = 1 + K_{1,1}[PH_2O_2^-] + \cdots. \quad (5)$$

In this the chromium sample was taken from the effluent for the $[Cr(PH_2O_2)(H_2O)_5]^{2+}$ peak in the Donnan exclusion chromatographic separation. A temperature of 20°C was used in the experiment to avoid an inner-sphere reaction. The D_{Cr}^o/D_{Cr} vs $[PH_2O_2^-]$ plot showed an approximately linear relation (Fig. 3), indicating only the outer-sphere formation of the singly-charged cationic complex $[Cr(PH_2O_2)(H_2O)_5\cdot(PH_2O_2)]^+$, which may correspond to the result in the foregoing section.

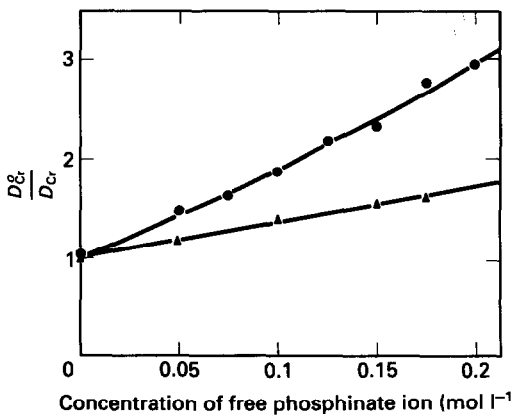


Fig. 3. Determination of stability constants of outer-sphere and inner–outer-sphere complexes by the cation-exchange equilibrium method: (●) outer-sphere complex, (▲) inner–outer-sphere complex.

Determination of the inner-sphere stability constants $K_{1,0}$–$K_{6,0}$

The analyses of $[Cr(H_2O)_6]^{3+}$, $[Cr(PH_2O_2)(H_2O)_5]^{2+}$ and $[Cr(PH_2O_2)_2(H_2O)_4]^{+}$ for the corresponding peaks in a chromatogram of the type in Fig. 2 do not give a direct calculation on the inner-sphere complex formation in the original sample solution. Instead, the following relationships hold:

$$\frac{m_{CrL}}{m_{Cr}} = \frac{[Cr(PH_2O_2)(H_2O)_5^{2+}] + [Cr(PH_2O_2)(H_2O)_5 \cdot (PH_2O_2)^{+}]}{[Cr(H_2O)_6^{3+}] + [Cr(H_2O)_6 \cdot (PH_2O_2)^{2+}] + [Cr(H_2O)_6 \cdot (PH_2O_2)_2^{+}]}$$

$$= \frac{K_{0,1}(1 + K_{1,1}[PH_2O_2^-])[PH_2O_2^-]}{1 + K_{0,1}[PH_2O_2^-] + K_{0,1}K_{0,2}[PH_2O_2^-]^2} \quad (6)$$

and

$$\frac{m_{CrL_2}}{m_{CrL}} = \frac{[Cr(PH_2O_2)_2(H_2O)_4^{+}]}{[Cr(PH_2O_2)(H_2O)_5^{2+}] + [Cr(PH_2O_2)(H_2O)_5 \cdot (PH_2O_2)^{+}]} = \frac{K_{2,0}[PH_2O_2^-]}{1 + K_{1,1}[PH_2O_2^-]}, \quad (7)$$

where L refers to the $[PH_2O_2]^-$ ligand and m is the total amount of chromium contained in each elution peak for the subscribed complex in the chromatogram. It may be reasonable to assume that the neutral complex $[Cr(PH_2O_2)_2(H_2O)_4 \cdot (PH_2O_2)]$ is negligible. Thus the inner-sphere constants $K_{1,0}$ and $K_{2,0}$ can be determined by:

$$K_{1,0} = \frac{m_{CrL}}{m_{Cr}} \cdot \frac{1 + K_{0,1}[PH_2O_2^-] + K_{0,1}K_{0,2}[PH_2O_2^-]^2}{(1 + K_{1,1}[PH_2O_2^-])[PH_2O_2^-]}, \quad (8)$$

$$K_{2,0} = \frac{m_{CrL_2}}{m_{CrL}} \cdot \frac{1 + K_{1,1}[PH_2O_2^-]}{[PH_2O_2^-]}, \quad (9)$$

when $K_{0,1}$, $K_{0,2}$, $K_{1,1}$ and $[PH_2O_2^-]$ are known.

The inner-sphere stability constants $K_{3,0}$, $K_{4,0}$, $K_{5,0}$ and $K_{6,0}$ for the higher complexes can be expressed in a simpler form, since no complexes involve outer-sphere binding with phosphinate anions:

$$K_{3,0} = \frac{m_{CrL_3}}{m_{CrL_2}[PH_2O_2^-]}, \quad (10)$$

$$K_{4,0} = \frac{m_{CrL_4}}{m_{CrL_3}[PH_2O_2^-]}, \quad (11)$$

$$K_{5,0} = \frac{m_{CrL_5}}{m_{CrL_4}[PH_2O_2^-]}, \quad (12)$$

$$K_{6,0} = \frac{m_{CrL_6}}{m_{CrL_5}[PH_2O_2^-]}. \quad (13)$$

The free phosphinate concentration, $[PH_2O_2^-]$, in the original sample solution containing the complex mixture can be expressed as:

$$[PH_2O_2^-]V_s = m_{\Sigma L} - 6m_{CrL_6} - 5m_{CrL_5} - 4m_{CrL_4} - 3m_{CrL_3} - 2m_{CrL_2} - m_{CrL} \times \left(1 + \frac{K_{1,1}[PH_2O_2^-]}{1 + K_{1,1}[PH_2O_2^-]}\right) - m_{Cr}K_{0,1}[PH_2O_2^-] \times \left(\frac{1 + 2K_{0,2}[PH_2O_2^-]}{1 + K_{0,1}[PH_2O_2^-] + K_{0,1}K_{0,2}[PH_2O_2^-]^2}\right), \quad (14)$$

where V_s is the sample solution volume injected into the column and $m_{\Sigma L}$ is the total amount of phosphinate injected.

Accordingly, all unknown six inner-sphere constants can be evaluated from all m values analyzed and the total ligand concentration using eqns (8)–(14). The experimental condition and analytical data are shown in Table 1. Three chromatographic runs were made with different compositions of chromium and phosphinate in order to obtain each complex component in reasonable abundance for analysis. A difference in the stability constant between different runs was not serious for such a complicated system (for instance, $\log K_{5,0} = 0.68$ and 0.74).

All the constants evaluated are shown in the whole complexation scheme (Fig. 4) with some additional constants calculated merely by numerical balancing (not experimentally determined). A general view concerning both the inner- and outer-

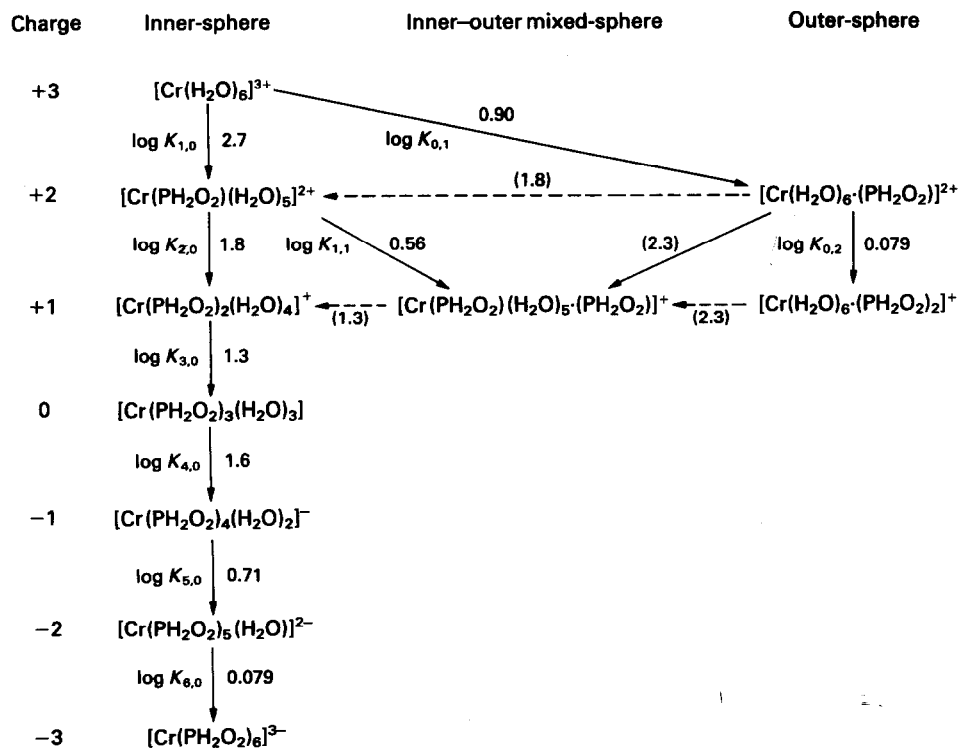


Fig. 4. Stability constants of chromium(III)–phosphinate complexes at 50°C and ionic strength 0.2.

sphere distribution of chromium(III)–phosphinate complexes has been reached, at least for the mononuclear system. The inner-sphere constants were mostly in the decreasing order: $K_{1,0} > K_{2,0} > K_{3,0} < K_{4,0} > K_{5,0} > K_{6,0}$, showing a normal behavior for the complexation reaction with the exception between $K_{3,0}$ and $K_{4,0}$. The irregularity $K_{3,0} < K_{4,0}$ might be ascribed to an easier displacement of H_2O molecules from the uncharged complex $[Cr(PH_2O_2)_3(H_2O)_3]$ in comparison with other charged complexes which can strongly attract H_2O dipoles by an electrostatic force.

Also, it was found that the outer-sphere constants are considerably lower than those for the corresponding inner-sphere ones, though this is a matter of course.

Characteristic absorption spectra for the inner-sphere chromium–phosphinate complexes

From the success of the isolation of each inner-sphere complex species, an absorption spectrum characteristic of the complex of each ligand number was obtained by measuring the absorbance of the effluent solution at each elution peak in the chromatogram, combined with the elemental analysis of chromium. Table 2 gives the wavelengths of the absorption maximum and the maximal molar

Table 2. Absorption spectrum characteristics of chromium(III)–phosphinate complexes

Complex	Maximal absorption wavelength (nm)		Molar absorption coefficient ($M^{-1}cm^{-1}$)	
	I	II	I	II
$[Cr(H_2O)_6]^{3+}$	410	580	15.3	12.8
$[Cr(PH_2O_2)(H_2O)_5]^{2+}$	419	594		
$[Cr(PH_2O_2)_2(H_2O)_4]^{+}$	430	614	19.2	15.7
$[Cr(PH_2O_2)_3(H_2O)_3]$	435	620		
$[Cr(PH_2O_2)_4(H_2O)_2]^{-}$	440	626	21.5	18.0
$[Cr(PH_2O_2)_5(H_2O)]^{2-}$	444	630		
$[Cr(PH_2O_2)_6]^{3-}$	447	634	25.2	23.0

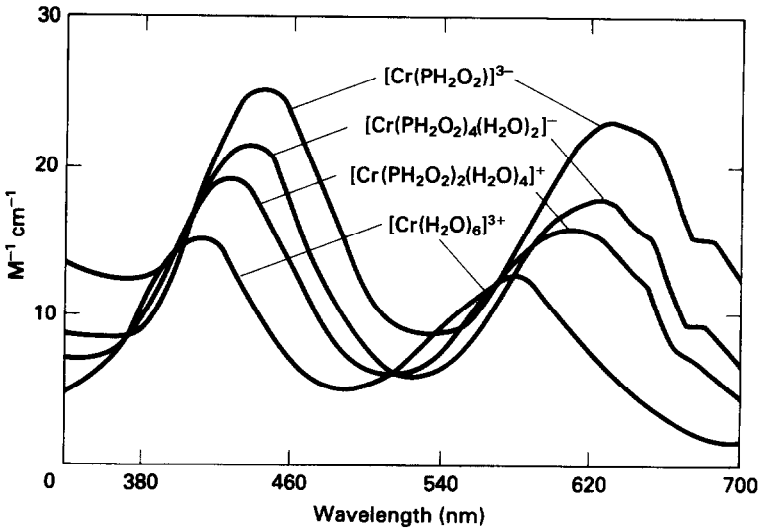


Fig. 5. Absorption spectra of chromium(III)–phosphinate complexes.

absorption coefficients and Fig. 5 shows four absorption spectra as examples. It was found that the wavelength shifts to longer wavelengths continuously and the molar absorption coefficient increases with increase in the ligand number, though this behavior can also be observed in most other systems of complex formation.

REFERENCES

1. J. H. Espenson and D. E. Binau, *Inorg. Chem.* 1966, **5**, 1365.
2. A. M. Lunyatskas and P. K. Norkus, *Zh. Neorg. Khim.* 1968, **13**, 665.
3. R. M. Smith and A. E. Martell (Eds), *Critical Stability Constants, Inorganic Complexes*, Vol. 4. Plenum Press, New York (1976).
4. E. Hogfeldt (Ed.), *Stability Constants of Metal–Ion Complexes. Part A: Inorganic Ligands.* Pergamon Press, Oxford (1982).
5. H. Waki and Y. Tokunaga, *J. Chromatogr.* 1980, **201**, 259.
6. H. Waki and Y. Tokunaga, *J. Liq. Chromatogr.* 1982, **5**, 105.
7. H. Waki, K. Tsuruta and Y. Tokunaga, *J. Liq. Chromatogr.* 1985, **8**, 2105.
8. J. Schubert, *J. Phys. Chem.* 1948, **52**, 340.

Polyhedron Vol. 5, No. 7, pp. 1247–1251, 1986
Printed in Great Britain

0277–5387/86 $3.00+.00
Pergamon Journals Ltd

EQUILIBRIA IN AQUEOUS SOLUTION BETWEEN Fe(II) AND *N*-METHYLIMINODIACETIC, *N*-ETHYLIMINODIACETIC AND *N*-PROPYLIMINODIACETIC ACIDS

A. MEDEROS,* S. DOMINGUEZ and A. M. MEDINA

Departamento de Química Inorgánica, Facultad de Química, Universidad de La Laguna, Canary Islands, Spain

and

F. BRITO and E. CHINEA

Laboratorio de Equilibrios en Solución, Escuela de Química, Facultad de Ciencias, Universidad Central de Venezuela, Caracas, Venezuela

(*Received* 23 *September* 1985; *accepted* 6 *November* 1985)

Abstract—The complex species formed in aqueous solution between Fe(II) and *N*-methyliminodiacetic acid (MIDA), *N*-ethyliminodiacetic acid (EIDA) and *N*-propyliminodiacetic acid (PIDA) were studied at 25°C and ionic strength 0.1 M in KCl. The experimental potentiometric data were analysed with the least-squares computer program LETAGROP, taking into account hydrolysis of the Fe(II) ion. The ionization constants of MIDA, EIDA and PIDA acids are determined for the corresponding ionic strength and temperature. The following complex species were found (ligands, H_2C): MIDA, $[FeHC]^+$, FeC and $[FeC_2]^{2-}$; EIDA, FeC and $[FeC_2]^{2-}$; PIDA, FeC, $[FeC_2]^{2-}$ and $[Fe(OH)C]^-$. The corresponding stability constants were determined.

Studies of the coordinating capacity in aqueous solution of Fe(II) with aminoacids or polyamicarboxylic derivatives have not been undertaken as frequently as those of other bivalent first-row transition-metal cations,[1–3] perhaps because of the precautions needed to avoid oxidation of Fe(II) to Fe(III).[4] The studies are of biological interest.[5] In the specific case of iminodiacetic acid (IDA) and its derivatives, *N*-methyliminodiacetic acid (MIDA), *N*-ethyliminodiacetic acid (EIDA) and *N*-propyliminodiacetic acid (PIDA), investigations have only been carried out with Fe(II) for IDA[6] at 25°C and ionic strength 0.5 M in $NaClO_4$ and for MIDA[7] at 20°C and ionic strength 0.1 M in KCl. The species FeY and $[FeY_2]^{2-}$ (H_2Y acids) were identified for both ligands. No studies have been reported on the ligands EIDA and PIDA. In the present work the coordinating capacity in aqueous solution of Fe(II) with the ligands MIDA, EIDA and PIDA at 25°C and ionic strength 0.1 M in KCl is studied. An example of the biological interest of IDA and ligand derivatives is the recent proposal[8] of the complex $VOL_2 \cdot 2H_2O$ (H_2L = IDA) as a model for Amavadina, a natural product of vanadium from the fungus *Amanita muscaria*.

EXPERIMENTAL

Reagents

The acids MIDA, EIDA and PIDA were synthesized by reacting methylamine, ethylamine and *n*-propylamine (Merck, products for synthesis), respectively with previously neutralized chloracetic acid, following the procedure described by Souchay *et al.*[9] The previously obtained barium salts gave the corresponding acid on adding conc. H_2SO_4. The acids were purified by recrystallization in water–isopropanol mixtures, and were identified by their potentiometric equivalents, NMR, mass spectra and IR.

* Author to whom correspondence should be addressed.

The Fe(II) solutions were freshly prepared using $FeSO_4 \cdot 7H_2O$ (Merck, analytical grade). The ferrous solution was stored out of contact with the air, in a vessel with an atmosphere of hydrogen. Possible traces of Fe(III) were reduced by means of a current of hydrogen and using palladium carbon, as indicated in an earlier work.[10] Before adding the solution of Fe(II) to the titration cell, Fe(II) concentration was determined by dichromatic titration,[11] and the absence of Fe(III) checked by means of thiocyanate. Carbonate-free sodium hydroxide solution was prepared according to the school of Sillén[12] and standardized against potassium hydrogen phthalate. The solution of HCl was prepared from hydrochloric acid (Merck, analytical grade). Potassium chloride was prepared by recrystallization of KCl (Merck, analytical grade).

Apparatus and titration procedures

The potentiometric titrations were carried out in argon inert atmosphere, at 25 ± 0.05°C, ionic strength 0.1 M in KCl, using a Radiometer Type PHM-64 potentiometer, a Radiometer G 202 B glass electrode and a K 401 calomel electrode. The free hydrogen ion concentration, $[H^+]$, was determined by measuring the e.m.f. of the cell Hg/Hg_2Cl_2, KCl sat//Fe^{2+}, ligand, KCl 0.1 M/glass electrode.

The cell constants were determined according to the method of Biedermann and Sillén,[13] the liquid junction potentials were found to be negligible within the margins of $[H^+]$ studied. It was found that $pK_w = 13.77$, in good agreement with reported data.[14]

The ligands were measured alone at the following concentrations: MIDA ($C_L = 3.00 \times 10^{-3}$); EIDA ($C_L = 3.94 \times 10^{-3}$), and PIDA ($C_L = 5.70 \times 10^{-3}$); the Fe(II) alone ($C_M = 5.00 \times 10^{-3}$ and 2.50×10^{-3}) in order to study hydrolysis by dilution of the solution of initial concentration at 25°C and ionic strength 0.1 M in KCl; and the ligands in the presence of Fe(II) at the following concentrations and ligand : metal ratios: MIDA 1 : 1 ($C_L = 3$ mM), 3 : 1 ($C_L = 3$ mM), 1 : 15 ($C_L = 1$ mM); EIDA 1 : 1 ($C_L = 4$ mM), 2.54 : 1 ($C_L = 3.74$ mM), 1 : 15 ($C_L = 1$ mM); and PIDA 1 : 1, 3 : 1, 5 : 1 ($C_L = 3$ mM), 1 : 15 ($C_L = 1$ mM).

Data treatment

The experimental potentiometric data were analysed by means of the NERNST/LETA/GRAFICA version[15] of the LETAGROP programme,[16] based on a generalized form of the least-squares method, that establishes the best model and best values of the β_{pqr} constants, minimizing the function $U = \Sigma (Z_{exp} - Z_{calc})^2$, Z being the average number of dissociated protons for the total concentration of ligand (Z_c) or for the total concentration of metal (Z_B). The LETAGROP calculations also give standard deviations $\sigma(Z)$ and $\sigma(\log \beta_{pqr})$.[17] The computations were performed on a Burroughs 6700 computer (Facultad de Ciencias, Universidad Central de Venezuela, Caracas).

RESULTS AND DISCUSSION

Hydrolysis of Fe(II)

Twenty-five experimental points of the two potentiometric titrations carried out were used for the calculations. For the equilibrium

$$qFe^{2+} + pH_2O \rightleftharpoons [Fe_q(OH)_p]^{(2q-p)+} + pH^+, \quad \beta_{-pq}$$

it is found that $\log \beta_{-11} = -7.301 \pm 0.185$, with a standard deviation $\sigma(Z) = 0.003$ (25°C and $I = 0.1$ M in KCl), that corresponds to the formation of the species $[Fe(OH)]^+$. The value found is in good agreement with that obtained by Gayer and Woontner at 25°C and $I = 0.5$ M in KCl, $\log \beta_{-11} = -7.17$.[18]

Ionization constants of the acids

Potentiometric titrations were carried out of each of the acids with NaOH 0.1 M and HCl 0.1 M, respectively. From the values obtained for the constants β_{pr}, corresponding to the equilibria

$$pH^+ + rH_2C \rightleftharpoons H_p(H_2C)_r,$$

the ionization constants of the acids, K_i, given in Table 1, could readily be determined.

For comparison purposes, values from the literature for other acids, at the same ionic strength and temperature, are also included, as well as those of acid IDA.[2] It is observed that the order of basicity of the N atom (equilibrium HC^-/C^{2-}) is IDA < MIDA < EIDA ≤ PIDA, which corresponds to the electrodonor effect of the corresponding alkyl radical.

The validity of the values found for the constants β_{pr} is proven in Fig. 1 by the excellent agreement between the experimental curves $Z(-\log[H^+])$ and those calculated from the β_{pr} values given in Table 1.

Stability constants of the complexes formed

The analysis of the experimental data of each of the three ligand–metal systems by the

Table 1. Ionization constants of MIDA, EIDA and PIDA acids (25°C, $I = 0.1$ M in KCl)

	$-\log \beta_{pr}$		
pr	MIDA	EIDA	PIDA
11	-1.916 ± 0.091	-1.569 ± 0.061	-1.532 ± 0.139
-11	2.314 ± 0.021	2.219 ± 0.042	2.244 ± 0.023
-21	11.925 ± 0.018	12.173 ± 0.010	12.256 ± 0.024
[a]	42	38	61
[b]	0.009	0.007	0.005

	Equilibrium (pK_i)			
	H_3C^+/H_2C	H_2C/HC^-	HC^-/C^{2-}	Reference
IDA	1.82	2.61	9.32	2
MIDA	1.92	2.31	9.61	[c]
		2.2	9.60	2
EIDA	1.57	2.22	9.95	[c]
PIDA	1.53	2.24	10.02	[c]
		2.44	10.09	9

[a] Number of experimental points.
[b] Standard deviations $\sigma(Z)$.
[c] Present work.

NERNST/LETA/GRAFICA version[15] of the LETAGROP programme[16] allowed us to calculate the β_{pqr} constants for the complex species formed for each ligand, defined by means of the equilibrium

$$pH^+ + qFe^{2+} + rH_2C \rightleftharpoons [H_pFe_q(H_2C)_r]^{(p+2q)+}, \quad \beta_{pqr}.$$

Taking into account the species resulting from the massive ionizations of the ligand (H_2C, HC^- and C^{2-}) and the species $[Fe(OH)]^+$ obtained from the hydrolysis of Fe(II), the results that best fit the experimental results are those given in Table 2, the validity of which is proven in Figs 2–4, where an

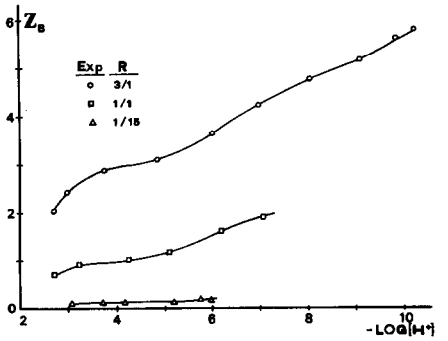


Fig. 2. $Z_B(-\log [H^+])$ curves of the system MIDA–Fe(II). Full curves have been calculated using the set of proposed constants β_{pqr} in Table 2.

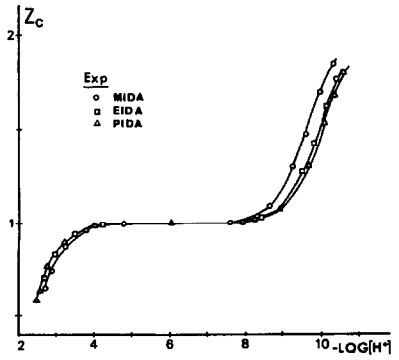


Fig. 1. $Z_c(-\log [H^+])$ curves corresponding to MIDA, EIDA and PIDA acids. Full curves have been calculated using the set of proposed constants β_{pr} in Table 1.

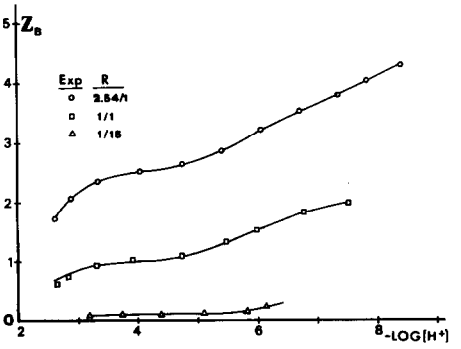


Fig. 3. $Z_B(-\log [H^+])$ curves of the system EIDA–Fe(II). Full curves have been calculated using the constants β_{pqr} in Table 2.

Table 2. Stability constants of the complexes of MIDA, EIDA and PIDA acids with Fe(II) (25°C, $I = 0.1$ M in KCl)

	$-\log \beta_{pqr}$		
pqr	MIDA	EIDA	PIDA
−111	0.027±0.152		
−211	5.215±0.091	5.456±0.068	5.661±0.034
−311			14.741±0.075
−412	12.090±0.117	12.669±0.119	12.622±0.050
[a]	3	3	4
[b]	93	93	153
[c]	0.021	0.026	0.019
[d]	2.7–10.2	2.6–8.5	2.6–11.0

	$\log K_1$	$\log K_2$	$\log K'$	$\log K''$	Reference
IDA	5.54[e]	4.27			6
	5.8[f]	4.3			20
MIDA	6.65[f]	5.37			7
	6.71	5.05	2.29		[g]
EIDA	6.72	4.96			[g]
PIDA	6.59	5.29		11.28	[g]

[a] Number of titrations.
[b] Number of experimental points.
[c] Standard deviations $\sigma(Z)$.
[d] $-\log [H^+]$, range.
[e] 25°C, $I = 0.5$ M in $NaClO_4$.
[f] 20°C, $I = 0.1$ M in KCl.
[g] Present work.

excellent fit can be observed between the experimental curves $Z(-\log [H^+])$ and those calculated from the β_{pqr} values given in Table 2.

From the β_{pqr} constants and taking into account the β_{pr} constants of the acids given in Table 1, the stability constants of the complex species formed can readily be calculated, according to the following equilibria:

$$Fe^{2+} + HC^- \rightleftharpoons [FeHC]^+, \qquad K';$$

$$Fe^{2+} + C^{2-} \rightleftharpoons FeC, \qquad K_1;$$

$$FeC + C^{2-} \rightleftharpoons [FeC_2]^{2-}, \qquad K_2;$$

$$Fe^{2+} + C^{2-} + OH^- \rightleftharpoons [Fe(OH)C]^-, \qquad K''.$$

The value of K_w at the same ionic strength and temperature must also be taken into account in order to calculate K''.

The results are also given in Table 2 and are compared with data for MIDA from the literature; for comparison purposes, in this series of ligands, they are also contrasted with data for IDA.

The complex $[FeHC]^+$ only appears in significant amounts for MIDA acid, and even here it is not well defined, as can be deduced from the data found for $-\log \beta_{-111}$ in Table 2. The value calculated for the pK corresponding to ionization of the complex ($[FeHC]^+ \rightleftharpoons FeC + H^+$) is 5.60, indicating that this

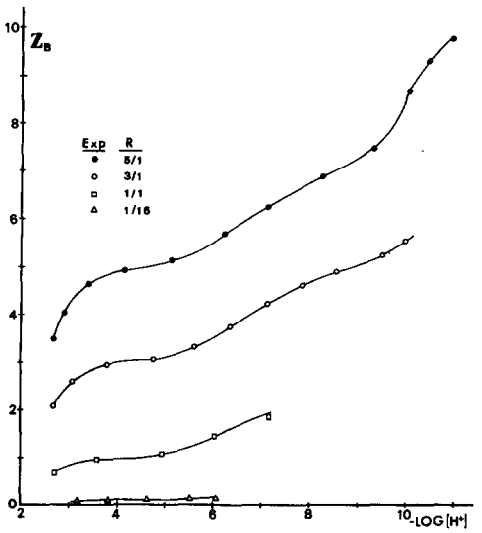


Fig. 4. $Z_B(-\log [H^+])$ curves of the system PIDA–Fe(II). Full curves have been calculated using the constants β_{pqr} in Table 2.

species has the proton over the N atom and that only the carboxylate groups will coordinate with the metal. The value of 5.60 also indicated that the proton is subjected to repulsion of the metallic cation, that tends to displace it in order to form the stable complex FeC. The species $[MHC]^+$ is of weak stability and for the acids EIDA and PIDA has only been found for divalent cations forming complexes more stable than Fe(II), such as Co(II), Ni(II), Zn(II) and Pb(II).[21]

The monohydroxycomplex $[Fe(OH)C]^-$ only appeared well defined for PIDA, probably resulting from the hydrolysis of the neutral complex, i.e. $FeC(H_2O) \rightleftharpoons [Fe(OH)C]^- + H^+$. The intervals referred to are, of course, those of $-\log [H^+]$ studied, which in the case of PIDA attained 11. The formation of this species was hindered, especially with excess of ligand, by the tendency to form the 2:1 complex, $FeC + C^2 \rightleftharpoons [FeC_2]^{2-}$. The species $[FeC_2]^{2-}$ was well defined in all the acids, because these ligands are tricoordinating and two ligands saturate the coordination index 6 of the central ion.[22] The neutral complex FeC, that in aqueous solution is really $FeC(H_2O)_3$, in order to fulfil the coordination index 6 of Fe(II),[22] coordinates the N atom and the two O atoms of the two carboxylate groups to the Fe(II). The order of stability found (Table 2), IDA < MIDA $\leqslant$ EIDA > PIDA, no longer corresponds to the expected basicity for the N atom, according to the electrodonor nature of the alkyl radical that became evident with respect to the H^+ (Table 1). Perhaps when the length of the alkyl radical increases, as is manifested in the *n*-propyl radical, steric repulsion effects that counteract the inductive effects are brought to bear on the metallic cation. These effects also become apparent with respect to other divalent transition cations.[21]

If the values of log *K* given in Table 2 for Fe(II) are compared with those found for Mn(II) and Co(II)[21]

	MIDA	EIDA	PIDA
Mn	5.39	5.33	5.32
Co	7.60	7.62	7.58

it is observed that the stability sequence of Irving and Williams is fulfilled.[23]

REFERENCES

1. A. E. Martell and R. M. Smith, *Critical Stability Constants*, Vol. 1, *Amino Acids*. Plenum Press, New York (1974).
2. A. E. Martell and R. M. Smith, *Critical Stability Constants*, Vol. 5, *First Supplement*. Plenum Press, New York (1982).
3. D. D. Perrin, *Stability Constants of Metal–Ion Complexes. Part B: Organic Ligands*. Pergamon Press, Oxford (1979).
4. F. A. Cotton and G. Wilkinson, *Advanced Inorganic Chemistry*, 4th edn, p. 756. John Wiley, New York (1980).
5. M. N. Hughes, *The Inorganic Chemistry of Biological Processes*. John Wiley, London (1972).
6. A. Napoli, *J. Inorg. Nucl. Chem.* 1972, **34**, 1347.
7. G. Schwarzenbach, G. Anderegg, W. Schneider and H. Senn, *Helv. Chim. Acta* 1955, **38**, 1147.
8. M. Asri Nawi and Th. L. Riechel, *Inorg. Chim. Acta* 1984, **93**, 131.
9. P. Souchay, N. Israily and P. Gouzerh, *Bull. Soc. Chim. Fr.* 1966, 3917.
10. E. Medina de la Rosa, A. Mederos, P. Martín Barroso and J. J. Alvarez Colomer, *An. Quím.* 1979, **75**, 799.
11. I. M. Kolthoff and E. B. Sandell, *Análisis Químico Cuantitativo*, p. 867. Nigar, Buenos Aires (1972).
12. F. Brito and N. Ingri, *An. R. Soc. Esp. Fis. Quím.* 1960, **56B**, 165.
13. G. Biedermann and L. G. Sillén, *Ark. Kemi* 1953, **5**, 425.
14. R. M. Smith and A. E. Martell, *Critical Stability Constants*, Vol. 4, *Inorganic Complexes*. Plenum Press, New York (1976).
15. F. Brito and J. M. Gonçalves, Project No. 51.78.31-S1-1228, CONICIT, Caracas, Venezuela (1981).
16. R. Arnek, L. G. Sillén and O. Wahlberg, *Ark. Kemi* 1969, **31**, 353.
17. L. G. Sillén, *Acta Chem. Scand.* 1962, **16**, 159; L. G. Sillén and B. Warnqvist, *Ark. Kemi* 1969, **31**, 341.
18. K. H. Gayer and L. Woontner, *J. Am. Chem. Soc.* 1953, **75**, 2476.
19. M. B. Jones and L. Pratt, *J. Chem. Soc., Dalton Trans.* 1976, 1207.
20. G. Anderegg, *Helv. Chim. Acta* 1964, **47**, 1801.
21. A. Mederos, S. Dominguez and A. M. Medina, *An. Quím.* (to be published).
22. J. Burgess, *Metal Ions in Solution*. Ellis Horwood, Chichester (1978).
23. H. Irving and R. J. P. Williams, *Nature (London)* 1948, **162**, 746; *J. Chem. Soc.* 1953, 3192.

Polyhedron Vol. 5, No. 7, pp. 1253–1257, 1986
Printed in Great Britain

0277–5387/86 $3.00+.00
Pergamon Journals Ltd

POTENTIOMETRIC STUDY ON THE COMPLEX EQUILIBRIA BETWEEN Ni(II), Co(II) AND Mn(II) AND 3-(2-FURYL)-2-MERCAPTOPROPENOIC AND 3-(2-FURYL)-2-MERCAPTOPROPANOIC ACIDS

A. IZQUIERDO* and L. GARCIA-PUIGNOU

Departament de Química Analítica, Facultat de Química, Universitat de Barcelona, 08028 Barcelona, Spain

and

J. GUASCH

Departament de Química Analítica, Facultat de Ciències Químiques, Universitat de Barcelona, 43005 Tarragona, Spain

(*Received* 5 *August* 1985; *accepted* 6 *November* 1985)

Abstract—Complex formation between Ni(II), Co(II) and Mn(II) and 3-(2-furyl)-2-mercaptopropenoic and 3-(2-furyl)-2-mercaptopropanoic acids has been studied using glass electrode potentiometry. Ligand–metal ion mixtures in 10% (v/v) ethanol–water containing 0.1 mol dm^{-3} KNO_3 were titrated with potassium hydroxide. The e.m.f. data obtained have been analyzed using the linearization method, and initial estimates of protonation constants for the ligands and complex formation constants have been refined with the MINIQUAD program.

The complexation of metals by 2-mercaptoacids has been widely studied,[1,2] but only a few studies of the complexation of 3-aryl-2-mercaptoacids with metal ions appear in the literature. The 3-aryl-2-mercaptoacids are compounds which act as complexing agents for metal ions. They have many analytical applications and they are also interest in relation to various biological systems. 3-(2-Furyl)-2-mercaptopropenoic acid has been used for the spectrophotometric determination of Ti(IV)[3] and Mo(IV),[4] and 3-(4-methoxyphenyl)-2-mercaptopropenoic acid for Ni(II).[5] Following administration of 3-(2-furyl)-2-mercaptopropenoic acid, blood plasma zinc concentration increases manyfold[6] and evidence for the formation of a ternary complex of plasma albumin, zinc and the furyl derivative has been obtained.[7] Foye and Lo[8] reported stability constant data for complexes of the phenyl derivative with Al(III), Cu(II) and Fe(III), and also found this compound to have antimicrobial activity. Wagner *et al.*[9] studied the inhibition of metaloenzymes by differents 3-aryl-2-mercaptopropenoic acids and the stability constants of metal complexes in 50% (v/v) dioxane–water were reported.

In order to compare the influence of the double bond in the complexing ability of 3-aryl-2-mercaptoacids we have determined potentiometrically the stability constants of 3-(2-furyl)-2-mercaptopropenoic and 3-(2-furyl)-2-mercaptopropanoic acids with the ions Ni(II), Co(II) and Mn(II) in 10% (v/v) ethanol–water.

EXPERIMENTAL

Reagents and solutions

3-(2-Furyl)-2-mercaptopropenoic acid (FMPE) was prepared by alkaline hydrolysis of the rhodanine derivative obtained from the condensation of furylaldehyde with rhodanine, following the procedure of Campaigne and Cline.[10] 3-(2-Furyl)-2-mercaptopropanoic acid (FMPA) was obtained by reduction of FMPE with sodium amalgam and puri-

* Author to whom correspondence should be addressed.

fied as described earlier.[11] Their purity were tested periodically by iodometric titrations.[12] Although FMPE and FMPA were found to be quite stable, freshly prepared solutions were used for each titration.

Standard stock solutions of metals were prepared as its nitrate salts. The Ni(II) (40.3 mmol dm^{-3}) and Co(II) (48.7 mmol dm^{-3}) stock solutions were standardized electrogravimetrically and the Mn(II) (55.4 mmol dm^{-3}) stock solution was standardized gravimetrically as Mn(II) pyrophosphate.[13]

Potassium hydroxide solution (0.05 mol dm^{-3}) was prepared frequently[14] and standardized by titration against standard grade potassium hydrogen phthalate.

Water used to prepare reagent solutions and in all dilutions was double deionized, Culligan Water Ultrapure, 0.08 μohm^{-1} cm^{-1} conductivity. All other reagents used were reagent grade, and all solutions were 10% (v/v) ethanol–water.

Apparatus

A radiometer compensator potentiometer PHM 64 was used. The indicator glass electrode (Radiometer G-202B) was conditioned for several hours in the mixed solvent and saturated calomel reference electrode (Radiometer K-401), with an external salt bridge containing saturated KCl solution. Indicator electrode calibration was performed without buffer solutions by application of Gran's technique.[15] Titration cells, which include pure nitrogen inlet and outlet, were thermostatted at 25 or 30 ± 0.1°C.

Procedure

Complex formation equilibria were studied through e.m.f. measurements along the course of titrations performed in a 10% ethanol–water medium containing 0.1 mol dm^{-3} KNO_3 under a nitrogen atmosphere. Ethanol was used because of the solubility limitations of metal complexes in water. Measurements of e.m.f. were performed according to the following procedure:

50 cm^3 of the test solution (TS) with the initial composition

TS = L_0 mol dm^{-3} FMPE or FMPA,

H_0 mol dm^{-3} HNO_3, M_0 mol dm^{-3} $M(NO_3)_2$,

0.1 mol dm^{-3} KNO_3, 10% ethanol

is titrated with 0.1 mol dm^{-3} KOH solution (T), containing the proper ethanol volume. The free hydrogen concentration was measured from a reading obtained with the glass electrode (GE), against the reference electrode (RE) in the cell:

GE/TS//saturated KCl/RE.

The e.m.f. measurements were taken, after the addition of titrant solution, when equilibrium was reached, i.e. as soon as the readings reached stable values. The stabilization of electrode potentials was achieved in every case within less than 5 min.

The free hydrogen ion concentration [H] is calculated from the expression: $E = E^{\ominus} - g \log [H]$ ($g = 59.16$ mV at 25°C and 60.15 mV at 30°C). Before starting the titration, the initial hydrogen ion concentration (H_0), the standard electrode potential for the glass electrode ($E^{\ominus}$) and the K_w under the experimental conditions were determined according to Gran's method.[15]

Absence of polynuclear species was proved from titrations of several TS solutions with different ligand : metal concentration ratios (see Figs 3–5). A wide range was not used because of solubility limitations of metal complexes.

DATA TREATMENT

The general equilibria studied can be written as

$$pM + qL + rH \rightleftharpoons M_pL_qH_r$$

and the overall formation constants are defined as

$$\beta_{pqr} = [M_pL_qH_r]/[M]^p[L]^q[H]^r,$$

where the square brackets indicate the concentration of free metal, ligand and hydrogen ions (charges are omitted for simplicity).

The experimental values $(V_T, E)_{L_0,M_0}$ obtained from the titrations of TS solutions with potassium hydroxide solution (T) are transformed[16] into pairs $(\bar{n}_L, -\log [L])_{L_0,M_0}$ in order to build the metal complex formation curve which corresponds to each experiment.

Analogously, the experimental values obtained from the titrations of the TS solutions without metal ion ($M_0 = 0$) permit the construction of ligand protonation curves ($\bar{n}_H$, $-\log [H]$). These curves are shown in Figs 1 and 2, and the metal complex formation curves in Figs 3–5.

Data pairs ($\bar{n}_H$, $-\log [H]$) or ($\bar{n}_L$, $-\log [L]$) have been treated graphically by the linearization method,[17] under the assumption that only mononuclear complexes are formed. Figure 6 shows, as an example, the straight line obtained from the application of this method to the data obtained with the Mn(II)–FMPA system. The stability constants β_{120} can be evaluated from the slope and the β_{110} from the intercept of the resulting straight line.

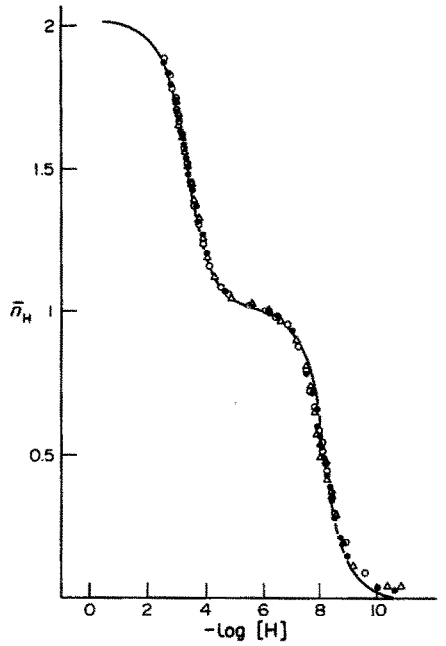


Fig. 1. Protonation curves of FMPE. (●) 3.972 mM, (○) 3.478 mM, (△) 4.419 mM. (—) Theoretical curve.

The experimental values of the ligand protonation constants and the overall formation constants of the metal complexes were refined by the least-squares program MINIQUAD.[18] All calculations were performed on an IBM 3083/XE01 computer.

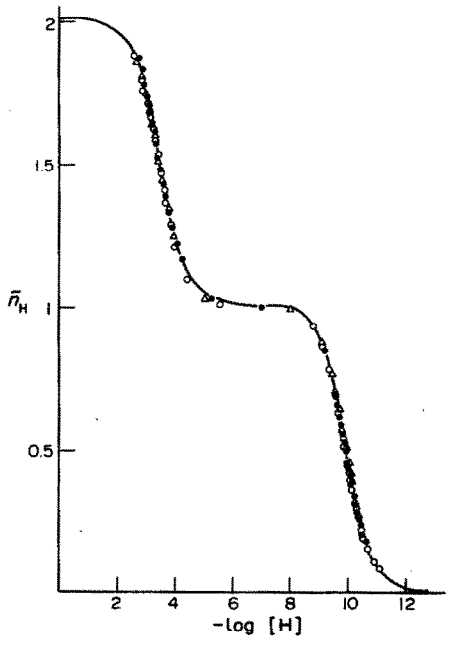


Fig. 2. Protonation curves of FMPA. (●) 2.904 mM, (○) 3.682 mM, (△) 4.710 mM. (—) Theoretical curve.

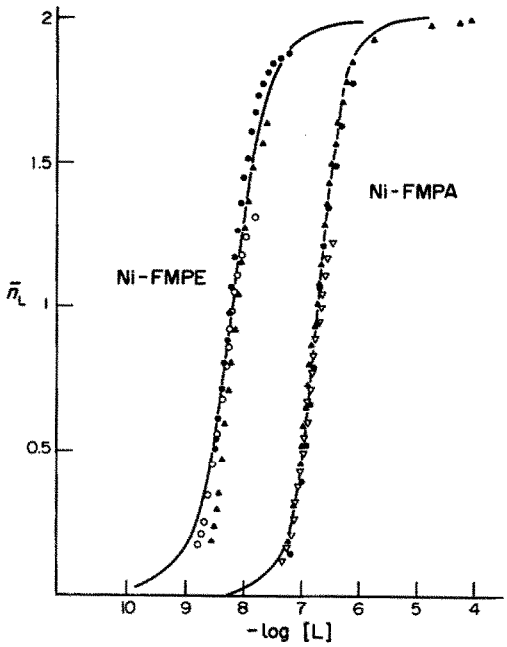


Fig. 3. Formation curves of Ni(II) complexes. Ni(II)–FMPE: (●) $L_0 = 3.855$ mM, $M_0 = 0.403$ mM; (△) $L_0 = 1.974$ mM, $M_0 = 0.403$ mM; (▲) $L_0 = 2.956$ mM, $M_0 = 2.014$ mM. Ni(II)–FMPA: (▲) L_0 2.816 mM, $M_0 = 0.806$ mM; (●) $L_0 = 3.926$ mM, $M_0 = 0.806$ mM; (△) $L_0 = 2.938$ mM, $M_0 = 2.014$ mM. (—) Theoretical curves.

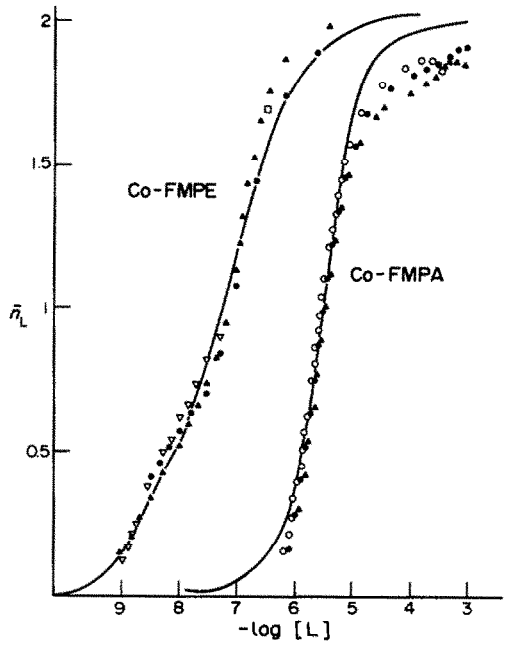


Fig. 4. Formation curves of Co(II) complexes. Co(II)–FMPE: (▲) $L_0 = 2.098$ mM, $M_0 = 0.487$ mM; (△) $L_0 = 2.415$ mM, $M_0 = 0.487$ mM; (●) $L_0 = 1.675$ mM, $M_0 = 0.244$ mM. Co(II)–FMPA: (▲) $L_0 = 3.310$ mM, $M_0 = 0.487$ mM; (●) $L_0 = 4.558$ mM, $M_0 = 0.974$ mM; (○) $L_0 = 2.596$ mM, $M_0 = 0.974$ mM. (—) Theoretical curves.

Table 1. Formation constants of metal complexes ($M_pL_qH_r$) of FMPE and FMPA: 0.1 mol dm^{-3}, 10% ethanol–water (v/v)

			log β_{pqr} (s)		
	pqr	*N*[a]	FMPA[b]	*N*	FMPE[c]
H	011	59	9.890 (0.003)	45	8.097 (0.001)
	012		13.337 (0.006)		11.490 (0.002)
Ni	110	48	6.02 (0.07)	56	7.50 (0.09)
	120		13.38 (0.01)		16.39 (0.02)
Co	110	56	5.48 (0.04)	42	8.12 (0.04)
	120		11.01 (0.02)		14.65 (0.07)
Mn	110	53	3.68 (0.02)	49	5.07 (0.01)
	120		6.58 (0.02)		8.90 (0.01)

[a] N = number of data points.
[b] 25°C.
[c] 30°C.

RESULTS AND DISCUSSION

FMPA and FMPE show two protonation constants that can be assigned to the carboxylate and thiol groups (Table 1). The values found are quite similar to those reported for other 3-aryl-2-mercaptoacids (Table 2). It can be observed that the carboxylic dissociation constants are not greatly influenced by either the nature of the aryl substituent or the presence of the double bond in the α-position, which is in accordance with Wagner *et al.*[6] Besides, this behavior is in agreement with the value obtained for the 2-mercaptopropanoic acid.[1,2]

Conversely, the thiol dissociation constant is strongly influenced because of the presence of the double bond, which allows further conjugation between both thiol and aryl groups. It can be observed that the 3-aryl-2-mercaptopropenoic acids show a higher acidity of the thiol group than the 2-mercaptopropanoic and 3-aryl-2-mercaptoproanoic acids.

In reference to the metal complexes studied, a comparison of their formation constants (Table 1) shows that the propenoic derivatives are more

Table 2. Literature ionization constants of some 2-mercaptoacids

	pK_1	pK_2	*T* (°C)	Solvent	*I* (mol dm^{-3})	Reference
3-Aryl-2-mercaptopropenoic acids						
3-Phenyl-	3.77	8.89	25	30% ethanol–water	0.1 (KNO_3)	16
	4.72	10.82	25	50% ethanol–water	0.1 ($NaClO_4$)	6
3-(2-Thienyl)-	3.63	7.38	19	Water	—	17
3-(2-Pyrrolyl)-	3.72	8.01	23	Water	—	17
3-(2-Hydroxyphenyl)-	3.59	7.48	27	Water	—	17
3-(1-Naphthyl)-	4.18	9.80	25	50% ethanol–water	0.2 ($NaClO_4$)	18
3-(2-Furyl)-	3.393	8.097	30	10% ethanol–water	0.1 (KNO_3)	[a]
3-Aryl-2-mercaptopropanoic acids						
3-Phenyl-	3.96	10.53	25	30% ethanol–water	0.1 (KNO_3)	16
3-(2-Thienyl)-	3.37	9.71	25	10% ethanol–water	0.1 (KNO_3)	8
3-(2-Hydroxyphenyl)-	3.58	9.85	25	10% ethanol–water	0.1 (KNO_3)	8
3-(2-Furyl)-	3.446	9.890	25	10% ethanol–water	0.1 (KNO_3)	[a]
2-Mercaptopropanoic acid	3.51	10.03	25	Water	0.2 ($NaClO_4$)	(2)

[a] This work.

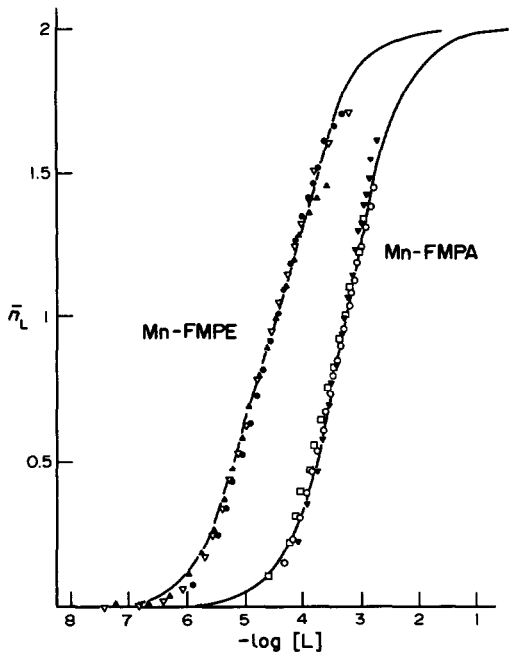


Fig. 5. Formation curves of Mn(II) complexes. Mn(II)–FMPE: (●) $L_0 = 3.038$ mM, $M_0 = 0.554$ mM; (△) $L_0 = 3.925$ mM, $M_0 = 1.108$ mM; (▲) $L_0 = 2.591$ mM, $M_0 = 1.108$ mM. Mn(II)–FMPA: (▲) $L_0 = 4.564$ mM, $M_0 = 0.554$ mM; (○) $L_0 = 4.036$ mM, $M_0 = 1.108$ mM; (□) $L_0 = 3.130$ mM, $M_0 = 1.108$ mM. (—) Theoretical curves.

stable than propanoic derivatives. This behavior is due in part to the double bond in the α-position and the inductive effect of the aryl substituent, which seems to confer greater stability to the complexes formed. With a given metal ion, but different 3-aryl-2-mercaptoacids, values of the complex formation constants vary with values of the protonation constants, as was to be expected. The results obtained shows that the affinity of complexation follows the Irving–Williams order, Ni(II) > Co(II) > Mn(II).

REFERENCES

1. IUPAC, *Stability Constants of Metal–Ion Complexes. Part B: Organic Ligands.* Pergamon Press, Oxford (1979).
2. A. E. Martell and R. M. Smith, *Critical Stability Constants*, Vol. 3. Plenum Press, New York (1977).
3. A. Izquierdo and J. Calmet, *Talanta* 1977, **25**, 56.
4. A. Izquierdo and J. Calmet, *Analysis* 1976, **4**, 200.
5. A. Izquierdo and J. Carrasco, *Analyst* 1984, **109**, 605.
6. N. J. Prakash, P. J. Schechter, E. Giroux and A. Sjoerdsma, *Clin. Exp. Pharmacol. Physiol.* 1977, **4**, 17.
7. E. Giroux, N. J. Prakash and P. J. Schechter, *Clin. Exp. Pharmacol. Physiol.* 1977, **4**, 27.
8. W. O. Foye and J. R. Lo, *J. Pharm. Sci.* 1972, **61**, 1209.
9. J. Wagner, P. Vitali, J. Schoun and E. Giroux, *Can. J. Chem.* 1977, **55**, 4028.
10. E. Campaigne and R. E. Cline, *J. Org. Chem.* 1956, **21**, 32.
11. A. Izquierdo, J. Guasch and J. Miquel, *An. Quim.* 1984, **80**, 382.
12. D. L. Leussing and I. M. Kolthoff, *J. Electrochem. Soc.* 1953, **100**, 334.
13. A. I. Vogel, *A Textbook of Quantitative Inorganic Analysis*, 4th edn. Longman, London (1978).
14. *Some Laboratory Methods.* Department of Inorganic Chemistry, The Royal Institute of Technology, Stockholm (1959).
15. G. Gran, *Analyst* 1952, **77**, 661.
16. F. J. C. Rossotti and H. S. Rossotti, *The Determination of Stability Constants.* McGraw-Hill, New York (1961).
17. H. Irving and H. S. Rossotti, *J. Chem. Soc.* 1953, 3397.
18. A. Sabatini, A. Bacca and P. Gans, *Talanta* 1974, **21**, 53.
19. A. Izquierdo and N. Garriga, *Talanta* (in press).
20. A. Izquierdo and M. Giné, *An. Quim.* 1978, **74**, 53.
21. A. Izquierdo, E. Bosch and J. L. Beltran, *Talanta* 1984, **31**, 475.

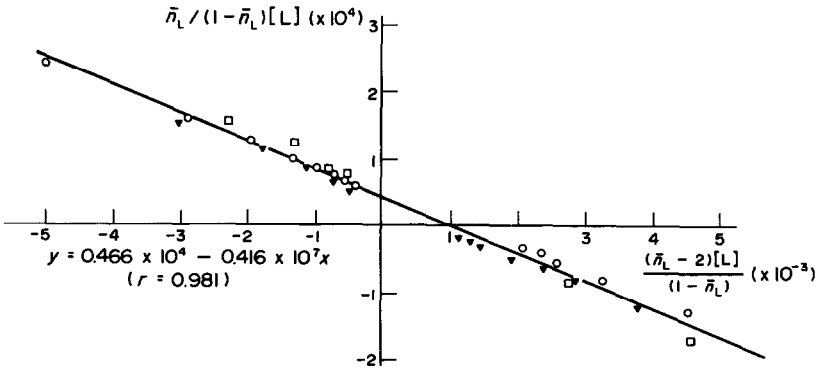


Fig. 6. Linearization method applied to the Mn(II)–FMPA system. (▲) $L_0 = 4.564$ mM, $M_0 = 0.554$ mM; (○) $L_0 = 4.036$ mM, $M_0 = 1.108$ mM; (□) $L_0 = 3.130$ mM, $M_0 = 1.108$ mM.

Polyhedron Vol. 5, No. 7, pp. 1259–1265, 1986
Printed in Great Britain

0277–5387/86 $3.00+.00
Pergamon Journals Ltd

REACTIONS OF ALKALINE EARTH METAL OR Al SLURRIES WITH BIS-CYCLOPENTADIENYL COMPLEXES OF SOME EARLY TRANSITION METALS

W. E. LINDSELL* and R. A. PARR

Department of Chemistry, Heriot-Watt University, Riccarton, Edinburgh EH14 4AS, U.K.

(*Received* 26 *August* 1985; *accepted* 11 *November* 1985)

Abstract—Slurries of Mg, Ca, Ba and Al, prepared by cocondensation of metal vapour with volatile organic solvents, especially toluene, at −196°C, reacted at ambient temperature with some bis-cyclopentadienyl complexes of Ti, Zr, Hf, V and Cr. $[TiCl_2Cp_2]$ ($Cp = \eta^5$-C_5H_5) with slurries of Al in hexane or toluene, or Mg or Ba, in toluene, formed $[TiClCp_2]_2$ accompanied by side-products. From related reactions with slurries of Mg in tetrahydrofuran (THF), $[TiCl_2Cp(THF)]$ was obtained and with Ca–toluene slurries an unstable paramagnetic dihydrido complex of Ti(III) was observed by using ESR spectroscopy. Reactions of $[TiPh_2Cp_2]$ with slurries of Al or Ba in toluene yielded a form of "titanocene" ($TiC_{10}H_{10}$) and ESR studies of these reactions revealed related paramagnetic species in solution. Reaction of slurries of Al, Mg or Ba with $[TiMe_2Cp_2]$ produced several different paramagnetic products which were studied by ESR spectroscopy, and the reaction of metal slurries with the complexes $[MR_2Cp_2]$ (M = Ti, R = OPh; M = Zr or Hf, R = Cl or Me), $[VRCp_2]$ (R = Cl or Me), and $[CrCp_2]$ are also reported.

In view of the wide application of systems containing Ti, Zr and related metals with Al or Mg as components in Ziegler–Natta catalysts,[1] we have undertaken a study of the products formed in reactions of finely divided slurries of alkaline earth metals or Al, suspended in organic solvents, with compounds of early transition metals. Such products might be expected to show useful catalytic activity in alkene polymerizations and could be interesting reduced oxidation state species, possibly of mixed metal composition.

Active metal slurries have found applications in synthesis in recent years and have been produced either by vaporization techniques[2] or by reduction of metal halides in solution, especially by using K or other alkali metals.[3] Of particular relevance to this work, slurries of Mg[4,5] and Al[6,7] have been previously reported. Such slurries exhibit superior reactivity to bulk metals, undergoing a number of previously unknown or difficult reactions.

Bis-cyclopentadienyl metal complexes of Ti, Zr, Hf, V, Nb and Cr have been shown to undergo reduction reactions with alkali metals, and in some cases metallic Zn, Mg or Al is an effective reducing agent, although products may be mixed bimetallic species.[8] By using finely divided slurries of Mg, Ca, Ba or Al we hoped to observe some variations on reactions of complexes of these early transition metals.

RESULTS AND DISCUSSION

Finely divided slurries of Mg, Ca, Ba or Al were produced by vaporization of the metal and cocondensation with inert organic solvent at −196°C, followed by warming to ambient temperature, using a method similar to that described by Klabunde and coworkers.[2,4,6] Slurries of Al in hexane or toluene[6] and of Mg in toluene or tetrahydrofuran (THF)[4] have been previously formed by this method and we have utilized the same slurries; in the course of this work we also produced slurries of Ca or Ba in toluene which were, respectively, brown or black-brown in colour. The size of particles in these slurries varied with the rate of warm-up of the cold metal–solvent matrix and nature of the organic medium, as noted earlier[9]—e.g. the slurry of Al in hexane was coarser than Al in toluene, and the former showed a lower reactivity.

* Author to whom correspondence should be addressed.

It has been recognized that the particles of metal slurries made by cocondensation include some carbonaceous material derived from the organic medium incorporated either by simple absorption or by chemical reactions to form organometallic species.[9] Microanalysis of vacuum-dried powders from representative slurries in toluene showed that the carbon content increased in the order Mg < Al < Ba < Ca and this must represent an increasing formation of organometallic species between metal atom and toluene during cocondensation, warm-up and/or on standing at ambient temperature. Formation of a benzyl–metal derivative is possible and the brown solid residue from a Ca–toluene slurry did show partial solubility in THF giving a brown-red solution with $\lambda_{max} \sim 330$ nm, similar to that observed for dibenzylcalcium.[10] This observation may explain a greater difference in the course of reactions using Ca slurries when compared to reactions of the other metal slurries.

Reactions with $[MCl_2Cp_2]$ (M = Ti, Zr *or* Hf)

Electrochemical studies on $[TiCl_2Cp_2]$ (Cp = η^5-cyclopentadienyl) in THF support primary reduction to a stable monoanion $[TiCl_2Cp_2]^-$, with an ESR g_{iso} signal of 1.9789, whereas two-electron reduction causes dissociation of Cl^-.[11] Chemical reduction by finely divided Zn in polar solvents gives bimetallic $[Cp_2Ti(\mu\text{-}Cl)_2Zn(\mu\text{-}Cl)_2TiCp_2]$ which can be cleaved by Lewis bases to $[TiClCp_2]_2$.[8] Reduction of $[TiCl_2Cp_2]$ by carefully activated Al foil in THF also yields $[TiClCp_2]_2$,[12] although in the presence of $AlCl_3$ the hydrocarbon soluble $[Cp_2Ti(\mu\text{-}Cl)_2AlCl_2]$ is formed;[13] moreover addition of water to THF causes Al to produce solvated $[TiCl_2Cp]$.[14] Mg metal may reduce $[TiCl_2Cp_2]$ to Ti(II) products[8,15] in a reaction comparable to reduction by Na to "titanocene".

Using metal slurries formed by vaporization, we find that Al suspensions in hexane or toluene form primarily $[TiClCp_2]_2$, identified by analysis and spectroscopy. In hexane, reduction by Al is slow and, even in the presence of added THF to improve solubility, conversion to Ti(III) product was only *ca* 30% after 2 days. In toluene, reduction was complete within a few hours and further stirring at ambient temperature for 3 days gave no reduction beyond oxidation state III; $[TiClCp_2]_2$ was isolated in 66% yield and the remaining product was mainly present as $[Cp_2Ti(\mu\text{-}Cl)_2AlCl_2]$, formed in the stoichiometric reaction:

$$3[TiCl_2Cp_2] + Al \rightarrow [TiClCp_2]_2 + [Cp_2TiCl_2AlCl_2].$$

Toluene slurries of Mg or Ba also produced $[TiClCp_2]_2$ as the main soluble product (isolated yield 26 or 38%, respectively), although much insoluble material was also formed. The insoluble brown solid obtained from the Mg–toluene slurry reaction incorporated toluene and reduced Ti, having a molar composition Ti : Mg : Cl of 2 : 3 : 6; a formulation $2(TiC_{10}H_{10}) \cdot 3(MgCl_2) \cdot 1.5(C_7H_8)$ is consistent with the analytical results but further characterization has not been attempted.

Reduction of $[TiCl_2Cp_2]$ by Mg–THF slurry gave the monocyclopentadienyl product $[TiCl_2Cp(THF)]$ as the only isolable product (deep blue-black crystals, 50%) from a dark-green solution. The THF used in this reaction had been carefully dried and to our knowledge no water had been admitted during handling under dry Ar or *in vacuo*. Thus, removal of either Cp or Cl ligand occurs by Mg in THF or toluene, respectively. ESR spectra of $[TiClCp_2]_2$ or $[TiCl_2Cp(THF)]$ in toluene (or THF) are very similar (Fig. 1a): singlets ($\Delta H_{pp} = 0.4$–0.5 mT) at $g_{iso} = 1.9785$ or 1.979, respectively, with satellites $A_{iso}(^{47/49}Ti) = 1.2$ mT.[13(a)]

Reaction of excess Ca–toluene slurry with $[TiCl_2Cp_2]$ over 16 days gave only a toluene-insoluble product; extraction of this brown product with THF gave a purple solution exhibiting a strong 1 : 2 : 1 triplet ESR signal [$g_{iso} = 1.992$, $A_{iso}(^1H) = 0.88$ mT with satellites $A_{iso}(Ti) = 0.74$ mT] (Fig. 1b). This spectrum is similar to those previously assigned to non-isolated $[Cp_2TiH_2]^-$ with various counter-ions, although coupling to cyclopentadienyl hydrogens was also reported.[16] The product obtained in our work may be $[Cp_2TiH_2]^-$ with a Ca^{2+} counter-ion, formed by hydrogen transfer from toluene (or THF), or a related dihydrido-titanium(III) complex. Attempted isolation of this species yielded a purple solid, itself sparingly soluble in THF, and this solid did not reproduce the former ESR spectrum on redissolution. Analytical data on this solid were inconsistent with a simple species so that some decomposition may have occurred.

Reduction of $[ZrCl_2Cp_2]$ is more difficult than for the Ti analogue, as shown by electrochemical studies.[11,17] Reductions by Na–$C_{10}H_8$ give a form of "zirconocene"[8] and an ESR study of reduction by Mg in THF demonstrates the formation of Zr(III) hydride by H-transfer from a cyclopentadienyl ring.[18] Recently diamagnetic $[ZrClCp_2]_2$ has been synthesized from $[Zr(CO)_2Cp_2]$ and $[ZrCl_2Cp_2]$.[19] We observed that Al–toluene slurries with $[ZrCl_2Cp_2]$ produced a red solution exhibiting a single ESR signal [$g_{iso} = 1.998$ ($\Delta H_{pp} = 1.5$ mT)] but attempted isolation of this product afforded much unreacted starting material and a small amount of uncharacterizable brown solid. It does appear that

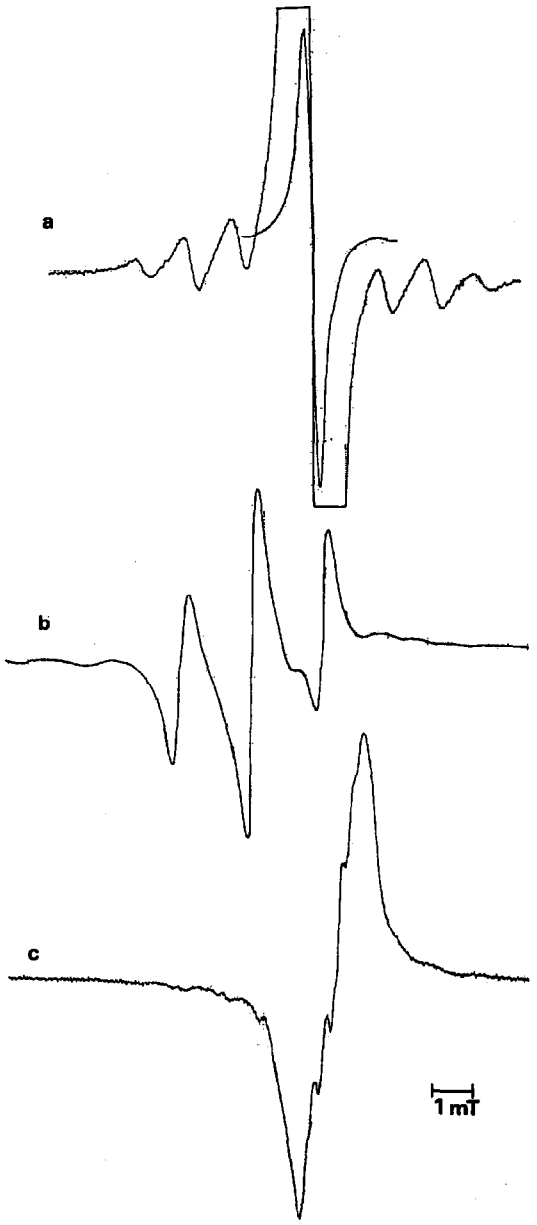


Fig. 1. *X*-band ESR spectra of: (a) $[TiClCp_2]_2$ in THF ($g = 1.979$); (b) product from $[TiCl_2Cp_2]+Ca$, in THF (probably $[TiH_2Cp_2]^- \cdot \frac{1}{2}Ca^{2+}$) ($g = 1.992$); and (c) product from $[Ti(OPh)_2Cp_2]+Al$-toluene ($g = 1.977$).

the Al–toluene slurry will partially reduce $[ZrCl_2Cp_2]$; on the other hand no reactions were observed between Al–toluene slurry and $[HfCl_2Cp_2]$, between Mg–toluene slurry and $[ZrCl_2Cp_2]$ or between Ba–toluene slurry and $[(ZrClCp_2)_2O]$.

Reaction with $[Ti(OPh)_2Cp_2]$

A slurry of Al–toluene readily reacted with $[Ti(OPh)_2Cp_2]$ to give a green solution. The filtered solution showed ESR signals from at least three paramagnetic species: singlets at $g_{iso} = 1.978$ and 1.976 ($\Delta H_{pp} = 0.3$–0.4 mT) and a broader underlying signal [$g_{iso} \sim 1.977$ ($\Delta H_{pp} \sim 1.5$ mT)]. Controlled aerial oxidation of an ESR sample caused the primary disappearance of the two sharper singlets and the broader signal was revealed as a poorly resolved multiplet (Fig. 1c); further oxidation caused the loss of this signal. The multiplet can be analysed as a sextet resulting from coupling to ^{27}Al[20] and may be tentatively assigned to a species $[Cp_2Ti(\mu\text{-}OPh)_2AlR_2]$ with R = OPh, or possibly Cp [$g_{iso} = 1.977$, $A_{iso}(Al) \simeq 0.25$ mT, $A_{iso}(Ti) \simeq 1.0 \pm 0.1$ mT]. Previous studies of electrochemical reductions of complexes $[Ti(OAr)_2Cp_2]$ support the formation of neutral species $[Ti(OAr)_2Cp]$ ($g_{iso} \simeq 1.977$ in THF) by Cp^- dissociation:[21] it thus seems highly likely that the other two ESR species observed in reaction with Al slurry are $[Ti(OPh)_2Cp]$ and $[Ti(OPh)Cp_2]$. Dimeric complexes $[Ti(OR)Cp_2]_2$ with magnetic moments varying with temperature have been studied[22] but ESR studies on these have not been reported.

Reactions with $[TiPh_2Cp_2]$

Both Al– and Ba–toluene slurries react with $[TiPh_2Cp_2]$ to give dark-green, toluene-soluble products, obtainable as dark microcrystalline solids on cooling concentrated solutions. Analysis of the percentage of C, H, Ti and, in the former case, Al established a stoichiometry corresponding reasonably to that of "titanocene", i.e. $TiC_{10}H_x$ ($x \sim 10$) (*ca* 65% yield). IR spectra of these samples showed no significant absorption around 1230 cm^{-1}, which has been assigned to a ν(Ti—H—Ti) vibration in the fulvalene derivative $[Ti_2(\mu\text{-}\eta^5,\eta^5\text{-}C_{10}H_8)(\mu\text{-}H_2)Cp_2]$.[23] The IR spectra were essentially identical to those attributed to metastable "$[TiCp_2]_2$" by Bercaw *et al.*[24] Other physical properties of the products accord with this species: the relation of this species to the black, microcrystalline "titanocene" $[Cp_2Ti(\mu\text{-}\eta^1,\eta^5\text{-}C_5H_4)TiCp]$, described by Pez,[25] is not clear—the published IR spectrum of the latter does show a significant band at 1224 cm^{-1} and, overall, less similarity to that of our dark-green product but, as discussed in previous reviews,[26] these products may basically be structurally the same.

ESR spectra of the products obtained from metal slurry reactions with $[TiPh_2Cp_2]$ have thrown more light on the reaction. Using an Al–toluene slurry, the filtered reaction solution after 7 days exhibited a dominant signal ($g_{iso} = 1.977_5$ with doublet-splitting $A_{iso} = 0.435$ mT), attributable to coupling with a single ^1H, accompanied by other weaker ESR

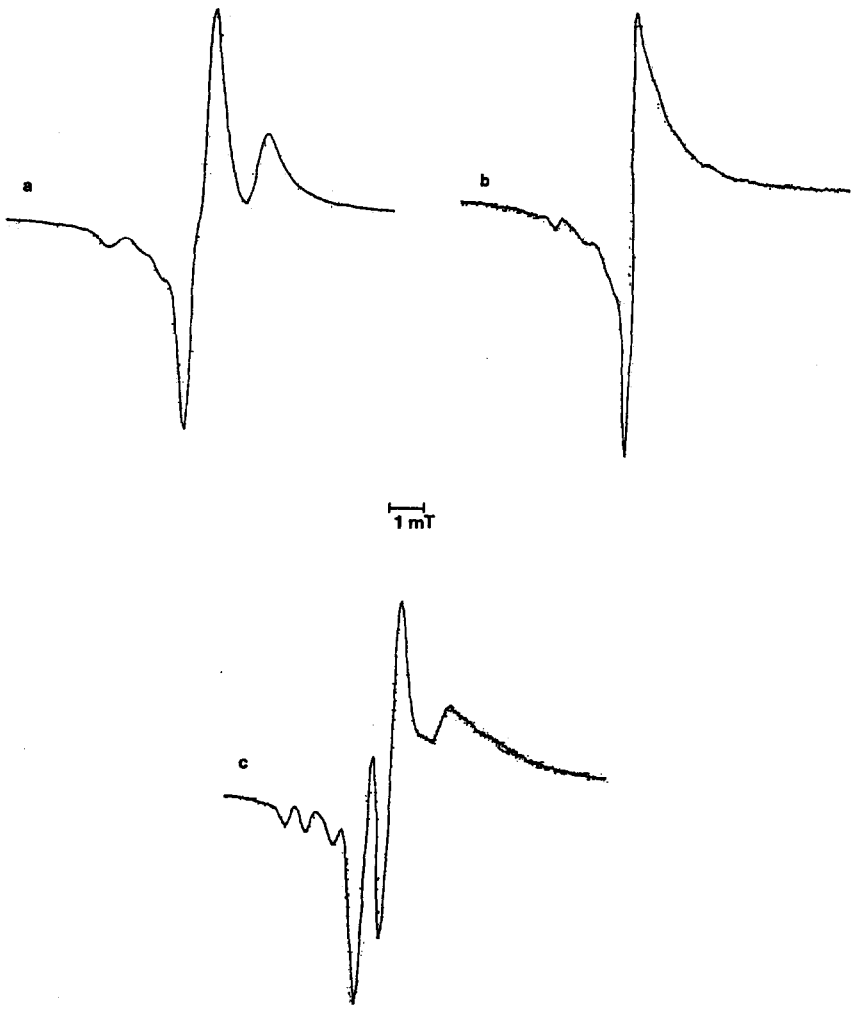


Fig. 2. *X*-band ESR spectra of: (a) reaction mixture of $[TiPh_2Cp_2]$+Al–toluene; (b) product, $TiC_{10}H_{10}$, obtained from $[TiPh_2Cp_2]$+Al reaction, in toluene ($g = 1.979$); and (c) reaction mixture of $[TiMe_2Cp_2]$+Al–toluene.

resonances varying in intensity with different experiments and including one at $g_{iso} = 1.968$ (Fig. 2a). Controlled aerial oxidation of these solutions initially increased the complexity of the ESR spectrum but finally produced a singlet ($g_{iso} = 1.979$) before giving an ESR inactive solution. The green microcrystalline solid obtained by careful addition of hexane under Ar to an unoxidized concentrated solution in toluene showed a broad ESR signal [$g_{iso} = 1.980$ ($\Delta H_{pp} = 6$ mT)]. Redissolution of this solid in toluene gave an apparent singlet [$g_{iso} = 1.979$, $A_{iso}(Ti) = 0.9$ mT] (Fig. 2b), coincidently similar to that produced by oxidation but, we believe, assignable to non-oxidized product. Similar ESR observations were made for reaction of Ba or Ca slurries in toluene, although more ESR active by-products were formed in solutions produced using Ca.

The ESR spectrum of unstable $[TiPhCp_2]$ is reported to show $g_{iso} = 1.95$ in toluene[27] and so is inconsistent with species formed during these slurry reactions. Photolysis of $[TiPh_2Cp_2]$ in benzene is reported to give a singlet ESR resonance ($g_{iso} = 1.979$) at ambient temperature assigned to a monomeric form of metastable "$[TiCp_2]_2$".[18] This latter report is in accord with the proposed nature of our isolated microcrystalline product; the doublet ESR observed in our work may be related to hydrido species such as $[TiHCp_2]_x$[24] or $[Ti_2HCp_4]$[29] (possibly identical—see Ref. 26) which are interconvertible with "titanocene" by loss or gain of hydrogen.

Reactions with $[MMe_2Cp_2]$ (M = Ti, Zr *or* Hf)

Dark-green toluene solutions were obtained by stirring slurries of Al, Mg or Ba with $[TiMe_2Cp_2]$. The products obtained from these reactions (>50% yields), however, appeared to differ and spectroscopic and analytical results suggest that

varying mixtures of two or more reduced organotitanium compounds were formed.

Reaction solutions or solid obtained from Al–toluene slurries gave an ESR spectrum with two equally intense single resonances (Fig. 2c); this spectrum could be assigned to a single species having $g_{iso} = 1.981$ and $A_{iso} = 0.75$ mT with doublet coupling to a single ^1H nucleus or, alternatively, to two species with singlets at $g_{iso} = 1.983$ and 1.979. IR spectra of this solid showed typical Cp bands but no strong band assignable to Ti—H—Ti vibrations apart from a weak absorption at 1155 cm^{-1} and analytical data supported an empirical formula TiC_6H_x ($x \sim 6$).

Filtered reaction solutions obtained from Mg–toluene slurries showed the same two ESR resonances as above superimposed on a strong, broad signal [$g_{iso} = 1.98$ ($\Delta H_{pp} \sim 4.5$ mT)], whereas the green solid isolated from solution showed only an ESR singlet [$g_{iso} = 1.979$ ($\Delta H_{pp} \sim 0.2$ mT)] on redissolution in toluene. This solid did exhibit a broad IR band of medium intensity at 1225 cm^{-1} and had analytical data consistent with the empirical formula $TiC_{6-7}H_x$ ($x \sim 7$).

The green solid isolated from Ba–toluene slurry reaction gave a dominant doublet ESR signal ($g_{iso} = 1.977$, $A_{iso} = 0.4$ mT) and a broad band at 1225 cm^{-1} in its IR spectrum. Analytical data supported an empirical formula TiC_9H_x ($x \sim 10$), i.e. close to $TiC_{10}H_{10}$.

[$TiMeCp_2$] is thermally unstable in ether solution at $> -50°C$,[30] although it may be more stable in toluene, in which solvent an ESR signal ($g_{iso} = 1.980$) has been assigned to this complex.[31] In THF, [$TiMeCp_2$] gives a quartet ESR signal at low temperatures.[30] Electrochemical reduction of [$TiMe_2Cp_2$] in THF may produce [$TiMe_2Cp_2$]$^-$ and/or [$TiMe_2Cp$]:[17,21] at $-20°C$ a septet ($g_{iso} = 1.986$) ([$TiCp_2Me_2$]$^-$) has been reported in one investigation[17] whereas a singlet resonance ($g_{iso} = 1.9789$) at $+20°C$ ([$TiMe_2Cp$]) is quoted in another report.[21] Electrochemical studies, however, do support some cleavage of Cp^- during reduction.[21]

Thus, possible products of our slurry reactions include [$TiMeCp_2$], [$TiMe_2Cp$], a form of "titanocene" and also related hydride species. [$TiMeCp_2$], although a possible intermediate detected in solution, is inconsistent with isolated products which appear to have undergone Cp cleavage by Al or Mg slurries: [$TiMe_2Cp$] or a product involving further transformation of methyl group(s) may be formed. Doublet ESR signals may arise from monohydrido complexes or from interaction of Ti with a C—H group as found in alkyl–metal compounds with agostic hydrogens.[32] The main product from reactions of Ba–toluene slurries more closely corresponds to a form of "titanocene" or a stoichiometrically similar species exhibiting a Ti–H coupling in its ESR spectrum (cf. reactions of [$TiPh_2Cp_2$] discussed above) but has not been isolated in a completely pure state.

It was found that Mg–toluene slurries were unreactive towards [MMe_2Cp_2] (M = Zr or Hf) after stirring for 14 days at ambient temperature. Al–toluene slurries did react to small extent with [MMe_2Cp_2] (M = Zr or Hf), but again much unreacted M(IV) complex was recovered. Thus, [$ZrMe_2Ph_2$] with Al–toluene slurry gave a solution containing ESR active Zr species—a doublet ($g_{iso} = 1.981$, $A_{iso} = 0.7$ mT), superimposed on a broad signal [$g \sim 1.98$ ($\Delta H_{pp} \sim 3$ mT)], and a smaller resonance at $g_{iso} = 2.000$; the brown solid isolated from this reaction (mainly [$ZrMe_2Cp_2$]) contained <0.1% Al and redissolved in THF to give a doublet ($g_{iso} = 1.986$, $A_{iso} \simeq 0.8$ mT) and a broader singlet ($g_{iso} = 1.996$). With an Al–toluene slurry, [$HfMe_2Cp_2$] gave a dark-red coloured solution which was ESR inactive and an attempted separation of this low-yield red product from starting material was unsuccessful. It may be noted that crimson [$ZrMeCp_2]_2$ has been reported[8] and that electrochemical reductions of species [ZrR_2Cp_2] involve Cp^- loss to give [ZrR_2Cp] complexes[17] with $g_{iso} \sim 1.984$–1.987. Photolysis of [$ZrMe_2Cp_2$] and related dialkyl complexes involves primary Me loss and resulting Zr(III) monohydride species have been observed by ESR spectroscopy ($g_{iso} \sim 1.984$–1.987, $A_{iso} \sim 0.65$–0.7 mT).[33]

Reactions with other bis-cyclopentadienyl complexes

Al slurries in toluene reduce [$VXCp_2$] (X = Cl or Me) to vanadocene, isolated in high yield as the only identified vanadium product. However, a Mg–toluene slurry was found to be unreactive towards [$VMeCp_2$] after stirring for 7 days at ambient temperature. Also, no reaction occurred between [$CrCp_2$] and Mg or Ba slurries in toluene; on addition of THF and continued stirring, the solution became dark brown but only small quantities of uncharacterized brown product were isolated and much unreacted [$CrCp_2$] was recovered.

EXPERIMENTAL

All reactions and manipulations were carried out using Schlenk techniques under an atmosphere of dry, dioxygen-free Ar or *in vacuo*. Reagent-grade solvents were subjected to preliminary purifications, followed by refluxing (>2 h) with $Na[OCPh_2]$ (toluene or THF), CaH_2 (hexane or

ether) or P_4O_{10} (dichloromethane) and distillation under dinitrogen. For slurry reactions these solvents were then purged with Ar for 5 min before use. For cocondensation to form slurries, these solvents were treated to at least three freeze–thaw degassing cycles and distilled *in vacuo* ($<10^{-3}$ torr) from appropriate drying reagents before introduction into the evacuated apparatus.

Elemental analyses were determined by Analytische Laboratorien, Engelskirchen, F.R.G., or by Butterworth Laboratories, Teddington, U.K. Aluminium analyses were carried out using a Pye–Unicam AA Spectrophotometer at 309.28 nm. ESR spectra were recorded on samples in evacuated tubes or under Ar at 12 ± 5°C with JEOL PEI-X X band spectrometer using dpph ($g = 2.0036$) as standard and a Bruker ER 035M Gaussmeter for field calibration. IR spectra were obtained from Nujol mulls made up under argon and recorded between CsI plates on a PE 580 spectrometer.

Some starting materials were purchased as follows: $[ZrCl_2Cp_2]$ (Aldrich Chemical Co.); $[HfCl_2Cp_2]$ and Ca, >99.5% (Alfa/Ventron GmbH); Al, >99.9% (BDH); Mg, >99.8% and Ba, >99% (Koch-Light) and VCl_3 (Fluka). Other compounds were prepared according to literature procedures: $[MR_2Cp_2]$ (M = Ti, R = Cl,[34] Ph,[35] Me[36] or OPh;[37] M = Zr or Hf, R = Me[38]), $[MCp_2]$ (M = V[34] or Cr[39]), and $[VRCp_2]$ (R = Cl[40] or Me[40]).

Preparation of metal slurries

The apparatus used comprised a rotating (*ca* 60 rpm) evacuated ($<10^{-3}$ torr) 3-dm^3 flask similar to that described by Timms[41] and used in previous investigations.[42] Mg, Ca or Ba were evaporated from conically wound, electrically heated (45–85-A) Mo wire furnaces and Al was evaporated from a boron nitride crucible wrapped in an alumina-coated, Mo wire heater. Cocondensation of metal (0.4–0.9 g) with solvent (120–200 cm^3) vapour at −196°C gave dark matrices which were then warmed slowly to ambient temperature. Dry Ar was admitted to the vessel during this latter process and the resulting slurry was then siphoned under Ar into a storage Schlenk tube for use in reactions.

Analysis of powders obtained by solvent removal *in vacuo* at 20°C from representative toluene slurries gave the following approximate M:C:H compositions: M = Mg, 10:1:1, M = Ba, 1:1:3; M = Ca, 1:3:3; M = Al, 2:1:2.

Reactions of bis-cyclopentadienyl metal complex with metal slurry

Typical reactions involved stirring the complex with metal slurry (25–70 cm^3; complex:metal ratio = *ca* 1:2, i.e. excess metal) at ambient temperature for several days. Periods of up to 22 days were employed for systems which showed negligible or zero reaction. Normally no additional solvent other than that present in slurry was introduced, except for reactions $[TiCl_2Cp_2]$ + hexane–Al slurry and $[CrCp_2]$ + toluene–Mg or Ba slurry, when THF (35 cm^3) was also added to some reactions. Reaction solutions were then filtered and solid, often crystalline or microcrystalline, product was isolated by

Table 1.

Reaction system	Product	Analyses (%)
$[TiCl_2Cp_2]$ + Al–toluene	$[TiClCp_2]_2$	Found: C, 55.8; H, 4.8; Cl, 18.1 Calc.: C, 56.2; H, 4.7; Cl, 16.6
$[TiCl_2Cp_2]$ + Mg–toluene	Brown solid (insoluble toluene)	Found: Cl, 27.2; Ti, 12.9; Mg, 9.0
$[TiCl_2Cp_2]$ + Mg–THF	$[TiCl_2Cp(THF)]$	Found: C, 42.5; H, 5.7; Cl, 27.4 Calc.: C, 42.2; H, 5.1; Cl, 27.4
$[TiCl_2Cp_2]$ + Ca–toluene	Purple solid (ex THF)	Found: C, 30.1; H, 4.3; Cl, 16.5; Ca, 9.0
$[TiPh_2Cp_2]$ + Al–toluene	$[TiC_{10}H_{10}]$	Found: C, 66.8; H, 5.5; Ti, 28.6; Al, < 0.4 Calc.: C, 67.4; H, 5.7; Ti, 26.9
$[TiPh_2Cp_2]$ + Ba–toluene	$[TiC_{10}H_{10}]$	Found: C, 66.6; H, 5.6 Calc.: C, 67.4; H, 5.7
$[TiMe_2Cp_2]$ + Al–toluene	"TiC_6H_6" (green)	Found: C, 57.0; H, 4.9 Calc.: C, 57.1; H, 4.8
$[TiMe_3Cp_2]$ + Mg–toluene	Green solid	Found: C, 59.0; H, 5.3
$[TiMe_2Cp_2]$ + Ba–toluene	Green solid	Found: C, 64.4; H, 5.8

concentration of solutions, addition of hexane and/or cooling, as appropriate. Further recrystallizations were carried out when necessary.

Analytical data for solid products, discussed in the text, are given in Table 1.

Acknowledgements—We thank the SERC and B.P. Chemicals Ltd for a CASE studentship (to RAP), and Drs J. G. Speakman and G. W. Downs for their interest and helpful discussions throughout the course of this work.

REFERENCES

1. e.g. H. Sinn and W. Kaminsky, *Adv. Organomet. Chem.* 1980, **18**, 99.
2. (a) K. J. Klabunde, *Acc. Chem. Res.* 1975, **8**, 393; (b) J. D. Blackborrow and D. Young, *Metal Vapour Synthesis in Organometallic Chemistry*. Springer, Berlin (1979).
3. (a) R. D. Rieke, *Acc. Chem. Res.* 1977, **10**, 301; (b) A. V. Kavalinnas, A. Taylor and R. D. Rieke, *Organometallics* 1983, **2**, 377 (and references therein).
4. K. J. Klabunde, H. F. Efner, L. Satek and W. Donley, *J. Organomet. Chem.* 1974, **71**, 309.
5. R. D. Rieke and S. E. Bales, *J. Am. Chem. Soc.* 1974, **96**, 1775.
6. K. J. Klabunde and T. O. Murdock, *J. Org. Chem.* 1979, **44**, 3901.
7. R. D. Rieke and L. Chao, *Synth. React. Inorg. Met.–Org. Chem.* 1974, **4**, 101.
8. e.g. (a) P. C. Wailes, R. S. P. Coutts and H. Weigold, *Organometallic Chemistry of Titanium, Zirconium and Hafnium*. Academic Press, London (1974). (b) *Comprehensive Organometallic Chemistry* (Edited by G. Wilkinson, F. G. A. Stone and E. W. Abel), Vol. 3. Pergamon Press, Oxford (1982).
9. S. C. Davis, S. J. Severson and K. J. Klabunde, *J. Am. Chem. Soc.* 1981, **103**, 3024 (and references therein).
10. K. Takahashi, J. Kondo and R. Asami, *J. Chem. Soc., Perkin Trans.* 2 1978, 577.
11. (a) N. El Murr, A. Chaloyard and J. Tirouflet, *J. Chem. Soc., Chem. Commun.* 1980, 446; (b) see also N. El Murr and A. Chaloyard, *J. Organomet. Chem.* 1982, **231**, 1 (and references therein).
12. R. S. P. Coutts and P. C. Wailes, *J. Organomet. Chem.* 1973, **47**, 375.
13. (a) G. Henrici-Olivé and S. Olivé, *Makromol. Chem.* 1969, **121**, 70; (b) see also G. Natta, P. Pino, G. Mazzanti and U. Giannini, *J. Inorg. Nucl. Chem.* 1958, **8**, 612.
14. R. S. P. Coutts, R. L. Martin and P. C. Wailes, *Aust. J. Chem.* 1971, **24**, 2533.
15. Cf. V. B. Shur, S. Z. Bernadyuk, V. V. Burlakov, V. G. Andrianov, A. I. Yanovsky, Yu. T. Struchkov and M. E. Vol'pin, *J. Organomet. Chem.* 1983, **243**, 157.
16. H. H. Brintzinger, *J. Am. Chem. Soc.* 1967, **89**, 6871; J. G. Kenworthy, J. Myatt and M. C. R. Symons, *J. Chem. Soc. A* 1971, 1020.
17. M. F. Lappert, C. J. Pickett, P. I. Riley and P. I. W. Yarrow, *J. Chem. Soc., Dalton Trans.* 1981, 805.
18. E. Samuel, *Inorg. Chem.* 1983, **22**, 2967.
19. G. Fochi, G. Guidi and C. Floriani, *J. Chem. Soc., Dalton Trans.* 1984, 1253.
20. G. Henrici-Olivé and S. Olivé, *J. Organomet. Chem.* 1970, **21**, 377.
21. A. Chaloyard, A. Dormond, J. Tirouflet and N. El Murr, *J. Chem. Soc., Chem. Commun.* 1980, 214.
22. M. F. Lappert and A. R. Sanger, *J. Chem. Soc. A* 1971, 1314.
23. H. H. Brintzinger and J. E. Bercaw, *J. Am. Chem. Soc.* 1970, **92**, 6182.
24. J. E. Bercaw, R. H. Marvich, L. G. Bell and H. H. Brintzinger, *J. Am. Chem. Soc.* 1972, **94**, 1219.
25. G. P. Pez, *J. Am. Chem. Soc.* 1976, **98**, 8072.
26. (a) G. P. Pez and J. N. Armor, *Adv. Organomet. Chem.* 1981, **19**, 1; (b) G. E. Toogood and M. G. H. Wallbridge, *Adv. Inorg. Chem. Radiochem.* 1982, **25**, 267.
27. J. H. Teuben and H.-J. de Liefde Meyer, *J. Organomet. Chem.* 1972, **46**, 313.
28. (a) M. Peng and C. H. Brubaker, *Inorg. Chim. Acta* 1978, **26**, 231; (b) see also: M. D. Rausch, W. H. Boon and E. A. Mintz, *J. Organomet. Chem.* 1978, **160**, 81.
29. G. P. Pez and S. C. Kwan, *J. Am. Chem. Soc.* 1976, **98**, 8079.
30. E. Klei and J. H. Teuben, *J. Organomet. Chem.* 1980, **188**, 97.
31. E. Samuel, P. Maillard and C. Gianotti, *J. Organomet. Chem.* 1977, **142**, 289.
32. M. Brookhart and M. L. H. Green, *J. Organomet. Chem.* 1983, **250**, 395.
33. A. Hudson, M. F. Lappert and R. Pichon, *J. Chem. Soc., Chem. Commun.* 1983, 374; J. M. Atkinson, P. B. Brindley, A. G. Davies and J. A.-A. Hawari, *J. Organomet. Chem.* 1984, **264**, 253.
34. R. B. King, *Organometallic Syntheses* (Edited by J. J. Eisch and R. B. King). Vol. 1. Academic Press, New York (1965).
35. L. Summers, R. L. Uloth and A. Holmes, *J. Am. Chem. Soc.* 1955, **77**, 3604.
36. K. Clauss and H. Bestion, *Liebigs Ann. Chem.* 1962, **654**, 8.
37. K. Andrä, *J. Organomet. Chem.* 1968, **11**, 567.
38. D. Samuel and M. D. Rausch, *J. Am. Chem. Soc.* 1973, **95**, 6263.
39. K. Handlir, J. Holecek and J. Klikorka, *Z. Chem.* 1979, **19**, 265.
40. F. H. Köhler and W. Prössdorf, *Chem. Ber.* 1978, **111**, 3464; H.-J. de Liefde Meyer and F. Jellinck, *Inorg. Chim. Acta* 1970, **4**, 651.
41. P. L. Timms, *Angew Chem., Int. Ed. Engl.* 1975, **14**, 273.
42. B. G. Gowenlock, W. E. Lindsell and B. Singh, *J. Chem. Soc., Dalton Trans.* 1978, 657.

Polyhedron Vol. 5, No. 7, pp. 1267–1271, 1986
Printed in Great Britain

0277–5387/86 $3.00+.00
Pergamon Journals Ltd

CATALYSIS BY HETEROPOLYACIDS—IX. PHOTOCATALYTIC OXIDATION OF ISOPROPYL ALCOHOL TO ACETONE UNDER OXYGEN USING TETRABUTYLAMMONIUM DECATUNGSTATE

KENJI NOMIYA, YOSHINOBU SUGIE, TOSHIAKI MIYAZAKI and MAKOTO MIWA*

Department of Industrial Chemistry, Faculty of Engineering, Seikei University, Musashino, Tokyo 180, Japan

(*Received* 2 *September* 1985; *accepted* 18 *November* 1985)

Abstract—Homogeneous photocatalytic oxidation of isopropyl alcohol by tetrabutylammonium decatungstate $(Bu_4N)_4[W_{10}O_{32}]$ in acetonitrile using O_2 as a reoxidizing reagent has been studied. The photocatalysis is interpreted on the basis of a rapid redox cycle between 2*e*-reduced species and the oxidized species of decatungstate; O_2 as a reoxidizing reagent is converted to water. The catalytic activity and the mechanism of the redox cycle of decatungstate are in contrast to those of Keggin-type heteropolytungstic acids. When the concentration of isopropyl alcohol is lowered by prolonged irradiation, pale yellow precipitates are produced by side reactions due to electron transfer from the counter-ion Bu_4^+ to the decatungstate.

Photosensitivity of heteropoly and isopoly compounds in the presence of organic compounds has been well known. Recently, the photocatalytic oxidations of alcohols using heteropolytungstates such as $[SiW_{12}O_{40}]^{4-}$, $[PW_{12}O_{40}]^{3-}$ and $[P_2W_{18}O_{62}]^{6-}$ have been reported by Papaconstantinou[1] and Darwent.[2] The former used oxygen whereas the latter used colloidal platinum for the reoxidation of the reduced heteropolyacid. In the latter experiment, evolution of H_2 has been confirmed in the reoxidation process. In view of the chemical conversion of solar energy, these experiments are of special interest and have more recently been studied in detail.[3,4] From a similar standpoint, Yamase *et al.*[5] have reported the photocatalytic H_2 evolution from alcohols by $[W_{10}O_{32}]^{4-}$ in the presence of heterogeneous catalysts such as RuO_2, IrO_2 and Pt. They have also shown a quantitative photochemistry of $(Bu_4N)_4[W_{10}O_{32}]$ in acetonitrile under deaerated conditions. On the other hand, Launay *et al.*[6] have investigated the electrochemical and photochemical reductions of $[W_{10}O_{32}]^{4-}$ and characterized one- (1*e*) and two-electron (2*e*) reduced species by optical and ESR spectra. Our attention has been devoted to the catalytic oxidation by hetero- and isopolyanions using O_2 as a reoxidizing reagent and to its application to organic synthesis. In this paper, we report a photocatalytic oxidation of isopropyl alcohol to acetone using $(Bu_4N)_4[W_{10}O_{32}]$ in acetonitrile under O_2, and show that its photocatalysis is more effective than that of the Keggin-type heteropolytungstic acids. The decatungstate is a unique isopolytungstate with color (pale yellow) and there is no isostructural polyanion. The polyhedral model is shown in Fig. 1.

EXPERIMENTAL

Tetrabutylammonium decatungstate was prepared according to a procedure previously described[6] and recrystallized twice from acetonitrile. Found: C, 23.0; H, 4.5; N, 1.8%. Calc. for $[(C_4H_9)_4N]_4[W_{10}O_{32}]$: C, 23.1; 4.4; N, 1.7%. The salt was identified by its characteristic absorption maxima at 324 (ε 14,000), 262 (ε 16,500) and 218 nm (ε 50,000) in acetonitrile, which correspond to oxygen-to-tungsten charge-transfer bands, and by IR bands (cm^{-1}): 990(vw), 954(vs), 941(s), 888(s), 802(vs),

* Author to whom correspondence should be addressed.

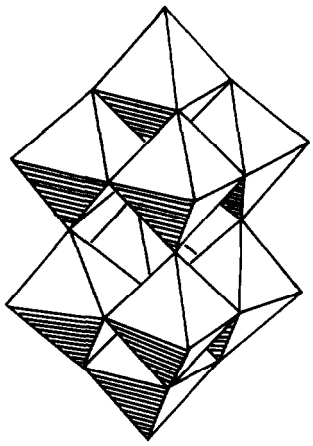


Fig. 1. Polyhedral model of $[W_{10}O_{32}]^{4-}$.

575(vw), 436(m), 420(m) and 405(s). All chemicals used were analytical grade.

A 75-W mercury lamp (SHL-100UV, Toshiba Corporation) in conjunction with a 5-cm cold water IR filter was used as a light source of an external irradiation. The apparatus is shown in Fig. 2. Sample solutions (50 cm^3) were prepared by dissolving decatungstate (5×10^{-3} mol dm^{-3}), isopropyl alcohol as a substrate (0.2–0.8 mol dm^{-3}), and benzene as an internal reference for the gas chromatographic analyses into acetonitrile as a solvent. The Pyrex flask containing the solution was purged with O_2 and irradiated while stirring thoroughly. For the experiment under excess O_2 environment the flask was joined through an inlet tube to a *ca* 5000-cm^3 balloon filled with O_2 before irradiation. Photooxidation of the alcohol was monitored by TCD gas chromatography (Shimadzu GC-8A) on a PEG 20M column. The sampling was performed at time intervals with a microsyringe through a rubber cap of the flask. A blank test of the photoreaction was checked under the system without the decatungstate.

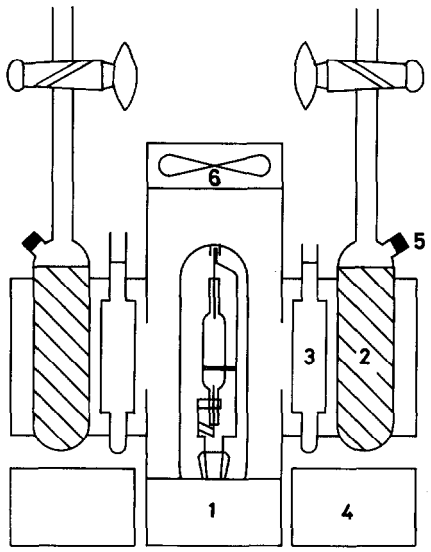


Fig. 2. Apparatus for the photoreaction: (1) light source (75-W mercury lamp); (2) Pyrex flask with a vacuum, stopcock; (3) cold-water IR filter; (4) stirring motor; (5) rubber cap for gas chromatographic sampling; and (6) fan for cooling. For the experiment under excess O_2 environment, a *ca* 5000-cm^3 balloon filled with O_2 is added to the flask.

Absorption spectra of the photoreduced decatungstate observed under N_2 were recorded on a Hitachi-340 spectrophotometer. The decatungstate in the acetonitrile solution was controlled to 1/80 of that in the reaction system described above and the measurements were performed with and without isopropyl alcohol in the region of 1200–300 nm.

RESULTS AND DISCUSSION

When the pale yellow solution of decatungstate (5×10^{-3} mol dm^{-3}) was irradiated under N_2 in the presence of isopropyl alcohol (0.4 mol dm^{-3}), it rapidly became deep blue and reduced decatungstate was formed. If the blue solution was degassed, and O_2 introduced, the initial colour was regenerated within a few minutes. O_2 in the 75-cm^3 Pyrex flask was completely consumed after irradiating for 1 h and the system became a reduced-pressure state—the solution turning deep blue again. O_2 plays an important role in the reoxidation of the reduced form of decatungstate. In conjunction with the redox cycle of decatungstate, isopropyl alcohol was oxidized to acetone. In the presence of O_2, the reaction proceeds with the initial colour being maintained. Under an excess O_2 environment in the Pyrex flask (attached to an oxygen-filled balloon), the gas chromatographic results shown in Fig. 3 were obtained. In each run, the molar amount of acetone produced is equivalent to that of decatungstate used within a few hours of irradiation and thereafter the former continues to increase. This shows that the oxidation of isopropyl alcohol to acetone is truly catalytic with respect to decatungstate. In these reactions, no H_2 evolution was observed; instead H_2O production was observed. Thus, O_2 consumed in the reoxidation of reduced decatungstate was converted into H_2O. The decrease in isopropyl alcohol could be treated as a psuedo-first-order reaction and its rate constant was 2.5×10^{-6} s^{-1}. The catalytic turnover, defined as the molar ratio of the produced acetone to the used catalyst, was 17.6 and the conversion of isopropyl alcohol to acetone was 22% after irradiating for 30 h with 5×10^{-3} mol dm^{-3} $(Bu_4N)_4[W_{10}O_{32}]$, 0.4

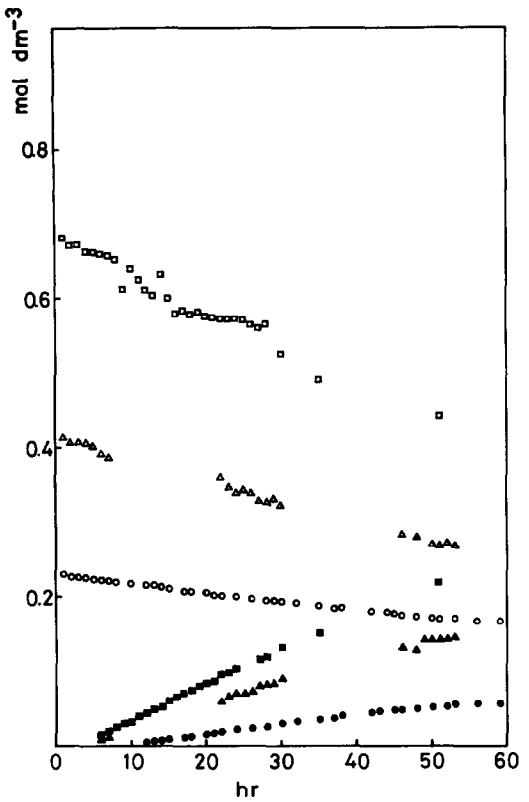


Fig. 3. Plots of decrease in isopropyl alcohol (□, △ and ○) and production of acetone (■, ▲ and ●) by photocatalysis of decatungstate in acetonitrile solutions under excess O_2 environment. Concentrations of isopropyl alcohol used are 0.68 (□), 0.40 (△) and 0.224 (○) mol dm^{-3}, and those of $\{Bu_4N\}_4[W_{10}O_{32}]$ as a catalyst and benzene as an internal reference are 0.5 and 0.256 mol dm^{-3}, respectively. The corresponding open and filled symbols result from the same experimental run.

mol dm^{-3} isopropyl alcohol and 0.287 mol dm^{-3} benzene as an internal reference in a 50-cm^3 acetonitrile solution. These values are larger than those of other polyanions as a photocatalyst; for instance, the turnover and the conversion to acetone were 6 and 7.5%, respectively, after irradiating for 70 h with 5×10^{-3} mol dm^{-3} $H_4[SiW_{12}O_{40}]$, 0.4 mol dm^{-3} isopropyl alcohol and 0.5 mol dm^{-3} H_2SO_4 in a 50-cm^3 aqueous solution. Some advantages of decatungstate as a photocatalyst were confirmed. (1) Both the formation of reduced species under N_2 and its reoxidation by O_2 are very rapid in comparison with other heteropolyanions such as Keggin-type $[PW_{12}O_{40}]^{3-}$ and $[SiW_{12}O_{40}]^{4-}$, and Dawson-type $[P_2W_{18}O_{62}]^{6-}$ under similar conditions. This leads to the high activity of the photocatalysis of decatungstate. (2) The reaction can be carried out under the entirely organic system and no addition of another acid is needed. The latter point is also in marked contrast to the photocatalysis of other heteropolyanions.[1,2,7]

The photoexcitation of the decatungstate is attributed to the absorption at 324 nm, which corresponds to the lowest-energy charge-transfer transition, because the excitations of the higher-energy charge-transfer bands are prevented by the Pyrex tube and the water filter.

The absorption spectra of photoreduced decatungstate in the presence of a large amount of isopropyl alcohol under N_2 are shown in Fig. 4(a). The absorbance increases with the irradiation time and the spectrum saturates after 4 h. Maximum absorptions at 625 and 960 nm are in agreement with those of electrochemically reduced 2*e* species, which have been reported by Launay *et al.*[6] The absorption bands are due to an intervalance charge-transfer (IVCT) transition between W^V—O—W^{VI} and W^{VI}—O—W^V.[8,9] In this experiment, 1*e* species could not be observed, whereas these could be detected in the system without the substrate at the early stage of the irradiation [Fig. 4(b)]. These facts are also consistent with the results reported by Launay's[6] and Yamase's[5] groups. Thus, only when an appropriate amount of substrate remains in the system, does a direct reduction to the 2*e* species presumably occur. The reoxidation of 2*e* species by O_2 was very rapid and could not be monitored by a usual scanning spectrophotometer. A redox cycle between the 2*e* species and the oxidized form is suggested to play a catalytic role for the photo-oxidation of the isopropyl alcohol. The 2*e* species will probably be a diprotonated form ($[H_2W_{10}O_{32}]^{4-}$).[5,6] The schematic diagram is depicted in Fig. 5. Incidentally, the redox cycle is also different from the case of the Keggin-type heteropolyacid. We have examined spectrophotometrically analogous experiments using $H_3[PW_{12}O_{40}]$ in acidic aqueous solution containing isopropyl alcohol. The spectral bands of electrochemically reduced 1*e* and 2*e* species of $[PW_{12}O_{40}]^{3-}$ have been previously reported by Pope *et al.*:[10] 490 (ε 1200), 750 (ε 2000) and 1250 nm (ε 1600) for the 1*e* species; and 490 (ε 3300), 654 (ε 4400) and 1110 nm (ε 3000) for the 2*e* species. It has been shown that there are two processes of reduced-species formation under N_2: the relatively rapid step due to 1*e* species formation and the following slow step due to 2*e*-species formation. Exposure to O_2 gave spectra comprising a rapid decrease in the 2*e* species followed by a gradual decrease in the 1*e* species. This suggests that the 1*e* species of $[PW_{12}O_{40}]^{3-}$ plays an important role in the photo-oxidation of isopropyl alcohol under O_2.

In the photo-oxidation by decatungstate, prolonged irradiation (more than 35 h) gave pale yellow

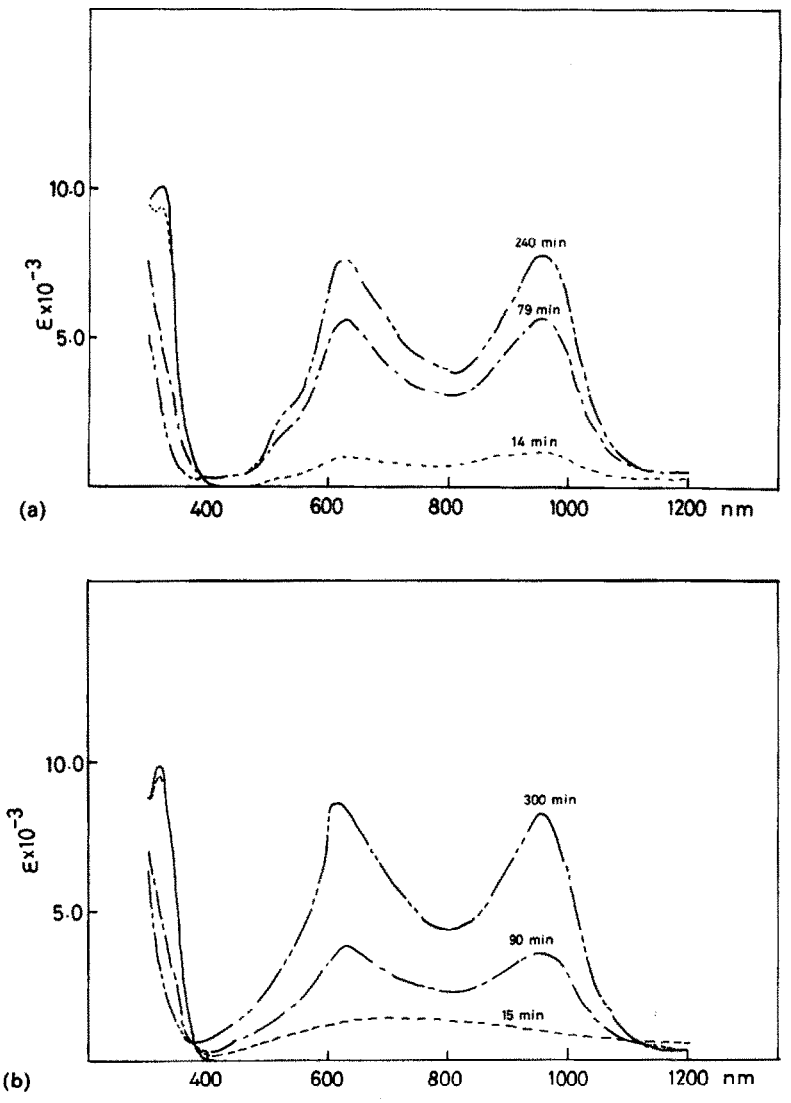


Fig. 4. Absorption spectra of photoreduced decatungstate under N_2 in acetonitrile solutions with (a) and without (b) isopropyl alcohol. Conditions are 4.37×10^{-5} (a) and 4.11×10^{-5} (b) mol dm^{-3} of $(Bu_4N)_4[W_{10}O_{32}]$ and 3.08×10^{-3} mol dm^{-3} (a) of isopropyl alcohol. The figures on the curves are times after irradiation. Full lines show the spectra before irradiation.

precipitates and the system became heterogeneous, even if enough O_2 was present. The IR and electronic absorption spectra showed the presence of the $[W_{10}O_{32}]$ structure and of the carbonyl group. The elemental analysis (found: C, 21.3; H, 3.5; N, 1.8%) indicated that some tetrabutylammonium counter-ions were converted to tributyl- and dibutylammoniums. Such precipitates were also obtained by irradiation both in the absence of any substrates and in the presence of other substrates such as cyclohexanol and ethyl lactate. Furthermore, an aldehyde was detected in the filtrate. These facts suggest that the formula of the precipitate obtained is $(Bu_4N)_2(Bu_3NH)(Bu_2NH_2)[W_{10}O_{32}] \cdot PrCHO$ (calc. C, 20.9; H, 4.0; N, 1.7%)

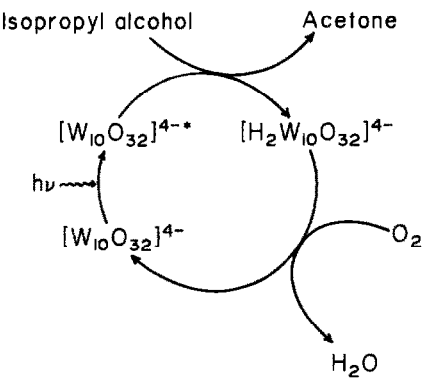


Fig. 5. Schematic diagram of photo-oxidation of isopropyl alcohol by decatungstate.

or $(Bu_3NH)_2(Bu_2NH_2)_2[W_{10}O_{32}]\cdot 5PrCHO$ (calc. C, 21.5; H, 4.1; N, 1.7%). This shows that decatungstate also promotes the photo-oxidation of the tetrabutylammonium counter-ion when the concentration of substrate is lowered. This leads necessarily to a decrease in the photocatalysis for isopropyl alcohol, because of interrupting the homogeneity. The photo-oxidation of tetrabutylammonium by decatungstate in acetonitrile has recently been investigated by Yamase *et al.* and a mechanism for the production of Bu_3N, Bu_2NH and PrCHO has been proposed.[5] The composition of the pale yellow precipitates obtained supports such a mechanism. Yamase *et al.*[5] have also revealed the production of 1*e* species by electron transfer from Bu_4N^+ to $[W_{10}O_{32}]^{4-}$ within the lifetime of the photoflash ($t_{1/2} = 50\,\mu s$), the protonation of $[W_{10}O_{32}]^{5-}$ and its disproportionation to diprotonated species of the 2*e* form $[H_2W_{10}O_{32}]^{4-}$. They have applied the same mechanism to the oxidation of BuOH in acetonitrile by decatungstate, which is based on the absorption kinetics at 780 and 630 nm for the flash photolysis. However, since the observation of 1*e* oxidation by decatungstate should be dependent upon the composition of the acetonitrile–alcohol system and the sort of alcohol, we prefer rather to adopt a different mechanism for decatungstate—namely direct 2*e* oxidation for the isopropyl alcohol and 1*e* oxidation for the ammonium.

REFERENCES

1. E. Papaconstantinou, *J. Chem. Soc., Chem. Commun.* 1982, 12.
2. J. R. Darwent, *J. Chem. Soc., Chem. Commun.* 1982, 798.
3. A. Iodannidis and E. Papaconstantinou, *Inorg. Chem.* 1985, **24**, 439.
4. R. Akid and J. R. Darwent, *J. Chem. Soc., Dalton Trans.* 1985, 395.
5. T. Yamase, N. Takabayashi and M. Kaji, *J. Chem. Soc., Dalton Trans.* 1984, 793.
6. A. Chemseddine, C. Sanchez, J. Livage, J. P. Launay and M. Fournier, *Inorg. Chem.* 1984, **23**, 2609.
7. E. Papaconstantinou, D. Dimotikali and A. Politou, *Inorg. Chim. Acta* 1980, **46**, 155.
8. S. C. Termes and M. T. Pope, *Inorg. Chem.* 1978, **17**, 500.
9. J. P. Launay and R. Massart, *J. Inorg. Nucl. Chem.* 1976, **38**, 1627.
10. G. M. Varga, E. Papaconstantinou and M. T. Pope, *Inorg. Chem.* 1970, **9**, 662.

Polyhedron Vol. 5, No. 7, pp. 1273–1276, 1986
Printed in Great Britain

0277–5387/86 $3.00+.00
Pergamon Journals Ltd

STABILITY CONSTANTS AND PROTONATION CONSTANTS OF TETRACYANO BIS(PHENANTHROLINE) MOLYBDATE(IV) AND TETRACYANO BIS(BIPYRIDYL) MOLYBDATE(IV)

S. I. ALI* and ZAKIR MURTAZA

Department of Chemistry, Jamia Millia Islamia, New Delhi 110025, India

(*Received* 13 *September* 1985; *accepted* 18 *November* 1985)

Abstract—1,10-Phenanthroline (phen) and 2,2′-bipyridyl (bipy) form 2:1 complexes with the dioxotetracyanomolybdate(IV) ion by substitution reactions. The stepwise stability constants and the protonation constants of the substituted products $Mo(CN)_4(phen)_2$ and $Mo(CN)_4(bipy)_2$ have been calculated using spectrophotometric and potentiometric methods. Two successive protonation steps have been found for these systems. Concentration protonation constants have been determined at different ionic strengths and the thermodynamic protonation constants were evaluated by extrapolation to infinite dilution. The dependence of log K_n^p (where $n = 1.5$ or 3.0) on ionic strength is given by the equation $\log K_n^p = \log {}^TK_n^p + B\sqrt{I}/(1+\sqrt{I})$. Thermodynamic parameters for the complex formation have been calculated and the results have been discussed. The protonated products have been isolated and analysed.

Numerous studies have been made on the dioxotetracyano complexes of rhenium(V),[1–5] molybdenum(IV)[6–11] and tungsten(IV),[8–10] regarding their structure and reactivity. Previously, the reported hydrolysis constants[12] calculated for tungsten(IV) and molybdenum(IV) complexes were based on limited data and were not suitable for quantitative treatment, but the mixed tetracyano complexes need more knowledge of proton transfer equilibria in solution. Extensive investigations have been carried out in order to assess quantitatively the importance of various proton transfer equilibria governing the behaviour of these mixed tetracyano complexes. The protonation constants have been recalculated[13] for these complexes and the $[MO_2(CN)_4]^{4-}$ ion (where M = Mo or W) has been treated as a Bronstead base. The corresponding base strength has been expressed conveniently in terms of the successive protonation constants:

$$[MO_2(CN)_4]^{4-} \underset{K_1^p}{\overset{H^+}{\rightleftharpoons}} [MO(OH)(CN)_4]^{3-} \underset{K_2^p}{\overset{H^+}{\rightleftharpoons}} [M(OH)_2(CN)_4]^{2-}.$$

In this study the complexes $Mo(CN)_4(phen)_2$ (phen = 1,10-phenanthroline) and $Mo(CN)_4(bipy)_2$ (bipy = 2,2′-bipyridyl) were investigated by physical methods. The stepwise stability constants (K_1 and K_2) for the reaction of dioxotetracyanomolybdate(IV) with AA ligands (where AA = phen or bipy), the concentration protonation constants (K_n^p) and the thermodynamic protonation constants ($^TK_n^p$) have been calculated. The thermodynamic parameters $\Delta G^\ominus$, $\Delta H^\ominus$ and $\Delta S^\ominus$ have also been evaluated. The protonated products were isolated and their composition determined by analysis.

EXPERIMENTAL

Materials

$K_4MoO_2(CN)_4 \cdot 6H_2O$ was prepared by the method of Samotus *et al.*[14] and its solution strength was determined potentiometrically against $K_3Fe(CN)_6$.[15] The ligands phen, bipy and potassium chloride were of A.R. grade.

Apparatus

The absorbance was recorded on the Spectromom 361 using quartz cells. The pH of the solutions was

* Author to whom correspondence should be addressed.

recorded on Toshniwal's digital pH meter (Cat. CL 46) using a combined glass electrode (Toshniwal's Moeller).

Preparation of compounds

The stoichiometry of the substitution reactions of dioxotetracyanomolybdate(IV) with AA ligands was determined spectrophotometrically by the method of continuous variation and the mole ratio method.

Tetracyano bis(phenanthroline) molybdate(IV) was prepared in solution by mixing a 0.01 M $K_4MoO_2(CN)_4 \cdot 6H_2O$ solution with a 0.02 M phen solution. The colour of the solution changed from blue to green and the mixture was kept for 30 min for completion of the reaction. Tetracyano bis(bipyridyl) molybdate(IV) was prepared in solution similarly.

For the extraction of the protonated product, a solution of HCl was added to a $Mo(CN)_4(AA)_2$ solution so that the pH is lowered to 4 or below, the brown precipitates were extracted by filtration and washed with water and alcohol, and then dried in a desiccator over calcium chloride. The dried complexes were analysed by standard gravimetric methods.[16] Water of crystallization was determined by heating the sample at 110°C. From the analysis the following results were obtained.

Found: Mo, 17.4; N, 13.6; C, 53.2; H_2O, 4.2%. Calc. for $Mo(OH)_3(CN)(phen)_2(H_2O)_2$: Mo, 17.5; N, 12.9; C, 54.8; H_2O, 3.3%. Found: Mo, 17.6; N, 13.7; C, 40.9; H_2O, 4.9%. Calc. for $Mo(OH)_3(CN)(bipy)_2(H_2O)_2$: Mo, 17.8; N, 13.0; C, 46.7; H_2O, 4.3%.

Determination of protonation constants

The protonation constants were determined by the method of Bjerrum.[17] Dilute aqueous solutions of known concentrations of tetracyano bis(phenanthroline) or (bipyridyl) molybdate(IV) were titrated with standard HCl and the pH values recorded. The ionic strength was maintained at levels of 0.0785, 0.125, 0.250 and 0.4 M for the phen system and at 0.039, 0.075, 0.15 and 0.25 M for the bipy system by adding the right amounts of KCl. The pH changes from 11 to 1.5. The glass electrode was standardized with the help of buffer solutions of pH 4.01 and 9.2. All the measurements were carried out at 30°C. Volume changes occuring during the titration were taken into account in calculating the protonation constants. The titration curves show sharp changes in pH of the solution at 1.5 and 3.0 mol of acid per mol of $Mo(CN)_4(phen)_2$ or $Mo(CN)_4(bipy)_2$.

RESULTS AND DISCUSSION

The stepwise stability constants were determined[18] by using spectroscopic techniques monitoring changes at 450 nm for both the systems. The stepwise equilibrium reactions for the 1:2 complex of $K_4MoO_2(CN)_4$ and AA ligands are represented by the following equations.

$$[MoO_2(CN)_4]^{4-} + 2H_2O \rightleftharpoons [Mo(OH)_4(CN)_4]^{4-},$$

$$[Mo(OH)_4(CN)_4]^{4-} + AA \overset{K_1}{\rightleftharpoons} [Mo(OH)_2(CN)_4(AA)]^{2-} + 2OH^-,$$

$$[Mo(OH)_2(CN)_4(AA)]^{2-} + AA \overset{K_2}{\rightleftharpoons} Mo(CN)_4(AA)_2 + 2OH^-.$$

The concentration protonation constants $K^p_{1.5}$ and K^p_3 of the complex $Mo(CN)_4(AA)_2$ were calculated[18] from the equations:

$$K^p_{1.5} = \left(\frac{\bar{n}-0.5}{1.5-\bar{n}}\right)\frac{1}{[H^+]} \quad \text{for} \quad 0 < \bar{n} < 1.5,$$

$$K^p_3 = \left(\frac{\bar{n}-2}{3-\bar{n}}\right)\frac{1}{[H^+]} \quad \text{for} \quad 3 > \bar{n} > 1.5,$$

where $\bar{n}$ = ratio of the concentration of proton bound, H_b, to complex C:

$$\bar{n} = \frac{[H_b]}{C} = \frac{[HCl]+[OH^-]-[H^+]}{C},$$

where C = concentration of the protonated complex and [HCl] = concentration of acid added at any stage of titration. The equilibrium concentrations of H^+ and OH^- ions were obtained from the pH at any stage of titration. The thermodynamic protonation constants ${}^TK^p_{1.5}$ and ${}^TK^p_3$ were calculated by using equation $\log K^p_n = \log {}^TK^p_n + B\sqrt{I}/(1+\sqrt{I})$. On plotting $\log K^p_n$ against $\sqrt{I}/(1+\sqrt{I})$ a straight line was obtained and values of B and $\log {}^TK^p_n$ were obtained from the slope and intercept, respectively.

The values of the changes in free energy ($\Delta G^\ominus$), enthalpy ($\Delta H^\ominus$) and entropy ($\Delta S^\ominus$) accompanying the complex formation have been calculated using the standard equations[19] at 31°C. The enthalpy change ($\Delta H^\ominus$) has been calculated by carrying out experiments at different temperatures (31–40°C). On plotting $\log \beta$ against $1/T$ a straight line was obtained. $\Delta H^\ominus$ was obtained from the slope of the curve. The values of these parameters are given in Table 1.

The AA ligands react with $[Mo(OH)_4(CN)_4]^{4-}$ to form the complexes $[Mo(OH)_2(CN)_4AA]^{2-}$ and $Mo(CN)_4(AA)_2$ with formation constants K_1 and

Table 1. Successive stability constants and thermodynamic parameters at 31°C and $I = 0.04$ M[a]

Complex	Temperature (°C)	log K_1	Mean log K_2	Mean log B	$\Delta G^\ominus$	$\Delta H^\ominus$	$\Delta S^\ominus \times 10^2$
$Mo(CN)_4(phen)_2$	31	3.56	4.00±0.01	7.56±0.05	−44.1±0.2	98	46.7±0.1
	35	3.57	4.13±0.20	7.70±0.13			
	40	3.75	4.30±0.30	8.05±0.20			
$Mo(CN)_4(bipy)_2$	31	3.40	3.67±0.02	7.07±0.03	−41.2±0.4	73	37.5±0.1
	35	3.50	3.70±0.16	7.20±0.12			
	40	3.53	3.92±0.10	7.45±0.21			

[a] $\Delta G^\ominus$, $\Delta H^\ominus$ and $\Delta S^\ominus$ are in kJ mol^{-1} K^{-1}.

K_2, respectively. Two species have been assumed in solution so the absorbance of the solution could be expressed as:

$$A = e_o[Mo(OH)_4(OH)_4^{4-}] + e_1[Mo(OH)_2(CN)_4AA^{2-}] + e_2[Mo(CN)_4(AA)_2],$$

where brackets represent the equilibrium concentrations and the e values are the molar absorptivities. The method of continuous variation and the mole ratio method give a 1:2 stoichiometry between dioxotetracyanomolybdate(IV) and the AA ligands. The reaction can be represented by the following equation:

$$[Mo(OH)_4(CN)_4]^{4-} + 2AA \rightarrow Mo(AA)_2(CN)_4 + 4OH^-.$$

The stepwise stability constants of the above reaction have been calculated and are given in Table 1. The small difference between log K_1 and log K_2 suggests the simultaneous formation of both 1:1 and 1:2 complexes in solution. The stability of the complex depends on the basicity of the ligand.[20] The lower stability of the bipy complex than that of phen may be attributed to the less basic character of bipy.

The typical pH titration curve can readily be interpreted in terms of the formation of $Mo(CN)_3(AA)_2OH$, $Mo(CN)_2(AA)_2(OH)_2$ and $Mo(CN)(AA)_2(OH)_3$, which can be represented by the following equation:

$$Mo(CN)_4(AA)_2 \underset{K_1^p}{\overset{H^+}{\rightleftharpoons}} Mo(CN)_3(AA)_2OH \underset{K_2^p}{\overset{H^+}{\rightleftharpoons}} Mo(CN)_2(AA)_2(OH)_2 \underset{K_3^p}{\overset{H^+}{\rightleftharpoons}} Mo(CN)(AA)_2(OH)_3. \quad (1)$$

After adding 1, 2 or 3 equivalents of acid per mol of the complex only two widely separated end points are observed, one at 1.5 (pH range 7–9) and the other at 3.0 (pH range 3–4). The value of $n = 1.5$ reveals the formation of a 1:1 as well as a 1:2 complex, and $n = 3.0$ shows the formation of a 1:3 complex. The above results show the replacement of three cyanide ions from $Mo(CN)_4(AA)_2$. Protonation curves ($\bar{n}$ vs pH) at various ionic strengths are plotted. The concentration protonation constants calculated from experimental data are given in Table 2. The protonation constants $K_{1.5}^p$ and K_3^p were calculated for a suitable range of pH and $\bar{n}$ values. A straight line was obtained on plotting log K_3^p vs $\sqrt{I}/(1+\sqrt{I})$. The intercept is equal to log K_3^p and the slope is equal to B. The dependence of K_3^p on the ionic strength can be expressed by the equation $\log K_n^p = \log {}^TK_n^p + B\sqrt{I}/(1+\sqrt{I})$, where $B = -1.0$ for the $K_{1.5}$ plot and -0.5 for the K_3^p plot for both the systems.

The values of the thermodynamic protonation constants are given in Table 3. The values of the protonation constants decrease with increasing ionic strength. This is in accordance with the earlier conclusions since in media of higher ionic strength the metal ions are shielded from the ligands by the other ions present.[21] The $\Delta G^\ominus$ values were found to be negative in the above case, showing the substitution reactions to be spontaneous processes. $\Delta G^\ominus$ values are higher for the phen complex than for the bipy complex. The $\Delta S^\ominus$ values are all positive, indicating that the change in entropy favours complex formation. The positive values of $\Delta H^\ominus$ predict the endothermic nature of the reaction. The plots of log β against T^{-1} in all the systems are linear and indicate that the values of $\Delta C_p^\ominus$ are equal to zero.[22] The colour of the $Mo(CN)_4(AA)_2$ solution changes from green to brown on acidification, and precipitates are obtained at pH < 4. The change of pH to <2 is very slow, which may be attributed to

Table 2. Comparison of the experimentally determined protonation constants (log $K^{p}_{1.5}$ and log K^{p}_{3}) at various ionic strengths (I) for $Mo(CN)_4(phen)_2$ and $Mo(CN)_4(bipy)_2$ at 30°C

	I			
	0.0785	0.125	0.250	0.4
$Mo(CN)_4(phen)_2$				
log $K^{p}_{1.5}$	9.14±0.18	9.35±0.21	9.05±0.18	8.98±0.25
log K^{p}_{3}	6.31±0.25	6.35±0.24	6.27±0.26	6.20±0.27
	I			
	0.039	0.075	0.150	0.250
$Mo(CN)_4(bipy)_2$				
log $K^{p}_{1.5}$	8.54±0.15	8.51±0.40	8.55±0.12	8.44±0.25
log K^{p}_{3}	5.60±0.29	5.68±0.52	5.68±0.36	5.53±0.32

Table 3. Thermodynamic protonation constants of $Mo(CN)_4(phen)_2$ and $Mo(CN)_4(bipy)_2$ at 30°C (at $I = 0$)

System	log $^{T}K^{p}_{1.5}$	log $^{T}K^{p}_{3}$
$Mo(CN)_4(phen)_2$	9.35±0.20	6.4±0.28
$Mo(CN)_4(bipy)_2$	8.70±0.24	5.7±0.40

the polynuclear species which become important at higher acidities. The brown precipitates were extracted and analysed. The results of analysis confirmed the products obtained by protonation [eqn (1)].

Acknowledgements—The financial assistance from UGC, New Delhi, and CSIR, New Delhi, for awarding a P.D.F. to Z.M. is thankfully acknowledged.

REFERENCES

1. R. K. Murmann and E. O. Schlemper, *Inorg. Chem.* 1971, **10**, 25.
2. R. H. Fenn and A. J. Graham, *J. Chem. Soc. A* 1971, 2880.
3. R. Shandles, E. O. Schlemper and R. K. Murmann, *Inorg. Chem.* 1971, **10**, 2785.
4. B. Jeżowska-Trzebiatowska, J. Hanuza and M. Baluka, *Spectrochim. Acta* 1971, **27A**, 1753.
5. M. C. Chakarvarti, *J. Inorg. Nucl. Chem.* 1972, **39**, 893.
6. V. W. Day and J. L. Hoard, *J. Am. Chem. Soc.* 1968, **90**, 3374.
7. J. Chojnacki, J. Ryerlowka and K. Standnicka, *Rocz. Chem.* 1969, **43**, 227.
8. S. J. Lippard and B. J. Russ, *Inorg. Chem.* 1967, **6**, 1943.
9. S. J. Lippard, H. Nozaki and B. J. Russ, *J. Chem. Soc., Chem. Commun.* 1967, **00**, 118.
10. J. Vande Peol and H. M. Neumann, *Inorg. Chem.* 1968, **7**, 2086.
11. W. Jakob and M. Dudek, *Zesz. Nauk. Uniw. Jagiellon. Pr. Chem.* 1971, **16**, 9.
12. W. M. Letvinchuk and C. M. Mikhelevich, *Russ. J. Inorg. Chem.* 1959, **00**, 800.
13. E. Hejmo, A. Kanas and A. Samotus, *Bull. Acad. Pol. Sci., Ser. Sci. Chem.* 1973, **21**, 31.
14. A. Samotus, M. Dudek and A. Kanas, *J. Inorg. Nucl. Chem.* 1975, **37**, 943.
15. Kabir-ud-din and M. A. Beg, *J. Indian Chem. Soc.* 1968, **45**, 455.
16. A. I. Vogel, *Quantitative and Inorganic Analysis*, 4th edn., p. 472. Longmans, London (1979).
17. J. Bjerrum, *Metal Amine Formation in Aqueous Solution*. P. Haase, Copenhagen (1941).
18. M. T. Beck, *Chemistry of Complex Equilibria*, pp. 49 and 87. Van Nostrand Reinhold, London (1970).
19. K. B. Yatsimirskii and V. P. Vasil'es, *Instability Constants of Complex Compounds*, p. 65. Constants Bureau, New York (1960).
20. M. M. Islam, R. S. Singh and B. G. Bhat, *Indian J. Chem.* 1982, **21A**, 751.
21. A. Gupta and B. S. Pannu, *J. Indian Chem. Soc.* 1961, **59**, 937.
22. A. Mcauley and G. H. Nancollas, *J. Chem. Soc.* 1961, 2215.

Polyhedron Vol. 5, No. 7, pp.1277–1284, 1986
Printed in Great Britain

0277–5387/86 $3.00 + .00
Pergamon Journals Ltd

ANALYTICAL PROPERTIES OF THE AMIDOXIME GROUP—XII. SPECTROPHOTOMETRIC STUDY OF SEVERAL METAL–AMIDOXIME COMPLEXES

F. BORRULL* and J. GUASCH

Departament de Química Analítica, Facultat de Ciències Químiques, Tarragona, Spain

E. CASASSAS

Departament de Química Analítica, Facultat de Químiques de Barcelona, Barcelona, Spain

and

V. CERDÁ

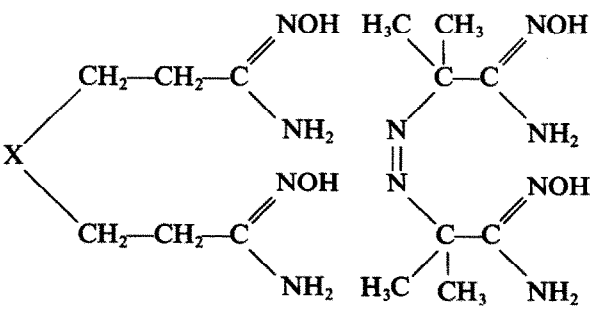
Departament de Química Analítica, Facultat des Ciències, Universitat de Palma de Mallorca, Palma de Mallorca, Spain

(*Received* 22 *October* 1985; *accepted* 2 *December* 1985)

Abstract—The spectrophotometric behaviour of a number of amidoxime–metal complexes is studied, mainly those formed by Cu(II). The influence of several variables (pH, time etc . . .) on complex formation is determined, together with the performance of Beer's law and the precision according to Ringbom. For the Cu(II) complexes of several polyamidoximes the conditional stability constants are calculated and refined by means of the MINISPEF program. These constants, after correction using the appropriate side-reaction coefficients, are used to draw the corresponding distribution diagrams.

In previous papers, the physico-chemical properties of several amidoximes, including their acid–base dissociation equilibria, were studied.[1–5] Some of these amidoximes have been proposed as analytical reagents,[6–9] on the basis either of their ability to form metal complexes or of their redox properties. The physico-chemical properties of the metal complexes of the amidoximes, however, have scarcely been studied.

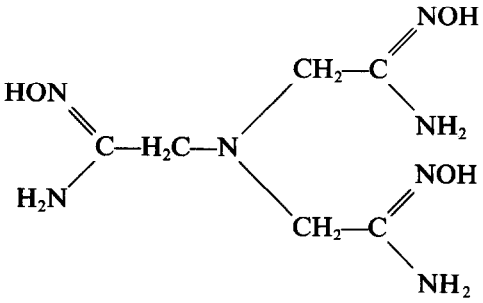
As a part of a research project directed towards the study of the analytical behaviour of the amidoxime group, some spectrophotometric properties were determined for the complexes formed in solution between several metal ions [Cu(II), Co(II), Ni(II), Fe(II), Fe(III), Pd(II), Mo(VI) and U(VI)] and the following polyamidoximes: 3,3′-imino-, 3,3′-oxy- and 3,3′-thiodipropioamidoxime (IDPA, ODPA and TDPA, respectively), α,α′-azobis(isobutyroamidoxime) (AIBA), nitrilotriacetoamidoxime (NTAA) and ethylenediaminotetraacetoamidoxime (EDTAA):



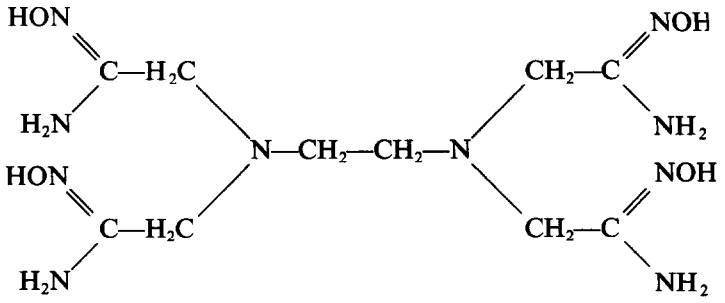
X = NH (IDPA)
X = O (ODPA)
X = S (TDPA)

AIBA

* Author to whom correspondence should be addressed.



NTAA



EDTAA

Although the tests for most of metal ions with these amidoximes do not show very low limits of detection and, as a consequence, these reagents are not, in principle, suitable for metal-ion determination at trace levels, the spectrophotometric study was performed in order to explore all possibilities and to correlate its results with data resulting from previous thermometric experiments. Among the several metal complexes reviewed, those of the Cu(II) ion, which give well-defined absorption bands with all the selected amidoximes, were selected for a more thorough study, which included the determination of their pH and time stability, and their stoichiometry, as well as the evaluation of their formation constants.

EXPERIMENTAL

Apparatus

A double-beam UV–VIS spectrophotometer, Beckman 5260, with 1.0-cm quartz cells was used for measurements.

A microcomputer, HP-85, with 32 kilobytes of RAM memory was used for computation of the results.

Chemicals and solutions

Amidoximes, obtained as described[2,10] and purified, were used to prepare stock 1% aqueous solutions. Test solutions were prepared from the stock solutions by appropriate dilution, as needed.

All metal-ion solutions were prepared from metal salts of analytical-reagent grade, at a concentration of 1000 ppm. These solutions were standardized by the usual recommended methods.[11]

Other chemicals (e.g. for buffer preparation) were also analytical-reagent grade. The buffer solution used was an universal buffer of a constant 0.1 mol l^{-1} ionic strength.[12]

Procedure

Absorption spectra. 1 cm^3 of the metal-ion solution and 1 cm^3 of the buffer of the appropriate pH were introduced into a 10-cm^3 volumetric flask, the amidoxime solution was then added in excess in order to ensure quantitative complex formation, and then water was added up to the mark. The spectra of these solutions were recorded from 300 to 900 nm against a reference blank containing the same metal ion and buffer components. Spectra of the pure amidoximes at the same concentration and in the same buffer were also recorded (against the buffer solution as a blank). Wavelengths of maximum absorption and molar absorptivity for the complexes at these wavelengths were measured in all cases where their absorption bands did not overlap with those of the amidoximes. For each metal ion and amidoxime, optimum pH conditions to record the spectra were found in a previous qualitative study performed by the usual procedures.[10]

The pH and time dependence of the spectra of the Cu(II) complexes, the Beer's law range of linearity and the Ringbom's maximum-precision range were determined according to the standard procedures.

Stoichiometry. The stoichiometry of the Cu(II) complexes in aqueous solution was determined by the Yoe–Jones method in the presence of a selected buffer.[13]

Conditional formation constants. Approximate values of the conditional stability constants of the Cu(II)–amidoxime complexes were evaluated directly from the absorbance and concentration data obtained in the experiments done for the stoichiometry determination. These constants were then refined by means of the MINISPEF program,[14] as described later.

RESULTS AND DISCUSSION

Absorption spectra

Table 1 gives the results of the qualitative tests yielding coloured solutions, given by each of the

Table 1. Complexes initially selected for the spectrophotometric study: results of qualitative tests

Amidoxime	Metal ion	Medium	(pH)	Dilution limit	Colour
IDPA	Cu(II)	HAc	(~4)	1/25,000	Blue
	Fe(II)	HAc	(~4)	1/25,000	Rose
	Fe(III)	HAc	(~4)	1/25,000	Brown
	Co(II)	HAc	(~4)	1/25,000	Yellow
	Mo(VI)	HAc	(~4)	1/10,000	Green
ODPA	Cu(II)	NaAc	(~9)	1/5000	Brown
	Fe(II)	NaAc	(~9)	1/10,000	Green-brown
	Fe(III)	NaAc	(~9)	1/10,000	Brown
	Co(II)	NaAc	(~9)	1/10,000	Brown
	Ni(II)	NaAc	(~9)	1/100,000	Green
	Pd(II)	NaAc	(~9)	1/25,000	Yellow-green
TDPA	Cu(II)	NaAc	(~9)	1/1000	Green
	Fe(II)	NaAc	(~9)	1/1000	Blue
	Fe(III)	Water	(~7)	1/100,000	Green
	Ni(II)	NaAc	(~9)	1/100,000	Green
AIBA	Cu(II)	Water	(~7)		Blue
	Ni(II)	Water	(~7)		Yellow-orange
	Co(II)	Water	(~7)		Red-brown
	U(VI)	Water	(~7)		Orange
NTAA	Cu(II)	Water	(~7)	1/100,000	Green
	Fe(III)	HAc	(~4)	1/500,000	Brown
	Co(II)	HAc	(~4)	1/100,000	Rose
	Ni(II)	HAc	(~4)	1/20,000	Blue
EDTAA	Cu(II)	HAc	(~4)	1/100,000	Green
	Fe(III)	HAc	(~4)	1/500,000	Red-brown
	Co(II)	HAc	(~4)	1/50,000	Rose
	Ni(II)	Water	(~7)	1/1000	Violet
	U(VI)	Water	(~7)	1/50,000	Yellow

selected amidoximes with various metal ions, including the reaction medium, observed colour, and limit of detection (expressed as the dilution limit). The absorption spectra of each one of the coloured solutions, supposed to contain a soluble metal ion–amidoxime complex, together with the spectrum of the respective amidoxime, are shown in Figs 1–6.

All Cu(II)–amidoxime complexes gave well-defined absorption bands. The wavelength of their maxima clearly showed that the heteroatom in the amidoximes enters into the co-ordination sphere of the Cu(II) ion: for the ODPA complex (O, heteroatom), λ_{max} = 740 nm; for the IDPA and AIBA complexes (N, heteroatom), λ_{max} = 610 and 605 nm, respectively; for the TDPA complex (S, heteroatom), λ_{max} = 500 nm. The polyaminopolyamidoximes ligands, NTAA and EDTAA, gave, respectively, λ_{max} = 710 nm (absorbance grows towards the 850–900 nm end of the recorded spectrum) and λ_{max} = 690 nm.

Ni(II) complexes showed well-defined absorption bands with ligands containing an O heteroatom (with ODPA, λ_{max} = 645 nm, shoulder at 750 nm) or an S heteroatom (with TDPA, λ_{max} = 615 nm, shoulder at 770 nm), but not with those ligands containing an N heteroatom. The complexes with NTAA and EDTAA showed maxima at about 380 and 580 nm, both with a rather low absorptivity.

In the spectra of the Co(II) complexes with NTAA an absorption band was observed at 520 nm; for the Co(II) complex of EDTAA the band shifted to 505 nm. The spectra of the AIBA complex showed two shoulders, at about 500 and 650 nm, but not any well-defined band.

Only the ligands NTAA, EDTAA and TDPA yielded complexes with Fe(III) which showed well-defined absorption bands at 425, 435 and 575 nm,

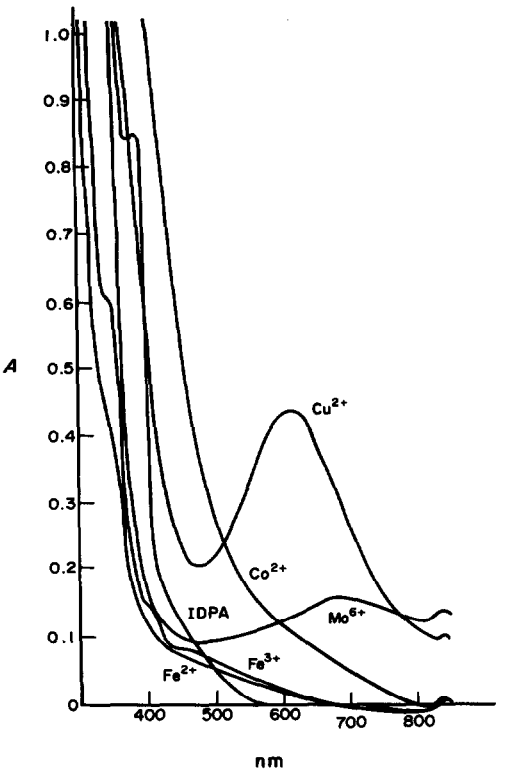


Fig. 1. IDPA–metal complexes

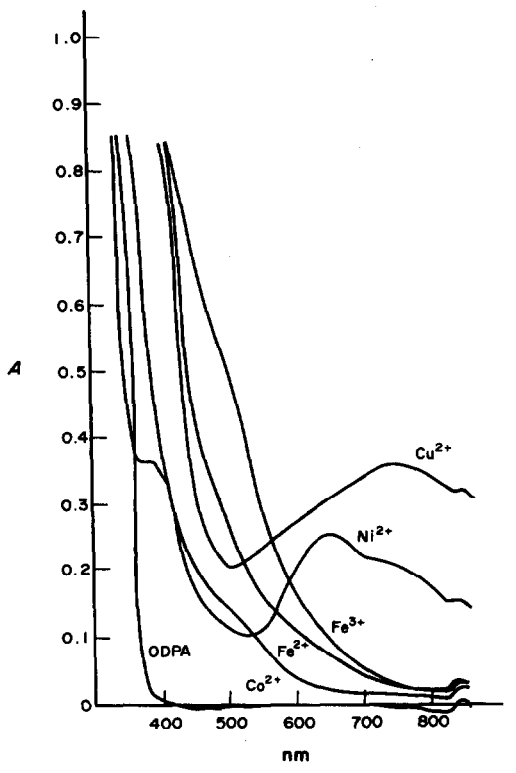


Fig. 2. ODPA–metal complexes

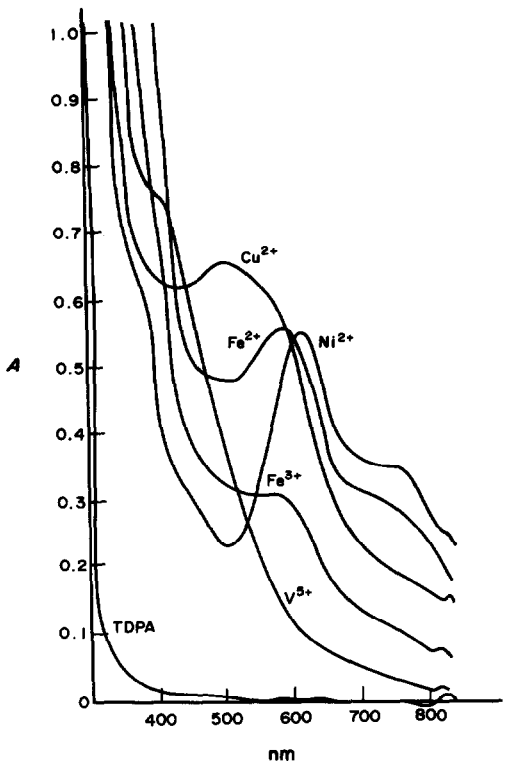


Fig. 3. TDPA–metal complexes.

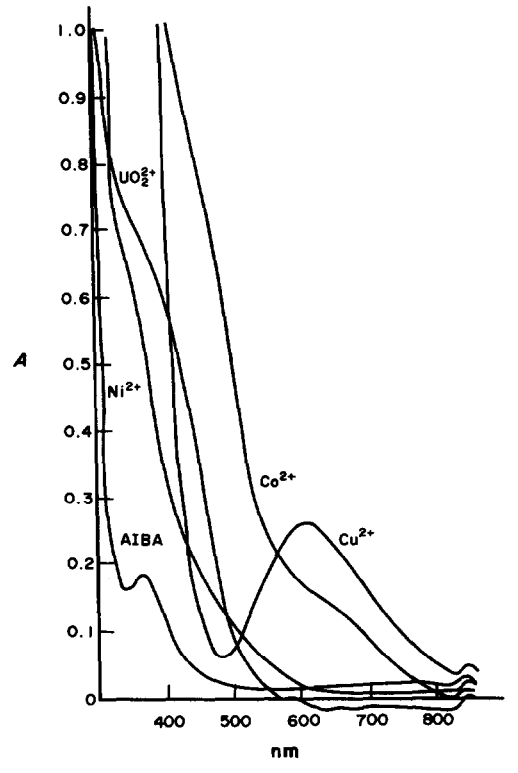


Fig. 4. AIBA–metal complexes.

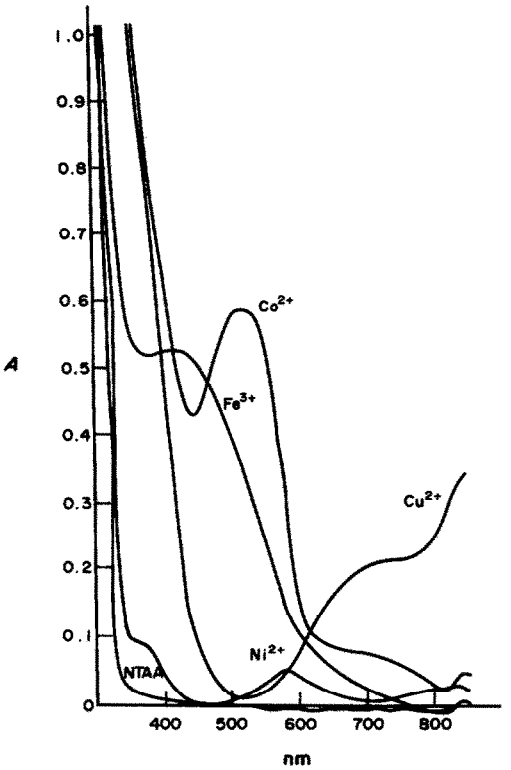


Fig. 5. NTAA–metal complexes.

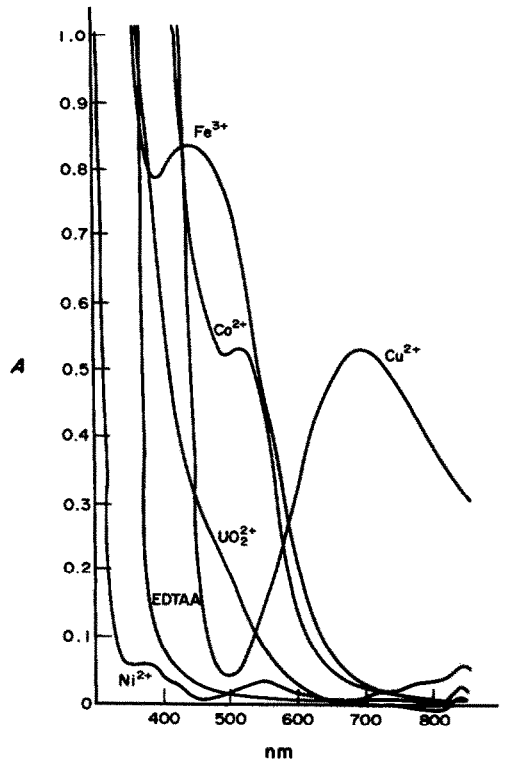


Fig. 6. EDTAA–metal complexes.

respectively. The absorption band of the Fe(III)–TDPA complex was a charge-transfer band which clearly results from a strong S–Fe interaction. For the Fe(II)–TDPA complex, this band appears at 585 nm.

The Mo(VI)–IDPA complex showed a band with $\lambda_{max} = 680$ nm.

All other complexes studied yielded spectra which strongly overlap with those of the respective amidoxime.

Cu(II) *complexes*

The formation equilibria of the Cu(II) complexes of amidoximes were quantitatively studied after the data in Table 2 were collected. Absorbance of each Cu(II) complex is pH-independent within the pH ranges given in Table 2. In these pH ranges, Beer's law is obeyed within a large Cu(II) ion concentration range, as shown by the empirical linear equation given in Table 2, together with their correlation coefficients. As is shown by these equations, none of the amixodimes studied can be adopted as a reagent for a new absorptiometric method for Cu(II) ion determination, since the molar absorptivity of the Cu(II) complexes formed is too low for a good limit of detection to be reached (Ringbom intervals of maximum precision of these potential methods, also given in Table 2, would have lower limits of about 40–50 ppm in the optimum cases).

The stoichiometry of the Cu(II)–amidoxime complexes was determined by use of the well-known Yoe–Jones method.[13] The results obtained yield a stoichiometric Cu(II) : amidoxime ratio equal to 1 : 1 for the complexes of the ligands which contain N heteroatoms, IDPA, AIBA, NTAA and EDTAA, and to 1 : 2 for the complexes of the ligands containing O or S heteroatoms, ODPA and TDPA.

Formation constants of the Cu(II) *complexes*

From the experimental data [absorbance, Cu(II) ion concentration, and ligand concentration] obtained in the course of the study of the stoichiometry, approximate values of the conditional stability constants were obtained as shown in Table 3(A) for the Cu(II)–IDPA complex. Results for log β_{11} for the 1 : 1 complexes are as follows: IDPA complex (at pH 4.1, buffer components : acetic acid and NaOH), 4.42; AIBA complex (at pH 4.1, buffer components : acetic acid and NaOH), 5.40; NTAA complex (at pH 5.8, buffer components : KH_2PO_4 and Na_2HPO_4), 4.87; EDTAA complex (at pH 3.9, buffer components : acetic acid and NaOH), 5.07; and for log β_{11} and log β_{12}, for the cases where the 1 : 2 complex is the dominant complex formed, are

Table 2. Absorptiometric behaviour of the Cu(II)–amidoxime complexes

Compound	pH range	Beer's law equation C (mol l^{-1})	r	Concentration range (ppm)	Linear Ringbom range (ppm)
IDPA	3.9–5.0	$A = 1.61 \times 10^{-3}C - 5.99 \times 10^{-3}$	1.0000	0–1000	100–800
ODPA	—	$A = 3.15 \times 10^{-3}C - 9.20 \times 10^{-4}$	0.9999	0–500	50–220
AIBA	4.2–5.6	$A = 2.40 \times 10^{-3}C - 9.99 \times 10^{-3}$	0.9999	0–500	40–300
NTAA	3.5–9.2	$A = 1.53 \times 10^{-3}C - 5.63 \times 10^{-3}$	0.9995	0–700	250–500
EDTAA	3.0–5.8	$A = 2.40 \times 10^{-3}C - 2.71 \times 10^{-3}$	1.0000	0–500	150–500

as follows: ODPA complexes [pH 6.5, water solution ($I = 0.1$ mol l^{-1} KNO_3)], 5.40 and 8.00 respectively; TDPA complexes [pH 6.5, water solution ($I = 0.1$ mol l^{-1} KNO_3)], 5.40 and 8.00 respectively.

These values of the constants were then refined by means of the computer program MINISPEF[14] which minimizes the sum of the residuals:

$$U(\log \beta_i, \varepsilon_i, \varepsilon_M, \varepsilon_L) = \sum_i (A_{\text{meas},i} - A_{\text{calc},i})^2 = \sum_i (A_{\text{meas},i} - \varepsilon_M[M] - \varepsilon_L[L] - \sum_j \varepsilon_j \beta_j [M]^{q_j} [L]^{p_j} [H^+]^{r_j})^2.$$

Values of ε_{11}, when only the 1 : 1 complex was formed, and of ε_{12} for the 1 : 2 complexes are experimentally determined by measuring the absorbance of solutions which contained a very large excess of amidoxime. Initial values of ε_{12} when both 1 : 1 and 1 : 2 complexes were simultaneously formed were arbitrarily taken as equal to ε_{12}, since the computer program MINISPEF has the advantage of not needing accurate values of ε_i and $\log \beta_i$ as starting parameters. In all cases, initial values for ε_M and ε_L were considered to be zero, since both metal and ligand are either non-absorbing or very slightly absorbing species in the wavelength range used for measurement. Table 3(B) shows the results obtained from an experiment in the study of the Cu(II)–IDPA complex.

Table 4 gives the conditional constants of the Cu(II) complexes of all the selected amidoximes, together with the molar absorptivities of all the implied species, as refined by use of MINISPEF program. The final values of the minimization function, U, and the standard deviations of the results, S, are also included in Table 4.

Once the conditional formation constants were known, they were corrected using the side-reaction coefficients defined by Ringbom[15] to account for the side-reaction effects produced mainly by the constituents of the buffer systems and by the hydroxide ions. To carry out the correction, the side-reac-

Table 3. Conditional stability constants of the Cu(II)–IDPA complex

(A) From absorbance readings in Yoe–Jones experiments

$\varepsilon_M = 0$, $\varepsilon_L = 0$

No.	A, m	A, c	D
1	0.060	0.046	+0.014
2	0.110	0.091	+0.019
3	0.157	0.136	+0.021
4	0.199	0.180	+0.019
5	0.240	0.222	+0.018
6	0.269	0.257	+0.012
7	0.284	0.279	+0.005
8	0.295	0.288	+0.007
9	0.300	0.297	+0.003

Q	P	R	$\log \beta_{11}$	ε_{11}
+1	+1	0	+4.422	9.44×10^{-1}

Square of residuals = 1.85×10^{-3}
Standard deviation = 1.63×10^{-2}

(B) After refinement according to MINISPEF

No.	Total M	Total L	A, m	A, c	D
1	3.179	0.492	0.060	0.068	−0.008
2	3.179	0.981	0.110	0.111	−0.001
3	3.179	1.477	0.157	0.153	+0.004
4	3.179	1.969	0.199	0.195	+0.004
5	3.179	2.461	0.240	0.234	+0.006
6	3.179	2.954	0.269	0.266	+0.003
7	3.179	3.446	0.284	0.286	−0.002
8	3.179	3.938	0.295	0.296	−0.001
9	3.179	7.384	0.300	0.307	−0.007

Q	P	R	$\log \beta_{11}$	ε_{11}
1	1	0	4.33	9.74×10

$\varepsilon_M = 7.65$, $\varepsilon_L = 0$

Square of residuals = 1.89×10^{-4}
Standard deviation = 5.62×10^{-3}

Error in parameter No. 2 = 8.27×10^{-1}
Error in parameter No. 1 = 2.04×10^{-2}

Table 4. Conditional stability constants of the Cu(II)–amidoxime complexes, as evaluated with MINISPEF program

Ligand		$\log \beta_{11}$[a]	$\log \beta_{12}$[a]	ε_{11}	ε_{12}	ε_M	ε_L	U	S	λ (nm)
IDPA	A	4.33±0.02	—	97.4±0.8	—	7.65	0	1.90×10^{-4}	5.62×10^{-3}	610
	B	11.7	—							
ODPA	A	5.52±0.06	8.01±0.16	122.3	273.7	0	0	2.1×10^{-2}	5.4×10^{-2}	740
	B	5.52	8.01							
TDPA	A	5.34±0.05	7.76±0.15	156.6	961.0	0	24.8	1.9×10^{-2}	4.6×10^{-2}	500
	B	5.34	7.76							
AIBA	A	6.05±0.05	—	148.0	—	3.19	0.95	1.00×10^{-4}	3.78×10^{-3}	605
	B	7.97	—							
NTAA	A	5.42±0.08	—	89.5	—	7.85	8.16	1.2×10^{-3}	1.4×10^{-2}	710
	B	5.88	—							
EDTAA	A	4.87±0.01	—	157.5	—	18.0	1.53	6.1×10^{-4}	8.7×10^{-3}	690
	B	10.07	—							

[a] A = log of the refined conditional stability constants by MINISPEF. B = log of the stability constants corrected by means of the side-reaction coefficients defined by Ringbom.

tion coefficients were calculated from the stability constants found in the literature[16] (for hydroxo-complex formation and for complexation with the buffer constituents) or from values previously determined[11] (for protonation of the ligands). Table 4 gives the corrected formation constants of the Cu(II)–amidoxime complexes.

Finally, from these formation constants, the protonation constants of the ligands and all other pertinent constants, the distribution diagrams for all the systems studied were calculated by use of the program COMPLEX, taking into account all possible species present. The resulting distribution diagrams are shown in Figs 7–12.

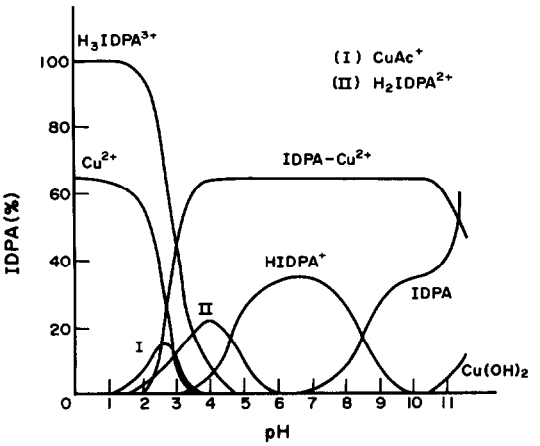


Fig. 7. Distribution diagram corresponding to the Cu–IDPA system. Total concentration ratio [Cu(II)/IDPA] = 0.65. Total acetate (HAc + Ac$^-$) in solution = 7.5×10^{-2} mol l^{-1}.

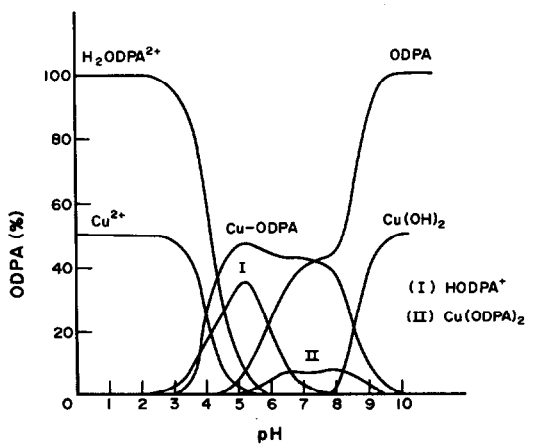


Fig. 8. Distribution diagram corresponding to the Cu(II)–ODPA system. Total concentration ratio [Cu(II)/ODPA] = 0.48.

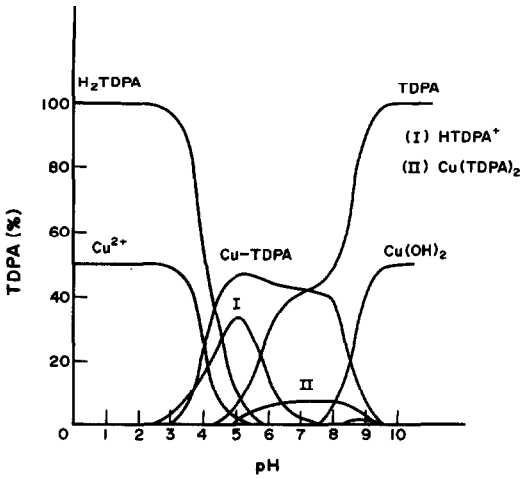


Fig. 9. Distribution diagram corresponding to the Cu(II)–TDPA system. Total concentration ratio [Cu(II)/TDPA] = 0.48.

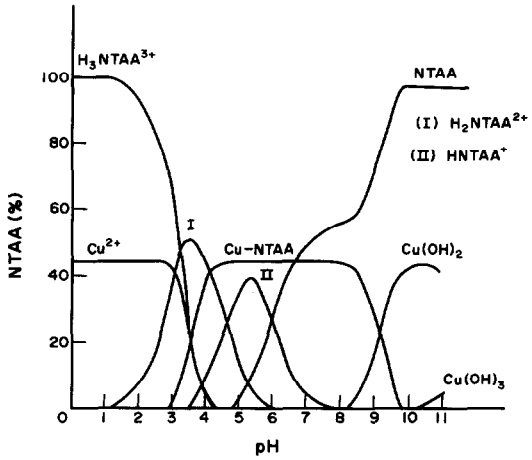


Fig. 11. Distribution diagram corresponding to the Cu(II)–NTAA system. Total concentration ratio [Cu(II)/NTAA] = 0.45.

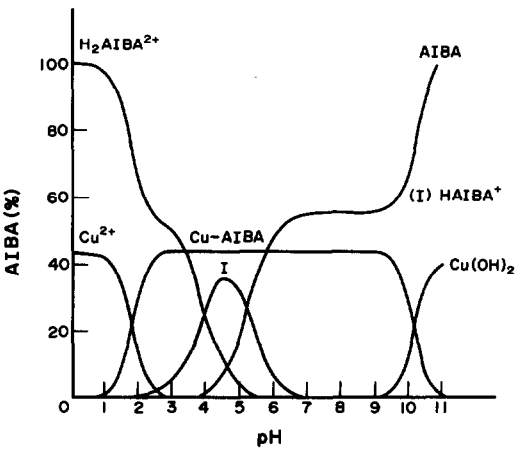


Fig. 10. Distribution diagram corresponding to the Cu(II)–AIBA system. Total concentration ratio [Cu (II)–AIBA] = 0.44. Total acetate ($HAc + Ac^-$) in solution = 3.9×10^{-2} mol l^{-1}.

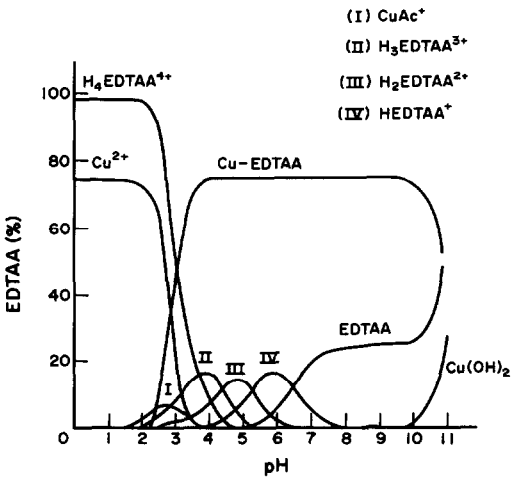


Fig. 12. Distribution diagram corresponding to the Cu(II)–EDTAA system. Total concentration ratio [Cu(II)/EDTAA] = 0.74. Total acetate ($HAc + Ac^-$) in solution = 7.5×10^{-2} mol l^{-1}.

REFERENCES

1. A. Mantecon, M. L. Albelda, V. Cádiz and V. Cerdá, *Afinidad* 1981, **38**, 143.
2. V. Cerdá, E. Casassas and F. Borrull, *Ann. Quim.* 1982, **78B**, 327.
3. V. Cerdá, E. Casassas and F. Borrull, *Thermochim. Acta* 1982, **57**, 195.
4. V. Cerdá, J. M. Estela and R. Jara, *Thermochim. Acta* 1985, **87**, 13.
5. V. Cerdá, J. Jara and R. Forteza, *J. Electroanul. Chem.* 1985, **195**, 335.
6. F. Eloy and R. Lenaers, *Chem. Rev.* 1962, **62**, 155.
7. M. Kuras, *Chem. Listy* 1944, **38**, 54; 1950, **44**, 90; 1951, **45**, 33; 1952, **46**, 482; 1954, **48**, 1275.
8. M. Kuras and E. Ruzicka, *Chem. Listy* 1953, **47**, 1870.
9. G. A. Pearse and R. T. Pflaum, *J. Am. Chem. Soc.* 1959, **81**, 6505.
10. V. Cerdá, E. Casassas, J. Guasch and F. Borrull, *Quim. Anal.* (in press).
11. A. Vogel, *A Textbook of Quantitative Inorganic Analysis*, 3rd edn. Longman, London (1961).
12. C. Mongay and V. Cerdá, *Talanta* 1977, **24**, 747.
13. J. H. Yoe and A. L. Jones, *Ind. Eng. Chem., Anal. Ed.* 1944, **16**, 111.
14. F. Gaizer and A. Puskás, *Talanta* 1981, **28**, 925.
15. A. Ringbom, *Complexation in Analytical Chemistry*. Interscience, New York (1963).
16. A. Martell and R. M. Smith, *Critical Stability Constants*, Plenum Press, New York (1974–1982) (five volumes).

Polyhedron Vol. 5, No. 7, pp. 1285–1290, 1986
Printed in Great Britain

0277–5387/86 $3.00+.00
Pergamon Journals Ltd

SYNTHESES, CHARACTERIZATION AND ADDUCT FORMATION OF CHLORIDE–2,4,6-TRIMETHYLPHENOXIDE DERIVATIVES OF TITANIUM AND ZIRCONIUM

A. SHAH, A. SINGH and R. C. MEHROTRA*

Chemical Laboratories, University of Rajasthan, Jaipur, India

(*Received* 26 *July* 1985; *accepted after revision* 9 *December* 1985)

Abstract—Chloride phenoxides of type $MCl_{4-n}(OAr')_n$ (where M = Ti or Zr; n = 1, 2 or 3) have been prepared by the interaction of the metal chlorides with 2,4,6-trimethylphenol (Ar'OH). The mixed chloride phenoxides showed considerable reactivity as Lewis acids towards bases, resulting in addition complexes of general formula $MCl_{4-n}(OAr')_nL_2$ (where L = primary or tertiary aromatic amines, or oxygen- or phosphorus-containing bases). These complexes have been characterized by IR and the ^1H NMR studies, conductivity measurements, molecular weight measurements (in the case of soluble products), thermogravimetric and mass spectral studies.

During the last few years, sterically crowded phenoxides have received considerable attention and have exhibited interesting features such as: (i) intramolecular C—H bond activation via metallation of the *t*-Bu group of the phenoxides,[1] (ii) isolation of hydrocarbon-soluble compounds in low coordination states,[2] (iii) accessibility of hydrocarbon-soluble mononuclear complexes,[3] and (iv) possible η^5-phenolate bonding.[4–6]

The interaction of titanium tetrachloride with simple phenol (1:4 equivalents) resulted in the tetrakis derivatives.[7] Similar tetrakis derivatives have also been obtained in the reaction of perfluorophenols with $TiCl_4$.[8] X-ray crystallography has shown the bis derivative of titanium with simple phenol to be dimeric phenoxy-bridged with titanium penta-coordinated in the form of a distorted trigonal bipyramid.[9] Following their observation[4] of the formation of an η^5-bonded phenoxide ion to platinum group metals (Ru or Rh), Wilkinson and coworkers synthesized $TiCl_2(OPh)_2$ to examine any η^5-bonding in the case of this earlier transition metal derivative also. Although no evidence was found for η^5-bonding in the above derivative, yet these workers made a detailed study of its reactions with reducing agents,[10] which aroused considerable interest due to the observation that the reduction of $TiCl_2(OPh)_2$ with sodium naphthalenide or potassium under nitrogen gave appreciable quantities of ammonia.

The tetra-alkoxides (and phenoxides) of titanium and zirconium generally attain higher coordination numbers through oligomerization, and generally do not show Lewis acid character, whereas chloride alkoxides exhibit considerable Lewis acid character, leading to the formation of a large number of adducts.[11–14]

In contrast to the chloride alkoxides, the Lewis acid character of phenoxide derivatives of titanium and zirconium has received scanty attention. Recently reports have appeared in the literature describing the Lewis acidic nature of titanium naphthyloxides.[15,16]

X-ray crystallographic studies of sterically hindered phenoxide derivatives of early transition metals have shown that phenolate ions can also behave as π-donor ligands, M⇐OAr, which would in effect reduce the electrophilicity of the metal atom.

In view of the above interesting findings, it was considered worthwhile to synthesize derivatives of titanium and zirconium with a moderately hindered phenol, i.e. 2,4,6-trimethylphenol, and to study the Lewis acidic behaviour of these phenoxide derivatives.

* Author to whom correspondence should be addressed.

EXPERIMENTAL

Titanium and zirconium tetrachlorides were purified by distillation and sublimation, respectively, under reduced pressure. Solvents and the various bases were made anhydrous before use. Molecular weights were measured either ebullioscopically (Gallenkamp apparatus) or cryoscopically. IR spectra were recorded (4000–200 cm^{-1}) on a Perkin–Elmer grating spectrometer 577. PMR spectra of the compounds were recorded on a 60-MHz Perkin–Elmer instrument. Molar conductances of the addition complexes were measured on a conductivity bridge type 302 Sr No. 471. TGA, DTA and mass spectrum were recorded in air on a thermal balance and under reduced pressure on a mass spectrometer.

Synthetic procedures

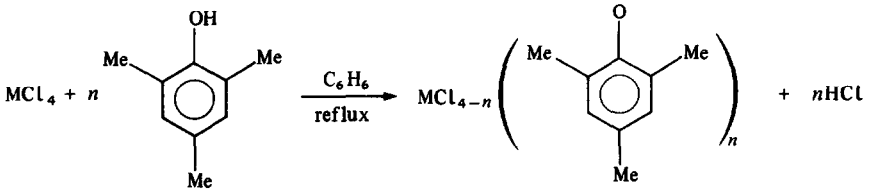
$MCl_{4-n}(OAr')_n$ derivatives were synthesized in general by the reaction of the tetrachlorides of titanium and zirconium (M) with 2,4,6-trimethylphenol in different stoichiometric ratios using benzene or toluene as the solvent. Their adducts were synthesized by stirring the benzene solution of $MCl_{4-n}(OAr')_n$ derivatives with various bases. For brevity, details of one reaction each of the above types are given below and the data for these reactions are summarized in Table 1.

Synthesis of titanium bis(2,4,6-trimethylphenoxide)dichloride, $TiCl_2(C_9H_{11}O)_2$. To a solution of titanium tetrachloride (1.92 g, 6.63 mmol) in benzene (~ 40 cm^3) was added 2,4,6-trimethylphenol (2.75 g, 13.27 mmol). The reaction mixture was refluxed for about 15 h till the evolution of HCl gas had ceased. After removal of the solvent under reduced pressure, the product was recrystallized to give a brown-red crystalline solid, $TiCl_2(OAr')_2$.

Synthesis of the bipyridyl adduct of titanium (2,4,6-trimethylphenoxide)trichloride. The addition of bipyridyl (1.03 g, 6.63 mmol) to a benzene (~40 cm^3) solution of $TiCl_3(C_9H_{11}O)$ (1.92 g, 6.63 mmol) resulted in an exothermic reaction with instantaneous precipitation of a red solid. The reaction mixture was stirred for about 8–10 h at room temperature. The product was filtered off, washed with benzene and finally dried under reduced pressure.

RESULTS AND DISCUSSION

The reactions of the tetrachlorides of titanium and zirconium with stoichiometric amounts of 2,4,6-trimethylphenol resulted in the formation of mono-, bis-, tris- and tetrakis derivatives:



The reactions are rather slow and required ~8, ~15, ~22 and ~28 h, respectively, of refluxing in benzene; in a higher boiling solvent such as toluene, the completion time for the tetrakis derivatives could be reduced considerably (20 h).

Although the zirconium derivatives are generally less soluble than their titanium analogues, the solubility of the mixed chloride–phenoxide derivatives of both metals increases with the number of phenoxide groups attached to the metal atom.

The phenoxides of titanium are reddish brown in colour whereas the zirconium analogues are pale-yellow or white in colour. The reddish-brown colour of the substituted phenoxides of titanium is probably due to a charge-transfer transition tailing into the visible region of the spectrum. Measurements (cryoscopic as well as ebullioscopic) of molecular weights of chloride phenoxides which are soluble in organic solvents showed that they were monomeric.

The addition complexes were synthesized by the following reaction:

$$MCl_{4-n}(OAr')_n + 2L \xrightarrow[8\text{–}10\,h]{C_6H_6,\ stir} MCl_{4-n}(OAr')_nL_2,$$

where M = Ti or Zr; OAr′ = 2,4,6-trimethylphenoxy; L = aromatic primary or tertiary nitrogenous bases, tetrahydrofuran (thf) or bis(1,2-diphenylphosphino)ethane.

The reactions with nitrogenous bases were fast and exothermic as they led to the instantaneous precipitation of the adduct, whereas reactions with other bases were comparatively slow. Elemental analysis indicated the addition of 2 mol of various bases to the chloride phenoxides but the tetrakis derivatives formed an adduct with only 1 mol of the base. This may be due either to steric crowding or electronegativity differences. The molecular weight measurements (in the case of soluble complexes)

show them to be monomeric in freezing nitrobenzene or refluxing acetonitrile.

Conductivity measurements

The molar conductance values (in the case of soluble addition complexes) in nitrobenzene were found to lie in the range 1.6–3.5 Ω^{-1} cm^2 mol^{-1}, indicating their non-ionic nature.

IR spectral studies

The chloride phenoxides of titanium, $TiCl_3(OAr')$ and $TiCl_2(OAr')_2$, showed two ν(M—Cl) around 330–365 cm^{-1}, whereas in the zirconium analogues these appear around 320–340 cm^{-1}. As expected, ν(C—O), observed at 1228 cm^{-1} in the free phenol, shifts to lower frequency (by ~75 cm^{-1}) in the metal phenoxides. The alternative η^5-bonding of the phenolic moiety with some later transition metals such as rhodium and iridium has been established by single-crystal X-ray studies,[6] and further corroborated by the appearance of a carbonyl absorption in complexes of type (η^5-2,6-*t*-Bu-4-MeC_6H_2O)$Rh(PPh_3)(CO)$ around 1576 cm^{-1}. However, the absence of absorption around 1580 cm^{-1} and the appearance of ν(M—O) around 440–560 cm^{-1} rules out η^5-bonding and confirms the simple M—O—C bonding in the present titanium and zirconium complexes.

Addition complexes

In the addition complexes $MCl_{4-n}(OAr')_nL_2$ [where L = pyridine or picoline (α, β or γ)], ν(M—Cl) stretching vibrations were observed in the region 320–370 cm^{-1}, which is higher (~10–30 cm^{-1}) than that of the parent chloride–phenoxide derivatives. Although such an increase was considered earlier[17] to be indicative of enhancement of the coordination state of the metal, more recent work[18–20] on early transition metal halide complexes has revealed instances of the shifting of ν(M—Cl) in the reverse direction. However, the latter trend may be reversed by factors such as steric interactions and double bonding.[19]

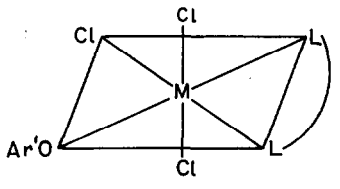
The bands which emerge around 285 ± 5 cm^{-1} could be assigned to M←N bonds.[20] ν(Ti—O) and ν(Zr—O) bands were observed around 460 ± 20 and 545 ± 10 cm^{-1}, respectively. The ν(C=N) which occurs at 1578 cm^{-1} in the free pyridine molecule exhibits a shift to higher frequency in the addition complexes with phenoxide derivatives. Such a shift towards higher wavenumbers is characteristic of coodination through nitrogen.[21] In a series of pyridine adducts with titanium phenoxide derivatives the values for ν(C=N) (in parentheses) follow the order: $TiCl_3(OAr')L_2$ (1605) > $TiCl_2(OAr')_2L_2$ (1600) > $TiCl(OAr')_3L_2$ (1585) > $Ti(OAr')_4L$ (1582). The above trend in the variation in ν(C=N) can be explained in terms of a decrease in Lewis acidic behaviour of titanium phenoxide derivatives. A similar trend has been observed in the case of the zirconium derivatives also.

The aniline free ligand showed two N—H stretching vibrations at 3400 and 3320 cm^{-1} due to asymmetrical and symmetrical vibrations, respectively.[22] In the complexes $MCl_3(OAr')(ArNH_2)_2$, $MCl_2(OAr')_2(ArNH_2)_2$ and $MCl(OAr')_3(ArNH_2)_2$, the N—H vibrations appeared around 3380 ± 5 and 3300 ± 5 cm^{-1}, indicating a shift of ~20 cm^{-1} to a lower frequency. ν(M—Cl) bands were observed around 345 cm^{-1} and M←N around 285 ± 5 cm^{-1}. The formation of substitution products is ruled out on the basis of the absence of bands for $[ArNH_3]^+Cl^-$ in the region 1520–1600 cm^{-1}.

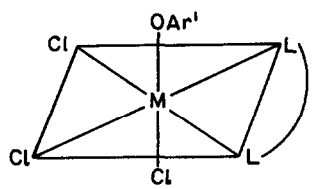
In the thf adducts $MCl_{4-n}(OAr')_n(thf)_2$ (where n = 1 or 2), ν(M—Cl) appeared around 350 cm^{-1}. The C—O—C vibrational mode which occurred at 1070 cm^{-1} in the free thf molecule was lowered ~70 cm^{-1}, indicating coordination through the oxygen atom of the thf molecule.[23].

Bipyridyl adducts, $MCl_3(OAr')(L–L)$ [where L–L = bipyridyl or bis (1,2-diphenylphosphino) ethane], showed ν(M—Cl) stretching vibrations as a triplet around 320–370 cm^{-1}, ν(M—O) around 445–555 cm^{-1}, and ν(C=N) around 1610 cm^{-1} showed a shift of 30 cm^{-1} to a higher frequency than the ligand bipyridyl [ν(C=N) at 1580 cm^{-1}], indicating coordination through a nitrogen atom. ν(M—P) in diphos adducts were observed around 400 ± 5 cm^{-1}.[24]

The appearance of three bands due to ν(M—Cl) in these complexes is suggestive of an octahedral environment around the central metal atom.[25] Two *cis* chlorine atoms on the metal give rise to a doublet, whereas the *trans* chlorine atoms give rise to a singlet. These octahedral complexes may exist in the meridional (*mer*) and facial (*fac*) forms as illustrated below:



mer



fac

Table 1. Analytical data

No.	Compound	% Metal		% Cl		Molecular weight		Conductivity in nitrobenzene (Ω^{-1} cm^2 mol^{-1})	Colour and appearance
		Found	Calc.	Found	Calc.	Found	Calc.		
1	$TiCl_3(C_9H_{11}O)$	16.8	16.6	36.9	36.8	289	289		Brown crystalline solid
2	$TiCl_2(C_9H_{11}O)_2$	12.3	12.3	18.4	18.3	380	389		Dark brown solid
3	$TiCl(C_9H_{11}O)_3$	9.9	9.8	7.2	7.3				Dark brown solid
4	$Ti(C_9H_{11}O)_4$	8.3	8.1	0.0	0.0				Brown solid
5	$ZrCl_3(C_9H_{11}O)$	27.6	27.4	31.9	32.0				White solid
6	$ZrCl_2(C_9H_{11}O)_2$	21.4	21.1	16.3	16.4				White solid
7	$ZrCl(C_9H_{11}O)_3$	17.2	17.2	6.7	6.7				Cream white solid
8	$Zr(C_9H_{11}O)_4$	14.6	14.5	0.0	0.0				Brownish white solid
9	$TiCl_3(C_9H_{11}O)(py)_2$	10.9	10.7	23.7	23.8	459	447	3.5	Brownish yellow solid
10	$TiCl_2(C_9H_{11}O)_2(py)_2$	8.8	8.8	12.9	13.0				Brownish yellow solid
11	$TiCl(C_9H_{11}O)_3(py)_2$	7.5	7.4	5.4	5.5				Light brown solid
12	$Ti(C_9H_{11}O)_4(py)$	7.3	7.2	0.0	0.0				Brown solid
13	$TiCl_3(C_9H_{11}O)(bipy)$	10.9	10.8	23.6	23.8	452	445	2.5	Red solid
14	$TiCl_3(C_9H_{11}O)(\alpha\text{-pic})_2$	10.2	10.1	22.5	22.5				Reddish brown solid
15	$TiCl_3(C_9H_{11}O)(\beta\text{-pic})_2$	10.2	10.1	22.5	22.5	491	475	1.9	Yellowish brown solid
16	$TiCl_3(C_9H_{11}O)(\gamma\text{-pic})_2$	10.2	10.1	22.5	22.5			2.2	Brownish yellow solid
17	$TiCl_3(C_9H_{11}O)(ArNH_2)_2$	10.1	10.0	22.2	22.2			1.8	Brown red solid
18	$TiCl_2(C_9H_{11}O)_2(ArNH_2)_2$	8.3	8.3	12.3	12.3			1.9	Red yellow solid
19	$TiCl(C_9H_{11}O)_3(ArNH_2)_2$	7.1	7.1	5.3	5.3				Brownish sticky solid
20	$TiCl_3(C_9H_{11}O)(thf)_2$	11.1	11.1	24.6	24.6				Dark brown pasty solid
21	$TiCl_2(C_9H_{11}O)_2(thf)_2$	8.9	9.0	13.3	13.3	520	533	1.6	Dark brown pasty solid
22	$TiCl_3(C_9H_{11}O)(Ph_2PCH_2CH_2PPh_2)$	6.4	6.2	13.8	13.8				Brick red solid
23	$ZrCl_3(C_9H_{11}O)(py)_2$	18.8	18.6	21.7	21.7				White solid
24	$ZrCl_2(C_9H_{11}O)_2(py)_2$	15.7	15.5	12.2	12.0				White solid
25	$ZrCl(C_9H_{11}O)_3(py)_2$	13.4	13.2	5.1	5.1				White solid
26	$Zr(C_9H_{11}O)_4(py)$	13.0	12.8	0.0	0.0				Dirty white solid
27	$ZrCl_3(C_9H_{11}O)(bipy)$	21.0	20.3	23.6	23.7				White solid
28	$ZrCl_3(C_9H_{11}O)(\gamma\text{-pic})_2$	17.8	17.6	20.5	20.5				White solid
29	$ZrCl_3(C_9H_{11}O)(ArNH_2)_2$	17.6	17.5	20.3	20.4				Pale yellow solid
30	$ZrCl_3(C_9H_{11}O)(thf)_2$	19.1	19.3	22.3	22.4	492	477	2.1	Light brown sticky solid
31	$ZrCl_2(C_9H_{11}O)_2(thf)_2$	15.8	16.0	12.3	12.3	562	576	2.4	Light brown sticky solid
32	$ZrCl_3(C_9H_{11}O)(Ph_2PCH_2CH_2PPh_2)$	12.6	12.6	14.6	14.6				Yellow creamy solid

		IR spectral data			
		ν(M—Cl) (cm^{-1})	ν(M←N) ν(M←O) ν(M←P) (cm^{-1})	ν(M—O) (cm^{-1})	ν(C—O) (cm^{-1})
1	$TiCl_3(C_9H_{11}O)$	330, 360	—	445	1155
2	$TiCl_2(C_9H_{11}O)_2$	330, 365	—	440	1160
3	$TiCl(C_9H_{11}O)_3$	335	—	450	1150
4	$Ti(C_9H_{11}O)_4$	—	—	450	1150
5	$ZrCl_3(C_9H_{11}O)$	320, 340	—	540	1155
6	$ZrCl_2(C_9H_{11}O)_2$	320, 340	—	550	1160
7	$ZrCl(C_9H_{11}O)_3$	335	—	560	1145
8	$Zr(C_9H_{11}O)_4$	—	—	550	1150
9	$TiCl_3(C_9H_{11}O)(py)_2$	343	280	450	1170
10	$TiCl_2(C_9H_{11}O)_2(py)_2$	335	280	445	1155
11	$TiCl(C_9H_{11}O)_3(py)_2$	335	285	440	1150
12	$TiCl_3(C_9H_{11}O)$(bipy)	335, 350, 370	275	445	1160
13	$TiCl_3(C_9H_{11}O)(\alpha\text{-pic}_2$	345	280	460	1145
14	$TiCl_3(C_9H_{11}O)(\beta\text{-pic})_2$	340	290	455	1135
15	$TiCl_3(C_9H_{11}O)(\gamma\text{-pic})_2$	345	275	460	1160
16	$TiCl_3(C_9H_{11}O)(ArNH_2)_2$	344	280	470	1140
17	$TiCl_2(C_9H_{11}O)_2(ArNH_2)_2$	342	290	480	1150
18	$TiCl(C_9H_{11}O)_3(ArNH_2)_2$	350	280	480	1145
19	$TiCl_3(C_9H_{11}O)(thf)_2$	350	530	460	1155
20	$TiCl_2(C_9H_{11}O)_2(thf)_2$	350	535	455	1150
21	$TiCl_3(C_9H_{11}O)(Ph_2PCH_2CH_2PPh_2)$	320, 335, 345	395	450	1155
22	$ZrCl_3(C_9H_{11}O)(py)_2$	350	280	540	1140
23	$Zr(C_9H_{11}O)_4(py)$	340	285	550	1160
24	$ZrCl_3(C_9H_{11}O)$(bipy)	340, 350, 360	290	555	1150
25	$ZrCl_3(C_9H_{11}O)(\gamma\text{-pic})_2$	340	290	540	1160
26	$ZrCl_3(C_9H_{11}O)(ArNH_2)_2$	350	295	535	1140
27	$ZrCl_2(C_9H_{11}O)_2(thf)_2$	350	520	540	1150
28	$ZrCl_3(C_9H_{11}O)(Ph_2PCH_2CH_2PPh_2)$	330, 340, 350	405	550	1145

where M = Ti or Zr, OAr′ = 2,4,6-trimethylphenoxide, and L–L = bipyridyl or bis(1,2-diphenylphosphino)ethane.

On the basis of only IR spectra, no conclusive distinction can be made between the *mer* and *fac* configurations.

^1H NMR spectral studies

Free 2,4,6-trimethylphenol exhibits a singlet at δ 2.05 ppm for the methyl protons. However, $TiCl_3(C_9H_{11}O)$ exhibits a doublet [2.2(s), 2.3(s)] centred at δ 2.25 ppm, indicating that the *ortho* and *para* methyl protons are not chemically equivalent (integrating in a 2:1 ratio). The downfield shift is possibly associated with delocalization of electrons from the aromatic nucleus to the titanium atom. In the thf adducts of the titanium and zirconium compounds, the methyl protons on the phenolic ring exhibit a singlet around 2.2 ppm. The CH_2 and OCH_2 protons in the free thf ligand appearing around 1.85 and 3.75 ppm shifted slightly downfield on coordination, and appear around 1.90 and 3.80 ppm, respectively.

Thermogravimetric and mass spectrometric analysis

The TG and DT analyses (in the range 40–990°C) of $[TiCl_3\{2,4,6\text{-}(CH_3)_3C_6H_2O\}(py)_2]$ and $[TiCl_3\{2,4,6\text{-}(CH_3)_3C_6H_2O\}(bipy)]$, indicated an initial decomposition (endothermic) to $TiOCl_2$, which appears to undergo exothermic disproportionation into TiO_2 and $TiCl_4$.

The mass spectral study of $TiCl_3(OAr')(py)_2$ indicated a base peak corresponding to the monoadduct $TiCl_3(OAr')(py)$, suggesting the lower stability of the parent diadduct $[P]^+$. Other metal-containing peaks were observed at m/z 289 $[P-2py]^+$, 238 $[P-2py\text{-}Cl\text{-}CH_3]^+$ and 208 $[P-2py\text{-}Cl\text{-}2CH_3]^+$.

Acknowledgement—One of us, A. Shah, gratefully acknowledges financial assistance from CSIR, New Delhi.

REFERENCES

1. L. R. Chamberlain and I. P. Rothwell, *J. Am. Chem. Soc.* 1983, **105**, 1965.
2. P. B. Hitchcock, M. F. Lappert and A. Singh, *J. Chem. Soc., Chem. Commun.* 1983, 1499.
3. P. B. Hitchcock, M. F. Lappert, A. Singh, R. G. Taylor and D. Brown, *J. Chem. Soc., Chem. Commun.* 1983, 56.
4. D. J. Cole-Hamilton, R. J. Young and G. Wilkinson, *J. Chem. Soc., Dalton Trans.* 1976, 1995.
5. B. Cetinkaya, P. B. Hitchcock, M. F. Lappert and S. Torroni, *J. Organomet. Chem.* 1980, **188**, C31.
6. L. Dahlenburg and N. Höck, *J. Organomet. Chem.* 1985, **284**, 129.
7. I. D. Verma and R. C. Mehrotra, *J. Indian Chem. Soc.* 1961, 38, 147.
8. V. S. V. Nayar and R. D. Peacock, *J. Chem. Soc.* 1964, 2827.
9. K. Watenpaugh and C. N. Caughlan, *Inorg. Chem.* 1966, **5**, 1782.
10. A. Flamini, D. J. Cole-Hamilton and G. Wilkinson, *J. Chem. Soc., Dalton Trans.* 1978, 454.
11. D. C. Bradley, E. M. A. Halim, E. A. Sadek and W. Wardlaw, *J. Chem. Soc.* 1952, 2032.
12. D. C. Bradley, A. K. Chatterjee and W. Wardlaw, *J. Chem. Soc.* 1957, 2600.
13. R. C. Paul, P. K. Gupta, K. Bindra and S. L. Chadha, *Indian J. Chem.* 1976, **14**, 776.
14. R. C. Paul, P. K. Gupta, K. Kaur and S. L. Chadha, *Indian J. Chem.* 1979, **18A**, 366.
15. K. C. Malhotra, K. C. Mahajan and S. C. Chaudhary, *Polyhedron* 1984, **3**, 125.
16. K. C. Malhotra, K. C. Mahajan and S. C. Chaudhary, *Indian J. Chem.* 1984, **23A**, 614.
17. I. R. Beattie and M. Webster, *J. Chem. Soc.* 1964, 3507.
18. R. J. H. Clark and A. J. McAlees, *J. Chem. Soc. A* 1970, 2026.
19. R. J. H. Clark, *Spectrochim. Acta* 1965, **21**, 955.
20. D. Horley and E. G. Torrible, *Can. J. Chem.* 1965, **43**, 3201.
21. T. J. Quellette and H. M. Haendler, *Inorg. Chem.* 1969, **8**, 1777.
22. R. M. Silverstein, G. C. Bassler and T. C. Morrill, *Spectroscopic Identification of Organic Compounds.* 4th edn, p. 127. John Wiley, New York.
23. L. S. Benner and C. A. Root, *Inorg. Chem.* 1972, **11**, 652.
24. V. G. Myers, F. Basolo and K. Nakamoto, *Inorg. Chem.* 1969, **8**, 1204.
25. R. J. H. Clark and A. J. McAlees, *Inorg. Chem.* 1972, **11**, 342; *J. Chem. Soc., Dalton Trans.* 1972, 640.

Polyhedron Vol. 5, No. 7, pp. 1291–1295, 1986
Printed in Great Britain

0277–5387/86 $3.00 + .00
Pergamon Journals Ltd

EXTRACTION OF MOLYBDENUM(VI) BY BIS-(DIOCTYLPHOSPHINYL)-ALKANES

YUKO YAMASHOJI,* TAKAYUKI MATSUSHITA and TOSHIYUKI SHONO

Department of Applied Chemistry, Faculty of Engineering, Osaka University, Yamadaoka, Suita, Osaka 565, Japan

(*Received* 23 *September* 1985; *accepted* 9 *December* 1985)

Abstract—A series of bis-(dioctylphosphinyl)-alkanes [$(DOPO)_2R$], has been prepared and employed as liquid–liquid extractants for molybdenum(VI) from hydrochloric acid solutions [R = p-$CH_2C_6H_4CH_2$ or $—(CH_2)_n—$ (n = 2, 3, 4, 5, 8 or 10)]. These bis-type ligands were found to be much more efficient extractants than trioctylphosphine oxide and benzyldioctylphosphine oxide. The formula of the molybdenum(VI) extracted by $(DOPO)_2(CH_2)_5$ into the organic phase was determined to be $MoO_2[(DOPO)_2(CH_2)_5](Cl)_2$.

Organophosphorus compounds such as alkylphosphonic acid,[1–5] trialkyl phosphates,[6,7] trialkylphosphine oxides[8–10] and bis-(tertiaryphosphine oxide)s[11,12] have been utilized as practical extractants for various metal ions. For example, trioctylphosphine oxide (TOPO) can extract molybdenum(VI) from highly acidic solutions.

In this paper, we describe the preparation of novel bis(dioctylphosphinyl)-alkanes [$(DOPO)_2R$] and their efficiency as extractants for molybdenum(VI). The bis-type ligands were found to extract molybdenum(VI) much more efficiently than TOPO and benzyldioctylphosphine oxide [(Bz)DOPO]. Moreover, among these bis-type ligands, $(DOPO)_2(CH_2)_n$ is a more efficient extractant compared to $(DOPO)_2(p\text{-Xyl})$ (p-Xyl = p-$CH_2C_6H_4CH_2$) (see Fig. 1).

EXPERIMENTAL

Reagents

All reagents were of reagent grade. Chloroform was refluxed over P_4O_{10} and distilled. Water was deionized. An aqueous solution of molybdenum(VI) was prepared by dissolving $Na_2MoO_4 \cdot 2H_2O$ in a hydrochloric acid solution of appropriate concentration.

Preparation of $(DOPO)_2R$

$(DOPO)_2R$ were prepared according to the method described by N'guyen *et al.*[13] as follows. A toluene solution (30 cm^3) of dioctylphosphine oxide (2.0 g, 7.3 mmol) and α,α'-dichloro-p-xylene (1.0 g, 5.7 mmol) was added to a 50% aqueous solution of sodium hydroxide (10 cm^3) containing a phase-transfer catalyst, tetrabutylammonium hydrogensulphate (TBAH) (0.2 g). This heterogeneous mixture was stirred vigorously at 65°C for 10 h under a nitrogen atmosphere. After cooling, the organic phase was separated by a separatory funnel, washed with diluted hydrochloric acid (0.01 M, 50 cm^3) and then water, dried over magnesium sulphate, and evaporated to dryness under reduced pressure. The resulting white precipitate was recrystallized from an acetone–water (1 : 1) mixture. The yield was 80%.

Other $(DOPO)_2R$ were obtained in a similar way to the method described above by using an appropriate alkyl dihalide in place of α,α'-dichloro-

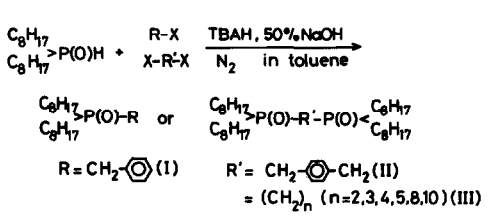


Fig. 1. Preparation scheme for $(DOPO)_2R$ studied.

* Author to whom correspondence should be addressed.

p-xylene. These were recrystallized from acetone and further purified by gel-permeation chromatography. Their yields were 15–20%.

(Bz)DOPO was obtained by the reaction of dioctylphosphine oxide and benzyl chloride in a similar way to that described above. It was recrystallized from an acetone–water (1 : 1) mixture. The yield was 30%.

The preparation scheme for these extractants is shown in Fig. 1.

Extraction and analytical procedures

A chloroform solution (5 cm^3) of a ligand and a molybdenum(VI) solution in hydrochloric acid (5 cm^3) were placed into a 10-cm^3 test-tube with a stopper. This was placed in a water bath thermostatted at 25±0.1°C and shaken for 1 h, and then centrifuged for separation. Preliminary experiments confirmed that a shaking time of 30 min was enough to attain an extraction equilibrium. The concentration of molybdenum(VI) remaining in the aqueous phase was determined by atomic absorption spectrometry. The concentration of molybdenum(VI) in the organic phase was calculated from the mass balance using that determined in the aqueous phase.

Isolation of molybdenum(VI) complexes with TOPO *or* $(DOPO)_2(CH_2)_5$

A chloroform solution (20 cm^3) of TOPO (0.1 M) was mixed with a 6.0 M hydrochloric acid solution (10 cm^3) containing excess amounts of molybdenum(VI) over TOPO. The mixture was stirred vigorously for 2 h at room temperature. The chloroform solution was separated by a separatory funnel, washed with water, and then evaporated to give a yellow oil. This oily product was washed with a methanol–water (1 : 50) mixture (20 cm^3) by decantation and dried *in vacuo* for 48 h. The yield was 80%, based on TOPO. IR (direct): ν(P=O), 1117 cm^{-1}; ν(Mo=O), 938 and 896 cm^{-1}. Found: C, 59.7; H, 10.8; Cl, 6.9%. Calc. for $MoO_2(C_{24}H_{51}PO)_2Cl_2$: C, 59.3; H, 10.5; Cl, 7.3%.

The other molybdenum(VI) complex with $(DOPO)_2(CH_2)_5$ was obtained in a similar way to the above complex as pale-yellow crystals. The yield was 85%, based on the ligand. IR (in KBr disc): ν(P=O), 1106 cm^{-1}, ν(Mo=O), 938 and 896 cm^{-1}. Found: C, 54.7; H, 10.3; Cl, 8.3%. Calc. for $MoO_2(C_{37}H_{78}P_2O_2)Cl_2$: C, 54.5; H, 9.6; Cl, 8.7%.

Physical measurements

UV absorption spectra were recorded on a Hitachi 340 recording spectrophotometer. IR spectra of chloroform solutions were recorded on a JASCO 910 grating spectrophotometer with a 0.1-mm light-pass. Atomic absorption analyses were made with a Nippon Jarrell Ash AA-1 spectrophotometer using a N_2O–C_2H_2 flame. Mass spectra were obtained with a Hitachi RMU-6E mass spectrometer.

RESULTS AND DISCUSSION

Preparation of $(DOPO)_2R$

A series of $(DOPO)_2R$ has been prepared and characterized by melting points, elemental analyses, and mass and IR spectra. These data are summarized in Table 1.

Extraction isotherm

In the present study, we have investigated extractabilities of the $(DOPO)_2R$ for molybdenum(VI) in

Table 1. Elemental analyses, melting points (m.ps), mass spectral data and characteristic IR bands for mono- and bis-type tertiaryphosphine oxides

Compound	Found (%)		Calc. (%)		M.p. (°C)	Mass spectrum [M^+]	ν(P=O) (cm^{-1})
	C	H	C	H			
(Bz)DOPO	75.7	11.4	75.8	11.3	58–59	364	1174
$(DOPO)_2$(*p*-Xyl)	73.3	12.0	73.8	11.7	126–127	650	1172
$(DOPO)_2(CH_2)_2$	70.5	12.7	71.1	12.5	154–155	574	1143
$(DOPO)_2(CH_2)_3$	71.2	13.0	71.1	12.5	90–91	588	1153, 1145
$(DOPO)_2(CH_2)_4$	71.2	13.2	71.8	12.6	88–89	602	1158
$(DOPO)_2(CH_2)_5$	71.8	12.9	72.1	12.7	101–102	616	1151, 1145
$(DOPO)_2(CH_2)_8$	72.6	13.3	72.9	12.8	88–98	658	1146
$(DOPO)_2(CH_2)_{10}$	73.0	13.1	73.5	12.8	64–65	686	1148

comparison with those of the corresponding monophosphine oxides. Figure 2 shows the percentage extractions of molybdenum(VI) by these extractants with various concentrations (1.0–9.3 M) of hydrochloric acid in the aqueous phase. They strongly depend on the concentration of hydrochloric acid for all extractants. The efficiency of extraction increases steeply with increasing concentration of hydrochloric acid, and the maximal values are obtained in the range of 5.0–7.0 M hydrochloric acid. They decreased above 7.0 M hydrochloric acid. It should be noticed that all the bis-type ligands are better extractants than the corresponding monophosphine oxides: the percentage extraction obtained for $(DOPO)_2(CH_2)_5$ (5×10^{-3} M) is 93% under the optimum conditions (5.4 M HCl), whereas that for TOPO (1×10^{-2} M) is 72.5% at 5.4 M HCl.

These results suggest that the bis-type ligands may act as a bidentate ligand to form relatively stable complexes with molybdenum(VI) compared to those of the monodentate ones.

Effect of additional lithium chloride on extraction of molybdenum(VI)

It has been reported that the extraction of molybdenum(VI) by trialkylphosphine oxides depends on the concentration of chloride ion in the aqueous phase. Figure 3 shows the effect of additional chloride ion on the extractions of molybdenum(VI) by $(DOPO)_2(CH_2)_4$ and TOPO when lithium chloride (2.0–6.0 M) was added to aqueous solutions of 1.0 M hydrochloric acid. It can be seen that the concentration of total chloride ions strongly affects the extraction of molybdenum(VI). The percentage extractions of molybdenum(VI) are increased with

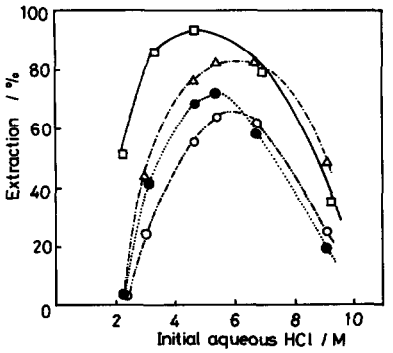


Fig. 2. Effect of hydrochloric acid concentration on extraction of molybdenum(VI) by mono- and bis-type tertiaryphosphine oxides. (●) TOPO (1×10^{-2} M), (○) (Bz)DOPO (1×10^{-2} M), (△) $(DOPO)_2$(*p*-Xyl) (1×10^{-2} M), and (□) $(DOPO)_2(CH_2)_5$ (5×10^{-3} M). Molybdenum(VI) concentration = 5×10^{-4} M.

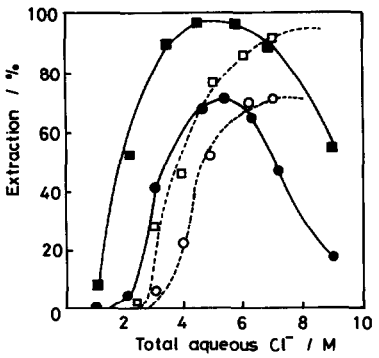


Fig. 3. Additive effect of lithium chloride on extraction of molybdenum(VI). TOPO concentration = 1×10^{-2} M, $(DOPO)_2(CH_2)_4$ concentration = 5×10^{-3} M, and molybdenum(VI) concentration = 5×10^{-4} M. (●) TOPO (hydrochloric acid alone), (○) TOPO (1.0 M hydrochloric acid + lithium chloride), (■) $(DOPO)_2(CH_2)_4$ (hydrochloric acid alone), and (□) $(DOPO)_2(CH_2)_4$ (1.0 M hydrochloric acid + lithium chloride).

increasing concentration of additional lithium chloride: the maximal values are obtained at about 7.0 M of total chloride ion concentration for both extractants. These concentrations of total chloride ions are higher than those observed in hydrochloric acid only systems. This may arise from differences in the activities of the chloride ion between hydrochloric acid and lithium chloride in aqueous phases.

In the present work, the following experiments were conducted in order to identify the species of molybdenum(VI) extracted by the bis-type extractants.

IR spectra

Figure 4 shows the IR spectra of chloroform solutions of TOPO (0.05 M) and $(DOPO)_2(CH_2)_4$ (0.1 M) after extraction of molybdenum(VI) from an aqueous solution of hydrochloric acid (6.0 M) containing molybdenum(VI) (0.2 M). With TOPO, an absorption band due to ν(P═O) observed at 1147 cm^{-1} decreases in intensity after extraction of molybdenum(VI), and a new absorption band appears at 1117 cm^{-1}. Its intensity is greater than that observed for the spectrum of the blank, which was prepared by shaking a chloroform solution of TOPO with 6.0 M hydrochloric acid. Therefore, the new absorption band can be assigned to the ν(P═O) of the TOPO coordinated to molybdenum(VI). Similar spectral changes are observed for the IR spectrum of the chloroform solution of $(DOPO)_2(CH_2)_4$: after extraction of molybdenum(VI), the absorption band due to the ν(P═O) of the free ligand is shifted from 1158 to 1117 cm^{-1}.

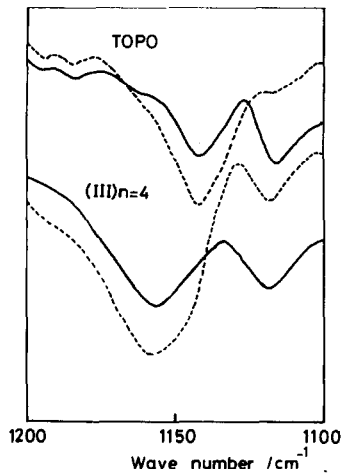


Fig. 4. IR spectra of chloroform solutions of TOPO and $(DOPO)_2(CH_2)_4$ (5×10^{-2} M) before (---) and after (——) extraction of molybdenum(VI) from 6.0 M hydrochloric acid solution.

UV absorption spectra

Figure 5 shows the absorption spectra of the aqueous and chloroform solutions of molybdenum(VI) in the UV region. The spectrum of molybdenum(VI) in water curve (a) shows an absorption maximum at 226 nm with a shoulder band around 240 nm. Its spectrum changes remarkably in 6.0 M hydrochloric acid to the spectrum shown by curve (b) in Fig. 5, which exhibits an absorption maximum at 240 nm and a shoulder band around 260 nm. Previously, Neumann and Cook[14] have reported that all the molybdenum(VI) compounds coordinated with chlorine atoms have an absorption maximum at 226 nm and that the 1 : 2 (molybdenum : chlorine) species particularly can be characterized by the shoulder band observed around 240–250 nm. Moreover, they have pointed out that the amount of the 1 : 2 species formed in aqueous solutions of hydrochloric acid depend on its concentration and is maximum at 6.0 M hydrochloric acid.

On the other hand, the absorption spectra of the chloroform solutions of TOPO (1.0×10^{-2} M) [Fig. 5, curve (c)] and $(DOPO)_2(CH_2)_4$ (1.0×10^{-2} M) [fig. 5, curve (d)] after extraction of molybdenum(VI), at 6.0 M hydrochloric acid, possess shoulder bands around 260 nm. These bands may arise from the same origin as that observed for curve (b) in Fig. 5, because TOPO and $(DOPO)_2(CH_2)_4$ themselves have no absorption bands in this region. Therefore, we have speculated that the complexes of molybdenum(VI) extracted by these ligands from 6.0 M hydrochloric acid may be composed of the 1 : 2 molybdenum : chlorine ratio species.

Relationship between extractant concentration and distribution ratio

Figure 6 shows the log–log plots for extractant concentration vs distribution ratio in the extractions of molybdenum(VI) by the various extractants from 6.0 M hydrochloric acid. With (Bz)DOPO and TOPO, the slopes of their straight lines are 1.6, suggesting that the extractant : molybdenum(VI) ratio in the extracted species is 2 : 1. On the other hand, with $(DOPO)_2(p\text{-Xyl})$ and $(DOPO)(CH_2)_n$ ($n = 2$ or 5), the slopes of the straight lines are nearly unity, suggesting that the extracted species for these systems are in a 1 : 1 extractant : molybdenum(VI) molar ratio.

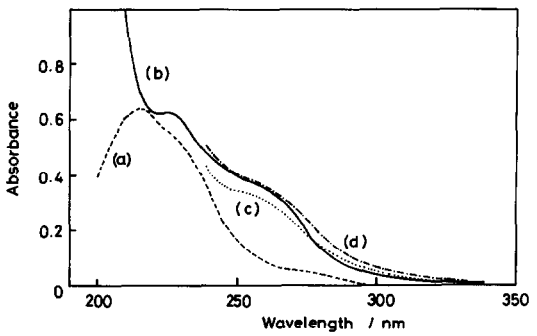


Fig. 5. Absorption spectra of molybdenum(VI) in the UV region. Molybdenum(VI) concentration = 1×10^{-4} M. (a) In water, (b) in 6.0 M HCl, (c) a chloroform solution of TOPO (1×10^{-2} M) after extraction of molybdenum(VI), and (d) a chloroform solution of $(DOPO)_2(CH_2)_4$ (1×10^{-2} M) after extraction of molybdenum(VI). Cell length = 1.0 cm.

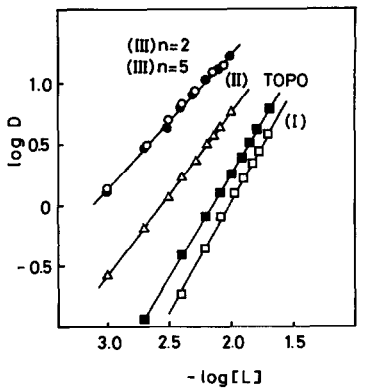


Fig. 6. Log–log plots of distribution ratio vs extractant concentration. Molybdenum(VI) concentration = 5×10^{-4} M, and hydrochloric acid concentration = 6.0 M. (■) TOPO, (□) (BzDOPO), (△) $(DOPO)_2(p\text{-Xyl})$, (○) $(DOPO)_2(CH_2)_2$, and (●) $(DOPO)_2(CH_2)_5$.

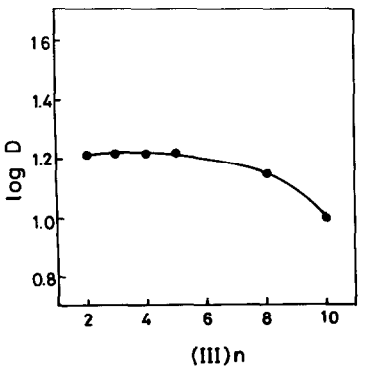


Fig. 7. Effect of the chain length of the methylene group on the distribution ratio of molybdenum(VI). Molybdenum(VI) concentration = 5×10^{-4} M, hydrochloric acid concentration = 6.0 M, and $(DOPO)_2(CH_2)_n$ concentration = 1×10^{-2} M.

Identification of the extracted molybdenum(VI) complexes

We have isolated two molybdenum(VI) complexes with TOPO or $(DOPO)_2(CH_2)_5$ in order to identify the species of molybdenum(VI) extracted by the extractants investigated here. The analytical data for these complexes are fairly in agreement with the calculated values for the formulae $MoO_2(TOPO)_2Cl_2$ and $MoO_2[(DOPO)_2(CH_2)_5]Cl_2$. In their IR spectra, only one absorption band due to ν(P=O) was observed at 1117 and 1106 cm^{-1}, respectively, indicating that all P=O groups of the ligands in these complexes are coordinated to the molybdenum ion. These results are consistent with those obtained from the log–log plots (Fig. 6) and the spectroscopic data (Figs 4 and 5). Thus, it is concluded that the extracted complexes of molybdenum(VI) have the formulae $MoO_2(L^1)_2Cl_2$ and $MoO_2(L^2)Cl_2$, where L^1 and L^2 denote the tertiaryphosphine oxides and $(DOPO)_2R$, respectively.

Effect of the chain length of the methylene group in $(DOPO)_2(CH_2)_n$ on distribution ratio of molybdenum(VI)

Figure 7 shows the effect of the chain length of the methylene group in $(DOPO)_2(CH_2)_n$ on the distribution ratio of molybdenum(VI) in the extraction at 6.0 M hydrochloric acid. The distribution ratios were found to be almost constant for the extractants with $n = 2$, 3, 4 or 5, and to decrease gradually for those with $n = 8$ or 10. These results may reflect the relative stabilities of the extracted species, although the formation constants have not been determined in the present work.

REFERENCES

1. K. Kimura, *Bull. Chem. Soc. Jpn* 1960, **33**, 1038.
2. T. Sato, *Z. Anorg. Allg. Chem.* 1968, **358**, 296.
3. T. Sato, *Anal. Chim. Acta* 1970, **52**, 183.
4. F. Nakashio, K. Kondo, A. Murakami and Y. Akiyoshi, *J. Chem. Eng. Jpn* 1982, **15**, 274.
5. F. Nakashio, K. Kondo, Y. Sato, F. Valenzuela and T. Tsuneyuki, In *Proceedings of the Symposium on Solvent Extraction*, 1983, *Hamamatsu*, p. 35. Japanese Association of Solvent Extraction (1983).
6. T. Ishimori, K. Watanabe and E. Nakamura, *Bull. Chem. Soc. Jpn* 1960, **33**, 636, 1443.
7. S. P. Vorob'ev, I. P. Davydov and I. V. Shilin, *Russ. Inorg. Chem.* 1967, **12**, 1406.
8. T. Ishimori, K. Kimura, T. Fujino and H. Murakami, *J. At. Energy Jpn* 1962, **4**, 117 (in Japanese).
9. T. Sato and M. Yamatake, *Z. Anorg. Allg. Chem.* 1972, **391**, 174.
10. Y. Hasegawa, T. Shimada and M. Niitsu, *J. Inorg. Nucl. Chem.* 1980, **42**, 1487.
11. Z. A. Berkman, L. E. Bertina, G. M. Vol'dman, A. N. Zelikman, M. I. Kabachnik, V. G. Kossykh, T. Ya. Medved, N. P. Nesterova, A. M. Rozen and K. S. Yudina, *Zh. Neorg. Khim.* 1974, **19**, 2839.
12. T. S. Lobana and S. S. Sandhu, *Coord. Chem. Rev.* 1982, **47**, 283.
13. T. D. N'guyen, S. Boileau and J. C. Gautier, *Bull. Soc. Chim. Fr.* **1982**, II-288.
14. H. M. Neumann and N. C. Cook, *J. Am. Chem. Soc.* 1957, **79**, 3026.

Polyhedron Vol. 5, No. 7, pp. 1297–1301, 1986
Printed in Great Britain

0277–5387/86 $3.00+.00
Pergamon Journals Ltd

PHOTOREDUCTION OF Fe(III) PROTOPORPHYRIN IX IN ETHANOL–WATER SOLUTIONS CONTAINING BIFUNCTIONAL LIGANDS

CARLO BARTOCCI,* ROSSANO AMADELLI, ANDREA MALDOTTI and VITTORIO CARASSITI

Centro Studio sulla Fotochimica e Reattività degli Stati Eccitati dei Composti di Coordinazione del C.N.R., Dipartimento di Chimica dell'Università di Ferrara, Via L. Borsari 46, I 44100 Ferrara, Italy

(*Received* 30 *October* 1985; *accepted* 19 *December* 1985)

Abstract—The irradiation of Fe(III) protoporphyrin IX [Fe(III)PPIX] in a thoroughly deoxygenated 35% ethanol–water solution containing pyrazine (pyz) leads to changes in the visible spectrum that are indicative of Fe(II)PP species formation. With a large excess of pyz the spectrum is similar to that of the Fe(II) pyridine hemochrome, suggesting that the monomer Fe(II)PP(pyz)$_2$ is formed. With a lower pyz content, the photochemically formed bis-pyz complex converts to a polymeric Fe(II)PP species. A similar photochemical behaviour is observed when piperazine or 4,4′-bipyridine are used as bridge ligands instead of pyz. The origin of the absorptions characteristic of the photoreaction products is discussed on the basis of the dependence of the spectra on the nature of the bridge ligands.

The photochemical reduction of chlorohemin {Fe(III)protoporphyrin IX chloride [Fe(III)PP Cl]} in pyridine–ethanol–water mixtures has been the object of previous investigations.[1] The results have shown that the primary act is an electron transfer from an ethanolate axial ligand to Fe(III). An ethoxy radical and a co-ordinatively unsaturated Fe(II)PP species were the primary photoproducts from which a bis-pyridine Fe(II)PP complex and acetaldehyde were formed.

Pyrazine (pyz), piperazine (pip) and 4,4′-bipyridine (bipy) were known to function as bridging ligands in a number of polynuclear transition-metal complexes.[2] Since they, like pyridine, are good ligands for Fe(II) porphyrin complexes, it was of interest to check the possibility of photochemically obtaining ligand-bridged Fe(II) protoporphyrin species.

The formation of square planar Fe(II) macrocyclic complexes bisaxially linked through bifunctional ligands have been prepared recently.[3] In particular, ligand-bridged phtalocyaninate Fe(II) polymeric complexes have been studied in detail.[3,4] Although these polymers are studied especially in view of their properties as monodimensional electrical conductors, they could be of some utility in studies aiming at elucidating the photosynthesis mechanism. In fact, it has been reported[5] that chlorophyll is able to form, with bifunctional ligands, bridged oligomeric adducts which give rise to substantial red shifts in the visible absorption spectrum. The spectral behavior of these models was found to be useful for clarifying the nature of the chlorophyll red absorptions, which seem to result from interactions between several chlorophyll molecules in an assembly where the macrocyclic planes are close to each other.

In the present paper we report evidence for the photochemical formation of ligand-bridged polymeric Fe(II)PP species from Fe(III)PP Cl in a water–ethanol solvent containing bifunctional ligands. The photoreaction mechanism and the differences in the electronic spectrum between the monomeric and the polymeric species are also discussed.

EXPERIMENTAL

Chlorohemin was obtained from Fluka and recrystallized following the reported glacial acetic acid method.[6] All the other chemicals were reagent

* Author to whom correspondence should be addressed.

grade commercial products. UV–VIS spectra were recorded with a Jasco Uvidec 650 spectrophotometer. Irradiations were carried out at room temperature with a Hanau Q 400 mercury vapor lamp. Light of wavelength below 360 nm was cut off with suitable glass filters. Solutions of 2×10^{-5} mol dm^{-3} Fe(III)PP Cl in 35% (v/v) ethanol–water at pH 11 were employed. All solutions were deaerated by means of at least four vacuum line freeze–thaw pump cycles ($> 10^{-6}$ torr) prior to irradiation.

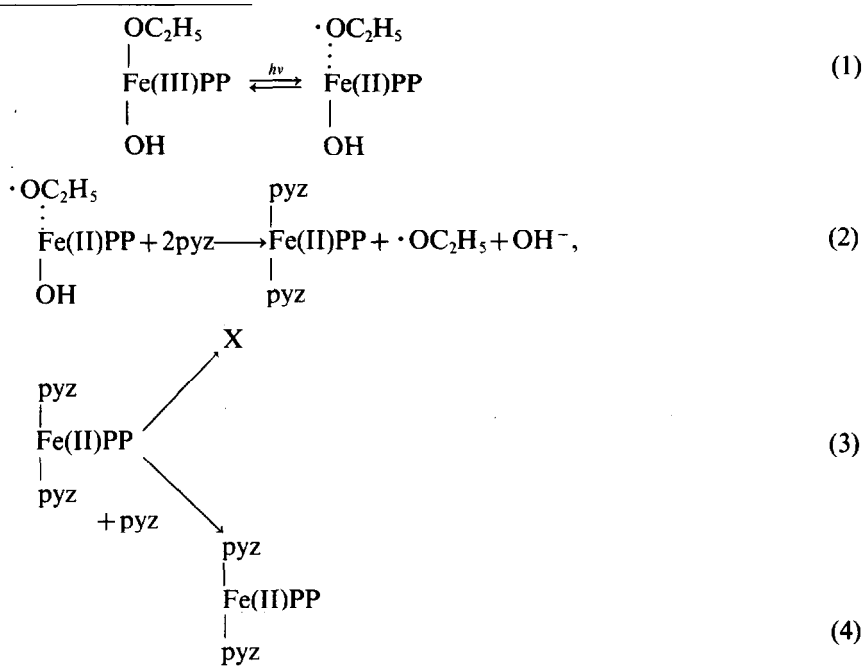
RESULTS AND DISCUSSION

Reaction mechanism

The electronic spectrum obtained following the irradiation of a Fe(III)PP Cl solution (see Experimental) containing a 5000-fold excess of pyz* shows a Soret band (415 nm) and Q-bands (520 and 550 nm) at the same wavelengths as the bis-pyridine Fe(II)PP complex, indicating that the photoproduct in the above conditions is $(pyz)_2$Fe(II)PP. This compound is stable in the absence of oxygen, but is rapidly reoxidized to the initial Fe(III)PP complex when air is let into the reaction vessel.

When the pyz:Fe concentration ratio is decreased, the electronic spectrum obtained after irradiation shows, in addition to the bands characteristic of $(pyz)_2$Fe(II)PP, absorptions at 455, 530, 575 and 805 nm, which are indicative of the formation of another Fe(II)PP product. With the aim of verifying if the two photoproducts were formed through parallel or consecutive processes, an experiment was carried out in which Fe(III)PP Cl was irradiated for a long enough time to obtain spectral evidence of $(pyz)_2$Fe(II)PP, but not sufficient to allow an eventual additional product to build up in a detectable amount. Spectral changes in time were then followed in the dark at constant temperature (22°C). The result (Fig. 1) was that the bands at 415, 520 and 550 nm decreased while, at the same time, new bands at 455, 530, 575 and 805 nm increased. This behavior is a clear evidence that the photochemical formation of $(pyz)_2$Fe(II)PP is followed by a thermal process which converts the bis-pyz complex to a new Fe(II)PP species. The rate of the secondary thermal reaction increases with decreasing pyz concentration and the process becomes spectrophotometrically undetectable at a pyz:Fe concentration ratio less than 10:1.

On the basis of the above results we propose the following reaction scheme:



Scheme 1.

When the pyz:Fe concentration ratio is decreased, the electronic spectrum obtained after irradiation shows, in addition to the bands characteristic of $(pyz)_2$Fe(II)PP, absorptions at 455, 530, 575 and 805 nm, which are indicative of the formation of another Fe(II)PP product. With the aim of verifying if the two photoproducts were formed through parallel or consecutive processes, an experiment was carried out in which Fe(III)PP Cl was irradiated for a long enough time to obtain spectral evidence of $(pyz)_2$Fe(II)PP, but not sufficient to allow an eventual additional product to build up in a detectable amount. Spectral changes in time were then followed in the dark at constant temperature (22°C). The result (Fig. 1) was that the bands at 415, 520 and 550 nm decreased while, at the same time, new bands at 455, 530, 575 and 805 nm increased. This behavior is a clear evidence that the photochemical formation of $(pyz)_2$Fe(II)PP is followed by a thermal process which converts the bis-pyz complex to a new Fe(II)PP species. The rate of the secondary thermal reaction increases with decreasing pyz concentration and the process becomes spectrophotometrically undetectable at a pyz:Fe concentration ratio less than 10:1.

On the basis of the above results we propose the following reaction scheme:

$$\text{Fe(III)PP(OH)} \overset{h\nu}{\rightleftharpoons} \text{Fe(II)PP(OH)}\cdot OC_2H_5 \qquad (1)$$

$$\text{Fe(II)PP(OH)}\cdot OC_2H_5 + 2\text{pyz} \longrightarrow \text{Fe(II)PP(pyz)}_2 + \cdot OC_2H_5 + OH^-, \qquad (2)$$

$$\text{Fe(II)PP(pyz)}_2 \longrightarrow \text{X} \qquad (3)$$

$$\text{Fe(II)PP(pyz)}_2 + \text{pyz} \longrightarrow \text{Fe(II)PP(pyz)}_3 \qquad (4)$$

Scheme 1.

$(pyz)_2$Fe(II)PP is formed through the same mechanism [eqns (1) and (2)] previously proposed for the photochemical formation of $(py)_2$Fe(II)PP.[1] The formation of X from the bis-pyz complex [eqn (3)] occurs in competition with a pyz exchange process [eqn(4)], thus accounting for the dependence

* The addition of this excess of ligand does not appreciably change the spectrum of the Fe(III)PP Cl solution.

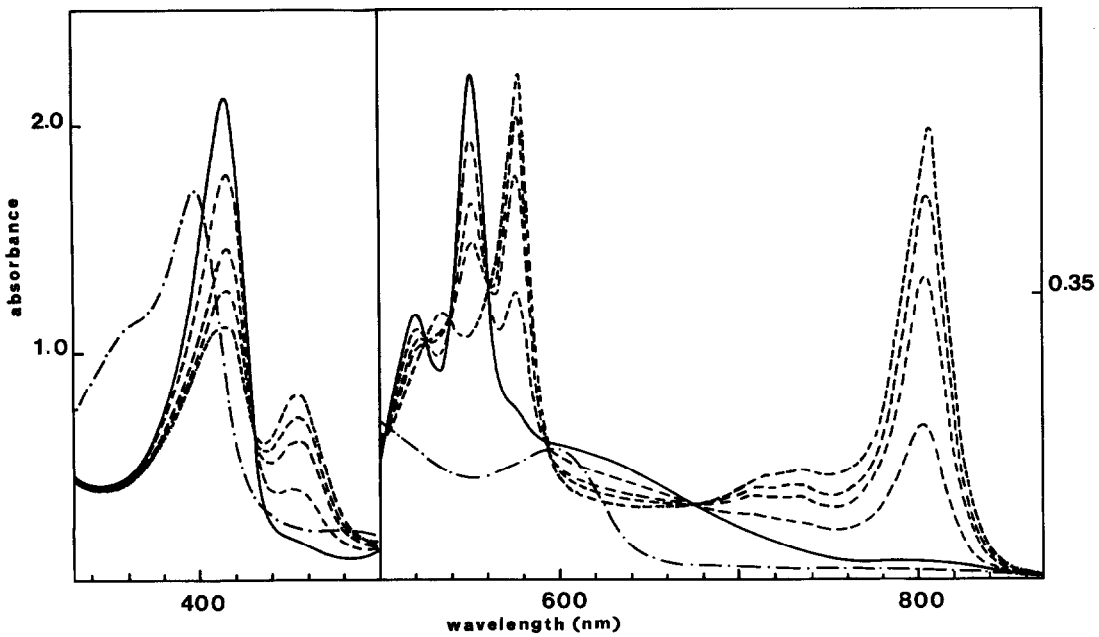


Fig. 1. Electronic spectra obtained from deaerated solutions (see Experimental) of Fe(III)PP Cl, containing a100-fold excess of pyrazine: (–·–·–) before irradiation; (——) immediately after 90 s of irradiation with $\lambda > 360$ nm; and (– – –) 15, 30, 45 and 120 min in the dark at 22°C, after irradiation.

of the rate of process (3) on the pyz:Fe concentration ratio.

As far as the nature of species X is concerned, the bifunctional character of the pyz ligand is in favour of a binuclear or polynuclear pyz-bridged Fe(II)PP species. The formation of mixed-valence [Fe(II)–Fe(III)] polynuclear species can be ruled out by the fact that the absorption spectrum of the irradiated solution does not undergo appreciable changes when dithionite is added.

An electronic spectrum quite similar to that of species X has been obtained by Furhop *et al.*[7] by reducing chlorohemin with an excess of dithionite in a pyz-containing alkaline aqueous solution. The authors suggested that a pyz-bridged Fe(II)PP dimer was the reduction product. Following the method used by Furhop *et al.*,[7] we have titrated with pyz a 35% ethanol–water solution of Fe(II)PP Cl at pH 11, which had been previously reduced with an excess of dithionite. We observed that the maximum intensity of the 805-nm band corresponds to a pyz:Fe concentration ratio of 1:1 rather than 1:2 obtained by the above-cited authors. On the basis of this result, we expect that in an eventual dimer compound the axial positions *trans* to the bridge are also occupied by pyz. The known enhancement in the basicity of the non-coordinated terminal nitrogen in this complex would favor the lengthening of the chain to form a polymeric species. This is supported by the isolation and characterization of bridged phthalocyaninate Fe(II) polynuclear compounds.[3,4]

Any attempt to isolate and then characterize the porphyrin polymeric compound was unsuccessful due to the extremely high sensitivity of the product towards the oxygen.

Electronic spectra

The electronic spectrum of the $(pyz)_2$Fe(II)PP monomer is similar to that of $(py)_2$Fe(II)PP, as far as the position and the intensity of the Soret and Q-bands are concerned (Fig. 1). The bis-pyridine complex, however, presents a band at 480 nm which has been attributed to an Fe(II) → pyridine charge-transfer (CT) transition.[8] This 480-nm absorption disappears in the bis-pyz complex which, in turn, exhibits a band at about 650 nm (Fig. 1). It seems plausible that this absorption corresponds to an Fe(II) → pyz CT transition, shifted to longer wavelengths with respect to the Fe(II) → pyridine transition, because pyz has π^*-orbitals at a lower energy than pyridine.[9]

Besides the presence of a sharp and intense absorption band at 805 nm, other features distinguish the spectrum attributed to the polymer from that of the monomer; that is, a less intense Soret band shifted from 415 to 455 nm, and a shift in the Q-bands from 520 to 530 and from 550 to 575 nm, respectively.

In order to investigate the role played by the bridge ligand in determining the observed spectral behavior, the above-described photochemical experiments were repeated in the same experimental conditions except that pip was used instead of pyz. The results indicate that: (i) in strong excess (5000-fold) of pip† the spectrum shows the Soret and Q-bands in the same positions as observed for $(pyz)_2Fe(II)PP$, indicating that $(pip)_2Fe(II)PP$ was the photoproduct; on the other hand, no evidence of bands attributable to CT transitions are observed in the visible region of the spectrum, in accordance with the lack of low-energy π^*-orbitals in the pip molecule; (ii) with a pip : Fe of 100 : 1, the spectrum changes in the dark after irradiation. The spectral variations are the same as those observed for the pyz complex as far as the Soret and Q-bands are concerned, but differ from them in that no absorptions are observed to increase in the red spectral region.

The fact that the same shift of the Soret and Q-bands is observed with pyz and pip can be taken as an indication of the formation also of polymeric species with the latter ligand.

The intense band observed at 805 nm in the case of the pyz Fe(II)PP polymer is likely to be due to a Fe(II) → pyz CT transition which, as a consequence of the polymerization, appears at longer wavelengths (805 nm) with respect to the monomeric species (650 nm) (Fig. 1). Similar shifts of d–π^* bands have been previously reported for ruthenium and iron ligand-bridged polynuclear complexes.[10] On the other hand, the shifts in the bands for these complexes are generally less dramatic, and the bands tend to be broader than in the present case.

Another potential explanation may be that of Fuhrop *et al.*[7] who ascribe the 805-nm band to a direct electron transfer involving two porphyrin chromophores, which should be favored in some way by the aromaticity of the bridge ligand.

As far as the Soret and Q-bands are concerned, the shift caused by the polymerization appears to be quite similar in both the pyz and pip complexes. Since these bands are π–π^* in origin, the shift is likely to be caused by a perturbation of the π-system of the porphyrin macrocycle, due to the face-to-face approach of the tetrapyrrolic rings. This statement is confirmed by the results obtained from photochemical runs carried out with bipy as the bifunctional ligand, in entirely identical conditions as those described above for pyz and pip. The absorption spectrum obtained after irradiation of Fe(III) PP Cl solutions (see Experimental) containing a 10-fold excess of bipy‡ is reported in Fig. 2 (spectrum a). Spectrum b in Fig. 2 represents the monomeric $(bipy)_2Fe(II)PP$ species, obtained by chemical (dithionite) reduction of Fe(III)PP Cl in an ethanol–water solution containing a 5000-fold excess of bipy. The red shifts of the Q-bands, which are attributable to polymer formation, are smaller than

† See footnote * on p. 1298.

‡ Spectral evidence of axial coordination of bipy is observed with a higher excess of ligand.

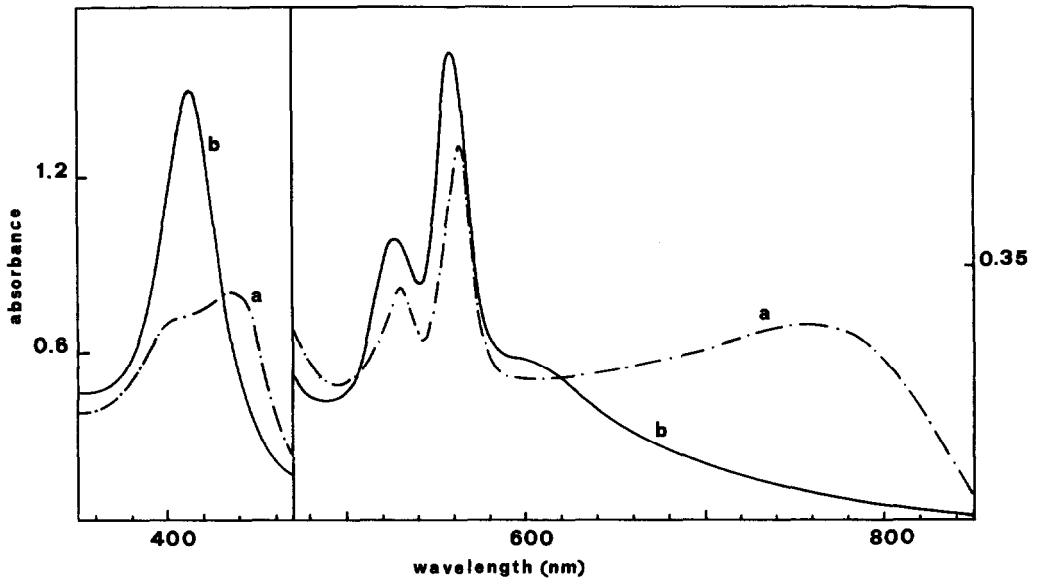


Fig. 2. (——) Electronic spectrum of $(bipy)_2Fe(II)PP$ obtained by addition of an excess of sodium dithionite to a Fe(III)PP Cl solution (see Experimental) in the presence of a 5000-fold excess of bipy, and (–·–·–) electronic spectrum obtained after irradiation with light of $\lambda > 360$ nm of Fe(III)PP Cl solution (see Experimental) containing a 10-fold excess of bipy.

those observed for pyz and pip polymers. This may be explained by a minor perturbation effect on the transitions due to an increased length of the bridge.

Owing to the aromaticity of the bridge molecule, the bipy Fe(II)PP polymer presents, as expected, an absorption in the red region of the spectrum, as observed for the analogous pyz compound. The shape of this band, however, appears to be strongly dependent on the nature of the bridge ligand.

REFERENCES

1. C. Bartocci, F. Scandola, A. Ferri and V. Carassiti, *J. Am. Chem. Soc.* 1980, **102**, 7067; A. Maldotti, C. Bartocci, R. Amadelli and V. Carassiti, *Inorg. Chim. Acta* 1983, **74**, 275.
2. C. Creutz, *Prog. Inorg. Chem.* 1983, **30**, 1 (and references therein).
3. O. Schneider and M. Hanack, *Angew. Chem., Int. Ed. Engl.* 1980, **19**, 392 (and references therein).
4. O. Schneider and M. Hanack, *Chem. Ber.* 1983, **116**, 2088.
5. J. J. Katz, In *Inorganic Biochemistry* (Edited by G. L. Eichhorn), Vol. 2, p. 1057. Elsevier, Amsterdam (1973).
6. J. H. Fuhrop and K. M. Smith, In *Porphyrins and Metalloporphyrins* (Edited by K. M. Smith), p. 809. Elsevier, Amsterdam (1975).
7. J. H. Fuhrop, M. Baccouche and M. Bunzel, *Angew. Chem.* 1980, **92**, 300; *Angew. Chem., Int. Ed. Engl.* 1980, **19**, 322.
8. M. Gouterman, In *The Porphyrins* (Edited by D. Dolphin), Vol. 3, p. 51. Academic Press, New York (1978).
9. H. H. Jaffè and M. Orchin, *Theory and Applications of Ultraviolet Spectroscopy*, p. 364. John Wiley, New York (1966).
10. R. W. Callahan, F. R. Keene, T. J. Meyer and D. J. Salmon, *J. Am. Chem. Soc.* 1977, **99**, 1064; F. Felix and A. Ludi, *Inorg. Chem.* 1978, **27**, 1782; A. Von Kameke, G. M. Tom and H. B. Taube, *Inorg. Chem.* 1978, **17**, 1790.

Polyhedron Vol. 5, No. 7, pp. 1303–1305, 1986
Printed in Great Britain

0277–5387/86 $3.00+.00
Pergamon Journals Ltd

SUBSTITUTION OF *ARACHNO*-4,6-$C_2B_7H_{13}$ CARBORANE

TOMÁŠ JELINEK, STANISLAV HEŘMÁNEK, BOHUMIL ŠTIBR* and JAROMIR PLEŠEK

Institute of Inorganic Chemistry, Czechoslovak Academy of Sciences, 250, 68 Řež near Prague, Czechoslavakia

(*Received* 25 *November* 1985; *accepted* 19 *December* 1985)

Abstract—Substitution of the 4,6-$C_2B_7H_{13}$ cluster yields a series of 3-X-4,6-$C_2B_7H_{12}$ (X = Cl, Br, I or HS), 5-X-4,6-$C_2B_7H_{12}$ (X = Br, I, HS or Bu), and 3,5-X_2-4,6-$C_2B_7H_{11}$ (X = D, Cl, Br or I) derivatives whose ^1H and ^{11}B NMR spectra are reported and discussed.

The 4,6-dicarba-*arachno*-nonaborane(13), 4,6-$C_2B_7H_{13}$ (Fig. 1), and its *C*-alkylderivatives have been used for the synthesis of a relatively large number of metallacarboranes and *closo*-boranes. The parent compound is available in high yields either by the oxidation of the *nido*-[7,9-$C_2B_9H_{12}$]$^-$ anion[1] or by acid hydrolysis of the *nido*-[6,9-$C_2B_8H_{10}$]$^{2-}$ dianion.[2] Surprisingly, no attention has so far been paid to boron substitution of the 4,6-$C_2B_7H_{13}$ cluster. We wish to report in this paper our preliminary results obtained in studying its electrophilic and, in part, nucleophilic substitution reactions.

Direct $AlCl_3$-catalyzed halogenation and/or sulphydrylation of 4,6-$C_2B_7H_{13}$ with CCl_4 (25°C, 4 h), Br_2 (CS_2, 25°C), I_2 (benzene, reflux, 6 h), and elemental sulphur (130°C, melt, 3 h) gives rise to mixtures of monosubstituted 3-X-4,6-$C_2B_7H_{12}$ (X = Cl, Br, I or HS), 5-X-4,6-$C_2B_7H_{12}$ (X = Br, I or HS), and disubstituted 3,5-X_2-4,6-$C_2B_7H_{11}$ (X = Cl or Br) derivatives. Uncatalyzed iodination (sealed tube, 100°C, 4 h) produced a mixture of 3-I, 5-I and 3,5-I_2 derivatives in which the disubstituted derivatives prevails. The mixtures were separated by column chromatography on silica gel in benzene–hexane (1 : 2). Prolonged deuteration of 4,6-$C_2B_7H_{13}$ in a DCl–$AlCl_3$–CS_2 system is ambient temperature afforded the 3,5-dideuterioderivative.

Of some interest is the observed 3-X-4,6-$C_2B_7H_{12}$: 5-X-4,6-$C_2B_7H_{12}$ ratio in the $AlCl_3$-catalyzed reactions varying with the substitution agent used and sharply descending in the series Cl (only 3-isomer is formed) > Br ~ HS (3 : 2) > I (1 : 10), while a reverse (10 : 1) ratio of 3-I and 5-I derivatives was observed in the uncatalyzed iodination. Quantum chemical calculations on 4,6-$C_2B_7H_{13}$ suggest a preference for electrophilic substitution at the B(3) and B(8) sites.[3] The observed substitution of the relatively positive B(5) vertex, however, contrasts with the calculated data, which is indicative of an alternative substitution mechanism.

In fairly good agreement with the quantum chemical results is the reaction of 4,6-$C_2B_7H_{13}$ with butyllithium in ether–hexane (3 : 2) to produce 5-Bu-4,6-$C_2B_7H_{12}$ on decomposing the reaction mixture with anhydrous HCl. The result is consistent with a nucleophilic addition of the [C_4H_9]$^-$ anion at the B(5) atom to form an intermediate [5-Bu-4,6-$C_2B_7H_{13}$]$^-$ anion which loses H_2 on proton attack and generates 5-Bu-4,6-$C_2B_7H_{12}$.

Substitution of the B(3) and B(5) vertices in 4,6-$C_2B_7H_{13}$ does not bring any symmetry change and therefore the number and intensity of individual ^1H and ^{11}B NMR signals are the same as in the parent

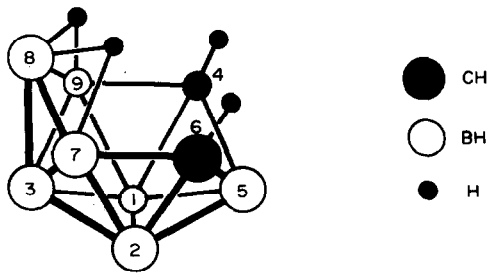


Fig. 1. Simplified structure and numbering system of *arachno*-4,6-$C_2B_7H_{13}$.

* Author to whom correspondence should be addressed.

Table 1. Some properties of substituted derivatives of $4,6\text{-}C_2B_7H_{13}$

Substituent	R_F[a]	m/z	M.p.[b] (°C)	^{1}H NMR[c] CH(eq)	CH(ax)	μH
H[d]	0.75	114	50–52	0.204	−0.788	−2.14
3-Cl	0.50	150	104–106	0.555	−0.643	−1.27
3-Br	0.64	193	72–74	0.579	−0.555	−1.68
3-I	0.60	240	55–58	0.560	−0.466	−1.79
3-HS	0.58	146	112–113	0.504	−0.540	−1.44
5-Bu	0.82	170	39–41	0.193	−0.952	−2.18[e]
5-Br	0.48	193	90–93	0.587	−0.101	−1.91
5-I	0.47	240	67–69	0.637	0.018	−1.85
5-HS	0.35	146	106–108	0.426	−0.296	−1.99
$3,5\text{-}D_2$	0.75	116	51–53	0.205	−0.800	−2.19
$3,5\text{-}Cl_2$	0.40	186	126–129	0.864	−0.114	−1.14
$3,5\text{-}Br_2$	0.36	272	179–181	0.923	−0.020	−1.16
$3,5\text{-}I_2$	0.30	366	203–205	0.900	0.180	−1.17

[a] TLC on Silufol [silica gel on aluminium foil (Kavalier, Czechoslovakia)] in benzene.

[b] Measured in sealed capillaries, uncorrected.

[c] δ in ppm relative to TMS internal standard, measured at 200 MHz in $CDCl_3$, all singlets of equal intensity.

[d] Relevant data for the parent compound for comparison.

[e] Three additional signals at δ 2.17 (t, CH_3), 1.13 and 1.41 (m, CH_2 groups) ppm.

compound. Assignments of signals (Tables 1 and 2) are based on previous works[3,4] and the recent[5] two-dimensional $\{^{11}B\text{–}^{11}B\}$ NMR study of $4,6\text{-}C_2B_7H_{13}$.

For monohalogenated compounds, inspection of Table 2 immediately reveals a trend of decreasing shielding of the substituted atoms in the order $\sigma(I) > \sigma(HS) > \sigma(Br) > \sigma(Cl)$. There is a fairly good linear correlation of relevant $\Delta\delta$ values (δ_i^s for substituted $-\delta_i^p$ for parent compound) for 3- and 5-substituted compounds with the electronegativity of the substituent, the low-field shift being more pronounced in the 3-substituted series due to a higher electron density at B(3).

Taking into account the mean effect of halogen

Table 2. Assignments of the ^{11}B NMR signals of substituted derivatives of $4,6\text{-}C_2B_7H_{13}$

Substituent	B(7,9)	B(5)	B(1,2)	B(8)	B(3)
H	0.87[a] (156)[b]	0.16 (166)	−17.36 (166)	−27.84 (156/42)	−52.55 (151)
3-Cl	1.78 (168)	2.43 (170)	−16.69 (166)	−26.90 (156/48)	−32.29[c]
3-Br	1.66 (158)	2.64 (169)	−16.80 (165)	−26.28 (154/49)	−39.45[c]
3-I	1.50 (158)	2.69 (170)	−16.50 (168)	−25.16 (157/46)	−57.35[c]
3-HS	1.97 (166)	1.97 (166)	−16.58 (167)	−26.09 (156/49)	−40.69[c]
5-Bu	−1.95 (147)	14.94[c]	−19.00 (164)	−31.66 (167/44)	−51.26 (149)
5-Br	0.34 (164)	0.17[c]	−14.26 (180)	−29.19 (162/44)	−52.37 (154)
5-I	2.08 (158)	−15.03[c]	−13.37 (153)	−27.16 (166/43)	−52.07 (147)
5-HS	0.38 (156)	7.18[c]	−15.70 (165)	−29.98 (156/45)	−51.20 (153)
$3,5\text{-}D_2$	−0.29 (157)	−0.78[c]	−17.40 (164)	−27.88 (155/42)	−52.70[c]
$3,5\text{-}Cl_2$	−0.10 (159)	−8.69[c]	−15.22 (173)	−30.35 (151/46)	−32.21[c]
$3,5\text{-}Br_2$	1.02 (166)	2.33[c]	−14.23 (173)	−28.11 (162/40)	−39.60[c]
$3,5\text{-}I_2$	2.59 (167)	−12.86[c]	−12.86 (171)	−24.83 (147/30)	−57.54[c]

[a] In ppm relative to $BF_3 \cdot OEt_2$, all doublets, measured at 64.18 MHz in $CDCl_3$, positive values of δ_B downfield.

[b] $J_{^{11}B\text{–}^1H}/J_{^{11}B\text{–}\mu^1H}$ in parentheses.

[c] Singlets of substituted atoms.

substituents on the shielding of adjacent and *meta*-atoms, a general trend for a decrease in shielding in the order $\sigma(Cl) > \sigma(Br) > \sigma(I)$, i.e. in the order of decreasing ability of the substituent nonbonding electron pairs to share their electron density with the cluster, is readily seen from Table 2. Due to a lower electron density at the B(5) site, both effects are more pronounced in the 5-substituted series in which a remarkable antipodal shielding[6] of the B(8) atom, decreasing in the same order, is observed. The same trends caused by combined effects of the two substituents are clearly seen in the 3,5-dihalogenated series.

To draw more general conclusions on the effect of substituents on the NMR shielding in the 4,6-$C_2B_7H_{13}$ framework, we are presently engaged in developing methods for obtaining derivatives substituted on other cluster atoms.

REFERENCES

1. P. M. Garret, T. A. George and M. F. Hawthorne, *Inorg. Chem.* 1969, **8**, 2008.
2. B. Štibr, J. Plešek and S. Heřmánek, *Collect. Czech. Chem. Commun.* 1973, **38**, 338.
3. J. Dolanský, S. Heřmánek and R. Zahradnik, *Collect. Czech. Chem. Commun.* 1981, **46**, 2479.
4. F. N. Tebbe, P. M. Garret, M. F. Hawthorne, *J. Am. Chem. Soc.* 1968, **90**, 869.
5. S. Heřmánek, J. Fusek, T. Jelínek, J. Plešek and B. Štibr, to be submitted for publication.
6. S. Heřmánek, V. Gregor, B. Štibr, J. Plešek, Z. Janoušek and V. V. Antonovich, *Collect. Czech. Chem. Commun.* 1976, **41**, 1492.

Polyhedron Vol. 5, No. 8, pp. 1307–1310, 1986
Printed in Great Britain

0277–5387/86 $3.00+.00
Pergamon Journals Ltd

SPECTROPHOTOMETRIC INVESTIGATIONS OF BINARY AND TERNARY COMPLEXES OF Cd(II), METHYLTHIOUREA AND HALIDE IONS IN AQUEOUS SOLUTION

JOANNA MASŁOWSKA* and ELŻBIETA CHRUŚCIŃSKA

Institute of General Food Chemistry, Technical University of Łódź, 90-924 Łódź, Stefanowskiego 4/10, Poland

(*Received* 20 *September* 1985; *accepted* 6 *November* 1985)

Abstract—The results of spectrophotometric investigations of mixed-complex formation equilibria of Cd(II), methylthiourea (MeTU) and halide ions (Cl^-, Br^- and I^-) in aqueous solution have been reported. The formation of binary and ternary complexes has been found. The values of the equilibrium constants (log units) for the reaction $MA_2+MB_2 \rightleftharpoons 2MAB$, are 1.03 ± 0.10, 1.17 ± 0.12 and 1.34 ± 0.08 for $[CdMeTUCl]^+$, $[CdMeTUBr]^+$ and $[CdMeTUI]^+$, respectively. It was found that the stability of ternary complexes depends on the values of the normal redox potential of halide ions.

The spectrophotometric method was used to determine the equilibrium constants of the mixed complexes of mercuric halides[1] and the mixed complexes of Cu(II) with pyrophosphate and ethylenediamine,[2] ethylenediamine and iminodiacetate[3] and ethylenediamine and oxalate.[4] Because of lack of data for the mixed complexes of Cd(II) with methylthiourea (MeTU) and halide ions, we undertook the studies in this field. In our previous papers[5,6] we proved the formation of the mixed complexes of Cd(II) with derivatives of thiourea and halide ions using electrochemical methods: potentiometry and polarography. Thus it seemed to be appropriate to use the spectrophotometric method to study the equilibrium reaction of the formation of mixed complexes in similar systems, in order to find new experimental data and extend the information about these little known complexes.

EXPERIMENTAL

Reagents

Triply distilled water was used. *N*-methylthiourea was recrystallized from water–ethanol mixtures and dried *in vacuo* over P_4O_{10}. Cadmium perchlorate was prepared by treating cadmium oxide with perchloric acid. $Cd(ClO_4)_2$ solution was standardized by a complexometric method.[7] Sodium chloride, bromide and iodide were purified by crystallization from aqueous solution. NaCl, NaBr and NaI solutions were standardized by argentometric methods. All stock solutions were acidified with $HClO_4$ to pH = 2.0 to prevent any hydrolysis of the complexes. The concentrations used were selected according to Spiro and Hume's data.[1] The concentration of Cd(II) was kept constant, 5×10^{-5} M; total concentration of NaCl (NaBr, NaI) and that of MeTU was about 0.01 M. The ionic strength of solutions was $\mu = 0.02$.

Apparatus

The measurements were recorded on a Specord UV–Vis (Carl Zeiss, Jena) spectrophotometer in the range of λ = 200–300 nm with 1-cm quartz cells.

Measurement method and calculation procedure

Spiro and Hume[1] described a spectrophotometric method for the determination of the equilibrium constant, K, for the reaction of the mixed-complex formation [(1)]:

$$MA_2+MB_2 \rightleftharpoons 2MAB. \quad (1)$$

The equilibrium constant K for the reaction (1) is

* Author to whom correspondence should be addressed.

given by eqn (2):

$$K = \frac{4\alpha_{11}^2}{(1-\alpha_{11})^2-(1-R/1+R)^2}, \quad (2)$$

hence:

$$\alpha_{11} = \frac{1}{1-4K^{-1}}\left(1 \pm \sqrt{1-\frac{4R}{(1+R)^2}(1-4K^{-1})}\right), \quad (2')$$

where

$R = c_{MB_2}/c_{MA_2}$,
$\alpha_{11} = [MAB]/c_M$ (the mole fraction of metal ion present as the complex MAB),
c_M = the total concentration of metal,
c_{MA_2} and c_{MB_2} = the total concentrations of binary complexes, MA_2 or MB_2.

The equilibrium constant K can be calculated for each value of R, if the value of α_{11} is known. The value of α_{11} can be determined from the spectrophotometric data. The total absorbance of solution of three species MA_2, MB_2 and MAB is given by eqn (3):

$$A = \varepsilon_{20}[MA_2]+\varepsilon_{11}[MAB]+\varepsilon_{02}[MB_2], \quad (3)$$

where ε_{20}, ε_{11} and ε_{02} are the molar absorptivities of MA_2, MAB and MB_2, respectively. From the stoichiometry of the reaction (1) and eqn (3), the result is:

$$\varepsilon = \varepsilon_{11} - \frac{\varepsilon_{20}+\varepsilon_{02}}{2}, \quad (4)$$

$$\Delta A = A-(\varepsilon_{20}c_{MA_2}+\varepsilon_{02}c_{MB_2}), \quad (5)$$

$$\alpha_{11} = \frac{\Delta A}{\Delta\varepsilon c_M}. \quad (6)$$

If the absorptivity of the mixed complex is the same as the absorptivity of the binary complexes, $\Delta\varepsilon = 0$, then there is no spectrophotometric evidence of mixed-complex formation. On the other hand, the greater the value of $\Delta\varepsilon$ which can be obtained relative to the total molar absorbance, the greater will be the sensitivity of the measurements. Therefore, the calculations should be carried out at those wavelengths where $\Delta\varepsilon$ is greatest. In eqn (5), c_{MA_2} and c_{MB_2} are known and values of ε_{20} and ε_{02} can be measured, while values of ε_{11} can be determined at low or high values of R. For those values of R one of the binary complexes is present in excess, and the other is converted to the mixed complex. The result is a two-component mixture, for which the single unknown α_{11} can be easily determined. Equations (7) and (8) can be obtained for these conditions:

(for low R)

$$A-\varepsilon_{20}c_{MA_2} = (2\varepsilon_{11}-\varepsilon_{20})c_{MB_2}, \quad (7)$$

(for high R)

$$A-\varepsilon_{02}c_{MB_2} = (2\varepsilon_{11}-\varepsilon_{02})c_{MA_2}. \quad (8)$$

The plots of the left-hand side of eqns (7) and (8) against c_{MB_2} or c_{MA_2}, respectively, should be straight lines passing through the origin. From their slopes ε_{11} can be calculated. As R approaches unity, the solutions change from two- to three-component systems, and the above plots then deviate from linearity (provided $\Delta\varepsilon \lesssim 0$). The statement of this deviation is very important because it is the evidence for mixed-complex formation. If no deviation occurs, the solutions always contain two components, and the plots are linear over the entire concentration range. In the present paper, absorptivities of the mixed complexes were calculated from linear plots of $A-\varepsilon_{20}c_{MB_2}$ vs c_{MB_2} at low R and of $A-\varepsilon_{02}c_{MA_2}$ against c_{MA_2} at high R. The resulting spectra are shown in Figs 1–3. For each system, the absorptivities were determined at maximal values of $\Delta\varepsilon$. Values of ε_{20} and ε_{02} were calculated as the slopes of absorbance vs concentration plots for the binary complexes, while ε_{11} was determined from linear plots at low and high R. The results are shown in Table 1.

RESULTS AND DISCUSSION

For formation of mixed complexes, of type $[CdMeTUX]^+$, where X = Cl, Br or I, has been

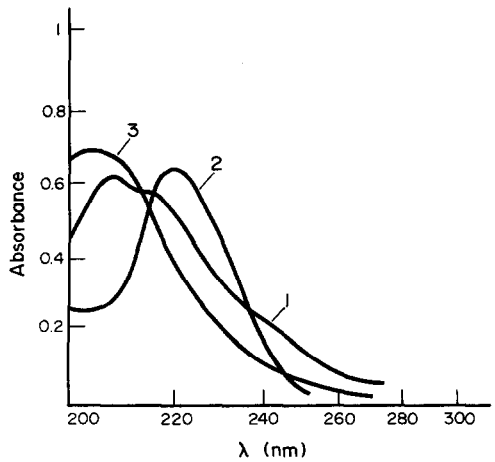


Fig. 1. Absorption spectra of binary and ternary complexes of Cd(II) with MeTU and Cl^- at various molar fractions of MeTU and Cl^-. (1) 1:0; (2) 9:1; (3) 0:1. $c_{Cd} = 5\times10^{-5}$ M, pH = 2.00.

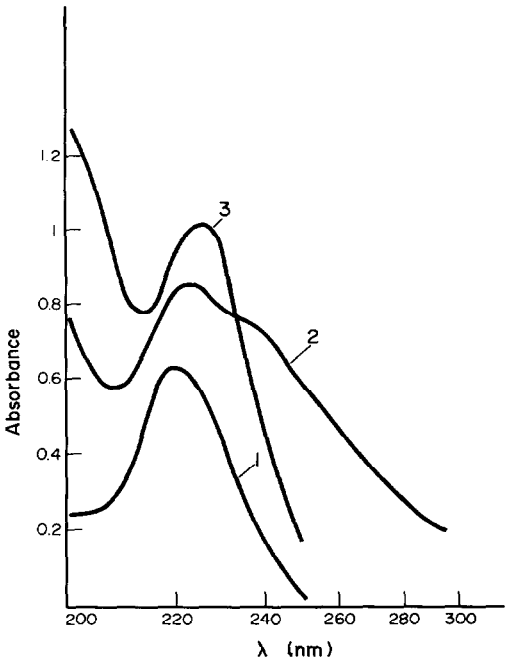


Fig. 2. Absorption spectra of binary and ternary complexes of Cd(II) with MeTU and Br^- at various molar fractions of MeTU and Br^-. (1) 1:0; (2) 9:1; (3) 0:1. $c_{Cd} = 5 \times 10^{-5}$ M, pH = 2.00.

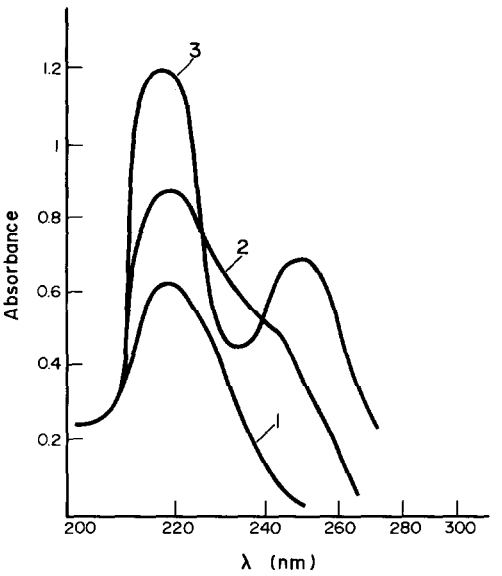


Fig. 3. Absorption spectra of binary and ternary complexes of Cd(II) with MeTU and I^- at various molar fractions of MeTU and I^-. (1) 1:0; (2) 9:1; (3) 0:1. $c_{Cd} = 5 \times 10^{-5}$ M, pH = 2.00.

found. Values of α_{11} were calculated for each point in the vicinity of R equal to unity and plotted vs log R (Fig. 4). The equilibrium constant was calculated for each point and log K was averaged for all points in each researched system (Table 2).

An analysis of the plots, presented on Fig. 4, indicates a scatter in the points resulting from different wavelengths of the research solutions. This is a reflection of inaccuracies in the spectrophotometric measurements. There are two principal sources of error in the above spectrophotometric method. One is the uncertainty in the determination of α_{11}, which depends on the experimental technique used and which is increased in the subsequent calculation of K. Differentiation of eqn (2′) with respect to α_{11} at $R = 1$ (where the highest accuracy in determining K is to be expected) provides eqn (9):

$$\frac{dK}{K} = (K^{1/2}+2)\frac{d\alpha_{11}}{\alpha_{11}}, \qquad (9)$$

which means that a small relative error in the determination of α_{11} is magnified by a factor of $(K^{1/2}+2)$ in calculating K even at the point of greatest accuracy. Clearly, the determination of large constants involves a considerable uncertainty on theoretical considerations alone.

The other possible and serious source of error is the assumption that the equilibrium reaction of the formation of the mixed complex is mainly fixed and

Table 1. Molar absorptivities ε (10^3 mol^{-1} cm^{-1}) of the binary and ternary complexes of Cd(II)

Complex	ε_{20}	ε_{20}	ε_{11}	
$[CdMeTU_2]^{2+}$	3.60±0.01	15.02±0.06	5.29±0.06	−4.02±0.06
$CdCl_2$	3.65±0.01	13.43±0.05	5.02±0.05	−3.53±0.05
$[CdMeTU_2]^{2+}$	2.92±0.02	3.07±0.01	3.75±0.02	0.76±0.02
$CdBr_2$	2.59±0.02	3.16±0.01	3.60±0.02	0.72±0.02
$[CdMeTU_2]^{2+}$	3.41±0.01	27.06±0.11	8.95±0.11	−6.29±0.11
CdI_2	3.30±0.01	26.76±0.09	8.87±0.09	−6.16±0.09

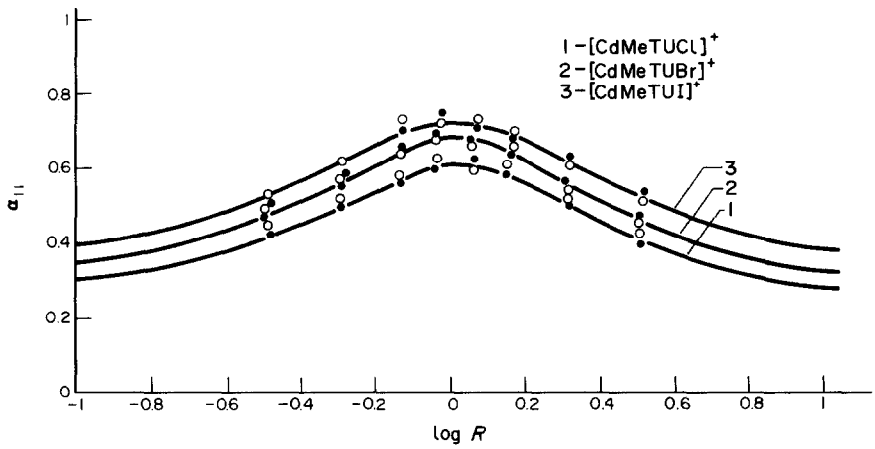


Fig. 4. Plots of the relationship $\alpha_{11} = f(\log R)$: (1) (●) $\lambda = 219$ nm, (○) $\lambda = 222$ nm (for $[CdMeTUCl]^+$); (2) (●) $\lambda = 225$ nm, (○) $\lambda = 227$ nm (for $[CdMeTUBr]^+$); (3) (●) $\lambda = 221$ nm, (○) $\lambda = 224$ nm (for $[CdMeTUI]^+$).

Table 2. Equilibrium constants of mixed complexes ($[CdMeTUX]^+$): $T = 298$ K, pH = 2.00

Complex	log K
$[CdMeTUCl]^+$	1.03±0.10
$[CdMeTUBr]^+$	1.17±0.12
$[CdMeTUI]^+$	1.34±0.08

that both the dissociation and disproportionation of the binary complexes are not being considered. This means that the accepted concentrations of species can differ considerably from those existing in the researched solutions.

We conclude that the present method is less precise than the potentiometric and polarographic methods described in our previous papers.[5,6] In order to explain the relations existing between changes of mixed complex stability and redox properties of halide ions, the plot of log K vs the normal redox potential of halide ions has been drawn (Fig. 5). The above relation shows the mixed-complex stability increases after the addition of halide ion with the greater reducing action, in the following order:

$$[CdMeTUCl]^+ < [CdMeTUBr]^+ < [CdMeTUI]^+.$$

This indicates that Cd(II) forms mixed complexes in which a significant contribution of the covalent bond between Cd(II) and halide ions occurs with a small E_x°.[8]

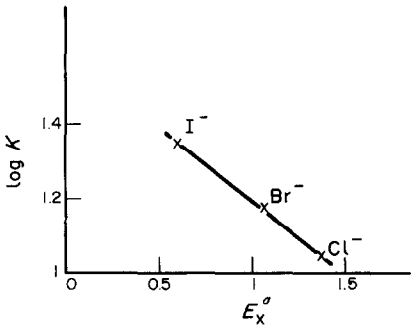


Fig. 5. The equilibrium constants (log K) of $[CdMeTuX]^-$, X = Cl, Br or I, as a function of the normal redox potential of halide ions (E_x°).

REFERENCES

1. T. G. Spiro and D. N. Hume, *J. Am. Chem. Soc.* 1961, **83**, 4305.
2. J. I. Watters and E. D. Loughran, *J. Am. Chem. Soc.* 1953, **75**, 4819.
3. W. E. Bennet, *J. Am. Chem. Soc.* 1957, **79**, 1291.
4. R. De Wit and J. I. Watters, *J. Am. Chem. Soc.* 1954, **76**, 3810.
5. J. Masłowska and E. Chruścińska, *Pol. J. Chem.* 1983, **57**, 399.
6. J. Masłowska and E. Chruścińska, *Pol. J. Chem.* 1982, **56**, 617.
7. F. J. Welcher, *The Analytical Uses of Ethylenediamine Tetraacetic Acid.* Van Nostrand, Amsterdam (1958).
8. Y. Marcus, *Coord. Chem. Rev.* 1969, **4**, 273.

Polyhedron Vol. 5, No. 8, pp. 1311–1315, 1986
Printed in Great Britain

0277-5387/86 $3.00+.00
Pergamon Journals Ltd

SPECTROSCOPIC AND STRUCTURAL PROPERTIES OF HOMONUCLEAR Fe(II) POLYMERIC COMPOUNDS—II. THERMAL DECOMPOSITION PRODUCTS OF $[Fe(PYRAZINE)_2X_2]_n$

K. RACHLEWICZ*, J. PIETRZYK and K. DRABENT

Institute of Chemistry, University of Wrocław, 50-383 Wrocław, F. Joliot-Curie 14, Poland

(*Received* 22 *July* 1985; *accepted* 6 *November* 1985)

Abstract—The thermal decomposition of $[Fe(pyz)_2X_2]_n$ (where pyz = pyrazine and X = Cl, Br or I) was investigated. For the chloride and bromide complexes the decomposition proceeds in two stages in which two pyrazine molecules dissociate successively, whereas in the iodide complex both pyrazine molecules dissociate in a single stage. Spectroscopic measurements (UV, Vis, Raman and Mössbauer spectra) indicate that intramolecular rearrangement resulting from dissociation of one pyrazine molecule leads to a change in coordination from FeN_4X_2 characteristic of initial compounds, $[Fe(pyz)_2X_2]_n$, to FeX_4N_2 characteristic of $[Fe(pyz)X_2]_n$ which is accomplished through both pyrazine and halide bridges. Thus, polymers are being formed in which the $(FeX_2)_n$ chains are being bridged by the pyrazine molecules. The magnetic moments of monopyrazine intermediate compounds are independent of temperature and low-temperature magnetic measurements do not indicate any magnetic ordering above 4.2 K.

The FeL_4X_2 compounds (where L = pyridine and its derivatives),[1,2] and FeL_2X_2 compounds (where L = 2,2′-bipyridyl, 1,10-phenanthroline and its derivatives, and X = Cl, Br, I, NCS or NCO),[3–6] undergo thermal decomposition at temperatures above 100°C. In the first stage of thermal dissociation two coordination positions are liberated and—as a result of intramolecular rearrangement—polymeric compounds with the halide or pseudohalide bridges of the FeL_2X_2 and $FeLX_2$ formulae, respectively, are formed. The FeL_2X_2 compounds (L = ligands coordinating through nitrogen and sulphur) with the polymeric pseudo-octahedral and monomeric pseudotetrahedral structures may also be prepared by wet synthesis. This group of compounds attracts attention because of the existence of metamagnetic transitions and a structural-phase transition in certain of these complexes.

The compounds with pyrazine of formula $[Fe(pyz)_2X_2]_n$ (X = Cl, Br or I) were prepared by direct synthesis.[7] The structure of these compounds was defined as pseudo-octahedral polymeric with pyrazine bridges. Thermal decomposition of $[Fe(pyz)_2Cl_2]_n$ was investigated by Beech *et al.*[8] The authors found this compound to decompose in two stages in which the pyrazine molecules are being released successively:

$$Fe(pyz)_2Cl_2 \rightarrow Fe(pyz)Cl_2 \rightarrow FeCl_2.$$

The authors have incorrectly determined the structure of the initial compound and did not attempt to determine the structure of the monopyrazine intermediate compound.

The present paper deals with spectroscopic (UV, Vis, IR, FIR, Raman and Mössbauer) and magnetochemical studies of intramolecular rearrangement resulting from dissociation of the ligand molecule and with determination of the product structure.

EXPERIMENTAL

The products of the first stage of thermal decomposition of $Fe(pyz)_2X_2$ (where X = Cl or Br) were analysed as $Fe(pyz)X_2$.

$Fe(pyz)Cl_2$. Found: Fe, 27.0; C, 23.3; H, 2.0; N, 13.5; Cl, 34.3%. Calc. for $Fe(pyz)Cl_2$: Fe, 27.0; C, 23.2; H, 1.9; N, 13.5; Cl, 34.3%.

* Author to whom correspondence should be addressed.

$Fe(pyz)Br_2$. Found: Fe, 18.8; C, 16.3; H, 1.4; N, 9.5; Br, 54.1%. Calc. for $Fe(pyz)Br_2$: Fe, 18.9; C, 16.2; H, 1.4; N, 9.5; Br, 54.0%.

Physical measurements

Diffuse-reflectance electronic spectra in magnesium oxide were recorded on a Beckman 5240.

The IR spectra in the region 4000–20 cm^{-1} were obtained on a Perkin–Elmer 180 spectrometer in both KBr pressed pellets and Nujol mulls.

The Raman spectra were measured by means of a JEOL IRS-S1 spectrophotometer using the 488- and 514.5-nm exciting lines of an Ar-ion laser. The magnetic measurements were made on either a Gouy or a Faraday balance calibrated with $HgCo(NCS)_4$. The diamagnetic corrections were applied using Pascal's constants. The Mössbauer effect measurements of powders were done on a Mössbauer 2330 spectrometer (Polon, Poland). Measurements were made at 80 and 295 K. The isomer shift (IS) values was related to a sodium nitroprusside (SNP) standard. ^{57}Co in a chromium matrix of 20-mCi activity was used as the source. The source and SNP during all measurements were stored at room temperature. The spectra were processed numerically by distribution into Lorentz curves.

Carbon, hydrogen, nitrogen and halide analyses were performed by the Analytical Laboratory of the Institute of Chemistry, University of Wrocław.

Iron was determined by using dichromate titrimetry.

RESULTS AND DISCUSSION

The $[Fe(pyz)_2X_2]_n$ complexes (X = Cl or Br) undergo thermal decomposition according to the scheme suggested by Beech *et al.*,[8] whereas the iodide compound decomposes in a single stage with simultaneous detachment of both pyrazine molecules. The TG and DTG curves are shown in Fig. 1. Depending on process conditions up to 1000°C the final product is FeX_2 or Fe_2O_3.

Elementary analysis and physicochemical studies of intermediate monopyrazine compounds indicate that they are sufficiently pure for spectroscopic and magnetic studies.

The magnetic susceptibility was examined as a function of temperature over the 4.2–293 K range. Over this temperature range the monopyrazine chloride and bromide complexes obey the Curie–Weiss law. The magnetic moment is independent of temperature and characteristic of the pseudo-octahedral, high-spin iron(II) complexes.

The electronic spectra of the compounds investigated exhibit two well-resolved bands in the NIR region and a CT band at 20,800 cm^{-1} whose energy is independent of the X substituent. The bands found in the NIR region should be assigned to intraconfigurational *d–d* transitions which are typical of Fe(II) with the high-spin d^6 structure in the distorted octahedral field.[9,10] These are transitions from the ground state $^5T_{2g}$ to the excited state E_g which becomes split in the low-symmetry field into $^5B_{1g}$ and $^5A_{1g}$. The parameters of the *d–d* bands are presented in Table 1. The $\nu_1 - \nu_2$ parameter deter-

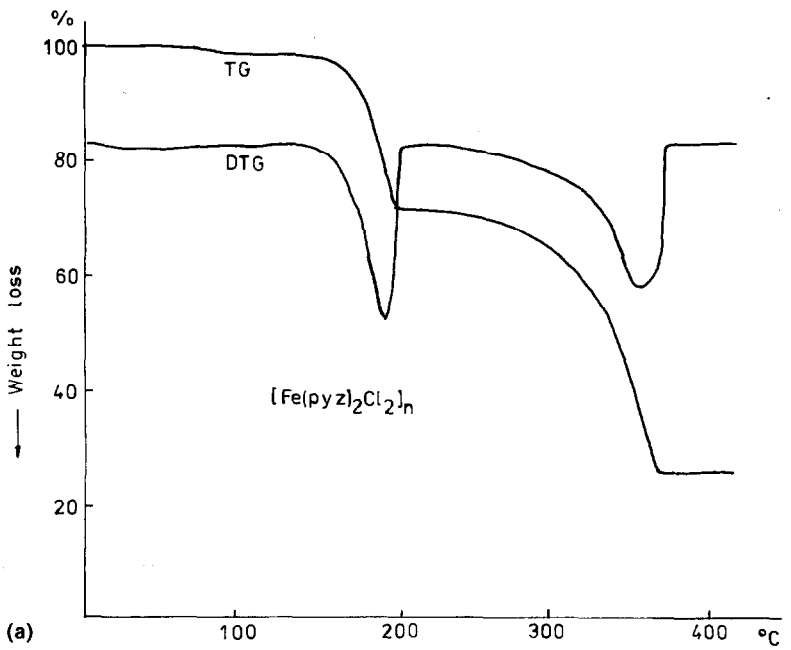


Fig. 1. TG and DTG curves of $[Fe(pyz)_2X_2]_n$ complexes.

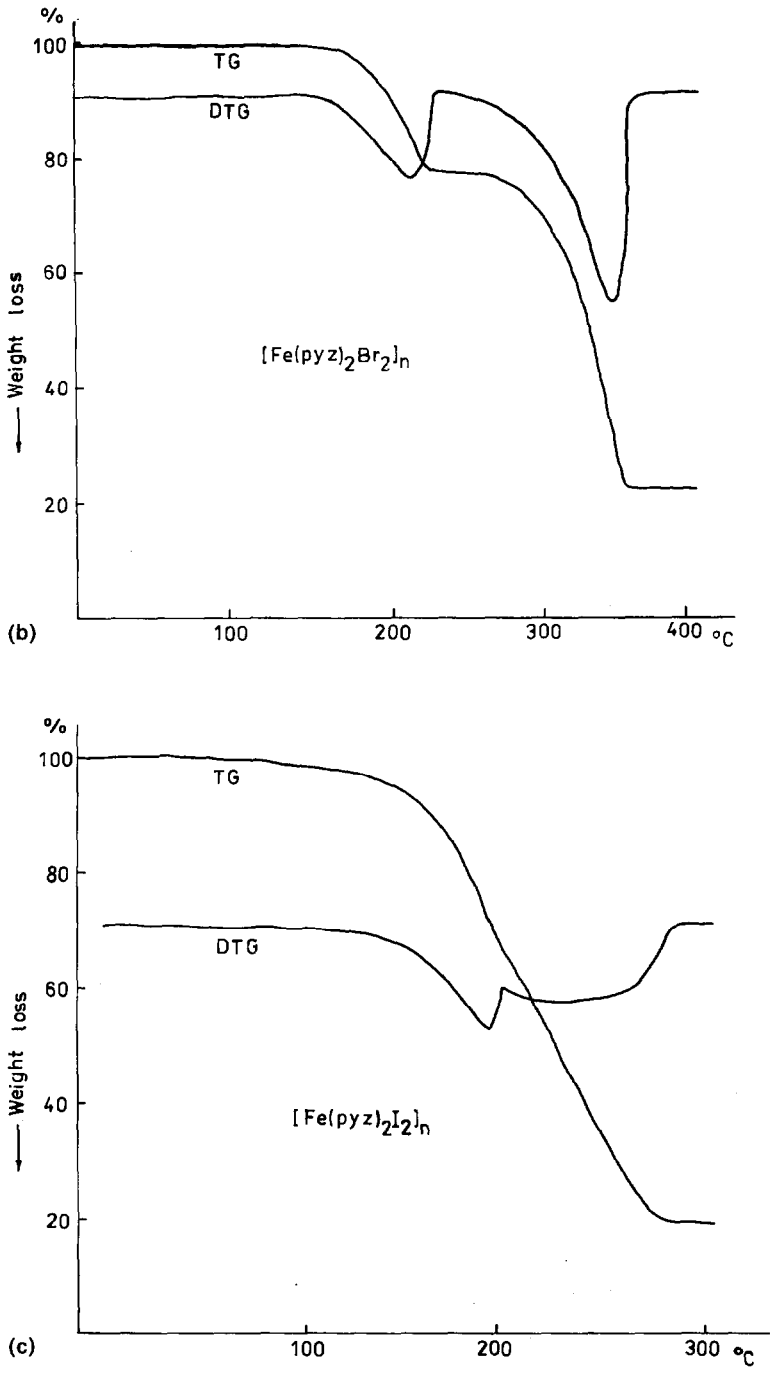


Fig. 1. (*Cont.*)

Table 1. Experimental electronic spectral results[a]

Compound	ν_1 ($^5T_{2g} \rightarrow {}^5A_{1g}$)	ν_2 ($^5T_{2g} \rightarrow {}^5B_{1g}$)	$\nu_1 - \nu_2$	ν_{av}
$Fe(pyz)Cl_2$	10,100	7000	3100	8550
$Fe(pyz)Br_2$	9500	6000	3500	7750

[a] All data in cm^{-1}.

mines the value of splitting for the ^5E_g state, whereas ν_{av} is the arithmetic mean of the energy values for both bands. A considerable increase in $\nu_1-\nu_2$ and a decrease in ν_{av} with respect to those found for the initial $[Fe(pyz)_2X_2]_n$ complexes[7] indicates a molecular rearrangement resulting from thermolysis and leading to a change in the coordination type from FeN_4X_2 to FeX_4N_2. This type of chromophore is characteristic of the polymeric compounds containing halide bridges, for instance $[Fe(py)_2X_2]_n$.[1] In comparison with the pyridine compounds the monopyrazine compounds with the same type of FeX_4N_2 chromophore exhibit lower values of $\nu_1-\nu_2$ splitting, an increase in the value of that parameter on changing from the chloride compounds to bromide compounds being comparable in both types of compounds. On the other hand, higher values of the ν_{av} parameter (which is equivalent to the $10Dq$ parameter in the crystal field approximation) are observed. The differences found may be explained as due to stronger π-acceptor properties of pyrazine as compared to pyridine. According to the Jørgensen's principle[11] of mean environment the effect of π-acceptor properties of pyrazine is weaker for $[Fe(pyz)X_2]_n$ than that observed for the $[Fe(pyz)_2X_2]_n$ compounds.

The IR and Raman spectra of the compounds investigated over the medium IR range exhibit bands of pyrazine which become slightly shifted with respect to those found for the parent complexes.[12-14,7] As in the case of the initial $[Fe(pyz)_2X_2]_n$ compounds, also in their thermal decomposition products no band coincidence in the IR and Raman spectra occurs.[7] This is evidence for the presence of the symmetry centre in the coordinated pyrazine molecule[16,17] and indicates that the pyrazine bridges appear in the compounds under investigation. A decrease in the ν(Fe—X) frequency found in the FIR spectra in comparison to those found for $[Fe(pyz)_2X_2]_n$[7] by 20 cm^{-1} for the chloride compound and 30 cm^{-1} for the bromide compound suggests that halide bridges occur also in the monopyrazine complexes.

The results obtained indicate that the FeX_4N_2-type coordination in the compounds under investigation is accomplished through both the halide and pyrazine bridges.

Mössbauer spectroscopy is considered to be particularly useful for investigation of intramolecular rearrangement in the solid phase.[18] Mössbauer spectra of the monopyrazine compounds that result from thermal decomposition of the $[Fe(pyz)_2X_2]_n$ compounds consist of well-formed quadrupole doublets with narrow lines; their quadrupole splitting parameters (QS) and IS parameters are presented in Table 2. The values of IS are characteristic of the suggested structure containing hexacoordinated, high-spin Fe(II). The values of IS are about 1.3 mm s^{-1} and are almost identical to those for the polymeric compounds $Fe(py)_2X_2$,[1] $Fe(phen)X_2$[6] and $Fe(bipy)X_2$[3-5] investigated earlier which contain iron surrounded by FeX_4N_2. A comparison of this parameter for the initial compounds and thermolysis products shows that the parameter decreases in the series:

$$FeX_2 > Fe(pyz)X_2 > Fe(pyz)_2X_2.$$

A decrease in the IS parameter results from an increase in electron density on the iron nucleus as a result of electron descreening by the *d*-electrons whose density on the iron atom decreases because of the π-acceptor effect of pyrazine. This interaction is most effective for $Fe(pyz)_2X_2$ and is confirmed

Table 2. The Mössbauer parameters and magnetic moments

Compound	T (K)	QS[a] (mm s^{-1})	IS[a,b] (mm s^{-1})	Γ_-^a (mm s^{-1})	Γ_+^a (mm s^{-1})	μ_B^c
$Fe(pyz)Cl_2$	295	1.80	1.32	0.34	0.33	5.30
	80	2.53	1.42	0.40	0.39	5.25
	4.2	—	—	—	—	4.90
$Fe(pyz)Br_2$	295	1.02	1.28	0.27	0.26	5.32
	80	1.49	1.40	0.39	0.36	5.25
	4.2	—	—	—	—	4.95
$FeCl_2$	295	0.76	1.35	0.26	0.26	—
$FeBr_2$[d]	295	1.30	1.43	—	—	—

[a] Error in QS, IS and $\Gamma_\pm$ estimated as ± 0.01 mm s^{-1}.
[b] IS relative to sodium nitroprusside.
[c] Magnetic moments in Bohr magnetons.
[d] Data from Reference 19.

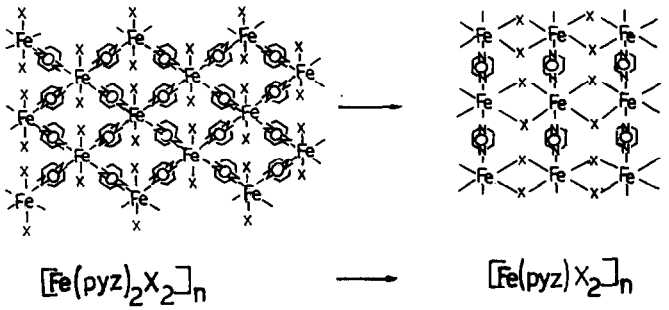


Fig. 2. Polymeric structures of $[Fe(pyz)_2X_2]_n$ and $[Fe(pyz)X_2]_n$ complexes.

by the conclusions resulting from interpretation of the electronic spectra.

The values of QS are characteristic of the compounds with the FeX_4N_2 type of coordination.[1-6] This confirms the conclusion that—as a result of thermal dissociation of one pyrazine molecule—intramolecular rearrangement takes place leading to the formation of a spatial polymer in which the $(FeX_2)_n$ chains are bridged by the pyrazine molecules (Fig. 2).

In comparison with the initial compounds, the products of their thermal decomposition exhibit a considerable difference in the value of QS on changing from the chloride compound to the bromide compound. This might also be explained by the reduced effect of the π-acceptor interactions of pyrazine in the monopyrazine complexes.

The temperature dependence of the QS observed results from the Boltzman population effect; magnetic studies over the temperature range 4.2–298 K are not indicative of any phase transitions in the complexes under investigation as is the case for $[Fe(py)_2Cl_2]_n$.[1] This transition is related to the transformation of a symmetric chloride bridge into an asymmetric one, something that cannot occur in the monopyrazine compounds because of the increased stiffness of the molecule that is afforded by the additional pyrazine bridges.

REFERENCES

1. B. L. Little and G. J. Long, *Inorg. Chem.* 1978, **17**, 3401.
2. M. Takeda, T. Tominaga and N. Saito, *J. Inorg. Nucl. Chem.* 1974, **36**, 2459.
3. E. König, K. Madeja and K. J. Watson, *J. Am. Chem. Soc.* 1968, **90**, 1146.
4. B. W. Dockum and W. M. Reiff, *Inorg. Chem.* 1982, **21**, 1406.
5. W. M. Reiff, B. Dockum, M. A. Weber and R. B. Frankel, *Inorg. Chem.* 1975, **14**, 800.
6. W. M. Reiff and S. Foner, *J. Am. Chem. Soc.* 1973, **95**, 260.
7. K. Rachlewicz, J. Pietrzyk and K. Drabent, *Polyhedron* 1985, **4**, 1777.
8. C. Beech and C. T. Mortimer, *J. Chem. Soc.* (*A*) 1967, 1115.
9. C. E. Schäffer, *Struct. Bonding* (*Berlin*) 1968, **5**, 68.
10. M. Gerloch and R. C. Slade, *Ligand-field Parameters*, p. 173. Cambridge University Press, London (1973).
11. C. K. Jørgensen, *Absorption Spectra and Chemical Bonding in Complexes*. Pergamon Press, Oxford (1962).
12. R. C. Lord, A. L. Marston and F. A. Miller, *Spectrochim. Acta* 1957, **9**, 113.
13. S. Kalifano, G. Adembri and G. Sbana, *Spectrochim. Acta* 1964, **20**, 385.
14. J. D. Simmons, K. K. Innes and G. M. Begum, *J. Mol. Spectrosc.* 1964, **14**, 190.
15. J. R. Ferraro, J. Zipper and W. Wozniak, *Appl. Spectrosc.* 1969, **23**, 160.
16. M. Goldstein and W. D. Unsworth, *Spectrochim. Acta* 1971, **27A**, 1055; 1972, **28A**, 1297.
17. M. Goldstein, F. B. Taylor and W. D. Unsworth, *J. Chem. Soc., Dalton Trans.* 1972, 418.
18. P. Gütlich, R. Link and A. Trautwein, *Mössbauer Spectroscopy and Transition Metal Chemistry*, p. 224. Springer, Berlin (1978).
19. R. C. Axtmann, Y. Hazony and J. W. Hurley, Jr, *Chem. Phys. Lett.* 1968, **2**, 673.

Polyhedron Vol. 5, No. 8, pp. 1317–1320, 1986
Printed in Great Britain

0277–5387/86 $3.00+.00
Pergamon Journals Ltd

METAL COMPLEXES OF PYRIMIDINE-DERIVED LIGANDS—V.* Co(II) AND Cu(II) COMPLEXES WITH 6-GUANIDINO-2,4-DIMETHYL-1,3-DIAZINE AND 6-PHENYLGUANIDINO-2,4-DIMETHYL-1,3-DIAZINE

NITYANANDA SAHA† and DURGADAS MUKHERJEE

Department of Chemistry, University College of Science, 92, A.P.C. Road, Calcutta 700009, India

(*Received* 24 *June* 1985; *accepted after revision* 11 *November* 1985)

Abstract—The synthesis and physicochemical characterization of Co(II) and Cu(II) complexes of the title ligands are reported. Effective magnetic moment values and electronic diffuse-reflectance and solution spectral features along with ligand field parameters classify the Co(II) and Cu(II) complexes as six-coordinated. Vibrational spectral data furnish meaningful information regarding the bonding sites of the title ligands.

In view of the significant importance of pyridimidine derivatives in many bio-systems, we report herein, in continuation of our recent publication,[1] the synthesis and characterization of Co(II) and Cu(II) complexes of the title ligands.

EXPERIMENTAL

[GPym = 6 - guanidino - 2,4 - dimethyl - 1,3 - diazine (pyrimidine), and PGPym = 6 - phenylguanidino - 2,4 - dimethyl - 1,3 - diazine (pyrimidine)] $M(GPym/PGPym)_2X_2 \cdot (H_2O)_n$[M = Co(II); X = Cl, Br, I, ClO_4 or BF_4; $n = 0$ or 2: M = Cu(II), X = CH_3COO, $n = 0$]. The general preparative method consisted of refluxing an ethanolic solution of a mixture of the ligand and the corresponding hydrated M(II) salt in 1:2 ratio at water-bath temperatures for 30 min. The resultant solution was concentrated to half its original volume by heating on a steam bath and then kept at room temperature in a desiccator over fused $CaCl_2$. The coloured microcrystalline solid which separated out was filtered off, washed with cold ethanol and dried over silica gel. The complex species on recrystallization from methanol did not afford crystals large enough for X-ray diffraction work.

The complexes of Cu(II), namely $Cu(GPym/PGPym)_2X_2$ (X = Cl, Br or SCN) were prepared by refluxing an ethanolic solution of $Cu(GPym/PGPym)(CH_3COO)_2$ with a saturated solution of the ammonium salt of the corresponding anion for 30 min. The deep-brown solution was, in each case, concentrated to a smaller bulk by heating on a steam bath. On cooling to room temperature (31°C) the brown compounds separated out and were filtered off. Upon recrystallization from water–ethanol mixtures the complexes were obtained in a brownish, microcrystalline state, but no single crystals could be isolated. Co(II) thiocyanate complexes of both the ligands were obtained by metathesis reactions of the corresponding chloro complex with potassium thiocyanate in dry ethanolic medium for 15 min at water bath temperatures; in each case a reddish-violet product was isolated. The metals were analysed by standard analytical procedures. Carbon and nitrogen were estimated by the departmental microanalytical laboratory. Different physicochemical measurements were carried out as described earlier.[1]

RESULTS AND DISCUSSION

The characterization of both ligands has been reported in a previous paper[1] from mass spectral and PMR data. All the metal complexes of Co(II) and Cu(II) give satisfactory C, N and metal analysis (Table 1). The room-temperature magnetic-moment values (Table 1) of Co(II) are above the spin-only value of 3.89 BM for high-spin, octahedral complexes due to a high orbital contribution.[2] The observed magnetic moments, in the

* For Part IV, see Ref. 1.

† Author to whom correspondence should be addressed.

Table 1. Analytical data and pertinent physicochemical properties of the complexes

Compound	Elemental analyses Found (calc.) % C	% N	% M	Conductivity (Λ_M) (cm^2 ohm^{-1} mol^{-1})	μ_{eff} (302 K)	Far-IR data (cm^{-1}) ν(M—X)	ν(M—N)[a]	ν(M—N)[b]
$Co(GPym)_2Cl_2$ (pink-violet)	37.4 (37.5)	30.8 (30.6)	12.6 (12.7)	66.92	4.82	285(m)	244(m)	538(ms)
$Co(GPym)_2Br_2$ (reddish violet)	30.4 (30.6)	25.8 (25.6)	10.6 (10.5)	64.37	4.74	260(m)	240(m)	525(s)
$Co(GPym)_2I_2$ (pink-violet)	25.9 (26.1)	21.9 (21.8)	9.1 (9.2)	60.40	4.70	—	—	—
$Co(GPym)_2(SCN)_2$ (rose red)	33.1 (33.2)	33.6 (33.5)[c]	11.5 (11.6)	71.25	4.57	—	245(w)	536(s)
$Co(GPym)_2(ClO_4)_2(H_2O)_2$ (pink)	26.7 (27.0)	21.6 (21.5)	9.0 (8.9)	157.80	4.32	—	248(w)	532(s)
$Co(GPym)_2(BF_4)_2(H_2O)_2$ (pink)	33.5 (33.6)	23.5 (23.4)	9.8 (9.7)	154.60	4.39	—	—	—
$Cu(GPym)_2Cl_2$ (brown)	36.3 (36.5)	30.8 (30.9)	13.8 (13.7)	61.92	1.85	280(s)	265(m)	532(m)
$Cu(GPym)_2Br_2$ (brown)	30.2 (30.3)	25.3 (25.4)	11.6 (11.5)	56.67	1.74	265(m)	248(m)	535(m)
$Cu(GPym)_2I_2$ (brown)	25.7 (26.0)	20.6 (20.7)	9.4 (9.2)	44.21	1.80	—	—	—
$Cu(GPym)_2(SCN)_2$ (brown)	32.6 (33.0)	33.2 (33.0)	12.6 (12.4)	64.97	1.82	—	252(m)	542(s)
$Co(PGPym)_2Cl_2$ (violet-pink)	50.6 (51.0)	22.9 (23.0)	9.6 (9.7)	67.2	4.82	285(s)	248(w)	530(m)
$Co(PGPym)_2Br_2$ (pink)	44.3 (44.5)	22.1 (22.0)	8.5 (8.4)	62.5	4.78	280(s)	245(m)	528(s)
$Co(PGPym)_2I_2$ (pink)	39.0 (39.2)	17.5 (17.6)	7.9 (8.0)	60.3	4.74	—	—	—
$Co(PGPym)_2(SCN)_2$ (pink-violet)	47.0 (47.2)	24.4 (24.3)[c]	8.6 (8.5)	64.6	4.70	—	238(m)	540(s)
$Co(PGPym)_2(ClO_4)_2(H_2O)_2$ (pink)	40.0 (40.2)	18.2 (18.0)	7.7 (7.6)	142.7	4.80	—	—	—
$Co(PGPym)_2(BF_4)_2(H_2O)_2$ (pink)	47.6 (47.8)	18.8 (18.7)	7.8 (7.9)	146.8	4.79	—	—	—
$Cu(PGPym)_2Cl_2$ (brown)	50.4 (50.6)	22.9 (22.8)	10.3 (10.4)	65.27	1.82	280(s)	265(m)	532(m)
$Cu(PGPym)_2Br_2$ (brown)	44.0 (44.2)	19.9 (19.9)	9.1 (9.0)	63.20	1.80	265(m)	248(m)	535(m)
$Cu(PGPym)_2I_2$ (brown)	38.7 (39.0)	17.7 (17.5)	8.0 (7.9)	59.18	1.78	—	—	—
$Cu(PGPym)_2(SCN)_2$ (brown)	47.0 (47.1)	25.5 (25.4)[c]	9.5 (9.6)	64.12	1.79	—	252(m)	542(s)

[a] M—N (pyrimidine).
[b] M—N (guanidine).
[c] Including nitrogen present in thiocyanate.

range 1.70–1.80 BM at room temperature for Cu(II) complexes, are consistent with the presence of a single unpaired electron and furnish no other stereochemical information unlike other first-row divalent transition metal complexes. Molar-conductance values[3] (Table 1) suggest that these complexes are either 1 : 1 or 1 : 2 in nature, depending on the counter-ion (X), and the data may be reconciled in terms of equilibria of the following types:

$$M(GPym/PGPym)_2X_2 + DMF \rightleftharpoons [M(GPym/PGPym)_2 \cdot X \cdot DMF]^+ + X^-, \quad (1)$$

where M = Co(II) or Cu(II); X = Cl, Br, I or SCN.

$$M(GPym/PGPym)_2X_2 + 2DMF \rightleftharpoons [M(GPym/PGPym)_2(DMF)_2]^{2+} + 2X^-, \quad (2)$$

where M = Co(II), X = ClO_4 or BF_4.

In the diffuse-reflectance spectra of Co(II) complexes, two principal bands are observed in the range 8000–9600 and 18,400–21,000 cm^{-1}, respectively, and these are assigned to ν_1 and ν_3 transitions for an octahedral ligand environment around the Co(II) ion. There are two other weak bands in the region of 17,800 and 20,400 cm^{-1} (on both the low- and the high-energy side of ν_3) and they may be the result of splitting the $^4T_{1g}(P)$ state due to spin–orbit coupling or tetragonal distortion.[4] Hence, the pink variety of Co(II) complexes may have a pseudo-octahedral configuration. This proposition is further substantiated by calculated values of Dq, B and β from standard relationships and low values of molar extinction coefficients (ε_{molar} 1.01–13.65) of the main spectral bands in DMF solutions of the species. Additional shoulders around 14,200 cm^{-1} in the cases of $Co(PGPym)_2X_2$ (X = Cl or Br) are likely to be of symmetry-split–spin-allowed transitions[5] in a lower symmetry field.

Six-coordinate Cu(II) complexes might exist in either D_{4h}- or C_{4v}-symmetry, and the d_γ- and d_ε-levels of the ^2D free ion term will further split into B_{1g}, A_{1g} and B_{2g}, E_g levels, respectively. Thus, three spin-allowed transitions [ν_1 ($^2B_1 \rightarrow {}^2A_1$), ν_2 ($^2B_1 \rightarrow {}^2B_2$) and ν_3 ($^2B_1 \rightarrow {}^2E$)], predicted for Cu(II) complexes of D_{4h}-symmetry,[6] are observed in the examined Cu(II) complexes as a broad maxima in the range around 14,700–17,000 cm^{-1} with poorly resolved shoulders on the low-frequency side in the diffuse-reflectance spectra of the Cu(II) complexes. In DMF, absorption peaks are shifted to lower-frequency regions as compared to the solid-state spectrum—suggesting a considerable degree of solvation. In the absence of single-crystal polarized spectra[7] or magnetic circular dichroism studies[8] no definite conclusion regarding spectral assignments can be made.

In the IR spectra of all these metal complexes, the bands in the 3μ region arising due to ν_{asy}(N—H) (3300–3390 cm^{-1}) and ν_{sy}(N—H) (3100–3140 cm^{-1}) modes of vibration of the guanyl group[9] remain practically unaltered as compared to those of the uncomplexed ligands, with only slight decreases in intensities, suggesting participation of the ligands

Table 2. Anion frequencies with probable assignments[a]

Compound	Anion band (cm^{-1})	Assignment
$Co(GPym)_2(ClO_4)_2(H_2O)_2$	1150(w) 1110(s) 1080(s)	Components of ν(Cl—O) with C_{3v}-symmetry
$Co(GPym)_2(BF_4)_2(H_2O)_2$	1100(s) 1070(ms) 1040(s)	Split components of ν_3 with C_{3v}-symmetry
$Co(GPym)_2(SCN)_2$	2100(vs) 780(s) 485(m)	ν(C≡N) ν(C—S) δ(NCS)
$Cu(GPym)_2(SCN)_2$	2110(s) 790(ms) 480(m)	ν(C≡N) ν(C—S) δ(NCS)
$Co(PGPym)_2(ClO_4)_2(H_2O)_2$	1145(m) 1115(s) 1085(s)	Components of ν(Cl—O) with C_{3v}-symmetry
$Co(PGPym)_2(BF_4)_2(H_2O)_2$	1105(s) 1080(m) 1030(s)	Split components of ν_3 with C_{3v}-symmetry
$Co(PGPym)_2(SCN)_2$	2115(s) 790(m) 478(m)	ν(C≡N) ν(C—S) δ(NCS)
$Cu(PGPym)_2(SCN)_2$	2105(vs) 785(s) 482(m)	ν(C≡N) ν(C—S) δ(NCS)

[a] vs = very strong, s = strong, m = medium, w = weak.

in complex formation without deprotonation. The most probable involvement of the imino nitrogen (>NH) of the guanidine moiety of the title ligands in complex formation with Co(II) and Cu(II) is substantiated by a negative shift of the order of 10 ± 5 cm^{-1} of the ν(C≡N) stretching band of the guanidine part of both the ligands appearing around 1650 cm^{-1} in the free ligands.[10] IR bands due to the 1:3 diazine (pyrimidine) system have been found to experience shifts in the higher-energy side ($\Delta\nu \sim 10\pm5$ cm^{-1}) in the metal complexes, indicating expected involvement of the pyrimidyl ring nitrogen in complexation;[11] this is in agreement with our earlier observations.[12] The above proposition has been further substantiated by far-IR data (down to 200 cm^{-1}) of some of the metal complexes (Table 1) through appearance of new bands (absent in the free ligands) in the ranges 238–265 cm^{-1} and 530–542 cm^{-1} which may safely be assigned to ν(M—N)(Pym)[13] and ν(M—N)(guanidine),[14] respectively. The diagnostic band frequencies of the polyatomic counterions with probable assignments (Table 2) indicate their monodentate nature.

The IR bands appearing around 340–295 cm^{-1} assigned to ν(M—Cl) and around 280–265 cm^{-1} due to ν(M—Br) [M = Co(II) and Cu(II)] indicate the coordinated nature of the chloro and bromo groups,[15] respectively. The absence of any recognizable bands for rocking and wagging modes of vibrations due to water molecules indicates their non-coordinating nature. The lattice nature of water molecules is further substantiated by the appearance of a broad diffuse band around 3500 cm^{-1} in the IR spectra of those complexes. Mass-loss data on heating samples with attached water molecules at 120°C may be considered as additional evidence for the lattice water molecules.

Acknowledgements—We are thankful to Sri Subhas Maikup, R.S.I.C., Eastern Zone, India, for providing diffuse-reflectance and solution spectra of the metal complexes.

REFERENCES

1. N. Saha and D. Mukherjee, *Polyhedron* 1984, **3**, 983 (and references therein).
2. J. Lewis and R. J. Wilkins, *Modern Coordination Chemistry*, p. 400. Interscience, New York (1960).
3. W. J. Geary, *Coord. Chem. Rev.* 1971, **7**, 81.
4. J. Reedijk, *React. Trav. Chem.* 1970, **89**, 993.
5. F. A. Cotton and G. Wilkinson, *Advanced Inorganic Chemistry*, 3rd edn, p. 881, Interscience, New York (1972).
6. M. Biddau, M. Massacesi, R. Pinna and G. Pontichelli, *Transition Met. Chem.* 1978, **3**, 153.
7. J. Ferguson and T. E. Wood, *Inorg. Chem.* 1975, **14**, 184; 190.
8. T. E. Kaden, B. Holmquist and B. L. Vallee, *Inorg. Chem.* 1974, **13**, 2585.
9. A. Albert and E. Spinner, *J. Chem. Soc.* 1960, 1221.
10. N. Nakanishi and P. H. Solomon, *Infrared Absorption Spectroscopy*, 2nd edn, p. 257. Holden-Day, San Francisco (1977).
11. I. A. Brownlie, *J. Chem. Soc.* 1950, 3062.
12. N. Saha and D. Mukherjee, *Polyhedron* 1983, **2**, 47.
13. I. A. Dorrity and K. G. Orrel, *J. Inorg. Nucl. Chem.* 1974, **36**, 230.
14. A. D. Alien and T. Theophanides, *Can. J. Chem.* 1964, **42**, 1551.
15. D. M. Adams, *Metal–Ligand and Related Vibrations*, p. 248. Edward Arnold, London (1968).

Polyhedron Vol. 5, No. 8, pp. 1321–1328, 1986
Printed in Great Britain

0277–5387/86 $3.00+.00
Pergamon Journals Ltd

MIXED ALKYL ISOCYANIDE–1,4-DIAZA-1,3-BUTADIENE COMPLEXES OF CHROMIUM—II.* SECONDARY-ION, ELECTRON IMPACT AND CHEMICAL-IONIZATION MASS SPECTROMETRY OF THE 18-ELECTRON SPECIES $Cr(CO)_3(CNR)(R'\text{-DAB})$

LISA D. DETTER and RICHARD A. WALTON†

Department of Chemistry, Purdue University, West Lafayette, IN 47907, U.S.A.

(*Received* 11 *October* 1985; *accepted* 14 *November* 1985)

Abstract—Mass analysis of the 18-electron mixed isocyanide–1,4-diaza-1,3-butadiene complexes $[Cr(CO)_3(CNR)(R'\text{-DAB})]$ (R = Me, $CHMe_2$, CMe_3 or xylyl; R′ = *i*-Pr, *t*-Bu or Cy) was undertaken using secondary-ion mass spectrometry (SIMS), electron impact (EI) mass spectrometry and both positive- and negative-ion chemical-ionization (CI) (PICI and NICI) mass spectrometry. With the exception of the PICI spectra, abundant molecular ions were not present. In all instances, well-defined, structurally informative fragment ions were identified which arise by loss of CO and/or the intact RNC and R′-DAB ligands. Cleavage of the RNC ligands (dealkylation) occurs in the SIMS and EI spectra to give fragment ions containing $[Cr(CNH)]^+$, whereas only in NICI are fragments observed in which the cyano moiety $[Cr(CN)]^+$ is present. High-abundance carbonyl-containing fragments are seen only in the case of the CI spectra and are most common in the NICI measurements. These trends are discussed in the light of the Cr–ligand bonding.

Fast atom bombardment (FAB), secondary-ion mass spectrometry (SIMS) and allied techniques are being increasingly applied to the characterization of non-volatile and/or thermally labile coordination complexes and organometallics.[2] While other groups have focused their attention upon the use of the FAB–MS technique using liquid matrices,[3] we have employed SIMS with solid-phase samples. Previous studies have involved a general survey of organometallic and coordination complexes,[4] β-diketone complexes of the transition metals,[5] phosphine complexes and phosphonium salts,[6] nickel(II) complexes on oxide supports,[7] Ag(I) complexes,[8,9] and various isocyanide complexes of Cu,[10] Ag,[8,10] Cr[11,12] and Mo.[11]

In the SIMS experiment the secondary ions ejected upon surface bombardment are mass analyzed using conventional methods. Although it is formally a surface-sensitive technique, SIMS can clearly be used for the bulk analysis of inorganic complexes. With our understanding of the general types of processes which can lead to the formation of secondary ions now well-established,[4] we have increasingly turned our attention to a comparison of results obtained by this technique with those emanating from related types of mass spectrometry. Our previous study of the SIMS and laser desorption mass spectra of β-diketonate complexes[5] is a case in point. We now report the results of a comparative SIMS, electron impact (EI) mass spectrometry, and chemical-ionization (CI) (both positive and negative ions) study of a series of mixed alkyl isocyanide–1,4-diaza-1,3-butadiene complexes of chromium of stoichiometry $Cr(CO)_3(CNR)(R'\text{-DAB})$ [R = Me, $CHMe_2$, CMe_3 or xylyl; R′-DAB = R′N=CH—CH=NR′, where R′ = *i*-Pr, *t*-Bu or Cy (cyclohexyl)]. These complexes were available from an earlier study[1] in which we had examined the preparation and characterization of the series of 17-, 18- and 19-electron species of type $[Cr(CO)_3(CNR)(R'\text{-DAB})]^{+,0,-}$.

* For Part I, see Ref. 1.

† Author to whom correspondence should be addressed.

EXPERIMENTAL

Materials

All the Cr compounds used in this study were provided by Dr Andrew Bell.

Instrumentation

SIMS spectra were obtained on a Riber Instrument (Model SQ 156L) in the positive ion mode by using an energy selector, a quadrupole mass filter, a channeltron electron multiplier and pulse-counting electronics. An argon ion beam was used at 4 keV with a primary-ion (PI) current of 5.0×10^{-9} A cm^{-2} or less and was focused to a beam size of 0.1 cm^{-2}. Under these conditions, the static SIMS condition can be assumed.[13] The main-chamber pressure during analysis was 1.0×10^{-8} torr or less. In most cases the SIMS samples were admixed 1 : 10 with excess ammonium chloride[14] and were burnished directly onto an abrasively cleaned 1-cm^2 graphite foil. No charge compensation was used in any of the experiments.

The EI and CI experiments were performed utilizing a Finnigan model 4000 mass spectrometer with an INCOS data system. The source was maintained at 250°C, the average probe temperature was 120°C and the primary-ion beam for EI and CI was 70 eV. The reagent gas for positive- and negative-ion CI (PICI and NICI) was isobutane.

The FAB spectrum of $Cr(CO)_3(CNCMe_3)$(*t*-Bu-DAB) was recorded in a dithiothreitol matrix using a Kratos MS-50 spectrometer.

RESULTS AND DISCUSSION

Mass spectral measurements were carried out on the complexes $[Cr(CO)_3(CNR)$(R′-DAB)]. Key spectral data are summarized in Tables 1–3. Measurements of the FAB spectrum of $Cr(CO)_3(CNCMe_3)$(*t*-Bu-DAB) showed that it resembled very closely the related SIMS spectrum, with the single important exception that the molecular ion (M^+, *m/z* 388) was present in higher relative abundance in the FAB spectrum. In view of the similarity between the SIMS and FAB spectral results, we decided to concentrate our attention upon the SIMS measurements to the exclusion of FAB. Additionally, the striking similarity that we found existed between the SIMS spectrum

Table 1. Summary of SIMS data for complexes of type $Cr(CO)_3(CNR)$(R′-DAB)[a]

	R =	Me		$CHMe_2$	CMe_3			xylyl
Fragment	R′ =	*i*-Pr[b]	*t*-Bu[c]	*i*-Pr[b]	*i*-Pr[b]	*t*-Bu[c]	Cy	*i*-Pr[b]
$[Cr(CO)_3(CNR)(R'\text{-DAB})]^+$		1		1	1			
$[Cr(CO)_3(R'\text{-DAB})]^+$					1			
$[Cr(CO)(CNR)(R'\text{-DAB})]^+$		3		1				
$[Cr(CNR)(R'\text{-DAB})]^+$		100	40	100	40	59	13	75
$[Cr(CNR)(R'NCHCHN)]^+$		60						
$[Cr(CNR)(R'NCH)]^+$		40						
$[Cr(CNR)(NCH)]^+$		50						
$[Cr(CNH)(R'\text{-DAB})]^+$					30	31		
$[Cr(R'\text{-DAB})]^+$		90	48	42	45	97	39	62
$[Cr(R'NCHCHN)]^+$		50		38	55	56		46
$[Cr(R'NCH)]^+$		50		52	33	28		45
$[Cr[CNR)]^+$		85	52	55	33	56		40
$[Cr(CNH)]^+$		65	38	54	24	59	68	32
Cr^+		90	100	75	79	73	100	100
$C_3H_5^+$		75	90	92	100			
$C_3H_7^+$		75		92	100	73		19
$C_4H_9^+$			71		67	100	12	
$C_6H_{11}^+$							12	

[a] Numbers in the table refer to the relative abundances of the identified positive ions in the SIMS spectrum, where 100 represents the maximum relative abundance.

[b] Peaks at *m/z* 175 and 176 (see Fig. 1) may arise from loss of CH_4 from $[Cr(i\text{-Pr-DAB})]^+$ to give $[Cr(i\text{-PrNCH-CHNCMe})]^+$ (*m/z* 176) followed, subsequently, by loss of $H^\cdot$. There is ample precedence in the literature for this (see, for example, M. L. Sigsby, R. J. Day and R. G. Cooks, *Org. Mass Spectrom.* 1979, **14**, 556).

[c] Peaks at *m/z* 205 and 189 may be due to sequential loss of $CH_3^\cdot$ and CH_4 from $[Cr(t\text{-Bu-DAB})]^+$ (*m/z* 220).

Table 2. Summary of PICI mass spectral data for complexes of type $Cr(CO)_3(CNR)(R'\text{-DAB})$[a]

	R =	Me		$CHMe_2$[b]	CMe_3			xylyl
Fragment	R′ =	*i*-Pr	*t*-Bu	*i*-Pr	*i*-Pr	*t*-Bu	Cy	*i*-Pr
$[Cr(CO)_3(CNR)(R'\text{-DAB})+H]^+$		23		1	31			
$[Cr(CO)_3(CNR)(R'\text{-DAB})]^+$		100		1	97	32	19	24
$[Cr(CO)_3(R'\text{-DAB})+H]^+$			1	1				
$[Cr(CO)_2(CNR)(R'\text{-DAB})+H]^+$				1	12			
$[Cr(CO)_2(R'\text{-DAB})+H]^+$			1					
$[Cr(CO)(CNR)(R'\text{-DAB})+H]^+$				1				
$[Cr(CNR)(R'\text{-DAB})+H]^+$		1		2	16			
$[Cr(CNR)(R'\text{-DAB})]^+$		21	3		38		39	37
$[Cr(R'\text{-DAB})]^+$			4			20		
$[RNC+H]^+$				100	63	44	43	100
$[(R'\text{-DAB})+H]^+$		20	100	92	100	100	100	46
$[Cr(R'\text{-DAB})_2]^+$			1	8	12	32	5	1

[a] Numbers in the table refer to the relative abundances of the positive ions in the mass spectrum, where 100 represents the maximum relative abundance.

[b] Clusters corresponding to $[Cr_2(CO)_3(CNCHMe_2)(i\text{-Pr-DAB})_2]^+$ (*m/z* 537), $[Cr_2(CO)_2(CNCHMe_2)(i\text{-Pr-DAB})_2]^+$ (*m/z* 509), $[Cr_2(CO)_3(i\text{-Pr-DAB})_2]^+$ (*m/z* 468), and $[Cr_2(CNCHMe_2)(i\text{-Pr-DAB})_2]^+$ (*m/z* 453) were observed in low abundance.

of $Cr(CO)_3(CNCMe_3)(t\text{-Bu-DAB})$ and that of its 17-electron derivative $[Cr(CO)_3(CNCMe_3)(t\text{-Bu-DAB})]PF_6$ (the latter was recorded with and without the presence of added NH_4Cl using a PI current of 2×10^{-9} A cm^{-2}), led us to focus our attention upon the more easily prepared, neutral 18-electron species.

(a) SIMS data

The essential features of these spectra are summarized in Table 1 where relative abundances (relative to 100 as the maximum) are compared. Note that abundant organic-fragment ions are seen at low *m/z* values. In some instances these are the most

Table 3. Summary of NICI mass spectral data for complexes of type $Cr(CO)_3(CNR)(R'\text{-DAB})$[a]

	R =	Me		$CHMe_2$[b]	CMe_3			xylyl
Fragment	R′ =	*i*-Pr	*t*-Bu	*i*-Pr	*i*-Pr	*t*-Bu	Cy	*i*-Pr
$[Cr(CO)_3(CNR)(R'\text{-DAB})]^-$						2		
$[Cr(CO)_3(R'\text{-DAB})]^-$		100	51	100	29		66	5
$[Cr(CO)_3(R'\text{-NCHCHN})]^-$							5	
$[Cr(CO)_2(CNR)(R'\text{-DAB})]^-$		6	17	71	48	36	71	100
$[Cr(CO)_2(CN)(R'\text{-DAB})]^-$				24	100		100	
$[Cr(CO)_2(R'\text{-DAB})]^-$		60	33	5	2	18		
$[Cr(CO)(CNR)(R'\text{-DAB})]^-$			2					1
$[Cr(CO)(R'\text{-DAB})]^-$			1	2				
$[Cr(CNR)(R'\text{-DAB})]^-$						19		1
$[Cr(CN)(R'\text{-DAB})]^-$					11	19	28	
$[Cr(CNR)(R'\text{-DAB})-H]^-$						84		
$[Cr(R'\text{-DAB})_2]^-$			100	3	58	100	5	4

[a] Numbers in the table refer to the relative abundances of the negative ions in the mass spectrum, where 100 represents the maximum relative abundance.

[b] Clusters corresponding to $[Cr_2(CO)_2(CNCHMe_2)(i\text{-Pr-DAB})_2]^-$ (*m/z* 509), $[Cr_2(CO)_3(i\text{-Pr-DAB})_2]^-$ (*m/z* 468), and $[Cr_2(CNCHMe_2)(i\text{-Pr-DAB})_2]^-$ (*m/z* 453) were observed in low abundance.

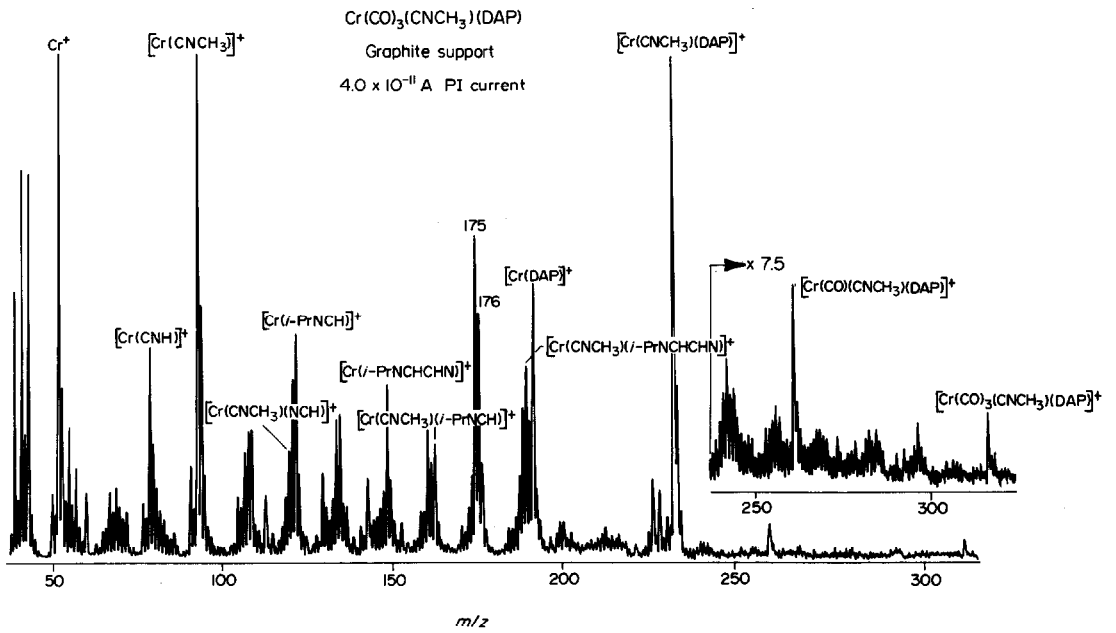


Fig. 1. SIMS spectrum of $Cr(CO)_3(CNMe)(DAP)$ admixed with NH_4Cl on graphite foil showing the molecular cation and additional fragmentation. DAP is used as an abbreviation for *i*-Pr-DAB. Inset shows region from *m/z* 240 to 320 recorded with 7.5-fold increase in PI current.

abundant ions in the SIMS. Powdered samples of the complexes were admixed with an excess of NH_4Cl as has been our usual practice[4,14] and recorded using a graphite support. A representative SIMS spectrum, that of $Cr(CO)_3(CNMe)$(*i*-Pr-DAB), is shown in Fig. 1. In one instance, difficulty was experienced in causing samples of the complex $Cr(CO)_3(CNCHMe_2)$(*i*-Pr-DAB) to adhere to the graphite support. Although this problem was eventually overcome, we found that a satisfactory alternative was a copper support (see Fig. 2); under these conditions the spectrum was very similar to that recorded from graphite foil.

Molecular cations (M^+) were obtained in very low abundance at best (Table 1). This result accords with our previous results for the SIMS of neutral β-diketonate complexes of the transition metals[5] where only in the case of the vanadyl complex $VO(CH_3COCHCOCH_3)_2$ did we see evidence for the molecular ion (albeit of low intensity). Note that for the β-diketonate complexes the intact molecular complex is only encountered under conditions

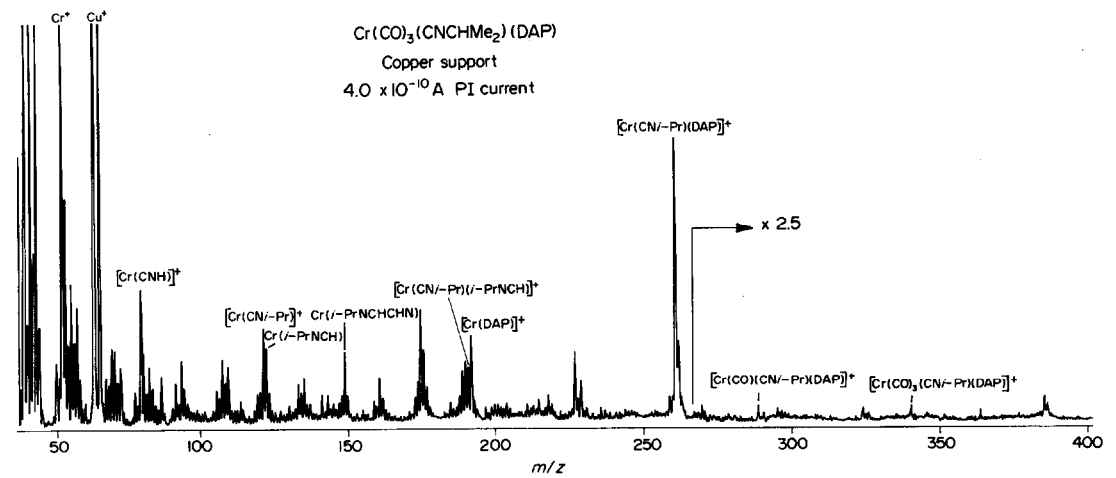


Fig. 2. SIMS spectrum of $Cr(CO)_3(CNCHMe_2)(DAP)$ admixed with NH_4Cl on copper. This spectrum is very similar to that obtained using a graphite foil support. The molecular cation and additional fragmentation are shown. DAP is used as an abbreviation for *i*-Pr-DAB. For *m/z* above 270 spectrum recorded using a 2.5-fold increase in PI current.

where cationization can occur, i.e. to give CM^+, where C^+ represents a suitable cationizing agent (e.g. Ag^+ or Na^+) and M is the molecular complex. We found no evidence for significant levels of "self-cationization", to give $[Cr_2(CO)_3(CNR)(R'\text{-DAB})]^+$, as has been encountered in other systems.[5] The samples apparently do not form higher mass polymetallic ions, which can subsequently fragment to give such bimetallic fragment ions, or undergo $Cr^+ + Cr(CO)_3(CNR)(R'\text{-DAB})$ combination reactions in the selvedge region. These results contrast with those for β-diketonate complexes in which bimetallic and higher cluster ions have been observed using a silver support (in conjunction with an NH_4Cl matrix).[5]

Several characteristic fragmentation sequences were observed in the SIMS spectra for all the complexes. Fragmentation is seen to occur by the loss of the three carbonyl ligands, to give in most instances $[Cr(CNR)(R'\text{-DAB})]^+$ as a very abundant species. This loss of carbonyls from the molecular cations $[Cr(CO)_3(CNMe)(i\text{-Pr-DAB})]^+$ and $[Cr(CO)_3(CNCMe_2)(i\text{-Pr-DAB})]^+$ yields the base peak in these two instances (see Fig. 1). Further fragmentation of $[Cr(CNR)(R'\text{-DAB})]^+$ occurs by loss of the isocyanide ligand to give the $[Cr(R'\text{-DAB})]^+$ ion. Likewise, species were present due to loss of the intact R′-DAB ligand thereby yielding the chromium isocyanide cations, $[Cr(CNR)]^+$. The ions $[Cr(CNR)]^+$ and $[Cr(R'\text{-DAB})]^+$ are seen in comparable abundance (Table 1 and Figs 1 and 2) thereby affirming the similar stabilities of these species. Subsequent loss of RNC and R′-DAB from $[Cr(CNR)]^+$ and $[Cr(R'\text{-DAB})]^+$ yields the intense Cr^+ ion.

These fragmentation patterns accord in a general way with those reported previously[15] in the EI mass spectra of mixed carbonyl–isocyanide complexes of type $M(CO)_{3+n}(CNR)_{3-n}$ (M = Cr or Mo; R = Me, Et, $CHMe_2$, CMe_3, p-MeC_6H_4 or p-ClC_6H_4; n = 0, 1 or 2). In these systems, carbonyl ligands are lost in preference to RNC and the homoleptic isocyanide cations $[M(CNR)_n]^+$ (n = 2 and/or 1) were abundant species. The preferential loss of CO indicates that the $[Cr(CNR)(R'\text{-DAB})]^+$ ions which are formed after fragmentation are more stable than the fragment ions $[Cr(CO)_{3-x}(CNR)(R'\text{-DAB})]^+$. While relative bond strengths are certainly important in determining initial ligand loss from large molecular cations,[11] the subsequent fragmentation of the smaller cations is governed by their ability to delocalize charge. Thus, these observations seem to reflect the greater ability of the RNC and R′-DAB ligands to delocalize the positive charge compared to CO. However, note that in SIMS studies on mixed nitrosyl–isocyanide complexes of type $[Cr(NO)(CNR)_4L]^+$ (L = RNC or an amine or tertiary phosphine ligand) and some closely related species[11,12] loss of NO is competitive with loss of RNC.

Fragmentation of the bound R′-DAB ligand is seen to give rise to ions in which dealkylation (loss of R′) and/or cleavage (C—C bond breaking) has formally occurred (see Table 1 and Figs 1 and 2). These results, which appear to be consistent with prior mass spectral results on R′-DAB ligands,[16] are of little direct structural interest to us. However, a much more significant and interesting process is encountered in the dealkylation of the isocyanide ligands. In all instances, dealkylation occurs to give $[Cr(CNH)]^+$ in quite high abundance and, in a couple of instances, also fragment ions with m/z values corresponding to $[Cr(CNH)(R'\text{-DAB})]^+$. Note that while we write the ion as $[Cr(CNH)]^+$ we cannot distinguish between this formulation as the isocyanic acid complex and the alternative hydrocyanic acid form $[Cr(NCH)]^+$. We found no evidence for the formation of the corresponding cyano species $[Cr(CN)]^+$ and $[Cr(CN)(R'\text{-DAB})]^+$. The latter type of process (to give cyanide) has been encountered in the field desorption (FD) mass spectrometry of $[M(CNCMe_3)_6X](PF_6)_2$ and $[M(CNCMe_3)_5(CN)X]PF_6$ (M = Tc or Re, X = Cl or Br) where dealkylation of the Me_3CNC ligands occurs quite easily.[17] While dealkylation has been found to give the fragment ion $[Cr(CN)]^+$ (and in some instances $[Cr(CN)(CNR)_2]^+$ as well) in the EI mass spectra of the series of complexes $Cr(CO)_{3+n}(CNR)_{3-n}$ (n = 0, 1, or 2), the ion $[Cr(CNH)]^+$ is also encountered in the EI spectra of $Cr(CO)_5(CNR)$[15] and is present in high relative abundance in the case of the t-butyl isocyanide complex. The generality of our own observations suggests that the loss of olefin (formally speaking at least) from MCNR to give MCNH (+alkene) may be a favored pathway in SIMS over that observed with the more energetic EI and, possibly, FD mass spectroscopic techniques. Thus, the loss of butene and propene from some mixed nitrosyl–isocyanide complexes of chromium and molybdenum which contain the $CNCMe_3$ and $CNCHMe_2$ ligands, respectively, has been well documented.[11] Such is the case also for Cu(I) and Ag(I) complexes that contain methyl, cyclohexyl and t-butyl isocyanide ligands.[8,10,11] While the formation of an MCNH moiety can arise through an intramolecular mechanism by loss of olefin, other pathways include: (1) the loss of carbonium ion from MCNR (clearly favored in the case of Me_3C^+) to generate MCN^-, and (2) homolytic bond cleavage to give M—CN$^\cdot$ and R$^\cdot$. The latter two processes then require sub-

sequent protonation, or abstraction of H$^{\bullet}$ (perhaps involving an adventitious source of hydrogen), respectively, in order to form MCNH. While we are uncertain of the mechanistic details in the case of the Cr complexes listed in Table 1, such studies are currently underway in the case of the homoleptic isocyanide complexes of Cu(I) and Ag(I).[10]

(b) EI mass spectra

These spectra, which were not especially informative, were dominated by intense peaks due to organic cations ($C_3H_5^+$, $C_3H_7^+$ or $C_4H_9^+$). Molecular cations were very weak (< 5% relative abundance) and other carbonyl-containing fragments, if present, also exhibited very low relative abundances (< 3%). Fragmentation to give [Cr(CNR)(R′-DAB)]$^+$, [Cr(CNH)(R′-DAB)]$^+$, [Cr(R′-DAB)]$^+$, [Cr(CNR)]$^+$, [Cr(CNH)]$^+$ and Cr$^+$ was observed, thereby revealing a basic similarity to the SIMS results, although with much lower abundance. Thus, the most intense [Cr(CNR)(R′-DAB)]$^+$ ion in the EI spectra was [Cr(CNCHMe$_2$)(*i*-Pr-DAB)]$^+$ (26% abundance relative to $C_3H_7^+$ as 100%) whereas in the SIMS spectrum it was the base peak. These observations seem reasonable since EI mass spectrometry is a more energetic process relative to the SIMS methodology.[13] As in the SIMS experiment, the N—C bonds of the RNC and R′-DAB ligands were easily cleaved and deakylation occurred from both the isocyanide and the diimine moieties. No fragments formally containing CN$^-$ were detected.

The most noteworthy differences between the SIMS and EI spectral results were seen in the presence of low-abundance peaks corresponding to [Cr(*i*-Pr-DAB)$_2$]$^+$ (*m/z* 332) and [Cr(*t*-Bu-DAB)$_2$]$^+$ (*m/z* 388) in the EI mass spectra of Cr(CO)$_3$(CNR)(R′-DAB) in the cases of R = CHMe$_2$, CMe$_3$ or xylyl when R′ = *i*-Pr, and R = Me or CMe$_3$ when R′ = *t*-Bu. These ions may result from fragmentation of higher clusters, such as [Cr$_3$(*i*-Pr-DAB)$_3$]$^+$ (*m/z* 576) and [Cr$_2$(*i*-Pr-DAB)$_2$]$^+$ (*m/z* 384), which are seen (< 10% relative abundance) in the spectra of the *i*-Pr-DAB complexes.

(c) CI mass spectra

In the CI measurements, ionization was effected by chemical reaction with *iso*-butane. The internal energy content of the pseudomolecular ion, e.g. MH$^+$ produced by isobutane CI, is generally much less if compared to the excess energy imparted to M$^+$ via EI. Therefore, the MH$^+$ ions, formed in PICI, are usually more stable towards dissociation than are the odd-electron ions, generated by EI.[18] A smaller degree of fragmentation relative to EI and SIMS is therefore expected and, indeed, observed (see Table 2). This is especially noticeable in the occurrence of fragments (many of high abundance) which contain CO ligands. Most noteworthy are the molecular cations [Cr(CO)$_3$(CNMe)(*i*-Pr-DAB)]$^+$ and [Cr(CO)$_3$(CNCMe$_3$)(*i*-Pr-DAB)]$^+$ which are present in 100% abundance or close to it. Only in the case of Cr(CO)$_3$(CNMe)(*t*-Bu-DAB) and Cr(CO)$_3$(CNCHMe$_2$)(*i*-Pr-DAB) were the relative abundances of Cr-containing ions uniformly low. We have no simple explanation for this observation.

In addition to the occurrence of some of the same fragments as found in the SIMS studies, the protonated forms of many species were observable in PICI, e.g. [Cr(CO)$_3$(CNR)(R′-DAB)+H]$^+$, [Cr(CO)$_3$(R′-DAB)+H]$^+$ and [Cr(CNR)(R′-DAB)+H]$^+$ (Table 2). Unlike the SIMS and EI mass spectra, a total of six carbonyl-containing ions were identified. However, that loss of the carbonyl ligands is still a favorable process is seen by the rather high relative abundance of the [Cr(CNR)(R′-DAB)]$^+$ ion in some of the spectra. The resistance of this ion to further fragmentation is reflected by the absence of [Cr(CNR)]$^+$ and Cr$^+$. The base peaks in the PICI mass spectra are generally due to the protonated isocyanide ligand and the intact protonated α-diimine ligand. The only exception was in the case of Cr(CO)$_3$(CNMe)(*i*-Pr-DAB), where the molecular cation was the base peak (Table 2).

A resemblance to the EI mass spectral results is seen in the presence of [Cr(R′-DAB)$_2$]$^+$ ions (Table 2). In the case of Cr(CO)$_3$(CNCHMe$_2$)(*i*-Pr-DAB), this is accompanied by the presence of higher clusters (see footnote *b* in Table 2) which may be the parents of [Cr(R′-DAB)$_2$]$^+$.

In the case of the NICI spectral results, the majority of fragments contain CO ligands (Table 3). Although the 19-electron molecular anion [Cr(CO)$_3$(CNR)(R′-DAB)]$^-$ was observed only in the case of [Cr(CO)$_3$(CNCMe$_3$)(*t*-Bu-DAB)]$^-$ (2% relative abundance), other structurally informative ions were present, many in high abundance, in these spectra. Of special note is the presence of carbonyl-containing fragment ions in high abundance. Thus, the loss of RNC from [Cr(CO)$_3$(CNR)(R′-DAB)]$^-$ gives [Cr(CO)$_3$(R′-DAB)]$^-$ as a highly abundant anion in the majority of the spectra (Table 3). A competitive loss of one CO vs the intact isocyanide ligand from the parent molecule yields high relative abundances of the following ions:

[Cr(CO)$_2$(CNCMe$_3$)(*t*-Bu-DAB)]$^-$ (36%),
[Cr(CO)$_2$(CNCMe$_3$)(*i*-Pr-DAB)]$^-$ (48%),

$[Cr(CO)_2(CNCMe_3)(Cy\text{-}DAB)]^-$ (71%),
$[Cr(CO)_2(CNCHMe_2)(i\text{-}Pr\text{-}DAB)]^-$ (71%)

and

$[Cr(CO)_2(CNxylyl)(i\text{-}Pr\text{-}DAB)]^-$ (100%).

Dealkylation occurs from $[Cr(CO)_2(CNCMe_3)(i\text{-}Pr\text{-}DAB)]^-$ and $[Cr(CO)_2(CNCMe_3)(Cy\text{-}DAB)]^-$ to yield the cyano-containing anions $[Cr(CO)_2(CN)(R'\text{-}DAB)]^-$ in 100% abundance. This result is very important since it reveals the first instances where dealkylation of these chromium complexes gives the $[Cr(CN)]^+$ moiety rather than $[Cr(CNH)]^+$ as we have seen in the SIMS and EI mass spectra. The restriction of this process to complexes which contain Me_2CHNC and Me_3CNC ligands supports the notion that simple cleavage is favored in those instances where the more stable radicals ($Me_2CH^\cdot$ and $Me_3C^\cdot$) are eliminated.[15] Further loss of two CO ligands can give rise subsequently to $[Cr(CN)(R'\text{-}DAB)]^-$, as seen in the case of $[Cr(CO)_2(CN)(R'\text{-}DAB)]^-$ for $R' = i$-Pr or Cy (Table 3).

The loss of a CO from $[Cr(CO)_3(R'\text{-}DAB)]^-$, where $R' = i$-Pr or t-Bu, gives $[Cr(CO)_2(t\text{-}Bu\text{-}DAB)]^-$ (33% abundance) and $[Cr(CO)_2(i\text{-}Pr\text{-}DAB)]^-$ (60% abundance). The high abundance of $[Cr(R'\text{-}DAB)_2]^-$ fragments in certain of the spectra again argues for the formation of putative cluster species (see, for example, footnote *b* in Table 3) which can fragment further. While the intensities of the $[Cr(R'\text{-}DAB)_2]^-$ anions are surprisingly high in some instances, it is reasonable that they exceed those of the analogous electron-deficient cations $[Cr(R'\text{-}DAB)_2]^+$ which are seen in the PICI spectra (see Table 2).

The fact that isocyanide is lost competitively with the carbonyl in the NICI spectra indicates that $[Cr(CO)_3(R'\text{-}DAB)]^-$ is of comparable stability to the corresponding $[Cr(CO)_2(CNR)(R'\text{-}DAB)]^-$ ions. This would appear reasonable since CO ligands can be very effective at delocalizing negative charge of the molecule through Cr-to-CO π-backbonding.

CONCLUSIONS

This work represents the first comparative study of the SIMS, EI and CI mass spectra of a group of inorganic or organometallic complexes. The absence of intense 17-electron molecular cations $[Cr(CO)_3(CNR)(R'\text{-}DAB)]^+$ in the SIMS and EI spectra is perhaps surprising in view of the stability of such species in solution and the solid state.[1] On the other hand, abundant molecular cations are seen in the PICI spectra. This difference presumably reflects the low internal energy content of these ions as produced by CI. In addition to the parent ions, well-defined fragment species are formed by loss of the carbonyl groups, by loss of the intact RNC and R′-DAB ligands, and by fragmentation of the latter. Similar fragmentation patterns were observed in the SIMS, and the EI and PICI spectra. Of greatest interest in the case of ligand fragmentation are the cleavage reactions of the bound RNC ligands which give rise to fragment ions that contain the $[Cr(CN)]^+$ or $[Cr(CNH)]^+$ moieties. The formation of fragment ions containing $[Cr(CNH)]^+$ is favored in the case of the SIMS and EL spectra, whereas the cyano species (i.e. $[Cr(CN)]^+$ are observed in the fragmentation patterns encountered in the NICI spectra. Another important and interesting difference which is seen in the NICI spectra (and to a certain extent in PICI) is the high relative abundance of carbonyl-containing fragments. This feature makes the CI spectra the most structurally diagnostic of the methods we have investigated. The paucity of CO fragments in the SIMS and EI spectra reflects the higher internal energies encountered with these techniques, and the enhanced ability of the RNC and R′-DAB ligands (compared to CO) to delocalize the positive charge in the cations. However, CO is lost competitively with RNC from the anions that are produced in the NICI measurements. This difference arises because the CO ligands are now very effective in delocalizing the negative charge (through Cr-to-CO π-backbonding) and, as a consequence, CO-containing fragments are much more stable.

Acknowledgements—This work was supported by the NSF-MRL Program, Grant DMR 83-16988. We are most grateful to Professor R. Graham Cooks for stimulating discussions and to Dr Andrew Bell for the preparation of the Cr complexes.

REFERENCES

1. A. Bell and R. A. Walton, *Polyhedron* 1986, **5**, 951.
2. For an excellent recent review with a focus on FAB–MS, see J. M. Miller, *Adv. Inorg. Chem. Radiochem.* 1984, **28**, 1.
3. For a selection of important references published over the last couple of years see (a) S. E. Unger, *Anal. Chem.* 1984, **56**, 363; (b) T. R. Sharp, M. R. White, J. F. Davis and P. J. Stang, *Org. Mass Spectrom.* 1984, **19**, 107; (c) B. Gregory, C. R. Jablonski and Y.-P. Wang, *J. Organomet. Chem.* 1984, **269**, 75; (d) T. Blumenthal, M. I. Bruce, O. B. Shawkataly, B. N. Green and I. Lewis, *J. Organomet. Chem.* 1984, **269**, C10; (e) R. L. Cerny, M. M. Bursey, D. L. Jameson,

M. R. Malachowski and T. N. Sorrell, *Inorg. Chim. Acta* 1984, **80**, 89; (f) D. Dalietos, A. Furst, D. Theodoropoulos and T. D. Lee, *Int. J. Mass Spectrom. Ion Phys.* 1984, **61**, 141; (g) R. B. Freas and J. E. Campana, *Inorg. Chem.* 1984, **23**, 4654; (h) B. J. Brisdon and A. J. Floyd, *J. Organomet. Chem.* 1985, **288**, 305; (i) B. Divisia-Blohorn, G. Kyriakakou and J. Ulrich, *Org. Mass Spectrom.* 1985, **20**, 463; (j) R. L. Cerny, B. P. Sullivan, M. M. Bursey and T. J. Meyer, *Inorg. Chem.* 1985, **24**, 397; (k) G. Bojesen, *Org. Mass Spectrom.* 1985, **20**, 413.

4. J. Pierce, K. L. Busch, R. A. Walton and R. G. Cooks, *J. Am. Chem. Soc.*, 1981, **103**, 2583.
5. J. L. Pierce, K. L. Busch, R. G. Cooks and R. A. Walton, *Inorg. Chem.* 1982, **21**, 2597.
6. J. L. Pierce, D. DeMarco and R. A. Walton, *Inorg. Chem.* 1983, **22**, 9.
7. J. L. Pierce and R. A. Walton, *J. Catal.* 1983, **81**, 375.
8. J. L. Pierce, K. L. Busch, R. G. Cooks and R. A. Walton, *Inorg. Chem.* 1983, **22**, 2492.
9. K. L. Busch, R. G. Cooks, R. A. Walton and K. V. Wood, *Inorg. Chem.* 1984, **23**, 4093.
10. L. D. Detter, R. G. Cooks and R. A. Walton, unpublished results.
11. J. L. Pierce, D. E. Wigley and R. A. Walton, *Organometallics* 1982, **1**, 1328.
12. D. E. Wigley and R. A. Walton, *Inorg. Chem.* 1983, **22**, 3138.
13. A. Benninghoven, *Surf. Sci.* 1973, **35**, 427.
14. L. K. Liu, K. L. Busch and R. G. Cooks, *Anal. Chem.* 1981, **53**, 109.
15. J. A. Connor, E. M. Jones, G. K. McEwen, M. K. Lloyd and J. A. McCleverty, *J. Chem. Soc., Dalton Trans.* 1972, 1246.
16. A. T. T. Hsieh and B. O. West, *J. Organomet. Chem.* 1976, **112**, 285.
17. J. P. Farr, M. J. Abrams, A. D. Costello and S. J. Lippard, *Organometallics* 1985, **4**, 139.
18. I. P. Howe, D. H. Williams and R. D. Bowen, *Mass Spectrometry Principles and Applications*. 2nd edn, p. 6. McGraw-Hill, New York (1981).

Polyhedron Vol. 5, No. 8, pp. 1329–1333, 1986
Printed in Great Britain

0277–5387/86 $3.00+.00
Pergamon Journals Ltd

^{133}Cs NMR STUDY OF Cs^+ ION COMPLEXES WITH DIBENZO-21-CROWN-7 AND DIBENZO-24-CROWN-8 IN SOME MIXED SOLVENTS

GHOLAMHOSSEIN ROUNAGHI and ALEXANDER I. POPOV*

Department of Chemistry, Michigan State University, East Lansing, MI 48824, U.S.A.

(*Received* 23 *September* 1985; *accepted* 18 *November* 1985)

Abstract—Complexation of the cesium ion with macrocyclic ligands, dibenzo-21-crown-7 and dibenzo-24-crown-8, was studied in binary solvent mixtures of dimethylsulfoxide with acetone, acetonitrile, propylene carbonate, pyridine and hexamethylphosphoramide (HMPA) as well as in pyridine–methanol mixtures. In the first four binary mixtures the complexation constants increased with decreasing amounts of dimethylsulfoxide (DMSO), the trend is reversed in the DMSO–HMPA system. In all of the above cases, the variation of the stability constant with composition was monotonic and showed good correlation with the inherent solvating ability of the neat solvents which form the mixture. In the pyridine–methanol system, however, for both complexes, the log K_f vs composition plots show several changes in direction. This behavior is probably due to a change in the structure of this binary solvent as the composition of the medium is varied.

While macrocyclic complexes of the alkali and alkaline earth cations have been extensively investigated in aqueous solutions and in a wide variety of neat nonaqueous solvents,[1,2] complexation reactions in mixed solvent systems have been investigated only to a very limited extent and seem to have been essentially restricted to water–methanol (MeOH) mixtures.[2,3] Yet it is well known that the selectivity of complexations strongly depends on the solvating ability of the solvent not only with respect to the cation but also with respect to the ligand.[4] It was of interest to us to investigate the dependence of complex stabilities on the composition of several binary solvent mixtures in order to see how this variation in solvent composition affects the selectivity of complexation.

For our initial studies we selected the Cs^+ ion as the probe cation and used ^{133}Cs NMR measurements to determine stability constants of the cesium complexes with the crown ethers dibenzo-21-crown-7 (DB21C7) and dibenzo-24-crown-8 (DB24C8). The cavities of these ligands are sufficiently large to accommodate the cesium ion, and, in contrast to 18-crown-6 and smaller crown ethers, only 1 : 1 complexes are formed.

* Author to whom correspondence should be addressed.

EXPERIMENTAL

Reagents and solvents

The complexing agents, DB24C8 and DB21C7 (Parish), were recrystallized from normal heptane and then dried in a vacuum oven for 3 days at room temperature. Cesium thiocyanate (Pfaltz & Bauer) was recrystallized in absolute MeOH and dried in a vacuum oven at 50°C for 4 days.

Hexamethylphosphoramide (HMPA), dimethylsulfoxide (DMSO), acetonitrile (AN), propylene carbonate (PC), acetone (AC) and pyridine (Py) were refluxed for several days over dehydrating agents (calcium hydride for the first four, anhydrous calcium sulfate and barium oxide for AC and Py, respectively) and then fractionally distilled. MeOH was refluxed over magnesium turnings and iodine, and then fractionally distilled. CCl_4 was dried over activated molecular sieves. All of these solvents were transferred into a dry box under a nitrogen atmosphere and further dried over activated molecular sieves (Lind type 4 A). Water contents of the solvents were tested either by Karl Fischer titration using an automatic Karl Fischer Aquatest (Photovolt Corp.) titrator, or by using a Varian Aerograph Model 490 gas chromatograph with a propak Q column. In all cases the water content of the purified solvents was below 100 ppm.

Instrumental measurements

Most of the ^{133}Cs NMR measurements were performed on a Bruker WH-180 spectrometer in the Fourier transform mode, operating at a field of 42.3 kG and a frequency of 23.62 MHz. Spinning 10-mm-o.d. NMR tubes (Wilmad) were used for samples. A 5-mm coaxially insert NMR tube, containing a solution of 0.5 M CsBr in D_2O (lock) was used as an external standard. The chemical shifts, obtained at $22 \pm 1°C$ (probe temperature), were referenced to a 0.5 M solution of cesium bromide in deuterium oxide.

Some of the ^{133}Cs data were obtained with a Varian DA-60 spectrometer operating at a field of 14.09 kG and a frequency of 7.87 MHz in the pulsed Fourier transform mode. This spectrometer was equipped with a wide-band probe capable of multinuclear operation and with a homebuilt lock which used the DA-60 console to lock the magnetic field on an external proton resonance. Measurements were made in nonspinning 10-mm NMR tubes at $30 \pm 1°C$. A 0.5 M aqueous solution of CsBr was used as the reference.

All of the chemical-shift values obtained with both instruments were subsequently referenced to the infinitely dilute aqueous solution of cesium ions, and they were corrected for the difference in the bulk diamagnetic susceptibility of the pure or mixed nonaqueous solvents and the aqueous reference solution. The paramagnetic (downfield) shifts are designated as *positive*.

Proton NMR measurements were carried out on a Bruker WM-250 spectrometer, operating at a field of 58.7 kG and at 250 MHz. Spinning 5-mm-o.d. NMR tubes were used for the samples. A 2-mm coaxially insert NMR tube, containing a solution of a 0.28-mol fraction of TMS (Aldrich) in acetone-d_6 (Aldrich, gold label) was used as an external standard. All of the proton chemical shifts were referenced to the external Me_4Si resonance in acetone-d_6 and they were corrected for the difference in the bulk diamagnetic susceptiblity of the pure or mixed solvents. The probe temperature was $22 \pm 1°C$.

Data handling

Analysis of the data and calculations of the complexation constants were carried out by previously described procedures.[5]

RESULTS AND DISCUSSION

The $Cs^+ \cdot$ DB21C7 complex was studied in AC–DMSO and Py–MeOH systems, while its DB24C8 analog was studied in binary DMSO mixtures with AC, AN, PC and HMPA, as well as in the Py–MeOH system. In all cases the exchange was fast and only one, population-averaged, signal was observed at the probe temperature. An example of the variation of the ^{133}Cs chemical shift for the different DMSO–AN mixtures, as a function of the [DB24C8]/[Cs^+] mole ratio, is illustrated in Fig. 1. It is seen that the curvature of the plots increases with increasing concentrations of AN giving a qualitative indication that the stability of the complex increases with increasing concentration of AN. Similar plots were obtained for the DMSO mixtures with AC, PC and Py. In the case of the DMSO–HMPA mixtures, however, the curvature of the plots decreased with increasing concentration of HMPA.

The formation constants of the two macrocyclic complexes in different solvent mixtures and in neat solvents are listed in Table 1. The observed trends are not particularly surprising and, with the exception of Py (Table 2), show that the donor abilities of the solvents, as expressed by the Gutmann donor number,[6] play a very important role in determining the stabilities of the complexes. We have previously observed similar, seemingly exceptional, behavior of Py[7] and ascribed it to the fact that, although it

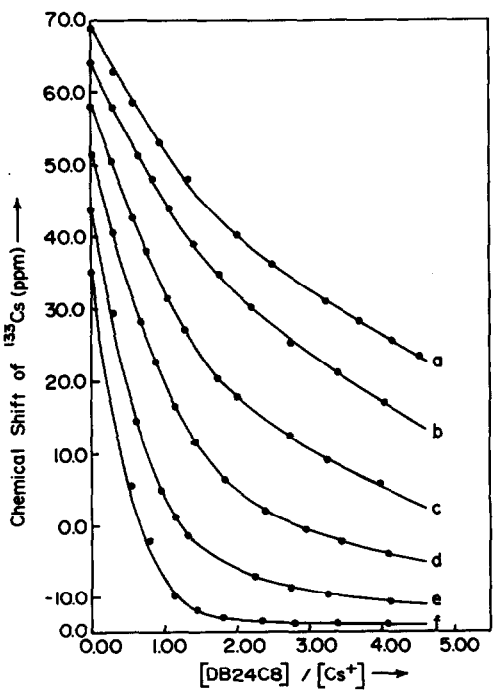


Fig. 1. ^{133}Cs chemical shifts as a function of [DB24C8]/[Cs^+] mole ratio in DMSO–AN binary mixtures. Mol % AN: a = 0, b = 25.2, c = 47.4, d = 67.0, e = 84.4, f = 100.0.

Table 1. Log K_f values of the $Cs^+ \cdot$ DB21C7 and $Cs^+ \cdot$ DB24C8 complexes in some binary solvent mixtures at 22 ± 1°C

DB21C7		DB24C8									
DMSO–AC system[a]		DMSO–AN system[a]		DMSO–AC system[b]		DMSO–Py system[c]		DMSO–PC system[a]		DMSO–HMPA system[a]	
mol % AC	Log K_f	mol % AN	Log K_f	mol % AC	Log K_f	mol % Py	Log K_f	mol % PC	Log K_f	mol % HMPA	Log K_f
100	4.04 ± 0.10	100	3.92 ± 0.06	100	2.91 ± 0.02	100	4.41 ± 0.02	100	3.37 ± 0.01	100	1.23 ± 0.02
79.4	3.12 ± 0.02	84.4	2.94 ± 0.03	84.5	2.38 ± 0.02	78.0	3.02 ± 0.01	77.1	2.74 ± 0.02	62.1	1.32 ± 0.02
59.1	2.71 ± 0.02	66.9	2.34 ± 0.01	69.2	1.99 ± 0.01	57.1	2.41 ± 0.02	55.8	2.31 ± 0.01	38.0	1.41 ± 0.02
39.1	2.44 ± 0.01	47.4	1.99 ± 0.02	49.1	1.73 ± 0.03	37.1	1.94 ± 0.02	36.0	1.97 ± 0.01	0	1.44 ± 0.04
19.4	2.23 ± 0.05	25.2	1.70 ± 0.01	24.2	1.44 ± 0.07	18.2	1.71 ± 0.01	17.4	1.80 ± 0.02		
0	2.22 ± 0.02	0	1.44 ± 0.04	14.6	1.44 ± 0.04	0	1.44 ± 0.04	0	1.64 ± 0.04		

[a] [CsNCS] = 0.0100 M.
[b] [CsNCS] = 0.0050 M.
[c] [CsNCS] = 0.0070 M.

has a high donor number, it is a "softer" base than the other solvents and does not solvate strongly the cesium ion ("hard" acid). Consequently its solvation shell is easily replaced by the ether oxygens of the crown ethers. On the other hand, it reacts strongly with a "soft" acid, $SbCl_5$, thus giving a high donor number on the Gutmann scale.

The variation of the stability constants with solvent composition is illustrated in Fig. 2. Several reversals of stability can be observed, e.g. the complex is more stable in a 75–25 mol % DMSO–AN mixture than in the 75–25 mol % DMSO–PC system; however, with a 10–90 mol % composition of the two mixtures, the stabilities are reversed. The above and the other reversals of stabilities shown in Fig. 2 are not large, but they do indicate the possibility that more substantial changes in stabilities and reversals of cation selectivities may be obtained in more optimally selected mixed solvent systems.

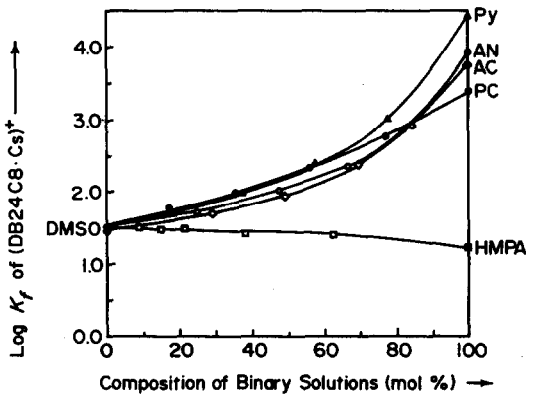


Fig. 2. Variation of the stability constant of the $Cs^+ \cdot$ DB24C8 complex with the solvent composition in binary solvent mixtures.

A very different behavior was observed in the MeOH–Py system. As shown in Fig. 3, the change in the formation constant is certainly not mono-

Table 2. Some physical properties of neat solvents and log K_f values obtained in these media

Solvent	Dielectric constant	Dipole moment (D)	Donor number	Log K_f of $Cs^+ \cdot$ DB24C8
AN	37.5	3.44	14.1	3.96 ± 0.06
PC	64.4		15.1	3.37 ± 0.01
AC	20.7	2.69	17.0	3.97 ± 0.02
MeOH	32.7	2.87	25.7[a]	3.65 ± 0.05
DMSO	46.7	3.9	29.8	1.44 ± 0.04
Py	12.4	2.37	33.1	4.41 ± 0.02
HMPA	30.0	4.31	38.8	1.23 ± 0.04

[a] From ^{23}Na NMR measurements: A. I. Popov, *Pure Appl. Chem.* 1975, **41**, 275.

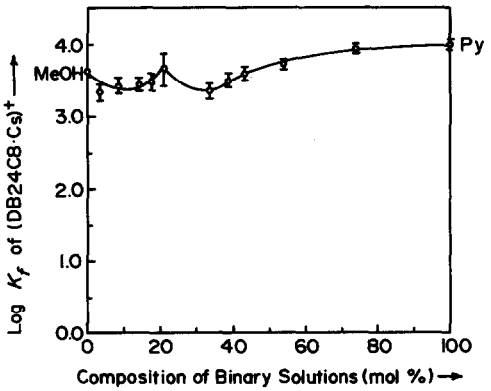


Fig. 3. Variation of the stability constant of the $Cs^+ \cdot$ DB24C8 complex with the solvent composition in MeOH–Py mixture.

Table 3. Study of the $Cs^+ \cdot$ DB21C7 and $Cs^+ \cdot$ DB24C8 complexes in MeOH–Py mixtures

DB21C7[a]		DB24C8[b]	
mol % Py	Log K_f	mol % Py	Log K_f
100	4.76±0.11	100	4.41±0.02
66.8	3.98±0.16	74.1	3.44±0.06
43.2	4.32±0.13	54.0	3.69±0.07
25.1	4.27±0.08	43.0	3.59±0.11
11.2	4.08±0.09	38.1	3.52±0.09
0	4.03±0.08	33.5	3.31±0.12
		21.3	3.71±0.24
		17.8	3.45±0.10
		14.4	3.47±0.10
		8.1	3.42±0.11
		3.7	3.32±0.08
		0	3.65±0.05

[a] [CsNSC] = 0.0100 M.
[b] [CsNSC] = 0.0070 M.

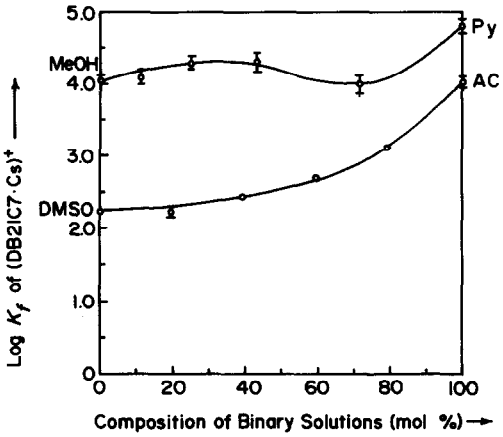


Fig. 4. Variation of the stability constant of the $Cs^+ \cdot$ DB21C7 complex in DMSO–AC and MeOH–Py binary mixtures.

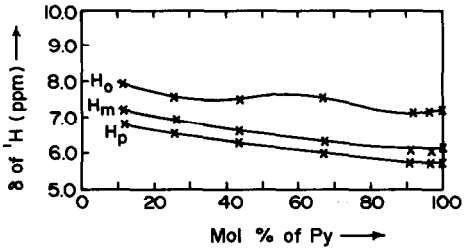


Fig. 5. Variation of the proton chemical shifts of the *ortho-*, *meta-* and *para*-protons of Py in Py–MeOH mixtures.

tonic. As the concentration of Py increases, the complex stability first goes down, then increases to a maximum value at about 20 mol % Py, then decreases only to rise again very gradually after 40 mol % Py. Somewhat similar results were obtained with the $Cs^+ \cdot$ DB21C7 complex in the same solvent mixtures (Fig. 4). The data are given in Table 3.

Proton NMR measurements on the Py moiety in the binary mixtures (Fig. 5) show that the variation of the chemical shift of the *ortho-* proton is not monotonic and in fact, strongly resembles the behavior of the complexity constants (Figs 3 and 4) in the same solvent mixture. On the other hand, the resonances of the *meta-* and *para*-protons show only a minor monotonic variation with the change in the composition of the medium. Similar monotonic variation for *all three protons* was observed in Py–CCl_4 mixtures. Of course, in the first case we have two associated dipolar solvents both with substantial dipole moments (2.87 D for methanol and 2.23 D for pyridine). In addition neat MeOH is strongly hydrogen-bonded. There is little doubt that as the two solvents are mixed the homo-dimers (and/or higher aggregates) are broken up with the formation of hetero-aggregates. We have previously observed such behavior in DMSO–Py mixtures, where the solvating abilities of DMSO are considerably enhanced as compared to the neat solvent.[8,9] Our knowledge of the structure and properties of solvent mixtures is still very rudimentary and a more detailed study is needed (in this case) of the Py–MeOH system to elucidate the details of the intermolecular interactions in these systems.

Acknowledgement—We gratefully acknowledge the support of this work by the National Science Foundation Grant No. CHE-8515474.

REFERENCES

1. A. I. Popov and J.-M. Lehn, In *Coordination Chemistry of Macrocyclic Compounds* (Edited by G. A. Melson), Chap. 9. Plenum Press, New York (1979).
2. M. Hiroaka, *Crown Compounds*. Elsevier, New York (1982).
3. J. D. Lamb, R. M. Izatt, J. J. Christensen and D. J. Eatough, In *Coordination Chemistry of Macrocyclic Compounds* (Edited by G. A. Melson), Chap. 3. Plenum Press, New York (1979).
4. P. A. Mosier-Boss and A. I. Popov, *J. Am. Chem. Soc.* 1985, **107**, 6168.
5. Y. Lee, J. Allison and A. I. Popov, *Polyhedron* 1985, **4**, 441 (and references therein).
6. V. Gutmann, *Coordination Chemistry in Nonaqueous Solutions*. Springer, New York (1968).
7. A. Hourdakis and A. I. Popov, *J. Solution Chem.* 1977, **6**, 299; N. Ahmad and M. C. Day, *J. Am. Chem. Soc.* 1974, **99**, 941.
8. R. H. Erlich, M. S. Greenberg and A. I. Popov, *Spectrochim. Acta* 1973, **29A**, 543.
9. J. B. Kinsinger, M. M. Tannahill, M. S. Greenberg and A. I. Popov, *J. Phys. Chem.* 1973, **77**, 2444.

Polyhedron Vol. 5, No. 8, pp. 1335–1339, 1986
Printed in Great Britain

0277–5387/86 $3.00+.00
Pergamon Journals Ltd

COMPLEX FORMATION OF Ni(II) AND Fe(III) WITH THE NITRITE ANION

EFRAIM AVSAR* and F. BEDIA ERIM

Department of Chemistry, Technical University of Istanbul, Istanbul, Turkey

(*Received* 3 *July* 1985; *accepted* 6 *November* 1985)

Abstract—The stepwise stabilities of the complexes formed by Ni(II) and Fe(III) with the nitrite anion have been determined potentiometrically in an aqueous sodium perchlorate medium of unit ionic strength at 25.0°C. Two fairly weak mononuclear complexes are formed in the Ni(II)–nitrite system with the overall formation constants as $\beta_1 = 5.9 \pm 0.9$ M^{-1} and $\beta_2 = 12 \pm 2$ M^{-2}, while for the Fe(III)–nitrite system three mononuclear complexes of moderate strengths, namely $\beta_1 = (3.9 \pm 0.7) \times 10^2$ M^{-1}, $\beta_2 = (5 \pm 2) \times 10^3$ M^{-2} and $\beta_3 = (2.8 \pm 0.6) \times 10^5$ M^{-3}, are found. No evidence has been found for the formation of polynuclear or acid complexes in the concentration range studied.

Much of the interest in transition-metal–nitrite complexes in solution concerns the fact that the nitrite ligand can be bonded to a metal ion via either the nitrogen or the oxygen atom. The electronic structure of the metal ion has a dominant influence on this bonding.

Studies on the formation of metal–nitrite complexes in aqueous solution have been carried out by different techniques. Data pertaining to the equilibrium measurements on the nitrite complexes are, however, scarce.[1] The nitrite system of Fe(III) has already been studied spectrophotometrically at 25°C in a 0.01 M perchloric acid medium.[2] However, only the first formation constant was evaluated. For the Ni(II)–nitrite system, on the other hand, no such measurements seem to have been made so far.

The potentiometric measurements have been carried out by means of a glass electrode. Thus, the free ligand concentration ([L]), has been determined via pH measurements in metal ion solutions containing nitrite–nitrous acid buffers.[3] This method can, generally, be applied for the numerous ligands which are anions of weak acids. To do this, the acidity constant of nitrous acid has to be known under the same conditions. This has therefore been determined in separate measurements with solutions which are free from the metal ion.

All measurements have been performed at 25.0°C and in an aqueous medium of unit ionic strength with sodium perchlorate as inert salt.

EXPERIMENTAL

Chemicals

Ni(II) perchlorate was prepared by dissolving $NiCO_3 \cdot 2Ni(OH)_2 \cdot 4H_2O$ (Merck, p.a.) in perchloric acid (Merck, p.a.) and recrystallized once from an acidic aqueous solution. The concentration of Ni(II) was determined gravimetrically by dimethylglyoxime. Fe(III) perchlorate solutions were prepared as before.[4] The free-acid concentrations in the stock solutions were determined both potentiometrically and by passing aliquots through a column containing Dowex 50 W cation exchange resin in the hydrogen form and titrating the eluate with standard sodium hydroxide. The perchloric acid (Merck, p.a.) solutions were standardized against borax. Sodium perchlorate was prepared and analyzed as described before.[5] Sodium nitrite solution was made from $NaNO_2$ (Merck, p.a.) without further purification. Analysis for $NaNO_2$ was made volumetrically by standard $KMnO_4$.[6] The Ag–AgCl electrodes were prepared according to Brown.[7]

Apparatus and procedure

A Metrohm E500 Digital pH meter equipped with a Metrohm EA 109 glass electrode has been

* Author to whom correspondence should be addressed.

used for the potentiometric measurements. The glass electrode has been checked, before and after each titration series, and gave a slope of 59.2 ± 0.2 mV. A magnetic stirrer was used for mixing. Stable e.m.fs were reached in a few minutes. The reproducibility was generally within ± 0.4 mV and even better for the Fe(III)–nitrite system. The e.m.fs of the following cell were measured:

$$-\mathrm{RE}//C_M\mathrm{M\ Me(ClO_4)_v}, C_H\mathrm{M\ HClO_4},$$
$$C_L\mathrm{M\ NaNO_2, NaClO_4\ to}\ I = 1\ \mathrm{M/GE}+,$$

where

$$\mathrm{RE}// = \mathrm{Ag,AgCl/0.025\ M\ NaCl},$$
$$0.975\ \mathrm{M\ NaClO_4/1.00\ M\ NaClO_4/}.$$

Here, Me denotes Ni or Fe, and v is the valency.

The measurements have been performed as titrations at constant metal ion and constant acid concentrations, C_M and C_H, respectively. Equal volumes of solutions T_1 and T_2 were added from piston burettes to V_0 ml of solution S. These solutions had the following compositions:

S: C_M M $Ni(ClO_4)_2$, C_H M $HClO_4$, $(1.0–3C_M)$ M $NaClO_4$,

T_1: 1.00 M $NaNO_2$,

T_2: $2C_M$ M $Ni(ClO_4)_2$, $2C_H$ M $HClO_4$, $(1.0–6C_M)$ M $NaClO_4$,

for the Ni(II)–nitrite system. In the case of Fe(III), the compositions were:

S: C_M M $Fe(ClO_4)_3$, C_H M $HClO_4$, $(1.0–6C_M)$ M $NaClO_4$,

T_1: 1.00 M $NaNO_2$,

T_2: $2C_M$ M $Fe(ClO_4)_3$, $2C_H$ M $HClO_4$, $(1.0–12C_M)$ M $NaClO_4$.

Thus, up to $C_L = C_H$ the ionic strength is higher than 1 M. But when $C_L = C_H$, which is reached soon in the titrations, practically all the free acid will be converted into HNO_2. The ionic strength of the resulting solution will then be 1 M.

Calculation of constants from measurements

The e.m.f. of the above cell is given, in mV, at 25.0°C by:

$$E_H = E_H^\circ + E_j + 59.16 \log h \qquad (1)$$

where E_H° is the cell constant, E_j the liquid junction potential, and h the free hydrogen ion concentration. E_j depends almost only on h and can therefore be determined separately.[8]

By measuring the values of h, the free ligand concentration ([L]) and the average ligand number ($\bar{n}$) can be calculated from:

$$[L] = K_a(C_H - h)/h \qquad (2)$$

and

$$\bar{n} = (C_L - C_H + h - |L|)/C_M, \qquad (3)$$

respectively.

Once corresponding values of $\bar{n}$ and [L] are known the function

$$X = 1 + \sum_{j=1}^{N} \beta_j [L]^j$$

can be evaluated from a graphical integration of an $\bar{n}/[L]$ vs [L] plot. The constants are then obtained graphically[9] by plotting the functions $X_j = (X_{j-1} - \beta_{j-1})/[L]$ vs [L], where $1 \leqslant j \leqslant N$; $X_0 = X$; $\beta_0 = 1$.

RESULTS AND DISCUSSION

Proton–nitrite system

The measurements were carried out as a series of titrations of a solution $C_H = 100$ mM ($I = 1.0$ M) into a solution containing sodium nitrite in different concentrations, i.e. 10, 20 and 40 mM. In another series, titrations were performed where a solution of nitrite–nitrous buffer was added to various perchloric acid solutions of the same ionic strength of 1.0 M. From these measurements the acidity constant of nitrous acid can be calculated by the relation:

$$K_a = \frac{h(C_L - C_H + h)}{C_H - h}, \qquad (4)$$

where C_L is the ligand concentration, C_H the total acid concentration and h is found according to eqn (1).

The value of $K_a = (1.03 \pm 0.06) \times 10^{-3}$ M obtained from these measurements agrees excellently with that reported in literature under the same conditions.[1]

Ni(II)–*nitrite system*

The potentiometric titrations were performed with three different values of C_M, i.e. 40, 60 and 80 mM. The acid concentrations, constant during the titrations, were 40 mM for $C_M = 40$, 30, 60 and 120 mM for $C_M = 60$, 80 and 40 mM for $C_M = 80$ mM. Thus, various ratios of C_M/C_H have been used for

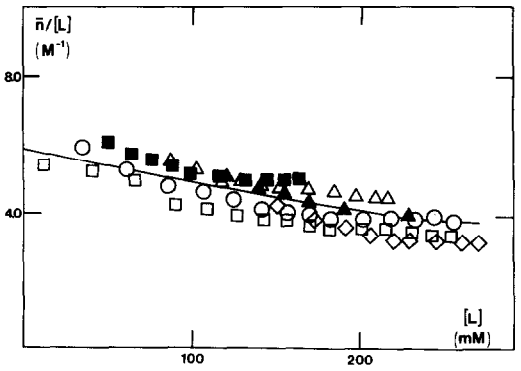


Fig. 1. Plot of $\bar{n}/[L]$ vs [L] for the Ni(II)–nitrite system. (○) $C_M = 40$ mM, $C_H = 40$ mM; (□) $C_M = 60$ mM, $C_H = 30$ mM; (◇) $C_M = 60$ mM, $C_H = 60$ mM; (■) $C_M = 60$ mM, $C_H = 120$ mM; (△) $C_M = 80$ mM, $C_H = 40$ mM; (▲) $C_M = 80$ mM, $C_H = 80$ mM. The full-drawn curve has been calculated from the values of β_j listed in Table 1. Only half of the experimental points, chosen at random, have been plotted.

each series. A free ligand ion concentration up to $\simeq 300$ mM could be reached in the measurements. In spite of the fairly large variation of both C_M and C_H during the measurements, no systematic deviations can be observed between the various titrations series, which proves that neither polynuclear nor acid complexes are formed (Figs 1 and 2).

The formation constants of the complexes formed in the concentration range studied were evaluated both graphically[9] and numerically by a high-speed computer using a program written for this purpose.[10] Both the methods gave the same results: $\beta_1 = 5.9 \pm 0.9\ M^{-1}$, $\beta_2 = 12 \pm 2\ M^{-2}$.

The errors given correspond to confidence limits on the 99.9% level of significance.

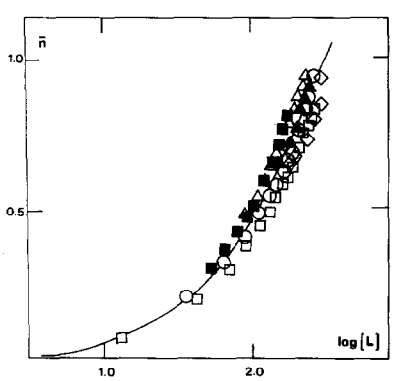


Fig. 2. Complex formation function of the Ni(II)–nitrite system. For symbols refer to Fig. 1. [L] in mM.

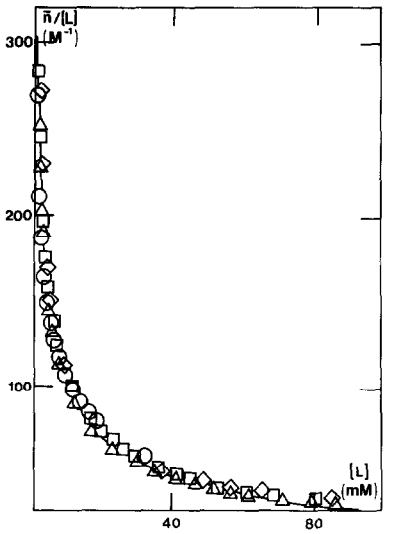


Fig. 3. Plot of $\bar{n}/[L]$ vs [L] for the Fe(III)–nitrite system. (○) $C_M = 5$ mM, $C_H = 60.35$ mM; (□) $C_M = 10$ mM, $C_H = 114.70$ mM; (△) $C_M = 15$ mM, $C_H = 156.97$ mM; (◇) $C_M = 20$ mM, $C_H = 214.32$ mM. The full-drawn curve has been calculated from the values of β_j listed in Table 1. Only half of the experimental points, chosen at random, have been plotted.

Fe(III)–*nitrite system*

For this system four different values of C_M, namely 5, 10, 15 and 20 mM, were used. In order to prevent the initial hydrolysis of the Fe(III) ion, the concentration of perchloric acid was kept high for each series, i.e. 60, 115, 157 and 214 mM, respectively. Once the formation of nitrite complexes proceeds the hydrolysis is virtually suppressed even in buffers containing a fairly high proportion of the ligand.

The $\bar{n}/[L]$ vs [L] plot is shown in Fig. 3 and the complex formation function is presented in Fig. 4.

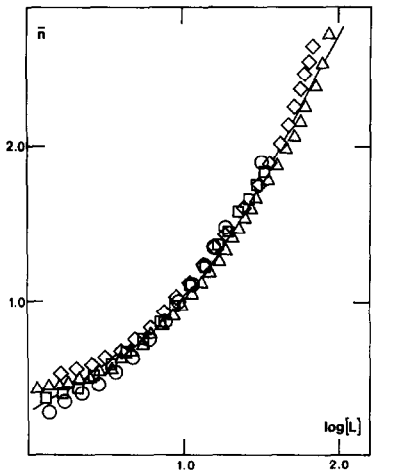


Fig. 4. Complex formation function of the Fe(III)–nitrite system. For symbols refer to Fig. 3. [L] in mM.

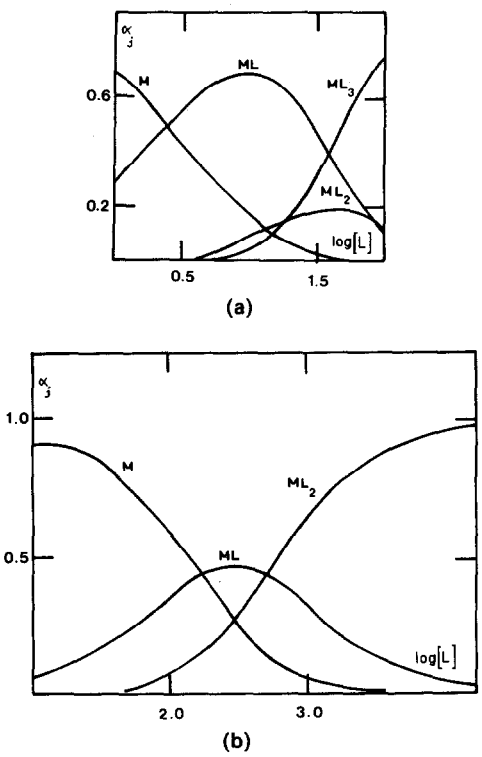


Fig. 5. Distribution of nickel(II) (a) and iron(III) (b) between the different ML_j complexes with varying nitrite ion concentration ([L] in mM).

The complex formation function is independent of both C_M and C_H, which indicates that no polynuclear and acid complexes exist.

In the graphical determination of the constants, the plot of the function $X_3([L])$ against [L] shows a slight positive curvature. This may, of course, be interpreted in terms of the formation of a fourth complex. It is more likely, however, that this slight deviation from linearity is due to the changes in the activity coefficients at high ligand concentrations. In the numerical calculations models including three and four, as well as two, mononuclear complexes have been tried. For a model containing four mononuclear complexes a value of $(1 \pm 1) \times 10^5\ M^{-3}$ is found for β_3. The value of β_4 becomes $(1.3 \pm 0.6) \times 10^6\ M^{-4}$ in this case. Thus, introducing the fourth complex in the evaluation increases the uncertainty in β_3. For a model including only three mononuclear complexes a good fit of experimental data is obtained with estimates, $\beta_1 = (3.9 \pm 0.7) \times 10^2\ M^{-1}$, $\beta_2 = (5 \pm 2) \times 10^3\ M^{-2}$ and $\beta_3 = (2.8 \pm 0.6) \times 10^5\ M^{-3}$. A model with only two mononuclear complexes, on the other hand, should be discarded since only a very poor fit to the potentiometric data can be obtained.

The results of this study are collected in Table 1. Considering the different media and techniques used in the determination of β_1 for $[FeNO_2]^{2+}$, the agreement with the value found by Zhuravleva and Berdnikov is fairly good.[2] Nitrogen- and oxygen-containing ligands form complexes in aqueous solution with most acceptors. Nitrogen should be classified as a considerably softer donor atom than oxygen. The nitrite ion, as both an oxygen and a nitrogen donor, shows linkage isomerism in its complexes. The best known complexes of this kind are those formed by Co(III), Rh(III), Ir(III) and Pt(IV).[11] In fact, the nitrite anion acts as a strong σ-donor when bonded through the nitrogen atom compared to oxygen bonding. In agreement with this, metal complexes involving only nitrogen donors are more stable than those involving oxygen donors as well.[4,12] When π-interactions are involved, however, the non-bonding orbital is mainly localized on the two oxygen atoms. As a result of that, the nitrite ligand acts as a π-donor when bonding takes place over oxygen.[11]

Acknowledgement—We are most grateful to Dr Arvid Sandell of the University of Lund, Lund, Sweden, for good advice on discussions of the results and for invaluable help with computer calculations.

Table 1. Overall formation constants and values of $\Delta G_j^\ominus$ for the consecutive steps of the Ni(II)– and Fe(III)–nitrite systems at 25.0°C and $I = 1.0$ M: errors given correspond to confidence limits at the 99.9% level of significance

System	j	β_j (M^{-j})	$-\Delta G_j^\ominus$ (kJ mol^{-1})
Ni(II)–nitrite	1	5.9 ± 0.9	4.4 ± 0.4
	2	12 ± 2	1.8 ± 0.6
Fe(III)–nitrite	1	$(3.9 \pm 0.7) \times 10^2$	14.8 ± 0.5
	2	$(5 \pm 2) \times 10^3$	6 ± 1
	3	$(2.8 \pm 0.6) \times 10^5$	10 ± 1

REFERENCES

1. R. M. Smith and A. E. Martell, *Critical Stability Constants*, Vol. 4. Plenum, New York (1976).
2. O. S. Zhuravleva and V. M. Berdnikov, *Koord. Khim.* 1976, **2**, 9.
3. E. Avsar, *J. Inorg. Nucl. Chem.* 1980, **42**, 881.
4. E. Avsar, *Acta Chem. Scand.* 1980, **A34**, 405.
5. S. Ahrland and E. Avsar, *Acta Chem. Scand.* 1975, **A29**, 881.
6. A. I. Vogel, *A Textbook of Quantitative Inorganic Analysis*. Longmans, London (1961).
7. A. S. Brown, *J. Am. Chem. Soc.* 1934, **56**, 646.
8. S. Ahrland and L. Kullberg, *Acta Chem. Scand.* 1971, **25**, 3457.
9. S. Fronaeus, In H. B. Jonassen and A. Weisberger, *Techniques of Inorganic Chemistry*, Vol. 1, Chap. 1. Interscience, New York (1963).
10. J. P. Chandler, STEPIT 5. Quantum Chemistry Program Exchange, Department of Chemistry, Indiana University, Bloomington, IN (1965).
11. M. A. Hitchman and G. L. Rowbottom, *Coord. Chem. Rev.* 1982, **42**, 55.
12. S. Ahrland and E. Avsar, *Acta Chem. Scand.* 1975, **A29**, 881.

Polyhedron Vol. 5, No. 8, pp. 1341–1344, 1986
Printed in Great Britain

0277–5387/86 $3.00+.00
Pergamon Journals Ltd

ADDUCTS OF BIS(8-QUINOLINATE) OXOVANADIUM(IV) WITH ORGANIC BASES

R. LOZANO*, J. MARTÍNEZ, J. ROMÁN, A. MARTÍNEZ and A. DOADRIO

Departamento de Química Inorgánica y Analítica, Facultad de Farmacia, Universidad Complutense de Madrid, 28040 Madrid, España

and

J. L. PEÑA

Departamento de Química Inorgánica y Analítica, Colegio Universitario Toledo, España

(*Received* 26 *July* 1985; *accepted after revision* 18 *November* 1985)

Abstract—We report the synthesis and study of bis(8-quinolinol) oxovanadium(IV) adducts with pyridine and substituted pyridines. These complexes were identified by IR and electronic spectra, magnetic susceptibility measurements and analytical data. The relation between the basicity of the pyridines and the V=O stretching frequency has also been studied. The effects of steric hindrance and the inductive effects exercised by the functional groups, amino and methyl of the pyridine, in the formation of the adducts are discussed.

Henry *et al.*[1] reported the synthesis of the adducts of bis(8-quinolinol) oxovanadium(IV) with several organic bases whose formulae correspond to VOQ_2B and $BH^+[VOQ_3]^-$, in which Q = 8-quinolinol and B = organic base, by means of the reactions:

$$VO^{2+} + HQ + B \rightarrow VOQ_2B + 2H^+,$$

$$VO^{2+} + 3HQ + B \rightarrow [VOQ_3]^- + BH^+ + 2H^+.$$

These authors also reported the impossibility of obtaining these adducts by the direct reaction between the complex VOQ_2 and the organic base B, because the complex presents a trigonal bipyramid structure.

In this paper we describe the synthesis of the bis(8-quinolinol) oxovanadium(IV) adducts with substituted pyridines (3-methyl-, 4-methyl-, 3,5-dimethyl-, 3-amino- and 4-aminopyridine) by the direct reaction between the complexes and the pyridines. The study of these complexes by IR and electronic spectroscopy, magnetic susceptibilities and analytical data, shows that stoichiometry of the complex is 2:1 (ligand:metal) and 1:1 (base:complex) for these adducts.

From IR and electronic spectral data, we assign a square pyramidal structure for the complex and a distorted octahedral structure for the adducts. We have also obtained a relationship between the pyridine's basicity (pK_b values), and V=O stretching mode and the $^2B_2 \rightarrow {}^2B_1$, $^2B_2 \rightarrow {}^2E(I)$ transition frequencies.

EXPERIMENTAL

Materials

8-Quinolinol, vanadyl-oxosulphate and the organic bases were Merck commercial products. The solvents used to prepare the complexes were Carlo Erba or Merck.

Analytical procedures

Elemental analyses were performed with a Perkin–Elmer model 240B. Vanadium was determined by atomic absorption with a Perkin–Elmer 430 atomic absorption spectrophotometer after decomposing the compounds with a concentrated HNO_3 and H_2SO_4 mixture (1:1).

The analytical data for the compounds are shown in Table 1.

Methods

Magnetic susceptibilities were measured by the Gouy[2] method at room temperature on a

* Author to whom correspondence should be addressed.

Table 1. Analytical data and magnetic properties

Compound[a]	% Calculated				% Found				μ (BM)
	C	H	N	V	C	H	N	V	
$VO(ox)_2$	60.9	3.4	7.9	13.3	60.7	3.3	8.2	13.9	1.7
$VO(ox)_2(Py)$	63.6	4.0	9.7	11.6	63.7	4.0	9.8	11.8	1.7
$VO(ox)_2(3MP)$	64.3	4.3	9.4	11.4	64.0	4.3	9.3	11.3	1.7
$VO(ox)_2(4MP)$	64.3	4.3	9.4	11.4	64.6	4.5	9.5	11.5	1.7
$VO(ox)_2(3,5DMP)$	64.9	4.6	9.1	11.0	65.2	4.8	9.2	11.6	1.7
$VO(ox)_2(3AP)$	61.5	4.0	12.5	11.3	61.5	4.1	12.6	11.7	1.7
$VO(ox)_2(4AP)$	61.5	4.0	12.5	11.3	61.7	4.1	12.6	11.5	1.6

[a] Py, pyridine; 3MP, 3-methylpyridine; 4MP 4-methylpyridine; 3,5DMP, 3,5-dimethylpyridine; 3AP, 3-aminopyridine; 4AP, 4-aminopyridine.

Mettler H-51 A.R. balance and a type C-Oxford electromagnet. Molar susceptibilities have been corrected for the diamagnetism of the constituent molecules.[3,4] The magnetic moments were calculated according to the formula $\mu = 2.84(\chi'_M T)^{0.5}$ BM, where χ'_M is the corrected molar susceptibility. The values of the magnetic moments are given in Table 1.

The IR spectra were taken on a Perkin–Elmer 283 recording spectrophotometer. The samples were run as KBr pellets. The IR absorption peaks for the compounds prepared in this study are listed in Table 2.

The visible–near-UV spectra of the compounds were carried out in the range 220–1000 nm on a Beckman 5240 recording spectrophotometer using solutions of the complexes in dichloromethane. The results obtained are given in Table 3.

Preparation

$VO(C_9H_4NO)_2$: 1.27 g (5 mmol) of $VOSO_4 \cdot 5H_2O$ was dissolved in 5 cm^3 of water. Another solution of 1.45 g (10 mmol) of 8-quinolinol in 10 cm^3 of absolute ethanol was prepared. This solution was added to the previous one stirring continuously and a greenish-black precipitate was formed. The precipitate was separated by filtration *in vacuo*, washed repeatedly with a boiling water–ethanol mixture and dried over P_4O_{10} in a nitrogen atmosphere to avoid oxidation. Yield 80%.

$VO(C_9H_4NO)_2 \cdot B$: The complex previously obtained was dissolved in the organic base (3-methyl-, 4-methyl- and 3,5-dimethylpyridine, and pyridine) or in an ethanolic solution of 3-amino- and 4-aminopyridine with continuous stirring. After cooling for 2 days, the adducts—obtained as green crystals—were separated by filtration *in vacuo* and dried over P_4O_{10} in a nitrogen atmosphere. Yield 42%.

DISCUSSION

The complexes obtained in this study gave analytical results which are concordant with the formulas assigned: $VO(ox)_2$ and $VO(ox)_2 \cdot B$ (ox = 8-quinolinol; B = pyridine, 3-methyl-, 4-methyl-, 3,5-dimethyl-, 3-amino- and 4-aminopyridine).

The complex $VO(ox)_2$ is less stable to vanadium(V) oxidation than the new adducts.

Table 2. IR absorption maxima (cm^{-1}) of vanadium(IV) oxocomplexes and pK_b values of substituted pyridines

Compound[a]	ν(V=O)	ν(C—O—V)	ν(V—N_{lig})	ν_a(V—O_{lig})	ν_s(V—O_{lig})	ν(V—N_{base})	pK_b
$VO(ox)_2$	970	1100	349	550	365	—	—
$VO(ox)_2(Py)$	935–945	1109	357	568	373	335	8.87
$VO(ox)_2(3MP)$	930	1100	358	570	375	339	8.37
$VO(ox)_2(4MP)$	965	1105	351	553	368	332	7.98
$VO(ox)_2(3,5DMP)$	960	1103	353	560	371	330	7.85
$VO(ox)_2(3AP)$	924	1112	364	573	379	348	7.49
$VO(ox)_2(4AP)$	920	1115	366	572	375	350	4.88

[a] Abbreviations as in Table 1.

Table 3. Electronic absorption spectra: transition ν (kK) (ε)

Compound[a]	$^2B_2 \rightarrow {}^2E(I)$	$^2B_2 \rightarrow {}^2B_1$	$^2B_2 \rightarrow {}^2A_1$	Intraligand
$VO(ox)_2$	14.0 (73)	18.0 (84)	20.2 (153)	38.3 (39,406)
$VO(ox)_2$(Py)	14.0 (61)	18.6 (98)	21.0 (184)	37.7 (42,572)
$VO(ox)_2$(3MP)	13.9 (60)	18.8 (103)	21.2 (192)	37.4 (37,743)
$VO(ox)_2$(4MP)	14.0 (68)	18.1 (93)	21.3 (187)	37.7 (30,504)
$VO(ox)_2$(3,5DMP)	14.0 (52)	18.4 (99)	21.2 (202)	37.0 (38,586)
$VO(ox)_2$(3AP)	13.8 (48)	19.3 (118)	20.7 (198)	38.0 (42,327)
$VO(ox)_2$(4AP)	13.8 (59)	19.0 (58)	20.8 (311)	37.4 (38,891)

[a] Abbreviations as in Table 1.

All these compounds are paramagnetic with values of magnetic moments between 1.65 and 1.72 BM. These results show the existence of monomeric species of vanadium(IV) (ion d^1).

IR spectra exhibit a very strong band at 920–970 cm^{-1}, which is attributed to the stretching vibration of the terminal V=O bond. If we compare the complex $VO(ox)_2$ with the adducts $VO(ox)_2 \cdot B$, one observes that the adducts show the V=O band displaced to lower frequencies (920–965 cm^{-1}) than the complex (970 cm^{-1}). This displacement can be attributed to the different basicity of the pyridine or substituted pyridine employed. The pK_b value reflects the basicity of the ligand towards the proton. It may be assumed that the pK_b of the ligand provides a measure of the ability of the ligand to form σ-bonds to metal ions. In general (see Table 2), the greater the basicity the lower the frequency of the V=O vibration. The outstanding exceptions are the 3,5-dimethyl- and 4-methylpyridine adducts. The explanation of this behaviour may be due to the existence of resonance forms to the complex with 4-methylpyridine and to the steric effects to the complex with 3,5-dimethylpyridine as has been reported previously.[5–7]

The IR spectra of the adducts exhhibit a band at 330–350 cm^{-1}, which is assigned to the stretching vibration of the V—N(base)[8] bond. The frequencies of this band listed in decreasing order are:

$$VO(ox)_2(4AP) > VO(ox)_2(3AP) > VO(ox)_2(3MP) > VO(ox)_2(Py),$$
$$VO(ox)_2(4MP) > VO(ox)_2(3,5DMP).$$

These differences can be attributed to the electronic donation of the pyridine or substituted pyridine to the vanadium (N → V) which increases the electron density on the metal *d*-orbitals and consequently the $p_\pi \rightarrow d_\pi$ donation from the oxygen atom to vanadium is expected to be reduced to an extent which depends upon the donor ability of the base. As a result there will be a lowering of the V=O bond [hence ν(V=O)] and a greater frequency of the V—N bond.

The IR spectra of all the compounds obtained in this work show two bands at 550–573 and 365–379 cm^{-1}, which are assigned to the antisymmetrical and symmetrical vibration, respectively, of the stretching V—O ligand. Both bands are displaced to greater frequencies in the adducts than in the complex $VO(ox)_2$ (see Table 2).[8]

All the compounds exhibit a very strong band in the 1100-cm^{-1} region and another band of lower intensity in the 350-cm^{-1} region. We attribute the first band to C—O—V vibration and this indicates the formation of a vanadium chelate, while the second band corresponds to the stretching of the V—N bond as also happens in other complexes that were studied previously. These bands appear at higher frequencies in the adducts than in the complex $VO(ox)_2$.[9,10]

The electronic spectra of the compounds obtained here is in accordance with the Ballhausen–Gray scheme for a square pyramidal structure for the complex and a distorted octahedral structure for the adducts.[11]

The electronic spectra of the compounds obtained here exhibit three bands in the visible zone at 13,793–13,986, 18,018–19,379 and 20,242–21,276 cm^{-1}. The first band can be attributed to a $^2B_2 \rightarrow {}^2E(I)$ transition and it is displaced to lower frequencies in the adducts. This displacement is greater for lower values of the pK_b value of the pyridine or substituted pyridine, which is indicative that the $^2B_2 \rightarrow {}^2E(I)$ transition is very sensitive to the electronic donation V → O (see Table 3).

The second band can be assigned to a $^2B_2 \rightarrow {}^2B_1$ transition. This band shows the greater or lesser bonding force from the vanadium to the ligands. Therefore the band is displaced to higher frequencies in the adducts, because the introduction of the base in the six-coordination position and the "*trans*" effect strengthen the

8-quinolinol–vanadium σ-bond, as we have observed in the IR spectra.

The last band (20,242–21,276 cm^{-1}) corresponds to a ligand-to-metal charge transfer and generally is displaced to higher frequencies in the adducts.

In the UV region one observed an intense band between 37,037 and 38,314 cm^{-1}, which is attributed to an intraligand transition.

REFERENCES

1. R. J. Henry, P. C. Mitchell and J. E. Prue, *Inorg. Chim. Acta* 1973, **7**, 125.
2. L. G. Gouy, *C. R. Hebd. Seanc., Paris* 1889, **109**, 935.
3. N. F. Curtis, *J. Chem. Soc.* 1961, **3**, 147.
4. P. W. Selwood, *Magnetochemistry*, p. 78. Interscience, New York (1956).
5. R. Lozano, J. Martínez, A. Martínez and A. Doadrio, *Polyhedron* 1983, **3**, 977.
6. J. Martínez, R. Lozano, A. Martínez and A. Doadrio, *An. Quim.* 1983, **79B**, 486.
7. J. Martínez, R. Lozano, A. Martínez and A. Doadrio, *An. Quim.* 1984, **80**, 271.
8. A. Doadrio and J. Martínez, *An. Quim.* 1970, **4**, 325.
9. R. Lozano, A. Doadrio and A. L. Doadrio, *Polyhedron* 1982, **1**, 163.
10. R. Lozano, J. Román, E. Alarcón, A. L. Doadrio and A. Doadrio, *Rev. Chim. Miner.* 1983, **20**, 173.
11. C. J. Ballhausen and H. B. Gray, *Molecular Orbital Theory*. Benjamin, New York (1965).

Polyhedron Vol. 5, No. 8, pp. 1345–1350, 1986
Printed in Great Britain

0277–5387/86 $3.00+.00
Pergamon Journals Ltd

KINETICS AND MECHANISM OF SUBSTITUTION REACTION WITH ETHYLENEDIAMINE OF COORDINATED GLYCINATE LIGAND IN BIS(ETHYLENEDIAMINE)GLYCINATOCOBALT(III) COMPLEX

MASAHIKO ISHIKAWA, KEN-ICHI OKAMOTO and JINSAI HIDAKA

Department of Chemistry, University of Tsukuba, Niihari, Ibaraki 305, Japan

and

HISAHIKO EINAGA*

Institute of Materials Science, University of Tsukuba, Niihari, Ibaraki 305, Japan

(*Received* 28 *August* 1985; *accepted after revision* 18 *November* 1985)

Abstract—The substitution reaction with ethylenediamine of the coordinated glycinate ligand of bis(ethylenediamine)glycinatocobalt(III) complex has been studied at 60–70°C in a weakly alkaline aqueous solution (buffered around pH 12) of 1.0 mol dm^{-3} chloride concentration. The reaction was studied under the pseudo-first-order kinetic condition with respect to ethylenediamine and followed by means of electronic absorption spectra for the racemate and by circular dichroism spectra for the optically active isomers. The reaction proceeds stepwise with three rate-determining steps: the first step is dependent neither on ethylenediamine nor on hydroxide ion concentration but is accompanied by loss of optical activity, while the second one is dependent both on ethylenediamine and on hydroxide ion concentrations. Mechanisms of the ligand substitution reaction are discussed.

Elucidation of the substitution reaction mechanism of a coordinated multidentate ligand in a chelated cobalt(III) complex of octahedral or pseudo-octahedral coordination with another multidentate ligand is of fundamental importance, not only in stereochemistry but also in synthetic chemistry of the substitution-inert metal complexes. There have been vast numbers of studies concerning kinetics and mechanisms of the cobalt(III) complexes; however these studies are largely centered around aquation, acid or base hydrolysis, anation etc.[1] It has been reported[2] that the ligand substitution reaction with ethylenediamine of the carbonatobis(ethylenediamine)cobalt(III) complex $\{[Co(CO_3)(en)_2]^+$ (en = ethylenediamine)$\}$ proceeds with two successive rate-determining steps, where the first rate-determining step corresponds to the parallel aquation and base-catalyzed hydrolysis pathways and accompanies loss of optical activity and the second one corresponds to the ethylenediamine coordination pathway. In order to get further information on this sort of ligand substitution reaction, we investigated the substitution with ethylenediamine of coordinated glycinate ligand in the racemate and the optically active isomers of the bis(ethylenediamine)glycinatocobalt(III) complex $\{[Co(gly)(en)_2]^{2+}$ (gly = glycinate)$\}$ at 60–70°C in weakly alkaline aqueous solution (buffered around pH 12) of 1.0 mol dm^{-3} chloride concentration.

* Author to whom correspondence should be addressed.

EXPERIMENTAL

$[Co(gly)(en)_2]Cl_2$ was prepared from *trans*-$[CoCl_2(en)_2]Cl$ and glycine.[3,4] Its optical resolution was carried out by using $K_2[Sb_2(d\text{-}(+)\text{-tart})_2]\cdot H_2O$ (tart = tartrate) according to the literature procedure.[4] The complex and its optically active isomers were characterized by elemental analysis and electronic absorption and circular dichroism (CD) spectra. Ethylenediamine of analytical reagent grade was used. All the other reagents used were also of analytical grade.

The absorption and CD spectra were recorded

on JASCO spectrophotometers, models UVIDEC-1 and 610 C, and on JASCO spectropolarimeters, models J-20 and 500 C, respectively. The pH of the solution was measured with a Horiba glass electrode pH meter, model F7-SS. The pH meter reading was converted to the hydroxide ion concentration by defining $-\log [OH^-]$ of a solution containing 0.0100 mol dm^{-3} sodium hydroxide and 0.9900 mol dm^{-3} sodium chloride to be 2.00.

Kinetic runs were made in a weakly alkaline aqueous solution of 1.0 mol dm^{-3} chloride concentration under the pseudo-first-order reaction condition with respect to ethylenediamine (at a temperature between 60 and 70°C) by following absorbance changes with time (at 515 nm) for the racemate and CD intensity changes with time (at 510 nm) for the optically active isomers. The sample solution was highly buffered for $[OH^-]$ owing to the large concentration of ethylenediamine; no other buffer systems were necessary for its control. The temperature was regulated at a specified value within ±0.1°C. The observed rate constant, k_{obsd}, was calculated from the net absorbance and from CD intensity changes with time—as will be described in the following section.

RESULTS

The ligand substitution reaction of $[Co(gly)(en)_2]^{2+}$ with ethylenediamine does not proceed noticeably at room temperature (25°C) but does proceed at an elevated temperature of 60–70°C. A typical example of absorbance change at a fixed wavelength with time of the reaction system at 70°C is shown in Fig. 1. The absorbance vs time plots consist of three exponential parts. Absorption spectral measurements of the reaction system in the *d–d* transition $[^1T_{1g}(O_h) \leftarrow {}^1A_{1g}(O_h)]$ region on the time course revealed that the starting complex with an absorption maximum at 487 nm changed successively—via two intermediate states—to the final complex with an absorption maximum at 469 nm, which corresponds to $[Co(en)_3]^{3+}$. Liquid column chromatography on the reaction product with a column of SP Sephadex C-25 (Na^+ form) and elution with 0.1–0.5 mol dm^{-3} aqueous sodium chloride solution (programmed concentration) showed quantitative formation of $[Co(en)_3]^{3+}$. Hence, it is concluded that the ligand substitution reaction proceeds through three rate-determining steps to give $[Co(en)_3]^{3+}$.

The rate equation of the consecutive system $S \xrightarrow{k_1} I_1 \xrightarrow{k_2} I_2 \xrightarrow{k_3} P$ can be given as follows:

$$A_t = B_1 \exp(-k_1 t) + B_2 \exp(-k_2 t) + B_3 \exp(-k_3 t) + A_\infty,$$

$$B_1 \equiv [S]_0\{\varepsilon_S(k_2-k_1)+\varepsilon_{I_1}k_1-\varepsilon_P k_2\}/(k_2-k_1), \quad (1)$$

$$B_2 \equiv [S]_0\{\varepsilon_{I_1}k_1(k_2-k_3)-\varepsilon_{I_2}k_1k_2+\varepsilon_P k_1k_3\}/(k_3-k_2)(k_2-k_1),$$

$$B_3 \equiv [S]_0\{(\varepsilon_{I_2}-\varepsilon_P)k_1k_2\}/(k_3-k_2)(k_2-k_1).$$

Here, k_1, k_2 and k_3 are the rate constants for the first, the second and the third rate-determining steps; S, I_1, I_2 and P are the starting, the first and second intermediate and the final complexes; $[S]_0$ is the initial concentration of the starting complex; ε_S, ε_{I_1}, ε_{I_2} and ε_P are the molar absorption coefficients of S, I_1, I_2 and P; and A_t and A_∞ are the absorbances at the fixed wavelength at time t and at equilibrium, respectively. When the magnitudes of these rate constants differ sufficiently to give three linear portions in the logarithmic net absorbance changes vs time plots, these rate constants can be estimated

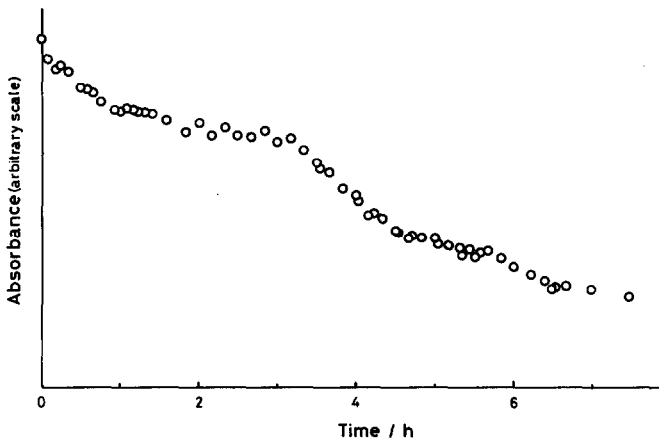


Fig. 1. Absorbance change with time of $[Co(gly)(en)_2]^{2+}$. $[[Co(gly)(en)_2]^{2+}] = 1.00 \times 10^{-2}$ mol dm^{-3}. [en] = 2.00 mol dm^{-3}. $[OH^-] = 1.58 \times 10^{-2}$ mol dm^{-3} (buffered). $[Cl^-] = 1.0$ mol dm^{-3}. 70°C. Wavelength = 515 nm.

from the slope of the corresponding linear portions and refined by simulation of the experimental absorbance vs time plots by using the estimated rate constants. In the $[Co(gly)(en)_2]^{2+}$ complex, k_3 was considerably smaller than k_2 with small net absorbance changes and much scattered experimental data on the plots; this is because fluctuations in the preceding two kinetic processes were superimposed directly on the third kinetic process. Hence, no reliable estimation of k_3 was possible; but it may not exceed the order of 10^{-7} s^{-1} based on the simulation. The constant k_2 was calculated from the linear portion of $\ln\{A_t - B_3\exp(-k_3t) - A_\infty\}$ vs t plots by assuming the contribution of the second term in the logarithm to be constant and small and by estimating B_3 from the absorbance change after the second kinetic step and A_∞ from the molar absorption coefficient of $[Co(en)_3]^{3+}$. The validity of this treatment was checked by determining k_2 from the Guggenheim plots[5] on a $\ln\{A_t - A_\infty\}$ vs t curve. The constant k_1 can be determined in the same way as k_2 from the linear portion of $\ln\{A_t - B_2\exp(-k_2t) - B_3\exp(-k_3t) - A_\infty\}$ vs t plots by assuming that the contribution of the second and the third terms in the logarithm to be constant and by estimating B_2 from the absorbance change during the second kinetic step. The values thus obtained were less reliable than k_2 because the time interval giving linearity was rather narrow as compared with the second rate-determining step, where linearity was found for more than two half-lives. Therefore, the magnitude of k_1 was calculated to only one significant figure.

Figures 2 and 3 show the hydroxide ion and ethylenediamine concentration dependencies on the observed rate constant in the second rate-determining step, k^2_{obsd}. The first step (k^1_{obsd}) was dependent neither on the hydroxide ion nor on the ethylenediamine concentration. It should be emphasized that the second step depends both on the hydroxide ion and on the ethylenediamine concentration. Hence, the following relations can be deduced from Figs 2 and 3:

$$k^1_{obsd} = k^1_{H_2O},$$
$$k^2_{obsd} = (k^2_{en} + k^2_{OH,en}[OH^-])[en]. \quad (2)$$

Here, $k^1_{H_2O}$, k^2_{en} and $k^2_{OH,en}$ denote the rate constants for the aquation, the ethylenediamine coordination and the hydroxide-assisted ethylenediamine coordination pathways, respectively.

These spectrochemical and kinetic results indicate that, in the first step, $[Co(gly)(en)_2]^{2+}$ undergoes the aquation uniquely to give the first intermediate species having a unidentate glycinate ligand, and that the first intermediate species then—in the second step—undergoes ligand substitution by ethylenediamine and hydroxide-assisted ethylenediamine coordination in a parallel way to give the second intermediate species. This then changes in the third step to give $[Co(en)_3]^{3+}$ with liberation of the unidentate glycinate ligand followed by the ethylenediamine chelate ring closure. Kinetic par-

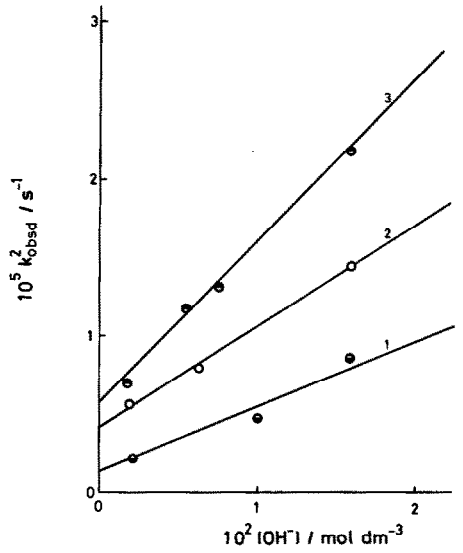


Fig. 2. Relation between k^2_{obsd} and $[OH^-]$. $[[Co(gly)(en)_2]^{2+}] = 1.00\times10^{-2}$ mol dm^{-3}. [en] = 2.00 mol dm^{-3}. $[Cl^-] = 1.0$ mol dm^{-3}. Temperature: 1, 60; 2, 65; and 3, 70°C. k^1_{obsd} was independent of $[OH^-]$.

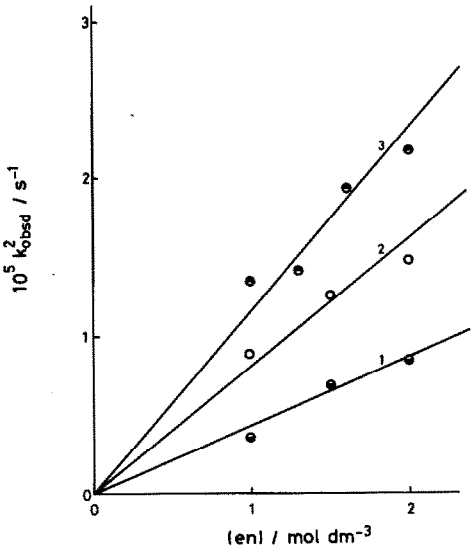


Fig. 3. Relation between k^2_{obsd} and [en]. $[[Co(gly)(en)_2]^{2+}] = 1.00\times10^{-2}$ mol dm^{-3}. $[OH^-] = 1.58\times10^{-3}$ mol dm^{-3} (buffered). $[Cl^-] = 1.0$ mol dm^{-3}. Temperature: 1, 60; 2, 65; and 3, 70°C. k^1_{obsd} was independent of [en].

Table 1. Kinetic parameters of ligand substitution reaction: $[Cl^-] = 1.0$ mol dm^{-3}, 65°C

	Electronic absorption spectral method			CD spectral method		
Pathway[a]	Rate constant	ΔH^* (kJ mol^{-1})	ΔS^* (J mol^{-1} K^{-1})	Rate constant	ΔH^* (kJ mol^{-1})	ΔS^* (J mol^{-1} K^{-1})
I	1×10^{-5}[b,c]	70	−140	$(3.54\pm0.26)\times10^{-5}$[b]	79.8±2.3	−95.2±13.6
				$(3.56\pm0.25)\times10^{-5}$[d]	—	—
				$(3.38\pm0.35)\times10^{-5}$[e]	—	—
IIa	$(2.08\pm0.16)\times10^{-6}$[f]	168±3	142±9			
IIb	$(3.35\pm0.25)\times10^{-4}$[g]	73.6±1.6	−94.9±9.5			

[a] I, aquation; IIa, ethylenediamine coordination; and IIb, hydroxide-assisted ethylenediamine coordination.
[b] $k^1_{H_2O}$ (s^{-1}).
[c] CD spectral data are much more reliable than absorption spectral data (consult the text).
[d] Λ-(+)$_{589}$-[Co(gly)(en)$_2$]$^{2+}$.
[e] Δ-(−)$_{589}$-[Co(gly)(en)$_2$]$^{2+}$.
[f] k^2_{en} (mol^{-1} dm^3 s^{-1}).
[g] $k^2_{OH,en}$ (mol^{-2} dm^6 s^{-1}).

ameters of these reaction pathways are summarized in Table 1.

The kinetic study was made on the optically active isomer, Λ-(+)$_{589}$-[Co(gly)(en)$_2$]$^{2+}$,[4] under otherwise the same experimental conditions as those adopted for the racemate. Figure 4 shows CD spectral change with time of the Λ-(+)$_{589}$ isomer in the *d–d* transition region. The CD intensity decreased with time without any changes in the spectral pattern. The CD spectral changes with time of the Δ-(−)$_{589}$ isomer were antipodal to those of the Λ-(+)$_{589}$ isomer. The half-life of this stereochemical step was of the same magnitude as that of the first rate-determining step of the racemate. These CD spectral features imply that the first rate-determining step in the reaction of [Co(gly)(en)$_2$]$^{2+}$ with ethylenediamine accompanies the racemization into the first intermediate species.

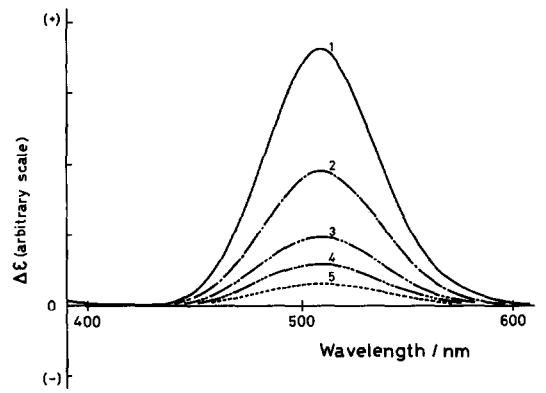


Fig. 4. CD spectral change with time of Λ-(+)$_{589}$-[Co(gly)(en)$_2$]$^{2+}$. $[[Co(gly)(en)_2]^{2+}] = 1.00\times10^{-2}$ mol dm^{-3}. [en] = 2.00 mol dm^{-3}. $[OH^-] = 1.58\times10^{-2}$ mol dm^{-3}. $[Cl^-] = 1.0$ mol dm^{-3}. 70°C. Time: 1, 0; 2, 120; 3, 240; 4, 360; and 5, 480 min.

In the case where the starting optically active isomer, $S_{\Lambda(or\Delta)}$, changes to enantiomers of the first intermediate complex, $I_{1\Lambda}$ and $I_{1\Delta}$, $S_{\Lambda(or\Delta)} \xrightarrow{k_{1\Lambda(or\Delta)}} I_{1\Lambda} + I_{1\Delta}$ the rate equation can be given in logarithmic form as follows:

$$\ln\{(\Delta\varepsilon_0-\Delta\varepsilon_\infty)/(\Delta\varepsilon_t-\Delta\varepsilon_\infty)\} = k_{1\Lambda(or\Delta)}t. \quad (3)$$

Here, $k_{1\Lambda(or\Delta)}$ is the rate constant of the starting Λ (or Δ) isomer and $\Delta\varepsilon_0$, $\Delta\varepsilon_t$ and $\Delta\varepsilon_\infty$ are total CD intensities in the initial state, at time t and at equilibrium, respectively. A linear relation was obtained on the $-\ln(\Delta\varepsilon_t-\Delta\varepsilon_\infty)$ vs t plots, from which the observed rate constant, $k^1_{obsd,\Lambda}$, was estimated for the Λ-(+)$_{589}$ isomer.

It was found that, in the concentration range $(0.20\text{–}1.58)\times10^{-2}$ mol dm^{-3} for the hydroxide ion and 1.00–2.00 mol dm^{-3} for the ethylenediamine concentration, $k^1_{obsd,\Lambda}$, was dependent on neither of them and it was the same magnitude as $k^1_{H_2O}$ for the racemate

$$k^1_{obsd,\Lambda} = k^1_{H_2O,\Lambda}. \quad (4)$$

Hence, it is concluded that the stereochemical change is accompanied solely in the aquation pathway. Kinetic parameters of the reaction pathway is given in Table 1.

DISCUSSION

The ligand substitution reaction of [Co(gly)(en)$_2$]$^{2+}$ with ethylenediamine proceeds with three rate-determining steps. This evidence rules

out a ligand substitution reaction mechanism in which the coordinated glycinate ligand dissociates from the starting complex to form an intermediate complex species such as di(aqua or hydroxo)bis(ethylenediamine)cobalt(III) or a related complex followed by coordination of ethylenediamine because this mechanism necessitates two rate-determining steps.

Presence of the third rate-determining step implies that slow liberation of unidentately coordinated ligand before the rapid ethylenediamine chelate ring closure[2] is expected as a mechanistic rate-determining step; the ligand may be glycinate coordinated through the oxygen donor atom (*vide infra*).

The reaction mechanism with three rate-determining steps can be modelled either by $S \underset{k_{-1}}{\overset{k_1}{\rightleftharpoons}} I_1 \underset{k_{-1}}{\overset{k_2}{\rightleftharpoons}} I_2 \xrightarrow{k_3} P$ or by $S \xrightarrow{k_1} I_1 \xrightarrow{k_2} I_2 \xrightarrow{k_3} P$, where the ks are the rate constants for the corresponding kinetic steps. Of these two model expressions, the former was rejected because we could not obtain any absorption and CD spectral evidence supporting backward processes ($I_2 \rightarrow I_1$ and $I_1 \rightarrow S$) and because no attempts to determine equilibrium constants for the processes $S \rightleftharpoons I_1$ and $I_1 \rightleftharpoons I_2$ were successful for the substitution-inert cobalt(III) complex species in the present system. Hence, the latter was adopted for the analysis of experimental data.

The first rate-determining step, which depends neither on the hydroxide ion nor on the ethylenediamine concentration and which accompanies the loss of optical activity when the optically active isomer is used as the starting complex, corresponds to the aquation with dissociative chelate ring opening[2] of the coordinated glycinate ligand. The first intermediate complex species thus formed is expected to have a glycinate ligand coordinated through the *O* donor atom and an aqua ligand *cis* to each other. This configuration occurs because glycinate tends to coordinate more easily through the *O* than through the *N* donor atom[6]* and because the intermediate species gave no splitting pattern in the first *d–d* transition band [$^1T_{1g}(O_h) \leftarrow {}^1A_{1g}(O_h)$].[7] Among three possible geometrical configurations[2] in the glycinate ring-opened, five-coordinate, transitional species are: a square planar configuration with a $(N)_3(O)$ basal plane (**I**); a trigonal bipyramidal configuration with a $(N)_3$ trigonal basal plane (**II**); and a trigonal bipyramidal one with a $(N)_2(O)$ basal plane (**III**); the species **II** is expected for the present kinetic step because the starting optically active isomer changes into racemic first intermediate complex species. Species **I** requires complete configurational retention and **III** configurational retention and conversion to *trans*-(O) isomer; hence, optical activity after the first kinetic step is anticipated for these two species. The first intermediate monoaqua complex with unidentate glycinate ligand may be subjected—before the second kinetic step—to rapid deprotonation of the coordinated water molecule in a weakly alkaline solution to give *cis*-(*O*)-[Co(gly-*O*)(OH)$(en)_2]^+$ (racemates in the case of the optically active isomer as the starting complex), where gly-*O* denotes glycinate ligand coordinated through the *O* donor atom.

The second rate-determining step corresponds to reaction of *cis*-(*O*)-[Co(gly-*O*)(OH)$(en)_2]^+$ with ethylenediamine because k^2_{obsd} is directly proportional to the ethylenediamine concentration with zero intercept (cf. Fig. 3). This step proceeds via two parallel pathways: one is independent of and the other is dependent on the hydroxide ion concentration (cf. Fig. 2). The second intermediate complex may be of a form of *cis*-(*O*,*N*)-[Co(gly-*O*)(en-*N*)$(en)_2]^{2+}$ with two unidentate ligands at the *cis* position each other, where en-*N* denotes ethylenediamine ligand unidentately coordinated. A large positive value of the activation entropy in the ethylenediamine coordination pathway of $[Co(gly)(en)_2]^{2+}$, which can be compared with that of the related pathway in the reaction of $[Co(CO_3)(en)_2]^+$,[2] implies that the mechanistic ligand substitution reaction process of the former is intrinsically analogous to that of the latter. The hydroxide-assisted ethylenediamine coordination pathway can be explained as follows; deprotonation of amino group of bidentately coordinated ethylenediamine *trans* to the hydroxide ligand in *cis*-(*O*)-[Co(gly-*O*)(OH)$(en)_2]^+$ takes place rapidly to give *cis*-(*O*)-[Co(gly-*O*)(OH)(en(−H))(en)]$^+$, where en(−H) denotes ethylenediamine in the conjugate base form, then the ligand substitution of coordinated hydroxide ligand with ethylenediamine takes place as a mechanistic rate-determining step to give *cis*-(*O*,*N*)-[Co(gly-*O*)(en-*N*)(en(−H))(en)]$^+$, to which protonation occurs rapidly to give *cis*-(*O*,*N*)-[Co(gly-*O*)(en-*N*)$(en)_2]^{2+}$.

On the basis of the discussion given above, the second rate-determining step can be expressed as eqn (5):

$$k^2_{obsd} = \{k^2_{en} + k^{2\prime}_{OH,en}(K_a/K_w)[OH^-]\}[en]/\{1+(K_a/K_w)[OH^-]\}, \quad (5)$$

* Boreham *et al.*[10] reported on base hydrolysis of *cis*-$[CoX(gly\text{-}N)(en)_2]^+$ (X = Cl and Br) to form *cis*-[Co(gly-*N*)(OH)$(en)_2]^+$ with glycinate coordinated through the *N* donor atom (gly-*N*), but the starting complex was prepared specifically from *cis*-$[CoX(gly\text{-}CH_3)(en)_2]^{2+}$,[11,12] where gly-$CH_3$ denotes methyl ester of glycine.

where K_a and K_w are the deprotonation constant of coordinated ethylenediamine to its conjugate base and the ionic product of water, respectively, and $k^{2'}_{OH,en}$ is the rate constant for the hydroxide-assisted ethylenediamine coordination pathway in its intrinsic sense. Figures 2 and 3 indicate that $(K_a/K_w)[OH^-]$ does not contribute to the denominator in eqn (5); and eqn (6) holds for the present second rate-determining step:

$$k^2_{obsd} \doteqdot \{k^2_{en} + k^{2'}_{OH,en}(K_a/K_w)[OH^-]\}[en]. \quad (6)$$

$k^2_{OH,en}$ in Table 1 may be a composite constant in which K_a and K_w are incorporated. If the tentative assumption is made that $(K_a/K_w)[OH^-] \leqslant 0.1$, then $k^{2'}_{OH,en}$ should be larger than 10^{-5} mol^{-1} dm^3 s^{-1} and K_a should not exceed 10^{-12} because K_w is of the order of 10^{-13} at 65°C[9] and $[OH^-]$ is of the order of 10^{-2} mol dm^{-3} under the experimental conditions. This estimated K_a is very small; it implies high basicity of the conjugate base because deprotonation constant of coordinated water molecule has been reported to be *ca* 10^{-8} at 25°C {*cis*-(*O*)-$[Co(OH)(H_2O)(en)_2]^{2+}$}.[10]

We could not estimate the rate constant for the third rate-determining step owing to large experimental errors accumulated from the previous two kinetic steps. However, we can safely state {from the results of $[Co(CO_3)(en)_2]^+$}[2] that the third rate-determining step corresponds to liberation of the unidentately coordinated glycinate ligand as a mechanistic rate-determining step followed by rapid chelate ring closure to give $[Co(en)_3]^{3+}$.

In conclusion, the ligand substitution reaction of $[Co(gly)(en)_2]^{2+}$ with ethylenediamine proceeds according to the following mechanism: $[Co(gly)(en)_2]^{2+}$ becomes in the first kinetic step with stereochemical structural change followed by rapid deprotonation in alkaline medium to the first intermediate *cis*-(*O*)-$[Co(gly\text{-}O)(OH)(en)_2]^+$ complex, which then reacts in the second kinetic step by hydroxide-dependent and independent parallel pathways to give the second intermediate *cis*-(*O*,*N*)-$[Co(gly\text{-}O)(en\text{-}N)(en)_2]^{2+}$ complex. This second intermediate complex finally changes in the third kinetic step to the $[Co(en)_3]^{3+}$ complex with liberation of the unidentately coordinated glycinate ligand followed by ethylenediamine chelate ring closure.

REFERENCES

1. For example: F. Basolo and R. G. Pearson, *Mechanisms of Inorganic Reactions*, 2nd edn, Chaps 3 and 4. Wiley, New York (1967). R. G. Wilkins, *The Study of Kinetics and Mechanism of Reactions of Transition Metal Complexes*, Chaps 4 and 8. Allyn & Bacon, Boston (1974).
2. H. Fushimi, K. Okamoto, J. Hidaka and H. Einaga, *Inorg. Chim. Acta* 1985, **98**, 47.
3. J. Meisenheimer, *Ann.* 1924, **438**, 217.
4. C. T. Liu and B. E. Douglas, *Inorg. Chem.* 1964, **3**, 1356. Absolute configurations of the complexes are designated by the IUPAC tentative rule, *Inorg. Chem.* 1970, **9**, 1.
5. E. A. Guggenheim, *Philos. Mag.* 1926, **2**, 538.
6. J. Fujita, T. Yasui and Y. Shimura, *Bull. Chem. Soc. Jpn* 1965, **38**, 654.
7. H. Yamatera, *Bull. Chem. Soc. Jpn* 1958, **31**, 95.
8. This magnitude was estimated from data in the monographs, G. Schwarzenbach, L. G. Sillén and A. E. Martell, *Stability Constants of Metal–Ion Complexes*, Special Publication No. 17 (1964) and No. 25 (1971). Chemical Society, London.
9. J. Bjerrum and S. E. Rasmussen, *Acta Chem. Scand.* 1952, **6**, 1265.
10. C. J. Boreham, D. A. Buckingham and C. R. Clark, *Inorg. Chem.* 1979, **18**, 1990.
11. R. T. M. Fraser, *Inorg. Chem.* 1964, **3**, 1561.
12. M. D. Alexander and D. H. Busch, *Inorg. Chem.* 1966, **5**, 602.

Polyhedron Vol. 5, No. 8, pp. 1351–1355, 1986
Printed in Great Britain

0277–5387/86 $3.00+.00
Pergamon Journals Ltd

A PROTON MAGNETIC RESONANCE STUDY OF LIGAND EXCHANGE ON HEXAKIS(1,1,3,3-TETRAMETHYLUREA)THULIUM(III)

STEPHEN F. LINCOLN* and ALEX WHITE

Department of Physical and Inorganic Chemistry, University of Adelaide, South Australia 5001, Australia

(*Received* 9 *October* 1985; *accepted* 25 *November* 1985)

Abstract—A ^1H NMR study of the rate of exchange of 1,1,3,3-tetramethylurea (tmu) on $[Tm(tmu)_6]^{3+}$ is found to be independent of [tmu] over a five-fold variation in CD_3CN solution, and to be characterized by $k(298.2\ K) = 145 \pm 1\ s^{-1}$, $\Delta H^{\#} = 29.3 \pm 0.3\ kJ\ mol^{-1}$, and $\Delta S^{\#} = 105 \pm 1\ J\ K^{-1}\ mol^{-1}$. These data are discussed in conjunction with data from related lanthanide and pseudo-lanthanide systems and the mechanistic implications are considered.

The trivalent lanthanide $[Ln(solvent)_n]^{3+}$ species are characterized by $n = 9$ for water,[1] $n = 8$ for dimethylformamide (dmf),[2,3] and $n = 6$ for trimethylphosphate (tmp)[3] and 1,1,3,3-tetramethylurea (tmu).[4,5] This decrease in coordination number also appears to be characterized by a decrease in the lability of $[Ln(solvent)_n]^{3+}$ towards solvent exchange as exemplified by $[Gd(OH_2)_9]^{3+}$ and $[Lu(tmu)_6]^{3+}$ for which the exchange rate constants [k(298.2 K)] for one solvent molecule $= 1.06 \times 10^9$ and 41.9 s^{-1}, respectively.[4,6] Such variations indicate the opportunity offered by the trivalent lanthanides for the study of the factors controlling the lability and mechanism of ligand substitution processes on metal ions in the absence of significant ligand field and directional bonding effects.[7] However, at present there are no reported studies of solvent exchange or ligand substitution on a given trivalent lanthanide exhibiting different coordination numbers. Accordingly we have undertaken a study of tmu exchange on six-coordinate $[Tm(tmu)_6]^{3+}$ in order to make a comparison of the lability of this species with that of eight-coordinate $[Tm(dmf)_8]^{3+}$ and other lanthanide and pseudo-lanthanide (Sc^{3+} and Y^{3+}) species.

EXPERIMENTAL

Materials

$[Tm(tmu)_6](ClO_4)_3$ was prepared by literature methods.[8,9] Found: C, 30.7; H, 6.3; N, 14.7; Tm, 14.5%. Calc. for $[Tm(tmu)_6](ClO_4)_3$: C, 30.9; H, 6.2; N, 14.4; Tm, 14.5%. Tm(III) was determined as a trivalent cation using an ion-exchange technique,[10] and other elemental analyses were carried out by the Australian Microanalytical Service, Melbourne. (*Caution—perchlorate salts of metal complexes may be explosive under some conditions and should be handled with care. No explosion hazard was encountered during the course of this study.*) The IR spectrum of the complex in a Nujol mull exhibited no absorptions attributable to coordinated perchlorate or the presence of trace amounts of water. Hydrated thulium perchlorate was obtained through the reaction of Tm(III) oxide (Spex) with the stoichiometric amount of concentrated perchloric acid. Tmu (Fluka) and CD_3CN (99% deuterated, Aldrich) were distilled and stored over Linde 4A molecular sieves prior to use. Solutions of $[Tm(tmu)_6](ClO_4)_3$ and tmu in CD_3CN were prepared in a dry nitrogen flushed glove box, and were sealed *in vacuo* in 5-mm NMR tubes.

NMR spectroscopy

Variable-temperature 90-MHz ^1H NMR studies were carried out on a Bruker HX-90E spectrometer.

* Author to whom correspondence should be addressed.

Depending on the concentration and temperature of the sample up to 1200 transients were collected and stored as 8192 datum point blocks prior to Fourier transformation and lineshape analysis[11] on a Nicolet BNC-12 computer. Probe temperature control was ±0.03 K and the Bruker B-VT 1000 temperature controller was calibrated with a copper–constantan thermocouple.

RESULTS AND DISCUSSION

Stoichiometry of the complex in solution

The compositions of the four solutions studied are shown in Table 1. In the temperature range 235–260 K well-resolved singlet ^1H resonances were observed for coordinated and free (upfield) tmu, and comparisons of the integrated resonance areas showed that Tm(III) retains a coordination number of 6.0 ± 0.1 in solution consistent with $[Tm(tmu)_6]^{3+}$ being the greatly predominant Tm(III) species in solution. (Under the conditions of this study rotation about the C—N bonds in both coordinated and free tmu is rapid on the NMR time scale and in consequence singlet resonances are observed.[12]) Similar observations have been made for $[Lu(tmu)_6]^{3+}$ and $[Y(tmu)_6]^{3+}$ in CD_3CN solution, which indicates that CD_3CN does not compete significantly with tmu for coordination sites, and that the larger size of tmu restricts the coordination number of these metal ions to 6 in contrast to the smaller H_2O and dmf molecules, which allow coordination numbers of 9 and 8, respectively, to be attained.[1-3,7]

NMR kinetic measurements

The ^1H singlets arising from coordinated and free tmu coalesce to an environmentally averaged singlet as the temperature is increased and tmu exchange between these two environments becomes increasingly rapid (Fig. 1). The mean site lifetime of a single coordinated tmu, τ, is readily derived through lineshape analysis,[11] and some examples of the calculated lineshapes and the corresponding τ values are shown in Fig. 1. For each of the four solutions

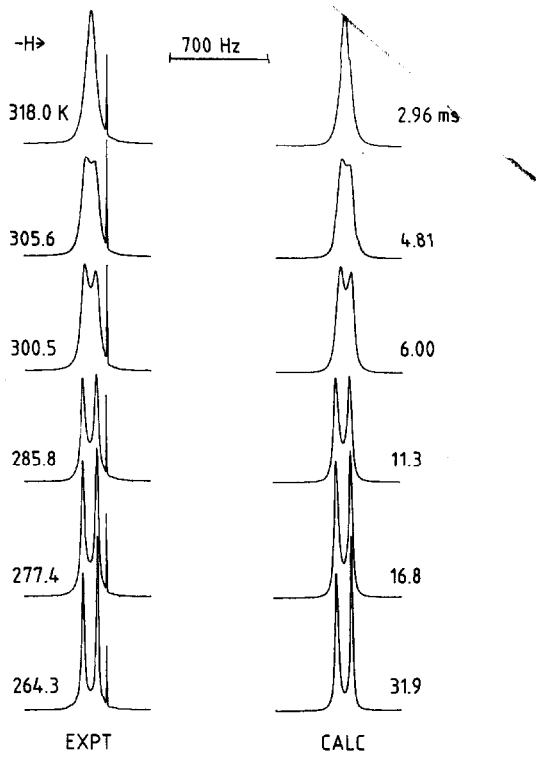


Fig. 1. ^1H NMR (90-MHz) spectra of a CD_3CN solution of $[Tm(tmu)_6](ClO_4)_3$ (0.09220 mol dm^{-3}) and tmu (0.5167 mol dm^{-3}). The downfield resonance arises from $[Tm(tmu)_6]^{3+}$. The experimental spectra and temperatures (K) are shown on the left, and the best-fit calculated lineshapes and τ (ms) values derived through complete lineshape analyses are shown on the right. The narrow multiplet appearing at high field arises from the CD_3CN proton impurity.

Table 1. Solution compositions and kinetic parameters for ligand exchange on hexakis(1,1,3,3-tetramethylurea)thulium(III)[a]

Solution	$[Tm(tmu)_6^{3+}]$ (mol dm^{-3})	[tmu] (mol dm^{-3})	k(298.2 K) (s^{-1})	$\Delta H^{\#}$ (kJ mol^{-1})	$\Delta S^{\#}$ (J K^{-1} mol^{-1})
1	0.1188	0.8675	141 ± 1	31.6 ± 0.3	−97.8 ± 1.1
2	0.09220	0.5167	153 ± 1	28.6 ± 0.2	−107 ± 1
3	0.06367	0.3568	147 ± 1	28.1 ± 0.4	−109 ± 1
4	0.03006	0.1753	141 ± 2	29.4 ± 0.5	−105 ± 2
1–4	—	—	145 ± 1	29.3 ± 0.3	−105 ± 1

[a] Quoted errors represent standard deviations obtained from a linear regression fit of the experimental data to the Eyring equation.

τ values were determined for at least 10 temperatures in the range 260–315 K. The relationship between τ and the rate of tmu exchange is given by eqn (1) in which k is the first-order exchange rate constant and all other symbols have their usual meaning.

$$1/\tau = k = \text{exchange rate}/6[\text{Tm(tmu)}_6^{3+}] = k_B T/h \exp(-\Delta H^{\#}/RT + \Delta S^{\#}/R). \quad (1)$$

The derived k, $\Delta H^{\#}$ and $\Delta S^{\#}$ values for the four solutions appear in Table 1 from which it is seen that they exhibit no significant variation over the approximately five-fold variation in [tmu]. This independence of k of [tmu] is consistent with the operation of either a dissociative (D) mechanism for tmu exchange in which the rate-determining step is the formation of the reactive five-coordinate intermediate $[Tm(tmu)_5]^{3+}$ as shown in eqn (2):

$$[Tm(tmu)_6]^{3+} \xrightarrow{k} [Tm(tmu)_5]^{3+} + tmu$$
$$[Tm(tmu)_5]^{3+} + *tmu \xrightarrow{\text{fast}} [Tm(tmu)_5(*tmu)]^{3+}. \quad (2)$$

Alternatively these observations are consistent with the operation of an interchange (I) mechanism [eqn (3)] in the limit in which all of the $[Tm(tmu)_6]^{3+}$ exists in the encounter complex form, $[Tm(tmu)_6]^{3+} \ldots tmu$, in which one tmu resides in the second coordination sphere, such that $k = k_i$.

$$[Tm(tmu)_6]^{3+} + *tmu \underset{\text{fast}}{\overset{K_0}{\rightleftharpoons}} [Tm(tmu)_6]^{3+} \ldots *tmu \quad (3)$$
$$[Tm(tmu)_6]^{3+} \ldots *tmu \xrightarrow{k_i} [Tm(tmu)_5(*tmu)]^{3+} \ldots tmu.$$

For the latter mechanism to operate the encounter complex would need to be characterized by an apparent stability constant (K_0) of ~ 100 dm^3 mol^{-1}, which is approximately 100 times greater than that determined for the formation of the $[Tb(dmf)_8]^{3+} \ldots$ dmf encounter complex in CD_3NO_2 solution[3] and also that calculated through the Fuoss equation.[13] (The concentration of CD_3CN ranges from 15.474 to 17.839 mol dm^{-3} in solutions 1–4 in Table 1, and hence on a statistical basis the expectation of finding one tmu in the second coordination sphere of $[Tm(tmu)_6]^{3+}$ ranges from 95 to 20% for solutions 1–4, assuming 15–20 solvent molecules in the second coordination sphere.) Hence it appears that tmu exchange on $[Tm(tmu)_6]^{3+}$ proceeds through a D-mechanism, but the further ramifications of this conclusion are considered later.

It is now appropriate to consider the 2×10^5-fold difference in lability between $[Tm(tmu)_6]^{3+}$ and $[Tm(dmf)_8]^{3+}$ (Table 2). Tmu and dmf are both oxygen donor ligands of similar electron-donating ability, as judged from their respective Gutmann donor numbers[14] of 29.6 and 26.6, and accordingly the greater lability of $[Tm(dmf)_8]^{3+}$ must be largely attributable to its higher coordination number. The coordination of eight oxygens to Tm(III) should result in greater steric crowding close to the metal centre and therefore longer and weaker Tm—O bonds in $[Tm(dmf)_8]^{3+}$ by comparison with those in $[Tm(tmu)_6]^{3+}$. (Evidence for an increase in bond length may be adduced from the observation that in the solid state Er—O bond distances in tricapped trigonal prismatic $[Er(OH_2)_9]^{3+}$ are 2.52 and 2.37 Å for the capping and prismatic waters, respectively,[15] which compare with Er—O distances of 2.25(2) and 2.185(9)–2.198(8) Å observed in octahedral $[Er(OH_2)_6]^{3+}$ and $[Er(tmu)_6]^{3+}$, respectively.[4,16]) Thus for a dissociatively (d) activated solvent exchange process it is anticipated that for similarly bonding ligands the lability of a given metal ion should increase with increase in coordination number as is seen here for $[Tm(tmu)_6]^{3+}$ and $[Tm(dmf)_8]^{3+}$, which is seemingly the first such observation for a single metal ion.

The data in Table 2 show that as the effective ionic radius[17] of M^{3+}, r, decreases from Sc^{3+} to Y^{3+} the following systematic variations occur in the parameters characterizing tmu exchange on $[M(tmu)_6]^{3+}$: k(298.2 K) increases, $\Delta H^{\#}$ decreases and $\Delta S^{\#}$ becomes more negative. (On the basis of the observed first-order rate law all four of these exchange processes are considered to proceed through a D-mechanism.[5,8,18] As a consequence of the smaller chemical shifts exhibited by the $[Y(tmu)_6]^{3+}$ and $[Lu(tmu)_6]^{3+}$ systems[8,5] it was possible to study the tmu exchange at 270 MHz and the consequently increased sensitivity permitted the establishment of the first-order exchange rate law over [tmu] ranges of 15.3 and 19.6, respectively, and at lower [tmu] values than was possible for $[Tm(tmu)_6]^{3+}$.) A major cause of the decrease in $\Delta H^{\#}$ is probably the increase in r and the consequent decrease in the electrostatic interaction between tmu and M^{3+}, and the resultant decrease in bond strength in the ground state. The large negative $\Delta S^{\#}$ values observed for $[Tm(tmu)_6]^{3+}$ and its Lu^{3+} and Y^{3+} analogues are unexpected for a d-activated exchange process unless there is a substantial contribution to $\Delta S^{\#}$ arising from interactions outside the first coordination sphere. In the case of these species such interactions seem particularly feasible. The tricapped trigonal prismatic structure[1] in which the three capping waters are up to 9% more distant from M^{3+} than the six prismatic waters is well established for the $[Y(OH_2)_9]^{3+}$ and

Table 2. Parameters for ligand exchange on some trivalent metal ions

M^{3+}	r^a (pm)	k(298.2 K) (s^{-1})	$\Delta H^{\#}$ (kJ mol^{-1})	$\Delta S^{\#}$ (J K^{-1} mol^{-1})	$\Delta V^{\#}$ (cm^3 mol^{-1})
			$[M(tmu)_6]^{3+}$ [b]		
Sc^{3+} [c]	74.5	0.90	68.6	−15.7	—
Lu^{3+} [d]	86.1	41.9	41.7	−74	—
Tm^{3+} [e]	88.0	145	29.3	−105	—
Y^{3+} [f]	90.0	253	27.1	−108	—
			$[M(dmf)_8]^{3+}$ [g]		
Tm^{3+} [h]	99.4	3.1×10^7	33.19	9.85	7.4
Tb^{3+} [h]	104.0	1.9×10^7	14.09	−58.25	5.2

[a] Six- and eight-coordinate radii from Ref. 17.
[b] In CD_3CN solution.
[c] Reference 18.
[d] Reference 5.
[e] This work.
[f] Reference 8.
[g] In CD_3NO_2 solution.
[h] Reference 3.

$[Ln(OH_2)_9]^{3+}$ species, and it is considered that these waters may rapidly interchange between the two types of coordination sites through a capped square antiprism intermediate in solution.[7] In view of this propensity of the trivalent lanthanides for high coordination numbers it seems probable that this may be reflected in the six-coordinate $[Ln(tmu)_6]^{3+}$ exchange mechanism. Taking the tricapped trigonal prism as the reference geometry it may be envisaged that as one Ln—tmu bond lengthens (and thereby assumes some of the character of a capping ligand) to form the dissociative transition state or intermediate, there will also be a change in the bond distances and angles of the remaining five tmu ligands towards a trigonal prismatic geometry simultaneously with the positioning of the incoming tmu to take up the incipient vacancy in the sixth prismatic position. The two remaining capping positions will be occupied by acetonitrile. Because of the bulkiness of tmu it is unlikely that acetonitrile in the two capping positions could approach the metal centre as closely as water in $[Ln(OH_2)_9]^{3+}$, and in consequence the interaction between these two acetonitriles and Tm(III) will be weak at best. Nevertheless such a mechanism would produce considerable ordering into the second coordination sphere and a substantial negative entropy contribution leading to a negative $\Delta S^{\#}$ whilst retaining the dissociative character of the tmu exchange process. This proposal is highly idealized but it does suggest that the mechanistic schemes which seem to work well for the lighter six-coordinate metal ions may need modification to incorporate a more active role of the second coordination sphere in the ligand exchange processes of six-coordinate trivalent lanthanides. In the case of the smaller Sc(III) ion there appears to be no reported case of a coordination number >6 observed in the presence of monodentate ligands, and it seems unlikely that the involvement of the second coordination sphere in the $[Sc(tmu)_6]^{3+}$ exchange process will be as significant as that for its heavier analogues in Table 2.

For dmf exchange on $[Ln(dmf)_8]^{3+}$ it has also been reported that $\Delta H^{\#}$ decreases and $\Delta S^{\#}$ changes from positive to negative as r increases (Table 2). The positive $\Delta V^{\#}$ values and the rate laws for dmf exchange are consistent with the operation of D and I_d dmf exchange mechanisms for $[Tm(dmf)_8]^{3+}$ and $[Tb(dmf)_8]^{3+}$, respectively, with the negative $\Delta S^{\#}$ for the latter species being largely attributed to the involvement of a ninth dmf in the transition state.[3]

REFERENCES

1. J. McB. Harrowfield, D. L. Kepert, J. M. Patrick and A. H. White, *Aust. J. Chem.* 1983, **36**, 483.
2. D. L. Pisaniello and A. E. Merbach, *Helv. Chem. Acta* 1982, **65**, 573.
3. D. L. Pisaniello, L. Helm, P. Meier and A. E. Merbach, *J. Am. Chem. Soc.* 1983, **105**, 4528.
4. L. A. Aslanov, V. M. Ionov and S. S. Sotman, *Kristallografiya* 1976, **21**, 1200.
5. S. F. Lincoln, A. M. Hounslow and A. J. Jones, *Aust. J. Chem.* 1982, **35**, 2393.
6. R. V. Southwood-Jones, W. L. Earl, K. E. Newman and A. E. Merbach, *J. Chem. Phys.* 1980, **73**, 5909.
7. S. F. Lincoln, In *Advances in Inorganic and Bioinor-*

ganic Mechanisms (Edited by A. G. Sykes), Vol. 4, p. 217. Academic Press, London (1986).
8. D. L. Pisaniello, S. F. Lincoln, E. H. Williams and A. J. Jones, *Aust. J. Chem.* 1981, **34**, 495.
9. P. W. N. M. van Leeuwen and W. L. Groeneveld, *Inorg. Nucl. Chem. Lett.* 1967, **3**, 145.
10. A. I. Vogel, *Quantitative Inorganic Analysis*, 3rd edn, p. 702. Longmans Green, London (1961).
11. S. F. Lincoln, *Prog. React. Kinet.* 1977, **9**, 1.
12. P. Stilbs and M. E. Moseley, *J. Magn. Reson.* 1978, **31**, 55.
13. (a) R. J. Fuoss, *J. Am. Chem. Soc.* 1958, **80**, 5059; (b) R. J. Fuoss, *J. Phys. Chem.* 1978, **82**, 2427.
14. V. Gutmann, In *Coordination Chemistry in Non-Aqueous Solvents*. Springer, Wien (1968).
15. D. R. Fitzwater and R. E. Rundle, *Z. Kristallogr. Kristallgeom. Kristallchem.* 1959, **112**, 362.
16. J. Glaser and G. Johansson, *Acta Chem. Scand.* 1981, **A35**, 639.
17. R. D. Shannon, *Acta Cryst.* 1976, **A32**, 751.
18. D. L. Pisaniello and S. F. Lincoln, *J. Chem. Soc., Dalton Trans.* 1980, 699.

Polyhedron Vol. 5, No. 8, pp. 1357–1361, 1986
Printed in Great Britain

0277–5387/86 $3.00+.00
Pergamon Journals Ltd

Cu(II) HALIDE AND PRIMARY AMINE COMPLEXES OF GUANINE AND XANTHINE

W. J. BIRDSALL,* B. W. PFENNIG and J. L. TOTO

Department of Chemistry, Albright College, Reading, PA 19604, U.S.A.

(*Received* 28 *September* 1985; *accepted* 26 *November* 1985)

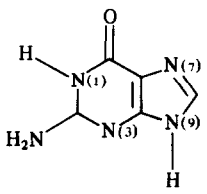
Abstract—Guanine (Gua) and xanthine (Xan) complexes of copper halides of types Cu(Gua)Cl_2, Cu(Gua)Br_2, Cu(Xan)$_2Cl_2 \cdot 2H_2O$ and Cu(Xan)$_2Br_2$ were synthesized by the interaction of the ligand and respective metal halide in methanol. In addition, Cu(Gua)$(CH_3NH_2)_2 \cdot 2H_2O$ and Cu(Xan)$(CH_3CH_2NH_2)_2 \cdot 2H_2O$ were prepared by reacting $CuSO_4 \cdot 5H_2O$ with the respective purine in the indicated primary amine. IR spectra of the halide complexes suggest that their stereochemistry is distorted tetrahedral, in keeping with previously reported complexes of this type. The amine compounds exhibit significant carbonyl IR shifts, indicating hydrogen bonding is present between purine carbonyl and the primary amine. Room-temperature magnetic susceptibilities are normal for related Cu(II) complexes. Comparison of these compounds with known complexes suggests the possibility of N(7)–N(9) purine bridging between copper atoms leading to polymer formation.

The interaction of metal ions with nucleic acids and nucleic acid constituents has been actively studied in recent years.[1,2] Research has provided information as to how certain metal ions bind to and influence DNA and RNA, as well as the mode of action of anti-cancer drugs containing metal ions such as *cis*-$PtCl_2(NH_3)_2$.[3,4] We have prepared a number of complexes with theophylline, a purine derivative with structural similarities to guanine and xanthine.[5] We report now the synthesis and structural study of halide adducts of Cu(II) with guanine and xanthine, with the general formulae Cu(Gua)X_2 (Gua = guanine) and Cu(Xan)$_2X_2$ (Xan = xanthine), where X = Cl and Br. We have also synthesized Cu(II) complexes of xanthine and guanine with primary amines, namely Cu(Xan)$(CH_3CH_2NH_2)_2 \cdot 2H_2O$ and Cu(Gua)$(CH_3NH_2)_2 \cdot 2H_2O$.

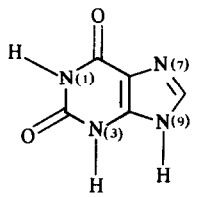
Cu(Gua)Cl_2 and Cu(Xan)$_2Cl_2 \cdot 2H_2O$ have been prepared previously but not structurally characterized.[6] X-ray structural determinations have been performed on Zn(Gua)Cl_3,[7] a monomer with Zn–N(9) bonding, and on Cu(Gua)$Cl_3 \cdot 2H_2O$,[8] a dimer with Cu–N(9) bonding and copper bridging by chlorine atoms. Structures of Cu(II) complexes with xanthine and hypoxanthine have been reported with metal coordination to the ligand N(9) nitrogen, as well as N(3) nitrogen in bidentate complexes.[9,10] Related Cu(II) complexes of xanthine and guanine have been reported,[11] as well as 3*d* metal perchlorate complexes of guanine,[12,13] guanine metal chloride adducts,[14–17] and xanthine 3*d* metal complexes.[18] The syntheses of guanine adducts with Co(II), Cu(II) and Zn(II) of general formula M(Gua)Cl_2 have recently been reported,[19] and a linear polymeric structural type with metal centers of tetrahedral symmetry bridged by guanine ligands has been proposed for these complexes.

Vestues and Sletten have reported the X-ray structure of the copper–purine complex, [Cu(Pur)$(H_2O)_4$]$SO_4 \cdot 2H_2O$ (Pur = purine), to be a polymeric chain with copper atoms in an octahedral coordination binding to N(7) and N(9) of two purine rings, a mode of bonding known for imidazole and benzimidazole complexes.[20] Many other purine metal complexes do not exhibit this N(7)–N(9) purine bridging, however; the dimeric nature of Cu(Gua)$Cl_3 \cdot 2H_2O$ and the monomeric Cu(Tp)$_2Cl_2$ (Tp = theophylline)[21] illustrate that a wide variety of bonding is present in compounds of

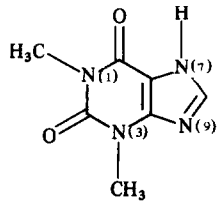
* Author to whom correspondence should be addressed.



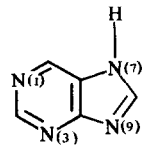
Guanine



Xanthine



Theophylline



Purine

this type. We have used IR (4000–200 cm^{-1}) and room-temperature magnetic susceptibility measurements to study the presently reported guanine and xanthine complexes, in an attempt to better understand their structures.

EXPERIMENTAL

Preparation of $Cu(Gua)Cl_2$, $Cu(Gua)Br_2$, $Cu(Xan)_2Cl_2 \cdot 2H_2O$ *and* $Cu(Xan)_2Br_2$

The synthetic procedure was similar to that used in the preparation of theophylline–copper halide complexes reported previously.[5] 5.0 mmol of the purine and 5.0 mmol of either $CuCl_2 \cdot 2H_2O$ or $CuBr_2$ were refluxed in methanol for 24 h, and allowed to cool to room temperature before filtration of the solid product. A 4:1 molar ratio of $CuBr_2$–xanthine was employed to form $Cu(Xan)_2Br_2$; this eliminated the need to separate unreacted xanthine at the conclusion of the reflux period. Found: C, 16.2; H, 1.5; N, 18.9; Cu, 16.7%. Calc for $Cu(C_5H_4N_5O)Br_2$ (dark brown): C, 16.1; H, 1.1; N, 18.7; Cu, 17.0%. Found: C, 23.1; H, 1.1; N, 21.5; Cu, 11.9%. Calc. for $Cu(C_5H_3N_4O_2)_2Br_2$ (orange–yellow): C, 22.8; H, 1.1; N, 21.2; Cu, 12.0%. $Cu(Gua)Cl_2$ (dark brown) and $Cu(Xan)_2Cl_2 \cdot 2H_2O$ (green) have been prepared previously by another method,[6] but the present synthetic procedure produced identical compounds, as evidenced by identical IR spectra and Cu analyses.

Preparation of $Cu(Xan)(CH_3CH_2NH_2)_2 \cdot 2H_2O$ *and* $Cu(Gua)(CH_3NH_2)_2 \cdot 2H_2O$

These compounds were synthesized in a similar fashion to previously reported copper–theophylline adducts with primary amines.[22,23] Because of the low solubility of guanine in methylamine, 5.0 mmol $CuSO_4 \cdot 5H_2O$ and 5.0 mmol guanine were stirred for 24 h in 25% methylamine–H_2O to produce a blue powder. Found: C, 31.9; H, 5.8; N, 24.5; Cu, 18.6%. Calc. for $(C_5H_3N_4O_2)Cu(C_2H_7N)_2 \cdot 2H_2O$ (blue): C, 31.7; H, 6.2; N, 24.7; Cu, 18.6%. Found: C, 26.9; H, 5.5; N, 31.5; Cu, 20.1%. Calc. for $(C_5H_4N_5O)Cu(CH_5N)_2 \cdot 2H_2O$ (blue): C, 27.0; H, 5.8; N, 31.5; Cu, 20.4%.

IR spectra were obtained as Nujol mulls between high-density polyethylene windows (600–200 cm^{-1}) and as KBr pellets (4000–500 cm^{-1}) on a Perkin–Elmer 1430 spectrophotometer. Room-temperature magnetic susceptibility measurements were made on a Gouy balance of standard design. Elemental analyses (C, H and N) were performed by Galbraith Laboratories.

RESULTS AND DISCUSSION

The crystal structure of $Cu(Tp)_2Cl_2$ has recently been reported.[21] Copper is coordinated to two imidazole N(7) atoms from theophylline ligands and two chlorine atoms. The stereochemistry about copper is a flattened tetrahedron, intermediate between tetrahedral and *cis*-square-planar. Monomeric $Cu(Tp)_2Cl_2$ units are hydrogen bonded to one another through N(9) hydrogen donor atom from one complex and the O(6) exocyclic oxygen atom from another complex. A distorted tetrahedral stereochemistry was also reported for this complex as well as for $Cu(Tp)_2Br_2 \cdot H_2O$ on the basis of low-frequency IR analysis.[5] Prominent doublets could be assigned to Cu—Cl and Cu—Br stretching, suggesting a tetrahedral or *cis*-square-planar symmetry about the copper atom.

Table 1 lists selected IR frequencies for the guanine and xanthine complexes. Prominent doublets are observed for $Cu(Gua)Cl_2$ and $Cu(Gua)Br_2$ at 285 and 258, and 245 and 220 cm^{-1}, respectively. The Cu—Br/Cu—Cl frequency ratio is 0.86, in keeping with ratios of other reported complexes of this sort, and confirming their assignments. This was the only region of the 4000–200-cm^{-1} IR spectra where significant differences were observed in these two compounds. Two low-frequency guanine bands at 345 and 398 cm^{-1} are slightly shifted to higher frequencies upon complexation, similar to but not to the same extent as low-frequency bands of compounds of theophylline and pyridine.[5,24] Guanine exhibits strong absorbances at 1698 and 1672 cm^{-1}, primarily due to $\nu(C{=}O)$ and $\delta(NH_2)$, respectively;[25] the carbonyl frequency at 1698 cm^{-1} does not change appreciably in the halide complexes, but two intense absorbances replace the peak at 1672 cm^{-1} [1698, 1645 and 1605 cm^{-1} in

Table 1. Selected IR frequencies (cm^{-1}) of Cu(II) halide and Cu(II) primary amine complexes of guanine and xanthine

Compound	ν(C=O)	ν(Cu—X)	ν(Cu—N)	Ligand bands
Gua	1698vs, 1672vs			398s, 345m
$Cu(Gua)Cl_2$	1698vs, 1645vs, 1605vs	285s, 258s		411s, 355m
$Cu(Gua)Br_2$	1695vs, 1642vs, 1600vs	245s, 220s		410s, 355m
$Cu(Gua)(CH_3NH_2)_2 \cdot 2H_2O$	1638vs, 1588vs		280w, 227w	408m, 355w
Xan	1700vs, 1660vs			353s
$Cu(Xan)_2Cl_2 \cdot 2H_2O$	1720vs	334s, 298s	258m	369s
$Cu(Xan)_2Br_2$	1728vs, 1700vs	234s	250sh	362s
$Cu(Xan)(CH_3CH_2NH_2)_2 \cdot 2H_2O$	1651vs, 1600vs		283m, 250m	375s

$\delta(NH_2)$ and δ(OH) also present in guanine and xanthine, respectively.

$Cu(Gua)Cl_2$; and 1695, 1642 and 1600 cm^{-1} in $Cu(Gua)Br_2$]. Methylmercury(II) complexes of 9-methylguanine with metal coordination to N(7) exhibit similar changes in this spectral region, but X-ray analysis demonstrates that the C(6) carbonyl of 9-methylguanine is not involved in chelate formation with the metal and hydrogen bonding does not occur between guanine molecules.[26]

The binuclear $Cu(Gua)Cl_3 \cdot 2H_2O$ complex is a dimer consisting of chlorine-bridged copper atoms, each having a trigonal-bipyrimidal environment.[8] Copper is bonded to the N(9) of guanine and to one of the bridge chlorines in the axial direction. The trigonal plane consists of three Cu—Cl bonds. Other halogen-bridged Cu(II) guanine dimers include $Cu(Gua)Cl_3$, $Cu(Gua)Br_3$ and $Cu(Gua)F_3 \cdot 2H_2O$.[27] The C(6) carbonyl IR frequency for these compounds does not change upon coordination, suggesting that carbonyl is not involved in bonding.

Mikulski *et al.* have recently reported the synthesis of $Cu(Gua)Cl_2$, a green solid obtained by refluxing a 2:1 molar ratio of guanine and $CuCl_2$ for 2–3 days in a 7:3 (v/v) mixture of ethanol–triethylorthoformate.[19] This complex is physically different from the presently reported dark brown $Cu(Gua)Cl_2$, which is identical to that reported by Weiss and Venner.[6] However, the structure of the green $Cu(Gua)Cl_2$ is proposed to be a linear chain-like polymer with copper atoms of tetrahedral symmetry bridged by bidentate guanine molecules, a structure which is also possible for the present compound. Cu—Cl and Cu—N doublets are assigned at 329 and 313 and 292 and 253 cm^{-1}, respectively, and C(6) carbonyl frequencies do not shift appreciably upon complexation, suggesting that the C(6) carbonyl does not participate in coordination. However, this complex is not identical to the presently discussed $Cu(Gua)Cl_2$;[6] its color and IR spectrum are significantly different.

Vestues and Sletten have obtained the crystal structure of the purine complex $[Cu(Pur)(H_2O)_4]SO_4 \cdot 2H_2O$, and report that the copper ion is octahedrally surrounded, binding equatorially to N(7) and N(9) in two symmetry-related purine rings, producing a polymeric chain.[20] This bonding is known for imidazole– and benzimidazole–metal complexes, and Vestues and Sletten suggest that this mode of bonding is probably also present in other metal halide complexes of purine.[28] In fact, the authors assign a Cu—Cl stretching frequency in $Cu(Pur)Cl_2 \cdot H_2O$ at 298 and 284 cm^{-1},[28] an assignment which could suggest distorted tetrahedral coordination about the copper atoms linking purine molecules through N(7)–N(9) bridges. N(7)–N(9) bridging in platinum complexes of theophylline has also been reported;[29] theophylline anions are reported to form a trimeric complex with trimethylplatinum(IV) containing Pt–N(7)–N(9)–Pt bridges and O(6)–Pt bonds.

Table 1 lists several IR frequencies for $Cu(Gua)(CH_3NH_2)_2 \cdot 2H_2O$. Guanine carbonyl frequencies at 1698 and 1672 cm^{-1} are shifted to 1638 and 1588 cm^{-1} in this complex, demonstrating significant hydrogen bonding between methylamine and the C(6) carbonyl. The magnitude and direction of this shift is similar to those noticed in copper amine complexes of theophylline.[30] Intramolecular hydrogen bonding between the C(6) carbonyl and other metal-coordinated ligands has been documented through several X-ray structural determinations of theophylline–metal complexes.[1,2,31] Cu–N absorbances can be tentatively assigned at 280 and 227 cm^{-1}, which is consistent with those reported for other guanine–copper complexes;[11] these weak absorbances, however, could arise from either copper–methylamine or copper–guanine nitrogen stretching. Metal halide bands obscure this region in $Cu(Gua)Cl_2$ and $Cu(Gua)Br_2$. Low-frequency ligand bands in Cu(Gua)

$(CH_3NH_2)_2 \cdot 2H_2O$ are similar to those of the guanine halide complexes.

Room-temperature magnetic susceptibility measurements for the guanine and xanthine complexes are normal for Cu(II) compounds, with the bromide and amine derivatives of both xanthine and guanine slightly subnormal. X-ray structure determinations of adenine and hypoxanthine Cu(II) compounds with room-temperature magnetic susceptibilities between 1.38–1.74 BM[6,32] show that they consist of quadruple bridges of bidentate purine connecting two Cu(II) centers through N(3) and N(9) ring nitrogen atoms.[9,33–35] Mikulski *et al.*[11] have prepared $Cu(Xan)_2 \cdot 2C_2H_5OH$ (μ_{eff} 1.60 BM) and $Cu(Gua)_2 \cdot H_2O$ (μ_{eff} 1.57 BM), and propose that they are binuclear complexes with copper atoms bridged by purine nitrogen atoms.

Selected IR frequencies for the isomorphous xanthine–copper halide complexes (Table 1) exhibit a low-frequency doublet for the copper compound in keeping with that observed for the above guanine derivatives, but a single peak for the bromide compound. The bromide absorption, 234 cm^{-1}, may be the high-frequency peak of a doublet extending below 200 cm^{-1}, or it may suggest a different stereochemistry in this complex. Tentative assignments can be made for Cu—N stretching at 258 cm^{-1} for $Cu(Xan)_2Cl_2 \cdot 2H_2O$ and at 250 cm^{-1} for $Cu(Xan)_2Br_2$; these absorbances are not observed for the above guanine halide complexes. A low-frequency xanthine band at 353 cm^{-1} shifts slightly to higher frequency upon complexation. Broad absorbances in xanthine at 1700 and 1660 cm^{-1}[11] sharpen and shift slightly to higher energy in $Cu(Xan)_2Cl_2 \cdot 2H_2O$ (1720 cm^{-1}) and $Cu(Xan)_2Br_2$ (1728 and 1700 cm^{-1}); this suggests that carbonyl is not involved in extensive hydrogen bonding in these complexes, perhaps even less than in free xanthine. Carbonyl frequencies shift considerably in $Cu(Xan)(CH_3CH_2NH_2)_2 \cdot 2H_2O$, however, from 1700 and 1660 to 1651 and 1600 cm^{-1}; this indicates that xanthine carbonyl is involved in hydrogen bonding with ethylamine in this complex, similar to the situation in the above $Cu(Gua)(CH_3NH_2)_2 \cdot 2H_2O$ and also in theophylline–copper(II) amine adducts.[30] Cu—N absorbances can be tentatively assigned at 283 and 250 cm^{-1}.

Copper halide complexes of guanine and xanthine exhibit low-frequency IR spectra which suggest that their stereochemistry is tetrahedrally distorted, similar to that observed in $Cu(Tp)_2Cl_2$.[5,21] Tetrahedral coordination about the metal center cannot be assigned with certainty to the primary amine complexes of guanine and xanthine; significant carbonyl hydrogen bonding with the primary amines is noticed in these adducts, however. Normal to slightly low room-temperature magnetic moments are present, suggesting bridged polymeric structures may occur in at least some of the complexes. These observations are similar to those of Cu(II) halide and amine complexes of theophylline.[5,30]

Crystal structure determinations of metal complexes of guanine reveal metal ion–N(9) coordination,[7,8] and N(9)–metal coordination is also observed in xanthine–metal complexes whose structures have been determined.[9,10] If N(9) coordination is assumed for the present compounds on the basis of previous structures, copper bonding may also occur to N(7) [or possibly N(1)] in $Cu(Gua)(CH_2NH_2)_2 \cdot 2H_2O$ and $Cu(Xan)(CH_3CH_2NH_2)_2 \cdot 2H_2O$, as evidenced by purine carbonyl hydrogen bonding to coordinated amines. On the basis of the known structure of polymeric $[Cu(Pur)(H_2O)_4]SO_4 \cdot 2H_2O$, where copper centers are bridged by purine N(7) and N(9) atoms,[20] N(7)–Cu–N(9) bridging for polymer formation may occur as well in the present complexes.

REFERENCES

1. L. G. Marzilli, *Prog. Inorg. Chem.* 1977, **23**, 255.
2. D. J. Hodgson, *Prog. Inorg. Chem.* 1977, **23**, 211.
3. T. G. Spiro (Ed.), *Nucleic Acid–Metal Ion Interactions*, Vol. 1. Wiley, New York (1980).
4. S. J. Lippard, *Science* 1982, **218**, 1075.
5. W. J. Birdsall, *Inorg. Chim. Acta* 1985, **99**, 59.
6. R. Weiss and H. Venner, *Hoppe-Seyler's Z. Phys. Chem.* 1965, **340**, 138.
7. L. Srinivasan and M. R. Taylor, *J. Chem. Soc., Chem. Commun.* 1970, 1668.
8. J. A. Carrabine and M. S. Sundaralingam, *J. Am. Chem. Soc.* 1970, **92**, 369.
9. E. Sletten, *Acta Cryst.* 1970, **B26**, 1609.
10. L. G. Marzilli, L. A. Epps, T. Sorrell and T. J. Kistenmacher, *J. Am. Chem. Soc.* 1975, **97**, 3351.
11. C. M. Mikulski, T. B. Tran, L. Mattucci and N. M. Karayannis, *Inorg. Chim. Acta* 1983, **78**, 211.
12. C. M. Mikulski, L. Mattucci, Y. Smith, T. B. Tran and N. M. Karayannis, *Inorg. Chim. Acta* 1983, **80**, 127.
13. C. M. Mikulski, L. Mattucci, L. Weiss and N. M. Karayannis, *Inorg. Chim. Acta* 1984, **92**, 275.
14. C. M. Mikulski, L. Mattucci, L. Weiss and N. M. Karayannis, *Inorg. Chim. Acta* 1984, **92**, L29.
15. C. M. Mikulski, L. Mattucci, Y. Smith, T. B. Tran and N. M. Karayannis, *Inorg. Chim. Acta* 1982, **66**, L71.
16. C. M. Mikulski, S. Cocco, L. Mattucci, N. DeFranco, L. Weiss and N. M. Karayannis, *Inorg. Chim. Acta* 1982, **67**, 173.
17. C. M. Mikulski, L. Mattucci, L. Weiss and N. M. Karayannis, *Inorg. Chim. Acta* 1984, **92**, 181.

18. C. M. Mikulski, M. Kurlan and N. M. Karayannis, *Inorg. Chim. Acta* 1985, **106**, L25.
19. C. M. Mikulski, L. Mattucci, L. Weiss and N. M. Karayannis, *Inorg. Chim. Acta* 1985, **107**, 81.
20. P. I. Vestues and E. Sletten, *Inorg. Chim. Acta* 1981, **52**, 269.
21. M. B. Cingi, A. M. M. Lanfredi and A. Tiripicchio, *Acta Cryst.* 1983, **C39**, 1523.
22. M. S. Zitzman, R. R. Krebs and W. J. Birdsall, *J. Inorg. Nucl. Chem.* 1978, **40**, 572.
23. W. J. Birdsall and M. S. Zitzman, *J. Inorg. Nucl. Chem.* 1979, **41**, 117.
24. R. J. H. Clark and C. S. Williams, *Inorg. Chem.* 1965, **4**, 350.
25. J. M. Delabar and M. Majoube, *Spectrochim. Acta* 1978, **34A**, 129.
26. A. J. Canty, R. S. Tobias, N. Chaichit and B. M. Gatehouse, *J. Chem. Soc., Dalton Trans.* 1980, 1693.
27. J. F. Villa, R. Doyle, H. C. Nelson and J. L. Richards, *Inorg. Chim. Acta* 1977, **25**, 49.
28. A. N. Speca, C. M. Mikulski, F. J. Iaconianni, L. L. Pytlewski and N. M. Karayannis, *Inorg. Chim. Acta* 1980, **46**, 235.
29. N. H. Agnew, T. G. Appleton, J. R. Hall, G. F. Kilmister and I. J. McMahon, *J. Chem. Soc., Chem. Commun.* 1979, 324.
30. B. J. Acken, D. A. Cole and W. J. Birdsall, *Synth. React. Inorg. Met.-Org. Chem.* 1983, **13**, 659.
31. L. G. Marzilli, T. J. Kistenmacher and G. L. Eichhorn, in *Nucleic Acid–Metal Ion Interactions* (Edited by T. G. Spiro), Vol. 1. Wiley, New York (1980).
32. R. Weiss and H. Venner, *Hoppe-Seyler's Z. Physiol. Chem.* 1963, **333**, 169; 1966, **345**, 122.
33. E. Sletten, *Acta Cryst.* 1969, **B25**, 1480.
34. P. de Meester and A. C. Skapski, *J. Chem. Soc. A* 1971, 2167.
35. A. Terzis, A. L. Beauchamp and R. Rivest, *Inorg. Chem.* 1973, **12**, 1166.

Polyhedron Vol. 5, No. 8, pp. 1363–1370, 1986
Printed in Great Britain

0277–5387/86 $3.00+.00
Pergamon Journals Ltd

MONO-η-ARENEBIS(TRIMETHYLPHOSPHINE)RHENIUM CHEMISTRY: ALKYL, HYDRIDO, HALOGENO AND OLEFIN DERIVATIVES

MALCOLM L. H. GREEN,* DERMOT O'HARE and JULIAN M. WALLIS

Inorganic Chemistry Laboratory, South Parks Road, Oxford OX1 3QR, U.K.

(*Received* 22 *November* 1985; *accepted* 27 *November* 1985)

Abstract—Co-condensation of rhenium atoms with a benzene–trimethylphosphine mixture gives the dimer $[Re(\eta\text{-}C_6H_6)(PMe_3)_2]_2$ which is a precursor to the new compounds $Re(\eta\text{-}C_6H_6)(PMe_3)_2R$ (R = H, Cl, I, Me, Et, CH=CH$_2$ or Ph), $[Re(\eta\text{-}C_6H_6)(PMe_3)_2X_2]BF_4$ ($X_2 = H_2$ or HI), $[Re(\eta\text{-}C_6H_6)(PMe_3)_2H_2][BF_4]_2$, and $[Re(\eta\text{-}C_6H_6)(PMe_3)_2L]BF_4$ (L = $\eta\text{-}C_2H_4$ or CO). Co-condensation of manganese atoms with benzene–trimethylphosphine gives $Mn(\eta\text{-}C_6H_6)(PMe_3)_2H$.

There are relatively few mono-η-arene rhenium complexes known, with the majority of these being members of the class of cations $[(\eta\text{-arene})Re(CO)_3]^+$.[1] Recently, the η-arene complex $(\eta\text{-}C_6H_6)Re(PPh_3)_2H$, synthesized from $Re(PPh_3)_2H_7$, has been described.[2] Co-condensation of rhenium atoms with a mixture of benzene and alkanes, or with alkyl-substituted benzenes gives binuclear compounds in the class $(\eta\text{-arene})Re(\mu\text{-}H)_2(\mu\text{-alkylidene})Re(\eta\text{-arene})$.[3,4] The compounds $Re(\eta\text{-}C_6H_6)(\eta\text{-}C_6H_8)H$ and $(\eta\text{-}C_6H_6)Re(\mu\text{-}H)_2Re(\eta\text{-}C_6H_8)_2$ have also been synthesised via rhenium atom reactions.[5,6] In a further development of η-arene rhenium chemistry we explored the reaction between rhenium atoms and a mixture of benzene and trimethylphosphine and found that the dimer $[Re(\eta\text{-}C_6H_6)(PMe_3)_2]_2$ could be prepared on a 1–2-g scale. Here we describe the chemistry of the $Re(\eta\text{-}C_6H_6)(PMe_3)_2$ system. A brief report of part of this work has been communicated previously.[7]

RESULTS

Co-condensation of rhenium atoms with a benzene–trimethylphosphine mixture (5:1) gives a red oil. Chromatography on alumina separated three rhenium compounds. Elution with toluene separated a small yellow band from which the compound $Re(\eta\text{-}C_6H_6)(PMe_3)_2Ph$ (**1**) was isolated. Further elution with diethyl ether separated a second band from which orange crystals of the dimer $[Re(\eta\text{-}C_6H_6)(PMe_3)_2]_2$ (**2**) were obtained. Finally, elution with acetone–water followed by addition of sodium tetrafluoroborate to the eluate gave the dihydride $[Re(\eta\text{-}C_6H_6)(PMe_3)_2H_2]BF_4$ (**3**).

Elemental analysis, NMR spectroscopic data and other characterizing data for compounds **1**–**3**, and for all the other new compounds described below, are given in Table 1 and, except where interpretation is not straightforward, the data are not further discussed.

The $^{13}C\text{-}\{^1H\}$ NMR spectrum of **1** shows a virtual triplet at δ 23.5 assigned to two trimethylphosphine ligands, and a triplet η-benzene resonance at δ 72.9 ($J = 2.08$ Hz). Resonances at δ 120.0, 126.1 and 144.2 are, respectively, assigned to the *para*-, *meta*- and *ortho*-carbons of the phenyl group: the *ipso*-carbon was not observed. The ^1H NMR spectrum of **3** showed the two Re-hydrogens to be equivalent and the data are consistent with either a *trans*- or a fluxional *cis*-structure. Compound **3** is presumed to be formed from the protonation on the chromatography column of the neutral hydride $Re(\eta\text{-}C_6H_6)(PMe_3)_2H$, which is described below. Evidence for this comes from the fact that the ^1H NMR spectrum of the sublimate from a crude sample of the co-condensation mixture showed a triplet hydride at δ 8.70, assignable to $Re(\eta\text{-}C_6H_6)(PMe_3)_2H$.

Treatment of **2** with iodine gave no tractable product, neither did **2** react with sodium amalgam (2%). However, stirring a tetrahydrofuran (thf) solution of **2** in the presence of a K film caused the

* Author to whom correspondence should be addressed.

Table 1. Analytical and spectroscopic data

Compound	Colour	Analysis[a] (%)		NMR data[b]
(1) $Re(\eta\text{-}C_6H_6)(PMe_3)_2Ph$	Yellow	43.9 (43.8)	5.9 (5.9)	^1H: 7.74 (2H, m, 2*ortho*-H), 7.08 (3H, m, *meta*- and *para*-H), 4.02 [6H, t, *J*(P–H) 1.5, η-C_6H_6], 1.16 (18H, vt, $2PMe_3$).[c] ^{31}P–{^1H}: −46.7 (s, $2PMe_3$).[c] ^{13}C–{^1H}: 23.5 (6C, vt, $2PMe_3$), 72.9 [6C, t, *J*(P–C) 2.08, η-C_6H_6], 120.0 (1C, s, *para*-C), 126.1 (2C, s, *meta*-C), 144.2 [2C, t, *J*(P–C) 6.8, *ortho*-C].[c]
(2) $[Re(\eta\text{-}C_6H_6)(PMe_3)_2]_2$	Orange	33.6 (34.6)	5.5 (5.8)	^1H: 4.26 [12H, t, *J*(P–H) 1.5, 2η-C_6H_6], 1.23 (36 H, vt, $4PMe_3$).[c] ^{31}P–{^1H}: −45.8 (s, $4PMe_3$).[c]
(3) $[Re(\eta\text{-}C_6H_6)(PMe_3)_2H_2]BF_4$[d]	Orange	25.6 (25.6)	4.4 (4.7)	^1H: 5.88 (6H, s, η-C_6H_6), 1.83 (18H, vt, $2PMe_3$), −9.93 [2H, t, *J*(P–H) 41.43 2Re-H].[e] ^{31}P–{^1H}: −40.6 (s, $2PMe_3$).[e]
(5) $Re(\eta\text{-}C_6H_6)(PMe_3)_2I$	Orange	27.1 (26.5)	4.6 (4.5)	^1H: 4.23 [6H, t, *J*(P–H) 1.7, η-C_6H_6], 1.33 (18H, vt, $2PMe_3$).[c] ^{31}P–{^1H}: −61.7 (s, $2PMe_3$).[c]
(6) $[Re(\eta\text{-}C_6H_6)(PMe_3)_2H]_2(BF_4)_2$	Orange-pink	25.6 (25.6)	4.4 (4.5)	^1H: 6.06 (12H, s, 2η-C_6H_6), 1.87 (36H, vt, $4PMe_3$), −8.74 [2H, t, *J*(P–H) 48.1, 2ReH].[e] ^{31}P–{^1H}: −36.6 (s, $4PMe_3$).[e]
(7) $Re(\eta\text{-}C_6H_6)(PMe_3)_2Me$	Yellow[f]			^1H: 4.05 [6H, t, *J*(P–H) 1.5, η-C_6H_6], 1.24 (18H, vt, $2PMe_3$), 0.49 [3H, t, *J*(P–H) 9.47, ReMe].[c] ^{31}P–{^1H}: −47.5 (s, $2PMe_3$).[c] ^{13}C: 70.83 (6C, d, η-C_6H_6), 22.21 (6C, q of m, $2PMe_3$), 1.41 (C, q, ReMe).[c]
(8) $Re(\eta\text{-}C_6H_6)(PMe_3)_2Et$	Yellow	37.5 (37.7)	6.4 (6.6)	^1H: 4.08 [6H, t, *J*(P–H) 1.5, η-C_6H_6], 1.85 [3H, t, *J*(H–H) 7.68, CH_3], 1.38 [2H, q, *J*(H–H) 7.67, CH_2], 1.17 (18H, vt, $2PMe_3$).[c] ^{31}P–{^1H}: −47.0 (s, $2PMe_3$).[c] ^{13}C–{^1H}: 70.9 (6C, s, η-C_6H_6), 32.2 (1C, s, $ReCH_2$), 22.7 (6C, m, $2PMe_3$), 12.95 (1C, s, CH_3).[c]

(9)	$Re(\eta\text{-}C_6H_6)(PMe_3)_2(CH{=}CH_2)$	Yellow[f]			^1H: 8.63 [1H, ddt, $J(H_a\text{–}H_{trans})$ 18.7, $J(H_a\text{–}H_{cis})$ 12.2, J(P–H) 9.9, H_a], 6.87 [1H, ddt, $J(H_a\text{–}H_{cis})$ 12.2, $J(H_{cis}\text{–}H_{trans})$ 5.6, J(P–H) 2.7, H_{cis}], 5.82 [1H, ddt, $J(H_a\text{–}H_{trans})$ 18.5, $J(H_{cis}\text{–}H_{trans})$ 5.6, J(P–H) 1.7, H_{trans}], 4.10 [6H, t, J(P–H) 1.5, $n\text{-}C_6H_6$], 1.21 (18H, vt, $2PMe_3$).[c] $^{31}P\text{–}\{^1H\}$: −58.1 (s, $2PMe_3$).[c]
(10)	$Re(\eta\text{-}C_6H_6)(PMe_3)_2H$[g]	Yellow	34.3 (34.5)	5.9 (6.0)	^1H: 4.28 (6H, s, $\eta\text{-}C_6H_6$), 1.39 (18H, vt, $2PMe_3$), −8.70 [1H, t, J(P–H) 36.8, ReH].[c] $^{31}P\text{–}\{^1H\}$: −45.5 (s, $2PMe_3$).[c]
(11)	$Re(\eta\text{-}C_6H_6)(PMe_3)_2HI]BF_4$	Red	23.7 (22.8)	4.2 (4.0)	^1H: 6.20 (6H, s, $\eta\text{-}C_6H_6$), 2.06 (18H, vt, $2PMe_3$), −10.43 [1H, t, J(P–H) 49.4, ReH].[e] $^{31}P\text{–}\{^1H\}$: −51.9 (s, $2PMe_3$).[e]
(12)	$[Re(\eta\text{-}C_6H_6)(PMe_3)_2(CH_2{=}CH_2)]BF_4$	Yellow[f]			^1H: 5.48 [6H, t, J(P–H) 1.1, $\eta\text{-}C_6H_6$], 2.30 [4H, t, J(P–H) 5, $\eta\text{-}CH_2{=}CH_2$], 1.65 (18H, vt, $2PMe_3$).[e] $^{31}P\text{–}\{^1H\}$: −52.1 (s, $2PMe_3$).[e] $^{13}C\text{–}\{^1H\}$: 85.04 (6C, s, $\eta\text{-}C_6H_6$), 22.98 (2C, s, $n\text{-}CH_2{=}CH_2$), 20.94 (6C, vt, $2PMe_3$).[e]
(13)	$[Re(\eta\text{-}C_6H_6)(PMe_3)_2CO]BF_4$[h]	Colourless[f]			^1H: 5.74 (6H, s, $\eta\text{-}C_6H_6$), 1.83 (18H, vt, $2PMe_3$).[e]
(14)	$Re(\eta\text{-}C_6H_6)(PMe_3)_2Cl$	Yellow	32.4 (31.9)	5.3 (5.4)	^1H: 4.26 [6H, t, J(P–H) 2.44, $\eta\text{-}C_6H_6$], 1.24 (18H, vt, $2PMe_3$). $^{31}P\text{–}\{^1H\}$: −45.8 (s, $2PMe_3$).[c]
(15)	$Mn(\eta\text{-}C_6H_6)(PMe_3)_2H$[i]	Orange-red	49.2 (50.4)	8.5 (8.8)	^1H: 4.36 (6H, s, $\eta\text{-}C_6H_6$), 1.04 (18H, vt, $2PMe_3$), −10.39 [1H, t, J(P–H) 82.8, MnH]. $^{31}P\text{–}\{^1H\}$: 24.3 (s, $2PMe_3$).

[a] Found (required) (%).

[b] Given as: chemical shift (δ) [relative intensity, multiplicity, J (in Hz), assignment]. Spectra were referenced using tetramethylsilane (^1H and ^{13}C) or trimethylphosphate in D_2O (^{31}P).

[c] In C_6D_6.

[d] ν(Re–H) = 1997 cm^{-1}.

[e] In CD_3COCD_3.

[f] Characterized spectroscopically only.

[g] ν(Re–H) = 1814 cm^{-1}.

[h] ν(C=O) = 1912 cm^{-1}.

[i] ν(Mn–H) = 1722 cm^{-1}.

initial orange solution to darken gradually to deep red; this reaction could be facilitated by addition of a catalytic amount of naphthalene. The red thf solution was very air- and water-sensitive, and this intermediate species, which we presume to be the K salt of the 18-electron anion $[Re(\eta\text{-}C_6H_6)(PMe_3)_2]^-$ (**4**), was not characterized. Indirect evidence for the nature of **4** comes from its reaction with water; dropwise addition of the red thf solution into wet Et_2O causes an immediate decolorization to give a bright yellow solution. Chromatography of the solution gave **3** as the only isolated complex.

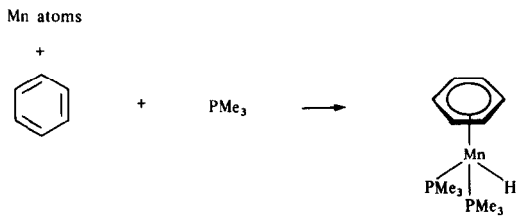
Treatment of the red solution (**4**) with MeI gave orange crystals of $Re(\eta\text{-}C_6H_6)(PMe_3)_2I$ (**5**). Addition of HBF_4 in Et_2O to **2** gives orange-pink crystalline $[Re(\eta\text{-}C_6H_6)(PMe_3)_2H]_2[BF_4]_2$ (**6**). The protonation may be reversed by treatment of **6** with $NaOH_{aq.}$ or potassium hydride (KH).

The iodo compound **5** is a useful synthetic intermediate for development of the chemistry of the $Re(\eta\text{-}C_6H_6)(PMe_3)_2$ radical. Thus, treatment of **5** with Grignard reagents (RMgX) (RX = MeI, EtI or $CH_2{=}CHBr$) or PhLi gives the compounds $Re(\eta\text{-}C_6H_6)(PMe_3)_2Me$ (**7**), $Re(\eta\text{-}C_6H_6)(PMe_3)_2Et$ (**8**), $Re(\eta\text{-}C_6H_6)(PMe_3)_2(CH{=}CH_2)$ (**9** and **1**), respectively. Treatment of **5** with lithium tetrahydridoaluminate(III) gives the hydrido derivative $Re(\eta\text{-}C_6H_6)(PMe_3)_2H$ (**10**).

Treatment of the iodo compound **5** with HBF_4 in Et_2O gives the iodohydride $[Re(\eta\text{-}C_6H_6)(PMe_3)_2HI]BF_4$ (**11**). The η-ethylene compound $[Re(\eta\text{-}C_6H_6)(PMe_3)_2(\eta\text{-}C_2H_4)]BF_4$ (**12**), is formed by treatment of **5** with $TlBF_4$ in the presence of 1 atm ethylene; by abstraction of a hydride ion from the β-hydrogen of **8** using trityl tetrafluoroborate and also by protonation of **9** with HBF_4in Et_2O. The ^1H and ^{13}C NMR spectra of **12** show the hydrogen and carbon atoms to be equivalent and coupled to two ^{31}P nuclei. This suggests that the ethylene hydrogens are made equivalent by rotation of the ethylene ligand about the Re–ethylene bond.

Treatment of **5** with $TlBF_4$ in the presence of CO gives colourless crystals of the monocarbonyl $[Re(\eta\text{-}C_6H_6)(PMe_3)_2CO]BF_4$ (**13**), for which the IR spectrum shows a strong band assignable to $\nu(C{=}O)$ at 1912 cm^{-1}.

The hydride **10** is highly reactive towards CH_2Cl_2, giving the chloro compound $Re(\eta\text{-}C_6H_6)(PMe_3)_2Cl$ (**14**), in excellent yields. Treatment of **10** with triethyloxonium tetrafluoroborate gives the dihydride $[Re(\eta\text{-}C_6H_6)(PMe_3)_2H_2]BF_4$ (**3**); it is possible that protonation resulted from adventitious water. Compound **3** is stable in aqueous base but may be deprotonated using potassium hydride.



15

Scheme 1.

Co-condensation of manganese atoms with benzene–trimethylphosphine (5 : 1) affords, on work-up, volatile, orange-red, petroleum ether soluble crystals of $Mn(\eta\text{-}C_6H_6)(PMe_3)_2H$ (**15**). The ^1H NMR spectrum of **15** shows three resonances; a singlet at δ 4.36 may be assigned to a coordinated η-benzene ring, a virtual triplet at δ 1.04 is assignable to the two trimethylphosphine ligands, and a high-field triplet at δ 10.39 ($J = 82.8$ Hz) is attributable to a single metal hydride ligand (see Scheme 1).

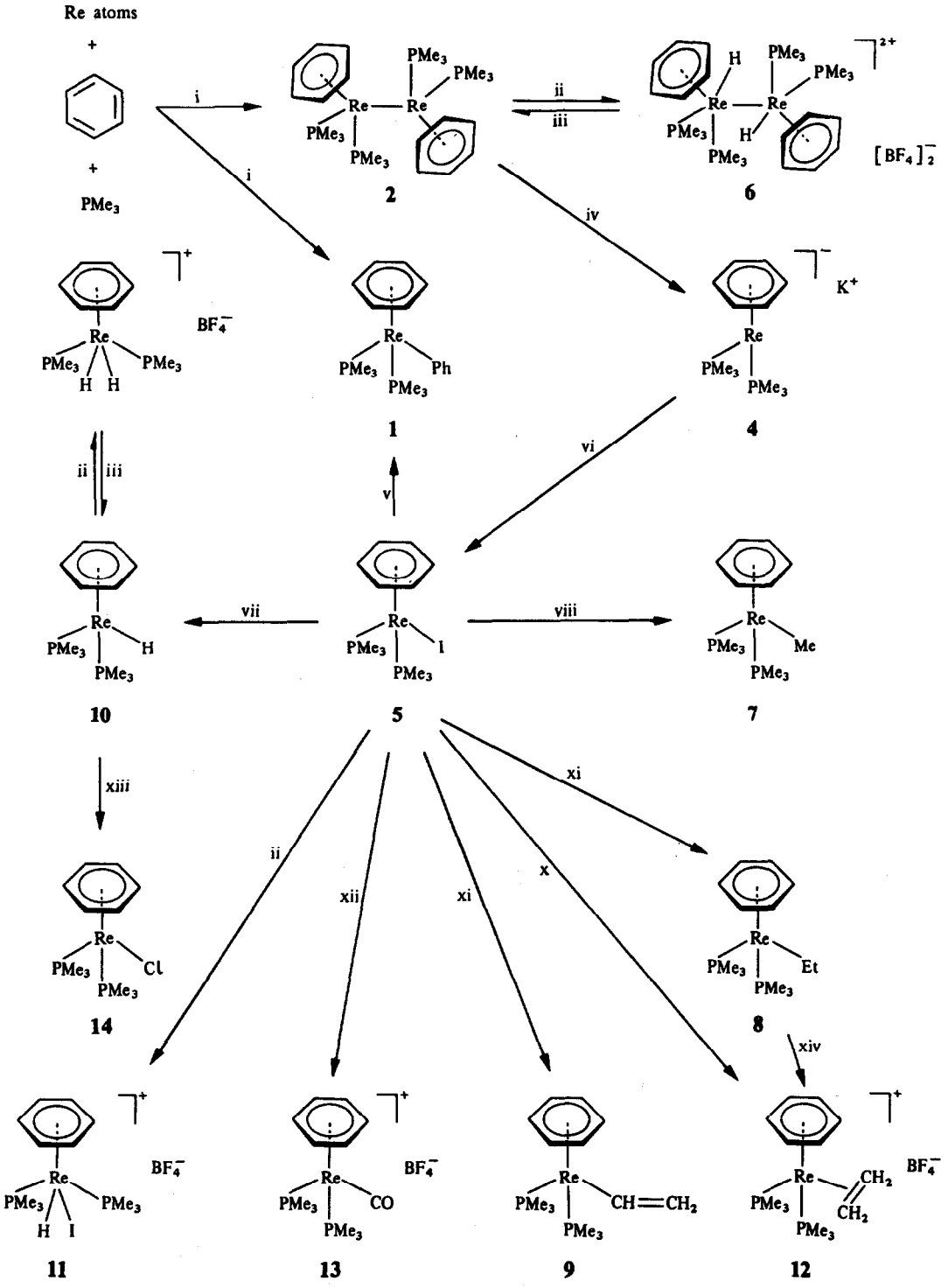
The photoelectron spectra of **2**, **5**, **10** and **15** show the first ionization potentials to be 6.18, 6.40, 6.21 and 6.06 eV, respectively.[8]

DISCUSSION

The structures proposed for compounds **1–14** are shown in Scheme 2. The low ionization energies for the compounds **2**, **5** and **10** show them to be classifiable as high-energy (electron-rich) compounds. This is supported by the basicity of these compounds as exemplified by their ease of protonation. Unlike the well-known dimer $[Fe(\eta\text{-}C_5H_5)(CO)_2]_2$, the dimer **2** is not cleaved by sodium amalgam but requires more vigorous conditions, namely a K film. The formation of the iodo compound from the reaction between the anion $[Re(\eta\text{-}C_6H_6)(PMe_3)_2]^-$ and iodomethane may be presumed to proceed via a radical process and contrast with the reaction between methyl iodide and the anion $[Fe(\eta\text{-}C_5H_5)(CO)_2]^-$, in which the methyl derivative $Fe(\eta\text{-}C_5H_5)(CO)_2Me$ is formed. In other respects the chemistry of the radical $Re(\eta\text{-}C_6H_6)(PMe_3)_2$ follows expected patterns.

EXPERIMENTAL

All preparations and reactions described were carried out under an atmosphere of dinitrogen using standard Schlenk vessel and vacuum line techniques. Solvents were pre-dried over molecular sieves and then distilled from K (toluene, benzene, cyclohexane or thf), Na–K alloy [pentane, petroleum ether (40–60°C) or Et_2O] or phosphorus pentoxide (CH_2Cl_2), under dinitrogen.



Scheme 2. (i) Rhenium atoms with benzene–trimethylphosphine, 2% for **1**, 20% for **2**, (ii) HBF_4 in Et_2O (90%), (iii) $NaOH_{aq.}$ (> 90%), (iv) K metal film in thf (> 90%), (v) PhLi in Et_2O at rt (> 70%), (vi) MeI in thf at rt for 30 min (62%), (vii) $LiAlH_4$ in thf at rt for 3 h (85%), (viii) MeMgBr in thf at 50°C for 2 h (70%), (ix) EtMgBr in Et_2O at rt for 1 h (49%), (x) $TlBF_4$ and ethylene (2 atm) in thf for 2 days (30%), (xi) vinylmagnesium bromide in thf at rt (49%), (xii) $TlBF_4$ and CO (2 atm) in thf at rt for 16 h (20%), (xiii) CH_2Cl_2 at rt for 2 h (93%), (xiv) $[Ph_3C][BF_4]$ in CH_2Cl_2 at rt (21%).

Elemental analyses were performed by the Analysis Department in this laboratory, or, in the case of very air-sensitive materials, by the Analytische Laboratorien, 5270 Gummersbach 1 Elbach, F.R.G.

IR spectra were recorded on a Pye–Unicam SP2000 double-beam grating spectrophotometer, or on a Perkin–Elmer 457 double-beam grating spectrophotometer. NMR spectra were recorded on a JEOL PMX60 (^{1}H NMR 60 MHz, c.w.), a Bruker WH300 (^{1}H NMR, 300 MHz) or a Bruker AM250 (heteronuclear NMR, 250 MHz). ^{13}C NMR and ^{31}P NMR spectra were run at frequencies of 62.9 and 101.2 MHz, respectively. Low-resolution mass spectra were recorded on an AEI MS902 mass spectrometer. Photoelectron spectra were recorded on a PES Laboratories 0078 spectrometer using a heated inlet system. The spectrometer was calibrated using He, Xe and N_2 ionization potentials. Syntheses with metal atoms were carried out using the apparatus described elsewhere,[9] metals were vaporized from a positive-hearth, electron-gun furnace, based on designs provided by G. V. Planer Co. Ltd.

Reaction of rhenium atoms with benzene–trimethylphosphine: *η-benzenebis(trimethylphosphine)phenylrhenium* (**1**), *bis[η-benzene-bis(trimethylphosphine)rhenium* (**2**) *and η-benzenebis(trimethylphosphine)dihydridorhenium tetrafluoroborate* (**3**)

A sample of rhenium powder (*ca* 12 g) was melted in an electron-gun furnace giving a rhenium ingot free of volatiles. This sample was then heated to *ca* 2600°C at which temperature rhenium vaporizes steadily. The vacuum in the reaction chamber, measured at a point below the furnace was *ca* 10^{-4} torr. The input power to the electron-gun furnace was maintained at 6 kV and 450 mA throughout. Rhenium atoms (4.1 g, 22 mmol) were co-condensed with a 5:1 molar mixture of benzene and trimethylphosphine (100 cm^3) for 4 h. After warming to room temperature (rt) the red-brown mixture was washed out of the machine with toluene (750 cm^3), filtered through a bed of Celite and reduced to a brown oil under reduced pressure at 50°C. The oil was extracted with petroleum ether (40–60°C, 5 × 300 cm^3), filtered through Celite and reduced in volume to 50 cm^3, giving a deep red solution. The red solution was adsorbed onto a chromatography column (neutral alumina, 6% water by weight, 50 × 4 cm).

Elution with toluene gave an orange band, which upon concentration of the eluate gave a deep red oil. Extraction with petroleum ether (40–60°C, 50 cm^3) gave an orange solution, which, on cooling to −80°C, yielded yellow crystals of **1**. Yield 0.2 g (2%).

Further elution with Et_2O produced a yellow band, which upon reduction in volume of the eluate and cooling to −20°C gave orange crystals of **2**. Yield 1.8 g (20%), based on rhenium evaporated from the furnace.

Further elution with aqueous acetone (1 : 1) gave a quickly moving brown band. Removal of the acetone under reduced pressure, followed by the addition of excess aqueous ammonium tetrafluoroborate produced an orange precipitate, which was collected and dried. Recrystallization from acetone (20 cm^3) gave yellow microcrystals of **3**. Yield 0.2 g (2%).

10 (50 mg, 0.12 mmol) was dissolved in Et_2O (30 cm^3), and three drops of ethereal HBF_4 were added. An immediate orange precipitate formed, which was washed with Et_2O (3 × 20 cm^3), and dried *in vacuo*. Recrystallization from acetone–water afforded orange crystals of (η-benzene) bis(trimethylphosphine)dihydridorhenium tetrafluoroborate. Yield 58 mg (95%).

Reaction beween **2** *and* K *metal*: *synthesis of* **4**

2 (1.0 g, 1.2 mmol) in thf (70 cm^3) was transferred on to a freshly prepared K film. One crystal of naphthalene was added to the orange solution. The solution was stirred and turned to deep red after 10 min. The colour deepened markedly over 8 h. The resulting solution was filtered and used immediately in subsequent reactions.

η-Benzenebis(trimethylphosphine)iodorhenium (**5**)

2 (1.0 g, 1.2 mmol) was used to prepare a red solution, as described above. Freshly distilled MeI (0.5 cm^3, 8.0 mmol) was added dropwise to the deep red solution with stirring. A white precipitate immediately developed and the solution changed from deep red to orange. The mixture was stirred for 30 min and then reduced to an oily solid under reduced pressure. Extraction with toluene (3 × 20 cm^3), followed by filtration and concentration produced a red oil. Extraction with petroleum ether (40–60°C, 3 × 20 cm^3) yielded, on concentration and cooling to −20°C, orange crystals of Re(η-C_6H_6)$(PMe_3)_2$I. Yield 0.8 g (62%).

Bis[(η - benzenebis(trimethylphosphine)hydridorhenium] bis-tetrafluoroborate (**6**)

The (η-benzene)bis(trimethylphosphine)rhenium dimer (70 mg, 0.08 mmol) was dissolved in Et_2O (30 cm^3), and excess of HBF_4 in Et_2O was added dropwise. An immediate orange-pink precipitate

formed, leaving a colourless solution. After washing with ether (3×20 cm^3), the solid was collected and dried *in vacuo*. Recrystallization from acetone–water gave orange crystals of **6**. Yield 76 mg (90%).

Reaction of **6** *with* $NaOH_{aq.}$

6 (50 mg, 0.05 mmol) in thf (10 cm^3) was treated wih $NaOH_{aq.}$ solution (5 cm^3). The mixture was stirred at rt for 3 h and the organic layer developed a yellow colour. Addition of pentane (30 cm^3), followed by separation of the organic layer, and partial removal of solvent under reduced pressure gave yellow crystals of **2** (^{1}H NMR). Yield > 80%.

5 (50 mg, 0.09 mmol) in petroleum ether (40–60°C, 30 cm^3) was treated with an excess of PhLi (3 cm^3, 1 M solution in Et_2O) at −78°C. After warming to rt the solvent was removed under reduced pressure. The residue was extracted with petroleum ether (40–60°C, 50 cm^3), the extract was filtered and the orange filtrate was cooled to −80°C giving yellow crystals which were collected, washed and dried *in vacuo*. Yield > 70%.

η-Benzenebis(trimethylphosphine)methylrhenium (**7**)

A solution of **14** (*vide infra*) (20 mg, 0.044 mmol) in thf (20 cm^3) was stirred while a saturated solution of MeMgBr in thf (1 cm^3) was added dropwise. No colour change was observed in the yellow-orange solution. Warming to 50°C for 2 h, followed by removal of solvent, gave a white powder and a yellow solid. Extraction with petroleum ether (40–60°C, 2×20 cm^3) and removal of the solvent under reduced pressure gave a yellow solid. This was recrystallized from light petroleum ether yielding yellow microcrystals of $Re(\eta\text{-}C_6H_6)(PMe_3)_2Me$. Yield 13 mg (70%).

η-Benzenebis(trimethylphosphine)ethylrhenium (**8**)

5 (50 mg, 0.09 mmol) in petroleum ether (40–60°C, 30 cm^3) was treated with an excess of EtMgBr (4 cm^3, 1 M solution in Et_2O) at −78°C. On warming to rt an off-white precipitate developed in a yellow solution. The solution was filtered, and the remaining solid was washed with petroleum ether (40–60°C, 2×20 cm^3). The combined extracts were reduced to a yellow oil under reduced pressure. Sublimation at 90°C (2×10^{-2} mmHg) gave yellow microcrystals of **8**. Yield 20 mg (49%).

η-Benzenebis(trimethylphosphine)vinylrhenium (**9**)

5 (50 mg, 0.09 mmol) was dissolved in petroleum ether (40–60°C, 30 cm^3) and cooled to −78°C. Dropwise addition of vinylmagnesium bromide (3 cm^3, 1.3 M solution in thf), followed by warming to rt, gave an orange solution and a white precipitate. Petroleum ether (40–60°C, 40 cm^3) was added, and the solution was filtered. Degassed water (30 cm^3) was added to the orange petroleum ether solution, and the two phases were shaken vigorously. The organic layer was decanted off, and upon removal of the solvent an orange oil remained. Repeated extraction with petroleum ether (40–60°C) yielded orange crystals of **9**. Yield 20 mg (49%).

η - Benzenebis(trimethylphosphine)hydridorhenium (**10**)

5 (70 mg, 0.13 mmol) was dissolved in thf (40 cm^3) and transferred on to excess $LiAlH_4$ (150 mg, 4.0 mmol). After stirring for 3 h at rt, the mixture was reduced to an oily yellow solid *in vacuo*. Extraction with toluene (2×20 cm^3), followed by removal of solvent gave an oily solid. Extraction with pentane (2×20 cm^3), and concentration (to 10 cm^3) and cooling to −20°C gave yellow crystals of **10**. Yield 46 mg (85%).

Reaction of **3** *with potassium hydride*

3 (40 mg, 0.08 mmol) was suspended in thf (30 cm^3), and a suspension of potassium hydride (excess, 1.2 g) in petroleum ether (60–80°C) was added with stirring. Over 4 h the orange solid dissolved, forming a yellow solution. Removal of solvent, followed by extraction with petroleum ether (40–60°C, 2×20 cm^3) gave a bright yellow solution. Concentration to low volume gave a high yield of yellow crystals. Comparison of the ^{1}H NMR data with that of an authentic sample of **10** showed them to be identical.

η - Benzenebis(trimethylphosphine)hydridoiodorhenium tetrafluoroborate (**11**)

5 (40 mg, 0.07 mmol) was dissolved in Et_2O (30 cm^3), giving an orange solution. Dropwise addition of ethereal HBF_4 produced an immediate orange precipitate, and the colour of the solution was completely discharged. The solution was decanted, and the residual solid was washed with Et_2O (3×20 cm^3). Recrystallization from acetone–water afforded orange-red microcrystals of **11**. Yield 40 mg (86%).

Reaction of **5** *with silver tetrafluoroborate*

Dropwise addition of silver tetrafluoroborate (10 mg, 0.05 mmol) in thf (10 cm^3) to an orange solution

of **5** (20 mg, 0.04 mmol) in thf (20 cm^3) at −78°C, followed by slow warming to rt produced a black precipitate and a bright red solution. Filtration of the solution followed by careful removal of the solvent under reduced pressure gave red crystals, which were shown to be **11** by ^1H NMR spectroscopy. Yield *ca* 30%.

η - Benzenebis(trimethylphosphine)(η - ethylene) rhenium tetrafluoroborate (**12**)

Method A. **5** (70 mg, 0.13 mmol) was dissolved in thf (30 cm^3) and $TlBF_4$ (200 mg, 0.69 mmol) was added with stirring. The solution was saturated with ethylene, and the Schlenk vessel was pressurized to 2 atm with ethylene. The orange solution containing a suspension of $TlBF_4$ was stirred at rt for 2 days. After that time a white solid remained suspended in a yellow-green solution. The solution was filtered, and the solvent was removed from the filtrate under reduced pressure, giving a yellow solid, which was washed with petroleum ether (40–60°C, 2 × 20 cm^3). Recrystallization from aetone–water afforded yellow microcrystals of **12**. Yield 20 mg (30%).

Method B. A solution of trityl hexafluorophosphate in CH_2Cl_2 was added dropwise to a stirred solution of **8** (20 mg, 0.045 mmol) in CH_2Cl_2 (20 cm^3). An immediate fine purple precipitate formed, and the solution became completely decolorized. The solvent was removed under reduced pressure, and the resulting pink solid was washed with petroleum ether (40–60°C, 2 × 20 cm^3). The solid was redissolved in thf (2 × 20 cm^3), filtered, and concentrated to *ca* 10 cm^3. Addition of petroleum ether (40–60°C, 30 cm^3) caused the pink solution to decolorize, and deposit a pale pink powder, which was collected and dried *in vacuo*. A ^1H NMR spectrum of the pink solid showed it to be identical to that of an authentic sample of the $[Re(\eta\text{-}C_6H_6)(PMe_3)_2(\eta\text{-}CH_2{=}CH_2)]^+$ cation. Yield 5 mg (21%).

Method C. Two drops of ethereal HBF_4 were added to an orange solution of **9** (15 mg, 0.03 mmol) in petroleum ether (40–60°C, 10 cm^3). An immediate pale orange precipitate formed. The orange solid was washed with Et_2O (3 × 20 cm^3), collected, and dried *in vacuo*. Yield 5 mg (28%). The ^1H NMR spectrum showed the product to be the $[Re(\eta\text{-}C_6H_6)(PMe_3)_2(CH_2{=}CH_2)]^+$ cation, by comparison with that of a known sample.

η - Benzenebis(trimethylphosphine)carbonylrhenium tetrafluoroborate (**13**)

5 (50 mg, 0.09 mmol) was dissolved in thf (30 cm^3) and a suspension of $TlBF_4$ (150 mg, 0.52 mmol) in thf (20 cm^3) was added. The atmosphere and solution were charged with CO to 2-atm pressure. The orange solution and white suspension was stirred at rt for 16 h, and then the atmosphere was repressurized to 2 atm, and stirred for a further 16 h. After this time the solution had become almost colourless, and was filtered off the white insoluble material. The solution was reduced to a white solid *in vacuo*. This solid was re-extracted with thf (2 × 20 cm^3), filtered, and concentrated; on cooling to −20°C a white powder precipitated. This was collected and dried. Yield 10 mg (20%).

η-Benzenebis(trimethylphosphine)chlororhenium (**14**)

8 (30 mg, 0.07 mmol) was dissolved in dry, distilled CH_2Cl_2 (20 cm^3) giving a yellow solution, which on extraction with petroleum ether (40–60°C, 2 × 20 cm^3) and filtration yielded a bright yellow solution. Concentration and cooling to −20°C afforded yellow microcrystals (30 mg, 93%) of $(\eta\text{-}C_6H_6)Re(PMe_3)_2Cl$.

Acknowledgements—We thank the S.E.R.C. for a studentship (to J.M.W.) and the Donors of the Petroleum Research Fund, administered by the American Chemical Society, for partial support.

REFERENCES

1. T. H. Coffield, V. Sandel and R. D. Closson, *J. Am. Chem. Soc.* 1957, **79**, 5826.
2. D. Baudry and M. Ephritikhine, *J. Chem. Soc., Chem. Commun.* 1980, 249.
3. F. G. N. Cloke, A. E. Derome, M. L. H. Green and D. O'Hare, *J. Chem. Soc., Chem. Commun.* 1983, 1312.
4. J. A. Bandy, F. G. N. Cloke, M. L. H. Green, D. O'Hare and K. Prout, *J. Chem. Soc., Chem. Commun.* 1984, 240.
5. M. L. H. Green, D. O'Hare, J. A. Bandy and K. Prout, *J. Chem. Soc., Chem. Commun.* 1984, 884.
6. A. E. Derome, M. L. H. Green and D. O'Hare, *J. Chem. Soc., Dalton Trans.* (in press).
7. M. L. H. Green, D. O'Hare and J. M. Wallis, *J. Chem. Soc., Chem. Commun.* 1984, 233.
8. J. Wallis, D.Phil. thesis, Oxford (1984); J. C. Green, unpublished work.
9. M. L. H. Green, *J. Organomet. Chem.* 1980, **200**, 119; F. G. N. Cloke and M. L. H. Green, *J. Chem. Soc., Dalton Trans.* 1981, 1938; M. L. H. Green, U.K. Patents 5953/74 and 53675/74, U.S. Patent 7,182,742 (1980); M. L. H. Green and V. J. Hammond, U.K. Patent, 1,597,825 (1981); M. L. H. Green and P. J. Norgate, U.K. Patent 1,597,822 (1981); M. L. H. Green and V. J. Hammond, U.S. Patent 4,182,749 (1980).

Polyhedron Vol. 5, No. 8, pp. 1371–1376, 1986
Printed in Great Britain

0277–5387/86 $3.00+.00
Pergamon Journals Ltd

OCTAKIS(DI-*p*-METHYLPHENYL SULFOXIDE)LANTHANIDE(III) PERCHLORATES AND THEIR DECOMPOSITION

M. A. BAÑARES, M. GONZALEZ, M. E. PEREZ and R. J. RUANO*

Departamento de Química Inorgánica, Facultad de Ciencias Químicas,
Universidad de Salamanca, Salamanca, 37008, Spain

(*Received* 14 *October* 1985; *accepted* 19 *December* 1985)

Abstract—Lanthanide(III) complexes of general composition $Ln(p\text{-}TSO)_8(ClO_4)_3$ (where Ln = Tb–Lu or Y and *p*-TSO = di-*p*-methylphenyl sulfoxide) were synthesized and characterized by chemical and thermal analysis, magnetic moments and IR spectra in the solid phase, and by molar conductance and molecular weights in solution studies. The thermal decomposition, in an air stream, of these complexes leads to the formation of pure lanthanide oxysulfates at 900°C. The formation of these species requires the transformation of part of the ligand sulfoxide and this process is discussed in terms of the identification of the solid and gaseous products obtained after heating to different temperatures by X-ray diffraction, IR spectroscopy and mass spectrometry.

The coordination chemistry of the transition metals with sulfoxides was developed in the 1960s and began with the use of dimethylsulfoxide (DMSO) as an appropriate ligand for all the transition metals in view of its ambidentate nature.[1]

More recently, the coordination chemistry of DMSO and of the higher sulfoxides has been reviewed, the main advances in the field being due to the application of such complexes in extraction processes, in preparative chemistry, in homogeneous catalysis and even in bioinorganic chemistry.[2]

Later work[3] examined the thermochemistry of the sulfoxide complexes of the transition metals and the application of thermoanalytical methods in the area of coordination chemistry, and underlined the impossibility of using thermal analysis in such complexes if they contain oxidizing anions, mainly the perchlorate ion, due to the explosive nature of the labile complexes formed after losing one or several ligand molecules of the original complex following a rise in temperature. Even then, the available information is scanty and only in one case has an attempt been made to represent the decomposition mechanism.[4]

Regarding the halo-complexes, thermal degradation takes place with the more or less gradual loss of the ligands at temperatures close to that of the boiling point of the complex-forming sulfoxide, the solid products found being those expected in the decomposition in air of anhydrous halides; oxohalides or oxides. Only in the case of copper(II) complexes does a so-called catalytic combustion yield Cu_2S, which is later oxidized to copper(II) sulfate.[5]

The aim of the present work was to prepare a series of complexes where the nature of the sulfoxide ligand itself minimizes the explosive nature of the perchlorate complexes with sulfoxide ligands in order to establish the reaction by which their decomposition takes place.

EXPERIMENTAL

The perchlorates of the hydrated lanthanides were prepared from the corresponding oxides supplied by BDH (U.K.). They were obtained by dissolving the oxide in 30% warm perchloric acid, and then evaporating to dryness. Following this, the product was dissolved in 10 cm^3 of dry methanol.

Di-*p*-methylphenyl sulfoxide (*p*-TSO), melting point 94°C, was supplied by Aldrich-Europe.

* Author to whom correspondence should be addressed.

Synthesis

The $Ln(ClO_4)_3 \cdot 8p$-TSO complexes, where Ln = Tb–Lu or Y, were prepared by dropwise addition at 0°C of a solution of 5 g of *p*-TSO in 20 cm^3 of methanol onto a solution of the corresponding lanthanide perchlorate in this medium, with continuous shaking. The precipitates obtained were washed with dry, cold methanol and with carbon tetrachloride, and then dried *in vacuo* over P_4O_{10} at room temperature.

Methods

The conductivity measurements were carried out in 10^{-3} M solutions of DMSO and nitrobenzene, using a Radiometer CDM 2E conductimeter with a CDC 104 immersion cell.

Magnetic susceptibilities were obtained at room temperature using a Stanton MC-5 microbalance, according to the Gouy method.

IR spectra were recorded with a Beckman Acculab 10 spectrophotometer in the 4000–400-cm^{-1} range in KBr discs.

Differential thermal analysis was carried out with a Perkin–Elmer DTA 1700 high-temperature differential thermal analyzer with a model 3600 data station.

Thermogravimetry was conducted with a Perkin–Elmer mod. TGS-2 thermobalance.

X-ray debyegrams were recorded with a Siemens Kristalloflex 810 apparatus with Cu-K_α radiation (λ = 154.050 pm) with a nickel filter.

Mass spectra were registered on a Hewlett–Packard mod. 5930-A spectrometer. In each case, samples were introduced in the chromatograph of the apparatus on an empty column, using He as the support gas at a rate of 60 cm^3 min^{-1}. The ion source temperature was 170°C and the ionization energy was 60 eV.

RESULTS AND DISCUSSION

According to the quantitative determinations of the contents of ligand, perchlorate and lanthanide ions and from the results deduced from the study of molar conductivity, molecular weights (Table 1), IR and thermogravimetric analysis, the general formula of $Ln(p\text{-TSO})_8(ClO_4)_3$ has been assigned to all the complexes.

The complexes are stable at room temperature, they melt without decomposing (Table 1) and are very insoluble in non-polar solvents. They decompose rapidly in water with precipitation of the ligand, though the increase in temperature favours their complete decomposition. They are soluble in DMSO, nitrobenzene, acetone, acetonitrile and nitromethane, among other polar solvents. Their colours are similar to those of the hydrated lanthanide perchlorates, though there is an appreciable decrease in intensity.

Quantitative analyses were carried after decomposing the complexes in water at 80°C. The white precipitate obtained, characterized by its IR spectrum as *p*-TSO, was dried to constant weight in an oven at 85°C. Using aqueous solutions, the lanthanide elements were determined by complexiметric evaluation with EDTA and using xylenol orange as indicator. The perchlorate anion was determined by precipitation with nitron and weighing the $C_{20}H_{17}N_4ClO_4$ compound.

The molar conductivities of the solutions of the complexes in DMSO and nitrobenzene at a concentration of 10^{-3} M revealed 3:1 and 2:1 electrolyte behaviour, respectively.[6]

Determination of molecular weights by studying the cryoscopic decreases of the complexes in DMSO and nitrobenzene revealed the presence of 12 and three particles in solution, respectively, per molecule of complex.

The IR spectra of all the complexes are very similar. A comparison of their spectra with that of free *p*-TSO (Table 2) reveals that the complexing affects the bands assigned to the stretching vibration of the S—O bond (1040 cm^{-1}) and those of the CH bending vibrations outside the plane (820 and 805 cm^{-1}).[7] The former undergoes a shift towards lower wavenumbers by a magnitude of 60 cm^{-1}, which shows that the coordination of the ligand takes place through the oxygen atom and that the bonding strength in all the complexes is the same.[8] The out-of-plane CH bending vibration appears as a doublet with the two bands separated by about 20 cm^{-1} in those compounds having two phenyl groups bound to a common atom which, in turn, is multiple bonded to another adjacent one. This is due to a mode coupling, originated by the great proximity of the *o*-hydrogen atoms and the aforementioned common atom.[9] In the spectrum of the complexes, this vibration appears as a single band at 810 cm^{-1} which, taking into account the nature of the bond of the sulfoxide group, confirms the coordination of the *p*-TSO through the oxygen atom, since it implies a decrease in the p_π–d_π bond strength and, in turn, a decrease in the order of such a bond. The T_d-symmetry of the perchlorate ion is conserved since only two bands appear in the spectrum, showing that this ion is not coordinated to tripositive lanthanides.[10]

The differential thermal analysis shows that heat decomposition in air of these complexes is identical in energy terms. In all the diagrams a first peak was

Table 1. Characterizing data for $Ln(p\text{-}TSO)_8(ClO_4)_3$ complexes

Complex	M.p. (°C)	% Ln[a]	% ClO_4^-[a]	% *p*-TSO[a]	μ_{eff} (BM)	Λ (Ω^{-1} cm^2 mol^{-1}) DMSO	Λ (Ω^{-1} cm^2 mol^{-1}) Nitrobenzene	M_{exp}[b] DMSO	M_{exp}[b] Nitrobenzene
$Y(p\text{-}TSO)_8(ClO_4)_3$	214	4.0	13.3	82.5	—	107.9	46.8	186.3	740.2
		(4.0)	(13.4)	(82.6)				(11.95)	(3.01)
$Tb(p\text{-}TSO)_8(ClO_4)_3$	214	6.6	12.1	80.7	9.6	111.1	46.2	197.4	742.3
		(6.9)	(13.0)	(80.1)				(11.64)	(3.09)
$Dy(p\text{-}TSO)_8(ClO_4)_3$	217	7.4	12.3	80.0	9.9	111.8	47.2	198.2	750.7
		(7.1)	(13.0)	(80.0)				(11.61)	(3.06)
$Ho(p\text{-}TSO)_8(ClO_4)_3$	216	7.1	12.6	79.2	10.2	123.9	45.6	190.9	749.8
		(7.2)	(13.0)	(79.9)				(12.06)	(3.07)
$Er(p\text{-}TSO)_8(ClO_4)_3$	218	7.7	13.2	79.0	9.3	117.5	47.1	194.4	785.6
		(7.2)	(12.9)	(79.8)				(11.86)	(2.93)
$Tm(p\text{-}TSO)_8(ClO_4)_3$	216	7.6	12.7	79.5	7.8	121.8	47.3	192.9	756.2
		(7.3)	(12.9)	(79.9)				(11.96)	(3.05)
$Yb(p\text{-}TSO)_8(ClO_4)_3$	215	7.6	13.0	79.6	4.8	121.4	48.3	198.5	781.7
		(7.5)	(12.9)	(79.6)				(11.65)	(2.96)
$Lu(p\text{-}TSO)_8(ClO_4)_3$	200	7.6	13.0	78.9	—	115.8	49.2	193.8	759.8
		(7.6)	(12.9)	(79.5)				(11.93)	(3.04)

[a] Calculated values in parentheses.
[b] Van't Hoff factors in parentheses.

Table 2. IR data for *p*-TSO and its lanthanide complexes (cm^{-1})[a]

1910 (w)	1910 (w)	Combination bands and aromatic 1:4
1800 (w)	1800 (w)	disubstitution
1650 (w)	—	Overtone band of CH out-of-plane deformation
1590 (m)	1590 (m)	C—C stretching
1490 (m)	1490 (m)	C—C stretching
1455 (w)	1455 (w)	C—C stretching and asymmetrical CH
1450 (w)	1450 (w)	deformation of the methyl group
1400 (m)	1400 (m)	C—C stretching
1380 (m)	1380 (w)	Symmetrical CH deformation of the methyl group
1350 (w)	—	C—C stretching
1305 (m)	1305 (m)	
1285 (w)	1285 (w)	
1210 (w)		
1210 (w)		
1180 (m)	1180 (m)	CH in-plane deformation
1120 (w)	—	CH in-plane deformation
1090 (s)		Fermi resonance band and ν_3 of the
1075 (s)	1090 (s)	perchlorate ion
1040 (s)	980 (s)	S—O stretching
1014 (s)	1014 (s)	CH in-plane deformation
970 (w)	—	
945 (w)	—	
850 (w)	850 (w)	
820 (s)	810 (s)	CH out-of-plane deformation
805 (s)		
710 (m)	710 (m)	S—C stretching
635 (m)	635 (w)	
625 (m)	615 (s)	ν_4 of the perchlorate ion
605 (m)		

[a] Abbreviations: s, strong; m, medium; w, weak.

obtained, which was endothermic, whose minimum appears within a temperature range of 220–225°C and is attributed to the melting of the complexes. A second, exothermic peak is located between 280 and 400°C, with a maximum in the 340–350°C range, and corresponds to the rapid decomposition of the complexes. The third peak, also exothermic, has a maximum in the 530–545°C range (Fig. 1).

The thermogravimetric curves of all the complexes are similar and show that the complexes are stable, in air, until temperatures in the region of their melting points. Thereafter their decomposition abruptly begins to take place accompanied by a huge loss of weight up to a temperature close to 360°C where the mass of the residues ranges between 32 and 35% of the initial amount of the complex.

From this temperature onwards and up to 560°C the loss of mass is very slow and gradual; in an interval of 200°C, the variation in mass is only 7–8% of the initial amount of the complex.

Between 560 and 750°C, an important decrease

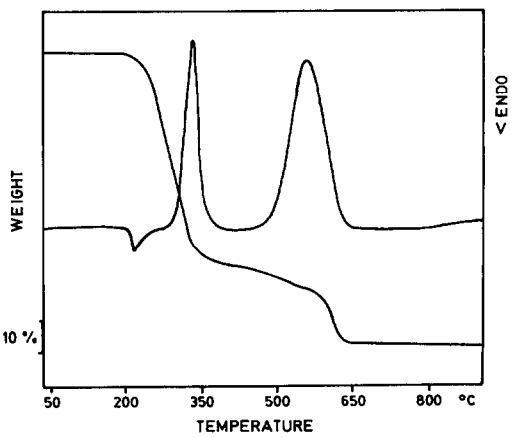


Fig. 1. TG–DTA curves of $Yb(p\text{-}TSO)_8(ClO_4)_3$.

in mass takes place in the residues (16–18%) after which their mass remains stable until the maximum heating temperature of 900°C (Fig. 1).

The residues of the calcination of the complexes at 750°C are white solids which are insoluble in water but will dissolve in dilute hydrochloric acid. Their IR spectrum exhibits active absorptions in the IR range, corresponding to a point group C_{2v}. The frequencies of the absorption maxima are in good agreement with those assigned for the sulfate ion in the oxysulfates of the lanthanides.[11] Likewise, the interlayer spaces deduced from the measurement of the X-ray diffraction diagrams are in accordance with those calculated from the reticular parameters published in the literature for the lanthanide oxysulfates.[12] Finally, the percentages of the residuals found at the end of the thermal decomposition ($Ln_2O_2SO_4$) are those corresponding to an initial complex composition identical to the formulation proposed and hence confirm the results obtained from the quantitative analyses and those of the molecular weight.

The IR spectra of the calcination residues of the complexes up to 560°C show a strong band with a maximum close to 1130 cm^{-1} and a sharp band at 610 cm^{-1} which are the active bands in the IR range of a T_d point group to which the undistorted sulfate belongs. The X-ray diffraction diagrams display interlayer spaces in agreement with those published in the literature for the anhydrous sulfates of lanthanum, cerium, gadolinium and lutetium.[13] The residue is black.

The gaseous products of the thermal decomposition of the complexes up to 360°C have been identified in two fractions; in the first, using mass spectrometry, are included those which remain in the gaseous state at room temperature. The second fraction, by IR spectroscopy, includes those gases which condense on the collecting flask on cooling. These latter residues are insoluble in water but soluble in dry methanol and their IR spectrum contains all the bands assigned to the uncoordinated *p*-TSO. Besides these bands, the spectrum also shows another with a medium intensity at 1700 cm^{-1} together with a further three bands at 1320, 1150 and 550 cm^{-1}. These latter three bands can be assigned, respectively, to $\nu(SO_2)$(asym), $\nu(SO_2)$ (sym) and scissoring modes active in IR of the aromatic sulfones.[7] The band at 1700 cm^{-1} must be the result of the combination of those taking place at 1150 and 550 cm^{-1}.

The mass spectra of the gases, the product of the thermal decomposition of the complexes up to temperatures of about 360°C, show peaks with the following mass/charge ratios [m/z (%)]: 44 (28) attributable to carbon dioxide, 48 (31) assignable to SO^+, 64 (100) due to sulfur dioxide, and 79 (30), 91 (15) and 92 (9), all ionization fragments of methylbenzene, together with the peaks which permit the identification of the presence of chlorine molecules in the gaseous mixture.

The solid residues of the pyrolysis of the complexes up to a temperature of 360°C are black in colour and it is not possible to identify them by X-ray diffraction owing to the poor resolution of the lines present in the diagrams. The IR spectra of these residues display the absorptions assigned to the ν(OH) stretching vibration (3400 cm^{-1}) and the δ(HOH) bending vibration (1600 cm^{-1}) of the water, together with a very wide band with two well-defined maxima at 1150 and 1100 cm^{-1}, and an another maximum of lower intensity at 1000 cm^{-1}, two strong bands at 630 and 605 cm^{-1}, and a band of medium intensity at 435 cm^{-1}. All of them correspond to active absorptions in the IR of a point group C_{3v} generated by a decrease in the T_d-symmetry of the sulfate ion due to an effect of the crystallization water. From this it is deduced that the weight loss observed between 360 and 560°C (7–8%) is due to the loss of the water present in the residues and the consequent stabilization of the corresponding anhydrous lanthanide sulfates.

Accordingly, the study of the thermal decomposition in air of the complexes examined here shows that, contrary to what has been reported by other authors, the loss of the sulfoxide ligand in them is not total; rather, part of the ligand is present in the residues in a number of sulfate ions sufficient to neutralize the existing lanthanide ions. Likewise, the oxidation of this sulfoxide to sulfate ion also gives rise to amorphous carbon which is only eliminated from the residues, as carbon dioxide, at temperatures greater than 560°C. The presence of this carbon accounts for the colouring of the solids and for the lack of resolution in the X-ray diagrams. In turn the combustion of this carbon induces the transformation of the anhydrous lanthanides sulfates into oxysulfates at temperatures substantially lower than that normally considered as their normal decomposition temperature in air.

REFERENCES

1. W. L. Reynolds, *Prog. Inorg. Chem.* 1970, **12**, 1.
2. J. A. Davies, *Adv. Inorg. Chem. Radiochem.* 1981, **24**, 115.
3. J. A. Davies and G. A. Miller, *Thermochim. Acta* 1983, **62**, 35.
4. H. Dehn, U.S. Patent 3,463,684; *Chem. Abstr.* 1969, **71**, 126729d.

5. M. Glavas and T. Skerlak, *Glas. Hem. Tehnol. Bosne Hercegovine* 1967, **15**, 31; *Chem. Abstr.* 1968, **69**, 48796r.
6. W. J. Geary, *Coord. Chem. Rev.* 1971, **7**, 81.
7. L. J. Bellamy, *The Infra-red Spectra of Complex Molecules*, 3rd edn, Vol. 1. Chapman & Hall, London (1978).
8. W. F. Currier and J. H. Weber, *Inorg. Chem.* 1967, **6**, 1539.
9. M. F. Lappert and I. K. Smith, *J. Chem. Soc.* 1961, 3224.
10. B. J. Hathaway and A. E. Underhill, *J. Chem. Soc.* 1961, 3091.
11. V. P. Surgustskii, V. I. Gaivoronskii and V. W. Serebrennikov, *Russ. J. Inorg. Chem.* 1968, **13**, 527.
12. J. A. Fahey, In *Proceedings of the* 12*th Rare Earth Research Conference Vail, Colorado*, p. 762, Vol 2 (1976).
13. L. G. Berry (Ed.), *Powder Diffraction File*. Joint Committee on Powder Diffraction Standards, Philadelphia, PA (1976).

Polyhedron Vol. 5, No. 8, pp. 1377–1380, 1986
Printed in Great Britain

0277-5387/86 $3.00+.00
Pergamon Journals Ltd

COMMUNICATION

UNEXPECTED PRODUCTS FORMED BY THE ADDITION OF HALOGENS [X_2 (= I_2 OR Br_2)] TO $W_2(O_2CBu^t)_4$ (M≡M): THE X-RAY CRYSTAL STRUCTURES OF $[W_2(O_2CBu^t)_5 \cdot 2Bu^tCONMe_2]^+[W_2I_4(O_2CBu^t)_2]^-$ AND $W_2Br_2(O_2CBu^t)_3 \cdot 2THF$

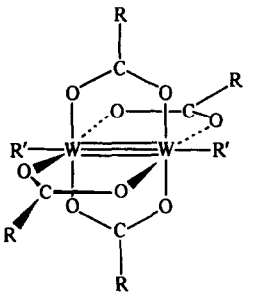
M. H. CHISHOLM,* H. T. CHIU and J. C. HUFFMAN

Department of Chemistry and Molecular Structure Center, Indiana University, Bloomington, IN 47405, U.S.A.

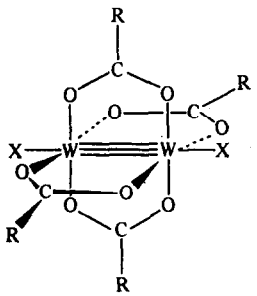
(*Received* 17 *September* 1985; *accepted* 7 *January* 1986)

Abstract—Addition of halogens, X_2 (X = I or Br), to hydrocarbon solutions of $W_2(O_2CBu^t)_4 \cdot 2L$, where L = THF or Bu^tCONMe_2, does not lead to simple oxidative-addition products of formula $W_2X_2(O_2CBu^t)_4$ having axially aligned halogen–tungsten bonds [cf. $W_2R_2(O_2CR')_4$ compounds, where R = CH_2CMe_3 or CH_2Ph, and R' = Me, Et, Bu^t or Ph] but rather leads to facile carboxylate group exchange. The overall reactions are thus complex and two crystalline products isolated in *ca* 20% crystalline yield have been characterized by X-ray studies. Addition of I_2 has allowed isolation of the salt $[W_2(O_2CBu^t)_5 \cdot 2L]^+[W_2I_4(O_2CBu^t)_2]^-$, where L = Bu^tCONMe_2, while addition of Br_2 gave $W_2Br_2(O_2CBu^t)_3 \cdot 2L$, where L = THF.

It is now a well-recognized aspect of the reactivity of multiple bonds between metal atoms that the bonds between elements of the 3rd transition series are more easily oxidized than those involving the 2nd transition series.[1,2] Our discovery of the axially bound (R') d^3–d^3 compounds $W_2(O_2CR)_4R'_2$ (**I**), where R = Me, Et, Bu^t or Ph, and R' = CH_2Ph or CH_2CMe_3,[3,4] prompted us to see whether or not the quadruply bonded compounds $W_2(O_2CR)_4$[5,6] or their lightly ligated adducts $W_2(O_2CR)_4L_2$ (e.g. L = THF or Me_2NCOR[7]) might react with halogens to give by oxidative-addition axially bound (X) compounds $W_2(O_2CR)_4X_2$ (**II**).



I



II

It should be noted that earlier work by Katovicc and McCarley[8] had shown that the addition of ½ equivalent of I_2 to $MoW(O_2CBu^t)_4$ (M ≡ M) in CH_3CN gave the mixed-valence compound of formal bond order 3.5, $MoW(O_2CBu^t)_4(I)(MeCn)$, where the iodo ligand was bound to W and the MeCN molecule ligated to Mo. Also recently Santure *et al.*[9] reported the preparation of $W_2(O_2CBu^t)_4I$ in a similar oxidative-addition reaction, though little was reported on this compound. We show here that compounds of type **II** are not readily prepared by the addition of halogens to $W_2(O_2CBu^t)_4$ because of facile carboxylate ligand scrambling.

In typical experiments $W_2(O_2CBu^t)_4 \cdot 2L$, *ca* 0.4 mmol, where L = Bu^tCONMe_2 or THF, was allowed to react with 1 equivalent of I_2 or Br_2 in toluene/hexane solutions at room temperature. Note the use of dry and oxygen-free atmospheres

* Author to whom correspondence should be addressed.

(N_2) and solvents. Crystals formed and were separated from the solution by filtration. In both instances the isolated yield based on tungsten was *ca* 20%. From the formula established by X-ray analyses* and elemental analyses it is evident that other species must also be formed.

$W_2(O_2CBu^t)_5 \cdot 2Bu^tCONMe_2]^+[W_2I_4(O_2CBu^t)_2]^-$ is formulated as a salt because: (i) the overall sample is paramagnetic (detailed magnetic studies have yet to be performed), and (ii) ^1H NMR spectroscopy reveals a spectrum entirely consistent with expectations for the d^3–d^3 (M≡M) cation based on the solid structure which contains two independent but essentially equivalent cations. Similarly there are are two independent $W_2I_4(O_2CBu^t)_2$ anions in the unit cell. The structure of $[W_2(O_2CBu^t)_5 \cdot 2Bu^tCONMe_2]^+$ is shown in Fig. 1, and can be seen to be related to the previously characterized d^3–d^3 triple bonded compounds $W_2(O_2CNMe_2)_6$[10] and $W_2(O_2CBu^t)_6$.[11] Specifically there are five relatively short W—O bonds in a pentagonal plane at each tungsten center and one long axial W---O bond involving here the Bu^tCONMe_2 molecules. The W–W distance, 2.28 Å (averaged), for the two cations is also essentially identical to that seen for the other d^3–d^3 compounds mentioned above. The anion $[W_2I_4(O_2CBu^t)_2]^-$ is NMR-silent and has a slightly shorter W–W distance, 2.24 Å (averaged), consistent with its formal bond order 3.5 and M–M bonding configuration $\sigma^2\pi^4\delta^1$. The gross structural features are similar to those seen in $[Ph_4As]_2[Mo_2(O_2CMe)_2Cl_4] \cdot 2MeOH$[12] and $Re_2(O_2CPh)_2I_4$[13] (see Fig. 2).

*(i) Crystal data for $[W_2(O_2CBu^t)_5 \cdot 2Bu^tCONMe_2]^+[W_2I_4(O_2CBu^t)_2]^-$ at −161°C: $a = 33.275(9)$ Å, $b = 24.600(11)$ Å, $c = 17.474(5)$ Å, $Z = 8$, $d_{calc} = 2.06$ g cm^{-3}, and space group $P2_12_12_1$. Of the 10,199 unique intensities collected (Mo-K_α, $6° \leq 2\theta \leq 45°$) the 6151 having $F > 2.33\sigma(F)$ were used in the refinement. Patterson techniques indicated that there were up to four W–W vectors and further indicated that there were numerous heavy atoms. Several direct approaches were used to obtain trial positions for the metal atoms. It was finally possible to get a MULTAN solution which agreed with the Patterson solution, and subsequent refinement of six W atoms thus revealed not only the remaining W atoms but also the eight I atoms. Subsequent difference Fourier synthesis were used to locate all 150 non-hydrogen atoms in the cell. Refinement was by block with each ion representing a block. No attempt was made to include the 206 H atoms in the least-squares refinement and no absorption correction was made. Final residuals are $R(F) = 0.071$ and $R_w(F) = 0.069$.

(ii) Crystal data for $W_2Br_2(O_2CBu^t)_3 \cdot 2THF$ at −160°C: $a = 18.694(7)$ Å, $b = 17.106(6)$ Å, $c = 9.437(3)$ Å, $\beta = 95.55(2)°$, $Z = 4$, $d_{calc} = 2.16$ g cm^{-3}, and space group $P2_1/a$. Of the 3943 unique intensities collected (Mo-K_α, $6° < 2\theta < 45°$) the 3218 having $F > 3\sigma(F)$ were used in the refinement.

The crystal used in the study was cleaved from a larger crystal. ψ scans indicated a severe absorption and the data were corrected accordingly. Due to the irregular shape of the faces (resulting from crystal cleavage), the absorption correction is not as precise as one might wish. The agreement between "equivalent" reflections for a subshell of 485 reflections decreased from 0.145 to 0.048 after correction. Because of the imperfect nature of the absorption coefficient, no attempt to refine the model anisotropically (except for Br and W atoms) was made. The structure was solved using a combination of direct methods (MULTAN 78) and Fourier techniques, and refined by full-matrix least squares. H atoms were located in fixed idealized positions. Final residuals are $R(F) = 0.070$ and $R_w(F) = 0.069$.

Supplementary materials available. Tables of fractional coordinates and thermal parameters have been deposited with the Cambridge Crystallographic Data Centre. Complete structural information is available from the Editor at Queen Mary College and, in microfiche form only, from the Indiana University Library, Bloomington, IN 47405, U.S.A. at a cost of $2.50 per copy. For $[W_2(O_2CBu^t)_5 \cdot 2Bu^tCONMe_2]^+[W_2I_4(O_2CBu^t)_2]^-$ request MSC Report No. 84024 and for $W_2Br_2(O_2CBu^t)_3 \cdot 2THF$ request MSC Report No. 84082.

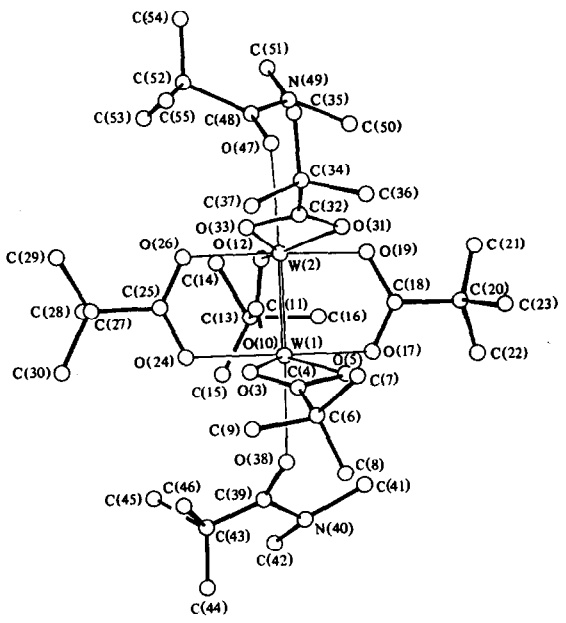


Fig. 1. A view of one of the $[W_2(O_2CBu^t)_5 \cdot 2Bu^tCONMe_2]^+$ cations showing the atom-numbering scheme. The central portion of the cation, $W_2(O_2CBu^t)_5$ has virtual C_{2v}-symmetry with three bridging carboxylate ligands and two bidentate ligands. The W–W distance is 2.29 Å (averaged) and the W—O bond distances in the pentagonal plane to the carboxylate oxygen atoms fall in the range 2.04–2.15 Å while the axially aligned W---O bonds involving the Bu^tCONMe_2 ligands are in the range 2.36–2.46 Å.

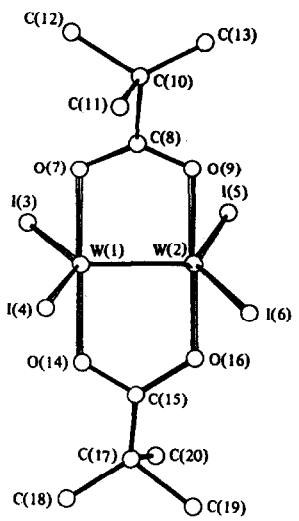


Fig. 2. A view of one of the $[W_2I_4(O_2CBu^t)_2]^-$ anions giving the atom-numbering scheme. The anion has virtual D_{2h}-symmetry. Pertinent distances (Å) and angles (°) (averaged) are W–W = 2.237, W—I = 2.68, and W—O ranges from 2.00 to 2.12; W–W—I = 109, and W–W—O = 90.

$W_2Br_2(O_2CBu^t)_3 \cdot 2THF$ forms dark brown crystals from hexane solutions and in toluene-d_8 shows only broadened ^1H NMR signals centered at *ca* 7 ppm for the Bu^t protons. We believe that this is also indicative of the paramagnetic nature of the species which contains a central W_2^{5+} center. An ORTEP view of the molecule is shown in Fig. 3 which reveals the virtual C_{2v}-symmetry. Again the axial W---O (THF) bonds are long, 2.45 Å (averaged), and the W–W distance, 2.31 Å, is in the range typically found for W≡W bonds of configuration $\sigma^2\pi^4$, though in this instance the W–W bond is formally of order 3.5 and of configuration $\sigma^2\pi^4\delta^1$. Ignoring the THF molecules the structure is somewhat related to that seen for $Re_2(O_2CBu^t)_3Cl_3$.[14]

Clearly more work is needed to characterize these paramagnetic W_2-containing centers. What is clear from this work is that compounds of type **II** are not readily accessible by oxidative-additions of halogens to $W_2(O_2CR)_4$ compounds because of facile carboxylate exchange reactions. To our knowledge this communication reports the first example of a cationic $(W{\equiv}W)^{6+}$-containing compound. Further studies are in progress.

Acknowledgements—We thank the National Science Foundation and the Wrubel Computing Center for support.

REFERENCES

1. F. A. Cotton and R. A. Walton, In *Multiple Bonds between Metal Atoms*. John Wiley, New York (1982).
2. F. A. Cotton, *J. Chem. Educ.* 1983, **60**, 713.
3. M. H. Chisholm, D. M. Hoffman, J. C. Huffman, W. G. Van Der Sluys and S. Russo, *J. Am. Chem. Soc.* 1984, **106**, 5386.
4. M. H. Chisholm, D. L. Clark, J. C. Huffman, W. G. Van Der Sluys, E. M. Kober and D. Lichtenberger, manuscript in preparation.

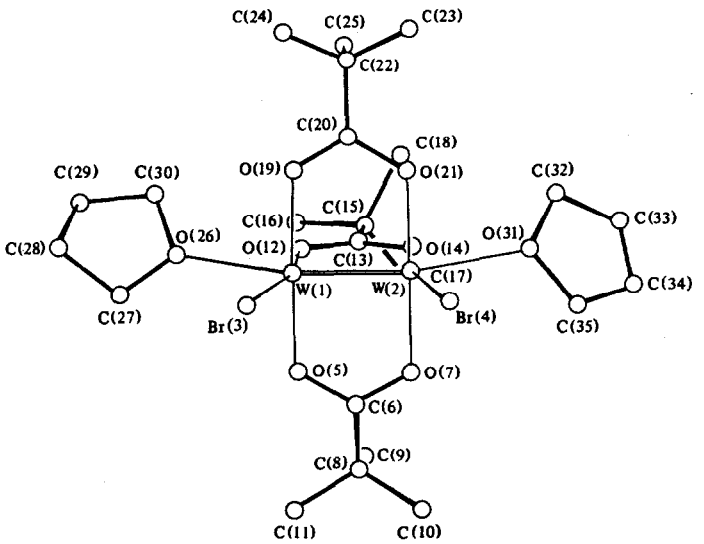


Fig. 3. A view of the $W_2Br_2(O_2CBu^t)_3 \cdot 2THF$ molecule giving the atom-numbering scheme. The central $W_2Br_2(O_2CBu^t)_3$ skeleton has virtual C_{2v}-symmetry. Pertinent distances (Å) and angles (°), averaged where appropriate, are W–W = 2.313, W—Br = 2.50, W—O (carboxylate) ranges from 2.04 to 2.09, W–W—Br = 110, W–W—O = 89; W---O (THF) = 2.45, and W–W---O (THF) = 162.

5. A. P. Sattelberger, K. W. McLaughlin and J. C. Huffman, *J. Am. Chem. Soc.* 1981, **103**, 2880.
6. F. A. Cotton and W. Wang, *Inorg. Chem.* 1982, **21**, 3861.
7. M. H. Chisholm, H. T. Chiu and J. C. Huffman, *Polyhedron* 1984, **3**, 759.
8. V. Katovic and R. E. McCarley, *J. Am. Chem. Soc.* 1978, **100**, 5586.
9. D. J. Santure, J. C. Huffman and A. P. Sattelberger, *Inorg. Chem.* 1985, **24**, 371.
10. M. H. Chisholm, F. A. Cotton, M. W. Extine and B. R. Stults, *Inorg. Chem.* 1977, **16**, 603.
11. M. H. Chisholm, J. A. Heppert, D. M. Hoffman and J. C. Huffman, *Inorg. Chem.* 1985, **24**, 3214.
12. W. Clegg, C. D. Garner, S. Parkes and I. B. Walton, *Inorg. Chem.* 1979, **18**, 2250.
13. W. K. Bratton and F. A. Cotton, *Inorg. Chem.* 1969, **8**, 1299.
14. F. A. Cotton, L. D. Gage and C. E. Rice, *Inorg. Chem.* 1979, **18**, 1138.

Polyhedron Vol. 5, No. 8, pp. 1381–1382, 1986
Printed in Great Britain

0277–5387/86 $3.00+.00
Pergamon Journals Ltd

COMMUNICATION

SYNTHESIS, SPECTRAL PROPERTIES AND REACTIONS OF THE NOVEL ACETONITRILE DIIODOTRICARBONYLTRIPHENYL PHOSPHINE, ARSINE AND ANTIMONY COMPLEXES OF MOLYBDENUM(II) AND TUNGSTEN(II)

PAUL K. BAKER* and STUART G. FRASER

Department of Chemistry, University College of North Wales, Bangor, Gwynedd LL57 2UW, U.K.

(*Received* 24 *January* 1986; *accepted* 10 *February* 1986)

Abstract—The bisacetonitrile complexes $[MI_2(CO)_3(NCMe)_2]$ (M = Mo or W) react with L (L = PPh_3, $AsPh_3$ or $SbPh_3$) to give the novel compounds $[MI_2(CO)_3(NCMe)L]$, which undergo acetonitrile displacement reactions to afford a variety of new mixed complexes.

The complexes $[MX_2(CO)_3L_2]$ (M = Mo or W, L = PPh_3 or $AsPh_3$, X = Cl or Br) are currently under investigation as catalysts for the ring-opening polymerization of norbornene,[1,2] and it is proposed that it is the ease of phosphine or arsine dissociation in these complexes which is the rate-determining step in the mechanism. Although a wide variety of bisphosphine complexes of the type $[MX_2(CO)_3L_2]$ (L = phosphine) have been prepared,[3] until now no mixed seven-coordinate complexes of this type have been reported with a labile ligand such as acetonitrile attached to the metal which should enhance the catalytic activity of these complexes in view of the work of Bencze *et al.*[1,2] In this communication the synthesis of the new mixed compounds $[MI_2(CO)_3(NCMe)L]$ (M = Mo or W; L = PPh_3, $AsPh_3$ or $SbPh_3$) and preliminary studies of their reactivity are reported.

Equimolar quantities of $[MI_2(CO)_3(NCMe)_2]$,[4] and L (L = PPh_3, $AsPh_3$ or $SbPh_3$) react in CH_2Cl_2 to afford high yields of the crystalline compounds $[MI_2(CO)_3(NCMe)L]$, which have been fully characterized by elemental analysis (C, H and N) and IR spectroscopy (Table 1) and ^1H NMR spectroscopy.† All the complexes are stable in the solid state when stored under argon, but decompose rapidly in solution when exposed to air. Several X-ray crystal structures of the known seven-coordinate bisphosphine compounds $[MX_2(CO)_3L_2]$ have been carried out,[5–16] all having capped octahedral geometry. Since the spectral properties of $[MI_2(CO)_3(NCMe)L]$ closely resemble those of the analogous bisphosphine compounds it is likely that they will have a similar geometry.

It is interesting to note that $[MoI_2(CO)_3(NCMe)_2]$ reacts with $SbPh_3$ to initially afford $[MoI_2(CO)_3(NCMe)(SbPh_3)]$, which rapidly loses acetonitrile to afford the iodide-bridged dimer $[Mo(\mu\text{-}I)I(CO)_3(SbPh_3)]_2$, whereas the other complexes $[MI_2(CO)_3(NCMe)L]$ are fairly stable to loss of acetonitrile. We are currently investigating the electronic and steric effects of different phosphine and phosphite ligands on the rate of dimerization of the complexes $[MI_2(CO)_3(NCMe)L]$ (L = phosphine or phosphite). The chemistry of these complexes is dominated by acetonitrile displacement (Scheme 1).

Acknowledgement—S.G.F. thanks the S.E.R.C. for support.

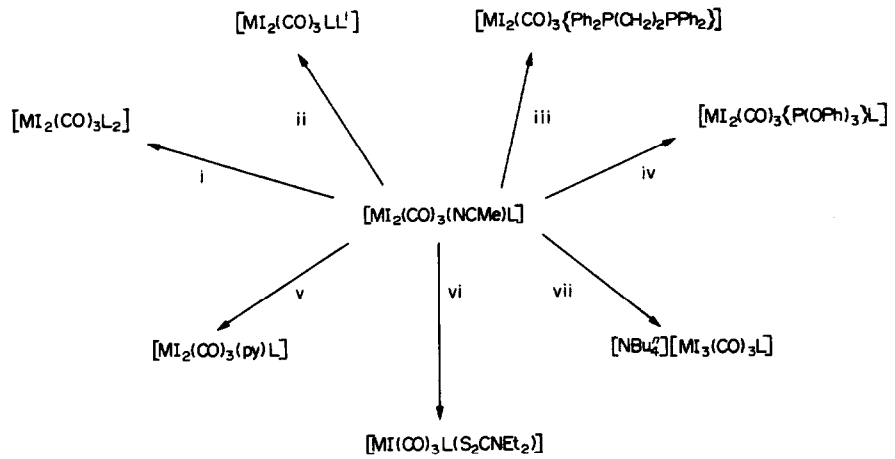
* Author to whom correspondence should be addressed.

† ^1H NMR spectra (δ) of **1–6** (see Table 1) all recorded in $CDCl_3$ referenced to tetramethylsilane. (**1**) 7.72 (m, 15H, Ph), 2.02 (*s*, 3H, NCMe). (**2**) 7.47 (*m*, 15H, Ph), 1.9 (*s*, 3H, NCMe). (**3**) 7.48 (*m*, 15H, Ph), 1.99 (*s*, 3H, NCMe). (**4**) 7.52 (*m*, 15H, Ph), 1.96 (*s*, 3H, NCMe). (**5**) 7.50 (*m*, 15H, Ph), 1.94 (*s*, 3H, NCMe). (**6**) 7.53 (*m*, 15H, Ph), 2.01 (*s*, 3H, NCMe).

Table 1. Analytical (C, H and N)[a] and IR[b] data of $[MI_2(CO)_3(NCMe)L]$

	M	L	C	H	N	ν(CO) (cm^{-1})	ν(CN) (cm^{-1})
1	Mo	PPh_3	37.3 (37.5)	2.2 (2.5)	1.9 (2.2)	2045(s), 1965(s), 1930(s)	2320(w)
2	Mo	$AsPh_3$	35.6 (35.4)	2.5 (2.3)	2.0 (1.8)	2049(s), 1985(s), 1921(m)	2315(w)
3	Mo	$SbPh_3$	33.5 (33.4)	2.4 (2.2)	1.2 (1.7)	2049(s), 1990(s), 1919(s)	2310(w)
4	W	PPh_3	33.7 (33.5)	2.3 (2.2)	1.7 (1.5)	2040(s), 1950(s), 1918(s)	2325(w)
5	W	$AsPh_3$	32.0 (31.8)	2.3 (2.1)	1.5 (1.6)	2040(s), 1970(s), 1909(s)	2325(w)
6	W	$SbPh_3$	30.3 (30.2)	2.2 (2.0)	1.3 (1.5)	2035(s), 1975(s), 1905(s)	2315(w)

[a] Calculated values in parentheses.
[b] Spectra recorded in $CHCl_3$ unless stated: s = strong, m = medium, w = weak.



Scheme 1. M = Mo or W; L = PPh_3, $AsPh_3$ or $SbPh_3$. Reagents: L, L^1 = PPh_3, $AsPh_3$ or $SbPh_3$ in CH_2Cl_2 [(i) and (ii)]; $Ph_2P(CH_2)_2PPh_2$ in CH_2Cl_2 (iii); $P(OPh)_3$ in CH_2Cl_2 (iv); pyridine in CH_2Cl_2 (v); $NaS_2CNEt_2 \cdot 3H_2O$ in CH_2Cl_2 (vi); and $[NBu^n_4]I$ in CH_2Cl_2 (vii).

REFERENCES

1. L. Bencze and A. Kraut-Vass, *J. Mol. Catal.* 1985, **28**, 369.
2. L. Bencze, A. Kraut-Vass and L. Prókai, *J. Chem. Soc., Chem. Commun.* 1985, 911.
3. R. Colton, *Coord. Chem. Rev.* 1971, **6**, 269 (and references cited therein).
4. P. K. Baker, S. G. Fraser and E. M. Keys, *J. Organomet. Chem.* (in press).
5. A. Mawby and G. E. Pringle, *J. Inorg. Nucl. Chem.* 1972, **34**, 517.
6. M. G. B. Drew, *J. Chem. Soc., Dalton Trans.* 1972, 1329.
7. M. G. B. Drew and J. D. Wilkins, *J. Chem. Soc., Dalton Trans.* 1973, 2664.
8. M. G. B. Drew, *J. Chem. Soc., Dalton Trans.* 1972, 626.
9. M. G. B. Drew, *J. Chem. Soc., Dalton Trans.* 1975, 1984.
10. M. G. B. Drew, I. B. Tomkins and R. Colton, *Aust. J. Chem.* 1970, **23**, 2517.
11. G. Schmid, R. Boese and E. Welz, *Chem. Ber.* 1975, **108**, 260.
12. R. Boese and U. Müller, *Acta Cryst.* 1976, **B32**, 582.
13. M. G. B. Drew and J. D. Wilkins, *J. Chem. Soc., Dalton Trans.* 1977, 557.
14. M. G. B. Drew, A. P. Wolters and I. B. Tomkins, *J. Chem. Soc., Dalton Trans.* 1977, 974.
15. J. C. Dewan, K. Henrick, D. L. Kepert, K. R. Trigwell, A. H. White and S. B. Wild, *J. Chem. Soc., Dalton Trans.* 1975, 546.
16. M. G. B. Drew and J. D. Wilkins, *J. Chem. Soc., Dalton Trans.* 1977, 194.

Polyhedron Vol. 5, No. 9, pp. 1383–1386, 1986
Printed in Great Britain

0277–5387/86 $3.00+.00
Pergamon Journals Ltd

DIFFERENTIAL-PULSE VOLTAMMETRIC STUDIES ON SOME BINARY AND TERNARY COPPER(II) AMINO ACID COMPLEXES

P. S. ZACHARIAS,* T. SREENIVAS and J. MARY ELIZABATHE

School of Chemistry, University of Hyderabad, Hyderabad 500134, India

(*Received* 20 *August* 1985; *accepted* 6 *November* 1985)

Abstract—Some selected binary and ternary copper(II) amino acid complexes are investigated by differential-pulse voltammetry and the results are discussed. These results are compared with cyclic voltammetric results of the same systems.

The electrochemical behaviour of several binary and ternary copper(II) amino acid complexes in aqueous media has been investigated recently by cyclic voltammetry and an electrode reaction mechanism has been proposed.[1,2] An important step in this mechanism is the electrochemical generation of a copper(I) intermediate species by a one-electron reduction of the starting amino acid complex. Since the eletrochemical identification of such an intermediate for the amino acid complexes had been reported for the first time, further evidence to show the generation of this species seemed desirable. Hence differential-pulse voltammetry (DPV), another sensitive electrochemical technique,[3,4] is used in the investigation of the electrochemical behaviour of some selected binary and ternary copper(II) amino acid complexes. For a reversible electrochemical process, the number of electrons (n) involved is related to the width (in mV) at the half-height of the DPV peak.[5] Since the first step in the electrode mechanism of the binary and ternary system is nearly reversible, this relationship is employed to find out the value of n for this step.

The binary copper(II) complexes are of general composition $Cu(AA)_2$ and ternary systems of composition Cu(BPY)(AA), where AA represents an amino acid ligand and BPY is the 2,2′-bipyridyl ligand. The interest in the study of copper(II) amino acid complexes is due to their reported participation in the catalysis of superoxide dismutation[6,7] and to the observation that the type 2 copper centres of copper enzymes undergo a one-electron reduction.[8] Ternary complexes containing an amino acid and another ligand system are similar to biologically important copper(II) mixed amino acid complexes.[9] Hence these binary and ternary copper(II) amino acid systems are selected for the investigation. The DPV data on these systems are presented and discussed.

EXPERIMENTAL

The binary and ternary complexes were prepared by reported methods.[1,10] The ternary systems were purified by preparative TLC on silica gel with an n-butanol–water–methanol (20 : 40 : 40) solvent system. Differential-pulse voltammograms were recorded with a three-electrode system consisting of an HMDE working electrode, PAR model 9331 SCE reference electrode and a platinum wire auxiliary electrode on a PAR 370 electrochemistry system. Aqueous solutions of 10^{-3} M concentration range with TEAP as the supporting electrolyte were used. Solution pH was changed by the addition of μl quantities of pure perchloric acid and determining the pH value by a sensitive pH meter.

RESULTS AND DISCUSSION

The DPV data on the binary and ternary complexes are presented in Tables 1 and 2, respectively. The n values calculated for the C, D Peaks are also given in Tables 1 and 2. Figure 1 represents the differential-pulse voltammograms from a repetitive scan for a representative binary compound at neutral pH conditions (neutral pH is taken to be the pH of the solution on dissolving the compound).

* Author to whom correspondence should be addressed.

Table 1. Differential-pulse voltammetry data for $Cu(AA)_2$ complexes

Compound	pH	E_p (V)				$W_{1/2}$ (mV)		n^a	
		A	B	C	D	C	D	C	D
$Cu(Gly)_2$	8.03	[b]	0.02	−0.27	−0.25	95	90	0.952	1.004
	6.14	−0.05	−0.01	−0.27	−0.25	95	90	0.952	1.004
	5.08	−0.05	−0.02	−0.27	−0.25	90	90	1.004	1.004
	3.78	−0.03	−0.07	[b]	[b]	[b]	[b]	—	—
$Cu(Ser)_2$	7.86	[b]	0.00	−0.25	−0.23	100	100	0.904	0.904
	6.22	[b]	0.00	−0.25	−0.23	100	100	0.904	0.904
	4.77	−0.06	−0.02	−0.25	−0.23	90	90	1.004	1.004
	3.83	−0.04	−0.06	[b]	[b]	[b]	[b]	—	—
$Cu(Ala)_2$	8.30	[b]	+0.01	−0.26	−0.24	100	100	0.904	0.904
	6.22	−0.05	+0.01	−0.26	−0.24	95	95	0.952	0.952
	4.87	−0.05	−0.01	−0.26	−0.24	95	90	0.952	1.004
	3.80	−0.05	−0.01	[b]	[b]	[b]	[b]	—	—
$Cu(Ile)_2$	7.91	[b]	0.02	−0.25	−0.23	100	100	0.904	0.904
	6.49	[b]	0.02	−0.25	−0.23	100	95	0.904	0.952
	5.20	−0.04	−0.01	−0.25	−0.23	95	95	0.952	0.952
	3.86	−0.04	0.00	[b]	[b]	[b]	[b]	—	—

[a] $W_{1/2} = 90.4/n$. [b] Peak not observed.

Table 2. Differential-pulse voltammetry data for Cu(BPY)(AA) complexes

Compound	pH	E_p (V)						n^a	
		A	B	C′	D′	C	D	C	D
Cu(BPY)(Gly)	6.80	−0.060	−0.030	—	—	−0.240	−0.185	0.90	0.90
	6.10	−0.060	−0.030	—	—	−0.240	−0.185	0.86	0.86
	3.10	—	—	−0.120	−0.085	—	—		
Cu(BPY)(Ser)	7.10	−0.045	−0.010	—	—	−0.215	−0.180	0.95	1.0
	5.25	−0.040	0.0	—	—	−0.215	−0.180	0.90	1.0
	4.85	—	—	−0.080	0.0	−0.220	−0.180	0.86	0.90
	4.20	—	—	−0.095	−0.010	—	—		
Cu(BPY)(Ala)	6.80	0.015	0.0	—	—	−0.210	−0.185	0.86	0.86
	5.35	0.010	−0.005	—	—	−0.210	−0.185	0.82	0.82
	4.20	—	—	−0.100	−0.070	—	—		
Cu(BPY)(Ile)	6.70	−0.040	−0.010	—	—	−0.175	−0.155	0.90	0.86
	5.30	−0.045	−0.020	—	—	−0.180	−0.160	0.90	0.90
	4.30	—	—	−0.080	−0.010	−0.170	−0.135	0.86	0.86
	3.80	—	—	−0.080	−0.020	—	—		
Cu(BPY)(Val)	7.80	−0.040	−0.020	—	—	−0.220	−0.175	0.90	0.95
	6.40	−0.035	−0.015	—	—	−0.240	−0.175	0.90	1.0
	5.40	—	—	−0.090	−0.010	−0.235	−0.170		
	4.10	—	—	−0.095	0.0	—	—		
Cu(BPY)(Thr)	7.0	−0.030	0.0	—	—	−0.205	−0.175	0.90	1.0
	5.65	[b]	−0.045	—	—	−0.205	−0.165	0.86	0.86
	5.15	—	−0.050	—	—	−0.200	−0.155	0.82	0.82
	4.25	—	—	−0.095	−0.050	—	—		

[a] $W_{1/2} = 90.4/n$. [b] Peak not observed.

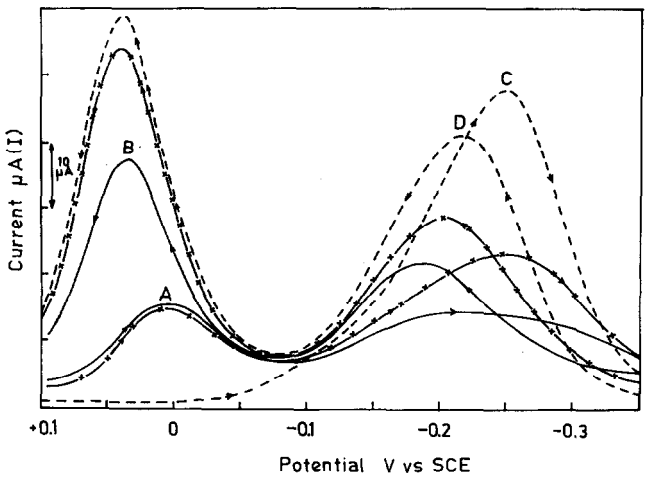


Fig. 1. Multiscan differential-pulse voltammograms of $Cu(Ser)_2$: (----) first scan, (—×—) second scan, (——) third scan.

The DPV profiles of the ternary systems at neutral pH conditions for slow scan rates are similar to the binary systems and hence will be discussed in relation to Fig. 1.

Before discussing the DPV results, the cyclic voltammetric results of the binary and ternary systems will be briefly mentioned here. The CV results can be summarized on the basis of a three-step electrode reaction mechanism. The first step involves a one-electron reduction (peak C) of the starting copper(II) complex to give an intermediate copper(I) species. Reoxidation of this to the starting complex gives peak D. The second step is the chemical reaction involving a fraction of the intermediate copper(I) species, eventually generating copper(0) species. The third step involves a two-electron oxidation of the Cu^0 to Cu^{2+} ions and its subsequent reduction, and is responsible for the B–A couple. These steps have been discussed in detail.[1,2]

The differential-pulse voltammograms (Fig. 1) show four peaks (C,D and A,B) and the potentials are listed in Tables 1 and 2. The n value of approximately 1 for the peaks C and D suggests that the redox process for this step involves a single electron. This suggests that the intermediate generated is the copper(I) species. Thus the peak C results from a single electron reduction of the starting complex while D results from the reoxidation of the generated copper(I) species. In a reversible electron transfer process, the DPV peak should be traced back in the reverse scan. The slight separation observed in peaks C and D implies that the electron transfer is only close to reversibility. A,B forms the other redox couple and involves a two-electron process between Cu^0 and Cu^{2+} species. It is clear that peak A is absent in the first scan but increases in magnitude as the scan number increases with the simultaneous decrease of C and D. This is expected as more and more Cu^{2+} is generated at the electrode on repetitive scan and this is compatible with the reaction mechanism discussed earlier. The DPV features mentioned here are observed for all the binary systems and for the ternary systems at slow scan rates. However, for the ternary systems at faster scan rates ($v > 0.01$ V s^{-1}), the A,B, couple is absent. This suggests that the chemical reactions of the intermediate species are not fast enough to generate Cu^0 species. In other words, intermediate Cu(I)(BPY)(AA) has a longer lifetime than the corresponding copper(I) binary amino acid complexes.

Protonation

The differential-pulse voltammetric characteristics of binary and ternary systems have been investigated in low pH (acidic) conditions. It is known that the binary amino acid complexes get protonated as the pH is lowered and the protonated species disproportionate to give free Cu^{2+} ions.[11] When this happens, the peaks C and D should decrease while A and B should increase in magnitude—if the earlier proposed mechanism is correct. Figure 2 shows these features clearly. However, the ternary systems behave differently. Figure 3 shows the pH-dependent DPV profiles of a representative ternary system. Peaks C and D start decreasing as pH is decreased. Simultaneously a new peak C′ starts appearing and peak A is absent. The position of peak C′ is in between that of C and A indicating that the origin of C′ is different from that of C and A. C′ does not correspond to the reduction peak of free copper ions. It is known that monobipyridyl copper(II) complex is stable at low pH conditions[12] and hence it can be believed that the

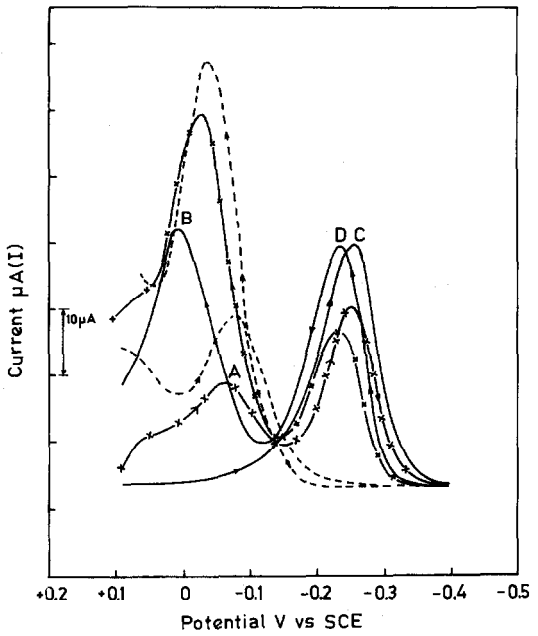


Fig. 2. Differential-pulse voltammograms at different pH values of $Cu(Ser)_2$ compound: (——) 7.86, (—×—) 4.77, (– – – –) 3.83.

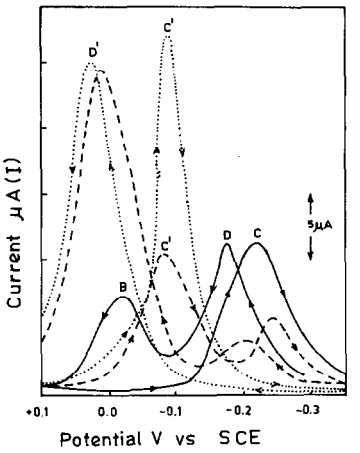


Fig. 3. Differential-pulse voltammograms at different pH values of Cu(BPY)(Val) compound: (——) 7.80, (– – – –) 4.60, (· · · ·) 3.20.

end product of protonation of the ternary systems is this species and not Cu^{2+} ions. Then peak C′ should be related to the reduction of this species. This explains the shift in the potential of C′ compared to peak A.

Thus the differential-pulse voltammetric experiments clearly support the cyclic voltammetric results on the binary and ternary systems. These experiments give additional proof to the one-electron reduction of the starting copper(II) complex, thereby confirming the electrochemical generation of the copper(I) intermediate.

REFERENCES

1. G. Thomas and P. S. Zacharias, *Polyhedron* 1985, **4**, 811.
2. G. Thomas and P. S. Zacharias, *Polyhedron* 1985, **4**, 299.
3. J. B. Flato, *Anal. Chem.* 1972, **44**, 75A.
4. A. Weissberger and B. W. Rossitter, *Techniques of Chemistry*, Vol. 1, Part IIA. Wiley Interscience, New York (1981).
5. A. J. Bard and L. R. Faulkner, *Electrochemical Methods, Fundamentals and Applications*, p. 190. Wiley, New York (1980).
6. U. Weser, *Struct. Bonding (Berlin)* 1973, **17**, 1.
7. R. Brigelius, R. Spottl, W. Bors, E. Lengfelder, M. Saran and U. Weser, *FEBS Lett.* 1974, **47**, 72.
8. B. Reinhammer, *Biochim. Biophys. Acta* 1972, 275.
9. B. Sarkar and T. P. A. Kruck, In *Biochemistry of Copper* (Edited by J. Peisach, P. Aisen and W. E. Bhimberg), p. 183. Academic Press, New York (1966).
10. W. L. Kwik, K. P. Ang and G. Chen, *J. Inorg. Nucl. Chem.* 1980, **42**, 303.
11. R. H. Carlson and T. L. Brown, *Inorg. Chem.* 1966, **5**, 268.
12. F. Debreczeni and I. Nagypal, *Inorg. Chim. Acta* 1982, **57**, 135.

Polyhedron Vol. 5, No. 9, pp. 1387–1392, 1986
Printed in Great Britain

0277-5387/86 $3.00+.00
Pergamon Journals Ltd

REACTIONS OF TETRAALKYLDIPHOSPHINES AND OF TETRAMETHYLDIPHOSPHINE MONOXIDE WITH HEXAFLUOROACETONE*

GERD-VOLKER RÖSCHENTHALER and UDO VON ALLWÖRDEN

Fachbereich 2 (Biologie/Chemie) der Universität, Leobener Strasse, 2800 Bremen 33, F.R.G.

and

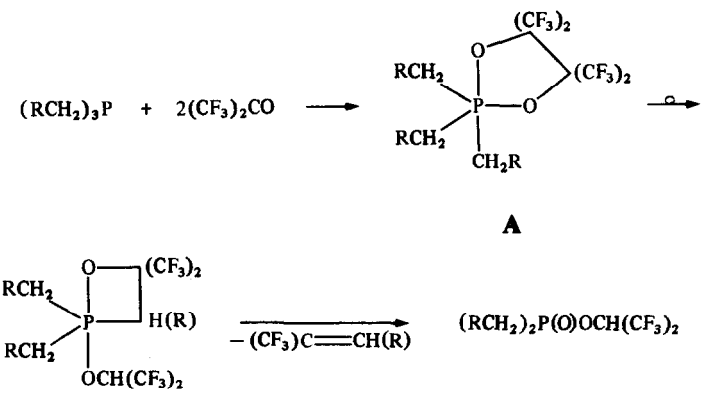
REINHARD SCHMUTZLER†

Institut für Anorganische und Analytische Chemie der Technischen Universität, Hagenring 30, 3300 Braunschweig, F.R.G.

(*Received* 4 *September* 1985; *accepted* 18 *November* 1985)

Abstract—The diphosphorus compounds $R^1R^2PPR^1R^2$ ($R^1 = R^2 = Me$ or Et; $R^1 = Me$, $R^2 = Bu^t$) and $Me_2P(:O)PMe_2$ were found to react with hexafluoroacetone (HFA) to give 1,2-λ^5-oxaphosphetanes, phosphonates and phosphinates. For $R^1 = R^2 = Et$ and $R^1 = Me$, $R^2 = Bu^t$ 1,3,2-λ^5-dioxaphospholanes were obtained. For $R^1 = R^2 = Et$, in addition, a 1,3,4-λ^5-dioxaphospholane was found. With tetramethyldiphosphine a thermally stable compound was formed containing a P(III)$C(CF_3)_2$OP(V) moiety which could be bound to a $(OC)_4Mo$ fragment. No reaction has been observed between HFA and $Bu^t_2PPBu^t_2$ and Ph_2PPPh_2.

The reactions of trimethylphosphine and triethylphosphine with hexafluoroacetone (HFA) give indications of the presence of two centres of reactivity in the molecules—the lone pair and the methyl or methylene group at phosphorus—furnishing 1,3,2-λ^5-dioxaphospholanes[1] (**A**) and 1,2-λ^5-oxaphosphetanes[1] (**B**), respectively. From the thermal decomposition of the products phosphinates (**C**) and bis(trifluoromethyl)ethene are obtained [eqn (1)]:



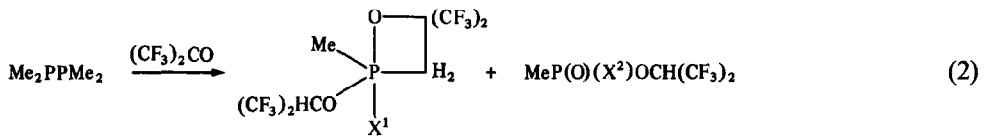
(1)

The P—P bond in tetraalkyldiphosphines may be considered a third centre of reactivity; tetrafluorodiphosphine and tetraethyldiphosphite[3]

* Dedicated to Professor Hans-Herloff Inhoffen on the occasion of his 80th birthday.

† Author to whom correspondence should be addressed.

are known to react with HFA to form a P(III)C$(CF_3)_2$OP(III) system. In the case of tetramethyldiphosphine apparently all three centres of reactivity are active [eqn (2)]:



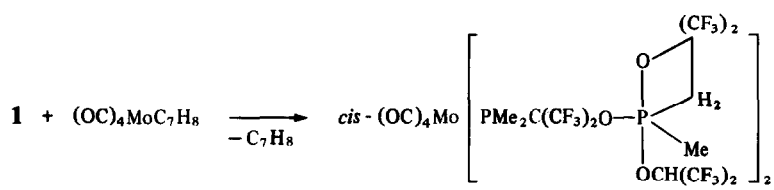
(2)

1 $X^1 = OC(CF_3)_2PMe_2$
2 $X^1 = OCH(CF_3)_2$
3 $X^1 = F$
4 $X^2 = OCH(CF_3)_2$
5 $X^2 = F$

In addition to the phosphinophosphorane (**1**), involving a P(III)C$(CF_3)_2$OP(V) bridge, phosphetanes **2** and **3** are found,[4] proving that abstraction of fluorine *and* hydrogen has occurred, as well as fission of the P—P bond. Further products were the phosphonates **4** and **5**,[5] the formation of which may be rationalized by assuming a formal loss of bis(trifluoromethyl)ethene[6] from **2** and **3**. Here we describe some properties of compound **1** and products of the reaction of diphosphines, $R^1R^2PPR^1R^2$ ($R^1 = R^2 =$ Et, Bu^t or Ph; $R^1 =$ Me, $R^2 =$ Bu^t) with HFA. The change in substituent size should provide some insight into the reaction pathway.

RESULTS AND DISCUSSION

Compound **1**[2] with its phosphine portion is able to function[1] as a ligand in a carbonyl complex [eqn (3)]:



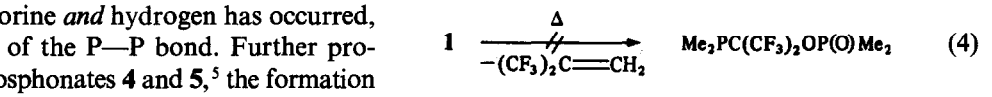
(3)

6

In norbornadiene tetracarbonyl molybdenum the olefin was readily displaced by **1** with formation of the *cis* complex (**6**), a yellow, air-sensitive solid. The IR spectrum of **6** in the CO region showed three absorptions. For a C_{2v} arrangement four ν(CO) bands are expected, two of which are apparently overlapping. HFA did not oxidize the phosphine part of the molecule of **1** with formation of a $C(CF_3)_2O$-bridged diphosphorane.

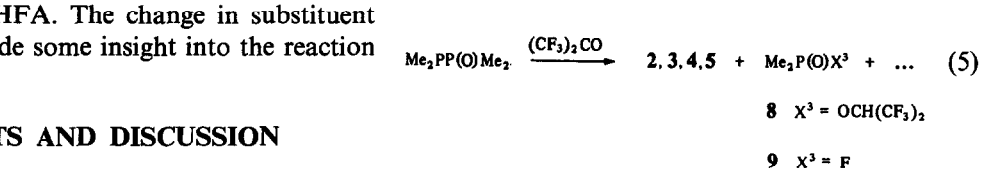
The thermal decomposition of **1** with the expected formation of **7** was not straightforward.*

In order to obtain the product of oxidation of **1**, involving the $Me_2P(O)C(CF_3)_2O$ moiety tetramethyldiphosphine monoxide[7] was allowed to react with HFA but compounds **2**, **3**, **4** and **5**, and the phosphinates **8**[1] and **9**[8] were formed [eqn (5)]:



(4)

7



(5)

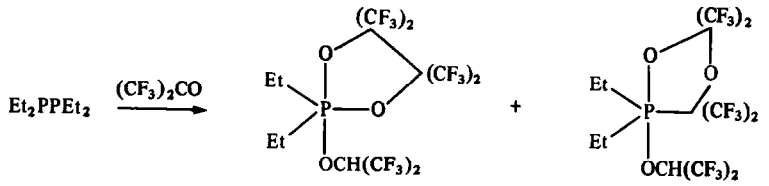
8 $X^3 = OCH(CF_3)_2$
9 $X^3 = F$

A small amount of bis(trifluoromethyl)ethene was also detected.

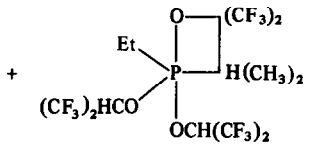
The products of the reaction of tetraethyldiphosphine[9] with HFA [eqn (6)] were three isomeric phosphoranes,[10] the 1,3,2-λ^5- and 1,3,4-λ^5-dioxaphospholanes (**10** and **11**), the 1,2-λ^5-oxaphosphetane (**12**), and the phosphinate **13**,[1] respectively, in the ratio 1:4:28:57. From the monochlorophosphines, R_2PCl (R = Me or Et), and HFA 1,3,4-λ^5-dioxaphospholanes were also obtained.[11,12]

In the case of Me(Bu^t)PP(Bu^t)Me[13] the 1,3,2-λ^5-dioxaphospholane (**14**), the 1,2-λ^5-oxaphosphetane (**15**),[14] the phosphonate **4**, and the phosphinate **16**

*A non-separable mixture of **2** (10%), **3** (10%), **4** (15%), **5** (10%), **8** (20%) and **9** (7%), and other, unidentified, products was observed.



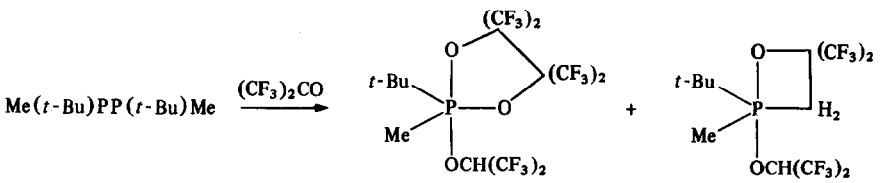
10 11



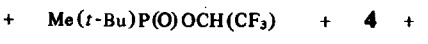
12 13

(6)

were observed in the reaction mixture in a ratio 1:35:36:22 [eqn (7)]:



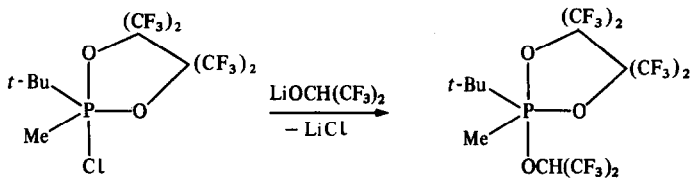
14 15



16

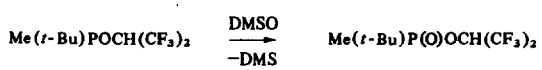
(7)

Formation of the 1,3,4-λ^5-dioxaphospholane system was not observed, presumably for steric reasons. Compound **15** could be separated from **14**, **4** and **16** by means of preparative thin-layer chromatography while **14**, **4** and **16** could not be isolated in a pure state. **14** was prepared via a different route [eqn (8)]:



17 14

Starting from **17**[11] chlorine was substituted by lithium - [2,2,2 - trifluoro - 1 - (trifluoromethyl)]-ethylate to furnish **14** in good yield. **16** was obtained by oxidation of the phosphinate $Me(Bu^t)POCH(CF_3)_2$[15] with dimethylsulfoxide [eqn (9)]:

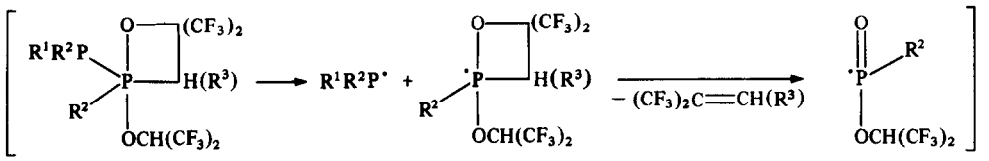


16

Tetra-*tert*-butyldiphosphine[16] and tetraphenyldiphosphine did not react with HFA under the conditions employed. In the reaction of the diphosphine monoxide, $Me_2P(O)PMe_2$, and of the diphosphine, $Me(Bu^t)PP(Bu^t)Me$, with HFA small amounts of $(CF_3)_2C{=}CH_2$, in the case of Et_2PPEt_2 traces of $(CF_3)_2C{=}CHCH_3$,[1] were formed and were characterized by IR and NMR spectroscopy. As a result of the formation of phosphonates and phosphinates the observation of the corresponding olefins was to be expected if the Wittig-type products, the oxaphosphetanes are the precursors. On the other hand the phosphoryl group may also be created by oxygen transfer from HFA which is not observed in the case of Me_3P or Et_3P but is with $(Me_2N)_3P$.[17] When Et_2PPEt_2 and $(CF_3)_2C{=}CH_2$ are allowed to react a red, viscous oil is formed. A red, non-distillable liquid was found to be left as a residue in all cases, after the more volatile products

had been removed by distillation. It was *not* formed during the separation process.

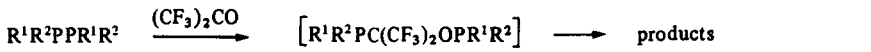
The reaction mechanism operative here is not clear. There is the possibility of the formation of a phosphinophosphorane (**D**), which may serve as a source of radicals [eqn (10)]:



(10)

D $R^3 = H$ or CH_3

yielding further products. It also seems likely that an insertion of HFA into the P—P bond is taking place giving species **E** which is decomposed in a fashion similar to that of $Ph_2PC(CF_3)_2OH$ to yield the products observed [eqn (11)]:



(11)

E

The mass spectrum of **6** showed ions formed due to a successive loss of CO: M^+, M^+-CO, M^+-2CO, M^+-4CO and M^+-CO-L, $M^+-2CO-L$, $M^+-3CO-L$ and $M^+-4CO-L$. The fragment of highest abundance is CF_3^+. The mass spectrum of **14** did not exhibit a molecular ion but fragments due to M^+-F, M^+-Bu^t, M^+-CF_3, $M^+-OCH(CF_3)_2$, CF_3^+ and Bu^t (100%) were observed.

The ^1H and ^{19}F NMR data for the ligand in **6** were found not to differ significantly from those of the non-coordinated species.[4] The ^{19}F NMR spectrum of **14** proves clearly that the phosphorane structure is rigid, relative to the NMR time scale. Four multiplets for the ring–CF_3 groups and two doublets of quartets for the $OCH(CF_3)_2$ grouping are observed, due to the presence of chiral phosphorus (five different groups are bonded to λ^5-phosphorus). The phosphorus atom in **16** is also chiral and induces magnetic inequivalence on the CF_3 groups.

EXPERIMENTAL

All manipulations were carried out in an atmosphere of dry nitrogen using standard techniques. Literature procedures were employed for the preparation of the phosphorane **1**,[4] norbornadiene molybdenum tetracarbonyl,[18] tetramethyldiphosphine monoxide,[7] tetraethyldiphosphine,[9] 1,2-dimethyl-1,2-di-*t*-butyldiphosphine,[13] tetra-*t*-butyldiphosphine,[16] and hexafluoroisopropyl methyl-*t*-butylphosphinate.[4]

NMR spectra were recorded on a Bruker WH-360 instrument. Chemical shifts are referenced to internal TMS for ^1H, external CCl_3F for ^{19}F, and external 85% H_3PO_4 for ^{31}P. High-field chemical shifts are listed with a negative sign. IR spectra were obtained on solutions using a Perkin–Elmer 577 instrument. Mass spectra (at 70 eV) were recorded on a Varian MAT-CH 7 spectrometer. Elemental analyses were performed by Mikroanalytisches Laboratorium Beller, Göttingen.

Preparation of bis-{2 - [2,2,2 - trifluoro - 1 - (trifluoromethyl)ethoxy - 2 -]2,2,2 - trifluoro - 1 - (trifluoromethyl) - 1 - (dimethylphosphino)ethoxy - 2 - methyl - 4,4 - bis(trifluoromethyl) - 1,2 - λ^5 - oxaphosphetan}tetracarbonylmolybdenum (**6**)

A mixture of **1** (12.40 g; 0.02 mol) in 50 cm^3 of methylcyclohexane and 3.00 g (0.01 mol) of norbornadiene tetracarbonylmolybdenum was stirred at room temperature for 6 days. After solvent and norbornadiene were distilled off a residue of 14.00 g (95%) of **6** (m.p. 114°C) remained.

IR spectrum (*n*-hexane): 2040(m), 1985(s), 1950(s) [ν(CO)].

Mass spectrum [proposed fragment and relative abundance (^{98}Mo) in parentheses]: *m/z* 1450 (M^+, 11%); 1422 (M^+-CO, 2); 1394 (M^+-2CO, 1); 1338 (M^+-4CO, 2); 930 (M^+-L, 23); 802 (M^+-CO-L, 30); 774 ($M^+-2CO-L$, 15); 744 ($M^+-3CO-L$, 35); 716 ($M^+-4CO-L$, 41); 620 (L^+, 71); 69 (CF_3^+, 100).

NMR spectra—^1H: δ 1.25 [6H, P(III)Me_2; ^2J(PH) 4.00]; 2.20 [3H, P(V)Me; ^2J(PH) 16.50]; 4.50 (2H, CH_2, ABX spin system); 5.85 (1H, CH, not resolved multiplet). ^{19}F: δ −64.10 [3F, multiplet, P(III)$C(CF_3)_2$], −65.10 [3F, multiplet; P(III)$C(CF_3)_2$], −74.00 [6F, $OCH(CF_3)_2$, broad signal], −77.90 (3F, multiplet), −79.50

(3F, multiplet). ^{31}P: δ_P[P(III)] 20.3 (multiplet); δ[P(V)] −10.5 (multiplet), {^1H}.

Analysis. $C_{30}H_{24}F_{36}MoO_{10}P_4$ (1448.30): Calc. C, 24.9; H, 1.7; F, 47.2%. Found C, 24.9; H, 1.6; F, 47.1%.

Attempted reaction of **1** *with HFA*

A mixture of **1** (12.40 g, 0.02 mol) and HFA (6.60 g, 0.04 mol) was sealed in a heavy-wall glass tube. After 1 week the two compounds were recovered unreacted.

Reaction of tetramethyldiphosphine monoxide with HFA

A mixture of 1.38 g (0.01 mol) of tetramethyldiphosphine monoxide and 3.32 g (0.02 mol) of HFA was allowed to react for 1 day at room temperature. The olefin, $(CF_3)_2C{=}CH_2$ (0.10 g), was recovered from the reaction mixture which was found to contain compounds **2**,[4] **3**,[4] **4**,[5] **7**[1] and **8**[8] in the ratio 3:2:1:1:2. All compounds could be removed from the red oily residue by distillation at 100°C (0.001 mm).

Reaction of tetraethyldiphosphine with HFA

A mixture of 2.70 g (0.015 mol) of tetraethyldiphosphine and 10.00 g (0.06 mol) of HFA was allowed to react at −50°C for 2 days and was subsequently warmed up to room temperature over 1 day. The attempted separation of the reaction mixture into its components by distillation was unsuccessful. ^{31}P NMR spectroscopy revealed the presence of **9**,[10] **10**,[10] **11**,[10] and **12**[1] in a ratio of 1:4:28:57. All compounds were found to be distillable from the viscous, red reaction mixture at 100°C (0.001 mm). The olefin $(CF_3)_2C{=}CHCH_3$ could be separated and was characterized by its IR and NMR spectra.

Reaction of 1,2 - *dimethyl* - 1,2 - *di* - tert - *butyldiphosphine with HFA*

1,2 - Dimethyl - 1,2 - di - *tert* - butyldiphosphine (4.00 g, 0.02 mol) and 13.30 g (0.08 mol) of HFA were allowed to react for 3 h at −50°C. Over a period of 5 h the mixture was allowed to warm up to room temperature. Compound **14** could be separated by preparative thin-layer chromatography (Al_2O_3, 150*F*; benzene; R_f 1.0). The ^{31}P NMR investigation of the reaction mixture revealed the presence of **13**, **14**,[4] **15** and **5**[5] in a ratio of 1:35:36:22. All compounds could be removed by distillation from the reaction mixture—a red, viscous oil—at 100°C (0.001 mm) but their separation was not possible.

Preparation of 2 - [2,2,2 - *trifluoro* - 1 - (*trifluoromethyl*)*ethyl*] - 2 - *methyl* - 2 - tert - *butyl* - 4,4,5,5 - *tetrakis*(*trifluoromethyl*) - 1,3,2 - λ^5 - *dioxaphospholane* (**13**)

2 - Chloro - 2 - methyl - 2 - *tert* - butyl - 4,4,5,5 - tetrakis(trifluoromethyl) - 1,3,2 - λ^5 - dioxaphospholane (**16**)[15] (2.00 g, 0.004 mol) was added to 1.10 g (0.06 mol) of lithium - 2,2,2 - trifluoro - 1 - (trifluoromethyl)ethylate. After the mixture had been warmed up to 40°C for 30 min, 10 cm^3 of pentane were added. in order to separate the lithium chloride formed. The solvent was removed and the remaining liquid was distilled at 128°C (2 mm). Compound **14** was obtained in a yield of 1.10 g (43%).

IR spectrum: 2998(m), 2948(s), 2930(m), 2900(m), 2862(m) [ν(CH)], 1475(m), 1460(m), 1415(w), 1398(m), 1362(s), 1350(s), 1300(vs), 1260(vs), 1180(vs), 1100(vs) [ν(CF)], 1017(m), 990(m), 954(s), 936(s), 878(s), 816(s), 755(s), 740(s), 705(s), 680(s).

Mass spectrum: *m/z* 583 (M^+-F, 2%); 545 (M^+-Bu^t, 48); 533 (M^+-CF_3, 12); 435 [$M^+-OCH(CF_3)_2$, 20]; 69 (CF_3^+, 57); 57 (Bu^t, 100).

NMR spectra—^1H: δ 2.05 [9H, Bu^t; ^3J(PH) 25.00]; 2.60 [3H, Me; ^2J(PH) 12.40]; 5.10 [1H, $CH(CF_3)_2$; ^3J(HF) 5.80]. ^{19}F: δ −66.98 (3F, multiplet); −67.47 (3F, multiplet); −69.00 (3F, multiplet); −70.09 (3F, multiplet); −74.27 (3F, multiplet); −74.82 (3F, multiplet). ^{31}P: δ +12.30.

Analysis. $C_{14}H_{13}F_{18}O_3P$ (602.21). Calc. C, 27.9; H, 2.2; F, 56.8%. Found C, 28.0; H, 2.3; F, 56.5%.

Preparation of methyl - tert - *butyl* - [2,2,2 - *trifluoro* - 1 - (*trifluoromethyl*)*ethyl*]*phosphinate* (**16**)

Dimethylsulfoxide (1.50 g, 0.02 mol) in 20 cm^3 of diethylether was added to 5.30 g (0.02 mol) of methyl - *tert* - butyl[2,2,2 - trifluoro - 1 - (trifluoromethyl)ethyl]phosphinate,[16] and the mixture was stirred for three days at 70°C. The solvent was removed and the remaining liquid (dimethylsulfoxide) was distilled at 50°C (0.3 mm); m.p. 28°C. **16** [4.20 g (77%)] remained as a residue.

IR spectrum: 2970(m), 2932(m), 2868(m) [ν(CH)], 1460(m), 1372(s), 1290(s), 1260(s), 1255(vs), 1200(vs), 1105(vs) [ν(CF)], 1011(m), 940(w), 890(s), 868(m), 820(m), 755(m), 723, 682(m).

NMR spectra—^1H: δ 1.04 [9H, Bu^t; ^3J(PH) 16.00]; 1.40 [3H, Me; ^2J(PH) 13.00]; 5.10 [1H,

$CH(CF_3)_2$; ^3J(HF) 5.80]. ^{19}F: δ −73.50 (3F, multiplet); −74.36 (3F, multiplet). ^{31}P: δ +49.30.

Analysis. $C_8H_{13}F_6O_2P$ (286.15). Calc. C, 33.6; H, 4.6; F, 39.8%. Found C, 33.5; H, 4.6; F, 40.1%.

*Attempted reaction of tetra-*tert*-butyldiphosphine and tetraphenyldiphosphine with HFA*

A mixture of the diphosphine (0.01 mol) and HFA (6.64 g, 0.04 mol) was heated for 3 days at 100°C in a steel cylinder. The starting compounds were recovered unreacted.

Reaction of tetraethyldiphosphine with 3,3,3 - trifluoro - 2 - (trifluoromethyl)propene (2)

Tetraethyldiphosphine (1.80 g, 0.01 mol) and 1.60 g (0.01 mol) of 3,3,3 - trifluoro - 2 - (trifluoromethyl)propene were sealed together into a heavy-wall glass tube. After 2 days at room temperature a red, viscous oil was obtained after removal of the unreacted tetraethyldiphosphine. The ^{19}F and ^1H NMR spectra showed very broad signals at δ_F −67.0 and δ_H 5.3.

Acknowledgements—The support of Fonds der Chemischen Industrie is gratefully acknowledged. Hexafluoroacetone was kindly supplied by Dr S. Misaki of Daikin Kogyo Ltd, Osaka, Japan. I. Erxleben and J. Stelten are thanked for recording NMR and mass spectra.

REFERENCES

1. F. Ramirez, C. P. Smith and J. F. Pilot, *J. Am. Chem. Soc.* 1968, **90**, 6772.
2. G. N. Bokerman and R. W. Parry, *J. Fluorine Chem.* 1976, **7**, 1.
3. V. L. Foss, N. V. Lukashev, Yu. E. Tsvetkov and I. F. Lutsenko, *Zh. Obshch. Khim.* 1982, **52**, 2183.
4. G.-V. Röschenthaler, J. A. Gibson and R. Schmutzler, *Z. Naturforsch.* 1977, **32B**, 599.
5. G.-V. Röschenthaler, *Z. Naturforsch.* 1978, **33B**, 131.
6. M. H. Kauffman and J. D. Braun, *J. Org. Chem.* 1966, **31**, 3090.
7. M. Volkholz, O. Stelzer and R. Schmutzler, *Chem. Ber.* 1978, **111**, 890.
8. (a) J. F. Nixon and R. Schmutzler, *Spectrochim. Acta* 1964, **20**, 1835; (b) R. Schmutzler, *J. Chem. Soc.* 1964, 4551.
9. K. Issleib and W. Seidel, *Chem. Ber.* 1965, **92**, 2681.
10. U. v. Allwörden, I. Tzeggai and G.-V. Röschenthaler, *Phosphorus Sulphur* 1984, **21**, 177.
11. J. A. Gibson, G.-V. Röschenthaler, K. Sauerbrey and R. Schmutzler, *Chem. Ber.* 1977, **110**, 3214.
12. V. N. Volkovitskii, I. L. Knunyants and E. G. Bykhovskaya, *Zh. Vses. Khim. Ova* 1973, **18**, 112.
13. O. J. Scherer and W. Gick, *Chem. Ber* 1970, **103**, 71.
14. D. Dakternieks, G.-V. Röschenthaler, K. Sauerbrey and R. Schmutzler, *Chem. Ber.* 1979, **112**, 2382.
15. D. Dakternieks, G.-V. Röschenthaler and R. Schmutzler, *Z. Naturforsch.* 1978, **33B**, 507.
16. K. Issleib and W. Hoffmann, *Chem. Ber.* 1966, **99**, 1320.
17. F. Ramirez, A. S. Gulati and C. P. Smith, *J. Am. Chem. Soc.* 1967, **89**, 6283.
18. R. Pettit, *J. Am. Chem. Soc.* 1959, **81**, 1266.
19. E. Evangelidou-Tsolis, F. Ramirez, J. F. Pilot and C. P. Smith, *Phosphorus* 1974, **4**, 109.

Polyhedron Vol. 5, No. 9, pp. 1393–1403, 1986
Printed in Great Britain

0277–5387/86 $3.00+.00
Pergamon Journals Ltd

RAMAN SPECTROSCOPIC STUDIES OF VAPOR COMPLEXATION IN THE MCl_4–$POCl_3$ AND MCl_4–$AlCl_3$ (M = Zr OR Hf) BINARY SYSTEMS

S. BOGHOSIAN and G. N. PAPATHEODOROU*

Institute of Chemical Engineering and High Temperature Chemical Processes, University of Patras, GR-26110 Patras, Greece

and

R. W. BERG and N. J. BJERRUM

Chemistry Department A, The Technical University of Denmark, DK-2800 Lyngby, Denmark

(*Received* 30 *September* 1985; *accepted* 25 *November* 1985)

Abstract—Raman spectra of vapor mixtures $ZrCl_4$–$POCl_3$, $HfCl_4$–$POCl_3$, $ZrCl_4$–$AlCl_3$ and $HfCl_4$–$AlCl_3$ are obtained in the temperature range 300–500°C. The spectra consist of superposition of bands due to the component gases plus a few new bands which were attributed to vapor complexation. A comparison of the spectra features in the systems MCl_4–$POCl_3$ (M = Zr or Hf) with the spectra of the 1:1 liquid and glass $MCl_4 \cdot POCl_3$ (M = Zr or Hf) with the spectra of the 1:1 liquid and glass $MCl_4 \cdot POCl_3$ indicate that the vapor complexes also have a 1:1 stoichiometry and that complexing occurs through oxygen bridging. The strongest Raman bands for the Zr–O–P and the Hf–O–P complex are at 508 and 512 cm^{-1}, respectively. For the MCl_4–$AlCl_3$ systems two possible vapor complexes, MAl_2Cl_{10} and $MAlCl_7$, are considered. Temperature dependence measurements of the Raman spectra of the $ZrCl_4$–$AlCl_3$ systems indicate that the predominant vapor complex is probably 1:1 and permit the estimation of the enthalpy of the reaction: $ZrCl_4(g) + \frac{1}{2}Al_2Cl_6(g) = ZrAlCl_7(g)$; $\Delta H^0 = -34.9 \pm 2.5$ kJ mol^{-1}. The strongest Raman bands for the Zr–Cl–Al and the Hf–Cl–Al complex are at 401 and 391 cm^{-1}, respectively, and is assigned to M—Cl (terminal) stretching.

It has been established that inorganic salt vapors at elevated temperatures (typically above 150°C) react with condensed-phase compounds or other vapors to form vapor complexes.[1–3] Vapor complexation appears to be a general phenomenon for many metal-halide salts as well as oxides and sulfides and is important in determining the vapor pressures, rates of vaporization and apparent volatilities of materials. A large number of vapor complexes involving mainly metal halides have been reported and extensive reviews on their structural[4–7] and thermodynamic[8–10] properties are available. The most important of the complex-forming agents are the chlorides and bromides of tervalent Al, Ga, In and Fe. Reactions of these trihalides with many monovalent, divalent and tervalent metal halides have been reported and the structural properties of the vapor complexes have been studied by means of electronic and vibrational (mainly Raman) spectroscopy.[4,5] Raman spectroscopy has also been used for investigating the vapor complexes of $AlCl_3$ with $ZrCl_4$[11] and $NbCl_5$,[12] and for studying the structures of the "adduct"-type molecules $AlX_3 \cdot NH_3$ (X = F, Cl or Br).[13]

Like Al, Ga, In and Fe trihalides the $POCl_3$ has

*Author to whom correspondence should be addressed.

"acid"-like properties and is known to react with metal halides to form complexes (adducts) in the liquid, solid and vapor phase.[14-16] The formation of vapor complexes of $POCl_3$ with $ZrCl_4$ and $HfCl_4$ has been carefully investigated due to the potential use of these systems for separation by distillation of Zr from Hf in nuclear reactor materials.[17]

The present work is concerned with the characterization of the vibrational spectra of equilibrium vapor complexes of the tetravalent chlorides of Zr and Hf with $POCl_3$ and $AlCl_3$. Raman spectroscopy is used to study the vapors over the liquid $POCl_3$–MCl_4 and $AlCl_3$–MCl_4 mixtures (M = Zr or Hf). Certain vibrational band wavenumbers of the vapor complexes in these systems are determined and, for the $ZrCl_4$–$AlCl_3$ system, the enthalpy of complex formation is measured from the spectral data. Finally, the vibrational band wavenumbers in the 1:1 "adduct molecules" $MCl_4 \cdot POCl_3$ in the liquid and glass state are determined by Raman spectroscopy.

EXPERIMENTAL

High-purity $AlCl_3$, $ZrCl_4$ and $HfCl_4$ were prepared from "Cerac Pure" reagents by repeated slow sublimations in fused silica tubes sealed *in vacuo*. Liquid $POCl_3$ was purchashed from Cerac Pure and used without further purification.

The Raman (optical) cells containing the salt vapors were made of 20-mm o.d. fused silica tubing.[18] All cells were approximately of the same dimensions with a volume of ~ 5 cm^3. Before use all cells were carefully cleaned, rinsed well, flamed to red-heat with a propane–oxygen torch and degassed by evacuating while hot.

The cells for recording the vapor-phase Raman spectra of MCl_4–$POCl_3$ (M = Zr or Hf) were loaded using dry-box techniques as follows. Preweighed amounts of MCl_4 were transferred into a cell of known volume which was then attached to a vacuum line. The desired amounts of $POCl_3$ were fed into the evacuated cell by connecting it with a spherical flask containing known quantities of $POCl_3$. The bottom of the Raman cell was then cooled with liquid nitrogen to condense all the $POCl_3$ from the flask, and the neck of the cell was sealed *in vacuo*.

The amount of $POCl_3$ added was more than 50 mol %. By heating up a cell, low-melting glass-forming liquids, $MCl_4 \cdot 2POCl_3$ and $MCl_4 \cdot POCl_3$, were formed.[14] At temperatures above 150°C a stable liquid, presumably the 1:1 adduct, was always present in the cell in equilibrium with the vapor phase. Raman spectra of the vapors over this liquid are presented here.

Raman spectra of the 1:1 adduct liquid at 200°C and its glass at 25°C were also measured by fast cooling of the cell and by condensing and isolating the vapors away from the liquid glass. Additional cells containing pure $POCl_3$, $ZrCl_4$ and $HfCl_4$ were also prepared for recording the vapor-phase Raman spectra of the pure compounds. Detailed spectra for all three compounds have been measured and reported previously[19,20] but it was necessary to repeat these measurements so to compare the relative intensities of the vapor mixtures with those of the pure compounds.

The cells for measuring the Raman spectra of the MCl_4–$AlCl_3$ (M = Zr or Hf) vapors were prepared by adding preweighed amounts of MCl_4 and $AlCl_3$ into the neck of the cell then subliming the chemicals into the cell *in vacuo*. Several cells were also made having largely varying molar ratios of $AlCl_3$ and MCl_4 to be able to obtain the spectra of vapor in equilibrium with the liquid mixture.

For the $POCl_3$–MCl_4 systems the spectra were measured in cells where the vapors were in equilibrium with the liquid phase. For the $AlCl_3$–MCl_4 systems measurements from two cells (I and II) containing vapor mixtures and no condensed phases, as well as gas over liquid spectra concerning the $ZrCl_4$–$AlCl_3$ (cell III) will be presented here. Other gas–liquid-containing cells for both sets of systems, $POCl_3$–MCl_4 and $AlCl_3$–MCl_4, gave similar results and do not contribute much to the discussion.

Cell I had 171 mg $AlCl_3$ plus 36 mg $ZrCl_4$. Cell II had 116 mg $AlCl_3$ plus 20 mg $HfCl_4$. Cell III had 110 mg $AlCl_3$ plus 170 mg $ZrCl_4$ but its total volume was less than 1 cm^3. At temperatures above 220°C, all the $AlCl_3$ contained in cells I and II was in the vapor phase (mainly as Al_2Cl_6) giving rise to "ideal-gas" Al_2Cl_6 pressures of ~ 3.5 and ~ 2 atm, respectively. At the same temperature the partial pressures of $ZrCl_4$ (cell I) and $HfCl_4$ (cell II) should be ~ 0.5 and ~ 2 atm, respectively (values calculated assuming that all $ZrCl_4$ or $HfCl_4$ should be in an "ideal gas" gas phase). At 220°C or higher temperatures no formation of solid compounds could be observed.

The procedures and techniques for obtaining the Raman spectra at elevated temperatures have been described before.[18] By stabilizing the laser power and frequency, the same optical geometry and the same size cells, the relative Raman intensities could be reproduced to within less than 5%. Relative Raman intensities of gases obtained from the same cell at different temperatures could be also obtained within the same error.[18]

RESULTS AND DISCUSSION

MCl_4–$POCl_3$ (M = Zr *or* Hf) *systems*

A series of Raman spectra of vapors over the MCl_4–$POCl_3$ liquid mixtures were obtained. Representative spectra for the $ZrCl_4$–$POCl_3$ and $HfCl_4$–$POCl_3$ systems are shown in Figs. 1 and 2, respectively. A comparison with the spectra of the pure gases, $POCl_3$(g) and MCl_4(g) (see, for example, Fig. 2), shows that the vapor spectra over the liquid mixtures are mainly a superposition of bands due to the component gases plus certain new bands which are attributed to vapor complexation. The wavenumbers of these new bands are given in Table 1 which shows all the measurements including the wavenumbers of the 1 : 1 liquids and glasses, as well as the wavenumbers of the pure component gases. The glass–liquid spectra are shown in Fig. 1 for the $ZrCl_4$–$POCl_3$ mixture. Spectra of similar quality were also obtained for the $HfCl_4$–$POCl_3$ glass–liquid mixture and the Raman wavenumbers are

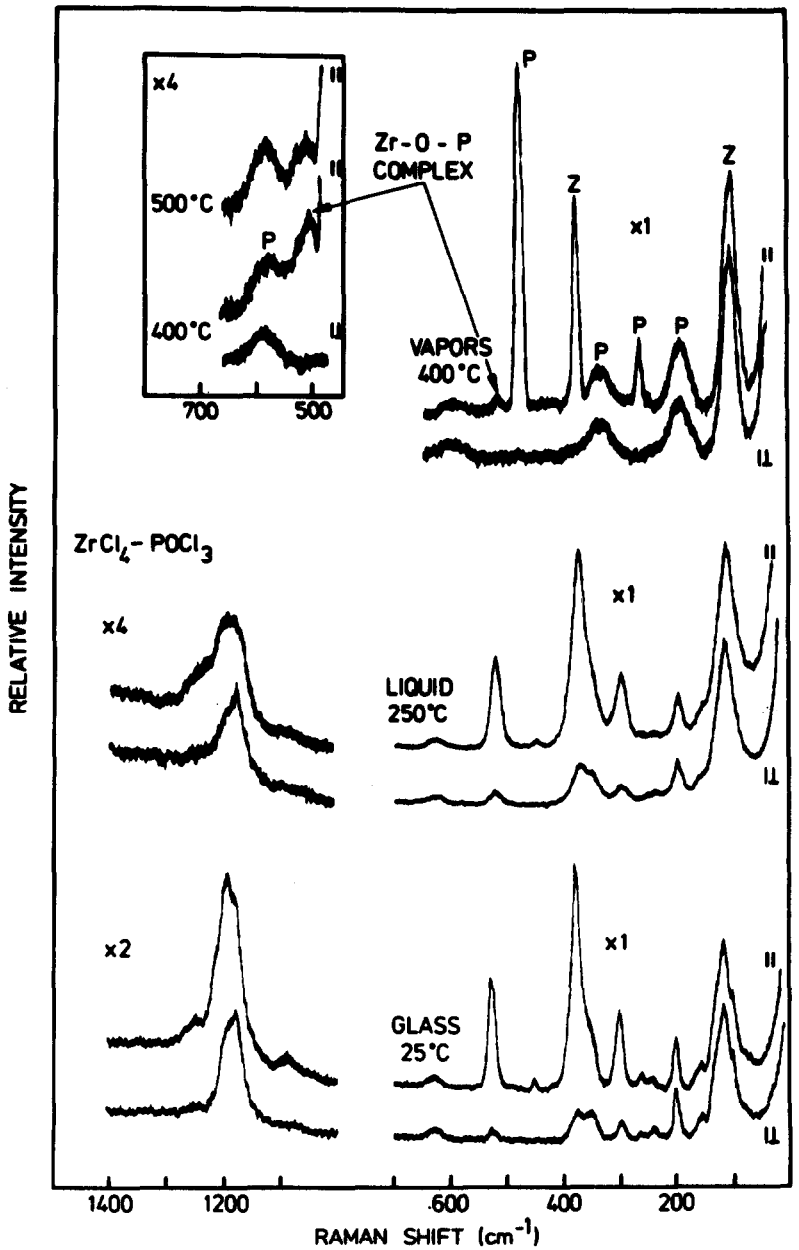


Fig. 1. Raman spectra of $ZrCl_4$–$POCl_3$ system. $\lambda_0 = 514.5$ nm, laser power = 1 W for the upper part (vapors); $\lambda_0 = 488.0$ nm, laser power 220 mW for the liquid and glass. Spectral slit width: 8 cm^{-1} for vapors and liquid, 2 cm^{-1} for glass.

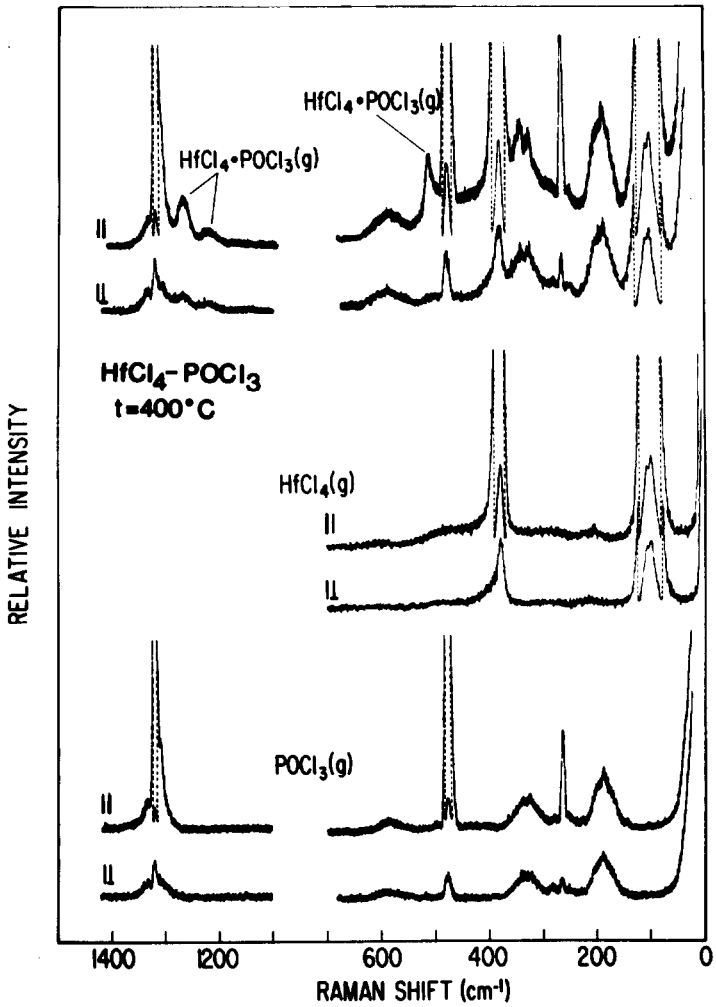


Fig. 2. Raman spectra of $POCl_3$ and $HfCl_4$ vapors, and vapors over $POCl_3$–$HfCl_4$ liquid mixtures at 400°C. $\lambda_0 = 514.5$ nm, laser power = 1 W. Spectral slit width = 4 cm^{-1}.

reported in Table 1. Presumably the spectra of the 1 : 1 liquid or glass mixture are due to the formation of the $MCl_4 \cdot POCl_3$ "adduct" molecules.[14,17]

In the $ZrCl_4$–$POCl_3$ system the data in Table 1 and Fig. 1 show a vapor complex band at 508 cm^{-1}. Three bands at 512, 1221 and 1263 cm^{-1} are seen for the complex in the $HfCl_4$–$POCl_3$ system (Table 1, Fig. 2). In the wavenumber region 1110–1500 cm^{-1} the vapor Raman cells with $ZrCl_4$–$POCl_3$ gave a strong fluorescence background and the probable bands due to the complex in that range were not seen, presumably due to the low signal : noise ratio. It should be noticed that most of the strong bands due to $MCl_4(g)$ and $POCl_3(g)$ are also present as strong bands in the spectra of the adduct liquid or glass with wavenumbers shifted to higher or lower energies. Thus, it is expected that in the vapor-phase spectra only those bands of the complex with strong intensities and with wavenumbers far away from those of the component gases will be seen.

With increasing temperature the intensities of the Raman bands due to the vapor complexes decreased relative to the bands of the component gases, indicating decomposition of the complex. An example of the temperature effect on the vapor spectra is shown in the insert of Fig. 1. The most probable equilibrium established in the gas phase[15,17] and also compatible with the spectral behavior here is:

$$MCl_4(g) + POCl_3(g) = MCl_4 \cdot POCl_3(g). \quad (1)$$

The formation of $(MCl_4 \cdot POCl_3)_2$ dimers[21(a)] as well as $MCl_4 \cdot 2POCl_3$ molecules[14] can be excluded from the previously reported vapor density measurements.[14,17]

The bonding in the "adduct" vapor complex $MCl_4 \cdot POCl_3$ (I) presumably occurs[14] by bridging the oxygen of $POCl_3$ (C_{3v} molecular symmetry)[19] to the metal atom through the face of the MCl_4 tetrahedron (T_d molecular symmetry in the gas[20,21(b)] phase).

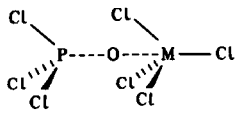
Table 1. Vibrational band wavenumbers (cm^{-1}) of the $ZrCl_4$–$POCl_3$ and $HfCl_4$–$POCl_3$systems[a]

$POCl_3$	$ZrCl_4$	$HfCl_4$	$ZrCl_4$–$POCl_3$			$HfCl_4$–$POCl_3$			
Vapor (400°C)	Vapor (400°C)	Vapor (400°C)	Glass (25°C)	Liquid (250°C)	Vapor[a] (400°C)	Glass (25°C)	Liquid (250°C)	Vapor[b] (400°C)	Assignment
	98s, $\nu_2(E)$	102.1s, $\nu_2(E)$	110sh			105m	101m		E
	113s, $\nu_4(T_2)$	109.5s, $\nu_4(T_2)$	125s	119s		133s	123s		E
186.5m, $\nu_6(E)$			162w	160w					E
			210m	205m		207m	205m		E
265.5s(p), $\nu_3(A_1)$									
			250w	245w					
			270w(p)	265w(p)					
			311m(p)	309m(p)		307m(p)	305m(p)		A_1
325.7w, 341.6w $\nu_5(E^c)$			357sh	365sh		358sh			E
	377s(p), $\nu_1(A_1)$	380.7s(p), $\nu_1(A_1)$	387s(p)	380s(p)		371m(p)	367s(p)		A_1: ν_{M-Cl}
	418w, $\nu_3(T_2)$	392sh, $\nu_3(T_2)$							
			461w(p)	458w(p)		465w(p)	453w(p)		A_1
478.5s(p), $\nu_2(A_1)$			537s(p)	532s(p)	508w(p)	536s(p)	534s(p)	512m(p)	A_1: ν_{P-Cl}
587.2w, $\nu_4(E)$			637w	632w			640w		E
			1095w(p)						
			1185m	1186m		1200w	1200w	1221w	E
			1200m(p)	1197m(p)			1200w(p)	1263w(p)	A_1: ν_{P-O}
			1257w(p)	1251w(p)					A_1
1319.4s(p), $\nu_1(A_1)$									

[a] Intensity code: s = strong, m = medium, w = weak, v = very, sh = shoulder, (p) = polarized.

[b] Due to high partial pressures of MCl_4 and $POCl_3$, the Raman bands of the vapor complex are contained in the strong bands of the component gases.

[c] Vibrational–rotational contour.



I

The molecular symmetry of the vapor-complex is C_{3v}. Rotation of the component molecules around the P–O–M axis does not alter this symmetry. The distribution of the 24 vibrational degrees of freedom of the complex can be classified by group theory into 16 modes as follows:

$$\Gamma_{\text{complex}} = 7A_1(\text{R, IR}) + 8E(\text{R, IR}) + A_2(\text{IR}).$$

An assignment of the observed bands is given in Table 1.

It is noteworthy that the ν(P—Cl) stretching frequency in the vapor complex is blue-shifted relative to the corresponding band of the free $POCl_3$(g). On the other hand, the ν(P—O) stretching frequency of the complex is red-shifted. These shifts are compatible with the above-proposed structure, indicating that the formation of the P—O—M bridging bond weakens the P—O and M—Cl bonds and strengthens the P—Cl bonds.

MCl_4–$AlCl_3$ (M = Zr *or* Hf) *systems*

Typical vapor Raman spectra from cells containing $ZrCl_4$–$AlCl_3$ and $HfCl_4$–$AlCl_3$ are presented in Figs 3 and 4. In Figs 3 and 4 the spectra of $ZrCl_4$, $HfCl_4$ and Al_2Cl_6 are included for comparison and are in agreement with the previously reported spectra of Clark *et al.*[20] and Tomita *et al.*[22]

It is evident that the spectra of $ZrCl_4$–$AlCl_3$ (Fig. 3C) consist mainly of a superposition of bands due

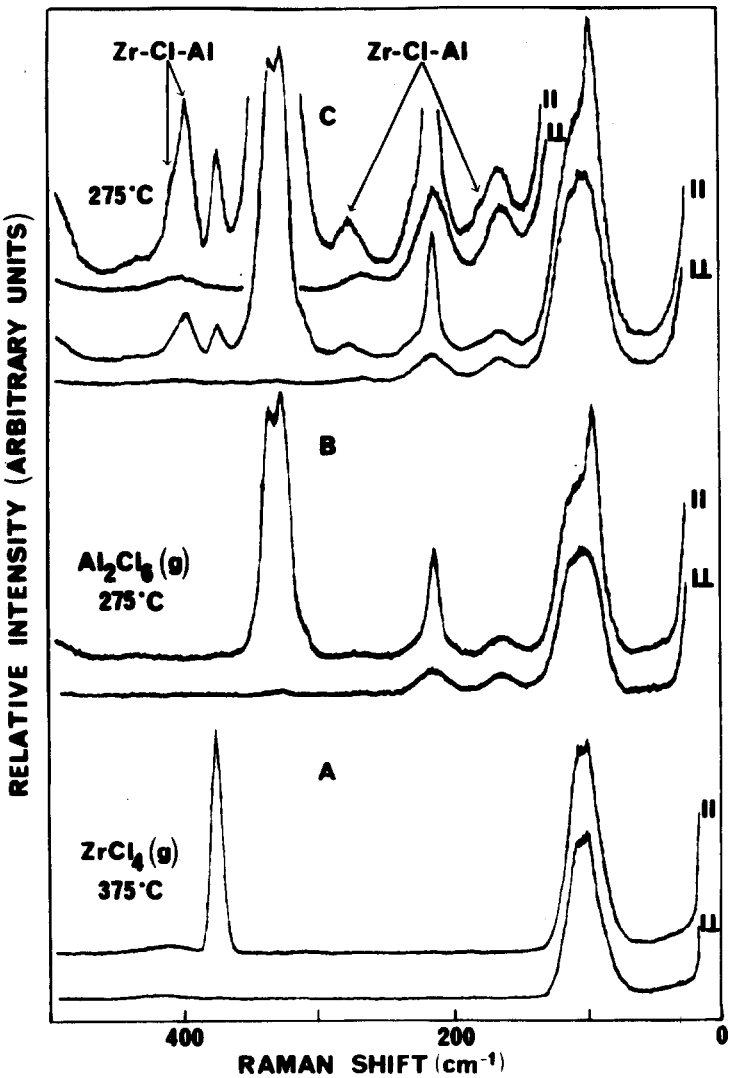


Fig. 3. Vapor Raman spectra of: (A) $ZrCl_4$ at 375°C, (B) Al_2Cl_6 at 275°C, and (C) mixtures of $ZrCl_4$–$AlCl_3$ from cell I at 275°C; λ_0 = 514.5 nm, laser power = 700 mW. Spectral slit width = 6 cm^{-1}.

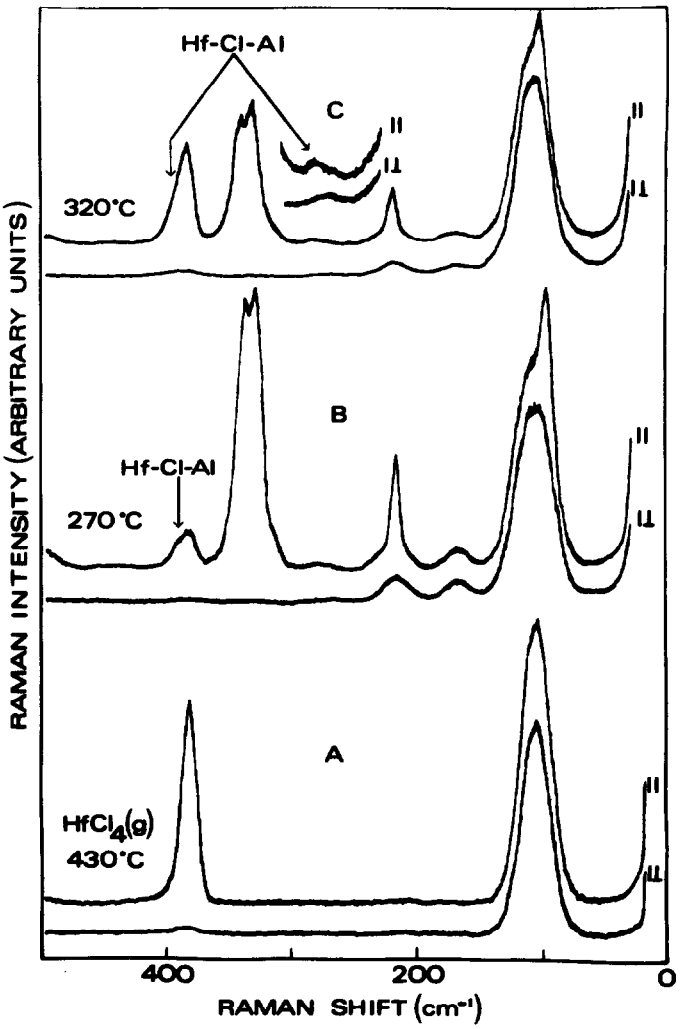


Fig. 4. Vapor Raman spectra of: (A) $HfCl_4$ at 430°C, (B) mixtures of $HfCl_4$ and Al_2Cl_6 from cell II at 270°C, and (C) mixtures of $HfCl_4$ and Al_2Cl_6 from cell II at 320°C. $\lambda_0 = 514.5$ nm; laser power = 700 mW. Spectral slit width = 6 cm^{-1}.

to $ZrCl_4$(g) and Al_2Cl_6(g). At 375°C, zirconium tetrachloride has its strongest ν_1 band at 377 cm^{-1} and a doublet (ν_2, ν_4) at ~100 cm^{-1}. At temperatures below 550°C and pressures near 1 atm the $AlCl_3$ vapors consist primarily of Al_2Cl_6 dimers,[18(a),22] having the strongest characteristic bands at ~335 (doublet), ~218 and ~100 cm^{-1}. In the spectra of the vapor mixture a new "strong" band at 401 cm^{-1} can be recognized which has also been observed by Taylor and Larsen[11] and is attributed to Zr–Cl–Al vapor complex(es). Careful examination of the polarization characteristics of the Raman bands established the presence of two additional bands at 281 and 188 cm^{-1} and a shoulder band with wavenumber near 412 cm^{-1}. The latter bands were best observed in the spectra of cell III (investigation of vapors over the liquid mixture) and are shown in Fig. 5. The wavenumbers and polarizations of the Raman bands measured for the Zr–Cl–Al complex(es) are listed in Table 2.

A comparison of the spectra of the $HfCl_4$–Al_2Cl_6 vapor mixtures (Fig. 4B and C) with the spectra of $HfCl_4$ (Fig. 4A) and Al_2Cl_6 (Fig. 3B) vapors shows that vapor complex bands are difficult to recognize. Gaseous $HfCl_4$ has a strong polarized band (ν_1) at 380.7 cm^{-1} and a very weak band (ν_2) at ~392 cm^{-1}. In the vapor mixture, however, a shoulder band appears at ~391 cm^{-1}, whose intensity at temperatures near 270°C is comparable with that of the ν_1 of $HfCl_4$(g). This band and the weak polarized band at 281 cm^{-1} are attributed to the Hf–Cl–Al vapor complex. The correspondence of the bands for the two complexes of Zr and Hf, and a tentative assignment is given in Table 2.

Vapor complexation of bivalent or tervalent metal chlorides with aluminum chloride usually

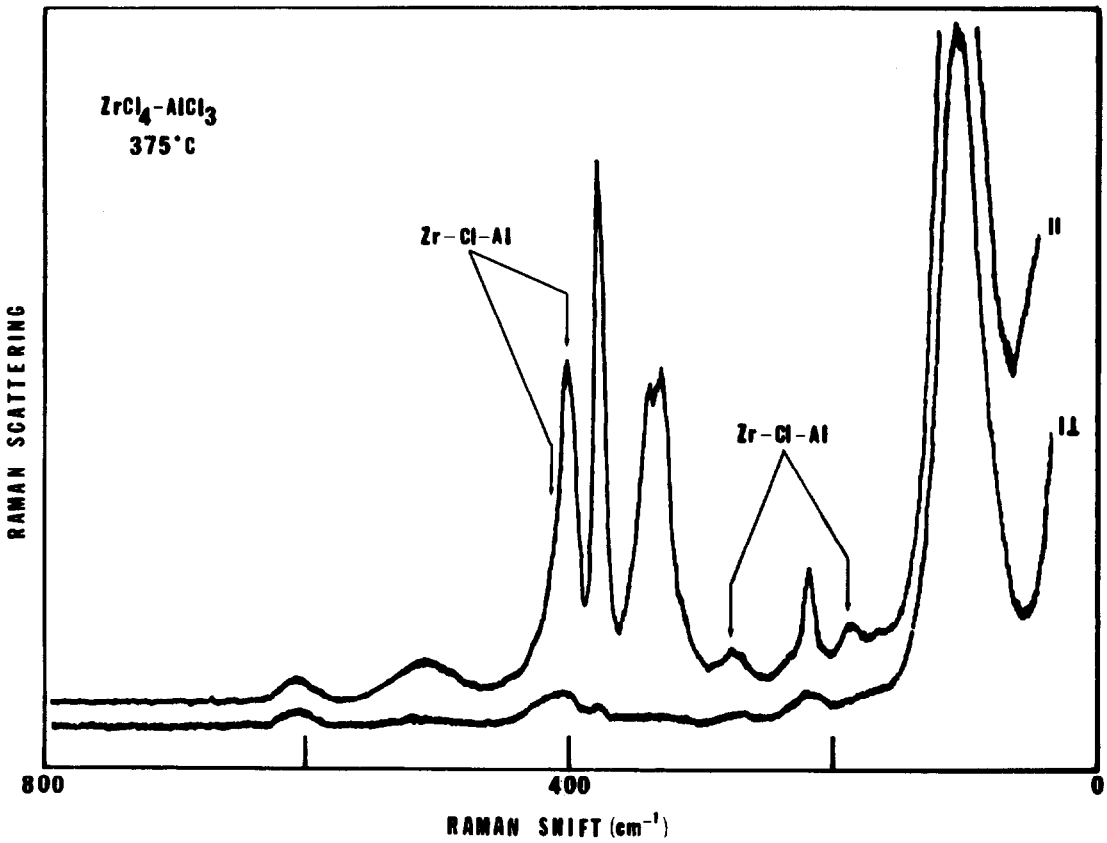


Fig. 5. Raman spectra of vapors over molten $ZrCl_4$–$AlCl_3$ mixtures (cell III) at 375°C. $\lambda_0 = 514.5$ nm; laser power = 700 mW. Spectral slit width = 6 cm^{-1}.

involves one molecule of the metal chloride and one, two, three or more molecules of $AlCl_3$.[5,23] Thus, it is more likely that the vapor complexation of tetravalent chlorides occurs with the general reaction:

$$MCl_4(g) + nAl_2Cl_6(g) = MAl_{2n}Cl_{6n+4}(g). \quad (2)$$

In the case of $ZrCl_4$, Taylor and Larsen[11] suggested that the vapor complex is $ZrAl_2Cl_{10}$, while the mass spectrometric measurements of Schäfer and Flörke[24] indicated that both $ZrAlCl_7$ and $ZrAl_2Cl_{10}$ are present in the gas-phase equilibrium. The thermodynamic functions of reaction (2) involving the $n = \frac{1}{2}$ and $n = 1$ Zr complexes are listed in Table 3.[24]

An average value of the enthalpies of reaction (2) can also be calculated from measurements of the relative Raman intensities of the gaseous species participating in the equilibrium [i.e. $ZrCl_4(g)$, $Al_4Cl_6(g)$ and the complexes]. The basic assumption

Table 2. Vibrational band wavenumbers (cm^{-1}) of vapor complexes in the $ZrCl_4$–Al_2Cl_6 and $HfCl_4$–Al_2Cl_6 systems[a]

$ZrCl_4$–Al_2Cl_6		$HfCl_4$–Al_2Cl_6	
This work	Reference 11	This work	Assignment[b]
188w(p)			
281w(p)		281vw(p)	ν(M—Cl)$_b$
401s(p)	408	391w(p)	ν(M—Cl)$_t$
412sh(p)	412		

[a] Intensity code: see Table 1.
[b] b = bridging, t = terminal.

Table 3. Thermodynamic functions of reactions in the temperature range 300–500°C

n	Reaction	ΔS^0 (J K^{-1} mol^{-1}) (Ref. 24)	ΔH^0 (kJ mol^{-1}) (Ref. 24)	ΔH^0 (kJ mol^{-1}) (this work)
$\frac{1}{2}$	$ZrCl_4(g)+0.5Al_2Cl_6(g) = ZrAlCl_7(g)$	−75.4	−36.0	−34.9±2.5
1	$ZrCl_4(g)+Al_2Cl_6(g) = ZrAl_2Cl_{10}(g)$	−140.7	−65.3	−35.6±3.1

made is that the partial pressures (P_i) of the species are proportional to the Raman intensity (I_i). Thus, for each cell at temperature T, the equilibrium constant of reaction (2) is:

$$k_p = \frac{P_C}{P_A^n P_M} = \lambda \frac{I_C}{I_A^n I_M} \quad (3)$$

where C, A and M are subscripts indicating the vapor complex, Al_2Cl_6 and MCl_4, respectively, and λ is a proportionality constant. The relation leads to:

$$\ln\left(\frac{I_C}{I_A^n \cdot I_M}\right) = -\frac{\Delta H}{R}\left(\frac{1}{T}\right) + [\Delta S - \ln \lambda], \quad (4)$$

and $\Delta H/R$ is determined as the slope of the logarithmic function vs $1/T$.

Measurements of the relative Raman intensities I_C, I_A and I_M for the $ZrCl_4$–$AlCl_3$ system were obtained at different temperatures from four cells. Variable amounts of $ZrCl_4$ and $AlCl_3$ were added into the cell and the measurements were obtained for each cell in the temperature range where all species (i.e. $ZrCl_4$, Al_2Cl_6 and complex) were in the gas phase. Figure 6 shows the temperature dependence of the relative intensities from 275 to 525°C. At temperatures above 450°C, small amounts of $AlCl_3(g)$ monomers are also present, giving rise to a Raman band at ~370 cm^{-1} [22] which overlaps with the $ZrCl_4(g)$ ν_1-band. However, based on previous work[22] the expected intensity of $\nu_1[AlCl_3(g)]$ could be estimated relative to the $\nu_2[Al_2Cl_6(g)]$ intensity and subtracted from the total intensity of the band observed at ~370 cm^{-1}. Thus, an intensity solely due to $\nu_1(ZrCl_4)$ could be measured.

Plots of the logarithmic function [eqn (4)] vs $1/T$ for each Raman cell gave straight lines with $n = \frac{1}{2}$ (Fig. 7) and values of ΔH very close to each other with a mean value of −34.9±2.5 kJ mol^{-1}. Similar plots were obtained with $n = 1$ and the mean enthalpy is −35.6±3.1 kJ mol^{-1}. The proximity of the ΔH^0 values of the $n = \frac{1}{2}$ reaction (1) (Table 3) relative to those of the $n = 1$ reaction measured by mass spectrometry[24] and by Raman experiments suggests that $ZrAlCl_7$ is the predominant vapor complex in the $ZrCl_4$–$AlCl_3$ system. On the other hand the accuracy of the data and the method used cannot completely exclude any possible formation of $ZrAl_2Cl_{10}$. Finally, it should be noticed that the

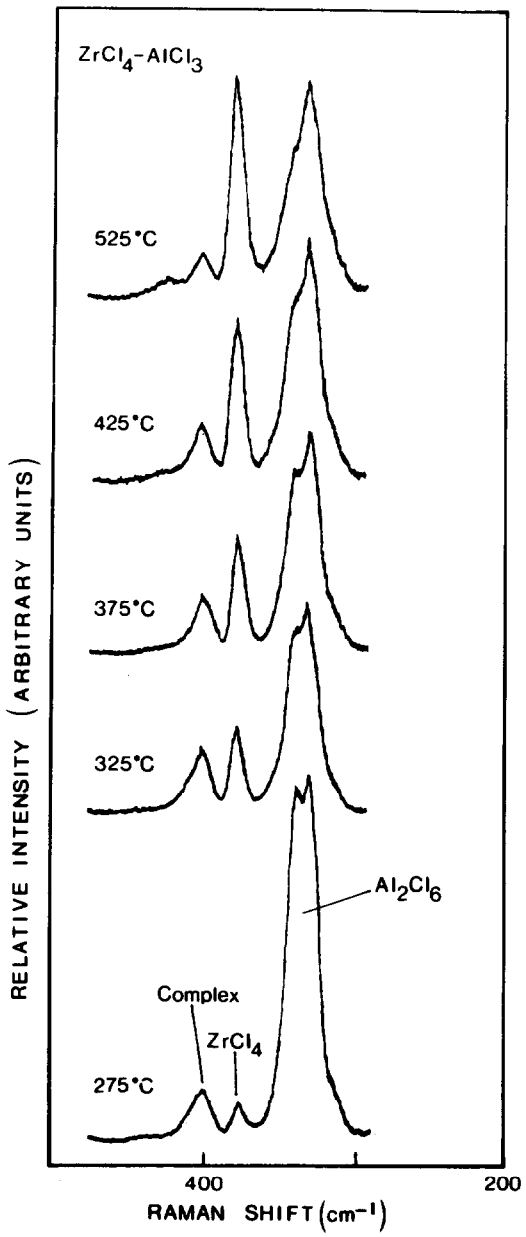


Fig. 6. Temperature dependence of vapor Raman spectra from cell I. λ_0 = 514.5 nm; laser power = 700 mW. Spectral slit width = 6 cm^{-1}.

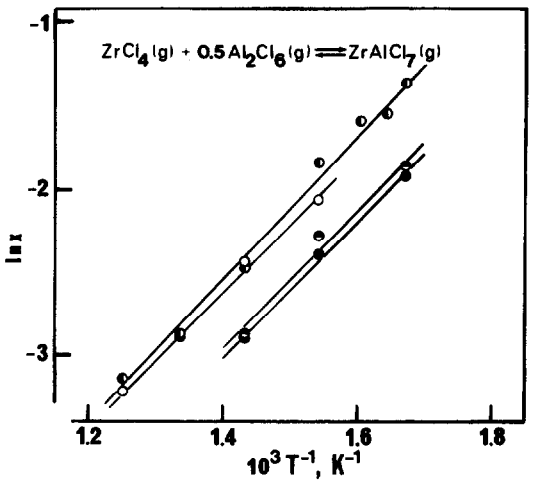


Fig. 7. Plots of

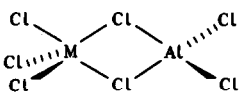
$$\ln x\left(x = \frac{I_C}{I_Z I_A^{0.5}}\right) \text{ vs } 1/T.$$

Points indicate molar ratios of Al_2Cl_6 to $ZrCl_4$: cell A (◑) $Al_2Cl_6/ZrCl_4 = 7$, cell B (○) $Al_2Cl_6/ZrCl_4 = 1$, cell C (◓) $Al_2Cl_6/ZrCl_4 = 4$, cell D (●) $Al_2Cl_6/ZrCl_4 = 4$.

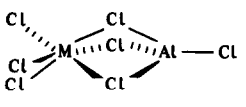
intensity of the shoulder band at 412 cm^{-1} relative to that at 401 cm^{-1} remained unchanged with temperature and total pressure. This is an indication that both bands are due to the same species (i.e. $ZrAlCl_7$) and not due to species with different structural conformations or stoichiometries.

From a structural point of view the MAl_2Cl_{10} complex is more likely to have a D_{2h} molecular symmetry with M as the central atom in a six-fold coordination and two bidentate $AlCl_4$ tetrahedra.[11,5] From the 33 vibrational modes, six are expected[5] with A_1-symmetry and are Raman-active only.

There are two possible structures concerning the



II



III

molecule $MAlCl_7$: Structure **II** has C_s-symmetry and a five-fold coordination [as in the case of the $M_2Cl_8(g)$ dimer] while structure **III** has C_{3v}-symmetry with triple chloride bridging and a six-fold coordination for M. The distribution of vibrational modes for these molecules are:

$$\Gamma_{C_s} = 13A'(R, IR) + 8A''(R, IR),$$

$$\Gamma_{C_{3v}} = 5A_1(R, IR) + 8E(R, IR).$$

The small number (four) of polarized bands seen for the Zr–Cl–Al complex points to a C_{3v} rather than a C_s-symmetry, but no definite conclusion can be made on this basis.

REFERENCES

1. J. W. Hastie, *High Temperature Vapors*. Academic Press, New York (1975).
2. J. L. Margrave (Ed.), *The Characterization of High Temperature Vapors*. Wiley, New York (1967).
3. H. Schäfer, *Chemical Tansport Reactions*. Academic Press, New York (1964).
4. M. Brooker and G. N. Papatheodorou, In *Advances in Molten Salt Chemistry* (Edited by G. Mamantov), Vols 5 and 6, p. 27. Elsevier, New York (1983).
5. G. N. Papatheodorou, *Curr. Top. Mater Sci.* 1982, **10**, 249.
6. J. W. Hastie (Ed.), *Proceedings of the 10th Materials Research Symposium on Characterization of High Temperature Vapors and Gases*. National Bureau of Standards Publication 561, Washington, DC (1979).
7. D. L. Hildebrand and D. D. Cubicioti (Eds), *Proceedings of the Symposium on High Temperature Metal Halide Chemistry*. The Electrochemical Society Inc. Proceedings 78-1, Princeton, NJ (1978).
8. H. Schäfer, *Adv. Inorg. Chem. Radiochem.* 1983. **26**, 201.
9. G. N. Papatheodorou, In *Metal Bonding and Interactions in High Temperature Systems* (Edited by J. L. Cole and W. C. Stwalley), ACS Symposium Series No. 179, p. 309. American Chemical Society, Washington, DC (1982).
10. H. Schäfer, *Angew. Chem., Int. Ed. Engl.* 1976, **15**, 713.
11. D. R. Taylor and E. M. Larsen, *J. Inorg. Nucl. Chem.* 1979, **41**, 481.
12. B. Krebs, H. Janssen, N. J. Bjerrum, R. W. Berg and G. N. Papatheodorou, *Inorg. Chem.* 1984, **23**, 164.
13. (a) G. N. Papatheodorou, L. A. Curtiss and V. A. Maroni, *J. Chem. Phys.* 1983, **78**, 3303; (b) T. Østvold, E. Rytter and G. N. Papatheodorou, *Polyhedron* 1986, **5**, 821.
14. R. H. Tomlinson, In *Mellor's Comprehensive Treatise on Inorganic and Theoretical Chemistry*, Vol. 8, Supplement 3, p. 508. Longmans, London (1971).
15. A. V. Suvorov, *Zh. Koord. Khim.* 1977, **3**, 1146.
16. Y. Kawano, Y. Gushikem and Y. Hase, *J. Mol. Struct.* 1977, **36**, 183.
17. See, for example, Ref. 1, p. 128.
18. For further experimental details see: (a) G. N. Papatheodorou and M. A. Capote, *J. Chem. Phys.* 1978, **69**, 2067; (b) G. N. Papatheodorou, NBS Special Publication (U.S.), No. 561, p. 647 (1979).
19. R. J. H. Clark and D. M. Rippon, *Mol. Phys.* 1974, **28**, 305.

20. R. J. H. Clark, B. K. Hunter and D. M. Rippon, *Inorg. Chem.* 1972, **11**, 59.
21. (a) A. F. Wells, *Structural Inorganic Chemistry*, p. 681. Clarendon Press, Oxford (1975). (b) E. M. Larsen, *Adv. Inorg. Radiochem.* 1970, **13**, 1, 87.
22. T. Tomita, C. E. Sjøgren, P. Klaeboe, G. N. Papatheodorou and E. Rytter, *J. Raman Spectrosc.* 1983, **14**, 415.
23. R. W. Berg and G. N. Papatheodorou, *Inorg. Chim. Acta* 1980, **45**, L211.
24. H. Schäfer and U. Flörke, *Z. Anorg. Allg. Chem.* 1981, **479**, 89.

Polyhedron Vol. 5, No. 9, pp. 1405–1411, 1986
Printed in Great Britain

0277–5387/86 $3.00+.00
Pergamon Journals Ltd

CHARACTERIZATION OF COPPER(II) COORDINATION COMPOUNDS OF 5,7-DIMETHYL[1,2,4]TRIAZOLO[1,5-*a*]PYRIMIDINE: THE CRYSTAL STRUCTURE OF DIAQUATETRAKIS(5,7-DIMETHYL[1,2,4]TRIAZOLO[1,5-*a*]PYRIMIDINE-N^3)-COPPER(II) HEXAFLUOROPHOSPHATE*

T. L. F. FAVRE, J. G. HAASNOOT† and J. REEDIJK

Department of Chemistry, Gorlaeus Laboratories, State University Leiden, P.O. Box 9502, 2300 RA Leiden, The Netherlands

(*Received* 17 *October* 1985; *accepted* 25 *November* 1985)

Abstract—Copper(II) coordination compounds of several CuA_2 salts (A = PF_6, BF_4, ClO_4, CF_3SO_3 or NO_3) with 5,7-dimethyl[1,2,4]triazolo[1,5-*a*]pyrimidine (dmtp) as a ligand have been studied. The crystal structure of $[Cu(dmtp)_4(H_2O)_2](PF_6)_2$ is described. This compound is monoclinic, space group $P2_1/c$, $a = 11.826(2)$ Å, $b = 9.463(2)$ Å, $c = 17.673(3)$ Å, $\beta = 97.50(1)°$, $Z = 2$, $d_{calc.} = 1.66$ Mg m^{-3}, and has been refined to a final discrepancy factor (R) of 0.0382 based on 2316 reflections. The structure consists of PF_6^- anions and centrosymmetric mononuclear $[Cu(dmtp)_4(H_2O)_2]^{2+}$ cations, Cu^{2+} being coordinated by four equatorial N(3)-bonded dmtp molecules with Cu—N = 2.019 and 2.050 Å, and by two axial water molecules with Cu—O = 2.650 Å. The water molecules form intramolecular hydrogen bonds with the dmtp N(4) atoms.

The coordination chemistry of purines, pyrimidines and imidazole-type ligands has recently been subjected to intensive studies, because of the importance of the interactions between such ligands and metal ions in many biological systems.[1]

With a few exceptions these purines appear to have either a monodentate coordination via the N(9) or a bidentate bridging coordination via the N(3) and N(9) nitrogen atoms.[2–7] If the N(9) nitrogen atom has been blocked, as, for example, in 9-methyladenine, the respective coordination sites are N(7) in the case of monodentate coordination or N(1) and N(7) in the case of bidentate bridging coordination.[8]

In the present study the ligand 5,7-dimethyl-[1,2,4]triazolo[1,5-*a*]pyrimidine, hereafter abbreviated as dmtp, is considered as a model for the naturally-occurring purines. In this paper the IUPAC ring numbering[9] has been used, which is shown in Fig. 1.

The main structural modifications of [1,2,4]triazolo[1,5-*a*]pyrimidines with respect to the purines are as follows. Firstly, none of the nitrogen atoms in these triazolopyrimidines are protonated in neutral or even weakly acidic solvents, which is in contrast with the purines.[6–8] Secondly, coordination via the purine N(1) nitrogen atom is ruled out due to the N(8) bridge-head position in [1,2,4]triazolo[1,5-*a*]pyrimidine, leaving three possible coordination sites at pH > 4, viz. N(1), N(3) and N(4). The coordination properties of [1,2,4]triazolo[1,5-*a*]pyrimidines can further be modified by steric or electronic effects due to the presence of substituents, as the two methyl groups in dmtp. This ligand was selected for a first study.

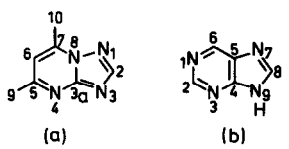


Fig. 1. IUPAC ring numbering of dmtp (a) and purine molecules (b).

* Dedicated to the memory of Dr Gerrit C. Verschoor, who died on 29 September 1985.

† Author to whom correspondence should be addressed.

Earlier work from this laboratory has shown that interesting coordination compounds can be obtained with dmtp and metal(II) thiocyanates.[10–12] We now extend this to the use of "non-coordinating" anions, like PF_6^-, ClO_4^- and BF_4^-, to see whether or not more than two dmtp ligands can be coordinated to Cu^{2+}. Results of coordination compounds with dmtp and copper(II) salts with relatively strong coordinating anions, like halides, will be published later.[13]

In addition, the present paper contains the description of the crystal structure determined by X-ray analysis of $[Cu(dmtp)_4(H_2O)_2](PF_6)_2$ to demonstrate how the ligand is coordinated.

EXPERIMENTAL

Preparations

Triazolopyrimidines can be obtained by reaction of two out of three possible tautomers of 3-amino-1,2,4-triazole, viz. the 2H and 4H tautomers, resulting in the [1,5-*a*] and [4,3-*a*] isomers, respectively.[14,15] The ligand dmtp was prepared according to the method of Bülow and Haas[16] from 3-amino-1,2,4-triazole and pentanedion-2,4. Melting point (136–137°C) and ^1H NMR [2.64(s), 2.78(s), 6.85(s), 8.44(s)] confirm that the [1,5-*a*] isomer was obtained.

$Cu(dmtp)_4(H_2O)_2(PF_6)_2$ was prepared by adding ammonium hexafluorophosphate (4.0 mmol) in water (5 cm^3) to a mixture of copper(II) perchlorate (2.0 mmol) and dmtp (3.0 mmol) in water (20 cm^3). The precipitate was separated by filtration and recrystallized from hot water, yielding blue crystals (m.p. = 158–159°C). Found: C, 34.1; Cu, 6.9; H, 3.8; N, 22.5%. Calc. for $C_{28}CuF_{12}H_{36}N_{16}O_2P_2$: C, 34.2; Cu, 6.5; N, 22.8%.

$Cu(dmtp)_4(C_2H_5OH)_2(BF_4)_2$ was obtained by adding dmtp (4.0 mmol) in ethanol (25 cm^3) to a filtered solution of copper(II) tetrafluoroborate (2.0 mmol) in ethanol (20 cm^3). After adding triethylorthoformate (teof) blue crystals could be isolated (m.p. = 155–117°C). Found: C, 41.1; Cu, 6.8; H, 4.8; N, 24.0%. Calc. for $B_2C_{32}CuF_8H_{44}N_{16}O_2$: C, 41.6; Cu, 6.9; H, 4.8; N, 24.3%.

$Cu(dmtp)_4(ClO_4)_2(H_2O)_1(C_2H_5OH)_{1.5}$ was prepared from copper(II) perchlorate and dmtp (1 : 1.5) in ethanol. After adding some diethylether and standing for one night, dark blue crystals were isolated by filtration (m.p. = 111–113°C). Found: C, 40.1; Cu, 6.8; H, 4.6; N, 23.5%. Calc. for $C_{31}Cl_2CuH_{43}N_{16}O_{10.5}$: C, 39.5; Cu, 6.7; H, 4.6; N, 23.8%.

$Cu(dmtp)_{3.67}(ClO_4)_2(H_2O)_{2.67}$ was prepared by reacting copper(II) perchlorate with dmtp (1 : 1.5) in water. Bluish purple crystals were isolated by filtration (m.p. = 133–134°C). Found: C, 35.8; Cu, 7.6; H, 4.1; N, 24.0%. Calc. for $C_{77}Cl_6Cu_3H_{104}N_{44}O_{32}$: C, 35.8; Cu, 7.5; H, 4.1; N, 23.9%.

$Cu(dmtp)_3(CF_3SO_3)_2(C_2H_5OH)_1$ was prepared from copper(II) triflate and dmtp (1 : 1.5) in ethanol–teof (1.5 : 1). After addition of some diethylether and standing at −20°C dark and light blue crystals formed. After dissolving the light-coloured product at room temperature, the dark blue crystals were obtained by filtration (m.p. = 153–155°C). Found: C, 34.8; Cu, 7.6; H, 3.4; N, 19.9%. Calc. for $C_{25}CuF_6H_{30}N_{12}O_7S_2$: C, 35.2; Cu, 7.5; H, 3.6; N, 19.7%.

$Cu(dmtp)_2(NO_3)_2$ was prepared from copper(II) nitrate and dmtp (1 : 1.5) in ethanol. The precipitate was isolated by filtration and recrystallized from hot ethanol, yielding blue crystals (m.p. = 180–181°C). Found: C, 34.9; Cu, 13.1; H, 3.6; N, 28.5%. Calc. for $C_{14}CuH_{16}N_{10}O_6$: C, 34.8; Cu, 13.1; H, 3.3; N, 28.9%.

Measurements

IR spectra were recorded on a Perkin–Elmer model 580B IR spectrophotometer as Nujol mulls between KRS-5 (4000–400 cm^{-1}) and polyethene (400–180 cm^{-1}) windows and as KBr, CsCl or CsI disks (concentration about 2%). Ligand field spectra (Table 1) were recorded in the solid state on a Beckman DK2A UV–vis–NIR spectrophotometer, by means of the diffuse reflectance technique using MgO as a reference. ^1H NMR spectra were taken on a JEOL PS 100 spectrometer using $Si(CH_3)_4$ as an internal standard. ESR spectra of powdered samples were measured on a Varian E3 instrument (X-band) or on a Varian V4500 instrument (Q-band) at either 77 K or ambient temperature. Magnetic measurements were obtained on a model 150A PAR instrument (2–80 K) and on a automated Faraday balance (80–300 K), using $Hg[Co(NCS)_4]$ as a calibration agent. Magnetic susceptibilities per copper(II) ion were corrected for diamagnetism using Pascal's constants[17] and for temperature-independent paramagnetism, equal to 60×10^{-6} $cm^3\ mol^{-1}$.

C, H and N analyses were performed by the Microanalytical Laboratory of Pascher (Bonn) and University College of Dublin. Copper was determined by indirect titrations with EDTA and zinc acetate using xylenol orange as an indicator. Experimental densities were determined by flotation in a mixture of 1,2-dibromoethane and trichloromethane.

Table 1. Ligand field and ESR data of the coordination compounds with dmtp as a ligand

Compound[a]	Ligand field maxima ($\times 10^3$ cm^{-1})	ESR parameters	
		g values	$A_\parallel$ (mT)
$CuL_4(H_2O)_2(PF_6)_2$	16.1	2.34, 2.09	14.9
$CuL_4(C_2H_5OH)_2(BF_4)_2$	16.3	2.30, 2.07	15.3
$CuL_4(ClO_4)_2(H_2O)_1(C_2H_5OH)_{1.5}$	16.1	[b]	[b]
$CuL_{3.67}(ClO_4)_2(H_2O)_{2.67}$[c]	16.8	2.27, 2.17, 2.08[d]	—
$CuL_3(CF_3SO_3)_2(C_2H_5OH)_1$	15.6	2.29, 2.10	13.4
$CuL_2(NO_3)_2$	15.2	2.28, 2.14, 2.09	—

[a] L = dmtp.
[b] Not recorded.
[c] The molecular formula of this compound can be written as $[CuL_4(H_2O)_2][CuL_4(H_2O)_1][CuL_3(H_2O)_2](ClO_4)_6(H_2O)_3$.
[d] Complicated pattern.

X-ray structure determination

X-ray analysis on a blue monocrystal of $[(Cu(dmtp)_4(H_2O)_2](PF_6)_2$ of dimensions $0.25 \times 0.20 \times 0.15$ mm was done on an Enraf–Nonius CAD-4 diffractometer. Intensities were collected at room temperature using Mo-K_α radiation ($\lambda = 0.71073$ Å) monochromated by graphite. No absorption or extinction corrections were applied. Relevant crystallographic and experimental data are tabulated in Table 2. All 2316 measured independent reflections with $I > 2\sigma(I)$ in the range of $2° < 2\theta < 24°$ were used in the analysis. The structure was solved by standard Patterson and Fourier methods. Calculations were carried out on an Amdahl V7B computer. Refinements were carried out by least-squares full-matrix cycles using unit weights, first with isotropic and later with anisotropic thermal parameters for all non-hydrogen atoms.Two positions of PF_6 with occupation ratios of 1.0 and 0.90, respectively, were introduced, because of disorder in the anion, treating all P—F bond distances and F—P—F valence angles with constraints.[18]

Most hydrogen atoms were directly located from a difference synthesis, except for a few hydrogen atoms of the dmtp methyl groups, which were placed in the geometrically calculated positions and included in the final structure factor calculations with fixed isotropic thermal parameters and fractional atomic coordinates. No significant peaks were present in the final difference map. The final residual indices are defined as $R = \Sigma(\|F_c| - |F_o\|)/\Sigma|F_o|$ and $R_w = \{\Sigma w(|F_o| - |F_c|)^2/\Sigma w|F_o|_2\}^{1/2}$.

Lists of structure factors, fractional coordinates and anisotropic thermal parameters have been deposited as supplementary material with the Editor, from whom copies are available on request. Atomic coordinates have also been deposited with the Cambridge Crystallographic Data Centre.[19]

RESULTS AND DISCUSSION

Description of the structure of $[Cu(dmtp)_4(H_2O)_2](PF_6)_2$

The compound consists of centrosymmetric mononuclear $[Cu(dmtp)_4(H_2O)_2]^{2+}$ units, as depicted in Fig. 2, and PF_6^- anions. The copper(II) ion, which is situated on an inversion centre, has an elongated tetragonally-distorted octahedral configuration, being coordinated by four equatorial dmtp molecules and two axial water molecules. The ligand dmtp is monodentately coordinated via the N(3) nitrogen atom to copper, the Cu—N(3) bond lengths of 2.019 and 2.050 Å being in agreement with the values of 2.000 and 2.019 Å in α-$Cu(dmtp)_2(NCS)_2]_2$,[11] with 1.995 and 2.058 in β-$[Cu(dmtp)_2(NCS)_2]_2$,[12] and with 1.962 and 2.016 Å in copper(II) compounds with 5-methyl-[1,2,4]triazolo[1,5-*a*]pyrimidine-7-ol as a ligand.[21]

The ligand dmtp has a planar geometry, as deduced from the maximum distances from the ring atoms to the least square planes, which are 0.03 and 0.02 Å for the odd and even numbered dmtp molecules, respectively. The Cu—O bond length of 2.456 Å is shorter than in most compounds with similarly axially coordinated water molecules, e.g. the value of 2.638 Å in $[Cu(Him)_4(H_2O)_2]F_2$ (Him = imidazole).[22]

Both hydrogen atoms of the water molecule

Table 2. Relevant crystallographic and experimental data of $[Cu(dmtp)_4(H_2O)_2](PF_6)_2$

Empirical formula	$C_{28}CuF_{12}H_{36}N_{16}O_2P_2$
Molecular weight	982.2
Space group	$P2_1/c$ (monoclinic)
Cell dimensions	$a = 11.826(2)$ Å
	$b = 9.463(2)$ Å
	$c = 17.673(3)$ Å
	$\alpha = \gamma = 90°$
	$\beta = 97.50(1)°$
Cell volume	$V = 1960.8$ Å^3
Packing	$Z = 2$
Absorption coefficient	$\mu = 7.43$ cm^{-1}
Density	$d_{calc.} = 1.66$ g cm^{-3}
	$d_{obs.} = 1.64(2)$ g cm^{-3}
No. of independent reflections measured	3068
No. of significant independent reflections	2316 [$I > 2\sigma(I)$]
Limits of data collection	$2° < 2\theta < 24°$
	$-13 < h < 13$
	$0 < k < 10$
	$-20 < l < 20$
$F(000)$	998
Final R	0.0382
Final R_w	0.0418

appear to form intramolecular hydrogen bonds to the N(4) nitrogen atoms of dmtp: H---N(4) = 1.909 and 2.113 Å, O---N(4) = 2.787 and 2.902 Å, OW—H---N(4) = 163.2 and 148.0°. The constrained octahedral PF_6^- ions are neither bonded to the metal ions nor hydrogen-bonded to the water molecules, which explains the disorder in the anions. The P—F bond lengths are in the range of 1.559–1.570 Å and the F—P—F valence angles in the range of 88.6–91.0°.

Bond distances and relevant valence angles are listed in Table 3.

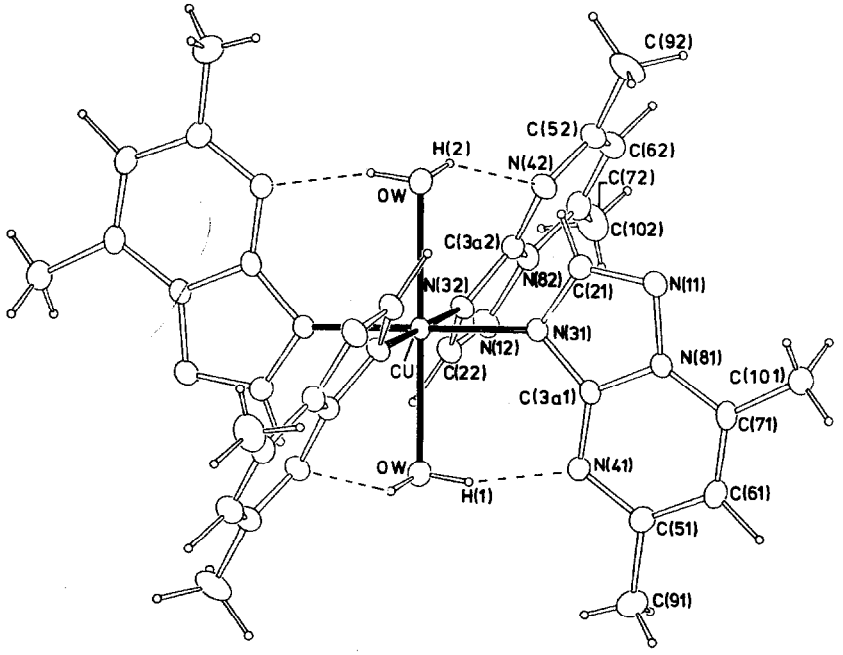


Fig. 2. ORTEP[20] perspective view of the $[Cu(dmtp)_4(H_2O)_2]^{2+}$ cation.

Table 3. Bond distances (Å) and valence angles (°) for $[Cu(dmtp)_4(H_2O)_2](PF_6)_2$

Cu—N(31)	2.050(3)	Cu—N(32)	2.019(3)
Cu—OW	2.456(3)		
N(11)—N(81)	1.375(4)	N(12)—N(82)	1.375(5)
N(11)—C(21)	1.310(5)	N(12)—C(22)	1.316(5)
C(21)—N(31)	1.356(5)	C(22)—N(32)	1.353(5)
N(31)—C(3a1)	1.335(5)	N(32)—C(3a2)	1.343(5)
C(3a1)—N(41)	1.329(5)	C(3a2)—N(42)	1.335(5)
C(3a1)—N(81)	1.366(5)	C(3a2)—N(82)	1.364(5)
N(41)—C(51)	1.335(5)	N(42)—C(52)	1.334(5)
C(51)—C(61)	1.408(6)	C(52)—C(62)	1.410(6)
C(51)—C(91)	1.483(6)	C(52)—C(92)	1.493(6)
C(61)—C(71)	1.358(6)	C(62)—C(72)	1.354(6)
C(71)—N(81)	1.372(5)	C(72)—N(82)	1.371(5)
C(71)—C(101)	1.487(6)	C(72)—C(102)	1.484(6)
OW—H(1)	0.904(3)	OW—H(2)	0.885(3)
H(1)—N(41)	1.909(3)	H(2)—N(42)	2.113(3)
OW—N(41)	2.787(4)	OW—N(42)	2.902(4)
N(31)—Cu—N(32)	90.1(1)		
N(31)—Cu—OW	94.7(1)		
N(32)—Cu—OW	92.2(1)		
N(81)—N(11)—C(21)	101.1(3)	N(82)—N(12)—C(22)	101.4(3)
N(11)—C(21)—N(31)	116.7(4)	N(12)—C(22)—N(32)	116.4(4)
C(21)—N(31)—C(3a1)	103.3(3)	C(22)—N(32)—C(3a2)	103.4(3)
N(31)—C(3a1)—N(41)	128.6(3)	N(32)—C(3a2)—N(42)	128.1(4)
N(31)—C(3a1)—N(81)	108.2(3)	N(32)—C(3a2)—N(82)	108.2(3)
N(41)—C(3a1)—N(81)	123.2(3)	N(42)—C(3a2)—N(82)	123.8(4)
C(3a1)—N(41)—C(51)	116.1(3)	C(3a2)—N(42)—C(52)	115.6(4)
N(41)—C(51)—C(61)	122.3(4)	N(42)—C(52)—C(62)	122.4(4)
N(41)—C(51)—C(91)	117.1(4)	N(42)—C(52)—C(92)	115.9(4)
C(61)—C(51)—C(91)	120.6(4)	C(62)—C(52)—C(92)	121.7(4)
C(51)—C(61)—C(71)	121.5(4)	C(52)—C(62)—C(72)	121.2(4)
C(61)—C(71)—N(81)	114.5(4)	C(62)—C(72)—N(82)	115.3(4)
C(61)—C(71)—C(101)	127.1(4)	C(62)—C(72)—C(102)	127.0(4)
N(81)—C(71)—C(101)	118.4(4)	N(82)—C(72)—C(102)	117.8(4)
N(11)—N(81)—C(3a1)	110.7(3)	N(12)—N(82)—C(3a2)	110.7(3)
N(11)—N(81)—C(71)	126.7(3)	N(12)—N(82)—C(72)	127.6(4)
C(3a1)—N(81)—C(71)	122.5(3)	C(3a2)—N(82)—C(72)	121.7(4)
H(1)—OW—H(2)	96.9(3)		
OW—H(1)—N(41)	163.2(2)	OW—H(2)—N(42)	148.0(2)

General

Table 1 lists the results of ligand field and ESR spectra of the coordination compounds. The IR absorptions of dmtp appeared to be similar in all the copper(II) compounds described here, indicating similar coordination of this ligand.

$[Cu(dmtp)_4L_2]A_2$ ($A = PF_6$, BF_4 *or* ClO_4; $L = H_2O$ *or* C_2H_5OH)

The presence of water and/or ethanol in these compounds with four dmtp ligands and two solvent molecules per copper(II) ion is confirmed by the IR O—H absorption bands at 3200–3300 cm^{-1}. The anions will be non-coordinated, as can be seen from the broad but single band at 1060 cm^{-1} of BF_4^- and the sharp single band at 1100 cm^{-1} of ClO_4^-.[23,26] The very similar ligand field spectra of the three compounds show a broad band at about 16,200 cm^{-1} which is indicative of an elongated tetragonally-distorted octahedral geometry.[24,25] This conclusion is supported by the axial ESR spectra, of which the results are summarized in Table 1. The clear hyperfine splitting of about 15.0 mT ($A_\parallel$) points to the absence of significant magnetic interactions between the Cu^{2+} ions, confirming the presence of mononuclear copper(II).[25]

From comparison of the spectral results it can be concluded that these three compounds will have a very similar coordination geometry, copper(II) being coordinated by four equatorial dmtp ligands and two axial solvent molecules, which has been confirmed by X-ray analysis on $[Cu(dmtp)_4(H_2O)_2](PF_6)_2$ (*vide supra*).

$Cu(dmtp)_{3.67}(ClO_4)_2(H_2O)_{2.67}$

The broad and unsplit IR absorption band at 1100 cm^{-1} is indicative of non-coordination of perchlorate.[23,26] The presence of water is confirmed by a broad band at 3380 cm^{-1}. The broad band at 16,800 cm^{-1} in the ligand field spectrum points to an elongated tetragonally-distorted octahedral or square pyramidal geometry of copper(II).

Both the X- and Q-band ESR spectra were complicated and could not be interpreted as just a rhombic distorted Cu^{2+} species and suggest the presence of more than one species containing Cu^{2+}. Therefore X-ray analysis on a monocrystal of this compound was attempted, of which the first results indicate that this compound does not consist of trimers as might be expected from the molecular formula, but of different monomeric units. One third of the copper ions appears to be six-coordinated by four dmtp ligands and two water molecules, having the same coordination geometry as $[Cu(dmtp)_4(H_2O)_2](PF_6)_2$, whereas two-thirds of the copper ions are five-coordinated, one third being surrounded by four equatorial dmtp ligands and one axial water molecule, and one third by three dmtp ligands and two water molecules.

The non-coordinated perchlorate anions and water molecules appear to be partly in disorder. This very complicated structure will be described elsewhere in detail.[27]

$Cu(dmtp)_3(CF_3SO_3)_2(C_2H_5OH)_1$

The IR $\nu_{as}(E)$ SO_3 band at triflate is split into two peaks at 1263 and 1292 cm^{-1}, which is clearly indicative of a monodentate coordination of the anions.[28–30] The presence of ethanol is confirmed by the absorption at 3250 cm^{-1}. The broad band at 15,600 cm^{-1} in the ligand field spectrum points to a tetragonally-distorted octahedral geometry.[24,25] This conclusion is supported by the axial ESR spectrum.

The absence of significant interactions between the Cu^{2+} ions has been demonstrated by magnetic measurements at 4–80 K. Extrapolation of the inverse susceptibility $1/\chi$ against the temperature resulted in a straight line with intercept (θ) of 0 K. So, $Cu(dmtp)_3(CF_3SO_3)_2(C_2H_5OH)_1$ appears to be a mononuclear compound, Cu^{2+} having a tetragonally-distorted octahedral configuration with three dmtp $N(3)$ ligands, two monodentately coordinated trifluoromethanesulfonate ions and one ethanol molecule. It is not clear from the spectral data whether or not $[CF_3SO_3]^-$ or EtOH forms the fourth equatorial ligand.

$Cu(dmtp)_2(NO_3)_2$

The absorption bands of the nitrate group in the IR spectrum clearly indicate the presence of both bidentately (1484 and 1293 cm^{-1}) and monodentately (1433 and 1306 cm^{-1}) coordinated nitrate.[23,31,32] From this result combined with the results from the ligand field spectrum and Q-band ESR spectrum (see Table 1) it can be concluded that Cu^{2+} has a rhombic geometry, and is coordinated by two dmtp $N(3)$ ligands and one monodentate and one bidentate nitrate group, resulting in a five-coordinated species.

CONCLUSIONS

The nature of coordination compounds with dmtp appears to be strongly influenced by the coordination properties of the used anions. It has been demonstrated that four dmtp ligands in the equatorial positions can be coordinated to copper(II) in the presence of non-coordinating anions, like PF_6, BF_4 and ClO_4. The axial positions can be occupied by solvent molecules, resulting in an elongated tetragonally-distorted octahedral or square pyramidal copper(II) configuration.

The number of dmtp ligands coordinated to copper(II) becomes less, when anions with an increasing tendency for coordination are used, as appears from the compounds with weak coordinating triflate and stronger coordinating nitrate. From the IR spectra it can be concluded, that the coordination mode of dmtp will be similar in all copper(II) compounds described here, being monodentate via the N(3) nitrogen atom, which has been proven by the crystal structure of $[Cu(dmtp)_4(H_2O)_2](PF_6)_2$.

Coordination via the N(4) nitrogen atom of dmtp will be hindered (but not excluded) by the presence of the methyl group at the C(5) position. In order to favour coordination via N(4), coordination compounds with unsubstituted [1,2,4]triazolo[1,5-*a*]pyrimidine and 6-methyl[1,2,4]-triazolo[1,5-2]pyrimidine will be studied.

From the hydrogen bonding of the N(4) nitrogen atom in $[Cu(dmtp)_4(H_2O)_2](PF_6)_2$ it can be concluded that coordination via this atom is negatively influenced by the presence of protic molecules like

water and ethanol. The use of aprotic solvents will presumably favour coordination via the atom.

The coordination properties of dmtp can be summarized as:

(1) coordination via N(3) is obviously preferred, since dmtp coordinates via this nitrogen atom in all coordination compounds known so far;

(2) coordination via N(4) will be probably favoured by using triazolopyrimidines unsubstituted at C(5) and/or by using aprotic solvents;

(3) no indications for coordination via N(1) have been found.

Acknowledgements—We wish to thank W. G. Haije, R. C. M. de Groot and G. Renes for operating the magnetic susceptibility instruments and assistance with the measurements.

REFERENCES

1. D. J. Hodgson, *Progress in Inorganic Chemistry* (Edited by S. J. Lippard), Vol. 23. Wiley, New York (1977).
2. P. M. Colman, H. C. Freeman, J. M. Guss, M. Murata, V. A. Norris, J. A. M. Ramshaw and M. P. Venkatappa, *Nature (London)* 1978, **272**, 319.
3. E. T. Adman, R. E. Stenkamp, L. C. Sieker and L. H. Jensen, *J. Mol. Biol.* 1978, **123**, 35.
4. E. Sletten, *Acta Cryst.* 1970, **B26**, 1609.
5. P. de Meester and A. C. Skapski, (a) *J. Chem. Soc. A* 1971, 2167; (b) *J. Chem. Soc., Dalton Trans.* 1972, 2400.
6. A. N. Speca, C. M. Mikulski, F. J. Iaconianni, L. L. Pytlewski and N. M. Karayannis, (a) *Inorg. Chem.* 1980, **19**, 3491; (b) *Inorg. Chim. Acta* 1980, **46**, 235; (c) *J. Inorg. Nucl. Chem.* 1981, **43**, 2771.
7. C. M. Mikulski, T. B. Tran, L. Mattucci and N. M. Karayannis, *Inorg. Chim. Acta* 1983, **78**, 211.
8. M. A. Guichelaar and J. Reedijk, *Recl Trav. Chim. Pays-Bas* 1978, **97**, 295.
9. IUPAC, *Nomenclature of Organic Chemistry*, 1979 edn, Section B, Rule B-3 (1979).
10. J. Dillen, A. T. H. Lenstra, J. G. Haasnoot and J. Reedijk, *Polyhedron* 1983, **2**, 195.
11. M. Biagini-Cingi, A. M. Manotti-Lanfredi, A. Tiripicchio, J. G. Haasnoot and J. Reedijk, (a) *Inorg. Chim. Acta* 1983, **72**, 81; (b) *Inorg. Chim. Acta* 1984, **86**, 137.
12. J. G. Haasnoot, W. L. Driessen and J. Reedijk, *Inorg. Chem.* 1984, **23**, 2803.
13. T. L. F. Favre, J. G. Haasnoot, W. Hinrichs and J. Reedijk, in preparation.
14. W. L. Mosby, *Heterocyclic Systems with Bridgehead Nitrogen Atoms*, Part II, p. 878. Interscience, New York (1961).
15. D. J. Brown and T. Nagamatsu, *Aust. J. Chem.* 1977, **30**, 2515.
16. C. Bülow and K. Haas, *Ber. Dtsch. Chem. Ges.* 1909, **42**, 4638.
17. A. Earnshaw, *Introduction to Magnetochemistry*. Academic Press, London (1968).
18. J. Waser, *Acta Cryst.* 1963, **16**, 1091.
19. Cambridge Crystallographic Data Centre, University Chemical Laboratory, Cambridge, U.K.
20. C. K. Johnson, Report ORNL-5138, Oak Ridge National Laboratory, Tennessee (1965).
21. E. J. Dirks, J. G. Haasnoot, A. J. Kinneging and J. Reedijk, *Inorg. Chem.* (submitted).
22. W. Vreugdenhil, P. J. M. W. L. Birker, R. W. M. ten Hoedt, G. C. Verschoor and J. Reedijk, *J. Chem. Soc., Dalton Trans.* 1984, 429.
23. K. Nakamoto, *Infrared and Raman Spectra of Inorganic and Coordination Compounds*, 3rd edn. Wiley, New York (1978).
24. J. Reedijk, *Transition Met. Chem.* 1981, **6**, 195.
25. B. J. Hathaway and D. E. Billing, *Coord. Chem. Rev.* 1970, **5**, 143.
26. M. R. Rosenthal, *J. Chem. Educ.* 1973, **50**, 331.
27. J. G. Haasnoot, T. L. F. Favre, G. C. Verschoor and J. Reedijk, in preparation.
28. M. G. Miles, G. Doyle, R. P. Cooney and R. S. Tobias, *Spectrochim. Acta* 1969, **25A**, 1515.
29. A. L. Arduini, M. Garnett, R. C. Thompson and T. C. T. Wong, *Can. J. Chem.* 1975, **53**, 3812.
30. P. L. Dedert, J. S. Thompson, J. A. Ibers and T. J. Marks, *Inorg. Chem.* 1982, **21**, 969.
31. B. M. Gatehouse, S. E. Livingstone and R. S. Nyholm, *J. Chem. Soc.* 1957, 4222.
32. N. F. Curtis and Y. M. Curtis, *Inorg. Chem.* 1965, **4**, 804.

Polyhedron Vol. 5, No. 9, pp. 1413–1421, 1986
Printed in Great Britain

0277–5387/86 $3.00+.00
Pergamon Journals Ltd

CHEMISTRY OF 3,4-DIMETHYLPHOSPHOLYL ANION IN THE COORDINATION SPHERE OF TUNGSTEN: SYNTHESIS AND X-RAY CRYSTAL STRUCTURE ANALYSIS OF (η^5-3,4-DIMETHYLPHOSPHOLYL)TRICARBONYL-IODOTUNGSTEN

SERGE HOLAND and FRANÇOIS MATHEY*

Laboratoire CNRS–SNPE, 2–8 rue Henry Dunant, 94320 Thiais, France

and

JEAN FISCHER

Laboratoire de Cristallochimie, Institut Le Bel, Université Louis Pasteur, 67070 Strasbourg, France

(*Received* 9 *September* 1985; *accepted* 25 *November* 1985)

Abstract—The reaction of the 3,4-dimethylphospholyl anion with $W(CO)_6$ and $W(CO)_5THF$ yields, according to the experimental conditions and stoichiometries, the η^1-P complex $(Me_2C_4H_2\bar{P})W(CO)_5$ or the μ^2-P complex $(Me_2C_4H_2\bar{P})[W(CO)_5]_2$. We have compared the reactivities of the free phospholyl anion and its P–$W(CO)_5$ and P–$[W(CO)_5]_2$ complexes toward H^+, $ClSnR_3$, S_8 and iodine. The most spectacular result has been observed when allowing iodine to react with the P–$[W(CO)_5]_2$ complex. The new η^5-$(Me_2C_4H_2P)W(CO)_3I$ complex has been obtained and characterized by X-ray crystal structure analysis. A typical nucleophile such as hydroxide ion attacks this η^5-complex not at the W—I bond as expected, but at the P atom with breaking of the P—W bond and formation of a η^4-diene complex. The lone pair at P remains able to coordinate with another metallic centre.

In a series of preceding papers, we have shown that complexation of the phosphorus lone pair by a pentacarbonyltungsten unit drastically alters the chemistry of tervalent phosphorus compounds. For example, strained phosphorus heterocycles gain additional stability[1–3] and decomposition of RP(H)X species through reductive elimination at phosphorus is quenched in many cases.[4–6] From another standpoint, if η^5-phospholyl complexes have been described with transition metals of the titanium (Zr[7]), manganese (Mn[8,9] or Re[9]), iron[10,11] and cobalt[12] families, no such complex has been reported till now with a metal of the chromium subgroup. These two kinds of considerations prompted us to study the chemistry of the well-known phospholyl anions[13] in the coordination sphere of tungsten.

EXPERIMENTAL

NMR spectra (chemical shifts in ppm from internal Me_4Si for ^1H and ^{13}C, and from external H_3PO_4 for ^{31}P; δ positive for downfield shifts in all cases) were recorded on a Bruker WP 80 instrument respectively at 80.13, 20.15, and 32.44 MHz. Mass spectra [electronic impact desorption (EID) or chemical ionization desorption (CID)] were recorded on a Nermag R10-10 spetrometer by Mr Charré (SNPE). All reactions were carried out under argon. Chromatographic separations were performed on deoxygenated silical gel columns (70–230-mesh, Riedel de Haën).

* Author to whom correspondence should be addressed.

Preparation of phospholyllithium–tungsten complexes

[η^1 - P - 3,4 - *dimethylphospholyllithium*]*pentacarbonyltungsten* (**3**). Solid tungsten hexacarbonyl (3.5 g, 10 mmol) was added to 10 mmol of 3,4-dimethylphospholyllithium (**2**) (see Ref. 14) in THF (80 cm^3). After stirring at room temperature for 8 h, the ^{31}P NMR spectrum of the reaction mixture showed a single signal at −54.8 ppm corresponding to the monotungsten complex. To a sample of the solution in a NMR tube was added an excess of methyl iodide. After 10 min at room temperature, the ^{31}P NMR spectrum showed a single signal corresponding to the known [1,3,4-trimethylphosphole]pentacarbonyltungsten complex (**4**) at −8.4 ppm [$^1J(^{31}P–^{183}W)$ 207.5 Hz].

[μ^2 - P - 3,4 - *dimethylphospholyllithium*]*decacarbonylditungsten* (**5**). To the preceding solution of phospholyllithium complex **3** (10 mmol) was added one equivalent of tungsten hexacarbonyl (3.5 g). After 5 h of reflux, the ^{31}P NMR spectrum showed a single signal at −99.5 ppm [$^1J(^{31}P–^{183}W)$ 141.5 Hz, intensities 1:6:1]. The same result was obtained by refluxing one equivalent of phospholyllithium (**2**) for 8 h with two equivalents of $W(CO)_6$, or by reaction of anion **2** with $W(CO)_5THF$.[5]

Preparation of [η^1-P-3,4-*dimethylphosphole*]*pentacarbonyltungsten* (**6**)

Methane sulfonic acid (1.9 g, 20 mmol) in 20 cm^3 of CH_2Cl_2 was treated at room temperature by a solution of 10 mmol of the phospholyllithium complex **3**. After vacuum distillation of the THF, the residue was chromatographed with toluene leading to a mixture which was dissolved in 1 cm^3 of CH_2Cl_2 and 50 cm^3 of hexane. Filtration over diatomaceous silica and distillation of the solvents gave a partially crystallized oil. Yield 2.5 g (ca 47%). The ^{31}P NMR spectrum in CH_2Cl_2 showed a major signal at −46.1 ppm [$^1J(^{31}P–^{183}W)$ 232 Hz, ^1J(P–H) 322 Hz] and a minor signal at 20.2 ppm [$^1J(^{31}P–^{183}W)$ 224.5 Hz]. A recrystallized sample at EtOH (pale yellow solid) gave the same spectrum.

[η^1 - P,η^1 - P′ - 3,3′,4,4′ - *tetramethyl* - 2,5 - *dihydro* - 1,1′ - *biphospholyl*]*decacarbonylditungsten* (**7**)

To a solution of **3** (10 mmol in THF), cooled at about −40°C, was added 3.4 g (20 mmol) of 4-toluene sulfonic acid monohydrate. The solvent was vacuum distilled and the residue chromatographed with CH_2Cl_2 leading to 7.4 g of a solid; m.p. 190°C (yield 85%). An analytical sample was recrystallized in acetone; pale yellow crystals; m.p. 195°C; ^{1}H NMR ($CDCl_3$) phosphole ring: δ 2.20 [pseudo t, ^4J(H–P) ~ 1 Hz, 6H, CH_3], 6.20 [d, ^2J(H–P) 37.4 Hz, 2H, =CH]; phospholene ring: δ 1.7 (s, 6H, CH_3), 2.53 and 2.96 [AB system, $^2J(H_A–H_B)$ 17.6 Hz, 4H, CH_2]; ^{13}C–{^{1}H} NMR ($CDCl_3$) phosphole ring: δ 17.7 [d, ^3J(C–P) 11 Hz, CH_3], 128.8 [pseudo q, ^1J(C–P) 30.5 Hz, ^2J(C–P) 2.5 Hz, =CH], 154.0 [pseudo q, ^2J(C–P) 6.1 Hz, ^3J(C–P) 3.7 Hz, =C<]; phospholene ring: δ 16.2 [d, ^3J(C–P) 6 Hz, CH_3], 43.3 [pseudo q, ^2J(C–P) 18.3 Hz, ^3J(C–P) 4.9 Hz, CH_2], 131.9 (s, =C<) and δ 196.1 (d, CO), 197.0 (d, CO); IR ($CHCl_3$) ν(CO) 2080, 2070, 1950, 1930 cm^{-1}; mass spectrum (EID, 70 eV, ^{184}W) m/z (relative intensity): 872 [M (50%)], 437 [M − phosphole ring (50%)], 435 [M − phospholene ring (40%)]. Found: C, 30.4; H, 2.1; P, 7.0; W, 42.1%. Calc. for $C_{22}H_{18}O_{10}P_2W_2$: C, 30.3; H, 2.1; P, 7.1; W, 42.2%.

[η^1 - P - 3,4 - *dimethyl* - 1 - *triphenylstannyl phosphole*]*pentacarbonyltungsten* (**9**)

To the phospholyllithium complex (**3**) (10 mmol in 80 cm^3 of THF) was added at room temperature triphenyltin chloride (4.25 g, 11 mmol) in 20 cm^3 of THF. After 30 min of stirring, the solvent was vacuum distilled and the residue chromatographed in toluene on silica gel dried at ca 150°C under 10^{-2} mmHg. Evaporation of the solvent led to 5.4 g (yield 68.5%) of an orange oil. ^{1}H NMR ($CDCl_3$): δ 1.82 (poorly resolved d, 6H, CH_3), 6.60 [d, ^2J(H–P) 41.2 Hz, 2H, CH], 7.4 (m, 15H, Ph); ^{13}C–{^{1}H} NMR: δ 17.8 [d, ^3J(C–P) 9.7 Hz, CH_3], 129.7 [d, ^1J(C–P) 40.3 Hz, =CH], 128.5–132.2 (m, aromatic CH), 135.8–138.9 (m, arom. =C<), 152.9 [d, ^2J(C–P) 4.9 Hz, =C<], 196.5 [d, ^2J(C–P) 6.1 Hz, CO], 200.1 [d, ^2J(C–P) 20.7 Hz, CO], ^{119}Sn–{^{1}H} NMR (C_6D_6): δ Me_4Sn (neat) −88.4 [d, $^1J(^{119}Sn–^{31}P)$ 92.8 Hz]; IR (hexane): ν(CO) 2068, 1985, 1950 cm^{-1}.

[η^1 - P - 3,4 - *dimethyl* - 1 - *methylthiophosphole*]*pentacarbonyltungsten* (**10**)

Solid sulphur (0.35 g, 11 mmol) was added to the THF solution of complexed phospholyllithium (10 mmol) at room temperature. After 30 min of stirring the thioanion formation was checked by ^{31}P NMR (resonance at 14.9 ppm in THF). Methyl iodide (1.56 g, 11 mmol) was then added. The reaction

mixture was stirred 30 min more and the THF was distilled under vacuum. Chromatography of the residue with toluene followed by solvent distillation led to 3.25 g (yield ca 70%) of complex **10**; m.p. 105°C (orange yellow crystals). ^{1}H NMR ($CDCl_3$): δ 1.77 [d, ^3J(H–P) 9.0 Hz, 3H, SCH_3], 2.2 [d, ^4J(H–P) 1.0 Hz, 6H, CH_3], 6.13 [dd, ^2J(H–P) 38.8 Hz, ^4J(H–H) 1.0 Hz, 2H, =CH]; ^{13}C–{^{1}H} NMR ($CDCl_3$): δ 13.65 [d, ^2J(C–P) 2.4 Hz, SMe], 16.75 [d, ^3J(C–P) 12.2 Hz, C–Me], 127.6 [d, ^1J(C–P) 37.6 Hz, =CH], 151.45 [d, ^2J(C–P) 9.7 Hz, =C<], 195.4 [d, ^2J(C–P) 7.3 Hz, CO]; IR (hexane): ν(CO) 2073, 1947 cm^{-1}. Found: C, 30.0; H, 2.0; P, 6.3; S, 6.4%. Calc. for $C_{12}H_{11}O_5PSW$: C, 29.9; H, 2.3; P, 6.4; S, 6.6%.

3,4-*Dimethyl*-1-*methylthiophosphole* P-*sulphide* (13)

To a solution of 10 mmol of **2** in THF, was added 2.2 equivalents of solid sulphur. After 10 min, the formation of the intermediate thioanion **13a** was controlled by ^{31}P NMR [δ(^{31}P) 63.9, t, ^2J(P–H) 29.3 Hz] and then 1.7 g (ca 12 mmol) of methyl iodide in 5 cm^3 of THF was added. The reaction mixture was vacuum concentrated and the residue chromatographed with hexane–CH_2Cl_2 (80 : 20) leading to 1.3 g (yield 65.5%) of **13**; m.p. 85°C (pale yellow crystals); ^{1}H NMR ($CDCl_3$): δ 2.1 [q, ^4J(H–P) 2 Hz, ^4J(H–H) 1 Hz, 6H, C—CH_3], 2.3 [d, ^3J(H–P) 14.5 Hz, 3H, SCH_3], 6.0 [dd, ^2J(H–P) 33.0 Hz, 2H, =CH]; ^{13}C–{^{1}H} NMR ($CDCl_3$): δ 12.7 [d, ^3J(C–P) 2.9 Hz, C–CH_3], 16.8 [d, ^2J(C–P) 19.5 Hz, S–CH_3], 123.2 [d, ^1J(C–P) 82.0 Hz, =CH], 151.7 [d, ^2J(C–P) 20.5 Hz, =C<]; mass spectrum (EID) m/z (relative intensity): 190 [M (26%)], 143 [M – SMe (100%)]. Found: C, 44.3; H, 5.8; P, 16.3%. Calc. for $C_7H_{11}PS_2$: C, 44.2; H, 5.8; P, 16.3%.

[η^1 - P,η^1 - P′ - 3,3′,4,4′ - *tetramethyl* - 1,1′-*biphospholyl*]*decarbonylditungsten* (14)

A solution of iodine (1.27 g, 5 mmol) in 10 cm^3 of THF was slowly added at room temperature to **3** (10 mmol in THF). The reaction mixture was vacuum contentrated and the residue chromatographed with first CH_2Cl_2 and then ethyl acetate. Distillation of the solvents led to 2.4 g (yield 55%) of yellow orange crystals; m.p. (dec.) 230°C. An analytical sample was recrystallized in THF; m.p. (dec.) 233–236°C; ^{1}H NMR (THF-d_8): δ 2.24 (pseudo t, 12H, CH_3), 6.63 [m, ^2J(H–P) 39.5 Hz, 4H, CH]; ^{13}C–{^{1}H} NMR (THF-d_8): δ 17.45 (pseudo t, CH_3), 130.9 (pseudo t, =CH), 156.2 (pseudo t, =C<), 195.5 (d, CO); IR ($CHCl_3$), ν(CO) 2065, 1980, 1950 cm^{-1}; mass spectrum (EID, ^{184}W) m/z (relative intensity): 870 [M (50%)], 590 [M – 10CO (20%)], 435 [M/2 (100%)]. Found: C, 30.4; H, 1.8; W, 42.5%. Calc. for $C_{22}H_{16}O_{10}P_2W_2$: C, 30.4; H, 1.8; W, 42.3%.

Complex **14** was also obtained by reaction of 3,3′,4,4′-tetramethyl-1,1′-biphospholyl[4] with two equivalents of $W(CO)_5$THF in THF.

[η^5 - 3,4 - *Dimethylphospholyl*]*tricarbonyliodotungsten* (15) *and* [η^1 - P - (η^5 - 3,4 - *dimethylphospholyl*) *tricarbonyliodotungsten*]*pentacarbonyltungsten* (17)

To a solution of 10 mmol of the ditungsten complex **5** was added iodine (11 mmol in 10 cm^3 of THF) at room temperature. After 2 h of stirring, the reaction mixture gave a single or major ^{31}P NMR signal at –31.5 ppm. The solvent was vacuum distilled and the residue dissolved in a small amount of CH_2Cl_2. In this solution, the ^{31}P NMR resonance at –31.5 decreased to the benefit of a new signal at –11.2 ppm. A large amount of hexane was then added and the mixture was filtered through a column of diatomaceous silica. The solvent was removed and the residue chromatographed on acidic silica gel giving first, by elution with hexane + 20% of CH_2Cl_2, complex **15**, then, with CH_2Cl_2, complex **17**.

Complex **15**: 1.9–2.7 g (yield 37.5–53.5%), dark purple crystals; m.p. 112°C; ^{1}H NMR ($CDCl_3$): δ 2.48 (s, 6H, CH_3), 5.16 [d, ^2J(H–P) 35.2 Hz, 2H, =CH]; ^{13}C–{^{1}H} NMR ($CDCl_3$): δ 16.6 (s, CH_3), 100.1 [d, ^1J(C–P) 67.1 Hz, =CH], 126.8 [d, ^2J(C–P) 8.5 Hz, =C<], 207.7 and 221.5 (CO); IR (hexane) ν(CO) 2037, 1968, 1957, 1945 cm^{-1}; mass spectrum (EID, ^{184}W) m/z (relative intensity): 506 [M (15%)], 478 [M – CO (50%)], 450 [M – 2CO (30%)], 422 [M – 3CO (75%). Found: C, 21.6; H, 1.5; I, 25.0; P, 6.1%. Calc. for $C_9H_8IO_3PW$: C, 21.4; H, 1.6; I, 25.1; P, 6.1%.

Complex **17**: in addition to the chromatographed product, another fraction of complex **17** was recovered by washing the celite column with CH_2Cl_2. Recrystallization of the two fractions gave 1–3 g (yield 12–36%) of orange crystals; m.p. (dec.) 185–187°C; ^{1}H NMR ($CDCl_3$): δ 2.60 (s, 6H, Me), 5.10 [d, ^2J(H–P) 32.0 Hz, 2H, =CH]; ^{13}C–{^{1}H} NMR (CD_3COCD_3): δ 15.75 [d, ^3J(C–P) 3.6 Hz, CH_3], 94.4 [d, ^1J(C–P) 7.3 Hz, =CH], 124.8 (s, =C<), 193.4 [d, ^2J(C–P) 7.3 Hz, W(CO)$_5$]; IR ($CHCl_3$): ν(CO) 2085, 2040, 2000 (sh), 1975, 1957 cm^{-1}; mass spectrum (CID, iso-C_4H_{10}, ^{184}W) m/z (relative intensity): 830 [M (90%)], 703 [M – I (40%)], 506

[M – $W(CO)_5$ (100%)]. Found: C, 20.4; H, 0.9; I, 15.2; P, 3.7; W, 44.4%. Calc. for $C_{14}H_8IO_8PW_2$: C, 20.3; H, 1.0; I, 15.3; P, 3.7; W. 44.3%.

The ditungsten complex **17** was also obtained by allowing the η^5-phospholyltungsten complex **15** to react with $W(CO)_5$THF in THF.

Tetramethylammonium [η^4 - C_4 - 3,4 - *dimethyl* - 1 - *oxophosphole*]*tricarbonyliodotungstate* (**16**)

To the η^5-phospholyl complex **15** (1.02 g, 2 mmol) in 30 cm^3 of CH_2Cl_2 was added 1.03 cm^3 (2 mmol) of a 20% methanolic solution of tetramethylammonium hydroxide. The reaction mixture turned from dark red to orange. Filtration on diatomaceous silica followed by vacuum concentration of the filtrate led to an orange oil which crystallized. The solid was sucked dry on sintered glass after washing with a mixture of hexane and CH_2Cl_2 (50:50). Yield 0.9 g (75%) orange crystals; m.p. 188°C; ^{1}H NMR (CD_3COCD_3): δ 2.26 (s, 6H, CH_3), 3.01 [dd, ^2J(H–P) 14.1 Hz, ^3J(H–H) 0.95 Hz, 2H, =CH], 3.43 [t, $^1J(^1H-^{14}N)$ 0.6 Hz, 12H, NCH_3], 7.36 [dt, ^1J(H–P) 530.2 Hz, 1H, PH]; ^{13}C–{^{1}H} NMR (CD_3COCD_3): δ 16.7 [d, ^3J(C–P) 3.6 Hz, CH_3], 52.4 [d, ^1J(C–P) 78.1 Hz, =CH], 56.0 [t, $^1J(^{13}C-^{14}N)$ 3.6 Hz, NCH_3], 90.1 [d, ^2J(C–P) 14.6, =C<], 218.2 and 228.6 (CO); IR (KBr): ν(PH) 2380 cm^{-1}; ν(PO) 1177 cm^{-1}; ν(CO) 1990, 1915, 1880 cm^{-1}. Found: C, 26.7; H, 3.9; N, 2.3; P, 5.0%. Calc. for $C_{13}H_{21}INO_4PW$: C, 26.1; H, 3.5; N, 2.3; P, 5.2%.

X-ray data collection and processing

Suitable single crystals of **15** were obtained by slow evaporation of CH_2Cl_2–hexane solutions at room temperature under argon. A systematic search in reciprocal space using a Philips PW 1100/16 automatic diffractometer showed that crystals of **15** belong to the monoclinic system. The unit-cell dimensions and their standard deviations were obtained and refined at –100°C with Mo-K_α radiation (λ = 0.71073 Å) by using 25 carefully selected reflections and the standard Philips software. Crystal data: $C_9H_8O_3PIW$, M = 506, a = 7.325(3) Å, b = 14.545(6) Å, c = 12.169(5) Å, β = 103.46(2), V = 1261 Å^3, Z = 4, d_c = 2.665 g cm^{-3}, d_o = 2.63 ± 0.02 g cm^{-3}, μ = 118.93 cm^{-1}, F(000) = 912, space group $P2_1/n$.

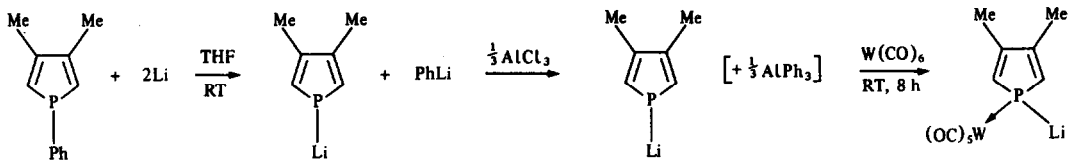
A parallelepipedic crystal of dimensions 0.15 × 0.22 × 0.26 mm was glued at the end of a glass fibre and mounted on a rotation free goniometer head. All quantitative data were obtained using the same diffractometer, graphite-monochromated radiation and standard software in a cold nitrogen gas stream (–100°C). The vertical and horizontal apertures in front of the scintillation counter were adjusted so as to minimize the background counts without loss of net peak intensity at the 2σ level. The total scan width in the θ–2θ flying step-scan used was $\Delta\theta = 1.0 + 0.343\ \mathrm{tg}(\theta)°$, with a step width of 0.05° and a scan speed of 0.02° s^{-1}. 7631 *hkl*, $\bar{h}kl$, $h\bar{k}l$ and $\bar{h}\bar{k}l$ reflections were recorded ($3° < \theta < 30°$). Three standard reflections measured every hour during the entire data-collection period showed no significant trend. The resulting data-set was transferred to a PDP 11/60 computer, and for all subsequent computations, the Enraf–Nonius SDP/V18 package was used,[16] with the exception of a local data-reduction program.

The raw step-scan data were converted to intensities using the Lehmann–Larson method[17] and then corrected for Lorentz, polarization and absorption factors, the latter computed by the empirical method of Walker and Stuart[18] (transmission factors between 1.00 and 0.81). Averaging of equivalent reflections (R_i = 0.019) led to a unique data set of 2942 reflections having $I > 3\sigma(I)$ used for determining and refining the structure.

The structure was solved using the heavy-atom method. After refinement of the heavy atoms, a difference-Fourier map revealed maxima of residual electronic density close to the positions expected for hydrogen atoms; they were introduced in structure factor calculations with computed coordinates (C—H = 0.95 Å) and isotropic temperature factors [B_{eqv}(C)] of +1 Å^2 but not refined. Full least-squares refinement converged to $R(F)$ = 0.029 and $R_w(F)$ = 0.060 $\{\alpha(F^2) = [\sigma^2(\mathrm{count}) + p(I)^2]^{1/2}\}$. The unit-weight observation was 1.32 for p = 0.08. A final difference map revealed no significant maxima. The scattering factors coefficients and anomalous dispersion coefficients come, respectively, from Refs 19 and 20.

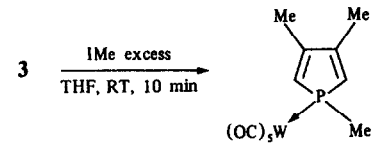
RESULTS AND DISCUSSION

Throughout this study, our starting product has been the readily available 1-phenyl-3,4-dimethylphosphole (**1**).[21] The cleavage of the P–phenyl bond of **1** is achieved by reaction with lithium in THF as usual. Then, phenyllithium is selectively destroyed by adding a stoichiometric amount of anhydrous aluminium trichloride (see Ref. 14). The solution of 3,4-dimethylphospholyllithium (**2**) thus obtained is then allowed to react at room temperature with one equivalent of hexacarbonyltungsten:



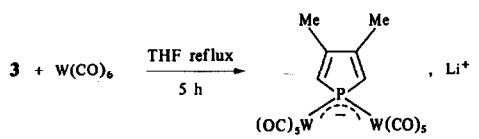
1 2 3

The ^{31}P NMR resonance of **2** at ca +55 ppm (vs external 85% H_3PO_4) slowly disappears and is replaced by a new resonance at −54.8 ppm corresponding to the complexed anion (**3**). The structure of **3** is established by methylation with methyl iodide which gives the already known 1,3,4-trimethylphosphole complex (**4**) [$\delta(^{31}P)$(**4**) −8.4 ppm in THF, $^1J(^{31}P-^{183}W)$ 207.5 Hz].



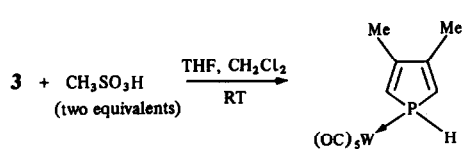
4

At room temperature, the reaction of **2** with $W(CO)_6$ stops at the level of the monocomplexed anion (**3**) but in refluxing THF, **3** is in turn able to react with another equivalent of $W(CO)_6$ to afford the already described[15] and almost unreactive dicomplexed anion (**5**) which has been previously obtained by allowing **2** to react directly with two equivalents of $W(CO)_5THF$ [$\delta(^{31}P)$(**5**) −99.5 ppm in THF].



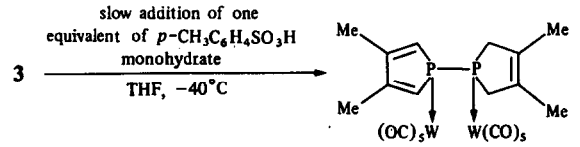
5

The protonation of **3** is very interesting. When pouring a THF solution of **3** into a CH_2Cl_2 solution of a strong acid such as methanesulfonic acid at room temperature, the sole product is the P–H phosphole complex (**6**) [$\delta(^{31}P)$(**6**) −46 ppm, $^1J(^{31}P-^{183}W)$ 232 Hz, ^1J(P–H) ≃ 322 Hz].



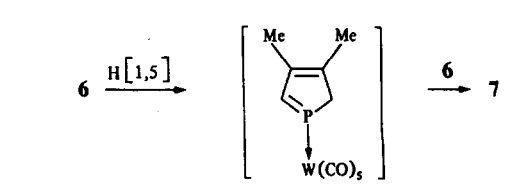
6

Complex **6** has only a limited stability in THF at room temperature and decomposes completely in ca 4 h to give two dimers (**6a** and **6b**) [$\delta(^{31}P)$ (**6a**) +25.6 ppm, $^1J(^{31}P-^{183}W)$ 237 Hz; and +15.6 ppm, $^1J(^{31}P-^{183}W)$ 229.5 Hz, J(P–P) 14.6 Hz, ^1J(P–H) 285.5 Hz. $\delta(^{31}P)$ (**6b**) −1.8 ppm, $^1J(^{31}P-^{183}W)$ 239.5 Hz; and −29.8 ppm, $^1J(^{31}P-^{183}W)$ 229.5 Hz, J(P–P) 7.3 Hz, ^1J(P–H) 325 Hz]. Both dimers contain one P—H bond and no P—P bond. We suspect that they are formed through addition of the P—H bond of one molecule of **6** to the dienic system of another molecule of **6**. Such dimerizations have been encountered during a study of the protonation of **1** (Quin *et al.*, to be published). Complex **6** can be also prepared by acidic cleavage of the P–$SnPh_3$ complex (**9**) by HCl in methanol (*vide infra*). If the protonation of **6** is either carried out with a weak acid (acetic acid, silica gel) or at low temperature, then the course of the reaction changes and the main product becomes the phospholenophosphole complex (**7**) [$\delta(^{31}P)$ (**7**) +6.0 ppm in THF, $^1J(^{31}P-^{183}W)$ 202 Hz (phosphole cycle); −8.65 ppm, $^1J(^{31}P-^{183}W)$ 220 Hz, ^1J(P–P) 178 Hz (phospholene cycle)] which is sufficiently stable to be isolated in the pure state and completely characterized contrary to **6**, **6a** and **6b**.



7

The formation of **7** deserves some comments. We have shown previously[17] that P–H phospholes tend to rearrange through hydrogen [1, 5] sigmatropic shifts to give the very reactive 2H-phospholes. This tendency still exists when P–H phospholes are complexed at phosphorus. Thus the mechanism through which **7** is formed simply involves the addition of the P—H bond of **6** onto the P=C double bond of the corresponding 2H-phosphole complex (**8**).

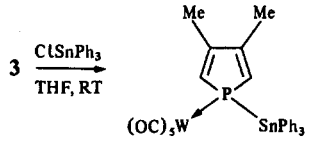


8

Such a dimerization has already been described in the case of the uncomplexed 2,3,4,5-tetraphenylphosphole.[22]

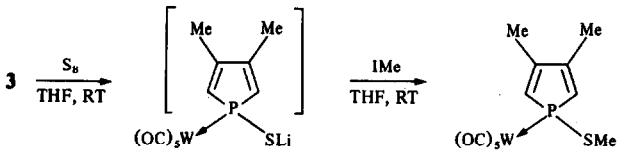
As mentioned earlier, it is possible to prepare

the P–$SnPh_3$ complex (**9**) [$\delta(^{31}P)$ (**9**) −66 ppm in THF, $^1J(^{31}P–^{183}W)$ 190 Hz, $^1J(^{31}P–^{119}Sn)$ 88 Hz] by reaction of the appropriate tin chloro derivative with **3**.



9

Complex **9** can be purified by chromatography and is obtained in ca 68% yield. Complex **3** is also able to react cleanly with sulphur at room temperature. The P–SLi complex thus obtained can be alkylated at sulphur by methyl iodide to give the P–SMe complex (**10**) in 70% yield [$\delta(^{31}P)$ (**10**) 19.6 ppm in THF, $^1J(^{31}P–^{183}W)$ 222 Hz].

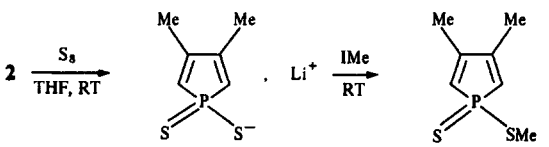


10

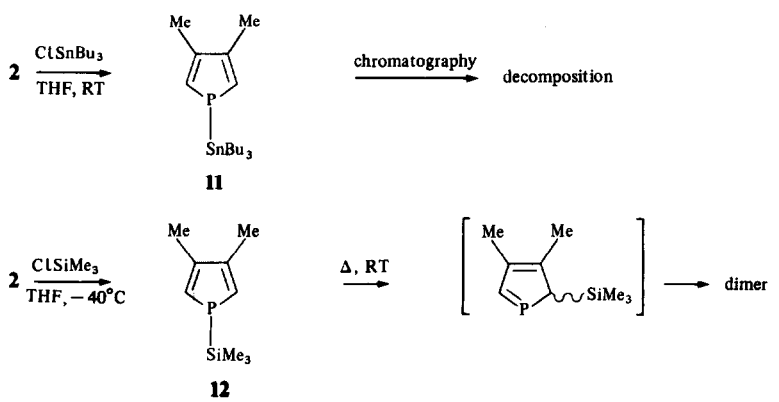
It is interesting to compare what occurs during the syntheses of **9** and **10** with what is observed when attempting similar reactions with the uncomplexed anion **2**. The reaction of **2** with *n*-Bu_3SnCl in THF gives the expected P–$SnBu_3$ phosphole (**11**) [$\delta(^{31}P)$ (**11**) −62.7 ppm in THF] but an attempted purification by chromatography led to decomposition. This decomposition probably occurs through hydrolysis and (or) oxidation of the P—Sn bond of **11** but can also involve a [1,5] migration of the $SnBu_3$ group similar to what happens when **6** is converted into **7** by chromatography on silica gel. Indeed, such a migration has been observed in a related case when attempting to prepare silylphosphole (**12**).

This silylphosphole [$\delta(^{31}P)$ (**12**) −50 ppm in THF] immediately rearranges to give a P—P bonded dimer [$\delta(^{31}P)$ +0.8 and −21.0 ppm in THF, ^1J(P–P) 195 Hz]. Even though we are unable to assign a precise formula to this dimer because it is very sensitive toward oxidation and hydrolysis and cannot be purified, the formation of a P—P bond necessarily involves a migration of the silyl group. Thus, the reasonable stabilities of both complexes **6** and **9** clearly demonstrate that P–$W(CO)_5$ complexation not only stabilizes phospholes toward oxidation and hydrolysis but also toward [1,5] sigmatropic shifts. It may be noted here that we[23] and Jutzi[24] have already demonstrated that P-complexation by $W(CO)_5$ or $Cr(CO)_5$ quenches the fluxionality of some selected cyclopentadienylphosphines which occurs through H and PR_2 [1,5] shifts. The freezing of these various types of migrations probably involves a common mechanism.

P-complexation also alters the course of the reaction of phospholyl anion with sulphur. Indeed, monosulphurization of **2** proved to be impossible. The reaction goes directly to the dithiophosphinic anion which can be easily alkylated by methyl iodide to give **13** [$\delta(^{31}P)$ (**13**) +62.9 ppm in THF].



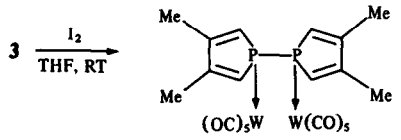
13a **13**



11

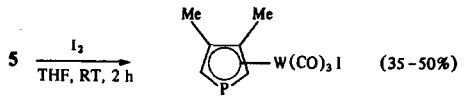
12

Finally, we have also studied the reaction of **3** with iodine. Here, the behaviour of **3** appears to be exactly similar to that of **2** (see Ref. 14): in both cases, a P—P bond is created. Complex **14** [$\delta(^{31}P)$ (**14**) +5.9 ppm in THF] is thus obtained in 55% yield.



14

The study of the reactivity of the dicomplexed anion (**5**) has been much less complete. In fact **5** is far less reactive than **3**. The protonation of **5** is difficult and requires a strong acid. It gives an interesting stable 2H-phosphole complex which has been described previously.[15] Quite unexpectedly, the reaction of **5** with iodine also affords a very interesting result: the first known η^5-phospholyltungsten complex (**15**) [$\delta(^{31}P)$ (**15**) −31.5 ppm in THF] is thus obtained.



15

The crystal structure of **15** was established by X-ray diffraction and consists of discrete molecules only linked by van der Waals' contacts; there are no non-usual intermolecular contacts.* Figure 1 displays one molecule of **15**. Table 1 gives selected bond lengths and angles with their estimated standard deviations. The tungsten atoms are nine-coordinated: three carbonyl and the iodine atom lie on one side whereas the η^5-phospholyl ring occupies the opposite side of the coordination polyhedron. C7, C8, C9 and I form a roof: I is outside the plane containing C7, C8 and C9 by 0.421(1) Å on the same side as W; the dihedral angle between the planes C7–C8–C9 and I–C8–C9 is 9.5°. The W—I bond length of 2.8331(5) Å is not significantly different from that reported for $WI_2(OCMe_3)_6$, 2.8293(8).[25] The three W—C (carbonyl) bond lengths range from 1.982(8) to 2.017(6) Å and the W—C≡O bond angles have values near to 180°. The W atom is not equidistant from the four

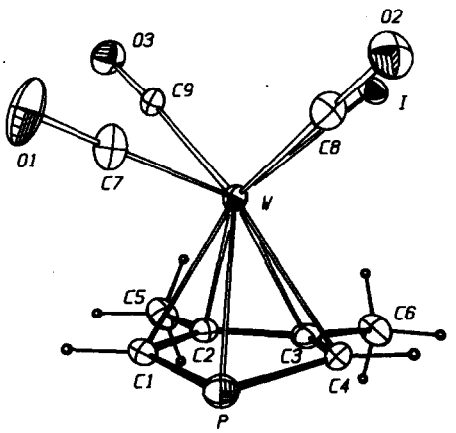


Fig. 1. Structure of complex **15**. The heavy-atom ellipsoids are scaled to enclose 50% of the electron density, hydrogen atoms have arbitrary radii.

C atoms of the phospholyl core: the W—C1 bond length is shorter than the three other bond lengths, thus the projection of W on the C1 → C4 plane is out of the line joining the P atom to the middle of the C2—C3 bond in the direction of C1.

The carbon atoms C1–C4 are coplanar within experimental error; the phosphorus atom is outside from this mean plane by 0.150(3) Å and the tungsten atom by 1.963(0) Å. As expected, the W—P bond length of 2.516(2) Å is greater than those found in pure W—P σ-bonds[2,15] but less than those in complexes having some π character in their W—P bond.[15] The dihedral angle between the mean planes of these four carbon atoms and P–C1–C4 is equal to 6.8°, a value greater than those found in η^5-phosphacymantrenes[8] or diphosphaferro-

Table 1. Selected bond lengths (Å) and angles (°) with their estimated standard deviations

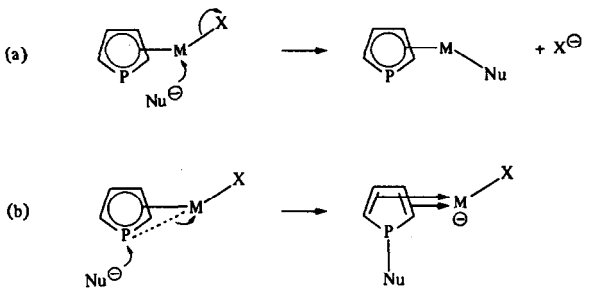
W—I	2.8331(5)	I—W—C7	131.6(3)
W—P	2.516(2)	I—W—C8	76.5(2)
W—C1	2.302(7)	I—W—C9	74.8(2)
W—C2	2.380(7)	C7—W—C8	78.3(3)
W—C3	2.443(7)	C7—W—C9	76.9(3)
W—C4	2.342(7)	C8—W—C9	110.1(3)
W—C7	1.982(8)	C1—P—C4	88.3(4)
W—C8	2.004(8)	P—C1—C2	113.7(6)
W—C9	2.017(6)	P—C4—C3	112.9(6)
P—C1	1.775(8)	C1—C2—C3	112.0(7)
P—C4	1.771(6)	C2—C3—C4	112.3(7)
C1—C2	1.41(1)	C1—C2—C5	122.8(7)
C3—C4	1.43(1)	C4—C3—C6	123.0(8)
C2—C3	1.40(1)	C3—C2—C5	125.0(7)
C2—C5	1.51(1)	C2—C3—C6	124.6(8)
C3—C6	1.51(1)	W—C7—O1	178.1(7)
C7—O1	1.14(1)	W—C8—O2	178.7(7)
C8—O2	1.13(1)	W—C9—O3	176.5(7)
C9—O3	1.121(8)		

* Tables of atomic positional parameters and thermal parameters and lists of F_o/F_c values have been deposited as supplementary data with the Editor, from whom copies are available on request. Atomic coordinates have also been deposited with the Cambridge Crystallographic Data Centre.

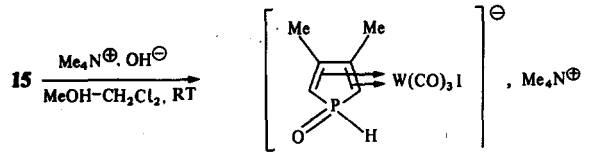
cenes,[11] suggesting some loss of aromaticity of the phospholyl ring in complex **15**. The bond lengths and angles in the phospholyl ring are not significantly different from those found in η^5-phosphacymantrenes.[8]

From a spectroscopic point of view, we have noted one very peculiar characteristic of this π-complex. No NMR coupling is visible between ^{31}P and ^{183}W nuclei, whereas the P—W bond length lies close to the normal value. This property seems to be characteristic of tungsten π-complexes involving P=C delocalized multiple bonds. Indeed, a similar situation has been encountered in the case of $\eta^2[CH_2{=}PCl]W(CO)_5$.[26]

Theoretical studies[27–29] have shown that the main difference between corresponding η^5-cyclopentadienyl and η^5-phospholyl complexes lies in the presence of a low-lying LUMO highly localized at phosphorus in the latter case. Since complex **15** is the first known η^5-phospholyl complex in which the P ring shares the coordination sphere of a metal with an halogen, it offered us the opportunity to compare the reactivities of P–metal and metal–halogen bonds toward nucleophiles. Two types of attacks could be envisaged: (a) the "normal" attack at the metal with loss of an halide ion; (b) the "abnormal" attack at phosphorus with cleavage of the phosphorus–metal bond.

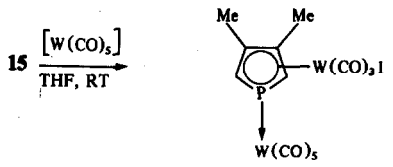


Apparently the "abnormal" attack is preferred at least in the case of the hydroxide ion.



16

Complex **16** [$\delta(^{31}P)$ (**16**) +38.8 ppm in acetone, ^1J(P–H) 532 Hz] is thus obtained in 75% yield. Finally, it is also interesting to note that, during the synthesis of **15**, a P → $W(CO)_5$ complex of **15** (**17**) is formed as a by-product [$\delta(^{31}P)$ (**17**) −14 ppm in $CDCl_3$, $^1J(^{31}P–^{183}W)$ 274 Hz].



17

Here of course, a normal ^1J coupling is observed between P and the $W(CO)_5$ tungsten. The formation of **17** from **15** is exactly similar to the various P-complexations observed with phosphamantrenes,[30] phosphaferrocenes[26] and diphosphaferrocenes.[32]

REFERENCES

1. A. Marinetti, F. Mathey, J. Fischer and A. Mitschler, *J. Chem. Soc., Chem. Commun.* 1982, 667.
2. A. Marinetti, F. Mathey, J. Fischer and A. Mitschler, *J. Am. Chem. Soc.* 1982, **104**, 4484.
3. A. Marinetti and F. Mathey, *Organometallics* 1984, **3**, 456.
4. A. Marinetti and F. Mathey, *Organometallics* 1982, **1**, 1488.
5. A. Marinetti and F. Mathey, *Phosphorus and Sulfur* 1984, **19**, 311.
6. F. Mercier and F. Mathey, *J. Chem. Soc., Chem. Commun.* 1984, 782.
7. P. Meunier and B. Gautheron, *J. Organomet. Chem.* 1980, **193**, C13.
8. F. Mathey, A. Mitschler and R. Weiss, *J. Am. Chem. Soc.* 1978, **100**, 5748.
9. E. W. Abel, N. Clark and C. Towers, *J. Chem. Soc., Dalton Trans.* 1979, 1552.
10. F. Mathey, *J. Organomet. Chem.* 1977, **139**, 77.
11. G. de Lauzon, B. Deschamps, J. Fischer, F. Mathey and A. Mitschler, *J. Am. Chem. Soc.* 1980, **102**, 994.
12. C. Charrier, H. Bonnard, F. Mathey and D. Neibecker, *J. Organomet. Chem.* 1982, **231**, 361.
13. E. H. Braye, I. Caplier and R. Saussez, *Tetrahedron* 1971, **23**, 5523.
14. S. Holand, F. Mathey, J. Fischer and A. Mitschler, *Organometallics* 1983, **2**, 1234.
15. S. Holand, C. Charrier, F. Mathey, J. Fischer and A. Mitschler, *J. Am. Chem. Soc.* 1984, **106**, 826.
16. B. A. Frenz, In *Computing in Crystallography* (Edited by H. Schenk, R. Olthof-Hazekamp, H. van Koningsveld and G. C. Bassi), p. 64. Delft University Press, Delft, The Netherlands (1978).
17. M. S. Lehmann and F. K. Larsen, *Acta Cryst.* 1974, **A30**, 580.
18. N. Walker and D. Stuart, *Acta Cryst.* 1983, **A39**, 159.
19. D. T. Cromer and J. T. Waber, *International Tables for X-ray Crystallography*, Vol. 4, Table 2.2b. The Kynoch Press, Birmingham, U.K. (1974).
20. D. T. Cromer, *International Tables for X-ray Crys-*

tallography, Vol. 4, Table 2.3.1. The Kynoch Press, Birmingham, U.K. (1974).
21. A. Breque, F. Mathey and Ph. Savignac, *Synthesis* 1981, 983.
22. C. Charrier, H. Bonnard, G. de Lauzon and F. Mathey, *J. Am. Chem. Soc.* 1983, **105**, 6871.
23. B. Deschamps and F. Mathey, *Phosphorus and Sulfur* 1983, **17**, 317.
24. P. Jutzi, H. Saleske and D. Nadler, *J. Organomet. Chem.* 1976, **118**, C8.
25. F. A. Cotton, W. Schwotzer and E. S. Shamshoum, *Inorg. Chem.* 1984, **23**, 4111.
26. B. Deschamps and F. Mathey, *J. Chem. Soc., Chem. Commun.* 1985, 1010.
27. C. Guimon, G. Pfister-Guillouzo and F. Mathey, *Nouveau J. Chim.* 1979, **3**, 725.
28. N. M. Kostic and R. F. Fenske, *Organometallics* 1983, **2**, 1008.
29. C. Guimon, D. Gonbeau, G. Pfister-Guillouzo, G. de Lauzon and F. Mathey, *Chem. Phys. Lett.* 1984, **104**, 560.
30. A. Breque, F. Mathey and C. Santini, *J. Organomet. Chem.* 1979, **165**, 129.
31. J. Fischer, A. Mitschler, L. Ricard and F. Mathey, *J. Chem. Soc., Dalton Trans.* 1980, 2522.
32. B. Deschamps, F. Mathey, J. Fischer and J. H. Nelson, *Inorg. Chem.* 1984, **23**, 3455.

Polyhedron Vol. 5, No. 9, pp. 1423–1427, 1986
Printed in Great Britain

0277–5387/86 $3.00+.00
Pergamon Journals Ltd

BINUCLEAR PLATINUM(I) COMPLEXES WITH BIS(DIMETHYLPHOSPHINO)METHANE LIGANDS: EVIDENCE FOR BOTH SHORT- AND LONG-RANGE NMR *TRANS*-INFLUENCES

SAMSON S. M. LING and RICHARD J. PUDDEPHATT*

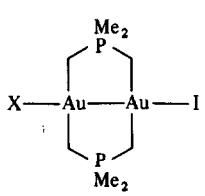
Department of Chemistry, University of Western Ontario, London, Ontario, Canada N6A 5B7

(*Received* 9 *August* 1985; *accepted* 26 *November* 1985)

Abstract—The diplatinum(I) complexes or complex ions $[Pt_2X_2(\mu\text{-dmpm})_2]$ (X = Cl or I), $[Pt_2X(PPh_3)(\mu\text{-dmpm})_2]^+$ (X = I, Br or Me), and $[Pt_2(PPh_3)_2(\mu\text{-dmpm})_2]^{2+}$, where dmpm = $Me_2PCH_2PMe_2$, have been prepared and characterized by ^1H and ^{31}P NMR spectroscopy. In the linear X–Pt–Pt–Y unit the *trans*-influence of X is felt primarily at the Pt–Pt bond, but groups X having a very high *trans*-influence (X = H or Me) can also exert a weaker long-range *trans*-influence on the Pt–Y bond.

Diplatinum(I) complexes with bridging bis(diphenylphosphino)methane (dppm) ligands are now well-known and have been important in investigations of the reactivity of the Pt–Pt bond.[1,2] The bulky phenyl substituents limit the reactivity of such complexes since only small molecules can approach the Pt–Pt bond.[3] We were therefore interested in preparing similar complexes with the small bis(dimethylphosphino)methane (dmpm) ligand in order to compare the reactivities with those of the known dppm analogues.

A feature of diplatinum(I) complexes is the transmission of electronic effects through the linear X–Pt–Pt–Y framework.[4–6] Fackler has described this effect in terms of a long-range *trans*-influence based on bond length determinations in gold–gold-bonded complexes[7] (1) in which gold(II) may be considered isoelectronic with platinum(I).



1a X = I
1b X = Me

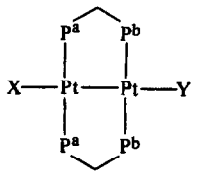
The Au–Au distances were similar in the two complexes (2.660 Å for **1a**, 2.695 Å for **1b**) but the Au–I distance was much longer in **1b** (2.699 Å for **1a**, 2.894 Å for **1b**). It was noted that the *trans*-influence[8] of the methyl group was not attenuated by the Au–Au bond, and the result was rationalized in terms of a qualitative MO diagram.[9] In contrast, both bond distances and $^1J(PtX)$ or $^1J(PtY)$ coupling constants indicate that increasing the *trans*-influence of X in the linear X–Pt–Pt–Y system (e.g. X and Y = H, Me, Ph_3P or Cl) significantly weakens both the Pt–Pt bond and the Pt–Y bond.[3–6] It is difficult to distinguish between these electronic effects and bond weakening due to steric effects in $[Pt_2XY(\mu\text{-dppm})_2]^{n+}$ complexes since, for example when X or Y = PPh_3, very large steric effects between phenyl substituents on the PPh_3 and μ-dppm ligands are observed.[6,10,11] It was expected that this complicating factor would be less severe in the analogous dmpm derivatives. A preliminary account of part of this work has been published.[12]

RESULTS

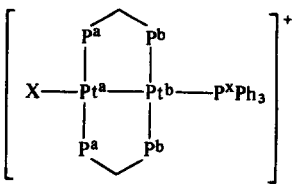
The first successful synthesis of a dmpm complex of platinum(I) involved reaction of $[\{PtCl_2(dmpm)\}_n]$[13] with $Na[BH_4]$ to give $[Pt_2Cl_2(\mu\text{-dmpm})_2]$ (**2a**). However, the yield of **2a** was low and so alternative synthetic methods were sought.

The most general route found involved oxidative addition to the diplatinum(0) complex $[Pt_2(\mu\text{-dmpm})_3(PPh_3)]$, which could be isolated or prepared *in situ* by reaction of dmpm with

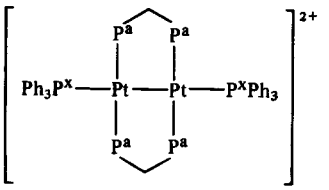
* Author to whom correspondence should be addressed.

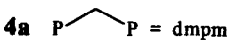


2a X = Y = Cl
2b X = Y = I
2c X = Me, Y = I



3a X = I
3b X = Br
3c X = Me





4a P^P = dmpm
4b P^P = dppm

$[Pt(PPh_3)_3]$.[14] Reaction with iodine gave **2b** in high yield and **2b** with triphenylphosphine gave the ionic **3a** and **4a** which were isolated as the hexafluorophosphate salts. Reaction with methyl iodide gave **2c** and **3c** as a mixture. It was not possible to isolate **2c** in pure form, and it was characterized spectroscopically in the mixture, but **3c** could be isolated as the hexafluorophosphate salt. Other alkyl halides failed to give alkyldiplatinum(I) derivatives. For example, $I(CH_2)_nI$, where $n = 3$, 4 or 5, gave only the iodo derivatives **2b** or **3a** and $1,2\text{-}C_6H_4(CH_2Br)_2$ gave the bromo derivative **3b**, isolated as the $[PF_6]^-$ salt.

The above oxidative additions and ligand substitutions are, in general, very similar to those of the analogous dppm complexes.[4,5,10] However, we note that in these oxidative addition reactions one of the three dmpm ligands is always lost whereas, in the corresponding dppm chemistry, the third dppm is retained as a monodentate ligand in place of the triphenylphosphine in **3** and **4**.[4,5] This difference is probably a result of the lower steric requirement of the $Pt_2(\mu\text{-dmpm})_2$ unit which allows the bulky triphenylphosphine to coordinate without undue strain (see later).

Structural characterization of these complexes was by ^1H, $^1H\text{-}\{^{31}P\}$ and $^{31}P\text{-}\{^1H\}$ NMR spectroscopy, and full details of spectra are given in Experimental. The spectra were complex but very characteristic as discussed in detail for the μ-dppm analogues, whose spectra are similar and have been discussed in detail elsewhere.[4,5,10,15,16]

DISCUSSION

In these complexes $[Pt_2XY(\mu\text{-LL})_2]^{n+}$, μ-LL = dmpm or dppm, the *trans*-influence of the terminal ligand X affects both the Pt–Pt and Pt–Y bonds, but the major effect is on the Pt–Pt bond. This is illustrated by bond length data given in Table 1 for monocationic complexes. For example, substituting PPh_3 for CO in $[Pt_2Cl(CO)(\mu\text{-dppm})_2]^+$ increases the Pt–Cl distance by 0.02 Å but the Pt–Pt distance by 0.045 Å.

Confirmation of this effect can be obtained by consideration of PtP and PtH coupling constants (Tables 2 and 3) bearing in mind that, at least within closely related families of complexes, there is an approximately linear correlation of $^1J(PtP)$ with the Pt–P bond distance.[8,17] In the complexes $[Pt_2X(PPh_3)(\mu\text{-dmpm})_2]^+$, there is a correlation of $J(PtPPh_3)$ with the *trans*-influence of X but the range is relatively small, from 2336 Hz for X = I to 2048 Hz for X = Me. Differences are much greater in mononuclear complexes with the phosphine directly *trans* to X as, for example, in *cis*-$[PtMeBr(PEt_3)_2]$ which has $^1J(PtP)$ values of 4178 and 1743 Hz for the phosphines *trans* to halogen and methyl, respectively. On the other hand, the long-range couplings $^2J(PtPtPPh_3)$ cover a very wide range (Table 2), from 1152 Hz for X = I to 416 Hz for X = Me. This coupling operates through the Pt–Pt bond, which is greatly weakened by the *trans*-influence of the terminal methyl group, and so the trend in coupling constants is greatly amplified.

A number of complexes of formula $[Pt_2HL(\mu\text{-dppm})_2]^+$ have been prepared recently and some coupling constants $[^1J(PtH)]$ are given in Table 3.[5,18,19] The magnitude of $^1J(PtH)$ is only slightly affected by the *trans*-influence of L and the coupling constant actually increases slightly as the *trans*-influence of L increases. Compare, for example, the values of $^1J(PtH)$ in Table 3 for L = PPh_3, CO and

Table 1. Bond distances (Å) in $[Pt_2XY(\mu\text{-dppm})_2]^+$ complexes

X	Y	r(Pt–Pt)	r(Pt–Cl)	r(Pt–P)	Reference
Cl	CO	2.620(1)	2.384(5)	—	3
Cl	PPh_3	2.665(2)	2.403(14)	2.333	11
H	η^1-dppm	2.769(2)	—	2.347	6

Table 2. Coupling constants $^1J(PtPR_3)$ and $^2J(PtPR_3)$ (Hz) in $[Pt_2X(PR_3)(\mu\text{-LL})_2]^{n+}$ complexes

Complex	μ-LL	^1J(PtP)	^2J(PtP)
$[I\text{–}Pt\text{–}Pt\text{-}PPh_3]^+$	dmpm	2336	1152
	dppm	2213	1258
$[Br\text{–}Pt\text{–}Pt\text{–}PPh_3]^+$	dmpm	2240	1120
$[Cl\text{–}Pt\text{–}Pt\text{–}PPh_3]^+$	dppm	2186	1232
$[Ph_3P\text{–}Pt\text{–}Pt\text{–}PPh_3]^{2+}$	dmpm	2125	696
	dppm	1680	
$[Ph_2MeP\text{–}Pt\text{–}Pt\text{–}PMePh_2]^{2+}$	dppm	1914	750
$[PhMe_2P\text{–}Pt\text{–}Pt\text{–}PMe_2Ph]^{2+}$	dppm	1938	650
$[H\text{–}Pt\text{–}Pt\text{–}PPh_3]^+$	dppm	2181	596
$[H\text{–}Pt\text{–}Pt\text{–}PMePh_2]^+$	dppm	2162	592
$[Me\text{–}Pt\text{–}Pt\text{–}PPh_3]^+$	dmpm	2048	416
$[Me\text{–}Pt\text{–}Pt\text{–}PPh_3]^+$	dppm	2040	490

Table 3. Coupling constants $^1J(PtH)$ and $^2J(PtH)$ (Hz) in hydrido $[Pt_2HL(\mu\text{-dppm})_2]^+$ complexes

	L					
	PPh_3	PMe_2Ph	CO	η^1-dppm	C_5H_5N	CD_3CN
$^1J(PtH)$	1005	999	990	980	975	963
$^2J(PtH)$	—	66	61	—	73	76

C_5H_5N of 1005, 990 and 975 Hz with the corresponding values in *trans*-$[PtHL(PMe_2Ph)_2]^+$ of 890, 967 and 1106 Hz, respectively.[8] A weak inverse long-range *trans*-influence is observed for the platinum(I) compounds.

Together, these bond length and coupling constant data provide strong evidence that, in these diplatinum(I) complexes with linear X–Pt–Pt–Y groups, the *trans*-influence of X and Y has its primary effect on the Pt–Pt bond, in contrast to the effect observed in digold(II) complexes.[7] In these platinum complexes the *trans*-influence of X on the Pt–Y bond is attenuated by the Pt–Pt bond and the usual *trans*-influence series may even be reversed in some situations (e.g. when Y = H).

The coupling constant $^1J(Pt\text{–}PPh_3) = 2125$ Hz in $[Pt_2(PPh_3)_2(\mu\text{-dmpm})_2]^{2+}$ (**4a**) is in the region expected from the *trans*-influence of PPh_3,[8] and can be compared to the anomalously low value for $^1J(Pt\text{–}PPh_3)$ of 1680 Hz in the corresponding μ-dppm complex **4b**.[10] The latter value is now clearly due to steric effects in $[Pt_2(PPh_3)_2(\mu\text{-dppm})_2]^+$ leading to anomalously weak $Pt\text{–}PPh_3$ bonds, and illustrates the advantages of using the smaller dmpm ligand in studies of this kind.

EXPERIMENTAL

General techniques have been described elsewhere, as have the syntheses of $[\{PtCl_2(dmpm)\}_n]$ and $[Pt_2(\mu\text{-dmpm})_3(PPh_3)]$.[12–14]

$[Pt_2Cl_2(\mu\text{-dmpm})_2]$ (2a)

To a suspension of $[\{PtCl_2(dmpm)\}_n]$ (0.25 g) in MeOH (8 cm^3) was added a solution of $NaBH_4$ (0.15 g) in MeOH (4 cm^3). After 30 min, the mixture was filtered, the solvent was evaporated from the

filtrate and the residue was extracted with CH_2Cl_2 (20 cm^3). Evaporation of the solvent gave the product. Yield 0.02 g, m.p. 252°C (decomp.). NMR (CD_2Cl_2): ^1H; 1.70 [m, $^2J+^4J(PH) = 7$ Hz, $^3J(PtH) = 28.5$ Hz, *Me*P]; 2.80 [m, $^2J(PH) = 7$ Hz, $^3J(PtH) = 43$ Hz]; ^{31}P; −43.4 [s, $^1J(PtP) = 2674$ Hz, $^3J(PtP) = 148$ Hz, $J(PP) = 50$ and 29 Hz, Pt*P*]. Found: C, 16.2; H, 3.8%. Calc. for $C_{10}H_{28}Cl_2P_4Pt_2$: C, 16.4; H, 3.8%.

$[Pt_2I_2(\mu\text{-dmpm})_2]$ (**2b**)

A solution of I_2 (0.053 g) in benzene (4 cm^3) was added to a solution of $[Pt_2(\mu\text{-dmpm})_3(PPh_3)]$ (0.21 mmol) in benzene (4 cm^3). The product precipitated as a brown solid and was purified by precipitation from CH_2Cl_2 solution using pentane. Yield 0.23 g, m.p. 232°C. NMR ($CDCl_3$): ^1H; 1.88 [m, $^3J(PtH) = 29$ Hz, *Me*P]; 2.88 [quintet, $^2J(PH) = 4$ Hz, $^3J(PtH) = 40$ Hz, CH_2P_2]; ^{31}P; −32.5 [s, $^1J(PtP) = 2630$ Hz, $^2J(PtP) = -150$ Hz, $J(PP) = 44$ and 27 Hz, Pt*P*]. Found: C, 12.8; H, 3.0%. Calc. for $C_{10}H_{28}I_2P_4Pt_2$: C, 13.1; H, 3.1%.

Reaction with excess I_2 gave the known *trans,trans*-$[Pt_2I_4(\mu\text{-dmpm})_2]$.[13]

$[Pt_2(PPh_3)_2(\mu\text{-dmpm})_2][PF_6]_2$ (**4a**)

PPh_3 (0.07 g) was added to a stirred solution of $[Pt_2I_2(\mu\text{-dmpm})_2]$ (0.04 g) in MeOH (120 cm^3), followed by addition of $NH_4[PF_6]$ (0.075 g). The solvent was evaporated *in vacuo*, the residue was washed with water and then recrystallized from acetone–pentane. Yield 0.022 g; m.p. 265°C (decomp.); NMR [$(CD_3)_2CO$]: ^1H: 1.3 (broad, *Me*P); 3.32 [m, $^2J(P^aH) = 8.0$ Hz, $^4J(P^xH) = 8.8$ Hz, $^3J(PtH) = 56$ Hz, CH_2P_2]; 7.32–7.50 (complex, *Ph*); ^{31}P: −33.3 [t, $^1J(PtP) = 2460$ Hz, $^2J(PtP) = 90$ Hz, $J(PP) = 27$ Hz, PtP^a]; 17.3 [quintet, $^1J(PtP) = 2125$ Hz, $^2J(PtP) = 696$ Hz, $J(P^xP^x) = 175$ Hz, PtP^x]. Found: C, 37.7; H, 4.1%. Calc. for $C_{46}H_{58}F_{12}P_8Pt_2$: C, 37.4; H, 3.9%.

$[Pt_2MeI(\mu\text{-dmpm})_2]$ (**2c**) *and* $[Pt_2Me(PPh_3)(\mu\text{-dmpm})_2][PF_6]$ (**3c**)

To a solution of $[Pt_2(\mu\text{-dmpm})_3(PPh_3)]$ (0.16 mmol) in toluene (8 cm^3) was added a solution of MeI in benzene (0.12 cm^3, 1.46 M). The yellow precipitate (0.11 g) was identified as a mixture containing **2c** and $[\mathbf{3c}]^+I^-$ in approximately equal amounts by ^{31}P and ^{31}H NMR spectroscopy. This precipitate was dissolved in CH_2Cl_2 (10 cm^3) and converted to $[\mathbf{3c}]^+[PF_6]^-$ by addition of $NH_4[PF_6]$ and PPh_3. Yield 0.144 g. NMR of **2c** (acetone-d_6): ^1H: 0.58 [t, $^2J(PtH) = 76$ Hz, $^3J(PH) = 7$ Hz, *Me*Pt]; 1.24–1.78 (m, *Me*P); 3.35 [m, $^2J(PH) = 9$ Hz, $^3J(PtH) = 30$ and 44 Hz, CH_2P_2]; ^{31}P: −6.5 [m, $^1J(PtP) = 2592$ Hz, $J(P^aP^b) = 65$ Hz, P^a]; −11.6 [m, $^1J(PtP) = 2208$ Hz, P^b]. NMR of **3c** (acetone-d_6): ^1H: 0.44 [m, $^2J(PtH) = 67$ Hz, $J(P^aH) = 3$ Hz, $J(P^xH) = 6$ Hz, *Me*Pt]; 1.53–1.98 (m, CH_3P); 2.94 [m, $J(PH) = 7$ Hz, $J(PtH) = 33$ Hz, CH_2P_2]. Reaction of **3c** with excess MeI gave the known $[Pt_2Me_2(\mu\text{-I})(\mu\text{-dmpm})_2][PF_6]$.

$[Pt_2I(PPh_3)(\mu\text{-dmpm})_2]I$

To a solution of $[Pt_2(\mu\text{-dmpm})_3(PPh_3)]$ (0.08 mmol) in benzene (4 cm^3) was added a solution of CH_2I_2 in benzene (0.136 cm^3, 1.13 M). An intense red coloration developed and a yellow precipitate formed. The precipitate of the product was filtered off and washed with hexane. Yield 0.088 g. NMR (acetone-d_6); ^1H: 1.86–1.98 (m, CH_3P); 3.14 [m, $^3J(PtH) = 37$ Hz, CH_2P_2]; ^{31}P: −31.2 [m, $^1J(PtP) = 2568$ Hz, $^3J(P^aP^x) = 5$ Hz, $J(P^aP^b) = 64$ Hz, P^a]; −34.8 [m, $^1J(PtP) = 2528$ Hz, $^2J(PtP) = 176$ Hz, $^2J(P^bP^x) = 24$ Hz, P^b]; 10.7 [m, $^1J(PtP) = 2336$ Hz, $^2J(PtP) = 1152$ Hz, P^x].

A similar reaction between $[Pt_2(\mu\text{-dmpm})_3(PPh_3)]$ and $C_6H_4(CH_2Br)_2$ gave $[Pt_2Br(PPh_3)(\mu\text{-dmpm})_2]Br$. NMR ($CD_2Cl_2$): ^1H: 1.76–2.30 (m, CH_3P); 3.14 [m, $^2J(PH) = 8.5$ Hz, $^3J(PtH) = 38$ and 80 Hz, CH_2P_2]; ^{31}P: −26.1 [m, $^1J(PtP) = 2576$ Hz, $J(P^aP^x)] = 8$ Hz $J(P^aP^b) = 64$ Hz, P^a]; −33.6 [m, $^1J(PtP) = 2528$ Hz, $^2J(PtP) = 160$ Hz, $^2J(P^bP^x) = 23$ Hz, P^b]; 27.7 [m, $^1J(PtP) = 2240$ Hz, $^2J(PtP) = 1120$ Hz, P^x].

Acknowledgement—We thank NSERC (Canada) for financial support.

REFERENCES

1. R. J. Puddephatt, *Chem. Soc. Rev.* 1982, 99.
2. A. L. Balch, in *Homogeneous Catalysis with Metal Phosphine Complexes* (Edited by L. Pignolet). Plenum, New York (1983).
3. Lj. Manojlovic-Muir, K. W. Muir and T. Solomon, *Acta Cryst.* 1979, **B35**, 1237.
4. K. A. Azam, M. P. Brown, R. H. Hill, R. J. Puddephatt and A. Yavari, *Organometallics* 1984, **3**, 697.
5. M. P. Brown, J. R. Fisher, R. H. Hill, R. J. Puddephatt and K. R. Seddon, *Inorg. Chem.* 1981, **20**, 3516.
6. Lj. Manojlovic-Muir and K. W. Muir, *J. Organomet. Chem.* 1981, **219**, 129.
7. J. P. Fackler, Jr and J. D. Basil, in *Inorganic Chemistry: Toward the 21st Century* (Edited by M. H. Chisholm), p. 201. ACS Symposium Series No. 211 (1983).

8. T. G. Appleton, H. C. Clark and L. E. Manzer, *Coord. Chem. Rev.* 1973, **10**, 335.
9. D. M. Hoffman and R. Hoffmann, *Inorg. Chem.* 1981, **20**, 3543.
10. M. P. Brown, S. J. Franklin, R. J. Puddephatt, M. A. Thomson and K. R. Seddon, *J. Organomet. Chem.* 1979, **178**, 281.
11. R. J. Blau, J. H. Espenson, S. Kim and R. A. Jacobson, *Inorg. Chem.* 1986, **25**, 757.
12. S. S. M. Ling, R. J. Puddephatt, Lj. Manojlovic-Muir and K. W. Muir, *Inorg. Chim. Acta* 1983, **77**, L95.
13. K. A. Azam, G. Ferguson, S. S. M. Ling, M. Parvez, R. J. Puddephatt and D. Srokowski, *Inorg. Chem.* 1985, **24**, 2799.
14. S. S. M. Ling, I. R. Jobe, A. J. McLennan, Lj. Manojlovic-Muir, K. W. Muir and R. J. Puddephatt, *J. Chem. Soc., Chem. Commun.* 1985, 566.
15. M. P. Brown, J. R. Fisher, S. J. Franklin, R. J. Puddephatt and K. R. Seddon, *J. Organomet. Chem.* 1978, **161**, C46.
16. M. P. Brown, R. J. Puddephatt, M. Rashidi and K. R. Seddon, *J. Chem. Soc., Dalton Trans.* 1977, 951.
17. A. Pidcock, in *Catalytic Aspects of Metal Phosphine Complexes* (Edited by E. C. Alyea and D. W. Meek), Vol. 196, p. 1. ACS Advances in Chemistry Series (1982).
18. H. C. Foley, R. H. Morris, T. S. Targos and G. L. Geoffroy, *J. Am. Chem. Soc.* 1981, **103**, 7337.
19. R. H. Hill, P. de Mayo and R. J. Puddephatt, *Inorg. Chem.* 1982, **21**, 3642.

Polyhedron Vol. 5, No. 9, pp. 1429–1436, 1986
Printed in Great Britain

0277–5387/86 $3.00+.00
Pergamon Journals Ltd

CATALYTIC BEHAVIOR OF SOME COPPER(II) COMPLEXES WITH MIXED LIGANDS IN THE DECOMPOSITION OF HYDROGEN PEROXIDE

H. BOBADILLA,* A. DECINTI and L. GIL

Departamento de Análisis Químico, Facultad de Ciencias Químicas y Farmacéuticas, Universidad de Chile, Santiago, Chile

(*Received* 1 *October* 1985; *accepted* 26 *November* 1985)

Abstract—A comparative study of the catalyzed decomposition of hydrogen peroxide using the following copper(II) complex salts, Cu(bipy)(*S*-threo)Cl·$3H_2O$, Cu(phen)(*S*-threo)Cl·$2H_2O$, Cu(bipy)(*S*-prol)Cl·$2H_2O$ and Cu(phen)(*S*-prol)Cl·$2H_2O$ has been made. Kinetic parameters were experimentally determined by the polarographic method at 25°C, pH 7.7 and constant ionic strength (μ = 0.1 M $NaNO_3$). The catalytic behavior of the chelate with 2,2′-bipyridine and *S*-prolinate was also studied at pH 6.5 and 8.5. The reactivity follows the sequence: [Cu(bipy)*S*-prol] > [Cu(phen)*S*-prol] > [Cu(bipy)*S*-threo] > [Cu(phen)*S*-threo]. Activation energies are very similar to each other. The pH-dependent exchange of the amino acid ligand with hydrogen peroxide seems to be a critical factor in the reaction pathway. Several reaction mechanisms are proposed.

The catalytic activity of copper(II), iron(III) and cobalt(III) binary metal complexes on the disproportionation of hydrogen peroxide in aqueous solution has already been well studied.[1–3] Sigel *et al.*[1,4] investigated the catalase-like activity of copper(II) promoted by the coordination of 2,2′-bipyridine and showed that increasing concentrations of chelating agent inhibit the catalytic activity of the Cu(II)–bipy (1:1) system on account of an increase in the concentration of the *cis*-diaquobis(2,2′-bipyridine)copper(II) complex. This species behaves as less active a catalyst than the 1:1 species owing to the higher degree of saturation of its coordination sphere, which becomes less accessible for hydrogen peroxide.[1,4] In this respect a study of the catalytic properties of ternary complexes of copper(II) with aromatic heterocyclic bases and optically active α-amino acid in aqueous solution appeared to be interesting for comparative purposes since these complexes would consist essentially of *trans*-diaqua tetragonally distorted octahedral species[5–7] and, hence, they would present accessible coordination positions somewhat different from those of the 1:2 Cu(II)–2,2′-bipyridine *cis*-diaqua species. Moreover, the accessible apical coordination positions of the above ternary complexes are not strictly equivalent as the presence of an α-carbon substituent would provide some degree of "out-of-plane" hydrophobic environment close to the coordination sphere. On the other hand the presence of a chiral center in these potential catalysts could constitute an advantage in further studies of a system containing, for instance, chiral organic peroxides. This work includes data on the catalytic activity of this kind of ternary complex in the decomposition of hydrogen peroxide in aqueous solution as well as a study of the influence upon the reaction rate of the dissociation equilibria involving the secondary ligand, i.e. the chiral amino acid. The kinetic parameters of the reaction are comparatively studied by using the complex ions [Cu(bipy)*S*-prol$(H_2O)_2]^+$, [Cu(phen)*S*-prol$(H_2O)_2]^+$, [Cu(bipy)*S*-threo$(H_2O)_2]^+$ and [Cu(phen)*S*-threo$(H_2O)_2]^+$ as catalysts since preliminary work indicated that they exhibit fairly different catalytic behavior. For convenience, coordinated water molecules will be hereafter omitted in all of the complex species formulae. However, a distorted octahedral structure will be reasonably assumed for all the explicit mononuclear species involved in the proposed reaction mechanisms.

EXPERIMENTAL

The mixed-ligand copper(II) complexes used in this work were synthesized in our laboratory

* Author to whom correspondence should be addressed.

according to Dutta and Dé's technique[8] with some modifications. The analytical data of the resulting compounds agreed with a 1:1:1 stoichiometry. Found: C, 44.3; N, 10.3; H, 4.5; Cu, 15.5%. Calc. for Cu(bipy)(*S*-prol)Cl·$2H_2O$: C, 44.6; N, 10.4; H, 5.0; Cu, 15.7%. The other analytical data have a similar agreement. The kinetic experiments were done by using different concentration ranges for each reactant. The complex salt concentration was varied from 10^{-3} to 10^{-5} M according to the degree of catalytic activity exhibited by each of the mixed-ligand complexes. The hydrogen peroxide concentration was varied from 10^{-1} to 10^{-2} M and was periodically checked against a standard solution of $TiOSO_4$ on a Carl Zeiss DMR 21 spectrophotometer (the resulting compound exhibits an absorption maximum at 410 nm[9]). In the determination of the order of reaction with respect to hydronium ion concentration the pH was varied from 6 to 9. However, both for the determinations of the orders of reaction of the other reacting species as for the activation energy measurements the initial pH was adjusted to 7.7 Moreover, since the concentrations of the catalytically active species depend upon the hydronium ion concentration, further kinetic experiments were performed at pH 6.5 and 8.5 by employing [Cu(bipy)*S*-prol]$^+$ as a catalyst. The solutions were freshly prepared. In all the determinations the system was deoxygenated by flushing pure N_2, before addition of the hydrogen peroxide solution. In all the cases the pH was adjusted with diluted NaOH or HCl, since the use of the appropriate buffers (phosphate, borate or Tris buffer) strongly inhibits the catalytic activity of these ternary complexes.[4] In the activation energy determinations the temperature was varied from 15 to 45°C. On the other hand, in the determinations of the orders of reaction the temperature was kept constant at 25°C. In all the cases the ionic strength was kept constant by using 0.1 M $NaNO_3$. The kinetics of the disproportionation of hydrogen peroxide were followed by measuring the oxygen concentration in the reaction solution, using a Fieldlab Oxygen Analyzer Model 123309 coupled with a Servogor recorder.

RESULTS AND DISCUSSION

The results obtained in the different kinetic determinations are illustrated in Figs 1–5 and are collected in Tables 1 and 2. The four complex salts under study exhibit reaction orders with respect to the complex ion less than 1, the *S*-threoninates compounds showing the lowest values. This would be attributed to the fact that the first dissociation equilibrium of the catalyst strongly influences the reaction pathway, as will be shown subsequently in the proposed reaction mechanisms. The reaction orders with respect to hydrogen peroxide, slightly greater than 1, do no differ too much from those obtained by other authors under conditions of rela-

Table 1. Partial orders of reaction for the catalytic activity of ternary copper(II) complexes, at 25°C and μ = 0.1 M $NaNO_3$[a]

	x	pH	y	pH	z
[Cu(bipy)*S*-prol]$^+$	0.9 (0.87)	7.7	1.1 (1.05)	7.7	−0.3 (−0.33)
[Cu(phen)*S*-prol]$^+$	0.9 (0.89)	7.7	1.3 (1.29)	7.7	−0.3 (−0.25)
[Cu(bipy)*S*-threo]$^+$	0.5 (0.54)	7.7	1.0 (1.01)	7.7	−0.4 (−0.43)
[Cu(phen)*S*-threo]$^+$	0.7 (0.70)	7.8	1.1 (1.08)	7.8	−0.4 (−0.36)

[a]The slopes of the best straight lines are in parentheses. $V_o = k[CuBA^+]^x[H_2O_2]^y[H^+]^z$.

Table 2. Specific rate constants and activation energies for the catalytic activity of ternary copper(II) complexes, at pH 7.7, 25°C and μ = 0.1 M $NaNO_3$

	k	ΔE (kJ mol^{-1})
[Cu(bipy)*S*-prol]$^+$	1.28×10^{-2} M$^{-0.7}$ s^{-1}	58.60
[Cu(phen)*S*-prol]$^+$	4.12×10^{-3} M$^{-0.9}$ s^{-1}	56.48
[Cu(bipy)*S*-threo]$^+$	7.61×10^{-6} M$^{-0.1}$ s^{-1}	58.93
[Cu(phen)*S*-threo]$^+$	1.23×10^{-5} M$^{-0.4}$ s^{-1}	62.08

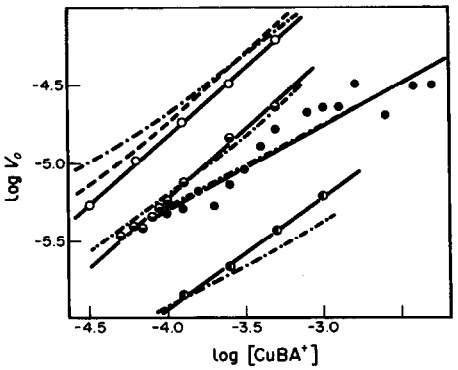


Fig. 1. Catalytic activity of ternary copper(II) complexes as a function of the analytic concentration of complex ion, at 25°C and $\mu = 0.1$ M $NaNO_3$. (○) [Cu(bipy)*S*-prol]$^+$, $[H_2O_2]_{tot(t=0)} = 0.064$ M, $pH_{(t=0)} = 7.7$; (◒) [Cu(phen)*S*-prol]$^+$, $[H_2O_2]_{tot(t=0)} = 0.064$ M, $pH_{(t=0)} = 7.7$; (●) [Cu(bipy)*S*-threo]$^+$, $[H_2O_2]_{tot(t=0)} = 0.060$ M, $pH_{(t=0)} = 7.7$; (◐) [Cu(phen)*S*-threo]$^+$, $[H_2O_2]_{tot(t=0)} = 0.0567$ M, $pH_{(t=0)} = 7.8$; (·–·–·–·–) calc. from eqn (1) and k'_1 and k'_2 of Table 4; (––––––) calc. from eqn (2) and k''_1 and k''_2 of Table 4.

tively high concentration of substrate.[4,10] The reaction orders with respect to hydronium ion concentration are less negative than the ones found in the catalase-like activity of binary copper(II) complexes.[1,4] This behaviour would be ascribed to the presence of the *S*-amino acid ligand, since the tendency of this species to adopt the zwitterionic form renders the first dissociation equilibrium of the ternary complex strongly pH-dependent. Furthermore, additional experiments showed that increasing concentrations of free amino acid inhibit the

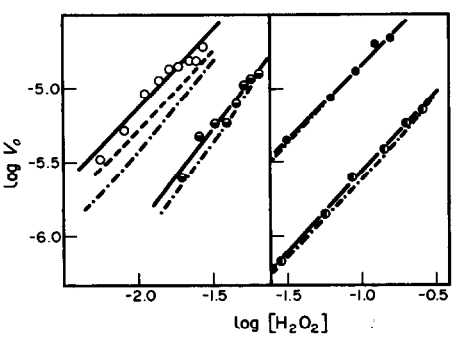


Fig. 2. Catalytic activity of ternary copper(II) complexes as a function of the initial concentration of hydrogen peroxide, at 25°C and $\mu = 0.1$ M $NaNO_3$. (○) [[Cu(bipy)*S*-prol]$^+$]$_{tot} = 2.5 \times 10^{-4}$ M, $pH_{(t=0)} = 7.7$; (◒) [[Cu(phen)*S*-prol]$^+$]$_{tot} = 2.5 \times 10^{-4}$ M, $pH_{(t=0)} = 7.7$; (●) [[Cu(bipy)*S*-threo]$^+$]$_{tot} = 2.5 \times 10^{-4}$ M, $pH_{(t=0)} = 7.7$; (◐) [[Cu(phen)*S*-threo]$^+$]$_{tot} = 1.25 \times 10^{-4}$ M, $pH_{(t=0)} = 7.8$; (·–·–·–·–) calc. from eqn (1) and k'_1 and k'_2 of Table 4; (––––––) calc. from eqn (2) and k''_1 and k''_2 of Table 4.

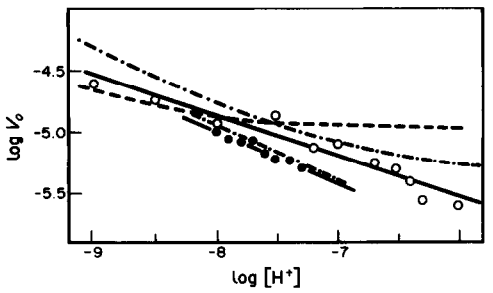


Fig. 3. Catalytic activity of ternary copper(II) complexes as a function of the initial concentration of hydrogen ion, at 25°C and $\mu = 0.1$ M $NaNO_3$. (○) [[Cu(bipy)*S*-prol]$^+$]$_{tot} = 1.25 \times 10^{-4}$ M, $[H_2O_2]_{tot(t=0)} = 0.0415$ M; (●) [[Cu(bipy)*S*-threo]$^+$]$_{tot} = 2.5 \times 10^{-4}$ M, $[H_2O_2]_{tot(t=0)} = 0.060$ M; (·–·–·–·–) calc. from eqn (1) and k'_1 and k'_2 of Table 4; (––––––) calc. from eqn (2) and k''_1 and k''_2 of Table 4.

catalytic activity of the complex [Cu(bipy)*S*-prol]$^+$. These data gave for the log V_o vs log [*S*-prolH] plot a straight line with a slope of about -1.3. They also showed that the amino acid behaves as a competitive inhibitor.

The specific constants of reaction rate, k, were calculated by using the reaction orders obtained from experimental data by regression analysis (Table 2). The resulting activation energy values are very similar to each other, suggesting that at pH 7.7 the four complexes are involved in similar reaction mechanisms (Table 2). The ternary complexes having *S*-prolinate as a secondary ligand exhibit higher catalytic activity than the ones having *S*-threoninate. This result would be accounted for by a more easy exchange of the *S*-prolinate ligand with hydrogen peroxide. Indeed the peculiar kinetic behavior of these ternary complexes would be precisely ascribed to their lack of accessible coordination positions appropriate for catalytic activity, these being generated only by dissociation. This fact

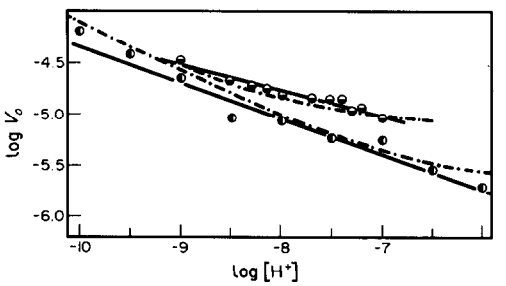


Fig.4. Catalytic activity of ternary copper(II) complexes as a function of the initial concentration of hydrogen ion, at 25°C and $\mu = 0.1$ M $NaNO_3$. (◒) [[(Cu(phen)*S*-prol]$^+$]$_{tot} = 2.5 \times 10^{-4}$ M, $[H_2O_2]_{tot(t=0)} = 0.064$ M; (◐) [[Cu(phen)*S*-threo]$^+$]$_{tot} = 2.5 \times 10^{-4}$ M, $[H_2O_2]_{tot(t=0)} = 0.1983$ M; (·–·–·–·–) calc. from eqn (1) and data of Table 4.

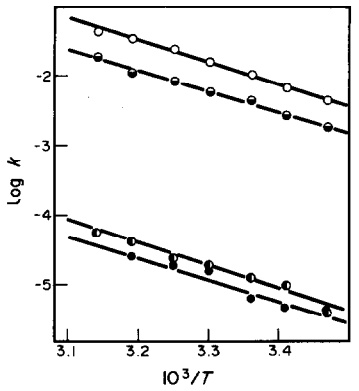


Fig. 5. Catalytic activity of ternary copper(II) complexes at different temperatures and $\mu = 0.1$ M $NaNO_3$. (○) $[[Cu(bipy)S\text{-prol}]^+]_{tot} = 3.13 \times 10^{-5}$ M, $[H_2O_2]_{tot(t=0)} = 0.064$ M, pH 7.7; (◒) $[[(Cu(phen)S\text{-prol}]^+]_{tot} = 2.5 \times 10^{-4}$ M, $[H_2O_2]_{tot(t=0)} = 0.064$ M, pH 7.7; (●) $[[Cu(bipy)S\text{-threo}]^+]_{tot} = 2.5 \times 10^{-4}$ M, $[H_2O_2]_{tot(t=0)} = 0.06$ M, pH 7.7; (◐) $[[Cu(phen)S\text{-threo}]^+]_{tot} = 2.5 \times 10^{-4}$ M, $[H_2O_2]_{tot(t=0)} = 0.0567$ M, pH 7.7; k values calc. with partial reaction orders of Table 1.

agrees with the inhibitory properties of the free amino acid previously mentioned. However, the apical accessible coordination positions of these complexes should be considered inadequate for catalysis only in the sense of the scarce possibility of formation of quaternary peroxo complexes, since it is not indispensable a *cis* bicoordination for a fast electron transfer through the metal ion.[11] On the other hand, if the assumption that such a ligand exchange greatly influences the reaction rate were relevant, [Cu(phen)*S*-threo]$^+$ should be the most stable of the mixed-ligand complexes under study. This inference does not agree with the relative stability of the binary species [Cu*S*-threo]$^+$ and [Cu*S*-prol]$^+$ whose formation constants, K_{Cu}^{CuA}, are 1.02×10^8 and 6.8×10^8, respectively.[12] Nevertheless, at the pH conditions of our experiments the free chiral ligand must be mainly in the form of a zwitterion. Hence, at pH 7.7 $[CuA^+]/[Cu^{2+}][HA]$ has values of 5.6×10^6 and 1.4×10^6 for *S*-threoninate and *S*-prolinate, respectively, i.e. the prolinate complex turns out to be of lower stability. Furthermore, the formation constants of ternary complexes of copper(II) with 2,2′-bipyridine or 1,10-phenanthroline and *S*-amino acid, K_{CuB}^{CuBA}, are very similar for a series of *S* amino acids, the small differences observed being independent upon pK_{HA}^{A}.[13] If the value for log $K_{Cu,bipy}^{Cu,bipy,prol} - \log K_{Cu,bipy}^{Cu,bipy,threo}$ were assumed to be similar to the greater difference of log K_{CuB}^{CuBA} values found in Malik's work,[13] i.e. about 0.5, the ratio $[S$ - prolH)[Cu(bipy)*S* - threo]$^+]/[S$ - threo] [(Cu(bipy)*S* - prol]$^+$] should be approximately 8.1, that is, the ternary complex of *S*-threoninate should be of higher stability.

The kinetic parameters for the reaction in the presence of [Cu(bipy)*S*-prol]$^+$ at pH 6.5 and 8.5 are found in Figs 6–8 and arranged in Table 3. According to these data both the reaction order with respect to the ternary complex and hydrogen peroxide appear to be pH-dependent. This would be accounted for by the presence of two or more reaction mechanisms occurring simultaneously, whose contribution to the reaction rate depends

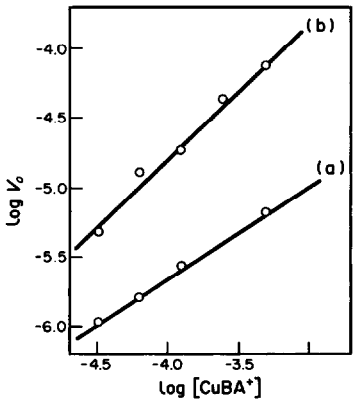


Fig. 6. Catalytic activity of [Cu(bipy)*S*-prol]$^+$ as a function of the analytical concentration of complex ion at different initial concentrations of hydrogen ion and $\mu = 0.1$ M $NaNO_3$; (a) pH 6.5, $[H_2O_2]_{tot(t=0)} = 0.064$ M; (b) pH 8.5, $[H_2O_2]_{tot(t=0)} = 0.064$ M. Temperature 25°C.

Table 3. Kinetic parameters for the catalytic activity of [Cu(bipy)*S*-prol]$^+$ at different initial concentrations of hydrogen ion[a]

	pH 6.5	pH 7.7	pH 8.5
x	0.7 (0.65)	0.9 (0.87)	1.0 (0.97)
y	1.7 (1.73)	1.1 (1.05)	1.2 (1.19)
z	−0.5	−0.3	−0.2
k	3.01×10^{-3} $M^{-0.9}$ s^{-1}	1.28×10^{-2} $M^{-0.7}$ s^{-1}	5.05×10^{-1} M^{-1} s^{-1}
ΔE (kJ mol^{-1})	69.0	58.6	54.4

[a] The slopes of the best straight lines are in parentheses. $V_0 = [CuBA^+]^x[H_2O_2]^y[H^+]^z$.

Table 4. Specific rate constants for eqns (1) and (2) at 25°C and $\mu = 0.1$ M $NaNO_3$

	k'_1 (s^{-1})	k'_2 ($M^{-2}s^{-1}$)	k''_1 ($M^{-1}s^{-1}$)	k''_2 ($M^{-1}s^{-1}$)
[Cu(bipy)*S*-prol]$^+$	2.9×10^{-6}	18.8	1.8×10^{-5}	2.0
[Cu(phen)*S*-prol]$^+$	7.1×10^{-7}	7.3	1.1×10^{-5}	0.4
[Cu(bipy)*S*-threo]$^+$	1.2×10^{-6}	0.4	—	—
[Cu(phen)*S*-threo]$^+$	2.5×10^{-7}	0.2	—	—

upon the pH conditions. The activation energy turned out to be also pH-dependent, probably on account of the same reasons.

At pH 7.7 the kinetic behavior of the four complexes studied fit acceptably with the rate expression:

$$V_o = \frac{k'_1[\mathrm{CuBA}^+]^{0.5}[\mathrm{H_2O_2}]}{[\mathrm{H}^+]^{0.5}} + k'_2[\mathrm{CuBA}^+][\mathrm{H_2O_2}]^2, \quad (1)$$

where B and A stand for the heterocyclic base and the amino acid ligand, respectively. An appropriate set of rate constants, k'_1 and k'_2, is listed in Table 4. These figures were obtained by averaging k'_1 and k'_2 values calculated from the regression equations of the different experimental determinations of reaction orders. Theoretical log V_o vs log [CuBA$^+$], log V_o vs log [H_2O_2] and log V_o vs log [H^+] plots, calculated from eqn (1), are included in Figs 1–4. As can be seen, the agreement between the theoretical plots and the experimental points is somewhat smaller for [Cu(bipy)*S*-prol]$^+$. Indeed the data of this complex fit better with the rate equation:

$$V_o = \frac{k''_1[\mathrm{CuBA}^+]^{0.5}[\mathrm{H_2O_2}]^2}{[\mathrm{H}^+]^{0.5}} + k''_2[\mathrm{CuBA}^+][\mathrm{H_2O_2}], \quad (2)$$

whereas [Cu(phen)*S*-prol]$^+$ fits both eqn (1) and eqn (2) well. The values of k''_1 and k''_2 for the *S*-prolinate complexes were calculated in the same way as k'_1 and k'_2, and are also included in Table 4. The log V_o values for [Cu(bipy)*S*-prol]$^+$ calculated from eqn (2) are included in Figs 1–3. The quantities k'_1, k'_2, k''_1 and k''_2 depend upon the equilibrium reactant concentrations and hence upon pH. Therefore it should not be expected that they are valid for wide ranges of concentration. These "constants" correspond rather to $k'_1 = k_{11}(1-\alpha_c)^{0.5}(1-\alpha_s)$, $k'_2 = k_{21}(1-\alpha_c)(1-\alpha_s)^2$, $k''_1 = k_{12}(1-\alpha_c)^{0.5}(1-\alpha_s)^2$ and $k''_2 = k_{22}(1-\alpha_c)(1-\alpha_s)$, where α_c and α_s are the degree of dissociation of the ternary complexes and the hydrogen peroxide, respectively. If it was assumed that the ternary complex dissociation mainly occurs according to the fast equilibrium:

$$[\mathrm{CuBA}]^+ + \mathrm{H}^+ \overset{K_1}{\rightleftharpoons} [\mathrm{CuB}]^{2+} + \mathrm{HA},$$

at t = 0 α_c should be given approximately by:

$$\alpha_c^2 + \frac{K_1[\mathrm{H}^+]\alpha_c}{[\mathrm{CuBA}^+]_{tot}} - \frac{K_1[\mathrm{H}^+]}{[\mathrm{CuBA}^+]_{tot}} = 0.$$

In order to verify the validity of rate expressions (1) and (2), the experimental data obtained from the determination of the reaction order with respect

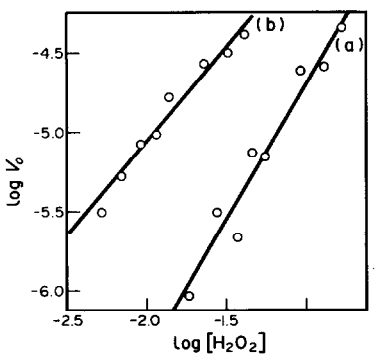


Fig. 7. Catalytic activity of [Cu(bipy)*S*-prol]$^+$ as a function of the total initial concentration of hydrogen peroxide at different initial concentrations of hydrogen ion and $\mu = 0.1$ M $NaNO_3$; (a) pH 6.5, $[[\mathrm{Cu(bipy)}S\text{-prol}]^+]_{tot} = 2.5\times10^{-4}$ M; (b) pH 8.5, $[[\mathrm{Cu(bipy)}S\text{-prol}]^+]_{tot} = 2.5\times10^{-4}$ M. Temperature 25°C.

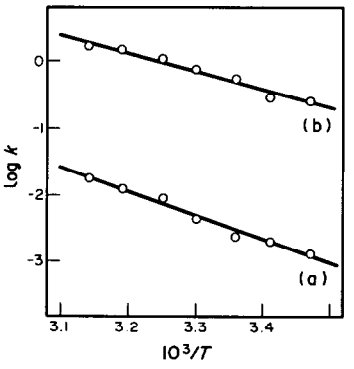


Fig. 8. Catalytic activity of [Cu(bipy)*S*-prol]$^+$ at different temperatures and concentrations of hydrogen ion. $\mu = 0.1$ M $NaNO_3$. (a) pH 6.5, $[[\mathrm{Cu(bipy)}S\text{-prol}]^+]_{tot} = 5\times10^{-4}$ M, $[\mathrm{H_2O_2}]_{tot(t=0)} = 9.23\times10^{-3}$ M; (b) pH 8.5, $[[\mathrm{Cu(bipy)}S\text{-prol}]^+]_{tot} = 1.25\times10^{-4}$ M, $[\mathrm{H_2O_2}]_{tot(t=0)} = 9.23\times10^{-3}$ M.

to hydrogen ion concentration for [Cu(bipy)*S*-prol]$^+$ and [Cu(phen)*S*-threo]$^+$ as catalyst were further analyzed. The above k' and k'' expressions were, respectively, substituted in eqns (1) and (2). The corresponding values of k' and k'' listed in Table 4 were used as a starting point for the calculation of the pH-independent rate constants by assuming an appropriate value for K_1. Reasonable K_1 values were successively iterated until an acceptable fitting with experimental data was reached. For H_2O_2 pK_a = 11.62 was employed. The results obtained from these calculations are shown in Figs 9 and 10. In the case of *S*-prolinate complex results from the application of eqn (1) are also included. According to this analysis the kinetics summarized by eqn (2) agrees with the experimental data of [Cu(bipy)*S*-prol]$^+$ over almost all the pH range studied, whereas eqn (1) agrees only up to pH 7.7. However, the log K_{CuB}^{CuBA} value resulting from the fitting with eqn (1) seems to be somewhat more realistic than the one obtained from eqn (2), i.e. log K_{CuB}^{CuBA} = log $K_A^{HA} - K_1$ = 8.30 from eqn (1) and 7.54 from eqn (2).[13] The application of eqn (2) to the data of [Cu(phen)*S*-threo]$^+$ was not attempted since previous calculations of k_1'' and k_2'' for the reaction in the presence of this species showed a rather poor accordance between the different reaction order experiments. On the contrary, eqn (1) showed a moderate agreement between the different kinetic determinations (Figs 1, 2 and 4). Since the starting point of these calculations were the average values of k_1' and k_2', an improvement of the fitting between the theoretical curve and the experimental data of Fig. 10 by decreasing k_{11} and k_{21} impairs the agreement with the experiments at variable concentrations of complex ion and hydrogen peroxide. A somewhat low value for the log K_{CuB}^{CuBA} of

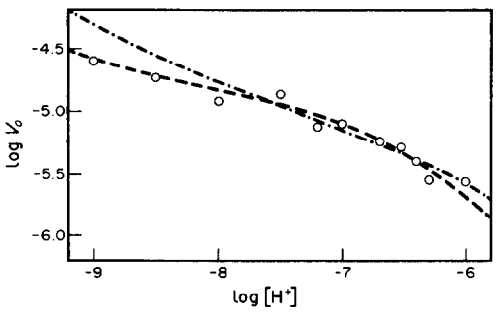


Fig. 9. Theoretical rate equations for catalytic activity of [Cu(bipy)*S*-prol]$^+$. $[[Cu(bipy)S\text{-prol}]^+]_{tot} = 1.25 \times 10^{-4}$ M, $[H_2O_2]_{tot(t=0)} = 0.0415$ M, $\mu = 0.1$ M $NaNO_3$, 25°C; (○) experimental values; (–·–·–·–) eqn (1) with $k_{11} = 3.02 \times 10^{-6}$ s^{-1}, $k_{21} = 20.37$ M^{-2} s^{-1} and $K_1 = 120$; (––––––) eqn (2) with $k_{12} = 2.13 \times 10^{-5}$ M^{-1} s^{-1}, $k_{22} = 2.792$ M^{-1} s^{-1} and $K_1 = 700$.

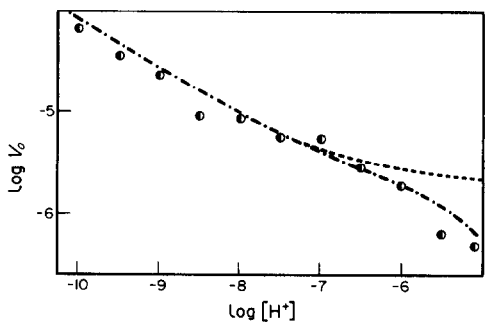


Fig. 10. Theoretical rate equations for catalytic activity of [Cu(phen)*S*-threo]$^+$. $[[Cu(phen)S\text{-threo}]^+]_{tot} = 2.5 \times 10^{-4}$ M, $[H_2O_2]_{tot(t=0)} = 0.1983$ M, $\mu = 0.1$ M $NaNO_3$, 25°C; (●) experimental values; (–·–·–·–) eqn (1) with $k_{11} = 2.56 \times 10^{-7}$ s^{-1}, $k_{12} = 0.21$ M^{-2} s^{-1} and $K_1 = 40$; (·····) eqn (1) with $k_1' = 2.5 \times 10^{-7}$ (pH 7.8), $k_2' = 0.2$ (pH 7.8) and $K_1 = 0$.

[Cu(phen)*S*-threo]$^+$ was obtained from the calculations summarized in Fig. 10. This value is, however, of the same order as the ones found for similar ternary complexes,[13] i.e. log K_A^{HA} – log K_1 = 7.37 (μ = 0.1).

From the above considerations it seems that kinetics of eqn (1) is predominant at lower values of K_1, i.e. at lower degrees of dissociation of the ternary complex; the one of eqn (2) being seemingly predominant at higher degrees of dissociation. Moreover, it is possible that the four mechanisms involved in eqns (1) and (2) were occurring simultaneously in these systems but with different degrees of importance, according to the concentration of the catalytically active species,[4] which in the present case depends upon both the tendency of the chiral ligand to adopt the zwitterionic form and the stability of the ternary complex, i.e. upon K_1. The following simultaneous fast equilibria would be considered as a starting point for the different possible mechanisms:

$$[CuBA]^+ + H^+ \overset{K_1}{\rightleftharpoons} [CuB]^{2+} + HA, \quad (3)$$

$$[CuB]^{2+} + H_2O_2 \overset{K_2}{\rightleftharpoons} [CuB(H_2O_2)]^{2+}, \quad (4)$$

$$[CuB(H_2O_2)]^{2+} \overset{K_3}{\rightleftharpoons} [CuB(HO_2)]^+ + H^+. \quad (5)$$

Equilibria (4) and (5) have been previously proposed by Sigel *et al.*[4] in order to account for the catalase-like activity of [Cu(bipy)]$^{2+}$. Starting from eqn (5), the reaction course would go on through different simultaneous pathways.

Mechanism (I-1)

$$[CuB(HO_2)]^+ \xrightarrow{k_4} \text{intermediate products}, \quad (6)$$

$$\text{Intermediate products} + H_2O_2 \xrightarrow{\text{fast}} [CuB]^{2+} + OH^- + H_2O + O_2.$$

Since at t = 0 $[CuB^{2+}] \cong [HA]$:

$$[CuB^{2+}] \cong K_1^{0.5}[CuBA^+]^{0.5}[H^+]^{0.5}. \quad (7)$$

Hence:

$$V_o = \frac{k'_1[CuBA^+]^{0.5}[H_2O_2]}{[H^+]^{0.5}},$$

where $k'_1 = K_1^{0.5}K_2K_3k_4$.

Mechanism (I-2)

$$[CuB(HO_2)]^+ + [CuB(H_2O_2)]^{2+} \rightleftharpoons^{K_4} [(CuB)_2(HO_2)(H_2O_2)]^{3+}, \quad (8)$$

$$[(CuB)_2(HO_2)(H_2O_2)]^{3+} \xrightarrow{k_5} 2[CuB]^{2+} + OH^- + H_2O + O_2. \quad (9)$$

From eqns (4), (5), (7), (8) and (9):

$$V_o = k'_2[CuBA^+][H_2O_2]^2,$$

where $k'_2 = K_1K_2^2K_3K_4k_5$. This mechanism is similar to the one proposed by Nishida *et al.*[14,15] with respect to the binuclear nature of the intermediate species. Although eqn (8) is not the only possible route of formation of such an intermediate, other suitable pathways originate the same rate equation, unless it were supposed that the amino acidate ligand plays some bridging role in the binuclear species.

Mechanism (II-1)

$$[CuB(HO_2)]^+ + H_2O_2 \rightleftharpoons^{K_5} [CuB(HO_2)(H_2O_2)]^+, \quad (10)$$

$$[CuB(HO_2)(H_2O_2)]^+ \xrightarrow{k_6} [CuB]^{2+} + OH^- + H_2O + O_2. \quad (11)$$

From eqns (4), (5), (7), (10) and (11) it can be deduced that:

$$V_o = \frac{k''_1[CuBA^+]^{0.5}[H_2O_2]^2}{[H^+]^{0.5}},$$

where $k''_1 = K_1^{0.5}K_2K_3K_5k_6$. This mechanism is essentially the same one proposed by Sigel *et al.*[4] for the catalase-like activity of $[Cu(bipy)]^{2+}$.

Mechanism (II-2)

$$[CuB(HO_2)]^+ + [CuB]^{2+} \rightleftharpoons^{K_7} [(CuB)_2(HO_2)]^{3+}, \quad (12)$$

$$[(CuB)_2(HO_2)]^{3+} + H_2O_2 \xrightarrow{k_8} \text{intermediate products}, \quad (13)$$

$$\text{Intermediate products} \xrightarrow{\text{fast}} 2[CuB]^{2+} OH^- + H_2O + O_2.$$

From eqns (4), (5), (7), (12) and (13):

$$V_o = k''_2[CuBA^+][H_2O_2],$$

where $k''_2 = K_1K_2K_3K_7k_8$.

Discussion on the possible nature of the intermediate species involved in the above proposed mechanisms has been already provided by other authors on similar systems.[1,2,14] However in mechanism (II-2) a mixed-valence intermediate, i.e. Cu(I) and Cu(II), might be also proposed.

The pH dependence of the reaction orders (Table 3) seems to be agreeing with the simultaneous occurrence of these kinetic pathways, since at low pH values the experimental rate law tends to be similar to the equation obtained from mechanism (II-1), which should predominate at relatively higher concentration $[Cu(bipy)]^{2+}$. On the other hand, at higher pH values the experimental rate equation tends to adopt the form of the equation obtained from mechanism (I-2), which was previously assigned to the catalysis by threoninate complexes. Again, this seems to agree with the increasing stability of the prolinate complexes on increasing pH, which lowers the concentration of $[Cu(bipy)]^{2+}$.

The second term of eqns (1) and (2) would be also accounted for by reaction pathways involving the ternary complex itself acting as a catalyst; for instance:

$$[CuBA]^+ + H_2O_2 \rightleftharpoons^{K'} [CuBA(H_2O_2)]^+,$$

$$[CuBA(H_2O_2)]^+ + H_2O_2 \rightleftharpoons^{K''} [CuBA(H_2O_2)_2]^+,$$

$$[CuBA(H_2O_2)_2]^+ \xrightarrow{k'} [CuBA]^+ + 2H_2O + O_2,$$

$$V_o = k[CuBA^+][H_2O_2]^2, \quad k = K'K''k',$$

where the intermediate species would be a quaternary complex with two hydrogen peroxide molecules coordinated to the apical positions [or one molecule in the case of eqn (2)]. Another possible intermediate would consist of a *cis* apical–equatorial coordination of two hydrogen peroxide molecules, the amino acid remaining as monodentate a ligand. However, as were already pointed out, these reac-

tion pathways disagree with the competitive inhibitory properties of the free amino acid. Moreover, the reaction order for this species, -1.3, strongly suggests that a simultaneity of the above proposed mechanisms would be feasible.

On summary, although it is possible that there exist some steric effects on these catalytic reactions, arising from the particular coordination environments provided by the chiral ligands, evidence with respect to this point was not found. The structural features of the secondary ligand seem to influence the catalytic behavior mainly by thermodynamic stability effects which rule the availability of accessible coordination sites on the metal ion.

Acknowledgement—This work was supported by Departamento de Investigación y Bibliotecas, Dirección General Académica y Estudiantil, Universidad de Chile (P.Q 1870-8524).

REFERENCES

1. H. Sigel, C. Flierl and R. Griesser, *J. Am. Chem. Soc.* 1969, **91**, 1061.
2. E. N. Rizkalla, O. H. El-Shafey and N. M. Guindy, *Inorg. Chim. Acta* 1982, **57**, 199.
3. P. Waldmeier and H. Sigel, *Inorg. Chem.* 1972, **11**, 2174.
4. H. Sigel, K. Kyss, B. E. Fischer and B. Prijs, *Inorg. Chem.* 1979, **18**, 1354.
5. H. Sigel, *Metal Ions in Biological Systems, Vol. 2, Mixed Ligand Complexes.* Marcel Dekker, New York (1973).
6. L. Gil, E. Moraga, H. Bobadilla, S. Bunel and C. A. Bunton, *J. Inorg. Nucl. Chem.* 1975, **37**, 2509.
7. W. L. Kwik, K. P. Ang and G. Chen, *J. Inorg. Nucl. Chem.* 1980, **42**, 303.
8. R. L. Dutta and D. Dé, *J. Indian Chem. Soc.* 1969, **46**, 74.
9. H. Brintzinger and H. Erlenmayer, *Helv. Chim. Acta* 1965, **48**, 826.
10. H. Sigel and B. Prijs, *J. Inorg. Nucl. Chem.* 1977, **39**, 179.
11. S. Fallab, *Chimia* 1961, **15**, 576.
12. A. Martell and R. Smith, *Critical Stability Constants.* Plenum Press, New York (1974).
13. G. S. Malik, S. P. Singh and J. P. Tandon, *Monatsh. Chem.* 1979, **110**, 149.
14. N. Oishi, M. Takeuchi, Y. Nishida and S. Kida, *Polyhedron* 1984, **3**, 157.
15. Karlin and Zubieta, *Copper Coordination Chemistry: Biochemical and Inorganic Perspectives*, p. 440. Adenine Press, New York (1983).

Polyhedron Vol. 5, No. 9, pp. 1437–1447, 1986
Printed in Great Britain

0277–5387/86 $3.00+.00
Pergamon Journals Ltd

BOND INDICES, ENTHALPIES AND RELATIVE STABILITIES OF REAL AND HYPOTHETICAL *CLOSO*-$B_nH_n^{c-}$ CLUSTERS ($n = 5$–12; $c = 0$, 2 OR 4) AS REVEALED BY THE MOLECULAR-ORBITAL BOND INDEX METHOD

ROBERT E. MULVEY, MARION E. O'NEILL and KENNETH WADE*

Chemistry Department, Durham University Science Laboratories,
South Road, Durham DH1 3LE, U.K.

and

RONALD SNAITH

Department of Pure and Applied Chemistry, University of Strathclyde,
295 Cathedral Street, Glasgow G1 1XL, U.K.

(*Received* 14 *November* 1985; *accepted* 19 *December* 1985)

Abstract—Bond indices (I) have been calculated, using the CNDO-based molecular-orbital bond index method, for real and hypothetical *closo* borane species, $B_nH_n^{c-}$ ($n = 5$–12; $c = 0$, 2 or 4), and used to infer their relative stabilities by means of the bond index (I)–bond enthalpy [E (kJ mol^{-1})] equations E(B—B) = 297.9I(B—B), and E(B—H) = 374.8I(B—H). For the species able to tolerate $n+2$ skeletal electron pairs ($n = 8$, 9 or 11) in closed-shell electronic configurations, estimates of the relative stabilities of alternative *nido* structures for the anions $B_nH_n^{4-}$ have been made. Detailed assessments of the changes in bond index with electron numbers for particular edge types for $B_nH_n^{c-}$ species ($n = 8$, 9 or 11; $c = 0$, 2 or 4) have been carried out, providing quantitative confirmation of earlier qualitative predictions, and showing that generally for the "normal" *closo* $B_nH_n^{2-}$ species addition or removal of an electron pair leads to the same type of polyhedral distortion, because, where the HOMO of $B_nH_n^{2-}$ is bonding for a particular edge, the LUMO is antibonding.

This paper is concerned with the strength of the cluster bonding in some systems that may be regarded as exceptions to the general rules linking boron cluster shapes to formula types and so to skeletal electron numbers. In particular, we shall consider some clusters in which n skeletal atoms are held together in a *closo* polyhedral arrangement even though bound by other than the usual ($n+1$) skeletal electron pairs, and shall probe quantitatively the bonding consequences of their electron deficits or surpluses, testing the qualitative predictions we have made earlier about such systems.[1–3]

The well-established link between the skeletal shapes and electron numbers of borane clusters[4–12] can be summarized as follows. $B_nH_n^{2-}$ anions ($n = 6$–12), neutral carboranes [$C_2B_{n-2}H_n$ ($n = 5$–12)] and related clusters, with $n+1$ skeletal bond pairs to hold their n skeletal atoms together, have *closo* deltahedral structures whose symmetries (as many MO treatments[13–19] have shown) generate $n+1$ strongly bonding MOs with substantial HOMO–LUMO energy gaps. Figure 1 shows these *closo* shapes of the $B_nH_n^{2-}$ species ($n = 5$ as yet unknown, $n = 6$–12) and gives the edge distances used in calculations. More open *nido* or *arachno* structures, based on the deltahedra with $n+1$ or $n+2$ vertices, are generally found for n-atom clusters with $n+2$ or $n+3$ skeletal bond pairs, respectively, one or two vertices (respectively) being left vacant. Their polyhedral fragment structures generate the same number of bonding MOs as the complete deltahedra.

Here, we shall be concerned with exceptions to these generalizations in which n-atom clusters with *closo* shapes are held together by n or $n+2$ skeletal electron pairs. Examples of the former include

* Author to whom correspondence should be addressed.

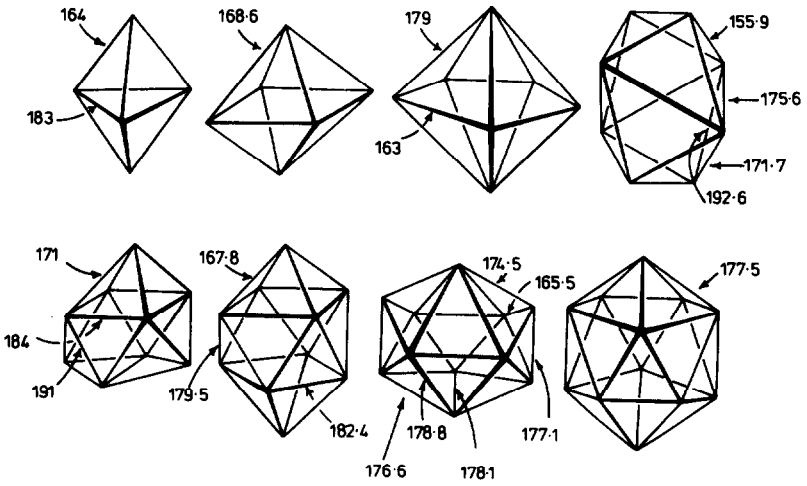


Fig. 1. All *closo* polyhedra showing interatomic distances used in calculations.

B_8Cl_8,[20] B_9Cl_9[21] and $(\eta^5\text{-}C_5H_5)_4Co_4B_4H_4$,[22] held together by one pair of electrons fewer than the norm. On the other hand, Bi_9^{5+} [23] and $(\eta^5\text{-}C_5H_5)_4Ni_4B_4H_4$[24,25] are of the latter type, with *closo* structures rather than the *nido* shapes expected. We have elsewhere[1-3] noted that the frontier orbital degeneracies of these D_{2d} dodecahedral and D_{3h} tricapped trigonal prismatic clusters allow them to be compatible with n, $n+1$ or $n+2$ skeletal electron pairs (the same being true in principle for C_{2v} octadecahedral clusters shaped like $B_{11}H_{11}^{2-}$) although the most effective bonding is presumably achieved with $n+1$ skeletal electron pairs (though calculations to test this quantitatively have not to our knowledge previously been carried out). We also pointed out that the subtle differences in bond lengths between $B_8H_8^{2-}$ and B_8Cl_8, or between $B_9H_9^{2-}$ and B_9Cl_9, were qualitatively explicable in terms of the bonding or antibonding nature of particular B–B edge links in the HOMOs of $B_8H_8^{2-}$ or $B_9H_9^{2-}$.

Below, we attempt to place on a quantitative basis the consequences, for *closo* clusters, of having n or $n+2$ instead of $n+1$ skeletal electron pairs. For the purpose, we use the CNDO-based molecular-orbital bond index (MOBI) method developed by Armstrong *et al.*[26] which in a previous paper[27] we employed to estimate skeletal bond enthalpies [E(B—B)] for the *closo* borane anions, $B_nH_n^{2-}$ (n = 5–12), using the following relationships (already known to be compatible with published thermochemical data for various boranes[28]) to link E(B—B) (kJ mol^{-1}) to bond indices (I):

$$E(\text{B—B}) = 297.9I(\text{B—B})$$

and

$$E(\text{B—H}) = 374.8I(\text{B—H}).$$

RESULTS AND DISCUSSION

In reporting and discussing the results of our MOBI calculations, we consider in turn the following issues:

(a) the degeneracies of the frontier orbitals of *closo*-$B_nH_n^{2-}$ anions;

(b) the variations in total $I(\Sigma I)$ and enthalpies (ΣE) of *closo*-$B_nH_n^{c-}$ species (c = 0, 2 or 4) with their skeletal electron pair numbers $\left(n+\frac{c}{2}\right)$;

(c) the influence of $\left(n+\frac{c}{2}\right)$ on individual bond lengths and indices; and

(d) the relative energies of *closo* and *nido* structures for $B_nH_n^{4-}$ anions (n = 7, 8, 9 or 11).

Frontier-orbital degeneracies

Figure 1 shows the D_{2d}-, D_{3h}- and C_{2v}-skeletons of the *closo* borane anions $B_8H_8^{2-}$, $B_9H_9^{2-}$ and $B_{11}H_{11}^{2-}$. For our calculations, atomic coordinates for $B_8H_8^{2-}$ and $B_9H_9^{2-}$ were taken from published structures of salts of these anions.[15] For the hypothetical neutral hydrides B_8H_8 and B_9H_9 we used the boron coordinates found in X-ray crystallographic studies of B_8Cl_8[20] and B_9Cl_9,[21] substituting B—H bonds of length 116 pm for the B—Cl bonds. Atomic coordinates for $B_{11}H_{11}^{2-}$ were derived from the published structure of the $[B_{11}H_{10}SMe_2]^-$ anion,[29] with a B—H unit (bond length 116 pm) replacing the $BSMe_2$ unit. The non-degeneracy of the frontier orbitals that allows these systems to tolerate n, $n+1$ or $n+2$ skeletal electron

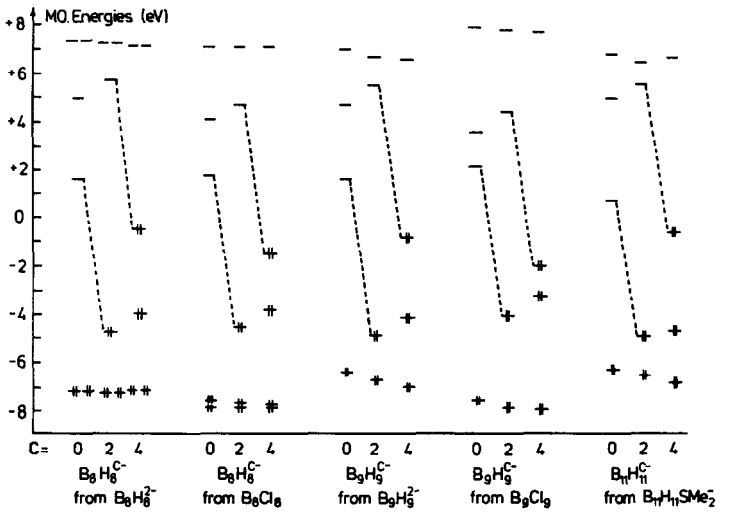


Fig. 2. Frontier-orbital energies of $B_8H_8^{2-}$, $B_9H_9^{2-}$ and $B_{11}H_{11}^{2-}$.

pairs is confirmed by our calculations (Fig. 2). Removal of electron pairs from these anions to generate neutral B_nH_n species (n atoms, n pairs) or addition of electron pairs to them, to generate $B_nH_n^{4-}$ anions (n atoms, $n+2$ pairs) would leave closed-shell, spin-paired electronic configurations and hence give rise to potentially stable species.

As expected for colourless species that are not easily reduced, the HOMO–LUMO gaps for the $B_nH_n^{2-}$ dianions are large (8.3–10.4 eV). If one bonding MO is left unfilled, as in the case of neutral B_nH_n molecules, the $(n+1)$th skeletal bonding MO, formerly the HOMO of $B_nH_n^{2-}$, increases markedly in energy relative to the nth skeletal bonding MO, so preserving a significant HOMO–LUMO energy gap of *ca* 7.4–9.6 eV for the hypothetical neutral B_nH_n species (Fig. 2).

In order to check the sensitivity of MO energies and degeneracies to the atomic coordinates used, we also calculated the energies of the MOs of hypothetical B_nH_n species using the atomic coordinates found experimentally for $B_nH_n^{2-}$ anions. As expected, the degeneracies (which reflect the symmetries) were unaffected, though orbital energies changed slightly. For example, the HOMO of B_8H_8 is calculated to have an energy of -7.62 eV using the boron coordinates of B_8Cl_8, but of -7.06 eV using the boron coordinates of $B_8H_8^{2-}$.

Addition of an electron pair to a *closo*-$B_nH_n^{2-}$ species to generate a hypothetical *closo*-$B_nH_n^{4-}$ anion fills the former's slightly antibonding LUMO. Again, orbital energy changes with occupancy leave substantial (7.0–9.3 eV) HOMO–LUMO gaps for these hypothetical $B_nH_n^{4-}$ species ($n = 8$, 9 or 11).

By contrast, MOBI calculations[27] on other *closo*-$B_nH_n^{2-}$ anions ($n = 5$, 6, 7, 10 or 12) using experimentally determined[30–32] or estimated[27] ($n = 5$ or 7) atomic coordinates confirmed that their frontier orbitals are degenerate. Adding an electron pair to any of these dianions, or removing an electron pair, would generate a paramagnetic species prone to distortion to remove the HOMO degeneracy. (Actually, use of the published atomic coordinates for $B_{10}H_{10}^{2-}$ [31] and $B_{12}H_{12}^{2-}$,[32] which show slight departures from idealized D_{4d}- and I_h-symmetries, respectively, causes a slight splitting of the frontier orbitals that vanishes if idealized symmetries are used.)

ΣI *and* ΣE *of* closo-$B_nH_n^{c-}$ *species* (c = 0, 2 *or* 4)

Tables 1 and 2 list the B—B and B—H I calculated for the real and hypothetical *closo*-$B_nH_n^{c-}$ systems considered in this work. Table 1 presents data for systems with $n = 8$, 9 or 11, i.e. those systems that are either known to tolerate other than $n+1$ skeletal electron pairs, or may reasonably be expected to do so for the orbital degeneracy reasons just outlined. Table 2 presents data for systems with $n = 5$, 6, 7, 10 or 12, for which the presence of n or $n+2$ skeletal electron pairs (i.e. when $c = 0$ or 4) would leave frontier orbitals incompletely filled.

Entries in the second, third and fourth columns in both tables record the following: $\Sigma I(\text{B—B})_{\text{adj}}$, the sum of the bond indices between nearest neighbour (adjacent) boron atoms, i.e. for all of the boron–boron polyhedral edge bonds; $\Sigma I(\text{B—B})_{\text{all}}$, the sum of *all* of the (skeletal) boron–boron links, including pairwise cross-polyhedral interactions as well as polyhedral edge interactions; and $\Sigma I(\text{B—H})$, the sum of the n B—H I for each species.

The fifth column in each table lists figures that

Table 1. Bond indices (I) and enthalpies (E_I) (kJ mol^{-1}), for *closo* $B_nH_n^{c-}$ species (n = 8, 9 or 11; c = 0, 2 or 4)

Species	ΣI(B—B)$_{adj}$	ΣI(B—B)$_{all}$	ΣI(B—H)	ΣI(B—B)$_{all}/\left(n+\frac{c}{2}\right)$	ΣI(B—H)/n	ΣE(B—B)$_{all}$	ΣE(B—H)	E_{total}
B_8H_8	10.18	10.59	7.96	1.32	0.995	3154	2983	6137
$B_8H_8^{2-}$	10.74	10.91	7.72	1.21	0.965	3250	2895	6142
$B_8H_8^{4-}$	10.70	11.61	7.23	1.12	0.903	3324	2708	6032
B_9H_9	11.34	11.84	8.96	1.32	0.996	3528	3358	6886
$B_9H_9^{2-}$	12.02	12.27	8.73	1.23	0.970	3655	3272	6927
$B_9H_9^{4-}$	11.96	12.50	8.22	1.14	0.913	3724	3081	6805
$B_{11}H_{11}$	13.98	14.56	10.95	1.32	0.995	4338	4104	8441
$B_{11}H_{11}^{2-}$	14.67	15.00	10.71	1.25	0.974	4468	4013	8480
$B_{11}H_{11}^{4-}$	14.70	15.28	10.19	1.18	0.926	4550	3817	8367

Table 2. Bond indices (I) and enthalpies (E_I) (kJ mol^{-1}), for *closo* $B_nH_n^{c-}$ species (n = 5, 6, 7, 10 or 12; c = 0, 2 or 4)

Species	ΣI(B—B)$_{adj}$	ΣI(B—B)$_{all}$	ΣI(B—H)	ΣI(B—B)$_{all}/\left(n+\frac{c}{2}\right)$	ΣI(B—H)/n	ΣE(B—B)$_{all}$	ΣE(B—H)	E_{total}
B_5H_5	5.61	5.63	4.99	1.13	0.998	1676	1870	3545
$B_5H_5^{2-}$	6.83	6.90	4.79	1.15	0.958	2054	1795	3849
$B_5H_5^{4-}$	6.26	6.28	4.09	0.90	0.818	1871	1533	3404
B_6H_6	7.26	7.58	5.95	1.26	0.992	2259	1892	4151
$B_6H_6^{2-}$	8.17	8.31	5.73	1.19	0.955	2476	2148	4625
$B_6H_6^{4-}$	6.95	7.06	5.21	0.88	0.868	2103	1952	4055
B_7H_7	8.44	8.57	6.70	1.22	0.957	2554	2511	5066
$B_7H_7^{2-}$	9.51	9.59	6.74	1.20	0.963	2859	2526	5384
$B_7H_7^{4-}$	8.51	8.65	6.25	0.96	0.893	2577	2342	4919
$B_{10}H_{10}$	12.46	13.07	9.96	1.31	0.996	3893	3732	7624
$B_{10}H_{10}^{2-}$	13.41	13.65	9.76	1.24	0.976	4067	3658	7725
$B_{10}H_{10}^{4-}$	12.71	13.00	9.20	1.09	0.920	3873	3446	7319
$B_{12}H_{12}$	15.03	15.52	11.16	1.28	0.930	4623	4182	8806
$B_{12}H_{12}^{2-}$	16.17	16.39	11.73	1.26	0.978	4884	4395	9278
$B_{12}H_{12}^{4-}$	15.87	16.56	11.32	1.18	0.943	4932	4243	9175

reflect the efficiency with which the $2n+c$ electrons formally available for skeletal bonding are used in these systems, by listing the mean boron–boron I per skeletal electron pair. The next column shows how effectively the n electron pairs notionally available for B–H bonding are used, and the final three columns convert these total bond indices into total bond enthalpies using the equations[28] already referred to, i.e. E(B—B) = 297.9I(B—B), and E(B—H) = 374.8I(B—H).

Considering first the data in Table 1, and comparing entries for the "normal" $(n+1)$ skeletal pair systems ($B_nH_n^{2-}$) with those (B_nH_n) containing only n skeletal electron pairs, we see that:

(i) the $n+1$th skeletal electron pair does indeed contribute significantly to the skeletal bonding, albeit to a lesser extent than the other n "skeletal" pairs already present;

(ii) this same $(n+1)$th electron pair, formally a skeletal bond pair, apparently has slight B–H *antibonding* character in that its presence correlates with a slight (2–3%) decrease in ΣI(B—H);

(iii) the cross-polyhedral boron–boron interactions in these systems, as represented by the difference between $\Sigma I(\text{B—B})_{\text{all}}$ and $\Sigma I(\text{B—B})_{\text{adj}}$, are of little significance [$<2.5\%$ of $\Sigma I(\text{B—B})_{\text{all}}$] for the normal $B_nH_n^{2-}$ anions but of rather more significance [still $<5\%$ of $\Sigma I(\text{B—B})_{\text{all}}$] for the neutral B_nH_n species; and

(iv) the total energy of the B—B and B—H bonds in the $B_nH_n^{2-}$ anions is greater than that of the hypothetical B_nH_n species, though only marginally so (difference $<0.6\%$).

The entries in Table 1 relating to hypothetical $B_nH_n^{4-}$ anions show that the extra electron pair such species possess compared to the normal *closo*-$B_nH_n^{2-}$ anions strengthens the cross-polyhedral boron–boron interactions while leaving the polyhedral edge bonding essentially little changed overall, though individual edge bonds change markedly in strength, as shown below. However, the concomitant *decrease* in the total boron–hydrogen I (and consequent loss of boron–hydrogen bond energy) is more than sufficient to offset completely the marginal strengthening of the skeletal bonding, leaving the overall effect of this $(n+2)$th pair of electrons *anti*bonding.

A qualitatively similar but quantitatively more pronounced picture emerges from an examination of the data in Table 2, which show, as expected, that the *closo*-$B_nH_n^{2-}$ clusters, containing $n+1$ bond pairs that are attributable to skeletal (boron–boron) bonding and n bond pairs attributable to boron–hydrogen bonding, are those that make best use of their electrons. The relatively strongly bonding nature of the $(n+1)$th pair of skeletal electrons is reflected in the marked reduction in bond energy when this pair is removed going from $B_nH_n^{2-}$ to the hypothetical neutral B_nH_n species though since the bond indices and enthalpies of the latter were calculated using the atomic coordinates of the dianions, not on optimized structures, the bonding nature of the $(n+1)$th skeletal pair will actually be rather less than the figures in Table 2 suggest.

An interesting implication of the figures in Table 2 is that, of the $B_nH_n^{2-}$ anions therein, $B_{10}H_{10}^{2-}$ appears to be the best candidate for oxidation to a neutral B_nH_n species, in that it is calculated to lose the least bond energy on removal of two electrons.

The influence of skeletal electron numbers on individual polyhedral edge lengths and I

Earlier[1-3] we pointed out that the differences between the skeletal geometries of the dodecahedral $B_8H_8^{2-}$ [15] and B_8Cl_8,[20] or of the tricapped trigonal prismatic $B_9H_9^{2-}$ [15] and B_9Cl_9,[21] could qualitatively be understood in terms of the polyhedral edge-bonding or edge-antibonding characteristics of their $(n+1)$th skeletal bonding MOs, which are occupied, as the HOMOs, in the hydride $B_nH_n^{2-}$ dianions but empty in the neutral halides, B_nCl_n: loss of electrons that bond specific edges causes those edges to lengthen on going from $B_nH_n^{2-}$ to B_nCl_n; on the other hand, edges for which those same electrons were antibonding contract. The bond indices calculated in the present study confirm these qualitative changes, and reveal the extent to which specific edge bonds are strengthened or weakened. Results for systems with 8, 9 or 11 skeletal atoms are discussed in turn below.

D_{2d} *dodecahedral* closo *octaboranes*, $B_8H_8^{c-}$ (c = 0, 2 *or* 4)

The four distinct types of polyhedron edge in the D_{2d} dodecahedral octaborane clusters B_8Cl_8[20] and $B_8H_8^{2-}$,[15] labelled w, x, y and z in Fig. 3, differ in length as summarized in Table 3. Figure 3 and Table 3 also illustrate the edge-bonding or edge-antibonding characteristics of the frontier orbitals. The HOMO of $B_8H_8^{2-}$, empty in B_8Cl_8, is *bonding* for edges of types w, y and z, but *antibonding* for those of type x. Conversely, the LUMO of $B_8H_8^{2-}$, which would be filled in a hypothetical D_{2d} $B_8H_8^{4-}$ cluster (or in an isoelectronic neutral D_{2d} dodecahedral carborane, $C_4B_4H_8$) is *antibonding* for edges of types w, y and z, but *bonding* for edges of type x. Whether a pair of electrons is added to or

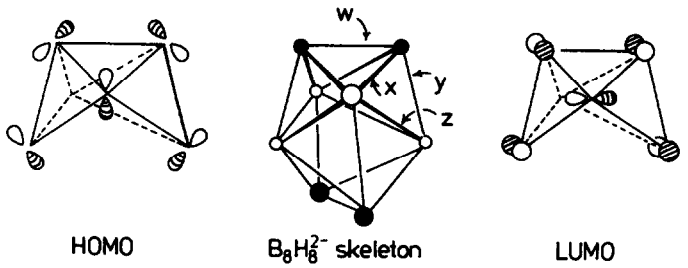


Fig. 3. $B_8H_8^{2-}$ shape, and HOMO and LUMO.

removed from $B_8H_8^{2-}$, provided the D_{2d} *closo* dodecahedral shape is retained, the same type of distortion is expected. Edges of types *w*, *y* and *z* will lengthen, while those of type *x* will contract.

Such changes in edge bond strengths, which incidentally make the skeletal atom geometry of B_8Cl_8 a realistic model for that of the hypothetical $B_8H_8^{4-}$ anion, are clearly reflected in the *I* calculated for the four edge types and listed in Table 3. Calculations of edge *I* were carried out for B_8H_8, $B_8H_8^{2-}$ and $B_8H_8^{4-}$ using both B_8Cl_8[20] and $B_8H_8^{2-}$[15] skeletal atom geometries, to explore the extent to which the *I* were dependent on the interatomic distance used. The *I* calculated for B_8H_8 and $B_8H_8^{4-}$ using the B_8Cl_8 skeletal atom coordinates, and those calculated for $B_8H_8^{2-}$ using its measured skeletal atom coordinates, are the *I* considered the more apt of the pair listed for each system.

That the calculated *I* are influenced more by changes in electron numbers than by subtle changes in interatomic distances is shown by the sets of data in Table 3 that relate to a common structure for B_8H_8, $B_8H_8^{2-}$ and $B_8H_8^{4-}$, whether that structure be that of the B_8Cl_8 or the $B_8H_8^{2-}$ skeleton.

The structural changes expected to accompany two-electron oxidation or reduction of D_{2d} dodecahedral $B_8H_8^{2-}$ with retention of *closo* geometry incidentally result in an overall *expansion* of the dodecahedron, the atoms of lower coordination number (those connected to each other by edges of type *w*) moving out from the centre more than those of higher coordination number, stretching the polyhedron along the two-fold axis connecting the midpoints of the edges of type *w*.

D_{3h} *tricapped trigonal prismatic* closo *nonaboranes*, $B_9H_9^{c-}$ (c = 0, 2 *or* 4)

The three distinct types of polyhedron edge in the D_{3h} tricapped trigonal prismatic nonaborane clusters B_9Cl_9[21] and $B_9H_9^{2-}$,[15] labelled *f*, *g* and *h* in Fig. 4, differ in length as summarized in Table 4. Figure 4 and Table 4 also illustrate the edge-bonding or edge-antibonding characteristics of the frontier orbitals. The HOMO of $B_9H_9^{2-}$, empty in B_9Cl_9, is clearly *bonding* for edges of types *g* and *h*, but *antibonding* for those of type *f*. Conversely, the LUMO of $B_9H_9^{2-}$, which would be occupied in a hypothetical

Table 3. Bond lengths (pm) and indices, and frontier-orbital bonding/antibonding (b/ab) characteristics for $B_8H_8^{c-}$ (*c* = 0, 2 or 4)

Edge type[a]	*w*	*x*	*y*	*z*
Bond length				
B_8Cl_8[20]	168.1	174.4	181.4	200.1
$B_8H_8^{2-}$[15]	155.9	175.6	171.7	192.6
Bond index[b]				
B_8H_8	0.66 (**0.62**)	0.61 (**0.64**)	0.55 (**0.53**)	0.45 (**0.43**)
$B_8H_8^{2-}$	**0.93** (0.87)	**0.53** (0.56)	**0.70** (0.69)	**0.46** (0.43)
$B_8H_8^{4-}$	0.72 (**0.67**)	0.70 (**0.74**)	0.56 (**0.55**)	0.39 (**0.33**)
Frontier orbital				
$B_8H_8^{2-}$ HOMO	b	ab	b	b
$B_8H_8^{2-}$ LUMO	ab	b	ab	ab

[a] See Fig. 3.

[b] Figures in parentheses relate to B_8Cl_8 skeletal geometry, others to $B_8H_8^{2-}$ geometry; the more apt are in **bold print**.

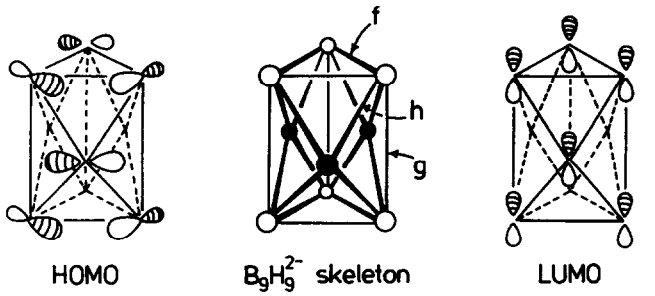


Fig. 4. $B_9H_9^{2-}$ shape, and HOMO and LUMO.

$B_9H_9^{4-}$ cluster, and is indeed occupied by one electron in the tricapped trigonal prismatic Sn_9^{3-} anion,[33] and by two electrons in the tricapped trigonal prismatic Bi_9^{5+} cation,[23] is clearly *bonding* for edges of type *f* but *antibonding* for those of type *g*. Its bonding/antibonding character with respect to edges of type *h* is less clearly deducible from the lobal characteristics of its AOs, and was referred to earlier by us[1-3] as *antibonding*, in contrast to the description of Critchlow and Corbett[33] who in considering the Sn_9^{3-} anion found the singly-occupied HOMO to be *bonding* with respect to edges of type *h*.

The *I* data in Table 4 shed useful light on this and other issues. Whatever the bonding or antibonding character of the LUMO for edges of type *h*, one feature is clear. This is that two-electron oxidation *or* reduction of a cluster such as $B_9H_9^{2-}$, provided that a tricapped trigonal prismatic structure is retained, will cause the trigonal prism to become elongated along its three-fold axis, but thinner. This conclusion is reinforced by the *I* for edges of types *f* and *g* given in Table 4, which increase and decrease, respectively, on going from $B_9H_9^{2-}$ to B_9H_9 or $B_9H_9^{4-}$, when appropriate sets of skeletal atom coordinates are used. (If a particular structure, whether using the atomic coordinates of B_9Cl_9 or of $B_9H_9^{2-}$, is retained for all the calculations of bond indices, the *I* calculated for edges of type *g* remains essentially unchanged going from $B_9H_9^{2-}$ to B_9H_9.)

As regards edges of type *h*, these are clearly weakened going from $B_9H_9^{2-}$ to B_9H_9 as the edge-bonding power of two electrons is lost. Going from $B_9H_9^{2-}$ to $B_9H_9^{4-}$, these same edges are calculated to be strengthened a little if a B_9Cl_9-type structure

Table 4. Bond lengths (pm) and indices, and frontier-orbital bonding/antibonding (b/ab) characteristics for $B_9H_9^{c2}$ ($c = 0$, 2 or 4) and related 9-atom clusters

Edge type[a]	*f*	*g*	*h*	*f*/*g*
Bond length (number of skeletal electron pairs)				
B_9Cl_9 (9)[21]	180	208	175	0.87
$B_9H_9^{2-}$ (10)[15]	191	184	171	1.04
$C_2B_7H_9$ (10)[34]	197	177	170[b]	1.11
Ge_9^{2-} (10)[35]	267	295[c]	256	0.91[c]
Sn_9^{3-} (10.5)[33]	306	330	294	0.93
Bi_9^{5+} (11)[23]	324	374	309	0.87
Bond index[d]				
B_9H_9	0.50 (**0.54**)	0.45 (**0.39**)	0.58 (**0.58**)	1.11 (**1.39**)
$B_9H_9^{2-}$	**0.45** (0.50)	**0.46** (0.38)	**0.66** (0.65)	**0.97** (1.31)
$B_9H_9^{4-}$	0.50 (**0.57**)	0.39 (**0.25**)	0.65 (**0.67**)	1.29 (**2.29**)
Frontier orbital				
$B_9H_9^{2-}$ HOMO	ab	b	b	
$B_9H_9^{2-}$ LUMO	b	ab	ab	

[a] See Fig. 4.

[b] Distance to capping boron; *h* for capping carbon is 161 pm.

[c] This anion is very distorted,[35] with one long prism edge, *g*. For the others, the *f*/*g* ratio is 0.94.

[d] Figures in parentheses relate to B_9Cl_9 skeletal geometry, others to $B_9H_9^{2-}$ geometry; the more apt are in **bold print**.

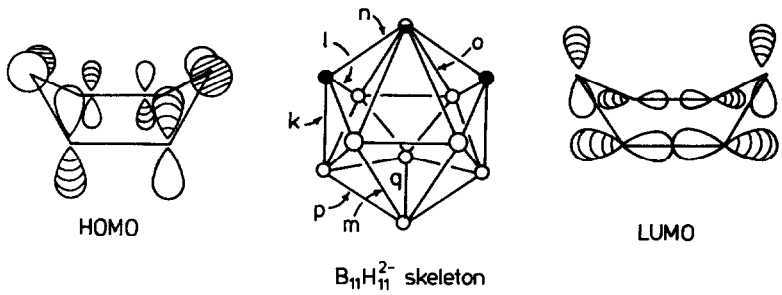


Fig. 5. $B_{11}H_{11}^{2-}$ shape, and HOMO and LUMO.

is assumed for both species, but to be weakened a little if the $B_9H_9^{2-}$ structure is assumed for both species. Making the more reasonable comparison between $B_9H_9^{2-}$, with its known structure, and $B_9H_9^{4-}$ with a skeletal atom arrangement like that of B_9Cl_9, we find the edges of type *h* to suffer negligible change in bond index—the increase from 0.663 for $B_9H_9^{2-}$ to 0.667 for $B_9H_9^{4-}$ cannot be regarded as significant. We conclude that the LUMO of $B_9H_9^{2-}$ is essentially *nonbonding* for these edges.

In addition to the interatomic distances for B_9Cl_9 and $B_9H_9^{2-}$ given in Table 4, structural data for the related tricapped trigonal prismatic clusters $C_2B_7H_9$,[34] Ge_9^{2-},[35] Sn_9^{3-} [33] and Bi_9^{5+} [23] are included for purposes of comparison. Direct comparison of interatomic distances for clusters of atoms of such different sizes as boron, germanium, tin and bismuth is of little value, so the ratio, *f*/*g*, of the prism edge lengths is given to facilitate comparison. The longer, thinner prism of B_9Cl_9 compared with $B_9H_9^{2-}$ is reflected in its smaller *f*/*g* ratio (0.87, cf. 1.04 for $B_9H_9^{2-}$); Sn_9^{3-} and Bi_9^{5+} likewise have low *f*/*g* ratios. However, values of *f*/*g* less than unity cannot be taken as uniquely characteristic of tricapped trigonal prismatic clusters with "anomalous" electron numbers, as shown by the *f*/*g* ratio of 0.91 for the "normal" *closo* cluster Ge_9^{2-} anion,[35] though it should be acknowledged that this ion is significantly distorted from idealized D_{3h}-symmetry in the crystal.

C_{2v} *octadecahedral* closo *enneaboranes*, $B_{11}H_{11}^{c-}$ (c = 0, 2 *or* 4)

The 11-vertex *closo* borane systems are far less well documented than the 8- and 9-vertex systems just considered. The structure of the anion $B_{11}H_{11}^{2-}$ has not yet been determined crystallographically, though that of the derivative $[B_{11}H_{10}SMe_2]^-$ [29] provides a good guide to its likely interatomic distances (Fig. 5, Table 5).

In principle, because its frontier orbitals (Fig. 5) are nondegenerate, the $B_{11}H_{11}^{2-}$ anion could tolerate two-electron oxidation or reduction while retaining its *closo* deltahedral shape, albeit with modified interatomic distances, though no 11-atom *closo*-shaped clusters with 11 or 13 skeletal electron pairs have to our knowledge been characterized to date. In order to get some feeling for the manner in which

Table 5. Bond lengths (pm) and indices, and frontier-orbital bonding/antibonding (b/ab) characteristics for $B_{11}H_{11}^{c-}$ (*c* = 0, 2 or 4)

Edge type[a]	*k*	*l*	*m*	*n*	*o*	*p*	*q*
Edge length[b]	177.1	165.5	178.8	174.5	201.2	176.6	178.1
Bond index							
$B_{11}H_{11}$	0.521	0.573	0.532	0.603	0.366	0.537	0.517
$B_{11}H_{11}^{2-}$	0.510	0.772	0.527	0.576	0.376	0.561	0.501
$B_{11}H_{11}^{4-}$	0.664	0.633	0.543	0.705	0.320	0.520	0.597
Frontier orbital							
$B_{11}H_{11}^{2-}$ HOMO	ab	b	ab	ab	b	b	ab
$B_{11}H_{11}^{2-}$ LUMO	b	ab	b	b	ab	ab	b

[a] See Fig. 5.

[b] Skeletal atom coordinates as for $[B_{11}H_{10}SMe_2]^-$.[29]

they would be expected to differ from $B_{11}H_{11}^{2-}$, we carried out *I* calculations on $B_{11}H_{11}$, $B_{11}H_{11}^{2-}$ and $B_{11}H_{11}^{4-}$, assuming for each a structure like that of $B_{11}H_{11}^{2-}$, itself deduced from the published structure[29] of $[B_{11}H_{10}SMe_2]^-$ by replacement of the SMe_2 ligand by a hydrogen ligand. The results are given in Table 5.

Detailed interpolation of the data in Table 5 is not justified, since the calculations for $B_{11}H_{11}$ and $B_{11}H_{11}^{4-}$ have been carried out using the structure of $B_{11}H_{11}^{2-}$, making no allowance for the expected distortions. Nevertheless, the nature of these distortions can be inferred from the calculated *I*, in that edges experiencing an increase in *I* on electron pair addition or removal may be expected to shorten relative to those of $B_{11}H_{11}^{2-}$, while those experiencing a decrease in *I* may be expected to lengthen.

Thus, in the hypothetical *closo* hydride, $B_{11}H_{11}$, or chloride, $B_{11}Cl_{11}$, the edges of types *k*, *m*, *n* and *q* are expected to be slightly shorter than their counterparts in $B_{11}H_{11}^{2-}$, while edges of types *l*, *o* and *p* are expected to be longer, type *l* showing the most marked change.

Qualitatively similar changes relative to $B_{11}H_{11}^{2-}$ are expected for a *closo* $B_{11}H_{11}^{4-}$ species, i.e. edges of types *k*, *m*, *n* and *q* shorter than in the parent $B_{11}H_{11}^{2-}$, edges of types *l*, *o* and *p* longer. From this we can infer that, as with $B_8H_8^{2-}$ and $B_9H_9^{2-}$, so with $B_{11}H_{11}^{2-}$, for the edges for which the HOMO is bonding, the LUMO is antibonding, and vice versa.

Our data incidentally allow the symmetries of the frontier orbitals of $B_{11}H_{11}^{2-}$ to be identified for the first time. The HOMO is A_2, the LUMO A_1.

Relative energies of closo *and* nido *structures for* $B_nH_n^{4-}$ *anions* (n = 8, 9 *or* 11)

So far in this paper we have been considering the bonding consequences of changing the numbers of electrons of *closo* clusters while retaining *closo* geometries, paying particular attention to systems with 8, 9 or 11 skeletal atoms whose nondegenerate frontier orbitals allow closed-shell electronic configurations for neutral B_nH_n entities (effectively already known in the form of the chlorides B_8Cl_8 and B_9Cl_9) and for $B_nH_n^{4-}$ tetra-anions (unknown as *closo* species, but known in protonated or metallated form as *nido* species based on deltahedra with $n+1$ vertices). In this final section we use the MOBI method to compare the energies of such hypothetical *closo* structures with likely alternative *nido* structures for $B_8H_8^{4-}$, $B_9H_9^{4-}$ and $B_{11}H_{11}^{4-}$.

Our results are summarized in Table 6, which lists the total B—B and B—H *I* calculated for the various possible structures for these tetra-anions, and the *E* they imply, calculated using the relationships $E(B—B) = 297.9I(B—B)$ kJ mol^{-1}, and $E(B—H) = 374.8I(B—H)$ kJ mol^{-1}.[28]

For $B_8H_8^{4-}$, we compare the results for a *closo* species with what we regard as the most plausible skeletal structure (like that of B_8Cl_8), with *nido* structures derived from the $B_9H_9^{2-}$ skeleton by removal of one or other of the two types of capping BH^{2+} units, or by removal of one of the more highly coordinated BH^{2+} units from a prism vertex site (Fig. 6) (*nido* boranes are generally found to have skeletons based on deltahedra with the *most highly* coordinated vertex vacated). Interestingly, in all

Table 6. Relative energies of *closo* and *nido* structures for borane anions, $B_8H_8^{4-}$, $B_9H_9^{4-}$ and $B_{11}H_{11}^{4-}$

Species	Skeletal structure	ΣI(B—B)	ΣI(B—H)	ΣE(B—B) (kJ mol^{-1})	ΣE(B—H) (kJ mol^{-1})	E_{total} (kJ mol^{-1})
$B_8H_8^{4-}$	*closo* (B_8Cl_8)	11.10	7.26	3306	2720	6026
$B_8H_8^{4-}$	*nido* ($B_9H_9^{2-}$)[a]	11.13	7.27	3314	2724	6038
$B_8H_8^{4-}$	*nido* ($B_9H_9^{2-}$)[b]	11.08	7.24	3302	2713	6014
$B_8H_8^{4-}$	*nido* ($B_9H_9^{2-}$)[c]	11.09	7.20	3303	2698	6001
$B_9H_9^{4-}$	*closo* (B_9Cl_9)	12.50	8.22	3724	3081	6805
$B_9H_9^{4-}$	*nido* ($B_{10}H_{10}^{2-}$)[d]	12.49	8.35	3720	3128	6848
$B_9H_9^{4-}$	*nido* ($B_{10}H_{10}^{2-}$)[e]	12.49	8.34	3720	3125	6845
$B_{11}H_{11}^{4-}$	*closo* ($[B_{11}H_{10}SMe_2]^-$)	15.28	10.19	4550	3817	8367
$B_{11}H_{11}^{4-}$	*nido* ($B_{12}H_{12}^{2-}$)[f]	15.18	10.32	4521	3869	8389

[a] With BH^{2+} removed from smaller cap.
[b] With BH^{2+} removed from larger cap.
[c] With BH^{2+} removed from a prism vertex.
[d] With BH^{2+} removed from a polar site.
[e] With BH^{2+} removed from a tropical site.
[f] With BH^{2+} removed.

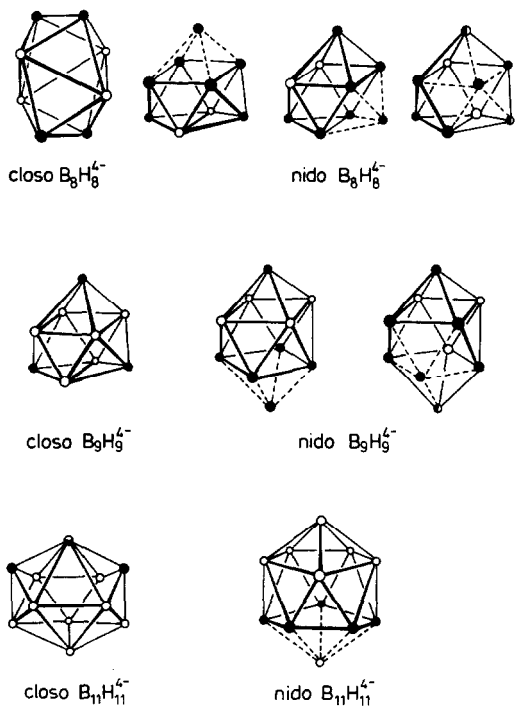


Fig. 6. Alternative *nido* shapes for $B_8H_8^{2-}$, $B_9H_9^{2-}$ and $B_{11}H_{11}^{2-}$.

cases, the skeletal I, ΣI(B—B), are very similar, as are the BH I, ΣI(B—H), and when these are converted into E, we find only very small differences in total E, E_{total}, between these alternative structures. Our conclusion is that the hypothetical *closo* structure we have been considering for $B_8H_8^{4-}$ may indeed by a plausible possible structure for such an anion or isoelectronic analogues such as $C_4B_4H_8$, Sn_8^{4-} etc., even if slightly more stable *nido* alternatives exist, so the *closo* geometry could provide at least a low-energy intermediate/transition state through which *nido* species might readily rearrange.

Similar conclusions can be drawn concerning the feasibility of a *closo* structure for $B_9H_9^{4-}$. Indeed, the *closo* structures already known for salts of the Sn_9^{3-} anion and the Bi_9^{5+} cation show that in certain systems the *closo* structure may actually be preferred to *nido* alternatives, though the influence of the counter-ions in such salts should not be ignored.

For $B_{11}H_{11}^{4-}$, since in icosahedral *closo*-$B_{12}H_{12}^{2-}$ all 12 BH units are equivalent, there is only one feasible *nido* structure with which to compare our hypothetical *closo* structure. Again, the difference in E_{total} is calculated to be very small, surprisingly so since the skeleton assumed for the calculation on *closo*-$B_{11}H_{11}^{4-}$ was that of the normal $(n+1)$-skeletal pair species $[B_{11}H_{10}SMe_2]^-$,[29] no allowance being made for the expected distortions.

The above results for $B_nH_n^{4-}$ species (n = 8, 9 or 11) for which *closo* structures are feasible alternatives to *nido* ones can be contrasted with those for other $B_nH_n^{4-}$ species (n = 5, 6, 7, 10 or 12) for which they are not. For example, comparing the results for a *closo*-$B_7H_7^{4-}$ species (using bond lengths predicted earlier[27] for $B_7H_7^{2-}$) with those for a *nido*-$B_7H_7^{4-}$ one (derived from *closo*-$B_8H_8^{2-}$ by removal of the high-coordinate BH^{2+} capping unit) shows severe weakening of cluster bonding in the former [ΣI(B—B) = 8.65 and 9.81, respectively]. As the exo-B—H bonding is of very comparable strength in both [ΣI(B—H) = 6.25 and 6.26, respectively], the effect of this is to make the *closo* structures energetically extremely unfavourable (E_{total} = 4919 and 5267 kJ mol^{-1}, respectively).

Acknowledgements—We thank Professor P. G. Perkins for permission to use his MOBI programs and the SERC for financial support.

REFERENCES

1. M. E. O'Neill and K. Wade, *Inorg. Chem.* 1982, **21**, 461.
2. M. E. O'Neill and K. Wade, *Polyhedron* 1983, **2**, 963.
3. M. E. O'Neill and K. Wade, *J. Mol. Struct. Theochem.* 1983, **103**, 259.
4. R. E. Williams, *Inorg. Chem.* 1971, **10**, 210.
5. K. Wade, *J. Chem. Soc. D* 1971, 792.
6. R. W. Rudolph and W. R. Pretzer, *Inorg. Chem.* 1972, **11**, 1974.
7. D. M. P. Mingos, *Nature (London), Phys. Sci.* 1972, **236**, 99.
8. R. N. Grimes, *Ann. N. Y. Acad. Sci.* 1974, **239**, 180.
9. K. Wade, *Advan. Inorg. Chem. Radiochem.* 1976, **18**, 1.
10. R. W. Rudolph, *Acc. Chem. Res.* 1976, **9**, 446.
11. R. N. Grimes (Ed.), *Metal Interactions with Boron Clusters*. Plenum, New York (1982).
12. D. M. P. Mingos, *Acc. Chem. Res.* 1948, **17**, 311.
13. H. C. Longuet-Higgins, *Quart. Rev. Chem. Soc.* 1957, **11**, 121.
14. W. N. Lipscomb, *Boron Hydrides*. W. A. Benjamin, New York (1963).
15. L. J. Guggenberger, *Inorg. Chem.* 1968, **7**, 2260; 1969, **8**, 2771.
16. D. A. Kleir and W. N. Lipscomb, *Inorg. Chem.* 1979, **18**, 1312.
17. S. F. A. Kettle and V. Tomlinson, *J. Chem. Soc. A* 1969, 2002.
18. D. R. Armstrong, P. G. Perkins and J. J. P. Stewart, *J. Chem. Soc., Dalton Trans.* 1973, 627.
19. M. J. S. Dewar and M. L. McKee, *Inorg. Chem.* 1978, **17**, 1569.
20. G. S. Pawley, *Acta Cryst.* 1966, **20**, 631.
21. M. B. Hursthouse, J. Kane and A. G. Massey, *Nature (London)*, 1970, **228**, 659; M. B. Hursthouse, personal communication.

22. J. R. Pipal and R. N. Grimes, *Inorg. Chem.* 1979, **18**, 257.
23. J. D. Corbett, *Prog. Inorg. Chem.* 1976, **21**, 140.
24. J. R. Bowser, A. Bonny, J. R. Pipal and R. N. Grimes, *J. Am. Chem. Soc.* 1979, **101**, 6229.
25. D. N. Cox, D. M. P. Mingos and R. Hoffmann, *J. Chem. Soc., Dalton Trans.* 1981, 1788.
26. D. R. Armstrong, P. G. Perkins and J. J. P. Stewart, *J. Chem. Soc., Dalton Trans.* 1973, 838, 2273.
27. C. E. Housecroft, R. Snaith, K. Moss, R. E. Mulvey, M. E. O'Neill and K. Wade, *Polyhedron* 1985, **4**, 1875.
28. D. Laurie and P. G. Perkins, *Inorg. Chim. Acta* 1982, **63**, 53.
29. E. H. Wong, L. Prasad, E. J. Gabe and M. G. Gatter, *Inorg. Chem.* 1983, **22**, 1143.
30. R. Schaeffer, Q. Johnson and G. S. Smith, *Inorg. Chem.* 1965, **4**, 917.
31. J. T. Gill and S. J. Lippard, *Inorg. Chem.* 1975, **14**, 751.
32. J. A. Wunderlich and W. N. Lipscomb, *J. Am. Chem. Soc.* 1960, **82**, 4427.
33. S. C. Critchlow and J. D. Corbett, *J. Am. Chem. Soc.* 1983, **105**, 5715.
34. T. F. Koetzle, F. E. Scarbrough and W. N. Lipscomb, *Inorg. Chem.* 1968, **7**, 1076.
35. C. H. E. Belin, J. D. Corbett and A. Cisar, *J. Am. Chem. Soc.* 1977, **99**, 7163.

Polyhedron Vol. 5, No. 9, pp. 1449–1458, 1986
Printed in Great Britain

0277–5387/86 $3.00+.00
Pergamon Journals Ltd

MODES OF COORDINATION OF 1,2-AMINOTHIOLS IN ORGANOTIN(IV) COMPLEXES, AS DEMONSTRATED BY ^{119}Sn, ^{15}N AND ^{13}C NMR SPECTROSCOPY

BHIM SEN SARASWAT* and JOAN MASON†

Department of Chemistry, The Open University, Milton Keynes MK7 6AA, U.K.

(*Received* 29 *November* 1985; *accepted* 19 *December* 1985)

Abstract—Three series of organotin(IV) cysteamine complexes have been prepared in which the 1,2-aminothiol may be monodentate, chelating or bridging, on the ^{119}Sn, ^{15}N or ^{13}C NMR spectroscopic and other physical evidence. Triorganotin(IV) complexes $[SnR_3(SCH_2CH_2NR'_2)]$ (R = Me, Bu^n or Ph; R′ = H, Me or Et) are monomeric and the aminothiol monodentate in non-coordinating solvents. Dialkyltin(IV) chloro complexes $[SnR_2Cl(SCH_2CH_2NR'_2)]$ (R = Me, Et, Bu^n or Oct^n; R′ = H, Me or Et), however, are monomeric with chelation of the aminothiol, like the SnR_2Cl complex of ethyl cysteinate, although nitrogen ligation is hindered by *N,N*-dialkylation. These solution properties contrast with the polymeric solid structures that are likely for $[SnR_2Cl(SCH_2CH_2NH_2)]$ complexes with R = Me or Et, though not for R = Bu^n or Oct^n. Dialkyltin bis-cysteamine complexes $[SnR_2(SCH_2CH_2NR'_2)_2]$ (R = Me, Et, Bu^n or Oct^n; R′ = H or Et) show an intermolecular association as neat liquids and in non-coordinating solvents, increasingly with concentration, but again, nitrogen ligation is hindered by tertiary amino groups. The ^{15}N results usefully complement those from ^{119}Sn and ^{13}C NMR spectroscopy.

The chemistry of organotin(IV) compounds with strongly ligating sulphur and possibly ligating nitrogen is of interest in view of the biocidal activity of triorgano-$[R_3SnX]$ and diorgano-$[R_2SnX_2]$ tin compounds.[1,2] Particularly effective R groups in $[R_3SnX]$ are Me, Et, Pr^n, Bu^n and Ph. Remarkably, each is effective against different living species, the toxicity decreasing with increase in alkyl-chain length beyond C_4. Detailed mechanisms are obscure, but $[R_3SnX]$ compounds (which inhibit mitochondrial oxidative phosphorylation) and $[R_2SnX_2]$ compounds (which inhibit α-ketoacid oxidation) are known to combine with thiol and dithiol groups, respectively, in proteins and enzymes. There is interest also in organotin compounds with nitrogen ligands for cancer chemotherapy.[1,2] Some organotin(IV) complexes with sulphur-containing aminoacid or other biological ligands have been studied,[3–7] and corresponding inorganic complexes.[8] Less information is available, however, on aminothiol complexes, although certain cysteamine (2-aminoethanethiol) derivatives are reported, $[SnMe_2Cl(SCH_2CH_2NH_2)]$[4,5] and $[SnR_3(SCH_2CH_2NH_2)]$, with R = Me[5] or Bu^n.[6]

To explore effects of changes in the coordination sphere and in the organo groups, we undertook the preparation and characterization of three series of organotin(IV) cysteamine compounds, $[SnR_2Cl(SCH_2CH_2NR'_2)]$, $[SnR_3(SCH_2CH_2NR'_2)]$ and $[SnR_2(SCH_2CH_2NR'_2)_2]$, with R = Me, Et, Bu^n, Oct^n or Ph, and R′ = H, Me or Et (cf. Table 1), and related compounds of known structure for comparison, the cysteinato complex (**1**),[9,10] and $[SnR_2(SAT)]$ (**3**).[3] Depending on the balance of steric and electronic effects the aminothiol may be mono- or bidentate, chelating or bridging, and the tin may increase its coordination number with electronegative substituents, but not if the ligands are too bulky. Information on solid-state structures is available from X-ray crystallography, vibrational spectroscopy, and Mössbauer quadrupole splittings.[2,11] In solution, however, the structures may differ, they may depend

* Present address: Chemistry Department, Malaviya Engineering College, Jaipur 302004, Rajasthan, India.

† Author to whom correspondence should be addressed.

Table 1. Analysis of new organotin(IV) complexes

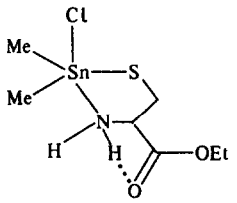
	Compound	Analysis % found (calc.) C	H	N	M.p. (°C)	B.p. (°C) [pressure (mb)]
1	$[SnMe_2Cl(SCH_2CH_2NMe_2)]$	24.9 (25.0)	5.7 (5.6)	4.8 (4.8)	112	
2	$[SnMe_2Cl(SCH_2CH_2NEt_2)]$	29.7 (30.4)	6.3 (6.4)	4.3 (4.4)	153	
3	$[SnEt_2Cl(SCH_2CH_2NH_2)]$	25.1 (25.0)	5.9 (5.6)	4.8 (4.8)	186	
4	$[SnBu^n_2Cl(SCH_2CH_2NH_2)]$	34.7 (34.9)	7.2 (7.0)	4.0 (4.1)	47	190–194 (0.02)
5	$[SnBu^n_2Cl(SCH_2CH_2NEt_2)]$	41.0 (42.0)	8.3 (8.0)	3.7 (3.5)	63	
6	$[SnOct^n_2Cl(SCH_2CH_2NH_2)]$	46.0 (47.3)	8.9 (8.8)	3.1 (3.1)	59	
7	$[SnMe_2(SCH_2CH_2NH_2)_2]$	24.0 (23.9)	6.1 (6.0)	9.2 (9.3)		
8	$[SnEt_2(SCH_2CH_2NH_2)_2]$	30.1 (29.2)	6.9 (6.7)	8.3 (8.5)		165–170 (0.04)
9	$[SnBu^n_2(SCH_2CH_2NH_2)_2]$	37.4 (37.4)	7.8 (7.8)	7.1 (7.3)		166–170 (0.03)
10	$[SnBu^n_2(SCH_2CH_2NEt_2)_2]$	48.3 (48.3)	9.3 (9.3)	5.6 (5.6)		162–164 (0.03)
11	$[SnOct^n_2(SCH_2CH_2NH_2)_2]$	49.5 (48.3)	9.6 (9.3)	5.9 (5.6)		
12	$[SnMe_3(SCH_2CH_2NH_2)]$[a]	25.1 (25.0)	6.1 (6.3)	5.4 (5.8)		56–58 (0.08)
13	$[SnBu^n_3(SCH_2CH_2NH_2)]$	46.1 (46.0)	9.0 (9.1)	3.9 (3.8)		128–130 (0.05)
14	$[SnBu^n_3(SCH_2CH_2NEt_2)]$	51.6 (51.1)	10.3 (9.8)	3.8 (3.3)		138–140 (0.02)
15	$[SnPh_3(SCH_2CH_2NH_2)]$	55.9 (56.4)	5.0 (5.0)	3.4 (3.3)	113	
16	$[SnPh_3(SCH_2CH_2NMe_2)]$	58.2 (58.2)	5.5 (5.5)	3.1 (3.1)	42	

[a] Reported without analytical data.[5]

on the solvent, and there may be fluxionality. We have used the ^{119}Sn shift and one-bond coupling to carbon as evidence for the tin coordination number,[12] and the nitrogen coordination shift for the nitrogen ligation.[13] The tin shielding increases markedly with increase in coordination number,[14–17] from $\delta = 50$–100 ppm for trialkyltin thiolates with four-coordinate tin[18] to -204 ppm for $[SnMe_2Cl(S_2CNEt_2)]$ with five-coordinate tin and to -336 ppm for $[SnMe_2(S_2CNEt_2)_2]$ with six-coordinate tin.[16] There is a similar marked increase in $^1J(^{119}Sn$–$^{13}C)$: in trialkyltin compounds, from 330–390 Hz for four-coordinate to 450–480 Hz for five-coordinate tin, and in dialkyltin compounds, from 370–480 Hz for four-coordinate to 900–970 Hz for six-coordinate tin.[19] The absolute $J(^{119}Sn$–$^{13}C)$ values in alkyltin groups usually decrease as $^1J > {}^3J > {}^2J > {}^4J$.[12] Little nitrogen NMR work has been reported for nitrogen attached to tin: some ^{15}N shifts and $^1J(^{119}Sn$–$^{15}N)$ values for stannatranes[20] and $SnMe_3$ derivatives of aniline,[21] and ^{14}N shifts in trimethylstannylamines.[22]

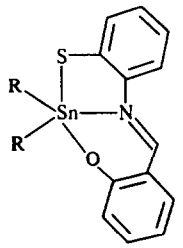
RESULTS AND DISCUSSION

The organotin cysteamine complexes are thermally stable but slowly oxidize in air to give organic sulphides, signalled by extra ^{13}C peaks.



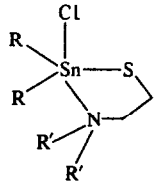
1

Ethyl L-cysteinato *S,N*-(chlorodimethyl)stannate(IV)



2

$[SnR_2SAT]^*$



3

$[SnR_2Cl(SCH_2CH_2NR'_2)]$

*SAT is the anion of the Schiff base form of 2-(2-hydroxyphenyl)benzothiazoline

Triorganotin(IV) cysteamine complexes

As shown in Table 2, the ^{119}Sn shifts do not vary greatly with concentration, and fall in the range 70–90 ppm as for trialkyltin thiolates,[17,18] in which tin is four-coordinate. Similarly the $^1J(^{119}Sn–^{13}C)$ values resemble those for four-coordinate compounds such as $[SnMe_3Cl]$ (386 Hz) and $[SnBu_3Br]$ (330 Hz), decreasing slightly with increase in alkyl-chain length.[19] Four-coordination of tin is supported also by the small differences ($\Delta\delta$) in ^{15}N shift from the free to the coordinated ligand, measured in saturated solutions (cf. Table 5). These differences, however, are all in the direction of deshielding, consistent with very weak coordination to tin (although hydrogen bonding was suggested[23] for the aminostannanes $[SnMe_{4-n}(NR_2)_n]$, with R = Me or Et). The neat liquids are not particularly viscous, but show increases in tin shielding and in $^1J(^{119}Sn–^{13}C)$ which suggest some associative process. The increase in shielding is largest (32 ppm) for the least hindered compound, $[SnMe_3(SCH_2CH_2NH_2)]$; it is 15 ppm for $[SnMe_3(SCH_2CH_2NMe_2)]$, in which the nitrogen is less basic and more hindered, the butyltin compounds showing smaller increases. For comparison, the addition of excess pyridine to $[SnMe_3Cl]$ (these forming a trigonal bipyramidal adduct in the solid state) increases the tin shielding[24] by 170 ppm and $^1J(^{119}Sn–^{13}C)$ by 100 Hz.[19] Thus weak and exchanging coordination of nitrogen to tin is likely for these cysteamine complexes as neat liquids.

The phenyltin compounds, also, are seen to be four-coordinate in Table 2. Tin shifts and coupling constants are normally higher with phenyl compared to alkyl substituents:[15,25] e.g. $\delta(Sn)$ −40 to −120 ppm and $^1J(^{119}Sn–^{13}C)$ 550–660 Hz for four-coordinate tin, cf. −180 to −250 ppm and 750–850 Hz for five-coordinate tin (or 600–650 Hz, depending on the coordination geometry).[15] The ^{119}Sn parameters resemble those for thiolates, e.g. −62 ppm for $[SnPh_3SPr^i]$[25] and 566 Hz for $[SnPh_3SPr^n]$.[15] The increaase in tin shielding in thf solvent probably reflects some thf coordination, and the nitrogen deshielding (by 4 ppm) is likely to arise from hydrogen bonding to thf.

Diorganochlorotin(IV) cysteamine complexes

The presence of the electronegative chloro substituent is expected to favour five-coordinate tin for the compounds in Table 3. A chelate structure in the solid state has been demonstrated for **1**,[3] as for **2**.[9,10] An amino-bridged polymeric structure, however, is likely for $[SnMe_2Cl(SCH_2CH_2NH_2)]$ on the Mössbauer and IR evidence.[5] We could not dissolve this or the analogous diethyltin compound in non-coordinating solvents, including chloroform or benzene. They are sparingly soluble in methanol, but fairly soluble in dmf and dmso. With longer alkyl chains, however (R = Bu^n or Oct^n) the compounds are soluble in chloroform and benzene, and our experiments showed them to be monomeric in freezing benzene.

The tin shifts and coupling constants of all the $(SCH_2CH_2NH_2)$ compounds in Table 3 are consistent with five-coordination and chelation. A tin shift of −92 ppm is observed[14] for the chelate complex of 8-quinolinol, $[SnMe_2Cl(8\text{-quin})]$, in which tin forms part of a five-membered ring. Four-coordinate tin is deshielded by *ca* 60 ppm in a five-membered stanna-alkane or stanna-thioalkane ring as in $[SnMe_2(CH_2)_4]$ or $[SnMe_2(SCH_2CH_2S)]$, relative to open-chain analogues such as $[SnMe_2(SEt)_2]$;[26] but effects of angular distortion should be smaller in trigonal bipyramidal geometry, since the relevant (equatorial–axial) angle is already reduced from the tetrahedral angle. There is some additivity of substituent effects (for four-coordinate tin), e.g. the tin shifts for Me_2Sn bound to nitrogen

Table 2. NMR measurements of $[SnR_3(SCH_2CH_2NR'_2)]$ compounds

Compound	Concentration (mol l^{-1})	Solvent	$\delta(^{119}Sn)^a$ (ppm)	$W_{1/2}{}^b$ (Hz)	$^1J(^{119}Sn-^{13}C)^c$ (Hz)	$\Delta\delta(^{15}N)^d$ (ppm)
$[SnPh_3(SCH_2CH_2NH_2)]$	0.33	thf	−111.8	60		4.4
	0.33	$CDCl_3$	−86.3	15		
	1.0	$CDCl_3$	−71.2	10	566	3.8
	0.33	$CDCl_3$	−68.1	4		
$[SnPh_3(SCH_2CH_2NMe_2)]$	0.87	$CDCl_3$	−61.7	7	562	*ca* 0.5
	0.1	$CDCl_3$	−60.5	7		
$[SnMe_3(SCH_2CH_2NH_2)]$	Neat liquid		59.7	17	375	
	0.24	$CDCl_3$	91.4	8		1.3
	4.3	CD_3CN			374	
$[SnMe_3(SCH_2CH_2NMe_2)]$	Neat liquid		74.3	22		
	0.22	$CDCl_3$	89.6	13		
	3.7	$CDCl_3$			357	*ca* 1.2
$[SnBu^n_3(SCH_2CH_2NH_2)]$	Neat liquid		74.9	45		
	0.1	$CDCl_3$	78.2	18	331	1.1
$[SnBu^n_3(SCH_2CH_2NEt_2)]$	Neat liquid		75.9	20		
	0.25	$CDCl_3$	81.3	6	332	2.7

[a] Relative to external $SnMe_4$, high-frequency positive.
[b] Line-width at half height.
[c] Observed in ^{13}C spectrum.
[d] Shift (high-frequency positive) relative to the appropriate free ligand $HSCH_2CH_2NR_2$ (R = H, Me or Et), measured in the solvent recorded, usually in saturated solution. Only one ^{15}N resonance was observed in each case (cf. Table 5).

and sulphur in six-membered ring compounds $[Me_2SnZ]_3$, where Z is NEt or S, are intermediate between those in $[Me_2SnS]_3$ (128 ppm) and $[Me_2SnNEt]_3$ (76 ppm).[16]

The nitrogen coordination shifts of 10–13 ppm are as expected for bonding to tin: nitrogen in amines is commonly deshielded by a few ppm on replacement of Me by $SnMe_3$,[20–22] a similarly small deshielding being observed on quaternization by H or R[27] (cf. also Table 5). The $^1J(^{15}NH)$ coupling constant of 54 Hz observed for the dibutyltin compound clearly shows coordination to tin: it is larger than any two- or three-bond ^{15}NH coupling constant, but smaller than those observed for free amines (*ca* 65 Hz) or alkylammonium (*ca* 75 Hz). The reduced ^1J value is consistent with reduction in *s*-character of the NH bonding orbitals and in the effective nuclear charge of the nitrogen when bonded to an electropositive atom; cf. $^1J(^{15}NH) = 66$ Hz in $[(Me_3Si)_2NH]$,[28] also the increase in $^1J(SnC)$ with a chloro substituent on tin.[19] The failure to resolve fine structure for the homologous compounds is most likely due to exchange. This is found to be twice as fast for NH_2 as for NH groups in phenylhydrazines, for which a dimeric transition state with a four-membered N_2H_2 ring was proposed.[29] Interactions with a polar solvent, also, may wash out fine structure.

For the $[SnR_2Cl(SCH_2CH_2NH_2)]$ complexes, therefore, the NMR parameters show nitrogen coordinating to tin, and their insensitivity to concentration in non-coordinating solvents, and the evidence for monomolecularity, suggest a chelate structure (**3**), as found for **1** in the solid.[3] This has a distorted trigonal bipyramidal configuration with the more electronegative ligating atoms in the apical positions, as generally found for $[SnR_3X_2]$ compounds, following Bent's rule.[1] The $[SnR_2Cl(SCH_2CH_2NH_2)]$ compounds with R = Me or Et are then polymeric in the solid and monomeric in solution, the tin shifts and coupling constants indicating further coordination to tin in dmf solution.

The complexes in which the amino group is dialkylated clearly differ. With *N,N*-diethylation of

Table 3. NMR measurements of $[SnR_2Cl(SCH_2CH_2NR'_2)]$ and related compounds

Compound	Concentration (mol l^{-1})	Solvent	$\delta(^{119}Sn)^a$ (ppm)	$W_{1/2}{}^b$ (Hz)	$^1J(^{119}Sn-^{13}C)^c$ (Hz)	$\Delta\delta(^{15}N)^d$ (ppm)
$[SnMe_2(SC_6H_4N{=}CHC_6H_4O)]$ (2)	0.50	$CDCl_3$	−105.7	20	591	
$[SnBu^n_2Cl(SCH_2CH_2NH_2)]$	0.39	dmf	−91.7	45		
	1.13	$CDCl_3$	−78.9	56	555	12.6[e]
	0.39	$CDCl_3$	−77.4	60		
$[SnMe_2Cl(SCH_2CH_2NH_2)]$	0.52	dmf	−86.4	50	603	
	0.50	dmso	−87.8	35	601	12.6
	0.09	CD_3OD	−44.3	70		
$[SnEt_2Cl(SCH_2CH_2NH_2)]$	0.50	dmso	−84.2	30	590	10.2
	0.49	dmf	−79.4	38		
$[SnOct^n_2Cl(SCH_2CH_2NH_2)]$	0.73	$CDCl_3$	−75.6	42	544	12.8
	0.20	$CDCl_3$	−72.4	32		
$[SnMe_2Cl(SCH_2CHNH_2COOEt)]$ (1)	0.50	dmf	−78.9	25		
	0.34	$CDCl_3$	−51.4	15	581[f]	
$[SnMe_2Cl(SCH_2CH_2NMe_2)]$	0.48	dmf	−43.8	55		
	0.41	CD_2Cl_2	−37.7	55	550	*ca* 5.0
	0.10	CD_2Cl_2	−37.5	50		
$[SnMe_2Cl(SCH_2CH_2NEt_2)]$	1.0	CD_2Cl_2	−35.1	39	555	−0.7
	0.2	CD_2Cl_2	−34.9			
$[SnBu^n_2Cl(SCH_2CH_2NEt_2)]$	1.0	$CDCl_3$	−34.5	110	404	−0.2
	0.2	$CDCl_3$	−33.8			

[a–d] As for Table 2.
[e] Triplet, $^1J(^{15}NH) = 54$ Hz.
[f] Reference 4.

$[SnBu^n_2Cl(SCH_2CH_2NH_2)]$, tin is deshielded by 44 ppm, the nitrogen coordination shift vanishes, and $^1J(^{119}Sn-^{13}C)$ is reduced from 555 to 404 Hz, as appropriate for four-coordinate tin. The carbon bonded to tin also reflects a change in the coordination sphere (Table 6): the shielding increases by 2.7 ppm, whereas dialkylation of nitrogen has little effect on the α-carbon shielding in four-coordinate $[SnR_3(SCH_2CH_2NH_2)]$ compounds. Comparable results are obtained with *N,N*-diethylation of $[SnMe_2Cl(SCH_2CH_2NH_2)]$, but interestingly, the NMe_2 compound shows evidence of some *N*-ligation. The presence of the alkyl groups would be expected to reduce the basicity of the amino group, and sterically hinder the coordination, as before. Again, the shifts are insensitive to dilution in non-coordinating solvents, so intermolecular interactions are unimportant. The broadening of the tin resonance in the dibutyltin complex suggests some fluxional process.

Diorganotin(IV) bis-cysteamine complexes

The *bis*-cysteamine complexes differ from both categories of *mono*-cysteamine complexes. Only one tin resonance is observed, but the shielding decreases with dilution, by up to 70 ppm from the neat liquid to 0.05 M solution (Table 4). The neat liquids are very viscous. In freezing benzene, 0.06 M $[SnBu^n_2(SCH_2CH_2NH_2)_2]$ shows evidence of intermolecular association, which increases with concentration, whereas the corresponding *N,N*-diethyl compound is monomeric at 0.08 M. Similarly, at higher concentrations of the ($SCH_2CH_2NH_2$) compounds the tin shifts and tin–carbon coupling constants are appropriate for five-

Table 4. NMR measurements of $[SnR_2(SCH_2CH_2NR'_2)_2]$ compounds

Compound	Concentration (mol l^{-1} in $CDCl_3$)[a]	$\delta(^{119}Sn)$[b] (ppm)	$W_{1/2}$[c] (Hz)	$^1J(^{119}Sn-^{13}C)$[d] (Hz)	$\Delta\delta(^{15}N)$[e] (ppm)
$[SnMe_2(SCH_2CH_2NH_2)_2]$	3.30	−68.3	54	560	7.1
	1.30	−55.5	20		
	0.10	−25.6	20		
$[SnBu^n_2(SCH_2CH_2NH_2)_2]$	Neat liquid	−68.4	45		
	1.9	−58.7	40	531	5.6
	0.34	−18.0	25		
	0.11	−7.5	28		
	0.05	−3.6	28		
$[SnOct^n_2(SCH_2CH_2NH_2)_2]$	Neat liquid	−66.9	25		
	1.0	−40.5	40	488	5.4
	0.1	−5.3	20		
$[SnEt_2(SCH_2CH_2NH_2)_2]$	Neat liquid	−62.0	32		
	2.31 (300 K)	−53.9		542	4.9
	2.31 (273 K)	−59.3			
	2.31 (230 K)	−69.0			
	0.82	−25.5	48		
	0.14	−4.9	32		
$[SnEt_2(SCH_2CH_2NH_2)_2]$ $+OP(NMe_2)_3$ (1 : 1)	0.82	−34.6	30		
	0.63[f]	−77.9	12		
	0.31[f]	−77.5	15		
$[SnBu^n_2(SCH_2CH_2NEt_2)_2]$	Neat liquid	122.8	18	381	1.7
	0.1	122.5	10		

[a] Unless otherwise specified.
[b–e] As [a–d] in Table 2.
[f] In $OP(NMe_2)_3$.

coordination, but with dialkylation of the amino group the ^{119}Sn shift shows the dibutyltin compound to be four-coordinate in the neat liquid and in 0.1 M solution in chloroform.

Again, the singularity of the ^{119}Sn, ^{13}C and ^{15}N spectral lines can be explained by sufficiently fast exchange, as can the variation in ^{119}Sn and ^{15}N shifts with concentration. There is some trend towards broader lines at higher concentrations. The ^{15}N shifts fall midway between the values for coordinated and uncoordinated nitrogen (cf. Tables 3 and 5). The presence of a dynamic equilibrium is supported also by the increase in tin shielding by 15 ppm when a concentrated solution of the diethyltin complex is cooled to 230 K.

As shown in Table 4, $[SnEt_2(SCH_2CH_2NH_2)_2]$ forms an adduct in solution in $(Me_2N)_3PO$ in which the tin shielding ($\delta - 78$ ppm) is comparable with that in the self-associated systems. The increase of 201 ppm in the shielding relative to the four-coordinate NEt_2 complex with $\delta = 123$ ppm, resembles the increase of 207 ppm when $[SnMe_3Cl]$ is dissolved in $(Me_2N)_3PO$.[12]

EXPERIMENTAL

Organotin chlorides, cysteamine hydrochloride, *N*-dimethyl- and *N*-diethylcysteamine hydrochlorides, L-cysteine ethyl ester hydrochloride and *S*-methylcysteamine were commercial samples. All solvents were dried by standard methods and moisture was excluded throughout the manipulations. Free ligands were obtained by the reaction of ligand hydrochlorides with sodium methoxide in dry methanol under nitrogen. After filtration of sodium chloride, the ligands were purified by subli-

Table 5. ^{15}N NMR measurements

Compound	Solvent[a]	δN^b (ppm)
$[SnBu^n_3(SCH_2CH_2NH_2)]$	$CDCl_3$	−360.4
$[SnMe_3(SCH_2CH_2NH_2)]$	$CDCl_3$ (0.5 M)	−360.2
$[snPh_3(SCH_2CH_2NH_2)]$	$CDCl_3$	−357.7
	thf-d^4	−355.4
$[SnPh_3(SCH_2CH_2NMe_2)]$	$CDCl_3$	−354.6
$[SnMe_3(SCH_2CH_2NMe_2)]$	$CDCl_3$	−353.8
$[SnBu^n_3(SCH_2CH_2NEt_2)]$	$CDCl_3$	−332.6
$[SnEt_2Cl(SCH_2CH_2NH_2)]$	dmso-d^6	−351.3
$[SnMe_2Cl(SCH_2CH_2NMe_2)]$	$CDCl_3$	−349.9
$[SnBu^n_2Cl(SCH_2CH_2NH_2)]$	$CDCl_3$	−348.9[c]
$[SnMe_2Cl(SCH_2CH_2NH_2)]$	dmso-d^6	−348.9[d]
$[SnOct^n_2Cl(SCH_2CH_2NH_2)]$	$CDCl_3$	−348.7
$[SnMe_2Cl(SCH_2CH_2NEt_2)]$	$CDCl_3$	−336.0
$[SnBu^n_2Cl(SCH_2CH_2NEt_2)]$	$CDCl_3$	−334.5
$[SnEt_2(SCH_2CH_2NH_2)_2]$	$CDCl_3$	−356.6
$[SnOct^n_2(SCH_2CH_2NH_2)_2]$	$CDCl_3$	−356.1
$[SnBu^n_2(SCH_2CH_2NH_2)_2]$	$CDCl_3$	−355.9
$[SnMe_2(SCH_2CH_2NH_2)_2]$	$CDCl_3$	−353.5
$[SnBu^n_2(SCH_2CH_2NEt_2)_2]$	$CDCl_3$	−332.6
$HSCH_2CH_2NH_2$	$CDCl_3$	−361.5
	CD_3OD	−359.8
$MeSCH_2CH_2NH_2$	$CDCl_3$	−360.6
$HSCH_2CH_2NMe_2$	$CDCl_3$	−355.9
$HSCH_2CH_2NEt_2$	$CDCl_3$	−335.3
	CD_3OD	−331.6
$MeSCH_2CH_2NEt_2$	$CDCl_3$	−334.3
$HSCH_2CH_2NH_3Cl$	CD_3OD	−349.1
$HSCH_2CH_2NEt_2HCl$	CD_3OD	−325.4

[a] Saturated solutions unless otherwise specified.

[b] Relative to neat liquid CH_3NO_2, high-frequency positive; corrected for susceptibility differences due to addition of $[Cr(pd)_3]$ to promote relaxation.

[c] $^1J(^{15}NH) = 54$ Hz.

[d] Weak signal.

mation or distillation under a nitrogen atmosphere. $[MeSCH_2CH_2NEt_2]$,[30]

$[S\overline{nMe_2(SC_6H_4N{=}CHC_6H_4O}]$

and

$[S\overline{nMe_2Cl(SCH_2CHNH_2COOEt)}]$

were prepared by reported methods. Microanalyses were done at the Open University and at Butterworth laboratories.

Synthesis of complexes

Complexes **1**–**3** in Table 1, **15** and **16** were prepared by the reaction in methanol of organotin(IV) chlorides with equimolar amounts of the sodium salt of the ligand prepared *in situ*. After the filtration of the sodium chloride the complexes crystallized out on standing overnight, in 60–80% yield. $[SnMe_2Cl(SCH_2CH_2NH_2)]$[4,5] also was prepared by this method. Complexes **4**–**6** were prepared similarly with Pr^iOH as solvent. After the filtration of sodium

Table 6. ^{13}C NMR shifts, with $J(^{119}Sn-^{13}C)$ values in parentheses

Compound	Concentration (mol l^{-1})	Solvent	SnR or SnPh C-1	C-2	C-3	C-4	—SCH_2—	—CH_2N	NR_2
$[SnMe_3(SCH_2CH_2NH_2)]$	4.30	CD_3CN	−4.0 (374)				31.0	45.8	
$[SnMe_3(SCH_2CH_2NMe_2)]$	3.70	$CDCl_3$	−4.8 (357)				24.4	63.4	45.3 (38)
$[SnBu^n_3(SCH_2CH_2NH_2)]$	0.50	$CDCl_3$	13.7 (331)	28.7 (22)	27.1 (60)	13.7	31.0	45.7	
$[SnBu^n_3(SCH_2CH_2NEt_2)]$	1.0	$CDCl_3$	13.4 (332)	28.8 (22)	27.2 (59)	13.7	24.5 (14)	58.1 (16)	47.4, 12.4
$[SnPh_3(SCH_2CH_2NH_2)]$	1.0	$CDCl_3$	139.3 (566)	136.4 (42)	128.7 (55)	129.4 (13)	30.8 (16)	44.8 (16)	
$[SnPh_3(SCH_2CH_2NMe_2)]$	0.87	$CDCl_3$	138.2 (562)	136.5 (42)	128.7 (57)	129.5 (13)	24.7 (16)	62.7 (17)	45.0 (38)
$[SnMe_2Cl(SCH_2CH_2NH_2)]$	0.52	dmf+$CDCl_3$	4.0 (603)				26.0 (17)	41.6 (22)	
		dmso-d^6	6.3 (601)				27.5 (16)	42.8 (21)	
$[SnMe_2Cl(SCH_2CH_2NMe_2)]$	0.41	CD_2Cl_2	5.4 (550)				25.1	61.2	44.8
$[SnMe_2Cl(SCH_2CH_2NEt_2)]$	1.0	CD_2Cl_2	6.5 (555)				24.3	54.3	43.0, 8.2
$[SnEt_2Cl(SCH_2CH_2NH_2)]$	1.0	dmso-d^6	16.5 (590)	10.0 (39)			27.5 (14)	43.3 (18)	
$[SnBu^n_2Cl(SCH_2CH_2NH_2)]$	0.65	$CDCl_3$	26.6 (555)	28.2 (36)	25.9 (68)	13.7	28.7	44.3	
$[SnBu^n_2Cl(SCH_2CH_2NEt_2)]$	1.0	$CDCl_3$	23.9 (40.4)	28.1 (34)	26.7	13.7	24.2	55.0	43.5, 8.7
$[SnOct^n_2Cl(SCH_2CH_2NH_2)]$	0.68	$CDCl_3$	26.1 (544)				28.6	44.3	
$[SnMe_2(SCH_2CH_2NH_2)_2]$	3.30	$CDCl_3$	4.0 (560)				29.6	43.9	
$[SnEt_2(SCH_2CH_2NH_2)_2]$	2.50	$CDCl_3$	15.2 (542)	10.8 (45)			30.0	44.6	
$[SnBu^n_2(SCH_2CH_2NH_2)_2]$	1.90	$CDCl_3$	23.2 (531)	28.6 (30)	26.7 (90)	13.7	30.0	44.5	
$[SnBu^n_2(SCH_2CH_2NEt_2)_2]$	2.10	$CDCl_3$	18.1 (381)	28.3 (25)	26.7	13.6	24.9	57.2	47.1, 12.2
$[SnOct^n_2(SCH_2CH_2NH_2)_2]$	1.0	$CDCl_3$	22.7 (488)				30.1	44.6	
$HSCH_2CH_2NH_2$	1.70	$CDCl_3$					28.8	45.0	
$HSCH_2CH_2NMe_2$	1.20	$CDCl_3$					22.6	62.3	45.1
$HSCH_2CH_2NEt_2$	1.50	$CDCl_3$					22.7	56.1	46.9, 11.9
$MeSCH_2CH_2NEt_2$	1.50	$CDCl_3$					31.8	52.4	47.0, 11.8
							—SMe 15.7		

chloride the complexes were isolated by evaporation of the filtrate under reduced pressure. Complexes **7–14** are somewhat air-sensitive, and were synthesized by the reaction of organotin(IV) chlorides with the sodium salt of the ligand in stoichiometric ratio under a nitrogen atmosphere in a mixture of methanol and benzene as solvent. After filtration of sodium chloride the excess solvent was removed under reduced pressure. Complexes **8–10** were further purified by distillation under reduced pressure. Complexes **7** and **11** decompose on distillation and so were used undistilled for spectral measurements. Complex $[SnMe_3(SCH_2CH_2NMe_2)]$[31] also was prepared by this method and purified by distillation under reduced pressure.

Molar masses were determined (as appropriate) by depression of the melting temperature of benzene.

NMR spectroscopy

Non-coordinating solvents were used unless a coordinating solvent was necessary for solubility. ^{119}Sn and ^{13}C spectra were measured on a JEOL FX90Q spectrometer at 27°C in 10-mm sample tubes. The ^{119}Sn–^{13}C coupling constants were obtained from satellites in the carbon spectra in about 250 pulses for neat liquids, or up to 6000 pulses for concentrated solutions. ^{117}Sn–^{13}C couplings were observed at the same time in the expected ratios. ^{15}N spectra were measured in natural abundance on 15-cm^3 samples on a Bruker WH180 spectrometer, in 25-mm sample tubes.

CONCLUSION

The sensitive balance of electronic and steric factors involved in the coordination of 1,2-aminothiol ligands to organotin(IV) is demonstrated by the differences between the three series of complexes reported here, between the primary and tertiary amino groups, and, interestingly, between complexes of the same type but with different alkyl-chain lengths. Although the nitrogen coordination shifts are not very large they are characteristic of the coordination mode; there is a periodic dependence of nitrogen shielding on the nature of the ligating atom, such that larger shifts are observed with other metals.[13] Nitrogen NMR spectroscopy is therefore a useful indicator of ligation, particularly with metals less amenable than tin to NMR spectroscopy, and if coupling to nitrogen can be observed.

Acknowledgements—We thank Dr P. J. Smith of the International Tin Research Institute for gifts of organotin chlorides, Dr Fred Armitage for a recipe for $[SnMe_3Cl]$, the S.E.R.C. for the provision of widebore 180-MHz facilities for natural-abundance ^{15}N NMR, Mr Maurice Cooper for running the ^{15}N spectra, and Mr Gordon Howell for ^{119}Sn and ^{13}C spectra run at the Open University.

REFERENCES

1. J. J. Zuckerman (Ed.), *Organotin Compounds: New Chemistry and Applications*, *Adv. Chem. Ser.* 1976, **157**, 227.
2. A. G. Davies and P. J. Smith, In *Comprehensive Organometallic Chemistry* (Edited by G. Wilkinson), Vol. 11, p. 608. Pergamon Press, Oxford (1982).
3. G. Domazetis, M. F. Mackay, R. J. Magee and B. D. James, *Inorg. Chim. Acta* 1979, **34**, L247; G. Domazetis and M. F. Mackay, *J. Cryst. Mol. Struct.* 1979, **9**, 57.
4. G. Domazetis, R. J. Magee and B. D. James, *J. Organomet. Chem.* 1978, **162**, 239.
5. G. Domazetis, R. J. Magee, B. D. James and J. D. Cashion, *J. Inorg. Nucl. Chem.* 1981, **43**, 1351; J. D. Cashion, G. Domazetis and B. D. James, *J. Organomet. Chem.* 1980, **185**, 433.
6. G. Domazetis, R. J. Magee and B. D. James, *J. Organomet. Chem.* 1978, **148**, 339.
7. G. Domazetis, R. J. Magee and B. D. James, *J. Organomet. Chem.* 1979, **173**, 357.
8. P. A. Cusack, P. J. Smith and J. D. Donaldson, *J. Chem. Soc., Dalton Trans.* 1982, 439; S. Calogero, G. Valle, P. A. Cusack, P. J. Smith and J. D. Donaldson, *Inorg. Chim. Acta* 1982, **67**, 95.
9. R. Cefalu, R. Bosco, F. Bonati, F. Maggio and R. Barbieri, *Z. Anorg. Allg. Chem.* 1970, **376**, 180.
10. H. Preut, H.-J. Haupt, F. Huber, R. Cefalu and R. Barbieri, *Z. Anorg. Allg. Chem.* 1974, **407**, 257.
11. J. A. Zubieta and J. J. Zuckerman, *Prog. Inorg. Chem.* 1978, **24**, 251; B. Y. K. Ho and J. J. Zuckerman, *J. Organomet. Chem.* 1973, **49**, 1.
12. J. D. Kennedy and W. McFarlane, In *NMR and the Periodic Table* (Edited by R. K. Harris and B. E. Mann), p. 342 (and references therein). Academic Press, London (1978).
13. J. Mason, *Chem. Rev.* 1981, **81**, 205; *Chem. Br.* 1983, 654.
14. J. Otera, *J. Organomet. Chem.* 1981, **221**, 57.
15. J. Holeček, M. Nádvorník, K. Handlíř and A. Lyčka, *J. Organomet. Chem.* 1983, **241**, 177.
16. A. G. Davies, P. G. Harrison, J. D. Kennedy, T. N. Mitchell, R. J. Puddephatt and W. McFarlane, *J. Chem. Soc. (C)* 1969, 1136.
17. J. D. Kennedy and W. McFarlane, *J. Chem. Soc., Perkin Trans.* 2 1974, 146.
18. E. V. van den Berghe and G. P. van der Kelen, *J. Organomet. Chem.* 1971, **26**, 207.
19. T. N. Mitchell, *J. Organomet. Chem.* 1973, **59**, 189.
20. K. Jurkschat, C. Mugge, A. Tzschach, A. Zschunke, G. Englehardt, E. Lippmaa, M. Mägi, M. F. Larin, V. A. Pestunovich and M. G. Voronkov, *J. Organomet. Chem.* 1979, **171**, 301.

21. J. D. Kennedy, W. McFarlane, G. S. Pyne and B. Wrackmeyer, *J. Organomet. Chem.* 1980, **195**, 285.
22. K. Barlos, G. Hubler, H. Nöth, P. Wanninger, N. Wiberg and B. Wrackmeyer, *J. Magn. Reson.* 1978, **31**, 363.
23. P. J. Smith and L. Smith, *Inorg. Chim. Acta, Rev.* 1973, **7**, 11.
24. E. V. van den Berghe and G. P. van der Kelen, *J. Organomet. Chem.* 1973, **61**, 197.
25. J. D. Kennedy, W. McFarlane, G. S. Pyne, P. L. Clarke and J. L. Wardell, *J. Chem. Soc., Perkin Trans.* 2 1975, 1234.
26. J. D. Kennedy, W. McFarlane and G. S. Pyne, *Bull. Soc. Chim. Belg.* 1975, **84**, 289.
27. R. O. Duthaler and J. D. Roberts, *J. Am. Chem. Soc.* 1978, **100**, 3889.
28. A. H. Cowley and J. R. Schweiger, *J. Am. Chem. Soc.* 1973, **95**, 4179.
29. I. Yavari and J. D. Roberts, *J. Am. Chem. Soc.* 1978, **100**, 4662.
30. F. Yu. Rachinskii and N. M. Slavachevskaya, *Tiolovye Soedinen V. Med. Ukrain. Nauch.-Issledovatel. Sanit.-Khim. Inst., Trudy Nauch. Konf. Kiev.* 1957, 23; *Chem. Abstr.* 1960, **54**, 24368g.
31. G. Chandra, A. D. Jenkins, M. F. Lappert and R. C. Srivastava, *J. Chem. Soc.* (*A*) 1970, 2550.

Polyhedron Vol. 5, No. 9, pp. 1459–1465, 1986
Printed in Great Britain

0277–5387/86 $3.00+.00
Pergamon Journals Ltd

CATIONIC COMPLEXES OF TRIMETHYLPLATINUM(IV) WITH TRIDENTATE LIGANDS—I. PREPARATION AND CHARACTERIZATION OF COMPLEXES FROM A RANGE OF THIO, SELENO, THIO-SELENO, AMINO-THIO AND AMINO-SELENO LIGANDS

EDWARD W. ABEL, KENNETH KITE* and PHILLIP S. PERKINS

Department of Chemistry, University of Exeter, Exeter EX4 4QD, U.K.

(*Received* 6 *December* 1985; *accepted* 20 *December* 1985)

Abstract—The new ionic complexes $[PtMe_3\{MeE(CH_2)_nE'(CH_2)_nEMe\}]^+X^-$ [$n = 3$; E = E′ = S: $n = 2$; E = Se or S; E′ = O, S, Se or —SS—: X = I, BPh_4 or BF_4] and $[PtMe_3(H_2NCH_2CH_2)_2E']^+BF_4^-$ [E′ = O or —SS—] have been prepared and characterized by molar-conductivity measurements and ^1H NMR spectroscopy. The hitherto unreported ligands $[(MeE(CH_2)_n)_2E']$ ($n = 3$; E = E′ = S: $n = 2$; E = Se; E′ = O or S or Se: $n = 2$; E = S; E′ = Se] have been characterized by ^1H NMR and ^{77}Se NMR (where appropriate), and by mass spectroscopy.

Extensive studies in this department on the fluxional properties of complexes of trimethylplatinum(IV) with bidentate chalcogen donors[1] have been exclusively concerned with neutral systems in which a halide counter ion has been coordinated to the metal. The extension to tridentate chalcogen donor ligands is appealing for a number of reasons. The comparatively few reported complexes of *fac*-$PtMe_3$(IV) in which one ligand occupies all three *trans* sites are limited to nitrogen and oxygen donors, i.e. with pyrazolylborates[2] $\{[(C_3H_3N_2)_nBH_{4-n}]^-\}$ ($n = 3$ or 4), with tris(1-pyrazolyl)methane and tris(2-pyridyl)methane,[3] and with imidodiacetate, its *N*-methyl analogue, and nitrilotriacetate.[4] Complexes with two tridentate Schiff base ligands containing one SMe and two nitrogen donor groups have been shown to lead to interesting stereochemistry at the metal.[5] The steric requirement that the methyl groups have a *fac*-orientation,[6] and therefore a *fac*-disposition of *trans* ligands might be expected to impose constraints on the fluxionality which are not observed in the bidentate system. We have explored these possibilities using ligands of general formula $MeE(CH_2)_nE'(CH_2)_nEMe$, where E and E′ are chalcogen donor atoms, with three potential inverting centres, and for comparative purposes the ligands $(H_2NCH_2CH_2)_2E'$, where E′ = O or —SS—, having only one such centre. In this paper we report the preparation and characterization of the ligands and their $PtMe_3$(IV) complexes with appropriate counter ions.

EXPERIMENTAL

The following were made by literature methods: trimethylplatinum iodide[7] and sulphate,[8] dimethyldiselenide,[9] 2-chloro-1-methylthioethane,[10] β,β′-dichloroethylsulphide[11] and β-methylthioethylmercaptan.[12] 3-Chloro-1-methylthiopropane was prepared in 70% yield (b.p. 163–165°C) in an analogous manner to 2-chloro-1-methylthioethane but using 3-hydroxy-1-methylthiopropane in place of 2-hydroxy-1-methylthioethane. β,β′-Dichloroethyloxide [b.p. 66–70°C (15 mmHg)] and β,β′-dichloroethylselenide [b.p. 95–97°C (15 mmHg)] were made in 47 and 45% yield in a similar manner to β,β′-dichloroethylsulphide, using the oxygen and selenium analogues of β-thiodiglycol, respectively, and HCl in place of $SOCl_2$ in the selenide preparation. The characterization of these precursors is summarized in Table 1. The ligands 2,5,8-trithianonane {b.p. 113°C (0.5 mmHg) [lit.[13] 118°C (1.0 mmHg)]} and 2,5,6,9-tetrathiadecane {b.p. 117°C (0.02 mmHg)

* Author to whom correspondence should be addressed.

Table 1. Boiling points and ^{1}H NMR data for the precursors

Compound	B.p.[a] (°C)		^{1}H NMR data[b] δ (ppm)	J (Hz)
$(ClCH_2CH_2)_2O$	176–185	a, b	3.71	—
$(ClCH_2CH_2)_2S$	210	a	3.64	7.0
		b	2.89	7.0
$(ClCH_2CH_2)_2Se$	215	a	3.74	8.25
		b	2.94	8.06
$MeSCH_2CH_2SH$	168	a	2.12	—
		b	2.70	—
		c	2.73	—
		d	1.73	4.0
$MeSCH_2CH_2CH_2Cl$	163–165	a	2.14	—
		b	2.68	6.85
		c	2.06	6.15
		d	3.67	6.25

[a] At 1 atm.
[b] In $CDCl_3$ with TMS as reference.

[lit.[14] 160–162°C (<0.5 mmHg)]} were made by literature methods. 2,6,10-Trithiaundecane [b.p. 111°C (0.02 mmHg)] and 2,8-dithia-5-selenononane [b.p. 82°C (0.005 mmHg)] were prepared in 35 and 70% yield, respectively, in a similar manner to 2,5,8-trithianonane,[13] but using 3-chloro-1-methylthiopropane instead of 2-chloro-1-methylthioethane for the formed ligand, and sodium selenide in place of sodium sulphide for the latter.

2,8-*Diseleno-5-oxynonane.* To approximately 300 cm^3 of freshly distilled, anhydrous liquid ammonia was added dimethyldiselenide (4.56 g, 48.5 mmol) followed by sodium metal (2.27 g, 98.7 mmol), and the mixture stirred under reflux until a permanent blue tinge was observed. To this mixture was added β,β'-dichloroethyloxide (6.45 g, 45.1 mmol) over 20 min, and stirring was continued with slow ammonia evaporation until a slurry remained. Water and chloroform (100 cm^3 of each) were added, and the organic layer was removed and dried over magnesium sulphate. Removal of the solvent followed by vacuum distillation gave a malodorous pale yellow oil [b.p. 45–49°C (0.03 mmHg)] (4.7 g, 63%).

The following were prepared similarly with the modifications noted: 2,8-diseleno-5-thianonane [b.p. 112°C (0.175 mmHg), 93%] using β,β'-dichloroethylsulphide for β,β'-dichloroethyloxide; 2,5,8-triselenononane [b.p. 91°C (0.017 mmHg), 43%] using β,β'-dichloroethylselenide for β,β'-dichloroethyloxide; and 2,8-dithia-5-oxynonane [b.p. 45–49°C (0.03 mmHg), 63%] [lit.[15] 97°C (4 mmHg)] using dimethyldisulphide instead of dimethyldiselenide.

2,2′-*Oxybis(ethylamine) and cystamine.* These ligands were obtained as their dihydrochloride salts from Aldrich Chemical Co. Ltd, the free amine being recovered by bubbling dry ammonia gas through a suspension of the salt in chloroform, maintaining anhydrous conditions throughout. Subsequent filtration and removal of solvent gave the product. The amines gave molecular ions at m/z 105 and 152, respectively.

The same general method was used for the preparation of each of the iodide salts, the following being typical.

[(2,5,8-*Trithianonane*)*trimethylplatinum*(IV) *iodide*]. A solution of trimethylplatinum(IV) iodide (500 mg, 1.36 mmol*) and 2,5,8-trithianonane (250 mg, 1.37 mmol) in chloroform (27 cm^3) was refluxed overnight. Concentration to *ca* 5 cm^3 and addition of light petroleum (40–60°C) precipitated a pale yellow solid. Recrystallization from dichloromethane–light petroleum gave the pure product (190 mg, 25%).

The tetrafluoroborate salts were prepared by the following general method.

[(2,8 - *Dithia* - 5 - *oxynonane*)*trimethylplatinum*(IV) *tetrafluoroborate*]. To a solution of trimethylplatinum(IV) sulphate tetrahydrate (170 mg,

* Based on the molar unit $PtMe_3I$.

0.262 mmol) in acetone (10 cm^3) was added 2,8-dithia-5-oxynonane (90 mg, 0.54 mmol), producing a dense white precipitate. A solution of sodium tetrafluoroborate (80 mg, 0.73 mmol) in water (4 cm^3) was added, and the mixture refluxed for 8 h, then concentrated to *ca* 7 cm^3. Addition of water (10 cm^3) and dichloromethane (10 cm^3) gave a two-phase system. The lower organic layer was removed and dried over magnesium sulphate. Removal of the solvent gave a white solid, which was recrystallized from dichloromethane–carbon tetrachloride to give the pure product (110 mg, 42%). For the nitrogen-containing ligands, methanol replaced acetone, and the products were recrystallized from chloroform.

The tetraphenylborate salts were made by an analogous method, using sodium tetraphenylborate for sodium tetrafluoroborate. The crystalline salts were sparingly soluble in chlorocarbons and acetone, but dissolved readily in dimethylsulphoxide and dimethylformamide.

100-MHz ^1H NMR spectra were obtained using either a JEOL MH-100 spectrometer operating in the continuous-wave mode under internal field-frequency lock conditions, or a JEOL PS/PFT-100 spectrometer operating in the Fourier transform mode. The latter instrument was also used to obtain the ^{77}Se NMR spectra at 19 MHz. A JES-VT-3 variable-temperature unit was used to control the probe temperature.

Mass spectra were obtained on a single-focusing VG-Micromass MM-30 spectrometer interfaced with a Pye 104 gas chromatograph. Electron ionization was employed using potentials of 70 and 18 eV with probe temperature of 200 or 145°C. Chemical ionization was used to observe molecular ions for the amine ligands.

Conductivity measurements were made on approximately 1×10^{-3} M solutions in acetone using a Doran conductivity bridge.

RESULTS AND DISCUSSION

The ligands $[MeE(CH_2)_n]_2E'$ ($n = 3$, E = E′ = S; $n = 2$, E = S, E′ = O, S, —SS— or Se; $n = 2$, E = Se, E′ = O, S or Se), and $[(H_2NCH_2CH_2)_2E']$ (E′ = O or —SS—) are malodorous viscous oils with high boiling points. They were characterized by mass spectroscopy, and by ^1H NMR and ^{77}Se NMR spectra (Table 2). Characteristic resonances for the SMe and SeMe protons were seen at *ca* 2.15 and *ca* 2.03 ppm, respectively, the latter showing coupling to ^{77}Se ($^2J = 11$ Hz, intensity 7%). The ^{77}Se NMR data showed that Se nuclei in CH_2SeCH_3 groups ($\delta = 60$–129 ppm) invariably resonate at lower frequencies than in $—CH_2SeCH_2—$ groups ($\delta = 211$–253 ppm). The $—CH_2—$ protons in both S and Se mixed ligands give non-first-order multiplets, showing that these chemically different groups exhibit magnetic equivalence at 100 MHz. The mass spectra showed excellent correlation between theoretical and observed fragments. An ionization potential of 18 eV was necessary to observe the molecular ion of the disulphide ligands, as a potential of 70 eV gave spectra whose most intense signals corresponded to fragments resulting from the cleavage of the disulphide bond. Electron ionization on the amine ligands produced typical primary amine fragments, but chemical ionization was needed to observe the molecular ion of $(H_2NCH_2CH_2)_2O$.

The $PtMe_3$(IV) complexes (Table 3) were made initially as iodide salts by refluxing $[PtMe_3I]_4$ with the ligands in chloroform. These salts readily dissolve in spectroscopic solvents, but dissociate in solution on heating to give covalent species with coordinated iodide. The BPh_4^- salts made from $[(PtMe_3)_2SO_4 \cdot 4H_2O]$ showed no tendency to dissociate in solution, but had limited solubility. Changing the counter ion to BF_4^- gave complexes which had good solubility and high temperature stability. This type of non-coordinating anion was also necessary to observe oxygen coordination with the O-containing ligands. Ether-type oxygen does not usually bond to transition metals unless it is part of a chelate ligand.[16–18] Attempts to make tridentate O-coordinated complexes were not successful with I^- or SO_4^{2-} as counter ions, the ligand coordinating in a bidentate manner with non-bonded oxygen. However, when the anion-bound complexes were refluxed with $NaBF_4$, oxygen replaced the anion to give the ionic tridentate complexes. All the compounds are pale yellow or white crystalline solids with sharp melting points. Molar-conductivity measurements in acetone gave values lying within the range for typical 1:1 electrolytes (92–199 Ω^{-1} cm^2 mol^{-1}),[19] and elemental analyses are also consistent with the ionic formulation in Fig. 1.

Structural confirmation was provided by ^1H

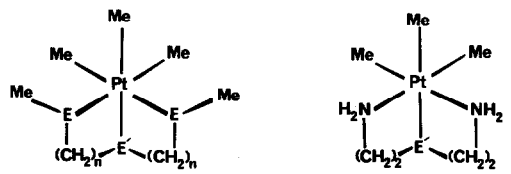


Fig. 1. Structures of the cationic complexes $[PtMe_3\{MeE(CH_2)_nE'(CH_2)_nEMe\}]^+$ [$n = 3$; E = E′ = S; $n = 2$; E = S or Se, E′ = O, S or Se: $n = 2$; E = S, E′ = —SS—] and $[PtMe_3(H_2NCH_2CH_2)_2E']^+$ [E′ = O or —SS—].

Table 2. Boiling points, ^1H and ^{77}Se NMR, and mass spectroscopic data for the ligands

Compound	Colour B.p. [°C (mmHg)]	^1H and ^{77}Se NMR data[a]			Molecular ion[b] *m/z*
			δ (ppm)	J (Hz)	
$(MeSCH_2CH_2CH_2)_2S$	Pale yellow	a	2.10		210 (210)
	111 (0.02)	b	2.61	6.65	
		c	1.87	6.85	
		d	2.61	6.65	
$(MeSCH_2CH_2)_2O$	Colourless	a	2.14		166 (166)
	45–49 (0.03)	b	2.68	13.3	
		c	3.65	13.3	
$(MeSCH_2CH_2)_2S$	Colourless	a	2.12		182 (182)
	113 (0.5)	b	2.73		
		c	2.73		
$(MeSCH_2CH_2)_2Se$	Pale yellow	a	2.13		226–232 (229)
	82 (0.005)	b	2.80		
		c	2.80	7.8[c]	
		y	211.5		
$(MeSeCH_2CH_2)_2O$	Yellow	a	2.03	10.5[c]	256–264 (260)
	45–49 (0.03)	b	2.68	7.6	
		c	3.69	8.2	
		x	60.3		
$(MeSeCH_2CH_2)_2S$	Pale yellow	a	2.04	13.0[c]	272–280 (276)
	112 (0.175)	b	2.80		
		c	2.80		
		x	106.6		
$(MeSeCH_2CH_2)_2Se$	Orange	a	2.04	10.6[c]	320–328 (323)
	91 (0.017)	b	2.87		
		c	2.87		
		x	129.2		
		y	253.1		
$(MeSCH_2CH_2S)_2$	Yellow	a	2.14		215 (214)
	117 (0.02)	b	2.86		
		c	2.86		
$(NH_2CH_2CH_2)_2O$	Pale green	a	1.45		105 (104)
	233–234[d]	b	2.84	10.1	
		c	3.48	10.5	
$(NH_2CH_2CH_2S)_2$	Pale yellow	a	1.32		152 (152)
	85–88 (0.01)	b	2.74	5.0	
		c	2.98	5.0	

[a] In $CDCl_3$ with TMS and Me_2Se as references, respectively.
[b] Theoretical values in parentheses.
[c] Coupled to ^{77}Se.
[d] Melting point of dihydrochloride salt.

NMR spectra at temperatures where chalcogen–methyl inversion is fast (for **I–IV** and **VI–VIII**) (Table 4). For compound **V** the central O atom dissociates before Se inversion is fast, and the spectrum at low temperatures is complicated by the presence of four configurational isomers. The spectra of the complexes in Table 4 consist of three regions associated with the —CH_2— protons (δ = 3.0–4.2 ppm), the E–Me protons (δ = 2.3–2.5 ppm) and the Pt–Me protons (δ = 0.8–1.3 ppm). The methylene protons give non-first-order multiplets. Chalcogen–methyl signals show the typical three-bond coupling to ^{195}Pt ($^3J \sim 14$ Hz) and are easily identified. Se–Me signals are also coupled to ^{77}Se ($^2J \sim 8.0$ Hz).

Table 3. Analytical data, colour, melting points and molar conductivities of the complexes

No.	Complex	Variables in Fig. 1			Colour	M.p. (°C)	Elemental analysis [found (calc.) %)]		Molar conductance (Ω^{-1} cm^{-2} mol^{-1})
		E	E′	*n*					
I	$[PtMe_3(MeSCH_2CH_2CH_2)_2S]^+BF_4^-$	S	S	3	Pale yellow	86.7–87.5	24.37 (24.59)	5.02 (5.06)	165.3
II	$[PtMe_3(MeSCH_2CH_2)_2O]^+BF_4^-$	S	O	2	White	161.1–161.8	22.00 (21.92)	4.67 (4.70)	169.4
III	$[PtMe_3(MeSCH_2CH_2)_2S]^+BPh_4^-$	S	S	2	White	238.0–242.0	53.29 (53.44)	5.81 (5.84)	118.0
IIIa	$[PtMe_3(MeSCH_2CH_2)_2S]^+I^-$	S	S	2	Pale yellow	133.7–134.5	19.34 (19.68)	4.14 (4.20)	147.1
IV	$[PtMe_3(MeSCH_2CH_2)_2Se]^+I^-$	S	Se	2	Pale yellow	144.5–145.5	17.93 (18.12)	3.71 (3.82)	139.3
V	$[PtMe_3(MeSeCH_2CH_2)_2O]^+BF_4^-$	Se	O	2	Pale yellow	78.0–80.0	17.84 (18.40)	3.54 (3.95)	161.9
VI	$[PtMe_3(MeSeCH_2CH_2)_2S]^+BF_4^-$	Se	S	2	White	196.5–197.0[a]	17.83 (17.92)	3.68 (3.84)	168.5
VII	$[PtMe_3(MeSeCH_2CH_2)_2Se]^+BF_4^-$	Se	Se	2	White	182.5–182.7	15.57 (16.63)	3.00 (3.57)	135.9
VIII	$[PtMe_3(MeSCH_2CH_2S)_2]^+BF_4^-$	S	—SS—	2	White	165.6–166.1[a]	20.18 (19.97)	4.25 (4.28)	131.5
VIIIa	$[PtMe_3(MeSCH_2CH_2S)_2]^+BPh_4^-$	S	—SS—	2	White	> 300.0	51.30 (51.22)	5.56 (5.60)	—
IX	$[PtMe_3(H_2NCH_2CH_2)_2O]^+BF_4^-$	NH_2	O	2	White	211.0–212.0[a]	19.38 (19.50)	4.96 (4.91)[b]	132.8
X	$[PtMe_3(H_2NCH_2CH_2S)_2]^+BF_4^-$	NH_2	—SS—	2	Pale yellow	140.5–141.0	17.63 (17.54)	4.35 (4.40)[c]	100.1

[a] Melts with decomposition.
[b] % N 6.09 (6.50).
[c] % N 5.03 (5.82).

Table 4. ^{1}H NMR data[a] for the complexes

Complex[b]	T (°C)	Chemical shift (ppm) [coupling constant (Hz)] Pt–Me (*trans* to E)		Pt–Me (*trans* to E′)		E–Me
I	26.0	1.05 (65.9)	S	0.82 (66.4)	S	2.30 (15.3)
II	1.3	1.08 (66.2)	S	1.21 (81.6)	O	2.49 (15.1)
IIIa	16.8	0.94 (67.0)	S	1.03 (67.0)	S	2.44 (14.8)
IV	29.0	0.95 (67.1)	S	1.08 (66.9)	Se	2.43 (14.7)
VI	78.4	1.02 (67.1)	Se	1.16 (67.4)	S	2.30 (11.0)
VII	83.2	1.01 (67.3)	Se	1.18 (67.3)	Se	2.30 (12.0)
VIII	33.0	1.27 (66.0)	S	1.07 (68.8)	—SS—	2.45 (15.3)
		0.89 (66.2)	S			2.40 (15.4)
IX	11.5	0.77 (68.4)	N	1.27 (83.4)	O	2.08[c]
X	27.5	0.86 (67.9)	N	0.42 (67.9)	—SS—	1.99[c]
		1.06 (68.6)	N			

[a] In CD_2Cl_2 (sealed tube) except for **IX** and **X**, for which $C_6D_5NO_2$–C_6D_6 was used.

[b] Numbering as in Table 3.

[c] Signals for the NH_2 protons.

The Pt–Me signals at highest field are most diagnostically useful, as the $^2J(^{195}Pt–^1H)$ values are highly sensitive to the *trans* ligand.[6] In all but the disulphide complexes a mirror plane relates two of the Pt–Me groups, as the chelate rings will be in an averaged planar conformation,[20] so that two signals (ratio 2 : 1) are seen. The ^2J values for Me *trans* to S and Se are in the same narrow range (65.9–67.3 Hz), as was found for the complexes with the bidentate ligands $[PtMe_3(MeE(CH_2)_nEMe)X]$ (E = S or Se, n = 2 or 3, X = halide). Where direct comparison is possible (compounds **I**, **IIIa** and **VII**) the values are significantly lower for the tridentate ligands, indicating stronger Pt–chalcogen bonding.[21] Comparison of **I** with **IIIa** also shows that ^2J is slightly lower for the six-membered ring complexes, just as was found for the bidentate compounds. There is practically no difference between the ^2J values for Pt–Me groups *trans* to the same chalcogen when that atom is terminal compared to when it is in the middle of the chain.

When oxygen is the *trans* atom (**II** and **IX**), the expected[22,23] much higher ^2J values for the Pt–Me signals (81.6 and 83.4 Hz) demonstrate the inherent weakness of the Pt–O bond evident in its ready displacement by coordinating anions (see above). When a disulphide S atom is the donor (**VIII** and **X**), ^2J values of 68.8 and 67.9 Hz show the somewhat weaker Pt–S bonds compared to Pt–S(thioether), though they are stronger than those found in the dinuclear complexes $[(PtMe_3X)_2MeSSMe]$[6] for which ^2J is 71.6–73.8 Hz. No evidence for a 1,2-shift was found in the spectra of the disulphide complexes (E′ = —SS—). This would necessarily introduce a plane of symmetry, and in both **VIII** and **X** all three Pt–Me groups are distinct, as are the two S–Me groups in **VIII** and the NH_2 groups in **X**. Separate five- and six-membered rings are clearly present. Coupling constants for Pt–Me *trans* to sp^3-hybridized nitrogen are in the expected range[23] {e.g. 69.8 Hz in $[PtMe_3(H_2NCH_2CH_2)_2NH]^+$}.[5]

A full DNMR study of the complexes shows the presence of configurational isomers at temperatures where inversion at the chalcogen atoms is slow, and their fluxional behaviour will be discussed in detail elsewhere.

REFERENCES

1. E. W. Abel, S. K. Bhargava and K. G. Orrell, *Prog. Inorg. Chem.* 1984, **32**, 62.
2. R. B. King and A. Bond, *J. Am. Chem. Soc.* 1974, **96**, 1338.
3. H. C. Clark, G. Ferguson, V. K. Jain and M. Parvez, *J. Organomet. Chem.* 1984, **270**, 365.
4. J. G. Appleton, J. R. Hall and L. Lambert, *Inorg. Chim. Acta* 1978, **29**, 89.
5. D. H. Goldsworthy and K. Kite, unpublished results.
6. E. W. Abel, A. R. Khan, K. Kite, K. G. Orrell and V. Sik, *J. Chem. Soc., Dalton Trans.* 1980, 1169.
7. J. C. Baldwin and W. C. Kaska, *Inorg. Chem.* 1975, **14**, 2020.
8. D. E. Clegg and J. R. Hall, *Spectrochim. Acta* 1965, **21**, 357.
9. L. Brandsma and H. E. Wijers, *Recl Trav. Chim.* 1963, **82**, 68.

10. W. R. Kirner and W. Windus, *Org. Synth. Coll.* 1943, **2**, 136.
11. M. Gomberg, *J. Am. Chem. Soc.* 1919, **41**, 1414.
12. B. C. Newman and E. L. Eliel, *J. Org. Chem.* 1970, **35**, 3641.
13. E. M. Mead and R. C. G. Moggridge, *J. Chem. Soc.* 1946, 813.
14. T. B. Rauchfuss and D. M. Roundhill, *J. Am. Chem. Soc.* 1975, **97**, 3386.
15. W. von E. Goering and K. C. Schreiber, *J. Am. Chem. Soc.* 1955, **77**, 514.
16. J. R. Lotz, B. P. Block and W. C. Fernelius, *J. Phys. Chem.* 1959, **63**, 541.
17. M. Ciampolini and N. Nardi, *Inorg. Chem.* 1967, **6**, 445.
18. R. Barbucci and A. Vacca, *J. Chem. Soc., Dalton Trans.* 1974, 2363.
19. W. J. Geary, *Coord. Chem. Rev.* 1971, **7**, 81.
20. E. W. Abel, A. R. Khan, K. Kite, K. G. Orrell and V. Sik, *J. Chem. Soc., Dalton Trans.* 1980, 1175.
21. D. E. Clegg, J. R. Hall and G. A. Swile, *J. Organomet. Chem.* 1972, **38**, 403.
22. K. Kite, J. A. S. Smith and E. W. Wilkins, *J. Chem. Soc.* 1966, 1744.
23. T. G. Appleton, H. C. Clark and L. E. Manzer, *Coord. Chem. Rev.* 1973, **10**, 335.

Polyhedron Vol. 5, No. 9, pp. 1467–1473, 1986
Printed in Great Britain

0277–5387/86 $3.00+.00
Pergamon Journals Ltd

POLAROGRAPHIC REDUCTION OF AQUEOUS SULFUR DIOXIDE

W. L. REYNOLDS* and YU YUAN

Chemistry Department, University of Minnesota, Minneapolis, MN 55455, U.S.A.

(*Received* 23 *September* 1985; *accepted* 7 *January* 1986)

Abstract—Direct- and alternating-current polarograms of aqueous $SO_2 \cdot OH_2$ solutions show four reduction waves, more than previously reported. Waves I and II probably result from the electroreduction of $SO_2 \cdot OH_2$ and HSO_3^-, respectively; these two waves completely overlap at pH 1 but are partially resolved at higher pH values due to different pH dependence. Reduction of $SO_2 \cdot OH_2$ involves two electrons and two H^+ ions and the initial product is probably sulfoxylic acid, H_2SO_2. This product can disproportionate to S^0 and $SO_2 \cdot OH_2$ in very acidic media (pH $\leqslant$ 1) and, in the limit, double the reduction current of $SO_2 \cdot OH_2$. Reduction of HSO_3^- appears to occur via two paths: one is a two-electron three-H^+ ion path and the other is a one-electron one-H^+ ion path. The former dominates at pH $\leqslant$ 3 and probably produces H_2SO_2; the latter dominates at pH > 4 and may produce SO_2^-. H_2SO_2 in less acidic media can react with HSO_3^- to yield dithionite species (such as $H_2S_2O_4$, $HS_2O_4^-$ and $S_2O_4^{2-}$) and HSO_2 and SO_2^- by dissociation of the dithionite species. Waves III and IV are believed to result from reduction of HSO_2 and SO_2^-, respectively, to H_2SO_2 species.

Several investigations on the reduction of sulfur dioxide, $SO_2 \cdot OH_2$, in aqueous solution at a mercury electrode have reported two waves in acidic media and no waves in neutral or slightly alkaline media. There has been much disagreement in the interpretation of these results. Gosman[1] postulated that in acidic media only undissociated sulfurous acid, i.e. $SO_2 \cdot OH_2$, is reduced, that it is reduced by a one-electron reduction to the S(III) state with subsequent dimerization to $H_2S_2O_4$, that in neutral or alkaline solutions $S_2O_4^{2-}$ disproportionates to SO_2^{2-} and SO_2 and that the SO_2 so produced is reduced by a two-electron reduction directly to SO_2^{2-} in the second wave. This explanation for the second wave is incorrect for the following reason: the pH controls the disproportionation of 2S(III) to S(II) and SO_2, and at the pH values where the disproportionation occurs the limiting current due to S(IV) → S(III) reduction in the first wave will be increased (doubled in the limit) by a kinetic current contribution from the disproportionation. At the limit all SO_2 reaching the electrode is effectively reduced to S(II) at potentials more positive than the potential where the second wave is observed. Consequently when the potential of the second wave is reached and direct reduction of SO_2 to S(II) can occur there will be little change in the current due to SO_2 → S(II) reduction. Experimentally there is no evidence of the limiting current in the first wave increasing with increasing pH as the disproportionation increasingly produces more SO_2.

Kolthoff and Miller[2] found that the first wave in 0.1 M HNO_3 was a two-electron reduction and postulated reaction (1) as the electrode reduction:

$$SO_2 + 2H^+ + 2e^- \rightarrow H_2SO_2. \qquad (1)$$

They also postulated that, of the two waves seen at pH 6, the first was due to reduction of HSO_3^- to HSO_2 and the second to reduction of $S_2O_4^{2-}$ (from dimerization and ionization of HSO_2) to thiosulfate, $S_2O_3^{2-}$.

Čermak[3] postulated that the first wave was a one-electron reduction of SO_2 to HSO_2 followed by a rapid disproportionation of $2HSO_2 \rightarrow SO_2 + H_2SO_2$ to make it appear that the first wave was a two-electron reduction of SO_2 to H_2SO_2 and that the second wave was a direct two-electron reduction of SO_2 to H_2SO_2. The objection to this explanation

* Author to whom correspondence should be addressed.

of the waves follows much the same lines as the objection to Gosman's explanation: if the disproportionation of the S(III) electroreduction product to H_2SO_2 and SO_2 is so rapid as to make the first wave appear to be a two-electron reduction then there will be little or no current increase when the potential for the direct two-electron reduction is reached.

Jacobsen and Sawyer[4] postulated that the first wave was a two-electron reduction as given in reaction (1) and that the second wave was due to adsorption of a reduction product of SO_2 with partial inhibition of SO_2 reduction.

Here we report the detection of four polarographic reduction waves and their interpretation.

EXPERIMENTAL

Chemicals

Reagent-grade sodium metabisulfite, $Na_2S_2O_5$, was used as a source of SO_2 and HSO_3^- and was obtained from Matheson, Coleman & Bell. It was analysed using an excess of standard iodine solution which was back-titrated with standard sodium thiosulfate solution; it was found to be $99.7 \pm 0.66\%$ pure in seven analyses. All other acids and salts used as supporting electrolytes, buffer components or to establish ionic strength were reagent-grade and were used without further purification. The de-ionized water used in preparing solutions gave typical residual currents.

Apparatus

A Princeton Applied Research Model 170 Electrochemistry System was used to record current–voltage data. An IBM Instruments Inc. electrolysis cell with a saturated calomel electrode (SCE) as the reference electrode, a dropping mercury electrode (dme) as the indicator electrode and a Pt wire as the third electrode were used. All solutions in this cell were de-aerated by passage of N_2 gas prior to the addition of a known quantity of sulfite by microsyringe through a port sealed with a self-sealing rubber septum. The rate of N_2 gas flow over the solution after sulfite addition was reduced to minimize SO_2 loss but yet maintain a positive N_2 gas pressure inside the cell. The loss of SO_2 from the cell during the recording of any one polarogram was not sufficient to invalidate the results but was detectable in very acidic solutions over a half-hour period. Consequently measurements of limiting currents at a series of sulfite concentrations or mercury column heights were performed in times much less than half an hour or a series of freshly prepared solutions was used. All currents used in calculations were corrected for residual current.

At a mercury column height of 70.0 cm the mercury flow rate was 2.650 mg s^{-1} with the capillary tip on the mercury pool surface, the drop time was 3.84_6 s at -0.50 V vs (SCE), and the drop surface area was 0.0400 cm^2 at the maximum drop size.

Maximum suppressors were not used and maxima did not occur. Sodium dodecylsulfate, a surfactant, was added only to test the effect, if any, on polarographic waves suspected of being due to adsorption effects.

RESULTS AND DISCUSSION

Direct-current (dc) polarography

$pH < 1.3$. At H^+ concentrations in the range 0.10–4.0 M HCl at a constant ionic strength of 4.0 M or at variable ionic strength in the range 1.0–4.0 M, there was only one reversible two-electron reduction wave, hereafter referred to as wave I. The customary plots of $\log [i/(i_l - i)]$ vs $-E$ gave slopes of approximately $+33.8$ V^{-1}, i.e. the inverse of 0.05915/2, where i and i_l are the maximum current at voltage E and the maximum limiting current, respectively, corrected for the residual current.

In a 0.10 M HCl + 3.90 M KCl medium the value of I_{max}, the diffusion current constant at maximum current, for SO_2 was 7.14 ± 0.09. Although the slope of the $\log [i/(i_l - i)]$ vs E plot was independent of pH in the pH range under discussion, the height of the SO_2 reduction wave was dependent on the pH. The height of the wave rapidly increased with increasing H^+ concentration at constant ionic strength and reached a limiting value in 4.0 M HCl of approximately twice its height in 0.10 M HCl. Hence it is likely that electrode reaction (1) is followed by the overall disproportionation reaction (2):

$$2H_2SO_2 \rightarrow S^0 + SO_2 + 2H_2O, \qquad (2)$$

which is acid-catalysed so that the wave height asymptotically approaches twice the height of wave I in the absence of reaction (2). Thus, at pH < 1.3 the mechanism of SO_2 reduction is EC_{dis} where the electrode reaction is followed by disproportionation of S(II) to S(0) and S(IV). The classic example of this mechanism is the reduction[5] of U(VI) to U(V) at the dme followed by disproportionation of U(V) to U(IV) and U(VI); the limiting current for the $U(VI) + e^- \rightarrow U(V)$ reduction wave is doubled by quantitative disproportionation of U(V).

The value of i_l in 1.0 M HCl increased somewhat more slowly than $h^{1/2}$, the square root of the mer-

cury column height, as expected if reaction (2) was partly limiting the SO_2 supply at this acidity.

Orlemann and Kern[6] have given a quantitative treatment, subject to some assumptions, of the EC_{dis} mechanism and derived equation (3):

$$\frac{1}{(\bar{i}_l-\bar{i}_d)^{1/2}}=\left(\frac{0.2tk}{\bar{K}_R}\right)^{1/2}\left(\frac{\bar{i}_l}{\bar{i}_i-\bar{i}_d}-2\right), \qquad (3)$$

where $\bar{i}_d$ is the diffusion current, averaged over the lifetime of the drop, that would be obtained in the absence of the disproportionation reaction, $\bar{i}_l$ is the limiting current in the presence of the disproportionation averaged over the drop lifetime, t is the drop time, k is a rate constant for the disproportionation reaction and $\bar{K}_R$ is the Ilkovic constant for the product of the electrode reaction (calculated using average diffusion currents). It was assumed in the derivation, and it is assumed here, that the diffusion coefficients of oxidized and reduced species in the electrode reaction are equal so that $\bar{K}_R = \bar{K}_0$. The experimental values of i_l, i_d, t, K_R and HCl concentration are given in Table 1, as are the value of k calculated from eqn (3). The maximum values of i_l, $i_l - i_d$ and K_R for currents at the end of the droplife were converted to average values for use in eqn (3) as explained in the original derivation.[6] When the rate constants in Table 1 were expressed as:

$$\log k_j = \log k_o + n \log [H^+]_j$$

a least-squares treatment of the data gave $n = 2.93 \pm 0.03$ and $k_o = 21.9 \pm 0.5$ (mmol dm^{-3})$^{-4}$ s^{-1}, so that k is approximately given by:

$$k = k_o[H^+]^3 \text{ (mmol dm}^{-3})^{-1}\text{ s}^{-1}.$$

This dependence on the cube of the H^+ concentration accounts for the rapid decrease in the rate of the disproportionation reaction with increasing pH so that at pH > 1.3 reaction (2) contributes negligibly to the electrochemical behavior of SO_2.

The value of I_{max} in 4.00 M HCl was 13.98 ± 0.29. If this number is divided by 2 to give I_{max} for SO_2 reduction in the absence of reaction (2) then one obtains:

$$I_{max} = 6.99 \pm 0.15 = 708nD^{1/2}.$$

Thus D, the diffusion coefficient of SO_2, in this medium is found to be $(2.44 \pm 0.10) \times 10^{-5}$ cm^2 s^{-1}. This value is somewhat larger than the value of 2.04×10^{-5} cm^2 s^{-1} reported by Kolthoff and Miller[2] for 0.10 M HNO_3. Some uncertainties surround the latter value because in 0.10 M H^+ the SO_2 is approximately 12% ionized and because the behavior of the very unstable H_2SO_2 in reducible HNO_3 is unknown. In 4.0 M HCl there is an entirely negligible amount of SO_2 ionized and there is no evidence that Cl^- affects the stoichiometry of reaction (2). The value of the limiting current was not affected by ionic strength changes or by Cl^- ion concentration changes when the KCl concentration was increased from 0.0 to 3.0 M in SO_2 solutions containing 1.00 M HCl.

Table 1. Kinetic data for disproportionation reaction (2)[a]

[HCl] (mol dm^{-3})	i_l (μA)	k [(mmol dm^{-3})$^{-1}$ s^{-1}]
4.00	33.5	—
2.00	31.5	165.3
1.00	28.7	21.9
0.75	26.9	9.73
0.50	23.5	2.80

[a] $t = 3.846$ s, $i_d = 16.7$ μA, $K_R = 16.7$ μA (mmol dm^{-3})$^{-1}$.

In chronopotentiometric studies Jacobsen and Sawyer[4] found that the quantity $i\tau^{1/2}$ increased linearly with τ, the transition time, at pH < 1.5 and that this increase became more pronounced at pH 0. These authors also observed elemental sulfur formation, as did we, in the electrolysis cell in these very acidic solutions. Hence they suggested reaction (2) as an explanation.

1.3 < pH < 3. As noted by previous investigators the SO_2 reduction wave lost its reversible character at pH values somewhat greater than 1.0. The cause of this irreversibility in the reduction does not appear to have been determined. We found that, as the pH increased, the plots of log $[i/(i_l - i)]$ vs $-E$ became S-shaped, that the S-character of the plot increased at first, that the slope of the upper branch of the plot decreased faster than the slope of the lower branch and that at approximately pH 4.5–5.0 the plot became linear again. There were two overlapping waves present, namely waves I and II, both of which shift to more negative potentials as pH increases. The overlapping waves can be analysed by the methods of Ružić and co-workers.[7] The $E_{1/2}$ values for the two waves and the corresponding pH values are given in Table 2. When these $E_{1/2}$ values were plotted against pH it was found that the least-squares straight-line relationships were given by:

$$(E_{1/2})_I = (-0.272 \pm 0.007) - (0.065 \pm 0.003)\text{pH}$$

for wave I and by:

$$(E_{1/2})_{II} = (-0.254 \pm 0.006) - (0.099 \pm 0.002)\text{pH}$$

for wave II. Thus wave I involves two protons in the reduction; this is evidence in support of reaction

Table 2. Half-wave potentials of waves I and II as a function of pH

pH	Supporting electrolyte	$(E_{1/2})_I^c$ (V)	$(E_{1/2})_{II}^c$ (V)
1.30	0.984 M KNO_3+0.016 M PTSA+NaPTS[a]	−0.357	−0.389
1.68	0.931 M KNO_3+0.069 M PTSA+NaPTS[a]	−0.382	−0.417
1.98	0.914 M KNO_3+0.086 M PTSA+NaPTS[a]	−0.403	−0.452
2.14	0.990 M KNO_3+0.010 M HNO_3	−0.410	−0.463
2.32	0.996 M KNO_3+0.004 M ClAcOH[b]+KOH	−0.421	−0.480$_5$
2.72	0.992 M KNO_3+0.008 M ClAcOH[b]+KOH	−0.441	−0.520
3.00	0.991 M KNO_3+0.009 M ClAcOH[b]+KOH	−0.460	−0.550

[a] *p*-Toluenesulfonic acid and sodium *p*-toluenesulfonate buffer of the indicated ionic strength.
[b] Chloroacetic acid and potassium hydroxide buffer of the indicated ionic strength.
[c] Voltage vs the SCE.

(1) which has not been forthcoming heretofore. Wave II involves three protons and we propose reaction (4) for this reduction:

$$HSO_3^- + 3H^+ + 2e^- \rightarrow H_2SO_2 + H_2O. \quad (4)$$

The reduction waves for SO_2 and its conjugate base HSO_3^- can be treated in the manner in which the reduction waves for pyruvic acid and its conjugate base, the pyruvate ion, have been treated.[8-10] The pH at which i_{l1}, the limiting current for wave I, is reduced to one-half its value at pH 1.2 (where only wave I is present) is approximately 2.7. This pH value yields[8,9] $k_{h,r}$, the heterogeneous second-order rate constant for recombination of H^+ and HSO_3^-, equal to 792 cm mol dm^{-3} s^{-1}. The homogeneous second-order rate constant, k_r, for the recombination is related to $k_{h,r}$ by the equation:

$$k_r = \frac{K_{a1}}{D} k_{h,r}^2$$

where K_{a1} is the first acid ionization constant of SO_2. The values of 1.4×10^{-2} mol dm^{-3} for K_{a1}^{11} and 2.4×10^{-5} cm^2 s^{-1} for D yield $k_r = 3.7 \times 10^8$ (mol dm^{-3})$^{-1}$ s^{-1}, which is between the values of 2×10^8 (mol dm^{-3})$^{-1}$ s^{-1} reported by Eigen *et al.*[12] from relaxation measurements and 2.5×10^9 (mol dm^{-3})$^{-1}$ s^{-1} reported by Betts and Voss[13] from isotope exchange rate measurements.

$5.8 \leqslant pH \leqslant 7.4$. In this pH range in KH_2PO_4+NaOH and $Na_2B_4O_7$+HCl buffers we observed three waves which we designated waves II, III and IV. Kolthoff and Miller[2] used the former buffer to obtain pH 6.0 but reported only two waves. Wave I due to undissociated $SO_2 \cdot OH_2$ had completely disappeared because the SO_2 content was entirely negligible. Wave II due to HSO_3^-, the major sulfite species, had so decreased in height as to strongly suggest that the electrode reaction was now a one-electron reduction so that reaction (4) no longer represents the HSO_3^- electrode reaction in this pH range. The change in the electroreduction reaction of HSO_3^- is discussed further in the section on alternating-current (ac) polarography. Reaction (2) has become entirely negligible and reactions (5) and (6) are now important for any H_2SO_2 formed by two-electron reduction of HSO_3^-:

$$H_2SO_2 + HSO_3^- \rightarrow HS_2O_4^- + H_2O, \quad (5)$$

$$H_2SO_2 + SO_3^{2-} \rightarrow S_2O_4^{2-} + H_2O. \quad (6)$$

In addition to proton transfer reactions between $S_2O_4^{2-}$, $HS_2O_4^-$ and $H_2S_2O_4$ there exist the dissociations of $H_2S_2O_4$ in reaction (7) and/or $S_2O_4^{2-}$ in reaction (8), and proton transfer between HSO_2 and SO_2^- to be considered:

$$H_2S_2O_4 \rightleftarrows 2HSO_2, \quad (7)$$

$$S_2O_4^{2-} \rightleftarrows 2SO_2^-. \quad (8)$$

The S–S bond length in $S_2O_4^{2-}$ is[14,15] 239 pm and is much longer than the S–S bond length[15] of 221 pm in $S_2O_5^{2-}$ which dissociates completely[16] and rapidly at millimolar concentrations in aqueous solutions according to reaction (9):

$$S_2O_5^{2-} + H_2O \rightleftarrows 2HSO_3^-. \quad (9)$$

The first-order rate constant for dissociation of $S_2O_4^{2-}$ at 25°C was found to be[17] 2.5 s^{-1} at pH 6.5 and 1.8 s^{-1} in 0.1 M NaOH, so that the half-life for dissociation to $2SO_2^-$ is of the order of 0.28 s and the drop time of the electrode was approximately 14 half-lives. During the formation of each drop at potentials where all SO_2^- reaching the electrode is reduced, the dissociation in reaction (8) could be

displaced sufficiently to the right to yield an easily observable current depending on the concentration of $S_2O_4^{2-}$ in the reaction volume near the electrode surface. We postulate that polarographic waves III and IV are due to electroreduction of HSO_2 and SO_2^-, respectively, according to overall reactions (10) and (11):

$$HSO_2 + H^+ + e^- \rightarrow H_2SO_2, \quad (10)$$

$$SO_2^- + e^- \rightarrow SO_2^{2-}. \quad (11)$$

Because the undissociated form of a weak acid is usually reduced at a more positive potential than the conjugate base form we believe that pH-dependent wave III is due to reaction (10) and that pH-independent wave IV is due to reaction (11). Since wave IV is independent of pH over a wide pH range the electroreduction does not involve any protons in the rate-determining step. Furness[18] observed a small reduction wave at approximately the potential of wave IV in 0.1 M NaOH solutions of $Na_2S_2O_4$ which he concluded was due to a reducible species derived from $Na_2S_2O_4$, and which had a large temperature dependence typical of a kinetically controlled wave.

We were unable to quantitatively obtain the pH dependence of wave III by dc polarography because of the spread-out nature of wave III and its overlapping with wave II.

The wave labelled IV here was assigned by Jacobsen and Sawyer[4] to an inhibited electrode reaction because the presence of 0.001% dodecylamine perchlorate eliminated the wave. We found that the presence of 0.001% sodium dodecylsulfate, which is also a surfactant, did not eliminate or decrease either wave III or wave IV. It is unlikely that either of these waves is due to an adsorbed layer of a reduction product which is either desorbed at the potential of the waves or penetrated by the electroactive species. A further argument against the adsorption origin of waves III and IV is that the waves do not appear when their potential is reached until the pH is sufficiently high for reactions such as (5) and (6) to occur.

Ac polarography

For 3.0 mmol dm^{-3} SO_2 in 1.00 M HCl and 1.00 M ionic strength the peak current, I_p, in an ac polarogram was proportional to $v^{1/2}$, the square root of the frequency, up to 25 Hz, then increased less rapidly than $v^{1/2}$ and was independent of frequency above *ca* 640 Hz. Since I_p is proportional to $v^{1/2}$ for reversible waves and independent of v for irreversible waves[19] the electrode reaction for SO_2 reduction apparently becomes irreversible within the approximate range of times set by these frequency limits. However there seems to be some degree of irreversibility even at a frequency of 10 Hz because the peak width at half-height is approximately 70 mV, greater than $90/n$ or 45 mV for a reversible two-electron reduction.

At pH 2.27 the peaks for waves I and II for SO_2 and HSO_3^- reduction, respectively, are plainly evident (although overlapping) and no peaks for waves III and IV are present.

At pH 2.86 a low, broad peak for wave III appears in the ac polarogram but a peak for wave IV does not.

At pH 4.00 the four peaks for waves I–IV inclusive can be seen as shown in Fig. 1. The peaks for waves I–III overlap. The SO_2 reduction occurring in wave I now makes only a modest contribution. The HSO_3^- reduction occurring in wave II makes

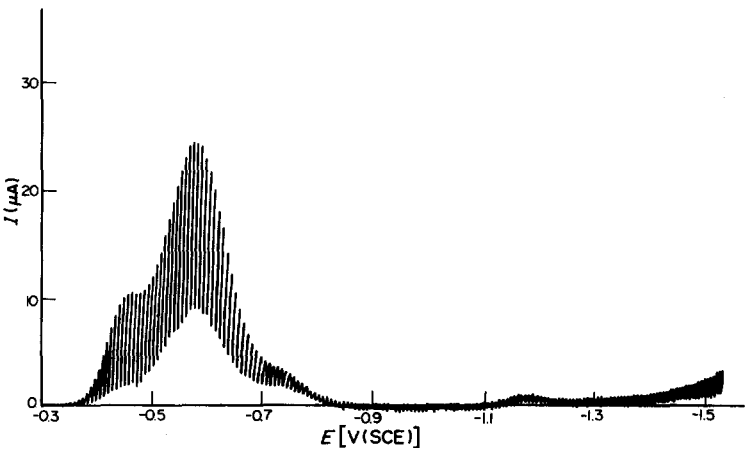


Fig. 1. Ac polarogram of 0.020 mol dm^{-3} sulfur dioxide in acetic acid–KOH buffer: pH 4.0, ionic strength 4.0 M, 25°C.

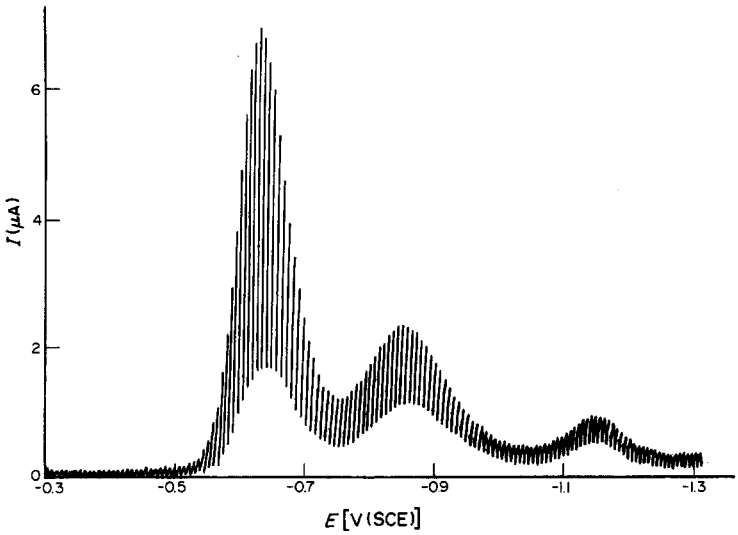


Fig. 2. Ac polarogram of 0.020 mol dm^{-3} sulfur dioxide in acetic acid–KOH buffer: pH 5.89, ionic strength 4.0 M, 25°C.

the major contribution to the current because at this pH sulfite is virtually all present as HSO_3^-. The product H_2SO_2 of the electroreduction of HSO_3^- reacts with HSO_3^- to yield some HSO_2 via reactions (5) and (7). The HSO_2 produced in this way and its conjugate base SO_2^- are reduced via reactions (10) and (11), and so contribute to waves III and IV, respectively. More HSO_2 and SO_2^- can be formed in another manner and also contribute to waves III and IV. Apparently the electroreduction of HSO_3^- can proceed by more than one path, the different paths having different H^+ ion dependencies and different numbers of electrons. The path with $[H^+]^3$ dependence in the pH range 1.3–3 was not experimentally detectable at pH 4. Instead the H^+ ion dependence became approximately first-order because $(E_{1/2})_{II}$ for wave II shifted from −0.55 V at pH 3.0 to approximately −0.583 V at pH 4.0, or −0.033 V per pH unit. At pH 5.89 the peak for wave II was shifted to −0.638 V (as shown in Fig. 2) or by −0.029 V per pH unit from its position at pH 4.0. At the same time the height of wave II is greatly decreased as observed by Kolthoff and Miller[2] for this pH range. It is clear that reaction (4) no longer represents the electroreduction of HSO_3^- in this pH range. Instead we suggest reaction (12):

$$HSO_3^- + H^+ + e^- \rightarrow SO_2^- + H_2O, \qquad (12)$$

a one-electron reduction (as suggested by Kolthoff and Miller[2]) with first-order H^+ ion dependence.

At pH 4.0 the peak for wave III was at −0.72 V and at pH 5.89 it was at −0.85 V. The shift was approximately −0.069 V per pH unit, indicating a $[H^+]^2$ dependence for the electrode reaction. The product of the HSO_3^- reduction in these very weakly acidic solutions must pick up two H^+ ions for the electrode reaction to occur so we suggest reaction (13) for wave III:

$$SO_2^- + 2H^+ + e^- \rightarrow H_2SO_2. \qquad (13)$$

Reaction (13) is really reaction (10) written differently. Therefore the SO_2^- produced from both the two-electron three-H^+ and one-electron one-H^+ reductions of HSO_3^- will be reduced in wave III by the same electrode process. It is expected that the recombination reaction between H^+ and SO_2^- can proceed at rates comparable to the rates of recombination of H^+ with other mononegative conjugate bases. The shift from a two-electron to a one-electron reduction of HSO_3^- should not be too surprising since one-electron reductions of SO_2 take place at a dme in dimethyl sulfoxide,[20] an aprotic solvent. Perhaps the shift can occur in water when the proton concentration is sufficiently small.

The peak for wave IV is not shifted by the pH change from 4.0 to 5.89.

At pH 7.4 all peaks have disappeared, as have all dc polarographic waves because reducible SO_2 and HSO_3^- are not present at sufficiently high concentrations.

REFERENCES

1. B. Gosman, *Coll. Czech. Chem. Commun.* 1930, **2**, 185.
2. I. M. Kolthoff and C. S. Miller, *J. Am. Chem. Soc.* 1941, **63**, 2818.

3. V. Čermak, *Coll. Czech. Chem. Commun.* 1958, **23**, 1871.
4. E. Jacobsen and D. T. Sawyer, *Electroanal. Chem. Interfacial Electrochem.* 1967, **15**, 181.
5. I. M. Kolthoff and W. E. Harris, *J. Am. Chem. Soc.* 1946, **68**, 1175.
6. E. F. Orlemann and D. M. H. Kern, *J. Am. Chem. Soc.* 1953, **75**, 3058.
7. I. Ruzic and M. Branica, *Electroanal. Chem. Interfacial Electrochem.* 1969, **22**, 243, 422 (and references therein).
8. P. Delahay, *J. Am. Chem. Soc.* 1951, **73**, 4944.
9. P. Delahay and J. E. Strassner, *J. Am. Chem. Soc.* 1951, **73**, 5219.
10. P. Delahay, *J. Am. Chem. Soc.* 1952, **74**, 3506.
11. A. Huss, Jr and C. A. Eckert, *J. Phys. Chem.* 1977, **81**, 2268.
12. M. Eigen, K. Kustin and G. Maass, *Z. Physik. Chem.* 1961, **30**, 130.
13. R. H. Betts and R. H. Voss, *Can. J. Chem.* 1970, **48**, 2035.
14. J. D. Dunitz, *Acta Cryst.* 1956, **9**, 579.
15. *Tables of Interatomic Distances and Configuration in Molecules and Ions.* The Chemical Society Special Publication No. 18, Supplement 1956–1959. The Chemical Society, London (1965).
16. R. E. Connick, T. M. Tamm and E. von Deuster, *Inorg. Chem.* 1982, **21**, 103.
17. N. Sutin and C. Creutz, *Inorg. Chem.* 1974, **13**, 2041.
18. W. Furness, *J. Soc. Dyers Colour.* 1950, **66**, 270.
19. A. J. Bard and L. R. Faulkner, *Electrochemical Methods*, p. 336. John Wiley, New York (1980).
20. P. Bruno, M. Caselli and M. Traini, *J. Electroanal. Chem.* 1980, **113**, 99.

Polyhedron Vol. 5, No. 9, pp. 1475–1478, 1986
Printed in Great Britain

0277–5387/86 $3.00+.00
Pergamon Journals Ltd

PREPARATION AND X-RAY CRYSTAL STRUCTURE OF $[Pd_2(\mu\text{-}O_2CMe)_2(C_6H_5)_2(PPh_3)_2]$, A BINUCLEAR ACETATE-BRIDGED PALLADIUM(II) PHENYL COMPLEX FORMED BY P—C BOND CLEAVAGE OF TRIPHENYLPHOSPHINE

MICHAEL B. HURSTHOUSE,* OLIVIER D. SLOAN, PETER THORNTON* and NIGEL P. C. WALKER

Department of Chemistry, Queen Mary College, Mile End Road, London E1 4NS, U.K.

(*Received* 10 *January* 1986; *accepted* 27 *January* 1986)

Abstract—The new binuclear complex $[Pd_2(\mu\text{-}O_2CMe)_2(C_6H_5)_2(PPh_3)_2]$ is formed when $[Pd_3(O_2CMe)_6]$ reacts with PPh_3 in methanol. An X-ray crystal structure analysis shows the complex to comprise two square planar palladium(II) atoms bridged by two acetate ligands in a *cis* fashion. The phosphine and phenyl ligands on each metal atom adopt positions which are mutually *trans* to the equivalent ligand on the other metal atom, so that the complex has an approximate two-fold axis perpendicular to the plane of the four acetate oxygens. The NMR (^1H, ^{13}C and ^{31}P) spectra are reported.

The comparatively few reports of P—C bond cleavage of triaryl phosphines in the presence of metal compounds have usually involved reactions which can be considered as oxidative additions, so that a zerovalent metal is oxidized to the bivalent state with the formation of complexes of aryl and/or dialkylphosphido ligands.[1] The formation of aryl intermediates has also been suggested during the alkylation of alkenes[2] and during the formation of biphenyl in reactions involving $[NiClR'(PR_3)_2]$,[3] $[NiCl_2(PPh_3)_2]$[4] or $[Pd(O_2CMe)_2(PPh_3)_2]$,[5] and must also occur when the latter complex is used to phenylate styrene.[6]

These suggestions are now confirmed by our finding that the solution obtained by the reaction of $[Pd_3(O_2CMe)_6]$ with triphenylphosphine in methanol produces the new binuclear aryl complex $[Pd_2(\mu\text{-}O_2CMe)_2(C_6H_5)_2(PPh_3)_2]$, which has been characterized by NMR spectroscopy and X-ray crystallography. The ^1H NMR spectrum ($CDCl_3$) shows only a broad singlet, δ 1.32, for acetate protons and a complex multiplet, δ 6.5–7.5, for phenyl protons, but in the broad-band-decoupled ^{13}C spectrum the acetate carbons are found at δ 24.04 ($\underline{C}H_3CO_2$) and 147.4 ($CH_3\underline{C}O_2$), the triphenylphosphine carbons at 127.9 (*m*), 130.0 (*p*), 132.0 (P—$\underline{C}$) and 134.7 (*o*), and the phenyl carbons at 123.2 (*p*), 126.8 (*m*) and 137.3 (*o*), though the carbon bound to palladium was not detected. The ^{31}P spectrum shows a singlet (δ 29.03, with reference to H_3PO_4).

EXPERIMENTAL

NMR spectra were obtained on Bruker WP-80 (^1H) and WM-250 (^{13}C and ^{31}P) spectrometers, and the IR spectrum on a Perkin–Elmer 577 spectrophotometer.

Di-μ-acetatodiphenylbis(triphenylphosphine)dipalladium(II)

$[Pd_3(O_2CMe)_6]$ (0.19 g, 0.30 mmol) and triphenylphosphine (0.67 g, 2.6 mmol) were dissolved in methanol (75 cm^3) and the solution refluxed for 10 min. The red-brown solution was cooled and allowed to evaporate slowly in air until a black crystalline solid was deposited and a clear solution remained (approximately 36 h). Yield 0.19 g (41%). Found: C, 61.1; H, 4.5; P, 6.8; Pd, 22.0%. $C_{26}H_{23}O_2PPd$ requires: C, 61.9; H, 4.6; P, 6.1; Pd, 21.1%. IR spectrum: 3050(m) (aromatic C—H), 1575(vs) [$\nu_{as}(CO_2)$], 1440(s) (P—Ph), 1414(vs) [$\nu_s(CO_2)$], 1376(s) (C—H sym. def.), and 750–690(s) (aromatic o.o.p. bending).

* Authors to whom correspondence should be addressed.

Crystal data

$C_{52}H_{46}O_4P_2Pd_2$, $M = 1008.8$, monoclinic, $a = 11.104(2)$ Å, $b = 24.135(5)$, Å, $c = 17.193(3)$ Å, $\beta = 99.51(2°)$, $U = 4544.3$ Å^3, space group $P2_1/n$, $Z = 4$, $D_c = 1.474$ g cm^{-3}, $F(000) = 2048$, λ(Mo-K_α) = 0.71069 Å, μ(Mo-K_α) = 8.11 cm^{-1}.

Data collection

Unit cell parameters were determined and intensity data collected at room temperature on an Enraf–Nonius CAD4 diffractometer using graphite-monochromated Mo-K_α radiation and an ω–2θ scan procedure.[7] 8634 data ($1.5 \leqslant \theta \leqslant 25°$) were measured of which 7983 were unique and 6096 considered observed [$I \geqslant 1.5\sigma(I)$]. Monitoring of three intensity control reflections showed no crystal decomposition.

Structure solution and refinement

The structure was solved via the heavy-atom method. After least-squares refinement with isotropic temperature factors for all non-hydrogen atoms the DIFABS empirical method of absorption correction[8] was applied. Following refinement using anisotropic thermal parameters for all atoms and with constraints on the phosphine phenyl rings to retain regular hexagonal geometry a difference-Fourier map revealed the location of most of the hydrogen atoms on the phenyl and methyl groups. All hydrogen atoms on the phenyl rings were included in refinement with a common refined isotropic temperature factor for each ring and constaints to main regular geometry. The methyl-group hydrogens were also subjected to constraints to retain tetrahedral geometry and assigned group isotropic temperature factors.

The final full-matrix least-squares refinement was carried out with unit weights and gave the following R-factor values: $R = \Sigma|\Delta F|/\Sigma|F_o| = 0.056$ and $R_w = [\Sigma|\Delta F|^2/\Sigma|F_o|^2] = 0.069$.

All computations were made using SHELX76[9] on a DEC VAX-11/750. Fractional atomic coordinates, thermal parameters, full lists of bond lengths and angles, and lists of F_o/F_c values have been deposited as supplementary material with the Editor, from whom copies are avilable on request. Atomic coordinates have also been deposited with the Cambridge Crystallographic Data Centre.

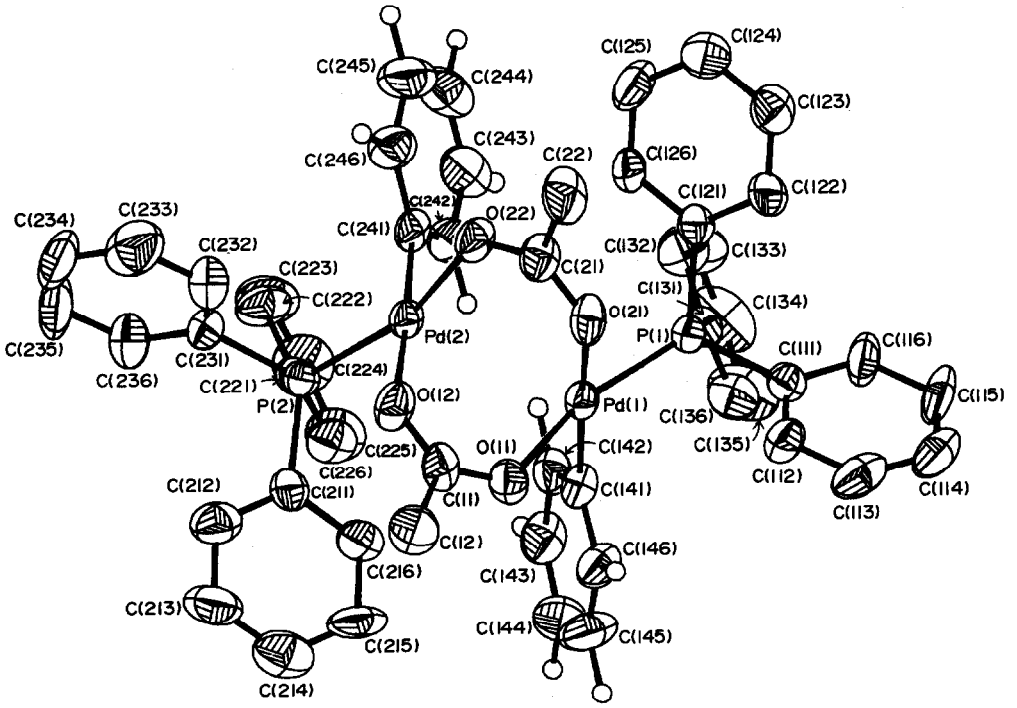


Fig. 1. The crystal structure of $[Pd_2(O_2CMe)_2(C_6H_5)_2(PPh_3)_2]$ with hydrogens on the phosphine phenyl rings and methyl groups omitted for clarity. The thermal ellipsoids are drawn to include 50% probability [E. K. Davies, SNOOPI program for drawing crystal structures, University of Oxford (1983)].

DISCUSSION

The molecular structure is illustrated in Fig. 1. Selected bond lengths and angles are given in Table 1. The two palladium atoms are linked by two *syn–syn* acetate bridges, with the acetate oxygens adopting a *cis*-configuration at the square planar palladium(II) atoms, as in $[Pd_2(O_2CMe)_2Cl_2(Me_2PPh)_2]$.[10] The other two coordination sites on each palladium are occupied by a phenyl group and a triphenylphosphine ligand with the coordinated atoms remaining within 0.4 Å of planarity at both palladiums. The bulky phosphines are kept well apart by these two PdO_2CP planes being splayed at an angle of 38° and a torsion angle between the phosphorus atoms across the Pd–Pd axis of 115°. By comparison the torsion angle between the bonded carbon atoms of the phenyl groups [C(141) and C(241)] is 85°. There is no question of a Pd—Pd bond with these atoms 3.079 Å apart.

Concerning the formation of our compound, we

Table 1. Selected bond lengths (Å) and angles (°) for $[Pd_2(\mu\text{-}O_2CMe)_2(C_6H_5)_2(PPh_3)_2]$

		Bond lengths	
Pd(2)—Pd(1)	3.079(4)	O(11)—Pd(1)	2.092(8)
O(21)—Pd(1)	2.136(8)	P(1)—Pd(1)	2.223(4)
C(141)—Pd(1)	1.969(10)	O(12)—Pd(2)	2.126(9)
O(22)—Pd(2)	2.100(9)	P(2)—Pd(2)	2.221(4)
C(241)—Pd(2)	1.953(11)	C(11)—O(11)	1.260(12)
C(11)—O(12)	1.234(13)	C(12)—C(11)	1.497(16)
C(21)—O(21)	1.265(13)	C(21)—O(22)	1.251(13)
C(22)—C(21)	1.525(16)	C(111)—P(1)	1.821(9)
C(121)—P(1)	1.824(8)	C(131)—P(1)	1.837(9)
C(211)—P(2)	1.828(9)	C(221)—P(2)	1.817(9)
C(231)—P(2)	1.814(9)		
		Bond angles	
O(11)—Pd(1)—Pd(2)	76.4(3)	O(21)—Pd(1)—Pd(2)	78.5(3)
O(21)—Pd(1)—O(11)	87.3(3)	P(1)—Pd(1)—Pd(2)	119.3(2)
P(1)—Pd(1)—O(11)	163.6(2)	P(1)—Pd(1)—O(21)	91.4(3)
C(141)—Pd(1)—Pd(2)	105.4(4)	C(141)—Pd(1)—O(11)	88.0(4)
C(141)—Pd(1)—O(21)	173.0(3)	C(141)—Pd(1)—P(1)	91.6(4)
O(12)—Pd(2)—Pd(1)	78.2(3)	O(22)—Pd(2)—Pd(1)	76.7(3)
O(22)—Pd(2)—O(12)	88.3(4)	P(2)—Pd(2)—Pd(1)	120.9(2)
P(2)—Pd(2)—O(12)	91.6(3)	P(2)—Pd(2)—O(22)	162.0(2)
C(241)—Pd(2)—Pd(1)	105.5(4)	C(241)—Pd(2)—O(12)	174.4(3)
C(241)—Pd(2)—O(22)	88.5(4)	C(241)—Pd(2)—P(2)	90.0(4)
C(11)—O(11)—Pd(1)	128.9(7)	C(11)—O(12)—Pd(2)	125.9(7)
O(12)—C(11)—O(11)	125.3(10)	C(12)—C(11)—O(11)	116.6(10)
C(12)—C(11)—O(12)	118.1(9)	C(21)—O(21)—Pd(1)	124.2(7)
C(21)—O(22)—Pd(2)	128.2(7)	O(22)—C(21)—O(21)	126.4(9)
C(22)—C(21)—O(21)	117.0(10)	C(22)—C(21)—O(22)	116.6(10)
C(111)—P(1)—Pd(1)	109.3(3)	C(121)—P(1)—Pd(1)	111.4(3)
C(121)—P(1)—C(111)	104.8(4)	C(131)—P(1)—Pd(1)	123.9(4)
C(131)—P(1)—C(111)	102.1(4)	C(131)—P(1)—C(121)	103.6(4)
C(112)—C(111)—P(1)	118.8(5)	C(116)—C(111)—P(1)	121.2(6)
C(122)—C(121)—P(1)	121.2(5)	C(126)—C(121)—P(1)	118.7(6)
C(132)—C(131)—P(1)	120.9(5)	C(136)—C(131)—P(1)	119.1(6)
C(142)—C(141)—Pd(1)	124.9(8)	C(146)—C(141)—Pd(1)	117.7(8)
C(211)—P(2)—Pd(2)	111.6(4)	C(221)—P(2)—Pd(2)	121.8(4)
C(221)—P(2)—C(211)	104.7(4)	C(231)—P(2)—Pd(2)	107.1(3)
C(231)—P(2)—C(211)	104.8(4)	C(231)—P(2)—C(221)	105.4(4)
C(212)—C(211)—P(2)	122.9(5)	C(216)—C(211)—P(2)	117.0(6)
C(222)—C(221)—P(2)	119.5(5)	C(226)—C(221)—P(2)	120.1(6)
C(232)—C(231)—P(2)	118.2(7)	C(236)—C(231)—P(2)	121.7(6)
C(242)—C(241)—Pd(2)	124.3(8)	C(246)—C(241)—Pd(2)	119.2(8)

note that the P—C bond fission has, unusually, not come from an oxidative addition. Our reaction has similarities to the recent finding[11] that triphenylphosphine is cleaved by $[Ru_2(PhCONH)_4Cl]$ to give $[Ru_2Ph_2(PhCONH)_2\{Ph_2POC(Ph)N\}_2]$. In that example the diphenylphosphido group becomes attached to the benzamide residue, but in our reaction the Ph_2P units must form some soluble compound, possibly a palladium complex (our yield is 41%), which we have not identified. We have also found that the assertion[12] that palladium(II) carboxylates decompose when warmed in alcohols is incorrect.

Acknowledgements—We thank the S.E.R.C. for financial support, including provision of instruments and computing facilities and a C.A.S.E. studentship (O.D.S.) with the valued collaboration of ICI Petrochemicals and Plastics Division. We are also grateful to Ms J. Elliott (King's College, London) for ^{13}C and ^{31}P NMR spectra, and to Dr R. J. Errington for helpful discussions.

REFERENCES

1. D. R. Coulson, *J. Chem. Soc., Chem. Commun.* 1968, 1530; C. W. Bradford, R. S. Nyholm, G. J. Gainsford, J. M. Guss, P. R. Ireland and R. Mason, *J. Chem. Soc., Chem. Commun.* 1972, 82; C. W. Bradford and R. S. Nyholm, *J. Chem. Soc., Dalton Trans.* 1973, 529; J. R. Blickensderfer and H. D. Kaesz, *J. Am. Chem. Soc.* 1975, **97**, 2681; D. R. Fahey and J. E. Mahan, *J. Am. Chem. Soc.* 1976, **98**, 4499; D. G. Evans, G. R. Hughes, D. M. P. Mingos, J.-M. Bassett and A. J. Welch, *J. Chem. Soc., Chem. Commun.* 1980, 1255; W. Beck, M. Keubler, E. Leidl, U. Nagel, M. Schaal, S. Cenini, P. del Buttero, E. Licandro, S. Maiorana and A. Chiesi Villa, *J. Chem. Soc., Chem. Commun.* 1981, 446.
2. T. Yamane, K. Kikukawa, M. Takagi and T. Matsuda, *Tetrahedron* 1973, **29**, 955.
3. A. Nakamura and S. Otsuka, *Tetrahedron Lett.* 1974, 463.
4. M. L. H. Green, M. J. Smith, H. Felkin and G. Swierczewski, *J. Chem. Soc., Chem. Commun.* 1971, 158.
5. A. B. Goel, *Inorg. Chim. Acta* 1984, **84**, L25.
6. K. Kikukawa and T. Matsuda, *J. Organomet. Chem.* 1982, **235**, 243.
7. M. B. Hursthouse, R. A. Jones, K. M. A. Malik and G. Wilkinson, *J. Am. Chem. Soc.* 1979, **101**, 4128.
8. N. Walker and D. Stuart, *Acta Cryst.* 1983, **A39**, 158.
9. G. M. Sheldrick, *SHELX76 Program for Crystal Structure Determination.* University of Cambridge (1976).
10. J. Powell and T. Jack, *Inorg. Chem.* 1972, **11**, 1039.
11. A. R. Chakravarty, F. A. Cotton and D. A. Tocher, *J. Am. Chem. Soc.* 1984, **106**, 6409.
12. T. A. Stephenson, S. M. Morehouse, A. R. Powell, J. P. Heffer and G. Wilkinson, *J. Chem. Soc.* 1965, 3632.

Polyhedron Vol. 5, No. 9, pp. 1479–1482, 1986
Printed in Great Britain

0277-5387/86 $3.00+.00
Pergamon Journals Ltd

SOLVENT EXTRACTION OF METAL IONS FROM AQUEOUS SOLUTIONS CONTAINING *N,N,N',N'*-ETHYLENEDIAMINETETRAACETIC AND RELATED ACIDS—II.* La(III) AND DIETHYLENETRIAMINEPENTAACETIC ACID

FAWZI H. AL-DABBAGH and JOSEPH I. BULLOCK†

Department of Chemistry, University of Surrey, Guildford GU2 5XH, U.K.

(*Received* 23 *January* 1986; *accepted* 10 *February* 1986)

Abstract—In the absence of a competing anion, $[La(DTPA)]^{2-}$ was extracted from aqueous phases in the pH ranges 1–3 by the perchlorate salt of the primary amine Primene JM-T. The addition of small amounts of SO_4^{2-} to the aqueous phases depressed the extraction of La to near zero. As the SO_4^{2-} concentration was increased further, D_{La} increased to values greater than that found in the absence of SO_4^{2-}; this was caused by a change in the mechanism of extraction and $[La(SO_4)_2]^-$ became the extracted species.

The extraction of lanthanides(III) from aqueous phases containing aminepolycarboxylic acids at low pH into Primene JM-T and other amines in the absence of a complexing inorganic anion has long been supposed[1–3] to occur through anions such as $[Eu(DTPA)]^{2-}$. If much SO_4^{2-} is also present then the $[Ln(SO_4)_2]^-$ complexes are said to be extracted[4] with the organic acids acting as aqueous-phase masking agents since, for example, an increase in the complexone concentration actually depressed the extraction of the lanthanide. The present study was aimed at demonstrating these assertions using, as example, the extraction of La from H_5DTPA solution. Throughout the abbreviation DTPA refers to a non-specific form; for specific cases charges are included. A comparison with the U(IV) system is offered.

EXPERIMENTAL

Materials

Primene JM-T was described before.[5] All other materials, including diluents, were of high quality.

Extraction experiments

All were repeated at least twice and two samples for analysis were taken from each aqueous phase. The reproducibility of the D_{La} values was 10% or better. D_{La} was determined by analysis of the initial and equilibrium aqueous phases only using xylenol orange.[6] All concentrations of La were determined in the presence of the same aqueous-phase components as used in the extractions.

Solutions of Primene JM-T and its salts were made up as before.[5] La solutions were prepared by dissolving La_2O_3 in perchloric acid and, after dilution, adjusting the pH with sodium or ammonium hydroxides; pH was measured with calibrated Philips PW 9148 or 9409 meters. All quoted pH values refer to the equilibrium aqueous phases.

RESULTS AND DISCUSSION

There are major differences between the species formed by La(III) and U(IV) with amine-polycarboxylate anions in the pH range 1–3. The formation constants for La(III) are much smaller, giving rise to a considerable amount of free La ion; it is thus possible that a second complexing agent could, by interacting with the free La ion, produce a competing mechanism of extraction which would be unimportant in the U(IV) systems.[5] Also, protonated forms such as $[La(H \cdot DTPA)]^-$ are found but similar U(IV) species are unknown. Further, hydrolysis of the complexes will occur at a lower pH for U(IV) than La(III). With regard to the formation of ternary complexes with a second

* For Part I see Ref. 5.

† Author to whom correspondence should be addressed.

Table 1. Species distribution (%) in La(III) and U(IV) solutions containing DTPA[a]

			pH			
			1	2	3	4
$[DTPA]^{5-}$	$\log K = 19.48$[a]	La^{3+}	—	95.5	10.8	0.4
$[H\cdot DTPA]^{4-}$	$\log K = 2.60$[ab]	$[La(DTPA)]^{2-}$	—	0.9	63.8	95.8
		$[La(H\cdot DTPA)]^{-}$	—	3.6	25.4	3.8
$[DTPA]^{5-}$	$\log K = 28.76$[c]	U^{4+}	4.6	0.02	1×10^{-3}	—
		$[U(DTPA)]^{-}$	95.4	99.98	99.99	—

[a] Total metal ion = total H_5DTPA; for log K values, see Ref. 9.
[b] For $[La(DTPA)]^{2-} + H^+ \rightleftharpoons [La(H\cdot DTPA)]^-$.
[c] Reference 10.

Table 2. Extraction data for La(III): variation of D_{La} with pH and SO_4^{2-} concentration

Series 1.	Primene JM-T perchlorate[a] [La(III)–$HClO_4$, pH 2, $D_{La} = 0.00$] $H_5DTPA = La(III) = 5.00\times10^{-4}$ mol dm^{-3}						
pH	1.45	1.70	2.00	2.40	2.70		
D_{La}	0.02	0.09	0.13	0.18	0.23		
Series 2.	Primene JM-T perchlorate[a] (H_5DTPA absent) $SO_4^{2-} = 0.05$ mol dm^{-3}; $La(III) = 5.00\times10^{-4}$ mol dm^{-3}						
pH	1.68	2.23	2.90	3.58			
D_{La}	0.24	0.29	0.83	1.06			
Series 3.	Primene JM-T perchlorate[a]; pH 2.80 $La = H_5DTPA = 5.02\times10^{-4}$ mol dm^{-3}						
SO_4^{2-}	0.000	0.005	0.010	0.020	0.030	0.040	0.050
D_{La}	0.19	0.13	0.04	0.25	0.48	0.54	0.67

[a] Primene JM-T = 0.033 mol dm^{-3}.

ligand, for example SO_4^{2-}, the formation constants:

$$M^{n+} + xSO_4^{2-} \rightleftharpoons [M(SO_4)_x]^{(2x-n)-}$$

are about two orders of magnitude smaller for La(III) ($I = 0.5$ mol dm^{-3}; La(III):[7] $\log K_1 = 1.77$, $\log \beta_2 = 2.66$; U(IV):[8] $\log K_1 = 3.42$, $\log \beta_2 = 5.82$). By analogy the formation constants for mixed-ligand complexes, e.g. $[M(DTPA)SO_4]^{a-}$, are likely to be lower for M = La ($a = 4$) than for M = U ($a = 3$). Speciation in the La and U(IV) systems is shown in Table 1.

Extraction of La(III) *from DTPA solution by Primene JM-T perchlorate (solvent xylene)*

As expected no extraction was found at pH 2 from a solution of La(III) in perchloric acid. Extraction was found from La(III)–DTPA solution and increased as the pH was raised towards 3 (Table 2, series 1) in keeping with the results given in Table 1. Extraction[5] from U(IV)–DTPA was more marked at the lower pH values. An amine dependence experiment (Table 3, series 1) gave a plot of log D_{La} against log [Primene JM-T] with a slope of 1.81 which would suggest that $[La(DTPA)]^{2-}$ was the extracted species.

Table 3. Primene JM-T concentration dependencies[a]

Series 1.	Primene JM-T perchlorate (JM-T) (mol dm^{-3}) (pH 2.80)				
JM-T	0.033	0.030	0.028	0.025	0.020
D_{La}	0.238	0.197	0.177	0.143	0.102
Series 2.	JM-T (mol dm^{-3}) (pH 2.80)				
	(a) $SO_4^{2-} = 0.005$ mol dm^{-3}				
JM-T	0.033	0.030	0.028	0.025	0.020
D_{La}	0.131	0.112	0.092	0.074	0.056
	(b) $SO_4^{2-} = 0.050$ mol dm^{-3}				
JM-T	0.033	0.030	0.028	0.025	0.020
D_{La}	0.639	0.578	0.536	0.479	0.384

[a] $La(III) = H_5DTPA = 5.02\times10^{-4}$ mol dm^{-3}.

Table 4. Equilibrium H_5DTPA concentrations[a]

Series 1. Total La = 5.02×10^{-4} mol dm^{-3} = total H_5DTPA [see Table 2 (series 3)]						
SO_4^{2-}	0.005	0.010	0.020	0.030	0.030	0.050
$[DTPA]_{AQ}$[b]	28	30	33	40	41	46
$[DTPA]_{ORG}$	22	20	17	10	9	4
$[La]_{ORG}$	5.62	1.98	10.1	16.4	17.6	20.1
Series 2. Total H_5DTPA = 5.01×10^{-4} mol dm^{-3}, total La = 0.00						
SO_4^{2-}	0.005	0.010	0.020	0.030	0.040	0.050
$[DTPA]_{AQ}$	36.0	35.2	34.8	34.0	33.6	33.2
$[DTPA]_{ORG}$	14.1	14.9	15.3	16.1	16.5	16.9

[a] Primene JM-T perchlorate = 0.033 mol dm^{-3} (pH 2.80).

[b] $[DTPA]_{AQ}$, $[DTPA]_{ORG}$ and $[La]_{ORG}$: multiply value quoted by 10^{-5} mol dm^{-3}; SO_4^{2-} in mol dm^{-3}.

Extraction of La(III) *from solutions containing* SO_4^{2-} *by Primene JM-T perchlorate or sulphate (solvent xylene)*

La(III)–SO_4^{2-}. In the presence of 0.05 mol dm^{-3} SO_4^{2-}, La(III) was more strongly extracted into Primene JM-T perchlorate at a given pH (Table 2, series 2) than from DTPA solution containing no SO_4^{2-}. Further, when Primene JM-T sulphate was used with an aqueous phase containing 0.5 mol dm^{-3} SO_4^{2-} at pH 2 there was no detectable La present in the equilibrium aqueous phase. The results strongly suggest the extraction of $[La(SO_4)_2]^-$ {there is evidence[11] for the extraction of both $[La(SO_4)_2]^-$ and $[La(SO_4)_3]^{3-}$}.

La(III)–DTPA–SO_4^{2-}. The addition of small amounts of SO_4^{2-} to aqueous phases containing La(III)–DTPA at pH 2.80 reduced D_{La} (Table 2, series 3) for extraction into Primene JM-T perchlorate to almost zero near 0.01 mol dm^{-3} SO_4^{2-}. It is possible that a non-extractable, mixed-ligand complex, e.g. $[La(DTPA)(SO_4)]^{4-}$, was formed. In an earlier study,[12] lanthanide(III) mixed-ligand complexes with DTPA and iminodiacetate were not found but subsequent[13,14] studies identified such complexes with phthalate, malonate, tartrate and malate. Since $[La(EDTA)(H_2O)_3]^-$ is nine-coordinate,[15] coordination numbers greater than 8 involving DTPA are possible. The slope of an amine dependence plot [0.005 mol dm^{-3} SO_4^{2-} (Table 3, series 2a)] was 2.13 which implied that $[La(DTPA)]^{2-}$ was extracted at low SO_4^{2-}. On increasing the SO_4^{2-} concentration further (Table 2, series 3), D_{La} began to increase to values greater than that found in the absence of SO_4^{2-}. The slope of the amine dependence plot [0.05 mol dm^{-3} SO_4^{2-} (Table 3, series 2b)] became 1.01. This suggested a change in the extraction mechanism with $[La(SO_4)_2]^-$ as the new extracted species. This was confirmed by bringing the SO_4^{2-} concentration in each of the equilibrium aqueous phases at pH 2.80 from Table 2 (series 3) to 0.5 mol dm^{-3} and re-extracting with Primene JM-T sulphate when all the residual La was extracted. Titration of the new equilibrium aqueous phases for DTPA with zinc ions clearly showed (Table 4, series 1) that, in the initial extractions from the higher SO_4^{2-} concentrations, the equilibrium organic-phase La concentration was much greater than that of DTPA. $[La(DTPA)]^{2-}$ cannot be the only extracted species across the whole SO_4^{2-} concentration range and a change in mechanism to give predominantly organic-phase $[La(SO_4)_2]^-$ must occur. It is of interest to note that the weakly complexing SO_4^{2-} can compete so successfully with DTPA for the metal ion in the solvent extraction system. In our experiments, La and H_5DTPA were introduced at the same concentration and so, if free La is present at the prevailing pH (Table 1), so must free DTPA. In the absence of La and SO_4^{2-}, DTPA species exchange to a considerable extent with organic-phase perchlorate (Table 4, series 2) and this might well have a synergic influence on the successful competition of SO_4^{2-} over DTPA for the available aqueous-phase La. The reextraction experiments (Table 4, series 1), showed that at low SO_4^{2-} concentrations the initial, equilibrium organic phases contained more DTPA than La. Such exchanges of DTPA and perchlorate are not important in the U(IV) systems since the aminepolycarboxylate complexes are completely formed at the prevailing aqueous-phase pH.

REFERENCES

1. F. L. Moore, *Anal. Chem.* 1965, **37**, 1235.
2. D. Kuiper, In *Solvent Extraction Chemistry of Metals* (Edited by H. A. C. McKay, T. V. Healy, I. L.

Jenkins and A. Naylor), p. 421. McMillan, London (1965).
3. F. L. Moore, *Anal. Chem.* 1966, **38**, 905.
4. A. C. Rice, *U.S. Bur. Mines, Rep. Invest.* 6205 (1963).
5. F. H. Al-Dabbagh and J. I. Bullock, *Inorg. Chim. Acta* 1985, **110**, 69.
6. V. Svoboda and V. Chromy, *Talanta* 1966, **13**, 237.
7. A. Aziz and S. J. Lyle, *J. Inorg. Nucl. Chem.* 1970, **32**, 1925.
8. J. C. Sullivan and J. C. Hindman, *J. Am. Chem. Soc.* 1952, **74**, 6091.
9. A. E. Martell and R. M. Smith, *Critical Stability Constants*, Vol. 1, p. 281. Plenum, New York (1974).
10. E. M. Piskunov and A. G. Rykov, *Sov. Radiochem.* 1972, **14**, 265.
11. A. I. Sherchuk, Z. M. Ivanova and L. N. Stepanova, *Russ. J. Inorg. Chem.* 1969, **14**, 1495.
12. C. L. Thompson and J. A. Loraas, *Inorg. Chem.* 1963, **2**, 89.
13. R. Kumar, R. C. Sharma and G. K. Chaturvedi, *Monatsh. Chem.* 1979, **110**, 907.
14. S. P. Tripathi, R. C. Sharma and G. K. Chaturvedi, *J. Indian Chem. Soc.* 1980, **52**, 203.
15. J. L. Hoard, B. Lee and M. D. Lind, *J. Am. Chem. Soc.* 1965, **87**, 1612.

Polyhedron Vol. 5, No. 9, pp. 1483–1485, 1986
Printed in Great Britain

0277-5387/86 $3.00+.00
Pergamon Journals Ltd

COMMUNICATION

SYNTHESIS, FORMATION CONSTANTS AND REACTIONS OF CATIONIC RHODIUM(I) COMPLEXES OF NITRILES

MYOUNG KIE LEE, IN BUM KIM, HWA-KUN PARK, SOON HEUM PARK and CHONG SHIK CHIN*

Department of Chemistry, Sogang University, CPO Box 1142, Seoul 121, Korea

(*Received* 29 *July* 1985; *accepted after revision* 20 *January* 1986)

Abstract—Reactions of $Rh(ClO_4)(CO)(PPh_3)_2$ with nitriles produce new cationic rhodium(I) complexes, $[RhL(CO)(PPh_3)_2]ClO_4$ [L = CH_3CN (**1**), $CH_3CH_2CH_2CN$ (**2**) or C_6H_5CN (**3**)], whose spectral data suggest that the nitriles are coordinated through the nitrogen atom. Formation constants for the reaction $Rh(ClO_4)(CO)(PPh_3)_2 + L \rightleftharpoons [RhL(CO)(PPh_3)_2]ClO_4$, have been measured to be 1.01×10^5 M^{-1} (CH_3CN), 1.07×10^5 M^{-1} ($CH_3CH_2CH_2CN$) and 2.59×10^4 M^{-1} (C_6H_5CN) at 25°C in monochlorobenzene. The differences in the formation constants for the different nitriles seem to be predominantly due to differences in ΔH (not to differences in ΔS). The nitriles in **1–3** are readily replaced with nitrogen base ligands (unsaturated nitriles and pyridine) and PPh_3.

The synthesis, physical properties and chemical reactivities of cationic rhodium(I) complexes of saturated nitriles[1–3] and iridium(I) complexes of unsaturated[4–6] and saturated[7] nitriles, $[ML(CO)(PPh_3)_2]ClO_4$ (M = Rh or Ir, L = unsaturated or saturated nitriles), have been reported recently. This communication reports the synthesis, formation constants with thermodynamic parameters, and reactions of new cationic rhodium(I) complexes of saturated and aromatic nitriles.

Addition of nitriles (L) into the yellow solution of $Rh(ClO_4)(CO)(PPh_3)_2$ in benzene at 25°C under nitrogen resulted within 5 min in yellow-orange microcrystals of $[RhL(CO)(PPh_3)_2]ClO_4$ [eqn (1)]:†

$$Rh(ClO_4)(CO)(PPh_3)_2 + L \rightarrow [RhL(CO)(PPh_3)_2]ClO_4, \quad (1)$$

where L = CH_3CN (**1**), $CH_3CH_2CH_2CN$ (**2**) or C_6H_5CN (**3**). Complexes **1–3** are stable in the solid state in air and in solution under nitrogen at 25°C, and soluble in polar solvents (chloroform, dichloromethane and acetonitrile) and insoluble in non-polar solvents (benzene and hexane). The molar-conductance values (110–120 Ω^{-1} cm^2 mol^{-1}) of **1–3** (5.0×10^{-5} M in dichloromethane) suggest that the complexes are 1 : 1 electrolytes.‡

IR spectral data (Table 1) unambiguously show that nitriles in complexes **1–3** are coordinated to rhodium through the nitrogen atom, and not through the π-system of the nitrile group. It is well-known that ν(CN) for a nitrile increases upon coordination through the nitrogen atom,[8–10] while it decreases significantly upon coordination through the π-system of the nitrile group.[10] A broad and strong absorption band at *ca* 1100 cm^{-1} (not listed in Table 1) observed for all the complexes is attributable to the anionic tetrahedral ClO_4 (T_d) group,[11]

* Author to whom correspondence should be addressed.

† One drop (*ca* 0.75 mmol) of a nitrile (CH_3CN, $CH_3CH_2CH_2CN$ or C_6H_5CN), 1.20 g (0.26 mmol) of $Rh(ClO_4)(CO)(PPh_3)_2$ and 10 cm^3 of benzene were used. The yellow-orange crystals were collected by filtration, washed with benzene (5 cm^3) and hexane (15 cm^3), and dried *in vacuo*. The yield was *ca* 85% based on $[RhL(CO)(PPh_3)_3]ClO_4$ [L = CH_3CN (**1**), $CH_3CH_2CH_2CN$ (**2**) or C_6H_5CN (**3**)]. Found: C, 59.5; H, 4.8; N, 1.6%. Calc. for $RhC_{39}H_{33}NClO_5P_2$ (**1**): C, 58.8; H, 4.2; N, 1.8%. Found: C, 60.7; H, 4.4; N, 1.7%. Calc. for $RhC_{41}H_{37}NClO_5P_2$ (**2**): C, 59.8; H, 4.5; N, 1.7%. Found: C, 62.6; H, 3.9; N, 1.7%. Calc. for $RhC_{44}H_{35}NClO_5P_2$ (**3**): C, 61.6; H, 4.1; N, 1.6%.

‡ The molar conductance of a standard 1 : 1 electrolyte, $[(C_3H_7)_4N]PF_6$, in dichloromethane at 25°C was measured to be 110 Ω^{-1} cm^2 mol^{-1}.

Table 1. IR (in Nujol), electronic absorption (in monochlorobenzene) and ^1H NMR (in $CDCl_3$) spectral data for $[RhL(CO)(PPh_3)_2]ClO_4$ [L = CH_3CN (**1**), $CH_3CH_2CH_2CN$ (**2**) or C_6H_5CN (**3**)]

Compound	IR absorption (cm^{-1})		Electronic absorption (nm)
	ν(CN) [$\Delta\nu$(CN)][a]	ν(CO)[b]	λ_{max} (ε)[c]
1	2291 (36)	2000	374 (3500)
2	2291 (40)	2020	375 (3550)
3	2270 (40)	2026	379 (3460)
	^1H NMR chemical shift (ppm)[d]		
CH_3CN	1.73 (s, CH_3)		
$CH_3CH_2CH_2CN$	0.77 (t, CH_3), 1.35 (m, CH_3CH_2), 2.09 (t, CH_2CN)		
C_6H_5CN	*ca* 7.5 (m, C_6H_5)		
1	1.55 (s, CH_3)		
2	0.23 (t, CH_3), 0.75 (m, CH_3CH_2), 1.83 (t, CH_2CN)		
3	*ca* 7.5 (m, C_6H_5)		

[a] Weak. $\Delta\nu$(CN) = ν(CN) of coordinated nitrile − ν(CN) of free nitrile.
[b] Very strong.
[c] At 25°C under nitrogen in the presence of excess corresponding L.
[d] At 25°C at 60 MHz. All complexes (**1–3**) show a multiplet due to the phenyl protons of PPh_3 at *ca* 7.5 ppm. Relative to TMS.

which supports the view that the complexes are 1 : 1 electrolytes as confirmed by the conductance measurements. It is noticed in Table 1 that ν(CO) for the CH_3CN complex (**1**) is lower than those of other nitrile complexes.

Electronic absorption spectral data (Table 1) also suggest that **1–3** are four-coordinated rhodium(I) complexes and the nitriles in **1–3** are coordinated through the nitrogen atom. It is well-known that the four-coordinated rhodium(I) complexes $RhA(CO)(PPh_3)_2$ [A = monodentate nitrogen base ligand such as NCO, NO_2, NCS or $N(CN)_2$][12] and $[RhL(CO)(PPh_3)_2]ClO_4$ (L = monodentate nitrile coordinated through the nitrogen atom)[3] show an absorption band at 365–383 nm (ε 3400–4300).

The observed chemical shifts of the nitrile protons in **1** and **2** (Table 1) and the ratios (not given in Table 1) of the phenyl protons of PPh_3 to nitrile protons clearly indicate a $RhL(PPh_3)_2$ (L = CH_3CN or $CH_3CH_2CH_2CN$) moiety in **1** and **2**. It is seen in Table 1 that all protons of nitriles in **1** and **2** showed upfield shifts relative to those of the free nitriles as observed for related rhodium(I) and iridium(I) complexes of nitriles coordinated through the nitrogen atom.[2,3,6] The spin coupling between ^{103}Rh and the protons of coordinated nitriles has not been observed for the complexes prepared in this study.

Formation constants and thermodynamic parameters have been determined for eqn (2):*

$$Rh(ClO_4)(CO)(PPh_3)_2 + L \rightleftharpoons [RhL(CO)(PPh_3)_2]ClO_4 \quad (2)$$

where L = CH_3CN, $CH_3CH_2CH_2CN$, C_6H_5CN.

It is noticed in Table 2 that the formation constant of **3** is smaller than those of **1** and **2**, which seems to be predominantly due to differences in ΔH (not to differences in ΔS).

Nitriles in **1–3** are readily replaced by nitrogen and phosphorus base ligands according to eqn (3):

$$[RhL(CO)(PPh_3)_2]ClO_4 + L' \rightarrow [RhL'(CO)(PPh_3)_2]ClO_4 + L, \quad (3)$$

where L = CH_3CN, $CH_3CH_2CH_2CN$ or C_6H_5CN; and L′ = $CH_2{=}CHCN$,[1] $CH_2{=}C(CH_3)CN$,[3]

* Formation constants for eqn (2) were determined in the same manner as described for the formation constants of $[RhL(CO)(PPh_3)_2]ClO_4$ (L = unsaturated nitriles coordinated through the nitrogen atom).[3] The molar conductances of **1–3** in monochlorobenzene are practically zero, indicating that the ionization $[RhL(CO)(PPh_3)_2]ClO_4 \rightarrow [RhL(CO)(PPh_3)_2]^+ + ClO_4^-$ is negligible, while that in dichloromethane is 110–120 Ω^{-1} cm^2 mol^{-1}, suggesting that the complexes undergo complete ionization. A similar observation was previously reported for the related complexes of unsaturated nitriles[3] and $Rh(ClO_4)(CO)(PPh_3)_2$.[11]

Table 2. Formation constants and thermodynamic parameters for the reaction $Rh(ClO_4)(CO)(PPh_3)_2 + L \rightleftharpoons [RhL(CO)(PPh_3)_2]ClO_4$ (L = CH_3CN, $CH_3CH_2CH_2CN$ or C_6H_5CN) in monochlorobenzene

L	Formation constant[a] (M^{-1})	ΔH^b (kcal mol^{-1})	ΔS (cal mol^{-1} deg^{-1})
CH_3CN	1.01×10^5	-7.3 ± 0.8	-2 ± 3
$CH_3CH_2CH_2CN$	1.07×10^5	-7.3 ± 0.4	-1 ± 1
C_6H_5CN	2.59×10^4	-6.7 ± 0.1	-2 ± 0.3

[a] At 25°C.
[b] In the region of 25–55°C.

$CH_2{=}CHCH_2CN$,[3] *cis,trans*-$CH_3CH{=}CHCN$,[3] PPh_3[13] or C_5H_5N.[13]

The reactions of **1–3** with unsaturated aldehydes, however, do not produce $[Rh(RCH{=}CHCHO)(CO)(PPh_3)_2]ClO_4$ (R = H or CH_3), which are readily formed by the reactions of $Rh(ClO_4)(CO)(PPh_3)_2$ with $RCH{=}CHCHO$.[14]

Acknowledgement—We wish to thank the Korean Science and Engineering Foundation for financial support.

REFERENCES

1. T. Kwon, J. C. Woo and C. S. Chin, *Polyhedron* 1983, **2**, 1225.
2. M. K. Lee, T. Kwon and C. S. Chin, *Bull. Korean Chem. Soc.* 1984, **5**, 88.
3. M. K. Lee, I. B. Kim and C. S. Chin, *J. Organomet. Chem.* 1985, **290**, 115.
4. J. C. Woo, S. H. Kim and C. S. Chin, *J. Polym. Sci., Chem. Educ.* 1982, **20**, 1947.
5. S. H. Park, H.-K. Park and C. S. Chin, *Bull. Korean Chem. Soc.* 1984, **5**, 167.
6. S. H. Park, H.-K. Park and C. S. Chin, *Inorg. Chem.* 1985, **24**, 1120.
7. C. S. Chin, H.-K. Park and W.-C. Joo, *Polyhedron* 1985, **4**, 1673.
8. S. J. Bryan, P. G. Hugget K. Wade, J. A. Daniels and J. R. Jennings, *Coord. Chem. Rev.* 1982, **44**, 149.
9. M. Klinger, *Adv. Organomet. Chem.* 1972, **10**, 115.
10. K. Nakamoto, *Infrared and Raman Spectra of Inorganic and Coordination Compounds*, p. 259. John Wiley, New York (1978).
11. J. Peone, Jr and L. Vaska, *Angew. Chem., Int. Ed. Engl.* 1971, **10**, 511.
12. R. Brady, B. R. Flynn, G. L. Geoffroy, H. B. Gray, J. Peone, Jr and L. Vaska, *Inorg. Chem.* 1976, **15**, 1485.
13. L. Vaska and J. Peone, Jr, *Suom. Kemistil.* 1971, **B44**, 317.
14. I. B. Kim and C. S. Chin, *Polyhedron* 1984, **3**, 1151.

Polyhedron Vol. 5, No. 9, pp. 1487–1488, 1986
Printed in Great Britain

0277–5387/86 $3.00+.00
Pergamon Journals Ltd

COMMUNICATION

CRYSTAL STRUCTURE OF $Ni(NCS)_2 \cdot 2Ph_3P$

T. TUNDE BAMGBOYE

Department of Chemistry, University of Ilorin, Ilorin, Nigeria

and

D. BRYAN SOWERBY*

Department of Chemistry, University of Nottingham, Nottingham, U.K.

(*Received* 10 *December* 1985; *accepted* 28 *February* 1986)

Abstract—Crystals of the complex $Ni(NCS)_2 \cdot 2Ph_3P$ are triclinic with $a = 7.939(4)$ Å, $b = 10.457(5)$ Å, $c = 11.474(5)$ Å, $\alpha = 111.08(3)°$, $\beta = 74.56(3)°$ and $\gamma = 92.25(3)°$. X-ray data for 2692 independent observed reflections were collected and the structure determined by Fourier methods and refined to $R = 0.038$. The nickel geometry is square planar with the triphenylphosphine ligands occupying *trans* positions. A feature of the structure is the large value (173.3°) for the Ni–N–C angles.

Structures have previously been determined for a number of nickel complexes containing tertiary phosphine ligands showing the presence of tetrahedral coordination about the central atom for the halide complexes.[1,2] The related thiocyanates are often square planar,[3] but, in a number of cases, octahedral coordination has been found as a result of both intra- and intermolecular interactions.[4] No data are available for the simple bis(triphenylphosphine) adduct of nickel thiocyanate and, in the context of general nickel stereochemistry, it was of interest to investigate its structure.

EXPERIMENTAL

The compound was prepared by treating a mixture of $Ni(NO_3)_2 \cdot 6H_2O$ with 2 mol of potassium thiocyanate in ethanol with an excess of triphenylphosphine. Crystals suitable for X-ray analysis were obtained by slow recrystallization from ethanol solution. Found: C, 65.2; H, 4.3; N, 4.0%. Calc. for $C_{38}H_{30}N_2NiP_2S_2$: C, 65.3; H, 4.2; N, 4.0%.

Crystal data

$C_{38}H_{30}N_2NiP_2S_2$, $M = 698.7$, triclinic, $a = 7.939(4)$ Å, $b = 10.457(5)$ Å, $c = 11.474(5)$ Å, $\alpha = 111.08(3)°$, $\beta = 74.56(3)°$, $\gamma = 92.25(3)°$, $U = 855$ Å^3, $Z = 1$, $D_c = 1.36$ g cm^{-3}, $F(000) = 362$, space group $P\bar{1}$, Mo-K_α radiation, $\lambda = 0.7107$ Å, $\mu = 8.07$ cm^{-1}, crystal size $1.3 \times 0.2 \times 0.35$ mm^3, rotating about *a*.

Structure determination

Data were collected using a Hilger and Watts four-circle diffractometer for 3211 reflections of which 2692 with $I > 3\sigma(I)$ were observed. Data reduction and subsequent crystallographic calculations used the CRYSTALS programs;[5] scattering factors were those for neutral atoms.[6] As the unit cell contains one molecule of the complex, the nickel atom lies on a centre of symmetry ($\frac{1}{2}, \frac{1}{2}, \frac{1}{2}$). The refinement converged at $R = 0.112$ with isotropic and $R = 0.038$ with anisotropic thermal parameters, and the hydrogen atoms placed (but not refined) at their calculated positions. The final atomic co-ordinates, temperature factors, observed and calculated structure factors, and torsion angles have been deposited as supplementary data with the

* Author to whom correspondence should be addressed.

Table 1. Bond lengths (Å) and angles (°) for $Ni(NCS)_2 \cdot 2Ph_3P$

Ni(1)–N(1)	1.819(3)
Ni(1)–P(1)	2.245(1)
N(1)–C(1)	1.161(4)
C(1)–S(1)	1.606(4)
P(1)–C(11)	1.818(3)
P(1)–C(21)	1.816(3)
P(1)–C(31)	1.816(3)
N(1)–Ni(1)–P(1)	92.1(1)
Ni(1)–N(1)–C(1)	173.3(3)
N(1)–C(1)–S(1)	179.5(3)
Ni(1)–P(1)–C(11)	117.9(1)
Ni(1)–P(1)–C(21)	111.2(1)
Ni(1)–P(1)–C(31)	111.1(1)
C(11)–P(1)–C(21)	104.4(1)
C(11)–P(1)–C(31)	104.3(1)
C(21)–P(1)–C(31)	107.1(2)

Editor, from whom copies are available on request.*

DISCUSSION

Important bond distance and angle data are collected in Table 1 and Fig. 1 shows the molecular structure and atom-numbering scheme. The complex forms isolated molecules; there are no intermolecular Ni...S interactions within 3.8 Å. The geometry about nickel is square planar [N(1)–Ni(1)–P(1) 92.08° and N(1)–Ni(1)–P(1′) 87.92°] and, as the metal atom lies on a centre of symmetry, the complex is necessarily the *trans* isomer. In keeping with the hardness of Ni^{2+}, the thiocyanate group is bonded via nitrogen. Surprisingly, the softer Pd^{2+} ion also bonds via nitrogen in $Pd(NCS)_2 \cdot 2Ph_3P$,[7] but via sulphur in $Pd(SCN)_2 \cdot 2Ph_2MeP$.[3]

Important features of the structure are the closeness to planarity of the $NiP_2(NCS)_2$ system and the large value (173.7°) for the Ni(1)–N(1)–C(1) angle. In the former, the maximum deviation of any atom [N(1) and N(1′)] from the best plane through the nine atoms is 0.01 Å. Both features can be interpreted in terms of π-bonding between nickel and nitrogen and, in agreement, the Ni(1)–N(1) bond length is short (1.819 Å). The isothiocyanate group is linear with distances in the expected ranges; the Ni–P distance is also as expected.

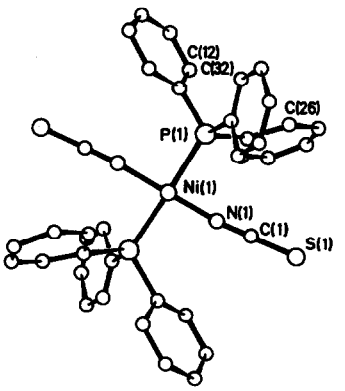


Fig. 1. Structure of $Ni(NCS)_2 \cdot 2Ph_3P$ showing the atom-numbering scheme.

* Atomic co-ordinates have also been deposited with the Cambridge Crystallographic Data Centre.

REFERENCES

1. G. Garton, D. E. Henn, H. M. Powell and L. M. Venanzi, *J. Chem. Soc.* 1963, 3625.
2. J. A. J. Jarves, R. H. B. Mais and P. G. Owston, *J. Chem. Soc. A* 1968, 1473.
3. J. J. Macdougall, J. H. Nelson, M. W. Babich, C. C. Fuller and R. A. Jacobson, *Inorg. Chim. Acta* 1978, **27**, 201.
4. B. M. Foxman, P. L. Goldberg and H. Mazurek, *Inorg. Chem.* 1981, **20**, 4368.
5. J. R. Carruthers, *CRYSTALS, the Oxford Crystallographic Programs* (1975).
6. *International Tables for X-ray Crystallography*, Vol. 4. Kynoch Press, Birmingham (1974).
7. A. J. Carty, P. C. Chien, N. J. Taylor and T. S. Wong, *J. Chem. Soc., Dalton Trans.* 1976, 572.

Polyhedron Vol. 5, No. 9, p. 1489, 1986
Pergamon Journals Ltd. Printed in Great Britain

BOOK REVIEW

Gmelin Handbook of Inorganic Chemistry, 8th Edition. Cu—Organocopper Compounds, Part 1, Organocopper Compounds. 1985, 2 illus., x + 470 pp., hard cover, DM1725, Springer, Berlin, ISBN 3-540-93517-7.

This is the second Gmelin Handbook on Organocopper compounds. Part 2, published in 1983, dealt with the metal dialkylcuprates, or "homocuprates", R_2CuM. Part 1 now covers the mono-organic copper(I) compounds RCu and RCu,MX or RCuX,M (the "heterocuprates").

These organocopper compounds have become widely used as sources of nucleophilic organic groups, particularly in substitution reactions with alkyl, vinyl or acyl halides, or propargyl sulphonates or carboxylates, or in conjugate additions to enones, and the reactivity can be modulated by the addition of metal halides such as BF_3, or of ligands such as sulphides or amines.

However, these compounds are often thermally unstable and very reactive towards oxygen and moisture, and few have been isolated and fully characterized. More usually the heterocuprates are formed in solution from an equimolar mixture of CuX and MR (organolithium or Grignard reagent), and their composition and degree of aggregation in solution may vary with the reaction conditions. In this volume, the compounds are therefore assigned the simplest formula as derived from the stoichiometry of the preparation, unless there is firm evidence for a different specific structure.

The first major section covers the compounds RCu (R = alkyl, alkenyl and aryl). These compounds often separate from organic solvents at low temperatures as coloured (often yellow to red), sometimes explosive solids. The perfluoroalkyl compounds are unusual in that they can be prepared from the perfluoralkyl iodides and activated copper, and, once formed, are not readily hydrolysed. The preparation, spectra, structure and chemical behaviour are clearly presented; for example the section on MeCu covers 8 pp. and includes 66 references. Families of related compounds are tabulated, and information on the more important members is amplified by extensive footnotes.

The next sections then deal in a similar way with the complexes with lithium salts, RCu,LiX (154 pp.) and with magnesium salts, RCu,MgX_2 (118 pp.). The most important part here is the extensive tabulation of the synthetic applications of these compounds in their reactions with organic halides, R′Y, to couple together the two organic groups to form RR′ (often with allylic or propargylic rearrangement within R′).

The complexes formed with salts of copper, silver, gold, zinc, tin, aluminium and titanium are then covered more briefly, then there is a substantial section (23 pp.) on the enhancement of reactivity which is obtained in the presence of boron compounds. The final sections deal with the modulation of the reactivity of the organocopper compounds by ligands such as dioxane, dialkylsulphides, amines and phosphines.

The text, as in all current volumes of Gmelin, is wholly in English, and the layout of the text and tables is excellent in the usual sanserif typeface. The formal literature closing date is the end of 1983, but some 1985 references are included. The authors are J. Faust, J. Füssel and H. Somer, and the editors J. Füssel and A. Slawisch.

This will be an invaluable source of reference to anyone who becomes involved in the application of organocopper compounds in organic synthesis, which is a rapidly expanding field. Unfortunately, at a price of DM1725 (£530, U.S. $750) it will be beyond the reach of many libraries.

A. G. DAVIES

Department of Chemistry
University College London
20 *Gordon Street*
London WC1H 0AJ, U.K.

Polyhedron Vol. 5, No. 10, pp. 1491–1497, 1986
Printed in Great Britain

0277–5387/86 $3.00+.00
Pergamon Journals Ltd

SYNTHESES AND CHARACTERIZATION OF $[Ru(\eta^5\text{-}C_5H_5)(AsPh_3)(L)X]$ AND $[Ru(\eta^5\text{-}C_5H_5)(AsPh_3)(L)(MeCN)]^+_mY^-$ (L = PPh_3 OR $AsPh_3$; X = F, Cl, Br, I, CN, H OR $SnCl_3$; Y = $HgCl_3$, Zn_2Cl_6 OR BPh_4; m = 1 OR 2)

KOLLIPARA MOHAN RAO, LALLAN MISHRA* and UMESH CHANDRA AGARWALA†

Department of Chemistry, Indian Institute of Technology, Kanpur 208016, India

(*Received* 23 *September* 1985; *accepted* 19 *December* 1985)

Abstract—The syntheses of the complexes $[(\eta^5\text{-}C_5H_5)Ru(AsPh_3)(L)X]$ (L = PPh_3 or $AsPh_3$; X = Cl, F, Br, I, H, CN or $SnCl_3$) and $[(\eta^5\text{-}C_5H_5)Ru(AsPh_3)(L)(MeCN)]^+Y^-$ (Y = $HgCl_3$, BPh_4 or Zn_2Cl_6) are described. They were characterized by elemental analyses, IR, UV and visible, PMR spectroscopy, X-ray powder diffraction, and mass spectral studies.

The potential chemical reactivities of the complexes $[(\eta^5\text{-}C_5H_5)RuX(PR_3)_2]$ (X = Cl, Br or I; R = Me or Ph) with various heterocyclic bases, dienes, trienes, NOX (X = Cl, Br, Br_3 or NO_2) etc. have recently received considerable attention in the chemical literature.[1–10] Interest in these molecules stems from the reactions of the substitution-reaction products which they show because of the close proximity of sterically hindered two trialkyl or triaryl phosphine molecules. It has recently been demonstrated that $[(\eta^5\text{-}C_5H_5)RuCl(PPh_3)_2]$ undergoes a substitution reaction under refluxing conditions for a very long period, giving $[(\eta^5\text{-}C_5H_5)RuCl(AsPh_3)_2]$ in good yield. Since, in our previous papers,[8,9] the substitution of one molecule of PPh_3 by a heterocyclic base like pyridine has been reported, it is anticipated that substitution reactions should proceed through stepwise replacement of one molecule by another. It was, therefore, of interest to extend our investigations of substitution reactions and to attempt to synthesize mixed complexes $\{[(\eta^5\text{-}C_5H_5)RuX(A)(B)]$ (A = PPh_3, $AsPh_3$ or $SbPh_3$; B = PPh_3, $AsPh_3$ or $SbPh_3$)$\}$, and to interconvert them. In this paper we describe the syntheses of these complexes, which have been characterized by chemical analyses, spectroscopic studies (IR, PMR and mass), the powder X-ray method, and by magnetic-susceptibility measurements.

EXPERIMENTAL

All the reagents were Analar or of chemically pure grade. All the solvents were dried and distilled before use. The reactions were carried out under a dry and pure nitrogen atmosphere. $[(\eta^5\text{-}C_5H_5)RuCl(PPh_3)_2]$, $[(\eta^5\text{-}C_5H_5)RuCl(AsPh_3)_2]$ and $[(\eta^5\text{-}C_5H_5)Ru(AsPh_3)_2H]$ were prepared by the literature methods.[7,11]

Preparation of complexes

(*A*) *Preparation of monochloromonocyclopentadienylmonotriphenylphosphine monotriphenylarsine ruthenium(II)* $\{[(\eta^5\text{-}C_5H_5)RuCl(AsPh_3)(PPh_3)]\}$ (**1**). A solution of $[(\eta^5\text{-}C_5H_5)RuCl(PPh_3)_2]$ (0.500 g, 7.0×10^{-4} mol) and $AsPh_3$ (0.4 g, 1.3×10^{-4} mol) in 60 cm^3 benzene was heated to reflux for 25 h. The resulting solution was concentrated to near dryness, the residue extracted by CH_2Cl_2 and the complex precipitated from the extract by using petroleum ether. It was centrifuged and purified by recrystallization from CH_2Cl_2–petroleum ether. It was filtered, washed with petroleum ether, and dried. The orange-yellow complex **1** was analysed (yield *ca* 78%).

(*B*) *Preparation of monohydridomonocyclopentadienylmonotriphenylarsine monotriphenylphosphine ruthenium(II)* $\{[(\eta^5\text{-}C_5H_5)Ru(AsPh_3)(PPh_3)H]\}$. (i) *Using* NaOMe–MeOH. A mixture of the orange-yellow coloured complex **1** (0.1 g, 1.3×10^{-4} mol) and sodium metal (0.20 g, *ca* 0.009 g atm) in 15

*Present address: S.C.P.G. College, Ballia 277001, India.
†Author to whom correspondence should be addressed.

cm^3 methanol was heated to reflux until all the starting material was dissolved (*ca* 20 min) with the simultaneous formation of a precipitate from the solution near the glass surface, which was separated by centrifugation, washed with small quantities of methanol, and dried *in vacuo*. It was identified as $[(\eta^5\text{-}C_5H_5)Ru(AsPh_3)(PPh_3)H]$ by analyses (yield *ca* 50%).

(ii) *Using* NaOEt–EtOH. The hydrido derivative was also prepared by the same procedure as given in B(i), except that ethanol (15 cm^3) was used in place of methanol. The yellow complex was collected and identified by chemical analyses and by comparing it with that prepared in B(i). Both samples were found to be identical.

(*C*) *Preparation of mono(fluoro, bromo or iodo)-monocyclopentadienylmonotriphenylarsine monotriphenylphosphine ruthenium(II)* $\{[(\eta^5\text{-}C_5H_5)Ru(AsPh_3)(PPh_3)X]$ (X = F, Br *or* I)$\}$. (i) *Using* HX (X = F, Br *or* I). A yellow suspension of $[(\eta^5\text{-}C_5H_5)Ru(AsPh_3)(PPh_3)H]$ (0.1 g, 1.4×10^{-3} mol) in methanol (15 cm^3) was treated with concentrated HX (five or six drops). Immediately, the yellow suspension dissolved to form a light yellowish-orange coloured solution which was stirred for about 10 min, whereby a brownish-orange precipitate deposited. It was collected by centrifuging the solution, washed with methanol and ether, and dried *in vacuo*. On analysis it was identified as $[(\eta^5\text{-}C_5H_5)Ru(AsPh_3)(PPh_3)X]$ (yield *ca* 90%).

(ii) *Using* KX (X = Br *or* I). Complexes of $[(\eta^5\text{-}C_5H_5)RuX(AsPh_3)(PPh_3)]$ (X = Br or I) were also prepared by heating under reflux a solution of $[RuCl(AsPh_3)_4(PPh_3)(\eta^5\text{-}C_5H_5)]$ (0.1 g, 1.3×10^{-4} mol) in ethanol (20 cm^3) with KX (0.200 g, *ca* 0.17 mol) for 1 h, whereupon brownish-orange crystals were deposited. These were separated by centrifuging the solution, washed with water, methanol and diethyl ether, and dried. On analysis the complex was identified as $[(\eta^5\text{-}C_5H_5)Ru(AsPh_3)(PPh_3)X]$ (X = Br or I) (yield *ca* 80%).

(iii) *Using* MeI. The iodo analogue of the complex was prepared by the procedure described in C(i) by treating $[(\eta^5\text{-}C_5H_5)Ru(AsPh_3)(PPh_3)H]$ (0.1 g, 1.4×10^{-4} mol) with methyl iodide (five or six drops) in methanol (10 cm^3). The resulting complex was identified as $[(\eta^5\text{-}C_5H_5)Ru(AsPh_3)(PPh_3)I]$.

(iv) The bromo analogue $[(\eta^5\text{-}C_5H_5)Ru(AsPh_3)(PPh_3)Br]$ was also prepared by heating to reflux a solution of $[(\eta^5\text{-}C_5H_5)Ru(PPh_3)_2Br]$ (0.1 g, 1.2×10^{-4} mol) in ethanol (30 cm^3) with $AsPh_3$ (0.1 g, 3.3×10^{-4} mol) for 15 h, whereupon brown crystals were deposited. These were separated by centrifuging the suspension, washed with ethanol, diethyl ether and petroleum ether. The complex was dried and identified as the bromo derivative (yield *ca* 70%).

(*D*) *Preparation of monocyclopentadienylmonotriphenylarsine monotriphenylphosphinetrichlorotin ruthenium(II)* $\{[(\eta^5\text{-}C_5H_5)Ru(AsPh_3)(PPh_3)SnCl_3]\}$. A mixture of $[(\eta^5\text{-}C_5H_5)Ru(AsPh_3)(PPh_3)Cl]$ (0.1 g, 1.3×10^{-4} mol) and tin(II) chloride (0.05 g, 2.5×10^{-4} mol) was heated to reflux in 15 cm^3 of benzene to which 20 cm^3 of methanol was added. After about half an hour yellow crystals had appeared, which were separated by centrifugation. The centrifugate was further concentrated by heating on a water bath whereby more compound appeared in the concentrate. It was centrifuged, recrystallized from CH_2Cl_2–petroleum ether, washed with petroleum ether, and dried *in vacuo*. The complex was identified as $[(\eta^5\text{-}C_5H_5)Ru(AsPh_3)(PPh_3)SnCl_3]$ (yield *ca* 60%).

(*E*) *Preparation of monocyanomonocyclopentadienylmonotriphenylarsine monotriphenylphosphine ruthenium(II)* $\{[(\eta^5\text{-}C_5H_5)Ru(AsPh_3)(PPh_3)CN]\}$. A mixture of $[(\eta^5\text{-}C_5H_5)Ru(AsPh_3)(PPh_3)Cl]$ (0.1 g, 1.3×10^{-4} mol) and excess KCN (0.2 g, 3.3×10^{-3} mol) was heated under reflux for 4–5 h in methanol (20 cm^3), whereupon greenish-yellow crystals separated, which were centrifuged. The centrifugate was further concentrated, yielding more of the complex as precipitate. The complex was centrifuged, washed with water, methanol and ether, and dried *in vacuo*. It was identified as $[(\eta^5\text{-}C_5H_5)Ru(AsPh_3)(PPh_3)CN]$ (yield *ca* 50%).

(*F*) *Preparation of monocyclopentadienylmonotriphenylarsine monotriphenylhosphineacetonitrile ruthenium(II) cationic salts* $\{[(\eta^5\text{-}C_5H_5)Ru(AsPh_3)(PPh_3)(MeCN)]^+X^-$ (X = BPh_4, $HgCl_3$ *or* Zn_2Cl_6)$\}$. (i) *Tetraphenylborate salt.* Addition of sodium tetraphenylborate (0.05 g, 1.1×10^{-4} mol) to a solution of $[(\eta^5\text{-}C_5H_5)Ru(AsPh_3)(PPh_3)Cl]$ (0.07 g, 1.0×10^{-4} mol) in 20 cm^3 acetonitrile, followed by heating for about 20 min under reflux, yielded a yellow solution, which was filtered. The filtrate was concentrated to nearly one-third of the volume ($\sim$5 cm^3). Ether was then added to the concentrate, whereby the complex precipitated. It was then centrifuged and recrystallized from acetonitrile–ether. It was washed with ether and dried *in vacuo*. The complex was identified as $[(\eta^5\text{-}C_5H_5)Ru(AsPh_3)(PPh_3)(MeCN)]BPh_4$.

(ii) *Trichloromercurate salt.* The reaction was carried out by a procedure similar to that described in F(i) except that mercury(II) chloride was used instead of sodium tetraphenylborate to obtain $[(\eta^5\text{-}C_5H_5)Ru(AsPh_3)(PPh_3)(MeCN)]HgCl_3$.

(iii) *Hexachlorodizincate salt.* The reaction was carried out by a procedure similar to that described

in F(i) except that zinc(II) chloride was used instead of tetraphenylborate to obtain $[(\eta^5\text{-}C_5H_5)Ru(AsPh_3)(PPh_3)(MeCN)]_2Zn_2Cl_6$.

The corresponding $[(\eta^5\text{-}C_5H_5)Ru(AsPh_3)_2X]$ (X = Cl, Br, I, CN or $SnCl_3$) complexes have also been prepared using the same procedures as described in the above sections.

Interconversions (*Scheme* 1)

Conversion of $[(\eta^5\text{-}C_5H_5)Ru(SbPh_3)_2Cl]$ *to* $[(\eta^5\text{-}C_5H_5)Ru(AsPh_3)_2Cl]$. A mixture of $[(\eta^5\text{-}C_5H_5)Ru(SbPh_3)_2Cl]$ (prepared by a method described elsewhere)[13] (0.1 g, 1.1×10^{-4} mol) and triphenylarsine (0.1 g, 3.3×10^{-4} mol) was refluxed in 20 cm^3 benzene for 12 h. The resulting orange solution was evaporated to dryness, and the residue extracted with 10 cm^3 of dichloromethane. Excess petroleum ether was added to the extract to give the corresponding arsine complex. It was identified by comparing its spectral and analytical data with those of the authentic sample, and by determining the mixed melting point.

Conversion of $[(\eta^5\text{-}C_5H_5)Ru(SbPh_3)_2Cl]$ *to* $[(\eta^5\text{-}C_5H_5)Ru(PPh_3)_2Cl]$. A mixture of $[(\eta^5\text{-}C_5H_5)Ru(SbPh_3)_2(Cl]$ (0.1 g, 1.1×10^{-4} mol) and triphenylphosphine (0.1 g, 3.8×10^{-4} mol) was refluxed in 30 cm^3 of ethanol for 10 h. The resulting solution was evaporated to nearly 5 cm^3, whereby an orange crystalline precipitate appeared. It was centrifuged, washed with ethanol, recrystallized from CH_2Cl_2–petroleum ether, and dried *in vacuo*. The complex was identified as $[(\eta^5\text{-}C_5H_5)Ru(PPh_3)_2Cl]$.

Conversion of $[(\eta^5\text{-}C_5H_5)Ru(AsPh_3)(PPh_3)Cl]$ *to* $[(\eta^5\text{-}C_5H_5)Ru(PPh_3)_2Cl]$. A mixture of $[(\eta^5\text{-}C_5H_5)Ru(AsPh_3)(PPh_3)Cl]$ (0.1 g, 1.3×10^{-4} mol) and triphenylphosphine (0.1 g, 4.0×10^{-4} mol was refluxed in 20 cm^3 ethanol for 12 h. The resulting solution was filtered and the filtrate was concentrated to 5 cm^3, whereby an orange crystalline precipitate appeared. It was filtered, washed with ethanol and diethyl ether, and dried *in vacuo*. The complex was identified as $[(\eta^5\text{-}C_5H_5)Ru(PPh_3)_2Cl]$.

Conversion of $[(\eta^5\text{-}C_5H_5)Ru(AsPh_3)(PPh_3)Cl]$ *to* $[(\eta^5\text{-}C_5H_5)Ru(AsPh_3)_2Cl]$. A mixture of $[(\eta^5\text{-}C_5H_5)Ru(AsPh_3)(PPh_3)Cl]$ (0.5 g, *ca* 6.5×10^{-4} mol and triphenylarsine (0.2 g, 6.4×10^{-4} mol) was refluxed in benzene (20 cm^3) for 24 h. The solution was then centrifuged and the centrifugate evaporated to near dryness. The residue was extracted with CH_2Cl_2, and excess petroleum ether was added to the extract to yield a crystalline product which was identified as $[(\eta^5\text{-}C_5H_5)Ru(AsPh_3)_2Cl]$.

Physical measurements

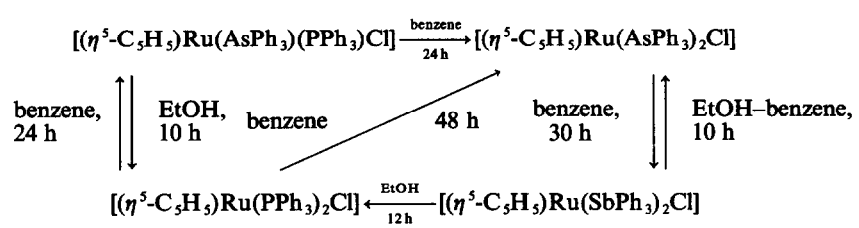
Carbon, hydrogen and nitrogen analyses were carried out by the Microanalytical Laboratory of the I.I.T., Kanpur, India. The percentage of halide in the sample was determined by the standard method[12] in the filtrate obtained after fusing the sample with the fusion mixture, extracting it with distilled water and filtering it. IR, UV and visible, ^1H NMR, ^{31}P NMR and mass spectra, magnetic measurements and powder X-ray data were determined by the methods described elsewhere.[13] The results are given in Table 1. All the complexes were found to be diamagnetic. The molecular weight of complex **1** was determined by using a Knauer vapour pressure osmometer.

RESULTS AND DISCUSSION

The analytical data of the yellowish-orange, air-stable complex **1** and other substitution products suggested that their formula was $[(\eta^5\text{-}C_5H_5)Ru(AsPh_3)(PPh_3)X]$. Complex **3** was obtained as a result of the substitution reaction of $[(\eta^5\text{-}C_5H_5)Ru(PPh_3)_2Cl]$ with triphenylarsine. It was found to be highly soluble in $CHCl_3$ and CH_2Cl_2, partially soluble in ethanol, methanol and diethyl ether, and insoluble in petroleum ether and *n*-hexane. This formulation was further confirmed by the results of the following experiments:

(i) Its experimentally determined molecular weight (752) by osmometer as against the theoretical value of 770.

(ii) By the presence of peaks in its mass spectrum



Scheme 1. Interconversion of various complexes.

Table 1. Characterization data

	Complex (molecular weight)	M.p.[a] (°C)	Colour[b]	Analysis [found (calc.)] (%) C	H	N	X/S	IR bands (cm^{-1}) (C_5H_5)	C_5H_5 ^1H NMR [δ (ppm)][c]
1	$[(\eta^5\text{-}C_5H_5)Ru(AsPh_3)(PPh_3)Cl]$ (770)	140d	YO	63.1 (63.8)	4.8 (5.1)	— —	5.0 (4.6)	843	4.10
2	$[(\eta^5\text{-}C_5H_5)Ru(AsPh_3)(PPh_3)F]$ (753)	138d	YO	65.5 (65.3)	4.2 (4.6)	— —	— —	843	4.10
3	$[(\eta^5\text{-}C_5H_5)Ru(AsPh_3)(PPh_3)Br]$ (814)	145d	B	62.3 (60.4)	3.4 (4.3)	— —	10.0 (9.8)	843	4.15
4	$[(\eta^5\text{-}C_5H_5)Ru(AsPh_3)(PPh_3)I]$ (861)	150d	OR	57.2 (57.1)	4.3 (3.7)	— —	13.4 (14.6)	843	4.12
5	$[(\eta^5\text{-}C_5H_5)Ru(AsPh_3)(PPh_3)H]$ (735)	135d	Y	66.4 (66.9)	5.2 (4.9)	— —	— —	845, 1950 ν(Ru—H)	4.10
6	$[(\eta^5\text{-}C_5H_5)Ru(AsPh_3)(PPh_3)SnCl_3]$ (959)	198	YO	51.4 (51.2)	3.6 (3.6)	— —	12.0 (11.1)	840	4.45
7	$[(\eta^5\text{-}C_5H_5)Ru(AsPh_3)(PPh_3)CN]$ (760)	240	YG	65.5 (66.3)	4.1 (4.6)	2.3 (1.9)	— —	845, 2050 ν(CN)	4.45
8	$[(\eta^5\text{-}C_5H_5)Ru(AsPh_3)(PPh_3)(MeCN)]BPh_4$ (1104)	140d	YG	73.2 (72.8)	5.6 (5.2)	1.5 (1.3)	— —	850	
9	$[(\eta^5\text{-}C_5H_5)Ru(AsPh_3)(PPh_3)(MeCN)]HgCl_3$	145d	YG	47.5 (47.7)	4.1 (3.5)	1.5 (1.3)	10.6 (9.8)	850	
10	$[(\eta^5\text{-}C_5H_5)Ru(AsPh_3)(PPh_3)(MeCN)]_2Zn_2Cl_6$ (1894)	180	YG	55.4 (54.5)	4.5 (4.0)	1.7 (1.5)	11.9 (11.3)	850	
11	$[(\eta^5\text{-}C_5H_5)Ru(AsPh_3)_2F]$ (797)	140d	BR	62.3 (61.7)	5.0 (4.4)	— —	— —	840	4.10
12	$[(\eta^5\text{-}C_5H_5)Ru(AsPh_3)_2Br]$ (858)	146d	B	58.0 (57.2)	3.6 (4.0)	— —	10.6 (9.3)	840	4.20
13	$[(\eta^5\text{-}C_5H_5)Ru(AsPh_3)_2I]$ (905)	152	OR	55.2 (54.4)	3.5 (3.8)	— —	13.5 (14.0)	840	4.20
14	$[(\eta^5\text{-}C_5H_5)Ru(AsPh_3)_2SnCl_3]$ (1003)	203–205	OY	49.8 (49.1)	3.6 (3.4)	— —	11.2 (10.6)	840	4.50
15	$[(\eta^5\text{-}C_5H_5)Ru(AsPh_3)_2CN]$ (804)	250	YG	63.2 (62.7)	4.5 (4.3)	2.1 (1.7)	— —	843, 2050 ν(CN)	4.50
16	$[(\eta^5\text{-}C_5H_5)Ru(AsPh_3)_2(MeCN)]BPh_4$ (1148)	138	YG	71.0 (70.3)	5.4 (5.0)	1.5 (1.2)	— —	850	
17	$[(\eta^5\text{-}C_5H_5)Ru(AsPh_3)_2(MeCN)]HgCl_3$ (1125)	148	YG	46.2 (45.8)	4.5 (3.4)	1.6 (1.2)	11.0 (9.5)	850	
18	$[(\eta^5\text{-}C_5H_5)Ru(AsPh_3)_2(MeCN)]_2Zn_2Cl_6$ (1982)	180	YG	52.5 (52.1)	4.2 (3.5)	1.6 (1.4)	12.1 (10.7)	850	

[a] d = decomposition.
[b] YO = yellowish-orange, B = brown, OR = orange-red, Y = yellow, YG = yellowish-green, BR = brick-red.
[c] Solvent $CDCl_3$. Aromatic protons of the other coligands appeared in the region of δ 7–8 as broad multiplets, and in the case of acetonitrile additional signals in the δ-1.8–2.0 region were observed due to the methyl protons.

with m/z values of 306, 262 and 201, corresponding to $AsPh_3$, PPh_3 and [RuCpCl], respectively. (Since the purpose of this study was just to detect the presence of $AsPh_3$ and PPh_3 fragments, no attempt has been made to explain other relatively less intense peaks.)

(iii) Complex **1** was subjected to substitution reactions which led to the scission of the Ru—Cl bond and yielded $[(\eta^5\text{-}C_5H_5)Ru(AsPh_3)(PPh_3)X]$ as substituted products (X = Br, I, F, CN or $SnCl_3$) (Table 1).

(iv) Reactions between complex **1** and zinc or mercury(II) chlorides in acetonitrile produced a rapid colour change from orange to yellow of the solution from which stable yellow complexes were isolated. They were initially thought to be 1:1 adducts of the Ru complex acting as a Lewis base. Further investigations revealed that the products were salts of the cation $[(\eta^5\text{-}C_5H_5)Ru(AsPh_3)(PPh_3)(MeCN)]^+$. The cationic nature has been tested by ion exchange studies.

It has been observed that, by refluxing a solution of $[(\eta^5\text{-}C_5H_5)Ru(AsPh_3)(PPh_3)Cl]$ with either PPh_3 or $AsPh_3$, it was possible to convert them to the known compounds $[(\eta^5\text{-}C_5H_5)Ru(MPh_3)_2Cl]$ (M = P or As). These reactions have been further extended and the PPh_3 or $AsPh_3$ can easily be substituted by triphenylstibine ($SbPh_3$) simply by refluxing the solution of $[(\eta^5\text{-}C_5H_5)Ru(MPh_3)_2Cl]$ (M = P or As) with $SbPh_3$. It has, however, been observed that the time of refluxing for the substitution reaction of the complex having PPh_3 as a coligand with $AsPh_3$, was much longer compared to the complex having a $AsPh_3$ as coligand. This could possibly be due to the similarity of some of the chemical properties of the alternate elements in a group.[14] This is, however, a tentative explanation.

The properties of the substitution products of $[(\eta^5\text{-}C_5H_5)Ru(AsPh_3)(PPh_3)Cl]$ and $[(\eta^5\text{-}C_5H_5)Ru(AsPh_3)(PPh_3)(MeCN)]^+$ are given in Table 1. Their formulae have been assigned on the basis of the chemical analyses and other properties discussed below.

IR spectra

The IR spectra of all the complexes exhibited two bands of medium intensity in the 840–850- and 420-cm^{-1} regions, corresponding to the C—H out-of-plane and skeletal bending modes of the C_5H_5 ring, respectively, besides the characteristic bands[15] of triphenylphosphine and triphenylarsine (1490, 1440, 1100, 750, 700 and 535 cm^{-1}). Since the band positions due to the phenyl groups of $AsPh_3$ and PPh_3 in their IR spectra do not appreciably vary it was difficult to distinguish the presence of both triphenylarsine and triphenylphosphine in the same complexes by the IR spectra. However, it has been observed that all the phenyl bands in the IR spectra of the complexes $[(\eta^5\text{-}C_5H_5)Ru(AsPh_3)(PPh_3)X]$ were relatively broader compared to those found in $[(\eta^5\text{-}C_5H_5)Ru(MPh_3)_2X]$ (M = P or As). This broadness could possibly be taken tentatively as evidence for the presence of both $AsPh_3$ and PPh_3 in the complexes, as indicated by other experiments. The IR spectra of all the complexes displayed a characteristic pattern of three bands decreasing in intensity from 535 to 495 cm^{-1}, which suggests the presence of a triphenylphosphine- or triphenylarsine-coordinated ligand.[16] Spectra of the cyanato and hydrido complexes exhibited medium-intensity, slightly broad bands at 2050 and 1950 cm^{-1}, assigned to ν(CN) and ν(Ru—H), respectively,[7,8,17] confirming the presence of a CN^- or H^- ion bonded to ruthenium in the complexes.

It is interesting to observe that the ν(CN) band in all complexes having a coordinated isonitrile around 2100 cm^{-1} is very weak. A low value of the transition moment is usually observed in these type of complexes.[18,19] In the 400–200-cm^{-1} region bands assignable to $[Zn_2Cl_6]^{2-}$ and $[HgCl_3]^-$ anions, besides those due to ν(Ru—Cl), have been observed. In the spectrum of the mercury derivative a band at 285 cm^{-1}, assigned to the asymmetric mode in $[HgCl_3]^-$, and for the zinc complex the characteristic bands of $[Zn_2Cl_6]^{2-}$ at 335, 305, 252 and 242 cm^{-1}, were present. The positions and relative intensities of the $[Zn_2Cl_6]^{2-}$ bands were found to be similar to those observed in the IR spectra of the solutions of the complexes B^+MCl_3 (B = bipyBPh$_2$, M = Zn or Hg), where it has been suggested[20] that the zinc is present as the bridged $[Zn_2Cl_6]^{2-}$ rather than the mononuclear $[ZnCl_3]^-$ anion.[21]

^{1}H *NMR spectra*

^{1}H NMR spectra of all the complexes showed a sharp resonance in the δ-4.0–4.5 region. The sharp singlet in this region is characteristic of π-bonded cyclopentadiene. The aromatic group on the triphenylphosphine and triphenylarsine ligands showed broad complex resonances in the usual range of δ 7.0–8.0 for the C_6H_6 protons. The integrated intensity ratio of the signals of C_5H_5 and MPh_3 (M = P or As) (1:6) corresponded to the ratio of the number of hydrogen atoms of the cyclopentadienyl anion and the sum of those present in triphenylphosphine and triphenylarsine. It was reported earlier that a sharp resonance in the NMR spectra of $[(\eta^5\text{-}C_5H_5)Ru(PPh_3)_2Cl]$ and $[(\eta^5\text{-}C_5H_5)Ru(AsPh_3)_2Cl]$ appears at δ 4.0 and 4.2 (Fig. 1), respectively.[1] The presence of a peak at δ 4.1 in

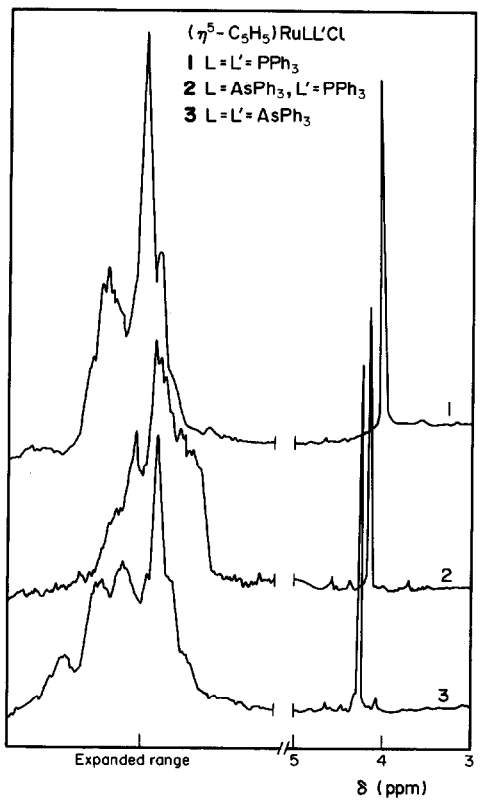


Fig. 1. ^{1}H NMR spectra of Ru complexes.

the complex $[(\eta^5\text{-}C_5H_5)Ru(AsPh_3)(PPh_3)Cl]$, therefore, suggests the environment of the cyclopentadienyl protons to be different from that in the former two complexes. Furthermore, the presumption that the complex $[(\eta^5\text{-}C_5H_5)Ru(AsPh_3)(PPh_3)Cl]$ is a 1.1 mixture of $[(\eta^5\text{-}C_5H_5)Ru(PPh_3)_2Cl]$ and $[(\eta^5\text{-}C_5H_5)Ru(AsPh_3)_2Cl]$ is also not tenable because of the fact that the NMR spectra of the mixture is expected to exhibit two independent peaks due to cyclopentadienyl protons at δ 4.0 and 4.2, one for each component of the mixture. The presence of only one sharp peak at δ 4.1 suggests only one type of electronic environment around the cyclopentadienyl protons. Further, the spectra of all the complexes showed a broad multiplet in the region of δ 7.8 different from the one present in the spectra of triphenylphosphine and triphenylarsine complexes. The spectra of latter two together did not match the one of complex **1** in the region of δ 7.0, indicating again that it is not a mixture of the phosphine and arsine complexes. In the case of the acetonitrile complexes, an additional signal in the δ-1.8–2.0 region was observed for the methyl protons. ^{31}P NMR exhibited a sharp resonance at δ 39.01, indicating the presence of at least one triphenylphosphine molecule in our complex. The literature indicates one single sharp ^{31}P signal in $[(\eta^5\text{-}C_5H_5)Ru(PPh_3)_2Cl]$ at δ 38.6, indicating the presence of two symmetrical triphenylphosphine molecules.[22] The shifting of the signal in our complex towards a lower value by about δ 0.5 suggests that triphenylphosphine in our complex has different surroundings than in $[(\eta^5\text{-}C_5H_5)Ru(PPh_3)_2Cl]$. These data, along with those of other physical measurements, further confirm the formula to contain one molecule each of triphenylphosphine and triphenylarsine.

Magnetic moments and electronic spectra

All the complexes were found to be diamagnetic, indicating spin pairing. The symmetry of the donor atoms around the metal centre in all these complexes may be considered to be distorted octahedral, based upon the assumption that the cyclopentadienyl group occupies three coordinate sites, or distorted tetrahedral if the perpendicular axis of the C_5-ring is considered to occupy one position. The diamagnetism of the complexes is, however, strongly suggestive of the former alternative, because of the definite possibility of there being spin-free complexes in a tetrahedral environment.

The position of the absorption bands shown in the UV and visible region of the electronic spectra of complex **1** were at 375 nm and a shoulder at 455 nm due to a M → L charge-transfer band. When we compared complex **1** with the $[(\eta^5\text{-}C_5H_5)Ru(PPh_3)_2Cl]$ complex the absorption band showed red shifts.

The powder X-ray photograph of complex **1** is found to be identical to that of $[(\eta^5\text{-}C_5H_5)Ru(PPh_3)_2Cl]$ and $[(\eta^5\text{-}C_5H_5)Ru(AsPh_3)_2Cl]$ as far as peak positions are concerned. However, the peak intensities were different from those of the phosphine and arsine analogues as expected because of the difference in the scattering power of P and As. It suggests that these three complexes are isomorphous and the same structure may be assigned to the complex $[(\eta^5\text{-}C_5H_5)Ru(AsPh_3)(PPh_3)Cl]$ as to $[(\eta^5\text{-}C_5H_5)Ru(PPh_3)_2Cl]$.

CONCLUSIONS

From the above discussion it is postulated that, during the substitution reaction of $[(\eta^5\text{-}C_5H_5)Ru(PPh_3)_2Cl]$ by $AsPh_3$ to yield $[(\eta^5\text{-}C_5H_5)Ru(AsPh_3)_2Cl]$ the phosphine molecules are not both simultaneously substituted by two molecules of triphenylarsine, but the reaction proceeds by a stepwise mechanism with the formation of a stable intermediate complex having one molecule of phosphine and one molecule of arsine as coligands. Various derivatives of the $[(\eta^5\text{-}C_5H_5)Ru(AsPh_3)$

$(PPh_3)X]$ (X = Br, I, CN or $SnCl_3$) have been prepared and characterized. Their structures are assumed to be the same as those of their respective phosphine analogues. Although it has also been observed that phosphine, arsine and stibine analogues of the complexes $[(\eta^5\text{-}C_5H_5)Ru(MPh_3)_2Cl]$ (M = P, As or Sb) can be interconverted simply by refluxing the complex with the appropriate compound (MPh_3), the substitution of phosphine or stibine involves a much shorter time of refluxing compared to that of arsine.

REFERENCES

1. T. Blackmore, M. I. Bruce and F. G. A. Stone, *J. Chem. Soc. A* 1971, 2376.
2. M. I. Bruce, R. C. F. Gardner and F. G. A. Stone, *J. Chem. Soc., Dalton Trans.* 1976, 81.
3. M. I. Bruce and R. Wallis, *Aust. J. Chem.* 1979, **32**, 1471.
4. G. S. Ashby, M. I. Bruce, I. B. Tomkins and R. Wallis, *Aust. J. Chem.* 1979, **32**, 1003.
5. M. I. Bruce and F. S. Wong, *J. Chem. Soc., Dalton Trans.* 1981, 1398.
6. M. I. Bruce, F. S. Wong, B. W. Skelton and A. H. White, *J. Chem. Soc., Dalton Trans.* 1982, 687.
7. M. I. Bruce, M. G. Humphrey, A. G. Swincer and R. C. Walls, *Aust. J. Chem.* 1984, **37**, 1747.
8. R. F. N. Ashok, M. Gupta, K. S. Arulsamy and U. C. Agarwala, *Inorg. Chim. Acta* 1985, **98**, 161.
9. R. F. N. Ashok, M. Gupta, K. S. Arulsamy and U. C. Agarwala, *Inorg. Chim. Acta* 1985, **98**, 169.
10. H. Nagasimha, K. Yamaguchi, K. Mukai and K. Itoh, *J. Organomet. Chem.* 1985, **191**, C20.
11. M. I. Bruce and N. J. Windsor, *Aust. J. Chem.* 1977, **30**, 1601.
12. A. I. Vogel, *A Textbook of Quantitative Inorganic Analysis*, 4th Edn, p. 491. Longmans Green, London (1978).
13. K. Mohan Rao, Lallan Misra and U. C. Agarwala, *J. Organomet. Chem.* (communicated).
14. J. E. Huheey, *Inorganic Chemistry*, 3rd Edn, p. 841 (1983).
15. L. Maier, *Proc. Inorg. Chem.* 1963, **5**, 27.
16. R. Uson *et al.*, *J. Organomet. Chem.* 1983, **256**, 331.
17. S. D. Ross, *Infrared and Raman Spectra*, p. 136. McGraw-Hill, London (1971).
18. P. M. Treichel, R. L. Shubkin, K. W. Barnett and D. Reichard, *Inorg. Chem.* 1966, **5**, 1171.
19. S. G. Davies and F. Schott, *J. Organomet. Chem.* 1980, **188**, C41.
20. G. E. Coats and Ridley, *J. Chem. Soc.* 1964, 166.
21. H. Bloom *et al.*, *Aust. J. Chem.* 1970, **23**, 843.
22. T. Wilczewski, M. Bochenska and J. F. Biernat, *J. Organomet. Chem.* 1981, **215**, 87.

Polyhedron Vol. 5, No. 10, pp. 1499–1501, 1986
Printed in Great Britain

0277–5387/86 $3.00+.00
Pergamon Journals Ltd

STUDIES ON HOMO-TRINUCLEAR COMPLEXES OF Mn(II), Co(II) AND Ni(II) WITH A NONADENTATE LIGAND

D. L. ARORA, KEEMTI LAL,* S. P. GUPTA and S. K. SAHNI†

Department of Chemistry, D.N. College, Meerut 250002, India

(*Received* 28 *January* 1985; *accepted after revision* 19 *December* 1985)

Abstract—Homo-trinuclear complexes of general formula $[M_3LCl_2(H_2O)_3]$ [M = Mn(II), Co(II) or Ni(II); H_4L = bis-(resacetophenone)-2,6-dipicolinoyldihydrazone] have been synthesized. The ligand acts as a tetrabasic nonadentate (N_5O_4) chelating agent. The complexes have been characterized on the basis of elemental-analysis, electrical-conductance and IR spectral data.

In recent years, an increasing number of homo-binuclear or homo-bimetallic complexes of first-row-transition metal ions with a variety of binucleating ligands have been studied.[1,2] The majority of these complexes involve two metal ions in similar environments of four-, five- or six-coordination. Very few examples are known in which each of the two metal ions possesses a different stereochemistry and spin-state.[3,4] A number of trimeric or tetrameric bivalent metal complexes involving multidentate ligands of varied denticity are known.[4,5] All these complexes could be obtained as a result of the tendency of the metal ions to polymerize the organic-ligand systems. However, it appears that no trinuclear or trimetallic complexes of trinucleating ligands of type M_3L, $M_2M'L$ or $MM'M''L$ are known in which one ligand molecule coordinates three ions of the same or different metal ions. In this paper we report the isolation of homo-trinuclear complexes of Mn(II), Co(II) and Ni(II) with bis-(resacetophenone)-2,6-dipicolinoyldihydrazone ($rdphH_6$). The complexes are characterized on the basis of elemental-analysis, electrical-conductance and IR spectral data.

EXPERIMENTAL

The dimethyl ester of dipicolinic acid was procured from Midland Yorkshire Tar Distillers Ltd, U.K. All other chemicals used were of A.R. grade and the solvents were purified before use.

The molar-conductance and magnetic measurements, and IR spectra, were recorded as earlier.[6] The elemental analyses were carried out at I.I.T., New Delhi.

2,6-Dipicolinoyldihydrazine ($dphH_2$) was synthesized by refluxing the dimethyl ester of dipicolinic acid (0.1 mol) with hydrazine hydrate (0.2 mol, 99%) for 2 h on a water bath. The product, on repeated crystallization from hot water, gave colourless needles (m.p. 285°C). The ligand, $rdphH_6$, was prepared by the condensation of $dphH_2$ with resacetophenone in methanol on a water bath for 2 h (Fig. 1). Straw-coloured crystals of $rdphH_6$ were formed with a sharp m.p. at 340°C. Found: C, 59.5; H, 4.5; N, 15.1%. Calc. for $C_{23}H_{21}N_5O_6$: C, 59.6; H, 4.5; N, 15.1%. The purity of the ligand was confirmed by thin-layer chromatography.

For trinuclear complexes, the metal salt (0.003 mol) was dissolved in ethanol (50%, 75 cm^3) and the ligand (0.001 mol) was added to it slowly with constant stirring. The mixture was refluxed for about 4 h on a water bath. The pH of the mixture was then raised to ~8 by adding alcoholic potassium hydroxide and the mixture was then digested on a water bath for about 1 h. The solid complex that separated was filtered, washed successively with water and ethanol (50%), and dried *in vacuo* at room temperature.

RESULTS AND DISCUSSION

The analytical results for the complexes (Table 1) indicate that they possess a 3:1 metal–ligand stoichiometry. The molar-conductance values in

* Author to whom correspondence should be addressed.
† Present address: Department of Chemistry, State University of Leiden, Leiden, The Netherlands.

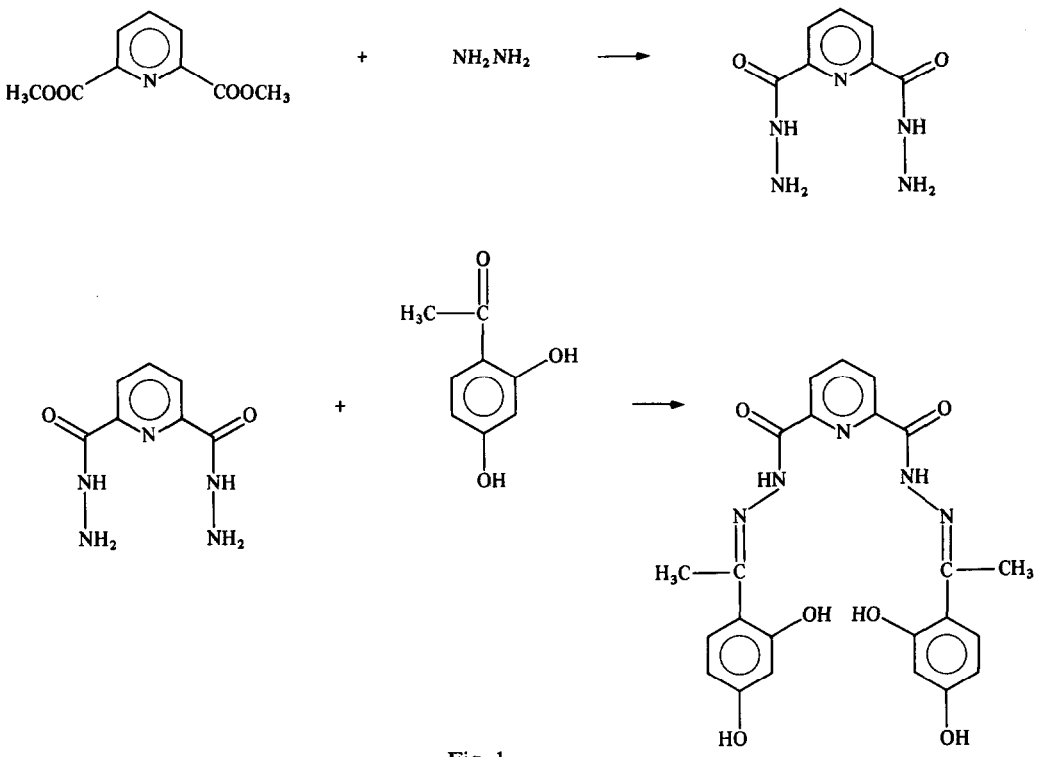


Fig. 1.

DMF are consistent with the non-electrolytic nature of the complexes.

The magnetic moments (Table 1) at 293 K indicate that the values are appreciably lower than those observed for the high-spin metal ions, possibly due to metal–metal interaction and anti-ferromagnetic exchange in the complexes,[7] but measurements over a temperature range are required.

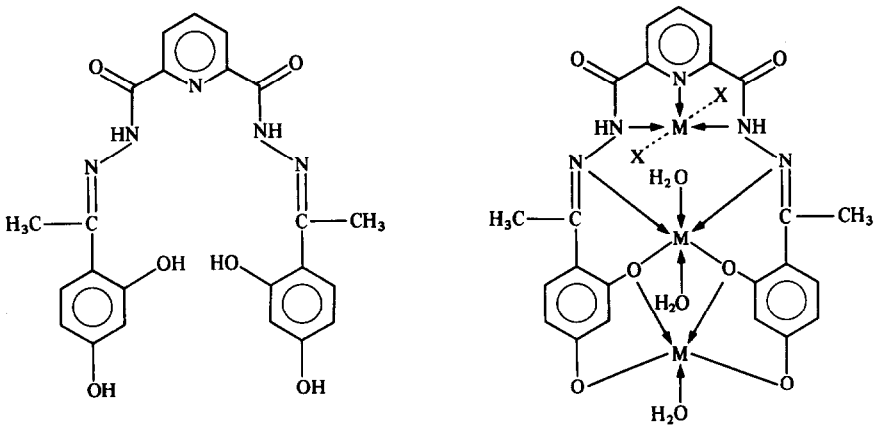
The important IR spectral bands along with their assignments for the ligand and their complexes are discussed here. These assignments are based on the study of the metal complexes of 2,6-dphH_2 and its hydrazones.[8,9] The IR spectra of the ligand show two bands at 3360 and 2625 cm^{-1} assigned to ν(OH) phenolic groups and ν(OH---N=C) intramolecular hydrogen bonding,[10] respectively. These bands disappear in the complexes, indicating bond formation between metal and phenolic oxygen atoms after deprotonation. Two other bands occurring at 1550 and 1260 cm^{-1}, due to phenolic ν(C—O) and δ(C—O), respectively, in the ligand, shift to ~1580 and ~1300 cm^{-1}, respectively, in the complexes. This indicates that these complexes possess oxo-bridges provided by the phenolic oxygen atoms. The presence of oxo-bridging is further supported by the presence of weak-intensity bands in the 790–810-cm^{-1} region in the complexes.[11] A weak band at ~515 cm^{-1} may be assigned to ν(M–O) vibrations.[11]

The bands appearing at 1670, 1480, 1290, 690 and 450 cm^{-1} may be assigned to amide-**I** [ν(CO)], amide-**II** [ν(CN)+δ(NH)], amide-**III**

Table 1. Analytical data, conductances and magnetic moments of the complexes of rdphH_6 (L = rdphH_2 = $C_{23}H_{17}N_5O_6$)

Complex	Colour	M.p. (°C)	Found (calc.) (%) C	H	N	Cl	Metal	Λ_M (Ω^{-1} cm^2 mol^{-1})	μ_{eff} (BM)
$[Mn_3LCl_2(H_2O)_3]$	Dark brown	325	36.4 (36.9)	3.1 (3.1)	9.4 (9.3)	9.6 (9.5)	21.9 (22.0)	30.5	3.98
$[Co_3LCl_2(H_2O)_3]$	Dark brown	315	36.1 (36.3)	3.1 (3.0)	9.0 (9.2)	9.4 (9.3)	23.1 (23.3)	25.1	3.6
$[Ni_3LCl_2(H_2O)_3]$	Green	309[a]	36.1 (36.3)	3.0 (3.0)	9.3 (9.2)	9.2 (9.3)	23.3 (23.1)	29.4	1.67

[a] Decomposed.



Ligand

Fig. 2.

[ν(CN)+δ(NH)], amide-**IV** (C=O in-plane deformation) and amide-**VI** (C=O out-of-plane deformation) vibrations, respectively,[8,9] in the free ligand. These bands appear in the 1680–1685-, 1440–1450-, 1305–1310-, 705–710- and 465–470-cm^{-1} regions, respectively, in the complexes. The upward shift in amide-**I**, amide-**III**, amide-**IV** and amide-**VI**, and downward shift in amide-**II** bands are compatible with a secondary amide-nitrogen coordination to a metal atom. A broad band at 3300 cm^{-1} in the free ligand and the complexes due to ν(NH) indicates that this group remains intact during complexation. A medium band at 1620 cm^{-1} attributable to ν(C=N) of the azomethine group in the ligand appears at a lower frequency (1605 cm^{-1}) in the complexes, indicating the coordination of imino-nitrogen to the metal atom.[12] The bands appearing at 440, 435 and 450 cm^{-1} may be assigned to ν(Mn–N), ν(Co–N) and ν(Ni–N) vibrations, respectively.

The pyridine-ring vibrations most affected on its coordination to a metal atom include 8a (pyridine-ring deformation), 8b (pyridine-ring breathing), 6a (in-plane ring deformation) and 16b (out-of-plane ring deformation).[13] In the free ligand, these vibrations occur at 1595, 1060, 640 and 420 cm^{-1}, respectively. These bands appear at higher frequencies (*ca* 1600, 1080, 660 and 450 cm^{-1}, respectively) in the complexes. The upward shift in these vibrations of the pyridine ring indicates its coordination with a metal atom.[14] The medium bands appearing at 250, 265 and 260 cm^{-1} may be assigned to ν(Mn–Py), ν(Co–Py) and ν(Ni–Py) vibrations, respectively.

The bands appearing at 300, 310 and 305 cm^{-1} may be assigned to ν(Mn–Cl), ν(Co–Cl) and ν(Ni–Cl) vibrations, respectively.[10] Four new bands appear in the 3430–3440-, 1615–1620-, 795–800- and 520–545-cm^{-1} regions attributable to ν(OH), δ(OH), $\delta\nu$(H_2O) and $\delta\omega$(H_2O) vibration modes, respectively, of the coordinated water molecules in the complexes.[10]

On the basis of the preceding discussion it appears that the ligand acts as a nonadentate chelating agent having coordination sites at one pyridine-nitrogen, two azomethine-nitrogen, two secondary-amide-nitrogen and four phenolic oxygen atoms (Fig. 2).

Acknowledgement—We thank the Head of the Chemistry Department, I.I.T., New Delhi, India, for providing laboratory facilities.

REFERENCES

1. U. Casellato, P. A. Vigate, D. E. Fenton and M. Vidali, *Chem. Soc. Rev.* 1979, **8**, 199.
2. S. E. Groh, *Israel J. Chem.* 1976–1977, **15**, 277.
3. K. S. Murray, *Coord. Chem. Rev.* 1974, **12**, 1.
4. E. Sinn, *Coord. Chem. Rev.* 1971, **5**, 45.
5. C. M. Harris and E. Sinn, *Coord. Chem. Rev.* 1969, **4**, 39.
6. K. Lal and S. R. Malhotra, *J. Macromol. Sci. Chem.* 1984, **21A**, 825.
7. S. F. A. Kettle, *Coordination Compounds*. Thomas Nelson, Canada (1969).
8. V. B. Rana, S. K. Sahni and S. K. Sangal, *J. Inorg. Nucl. Chem.* 1979, **41**, 1498.
9. S. K. Sahni, S. P. Gupta, S. K. Sangal and V. B. Rana, *J. Inorg. Nucl. Chem.* 1977, **39**, 1098; *J. Indian Chem. Soc.* 1977, **54**, 200.
10. K. Nakamoto, *Infrared Spectra of Inorganic and Coordination Compounds*. Wiley Interscience, New York (1970).
11. D. K. Rastogi, S. K. Sahni, V. B. Rana and S. K. Dua, *J. Coord. Chem.* 1978, **8**, 97.
12. S. K. Sahni, *Transition Met. Chem.* 1978, **3**, 56; 1979, **4**, 73.
13. D. P. Madden and S. M. Nelson, *J. Chem. Soc.* (*A*) 1968, 2342.
14. R. C. Agarwal and T. R. Rao, *Transition Met. Chem.* 1977, **2**, 201.

Polyhedron Vol. 5, No. 10, pp. 1503–1508, 1986
Printed in Great Britain

0277–5387/86 $3.00+.00
Pergamon Journals Ltd

KINETIC STUDIES ON THE REACTIONS OF Ru(II) TETRAAMMINES WITH $CS_2N_3^-$

ELIZEU TRABUCO*

Instituto de Biociências, Letras e Ciências Exatas de São José do Rio Preto, UNESP, 15100 São José do Rio Preto, SP, Brazil

and

DOUGLAS WAGNER FRANCO

Instituto de Física e Química de São Carlos, Universidade de São Paulo, P.O. Box 369, 13560 São Carlos, SP, Brazil

(*Received* 10 *July* 1985; *accepted after revision* 2 *January* 1986)

Abstract—The kinetics of the reactions of Ru(II) complexes with $CS_2N_3^-$ ions were studied spectrophotometrically. The formation rate constants data for *trans*-$[Ru(NH_3)_4L(CS_2N_3)]$ are 2.2×10^2, 1.8×10 and $1.3 \times 10^2\ M^{-1}\ s^{-1}$ for L = SO_3^{2-}, HSO_3^- and $P(OEt)_3$), respectively [μ = 1.0 M ($NaCF_3COO$), 25°C]. Under the same experimental conditions, the values of k^{-1} (specific rate for the aquation reaction) are 1.5×10^{-2}, 5.0×10^{-2} and $4.5 \times 10\ s^{-1}$ for L = SO_3^{2-}, HSO_3^- and $P(OEt)_3$, respectively. The free-energy change (ΔG^+) for the systems where L = $P(OEt)_3$ and SO_3^{2-} are in agreement within the experimental error. It was observed that the affinity of the $CS_2N_3^-$ ion decreases with the increasing π-acidity of the auxiliary ligand L. The order of affinity of the $CS_2N_3^-$ ion for the Ru(II) center studies is $SO_3^{2-} > HSO_3^- > P(OEt)_3 > SO_2$.

The compound 1,2,3,4-thiatriazole-5-thiolate acid [HCS_2N_3] (pK = 1.5, μ = 1.0) is the first member of the thiatriazole series. Its chemistry is worthy of study.

After the development of adequate preparation, storage[1] and analytical determination methods[2,3] for the 1,2,3,4-thiatriazole-5-thiolate ion ($CS_2N_3^-$) (Fig. 1), studies have been carried out on its complexing properties[3,4] and electron-transfer reactions.[5]

The data obtained thus far on formation constants,[4] electrochemical measurements[5–8] and chemical reactivity[9–11] suggest a soft-base character for the $CS_2N_3^-$ anion.

The Ru(II) centers (soft acids) are inert to substitution reactions. The substitution of the NH_3 group from the $[Ru(NH_3)_5(H_2O)]^{2+}$ complex from a position *trans* to water by an auxiliary ligand L, with π-acid character transforms the π-electron density of the central atom, strikingly affecting the metal capacity for back-donation.[12–15] Because of this characteristic, Ru(II) tetraammines represent excellent models for the study of the chemical behaviour of the $CS_2N_3^-$ ion as a ligand towards metal centers of different acidity.

In the course of the investigation of the reactivity of Ru(II) ammines, soft acids, and of HCS_2N_3 chemistry, we report here some results on the $[Ru(NH_3)_5(H_2O)]^{2+}$–$CS_2N_3^-$ and *trans*-$[Ru(NH_3)_4L(H_2O)]$–$CS_2N_3^-$ systems, where L = SO_3^{2-} and $P(OEt)_3$.

EXPERIMENTAL

Solvents and reagents

(a) Imidazole (imN): *puriss* grade 99% (Aldrich) was used as supplied. (b) Triethyl phosphite

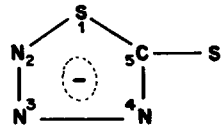


Fig. 1. Structure of the $CS_2N_3^-$ ion.

* Address to whom correspondence should be addressed.

$[P(OEt)_3]$ (Aldrich) was purified by distillation over metallic sodium as usual.[16]

The purification of carbon disulphide and sodium azide and the preparation and storage of sodium 1,2,3,4-thiatriazole-5-thiolate have been previously described.[1,4,6] Solvents were purified and dried by standard methods.[17,18] All other chemicals were of analytical purity and used as supplied.

Ru *complexes*

$[Ru(NH_3)_5(H_2O)](PF_6)_2$,[19] $[Ru(NH_3)_6]Cl_2$,[20] $[Ru(NH_3)_5Cl]Cl_2$,[21] *trans*-$[Ru(NH_3)_4SO_2Cl]Cl$[22] and *trans*-$[Ru(NH_3)_4(P(OEt)_3)_2](PF_6)_2$[14] were synthesized as described in the literature.

Apparatus and methods

Spectra. UV and visible spectra were recorded on a Varian–Tectron spectrophotometer, model 635.

Kinetic experiments. Slow reactions were followed using the same spectrophotometer. An Aminco–Morrow stopped-flow apparatus was used for rapid reactions. The reactions were studied with ligand concentrations $\geqslant$ 10-fold that of the complex. Under these conditions, in all experiments, pseudo-first-order rate constants (k_{obs}) were obtained. These were determined graphically by plotting $\log(A_\infty - A_t)$ vs time, where A_∞ was the final absorbance value and A_t the absorbance at time t. Rate constants were reproducible to within $\pm 5\%$. The plots of k_{obs} vs $[CS_3N_3^-]$ are linear with a positive intercept. The observed pseudo-first-order rate constant for approach to equilibrium in reaction (1):

$$\textit{trans}\text{-}[Ru(NH_3)_4L(H_2O)] + CS_2N_3^- \underset{k_{-1}}{\overset{k_1}{\rightleftharpoons}} \textit{trans}\text{-}[Ru(NH_3)_4L(CS_2N_3)] + H_2O, \quad (1)$$

where L = SO_3^{2-}, $P(OEt)_3$, HSO_3^- or NH_3, is given by the expression:

$$k_{obs} = k_1[CS_2N_3^-] + k_{-1}.$$

Values of k_1 and k_{-1} were calculated from the slope and intercept of plots of k_{obs} vs $[CS_2N_3^-]$.

The rate constant for aquation of *trans*-$[Ru(NH_3)_4L(CS_2N_3)]$ in some cases was measured using a high excess (100 times) of a competitor ligand, imN, to eliminate the reverse reaction according to the following scheme:

$$\textit{trans}\text{-}[Ru(NH_3)_4L(CS_2N_3)] + H_2O \xrightarrow[\text{slow}]{k_{-1}} \textit{trans}\text{-}[Ru(NH_3)_4L(H_2O)] + CS_2N_3^-, \quad (2)$$

$$\textit{trans}\text{-}[Ru(NH_3)_4L(H_2O)] + \text{imN} \xrightarrow{\text{fast}} \textit{trans}\text{-}[Ru(NH_3)_4L(\text{imN})] + H_2O. \quad (3)$$

The pH was adjusted by using buffers as follows. For $[Ru(NH_3)_4P(OEt)_3(H_2O)]^{2+}$, pH = 3.0 ($HCF_3COO$); $[Ru(NH_3)_4(SO_3)(H_2O)]^{2+}$, pH = 9.0 ($NaHCO_3$) and $[Ru(NH_3)_4(HSO_3)(H_2O)]^{2+}$, pH = 3.7 and 4.7 ($NaCH_3COO$–$HCH_3COO$). Ionic strengths (1.0 M) were adjusted in all cases with sodium trifluoroacetate. The temperature was adjusted before each experiment. Due to the air sensitivity of Ru(II) complexes all manipulations were carried out in an inert atmosphere of argon or nitrogen.

The equilibrium constants (K_{eq}) were evaluated by the k_1/k_{-1} ratio. For some cases, K_{eq} were calculated also by using the method described by Babko and Pilipenko,[23] employing the following expressions:

$$P = \frac{C_z''}{C_z'} = \frac{A_2}{A_1}, \quad C_z' = \frac{C_x(C_L'' - PC_L')}{P(C_L'' - C_L')},$$

and (4)

$$K_{eq} = \frac{PC_z'}{(C_x - PC_z')C_L''},$$

where C_x = initial concentration of metallic ion, C_L' and C_L'' = the ligand concentrations, C_z' and C_z'' = the complex concentration in the ligand's solutions where the concentrations are C_L' and C_L'', respectively, and A_1 and A_2 = the absorbance values of complex solutions C_z' and C_z''.

The activation parameters quoted were calculated by unweighted least-squares analysis of specific rate data over three temperatures, employing Eyring's equations[24,25] from plots of $\log(k/T)$ vs $1/T$.

RESULTS

The reactions of *trans*-$[Ru(NH_3)_4L(H_2O)]$ and the $CS_2N_3^-$ ion were studied under pseudo-first-order conditions. The experimental data for the k_{obs} are summarized in Table 1. The values of k_1, k_{-1} and K_{eq} are listed in Table 2.

For L = SO_2, HSO_3^- and SO_3^{2-}, the substitution reactions were studied over a wide range of hydrogen ion concentrations.

The coordinated sulfite adopts several forms as a function of pH,[21] according to the scheme:

$$[Ru(NH_3)_4SO_2(H_2O)]^{2+} \underset{+H^+}{\overset{-H^+}{\rightleftharpoons}} [Ru(NH_3)_4HSO_3(H_2O)]^+ \underset{+H^+}{\overset{-H^+}{\rightleftharpoons}} [Ru(NH_3)_4SO_3(H_2O)]. \quad (5)$$

Table 1. Pseudo-first-order rate constants[a] for the approach to equilibrium in the reaction[b] of $[Ru(NH_3)_4L(H_2O)]$ with the $CS_2N_3^-$ ion

	$P(OEt)_3$[c]		SO_3^{2-}[d]		HSO_3^-			
Temperature (°C)	$[CS_2N_3^-]$ (M)	k_{obs} (s^{-1})	$[CS_2N_3^-]$ (M)	k_{obs} (s^{-1})	$[CS_2N_3^-]$ (M)	k_{obs}[e] (s^{-1})	$[CS_2N_3^-]$ (M)	k_{obs}[f] (s^{-1})
25.0±0.5	0.025	4.3	0.020	5.0	0.05	1.5	0.025	0.5
	0.050	5.9	0.050	12.4	0.10	2.5	0.050	0.9
	0.080	10.0	0.075	17.3	0.15	3.7	0.075	1.5
	0.10	12.0	0.100	23.0	0.20	3.9	0.10	1.9
	0.20	25.4	0.150	35.0	0.30	7.0	0.15	2.8
	0.30	39.2	0.200	39.0	0.40	9.4	0.20	3.7
	0.40	49.4	0.250	60.0	0.50	13.7	0.30	6.5
			0.350	79.0			0.40	7.2
15.0±0.5	0.015	1.6	0.020	2.3				
	0.025	2.4	0.025	2.7				
	0.040	3.0	0.050	4.6				
	0.080	6.0	0.075	5.4				
	0.10	7.7	0.100	8.7				
	0.15	13.5	0.150	12.6				
	0.20	16.0	0.200	17.3				
	0.30	22.5	0.300	24.5				
5.0±0.5	0.025	1.5	0.025	1.5				
	0.050	2.3	0.050	2.4				
	0.075	2.6	0.075	3.5				
	0.095	4.6	0.100	4.1				
	0.15	7.3	0.150	6.9				
	0.20	9.0	0.200	7.9				
	0.30	14.0	0.300	11.0				
			0.400	17.3				

[a] Each value is the mean of at least three independent determinations with better than 95% agreement.
[b] $\mu = 1.0$ M ($NaCF_3COO$), $[Ru] = 1.0 \times 10^{-3}$ M.
[c] pH = 3.0 (HCF_3COO).
[d] pH = 9.0 ($NaHCO_3$).
[e] pH = 3.7 ($NaCH_3COO$–HCH_3COO).
[f] pH = 4.7 ($NaCH_3COO$–HCH_3COO).

Table 2. Data on substitution reactions[a] of *trans*-$[Ru(NH_3)_4L(H_2O)]^{2+}$ and the $CS_2N_3^-$ ion, where L = SO_3^{2-}, HSO_3^-, SO_2 or $P(OEt)_3$

L	k_1 ($M^{-1}\,s^{-1}$)	k_{-1} (s^{-1})	K_{eq} (M^{-1})	λ_{max} (nm)
SO_3^{2-}	225	0.015	1.5×10^4	420
HSO_3^-[b]	18	0.05	360	410
HSO_3^-[c]	22	0.30	75	410
SO_2	—	—	<10	390
$P(OEt)_3$	127	0.45	280	390
			350[d]	

[a] $\mu = 1.0$ M ($NaCF_3COO$), 25°C, $[Ru] = 1.0 \times 10^{-3}$ M.
[b] pH = 4.7.
[c] pH = 3.7.
[d] Determined by the method described by Babko and Pilipenko.[23]

Within a low-pH range (1.15–3.15) the Ru complex is present as sulphur dioxide, whereas the predominant form at pH values higher than 6.0 is the sulfite.

In order to obtain more accurate data, the k_{-1} values were also determined from the aquation reactions on $[Ru(NH_3)_4SO_3(CS_2N_3)]^-$, using imN as the competitor ligand.

The *trans*-$[Ru(NH_3)_4SO_2(H_2O)]^{2+}$ complex ion exists[13] in aqueous solutions since $C_{H^+} > 10^{-3}$ M. The complete conversion of the HSO_3^- into the SO_2 form occurs in the medium where $C_{H^+} = 0.5$ M. Under these conditions, the $CS_2N_3^-$ ion is protonated.[4] The solution formed by mixing the above reagents as $C_{H^+} = 10^{-1.8}$ M and $C_{H^+} = 1.0$ M shows an absorption band at 390 nm ($\varepsilon = 2 \times 10^3$ $M^{-1}\,cm^{-1}$). In the case where $C_{H^+} = 10^{-1.8}$ M, the

first possibility is coordination either by nitrogen N-4 or by the extracyclic sulphur atom, whereas, when $C_{H^+} = 1.0$ M, with the sulphur atom protonated,[4] coordination must occur by nitrogen (Fig. 1).

Spectrophotometric measurements at 390 nm in solutions where $C_{H^+} = 10^{-1.8}$ permit estimation of the order of magnitude of the equilibrium constant:

$$trans\text{-}[Ru(NH_3)_4SO_2(H_2O)]^{2+} + HSCSN_3 \rightleftharpoons [Ru(NH_3)_4SO_2(HSCSN_3)]^{2+} + H_2O, \quad (6)$$

which must be lower than 10 M^{-1}.

Since the pseudo-halide $CS_2N_3^-$ is unstable in acidic media[1] where $C_{H^+} > 10^{-3}$ M, these studies were discontinued.

For L = $P(OEt)_3$, the reactions were studied at pH = 3.0 and at temperatures of 5.0, 15.0 and 25.0°C. Figure 2 shows a plot of k_{obs} vs $[CS_2N_3^-]$. The results are summarized in Table 3. As for the SO_3^{2-} system, the k_{-1} values obtained from graphic extrapolation were too close to the origin (Fig. 3).

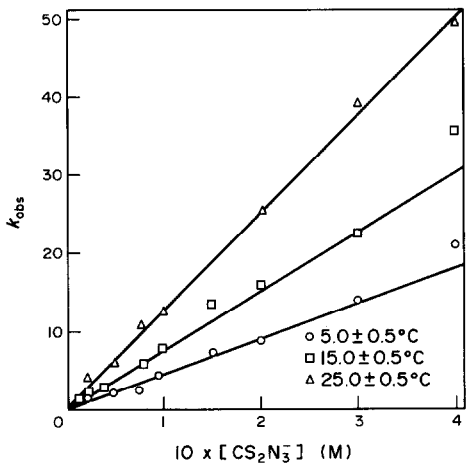


Fig. 2. Dependence of the observed constant, k_{obs} on the concentration of the ligand for the formation of the *trans*-$[Ru(NH_3)_4P(OEt)_3(CS_2N_3)]^+$ complex. $\mu = 1.0$ M, pH = 3.0.

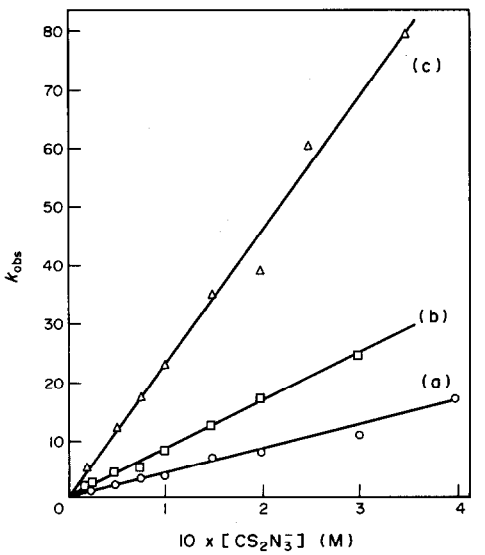


Fig. 3. Dependence of the observed constant, k_{obs} on the concentration of the ligand for the formation of the *trans*-$[Ru(NH_3)_4SO_3(CS_2N_3)]^-$ complex, $\mu = 1.0$ M, pH = 9.0. (a) 5.0±0.5°C. (b) 15.0±0.5°C. (c) 25.0±0.5°C.

Thus, to obtain better data for k_{-1}, the aquation of *trans*-$[Ru(NH_3)_4P(OEt)_3(CS_2N_3)]^+$ was studied in the presence of imN as the competitor ligand. The results of this method are in good agreement with those obtained by *trans*-$[Ru(NH_3)_4P(OEt)_3(CS_2N_3)]^+$ aquation.

In the case where L = NH_3, solutions of $CS_2N_3^-$ and $[Ru(NH_3)_5H_2O]^{2+}$ mixed in acidic medium in the absence of oxygen develop a reddish colour.

The electronic spectrum exhibits two peaks at 510 and 430 nm. However, when the spectrum is taken on the stopped-flow time scale, another peak is observed at 460 nm. This absorption band at 460 nm does not grow in the same proportion as the other two but disappears after 10 s.

DISCUSSION

The free-energy variations ΔG^+ and $\Delta G^{\pm}_1$ (Table 3) for the systems where L = $P(OEt)_3$ and

Table 3. Thermodynamic parameters for the reaction:[a] *trans*-$[Ru(NH_3)_4L(H_2O)] + CS_2N_3^- \rightleftharpoons [Ru(NH_3)_4L(CS_2N_3)] + H_2O$

L	$\Delta H_1^{\ddagger}$ (kcal mol^{-1})	$\Delta S_1^{\ddagger}$ (cal K^{-1} mol^{-1})	$\Delta G_1^{\ddagger}$ (kcal mol^{-1})	$\Delta H^{\pm}_1$ (kcal mol^{-1})	$\Delta S^{\pm}_1$ (cal K^{-1} mol^{-1})	$\Delta G^{\pm}_1$ (kcal mol^{-1})
SO_3^{2-} [b]	16.2	1.3	16.6	18.8	−3.9	20.5
$P(OEt)_3$ [c]	8.7	−19.4	14.5	10.3	−26.3	18.1

[a] $\mu = 1.0$ M ($NaCF_3COO$), [Ru] = 1.0×10^{-3} M.
[b] pH = 9.0 ($NaHCO_3$).
[c] pH = 3.0 (HCF_3COO). The $\Delta G^{\pm}_1$ and $\Delta G_1^{\ddagger}$ data have an uncertainty of ±2 kcal mol^{-1}.

SO_3^{2-} are in agreement within the experimental error. The substitution reactions for the Ru(II) ammines, 18-electron systems, are governed mainly by dissociative activation. Thus, although no evidence for rate saturation has been observed for the systems dealt with in the present study, these reactions, by analogy with data observed for other Ru(II) systems,[13,14] are supposed to occur by a dissociative mechanism.

Except for the pentaammineaquoruthenium(II) complex ion, all other Ru(II) complexes behave as a monocoordinative center, mainly owing to the *cis*-delabilizing effects of the SO_2, HSO_3^-, SO_3^{2-} and $P(OEt)_3$ ligands. For the $[Ru(NH_3)_5(H_2O)]^{2+}$–$CS_2N_3^-$ system, two bands are initially observed at 428 and 514 nm, probably due to the *cis*-ammonia labilization.

As judged from continuous-variation plots at several wavelengths, the product of the reaction between $[Ru(NH_3)_5(H_2O)]^{2+}$ and $CS_2N_3^-$ has a stoichiometry of 1:1. The labilization of the *cis*-ammonia and the decomposition of the ligand, probably assisted by the metal center, are additional complications in the substitution process of the $[Ru(NH_3)_5(H_2O)]^{2+}$ complex ion. This system is currently under study and the results will be published elsewhere.

The λ_{max} for the metal–ligand charge-transfer band (MLCT) observed for the P(III)–Ru(II)–$CS_2N_3^-$ and S(IV)–Ru(II)–$CS_2N_3^-$ complexes are 390, 390, 410 and 420 nm for $P(OEt)_3$, SO_2, HSO_3^- and SO_3^{2-}, respectively. The shift on the λ_{max} for the MLCT band in such complexes is related to the availability of the Ru(II) $4d_\pi$-electrons for back-bonding with $CS_2N_3^-$: the lower the energy of the transition, the stronger the back-bonding Ru(II) → $CS_2N_3^-$.

Based on the energy of MLCT bands, the order of the π-acidity of the auxiliary ligands L coordinated to the Ru(II) center in L–Ru(II)–$CS_2N_3^-$ complexes is:

$$NH_3 < SO_3^{2-} < HSO_3^- < SO_2 \sim P(OEt)_3.$$

The affinity of the L–Ru(II) centers with respect to the $CS_2N_3^-$ ion, measured by the formation constants of derivatives L–Ru(II)–$CS_2N_3^-$ decreases with increasing π-acidity of the auxiliary ligand L, and the affinity order is

$$SO_3^{2-} > HSO_3^- > P(OEt)_3 > SO_2.$$

The studies on Ru(II) and Ru(III) aquopentaammine systems, although limited, showed that the mercaptide ligands, RS^-, are very strong σ-donors and weak π-acids. However, this does not seem to be the behaviour of $CS_2N_3^-$, a weak σ-base. The HCS_2N_3 acid has a pK_a of 1.5 and exhibits properties of mercaptans. The order of Ru(II) center affinity towards $CS_2N_3^-$ strongly suggests that the π-bonding is important in such systems.

Comparing $CS_2N_3^-$ with other pseudo-halides,[27] with respect to the *trans*-$[Ru(NH_3)_4P(OEt)_3(H_2O)]^{2+}$ ion affinity the following order can be established: $SCN^- < N_3^- < CS_2N_3^- \ll CN^-$. The position of 1,2,3,4-thiatriazole-5-thiolate in this series is close to CN^-, a biphilic ligand, a strong σ-base and a strong π-acid.

Another point that deserves comment is the binding site of the $CS_2N_3^-$ anion. The affinity of $CS_2N_3^-$ toward several metal cations and the chemical reactivity of this anion suggest the sulphur atom to be the reactive center.[4,6] Quantum mechanical calculations for this molecule[28] have shown that the electron density in N-4 and the extracyclic sulphur are not very different. Although the sulphur is more basic than the nitrogen atom, and considering the soft-base character of $CS_2N_3^-$ in the $[Ru(NH_3)_5(H_2O)]^{2+}$ system, the possibility of coordination also through nitrogen with the formation of a chelate ring should not be ruled out. Investigations in this direction are currently in progress and will be reported later.

Acknowledgements—We are grateful to FAPESP, CNPq and CAPES for financial support.

REFERENCES

1. D. W. Franco and E. F. A. Neves, *J. Inorg. Chem.* 1974, **36**, 3851.
2. E. F. A. Neves, D. W. Franco and P. F. Romanelli, *Anal. Chem. Acta* 1977, **92**, 393.
3. E. F. A. Neves and D. W. Franco, *Talanta* 1979, **26**, 81.
4. D. W. Franco, E. F. A. Neves and N. Milcken, *J. Inorg. Nucl. Chem.* 1981, **43**, 2081.
5. E. F. A. Neves, D. W. Franco, W. L. Polito and V. L. Moraes, *Talanta* 1981, **28**, 867.
6. D. W. Franco and E. F. A. Neves, *J. Inorg. Nucl. Chem.* 1975, **37**, 277.
7. W. L. Polito, E. F. A. Neves, D. W. Franco and T. Tamura, *Simpósio de Electroquímica e Electroanalítica* 1978, **1**, 127.
8. W. L. Polito, Ph.D. thesis, Instituto de Química, USP, São Paulo (1983).
9. K. A. Jensen and C. Pedersen, *Adv. Heterocycl. Chem.* 1964, **3**, 263.
10. C. Christophensen and A. Holm, *Acta Chem. Scand.* 1971, **25**, 2015.
11. K. Pilgram and F. Gorgen, *J. Heterocycl. Chem.* 1971, **8**, 899.
12. H. Taube, *Surv. Prog. Chem.* 1973, **6**, 1.
13. S. Isied and H. Taube, *Inorg. Chem.* 1976, **15**, 3070.

14. D. W. Franco and H. Taube, *Inorg. Chem.* 1978, **17**, 577.
15. D. W. Franco, *Inorg. Chim. Acta* 1979, **32**, 273.
16. A. H. Ford-Moore and B. J. Perry, *Org. Synth. Coll.* 1963, **4**, 955.
17. A. Vogel, *Química Orgânica*, Vol. 1, p. 191. Ao Livro Técnico, Rio de Janeiro (1980).
18. P. G. Douglas and B. L. Shaw, *J. Chem. Soc.* 1970, 1556.
19. C. G. Kvehn and H. Taube, *J. Am. Chem. Soc.* 1976, **98**, 689.
20. J. F. Fergusson and J. L. Love, *Inorg. Synth.* 1972, **13**, 208.
21. L. H. Vogt, J. L. Katz and S. E. Wiberley, *Inorg. Chem.* 1965, **4**, 1157.
22. S. S. Isied and H. Taube, *Inorg. Chem.* 1974, **13**, 1544.
23. A. R. Babko and A. T. Pilipenko, *Photometric Analysis*. Mir Publishers, Moscow (1971).
24. H. Eyring, *Chem. Rev.* 1935, **17**, 65.
25. J. F. Bunnett, In *Techniques of Chemistry* (Edited by E. S. Lewis), Vol. 6, Chap. 4. Wiley, New York (1974).
26. J. C. Bailar and D. F. Peppard, *J. Am. Chem. Soc.* 1940, **62**, 105.
27. D. W. Franco, S. M. Neiva, L. S. Santos, S. B. Araújo and J. C. Nascimento, *Can. J. Chem.* (in press).
28. M. Trsic, D. W. Franco and M. Conti, *Inorg. Chim. Acta* 1986, **113**, 71.

Polyhedron Vol. 5, No. 10, pp. 1509–1511, 1986
Printed in Great Britain

0277-5387/86 $3.00+.00
Pergamon Journals Ltd

REACTIONS OF 2,5-PYRROLEDIYLBIS[*N*-(*o*-HYDROXYPHENYLALDIMINE)] WITH SOME METAL IONS

H. A. TAYIM,* A. S. SALAMEH† and U. S. I. MERI

Department of Chemistry, University of Petroleum and Minerals, Dhahran, Saudi Arabia

(*Received* 20 *August* 1985; *accepted after revision* 2 *January* 1986)

Abstract—The novel Schiff-base 2,5-pyrrolediylbis[*N*-(*o*-hydroxyphenylaldimine)] (SBH_2) has been synthesized by the condensation of 2,5-pyrroledicarboxaldehyde and *o*-aminophenol. The reactions of the Schiff-base with several transition- and post-transition-metal ions have been investigated. The Schiff-base reacts as a tetradentate dianion without deprotonation of the pyrrole. The complexes $M(SB)\cdot nH_2O$ have been isolated and characterized with $n = 1$, 2 or 3; SB is the dianion of the Schiff-base; and M = divalent Mn, Co, Ni, Cu, Zn, Pd, Cd, Pb or UO_2. The binuclear complexes $M(SB)MX_2$ for M = Cu, X = NO_3, and M = Ni or Pd, X = Cl, have also been isolated.

We have recently reported the reactions of 2,5-pyrroledicarboxaldehyde with several transition-metal ions as an introduction to the investigation of the chemistry of the Schiff-base derived from the condensation of this dialdehyde with *o*-aminophenol and *o*-aminobenzenethiol.[1] The present report deals with the reactions of metal ions with 2,5-pyrrolediylbis[*N*-(*o*-hydroxyphenylaldimine)] synthesized from the reaction of 2,5-pyrroldicarboxyaldehyde with *o*-aminophenol.

EXPERIMENTAL

Preparation of 2,5-*pyrrolediylbis*[N-(o-*hydroxyphenylaldimine*)] (SBH_2)

To a solution of 3.00 g 2,5-pyrroledicarboxaldehyde[2] in 50 cm^3 of hot water a solution of 6.11 g *o*-aminophenol in 50 cm^3 hot water was added dropwise through a dropping funnel with continuous stirring of the reaction mixture. The reaction temperature was kept at about 85°C throughout the reaction time of 2 h. The crude solid product that separated was filtered off and recrystallized from hot benzene. The product is golden yellow (m.p. 184–185°C). Yield 5.00 g (67%). It is insoluble in water, ether and hexane; and soluble in DMF, DMSO, chloroform, ethanol, hot benzene, toluene, dioxane and methylene chloride.

Reaction of the Schiff-base SBH_2 *with some metal ions*

The following general procedure was followed in the reactions of the Schiff-base with each of $MnCl_2\cdot 4H_2O$, $CoCl_2\cdot 6H_2O$, $NiCl_2\cdot 6H_2O$, $Ni(acac)_2\cdot(H_2O)_2$, $Cu(NO_3)\cdot 3H_2O$, Cu(acac)OCH_3, $Zn(CH_3COO)_2\cdot 2H_2O$, $Zn(acac)_2\cdot 2H_2O$, $PdCl_2$, $Pd(PhCN)_2Cl_2$, $Cd(CH_3COO)_2\cdot 2H_2O$, $SnCl_2\cdot 2H_2O$, $Pb(CH_3COO)_2$ and $UO_2(CH_3COO)_2\cdot 2H_2O$. To a stirred solution of 0.400 g (1.31 mmol) of SBH_2 in 50 cm^3 ethanol, a solution of an equimolar amount of the reactant metal salt or complex was added slowly. An immediate reaction took place as indicated by the change in colour or the formation of a precipitate. The reaction mixture was stirred overnight. The product was then filtered off and washed with ethanol and petroleum ether, respectively.

Dioxane was used as a solvent for the Schiff-base in the reaction of $Cu(NO_3)_2\cdot 3H_2O$. The salt was dissolved in the minimum amount of water. In the few cases where the salt did not dissolve in ethanol, the solid salt was added slowly to the solution of the Schiff-base. The colours of the products were dark red, dark brown or reddish brown. The Mn(II) complex was deep orange. The yields ranged between 50 and 62% except for $PdCl_2$ and

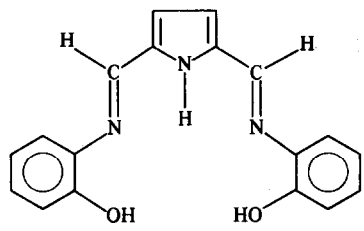
* Author to whom correspondence should be addressed.
† Present address: Department of Chemistry, Faculty of Sciences, Lebanese University, Beirut, Lebanon.

$MnCl_2 \cdot 4H_2O$ where the yield was only 15%. The molecular mass was determined for the product from the reaction of the Schiff-base with $Cu(NO_3)_2 \cdot 3H_2O$ by mass spectrometry using a JEOL DX 300 instrument. Calc. for $C_{18}H_{11}N_5O_8Cu_2$: 552; found: 551.

RESULTS AND DISCUSSION

The investigation of Schiff-bases derived from 2,5-pyrroledicarboxaldehyde has only recently been started,[3] apparently due to the difficulty of synthesizing the dialdehyde.[2] The reaction of the dialdehyde with *o*-aminophenol readily yields the corresponding Schiff-base SBH_2. The proposed structure (**I**) of the Schiff-base is substantiated by elemental analysis and physico-chemical evidence. Found: C, 71.0; H, 5.1; N, 13.8%: Mol. wt (in $CHCl_3$) 301. Calc. for $C_{18}H_{15}N_3O_2$: C, 70.8; H, 4.9; N, 13.8%; mol. wt 305. The IR spectrum shows ν(OH) at 3400(m), ν(NH) at 3300(s), ν(C=C) at 1650(s) and ν(C=N) at 1615(s).

The Schiff-base has four potential donor atoms: the two azomethine nitrogens and the two phenolate oxygens. Models show that all these donor atoms are simultaneously accessible to a metal ion when the phenolate hydrogens are ionized. The pyrrole nitrogen is another potential donor site if it were deprotonated. Investigation of the reactions of 2,5-pyrroledicarboxaldehyde has shown that this may happen only in appreciably basic media. The dialdehyde itself did not afford transition-metal complexes in neutral media, i.e. under reaction conditions similar to those used in the present investigation. It was not surprising, therefore, to find that the Schiff-base behaved in its reaction with all the metal ions that have been investigated as a dianionic tetradentate ligand $(SB)^{2-}$. Complexes of



SBH_2

I

Table 1. Elemental analyses and melting points of the complexes of 2,5-pyrrolediylbis[*N*-(*o*-hydroxyphenylaldimine)] (SBH_2)

Compound	M.p. (°C) (with decomposition)	Analyses[a] (%) C	H	N
$Mn(SB) \cdot H_2O$	>360	57.2 (57.4)	3.8 (4.0)	10.8 (11.2)
$Co(SB) \cdot 3H_2O$	>360	51.7 (51.9)	4.3 (4.6)	9.2 (10.1)
$Ni(SB) \cdot H_2O$[b]	295	56.7 (56.8)	3.7 (3.9)	10.6 (11.1)
$Ni_2(SB)Cl_2 \cdot 4H_2O$[c]	212	38.9 (38.3)	3.6 (3.7)	7.0 (7.4)
$Cu(SB) \cdot H_2O$[d]	235	56.0 (56.1)	3.8 (3.9)	10.6 (10.9)
$Cu_2(SB)(NO_3)_2 \cdot$ dioxane	194	41.8 (41.2)	3.5 (3.3)	11.1 (10.9)
$Zn(SB) \cdot H_2O$[e]	245	55.4 (56.0)	3.8 (3.9)	9.9 (10.9)
$Zn(SB) \cdot 2H_2O$[f]	213	52.9 (53.5)	3.9 (4.2)	10.2 (10.4)
$Pd(SB) \cdot 3H_2O$[g]	207	45.8 (46.7)	3.8 (4.1)	9.3 (9.1)
$Pd_2(SB)Cl_2 \cdot EtOH$[h]	141	38.7 (37.9)	3.0 (3.0)	7.2 (6.6)
$Cd(SB) \cdot H_2O$	164	49.4 (49.9)	3.4 (3.5)	9.3 (9.7)
$Sn(SB)Cl_2$[i]	>360	43.3 (43.9)	2.8 (2.6)	8.2 (8.5)
$Pb(SB) \cdot H_2O$	>360	40.7 (40.9)	2.9 (2.8)	7.7 (8.0)
$UO_2(SB) \cdot 4H_2O$	>360	33.4 (33.5)	3.3 (3.3)	6.4 (6.5)

[a] Calculated values in parentheses.
[b] From $Ni(H_2O)_2(acac)_2$.
[c] Cl, 12.9 (12.6).
[d] From $Cu(acac)OCH_3$.
[e] From $Zn(acac)_2 \cdot 2H_2O$.
[f] From $Zn(CH_3COO)_2 \cdot 2H_2O$.
[g] From $PdCl_2$.
[h] From $Pd(PhCN)_2Cl_2$. Cl, 10.8 (11.2).
[i] Cl, 14.8 (14.4).

divalent metal ions have thus been isolated and characterized. They are formulated as $M(SB)\cdot nH_2O$ (M = Mn, Ni, Cu, Zn, Cd or Pd; $n = 1$: M = Zn; $n = 2$: M = Co or Pd; $n = 3$). The uranyl complex $UO_2(SB)\cdot 4H_2O$ and the tin complex $Sn(SB)Cl_2$ have also been synthesized. The formulae of these complexes are supported by elemental analyses (Table 1) and by spectral evidence. In all these complexes the ligand is tetradentate bonded to the metal through the azomethine nitrogens and the phenolate oxygens. The C=N stretching band in the complexes is lowered by 10–30 cm^{-1} relative to its value in the free Schiff-base, suggesting bonding of the azomethine nitrogens to the metal atom. The ν(NH) observed in the IR spectra of all the complexes around 3300 cm^{-1} supports the fact that the pyrrole is not deprotonated. Moreover, a ν(OH) around 3400 cm^{-1} was observed in the IR spectra of the hydrated complexes.

The colours of the complexes are all intense and dark, varying between red and brown. Even the Mn(II) complex has a deep orange color. This may be due to extensive delocalization of electrons over the skeleton of the planar Schiff-base dianion. The coordination sphere may be completed by solvent molecules or by ions [e.g. $Sn(SB)Cl_2$], whenever this is called for by the nature of the metal ion involved.

Cu(II), Ni(II) and Pd(II) also afforded solvated binuclear complexes of the form $[M(SB)MX_2\cdot$ solvent], where X = NO_3 for Cu(II), and Cl for Ni(II) and Pd(II). In these complexes the species M(SB) behaves as a neutral bidentate ligand that bonds to the other metal atom through the two phenolate oxygens, each of which still has two lone pairs of electrons, even after forming the M(SB) species. In other words, the phenolate oxygens bridge the two metal atoms. The binuclear nature of these complexes is confirmed by molecular weight determination by mass spectrometry.

The behaviour of SBH_2 is similar to the behaviour of the analogous Schiff-base derived from 2,6-pyridinedicarboxaldehyde in every aspect,[4] including the formation of the binuclear complexes. Even the colours, solubilities and melting points of the complexes of both Schiff-bases are very similar. This supports our previous suggestion[4] that the pyridine nitrogen is not involved in bonding to the metal in the complexes of the Schiff-base derived from 2,6-pyridinedicarboxaldehyde.

Acknowledgement—This work has been supported by the Department of Chemistry of the University of Petroleum and Minerals for which we are grateful.

REFERENCES

1. H. A. Tayim and A. S. Salameh, *Polyhedron* 1986, **5**, 687–689.
2. R. Miller and K. Olsson, *Acta Chem. Scand.* 1981, **B35**, 303.
3. H. A. Tayim and A. S. Salameh, *Polyhedron* 1986, **5**, 691–693.
4. H. A. Tayim, M. Absi, A. Darwish and S. K. Thabet, *Inorg. Nucl. Chem. Lett.* 1975, **11**, 395.

Polyhedron Vol. 5, No. 10, pp. 1513–1518, 1986
Printed in Great Britain

0277–5387/86 $3.00+.00
Pergamon Journals Ltd

SYNTHESIS AND CHARACTERIZATION OF Bi(III) COMPLEXES OF 2-AMINOBENZENETHIOL

E. CASASSAS* and T. VISA

Department of Analytical Chemistry, Facultat de Química, Universitat de Barcelona, Av. Diagonal, 647, Barcelona 08028, Spain

(*Received* 17 *September* 1985; *accepted* 7 *January* 1986)

Abstract—Bi(III) complexes with 2-aminobenzenethiol were studied, and the preparation and properties of the new compound tris(2-ammoniumbenzenethiolato)bismuth(III) chloride are reported. Spectral and emf data are consistent with the zwitterionic nature of the ligand. A mercury-bis(2-aminobenzenethiolato)mercury(II) electrode is proposed and used to follow the relative changes in 2-aminobenzenthiol concentration along the course of the complexometric titration of Bi(III) ion with this ligand.

Several solid metal derivatives (normal salts, complex salts and chelates) of 2-aminobenzenethiol (2-abt) are described in the literature. Water-insoluble complexes formed by the Bi(III) ion and 2-abt have been studied by different authors,[1–4] although only Alonzo isolated and analyzed a compound with a well-defined stoichiometry. According to Alonzo, this complex compound is obtained by reacting Bi(III) carbonate suspended in methanol with 2-abt. Other inorganic Bi(III) salts, particularly the trihalides, yield several different products, coloured from orange to red, which have various melting points and lack a defined stoichiometry. In this paper, the preparation of two different Bi(III)–2-abt compounds is described. They are obtained from strongly acidic solutions (hydrochloric acid containing) of Bi(III) nitrate, and are formed within narrow pH ranges during the progressive neutralization of these solutions with sodium hydroxide. The characterization of the two Bi(III)–2-abt compounds and some of their properties (solubility in different solvents, and UV and IR absorption spectra) are also described.

The equilibria in solution which lead to the formation of both bismuth complexes cannot be studied from emf measurements if an indicator glass electrode is used, because it lacks the required precision since, in the strongly acidic reaction medium, the deprotonation of the mercapto group due to its binding to the bismuth atom does not yield any significant acidity change. An emf-based study requires, then, the direct measurement of either the free-ligand concentration or the free-metal-ion concentration during the course of the complexation, and this requires the use of an electrode in the presence of a mercury complex of the implied ligand. An electrode of this type was introduced by Reilley and Schmid[5] to follow potentiometrically a wide variety of complexometric titrations using EDTA in which the electrode was used as an indicator either for the free ligand or for a metal ion different from mercury. This type of electrode has been used with other complexing agents than EDTA. Thus, Galkina *et al.*[6] used a mercury electrode in the presence of 2-mercaptobenzothiazole (HR) or, better, in the presence of the complex HgR_2, for the potentiometric determination of metal ions such as those of nickel, cadmium and lead. They showed that the measured electrode potential is linearly related to the free-ligand concentration. Later, Rusina *et al.*[7] used the same electrode for the determination of several other ions with HR, and established that the electrode potential is determined by the equilibrium $Hg + HR = HgR + H^+ + e^-$.

Similarly, a mercury electrode in the presence of 2-abt is now shown to be useful for following the complexometric titration of the Bi(III) ion (in a citrate-containing medium) with 2-abt as the titrant, since its potential is a linear (although not fully Nernstian) function of the free-ligand concentration. The electrode behaviour allows the confirmation of the 1 : 3 stoichiometry of the new Bi complexes.

* Author to whom correspondence should be addressed.

EXPERIMENTAL

Commercially available reagents and solvents were used without further purification, except when otherwise stated.

Bi(III) nitrate solution

5.224 g (1.077×10^{-2} mol) of bismuth nitrate pentahydrate (Merck, analytical-reagent grade) is dissolved in 25 cm^3 of conc. hydrochloric acid (approx. 0.30 mol), and 100 cm^3 of water are added. From the resulting solution, which is 8.64×10^{-2} mol l^{-1} in Bi(III) and 2.40 mol l^{-1} in hydrochloric acid, bismuth basic salts do not precipitate.

2-abt solution

8.85 g (7.07×10^{-2} mol) of 2-abt (Aldrich, analytical-reagent grade), previously distilled under nitrogen atmosphere, at reduced pressure (less than 1 mmHg), is dissolved in 250 cm^3 of ethanol plus 250 cm^3 of water, both solvents previously deaerated by prolonged bubbling of nitrogen gas into them. The resulting solution is 14.14×10^{-2} mol l^{-1} in 2-abt (as determined iodatometrically) and it is colourless. It is stored in a nitrogen atmosphere and sheltered from light.

*C and H were analyzed by automated microanalytical techniques, and S, N, Cl and Bi by the following methods:

Mercapto sulphur. After destruction of the complexes by strong acid attack, the HS group was titrated with potassium iodate in the presence of excess iodide and starch as indicator.[8]

Nitrogen. Semimicro-Kjeldahl mineralization and titration.

Bismuth. This was gravimetrically determined as Bi_2O_3. Semimicro samples were calcined to 750°C and the residue was weighed as Bi_2O_3.

Chloride. Chloride was potentiometrically titrated with silver nitrate as a titrant and a Ag–AgCl indicator electrode. A weighed amount of the complex trichloride was decomposed by treatment in the cold with 15 cm^3 of 1.0 mol l^{-1} sodium hydroxide solution, with constant stirring by nitrogen bubbling, for several hours. A dirty pale-yellow insoluble residue, supposed to be mainly bismuth(III) hydroxide, was filtered off and the pure yellow filtrate, once acidified with 10 cm^3 of conc. nitric acid, was titrated with silver nitrate solution. Two potential steps are obtained in the titration curve; the amount of chloride was calculated from the titrant volume needed to proceed from the first to the second potential step.

Synthesis of 2-abt–Bi(III) complexes from hydrochloric acid containing solutions

The solid 2-abt–Bi(III) complexes were obtained through neutralization with sodium hydroxide of the strongly acidic solution resulting from mixing the two solutions described before, according to the following procedures:

Preparation of the complex salt tris(2-ammoniumbenzenethiolato)bismuth(III)chloride [$Bi(SC_6H_4NH_3)Cl_3$] (*complex* I). Into a 1:1 mixture of the two solutions described before, which is of a very intense orange colour, stirred by nitrogen bubbling and maintained in a nitrogen atmosphere, a 1.00 mol l^{-1} sodium hydroxide solution was slowly added, until a microcrystalline orange-yellow precipitate formed. This precipitate was rapidly filtered through a No. 3 sintered-glass filter. The clear and transparent filtrate has a pH lower than 2.0 and is also orange-coloured, but much weaker in colour than before precipitation. The solid collected on the filter was repeatedly washed with a water–ethanol mixture [3:2 (v/v)]. Without any recrystallization it is dried in a vacuum desiccator.

*Elemental analysis.** Found: C, 31.3; H, 3.3; N, 5.7; S, 14.1; Cl, 15.2; Bi, 30.8%. Calc for $Bi(SC_6H_4NH_3)Cl_3$: C, 31.3; H, 3.1; N, 6.1; S, 13.9; Cl, 15.4; Bi, 30.2%.

Preparation of the complex tris(2-aminobenzenethiolato)bismuth(III) [$Bi(SC_6H_4NH_2)_3$] (*complex* II). To the filtrate from the precipitation of the later complex trichloride, further additions of 1.00 mol l^{-1} sodium hydroxide solution were slowly made, while the stirring by nitrogen bubbling was continued, until a spongy orange-red precipitate formed. Additions of sodium hydroxide solution were continued drop by drop until the precipitation was complete, but care must be taken not to exceed pH 4.0. The solid was filtered off through a No. 4 sintered-glass filter, repeatedly washed with a water–ethanol mixture [3:2 (v/v)], and dried in a vacuum desiccator.

Elemental analysis. Found: C, 37.3; H, 3.1; N, 7.5; S, 16.1; Cl, traces: Bi, 35.2%. Calc for $Bi(SC_6H_4NH_2)_3$: C, 37.2; H, 3.1; N, 7.2; S, 16.5; Cl, 0.0; Bi, 35.9%.

The chemical process in chloride determination as described is as follows. The yellow colour of the acidified solution is due to the presence of organic matter proceeding from the 2-abt in the complex. During the sodium hydroxide treatment, the ligand 2-abt is set free and is first quantitatively oxidized to disulphide; later on in the strongly basic medium the latter dismutates into the mercaptide anion RS^-, and a higher oxidation product, e.g. the sulphenate anion RSO^-. The UV spectrum of the final

basic solution, actually, shows the absorption maximum at 297.5 nm which is characteristic of 2-abt. The presence of 2-abt in the acidified solution used for the chloride titration with silver nitrate is also shown by the potentiometric results: the titration curve shows two potential steps, the first one corresponding to the end-point of the precipitation of the silver mercaptide and the second one which is the end-point of the precipitation of silver chloride. In this way, the sulfur content in the complex can be also evaluated. A mean value for the sulfur content in the complex trichloride of 13.2% resulted, with a relative error of 4% be defect, losses being assignable to 2-abt oxidation during the acidification process.

RESULTS AND DISCUSSION

Some physical properties of both bismuth complexes have been determined (solubility in several solvents of different polarities, and spectral properties in the UV–VIS and IR ranges) and emf measurements have been used to study complex formation as well as the conversion of complex I into complex II. The results are discussed as follows.

Solubility

The following solvents were tested: benzene, carbon tetrachloride, chloroform, ethanol, dioxane, carbon disulphide, pyridine, dimethylformamide, dimethyl sulphoxide and water. At a concentration of 1 mg ml^{-1} both complexes are soluble in pyridine, dimethylformamide and dimethyl sulphoxide; complex II is also soluble in dioxane.

UV–VIS absorption spectrophotometry

Solutions of complex I in pyridine show absorption maxima at 400 and 305 nm, in DMF at 387.5, 300 and 267.5 nm, and in DMSO at 400 and 290 nm. The absorption maxima of solutions of complex II are: in pyridine at 400 and 301 nm, in DMF at 400, 277.3 and 267.5 nm, in DMSO at 400 and 295 nm, and in dioxane at 400, 280, 226 and 215.4 nm. Both complexes seem to have the same chromophore group, responsible for the absorption maxima at 400 nm. In complex I the amino group is protonated and cannot coordinate to the metal ion, whereas, in principle, in complex II the situation is the reverse. The evidence afforded by Alonzo[4] and the observed spectral behaviour discount the participation of the amino group in the binding of bismuth in complex II and, therefore, invalidate a chelate structure for this complex. The constancy of the absorption band at 400 nm in the different solvents can be taken as a proof that both complexes have a common mercaptide structure, and that the actual common chromophore must be $[BiS_3]$.

IR absorption spectra

The IR spectrum of complex II was described by Alonzo:[4] that of complex I (obtained either from a KBr pellet or a Nujol mull) shows significant differences, all of which can be assigned to the protonation of the amino group.

Thus, the two bands at 3440 and 3320 cm^{-1} in the spectrum of complex II, which appear at 3440 and 3360 cm^{-1} in the 2-abt spectrum, and which are assigned to the stretching vibrations of NH_2 in the spectrum of complex I are changed into a set of three bands at 3440, 2900 and 2600 cm^{-1}, characteristic of the protonated amino group.[9] Similarly, the zone of the NH_2-deformation bands is changed as a result of protonation: thus, whereas the 2-abt spectrum shows a very strong band at 1618 cm^{-1} and complex II one strong band at 1598 cm^{-1} and a medium-intensity band at 1580 cm^{-1}, the spectrum of complex I has a family of bands at 1610 cm^{-1} (strong), 1555 cm^{-1} (medium), 1540 cm^{-1} (medium) and 1511 cm^{-1} (medium). It must be mentioned that the symmetry properties of complex I, which is a chloride, can be changed on compacting it with potassium bromide to form the pellet used for IR measurements, as observed by Burger[10] in several cases, as a result not only of chloride substitution but even of the entering of bromide into the co-ordination sphere of the metal ion. In the spectrum from the Nujol mull, the mentioned family of bands appears at 1600, 1543, 1538 and 1500 cm^{-1}.

Features which are common to the spectra of both complexes are the following: the band assigned to stretching of the C–S bond (at 680 cm^{-1} in 2-abt), appearing at 675 cm^{-1}; the lack of a band due to SH stretching (which appears at 2537 cm^{-1} in the spectrum of 2-abt); the series of weak bands between 290 and 250 cm^{-1}, which has been assigned for complex II[4] to the Bi–S bond; and, finally, an unassigned band of medium intensity at 815 cm^{-1} (complex I) or at 801 cm^{-1} (complex II).

Potentiometric study of the reaction of Bi(III) with 2-abt

The amount of mercury suitable to form the pool which will act as electrode was left during several hours in contact with an acidic 2-abt solution (about 0.02 mol l^{-1} in 2-abt and between 1.0 and 2.0 M in perchloric acid) in 1 : 1 (v/v) water–ethanol, with constant bubbling of a nitrogen-gas stream.

The contact solution was then extracted, the pool washed with a diluted perchloric acid solution in water–ethanol and the following cell assembled:

$$\text{Treated Hg} \left| \begin{matrix} \text{test solution in} \\ \text{water–ethanol} \end{matrix} \right| \left| \text{NaCl, AgCl} \right| \text{Cl}$$

The cell contains a measured volume of test solution, which contains A mol l^{-1} 2-abt and H mol l^{-1} perchloric acid, was kept under a nitrogen atmosphere, and was connected to the reference half-cell through a Wilhelm-type salt bridge containing 1 M $NaClO_4$ in 1 : 1 water–ethanol. The concentration of 2-abt in the test solution was initially zero, and was increased by successive additions of a 10^{-1}–10^{-2} mol l^{-1} 2-abt solution from a buret. The cell emf was measured with a Radiometer pH-meter PHM64 (precision ± 0.1 mV). After each 2-abt addition the emf reading was taken when stabilized, which happens in less than 1 min (if the mercury has been pretreated as prescribed, but not if clean mercury was used for the electrode construction).

The following behaviour was observed. For each of the potentiometric runs successively done using the same mercury electrode, emf readings showed a linear dependence on log [2-abt] within the 2-abt concentration ranges shown in Table 1. The values of the parameters m and n in the expression $E = m + n \log$ [2-abt] which produce the best fit to the experimental points for each one of the potentiometric runs in a series, together with their correlation coefficients, are given at Table 1. It is observed that in each case linearity is acceptable, but that reproducibility is not. In the first runs, the slope n lies usually in the range of 100–130 mV; when the same mercury pool is used again the numerical value of the slope in each run falls to a value of about 60 mV. The value of the standard potential of the electrode is not wholly reproducible: after the abnormal first run, E^o stabilizes at about 320–340 mV, as is also shown in Table 1.

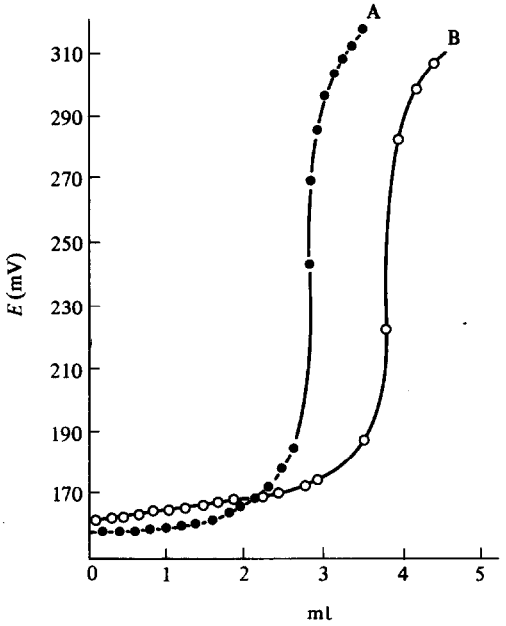


Fig. 1. Titration curves of Bi(III) aqueous solutions, in a citrate buffer of pH 3.50, with a 2-abt titrant solution in 1 : 1 (v/v) water–ethanol, as followed with a treated-mercury indicator electrode. (A) Titration of 20.0 cm^3 of 6.214×10^{-3} mol l^{-1} Bi(III). Titrant: 0.1395 mol l^{-1} 2-abt. (B) Titration of 20.0 cm^3 of 5.579×10^{-3} mol l^{-1} Bi(III). Titrant: 0.0901 mol l^{-1} 2-abt.

The observed behaviour clearly shows that, although the cell employing a treated-mercury electrode cannot be used to calculate the free concentration of ligand in equilibrium with the Bi ion, for instance, because the values of the parameters m and n show slight changes from run to run, it can actually be used to follow the *relative* changes in 2-abt concentration along the course of a potentiometric titration of the Bi ion with 2-abt solution as a titrant. That this is actually the case is shown by the two curves in Fig. 1, which are examples of the titration curves of bismuth(III) chloride solutions which contain excess chloride ion buffered

Table 1. Observed response of a treated-mercury electrode in 2-abt solutions (1.0 mol l^{-1} in $HClO_4$) in 1 : 1 (v/v) water–ethanol

Experiment No.	2-abt concentration range (10^{-3} mol l^{-1})	No. of points	E^o (mV) m	Slope (mV) n	Correlation coefficient
1	2.60–7.40	13	441.9	105.84	0.9980
2	3.00–5.40	6	337.7	59.29	0.9952
3	1.46–7.30	9	340.6	67.27	0.9926
4	2.03–9.62	16	343.2	67.71	0.9986
5	2.40–7.50	7	321.3	63.15	0.9953

Table 2. 2-abt/Bi(III) ratio in complex **II**, as determined from potentiometric titrations with 2-abt of 20.0 cm^3 of a Bi(III) solution buffered with citrate

Experiment No.	pH	Bi(III) concentration (mmol l^{-1})	2-abt concentration (mol l^{-1})	Titrant volume (cm^3)	2-abt/Bi(III) ratio
1	3.5	6.214	0.1395	2.80	3.14
2	3.5	5.579	0.0901	3.80	3.06
3	3.5	5.579	0.0901	3.90	3.14
4	3.9	5.432	0.0400	8.64	3.18
5	4.0	7.390	0.0400	11.80	3.19

with citrate at pH 3.5. The potential jump at the end-point is very steep and covers a potential range of over 100 mV.

These properties were used to check the stoichiometric ratio 2-abt : Bi in the new complexes. Complex **I** formation, occurring at pH lower than 2.0 and producing a non-quantitative precipitation of bismuth ion, cannot be followed by potentiometric means with this aim. Complex **II** formation, which is quantitative, occurs at a higher pH and, in order to avoid bismuth hydrolysis or hydroxocomplex precipitation, the potentiometric study must be done in the presence of a suitable complexing agent, such as citrate. The experiment was performed as follows.

Bi(III) solutions were prepared from samples of pure Bi_2O_3 accurately weighed and dissolved in the minimum amount of conc. hydrochloric acid. The resulting solution was made 2.0 mol l^{-1} in sodium citrate, and sodium hydroxide and water were added until the desired pH (in the range 3.5–4.0) was reached and up to volume. This solution was introduced into the potentiometric cell, deaerated with nitrogen gas and titrated with a 2-abt solution in 1 : 1 (v/v) water–ethanol that was previously adjusted to the same pH. The concentration of the titrant was previously determined by titration with potassium iodate.[8] After each titrant addition, emf readings were taken when stabilized. An orange-red spongy precipitate of complex **II** formed during the titration. From the end-point detected in the titration curve the amount of 2-abt reacted and the stoichiometric ratio of reactants in complex **II** were evaluated, as shown in Table 2. The results for the 2-abt/Bi ratio, although they are a little too high, due perhaps to 2-abt co-precipitation or auto-oxidation, confirm the 3 : 1 stoichiometry previously found from the results of elemental analysis.

Conversion of complex **I** *into complex* **II**

The major chemical difference between the two bismuth complexes stems from the amino group of 2-abt, which is protonated in complex **I** and unprotonated in complex **II**. In free 2-abt, the log of the protonation constant for the amino group is $\log K_{H2} = 2.63$.[11] In complexed 2-abt the value of this protonation constant cannot be very different. Then, if the solid complex **I** is suspended in water and shaken for some minutes, an acid–base equilibrium is established (pH is stabilized at about 2.5). The equilibrium can be shifted by titration with sodium hydroxide and complex **I** will be converted into complex **II**.

Three samples of complex **I** (55.0, 50.5 and 35.9 mg) were suspended in water and, after shaking for 30 min, the suspension was potentiometrically titrated with sodium hydroxide solution using a glass-electrode indicator. During the course of the titration, the aspect of the suspended solid actually changes to that of complex **II**, but near the end-point a new change begins to be apparent to a brown denser solid. Since at the end-point emf readings show a steep jump in pH from about 4 to about 11, it is likely that some mixed hydroxocomplex formation takes place. The amounts of sodium hydroxide reacted in the titration of the three mentioned samples were 0.1653, 0.1820 and 0.1199 mmol, respectively, leading to ratios of hydrogen ion titrated per mol of complex **I** equal to 2.08, 2.49 and 2.29, respectively. The conversion into complex **II** is not quantitative in any case, the theoretical value of 3.0 not being reached due to the heterogeneous nature of the phases implied in the acid–base equilibrium.

REFERENCES

1. N. Steiger, U.S. Patent 2,490,717, 6 December (1949) (*Chem. Abs.* 1950, **44**, 3526i).
2. E. J. Olzewski and M. J. Albinak, *J. Inorg. Nucl. Chem.* 1965, **27**, 1431.
3. R. G. Charles and H. Freiser, *J. Am. Chem. Soc.* 1952, **74**, 1383.
4. G. Alonzo, *Inorg. Chim. Acta* 1983, **73**, 141.

5. C. N. Reilley and R. W. Schmid, *J. Am. Chem. Soc.* 1955, **78**, 1294; *Anal. Chem.* 1957, **29**, 264.
6. E. I. Galkina, K. N. Bagdasarov and V. I. Man'ko, *Fiz.-Khim. Metody Anal. Kontrolya Proizvod., Mezhvuz. Sb.* 1976, **21**, 2.
7. O. N. Rusina, P. N. Kovalienko and S. I. Ivanova, *Z. Anal. Chim.* 1965, **20**, 44.
8. N. D. Cheronis and T. S. Ma (Eds), *Organic Functional Analysis by Micro and Semimicro Methods*, p. 324. Interscience, New York (1964).
9. J. B. Lambert, H. F. Shurvell, L. Verbit, R. G. Cooks and G. H. Stout, *Organic Structural Analysis*, p. 178. Collier-Macmillan, London (1976).
10. K. Burger, in *Coordination Chemistry, Experimental Methods*, p. 76. Butterworths, London (1973).
11. E. Casassas and T. Visa, *J. Chim. Phys.* (in press).

Polyhedron Vol. 5, No. 10, pp. 1519–1523, 1986
Printed in Great Britain

0277–5387/86 $3.00+.00
Pergamon Journals Ltd

RUTHENIUM(II) COMPLEXES WITH 2-METHYL-3-SUBSTITUTED (3*H*)-QUINAZOLIN-4-ONES

K. LAXMA REDDY and P. LINGAIAH

Department of Chemistry, Kakatiya University, Warangal 506 009, India

and

K. VEERA REDDY*

Department of Chemistry, University College of Science, Osmania University, Hyderabad 500007, India

(*Received* 16 *October* 1985; *accepted after revision* 20 *January* 1986)

Abstract—A number of ruthenium(II) complexes of some polydentate O–N, O–O and O–N–O donors in the form of 2-methyl-3-substituted (3*H*)-quinazolin-4-ones have been synthesized and studied. The reaction between $RuCl_2(DMSO)_4$ and the uninegative bidentate ligands yielded complexes of the type $Ru(DMSO)_2(O–O)_2$ (O–O = MHQ, PHQ, MHEQ, MHPQ or MCMQ), displacing only two DMSO groups along with chlorides, whereas the neutral bidentate ligands gave $RuCl_2(O–N)_2$ (O–N = MAQ, PAQ, MANQ, PANQ, MAAQ, MAPQ, MPQ or PPQ), displacing all the DMSO groups. A uninegative terdentate ligand (MHAQ) with O–N–O donors, however, yielded a bis chelate of ruthenium(II).

Quinazolone and its derivatives are widely known for their anti-tubercular,[1] anti-convulsant,[2] anti-amoebic[3] and anti-allergic[4,5] properties. The chelating tendency of these compounds is little known except for a few publications involving similar ligands.[6–8] We report here the synthesis of a series of neutral ruthenium(II) complexes obtained by the reaction of $RuCl_2(DMSO)_4$ with various 2,3-disubstituted quinazolones represented in Fig. 1, where X is invariably a donor group and R a methyl or phenyl group.

EXPERIMENTAL

All analytical data are collected in Table 1. IR and proton NMR spectral data are presented in Tables 2 and 3. The ligands were prepared by reported methods[9–17] (Table 1). The complex $RuCl_2(DMSO)_4$ was prepared by a published method.[18] Elemental analyses and other physical measurements were carried out as reported earlier.[19]

General method for the preparation of ruthenium(II) complexes

The complex, $RuCl_2(DMSO)_4$ (0.2 g) was suspended in toluene (30 cm^3) and refluxed for 1 h with about 4 mol excess of the appropriate ligand in methanol (10 cm^3). During the period of refluxing the whole suspension dissolved, resulting in a clear solution, which was then evaporated under reduced pressure to remove the excess solvent. The residue was treated with diethylether, when the solid complex precipitated. This was filtered off, washed several times with diethylether, dried and recrystallized from methanol–ether to give a pure complex. Yields 50–70%. The complexes are highly soluble in methanol, ethanol and other organic solvents.

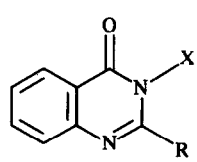


Fig. 1.

*Author to whom correspondence should be addressed.

Table 1. Analytical and physical data of ruthenium(II) complexes

No.	Complex	R[a]	X[a]	Colour	M.p.[b] (°C)	Analyses (%)[c] C	H	N	S/Cl	Molar conductance[d] (mho cm^2 mol^{-1})
1	$Ru(DMSO)_2(MHQ)_2$	CH_3	OH[9]	Brown	230	43.8 (43.5)	4.3 (4.3)	9.3 (9.2)	10.9 (10.5)	18
2	$Ru(DMSO)_2(PHQ)_2$	C_6H_5	OH[9]	Brown	228	52.9 (52.5)	4.3 (4.1)	7.6 (7.7)	8.8 (8.7)	20
3	$Ru(DMSO)_2(MHEQ)_2$	CH_3	CH_2CH_2OH[10]	Red brown	225	47.2 (47.0)	5.3 (5.1)	8.6 (8.5)	9.7 (9.6)	16
4	$Ru(DMSO)_2(MHPQ)_2$	CH_3	*o*-$C_6H_4(OH)$[11]	Orange yellow	225	53.4 (53.8)	4.3 (4.5)	7.5 (7.4)	8.7 (8.4)	22
5	$Ru(DMSO)_2(MCMQ)_2$	CH_3	CH_2COOH[12]	Yellow	228	45.3 (45.1)	4.4 (4.3)	8.2 (8.1)	9.3 (9.3)	20
6	$RuCl_2(MAQ)_2$	CH_3	NH_2[13]	Pink	240	41.5 (41.4)	3.5 (3.5)	16.2 (16.0)	13.7 (13.6)	20
7	$RuCl_2(PAQ)_2$	C_6H_5	NH_2[14]	Pink	235	52.2 (52.0)	3.5 (3.4)	13.3 (13.10)	11.0 (10.9)	18
8	$RuCl_2(MANQ)_2$	CH_3	$NH(C_6H_5)$[13]	Brown	232	53.9 (53.4)	3.9 (3.9)	12.5 (12.4)	10.7 (10.5)	22
9	$RuCl_2(PANQ)_2$	C_6H_5	$NH(C_6H_5)$[14]	Red brown	230	60.3 (60.1)	3.9 (3.7)	10.6 (10.5)	8.8 (8.9)	14
10	$RuCl_2(MAAQ)_2$	CH_3	$NHC(O)CH_3$[15]	Brown	230	43.2 (43.6)	3.7 (3.6)	13.8 (13.9)	11.9 (11.7)	20
11	$RuCl_2(MAPQ)_2$	CH_3	*o*-$C_6H_4(NH_2)$[10]	Green	233	53.9 (53.4)	3.9 (3.9)	12.6 (12.5)	11.0 (10.5)	16
12	$RuCl_2(MPQ)_2$	CH_3	2-C_5H_4N[16]	Brown	238	52.3 (52.0)	3.6 (3.4)	13.2 (13.0)	11.0 (10.8)	18
13	$RuCl_2(PPQ)_2$	C_6H_5	2-C_5H_4N[17]	Brown	230	59.4 (59.2)	3.5 (3.4)	10.8 (10.9)	9.8 (9.2)	20
14	$Ru(MHAQ)_2$	CH_3	$CH_2CH_2NH(CH_2)_2OH$[14]	Green	250	53.0 (52.6)	5.7 (5.4)	14.2 (14.2)	—	16

[a] R and X are the substituents at the 2- and 3-positions, respectively, on quinazolin-(3*H*)-4-one.
[b] All the complexes decompose above the temperatures cited.
[c] Calculated values in parentheses.
[d] 10^{-3} M solutions in methanol at room temperature.

Table 2. Some IR spectral data of 2-methyl-3-substituted (3*H*)-quinazolin-4-ones and their ruthenium(II) complexes

	Stretching frequencies (cm^{-1})[a]				
		ν(N—H)			
Complex	ν(C=O)	—NH_2	—NH	ν(OH)	ν(S=O)
1	1660s	—	—	—	1060s
	(1700s)			(3100br)	—
2	1665s	—	—	—	1070s
	(1700s)			(3100br)	—
3	1650s	—	—	—	1080s
				(3300br)	—
4	1660s	—	—	—	1050s
	(1700s)			(3300br)	—
5	1670s	—	—	—	1060s
	(1700s)			(2500br)[b]	—
6	1660s	3300s	—	—	—
	(1700s)	(3340s)			
7	1650s	3320s	—	—	—
	(1700s)	(3360s)			
8	1650s	—	3150s	—	—
	(1700s)		(3200s)		
9	1660s	—	3160s	—	—
	(1700s)		(3200s)		
10	1650s, 1640s[c]	—	3120s	—	—
	(1690s, 1640s)		(3200s)		
11	1650s	3300s	—	—	—
	(1690s)	(3340s)			
12	1660s	—	1640s, 1570s	—	—
	(1700s)		(1640s, 1610s)[d]		
13	1650s	—	1640s, 1560s	—	—
	(1700s)		(1640s, 1610s)[d]		
14	1660s	—	3130s	—	—
	(1690s)		(3180s)	(3300br)	

[a] Free-ligand absorptions are given in parentheses: s, strong; m, medium; w, weak; br, broad.

[b] The ν(OH) of the carboxylic group of the MCMQ ligand.

[c] The ν(C=O) of the amide group of the MAAQ ligand.

[d] The ν(C=N) of quinazoline and pyridyl rings in the MPQ and PPQ ligands.

RESULTS AND DISCUSSION

The complex, $RuCl_2(DMSO)_4$ is an excellent precursor for the synthesis of many new ruthenium(II) complexes and the reactions involving this complex are mainly of the displacement type.[18,19] The reaction of this complex with 2-methyl-3-substituted (3*H*)-quinazolin-4-ones at reflux temperature in toluene was rapid and gave good yields of the complexes. Depending on the nature of the chelate this complex undergoes a variety of reactions. Uninegative bidentate ligands such as MHQ, PHQ, MHEQ, MHPQ and MCMQ yielded $Ru(DMSO)_2(O–O)_2$ and neutral bidentate ligands such as MAQ, PAQ, MANQ, PANQ, MAAQ, MAPQ, MPQ and PPQ gave $RuCl_2(O–N)_2$. A bis chelate of type $Ru(O–N–O)_2$ was also obtained when $RuCl_2(DMSO)_4$ was reacted with a large excess of uninegative terdentate ligand MHAQ. All the complexes were isolated as crystalline, air-stable compounds. The yields are high and the reactions generally faster when the 2-position is substituted by a methyl rather than a phenyl group. Molar conductivities are found in the range of 16–22 mho $cm^2 mol^{-1}$, indicating their non-electrolytic nature[20] (Table 1). All are diamagnetic ruthenium(II) complexes.

The most important bands occurring in the IR

Table 3. Proton NMR spectra of ligands and their complexes of ruthenium(II)[a]

Complex	Chemical shifts [δ (ppm)][b]			
	—CH_3(s)[c]	Aromatic protons(m)	—NH(br)/ —NH_2(br)/ —OH(s)	—CH_2—(s)
1	2.4 (2.5)	7.2–9.0	—	
	3.0–3.3	(7.1–8.9)	(10.5)	
2	3.0–3.5	7.15–8.99		
		(7.10–8.90)	(10.3)	
3	2.65 (2.75)	7.2–9.1		6.6
		(7.1–8.9)	(9.9)	(4.8, 5.0)
4	2.55 (2.65)	7.15–8.95		
	3.0–3.3	(7.1–8.9)	(9.6)	
5	2.65 (2.80)	7.25–9.12		6.8
	3.0–3.4	(7.20–8.99)	(10.8)[d]	(4.75)
6	2.55 (2.65)	7.20–9.10	8.2[e]	
		(7.10–8.95)	(6.2)	
7	—	7.15–9.10	8.1[e]	
		(7.1–9.0)	(6.2)	
8	2.8 (2.95)	7.12–8.92	8.3[e]	
		(7.1–8.9)	(6.5)	
9	—	7.22–9.12	8.4[e]	
		(7.1–9.1)	(6.6)	
10	2.65 (2.75)	7.25–9.10	8.4[e]	
	3.0 (2.9)[f]	(7.2–9.0)	(4.2)[f]	
11	2.65	7.16–9.15	8.2	
		(0.1–9.0)	(6.2)	
12	2.68 (2.90)	7.12–9.10	—	
		(7.10–8.95)		
13	—	7.15–9.15	—	
		(7.1–9.0)		
14	2.65 (2.85)	7.22–9.00	8.4[e]	6.4
		(7.15–8.95)	(6.2) (9.8)[g]	(4.4, 4.95)

[a] Free-ligand values are given in parentheses. 100-MHz spectra in $CDCl_3$ solutions with $Si(CH_3)_4$ as internal reference.

[b] s, singlet; m, multiplet; br, broad.

[c] The peaks in the range δ 3.0–3.5 are broad and correspond to CH_3 protons of DMSO in complexes **1–5**.

[d] Due to the OH of the carboxylic group in the MCMQ ligand.

[e] Due to NH/NH_2.

[f] Due to the amide CH_3 (δ 2.9) and —NH— (δ 4.2) protons of the MAAQ ligand.

[g] Due to the OH group.

of the free ligands and their metal complexes have been compared in order to ascertain the bonding sites in ligands (Table 2). A strong band corresponding to ν(C=O) at 1700 cm^{-1} of the quinazolone ring is shifted to lower wavenumbers by 35–50 cm^{-1} in the IR of all the complexes, indicating that the carbonyl oxygen is invariably coordinated to ruthenium(II).[21]

The bands due to ν(OH) observed in the IR of MHQ, PHQ, MHEQ, MHPQ and MCMQ disappeared completely in their complexes, confirming the coordination of these ligands by deprotonation.[22,23] The presence of DMSO in complexes **1–5** was characterized by its ν(S=O), which occurs as a strong band in the 1050–1100-cm^{-1} region, corresponding to the S-bonded DMSO ligands[18,24] (Table 2).

The NMR spectra of complexes **1–5** bear general resemblances to those of free ligands; nevertheless some differences are evident because of co-

ordination (Table 3). A single intense signal in the δ-3.0–3.5 region in complexes **1–5** with a downfield shift of about 0.7–0.9 ppm from that of free DMSO may be assigned to the S-bonded DMSO ligands coordinated in a *trans* manner.[18] The resonances due to OH groups of MHQ, PHQ, MHEQ, MHPQ and MCMQ totally disappear in their complexes.

The ligands MAQ, PAQ, MANQ, PANQ, MAAQ, MAPQ, MPQ and PPQ with mixed-donor centres (O–N) are neutral and react with $RuCl_2(DMSO)_4$ to give neutral complexes of type $RuCl_2(O–N)_2$ (**6–13**). The IR spectra confirms the absence of DMSO groups in all these complexes. The ν(N—H) frequencies of the NH_2 group in MAQ, PAQ and MAPQ were reduced by about 40 cm^{-1} upon coordination in complexes **6**, **7** and **11**.[25] On the other hand, the ν(N—H) of —NH— in MANQ, PANQ and MAAQ were lowered by 40–80 cm^{-1} in complexes **8–10**[26] (Table 2). In complex **10**, the shift in the ν(N—H) band to the lower side is more pronounced, supporting coordination through the amide nitrogen.[27] The band at 1640 cm^{-1} due to the ν(C=N) of quinazolone remains unaltered in the IR of complexes **12** and **13**, whereas the band at 1610 cm^{-1} due to the ν(C=N) of pyridine undergoes a lower shift of 40–50 cm^{-1}, suggesting coordination through the pyridine nitrogen.[28]

A broad signal around δ 6.2 in the proton NMR spectra of MAQ, PAQ and MAPQ due to $—NH_2$ protons undergoes a downfield shift to δ 8.1–8.2 in complexes **6**, **7** and **11**, as the primary amine nitrogen is bonded to the metal ion. Similarly, a large downfield shift of 1.8 ppm is observed in complexes **8** and **9**, compared to the free-ligand values at δ 6.5 and 6.6, respectively. Further, a very large downfield shift of δ 4.2 was observed when coordination occurred via the amide nitrogen in complex **10**.

MHAQ binds as a uninegative terdentate ligand in the complex $Ru(MHAQ)_2$ (**14**). Besides IR evidence, proton NMR data also confirm this type of coordination (Table 3). There is a large downfield shift observed for the —NH— proton in MHAQ and the signal merged with those of aromatic protons at δ 7.22–9.00 has been identified by means of D_2O exchange studies.

Acknowledgement—One of us (KLR) is thankful to CSIR, New Delhi, for the award of a Research Associateship.

REFERENCES

1. N. P. Bu-Hoi, N. D. Xyong and C. R. Nami, *C. R. Acad. Sci.* 1954, **1**, 238, 295.
2. S. H. Zaheer, G. S. Sidhu, P. B. Sattur, S. S. Mandrekar, V. K. Seth and V. H. Seth, *Symposium on CNS Drugs*, p. 170. CSIR, New Delhi (1966).
3. W. Merillus, *J. Med. Chem.* 1968, **11**, 171.
4. (a) C. F. Schwender, B. R. Sunday, D. J. Herzig, E. K. Kusner, P. R. Schumann and D. L. Gawlak, *J. Med. Chem.* 1979, **22**, 748; (b) J. W. Tilley, R. A. LeMahien, M. Carson, R. W. Kierstead, H. W. Baruth and B. Yaremko, *J. Med. Chem.* 1980, **23**, 92.
5. R. A. LeMahieu, M. Carson, W. C. Nason, D. R. Parrish, A. F. Welton, H. W. Baruth and B. Yaremko, *J. Med. Chem.* 1983, **26**, 420.
6. B. Singh, Lakshmi Agarwala and U. Agarwala, *Inorg. Chem.* 1969, **8**, 2341.
7. U. Agarwala and Lakshmi Agarwala, *J. Inorg. Nucl. Chem.* 1971, **34**, 241.
8. B. Singh, R. N. Pandey, D. K. Sharma, U. S. Sharma and Uday Bhanu, *Indian J. Chem.* 1981, **20A**, 1097.
9. L. Legrand and N. Lozach, *Bull. Soc. Chim. Fr.* 1961, 618.
10. K. Kishor, R. C. Arora and S. S. Parmar, *J. Med. Chem.* 1965, **8**, 550.
11. K. H. Boltz, H. D. Bell, H. Lehwald, D. Lorenz and M. Rueberg, *Arzneim.-Forsch.* 1963, **13**, 688; *Chem. Abstr.* 1965, **63**, 4289d.
12. R. Soliman and F. S. G. Soliman, *Synthesis* 1979, 803.
13. L. Legrand and N. Lozach, *Bull. Soc. Chim. Fr.* 1961, 1400.
14. A. P. Bhaduri and N. M. Khanna, *Indian J. Chem.* 1966, **4**, 447.
15. S. Anjaneyulu, M.Phil. dissertation, Kakatiya University, A.P., India (1979).
16. K. Kishor, R. Kumar and S. S. Parmar, *J. Med. Chem.* 1964, **7**, 831.
17. S. Somashekhara, V. S. Dighe, P. V. Arur and S. L. Mukherjee, *Curr. Sci.* 1964, **33**, 746.
18. I. P. Evans, A. Spencer and G. Wilkinson, *J. Chem. Soc., Dalton Trans.* 1973, 204.
19. V. Ravindar, P. Lingaiah and K. Veera Reddy, *Inorg. Chim. Acta* 1984, **87**, 35.
20. W. J. Geary, *Coord. Chem. Rev.* 1971, **7**, 81.
21. R. Sahai, R. S. Agarwal and S. S. Kushwaha, *J. Indian Chem. Soc.* 1982, **7**, 853.
22. A. Sammour, A. F. M. Fammoy and M. Mahmoud, *Indian J. Chem.* 1973, **13**, 272.
23. B. Singh, V. Banerjee, B. V. Agarwala and K. Dey Arun, *J. Indian Chem. Soc.* 1980, **57**, 365.
24. W. L. Reynolds, *Prog. Inorg. Chem.* 1970, **12**, 1.
25. J. V. Quagliano, G. V. Svatos and B. C. Curran, *Anal. Chem.* 1954, **26**, 429.
26. Senguptha, S. K. Sahni and R. N. Kapoor, *Indian J. Chem.* 1981, **20A**, 692.
27. S. S. Sandhu, B. S. Manhas, M. R. Mittal and S. S. Parmar, *Indian J. Chem.* 1969, **7**, 286.
28. C. P. Prabhakaran and C. C. Patel, *J. Inorg. Nucl. Chem.* 1972, **34**, 3485.

Polyhedron Vol. 5, No. 10, pp. 1525–1530, 1986
Printed in Great Britain

0277–5387/86 $3.00+.00
Pergamon Journals Ltd

STABILITY AND SPECTRAL CHARACTERISTICS OF THE U(VI)–ALIZARIN MAROON–THIOSALICYLIC ACID TERNARY COMPLEX

MOHAMED M. SELEIM, KAMAL A. IDRISS,* MAGDA S. SALEH and ELHAM Y. HASHEM

Department of Chemistry, Faculty of Science, Assiut University, Assiut, Egypt

(*Received* 15 *July* 1985; *accepted after revision* 27 *January* 1986)

Abstract—The stability constant of the ternary U(VI) complex containing alizarin maroon (azm) and, as a second ligand, thiosalicylic acid (tsa) in a 1 : 1 : 1 molar ratio was determined by potentiometric titration in 40% (v/v) ethanol–water medium [$I = 100$ mmol dm^{-3} ($NaClO_4$), 25 ± 0.1°C]. For the equilibrium, $U(azm)_2 + U(tsa)_2 \rightleftharpoons 2U(azm)(tsa)$, the corresponding constant, $\log X$, was found to be 2.80 (0.27). The constant given in parentheses is due to $\Delta \log K = \log K^{U(tsa)}_{U(azm)(tsa)} - \log K^{U}_{U(azm)}$. The absorption spectra of the U(azm)(tsa) ternary complex were investigated and a sensitive method was developed for the microdetermination of uranium based on the formation of this complex. The solution spectrum of the ternary complex gave an absorption band at 630 nm over the pH range 5.8–7.4. The ternary system conformed Beer's law between 5.9 and 66.6 μg cm^{-3} uranium with a molar absorptivity of 2×10^4 l mol^{-1} cm^{-1}. The IR spectra of the mono- and biligand complexes were also studied.

It has already been recognized that the stability of mixed-ligand complexes is strongly dependent on the kind of donor atoms available and the possibility of π-bond formation.[1] Since S is one of the more important donor atoms, being able to form σ- and π-bonds,[2] it seems of interest to study the binding behaviour of this atom in ternary complexes. The strongest and most common binding site in this respect is proffered by the thiol group.

Thiosalicylic acid (tsa), widely known for its analytical applications, has two possible coordination sites, namely the sulphydryl (SH) and carboxyl (COOH) groups. Although it was reported that tsa forms stable binary complexes with some metal ions[3–5] yet mixed-ligand complexes involving this reagent as one of the ligands are scarce. No studies have yet been reported on ternary systems containing tsa and an acid anthraquinone dye.

In this paper, the mixed-ligand complex of U(VI) with azm (3-amino-1,2-dihydroxyanthraquinone) and tsa was investigated potentiometrically. An Irving and Rossotti pH-titration technique[6] and its modifications[7,8] were employed, the aim being to establish the equilibria existing in solution and to characterize the ternary stability constant of the U(VI)–azm–tsa complex. Measurements were made at 25 ± 0.1°C, and $I = 100$ mmol dm^{-3} ($NaClO_4$) in 40% (v/v) ethanol. The absorption and vibrational spectra of the mixed-ligand complex were also investigated. Fundamental conditions for the spectrophotometric determination of U(VI) using the U(VI)–azm–tsa ternary system were established.

EXPERIMENTAL

Analytical-grade reagents and deionized water (or pure ethanol) were used for preparation of solutions. 10^{-3} mol dm^{-3} stock solutions of azm or tsa were prepared by dissolving the accurately weighed amount of the reagent in ethanol. A solution of U(VI) (5×10^{-3} mol dm^{-3}) was prepared using AnalaR uranyl nitrate and standardized as recommended.[9] Standard solutions of NaOH (0.1 mol dm^{-3}) and $HClO_4$ (2.5×10^{-2} mol dm^{-3}) were also prepared. More dilute solutions of the reagents were obtained as required by accurate dilution. Buffer solutions and solutions of diverse ions used for interference studies were all prepared as mentioned elsewhere.[10]

* Author to whom correspondence should be addressed.

All pH-metric titrations were carried out at 25±0.1°C using an Orion (M 601 A) digital pH-meter with a combined glass–calomel electrode. The ionic strength of solutions was kept constant at 100 mmol dm^{-3} ($NaClO_4$). Measurements were carried out in a 40% (v/v) ethanol–water medium. Correction of pH readings in this medium was made as described previously.[11] The absorption spectra of solutions were recorded on a Pye–Unicam SP 8000 spectrophotometer in the range 350–750 nm using 1-cm matched stoppered quartz cells. IR spectra of organic ligands and their solid chelates were recorded as CsBr discs on a Perkin–Elmer 251 IR spectrophotometer.

Dissociation constants of the ligands and stability constants of the binary and ternary complexes

The previous work[12,13] from this laboratory on the acid dissociation of azm in aqueous solution and in water–organic solvent mixtures indicated that the predominate form of this reagent in acid solutions of pH 2–6 is the monocationic species (H_3A^+), which undergoes stepwise ionization on increasing the pH of solution. In this work, the proton association constant $pK^H_{H_3A}$ and the dissociation constant $pK^H_{H_2L}$ of azm in 40% (v/v) ethanol were determined by titrating 50 cm^3 of 2.5×10^{-3} mol dm^{-3} $HClO_4$ and $NaClO_4$ (I = 100 mmol dm^{-3}) in the presence and absence of the ligand (10^{-4} mol dm^{-3}) with standard carbonate-free NaOH (1.05×10^{-2} dm^{-3}).

The dissociation constant of tsa ($pK^H_{H_2L}$) corresponding to the ionization of the carboxyl hydrogen was also determined under the same experimental conditions. The value for pK^H_{HL} as reported by Kumar *et al.*[14] was 9.52. Table 1 gives the values of dissociation constants of azm and tsa as depicted from the titration graphs. The stability constant of the binary complexes were calculated from titration graphs in which the metal : ligand ratio was 1 : 2. The conditions for the measurements were the same as for the acidity constants. Titrations of solutions without ligand were used as a basis for the evaluation. The conditions of measurements for the titrations of the ternary complex were the same as for the binary ones, but the solutions contained equivalent amounts of azm, U(VI) and tsa. The evaluation of the titration curves was done using curves obtained using the same solutions but without tsa. Multiple titrations were carried out for each system. The uncertainties given in Tables 2 and 3 are 3 times the standard deviation.

Table 1. Negative logarithms of the acidity constants of the ligands

Ligand (L)	$pK^H_{H_2L}$	pK^H_{HL}
tsa	4.3±0.01	9.15±0.02
azm[a]	9.1±0.03	11.2[b]

[a] $pK^H_{H_3L}$ for azm = 6.75±0.02.
[b] Reference 12.

Table 2. Logarithms of the stability constants of the binary U(VI) complexes with azm and tsa [I = 0.1, 25±0.1°C, 40% (v/v) ethanol]

Ligand (L)	$\log K^M_{ML}$	$\log K^{ML}_{ML_2}$	$\log \beta^M_{ML_2}$
azm	6.45±0.03	5.07	11.52
tsa	4.60±0.02	3.72	8.32

RESULTS AND DISCUSSION

The stoichiometry of the complexes formed during the interaction of U(VI) with azm (H_3A^+) was established from the magnitude of the proton displacement, which was determined by titrating solutions containing the ligand against standard alkali in the absence and presence of different molar quantities of U(VI). The potentiometric titration graph for azm in the cationic form (H_3A^+) (Fig. 1) shows

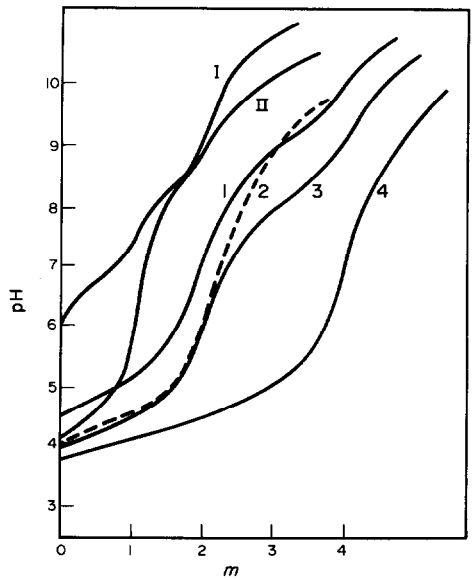


Fig. 1. Potentiometric titration curves of binary and ternary complex systems of U(VI) [I = 100 mmol dm^{-3} ($NaClO_4$), 25±0.1°C, 40% (v/v) ethanol]. For curves I and II, the abscissa represents mol of alkali added per mol of ligand (*a*). (I) azm, (II) tsa, (1) 1 : 1 U(VI)–azm, (2) 1 : 1 U(VI)–tsa, (3) 1 : 2 U(VI)–tsa, (4) 1 : 1 : 1 U(VI)–azm–tsa.

Table 3. Logarithms of the equilibrium constants of the ternary U(VI)–azm–tsa complex and some related data [$I = 0.1$, 25 ± 0.1°C, 40% (v/v) ethanol]

$\log \beta^{M}_{M(azm)(tsa)}$ [a]	$\log K^{M(azm)}_{M(azm)(tsa)}$ [b]	$\log K^{M(tsa)}_{M(tsa)(azm)}$ [c]	$\log X$ [d]	$\Delta \log K$ [e]
11.32 ± 0.04	4.87	6.72	2.80	0.27

[a] Equation (6).
[b] Equation (8).
[c] Equation (7).
[d] Equations (13) and (14).
[e] Equation (11).

a moderate inflection at $a = 1$ followed by a steep inflection at $a = 2$ (where a is the number of mol of base added per mol of ligand). The constants $pK^{H}_{H_3A}$ and $pK^{H}_{H_2A}$ corresponding to the stepwise dissociation of the ligand are given in Table 1.

The titration graph for a system containing a 1:2 molar ratio of U(VI) and azm exhibits two inflections at $m = 2$ and 4 (m = mol of base added per mol of metal ion), indicating the formation of mono and bis-binary complexes, the corresponding equilibria may be represented as follows

$$U + azm \rightleftharpoons U(azm), K^{U}_{U(azm)}; \quad (1)$$

$$U(azm) + azm \rightleftharpoons U(azm)_2, K^{U(azm)}_{U(azm)_2}. \quad (2)$$

The formation constants were calculated taking into account the species H, H_3A, H_2A, HA, U, U(HA) and $U(HA)_2$, where H_2A is the neutral form of azm.

The titration curve for a system containing a 1:2 molar ratio of U(VI) and tsa (H_2L), exhibits two inflections at values of $m = 2$ and 4, respectively, indicating the stepwise formation of 1:1 and 1:2 binary complexes. The corresponding constants for equilibria (3) and (4) were calculated:

$$U + tsa \rightleftharpoons U(tsa), K^{U}_{U(tsa)}; \quad (3)$$

$$U(tsa) + tsa \rightleftharpoons U(tsa)_2, K^{U(tsa)}_{U(tsa)_2}. \quad (4)$$

The potentiometric titration graph for the ternary system containing U(VI), azm and tsa in a 1:1:1 molar ratio exhibits a single steep inflection at $m = 4$. The overall stability constant for the complexation equilibrium (5) was calculated taking into account the species H, H_3A, H_2A HA, H_2L, HL, L, U, U(HA), $U(HA)_2$, UL, UL_2 and U(HA)L:

$$U + azm + tsa \rightleftharpoons U(azm)(tsa), \beta^{U}_{U(azm)(tsa)}. \quad (5)$$

However, most of the species already taken into account occur only at a very low concentration. Calculations were carried out only with the species H, H_2L, HL, L, U(HA) and U(HA)L, assuming that, in a 1:1 mixture of the metal ion and azm, the formation of a U(azm) (1:1) complex is complete.

The stability constants of a ternary system are defined by eqns (6)–(8). The overall stability constant $\beta^{U}_{U(azm)(tsa)}$, which was determined experimentally, is connected with $K^{U(tsa)}_{U(azm)(tsa)}$ and $K^{U(azm)}_{U(azm)(tsa)}$ by eqns (9) and (10), respectively:

$$U + azm + tsa \rightleftharpoons U(azm)(tsa), \quad \beta^{U}_{U(azm)(tsa)} = [U(azm)(tsa)]/[U][azm][tsa]; \quad (6)$$

$$U(tsa) + azm \rightleftharpoons U(tsa)(azm), \quad K^{U(tsa)}_{U(tsa)(azm)} = [U(tsa)(azm)]/[U(tsa)][(azm)]; \quad (7)$$

$$U(azm) + tsa \rightleftharpoons U(azm)(tsa), \quad K^{U(azm)}_{U(azm)(tsa)} = [U(azm)(tsa)]/[U(azm)][tsa]; \quad (8)$$

$$\log K^{U(tsa)}_{U(tsa)(azm)} = \log \beta^{U}_{U(tsa)(azm)} - \log K^{U}_{U(tsa)}; \quad (9)$$

$$\log K^{U(azm)}_{U(azm)(tsa)} = \log \beta^{U}_{U(azm)(tsa)} - \log K^{U}_{U(azm)}. \quad (10)$$

Stability of U(VI)–azm–tsa ternary complex

One way to quantify the stability of ternary complexes is according to eqn (11):[15]

$$\Delta \log K_U = \log K^{U(tsa)}_{U(tsa)(azm)} - \log K^{U}_{U(azm)} = \log K^{U(azm)}_{U(azm)(tsa)} - \log K^{U}_{U(tsa)}. \quad (11)$$

i.e. by comparing the differences in stability, e.g. for the reaction between U(tsa) and azm.

The value of $\Delta \log K_U$ is the logarithm of the equilibrium constant of eqn (12):

$$U(tsa) + U(azm) \rightleftharpoons U(azm)(tsa) + U. \quad (12)$$

In general, negative value for $\Delta \log K_U$ [eqn (11)] is expected, since usually $K^{M}_{ML} > K^{ML}_{ML_2}$. This is in accordance with the statistical values obtained for the coordination of two different bidentate ligands to a regular and to a distorted octahedral coordination sphere, i.e. $\Delta \log K_{oh} = -0.4$ and $\Delta \log K_{do} \simeq -0.9$, respectively.[16]

The other approach commonly used to quantify the stability of a ternary complex is based on the equilibrium constant, X, as defined by eqn (13)[17,18]

[log X may be calculated according to eqn (14)]:

$$\begin{aligned} &U(azm)_2 + U(tsa)_2 \rightleftharpoons 2U(azm)(tsa), \\ &X = [U(azm)(tsa)]^2/[U(azm)_2][U(tsa)_2]; \end{aligned} \quad (13)$$

$$\begin{aligned} \log X &= 2\log \beta^{U}_{U(tsa)(azm)} - [\log \beta^{U}_{U(azm)_2} \\ &\quad + \log \beta^{U}_{U(tsa)_2}] \\ &= [\log K^{U(azm)}_{U(azm)(tsa)} - \log K^{U(tsa)}_{U(tsa)_2}] \\ &\quad + [\log K^{U(tsa)}_{U(tsa)(azm)} - \log K^{U(azm)}_{U(azm)_2}]. \end{aligned} \quad (14)$$

The statistical value for log X is for all geometries of the coordination sphere of a metal ion the same and is 0.6.[18,19]

According to our results, the formation of U(VI)–azm and U(VI)–tsa binary complexes and the complex equilibrium for the U(VI)–azm–tsa ternary system can be represented by the following schemes:

U(VI)–azm complexes:

$$UO_2^{2+} + H_3A^+ \rightleftharpoons [UO_2(HA)]^+ + 2H^+, \quad K^{U}_{U(azm)}; \quad (15)$$

$$[UO_2(HA)]^+ + H_3A^+ \rightleftharpoons [UO_2(HA)_2] + 2H^+, \quad K^{U(azm)}_{U(azm)_2}. \quad (16)$$

U(VI)–tsa complexes:

$$UO_2^{2+} + H_2L \rightleftharpoons [UO_2(L)] + 2H^+, \quad K^{U}_{UL}; \quad (17)$$

$$[UO_2(L)] + H_2L \rightleftharpoons [UO_2(L)_2]^{2-} + 2H^+, \quad K^{UL}_{UL_2}. \quad (18)$$

U(VI)–azm–tsa ternary system:

$$UO_2^{2+} + H_3A^+ + H_2L \rightleftharpoons [UO_2(HA)L]^- + 4H^+, \quad \beta^{U}_{U(azm)L}; \quad (19)$$

$$[UO^2(HA)]^+ + H_2L \rightleftharpoons [UO_2(HA)L]^- + 2H^+, \quad K^{U(azm)}_{U(azm)L}; \quad (20)$$

$$[UO_2(HA)_2] + [UO_2L_2]^{2-} \rightleftharpoons 2[UO_2(HA)(L)]^-, \quad X. \quad (21)$$

Comparing the curves resulting from the titration of U(VI) and tsa in a molar ratio of 1 : 1 with that where, in addition, azm was present (ratio 1 : 1 : 1) one can observe that the deprotonation of tsa in the ternary system occurs at a lower pH. This means that the ternary complex is more stable than the corresponding binary one, and we shall obtain a positive Δ log K value in this case. The results obtained for the formation of the U(VI)–azm–tsa ternary complex are given in Table 3. The constant log $\beta^{U}_{U(azm)L}$, which is due to the overall equilibrium [eqn (19)] was determined from the experimental data. By using the results given in Table 3, the values of $\Delta \log K_U$ [eqn (11)] and log X [eqns (13) and (14)] were calculated.

Spectrophotometric study of the ternary complex of U(VI) *with azm and tsa*

Absorption spectra and optimum pH. The visible spectra of azm exhibit a main absorption band at $\lambda = 470$ nm within the pH range 4–6.5. This band undergoes a reasonable shift to longer wavelengths on adding a U(VI) solution. The spectra of the U(VI)–azm 1 : 1 complex with reagent blank as reference are characterized by an absorption band at $\lambda = 590$ nm. A tsa solution (10^{-4} mol dm^{-3}) shows no measurable absorbance above 400 nm. In the pH range 4.5–6.5, the absorption spectrum of the U(VI)–tsa 1 : 1 complex was characterized by an absorption band at $\lambda = 420$ nm. The solution containing equimolar concentrations of azm and tsa undergoes a change in colour, from yellow to pink, when mixed with the U(VI) solution. The spectrum of the reaction mixture against a blank solution containing the same concentration of the two ligands shows an apparent decrease in the absorption at 470 nm and exhibits a new band at 630 nm (cf. Fig. 2). The latter band is unambiguously due to the formation of a mixed-ligand complex of U(VI) with the maximum colour development attained in the pH range 5.8–7.4. Job's method of continuous variation[20,21] was applied to establish the composition of the ternary U(VI)–azm–tsa complex. The molar fractions of two of the components were varied continuously, keeping their combined concentration constant, and keeping the third component in a large excess for all solutions

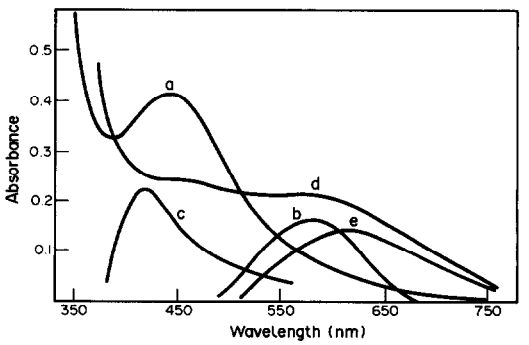


Fig. 2. Absorption spectra of U(VI)–azm–tsa ternary complex in 40% (v/v) ethanol [pH = 6.0, U(VI) = 1×10^{-4} mol dm^{-3})]: (a) azm and azm–tsa (both give the same spectrum), (b) 1 : 1 U(VI)–azm (vs azm), (c) U(VI)–tsa (vs tsa), (d) 1 : 1 : 1 U(VI)–azm–tsa (vs buffer containing 40% ethanol), (e) 1 : 1 : 1 U(VI)–azm–tsa (vs reagent blank).

in the series. Under these conditions, the ternary system was modified to a quasi binary system. The results graphically shown in Fig. 3 indicate that the overall U(VI)–azm–tsa complex has a 1 : 1 : 1 composition at the pH of the study. The stoichiometry of the ternary system was also determined by applying the mole-ratio method.[22]

Spectrophotometric determination of U(VI)

An aliquot of an acidic sample solution containing 148–714 μg of U(VI) was transferred to a 25-cm^3 calibrated flask and subsequently 2 ml of 10^{-3} mol dm^{-3} azm were added. The pH was adjusted to pH 6.2 with buffer solution and then 2 ml of 10^{-3} mol dm^{-3} tsa was introduced. The solution was diluted to volume with doubly distilled water and the requisite amount of pure ethanol. After thoroughly mixing the reaction mixture, the absorbance was measured at 630 nm against a reagent blank similarly prepared but containing no uranium.

Effect of diverse ions. To determine the effect of diverse ions on the determination of uranium, solutions were prepared containing 178.5 μg of U(VI) and varying concentrations of each ion to be tested. The uranium was then determined under the optimum conditions as described in the given procedure. The presence of 18 mg (100-fold excess) of the following ions caused no interference: Li^+, K^+, Na^+, Ba^{2+}, Ca^{2+}, Sr^{2+}, Mg^{2+}, Zn^{2+}, Mn^{2+}, Cd^{2+}, Pb^{2+}, Br^-, Cl^-, SO_4^{2-}, SO_3^{2-}, NO_3^-, NO_2^-, CN^-, tartarate, citrate, tetraborate and oxalate. The negative interference due to Al^{3+}, Cu^{2+}, Fe^{3+} and Ni^{2+} was completely eliminated by the addition of 1.0 ml M EDTA solution. Of the anions investigated, F^-, HPO_4^{2-} and S^{2-} caused a serious negative error even when reduced to only 10-fold excess.

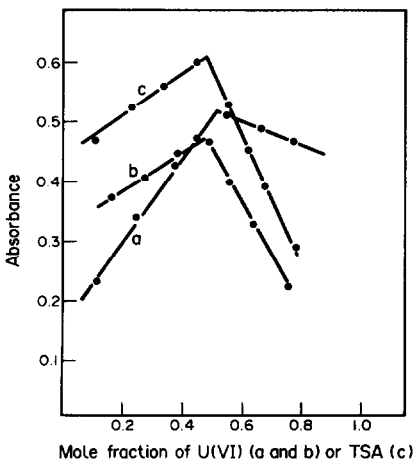


Fig. 3. Job's plots: (a) U(VI)–tsa (in presence of excess azm), (b) U(VI)–azm (in presence of excess tsa), (c) tsa–azm [in present of excess U(VI)].

Calibration graph and reproducibility. The system followed Beer's law over the range 2.5×10^{-5}–2.8×10^{-4} mol dm^{-3} of U(VI). The molar absorptivity was 2×10^4 l mol^{-1}. Eight identical samples each with a final U(VI) concentration of 1.5×10^{-4} mol dm^{-3} were treated according to the recommended procedure and their absorbance were measured. The mean absorbance was 0.350, with a standard deviation of 0.005 absorbance units.

IR spectra of the single and mixed-ligand complexes of U(VI) *with azm and/or tsa*

The solid 1 : 1 chelates of uranyl ion with azm or tsa as well as the 1 : 1 : 1 UO_2^{2+}–azm–tsa ternary complex were isolated and characterized. The IR spectra of the pure ligands were also recorded. The aim is to examine the salient features of the IR spectrum of the mixed-ligand complex (Fig. 4).

The IR spectrum of the UO_2^{2+}–azm (1 : 1) complex exhibits a band in the vicinity of 3480 cm^{-1}, which denotes the assignment of ν(NH). The band at 3380 cm^{-1} which corresponds to the ν(OH) of the bonded group is shifted to a lower frequency (3300 cm^{-1}) in the complexed ligand. The band becomes broadened and less intense. The spectrum indicates an overlap of the bounded ν(C=O) with ν(C=C) near 1600 cm^{-1}, and a red shift is observed. This indicates that the quinone structure is influenced by the substituents, that is to say it lowers the C=O character and increases the C=C bond order. The bands observed at 1440 and 1270 cm^{-1} in the spectrum of the free ligand, azm, suffer a red shift on complexation with the metal ion. The frequency shift of the former band was more or less in good agreement with the change in the reduced mass of the vibrating atoms. The intensity of this band decreases due to the displacement of a proton from one OH group on complex formation.

The band at 2520 cm^{-1} in the spectrum of tsa corresponds to the ν(S—H) stretching vibration. The disappearance of this band in the UO_2^{2+}–tsa and UO_2^{2+}–azm–tsa complexes confirms that the sulphydryl hydrogen is replaced by the metal and, consequently, coordination through sulphur is achieved in these complexes. The carbonyl stretching frequency at 1876 cm^{-1} in tsa appears at 1620–1650 cm^{-1} in its binary and ternary chelates, respectively, whereas the ν(C=O) band position is blue-shifted. The coordination of the uranyl ion with tsa in the ternary complex seems, therefore, to be carried out through the carbonyl oxygen of the

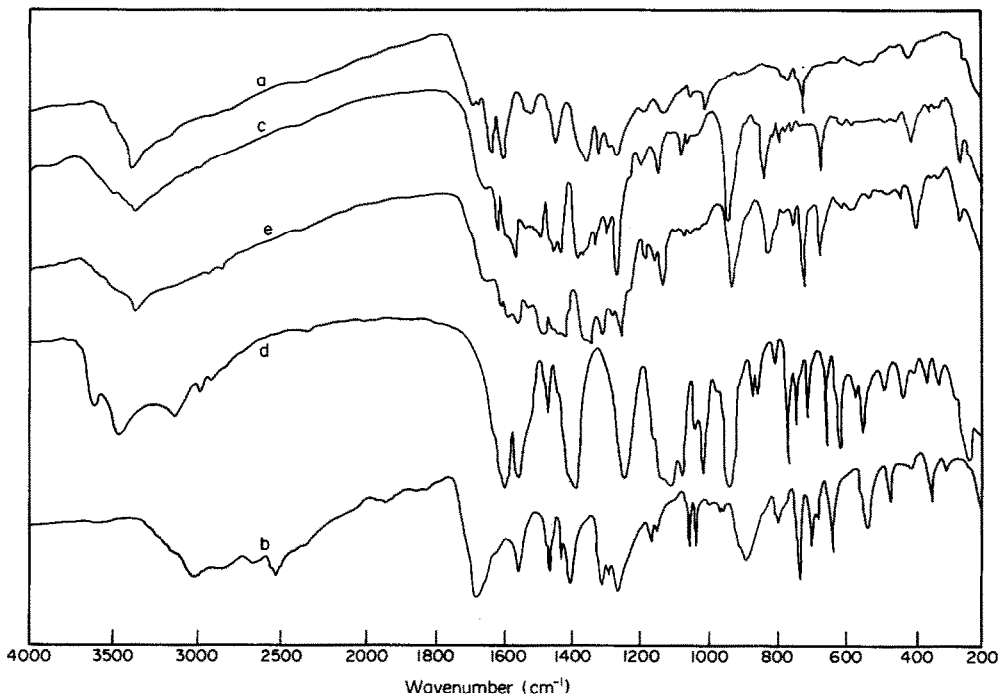


Fig. 4. IR spectra of binary and ternary complexes of U(VI): (a) U(VI)–azm, (b) U(VI)–tsa, (c) 1 : 1 U(VI)–azm, (d) 1 : 1 U(VI)–tsa, (e) 1 : 1 : 1 U(VI)–azm–tsa.

carboxyl group. Similar behaviour was reported elsewhere[23,24] for the Ni(II) complexes of tsa.

The IR spectrum of the ternary complex exhibits a band at 3300 cm^{-1}, which denotes the assignment of ν(OH). The appearance of the hydroxyl stretching frequency in the spectrum of UO_2^{2+}–tsa complex give additional evidence that the coordination through the hydroxyl oxygen of the carboxyl group is not taking place in the complex under investigation.

REFERENCES

1. H. Sigel, R. Griesser and B. Prijs, *Z. Naturforsch.* 1972, **27B**, 353; R. Griesser and H. Sigel, *Inorg. Chem.* 1971, **10**, 2229; *ibid.* 1970, **9**, 1238; P. R. Huber, R. Griesser and H. Sigel, *ibid.* 1971, **10**, 945.
2. H. Sigel and D. B. McCormick, *Acc. Chem. Res.* 1970, **3**, 201.
3. M. V. Reddi and P. K. Bhattachrya, *J. Inorg. Nucl. Chem.* 1970, **32**, 2321.
4. R. S. Ramkrishna and M. E. Bernandopulle, *J. Inorg. Nucl. Chem.* 1971, **33**, 2071.
5. A. N. Kumar and H. L. Nigam, *J. Prakt. Chem.* 1966, **33**, 160.
6. H. M. Irving and H. S. Rossotti, *J. Chem. Soc.* 1953, 3397; 1954, 2904.
7. M. V. Chidambaram and P. K. Bhattacharya, *J. Inorg. Nucl. Chem.* 1970, **32**, 3271.
8. B. H. Agrawal, K. Dwivedi, M. Chandra, B. Agrawala and A. K. Dey, *J. Indian Chem. Soc.* 1977, **54**, 931.
9. W. Scott and H. Furman, *Standard Methods of Chemical Analysis*, 6th Edn. Van Nostrand, New York (1962).
10. K. A. Idriss, M. M. Seleim, M. S. Abu-Baker and M. S. Saleh, *Analyst* 1982, **107**, 12.
11. K. A. Idriss, M. K. Hassan, M. S. Abu-Baker and H. Sedaira, *Analyst* 1984, **109**, 1389.
12. K. A. Idriss, M. M. Seleim and M. S. Abu-Baker, *Bull. Soc. Chim. Fr.* 1981, **5–6**, 180.
13. K. A. Idriss, M. M. Seleim, M. S. Abu-Baker and M. S. Saleh, *Indian J. Chem.* 1982, **21A**, 395.
14. A. N. Kumar, H. L. Nigam and T. D. Seth, *J. Polarogr. Soc.* 1966, **3**, 83.
15. B. E. Fisher and H. Sigel, *Inorg. Chem.* 1979, **18**, 425.
16. H. Sigel, In *Artificial Enzymes* (Edited by A. E. Martell), Vol. 2. Dekker, New York (1973).
17. R. B. Martin and R. Prados, *J. Inorg. Nucl. Chem.* 1974, **36**, 1665.
18. R. Dewitt and J. I. Watters, *J. Am. Chem. Soc.* 1954, **76**, 3810.
19. S. Kida, *Bull. Chem. Soc. Jpn* 1956, **29**, 805.
20. P. Job, *Ann. Chim. (Rome)* 1928, **10**, 113.
21. F. G. Shirif and A. M. Awad, *J. Inorg. Nucl. Chem.* 1962, **24**, 79.
22. G. H. Yoe and A. L. Jones, *Ind. Eng., Chem. Anal. Ed.* 1944, **16**, 111.
23. H. L. Nigam, A. N. Kumar and K. B. Pandeya, *Proc. 1st Chem. Symp.* 1970, **2**, 53.
24. C. Nair and H. L. Nigam, *Indian J. Chem.* 1974, **12**, 769.

Polyhedron Vol. 5, No. 10, pp. 1531–1536, 1986
Printed in Great Britain

0277-5387/86 $3.00+.00
Pergamon Journals Ltd

ESR STUDIES ON THE REACTIONS OF THE SULPHITE RADICAL ANION, $SO_3^{\bar{\cdot}}$, WITH OLEFINIC COMPOUNDS IN AQUEOUS SOLUTIONS

TOSHIHIKO OZAWA*

National Institute of Radiological Sciences, 9-1, Anagawa-4-chome, Chiba-shi 260, Japan

and

TAKAO KWAN

Faculty of Pharmaceutical Sciences, Teikyo University, Sagamiko-cho, Tsukui-gun, Kanagawa 199-01, Japan

(*Received* 20 *August* 1985; *accepted after revision* 27 *January* 1986)

Abstract—The reactions of the sulphite radical anion, $SO_3^{\bar{\cdot}}$, which was generated either from a Ce^{4+}–$NaHSO_3$ system at pH 2.5 or from a Ti^{3+}(ethylenediaminetetraacetic acid)–H_2O_2–Na_2SO_3 system at pH 9 in aqueous solutions, with some olefinic compounds were investigated by use of a rapid-mixing flow technique coupled with ESR which can detect the radicals having a lifetime of 5–100 ms. The $SO_3^{\bar{\cdot}}$ radical could add to the C=O double bond in the olefinic compounds in both acidic and alkaline aqueous solutions, although the $SO_3^{\bar{\cdot}}$ radical is more active in acidic conditions than in alkaline conditions. From the observed hyperfine splitting constants of the $SO_3^{\bar{\cdot}}$ adducts of the olefinic compounds, the preferred conformation of the adducts was discussed.

It is well known that the rapid-mixing flow technique coupled with electron spin resonance (ESR) is very useful to detect the short-lived radicals having a lifetime longer than a few milliseconds. By use of this technique we have reported that the sulphite radical anion, $SO_3^{\bar{\cdot}}$, which is generated from a Ce^{4+}–$NaHSO_3$ system in acidic aqueous solutions, can add to compounds having C=C[1], C≡C[2] and C=S[3] bonds to give the corresponding secondary radicals. Also, in alkaline aqueous solutions at pH 9, the same radical species, $SO_3^{\bar{\cdot}}$, which is obtained from a Ti^{3+}(ethylenediaminetetraacetic acid)–H_2O_2–Na_2SO_3 system, can add to uracil derivatives having a C=S bond[4] and to nitroalkane *aci*-anions having C=N bonds.[5] Further, we have found that the reactive characteristics of the oxy anion radicals of sulphur ($SO_2^{\bar{\cdot}}$, $SO_3^{\bar{\cdot}}$ and $SO_4^{\bar{\cdot}}$) are different from each other and reported that these differences of the reactivity towards the organic substrates may be caused by the difference in the distribution of the unpaired electron density of each radical anions.[6]

In previous papers,[1,6] we briefly described that the $SO_3^{\bar{\cdot}}$ radical can add some olefinic compounds in acidic aqueous solutions. We have further examined the reactions of the $SO_3^{\bar{\cdot}}$ radical with olefinic compounds in both acidic and alkaline aqueous solutions by use of the rapid-mixing flow technique coupled with ESR in order to discuss the preferred conformation of the $SO_3^{\bar{\cdot}}$ adducts of the olefinic compounds. In this paper, we would like to report these results.

EXPERIMENTAL

Materials

$Ce(NO_3)_4 \cdot 2NH_4NO_3$, $NaHSO_3$, $TiCl_3$ [20% (v/v)], ethylenediaminetetraacetic acid (EDTA) and Na_2SO_3 were purchased from Wako Pure Chemical Industries Ltd and used without further purification. H_2O_2 (30%) was obtained from Mitsubishi Gas Chemical. Organic substrates were purchased from a commercial source and used without further purification. Sulphuric acid, NaOH, NH_4OH and

* Author to whom correspondence should be addressed.

other chemical reagents were of commercial GR grade.

ESR measurements

ESR measurements were carried out on a JEOL-PE-1X ESR spectrometer (X-band) with 100-kHz field modulation in conjunction with a JEOL mixing chamber. In the Ti^{3+}(EDTA)–H_2O_2–Na_2SO_3 system a T-shaped cell which enabled three reagents to mix almost simultaneously was used.[4] This apparatus enabled us to detect radicals having a lifetime of 5–100 ms. The hyperfine coupling constants and g values were calibrated by comparison with an aqueous solution of Fremy's salt ($g = 2.0055$, $a^N = 13.0$ G),[7,8] in a capillary tube attached to the sample.

Procedure

All solutions were prepared from triply distilled water, and their pH was adjusted by an aqueous solution of sulphuric acid, NaOH or NH_4OH.

For the generation of the SO_3^- radical in acidic aqueous solutions, $Ce(NO_3)_4 \cdot 2NH_4NO_3$ and $NaHSO_3$ were used. To investigate the reactions of the SO_3^- radical with organic substrates, two aqueous solutions were mixed: one (a) contained 0.01 M Ce^{4+} acidified by sulphuric acid and the other (b) 0.1 M $NaHSO_3$ containing various organic substrates of 0.02–0.3 M concentrations.

For the generation of the SO_3^- radical in alkaline aqueous solutions,[4,5,9] $TiCl_3$ (20%), H_2O_2 (30%) and Na_2SO_3 were used. The conditions for oxidation with and without an added organic substrate were the same except that, in the latter case, only two of the three entry ports into the mixing chamber were employed and the third solution referred to below was omitted. Three solutions were prepared: the first solution (c) contained 0.01 M Ti^{3+}, 0.01 M EDTA and 0.1 M Na_2SO_3; the second (d) contained 0.05 M H_2O_2; the third (e) contained the organic compounds (0.1 M). Aqueous ammonia was added to the first and the third solution to give a pH of 9.

RESULTS

Reactions of the SO_3^- radical with olefinic compounds in an acidic medium

The secondary radicals were detected when maleic acid, acrylic acid, methacrylic acid, crotonic acid, 3,3-dimethylacrylic acid and vinyl acetate, respectively, were added to the Ce^{4+}–$NaHSO_3$ system, as described previously.[1,6] The assigned structures and the ESR parameters were summarized in Table 1, along with those of the OH adducts of the corresponding olefinic compounds, which were obtained by oxidation with the Ti^{3+}–H_2O_2 system. For comparison, Fig. 1 shows the ESR spectrum observed by the reaction of SO_3^- with maleic acid.

Under the same experimental conditions, only very weak unanalysable resonance was detected with allyl alcohol, styrene and cinnamyl alcohol, and there was no detectable ESR absorption with the following compounds: acrylamide, acrolein, crotonaldehyde and acrylic acid methyl ester.

Reactions of the SO_3^- radical with olefinic compounds in an alkaline medium

When solutions of Ti^{3+} and EDTA, H_2O_2 and Na_2SO_3 were mixed in the cavity of the ESR spectrometer, the pH after mixing being 9, a singlet absorption line due to the SO_3^- radical was observed.[4] Since, when either Ti^{3+} or H_2O_2 was omitted, no ESR spectrum could be observed, the SO_3^- radical may be formed by one-electron oxidation of the sulphite ion by the hydroxyl radical (OH·) which is generated by the reaction of Ti^{3+} ion with H_2O_2[11] [eqns (1)–(4)], taking into consideration the pK of HSO_3^-:[12]

$$Ti^{3+} + H_2O_2 \rightarrow Ti^{4+} + HO^- + HO\cdot, \quad (1)$$

$$HO\cdot + HSO_3^- \rightarrow H_2O + SO_3^-, \quad (2)$$

$$HSO_3^- \rightleftarrows SO_3^{2-} + H^+, \quad (3)$$

$$HO\cdot + SO_3^{2-} \rightarrow HO^- + SO_3^-. \quad (4)$$

Maleate ion. When the maleate ion was added as the third solution and allowed to react with the solution mentioned above, the signal intensity of

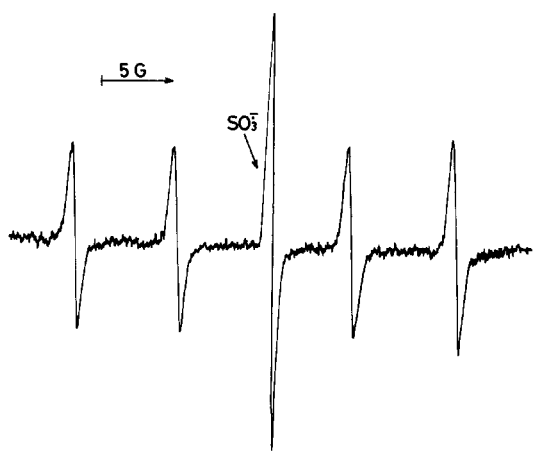


Fig. 1. ESR spectrum observed by the reaction of the SO_3^- generated from Ce^{4+}–$NaHSO_3$ with maleic acid at pH 2.5.

Table 1. ESR spectra of radicals formed by addition of the SO_3^- radical to olefinic compounds

Substrate	Added	Radical	Splitting constant (G) $a(\alpha\text{-H})$	$a(\beta\text{-H})$	a^H_{Me}	g
$HO_2CCH{=}CHCO_2H$	SO_3^-	$^-O_3SCH(CO_2H)\dot{C}HCO_2H$	19.8	7.1	—	2.0033
	OH·	$HOCH(CO_2H)\dot{C}HCO_2H$	20.8	12.5	—	2.0032
$^-O_2CCH{=}CHCO_2^-$	SO_3^-	$^-O_3SCH(CO_2^-)\dot{C}HCO_2^-$	20.4	5.2	—	2.0034
	OH·	$HOCH(CO_2^-)\dot{C}HCO_2^-$	20.4	15.6	—	2.0031
$CH_2{=}CHCO_2H$	SO_3^-	$^-O_3SCH_2\dot{C}HCO_2H$	20.4	15.9	—	2.0034
	OH·	$HOCH_2\dot{C}HCO_2H$	20.4	27.1	—	2.0031
	OH·	$\dot{C}H_2CH(OH)CO_2H$	22.5	25.5	—	2.0025
$CH_2{=}CHCO_2^-$	SO_3^-	$^-O_3SCH_2\dot{C}HCO_2^-$	13.0	11.25	—	2.0033
	OH·	$HOCH_2\dot{C}HCO_2^-$	20.5	27.7	—	2.0031
$CH_2{=}CMeCO_2H$	SO_3^-	$^-O_3SCMe(CO_2H)\dot{C}H_2$	23.1	—	—	2.0032
	OH·	$HOCH_2\dot{C}MeCO_2H$	—	20.0	23.1	2.0030[a]
	OH·	$HOCMe(CO_2H)\dot{C}H_2$	23.2	—	—	2.0025[a]
$MeCH{=}CHCO_2H$	SO_3^-	$^-O_3SCH(Me)\dot{C}HCO_2H$	20.3	6.6	0.74	2.0033
	OH·	$Me\dot{C}HCH(CO_2H)OH$	21.6	16.1	25.8	2.0032
	OH·	$HOCH(Me)\dot{C}HCO_2H$	20.4	15.6	1.5	2.0026
$MeCH{=}CHCO_2^-$	SO_3^-	$^-O_3SCH(Me)\dot{C}HCO_2^-$	19.6	6.1	0.95	2.0033
	OH·	$HOCH(Me)\dot{C}HCO_2^-$	20.4	15.9	1.4	2.0032
$Me_2C{=}CHCO_2H$	SO_3^-	$^-O_3SCMe_2\dot{C}HCO_2H$	20.5	—	—	2.0033
	OH·	$HOCMe_2\dot{C}HCO_2H$	20.8	—	—	2.0031[a]
	OH·	$HOCH(CO_2H)\dot{C}Me_2$	—	8.5	23.6	2.0026[a]
$CH_2{=}CHOCOCH_3$	SO_3^-	$^-O_3SCH_2\dot{C}HOCOCH_3$	20.0	13.7	1.4	2.0035
	OH·	$HOCH_2\dot{C}HOCOCH_3$	19.8	12.3	1.6	2.0025

[a] A. L. J. Beckwith, *Aust. J. Chem.* 1972, **25**, 1887.

the SO_3^- radical considerably decreased, and another two ESR signals due to the different radical species were observed as shown in Fig. 2. The ESR spectrum of a doublet of a doublet [$a^H(1) = 20.4$ G and $a^H(1) = 15.6$ G] shown by the arrows (Fig. 1) is almost identical to that of the radical (**I**) formed by the reaction of the OH radical with maleate ion.[13] Thus, the radical species giving the ESR spectrum shown by the arrows was identified as the OH adduct (**I**).

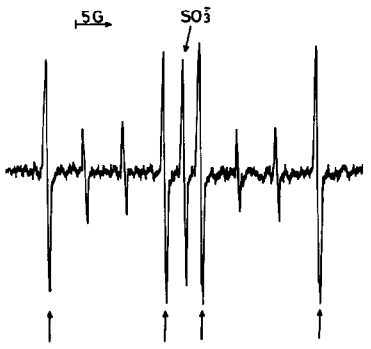
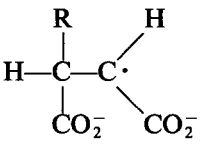


Fig. 2. ESR signal observed when the SO_3^- radical is generated in the presence of the maleate ion. It comprises overlapping spectra for $^-O_3SCH(CO_2^-)\dot{C}HCO_2^-$ and $HOCH(CO_2^-)\dot{C}HCO_2^-$ (marked ↑).

Since the other ESR spectrum consisting of a doublet of a doublet [$a^H(1) = 20.4$ G and $a^H(1) = 5.2$ G] resembles that of the SO_3^- adduct of maleic acid observed in acidic medium,[6] this radical species was identified as the SO_3^- adduct (**II**).



I: R = OH
II: R = SO_3^-

The fact that the two radical species, the OH adduct (**I**) and the SO_3^- adduct (**II**), could be observed in the Ti^{3+}(EDTA)–H_2O_2–Na_2SO_3 system indicates that the rate of addition of the OH radical to the maleate ion is almost the same as that of the oxidation of SO_3^{2-} by the OH radical, and that the decay rates are similar.

Acrylate ion. When the acrylate ion was mixed with the SO_3^- radical, the ESR signal intensity of the SO_3^- radical decreased and a new ESR signal was observed at $g = 2.0033$ (Fig. 3). This spectrum can be analysed in terms of the following parameters: $a^H(1) = 13.0$ G and $a^H(2) = 11.25$ G.

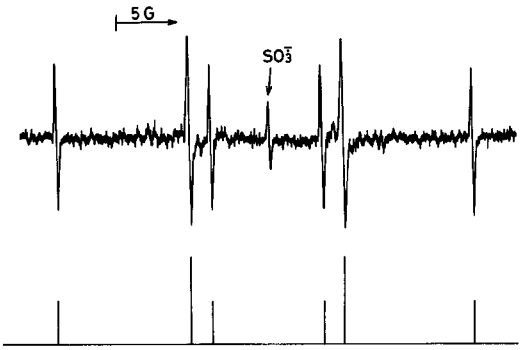
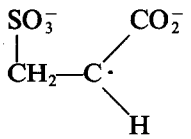


Fig. 3. ESR spectrum obtained by the reaction of the acrylate ion with the SO_3^- radical generated from Ti^{3+}(EDTA)–H_2O_2–Na_2SO_3 at pH 9.0.

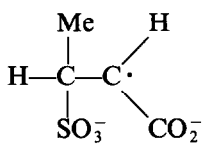
Since the spectral pattern is similar to that of the SO_3^- adduct of acrylic acid,[6] the radical species can be assigned to the SO_3^- adduct (**III**).



III

Methacrylate ion. When the methacrylate ion was added to the Ti^{3+}(EDTA)–H_2O_2–Na_2SO_3 system, an unanalysable ESR spectrum was observed, although the SO_3^- adduct of methacrylic acid was observed in an acidic medium (Table 1).

Crotonate ion. When the crotonate ion was reacted with the SO_3^- radical, a weak ESR spectrum similar to that obtained by the same reaction in acidic medium was observed. This spectrum was analysed as follows: $a^H(1) = 19.6$ G, $a^H(1) = 6.1$ G and $a^H(3) = 0.95$ G. This radical species was assigned to the SO_3^- adduct (**IV**).



IV

3,3-*Dimethylacrylate ion.* No ESR spectrum was observed for the reaction of the SO_3^- radical with the 3,3-dimethylacrylate ion, although the SO_3^- adduct was observed in an acidic medium (Table 1).

Vinyl acetate. The same ESR spectrum as observed in acidic medium was obtained by the reaction of the SO_3^- radical with vinyl acetate at pH 9.

Under the same experimental conditions, there was no detectable ESR absorption with the following compounds: styrene, cinnamyl alcohol, acrylamide, acrolein, crotonaldehyde and acrylic acid methyl ester.

The ESR parameters observed during the reaction of the SO_3^- radical with olefinic compounds are summarized in Table 1, along with the OH adducts of the corresponding olefinic compounds for comparison.

DISCUSSION

From Table 1, it is apparent that the SO_3^- radical can easily add to the C=C double bond of olefinic compounds to yield SO_3^- adducts. Further, it is indicated from Table 1 that the SO_3^- radical is more active in an acidic medium than in an alkaline medium.

From the radical structures assigned here (Table 1), it is also suggested that the addition reactions of the SO_3^- radical are influenced by the steric hindrance. That is, for acrylic acid and its anion, crotonic acid and its anion, and 3,3-dimethylacrylic acid, the SO_3^- radical adds to the *C*-terminal of the C=C bond far from the carboxyl or carboxylate group, whereas the OH radical adds to both sides of the C=C bond. These results indicate that the bulky SO_3^- radical is more sensitive to steric hindrance than the OH radical.

The facts that the radical concentration of the SO_3^- adduct obtained by the reaction of the SO_3^- radical with the crotonate ion was very low and that no secondary radical was observed from the reaction of the SO_3^- radical with the 3,3-dimethylacrylate ion indicate that the addition reactions of the SO_3^- radical in an alkaline medium are affected by the electrostatic repulsion between the SO_3^- and the carboxylate group.

The α-proton-splitting constants of the SO_3^- adducts are almost the same as those of the OH adducts (Table 1). However, the β-proton-splitting constants of the SO_3^- adducts are less than those of the OH adducts, except for that of vinyl acetate (Table 1). Since the hyperfine splitting constants of the β-proton reflect the radical conformation,[14,15] it is suggested that the conformations of the SO_3^- adducts are different from those of the OH adducts.

It is known that the sensitivity of the hyperfine splitting from the β-proton to the dihedral angle between the orbital of the unpaired electron and the β-C—H bond has continued to provide a useful probe for the study of the radical conformation.

Generally, the hyperfine splitting constant due to the β-proton could be represented by eqn (5):

$$a(\beta\text{-H}) = B_0 + B\cos^2\theta, \qquad (5)$$

where θ is the dihedral angle between the orbital of

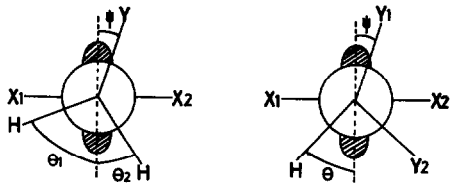


Fig. 4. Sterical conformation: $YCH_2\dot{C}X_1X_2$ (a) and $Y_1Y_2CH\dot{C}X_1X_2$ (b).

the unpaired electron and the β-C—H bond, and B_0 and B are constants. In this equation, since B_0 is approximately zero, $a(\beta\text{-H})$ is mainly dependent on $\cos^2\theta$.

From Table 1, we can divide the conformations of the SO_3^- adducts into two groups: one is the conformation having two protons, such as acrylic acid, its anion and vinyl acetate, as shown in Fig. 4(a), and the other having one proton such as maleic acid, its anion, and crotonic acid and its anion, as shown in Fig. 4(b). Thus, we consider the representative example for each group.

First, we consider the SO_3^- adduct of the acrylate ion ($X_1 = H$, $X_2 = CO_2^-$) as the radical shown in Fig. 4(a). Each dihedral angle of the SO_3^- adduct ($Y = SO_3^-$) is represented by ψ, θ_1 and θ_2, and the corresponding dihedral angles of the OH adduct ($Y = OH$) are represented by ψ', θ'_1 and θ'_2, as shown in Fig. 4(a). Since the SO_3^- group is larger than the OH group, the steric hindrance towards the carboxylate group is larger in the SO_3^- group than in the OH group. Then, $\psi < \psi' < 90°$. These results lead to $\cos^2\psi' < \cos^2\psi$, and, then, for the dihedral angle of the two β-protons of the rest, the following equation is obtained:

$$\frac{1}{2}(\cos^2\theta_1+\cos^2\theta_2) = \cos^2\theta < \cos^2\theta'$$

$$= \frac{1}{2}(\cos^2\theta'_1+\cos^2\theta'_2), \qquad (6)$$

where θ and θ' are the average dihedral angle of the SO_3^- adduct and the OH adduct, respectively. When eqn (6) is substituted in eqn (5), we obtain $a(\beta\text{-H})$ for the SO_3^- adduct $< a(\beta\text{-H})$ for the OH adduct.

The conformation of the SO_3^- adduct of acrylic acid is considered to be the same as mentioned above.

For the SO_3^- adduct of the vinyl acetate, no difference in the values of $a(\beta\text{-H})$ for both adducts can be detected. This result suggests that the conformations of both adducts are almost the same.

In these radicals, represented as $YCH_2\dot{C}X_1X_2$, we can calculate the ψ value from the observed $a(\alpha\text{-H})$ and $a(\beta\text{-H})$, according to Fischer's method.[14] As a result, in the acrylate ion, the calculated ψ value is 28 and 52° for the SO_3^- adduct and the OH adduct, respectively. In acrylic acid, ψ is 23 and 23° for the SO_3^- adduct and the OH adduct, respectively. In vinyl acetate, ψ is 9 and 5° for the SO_3^- adduct and the OH adduct, respectively. These results indicate that, when the C—S bond of the SO_3^- adduct approaches the orbital of the unpaired electron, the conformation of the SO_3^- adduct is energetically most stable.

Next, we consider the conformation of the SO_3^- adduct of the crotonate ion ($X_1 = H$, $X_2 = CO_2^-$) as the radical shown in Fig. 4(b). The dihedral angles of the SO_3^- adduct ($Y_1 = SO_3^-$, $Y_2 = CH_3$) are represented by ψ and θ, and the corresponding dihedral angles of the OH adduct ($Y_1 = OH$, $Y_2 = CH_3$) are represented by ψ' and θ', respectively, as shown in Fig. 4(b). Since the results for the adduct from the crotonate ion and the SO_3^- radical can be understood in a similar way as explained by the SO_3^- adduct of the acrylate ion, $\psi < \psi' < 90°$. Then, since $\cos^2\psi > \cos^2\psi'$, for the remaining dihedral angles $\cos^2\theta < \cos^2\theta'$. Therefore, from eqn (5), the $a(\beta\text{-H})$ of the SO_3^- adduct $< a(\beta\text{-H})$ of the OH adduct. The results for the SO_3^- adducts from maleic acid, maleate ion and crotonic acid can be understood similarly.

In these adducts, represented by $Y_1Y_2CH\dot{C}X_1X_2$, since there are two β-substituents without a proton, it is difficult to calculate the value of the ψ.[16] However, the fact that a large reduction in the hyperfine splitting of the β-proton in the SO_3^- adduct was observed indicates that in these adducts the conformation in which the dihedral angle between the C_β—H bond and the orbital of the unpaired electron approaches 90° is energetically lowest.

REFERENCES

1. T. Ozawa, M. Sato and T. Kwan, *Chem. Lett.* 1972, 591.
2. T. Ozawa and T. Kwan, *J. Chem. Soc., Chem. Commun.* 1983, 80.
3. T. Ozawa, M. Setaka, H. Yamamoto and T. Kwan, *Chem. Pharm. Bull.* 1974, **22**, 962.
4. T. Ozawa and T. Kwan, *J. Chem. Soc., Chem. Commun.* 1983, 1295.
5. T. Ozawa and T. Kwan, *Polyhedron* 1985, **4**, 1425.
6. T. Ozawa and T. Kwan, *Polyhedron* 1983, **2**, 1019.
7. J. Q. Adams, S. W. Nicksick and J. R. Thomas, *J. Chem. Phys.* 1966, **45**, 654.
8. T. Ozawa and T. Kwan, *J. Chem. Soc., Chem. Commun.* 1985, 54.
9. R. O. C. Norman and P. M. Storey, *J. Chem. Soc. B* 1971, 1009.
10. T. Ozawa, M. Setaka and T. Kwan, *Bull. Chem. Soc. Jpn* 1971, **44**, 3473.

11. W. T. Dixon and R. O. C. Norman, *J. Chem. Soc.* 1963, 3119.
12. A. Albert and E. P. Serjent, *Ionization Constants of Acids and Bases*, p. 151. Methuen, London (1962).
13. A. L. J. Beckwith and R. O. C. Norman, *J. Chem. Soc. B* 1969, 403.
14. H. Fischer, *Z. Naturforsch.* 1964, **19A**, 866.
15. E. W. Stone and A. H. Maki, *J. Chem. Phys.* 1962, **37**, 1326.
16. R. O. C. Norman and B. C. Gilbert, *Adv. Phys. Org. Chem.* 1967, **5**, 53.

Polyhedron Vol. 5, No. 10, pp. 1537–1542, 1986
Printed in Great Britain

0277–5387/86 $3.00+.00
Pergamon Journals Ltd

SINGLE-HALIDE ANIONS IN PHOSPHORUS(V) HALIDE COMPLEXES: A RAMAN INVESTIGATION

ARTHUR FINCH, PETER N. GATES* and ALAN S. MUIR

Department of Chemistry, Royal Holloway and Bedford New College, Egham Hill, Egham, Surrey TW20 0EX, U.K.

(*Received* 27 *November* 1985; *accepted* 27 *January* 1986)

Abstract—Phosphorus(V) chloride and bromide complexes containing single-halide anions are surveyed in terms of characteristic phosphonium ion Raman shift patterns. Methods of preparation of Phase III phosphorus pentachloride are reviewed and some modes of formation proposed. The nature of the phosphonium cation–single-halide anion interaction is discussed on the basis of observed Raman shifts. With trihalide anions, similar shifts are observed but are strongly dependent on anion symmetry.

Structurally, solid phosphorus pentachloride and phosphorus pentabromide are very different, viz. $[PCl_4^+][PCl_6^-]$[1–3] and $[PBr_4^+][Br^-]$[4–6] respectively. The significant difference is the presence of the single-bromide ion in the pentabromide, the PBr_6^- ion being unknown. In addition, a well-documented modification (Phase III) of phosphorus pentachloride exists, in which the presence of a single-chloride anion is inferred,[7–16] i.e. $[PCl_4^+]_2[PCl_6^-][Cl^-]$. Raman spectroscopy affords a convenient and clear distinction between the two forms of PCl_5; the chief differences on passing from $[PCl_4^+][PCl_6^-]$ to $[PCl_4^+]_2[PCl_6^-][Cl^-]$ are: (i) a large increase in the intensities of the PCl_4^+ modes relative to those of PCl_6^- (Fig. 1) and, (ii) a low-frequency shift of *ca* 20 cm^{-1} in the $\nu_1(a_1)$ (symmetric) and $\nu_3(e)$ (antisymmetric) stretching frequencies of the PCl_4^+ ion (Table 1). In phosphorus pentabromide, which already contains a single-bromide ion, formation of PBr_4^+ complexes with polyatomic anions leads to *high*-frequency shifts in the ν_1- and ν_3-modes of the cation. Examples of this effect for PCl_4^+ and PBr_4^+ are summarized in Table 1.

EXPERIMENTAL

All preparations and manipulations were carried out in an atmosphere of dry nitrogen. Chemicals of the best available commercial grade were used, generally without further purification, except for Et_4NCl which was recrystallized from ethanol by addition of diethyl ether, followed by drying at 50°C and storage *in vacuo* over P_4O_{10} until required.[17] Halogenated solvents were dried over 4-Å molecular sieves.

$[PCl_4^+][SbCl_6^-]$ and $[PCl_4^+][AlCl_4^-]$ were prepared from PCl_5, with $SbCl_5$ and $AlCl_3$, respectively, in CH_2Cl_2 as solvent, using modifications of established methods.[18,19] $[PBr_4^+][BBr_4^-]$ was prepared by reaction of PBr_5 and BBr_3 in CH_2Cl_2 as previously described.[20] A novel complex, $[PCl_4^+]_2[BCl_4^-][Cl^-]$, was prepared by reaction of PCl_3, BCl_3 and Cl_2 (in 2:1:1 molar ratio) in $AsCl_3$, and is described in detail elsewhere.[21,22] Phase III phosphorus pentachloride ($[PCl_4^+]_2[PCl_6^-][Cl^-]$) was usually prepared by recrystallization of Phase II PCl_5 from CH_2Cl_2 in the presence of a small quantity of Br_2.[15] Several other methods of obtaining this complex were found during the course of this work, and are summarized in Table 2. On one occasion, use of a larger quantity of Br_2 during recrystallization of Phase II PCl_5 from CH_2Cl_2, followed by sudden cooling, yielded a very unstable yellow aggregate which could not be analysed.

Halide analyses were performed potentiometrically following hydrolysis; in all cases, analytical results were within 0.4% of calculated values.

Raman spectra were obtained on solid samples sealed in glass capillaries using a Coderg PHO spectrometer equipped with a Coherent Radiation argon laser with excitation at 514.5 nm.

* Author to whom correspondence should be addressed.

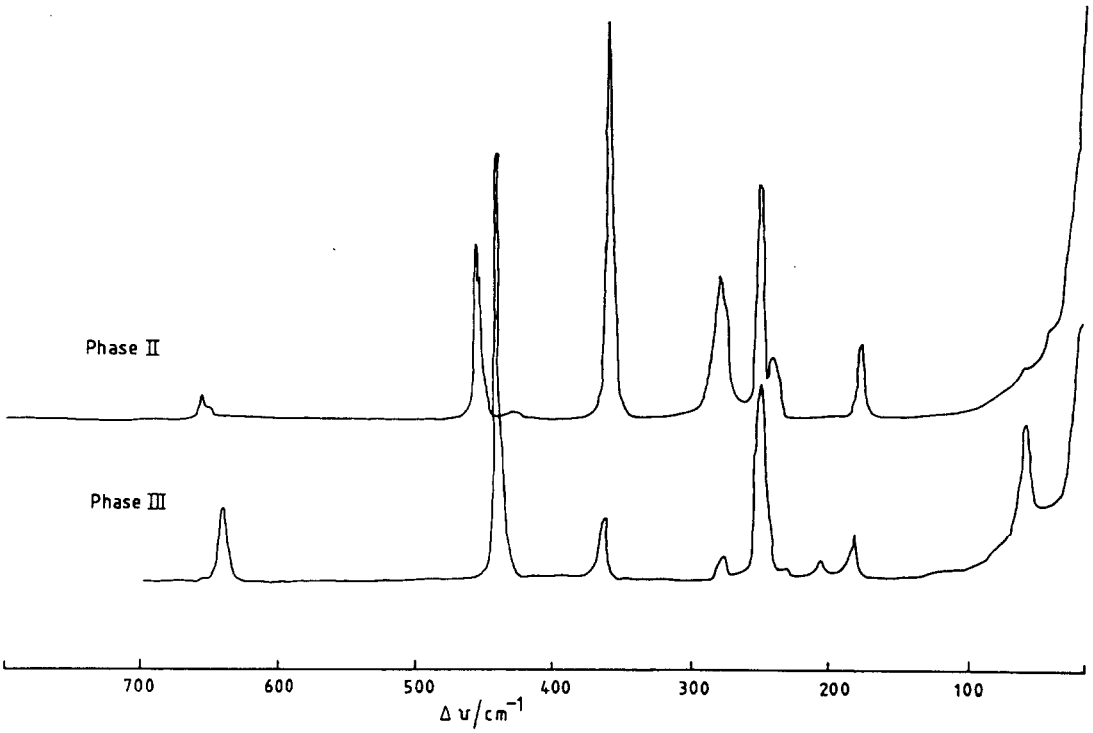


Fig. 1. Solid-state Raman spectra of Phase II and Phase III PCl_5.

RESULTS AND DISCUSSION

Formation of Phase III PCl_5

Although a variety of procedures (Table 2) have yielded Phase III (metastable) PCl_5 very little is understood about the mechanism of formation of the isomer. ^{31}P NMR studies[14] have suggested that the conversion of Phase II to Phase III may proceed *via* a selective decomposition of PCl_6^-, ions at least in the solid state.

The present Raman study has provided some insight into the mode of formation involved in some of the chemical methods of preparation. Probably the most convenient reliable method is the recrystallization of Phase II PCl_5 from CH_2Cl_2 in the presence of small (typically $< 5\%$) quantities of Br_2. The Raman spectrum of a typical sample prepared in this way is compared with that for Phase II PCl_5 in Fig. 1. In one experiment, where a stoichiometric quantity of Br_2 was present, a very unstable yellow solid was isolated. Raman wavenumbers and assignments for these species are given in Table 3, together with those of saturated solutions of PCl_5 and Et_4NCl in Br_2. Spectra are shown in Figs 2 and 3. Earlier ^{31}P NMR work has shown that PCl_4^+ is the only phosphorus-containing moiety in a solution of PCl_5 in Br_2,[23] and this is supported by the present observation of bands at 178, 250, 452 and 655 cm^{-1} in the Raman spectrum. The only additional band, a strong, broad scattering centred at 278 cm^{-1}, is reasonably assigned to a species such as Br_2Cl^-. This is supported by an almost identical feature in the spectrum of Et_4NCl in Br_2. It should be noted that the $\nu_1(a_1)PCl_4^+$ mode occurs at 452 cm^{-1} in the PCl_5 in Br_2 solution, consistent with those of other complexes containing a polyhalide counter ion (Table 1). On this basis the Raman spectrum clearly indicates the presence of PCl_4^+, PCl_6^- and Br_2Cl^- ions in the unstable material. This complex underwent progressive decomposition in the laser beam, resulting in the formation of Phase III PCl_5; this was evident from the reduction in intensity of bands at 360 cm^{-1} (ν_1 PCl_6^-) and 280–284 cm^{-1} (ν_2 PCl_6^- and ν_1 Br_2Cl^-) together with a shift in $\nu_1(a_1)$ PCl_4^+ from 450 to 440 cm^{-1}. These observations strongly suggest that the unstable yellow complex is an intermediate species in the formation of Phase III from Phase II PCl_5. This process could be represented as follows:

$$PCl_5 + Br_2 \rightarrow [PCl_4^+][ClBr_2^-],$$

$$[PCl_4^+][ClBr_2^-] + [PCl_4^+][PCl_6^-] \rightarrow [PCl_4^+]_2[PCl_6^-][Cl^-] + Br_2. \quad (1)$$

Such a scheme seems reasonable, assuming the instability of the Br_2Cl^- ion in an environment

Table 1. Variation of some PCl_4^+ and PBr_4^+ frequencies cm^{-1} with different anions

Mode	$PCl_4^+PCl_6^-$ [a]	$PCl_4^+SbCl_6^-$ [a]	$PCl_4^+AlCl_4^-$ [a]	$PCl_4^+ICl_2^-$ [b]	$(PCl_4^+)_2PCl_6^-Cl^-$ [a]	$(PCl_4^+)_2BCl_4^-Cl^-$ [a]
$\nu_1(a_1)$	458	458	458	449	440	441
$\nu_3(t_2)$	658	657	657	646	639	637

Mode	$PBr_4^+Br^-$ [a]	$PBr_4^+Cl^-$ [c]	$PBr_4^+Br_3^-$ [d]	$PBr_4^+IBr_2^-$ [b]	$PBr_4^+BBr_4^-$ [a]	$PBr_4^+TaBr_6^-$ [c]
$\nu_1(a_1)$	229	224 231	228 231	238	253	254 496
$\nu_3(t_2)$	469 475 481	471 473 477	479 480 481	484	497	503

[a] All frequencies obtained in current study.
[b] R. Rafaeloff and J. Shamir, *Spectrochim. Acta* 1974, **30A**, 1305.
[c] W. Gabes, K. Olie and H. Gerding, *Recl. Trav. Chim. Pays-Bas* 1972, **91**, 1367.
[d] P. Dhamelincourt and M. Crunelle-Cras, *Compt. Rendu* 1971, **272B**, 124.
[e] M. Delhaye, P. Dhamelincourt and J. C. Merlin, *Compt. Rendu* 1971, **272B**, 370.

Table 2. Summary of synthetic routes to Phase III PCl_5

	References
(A) Application of high pressure to Phase II PCl_5	12, 13, 14
(B) Sublimation of Phase II PCl_5 under a variety of conditions	7, 8, 9, 10
(C) Chemical methods	
(i) Recrystallization of Phase II PCl_5 from CH_2Cl_2 in the presence of catalytic quantities of Br_2 or SCl_2	11, 15, 21
(ii) Recrystallization of Phase II PCl_5 from CH_2Cl_2 under UV irradiation	21
(iii) Recrystallization of Phase II PCl_5 from $CHCl_3$ or CCl_4	21
(iv) Recrystallization of Phase II PCl_5 anhydrous HCl	21
(v) Recrystallization of Phase II PCl_5 from PCl_3	21
(vi) Recrystallization of the complex P_2Cl_9Br from CH_2Cl_2	21
(vii) Reaction of PCl_3 and Cl_2 in anhydrous HCl	21

other than Br_2. In an additional experiment, Phase II PCl_5 was recrystallized from Br_2 alone, resulting in a dark red unstable aggregate, the Raman spectrum of which could not be obtained; pumping of this material yielded a pale yellow solid with a Raman spectrum identical to that of Phase III PCl_5. In an earlier report,[7] powder X-ray analysis of a yellow material, $PCl_{4.66}Br_{0.33}$, was consistent with a formulation $8PCl_4^+4PCl_6^-4Br^-$ per unit cell. This is probably an analogue of Phase III PCl_5, with Br^- substituted for Cl^-, i.e. $[PCl_4^+]_2[PCl_6^-][Br^-]$ Unfortunately no Raman data for this are reported and attempts to repeat the synthesis in this laboratory were unsuccessful.

It is interesting to compare the effects of the different halogens on the recrystallization of Phase II PCl_5 from CH_2Cl_2. Cl_2 has no effect, and I_2 leads to the formation of $[PCl_4^+][ICl_2^-]$. In terms of the proposed trihalide intermediate (see above for the Br_2 case), Cl_2 interacts negligibly at ambient temperatures, where the Cl_3^- ion is relatively unstable, whereas I_2 leads to the formation of the well-known ICl_2^- salt. Thus, in terms of intermediate trihalide ion stability, Br_2Cl^- probably represents a borderline case. When Phase II PCl_5 was recrystallized from liquid Cl_2 no change to Phase III occurred, consistent with the extreme instability of any intermediate.

Recrystallization of Phase II PCl_5 from anhy-

drous liquid HCl also produced Phase III. A previous Raman study[24] of PCl_5 dissolved in liquid HCl indicated that the ions present in solution are PCl_4^+ and HCl_2^-. The cation is characterized by bands at *ca* 188, 244, 445 and 645 cm^{-1}, and the anion by a strong band at *ca* 2600 cm^{-1} (frequencies estimated from Fig. 3 in Ref. 24). A similar scheme to (1) could account for the formation of Phase III:

$$PCl_5 + HCl \rightarrow [PCl_4^+][HCl_2^-],$$

$$[PCl_4^+][HCl_2^-] + [PCl_4^+][PCl_6^-] \rightarrow [PCl_4^+]_2[PCl_6^-][Cl^-] + HCl. \quad (2)$$

The instability of the HCl_2^- with loss of HCl during the recrystallization would provide the driving force for the process.

Recrystallization from CCl_4 can also produce Phase III PCl_5, although in this case the nature of any analogous intermediate is less clear. An adduct $2PCl_5 \cdot CCl_4$ has been reported[25] but attempts to isolate it in these laboratories have so far been unsuccessful. The preparations of P_2Cl_9Br (formulated as $[PCl_4^+]_6[PCl_3Br^+]_2[PCl_6^-]_4[Br^-]_4$[26]), and of $[PCl_4^+]_2[BCl_4^-][Cl^-]$,[21,22] are both solvent-dependent; both complexes can be prepared in $AsCl_3$ but not in CH_2Cl_2, and it seems probable that some intermediate species involving PCl_5 and $AsCl_3$ are involved.

Nature of the interaction between a cation and a single-halide or trihalide anion

As mentioned above, the chief manifestations of cation perturbation when a single-halide or trihalide anion is present are low-frequency shifts and intensity changes. When PCl_5 changes from Phase III to Phase II the intensity (I) ratio, $[I(\nu_1\, PCl_4^+)]/[I(\nu_1\, PCl_6^-)]$, decreases by a factor of approximately 10; this cannot be accounted for simply on the basis of the change in the $PCl_4^+ : PCl_6^-$ ratio (2 : 1 in Phase III and 1 : 1 in Phase II). These effects seem to be general in these types of compounds, having also been observed in mixed-halogen phosphonium cations ($PCl_nBr_{4-n}^+$, $1 \leqslant n \leqslant 3$)[11,20,26] and mono-, di- and trimethylphosphoranes and derivatives.[21] Unfortunately there is a paucity of X-ray data, which exist only for PBr_4Br and $PBr_4^+Br_3^-$.

In PBr_5, the PBr_4^+ ion is a nearly regular tetrahedron with all PBr distances in the range 213–217 pm,[6] consistent with earlier work.[4,5] Each Br^- ion is surrounded by four Br atoms, each from a different cation, with interaction distances averaging 312 pm, i.e. less than the van der Waals' separation, thus indicating a significant anion–cation interaction but with no reduction of the T_d-symmetry of the cation. In $PBr_4^+Br_3^-$ a tetrahedral cation (angles in the range 107–110°) with all P—Br distances between 216 and 218 pm is found.[27] The Br_3^- ion is almost linear but with one bond of 239 pm (cf. 228 pm in Br_2) and the other of 291 pm. The extended terminal Br atom is much closer to the Br atoms of surrounding cations than to the other two anion Br atoms. Each elongated end of the Br_3^- ion has four close Br neighbours (each from a different cation) within the 310–340 pm range, whereas all other nearest approaches were *ca* 390 pm. As the van der Waals' radius of Br is 195 pm, significant interaction is indicated, although again there is no perturbation

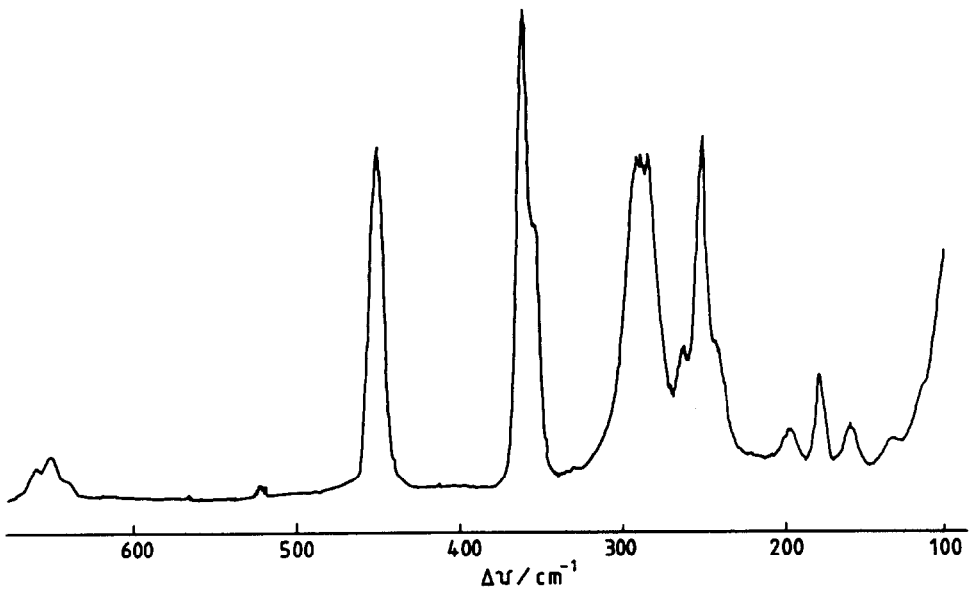


Fig. 2. Raman spectrum of unstable yellow solid from 1 : 1 reaction of PCl_5 with Br_2 in CH_2Cl_2.

Table 3. Raman wavenumbers (cm^{-1}) for: (a) Phase II PCl_5. (b) Phase III PCl_5, (c) Et_4NCl in Br_2, (d) PCl_5 in Br_2 and (e) yellow product isolated from a cooled PCl_5–Br_2 reaction[a]

(a) $PCl_4^+PCl_6^-$	(b) $(PCl_4^+)_2PCl_6^-Cl^-$	(c) Et_4NCl–Br_2[b]	(d) PCl_5–Br_2	(e) Unstable product	Assignment
				160(w)	?
177(w)	184(m/w)		178(w)	177(w)	$\nu_2(e)$ PCl_4^+
				193(w)	?
240(w)	239(w,sh)			240(w,sh)	$\nu_5(t_{2g})$ PCl_6^-
250(s)	245(s)		250(m,sh)	248(m/s)	$\nu_4(t_2)$ PCl_4^+
				260(w,sh)	?
279(s)	276(w)			280(m,sh)	$\nu_2(e_g)$ PCl_6^-
		279(vs)	278(vs)	284(s,br)	$\nu_1(\Sigma_g^+)$ Br_2Cl^-
				355(m,sh)	?
360(vs)	360(m)			360(s)	$\nu_1(a_{1g})$ PCl_6^-
458(s)	440(vs)		452(m/w)	450(s,br)	$\nu_1(a_1)$ PCl_4^+
	639(m)			640(w)	
656(w)			655(vw)	650(w)	$\nu_3(t_2)$ PCl_4^+
				660(w)	

[a] All frequencies obtained in current study.
[b] Band at ~305 cm^{-1} observed due to elemental bromine.

of the T_d-symmetry of PBr_4^+, consistent with the observed Raman spectra. These data give a clue to the origin of the shifted Raman frequencies. The close approach of the single-halide[4–6] or polyhalide[27] anion indicates some interaction, probably resulting in weakening of the P—X bonds and consequent reduction in stretching frequencies. From Table 1 it can be seen that the low-frequency shifts (relative to $[PBr_4^+][BBr_4^-]$) for both $[PBr_4^+][Br^-]$ and $[PBr_4^+][Br_3^-]$ are very similar (24 and 22 cm^{-1},

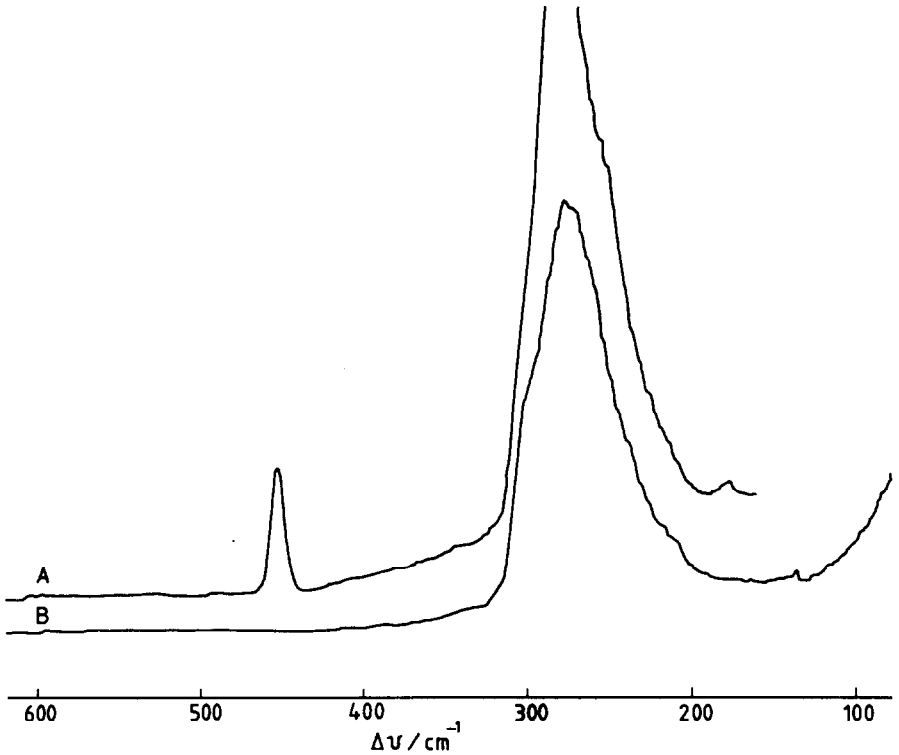


Fig. 3. Raman spectra of Br_2 solutions of PCl_5 (A) and Et_4NCl (B).

respectively), suggesting a similar anion–cation interaction. However, when the symmetric ($D_{\infty h}$) IBr_2^- ion replaces the asymmetric Br_3^- species, the shift is reduced to 15 cm^{-1}, suggesting a weaker anion–cation interaction. A similar trend in shifts can be seen in the series $[PCl_4^+][PCl_6^-]$, $[PCl_4^+][ICl_2^-]$ (where the ICl_2^- is symmetric) and $[PCl_4^+]_2[PCl_6^-][Cl^-]$, presumably arising from similar interactions, although the structures of these species must be quite different from the Br analogues. The very significant intensity increases of the PCl_4^+ stretching modes in Phase III PCl_5 must reflect an enhanced P—Cl bond polarizability derivative arising from interaction of PCl_4^+ with the single Cl^- ion. Another manifestation of the interaction is observed in the ^{31}P magic angle rotation NMR spectra of some of the complexes, in which very significantly broader phosphonium ion resonances occur when single-halide ions are present.[21,28] This is probably due to a closer cation–single halide approach, leading to increased dipolar interaction and consequent line-broadening.

The stretching frequencies of the trihalide ion in some complexes are also informative. In $[PBr_4^+][Br_3^-]$, a Br—Br stretching mode of the Br_3^- ion ($C_{\infty v}$-symmetry) occurs at 252 cm^{-1}, only *ca* 50 cm^{-1} less than that in liquid Br_2 at 308 cm^{-1}.[29–31] Symmetric ($D_{\infty h}$) Br_3^- ions are also known in which the Br—Br symmetric stretch (ν_1, Σ_g^+) occur at a much lower frequency, typically 168 cm^{-1}.[31] Hence in the less symmetric ($C_{\infty v}$) Br_3^- ion, the mode at 252 cm^{-1} may be regarded as essentially a weakened Br—Br stretching mode in the species Br—Br...Br^-. The proposed Br_2Cl^- ion in the PCl_5–Br_2 and Et_4NCl–Br_2 systems is probably similar to this. The strongest mode is at 280 cm^{-1} (Table 3) which is even closer to that in Br_2, suggesting that the Cl^-------Br—Br interaction is very weak, consistent with its apparent instability.

Acknowledgements—We thank Professor R. K. Harris and Mr A. Root (University of East Anglia) for solid-state NMR data, and Humberside County Council for provision of a Research Assistantship (A.S.M.).

REFERENCES

1. H. M. Powell, D. Clark and A. F. Wells, *Nature* (*London*) 1940, **145**, 149.
2. D. Clark, H. M. Powell and A. F. Wells, *J. Chem. Soc.* 1942, 642.
3. H. Preiss, *Z. Anorg. Allg. Chem.* 1971, **380**, 51.
4. H. M. Powell and D. Clark, *Nature* (*London*) 1940, **145**, 1971.
5. M. van Driel and C. H. MacGillavray, *Recl Trav. Chim. Pays-Bas* 1941, **60**, 869.
6. W. Gabes and K. Olie, *Acta Cryst.* 1970, **B26**, 443.
7. I. Popov, D. H. Geske and N. C. Baenziger, *J. Am. Chem. Soc.* 1956, **78**, 1793.
8. R. Baumgartner, W. Sawodny and J. Goubeau, *Z. Anorg. Allg. Chem.* 1966, **331**, 171.
9. H. Chihara, M. Nakamura and K. Muskane, *Bull. Soc. Chem. Jpn* 1967, **40**, 50.
10. S. G. Shore and H. Knachel, personal communication.
11. A. Finch, P. N. Gates, F. J. Ryan and F. F. Bentley, *J. Chem. Soc., Dalton Trans.* 1973, 1863.
12. R. Cahay and E. Whalley, *J. Chem. Phys.* 1979, **70**, 5534.
13. R. Cahay, P. T. T. Wong and E. Whalley, *J. Chem. Phys.* 1979, **70**, 5539.
14. J. A. Ripmeester, P. T. T. Wong, D. W. Davidson and E. Whalley, *J. Chem. Phys.* 1979, **70**, 5545.
15. A. Finch, P. N. Gates, H. D. B. Jenkins and K. P. Thakur, *J. Chem. Soc., Chem. Commun.* 1980, 579.
16. H. D. B. Jenkins, K. P. Thakur, A. Finch and P. N. Gates, *Inorg. Chem.* 1982, **21**, 423.
17. D. D. Perrin, W. L. F. Armarego and D. R. Perrin, *Purification of Laboratory Chemicals*. Pergamon Press, Oxford (1982).
18. I. R. Beattie and M. Webster, *J. Chem. Soc.* 1963, 38.
19. V. P. Petro and S. G. Shore, *J. Chem. Soc.* 1964, 326.
20. F. J. Ryan, Ph.D. thesis, University of London (1972).
21. A. S. Muir, Ph.D. thesis, University of London (1985).
22. A. Finch, P. N. Gates and A. S. Muir, *J. Chem. Res.* (S) 1986, 68.
23. K. B. Dillon, personal communication.
24. P. Van Huong and B. Desbat, *Bull. Soc. Chim. Fr.* 1972, 2631.
25. S. Krakowiecki, *Rocz. Chem.* 1930, **10**, 197.
26. F. F. Bentley, A. Finch, P. N. Gates, F. J. Ryan and K. B. Dillon, *J. Inorg. Nucl. Chem.* 1974, **36**, 457.
27. G. L. Breneman and R. D. Willet, *Acta Cryst.* 1967, **B23**, 467.
28. R. K. Harris and A. Root, personal communication.
29. P. Dhamelincourt and M. Crunelle-Cras, *Bull. Soc. Chim. Fr.* 1970, 2470.
30. W. Gabes and H. Gerding, *Recl Trav. Chim. Pays-Bas* 1971, **90**, 157.
31. W. Gabes, Ph.D. thesis, University of Amsterdam (1973).

Polyhedron Vol. 5, No. 10, pp. 1543–1545, 1986
Printed in Great Britain

0277–5387/86 $3.00+.00
Pergamon Journals Ltd

THERMODYNAMIC STUDIES ON IODINE(III) COMPOUNDS

B. M. DERAKHSHAN, A. FINCH* and P. N. GATES

Chemistry Department, Royal Holloway and Bedford New College, Egham, Surrey TW20 0EX, U.K.

(*Received* 27 *November* 1985; *accepted* 28 *February* 1986)

Abstract—The standard enthalpies of aqueous hydrolysis of $I_2Cl_6(c)$ and $I_2(CH_3COO)_6(c)$ have been determined as -59.3 ± 3.4 and -57.1 ± 2.0 kJ mol^{-1}, respectively, leading to the estimates of the standard enthalpies of formation $\{\Delta H_f^{\ominus}[I_2Cl_6(c)] = -179.8 \pm 4.0$ and $\Delta H_f^{\ominus}[I_2(CH_3COO)_6(c)] = -2101.6 \pm 9.0$ kJ mol^{-1}, respectively$\}$. A thermometric titration of I_2Cl_6 with aqueous $AgNO_3$ has been used to investigate the mechanism of the hydrolysis reaction.

Notwithstanding its electronegative character, iodine forms numerous species in which formal positive oxidation states are found. Thus I_n^+ ($n = 2, 3$ or 5) species in non-aqueous solutions, interhalogen cations (e.g. $ICl_2^+AlCl_4^-$), neutral polyhalogens (e.g. I_2Cl_6) and crystalline polyhalides (e.g. $MICl_2$ and $MICl_4$ where M = Group I metal or alkylammonium) are well documented;[1] considerable synthetic, structural and thermodynamic data are available. In addition, several tervalent iodine compounds such as the iodine triacylates $(RCOO)_3I$ and IPO_4[2,3] are known. $(CH_3COO)_6I_2$, in particular, has been used as a regio- and stereospecific reagent in alkene synthesis;[4,5] indications of a bridged, dimeric structure for this compound have been adduced from Mössbauer studies.[6] Thermodynamic data on these species are limited to an early, but meticulous, study of I_2Cl_6,[7] and to some polyhalide species.[8] We report here measurements leading to an estimation of the standard enthalpy of formation ($\Delta H_f^{\ominus}$) of iodine(III) chloride (I_2Cl_6) and $(CH_3COO)_6I_2$. Further, via a thermometric titration procedure, we define the sequential stages of hydrolysis of I_2Cl_6.

EXPERIMENTAL

Preparation of compounds

I_2Cl_6. Chlorine gas was liquefied at −78°C and powdered iodine added with stirring (2 h). Excess chlorine was allowed to evaporate at room temperature to leave orange-yellow needles of I_2Cl_6. Found: Cl, 44.7; I, 54.2%. Calc.: Cl, 45.6; I, 54.4%.

$(CH_3COO)_6I_2$. Powdered iodine (7.05 g, 0.05 mol) was added to glacial acetic acid (10.0 g, 0.16 mol) in the presence of acetic anhydride (15 cm^3). On addition of fuming nitric acid (6 cm^3) a yellow solution developed, from which yellow iodine triacetate precipitated on cooling. The compound was filtered and dried *in vacuo*, and stored in the absence of light. Found: I, 42.0%. Calc.: I, 41.8%.

Calorimetry

Enthalpies of aqueous hydrolysis ($\Delta H_h^{\ominus}$) were measured in the ampoule-breaking mode using a commercial isoperibol calorimetric system (LKB model 8700), the performance of which was periodically checked using the enthalpy of neutralization of tris(hydroxymethyl) methylamine in an excess of HCl. The apparatus for the thermometric titration of I_2Cl_6 with $AgNO_3$(aq) has been described previously.[9]

RESULTS

Values for $\Delta H_h^{\ominus}$ are summarized in Table 1 for reactions (1) and (2), and $\Delta H_f^{\ominus}$ of the compounds were calculated on the basis of eqns (3) and (4):

$$5I_2Cl_6(c) + 18H_2O(l) \rightarrow 2I_2(c) + 6IO_3^-(aq) + 36H^+(aq) + 30Cl^-(aq), \quad (1)$$

* Author to whom correspondence should be addressed.

Table 1. Standard enthalpies of aqueous hydrolysis ($\Delta H_h^\ominus$) and formation ($\Delta H_f^\ominus$) of crystalline I_2Cl_6 and $I_2(CH_3COO)_6$

Compound	Dilution[a]	No. of values	Mean $-\Delta H_h^\ominus$ (kJ mol^{-1})	$-\Delta H_f^\ominus$[b] (kJ mol^{-1})
I_2Cl_6	2886:8140	4	59.3±3.4	179.8±4.0
$I_2(CH_3COO)_6$	5349:10,833	7	57.1±2.0	2101.6±9.0

[a] Water : compound mole ratio.

[b] Uncertainties calculated using a Student's *t*-distribution at the 99.5% level.

$$5(CH_3COO)_6I_2(c)+18H_2O(l) \rightarrow 2I_2(c) + 6IO_3^-(aq)+6H^+(aq)+30CH_3COOH(aq), \quad (2)$$

$$5\Delta H_f^\ominus[I_2Cl_6(c)] = 6\Delta H_f^\ominus[IO_3^-(aq)] + 30\Delta H_f^\ominus[Cl^-(aq)]+2\Delta H_f^\ominus[I_2(c)] + 36\Delta H_f^\ominus[H^+(aq)]-18\Delta H_f^\ominus[H_2O(l)]-5\Delta H_h^\ominus, \quad (3)$$

$$5\Delta H_f^\ominus[(CH_3COO)_6I_2(c)] = 6\Delta H_f^\ominus[IO_3^-(aq)] + 2\Delta H_f^\ominus[I_2(c)]+30\Delta H_f^\ominus[CH_3COOH(aq)] + 6\Delta H_f^\ominus[H^+(aq)]-18\Delta H_f^\ominus[H_2O(l)]-5\Delta H_h^\ominus, \quad (4)$$

using the following ancillary data (all values in kJ mol^{-1}):

$$\Delta H_f^\ominus[IO_3^-(aq)] = -221.3\pm4.0;^{10}$$

$$\Delta H_f^\ominus[Cl^-(aq)] = -167.08\pm0.004;^{10}$$

$$\Delta H_f^\ominus[H_2O(1)] = -285.83\pm0.004;^{11}$$

$$\Delta H_f^\ominus(CH_3COOH)(3000H_2O) = -487.0\pm1.0.^{12}$$

DISCUSSION

Hydrolysis of I_2Cl_6

The excellent agreement between the definitive value (based on heat capacity measurements) of Lamoureaux and Giauque[7] for the $\Delta H_f^\ominus$ of I_2Cl_6 and that calculated from the present solution calorimetric measurements (-89.29 ± 0.10 and -89.89 ± 1.9 kJ mol^{-1}, respectively) supports the view that the hydrolytic reaction proceeds as in eqn (1). The possibility of significant polyhalide formation, e.g. ICl_2^-, and reversibility under the prevailing experimental conditions, is unlikely.

Sequential reaction of I_2Cl_6 *with* $AgNO_3$

As shown in Fig. 1, the aqueous reaction between I_2Cl_6 and $AgNO_3$ is clearly sequential and may be quantitatively rationalized as follows. All the chloride ions are first precipitated, followed by reaction of iodine to give iodide and iodate ions. AgI then precipitates immediately ($K_{sp} \sim 10^{-16}$), together with some $AgIO_3$ ($K_{sp} \sim 10^{-8}$). This is followed by precipitation of the remaining iodate when conditions, e.g. pH, allow the solubility product to be exceeded. These processes may be summarized as follows:

$$30Cl^- + 30Ag^+ \rightarrow 30AgCl\downarrow, \quad (i)$$

$$2I_2+2H_2O+4Ag^+ \rightarrow \frac{10}{3}AgI\downarrow+\frac{2}{3}AgIO_3\downarrow+4H^+, \quad (ii)$$

$$6IO_3^- + 6Ag^+ \rightarrow 6AgIO_3\downarrow. \quad (iii)$$

The overall reaction is hence:

$$3I_2Cl_6+24AgNO_3+12H_2O \rightarrow 18AgCl+2AgI+4AgIO_3+24HNO_3. \quad (iv)$$

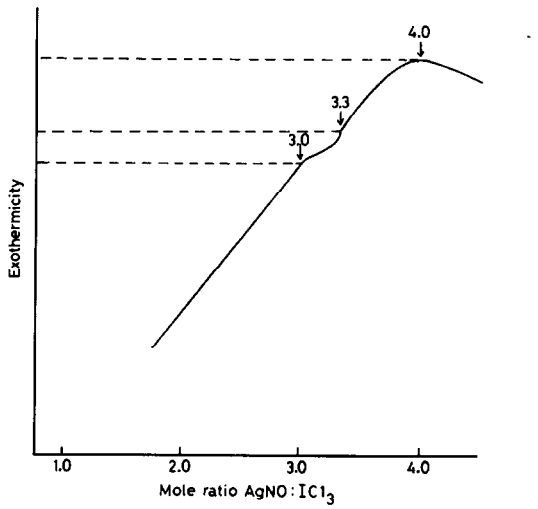


Fig. 1. Thermometric titration of ICl_3 with aqueous $AgNO_3$.

That reactions (i)–(iii) proceed discretely and sequentially is shown by the positions of the projections of the inflections on the abscissa of the thermometric reaction trace at $Ag^+ : IO_3^-$ mole ratios of 3 : 1, 3.33 : 1 and 4 : 1, respectively. In each case the position on the ordinate (energy) axis relevant to these points was quantitatively and unequivocally assignable to the precipitation of the appropriate mass of product, viz. AgCl, AgI and $AgIO_3$, respectively, via the literature values of the appropriate $\Delta H_f^\ominus$; details are given elsewhere.[13] Finally, the validity of eqn (iv) was further confirmed by acidimetric back titration of the nitric acid produced.

Hydrolysis of $(CH_3COO)_6I_2$

Combustion studies, routinely applied to organic compounds using a conventional static bomb calorimeter, cannot be applied to iodine(III) organic compounds in view of the uncertainties in defining the final state. The good agreement in results reported above for I_2Cl_6, compared with independent measurements,[7] and its clear chemical similarity to $(CH_3COO)_6I_2$ on hydrolysis, give confidence that a solution–reaction procedure is appropriate for determination of $\Delta H_f^\ominus$. Presumably comparable sequential processes are likely in reductive hydrolyses, as with $AgNO_3$ and I_2Cl_6. The substantial negative value for $\Delta H_f^\ominus (CH_3COO)_6I_2$ does not, of course, reflect reactive stability.

REFERENCES

1. N. N. Greenwood and A. Earnshaw, *Chemistry of the Elements*, Chap. 17, p. 920. Pergamon Press, Oxford (1984).
2. F. Fichter and S. Stern, *Helv. Chim. Acta* 1928, **11**, 1256.
3. G. B. Badman, G. F. Kite, S. Tuccarbasu and G. M. Tullman, *J. Org. Chem.* 1970, **35**, 3167.
4. R. C. Cambie, D. Chambers, P. S. Rutledge and P. D. Woodgate, *J. Chem. Soc., Perkin Trans.* 1 1977, 2231.
5. R. C. Cambie, D. Chambers, P. S. Rutledge and P. D. Woodgate, *J. Chem. Soc., Perkin Trans.* 1 1978, 1483.
6. C. H. W. Jones, *J. Chem. Phys.* 1975, **62**, 4343.
7. R. H. Lamoreaux and W. F. Giauque, *J. Phys. Chem.* 1969, **73**, 755.
8. B. M. Derakhshan, A. Finch and P. N. Gates, *J. Chem. Soc., Dalton Trans.* 1985, 997 (and references therein).
9. A. Finch, P. N. Gates and S. J. Peake, *Thermochim. Acta* 1977, **19**, 213.
10. J. B. Pedley, A. Kirk, S. Seilman and L. G. Heath, *Computer Analysis of Thermochemical Data, Halogen Compounds*. University of Sussex (1972).
11. *CODATA Recommended Key Values for Thermodynamics*, 1975; *J. Chem. Thermodyn.* 1976, **8**, 603.
12. D. D. Wagman, W. H. Evans, V. B. Parker, I. Halow, S. M. Bailey and R. H. Schumm, *Selected Values of Chemical Thermodynamic Properties*. Technical Note 270-4, U.S. Government Printing Office, Washington, DC (1969).
13. B. M. Derakhshan, Ph.D. Thesis, University of London (1981).

Polyhedron Vol. 5, No. 10, pp. 1547–1551, 1986
Printed in Great Britain

0277–5387/86 $3.00+.00
Pergamon Journals Ltd

SYNTHESIS, CHARACTERIZATION AND ^{1}H NMR STUDIES OF $[Co(en)_2(malH)_2]ClO_4 \cdot H_2O$

C. CHATTERJEE,* MARIE STEPHEN, RAKESH KUMAR and SUBROTO DAS

Department of Chemistry, Indian Institute of Technology, Powai, Bombay 400076, India

(*Received* 9 *December* 1985; *accepted* 27 *January* 1986)

Abstract—The *trans*-$[Co(en)_2(malH)_2]ClO_4 \cdot H_2O$ complex was prepared by the reaction of sodium hydrogen malonate with $[Co(en)_2(H_2O)_2](ClO_4)_3$ in the presence of a large concentration of perchlorate ion. It showed a three-band visible spectrum ($\lambda\lambda_{max}$ 357, 448 and 542.6 nm), diagnostic of a *trans*-MA_4B_2 system and gave characteristic IR bands as expected for a *trans*-bisethylenediamine cobalt(III) complex. The ^{1}H NMR spectrum in DMSO-d_6 revealed a broad band at 5.8 ppm assignable to the amino hydrogen and a single band at 2.68 for the ethylene group of the chelate ring. The $\rangle CH_2$ group of the hydrogen malonate ion appeared as a sharp singlet at 2.95 ppm and integration showed the presence of two bimalonate groups. The reactive methylene protons were found to be exchangeable. Ion association by counter ions of the complex ion in DMSO-d_6 showed no preference among amino protons. This is as expected for *trans* complexes with D_{2h}-symmetry.

In the anation reaction of *cis*-$[Co(en)_2(OH_2)_2]^{3+}$ with the bimalonate ion[1] the product expected is $[Co(en)_2(mal)]^+$. However, at low pH (~2.5), instead of getting complete conversion the absorbance at the end of the reaction does not match the spectral data of $[Co(en)_2(mal)]^+$. Some side reactions occur which could be due to formation of the *trans* product. The *trans* product separates out on standing for a long time from the reactant solution containing excess sodium perchlorate.

The synthesis of *trans* compounds with dicarboxylate as the unidentate group are very rare and hence justifies detailed characterization. Carunchio *et al.*[2] reported the synthesis of *trans*-$[Co(en)_2(malH)(H_2O)]^{2+}$ in solution and hence characterization was confined to the liquid phase only. The isolation of the title complex in the solid state allowed extensive and systematic structural investigations.

EXPERIMENTAL

Preparation of the complexes

$[Co(en)_2(CO_3)]ClO_4$ was prepared following the method described in the literature.[3] *cis*-$[Co(en)_2(H_2O)_2](ClO_4)_3$ was obtained by acidifying $[Co(en)_2(CO_3)]ClO_4$ with a slight excess of perchloric acid.

trans-$[Co(en)_2(malH)_2]ClO_4 \cdot H_2O$

This was synthesized by the addition of excess sodium hydrogen malonate (0.1 M) to an aqueous solution (50 cm^3) of *cis*-$[Co(en)_2(H_2O)_2]ClO_4$ (0.005 M). The pH of the solution was adjusted to ~2.5 followed by addition of the requisite quantity of sodium perchlorate such that the final concentration of perchlorate ion in the solution was $\geqslant$ 2.0 M. After digesting the reaction mixture at 70°C for 4 h the solution was allowed to evaporate slowly at room temperature. The reddish violet crystals of *trans*-$[Co(en)_2(malH)_2]ClO_4 \cdot H_2O$ separated out on standing. The product was recrystallized twice from acidified aqueous solution and washed successively with water, ethanol and ether and finally dried in air. Found: C, 23.6; H, 4.7; N, 11.2%. Calc. for $[CoC_{10}H_{22}N_4O_8]ClO_4 \cdot H_2O$: C, 23.9; H, 4.4; N, 11.4%.

Physical measurements

IR spectra of the complex in KBr were recorded using Nicolet model FTIR Spectrometer. A. Shimadzu 260 UV–visible spectrophotometer was

* Author to whom correspondence should be addressed.

employed for recording electronic absorption spectra. ^{1}H NMR spectra were recorded on a Varian-XL 100 spectrometer operating at 100 MHz. The spectra were obtained either in deuterium oxide (Aldrich, 99.8 atom % D minimum) or in perdeuteriodimethyl sulphoxide (Me_2SO-d_6, 99.9 atom % D minimum) with an internal reference of sodium 2,2-dimethyl-2-siliapentane-5 sulfonate or tetramethyl silane, respectively. Thermogravimetric analysis (TGA) was carried out using a Dupont thermal balance at a heating rate of 5°C min^{-1} under a nitrogen atmosphere.

RESULTS AND DISCUSSION

Carunchio *et al.*[2] isolated a mixture of *cis*- and *trans*-$[Co(en)_2(mal)(OH)]$ during the base hydrolysis of the $[Co(en)_2(mal)]^+$ ion. The *trans* species was separated from the *cis* isomer chromatographically. Acidification of the *trans*-hydroxo species led to the synthesis of the *trans*-$[Co(en)_2(malH)(H_2O)]^{2+}$ ion characterized in the solution phase. The complex in the present investigation contains two hydrogen malonate ions in the *trans* position. Preliminary investigation reveals that the aquation of the complex in weakly acidic medium leads to the initial formation of *trans*-$[Co(en)_2(malH)(H_2O)]^{2+}$ followed by the isomerization of the latter to the *cis*-$[Co(en)_2(malH)(H_2O)]^{2+}$ product. The isolation of the title complex in the solid state thus enabled detailed characterization by various physical techniques. The present data will add knowledge in the chemistry of *trans*-dicarboxylate bisethylenediamine complexes.

Protonation equilibrium studies

Acid dissociation constants of the *trans*-$[Co(en)_2(malH)_2]ClO_4 \cdot H_2O$ complex at 25°C and ionic strength 1.0 mol dm^{-1} were determined from conventional pH-metric titrations against a carbonate-free sodium hydroxide solution using pH M-64 research pH meter (Radiometer, Copenhagen). The pK_a values computed were $pK_1 = 3.0 \pm 0.05$ and $pK_2 = 4.10 \pm 0.1$, respectively.

Electronic absorption spectrum

Wilkins and Williams[4] have summarized the use of electronic absorption spectroscopy to distinguish between *cis*- and *trans*-cobalt(III) isomers based on crystal field considerations as established by Ballhausen and Jorgensen,[5] Moffit and Ballhausen,[6] and Yamatera.[7] The visible spectrum of the complex *trans*-$[Co(en)_2(malH)_2]^+$ in dilute perchloric acid showed absorption maxima corresponding to *d–d* transitions at 357, 448 and 542.6 nm respectively. The three absorption band spectrum (Fig. 1 and Table 1) is diagnostic of a *trans* configuration for the hexacoordinate complex of type MA_4B_2. In the *trans* isomer the $^1A_1 \rightarrow {}^1T_1$ transition was split and the principal band shifted to a lower energy. The low extinction coefficients of *d–d* bands (Table 1) also suggests the *trans* configuration for the complex. For the present system and for the *trans*-$[Co(en)_2(H_2O)(malH)]^{2+}$ ion the extinction coefficient corresponding to the shorter wavelength (357 nm) is higher than that of the longest-wavelength band (542–546 nm) while for *cis*-$[Co(en)_2(H_2O)(malH)]^{2+}$ and *cis*-$[Co(en)_2(mal)]^+$ ions the reverse trend is observed.[2]

IR spectrum

The IR spectrum of the complex in KBr pellets (Fig. 2) revealed two strong bands at 1581 and 1729 cm^{-1} attributable to the carbonyl stretching frequencies of the coordinated and free carboxyl groups, respectively. Morris and Busch[8] while

Table 1. Spectral data

trans-$[Co(en)_2(malH)_2]^{+a}$		*cis*-$[Co(en)_2(mal)]^{+b}$	
Wavelength (nm)	Molar extinction coefficient (M^{-1} cm^{-1})	Wavelength (nm)	Molar extinction coefficient (M^{-1} cm^{-1})
542.6	62.1	498	116
448	31.5	370	109
357.4	75.0		

[a] The spectrum was taken in 0.05 M perchloric acid.
[b] M. E. Farago and I. M. Keefe, *Inorg. Chim. Acta* 1975, **15**, 5.

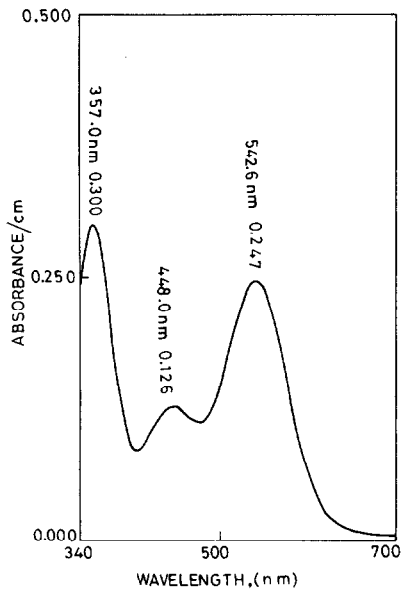


Fig. 1. Electronic spectrum of *trans*-$[Co(en)_2(malH)_2]ClO_4 \cdot H_2O$ in 0.05 mol dm^{-3} $HClO_4$. [Complex] = 0.004 mol dm^{-3}.

studying the IR spectra of *cis*- and *trans*-dichloro- and dinitro-bisethylenediamine cobalt(III) complexes, observed a characteristic difference in the N—H bending mode between the isomers. *Cis* complexes showed splitting of the band in the region 1640–1570 cm^{-1} while no splitting is observed for the corresponding *trans* isomer. The title complex $[Co(en)_2(malH)_2]^+$ shows only one peak at 1581 cm^{-1}, whereas *cis*-$[Co(en)_2(mal)]^+$ shows two absorptions at 1571 and 1621 cm^{-1}. On the basis of

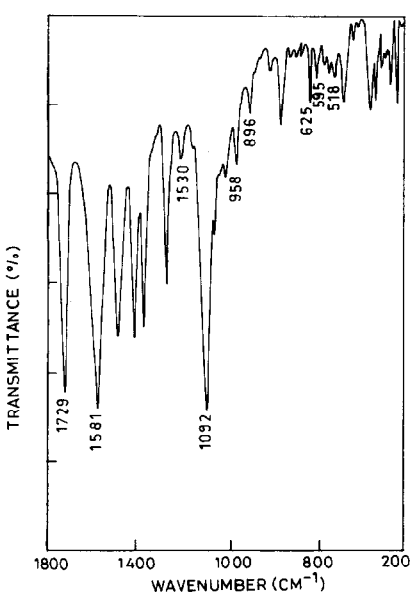


Fig. 2. IR spectrum of *trans*-$[Co(en)_2(malH)_2]ClO_4 \cdot H_2O$.

IR spectra of several *cis*- and *trans*-diacido bisethylenediamine cobalt(III) complexes, Chamberlain and Bailar[9] suggested that only one N—H wagging frequency appears in the range 1120–1150 cm^{-1} for the *trans* but two for the corresponding *cis* isomers. A single peak at 1130 cm^{-1} for the complex under investigation strongly suggests the *trans* configuration. The peak at 1130 cm^{-1} appears as a shoulder along with the major absorption band due to the perchlorate ion at 1092 cm^{-1}. Baldwin[10] in the course of their spectral studies on *cis*- and *trans*-bisethylenediamine cobalt(III) complexes noted a consistent variation of spectra with configuration in the CH_2 rock region (870–910 cm^{-1}) of the chelate ring. Here again, the complexes with the *cis* configuration showed two bands whereas a single band was observed for the *trans* isomers. In accordance with a *trans* configuration the title complex exhibited only one band at 896 cm^{-1}. Hughes and McWhinnie[11] obtained a satisfactory correlation with the number of peaks and the configuration of the isomers in the region 500–610 cm^{-1} where Co–N stretching modes occur. In this region no *trans* isomer has more than three strong bands whereas four bands were exhibited by the *cis* isomers. The bands for the *trans* isomers are generally evenly spaced, whereas in the *cis* complexes they appear in two separate groups. The band at 561 cm^{-1} is attributable to the Co—O of the Co–malH bond. It is evident from Fig. 2 that the *trans* complex reveals only three bands at 595, 540 and 518 cm^{-1}, whereas four bands at 592, 580, 533 and 520 cm^{-1} are exhibited by *cis*-$[Co(en)_2(mal)]ClO_4$. Prominent IR peaks due to perchlorate ions are observed at 1092, 958 and 625 cm^{-1} and the evidence obtained from IR studies is thus consistent with a *trans* configuration for the title complex.

^{1}H NMR *spectrum*

The ^{1}H NMR spectrum offers conclusive proof of the configuration of the isomers in solution. The *cis* and *trans* isomers of $[Co(en)_2X_2]^+$ ions have different symmetry properties, and this factor appears to govern the difference in their NMR spectra. The *cis* isomers possess C_2-symmetry with the two-fold axis in the plane of cobalt and the two X groups. As a result the $\diagdown CH_2$ protons become equivalent provided the cobalt–ethylenediamine rings have the same conformation. In case of relatively rigid conformers an ABCD pattern could be seen in D_2O. If an average conformer is observed an A_2B_2 system should appear since the protons on

either side of each cobalt–ethylenediamine ring would experience different fields. The amine hydrogens in the *cis* configuration also undergoes splitting and gives rise to four peaks in ideal situations. In *trans* isomers, however, with D_{2h}-symmetry, the amine protons and methylene protons of ethylenediamine appear as singlets. A similar situation is observed in dipolar aprotic solvents, such as DMSO-d_6. Both the number and the intensity of NH signals may be rationalized in terms of overall stereochemistry. In the *trans* complexes all the protons are equivalent due to the rapid conformational interchange and hence only one signal is observed. For the *cis* compound the different NH absorption are attributed to the orientation of the NH protons with respect to the rest of the ions.

Figure 3 illustrates the NMR spectra of the title complex in DMSO-d_6 and D_2O solvents. The spectrum of the title complex in DMSO-d_6 exhibited a broad band of eight-proton intensity at δ 5.8 ppm which is assignable to the amine hydrogens of ethylenediamine. The absorptions at δ 2.95 and 2.68 ppm are assigned to the CH_2 absorptions of hydrogen malonate and ethylenediamine, respectively, on the basis of their integrated intensities (1 : 2). The sharp signal at 2.95 ppm is indicative of the equivalence of the two protons of the methylene moiety of the hydrogen malonate ion. A similar pattern was also observed in D_2O (Fig. 3b).

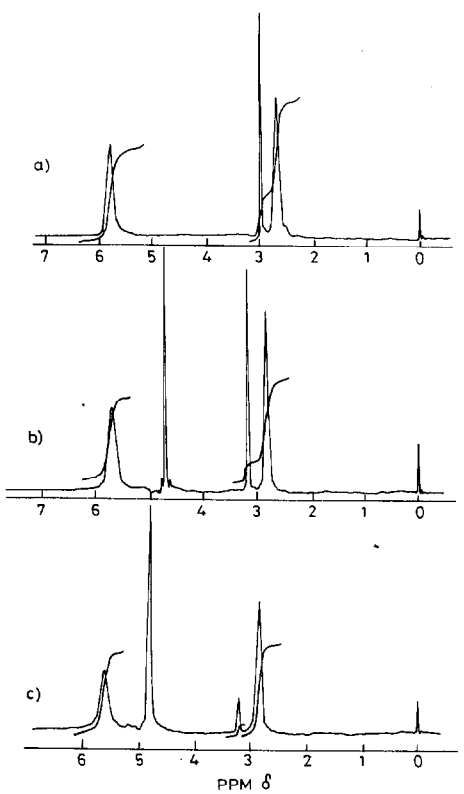


Fig. 3. PMR spectra of *trans*-$[Co(en)_2(malH)_2]ClO_4 \cdot H_2O$ in: (a) DMSO-d_6, (b) D_2O, and (c) D_2O and DCl.

Proton exchange

The amine protons of metal amine complexes undergo fast H–D exchange when dissolved in D_2O. In contrast, no appreciable exchange of amine protons in the title complex was observed under identical conditions. As the H–D exchange of the amine proton is always base-catalysed the lack of proton exchange can be attributed to the presence of free carboxylic acid groups contribution to the residual acidity. The reactive methylene protons of the malonate groups are found to exchange at a fast rate in both acidic and alkaline D_2O. Such an exchange of methylene hydrogen in the coordinated malonate group has been reported by several workers.[12]

Ion association

Directional association of ions with amine protons in metal complexes as inferred from NMR spectra is a fascinating subject and yields valuable information as regards the three-dimensional structure of the complex in solution. Ion association occurs when counter anions bind with an ionizable hydrogen of the coordinated ligands in the complex ion. The counter ions are known to associate with amine hydrogens via hydrogen bonding. Association by hydrogen bonding causes a reduction in electron density on the bonded hydrogen atom and the NMR signal moves downfield. The downfield shift increases with increasing amount of counter ions. The most interesting and important fact is that the association of the counter anion with a complex cation is stereoselective. The selection based on electrostatic consideration suggests that, since the anion carries a negative charge, it will approach the complex cation along the C_2-axis from the side opposite to the acido group present in the complex. Yoneda *et al.*,[13] while studying the ion association of amine hydrogens in *cis*-$[Co(en)_2X_2]^+$ systems, found that the NH *trans* to X was most sensitive to ion association. In *trans*-$[Co(en)_2X_2]^+$ such a preference is not expected since all the amine hydrogens are *cis* to X. In order to test the above generalization for differentiating the *cis* and *trans* configurations, ion association studies were carried out by the addition of lithium chloride to the complex ion dissolved in DMSO-d_6. As expected all the amine hydrogens

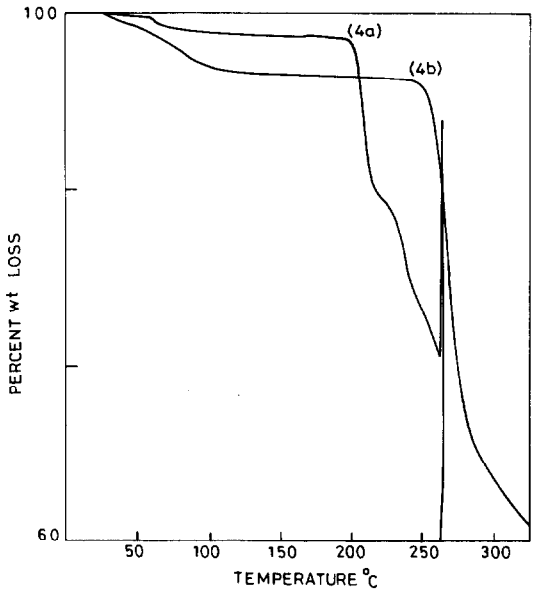


Fig. 4. Thermal analysis of: (a) *trans*-$[Co(en)_2(malH)_2]ClO_4 \cdot H_2O$, and (b) $[Co(en)_2mal]Cl \cdot 2H_2O$.

moved downfield together. The downfield shift was only 0.3 ppm even in the presence of a large excess of lithium chloride as against a 1–2-ppm shift of amine protons *trans* to X in *cis*-$[Co(en)_2X_2]^+$. A larger downfield shift is indicative of a higher association constant of *cis* complexes in a dipolar aprotic solvent.

Thermal studies

The thermal data (Fig. 4) show that the title compound decomposed in multiple steps. The first step was due to the loss of one water molecule at 75°C (found = 3.3%, calculated for % water in $[Co(en)(malH)_2]H_2O_4 \cdot H_2O$ = 3.58). The second step at 215°C could be attributed to the loss of two CO_2 molecules. This most probably occurred due to decarboxylation from free carboxylic acid groups in the complex [found (% loss) = 17.6, calculated for loss of two CO_2 molecules = 17.51]. The third step at 255°C is decarboxylation of the coordinated carboxylate group with total decomposition of the complex which occurred through an *explosion* as shown by the break in the line in Fig. 4a. The TGA of the chelated malonate complex $[Co(en)_2(mal)]Cl \cdot 2H_2O$ (Fig. 4b) shows a one-step decomposition at 267°C. In the chelated complex it shows that decarboxylation occurs at a higher temperature.[14]

REFERENCES

1. C. Chatterjee and S. Das, to be communicated.
2. V. Carunchio, G. R. Strassa and T. Prosperi, *Gazz. Chim. Ital.* 1974, **104**, 903.
3. F. P. Dwyer, A. M. Sargeson and J. K. Reid, *J. Am. Chem. Soc.* 1963, **85**, 1213.
4. R. G. Wilkins and M. J. G. Williams, In *Modern Coordination Chemistry* (Edited by J. Lewis and R. G. Wilkins), p. 187. Interscience, New York (1960).
5. G. C. Ballhausen and C. K. Jorgensen, *Kgl. Darrske, Videnskab. Salskab Mat. Fys. Medd.* 1955, **29**, 14.
6. W. J. Moffit and C. J. Ballhausen, *J. Inorg. Nucl. Chem.* 1956, **3**, 178.
7. H. Yamatera, *Bull. Chem. Soc. Jpn* 1958, **31**, 95.
8. M. L. Morris and D. H. Busch, *J. Am. Chem. Soc.* 1960, **82**, 1521.
9. M. M. Chamberlain and J. C. Bailar, *J. Am. Chem. Soc.* 1959, **81**, 6412.
10. M. E. Baldwin, *J. Chem. Soc.* 1960, 4369.
11. M. N. Hughes and W. R. McWhinnie, *J. Inorg. Nucl. Chem.* 1966, **28**, 1659.
12. M. E. Farago and M. A. R. Smith, *Inorg. Chim. Acta* 1975, **14**, 21.
13. H. Nakazawa, H. Sakaguchi, H. Yoneda and Y. Morimoto, *Inorg. Chem.* 1981, **20**, 973.
14. T. R. Bhatt and R. K. Iyyer, *J. Inorg. Nucl. Chem.* 1967, **29**, 179.

Polyhedron Vol. 5, No. 10, pp. 1553–1558, 1986
Printed in Great Britain

0277–5387/86 $3.00+.00
Pergamon Journals Ltd

PULSE RADIOLYSIS AND VOLTAMMETRY OF BIS(DIAMINE)DIOXORHENIUM(V) COMPLEXES

GEOFFREY A. LAWRANCE*

Department of Chemistry, The University of Newcastle, New South Wales 2308, Australia

and

DAVID F. SANGSTER

Division of Chemical Physics, CSIRO, Lucas Heights Research Laboratories, Private Bag 7, Sutherland 2232, Australia

(*Received* 10 *December* 1985; *accepted* 24 *February* 1986)

Abstract—The Re(V) complexes $[Re(L)_2O_2]^+$ [L = en (1,2-diaminoethane) or pn (1,3-diaminopropane)] are reduced irreversibly near −1.5 V (SCE) in a neutral or basic aqueous solution, but protonation causes a significant anodic shift of ~+1 V. No oxidation is observed in aqueous solution before the solvent limit (~+1 V) at solid electrodes but oxidation of $[Re(en)_2O_2]^+$ with OH in pulse radiolysis experiments generates a Re(VI) intermediate which decays by first-order kinetics (k_d 2.5×10^4 s^{-1}), apparently by rate-determining ligand loss. Reduction with e_{aq}^- likewise forms transient d^3-Re(IV) complexes which show first-order decay (6×10^3 s^{-1} for en, 9×10^3 s^{-1} for pn), ultimately to ReO_2. Transient intermediates were characterized by their electronic spectra, which for d^3-Re(IV) complexes are qualitatively similar to Cr(III) and known octahedral Re(IV) complexes with different donor ligands.

The known chemistries of rhenium and technetium are similar.[1,2] The latter element has attracted a deal of recent interest, largely as a result of the importance of compounds of technetium as radiopharmaceuticals.[2,3] This interest has caused the coordination chemistry of this synthetic element to be investigated more extensively than that of rhenium. Nevertheless, the latter element is inherently easier to work with on a large scale and the study of its chemistry and reactions may have implications for reactions of the former. With simple saturated multidentate amines, both elements form hexacoordinate dioxo complexes with the metal in oxidation state V. Although various amines have been coordinated to Tc(V),[2] only the 1,2-diaminoethane (en) and 1,3-diaminopropane (pn) complexes of Re(V) are well-characterized.[4–9]

The dioxorhenium(V) diamine compounds are known to protonate in aqueous acid (presumably oxo to hydroxo),[4,8] and appear to undergo a one-electron reduction below −1 V in aqueous solution,[9] although redox properties have not been investigated extensively. Since a one-electron reduction would lead to d^3-Re(IV), and this electronic configuration is inherently inert, it was of interest to investigate this reduction in detail by electrochemical and pulse radiolytic means. Further, the prospect of oxidation to presumably labile d^5-Re(VI) exists. This paper reports the pulse radiolysis and pH-dependent voltammetry of dioxobis(diamine)rhenium(V) cations in aqueous solution.[10]

EXPERIMENTAL

Syntheses

Bis(1,2-*diaminoethane*)*dioxorhenium*(V) *chloride*. This complex was prepared by the oxidation of a mixture of K_2ReCl_6 (3 g) in 90% en (15 cm^3) with air as previously described,[4] and recrystallized from water and alcohol as yellow-green microcrystals (1.6 g, 70%). Found: C, 13.0; H, 4.3; N, 14.9%. Calc. for $C_4H_{16}ClN_4O_2Re$: C, 12.8; H, 4.3; N, 15.0%.

Bis(1,3 - *diaminopropane*)*oxohydroxorhenium*(V) *chloride*. This complex was prepared as above,

* Author to whom correspondence should be addressed.

except that recrystallization from dilute acidic solution (pH ~ 2) gave the purple oxohydroxo complex in similar yield. Found: C, 16.7; H, 4.9; N, 12.8%. Calc. for $C_6H_{21}Cl_2N_4O_2Re$: C, 16.4; H, 4.8; N, 12.8%.

Bis(1,4 - *diaminobutane*)*dichlorotetraoxodirhenium*(V). Attempts to reproduce the above syntheses with 1,4-diaminobutane (bn) yielded a black neutral product in the initial step following addition of acetone. Spectroscopy and microanalysis were most consistent with formulation as a dimer, the complex being isolated with the ·KCl·acetone formulation. Found: C, 16.0; H, 3.8; N, 7.2; Cl, 12.8%. Calc. for $C_8H_{24}Cl_2N_4O_4Re_2 \cdot KCl \cdot (CH_3)_2CO$: C, 16.2; H, 3.7; N, 6.9; Cl, 13.0%.

Physical methods

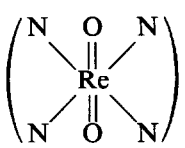
IR spectra were recorded as KBr discs using a Perkin–Elmer 3-300 spectrometer. Electronic spectra were recorded using an Hitachi 220A spectrophotometer. The pK_a values for the hydroxo/oxo forms of the pn complex were determined spectrophotometrically at several wavelengths in the visible region using either a range of acids of known concentration or a range of buffers of known pH.

Polarography at a dropping mercury (DME) or a static mercury drop electrode, and cyclic voltammetry at either a hanging mercury drop electrode (HMDE) or a glassy carbon electrode, was performed on dilute aqueous solutions ($\sim 10^{-3}$ M) under an inert argon atmosphere. A conventional three-electrode system was employed with a platinum wire auxiliary electrode and a silver–silver chloride or SCE reference electrode. Electrochemical controllers employed were either BAS Model 27 or Amel Model 457 units.

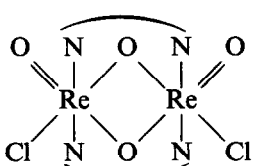
Pulse radiolysis experiments were conducted using the 1-MeV electron accelerator facility and optical system previously described.[11] The system was calibrated by thiocyanate dosimetry.[12] Complexes in triply-distilled water at concentrations $\leqslant 10^{-3}$ M were reacted with e_{aq}^- or OH radical. For e_{aq}^-, an N_2-purged solution containing 0.1 M *t*-butyl-alcohol as an OH radical scavenger was used; for OH, the solution was purged with N_2O to capture e_{aq}^- by converting e_{aq}^- to OH, thus effectively doubling the yield of OH radical. Initial and final optical-density changes were measured at 5–25-nm intervals from signal-averaged data over the range 220–700 nm. This permitted construction of the absorption spectra of intermediate and decay products. Kinetics of the decay processes were followed at several wavelengths in the UV–visible region. Formation rate constants for reaction with e_{aq}^- ($G_e = 2.7$) were determined by monitoring the decay kinetics of e_{aq}^- at 580 nm in the presence of different concentrations of complex. The rate constant for formation with OH ($G_{OH} = 5.5$) was determined by competition kinetics with KSCN. The radiolytically generated e_{aq}^- is a powerful reducing agent ($E^\ominus = -2.8$ V), while the OH radical is a powerful oxidizing agent ($E^\ominus = \sim +2$ V); the reaction conditions in these experiments determine that the oxidation and reduction processes initiated are definitively one-electron in character.

RESULTS AND DISCUSSION

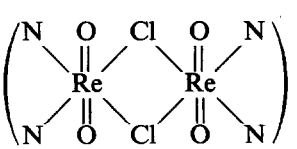
Reaction of $ReCl_6^{2-}$ with en or pn and oxygen at room temperature yields the bis(diamine)dioxorhenium(V) compounds in high yield. The crystal structure of $[Re(en)_2O_2]^+$ has been determined,[7] and the Re(V) ion is monomeric and essentially octahedral, with a *trans*-dioxo configuration and chelated diamines (**I**). While five- and six-membered chelates readily lead to monomers with structure **I**, attempts to repeat the synthesis with bn yielded a black and possibly polymeric compound. Although detailed characterization was not pursued, IR spectroscopy is indicative of diamine coordination and bound oxo groups, and microanalysis best fits a formulation as a dimer of stoichiometry $[Re_2(bn)_2Cl_2O_4]$. Possible structures are **II**, where the bridging diamine may be appropriate with the longer-chain bn, or else a bridging chloro species such as **III**. Both



I



II



III

oxo and chloro bridges are known for rhenium,[1] and a structure like **III** could be viewed as an intermediate in the synthesis of **I**. Further work with this compound is warranted, but in this case we intended to concentrate on the definitive monomeric Re(V) diamines formed with en and pn.

The electronic spectra of the dioxorhenium(V) monomers are markedly pH-dependent, as observed previously.[8] Maxima for both diamine complexes at three different acidities apparently corresponding to three different species are collected in Table 1. From these spectra, at least two acid dissociation steps are apparent in aqueous solution; spectroscopic pK values determined were $pK_1 = 3.2$ and $pK_2 = -0.7$ for the pn complex, which agree well with values of 3.26 and -0.9 previously determined for the en complex.[8] The complexes decompose only very slowly in aqueous acid at room temperature, but decompose more rapidly in strong aqueous base. Allowed electronic transitions for octahedral d^2 are $^3T_{1g}(F) \rightarrow {}^3T_{2g}(F)$, $^3T_{1g}(F) \rightarrow {}^3T_{1g}(P)$ and $^3T_{1g}(F) \rightarrow {}^3A_{2g}(F)$; the latter probably does not contribute to transitions in the visible region for first-row V(III).[113] Observed transitions in third-row Re(V) may relate to the first-row case, and should be similar in octahedral d^2-W(IV), although electronic spectroscopy of neither third-row metal ion has been extensively studied.[1] The significant shifts in absorption maxima with acidity fit best with protonation of the O^{2-} ligand to OH^-, since these ligands differ in their position in the spectrochemical series. Considerable diminution in $d\pi$–$p\pi$ interactions to the M—O bonding is also expected from O^{2-} to OH^-.[14] The pH-dependent polarography supports in part ligand protonation. Previously, protonation/deprotonation shifts in metal-centred redox couples of approximately 1 V have been observed for octahedral third-row metal complexes of Pt(IV) and Os(IV).[15,16] Here, the $[Re(en)_2O_2]^+$ complex at neutral pH exhibits an irreversible reduction near -1.5 V (SCE) at the DME; this shifts to a quasi-reversible couple at -0.5 V at pH $\sim$ 1, paralleling the earlier observations.

Voltammetry of the dioxorhenium(V) complexes (Table 2) shows that reduction occurs well below -1 V on both mercury and solid-billet electrodes in neutral solution. Previously, polarography in aqueous chloride media of the $[Re(en)_2O_2]^+$ complex, some with added ethylenediamine, reported a reversible one-electron couple at or near -1.15 V (SCE).[9] This does not agree completely with the current results in ClO_4^- media, nor does the assertion in that note that the $Re(en)Cl_4$ compound is formed equate with the concept of reversibility. Notably, the polarography in acid defined a quasi-reversible couple which is a volt more cathodic than the wave in neutral solution (Fig. 1) for both complexes. The significant shift in potential observed at the mercury electrode was not reproduced clearly at a glassy carbon electrode where the wave is poorly-defined and irreversible, so it is likely that the former couple is not a simple metal-centred process, but involves some specific interaction with the metal electrode surface. In aqueous solution, no oxidation of Re(V) is observed at solid electrodes before the solvent limits of $\sim +1$ V.

It is only with the powerful oxidant OH in the pulse radiolysis experiments that an oxidation reaction is observed. Rapid formation (Table 3) of an apparently Re(VI) complex occurs upon reaction of OH with $Re(en)_2O_2^+$. The transience exhibits an absorbance maximum at 320 nm, with no detectable absorbances in the visible region (Fig. 2). The decay of this transience is quite rapid, and first-order in nature. Disproportionation of Re(VI) with second-order kinetics is the expected mode of decay, and has been observed for Re(VI) generated by reduction of ReO_4^- with e_{aq}^-.[17] The first-order process observed here implies that ligand loss is the

Table 1. Electronic absorption maxima of the $[Re(L)_2O_2]^+$ complexes in aqueous solution

Complex	Acidity	λ_{max} (nm) [ε (M^{-1} cm^{-1})]
$[Re(en)_2O_2]^+$	pH $\sim$ 5	550sh (6.0), 439 (27.5), 276sh (630), 255 (1070), 203 (18,500)
$[Re(en)_2(O)(OH)]^{2+}$	pH $\sim$ 1	625 (7.9), 485 (25.7), 257sh (520), 212 (4500)
$[Re(en)_2(OH)_2]^{3+}$	12 M HCl	835 (10.2), 602 (24.0), 252 (1280)
$[Re(pn)_2O_2]^+$	pH $\sim$ 6	545sh (5.5), 447 (26.5), 277sh (395), 253 (865), 204 (12,500)
$[Re(pn)_2(O)(OH)]^{2+}$	pH $\sim$ 1	653 (6.0), 492 (23.0), 255sh (350), 212 (3600)
$[Re(pn)_2(OH)_2]^{3+}$	12 M HCl	850 (8.8), 621 (22.4), 251 (2500)

Table 2. Reduction potentials for the Re(V)–(IV) couple of the $[Re(L)_2O_2]^+$ complexes in aqueous solution[a]

L ligand	pH	d.c. $E_{1/2}$ (V)	Cyclic voltammetry HMDE $E_{1/2}$ (V) [ΔE (mV)]	Cyclic voltammetry Glassy C $E_{1/2}$ (V)
en	~1	−0.50	−0.48 (120)	[b]
	~6	~−1.4	−1.45[c]	−1.52[c]
	~10	−1.45	~−1.5[c]	−1.55[c]
pn	~1	−0.49	−0.48 (60)	−0.60[c]
	~6	~−1.3	~−1.4[c]	−1.38[c]
	~10	−1.36	−1.34 (180)[d]	−1.42[c]

[a] 0.1 M $NaClO_4$, ambient temperature, V (SCE).
[b] Not observed.
[c] Irreversible, cathodic E_p reported.
[d] Poorly defined anodic wave, E_p (cathodic) = −1.43 V.

rate-determining process, i.e.:

$$[Re(en)_2O_2]^+ + OH \xrightarrow{k_f} [Re(en)_2O_2]^{2+} + OH^-$$

$$\downarrow k_{dissoc}$$

$$\text{oxo Re species} \xrightarrow{fast} Re(V) + Re(VII).$$

Alternatively, hydrogen abstraction from the amine ligand may be the first step, with intramolecular electron transfer to form an Re(VI) species which then undergoes ligand dissociation and disproportionation reactions. Like ReO_4^{2-}, the Re(VI) species generated in this reaction is not stable. Earlier studies of chemical oxidation of $[Re(en)_2O_2]^+$ to Re(VII) showed that the ReO_2 core remains intact,[5] so a like process probably holds in this one-electron oxidation, with amine loss the possible kinetically significant process.

While stable hexacoordinate Re(VI) is unlikely and its instability therefore not unexpected, the case for Re(IV) complexes is much stronger. Firstly, Re(IV) is a member of the d^3-family, and this is an inherently inert electronic configuration. Secondly, the present and previous voltammetry experiments lend some support to the existence of oxorhenium(IV) diamines. Finally, there are extant a range of examples of monomeric, octahedral Re(IV) compounds,[1,18–20] albeit not commonly with *N*-donor ligands. Known Re(IV) compounds usually contain

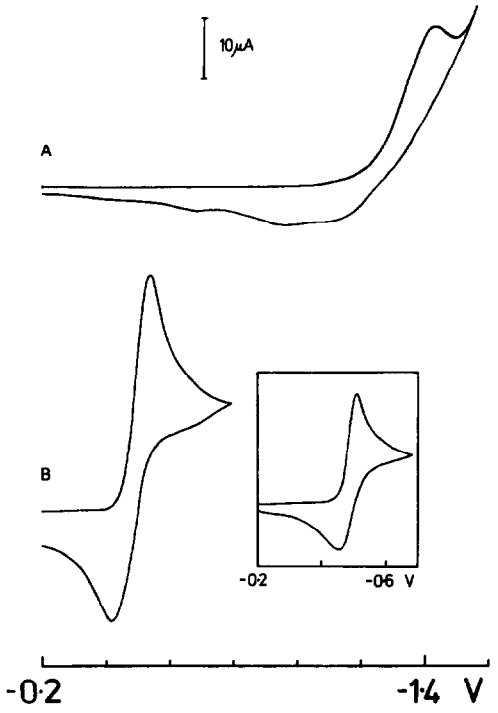


Fig. 1. Cyclic voltammetry at an HMDE of the $[Re(en)_2O_2]^+$ complex in aqueous solution: (A) at neutral pH, and (B) at pH ~ 1. Inset is the response for $[Re(pn)_2O_2]^+$ at pH ~ 1.

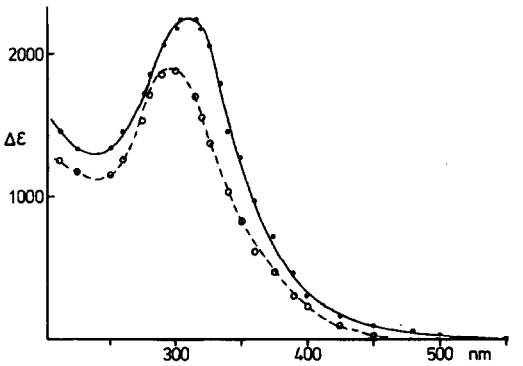


Fig. 2. Electronic spectrum of the transient (at 3 μs) (——) and the immediate decay product (at 0.2 ms) (– – – –) from reaction of the $[Re(en)_2O_2]^+$ ion with OH in neutral aqueous solution

Table 3. Formation and decay rate constants and electronic absorption maxima of transient intermediates formed from pulse radiolysis of $[Re(L)_2O_2]^+$ complexes in neutral aqueous solution

Process	k_f ($M^{-1}\,s^{-1}$)	λ_{max} (nm) [ε ($M^{-1}\,cm^{-1}$)]	k_d (s^{-1})
$[Re(en)_2O_2]^+ + OH$	7.8×10^9	320 (2200)	2.5×10^4
$[Re(en)_2O_2]^+ + e_{aq}^-$	2.3×10^{10}	500 (150), 330 (850)	6×10^3
$[Re(pn)_2O_2]^+ + e_{aq}^-$	2.4×10^{10}	500 (120), 325 (1100)	9×10^3

a halide or mixed halide, and O- or P-donors. The *trans*-$Re(acac)_2Cl_2$[19] and $Re(diphos)Cl_4$ [diphos = 1,2-bis(diphenylphosphino)ethane][20] compounds have been characterized by X-ray crystal structure analyses, and exhibit octahedral or distorted octahedral geometries. Since both Re(V) and Re(IV) commonly occur as hexacoordinated species, the addition of an electron to Re(V) should be accommodated without any requirement for marked geometric change.

Addition of e_{aq}^- to $[Re(en)_2O_2]^+$ and $[Re(pn)_2O_2]^+$ is rapid (Table 3), generating an intermediate which absorbs in the visible region. Two maxima are observed in each case (Fig. 3), and the spectra are qualitatively similar to those of octahedral d^3-Cr(III), and resemble somewhat the spectrum of *trans*-$Re(acac)_2Cl_2$ [maxima at 500 nm ($\varepsilon = 260$ M^{-1} cm^{-1}), 420 nm ($\varepsilon = 810$) and 330 nm ($\varepsilon = 1600$) reported,[18] the two low-energy maxima possible arising from splitting in the tetragonal field] despite the variation from a distorted O_4Cl_2 chromophore to a presumably N_4O_2 chromophore. Rapid formation of an Re(IV) complex is also supported by the expectation that the alternative of a saturated ligand radical would not absorb in the visible region. Decay of the intermediate Re(IV) complex occurs on the millisecond timescale by a first-order process which is presumed to involve amine ligand dissociation. Disproportionation is not consistent with the observed kinetic behaviour, nor is it expected for d^3-Re(IV), given the stability of ReO_2.

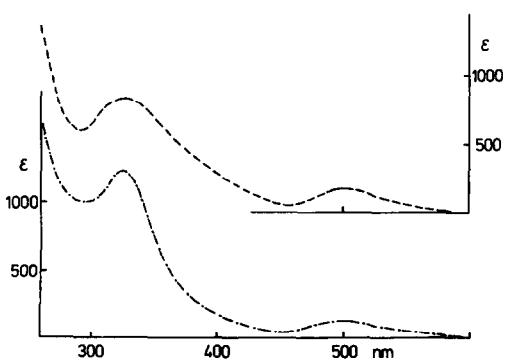


Fig. 3. Electronic spectra of the transient d^3-Re(IV) complexes formed from reaction of $[Re(en)_2O_2]^+$ (upper) and $[Re(pn)_2O_2]^+$ (lower) with e_{aq}^- in neutral aqueous solution.

The ultimate decomposition product was expected to be the cinnamon-coloured hydrate of ReO_2, and absorbance of visible light in aged solutions from continuous-pulse experiments is consistent with the expectation. It is known that decay of radiolytically-generated Mn(IV) amine complexes produces MnO_2 following decay,[21] so an analogy can be drawn. Further, decomposition of Re(IV) compounds such as $[Re(OH)Cl_5]^{2-}$ in aqueous solutions yield ReO_2 as the only stable product.[22] The immediate product of the decay in this case does not absorb in the visible region, however, so ReO_2 is not the initial decay product. Complexed species such as $Re(en)(OH)_4$, $Re(enH)(OH)_5$, $Re_2(en)(OH)_8$ or oxo analogues may form initially. The amine coordination chemistry of rhenium is strictly limited, so we are unable to establish the structure of this unstable species. It is notable that d^3-complexes of both Mn(IV)[21] and Re(IV) with saturated *N*-donor ligands apparently occupying four coordination sites decay relatively quickly. Apparently *N*-donor-saturated ligands do not form stable complexes with any metal in the +4 oxidation state in the manganese triad. This accords with the known chemistry, although whether this instability extends to unsaturated imine *N*-donors remains untested.

Acknowledgement—Support for this research from the Australian Institute of Nuclear Science and Engineering is gratefully acknowledged.

REFERENCES

1. J. E. Fergusson, *Coord. Chem. Rev.* 1966, **1**, 459; *Specialist Periodical Reports, Inorganic Chemistry of the Transition Elements*, Vols 1–6. Chemical Society, London.

2. E. Deutsch, K. Libson, S. Jurisson and L. F. Lindoy, *Prog. Inorg. Chem.* 1983, **30**, 75.
3. M. J. Clarke and P. H. Fackler, *Struct. Bonding (Berlin)* 1982, **50**, 55.
4. R. K. Murmann, *Inorg. Synth.* 1966, **8**, 173.
5. L. B. Kriege and R. K. Murmann, *J. Am. Chem. Soc.* 1972, **94**, 4557.
6. M. C. Chakravorti and C. K. Das, *Transition Met. Chem.* 1978, **3**, 133.
7. C. J. L. Lock and G. Turner, *Acta Cryst.* 1978, **B34**, 923.
8. R. K. Murmann and D. R. Foerster, *J. Phys. Chem.* 1963, **67**, 1383.
9. M. C. Chakravorti and C. K. Das, *J. Indian Chem. Soc.* 1978, **55**, 409.
10. Preliminary communication: G. A. Lawrance and D. F. Sangster, *J. Chem. Soc., Chem. Commun.* 1984, 1706.
11. H. A. Boucher, A. M. Sargeson, D. F. Sangster and J. C. Sullivan, *Inorg. Chem.* 1981, **20**, 379.
12. E. M. Fielden, In *The Study of Fast Processes and Transient Species by Electron Pulse Radiolysis* (Edited by J. H. Baxendale and F. Busi), p. 49. Reidel, Dordrecht (1982), pp. 49–62.
13. L. E. Orgel, *J. Chem. Phys.* 1955, **23**, 1004.
14. J. Hanuza, M. Baluka and B. Jesowska-Trzebiatowska, *Acta Phys. Pol. A* 1972, **42**, 537.
15. H. A. Boucher, G. A. Lawrance, P. A. Lay, A. M. Sargeson, A. M. Bond, D. F. Sangster and J. C. Sullivan, *J. Am. Chem. Soc.* 1983, **105**, 4652.
16. P. A. Lay, A. M. Sargeson, B. W. Skelton and A. H. White, *J. Am. Chem. Soc.* 1982, **104**, 6161.
17. G. A. Lawrance and D. F. Sangster, *Polyhedron* 1985, **4**, 1095.
18. W. D. Courrier, C. J. L. Lock and G. Turner, *Can. J. Chem.* 1972, **50**, 1797.
19. J. D. Brown, C. J. L. Lock and C. Wan, *Can. J. Chem.* 1973, **51**, 2073.
20. J. A. Jaecker, W. R. Robinson and R. A. Walton, *Inorg. Nucl. Chem. Lett.* 1974, **10**, 93.
21. T. W. Hambley, G. A. Lawrance, D. F. Sangster and C. B. Ward, *Inorg. Chim. Acta* 1985, **105**, L1.
22. M. Pavlova, N. Jordanov and N. Popova, *J. Inorg. Nucl. Chem.* 1974, **36**, 3845.

Polyhedron Vol. 5, No. 10, pp. 1559–1566, 1986
Printed in Great Britain

0277–5387/86 $3.00+.00
Pergamon Journals Ltd

THE DECOMPOSITION OF POTASSIUM BIS(CARBONATO)DIAMMINECOBALTATE(III) AND THE KINETICS OF THE BRIDGE CLEAVAGE REACTIONS OF A HYDROXY-BRIDGED DIMER IN AQUEOUS PERCHLORIC ACID*

XIAOHONG LING and KENNETH E. HYDE†

Department of Chemistry, State University of New York, College at Oswego, Oswego, NY 13126, U.S.A.

(*Received* 10 *September* 1985; *accepted after revision* 28 *January* 1986)

Abstract—The decomposition of the title complex in aqueous perchloric acid solution has been investigated. A rapid decarboxylation yields an unexpected product tentatively identified as a μ-hydroxo-dicobalt(III) complex by its cation exchange column and UV–vis spectral characteristics. A dimeric structure with two carbonate bridges is proposed for the title complex and it is suggested that each carbonate bridge uses only one oxygen atom for bridging. The di-μ-carbonato complex, similar to a monodentate carbonato complex, is suggested to decarboxylate with carbon–oxygen bond rupture, leaving the oxygen bridges intact. The product $[(NH_3)_2(H_2O)_2Co(OH)_2Co(H_2O)_2(NH_3)_2]^{4+}$ undergoes both water-induced and acid-catalyzed bridge cleavage reactions in two successive steps, ultimately forming *cis*-$[Co(NH_3)_2(H_2O)_4]^{3+}$ via a singly bridged intermediate. Under the experimental conditions $\{[H^+] = 0.1$–2.0 M; $I = 2.0$ M ($NaClO_4$), 40°C$\}$, the k_{obsd} for both steps shows the same form: $k_{fast} = (2.20 \pm 0.18) \times 10^{-4} + (3.70 \pm 0.15) \times 10^{-4}[H^+]$ and $k_{slow} = (2.90 \pm 1.02) \times 10^{-5} + (11.85 \pm 0.83) \times 10^{-5}[H^+]$. These results are compared with those for the acid-catalyzed bridge cleavage reactions of other μ-hydroxo complexes.

The current status of the work on carbonato metal complexes has been recently reviewed.[1] The kinetics and mechanisms for the decarboxylation of monodentate[1,2] and bidentate[1,3,4] monocarbonato complexes have been adequately investigated. Recent kinetic studies have dealt with the decarboxylation reactions of bis(carbonato) complexes[5–7] and complexes that contain a bridging carbonato[8] ligand.

It was the original objective of the present study to investigate in detail the kinetics of the acid-catalyzed decarboxylation reaction of another bidentate bis(carbonato)cobalt(III) complex *cis*-$K[Co(NH_3)_2(CO_3)_2]$. However, the first observable decarboxylation product has been found to be entirely different from those observed for the decarboxylation of the $[Co(py)_2(CO_3)_2]^-$ and $[Co(en)(CO_3)_2]^-$ ions. The unusual behavior of the ammine complex is that the decarboxylation reaction produces condensed complexes presumed to be hydroxy-bridged dimers. These undergo further decomposition in aqueous perchloric acid. As a result, we have turned our attention to the kinetic study of the acid-catalyzed bridge cleavage reaction of a μ-hydroxo-dicobalt(III) complex. Limited kinetic data have permitted us to obtain the experimental rate law for this reaction. The kinetic behavior of the ion investigated in this work has been compared with those of some other similar tri-, di- and monohydroxy-bridged cobalt(III) complexes and a possible mechanism is suggested.

EXPERIMENTAL

Synthesis of cis-$K[Co(NH_3)_2(CO_3)_2]$

The title complex was prepared by a method similar to that reported previously.[9–11] Since several modifications have been incorporated in our synthesis, it is reported in detail below.

Approximately 35 g of $KHCO_3$ was mixed with

* This article is based in part on the M.S. thesis of XL submitted to the State University of New York, College at Oswego (1985).

† Author to whom correspondence should be addressed.

30 cm^3 of water, and the resulting slurry was kept cool in an ice bath. Separately, 12 g of $CoCl_2 \cdot 6H_2O$ was dissolved in 10 cm^3 of hot water, and 27 cm^3 of cold 30% H_2O_2 was added to this solution after it had been cooled in an ice bath. The Co^{2+}–H_2O_2 solution was added dropwise, with constant stirring, to the cold $KHCO_3$ slurry. The resulting green solution was quickly filtered by suction and the filtrate, potassium tris(carbonato)cobaltate(III) solution, was kept at 0°C in an ice bath. To this cold green solution was added 6 g of ammonium carbonate and the mixture was warmed with stirring in a water bath at 45°C until the color of the solution changed from dark green to dark blue. This process took about 35 min. The vessel containing the warm solution was immediately dipped into an ice bath and kept at 0°C for 20 min. Addition of approximately 200 cm^3 of cold methanol to the cooled solution caused precipitation. The initial precipitate was removed by suction filtration and discarded. The filtrate stood for about 2 h at room temperature and additional precipitation occurred during this period. Filtration of this mixture gave the crude product. The crude product was dissolved in a minimum amount of water and was reprecipitated with pure methanol. Repeating this reprecipitation procedure yielded the final product.

The purity of the product was verified by the experimentally determined carbonate : cobalt(III) ratio of 2.02 : 1 and a good agreement between the obtained spectral parameters and the literature values (see Table 1). The result of chemical analysis for each element, with the exception of oxygen, was close to that calculated for $K[Co(NH_3)_2(CO_3)_2]$. (Found : Co, 23.2; C, 9.4 and 9.3; H, 2.5 and 2.6; N, 10.9; O, 26.5 and 23.9%. Calc. : Co, 23.4; C, 9.5; H, 2.4; N, 11.1; O, 38.1%.) We take this elemental analysis as additional evidence for the reasonable purity of the final product. The stoichiometry *cis*-$K[Co(NH_3)_2(CO_3)_2]$ is assigned to this compound.

Table 1. Spectral data for several cobalt(III) complexes

Complex	Medium	λ_{max} (ε_{max}) [nm (M^{-1} cm^{-1})]	λ_{min}(ε_{min}) [nm (M^{-1} cm^{-1})]	Reference
cis-$K[Co(NH_3)_2(CO_3)_2]$	1.0 M $KHCO_3$	579 394		10
	Distilled water	575 391		9
	1.0 M $KHCO_3$	578 (127) 393 (165)	474 (17) 355 (99)	This work
cis-$[Co(NH_3)_2(H_2O)_4]^{3+}$	$HClO_4$–$NaClO_4$	537 (42) 374 (42)		30
	1.0 M $HClO_4$	537 (48) 370 (46)	440 (9) 310 (7)	20
	1.0 M $HClO_4$	540 (41) 375 (40)		31
	1.5 M $HClO_4$	537 (44) 374 (42)	438 (8) 310 (9)	This work
"Condensed diammine species"	1.0 M $HClO_4$	540 310	452	18
$[(NH_3)_3(H_2O)Co(OH)_2Co(H_2O)(NH_3)_3]^{4+}$	1.0 M $HClO_4$	543 (170) 370 (170) 295 (2692)		32
$[(NH_3)_4Co(OH)_2Co(NH_3)_4]^{4+}$	$HClO_4$–$NaClO_4$	528 (187) 286 (2480)		21
$[(NH_3)_3Co(OH)_3Co(NH_3)_3]^{3+}$	Distilled water	526 (135) 364 (263) 296 (1778)		32
μ-Hydroxo dimer[a]	1.5 M $HClO_4$	542 (91) 315 (382)	442 (26) 285 (311)	This work

[a] The proposed decarboxylation product in this work. See the text for the stoichiometric assignment.

It indicates that there is no hydrate. The same complex has been reported to possess zero[9] or one[10] water of hydration.

Synthesis of cis-$[Co(NH_3)_2(H_2O)_4]^{3+}$

A small amount of *cis*-$K[Co(NH_3)_2(CO_3)_2]$ was dissolved in 1.5 M $HClO_4$. The resulting purple solution was kept at room temperature for 1 week. The *cis*-$[Co(NH_3)_2(H_2O)_4]^{3+}$ ion was purified by passing an acidic solution of this ion through a cold cation exchange column. The spectral parameters for *cis*-$[Co(NH_3)_2(H_2O)_4]^{3+}$ are reported in Table 1.

Cation exchange column procedures

A 1.5 × 3 cm column of Bio-Rad Dowex 50w-X2 cation exchange resin (200–400-mesh hydrogen form) with a cooling jacket 8 cm in length was employed for all the column chromatographic experiments. The column separation run started with prewashing the resin bed with at least two bed volumes of eluant and precooling the column to 0°C. All the exchange column experiments were performed at this temperature using 1.5 M $HClO_4$ as the eluant.

Analytical procedures

The cobalt concentration of a solution was determined spectrophotometrically using the procedure as described by Kitson.[12]

Carbon dioxide analysis was used in the determination of the stoichiometric carbonate content and in the estimate of the decarboxylation rate of the *cis*-$[Co(NH_3)_2(CO_3)_2]^-$ ion.

In the procedure for the investigation of decarboxylation rate, an amount (80–130 mg) of *cis*-$K[Co(NH_3)_2(CO_3)_2]$ was transferred to a dry flask previously thermostated to the desired temperature (0°C). This was followed by adding 20 cm^3 of 0°C 1.00 M $HClO_4$ [I = 2.0 M ($NaClO_4$)]. The start of the time measurement coincided with the addition of the acid. Dry nitrogen, free from carbon dioxide, passed through the reaction solution. The evolved carbon dioxide was carried by the nitrogen stream to the absorption system where it was absorbed by a standardized barium hydroxide solution. The absorption system was disconnected from the reaction system immediately after a selected time of 5 min. The excess barium hydroxide was titrated with standard hydrochloric acid to the phenolphthalein end point.[13]

By a slightly modified procedure, the bound carbonate content of the complex cations separated in the cation exchange column experiments was determined.

Kinetic measurements

The kinetic runs were followed by means of a CARY 14 spectrophotometer. Temperature control was maintained to within ±0.1°C by a thermostated circulating bath. A preliminary kinetic run was made at an acidity of 1.00 M [I = 2.0 M ($NaClO_4$)] and at 40°C by repeating the wavelength scan (from 600 to 280 nm) at certain time intervals. No isosbestic point was found.

Most kinetic data was obtained by recording the change in absorbance of the reaction solution at 315 nm as a function of time. To begin a run, a weighed sample (about 10 mg) of *cis*-$K[Co(NH_3)_2(CO_3)_2]$ was quickly dissolved in 20.0 cm^3 of $HClO_4$–$NaClO_4$ solution with appropriate acidity and at the temperature of the run. The resulting purple solution was immediately transferred to a cell contained in the thermostated cell compartment. In all kinetic runs, the reaction solution was monitored until the absorbance at 315 nm had decreased to a value below an A_∞ calculated from the known cobalt(III) concentration and the experimentally determined molar absorptivity of the product *cis*-$[Co(NH_3)_2(H_2O)_4]^{3+}$ (ε = 9.0 M^{-1} cm^{-1}).

RESULTS

The carbon dioxide analysis performed during the acid-catalyzed decomposition of the ammine–carbonato complex has shown conclusively that the loss of two carbon dioxides from each cobalt(III) center is complete in less than 5 min at 0°C and at an $[H^+]$ of 1.0 M. It is is assumed that the time span of 5 min corresponds to at least five half-lives, then an appropriate estimate of the pseudo-first-order rate constant would be 1×10^{-2} s^{-1}. This sets the lower limit for the decarboxylation rate constant at 0°C. This result is not unexpected. It has indicated that, under the experimental conditions of this work, the decarboxylation rate is too fast to be studied in detail by our techniques.

When *cis*-$K[Co(NH_3)_2(CO_3)_2]$ was dissolved in ~5 cm^3 of cold 1.5 M $HClO_4$ (0°C) and the resulting purple solution was immediately charged on the cold column, two bands appeared. A period of about 45 min was needed for removal of the first band from the column. Based on these experimental conditions and the observation that the loss of both carbonates from *cis*-$[Co(NH_3)_2(CO_3)_2]^-$ in 1.0 M $HClO_4$ is complete in less than 5 min at 0°C, we conclude that the species separated by our cold

column must not be a carbonato complex. In the spectrum of the very early portion of the band (leading 14 cm^3), there is a very strong absorbance peak at 315 nm. This peak around 300 nm has been proposed[14] to be indicative of the existence of hydroxy-bridged cobalt(III) dimers. The latter portions of the same band indicate the presence of a peak around 370 nm and a decrease in absorbance at 315 nm. This column experiment was repeated several times and the results were reproducible. They invariably indicated that the later the band portion was collected, the more evident was the peak at 370 nm and the less evident was the peak at 315 nm. This observation suggests poor separation and/or slight decomposition of the initial decarboxylation product during the cold column separation.

Compared with the column characteristics of the standard cations $[Co(NH_3)_4(H_2O)_2]^{3+}$, $[Co(NH_3)_5Cl]^{2+}$ and $[Co(NH_3)_4(NO_2)_2]^{+}$ the species contained in the first band appear to behave as 3+ charged cations. However, the components in this band need not have identical charges. It is not unreasonable for us to deduce that less eluant volume is required to elute a dimer (larger molecular size) than that needed for a same charged monomer (smaller size). It is therefore probable that a mixture of some hydroxy-bridged dimers with 3+ and/or higher charges are components of this first band.

The 620-cm^3 volume of eluant failed to elute the very small second band. No further attempts were made to obtain detailed information about the column and spectral characteristics of this very sluggish band which probably contains polymers with charges higher than 4+.

When the purple solution that resulted from dissolving *cis*-$K[Co(NH_3)_2(CO_3)_2]$ in ~ 5 cm^3 of 1.5 M $HClO_4$ was incubated for 1 week at room temperature, cold column separation showed only one band. This band behaved as a 3+ charged monomer. The leading, middle and trailing portions of this band exhibited nearly identical visible spectra and these spectra are in good agreement with that reported for *cis*-$[Co(NH_3)_2(H_2O)_4]^{3+}$.

Table 1 summarizes the spectral parameters in UV–vis range for the cobalt(III) complexes characterized in this work. The values previously published for some other similar cobalt(III) complexes are also listed in the same table for convenient comparison. Although caution has been used to minimize further decomposition of the initial decarboxylation product, the absorbance of the 315-nm peak still proved to be unreproducible. Therefore, the extinction coefficients reported in Table 1 for the proposed decarboxylation product (μ-hydroxo dimer) only can be assumed to be estimates.

In an extended kinetic run on the total decomposition of *cis*-$[Co(NH_3)_2(CO_3)_2]^{-}$, the observed A_∞ at 315 nm was smaller than the A_∞ calculated for the *cis*-$[Co(NH_3)_2(H_2O)_4]^{3+}$ ion ($\varepsilon = 9.0$ M^{-1} cm^{-1}), the expected final cobalt(III) product of the acid-catalyzed hydrolysis reaction. This observation suggests additional decomposition of *cis*-$[Co(NH_3)_2(H_2O)_4]^{3+}$. This further reaction is attributed to the slow reduction of the *cis*-$[Co(NH_3)_2(H_2O)_4]^{3+}$ ion to Co^{2+} species.

In the data treatment for a typical kinetic run, the calculated A_∞ was used and the plot of $\log(A_t - A_\infty)$ vs time showed a curvature at the beginning corresponding to an induction period, after which the plot became linear. These features suggest that the decomposition of the initial decarboxylation product occurs in two or more successive steps and that the relative rates of the slowest two steps (hereafter called fast step and slow step) are such that each step can be studied separately.

The pseudo-first-order rate constants for the slow step were obtained from the slopes of the later portions (linear for at least two half-lives) of the plots of $\log(A_t - A_\infty)$ vs time. An alternative method also was used to calculate the observed rate constants. This method involved a nonlinear least-squares computer fit of the absorbance–time data to the equation $A_t = (A_0 - A_\infty)e^{-kt} + A_\infty$. Both methods gave identical values within experimental uncertainty of the observed rate constants for the slow step. These values are shown as k_{slow} in Table 2. The A_∞ evaluated by the computer program agreed with the calculated A_∞ used in the conventional plot method to within 1.3%.

The observed rate constants that correspond to the fast step were extracted from the data as follows. The linear portions of the $\log(A_t - A_\infty)$ vs time plots

Table 2. Pseudo-first-order rate constants for the bridge cleavage reactions of $[(NH_3)_2(H_2O)_2Co(OH)_2Co(H_2O)_2(NH_3)_2]^{4+}$ in aqueous perchloric acid solutions at 40°C [$I = 2.0$ M ($NaClO_4$)]

$[H^+]$ (M)	k_{fast} (s^{-1})	k_{slow} (s^{-1})
0.1001	2.32×10^{-4}	5.29×10^{-5}
0.4010	3.90×10^{-4}	7.27×10^{-5}
1.002	5.94×10^{-4}	1.32×10^{-4}
1.507	7.94×10^{-4}	2.05×10^{-4}
2.006	9.45×10^{-4}	2.76×10^{-4}

$k_{fast} = k_a + k_b[H^+]$: $k_a = (2.20 \pm 0.18) \times 10^{-4}$
$k_b = (3.70 \pm 0.15) \times 10^{-4}$
$k_{slow} = k_c + k_d[H^+]$: $k_c = (2.90 \pm 1.02) \times 10^{-5}$
$k_d = (11.85 \pm 0.83) \times 10^{-5}$

were back extrapolated. The differences between the original values of $A_t - A_\infty$ and the back extrapolated values were plotted vs time in a semilogarithmic manner. These plots were linear for at least four half-lives and the corresponding slopes[15] gave the pseudo-first-order rate constants for the fast step (shown as k_{fast} in Table 2).

It is seen from Table 2 that, in the range of hydrogen ion concentration investigated, the observed rate constants for both steps show a simple first-order dependence on hydrogen ion concentration of the following forms:

$$k_{fast} = k_a + k_b[H^+], \quad (1)$$

$$k_{slow} = k_c + k_d[H^+]. \quad (2)$$

The values of k_a, k_b, k_c and k_d were evaluated by using a least-square computer program and are given in Table 2.

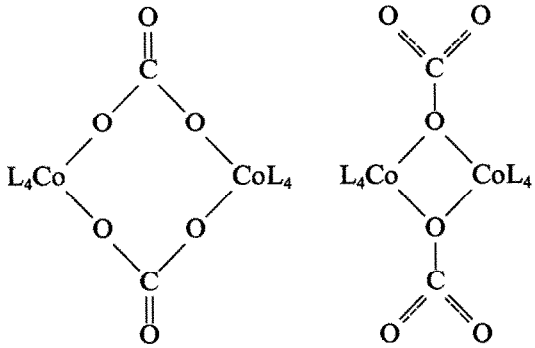
DISCUSSION

Our exchange column experiments have suggested a binuclear species, the μ-hydroxo-dicobalt(III) cation, as the first observable decarboxylation product of *cis*-$[Co(NH_3)_2(CO_3)_2]^-$. This behavior is in marked contrast to that of the $[Co(py)_2(CO_3)_2]^-$ and $[Co(en)(CO_3)_2]^-$ ions,[6,7] both of which give the corresponding monomeric tetraquo cobalt(III) complexes as the initial decarboxylation products. Now we concern ourselves with some possibilities for the structure of the reactant carbonato complex and the stoichiometry of the decarboxylation reaction that produces the hydroxy-bridged dimer.

One possibility is that the hydroxy-bridged dimer is produced from the acid-catalyzed decarboxylation reaction of a monomeric reactant, *cis*-$[Co(NH_3)_2(CO_3)_2]^-$. For the convenience of discussion, we have assumed this monomeric bis(carbonato)diamminecobaltate(III) ion earlier in this report. However, this proposal of a monomeric bidentate carbonato complex reactant may be refuted. The monomeric diaquo complex is always the observed decarboxylation product during the decomposition of a bidentate carbonato-cobalt(III) complex in acidic solution. Moreover, no precedent has been found for the formation of μ-hydroxo dimers from the corresponding monomeric aquo complexes in strongly acidic medium.

Another possibility is that the reactant carbonato complex is, itself, dimeric. Both monomeric and dimeric cobalt(III) complexes have been proposed to exist under the conditions usually used for the preparation of bis(carbonato) complexes[16] and it has been noted that acidification of these complexes yields hydroxy-bridged species.[17–20] These findings encourage us to propose a dimeric reactant with two carbonate bridges. However, there are two different binding modes for the carbonate bridges and hence two quite different structures for the dimeric reactant. One (structure **I**) may be thought to contain two triatomic bridging carbonate groups in a form that is somewhat analogous to that found in a bidentate carbonato complex. The other (structure **II**) contains carbonate groups with monoatomic oxygen bridges. These bridging carbonate groups may be viewed as being analogous to those found in a monodentate carbonato complex.

Previous work[8] on some μ-carbonato complexes in which the carbonate bridging is as shown in dimer **I** has indicated that the dimer possesses the same decarboxylation kinetic behavior as that of a bidentate carbonato complex.

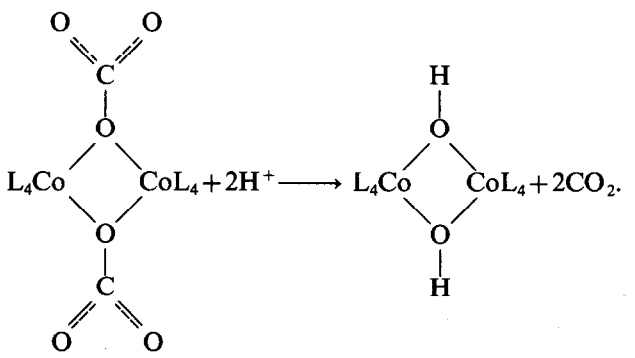


I **II**

Assuming that this conclusion is applicable in the present work, dimer **I** is not expected to behave differently from the monomeric carbonato complex in its acid-catalyzed decarboxylation reaction. Both carbonato bridges would decarboxylate with metal–oxygen bond breaking and a monomeric aquo product is to be expected.

To explain the formation of the binuclear μ-hydroxo product, dimer **II** seems to be a proper candidate. Although there has been no report of a cobalt(III) complex in which a single oxygen of a carbonate group bridges a pair of adjacent cobalt atoms, such a structure has been reported for several other metal ions.[1] It is also interesting to note that the μ-carbonatobis(pentaammine)cobalt(III) ion exhibits decarboxylation kinetics[21] similar to that observed for the monodentate $[Co(NH_3)_5CO_3]^+$ ion. The authors suggest the triatomic carbonate bridge (dimer **I**) for the complex of unknown structure. We suggest that the observed kinetic behavior of this complex is consistent with that expected for a monatomic carbonate oxygen bridge (dimer **II**). The following scheme [eqn (3)] is consistent with the decarboxylation mechanism of monodentate carbonato complexes and provides a

pathway which only involves oxygen–carbon bond breakage for the acid-catalyzed formation of the di-μ-hydroxo dimer:



$$L_4Co(O_2CO)CoL_4 + 2H^+ \longrightarrow L_4Co(OH)CoL_4 + 2CO_2. \quad (3)$$

The total reaction stoichiometry for the acid-catalyzed decarboxylation may be represented by eqn (4):

$$[(NH_3)_2(CO_3)Co(CO_3)_2Co(CO_3)(NH_3)_2]^{2-} + 6H^+ + 2H_2O \rightarrow [(NH_3)_2(H_2O)_2Co(OH)_2Co(H_2O)_2(NH_3)_2]^{4+} + 4CO_2. \quad (4)$$

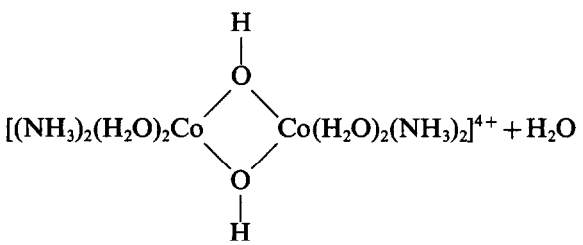
Our kinetic data obtained at 40°C are consistent with the hydrolysis of a hydroxy-bridged dimer formed as the initial decarboxylation product. The data suggests that the acid-catalyzed bridge cleavage reaction of $[(NH_3)_2(H_2O)_2Co(OH)_2Co(H_2O)_2(NH_3)_2]^{4+}$ takes place in two successive steps of the form:

$$\text{dimer} \xrightarrow{k_1} \text{intermediate} \xrightarrow{k_2} \text{monomer}. \quad (5)$$

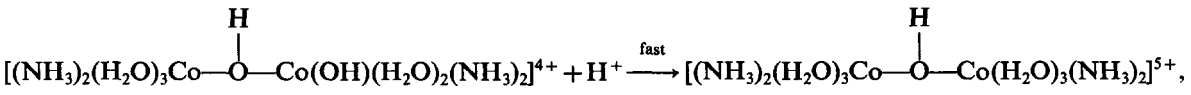
The relative rates of these two steps are such that each step can be treated separately. This type of stepwise bridge cleavage of di-μ-hydroxo complexes has been observed previously for the cationic species $N_4Co(OH)_2CoN_4]^{4+}$ (N ≡ NH_3[22] or $\frac{1}{2}$en[23,24]) and the anionic $[(NTA)Co(OH)_2Co(NTA)]^{2-}$ ion (NTA ≡ $[N(CH_2COO)_3]^{3-}$).[25] It has been suggested that simultaneous fission of two hydroxo bridges is improbable[23] and that the corresponding diaquo mono-μ-hydroxo dimeric species acts as an intermediate in the course of the complete cleavage reaction.[22–26] For the reaction of the $[(en)_2Co(OH)_2Co(en)_2]^{4+}$ ion, the existence of a short-lived singly bridged intermediate has been kinetically identified,[23] while the $[(NTA)(H_2O)Co(OH)Co(H_2O)(NTA)]^-$ ion produced as the intermediate during the bridge cleavage of the di-μ-hydroxo complex has been spectrally characterized.[25] In both cases, the singly bridged intermediates have been proven to exist in an appreciable concentration and the two consecutive cleavage steps can be treated separately.

In the present study, it is assumed that a similar situation exists for the $[(NH_3)_2(H_2O)_2Co(OH)_2Co(H_2O)_2(NH_3)_2]^{4+}$ ion where the mono-μ-hydroxo intermediate, $[(NH_3)_2(H_2O)_3Co(OH)Co(H_2O)_3(NH_3)_2]^{5+}$, is formed in an appreciable concentration as the product of the first hydroxo bridge fission. The similar mono-μ-hydroxo complex ion[27] $[(NH_3)_5Co(OH)Co(NH_3)_5]^{5+}$ undergoes an acid-catalyzed bridge cleavage reaction with a kinetic form[28] ($k_{obsd} = k_a + k_b[H^+]$) similar to that obtained in this work.

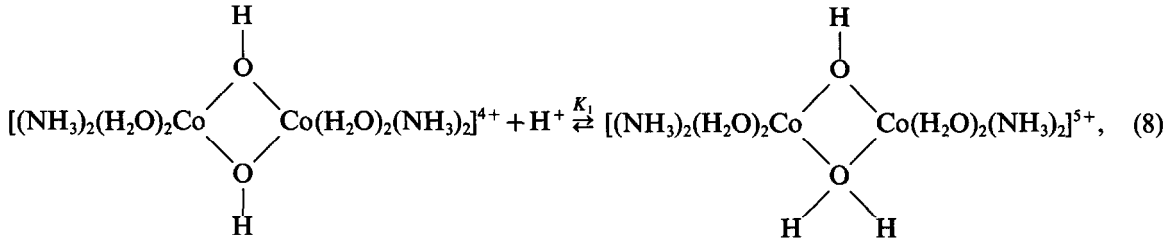
On the assumption that the singly bridged intermediate is produced in an appreciable concentration during the acid-catalyzed cleavage reactions of the di-μ-hydroxo complex, we suggest the following mechanism which is similar to that proposed by Harris and Meloon:[25]



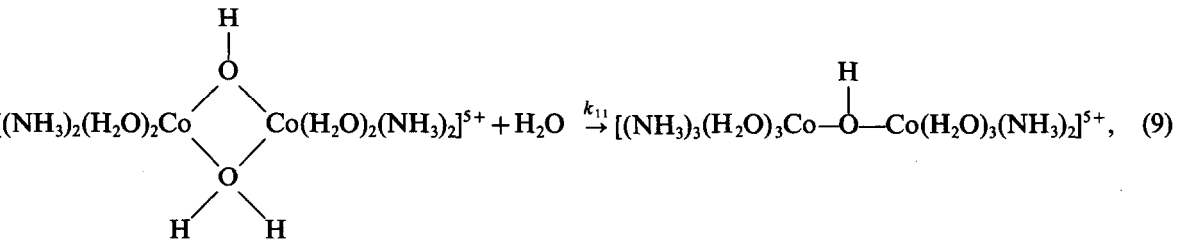
$$\xrightarrow{k_{10}} [(NH_3)_2(H_2O)_3Co{-}O{-}Co(OH)(H_2O)_2(NH_3)_2]^{4+}, \quad (6)$$



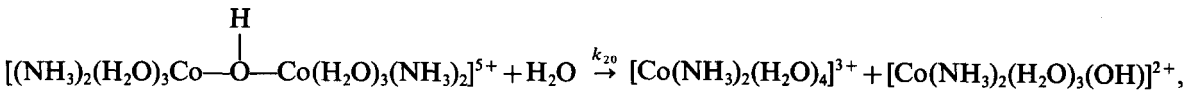
(7)



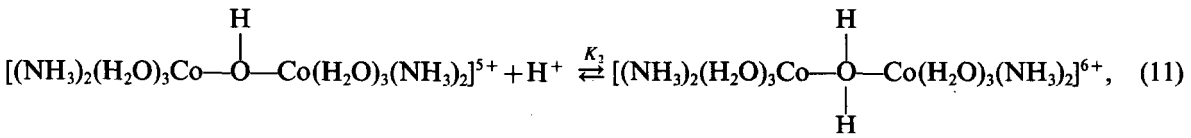
(8)



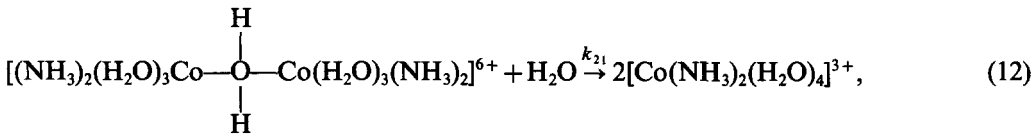
(9)



(10)



(11)



(12)



(13)

This mechanism leads to the simplified form of the observed rate constants:

$$k_1 = k_{10} + k_{11}K_1[H^+], \quad (14)$$

$$k_2 = k_{20} + k_{21}K_2[H^+]. \quad (15)$$

These have the same hydrogen ion concentration dependence as our experimental forms [eqns (1) and (2)].

By comparison of our simple first-order rate laws with the more complicated one generalized by Harris and Meloon[25] for the acid-catalyzed cleavage reactions of μ-hydroxo complexes:

$$k_{obsd} = (k_0 + k_1K_1[H^+ + k_2K_1[H^+]^2)/(1 + K_1[H^+]), \quad (16)$$

we can see the following kinetic features exhibited by the cleavage reactions of $[(NH_3)_2(H_2O)_2Co(OH)_2Co(H_2O)_2(NH_3)_2]^{4+}$ and $[(NH_3)_2(H_2O)_3Co(OH)Co(H_2O)_3(NH_3)_2]^{5+}$ in strong aqueous perchloric acid solution.

(a) For both the $[(NH_3)_2(H_2O)_2Co(OH)_2Co(H_2O)_2(NH_3)_2]^{4+}$ and the $[(NH_3)_2(H_2O)_3Co(OH)Co(H_2O)_3(NH_3)_2]^{5+}$ complex ions, the water-assisted paths symbolized by k_{10} and k_{20} [eqns (6) and (10)] play a significant role in the bridge cleavage reactions.

(b) The protonations of the highly charged cationic di-μ-hydroxo reactant and mono-μ-hydroxo intermediate are not very effective ($K_1[H^+] \ll 1$ and $K_2[H^+] \ll 1$). The same situation also exists for

the $[(NH_3)_3(H_2O)Co(OH)_2Co(H_2O)(NH_3)_3]^{4+}$ and $[(NH_3)_5Co(OH)Co(NH_3)_5]^{5+}$ ions.[28,29]

(c) In the rate-determining bridge cleavage steps, both protonated dimers (doubly bridged and singly bridged) undergo bridge fissions dominantly by the water-assisted paths represented by k_{11} and k_{21} [eqns (9) and (12)]. No contribution from the acid-catalyzed path represented by the $k_2K_1[H^+]^2$ term in eqn (16) is detected in the present cases.

The magnitudes of the rate constants obtained for the two successive bridge cleavage steps are such that one is slightly larger than the other. Moreover, both of the rate constants exhibit the same hydrogen ion concentration dependence. As a result, the assignment of the observed rate constants (k_{fast} and k_{slow}) to the individual cleavage steps [k_1 and k_2 in eqn (5)] is not obvious. However, there are two points noted by previous study[29] that can provide some basis for the rate constant assignment. Firstly, the cleavage rate of a singly bridged complex is comparable to or slightly faster than that of a doubly bridged complex. Secondly, in the cleavage reactions of singly bridged complexes, the water-assisted path usually makes a more significant contribution than that path makes in the cleavage reactions of multiply bridged complexes. This observation has been ascribed to the presence of additional bridge(s) that may help to retain the binuclear structure. Thus stretching of the metal–hydroxo bond is less likely to lead to bridge fission.

On inspection of the magnitudes of the rate constants for the water-induced and acid-catalyzed reactions, we should assign k_{slow} to the first bridge cleavage reaction of the di-μ-hydroxo reactant [k_1 in eqns (5) and (14), $k_{10}/k_{11}K_1 \simeq 0.255$] and k_{fast} to the bridge cleavage reaction of the mono-μ-hydroxo intermediate [k_2 in eqns (5) and (15), $k_{20}/k_{21}K_2 \simeq 0.60$]. In spite of these arguments, we must acknowledge the possibility that k_{fast} may correspond to the cleavage of the di-μ-hydroxo reactant and k_{slow} to the cleavage of the mono-μ-hydroxo intermediate. Usually the fast and slow reactions do conform to the first and second stages of a consecutive reaction sequence.

REFERENCES

1. D. A. Palmer and R. van Eldik, *Chem. Rev.* 1983, **83**, 651.
2. U. Spitzer, R. van Eldik and H. Kelm, *Inorg. Chem.* 1982, **21**, 2821.
3. G. M. Harris and K. E. Hyde, *Inorg. Chem.* 1978, **17**, 1892.
4. R. van Eldik and G. M. Harris, *Inorg. Chim. Acta* 1983, **70**, 147.
5. K. E. Hyde, E. W. Hyde, J. Moryl, R. Baltus and G. M. Harris, *Inorg. Chem.* 1980, **19**, 1603.
6. J. F. Glenister, K. E. Hyde and G. Davies, *Inorg. Chem.* 1982, **21**, 2331.
7. P. M. Coddington and K. E. Hyde, *Inorg. Chem.* 1983, **22**, 2211.
8. K. Wieghardt, W. Schmidt, R. van Eldik, B. Nuber and J. Weiss, *Inorg. Chem.* 1980, **19**, 2922.
9. M. Mori, M. Shibata, E. Kyuno and T. Adachi, *Bull. Chem. Soc. Jpn* 1956, **29**, 883.
10. O. Hyodo and R. D. Archer, *Inorg. Chem.* 1969, **8**, 2510.
11. M. Shibata, *Proc. Jpn Acad.* 1974, **50**, 779.
12. R. E. Kitson, *Analyt. Chem.* 1950, **22**, 664.
13. A. I. Vogel, *A Text-book of Quantitative Inorganic Analysis Including Elementary Instrumental Analysis*, pp. 246 and 249. John Wiley, New York (1961).
14. G. Schwarzenbach, J. Boesch and H. Egli, *J. Inorg. Nucl. Chem.* 1971, **33**, 2141.
15. R. G. Wilkins, *The Study of Kinetics and Mechanism of Reactions of Transition Metal Complexes*, p. 23. Allyn & Bacon, Boston (1974).
16. G. Davies and Y. Hung, *Inorg. Chem.* 1976, **15**, 704.
17. J. D. White and H. Taube, *J. Phys. Chem.* 1970, **74**, 4142.
18. J. D. White, Ph.D. thesis, Stanford University (1970).
19. I. Bodek, Ph.D. thesis, Northeastern University (1977).
20. I. Bodek, G. Davies and J. H. Ferguson, *Inorg. Chem.* 1975, **14**, 1708.
21. K. Koshy and T. P. Dasgupta, *Inorg. Chim. Acta* 1982, **61**, 207.
22. A. B. Hoffman and H. Taube, *Inorg. Chem.* 1968, **7**, 903.
23. A. A. El-Awady and Z. Z. Hugus, Jr, *Inorg. Chem.* 1971, **10**, 1415.
24. M. M. DeMaine and J. B. Hunt, *Inorg. Chem.* 1971, **10**, 2106.
25. D. R. Meloon and G. M. Harris, *Inorg. Chem.* 1977, **16**, 434.
26. J. D. Ellis, K. L. Scott, R. K. Wharton and A. G. Sykes, *Inorg. Chem.* 1972, **11**, 2565.
27. H. Siebert and H. Feuerhake, *Chem. Ber.* 1969, **102**, 2951.
28. W. Jentsch, W. Schmidt, A. G. Sykes and K. Wieghardt, *Inorg. Chem.* 1977, **16**, 1935.
29. R. K. Wharton and A. G. Sykes, *J. Chem. Soc., Dalton Trans.* 1973, 439.
30. W. D. Stanley, T. Davies, T. D. Tullius and C. S. Garner, *J. Inorg. Nucl. Chem.* 1973, **35**, 3857.
31. J. D. White, J. C. Sullivan and H. Taube, *J. Am. Chem. Soc.* 1970, **92**, 4733.
32. V. M. Linhard and H. Siebert, *Z. Anorg. Allg. Chem.* 1969, **364**, 24.

Polyhedron Vol. 5, No. 10, pp. 1567–1571, 1986
Printed in Great Britain

0277–5387/86 $3.00+.00
Pergamon Journals Ltd

NMR CHEMICAL SHIFT STUDIES OF ION ASSOCIATION IN ALUMINUM HALIDE–ORGANIC HALIDE MELTS

JOHN S. WILKES*

The Frank J. Seiler Research Laboratory, The United States Air Force Academy, Colorado Springs, CO 80840, U.S.A.

and

CHARLES L. HUSSEY and JOHN R. SANDERS

Department of Chemistry, The University of Mississippi, University, MS 38677, U.S.A.

(*Received* 14 *February* 1985; *accepted after revision* 28 *January* 1986)

Abstract—The anion–cation interactions that take place in several room-temperature haloaluminate molten salts were investigated by using NMR spectroscopy. The systems studied were $AlCl_3$–1-(1-butyl)pyridinium chloride, $AlCl_3$–1-methyl-3-ethylimidazolium chloride and $AlBr_3$–1-methyl-3-ethylimidazolium bromide. The ion–ion associations in these systems were examined by studying the ^1H and ^{13}C chemical shifts of the nuclei on the organic cations as a function of melt composition. Investigations conducted in basic melts, i.e. those melts with an aluminium halide mole fraction less than 0.5 and where the anion–cation interactions have been found to be most extensive, suggested that, in contrast to previous work, ion–ion interactions in these solvents involve more than just simple ion-pair formation. A model is proposed which considers that each cation may interact with two or more anions and vice versa to form oligomeric chains of alternating cations and anions. The latter model is shown to provide a more realistic interpretation of the experimental chemical shift data than a model based on simple ion-pair formation.

Mixtures of certain organic halide salts and $AlCl_3$ or $AlBr_3$ are liquid at room temperature. These ionic liquids have been used as electrolytes for electrochemical cells and as solvents for a variety of fundamental studies employing inorganic and organic solutes.[1–3] Raman spectroscopy[4] and ^{27}Al NMR spectroscopy[5,6] indicate that the melts consist of an organic cation and one or two anions (AlX_4^- and X^- or $Al_2X_7^-$), depending on the melt composition, i.e. the relative proportion of organic halide salt to aluminum halide. Structure imparted to these ionic liquids by associations between the organic cation and the anions may play an important role in transport processes[7] and the physical properties of the melts.[8]

In previous papers we showed that ^1H and ^{13}C NMR spectroscopy could be used to detect ion–ion interactions in the 1-methyl-3-ethylimidazolium chloride–$AlCl_3$ melt (MeEtImCl–$AlCl_3$).[6,9,10] Taulelle and Popov conducted similar studies in 1-(1-butyl)pyridinium chloride–$AlCl_3$ (BuPyCl–$AlCl_3$).[11] It was concluded from these investigations that changes in the chemical shifts of nuclei on the organic cations were best explained by extensive, probably complete, anion–cation associations.

Taulelle and Popov[11] observed a linear dependence of chemical shifts with changes in the apparent $AlCl_3$ mole fraction (N) over a small range of composition in basic melt. The greatest changes in chemical shifts with composition of the melt are observed in basic melts, i.e. compositions where the organic halide salt is in excess over the aluminum halide.[6,9–11] Therefore, only basic melts were considered here since the effects of interest are more pronounced in these than in acidic melts. In the present study we examined the ^1H and ^{13}C chemical

* Author to whom correspondence should be addressed.

shifts for the BuPyCl–$AlCl_3$, MeEtImCl–$AlCl_3$, and MeEtImBr–$AlBr_3$ melts over the entire basic composition range ($0 < N < 0.50$). In contrast to the results of Taulelle and Popov,[11] these measurements have indicated a decided non-linear dependence of chemical shifts on N in all of the systems that were examined. The impact of these observations on the formulation of models used to represent anion–cation interactions in room-temperature haloaluminate melts is described. This work also extends our earlier results in the MeEtImCl–$AlCl_3$ system[10] in which proton chemical shifts were reported over the limited composition range $0.33 < N < 0.50$.

EXPERIMENTAL

Reagents

BuPyCl,[12] MeEtImCl[13] and $AlCl_3$[14] were prepared and purified as previously described. MeEtImBr was synthesized by combining equal amounts of 1-methylimidazole and ethyl bromide in a flask fitted with a drying tube and allowing the mixture to react slowly. When the reaction was complete, the resulting salt was purified by the same procedure used to purify the chloride analog. $AlBr_3$ (Fluka, puriss grade) was sublimed *in vacuo* a minimum of 3 times before use. The melts were prepared by weighing and mixing the components in argon or nitrogen filled dry boxes.

NMR measurements

NMR spectra were obtained on a JEOL FX90Q spectrometer in 5-mm diameter tubes. Chemical shifts were externally referenced to dimethyl sulfoxide in a concentric capillary. In order to ensure that all samples remained liquid throughout the entire range of compositions that were studied the chloride melts were run at 150°C, and the bromide melts were run at 120°C. All spectra were qualitatively similar to those reported previously.[6,10,11]

RESULTS AND DISCUSSION

The variation in chemical shifts with N reported in previous studies[6,9–11] were explained by assuming that the organic cation was in fast exchange between more than one environment. Thus, the chemical shifts could be described by a population-weighted average:

$$\delta_{obs} = \sum_{i=1}^{n} \delta_i X_i \qquad (1)$$

where δ_i and X_i are the chemical shifts and mole fractions of the cations in the ith environment, respectively. Taulelle and Popov[11] attempted to explain this effect in the BuPyCl–$AlCl_3$ melt by considering two environments which resulted from ion-pair interactions between the $BuPy^+$ cation and the two different anions present in the basic melt (Cl^- and $AlCl_4^-$). In this case eqn (1) becomes:

$$\delta_{obs} = \delta_1 Y_1 + \delta_4 Y_4, \qquad (2)$$

where Y_1 and Y_4 are the anion fractions of Cl^- and $AlCl_4^-$ which may be calculated from the equations:

$$Y_1 = \frac{1-2N}{1-N}.$$

$$Y_4 = \frac{N}{1-N}.$$

Taulelle and Popov[11] state that Y_1 and Y_4 are essentially linear functions of N, which explains why they obtained linear chemical shifts as a function of N. However, eqn (2) is approximately linear for only small ranges of N. Figure 1 shows that Y_1 and Y_4 are both non-linear with N when the entire basic composition range is considered. The chemical-shift data for the $BuPy^+$ cations reported in Ref. 11 were taken over a range of N too small to permit detection of deviations from linearity.

Wilkes and coworkers[6,10] considered two associations for each anion and cation in the MeEtImCl–$AlCl_3$ melt which results in three environments for the $MeEtIm^+$ cation. In this case eqn (1) becomes:

$$\delta_{obs} = \delta_2 Y_1^2 + \delta_5 2 Y_1 Y_4 + \delta_8 Y_4^2. \qquad (3)$$

The subscripts associated with each δ denote the magnetic environment for the cation containing the nucleus under observations (*vide infra*).

The chemical shift behavior of the nuclei at the 2,6- and 4-positions on the $BuPy^+$ cation and the 2-position on the $MeEtIm^+$ cation in chloroaluminate

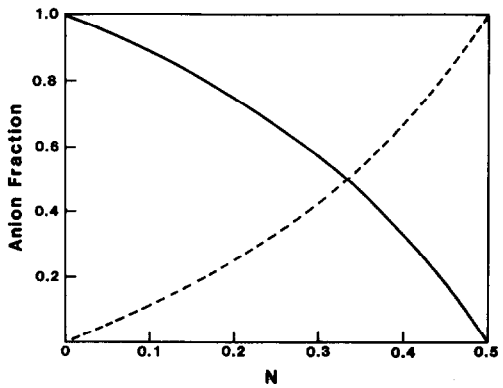


Fig. 1. Anion fractions of Cl^- (——) and $AlCl_4^-$ (– – – –) as a function of $AlCl_3$ mole fraction (N) calculated from the melt stoichiometry.

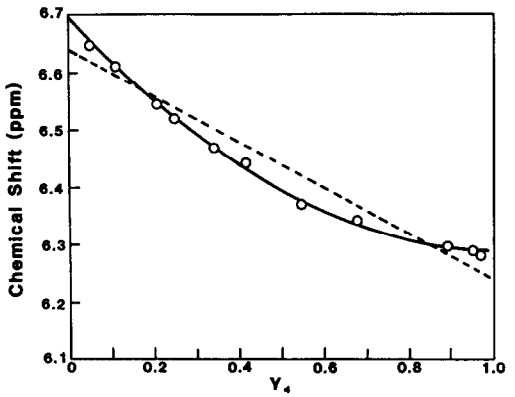


Fig. 2. Chemical-shift dependence on melt composition for ^1H at ring position 4 in BuPyCl–$AlCl_3$ binary melts. Lines are predicted according to eqn (4) (----) and eqn (5) (——). Y_4 is the anion fraction of $AlCl_4^-$.

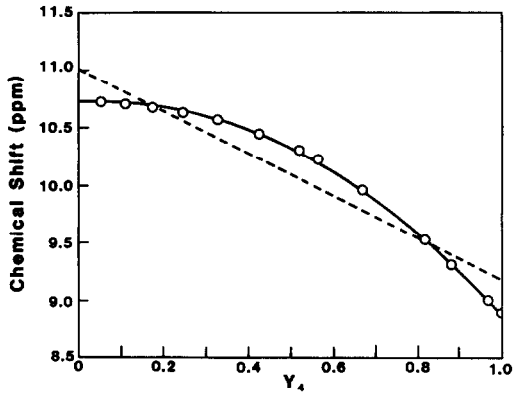


Fig. 4. Chemical-shift dependence on melt composition for ^1H at ring position 2 in MeEtImCl–$AlCl_3$ binary melts. Lines are predicted according to eqn (4) (----) and eqn (5) (——). Y_4 is the anion fraction of $AlCl_4^-$.

and bromoaluminate melts as a function of N are shown in Figs 2–7. In the past such data have been plotted with N as the abscissa. However, it is more advantageous to plot such data against the ion fraction of $AlCl_4^-$ as the abscissa. With this treatment eqn (2) becomes linear in Y_4:

$$\delta_{obs} = \delta_1 + (\delta_4 - \delta_1)Y_4, \quad (4)$$

while eqn (3) becomes quadratic in Y_4:

$$\delta_{obs} = \delta_2 + (2\delta_5 - 2\delta_2)Y_4 + (\delta_8 - \delta_5 + \delta_2)Y_4^2. \quad (5)$$

It should be noted that it is much easier to compare a linear equation like eqn (4) with a quadratic function like eqns (5) than to compare two non-linear, non-polynomial functions like eqns (2) and (3).

The chemical-shift data for the nuclei in Figs 2–7 are not linear in Y_4; thus, one can predict with relative certainty that eqn (4) will be inadequate for representing data that is obtained over a large composition range. In order to test this supposition statistically the data in Figs 2–7 were fitted to eqns (4) and (5). Two coefficients were adjustable in each equation. The parameter δ_2 in eqn (5) was calculated from the experimental chemical-shift data for the $N = 0$ composition, i.e. pure molten organic halide salt. The quality of the fits to eqns (4) and (5) was examined quantitively by calculating the Hamilton R-factors for each of the fits. The R-factor test is an accepted statistical method for comparing the quality of fits to different non-linear relationships and provides quantitive criteria that can be used to reject one model in favor of another.[15] One model may be selected over another at a specified confidence level by testing the ratio of R-factors against values appearing in statistical tables (see the appendix of Ref. 15). If the experimental value of the R-factor ratio exceeds the value listed in the statistical table, then it is possible to choose one model over the other. Table 1 compares the fits of the δ_{obs} data from Figs 2–7 to eqns (4) and (5). The

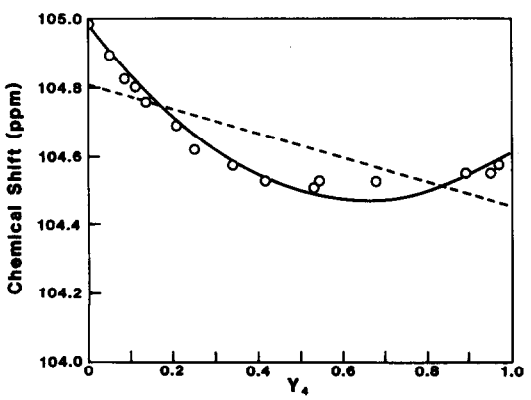


Fig. 3. Chemical-shift dependence on melt composition for ^{13}C at ring position 2,6 in BuPyCl–$AlCl_3$ binary melts. Lines are predicted according to eqn (4) (----) and eqn (5) (——). Y_4 is the anion fraction of $AlCl_4^-$.

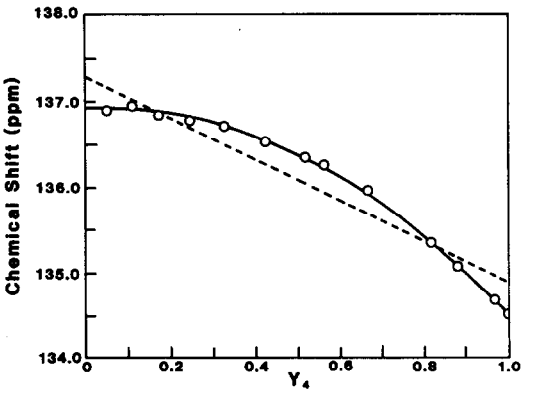


Fig. 5. Chemical-shift dependence on melt composition for ^{13}C at ring position 2 in MeEtImCl–$AlCl_3$ binary melts. Lines are predicted according to eqn (4) (----) and eqn (5) (——). Y_4 is the anion fraction at $AlCl_4^-$.

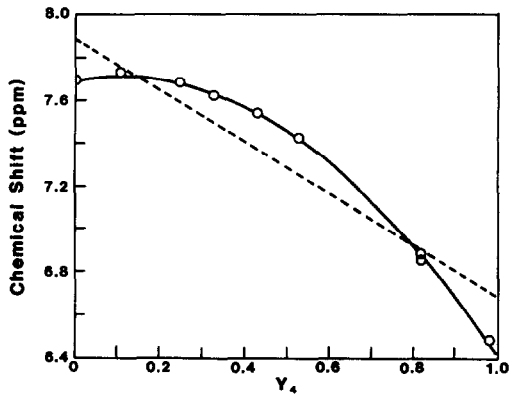


Fig. 6. Chemical-shift dependence on melt composition for ^1H at ring position 2 in MeEtImBr–$AlBr_3$ binary melts. Lines are predicted according to eqn (4) (----) and eqn (5) (——). Y_4 is the anion fraction of $AlBr_4^-$.

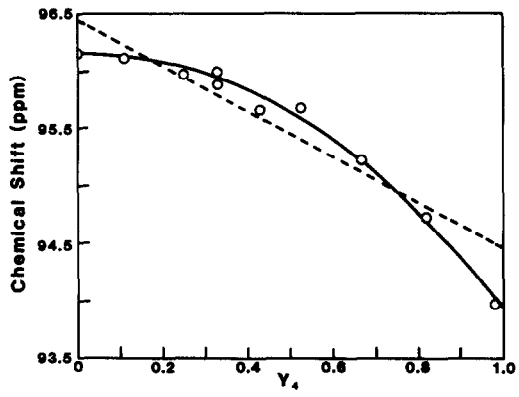
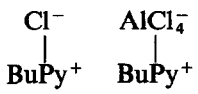


Fig. 7. Chemical-shift dependence on melt composition for ^{13}C at ring position 2 in MeEtImBr–$AlBr_3$ binary melts. Lines are predicted according to eqn (4) (----) and eqn (5) (——). Y_4 is the anion fraction of $AlBr_4^-$.

results given in this table clearly show that the fit to eqn (5) is superior to that for eqn (4). The nuclei that were examined in this study were chosen because they exhibit large changes in chemical shift with N. Other nuclei exhibit similar chemical shifts, but the dependences on N are less pronounced. In some cases the experimental error for measurement of the chemical shift is of the same order of magnitude as the observed change in the chemical shift with N. This makes comparison of the two models difficult, and the chemical shifts of these nuclei are not discussed here. However, in no case was the fit to eqn (4) found to be superior to that to eqn (5).

The important difference between data that fit eqns (2) or (4) and data that fit eqns (3) or (5) is in the number of ion–ion interactions that are considered for each ion. The data obtained by Taulelle and Popov, which appear to fit eqns (2) or (4) best, imply that simple ion-pairs are formed:



1 **4**

Table 1. Comparison of fits to eqns (4) and (5)

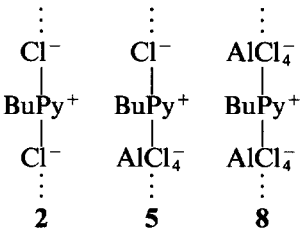
	Molten salt system					
	BuPyCl–$AlCl_3$		MeEtImCl–$AlCl_3$		MeEtImBr–$AlBr_3$	
Nucleus[a]	4–^1H	2,6–^{13}C	2–^1H	2–^{13}C	2–^1H	2–^{13}C
Data points	13	15	14	14	14	13
Equation (4) model						
δ_1 (ppm)	6.64	104.81	11.02	137.3	7.88	96.45
δ_4 (ppm)	6.24	104.45	9.17	134.9	6.69	94.45
R-factor[b]	5.0×10^{-3}	8.9×10^{-4}	1.9×10^{-2}	1.8×10^{-3}	1.8×10^{-2}	2.5×10^{-3}
Equation (5) model						
δ_2 (ppm)	6.7	104.99	10.73	136.92	7.69	96.15
δ_5 (ppm)	6.30	104.2	10.85	137.05	7.87	96.25
δ_8 (ppm)	6.29	104.61	8.89	134.54	6.42	93.94
R-factor[b]	9.1×10^{-4}	2.7×10^{-4}	1.5×10^{-3}	2.1×10^{-4}	2.0×10^{-3}	6.9×10^{-4}
R-factor ratio						
R [eqn(2)]/R [eqn (3)]	5.45	3.25	12.4	8.63	9.00	3.60
$R_{b,N,\alpha}$[c]	1.2×10^{-3}	4.4×10^{-4}	4.5×10^{-3}	3.4×10^{-4}	3.1×10^{-4}	4.8×10^{-4}

[a] Ring position–nucleus.

[b] Calculated according to Ref. 15.

[c] From tables in Ref. 15, b = number of adjustable parameters = 2, N = number of data points minus b, α = confidence level = 99.5%.

Our data for the $BuPy^+$ and $MeEtIm^+$ cations obtained in a variety of melts over a much larger composition range appear to fit best to the model represented by eqn (3). This implies that each cation interactions specifically with two anions and vice versa:



2 **5** **8**

These species need not be discrete but may be envisaged as portions of oligomeric chains of alternating cations and anions. The complexes proposed here are conceptually similar to the multi-ion pyridinium complexes which were reported by Angell and Schuppert[16] in the PyH–$AlCl_3$ system (PyH = hydropyridinium), e.g. $(PyH\ldots\ Cl\ldots HPy)^+$. However, the ion–ion interactions that occur in the systems studied here must arise via a purely electrostatic mechanism rather than through a hydrogen-bonding process since the latter is structurally precluded.

CONCLUSION

The chemical-shift data of Taulelle and Popov[11] were measured over too small a range of compositions to clearly establish the model represented by eqn (2). This is not to belie the importance of their conclusion that significant anion–cation interactions occur in the room-temperature chloroaluminate melts. Data which cover a wider composition range indicate that the anion–cation interactions that take place in these melts are considerably more complex than predicted by Taulelle and Popov. The "structures' represented by **2**, **5** and **8** appear more likely than those represented by **1** and **4** in the room-temperature haloaluminates melts examined in this study.

Acknowledgement—Work performed at the University of Mississippi was supported by the National Science Foundation through grant No. CHE-8412730.

REFERENCES

1. H. L. Chum and R. A. Osteryoung, In *Ionic Liquids* (Edited by D. Inman and D. G. Lovering), p. 407. Plenum Press, New York (1981).
2. C. L. Hussey, *Adv. Molten Salt Chem.* 1983, **5**, 185.
3. R. J. Gale and R. A. Osteryoung, In *Molten Salt Techniques* (Edited by D. G. Lovering and R. J. Gale), Vol. 1, p. 55. Plenum Press, New York (1983).
4. R. J. Gale, B. Gilbert and R. A. Osteryoung, *Inorg. Chem.* 1978, **17**, 2728.
5. J. L. Gray and G. E. Maciel, *J. Am. Chem. Soc.* 1981, **103**, 7141.
6. J. S. Wilkes, G. F. Reynolds and J. S. Frye, *Inorg. Chem.* 1983, **22**, 3870.
7. C. L. Hussey and H. A. Øye, *J. Electrochem. Soc.* 1984, **131**, 1621.
8. A. A. Fannin, Jr, D. A. Floreani, L. A. King, J. S. Landers, B. J. Piersma, D. J. Stech, R. L. Vaughn, J. S. Wilkes and J. L. Williams, *J. Phys. Chem.* 1984, **88**, 2614.
9. J. S. Wilkes, J. A. Levisky, J. L. Pflug, T. B. Scheffler and C. L. Hussey, *Anal. Chem.* 1982, **54**, 2378.
10. A. A. Fannin, Jr, L. A. King, J. A. Levisky and J. S. Wilkes, *J. Phys. Chem.* 1984, **88**, 2609.
11. F. Taulelle and A. I. Popov, *Polyhedron* 1983, **2**, 889.
12. R. A. Carpio, L. A. King, R. E. Lindstrom, J. C. Nardi and C. L. Hussey, *J. Electrochem. Soc.* 1979, **126**, 1644.
13. J. S. Wilkes, J. A. Levisky, R. A. Wilson and C. L. Hussey, *Inorg. Chem.* 1982, **21**, 1263.
14. D. W. Seegmiller, G. W. Rhodes and L. A. King, *Inorg. Nucl. Chem. Lett.* 1970, **6**, 885.
15. W. C. Hamilton, *Statistics in Physical Science*, p. 157. Ronald Press, New York (1964).
16. C. A. Angell and J. W. Schuppert, *J. Phys. Chem.* 1980, **84**, 538.

Polyhedron Vol. 5, No. 10, pp. 1573–1577, 1986
Printed in Great Britain

0277–5387/86 $3.00+.00
Pergamon Journals Ltd

X-RAY CRYSTAL AND MOLECULAR STRUCTURE OF SULPHATO AQUOTRIS(BENZOTRIAZOLE) COPPER(II)BENZOTRIAZOLE

MICHAEL B. HURSTHOUSE* and RICHARD L. SHORT

Department of Chemistry, Queen Mary College, Mile End Road, London E1 4NS, U.K.

and

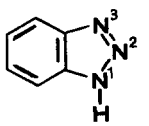
STEPHEN D. ROBINSON*

Department of Chemistry, King's College, Strand, London WC2R 2LS, U.K.

(*Received* 16 *December* 1985; *accepted* 28 *January* 1986)

Abstract—The complex "$Cu(SO_4)(btaH)_4 \cdot 2H_2O$" (btaH = benzotriazole) deposited as deep blue crystals from aqueous $CuSO_4 \cdot 5H_2O$–H_2SO_4–btaH solutions has been shown by X-ray diffraction methods to be a *mono*hydrate $[Cu(SO_4)(H_2O)(btaH)_3 \cdot btaH]$. The crystals contain five-coordinate, tetragonal pyramidal $Cu(SO_4)(H_2O)(btaH)_3$ units and bridging btaH molecules linked together by a three-dimensional array of H-bonding interactions.

The ability of benzotriazole (btaH) (I) to inhibit corrosion in copper and copper alloys has focused attention on btaH complexes of the transition metals in general, and of copper in particular.[1] Numerous copper–btaH complexes have been synthesized and several—notably $[Cu_5(bta)_6(acac)_4]$[2] and $[Cu_5(bta)_6(CNBu^t)_4]$[3]—have been shown to possess unusual structures in which btaH ligands adopt a variety of coordination modes. Copper–btaH complexes of indeterminate structure reported in the literature include the blue derivative "$Cu(SO_4)(btaH)_4 \cdot 2H_2O$" which crystallizes from aqueous solutions of $CuSO_4 \cdot 5H_2O$–H_2SO_4–btaH.[4] Vibrational, electronic and ESR spectra have been reported for this complex but only tenuous ideas, based on mono- and bidentate btaH ligands, have been advanced concerning its structure.[4] The fact that copper(II) complexes have a strong tendency to tetragonal distortion {cf. $[Cu(NH_3)_4(H_2O)_2]^{2+}$} coupled with the observation that btaH molecules participate readily in H-bonding led us to speculate that the complex $Cu(SO_4)(btaH)_4 \cdot 2H_2O$ might involve tetragonally distorted copper(II) with weakly bound axial water and/or sulphate ligands, as in the parent $CuSO_4 \cdot 5H_2O$, together with an equatorial set of four N^2-coordinated btaH ligands



Scheme 1.

linked via N^1—H---N^3 hydrogen bonds to form an N_4-macrocycle similar in shape and form to the very stable phthalocyanin ligand. To test this hypothesis we have undertaken an X-ray diffraction study of the complex as part of our current work on the coordination chemistry of btaH and related ligands. The results of this investigation, which are presented below, do not support our original hypothesis but establish that the complex is really a *mono*hydrate $[Cu(SO_4)(H_2O)(btaH)_3 \cdot btaH]$ with a novel structure based on $Cu(SO_4)(H_2O)(btaH)_3$ units and bridging non-coordinated btaH molecules linked together by a three-dimensional array of H-bonding interactions.

EXPERIMENTAL

The complex was prepared by the literature method,[4] crystallizing readily from aqueous $CuSO_4 \cdot 5H_2O$–H_2SO_4–btaH solutions as dark blue, air-stable plates. IR data were in good agreement with those originally reported.[4] Since the complex

* Authors to whom correspondence should be addressed.

is reported to react on attempted solubilization in water to form a green amorphous mass, recrystallization was not undertaken.

X-ray crystallography

The crystal used for X-ray work was sealed under nitrogen in a thin-walled glass capillary. After preliminary photography, unit cell and intensity data were obtained using a CAD4 diffractometer and graphite-monochromatized Mo-K_α radiation ($\lambda = 0.71069$ Å) following standard procedures.[5] The structure was solved via use of the heavy-atom method and full-matrix least-squares; non-hydrogen atoms were assigned anisotropic thermal parameters; hydrogen atoms were refined freely with isotropic thermal parameters, except those of the btaH ligands which were all assigned to a common refined μ_{iso} value.

Crystallographic data are as follows: $Cu(SO_4)(H_2O)(C_6H_5N_3)_4$, $C_{24}H_{22}N_{12}O_5SCu$, formula weight = 654.15, monoclinic, $a = 7.294(3)$ Å, $b = 19.744(3)$ Å, $c = 19.227(5)$ Å, $\beta = 82.97(3)°$, $U = 2748.1$ Å^3, space group $P2_1/c$, $Z = 4$, $D_c = 1.58$ g cm^{-3}, μ(Mo-K_α) = 9.3 cm^{-1}, $T = 295$ K. 5381 data were recorded, giving 4828 unique, 3207 observed [$I > 1.5\sigma(I)$]. Number of parameters = 462, weighting scheme $\omega = 1/[\sigma^2(F_o)+0.0005g(F_o)^2]$. Final R $(= \Sigma|\Delta F_o|/\Sigma F_o) = 0.0457$, $R_W = [\Sigma_W|\Delta F|^2/\Sigma_W F_o^2]^{1/2} = 0.0417$. Atomic scattering factors calculated from data in Ref. 6. Final atomic positional and thermal parameters, and lists of F_o/F_c values have been deposited as supplementary material with the Editor from whom copies are available on request.*

RESULTS AND DISCUSSION

The structures of the $Cu(SO_4)(H_2O)(btaH)_3$ unit and the associated btaH molecule are shown in Fig. 1, together with the atomic numbering scheme. Two views of the unit cell contents illustrating molecular packing and H-bonding interactions, are shown in Figs 2 and 3. Selected bond lengths and angles are given in Table 1.

Coordination about copper

The copper atom has a tetragonal pyramidal coordination (Fig. 1) with an apical H_2O ligand. The basal coordination positions are occupied by

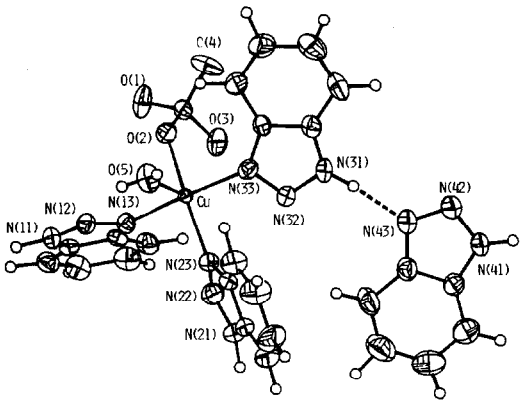


Fig. 1.

a monodentate sulphate and three N^3-coordinated btaH molecules. The copper atom is slightly displaced (0.157 Å) from the basal plane towards the apical H_2O ligand. The apical Cu—OH_2 bond [2.202(5) Å] is elongated relative to equatorial Cu—OH_2 bonds (*ca* 1.95–2.01 Å)[7] but less so than similar bonds in tetragonal bipyramidal copper(II) structures, values for which fall in the range *ca* 2.31–2.64 Å.[8,9] The Cu—OSO_3 distance [1.980(5) Å] is typical for equatorially coordinated sulphate[7] and the Cu—N distances [1.990(5), 2.009(5) and 2.019(5) Å] are similar to those previously recorded for related copper(II)–btaH structures.[10,11] An interesting feature of the structure is the co-existence of a non-coordinated btaH molecule and what would appear to be a relatively unhindered vacant coordination site at the copper

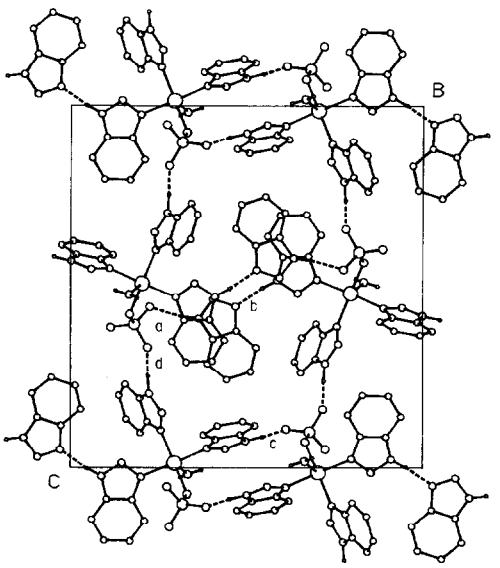


Fig. 2.

*Atomic coordinates have also been deposited with the Cambridge Crystallographic Data Centre.

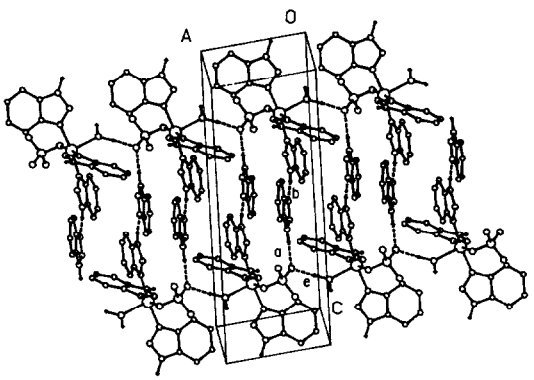


Fig. 3.

centre in the free molecule. However, in the crystal structure this site is partially blocked by the O(3) atom of the sulphate group [O(3)···Cu = 3.175 Å]. Presumably the presence of the fourth btaH is a requirement for the formation of this strong three-dimensional H-bonded crystal structure.

BtaH ligands

The molecular dimensions of the coordinated btaH ligands are in close agreement with those previously reported for related Cu(II)–btaH structures.[10,11] The most noticeable difference is a lengthening of the N^2—N^3 distances (1.326, 1.334 and 1.335 Å) in the N^3-coordinated btaH ligands relative to those found for the non-coordinated btaH in the present structure [1.300(6) Å] and for the free btaH molecule [1.310(4) Å].[12] Structural parameters recorded for the non-coordinated btaH are in good agreement with data previously reported for the free ligand.[12]

Sulphate ligand

The sulphate tetrahedra are irregular with the S—O bond length being greatest [1.489(4) Å] for the oxygen involved in coordination to the copper. For the terminal S—O bonds the bond lengths increase as participation of the oxygen in H-bonding interactions increases.

Table 1. Selected bond lengths (Å) and angles (°)

O(2)—Cu(1)	1.980(5)	N(13)—Cu(1)	2.009(5)
N(23)—Cu(1)	2.019(5)	N(33)—Cu(1)	1.990(5)
O(5)—Cu(1)	2.202(5)	O(1)—S(1)	1.448(4)
O(2)—S(1)	1.489(4)	O(3)—S(1)	1.472(4)
O(4)—S(1)	1.443(4)	C(19)—N(11)	1.366(7)
N(11)—N(12)	1.335(5)	N(12)—N(13)	1.319(6)
C(14)—N(13)	1.378(6)	C(14)—C(15)	1.396(7)
C(15)—C(16)	1.366(7)	C(16)—C(17)	1.423(8)
C(17)—C(18)	1.357(8)	C(14)—C(19)	1.388(6)
C(18)—C(19)	1.401(7)	C(29)—N(21)	1.353(7)
N(21)—N(22)	1.334(6)	C(24)—N(23)	1.382(6)
N(22)—N(23)	1.314(6)	C(24)—C(25)	1.394(7)
C(25)—C(26)	1.361(8)	C(26)—C(27)	1.412(9)
C(27)—C(28)	1.353(9)	C(24)—C(29)	1.391(6)
C(28)—C(29)	1.406(7)	C(39)—N(31)	1.351(6)
N(31)—N(32)	1.326(5)	N(32)—N(33)	1.314(5)
C(34)—N(33)	1.385(6)	C(34)—C(35)	1.392(7)
C(35)—C(36)	1.368(7)	C(36)—C(37)	1.416(8)
C(37)—C(38)	1.362(8)	C(34)—C(39)	1.389(6)
C(38)—C(39)	1.395(7)	N(42)—N(41)	1.339(6)
C(49)—N(41)	1.354(6)	N(43)—N(42)	1.300(6)
C(44)—N(43)	1.373(7)	C(45)—C(44)	1.400(8)
C(49)—C(44)	1.381(7)	C(46)—C(45)	1.358(9)
C(47)—C(46)	1.404(10)	C(48)—C(47)	1.354(9)
C(49)—C(48)	1.380(8)		
N(13)—Cu(1)—O(2)	87.4(2)	N(23)—Cu(1)—O(2)	170.1(1)
N(23)—Cu(1)—N(13)	90.6(2)	N(33)—Cu(1)—O(2)	91.3(2)
N(33)—Cu(1)—N(13)	171.5(1)	N(33)—Cu(1)—N(23)	89.3(2)
O(5)—Cu(1)—O(2)	90.0(2)	O(5)—Cu(1)—N(13)	91.8(2)
O(5)—Cu(1)—N(23)	99.7(2)	O(5)—Cu(1)—N(33)	96.6(2)

(*continued*)

Table 1. (*continued*)

O(2)—S(1)—O(1)	108.2(3)	O(3)—S(1)—O(1)	110.1(3)
O(3)—S(1)—O(2)	108.9(3)	O(4)—S(1)—O(1)	112.3(3)
O(4)—S(1)—O(2)	108.9(3)	O(4)—S(1)—O(3)	108.5(3)
S(1)—O(2)—CU(1)	127.8(3)	C(19)—N(11)—N(12)	111.1(4)
N(11)—N(12)—N(13)	107.8(4)	C(14)—N(13)—N(12)	109.1(4)
C(14)—N(13)—Cu(1)	129.9(4)	N(12)—N(13)—Cu(1)	120.5(3)
C(15)—C(14)—C(19)	121.2(4)	C(15)—C(14)—N(13)	131.4(3)
C(19)—C(14)—N(13)	107.4(4)	C(14)—C(15)—C(16)	117.0(5)
C(15)—C(16)—C(17)	121.0(5)	C(16)—C(17)—C(18)	122.9(5)
C(17)—C(18)—C(19)	115.5(5)	C(14)—C(19)—C(18)	122.5(5)
C(14)—C(19)—N(11)	104.6(4)	C(18)—C(19)—N(11)	132.9(4)
C(29)—N(21)—N(22)	110.7(4)	N(21)—N(22)—N(23)	108.5(4)
C(24)—N(23)—N(22)	108.7(4)	C(24)—N(23)—Cu(1)	131.8(3)
N(22)—N(23)—Cu(1)	118.9(4)	C(25)—C(24)—C(29)	120.8(5)
C(25)—C(24)—N(23)	132.2(4)	C(29)—C(24)—N(23)	107.0(4)
C(24)—C(25)—C(26)	116.8(5)	C(25)—C(26)—C(27)	122.1(6)
C(26)—C(27)—C(28)	122.2(6)	C(27)—C(28)—C(29)	115.9(6)
C(24)—C(29)—C(28)	122.2(5)	C(24)—C(29)—N(21)	105.1(4)
C(28)—C(29)—N(21)	132.6(4)	C(39)—N(31)—N(32)	111.2(4)
N(31)—N(32)—N(33)	108.3(4)	C(34)—N(33)—N(32)	108.7(4)
C(34)—N(33)—Cu(1)	132.5(2)	N(32)—N(33)—Cu(1)	118.7(3)
C(35)—C(34)—C(39)	121.6(5)	C(35)—C(34)—N(33)	131.7(3)
C(39)—C(34)—N(33)	106.7(4)	C(34)—C(35)—C(36)	116.3(5)
C(35)—C(36)—C(37)	121.5(6)	C(36)—C(37)—C(38)	122.9(6)
C(37)—C(38)—C(39)	115.2(5)	C(34)—C(39)—C(38)	122.6(5)
C(34)—C(39)—N(31)	105.1(4)	C(38)—C(39)—N(31)	132.3(4)
C(49)—N(41)—N(42)	110.7(4)	N(43)—N(42)—N(41)	108.5(4)
C(44)—N(43)—N(42)	108.4(4)	C(45)—C(44)—N(43)	130.5(4)
C(49)—C(44)—N(43)	108.1(4)	C(49)—C(44)—C(45)	121.4(5)
C(46)—C(45)—C(44)	115.8(6)	C(47)—C(46)—C(45)	122.3(6)
C(48)—C(47)—C(46)	121.8(6)	C(49)—C(48)—C(47)	116.6(6)
C(44)—C(49)—N(41)	104.3(5)	C(48)—C(49)—N(41)	133.6(4)
C(48)—C(49)—C(44)	122.1(5)		

Molecular packing and H-*bonding interactions*

The $Cu(SO_4)(H_2O)(btaH)_3$ polyhedra are linked by bridging non-coordinating btaH molecules which H-bond to coordinated sulphate [N(41)—H(41)···O(3), N···O = 2.764 Å] (a, Figs 2 and 3), and to coordinated btaH ligands [N(43)···H(31)—N(31), N···N = 2.731 Å] (b, Figs 2 and 3). The polyhedra are further linked by H-bonding interactions between coordinated sulphate and coordinated btaH [O(1)···H(11)—N(11), O···N = 2.687 Å (c, Fig. 2); O(4)···H(21)—N(21), O···N = 2.666 Å (d, Fig. 2)] and between coordinated sulphate and coordinated water [O(3)···H(52)—O(5), O···O = 2.764 Å] (e, Fig. 3) to generate a three-dimensional H-bonding network. The presence of a non-H-bonded hydrogen atom on the coordinated aquo ligand presumably accounts for the very characteristic strong, sharp IR absorption which occurs at *ca* 3620 cm^{-1}.

The preference shown for the observed structure over the macrocyclic alternative described above no doubt reflects in part the tendency of btaH to coordinate through N^3 rather than N^2. However, examples of N^2–btaH coordination are known: pertinent examples include the copper complexes $[Cu_5(bta)_6(acac)_4]$[2] and $[Cu_5(bta)_6(CNBu^t)_4]$.[3] It therefore seems probable that the very extensive H-bonding interactions found for the observed structure are a significant factor in tilting the thermodynamic balance against the "macrocyclic" structure in the present instance.

Acknowledgements—We thank Mr Bruce G. Olby and Miss M. Colette McGuire for preparation of crystals

used in this study, and the S.E.R.C. for support of the crystallographic work.

REFERENCES

1. J. Reedijk, G. Roelofsen, A. R. Siedle and A. L. Spek, *Inorg. Chem.* 1979, **18**, 1947 (and references therein); (b) P. G. Fox, G. Lewis and P. J. Boden, *Corros. Sci.* 1979, **19**, 457 (and references therein).
2. J. H. Marshall, *Inorg. Chem.* 1978, **17**, 3711.
3. V. L. Himes, A. D. Mighell and A. R. Siedle, *J. Am. Chem. Soc.* 1981, **103**, 211.
4. Z. Karwecka and L. Pajdowski, *Rocz. Chem.* 1976, **50**, 1251.
5. M. B. Hursthouse, R. A. Jones, K. M. A. Malik and G. Wilkinson, *J. Am. Chem. Soc.* 1979, **101**, 4128.
6. *International Tables for X-ray Crystallography*, Vol. 4. Kynoch Press, Birmingham (1974).
7. R. F. Zahrobsky and W. H. Baur, *Acta Cryst.* 1968, **B24**, 508.
8. J. Soldánová, F. Pavelčik and J. Majer, *Acta Cryst.* 1981, **B37**, 921.
9. F. Bigoli, M. Lanfranchi, E. Leporato and M. A. Pellinghelli, *Cryst. Struct. Commun.* 1980, **9**, 1255.
10. I. Søtofte and K. Nielsen, *Acta Chem. Scand.* 1984, **38A**, 253.
11. I. Søtofte and K. Nielsen, *Acta Chem. Scand.* 1981, **35A**, 733.
12. A. Escande, J. L. Galigné and J. Lapasset, *Acta Cryst.* 1974, **B30**, 1490.

Polyhedron Vol. 5, No. 10, pp. 1579–1580, 1986
Printed in Great Britain

0277–5387/86 $3.00+.00
Pergamon Journals Ltd

REACTIVITIES OF TETRAHALOSILANES AND SILANE WITH SULPHUR TRIOXIDE

B. S. SURESH and D. K. PADMA*

Department of Inorganic and Physical Chemistry, Indian Institute of Science, Bangalore 560012, India

(*Received* 30 *July* 1985; *accepted* 4 *February* 1986)

Abstract—Reactions of tetrahalosilanes [SiX_4 (X = F, Cl or Br)] and silane (SiH_4) with sulphur trioxide (SO_3) have been studied under different experimental conditions. Each of the silanes behaves differently in accordance with the bond energy of the Si—X bond. While SiF_4 remains unreactive even at 600°C, $SiCl_4$ reacts with SO_3 at 500°C giving rise to hexachlorodisiloxane [$(SiCl_3)_2O$] as the major product. In contrast $SiBr_4$ and SiH_4 react with SO_3 at room temperature and below room temperature, respectively, yielding silica as one of the products of reaction. In all cases the SO_3 is reduced to sulphur dioxide.

In continuation of our work on the reactions of silicon compounds, we found that silicon halides lend themselves for a good comparative study of their reactivities towards oxygen-containing compounds.[1–4] In the present system, a study has been made of the reactions of silicon tetrahalides [SiX_4 (X = F, Cl or Br)] and silane (SiH_4) towards sulphur trioxide (SO_3).

EXPERIMENTAL

Materials and methods

Standard methods of preparation were adopted for the preparation of SiH_4,[5] SiF_4,[5] $SiBr_4$[6] and SO_3.[7] Commercially available $SiCl_4$ was purified by repeated distillation and the fraction boiling at 55.5–56°C was collected and stored.

IR spectra of solids were recorded on a Perkin–Elmer Model 599 spectrophotometer, in a Nujol mull or a KBr matrix, and those of gases were recorded using a 10-cm gas cell fitted with KBr windows. IR spectra of liquids were recorded using conventional liquid cells.

Reaction of SiF_4 *with* SO_3. SiF_4 (~1.0 mmol) was placed in an evacuated reaction vessel and SO_3 (~5.0 mmol) was introduced into the vessel. The reactants were heated at various temperatures up to 600°C. The IR spectra shows only the reactants with a small amount of sulphur dioxide (SO_2) and complete absence of any other expected compounds such as sulphuryl fluoride and hexafluorodisiloxane.

Reaction of $SiCl_4$ *with* SO_3. $SiCl_4$ (~2.0 mmol) was introduced into the reaction vessel containing SO_3 (~8.0 mmol). SO_3 dissolved in $SiCl_4$ to give a clear solution. The reactants were heated to various temperatures. It was observed that no detectable reaction took place below 500°C. At 500°C (12 h), hexachlorodisiloxane [$(SiCl_3)_2O$] and SO_2 were formed as the volatile products. When the reaction was cooled to about −10°C the reaction mixture became yellow, indicating the presence of chlorine. This was further confirmed by separating chlorine at −30°C and reacting with solid potassium iodide to liberate iodine. All the volatile products were removed by gradual pumping till the IR (gas phase) showed no volatile compounds. A nonvolatile colourless liquid was left behind. The IR spectrum of its solution in CCl_4 showed absorption bands in the regions 630–650 and 1100–1250 cm^{-1} which could be assigned to ν(Si—Cl) and ν(Si—O) vibrations. These can be attributed to the formation of higher chlorosiloxanes in the reaction mixture. A white solid product deposited at the bottom of the reaction vessel was identified as silica by IR spectroscopy and chemical tests.

Reaction of $SiBr_4$ *with* SO_3. $SiBr_4$ (~2.0 mmol) was placed in a reaction vessel and SO_3 (~8.0 mmol) was introduced into the vessel. As soon as the two reactants came into contact with each other, brown fumes of bromine started evolving which

increased with time. The reaction mixture was kept at room temperature for about 12 h. The gas-phase IR spectra showed the presence of only SO_2. All the volatile products (SO_2, bromine and SO_3) were pumped off. A white solid was left behind in the reaction vessel. This was found to be silica by chemical tests and spectral analysis.

Reaction of SiH_4 *with* SO_3. SiH_4 (~4.0 mmol) was placed in a reaction vessel and kept frozen at liquid-nitrogen temperature. SO_3 (~20.0 mmol) was introduced into the vessel. The liquid-nitrogen bath was withdrawn and the reaction mixture was allowed to attain room temperature over a period of 1 h. The IR spectrum of the gaseous component shows only SO_2 and the complete absence of SiH_4 or any other higher siloxanes such as disiloxane. All the volatile products were transferred into another trap and treated with alkaline cadmium acetate solution and shaken well. No yellow precipitate was formed, indicating the absence of hydrogen sulphide (H_2S) among the reaction products. The reaction vessel was found to contain tiny droplets of a colourless nonvolatile liquid which was identified to be sulphuric acid (H_2SO_4) and a deposited white solid which was characterized as silica.

RESULTS AND DISCUSSION

From the experimental observations described above it can be seen that silicon tetrahalides and SiH_4 react differently with SO_3. SiF_4 remains unreactive even at elevated temperatures. This lack of reactivity can be attributed more to kinetic parameters rather than to thermodynamic feasibility as the reaction $SiF_4 + 2SO_3 \rightarrow SiO_2 + 2SO_2F_2$ is thermodynamically favourable ($\Delta G^{\ominus} = -42.3$ kcal mol^{-1}). This kind of nonreactivity by SiF_4 has been observed also with oxides of nitrogen.[8]

On the other hand, the other silicon compounds react with SO_3 with varying degrees of ease. $SiCl_4$ undergoes reaction only at 500°C giving rise to $(SiCl_3)_2O$ as the major product of the reaction. The minor products are polychlorosiloxanes and silica. The reactions should involve radical cleavage followed by oxidation and fragmentation to account for the formation of chlorine and higher siloxanes:

$$2SiCl_4 + SO_3 \xrightarrow{500°C} Cl_3Si{-}O{-}SiCl_3 + SO_2 + Cl_2,$$

$$3[Cl_3Si{-}O{-}SiCl_3] + SO_3 \xrightarrow{500°C} 2[SICl_3{-}O{-}SiCl_2{-}O{-}SiCl_3] + SO_2 + Cl_2,$$

$$SiCl_3{-}O{-}SiCl_2{-}O{-}SiCl_3 + 4SO_3 \xrightarrow{500°C} 3SiO_2 + 4SO_2 + 4Cl_2.$$

It is of interest to point out here that the formation of chlorine and SO_2 has been observed in reactions of sodium chloride with SO_3:[9]

$$SO_3 + 2NaCl \xrightarrow{350°C} Na_2S_2O_7 + SO_2 + Cl_2.$$

The reaction of $SiBr_4$ with SO_3 occurs at room temperature with the liberation of bromine and formation of silica, indicating that radical cleavage is not predominant. The SO_3 is reduced to SO_2 and the overall reaction may be represented as follows:

$$SiBr_4 + 2SO_3 \xrightarrow{25°C} SiO_2 + 2SO_2 + 2Br_2.$$

SiH_4 undergoes oxidation below room temperature with the formation of silica. The SO_3 is reduced only to SO_2 and not to H_2S. The hydrogen part of silane is oxidized to water, which further combines with unreacted SO_3 to form H_2SO_4:

$$SiH_4 + 4SO_3 \xrightarrow[\text{room temperature}]{\text{below}} SiO_2 + 2H_2O + 4SO_2,$$

$$2H_2O + 2SO_3 \rightarrow 2H_2SO_4.$$

It is clear from the above results that there is clear gradation in the ease with which the Si—X bonds (X = F, Cl, Br or H) are attacked and replaced by Si—O bonds. While Si—F is not attacked even at elevated temperatures, Si—Cl is cleaved at about 500°C. Si—Br is oxidized to Si—O at room temperature and the Si—H bond is converted to Si—O below room temperature. This trend is in accordance with the bond energies: Si—F > Si—Cl > Si—Br ~ Si—H.

Acknowledgement—One of us (BSS) wishes to thank the Department of Atomic Energy for financial assistance.

REFERENCES

1. B. S. Suresh and D. K. Padma, *J. Fluorine Chem.* 1984, **24**, 399.
2. B. S. Suresh and D. K. Padma, *Bull. Chem. Soc. Jpn* in press.
3. B. S. Suresh and D. K. Padma, *Polyhedron* 1985, **4**, 2067.
4. B. S. Suresh and D. K. Padma, *J. Chem. Soc., Dalton Trans.* 1984, 1779.
5. D. K. Padma, B. S. Suresh and A. R. Vasudeva Murthy, *J. Fluorine Chem.* 1979, **14**, 327.
6. W. C. Schumb, *Inorg. Synth.* 1946, **2**, 98.
7. R. W. Lovejoy, J. H. Colwell, D. F. Eggers, Jr and G. D. Halsey, Jr, *J. Chem. Phys.* 1962, **36**, 612.
8. B. J. Aylett, I. A. Ellis and J. R. Richmond, *J. Chem. Soc., Dalton Trans.* 1973, 1523.
9. D. J. Salley, *J. Am. Chem. Soc.* 1939, **61**, 834.

Polyhedron Vol. 5, No. 10, pp. 1581–1585, 1986
Printed in Great Britain

0277–5387/86 $3.00+.00
Pergamon Journals Ltd

SYNTHESIS OF ORGANOANTIMONY(V) AND μ-OXY-BIS(TRIARYLANTIMONY) SELENOCYANATES USING A PHASE-TRANSFER CATALYST

PREM RAJ,* RAJIV RASTOGI, KIRAN SINGHAL and A. K. SAXENA

Chemistry Department, Lucknow University, Lucknow 226007, India

(*Received* 17 *December* 1985; *accepted* 10 *February* 1986)

Abstract—Several new, pentacoordinated, triorganoantimony bis-selenocyanates [$R_3Sb(SeCN)_2$ (R = Me, Ph, *p*-$CH_3C_6H_4$, *p*-ClC_6H_4, *p*-F-C_6H_4 or C_6F_5)], tetraorganostibonium selenocyanates [$R_3R'Sb(SeCN)$ (R = R′ = Ph; R = Ph, and R′ = —CH_2—CH=CH_2)] and μ-oxy-bis(triarylantimony) bis-selenocyanates {[Ar_3Sb—O—$SbAr_3$]$(SeCN)_2$ (Ar = Ph, *p*-$CH_3C_6H_4$, *p*-ClC_6H_4 or *p*-FC_6H_4)} have been synthesized from potassium selenocyanate and the corresponding organoantimony halide (chloride and/or bromide) in the presence of the phase-transfer catalyst 18-crown-6, and characterized. Spectroscopic evidence suggested an *iso* structure (Sb—NCSe). The compounds were also obtained in the absence of 18-crown-6 but in lower yields. Some of these compounds were found to exhibit a significant biological activity.

Despite a considerable interest in the chemistry of selenocyanate derivatives of the main-group elements, and a variety of metal and metalloids for which such derivatives have been synthesized, synthetic routes for the corresponding selenocyanate compounds of group V elements (As, Sb and Bi) have been neglected.[1–9] During the course of our investigations on the oxidative addition, cleavage and metathetical reactions of tertiary aryl antimony(V) compounds,[10–12] it was observed that, except for a single reference by Challenger *et al.*[1] describing the synthesis and isolation of Ph_2Bi(III)SeCN obtained through the reaction of triphenyl bismuth and selenium bis-selenocyanate [$Se(SeCN)_2$], there are no references on any aspect of the selenocyanate derivatives of group V elements (P, As, Sb and Bi) in either oxidation state (+3 and +5).[8,9] Attempts to demonstrate the existence and isolation of $Ph_3Sb(V)(SeCN)_2$ by the same authors were unsuccessful.[1] In view of the scarcity of the data and the enhanced antimicrobial activity expected for such compounds, it was considered worthwhile to make a systematic study of organoantimony(V) selenocyanates.

The present work describes the synthesis of triarylantimony(V) bis-selenocyanates [$Ar_3Sb(SeCN)_2$ (Ar = Ph, *p*-FC_6H_4, *p*-$CH_3C_6H_4$ or C_6F_5)], and symmetrical and unsymmetrical tetraorganoantimony [$Ph_4Sb(V)$ and $Ph_3(CH_2$=CH—$CH_2)Sb(V)$] selenocyanate obtained using the phase-transfer catalyst (PTC) 18-crown-6. In addition to this, μ-oxy-bis(triarylantimony) bis-selenocyanates {[Ar_3Sb—O—$SbAr_3$]$(SeCN)_2$} have also been prepared.

On the basis of some previous studies and the present work it has been safely concluded that, except for the heaviest element in a group (Hg, Tl, Pb and Bi), all the preceding elements (In, Sn, Sb and Te), including other lighter members of the group studied so far, have the *iso* structure. A few compounds have been tested, and found to exhibit a significant biological activity.

EXPERIMENTAL

Triorganoantimony dihalides [R_3SbX_2 (R = Me, Ph, *p*-$CH_3C_6H_4$, *p*-ClC_6H_4, *p*-FC_6H_4 or C_6F_5; X = Cl and/or Br)[8,10–13] and μ-oxy-bis(triarylantimony) dihalides [(Ar_3Sb—O—$SbAr_3$)X_2 (Ar = Ph, *p*-$CH_3C_6H_4$, *p*-ClC_6H_4 or *p*-FC_6H_4)][14,15] were synthesized by the reported methods.

Tetraphenylstibonium bromide was obtained by the treatment of triphenyl stibine with bromobenzene in the presence of aluminium chloride[16] while triphenyl(allyl)stibonium bromide was prepared by the reactions of triphenylantimony dibromide with allyl magnesium bromide (1 mol) (m.p.

* Author to whom correspondence should be addressed.

204°C). Found: C, 52.1; H, 4.0%. Calc. for $C_{21}H_{20}SbBr$: C, 53.2; H, 4.2%.

Potassium selenocyanate and 18-crown-6 (used as a PTC) were Fluka products and dried before use.

All the solvents were purified and dried by standard procedures and reactions were carried out under strictly anhydrous conditions.

IR spectra were recorded in the range 4000–200 cm^{-1} by using KBr/CsI pellets on a Perkin–Elmer spectrophotometer. The molar conductance of 10^{-3} M solutions was determined at 25°C with a Phillips PR-9500 conductivity assembly. Molecular weights were determined cryoscopically in benzene using a Beckmann thermometer of accuracy ±0.01°C.

Typical experimental details of the reactions are described below. Relevant IR assignments and analytical data are listed in Tables 1–3.

Preparation of triorganoantimony(V) diselenocyanate

Triphenylantimony dichloride (0.424 g, 1 mol) and potassium selenocyanate (0.248 g, 2 mol) in benzene (60 cm^3) were stirred at room temperature in the presence of a catalytic amount of 18-crown-6 (0.01 mmol) for 4–6 h. Potassium chloride was filtered off and the solvent was removed *in vacuo* to afford a brownish pink solid, which was recrystallized from petroleum ether (40–60°C) and characterized as triphenylantimony bis-selenocyanate (m.p. 155–157°C, yield 83%).

Similarly, compounds **I–VI** were synthesized from triorganoantimony dihalide (chloride or bromide) and potassium selenocyanate in a 1:2 molar ratio in the presence of 18-crown-6.

Preparation of tetraorganostibonium selenocyanate

Tetraphenylstibonium bromide (0.510 g, 1 mol) and potassium selenocyanate (0.124 g, 1 mol) were mixed in anhydrous benzene and stirred for 3 h at room temperature in the presence of 18-crown-6 (0.01 mmol) under a nitrogen atmosphere. Potassium bromide was filtered off and the filtrate was concentrated to dryness *in vacuo* followed by the

Table 1. Analytical data of selenocyanate derivatives of antimony

	Compound	Yield (%)	M.p. (°C)	Colour	Analysis: found (calc.) (%) C	H	N
I	$Me_3Sb(SeCN)_2$	70	155	Red	15.8 (15.9)	2.1 (2.4)	6.5 (7.4)
II	$Ph_3Sb(SeCN)_2$	83	155–157	Pink	42.2 (42.6)	2.3 (2.7)	4.1 (5.0)
III	$(C_6F_5)_3Sb(SeCN)_2$	76	183–185	White	28.6 (28.8)	—	3.2 (3.4)
IV	$(p\text{-}CH_3C_6H_4)_3Sb(SeCN)_2$	81	91	Pink	45.3 (45.6)	3.0 (3.5)	4.4 (4.6)
V	$(p\text{-}ClC_6H_4)_3Sb(SeCN)_2$	80	109	White	35.9 (36.0)	3.0 (3.1)	4.0 (4.2)
VI	$(p\text{-}FC_6H_4)_3Sb(SeCN)_2$	78	103	Brown	38.6 (38.9)	1.9 (1.9)	4.4 (4.5)
VII	$Ph_4SbSeCN$	84	139	White	56.0 (56.1)	3.4 (3.7)	2.2 (2.6)
VIII	$Ph_3(CH_2—CH=CH_2)SbSeCN$	82	161	Pink	52.8 (52.9)	4.0 (4.1)	2.7 (2.8)
IX	$[Ph_3Sb—O—SbPh_3](SeCN)_2$	80	119	White	48.8 (48.9)	3.0 (3.2)	2.9 (3.0)
X	$[(p\text{-}CH_3C_6H_4)_3Sb—O—Sb(p\text{-}CH_3C_6H_4)_3](SeCN)_2$	79	229	Light yellow	51.8 (52.0)	4.0 (4.1)	2.5 (2.7)
XI	$[(p\text{-}ClC_6H_4)_3Sb—O—Sb(p\text{-}ClC_6H_4)_3](SeCN)_2$	76	83	White	40.0 (40.0)	2.0 (2.1)	2.2 (2.4)
XII	$[(p\text{-}FC_6H_4)_3Sb—O—Sb(p\text{-}FC_6H_4)_3](SeCN)_2$	74	126	Light yellow	43.0 (43.9)	2.2 (2.3)	2.6 (2.7)

Table 2. IR data for selenocyanate derivatives of antimony

Compound	ν_{as}(SeCN)	ν_{sy}(SeCN)	δ(SeCN) deformation	M—N	M—C
I	2040ms	610m	405v	370v	575
II	2030	635m	455as	385m	
III	2060	610m	420w 390w	370m	
IV	2047	580m	485ams 420vw 400w	360v	
V	2020	550vb	485ams	—	—
VI	2090	—	—	—	—
VII	2065	620	460	—	—
VIII	2040	630vw	460m	380w	—
IX	2040	635	455[a]	385	740 (Sb—O—Sb)
X	2050	—	—	—	740 (Sb—O—Sb)
XI	2060	—	—	—	740 (Sb—O—Sb)
XII	2045	—	—	—	740 (Sb—O—Sb)

[a] Overlapped with ν_{asy}(Sb—C) stretching (*Y*-mode).

addition of petroleum ether (20 cm^3) (40–60°C) to yield light brown crystals of tetraphenylstibonium selenocyanate (m.p. 139°C, yield 84%).

Triphenyl(allyl)antimony selenocyanate was also prepared in an analogous manner (m.p. 161°C, yield 80%).

Tetraphenylstibonium selenocyanate in 40% yield was also synthesized without the PTC from tetraphenylstibonium bromide and potassium selenocyanate in benzene. However, a crystal of NaOH was added at the beginning of the reaction to check the decomposition of KSeCN. The NaOH was recovered after the usual work up of the reaction.

Table 3. Molar conductance of representative selenocyanate derivatives of antimony(V)

Compound	Molar conductance (Λ_m) (Ω^{-1} cm^2 mol^{-1}) Nitrobenzene	Acetonitrile
II	10.25	20.54
III	9.86	19.62
IV	11.12	23.48
V	9.52	16.00
VI	8.86	24.56
VII	9.24	17.82

Preparation of μ-oxy-bis(triarylantimony) bis-selenocyanate

The title compounds (**IX–XII**) were synthesized from potassium selenocyanate and the corresponding μ-oxy-bis(triarylantimony) dichloride in a 1:2 molar ratio under conditions similar to those described for triphenylantimony bis-selenocyanate. The analytical data for the compounds are given in Table 1.

RESULTS AND DISCUSSION

Organoantimony(V) selenocyanates [$R_nSb(SeCN)_{5-n}$] are obtained in excellent yield by the interaction of potassium selenocyanate with the corresponding organoantimony dichloride or dibromide in a 1:2 molar ratio in the presence of the PTC 18-crown-6:

$$R_3SbX_2 + 2KSeCN \xrightarrow[\text{benzene}]{\text{PTC}} R_3Sb(SeCN)_2 + 2KX, \quad (1)$$

where R = Me, Ph, *p*-$CH_3C_6H_4$, *p*-ClC_6H_4, *p*-FC_6H_4 or C_6F_5; X = Cl or Br;

$$R_3R'SbX + KSeCN \xrightarrow[\text{benzene}]{\text{PTC}} R_3R'Sb(SeCN) + KX, \quad (2)$$

where R = R′ = Ph; R = Ph, and R′ = —CH_2—CH=CH_2. μ-Oxy-bis(triarylantimony) bis-selenocyanates are obtained in an analogous manner:

$$(R_3Sb—O—SbR_3)X_2 + 2KSeCN \xrightarrow[\text{benzene}]{\text{PTC}} (R_3Sb—O—SbR_3)(SeCN)_2 + 2KX, \quad (3)$$

where R = Ph, *p*-$CH_3C_6H_4$, *p*-ClC_6H_4 or *p*-FC_6H_4.

Compounds in equations (1)–(3) can also be obtained in the absence of the PTC but the yield of the product is invariably low. All the organometal selenocyanates in fact tend to decompose on prolonged stirring or heating without completion of the reaction, and the yields of the desired products are poor. However, the use of the PTC 18-crown-6 not only reduced the time of the reaction but also enhanced the yield considerably.

The analytical and molecular-weight data, and the melting points of the investigated compounds are recorded in Table 1. The compounds are, generally, coloured crystalline solids but are moisture-sensitive and tend to decompose on storage. Except for trimethylantimony bis-selenocyanate, they are moderately soluble in common organic solvents. $Me_3Sb(SeCN)_2$ (**I**) is insoluble in benzene and chloroform but soluble in acetonitrile. The molecular-weight data showed that all the compounds are monomeric in benzene. The equivalent conductances of these compounds in nitrobenzene (10^{-3} M solutions) and acetonitrile (Table 3) indicate their non-ionic nature.[17] The observed non-mass-sensitive frequencies associated with the various modes of vibration of aromatic groups are in conformity with the reported frequencies and hence are not discussed here.[9–12] IR absorptions associated with the various internal modes of vibration of the selenocyanate group have been identified and indicate the nature of the bonding.

IR spectra have been widely used to establish the distinction between the two isomeric forms. Selenocyanates, like thiocyanates, are capable of exhibiting bonding isomerism and can exist either in the normal or the *iso* form. They give rise to three fundamental modes of vibration in their IR spectra, two of which are ν(C=N) and ν(C—Se) while the third is due to a deformation mode of δ(NCSe). The observations made so far by the various groups of workers indicate that the position and intensity of the peaks vary with the nature of metal. Thus, Aynsley *et al.*[3] have shown that organolead selenocyanates have a sharp single ν(C=N) stretch at 2100 cm^{-1}, indicating that the selenocyanate group is selenium-bonded to the lead atom. On the other hand, the corresponding tin compounds show a broad band at 2108 cm^{-1}, which in $CHCl_3$ resolves into a weak band at 2144 cm^{-1} and a broad band of strong intensity at 2055 cm^{-1}, suggesting the *iso* structure for these compounds.[3] A similar conclusion has been arrived at in the case of $(CH_3)_3Si(NCSe)$.[4] Interestingly enough, on the basis of their ν_{as}(C=N) being a single sharp peak about 2100 cm^{-1}, $Ar_2Tl(III)SeCN$ are interpreted as having the normal[5] form while, in sharp contrast to this, $Bu_2M(III)SeCN$[6] (M = Ga, In or Te) have been shown to possess an *iso* form [ν_{as}(C=N) = 2040 cm^{-1})]. Organotellurium selenocyanates, irrespective of the nature of the organic group attached to the tellurium, have the *iso* structure.[7] Except for the synthesis of diphenylbismuth(III) selenocyanate[1] no synthetic route and IR data are available on the selenocyanate derivatives of group VB elements.[8,13]

In the IR spectra of all the selenocyanate derivatives of arylantimony(V) reported herein there is a sharp band of strong intensity in the range 2050–2090 cm^{-1}. No appreciable shifting was observed in ν_{as}(C=N) when the IR spectra were recorded in a $CHCl_3$ solution and thus the observed frequencies, both in the solid state and in chloroform, listed in Table 1 are consistent with an *N*-bonded NCSe group consonant with the usual *iso* structure of the thiocyanate counterpart of the antimony(V) derivatives.[9] In addition to this, absorption of medium-to-weak intensity in the region 610–650 cm^{-1} also supports the *iso* structure of the newly synthesized compounds.[18,19] In the case of aryl derivatives the deformation mode δ(NCSe) could not be assigned with certainty due to the overlapping of the Sb—C stretching (*Y*-mode) present in the same region. However, a tentative assignment has been made both for the δ(NCSe) deformation mode and for the Sb—N bending mode. Compound **I** exhibits a medium-intensity band at 575 cm^{-1}, which can safely be assigned to the equatorial ν_{as}(Sb—C) mode on the basis of a comparison with earlier studies on pentacoordinated methylantimony derivatives [Me_nSbX_{5-n} (n = 3 or 4, X = halide or pseudohalide)].[9]

A noticeable feature of the IR spectra of all the triarylantimony bis-selenocyanate compounds is the absence of an ν_{sym}(Sb—C) absorption corresponding to the *t*-mode which should be located in the region 250–300 cm^{-1} as reported by earlier workers.[9,10,20] The ν_{as}(Sb—C) absorption corresponding to the *Y*-mode is intermixed with the δ(NCSe) band and appears as a strong band in the range of 455–485 cm^{-1}. A medium-intensity band appearing at about 740 cm^{-1} in the case of μ-oxy-bis(triarylantimony) bis-selenocyanates may be assigned to Sb—O—Sb stretching.

The proton magnetic resonance spectra recorded

on an EM 360L Varian spectrometer in $CDCl_3$ containing TMS as an internal indicator, for a representative compound $(CH_3C_6H_4)_3Sb(SeCN)_2$ showed a singlet due to the CH_3 protons (δ 2.88 ppm) and a multiplet due to the phenyl-ring protons centred at δ 8.50–7.80 ppm. The integration of the peaks was consistent with the proposed formulation.

Thus, on the basis of the IR, NMR, molecular and conductance data, triarylantimony(V) bis-selenocyanates may be assigned a pentacoordinated trigonal bipyramidal structure with the two selenocyanate groups at the apical positions while the aryl groups occupy the equatorial positions. Stibonium selenocyanate [$R_4Sb(NCSe)$] may also be assigned a pentacoordinated covalent structure while a trigonal bipyramidal structure containing an oxygen bridge (Sb—O—Sb) can be proposed for the oxy-bridged organoantimony(IV) selenocyanates.

On the basis of the present and some previous studies on the selenocyanate derivatives of non-transition elements as discussed above, it may reasonably be concluded that the heaviest element organometal selenocyanates in a group, viz. Hg, Pb or Tl, have the normal structure (M—SeCN) while all the preceding elements, including the lighter elements (Sn, In, Sb, Te or Si) exist in the *iso* form (M—NCSe).

All the selenocyanate compounds of antimony have repulsive odours and cause headaches on exposure. A few representative compounds were tested for biocidal activity and were found to possess significant bactericidal and fungicidal activities, details of which will be published elsewhere.

Acknowledgement—We are thankful to the Head of the Chemistry Department, Lucknow University, Lucknow, for providing the necessary laboratory facilities, the Director RSIC, Lucknow, for obtaining IR spectra, and the Council of Scientific and Industrial Research, New Delhi, for a pool officership to K.S. and a JRF to R.R.

REFERENCES

1. F. Challenger, A. T. Peters and J. Hale'vy, *J. Chem. Soc.* 1926, 1648.
2. E. E. Aynsley, N. N. Greenwood and M. J. Sprague, *J. Chem. Soc.* 1965, 2395.
3. E. E. Aynsley, N. N. Greenwood, G. Hunter and M. J. Sprague, *J. Chem. Soc. A* 1966, 1344.
4. J. S. Thayer and R. West, In *Organometallic Pseudohalides* (Edited by F. G. A. Stone and R. West), *Adv. Organomet. Chem.* Vol. 5. p. 169. Academic Press, New York (1967).
5. T. N. Srivastava and K. K. Bajpaj, *J. Organomet. Chem.* 1971, **1**, 31.
6. T. N. Srivastava and Kiran Singhal, *Indian J. Chem.* 1979, **17A**, 611.
7. T. N. Srivastava, R. C. Srivastava and H. B. Singh, *Indian J. Chem. A* 1979, **18**, 71.
8. G. O. Doak and L. D. Freedman, *Organometallic Compounds of Arsenic, Antimony and Bismuth.* Wiley Interscience, New York (1970).
9. E. Maslowsky, *J. Organomet. Chem.* 1974, **70**, 153.
10. P. Raj, A. K. Saxena, K. Singhal and A. Ranjan, *Polyhedron* 1985, **4**, 251.
11. P. Raj, K. Singhal and R. Rastogi, *Polyhedron* 1986, **5**, 677.
12. P. Raj, K. Singhal and R. Rastogi, *Indian J. Chem.* (in press).
13. M. Dub (Ed.), *Organometallic Compounds of Arsenic, Antimony and Bismuth*, 2nd Edn, Vol. 3. Springer, New York (1968).
14. R. G. Goel and D. R. Ridley, *Inorg. Nucl. Chem. Lett.* 1971, **7**, 21.
15. P. Raj and R. Rastogi, *Synth. React. Inorg. Metal–Org. Chem.* 1985 (submitted).
16. J. Chatt and F. G. Mann, *J. Chem. Soc.* 1940, 1192.
17. W. J. Geary, *Coord. Chem. Rev.* 1971, **7**, 110.
18. A. H. Norbury, In *Advances in Inorganic Chemistry and Radiochemistry* (Edited by H. J. Emeleus and A. G. Sharpe), Vol. 17, p. 231. Academic Press, New York (1975).
19. R. A. Bailey, *Coord. Chem. Rev.* 1971, **6**, 407.
20. A. Otero and P. Royo, *J. Organomet. Chem.* 1978, **154**, 13.

Polyhedron Vol. 5, No. 10, pp. 1587–1591, 1986
Printed in Great Britain

0277–5387/86 $3.00+.00
Pergamon Journals Ltd

OXOVANADIUM(IV) COMPLEXES OF CARBOHYDRAZONES AND THIOCARBOHYDRAZONES

O. P. PANDEY

Department of Chemistry, University of Gorakhpur, Gorakhpur 273001, India

(*Received* 8 *May* 1985; *accepted* 24 *February* 1986)

Abstract—Oxovanadium(IV) complexes $\{[VOL_2(H_2O)]SO_4$ (L = ligand derived by the condensation of carbohydrazide or thiocarbohydrazide with benzaldehyde, *o*-nitrobenzaldehyde, anisaldehyde, cinnamaldehyde, acetophenone and 2-acetylpyridine)$\}$ have been synthesized and characterized by elemental analysis, room-temperature magnetic moment, electrical-conductance, electronic, IR and ESR studies. The complexes are hexacoordinate and have a distorted octahedral structure.

Metal complexes of semicarbazide and semicarbazones (thiosemicarbazide and thiosemicarbazones) have attracted much attention due to their activity against smallpox, virus diseases and certain kinds of tumour.[1] Some papers on oxovanadium(IV) complexes with these ligands have also reported certain striking structural features.[2–5] However, very little attention has been paid to the coordination behaviour of the next highest homolog in the series (carbohydrazide and thiocarbohydrazide).[6,7] Oxovanadium(IV) complexes of carbohydrazones and thiocarbohydrazones have been prepared and studied to learn whether coordination to the metal ion still occurs through the sulphur or oxygen atom (as in thiosemicarbazones and semicarbazones) or whether advantage is taken of the available nitrogen donors to form a coordination sheath consisting of only nitrogen atoms.

EXPERIMENTAL

Carbohydrazide and thiocarbohydrazides were prepared as reported in the literature.[7,8] The hydrazones were synthesized by the usual method using ethanol as the solvent.[9,10]

Preparation of complexes

The following general method was used. A hot ethanolic solution of the respective ligand (0.1 mol) and a hot water–ethanol solution of the metal salt (0.05 mol) were mixed together and boiled under reflux on a water bath for *ca* 2 h. The solution was then concentrated to half of its original volume and, on cooling, a brown, blue or green coloured precipitate separated out, which was filtered, washed with ethanol and dried in an oven at 80°C (yield 60–72%).

Analytical procedures

Microanalyses for carbon and hydrogen were performed by the C.D.R.I., Lucknow, and by the Department of Chemistry, B.H.U., Varanasi. Nitrogen was estimated by Kjeldahl's method. Vanadium was estimated as its oxide by the standard gravimetric method.

Physical measurements

Conductance measurements were done using a Toshniwal conductivity bridge type CL O1/O1A. Solid-state IR spectra were recorded with Beckman AccuLab-9 and Perkin–Elmer 621 spectrophotometers. Magnetic measurements were performed by the Faraday method using ferrous ammonium sulphate as the calibrant. The electronic spectra were recorded on Rissian C ϕ10 and Beckman DU-2 automatic recording spectrophotometers. The ESR spectra of polycrystalline samples were recorded on a Varian E_4-EPR spectrometer operating at 9.4-GHz and 100-KHz field modulation and phase-sensitive detection. The instrument was calibrated using DPPH powder.

RESULTS AND DISCUSSION

Elemental analyses (Table 1) reveal that all the complexes have the general composition $[VOL_2(H_2O)]SO_4$. The complexes are soluble in dimethylformamide, dimethylsulphoxide and nitrobenzene. Electrical-conductivity measurements in DMF show that the complexes behave as 1 : 2 electrolytes. The presence of one coordinated water molecule has been confirmed from the TGA studies which show weight loss at 170–180°C.

Magnetic moments and electronic spectra

The spin–orbit coupling (λ) for oxovanadium(IV) complexes is positive[11] and magnetically dilute oxovanadium(IV) complexes should exhibit magnetic moments very close to the spin-only magnetic moment of 1.73 BM[12] expected for an $S = \frac{1}{2}$ system. All the complexes exhibit magnetic moments in the 1.68–1.72 BM range corresponding to one unpaired spin.

Intepretation of the electronic spectra of oxovanadium(IV) complexes is a subject of continuing investigation and discussion. Three spin-allowed transitions, $b_2 \rightarrow e_\pi^* ({}^2B_2 \rightarrow E)$, $b_2 \rightarrow b_1 ({}^2B_2 \rightarrow {}^2B_1)$ and $b_2 \rightarrow a_1 ({}^2B_2 \rightarrow {}^2A_1)$, are expected for distorted octahedral oxovanadium(IV) complexes according to the energy level schemes suggested by Ballhausen and Gray,[13] Selbin[14] and Lever.[15] The present complexes exhibit all three *d–d* transitions in the 12,100–14,500-, 15,000–17,300- and 22,800–24,900-cm^{-1} regions which are assigned to the $b_2 \rightarrow e_\pi^* ({}^2B_2 \rightarrow E)$, $b_2 \rightarrow b_1 ({}^2B_2 \rightarrow {}^2B_1)$ and $b_2 \rightarrow a_1 ({}^2B_2 \rightarrow {}^2A_1)$ transitions, respectively, according to the above schemes.

On the basis of data available, it appears that these complexes have tetragonally distorted octa-

Table 1. Magnetic ESR and analytical data of the complexes[a]

Complex	Colour	Yield	Found (calc.) (%) C	H	N	N	μ_{eff} (300 K) (BM)	g
$[VO(BC_z)_2H_2O]SO_4$	Brown	60	50.3 (50.4)	4.1 (4.2)	15.7 (15.7)	7.1 (7.1)	1.68	1.947
$[VO(OBC_z)_2H_2O]SO_4$	Brown	68	40.3 (40.3)	2.8 (2.9)	18.6 (18.8)	5.7 (5.7)	1.68	1.945
$[VO(AC_z)_2H_2O]SO_4$	Blue	70	48.7 (48.9)	4.4 (4.5)	13.3 (13.4)	6.1 (6.1)	1.70	1.947
$[VO(CC_z)_2H_2O]SO_4$	Blue	72	55.7 (55.8)	4.6 (4.6)	13.6 (13.7)	6.1 (6.2)	1.72	1.948
$[VO(ACC_z)_2H_2O]SO_4$	Greenish blue	65	53.0 (53.0)	4.8 (4.9)	14.4 (14.5)	6.6 (6.6)	1.70	1.945
$[VO(PC_z)_2H_2O]SO_4$	Blue	60	46.5 (46.5)	4.2 (4.3)	21.6 (21.7)	6.5 (6.5)	1.69	1.947
$[VO(BTC_z)_2H_2O]SO_4$	Brown	60	48.3 (48.3)	4.0 (4.0)	14.8 (15.0)	6.7 (6.8)	1.70	1.991
$[VO(OBTC_z)_2H_2O]SO_4$	Brown	62	38.8 (38.9)	2.6 (2.8)	18.1 (18.1)	5.5 (5.5)	1.70	1.990
$[VO(ATC_z)_2H_2O]SO_4$	Green	65	47.0 (47.1)	4.2 (4.3)	12.9 (12.9)	5.8 (5.8)	1.68	1.993
$[VO(CTC_z)_2H_2O]SO_4$	Green	70	53.5 (53.7)	4.3 (4.4)	13.0 (13.1)	6.0 (6.0)	1.72	1.991
$[VO(ACTC_z)_2H_2O]SO_4$	Green	72	50.8 (50.9)	4.7 (4.7)	13.7 (13.9)	6.2 (6.3)	1.70	1.994
$[VO(PTC_z)_2H_2O]SO_4$	Green	68	44.6 (44.7)	4.0 (4.2)	20.8 (20.8)	6.3 (6.3)	1.70	1.992

[a] BC_z = benzaldehydecarbohydrazone; OBC_z = *o*-nitrobenzaldehydecarbohydrazone; AC_z = anisaldehydecarbohydrazone; CC_z = cinnamaldehydecarbohydrazone; ACC_z = acetophenonecarbohydrazone; PC_z = 2-acetylpyridinecarbohydrazone; BTC_z = benzaldehydethiocarbohydrazone; $OBTC_z$ = *o*-nitrobenzaldehydethiocarbohydrazone; ATC_z = anisaldehydethiocarbohydrazone; CTC_z = cinnamaldehydethiocarbohydrazone; $ACTC_z$ = acetophenonethiocarbohydrazone; PTC_z = 2-acetylpyridinethiocarbohydrazone.

hedral structures. Various ligand field parameters (*Dq*, *Ds* and *Dt*) have been calculated by making use of the energy level diagram suggested by Lever,[15] which are also consistent with a tetragonally distorted stereochemistry for the complexes. The negative *Dt* values may presumably be due to weak σ-bonding but still more to a π-bonding ability since *Dq* and *Ds* are positive. The thiocarbohydrazone derivatives have higher *Dq* values compared to corresponding carbohydrazone complexes. This is in line with the higher position of sulphur compared to oxygen in the spectrochemical series.

However, it may be pointed out that these parameters are inadequate, for *Dq* is the measure of the in-plane ligand field only and *Dt* does not take into account an off-diagonal fourth-order contribution. These shortcomings of classical Hamiltonian parameters have recently been overcome by Lever *et al.* by advancing a normalized spherical harmonic (NSH) Hamiltonian.[16,17] In the NSH Hamiltonian, all these parameters are capitalized to relate them to the corresponding crystal field parameters. The NSH and classical parameters are related as:[17]

$$DS = -7Ds,$$

$$DT = \left(\frac{7\sqrt{15}}{2}\right)Dt,$$

$$DQ = (6\sqrt{21})Dq - \left(\frac{7\sqrt{21}}{2}\right)Dt.$$

There are several advantages of NSH Hamiltonian theory: (a) the theory takes into account an off-diagonal contribution to *Dt*; (b) *DQ* is a measure of the average ligand field experienced by the metal ion, unlike the classical *Dq* which is the measure of in-plane field only; and (c) the parameters of the NSH theory are independent of the coordinate system used for the calculations and may be compared with the crystal field or angular overlap parameters to determine the restrictions of these values. The values of different NSH parameters for the present complexes are given in Table 2.

Further, the *DT*/*DQ* ratio has been shown to be a good measure of the degree of tetragonal distortion.[18] The values of *DT*/*DQ* for these complexes (Table 2) lie in the range 0.18–0.21. These values are much lower than the limiting value (0.4226), a value postulated for the square planar complexes, the limiting case of tetragonally distorted complexes. This small value indicates that the complexes are weakly distorted.

Table 2. Electronic spectral data (cm^{-1}) for oxovanadium(IV) complexes

Complex[a]	Assignment			*Dq*	*Ds*	*Dt*	*DQ*	*DS*	*DT*	*DT*/*DQ*
	$b_2 \rightarrow e_\pi^*$	$b_2 \rightarrow b_1$	$b_2 \rightarrow a_1$							
$[VO(BC_2)_2H_2O]SO_4$	12,100	16,050	23,000	1605	2715	−791	56,785	−19,005	10,742	0.19
$[VO(OBC_2)_2H_2O]SO_4$	12,100	16,000	23,000	1600	2715	−791	56,648	−19,005	10,742	0.19
$[VO(AC_2)_2H_2O]SO_4$	12,200	15,900	22,800	1590	2753	−788	56,325	−19,271	10,701	0.19
$[VO(CC_2)_2H_2O]SO_4$	12,150	15,000	22,900	1500	2850	−720	52,762	−19,950	9778	0.18
$[VO(ACC_2)_2H_2O]SO_4$	12,200	16,500	22,900	1650	2657	−826	58,583	−18,599	11,217	0.19
$[VO(PC_2)_2H_2O]SO_4$	12,500	16,300	23,000	1630	2743	−854	58,482	−18,201	11,597	0.20
$[VO(BTC_2)_2H_2O]SO_4$	12,800	17,300	24,500	1730	2857	−845	61,085	−18,999	11,475	0.19
$[VO(OBTC_2)_2H_2O]SO_4$	12,900	17,000	23,800	1700	2814	−891.6	61,008	−19,698	12,108	0.20
$[VO(ATC_2)_2H_2O]SO_4$	12,500	17,000	23,800	1700	2757	−845.8	60,274	−19,299	11,486	0.19
$[VO(CTC_2)_2H_2O]SO_4$	13,500	17,000	23,500	1700	3000	−900	61,143	−21,000	12,222	0.20
$[VO(ACTC_2)_2H_2O]SO_4$	12,900	17,200	24,000	1720	2814	−891.6	61,588	−19,698	12,108	0.20
$[VO(PTC_2)_2H_2O]SO_4$	14,500	17,200	24,900	1720	3171	−997	63,248	−22,197	13,539	0.21

[a] Abbreviations as in Table 1.

ESR spectra

ESR signals are observed readily for oxovanadium(IV) complexes because of the prevalence of a less than cubic symmetry, which results in a longer relaxation time. An isotropic spectrum is obtained at room temperature.

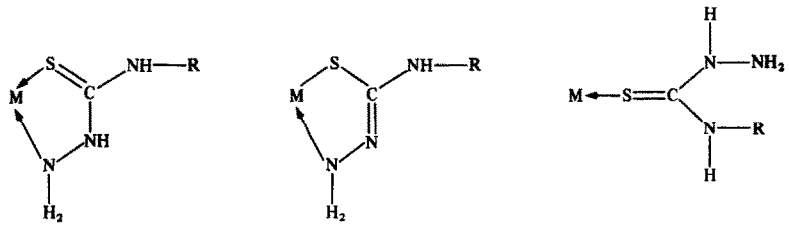
g values are listed in Table 1. They are lower than the free-electron value (2.0023) as expected for a d^1-system and this is related to the spin–orbit interaction of the ground state with a low-lying excited state. The decrease in the free-electron value is an approximate measure of the ligand field strength; the stronger the ligand field the smaller the decrease in the g value relative to the free-electron value. In the present study, the g-values of thiocarbohydrazone complexes are higher than those of carbohydrazone complexes. This also indicates the thiocarbohydrazone complexes possess a higher ligand field than carbohydrazone complexes. The line width is observed in the 240–260-G range.

IR spectra

Thiocarbohydrazone derivatives. The major interest in the preparation of these complexes is the attachment of the Schiff base ligand derived from thiocarbohydrazide. The IR spectra of thiocarbohydrazide and its complexes with several metals (Zn, Cd, Hg, Fe, Co, Ni and Pd) have been studied by Burns by carrying out a normal-coordinate analysis of the free ligand.[7] The thiocarbohydrazide molecule was treated as though it had C_{2v}-symmetry. X-ray crystallographic studies[19–21] have identified structures **1**–**3**. Recently, Singh *et al.*[22] and Srivastava *et al.*[23] have synthesized Mn(II), Ni(II), Cu(II), Zn(II), Pd(II), Pb(II) and Sn(IV) complexes with thiocarbohydrazones and concluded that the ligand can be pentadentate, quadridentate or tetradentate. The coordination behaviour of these ligands depends upon the nature of metal ion, the reaction conditions and the pH of the medium.

The ligands show one medium-intensity band and one weak band at *ca* 3270 and 1650 cm^{-1}, assignable to ν(NH) and δ(NH) of the secondary amine group.[7] These bands persist in the spectra of the complexes, indicating the non-coordination of the amino group. The ν(C=N) absorption at *ca* 1630–1600 cm^{-1} in the spectra of the ligands appears as a split band on complexation with one band located almost at the original position (due to uncoordinated C=N) and the other shifted to a lower frequency (*ca* 1590–1580 cm^{-1}), arising from the coordinated C=N. The splitting of ν(C=N) suggests that only one of the azomethine nitrogen atoms is involved in coordination.[24,25] The ν(C=S) band[22] appearing at 820–790 cm^{-1} in the spectra of the ligands is of medium intensity at 760–740 cm^{-1} in the spectra of the complexes. This shift to a lower wavenumber suggests that the thioamide sulphur is one of the bonding sites in the complexes.[25] Medium- or weak-intensity bands at *ca* 980, *ca* 460 and *ca* 400–380 cm^{-1} are tentatively assigned to ν(V=O), ν(V—N) and ν(V—S), respectively.

Carbohydrazone derivatives. Compared with thiocarbohydrazide derivatives, very few reports are available on the coordination behaviour of carbohydrazide[6,26–28] and, particularly, no study has been done on Schiff bases derived from carbohydrazide. The ligands carbohydrazones show one medium-intensity band at *ca* 3250 cm^{-1} due to ν(NH) of the secondary amino group which remains almost at the same position in oxovanadium(IV), indicating its non-involvement in coordination.[28] The carbohydrazones contain a —CONH— grouping and should show amide group vibrations. These are observed[27] at *ca* 1700 cm^{-1} [amide I, ν(C=O)], 1500 cm^{-1} [amide II, ν(CN)+δ(NH)], 1260–1220 cm^{-1} [amide III, δ(NH)] and 680–660 cm^{-1} [amide IV, ϕ(C=O)]. In the oxovanadium(IV) complexes, all these bands except amide I show upward shifts (~60–20 cm^{-1}), whereas the amide-I band shows a downward shift (~35–25 cm^{-1}). These changes in amide group vibrations indicate that the amide oxygen (ketonic) takes part in coordination to the metal atom.[27] This has further been confirmed by the appearance of new bands at *ca* 480–470 cm^{-1} assignable to ν(V—O).[29] The IR spectra of all carbohydrazones show a strong band at 1610–1600 cm^{-1} which may be due to the vibration of the azomethine linkages. In the complexes, this band is



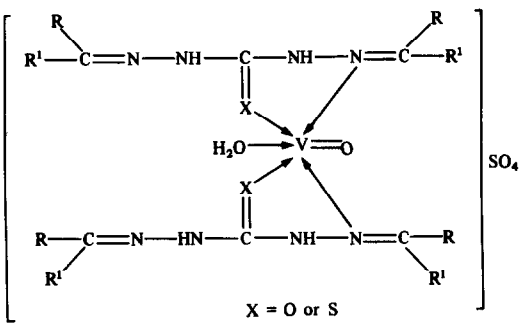
1 **2** **3**

found to be split into two with one almost at the same position and the other at a lower frequency (~1585–1570 cm^{-1}), indicating that only one of the azomethine nitrogens is involved in coordination.[25] The ν(V—N) vibration is observed at *ca* 460–440 cm^{-1}. The bands due to the ν(V=O) vibration occur in the 980–960 cm^{-1} region. The position of this band in different complexes clearly indicate that the ν(V=O) frequency depends upon the nature of substituent present in the ring, i.e. electron-withdrawing groups cause a lowering of the ν(V=O) frequency, and vice versa.

The carbohydrazone and thiocarbohydrazone derived from 2-acetylpyridine show bands at *ca* 1570, 600 and 420 cm^{-1} which may be assigned[27,30] to 8a (pyridine ring deformation), 6a (in-plane ring deformation) and 16b (out-of-plane ring deformation). In their complexes, all these bands persist, indicating the non-coordination of pyridine nitrogen to vanadium atoms.

In addition to these, the presence of an ionic sulphate group in these complexes has been confirmed[31] by the appearance of three bands at *ca* 1130 cm^{-1} (ν_3), 930 cm^{-1} (ν_1) and 650 cm^{-1} (ν_4). The absence of the ν_2-band and the non-splitting of ν_3-band indicates that T_d-symmetry still holds.[31]

Thus, on the basis of above discussion, the following structures may be assigned to the different complexes:



Acknowledgements—I am thankful to Professor S. C. Tripathi and Dr S. K. Sengupta for helpful discussions. Financial assistance from the Council of Scientific and Industrial Research is thankfully acknowledged.

REFERENCES

1. M. J. M. Campbell, *Coord. Chem. Rev.* 1975, **15**, 279 (and references therein).
2. Z. A. Saveleva, S. V. Laviorior, A. V. Nikolaev, L. T. Nasonava and G. N. Dubnlo, *Izv. Sib. Otd. Akad. Nauk. SSSR, Ser. Khim. Nauk* 1977, 73.
3. R. C. Aggarwal and B. S. Yadav, *Transition Met. Chem.* 1976, **1**, 136.
4. V. B. Rana, S. K. Sahni, M. P. Swami, P. C. Jain and A. K. Srivastava, *J. Inorg. Nucl. Chem.* 1976, **38**, 176.
5. V. B. Rana, P. C. Jain, M. P. Swami and A. K. Srivastava, *Indian J. Chem.* 1975, **13A**, 730.
6. F. Kurzer and M. Wilkinson, *Chem. Rev.* 1970, **70**, 145.
7. G. R. Burns, *Inorg. Chem.* 1968, **7**, 277.
8. E. B. Möhr, J. J. Brezinski and L. F. Audrieth, *Inorg. Synth.* 1953, **4**, 32.
9. H. W. Stephen and F. Wilson, *J. Chem. Soc., Dalton Trans.* 1976, 120.
10. L. F. Audrieth, E. S. Scott and P. S. Kippur, *J. Org. Chem.* 1954, **19**, 733.
11. A. Syamal, *Coord. Chem. Rev.* 1975, **16**, 309.
12. B. N. Figgis, *Introduction to Ligand Fields*, p. 266. Wiley, New York (1966).
13. C. J. Ballhausen and H. B. Gray, *Inorg. Chem.* 1962, **1**, 111.
14. J. Selbin, *Chem. Rev.* 1965, **65**, 153; *Coord. Chem. Rev.* 1966, **1**, 293; J. Selbin and L. Morpurgo, *J. Inorg. Nucl. Chem.* 1965, **27**, 673.
15. A. B. P. Lever, *Inorganic Electronic Spectroscopy*. Elsevier, Amsterdam (1968).
16. J. C. Donini, B. R. Hollebone, G. London, A. B. P. Lever and J. C. Hempel, *Inorg. Chem.* 1975, **14**, 455.
17. J. C. Donini, B. R. Hollebone and A. B. P. Lever, *Prog. Inorg. Chem.* 1977, **22**, 225.
18. S. K. Sahni and S. K. Sangal, *Synth. React. Inorg. Met.-Org. Chem.* 1978, **8**, 291.
19. M. Nardelli, G. F. Gasperri, G. G. Baltistini and A. Musatti, *J. Chem. Soc., Chem. Commun.* 1965, 187.
20. L. Cavalca, M. Nardelli and G. Fava, *Acta Cryst.* 1962, **15**, 1139.
21. R. Grnbaek and S. E. Rasmussen, *Acta Chem. Scand.* 1962, **16**, 2325.
22. R. Singh, J. P. Srivastava and L. K. Mishra, *Indian J. Chem.* 1977, **15A**, 805.
23. T. N. Srivastava and M. Agarwal, *Indian J. Chem.* 1979, **17A**, 613.
24. S. Satapathy and B. Sahoo, *J. Inorg. Nucl. Chem.* 1970, **32**, 2223.
25. O. P. Pandey, S. K. Sengupta and S. C. Tripathi, *Transition Met. Chem.* 1983, **8**, 362.
26. E. Campi, G. Ostacoli, A. Vanni and E. Casotati, *Ric. Sci. Rend.* 1964, **A6**, 344.
27. S. K. Sengupta, S. K. Sahni and R. N. Kapoor, *J. Coord. Chem.* 1982, **12**, 113.
28. O. P. Pandey, S. K. Sengupta and S. C. Tripathi, *Synth. React. Inorg. Met.-Org. Chem.* 1983, **13**, 867.
29. J. R. Ferraro, *Low Frequency Vibrations of Inorganic and Coordination Compounds*. Plenum, New York (1971).
30. D. P. Madden and S. M. Nelson, *J. Chem. Soc. A* 1968, 2342.
31. K. Nakamoto, *Infrared Spectra of Inorganic and Coordination Compounds*. Wiley, New York (1970).

Polyhedron Vol. 5, No. 10, pp. 1593–1596, 1986
Printed in Great Britain

0277–5387/86 $3.00+.00
Pergamon Journals Ltd

CRYSTAL STRUCTURE OF RUBIDIUM PENTABROMODISTANNATE(II)

ISAAC ABRAHAMS, JOHN D. DONALDSON and SUSAN GRIMES*

Department of Chemistry, The City University, Northampton Square, London EC1V 0HB, U.K.

GIOVANNI VALLE

Centro di Ricerche sui Biopolimeri del CNR, Via Marzolo, 35100, Padua, Italy

and

SANDRO CALOGERO

ICTR–CNR Corso Stati Uniti, 35100, Padua, Italy

(*Received* 20 *November* 1985; *accepted* 24 *February* 1986)

Abstract—The crystal structure of rubidium pentabromodistannate(II) ($RbSn_2Br_5$) is determined. The crystals are tetragonal and contain four formula units in a cell of dimensions $a = 8.442(2)$ Å, and $c = 14.754(3)$ Å with $D_c = 4.54$ g cm^{-3}, and $D_m = 4.44$ g cm^{-3}. The structure was solved in the space group *I*4/*mcm*. Unlike $NaSn_2F_5$, which contains discrete $[Sn_2F_5]^-$ ions, the structure is a layered lattice consisting of two-dimensional polymeric $(Sn_2Br_5)_n^{n-}$ layer units separated by Rb ions. The Sn and bridging Br atoms lie in planes perpendicular to the *c*-axis at $c = 0$ and $c = \frac{1}{2}$. Each Sn atom is surrounded by two bridging Br atoms, at 3.105(1) Å, in the plane of the polymer network and by two terminal Br atoms, at 2.755(3) Å, symmetrically above and below the network plane. The bridging Br atoms are surrounded by four equatorial Sn atoms and by two axial Rb atoms in the direction of the *c*-axis at 3.688(1) Å. The positions of the non-bonding orbitals on the Sn(II) atoms suggest that the lone pairs could be partly delocalized within the polymeric network. The ^{119}Sn Mössbauer data for $RbSn_2Br_5$ are interpreted in the light of its structural data.

The presence of stereochemically active lone pairs of electrons in Sn(II) species usually results in a distorted environment around the Sn atom.[1] The most common type of distortion found has a trigonal pyramidal distribution of three nearest-neighbour Sn–ligand bonds and three longer essentially non-bonding contacts completing a distorted octahedral environment. The longer contacts arise because close approach of the ligands to the tin is prevented along directions in which the lone pairs point. In the less common distorted four pyramidal environment, the Sn atom has two short bonds to ligands and two bonds of greater length than those normally found in Sn(II) compounds as nearest-neighbour contacts. Although most Sn(II) compounds have low-symmetry lattices, a few structures have tin in high-symmetry regular octahedral sites. Such environments are found in compounds containing heavier halide and chalcogenide ions, in which the distorting effects of the non-bonding electron pair, on the Sn atom, are removed by a population of solid-state bands arising from overlap of the empty halide or chalcogenide orbitals. Recent evidence has also shown that the direction in which lone-pair orbitals point can lead to some delocalization of the non-bonding electrons into cluster orbitals.[2]

In most examples in which Sn(II) forms complex ions with ligands, the triligandstannate(II) species

* Author to whom correspondence should be addressed.

is the stable and predominant ion. Crystal structures of a number of alkali metal trichloro- and trifluoro-stannates(II) have been determined.[3] The only known structure of a pentahalodistannate(II) complex, however, is that of $NaSn_2F_5$, in which an F atom bridges two SnF_2 groups to form discrete $[Sn_2F_5]^-$ ions.[4] There is, however, a considerable difference in the nature of bonds formed between Sn and F, and those formed between Sn and other halogen atoms.[1] We now describe the first structure determination of a pentahalogenodistannate(II) with a halide other than fluoride.

EXPERIMENTAL

Preparation

Rubidium pentabromodistannate(II) ($RbSn_2Br_5$) was prepared by mixing the appropriate quantities of RbBr and $SnBr_2$ dissolved in the minimum amount of boiling water containing tin metal and a few drops of HBr to minimize oxidation and hydrolysis, respectively. The resulting mixture was evaporated to give a clear yellow solution from which white rhomboid plates formed on cooling. These were collected and dried, *in vacuo*, over silica gel. The whole process was carried out under N_2 to minimize oxidation. A single crystal was selected from the bulk material to obtain the cell data.

X-ray crystal structure

Crystal data. $RbSn_2Br_5$, $M = 722.37$, tetragonal, space group $I4/mcm$ (No. 140), $a = b = 8.442(2)$ Å, $c = 14.754(3)$ Å, $U = 1051.48$ Å^3, $Z = 4$, $D_c = 4.56$ g cm^{-3}, $D_m = 4.44$ g cm^{-3}, $F(000) = 1248$. μ(Mo-K_α) = 275.31 cm^{-1}, $\gamma = 0.7107$ Å, $R = 0.058$. Intensity data were collected with a Philips PW1100 four-circle diffractometer by use of monochromatized Mo-K_α radiation. Intensity data for 365 independent tetragonal reflections were observed and of these 284 with $I > 3\sigma(I)$ were used in subsequent calculations. Data were corrected for Lorentz and polarization factors but not for absorption. The structure was solved via the heavy-atom method and refined successfully in the centrosymmetric space group $I4/mcm$. All atoms were refined with anisotropic temperature factor coefficients, giving a final R value of 0.058. Calculations were performed using "SHELX-76"[5] and unit-cell projections were obtained using "PLUTO".[6] The final atomic positions and anisotropic thermal parameters and lists of F_o/F_c values have been deposited with the Editor.* A projection of the unit cell is shown in Fig. 1. Bond lengths and angles are in Table 1.

^{119}Sn *Mössbauer spectra*

The ^{119}Sn Mössbauer data were recorded, at 80 K, using a $CaSnO_3$ source, on a Cryophysics MS102 spectrometer with a multi-channel analyser and fitted to Lorentzian distributions.

Thermal analysis

TG/DTA data were obtained over the temperature range, ambient to 600°C, using a Stanton Redcroft STA-780 Simultaneous Thermal Analyser. $RbSn_2Br_5$ decomposes above its melting point of 290°C.

RESULTS AND DISCUSSION

The arrangement of the Sn and bridging Br(1) atoms is such that they constitute a two-dimensional polymeric network perpendicular to the c-axes at $c = 0$ and $c = \frac{1}{2}$. The remaining Br(2) atoms lie symmetrically above and below the plane of the network forming terminal Sn—Br bonds. The resultant layer structure (Fig. 1) consists of two-dimensional polymeric $(Sn_2Br_5)_n^{n-}$ anionic layers separated by Rb ions lying symmetrically above and below Br(2) in the direction of the c-axis. The formation of the polymeric $(Sn_2Br_5)_n^{n-}$ network is in sharp contrast to the discrete $[Sn_2F_5]^-$ units found in $NaSn_2F_5$.

The Sn atoms in the structure are in distorted square pyrimidal environments with two long bonds to bridging Br(1) atoms within the plane of the polymeric network and two terminal bonds to Br(2) atoms symmetrically positioned above and below the plane of the network (Fig. 2). The distorted square pyramidal environment of the Sn atoms shown in Fig. 3 has an Sn—Br(2) bond length of 2.755(3) Å, typical of strong Sn—Br bonding interactions, and Sn—Br(1) bond lengths of 3.105(1) Å that are shorter than those found in Sn_3BrF_5[7] (3.29–3.35 Å) and which were considered to be non-bonding. The bridging Br(1) atoms are surrounded by four equatorial Sn atoms at distances of 3.105(1) Å and by two axial Rb atoms in the direction of the c-axis at 3.688(1) Å. The terminal Br atom, Br(2), is surrounded by one Sn at 2.75 Å, two Sn atoms at 3.49 Å, two Rb atoms at 3.60 Å, and two Br atoms at 3.84 and 3.97 Å.

The Sn–Br network perpendicular to the c-axis

* Atomic coordinates have also been deposited with the Cambridge Crystallographic Data Centre.

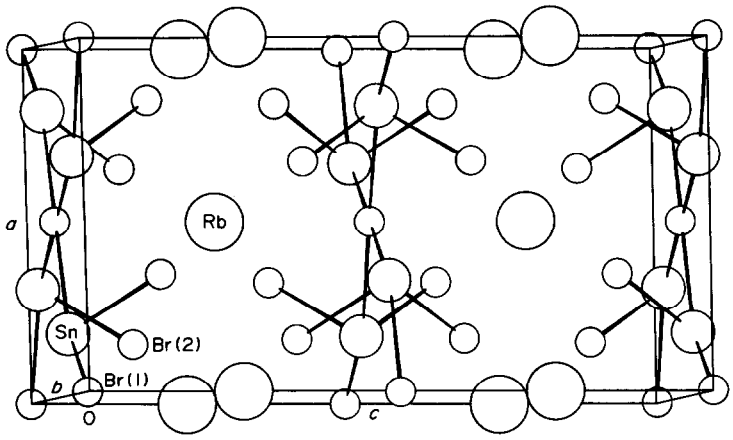


Fig. 1. Unit-cell contents of $RbSn_2Br_5$.

consists of interlocked puckered planar eight-membered Sn_4Br_4 rings. The Sn–Sn distances across the rings are 4.26 and 7.68 Å. The positions of the terminal Br atoms cause the lone pair orbitals on the Sn atoms to lie in the plane of the ring. It is interesting to note that the lone pairs on the Sn atoms point directly towards one another across the shortest Sn–Sn distance in the ring. This distance of 4.261(5) Å is too long to permit direct interaction between the filled non-bonding orbital on one Sn atom and the empty orbital on the opposite Sn atom, but they are close enough to the terminal Br atoms above and below the plane, directed along the longer Sn–Sn distance of the ring, to enable interaction between the lone-pair orbitals on Sn and the empty *d*-orbitals of Br. Taking the radius of the *s*-orbitals on the Sn atom as 2.05 Å and the empty *d*-orbitals on Br as 2.4 Å,[8] a significant overlap between the filled Sn orbitals and the Br *d*-orbitals is suggested. The effect of this would be to delocalize some of the lone-pair electron density on the Sn atoms into a two-dimensional band structure produced by overlap of empty Br *d*-orbitals within the planar ring network. The unusual Br(2)—Sn—Br(2) angle of approximately 90° is consistent with the suggested delocalization because it would provide the best arrangement of Br atoms to ensure a maximum overlap of the lone pairs on Sn and the empty Br *d*-orbitals. Such solid-state effects would not be possible in Sn–F networks because of the absence of suitable *d*-orbitals on the F to produce a delocalized band system and this may account for the formation of discrete $[Sn_2F_5]^-$ ions in $NaSn_2F_5$ rather than the polymeric network structure in $RbSn_2Br_5$.

The delocalization of non-bonding Sn electrons in $RbSn_2Br_5$ forms part of a range of interactions involving the non-bonding pairs that are known to have important consequences in certain Sn(II) compounds. The types of interactions range from dimer formation in $Sn[CH(SiMe_3)_2]_2$,[9] where the stability and structure of the material arises from interactions between the lone pair of one Sn atom with the empty orbital on the other Sn atom in the dimer, cluster formation of Sn atoms around the halogens in $K_3Sn_2(SO_4)_3X$ (X = Br or Cl),[2] where the distorting effects of the lone-pair orbitals pointing towards the halide ions are removed by delocalization of the Sn electron density into the cluster orbitals, to the population of solid-state bands by

Table 1. Bond lengths (Å), angles (°) and some significant contact distances (Å)

Sn—Br(1)	3.105(1)	Sn—Br(2)	2.755(3)
Rb...Br(1)	3.688(1)	Rb...Br(2)	3.600(1)
Br(1)...Br(2)	3.735(1)	Br(2)...Br(2)	3.844(5)
Sn...Sn	4.261(5)		
Br(1)—Sn—Br(2)	79.0(1)	Br(2)—Sn—Br(2)	91.8(1)
Br(1)—Rb—Br(2)	61.6(1)	Br(2)—Rb—Br(2)	68.0(1)
Rb—Br(1)—Br(2)	58.0(1)	Sn—Br(1)—Br(2)	46.4(1)
Sn—Br(2)—Rb	97.8(1)		

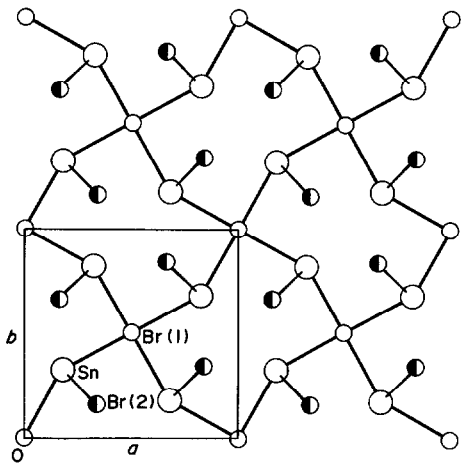


Fig. 2. $(Sn_2Br_5)_n$ layer at *110* (half-shaded atoms represent overlapping Br(2) sites).

non-bonding electrons that accounts for the optical and electrical properties of compounds such as $CsSnBr_3$[10] and SnO,[8] where the non-bonding orbitals are delocalized into three-dimensional and adjacent-layer Sn bands, respectively.

The ^{119}Sn Mössbauer shift of 3.91(6) mm s^{-1} for the complex $RbSn_2Br_5$ is only slightly lower than that of its parent compound $SnBr_2$ (δ = 3.98 mm s^{-1}). This slight decrease in shift can be described in terms of the existence of $SnBr_2$ units in the structure of $RbSn_2Br_5$ bridged by Br atoms. The quadrupole splitting of 0.89(5) mm s^{-1} is consistent with the unsymmetrical arrangement about the Sn atom with two short and two long Sn—Br bonds found in this structure.

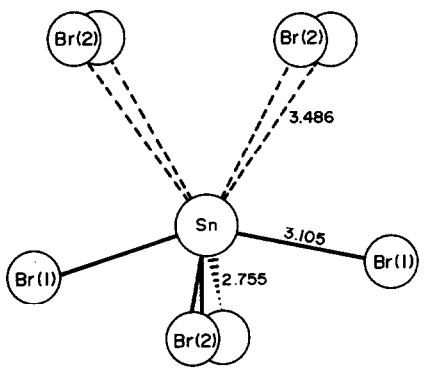


Fig. 3. Environment of the Sn atom.

Acknowledgements—We thank the S.E.R.C. and the International Tin Research Institute for a CASE award studentship (to IA). Financial support from the MSI, Rome, and from the bilateral projects of the CNR, Rome, is gratefully acknowledged.

REFERENCES

1. J. D. Donaldson and S. M. Grimes, *Rev. Silicon, Germanium, Tin Lead Compd.* 1985, **8**, 1.
2. J. D. Donaldson and S. M. Grimes, *J. Chem. Soc., Dalton Trans.* 1984, 1301.
3. P. A. Cusack, P. J. Smith, J. D. Donaldson and S. M. Grimes, *A Bibliography of X-ray Crystal Structures of Tin Compounds.* I.T.R.I. Publication No. 588, London (1980).
4. R. R. McDonald, A. C. Larson and D. T. Cromer, *Acta Cryst.* 1964, **17**, 1104.
5. G. M. Sheldrick, *Program for Crystal Structure Determination.* University of Cambridge (1975).
6. W. D. S. Motherwell, *Program of Plotting Molecular and Crystal Structures.* University of Cambridge (1979).
7. J. D. Donaldson, D. R. Laughlin and D. C. Puxley, *J. Chem. Soc., Dalton Trans.* 1977, 865.
8. J. D. Donaldson, J. Silver, S. Hadjiminolis and S. D. Ross, *J. Chem. Soc., Dalton Trans.* 1975, 1500.
9. J. D. Cotton, P. J. Davidson, M. F. Lappert, J. D. Donaldson and J. Silver, *J. Chem. Soc., Dalton Trans.* 1976, 2286.
10. S. J. Clark, C. D. Flint and J. D. Donaldson, *J. Phys. Chem. Solids* 1981, **42**, 133.

Polyhedron Vol. 5, No. 10, pp. 1597–1600, 1986
Printed in Great Britain

0277–5387/86 $3.00+.00
Pergamon Journals Ltd

COMPLEXATION OF SODIUM AND SILVER IONS BY THE CRYPTAND 4,7,13-TRIOXA-1,10-DIAZABICYCLO[8.5.5]EICOSANE IN A RANGE OF SOLVENTS

STEPHEN F. LINCOLN* and BARRY J. STEEL

Department of Physical and Inorganic Chemistry, University of Adelaide, South Australia 5001, Australia

and

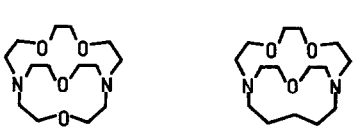
IAN M. BRERETON and THOMAS M. SPOTSWOOD

Department of Organic Chemistry, University of Adelaide, South Australia 5001, Australia

(*Received* 6 *January* 1986; *accepted* 24 *February* 1986)

Abstract—The apparent stability constants (K) of the cryptates $[Ag \cdot C21C_5]^+$ and $[Na \cdot C21C_5]^+$ ($C21C_5$ = 4,7,13-trioxa-1,10-diazabicyclo[8.5.5]eicosane) have been determined in a range of solvents. For $[Na \cdot C21C_5]^+$ log (K/dm^3 mol^{-1}) = 2.87, 3.72, 3.76, 3.98, 5.08 and 5.12 at 298.2 K in dimethylformamide, pyridine, methanol, acetone, acetonitrile and propylene carbonate, respectively, in the presence of 0.05 mol dm^{-3} tetraethylammonium perchlorate supporting electrolyte. These values are substantially lower than those observed for $[Na \cdot C211]^+$ (C211 = 4,7,13,18-tetraoxa-1,10-diazabicyclo-[8.5.5]eicosane) and this is attributed to the presence of one less oxygen atom in $C21C_5$ than in C211. A similar relationship is observed for $[Ag \cdot C211]^+$ and $[Ag \cdot C21C_5]^+$, where, for the latter cryptate, log (K/dm^3 mol^{-1}) = 5.19, <2, 7.62, 8.58 and 4.55 at 298.2 K in dimethylformamide, pyridine, methanol, acetone and acetonitrile, respectively.

As part of a study of cryptates[1–3] we have determined the apparent stability constants (K) of sodium and silver cryptates formed with the cryptand 4,7,13-trioxa-1,10-diazabicyclo[8.5.5]eicosane ($C21C_5$) in dimethylformamide, pyridine, methanol, acetone, acetonitrile and propylene carbonate in order to determine the effect on cryptate stability of the replacement of an oxygen atom in 4,7,13,18-tetraoxa-1,10-diazabicyclo[8.5.5]eicosane (C211) by a methylene unit. (The low solubilities of $C21C_5$ and $[Na \cdot C21C_5]ClO_4$ in water precluded a study in this solvent.) In the solid state both [Na(C211)NCS] and [Na($C21C_5$)NCS] exist in the *exclusive* form in which Na^+ resides above the face of the 15-membered ring delineated by two nitrogens and three oxygens (hereafter referred to as the N_2O_3 face), and the nitrogen of NCS^- is within bonding distance of Na^+.[2] ($[Li \cdot C211]I$[4] and $[Li \cdot C21C_5]NCS$[3] exemplify the *inclusive* form of cryptates in which the metal ion is totally encapsulated within the cryptand.) ^{13}C NMR spectra[1,2] of the perchlorate analogues of both of the above cryptates are consistent with the retention of the *exclusive* form of the cryptate in solution, and it is probable that solvent largely displaces perchlorate from the first coordination sphere of Na^+. Thus in this study $[Na(C211)]^+$ and $[Na(C21C_5)]^+$ denote the *exclusive* form of the cryptate in which Na^+ resides above the N_2O_3 face of the cryptand and at the same time retains part of its solvation shell. There appear to be no published structural studies of the analogous Ag^+ cryptates, but as the effective six-



C211 $C21C_5$

Scheme 1.

* Author to whom correspondence should be addressed.

coordinate ionic radius[5] of Ag^+ (1.15 Å) is greater than that of Na^+ (1.02 Å), and the diameters[6] of the C211 and $C21C_5$ cavities or crypts are 1.6 Å, it is expected that $[Ag \cdot C211]^+$ and $[Ag \cdot C21C_5]^+$ should exist in the *exclusive* form on the basis of these relative sizes.

EXPERIMENTAL

Materials

The cryptand $C21C_5$ was prepared as previously described and its purity was determined to be at least 98.5% by ^{13}C NMR spectroscopy.[2] Tetraethylammonium chloride (BDH) was converted to tetaethylammonium perchlorate through ion exchange of chloride on Amberlite IRA-400 resin in the hydroxide form followed by precipitation of the perchlorate with perchloric acid. This was followed by two recrystallizations from water, and vacuum drying at 335 K for 24 h to produce tetraethylammonium perchlorate which was stored over P_4O_{10} *in vacuo*. Sodium and silver perchlorate (Fluka) were dried *in vacuo* at 335 K for 48 h and were stored over P_4O_{10}. Dimethylformamide, pyridine, methanol, acetone, acetonitrile and propylene carbonate (BDH) were purified and dried as described in the literature[7] and were stored over Linde 3A molecular sieves under dry nitrogen.

Stability constant (K) *determinations*

K were determined titrimetrically at 298.2 ± 0.02 K in a water-jacketed Princeton Applied Research vessel under a dry nitrogen stream which both stirred the titration solution and prevented the ingress of moisture. Solutions for titration were 0.05 mol dm^{-3} in tetraethylammonium perchlorate background electrolyte, and were prepared in glove boxes under dry nitrogen. $[Ag \cdot C21C_5]^+$ K were determined from the potentiometric titration of 25 cm^3 of 10^{-3} mol dm^{-3} $AgClO_4$ solution with 10^{-2} mol dm^{-3} $C21C_5$ solution. The titration was monitored through a silver wire electrode and a reference electrode consisting of a silver wire in a 10^{-2} mol dm^{-3} $AgClO_4$ solution in the titration solvent. The titration vessel and the reference electrode were linked through a salt bridge containing 0.05 mol dm^{-3} tetraethylammonium perchlorate in the solvent under study. Cell potentials were measured using an Orion Research 701A digital analyser and were accurate to ±0.2 mV. The electrode response was calibrated in each solvent by measuring the potentials of solutions of known Ag^+ concentration in the presence of 0.05 mol dm^{-3} tetraethylammonium perchlorate, and encompassing the Ag^+ concentration range encountered in the $[Ag \cdot C21C_5]^+$ titration. Plots of potential (E) in mV against log$[Ag^+]$ were linear with slopes ($= k$) in the range 55–65 mV consistent with eqn (1):

$$E = E_o + k \log[Ag^+]. \quad (1)$$

K for $[Ag \cdot C21C_5]^+$ were determined from $[Ag^+]$ derived from the titrations by eqn (1) using methods of calculation described in the literature.[8] The derived K appear in Table 1.

In dimethylformamide, methanol, acetone and acetonitrile the K for $[Na \cdot C21C_5]^+$ were determined using a competitive-equilibrium method from the literature.[9,10] K_{Na} for the equilibrium

Table 1. Log (K/dm^3 mol^{-1}) for sodium and silver cryptates in the presence of 0.05 mol dm^{-3} tetraethylammonium perchlorate in a range of solvents at 298.2 K

Solvent	D_N[a]	Log (K/dm^3 mol^{-1}) at 298.2 K for the cryptates[b]			
		$[Na \cdot C21C_5]^+$[c]	$[Na \cdot C211]^+$[d]	$[Ag \cdot C21C_5]^+$[c]	$[Ag \cdot C211]^+$[d]
Dimethylformamide	26.6	2.87	5.2	5.19	8.6
Pyridine	33.1	3.72	—	<2	—
Methanol	19.0	3.76	6.1	7.62	10.6
Acetone	17.0	3.98	—	8.58	—
Acetonitrile	14.1	5.08	>9	4.55	7.7
Propylene carbonate	15.1	5.12	8.7	—	14.4

[a] Gutmann donor numbers from Ref. 13.

[b] Error in log (K/dm^3 mol^{-1}) is ±0.10 for data obtained in this study except for $[Ag \cdot C21C_5)^+$ in methanol where it is ±0.02.

[c] This study.

[d] Data from Ref. 12.

shown in eqn (2) may be determined by eqn (3) if K_{Ag} is known:

$$[Na \cdot C21C_5]^+ + Ag^+ \overset{K'}{\rightleftharpoons} [Ag \cdot C21C_5]^+ + Na^+, \quad (2)$$

$$K' = \frac{K_{Ag}}{K_{Na}} = \frac{[Ag \cdot C21C_5^+][Na^+]}{[Na \cdot C21C_5^+][Ag^+]}. \quad (3)$$

Thus, using the previously described apparatus, 25 cm^3 of 10^{-3} mol dm^{-3} $AgClO_4$ solution were titrated with a solution 10^{-2} mol dm^{-3} in both $NaClO_4$ and $C21C_5$. The derived K_{Na} data appear in Table 1.

Only a small potential change was observed for the $[Ag \cdot C21C_5]^+$ system in pyridine consistent with $\log (K_{Ag}/dm^3\ mol^{-1}) < 2$, and as a consequence K_{Ag} could not be accurately determined by the direct titration of Ag^+ employed in this study. Despite several purifications of propylene carbonate, $AgClO_4$ solutions in this solvent rapidly turned brown, and as a result no Ag^+ titrations were attempted.

The K of $[Na \cdot C21C_5]^+$ in pyridine and propylene carbonate were determined by direct Na^+ titration using the equipment employed in the Ag^+ titrations with the silver wire electrode replaced by a Radiometer G502 specific sodium ion electrode. The response of the electrode was calibrated and the $[Na \cdot C21C_5]^+$ titrations were carried out in a similar manner to that described for the $[Ag \cdot C21C_5]^+$ titrations, and the derived $\log (K_{Na}/dm^3\ mol^{-1})$ values appear in Table 1. All titrations were carried out in duplicate.

RESULTS AND DISCUSSION

In the solid state Na^+ is bound to the N_2O_3 face of the cryptand in $[Na \cdot C21C_5 \cdot NCS]$ with Na—N (cryptand) distances of 2.576(3) and 2.759(4) Å, and Na—O distances of 2.297(2), 2.340(3) and 2.356(2) Å.[2] In $[Na \cdot C211 \cdot NCS]$ Na^+ is also bound on the N_2O_3 face with Na—N(cryptand) distances of 2.492(17) and 2.478(13) Å, and Na—O distances of 2.289(14), 2.324(13) and 2.433(19) Å, and a fourth Na—O distance of 2.662(9) Å.[2] Thus although both cryptates exist in the *exclusive* form the fourth oxygen of $[Na \cdot C211 \cdot NCS]$ opposite the N_2O_3 face, above which Na^+ is sited, is still within bonding distance of Na^+. It is therefore expected that this fourth oxygen should have a significant influence on the stability of $[Na \cdot C211]^+$ in solution. Apart from the displacement of the anion (which in this study is perchlorate instead of thiocyanate) from its binding site with Na^+, it is anticipated that the *exclusive* structures observed in the solid state are largely retained in solution as indicated by ^{13}C NMR studies.[1,2] There are potentially two alternative forms of *exclusive* $[Na \cdot C211]^+$ in which Na^+ binds either to one of the equivalent 15-membered N_2O_3 faces of C211 (as observed in the solid state) or to the smaller 12-membered N_2O_2 face. The stability constants characterizing the crown ether complexes $[Na \cdot 12C4]^+$ in methanol and propylene carbonate are 10–100 times less than those observed for $[Na \cdot 15C5]^+$.[11] As the number of donor atoms and ring sizes of the two crown ethers are similar to those of the N_2O_2 and N_2O_3 faces of C211 it seems probable that these faces will exhibit similar relative propensities for binding Na^+ and hence that $[Na \cdot C211]^+$ will exist predominantly with Na^+ bound to a N_2O_3 face in solution. In the case of $C21C_5$ it is unlikely that the 12-membered N_2O or the 15-membered N_2O_2 faces will compete effectively with the 15-membered N_2O_3 face as Na^+-binding sites. Thus any differences in the stabilities of $[Na \cdot C21C_5]^+$ and $[Na \cdot C211]^+$ should predominantly reflect differences in binding of Na^+ on the N_2O_3 faces of the two cryptands.

Values of $\log (K/dm^3\ mol^{-1})$ for $[Na \cdot C21C_5]^+$ [eqn (4)] and $[Ag \cdot C21C_5]^+$, and $[Na \cdot C211]^+$ and $[Ag \cdot C211]^+$ from the literature[12] are given in Table 1. It is seen that the K characterizing $[Na \cdot C21C_5]^+$ [eqn (4)]:

$$Na^+ + C21C_5 \underset{k_d}{\overset{k_f}{\rightleftharpoons}} [Na \cdot C21C_5]^+ \quad (k_f/k_d = K) \quad (4)$$

is several orders of magnitude less than that characterizing $[Na \cdot C211]^+$ in the four common solvents studied, and that a similar relationship holds for $[Ag \cdot C21C_5]^+$ and $[Ag \cdot C211]^+$. This indicates the importance of the fourth oxygen in C211 in the competition between the cryptand and the solvent for Na^+- and Ag^+-binding sites. It is seen that K for $[Na \cdot C21C_5]^+$ increases as the Gutmann donor number (D_N)[13] decreases for the oxygen donor solvents in the sequence: dimethylformamide (26.6), methanol (19.0), acetone (17.0), and propylene carbonate (15.1), where D_N is shown in parentheses. A similar increase in K is seen for the nitrogen donor solvents pyridine (33.1) and acetonitrile (14.1), but whereas K observed in acetonitrile fits roughly into the sequence observed for the oxygen donor solvents, the K observed in pyridine is greater than expected on the basis of its high D_N. This is probably a consequence of the position of the *N*-donor atom in the pyridine ring causing substantial steric hindrance towards bonding with Na^+. In general it is expected that the electron-donating abilities indicated for the solvents by D_N will be modified by their steric characteristics. Similar variations of stability with the nature of the solvent have been observed for other cryptates.[12]

The kinetic origins of the differences in K for $[Na \cdot C21C_5]^+$ and $[Na \cdot C211]^+$ in dimethylformamide are apparent from the respective k_f (298.2 K) (2.14×10^7 and 1.92×10^6 $dm^3\ mol^{-1}\ s^{-1}$) and k_d (298.2 K) (2.88×10^4 and 12.1 s^{-1}) values.[1,2] Clearly the much greater dissociation rate of $[Na \cdot C21C_5]^+$ accounts predominantly for its lower stability in dimethylformamide, but a detailed mechanistic analysis must await the availability of kinetic data in other solvents.

In the oxygen donor solvents both silver cryptates are seen to be substantially more stable than their sodium analogues despite Na^+ being characterized by the smaller effective six-coordinate ionic radius[5] (1.02 Å), and therefore expected to fit further into the cryptand cavity and form a more stable cryptate than the larger Ag^+ (1.15 Å). This suggests that this difference in stability may arise from differences in bonding. While Na^+ has no directional bonding characteristics Ag^+ tends to form two strong coaxial bonds consistent with a greater degree of covalency in the bonding of the latter metal.[14] The reversal of the relative magnitudes of K for the sodium and silver cryptates with the change from oxygen donor solvents to nitrogen donor solvents indicates that the latter solvents compete more effectively with the cryptates for binding sites on Ag^+ than do the oxygen donor solvents. This is consistent with the known characteristic of Ag^+ for binding nitrogen donor atoms in preference to oxygen donor atoms in the formation of complexes;[14] and also with the observation that the ion–solvent interaction of Ag^+ (in comparison with Na^+) with acetonitrile is much stronger than with dimethylformamide, methanol or propylene carbonate.[12]

Acknowledgement—We thank the Australian Research Grants Scheme for partial support of this study.

REFERENCES

1. S. F. Lincoln, I. M. Brereton and T. M. Spotswood, *J. Chem. Soc., Faraday Trans.* 1, 1985, **81**, 1623.
2. S. F. Lincoln, E. Horn, M. R. Snow, T. W. Hambley, I. M. Brereton and T. M. Spotswood, *J. Chem. Soc., Dalton Trans.* 1986, 1075.
3. A. Abou-Hamdan, T. W. Hambley, A. M. Hounslow and S. F. Lincoln, *J. Chem. Soc., Dalton Trans.* (in press).
4. D. Moras and R. Weiss, *Acta Cryst.* 1973, **B29**, 400.
5. R. D. Shannon, *Acta Cryst.* 1976, **A32**, 751.
6. J.-M. Lehn and J. P. Sauvage, *J. Am. Chem. Soc.* 1975, **97**, 6700.
7. D. D. Perrin, W. L. F. Armarego and D. R. Perrin, *Purification of Laboratory Chemicals*, 2nd Edn. Pergamon Press, Oxford (1980).
8. F. J. Rossotti and H. Rossotti, *Determination of Stability Constants*. McGraw-Hill, New York (1961).
9. J. Gutknecht, H. Schneider and J. Stroka, *Inorg. Chem.* 1978, **17**, 3326.
10. B. G. Cox, H. Schneider and J. Stroka, *J. Am. Chem. Soc.* 1978, **100**, 4746.
11. R. M. Izatt, J. S. Bradshaw, S. A. Nielsen, J. D. Lamb and J. J. Christensen, *Chem. Rev.* 1985, **85**, 271.
12. B. G. Cox, J. Garcia-Rosas and H. Schneider, *J. Am. Chem. Soc.* 1981, **103**, 1384.
13. V. Gutmann, *Coordination Chemistry in Nonaqueous Solutions*. Springer, Wien (1968).
14. F. A. Cotton and G. Wilkinson, *Advanced Inorganic Chemistry*, 4th Edn, p. 970. Interscience, New York (1980).

Polyhedron Vol. 5, No. 10, pp. 1601–1605, 1986
Printed in Great Britain

0277–5387/86 $3.00+.00
Pergamon Journals Ltd

PREPARATION OF A NOVEL POLYMERIC LIGAND CONTAINING A TETRAAZA MACROCYCLE SUPPORTED ON POLYSTYRENE, AND SEPARATION OF COPPER(II) AND NICKEL(II)

YASUHIRO NAKAJIMA, MANABU FUJIWARA, TAKAYUKI MATSUSHITA and TOSHIYUKI SHONO*

Department of Applied Chemistry, Faculty of Engineering, Osaka University, Yamadaoka, Suita, Osaka 565, Japan

(*Received* 6 *January* 1986; *accepted* 24 *February* 1986)

Abstract—The novel polymeric ligand containing the tetraaza macrocycle as a pendant group was prepared by the reaction of 2,7,12,14-tetramethyl-1,4,8,11-tetraazacyclotetradeca-1,5,7,12-tetraene with iodomethylstyrene–divinylbenzene copolymer beads. The content of the ligand in the polymer was 0.75 mmol g^{-1} under the optimum conditions. The complexation of this polymer with copper(II) and nickel(II) in water under heterogeneous conditions in a batch system showed that it can bind copper(II) selectively by complex formation with the tetraaza macrocycle. The capacity for copper(II) was found to depend on the pH, ionic strength and ethanol content of the sample solutions. Moreover, the separation of nickel(II) and copper(II) was achieved in a column system.

Tetraaza macrocyclic compounds such as porphyrins and cyclam are important as models for metal enzymes in biological chemistry, so the properties of their metal complexes have been investigated in detail.[1–4] Recently, tetraaza macrocyclic compounds have been applied to selective extractants for transition-metal ions.[5–10] We have previously reported that the polymeric ligands, which were prepared by the reaction of 5,7,12,14-tetramethyl-1,4,8,11-tetraazacyclotetradeca-1,5,7,12-tetraene (L) with diisocyanates {OCN—R—NCO [R = $(CH_2)_6$ or $C_6H_5CH_2C_6H_5$]}, can be applied to a selective adsorbent for copper(II).[11]

In this paper, we describe the preparation and complexing ability of the polymeric ligand, in which L was incorporated covalently to polystyrene beads as a pendant group toward transition-metal ions such as copper(II) and nickel(II). In a column system, copper(II) and nickel(II) were found to be separated satisfactorily.

* Author to whom correspondence should be addressed.

EXPERIMENTAL

Materials

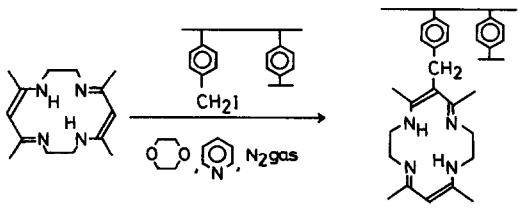
All reagents were of reagent grade. 1,4-Dioxane was refluxed over sodium and distilled. It was kept over sodium. Acetone was refluxed over calcium sulfate and distilled. Other solvents were purified in the usual manner. Water was deionized.

Measurements

IR spectra were recorded on a Hitachi 215 grating spectrophotometer. Atomic absorption spectra were obtained using a Nippon Jarrell Ash AA-1. The pH of the sample solution was measured with a Hitachi–Horiba F-8DP pH meter.

Preparation of polymeric ligand

The macrocyclic ligand was prepared according to the method of a previous paper.[12] The polymeric ligand was prepared as shown in Scheme 1.



Scheme 1. Preparation of the polymeric ligand.

Preparation of the iodomethylstyrene polymer

Five grams of chloromethylstyrene–5% divinylbenzene copolymer beads obtained from Mitsubishi Kasei Co. Ltd was suspended in acetone–1,4-dioxane (45 cm^3–15 cm^3) and stirred at room temperature for 3 h. To this suspension was added sodium iodide (5.0 g) and the mixture refluxed for 24 h in the dark. After cooling to room temperature, it was filtered and washed with acetone and water several times, and dried *in vacuo*. The reaction was found to occur almost quantitatively.

Incorporation of L into polymer beads

The iodomethylstyrene–divinylbenzene copolymer (10.0 g) was suspended in 1,4-dioxane (400 cm^3) and stirred at room temperature for 2 h under a nitrogen atmosphere. To this suspension was added a 1,4-dioxane solution (100 cm^3) of L (21.4 g) and dried pyridine (15 cm^3), which was then stirred at 70°C for 24 h. After cooling to room temperature, it was filtered and washed with chloroform and acetone several times. The resulting beads were dried *in vacuo*. Found: C, 48.8; H, 4.5; N, 4.2%.

Procedure for binding of metal ion in a batch system

Binding of metal ions in a batch system was carried out by using a 10-cm^3 test tube (with a stopper) which contained an aqueous solution of metal(II) acetate [copper(II) or nickel(II)] and polymer beads (*ca* 1×10^{-5} unit mol). The test tube was shaken for an appropriate time (from 1 to 48 h) at room temperature by using a shaker. After shaking, polymer beads were separated with decantation and the solution was diluted with water, and the concentration of the metal(II) ion remaining in it was determined by atomic absorption spectrometry. To investigate the effect of the ethanol content in the sample solution, the separated solution, with water added if necessary, was evaporated very slowly at 80°C to remove the ethanol. The residual solution was diluted with water, and the concentration of copper(II) remaining in it was determined by atomic absorption spectrometry.

Procedure for separation of metal(II) ions in a column system

Separation of copper(II) and nickel(II) ions in a column system was carried out under the following conditions. A column (i.d. = 10 mm) was packed with 3 g of the polymer beads which were fully swollen in advance. A mixed solution of copper(II) and nickel(II) {[metal(II)] = 1×10^{-3} M} was eluted at a flow rate of 0.2 $cm^3\ min^{-1}$. Eluates were fractionated into 2-cm^3 portions and diluted with water to determine the concentration of the eluted metal(II) ions.

RESULTS AND DISCUSSION

Characterization of the polymeric ligand

Figure 1 shows the IR spectra of the iodomethylstyrene–divinylbenzene copolymer, the tetraaza macrocycle and the polymeric ligand. The characteristic bands due to the tetraaza macrocycle were observed 1620, 1565 and 665 cm^{-1} for the spectrum of the polymeric ligand, indicating that the macrocycles were supported on the copolymer. The content of the macrocycle was calculated to be 0.75 mmol g^{-1}, based on the nitrogen content in the elemental analysis.

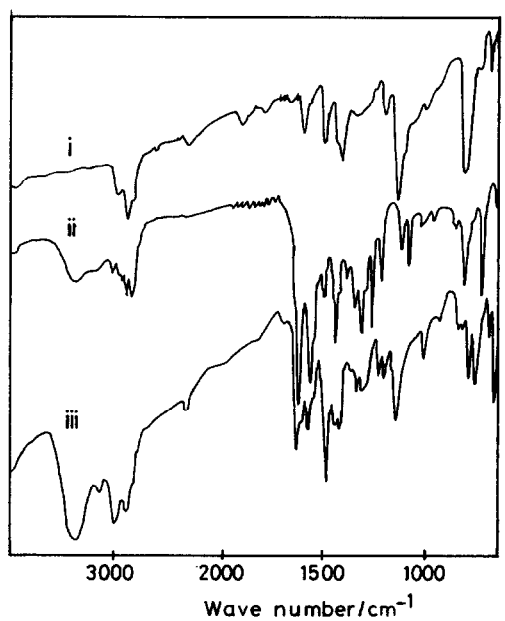


Fig. 1. IR spectra of iodomethylstyrene–divinylbenzene copolymer (i), tetraaza macrocycle (ii) and polymeric ligand (iii) in KBr disc.

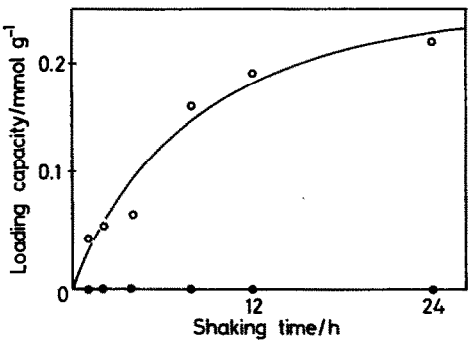


Fig. 2. Effects of shaking time on the loading capacity of the polymeric ligand for copper(II) (○) and nickel(II) (●). pH, 5.6; metal(II) acetate, 1×10^{-3} M (10 cm^3); polymeric ligand, 10 mg.

Effect of shaking time on the loading capacity in the batch system

Figure 2 shows the effect of shaking time on the loading capacity of the polymeric ligand for copper(II) and nickel(II) in the batch system at pH = 5.6 without a buffer solution. The loading capacity for copper(II) reached 0.23 mmol g^{-1} after shaking for 24 h. On the other hand, no nickel(II) was bound to the polymer after shaking for 24 h. This result indicates that this polymeric ligand possesses a high selectivity to copper(II). Thus, we have studied its binding ability for copper(II) in detail.

Effect of pH on the loading capacity

Figure 3 shows the effect of the pH of the sample solution on the loading capacity of the polymeric ligand for copper(II) ion. The pH values were adjusted by using acetate buffer solutions (0.02 M) from 3.5 to 5.6 and by the addition of appropriate amount of 0.25 M hydrochloric acid or sodium hydroxide solution below 3.5 or above 5.6, respectively.

The capacity for copper(II) increased gradually with increasing pH of the copper(II) solution. It should be noticed that a capacity of 0.12 mmol g^{-1} was obtained even at pH = 3.0. At this pH the corresponding monomeric tetraaza macrocycle could not bind copper(II).[8] This result can be explained as follows: the binding of copper(II) may take place on both the exterior and the interior of the polymer beads. The binding sites on the interior should be surrounded by a hydrophobic environment due to the polystyrene backbone. Thus, the hydrogen ion concentration on the interior is considered to be lower than those on the exterior and in the bulk solution. Therefore, a relatively slight effect of pH on the loading capacity was observed by lowering the pH of the bulk solution.

Effect of ionic strength

Figure 4 shows the effect of the ionic strength of the sample solution on the loading capacity for copper(II), which was carried out under the following conditions: the concentration of the copper(II) ion was 1.0×10^{-3} M, and the shaking time was 48 h. The ionic strength of the sample solution was varied from 0.0 to 3.0 by the addition of sodium nitrate.

The loading capacity for copper(II) decreased with increasing ionic strength and reached a constant value of 0.07 mmol g^{-1} above 2.5. The coexisting ionic salts in large amounts influence more or less the results for the solvent extraction and the adsorption on the resins: they exert a negative effect

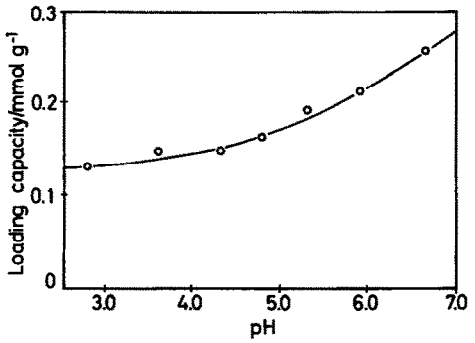


Fig. 3. Effect of pH on the loading capacity of the polymeric ligand for copper(II). Shaking time, 48 h; copper(II) acetate, 1×10^{-3} M (10 cm^3); polymeric ligand, 10 mg.

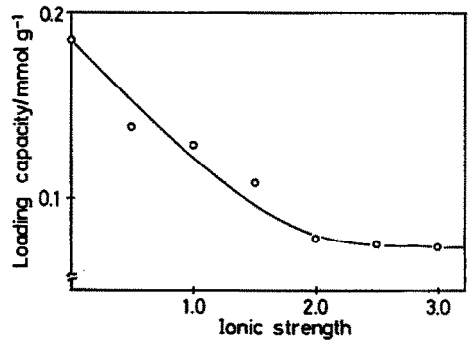


Fig. 4. Effect of ionic strength on the loading capacity for copper(II). Shaking time, 48 h; copper(II) acetate, 1×10^{-3} M (10 cm^3); polymeric ligand, 10 mg. Ionic strength was adjusted by the addition of sodium nitrate.

on the metal binding by weakening the interaction between the metal ion and the chelating agents, but they exert a positive effect on it by desolvation around the metal ion to be captured. In the present system, the former process may operate effectively.

Effect of the ethanol content in the sample solution

Figure 5 shows the effect of the ethanol content in the sample solution on the loading capacity for copper(II). The concentration of the copper(II) ion was 1.0×10^{-3} M and the ethanol content varied from 0 to 100 vol %. The shaking time was 48 h.

The loading capacity for copper(II) increased from 0.18 to 0.73 mmol g^{-1} as the ethanol content in the sample solution was increased from 0 to 100 vol %. These results indicate that the complexation of the polymeric ligand with copper(II) is accelerated by the addition of ethanol. It has been already pointed out that the addition of an appropriate organic solvent to an aqueous sample solution results in a strong retention of ions on ion-exchange resins.[13-15] Such behavior has been ascribed to a decreasing tendency for hydration in a mixed solvent, in which the metal ions can interact easily with the binding sites. In the present case, a similar effect operates and accelerates the complexation of copper(II) with the tetraaza macrocycles of the polymeric ligand. Of course, other factors, such as the swelling of the polymer beads, should increase the capacity.

Recovery of copper(II) ion from copper(II)-loading polymer beads with hydrochloric acid

We have examined the recovery of copper(II) bound in the polymeric ligand by treatment with hydrochloric acid. Figure 6 shows the effect of the shaking time on the recovery of copper(II) ion with 0.01 M hydrochloric acid. The recovery of copper(II) ion gradually increased and reached 21.4% after shaking for 24 h. The low percentage of recovery is explained by a slight pH dependence of the binding ability because of the hydrophobicity of the polymer support (see Fig. 3).

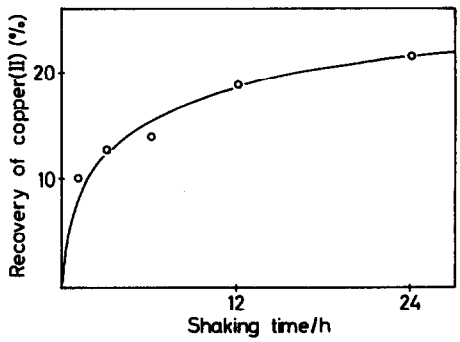


Fig. 6. Effect of shaking time on the recovery of copper(II) from copper(II)-loading polymer beads with 0.01 M hydrochloric acid.

Separation of copper(II) and nickel(II) in the column system

We have applied the polymeric ligand for separation of copper(II) and nickel(II) ions by using a column. Figure 7 shows the breakthrough curves of the copper(II) and nickel(II) ions under the conditions described in Experimental. The nickel(II) ion was rapidly eluted and the concentration in the effluents reached the feed concentration of 1×10^{-3} M. On the other hand, the copper(II) ion was completely adsorbed on the polymer beads and began to elute when the effluent volume exceeded 70 cm^3.

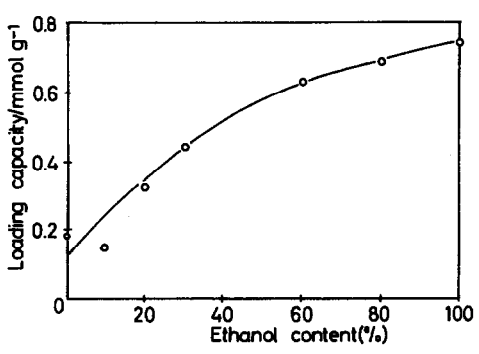


Fig. 5. Effect of ethanol content in the sample solution on the loading capacity for copper(II). Shaking time, 48 h; copper(II) acetate, 1×10^{-3} M (10 cm^3); polymeric ligand, 10 mg.

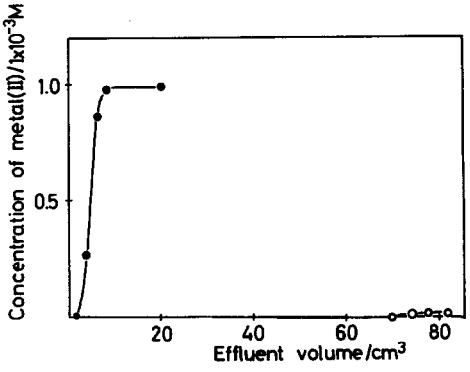


Fig. 7. Breakthrough curves for copper(II) (○) and nickel(II) (●) in the column system. Feed concentration of metal(II), 1×10^{-3} M; pH, 5.5; flow rate, 0.2 cm^3 min^{-1}; polymeric ligand, 3.0 g (dry).

This result indicates that this polymer ligand has a high selectivity to copper(II) ion, consistent with the results obtained in the batch system.

REFERENCES

1. T. J. Trux and R. H. Holm, *J. Am. Chem. Soc.* 1972, **94**, 4529.
2. S. C. Tang and R. H. Holm, *J. Am. Chem. Soc.* 1975, **97**, 3359.
3. A. M. Tait and D. H. Busch, *Inorg. Chem.* 1976, **15**, 197.
4. G. A. Melson, *Coordination Chemistry of Macrocyclic Compounds*. Plenum Press, New York (1979).
5. Yu. A. Zolotov, V. P. Bodnja, G. A. Larikova, N. V. Niz'eva, G. E. Vlasava and E. V. Rybakova, *Zh. Anal. Khim.* 1982, **37**, 1543.
6. Yu. A. Zolotov, N. V. Niz'eva, V. P. Ionov, D. M. Kumina and O. V. Ivanov, *Mikrochim. Acta* 1983, **1**, 381.
7. Yu. A. Zolotov, V. P. Ionov, N. V. Niz'eva and A. A. Formanovsky, *Dokl. Akad. Nauk SSSR* 1984, **277**, 1145.
8. M. Fujiwara, T. Matsushita and T. Shono, *Polyhedron* 1984, **3**, 1357.
9. N. Kubota, M. Fujiwara, T. Matsushita and T. Shono, *Polyhedron* 1985, **4**, 1051.
10. M. Fujiwara, Y. Nakajima, T. Matsushita and T. Shono, *Polyhedron* 1985, **4**, 1589.
11. M. Fujiwara, Y. Nakajima, T. Matsushita and T. Shono, *Polyhedron* 1985, **4**, 1859.
12. T. Tokumitsu and T. Hayashi, *Bull. Chem. Soc. Jpn* 1981, **54**, 2348.
13. A. Iguchi, *Bull. Chem. Soc. Jpn* 1958, **31**, 600.
14. A. Iguchi, *Bull. Chem. Soc. Jpn* 1958, **31**, 746.
15. J. S. Fritz and D. J. Pietrzyk, *Talanta* 1961, **8**, 143.

Polyhedron Vol. 5, No. 10, pp. 1607–1613, 1986
Printed in Great Britain

0277–5387/86 $3.00+.00
Pergamon Journals Ltd

THEORETICAL STUDY OF THE STATIC JAHN–TELLER EFFECT—III. TYPE OF VIBRONIC COUPLING IN HEXAHALO COMPLEXES*

MARTIN BREZA, PETER PELIKÁN and ROMAN BOČA†

Departments of Inorganic and Physical Chemistry, Slovak Technical University, CS-812 37 Bratislava, Czechoslovakia

(*Received* 14 *January* 1986; *accepted* 24 *February* 1986)

Abstract—Three types of vibronic coupling in hexacoordinate complexes are compared: the T_{ig}–$(a_{1g}+e_g)$ type in the group O_h, the E_g–$(a_{1g}+e_g)$ type in the group D_{3d}, and the E_g–$(a_{1g}+b_{1g})$ type in the group D_{4h}. It is shown that the group with the highest symmetry (O_h) does not imply the best model of vibronic coupling. Numerical applications were obtained for 29 complexes of the MX_6^q type having a triply degenerate electronic state in an octahedral geometry on the CNDO–UHF level of the MO–LCAO–SCF method. Characteristics of these Jahn–Teller active systems are calculated and discussed.

The Jahn–Teller effect (JTE) has been studied by many authors using various methods. Nevertheless, only a small number of publications deal with quantitative calculations in this field. In our previous papers[1–4] the hexahalo complexes of the first-row transition metals have been investigated by means of the semiempirical MO–LCAO–SCF methods in the CNDO and INDO versions. As a result, the vibronic coupling constants and the vibrational force constants have been calculated as parameters of the adiabatic potential surface (APS). Recently, using group theory, a complete classification of the possible symmetries, which may exist for the JTE, has been published.[5,6] We applied the principle of a step-by-step descent in symmetry (symmetry elements being lost) synchronous with a step-by-step splitting of degenerate electron terms. Accordingly, the symmetry group O_h with triple degenerate electron terms (T_{1g}, T_{2g}, T_{1u} and T_{2u}) is split to its first-level subgroups: cubic (T_h, T_d and O), hexagonal (D_{3d}) or tetragonal (D_{4h}). If the electronic terms still remain degenerate, the splitting continues to the corresponding second-, third- and fourth-level subgroups, respectively (Fig. 1). One possible pathway of distortion is shown in Fig. 2 for the tetragonal pattern. The central-atom effect [the proton number influence of the central atom M, as well as the oxidation state (q) and spin state (m) of the complex] and the ligand field effect represent factors which determine the final ground-state geometry of the system. The central problem of this paper may be formulated as follows. The vibronic coupling in hexacoordinate systems may be of the T_{2g}–$(a_{1g}+e_g+t_{2g})$ type within the O_h-group, the E–$(a_1+b_1+b_2)$ type for the D_4-group, the E–(a_1+e) type for the C_3-group etc. Many possibilities are relevant. Therefore the scope of this paper is to clear up which type of vibronic coupling actually operates in hexacoordinate complexes.

METHOD

The types of vibronic coupling have been studied by Griffith[7] who concluded that only three types (except icosahedral groups) may occur. They are:

(i) the three-mode coupling T–(a_1+e+t_2) for cubic groups with triple degenerate electron terms (T_d, T_h, T, O_h and O);

(ii) the three-mode coupling E–$(a_1+b_1+b_2)$ for groups D_{4h}, C_{4v}, C_{4h}, C_4, D_4, S_4 and D_{2d};

(iii) the two-mode coupling E–(a_1+e) for the remaining groups having doubly degenerate electron terms. Some subscripts (u or g and 1 or 2)

* For Part II see Ref. 4.

† Author to whom correspondence should be addressed.

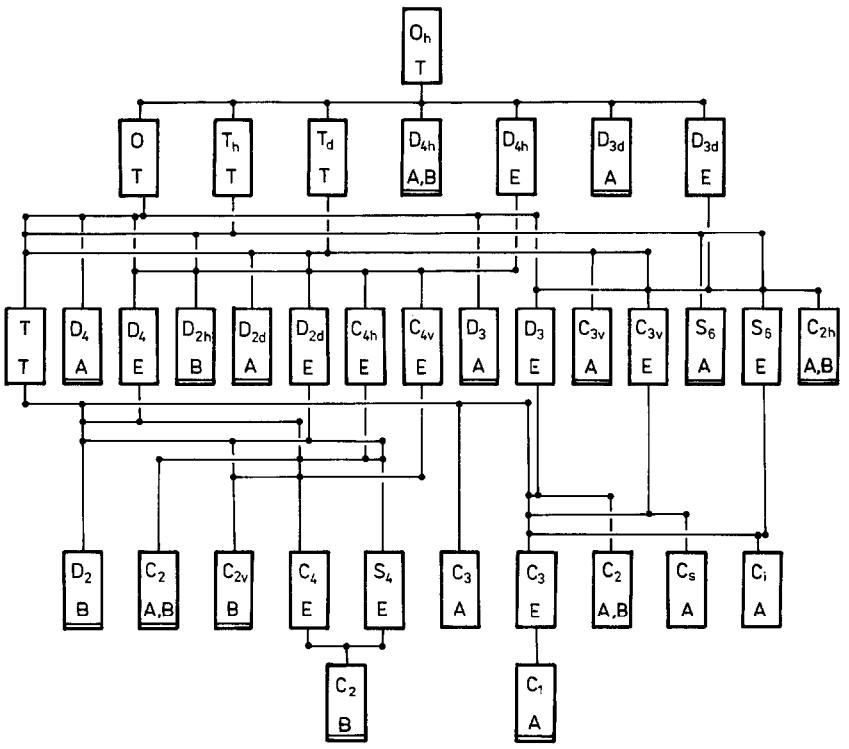


Fig. 1. Pattern of the octahedral system distortions.

for the symbols of irreducible representations are omitted here for simplicity. The a_1-mode (the totally symmetric coordinate) is usually deleted from consideration since it has no influence on the linear approximation of the electron–nuclear operator $\hat{V}(q, Q)$. Nevertheless, this mode is coupled with the other vibronic active modes in the quadratic approximation of $\hat{V}(q, Q)$, so that this degree of freedom has to be considered.

Using the degenerate perturbation theory an analytic formula for the APS can be derived:

$$W(\ldots Q_k \ldots) = E^0 + F(\ldots Q_k \ldots) + \varepsilon_i. \qquad (1)$$

The second term is the usual Taylor expansion along vibrational coordinates (Q_k) with the restriction that each component spans the totally symmetric representation. The vibronic correction term arises from the secular equation:

$$\det\{V_{mn} - \varepsilon_i \delta_{mn}\} = 0, \qquad (2)$$

with ε_i being the lowest eigenvalue of the electron–nuclear operator matrix (**V**) in the space of degenerate electronic functions. The actual shape of the APS depends on the individual type of vibronic interaction.

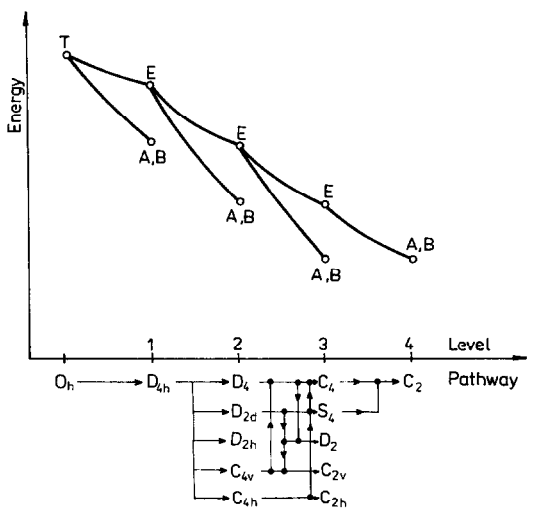


Fig. 2. Energy profile of octahedral system distortions for the tetragonal pattern.

Type 1

Vibronic interaction T_{ij}–$(a_{1g} + e_g + t_{2g})$ for the reference group O_h ($i = 1$ or 2, $j = u$ or g). The symmetrized normal coordinates span the a_{1g} (Q_1), e_g (Q_2 and Q_3) and t_{2g} (Q_4–Q_6) irreducible rep-

resentations. The APS adopts a form:

$$\begin{aligned}W(Q_1,Q_2,Q_3,Q_4,Q_5,Q_6)&=\varepsilon_i+E^0+K_aQ_1+\tfrac{1}{2}K_{aa}Q_1^2+\tfrac{1}{2}K_{ee}(Q_2^2+Q_3^2)\\&+T_{aaa}Q_1^3+T_{aee}Q_1(Q_2^2+Q_3^2)\\&+T_{att}Q_1(Q_4^2+Q_5^2+Q_6^2)\\&+T_{eee}Q_3(3Q_2^2-Q_3^2)+T_{ett}[Q_4^2(Q_3\\&-\sqrt{3}Q_2)+Q_5^2(Q_3+\sqrt{3}Q_2)\\&-2Q_3Q_6^2]+T_{ttt}Q_4Q_5Q_6.\end{aligned}\tag{3}$$

V is defined by the elements ($V_{mn}=V_{nm}$):

$$\begin{aligned}V_{11}&=\tfrac{1}{2}(A_e+Z_{ae}Q_1)(Q_3-\sqrt{3}Q_2)\\&+\tfrac{1}{2}B_{ee}(Q_2^2-Q_3^2-2\sqrt{3}Q_2Q_3)\\&+\frac{1}{\sqrt{6}}B_{tt}(-2Q_4^2+Q_5^2+Q_6^2),\\V_{12}&=(A_t+Z_{at}Q_1)Q_6+B_{tt}Q_4Q_5-Z_{et}Q_3Q_6,\\V_{13}&=(A_t+Z_{at}Q_1)Q_5+B_{tt}Q_4Q_6\\&+\tfrac{1}{2}Z_{et}Q_5(Q_3+\sqrt{3}Q_2),\\V_{22}&=\tfrac{1}{2}(A_e+Z_{ae}Q_1)(Q_3+\sqrt{3}Q_2)\\&+\tfrac{1}{2}B_{ee}(Q_2^2-Q_3^2+2\sqrt{3}Q_2Q_3)\\&+\frac{1}{\sqrt{6}}B_{tt}(Q_4^2-2Q_5^2+Q_6^2),\\V_{23}&=(A_t+Z_{at}Q_1)Q_4+B_{tt}Q_5Q_6\\&+\tfrac{1}{2}Z_{et}Q_4(Q_3-\sqrt{3}Q_2),\\V_{33}&=-V_{11}-V_{22}\\&=-(A_e+Z_{ae}Q_1)Q_3-B_{ee}(Q_2^2-Q_3^2)\\&-\frac{1}{\sqrt{6}}B_{tt}(Q_4^2+Q_5^2-2Q_6^2).\end{aligned}\tag{4}$$

The following parameters are contained in the APS: K_e = the linear vibration constant (it vanishes in equilibrium geometry), K_{ii} = harmonic force constants of ith vibration, T_{ijk} = cubic vibration constants, A_e and A_t = linear vibronic constants for e_g and t_{2g} active vibrations, B_{ee} and B_{tt} = quadratic vibronic constants, and Z_{ij} = quadratic vibronic constants which couple vibrations of different symmetry.

Type 2

Vibronic interaction E_i–$(a_{1g}+b_{1g}+b_{2g})$ for the reference group D_{4h} ($i=u$ or g). In this case the APS has the form:

$$\begin{aligned}W(Q_1,Q_2,Q_6)&=\varepsilon_i+E^0+K_aQ_1+\tfrac{1}{2}K_{11}Q_1^2\\&+\tfrac{1}{2}K_{22}Q_6^2+T_{aaa}Q_1^3\\&+T_{a11}Q_1Q_2^2+T_{a22}Q_1Q_6^2,\end{aligned}\tag{5}$$

with the vibronic correction originating from the explicit solution of the 2×2 secular equation:

$$\varepsilon_i=-[(A_1-Z_{a1}Q_1)^2Q_2^2+(A_2-Z_{a2}Q_1)^2Q_6^2]^{1/2}.\tag{6}$$

Its parameters have the same meanings as for type 1.

Type 3

Vibronic interaction E_i–$(a_{1g}+e_g)$ for the reference group O_h or D_{3d} ($i=u$ or g). For the APS it holds that:[3]

$$\begin{aligned}W(Q_1,Q_2,Q_3)&=\varepsilon_i+E^0+K_aQ_1\\&+\tfrac{1}{2}K_{aa}Q_1^2\\&+\tfrac{1}{2}K_{ee}(Q_2^2+Q_3^2)\\&+T_{aaa}Q_1^3+T_{aee}Q_1(Q_2^2+Q_3^2)\\&+T_{eee}(3Q_2^2-Q_3^2)Q_3,\end{aligned}\tag{7}$$

with the vibronic term:

$$\begin{aligned}\varepsilon_i=-[&(A_e-Z_{ae}Q_1)^2(Q_2^2+Q_3^2)\\&+B_{ee}^2(Q_2^2+Q_3^2)^2\\&+2B_{ee}(A_e-Z_{ae}Q_1)Q_3(Q_3^2-3Q_2^2)]^{1/2}.\end{aligned}\tag{8}$$

A significant simplification is obtained when restricting only to vibration coordinates Q_1 and $Q_x=Q_3$ ($Q_x=Q_22/\sqrt{3}$ for group D_{4h}). This means that only a certain cut of the APS will be considered. The APS adopts a uniform shape:

$$\begin{aligned}W(Q_1,Q_x)&=s(A_x-Z_{ax}Q_1)Q_x+sB_{xx}Q_x^2+E^0\\&+K_aQ_1+\tfrac{1}{2}K_{aa}Q_1^2\\&+\tfrac{1}{2}K_{xx}Q_x^2\\&+T_{aaa}Q_1^3+T_{axx}Q_1Q_x^2-T_{xxx}Q_x^3.\end{aligned}\tag{9}$$

In reality this represents:

(i) the vibronic interaction T_{2g}–$(a_{1g}+e_g)$ for the reference group O_h ($s=+1$ and -0.5, respectively; $Z_{ax}=-Z_{ae}$);

(ii) the vibronic interaction E_g–$(a_{1g}+b_{1g})$ for the reference group D_{4h} ($s=\pm1$, $Z_{ax}=Z_{a1}$, $T_{axx}=T_{a11}$, $T_{xxx}=0$, $B_{xx}=0$);

(iii) the vibronic interaction E_g–$(a_{1g}+e_g)$ for the reference group D_{3d} ($s=\pm1$, $Z_{ax}=Z_{ae}$).

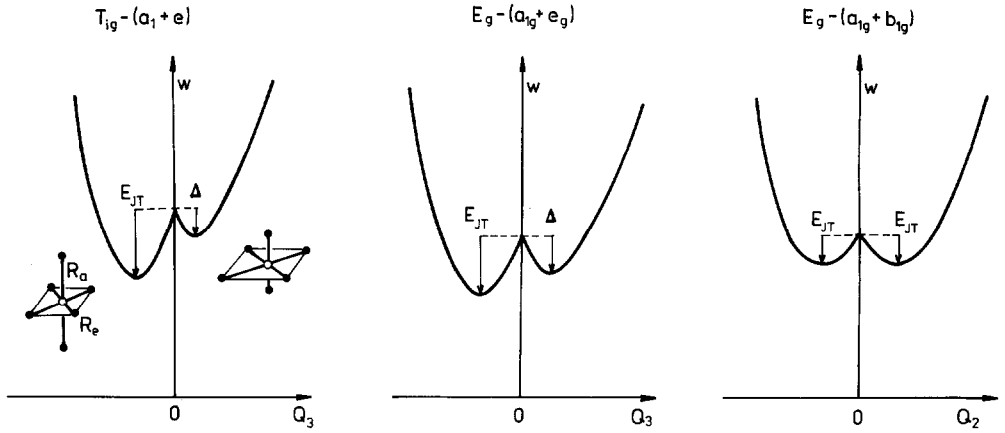


Fig. 3. Double-minimum form of the APS for three cases of vibronic coupling.

The positive values of s hold for an elongated bipyramid and the negative values for the compressed form (Fig. 3).

RESULTS AND DISCUSSION

A study of the type of vibronic coupling has been carried out for 29 complexes of the $^m[MX_6]^q$ type ($X = F^-$, Cl^- or Br^-). These systems are characterized in Table 1. The following procedure has been applied to each system.

(i) The total molecular energy was calculated for selected geometries of the complex so that a two-dimensional numerical map of $W^c(Q_1, Q_x)$ was obtained. The semiempirical CNDO–UHF version[8,9] of the MO–LCAO–SCF method was applied for this purpose. The energy cut-off was 10^{-5} eV.

(ii) A least-squares fitting was used so that the functional:

$$\mathscr{F} = \sum_i w_i^2[W_i^c(Q_1, Q_x) - W_i^q(Q_1, Q_x)]^2 = \min \tag{10}$$

was minimized. The metric weighting concept was applied with $w_i^2 = 1/(\sum_k Q_k^2)$. The procedure is fast owing to the simple (linearizable) form of function (9).

(iii) As a result of the least-squares method, the force constants (K_a, K_{aa}, K_{xx}, T_{aaa}, T_{axx} and T_{xxx}) and the vibronic constants (A_x, B_{xx} and Z_{ax}) have been calculated. They determine the extremal points of the APS (Q_1^0 and Q_x^0). Consequently, the Jahn–Teller stabilization energies (E_{JT}) were obtained: $E_{JT} = W(Q_1 = 0, Q_x = 0) - W(Q_1^0, Q_x^0)$.

The results of the least-squares fitting are collected in Table 2. 33–42 points of the APS were used in the regression. It is concluded that the best model of vibronic coupling corresponds to the highest value of N_ρ (the number of nines in the correlation coefficient ρ), the lowest value of the discrepancy factor and the highest E_{JT}. These conditions are fulfilled only for 11 complexes (from the total number of 29 systems) if the vibronic coupling $T_{ig}-(a_{1g}+e_g)$ within group O_h is considered. The vibronic coupling $E_g-(a_{1g}+e_g)$ within group D_{3d} is a better model for 15 complexes. This result is of great significance, because the group with the highest symmetry (O_h) does not imply the best model of vibronic coupling in each case. In the light of this conclusion Liehr's first postulate[10] needs

Table 1. Some characteristics of the systems under study

System	Electron configuration	Electron term in O_h-group
CrX_6^{4-}, MnX_6^{3-}	t_{2g}^4	$^1(A_{1g}+E_g+T_{2g})$
	t_{2g}^4	$^3T_{1g}$
MnX_6^{4-}, FeX_6^{3-}	t_{2g}^5	$^2T_{2g}$
FeX_6^{4-}, CoX_6^{3-}	$t_{2g}^4e_g^2$	$^5T_{2g}$
CoX_6^{4-}, NiX_6^{3-}	$t_{2g}^5e_g^2$	$^4T_{1g}$

Table 2. Results of the least-squares fitting[a]

		T_{ig}–$(a_{1g}+e_g)$ in O_h				E_g–$(a_{1g}+e_g)$ in D_{3d}				E_g–$(a_{1g}+b_{1g})$ in D_{4h}		
No.	System	N_ρ	R	E_{JT}	Δ	N_ρ	R	E_{JT}	Δ	N_ρ	R	E_{JT}
1	$^1CrF_6^{4-}$	6	0.049	0.25	0.06	3	1.128	0.20	0.11	3	2.950	0.14
2	$^1CrCl_6^{4-}$	6	0.066	0.28	0.07	4	0.950	0.24	0.13	3	3.098	0.17
3	$^1CrBr_6^{4-}$	7	0.041	0.51	0.13	3	1.630	0.46	0.20	2	4.109	0.29
4	$^1MnF_6^{3-}$	6	0.097	3.97	1.02	3	1.650	4.15	1.40	2	6.602	2.12
5	$^1MnCl_6^{3-}$	7	0.043	1.97	0.50	4	0.259	2.26	0.71	4	0.664	1.15
6	$^1MnBr_6^{3-}$	7	0.047	1.96	0.51	4	0.808	1.90	0.74	3	2.902	1.15
7	$^3CrF_6^{4-}$	4	0.883	0.04	0.02	4	0.456	0.04	0.03	3	1.326	0.04
8	$^3CrCl_6^{4-}$	3	1.066	0.04	0.02	4	0.533	0.04	0.03	3	1.568	0.04
9	$^3CrBr_6^{4-}$	3	1.152	0.08	0.05	4	0.566	0.10	0.07	3	1.886	0.08
10	$^3MnF_6^{3-}$	3	1.983	0.58	0.56	4	1.030	0.86	0.47	3	2.152	0.70
11	$^3MnCl_6^{3-}$	3	2.357	0.41	0.39	3	1.170	0.56	0.36	2	3.657	0.48
12	$^3MnBr_6^{3-}$	4	0.973	0.26	0.24	4	0.492	0.40	0.22	3	1.476	0.28
13	$^2MnF_6^{4-}$	2	10.009	0.05	0.03	2	6.507	0.03	0.03	2	6.338	0.03
14	$^2MnCl_6^{4-}$	4	0.564	0.07	0.03	4	0.521	0.06	0.06	4	0.602	0.06
15	$^2MnBr_6^{4-}$	5	0.271	0.14	0.04	5	0.294	0.12	0.07	4	0.875	0.08
16	$^2FeF_6^{3-}$	5	0.160	0.91	0.24	4	1.145	0.90	0.30	2	6.793	0.44
17	$^2FeCl_6^{3-}$	6	0.123	0.70	0.31	4	0.589	0.55	0.45	3	1.310	0.54
18	$^2FeBr_6^{3-}$	7	0.045	0.40	0.10	4	0.481	0.26	0.20	3	2.903	0.23
19	$^5FeF_6^{4-}$	4	0.660	0.05	0.02	5	0.331	0.06	0.04	4	0.561	0.05
20	$^5FeCl_6^{4-}$	5	0.343	0.06	0.03	5	0.160	0.06	0.05	4	0.805	0.05
21	$^5FeBr_6^{4-}$	3	1.547	0.07	0.04	4	0.807	0.08	0.06	3	1.775	0.06
22	$^5CoF_6^{3-}$	3	1.235	1.09	0.96	4	0.814	1.09	0.70	3	1.651	0.83
23	$^5CoCl_6^{3-}$	4	0.806	0.82	0.72	4	0.724	1.14	0.67	4	1.699	0.64
24	$^5CoBr_6^{3-}$	4	1.103	0.23	0.23	4	0.546	0.34	0.19	3	1.685	0.22
25	$^4CoF_6^{4-}$	3	1.797	0.19	0.04	3	1.387	0.15	0.10	3	1.835	0.14
26	$^4CoCl_6^{4-}$	5	0.349	0.10	0.03	5	0.152	0.09	0.06	5	0.356	0.09
27	$^4CoBr_6^{4-}$	4	0.852	0.14	0.04	4	0.421	0.08	0.07	4	1.098	0.07
28	$^4NiF_6^{3-}$	7	0.049	1.26	0.32	4	0.421	1.08	0.62	3	2.584	1.00
29	$^4NiCl_6^{3-}$	5	0.321	0.43	0.11	4	0.555	0.33	0.20	3	1.884	0.24

[a] N_ρ = number of nines in the correlation coefficient (e.g. $N_\rho = 6$ for $\rho = 0.9999998$), R = discrepancy factor $\{[\Sigma_i(W_i^c - W_i^a)^2/\Sigma_i(W_i^a)^2]^{1/2}\}$ in %, E_{JT} = Jahn–Teller stabilization energy in meV, Δ = stabilization energy of the second extremum (saddle point) in meV. The N_ρ value is underlined for the best description.

modification. The proposed statement is that the strong vibronic coupling operates in the presence of electron degeneracy within the group which is not necessarily of the highest symmetry. It implies the hypothesis of the existence of vibronic coupling in the group of lowest symmetry with degenerate electron terms. Moreover, our results represent excellent arguments for the theory of a step-by-step descent in symmetry by the classification of possible symmetries of the Jahn–Teller systems.[5,6]

The following conclusions can be drawn from Table 3.

(i) The non-zero values of K_a, Z_{ae} and Q_1^0 parameters are mutually interrelated. The greater the vibronic coupling constant Z_{ae} (this couples the vibration modes of different symmetry), the greater is the $|Q_1^0|$ value—a deviation from the optimum octahedron. This effect, however, is not substantial since Q_1^0 typically has values of 10^{-14} m.

(ii) The Jahn–Teller distortions may be characterized by the Q_3^0 parameter. Its values span the range of 10^{-13}–10^{-12} m. Higher distortions occur in M(III) complexes compared to M(II) systems. The values of $|Q_3^0|$ are also functions of the polarity of the metal–ligand bond: they decrease within the series M(III)—F, M(III)—Cl and M(III)—Br, and increase within the series M(II)—F, M(II)—Cl and M(II)—Br. Since the values of Q_3^0 are negative for the energy minimum, the elongated form of the tetragonal bipyramid represents the equilibrium geometry of the complexes under study.

(iii) $|Q_3^0|$ as well as E_{JT} are functions of the quadratic vibronic constant B_{ee} [$\sim \partial^2 \hat{V}(q, Q)/\partial Q_3^2$]. These

quantities are probably underestimated by the simple CNDO method used. Their trends, however, seem to be correct. A more sophisticated *ab initio* approach does not come into consideration at present, because of the large number of geometries—over 1000—in this study.

(iv) The harmonic force constants fulfil the relation $K_{ee} < K_{aa}$, so that the tetragonal distortion along the $Q_3(e_g)$ mode is much easier than the symmetric stretching $Q_1(a_{1g})$. Thus $Q_3(e_g)$ might be considered as a soft mode. The cubic force constants (T_{aaa}, T_{aee} and T_{eee}) adopt significant values so that the anharmonicity effects are not negligible.

These conclusions are valid not only for iron complexes included in Table 3 but also for the other systems characterized in Table 1.

Table 3. Calculated properties of iron complexes using various vibronic coupling schemes[a]

Quantity	$^2FeF_6^{3-}$	$^2FeCl_6^{3-}$	$^2FeBr_6^{3-}$	$^5FeF_6^{4-}$	$^5FeCl_6^{4-}$	$^5FeBr_6^{4-}$
R^o (pm)	204.355	235.702	251.035	217.635	245.821	259.742
Type 1—Vibronic coupling T_{ig}–$(a_{1g}+e_g)$ within the group O_h						
(a) Parameters of APS						
A_e (10^{10} eV m^{-1})	−0.212	−0.150	−0.135	−0.044	−0.045	−0.057
B_{ee} (10^{20} eV m^{-2})	−0.447	−0.374	−0.132	−3.040	−2.539	−4.010
Z_{ae} (10^{20} eV m^{-2})	−0.566	−0.295	−0.110	−0.26	−0.309	−0.213
K_a (10^{10} eV m^{-1})	0.009	0.104	0.002	0.006	−0.016	−0.002
K_{aa} (10^{20} eV m^{-2})	32.982	30.015	34.763	26.627	24.453	28.644
K_{ee} (10^{20} eV m^{-2})	24.039	21.069	22.414	15.437	13.774	14.492
T_{aaa} (10^{30} eV m^{-3})	−7.422	−6.891	−7.641	−6.88	−5.453	−2.34
T_{aee} (10^{30} eV m^{-3})	−23.44	−20.01	−18.77	−22.5	−19.3	−19.5
T_{eee} (10^{30} eV m^{-3})	−10.42	−5.29	−4.29	−34.06	−32.40	−59.6
(b) Minimum-point coordinates						
Q_1^0 (pm)	−0.037	−0.348	−0.007	−0.023	0.065	0.004
Q_3^0 (pm)	−0.858	−0.691	−0.598	−0.207	−0.243	−0.257
R_a^0 (pm)	205.33	236.36	251.72	217.86	246.13	260.04
R_e^0 (pm)	203.84	235.16	250.69	217.51	245.71	259.59
(c) Saddle-point coordinates						
Q_1^0 (pm)	−0.024	−0.315	−0.007	−0.022	0.066	0.005
Q_3^0 (pm)	0.446	0.361	0.303	0.175	0.198	0.259
R_a^0 (pm)	203.83	235.14	250.68	217.42	245.62	259.44
R_e^0 (pm)	204.60	235.77	251.21	217.73	245.96	259.89
Type 2—Vibronic coupling E_g–$(a_{1g}+b_{1g})$ within the group D_{4h}						
(a) Parameters of APS						
A_1 (10^{10} eV m^{-1})	−0.137	−0.124	−0.101	−0.042	−0.036	−0.047
K_a (10^{10} eV m^{-1})	0.023	0.103	0.007	0.006	−0.017	−0.000
Z_{a1} (10^{20} eV m^{-2})	1.56	−1.45	−0.37	0.40	−0.258	−0.125
K_{aa} (10^{20} eV m^{-2})	32.75	30.016	34.68	26.532	24.456	28.742
K_{11} (10^{20} eV m^{-2})	21.77	22.76	22.16	18.484	15.030	16.887
T_{aaa} (10^{30} eV m^{-3})	−16.0	−6.87	−9.0	−6.93	−5.45	−4.82
T_{a11} (10^{30} eV m^{-3})	140.0	−47.7	−19.0	−6.2	−23.6	−28.9
(b) First-minimum coordinates						
Q_1^0 (pm)	−0.058	−0.364	−0.023	−0.021	0.067	0.000
Q_2^0 (pm)	−0.631	−0.559	−0.456	−0.225	−0.241	−0.278
R_a^0 (pm)	205.06	236.20	251.55	217.89	246.13	260.06
R_e^0 (pm)	203.97	235.23	250.76	217.50	245.71	259.58
(c) Second-minimum coordinates						
R_a^0 (pm)	203.60	234.91	250.50	217.37	245.57	259.42
R_e^0 (pm)	204.69	235.88	251.29	217.76	245.99	259.90

(*continued*)

Table 3. (*continued*)

Quantity	$^2FeF_6^{3-}$	$^2FeCl_6^{3-}$	$^2FeBr_6^{3-}$	$^5FeF_6^{4-}$	$^5FeCl_6^{4-}$	$^5FeBr_6^{4-}$
Type 3—Vibronic coupling E_g–$(a_{1g}+e_g)$ within the group D_{3d}						
(a) Parameters of APS						
A_e (10^{10} eV m^{-1})	−0.149	−0.114	−0.101	−0.041	−0.038	−0.048
B_{ee} (10^{20} eV m^{-2})	8.383	1.749	1.471	−1.281	−1.098	−1.665
Z_{ae} (10^{20} eV m^{-2})	0.401	−0.91	0.137	−0.111	−0.425	−0.371
K_a (10^{10} eV m^{-1})	0.018	0.103	0.006	0.007	−0.017	−0.000
K_{aa} (10^{20} eV m^{-2})	32.959	29.958	34.765	26.684	24.474	28.734
K_{ee} (10^{20} eV m^{-2})	23.068	21.58	22.480	17.942	15.197	16.830
T_{aaa} (10^{30} eV m^{-3})	−14.27	−6.83	−7.27	−6.56	−5.40	−5.30
T_{aee} (10^{30} eV m^{-3})	7.5	−29.4	−16.88	−19.27	−23.30	−26.6
T_{eee} (10^{30} eV m^{-3})	275.4	10.81	7.11	19.07	20.87	35.48
(b) Minimum-point coordinates						
Q_1^0 (pm)	−0.044	−0.358	−0.014	−0.026	0.066	−0.003
Q_3^0 (pm)	1.012	0.634	0.515	0.265	0.287	0.346
R_a^0 (pm)	205.51	236.29	251.62	217.32	245.52	259.34
R_e^0 (pm)	203.75	235.19	250.73	217.78	246.01	259.94
(c) Saddle-point coordinates						
Q_1^0 (pm)	−0.050	−0.354	−0.015	−0.026	0.067	−0.002
Q_3^0 (pm)	0.407	0.467	0.399	0.202	0.219	0.241
R_a^0 (pm)	203.86	235.02	250.57	217.86	246.10	260.02
R_e^0 (pm)	204.57	235.85	251.26	217.51	245.72	259.60

[a] R_a^0 = axial (2×) metal–ligand distance, R_e^0 = equatorial (4×) metal–ligand distance, R^o = optimum metal–ligand distance for ideal octahedron.

REFERENCES

1. P. Pelikán, M. Breza and M. Liška, *Inorg. Chim. Acta* 1980, **45**, L1.
2. R. Boča, P. Pelikán, M. Breza and J. Gažo, *Polyhedron* 1983, **2**, 921.
3. P. Pelikán, M. Breza and R. Boča, *Polyhedron* 1985, **4**, 1543.
4. P. Pelikán, M. Breza and R. Boča, *Polyhedron* 1986, **5**, 753.
5. P. Pelikán and M. Breza, *Chem. Papers* 1985, **39**, 255.
6. P. Pelikán and M. Breza, *J. Mol. Struct. (Theochem.)* 1985, **124**, 231.
7. J. S. Griffith, *The Irreducible Tensor Method for Molecular Symmetry Groups*. Prentice-Hall, Englewood Cliffs, NJ (1962).
8. D. W. Clack, N. S. Hush and J. R. Yandle, *J. Chem. Phys.* 1972, **57**, 3503.
9. R. Boča, *Program MOSEM2*. Slovak Technical University, Bratislava (1980).
10. A. D. Liehr, *J. Phys. Chem.* 1963, **67**, 389, 471.

Polyhedron Vol. 5, No. 10, pp. 1615–1620, 1986
Printed in Great Britain

0277–5387/86 $3.00+.00
Pergamon Journals Ltd

SYNTHESIS AND CHARACTERIZATION OF $Rh_2\{Ph(2\text{-}pyr)N\}_4$: A PRECURSOR TO A DIRHODIUM(III) DICATION CONTAINING AN Rh–Rh BOND

DEREK A. TOCHER* and JOANNE H. TOCHER

Department of Chemistry, University College London, 20 Gordon Street, London WC1H 0AJ, U.K.

(*Received* 23 *January* 1986; *accepted* 24 *February* 1986)

Abstract—$Rh_2\{Ph(2\text{-}pyr)N\}_4$ has been prepared from hydrated rhodium trichloride and the sodium salt of 2-anilinopyridine in ethanol. The dark green air-stable compound has been characterized by analytical and spectroscopic measurements. The complex undergoes two facile one-electron oxidations at moderate potentials. The dication, $[Rh_2\{Ph(2\text{-}pyr)N\}_4]^{2+}$, formally contains two Rh(III) ions and a double Rh–Rh bond.

The one-electron oxidation of neutral binuclear Rh(II) compounds to the corresponding monocations, in which the mean oxidation state per Rh is 2.5, is well established[1–3] and results in a formal increase in Rh–Rh bond order from 1.0 to 1.5. The most extensively electrochemically studied series of dirhodium(II) complexes have been the tetracarboxylates ($Rh_2(O_2CR)_4L_2$).[4–14] Investigations into the electro-oxidation and electro-reduction reactions of $Rh_2(O_2CR)_4$ complexes in a number of solvents have shown that the midpoint potentials depended on the identify of both the carboxylate and the solvent.[9] Carboxylates possessing electron-withdrawing substituents were more difficult to oxidize than those with electron-donating substituents and a linear relationship between oxidation potentials and Taft polar substituents constants has been observed. The potential for electro-oxidation of a given $Rh_2(O_2CR)_4$ complex was inversely related to the solvent's donor ability.[9] Investigations into the 1:1 and 1:2 Lewis base adducts[10,14] of $Rh_2(O_2CR)_4$ complexes have shown that the 1:2 adducts are more easily oxidized than the corresponding 1:1 adducts. The shifts in potential observed in these studies are in accord with expectations based on the model of Rh–Rh interactions put forth by Kawamura and Nakatsuji.

The impetus for this work was the observation that, on replacing bridging carboxylate ions by amidates,[15–19] that is changing the immediate coordination sphere about the $[Rh_2]^{4+}$ core from one of eight oxygen atoms to one comprising four oxygen and four nitrogen atoms, a shift in oxidation potentials to values which are 700–1000 mV less positive is observed. For example, the parent acetate complex $Rh_2(O_2CCH_3)_4$ undergoes a quasi-reversible one-electron oxidation at a potential of +1.17 V (SCE) in acetonitrile, while the amidate $Rh_2(HNC(O)CH_3)_4$ undergoes a corresponding oxidation at +0.15 V (SCE).[19] Similar observations have been made for other pairs of dirhodium(II) compounds. In the two amidate-bridged compounds $Rh_2(C_6H_5NC(O)CH_3)_4$ and $Rh_2(HNC(O)CH_3)_4$ this shifting of oxidation potentials to less positive values is sufficiently dramatic that a second oxidation wave is brought into the available solvent range.[18,19] These new one-electron oxidations occur at potentials >1.40 V (SCE), unfortunately too close to the solvent background for any further characterization of the doubly oxidized products to be feasible.

The substitution of a further four nitrogen atoms for the remaining four oxygens of the amidates ought to result in the further shifting of the oxidation potentials to less positive values and an increase in the relative stability of both the singly and doubly oxidized products. To test this hypothesis we have prepared a new dirhodium(II) complex, $Rh_2\{Ph(2\text{-}pyr)N\}_4$, in which the immedi-

* Author to whom correspondence should be addressed.

ate coordination sphere about the $[Rh_2]^{4+}$ core comprises eight nitrogen atoms. This complex undergoes two facile one-electron oxidations at moderate potentials. Although we have been unable to isolate the cations, $[Rh_2\{Ph(2\text{-}pyr)N\}_4]^{+/2+}$, they have been characterized spectroelectrochemically. This paper reports the synthesis and full characterization of the dirhodium(II) precursor and discusses its electron-transfer behaviour. A preliminary report of the redox behaviour of this compound has already appeared.[20]

EXPERIMENTAL

Physical measurements

IR spectra were recorded in the region 4000–240 cm^{-1} on a Perkin–Elmer 983 spectrophotometer using Nujol mulls on CsI plates. The ^1H NMR spectrum was recorded on a Varian XL200 spectrometer. Electronic spectra were recorded in the range 1600–400 nm on a Varian 2390 spectrophotometer. Molecular weights were determined in acetone on a Perkin–Elmer Hitachi (model 115) osmometer calibrated with benzil. Mass spectra were by the University of London Intercollegiate Research Service at the School of Pharmacy.

Voltammetric studies employed a Metrohm E506 potentiostat interfaced with a Metrohm E505 cell-stand utilizing a three-electrode geometry. The working electrode consisted of either a dropping mercury electrode or a platinum wire electrode (Metrohm EA 285). A non-aqueous Ag–AgCl–Cl^-, CH_2Cl_2 electrode, separated from the bulk of the solution by a fritted glass disk, was used as a reference electrode (Metrohm EA 441/5), and a platinum wire as an auxiliary electrode. Cyclic voltammetric (CV) measurements also employed a Metrohm E612 VA Scanner in conjunction with a Hewlett–Packard 7035B XY recorder. Current–voltage curves were recorded at scan rates of 0.02–0.50 $V\,s^{-1}$. The solvents used for the electrochemical measurements were CH_2Cl_2 and dimethylsulphoxide. The solvents contained 0.5 M tetra-*n*-butylammonium tetrafluoroborate ($TBABF_4$) as supporting electrolyte. Deaeration of the solutions was carried out before commencing the experiment, and a stream of nitrogen was passed throughout. All potentials are reported with respect to the Ag–AgCl electrode, against which ferrocene is oxidized at a potential of +0.60 V. Spectroelectrochemistry was performed in an O.T.T.L.E. cell which had an optical path length of 0.10 cm. Time-resolved spectra were obtained using a Varian 2390 spectrophotometer.

Synthesis

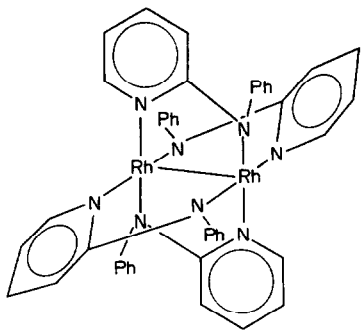
Sodium metal (0.46 g, 20.0 mol) was added to a solution of 2-anilinopyridine (3.42 g, 20.0 mmol) in ethanol (50 cm^3). The solution was stirred until all the sodium was dissolved (*ca* 15 min). To the homogeneous solution was added $RhCl_3 \cdot 3H_2O$ (0.50 g, 1.9 mmol). The resulting mixture was refluxed under N_2 for 3 h, after which time a microcrystalline dark green precipitate had formed. The precipitate was filtered off and recrystallized from MeOH. The final product was then extracted with the minimum volume of CH_2Cl_2 and then reprecipitated by addition of cold EtOH. The solid was dried *in vacuo* at room temperature. Yield 0.44 g (52%). Found: C, 59.4; H, 4.4; N, 12.7%. Calc. for $Rh_2(C_{11}H_9N_2)_4$: C, 59.8; H, 4.1; N, 12.7%. IR spectrum (Nujol mull, CsI plates); 1601 (s), 1584 (m), 1531 (w), 1508 (s), 1294 (s), 1229 (m), 1160 (w), 1015 (m), 858 (w), 743 (s), 709 (m), 529 (s), 506 (m), and 376 (w) cm^{-1} (s = strong, m = medium, w = weak). Electronic spectrum (1600–400 nm in CH_2Cl_2): 1015 ($\varepsilon = 2160\ dm^{-3}\ mol^{-1}\ cm^{-1}$), 579 (770), and 476 (sh). ^1H NMR [CD_2Cl_2 solvent, $(CH_3)_4Si$ reference]: δ 6.5–8.5 ppm (complex multiplets). Mass spectrum: *m/z* 882, $[Rh_2\{Ph(2\text{-}pyr)N\}_4]^+$; 713, $[Rh_2\{Ph(2\text{-}pyr)N\}_3]^+$; 544, $[Rh_2\{Ph(2\text{-}pyr)N\}_2]^+$; 441, $[Rh\{Ph(2\text{-}pyr)N\}_2]^+$; and 375, $[Rh_2\{Ph(2\text{-}pyr)N\}]^+$. Molecular weight (osmometrically in acetone): 864 (1.0×10^{-3}), and 894 (0.79×10^{-3} mol dm^{-3}), calc. 882. The complex is soluble in a wide range of common organic solvents.

RESULTS AND DISCUSSION

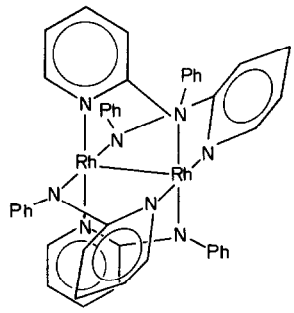
The anion derived from 2-anilinopyridine has previously been observed to coordinate across both Mo and W quadruple bonds,[21] across the Os–Os triple[22] bond, in the complex $Os_2\{Ph(2\text{-}pyr)N\}_3Cl_3$, and across the $Ru^{2.5}Ru$ bond[23] in the complex $Ru_2\{Ph(2\text{-}pyr)N\}_4Cl$. The geometry of the last complex was unusual in that all four of the asymmetric ligands adopted the same orientation about the $Ru^{2.5}Ru$ bond. Earlier attempts to prepare the Rh complex $Rh_2[Ph(2\text{-}pyr)N]_4$ by reaction of $RhCl_3 \cdot nH_2O$ with Na[Ph(2-pyr)N] were unsuccessful. When the reactants were combined in a 1 : 4 molar ratio a red solution was formed. Treatment of that solution with pyridine resulted in the deposition of orange crystals which were identified crystallographically as $RhCl_2py_2[(C_6H_4)(2\text{-}pyr)NH]$.[24] In this complex the 2-anilinopyridinato ligand is not only coordinated through the pyridine nitrogen atom but also through an *ortho* carbon atom of

the phenyl group, thus forming a six-membered metallocyclic ring. However when $RhCl_3 \cdot 3H_2O$ and Na[Ph(2-pyr)N] are refluxed in EtOH, in a molar ratio of *ca* 1:10, for 2–3 h a dark green solution is formed, together with a dark precipitate. The recrystallization and subsequent extraction of this precipitate leads ultimately to the isolation of a complex with the empirical formula $Rh\{Ph(2\text{-}pyr)N\}_2$. The ^1H NMR spectrum in CD_2Cl_2 solvent only contains signals in the region δ 6.5–8.5 ppm. Considerable overlapping of these multiplets is observed and we have not attempted to assign the resonances to individual protons on the phenyl or pyridyl rings. Importantly no N—*H* resonance was observed in the range 0–20 ppm. The absence of a proton on the amine nitrogen atom is confirmed by the IR spectrum. The free ligand 2-anilinopyridine contains a ν(N—H) stretching band at 3231 cm^{-1}, which is absent from the IR spectrum of the complex. The IR spectrum of the *ortho*-metallated complex, $Rh_2Cl_2py_2[(C_6H_4)(2\text{-}pyr)NH]$, contained bands at 1522 and 1570 cm^{-1} which were characteristic of the metallated phenyl ring.[24–26] Analogous bands are absent from the spectrum of this complex, although several other strong bands do occur in the region 1500–1600 cm^{-1}. A strong band at 1604 cm^{-1} can be assigned to the skeletal vibrations of the pyridyl rings. Strong bands in the regions 700–850 and 500–540 cm^{-1} are also characteristic of bridging 2-anilinopyridinato anions.[22,23]

The binuclear nature of the product has been confirmed by a variety of techniques. The mass spectrum contains a strong parent-ion peak at *m/z* 882 corresponding to the binuclear cation $[Rh_2\{Ph(2\text{-}pyr)N\}_4]^+$. The successive loss of three of the bridging ligands, to give peaks at *m/z* 713, 544 and 375, is also observed, together with peaks due to the mononuclear fragment cations $[Rh\{Ph(2\text{-}pyr)N\}_3]^+$ and $[Rh\{Ph(2\text{-}pyr)N\}_2]^+$, at *m/z* 610 and 441, respectively. The complex was sufficiently soluble in acetone for its molecular weight to be determined by osmometry. Values obtained agree well with the proposed dimeric formulation (see Experimental). When four asymmetric ligands bridge a dimetal unit a total of four different geometric isomers are possible.[23] However, as we have observed that $Rh_2\{Ph(2\text{-}pyr)N\}_4$ does not readily form axial adducts, this suggests that a close approach to the sixth coordination site of each rhodium is not facile. It is likely that the presence of two pendant phenyl groups would be sufficient to block axial coordination and hence it appears reasonable to suggest that the molecule adopts structure **1** or **2**. The former arrangement of bridging ligands has been observed for the Mo and W complexes $M_2\{Ph(2\text{-}pyr)N\}_4$,[21] while the *trans* disposition of two 2-anilinopyridine anionic ligands, both orientated in the same direction, has been observed in the mixed-ligand complex $Ru_2Cl(O_2CCH_3)_2\{Ph(2\text{-}pyr)N\}_2 \cdot Ph(2\text{-}pyr)NH$.[27]



1



2

CV and linear alternating-current voltammetric (ACV) measurements were made in several solvents at a Pt electrode. Figure 1 shows the voltammetric

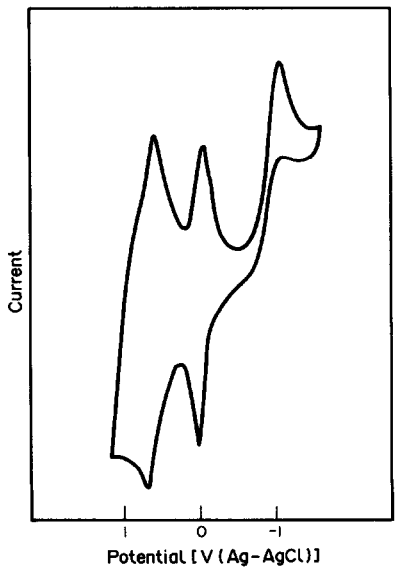


Fig. 1. Voltammetry of $Rh_2\{Ph(2\text{-}pyr)N\}_4$ in CH_2Cl_2. Scan rate = 100 mV s^{-1} (CV). Potentials vs Ag–AgCl reference electrode (against which ferrocene is oxidized at +0.60 V).

response of $Rh_2\{Ph(2\text{-}pyr)N\}_4$ in CH_2Cl_2. Clearly the complex undergoes two oxidation processes in the potential range 0.0–0.8 V as well as being reduced at −1.13 V. The electrochemical oxidation of $Rh_2\{Ph(2\text{-}pyr)N\}_4$ to the cation $[Rh_2\{Ph(2\text{-}pyr)N\}_4]^+$ is straightforward and uncomplicated at $E_{1/2} = +0.07$ V. Diagnostic plots of $E_p - E_{p/2}$ and $E_p^a - E_p^c$ are in the range predicted for a one-electron transfer.[28] The peak current is proportional to the square root of the scan rate and $i_{p,a}/i_{p,c} = 1$, indicating a diffusion-controlled one-electron transfer. The second oxidation, the mid-point potential of which is +0.72 V, is chemically reversible, although apparently characterized by sluggish heterogeneous charge-transfer kinetics. Hence, although $i_{p,a}/i_{p,c} = 1.0$ at all scan rates, ΔE_p $(E_p^a - E_p^c) = 100$ mV at $v = 50$ mV s^{-1}, and increases to 140 mV at 500 mV s^{-1}. In contrast to the oxidation behaviour of the dimer the reduction could be characterized as an irreversible process. A broad peak was obtained on the forward sweep and no peak was observed on the backward sweep. Neither scanning very rapidly nor recording the voltammograms at low temperatures improved the reversibility of this reduction wave. Analogous irreversible reduction waves have been reported for other dirhodium(II) complexes.[9,29] The one-electron nature of both oxidation processes was indicated by the ACV peak widths at half height and confirmed by comparison of the diffusion-limited currents with that of a known quantity of ferrocene, as measured by stirred voltammetry. On the basis of the observed data, the following description is proposed for the oxidation/reduction of $Rh_2\{Ph(2\text{-}pyr)N\}_4$:

$$\begin{array}{ccc} Rh_2\{Ph(2\text{-}pyr)N\}_4 & \xrightarrow{+e} & [Rh_2\{Ph(2\text{-}pyr)N\}_4]^- \\ {\scriptstyle +e}\uparrow\downarrow{\scriptstyle -e} & & \downarrow \\ [Rh_2\{Ph(2\text{-}pyr)N\}_4]^+ & & \text{decomposition products} \\ {\scriptstyle +e}\uparrow\downarrow{\scriptstyle -e} & & \\ [Rh_2\{Ph(2\text{-}pyr)N\}_4]^{2+} & & \end{array}$$

Repeated attempts to isolate the mono- and dication, through chemical or electrochemical oxidation, have generally been unsuccessful. Hence we have of necessity characterized the cations $[Rh_2\{Ph(2\text{-}pyr)N\}_4]^{+/2+}$ *in situ* by controlled potential oxidation of $Rh_2\{Ph(2\text{-}pyr)N\}_4$ in an optically transparent cell sited in the beam of an electronic spectrophotometer.

The steady-state spectra obtained at potentials of −0.10, +0.20 and +0.85 V are illustrated in Fig. 2. These spectra (1, 2 and 3) correspond to $Rh_2\{Ph(2\text{-}pyr)N\}_4$, $[Rh_2\{Ph(2\text{-}pyr)N\}_4]^+$ and $[Rh_2\{Ph(2\text{-}pyr)N\}_4]^{2+}$, respectively, the band maxima and extinction coefficients of which are presented in Table 1. The transitions which occur upon sequential oxidation are totally reversible since the spectra obtained upon controlled potential reduction of the oxidized species were identical with those observed initially. The appearance of two isosbestic points in the time-resolved spectra obtained in carrying out reduction/oxidations is consistent with the 1:1 interconversions of reduced and oxidized forms of the complex. For completeness we have carried out a controlled-potential reduction, at −1.2 V, in the spectroeletrochemical cell. The steady-state spectrum obtained is illustrated by curve 4 in Fig. 2. A

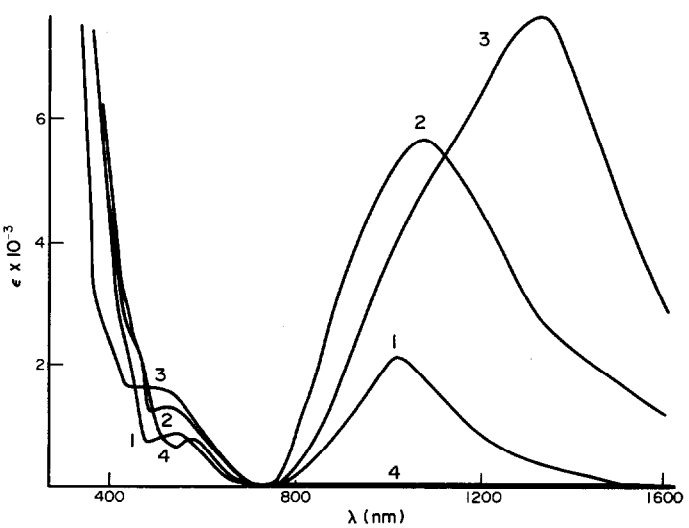


Fig. 2. Steady-state electronic absorption spectra obtained at potentials of −0.10 V (1), +0.20 V (2), +0.85 V (3), and −1.20 V (4), in CH_2Cl_2–0.5 M $TBABF_4$.

Table 1. Spectral characterization of $[Rh_2\{Ph(2\text{-}pyr)N\}_4]^n$ ($n = -1$, 0, 1 or 2) complexes

Complex	λ_{max} of major peaks (nm) [ε (dm^{-3} mol^{-1} cm^{-1})]
$Rh_2\{Ph(2\text{-}pyr)N\}_4$	1025 (2165), 579 (770), 476 (sh)
$[Rh_2\{Ph(2\text{-}pyr)N\}_4]^+$	1066 (5680), 525 (1235), 480 (sh)
$[Rh_2\{Ph(2\text{-}pyr)N\}_4]^{2+}$	1365 (7730), 500 (1545), 430 (sh)
"$[Rh_2\{Ph(2\text{-}pyr)N\}_4]^{1-}$"	595 (700)

controlled-potential reoxidization did not result in the quantitative regeneration of the spectrum of the neutral molecule. This observation together with the absence of isosbestic points in the time-resolved spectra are consistent with our earlier deductions on the irreversible nature of this electron-transfer step.

The electronic spectrum of each of the species $[Rh_2\{Ph(2\text{-}pyr)N\}_4]^{0/+/2+}$ contains a moderate-to-strong band in the near-IR region of the electronic spectrum. The magnitude of the associated extinction coefficients suggests that these bands are due to a charge-transfer process, and we will not discuss them further. The electronic spectrum of each of the species in question contains a single distinct band in the visible portion of that spectrum together with a series of shoulders at higher energy. The neutral molecule is characterized by a band at 579 nm ($\varepsilon = 770$ dm^{-3} mol^{-1} cm^{-1}). Upon oxidation to the monocation that band moves to a higher energy, 525 nm, and increases in intensity. Further shifting and gain in intensity, to 500 nm and $\varepsilon = 1545$ dm^{-3} mol^{-1} cm^{-1}, accompanies the formation of the dication.

To attempt to make a detailed assignment of the electronic transitions for this complex, based upon extrapolation from the theoretical results[13,30–34] obtained for the tetracarboxylates, $Rh_2(O_2CR)_4$, would be foolish. However, from the observations we have made, some useful general conclusions may be drawn. If the neutral dirhodium(II) complex, having no axial ligands, has the normal electronic ground state configuration $\sigma^2\pi^4\delta^2\delta^{*2}\pi^{*4}$, then the first electron to be removed by oxidation is likely to originate in the π^* molecular orbital. Thus the mono-oxidized product, $[Rh_2\{Ph(2\text{-}pyr)N\}_4]^+$, formally contains a $Rh\overset{1.5}{—}Rh$ bond, with the electronic configuration $\sigma^2\pi^4\delta^2\delta^{*2}\pi^{*3}$. In view of the smooth and reversible changes which occur in the electronic spectrum upon sequential oxidation, and which are consistent with the retention of the dimeric cage structure, we would suggest that the second electron removed also originated in the π^* molecular orbital. Hence the dication $[Rh_2\{Ph(2\text{-}pyr)N\}_4]^{2+}$ has the electronic configuration $\sigma^2\pi^4\delta^2\delta^{*2}\pi^{*2}$, and contains a $Rh\overset{2}{—}Rh$ bond.

Acknowledgement—We thank Johnson Matthey plc for their generous loans of rhodium trichloride.

REFERENCES

1. F. A. Cotton and R. A. Walton, *Multiple Bonds between Metal Atoms*. Wiley, New York (1982).
2. T. R. Felthouse, *Prog. Inorg. Chem.* 1982, **29**, 73.
3. E. B. Boyer and S. D. Robinson, *Coord. Chem. Rev.* 1983, **50**, 109.
4. K. M. Kadish, K. Das, R. A. Howard, A. M. Dennis and J. L. Bear, *Bioelectrochem. Bioenergy* 1978, **5**, 741.
5. C. R. Wilson and H. Taube, *Inorg. Chem.* 1975, **14**, 405.
6. C. R. Wilson and H. Taube, *Inorg. Chem.* 1975, **14**, 2276.
7. R. D. Cannon, D. B. Powell, K. Sarawek and J. S. Stillman, *J. Chem. Soc., Chem. Commun.* 1976, 31.
8. M. Moszner and J. J. Ziolkowski, *Bull. Acad. Pol. Sci., Ser. Sci. Chim.* 1976, **24**, 433.
9. K. Das, K. M. Kadish and J. L. Bear, *Inorg. Chem.* 1978, **17**, 930.
10. R. S. Drago, S. P. Tanner, R. M. Richman and J. R. Long, *J. Am. Chem. Soc.* 1979, **101**, 2897.
11. T. Kawamura, R. Fukamachi, T. Sowa, S. Hayashida and T. Yonezawa, *J. Am. Chem. Soc.* 1981, **103**, 364.
12. T. Sowa, T. Kawamura and T. Yonezawa, *Inorg. Chem.* 1983, **22**, 56.
13. H. Nakatsuji, Y. Onishi, J. Ushio and T. Yonezawa, *Inorg. Chem.* 1982, **22**, 1623.
14. L. A. Bottomley and T. A. Hallberg, *Inorg. Chem.* 1984, **23**, 1584.
15. A. M. Dennis, R. A. Howard, D. Lancon, K. M. Kadish and J. L. Bear, *J. Chem. Soc., Chem. Commun.* 1982, 399.
16. K. M. Kadish, A. M. Dennis and J. L. Bear, *Inorg. Chem.* 1982, **21**, 2982.
17. A. R. Chakravarty, F. A. Cotton, D. A. Tocher and J. H. Tocher, *Inorg. Chim. Acta* 1985, **101**, 185.
18. J. Duncan, T. Malinski, T. P. Zhu, Z. X. Hu, K. M.

Kadish and J. L. Bear, *J. Am. Chem. Soc.* 1982, **104**, 5507.
19. T. P. Zhu, M. Q. Absan, T. Malinski, K. M. Kadish and J. L. Bear, *Inorg. Chem.* 1984, **23**, 2.
20. D. A. Tocher and J. H. Tocher, *Inorg. Chim. Acta* 1985, **104**, L15.
21. A. R. Chakravarty, F. A. Cotton and E. S. Shamshoum, *Inorg. Chem.* 1984, **23**, 4216.
22. A. R. Chakravarty, F. A. Cotton and D. A. Tocher, *Inorg. Chem.* 1984, **23**, 4693.
23. A. R. Chakravarty, F. A. Cotton and D. A. Tocher, *Inorg. Chem.* 1985, **24**, 172.
24. A. R. Chakravarty, F. A. Cotton and D. A. Tocher, *Organometallics* 1985, **4**, 863.
25. M. I. Bruce, *Angew. Chem., Int. Ed. Engl.* 1977, **16**, 73.
26. Y. Fuchita, K. Hiraki and Y. Kage, *Bull. Chem. Soc. Jpn* 1982, **55**, 955.
27. A. R. Chakravarty and F. A. Cotton, *Inorg. Chim. Acta* 1985, **105**, 19.
28. R. S. Nicholson and I. Shain, *Anal. Chem.* 1964, **36**, 706.
29. A. R. Chakravarty, F. A. Cotton, D. A. Tocher and J. H. Tocher, *Organometallics* 1985, **4**, 8.
30. L. Dubiski and R. L. Martin, *Inorg. Chem.* 1970, **9**, 673.
31. J. G. Norman, Jr and H. J. Kolari, *J. Am. Chem. Soc.* 1978, **100**, 791.
32. J. G. Renzoni, J. G. Norman, Jr and D. A. Case, *J. Am. Chem. Soc.* 1979, **101**, 5256.
33. B. E. Bursten and F. A. Cotton, *Inorg. Chem.* 1981, **20**, 3042.
34. H. Nakatsuji, J. Ushio, K. Kanada, Y. Onishi, T. Kawamura and T. Yonezawa, *Chem. Phys. Lett.* 1978, **79**, 299.

Polyhedron Vol. 5, No. 10, pp. 1621–1623, 1986
Printed in Great Britain

0277–5387/86 $3.00+.00
Pergamon Journals Ltd

FACTORS AFFECTING THE FORMATION OF ALCOHOL AND ALKOXO COMPLEXES IN THE REACTIONS OF OXOMOLYBDENUM(V) TETRAPHENYLPORPHYRIN WITH VARIOUS ALCOHOLS IN DICHLOROMETHANE

MIYUKI MIURA, TAIRA IMAMURA* and MASATOSHI FUJIMOTO*

Department of Chemistry, Faculty of Science, Hokkaido University, Sapporo 060, Japan

(*Received* 6 *January* 1986; *accepted* 4 *March* 1986)

Abstract—The addition of alcohols to dichloromethane solution of Mo(V)O(tpp)Br (tpp = *meso*-tetraphenylporphinato) causes three-step reactions. The products in the first, second and third stages of the reactions are solvated, alcohol and alkoxo complexes, respectively. *t*-Butyl alcohol does not afford the corresponding alcohol complex. The most important factor controlling the formation of alcohol complexes is the bulkiness of the alcohol molecules.

Recently we reported the formation of an Mo(V) tetraphenylporphyrin (tpp) alcohol complex {[Mo(V)O(tpp)(ROH)]$^+$X$^-$ (X = Br or NCS)} and an alkoxo complex [Mo(V)O(tpp)OR] in the reaction of alcohols such as methanol and ethanol with Mo(V)O(tpp)X in dichloromethane.[1] In these reactions the following three factors are thought to be important: (1) the change in the values of the dielectric constants of the mixed solvents, (2) the basicity of the mixed solvents and the acidity of the coordinated alcohols, and (3) the bulkiness of the alcohol molecules.

In the present study, the reactions of Mo(V)O(tpp)Br with various alcohols and water were followed by electronic spectral measurements to find out the most important factors affecting the formation of the alcohol and alkoxo complexes, or driving those formation reactions.

EXPERIMENTAL

Mo(V)O(tpp)Br was prepared by the method previously reported.[1] Alcohols were purified by the usual methods. Dichloromethane was especially carefully purified. Visible absorption spectra were measured at 25±0.1°C with an Hitachi 808 spectrophotometer. ESR spectra were recorded on a JEOL JES-FE1X spectrometer at 25°C. All sample solutions were prepared and measured in the dark to avoid photochemical reductions of the complexes.[2,3]

RESULTS AND DISCUSSION

The addition of a trace amount of methanol [(0.02% (v/v)] to the dichloromethane solution of Mo(V)O(tpp)Br (1.1×10^{-5} mol dm^{-3}) causes a shift in the Soret band[4] from 510 to *ca* 508 nm (first stage of the reaction). This spectral shift was too small to confirm its presence in the previous study.[1] The presence of this first stage was confirmed in the present study by detailed electronic spectral measurements for the reaction systems between Mo(V)O(tpp)Br and various alcohols. Further addition of methanol yields a complex showing bands at 478, 600, and 645 nm (second stage). This spectral change shares isosbestic points with the final spectrum of the first stage. An Asmus plot[5] for this spectral change indicated that the complex formed in the first stage reacts with methanol with a 1:1 molar ratio. The absorption spectrum of the complex in the presence of a large excess of methanol (third stage) has bands at 454, 581 and 621 nm. This absorption spectrum agrees with that of the methoxo complex synthesized independently. The formation of the methoxo complex is accel-

* Authors to whom correspondence should be addressed.

erated by the addition of a trace amount of superoxide (O_2^-) which acts as a base to remove a proton from methanol.[1] ESR measurements showed that the oxidation state of the central molybdenum of the complexes formed in these three stages was +5: the ESR signal with nine lines due to the coupling of $^{92,94,96,98,100}Mo(d^1, I = 0)$ and four nitrogen atoms of the porphyrin ring was observed around $g = 1.967$. Therefore, there is no change in the oxidation state of molybdenum in these reactions with alcohols. These results suggest that the reaction of Mo(V)O(tpp)Br with alcohol in dichloromethane proceeds in three steps [(1)–(3)]:

$$\mathrm{Mo(V)O(tpp)Br} \overset{\mathrm{ROH}}{\rightleftharpoons} [\mathrm{Mo(V)O(tpp)Br}]_s \quad (\mathrm{s} = \text{solvation}), \quad (1)$$

$$[\mathrm{Mo(V)O(tpp)Br}]_s + \mathrm{ROH} \overset{K_1}{\rightleftharpoons} [\mathrm{Mo(V)O(tpp)(ROH)}]_s^+ \mathrm{Br}^-, \quad (2)$$

$$[\mathrm{Mo(V)O(tpp)(ROH)}]_s^+ \mathrm{Br}^- \overset{\mathrm{ROH}}{\rightleftharpoons} [\mathrm{Mo(V)O(tpp)OR}]_s + \mathrm{HBr}. \quad (3)$$

The solvation of the methoxo complex $Mo(V)O(tpp)OCH_3$ formed in the third stage is suggested by the shift of the UV-absorption peak of the synthesized complex $Mo(V)O(tpp)OCH_3$ from 341 to 322 nm when the dichloromethane solution contains 1% (v/v) methanol.

The electronic spectra of the alcohol and alkoxo complexes for various alcohol systems have almost the same peaks in the visible region. Table 1 shows the formation constants (K_1) obtained from the Asmus plots, the alcohol concentrations required for the 50% formation of alkoxo complexes, and the acidity and dielectric constants (D) of the pure alcohols. For the formation reactions of the alcohol complexes the difference in the acidity among those alcohols may not be the main consideration because dissociation of a proton from alcohols is unnecessary for the formation of the corresponding alcohol complexes. The methanol, ethanol and 1-propanol complexes are formed completely in dichloromethane containing 1, 10 and 2% (v/v) of the respective alcohols. The addition of these amounts of the alcohols causes only small changes in D [from 8.93 (pure CH_2Cl_2) to 9.2, 10.4 and 9.4 for the respective reaction systems]. This result suggests that the change in D is not an important factor in the formation of alcohol complexes. The smaller ligands such as water, methanol, ethanol and 1-propanol yield the aqua or alcohol complexes easily. The bulky *t*-butyl alcohol yields no alcohol complex, indicating that the bulkiness of the alcohol is the most important factor in the formation of alcohol complexes. This in turn suggests that the alcohol complexes have the structure shown in Fig. 1. The CPK model shows that alcohols which are longer and more bulky than 1-propanol destabilize the alcohol complexes.

More than 60% of the initial amount of the Mo(V) complex Mo(V)O(tpp)Br exists as alkoxo complexes under the conditions of 20% (v/v) methanol–dichloromethane or 40% (v/v) propanol–

Table 1. Data for the formation of alcohol and alkoxo complexes

Alcohol	K_1 ($mol^{-1}\,dm^3$)	Alcohol concentration for 50% formation of the alkoxo complex [% (v/v)]	pK_a[a]	pK_b[b]	Dielectric constant
			For pure alcohol at 25°C		
HOH	>10.8	<8	15.7	−1.7	78.5
CH_3OH	10.8±0.2	10.1±0.3	15.1	−2.2	32.6
CH_3CH_2OH	4.4±0.4	60.2±1.2	15.9	−2.4	24.3
$CH_3CH_2CH_2OH$	6.4±0.4	14.9±0.4	16.1		20.1
$CH_3(CH_2)_2CH_2OH$	4.6±0.4	[c]	16.1		17.1
$CH_3CH(OH)CH_3$	2.0±2.0[d]	[e]	17.1		18.3
$(CH_3)_3COH$	No formation	[f]	19.2	−3.8	10.9[g]

[a] $ROH \rightleftharpoons RO^- + H^+$.[6]
[b] $ROH_2^+ \rightleftharpoons ROH + H^+$.[7]
[c] Formation of 12% 1-butoxo complex in 90% (v/v) 1-butanol.
[d] The alcohol and alkoxo complexes form simultaneously.
[e] Formation of *ca* 8% of the 2-propoxo complex in 90% (v/v) 2-propanol.
[f] Formation of 24% of the *t*-butoxo complex in 90% (v/v) *t*-butyl alcohol.
[g] At 30°C.

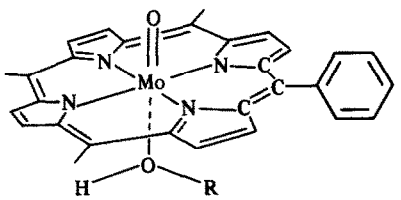


Fig. 1. Proposed structure of the alcohol complexes.

dichloromethane (D = 13.6 and 13.4, respectively). However, in 90% (v/v) butyl alcohol (D = 16), the yield of the alkoxo complex is only 12%. These results reveal also that the change in D of the mixed solvents is not an important factor for the formation of alkoxo complexes. Table 1 shows that smaller ligands such as water and methanol easily yield their aqua and methoxo complexes, respectively. 2-Propanol, presumed to be a bulky ligand, yields simultaneously alcohol and alkoxo complexes with a low concentration of alcohol. The more bulky *t*-butyl alcohol does not give an alcohol complex due to steric hindrance but gives an alkoxo complex with increasing concentration, which indicates that the *t*-butoxo complex is more stable sterically than the *t*-butyl alcohol complex. These results suggest that the size and bulkiness of the alcohol molecule are very important in determining the equilibria of reactions (2) and (3). The small size of the alcohol affects the formation of the alkoxo complex via the alcohol complex. The direct driving force for the formation of the alkoxo complex from the corresponding alcohol complex in the third stage may be a combined action of the acidity of the coordinated alcohol and the basicity of the solvent alcohol.

REFERENCES

1. T. Imamura, K. Hasegawa, T. Tanaka, W. Nakajima and M. Fujimoto, *Bull. Chem. Soc. Jpn* 1984, **57**, 194.
2. H. J. Ledon and M. Bonnet, *J. Am. Chem. Soc.* 1981, **103**, 6209.
3. T. Imamura, T. Jin, T. Susuki and M. Fujimoto, *Chem. Lett.* 1985, 847.
4. T. Imamura, T. Tanaka and M. Fujimoto, *Inorg. Chem.* 1984, **24**, 1038.
5. E. Asmus, *Fresenius' Z. Anal. Chem.* 1960, **178**, 104.
6. E. P. Serjeant and B. Dempsey, *Ionisation Constants of Organic Acids in Aqueous Solution.* IUPAC Chemical Data Series No. 23, Pergamon Press, New York (1978).
7. S. H. Pine, J. B. Hendrickson, D. J. Cram and G. S. Hammond, *Organic Chemistry*, 4th Edn. McGraw-Hill, Tokyo (1981).

Polyhedron Vol. 5, No. 10, pp. 1625–1628, 1986
Printed in Great Britain

0277–5387/86 $3.00+.00
© 1986 Pergamon Journals Ltd

HYDROGENATION OF IMINES BY RHODIUM–PHOSPHINE COMPLEXES

CINDY J. LONGLEY, TERENCE J. GOODWIN and GEOFFREY WILKINSON*

Chemistry Department, Imperial College, London SW7 2AY, U.K.

(*Received* 1 *May* 1986; *accepted* 19 *May* 1986)

Abstract—The hydrogenation of imines using $RhCl(PPh_3)_3$ and $[Rh(PPh_3)_2(diene)]PF_6$ as catalyst precursors is effective at room temperature under 1 atm of hydrogen, using alcohols as solvents. A water–diethylether phase-transfer system has been used for a solid imine. A catalytic cycle featuring hydrogen bonding between a coordinated alcohol and an imine, and involving a dialkylamido intermediate, is proposed.

Although rhodium–phosphine complexes have long been used in the reduction of carbon–carbon and carbon–oxygen double bonds by molecular hydrogen,[1] the reduction of carbon–nitrogen double bonds has been less well studied.[1,2] Rhodium–phosphine catalysts have been used to reduce imines via catalytic hydrosilylations,[3] but the use of metal carbonyl compounds has received more attention. For example, $Co_2(CO)_8$ under H_2+CO (1 : 1) at 100 bar and 95°C,[4] $Fe(CO)_5$ under CO (100 bar) at 100°C in the presence of NaOH or Et_3N,[5] Cr, Mo or W hexacarbonyls in MeOH containing NaOMe under H_2 (100 bar) at 60–160°C,[6] and $Fe(CO)_5$ in alcohols with and without organic bases under H_2 (100 bar) at 150°C[7] are found to be effective systems for the reduction. Rhodium–phosphine systems at temperatures above 40°C and > 10 bar pressure (H_2) have also been studied by Markó,[8] whilst $[Rh(diop)(nbd)]^+$ [diop = 2,3 - *O* - isopropylidene - 2,3 - dihydroxy - 1,4 - bis(diphenylphosphino)-butane, nbd = norbornadiene] has been employed without great success for asymmetric reduction.[9] Grigg *et al.*[10] have proposed a hydride-transfer mechanism for the reduction of imines by a $RhCl(PPh_3)_3$–Na_2CO_3 mixture in refluxing propan-2-ol, where $RhH(PPh_3)_4$ was suggested to be the effective catalyst.

We now show that $RhCl(PPh_3)_3$ or a cationic species, $[Rh(PPh_3)_2(diene)]^+$, can be used to reduce imines at 25°C and 1 atm H_2, provided that the solvent is an alcohol; large amounts (> 10 g) of imine can be reduced in a water–diethylether system using phase-transfer catalysis. $RhH(CO)(PPh_3)_3$, which has been used as a homogeneous hydrogenation catalyst in the selective reduction of carbon–carbon multiple bonds,[11] is effective in the reduction of imines under synthesis gas (1 : 1, 70 bar) in hot ethanol or toluene (95°C). Hydrogen alone was ineffective under these conditions, even in the presence of excess PPh_3.

RESULTS AND DISCUSSION

Hydrogenation of $RhCl(PPh_3)_3$ or $[Rh(PPh_3)_2(nbd)]PF_6$ in methanol, ethanol or higher alcohols gives a pale yellow or colourless solution, respectively, which on addition of imine becomes deep orange. On stirring under 1 atm H_2 at room temperature a stoichiometric amount of gas is absorbed and the imine reduced as in Table 1. For $RhCl(PPh_3)_3$ the orange solution reverts to yellow on completion of the reduction, but for the cationic species a brown solution is formed; such solutions tend to decompose and deposit rhodium metal, especially if fresh imine is added. No reduction occurs in acetone, dimethylformamide or acetonitrile, and addition of even small amounts (< 5%) of benzene to the alcohol severely inhibits reduction. Reductions in hexane–diethylether require temperatures > 50°C and pressures > 40 bar [cf. Ref. 8 where benzene–methanol (1 : 1) was used].

Although solvent effects in homogeneous hydrogenation are well-known,[1] the requirement for pure

* Author to whom correspondence should be addressed.

Table 1. Representative data for hydrogenation of imines with rhodium–phosphine catalysts

Precursor	Substrate[a]	Time[b] (min)
$RhCl(PPh_3)_3$[c]	*N*-BMA	160
	N-BIP	500
	N-BB	865
	N-BP	1250
	N-BMA[d]	125
	N-BMA[e]	1300
	N-BMA[f]	2195
$[Rh(PPh_3)_2(nbd)]PF_6$[g]	*N*-BMA	105
	N-BIP	210
	N-BB	270
	N-BP	360
	N-BMA[d]	95
	N-BP[d]	315
	N-BMA[e]	465
	N-BMA[f]	610
	N-BP[h]	600

[a] *N*-BMA, *N*-benzylidenemethylamine; *N*-BIP, *N*-benzylideneisopropylamine; *N*-BB, *N*-benzylidenebenzylamine; *N*-BP, *N*-benzylidenephenylamine.

[b] Time for complete hydrogenation. Average of three runs, error < 5%.

[c] Reaction conditions: Rh: substrate ratio = 1:50, *ca* 1 mmol of catalyst in ethanol (50 cm^3) at 25°C, 1 atm H_2.

[d] In methanol.

[e] In propan-1-ol.

[f] In propan-2-ol.

[g] Reaction conditions: Rh: substrate ratio = 1:120, *ca* 1 mmol of catalyst in ethanol (50 cm^3) at 25°C, 1 atm H_2.

[h] Reaction conditions: 10 cm^3 ether, 50 cm^3 H_2O, 0.1 cm^3 Triton X-100.

alcohols is unusual and the fact that other polar but non-hydrogen-bonding solvents are unsuitable suggests that hydrogen bonding may be important. Support is provided by observation of effective reduction even in aqueous alcohols.

A proposed cycle is shown in Fig. 1. It would normally be the N atom of the imine that would act as donor, but intramolecular hydrogen bonding as in **A** in Fig. 1 could lead to η^2-C,N bonding of the imine. Protonation of the imine nitrogen might be expected to have the same effect; however attempts to reduce $[RNH{=}CHR']^+$ failed probably because such a cationic substrate would have little tendency to bond a cationic metal species. H transfer to the imine in Fig. 1 would produce the dialkylamido species (**B**). This corresponds to the alkoxide intermediate species proposed in the reduction of ketones,[12] where we suggest that initial H-transfer occurs only to a η^2-ketone. A second hydride transfer to N would then give the coordinated amine complex (**C**), which, on oxidative addition of H_2, eliminates amine. The details of the cycle could, of course, differ from those in Fig. 1 in that the imine could coordinate to a rhodium(I) species which then undergoes oxidative addition of H_2, some of the species need not be solvated and the amine could be displaced by solvent etc. The rate of reduction is affected by the nature of the solvent alcohol, as illustrated in Table 1. For example, reduction is faster in propan-1-ol than in propan-2-ol, probably because steric crowding around the hydroxyl group in the latter restricts hydrogen bonding to the imine.

The formation of a dialkylamido intermediate, $[PhCH_2N(Ph)Cr(CO)_5]^-$, has also been proposed by Markó *et al.*[6] in the hydrogenation of imines using $[HCr(CO)_5]^-$; for $[HFe(CO)_4]^-$ it was suggested that interaction with $[PhCH{=}NHPh]^+$ gave an Fe—C σ-bonded species, $[Fe(PhCHNHPh)H(CO)_4]$.

The hydrogenolysis of a model dialkylamido complex is illustrated by the interaction of hydrogen with the complex $Rh[N(SiMe_3)_2](PPh_3)_2$.[13] A green solution of the complex immediately becomes yellow-brown on exposure to hydrogen, and $(Me_3Si)_2NH$ is formed quantitatively along with rhodium hydride species. Metal–nitrogen bond cleavage resulting in amine elimination has been established[14] in reactions of the type:

$$L_nM(NR_2)+L_mM'H \rightarrow L_nM{-}M'L_m+R_2NH,$$

but not previously, as far as we are aware, with dihydrogen.

Attempts to confirm the proposed reduction mechanism (Fig. 1) by performing the reaction under deuterium were not very successful. Only about 50% incorporation of D at the α-carbon atom in the product amine was observed; also the proportion of ROD in the solvent increased. This is due to D_2–ROH exchange processes, like those encountered by Schrock and Osborn[12] in ketone hydrogenation. Indeed such an exchange is observed on stirring alcohol solutions of the catalyst under D_2, in the absence of imine.

The results in Table 1 show that the rate of reduction decreases with increased steric crowding around the C=N bond. The higher activity of the cationic species relative to $RhCl(PPh_3)_3$ may be due to the possibility, in the former, of forming intramolecular hydrogen-bonded intermediates where both imine and alcohol are bound to the metal (as in **A**), whereas for $[RhCl(PPh_3)_2(H)_2(imine)]$ hydrogen bonding must be intermolecular. Also cationic

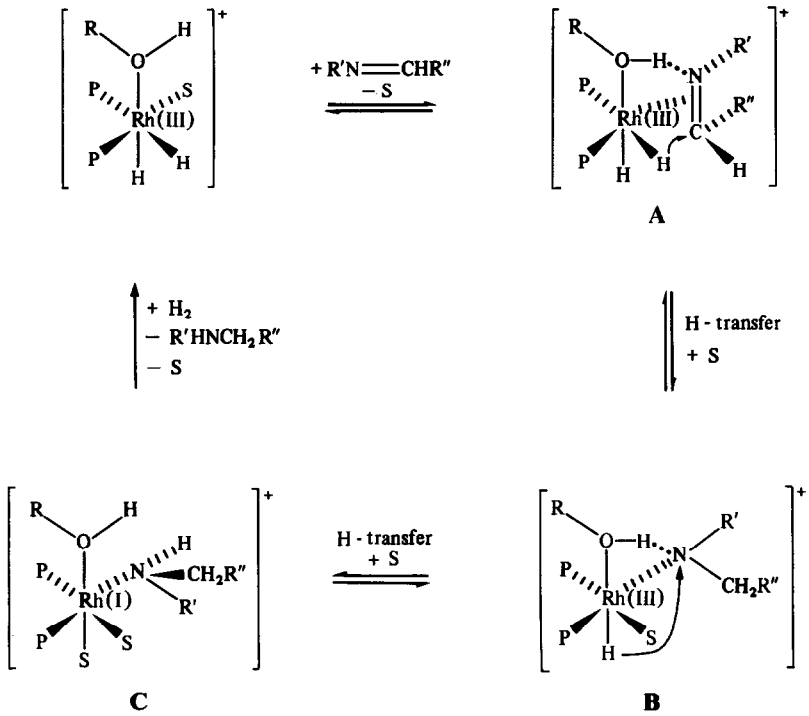


Fig. 1. Proposed cycle for catalytic hydrogenation of imines on cationic rhodium–triphenylphosphine complex. S = alcohol.

species are known to have a greater ability to reduce unsaturated linkages.

The relative insolubility of $RhCl(PPh_3)_3$ in alcohols precludes the use of this catalyst for reduction of large amounts of imine (> 10 g), since large volumes of solvent are required. The decomposition of the cationic catalysts in the presence of high concentrations of imine/amine makes them unsuitable for large-scale reductions. However, for the solid imine *N*-benzylidenephenylamine, phase-transfer permits the rapid reduction of relatively large amounts of imine. However, for liquid imines the reduction is very slow. Other two-phase systems such as polyethylene glycol–H_2O and toluene–H_2O were found to be ineffective.

EXPERIMENTAL

$RhCl(PPh_3)_3$,[15] $[Rh(PPh_3)_2(diene)]PF_6$[16] and $Rh[N(SiMe_3)_2](PPh_3)_2$[13] were prepared according to the literature. *N*-benzylidenemethylamine and *N*-benzylideneisopropylamine were from Lancaster Synthesis Ltd, *N*-benzylidenephenylamine and *N*-benzylidenebenzylamine were prepared by condensation of benzaldehyde with the appropriate amine in ethanol. Triton X-100 was from BDH Chemicals Ltd. Reagent grade solvents were purified by standard methods. Hydrogen was purified using an Englehard "Deoxo" catalyst.

Typical hydrogenation of imine in alcohols

$[Rh(PPh_3)_2(nbd)]PF_6$ (0.06 g, 0.07 mmol) in absolute ethanol was stirred vigorously under 1 atm hydrogen for 1 h. *N*-benzylidenemethylamine (1 g, 8.4 mmol) was added and the stirring continued until hydrogen uptake was complete (gas burette). Concentrated HCl (0.8 cm^3, 10 mmol) was added and the solution reduced to dryness. The solid was dissolved in the minimum amount of ethanol (*ca* 5 cm^3) and diethylether added dropwise until precipitation of the amine hydrochloride was complete; the white solid was collected, washed sparingly with ethanol–ether (1 : 1) and ether, and air dried. Yield 1.2 g (91%).

Free *N*-benzylmethylamine was liberated from the hydrochloride salt by dissolution in the minimum amount of 5 M NaOH (*ca* 5 cm^3) and extracting into ether. The ethereal extracts were dried over Na_2SO_4 and the ether removed under reduced pressure to give the amine. Yield 0.91 g (89%).

Hydrogenation using $RhH(CO)(PPh_3)_3$

$RhH(CO)(PPh_3)_3$ (0.06 g, 0.065 mmol) and *N*-benzylidenephenylamine (1 g, 5.52 mmol) were stirred in toluene (or ethanol) at 95°C under $CO+H_2$ (1 : 1, 70 bar) in a Berghof thermostatted autoclave for *ca* 48 h. The solution was cooled, evap-

orated and the solid dissolved in ethanol (*ca* 5 cm^3); concentrated HCl (1 cm^3, 13 mmol) was added followed by diethylether to precipitate the amine hydrochloride. The free amine was liberated as above.

Hydrogenation using phase-transfer catalysis

$[Rh(PPh_3)_2(cod)]PF_6$ (cod = cycloocta-1,5-diene) (0.2 g, 0.23 mmol) was stirred in diethylether (10 cm^3). Water (50 cm^3), then *N*-benzylidenephenylamine (5 g, 28 mmol) and Triton X-100 (0.1 cm^3) were added, and the mixture vigorously stirred under hydrogen until uptake was complete (*ca* 10 h). Concentrated HCl (3 cm^3, 36 mmol) was added and the solution evaporated under reduced pressure. The solid was dissolved in the minimum amount of hot ethanol (*ca* 20 cm^3) and after cooling precipitation of the amine hydrochloride was completed by slow addition of ether. The white crystals were collected, washed sparingly with ethanol–ether (1 : 1) and ether, and air dried. Yield 4.8 g (80%). The free amine was liberated as above.

Acknowledgements—We thank Johnson Matthey PLC for a loan of rhodium chloride and the S.E.R.C. for a studentship (C.J.L.).

REFERENCES

1. B. R. James, In *Comprehensive Organometallic Chemistry* (Edited by G. Wilkinson, F. G. A. Stone and E. W. Abel), Vol. 8, Chap. 51. Pergamon Press, Oxford (1982). B. R. James, *Homogeneous Hydrogenation*, Wiley Interscience, New York (1974).
2. B. Heil, L. Markó and S. Toros, In *Homogeneous Catalysis with Metal Phosphine Complexes* (Edited by L. H. Pignolet), Chap. 10. Plenum Press, New York (1983).
3. N. Langlois, T.-P. Dang and H. B. Kagan, *Tetrahedron Lett.* 1973, 4865.
4. A. Baranyai, F. Ungváry and L. Markó, *J. Mol. Catal.* 1985, **32**, 343.
5. M. A. Radhi, G. Pályi and L. Markó, *J. Mol. Catal.* 1983, **22**, 195.
6. J. Palágyi, Z. Nagy-Magos and L. Markó, *Transition Met. Chem.* 1985, **10**, 336.
7. M. A. Radhi and L. Markó, *J. Organomet. Chem.* 1984, **262**, 359.
8. S. Vastag, B. Heil, S. Toros and L. Markó, *Transition Met. Chem.* 1977, **2**, 58; Z. Nagy-Magos, S. Vastag, B. Heil and L. Markó, *ibid.* 1978, **3**, 123.
9. A. Levi, G. Modena and G. Scorrano, *J. Chem. Soc., Chem. Commun.* 1975, 6.
10. R. Grigg, T. R. B. Mitchell and N. Tongpenyai, *Synthesis* 1981, 442.
11. C. O'Connor and G. Wilkinson, *J. Chem. Soc. A* 1968, 2665.
12. R. R. Schrock and J. A. Osborn, *Chem. Commun.* 1970, 567.
13. B. Cetinkaya, M. F. Lappert and S. Torroni, *J. Chem. Soc., Chem. Commun.* 1970, 843.
14. W. J. Sartain and J. P. Selegue, *J. Am. Chem. Soc.* 1985, **107**, 5818; R. L. Geerts, J. C. Huffman and K. G. Caulton, *Inorg. Chem.* 1986, **25**, 591; M. H. Chisholm, J. C. Huffman and C. A. Smith, *J. Am. Chem. Soc.* 1986, **108**, 222.
15. J. A. Osborn, F. H. Jardine, J. F. Young and G. Wilkinson, *J. Chem. Soc. A* 1966, 1711.
16. R. R. Schrock and J. A. Osborn, *J. Am. Chem. Soc.* 1971, **93**, 2397.

Polyhedron Vol. 5, No. 10, pp. 1629–1634, 1986
Printed in Great Britain

0277-5387/86 $3.00+.00
Pergamon Journals Ltd

COMPARATIVE STUDY OF IRON(III) PHOSPHATE, ARSENATE, ANTIMONATE, SELENITE, MOLYBDATE AND TUNGSTATE

P. S. THIND and J. S. GANDHI*

Department of Chemistry, Guru Nanak Dev University, Amritsar 143005, India

(*Received* 24 *June* 1985; *accepted after revision* 28 *May* 1986)

Abstract—Six water-insoluble compounds of iron(III) have been synthesized by mixing solutions of ferric nitrate and the acidic oxides of elements of Groups V and VI. These compounds have been characterized on the basis of chemical-analysis, pH titration, thermogravimetry, solid-reflectance, IR and Mössbauer studies. Their chemical, thermal and ion-exchange characteristics have been compared.

Since the classical work of Amphlett,[1] numerous synthetic inorganic ion-exchangers have been synthesized and their properties studied. However, the methods of preparation of the same ion-exchanger by different workers are not always the same. It has been shown that the selectivity of an inorganic ion-exchanger depends not only upon its composition but also upon the pH at which the precipitation is performed. It is important that the various ion-exchangers should be synthesized again under the same conditions and their properties studied. Szirtes *et al.*,[2] as well as Qureshi *et al.*,[3,4] have made interesting studied of the phosphates of titanium, zirconium and chromium, and compared their ion-exchange properties. Furthermore, iron(III) phosphate,[5] arsenate,[6] antimonate,[7] tungstate[8] and molybdate have been synthesized and used for the separation of metal ions. In this investigation these iron(III)-based ion-exchangers have been used for a comparison of their spectroscopic, chemical, thermal and ion-exchange properties.

EXPERIMENTAL

Reagents

The ferric nitrate, ammonium dihydrogen phosphate, sodium tungstate, sodium selenite and sodium arsenate used were of L.R grade. Antimony pentachloride solution (sp. gr. 2.30) was diluted with 4 M hydrochloric acid to obtain solutions of the required concentration. All other reagents were of analytical grade.

Preparation

The iron(III) compounds have been synthesized under similar conditions to facilitate comparison (Table 1). The reagents given in column 2 were mixed in the volume ratios given in column 3. The pH of the reaction mixture was adjusted by adding an alkali or acid solution. Iron(III) hydroxide was prepared by adding ammonia solution to aqueous 0.10 M ferric nitrate. The gelatinous precipitates obtained were washed by decantation, filtered off, washed again with distilled water and then dried at 40°C. Aging always affects the properties of this type of inorganic ion-exchanger.[10] Therefore, all the precipitates were kept for 24 h with the reaction mixture at room temperature. The dried product was immersed in 0.1 M nitric acid to remove the foreign ions adsorbed during the preparation. Finally, the exchangers were washed with demineralized water to remove the excess acid, and dried again at 40°C.

Analytical procedures

A 0.20-g portion of the exchanger was dissolved in concentrated hydrochloric acid. Iron(III) was estimated as oxide, phosphate by the phospho-molybdate method, molybdate by the quinolinol

*Author to whom correspondence should be addressed.

Table 1. Synthesis and properties of some iron(III)-based ion-exchangers

Compound	Conditions of synthesis: Reagents used	Mixing-volume ratio	pH	Colour in H^+-form	Properties: Ion-exchange capacity (meq g^{-1})	Density (g cm^{-3})	Chemical composition (Fe:X)
Iron(III) phosphate	0.10 M $Fe(NO_3)_3 \cdot 9H_2O$ 0.10 M $(NH_4)H_2PO_4$	1:2	1.0	White	0.72	2.85	2.48:1.00
Iron(III) arsenate	0.10 M $Fe(NO_3)_3 \cdot 9H_2O$ 0.1 M $NaAsO_2$	6:8	1.0	Grey	0.80	3.09	1:2.52
Iron(III) antimonate	0.10 M $Fe(NO_3)_3 \cdot 9H_2O$ 0.1 M $SbCl_5$	2:1	0.0	Brown	0.82	4.62	1:2.98
Iron(III) molybdate	0.05 M $Fe(NO_3)_3 \cdot 9H_2O$ 0.05 M $(NH_4)_6Mo_7O_{24} \cdot 4H_2O$	2:1	1.0	Yellow	1.40	3.70	2:6.0
Iron(III) tungstate	0.10 M $Fe(NO_3)_3 \cdot 9H_2O$ 0.10 M $Na_2WO_2WO_4 \cdot 2H_2O$	1:1	0.0	Yellow	0.84	4.20	1:1
Iron(III) selenite	0.05 M $Fe(NO_3)_3 \cdot 9H_2O$ 0.05 M Na_2SeO_3	1:2	1.0	Brown	0.40	5.14	2:3.0

method, selenium by reducing it to the element, tungstate by the dithiol method, and arsenate and antimony by titrimetric methods.

To determine the solubility of the iron(III) compounds, 0.20 g of the exchanger was shaken for 24 h with 20 cm^3 of the solution concerned. The undissolved exchanger was filtered off and in the filtrate iron was determined spectrophotometrically by the 1,10-phenanthroline method. Phosphorus, molybdenum, tungsten, antimony and selenite were also determined spectrophotometrically. All the cations used for distribution studies were determined using EDTA.

RESULTS

Various properties of iron(III) compounds are given in Table 1. All these compounds remain as stable gels in water. The gels crack on immersion in water, with slight evolution of heat.

Ion-exchange capacity

The ion-exchange capacity of various iron(III)-based ion-exchangers was determined by column operation: 1 g of the exchanger in the H^+-form was loaded in a glass column with a glass wool support and washed with a 1.0 M sodium nitrate solution; 400 cm^3 of effluent was collected in each case, at the rate of 5–10 drops min^{-1}. The liberated hydrogen ions were titrated against standard alkali solution.

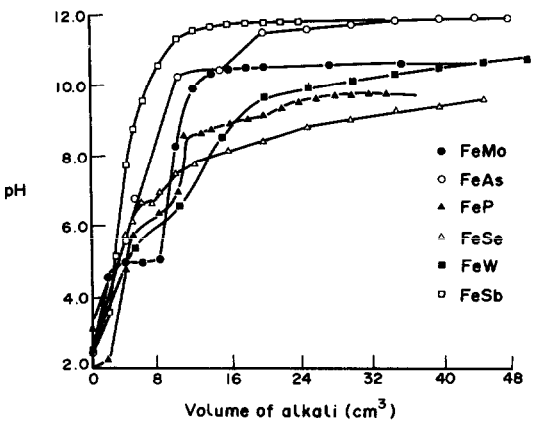


Fig. 1. pH titrations of different iron(III)-based ion-exchangers.

The ion-exchange capacity of different materials dried at various temperatures was also determined (Table 1).

pH titrations

The pH titrations with 0.1 N sodium hydroxide solutions were performed by the added-salt method: 0.2 g of the exchanger was kept in contact with varying volumes of the base and the salt solutions for about 24 h (Fig. 1).

Density measurements

The density (d) of the dry ion-exchanger has been calculated from the following formula[11] on the basis

of the measured data:

$$d = \frac{mS}{(M-M')+m},$$

where m is the weight of the exchanger, M is the weight of the pyknometer filled with water, M' is the weight of the pyknometer containing the ion-exchanger and water, and S is the density of water at the temperature of the measurements (25°C). The results of density measurements are given in Table 1.

Spectroscopic studies

The diffuse electronic spectra of the iron(III)-based ion-exchangers were recorded in the range 200–600 nm using magnesium oxide as the standard reflector.

The IR spectra of the ion-exchangers in the range 4000–200 cm^{-1} were recorded on a SP3-300 Pye-Unicam spectrophotometer using potassium bromide pellets.

Mössbauer spectra of the ion-exchangers were recorded at room temperature (25 ± 1°C) using a Mössbauer spectrometer MBS-35 (ECIL, India) having a multichannel analyser (480 channels, MCA-38B type using ^{57}Co source at constant acceleration). Sodium nitroprusside was used as the reference and the values of isomer shift have been quoted with respect to it. The results are given in Table 2.

X-ray photographs of the powder samples were taken using a Debye–Scherrer camera of radius 57.3 mm. A thick paste of the sample with "Quick-Fix" was shaped in the form of a thin solid rod of about 0.3 mm diameter and about 1 cm in length. It was mounted on the axis of the camera and the incident beam of X-rays was directed at right angles to this axis. The X-rays were produced from a Phillips generator of the type PW-1720. Cu-K_α radiation was used for taking the photographs.

Absorption studies

The K_d values for inorganic ions have been determined for the phosphate, molybdate, tungstate and selenite of iron(III) in demineralized water. The loading of cations for the system was less than 3% of the experimental ion-exchange capacity. The equation used was:

$$K_d = \frac{I-F}{F} \times \frac{20}{0.2} \text{ cm}^3 \text{ g}^{-1},$$

where I is the volume of 0.025 M EDTA needed to titrate the original cation solution, and F is the volume of 0.025 M EDTA needed for titration after equilibrium. The total volume of the equilibrating solution was 20 cm^3 and the amount of exchanger taken was 0.20 g. The results are given in Fig. 2.

DISCUSSION

All the six salts of iron(III) reported here were first prepared under varying conditions. The conditions of preparation finally chosen were those which appeared to give reproducible and fairly stable products. These conditions were adhered to in all preparations to facilitate comparison. The results for the chemical compositions of the phosphate, arsenate, antimonate, molybdate, tungstate and selenite are given in Table 1. Iron(III) arsenate, antimonate and tungstate have almost the same ion-exchange capacity but their chemical composition is quite different. Iron(III) molybdate has the highest ion-exchange capacity, which may be attributed to the hydrolysis of the exchanger in an aqueous system. Iron(III) selenite has the lowest ion-exchange capacity. The values of the ion-exchange capacity and chemical composition of all the iron(III) exchangers given in Table 1 are almost similar to those reported earlier.[5–9]

A comparison of the chemical stabilities of iron(III)-based ion-exchangers is presented in Fig.

Table 2. Isomer shifts and quadrupole splitting of various iron(III) compounds[a]

Compound	Drying temperature	Isomer shift (mm s^{-1})	Quadrupole splitting (mm s^{-1})
Iron(III) molybdate	RT[b]	0.68	0.48
Iron(III) selenite	RT	0.60	0.44
Iron(III) phosphate	RT	0.70	0.44
Iron(III) antimonate	RT	0.66	0.44
Iron(III) arsenate	RT	0.59	0.19

[a]The uncertainty in measurement is ±0.03 mm s^{-1}.
[b]Room temperature.

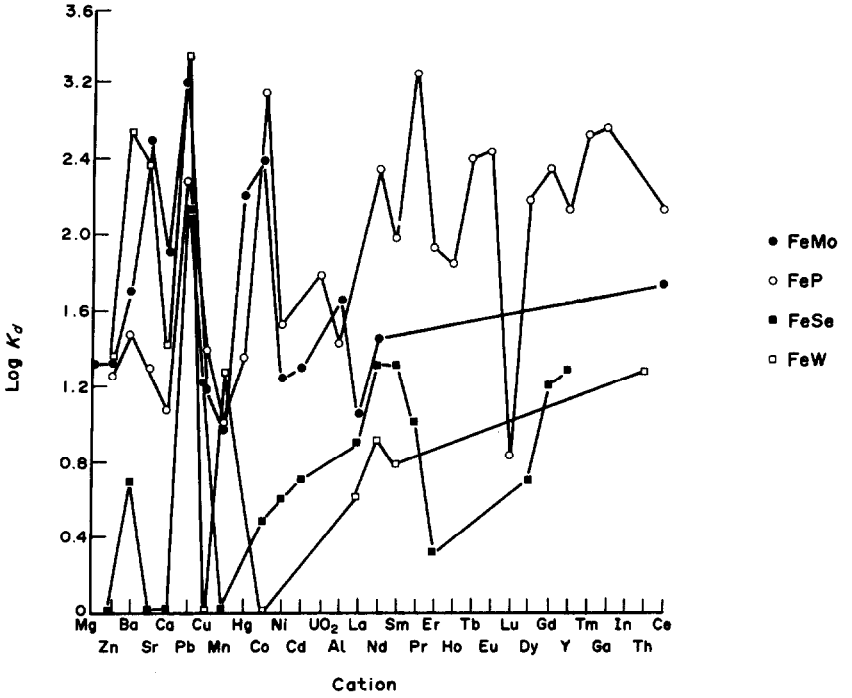


Fig. 2. Log K_d as function of metal ion.

2. Figure 3 gives an idea of the chemical stability of the materials. It is found that iron(III) tungstate is the most stable chemically in the lower-pH range while iron(III) selenite is the most stable in a neutral medium.

From Fig. 1, it can be seen that the exchange of sodium ions begins at acidic pH values and continues at the alkaline pH values. With iron(III) antimonate, no exchange of sodium ions takes place in acidic media, but it does at alkaline pH values.

The IR absorption bands observed for all six compounds are found to be identical. The materials show their characteristic bands in the range 350–700 cm^{-1}, in addition to the usual bands for interstitial water and the OH stretch. On increasing the drying temperature, the bands for water and the OH groups disappear, and this pattern is followed by all the exchangers discussed in the paper.

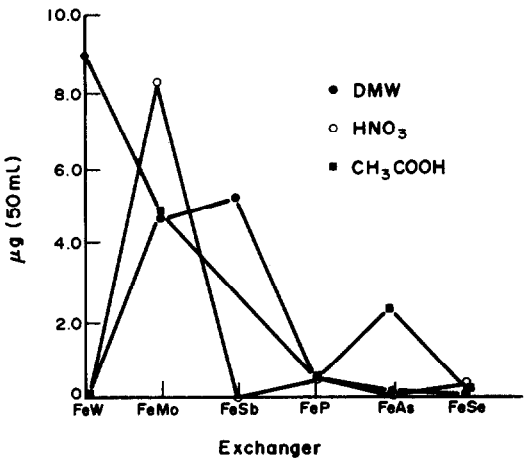


Fig. 3. Solubility as function of ion-exchanger.

The purpose of the present Mössbauer investigation of the amorphous substances of iron(III)-based ion-exchangers was to elucidate the bonding character between the iron and the anionic group in the material as shown in an earlier paper.[12]

The Mössbauer spectra of all the iron(III) compounds consist of a doublet at room temperature (25±2°C) (Table 2). The isomer shift values (0.59–0.70 mm s^{-1}) indicate that these compounds are high-spin with oxidation state +3. The quadrupole-splitting values show their distortion from the cubic symmetry around the iron nucleus. The peaks are broad (being 2–3 times the natural line width of the source), indicating more than one type of octahedral site. From Mössbauer data, it is concluded that iron atoms are surrounded predominantly by oxygen atoms. Therefore, relatively similar values of isomer shifts were observed for all the compounds.

X-ray powder photographs show that all the six compounds in hydrogen dried at 40°C are amorphous.

The Fe:Sb ratio by chemical analysis is 1:2.98. On heating, the oxides are produced, which should

Table 3. Possible separation on iron(III) compounds

Compound	Possible separations
Iron(III) phosphate	Th^{4+} from numerous metal ions; Pb^{2+} from Hg^{2+}, Cd^{2+}, Cu^{2+}, Ni^{2+} and Zn^{2+}
Iron(III) arsenate	Mg^{2+} from Ca^{2+}; Ba^{2+} from Sr^{2+} and Pb^{2+}; Ga^{3+} from Al^{3+}
Iron(III) antimonate	Sr^{2+} from Mg^{2+}; Ga^{3+} from Al^{3+}; Cd^{2+} from Zn^{2+} and Mg^{2+}; Sm^{3+} from Th^{4+}; La^{3+} from Y^{3+}
Iron(III) molybdate	Bi^{3+} from Zn^{2+}, Ni^{2+} and Cd^{2+}; Hg^{2+} from Cu^{2+} and Mn^{2+}; Co^{2+} from Ni^{2+}, Cu^{2+} and Cd^{2+}
Iron(III) selenite	Pb^{2+} from numerous metal ions
Iron(III) tungstate	Ba^{2+} from Mg^{2+}, Ca^{2+} and rare earth ions; Sr^{2+} from numerous metal ions

Table 4. Separation factors of some important pairs of cations on iron(III)-based ion-exchangers

Separation factor	Iron(III) molybdate	Iron(III) selenite	Iron(III) antimonate	Iron(III) tungstate	Iron(III) phosphate
α_{Pb}^{Sn}	30.4	132	8.2	38.2	10.5
α_{Pb}^{Ba}	13.0	26.4	2.0	2.5	6.3
α_{Pb}^{La}	56.6	16.5	0.0	220	—
α_{Pb}^{Cu}	42.2	7.7	0.0	879	7.8
α_{Pb}^{Ni}	36.9	33	1.2	—	5.7
α_{Sr}^{Hg}	15.3	—	1.4	—	—
α_{Sr}^{Cd}	15.8	5	0.6	—	—
α_{Sr}^{Mn}	33.6	0	2.9	12.7	1.9

be in the same mole ratio. Allowing for experimental error, this may be rounded off to a 1:3 ratio. Therefore, the empirical formula weight for $Fe_2O_3 \cdot 3Sb_2O_5$ is approximately 1130. The total weight loss on heating is 12.5%, so, if n is the number of mol of water per mol of "mixed oxide", then $1800n/(1130+18n) = 12.5$, and $n = 8.97$. Again, allowing for error in the TG work, we can write the formula as $Fe_2O_3 \cdot 3Sb_2O_5 \cdot 9H_2O$ (formula weight 1292). The cation exchange capacity on the basis of two protons per formula weight is $2000/1292 = 1.54$ meq g^{-1}. The Fe:W ratio by chemical analysis is 1:1, corresponding to a molecular formula of $Fe_2O_3(H_2WO_4)_2 \cdot 2H_2O$, and the Fe:As ratio by chemical analysis is found to be 2:5, corresponding to a molecular formula of $Fe_2O_3 \cdot 2.5As_2O_3 \cdot 5H_2O$. The structure of iron(III) phosphate, iron(III) molybdate and iron(III) selenite are similar, as reported earlier.[5,9]

A comparison of the K_d values of metal ions on these exchangers in demineralized water shows some outstanding features (Fig. 2). Thus, the antimonate has the highest ion uptake of the six exchange materials studied. This may be due to the fact that amorphous antimony oxide has the largest number of free exchange sites available for the metal ions to be adsorbed. The lanthanides have the lowest K_d values for iron(III) tungstate, their highest K_d values being for iron(III) antimonate as expected. In the case of the tungstate the highest K_d value is for Pb^{2+}, which shows high K_d values on almost all the exchangers. In the case of the phosphate, Th^{4+} is totally adsorbed. This is a characteristic feature of iron(III) phosphate because all the other exchangers have a very low affinity for Th^{4+}. Some possible separations on the basis of K_d values for iron(III) exchangers are given in Table 3. The arsenate and tungstate of iron(III) are useful for the separation of alkaline earth metal ions. The corresponding phosphate and antimonate are useful for the separation of thorium from other cations. The difficult separation of Ga^{3+} and Al^{3+} is possible on arsenate and antimonate columns. Separation factors of some important pairs of cations on these exchangers, given in Table 4, also prove the utility of these materials. Therefore, the insoluble iron(III) compounds may be used to achieve separation. Their chief advantage is that they are inexpensive and are easy to prepare.

Acknowledgement—J. S. Gandhi is thankful to the Guru Nanak Dev University for the award of a fellowship.

REFERENCES

1. C. B. Amphlett, *Inorganic Ion-Exchangers*. Elsevier, Amsterdam (1964).
2. L. Szirtes, L. Zsinks, K. B. Zaborenko and B. Z. Iofa, *Acta Chim. Acad. Sci. Hung.* 1971, **54**, 215.
3. M. Qureshi, R. Kumar and H. S. Rathore, *Talanta* 1972, **19**, 1377.
4. M. Qureshi, N. Zehra, S. A. Nabi and V. Kumar, *Talanta* 1973, **20**, 609.
5. J. P. Rawat and P. S. Thind, *Can. J. Chem.* 1976, **54**, 1892.
6. J. P. Rawat and J. P. Singh, *Can. J. Chem.* 1976, **54**, 2534.
7. J. P. Rawat and D. K. Singh, *Anal. Chim. Acta* 1977, **87**, 157.
8. J. P. Rawat, H. Shankar and T. Khatoon, *Ann. Chim.* 1978, **68**, 913.
9. P. S. Thind, Parveen and H. Singh, *Bull. Chem. Soc. Jpn* 1983, **56**, 1536.
10. M. Qureshi, K. Husain and J. P. Gupta, *J. Chem. Soc. A* 1971, 29.
11. J. Inczedy, *Analytical Applications of Ion-Exchangers*, Chap. 5, p. 116. Pergamon Press, New York (1966).
12. V. A. Bryokhanov, V. I. Gol Denskiv, N. N. Dalyagin and L. A. Kerytko, *Sov. Phys.—JETP* 1963, **16**, 361.

Polyhedron Vol. 5, No. 10, pp. 1635–1638, 1986
Printed in Great Britain

0277-5387/86 $3.00+.00
© 1986 Pergamon Journals Ltd

SPECTRAL, THERMAL AND MAGNETIC STUDIES OF BIACETYLMONOXIME ISONICOTINOYLHYDRAZONE COMPLEXES

K. M. IBRAHIM,* M. M. BEKHEIT, G. M. ABU EL-REASH and M. M. MOSTAFA

Chemistry Department, Faculty of Science, Mansoura University, Mansoura, A.R. Egypt

(*Received* 17 *December* 1985; *accepted after revision* 28 *May* 1986)

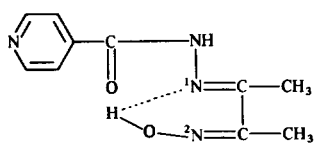
Abstract—The synthesis and characterization of Co(II), Ni(II), Cu(II), Zn(II), Cd(II) and UO_2^{2+} complexes of biacetylmonoxime isonicotinoylhydrazone (BMINH) are reported. Elemental-analysis, magnetic, thermal and spectral (IR, visible and NMR) measurements have been used to characterize the complexes. IR spectral data show that the ligand behaves in a bidentate and/or tridentate manner. An octahedral structure is proposed for the Ni(II) complexes, while a square-planar structure is proposed for both Co(II) and Cu(II) complexes, on the basis of magnetic and spectral measurements.

We reported earlier[1–3] on complexes of both aliphatic and aromatic hydrazone–oximes, but no work has been traced concerning a hydrazone–oxime containing a heterocyclic moiety. In this paper we report the preparation and characterization of some new metal complexes derived from biacetylmonoxime isonicotinoylhydrazone (BMINH), with dipositive transition metal ions. All the observations and data confirm that the behaviour of BMINH is quite different from those reported earlier.[1–3] In addition, the investigation of BMINH as a type of hydrazone–oxime-containing heterocyclic moiety as well as the importance of the isonicotonic acid residue for the treatment of tuberculosis provided an impetus for this study.

RESULTS AND DISCUSSION

The solid complexes isolated are quite stable in air and insoluble in common organic solvents, but easily soluble in dimethylformamide (DMF) and dimethylsulphoxide. The molar conductivities in DMF at 25°C are in the range indicating[4] a non-electrolytic nature for all complexes except the $[Ni(BMINH)(H_2O)_2(C_2H_5OH)]Cl_2$ and $[Mn(BMINH)(H_2O)_2]Cl_2$ complexes, which have high values which suggest that they are 1:2 electrolytes.

The most characteristic features of the IR spectrum of BMINH have been determined by a careful comparison of the spectrum of BMINH with both isonicotinic acid hydrazide and biacetylmonoxime. The spectrum of BMINH, in Nujol, shows three bands at 1675, 1635 and 1575 cm^{-1} assigned to $\nu(CO)$, $\nu(CN^1)$ and $\nu(CN^2)$, respectively. The strong band observed at 940 cm^{-1} in the spectrum of the ligand, which is absent in the spectrum of isonicotinic acid hydrazide is mainly attributed to the $\nu(NO)$ vibration. In addition, the two bands at 3320 and 3170 cm^{-1} in the spectrum of the ligand are assigned to the oxime NOH and NH groups, respectively. The presence of $\nu(OH)$ as a shoulder at a low wavenumber suggests intramolecular hydrogen bonding. The broad but weak bands in the 1910–2000- and 2200–2400-cm^{-1} regions can be taken as additional evidence for the presence of intramolecular hydrogen bonding (O—H . . N)[5] as shown below:



*Author to whom correspondence should be addressed.

The NMR spectrum of BMINH in d_6-DMSO shows two signals at δ 11.0 and 10.4 ppm (i.e. downfield from TMS), which disappear upon adding D_2O. These two signals are therefore assigned to *anti*- and *syn*-oxime NOH protons, respectively. The *syn*:*anti* ratio was found to be 1:1, indicating that the percentages of free and hydrogen-bonded OH are identical. Additionally, a signal at δ 8.25 ppm is assigned to the NH proton, and this also disappeared upon adding D_2O.

The IR spectra of the complexes [Cu(BMINH)Br_2]$2H_2O$ and [Mn(BMINH)$(H_2O)_2$]Cl_2 show that the ligand behaves as bidentate coordinating via the azomethine nitrogen (CN^1) and the carbonyl oxygen (CO) in the keto form, forming a five-membered ring around the metal ion. The mode of complexation is suggested by the negative shift of both ν(CO) and $\nu(CN^1)$ vibrations to a lower wavenumber as well as the positive shift of ν(N—N). The new bands observed at *ca* 470 and *ca* 410 cm^{-1} are assigned to ν(M—O)[6] and ν(M—N),[7] respectively.

In addition, the ligand acts as a bidentate in the complexes [Cd(BMINH)Cl_2]$2H_2O$ and [Cu(BMINH)Cl_2]C_2H_5OH, coordinating via the azomethine nitrogen of both the hydrazone (CN^1) and the oxime (CN^2) groups. The bonding sites are assigned on the basis of the following evidence: the negative shift of the CN^1 band to a lower wavenumber as well as the positive shift of the band due to CN^2; the CO band remains unaffected as observed in the IR spectrum of the free ligand; a new band is observed at *ca* 405 cm^{-1}, which is assigned to ν(M—N);[7] and the NMR spectrum of the [Cd(BMINH)Cl_2]$2H_2O$ complex shows signals due to the protons of the NOH and NH groups.

Moreover, the ligand coordinates in a bidentate manner via the azomethine nitrogen (CN^1) and the enolized carbonyl oxygen with the displacement of a hydrogen atom from the latter group. This behaviour is found in the [Co(BMINH–H)Ac]$4H_2O$ complex. This mode of complexation is supported by the following observations: the disappearance of ν(CO) with the simultaneous appearance of new bands at 1170 and 1620 cm^{-1}, assignable to ν(C—O)[8] and ν(C=N*), respectively; and the negative shift of $\nu(CN^1)$ together with the positive shift of ν(N—N). The new bands observed at *ca* 470 and *ca* 380 cm^{-1} are assigned to ν(M—O)[6] and ν(M—N),[7] respectively. The observation of two bands at 1590 and 1440 cm^{-1} attributable to ν_{as} and ν_s of the acetate group as well as the great difference (150 cm^{-1}) between those two bands indicates a bidentate nature for the acetate group.

The existence of water of hydration for [Co(BMINH–H)Ac]$4H_2O$ was confirmed by thermal analysis. The thermal-analysis results show that the mass loss up to 225°C corresponds to the removal of four water molecules. This indicates that the four water molecules are identical and exist in the outer coordination sphere.

On the other hand, the ligand may act in a tridentate way, coordinating via the azomethine nitrogen of both the hydrazone (CN^1), and the oxime (CN^2), and the carbonyl oxygen in the keto form. This behaviour is found in the case of the [Ni(BMINH)$(H_2O)_2(C_2H_5OH)$]Cl_2 complex. This mode of coordination is supported by the negative shifts of the CO group and the azomethine nitrogen of both the hydrazone (CN^1) and the oxime (CN^2) groups. The bands in the low-frequency region at *ca* 480 and *ca* 375 cm^{-1} are assigned to ν(M—O)[6] and ν(M—N)[7] vibrations, respectively.

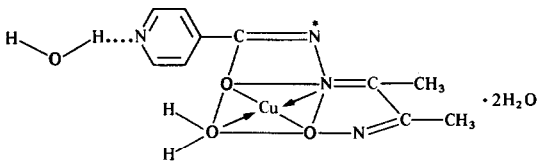
In addition, the ligand may behave in a tridentate way, coordinating via the azomethine nitrogen of the hydrazone (CN^1), the CO and the deprotonated NOH groups. This behaviour is found in [UO_2(BMINH–H)$_2$], [Cd(BMINH–H)$_2$] and [Zn(BMINH–H)Br]H_2O complexes. The mode of chelation is supported by the following evidence: the negative shifts of both the CO and the azomethine (CN^1) vibration bands to lower wavenumbers; the disappearance of ν(OH) together with the positive shift of ν(NO) to higher wavenumbers; the appearance of new bands in the 450–470- and 430–370-cm^{-1} regions, assignable to ν(M—O)[6] and ν(M—N),[7] respectively; and the disappearance of the signals due to the proton of the oxime group in the NMR spectra of those complexes.

The uranyl complex exhibits three bands at 930, 480 and 265 cm^{-1}, assigned to ν_3-, ν_1- and ν_4-vibrations, respectively, of the dioxouranium ion.[9] The force constant (F) for bonding sites of the U=O vibration is calculated by the method of McGlynn *et al.*[10] and the value (F_{UO}) is found to be 7.139 mdynes $Å^{-1}$.

The ligand may also behave in a tridentate way, coordinating via the azomethine nitrogen (CN^1), the oxime oxygen (NOH) and the carbonyl oxygen in the enol form (=C—OH), with displacement of two hydrogen atoms from the latter two groups. This behaviour is observed in the [Cu(BMINH–2H)$(H_2O)_2$]$2H_2O$ and [Ni(BMINH–2H)·$(H_2O)_2(C_2H_5OH)$] complexes. The mode of complexation is supported by the following evidence: the disappearance of the bands at 3320 and 1675 cm^{-1} attributable to ν(OH) and ν(CO) vibrations, respectively, with the simultaneous appearance of new bands at *ca* 1240 and

1645 cm^{-1}, assigned to ν(C—O)[8] and ν(C=N*), respectively; the negative shift of $\nu(CN^1)$ to a lower wavenumber and the positive shift of ν(NO) to a higher wavenumber; and the appearance of new bands in the low-frequency region at 440–420 and 395–375cm^{-1}, assigned to ν(M—O)[6] and ν(M—N),[7] respectively.

The presence of water molecules in the $[Cu(BMINH–2H)(H_2O)_2]2H_2O$ complex was confirmed by thermal analysis. The results show that there are three types of water molecules. Firstly, the mass loss up to 214°C corresponds to the removal of two loosely bound water molecules. Secondly, the mass loss up to 308°C corresponds to the removal of another water molecule. This water molecule may be hydrogen bonded to the pyridine nitrogen as shown in structure **I**. Thirdly, the mass loss up to 328°C corresponds to the removal of a water molecule of coordination.



I

The magnetic moments and electronic spectra of the complexes are listed in Table 1. The electronic spectra (Nujol) of the Ni(II) complexes, $[Ni(BMINH)(H_2O)_2(C_2H_5OH)]Cl_2$ and $[Ni(BMINH–2H)(H_2O)_2(C_2H_5OH)]$, show two bands in the 14,080–15,670- and 25,640–25,120-cm^{-1} regions, assignable to $^3A_{2g} \rightarrow {}^3T_{1g}(F)$ and $^3A_{2g} \rightarrow {}^3T_{1g}(P)$ transitions,[11] respectively. The calculated values of Dq, B, β and ν_2/ν_1 (Table 2) lie in the same range as reported for the octahedrally coordinated Ni(II) ion.[12] The position of ν_1 is calculated theoretically.[12] The values of the magnetic moment (3.15–2.96 BM) are additional evidence for an octahedral structure. The magnetic-moment value (2.37 BM) for $[Co(BMINH–H)Ac]4H_2O$ falls in the range reported for a square-planar structure. The presence of a characteristic band at *ca* 19,200 cm^{-1} further supports the square-planar configuration.[13] The electronic spectra of the complexes $[Cu(BMINH–2H)(H_2O)_2]2H_2O$, $[Cu(BMINH)Cl_2]C_2H_5OH$ and $[Cu(BMINH)Br_2]2H_2O$ show broad bands with maxima in the 14,800–13,700-cm^{-1} range, due to the $^2B_{1g} \rightarrow {}^2A_{1g}$ transition, and a shoulder in the 22,400–22,600-cm^{-1} range, in a square-planar configuration.[14] The band in the 25,900–25,600-cm^{-1} range may be due to a charge transfer, probably, d–π^*.[15] In addition, the magnetic-moment values (2.15–2.05 BM) can be taken as additional evidence of the square-planar configuration.[16] The low value of the magnetic moment (1.57 BM) for the complex $[Cu(BMINH–2H)(H_2O)_2]2H_2O$ may be explained on the basis of the existence of a polymeric structure including copper–copper interaction.

EXPERIMENTAL

All the chemicals were of analytical grade (BDH) and used as supplied. The ligand (BMINH) was prepared as reported earlier.[2] The metal complexes with the general formula $M(BMINH)X_2 \cdot nY$ [M = Ni(II), Cu(II), Cd(II) or Mn(II); X = Br or Cl; Y = H_2O or C_2H_5OH; and n = 0–2] were prepared by refluxing equimolar amounts of BMINH and hydrated metal salts in absolute ethanol for 0.5–1 h, whereas the complexes $[Zn(BMINH–H)Br]H_2O$ and $[Ni(BMINH–2H)(H_2O)_2(C_2H_5OH)]$ were prepared by the same method but in the presence of sodium acetate as a buffering agent. The complexes with the formulae $[Cd(BMINH–H)_2]$, $[Co(BMINH–H)Ac]4H_2O$, $[Cu(BMINH–2H)(H_2O)_2]2H_2O$ and $[UO_2(BMINH–H)_2]$ were prepared using the metal acetate or sulphate in doubly distilled water, except for the uranyl complex which was prepared in absolute ethanol.

Table 1. Spectral and magnetic data of BMINH complexes

Compound	Magnetic moment (μ_{eff}) (BM)	Electronic spectra ($cm^{-1} \times 10^3$); ligand field bands
$[Ni(BMINH)(H_2O)_2(C_2H_5OH)]Cl_2$	3.15	14.08, 25.64; Dq = 843, B = 963, β = 0.920, ν_2/ν_1 = 1.67
$[Ni(BMINH–2H)(H_2O)_2(C_2H_5OH)]$	2.96	15.67, 25.12; Dq = 990, B = 740, β = 0.71, ν_2/ν_1 = 1.58
$[Co(BMINH–H)Ac]4H_2O$	2.37	19.2
$[Cu(BMINH)Cl_2]C_2H_5OH$	2.05	13.7, 22.4 (sh), 25.9 (CT)
$[Cu(BMINH)Br_2]2H_2O$	2.15	14.8, 22.4 (sh), 25.6 (CT)
$[Cu(BMINH–2H)(H_2O)_2]2H_2O$	1.57	14.7, 22.6 (sh), 25.9 (CT)

Table 2. Analytical and physical data for the complexes

Compound	M.p. (°C)	Colour	% calculated				% found				Λ_m (Ω^{-1} cm^2 mol^{-1})
			C	H	M	X	C	H	M	X	
$[UO_2(BMINH-H)_2]$	290	Yellow	33.9	3.1	33.6	—	34.7	3.0	33.0	—	6
$[Zn(BMINH-H)Br]H_2O$	>300	Yellow	31.4	3.4	17.1	20.9	31.8	3.5	16.4	20.1	15
$[Cd(BMINH-H)_2]$	260	Yellow	43.6	4.0	20.4	—	44.2	3.8	20.0	—	2
$[Cd(BMINH)Cl_2]2H_2O$	250	Pale yellow	27.3	3.7	25.6	16.1	27.2	4.1	24.7	15.7	10
$[Mn(BMINH)(H_2O)_2]Cl_2$	>300	Pale yellow	31.4	4.2	14.4	18.6	30.6	4.2	15.1	19.4	67
$[Ni(BMINH)(H_2O)_2(EtOH)]Cl_2$	>300	Green	33.4	5.1	13.6	16.4	32.6	4.7	14.2	17.0	70
$[Ni(BMINH-2H)(H_2O)_2(EtOH)]$	>300	Brown	40.1	5.6	16.3	—	39.6	5.4	17.0	—	8
$[Cu(BMINH)Br_2]2H_2O$	183	Green	25.0	3.4	13.2	33.3	25.5	3.4	14.0	—	16
$[Cu(BMINH)Cl_2]C_2H_5OH$	180	Green	36.4	3.8	16.1	17.9	37.3	4.2	15.4	18.5	19
$[Cu(BMINH-2H)(H_2O)_2]2H_2O$	>300	Green	32.3	5.4	17.1	—	31.9	5.1	17.0	—	6
$[Co(BMINH-H)Ac]4H_2O$	>300	Red	35.2	5.4	14.4	—	35.6	5.7	13.75	—	12

The products were filtered off and washed with ethanol and diethyl ether, and finally dried in a vacuum desiccator over anhydrous calcium chloride. The results of elemental analysis together with some physical properties are listed in Table 2.

The analyses for the metals and halide were carried out by the standard method.[17] Carbon and hydrogen contents were performed by the Microanalytical Unit at Mansoura University. Magnetic moments were obtained at room temperature (25°C) by Gouy balance using $Hg[Co(SCN)_4]$ as a calibrating agent at Alexandria University. IR spectra were recorded on an SP 2000 IR spectrophotometer as Nujol mulls between CsI plates. Electronic spectra were recorded on an SP 1800 spectrophotometer. Molar conductivities in DMF at room temperature were measured using a Tacussel conductivity bridge type CD6NG. Proton magnetic resonance spectra were carried out on a Varian EM 360 (60-MHz) spectrophotometer. Thermal-analysis measurements were carried out with a thermoanalyser GDTD 16 (Setaram, Lyon, France) at Mansoura University.

REFERENCES

1. M. M. Mostafa, M. A. Khattab and K. M. Ibrahim, *Transition Met. Chem.* 1983, **8**, 212.
2. M. M. Mostafa, M. A. Khattab and K. M. Ibrahim, *Polyhedron* 1983, **2**, 583.
3. M. M. Mostafa, M. A. Khattab and K. M. Ibrahim, *Transition Met. Chem.* 1983, **8**, 282.
4. W. J. Geary, *Coord. Chem. Rev.* 1971, **7**, 81.
5. J. I. Bullock and H. A. Tajmir-Riahi, *J. Chem. Soc., Dalton Trans.* 1978, 34.
6. J. R. Ferraro, *Low Frequency Vibrations of Inorganic and Coordination Compounds.* Plenum Press, New York (1971).
7. J. R. Ferraro and W. R. Walkers, *Inorg. Chem.* 1965, **4**, 1382.
8. N. S. Biradar, B. R. Patil and V. H. Kulkarni, *J. Inorg. Nucl. Chem.* 1975, **37**, 1901.
9. A. T. T. Hsieh, R. M. Sheahan and B. O. West, *Aust. J. Chem.* 1975, **28**, 885.
10. S. P. McGlynn, J. K. Smith and W. C. Neely, *J. Chem. Phys.* 1961, **35**, 105.
11. C. K. Jørgensen, *Acta Chem. Scand.* 1956, **10**, 887.
12. A. B. P. Lever, *Inorganic Electronic Spectroscopy.* Elsevier, Amsterdam (1968).
13. A. B. P. Lever, J. Lewis and R. S. Nyholm, *J. Chem. Soc.* 1963, 2552.
14. M. Pulaniandavar and C. Natarajan, *Aust. J. Chem.* 1980, **33**, 737.
15. B. Bosnich, *J. Am. Chem. Soc.* 1968, **90**, 627.
16. M. Kato, H. B. Jonassen and J. C. Fanning, *Chem. Rev.* 1964, **64**, 99.
17. A. I. Vogel, *A Text Book of Quantitative Inorganic Analysis.* Longmans, London (1961).

Polyhedron Vol. 5, No. 10, pp. 1639–1643, 1986
Printed in Great Britain

0277–5387/86 $3.00+.00
© 1986 Pergamon Journals Ltd

^{11}B-^{11}B COSY NMR STUDIES OF DERIVATIVES OF THE OCTAHYDROTRIBORATE ANION, $[B_3H_7(X)]^-$ AND $[B_3H_6(X)_2]^-$

DOMINIC G. MEINA and JOHN H. MORRIS*

Department of Pure and Applied Chemistry, University of Strathclyde, 295 Cathedral Street, Glasgow G1 1XL, U.K.

and

DAVID REED

University of Edinburgh, West Mains Road, Edinburgh EH9 3JJ, U.K.

(*Received* 30 *January* 1986; *accepted* 28 *May* 1986)

Abstract—2-D ^{11}B–^{11}B correlation (COSY) spectra have been obtained on the series of monosubstituted and disubstituted octahydrotriborate anions, $[B_3H_7(X)]^-$ (X = Cl, NCS, NCSe, $NCBH_3$, $NCBH_2Cl$, $NCBPh_3$, $NCBH_2CN$, NCB_3H_7 or CNB_3H_6Cl) and $[B_3H_6(Cl)(X)]^-$ (X = Cl, NCS, $NCBH_2Cl$ or NCB_3H_7). All monosubstituted derivatives and $[B_3H_6(Cl)_2]^-$ showed a coupling correlation between the substituted and unsubstituted borons. The unsymmetrically disubstituted derivatives showed only one coupling correlation, between the borons carrying the substituents. The absence of other correlations is attributed to relaxation phenomena. The correlations are independent of the solid-state structural type.

The use of 2-D boron–boron correlation NMR spectroscopy (^{11}B–^{11}B COSY) as a probe in the study of boron hydride derivatives is now well established, and has been shown to give valuable information relating to boron atom connectivities.[1–4] Most of the published work has concentrated on polyhedral systems and it was found that generally only boron atoms which were directly bonded (by two-centre–two electron bonds) displayed couplings, whereas borons linked by bridging hydrogens usually showed no evidence for coupling. Only two compounds, 1,2,3-$[C_6Me_6]FeEt_2C_2B_3H_5$ and 2-$(C_5H_5)CoB_4H_8$, have shown evidence for coupling between borons linked by bridging hydrogens.[2]

In earlier work we prepared[5–7] a series of derivatives of the octahydrotriborate anion, of general types $[B_3H_7X]^-$ and $[B_3H_6X_2]^-$, in which several structural types were observed (Fig. 1).[8–11]

Evidence of ^{11}B–^{11}B couplings was only occasionally found in the previous 1-D ^{11}B NMR studies of these and related systems; in compounds in which the coupling could be observed, the coupling constants were found to be of the order of 8–20 Hz.[12] However, for most of the compounds, the quadrupolar relaxation mechanism resulted in broad lines without resolution of the ^{11}B–^{11}B couplings; indeed in many cases even the larger ^{11}B–^{1}H couplings of *ca* 35 Hz were only detectable after resolution enhancement techniques were applied to the free-induction decay signals prior to Fourier transformation.[12,13]

It was therefore apparent that this series of compounds, examined by the ^{11}B–^{11}B COSY technique, offered a unique opportunity to study the relationship of observation of ^{11}B–^{11}B coupling to the structural and bonding parameters in the triborate cage. In this work we have extended these NMR studies to include the results of ^{11}B–^{11}B COSY NMR spectra, and now compare the data with observed structures.

*Author to whom correspondence should be addressed.

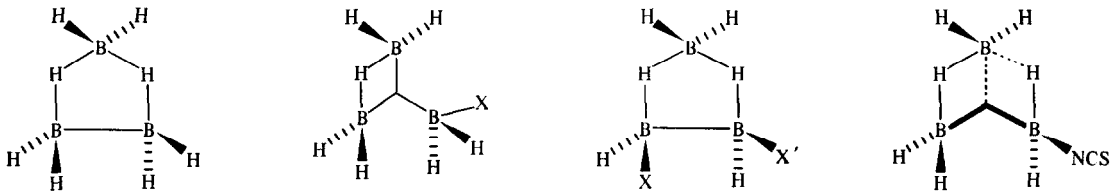


Fig. 1. Topological representations of crystallographically identified structures of substituted octahydrotriborate anions.

EXPERIMENTAL

115.55-MHz ^{11}B NMR spectra were recorded in $CDCl_3$ solutions using a Bruker WH 360 NMR spectrometer fitted with an Aspect 2000 computer. Homonuclear correlation spectra were obtained using the COSY-90 $D1$-90°-t_1-90°-AQ sequence,[14] where $D1$ is the recycling delay to allow complete relaxation (usually 0.1 s is adequate) and t_1 is the interpulse delay. The increment Δt_1, by which t_1 is successively increased during the COSY experiment, is controlled by the dwell time, and hence by the spectrum width. Broad-band decoupling was applied during runs.

Typically 128 FIDs were acquired with 512 words of data for each. Acquisition times ranging from 0.013 to 0.036 s were used. After Fourier transformation the spectra comprised a 256 × 256-word $F1 \times F2$ matrix. The COSY spectra are presented as contour maps. The contour levels were selected by examination of both the $F1$ and $F2$ projections, and setting the lowest contour threshold just above the average noise level. All COSY spectra were symmetrized.

The compounds, prepared as previously described,[5-7] were obtained as $[N(PPh_3)_2]^+$ salts of the $[B_3H_7(Cl)]^-$, $[B_3H_7(NCS)]^-$, $[B_3H_7(NCSe)]^-$, $[B_3H_7(NC)BH_3]^-$, $[B_3H_7(NC)BPh_3]^-$, $[B_3H_7(NC)BH_2(CN)]^-$, $[B_3H_7(NC)B_3H_7]^-$, $[B_3H_6(Cl)_2]^-$, $[B_3H_6(Cl)(NCS)]^-$ and $[B_3H_6(Cl)(NC)B_3H_7]^-$ anions.

RESULTS AND DISCUSSION

The recent advent of ^{11}B–^{11}B COSY as a viable technique in the study of boranes and their derivatives[1-4] has meant that it is now possible in many cases to study interactions between boron nuclei in the solution phase. Previously such interactions were rarely examinable by solution methods such as NMR, and any information was derived from solid-state studies such as X-ray crystallography. Clearly the possibility of carrying out such studies in both phases should provide an important insight into the nature of these materials. Since several structural types of compound had been established in the solid state by X-ray crystallography, it was of interest to determine whether the COSY spectra would distinguish these in solution, or whether fluxional character and quadrupolar relaxation effects would predominate and make solution characterization of structural type unfeasible. Previous 1-D NMR studies had yielded values of ^{11}B–^{11}B coupling constants for a few of the compounds in deuteroacetonitrile solution, but studies in deuterochloroform in general resulted in an increased efficiency of quadrupolar relaxation and hence a failure to resolve this coupling. Because many of the anionic triborane derivatives undergo reactions such as ligand–solvent exchange in acetonitrile solutions, the ability to derive coupling information from chloroform solutions would also be valuable. Homonuclear correlation spectroscopy provides a means by which such information may be derived.

The compounds which have been studied are listed in Tables 1 and 2, which also indicate the solid-state structure adopted by those compounds which have been examined crystallographically.

All the monosubstituted triborane derivatives have ^{11}B NMR spectra which comprise two signals of relative intensities 2:1, and correlations between these occur in all cases. A typical spectrum is given in Fig. 2 for the $[B_3H_7(NC)B_3H_7]^-$ anion, in which the two triborane units each give correlations, and are independent of each other. Since correlations are observed regardless of the solid-state structure, it is apparent that significant electron density exists between all three boron atoms, possibly as a result of the fluxional character.

In the disubstituted triboranes, the symmetrical $[B_3H_6(Cl)_2]^-$ anion showed a COSY correlation between the resonances of the unsubstituted boron (of intensity 1) and the two borons carrying substituents (of relative intensity 2) (Fig. 3). Each of

Table 1. Chemical shifts, COSY correlations and structural types of monosubstituted triborane anions, $[B_3H_7(X)]^-$

Monosubstituted anion	$\delta(1)$ (B—X)	$\delta(2,3)$ (B_2)	COSY correlation	Structure type[a]
$[B_3H_7(Cl)]^-$	−21.0	−14.5	1–(2,3)	
$[B_3H_7(NCS)]^-$	−32.5	−13.0	1–(2,3)	d
$[B_3H_7(NCSe)]^-$	−33.3	−10.0	1–(2,3)	d
$[B_3H_7(NC)BH_3]^-$	−36.1	−9.9	1–(2,3)	b
$[B_3H_7(NC)BH_2Cl]^-$	−34.8	−8.9	1–(2,3)	
$[B_3H_7(NC)BPh_3]^-$	−34.8	−9.2	1–(2,3)	
$[B_3H_7(NC)BH_2(CN)]^-$	−34.8	−8.9	1–(2,3)	
$[B_3H_7(NC)B_3H_7]^-$ (i)	−34.9	−9.5	1–(2,3)	b
(ii)	−49.5	−12.4	1–(2,3)	b
$[B_3H_7(CN)B_3H_6Cl]^-$	−49.8	−11.9	1–(2,3)	

[a]Determined crystallographically.

Table 2. Chemical shifts, COSY correlations and structural types of disubstituted triborane anions, $[B_3H_6(Cl)(X)]^-$

Disubstituted anion	$\delta(1)$ (B—Cl)	$\delta(2)$ (B—X)	$\delta(3)$ (B—H)	COSY correlation	Structure type[a]
$[B_3H_6(Cl)_2]^-$	−11.9	−11.9	−4.3	(1,2)–3	c
$[B_3H_6(Cl)(NCS)]^-$	−8.3	−25.1	−4.2	1–2	c
$[B_3H_6(Cl)(NC)BH_2Cl]^-$	0.6	−30.9	−4.1	1–2	
$[B_3H_6(Cl)(NC)B_3H_7]^-$	−0.2	−31.0	−3.8	1–2	

[a]Determined crystallographically.

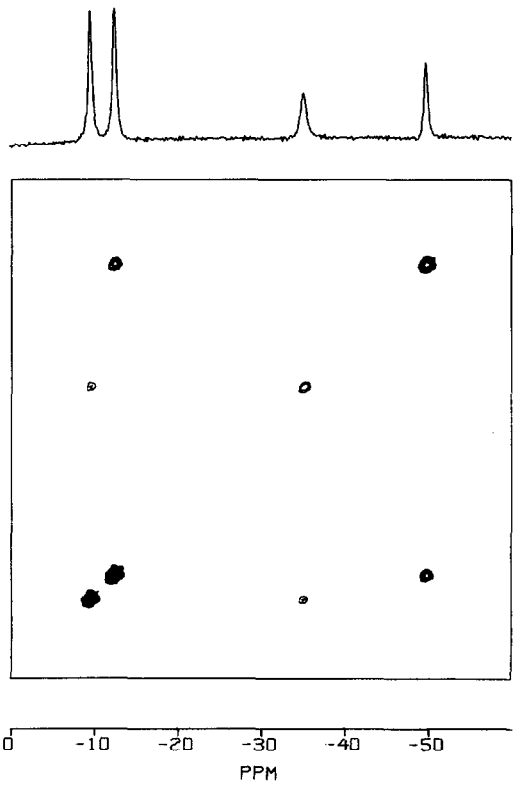


Fig. 2. 2-D COSY and 1-D ^{11}B–[^1H] spectra of $[B_3H_7(NC)B_3H_7]^-$.

the unsymmetrical disubstituted anions exhibited ^{11}B spectra which comprised three resonances of relative intensity 1:1:1. [See, for example, the spectrum of $[B_3H_6(Cl)NCS]^-$ in Fig. 4.] However, the COSY spectra revealed only one correlation; this occurs between the low-frequency resonance (which is assigned to the *N*-coordinated boron) and the sharper of the two high-frequency resonances.

The broad high-frequency resonance which occurred near δ 4.1 in all the compounds was earlier[6] assigned to the chlorine-substituted boron atom. However, it appears probable that it should rather be assigned to the unsubstituted boron since its shift varied very little over all the compounds. The fact that only one correlation is observed may at first sight be interpreted as evidence for a direct B—B bond between the substituted atoms, except for the fact that coupling is observed between the unsubstituted boron and those carrying chlorine substituents in $[B_3H_6Cl_2]^-$. The apparent absence of coupling with the broad boron resonance is the unsymmetric derivatives may be a result of the experimental COSY conditions, and in particular on the magnitude of the incremental time (Δt_1) by which the interpulse delay is successively increased. Δt_1 values, optimized between 2.5×10^{-4} and $5 \times$

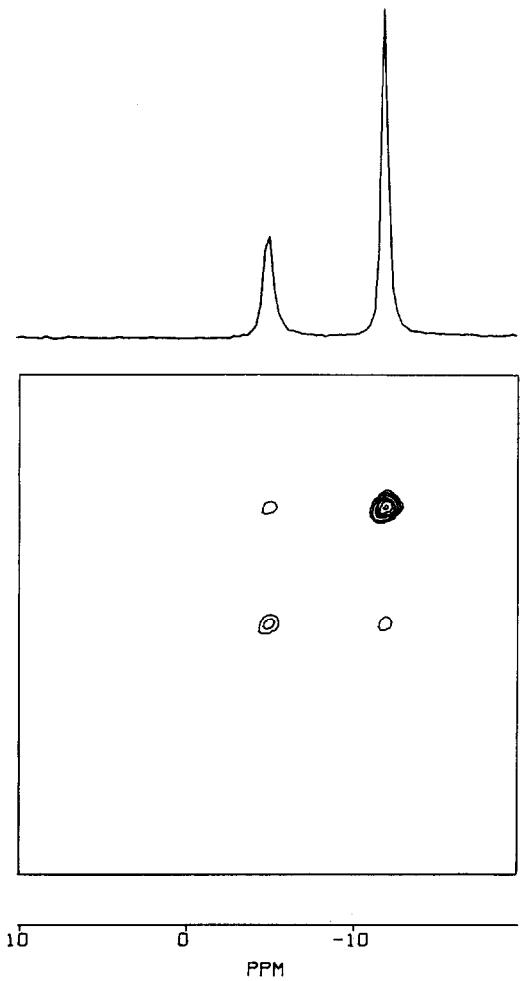


Fig. 3. 2-D COSY and 1-D ^{11}B–{^1H} spectra of $[B_3H_6(Cl)_2]^-$.

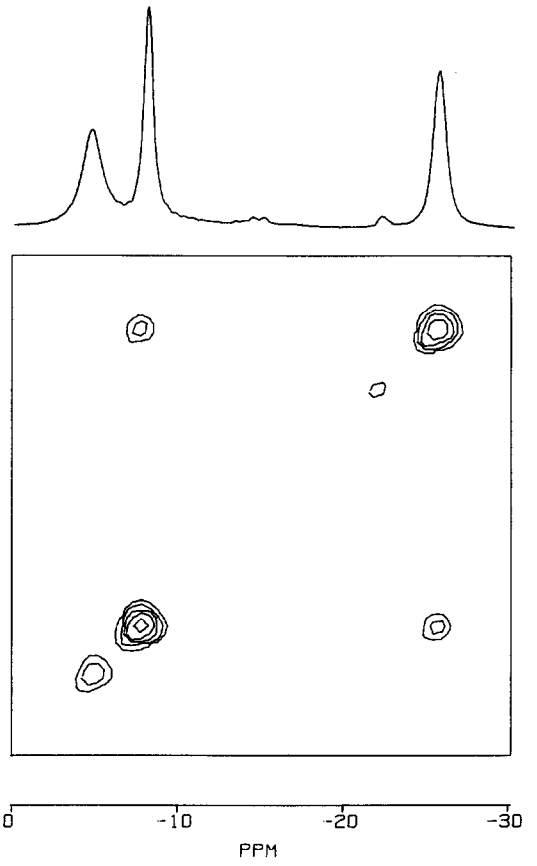


Fig. 4. 2-D COSY and 1-D ^{11}B–{^1H} spectra of $[B_3H_6(Cl)(NCS)]^-$.

10^{-5} s {for $[B_3H_7(NC)BPh_3]^-$} were found necessary in order to observe correlations with broad lines. It had been observed previously[3] that in the COSY spectra of the $[B_9H_{13}L]^-$ anions (L = NCS or NCSe) the high-frequency broad resonance of B(7) was not observed even along the diagonal. We have now reexamined the COSY spectra of $[B_9H_{13}(NCSe)]^-$ using a shorter value of Δt_1, and have now detected the resonance due to B(7) together with couplings from this signal. The COSY spectrum is now completely analogous to that of $B_9H_{13}(SMe_2)$.[3]

The COSY results for the triborane derivatives thus show that both mono- and disubstituted derivatives have significant *s*-electron density between all three boron atoms in the solution studies in which low-energy fluxional behaviour occurs. The failure to observe coupling with the broad resonance of the unsymmetrical disubstituted compounds is probably a result of fast relaxation resulting in broad, low-intensity signals, whose FIDs decay significantly in the time-scale of the pulse train. Effects of relaxations have been referred to previously by Grimes.[2]

The COSY spectra of the bridge-cyanide species $[B_3H_7(NC)B_3H_7]^-$ and $[B_3H_6(Cl)(NC)B_3H_7]^-$ also give unambiguous support for the structures and assignments of these compounds which were reported earlier on the basis of 1-D ^{11}B and ^{11}B–{^1H} measurements.[7]

Acknowledgement—We wish to thank the SERC for a studentship (DGM) and for the use of the high-field NMR service at Edinburgh University.

REFERENCES

1. W. C. Hutton, R. N. Grimes and T. L. Venable, *J. Am. Chem. Soc.* 1982, **104**, 4716.
2. T. L. Venable, W. C. Hutton and R. N. Grimes, *J. Am. Chem. Soc.* 1984, **106**, 29.
3. D. Reed, *J. Chem. Res. S* 1984, 198.
4. G. B. Jacobsen, D. G. Meina, J. H. Morris, C. Thomson, S. J. Andrews, D. Reed, A. J. Welch and D. F. Gaines, *J. Chem. Soc., Dalton Trans.* 1985, 1645.

5. G. B. Jacobsen and J. H. Morris, *Inorg. Chim. Acta* 1982, **59**, 207.
6. M. Arunchaiya, J. H. Morris, S. J. Andrews, D. A. Welch and A. J. Welch, *J. Chem. Soc., Dalton Trans.* 1984, 2525.
7. D. G. Meina and J. H. Morris, *J. Chem. Soc., Dalton Trans.* (in press).
8. S. J. Andrews, A. J. Welch, G. B. Jacobsen and J. H. Morris, *J. Chem. Soc., Chem. Commun.* 1982, 749.
9. S. J. Andrews and A. J. Welch, *Inorg. Chim. Acta* 1984, **88**, 153.
10. S. J. Andrews and A. J. Welch, *Inorg. Chim. Acta* 1985, **105**, 89.
11. (a) S. J. Andrews and A. J. Welch, *Acta Cryst. C* (in press); (b) P. C. Choi and J. H. Morris, *J. Chem. Soc., Dalton Trans.* 1984, 2119.
12. G. B. Jacobsen, J. H. Morris and D. Reed, *J. Chem. Res. S* 1983, 42; *J. Chem. Res. M* 1983, 0401.
13. M. Arunchaiya and J. H. Morris, *Inorg. Chim. Acta* 1985, **103**, 31.
14. R. Benn and H. Gunther, *Angew. Chem., Int. Ed. Engl.* 1983, **22**, 350.

Polyhedron Vol. 5, No. 10, pp. 1645–1646, 1986
Printed in Great Britain

0277-5387/86 $3.00+.00
© 1986 Pergamon Journals Ltd

COMMUNICATION

PERTURBED γ–γ DIRECTIONAL CORRELATIONS AND THE COORDINATION CHEMISTRY OF Hf: NEW ASPECTS OF THE BEHAVIOUR OF Hf IN THE PRESENCE OF HIGH FLUORIDE CONCENTRATIONS

P. BODE,* M. DE BRUIN and R. W. HOLLANDER†

Interuniversity Reactor Institute and †Delft University of Technology,
Department of Applied Physics, Mekelweg 15, 2629JB Delft, The Netherlands

(*Received* 24 *March* 1986; *accepted* 7 *May* 1986)

Abstract—In solutions of Hf at high fluoride concentrations, the γ–γ directional correlation of ^{181}Hf remains almost unperturbed. This result differed strongly from earlier observations of a strong perturbation in such systems, explained as a consequence of the formation of Hf–F polymers. It was shown that in these investigations the role of the Na^+ ion had been overlooked, and that these strong perturbations are due to the formation of $Na_5Hf_2F_{13}$.

Information on the chemical and/or physical environment of decaying radionuclides can be obtained by measuring the directional correlation between γ-rays emitted in cascade.[1] In an investigation of the relation between the observed γ–γ directional correlation and the chemical form of radioactive atoms in aqueous solutions, PDC experiments were carried out with ^{181}Hf in the presence of fluoride.‡ It was reported earlier[3,4] that with increasing F^-/Hf atomic ratios, the directional correlation becomes strongly perturbed. This was explained as a result of the formation of Hf–F polymers, either present as a macromolecule in solution, or as a precipitate.

However, recent measurements of Hf and F in solution yielded results which differ strongly from the observations mentioned above. Even for very high F^-/Hf atomic ratios up to 120 we found that the directional correlation remains almost unperturbed (Fig. 1), and no precipitation was observed. Closer examination of the experimental procedures showed that the essential difference between the two series of experiments was the way the fluoride was applied to the Hf solution. In our recent experiments, fluoride was added as an HF solution, whereas de Bruin *et al.* used an NaF solution. This indicates that, in their investigations of the Hf–F system, the role of the Na^+ ion might have been overlooked.

Therefore we have carried out a study of the nature of the precipitate as described by de Bruin *et al.* It was prepared by adding NaF to a solution of $HfOCl_2 \cdot 8H_2O$ in 1 N $HClO_4$; the crystals were isolated by centrifugation and rinsed with ethanol. After reactor irradiation, the time-differential PDC spectrum was recorded (Fig. 2). The interaction is obviously caused by a static, randomly oriented field gradient. Fitting of the experimental data leads to values of $\omega_Q = 87.9 \pm 0.8 \times 10^6\ s^{-1}$ and $\eta = 0.41 \pm 0.02$. These values are in agreement with the values reported by Hollander[4] for a similar precipitate, also assumed to be a Hf polyfluoride: $\omega_Q = 100.3 \pm 0.9 \times 10^6\ s^{-1}$ and $\eta = 0.37 \pm 0.01$. Mayer *et al.*[5] found similar results for single crystals of $(NH_4)_2HfF_6$: $\omega_Q = 80.3 \times 10^6\ s^{-1}$ and $\eta = 0.43$.

The existence of Na_xHfF_y compounds in Hf–Na–F systems has been described by different authors.[6–8] The agreement between our TDPDC results and the values found by Mayer for a compound of the M_xHfF_y type strongly suggests that the precipitate is a Na_xHfF_y compound.

*Author to whom correspondence should be addressed.

‡The PDC spectrometer has been described elsewhere.[2]

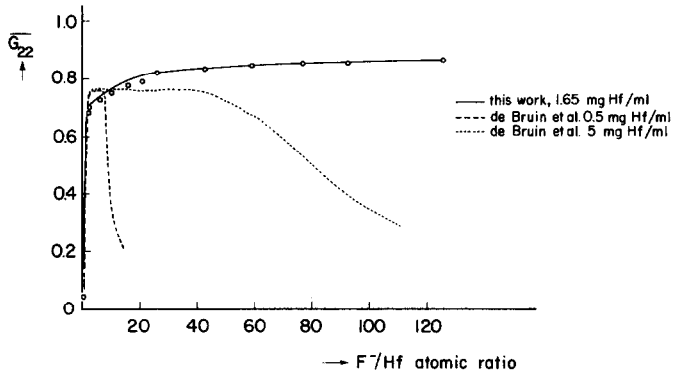


Fig. 1. Time-integral perturbation factor ($\overline{G_{22}}$) as function of the ratio of F^- to Hf atoms present in the source.

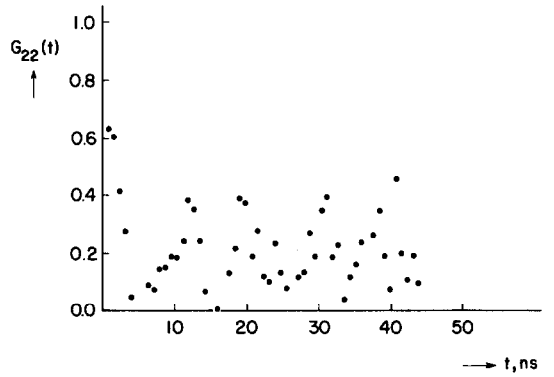


Fig. 2. Time-differential PDC spectrum of the precipitate.

Elemental analysis of the precipitate was carried out by instrumental neutron activation analysis. The major constituents were found to be Na (16.22%) and Hf (50.14%), corresponding to an Hf:Na atomic ratio of 2.5:1. In addition, the X-ray diffraction pattern was determined. From these data, the substance was identified as $Na_5Hf_2F_{13}$, which is in excellent agreement with the results from I.N.A.A.

The identification of the precipitate as $Na_5Hf_2F_{13}$ also explains the high-power relation between the inverse time constant of the change in the anisotropy after addition of F^- to the Hf solution, and the free fluoride concentration.[3,4] Under the experimental conditions used by these authors, $[F^-]$ almost equals $[Na^+]$, which makes $[F^-]$ proportional to $[Hf^{4+}]^{-9}$. The decrease in $[Hf^{4+}]$ due to precipitation of $Na_5Hf_2F_{13}$ is reflected by the anisotropy; the inverse time constant of the change in the anisotropy therefore corresponds to changes in the rate of decrease of $[Hf^{4+}]$, and is proportional to $[F^-]^9$.

CONCLUSIONS

The results from the work described in this paper strongly suggests that in the presence of fluoride ions no polymerization of Hf and F^- occurs at high F^-/Hf atomic ratios. Earlier reported suggestions of the existence of such an $(HfF_{x+1})_n$ polymer in Hf–F systems on the basis of results of directional correlation measurements can be associated with the formation of $Na_5Hf_2F_{13}$ due to the presence of Na^+ ions in the investigated systems.

Acknowledgement—We are indebted to Mr N. M. van der Pers of the Delft University of Technology, Department of Metallurgy, for carrying out the X-ray diffraction analysis.

REFERENCES

1. H. Frauenfelder and R. M. Steffen, In *Alpha, Beta and Gamma-ray Spectroscopy* (Edited by K. Siegbahn), Vol. 2, p. 997. North-Holland, Amsterdam (1965).
2. P. Bode and M. de Bruin, *Proceedings of the 5th International Conference on Nuclear Methods in Environmental and Energy Research, Mayaquez, Puerto Rico*, 1984, p. 540.
3. M. de Bruin and R. W. Hollander, *J. Inorg. Nucl. Chem.* 1976, **38**, 2149.
4. R. W. Hollander, Thesis, Delft University of Technology (1981).
5. L. Mayer, E. Bodenstedt and C. Gunther, In *Perturbed Angular Correlations, Supplement to Proceedings of the Uppsala Meeting on Extranuclear Perturbations in Angular Correlations* (Edited by E. Karlsson, E. Matthias and K. Siegbahn). North-Holland, Amsterdam (1964).
6. E. M. Larsen, In *Advances in Inorganic Chemistry and Radiochemistry* (Edited by H. J. Emeleus and A. G. Sharpe), Vol. 13, p. 106. Academic Press, New York (1970).
7. F. A. Cotton and G. Wilkinson, *Advances in Inorganic Chemistry*, p. 918. John Wiley, New York (1966).
8. I. V. Tananaev and L. S. Guzeeva, *Russ. J. Inorg. Chem.* 1966, **11**, 587.

Polyhedron Vol. 5, No. 10, pp. 1647–1650, 1986
Printed in Great Britain

0277–5387/86 $3.00+.00
Pergamon Journals Ltd

COMMUNICATION

UNUSUAL REACTIVITY OF A QUASI-AROMATIC Ni(II),2N,3C HETEROCYCLE

R. KENT MURMANN,* ELMER O. SCHLEMPER and MICHAEL S. TEMPESTA

Department of Chemistry, University of Missouri—Columbia, MO 65211, U.S.A.

(*Received* 27 *September* 1985; *accepted after revision* 20 *January* 1986)

Abstract—[Ni(PnAO)-6H]°, a Ni,2N,3C-pseudoaromatic heterocycle is shown to be highly reactive at the central carbon atom toward most aldehydes and ketones, giving with CH_2O, for example, a dimer having the formula [Ni(PnAO)-7H]$_2$-CH_2 whose X-ray crystal structure as well as ^{13}C and ^1H NMR spectra are presented.

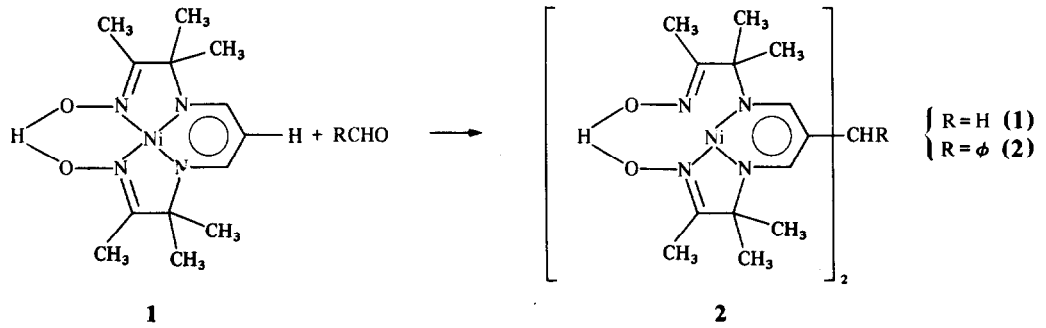
We recently reported[1] the X-ray crystal structure of [Ni(PnAO)-6H]° (**1**),† an "aromatic" Ni(II),2N,3C heterocycle and two products of its acid hydrolysis. These studies led to uncovering its remarkable reactivity towards aldehydes which we report herein. "Aromatic" behavior in complexes has been studied since about 1965.[2] A symposium on "aromaticity, pseudoaromaticity and antiaromaticity" was held in 1970,[3] and reactions involving delocalized M,2N,3C complexes with O_2,[4] nitriles,[5] alkynes[6] and isocyanates[7] are known. The present discovery is likely to revitalize this area because the planar complex described is much more reactive than any previously seen, and a reaction with aldehydes has not previously been reported. This also relates to the facile P alkylation for Ni,2N,2P complexes[8] and to the acylation of similar ligands.[9] The "aromatic" nature of **1** is indicated by the short Ni–N bond distances, the C–N and C–C distances, and the ^{13}C and ^1H NMR spectral data (Table 1). These are consistent with strong π-orbital overlap between the six ring atoms resulting in the downfield chemical shifts observed in ^{13}C and ^1H NMR caused by ring current effects. Comparison of the NMR chemical shift of **1** (11-H, δ 7.04; 12-H, δ 5.07; C-11, δ 147.7; C-12, δ 93.3) with the analogous pyrimidine δ values[10] (4-H, δ 8.78; 5-H, δ 7.36; C-4, δ 156.4; C-5, δ 121.4) indicates that 12-H and C-12 are found considerably upfield, the direct result of a high electron density at C-12.

The nucleophilic C-12 position of the Ni,2N,3C aromatic ring of **1** has a similar reactivity to that of the indole[11] C-3 (3-H, δ 6.45; C-3, δ 102.1[10]) position, and to other related organic molecules. The planar Ni(II) complex is very stable to dissociation or ligand replacement even in 1–2 M acid and reactions take place preferentially on the electron-rich C-12 site. Initial indication of this came with the preparation of the C-12 —NO_2, —NO, and —Cl derivatives (**2–4**) under mild conditions.[12,13] Additional evidence came with the discovery of the self-reaction of **1** in acid media at slightly elevated temperatures and long reaction times to give a 3C-bridged conjugated dimer.[1] The subsequent demonstration that malondialdehyde was the reactant (produced by the hydrolysis of the parent complex **1**) suggested that less reactive aldehydes and ketones might also condense under mild, acidic conditions.

Our recent discovery that formaldehyde and benzaldehyde react with **1** within a few minutes at room temperature in *ca* 0.002 M HCl [CH_3CN–H_2O (1 : 4) as the solvent] to give a single (2 : 1) product points out the unusual reactivity and the chemical potential for this remarkable complex compound (Scheme 1). We have isolated and identified the

* Author to whom correspondence should be addressed.

† [Ni(PnAO)-6H]°, (2,2,3,9,10,10 - hexamethyl - 5,7 - dioxa - 6 - hydra - 1,4,8,11 - tetraazacyclotetradeca - 3,8,11,13 - tetraene)nickel(II); [Ni(PnAO-H)]$^+$, [3,3′ - (1,3 - propanediamino)bis(3 - methyl - 2 - butanone oximato)]nickel(II) ion.



1

Scheme 1.

products of the reaction of **1** with CH_2O and ϕCHO and have shown the reaction to be analogous to that of aldehydes with indole.[11] The dimer is produced in a two-step reaction; under the conditions of preparation* the second reaction is very fast and no intermediate is found. The X-ray crystal structure† (Fig. 1) of product **5** shows the very planar nature of the mononuclear unit with a strong H-bond and aromatic type distances within the quasi-aromatic ring.‡ Except for the geminal methyls which are roughly mirrored across the planes, maximum deviations from least-squares planes thru the four coordinated nitrogen atoms are 0.060(7) and 0.139(6) Å for the atoms in each of the two subunits. The dihedral angle between those planes is 77° while the C12–C14–C12′ bond angle is 113.5(6)°. The twist as measured by the dihedral angles (89.1 and 86.5°) between the rings and the C12–C14–C12′ plane is minimal, indicative of a near mirror relationship of the monomers. The "aromatic" nature of the ring is reflected in the very short Ni–N distances [average 1.836(5) Å] which can be compared with the Ni–N(amine) distance of 1.937(5) Å in the unoxidized parent,[14] $[Ni(PnAO-H)]^+$, and with a comparable distance of 1.838(5) Å in the monomer.[1] The average C–N distance [1.313(6) Å] and the average C–C distance [1.397(14) Å] also reflect the aromatic nature of the very planar rings [maximum deviation 0.013(5) Å]. All other distances are normal including the short O—O hydrogen bonds between oxime hydrogens (2.398 Å).

Utilizing other reaction conditions we have determined that **1** is very reactive towards most aldehydes and ketones, to diazo reagents and to oxidized dimethylphenylenediamine. In some of the compounds we have prepared there is conjugation thru the bridge between the metal ion centers giving rise to intense charge-transfer bands in the visible region. These dye-like materials appear to be extremely stable both in solution and in the solid state. Some success has been obtained in replacing Ni(II) with other metal ions and further studies are now underway. Furthermore the unusual stability of this planar complex may allow the formation of styrene type polymers in which the stacked planar rings should give products with unique spectral and electronic properties. The oxidation–reduction properties of planar nickel complexes are of special interest in terms of their catalytic applications.[15] Of considerable significance is the expected facile conjugation thru C-12 of **1** to biologically interesting molecules.

* Preparation of **5** is accomplished by dissolving 80 mg of **1** in 5.0 cm^3 of CH_3CN and adding two drops (0.10 cm^3) of 1.0 M HCl. The slight change in color is due to protonation of the oxime intramolecular hydrogen bond. Addition of water to a volume of 25.0 cm^3 gives a clear orange solution which is treated with two–six drops (0.1–0.3 cm^3) of aqueous 37% CH_2O solution. Within a few minutes crystals of **5** begin to form and after a few hours are collected on a filter (yield *ca* 85% of theory). The product **5** can be recrystallized from CH_3CN–H_2O mixtures, giving well-formed orange-red crystals. The phenyl derivative **6** is prepared in an analogous fashion.

†Supplemental material available: Tables of fractional coordinates, thermal parameters, and bond distances and angles.

‡The dinuclear complex $[Ni_2O_4N_8C_{27}H_{44}]\cdot CH_3CN$ crystallizes from acetonitrile in space group $P2_12_12_1$ with $a = 8.241(3)$ Å, $b = 17.456(6)$ Å, $c = 23.919(7)$ Å, $V = 3441(2)$ Å^3, $Z = 4$, $D_c = 1.357$ g cm^{-3}, and $M_r = 703.2$. 4538 reflection intensities were measured by the θ–2θ scan technique with an Enraf–Nonius CAD-4 diffractometer using Mo-K_α radiation. Absorption correction involved a range of transmission from 0.927 to 1.0. The structure was solved by Patterson and Fourier methods, and refined by full-matrix least-squares methods with hydrogen atoms in "idealized", fixed positions (important hydrogen atoms including those on the bridging methylene were located from difference Fourier syntheses). The final agreement factors for 2949 observations with $F_o^2 > 2\sigma(F_o^2)$ on minimization of the $\Sigma w(|F_o|-|F_c|)^2$ were $R_F = 0.035$ and $R_{wF} = 0.037$. Additional structural details will be published with the structure of the ϕCHO product **6**.

Table 1. ^1H (300-MHz) and ^{13}C (62.9-MHz) NMR data on **1**, **5** and **6**

	1[a]		**5**[b]		**6**[b]	
	^1H	^{13}C	^1H[b]	^{13}C	^1H	^{13}C
C-1, C-2	—	161.4	—	161.2	—	161.3
C-3, C-4	1.98s	11.5	1.98s	11.6	1.96	11.7
C-5, C-6	—	69.4	—	68.9	—	69.2
C-7, C-9	1.33s	26.6	1.30s	26.7	1.22s	26.9
C-8, C-10	1.33s	26.6	1.30s	26.7	1.18s	26.9
C-11, C-13	7.04d (J = 6 Hz)	147.7	6.87s	148.2	6.78s	149.4
C-12	5.07t (J = 6 Hz)	93.3	—	104.5	—	108.5
C-14	—	—	3.36	33.7	4.94	61.5
Oxime *H*	19.10s	—	19.07s	—	19.09	
	—	—	—	—		
					o 7.11	129.0 × 3
					m 7.30	128.2 × 2
					p 7.18	126.1 × 1

[a] CD_3COCD_3–D_2O.
[b] $CDCl_3$.

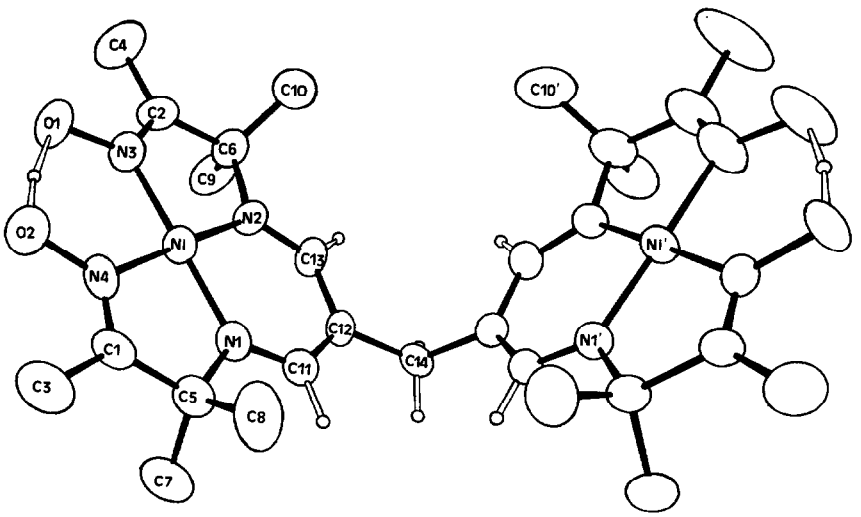


Fig. 1. Perspective drawing of **5** showing the atom numbering and selected H atoms. Important bond distances (Å) are: Ni1–N1 = 1.833(5), Ni1–N2 = 1.840(5), Ni1–N3 = 1.866(6), Ni1–N4 = 1.875(6), Ni2–N1′ = 1.844(5), Ni2–N2′ = 1.831(6), Ni2–N3′ = 1.863(6), Ni2–N4′ = 1.871(6), Cl2–Cl4 = 1.497(9), Cl2′–Cl4 = 1.503(9), C11–C12 = 1.387(9), C11′–C12′ = 1.378(9), C13–C12 = 1.417(9), C13′–C12′ = 1.406(9), N1–C11 = 1.313(8), N1′–C11′ = 1.324(8), N2–C13 = 1.303(8), and N2′–C13′ = 1.312(8).

REFERENCES

1. A. F. Ghiron, R. K. Murmann and E. O. Schlemper, *Inorg. Chem.* 1985, **24**, 3271.
2. J. P. Collman, *Angew. Chem., Int. Ed. Engl.* 1965, **4**, 132.
3. *Aromaticity, Pseudoaromaticity and Antiaromaticity*. Academic Press, New York (1971).
4. B. Durham, T. J. Anderson, J. A. Switzer, J. F. Endicott and M. D. Glick, *Inorg. Chem.* 1977, **16**, 1977.
5. K. Bowman, D. P. Riley and D. H. Busch, *J. Am. Chem. Soc.* 1976, **98**, 3389.
6. M. C. Weiss and V. L. Goedhen, *J. Am. Chem. Soc.* 1976, **98**, 3389.
7. R. P. Eckberg, J. H. Nelson, J. W. Kenney, P. N. Howells and R. A. Henry, *Inorg. Chem.* 1977, **16**, 3128.
8. C. W. G. Ansell, M. K. Cooper, K. P. Dancey, P. A. Duckworth, K. Henrick, M. McPartlin and P. A. Tasker, *J. Chem. Commun.* 1985, 439.
9. D. P. Fisher, V. Piermattie and J. C. Dabrowiak, *J. Am. Chem. Soc.* 1977, **99**, 2811.
10. E. Pretsch, T. Clerc, J. Seibl and W. Simon, *Spectral Data for Structure Determination of Organic Compounds*. Springer, New York (1983).
11. R. J. Sundberg, *The Chemistry of Indoles*, p. 39. Academic Press, New York (1970).
12. E. G. Vassian and R. K. Murmann, *Inorg. Chem.* 1967, **6**, 2043.
13. I. O. Urban and E. G. Vassian, *Inorg. Chem.* 1979, **18**, 867.
14. M. S. Hussain and E. O. Schlemper, *Inorg. Chem.* 1979, **18**, 2275.
15. J. D. Atwood, *Inorganic and Organometallic Reaction Mechanisms*, p. 200. Brooks Cole, Monterey, CA (1985).

Polyhedron Vol. 5, No. 10, pp. 1651–1653, 1986
Printed in Great Britain

0277–5387/86 $3.00+.00
Pergamon Journals Ltd

COMMUNICATION

A NOVEL DIPHOSPHORUS–MOLYBDENUM RING SYSTEM

ATTA M. ARIF, ALAN H. COWLEY,* MAREK PAKULSKI and GILLIAN J. THOMAS

Department of Chemistry, The University of Texas at Austin, Austin, TX 78712, U.S.A.

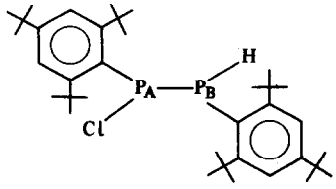
(*Received* 18 *November* 1985; *accepted after revision* 28 *January* 1986)

Abstract—The reaction of $ArPCl_2$ (Ar = 2,4,6-*t*-$Bu_3C_6H_2$) with $K[Mo(CO)_3(\eta\text{-}C_5H_5)]$ affords Ar(H)PP(Cl)Ar (**1**), $ArP[Mo(CO)_2(\eta\text{-}C_5H_5)]_2$ (**2**), ArP=PAr, $ArPH_2$ and Ar(H)PP(H)Ar. By means of X-ray crystallography, it was established that the Mo_2P ring of **2** involves a planar phosphorus geometry, a slight degree of Mo–P multiple bonding, and a Mo—Mo single bond. Thermolysis of the original reaction mixture produced the P_2Mo ring compound $ArPP(H)(Ar)[\mu^2\text{-}Mo(CO)_2(\eta\text{-}C_5H_5)]$ (**3**). The structure of **3** was determined by X-ray diffraction.

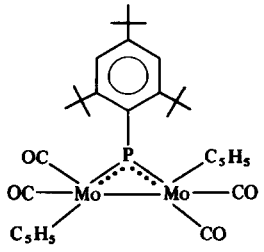
There are several examples of complexes of the type $R_2P{\cdots}ML_n$ which imply three-electron donation by phosphorus and thus a modicum of metal–phosphorus multiple bonding.[1] We describe a new type of interaction in which the $3e^-$ donation involves *two* phosphorus atoms.

A THF solution of $ArPCl_2$ (Ar = 2,4,6-*t*-$Bu_3C_6H_2$) was treated with two equivalents of $K[Mo(CO)_3(\eta\text{-}C_5H_5)]$ at −78°C and allowed to warm slowly to 25°C. ^{31}P NMR spectroscopic assay of the reaction mixture revealed the presence of ArP=PAr,[2] $ArPH_2$,[3] Ar(H)PP(H)Ar,[3] and two new compounds, ArP(H)PP(Cl)Ar (**1**) and $ArP[Mo(CO)_2(\eta\text{-}C_5H_5)]_2$ (**2**). Separation of the reaction mixture by column chromatography (silica gel–*n*-hexane) resulted in the isolation of **2** (22% yield), but caused the decomposition of **1**. However, the identity of **1** as ArP(H)PP(Cl)Ar was established by the following facts: (i) the ABX ^{31}P NMR spectrum for **1** ($\delta_{P_A}+111$, $\delta_{P_B}-30$, $^1J_{P_AP_B}=300$, $^1J_{P_BH}=224$, $^2J_{P_AH}=5$ Hz) is very similar to that of $(Me_3Si)_3CP(H)P(Cl)C(SiMe_3)_3$,[4] and; (ii) **1** can be produced (42% yield) (in admixture with smaller quantities of $ArPH_2$, ArP(H)PP(H)Ar and ArP=PAr) by slow addition of ArPHLi to $ArPCl_2$ in THF solution at 0°C. Compound **2** (δ_P+687) was identified as a bridging phosphinidene complex by X-ray crystallography (Fig. 1). Within experimental error, the geometry at phosphorus is trigonal planar and the Mo–P bond lengths [average 2.306(8) Å] are somewhat short and thus indicative of a slight degree of metal–phosphorus multiple bonding. The Mo–Mo bond length [3.220(8) Å], on the other hand, corresponds to a bond order of unity. The foregoing structural features for **2** are similar to those of $ArP[Co(CO)_3]_2$ (**4**).[5] While there are several

* Author to whom correspondence should be addressed.



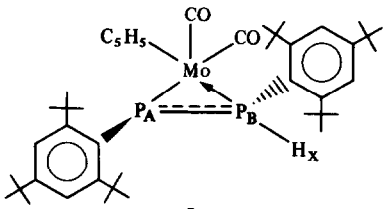
1



2

examples of complexes of the type $RP(ML_n)_2$ featuring $16e^-$ organometallic moieties,[7] the significance of **2** and **4** is that they involve $15e^-$ fragments.

Thermolysis of the original reaction mixture (refluxing toluene, 30 min) caused the disappearance of the ^{31}P resonance due to **1** and the emergence of a new ABX pattern attributed to **3** ($\delta_{P_A} - 151$, δ_{P_B} 0.2, $^1J_{P_AP_B} = 541$ Hz, $^1J_{P_AH} = 401$ Hz, $^2J_{P_AH} < 1$ Hz). Compound **3** can also be prepared



3

(in >90% yield) by the thermal reaction of **1** with $K[Mo(CO)_3(\eta\text{-}C_5H_5)]$, thus suggesting its origin in the previous reaction. Purification of **3** was effected by column chromatography (silica gel–*n*-hexane) and the compound was identified by X-ray crystallography (Fig. 2) and NMR spectroscopy.* Hydrogen H_x was not detected in the X-ray study due to poor crystal quality; however, its presence was clear from the ABX ^{31}P NMR spectrum. Examination of the geometry around P_B indicates that H_x is pointed away from the Mo–P_B bond. The simplest way to visualize the bonding in **3** is to consider it as a complex of the (as yet unprepared)[6] anion, $[ArP_A\text{–}P_B(H)(Ar)]^-$, in which P_A and P_B serve as one- and two-electron donors, respectively. The

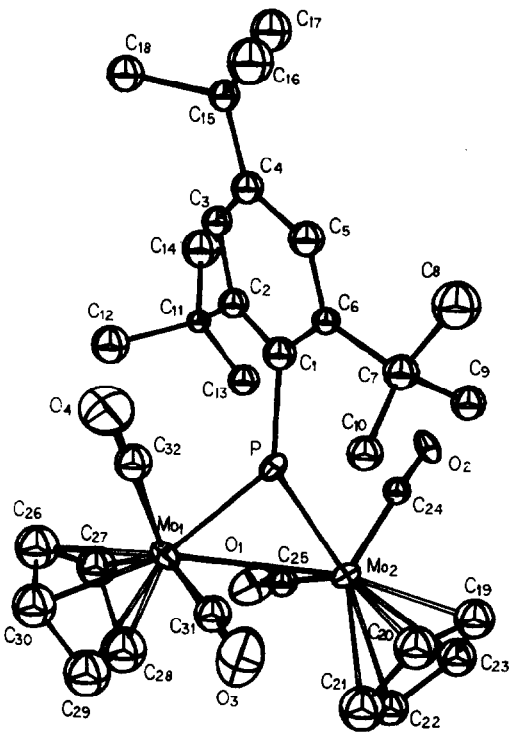


Fig. 1. ORTEP view of **2** showing the atom-numbering scheme. Important parameters: Mo(1)–Mo(2) = 3.220(8) Å, Mo(1)–P = 2.297(8) Å, Mo(2)–P = 2.315(8) Å, P–C(1) = 1.89(3) Å, Mo(1)–P–Mo(2) = 88.4(3)°.

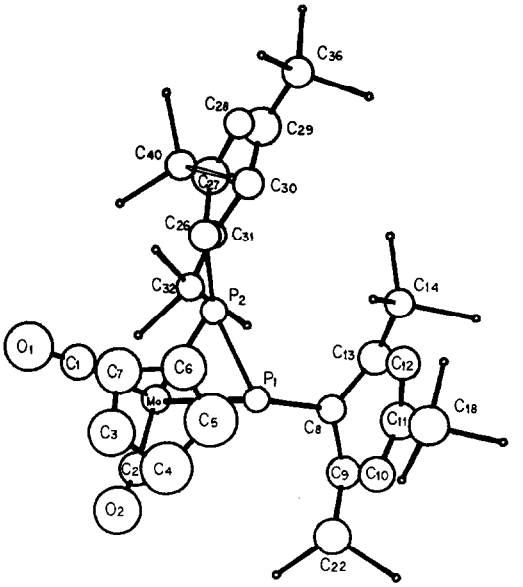


Fig. 2. ORTEP view of **3** showing the atom-numbering scheme. Important parameters: Mo–P(1) = 2.696(6) Å, Mo–P(2) = 2.389(7) Å, P(1)–P(2) = 2.145(8) Å, P(1)–Mo–P(2) = 49.4(2)°, P(2)–P(1)–Mo = 57.8(2)°, P(1)–P(2)–Mo = 72.8(3)°, P(2)–P(1)–C(8) = 103.0(8)°, P(1)–P(2)–C(26) = 124.2(7)°.

*Crystal data for **2**: $C_{32}H_{39}Mo_2O_4P$; $M = 710.52$. Crystal data: monoclinic, $P2_1/c$ (No. 14); $a = 13.429(2)$ Å, $b = 13.705(2)$ Å, $c = 17.072(2)$ Å, $\beta = 97.62(1)°$; $V = 3114$ Å^3, $Z = 4$, $D_c = 1.515$ g cm^{-3}.

Crystal data for **3**: $C_{43}H_{63}MoO_2P_2$; $M = 769.87$. Crystal data: monoclinic, $P2_1/c$ (No. 14); $a = 20.456(3)$ Å, $b = 11.501(3)$ Å, $c = 18.380(6)$ Å, $\beta = 97.80(2)°$; $V = 4284$ Å^3, $Z = 4$, $D_c = 1.194$ g cm^{-3}.

Intensity data: Enraf–Nonius CAD-4F diffractometer, ω–2θ scan modes in the range $2.0 \leqslant 2\theta \leqslant 50.0°$; 3007 and 3298 unique reflections for **2** and **3**, respectively. The structure of **2** was solved by direct methods while that of **3** was solved by Patterson and difference Fourier technqiues. The structures of **2** and **3** were refined (full matrix, least squares) by using 2127 and 2940 data, respectively. Final residuals (R) were 0.0870 and 0.1030 for **2** and **3**, respectively. Atomic positional and thermal parameter coefficients, full lists of bond lengths and angles and lists of F_o/F_c values for **2** and **3** have been deposited as supplementary material with the Editor, from whom copies are available on request. Atomic coordinates have also been deposited with the Cambridge Crystallographic Data Centre.

P_A–Mo distance [2.389(7) Å] corresponds to a bond order of unity. The P_B–Mo bond [2.696(6) Å] is somewhat longer than normal; nevertheless, the presence of such a bonding interaction is evident from, for example, the acute Mo–P_A–P_B angle [57.8(2)°]. Interestingly, the P_A–P_B distance [2.145(8) Å] is ~0.06 Å shorter than that of a P—P single bond, suggesting a slight multiple-bond character. This results should not be over-interpreted given the mediocre quality of the crystal structure. Nevertheless, it is interesting to note that the implication of modest multiple bonding is consistent with the large $^1J_{P_AP_B}$ coupling constant.[8]

Acknowledgements—We are grateful to the National Science Foundation and the Robert A. Welch Foundation for financial support.

REFERENCES

1. For representative references, see: (a) L. D. Hutchins, R. T. Paine and C. F. Campana, *J. Am. Chem. Soc.* 1980, **102**, 4521; (b) R. A. Jones, J. G. Lasch, N. C. Norman, B. R. Whittlesey and T. C. Wright, *J. Am. Chem. Soc.* 1983, **105**, 6184; (c) R. T. Baker, P. J. Krusic, T. H. Tulip, J. C. Calabrese and S. S. Wreford, *J. Am. Chem. Soc.* 1983, **105**, 6763; (d) E. Bross, K. Jörg, K. Fiederling, A. Göttlein, W. Malisch and R. Boese, *Angew. Chem., Int. Ed. Engl.* 1984, **23**, 738. For a more complete list of references, see A. H. Cowley and R. A. Kemp, *Chem. Rev.* 1985, **85**, 367.
2. M. Yoshifuji, I. Shima, N. Inamoto, K. Hirotsu and T. Higuchi, *J. Am. Chem. Soc.* 1981, **103**, 4587; *ibid.* 1983, **104**, 6167.
3. A. H. Cowley, J. E. Kilduff, T. H. Newman and M. Pakulski, *J. Am. Chem. Soc.* 1982, **104**, 5820.
4. A. H. Cowley, J. E. Kilduff, N. C. Norman, M. Pakulski, J. L. Atwood and W. E. Hunter, *J. Am. Chem. Soc.* 1983, **105**, 4845; J. Escudié, C. Couret, H. Ranaivonjatovo, J. Satgé and J. Jaud, *Phosphorus Sulfur* 1983, **17**, 221.
5. A. M. Arif, A. H. Cowley and M. Pakulski, *J. Chem. Soc., Chem. Commun.* 1985, 1707.
6. A. H. Cowley and M. Pakulski, *J. Am. Chem. Soc.* 1984, **106**, 1491.
7. See, for example: (a) K. M. Flynn, B. D. Murray, M. M. Olmstead and P. P. Power, *J. Am. Chem. Soc.* 1983, **105**, 7460; (b) G. Huttner, H.-D. Muller, A. Frank and H. Lorenz, *Angew. Chem., Int. Ed. Engl.* 1975, **14**, 705; (c) H. Lang, L. Zsolnai and G. Huttner, *ibid.* 1983, **22**, 976; (d) G. Huttner, J. Borm and L. Zsolnai, *J. Organomet. Chem.* 1984, **263**, C33; (e) H. Lang, G. Mohr, O. Scheidsteger and G. Huttner, *Chem. Ber.* 1985, **118**, 574.
8. (a) A. H. Cowley, *Acc. Chem. Res.* 1984, **17**, 386; (b) A. H. Cowley, J. E. Kilduff, J. G. Lasch, S. K. Mehrotra, N. C. Norman, M. Pakulski, B. R. Whittlesey, J. L. Atwood and W. E. Hunter, *Inorg. Chem.* 1984, **23**, 2582.

Polyhedron Vol. 5, No. 10, pp. 1655–1657, 1986
Printed in Great Britain

0277–5387/86 $3.00+.00
Pergamon Journals Ltd

COMMUNICATION

SYNTHESIS AND CHARACTERIZATION OF OXOMOLYBDATE CLUSTERS CONTAINING COORDINATIVELY BOUND ORGANO-DIAZENIDO UNITS: THE CRYSTAL AND MOLECULAR STRUCTURE OF THE HEXANUCLEAR DIAZENIDO-OXOMOLYBDATE, $(NBu^n_4)_3[Mo_6O_{18}(N_2C_6H_5)]$

TZE-CHEN HSIEH and JON A. ZUBIETA*

Department of Chemistry, State University of New York at Albany, Albany, NY 12222, U.S.A.

(*Received* 31 *October* 1985; *accepted after revision* 4 *March* 1986)

Abstract—$(NBu^n_4)_3[Mo_6O_{18}(N_2C_6H_5)]$ has been obtained by treating $(NBu^n_4)_2[Mo_6O_{19}]$ with an equivalent amount of phenylhydrazine in benzene. X-ray crystallography reveals the identity of the deep red crystalline material as a polymolybdate species incorporating a coordinatively bound organo-diazenido unit. The anion $[Mo_6O_{18}(N_2C_6H_5)]^{3-}$ is structurally similar to the precursor $[Mo_6O_{19}]^{2-}$, with the terminally bound phenyldiazenido group replacing a terminal oxo unit of the hexamolybdate moiety. $(NBu^n_4)_3[Mo_6O_{18}(N_2C_6H_5)]$ crystallizes in the orthorhombic space group *Pmcn* with $a = 17.162(3)$ Å, $b = 17.577(3)$ Å, $c = 23.860(4)$ Å, $V = 7197.7(8)$ Å^3, $Z = 4$, and $D_c = 1.56$ g cm^{-3} [$\mu = 10.60$ cm^{-1}, Mo–K_α ($\lambda = 0.71069$ Å)]. Solution and refinement based on 2118 reflections with $I_o \geqslant 3\sigma(I_o)$ gave a final reisdual of 0.080.

In view of their metal oxide like structures and high molecular weights, the interactions of isopolyanions with small organic molecules are of considerable interest in the development of models for the interactions of organic substrates with catalytic oxide surfaces.[1–3] Although a number of polymolybdate structures incorporating oxygen-donating organic ligands have been described,[4,5] examples of isopolymolybdates containing nitrogen-donating ligands are rare indeed.[6] We have shown that phenylhydrazine reacts with isopolymolybdate clusters in a condensation-type reaction to yeild organo-diazenido-polymolybdate species with tetranuclear, $[Mo_4O_8(OR)_2(N_2C_6H_5)_4]^{2-}$, or octanuclear, $[Mo_8O_{20}(N_2C_6H_5)_6]^{4-}$, frameworks, depending on reaction conditions.[7–9] Since the solvent often influences the stability of the various isopolymolybdate aggregates, it is not surprising that variation in reaction solvent should yield novel compositions for organo-diazenido-derivatized polymolybdates. Herein, we report the isolation and structural identification of the first example of a derivatized polymolybdate structurally related to the $[Mo_6O_{19}]^{2-}$ unit[10] through replacement of a terminal oxo group by an organodiazenido unit, $[Mo_6O_{18}(NNC_6H_5)]^{3-}$.

Reaction of a suspension of $(NBu^n_4)_2[Mo_6O_{19}]$ in dry benzene with an equivalent amount of phenylhydrazine and triethylamine results in an intense red solution after 3 h of reflux. Slow evaporation yields dark red crystals of rhombic habit. The material analyzed for $(NBu^n_4)_3[Mo_6O_{18}(NNC_6H_5)]$,† and exhibited an IR spectrum which confirmed the presence of the coordinated phenyldiazenido units [ν(N–N) 1588 cm^{-1}] and displayed a pattern characteristic of terminal and bridging oxo groups [ν(Mo–O$_t$) 935 cm^{-1}, ν(Mo–O$_b$) 790 cm^{-1}]. The electronic spectrum shows three bands in the UV, with maxima at 215, 295 and 335 mμ, and visible transitions at 390 and 525 mμ, the latter, presumably, associated with the $[Mo(NN_6H_5)]$ chromophore.

* Author to whom correspondence should be addressed.

† Elemental analysis: Found: C, 37.8; H, 6.5; N, 4.0%. Calc. for $C_{54}H_{113}Mo_6N_5O_{18}$: C, 38.2; H, 6.7; N, 4.3%.

Crystal data

$C_{54}H_{113}Mo_6N_5O_{18}$, $M = 1695.6$, orthorhombic space group *Pmcn*, $a = 17.162(3)$ Å, $b = 17.577(3)$ Å, $c = 23.860(4)$ Å, $U = 7197.7(8)$ Å, $Z = 4$ (based on the hexanuclear unit), $D_c = 1.56$ g cm^{-3}. 2118 reflections of 4321 collected were used in the structural analysis (Mo-K_α radiation, $R = 0.08$, error of fit = 1.67).*

The X-ray structure† confirms the presence of discrete hexanuclear units incorporating a single coordinatively bound phenyldiazenido group, $[Mo_6O_{18}(NNC_6H_5)]^{3-}$, as illustrated in Fig. 1. In contrast to the previously reported structures of phenyldiazenido-derivatized polymolybdates,[7-9] $[Mo_6O_{18}(NNC_6H_5)]^{3-}$ is structurally similar to the precursor hexamolybdate $[Mo_6O_{19}]^{2-}$.[10] While the structural integrity of the hexanuclear core is maintained, a single phenyldiazenido group has substituted for the terminal oxo unit of Mo3.

The geometry of the hexanuclear core of molybdenum atoms is distorted from the idealized octahedral symmetry displayed by the $[Mo_6O_{19}]^{2-}$ precursor as a consequence of phenyldiazenido substitution at Mo3. The Mo3–O1 bond distance is significantly shorter than the average of the the other Mo–O1 distances, 2.16(1) in contrast to 2.35 Å (average). A consequence of the Mo3–O1 bond contraction is a small lengthening of the Mo3–O(bridging) bond distances. The short Mo3–N1 distance and the linearity of the Mo3–N1–N3 valence angle are consistent with the description of the phenyldiazo linkage as the three-electron donation $-N_2R^+$ structure. However, the Mo3–N1 and N1–N2 distances imply a significant contribution of resonance form **II** to the overall structure of the [Mo–N_2R] unit, in contrast to other diazenido derivatives of polymolybdates which display metrical parameters approaching the idealized structure **I**.

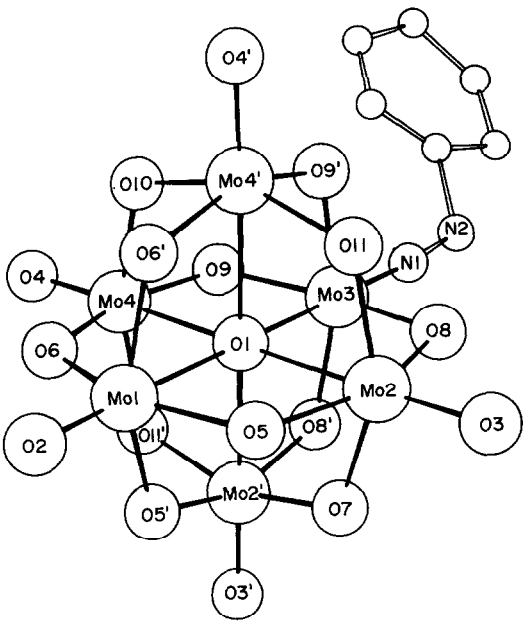
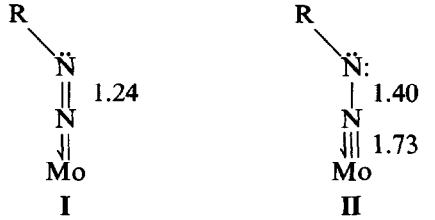


Fig. 1. ORTEP view of the structure of the molecular anion $[Mo_6O_{18}(NNC_6H_5)]^{3-}$, showing the atom-labelling scheme. Relevant bond lengths (Å) and angles (°): Mo3–O1 = 2.15(1), Mo3–O8 = 1.98(1), Mo3–O9 = 2.01(2), Mo3–N1 = 1.76(2), N1–N2 = 1.31(3), O1–Mo3–N1 = 179.2(10), O9–Mo3–N1 = 100.1(9), O8–Mo3–N1 = 101.8(9), O8–Mo3–O9 = 158.1(7), Mo3–N1–N2 = 178.7(19). Average values of the non-derivatized Mo sites: Mo–O_t = 1.68(2), Mo–O_b = 1.93(2), Mo–O_c = 2.35(1), O_c–Mo–O_t = 178.5(9), O_b–Mo–O_c = 76.9(7), and O_t–Mo–O_b = 103.2(9); where O_t, O_b and O_c refer to terminal, bridging, and central oxo groups, respectively. The atoms Mo1, Mo3, O1, O3, O7 and O10, and the entire phenyldiazenido unit, lie on a crystallographic mirror plane passing through the $[Mo_6O_{18}(NNC_6H_5)]^{3-}$ unit at $x = 0.2500$.



The complex is electrochemically active in common with type **I** polymolybdates, displaying a reversible one-electron oxidation at +0.076 V followed by a quasi-reversible one-electron oxidative process at +0.842 V.‡ Controlled-potential electrolysis at +0.3 V results in a dramatic color change from pale red to intense violet, accompanied in the

*The atomic coordinates for this work are available on request from the Director of the Cambridge Crystallographic Data Centre, Cambridge CB2 1EW. Any request should be accompanied by the full literature citation for this communication.

†One cation lies in the crystallographic mirror plane at $x = 0.2500$, such that N12 and C31–C38 occupy positions on the plane and C39–C42 rest in general positions. The cation exhibits disorder about the mirror plane, evidenced by significant residuals (1.5–1.8 e Å^{-3}) above and below the plane positions of C33, C34, C37 and C38. Thermal parameters associated with C41 and C42 also suggest a degree of disorder. Since various models assigning partial populations to these positions failed to yield a significantly improved fit, we have reported the model with carbon atoms located at the positions of major intensity with unit populations and unconstrained thermal parameters.

‡$[Mo_6O_{19}]^{2-}$ exhibits successive one-electron reductions at −0.85 and −1.70 V.[11]

electronic spectrum by the disappearance of the 390-mμ transition and the appearance of a band at 439 mμ. The electrochemically generated oxidized species $[Mo_6O_{18}(NNC_6H_5)]^{2-}$ is paramagnetic, and details of the magnetic properties and the EPR spectrum will be presented in subsequent publications.

REFERENCES

1. M. T. Pope, *Heteropoly and Isopoly Oxometalates.* Springer, New York (1983).
2. V. W. Day, M. F. Fredrick, W. G. Klemperer and R.-S. Liu, *J. Am. Chem. Soc.* 1979, **101**, 491.
3. E. M. McCarron III, R. H. Staley and A. W. Sleight, *Inorg. Chem.* 1984, **23**, 1043.
4. E. M. McCarron III and R. C. Harlow, *J. Am. Chem. Soc.* 1983, **105**, 6179.
5. R. D. Adams, W. G. Klemperer and R.-S. Liu, *J. Chem. Soc., Chem. Commun.* 1979, 256.
6. E. M. McCarron III, J. F. Whitney and D. B. Chase, *Inorg. Chem.* 1984, **23**, 3275.
7. T.-C. Hsieh and J. Zubieta, *Inorg. Chem.* 1985, **24**, 1287.
8. T.-C. Hsieh and J. Zubieta, *J. Chem. Soc., Chem. Commun.* 1985, 1749.
9. T.-C. Hsieh and J. A. Zubieta, *Polyhedron* 1986, **5**, 305.
10. O. Nagano and Y. Sasaki, *Acta Cryst.* 1979, **B35**, 2387.
11. M. Chi, M. Fournier and J. P. Launay, *J. Chem. Phys.* 1979, **71**, 1954.

Polyhedron Vol. 5, No. 10, p. 1659, 1986
Pergamon Journals Ltd. Printed in Great Britain

ANNOUNCEMENT

METALS IN OLEFIN POLYMERIZATION SYMPOSIUM

This symposium will be held in Denver, CO, U.S.A. (5–10 April 1987) at the 193rd American Chemical Society National Meeting. For further information or to submit contributions, contact: Dr Steven D. Ittel or Dr Andrew H. Janowicz, Central Research and Development Department, E. I. du Pont de Nemours & Co., Inc., Experimental Station, E328, Wilmington, DE 19898, U.S.A.

The symposium will focus on catalyst preparation, catalytic and stoichiometric reactions, mechanistic aspects, and novel applications of:

Coordination polymerization by late transition metals,

Effect of transition metals in free-radical polymerizations,

Group transfer polymerizations,

Ziegler–Nata catalysis,

Polymerizations by organolanthanides,

Main-group metals in polymerizations,

Other appropriate applications of metals in polymer chemistry.

POLYHEDRON REPORT NUMBER 16

TRANSITION-METAL COMPLEXES OF INORGANIC SULPHUR–NITROGEN LIGANDS

TRISTRAM CHIVERS* and FRANK EDELMANN

Department of Chemistry, The University of Calgary, Calgary, Alberta, Canada T2N 1N4

CONTENTS

I. INTRODUCTION 1662

II. COMPLEXES OF SULPHUR NITRIDES 1663
II.1. Thionitrosyl complexes 1663
II.1.A. Preparation 1663
II.1.B. Structure and bonding 1664
II.1.C. Spectroscopic studies 1664
II.1.D. Reactions 1666
II.2. Complexes of disulphur dinitride (S_2N_2) 1666
II.2.A. Preparation 1666
II.2.B. Structural studies 1667
II.3. Complexes of tetrasulphur tetranitride (S_4N_4) 1667
II.3.A. Preparation 1668
II.3.B. Structural studies 1669

III. COMPLEXES OF THIAZYL HALIDES 1670
III.1. Thiazyl fluoride (NSF) 1670
III.2. Thiazyl trifluoride (NSF_3) and the difluorosulphoximide anion $\{[NSOF_2]^-\}$ . . . 1671
III.3. Thiazyl chloride (NSCl) and thiazyl bromide (NSBr) 1671
III.3.A. Preparation 1672
III.3.B. Spectroscopic and structural studies 1674
III.3.C. Reactions 1674

IV. COMPLEXES OF SULPHUR–NITROGEN OXIDES 1676
IV.1. The thionylimide anion (NSO^-) and thionyl imide (HNSO) 1676
IV.2. Bis(thionylimino)sulphur [$S(NSO)_2$] 1677
IV.3. S_3N_2O and $S_4N_4O_2$ 1677

V. COMPLEXES OF SULPHUR IMIDES 1677
V.1. Sulphur imide (SNH) 1678
V.2. Tetrasulphur tetraimide ($S_4N_4H_4$) 1678

VI. CYCLOMETALLATHIAZENES AND RELATED COMPLEXES 1679
VI.1. MS_2N_2 1679
VI.1.A. Preparation 1679
VI.1.B. Structural studies 1681

* Author to whom correspondence should be addressed.

VI.2. MS_2N_2H 1681
VI.2.A. Preparation 1681
VI.2.B. Structural and spectroscopic studies 1683
VI.2.C. Reactions 1683
VI.3. MS_3N 1686
VI.3.A. Preparation 1686
VI.3.B. Structural studies 1688
VI.4. MS_2N_3 1688
VI.4.A. Preparation 1688
VI.4.B. Structural and spectroscopic studies 1690
VI.4.C. Reactions 1691
VI.5. MS_3N_4 1691
VI.6. MS_4N_3 1693
VI.7. $M_2S_2N_4$ 1693
VI.8. $M_2S_3N_2$ 1694
VI.9. Related complexes 1694

VII. SUMMARY AND FUTURE PROSPECTS 1694

I. INTRODUCTION

Complexes of transition metals with sulphur–nitrogen (S–N) ligands,* e.g. $MoCl_5 \cdot S_4N_4$[1] and $TiCl_4 \cdot S_4N_4$,[2] were first described in the early part of this century. The topic enjoyed some popularity in the 1950s, primarily due to the pioneering work of Becke-Goehring and co-workers in Germany and a review by Weiss was published in 1966.[3] The structural characterization of these compounds was a difficult task, however, due to the lack of suitable physical techniques, and progress was slow. Furthermore, unlike boron or phosphorus chemistry, the advent of NMR spectroscopy in the 1960s had little impact on the advancement of the subject since neither sulphur nor nitrogen have readily amenable NMR nuclei. In the 1970s there was a dramatic increase in interest in S–N chemistry.[4] X-ray crystallography has played the major role in providing essential structural information and, in the last 5 years, our knowledge of metal complexes has progressed to the point where a review of the subject is timely. It is particularly appropriate during the sesquicentennial anniversary (1985) of the discovery of tetrasulphur tetranitride S_4N_4,[5] the precursor of the first metal complexes with S–N ligands.

This review is limited to complexes of metals with *inorganic* S–N ligands such as binary sulphur nitrides and S–N anions, thiazyl halides (NSX), S–N oxides, and sulphur imides, $[(SNH)_x]$. It does not include complexes with *organic* ligands in which the donor sites are sulphur and nitrogen. Complexes between metals and the binary sulphur nitrides SN, S_2N_2 and S_4N_4, which are treated first, can be considered as typical Lewis acid–Lewis base adducts in which the ligand is bonded to the metal via a nitrogen atom. Complexes of thiazyl halides NSX (X = F, Cl or Br), which are covered in the next section, can be viewed in a similar way. A discussion of S–N oxides as ligands follows, for which coordination through oxygen or, less frequently, nitrogen is observed. Attachment to the metal via sulphur atoms is exhibited by sulphur imides, e.g. $S_4N_4H_4$, in which the nitrogen atoms are three-coordinate (cf. two-coordinate nitrogen in sulphur nitrides). The last section covers the important class of compounds known as cyclometallathiazenes, represented by the general formula MS_xN_y. In these complexes the metal ion is a constituent of an S–N ring and the ligand can be considered as a binary S–N anion.

In keeping with the current state of knowledge of the subject the major emphasis of the review will be on synthetic methods and structural information.

* The use of parentheses (or a period) in molecular formulae to distinguish between complexes in which the thiazene unit is bonded as a neutral ligand to the metal and those in which the metal is part of a thiazene ring should be noted. For example, $M(S_2N_2)$ (or $M \cdot S_2N_2$) represents an adduct of disulphur dinitride (Section II.2), whereas MS_2N_2 signifies a five-membered metallathiazene ring (Section VI.1). This distinction does not apply when the metal is part of more than one ring system, i.e. for a spirocyclic metal centre.

II. COMPLEXES OF SULPHUR NITRIDES

II.1. *Thionitrosyl complexes*

The chemistry of transition-metal–thionitrosyl complexes up to 1981 has been surveyed by Roesky and Pandey.[6] Accordingly, after a general introduction, this section will focus on publications that postdate that review. Recent investigations by Hursthouse *et al.*[7] have shown, however, that earlier claims of the preparation of a number of rhodium–thionitrosyl complexes[8–10] cannot be substantiated. Consequently, a reinterpretation of some of the earlier work is warranted and is included in this section.

II.1.*A. Preparation.* Unlike NO, the monomeric NS molecule has only a transient existence and it cannot be used to prepare thionitrosyl–metal complexes. The NS molecule is, however, stabilized by coordination to a transition metal. The following metals are known to form thionitrosyl complexes: Cr, Mo, W, Mn, Tc, Re, Fe, Ru, Os, Co, Rh and Ir.

The tetramer S_4N_4 is a potential source of the SN monomer, but there is only one example of the preparation of a metal–thionitrosyl complex from S_4N_4.[11] The reactions of S_4N_4 with certain transition-metal halides in methanol give complexes originally formulated as $M(NS)_4$ (M = Ni, Co or Fe),[12] but later shown to be $M(S_2N_2H)_2$[13,14] (see Section VI.2). Some poorly characterized products described as metal thionitrosyls, e.g. NiS_4N_4,[15] CoS_4N_4,[16] $Mo(CO)S_5N_5$,[17] $Fe(CO)(S_4N_4)$[18] and $Co_2(CO)(S_4N_4)$,[19] have been obtained from S_4N_4 and metal carbonyls, but structural information is lacking. In fact, treatment of the latter cobalt complex with NO gives the cyclometallathiazene $(NO)_2CoS_3N$ (Section VI.3).[20] The first M–NS complex was prepared in 1974 by the reaction of molybdenum nitrido complexes with sulphur or propylene sulphide.[21,22] Since then several other synthetic approaches to metal–thionitrosyl complexes have been discovered and examples of each of these are discussed below.

(a) *Reactions of nitrido complexes with* S_2Cl_2

This preparative route was first used for the synthesis of Re– and Os–thionitrosyl complexes.[23,24] It has recently been extended to the preparation of Tc(I) and Tc(II) complexes:[25]

$$L_3TcCl_2N + S_2Cl_2 \rightarrow L_3TcCl_x(NS),$$

where L = $PhMe_2P$ and $x = 2$ or 3.

(b) *Reactions of* NS^+ *salts with transition-metal complexes*

This approach has the potential to become a general method of synthesis but only a few thionitrosyl complexes have been obtained from NS^+ salts.[26,27] The latter can be generated *in situ* from $(NSCl)_3$ and $AgPF_6$:[26]

$$(C_6H_6)Cr(CO)_3 + [NS][PF_6] \xrightarrow{MeCN} [Cr(NS)(MeCN)_5][PF_6]_2,^{26}$$

$$[CpFe(CO)_2SO_2][AsF_6] + [NS][AsF_6] \longrightarrow [CpFe(CO)_2NS][AsF_6]_2 + SO_2,^{27}$$

$$[Re(CO)_5SO_2][AsF_6] + [NS][AsF_6] \longrightarrow [Re(CO)_5NS][AsF_6]_2 + SO_2.^{27}$$

(c) *Reactions of* $(NSCl)_3$ *with anionic metal–carbonyl complexes*

The first organometallic-thionitrosyl complex was prepared by the addition of $(NSCl)_3$ in THF to $[CpCr(CO)_3]^-$ at $-78°C$[28,29] and the corresponding C_5Me_5 derivative has been obtained in a similar way:[30]

$$Na[CpCr(CO)_3] + \tfrac{1}{3}(NSCl)_3 \rightarrow CpCr(CO)_2NS + CO + NaCl.$$

The analogous Mo or W complexes could not be prepared in this way, however, due to preferential oxidation of the $[CpM(CO)_3]^-$ anion to the dimer $[CpM(CO)_3]_2$ by $(NSCl)_3$.[28,29] This problem has

been overcome recently by replacement of Cp with the hydridotris(3,5-dimethylpyrazolyl)borate ligand:[31]

$$K[HB(Me_2Pz)_3M(CO)_3] + (NSCl)_3 \xrightarrow{THF} HB(Me_2Pz)_3M(CO)_2NS + [HB(Me_2Pz)_3M(CO)_2]_2S,$$

where M = Mo or W.

(d) *Halide abstraction from coordinated* NSF *or* NSCl

The reaction of $[Re(CO)_5NSF][AsF_6]$ with AsF_5 provides a source of $[Re(CO)_5NS]^{2+}$,[32] but method (b) is prefered for the preparation of this cation.[27] Complexes containing two NS ligands have been prepared by chloride abstraction from coordinated NSCl ligands:[33]

$$OsCl_4(NSCl)_2 + Ph_4AsCl \xrightarrow{CH_2Cl_2} [Ph_4As][OsCl_4(NS)(NSCl)]$$
$$GaCl_3\downarrow \uparrow Ph_4AsCl$$
$$OsCl_4(NS)_2$$

(e) *Reactions of* $(NSCl)_3$ *with transition-metal halides*

This method could be a versatile route to M–NS complexes and it has been applied recently to an improved synthesis of Ru and Os complexes:[33]

$$(Ph_3P)_3MCl_2 + \tfrac{1}{3}(NSCl)_3 \xrightarrow{THF} (Ph_3P)_2M(NS)Cl_3,$$

where M = Ru (55%) or Os (46%).

As indicated in subsequent sections, however, the reactions of transition-metal halides with $(NSCl)_3$ can give rise to a wide range of compounds including S_2N_2 adducts, NSCl complexes, cyclometallathiazenes or salts containing binary or chlorinated S–N cations. It should also be noted that the reactions of triphenylphosphine–rhodium complexes (or Ph_3P itself) with $(NSCl)_3$ produce Ph_3PNH and $[Ph_3PNH_2]Cl$,[7] not thionitrosyl complexes.[8–10]

(f) *Reactions of* S_4N_4 *with transition-metal halides or nitrides*

Very recently the first examples of the preparation of transition-metal–thionitrosyl complexes from S_4N_4 have been reported.[11] The reaction of $ReNCl_4$ with S_4N_4 in the presence of Ph_4AsCl gives $[Ph_4As]_2[ReCl_4(NS)(NSCl)] \cdot CH_2Cl_2$. In contrast, it should be noted that the reaction of $WNCl_3$ with S_4N_4 produces the cyclometallathiazene $[Cl_3WS_2N_3]_2$ (Section VI.4.A). The preparation of $[Ph_4As][Re(NS)Cl_5]$ from S_4N_4 and Re_2Cl_{10}, followed by treatment with Ph_4AsCl, has also been described:[11]

$$Re_2Cl_{10} + S_4N_4 \xrightarrow[CH_2Cl_2]{Ph_4AsCl} [Ph_4As][Re(NS)Cl_5].$$

The M–NS complexes that have been reported since 1981 and the methods used in their preparation are listed in Table 1.

II.1.*B. Structure and bonding.* Although more than 70 metal–thionitrosyl complexes have been described, X-ray structural data are available for only six (Table 2). The M—N≡S unit is essentially linear in all six compounds and, unlike metal nitrosyls, there are no confirmed examples of complexes containing either bent- or bridging-thionitrosyl ligands. From a comparison of the IR data [ν(CO) and ν(NX)] of the series of d^6-metal complexes $[CpM(CO)_2NX]^{n+}$ (M = Cr, $n = 0$; M = Mn, $n = 1$; M = Fe, $n = 2$; X = O or S) it is apparent that the comparative acceptor abilities of NO^+ and NS^+ depend on the charge density in the complex. The former behaves as a stronger π-acceptor in the Mn and Fe complexes.[27]

II.1.*C. Spectroscopic studies.* The bands attributed to the ν(NS) stretching mode of new metal–thionitrosyl complexes are given in Table 1. They fall within the broad range 1065–1390 cm^{-1}. Complexes that absorb in the 1110–1130-cm^{-1} region were considered earlier to contain bent, terminal NS ligands,[6] and a series of Rh complexes with an IR band at 1118 ± 3 cm^{-1} were claimed to be thionitrosyl complexes on the basis of analytical data and IR evidence.[8–10] However, the data

Table 1. Preparative methods and IR data for metal–thionitrosyl complexes

Complex	Preparative method[a]	ν(NS) (cm^{-1})	Reference
$(C_5Me_5)Cr(CO)_2NS$	c	1150	30
$HB(Me_2Pz)_3Mo(CO)_2NS$	c	1125, 1136	31
$Mo(NS)(N_3)(dppe)_2$	a	1065	22
$Mo(NS)Br(dppe)_2 \cdot 0.5CH_2Cl_2$	a	1065	22
$HB(Me_2Pz)_3W(CO)_2NS$	c	1127, 1140	31
$W(NS)(N_3)(dppe)_2$	a	1080	22
$[CpMn(CO)_2NS][AsF_6]$	b	1284	27
$[CpFe(CO)_2NS][AsF_6]_2$	b	1388	27
$[Re(CO)_5NS][AsF_6]_2$	b	1370	27
$[Ph_4As][Re(NS)Cl_5]$	f	1268	11
$[Ph_4As]_2[ReCl_4(NS)(NSCl)] \cdot CH_2Cl_2$	f	1222, 1270	11
$Ru(NS)Br_2Cl(PPh_3)_2$	e	1308	34
$Ru(NS)Br_2Cl(AsPh_3)_2$	e	1300	34
$Ru(NS)Cl_3(PPh_3)(SbPh_3)$	[b]	1300	34
$Ru(NS)Cl_3(AsPh_3)(SbPh_3)$	[b]	1299	35
$Ru(NS)Cl_3$	e	1290	35
$(NH_4)_2[Ru(NS)Cl_5]$	[c]		35
$[Ph_4P][Ru(NS)Cl_5]$	[c]	1300	35
$[Ph_4P][Ru(NS)Cl_4(H_2O)]$	[c]	1318	35
$Os(NS)Cl_3$	e	1290	36
$[Ph_4P]_2[Os(NS)Cl_5]$	[c]	1255	36
$[Ph_4P][Os(NS)Cl_4(H_2O)]$	[c]	1285	36
$Os(NS)Cl_4(POCl_3)$	e		37
$[Ph_4As][Os(NS)Cl_5]$	[c]	1340	37
$[Ph_4As][OsCl_4(NS)(NSCl)]$	d	1215, 1298	33
$OsCl_4(NS)_2$	d	1308, 1326, 1388	33

[a] See Section II.1.A for description of methods a–f.

[b] Prepared by ligand exchange reactions.

[c] Prepared by treatment of neutral complexes $M(NS)Cl_3$ (M = Ru or Os) with Ph_4ECl (E = P or As) or NH_4Cl.

given in Table 2 indicate that there is no correlation between ν(NS) and the MNS angle and more recent work has identified the source of this IR band to be $[Ph_3PNH_2]Cl$, an impurity that is formed from the reaction of triphenylphosphine–rhodium complexes with $(NSCl)_3$.[7]

A bridging-thionitrosyl group has been attributed to complexes of type $[Rh(NS)X_2L]_2$ (X = Cl or Br, L = Ph_3P or Ph_3As) on the basis of an IR band at 840 cm^{-1},[6] but a reinvestigation of the reaction of $[Rh(NO)(PPh_3)_3]$ with $(NSCl)_3$ gave Ph_3PO and $[Ph_3PNH_2]Cl$[7] and not

Table 2. X-ray structural and IR data for metal–thionitrosyl complexes

Complex	N–S (Å)	M–N (Å)	M–N–S (Å)	ν(NS) (cm^{-1})	Reference
$CpCr(CO)_2NS$	1.551(2)	1.694(2)	176.8(1)	1180	29
$Mo(NS)(S_2CNMe_2)_3$	1.59	1.73	172.0(7)	1100	38
$[Ph_4P][Ru(NS)Cl_4(H_2O)]$	1.504(4)	1.729(4)	170.9(5)	1318	35
$[Ph_4P][Os(NS)Cl_4(H_2O)]$	1.514(5)	1.731(4)	174.9(3)	1285	39
$Os(NS)Cl_3(PPh_3)_2$	1.503(10)	1.779(9)	180.0(1)	1310	39
$[Ph_4As][OsCl_4(NS)(NSCl)]$	1.46(1)	1.842(8)	169.9(5)	1298	37
	1.46(1)	1.828(8)	169.1(5)	1215	
$[Ph_4As]_2[ReCl_4(NS)(NSCl)]$	1.443(4)	1.894(4)	163.5(3)	1270	11
	1.456(4)	1.837(2)	177.1(3)	1222	

$[Rh(NS)Cl_2(Ph_3P)]_2$ as reported previously.[9] Thus the existence of Rh complexes containing bridging-thionitrosyl ligands is questionable.

^{13}C and ^{14}N NMR data have been reported for three pairs of metal–nitrosyl/thionitrosyl compounds.[40] Only small changes in the ^{13}C NMR chemical shifts of CO ligands are observed. However, the ^{14}N chemical shifts increase by as much as 49 ppm for an NS complex compared to the analogous NO complex and the ^{95}Mo chemical shift in $HB(Me_2Pz)_3Mo(CO)_2NX$ (X = O or S) increases by >550 ppm when NO is replaced by NS. This deshielding of both the ^{95}Mo and ^{14}N nuclei has been attributed to a decrease in the energies of the low-lying excited states for the M–NS complexes. The bathochromic shifts observed in the UV–visible spectra of M–NS complexes and earlier data from photoelectron spectra[41] provide support for this explanation of the NMR data.

II.1.*D. Reactions.* Several reactions of transition-metal–thionitrosyl complexes have been reported since 1981. Rh complexes containing the NSCl and NSF ligands were prepared by nucleophilic halide addition to the thionitrosyl ligand in the dicationic complex $[Re(CO)_5NS][AsF_6]_2$ (Section III.3.A). The reactivity of $Ru(NS)X_3L_2$ complexes (X = Cl or Br; L = PPh_3, $AsPh_3$, $SbPh_3$ or pyridine) towards NOCl, NOBr and N_2O_3 in the presence of excess L was investigated. In all cases displacement of the thionitrosyl group occurred and the products were nitrosyl and nitrosyl-nitrato (from N_2O_3) complexes of the general formulae $Ru(NO)X_3L_2$ and $Ru(NO)(NO_3)X_2L_2$.[34] Similarly, the reaction of $Co(NS)Cl_3(PPh_3)_2$ with NOCl or NOBr resulted in the formation of $Co(NO)XCl_2(PPh_3)_2$ (X = Cl or Br).[39]

II.2. *Complexes of disulphur dinitride* (S_2N_2)

The smallest cyclic sulphur nitride, S_2N_2, is usually prepared by pyrolysis of S_4N_4 in the vapour phase using a silver catalyst.[42] More recently, several alternative preparative routes have been reported.[43–45] Although S_2N_2 has attracted attention as the precursor of the conducting polymer $(SN)_x$,[46] the coordination chemistry of this simple ligand is not well developed, probably due to the difficulties involved in handling an explosively labile compound. In fact, the first transition-metal complex, polymeric $(\mu\text{-}S_2N_2)[Cu(CH_3CN)Cl_2]_2$, was not reported until 1980.[47]

II.2.*A. Preparation.* Complexes of S_2N_2 have been prepared by the reactions of transition-metal halides with a variety of S–N precursors. Examples of each preparative route are given below.

(a) *Direct reaction with* S_2N_2

This method has only been reported for $TiCl_4 \cdot S_2N_2$.[48]

(b) *Cleavage of* S_4N_4

The reaction of S_4N_4 with Lewis acids can result in cleavage of the eight-membered S_4N_4 ring to give S_2N_2 as a complex with the Lewis acid. This transformation occurs readily with aluminium trihalides [Al_2X_6 (X = Cl[49] or Br[50])]. It has also been reported for $CuCl_2$,[47] VCl_4[51] and the adduct $TiCl_4 \cdot S_4N_4$:[48]

$$2TiCl_4 \cdot S_4N_4 \xrightarrow{125°C} 2TiCl_4 \cdot S_2N_2 + S_4N_4.$$

The yield in the above reaction is quantitative, but the procedure is hazardous.

(c) *Ligand exchange*

This synthetic approach is potentially of general application but to date there is only one example:[48]

$$(Ph_3P)_2(CO)_2RuCl_2 + (\mu\text{-}S_2N_2)(AlCl_3)_2 \rightarrow [(Ph_3P)_2(CO)_2(S_2N_2)RuCl][AlCl_4] + \tfrac{1}{2}Al_2Cl_6.$$

(d) *Elimination of* SO_2 *from* $S(NSO)_2$

Although S_2N_2 cannot be obtained by pyrolysis of $S(NSO)_2$, the elimination of SO_2 from this

precursor in the presence of $TiCl_4$ gives $TiCl_4 \cdot S_2N_2$ in 95% yield:[48]

$$S(NSO)_2 + TiCl_4 \xrightarrow{CH_2Cl_2} TiCl_4 \cdot S_2N_2 + SO_2.$$

(e) *Reduction of* $(NSCl)_3$ *or* $S_3N_2Cl_2$

The reactions of chlorides of Groups 4–6 with $(NSCl)_3$ or $S_3N_2Cl_2$ have proved to be a rich source of transition-metal complexes with S–N ligands. In certain cases S_2N_2 complexes are obtained,[52,53] but this route can also give rise to cyclometallathiazenes (Section VI.4) or complexes of thiazyl chloride (Section III.3):

$$[Ph_4As][VCl_5] + (NSCl)_3 \xrightarrow{CH_2Cl_2} [Ph_4As]_2[(\mu\text{-}S_2N_2)(VCl_5)_2] \xrightarrow{(NSCl)_3} [Ph_4As][(S_2N_2)VCl_4]$$

(f) *Thermolysis of thiazyl chloride complexes*

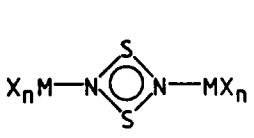
Thermolysis of the complexes $MCl_5(NSCl)$ (M = Nb or Ta) results in the reductive elimination of Cl_2 to give S_2N_2-bridged complexes:[54]

$$2MCl_5(NSCl) \xrightarrow{\Delta} (\mu\text{-}S_2N_2)(MCl_5)_2 + Cl_2,$$

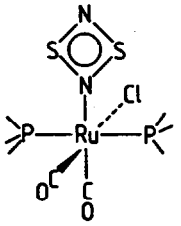
where M = Nb or Ta.

The known S_2N_2 complexes of transition metals and the methods used in their preparation are summarized in Table 3.

II.2.*B. Structural studies.* In Table 4 the pertinent X-ray structural data for S_2N_2 complexes of transition metals are compared with the corresponding data for S_2N_2 complexes of Lewis acids and the free ligand. In all but one of these complexes S_2N_2 acts as a bidentate, bridging ligand with nitrogen atoms as the donor sites **1**. The geometry of the coordinated S_2N_2 molecule is not substantially different from that of the square planar free ligand.[42] The S–N bond lengths remain essentially equal at *ca* 1.64 Å and the bond angles at S and N are *ca* 85 and *ca* 95°, respectively. The one exception is $[(Ph_3P)_2(CO)_2(S_2N_2)RuCl][AlCl_4]$ in which the S_2N_2 ligand is monodentate (**2**).[48] Significant differences in the S—N bond lengths are observed for this complex (Table 4), possibly due to a short, intramolecular S—Cl contact of 2.918(4) Å.



1



2

II.3. *Complexes of tetrasulphur tetranitride* (S_4N_4)

There have been numerous claims of the preparation of adducts of S_4N_4 with transition-metal halides, e.g. WCl_4,[1] $MoCl_5$[1] and $TiCl_4$,[2] in the early literature, and in 1978 these complexes were documented in a survey by Alange and Banister.[58] At that time structural assignments were based on IR spectra and chemical analyses. The fact that $WX_4 \cdot S_4N_4$ (X = Cl[1,58] or Br[59]) was obtained from the reactions of S_4N_4 with tungsten *hexa*halides suggests the occurrence of redox reactions. Indeed more recent investigations have revealed that, in addition to adduct formation, treatment of S_4N_4 with transition-metal halides can lead to fragmentation of the S_4N_4 ring to give S_2N_2 complexes (Section II.2), or redox reactions with the formation of S–N cations or cyclometallathiazenes (Section VI.4). Thus claims of the preparation of S_4N_4 complexes must be viewed with circumspection unless they are supported by X-ray structural characterization.

Table 3. Preparative methods for S_2N_2 complexes of transition metals

Complex	Preparative method[a]	Reference
$TiCl_4 \cdot S_2N_2$	a, b, d, e	48, 52
$VCl_4 \cdot S_2N_2$	b	51
$[Ph_4P][VCl_4(S_2N_2)]$	e	55
$[Ph_4As][VCl_4(S_2N_2)]$	e	55
$[Ph_4As]_2[(\mu\text{-}S_2N_2)(VCl_5)_2]$	e	53
$(\mu\text{-}S_2N_2)(NbCl_5)_2$	f	54
$(\mu\text{-}S_2N_2)(TaCl_5)_2$	f	54
$[(Ph_3P)_2(CO)_2(S_2N_2)RuCl][AlCl_4]$	c	48
$(\mu\text{-}S_2N_2)[Cu(CH_3CN)Cl_2]_2$	b	47
$(\mu\text{-}S_2N_2)[MoCl_4(NSCl)]_2$	e	56
$(\mu\text{-}S_2N_2)[WCl_4(NSCl)]_2$	e	56

[a] See Section II.2.A for description of methods a–f.

II.3.*A. Preparation.* Adducts of S_4N_4 with transition-metal halides may be prepared by direct combination of the components in inert solvents such as CH_2Cl_2 or CCl_4. In the case of the Cu complexes, $CuCl_2 \cdot S_4N_4$[60,61] and $CuX \cdot S_4N_4$ (X = Cl[60] or Br[62]), methanol or acetonitrile were used as solvents. However, the reactions of several other transition-metal halides with S_4N_4 in methanol result in the formation of five-membered MS_2N_2H rings [M = Co, Ni, Pd or Pt (see Section VI.2)].

The interaction of $FeCl_3$ with S_4N_4 in various solvents has been studied by several groups and provides a good example of the delicate balance between simple adduct formation and the occurrence of redox reactions. The adducts α- and β-$FeCl_3 \cdot S_4N_4$ have been prepared in CCl_4.[63,64] In CH_2Cl_2,

Table 4. X-ray structural data for S_2N_2 complexes

Complex	S–N (Å)	S–S (Å)	N–S–N (°)	S–N–S (°)	Reference
S_2N_2 (−130°C)	1.657(1) 1.651(1)	2.348	89.58(6)	90.42(6)	42
$(\mu\text{-}S_2N_2)(AlCl_3)_2$	1.648(3) 1.644(3)	2.425	85.1(2)	94.9(2)	49
$(\mu\text{-}S_2N_2)(AlBr_3)_2$	1.651(13) 1.629(13)		84.2(10)	95.8(10)	50
$(\mu\text{-}S_2N_2)(SbCl_5)_2$	1.616(7) 1.623(8)	2.390(5)	84.9(4)	95.4(6)	57
$[Ph_4P][(\mu\text{-}S_2N_2)(VCl_5)_2]$[a,b]	1.62(1) 1.66(1) 1.60(1) 1.64(1)		86.0(7) 85.6(7)	94.0(7) 94.4(7)	53
$[(Ph_3P)_2(CO)_2(S_2N_2)RuCl][AlCl_4]$	1.684(7) 1.656(9) 1.648(7) 1.612(8)	2.361(4)	90.0(4) 87.2(4)	92.5(4) 90.2(3)	48
$(\mu\text{-}S_2N_2)[Cu(CH_3CN)Cl_2]_2$[a]	1.633(8) 1.641(8)	2.410	85.2(5)	94.7(6)	47
$(\mu\text{-}S_2N_2)[MoCl_4(NSCl)]_2$	1.644(2) 1.643(2)		86.5(2)	93.5(2)	56

[a] These complexes are polymeric.

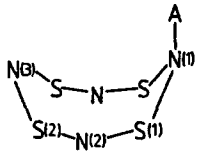
[b] The S_2N_2 ring exhibits positional disorder in this anion.

however, S_4N_4 is oxidized to give $[S_6N_4][FeCl_4]_2$ and other products.[65] The same reaction has also been reported to give a salt of the S_4N_4 radical cation, $[S_4N_4][FeCl_4]$,[66] but the structural parameters of the cation are very similar to those of $[S_4N_4H]^+$ in $[S_4N_4H][BF_4]$.[67]

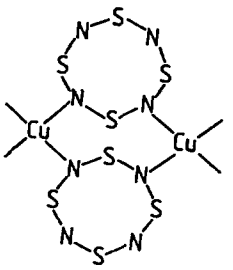
Treatment of S_4N_4 with VCl_4 in CH_2Cl_2 produces $VCl_4 \cdot S_2N_2$, but the primary product of this reaction is the cyclometallathiazene $[Cl_2VS_2N_3]_n$.[51] Similar redox reactions to give $[Cl_3MS_2N_3]_2$ (M = Mo or W) occur when S_4N_4 reacts with Mo_2Cl_{10} or WCl_6 in CH_2Cl_2 (Section VI.4).

The reaction of S_4N_4 with $IrCl(CO)(Ph_3P)_2$ in benzene gives the dark red crystalline complex $IrCl(CO)(Ph_3P)(S_4N_4)$ of unknown structure.[68] Two poorly characterized compounds, $L_2Pt(S_4N_4)$ [L = PPh_3 or $P(OPh)_3$], have been isolated from the interaction of S_4N_4 with the zero-valent Pt complexes, L_4Pt.[69]

II.3.*B. Structural studies.* The structures of five 1 : 1 adducts of S_4N_4 with transition-metal halides have been determined by X-ray crystallography: $TaCl_5 \cdot S_4N_4$,[70] $FeCl_3 \cdot S_4N_4$ (α- and β-modifications),[63,64] $CuCl \cdot S_4N_4$,[60] $CuBr \cdot S_4N_4$[62] and $CuCl_2 \cdot S_4N_4$.[60,61] The molecular structures of $TaCl_5 \cdot S_4N_4$ and $FeCl_3 \cdot S_4N_4$ are similar to those of adducts with Lewis acids, $S_4N_4 \cdot SbCl_5$,[59] $S_4N_4 \cdot BF_3$[71] and $S_4N_4 \cdot AsF_5$,[72] and the protonated species $[S_4N_4H]^+$.[67] In all cases the S_4N_4 ligand is coordinated via one of the nitrogen atoms. The structural consequence of this coordination is the disruption of the cross-ring S—S bonds of S_4N_4 to give a boat-shaped eight-membered ring with approximately coplanar sulfur atoms (**3**), and a remarkable regularity in S–N bond distances (Table 5). Oakley and co-workers have analyzed this structural rearrangement in the light of MNDO MO calculations on various conformations of $[S_4N_4H]^+$.[67] The effect of protonation is to localize π^*-electrons into the skeletal bonds to the protonated nitrogen as indicated by the relatively long S(1)–N(1) bonds. The resulting structure is susceptible to ring contraction reactions to give the five-membered ring $[S_3N_2NH_2]^+$,[73] cf. reactions of S_4N_4 with acid anhydrides to give S_3N_2NR (R = CF_3 or CCl_3).[4] In view of the structural resemblance between $[S_4N_4H]^+$ and $S_4N_4 \cdot A$ (A = an acceptor molecule), it is conceivable that the disruption of the S_4N_4 ring by transition-metal halides to give S_2N_2 complexes or cyclometallathiazenes is a related process.



3



4

A different coordination mode is exhibited by S_4N_4 in the three Cu complexes $CuCl \cdot S_4N_4$,[60] $CuBr \cdot S_4N_4$[62] and $CuCl_2 \cdot S_4N_4$ (**4**).[60,61] The first two are isostructural and form polymers in which $[Cu—X]_n$ chains (X = Cl or Br) are bridged via 1,3-bidentate S_4N_4 ligands. Surprisingly, the conformation and structural parameters for these bidentate ligands are not significantly different from those of uncoordinated S_4N_4. A very similar type of coordination was found for $CuCl_2 \cdot S_4N_4$. In

Table 5. Mean S–N bond lengths (Å) in S_4N_4 complexes of type $S_4N_4 \cdot A$ (**3**)[a]

A	N(1)–S(1)	S(1)–N(2)	N(2)–S(2)	S(2)–N(3)	Reference
H^+	1.650	1.589	1.538	1.562	67
BF_3	1.659	1.593	1.546	1.584	71
$SbCl_5$	1.69	1.59	1.57	1.58	59
AsF_5	1.659	1.584	1.540	1.567	72
α-$FeCl_3$	1.662	1.578	1.559	1.576	63
β-$FeCl_3$	1.654	1.571	1.558	1.516	64
$TaCl_5$	1.65	1.56	1.54	1.60	70

[a] Mean values are given for chemically equivalent S–N bonds.

this one-dimensional chain structure octahedrally surrounded Cu atoms are bridged by Cl and 1,3-bidentate S_4N_4 ligands.

III. COMPLEXES OF THIAZYL HALIDES

Four thiazyl halides, NSF, NSCl, NSBr and NSF_3, have been used as ligands in transition-metal complexes. In addition, a number of complexes with the related $[NSOF_2]^-$ ligand have been described.

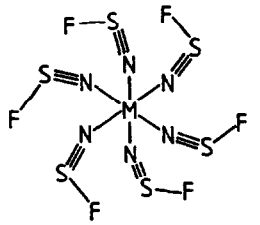
III.1. *Thiazyl fluoride* (NSF)

The chemistry of NSF and thiazyl trifluoride (NSF_3) has been surveyed in a recent review by Glemser and Mews.[74] The microwave spectrum of NSF indicates a bent structure,[75] cf. SO_2. It is most conveniently generated by decomposition of $FC(O)NSF_2$ or $Hg(NSF_2)_2$,[74] but the combination of moisture-sensitivity and thermal instability make it a difficult substance to handle. Thiazyl fluoride can be stabilized by coordination to a transition metal, however, and such complexes are conveniently prepared in liquid SO_2. This solvent is readily displaced from a metal site by weakly nucleophilic ligands and two homoleptic NSF complexes have been synthesized by this route:[76]

$$[M(SO_2)_2][AsF_6]_2 + 6NSF \rightarrow [M(NSF)_6][AsF_6]_2 + 2SO_2,$$

where M = Co or Ni.

Both complexes have been characterized by IR spectroscopy and X-ray diffraction (**5**) (Table 6).[77,78] The IR stretching frequencies ν(SN) and ν(SF) occur at higher wavenumbers and the S–N and S–F distances are significantly shorter than those in the free ligand, indicating an increase in S–N and S–F bond strength upon coordination.



5

An orange-red cationic NSF complex of Re has also been prepared by replacement of coordinated SO_2 with NSF:[79]

$$[Re(CO)_5SO_2][AsF_6] + NSF \xrightarrow[SO_2]{-30°C} [Re(CO)_5NSF][AsF_6] + SO_2.$$

This product has been used as a source of the corresponding thionitrosyl complex via halide abstraction (Section II.1.A).[32] It is also a useful intermediate for the synthesis of complexes of

Table 6. IR and structural data for NSF, $[Co(NSF)_6]^{2+}$ and $[Ni(NSF)_6]^{2+}$

	NSF(g)[a]	$[Co(NSF)_6]^{2+}$[b]	$[Ni(NSF)_6]^{2+}$[b]
ν(SN) (cm^{-1})	1361	1429	1438
ν(SF) (cm^{-1})	641	655	655
S–N (Å)	1.448	1.399(12)	1.404(5)
S–F (Å)	1.643	1.569(12)	1.581(13)
M–N (Å)		2.093(11)	2.054(3)
N–S–F (°)	116.5	115.0(7)	116.0(8)

[a] Reference 75.
[b] Reference 76.

other thiazyl halides, via halogen exchange,[41] and *N,N*-dialkylthiazylamides, by reaction with Me_3SiNMe_2:[81]

$$[Re(CO)_5NSF][AsF_6] + Me_3SiNMe_2 \xrightarrow[-30°C]{SO_2} [Re(CO)_5NSNMe_2][AsF_6] + Me_3SiF.$$

III.2. *Thiazyl trifluoride* (NSF_3) *and the difluorosulphoximide anion* $\{[NSOF_2]^-\}$

NSF_3 is more thermally stable and easier to handle than NSF. It can be obtained by fluorination of NSF or $FC(O)NSF_2$ with AgF_2.[74] On the basis of spectroscopic data, NSF_3 has a distorted tetrahedral structure.[74] The synthetic approach to transition-metal complexes of NSF_3 is similar to that described above for NSF derivatives:[82]

$$[M(SO_2)_2][AsF_6]_2 + 4NSF_3 \rightarrow [M(NSF_3)_4][AsF_6]_2 + 2SO_2,$$

where M = Mn, Fe, Co, Ni or Cu.

The IR spectra of NSF_3 complexes show a large increase in ν(SN) and ν(SF) compared to free NSF_3 (Table 7) and an X-ray structural determination of $[Mn(NSF_3)_4][AsF_6]_2$ has confirmed the proposed shortening of the S–N and S–F bonds in the coordinated NSF_3 ligands.[83] In fact the S–N bond distance in these complexes [1.365(11) Å] is essentially the same as that in the NS^+ cation [1.361(6) Å in $NS^+SbF_6^-$ at 293 K].[84] The vibrational spectra of $[Mn(NSF_3)_4][AsF_6]_2$ and $[Re(CO)_5NSF_3][AsF_6]$ have been discussed elsewhere in detail.[85]

The strengthening of S–N and S–F bonds in coordinated NSF and NSF_3 is in marked contrast to the behaviour of NS^+ and other ligands such as CO and PF_3. According to SCF calculations this effect can be ascribed to the increased net positive charge on sulphur resulting from removal of electrons from the thiazyl group.[86]

The synthesis of a cationic NSF_3 complex of Re has been reported and the product has been characterized by IR and ^{19}F NMR spectroscopy:[87]

$$[Re(CO)_5SO_2][AsF_6] + NSF_3 \xrightarrow{SO_2} [Re(CO)_5NSF_3][AsF_6].$$

The reaction of $AgAsF_6$ with excess NSF_3 affords unstable $[Ag(NSF_3)_2][AsF_6]$, which readily loses NSF_3 *in vacuo* to give the stable complex $[Ag(NSF_3)][AsF_6]$.[82]

The $[NSOF_2]^-$ anion is isoelectronic with NSF_3. The salts $[Ph_4E][NSOF_2]$ (E = P or As)[88] can be used for the preparation of anionic transition-metal complexes $[M(NSOF_2)_4]^{2-}$ (M = Hg, Co or Pt).[89] The reaction of $M(CO)_5Br$ (M = Mn or Re) with $AgNSOF_2$[90] at low temperature gives $M(CO)_5(NSOF_2)$,[91] which decompose at <20°C (M = Mn) and 90°C (M = Re) to give dinuclear compounds, $[M(CO)_4(\mu\text{-}NSOF_2)]_2$. The structures of $Re(CO)_5(NSOF_2)$[92] and $[Mn(CO)_4(\mu\text{-}NSOF_2)]_2$[92,93] have been shown by X-ray crystallography to contain terminal and bridging $NSOF_2$ groups, respectively. In both cases the ligand is coordinated to metal centres by the nitrogen atom.

III.3. *Thiazyl chloride* (NSCl) *and thiazyl bromide* (NSBr)

The first transition-metal complexes of NSCl were discovered by Dehnicke and co-workers in 1982[94] and within a few years these compounds have become a well-established group of S–N

Table 7. IR and structural data for NSF_3 derivatives

	NSF_3[a]	$[Mn(NSF_3)_4]^{2+}$[b]	$[Re(CO)_5NSF_3]^+$[b]
ν(SN) (cm^{-1})	1515	1576	1643
ν(SF) (cm^{-1})	811, 775	880, 836	890, 847
S–N (Å)	1.416	1.365(11)	
S–F (Å)	1.522	1.506(5)	
M–N (Å)		2.187(8)	

[a] Reference 74.
[b] Reference 82.

complexes. The bonding in metal–NSCl complexes can be described in terms of resonance structures **6** and **7**. Spectroscopic and X-ray structural data indicate that structure **6** is dominant in most transition-metal–NSCl complexes and that the metal–ligand interaction is stronger than in the transition-metal complexes of NSF.



6 **7**

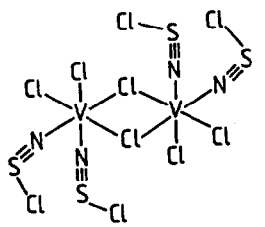
Monomeric NSCl is formed as a greenish-yellow gas by heating $(NSCl)_3$ *in vacuo* or in an inert-gas stream.[95] It has not been used for reactions with transition-metal complexes, probably due to its tendency to trimerize in the condensed state. In fact, the trimer $(NSCl)_3$ has proved to be a convenient starting material for the preparation of M–NSCl complexes. Monomeric NSBr has been prepared in the gas phase by the pyrolysis of S_4N_3Br and characterized by its IR spectrum.[96] The trimer $(NSBr)_3$ is unknown. The various routes available for the synthesis of M–NSX (X = Cl or Br) complexes are described below and summarized in Table 8.

III.3.*A*. *Preparation.*

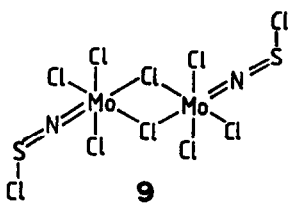
(a) *Reaction of* $(NSCl)_3$ *with metal halides*

The reaction of $(NSCl)_3$ with anhydrous metal chlorides in solvents such as CH_2Cl_2 or CCl_4 is the most general route to M–NSCl complexes. In some cases $POCl_3$ is used as a solvent to dissolve the metal chloride. Some MCl_n–$(NSCl)_3$ reactions are quite complicated and give rise to other S–N complexes, e.g. cyclometallathiazenes (Section VI.4).

Red crystalline 1 : 1 complexes, $MCl_5(NSCl)$ (M = Nb[97] or Ta[54]) are formed from MCl_5 (M = Nb or Ta) and $(NSCl)_3$, whereas VCl_4 yields a dimeric species $[VCl_3(NSCl)_2]_2$ (**8**).[55] $ReCl_5$ reacts with $(NSCl)_3$ in $POCl_3$ solution to give $ReCl_4(NSCl)(POCl_3)$[98] and $ReCl_3(NSCl)_2(POCl_3)$.[94,98]

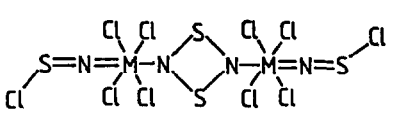


8



9

Several M–NSCl complexes have been isolated from reactions of molybdenum and tungsten chlorides with $(NSCl)_3$, but the nature of the products is dependent on subtle changes in reaction conditions (solvent, stoichiometry etc.). The dimeric complexes $[MCl_4(NSCl)]_2$ (M = Mo[99] or W[100]) (**9**) are obtained from $(NSCl)_3$ and Mo_2Cl_{10} or WCl_6, respectively, in CH_2Cl_2. In $POCl_3$ solution the solvated complex $MoCl_4(NSCl)(POCl_3)$ is formed.[99] When the $MoCl_5$: NSCl molar ratio is 1 : 2, a complex containing a bridging S_2N_2 ligand (**10**) (M = Mo) is obtained. [56] The W analogue $(\mu\text{-}S_2N_2)[WCl_4(NSCl)]_2$ (**10**) (M = W), is formed in addition to $[WCl_4(NSCl)]_2$[100] and $[Cl_3WS_2N_3]_2$ (Section VI.4) in the reaction of WCl_6 with $(NSCl)_3$ in CCl_4. A better synthesis of **10** (M = W) is the thermolysis of $[N(SCl)_2][WCl_5(NSCl)]$.[56]



10

An anionic NSCl complex, $[N(SCl)_2][MoCl_5(NSCl)]$ is also obtained in low yields from $(NSCl)_3$ and Mo_2Cl_{10} or $MoCl_4$ in CH_2Cl_2 suspension.[90] The cyclometallathiazene $[Cl_3MoS_2N_3]_2$ (Section VI.4) is formed as a by-product in this reaction.

Treatment of $OsCl_5$ with $(NSCl)_3$ in $CCl_4/POCl_3$ produces $OsCl_4(NSCl)$.[102]

Table 8. Preparative methods for M–NSX (X = Cl or Br) complexes

Complex	Preparative method[a]	Reference
$VCl_3(NSCl)_2$	a	55
$NbCl_5(NSCl)$	a	97
$TaCl_5(NSCl)$	a	54
$MoCl_4(NSCl)(POCl_3)$	a	99
$[MoCl_4(NSCl)]_2$	a	99
$[Ph_3MeP][MoCl_5(NSCl)]$	c	99
$[Ph_4As][MoCl_5(NSCl)]$	c	99
$[N(SCl)_2][MoCl_5(NSCl)]$	a	56, 101
$(\mu\text{-}S_2N_2)[MoCl_4(NSCl)]_2$	a	56
$[WCl_4(NSCl)]_2$	a	100
$[Ph_4P][WCl_5(NSCl)]$	c	56
$[Ph_4As][WCl_5(NSCl)]$	c	56,100
$[N(SCl)_2][WCl_5(NSCl)]$	b, c	56
$(\mu\text{-}S_2N_2)[WCl_4(NSCl)]_2$	a	56
$ReCl_4(NSCl)(POCl_3)$	a	98
$ReCl_3(NSCl)_2(POCl_3)$	a, b	94, 98, 103, 105
$[ReCl_3(NSCl)_2]_2$	b	94, 98, 103
$[Ph_4As][ReCl_4(NSCl)_2]\cdot CH_2Cl_2$	c	94, 98
$[Re(CO)_5NSCl][AsF_6]$	d, e, f	104
$OsCl_4(NSCl)_2$	a	102
$[Ph_4As][OsCl_4(NS)(NSCl)]$	c, d	102
$[Ph_4As]_2[ReCl_4(NS)(NSCl)]$	[b]	11
$[Re(CO)_5NSBr][AsF_6]$	d, e, f	104

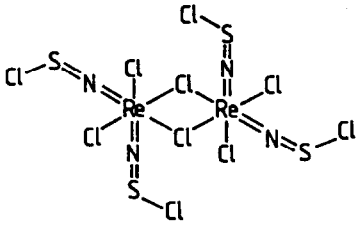
[a] See Section III.3.A for description of methods a–f.
[b] Reaction of S_4N_4 with a metal nitridochloride.

(b) *Reaction of* $S_3N_2Cl_2$ *with metal halides*

$S_3N_2Cl_2$ has been used less frequently than $(NSCl)_3$ for the synthesis of M–NSCl complexes, but the following reaction proceeds in high yield:[56]

$$WCl_6 + S_3N_2Cl_2 \xrightarrow{CCl_4} [N(SCl)_2][WCl_5(NSCl)].$$

The reaction of $ReCl_5$ with $S_3N_2Cl_2$ produces the dimeric species $[ReCl_3(NSCl)_2]_2$ (**11**) in CH_2Cl_2 suspension or $ReCl_3(NSCl)_2(POCl_3)$ in $POCl_3$ solution.[103] The latter complex has also been obtained from $ReCl_5(POCl_3)$ and $(NSCl)_3$.[94,98]



11

(c) *Halide addition to neutral* M–NSCl *complexes*

Some of the metal complexes prepared from $(NSCl)_3$ and anydrous metal chlorides [method (a)] are powdery, insoluble materials, e.g. $OsCl_4(NSCl)_2$[102] and $[ReCl_3(NSCl)_2]_2$.[103] They can, however,

be converted to soluble, more easily crystallized anionic NSCl complexes by treatment with R_4PCl or R_4AsCl (R = Me or Ph). A typical example is the reaction of $ReCl_3(NSCl)_2(POCl_3)$ with Ph_4AsCl in CH_2Cl_2 to give $[Ph_4As][ReCl_4(NSCl)_2] \cdot CH_2Cl_2$.[94,98] The neutral compound can be regenerated by treatment of the anionic complex with $GaCl_3$. Similarly, $MoCl_4(NSCl)(POCl_3)$ and $[WCl_4(NSCl)]_2$ yield $[R_4E][MoCl_5(NSCl)]$ (R_4E = Ph_3MeP or Ph_4As)[99] and $[Ph_4As][WCl_5(NSCl)]$,[94] respectively. The bridging S_2N_2 ligand in **10** (M = W) can also be displaced by chloride ion:[56]

$$(\mu\text{-}S_2N_2)[WCl_4(NSCl)]_2 + 2Ph_4PCl \rightarrow 2[Ph_4P][WCl_5(NSCl)] + S_2N_2.$$

A complex containing a thionitrosyl ligand in addition to coordinated NSCl, $[Ph_4As]$ $[OsCl_4(NS)(NSCl)]$, is prepared by the reaction of $OsCl_4(NSCl)_2$ with Ph_4AsCl.[33]

Halide addition also occurs in the reaction of $[WCl_4(NSCl)]_2$ with sulphur dichloride in boiling CCl_4:[56]

$$[WCl_4(NSCl)]_2 + SCl_2 \rightarrow [N(SCl)_2][WCl_5(NSCl)].$$

Hartmann *et al.*[81] have described three other synthetic approaches, which can be applied to the preparation of metal complexes of either NSCl or NSBr.

(d) *Halide addition to coordinated* NS

$$[Re(CO)_5NS][AsF_6]_2 + CsX \xrightarrow{SO_2} [Re(CO)_5NSX][AsF_6] + CsAsF_6,$$

where X = Cl or Br.

(e) *Insertion of* NS^+ *into metal–halogen bonds*

$$Re(CO)_5X + [NS][AsF_6] \xrightarrow{SO_2} [Re(CO)_5NSX][AsF_6],$$

where X = Cl or Br.

(f) *Halogen exchange at coordinated* NSF

$$[Re(CO)_5NSF][AsF_6] + \tfrac{1}{4}SiX_4 \xrightarrow{SO_2} [Re(CO)_5NSX][AsF_6] + \tfrac{1}{4}SiF_4,$$

where X = Cl or Br.

These methods, particularly (e), appear to be capable of wider application and preliminary studies have shown that other metal halides, e.g. $CpCr(NO)_2Cl$ and Cp_2TiCl_2, react similarly with $[NS][AsF_6]$, but crystalline products have not been isolated.[81]

III.3.*B. Spectroscopic and structural studies.* The IR spectra of M–NSCl complexes have been discussed in detail. Complexes in which the resonance structure **6** is dominant show a characteristic strong band at 900–1000 cm^{-1},[56,94,98–102] which has been assigned to ν_{as}(MNS). The IR spectra of compounds with a larger contribution from resonance form **7** show ν(N≡S) bands at 1290–1360 cm^{-1}. These include $NbCl_5(NSCl)$,[97] $TaCl_5(NSCl)$,[54] $[VCl_3(NSCl)_2]_2$[55] and $[Re(CO)_5(NSCl)][AsF_6]$.[41] The dimeric structures of $[ReCl_3(NSCl)_2]_2$,[103] $[VCl_3(NSCl)_2]_2$[55] and $[MoCl_4(NSCl)]_2$[99] were deduced from IR data.

X-ray structural data for six M–NSCl complexes are compared in Table 9 with the corresponding data for the free ligand determined by spectroscopic methods. Both the S–N bond length and the N–S–Cl angle for $NbCl_5(NSCl)$ are very similar to those of uncoordinated NSCl indicating that resonance form **7** is predominant for this complex. The average Nb–N distance of 2.264 Å is consistent with a weak interaction. By contrast, in four of the other complexes the S–N bond lengths are significantly longer and the N–S–Cl angle is smaller than those of free NSCl, suggesting that resonance form **6** is the best representation in these cases. The short metal–nitrogen distances support this interpretation.

III.3.*C. Reactions.* In this section only those reactions in which the NSCl ligand is replaced or modified will be mentioned.

Table 9. X-ray structural data for M–NSCl complexes

Complex	M–N (Å)	N–S (Å)	S–Cl (Å)	M–N–S (°)	N–S–Cl (°)	Reference
$NbCl_5(NSCl)$[a]	2.263(4) 2.264(4)	1.441(3) 1.434(3)	2.067(2) 2.078(2)	157.7(2) 163.6(2)	116.4(2) 116.4(2)	97
$[Ph_4As][ReCl_4(NSCl)_2]\cdot CH_2Cl_2$[b]	1.79(1) 1.766(10)	1.53(1) 1.555(10)	2.090(5) 2.065(6)	175.3(6) 175.9(6)	108.2(4) 107.9(6)	98
$(\mu\text{-}S_2N_2)[MoCl_4(NSCl)]_2$	1.745(2)	1.586(2)	2.013(1)	177.1(2)	101.7(1)	56
$[N(SCl)_2][MoCl_5(NSCl)]$	1.75(1)	1.59(1)	2.025(6)	171.2(9)	101.9(5)	101
$[WCl_4(NSCl)]_2$	1.76(2)	1.58(2)	2.013(8)	175(1)	104.0(7)	100
$[Ph_4As][OsCl_4(NS)(NSCl)]$[c]	1.842(8) 1.828(8)	1.46(1) 1.46(1)	2.28(1) 2.27(1)	169.9(5) 169.1(5)	104.2(4) 102.9(4)	102
$[Ph_4As]_2[ReCl_4(NS)(NSCl)]$	1.894(4) 1.837(2)	1.443(4) 1.456(4)	2.256(2)	163.5(3) 171.1(3)	112.6(2)	11
NSCl(g)[d]		1.450	2.161		117±3	86

[a] The two sets of data refer to two crystallographically independent molecules.

[b] The two sets of data refer to the two crystallographically inequivalent NSCl ligands.

[c] The Cl atom of the NSCl ligand is disordered and statistically belongs to both sulphur atoms with an occupation probability of 50%.

[d] The molecular dimensions of NSCl(g) were obtained from an analysis of its microwave spectrum.

(a) *Synthesis of nitrido compounds from* NSCl *complexes*

The conversion of coordinated NSCl into a nitrido ligand provides a useful new synthesis of transition-metal nitrides. The first example was the reaction of $ReCl_4(NSCl)(POCl_3)$ with Ph_4AsCl which affords the known complex $[Ph_4As][ReNCl_4]$ in good yield.[98] Treatment of $ReCl_4(NSCl)(POCl_3)$ with triphenylphosphine results in the formation of $ReNCl_2(PPh_3)_2$ (65% yield).[99] $[MoCl_4(NSCl)]_2$ was found to be an excellent precursor for the synthesis of nitrido complexes. Thermolysis leads to $MoNCl_3$ and anionic nitrido complexes are obtained by reaction with chloride ion:[99]

$$[MoCl_4(NSCl)]_2 \xrightarrow[10^{-3}\,\text{torr}]{130^\circ C} 2MoNCl_3 + 2SCl_2,$$

$$[MoCl_4(NSCl)]_2 + 2Cl^- \rightarrow 2[MoNCl_4]^- + 2SCl_2.$$

(b) *Formation of anionic halide complexes*

The weakly coordinated NSCl ligand in thiazyl chloride complexes of V, Nb and Ta is easily replaced by chloride ions:[54,55]

$$MCl_5(NSCl) + Ph_4AsCl \rightarrow [Ph_4As][MCl_6],$$

where M = Nb or Ta.

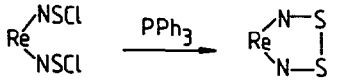
This reaction has no synthetic value, however, since the resulting anionic chloro complexes are more easily prepared directly from the corresponding metal chlorides.

(c) *Other reactions*

The NSCl ligands in $[VCl_3(NSCl)_2]_2$ are readily replaced by $POCl_3$ to give $[VCl_3(POCl_3)_2]_2$.[55] The thermolysis of $MCl_5(NSCl)$ (M = Nb or Ta) at 100°C under normal pressure yields dinuclear complexes containing a bridging S_2N_2 ligand (Section II.2.A).

The most interesting reaction of coordinated NSCl ligands has been reported for the complex

$ReCl_3(NSCl)_2(POCl_3)$. Reduction of the two NSCl ligands with triphenylphosphine results in the coupling of adjacent thionitrosyl groups with formation of a novel metallathiazene ring, $[Ph_3PCl][Cl_4ReN_2S_2]$[104] (Section IV.1).



IV. COMPLEXES OF SULPHUR–NITROGEN OXIDES

In contrast to the numerous reports of transition-metal complexes of NSCl and, to a lesser extent, NSF (Section III), there is only one confirmed example of a complex of the isoelectronic NSO^- ion. The S–N oxides $S(NSO)_2$, S_3N_2O and $S_4N_4O_2$ form adducts with silver(I) in which coordination occurs via oxygen or nitrogen (or both) atoms.

IV.1. *The thionylimide anion* (NSO^-) *and thionyl imide* (HNSO)

Potassium thionylimide (KNSO) is readily prepared from Me_3SiNSO and potassium *t*-butoxide in THF,[105] but this salt has not been used in the preparation of transition-metal derivatives. A complex described as $Co(NSO)Cl_2[P(OPh)_3]_2$, on the basis of elemental analyses and IR spectra, was isolated when the solution obtained from the reaction of $CoH[P(OPh)_3]_4$ with $(NSCl)_3$ in THF was oxidized in air.[106] The complicated IR spectrum was interpreted in terms of an *N*-bonded thionitrito ligand $\{(CoN(O)S]^-\}$,[106] but structural information is not available. The first confirmed example of a transition-metal complex of $[NSO]^-$ was reported in 1984.[107] The reaction of $CsNSO_2$[108] with $RhH(CO)(PPh_3)_3$ in acetonitrile yields *trans*-$Rh(CO)(NSO)(PPh_3)_2$ and Ph_3PO. The unbranched $[NSO]^-$ ligand is coordinated to rhodium via nitrogen with a bond angle of 122.5° at sulphur and N–S and S–O bond lengths of 1.480(12) and 1.509 (10)Å, respectively, indicative of double bonds.[107]

HNSO can be prepared by the reaction of $SOCl_2$ with ammonia in the gas phase.[109] It polymerizes rapidly in the condensed phase. The *cis*-thionylimide structure (**12**) is lower in energy than the isomeric thiazyl-*S*-hydroxide form, HOSN (**13**),[110] according to the best *ab initio* MO calculations.[111] The calculated isomerization energy is 9.5 ± 5.0 kcal mol^{-1}.[111]



12 **13**

The reaction of $(Ph_3P)_4$ Pt with $S_4N_4H_4$ in benzene–acetone gave a complex formulated as $(Ph_3P)_2Pt(S_2N_2H_2)$ on the basis of elemental analysis and UV–visible spectra,[69] but subsequently described as *cis*-bis(thionylimide-*O*)bis(triphenylphosphine)platinum(II), $(Ph_3P)_2Pt(OSNH)_2$, as a result of an X-ray structural determination.*[112,113] The bond lengths quoted for the coordinated OSNH ligands [d(SO) = 1.341(17) and 1.258(11) Å; d(SN) = 1.452(19) and 1.485(19) Å] are not very reliable, but they are remarkably short compared to those found by spectroscopic methods for the free ligand [d(SO) = 1.451 Å; d(SN) = 1.512 Å].[114]

The reaction of an aqueous solution of K_2PtCl_4 with $S_4N_4H_4$ in acetone is reported to give $Pt(OSNH)_2(S_2N_2H_2)$ on the basis of analytical data and IR and ^1H NMR spectra.[115] This compound would formally be a complex of the otherwise unknown $[S_2N_2H_2]^{2-}$ dianion and structural confirmation is awaited with interest.

Two approaches to the directed synthesis of thionylimide complexes have been reported recently.[116] The first involves quantitative displacement of coordinated SO_2 by preformed HNSO:

$$[M(CO)_5SO_2][AsF_6] + HNSO \xrightarrow[-50°C]{SO_2} [M(CO)_5HNSO][AsF_6] + SO_2,$$

where M = Mn or Re.

* The positions of the hydrogen atoms were not determined with certainty so the ligands could be either OSNH (**12**) or HOSN (**13**). However, the complex is a derivative of Pt(0) rather than Pt(II) since both **12** and **13** are neutral ligands.

The complex $[Ni(HNSO)_4][AsF_6]_2$ has also been prepared by this procedure.[116]

The second method involves nucleophilic displacement of fluoride ion from coordinated NSF by OH^- using trimethyltin hydroxide as the reagent:

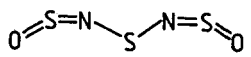
$$[Re(CO)_5NSF][AsF_6] + Me_3SnOH \xrightarrow[-30°C]{SO_2} [Re(CO)_5HNSO][AsF_6] + Me_3SnF.$$

The IR spectra of the Re complexes obtained by these two different routes are identical. Thus it seems reasonable to conclude that the ligand is present in the HNSO form. Furthermore, the second procedure would be expected to give an *N*-coordinated product.

The coordination chemistry of the organic ligands (ArNSO) and the related sulphur diimides (RNSNR) has been reviewed recently.[117]

IV.2. *Bis(thionylimino)sulphur* $[S(NSO)_2]$

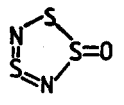
The acyclic S–N oxide $S(NSO)_2$ (**14**) is readily prepared from Me_3SiNSO and sulphur dichloride at reflux in the absence of a solvent.[118] The reaction of $S(NSO)_2$ with $AgAsF_6$ in SO_2 gives the polymeric complex $[Ag_4\{S(NSO)_2\}_9][AsF_6]_4 \cdot SO_2$ in which there are two crystallographically independent Ag atoms.[119] One is octahedrally coordinated by the terminal oxygens of six $S(NSO)_2$ ligands, while the other is unsymmetrically coordinated by the nitrogen atoms of three $S(NSO)_2$ ligands. The *cis,trans*-geometry of the two SNSO units of the free ligand[120,121] is unchanged upon coordination and the mean S(II)—N and S(IV)–N bond lengths of 1.649(21) and 1.530(23) Å, respectively, indicate that the localization of single and double bonds is also retained.[119]



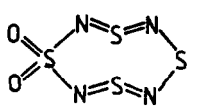
14

IV.3. S_3N_2O *and* $S_4N_4O_2$

The cyclic S–N oxides S_3N_2O (**15**) and $S_4N_4O_2$ (**16**) are obtained by the reaction of $S_3N_2Cl_2$ with formic acid or $SO_2(NH_2)_2$, respectively.[122] The former is a red liquid while the latter is an orange-yellow crystalline solid. In the octahedral complex $TiCl_4(S_3N_2O)_2$ coordination occurs through oxygen,[123] whereas in complexes with silver(I), $[Ag(S_3N_2O)_2][AsF_6]$[124] and $[Ag(S_4N_4O_2)_4][AsF_6]$,[125] the nitrogen atoms are bound to the metal. In the latter case all the coordinated nitrogen atoms are adjacent to the sulphur(VI) centre.



15



16

V. COMPLEXES OF SULPHUR IMIDES

The cyclic sulphur imides S_7NH, 1,3-, 1,4- and 1,5-$S_6(NH)_2$, 1,3,5- and 1,3,6-$S_5(NH)_3$, and $S_4N_4H_4$ are eight-membered rings derived formally from cyclo-S_8 by the replacement of one or more sulphur atoms by NH groups.[126] They differ fundamentally from the cyclic sulphur nitrides in that the nitrogen atoms are three-coordinate. These ring systems adopt a crown conformation, like cyclo-S_8, and the geometry about the nitrogen atoms in S_7NH[127] and $S_4N_4H_4$[128] is essentially planar suggesting that the lone pair of electrons on nitrogen is involved in π-bonding to neighbouring sulphur atoms. Consistent with this view the known coordination complexes of $S_4N_4H_4$ involve bonding to the metal via sulphur atoms. Transition-metal complexes of the other cyclic sulphur imides are unknown.

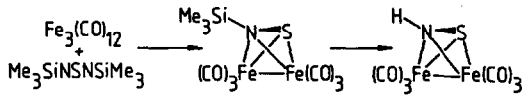
V.1. *Sulphur imide* (SNH)

SNH, the parent molecule of the unstable organic thionitroso compounds, is not known in the free state. *Ab initio* MO calculations suggest that the sulphur imide form (**17**) should be more stable than the thiazyl isomer (**18**).[129]



17 **18**

In 1984 Herberhold and Bühlmeyer[130] reported a complex in which HNS is stabilized by coordination as a six-electron ligand to two metal centres. The reaction of $Me_3SiNSNSiMe_3$ with $Fe_3(CO)_{12}$ in *n*-hexane at reflux gave $(Me_3SiNS)Fe_2(CO)_6$ (**19**) (51%), which was converted quantitatively to $(HNS)Fe_2(CO)_6$ (**20**) by chromatography on silica gel. Treatment of **20** with diazomethane yielded $(CH_3NS)Fe_2(CO)_6$ (92%), a member of a class of compounds, $(RNS)Fe_2(CO)_6$ (R = *t*-Bu, *p*-$CH_3C_6H_4$ or C_6H_5), that were discovered earlier.[131,132]

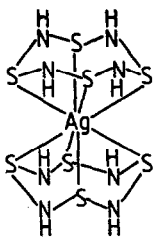


19 **20**

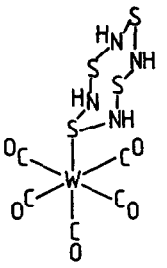
The mononuclear complexes $(RNS)Cr(CO)_5$ (R = Me_2N or Ph_2N), in which the ligand is bonded to the metal via sulphur, have been prepared and structurally characterized.[133,134]

V.2. *Tetrasulphur tetraimide* ($S_4N_4H_4$)

$S_4N_4H_4$ is easily made by reduction of S_4N_4 in benzene with methanolic $SnCl_2 \cdot 2H_2O$ at 80°C.[135] The coordination chemistry of $S_4N_4H_4$ is not well developed and only a few transition-metal derivatives have been described. A rather unstable silver(I) complex, $S_4N_4H_4 \cdot 2AgNO_3$, was reported by Meuwsen in 1931.[136] More recently adducts of $S_4N_4H_4$ with $AgClO_4$ in three different stoichiometries (2 : 1, 1 : 1 and 1 : 2) have been isolated.[137] The X-ray structure of $[Ag(S_4N_4H_4)_2][ClO_4] \cdot 1.5H_2O$ showed that the Ag atom is coordinated to all four sulphur atoms of two $S_4N_4H_4$ crowns in a sandwich-type structure (**21**).[138] The Ag atom is displaced sideways from the central position and the ligands are tilted with an angle of 20.4° between the two S_4 planes.



21



22

Organometallic derivatives of types $(S_4N_4H_4)M(CO)_5$ and μ-$(S_4N_4H_4)[M(CO)_5]_2$ (M = Cr or W) have been prepared by the reaction of $S_4N_4H_4$ with $(CO)_5M(THF)$:[139]

$$S_4N_4H_4 + 2(THF)M(CO)_5 \rightarrow (\mu\text{-}S_4N_4H_4)[M(CO)_5]_2 + 2THF.$$

An X-ray structural determination of $(S_4N_4H_4)W(CO)_5$ (**22**) showed that the monodentate $S_4N_4H_4$ is coordinated to the metal by a sulphur atom. Unlike the S_4N_4 adducts (Section II.3), coordination has little effect on the geometry or structural parameters of $S_4N_4H_4$. The crown conformation of the eight-membered ring is retained and the average S–N bond lengths [1.685(8) Å] and bond angles at sulphur [109.1(4)°] and nitrogen [120.9(4)°][12] are not substantially different from those reported for the free ligand [*d*(SN) = 1.665(1) Å; NSN = 109.3(1)°; SNS = 124.2(2)°].[128]

It should be mentioned that several compounds have been reported in which either two or

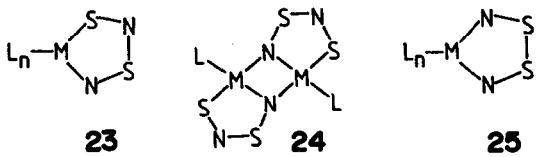
four hydrogen atoms of $S_4N_4H_4$ have been replaced by transition metals, e.g. $S_4N_4H_2(CuCl)_2$,[140] $S_4N_4H_2[Cu(NO_3)]_2$,[140] $Cu_4S_4N_4$,[140] $Ag_4S_4N_4$[140] and $Hg_4S_4N_4$.[141] However, it has not been established whether the S_4N_4 ring is retained in these complexes. It is conceivable that they are derivatives of the $[S_2N_2H]^-$ or $S_2N_2^{2-}$ anions, respectively (see Sections VI.1 and VI.2).

VI. CYCLOMETALLATHIAZENES AND RELATED COMPLEXES

A cyclometallathiazene is defined here as a ring system consisting only of sulphur and nitrogen, and one or more metal atoms.* As indicated in Table 10, cyclometallathiazenes can be formally considered as complexes between cationic-metal fragments and binary S–N anions in which both the sulphur and nitrogen atoms are two-coordinate.[142] With only two exceptions, S_3N^- [143,144] and SN_2^{2-},[145] these S–N anions have not been characterized as the free anion. Complexes of the hypothetical $[S_2N_2H]^-$ anion, which do not fall within this definition of cyclometallathiazenes, are also included in this section because of their close relationship to MS_2N_2 rings and historical importance (*vide infra*). The metals that are known to form a particular metallathiazene ring are also indicated in Table 10 together with the dates of the discovery and of the first X-ray structural determination for each system.

VI.1. MS_2N_2

The five-membered cyclometallathiazenes MS_2N_2 can be regarded as derivatives of the dianion of disulphur dinitride, $S_2N_2^{2-}$, for which simple salts are unknown. Several mononuclear MS_2N_2 rings (**23**) have been described, but the S_2N_2 unit can also be part of a binuclear structure (**24**). Very recently the first example of the isomeric heterocycle (**25**) has been reported (Section III.3).[104]



23 **24** **25**

VI.1.*A. Preparation.* With a few exceptions most rings of type **23** have been synthesized by the reaction of various metal complexes with S_4N_4. Indeed the first example of a cyclometallathiazene was of this type. In 1904 Ruff and Geisel[146] reported the reaction of S_4N_4 with PbI_2 in liquid ammonia and the isolation of green, crystalline $PbS_2N_2(NH_3)$. The coordinated NH_3 can be removed by heating at 80–90°C *in vacuo* to give red-brown, highly explosive PbS_2N_2.[140,147,148] Small amounts of crystalline PbS_2N_2 can also be obtained by the reaction of a mixture of $Pb(NO_3)_2$ and S_4N_4 in $CHCl_3$ suspension with NH_3.[149]

S_4N_4 is readily cleaved by complexes containing metals in low oxidation states to give MS_2N_2 rings. For example, the reaction of $CpCo(CO)_2$ or, preferably, CpCo(COD) with S_4N_4 in benzene produces $CpCoS_2N_2$ as black, air-stable crystals.[150,151] $(C_5Me_5)CoS_2N_2$ has been prepared from $(C_5Me_5)Co(CO)_2$ by a similar reaction:[151]

$$2CpCo(COD) + S_4N_4 \rightarrow 2CpCoS_2N_2 + 2COD.$$

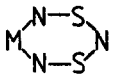
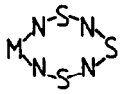
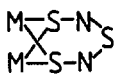
The mononuclear complex $(Ph_3P)_2PtS_2N_2$ is obtained on treatment of $(Ph_3P)_2Pt(C_2H_4)$ with S_4N_4 or $S(NSO)_2$:[152]

$$\left.\begin{array}{l}(Ph_3P)_2Pt(C_2H_4) + \tfrac{1}{2}S_4N_4 \\ (Ph_3P)_2Pt(C_2H_4) + S(NSO)_2\end{array}\right\} \xrightarrow{-SO_2} (Ph_3P)_2PtS_2N_2.$$

The cationic complex $[(Ph_2PCH{=}CHPPh_2)_2IrS_2N_2][BPh_4]\cdot 0.5Me_2CO$ was isolated in 60% yield from the reaction of $[(Ph_2PCH{=}CHPPh_2)_2Ir(CO)][BPh_4]$ with S_4N_4 in THF after recrystallization from acetone–*n*-Bu_2O.[153]

* See footnote on p. 1662.

Table 10. Metallathiazene ring systems and the corresponding S–N anions

Ring system[a]	Corresponding S–N anion[b]	Metal	Year of discovery (first X-ray structure)
	$S_2N_2^{2-}$	Co, Ir, Ni, Pd, Pt (Pb)	1982 (1982)
	$S_2N_2^{4-}$	Re	1984 (1984)
	$[S_2N_2H]^-$	Co, Ni, Pd, Pt	1953 (1958)
	$\boxed{S_3N^-}$	Co, Ni, Pd, Pt, Cu, Ag, Au	1958 (1966)
	$S_2N_3^{3-}$	V, Mo, W	1983 (1983)
	$S_3N_4^{2-}$	Ti	1983 (1983)
	$S_4N_3^-$	Pt	1981 (1981)
	$\boxed{SN_2^{2-}}$	Hg	1904 (1984)
	$S_3N_2^{2-}$	Pd	1966 (1982)

[a] The rings are represented as structural frameworks showing those atoms which are bonded to each other on the basis of X-ray structural data, since it is unlikely that valence bond structures give an adequate description of the bonding in these π-electron-rich systems.

[b] Only the species in boxes are known as the free anions.

It seems reasonable to conclude that the formation of mononuclear MS_2N_2 rings from low-valent metal complexes involves initial coordination of S_4N_4 to the metal centre, which promotes cleavage of S_4N_4 to S_2N_2 (Section II.2), followed by oxidative addition to the metal.

An anionic nickel complex containing two $S_2N_2^{2-}$ chelate ligands has been prepared by a different approach. $Ni(S_2N_2H)_2$ is deprotonated by KOH in methanol to give red $K_2[Ni(S_2N_2)_2]$.[154] Monoanions of $Ni(S_2N_2H)_2$, which also contain an $S_2N_2^{2-}$ ligand, will be discussed in Section VI.2.C.

Recently a number of complexes have been reported in which one of the metal-bonded nitrogens of each MS_2N_2 ring is also coordinated to a second metal centre to give a dimer (**24**). An anionic complex of this type, $K_2[(NiS_2N_2)_2(CN)_2]$, which is readily converted to the crystalline Ph_4As^+ salt, was prepared from $Ni(S_2N_2H)_2$ and KCN in MeOH in the presence of $KHCO_3$.[155] The mononuclear complex $K[(CN)_2NiS_2N_2H]$ is obtained in the absence of $KHCO_3$.

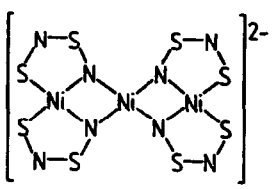
Neutral dinuclear MS_2N_2 complexes have been described for Ni, Pd and Pt. Treatment of $[(Ph_3P)_2Ni(C_3Ph_3)][ClO_4]$ with S_4N_4 in CH_2Cl_2 gives red-brown $[(Ph_3P)NiS_2N_2]_2$ (**24**) (M = Ni, L = Ph_3P) in low yield.[156] The analogous palladium complex is obtained in 50% yield from

$(Ph_3P)_2Pd(C_2H_4)$ and S_4N_4:[156]

$$2(Ph_3P)_2Pd(C_2H_4)+S_4N_4 \rightarrow [(Ph_3P)PdS_2N_2]_2+2Ph_3P+C_2H_4.$$

The products isolated from the platinum(0)–S_4N_4 system are dependent on reaction conditions. As indicated above, the yellow mononuclear complex $(Ph_3P)_2PtS_2N_2$ is formed from $(Ph_3P)_2Pt(C_2H_4)$ and S_4N_4 in a 2:1 molar ratio in CH_2Cl_2–ether.[152] When the reaction is carried out in THF or benzene using a 1:1 molar ratio, the red-brown dinuclear complex $[(Ph_3P)PtS_2N_2]_2$ (**24**) (M = Pt, L = Ph_3P) and a yellow complex, tentatively identified as $(Ph_3P)_3(PtS_2N_2)_2 \cdot C_6H_6$, were obtained.[156] By contrast, two poorly characterized compounds formulated as $(Ph_3P)_2PtS_2N_2$ and $(Ph_3P)_2Pt(S_4N_4)$ were obtained from the reaction of $(Ph_3P)_4Pt$ and S_4N_4 in benzene.[69*] It is well known, however, that $(Ph_3P)_4Pt$ dissociates to give free Ph_3P in solution and the reaction of Ph_3P with S_4N_4 in benzene produces the red compound $Ph_3P{=}N{-}S_3N_3$.[157] The formation of the latter compound as one of the products of the $(Ph_3P)_4Pt$–S_4N_4 reaction has been confirmed recently.[158]

An interesting trinuclear anion containing MS_2N_2 units (**26**) was described by Weiss in 1984. $Ni(S_2N_2H)_2$ reacts with $NiCl_2 \cdot 6H_2O$ in methanol in the presence of Ph_4POH to give crystalline $[Ph_4P]_2[Ni_3(S_2N_2)_4]$.[159]



26

VI.1.*B. Structural studies.* The structures of four transition-metal complexes of the $S_2N_2^{2-}$ ion have been determined by X-ray crystallography. The bond lengths and bond angles for these cyclometallathiazenes are compared in Table 11 with the corresponding data for PbS_2N_2 and $PbS_2N_2(NH_3)$, the latter being more reliable. Although the uncertainties are large for several of these structures, the S–N bond lengths exhibit similar trends with the exception of $(Ph_3P)_2PtS_2N_2$. The S(1)–N(1) distances (1.65–1.78 Å) are significantly longer than the S(2)–N(1) (1.56–1.58 Å) and S(2)–N(2) bond lengths (1.51–1.55 Å) indicating a localization of π-bonding within the thiazene unit. The former distance approximates to a single bond whereas the latter two are close to double-bond values.

VI.2. MS_2N_2H

Complexes of the hypothetical $[S_2N_2H]^-$ anion represent the largest and best characterized group of S–N ring systems containing a transition metal. The preeminent example is $Ni(S_2N_2H)_2$, which was discovered in 1953 by Goehring and Debo.[15] The reaction of $Ni(CO)_4$ with S_4N_4 produced an amorphous black material which, on extraction with organic solvents, yielded a soluble purple complex formulated as $Ni(NS)_4$, "nickel tetrathionitrosyl".[15,16] Subsequently, Piper[13,14] demonstrated the presence of N–H in this complex by IR and ^1H NMR spectroscopy. Chemical evidence was also consistent with the existence of an acidic proton.[13,14,160]

VI.2.*A. Preparation.* Complexes of the type $M(S_2N_2H)_2$ are known for Co, Ni, Pd and Pt. All four compounds are usually prepared from S_4N_4 and the anhydrous metal chlorides, but there are differences in the experimental details especially for the Pt derivative and some improvements in the established procedures have been reported recently.[161] $Ni(S_2N_2H)_2$ is readily obtained in 50–70% yields from the reaction of S_4N_4 with anhydrous $NiCl_2$ in methanol.[19,161,162] The hydrated salt, $NiCl_2 \cdot 6H_2O$, has also been used for this synthesis, but no yields were given.[163] In a similar manner $Co(S_2N_2H)_2$[15,19,160,161] and $Pd(S_2N_2H)_2$[161] are prepared in 23 and 26% yields, respectively, from $CoCl_2$

* The formulation $(Ph_3P)_2PtS_2N_2$ is based on analytical data (C, H, N and S) which are well outside of the normally acceptable limits for satisfactory analyses.

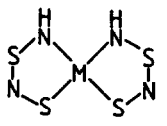
Table 11. X-ray structural data for MS_2N_2 rings

Bond distance (Å)	M = Pb[a]	M = Pb(NH$_3$)[a]	M = Co(C$_5$H$_5$)[b]	M = Pt(PPh$_3$)$_2$[c]	M–L = Ni–CN$^-$[d]	M–L = Pt(PPh$_3$)[e]
M–S(1)	2.71(1)	2.715(2)	2.066(1)	2.287(6)	2.07	2.225(13)
S(1)–N(1)	1.69(4)	1.717(7)	1.650(4)	1.54(2)	1.78	1.66(4)
N(1)–S(2)	1.56(4)	1.557(4)	1.579(4)	1.69(2)	1.58	1.58(4)
S(2)–N(2)	1.43(4)	1.508(7)	1.548(3)	1.45(2)	1.54	1.51(3)
M–N(2)	2.36(4)	2.295(4)	1.816(3)	2.14(2)	1.83	1.98(4)
Bond angle (°)						
M–S(1)–N(1)	102(1)	102.4(2)	107.6	108.2(7)	105	103.7(14)
S(1)–N(1)–S(2)	123(2)	119.2(4)	111.1	115(1)	110	117.6(24)
N(1)–S(2)–N(2)	115(2)	120.1(4)	112.7	118(1)	116	111.9(21)
S(2)–N(2)–M	125(2)	120.5(4)	117.8	114(1)	116	119.4(23)
N(2)–M–S(1)	74(1)	77.7(2)	90.9(1)	85.7(5)	93	87.3(11)

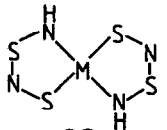
[a] Reference 149.
[b] Reference 150.
[c] Reference 152.
[d] Reference 155.
[e] Reference 156.

or $PdCl_2$ and S_4N_4 in methanol. The preparation of $Pt(S_2N_2H)_2$ from $PtCl_2$ and S_4N_4 was found to be unreliable because of the varying quality of commercial $PtCl_2$.[161] It was first prepared from H_2PtCl_6 and S_4N_4 in aqueous DMF,[164,165] but the most convenient synthesis involves the reaction of Na_2PtCl_6 with S_4N_4 in boiling methanol in the presence of $Na_2S_2O_4$. This method produces blue, crystalline $Pt(S_2N_2H)_2$ in 15% yield. The $M(S_2N_2H)_2$ complexes are usually isolated by preparative TLC or column chromatography on silica gel in order to separate them from the by-products $M(S_2N_2H)(S_3N)$ and $M(S_3N)_2$ (Section VI.3).

VI.2.*B. Structural and spectroscopic studies.* The structures of $Ni(S_2N_2H)_2$ (α-[166] and β-[163] modifications), $Pd(S_2N_2H)_2$[166] and $Pt(S_2N_2H)_2$[167,168] have been determined by X-ray crystallography. The MS_2N_2H units are planar and the hydrogen atom is bonded to the nitrogen atom that is coordinated to the metal. Two structural isomers, *cis* (**27**), and *trans* (**28**), are possible for $M(S_2N_2H)_2$ but only the *cis*-configuration has been found. The greater stability of the *cis* isomers is consistent with CNDO MO calculations for $Ni(S_2N_2H)_2$ and $Pd(S_2N_2H)_2$.[169]



27



28

Calculations of atomic-charge densities in $Ni(S_2N_2H)_2$ indicate that the nitrogen attached to Ni has a lower negative charge than the other nitrogen atom while the sulphur attached to the metal is less positively charged than the other sulphur. This prediction is in agreement with the core binding energies for $Ni(S_2N_2H)_2$ determined by X-ray photoelectron spectra.[170,171] For the palladium complex, however, there is a disagreement between the calculated and experimental charge densities.[169,172]

The mass spectra of $M(S_2N_2H)_2$ (M = Co, Ni, Pd or Pt) show the parent molecular ions, thus confirming the $M(S_2N_2H)_2$ stoichiometry. The predominant fragmentation pattern is the successive loss of SN units.[173]

An ESR spectrum has been obtained for $Co(S_2N_2H)_2$ and detailed studies have revealed the presence of a spin equilibrium between high- ($S = \frac{3}{2}$) and low-spin ($S = \frac{1}{2}$) cobalt(II).[161]

^1H and ^{13}C NMR spectra have been reported for a number of tricyclic derivatives of $Ni(S_2N_2H)_2$ in which the hydrogen atoms have been substituted by bridging organic groups.[174]

The near- and far-IR and Raman spectra of $M(S_2N_2H)_2$ (M = Co, Ni, Pd or Pt),[161,173,175,176] $Ni(S_2N_2H)(S_2N_2CH_3)$[176] and *trans*-$Ni(S_2N_2CH_3)_2$[176,177] have been studied in detail. Isotope shift data for $Co(S_2N_2D)_2$,[176] $Ni(S_2N_2D)_2$,[176,177] $^{62}Ni(S_2N_2H)_2$[177] and $^{62}Ni(S_2N_2CH_3)_2$[177] have been obtained to aid in the vibrational assignments.

The electronic spectra of $M(S_2N_2H)_2$ (M = Co, Ni, Pd or Pt) have been measured and the absorption maxima were found to be independent of solvent.[161] The high extinction coefficients suggest that the observed transitions arise from ligand-localized electrons. On the basis of studies of the resonance Raman spectrum of $Ni(S_2N_2H)_2$, the absorption maximum at 570 nm was assigned to a metal-to-ligand charge-transfer transition.[178] It should be noted that CNDO calculations for the free ligand $[S_2N_2H]^-$ indicate the presence of low-lying π^*-orbitals on the ligand.[161]

VI.2.*C. Reactions.* The $M(S_2N_2H)_2$ complexes undergo a variety of reactions that are largely dependent on the reactivity of the NH protons. These reactions are conveniently divided into three types: (a) deprotonation, (b) substitution of imide protons, and (c) displacement of $[S_2N_2H]^-$. Since $Ni(S_2N_2H)_2$ is more readily available in large quantities than the Co, Pd or Pt derivatives, most of the reactions have been carried out with the Ni complex. Only four derivatives of $Co(S_2N_2H)_2$ are known and no reactions of $Pd(S_2N_2H)_2$ or $Pt(S_2N_2H)_2$ have been reported.

(a) *Deprotonation*

The NH protons in $Ni(S_2N_2H)_2$ are acidic and can be determined quantitatively by titration with MeMgI.[160] Piper determined the pK_1 value to be 10.9 by titration of $Ni(S_2N_2H)_2$ with NaOH in ethanol–water (2:1).[13] The first crystalline products of deprotonation were described recently by Weiss.[154] Double deprotonation occurs with KOH in methanol to give the red salt $K_2[Ni(S_2N_2)_2]$ (Section VI.1). Crystalline brown salts of the monoanion $[Ni(S_2N_2H)(S_2N_2)]^-$ are obtained when

$Ni(S_2N_2H)_2$ is deprotonated with R_4NOH (R = Me, Et or *n*-Bu) or Ph_4EOH (E = P or As).[154] Protonation of the mono- or dianions regenerates $Ni(S_2N_2H)_2$:

$$Ni(S_2N_2H)_2 + OH^- \rightarrow [Ni(S_2N_2H)(S_2N_2)]^- + H_2O,$$

$$Ni(S_2N_2H)_2 + 2OH^- \rightarrow [Ni(S_2N_2)_2]^{2-} + 2H_2O.$$

The X-ray crystal structure of $[Ph_4As][Ni(S_2N_2H)(S_2N_2)]$ has been determined.[154] The structural parameters are very similar to those of the parent molecule $Ni(S_2N_2H)_2$.[163,166]

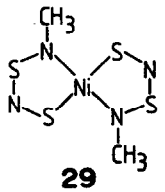
$Ni(S_2N_2H)_2$ also reacts with methyl-lithium[179,180] or silver nitrate,[179,181] to give uncharacterized lithium and silver salts of the anions $[Ni(S_2N_2H)(S_2N_2)]^-$ and $[Ni(S_2N_2)]^{2-}$, which have been used in substitution reactions (*vide infra*).

(b) *Substitution of imide protons*

The NH protons in $Ni(S_2N_2H)_2$ are readily substituted by organic groups and more than 30 derivatives have been synthesized. In addition to mono- and disubstitution products there are a number of tricyclic compounds in which both hydrogen atoms are replaced by a bridging organic group. These are all listed in Table 12, which also indicates those derivatives for which X-ray structural data are available.

Both $Ni(S_2N_2H)_2$ and $Co(S_2N_2H)_2$ can be deuterated by treatment with a large excess of D_2O in THF. The products, $Ni(S_2N_2D)_2$[175,176] and $Co(S_2N_2D)_2$[176] have been used in studies of the vibrational spectra of these complexes.

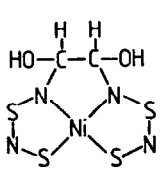
The simple alkyl derivatives $Ni(S_2N_2H)(S_2N_2CH_3)$, $Ni(S_2N_2H)(S_2N_2C_2H_5)$ and $Ni(S_2N_2CH_3)_2$ have been prepared by the reaction of an intermediate silver salt, formulated as "$(Ni(S_2N_2Ag)_2$", with the appropriate alkyl iodide.[180] The dimethyl derivative, $Ni(S_2N_2CH_3)_2$, is also obtained by treatment of $Ni(S_2N_2H)_2$ with KOH and methyl iodide in THF[177] and deserves special mention because it is the only structurally characterized $M(S_2N_2R)_2$ derivative with a *trans*-configuration (**29**).[180]



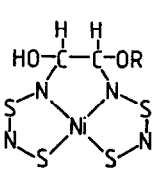
29

Both mono- and dibenzoyl derivatives, as well as small amounts of $Ni(S_2N_2C_6H_5)(S_2N_2H)$, are obtained on addition of benzoyl chloride to "$Ni(S_2N_2Li)_2$".[181] $Ni(S_2N_2C(O)NHC_6H_5)(S_2N_2H)$ has been synthesized from $Ni(S_2N_2H)_2$ and C_6H_5NCO and characterized by an X-ray structure analysis.[182] Two different monosubstitution products have been isolated from $Ni(S_2N_2H)_2$ and formaldehyde. In acetone solution $Ni(S_2N_2CH_2OH)(S_2N_2H)$ is formed.[183] When the reaction is carried out in methanol one solvent molecule is incorporated to give $Ni(S_2N_2CH_2OCH_3)(S_2N_2H)$, which has been characterized by X-ray diffraction.[184]

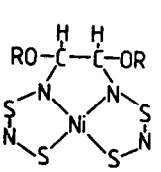
The largest group of $Ni(S_2N_2H)_2$ derivatives are tricyclic compounds in which the NH protons are replaced by a bridging group. The additional ring can have five, six or seven members. The tricyclic complexes **30**, **31** and **32** are obtained from $Ni(S_2N_2H)_2$ and glyoxal under various conditions (**31** and **32** are formed in the presence of alcohols).[174,183,185,186] The Co analogue of **30** has also been reported.[183] During chromatography on alumina the complexes **31** eliminate water to give **33**.



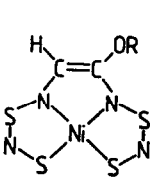
30



31 **a** R=CH_3 **b** R=C_2H_5

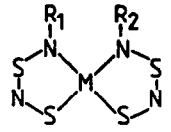
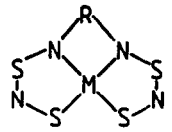


32 **a** R=CH_3 **b** R=C_2H_5

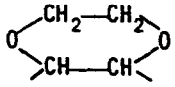


33 **a** R=CH_3 **b** R=C_2H_5

Table 12. Derivatives of $M(S_2N_2H)_2$ (M = Ni or Co)

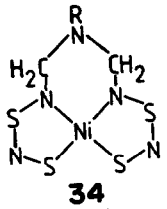



M	R_1	R_1	Reference	X-ray structure
Ni	H	H	13, 14, 15, 19, 160–163, 166, 170–173, 175, 176, 178	163, 164
	H	CH_3	14, 176, 180	
	H	C_2H_5	180	
	H	CH_2OH	183	
	H	CH_2OCH_3	183, 184	184
	H	C_6H_5	181	
	H	$C(O)—C_6H_5$	181	
	H	$C(O)—NHC_6H_5$	182	182
	D	D	175, 176	
	CH_3	CH_3 (*trans*)	14, 176, 177, 180	180
	$Si(CH_3)_3$	$Si(CH_3)_3$	170	
	$C(O)—C_6H_5$	$C(O)—C_6H_5$	181	
^{62}Ni	H	H	175	
	CH_3	CH_3 (*trans*)	177	
Co	H	H	16, 19, 160, 161, 172, 173, 175, 176	166
	D	D	176	
Pd	H	H	19, 160, 161, 164, 172, 173, 175, 176	
Pt	H	H	160, 161, 164, 165, 167, 168, 172, 175, 176	167, 168

M	R	Reference	X-ray structure
Ni	$—CH_2—N(CH_3)—CH_2—$	183, 187, 190	
	$—CH_2—N(C_2H_5)—CH_2—$	174, 183	
	$—CH_2—N(CH_2C_6H_5)—CH_2—$	183	
	$—CH_2—N(CH_2OCH_3)—CH_2—$	188, 189	
	$—CH(CH_3)—NH—CH(CH_3)—$	174, 183	
	—CH(OH)—CH(OH)—	174, 183, 185	
	$—C(OH)CH_3—CH(OH)—$	170	
	$—CH(OH)—CH(OCH_3)—$	185	
	$—CH(OH)—CH(OC_2H_5)—$	185	
	$—CH(OCH_3)—CH(OCH_3)—$ (*rac*)	174, 185, 186	
	$—CH(OCH_3)—CH(OCH_3)—$ (*meso*)	174, 185, 186	
	$—CH(OC_2H_5)—CH(OC_2H_5)—$ (*rac*)	185, 186	
	$—CH(OC_2H_5)—CH(OC_2H_5)—$ (*meso*)	185, 186	
	$—CH=C(OCH_3)—$	174, 185, 186	188
	$—CH=C(OC_2H_5—$	185, 186	
		185	
	$—Si(CH_3)_2—O—Si(CH_3)_2—$	191, 192	
	$—Si(CH_3)_2—NH—Si(CH_3)_2—$	192	
	$—Si(CH_3)_2—N(CH_3)—Si(CH_3)_2—$	191, 192	
	$—Si(CH_3)_2—N(C_2H_5)—Si(CH_3)_2—$	192, 193	195
	$—Si(CH_3)_2—N(CH_3)—N(CH_3)—Si(CH_3)_2—$	192	
Co	—CH(OH)—CH(OH)—	183	
	$—CH_2—N(CH_2OCH_3)—CH_2—$	189	191
	$—Si(CH_3)_2—O—Si(CH_3)_2—$	192, 193	195

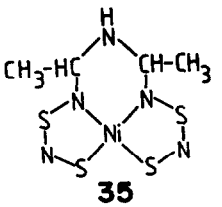
As a result of the two chiral carbons in the bridging group, the complexes **30–32** have diastereomers, which have been separated into their *meso* and *racemic* forms by chromatography on silica gel in the case of **32a**[174,185] and **32b**.[185]

Tricyclic compounds with a nitrogen-containing bridge (**34**) have been prepared by the condensation reaction of $Ni(S_2N_2H)_2$ with formaldehyde in the presence of primary amines[174,183,187–190] or methanol and ammonia [**34d** (R = CH_3OCH_2)].[188,189] Complex **35** is obtained similarly from $Ni(S_2N_2H)_2$ and acetaldehyde in the presence of ammonia.



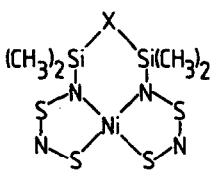
34

a R=CH_3
b R=C_2H_5
c R=$CH_2C_6H_5$
d R=CH_2OCH_3



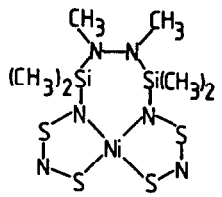
35

Finally, several tricyclic complexes with a silicon-containing bridging group have been reported.[191,192] Derivatives of type **36** are obtained by the reaction of $M(S_2N_2H)_2$ (M = Co or Ni) with 1,3-dichlorodisiloxanes or 1,3-dichlorodisilazanes in THF. Compound **37** was prepared similarly from $Ni(S_2N_2H)_2$ and 1,2-bis(chlorodimethylsilyl)dimethyl-hydrazine.



36

a M=Ni, X=O
b M=Ni, X=NH
c M=Ni, X=NCH_3
d M=Ni, X=NC_2H_5
e M=Co, X=O



37

(c) *Displacement of* $[S_2N_2H]^-$

There are a few examples of reactions in which the $[S_2N_2H]^-$ ligand is displaced from the metal site. A complex formulated as $(en)_2NiS_2N_2H$ has been obtained from the reaction of $Ni(S_2N_2H)_2$ with ethylenediamine (en) in acetone.[194] The monomeric nature of this complex is questionable in view of its insolubility in organic solvents. The anion $[(CN)_2NiS_2N_2H]^-$, prepared by treatment of $Ni(S_2N_2H)_2$ with KCN in methanol,[155] has been structurally characterized by X-ray crystallography.[195] It was first synthesized from $K_4[Ni_2(CN)_6]$ and S_4N_4 in methanol.[196]

Recently it was found that $Ni(S_2N_2H)_2$ can be a useful precursor for the synthesis of cyclic S–N compounds. The reaction of $Ni(S_2N_2H)_2$ with S_2Cl_2 affords S_4N_2 in 57% yield:[197]

$$Ni(S_2N_2H)_2 + S_2Cl_2 \xrightarrow[Et_3N]{THF} S_4N_2.$$

Similarly, $COCl_2$ and $SOCl_2$ react with $Ni(S_2N_2H)_2$ to give the five-membered ring systems S_2N_2CO and S_3N_2O, respectively.[197]

VI.3. MS_3N

Transition-metal complexes containing the five-membered MS_3N ring are an important and rapidly growing class of cyclometallathiazenes. With the exception of **25** they differ from the other ring systems discussed in this section in the presence of an S–S bond.

VI.3.*A. Preparation.* There are three approaches available for the systhesis of MS_3N derivatives.

(a) *Reactions of* S_4N_4 *with metal halides (or metal carbonyls) in methanol*

This method is not very satisfactory but it is of historical significance. The MS_3N ring system was first discovered in 1958 by Piper,[14] who isolated $Ni(S_2N_2H)(S_3N)$ and $Ni(S_3N)_2$, in addition to

the known complex $Ni(S_2N_2H)_2$ (Section VI.2), by chromatographic separation of the mixture obtained when S_4N_4 reacts with anhydrous $NiCl_2$ in methanol. The yield of $Ni(S_3N)_2$ from 10 g of S_4N_4 was 0.009 g (0.04% based on S)! Subsequently it was found that all preparations of $M(S_2N_2H)_2$ (M = Co, Ni, Pd or Pt) produce small amounts of $M(S_2N_2H)(S_3N)$ and $M(S_3N)_2$.[161,165,198] The following complexes have been isolated from the appropriate reaction mixtures by chromatography on silica gel: $Co(S_2N_2H)(S_3N)$,[165,198] $Co(S_3N)_2$,[165,198] $Pd(S_2N_2H)(S_3N)$,[165] $Pd(S_3N)_2$,[165,198] $Pt(S_2N_2H)(S_3N)$,[161,165] and $Pt(S_3N)_2$.[161,165] Although some improvements in the preparative procedures have been reported,[165] the yields are generally very low.

The unsymmetrical complexes $M(S_2N_2H)(S_3N)$ have been shown to disproportionate on contact with silica or alumina or on heating.[165,198] This disproportionation reaction has been used to prepare pure samples of $M(S_3N)_2$ (M = Co[198] or Pt[165]) that are not accessible by other routes:

$$2M(S_2N_2H)(S_3N) \rightarrow M(S_2N_2H)_2 + M(S_3N)_2.$$

The complex $(NO)_2CoS_3N$ was obtained in 12% yield on treatment of the insoluble black material obtained from the reaction of $Co_2(CO)_8$ and S_4N_4 with nitric oxide.[20]

(b) *Reactions of* S_3N^- *with metal halides*

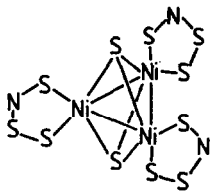
Crystalline salts of the S_3N^- anion are readily prepared by treatment of $[PPN][S_4N]$[199] or $[Ph_4As][S_4N]$[200] with triphenylphosphine in acetonitrile.[143,144] The metathetical reaction of this anion with metal halides represents the most direct synthesis of the MS_3N system, but this approach is frequently thwarted by competing redox reactions.[144] The reaction of $[PPN][S_3N]$ with $NiBr_2$ in acetonitrile does, however, produce $Ni(S_3N)_2$ in 30% yield, and smaller amounts of $Co(S_3N)_2$ have been obtained by this route.[144] The surprising feature of these reactions is that complexes of the $[S_2N_2H]^-$ anion are also formed as minor products.

Salts of the S_3N^- anion have been used for the synthesis of the first MS_3N rings containing copper or silver.[201] The reaction of $[PPN][S_3N]$ with CuCl in acetonitrile gives good yields of either $[PPN][ClCuS_3N]$ or $[PPN][Cu(S_3N)_2]$, depending on the stoichiometry. The corresponding Ag complex $[PPN][Ag(S_3N)_2]$ was prepared from $AgNO_3$ in a similar manner. Treatment of the anion $[ClCuS_3N]^-$ with triphenylphosphine gives the neutral complex $(Ph_3P)_2CuS_3N$ in 81% yield.[201] The same complexes are obtained when $[PPN][S_4N]$ is used instead of $[PPN][S_3N]$:[202]

$$[PPN][S_3N] + CuCl \rightarrow [PPN][ClCuS_3N] \xrightarrow{2Ph_3P} (Ph_3P)_2CuS_3N + PPNCl.$$

(c) *Reactions of* S_7NH *with metal halides in the presence of a base*

In view of the ready avilability of S_7NH (from the reaction of sodium azide with sulphur in HMPA),[203] this approach potentially provides the easiest access to the MS_3N ring system. It can be regarded as the *in situ* generation of S_4N^-, since this anion is produced on deprotonation of S_7NH with a base.[204] The first application of this method was reported by Weiss in 1982.[205] The trigonal–bipyramidal-cluster anion $[(NiS_3N)_3S_2]^-$ (**38**) was obtained from the reaction of S_7NH with $NiCl_2 \cdot 6H_2O$ in methanol in the presence of KOH. It was isolated and structurally characterized (X-ray) as the black *n*-Bu_4N^+ salt. When $Ni(CN)_2$ was used instead of $NiCl_2$ for this reaction, $K[(CN)_2NiS_3N]$ was isolated in addition to **38**.[206] The crystalline salt $[Me_4N][(CN)_2NiS_3N]$ was also prepared directly from $Ni(CN)_2$, S_7NH and Me_4NCl in methanol in the presence of aqueous ammonia.[206]



38

Simple syntheses of $[Ph_4As][ClCuS_3N]$ and $[Ph_4As][Cu(S_3N)_2]$ from S_7NH and $CuCl_2 \cdot 2H_2O$ in the presence of Ph_4AsOH have also been reported.[206] A trigonally coordinated copper complex, $(Ph_3PS)CuS_3N$, was isolated in low yield from the reaction of $(Ph_3P)CuCl$ with S_7NH in methylene chloride (without a base).[207] Finally the gold complex, Cl_2AuS_3N has been prepared in 21% yield by treatment of S_7NH with *n*-BuLi in the presence of $HAuCl_4$ in diethyl ether.[208]

VI.3.*B. Structural studies.* The structures of five MS_3N and two $M(S_3N)_2$ ring systems have been determined by X-ray crystallography and the pertinent bond lengths and bond angles are summarized in Table 13. The bidentate S_3N^- ligand is always bonded to the metal via two sulphur atoms. The MS_3N ring exhibits unequal S–N bond lengths. In most cases the S(1)–N distance is substantially longer than S(2)–N, but the opposite effect is observed for $(Ph_3P)_2CuS_3N$ and $[PPN][Cu(S_3N)_2]$.[201] The reversal of this trend in the latter complex is particularly puzzling since the more usual order, d[S(1)–N] > d[S(2)–N], was found for the Ph_4As^+ salt of the same anion.[206] The S–S bond distances fall within the range 1.95–2.06 Å.

VI.4. MS_2N_3

The discovery of complexes containing the six-membered MS_2N_3 ring is one of the most recent and significant developments in transition-metal S–N chemistry. The first example, polymeric $[Cl_2VS_2N_3]_n$, was reported in 1983 by Roesky *et al.*[51] and it has quickly become apparent that the MS_2N_3 system represents an important class of cyclometallathiazenes.

VI.4.*A. Preparation.* Six different methods have been used to prepare the MS_2N_3 ring and examples of each of these are discussed below and summarized in the following reaction scheme.

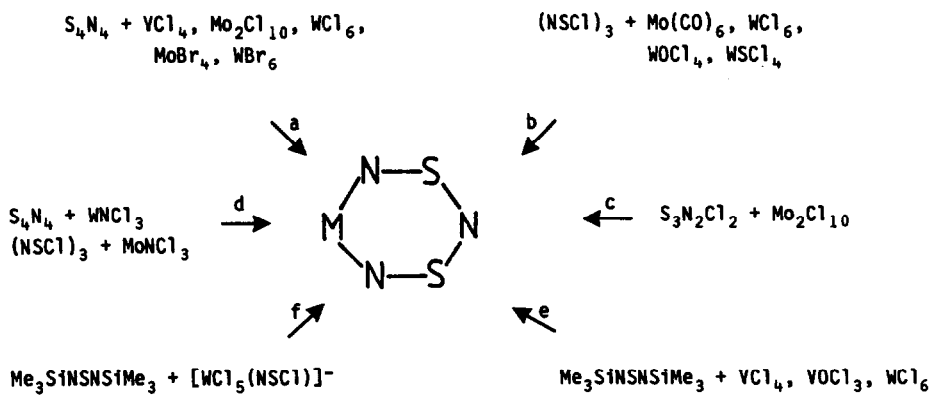
(a) *Reactions of* S_4N_4 *with transition-metal halides*

As indicated in previous sections, the reactions of S_4N_4 with transition-metal halides can give rise to a variety of S–N complexes including simple adducts (Section II.3), complexes of S_2N_2 (Section II.2) or cyclometallathiazenes (Sections VI.2, VI.3, VI.6 and VI.8). In certain cases, the MS_2N_3 ring system is formed as the major product.

A black, crystalline polymer $[Cl_2VS_2N_3]_n$ is obtained by heating the crude product from the reaction of VCl_4 with S_4N_4 at 110°C *in vacuo*.[51] The dark brown, microcrystalline dimers $[Cl_3MS_2N_3]_2$ (M = Mo or W) have been synthesized similarly from Mo_2Cl_{10} or WCl_6 and S_4N_4 in methylene dichloride.[210] The anionic complex $[PPN][Cl_4WS_2N_3]$ can be prepared from WCl_6 and S_4N_4 in the presence of PPNCl.[211]

(b) *Reactions of metal carbonyls or halides with* $(NSCl)_3$

The reaction of a metal carbonyl with $(NSCl)_3$ was first described by Wynne and Jolly in 1968.[17] Treatment of $Mo(CO)_6$ with $(NSCl)_3$ in CH_2Cl_2 yielded a dark brown, microcrystalline solid, formulated as $MoS_3N_3Cl_3$ on the basis of chemical analyses. Similar reactions with $Cr(CO)_6$ or

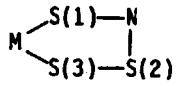


Scheme 1. Synthetic routes to the MS_2N_2 ring system (adapated from Ref. 210).

Table 13. X-ray structural data for MS_3N rings[a]

Bond length (Å)	MS_3N					$M(S_3N)_2$		
	M = $Co(NO)_2$	M = $[Ni(CN)_2]^-$	M = $CuCl^-$	M = $Cu(Ph_3PS)$	M = $Cu(PPh_3)_2$	M = Pd	M = Cu^{-b}	M = Cu^{-c}
M–S(1)	2.248(2)	2.131(4)	2.174(3)	2.191(3)		2.26 (2.25)	2.251(1) [2.255(2)]	2.290(2) [2.291(2)]
S(1)–N	1.629(5)	1.651(11)	1.666(8)	1.655(5)	1.541(13)	1.69 (1.65)	1.647(5) [1.614(5)]	1.512(11) [1.590(9)]
N–S(2)	1.553(5)	1.534(17)	1.599(7)	1.489(6)	1.593(12)	1.48 (1.58)	1.530(5) [1.570(5)]	1.652(9) [1.567(9)]
S(2)–S(3)	2.002(2)	2.020(4)	1.947(4)	2.007(3)	2.058(4)	1.96 (1.93)	1.961(2) [1.956(2)]	2.060(3) [2.044(4)]
S(3)–M	2.264(2)	2.134(6)	2.217(2)	2.200(3)	2.304(2)	2.29 (2.26)	2.362(2) [(2.317(2)]	2.291(2) [2.290(2)]
Bond angle (°)								
M–S(1)–N	109.0(2)	109.5(5)	105.5(3)	103.7(2)	107.9(5)	106.6 (108.2)	107.1(2) [107.3(2)]	111.1(3) [108.0(3)]
S(1)–N–S(2)	124.8(3)	122.3(5)	121.3(3)	125.5(3)	124.9(8)	126.1 (123.4)	125.2(3) [124.6(3)]	121.8(8) [122.1(6)]
N–S(2)–S(3)	110.9(2)	110.1(3)	115.8(3)	114.7(2)	114.9(5)	112.4 (111.9)	115.1(2) [114.1(2)]	114.6(4) [116.2(4)]
S(2)–S(3)–M	103.54(8)	103.1(3)	98.7(1)	97.8(1)	97.4(1)	103.1 (104.9)	99.8(1) [100.6(1)]	98.1(1) [98.0(1)]
S(3)–M–S(1)	91.80(5)	95.1(2)	98.6(1)	98.4(1)	94.90(8)	91.3 (91.5)	92.8(1) [93.1(1)]	94.28(6)
Reference	20	205	206	207	201	209	206	201

[a] Atomic-numbering scheme:



[b] In $[Ph_4As][Cu(S_3N)_2]$.
[c] In $[PPN][Cu(S_3N)_2]$.

$W(CO)_6$ were reported to give non-stoichiometric products.[17] A recent reinvestigation of these reactions revealed that "$MoS_3N_3Cl_3$" is in fact $[Cl_3MoS_2N_3]_2$.[210] This complex and the W analogue can be isolated in good yields from the reactions of $M(CO)_6$ (M = Mo or W) with $(NSCl)_3$. It appears, however, that the outcome of metal carbonyl–$(NSCl)_3$ reactions depends on subtle variations of experimental details since Dehnicke and co-workers obtained $(\mu\text{-}S_2N_2)[Cl_3MS_2N_3]_2$ (M = Mo or W) from the corresponding metal carbonyls and $(NSCl)_3$ under slightly different conditions.[212] The bromo derivatives $(\mu\text{-}S_2N_2)[Br_3MS_2N_3]_2$ have been prepared from $MoBr_4$ or WBr_6 and S_4N_4.[212]

A quantitative yield of $[Cl_3WS_2N_3]_2$ is obtained when $WOCl_4$ or $WSCl_4$ is allowed to react with $(NSCl)_3$ in CH_2Cl_2.[213] The reaction of $(NSCl)_3$ with excess $VOCl_3$ at 130°C in the absence of a solvent provides an improved synthesis of $[Cl_2VS_2N_3]_n$ in almost quantitative yield.[214] When $(NSCl)_3$ is present in excess, however, a thiazyl chloride adduct of $Cl_2VS_2N_3$ is obtained. This complex has been assigned a dimeric structure on the basis of IR spectroscopic data:[214]

$$VOCl_3 + \tfrac{4}{3}(NSCl)_3 \xrightarrow{CH_2Cl_2} \tfrac{1}{2}[Cl_2VS_2N_3(NSCl)]_2 + SOCl_2 + Cl_2.$$

(c) *Reactions of transition-metal halides with* $S_3N_2Cl_2$

Only one example of the preparation of an MS_2N_3 ring from $S_3N_2Cl_2$ has been reported. When Mo_2Cl_{10} is heated with $S_3N_2Cl_2$ in CH_2Cl_2 a low yield of $[Cl_3MoS_2N_3]_2$ is obtained.[210] In contrast, the analogous reaction of WCl_6 with $S_3N_2Cl_2$ yields $[WCl_4(NSCl)]_2$ (Section III.3.A).

(d) *Reactions of nitrido complexes with* S_4N_4 *or* $(NSCl)_3$

Transition-metal nitrido complexes have been used in two syntheses of MS_2N_3 rings. A quantitative yield of $[Cl_3MoS_2N_3]_2$ is obtained when $MoNCl_3$ is treated with $(NSCl)_3$ in CCl_4.[213] Although $MoNCl_3$ does not react with S_4N_4, the preparation of $[Cl_3WS_2N_3]_2$ from $WNCl_3$ and S_4N_4 in CH_2Cl_2 has been reported.[210] The formation of the WS_2N_3 ring in this reaction can be viewed as the cycloaddition of $WNCl_3$ with S_2N_2 (generated as an intermediate by cleavage of S_4N_4).[210]

(e) *Reactions of transition-metal halides with* $Me_3SiNSNSiMe_3$

Bis(trimethylsilyl)sulphur diimide ($Me_3SiNSNSiMe_3$) is a convenient reagent for the synthesis of certain MS_2N_3 rings from the appropriate transition-metal halide.[210] The reaction of WCl_6 with $Me_3SiNSNSiMe_3$ yields $[Cl_3WS_2N_3]_2$ as the major product, identified by conversion to the anion $[Cl_4WS_2N_3]^-$ by treatment with Ph_4AsCl (*vide infra*). Under identical conditions, Mo_2Cl_{10} gives $MoNCl_3$ and only a trace of $[Cl_3MoS_2N_3]_2$. The polymer $[Cl_2VS_2N_3]_n$ is obtained from $Me_3SiNSNSiMe_3$ and VCl_4 or $VOCl_3$ in CH_2Cl_2.[210]

(f) *Cyclization of transition-metal halide–*NSCl *complexes with* $Me_3SiNSNSiMe_3$

The cyclization of complexes of the type $MCl_x(NSCl)$ by treatment with $Me_3SiNSNSiMe_3$ potentially represents a controlled synthesis of the MS_2N_3 ring. One example, the reaction of $[Ph_4As][WCl_5(NSCl)]$ with $Me_3SiNSNSiMe_3$ in CH_2Cl_2 to give $[Ph_4As][Cl_4WS_2N_3]$ in 51% yield, has been reported.[210]

The known cyclometallathiazenes of type MS_2N_3 and the methods used in their preparation are summarized in Table 14.

VI.4.*B. Structural and spectroscopic studies.* The X-ray crystal structures of three monomeric (**39**) and two dimeric MS_2N_3 systems (**40** and **41**) have been reported. The structural data are compared with those of the related heterocycle $Ph_2PS_2N_3$ in Table 15. The thiazene segment of the ring in the three mononuclear complexes and in $[Cl_2VS_2N_3]_n$, like that in $Ph_2PS_2N_3$,[216] is planar while the metal atom is tilted out of the plane. The VS_2N_3 ring in $[Ph_4As]_2[\{VS_2N_3(N_3)_3\}_2] \cdot CH_2Cl_2$ is entirely planar.[214] The endocyclic bond angles at the metal in the MS_2N_3 are in the range 93–96° reflecting the octahedral geometry at the metal centre, whereas the bond angle at the approximately tetrahedral phosphorus atom in $Ph_2PS_2N_3$ is 115.8(2) Å. Consequently, the angles at the metal-bonded nitrogens in MS_2N_3 (129–141°) are substantially larger than the corresponding bond angles

Table 14. Preparative methods for MS_2N_3 rings

MS_2N_3 complex[a]	Method[b]	Reference
$[Cl_2VS_2N_3]_n$	a, b, e	51, 214
$[Cl_2VS_2N_3(NSCl)]_2$	b	214
$[Cl_3MoS_2N_3]_2$	a, b, c, d	210, 213
$(\mu\text{-}S_2N_2)[Cl_3MoS_2N_3]_2$	b	212
$[Cl_3WS_2N_3]_2$	a, b, d, e	210, 213
$[Ph_4As][Cl_4WS_2N_3]$	f	210, 213
$[PPN][Cl_4WS_2N_3]$	a	211
$(\mu\text{-}S_2N_2)[Cl_3WS_2N_3]_2$	b	212
$(\mu\text{-}S_2N_2)[Br_3MoS_2N_3]_2$	a	212
$(\mu\text{-}S_2N_2)[Br_3WS_2N_3]_2$	a	212

[a] Complexes obtained by the reactions of certain MS_2N_3 systems with Cl^- or MeCN are discussed in Section VI.4.C.

[b] See Section VI.4.A for description of methods a–f.

(120–121°) in $Ph_2PS_2N_3$. Nevertheless, the average S–N bond distance (1.58–1.59 Å) is similar to that in $Ph_2PS_2N_3$ [d(S–N) = 1.575 Å] for all MS_2N_3 systems and the bond angles at the unique nitrogen (125–129°) are uniformly larger than the bond angles at sulphur (108–118°). Calculations of the π-charge density in the model compound $H_2PS_2N_3$ suggest that the internal salt model $[H_2P]^+[S_2N_3]^-$ is a useful approximate description. However, NMR studies (^{51}V or ^{95}Mo) and magnetic susceptibility measurements of MS_2N_3 systems indicate oxidation states of +5 for V and +6 for Mo and W.[210] Thus these cyclometallathiazenes should be regarded as complexes of the hypothetical trianion $S_2N_3^{3-}$.

The IR spectra of MS_2N_3 complexes have been discussed elsewhere in detail.[210,213,214] This information has been used to deduce a dimeric structure for $[Cl_2VS_2N_3(NSCl)]_2$ {**40** [M = V(NSCl), X = Cl]},[214] and different dimeric structures [**40** (MX = $MoCl_3$, X = Cl) and **41** (M = WCl_3)], for $[Cl_3MS_2N_3]_2$.

VI.4.*C. Reactions.* A characteristic reaction of the cyclometallathiazenes $Cl_xMS_2N_3$ is the addition of chloride ions to give anionic complexes, which are frequently more tractable than their neutral precursors. Both mononuclear and dinuclear anionic complexes have been prepared in this way:[210,213,214]

$$[Cl_3MS_2N_3]_2 + 2Ph_4ECl \xrightarrow{CHCl_3} 2[Ph_4E][Cl_4MS_2N_3],$$

where M = Mo or W, and E = P or As.

$$\frac{2}{n}[Cl_2VS_2N_3]_n + 2Ph_4AsCl \rightarrow [Ph_4As]_2[(Cl_3VS_2N_3)_2].$$

On the basis of IR data the anion $[(Cl_3VS_2N_3)_2]^{2-}$ was assigned a nitrogen-bridged dimeric structure [**41** (M = VCl_3^-)], analogous to the structurally characterized azido complex {**41** [M = $V(N_3)_3]^-$}, which is obtained by treatment of $[Ph_4As]_2[(Cl_3VS_2N_3)_2]$ with a slurry of silver azide in CH_2Cl_2. The black, crystalline azido complex is not shock-sensitive, but explodes on heating.

The dimers $[Cl_2MS_2N_3]_2$ (M = Mo or W) also reacts with acetonitrile to give crystalline, monomeric adducts of type $Cl_3MS_2N_3(CH_3CN)$.[210,215]

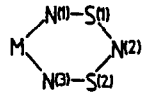
VI.5. MS_3N_4

The only example of the eight-membered MS_3N_4 ring system, in which one sulphur atom of S_4N_4 is replaced by a transition metal, was isolated from the following reaction in 16% yield (after chromatography) by Oakley *et al.* in 1983:[217]

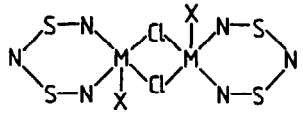
$$Cp_2Ti(CO)_2 + S_4N_4 \xrightarrow{THF} Cp_2TiS_3N_4.$$

Table 15. X-ray structural data for MS_2N_3 rings

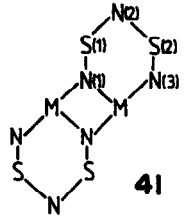
Bond length (Å)	39				40	41
	M = $MoCl_4^-$	M = WCl_4^-	M = $WCl_3(CH_3CN)$	M = PPh_2	M = V, X = Cl	M = $[V(N_3)_3]^-$
M–N(1)	1.807(11)	1.82(1)	1.827(14)	1.621(4)	1.841(3)	1.89(1)
N(1)–S(1)	1.581(14)	1.59(1)	1.585(15)	1.560(3)	1.580(3)	1.57(1)
S(1)–N(2)	1.597(13)	1.61(2)	1.571(17)	1.580(4)	1.578(3)	1.57(1)
N(2)–S(2)	1.605(14)	1.59(2)	1.590(17)	1.583(5)	1.606(3)	1.65(1)
S(2)–N(3)	1.548(14)	1.54(1)	1.575(16)	1.575(3)	1.585(3)	1.57(2)
N(3)–M	1.865(11)	1.88(1)	1.820(15)	1.625(3)	1.714(3)	1.72(1)
Bond angle (°)						
M–N(1)–S(1)		137.7(9)		121.3(2)	130.3(2)	129.4(5)
N(1)–S(1)–N(2)		111.4(8)		116.9(2)	115.3(1)	117.6(7)
S(1)–N(2)–S(2)		128.6(9)		124.6(3)	128.6(2)	125.5(11)
N(2)–S(2)–N(3)		113.1(8)		116.3(2)	108.1(2)	111.4(7)
S(2)–N(3)–M		136.1(8)		120.3(2)	140.9(2)	132.0(6)
N(3)–M–N(1)	92.6(5)	93.0(6)	94.7(7)	115.8(2)	96.3(1)	
Reference	215	213	215	216	51	214



39



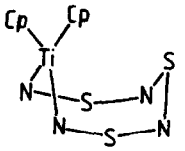
40



41

This synthesis can be viewed as an oxidative-addition reaction of a low-valent, early-transition-metal complex to give a titanium(IV) complex of the acyclic $S_3N_4^{2-}$ anion. The latter species is unknown as the free anion but the trimethylsilyl derivative, $Me_3SiNSNSNSNSiMe_3$, has been prepared.[218]

The cyclometallathiazene $Cp_2TiS_3N_4$ (**42**) is structurally related to $S_4N_4O_2$.[219] Both eight-membered rings adopt a boat conformation that is less puckered in $Cp_2TiS_3N_4$ than in $S_4N_4O_2$. The variations in S–N bond lengths suggest a somewhat different electronic structure in the two rings.[217]



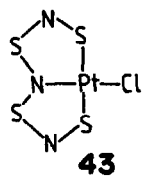
42

VI.6. MS_4N_3

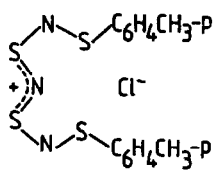
The only representative of the MS_4N_3 ring system, $ClPtS_4N_3$ (**43**), was prepared in 1981 in 10% yield by the following reaction:[220]

$$cis\text{-}PtCl_2(NCC_6H_5)_2 + S_4N_4 \xrightarrow[\text{reflux}]{\text{toluene}} ClPtS_4N_3.$$

The MS_4N_3 ring is formally derived from the hypothetical $S_4N_3^-$ ion, which is coordinated to platinum as a tridentate ligand via the two terminal sulphur atoms and the central nitrogen atom (**43**). A very similar geometry was found for the S_4N_3 unit in 1,7-di-*p*-tolyltetrasulphurtrinitrogen chloride (**44**).[221] The $ClPtS_4N_3$ molecule is planar and forms stacks along the *a* axis, but there are no significant interactions between neighbouring molecules.



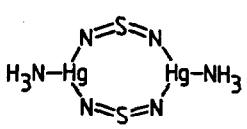
43



44

VI.7. $M_2S_2N_4$

In 1904 the reaction of HgI_2 with S_4N_4 in liquid ammonia was reported to give a yellow, crystalline product of empirical formula $HgN_2S \cdot NH_3$.[146] Eighty years later Weiss and Martan[222] showed that this product is in fact a mercury(II) derivative of the SN_2^{2-} anion, which has recently been characterized as its potassium salt, K_2SN_2.[145] The molecule consists of a planar eight-membered ring in which two Hg atoms are bridged by —NSN— units (**45**). Each Hg atom is bonded to an NH_3 ligand, and the nitrogen atoms of these ligands lie on opposite sides of the molecular plane. In addition, each Hg atom is linked to a nitrogen atom of an adjacent ring to give a two-dimensional network. The Hg–Hg distance of 3.106 Å is slightly longer than that in α-Hg.

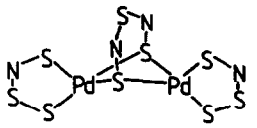


45

There are no transition-metal analogues of this ring system, but the recently described *cis*-$Pt(NSNSiMe_3)_2(PPh_3)_2$[223] could prove to be a useful precursor for the synthesis of such bimetallic cyclometallathiazenes.

VI.8. $M_2S_3N_2$

The reactions of transition-metal halides with S_4N_4 in methanol usually produce $M(S_2N_2H)(S_3N)$ and $M(S_3N)_2$ (M = Co, Ni, Pd or Pt) as minor products in addition to $M(S_2N_2H)_2$ (Section VI.2.A). In the case of Pd, Weiss and Thewalt[198] reported the formation of a red product formulated as "PdS_4N_2". The same product was also observed by other workers in the reaction of $PdCl_2$ with S_4N_4,[161] but it was not characterized further until an X-ray structural analysis in 1982 revealed it to have the composition $(S_3N)_2Pd_2S_3N_2$ (**46**).[224]



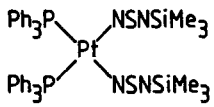
46

This molecule consists of two PdS_3N rings bridged by the two terminal sulphur atoms of a planar S_3N_2 unit. The coordination around the Pd atoms is approximately square planar, but the small PdSPd angles [77.1(1)°] and the Pd–Pd distance of 2.921(2) Å (cf. 2.751 Å in metallic Pd) indicate a significant Pd–Pd interaction.

No other complexes of the hypothetical $S_3N_2^{2-}$ ion have been described.

VI.9. *Related complexes*

The reaction of $(Ph_3P)_2Pt(C_2H_4)$ with $Me_3SiNSNSiMe_3$ in benzene produces the square planar complex *cis*-$Pt(NSNSiMe_3)_2(PPh_3)_2$ (**47**) in 44% yield.[223]



47

In view of the well-known reactivity of Si–N linkages towards metal halides, this complex offers obvious potential for the synthesis of novel cyclometallathiazenes.

Finally, it should be mentioned that a brown crystalline product formulated as $NiSN_3[P(OPh)_3]_2 \cdot 2H_2O$ (on the basis of analytical data) was isolated from the reaction of $Ni[P(OPh)_3]_4$ with S_4N_4 in benzene.[225] This compound is not well-characterized and awaits structural conformation. It is considered formally to be a Ni(II) complex of the hypothetical SN_3^{2-} ion,[225] and, as such, it would represent the only example of a cyclometallathiazene derived from a *paramagnetic*, binary S–N anion (Table 10).

VII. SUMMARY AND FUTURE PROSPECTS

Although considerable progress has been made in the synthesis and structural determination of transition-metal complexes of inorganic S–N ligands, particularly in the last 5 years, the subject is still at an early stage of development. A large number of complexes have been structurally characterized, but little is known about their electronic structures or chemical reactivity. A change in the emphasis of investigations from the synthesis of novel systems with unusual structures towards an understanding of the unique properties which S–N ligands confer on metal sites could advance the topic from the status of "chemical curiosities" to the forefront of coordination chemistry. The current interest in the role of coordination complexes of sulphur ligands in certain areas of bioinorganic chemistry and heterogeneous catalysis provides an incentive for such studies. The following avenues of investigation are likely to be fruitful in achieving a more prominent role for cyclometallathiazenes: (a) MO calculations of electronic structures; (b) electrochemical studies of redox behaviour; (c) investigation of reactivity towards electrophiles, nucleophiles and unsaturated substrates; and (d) preparation and catalytic activity of heterobimetallic or metal cluster complexes

containing S–N ligands. The directed synthesis of transition-metal–S–N polymers with interesting solid-state properties is another exciting possibility.

Acknowledgement—The financial support of the Natural Sciences and Engineering Research Council of Canada is gratefully acknowleged.

REFERENCES

1. O. C. M. Davis, *J. Chem. Soc.* 1906, **89**, 1575.
2. H. Wölbling, *Z. Anorg. Allg. Chem.* 1908, **57**, 286.
3. J. Weiss, *Fortschr. Chem. Forsch.* 1966, **5**, 635.
4. T. Chivers, *Chem. Rev.* 1985, **85**, 341.
5. W. Gregory, *J. Pharm.* 1835, **21**, 315; *ibid.* 1835, **22**, 301.
6. H. W. Roesky and K. K. Pandey, *Adv. Inorg. Chem. Radiochem.* 1982, **26**, 337; see also, M. Herberhold, *Nachr. Chem. Tech.* 1981, **29**, 365.
7. M. B. Hursthouse, N. P. C. Walker, C. P. Warrens and J. D. Woollins, *J. Chem. Soc., Dalton Trans.* 1985, 1043.
8. K. K. Pandey, S. Datta and U. C. Agarwala, *Z. Anorg. Allg. Chem.* 1980, **468**, 228.
9. K. K. Pandey and U. C. Agarwala, *Inorg. Chem.* 1981, **20**, 1308.
10. K. K. Pandey, U. C. Agarwala and K. C. Jain, *Inorg. Chim. Acta* 1981, **48**, 23.
11. J. Anhaus, Z. A. Siddiqi, H. W. Roesky, J. W. Bats and Y. Elerman, *Z. Naturforsch.* 1985, **40B**, 740.
12. M. Goehring, *Q. Rev., Chem. Soc.* 1956, **10**, 437.
13. T. S. Piper, *Chem. Ind.* 1957, 1101.
14. T. S. Piper, *J. Am. Chem. Soc.* 1958, **80**, 30.
15. M. Goehring and A. Debo, *Z. Anorg. Allg. Chem.* 1953, **273**, 319.
16. K.-W. Daum, M. Goehring and J. Weiss, *Z. Anorg. Allg. Chem.* 1955, **278**, 260.
17. K. J. Wynne and W. L. Jolly, *J. Inorg. Nucl. Chem.* 1968, **30**, 2851.
18. D. A. Brown and F. Frimmel, *Chem. Commun.* 1971, 579.
19. M. Goehring, K.-W. Daum and J. Weiss, *Z. Naturforsch.* 1955, **10B**, 298.
20. M. Herberhold, L. Haumaier and U. Schubert, *Inorg. Chim. Acta* 1981, **49**, 21.
21. J. Chatt and J. R. Dilworth, *J. Chem. Soc., Chem. Commun.* 1974, 508.
22. P. C. Bevan, J. Chatt, J. R. Dilworth, R. A. Henderson and G. J. Leigh, *J. Chem. Soc., Dalton Trans.* 1982, 821.
23. M. W. Bishop, J. Chatt and J. R. Dilworth, *J. Chem. Soc., Chem. Commun.* 1975, 780.
24. M. W. Bishop, J. Chatt and J. R. Dilworth, *J. Chem. Soc., Dalton Trans.* 1979, 1.
25. L. Kaden, B. Lorenz, R. Kirmse, J. Stach and U. Abram, *Z. Chem.* 1985, **25**, 29.
26. M. Herberhold and L. Haumaier, *Z. Naturforsch.* 1980, **35B**, 1277.
27. G. Hartmann and R. Mews, *Angew. Chem.* 1985, **97**, 218; *Angew. Chem., Int. Ed. Engl.* 1985, **24**, 202.
28. B. W. S. Kolthammer and P. Legzdins, *J. Am. Chem. Soc.* 1978, **100**, 2247.
29. T. J. Greenhough, B. W. S. Kolthammer, P. Legzdins and J. Trotter, *J. Chem. Soc., Chem. Commun.* 1978, 1036; T. J. Greenhough, B. W. S. Kolthammer, P. Legzdins and J. Trotter, *Inorg. Chem.* 1979, **18**, 3548.
30. W. A. Herrmann, J. Rohrmann, H. Nöth, C. K. Nanila, I. Bernal and M. Draux, *J. Organomet. Chem.* 1985, **284**, 189.
31. D. L. Lichtenberger and J. L. Hubbard, *Inorg. Chem.* 1984, **23**, 2718.
32. R. Mews and C. Liu, *Angew. Chem.* 1983, **95**, 156; *Angew. Chem., Int. Ed. Engl.* 1983, **22**, 158.
33. R. Weber, U. Müller and K. Dehnicke, *Z. Anorg. Allg. Chem.* 1983, **504**, 13.
34. K. N. Udupa, K. C. Jain, M. I. Khan and U. C. Agarwala, *Inorg. Chim. Acta* 1983, **74**, 191.
35. J. W. Bats, K. K. Pandey and H. W. Roesky, *J. Chem. Soc., Dalton Trans.* 1981, 2081.
36. K. K. Pandey, H. W. Roesky, M. Noltemeyer and G. M. Sheldrick, *Z. Naturforsch.* 1984, **39B**, 590.
37. R. Weber and K. Dehnicke, *Z. Naturforsch.* 1984, **39B**, 262.
38. M. B. Hursthouse and M. J. Motevalli, *J. Chem. Soc., Dalton Trans.* 1979, 1362.
39. H. W. Roesky, K. K. Pandey, W. Clegg, M. Noltemeyer and G. M. Sheldrick, *J. Chem. Soc., Dalton Trans.* 1984, 719.
40 M. Minelli, J. L. Hubbard, D. L. Lichtenberger and J. H. Enemark, *Inorg. Chem.* 1984, **29**, 2721.
41. J. L. Hubbard and D. L. Lichtenberger, *Inorg. Chem.* 1980, **19**, 1388.
42. C. M. Mikulski, P. J. Russo, M. S. Saran, A. G. MacDiarmid, A. F. Garito and A. J. Heeger, *J. Am. Chem. Soc.* 1975, **97**, 6358.
43. A. J. Banister and Z. V. Hauptmann, *J. Chem. Soc., Dalton Trans.* 1980, 731.

44. T. Chivers, A. W. Cordes, R. T. Oakley and P. N. Swepston, *Inorg. Chem.* 1981, **20**, 2376.
45. H. W. Roesky and J. Anhaus, *Chem. Ber.* 1982, **115**, 3682.
46. M. M. Labes, P. Love and L. F. Nichols, *Chem. Rev.* 1979, **79**, 1.
47. U. Thewalt and B. Müller, *Z. Anorg. Allg. Chem.* 1980, **462**, 214.
48. H. W. Roesky, J. Anhaus and W. S. Sheldrick, *Inorg. Chem.* 1984, **23**, 75.
49. U. Thewalt and M. Burger, *Angew. Chem.* 1982, **94**, 646; *Angew. Chem., Int. Ed. Engl.* 1982, **21**, 634.
50. U. Thewalt and K. Holl, *Z. Naturforsch.* 1984, **39B**, 145.
51. H. W. Roesky, J. Anhaus, H. G. Schmidt, G. M. Sheldrick and M. Noltemeyer, *J. Chem. Soc., Dalton Trans.* 1983, 1207.
52. J. Eicher, P. Klingelhöfer, U. Müller and K. Dehnicke, *Z. Anorg. Allg. Chem.* 1984, **514**, 79.
53. J. Hanich, M. Krestel, U. Müller and K. Dehnicke, *Z. Anorg. Allg. Chem.* 1985, **522**, 92.
54. J. Hanich and K. Dehnicke, *Z. Naturforsch.* 1984, **39B**, 1467.
55. G. Beber, J. Hanich and K. Dehnicke, *Z. Naturforsch.* 1985, **40B**, 9.
56. U. Kynast, P. Klingelhöfer, U. Müller and K. Dehnicke, *Z. Anorg. Allg. Chem.* 1984, **515**, 61.
57. R. L. Patton and K. N. Raymond, *Inorg. Chem.* 1969, **8**, 2426.
58. G. G. Alange and A. J. Banister, *J. Inorg. Nucl. Chem.* 1978, **40**, 203.
59. D. Neubauer and J. Weiss, *Z. Anorg. Allg. Chem.* 1960, **303**, 28.
60. U. Thewalt, *Angew. Chem.* 1976, **88**, 807; *Angew. Chem., Int. Ed. Engl.* 1976, **15**, 765.
61. U. Thewalt and B. Müller, *Z. Anorg. Allg. Chem.* 1980, **462**, 221.
62. U. Thewalt and B. Müller, *Z. Naturforsch.* 1982, **37B**, 828.
63. U. Thewalt, *Z. Naturforsch*, 1980, **35B**, 855.
64. U. Thewalt, *Z. Anorg. Allg. Chem.* 1981, **476**, 105.
65. U. Thewalt and M. Burger, *Z. Naturforsch.* 1981, **36B**, 293.
66. U. Müller, E. Conradi, U. Demant and K. Dehnicke, *Angew. Chem.* 1984, **96**; *Angew. Chem., Int. Ed. Engl.* 1984, **23**, 237.
67. A. W. Cordes, C. G. Marcellus, M. C. Noble, R. T. Oakley and W. T. Pennington, *J. Am. Chem. Soc.* 1983, **105**, 6008.
68. B. J. McCormick and B. M. Anderson, *J. Inorg. Nucl. Chem.* 1970, **32**, 3414.
69. A. A. Bhattacharyya, J. A. McLean, Jr and A. G. Turner, *Inorg. Chim. Acta* 1979, **34**, L199.
70. U. Thewalt and G. Albrecht, *Z. Naturforsch.* 1982, **37B**, 1098.
71. M. G. B. Drew, D. H. Templeton and A. Zalkin, *Inorg. Chem.* 1967, **6**, 1906.
72. R. J. Gillespie, J. P. Kent and J. G. Sawyer, *Acta Cryst.* 1980, **36B**, 655.
73. C. G. Marcellus, R. T. Oakley, A. W. Cordes and W. T. Pennington, *Can. J. Chem.* 1984, **62**, 1822.
74. O. Glemser and R. Mews, *Angew. Chem.* 1980, **92**, 904; *Angew. Chem., Int. Ed. Engl.* 1980, **19**, 883.
75. W. H. Kirchoff and E. B. Wilson, Jr, *J. Am. Chem. Soc.* 1963, **85**, 1726.
76. B. Buss, P. G. Jones, R. Mews, M. Noltemeyer and G. M. Sheldrick, *Angew. Chem.* 1979, **91**, 253; *Angew. Chem., Int. Ed. Engl.* 1979, **18**, 231.
77. B. Buss, P. G. Jones, R. Mews, M. Noltemeyer and G. M. Sheldrick, *Acta Cryst.* 1980, **36B**, 141.
78. G. Hartmann, P. G. Jones, R. Mews and G. M. Sheldrick, *Z. Naturforsch.* 1980, **35B**, 1191.
79. R. Mews, *Angew. Chem.* 1975, **87**, 669; *Angew. Chem., Int. Ed. Engl.* 1975, **14**, 640.
80. G. Hartmann and R. Mews, *Z. Naturforsch.* 1985, **40B**, 343.
81. G. Hartmann, R. Mews and G. M. Sheldrick, *Angew. Chem.* 1983, **95**, 753; *Angew. Chem., Int. Ed. Engl.* 1983, **22**, 723.
82. R. Mews, *J. Chem. Soc., Chem. Commun.* 1979, 278.
83. B. Buss, W. Clegg, G. Hartmann, P. G. Jones, R. Mews, M. Noltemeyer and G. M. Sheldrick, *J. Chem. Soc., Dalton Trans.* 1981, 61.
84. W. Clegg, O. Glemser, K. Harms, G. Hartmann, R. Mews, M. Noltemeyer and G. M. Sheldrick, *Acta Cryst.* 1984, **37B**, 548.
85. F. M. Schnepel, R. Mews and O. Glemser, *J. Mol. Struct.* 1980, **60**, 89.
86. C. Zirz and R. Ahlrichs, *Inorg. Chem.* 1984, **23**, 26.
87. R. Mews and O. Glemser, *Angew. Chem.* 1975, **87**, 208; *Angew. Chem., Int. Ed. Engl.* 1975, **14**, 186.
88. H. W. Roesky, O. Glemser, A. Hoff and W. Koch, *Inorg. Nucl. Chem. Lett.* 1967, **3**, 39.
89. R. Eisenbarth and W. Sundermeyer, *Z. Naturforsch.* 1978, **33B**, 1194.
90. M. Feser, R. Höfer and O. Glemser, *Z. Naturforsch.* 1974, **29B**, 716.
91. R. Mews and O. Glemser, *J. Chem. Soc., Chem. Commun.* 1973, 823.
92. B. Buss, D. Altena, R. Mews and O. Glemser, *Angew. Chem.* 1978, **90**, 287; *Angew. Chem., Int. Ed. Engl.* 1978, **17**, 280.
93. B. Buss and D. Altena, *Z. Anorg. Allg. Chem.* 1978, **440**, 65.
94. U. Müller, W. Kafitz and K. Dehnicke, *Naturwissenschaften* 1982, **69**, 503.
95. R. C. Patton and W. L. Jolly, *Inorg. Chem.* 1970, **9**, 1079.
96. T. Beppu, E. Hirota and Y. Morino, *J. Mol. Spectrosc.* 1970, **36**, 386.

97. J. Hanich, P. Klingelhöfer, U. Müller and K. Dehnicke, *Z. Anorg. Allg. Chem.* 1983, **506**, 68.
98. U. Müller, W. Kafitz and K. Dehnicke, *Z. Anorg. Allg. Chem.* 1983, **501**, 69.
99. U. Kynast and K. Dehnicke, *Z. Anorg. Allg. Chem.* 1983, **502**, 29.
100. U. Kynast, U. Müller and K. Dehnicke, *Z. Anorg. Allg. Chem.* 1984, **508**, 26.
101. U. Müller, P. Klingelhöfer, U. Kynast and K. Dehnicke, *Z. Anorg. Allg. Chem.* 1985, **520**, 18.
102. R. Weber, U. Müller and K. Dehnicke, *Z. Anorg. Allg. Chem.* 1983, **504**, 13.
103. H..G. Hauck, P. Klingelhöfer, U. Müller and K. Dehnicke, *Z. Anorg. Allg. Chem.* 1984, **510**, 180.
104. W. Hiller, J. Mohyla, J. Strähle, H. G. Hauck and K. Dehnicke, *Z. Anorg. Allg. Chem.* 1984, **514**, 72.
105. D. A. Armitage and J. C. Brand, *J. Chem. Soc., Chem. Commun.* 1979, 1078.
106. R. D. Tiwari, K. K. Pandey and U. C. Agarwala, *Inorg. Chem.* 1982, **21**, 845.
107. H. W. Roesky, K. K. Pandey, B. Krebs and M. Dartmann, *J. Chem. Soc., Dalton Trans.* 1984, 2271.
108. H. W. Roesky, W. Schmieder, W. Isenberg, D. Bohler and G. M. Sheldrick, *Angew. Chem.* 1982, **94**, 143; *Angew. Chem., Int. Ed. Engl.* 1982, **21**, 153.
109. P. W. Schenk, *Ber. Dtsch. Chem. Ges.* 1942, **75**, 94.
110. P. O. Tchir and R. D. Spratley, *Can. J. Chem.* 1975, **53**, 2318.
111. A. G. Turner, *Inorg. Chim. Acta* 1984, **84**, 85.
112. A. A. Bhattacharyya, A. G. Turner, E. M. Holt and N. W. Alcock, *Inorg. Chim. Acta* 1980, **44**, L185.
113. E. M. Holt, N. W. Alcock, A. A. Bhattacharyya and A. G. Turner, *Inorg. Chim. Acta* 1981, **47**, 255.
114. W. H. Kirchoff, *J. Am. Chem. Soc.* 1969, **91**, 2437.
115. A. A. Bhattacharyya and A. G. Turner, *Inorg. Chim. Acta* 1981, **53**, L89.
116. G. Hartmann, R. Hoppenheit and R. Mews, *Inorg. Chim. Acta* 1981, **76**, L201.
117. K. Vrieze and G. van Koten, *J. R. Netherlands Chem. Soc.* 1980, **99**, 145.
118. D. A Armitage and A. W. Sinden, *Inorg. Chem.* 1972, **11**, 1151.
119. H. W. Roesky, M. Thomas, P. G. Jones, A. Pinkert and G. M. Sheldrick, *J. Chem. Soc., Dalton Trans.* 1983, 1211.
120. R. Steudel, J. Steidel and N. Rautenberg, *Z. Naturforsch.* 1980, **35B**, 792.
121. G. MacLean, J. Passmore, P. S. White, A. J. Banister and J. A. Durrant, *Can. J. Chem.* 1981, **59**, 187.
122. H. W. Roesky, W. Schaper, O. Petersen and T. Müller, *Chem. Ber.* 1977, **110**, 2695.
123. H. W. Roesky, M. Kuhn and J. W. Bats, *Chem. Ber.*1982, **115**, 3025.
124. H. W. Roesky, M. Thomas, J. Schimkowiak, M. Schmidt, M. Noltemeyer and G. M. Sheldrick, *J. Chem. Soc., Chem. Commun.* 1982, 790.
125. H. W. Roesky, M. Thomas, H. G. Schmidt, W. Clegg, M. Noltemeyer and G. M. Sheldrick, *J. Chem. Soc., Dalton Trans.* 1983, 405.
126. H. G. Heal, *The Inorganic Heterocyclic Chemistry of Sulphur, Nitrogen, and Phosphorus*, p. 17. Academic Press, London (1980).
127. H. J. Hecht, R. Reinhardt, R. Steudel and H. Bradaczek, *Z. Anorg. Allg. Chem.* 1976, **426**, 43.
128. S. N. Nabi, M. B. Hursthouse and K. M. A. Malik, *Acta Cryst.* 1977, **33B**, 2309.
129. M. P. S. Collins and B. J. Duke, *J. Chem. Soc., Dalton Trans.* 1978, 277.
130. M. Herberhold and W. Bühlmeyer, *Angew. Chem.* 1984, **96**, 64; *Angew. Chem., Int. Ed. Engl.* 1984, **23**, 80.
131. S. Otsuka, T. Yoshida and A. Nakamura, *Inorg. Chem.* 1968, **7**, 1833.
132. R. Meij, D. J. Stufkens, K. Vrieze, A. M. F. Brouwers, J. D. Schagen, J. J. Zwinselman, A. R. Overbeek and C. H. Stam, *J. Organomet. Chem.* 1979, **170**, 337.
133. H. W. Roesky, R. Emmert, W. Clegg, W. Isenberg and G. M. Sheldrick, *Angew. Chem.* 1981, **93**, 623; *Angew. Chem., Int. Ed. Engl.* 1981, **20**, 591.
134. H. W. Roesky, R. Emmert, W. Isenberg, M. Schmidt and G. M. Sheldrick, *J. Chem. Soc., Dalton Trans.* 1983 (1983).
135. G. Brauer, *Handbook of Preparative Inorganic Chemistry*, 2nd edn, Vol. 1, p. 411. Academic Press, New York (1963).
136. A. Meuwsen, *Ber. Dtsch. Chem. Ges.* 1931, **64**, 2301.
137. S. N. Nabi, *J. Chem. Soc., Dalton Trans.* 1977, 1152.
138. M. B. Hursthouse, K. M. A. Malik and S. N. Nabi, *J. Chem. Soc., Dalton Trans.* 1980, 355.
139. G. Schmid, R. Greese and R. Boese, *Z. Naturforsch.* 1982, **37B**, 620.
140. M. Goehring, J. Weiss and G. Zirker, *Z. Anorg. Allg. Chem.* 1955, **278**, 1.
141. M. Goehring and G. Zirker, *Z. Anorg. Allg. Chem.* 1956, **285**, 70.
142. T. Chivers and R. T. Oakley, *Top. Curr. Chem.* 1982, **102**, 117.
143. J. Bojes and T. Chivers, *J. Chem. Soc., Chem. Commun.* 1980, 1023.
144. J. Bojes, T. Chivers, W. G. Laidlaw and M. Trsic, *J. Am. Chem. Soc.* 1982, **104**, 4837.
145. M. Herberhold and W. Ehrenreich, *Angew. Chem.* 1982, **94**, 637; *Angew. Chem., Int. Ed. Engl.* 1982, **21**, 633.
146. O. Ruff and E. Geisel, *Ber. Dtsch. Chem. Ges.* 1904, **37**, 1573.

147. M. Goehring, *Q. Rev., Chem. Soc.* 1956, **10**, 437.
148. D. T. Haworth and G. Y. Lin, *J. Inorg. Nucl. Chem.* 1980, **42**, 137.
149. H. Martan and J. Weiss, *Z. Anorg. Allg. Chem.* 1984, **514**, 107 (and references cited therein).
150. F. Edelmann, *J. Organomet. Chem.* 1982, **228**, C47.
151. T. Albright, F. Edelmann and G. Granozzi, unpublished results.
152. R. Drews, U. Behrens and F. Edelmann, unpublished results.
153. F. Cecconi, C. A. Ghilardi, S. Midollini, S. Moneti and A. Orlandini, *J. Organomet. Chem.* 1984, **275**, C22.
154. J. Weiss, *Z. Anorg. Allg. Chem.* 1983, **502**, 165.
155. K. Hornemann and J. Weiss, *Angew. Chem.* 1982, **94**, 645; *Angew. Chem., Int. Ed. Engl.* 1982, **21**, 633.
156. C. A. Ghilardi, S. Midollini, S. Moneti and A. Orlandini, *J. Organomet. Chem.* 1985, **286**, 419.
157. J. Bojes, T. Chivers, A. W. Cordes, G. MacLean and R. T. Oakley, *Inorg. Chem.* 1981, **20**, 16.
158. F. Edelmann, unpublished results.
159. J. Weiss, *Angew. Chem.* 1984, **96**, 232; *Angew. Chem., Int. Ed. Engl.* 1984, **23**, 225.
160. J. Weiss and M. Becke-Goehring, *Z. Naturforsch.* 1958, **13B**, 198.
161. J. D. Woollins, R. Grinter, M. K. Johnson and A. J. Thomson, *J. Chem. Soc., Dalton Trans.* 1980, 1911.
162. D. T. Haworth, J. D. Brown and Y. Chen, *Inorg. Synth.* 1978, **18**, 124.
163. K. F. Mayer and J. Weiss, *Acta Cryst.* 1978, **34B**, 1999.
164. E. Fluck, M. Goehring and J. Weiss, *Z. Anorg. Allg. Chem.* 1956, **287**, 51.
165. D. T. Haworth and G. Y. Lin, *J. Inorg. Nucl. Chem.* 1977, **39**, 1838.
166. J. Weiss and U. Thewalt, *Z. Anorg. Allg. Chem.* 1968, **363**, 159.
167. I. Lindquist and J. Weiss, *J. Inorg. Nucl. Chem.* 1958, **6**, 184.
168. I. Lindquist and R. Rosenstein, *J. Inorg. Nucl. Chem.* 1959, **7**, 421.
169. S. Millefiori, A. Millefiori and G. Granozzi, *Inorg. Chim. Acta* 1981, **48**, 233.
170. M. Bossa, C. Furlani, G. Mattogno and E. Paparazzo, *Inorg. Chim. Acta* 1978, **27**, L117.
171. R. Szargan, *Z. Chem.* 1982, **22**, 86.
172. R. Grinter and J. D. Woollins, *Inorg. Chim. Acta* 1980, **39**, 193.
173. I. S. Butler and T. Sawai, *Can. J. Chem.* 1977, **55**, 3838.
174. G. Y. Lin and D. T. Haworth, *J. Inorg. Nucl. Chem.* 1980, **42**, 1253.
175. D. T. Haworth, G. Y. Lin, J. D. Brown and Y. Chen, *Spectrochim. Acta* 1978, **34A**, 371.
176. D. B. Powell and J. D. Woollins, *Spectrochim. Acta* 1980, **36A**, 447.
177. D. T. Haworth and G. Y. Lin, *Spectrosc. Lett.* 1979, **12**, 451.
178. R. Czernuszewicz, G. Y. Lin, D. T. Haworth and K. Nakamoto, *Inorg. Chim. Acta* 1980, **44**, L167.
179. M. Becke-Goehring and E. Fluck, In *Developments in Inorganic Nitrogen Chemistry* (Edited by C. B. Colburn), Vol. 1, p. 150. Elsevier, Amsterdam (1966).
180. J. Weiss and M. Ziegler, *Z. Anorg. Allg. Chem.* 1963, **322**, 184.
181. J. Weiss and U. Thewalt, *Z. Naturforsch.* 1965, **20B**, 491.
182. J. Weiss and U. Thewalt, *Z. Anorg. Allg. Chem.* 1966, **343**, 274.
183. U. Thewalt and J. Weiss, *Z. Anorg. Allg. Chem.* 1966, **348**, 238.
184. U. Thewalt, *Z. Anorg. Allg. Chem.* 1979, **451**, 123.
185. U. Thewalt and J. Weiss, *Z. Anorg. Allg. Chem.* 1967, **352**, 225.
186. U. Thewalt and J. Weiss, *Z. Naturforsch.* 1968, **23B**, 1265.
187. U. Thewalt, *Z. Anorg. Allg. Chem.* 1969, **371**, 338.
188. U. Thewalt and C. E. Bugg, *Chem. Ber.* 1972, **105**, 1614.
189. U. Thewalt, *Z. Naturforsch.* 1974, **29B**, 308.
190. U. Thewalt, *Z. Anorg. Allg. Chem.* 1970, **374**, 259.
191. U. Wannagat and M. Schlingmann, *Chem.-Ztg* 1973, **97**, 447.
192. U. Wannagat and M. Schlingmann, *Z. Anorg. Allg. Chem.* 1974, **406**, 312.
193. U. Thewalt and M. Schlingmann, *Z. Anorg. Allg. Chem.* 1974, **406**, 319.
194. J. Weiss, *Z. Naturforsch.* 1957, **12B**, 480.
195. J. Weiss, *Acta Cryst.* 1978, **34B**, 1997.
196. J. Weiss, *Z. Naturforsch.* 1957, **12B**, 481.
197. A. Heitmann and F. Edelmann, *Z. Naturforsch.* 1983, **38B**, 521.
198. J. Weiss and U. Thewalt, *Z. Anorg. Allg. Chem.* 1966, **346**, 234.
199. T. Chivers, W. G. Laidlaw, R. T. Oakley and M. Trsic, *J. Am. Chem. Soc.* 1980, **102**, 5773.
200. N. Burford, T. Chivers, A.. W. Cordes, R. T. Oakley, W. Pennington and P. N. Swepston, *Inorg. Chem.* 1981, **20**, 4430.
201. J. Bojes, T. Chivers and P. W. Codding, *J. Chem. Soc., Chem. Commun.* 1981, 1171.
202. J. Bojes and T. Chivers, unpublished results.
203. J. Bojes, T. Chivers and I. Drummond, *Inorg. Synth.* 1978, **18**, 203.
204. T. Chivers and I. Drummond, *Inorg. Chem.* 1974, **13**, 1222.

205. J. Weiss, *Angew. Chem.* 1982, **94**, 719; *Angew Chem., Int. Ed. Engl.* 1982, **21**, 705.
206. J. Weiss, *Z. Anorg. Allg Chem.* 1985, **521**, 44.
207. H. W. Roesky, K. K. Pandey, M. Noltemeyer and G. M. Sheldrick, *Acta Cryst.* 1984, **40C**, 1555.
208. J. D. Woollins, *Polyhedron* 1984, **3**, 1365.
209. J. Weiss and H. S. Neubert, *Z. Naturforsch.* 1966, **21B**, 286.
210. J. Anhaus, Z. A. Siddiqi, J. Schimkowiak, H. W. Roesky and H. Lueken, *Z. Naturforsch.* 1984, **39B**, 1722.
211. J. Weiss and H. Martan, unpublished results quoted in Ref. 213.
212. A. Berg, E. Conradi, U. Müller and K. Dehnicke, *Chem.-Ztg* 1984, **108**, 292.
213. U. Kynast, E. Conradi, U. Müller and K. Dehnicke, *Z. Naturforsch.* 1984, **39B**, 1680.
214. J. Hanich, M. Krestel, U. Müller, K. Dehnicke and D. Rehder, *Z. Naturforsch.* 1984, **39B**, 1686.
215. J. Anhaus, P. G. Jones, M. Noltemeyer, W. Pinkert, H. W. Roesky and G. M. Sheldrick, *Inorg. Chim. Acta* 1985, **97**, L7.
216. N. Burford, T. Chivers, A. W. Cordes, W. G. Laidlaw, M. C. Noble, R. T. Oakley and P. N. Swepston, *J. Am. Chem. Soc.* 1982, **104**, 1282.
217. C. G. Marcellus, R. T. Oakley, A. W. Cordes and W. T. Pennington, *J. Chem. Soc., Chem. Commun.* 1983, 1451.
218. W. Lidy, W. Sundermeyer and W. Verbeek, *Z. Anorg. Allg. Chem.* 1974, **406**, 228.
219. P. G. Jones, W. Pinkert and G. M. Sheldrick, *Acta Cryst.* 1983, **39C**, 827.
220. H. Endres and E. Galantai, *Angew. Chem.* 1980, **92**, 644; *Angew. Chem., Int. Ed. Engl.* 1980, **19**, 653.
221. J. J. Mayerle, J. Kuyper and G. B. Street, *Inorg. Chem.* 1978, **17**, 2610.
222. H. Martan and J. Weiss, *Z. Anorg. Allg. Chem.* 1984, **515**, 225.
223. N. P. C. Walker, M. B. Hursthouse, C. P. Warrens and J. D. Woollins, *J. Chem. Soc., Chem. Commun.* 1985, 227.
224. U. Thewalt, *Z. Naturforsch.* 1982, **37B**, 276.
225. A. A. Bhattacharyya and A. G. Turner, *Inorg. Chim. Acta* 1983, **76**, L97.

Polyhedron Vol. 5, No. 11, pp. 1701–1707, 1986
Printed in Great Britain

0277–5387/86 $3.00+.00
Pergamon Journals Ltd

STUDIES ON THE MIXED-LIGAND COMPLEXES OF CADMIUM–IMIDAZOLE–CITRATE SYSTEMS USING DIFFERENTIAL-PULSE POLAROGRAPHY

A. M. Y. JABER

University of Petroleum and Minerals, UPM, Box No. 650, Dhahran 31261, Saudi Arabia

(*Received* 26 *September* 1985; *accepted* 6 *November* 1985)

Abstract—Differential-pulse polarography has been used to study the simple and mixed-ligand complexes of cadmium–imidazole–citrate systems in solution. Using the graphical DeFord–Hume and Schaap–McMasters treatments the overall stability constants, β_{ij}, for the mixed-ligand complexes were found to be: $\log \beta_{11} = 5.89$, $\log \beta_{12} = 6.38$, $\log \beta_{21} = 7.38$, $\log \beta_{22} = 7.08$, $\log \beta_{31} = 8.38$, and $\log \beta_{41} = 9.00$. The equilibria between the various mixed-ligand species coexisting in the solution together with their stepwise stability constants are also given.

Imidazole is an important material in biological systems since it is the nucleus in the amino acid histidine which, in turn, binds to metal ions in several metalloproteins, such as haemoglobin. The complexing properties have therefore been widely studied. For example, among the electroanalytical methods, successive association constants of imidazole with some transition-metal ions have been investigated using potentiometric[1–7] or polarographic methods.[8–13] Potentiometry was utilized for imidazole complexes with cadmium,[2–4], copper,[3–7] nickel,[1,3,7] cobalt,[3,7], zinc[3,5,7] and manganese(II).[3,7] On the other hand, conventional dc polarography was used to evaluate the consecutive stability constants of imidazole with cadmium[8–10] and copper.[8] The stability constants of the mixed-ligand complexes of cadmium,[11] copper[8] and europium[12] in the presence of tartrate and succinate, respectively, have also been reported.

This study concerns the consecutive stability constants for the simple and mixed-ligand complexes of Cd–imidazole–citrate systems using differential-pulse polarography. The graphical method of DeFord and Hume[14] has been used in assessing the stability constants of the simple complex (Cd–imidazole and Cd–citrate) systems, and the Schaap–McMasters[15] graphical method has been used to assess the stability constants of the mixed-ligand complexes (Cd–imidazole–citrate system).

THEORY OF STABILITY CONSTANT DETERMINATION

Heath and Hefter[16] have modified the DeFord–Hume treatment for determining the consecutive stability constants for the simple complexes for use with differential-pulse polarography instead of conventional dc polarography. In this modification, it is assumed that the shift in the half-wave potential, $(E_{1/2})_s - (E_{1/2})_c$, is equal to the shift in the differential-pulse peak potential, $(E_p)_s - (E_p)_c$ (the subscripts s and c refer to the simple and complex ions, respectively). Thus, the modified DeFord–Hume $F_0(X)$ is expressed as follows:

$$F_0(X) = \sum \beta_n C_L^n$$

$$= \text{antilog} \left\{ 0.434 \frac{nF}{RT} [(E_p)_s - E_p)_c] + \log (i_p)_s/(i_p)_c \right\},$$

where β_n is the overall stability constant for the nth complex, C_L is the analytical concentration of the ligand which is always taken in large excess over the metal ion concentration, and is, therefore, considered as the total ligand concentration, and i_p is the peak height of the differential-pulse wave. Apart from this modification, the DeFord–Hume treat-

ment for consecutive stability constant evaluation was followed.

Similarly, the Schaap and McMasters function, $F_{00}(XY)$,[15] might be modified for differential-pulse polarography:

$$F_{00}(XY) = \beta_{MX_iY_j}[X]^i[Y]^j$$

$$= \text{antilog}\left[\frac{0.434nF}{RT}\Delta E_p + \log\,(i_p)_s/i_p)_c\right],$$

where $\beta_{MX_iY_j}$ is the stability constant of the mixed-ligand complex, involving ligands X and Y. The concentration of one of the ligands is kept constant while the other is varied. The concentration of each ligand should individually be in excess with respect to the analytical concentration of the metal ion. i and j refer to the number of ligands associated in each mixed-ligand complex. Stability constants of the mixed-ligand complexes can then be determined as described by Schaap and McMasters.

EXPERIMENTAL

Polarograms were recorded by the Princeton Applied Research Polarographic Analyzer Model PAR 274A in conjunction with the EG and G Static Mercury Electrode Model 303 with a three-electrode system (Pt wire counter electrode and Ag–AgCl reference electrode) and X–Y recorder (Re 0074). The differential pulse mode was used with a modulation amplitude of 25 mV, scan rate of 2 mV s^{-1}, drop time of 0.5 s, and a full-scale sensitivity of 1 μA.

A glass double-walled cell was used with thermostated water circulating at 25±0.1°C. Sample solutions were purged with nitrogen gas for 8 min. The nitrogen was passed through a bottle containing vanadyl chloride solution followed by another containing distilled water for it to be saturated with water vapour.

General reagent grade imidazole, analytical reagent grade cadmium nitrate and trisodium citrate (Fischer), polarographic grade sodium nitrate and mercury (Merck), and deionized double distilled water were used.

Sample solutions (20.0 cm^3) were 1.0 mol dm^{-3} with respect to sodium nitrate for maintaining the ionic strength, 2.0×10^{-5} mol dm^{-3} with respect to cadmium nitrate, and of variable concentrations with respect to either imidazole (0.0–1.8 mol dm^{-3}) or trisodium citrate (0.0–0.90 mol dm^{-3}) for the simple complex systems. For the mixed-ligand complexes, polarograms were recorded for three series of solutions containing fixed citrate concentrations of 0.10, 0.20 and 0.45 mol dm^{-3}, with the imidazole concentration being varied in each case in the range 0.0–0.50 mol dm^{-3}. Imidazole of appropriate concentrations was either added to separate sample solutions or spiked into the same sample solution.

RESULTS AND DISCUSSION

Cd–imidazole system

E_p and i_p (for five sample solutions), were in the range 0.614–0.624 V (0.619±0.0043 V) and 120.7–129.5 divisions (125.8±3.2 divisions), respectively. Each 25.5 divisions correspond to 0.1 μA. It has been reported[8,11] that the polarographic reduction of Cd–imidazole complexes in potassium nitrate medium is reversible, with $n = 2$. The reversibility is confirmed in this study by measuring the half-peak width of the differential-pulse polarograms. Values of 51–52 mV were found for all of the polarograms recorded for either Cd or Cd–imidazole in 1.0 mol dm^{-3} sodium nitrate medium. This is consistent with the prediction of Parry and Osteryoung[17] where, for a fully reversible two-electron reduction with an applied-pulse amplitude of 25 mV, there will be a peak width of 49.5 mV.

Figure 1 shows that the maximum number of imidazole ligands associated with cadmium in the concentration range 0.0–1.8 mol dm^{-3} imidazole is 6, indicating that six stability constants can be determined. However, except for one[10] of the pre-

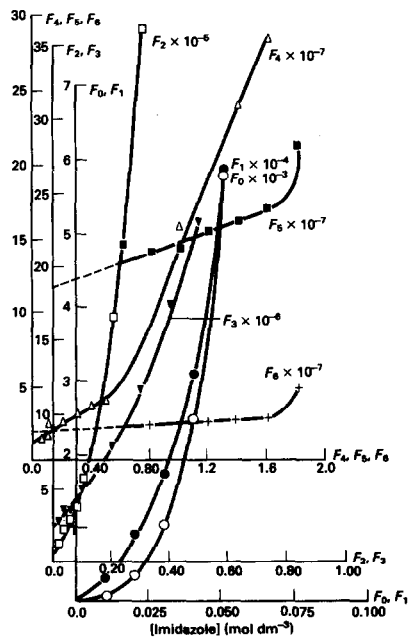


Fig. 1. Plots of the simple functions, F_i, vs imidazole concentration.

Table 1. Consecutive stability constants for the Cd–imidazole system

β_1	β_2	β_3	β_4	β_5	β_6	Reference
2.7	4.0	5.3	7.0	—	—	11, in 2.0 mol dm^{-3} $NaNO_3$ at 25°C
—	5.07	6.46	7.48	—	—	8, in 0.15 mol dm^{-3} KNO_3, at 25°C
2.80	4.90	6.45	7.58	—	—	4,[a] in nitrate medium
2.70	5.08	6.65	7.65	8.18	8.95	10, in 1.0 mol dm^{-3} $NaClO_4$ at 25°C
2.78	4.85	6.43	7.15	8.08	7.18	This study

[a]This study was carried out using potentiometry, while the remaining literature data were obtained with conventional dc polarography.

vious studies,[4,8,11] only four stability constants have been reported. Table 1 shows that the values of the consecutive stability constants obtained in this study are comparable with those obtained previously.[4,8,10,11] However, the β_6 for $Cd(imid)_6$ is much less than that obtained by Jensen.[10] This may be due to the activity effect, since Jensen's main concern was to determine the activity coefficients at the various imidazole concentrations and then to use them in calculating the stability constants.

Polarograms recorded on a sample solution containing 1.0 mol dm^{-3} sodium nitrate and 2.0×10^{-5} mol dm^{-3} cadmium nitrate, with spiked quantiaties of 1.0 mol dm^{-3} imidazole solution to yield imidazole concentrations of 0.0–9.5×10^{-2} mol dm^{-3} permitted the evaluation of just four stability constants owing to the low imidazole concentration. The log stability constants obtained are: $\beta_1 = 2.83$, $\beta_2 = 4.81$, $\beta_3 = 6.32$, and $\beta_4 = 7.36$, values which are consistent with those of the separate-solution method (Table 1).

Cd–citrate system

The half-peak width of each of the polarograms recorded for the Cd–citrate system over a citrate concentration range of 0.0–0.90 mol dm^{-3} in 1.0 mol dm^{-3} sodium nitrate medium is found to be in the range 51–52 mV, indicating a fully reversible two-electron reduction. It can be concluded from Fig. 2 that three species of the Cd–citrate complexes exist within the concentration range studied, namely, $[Cd(cit)]^-$, $[Cd(cit)_2]^{4-}$ and $[Cd(cit)_3]^{7-}$, with log stability constants of: $\beta_1 = 3.00$, $\beta_2 = 4.08$, and $\beta_3 = 4.47$.

The data were also treated according to Lingane,[18] whereby ΔE_p was plotted vs log $C_{citrate}$, when a line consisting of three segments was obtained. The log values of the consecutive stability constants deduced from the plot were: $\beta_1 = 3.11$, $\beta_2 = 4.08$, and $\beta_3 = 4.32$, with coordination numbers of 1.2, 1.8 and 2.3. This confirms the presence of three complex species. The log stability constants of cadmium with citric acid have previously been reported[19] as: $\beta_1 = 3.15$, and $\beta_2 = 4.54$. The existence of three Cd–citrate complexes have also been recently reported.[20]

Mixed-ligand Cd–imidazole–citrate system

Since the maximum number of imidazole species that can associate with cadmium is 6, and the maximum number of citrate ions is 3, imidazole can be considered as monodentate and the citrate ion as bidentate. Consequently, the Schaap and McMasters treatment for the mixed-ligand complexes can be written as follows:

$$F_{00}(XY) = A + B[X] + C[X]^2 + D[X]^3 + E[X]^4 + F[X]^5,$$

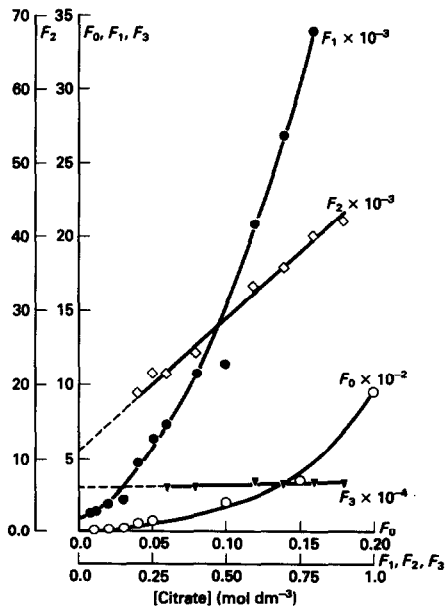


Fig. 2. Plots of the simple functions, F_j, vs citrate concentration.

where:

$$A = \beta_{00} + \beta_{01}[Y] + \beta_{02}[Y]^2 + \beta_{03}[Y]^3,$$

$$B = \beta_{10} + \beta_{11}[Y] + \beta_{12}[Y]^2,$$

$$C = \beta_{20} + \beta_{21}[Y] + \beta_{22}[Y]^2$$

$$D = \beta_{30} + \beta_{31}[Y],$$

$$E = \beta_{40} + \beta_{41}[Y],$$

$$F = \beta_{50}.$$

This predicts the coexistence of about 14 complexes in solutions containing both ligands. X and Y refer to imidazole and citrate ligands, respectively. In the stability constants β_{00}, the first subscript refers to the number of imidazole ligands while the second refers to the number of citrate ligands. According to Schaap and McMasters,[15] the function F_{00} is plotted vs imidazole, for calculating the parameter A. The other functions, F_{i0} ($i = 1, 2, 3, \ldots$ etc.) will also be calculated, and the other parameters (B, C, D, E and F) are evaluated. These parameters are calculated at three different citrate concentrations, that is, 0.10, 0.20 and 0.45 mol dm^{-3}. Calculation of the stability constants of the mixed-ligand complexes will then be possible.

The differential-pulse polarograms recorded for the mixed-ligand system at the concentration ranges of the ligands studied gave peak half-widths of 51–52 mV, and again suggests a two-electron reversible reduction. Polarograms also indicate that the negative shift, ΔE_p, for the mixed-ligand complex system is much more than those for the simple systems under the same conditions. For example, ΔE_p for the Cd–imidazole–citrate complex at 0.20 mol dm^{-3} imidazole and 0.20 mol dm^{-3} citrate is 179 mV, whereas ΔE_p for the simple Cd–imidazole and Cd–citrate systems at a ligand concentration of 0.20 mol dm^{-3} is 140 and 84 mV, respectively. This emphasizes that mixed-ligand complexes are formed.

The differential-pulse polarographic data at the three citrate concentrations are summarized in Table 2. Other data were obtained for two sample solutions containing 1.0 mol dm^{-3} sodium nitrate, 2.0×10^{-5} mol dm^{-3} cadmium nitrate, and a fixed citrate concentration of 0.10 mol dm^{-3} for one and 0.45 mol dm^{-3} for the other. Imidazole was spiked into the sample solution to give concentrations in the 0.0–9.5×10^{-2} mol dm^{-3} range and polarograms recorded for the mixed-ligand complexes after each addition. The results are reported in Table 3.

The values of F_{00}, F_{10}, F_{20} and F_{40} were calculated according to Schaap and McMasters and plotted vs the imidazole concentration. Graphs for the first set of data (the separate-solution method) are represented in Figs 3–5. The values for A, B, C, D, E and F estimated from the figures at the different citrate concentrations are given in Table 4. Values of parameter A given in Table 4 (5.5×10^2, 1.0×10^3 and 6.0×10^3) are in reasonable agreement with those calculated (2.5×10^2, 9.20×10^2 and 5.6×10^3, respectively) from the stability constants of the simple Cd–citrate system obtained in the experiment. Also, the value of parameter F obtained from Fig. 5 is in good agreement with that ex-

Table 2. Differential-pulse polarographic data for the Cd–citrate–imidazole system by the separate-solution method[a]

[Citrate]$^{3-}$ (mol dm^{-3})	[Imidazole] (mol dm^{-3})	$-(E_p)_c$ vs Ag–AgCl (V)	$(i_p)_c$ (divisions)
0.100	0.010	0.709	66.9
	0.020	0.719	75.6
	0.030	0.727	79.5
	0.040	0.735	85.2
	0.050	0.740	85.0
	0.100	0.760	90.0
	0.150	0.774	90.1
	0.200	0.784	90.0
	0.250	0.797	90.3
	0.300	0.804	91.3
	0.400	0.818	92.5
	0.500	0.828	91.0
0.200	0.010	0.715	68.9
	0.020	0.723	70.5
	0.050	0.729	74.6
	0.040	0.734	77.2
	0.050	0.740	77.4
	0.100	0.759	85.3
	0.150	0.773	88.3
	0.200	0.788	88.0
	0.250	0.796	84.0
	0.300	0.803	87.0
	0.400	0.817	85.1
	0.500	0.827	86.3
0.450	0.010	0.733	59.5
	0.020	0.740	61.6
	0.030	0.745	59.5
	0.040	0.750	66.1
	0.050	0.755	67.0
	0.100	0.773	74.2
	0.150	0.785	75.5
	0.200	0.798	75.6
	0.250	0.806	75.9
	0.300	0.814	76.0
	0.400	0.827	76.6
	0.500	0.838	77.0

[a] $[Cd^{2+}] = 2.0 \times 10^{-5}$ mol dm^{-3}, $(E_p)_s = 0.619$ V, $(i_p)_s = 125.8$ divisions.

Table 3. Differential-pulse polarographic data for the Cd–citrate–imidazole system by the imidazole-spiking method[a]

[Citrate]$^{3-}$ (mol dm^{-3})	[Imidazole] (mol dm^{-3})	$-(E_p)_c$ vs Ag–AgCl (V)	$(i_p)_c$ (divisions)
0.10	5.0×10^{-4}	0.699	89.5
	1.0×10^{-3}	0.700	89.5
	2.0×10^{-3}	0.701	90.8
	4.0×10^{-3}	0.704	91.6
	6.0×10^{-3}	0.707	92.7
	1.0×10^{-2}	0.711	93.7
	2.0×10^{-2}	0.720	94.5
	3.0×10^{-2}	0.727	95.1
	4.4×10^{-2}	0.736	93.9
	6.3×10^{-2}	0.747	92.4
	8.2×10^{-2}	0.755	91.0
	9.5×10^{-2}	0.760	91.0
0.45	5.0×10^{-4}	0.725	70.3
	1.0×10^{-3}	0.726	71.1
	2.0×10^{-3}	0.728	73.0
	4.5×10^{-3}	0.730	74.6
	8.0×10^{-3}	0.733	75.3
	1.0×10^{-2}	0.734	75.5
	2.0×10^{-2}	0.739	76.2
	3.9×10^{-2}	0.749	76.5
	5.4×10^{-2}	0.755	77.0
	7.2×10^{-2}	0.762	76.7
	9.5×10^{-2}	0.770	75.8

[a] $[Cd^{2+}] = 2.0\times10^{-5}$ mol dm^{-3}, $(E_p)_s = 0.619$ V, $(i_p)_s = 125.8$ divisions.

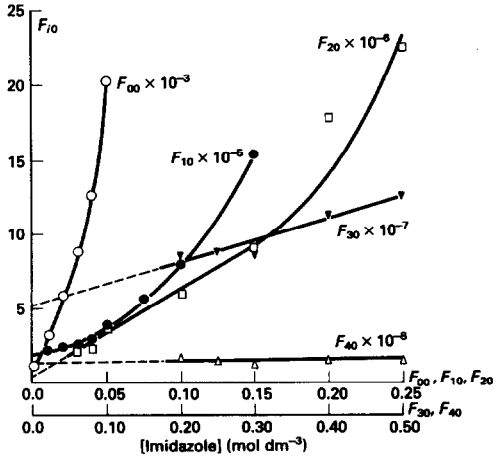


Fig. 4. Plots of the mixed-ligand complex functions, F_{ij}, vs imidazole concentration at [citrate]$^{3-}$ = 0.20 mol dm^{-3} (Table 2).

pected from the equation $F = \beta_{50}$ ($\beta_{50} = 1.2\times10^{8}$) (Table 1).

Stability constants of the mixed-ligand Cd–imidazole–citrate complex system were calculated using the parameter values estimated at three different citrate concentrations. The individual values of these stability constants and their log values are given in Table 5. Of course, the negative values of the stability constants for some complexes in Table 5 indicate that such complexes do not exist in the solution at the particular citrate concentration range. For example, the mixed-

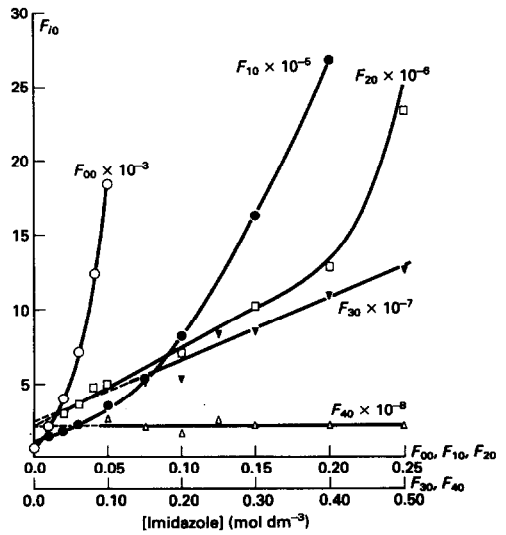


Fig. 3. Plots of the mixed-ligand complex functions, F_{ij}, vs imidazole concentration at [citrate]$^{3-}$ = 0.1 mol dm^{-3} (Table 2).

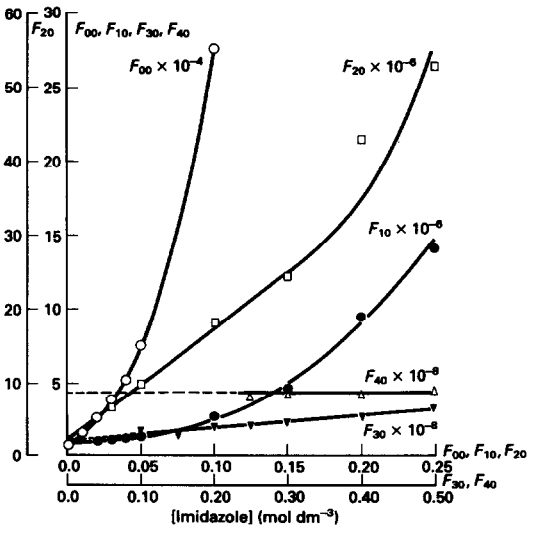


Fig. 5. Plots of the mixed-ligand complex functions, F_{ij}, vs imidazole concentration at [citrate]$^{3-}$ = 0.45 mol dm^{-3} (Table 2).

Table 4. Parameter values estimated at the different citrate concentrations

$[Citrate]^{3-}$ (mol dm^{-3})	A	B	C	D	E	F
0.10	6.5×10^{2}	1.1×10^{5}	2.1×10^{6}	2.4×10^{7}	2.1×10^{8}	—
0.20	1.0×10^{3}	2.0×10^{5}	4.1×10^{5}	5.2×10^{7}	1.3×10^{8}	—
0.45	6.0×10^{3}	9.0×10^{5}	2.2×10^{6}	1.0×10^{8}	3.6×10^{8}	1.8×10^{8}
0.10[a]	7.0×10^{2}	9.0×10^{4}	7.8×10^{5}	7.5×10^{7}	—	—
0.45[a]	8.0×10^{3}	4.8×10^{5}	3.2×10^{6}	1.2×10^{8}	3.6×10^{8}	—

[a]Values obtained from the imidazole-spiking method.

Table 5. Stability constants evaluated for the mixed-ligand complex Cd–imidazole–citrate system[a]

No.	β_{11}	β_{12}	β_{21}	β_{22}	β_{31}	β_{41}
1	1.2×10^{6}	-9.7×10^{5}	3.9×10^{7}	-1.9×10^{8}	2.1×10^{8}	2.0×10^{9}
2	8.4×10^{5}	2.6×10^{6}	2.5×10^{7}	-4.5×10^{7}	2.5×10^{8}	5.8×10^{8}
2a	8.5×10^{5}	4.9×10^{5}	7.5×10^{6}	-4.1×10^{6}	2.6×10^{8}	7.7×10^{8}
3	2.0×10^{5}	4.0×10^{6}	-7.0×10^{5}	1.2×10^{7}	2.2×10^{8}	7.7×10^{8}
Average and standard deviation	$(7.7\pm4.2)\times10^{5}$	$(2.4\pm1.8)\times10^{6}$	$(2.4\pm1.6)\times10^{7}$	1.2×10^{7}	$(2.4\pm0.2)\times10^{8}$	$(1.0\pm0.6)\times10^{9}$
$\log\beta_{ij}$	5.89	6.38	7.38	7.08	8.38	9.00

[a]Values shown in Nos 1, 2 and 3 are calculated from the data obtained at citrate concentrations of 0.10 and 0.20, 0.10 and 0.45, and 0.20 and 0.45 mol dm^{-3}, respectively. Values in No. 2a are derived from Table 3 at 0.10 and 0.45 mol dm^{-3} citrate.

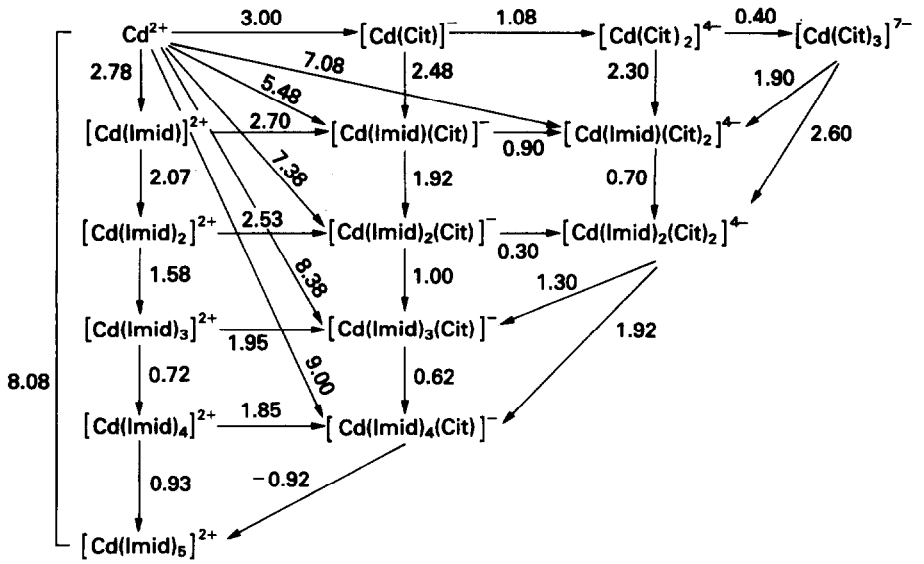


Fig. 6. Schematic diagram showing the equilibria in the mixed-ligand system and log k values for these equilibria.

ligand species $[Cd(imid)\cdot(cit)_2]^{2-}$ and $[Cd\cdot(imid)_2\cdot(cit)_2]^{4-}$ appeared in the solution only in high citrate concentration ranges.

The equilibria between the various species existing in the mixed-ligand system together with the log stepwise stability constant values (log k) are represented schematically in Fig. 6. The log k values indicate that it is easier to add the $[Cit]^{3-}$ ligand to the binary complex $[Cd(imid)]^{2+}$ (log $k = 2.70$) than to add it to the complex $[Cd(cit)]^{-}$ (log $k = 1.08$). However, addition of the imidazole ligand to the binary complex $[Cd(cit)]^{-}$ (log $k = 2.48$) is easier than adding it to the species $[Cd(imid)]^{2+}$ (log $k = 2.07$). This indicates that the tendency for formation of the mixed-ligand complex is favoured. It is also obvious from the schematic diagram (Fig. 6) that it is possible to replace citrate in the saturated mixed-ligand complex, while there is no tendency for replacing imidazole by citrate except for the species $[Cd(imid)_5]^{2+}$ (log k value is negative) which in any case probably does not coexist with the mixed-ligand complexes. This also indicates that the citrate ligand is much weaker than the neutral ligand, imidazole. These results are consistent with those reported earlier for other mixed-ligand complex systems, namely, Cd–imidazole–tartrate,[11] Cd–ethylenediamine–oxalate[15] and Cd–trimethylenediamine–succinate.[20]

Acknowledgements—I am grateful to the University of Petroleum and Minerals for supporting this research project (UPM proposed CY/Imidazole/83) and to Mr E. Michanowsky for assistance with the polarographic measurements. The constructive comments by Dr J. D. R. Thomas of UWIST, Cardiff, are much appreciated.

REFERENCES

1. W. Fosling, *Acta Chem. Scand.* 1979, **A33**, 641.
2. I. Gramberg and S. Sjoberg, *Acta Chem. Scand.* 1981, **A35**, 193.
3. N. Saha and H. Sigel, *J. Am. Chem. Soc.* 1982, **104**, 4100.
4. C. Tanford and M. L. Wagner, *J. Am. Chem. Soc.* 1953, **75**, 434.
5. J. T. Edsall, G. Felsenfold, D. S. Goodman and F. R. N. Guard, *J. Am. Chem. Soc.* 1954, **76**, 3054.
6. M. S. Nair and M. Santappa, *Indian J. Chem.* 1982, **21A**, 58.
7. T. R. Harkins and H. Frieser, *J. Am. Chem. Soc.* 1956, **78**, 1143.
8. N. C. Li, J. M. White and E. Doody, *J. Am. Chem. Soc.* 1954, **76**, 6219.
9. D. R. Grow, *J. Electroanal. Chem.* 1968, **16**, 137.
10. J. B. Jensen, *Acta Chem. Scand.* 1972, **A26**, 4031.
11. M. Shivhare and M. Singh, *J. Inorg. Nucl. Chem.* 1981, **43**, 1599.
12. M. Shivhare and M. Singh, *Indian J. Chem.* 1982, **21A**, 296.
13. C. Tanford, *J. Am. Chem. Soc.* 1952, **74**, 211.
14. D. D. DeFord and D. N. Hume, *J. Am. Chem. Soc.* 1951, **73**, 5321.
15. W. B. Schaap and D. L. McMasters, *J. Am. Chem. Soc.* 1961, **83**, 4699.
16. G. A. Heath and G. Hefter, *J. Electroanal. Chem.* 1977, **84**, 295.
17. E. P. Parry and R. A. Osteryoung, *Anal. Chem.* 1965, **37**, 1634.
18. J. J. Lingane, *Chem. Rev.* 1941, **29**, 1.
19. S. Kotrly and L. Sucha, *Handbook of Chemical Equilibria in Analytical Chemistry*. Ellis-Horwood, Chichester (1984).
20. H. M. Killa and M. Zaky, *Anal. Lett.* 1985, **18**, 167.

Polyhedron Vol. 5, No. 11, pp. 1709–1721, 1986
Printed in Great Britain

0277-5387/86 $3.00+.00
Pergamon Journals Ltd

LONG-RANGE NUCLEAR SPIN–SPIN COUPLING BETWEEN ^{11}B AND ^{13}C, ^{29}Si OR ^{119}Sn: A PROMISING TOOL FOR STRUCTURAL ASSIGNMENT

BERND WRACKMEYER

Institut für Anorganische Chemie, Meiserstraße 1, D-8000 München 2, F.R.G.

(*Received* 4 *June* 1985; *accepted* 20 *December* 1985)

Abstract—The influence of unresolved long-range nuclear spin–spin coupling [$^nJ(^{11}B–X)$ ($n > 1$; X = ^{13}C, ^{29}Si or ^{119}Sn)] on X resonances has been studied for aminoboranes (**1** and **2**), haloboration (**3** and **4**), hydroboration (**5**) and organoboration products of alkynes (**6** and **7**). The differential broadening of X resonances in the X NMR spectra arising from $^nJ(^{11}B–X)$ (most obvious for X = ^{119}Sn) shows a qualitatively useful pattern of various coupling pathways. $|^2J(^{13}CN–^{11}B)|$ in **1** and **2** appears to be sensitive to the nature of the *trans*-ligand and to the ring size. In many alkenylboranes (**3**, **4**, **5b** and **d**, **6** and **7**) the magnitude of the coupling constants across the C=C double bond follows the trend $|^2J(^{11}B–X)| \sim |^3J(^{11}B–X)|_{cis} < |^3J(^{11}B–X)|_{trans}$. An increasing number of electropositive substituents at the C=C double bond causes an increase in the magnitude of $|^3J(^{11}B–X)|_{cis,trans}$. If there are only organyl groups or hydrogen attached to the C=C double bond, as in the hydroboration products of alkynes (**5a** and **c**) $|^nJ(^{13}C–^{11}B)|$ appears to be too small with respect to $[T_{Q(^{11}B)}]^{-1}$, and the differential broadening was negligible under the experimental conditions used.

The ever increasing complexity of boron compounds under investigation requires efficient methods for rapid structural assignment. Multinuclear NMR methods, in addition to routine ^1H and ^{11}B NMR[1,2] measurements, appear to be particularly suitable for this purpose as they frequently provide decisive information on the composition and structure of the compounds in question.[3] Apart from chemical-shift data (δ) for various nuclei present in boron compounds in solution we are dealing with indirect nuclear spin–spin coupling (J) and relaxation phenomena (T_1 and T_2). Obviously, the δ values contain much structural information which can be used as soon as a sufficiently large set of data exists. The measurement of relaxation times (T_1 and T_2) for nuclei X (X = ^{13}C, ^{29}Si or ^{119}Sn) with $I = \frac{1}{2}$ is still a tedious non-routine procedure if one aims for accurate values, and their interpretation is not at all straightforward.

However, the relaxation behaviour of quadrupolar nuclei such as ^{11}B ($I = \frac{3}{2}$) in solution (assuming that the quadrupolar mechanism is dominant, $T_1 = T_2$, and that the motional narrowing limit applies) is somewhat more simple. Furthermore, the quadrupolar relaxation rate of the ^{11}B nucleus influences the appearance of the resonance of X with $I = \frac{1}{2}$[4] (scalar relaxation of the second kind).

That means that the scalar ^{11}B–X spin–spin coupling, $^nJ(^{11}B–X)$, will be completely averaged only by very rapid quadrupolar relaxation of the ^{11}B nucleus or if its absolute magnitude is very small [$|J(^{11}B–X)|T_{Q(^{11}B)}2\pi \ll 1$]. In the case of a slower quadrupolar relaxation or larger values of $|J(^{11}B–X)|$ more or less broadened X resonances [$|J(^{11}B–X)|T_{Q(^{11}B)}2\pi < 1$] or partially resolved ^{11}B–X spin–spin coupling [$|J(^{11}B–X)|T_{Q(^{11}B)}2\pi > 1$] will be observed. The main interest has been focused so far on values of $^1J(^{11}B–X)$[1–3,5,6] which frequently lead to partially resolved or to severely broadened X resonances. Except for favourable cases, such as a highly symmetric environment of boron (e.g. in borates[3,6,7]), the $^nJ(^{11}B–X)$ coupling constants ($n > 1$) are in general not resolved, neither in the ^{11}B nor in the X NMR spectra. In ^1H NMR spectra of boron compounds there are numerous examples

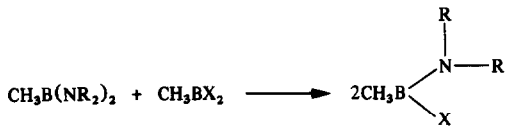
of slightly broadened ^1H resonances which can be sharpened in appropriate ^1H–$\{^{11}B\}$ heteronuclear double-resonance experiments. This has been used to evaluate $^nJ(^{11}B$–$^1H)$ coupling constants ($n = 2$ and 3),[8] to assign specific ^1H resonances in aryl- or alkenylboranes,[9] or to relate ^1H and ^{11}B resonances in mixtures of compounds.[10]

Bearing in mind the multinuclear NMR approach we have studied ^{13}C, ^{29}Si and ^{119}Sn NMR spectra of various boranes in order to obtain experimental evidence for the influence of long-range ^{11}B–X coupling [$^nJ(^{11}B$–X)] ($n > 1$). For this first systematic study we have selected compounds for which there is little or no doubt about the assignment of the ^{13}C, ^{29}Si and ^{119}Sn resonances. The compounds studied represent various active research areas in boron chemistry as they are aminoboranes (**1** and **2**) and products of haloboration (**3** and **4**), hydroboration (**5**) and organoboration (**6–8**).

RESULTS AND DISCUSSION

Synthesis

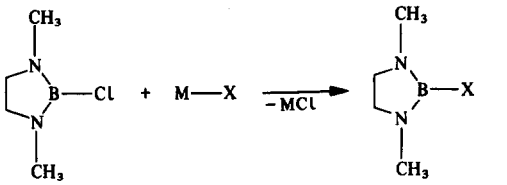
The aminoboranes **1** were prepared according to eqn (1):[11]



(1)

1	X	R
a	CH_3O	CH_3
b	CH_3S	CH_3
c	Br	C_2H_5

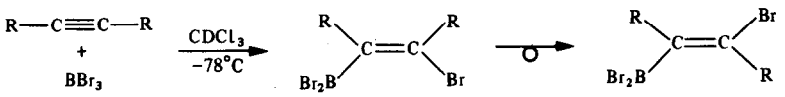
The reaction of **2c**[12] with metalated groups X led to the aminoboranes **2a**,[11(b),13] **b**,[14] **c**[15] and **d**[5] [eqn (2)]:



(2)

2	X	M
a	CH_3	Li
b	$Si(CH_3)_3$	Li
c	$NHCH_3$	Li
d	$SeCH_3$	Na

Haloborations[16–18] (**3** and **4**) were carried out by adding slowly a slight excess (10%) of BBr_3 in $CDCl_3$ to a $CDCl_3$ solution of the alkyne at $-78°C$. The reaction was monitored by NMR (^{11}B and ^{13}C). The haloboration products were not isolated.



(3)

3 **4**

R = C_2H_5 (**a**), C_3H_7 (**b**) or C_4H_9 (**c**)

Hydroboration of alkynes to compounds **5** was performed as described previously:[19–22]



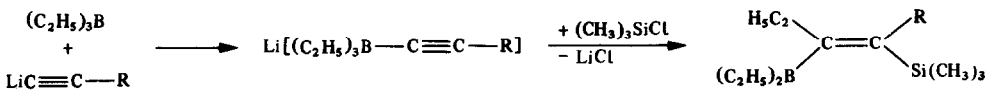
(4)

5

R = C_2H_5 (**a**), or $Si(CH_3)_3$ (**b**)

5	R^1	R^2
c	C_2H_5	C_2H_5
d	H	$Si(CH_3)_3$

Organoboration reactions were conducted either by the reaction of triethyl-alkynylborates with $(CH_3)_3SiCl$[23] [eqn (4)] or by direct organoboration of alkynylstannanes[24] [eqn (5)]:



(5)

6

R = CH_3 (**a**), or $Si(CH_3)_3$ (**b**)

$(C_2H_5)_3B + (CH_3)_3Sn{-}C{\equiv}C{-}R \longrightarrow$ **6** (6)

6

R = CH_3 (**c**), H (**d**), $Si(CH_3)_3$ (**e**), $Ge(CH_3)_3$ (**f**), or $Sn(CH_3)_3$ (**g**)

Isomers (**7**) of compounds **6** are either formed already during the synthesis of **6** (**7d** and **e**) or they can be obtained by UV irradiation or standing in daylight:[25]

7a (UV, 20 h, ~ 10%)

R = CH_3 (**b**), H (**c**), $Si(CH_3)_3$ (**d**), or $Ge(CH_3)_3$ (**e**) (7)

R = CH_3 (**f**), or H (**g**)

7h

All the relevant NMR data of the compounds studied are given in Tables 1–4.

^{13}C *NMR*

The origin of differential broadening in ^{13}C NMR spectra can be traced to the scalar interaction with the ^{11}B nucleus either by measuring the ^{13}C NMR spectra at different temperatures (affecting the quadrupolar relaxation rate) or by heteronuclear triple-resonance experiments (^{13}C–{^1H–^{11}B}). Since our NMR facilities enable us to perform the latter experiments, we can prove unambiguously the influence of the ^{11}B nucleus if there is another quadrupolar nucleus such as ^{14}N present. This is shown in Fig. 1 for compound **1c** and similar experiments have been carried out for the other compounds studied.

In the case of **1** it appears that the greater value of the geminal coupling constant $^2J(^{11}CN{-}^{11}B)$

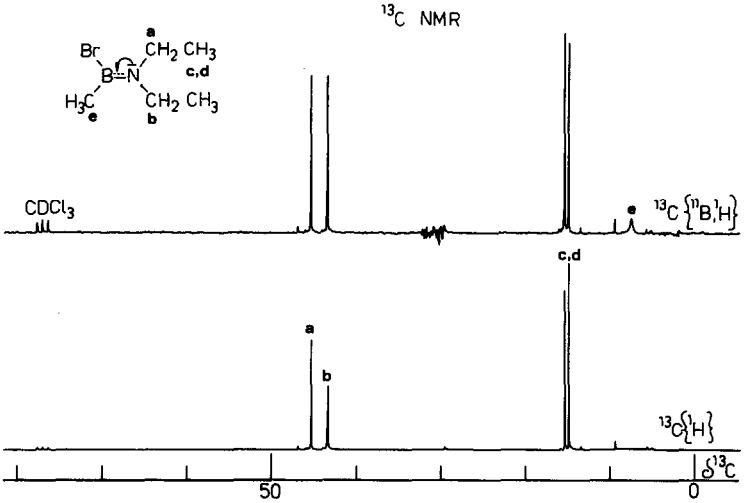
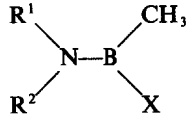
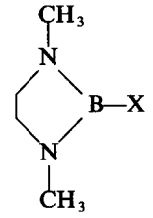
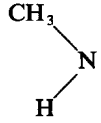


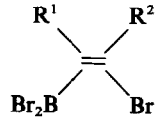
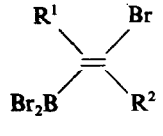
Fig. 1. 50.3-MHz ^{13}C NMR spectra of diethylamino-bromo-methylborane (**1c**). Simultaneous ^1H and ^{11}B decoupling leads to significant sharpening of the ^{13}C(b) resonance (and, of course, the $B\underline{C}H_3$–^{13}C resonance appears); the assignment of the ^{13}C(a and b) resonances is based upon the similarity between $\delta[^{13}C(a)]$ and $\delta[^{13}C(NCH_2)]$ in $Br_2BN(C_2H_5)_2$[36] and between $\delta[^{13}C(b)]$ and $\delta[^{13}C(NCH_2)]$ in $(CH_3)_2BN(C_2H_5)_2$.[36]

Table 1. ^{11}B and ^{13}C NMR data of some aminoboranes for the detection of long-range ^{11}B–^{13}C spin–spin coupling[a]

No.	Compound					$\delta(^{11}B)$	$\delta(^{13}C)$	Solvent
1		X	R^1	R^2				
		CH_3O	CH_3	CH_3	**(a)**	31.8	2.0 (BCH_3), *39.5* (R^1), 36.5 (R^2), 51.5 (OCH_3)	C_6D_6
		CH_3S	CH_3	CH_3	**(b)**	43.6	0.0 (BCH_3), *39.4* (R^1), 38.8 (R^2), 10.5 (SCH_3)	$CDCl_3$
		Br	C_2H_5	C_2H_5	**(c)**	37.8	7.4 (BCH_3), *43.4*, 15.2 (R^1), 45.3, 14.8 (R^2)	$CDCl_3$
2		X						
		CH_3			**(a)**	32.4	−5.0 (BCH_3), *33.8* (NCH_3), 51.6 (NCH_2)	C_6D_6
		$(CH_3)_3Si$			**(b)**	32.9	−0.1[b] ($SiCH_3$), *35.4* (NCH_3), 53.5 (NCH_2)	C_6D_6
					**(c)**	25.5	29.0 ($NHCH_3$), *34.1* (NCH_3), 52.0 (NCH_2)	$CDCl_3$
		CH_3Se			**(d)**	31.7	−2.4[c] ($SeCH_3$), *34.7* (NCH_3), 52.0 (NCH_2)	$CDCl_3$
		Cl			**(e)**	27.0	*32.9* (NCH_3), 50.3 (NCH_2)	C_6D_6

[a] Positions of ^{13}C resonances broadened most significantly by long-range ^{13}C–^{11}B spin–spin coupling are given in italics.
[b] $^1J(^{29}Si$–$^{13}C) = 47.3$ Hz.
[c] $^1J(^{77}Se$–$^{13}C) = 53.2$ Hz; $\delta(^{77}Se) = -240.0$ [neat $(CH_3)_2Se$ external reference compound]; $^1J(^{77}Se$–$^{11}B) = < 20$ Hz.

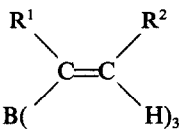
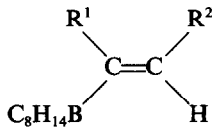
Table 2. ^{11}B and ^{13}C NMR data of some haloboration products of alkynes[a] for the detection of long-range ^{13}C–^{11}B spin–spin coupling[b]

No.	Compound	R^1	R^2		$\delta(^{11}B)$	$\delta(^{13}C)$	Solvent
3		H	C_4H_9	(a)	52.7	132.5 (BC=), 153.0 (=CBr), *46.8*, 30.2, 21.6, 13.9 (R^2)	$CDCl_3$
		C_2H_5	C_2H_5	(b)	55.7	144.2 (BC=), 129.7 (=CBr), 24.8, 13.9 (R^1) *30.2*, 13.2 (R^2)	$CDCl_3$
		C_3H_7	C_3H_7	(c)	55.8	145.0 (BC=), 128.2 (=CBr), 34.0, 21.4, 14.2 (R^1) *38.3*, 22.3, 13.1 (R^2)	$CDCl_3$
		C_4H_9	C_4H_9	(d)	55.6	145.2 (BC=), 128.4 (=CBr), 31.1, 31.7, 21.8, 14.0 (R^1) *36.4*, 30.3, 22.7, 13.8 (R^2)	$CDCl_3$
4		R^1	R^2				
		H	C_4H_9	(a)	50.1	138.0 (BC=), 161.3 (=CBr), *40.5*, 31.1, 22.9, 3.9 (R^2)	$CDCl_3$
		C_2H_5	C_2H_5	(b)	58.0	145.6 (BC=), 139.1 (=CBr), *29.9*, 13.6 (R^1) *36.3*, 12.8 (R^2)	$CDCl_3$
		C_3H_7	C_3H_7	(c)	57.8	144.5 (BC=), 138.1 (=CBr), *38.9*, 22.1, 14.2 (R^1) *44.4*, 21.9, 13.1 (R^2)	$CDCl_3$
		C_4H_9	C_4H_9	(d)	58.1	144.4 (BC=), 138.3 (=CBr), *36.7*, 31.0, 22.7, 14.0 (R^1) *42.4*, 30.5, 21.8, 13.9 (R^2)	$CDCl_3$

[a] Compounds **3** are observed in mixtures with **4**. A **3**:**4** ratio of 15:1 was observed at room temperature 1 h after preparation; after several days the **3**:**4** ratio had changed to 1:7, allowing for the unambiguous assignment of ^{11}B and various ^{13}C resonances.

[b] Positions of ^{13}C resonances most significantly broadened by long-range ^{13}C–^{11}B spin–spin coupling are given in italics.

Table 3. ^{11}B, ^{13}C and ^{29}Si NMR data of some hydroboration products of alkynes for the detection of long-range ^{11}B–X spin–spin coupling[ab]

No.	Compound	$\delta(^{11}B)$	$\delta(^{13}C)$	$\delta(^{29}Si)$	Solvent
					
5a	$R^1 = R^2 = C_2H_5$	68.6	23.4, 15.1 (R^1); 21.8, 14.1 (R^2); 150.7 (BC=); 144.6 (=CH)[c]	—	$CDCl_3$
5b	$R^1 = R^2 = (CH_3)_3Si$	70.0	2.2, 0.7 (R^1 and R^2) (51.1) (51.1) 174.1 (BC=); 158.9 (=CH)[e] (57.3) (63.4)	−10.3 (R^1)[d] *−10.6* (R^2)[d]	$CDCl_3$
					
5c	$R^1 = R^2 = C_2H_5$	78.6	28.4 (BCH); 33.9 ($CH\underline{C}H_2$); 23.4 (CH_2); 22.0, 15.5 (R^1); 22.2, 13.8 (R^2); 146.4 (BC=); 149.6 (=CH)[f]	—	$CDCl_3$
5d	$R^1 = H$, $R^2 = (CH_3)_3Si$	78.5	30.2 (BCH); 33.9 ($CH\underline{C}H_2$); 23.3 (CH_2); 1.6 (R^2); 151.8 (BC=); 157.2 (=CH)	−6.7	$CDCl_3$

[a] Assignment of ^{13}C (R^1 and R^2) resonances in **5a** and **c** is based on ^1H-coupled ^{13}C NMR spectra assuming $|^3J(^{13}C–^1H)| > |^2J(^{13}C–^1H)|$: $C_8H_{14}B$ = 9-borabicyclo[3.3.1]nonyl.

[b] Values of $J(^{29}Si–^{13}C)$ are given in parentheses.

[c] $^1J(^{13}C–^1H) = 152.5$ Hz.

[d] $^3J(^{29}Si–^{29}Si) = 6.2$ Hz.

[e] $^1J(^{13}C–^1H) = 126.8$ Hz.

[f] $^1J(^{13}C–^1H) = 151.5$ Hz.

can be assigned for ^{13}C *trans* to an electronegative substituent X. Considering the behaviour of $^2J(^{13}C^{\alpha}–^1H)$ in substituted alkenes, $XC^{\alpha}H=CH_2$,[26] large changes in the magnitude of $|^2J(^{13}CN–^{11}B)|$ are not entirely surprising. In contrast to **1**, there is no appreciable influence of electronegative groups X (Cl or N<) on the linewidth of the $^{13}C(NCH_2)$ resonance in 1,3-dimethyl-1,3,2-diazaborolidines (**2**). In all cases studied the $^{13}C(NCH_3)$ resonances exhibit much more residual broadening (removable by ^{11}B decoupling) than the $^{13}C(NCH_2)$ resonances. However, in the five-membered ring system it is conceivable that contributions from $^2J[^{13}C(NCH_2)–^{11}B]$ and $^3J[^{13}C(NCH_2)–^{11}B]$ cancel each other.

Recently, haloboration reactions have received renewed attention with respect to their stereochemistry[17] and their application in synthesis.[18] In this context we have already pointed out briefly the effect of ^{11}B decoupling for assignment purposes in ^{13}C NMR spectra[17(b)] and we report here on compounds **3** and **4** in more detail. The 1,2-haloboration proceeds stereospecifically *cis* to compounds **3** which slowly rearrange to the *trans*-products (**4**). Our $^{13}C–\{^1H–^{11}B\}$ experiments show that the magnitude of the coupling constants $|^{2,3}J(^{13}C–^{11}B)|$ across the C=C double bond increases in the order: $|^2J(^{13}C–^{11}B)| \sim |^3J(^{13}C–^{11}B)_{cis}| < |^3J(^{13}C–^{11}B)_{trans}|$.

Although many hydroboration products have been used *in situ* for conversion into other products by various procedures,[27] we note an increasing tendency for complete characterization of hydroboration products prior to further use in organic syntheses.[28,29] In general, ^{13}C NMR is very helpful in this respect[3,6] and we wanted to find out whether differential broadening by long-range coupling $[^nJ(^{13}C–^{11}B)]$ across C=C double bonds can be of diagnostic value. We have studied the boranes **5a** and **b**, which may be regarded as typical examples as far as the relaxation of the ^{11}B nucleus is concerned [$T_{Q(^{11}B)}$ for **5a** = 8.5×10^{-4} s, for **5b** = 4.3×10^{-4} s]. However, in both compounds we did not observe any appreciable line broadening originating from $^nJ(^{13}C–^{11}B)$ ($n > 1$). Since a digital resolution of 0.1 Hz/point was used and a linewidth of the $^{13}C(C_2H_5)$

signals of the order of 0.3–0.4 Hz was found we found an $^nJ(^{13}C-^{11}B)$ ($n = 2$ or 3) of < 5 Hz in **5a** and **b**.

It is well known that the magnitude of $^3J(HH)_{trans}$ or $^3J(HH)_{cis}$ increases with increasing number of electropositive groups attached to the C=C double bond. Therefore, we studied the organoboration products carrying one $Si(CH_3)_3$ or $Sn(CH_3)_3$ group at the C=C double bond. Indeed there is a distinct broadening (*ca* 0.3 Hz) of the ^{13}C-resonance signal of the methyl group *trans* to the ^{11}B nucleus in **6a** and **c**. In **7a**, **b**, **f** and **g** the linewidths of all relevant ^{13}C resonances are equal within the error of determination (± 0.2 Hz).

The ^{11}B quadrupolar relaxation rate in compounds **6a** and **c**, and **7a**, **b** and **f**, is similar to that in **5a** and **b**. Hence, it follows that $|^3J(^{13}C-^{11}B)|_{trans}$ increases in the presence of an $Si(CH_3)_3$ or $Sn(CH_3)_3$ group at the C=C double bond. Considering that it was possible to observe effects from $|^3J(^{13}C-^{11}B)|_{trans}$ in the haloboration compounds **3** [$T_{Q(^{11}B)}$ for **3d** (8.6×10^{-4} s) is very similar to $T_{Q(^{11}B)}$ for **5a** (8.5×10^{-4} s)] we conclude that electronegative substituents at the site of the boron atom also induce an increase in the magnitude of $|^3J(^{13}C-^{11}B)|_{trans}$.

In spite of the encouraging results the deduction of reliable data for $^nJ(^{13}C-^{11}B)$ coupling constants from these experiments is not straightforward. Several more or less convincing assumptions are involved: (i) the line shape of the ^{13}C resonances is exactly Lorentzian, (ii) relaxation time $T_{1(^{11}B)} = T_{2(^{11}B)} = T_{Q(^{11}B)}$, (iii) the contributions to the linewidth of the ^{13}C resonances in question arising from the species containing the ^{10}B isotope (*ca* 20%) can be evaluated accurately,[8(b)] (iv) different inhomogeneity broadening in two consecutive experiments (^{11}B-decoupled on-resonance and off-resonance) can be neglected, (v) digital resolution introduces small errors, and (vi) the values of the linewidth of the ^{11}B resonance are sufficiently accurate. Even if we believe that some of these assumptions [e.g. (i), (ii) and (iii)] are permissible in a semiquantitative treatment the error which is introduced considering all the other factors is fairly large. Thus, we calculate[8] a value of 9.5 ± 4 Hz for $|^3J(^{13}C-^{11}B)|_{trans}$ in **3a**. Clearly, some contributions to the error will become smaller with increasing values of $^nJ(^{13}C-^{11}B)$ and/or with decreasing linewidth of the ^{11}B resonance (e.g. **1c**: $h_{1/2} = 80$ Hz, **3a**: $h_{1/2} = 180$ Hz, and **3d**: $h_{1/2} = 370$ Hz). However, for the compounds studied we find that the values of $^nJ(^{13}C-^{11}B)$ ($n = 2$–4) range from 0 to *ca* 12 Hz, and that an error of *ca* ± 3–5 Hz is realistic. Therefore, we are left with the qualitative experimental evidence described.

However, as we aim primarily for the comparison of the absolute values of $|^nJ(^{13}C-^{11}B)|$ within the same molecule differential broadening effects as described may well serve as a guide for assignment. The comparison of effects arising from $|^nJ(^{13}C-^{11}B)|$ for different types of compounds is possible only in a crude qualitative way as pointed out for the haloboration, hydroboration and organoboration products.

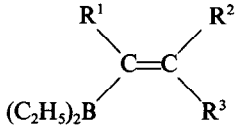
^{29}Si *NMR*

Silanes obtained via organoboration (**6a**, **b** and **e**, and **7d**) or hydroboration (**5b** and **d**) have been studied by ^{29}Si NMR using pulse sequences for refocused INEPT[30] or DEPT (with ^1H decoupling).[31] This helps to circumvent the problem of long and unpredictable ^{29}Si relaxation times and it guarantees an acceptable signal:noise ratio within a reasonably short time.[32] Figure 2 shows the ^{29}Si NMR spectrum for compound **5b** in $CDCl_3$ as a representative example. Running the ^{29}Si NMR spectrum of **5b** in pentane solution shows that both ^{29}Si resonances are more broadened owing to the slower quadrupolar relaxation rate in solvents of lower viscosity [$h_{1/2}(^{11}B) = 1450$ Hz in $CDCl_3$, 510 Hz in pentane]. Consequently, the ^{29}Si signals become equally broad if the spectrum of **5b** is recorded at -40°C, as the result of a much increased quadrupolar relaxation rate of the ^{11}B nucleus at lower temperature [$h_{1/2}(^{11}B) > 3000$ Hz in $CDCl_3$, -40°C].

Compound **5b** has been studied previously by ^1H, ^{11}B, ^{13}C and ^{29}Si NMR.[20] We observe very similar δ values but we find that several of the reported coupling constants are wrong. Thus, both ^1H and ^{29}Si NMR (^1H-coupled) show that, for the olefinic hydrogen atom, $|^3J(^{29}Si-^1H)|_{trans} = 21.3$ Hz and $|^2J(^{29}Si-^1H)| = 4.6$ Hz (the literature[20] gives a single value for $^2J(^{29}Si-^1H)$ of 26 Hz]. Both $^2J(^{29}Si-^1H)$ values for the $Si(CH_3)_3$ for groups are 6.55 ± 0.1 Hz. Very accurate values of $^1J(^{29}Si-^{13}C)$ can be obtained from the ^{29}Si NMR spectrum (Fig. 2). The value for $|^1J(^{29}Si-^{13}C)|$ of 57.3 Hz for the olefinic carbon atom attached to boron deviates significantly from the data in the literature (50 Hz[20]). There is no indication for a large geminal coupling [$^2J(^{29}SiC(B)-^{13}C)$], for which a value of 45 Hz has been given.[20] In addition, we can assign ^{29}Si satellites to $^3J(^{29}Si-^{29}Si)_{cis} = 6.2$ Hz, although these lines (AB-spin system) have a distorted phase in the DEPT experiment.

The amount of broadening of the ^{29}Si resonances in **5b** and **6b**, and **6a** and **7a**, together with the known quadrupolar relaxation rate of the ^{11}B nucleus suggests that $|^2J(^{29}Si-^{11}B)| \sim |^3J(^{29}Si-$

Table 4. ^{11}B, ^{13}C, ^{29}Si and ^{119}Sn NMR data of some organoboration products for the detection of long-range ^{11}B–X spin–spin coupling[ab]



No.	R^1	R^2	R^3	$\delta(^{11}B)$	$\delta(^{13}C)$	$\delta(^{29}Si)$	$\delta(^{119}Sn)$	Solvent
6a	C_2H_5	CH_3	$(CH_3)_3Si$	83.0	21.3, 9.4 (BC_2H_5); 22.5, 12.9 (R^1) (7.6) *15.5* (R^2); −0.8 (R^3); 161.7 (BC=); 130.4 (=CSi) (51.2) (70.9)	−6.0	—	C_6D_6
6b	C_2H_5	$(CH_3)_3Si$	$(CH_3)_3Si$	82.8	21.2, 9.4 (BC_2H_5); 30.0, 14.0 (R^1) (11.7) 3.5 (R^2); 2.2 (R^3); 184.0 (BC=); 140.0 (=CSi) (49.8) (50.1) (55.9, R^3) (53.4, R^2)	*−11.7* (R^2)[c] −5.9 (R^3)[c]	—	$CDCl_3$
6c	C_2H_5	CH_3	$(CH_3)_3Sn$	83.3	21.8, 8.9 (BC_2H_5); 23.1, 13.6 (R^1) [83.0] [10.5] *19.7* (R^2); −8.6 (R^3); 163.0 (BC=); 133.5 (=CSn) [66.0] [320.0] [540.0]	—	−47.9	$CDCl_3$
6d	C_2H_5	H	$(CH_3)_3Sn$	83.5	21.4, 8.5 (BC_2H_5); 32.3, 13.1 (R^1) [94.0] [10.6] −8.7 (R^3); 173.0 (BC=); 124.6 (=CSn) [336.5] [503.0]	—	−55.1	$CDCl_3$
6e	C_2H_5	$(CH_3)_3Si$	$(CH_3)_3Sn$	83.8	21.7, 9.5 (BC_2H_5); 32.1, 14.4 (R^1); [137.3] [9.8] 3.0 (R^2); −5.3 (R^3); 185.4 (BC=); 138.7 (=CSn) (50.7) [305.2] [332.0] [12.4]	−9.6[d]	−51.8	C_6D_6
6f	C_2H_5	$(CH_3)_3Ge$	$(CH_3)_3Sn$	84.0	21.6, 9.0 (BC_2H_5); 32.3, 14.3(R^1); [129.7] [9.6] 2.8 (R^2); −5.6 (R^3); 182.2 (BC=); 137.8 (=CSn) [12.7] [302.6] [347.1]	—	−51.5	C_6D_6
6g	C_2H_5	$(CH_3)_3Sn$	$(CH_3)_3Sn$	84.0	22.1, 9.4 (BC_2H_5); 36.9, 14.8 (R^1); [141.5 (R^3)] [9.1] [118.2 (R^2)] −5.3, −6.1 (R^2 and R^3); 185.0 (BC=); 138.0 (=CSn) [303.2] [310.4] [346.1, R^3] [10.4] [10.4] [298.0, R^2)	—	*−54.6*[e] (R^2) −48.0[e] (R^3)	C_6D_6

7a	C_2H_5	$(CH_3)_3Si$	CH_3	85.0	21.3, 8.9 (BC_2H_5); 22.2, 12.8 (R^1); 0.6 (R^2); 14.6 (R^3); 165.4 (BC═); 129.2 (═CSi) (51.2) (69.8)	*−8.8*	—	C_6D_6
7b	C_2H_5	$(CH_3)_3Sn$	CH_3	86.0	22.9, 8.7 (BC_2H_5); 31.2, 15.0 (R^1); [70.8] [9.8] −8.3 (R^2); 24.1 (R^3); 163.6 (BC═); 132.7 (═CSn) [320.1] [70.8] [493.5]	—	*−55.6*	$CDCl_3$
7c	C_2H_5	$(CH_3)_3Sn$	H	79.0	18.4, 8.4 (BC_2H_5); 32.2, 15.6 (R^1); [64.0] [9.4] −8.4 (R^2); 148.8 (BC═); 136.9 (═CSn) [336.5] [445.0]	—	*−61.4*	$CDCl_3$
7d	C_2H_5	$(CH_3)_3Sn$	$(CH_3)_3Si$	83.8	21.7, 9.5 (BC_2H_5); 34.8, 14.4 (R^1); [118.4] [8.5] −4.9 (R^2); 1.6 (R^3); 181.8 (BC═); 140.8 (═CSn) [302.7] (50.7) (59.2) [11.6] [304.6]	*−7.1*[f]	*−66.4*	C_6D_6
7e	C_2H_5	$(CH_3)_3Sn$	$(CH_3)_3Ge$	84.0	21.6, 9.2 (BC_2H_5); 34.7, 14.4 (R^1); [111.9] [8.4] −5.3 (R^2); 1.4 (R^3); 179.9 (BC═); 140.4 (═CSn) [305.2] [11.5] [335.7]	—	*−62.8*	C_6D_6
7f	CH_3	$(CH_3)_3Sn$	C_2H_5	86.5	20.9, 8.6 (BC_2H_5); 20.6 (R^1); −7.9 (R^2); [73.4] [318.2] 32.5, 15.8 (R^3); 155.5 (BC═); 141.8 (═CSn) [64.3] [12.3] [488.3]	—	*−58.4*	$CDCl_3$
7g	H	$(CH_3)_3Sn$	C_2H_5	84.0	21.1, 8.5 (BC_2H_5); −9.1 (R^2); 32.8, 15.6 (R^3); [326.4] [64.0] 148.8 (BC═); 162.1 (═CSn) [467.0]	—	*−37.4*	$CDCl_3$
7h	H	C_2H_5	$(CH_3)_3Sn$	84.0	21.1, 8.6 (BC_2H_5); 38.0, 14.5 (R^2); [64.0] −7.6 (R^3); 148.0 (BC═); 162.3 (═CSn) [329.0] [470.0]	—	−47.3	$CDCl_3$

[a] Positions of ^{13}C, ^{29}Si and ^{119}Sn resonances broadened most significantly by long-range ^{11}B–X spin–spin coupling are given in italics.
[b] Values of $^1J(^{29}Si–^{13}C)$ are given in parentheses, and values of $^1J(^{119}Sn–^{13}C)$ in square brackets.
[c] $^2J(^{29}Si–^{29}Si) = 8.6$ Hz.
[d] $^2J(^{119}Sn–^{29}Si) = 93.0$ Hz.
[e] $^2J(^{119}Sn–^{119}Sn) = 943.0$ Hz.
[f] $^2J(^{119}Sn–^{29}Si) = 92.1$ Hz.

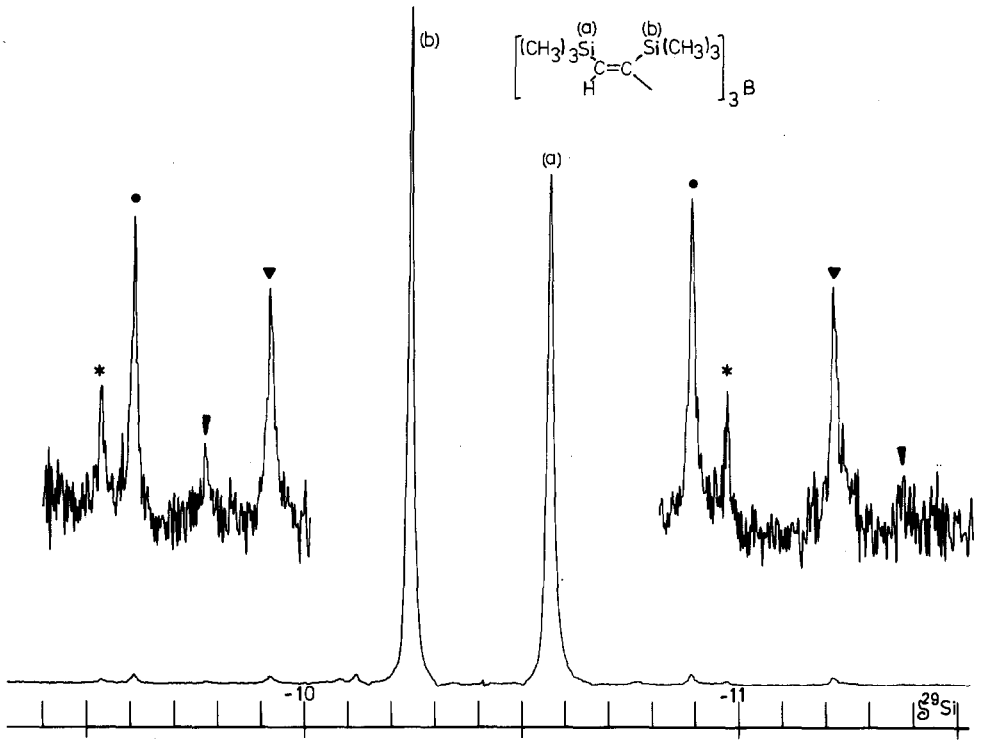


Fig. 2. 39.76-MHz ^{29}Si NMR spectrum [DEPT with ^{1}H decoupling,[31] $^{2}J(^{29}Si–^{1}H) = 6.5$ Hz] of tris[1,2-bis(trimethylsilyl)ethenyl]borane (**5b**); ^{13}C satellites are marked and serve for the assignment of the ^{29}Si resonances (a) and (b) by comparison with the values of $^{1}J(^{29}Si–^{31}C)$ from ^{13}C NMR spectra; the integral intensities of resonances (a) and (b) are 1:1 and the digital resolution was 0.02 Hz/point.

$^{11}B)|_{cis} > |^{3}J(^{29}Si–^{11}B)|_{trans}$, similar to the finding for $^{13}C–^{11}B$ long-range coupling. Furthermore, measurement of ^{29}Si and ^{11}B linewidths for **5d**, **6a** and **7a** indicate that the magnitude of $|^{3}J(^{29}Si–^{11}B)|_{cis,trans}$ is smaller than in compounds **5b** and **6b** with two $(CH_3)_3Si$ groups linked to the C=C double bond.

^{119}Sn *NMR*

The stannanes studied here showed significantly broadened ^{119}Sn resonances. The sharpening of these ^{119}Sn resonances at −40°C proves that $^{n}J(^{119}Sn–^{11}B)$ is the source of this broadening. Figure 3 shows the ^{119}Sn NMR spectrum of **6g** as a typical example. Since isomerization of the alkenylstannanes **6c–f** occurs readily in daylight or much faster with UV irradiation the application of ^{119}Sn NMR to follow these processes is clearly indicated. Figure 4 demonstrates this in the case of compound **6d**, which rearranges mainly into **7c**, **g** and **h**. The ^{119}Sn resonance of pure **6d** is known and the linewidth indicates that in **7g** the $Sn(CH_3)_3$ group and the boryl group are also in a mutual *cis*-position. In contrast, the greater linewidth of the ^{119}Sn resonances in **7c** and **h** suggest a mutual *trans*-position for both groups. Together with the pattern of $\delta(^{119}Sn)$ values[33] a preliminary assignment of the structures is possible. In the present examples we have confirmed all assignments by ^{1}H and ^{13}C NMR evidence. However, both ^{1}H and ^{13}C NMR suffer from a somewhat restricted choice of the solvent and sometimes there is a severe overlap of resonances in the spectral area of interest, in particular when mixtures of similar compounds are studied. Although, numerous techniques (such as 2D NMR[34]) are available today to deal with most of these shortcomings the NMR parameters of hetero-nuclei can be of great advantage for obtaining fast reliable information. In contrast to previous investigations [60-MHz ^{1}H NMR[24(a)]] it was easy now to prove that at ambient temperature the mixture of compounds **6e** and **7d** consists mainly (>95%) of **7d** rather than **6e**. The broad ^{119}Sn resonance of **7d** [$h_{1/2}(^{119}Sn) \sim 100$ Hz] with respect to **6e** [$h_{1/2}(^{119}Sn) \sim 30$ Hz) is convincing proof. In this case ^{119}Sn NMR is superior to ^{29}Si NMR because the much smaller differential broadening in the ^{29}Si

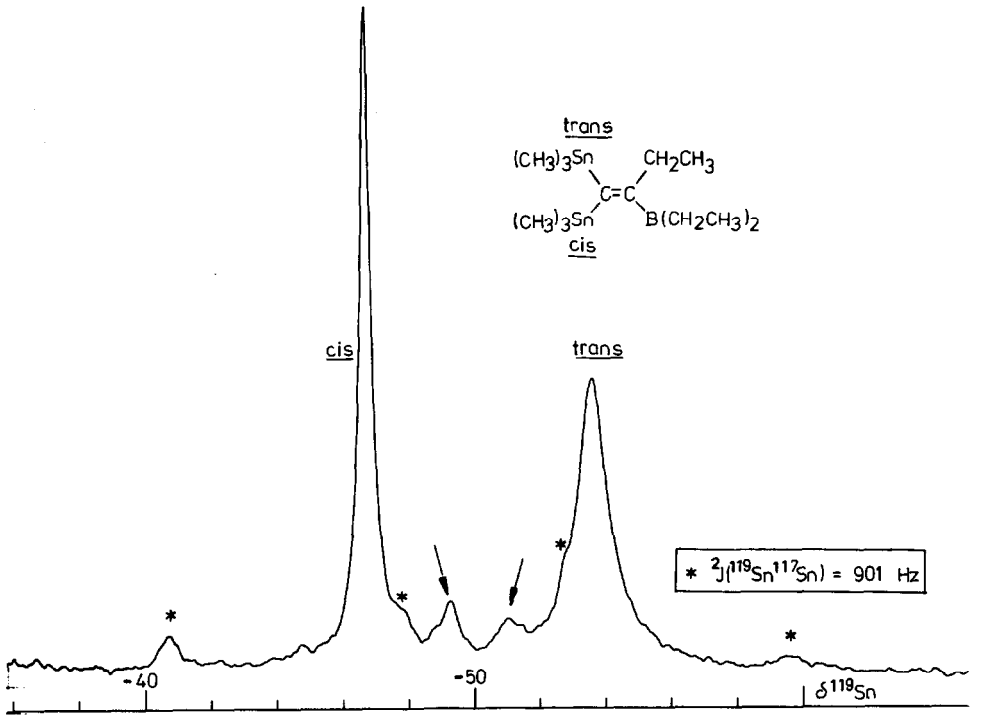


Fig. 3. 74.63-MHz ^{119}Sn NMR spectrum (^1H-decoupled) of 1,1-bis(trimethylstannyl)-2-diethylboryl-1-butene (**6g**); ^{117}Sn satellites are marked with asterisks. The inner lines of the ^{119}Sn satellite AB spectrum are marked with arrows; the calculation of the position of the other lines (low-intensity) agrees with a value for $^2J(^{119}Sn–^{119}Sn)$ of 943 Hz, obtained by multiplication of $^2J(^{119}Sn–^{117}Sn)$ with $\gamma_{(^{119}Sn)}/\gamma_{(^{117}Sn)} = 1.0465$.

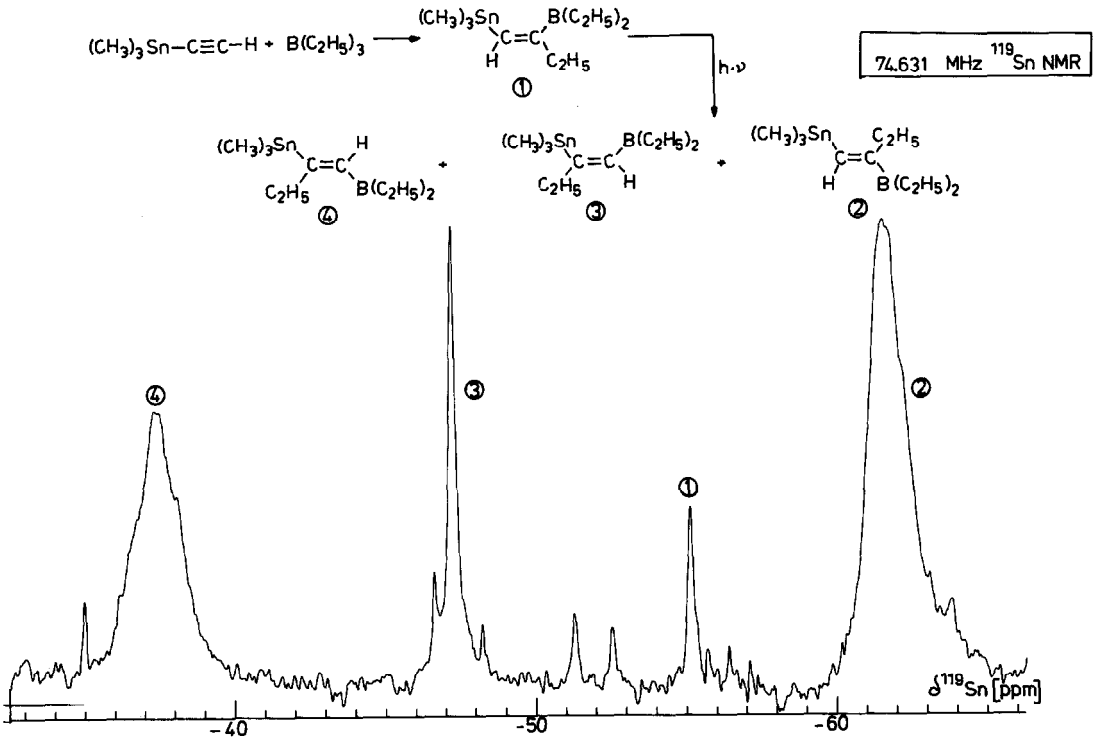


Fig. 4. 74.63-MHz ^{119}Sn NMR spectrum (^1H-decoupled) of the reaction mixture obtained from pure 1-trimethylstannyl-2-diethylboryl-1-butene[24(a)] (**6d**) signal ①, after standing in daylight for several weeks. The structural assignment of the main components, **7c**, ②, **7h**, ③, and **7g**, ④, of this mixture is based on conclusive information from ^1H and ^{13}C NMR.

NMR spectrum is difficult to observe owing to an isomer ratio > 9.5 : 1.

We evaluate[8] the magnitude of coupling constants $^3J(^{119}Sn-^{11}B)_{cis,trans}$ at the C=C double bond in the order of *ca* 40–50 Hz [$|^3J(^{119}Sn-^{11}B)|_{cis}$ in **6c** and **d**, and **7g**], *ca* 60–70 Hz [$|^3J(^{119}Sn-^{11}B)|_{cis}$ in **6e**, **f** and **g**], 75–85 Hz [$|^3J(^{119}Sn-^{11}B)|_{trans}$ in **6g**, and **7d** and **e**]. This is the same trend as has already emerged from ^{13}C and ^{29}Si NMR studies of similar types of compounds.

Conclusions

The experiments and results described and discussed show that long-range ^{11}B–X coupling is a promising tool for structural assignment, complementing the information from other NMR parameters. However, in general it is difficult to deduce accurate values of $^nJ(^{11}B-X)$ from linewidth measurements which is, probably, one of the reasons that these effects have not been discussed in detail for nuclei other than protons in the past. There is no need to emphasize the importance of the differential broadening arising from $^nJ(^{119}Sn-^{11}B)$ in the ^{119}Sn NMR spectra (see Figs 3 and 4). We have demonstrated that these effects, although they are much smaller, can be useful in ^{13}C and ^{29}Si NMR too. In this context, it is important to point out that the unambiguous assignment in the cases of ^{13}C and ^{29}Si NMR requires careful setting of the spectral parameters (see Experimental).

EXPERIMENTAL

Most of the compounds studied have been prepared following literature methods (**1a–c**;[11] **2a**,[11,13] **b**,[14] **c**,[15] **d**;[5] **5a**,[19] **b**,[20] **c**,[21] **d**;[22] **6a** and **b**,[23] **6c–g**[24]). The haloboration products **3** and **4** have been studied in the reaction solution and their structure was deduced from ^{11}B and ^{13}C NMR data. The compounds **7**, isomers of compounds **6**, were studied in the mixtures. The structural assignment of the isomers is based on combined ^1H, ^{11}B, ^{13}C, ^{29}Si or ^{119}Sn NMR evidence. In the case of **6a** 20 h of UV irradiation (Hg high-pressure lamp TQ 150, Hanau) was necessary for ~10% conversion into **7a**. In the case of **6c** standing in daylight for 60 days produced the isomers **7b** and **f** in a ratio of ~ 2 : 3. Similarly, in the case of **6d** standing in daylight for 5 days leads primarily to the formation of **7c**; **7g** and **h** are formed only after several weeks (see Fig. 4). The handling of all compounds required careful exclusion of oxygen and moisture.

All NMR spectra were recorded with a Bruker WP 200 NMR spectrometer, equipped with two frequency synthesizers, a multinuclear unit and a selective ^{13}C probehead, modified for ^{11}B decoupling. The ^{11}B-decoupling power used was 4–6 W and the efficiency of the experiment could be checked by the sharpening of ^{13}C resonances broadened by one-bond $^{13}C-^{11}B$ coupling. As the overall signal : noise ratio appeared to be somewhat dependent on the setting of the ^{11}B-irradiating frequency (probably a result of imperfect filtering of ^{13}C and ^{11}B frequencies in the decoupler and observe channel, respectively) no attempt was made to obtain quantitative data by comparison of ^{11}B-on-resonance- and ^{11}B-off-resonance decoupled spectra. Since the amount of residual broadening is dependent on all other experimental conditions (temperature, solvent and concentration) these data would not be very meaningful, anyhow.

The values of $h_{1/2}(^{11}B)$ increase with decreasing temperature as expected assuming that quadrupolar relaxation is dominant for the ^{11}B nucleus. The condition $T_{1(^{11}B)} = T_{Q(^{11}B)}$, with $T_Q = [\pi h_{1/2}(^{11}B)]^{-1}$ was checked by inversion recovery T_1 measurements[35] for several boranes (**1c**, **2c**, **3a**, **5a**, and **6a** and **c**). The values of $T_{1(^{11}B)}$ agreed within ±10%. In general, sharpening by ^{11}B decoupling, as shown in Fig. 1, was considered as proof for the origin of the broadening in ^{13}C NMR spectra. The digital resolution was selected according to the experimental linewidth in order to enable the correct assignment of broadened with respect to unbroadened or less broadened lines: ^{13}C: 0.2 Hz/point or better, ^{29}Si: 0.1 Hz/point; ^{119}Sn: 0.6 Hz/point.

The δ values given are referred to external BF_3–$O(C_2H_5)_2$ [$\delta(^{11}B)$]; to external $(CH_3)_4Si$ [$\delta(^{13}C)$ ($CDCl_3$) = 77.0, $\delta(^{13}C)$ (C_6D_6) = 128.0], [$\delta(^{29}Si)$]; to external $(CH_3)_4Sn$ [$\delta(^{119}Sn)$]. The spectra were recorded from samples in 10-mm tubes (o.d.) at 27–28°C in $CDCl_3$ or C_6D_6 [10–25% (w/v)].

Acknowledgements—Support of this work by the Deutsche Forschungsgemeinschaft and Fonds der Chemischen Industrie is gratefully acknowledged. I thank Prof. Dr R. Köster for a generous gift of triethylborane. I am also indebted to Prof. Dr H. Nöth and his group for samples of compounds **2b** and **c**.

REFERENCES

1. (a) G. R. Eaton and W. N. Lipscomb, *NMR Studies of Boron Hydrides and Related Compounds*. Benjamin, New York (1969); (b) H. Nöth and B. Wrackmeyer, In *NMR—Basic Principles and Progress* (Edited by P. Diehl, E. Fluck and R. Kosfeld). Springer, Heidelberg (1978).
2. (a) L. J. Todd and A. R. Siedle, *Prog. NMR Spectrosc.* 1979, **13**, 87; (b) A. R. Siedle, *Annu. Rep. NMR Spectrosc.* 1982, **12**, 177.

3. B. Wrackmeyer and R. Köster, In *Houben-Weyl, Methoden der Organischen Chemie* (Edited by R. Köster), Vol. XIII/3c, p. 377. Thieme, Stuttgart (1984).
4. (a) A. Abragam, *The Principles of Nuclear Magnetism*, p. 264. Oxford University Press, Oxford (1961); (b) M. Suzuki and R. Kubo, *Mol. Phys.* 1964, **7**, 201; (c) M. Kubo, M. Watanabe, T. Totani and M. Ohtsuru, *Mol. Phys.* 1968, **14**, 367.
5. H. Fussstetter, H. Nöth, B. Wrackmeyer and W. McFarlane, *Chem. Ber.* 1977, **110**, 3172.
6. B. Wrackmeyer, *Prog. NMR Spectrosc.* 1979, **12**, 227.
7. D. J. Hart and W. T. Ford, *J. Org. Chem.* 1974, **39**, 363.
8. (a) V. S. Bogdanov, A. V. Kessenikh and N. N. Negrebetskii, *J. Magn. Reson.* 1971, **5**, 145; (b) V. S. Bogdanov, A. V. Kessenikh, V. V. Negrebetskii and A. Ya. Shchteinshneider, *Zh. Strukt. Khim.* 1972, **44**, 1882; (c) V. V. Negrebetskii, V. S. Bogdanov, A. V. Kessenikh, P. V. Petrovskii, Yu. N. Bubnov and B. M. Mikhailov, *Zh. Obshch. Khim.* 1974, **44**, 1882.
9. (a) M. Wieber and W. Kunzel, *Z. Anorg. Allg. Chem.* 1974, **403**, 107; (b) Ref. 3, p. 450; (c) H.-O. Berger, H. Nöth and B. Wrackmeyer, *Chem. Ber.* 1979, **112**, 2866.
10. W. McFarlane, H. Nöth and B. Wrackmeyer, *Chem. Ber.* 1975, **108**, 3831.
11. (a) H. Vahrenkamp, Dissertation, University of Munich (1967); (b) H. Nöth and B. Wrackmeyer, *Chem. Ber.* 1973, **106**, 1145.
12. T.-T. Wang, P. J. Busse and K. Niedenzu, *Inorg. Chem.* 1970, **9**, 2150.
13. K. Niedenzu, H. Beyer and J. W. Dawson, *Inorg. Chem.* 1962, **1**, 738.
14. R. Schwerthöffer, Dissertation, University of Munich (1974).
15. H. Fussstetter, Dissertation, University of Munich (1977).
16. (a) M. F. Lappert and B. Prokai, *J. Organomet. Chem.* 1964, **1**, 384; (b) J. R. Blackborow, *J. Chem. Soc., Perkin Trans.* 2 1973, 1989; (c) J. R. Blackborow, *J. Organomet. Chem.* 1977, **128**, 161.
17. (a) R.-J. Binnewirtz, H. Klingenberger, R. Welter and P. Paetzold, *Chem. Ber.* 1983, **116**, 1271; (b) R. Schlögl and B. Wrackmeyer, *Polyhedron* 1985, **4**, 885.
18. (a) S. Hara, H. Dojo, S. Takinami and A. Suzuki, *Tetrahedron Lett.* 1983, 731; (b) S. Hara, Y. Satoh, H. Ishiguro and A. Suzuki, *Tetrahedron Lett.* 1983, 735.
19. H. C. Brown and G. Zweifel, *J. Am. Chem. Soc.* 1959, **81**, 1512.
20. N. S. Hosmane, N. N. Sirmokadam and M. N. Mollenhauer, *J. Organomet. Chem.* 1985, **279**, 359.
21. H. C. Brown, C. G. Scouten and R. Liotta, *J. Am. Chem. Soc.* 1979, **101**, 96.
22. K. Uchida, K. Utimoto and H. Nozaki, *J. Org. Chem.* 1976, **41**, 2941.
23. (a) P. Binger and R. Köster, *Synthesis* 1973, 309; (b) R. Köster, *Pure Appl. Chem.* 1977, **49**, 765.
24. (a) G. Menz and B. Wrackmeyer, *Z. Naturforsch.* 1977, **32B**, 1400; (b) B. Wrackmeyer, *Rev. Silicon, Germanium, Tin, Lead Compounds* 1982, **6**, 75.
25. B. Wrackmeyer, *J. Organomet. Chem.* 1981, **205**, 1.
26. D. F. Ewing, *Annu. Rep. NMR Spectrosc.* 1976, **6A**, 389.
27. H. C. Brown, G. W. Kramer, A. B. Levy and M. M. Midland, *Organic Synthesis via Boranes*. Wiley, New York (1975).
28. (a) R. Contreras and B. Wrackmeyer, *Z. Naturforsch.* 1980, **35B**, 1229, 1236; (b) R. Contreras and B. Wrackmeyer, *J. Organomet. Chem.* 1981, **205**, 15.
29. C. D. Blue and D. J. Nelson, *J. Org. Chem.* 1983, **48**, 4538.
30. (a) D. P. Burum and R. R. Ernst, *J. Magn. Reson.* 1980, **39**, 163; (b) G. A. Morris, *J. Magn. Reson.* 1980, **41**, 185.
31. D. T. Pegg, D. M. Doddrell and M. R. Bendall, *J. Chem. Phys.* 1982, **77**, 2745.
32. (a) D. M. Doddrell, D. T. Pegg, W. Brooks and M. R. Bendall, *J. Am. Chem. Soc.* 1981, **103**, 727; (b) B. J. Helmer and R. J. West, *Organometallics* 1982, **1**, 877.
33. B. Wrackmeyer, *Annu. Rep. NMR Spectrosc.* 1985, **16**, 73.
34. A. Bax, *Two-dimensional Nuclear Magnetic Resonance*. Delft University Press, Dordrecht (1982).
35. R. Freeman and H. D. W. Hill, *J. Chem. Phys.* 1969, **54**, 3140.
36. H. Nöth and B. Wrackmeyer, *Chem. Ber.* 1981, **114**, 1150.

Polyhedron Vol. 5, No. 11, pp. 1723–1732, 1986
Printed in Great Britain

0277–5387/86 $3.00+.00
Pergamon Journals Ltd

STUDIES ON AROMATIC AMINE BORANES BY ^{11}B AND ^{1}H NMR

C. CAMACHO, M. A. PAZ-SANDOVAL and R. CONTRERAS*

Centro de Investigación y de Estudios Avanzados del I.P.N., Departamento de Química, Apartado Postal 14-740, 07000—México, D.F. Mexico

(*Received* 2 *December* 1985; *accepted* 28 *January* 1986)

Abstract—^{1}H and ^{11}B NMR spectroscopy was applied to mono- and bisborane adducts derived from aryl-, benzyl-, phenethyl- and phenylenediamines, but no simple relationship was established between the spectroscopic data and the nature of the N—B bond. Comparative studies of the affinity of aromatic amines to BH_3 by equilibria reactions may be of great value in establishing a scale of relative basicity.

Although it is known that the order of reactivity among the BH_3–aliphatic amine adducts is closely related to their N—B bond strength[1] and that borane–arylamine complexes are rendered less stable due to steric and electronic effects,[2] there are, to our knowledge, no systematic studies of a series of aryl-, benzyl-, phenethyl- and phenylenediamine adducts.

Previous studies of aromatic amine borane complexes include bisdiphenylaminoborane,[3] the bifunctional hydride 1-pyrrolylborane–tetrahydrofuran complex,[4] pyrrolylborane–pyridine[4] and the exceptionally reactive diphenylamineborane,[5] where the aromatic groups were shown to weaken coordination of the nitrogen atom, thus making it more acidic and reactive as well as commercially attractive.[6] More recently, Brown[2] reported the use of phenylamine complexes as unique hydroborating and reducing agents, finding that the order of reactivity and consequently the stability of the adduct formed may be explained in terms of base strength.

It seemed of interest, therefore, to investigate the influence of *N*-alkyl, *N*-benzyl and *N*-aryl substituents on the strength of the N → B bond. Furthermore, these spectroscopic studies provide evidence for the relative affinity of these compounds to BH_3.

RESULTS AND DISCUSSION

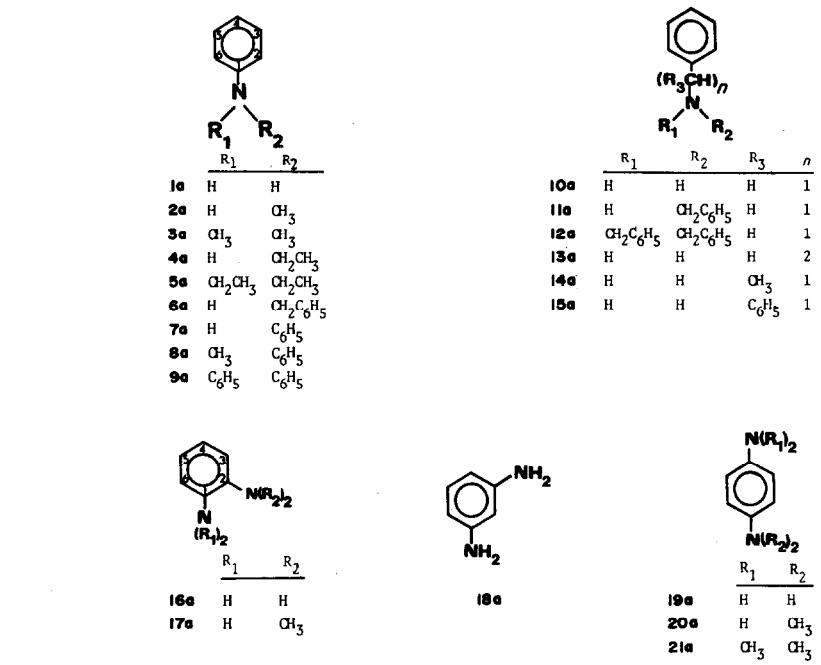
Reactions of amines **1a–21a** (Scheme 1) with borane or diborane were carried out and the resulting adducts were studied. Borane *N*-arylamine (**1b–7b**), *N*-benzylamine (**10b–12b**, **14b** and **15b**) and *N*-phenethylamine (**13b**) complexes were prepared by addition of a 1:1.25 BH_3:THF molar ratio to the corresponding amines (**1a–7a** and **10a–15a**) (Scheme 2). For compounds **1b** and **7b** immediate isolation is required to avoid formation of the bisaminoboranes **1d** and **7d**. On the other hand, compound **8b** was prepared by reaction of *N*-diphenylamine **8a** with diborane (~30:1) in benzene and was found to decompose upon evaporation to dryness, while compound **9b** was not obtained. Compound **12b** was not soluble enough to obtain NMR spectra.

Evidence of the formation of mono- (**16b–21b**) and bisborane adducts (**16c–21c**) (Scheme 2) derived from phenylenediamines (**16a–21a**) was provided by NMR when a 1:1 or 2:1 amine:BH_3 ratio was used. Complexes **19b**, **19c**, **21b** and **21c** were isolated as solid compounds. All of the borane derivatives were moisture-sensitive. Coordination of BH_3 to one of the nitrogen atoms allowed observation of electronic and steric effects induced at the aromatic ring. It was found that coordination causes a decrease in basicity of the remaining free amino group, thus rendering it less reactive to a second BH_3 molecule.

^{11}B *NMR studies*

Aryl-, benzyl- and phenethylamines. It has been described previously[7] that ^{11}B chemical shifts can be used as criteria for measuring the relative strength of the N—B dative bond. However, careful obser-

* Author to whom correspondence should be addressed.

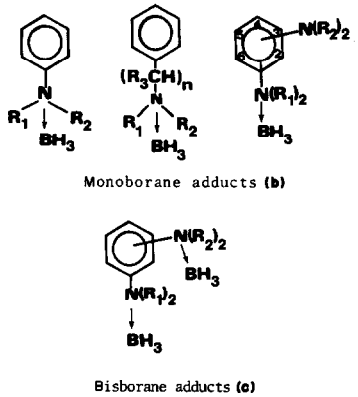


Scheme 1.

vation of Table 1 reveals that this does not hold for compounds **1b–8b**, **10b**, **11b** and **13b–15b**, since, for example, the **3b–8b** and **2b–4b** pairs, which differ considerably in basicity, show nearly identical ^{11}B chemical shifts.

Martin and coworkers[8] have also demonstrated that in the case of borane adducts of aniline and aminopyridines it is not only the density around the boron atom that exerts an influence on the ^{11}B δ but also paramagnetic anisotropic effects and hydrogen bonding.

Inspection of Table 1 shows clearly that for compounds **1b–8b**, **10b**, **11b** and **13b–15b** the shifts are not dependent on the nature of the substituent on the nitrogen atom, but rather tertiary amines (**3b** and **8b**) are shifted to lower fields than secondary (**2b**, **4b**, **7b** and **11b**) or primary (**1b**, **10b** and **13b–15b**) ones. A methyl (**3b**) or phenyl (**8b**) group produces the same variation on the chemical shift, indicating similar steric effects. This effect is considerably higher than those with an ethyl substituent group (**4b** and **5b**).



Scheme 2.

The importance of steric effects on the stabilities of the addition compounds is clearly established by considering **7a** and **8a**, which have pK_a values in water of 0.85[9(a)] and 0.86,[9(b)] respectively. It was found that **7a** reacts with BH_3·THF immediately, while complexation of **8a** must be carried out directly with diborane, implying the presence of greater steric hindrance.

Substitution at the β-carbon in primary benzyl- and phenethylamineboranes (**10b** and **13b–15b**) did not affect considerably the ^{11}B δ ($\Delta\delta = 1.3$ ppm). This observation is in contrast with cyclic systems[10] in which ^{11}B chemical shifts were highly dependent on steric effects.

Phenylenediamines. Table 1 summarizes the ^{11}B chemical shifts of phenylenediamineborane adducts (**16b** and **c**–**21b** and **c**). The data show that mono- or bisborane substitution has little effect on the shifts. As shown by ^1H, *o*-phenylenediamine (**16a**) on addition of BH_3·THF afforded mono- (**16b**) and bisborane (**16c**) adducts, both with a similar ^{11}B chemical shift (−18 ppm). Observation of the ^{11}B spectra of **16b** and **16c** showed that these adducts undergo an intramolecular reaction with

Table 1. $^{11}B^{a}$ NMR spectra of mono- and bisborane adducts

Compound	δ (ppm)	J (Hz)
1b	−16.2	94
2b	−11.9(c)	97
	−11.4(c)[b]	97
3b	−5.8(c)	100
4b	−12.6(c)[b]	77
5b	−11.8(c)	100
	−11.4(c)[c]	100
6b	−12.2(c)	81
7b	−11.8(c)	81
8b	−4.8(c)[b]	101
10b	−18.8(c)	93
	−18.5(c)[b]	93
11b	−14.6(c)	93
	−14.0(c)[b]	93
13b	−19.7(c)	88
14b	−20.1(c)	90
15b	−19.5	102
16b	−18.5(c)	87
16c	−18.0	
16e	+23.75(d)	134
17b[d]	−17(c)	80
	−7(c)	99
17c	−6	96
	−17	
17d	−6	97
	+26	
18b	−16.3	
18c	−16.3	
19b	−18(c)	90
19c	−18(c)	77
20b[d]	−17	83
	−7(c)	98
20c	−6	97
	−16.5	
20d	+26	
	−6	
21b	−6.7(c)	96
21c	−5.5(c)	100

[a] In THF relative to $BF_3 \cdot Et_2O$ (32.1 MHz).
[b] In C_6H_6.
[c] In toluene.
[d] See Scheme 4.

the formation of a cyclic compound (**16e**)[11] (23.75 ppm) (Scheme 3).

The ^{11}B spectra of the *o*-phenylenediamine derivative (**17b**) and the *p*-phenylenediamine derivative (**20b**) showed two quartets at −7 ppm ($(CH_3)_2N:BH_3$) and −17 ppm ($H_2N:BH_3$) in the ratios shown in Scheme 4. On standing at room temperature an additional broad signal at ~26 ppm was attributed to the bisaminoboranes **17d** and **20d** (Scheme 4). The bisborane adducts **17c** and **20c** obtained by addition of two equivalents of $BH_3 \cdot THF$ also decomposed in solution, giving **17d** and **20d** as shown by the appearance of the signal at ~26 ppm.

The initial ratios of **17b** to **17b′** (20:80%) and **20b** to **20b′** (45:55%) are different, probably due to structural effects.

The formation of a kinetic (**20b′**) and a thermodynamic (**20b**) product is suggested due to an increase in the size of the signal for **20b** (45 → 67%) and a decrease in **20b′** (55 → 33%) on standing for 3 h at room temperature.

Formation of mono- and bisadducts derived from *o*-phenylenediamines (**16a** and **17a**) suggests that there is no appreciable steric hindrance in such systems. On the other hand, the *m*- and *p*-phenylenediamine derivatives (**18b** and **c**, and **19b** and **c**) polymerize on standing in solution at room temperature and were not further investigated.

^{1}H *NMR studies*

Aryl-, benzyl- and phenethylamines. The ^{1}H NMR resonances of borane adducts **1b–7b**, **10b**, **11b** and **13b–15b** are summarized in Table 2 together with the literature values for **1a–15a**. The data show that the *N*-aryl-coordinated species **1b–7b** show a *considerable* downfield shift, particularly for the *o*-protons while the benzyl and phenethylamine derivatives (**10b**, **11b** and **13b–15b**) are essentially unaffected. In general δ for the aliphatic groups remained invariant ($\Delta\delta$ 0.05–0.2 ppm).

Freezing of N-inversion in **4b–6b**, **10b**, **11b** and **13b** was evident in the ^{1}H spectra which showed complex patterns due to the presence of diastereotopic protons. Also, an increased complexity of the aromatic proton multiplicities for **1b**, **2b**, **4b** and **6b** was observed.

N-dimethyl- and *N*-diethylaniline adducts (**3b** and **5b**) undergo large downfield shifts for the *o*-hydrogens, due to steric effects, while, the *m*- and *p*-hydrogens show shifts similar to benzene.

It has been shown that HCNH coupling constants are observed only when the nitrogen involved is a weak base[12] and the N—H dissociation is very slow ($pK_a < 1.3$).[13] In this study, although the HCNH couplings were observed for **2b**, **6b**, **11b**, **13b** and **15b**, the complexity of the systems allowed measurements only for **2b** and **15b** (Table 2).

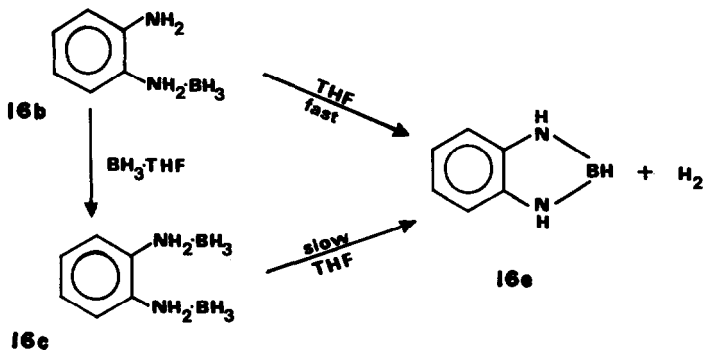
Phenylenediamines. As already mentioned, ^{1}H NMR spectroscopy allowed reliable detection of mono- and bisboranephenylenediamine adducts (**16b** and **c–21b** and **c**) (Table 3). In these cases adduct formation causes large downfield shifts of the aromatic and —NH($\Delta\delta \cong 3$ ppm) resonances

Table 2. $^1H^a$ spectra of *N*-arylamine, *N*-benzyl- and *N*-phenethylamine, and their borane adducts

	Aromatic proton			*N*-substituent	
Compound	2,6-H	3,5-H	4-H	R_1	R_2
1a[b]	6.4(d) 7 Hz	7.1(t) 7 Hz	6.7(t) 7 Hz	3.08(s)	3.08(s)
1b[b]		6.8–7.4(m)		6.8–7.4(m)	
2a[c]	6.4(d) 8 Hz	7.1(t) 8 Hz	6.6(t) 8 Hz	3.3(s)	2.7(s)
2b[c]		7.15–7.5(m)		6.5(br)	2.9(d) 6 Hz
3a	6.7(m)	7.2(m)	6.7(m)	2.9(s)	2.9(s)
3b	7.5–7.7(m)	7.1–7.4(m)	7.1–7.4(m)	3.0(s)	3.0(s)
4a[c]	6.4(d) 7 Hz	7.1(t) 7 Hz	6.6(t) 7 Hz	3.2(s)	3.0(C, 2H) 1.1(t, 3H) 7 Hz
4b[c]		7.2–7.4(m)		6.2(br)	2.9–3.6(m, 2H) 1.0(t, 3H) 7 Hz
5a[c]	6.9–7.2(m)	6.4–6.7(m)	6.4–6.7(m)	3.2(C, 2H) 1.05(t, 3H) 7 Hz	3.2(C, 2H) 1.05(t, 3H) 7 Hz
5b[c]	7.5–7.8(m)	7.1–7.5(m)	7.1–7.5(m)	3.3(C, 2H) 1.05(t, 3H) 7 Hz	3.3(c, 2H) 1.05(t, 3H) 7 Hz
6a	6.6(d) 8 Hz	7.2(t) 8 Hz	6.7(t) 8 Hz	3.9(s)	4.3(s, 2H) 7.3–7.5(m, 5H)
6b		6.8–7.4(m)		6.0(br)	3.9–4.8(m) 6.8–7.4(m)
7a[d]		6.6–7.4(m)		5.2–5.8(br)	6.6–7.4(m)
7b		6.8–7.6(m)		5.7(br)	6.8–7.6(m)
8a		6.8–7.43(m)		3.28(s)	6.8–7.43(m)
9a[d]		6.6–7.5(m)		6.6–7.5(m)	

				Other carbons	
				Cα	Cβ
10a	7.3(s)	1.35(s)	1.35(s)	3.8(s)	
10b	7.15–7.45(m)		3.7–4.5(m)	3.7–4.5(m)	
11a	7.15–7.45(m)	1.5(s)	3.75(s) 7.15–7.45(m)	3.75(s)	
11b	7.1–7.5(m)	3.5–4.3(m)	3.5–4.3(m) 7.1–7.5(m)	3.5–4.3(m)	
12a[d]	7.0–7.5(m)	3.6(s) 7.0–7.5(m)	3.6(s) 7.0–7.5(m)	3.6(s)	
13a	7.2(s)	1.0(s)	1.0(s)		2.8(m)
13b	7.0–7.4(m)	3.8(br)	3.8(br)		2.75–3.1(m)
14a[b]	7.0–7.4(m)	1.0(s)	1.0(s)	3.8(C, 1H) 1.15(d, 3H) 7 Hz	
14b[b]	6.7–7.3(m)		3.2–3.9(m)	3.2–3.9(m) 1.25(d, 3H) 7 Hz	
15a	7.1–7.5(m)	1.6(s)	1.6(s)	5.05(s) 7.1–7.5(m)	
15b	7.0–7.4(m)	4.6(br)	4.6(br)	5.0(t) 6 Hz 7.0–7.4(m)	

[a] All chemical shifts relative to TMS ($\delta = 0$) (90 MHz). In $CDCl_3$.
[b] In C_6D_6.
[c] In CCl_4.
[d] Reference 23.



Scheme 3.

of the **c** species, while the methyl signals are less affected. The aromatic protons in the *p*-substituted species **19b** and **21b** show A_2X_2 systems, while **19c** and **21c** are singlets, as are **19a** and **21a**.

The selective formation of the monoadduct is indicative of a decrease in the electron donating of nitrogen after monocoordination, thus rendering the remaining amino group less basic. This fact has also been observed in *p*-substituted aniline studies.[14]

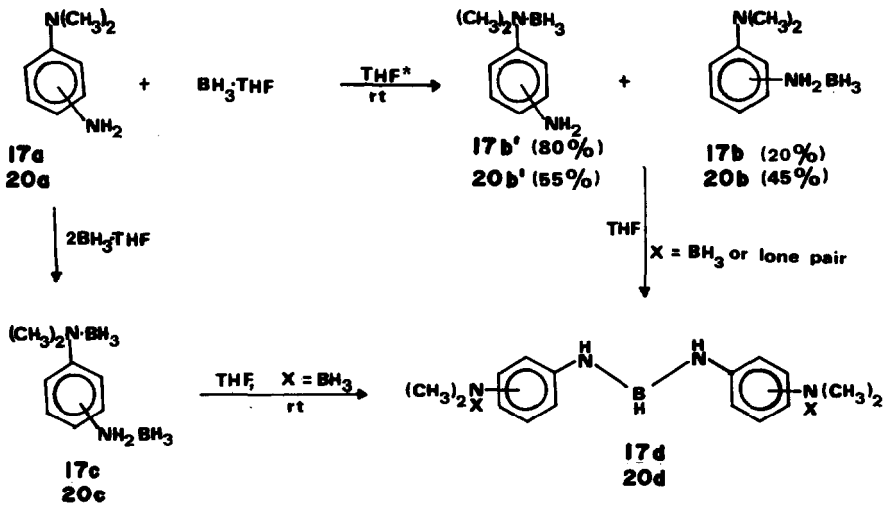
IR studies

As far as the IR spectra of the borane adducts are concerned (Table 4) the bands attributed to B—H (2200–2450 cm^{-1}), B—N (1100–1200 cm^{-1})[15] and N—H (3120–3324 cm^{-1}) were analyzed to obtain information concerning the influence of the charge on the boron and nitrogen atoms on the frequency of the corresponding vibrations[16] as well as the effect of various substituents on the nitrogen.

Table 4 shows that the asymmetric B—N stretching bands of borane adducts derived from primary amines (**10b**, **13b**, **14b** and **15b**) show very similar frequencies (1167–1170 cm^{-1}) while a delocalization effect is evident in the aniline derivative **1b**, where the corresponding band appears at 1139 cm^{-1}, the secondary amine derivatives (**2b**, **4b**, **6b**, **7b** and **11b**) being in the 1137–1165 cm^{-1} region. Arylamines having different electron-releasing alkyl substituents on the nitrogen (**2b**, **4b** and **6b**) showed identical B—N frequencies (1160 cm^{-1}).

In the case of tertiary amines (**3b**, **5b** and **12b**) the B—N frequency appeared between 1165 and 1176 cm^{-1}, except for the weakly basic complex **8b** (1100 cm^{-1}). This observation indicates that there is no direct correlation between absorption frequency and stability.

It is interesting to notice that the IR spectra of mono- (**19b** and **21b**) and bisborane adducts (**19c**



Scheme 4. *17c or **20c** could be another precursor of **17d** or **20d**, respectively, but according to monoboration selectivity may be less probable.

Table 3. $^{1}H^{a}$ NMR spectra of phenylenediamines and their corresponding borane adducts

Compound		Aromatic protons	*N*-protons			
			NH_2	NMe_2	NH_2BH_3	NMe_2BH_3
	H(3,4,5,6)					
16a[b]		6.54(s)	3.74(s)			
16b[c]		6.0–7.3(m)	4.3(br)		6.0–7.3(m)	
16c[c]		7.27(s)			6.9(br)	
17a		6.55(s)	4.35(br)	2.70(s)		
		6.4–6.75(m)[d]	2.80(br)	2.60(s)		
17c[c]		7.2–7.8(m)			6.8(br)	3.0(s)
	H(2,4,5,6)					
18a		6.0(m)	4.75(br)			
		7.0(m)				
18b[c]		5.9–7.4(m)	4.4(br)		5.9–7.4(m)	
18c[c]		7.0–8.0(m)			7.0–8.0(m)	
	H(2,3,5,6)					
19a		6.5(s)	4.3(s)			
19b	H(2,6)	7.1(d)	4.9(br)		[e]	
		8 Hz				
	H(3,5)	6.7(d)				
		8 Hz				
19c		7.3(s)			7.5(s)	
20a[f]		6.6–7.1(m)		2.80(s)		
20c[c]		6.8–7.4(m)			[e]	[g]
21a[f]		6.7(s)		2.80(s)		
21b[f]	H(2,6)	7.5(d)		3.0(s)		3.1(s)
		9 Hz				
	H(3,5)	6.7(d)				
		9 Hz				
21c[f]		7.6(s)				3.1(s)

[a] All chemical shifts are related to TMS ($\delta = 0$) (90 MHz). In $(CD_3)_2SO$.
[b] In TDF.
[c] In THF.
[d] In C_6D_6.
[e] Overlapped in aromatic region.
[f] In $CDCl_3$.
[g] Overlapped in THF region.

and **21c**) of phenylenediamines show distinct frequencies depending on whether one or two molecules of BH_3 are coordinated (Table 4). Also the free amino group in the monoborane adducts (**19b** and **21b**) produces a stronger N–B coordination with respect to the bisborane adducts (**19c** and **21c**). Compounds **16–18** and **20** were not analyzed due to superposition of solvent bands.

The data summarized in Table 4 allow us to conclude that, although the arylamine adducts are more affected than the benzyl or phenethyl derivatives, there is not a straightforward correlation between the strength of the B—N bond and the observed IR frequency.

Study of the relative affinity of aromatic amines to BH_3 *by equilibria reactions*

Early qualitative studies of molecular addition compounds of amine with BF_3[17] and $B(CH_3)_3$[18] established the importance of steric effects on the stabilities of the addition compounds. Subsequent equilibria studies by calorimetric measurements,[19] IR[20] and, more recently, ^{11}B NMR[21] techniques, have been helpful not only in studying steric effects, but also in understanding the mechanisms involved in these reactions.

Here, we have chosen arylamine adducts (**1b–7b**) for a detailed study of the base strength and steric

Table 4. IR data for amines and borane adducts

Compound	B—H	B—N	N—H	Phase
1a			3430(s), 3354(s) 3211(m)	Neat film
1b	2377(s), 2370(s) 2364(s), 2326(s) 2257(s)	1139(s)	3252(s), 3223(s) 3150(s)	KBr
2a			3442(m)	CCl_4
2b	2387(s), 2384(s) 2319(s), 2271(m)	1160(s)	3191(s)	CCl_4
3b	2387(s), 2325(m) 2278(m)	1165(s)		CCl_4
4a			3420(w)	CCl_4
4b	2393(s), 2326(s) 2273(s)	1160(s)	3189(s)	CCl_4
5b	3412(s), 2360(s) 2296(s)	1176(s)		CCl_4
6a			3418(s)	KBr
6b	2411(s), 2332(s) 2326(s), 2273(s)	1160(s)	3189(s)	KBr
7a			3330(m)	KBr
7b	2377(s), 2326(s) 2296(m)	1137(s)	3173(m)	KBr
8b	2410(m), 2430(m)	1100(s), 1085(s)		C_6H_6
10a			3377(m)	$CHCl_3$
10b	2381(s), 2329(s) 2275(s)	1167(s)	3324(m), 3226(m)	$CHCl_3$
11a			3347(w), 3317(w)	CCl_4
11b	2374(s), 2342(s) 2317(s), 2275(m)	1165(s)	3189(m)	CCl_4
12b	2391(s), 2340(s) 2292(m)	1170(s)		KBr
13a			3381(m)	CCl_4
13b	2381(s), 2322(s) 2272(s)	1168(s)	3234(s)	CCl_4
14a			3377(w), 3344(w)	C_6H_6
14b	2405(m), 2344(s) 2273(s)	1170(s)	3246(s), 3222(s)	KBr
15a			3374(m), 3304(w)	$CHCl_3$
15b	2385(s), 2355(s) 2322(s), 2283(m)	1168(s)	3323(m), 3307(m) 3276(m)	$CHCl_3$
19a			3409(m), 3383(m) 3374(s), 3308(m) 3302(m), 3204(m)	KBr
19b	2365(s), 2320(s) 2270(m)	1162(s)	3420(s), 3340(s) 3208(s), 3171(s)	KBr
19c	2388(s), 2380(s) 2376(s), 2335(s) 2261(m)	1132(s)	3246(s), 3212(s) 3134(m)	KBr
21b	2380(s), 2384(m) 2326(m), 2276(m)	1165(s)		KBr
21c	2387(s), 2376(s) 2316(m), 2275(m)	1146(s)		KBr

effects on NMR shifts. As mentioned before the base strength of the amines has little effect on ^{1}H and ^{11}B shifts. It can be shown, however, that a study of different equilibria in solution between arylaminoboranes (**1b–7b**) and aromatic amines (**1a–7a**) can be successfully carried out using NMR techniques. The results of equilibria are summarized (Table 5), the data showing that the extent of complexation reflects the relative basicity or affinity of each amine for BH_3.

The experiments were conducted by adding a stroichiometric amount of $BH_3 \cdot THF$ (2 M) to a solution of amine at $-78°C$ in THF (^{11}B NMR) or TDF (^{1}H NMR) under a nitrogen atmosphere, followed by addition of one equivalent of the second amine. The solution was then stirred until it reached room temperature. Exactly the same procedure using the reverse order of addition of the amines was also carried out as described in Scheme 5; a good agreement between both experiments was observed in all cases. Moreover, integration of the area under the ^{11}B NMR peak allowed us to obtain a rough estimate of the species present in solution. However, in some cases, the ^{11}B resonances of the adducts possessed similar chemical shifts or were too broad to allow a clear distinction of the aminoboranes. In such cases, a qualitative estimation of the equilibrium was made by ^{1}H NMR (Table 5).

Attempts to study the equilibrium reaction between benzyl- or phenethylamine and their borane derivatives were unsuccessful due to a strong $N \rightarrow BH_3$ coordination.

According to Table 5, it can be concluded that the base strength of the aromatic amine studied decreases in the following order: **2a**(130) > **1a**(100) > **4a**(90) > **3a**(30) > **7a**(5.6) ≅ **5a**(5) > **6a**(1) (relative to **6a**).

The above results clearly demonstrate that: (a) as the number of aryl substituents increases the affinity of the amine for the borane molecule decreases; and (b) in secondary amines, this N—B bond strength increases in the following order: $CH_3 > CH_2CH_3 > C_6H_5 > CH_2C_6H_5$; while in tertiary amines, the trend is $(CH_3)_2 > (CH_2CH_3)_2 > (CH_3)(C_6H_5) > (C_6H_5)_2$.

Table 5. Relative affinity of aromatic amines to BH_3 by equilibria reactions[a]

^{11}B NMR studies	
5b + **3a** ⇆ **3b** + **5a**	**7b** + **11a** ⇆ **11b** + **7a**
(14) (86)	(0) (100)
1b + **10a** ⇆ **10b** + **1a**	**7b** + **1a** ⇆ **1b** + **7a**
(0) (100)	(0) (100)
3b + **1a** ⇆ **1b** + **3a**	**3b** + **2a** ⇆ **2b** + **3a**
(24) (76)	(30) (70)
6b + **11a** ⇆ **11b** + **6a**	**1b** + **13a** ⇆ **13b** + **1a**
(0) (100)	(0) (100)
5b + **1a** ⇆ **1b** + **5a**	**6b** + **3a** ⇆ **3b** + **6a**
(0) (100)	(38) (62)
6b + **1a** ⇆ **1b** + **6a**	**3b** + **4a** ⇆ **4b** + **3a**
(0) (100)	(32) (68)
^{1}H NMR studies	
1b + **2a** ⇆ **2b** + **1a**	**4b** + **2a** ⇆ **2b** + **4a**
(44) (56)	(42) (58)
5b + **6a** ⇆ **6b** + **5a**	**7b** + **5a** ⇆ **5b** + **7a**
(83) (17)	(53) (47)
1b + **4a** ⇆ **4b** + **1a**	**3b** + **7a** ⇆ **7b** + **3a**
(55) (45)	(88) (12)

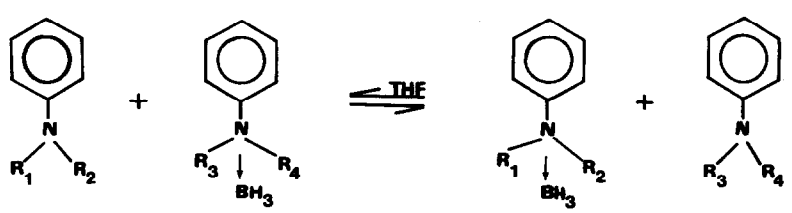
[a] As described in text and Scheme 5. Values in parentheses are % of the adduct formed.

In terms of base strength and the stability of the adduct formed, we can conclude that these aromatic adducts studied are more reactive than the aliphatic ones and therefore potentially useful reagents in synthesis.[1]

Finally, the spectroscopic methods employed suggest that we must be careful in the interpretation of the nature of the N—B bond since there is not a direct relationship between the chemical-shift or frequency data obtained and the basicity of the aromatic amines.

EXPERIMENTAL

^{11}B NMR spectra were recorded on a Varian XL-100A (32.1 MHz). ^{1}H NMR spectra were obtained with a Varian EM-390 spectrometer. Chemical shifts are relative to $BF_3 \cdot Et_2O$ and TMS. IR were



Scheme 5.

obtained on a Nicolet MX-1-FT spectrophotometer.

Dry solvents were distilled under dry nitrogen just before use: THF from $LiAlH_4$, hexane and benzene from sodium metal. Diborane and $BH_3 \cdot THF$ were prepared by published procedures.[22] Reagents were commercially available samples used without previous purification. All reactions were carried out under a dry nitrogen atmosphere.

General procedure for the preparation of N-*borane amine adducts* (**1–7b** *and* **10–15b**) *and the mono- and bisborane adducts* (**19b** *and* **c**, *and* **21b** *and* **c**)

To a stirred and ice-cooled solution of the amine (10 mmol) in 4 cm^3 of THF, a 2.0 M $BH_3 \cdot THF$ (15 mmol for amines **1a–7a** and **10a–15a**; 10 and 25 mmol for the mono- and bisadducts of phenylenediamines **19a** and **21a**, respectively) was added dropwise. Immediately, after the addition, the solvent and excess of $BH_3 \cdot THF$ were removed at reduced pressure, affording quantitative yields of the crude adducts.

The same procedure was carried out with phenylenediamines **16a–18a** and **20a**. However, attempts to isolate the corresponding adducts **16b** and **c**, **17c**, **18b** and **c** and **20c** were unsuccessful, and they were directly studied in THF solution.

N-*diphenylmethylamineborane* (**8b**)

Amine **8a** (0.13 g, 0.71 mmol) was dissolved in benzene (4 cm^3). The solution was stirred at 8°C and diborane 35:1 diborane:amine molar ratio was passed through the solution for ~3 h. Isolation was not carried out, because removal of the solvent under reduced pressure led to decomposition.

Acknowledgements—We are thankful to CONACYT—Mexico for providing financial support and also to Dr Rosa Santillán for reading the manuscript and for her helpful comments.

REFERENCES

1. R. O. Hutchins, K. Learn, B. Nazer, D. Pytlewski and A. Pelter, *Org. Preparations Procedures Int.* 1984, **16**, 335.
2. H. C. Brown and L. T. Murray, *Inorg. Chem.* 1984, **23**, 2746.
3. R. Köster, H. Bellut and S. Hattori, *Liebigs Ann. Chem.* 1968, **720**, 1.
4. M. Añez, G. Uribe, L. Mendoza and R. Contreras, *Synthesis* 1981, 214.
5. C. Camacho, G. Uribe and R. Contreras, *Synthesis* 1982, 1027.
6. Aldrich Catalog, 472 (1984–1985).
7. E. F. Mooney and M. A. Qaseem, *J. Inorg. Nucl. Chem.* 1968, **30**, 1439.
8. C. J. Foret, M. A. Chiusano, J. D. O'Brien and D. R. Martin, *J. Inorg. Nucl. Chem.* 1980, **42**, 165.
9. (a) N. F. Hall and M. R. Sprinkle, *J. Am. Chem. Soc.* 1932, **54**, 3469; (b) A. J. Hoefnagel, M. A. Hoefnagel and B. M. Wepster, *J. Org. Chem.* 1981, **46**, 4209.
10. R. Contreras, F. Santiesteban, M. A. Paz-Sandoval and B. Wrackmeyer, *Tetrahedron* 1984, **40**, 3829.
11. H. R. Morales, H. Tlahuext, F. Santiesteban and R. Contreras, *Spectrochim. Acta* 1984, **40A**, 855.
12. J. H. Clark, J. M. Miller and S. Paone, *J. Chem. Soc., Chem. Commun.* 1982, 63.
13. I. D. Rae, *Aust. J. Chem.* 1966, **19**, 409.
14. J. E. Parr and E. Wasylishen, *J. Mol. Struct.* 1977, **38**, 272.
15. (a) T. Mancilla, F. Santiesteban, R. Contreras and A. Klaébé, *Tetrahedron Lett.* 1982, **29**, 1561; (b) N. Farfán and R. Contreras, *Nouv. J. Chim.* 1982, **6**, 269.
16. B. Rice, R. J. Galiano and W. J. Lehman, *J. Phys. Chem.* 1957, **61**, 1222.
17. H. C. Brown, H. I. Schlesinger and S. Z. Cardon, *J. Am. Chem. Soc.* 1942, **64**, 325.
18. H. C. Brown, *J. Am. Chem. Soc.* 1945, **67**, 378, 1452.
19. H. C. Brown and L. Domash, *J. Am. Chem. Soc.* 1956, **78**, 5384.
20. H. C. Brown and K. K. Wang, *Recl Trav. Chim. Pays-Bas* 1979, **98**, 117.
21. H. C. Brown and G. G. Pai, *J. Org. Chem.* 1981, **46**, 4713 (and references therein).
22. H. C. Brown, *Organic Syntheses via Boranes*. John Wiley, New York (1975).
23. Ch. J. Pouchert and J. R. Campbell, *The Aldrich Library of NMR Spectra* (1974).

Polyhedron Vol. 5, No. 11, pp. 1733–1740, 1986
Printed in Great Britain

0277–5387/86 $3.00+.00
Pergamon Journals Ltd

PREPARATION AND CHARACTERIZATION OF OCTACYANOMOLYBDATES(IV AND V) AND OCTACYANOTUNGSTATES(IV AND V) WITH 2,2′-BIPYRIDYLIUM CATION

J. SZKLARZEWICZ, A. SAMOTUS* and A. KANAS

Faculty of Chemistry, Jagiellonian University, Kraków, Poland

(*Received* 8 *November* 1985; *accepted* 27 *January* 1986)

Abstract—Reaction of protonated 2,2′-bipyridine (bpy) with octacyanometalates(IV and V), $[M(CN)_8]^{n-}$ (M = Mo or W, $n = 3$ or 4), gave the following complexes: $\{(bpyH)_3[M(CN)_8]\cdot 4H_2O\}$, $\{(bpyH)_3(H_3O)[M(CN)_8]\cdot H_2O\}$, $\{(bpyH_2)_2[W(CN)_8]\cdot 3H_2O\}$ and $\{(bpyH_2)K_2[W(CN)_8]\cdot 2H_2SO_4\cdot 7H_2O\}$. These salts were characterized by electron absorption and reflectance spectrometry, IR, Raman and ESR spectrometry, thermogravimetry and differential thermal analysis, cyclic voltammetry and potentiometry. The solubility of the salts in water and some polar organic solvents has been measured. The intensively coloured salts of molybdenum(IV) and tungsten(IV) have been discussed in terms of the $bpyH^+$–$[M(CN)_8]^{4-}$ ion pairs, which exhibit an outer-sphere electron transfer between adjacent redox sites.

The ability of octacyanometalates(IV and V) (M = Mo or W) to form compounds with several metallic and organic cations is well-established.[1] These compounds are characterized by a cation-dependent crystal structure[2] and a strong tendency to ion-pair formation in solution.[3] In the course of a study on the photochemistry of octacyanometalates(IV and V) we became involved in an investigation of the interaction of complex anions with several cations.[4] By interaction of $[M(CN)_8]^{n-}$ ($n = 3$ or 4) with 2,2′-bipyridine (bpy) in acidic aqueous solution we obtained a series of new bipyridylium salts[5] and found evidence of a cation–anion association in aqueous and non-aqueous solutions. Accordingly, ion-pair or outer-sphere complexes of type $bpyH^+$–$[M(CN)_8]^{4-}$ which are characterized by an optical charge-transfer (CT) transition represent a new class of photochemically active systems. In this paper we have described the preparation and physicochemical properties of the salts $\{(bpyH)_3[M(CN)_8]\cdot 4H_2O\}$, $\{(bpyH)_3(H_3O)[M(CN)_8]\cdot H_2O\}$, $\{(bpyH_2)_2[W(CN)_8]\cdot 3H_2O\}$, and $\{(bpyH_2)K_2[W(CN)_8]\cdot 2H_2SO_4\cdot 7H_2O\}$.

* Author to whom correspondence should be addressed.

EXPERIMENTAL

Reagents and general procedure

All synthetic work was performed in red light under an argon atmosphere. Because of the low solubility of the 2,2′-bipyridylium salts in water the general method of preparation was the metathetical reaction of potassium octacyanides obtained as described earlier[6] with protonated bpy in aqueous solution of various acidity. Bpy (c.p.a. POCh) was recrystallized from 50% ethanol. The purity was checked by measuring the IR spectra before and after crystallization (m.p. = 70.5 ± 0.5°C).

Syntheses

Tris (2,2′-bipyridylium) octacyanomolybdate(V) tetrahydrate, $\{(bpyH)_3[Mo(CN)_8]\cdot 4H_2O\}$ (A). Method (a). To an aqueous solution of $K_3[Mo(CN)_8]$ (*ca* 0.02 M) 0.25 M bpy in 0.5 M H_2SO_4 was slowly added with mixing, resulting in the precipitation of light yellow crystals which were then filtered off and washed with water, methanol, and finally with diethyl ether.

Method (b). The saturated solution of $\{(bpyH)_3(H_3O)[Mo(CN)_8]\cdot H_2O\}$ (*vide infra*) in 0.5 M H_2SO_4 was oxidized with potassium per-

manganate resulting in the precipitation of the less soluble salt of molybdenum(V). The solid obtained was collected by filtration and recrystallised twice from water. Found: C, 53.4; H, 3.9; N, 23.7; Mo, 11.4; CN^-, 24.0; H_2O (1), 8.2; H_2O (2), 8.4; bpy, 55.1%. Calc.: C, 53.7; H, 4.2; N, 23.1; Mo, 11.3; CN^-, 24.5; H_2O, 8.4; bpy, 55.2%.

Tris (2,2′-*bipyridylium*) *octacyanotungstate*(V) *tetrahydrate*, $\{(bpyH)_3[W(CN)_8]\cdot 4H_2O\}$ (**B**). The procedure was analogous to the preparation of $\{(bpyH)_3[Mo(CN)_8]\cdot 4H_2O\}$ [methods (a) and (b)], resulting in the precipitation of white crystals. Found: C, 48.4; H, 3.5; N, 21.4; W, 19.9; H_2O (1), 7.7; H_2O (2), 8.0; bpy, 49.3%. Calc.: C, 48.6; H, 3.9; N, 20.9; W, 19.7; H_2O, 7.6; bpy, 50.0%.

Tris (2,2′-*bipyridylium*) *hydroxonium octacyanomolybdate*(IV) *monohydrate*, $\{(bpyH)_3(H_3O)[Mo(CN)_8]\cdot H_2O\}$ (**C**). In a typical preparation, 1.24 g (2.5 mmol) of $K_4[Mo(CN)_8]\cdot 2H_2O$ was dissolved in 50 cm^3 of water and a solution of 1.95 g (12.5 mmol) of bpy in 50 cm^3 of 0.5 M H_2SO_4 was added dropwise. The solution changed the colour from yellow to orange, and after stirring a yellow crystalline precipitate was formed. The product was filtered off, washed with water, methanol and ether, and dried at room temperature. The product when dried for about 3 days lost 8–10 water molecules, changing in colour from yellow to pale-orange. Found: C, 56.2; H, 3.9; N, 24.5; Mo, 11.7; CN^-, 25.4; bpy + H_2O, 62.3%. Calc.: C, 56.1; H, 3.9; N, 24.1; Mo, 11.8; CN^-, 25.5; bpy + H_2O, 62.0%.

$\{(bpyH)_3(H_3O)[Mo(CN)_8]\cdot H_2O\}$ when dried *in vacuo* over P_4O_{10} at room temperature lost 2.2% of its weight. This corresponds to the loss of one water molecule (calc. loss for one H_2O = 2.2%).

Tris (2,2′-*bipyridylium*) *hydroxonium octacyanotungstate*(IV) *monohydrate*, $\{(bpyH)_3(H_3O)[W(CN)_8]\cdot H_2O\}$ (**D**). To 1.46 g (2.5 mmol) of $K_4[W(CN)_8]\cdot 2H_2O$ in 50 cm^3 of water a solution of 1.95 g (12.5 mmol) of bpy in 50 cm^3 of water was slowly added, causing a change in colour from yellow to red and the precipitation of pale-red crystals. After 1 day the crystals were filtered off, washed 3 times with water, methanol and ether, and dried at room temperature. The crystals turn brown upon drying together with the loss of 6–7 mol of water per mol of complex. Found: C, 50.9; H, 3.6; N, 21.8; W, 20.4; CN^-, 22.6; bpy + H_2O, 55.3%. Calc.: C, 50.6; H, 3.6; N, 21.8; W, 20.4; CN^-, 23.1; bpy + H_2O, 56.1%. H_2O calc. for two water molecules should be 4.0% whereas the found H_2O (2) = 1.7%, which means that only one water molecule can be removed by isothermal dehydration.

Bis (2,2′-*bispyridinium*) *octacyanotungstate*(IV) *trihydrate*, $\{(bpyH_2)_2[W(CN)_8]\cdot 3H_2O\}$ (**E**). 2.0 g (7.7 mmol) of $K_4[W(CN)_8]\cdot 2H_2O$ was dissolved in approximately 5 cm^3 of water and a solution of 1.7 g (10.9 mmol) of bpy in 18 cm^3 of 7 M H_2SO_4 was slowly added. The solution changed in colour to a deep red-brown. After 3 days standing in a refrigerator (under argon) the resulting black crystals were filtered off, carefully washed with diethyl ether, and dried at room temperature. Found: C, 45.5; N, 21.3; W, 24.6; H_2O (2), 7.4; bpy, 44.3%.* Calc.: C, 45.1; N, 22.0; W, 24.1; H_2O, 7.2; bpy 41.0%.

$\{(bpyH_2)K_2[W(CN)_8]\cdot 2H_2SO_4\cdot 7H_2O\}$ (**F**). To 2.92 g (5 mmol) of $K_4[W(CN)_8]\cdot 2H_2O$ in 4 cm^3 of water a solution of 1.56 g (10 mmol) of bpy in 20 cm^3 of H_2SO_4 (1 : 1) was slowly added. Red-brown crystals were filtered off and carefully washed with diethyl ether. Found: C, 23.6; H, 3.0; N, 14.4; SO_4^{2-}, 22.2; WO_3+K_2O, 34.0; H_2O (2), 12.8%. Calc.: C, 22.7; H, 3.0; N, 14.8; SO_4^{2-}, 20.2; WO_3+K_2O, 34.3; H_2O, 12.2%.

Analytical methods

Carbon, nitrogen and hydrogen were determined by organic microanalysis (in the presence of $PbCrO_4$). Molybdenum and tungsten were determined gravimetrically as MO_3 after thermal decomposition of the sample (except for salt **F** for which the sum of the oxides WO_3+K_2O was determined gravimetrically). Water was determined by thermal gravimetric analysis, H_2O (1), and by isothermal dehydration *in vacuo* over P_4O_{10}, H_2O (2). Bpy was determined by thermal gravimetric analysis. In the case when water and bpy were removed together the sum, bpy + H_2O, was determined by thermal gravimetric analysis. Cyanide ions were determined by Volhard's method after photochemical decomposition of the sample in alkaline solution. Sulphate ions were determined gravimetrically as $BaSO_4$. The presence of potassium in salt **F** was found by flame photometry.

Solubility of the salts in water and organic solvents was determined at 21.5 (±0.5)°C in two ways: (i) by measuring UV–visible spectra of saturated solution and assuming for calculations molar extinction coefficients as given in Table 1, and (ii) gravimetrically by evaporation of the saturated solution to dryness.

Physical measurements

Electronic absorption and reflectance spectra were recorded on a Specord UV–visible spectrometer (Zeiss). IR spectra in the 400–4000- and 100–500-cm^{-1} ranges were recorded on a Zeiss

* Partial decomposition of the sample was observed.

Table 1. Summary of TG and DTA data

Salt	T_{max} (°C)	% weight loss	H_2O/M	bpy/M	(H_2O+bpy)/M
A	53	5.4	2.6	—	—
	76	2.1	1.0	—	—
	159	55.7	—	3.0	—
B	59	5.6	3.0	—	—
	82	2.1	1.1	—	—
	191	49.3	—	3.0	—
C	130, 134	20.5	—	—	2+0.8
	156	31.8	—	1.6	—
	231	10.0	—	0.5	—
D	126, 147	22.7	—	—	2+1.1
	189	22.7	—	1.3	—
	232	9.9	—	0.6	—
E	125	8.6	—	—	3.0+0.1
	148, 156, 189	44.2	—	2.1	—

UR-10 spectrophotometer and a "Digilab" interferometric spectrometer FTS-14,* respectively. Samples were prepared as Nujol mulls, KBr pellets and/or as thin films on polyethylene. Raman spectra were recorded with a Cary 82 spectrometer* using the 514.5-nm exciting line. The thermogravimetric (TG) and differential thermal analysis (DTA) analyses were performed under argon with a heating rate of 2 and 5°C min^{-1} on a Mettler thermoanalyser.* ESR spectra were recorded with a SE/X-25 spectrometer* (Poland) using $(bpyH)_3[M(CN)_8]\cdot 4H_2O$ as a standard for estimation of the content of M(V) in the M(IV) complexes. Potentiometric titrations were carried out by using a Radelkis pH-meter, Model OP-211 standardized in the usual way. Cyclic voltammograms† were scanned using approximately 10^{-3} M solutions of the complexes in 0.1 M KCl with a conventional three-electrode setup as described elsewhere.[7] A platinum working electrode was used. The formal reduction potentials for the reversible couples were taken as the means of the anodic and cathodic peaks. Formal reduction potentials reported are all vs a normal hydrogen electrode (NHE).

RESULTS AND DISCUSSION

Synthesis and analysis

It was found that by addition of bpy to an acidic aqueous solution of octacyanometalates(IV and V) various complexes with protonated bpy as a cation can be isolated. The reaction of $[M(CN)_8]^{3-}$ gave white (W) and pale-yellow (Mo) crystals of $(bpyH)_3[M(CN)_8]\cdot 4H_2O$. The complexes are paramagnetic with an ESR spectrum typical for d^1-M(V) octacyanides.[8] Salts **A** and **B** behave as strong acids giving, during titration with NaOH, a single potential jump (Fig. 1), corresponding to the simultaneous neutralization of all $bpyH^+$ cations. The presence of the $bpyH^+$ cation is clearly seen in the electronic spectra due to the intensive interligand bands in the UV region. The thermal decomposition of the organic cation which occurred at a lower temperature than for the complex anion can also be used for analytical purposes.

Interestingly, the reaction between $[M(CN)_8]^{4-}$ and bpy in an acidic aqueous medium gives an intensively coloured solution, orange (Mo) or

* Measurements were performed in the Regional Laboratory of Physicochemical Analyses and Structural Research of Jagiellonian University, Kraków, Poland.

† Measurements were performed in the Department of Inorganic Chemistry I of Ruhr University, Bochum, F.R.G.

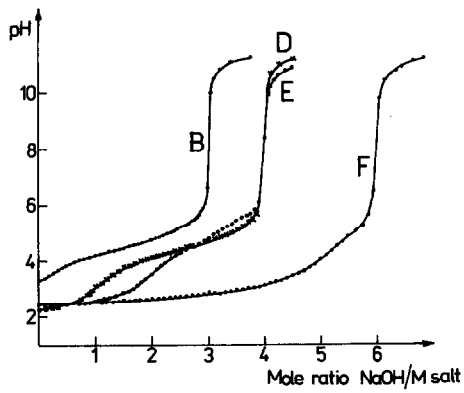


Fig. 1. Potentiometric pH titration of *ca* 0.001 M solution of salts **B**, **D**, **E** and **F** with 0.1 M NaOH.

red (W), from which coloured crystals of $\{(bpyH)_3(H_3O)[M(CN)_8]\cdot H_2O\}$ can be isolated. The d^2-$[M(CN)_8]^{4-}$ complexes should be diamagnetic but **C** and **D** contain *ca* 0.1 and 2.5%, respectively (see Table 2), of paramagnetic d^1-M(V). Potentiometric titrations with a standard NaOH solution clearly indicate two different types of protons with a molar ratio of 1:3 (Fig. 1). UV spectra give evidence of three protonated bpy per mol of salt. The assumption that the one additional proton is bound to one water molecule in the crystals was based on the following results: (i) under isothermal dehydration over P_4O_{10} only one water molecule was released, (ii) under thermal dehydration (see Table 1) the second water molecule was released together

Table 2. Selected IR frequencies[a] for $[M(CN)_8]^{n-}$ salts ($n = 3$ or 4)

Salt	ν(CN)	ν(MC) δ(MCN)	δ(CNC)	δ(HOH)	Some bands characteristic for protonated bpy
A	2110 vw 2130 w 2140 w 2132 vs[b] 2152 sh[b]	355 w 362 s 400 m 438 m 458 m 468 m	102 vw 136 w 152 w	1660 m	777 vs, 1228 w, 1281 w, 1436 s, 1461 s, 1476 s, 1532 s, 1587 vs, 1608 vs
B	2110 vw 2142 w 2156 w 2128 m[b] 2150 s[b]	336 w 378 s 398 m 440 m 447 m	102 vvw 140 m 175 w	1663 m	776 vs, 1230 w, 1281 m, 1436 m, 1461 m, 1476 m, 1532 vs, 1587 vs, 1608 vs
C	2120 vs 2141 vs 2150 sh	334 vw 346 vw 362 vw 375 w 398 vw 437 vw 457 vw 469 sh	102 m 152 vw 157 w 169 vw	1620 s 1700 vw, b	769 s, 1236 w, 1283 w, 1436 m, 1461 m, 1476 m, 1532 s, 1587 s, 1610 s
D	2118 vs 2141 vs 2150 s	334 vw 353 vw 374 sh 398 vw 437 vw 457 vw 469 sh	102 vvw 152 vw 168 vw	1620 s 1700 vw, b	768 s, 1236 w, 1283 w, 1436 m, 1461 m, 1476 m, 1532 s, 1587 vs, 1610 s
E	2118 vs 2140 s	—	—	1620 sh	772 m, 1275 m, 1432 m, b, 1522 m, 1596 s
F	2138 s	—	—	1620 sh	772 m, 1295 w

[a] The abbreviations v, s, m, w, sh and b denote very, strong, medium, weak, shoulder and broad.
[b] Bands in Raman spectrum.

with decomposition products of $bpyH^+$, and (iii) the IR spectra show the shoulder at 1700 cm^{-1} characteristic of the H_3O^+ bending mode. It should be mentioned that the X-ray structure determination of $\{[HN(C_2H_5)_3]_2[H_3O]_2[Mo(CN)_8]\}$[9] shows the existence of the H_3O^+ ion in the solid state.

Using more acidic solutions two other tungsten salts have been obtained: black **E** and red-brown **F**, the formulae of which are consistent with the analytical data, potentiometric (Fig. 1), TG (Table 1) and spectroscopic (Table 3) results. The last salt seems to be similar to a known adduct of tungstocyanide acid $\{H_4[W(CN)_8]\cdot 4HCl\cdot 12H_2O\}$.[10] Both salts contain some W(V): 28.8% (**E**) and 1.7% (**F**) (Table 3). The same synthetic procedure carried out to obtain molybdenum analogues of **E** and **F** caused the decomposition of the complex anion.

Several attempts were made to prepare the tetra(2,2′-bipyridylium) salts. However, such salts have not been obtained, most probably due to the steric reasons.

TG and DTA analyses

A summary of TG and DTA results is given in Table 1. In the temperature range investigated (20–350°C) the endothermic peaks and the weight loss are mainly due to the evolution of water and the decomposition of bpy. **A** and **B** began to lose water of hydration at about 40°C, giving two endothermic peaks in the temperature ranges 50–60 and 75–85°C, which correlates well with the loss of three and then one molecule of water per atom of metal (H_2O/M). The $bpyH^+$ cations decomposed at a much higher temperature with T_{max} (DTA peak maximum temperature) changing in the order W > Mo salt.

Table 3. UV–visible spectra and ESR data of complexes

		Solid		Solution	
Salt	Colour	λ_{max}[a]	% M(V)[b]	λ_{max}	ε_{max}[c]
A	Yellow	248	100	238	2.4×10^4
		310		300	3.8×10^4
		387		387	1.4×10^3
B	White	240	100	240	3.0×10^4
		310		300	4.1×10^4
		360		357	1.8×10^4
C	Orange	250	0.1	240	4.3×10^4
		310		300	4.4×10^4
		380		367	2.4×10^2
		420–440		420	1.0×10^2
		—		(490)[d]	8.3×10^0
D	Brown	256	2.5	246	4.6×10^4
		310		300	4.4×10^4
		370		362	3.3×10^2
		440–460		430	1.5×10^2
				(490)[d]	1.7×10^1
E	Black	—	28.8	246	3.5×10^4
				300	3.0×10^4
				362	2.9×10^2
				430	9.4×10^1
				(490)[d]	—
F	Brown	—	1.7	246	1.5×10^4
				300	1.3×10^4
				362	3.0×10^2
				430	1.6×10^0
				(490)[d]	—

[a] Reflectance spectra.
[b] Estimated from ESR spectra using **A** or **B** as standards.
[c] Apparent molar extinction coefficient.
[d] Band obtained from differential spectra.

There is a distinct difference in the behaviour of **A** and **B** and **C** and **D**. The latter salts seem to be strongly hydrogen bonded and on heating the release of water proceeded simultaneously with the decomposition of organic cations and even, at a higher temperature, complex anions. The separation between T_{max} for dehydration and decomposition of $bpyH^+$ for **E** is similar to that for **A** and **B**. This is consistent with the proposed formula with a diprotonated bpy and no H_3O^+ ion.

Spectra

Data for prominent bands in the IR and Raman* spectra are summarized in Table 2. The most characteristic bands are seen in the range 2180–2200 cm^{-1} (CN stretching), 1600–1700 cm^{-1} (H_2O and/or H_3O^+ bending), 1400–1600 cm^{-1} (ring C=N and C=C stretching, and ring H bending), 1200–1300 cm^{-1} (ring stretching and NH bending), 700–800 cm^{-1} (out-of-plane bending of the aromatic C—H), 300–500 cm^{-1} (M—C stretching and M—CN bending) and 100–200 cm^{-1} (C—M—C bending).

A and **B** show ν(CN) bands which are essentially identical to that of $M'[M(CN)_8]\cdot xH_2O$ ($M' = Na^+$, K^+, Rb^+, Cs^+ or $[(C_4H_9)_4N]^+$)[3(a),11] as well as the bands typical for $bpyH^+$ with a probable cissoid geometrical configuration.[12,13] The electronic spectra of the complexes in the solid state and in solution (Table 3) also exhibit bands characteristic of the component ions.[14,15] This clearly indicates that no significant interaction occurs between the $bpyH^+$ and $[M(CN)_8]^{3-}$ moieties.

C and **D** show a reduced number of ν(CN) bands and a shift of the maxima to higher frequencies in comparison with the $[M(CN)_8]^{4-}$ of D_{2d}-symmetry[16] (Table 2). The electronic spectrum of the complexes in the solid state exhibits a very broad band in the visible region, which may be due to an overlapping of the *d–d* band of $[M(CN)_8]^{4-}$ and the outer-sphere, intervalence CT (OSCT) band for the $bpyH^+$–$[M(CN)_8]^{4-}$ ion pair (Table 3 and Fig. 2). In solution the ion pair also exhibits a relatively low-energy absorption band visible to the eye as orange (Mo) or red (W) in a sufficiently concentrated solution of the ions. The band obtained from the differential spectrum is approximately Gaussian in shape and has a maximum at about 490 nm (Fig. 2). The extinction coefficient of the OSCT band for **D** seems to be higher than that of **C**, and at a higher concentration of both ions and in methanolic solution an increase in absorbance is observed in accordance with the increasing extent of ion-pair formation.

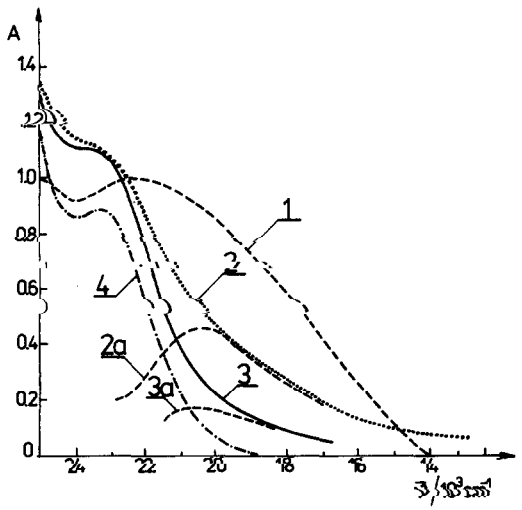


*Fig. 2. Reflectance spectrum (1) and absorption spectra of 0.0038 M solution of **B** ($d = 2$ cm) in CH_3OH (2) and H_2O (3) in comparison with the spectrum of $K_4[W(CN)_8]$ of the same concentration (4). The differential spectra 2a [(2)–(4)] and 3a [(3)–(4)] are given by dashed lines.*

The IR spectra in the solid state as well as the electronic spectra in solution clearly indicate the presence of monoprotonated bpy (the same bands as for **A** and **B**). On the other hand the IR spectra together with the potentiometric measurements are indicative of the H_3O^+ cation (weak band at *ca* 1700 cm^{-1}).

Salts **E** and **F** exhibit less IR bands in the 700–1600-cm^{-1} range than the other salts. This implies the presence of diprotonated bpy, $[bpyH_2]^{2+}$, which seems to occur in a transoid configuration[12,13] (the C_{2h} *trans*-configuration has a centre of symmetry, thus eliminating approximately half of the vibrational degrees of freedom from IR activity). After dissolution in water, the brown (**E**) and black (**F**) salts give electronic spectra identical to that of **D** due to the shift of the proton-transfer equilibria to the right

$$[bpyH_2]^{2+} + H_2O \rightleftharpoons bpyH^+ + H_3O^+.$$

Solubility

The solubility results for salts **A–D** in water and various polar organic solvents at 20 (±1)°C are shown in Table 4. The solubility of **A** and **B**

* The Raman spectra were obtained only for **A** and **B**. In the other cases decomposition of the complexes occurred under a 514-nm laser light.

Table 4. Solubility data (mmol dm^{-3}) and formal redox potentials (V) in various solvents at 20°C

	Solubility					
Solvent	A	B	C	D	E(A/C)	E(B/D)
H_2O	2.6	2.6	18.0	19.2	0.78	0.51
CH_3OH	3.3	8.6	2.8	8.4	0.58	0.32
C_2H_5OH	1.3	1.6	0.25	0.33	—	—
CH_3CN	2.6	2.6	0.06	0.21	0.51	0.26
DMSO	[a]	[a]	—	—	0.19	−0.06

[a] Solubility higher than 10 mmol dm^{-3}.

decreases in the order: DMSO > CH_3OH > H_2O ~ CH_3CN > C_2H_5OH, whereas that for **C** and **D** decreases in the order: H_2O > CH_3OH > C_2H_5OH > CH_3CN. In all cases the solubility of tungsten compounds is higher than that of molybdenum species.

Cyclic voltammetry

Electrochemical properties of octacyanometalates(IV) with protonated bpy as a cation in aqueous solution are in accord with those expected on the basis of existing data for $[M(CN)_8]^{n-}$.[17] The voltametric half-wave potentials vs NHE are presented in Table 4. The Mo and W complexes exhibit in water a couple, corresponding to a reversible one-electron oxidation at *ca* 0.78 and 0.51 V, respectively. Additionally these salts show an irreversible reduction at *ca* −0.38 V, most probably connected with a one-electron reduction of the $bpyH^+$ cation.

Standard redox potentials of the $[M(CN)_8]^{4-}$–$[M(CN)_8]^{3-}$ couple are solvent-dependent and decrease in the order: H_2O > CH_3OH > CH_3CN > DMSO. It seems that the changes are mainly due to preferential ion pairing with one redox component. The data in DMSO suggest that at least the W complex would be very air-sensitive because of the negative potential at which it is oxidized.

A fuller account of the electrochemical behaviour of $[M(CN)_8]^{n-}$ with various counter ions in water and in some polar organic solvents will be given elsewhere.[18]

Acknowledgements—We are greatly indebted to Prof. K. Wieghardt of Ruhr University, Bochum, F.R.G. for access to cyclic voltammetry equipment and stimulating discussion. This work was supported in part by the Polish Academy of Sciences.

REFERENCES

1. For reviews see, for example: (a) W. P. Griffith, *Chem. Rev.* 1975, **17**, 177; and (b) A. G. Sharpe, *The Chemistry of Cyano Complexes of the Transition Metals*. Academic Press, London (1976).
2. J. G. Leipoldt, S. S. Basson and L. D. C. Bok, *Inorg. Chim. Acta* 1980, **44**, L99 (and references therein).
3. H. Henning, A. Rehorek, D. Rehorek and Ph. Thomas, *Inorg. Chim. Acta* 1984, **86**, 41.
4. K. R. Butter, T. J. Kemp, B. Sicklucka and A. Samotus, *J. Chem. Soc., Dalton Trans.* 1986, 1217.
5. J. Szklarzewicz, A. Samotus and A. Kanas, *Proceedings of the 10th Conference on Coordination Chemistry, Smolenice-Bratislava, CSSR*, 1985, p. 393.
6. (a) A. Kosińska-Samotus and Z. Wilczewska-Stasicka, *Rocz. Chem.* 1957, **31**, 681; (b) Z. Jakób, *Rocz. Chem.* 1957, **31**, 681; (c) A. Samotus, *Rocz. Chem.* 1973, **47**, 265.
7. K. Wieghardt, U. Bossek, P. Chaudhuri, W. Hermann, B. Menke and J. Weiss, *Inorg. Chem.* 1982, **21**, 4308.
8. (a) B. R. McGarvey, *Inorg. Chem.* 1966, **5**, 476; (b) R. G. Hayes, *J. Chem. Phys.* 1966, **44**, 2210; (c) R. A. Pribush and R. D. Archer, *Inorg. Chem.* 1974, **13**, 2556; (d) P. M. Kiernan and W. P. Griffith, *J. Chem. Soc., Dalton Trans.* 1975, 2489; (e) C. D. Garner and F. E. Mabbs, *J. Inorg. Nucl. Chem.* 1979, **41**, 1125.
9. J. G. Leipoldt, S. S. Basson and L. D. C. Bok, *Inorg. Chim. Acta* 1980, **44**, L99.
10. L. D. C. Bok, J. G. Leipoldt and S. S. Basson, *Z. Anorg. Allg. Chem.* 1972, **392**, 303.
11. A. Kanas and A. Samotus, *Proceedings of* III *Symposium on Photo- and Thermal Reactions of Coordination Compounds, Kraków, Poland*, 1980, p. 37. Wydawnictwa, (1980).
12. D. Cook, *Can. J. Chem.* 1964, **42**, 2292.
13. J. S. Strukl and J. L. Walter, *Spectrochim. Acta* 1977, **27A**, 209.
14. (a) A. Gołębiewski and H. Kowalski, *Theor. Chim. Acta* 1968, **12**, 293; (b) A. Gołębiewski and R. Nale-

wajski, *Z. Naturforsch.* 1972, **27A**, 1672 (and references therein).
15. (a) J. H. Baxendale and R. George, *Trans. Faraday Soc.* 1950, **46**, 55; (b) F. H. Westheimer and W. T. Bentey, *J. Am. Chem. Soc.* 1956, **78**, 5309; (c) G. Nord and B. V. Agarwala, *Acta Chem. Scand.* 1981, **A35**, 231.
16. (a) K. O. Hartman and F. A. Miller, *Spectrochim. Acta* 1968, **24A**, 669; (b) R. V. Parish, P. G. Simms, M. A. Wells and L. A. Woodward, *J. Chem. Soc. A* 1968, 2882; (c) T. V. Long and G. A. Vernon, *J. Am. Chem. Soc.* 1971, **93**, 1919.
17. (a) O. Collenberg, *Z. Phys. Chem.* 1924, **109**, 353; (b) H. Baadsgaard and W. D. Treadwell, *Helv. Chim. Acta* 1955, **38**, 1669.
18. J. Szklarewicz and A. Samotus, to be published.

Polyhedron Vol. 5, No. 11, pp. 1741–1746, 1986
Printed in Great Britain

0277–5387/86 $3.00+.00
Pergamon Journals Ltd

THE ^{1}H NMR SPECTRA AND FLUXIONAL BEHAVIOUR OF $[Mo(\eta\text{-}C_5H_5)(CO)(CNR)_3][PF_6]$ COMPLEXES (R = Me, Et, Pr^i OR Bu^t): THE X-RAY STRUCTURE OF $[Mo(\eta\text{-}C_5H_5)(CO)(CNBu^t)_3][PF_6]$

GERARD LAWLESS, GERARD McNALLY and A. R. MANNING*

Department of Chemistry, University College, Belfield, Dublin 4, Ireland

and

DESMOND CUNNINGHAM and PATRICK McARDLE*

Department of Chemistry, University College, Galway, Ireland

(*Received* 16 *October* 1985; *accepted* 19 *February* 1986)

Abstract—A 3D X-ray diffraction study on a single crystal of $[Mo(\eta\text{-}C_5H_5)(CO)(CNBu^t)_3]^+[PF_6]^-$ shows that it contains an octahedral anion and a cation with a four-legged piano-stool ligand arrangement. The other $[Mo(\eta\text{-}C_5H_5)(CO)(CNR)_3][PF_6]$ salts (R = Me, Et or Pr^i) have similar spectra and hence similar structures to the above. Their ^{1}H NMR spectra at 270 MHz show that they are non-fluxional at room temperature with separate signals due to the CNR ligands *cis* to CO and that *trans* to it with the former always appearing at the greater δ values. The differences in chemical shifts are greater for the α- than for the β-protons, and decrease in the order: R = Me > Et > Pr^i. This suggests that, although a single resonance is observed for the Bu^t protons of $[Mo(\eta\text{-}C_5H_5)(CO)(CNBu^t)_3][PF_6]$ even at −60°C, it is due to identical ^{1}H chemical shifts for *cis* and *trans* ligands rather than to fluxionality. This conclusion is confirmed by the ^{13}C NMR spectra of the salts. However, at elevated temperatures fluxional interchange of these *cis*- and *trans*-CNR ligands is unambiguously observed for R = Et and Pr^i, with a coalescence temperature of 43°C when R = Et. The resonances due to the cyclopentadienyl protons are singlets, except when R = Me. Then it has two unequal components separated by 0.52 Hz which coalesce at *ca* 50°C.

Previously we reported the preparation of a series of $[Mo(\eta\text{-}C_5H_5)(CO)(CNR)_3][PF_6]$ salts which have IR spectra that are consistent with the four-legged piano-stool structure for the cations (Fig. 1). Their ^{1}H NMR spectra at 60 or 100 MHz in $CDCl_3$ solution indicated that these two types of alkyl isocyanide ligands interchanged rapidly on the NMR time-scale.[1] However a reinvestigation of the spectra at higher field has shown that the original data were of too low a quality to support such an interpretation, and that the cations are not fluxional at room temperature when R = Me, Et or Pr^i, and also probably not when R = Bu^t. ^{13}C NMR spectra confirm this viewpoint. On warming, $[Mo(\eta\text{-}C_5H_5)(CO)(CNEt)_3]^+$ and its CNPr^i counterpart become fluxional. The structure of $[Mo(\eta\text{-}C_5H_5)(CO)(CNBu^t)_3][PF_6]$ has been determined by a single-crystal X-ray diffraction study and shown to be that which was proposed previously.[1]

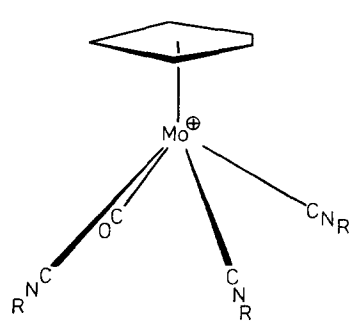


Fig. 1. Proposed structure of $[Mo(\eta\text{-}C_5H_5)(CO)(CNR)_3]^+$ cations.

EXPERIMENTAL

The preparation of the $[Mo(\eta\text{-}C_5H_5)(CO)(CNR)_3][PF_6]$ salts has been described for R = Me, Pr^i and Bu^t.[1] $[Mo(\eta\text{-}C_5H_5)(CO)(CNEt)_3][PF_6]$ was prepared similarly and isolated as an analytically pure, microcrystalline yellow solid.

NMR spectra were obtained using a JEOL GX-270 spectrometer in CD_2Cl_2, $CDCl_3$ or $(CD_3)_2CO$. All chemical shifts were measured with respect to Me_4Si or residual solvent peaks. The spectra are summarized in Table 1.

Crystal data

$C_{21}H_{32}F_6MoN_3OP$, $M = 583.47$, orthorhombic, $a = 11.438(3)$ Å, $b = 13.831(3)$ Å, $c = 17.631(4)$ Å, $\alpha = \beta = \gamma = 90°$, $U = 2789.2$ Å^3, $Z = 4$. $D_c = 1.39$ g cm^{-3}, $F(000) = 1191.99$, $\lambda(\text{Mo-}K_\alpha) = 0.71069$ Å, $\mu = 5.21$ cm^{-1}, space group $P2_12_12_1$. All intensity data were obtained as described by Alyea *et al.*[2] on a Hilger & Watts Y290 diffractometer. Unit-cell parameters were determined by a least-squares fit of θ values between 12 and 20° measured on the diffractometer. The data were collected by the θ–2θ method within the range $2 < \theta < 24°$. Intensities were corrected for Lorentz and polarization effects but not for extinction or absorption. Standard reflections showed an intensity variation of less than 2%. A total of 971 unique reflections with $I > 5\sigma(I)$ were obtained. The observed structure factors were placed on a common scale by the K curve method. Neutral atom-scattering factors were taken from Ref. 3 (hydrogen atoms) and Ref. 4 (others), whilst the anomalous dispersion correction factors for non-hydrogen atoms were taken from Ref. 5.

All calculations were carried out on a Dec-2060 computer. The structure was solved by direct methods (MULTAN)[6] which located both Fe atoms in the asymmetric unit. The other non-hydrogen atoms were located in difference-Fourier maps. Calculated hydrogen atom positions were included in the refinement which was carried out by full-matrix least-squares procedures (SHELX)[7] in which $\Sigma\ \omega(|F_o|-|F_c|)^2$ were minimized with weights (ω) for each reflection being given by $\omega = 0.4701(\sigma^2|F_o|+0.0064|F_o|^2)^{-1}$. The carbon atoms C_1–C_5 of the cyclopentadienyl ligand were constrained to a rigid pentagon during refinement; only the Mo and P atoms were allowed to vibrate anisotropically. The number of variable parameters was 135. The final R value was 0.0593 and R^1 $[= \{\Sigma\ \omega(|F_o|-|F_c|)^2/\Sigma\ \omega(|F_o|^2)\}^{1/2}] = 0.0633$. The final-difference map showed no electron densities >0.64 e Å^{-3}.

Final atom coordinates and isotropic thermal parameters, observed and calculated structure factors, and anisotropic atomic thermal parameters have been deposited as supplementary data with the Editor, from whom copies are available on request. Atomic coordinates have also been deposited with the Cambridge Crystallographic Data Centre.

RESULTS AND DISCUSSION

Structure of $[Mo(\eta\text{-}C_5H_5)(CO)(CNBu^t)_3][PF_6]$

An irregular single crystal of this compound was grown from hot benzene solution and subjected to

Table 1. NMR spectra of $[Mo(\eta\text{-}C_5H_5)(CO)(CNR)_3][PF_6]$ in $CDCl_3$ solution at 21°C[a]

	CNMe		CNEt[b]		CNPR^i[c]	CNBu^t	
	^{1}H	^{13}C	^{1}H	^{13}C	^{1}H	^{1}H	^{13}C
C_5H_5	5.338, 5.336(5)	90.63	5.347(5)	90.92	5.328(5)	5.360(5)	90.98
CO	—	241.34	—	241.18	—	—	240.75
CN	—	157.1[d]	—	157.5[d]	—	—	157.18[d]
	—	159.65	—	160.05	—	—	159.24
R (C_α or H_α)	3.654(3)	31.28	3.915 (q.2)	41.06	4.228 (p.1)	—	59.14
	3.629(6)	31.69	3.930 (q.4)	41.48	4.236 (p.2)	—	59.78
R (C_β or H_β)	—	—	1.417 (t.3)	15.54	1.446 (d.6)	1.541(27)	30.66
	—	—	11.425 (t.6)	15.52	1.463 (d.12)	—	30.70

[a] Resonance positions in ppm downfield from Me_4Si with integrations in parentheses for ^{1}H spectra only. d = doublet, t = triplet, q = quartet, p = quintet; otherwise resonances are singlets.

[b] For $C\underline{H}_2$–$C\underline{H}_3$ coupling $J = 7.14$ Hz for both types of CNEt ligands. At 51°C resonances for R are 3.927 (q.6) and 1.451 (t.9) with $J = 7.14$ Hz.

[c] CD_2Cl_2 solution for $C\underline{H}$–$C\underline{H}_3$ coupling. $J = 6.55$ Hz for both types of CNPr^i ligands.

[d] Broad resonances with multiplet character (see text).

an X-ray diffraction study. The unit cell contains discrete octahedral $[PF_6]^-$ anions and $[Mo(\eta\text{-}C_5H_5)(CO)(CNBu^t)_3]^+$ cations (Fig. 2), with no unusual anion–cation interactions as the shortest such contact is $F_6\cdots H(202)$ at 2.55 Å. The ligand distribution and interligand bond angles in the cation (Table 2) are similar to those found in a wide variety of $[Mo(\eta\text{-}C_5H_5)(L)_3X]$ complexes.[8] The Mo—CO distance of 1.90(2) Å is rather short {cf. 1.980(4)–2.009(6) Å in $[Mo(\eta\text{-}C_5H_5)(CO)_3Cl]$ in Ref. 8} which correlates well with the low ν(CO) frequency of 1928 cm^{-1},[1] indicative of extensive Mo to CO back-bonding. The Mo—CNBu^t distances are comparable with that found in $[Mo_2(\eta\text{-}C_5H_5)_2(CO)_5(CNMe)]$ [2.05(1)Å][9] and there are no significant differences between the two ligands *cis* to CO and the unique one *trans* to it.

NMR spectra of $[Mo(\eta\text{-}C_5H_5)(CO)(CNR)_3][PF_6]$

The ^1H NMR spectra of these salts in CD_2Cl_2 or $CDCl_3$ solutions show resonances due to alkyl and cyclopentadienyl protons (Table 1). The latter were usually singlets at *ca* δ 5, but for $[Mo(\eta\text{-}C_5H_5)(CO)(CNMe)_3][PF_6]$ in $CDCl_3$ solution two unequal ($\sim$100 : 85) resonances were observed, one at δ 5.3362 and the other at δ 5.3382. Although their separation of 0.52 Hz is very close to the limits of the resolution of the spectrometer, this does not appear to be an artifact. It is reproducible and is also observed in acetone-d^6 solution, but here the resonances are much broader and the weaker component is, apparently, much weaker than in $CDCl_3$ solution so that it appears only as a shoulder to lower δ on the stronger. A possible explanation for these observations is that it is due to the presence of ion-paired species in equilibrium with free anions and cations. Alternatively it may be due to isomerism within the cation arising as a consequence of the two different *trans*-MeNC—Mo—L angles (L = CO or CNMe). However, neither suggestion is completely convincing. In both cases the interconversion processes involved might be expected to have low energies of activation and to be fluxional on the NMR time-scale at room temperature, whereas the two cyclopentadienyl signals only coalesce at *ca* 50°C and do not change on cooling below 20°C.

Previously it was indicated that the ^1H resonances of the alkyl groups R were consistent with fluxional cations undergoing rapid interchange of *cis*- and *trans*-RNC ligand as two sets of such resonances

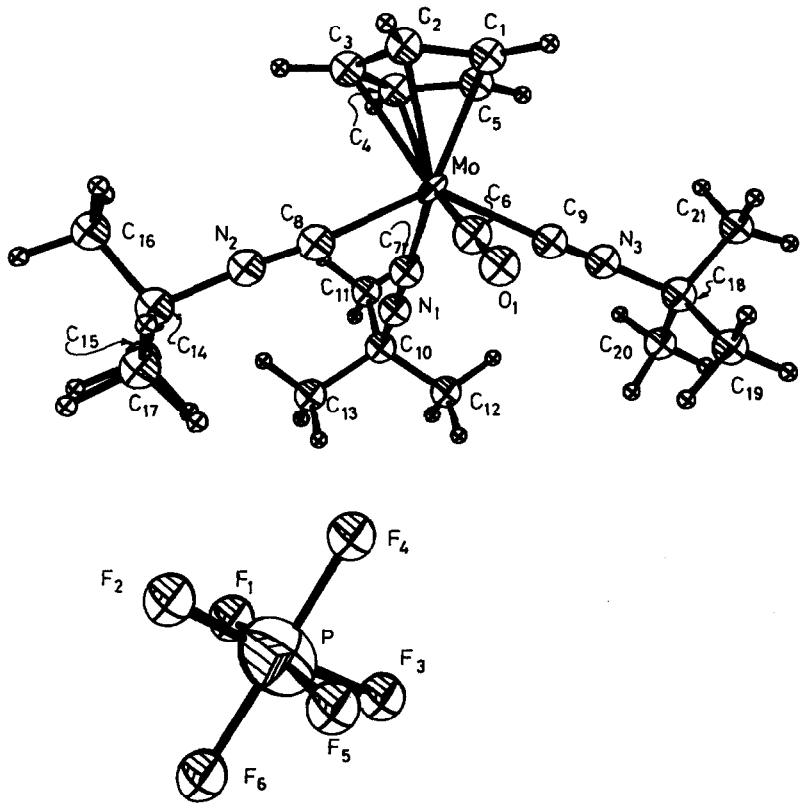


Fig. 2. Structure of $[Mo(\eta\text{-}C_5H_5)(CO)(CNBu^t)_3]^+$ and $[PF_6]^-$ in the crystal [C. K. Johnson, Oak Ridge National Laboratory (Report) ORNL (U.S.) 1986 ORNL-3794 (revised 1971)].

were not observed.[1] This is incorrect as at higher field in $CDCl_3$ solution at 21°C the ^1H NMR spectrum of $[Mo(\eta\text{-}C_5H_5)(CO)(CNMe)_3][PF_6]$ shows two well-defined singlets having relative intensities of 2:1 due to *cis*- and *trans*-MeNC ligands, respectively. In contrast, the alkyl protons of $[Mo(\eta\text{-}C_5H_5)(CO)(CNBu^t)_3]^+$ showed only a sharp singlet even at −60°C. The $[Mo(\eta\text{-}C_5H_5)(CO)(CNEt)_3]^+$ and $[Mo(\eta\text{-}C_5H_5)(CO)(CNPr^i)_3]^+$ cations occupy intermediate positions between these two extremes. In the first there are two resolved quartets due to the CH_2 and two triplets due to the CH_3 protons. Double-irradiation experiments cause both the quartets and triplets to each collapse to two singlets having an intensity ratio of 2:1. Those due to the CH_3 protons are less well resolved than those due to the CH_2. In the $CNPr^i$ cation the quintet due to the CH protons of the Pr^i group clearly have unequal components which are not completely resolved, whilst the doublet due to the CH_3 protons show shoulders. In all instances the less intense resonances due to the single RNC ligands *trans* to CO lie at lower δ than those due to the two which are *cis*.

On inspection of the spectra (Table 1) it can be seen that the differences in chemical shift between the corresponding protons of *cis*- and *trans*-RNC ligands is always greater for those on the α-carbon atoms ($\Delta\alpha$) than those on the β-carbon atoms ($\Delta\beta$), and for both they decrease along the series R = Me > Et > Pr^i. Thus it is very likely that when R = Bu^t $\Delta\beta$ is so small that it cannot be detected at the field strength employed, and that $[Mo(\eta\text{-}C_5H_5)(CO)(CNBu^t)_3]^+$ actually behaves in the same way as the other cations.

The conclusions are supported by the ^{13}C NMR spectra of the salts at 21°C (Table 1). Apart from the singlet resonances due to the cyclopentadienyl (*ca* δ 91) and carbonyl (*ca* δ 241) ligands, there are also resonances due to the α- and, where appropriate, β-carbon atoms of the R groups. There are always two of these with markedly unequal intensities.

Thus even when R = Bu^t there are two CNR environments which are not interchanging rapidly on the NMR time-scale. Again the chemical shift differences are always smaller for the β- than the α-carbon atoms. As for the protons, the former decrease

Table 2. Bond lengths (Å) and bond angles (°) for $[Mo(\eta\text{-}C_5H_5)(CO)(CNBu^t)_3][PF_6]$

Mo—C1	2.269(16)	Mo—C2	2.315(19)
Mo—C3	2.392(19)	Mo—C4	2.394(18)
Mo—C5	2.319(18)	Mo—C6	1.901(24)
Mo—C7	2.079(21)	Mo—C8	2.080(22)
Mo—C9	2.09(5)	O1—C6	1.182(24)
N1—C7	1.171(22)	N1—C10	1.468(25)
N2—C8	1.140(24)	N2—C14	1.48(3)
N3—C9	1.02(4)	N3—C18	1.50(4)
C1—C2	1.420(1)	C1—C5	1.420(1)
C2—C3	1.420(1)	C3—C4	1.420(1)
C4—C5	1.420(1)	C10—C11	1.51(3)
C10—C12	1.52(3)	C10—C13	1.52(3)
C14—C15	1.42(3)	C14—C16	1.47(4)
C14—C17	1.54(3)	C18—C19	1.48(4)
C18—C20	1.51(3)	C18—C21	1.48(4)
P—F1	1.576(20)	P—F2	1.62(3)
P—F3	1.57(4)	P—F4	1.538(20)
P—F5	1.499(25)	P—F6	1.560(23)
C2—Mo—C1	36.1(3)	C3—Mo—C1	59.0(4)
C3—Mo—C2	35.1(3)	C4—Mo—C1	59.0(4)
C4—Mo—C2	58.4(4)	C4—Mo—C3	34.5(3)
C5—Mo—C1	36.0(3)	C5—Mo—C2	59.4(4)
C5—Mo—C3	58.4(4)	C5—Mo—C4	35.0(3)
C6—Mo—C1	99.6(8)	C6—Mo—C2	97.5(8)
C6—Mo—C3	126.3(9)	C6—Mo—C4	155.6(8)
C6—Mo—C5	131.6(7)	C7—Mo—C1	138.0(7)
C7—Mo—C2	143.3(8)	C7—Mo—C3	108.5(8)
C7—Mo—C4	87.9(7)	C7—Mo—C5	102.1(7)
C7—Mo—C6	116(1)	C8—Mo—C1	133.4(9)
C8—Mo—C2	97.4(9)	C8—Mo—C3	83.7(9)
C8—Mo—C4	105.8(8)	C8—Mo—C5	140.0(9)

(*continued*)

Table 2. (*continued*)

C8—Mo—C6	79.7(9)	C8—Mo—C7	76.8(8)
C9—Mo—C1	91.9(8)	C9—Mo—C2	126.8(7)
C9—Mo—C3	143.1(8)	C9—Mo—C4	112.6(8)
C9—Mo—C5	84.7(8)	C9—Mo—C6	77(1)
C9—Mo—C7	77(1)	C9—Mo—C8	132(1)
C10—N1—C7	174(2)	C14—N2—C8	171(2)
C18—N3—C9	178(3)	C2—C1—Mo	73.7(5)
C5—C1—Mo	73.9(4)	C5—C1—C2	108.0(1)
C1—C2—Mo	70.2(5)	C3—C2—Mo	75.4(4)
C3—C2—C1	108.0(1)	C2—C3—Mo	69.5(3)
C4—C3—Mo	72.8(4)	C4—C3—C2	108.0(1)
C3—C4—Mo	72.7(5)	C5—C4—Mo	69.6(4)
C5—C4—C3	108.0(1)	C1—C5—Mo	70.1(4)
C4—C5—Mo	75.4(4)	C4—C5—C1	108.0(1)
O1—C6—Mo	179(2)	N1—C7—Mo	175(2)
N2—C8—Mo	176(2)	N3—C9—Mo	177(3)
C11—C10—N1	107(2)	C12—C10—N1	105(2)
C12—C10—C11	114(2)	C13—C10—N1	107(2)
C13—C10—C11	109(2)	C13—C10—C12	113(2)
C15—C14—N2	111(3)	C16—C14—N2	107(2)
C16—C14—C15	115(3)	C17—C14—N2	107(2)
C17—C14—C15	107(2)	C17—C14—C16	110(3)
C19—C18—N3	109(3)	C20—C18—N3	112(3)
C20—C18—C19	107(3)	C21—C18—N3	108(3)
C21—C18—C19	105(3)	C21—C18—C20	114(3)
F2—P—F1	84(1)	F3—P—F1	93(2)
F3—P—F2	174(1)	F4—P—F1	86(1)
F4—P—F2	95(1)	F4—P—F3	90(1)
F5—P—F1	176(1)	F5—P—F2	93(1)
F5—P—F3	90(2)	F5—P—F4	91(1)
F6—P—F1	93(1)	F6—P—F2	84(1)
F6—P—F3	91(2)	F6—P—F4	179(1)
F6—P—F5	90(1)		

in the order: R ⩭ Me ≫ Et > Bu^t, but the latter increase in the order: R = Et < Bu^t. The absolute ^{13}C chemical shifts (δ) for both α- and β-carbon atoms increase for R = Me < Et < Bu^t. The resonances due to the isocyanide carbon atoms are very weak but two can always be detected. Although one is sharp the other is much broader and when R = Bu^t at least it appears to be a triplet. Unfortunately, further studies on this unexpected and not readily explicable observation have been prevented by solubility and stability problems.

Fluxionality in $[Mo(\eta\text{-}C_5H_5)(CO)(CNEt)_3][PF_6]$

The site exchange of the ligands (L) in $[M(\eta\text{-}C_5H_5)(L)_4]$ derivatives has been shown to be a facile process especially for $[Mo(\eta\text{-}C_5H_5)(CO)_2(L)X]$ and $[Mo(\eta\text{-}C_5H_5)(CO)(L)_2X]$ systems.[10] Therefore the temperature dependence of the ^1H NMR spectrum of $[Mo(\eta\text{-}C_5H_5)(CO)(CNEt_3)][PF_6]$ was investigated. In $CDCl_3$ solution at 51°C the signals due to the CH_2 and CH_3 protons of the EtNC ligands are a sharp quartet and triplet, respectively. Double irradiation causes these to become sharp singlets. On cooling these broaden and separate each into the two components observed at 21°C (see above). The coalescence temperature for the CH_2 methylene protons, where the two signals were separated by 4.05 Hz, was 43°C. Faller and Anderson have suggested[10] that these site exchange processes proceed via intermediates which have a trigonal bipyramidal arrangement of the five ligands with η-C_5H_5 at an apical site. A similar mechanism probably operates in the $[Mo(\eta\text{-}C_5H_5)(CO)(CNR)_3]^+$ cations.

The two CNMe signals for $[Mo(\eta\text{-}C_5H_5)(CO)(CNMe)_3][PF_6]$ do not coalesce before the upper temperature limit for chloroform is reached (~55°C). However noticeable peak broadening, which is reversible, has taken place and it is clear that exchange of the two types of CNMe ligands is taking place.

REFERENCES

1. G. McNally and A. R. Manning, *Inorg. Chim. Acta* 1984, **85**, L7.
2. E. C. Alyea, G. Ferguson and R. J. Restivo, *Inorg. Chem.* 1975, **14**, 2491.
3. R. F. Stewart, E. R. Davidson and W. T. Simpson, *J. Chem. Phys.* 1965, **42**, 3175.
4. D. T. Cromer and J. B. Mann, *Acta Cryst.* 1968, **A24**, 321.
5. D. T. Cromer and D. J. Liberman, *J. Chem. Phys.* 1970, **53**, 1891.
6. P. Main, S. E. Fiske, S. L. Hull, G. Germain, J. P. Declerq and M. M. Woolfson, *MULTAN, A System of Computer Programs for Crystal Structure Determination from X-ray Diffraction Data.* Universities of York and Louvain (1980).
7. G. M. Sheldrick, *SHELX, A Computer Program for Crystal Structure Determination.* University of Cambridge (1976).
8. C. Bueno and M. R. Churchill, *Inorg. Chem.* 1981, **20**, 2194.
9. R. D. Adams, M. Brice and F. A. Cotton, *J. Am. Chem. Soc.* 1973, **95**, 6594.
10. J. W. Faller and A. S. Anderson, *J. Am. Chem. Soc.* 1969, **91**, 1550; *J. Am. Chem. Soc.* 1970, **92**, 5852.

Polyhedron Vol. 5, No. 11, pp. 1747–1753, 1986
Printed in Great Britain

0277–5387/86 $3.00+.00
Pergamon Journals Ltd

EXTRACTION EQUILIBRIUM BETWEEN PRIMARY AMINE PRIMENE 81R AND IRON(III) SULPHATE

F. J. ALGUACIL* and S. AMER

Centro Nacional de Investigaciones Metalúrgicas, Avda. Gregorio del Amo n° 8, Ciudad Universitaria, 28040 Madrid, Spain

(*Received* 6 *January* 1986; *accepted* 24 *February* 1986)

Abstract—The extraction equilibrium between aqueous iron(III) sulphate solutions and amine Primene 81R was studied. The results show that the free amine extracts iron(III) from these solutions. The extracted complex has been isolated and can be represented by the stoichiometric formula $4RNH_2 \cdot Fe_2(SO_4)_3$. The extraction reaction is almost independent of temperature and change in the diluent of the organic phase. On the basis of spectral studies a structure for the extracted complex is suggested.

The extraction of iron(III) from aqueous sulphate solutions by amines has been extensively studied before.[1–3] However, in all the above studies the extracting agent was the corresponding amine sulphate because it seems that the free amine can not extract iron(III) from these aqueous solutions.

Thus, the amine Primene 81R sulphate extracts iron(III) from aqueous sulphate solutions in the form of two well-defined complexes, depending on the extraction temperature,[4,5] although a previous study[5] has shown that as the sulphuric acid concentration in the aqueous phase decreases the amine Primene 81R extracts iron(III), and when no free sulphuric acid was present in the aqueous phase the amine also extracts this metallic ion. Thus, it can be concluded that the free amine extracts iron(III) because when there is no sulphuric acid the amine is in the free form.

It has been shown that several amines extract iron(III) and cobalt(III) from oxalate media when they are in the free form,[6] and also a primary amine named Primene JMT extracts uranium from sulphate solutions to form the complex $(RNH_3)_2UO_2(OH)_2SO_4$.[7] These results show that it is possible that the amines extract several metallic ions from aqueous solutions when they are acting in the free form and not as the amine salts.

The purpose of the present investigation was to study in detail the new liquid–liquid $Fe_2(SO_4)_3$–amine Primene 81R extraction system, when the amine is present as a free base. The objective was also to isolate and identify the compound extracted in the organic phase as a new contribution to understanding the extraction chemistry of amines.

EXPERIMENTAL

The amine Primene 81R used in this work was obtained as a commercial mixture from Rohm & Haas Co., Philadelphia, PA. This amine is a branched-chain, tertiary-carbon amine and its composition is >99% primary aliphatic amine, having the general structure $R_1R_2R_3$—C—NH_2, where the total carbon atom number is 12–14. The experimental molecular weight was 200, as calculated from the titration of various amine solutions, in ethanol, with standard hydrochloric acid using a Beckman 3560 pH-meter.

Kerosene was supplied by CAMPSA with the following specifications: % aromatics, ~20; density (20°C), 0.780 g cm^{-3}; boiling point, >140°C. All other chemicals were reagent grade.

Extractions were carried out by the following procedure. Equal volumes of Primene 81R solutions diluted in kerosene and iron(III) sulphate solutions were placed in separatory funnels, thermostatted at the required temperature, and mechanically shaken. On completion of the extraction the phases were separated and iron(III) in the organic phase was then stripped with 3 M sulphuric acid.

Iron(III) in both phases was determined volu-

* Author to whom correspondence should be addressed.

metrically with potassium dichromate. Sulphate was determined gravimetrically as barium sulphate.

The diluent of the saturated organic phases was evaporated under reduced pressure to yield a dark-red waxy solid residue. This was recrystallized from an ethanol–acetone mixture to yield an orange solid, which was dried in a desiccator over $CaCl_2$.

The solid melts at 140°C. Found: Fe, 9.2; SO_4^{2-}, 23.6; C, 51.3; N, 4.6; H, 9.0%. Calc. for $4RNH_2 \cdot Fe_2(SO_4)_3$: Fe, 9.3; SO_4^{2-}, 24.0; C, 52.1; N, 4.7; H, 10.0%.

IR measurements on the solid were carried out using Unicam SP3-200S and Perkin–Elmer 682 spectrophotometers with cesium iodide windows. Nujol and hexachlorobutadiene mulls were used. The UV spectra were obtained using a Beckman DB-GT spectrophotometer with 1-cm SiO_2 cells.

RESULTS AND DISCUSSION

Influence of sulphuric acid concentration

Figure 1 shows the results obtained by studying iron(III) sulphate extraction with organic phases of amine Primene 81R [10 and 5% (v/v) in kerosene] in dependence on the initial sulphuric acid concentration in the aqueous phase at temperatures of 25 and 50°C.

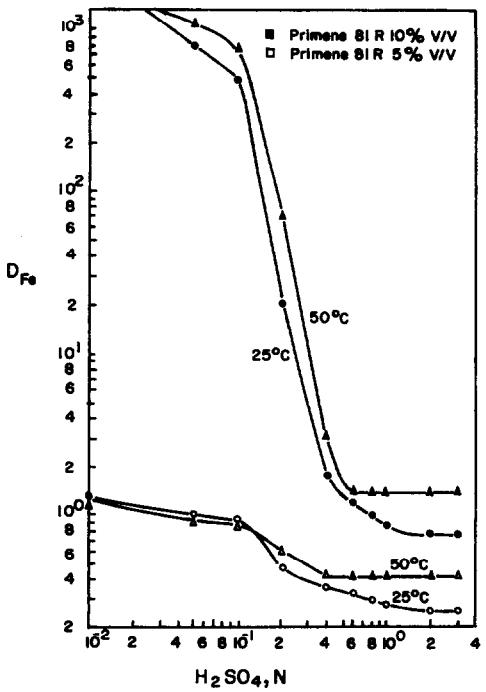


Fig. 1. Effect of sulphuric acid concentration on the extraction of iron(III) by amine Primene 81R. *Aqueous phase*: 0.179 M iron(III) solution.

It can be seen that in the extraction of $Fe_2(SO_4)_3$ with amine Primene 81R solutions the iron(III) concentration in the organic phases decreases with increasing sulphuric acid concentration in the aqueous phase. These results show that the amine bisulphate which formed at high acid concentration does not extract iron(III). The constancy of the results obtained at 50°C for a >6 N sulphuric acid concentration independent of the initial amine concentration is due to the formation of an amine salt that can be represented with the stoichiometric formula $5(RNH_3)_2SO_4 \cdot 3RNH_3HSO_4$, which is not formed at lower temperatures.[5,8]

Iron(III) extraction tends to be greatest when the sulphuric acid concentration is zero, that is in the case when all of the amine in the organic phase is in the form of the free base. This indicates that the extraction agent for iron(III) in the case of amine Primene 81R is the free amine in addition to the amine sulphate.

In order to achieve a clarification of this phenomenon the present investigation was carried out with aqueous solutions that contained no sulphuric acid.

Influence of the diluent

The present study was carried out with solutions of amine Primene 81R [10 and 5% (v/v)] in three diluents which present a great influence on the extraction of iron(III) sulphate by amine Primene 81R sulphate:[9] kerosene, benzene and chloroform. These organic phases were shaken for 10 min with an aqueous sulphate solution of 0.358 M iron(III) at 25°C. Time studies indicated that complete equilibration was obtained after about 5 min shaking, almost independent of the diluent.

The results obtained are shown in Table 1. It can be seen that in this system the change in the diluent of the organic phase does not have a great influence on the iron(III) extraction. The same result was

Table 1. Influence of diluent on the extraction of iron(III) by amine Primene 81R[a]

	Amine [5% (v/v)]	Amine [10% (v/v)]
Diluent	Fe(III) [g (l organic phase)$^{-1}$]	Fe(III) [g (l organic phase)$^{-1}$]
Kerosene	5.63	11.36
Benzene	5.63	11.36
Chloroform	5.63	11.36

[a] *Aqueous phase*: 0.358 M iron(III) solution. Temperature = 25°C.

obtained at higher temperatures. This behaviour is different from that observed with the amine Primene 81R sulphate.[10] From here onwards the only diluent studied for the organic phase was kerosene because it gave a better phase separation time when compared with the other diluents studied.

Influence of modifiers

The addition of a modifier to overcome the third-phase and emulsion tendencies in a solvent extraction system is a common practice. In this paper the use of *n*-alcohols as modifiers for the amine Primene 81R–iron(III) sulphate system was investigated, the alcohols chosen for this study were *n*-butanol, *n*-hexanol, *n*-octanol and *n*-decanol.

Table 2 presents the results obtained by shaking equal volumes of a 0.358 M iron(III) aqueous solution with an amine Primene 81R [10% (v/v) in kerosene] solution with different modifiers. The results show that the highest concentration values of iron(III) on the organic phase were obtained with *n*-decanol independent of the extraction temperature, it seems that the shorter the carbon organic chain of the modifier the less iron(III) is extracted by the amine. Table 2 shows the phase separation time at temperatures of 25 and 50°C. The best results are always obtained with *n*-decanol although at 50°C the experimental time is shorter than those obtained at the lower temperature for the four modifiers studied. Figure 2 shows the iron(III) concentration in the organic phase vs the *n*-decanol concentration in this phase. It can be seen that the presence of a small amount of *n*-decanol improves the extraction of iron(III) which is a new tendency found in this system because it is known that modifiers have a depressant effect on metal extraction.[11]

The maximum extraction was obtained when using 5% (v/v) *n*-decanol, although the differences in the range 4–7.5% (v/v) are small. This range of concentrations is independent of temperature and the initial amine Primene 81R concentration.

Thus, the following study was made using organic phases containing a concentration of *n*-decanol half that of the amine [expressed as % (v/v)].

Table 2. Effect of modifiers on the extraction of iron(III) by amine Primene 81R[a]

Modifier	% (v/v)	Fe(III) [g (l organic phase)$^{-1}$] 25°C	Fe(III) [g (l organic phase)$^{-1}$] 50°C	Phase separation time (min) 25°C	Phase separation time (min) 50°C
n-Butanol	5	6.01	6.00	5.15	2.00
n-Hexanol	5	6.42	6.40	5.17	1.89
n-Octanol	5	9.76	9.51	5.00	1.50
n-Decanol	5	11.35	11.20	4.00	1.27

[a] *Organic phase*: amine Primene 81R [10% (v/v) in kerosene]. *Aqueous phase*: 0.358 M iron(III) solution.

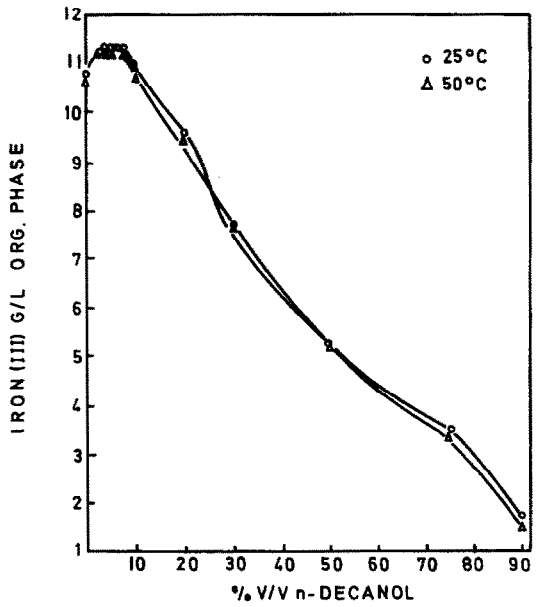


Fig. 2. Effect of *n*-decanol on the iron(III) loading in organic phase. *Aqueous phase*: 0.358 M iron(III) solution. *Organic phase*: Primene 81R [10% (v/v) in kerosene].

Study of extraction kinetics and influence of temperature

Kinetics studies have been carried out on the effect of various initial iron(III) sulphate concentrations on shaking time, keeping the iron(III) concentration constant.

The results obtained are shown in Fig. 3 for temperatures of 25 and 50°C, plotting the iron(III) concentration in the organic phases vs the equilibration time when an organic phase of amine Primene 81R [10% and 5% (v/v) in kerosene] was shaken with different aqueous iron(III) solutions.

An almost complete independence of temperature and amine concentration equilibrium was reached in 3 min, and from Fig. 3 can be seen that at 25°C in the organic phase a considerable amount of iron(III) is extracted compared to the extraction at the higher temperature, although there are no significant differences between the results obtained for the two temperatures when more diluted

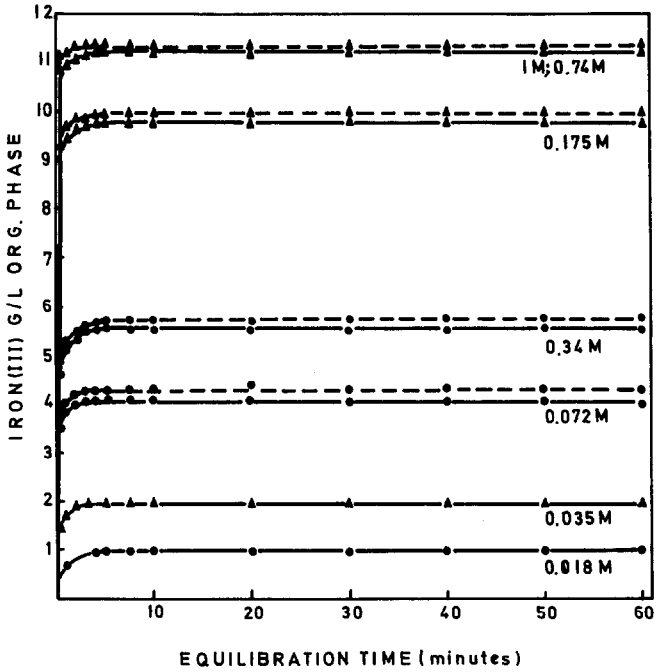


Fig. 3. Kinetics of iron(III) extraction by amine Primene 81R [(▲) 10% (v/v), and (●) 5% (v/v) in kerosene]. Influence of various iron(III) concentrations in the aqueous phase. Broken line, 25°C; continuous line, 50°C.

iron(III) concentrations were studied. Increasing iron(III) concentrations in the aqueous phase up to 1 M have no influence on the organic-phase load, indicating that there is not a species change in the organic phase at high aqueous iron(III) concentrations.

Figure 4 plots the relationship between the iron(III) loaded in the organic phase and the extraction temperature for organic phases which contain different amine Primene 81R concentrations in kerosene shaken with an aqueous phase of 0.358 M iron(III) for 10 min.

From Fig. 4 it can be seen that there is practically no change in the iron(III) concentration loaded in the organic phases at different temperatures, indicating that a complex with the same stoichiometry is extracted over the range of temperatures studied. This result differs from those obtained with amine Primene 81R sulphate which extracts two well-defined iron(III) complexes, depending on the extraction temperature.[4,12]

Temperature has a great influence on the phase separation time as can be seen in Fig. 5, in which this variable is plotted vs temperature for the experimental points obtained with 10% (v/v) amine Pri-

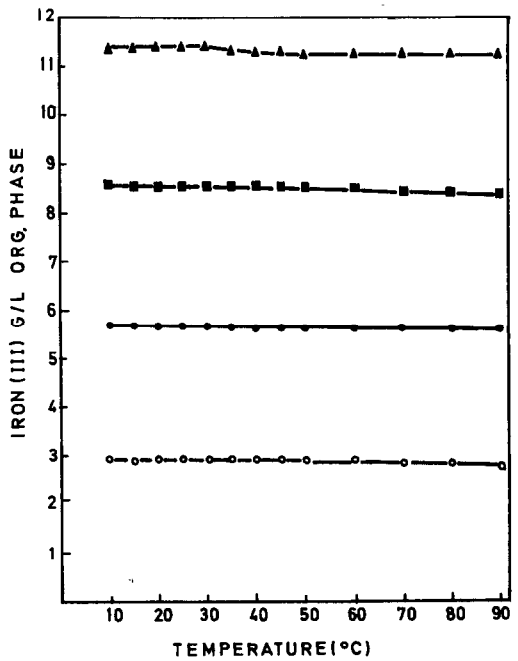


Fig. 4. Influence of temperature on the extraction of iron(III) by amine Primene 81R [(▲) 10% (v/v), (■) 7.5% (v/v), (●) 5% (v/v), and (○) 2.5% (v/v) in kerosene]. *Aqueous phase*: 0.358 M iron(III) solution.

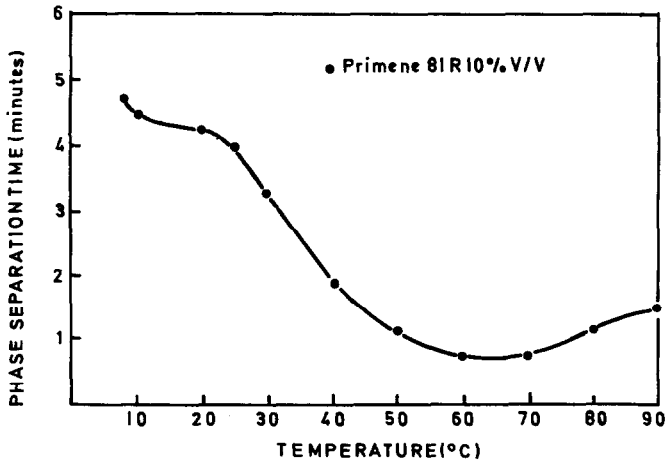


Fig. 5. Variation in the phase separation time with extraction temperature. *Aqueous phase*: 0.358 M iron(III) solution. *Organic phase*: Primene 81R [10% (v/v) in kerosene].

mene 81R. As the temperature increases the separation time decreases progressively until 70°C, at which a long time is required; similar results were also obtained with other initial amine concentrations.

Extraction equilibrium isotherms

Figure 6 shows loading isotherms for the extraction of iron(III) with amine Primene 81R [10 and 5% (v/v) in kerosene] in equilibrium with aqueous iron(III) sulphate solutions at 25 and 50°C; the shaking time in all cases was 10 min. At saturation loading the results show that the amine Primene 81R/iron(III) concentration ratio appears to approach 2 almost independently of temperature. Neither of the curves show an upward swing above the initial loading level as has been shown with amine sulphates.[12] This result supported the previous suggestion that there is no species change in the organic phase at high iron(III) concentrations.

Several sulphuric acid titrations on equilibrated aqueous phases show that no acid is liberated by iron(III) extraction as occurs with the extraction by means of amine Primene 81R sulphate; this result suggests that the extraction mechanism may differ from that proposed for the amine sulphate.

Figure 7 shows the relationship between the molar ratio of iron(III) concentration in the organic phase to the amine Primene 81R concentration vs the iron(III) concentration in the aqueous phase. From Fig. 7 it can be seen that the limiting ratio obtained is near to 0.5, corresponding to $[Fe(III)]_{org}/[RNH_2]_{org} = 0.5$. This ratio is similar to that obtained from extraction loading curves shown in Fig. 6.

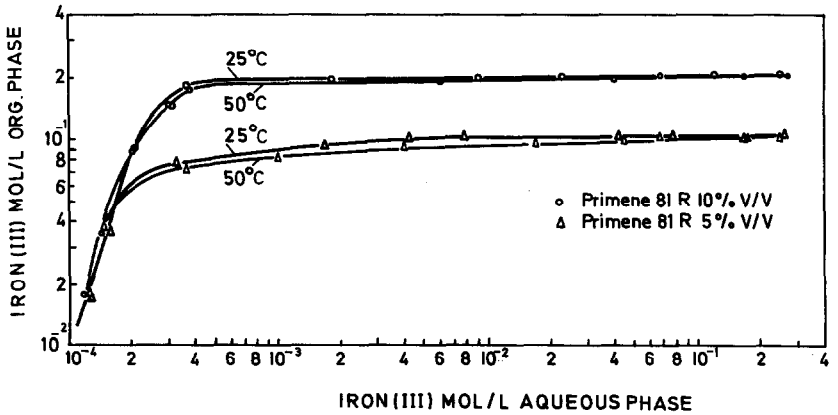


Fig. 6. Equilibrium extraction curves for iron(III) extracted by amine Primene 81R. Effect of the initial amine concentration. *Aqueous phase*: solutions containing various concentrations of iron(III) sulphate. *Organic phase*: Primene 81R [(○) 10% (v/v), and (△) 5% (v/v) in kerosene].

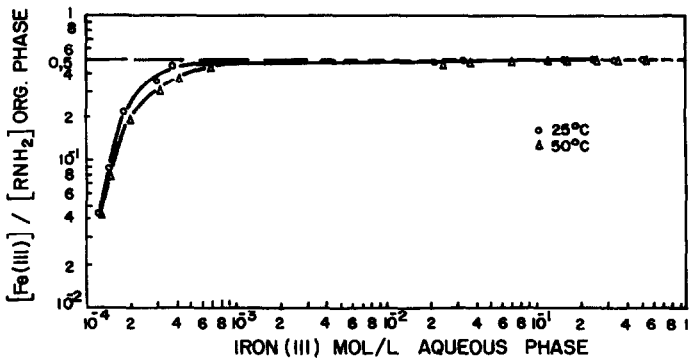


Fig. 7. Variation in the molar ratio [Fe(III)]/[RNH_2] in the organic phase with molar [Fe(III)] in the aqueous phase. *Organic phase*: Primene 81R [10% (v/v) in kerosene].

The sulphate analysis of the organic phase indicated that the molar ratio of the sulphate concentration to the iron(III) concentration in the organic phase is equal to 1.5.

According to the above experimental data the following extraction reaction of iron(III) sulphate by amine Primene 81R, acting as a free base, is suggested:

$$4RNH_{2org} + Fe_2(SO_4)_{3aq} \rightleftarrows 4RNH_2 \cdot Fe_2(SO_4)_{3org} \quad (1)$$

This extraction reaction being independent of temperature and different to those proposed with amine Primene 81R sulphate and other amine sulphates indicates that the amine acting as a free base extracts iron(III) sulphate by means of a well-defined complex.

Reagent concentration dependence

The study of the reagent dependence was carried out by shaking a 0.358 M iron(III) aqueous solution and different organic phases for 10 min at a temperature of 25°C. The results are shown in Fig. 8 in which the iron(III) concentration loaded in the organic phase is plotted against the initial amine concentration. There is a proportional relationship between the two values represented; thus, from Fig. 8 unknown amine Primene 81R concentrations can be determined by comparing values for the iron(III) concentration extracted with those shown in Fig. 8. The same result is obtained when the extraction is carried out at 50°C or other temperatures.

Spectra and structure of the complex

The UV spectrum obtained in kerosene of the isolated amine Primene 81R–iron(III) complex shows a band at about 307 nm ($\varepsilon \sim 3240$) that can be assigned to the species $[FeSO_4]^+$ and possibly $[Fe(SO_4)_2]^-$, as the $[FeSO_4]^+$ species absorbs at about 305–310 nm whereas the $[Fe(SO_4)_2]^-$ species appears to have an absorption maximum at 300 nm. Although it seems that the observed band is near to the $[FeSO_4]^+$ species it is possible that the spectrum of the compound in kerosene solution showed a contribution from both iron(III) species.

The molar extinction coefficient value is higher than those reported in aqueous solution for these species.[13] However, Good *et al.*[14] have found that in certain chloroform–amine solutions the spectra of ionic transition-metal complexes have higher extinction coefficients than the same ion in aqueous

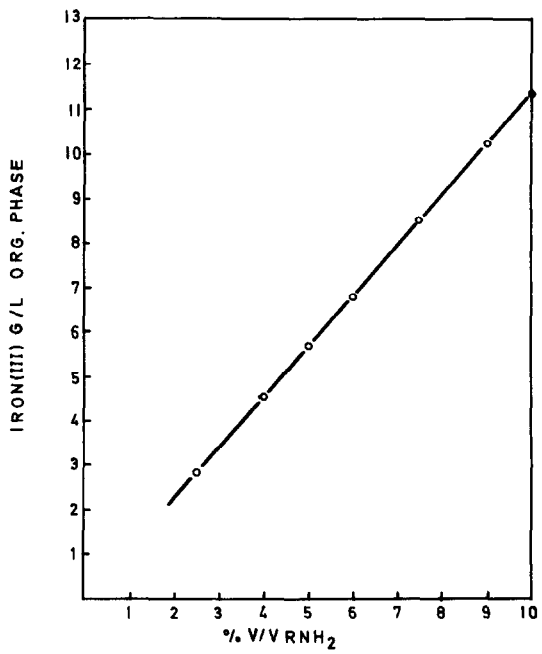


Fig. 8. Variation in iron(III) extracted in the organic phase with initial amine concentration in the organic phase. *Aqueous phase*: 0.358 M iron(III) solution.

solution. These will be probably due to certain interactions between the diluent and such species. This phenomenon has also been observed with the iron(III)–amine Primene 81R sulphate complexes extracted at different temperatures.[12]

The IR spectrum of the complex shows a band at 3400 cm^{-1} that can be assigned to the N—H stretching vibration of the amine group, and also two bands at 2950 and 2850 cm^{-1} assigned to the C—H stretching vibrations (antisymmetrical and symmetrical modes, respectively) of the carbon chains.

In the 1200–900-cm^{-1} zone the spectrum shows bands at 1175, 1135 (weak) and 1010 cm^{-1} that can be due to sulphate groups acting as bidentate ligands (C_{2v}-symmetry) and a band at 1105 cm^{-1} that can be assigned to the sulphate group with T_d-symmetry.[15] Also, a very weak band at 950 cm^{-1} can be assigned to the sulphate group with a C_{2v}-symmetry. This band is probably hidden by the broad band at 1010 cm^{-1}. At 1220 cm^{-1} there is a band which is probably due to the C—N vibration of the amine group and at about 1615 cm^{-1} a band assigned to the N—H deformation vibration of the amine group is also observed.

Molecular-weight values, obtained by cryoscopic measurements in benzene, of the iron(III) complex at various concentrations are presented in Table 3. They show that the complex is a monomer in benzene solution if based on the $4RNH_2 \cdot Fe_2(SO_4)_3$ formula.

From the data obtained the structure shown in Fig. 9 can be suggested for the amine Primene 81R–iron(III) complex. In this structure the stoichiometry of two iron(III) atoms for each of the four amine Primene 81R molecules deduced from the extraction reaction (1) and established by analysis remains constant and the iron(III) appears to

Table 3. Degree of association of the amine Primene 81R–iron(III) complex

Diluent	Molecular weight	Concentration (mM)	Degree of association[a]
Benzene	1195	57.19	1.0
Benzene	1203	28.60	1.0
Benzene	1210	14.20	1.0

[a] Based on the empirical formula $4RNH_2 \cdot Fe_2(SO_4)_3$ corresponding to a molecular weight of 1199.7.

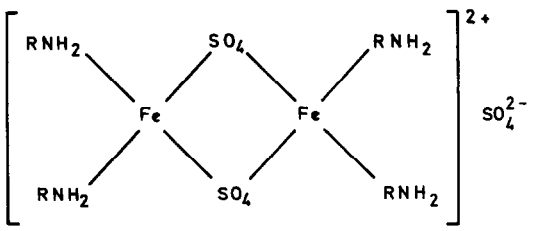


Fig. 9. Possible structure for the amine Primene 81R–iron(III) sulphate complex.

have a coordination number of 4. Also, in this structure there are sulphate groups acting as bidentate ligands (C_{2v}-symmetry) and a sulphate group acting as a free ion with a T_d-symmetry as suggested by the IR spectrum of the complex.

REFERENCES

1. R. W. Cattrall and B. O. West, *J. Inorg. Nucl. Chem.* 1966, **28**, 3035.
2. L. E. Schultze, J. A. Eisele, M. T. Morimoto and D. J. Bauer, *Bureau of Mines E.E.U.U., Report RI*-8353 (1979).
3. F. G. Seeley and W. J. McDowell, *J. Inorg. Nucl. Chem.* 1981, **43**, 375.
4. F. J. Alguacil and S. Amer, *Hydrometallurgy* 1986, **15**, 337.
5. F. J. Alguacil, Ph.D. Thesis, Universidad Complutense de Madrid, Madrid, Spain (1985).
6. S. E. Bryan and M. L. Good, *J. Inorg. Nucl. Chem.* 1961, **21**, 339.
7. M. Mrnka *et al.*, *International Solvent Extraction Conference* 1983, p. 333. EE.UU., Denver, CO (1983).
8. F. J. Alguacil and S. Amer, *Rev. Metal. (CENIM)* 1986, **22**, 55.
9. F. J. Alguacil, S. Amer and A. Luis, *XX Bienal de la Real Sociedad Española de Química*, 29-26. Castellón, Spain (1984).
10. F. J. Alguacil, S. Amer and A. Luis, *Anales de la Real Sociedad Española de Química* (in press).
11. G. M. Ritcey and A. W. Ashbrook, *Solvent Extraction*, Part I, Chap. 4. Elsevier, Amsterdam (1984).
12. F. J. Alguacil, S. Amer and A. Luis, *XX Bienal de la Real Sociedad Española de Química*, 29-25. Castellón, Spain (1984).
13. R. A. Whiteker and N. Davidson, *J. Am. Chem. Soc.* 1953, **75**, 3081.
14. M. L. Good, S. E. Bryan and F. Juge, *Inorg. Chem.* 1963, **2**, 963.
15. N. Nakamoto, *Infrared and Raman Spectra of Inorganic and Coordination Compounds*. John Wiley, New York (1978).

Polyhedron Vol. 5, No. 11, pp. 1755–1761, 1986
Printed in Great Britain

0277–5387/86 $3.00+.00
Pergamon Journals Ltd

STUDY OF THE AMINE PRIMENE 81R SULPHATE–$Fe_2(SO_4)_3$ EXTRACTION EQUILIBRIUM SYSTEM AT LOW TEMPERATURES

F. J. ALGUACIL* and S. AMER

Centro Nacional de Investigaciones Metalúrgicas, Avda. Gregorio del Amo n° 8, Ciudad Universitaria, 28040 Madrid, Spain

(*Received* 2 *December* 1985; *accepted* 28 *February* 1986)

Abstract—The extraction of iron(III) from aqueous sulphate solutions by Primene 81R sulphate at low temperatures was studied as a function of iron(III) and amine sulphate concentrations. In the range of temperatures between 8 and 5°C a complex with the stoichiometric formula $4(RNH_3)_2SO_4 \cdot [Fe(OH)SO_4]_2$ is extracted. The extraction reaction may occur by adduct formation between the amine sulphate and the species $[Fe(OH)SO_4]_2$ from the aqueous phase and not by an anion exchange reaction. The extracted complex is a monomer in benzene solution; the spectral study suggests that the $[Fe(OH)]_2^{4+}$ unit is present in its structure and the sulphate groups act as bidentate ligands.

The extraction of iron(III) from aqueous sulphate solutions with amine sulphates has been extensively studied. Baes[1] had studied the iron(III) extraction from acidic sulphate solutions by a secondary amine sulphate; Cattrall and West[2] have shown that the secondary amine di(3,5,5-trimethylhexyl)amine extracts iron(III) by means of a complex with the stoichiometric formula $(R_2NH_2)_2[FeOH(SO_4)]_2$, where R is 3,5,5-trimethylhexyl.

The extraction of iron(III) from aqueous solutions with primary amine sulphate has also been reported. Thus Cattrall and Reverill[3] investigated the extraction of iron(III) by means of the primary amines 3,5,5-trimethylhexylamine and *n*-dodecylamine. The extraction of iron(III) from sulphate solutions with primary amines has been reported by Seeley[4,5] and Ishimori[6] in extraction survey studies, and Schultze *et al.*[7] reported their investigations concerning the extraction of iron(III) from concentrated aluminium sulphate solutions by different types of amines.

The extraction of iron(III) by Primene 81R sulphate at 50°C or higher temperatures has been studied before,[8,9] showing that the extracted complex presents a stoichiometric formula represented by $3(RNH_3)_2SO_4 \cdot [Fe(OH)SO_4]_2$. All the above studies have been carried out at 20°C or higher temperatures and no data are available about the extraction of iron(III) at lower temperatures.

It has been shown, therefore, that the iron(III) extraction by the primary amine Primene 81R sulphate is temperature-dependent,[10] and in the range of temperatures between 8 and 5°C it seems that a complex with a different stoichiometry than that presented by the complex described above was extracted.

Thus, the purpose of the present paper was to study in detail the extraction equilibrium system between iron(III) sulphate and Primene 81R sulphate in kerosene at low temperatures as a new contribution to understanding the iron(III) extraction behaviour of amine sulphates, this being the first time that an extraction system at these temperatures has been described.

EXPERIMENTAL

Chemicals

The amine Primene 81R used in the investigation was obtained from Rohm & Haas Co., Philadelphia, PA; its composition is >99% primary aliphatic amine, having the general structure $R_1R_2R_3$—C—NH_2, where the total carbon atom number is 12–14. The experimental molecular weight was 200, as calculated from the titration of various amine solutions, in ethanol, by standard

* Author to whom correspondence should be addressed.

sulphuric and hydrochloric acid using a Beckman 3560 pH-meter.

Kerosene was supplied by CAMPSA with the following specifications: boiling point, >140°C; % aromatics, ~20; density (20°C), 0.780 g cm^{-3}. All other chemicals were reagent grade.

Procedure

Extractions were carried out by the following procedure. Equal volumes of Primene 81R solutions diluted in kerosene with *n*-decanol as modifier [in a proportion of half the initial amine concentration, expressed as % (v/v)] and iron(III) sulphate solutions containing the stoichiometric concentration of sulphuric acid to form the amine sulphate[8] were placed in separatory funnels, thermostatted at 8±0.1°C, and mechanically shaken. On completion of the extraction, the phases were separated and iron(III) in the organic phase was then back-extracted with 3 M sulphuric acid solutions.

Iron(III) in both phases was determined volumetrically with potassium dichromate; the acidity of the equilibrated aqueous phases was determined with sodium hydroxide solutions using methyl orange as indicator; the procedure followed was: an aliquot of the aqueous phase was treated with sufficient standard sodium hydroxide solution to precipitate all the iron(III) in the form of the hydroxide, and to neutralize free sulphuric acid formed in the extraction reaction. After filtration of the solid and carefully washing it, the solution was titrated with standard hydrochloric acid using methyl orange as indicator. Sulphuric acid concentrations were then calculated from all these values. The accuracy of this procedure was checked by the use of known-concentration solutions of either iron(III) or sulphuric acid. Sulphate was determined gravimetrically as barium sulphate.

The diluent of the saturated organic phases was evaporated under reduced pressure to yield a dark-red waxy solid residue. This was recrystallized from a methanol–acetone mixture to yield a dark-red solid. The compound was dried in a desiccator over $CaCl_2$ and P_4O_{10}.

The solid decomposes at 190°C. Found: Fe, 4.7; SO_4^{2-}, 23.1; C, 53.1; N, 4.7; H, 10.2%. Calc. for $4(RNH_3)_2SO_4 \cdot [Fe(OH)SO_4]_2$: Fe, 4.8; SO_4^{2-}, 24.7; C, 53.6; N, 4.81; H, 10.7; O, 1.4%.

IR measurements of the solid were carried out in Unicam SP-1100 and Perkin–Elmer 682 spectrophotometers using cesium iodide windows. Nujol and hexachlorobutadiene mulls were used. UV spectra were obtained in a Beckman DB-GT spectrophotometer using 1-cm SiO_2 cells.

RESULTS AND DISCUSSION

Study of extraction kinetics

Influence of the iron(III) concentration in the aqueous phase. Isotherms for the extraction of iron(III) by 0.203 M Primene 81R sulphate in kerosene and 5% (v/v) *n*-decanol from aqueous iron(III) sulphate solutions are presented in Fig. 1 (temperature of 8°C).

The experimental values obtained from these curves indicated that the equilibrium was reached within 10 min and the change between 10 min and 1 h is quite small, although at high iron(III) concentrations there are no significant differences between 1 and 10 min or 1 h.

The curves did not show the upward swing above the initial loading plateau shown in other amine systems.[5] Thus, it can be concluded that in the Primene 81R sulphate–iron(III) extraction system there is not a species change at high aqueous iron(III) concentration.

Influence of equilibration time. Kinetic studies have also been carried out on the effect of different initial aqueous iron(III) concentrations on the equilibration time, keeping the iron(III) concentration constant each time. The results obtained at 8°C are shown in Fig. 2, plotting the iron(III) concentration in the organic phase vs equilibration time, for an organic phase of 0.203 M amine Primene 81R sulphate in kerosene shaken with different aqueous iron(III) solutions.

At 8°C equilibrium was reached in 5 min for all compositions of the aqueous phase. Temperature has no influence on equilibrium extraction between 8 and 5°C. Increasing concentrations of iron(III) in the aqueous phase up to 1 M have no influence on the organic-phase composition. This result was in

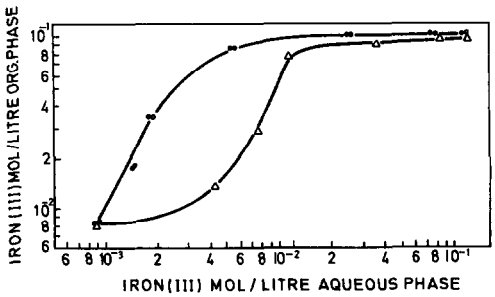


Fig. 1. Equilibrium loading curves for iron(III) extraction by Primene 81R sulphate in kerosene. *Organic phase*: 0.203 M Primene 81R sulphate in kerosene and 5% (v/v) *n*-decanol. *Aqueous phase*: solutions containing various concentrations of $Fe_2(SO_4)_3$. *Contact*: equal volumes equilibrated for: (△) 1 min, (●) 10 min, or (○) 1 h.

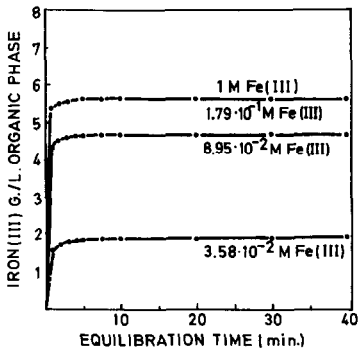


Fig. 2. Kinetics of iron(III) extraction by 0.203 M Primene 81R sulphate. Effect of varying initial iron(III) concentrations in the aqueous phase and equilibration time.

accordance with those obtained previously showing the absence of the upward swing of the curves in Fig. 1. Increasing equilibration time has no influence on the loading of the organic phase.

Extraction isotherms

Loading isotherms for the extraction of iron(III) with 0.0254, 0.0508, 0.1015 and 0.203 M amine Primene 81R sulphate in kerosene, in equilibrium with aqueous iron(III) sulphate solutions at 8 ± 0.1°C, are shown in Fig. 3. The results obtained show that at saturation loading the amine sulphate/iron(III) concentration ratio appears to approach 2. Neither of the curves shows an upward swing above this loading level as mentioned before.

Sulphuric acid titration of the equilibrated aqueous phase shows that 1 mol of sulphuric acid is liberated for every 2 mol of iron(III) extracted by Primene 81R sulphate as shown by experimental

Table 1. Experimental values of acid liberated by the extraction of iron(III) (organic phase: 0.203 M Primene 81R sulphate, temperature 8°C)

$[Fe(III)]_{org}$ (mM)	$[H_2SO_4]_{aq}$ (mM)	$[Fe(III)]_{org}/[H_2SO_4]_{aq}$
8.1	4.1	1.98
16.5	8.3	1.99
34.0	16.9	2.01
84.2	41.9	2.01
100.0	50.3	1.99
101.0	50.5	2.00
	Average	2.00

values in Table 1 for a 0.203 M amine sulphate concentration.

Figure 4 shows the relationship between the molar ratio of the iron(III) concentration in the organic phase to the Primene 81R concentration vs the iron(III) concentration in the aqueous phase; it can be seen that the limiting ratio obtained is equal to 0.25, corresponding to $[Fe(III)]_{org}/[RNH_2]_{org} = 0.25$. If the amine concentration is transformed into amine sulphate concentration, this value is 0.5, as $[RNH_2]_{org} = 2[(RNH_3)_2SO_4]_{org}$ for this system.[8] This molar ratio is similar to those obtained from curves in Fig. 3.

According to the experimental data, the following extraction reaction for iron(III) sulphate by Primene 81R sulphate in the range of temperatures between 8 and 5°C is suggested:

$$4(RNH_3)_2SO_{4(org)} + Fe_2(SO_4)_{3(aq)} + 2H_2O \rightleftarrows 4(RNH_3)_2SO_4 \cdot [Fe(OH)SO_4]_{2(org)} + H_2SO_{4(aq)}. \quad (1)$$

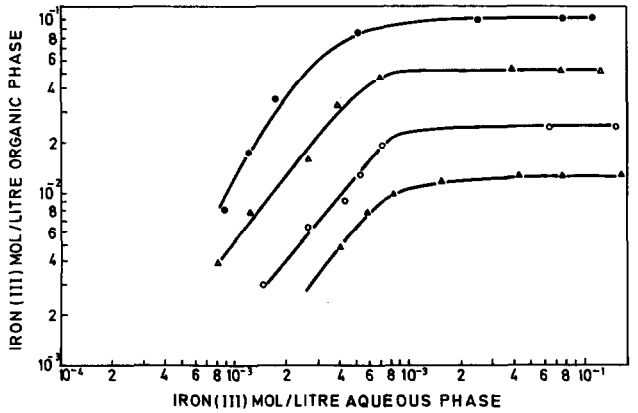


Fig. 3. Equilibrium loading curves for iron(III) extraction by Primene 81R sulphate. Effect of amine sulphate concentration. *Organic phase*: (●) 0.203 M, (△) 0.1015 M, (○) 0.0508 M, (▲) 0.0254 M amine sulphate in kerosene and *n*-decanol [5, 2.5, 1.25 and 0.63% (v/v), respectively]. *Aqueous phase*: aqueous solutions containing various concentrations of $Fe_2(SO_4)_3$. *Contact*: equal volumes were equilibrated for 10 min.

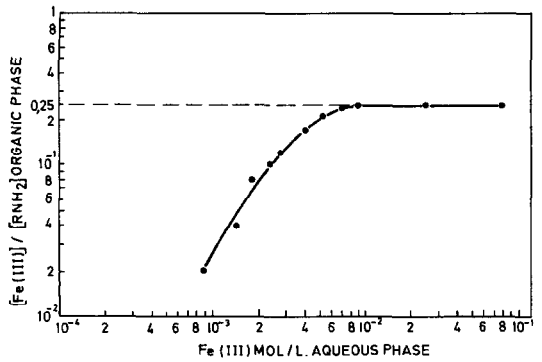


Fig. 4. Variation in the molar ratio [Fe(III)]/[RNH_2] in the organic phase with molar [Fe(III)] in the aqueous phase. *Organic phase*: 0.203 M Primene 81R sulphate.

It seems that an adduct is formed as suggested in other systems described by other authors, with the extraction of an iron(III) compound similar to those described before with other amine sulphates,[1-3] but different from the extracted species described for other primary amines.[5] The results obtained show that the structure of the amine sulphate will define the way in which iron(III) is extracted into the organic phase, and not the type of amine (i.e. primary, secondary, ...), because several primary and secondary amines (like those studied in this paper and in Refs 1–3 and 9) extract iron(III) in the form of a hydroxylated species of this metallic ion, whereas another primary amine named Primene JMT extracts iron(III) in a complex with no iron(III)-hydroxylated species.[5] The results obtained also show that the Primene 81R sulphate can extract iron(III) from aqueous sulphate solutions even at low temperatures, the mechanism of the extraction being similar to that described for the same amine sulphate at higher temperatures; the extraction reaction can be related as an adduct formation and not as an anion exchange reaction, this being the first time that the extraction behaviour of an amine sulphate at this temperature has been described.

Reagent concentration dependence

This study was carried out by shaking a 0.179 M iron(III) aqueous solution and different organic phases for 10 min at 8°C. The results obtained are shown in Fig. 5, in which the iron(III) concentration in the organic phase is plotted against the initial amine sulphate concentration. It can be seen that there is a proportional concentration relationship between both values until an approximately 0.2 M Primene 81R sulphate concentration. Thus, from Fig. 5 unknown amine sulphate concentrations can be determined by comparing values for the iron(III)

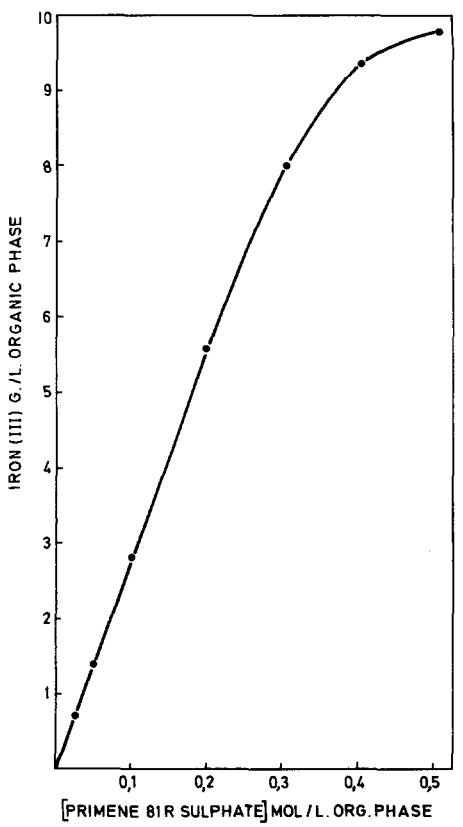


Fig. 5. Variation in iron(III) loading in the organic phase with initial Primene 81R sulphate concentration in the organic phase. *Aqueous phase*: 0.179 M iron(III) solution in sulphate media.

extracted in the organic phase with those shown in Fig. 5.

Figure 6 shows the relationship between the ratio of iron(III) to the amine sulphate concentration in the organic phase vs the initial Primene 81R sulphate concentration at 8°C. It shows that, when the organic phase is saturated with this metallic ion, the maximum value of this relationship is independent of the initial amine sulphate concentrations, this value being equal to the ratio 0.50 or 1/2. This maximum value is equal to that previously obtained from Fig. 4, indicating that, at least at saturation loading, an organic complex with constant stoichiometry was extracted. When there is an excess Primene 81R sulphate concentration the ratio decreases progressively.

The variation in the iron(III) distribution coefficient with the amine sulphate concentration is shown in Fig. 7 at 8°C (equilibrium time in all cases was 10 min). The results show that as the amine sulphate concentration increases the slope of the curves defined by $\log D_{Fe}$ vs log [Primene 81R sulphate] decreases progressively, indicating aggregation of the amine sulphate.

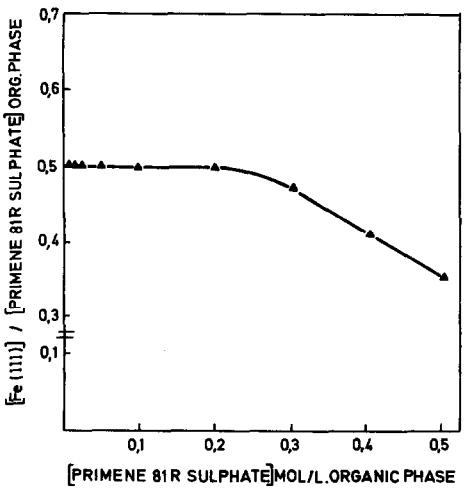


Fig. 6. Variation in the molar ratio [Fe(III)]/[Primene 81R sulphate] in the organic phase with initial amine sulphate concentration. *Aqueous phase*: 0.179 M iron(III) solution in sulphate media.

Equations describing the extraction equilibrium may be derived by considering the following equilibria:

(1) The formation of amine sulphate and distribution of the amine salt between the aqueous and the organic phases:

$$2RNH_{2(org)} + H_2SO_{4(aq)} \rightarrow (RNH_3)_2SO_{4(org)},$$

$$4(RNH_3)_2SO_{4(org)} \rightleftarrows 4(RNH_3)_2SO_{4(aq)},$$

$$K_1 = \frac{[(RNH_3)_2SO_4]^4_{aq}}{[(RNH_3)_2SO_4]^4_{org}}. \quad (2)$$

(2) The hydrolysis of iron(III) in the aqueous phase:

$$2Fe^{3+}_{(aq)} + 2H_2O \rightleftarrows [Fe(OH)]^{4+}_{2(aq)} + 2H^+_{(aq)},$$

$$K_2 = \frac{[[Fe(OH)]^{4+}_2]_{aq}[H^+]^2_{aq}}{[Fe^{3+}]^2_{aq}[H_2O]^2}. \quad (3)$$

(3) The formation of the species $[Fe(OH)SO_4]_2$ in the aqueous phase:

$$[Fe(OH)]^{4+}_{2(aq)} + 2SO^{2-}_{4(aq)} \rightleftarrows [Fe(OH)SO_4]_{2(aq)},$$

$$K_3 = \frac{[[Fe(OH)SO_4]_2]_{aq}}{[[Fe(OH)]^{4+}_2]_{aq}[SO^{2-}_4]^2_{aq}}. \quad (4)$$

(4) The formation of the complex in the aqueous phase:

$$4(RNH_3)_2SO_{4(aq)} + [Fe(OH)SO_4]_{2(aq)} \rightleftarrows 4(RNH_3)_2SO_4 \cdot [Fe(OH)SO_4]_{2(aq)},$$

$$K_4 = \frac{[4(RNH_3)_2SO_4 \cdot [Fe(OH)SO_4]_2]_{aq}}{[(RNH_3)_2SO_4]^4_{aq}[[Fe(OH)SO_4]_2]_{aq}}. \quad (5)$$

(5) And the distribution of the complex between the aqueous and the organic phases:

$$4(RNH_3)_2SO_4 \cdot [Fe(OH)SO_4]_{2(aq)} \rightleftarrows 4(RNH_3)_2SO_4 \cdot [Fe(OH)SO_4]_{2(org)},$$

$$K_5 = \frac{[4(RNH_3)_3SO_4 \cdot [Fe(OH)SO_4]_2]_{org}}{[4(RNH_3)_2SO_4 \cdot [Fe(OH)SO_4]_2]_{aq}}. \quad (6)$$

The combination of the expressions for the five equilibrium constants by rearrangement and substitution gives an expression of the equilibrium constant of the overall extraction reaction shown in eqn (1). This K may be deduced as:

$$K = \frac{[4(RNH_3)_2SO_4 \cdot [Fe(OH)SO_4]_2]_{org}[H^+]^2_{aq}[SO^{2-}_4]_{aq}}{[(RNH_3)_2SO_4]^4_{org}[Fe^{3+}]^2_{aq}[SO^{2-}_4]^3_{aq}[H_2O]^2}, \quad (7)$$

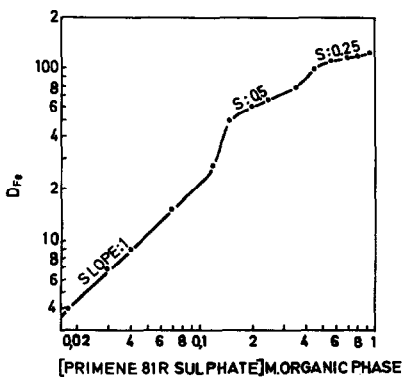


Fig. 7. Dependence of the iron(III) extraction coefficient on the organic-phase concentration of Primene 81R sulphate. *Aqueous phase*: aqueous solution of 0.179 M iron(III) in sulphate media.

in which K is the overall equilibrium constant and molar concentrations are used. If it is assumed that all the iron(III) in the organic phase is in the form of the complex given in eqn (7), and the iron(III) concentration in the aqueous phase is proportional to the iron(III) concentration as described in eqn (1), eqn (7) is transformed into eqn (8):

$$D_{Fe} = \frac{K[SO^{2-}_4]^2_{aq}[(RNH_3)_2SO_4]^4_{org}}{[H^+]^2_{aq}}. \quad (8)$$

From this equation eqn (9) is obtained:

$$\log D_{Fe} = 4\log[(RNH_3)_2SO_4]_{org} + \log K', \quad (9)$$

where K' is the overall constant.

It has been shown[5] that in the case of extraction by a primary amine this equation must be corrected by introducing a value named j, which represents

the number of free amine sulphate molecules per aggregate; hence:

$$\log D_{Fe} = \frac{n}{j}\log [(RNH_3)_2SO_4]_{org} + \log K', \quad (10)$$

in accordance with eqn (9). n is the number of amine Primene 81R sulphates associated with each iron(III).

Consequently, in a representation of $\log D_{Fe}$ vs log [Primene 81R sulphate] as in Fig. 7, the slope of the curves (n/j) will be dependent on the iron(III) complex stoichiometry and on the extractant aggregation. From Figs 3 and 6 is can be deduced that the value of n in this extraction system is 2 for the present complex stoichiometry [eight molecules of amine or four of the amine sulphate per two iron(III)]. Thus the slope $n/j = 1$ in Fig. 7 at low extractant concentrations gives an average Primene 81R sulphate aggregation of approximately 2, and the slope $n/j = 0.25$ at higher amine sulphate concentrations suggests an aggregation of approximately 8. These experimental data are in accordance with those obtained about the aggregation of primary amine sulphates.[11]

From the experimental values presented in this work it can be deduced that when iron(III) is extracted by Primene 81R sulphate at 8°C there is a deaggregation of the amine sulphate, which is much larger at low amine sulphate concentrations in the organic phase.

Spectra and structure of the complex

The IR spectrum of the complex shows four bands at 1180, 1125, 1035 and 985 cm^{-1}, which are consistent with those expected for the sulphate group acting as a bidentate ligand.[12] The spectrum also shows a band at 3025 cm^{-1} assigned to the N—H stretching vibration of the amine group and a band at 1220 cm^{-1} that can be assigned to the C—N vibration of the amine group. A band that can be assigned to the O—H group linked to iron(III) appears at about 3600 cm^{-1}, whilst the absence of a band in the region 1600–1650 cm^{-1} suggests the absence of water in the complex and implies that the band at 3600 cm^{-1} is only due to the O—H group.

The UV spectrum in kerosene of the isolated iron(III)–Primene 81R complex shows a band at about 335 nm. It has been suggested[13] that at certain iron(III) concentrations the iron(III)-hydroxylated species dimerizes to give the $[Fe(OH)]_2^{4+}$ species which shows an absorption peak at 335 nm. The dimer species must be considered with hydroxyl groups bridging two iron(III) ions.

Table 2. Degree of association of the amine Primene 81R sulphate–iron(III) complex extracted at 8°C

Solvent	Concentration (mM)	Molecular weight	Degree of association[a]
Benzene	12.51	2365	1.0
Benzene	25.01	2346	1.0
Benzene	50.02	2330	1.0

[a] Based on the empirical formula $4(RNH_3)_2SO_4 \cdot [Fe(OH)SO_4]_2$, corresponding to a molecular weight of 2330.

The value of the molar extinction coefficient at 335 nm is about 3887 (complex concentration = 3.91×10^{-5} M) which is different to that reported for these species in aqueous solutions. It has been shown[14] that in solutions of certain amines in chloroform, the spectra of several complexes of metals have higher extinction coefficients than those obtained in aqueous solutions, although the absorption maxima and character of the spectra will be constant. It is possible that this change is due to the different diluents and to certain interactions between the solvent and metallic species. The phenomenon observed in this paper has also been observed in other amine systems.[2,3,9]

Molecular-weight values, obtained by cryoscopic measurements in benzene of the iron(III) complex with Primene 81R sulphate, at various concentrations, are presented in Table 2. They show that the complex is a monomer in benzene solution if based on the $4(RNH_3)_2SO_4 \cdot [Fe(OH)SO_4]_2$ unit.

From the data obtained the structure shown in Fig. 8 can be suggested for the iron(III)–Primene 81R sulphate complex extracted in the range of temperatures between 8 and 5°C. In this structure the stoichiometry of two iron(III) atoms per four amine sulphate groups deduced above from the extraction reaction (1), and established by analysis, remains constant. Each iron(III) presents a coordination number of 6, similar to the coordination observed for this ion in similar complexes.[3,9]

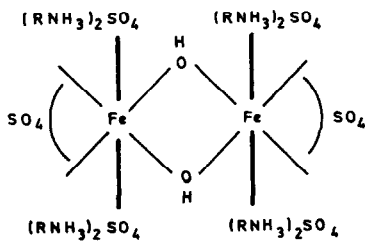


Fig. 8. A possible structure of the iron(III)–Primene 81R sulphate complex.

REFERENCES

1. C. F. Baes, *USAEC Report ORNL*-1930 (1955).
2. R. W. Cattrall and B. O. West, *J. Inorg. Nucl. Chem.* 1966, **28**, 3035.
3. R. W. Cattrall and K. I. Peverill, *J. Inorg. Nucl. Chem.* 1970, **32**, 663.
4. F. G. Seeley and D. J. Crouse, *J. Chem. Eng. Data* 1971, **16**, 393.
5. F. G. Seeley and W. J. McDowell, *J. Inorg. Nucl. Chem.* 1981, **43**, 375.
6. T. Ishimori, E. Akatsu, K. Tukuechi, T. Kobune, Y. Usuba, K. Kimura, G. Onawa and H. Uchyama, *Japan Atomic Energy Research Institute, Report JAERI*-1106 (1960).
7. L. E. Schultze, J. A. Eisele, M. T. Morimoto and D. J. Bauer, *Bureau of Mines EE.UU., Report RI*-8353 (1979).
8. F. J. Alguacil, Ph.D. Thesis, Universidad Complutense de Madrid, Madrid, Spain (1985).
9. F. J. Alguacil and S. Amer, *Hydrometallurgy* 1986, **15**, 337.
10. F. J. Alguacil, S. Amer and A. Luis, *XX Bienal de la Real Sociedad Española de Química*, 29-26. Castellón, Spain (1984).
11. K. A. Allen, *J. Phys. Chem.* 1958, **62**, 1119.
12. K. Nakamoto, *Infrared and Raman Spectra of Inorganic and Coordination Compounds*, 3rd edn. John Wiley, New York (1978).
13. L. N. Mulay and P. W. Selwood, *J. Am. Chem. Soc.* 1955, **77**, 2693.
14. M. L. Good, S. E. Bryan and F. Juge, Jr, *Inorg. Chem.* 1963, **2**, 963.

Polyhedron Vol. 5, No. 11, pp. 1763–1770, 1986
Printed in Great Britain

0277–5387/86 $3.00+.00
Pergamon Journals Ltd

PREDICTED STABILITIES OF MONATOMIC ANIONS IN WATER AND LIQUID AMMONIA AT 298.15 K

STEVEN G. BRATSCH* and J. J. LAGOWSKI

Department of Chemistry, The University of Texas, Austin, TX 78712, U.S.A.

(*Received* 3 *January* 1986; *accepted* 28 *February* 1986)

Abstract—Critically evaluated experimental and theoretical atomic electron affinities are assembled and used to derive thermodynamic properties of gas-phase monatomic anions throughout the Periodic Table. The stabilities (as ΔG_f^o) of these anions in water and liquid ammonia are calculated by a semiempirical electrostatic model. The predictions are compared with experimental observations where possible.

The ability of some metals to form "simple" anions represents a new and unusual area of inorganic chemistry. Monatomic metal anions (M^-) known in nonaqueous solvents and/or crystals include Na^-, K^-, Rb^-, Cs^-[1–3] and Au^-.[4,5(a),6]

Chemical intuition may serve as a guide in determining which metals should form anions. However, a significant advancement in our understanding of simple metal anions would be the calculation of their thermodynamics of formation in solution or crystals. In previous papers,[7–9] we have applied a semiempirical electrostatic model to the estimation of the stability of monatomic anions of the alkali metals, lanthanides and actinides in water and liquid ammonia at 298.15 K. In the present work we apply our model to the remaining elements of the Periodic Table. With the exception of about a dozen borderline cases, our results serve to identify those elements which are expected to form thermodynamically stable simple anions in solution under standard-state conditions.

The standard Gibbs free energy of formation of a solvated monatomic anion M^- [ΔG_f^o (M^-, solv)] is defined as the standard Gibbs free energy change for the reaction:

$$M(\text{std state}) + 0.5H_2(g) \rightarrow M^-(\text{solv}) + H^+(\text{solv}), \quad (1)$$

where H^+(solv) is a shorthand for the various cationic hydrogen species (e.g. H_3O^+, $H_9O_4^+$ etc., in water, and NH_4^+ in liquid ammonia). Based on experimental halide data,[7] we have previously derived the relationships:

$$\Delta G_f^o(M^-, \text{aq}) = \Delta G_f^o(M^-, \text{g}) - \frac{56.1}{r_{M^-} - 0.017} + 451, \quad (2)$$

$$\Delta G_f^o(M^-, \text{am}) = \Delta G_f^o(M^-, \text{g}) - \frac{50.3}{r_{M^-} - 0.017} + 354, \quad (3)$$

for anions in aqueous and ammonia solutions, respectively, at 298.15 K. In eqns (2) and (3), ΔG_f^o is in kJ mol^{-1} and r_{M^-} is the crystal anionic radius in nm.[10] The term in eqns (2) and (3) involving r_{M^-} represents a simple, semiempirical way of relating the standard Gibbs free energy of solvation of M^- in water or liquid ammonia to the ionic radius. In order to calculate the stability of a monatomic anion in water or liquid ammonia by eqn (2) or (3), we require ΔG_f^o (M^-, g) and an estimate for r_{M^-}.

THERMODYNAMICS OF GAS-PHASE ANIONS AT 298.15 K (TABLE 1)

Standard enthalpies of formation of monatomic gases [ΔH_f^o (M, g)] and standard entropies of the elements in their standard states [S^o (M, std state)] at 298.15 K have been taken from familiar references[11,12] and therefore have not been tabulated. Experimental atomic electron affinities [EA (M)] have been taken from the recent review by Hotop and Lineberger.[13]

* Author to whom correspondence should be addressed

Table 1. Thermodynamics of gas-phase anions at 298.15 K

M	EA (M)[a] [eV (0 K)]	e.c. (M^-)[b]	ΔH_f^o (M^-, g)[c] (kJ mol^{-1})	S^o (M^-, g)[d] (J K^{-1} mol^{-1})	ΔG_f^o (M^-, g)[e] (kJ mol^{-1})
e			0.0[f]	20.87	0.0[f]
H	0.7542	1*s*2	139.0	108.85	132.2
He	−0.5[g]	2*s*1	42	131.81	47
Li	0.6180	2*s*2	93.5	132.91	68.8
Be	−0.5[g]	2*p*1	366	141.93	333
B	0.277	2*p*2	527	138.43	494
C	1.2629	2*p*3	588.6	151.27	551.4
N	−0.07	2*p*4	473.2	155.05	461.7
O	1.4611	2*p*5	102.0	154.85	92.6
F	3.399	2*p*6	−254.8	145.47	−261.7
Ne	−1.2[g]	3*s*1	110	151.98	115
Na	0.5479	3*s*2	48.3	147.84	25.7
Mg	−0.4[g]	3*p*1	179	154.30	149
Al	0.441	3*p*2	281.0	149.84	251.0
Si	1.385	3*p*3	310	161.87	274
P	0.7465	3*p*4	238.3	164.94	207.6
S	2.0771	3*p*5	70.4	163.52	37.4
Cl	3.617	3*p*6	−233.9	153.25	−240.1
Ar	−1.0[g]	4*s*1	90	160.50	95
K	0.5015	4*s*2	34.7	154.47	14.2
Ca	−1.0[g]	3*d*1, 4*s*2	268	166.30	237
	−0.3[g]	4*s*2, 4*p*1	201	160.54	172
Sc	−0.3[g]	3*d*2, 4*s*2	401	169.59	367
	0.188	3*d*1, 4*s*2, 4*p*1	353.5	169.6	319.5
Ti	0.079	3*d*3, 4*s*2	456.1	168.53	421.2
V	0.525	3*d*4, 4*s*2	457.4	157.77	425.2
Cr	0.666	3*d*5, 4*s*2	326.1	172.92	287.9
Mn	−1.2[g]	3*d*6, 4*s*2	390	176.98	353
	−0.5[g]	3*d*5, 4*s*2, 4*p*1	323	174.9	287
Fe	0.163	3*d*7, 4*s*2	394.4	178.06	355.7
Co	0.661	3*d*8, 4*s*2	354.7	177.85	316.9
Ni	1.156	3*d*9, 4*s*2	312.0	174.43	275.1
Cu	1.228	3*d*10, 4*s*2	212.9	160.52	181.1
Zn	−0.6[g]	4*p*1	182	166.64	151
Ga	0.3	4*p*2	242	161.68	212
Ge	1.2	4*p*3	255	173.71	219
As	0.81	4*p*4	218.2	175.96	182.4
Se	2.0207	4*p*5	25.9	174.76	−7.3
Br	3.365	4*p*6	−219.0	163.38	−238.8
Kr	−1.0[g]	5*s*1	90	169.74	95
Rb	0.4859	5*s*2	27.8	164.22	8.0
Sr	−0.5[g]	4*d*1, 5*s*2	206	176.06	175
	−0.3[g]	5*s*2, 5*p*1	187	170.29	158
Y	0.0[g]	4*d*2, 5*s*2	415	178.09	381
	0.307	4*d*1, 5*s*2, 5*p*1	385.5	178.1	351.9
Zr	0.426	4*d*3, 5*s*2	561.5	176.56	526.7
Nb	0.893	4*d*4, 5*s*2	633.5	165.26	601.3
Mo	0.746	4*d*5, 5*s*2	579.9	180.56	540.8
Tc	0.6[g]	4*d*6, 5*s*2	556	184.06	517
Ru	1.05	4*d*7, 5*s*2	535.2	185.46	494.6
Rh	1.137	4*d*8, 5*s*2	441.0	184.81	401.5
Pd	0.557	4*d*10, 5*s*1	318.3	172.72	284.2
Ag	1.302	4*d*10, 5*s*2	153.1	167.12	122.2
Cd	−0.7[g]	5*p*1	173	173.40	143
In	0.3	5*p*2	208	167.90	181
Sn	1.2	5*p*3	179	179.84	147

(*continued*)

Table 1. (*continued*)

M	EA (M)[a] [eV (0 K)]	e.c. (M^-)[b]	ΔH_f^o (M^-, g)[c] (kJ mol^{-1})	S^o (M^-, g)[d] (J K^{-1} mol^{-1})	ΔG_f^o (M^-, g)[e] (kJ mol^{-1})
Sb	1.07	5*p*4	152.9	182.02	118.5
Te	1.9708	5*p*5	0.4	180.74	−32.4
I	3.0591	5*p*6	−194.6	169.15	−221.5
Xe	−0.8[g]	6*s*1	71	175.34	76
Cs	0.4716	6*s*2	24.4	169.73	5.4
Ba	−0.3[g]	5*d*1, 6*s*2	203	181.66	174
La	0.5	5*d*2, 6*s*2	377	183.66	345
Lu	0.0[g]	5*d*2, 6*s*2	421	186.54	387
	0.3[g]	5*d*1, 6*s*2, 6*p*1	392	186.5	358
Hf	0.1[g]	5*d*3, 6*s*2	603	184.93	567
Ta	0.322	5*d*4, 6*s*2	744.7	173.58	711.5
W	0.815	5*d*5, 6*s*2	764.6	188.67	724.3
Re	0.1[g]	5*d*6, 6*s*2	754	192.20	714
Os	1.1	5*d*7, 6*s*2	679	193.34	637
Ir	1.565	5*d*8, 6*s*2	508.1	192.60	467.5
Pt	2.128	5*d*9, 6*s*2	353.8	189.41	316.0
Au	2.3086	5*d*10, 6*s*2	137.2	174.63	105.5
Hg	−0.5[g]	6*p*1	103	180.62	78
Tl	0.2	6*p*2	157	175.09	130
Pb	0.364	6*p*3	153.9	186.79	123.8
Bi	0.946	6*p*4	109.6	188.75	76.5
Po	1.8[g]	6*p*5	0	186.90	−32
At	2.8	6*p*6	−176	175.43	−203
Rn	−0.7[g]	7*s*1	61	181.89	66

[a] Reference 13, except as noted.
[b] Anion electron configuration (Ref. 13 and this work).
[c] Equation (4). ΔH_f^o (M, g) from Ref. 11 or 12 except for M = Tc, Po and At [estimated (620, 180 and 100 kJ mol^{-1})] (this work).
[d] Equation (5).
[e] S^o (M, std state) from Ref. 11 or 12 except for M = Tc, Po and At [estimated (33, 60 and 65 J K^{-1} mol^{-1})] (this work). S^o (e^-) accounted for in $\Delta G_f^o = \Delta H_f^o - T\Delta S_f^o$.
[f] Arbitrary convention.
[g] Estimated (this work).

We have estimated the EAs where necessary by methods discussed by Zollweg.[14] All atomic ionization potentials [IP (M)] and atomic and cationic promotion energies (ΔE) required for these methods have been taken from Moore's tables.[15,16]

He, Ne, Ar, Kr *and* Xe

These were derived by quadratic extrapolation of isoelectronic sequences, correcting for ΔE [M^{2+}, $(n-1)d^1 \rightarrow ns^1$] for M = Sc, Y and La.

Be, Mg, Zn, Cd *and* Hg

These were derived by extrapolation of the EA of *p*-block elements by comparison with the IP of the following element (an isoelectronic process).

Ca (3d), Sc (3d), Mn (3d), Sr (4d), Y (4d), Tc, Lu (5d), Hf, Re *and* Po

These were calculated by horizontal analysis.[14]

Ca (4p), Sr (5p), Ba, Lu (6p) *and* Rn

These were estimated by vertical extrapolation.

Mn (4p)

This was assumed to lie between Ca (4*p*) and Zn.

The standard enthalpies of formation and standard entropies of gas-phase anions M^- have been calculated by:[17(a),(b)]

$$\Delta H_f^o(M^-, g) = \Delta H_f^o(M, g) - EA(M) - 2.5RT, \quad (4)$$

$$S^\circ(M^-, g) = 1.5R\ln(\text{at wt}) + R\ln(2J+1) + 108.745, \quad (5)$$

where ΔH_f° is in kJ mol^{-1} and S° is in J K^{-1} mol^{-1}. J in eqn (5) is the total angular-momentum quantum number (L–S coupling) and $2J+1$ is the electronic-spin multiplicity.[18,19]

Finally, ΔG_f° (M^-, g) values in Table 1 have been calculated by ΔH_f° (M^-, g) $- T\Delta S_f^\circ$ (M^-, g), using S° (e^-) = 20.87 J K^{-1} mol^{-1}.[17(c)]

CRYSTAL ANIONIC RADII AND PREDICTED STANDARD GIBBS FREE ENERGIES OF FORMATION OF ANIONS IN WATER AND LIQUID AMMONIA AT 298.15 K (TABLE 2)

Crystal anionic radii have been calculated by an extension of a method used for lanthanides and actinides:[8,9]

$$r_{M^-} = \frac{A}{q+B} + C, \quad (6)$$

where q equals the number of np, $(n-1)d$ or $(n-2)f$ electrons in the anion. The basis for q is the orbital type being filled in accordance with the Aufbau principle. B equals 6, 10 or 14 for anions of the p-, d- or f-block elements, respectively, and A and C are determined by fitting to certain "key" values. "Key" anionic radii have been assumed for the alkalides ($q = 0$) [Ref. 5(b) and this work], the halides ($q = 6$) (Ref. 10 and this work), and the copper and zinc subgroups ($q = 10$ and 1, respectively) [Ref. 5(c) and this work]. Irregularities in electron configurations (e.g. Pd^- is $4d^{10}5s^1$, not $4d^95s^2$) have been ignored in assigning q. Noble-gas anionic radii are probably the least certain because they have been extrapolated by using $q = -1$.

Pauling[10] has calculated the hydride ionic radius by the extrapolation of an isoelectronic sequence. Alternately, one may subtract the appropriate cationic radius from the measured metal–hydrogen distance in the alkali hydride crystals.[20(a)] Both results are given in Table 2.

Crystallographic measurements[21(a)] and spectroscopic correlations[5(c)] indicate that r_{Au^-} is about

Table 2. Predicted standard Gibbs free energies of formation of solvated anions and standard electrode potentials in water and liquid ammonia at 298.15 K

M	r_{M^-}[a] (nm)	ΔG_f° (M^-, aq)[b] (kJ mol^{-1})	$E^\circ_{H_2O}$ (M–M^-) (V)	ΔG_f° (M^-, am)[c] (kJ mol^{-1})	$E^\circ_{NH_3}$ (M–M^-) (V)
e	0.32[d]	266	−2.76	188	−1.95
H	0.208[e]	289	−3.0	223	−2.3
	0.15[f]	161	−1.7	108	−1.1
He	0.268	274	−2.8	201	−2.1
Li	0.230[g]	256	−2.7	187	−1.9
Be	0.203	482	−5.0	417	−4.3
B	0.183	607	−6.3	545	−5.6
C	0.167	628	−6.5	570	−5.9
N	0.155	506	−5.2	451	−4.7
O	0.145	105	−1.1	54	−0.6
F	0.136[g]	−282	2.92	−330	3.42
Ne	0.296	365	−3.8	289	−3.0
Na	0.263[g]	249	−2.6	175	−1.8
Mg	0.240	348	−3.6	277	−2.9
Al	0.222	428	−4.4	360	−3.7
Si	0.208	431	−4.5	365	−3.8
P	0.197	347	−3.6	282	−2.9
S	0.188	160	−1.7	97	−1.0
Cl	0.181[g]	−131	1.36	−193	2.00
Ar	0.336	370	−3.8	291	−3.0
K	0.308[g]	272	−2.8	195	−2.0
Ca	0.285	414[h]	−4.3	338[h]	−3.5
Sc	0.265	544[h]	−5.6	471[h]	−4.9
Ti	0.249	630	−6.5	558	−5.8
V	0.235	619	−6.4	548	−5.7
Cr	0.223	467	−4.8	398	−4.1
Mn	0.212	450[h]	−4.7	383[h]	−4.0
Fe	0.203	505	−5.2	439	−4.5

(continued)

Table 2. (*continued*)

M	r_{M^-}[a] (nm)	ΔG_f° (M^-, aq)[b] (kJ mol^{-1})	$E^\circ_{H_2O}$ (M–M^-) (V)	ΔG_f° (M^-, am)[c] (kJ mol^{-1})	$E^\circ_{NH_3}$ (M–M^-) (V)
Co	0.194	451	−4.7	387	−4.0
Ni	0.187	396	−4.1	333	−3.5
Cu	0.180[g]	288	−3.0	227	−2.4
Zn	0.220[g]	326	−3.4	257	−2.7
Ga	0.212	375	−3.9	308	−3.2
Ge	0.207	375	−3.9	308	−3.2
As	0.202	330	−3.4	265	−2.7
Se	0.198	134	−1.4	69	−0.7
Br	0.195[g]	−103	1.07	−167	1.73
Kr	0.343	374	−3.9	295	−3.1
Rb	0.316[g]	271	−2.8	194	−2.0
Sr	0.294	406[h]	−4.2	330[h]	−3.4
Y	0.276	586[h]	−6.1	512[h]	−5.3
Zr	0.260	747	−7.7	674	−7.0
Nb	0.247	808	−8.4	737	−7.6
Mo	0.235	734	−7.6	664	−6.9
Tc	0.225	698	−7.2	629	−6.5
Ru	0.216	664	−6.9	596	−6.2
Rh	0.208	559	−5.8	492	−5.1
Pd	0.201	430	−4.5	365	−3.8
Ag	0.195[g]	258	−2.7	194	−2.0
Cd	0.240[g]	342	−3.5	271	−2.8
In	0.233	372	−3.9	302	−3.1
Sn	0.227	331	−3.4	261	−2.7
Sb	0.223	297	−3.1	228	−2.4
Te	0.219	141	−1.5	73	−0.8
I	0.216[g]	−52	0.54	−120	1.24
Xe	0.364	365	−3.8	285	−3.0
Cs	0.352[g]	289	−3.0	209	−2.2
Ba	0.342	452	−4.7	373	−3.9
La	0.333	618	−6.4	540	−5.6
Lu	0.270	587[h]	−6.1	513[h]	−5.3
Hf	0.257	784	−8.1	711	−7.4
Ta	0.245	916	−9.5	845	−8.8
W	0.235	918	−9.5	848	−8.8
Re	0.227	898	−9.3	828	−8.6
Os	0.219	810	−8.4	742	−7.7
Ir	0.212	631	−6.5	564	−5.8
Pt	0.206	470	−4.9	404	−4.2
Au	0.201[g]	252	−2.6	186	−1.9
Hg	0.250[g]	288	−3.0	216	−2.2
Tl	0.242	332	−3.4	260	−2.7
Pb	0.236	319	−3.3	248	−2.6
Bi	0.231	265	−2.7	195	−2.0
Po	0.227	152	−1.6	82	−0.8
At	0.224[g]	−23	0.2	−92	1.0
Rn	0.37[g]	358	−3.7	278	−2.9

[a] Equation (6), except as noted.
[b] Equation (2)
[c] Equation (3)
[d] Reference 7.
[e] Reference 10.
[f] From metal–hydrogen distances in alkali hydrides.[20(a)]
[g] Assumed value for establishing periodic trends (see text).
[h] Using the more stable ΔG_f° (M^-, g) from Table 1.

0.02 nm *smaller* than r_{At^-} which occurs later in the same period. The difference is probably related to the presence of 6*p* electrons in the valence shell of the latter ion which are absent in Au^-. The isovalent cationic radii of the late *d*-block transition metals are also often somewhat smaller than those of the post-transition elements of the same period.[10,21(a)] Therefore, we postulate that a small (but possibly abrupt) increase in crystal anionic radius occurs on the initial filling of the *np* orbitals following the *d*-block transition metals, i.e. between the copper and zinc subgroups.

We estimate that anionic radii calculated by eqn (6) are probably reliable to about 0.02 nm; thus, the third decimal place in the anionic radius is significant only in a relative sense between adjacent elements.

Predicted standard Gibbs free energies of formation of monatomic anions M^- in water and liquid ammonia at 298.15 K are presented in Table 2 [calculated by eqns (2) and (3)]. The corresponding standard electrode potentials [E^o (M–M^-)] are also given.

DISCUSSION

The standard Gibbs free energy change at 298.15 K for the reaction:

$$0.5H_2(g) \rightarrow e^-(solv) + H^+(solv) \qquad (7)$$

is about 267 kJ mol^{-1} in water[22] and 186 kJ mol^{-1} in liquid ammonia.[5(d)] Therefore, for the reaction:

$$M(\text{std state}) + e^-(solv) \rightarrow M^-(solv) \qquad (8)$$

to be spontaneous at unit activity, ΔG_f^o (M^-, solv) must be less than these quantities. From Table 2, this requirement is met for the halogens, chalcogens, sodium and gold in either solvent, and also for lithium, silver and bismuth in water.

However, the formation of M^- from M depends not only on reaction (8) being both thermodynamically and kinetically feasible but also on all possible decomposition routes being prohibited for either thermodynamic or kinetic reasons. Thus, we expect anions of lithium, sodium, silver, gold and bismuth to be rapidly oxidized by water and not be detectable. Also, the existence of Na^- in liquid ammonia is doubtful, perhaps because the correction for activity effects in this solvent is very large (*vide infra*), but also perhaps because other combinations such as $Na^+ + 2e^-$, $Na^+e^- + e^-$ and/or $e^-Na^+e^-$ are thermodynamically favored.[1-3] Monatomic anions M^- of the chalcogens, although predicted to be stable in terms of reaction (8), should dimerize, forming O_2^{2-}, S_2^{2-} etc.

On the other hand, if ΔG^o for reaction (8) is positive, M^- might still be formed by an alternate route which does not involve the free element M, provided the decomposition kinetics are slow. In addition, other negative oxidation states may be stable (e.g. Pb_9^{4-} and Sb_7^{3-} in liquid ammonia) even if M^- is not.

The following values (in kJ mol^{-1}) are typical for the *d*-block transition metals:

$$\Delta H_f^o(M, g) = 500 \pm 200,$$

$$EA(M) = 60 \pm 70,$$

$$\Delta G_{solv}^o(M^-) = -260 \pm 30$$

[based on eqns (2) and (3)].

These figures indicate that the *variations* in transition-metal anion stability are determined mainly by ΔH_f^o (M, g), and that EA (M) and ΔG_{solv}^o (M^-) have a relatively minor influence. For example, although the electron affinity of platinum is only 0.2 eV less than that of gold, and the standard Gibbs free energies of solvation of the anions should be similar, Pt^- is predicted to be unstable in solution, because strong bonding in the metal forces reaction (8) to the left. On the other hand, anionic mercury is calculated to be almost stable in terms of reaction (8), the extreme volatility of the metal nearly compensating for the negative electron affinity.

The fictitious "rhenide" ion is known today to be a hydride species,[20(b),21(b)] although it is still incorrectly written as Re^- in some modern publications (e.g. Ref. 12). Table 2 indicates that authentic $Re^-(solv)$ should be extremely unstable.

Noble-gas anions are probably unstable in solution because the anionic radii are so large that solvation is not sufficiently exothermic to compensate for the negative electron affinities. If our EA (M) and anionic radius estimates are accurate, anionic helium is the most probable species. Zollweg[14] has derived noble-gas electron affinities from experimental excited-state EAs with estimated corrections to the ground state. By combining Zollweg's EA values with estimated anionic radii, Blake and Clack[23] have concluded that neon is the noble gas most likely to form anions (as Cs^+Ne^-).

Some of the information presented in this paper may have other applications in addition to predictions on anions in water and liquid ammonia. For example, Table 1 serves as a convenient reference of critically evaluated electron affinities and gas-phase anion thermodynamics for the entire Periodic Table (except the lanthanides and actinides). Table 2 offers an internally consistent set of anionic radii for all elements. These data may be used in structural predictions for solids containing metal anions or in crystal lattice energy calcu-

lations. Finally, for those who are interested only in qualitative trends, the standard electrode potentials provided in Table 2 should serve as approximate indicators of the stability of metal anions in other chemical systems (i.e. other solvents and crystals) because the *order* of anion stability is not expected to change radically in moving from one system to another.

Reliability of predictions of ΔG_f° (M^-, *solv*)

The atomic EAs which have been estimated in this work are mostly believed to be uncertain by about 0.2 eV, thereby contributing about 20 kJ mol^{-1} to the uncertainty in the standard Gibbs free energies of formation of M^- in solution. A similar contribution to the uncertainty is believed to be generated by the choice of crystal anionic radii.

We have not considered ligand field stabilization effects for transition-metal anions with partially filled $(n-1)d$ orbitals. Such effects should be small because the $(n-1)d$ electrons should be largely shielded from their environment by the overlying *ns* electrons. The situation is therefore not analogous to that found for transition-metal cations.[17(d),20(c)]

The validity of eqns (2) and (3) can be tested by comparison of our predicted ΔG_f° (M^-, solv) with experimental measurements or observations for those elements where errors due to the choice of EA (M) or r_{M^-} should be small. For example, Peer[5(e)] has reported E_{NH_3} [Au−Au(−I)] = −1.48 V (relative to the hydrogen electrode) in 0.1 M KI at 233 K. Because this potential does not take ion pairing (i.e. K^+Au^-) into account, the standard-state value $E^\circ_{NH_3}$ ($Au-Au^-$) must be more negative; thus ΔG_f° (Au^-, am) [reaction (1)] is greater than 143 kJ mol^{-1} at 233 K. By comparison with the standard entropies of the halides in liquid ammonia,[24] and correcting for the atomic weight of gold, we estimate ΔS_f° (Au^-, am) = -200 ± 20 J K^{-1} mol^{-1} at 298.15 K. Neglecting the unknown heat capacity correction, we derive ΔG_f° (Au^-, am) to be greater than 156 kJ mol^{-1} at 298.15 K. Therefore, our predicted value in Table 2 is probably in error by less than 30 kJ mol^{-1}.

Alkali metal anions are unknown in liquid ammonia,[1-3] despite the fact that ΔG_f° (Na^-, am) is calculated to be less than 186 kJ mol^{-1} (Table 2). However, a correction for activity effects[7] reveals that an impossibly high concentration of sodium metal would be required to produce a solution of Na^- under standard-state conditions (unit activity) in liquid ammonia.

On the basis of these considerations, we surmise that the uncertainty in our predictions of ΔG_f° (M^-, solv) could be as great as 50–60 kJ mol^{-1} in a few instances, but more typically about 30 kJ mol^{-1}. The greatest uncertainties in ΔG_f° (M^-, solv) are probably for hydride anion (due to the uncertainty in the anionic radius) and for the anions of the noble gases (due to the uncertainty in the anionic radii and the electron affinities). Nevertheless, with the exception of about a dozen borderline cases, one can predict whether a given metal anion should be thermodynamically stable in water or liquid ammonia. A more detailed approach which considers the specific anion–solvent interaction, perhaps as a sum of many terms, would be required to resolve the borderline cases.

Acknowledgement—We are grateful for the generous financial support provided by the Robert A. Welch Foundation (Grant No. F081).

REFERENCES

1. J. L. Dye, C. W. Andrews and S. E. Mathews, *J. Phys. Chem.* 1975, **79**, 3065.
2. J. L. Dye, *J. Chem. Educ.* 1977, **54**, 332.
3. J. L. Dye, *Angew. Chem., Int. Ed. Engl.* 1979, **18**, 587.
4. W. J. Peer and J. J. Lagowski, *J. Am. Chem. Soc.* 1978, **100**, 6260.
5. W. J. Peer, Ph.D. dissertation: (a) pp. 144–174, (b) p. 313, (c) p. 161, (d) p. 260, (e) pp. 159–160. The University of Texas, Austin, TX (1979).
6. J. J. Lagowski, *Gold Bull.* 1983, **16**, 8.
7. S. G. Bratsch and J. J. Lagowski, *J. Phys. Chem.* 1984, **88**, 1086.
8. S. G. Bratsch and J. J. Lagowski, *Polyhedron* 1984, **3**, 133.
9. S. G. Bratsch and J. J. Lagowski, *Polyhedron* 1985, **4**, 841.
10. L. Pauling, *The Nature of the Chemical Bond*, 3rd Edn, pp. 514 and 518. Cornell University Press, Ithaca, NY (1960).
11. *CODATA Recommended Key Values for Thermodynamics, J. Chem. Thermodyn.* 1978, **10**, 903.
12. NBS Technical Notes 270-3–270-8. National Bureau of Standards, Washington, DC (1968–1981).
13. H. Hotop and W. C. Lineberger, *J. Phys. Chem. Ref. Data* 1985, **14**, 731.
14. R. J. Zollweg, *J. Chem. Phys.* 1969, **50**, 4251.
15. C. E. Moore, National Standard Reference Data Series, NBS 34. National Bureau of Standards, Washington, DC (1970).
16. C. E. Moore, National Standard Reference Data Series, NBS 35. National Bureau of Standards, Washington, DC (1971).
17. D. A. Johnson, *Some Thermodynamic Aspects of Inorganic Chemistry*, 2nd Edn: (a) p. 251, (b) p. 8,

(c) p. 25, (d) pp. 141–150. Cambridge University Press, London (1982).
18. N. W. Gregory, *J. Chem. Educ.* 1956, **33**, 144.
19. V. P. Vasilev, E. K. Zolotarev and K. B. Yatsimirskii, *Zh. Fiz. Khim.* 1959, **33**, 328.
20. F. A. Cotton and G. Wilkinson, *Advanced Inorganic Chemistry*, 4th Edn: (a) p. 248, (b) pp. 899–900, (c) pp. 619–687. Wiley Interscience, New York (1980).
21. R. Rich, *Periodic Correlations*: (a) p. 36, (b) p. 105. W. A. Benjamin, New York (1965).
22. E. J. Hart and M. Anbar, *The Hydrated Electron*, p. 63. Wiley Interscience, New York (1970).
23. P. G. Blake and D. W. Clack, *J. Chem. Educ.* 1982, **59**, 637.
24. W. M. Latimer and W. L. Jolly, *J. Am. Chem. Soc.* 1953, **75**, 4147.

Polyhedron Vol. 5, No. 11, pp. 1771–1776, 1986
Printed in Great Britain

0277–5387/86 $3.00+.00
Pergamon Journals Ltd

VARIABLE-TEMPERATURE ^{119}Sn MÖSSBAUER STUDY OF TIN PHTHALOCYANINES

KIERAN C. MOLLOY*

School of Chemistry, University of Bath, Claverton Down, Bath BA2 7AY, U.K.

and

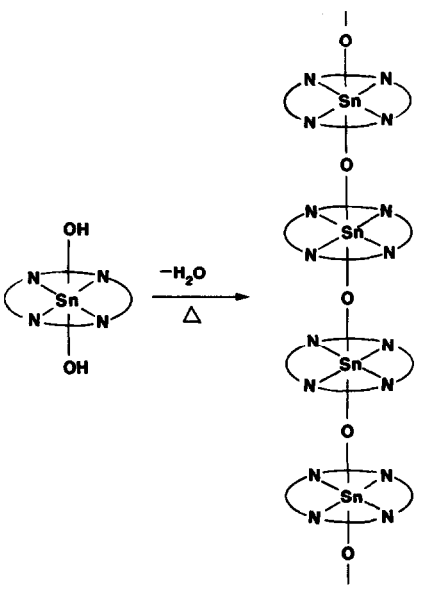
KIERAN QUILL

School of Chemical Sciences, National Institute for Higher Education, Glasnevin, Dublin 9, Ireland

(*Received* 5 *February* 1986; *accepted* 4 *March* 1986)

Abstract—Variable-temperature ^{119}Sn Mössbauer spectroscopic (VTMS) data for six tin phthalocyanine (pc) derivatives have been collected in order to ascertain the restrictions imposed by the macrocyclic ring on the vibrational motion of the tin atom. Thermal condensation of $[(t\text{-Bu})_4\text{pc}]\text{Sn(OH)}_2$ yields the co-facially stacked polymer $\{[(t\text{-Bu})_4\text{pc}]\text{SnO}\}_n$ which can be distinguished in the VTMS experiment by the enhanced rigidity of its structure.

A considerable amount of research effort has been directed towards the synthesis of organic and metal–organic molecular systems which have metal-like electrical, magnetic and optical properties.[1] Among the best known of the "1-D metals" are the organic charge-transfer compounds, e.g. tetrathiafulvalene–tetracyanoquinodimethane,[2] and square planar metal species, e.g. $K_2Pt(CN)_4$[3] and Ni(pc) (pc = phthalocyanine).[4] This latter class forms molecular stacks in the solid, yielding a conduction pathway by overlap of d_{z^2}-orbitals along the metal spine. More recent work has sought to overcome the unpredictable and largely uncontrollable intermolecular packing forces which determine whether or not stacks are formed by linking square planar metal complexes with axially-oriented bridging groups, e.g. M(pc)F (M = Al or Ga),[5] Fe(pc)pyrazine[6] and Co(pc)CN.[7] For main-group elements, Marks *et al.*[8] have shown that thermal condensation of silicon, germanium or tin phthalocyanine dihydroxide yields the oxo-bridged co-facial stack $[M(pc)O]_n$, e.g.



(1)

While these compounds are themselves semiconductors, partial oxidation with molecular halogens

* Author to whom correspondence should be addressed.

yields materials with metallic conductivities of *ca* $1\ \Omega^{-1}\ cm^{-1}$.

Our recent work utilizing variable-temperature Mössbauer spectroscopy (VTMS) as a lattice structure probe has shown that the technique is a good indicator of both polymer formation and the three-dimensional spacial disposition of atoms along the polymer backbone, i.e. rod, zig-zag, "S"-shaped and helical.[9] As such, VTMS seems ideally suited to assess reactions of the type shown in eqn (1), which leads to a stack of molecules linked by a central polymer strand. However such experiments cannot be viewed against the backdrop of systematics for simple molecular species[9,10] since the rigid macrocycle might itself be expected to significantly influence the lattice dynamics of the coordinated metal. In this report we quantify this "macrocyclic effect", and subsequently show how VTMS can be a useful probe of stack formation.

EXPERIMENTAL

The solvents quinoline and 1-chloronaphthalene were vacuum distilled from BaO before use; pyridine was dried over sodium hydroxide and distilled under a dry dinitrogen atmosphere. Anhydrous stannous chloride was obtained commercially (BDH) and used without further purification. (pc)$SnCl_2$,[11] (pc)SnI_2,[12] (pc)Sn[12] and [(*t*-Bu)$_4$pc]$SnCl_2$[13] were prepared by published procedures. IR, Mössbauer and (for the more soluble *t*-butylated compounds) ^{1}H NMR and UV–VIS spectroscopic data are in excellent agreement with those previously reported. The insolubility and involatility of the unsubstituted macrocyclic derivative makes purification of products difficult and microanalysis data* are on occasion low in carbon. The Mössbauer spectrum of (pc)Sn indicated that the presence of a resolved Sn(IV) impurity of *ca* 7% [assuming equal recoil-free fractions for the Sn(II) and Sn(IV) species], which could not be separated.

4-t-*Butyl*-o-*xylene* (2)

This was prepared by alkylation of *o*-xylene (**1**) with *t*-butyl chloride and iron(III) chloride as reported previously.[14] *o*-Xylene was removed from the reaction mixture by fractional distillation (15-cm packed column) at atmospheric pressure; the column was removed and the desired product distilled at 208°C (yield 52%).

4-t-*Butyl phthalic acid* (3)

The synthesis of this follows the general procedure of Hanack.[13] To a refluxing, mechanically stirred solution of **2** (32.8 g, 20 mmol) in a mixture of pyridine (250 cm^3) and water (80 cm^3) was added potassium permanganate (169.5 g, 1.07 mol) over a 1.5-h period such that reflux was maintained without external heating. At the conclusion of the addition, the solution was heated at reflux for a further 30 min. Ethanol (30 cm^3) was added to the hot solution, which was then allowed to cool to room temperature and filtered. The filtrate was concentrated to *ca* one-third its volume, treated with conc. HCl (80 cm^3), extracted with ether, and the extract washed with water and dried over anhydrous $MgSO_4$. The viscous oil which results after solvent evaporation was crystallized using a 1:1 chloroform–petroleum ether mixture (yield 24.6 g, 55%).

4-t-*Butyl phthalic anhydride* (4)

3 (24.6 g, 0.11 mol) was refluxed in acetic anhydride (70 cm^3) for 1 h. After cooling, the solution was filtered, the filtrate concentrated to *ca* 20 cm^3 and allowed to crystallize at −10°C. The resulting white solid was purified by sublimation at *ca* 80°C/1 mmHg to yield **4** (16.0 g, 71%).

(2,9,16,23 - *Tetra* - t - *butylphthalocyaninato)tin dihydroxide* (8)

[(*t*-Bu)$_4$pc]$SnCl_2$ (**7**) (500 mg) was heated at reflux for 6 h in a solution of NaOH (2.4 g) in 5:1 ethanol–water (60 cm^3). After cooling, a dark blue solid was isolated by filtration, redissolved in chloroform and washed several times with water. The organic phase was separated, dried over anhydrous $MgSO_4$, and the product [**8** (240 mg, 50%)] recovered by evaporation of the solvent. Found: C, 64.2; H, 5.7; N, 11.6%. Calc. for $C_{48}H_{50}N_8O_2Sn$: C, 64.8; H, 5.7; N, 12.6%.

Poly-(2,9,16,23-*tetra*-t-*butylphthalocyaninato)stannoxane* (10)

A sample of **8** (250 mg) was heated under dynamic vacuum at 330°C for 30 min. The resulting solid was washed with chloroform until the wash-

* (pc)$SnCl_2$: Found: C, 52.0; H, 2.1; N, 15.6%. Calc. for $C_{32}H_{16}Cl_2N_8Sn$: C, 54.8; H, 2.3; N, 16.0%. (pc)SnI_2: Found: C, 43.5; H, 1.9; N, 12.5%. Calc. for $C_{32}H_{16}I_2N_8Sn$: C, 43.4; H, 1.8; N, 12.6%. [(*t*-Bu)$_4$pc]$SnCl_2$: Found: C, 59.1; H, 5.3; N, 11.6%. Calc. for $C_{48}H_{48}Cl_2N_8Sn$: C, 62.2; H, 5.2; N, 12.1%.

ings were colourless. The black microcrystalline product was insoluble in organic solvents.

^{119}Sn *VTMS*

Details of our Mössbauer spectrometer, cryostat and temperature controller, along with the method of data manipulation, are given elsewhere.[15] Samples containing 0.5–1.0 mg ^{119}Sn cm^{-2} were used, and data acquisition was *ca* 12 h per spectrum; temperature stability was ± 0.1 K for the duration of data collection.

RESULTS AND DISCUSSION

Syntheses

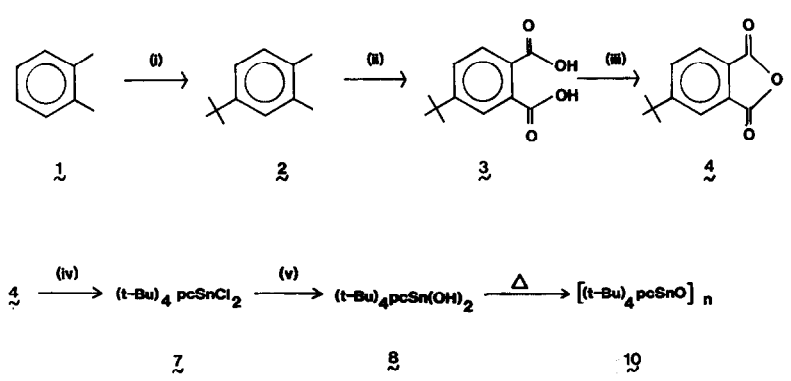
Tin phthalocyanine derivatives [(pc)Sn and (pc)SnX_2 (X = Cl or I)] were synthesized by published procedures. The dichloride is obtained from refluxing anhydrous $SnCl_2$ and *o*-phthalonitrite in 1-chloronaphthalene,[11] and can subsequently be reduced to the divalent species (pc)Sn by reaction with additional $SnCl_2$ in quinoline.[12] (Phthalocyaninato)tin diodide is prepared in an oxidative addition reaction between (pc)Sn and I_2 in 1-chloronaphthalene.[12] All three species are only sparingly soluble in organic solvents, and are hence difficult to purify and characterize. Their solubility in such media can be greatly enhanced by preparation of the peripherally substituted tetra-(*t*-butyl)phthalocyanine compounds, which follows the route used by Hanack and is shown in Scheme 1.[13] This increase in solubility also facilitates the hydrolysis of the dichloride (**7**) to the dihydroxy-species (**8**):

$$[(t\text{-Bu})_4\text{pc}]SnCl_2 + 2OH^- \rightarrow [(t\text{-Bu})_4\text{pc}]Sn(OH)_2 + 2Cl^- \quad (2)$$

The ν_a(Sn—Cl) absorption at 300 cm^{-1} for **7** is absent in the reaction product, and is replaced by a new band at 562 cm^{-1} which we assign to ν_a(Sn—O) on the basis of data for (pc)$Sn(OH)_2$ [ν_a(Sn—O) = 564 cm^{-1}].[11] The stannol (**8**) can be dehydrated to give the condensed polymer (**10**) by heating under a dynamic vacuum at 330°C:

$$[(t\text{-Bu})_4\text{pc}]Sn(OH)_2 \xrightarrow{330°C} \{[(t\text{-Bu})_4\text{pc}]SnO\}_n + H_2O. \quad (3)$$

The black, stannoxane polymer (**10**), unlike other *t*-butylated phthalocyanine derivatives studied, is totally insoluble in organic solvents. The dehydration process is accompanied by decomposition of the tin(IV) species, as noted by other workers for a similar reaction with (pc)$Sn(OH)_2$.[11,16] Decomposition is evidenced by the presence of an absorption of *ca* 10% of total intensity in the Mössbauer spectrum of **10**, with an isomer shift (IS) of 3.05 mm s^{-1} and a quadrupole spitting (QS) of 1.71 mm s^{-1}, indicative of tin in the +2 oxidation state. The similarity of these parameters, and indeed the temperature dependence of the Mössbauer recoil-free fraction (f) also, to data for (pc)Sn (Table 1) make it tempting to assign the decomposition product as [(*t*-Bu)$_4$pc]Sn; however other workers have found this compound to be soluble in organic solvents, and extremely light- and oxygen-sensitive.[13] Clearly, the exact nature of the decomposition product must remain as yet uncertain. Characterization of **10** is difficult. Its polymeric nature is suggested by its insolubility in common solvents, but its IR spectrum is very similar to that for **8**, other than that well-dispersed mulls proved difficult to obtain leading to a poor signal: background resolution. Our assignment of **10** as an oxo-bridged polymer rests largely on the temperature dependence of its Mössbauer spectrum, as described below.



Scheme 1. Preparative route to soluble tetra-(*t*-butyl)phthalocyanine compounds. Reagents: (i) $FeCl_3$ and *t*-BuCl, (ii) $KMnO_4$ and HCl, (iii) $(CH_3CO)_2O$, (iv) $SnCl_2$ and urea, and (v) NaOH.

Table 1. Mössbauer spectroscopic data for tin phthalocyanine (pc) derivatives[a]

	Compound	IS (mm s^{-1})	QS (mm s^{-1})	Γ_1[b]	Γ_2[b]	10^2a (K^{-1})
5	(pc)$SnCl_2$[c]	0.26	0.90	1.06	1.20	1.10
6	(pc)SnI_2[d]	0.45	1.21	1.26	1.17	0.67
7	[(*t*-Bu)$_4$pc]$SnCl_2$	0.25	0.89	1.00	1.10	1.06
8	[(*t*-Bu)$_4$pc]$Sn(OH)_2$	0.18	0.64	1.02	1.20	1.15
9	(TPP)$Sn(OH)_2$ · solv[e,f]	0.07	0.66	1.04	0.89	1.19
10	{[(*t*-Bu)$_4$pc]SnO}$_n$[g]	0.10	0.67	0.98	1.37	0.36
11	(pc)Sn[h,i]	2.80	1.43	1.28	1.26	1.40

[a] IS and QS data were recorded at 78 K, and are ±0.02 and 0.04 mm s^{-1}, respectively.
[b] Full width at half height for the low (Γ_1) and high (Γ_2) velocity wings of the doublet spectrum.
[c] Literature:[17] IS = 0.28, and QS = 0.99 mm s^{-1}.
[d] Literature:[17] IS = 0.45, and QS = 0.99 mm s^{-1}.
[e] α,β,γ,δ-Tetraphenylporphyrinatotin dihydroxide-bis(chloroform)-bis(carbon tetrachloride) solvate.
[f] Reference 19.
[g] Also contains a tin(II) impurity (~10%): IS = 3.05, and QS = 1.71 mm s^{-1}; 10^2a = 1.35 K^{-1}.
[h] Literature:[17] IS = 2.78, and QS = 1.40 mm s^{-1}.
[i] Also contains a tin(IV) impurity (<10%): IS = −0.10, and QS = 0.00 mm s^{-1}.

Mössbauer spectroscopy

Mössbauer spectroscopic data for tin phthalocyanine complexes are given in Table 1. IS and QS data for known compounds are in good agreement with literature values.[17] IS data for the series $(R_4pc)SnX_2$ (R = H or *t*-Bu; X = O, Cl or I) decrease with increasing electronegativity of X, concomitant with increasing *s*-electron density withdrawal from tin. Both IS and QS data for $(R_4pc)SnCl_2$ (R = H or *t*-Bu) are identical within experimental error, indicating, reasonably, that peripheral substitution of the macrocycle by alkyl groups has no appreciable effect on the electronic environment at the tin nucleus. The temperature dependence of *f* for compounds **5–11** is also given in Table 1, where:

$$a = -\frac{d\ln f}{dT} = -\frac{d\ln A}{dT}, \qquad (4)$$

and A is the area under the Mössbauer spectral envelope. Since:

$$f(T) = \exp[-\langle x(T)^2\rangle/\lambda\!\!\!^{-2}], \qquad (5)$$

and

$$\frac{df(T)}{dT} = \frac{d\exp[-6E_RT/k\theta_D^2]}{dT}, \qquad (6)$$

where $\langle x(T)^2\rangle$ is the mean-square amplitude of vibration of the tin at temperature T, $\lambda\!\!\!^{-}$ the wavelength of the Mössbauer transition divided by 2π, E_R the Mössbauer recoil energy and θ_D the Debye temperature of the lattice, plots of $\ln A$ vs T are linear and indicative of the tightness with which the tin atom is held in the lattice, with values of a decreasing with increasing lattice rigidity. Data for **8** and **10** are shown pictorially in Fig. 1, and typify the quality of data for all compounds.

Aided by a classification of tin polymers based upon the spacial disposition of atoms within the polymer backbone, we[9] and others[10] have shown broadly that non-associated lattices or lattices comprising "S"-shaped (Class 3) or helical (Class 4) polymers show $10^2a > 1.3$ K^{-1} and typically *ca* 1.8 K^{-1}. The value of a also depends on the strength of the intermolecular bond, and to a less well-defined extent the mass of the vibrating unit containing the Mössbauer atom (usually the whole molecule) although the variation due to this phenomenon is usually relatively small. VTMS data for **5–8**, all of which can be assumed to exist as discrete molecules within the solid lattice as has been shown for $(pc)SnCl_2$,[18] have $10^2a \sim 1.0$ K^{-1}, with $(pc)SnI_2$ somewhat lower at 0.67 K^{-1}. We ascribe this inhibition on the vibrational motion of the cavity-located tin in these monomers, which is akin to that in Class 2 or weakly-bridged Class 1 polymer systems,[9] to the restraining effect of the rigid, bulky phthalocyanine ring. The value of 10^2a for the related solvated tetraphenylporphyrin derivative $(TPP)Sn(OH)_2$ (1.19 K^{-1})[19] suggests that these findings can be generalized to a "*macrocyclic effect*". The lower 10^2a value for **6** (0.67 K^{-1}) is probably due to the mass effect of the two heavy iodine atoms in the axial sites on the metal coordination polyhedron. The structure of (pc)Sn is known, and

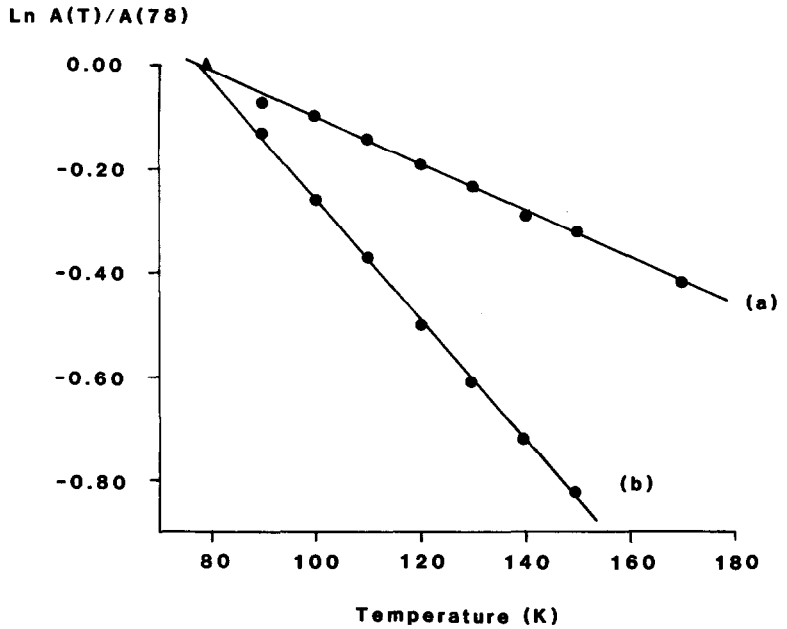


Fig. 1. Variable-temperature Mössbauer spectroscopic data for: (a) $\{[(t\text{-Bu})_4\text{pc}]\text{SnO}\}_n$, and (b) $[(t\text{-Bu})_4\text{pc}]\text{Sn(OH)}_2$. Normalization of the data is to facilitate intersample comparison. The point ▲ (78, 0.00) is common to both plots.

shows that the larger tin(II) atom cannot be accommodated within the macrocycle cavity, so that the metal lies 1.11 Å above the plane of the four isoindole nitrogens and that the macrocycle is slightly deformed away from tin to a "saucer" shape.[20] Such an environment for the metal "sitting-atop" the phthalocyanine reduces the *macrocyclic effect* and is entirely consistent with the increased 10^2a value of 1.40 K^{-1}.

The insoluble material $\{[(t\text{-Bu})_4\text{pc}]\text{SnO}\}_n$ has a significantly lower 10^2a value (0.35 K^{-1}) than any of the other compounds studied, and in particular its monomeric precursor (**8**) ($10^2a = 1.15$ K^{-1}). The reduction in vibrational freedom for tin in **10** clearly results from the formation of strong, covalent, single-atom linkages between tin–pc units to form a co-facially stacked polymer, which is rod-like (Class 1) with respect to the O—Sn—O—Sn—O backbone. In view of the difficulties encountered in monitoring the condensation reaction shown in eqn (1) (*vide supra*), VTMS seems a particularly useful diagnostic technique. Comparative VTMS data for other Class 1 tin polymers is unfortunately limited, due to the relative rareness of this architecture in tin chemistry. Class 1 polymers do seem a feature of associated tricyclohexyltin systems probably due to the steric demands of the bulky hydrocarbons, but while Cy_3SnCl ($10^2a = 1.40$ K^{-1}) and Cy_3SnF ($10^2a = 0.91$ K^{-1}) are both of this type[9] the rigidity of the lattice in each case is somewhat offset by a long Sn—X (X = Cl or F) bridging interaction (3.30 and 3.32 Å, respectively).[21,22] Cy_3SnOH appears to have a strongly bonded Class 1 mode of association ($10^2a = 0.66$ K^{-1})[9] but crystallographic confirmation of this assignment is still awaited.

CONCLUSIONS

In the light of the data presented, the effects of an embracing, rigid macrocycle on the vibrational freedom of the cavity-metal have been assessed and provide additional correlations between structure and VTMS behaviour. In addition, the VTMS technique has been shown to be a useful probe of the formation of co-facially stacked metallomacrocycle polymers, and should be applicable to a variety of such systems providing they contain a Mössbauer-active metal. We are currently pursuing this assertion with respect to coordination polymers of iron(II) phthalocyanine.

REFERENCES

1. For example, W. E. Hatfield (Ed.), *Molecular Metals*. Plenum Press, New York (1978); J. S. Miller (Ed.), *Extended Linear Chain Compounds*. Plenum Press, New York (1982).
2. F. Gutman and L. E. Lyons, *Organic Semiconductors*. Wiley, New York (1967).

3. A. E. Underhill and D. M. Watkins, *Chem. Soc. Rev.* 1980, **9**, 429.
4. C. J. Schramm, R. P. Scaringe, D. R. Stojakovic, B. M. Hoffman, J. A. Ibers and T. J. Marks, *J. Am. Chem. Soc.* 1980, **102**, 6702.
5. P. M. Kuznesof, K. J. Wynne, R. S. Nohr and M. E. Kenney, *J. Chem. Soc., Chem. Commun.* 1980, 121; R. S. Nohr, P. M. Kuznesof, K. J. Wynne, M. E. Kenney and P. G. Siebenman, *J. Am. Chem. Soc.* 1981, **103**, 4371.
6. O. Schneider and M. Hanack, *Angew. Chem., Int. Ed. Engl.* 1980, **19**, 392.
7. J. Metz and M. Hanack, *J. Am. Chem. Soc.* 1983, **105**, 828.
8. B. N. Diel, T. Inabe, J. W. Lyding, K. F. Schoch, C. R. Kannewurf and T. J. Marks, *J. Am. Chem. Soc.* 1983, **105**, 1551.
9. K. C. Molloy and K. Quill, *J. Chem. Soc., Dalton Trans.* 1985, 1417.
10. P. G. Harrison, R. C. Phillips and E. W. Thornton, *J. Chem. Soc., Chem. Commun.* 1977, 603.
11. C. W. Kirk, T. Inabe, K. F. Schoch and T. J. Marks, *J. Am. Chem. Soc.* 1983, **105**, 1539.
12. W. J. Kroenke and M. E. Kenney, *Inorg. Chem.* 1964, **3**, 251.
13. M. Hanack, J. Metz and G. Pawlowski, *Chem. Ber.* 1982, **115**, 2836.
14. D. Nightingale and J. R. Jones, *J. Am. Chem. Soc.* 1944, **66**, 154.
15. K. C. Molloy, T. G. Purcell, K. Quill and I. W. Nowell, *J. Organomet. Chem.* 1984, **267**, 237.
16. W. J. Kroenke, Ph.D thesis, Case Western Reserve University, U.S.A. (1963) (quoted in Ref. 11).
17. M. O'Rourke and C. Curran, *J. Am. Chem. Soc.* 1970, **92**, 1501.
18. D. Rogers and R. S. Osborn, *J. Chem. Soc., Chem. Commun.* 1971, 840.
19. P. G. Harrison, K. C. Molloy and E. W. Thornton, *Inorg. Chim. Acta* 1979, **33**, 137.
20. M. F. Friedel, B. F. Hoskins, R. L. Martin and S. A. Mason, *J. Chem. Soc., Chem. Commun.* 1970, 400.
21. S. Calogero, P. Ganis, V. Peruzzo and G. Tagliavini, *J. Organomet. Chem.* 1979, **179**, 145.
22. S. Calogero, P. Ganis, V. Peruzzo, G. Tagliavini and G. Valle, *J. Organomet. Chem.* 1981, **220**, 11.

Polyhedron Vol. 5, No. 11, pp. 1777–1784, 1986
Printed in Great Britain

0277–5387/86 $3.00+.00
Pergamon Journals Ltd

STABILITY CONSTANTS OF PALLADIUM(II) COMPLEXES WITH THIO- AND DITHIODIACIDS

J. COELLO, S. HERNÁNDEZ CASSOU* and H. ITURRIAGA MARTÍNEZ†

Departamento de Química Analítica, Facultad de Ciencias, Universidad Autónoma de Barcelona, Bellaterra, Barcelona, Spain

(*Received* 7 *February* 1986; *accepted* 4 *March* 1986)

Abstract—The formation of complexes between palladium(II) and 3,3′-thiodipropanoic (TDPA) and 3,3′-dithiodipropanoic (DTDPA) acids has been studied by using spectrophotometric methods in acidic aqueous media with a constant ionic strength of 0.5 M $(Na^+, H^+)ClO_4^-$. The stoichiometry of the detected complexes is 1 : 1 and 1 : 2 (metal : ligand) for the Pd–TDPA system, and 2 : 1 and 1 : 1 for the Pd–DTDPA system. The spectrophotometric characteristics and equilibrium constants for the different species have been calculated with the LETAGROP–SPEFO computer program.

A general survey of the methods for determining palladium indicates that sulphur compounds, thioether in particular, are commonly employed reagents,[1–3] while no attempt has been made to use 3,3′-thiodipropanoic (TDPA) and 3,3′-dithiodipropanoic (DTDPA) acids. Between these two ligand families and some divalent cations, a number of spectrophotometric studies have already been reported in the literature,[4–7] but no information exists about the palladium complex. Because of the increasing interest in platinum group metal compounds[3,8] and following our previous research with thio- and dithiodiacids,[9–11] a fundamental spectrophotometric study of the interaction between palladium(II) aqueous ion and the mentioned diacids was carried out in a perchlorate medium to establish the different complex species formed in acidic solution and evaluate their stability constants.

EXPERIMENTAL

Apparatus

The absorption spectra and quantitative absorbance measurements were obtained at 25°C with a Perkin–Elmer 554 spectrophotometer, employing 1-cm quartz cells. The reference cell solution had always the same matrix composition as the sample cell solution, except for the ligand and metal content.

The measurement of pH was done with a glass electrode (Radiometer G-202) using a Radiometer PHM-64 pH meter. The reference electrode was a saturated calomel electrode (Radiometer K-401) immersed in a salt bridge containing a 0.5 M $NaNO_3$ solution.

Reagents

TDPA (Merck for synthesis) was recrystallized twice from water, and DTDPA (Aldrich, analytical reagent grade) 3 times in the same manner from ethanol. The final purity of both ligands was 99.9%, as determined by acid–base titration of carboxylic groups with standardized sodium hydroxide. Sodium perchlorate was prepared from sodium carbonate and perchloric acid.[12] All other products were of analytical reagent grade. All solutions were prepared with double distilled water.

Standard palladium perchlorate solution. Palladium(II) perchlorate solution was prepared from $PdCl_2$ (Spanish Society of Noble Metals), precipitating palladium oxide twice and dissolving it in perchloric acid (Carlo Erba R.P.E.) as has been previously described.[13] The absence of chloride was checked by measuring the absorbance of the final

* Present address: Departamento de Química Analítica, Facultad de Química, Universidad de Barcelona, Barcelona, Spain.

† Author to whom correspondence should be addressed.

solution at 420 nm.[13] The chloride content was always less than 10^{-5} M. The concentration of palladium was determined gravimetrically by the dimethylglyoxime method and the total acidity was determined by passing the solution through a cationic resin column (Merck I) and titrating it with standard sodium hydroxide solution.

Preliminary studies

Spectral characteristics. Palladium perchlorate solutions showed two absorption bands, a small one at 370 nm and a higher and more intense one at around 200 nm.

Aqueous spectra of both ligands showed the carboxylic peak at 200–205 nm while the DTDPA solutions showed another peak corresponding to the disulphide group at 247 nm.

The Pd–TDPA system showed two peaks 225 and 270 nm, depending on the metal/ligand ratio, while Pd–DTDPA showed two broad bands about 260 and 330 nm; the solutions in both cases were acidic.

Variation of absorbance with pH. The study of the effect of pH changes on the absorbance of palladium complexes was done by adjusting the pH in the range 0.5–12 with sodium hydroxide and perchloric acid.

The absorbance values of solutions containing 9×10^{-5} M palladium and metal/ligand ratios of 1.3 and 0.1 for TDPA systems, and 2 and 0.5 for DTDPA systems, remained constant when pH = 3. The spectra from solutions with a pH greater than 3 showed shifts to lower wavelengths and new absorption bands that could be attributed to mixed complexes with hydroxide ion.

On this basis, a pC_H of 1.3 was chosen for the next studies in order to avoid problems with hydro complexes.

Variation of absorbance with time. The change in the absorbance was followed in solutions with Pd/TDPA ratios of 1.25, 0.3 and 0.1, and with Pd/DTDPA ratios of 1, 0.5 and 0.16. The total concentration of palladium was 1×10^{-4} M for TDPA complexes and 7.5×10^{-5} M for those of DTDPA. This study indicates that absorbances were stable for 6 h for Pd–TDPA system and for between 90 min and 5 h for DTDPA complexes.

Number and stoichiometry of complexes. The composition of different complexes formed was studied with a fixed pC_H of 1.3 by two well-known spectrophotometric methods: continuous-variation[14] and molar-ratio.[15] Because of the absorption of the metal and ligands at the complexes wavelengths, the experimental absorbances were corrected by subtracting the absorption corresponding to the metal and ligands as if they remained free in solution without complexation. These two graphical methods defined two complexes, 1 : 1 and 1 : 2 metal : ligand ratios and peaks at 225 and 275 nm, respectively, for Pd(II)–TDPA, and a polynuclear 2 : 1 and a mononuclear 1 : 1 complex for Pd(II)–DTDPA, this last one predominantly absorbing with a 340-nm band.

The TRIANG[16] numerical program was applied to confirm the number of absorbing species. Three species (which were assigned as 1 : 1 and 1 : 2 complexes and free ligand) were found for Pd–TDPA, and two (mononuclear 1 : 1 and polynuclear 2 : 1) for Pd–DTDPA, by employing an error matrix for both systems in the range of 0.002–0.008.

RESULTS AND DISCUSSION

Data were obtained from the absorbance measurements of solutions shown in Table 1. The ionic strength was always kept constant with perchloric acid and sodium perchlorate to 0.5 M (Na^+, H^+)ClO_4^-. Table 1 specifies the characteristics of these series and Figs 1 and 2 show the absorption spectra corresponding to one series of each system. The absorbance values were read at 275, 270, 240, 230 and 225 nm after 60 min for Pd–TDPA complexes, and at 340, 330, 267, 260 and 247 nm after 2 h for Pd–DTDPA.

Treatment of the experimental data

Some of the wavelengths which characterize the complexes were absorbed by palladium ion and ligands whose molar absorptivities had to be previously calculated under the same experimental conditions as the complexes. These were obtained from the slope of straight lines by representing the absorbance at each particular wavelength vs the metal (or ligand) concentrations. The values can be observed in Table 2. The molar absorptivities at wavelengths higher than 270 nm were averaged between the most and least concentrated solutions because of their very low absorbance values. The linearity ranges were 1×10^{-5}–1×10^{-4} M for palladium and 7×10^{-5}–2×10^{-3} M for TDPA and DTDPA.

Graphical methods. The small range of ligand concentration in which the absorbances of the complexes of the TDPA system grew induced us to think that the stepwise constants were high. On this basis, it was assumed that the whole ligand was complexed in the solutions with metal excess and its concentration was equal to that of the Pd(TDPA) species. Thus, an equation can be derived as

Table 1. Experimental conditions of the series needed to study Pd–TDPA and Pd–DTDPA systems [$I = 0.5$ M $(Na^+, H^+)ClO_4^-$, $T = 25°C$]

Total palladium (mol l^{-1})	Total hydrogen (mol l^{-1})	Total ligand (mol l^{-1})	Number of solutions
	TDPA		
3.5×10^{-5}–9.4×10^{-5}	5.31×10^{-2}	5.4×10^{-5}	9
1.7×10^{-5}–5.9×10^{-5}	5.31×10^{-2}	4.17×10^{-4}	8
5.9×10^{-5}	5.31×10^{-2}	1.2×10^{-5}–2.09×10^{-4}	11
7.0×10^{-5}	5.31×10^{-2}	1.2×10^{-5}–4.1×10^{-5}	8
7.4×10^{-5}	6.51×10^{-2}	5.2×10^{-5}–1.96×10^{-4}	6
4.4×10^{-5}	5.26×10^{-2}	4.1×10^{-5}–2.51×10^{-4}	6
7.4×10^{-5}	6.48×10^{-2}	6×10^{-6}–1.24×10^{-4}	16
	DTDPA		
1.3×10^{-5}	5.03×10^{-2}	1.0×10^{-5}–2.40×10^{-4}	11
2.7×10^{-5}	5.03×10^{-2}	1.0×10^{-5}–2.40×10^{-4}	13
5.3×10^{-5}	5.03×10^{-2}	1.0×10^{-5}–4.00×10^{-4}	15
6.7×10^{-5}	5.03×10^{-2}	1.0×10^{-5}–6.40×10^{-4}	16

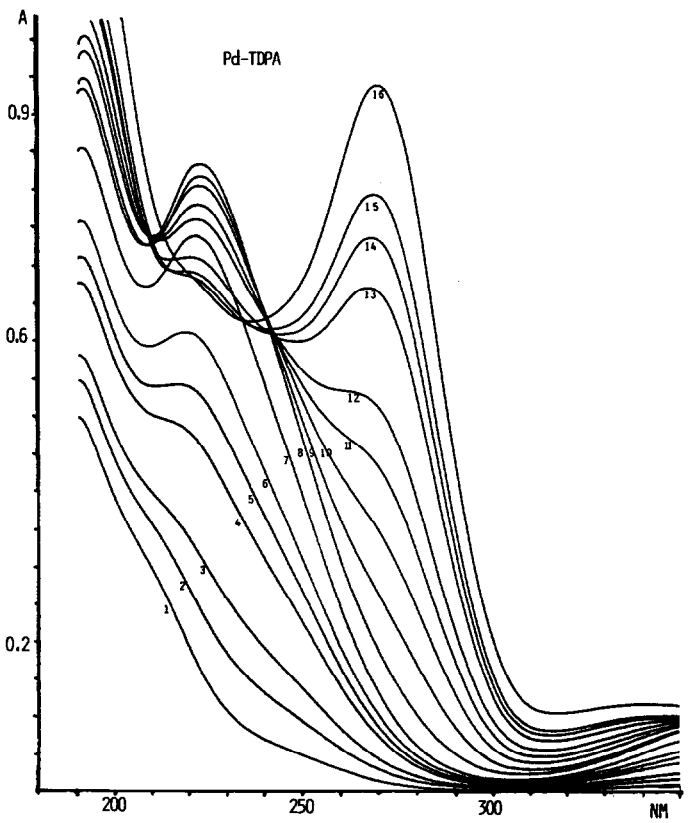


Fig. 1. Absorption spectra for the Pd–TDPA system. Palladium concentration was 7.4×10^{-5} M in all solutions and ligand concentration was: (1) 6×10^{-6} M, (2) 1.3×10^{-5} M, (3) 2.0×10^{-5} M, (4) 3.3×10^{-5} M, (5) 3.9×10^{-5} M, (6) 4.5×10^{-5} M, (7) 5.9×10^{-5} M, (8) 7.2×10^{-5} M, (9) 7.8×10^{-5} M, (10) 8.5×10^{-5} M, (11) 9.1×10^{-5} M, (12) 9.8×10^{-5} M, (13) 1.11×10^{-4} M, (14) 1.18×10^{-4} M, (15) 1.24×10^{-4} M, and (16) 1.44×10^{-4} M.

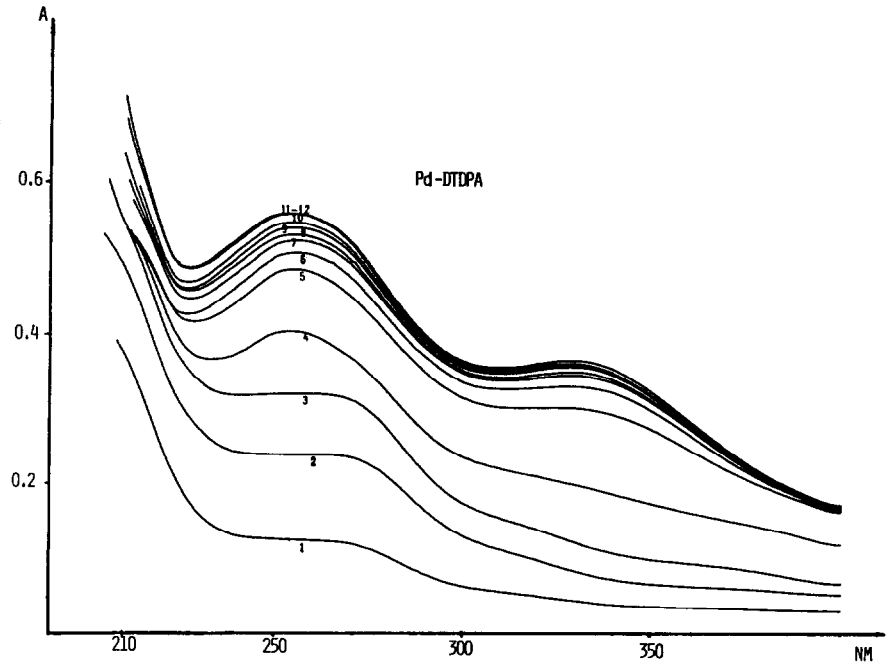


Fig. 2. Absorption spectra for the Pd–DTDPA system. Palladium concentration was 5.3×10^{-5} M in all solutions and ligand concentration was: (1) 1.0×10^{-5} M, (2) 2.0×10^{-5} M, (3) 3.0×10^{-5} M, (4) 4.0×10^{-5} M, (5) 6.0×10^{-5} M, (6) 8.0×10^{-5} M, (7) 1.00×10^{-4} M, (8) 1.20×10^{-4} M, (9) 1.40×10^{-4} M, (10) 1.60×10^{-4} M, (11) 1.80×10^{-4} M, and (12) 2.00×10^{-4} M.

follows:

$$A_{exp} - \varepsilon_{Pd}(C_{Pd} - C_{TDPA}) = A_1 = \varepsilon_{Pd(TDPA)}C_{TDPA}, \quad (1)$$

where C_{Pd} and C_{TDPA} are the total concentrations of palladium and ligand, respectively, and A_{exp} is the experimental absorbance of the solution. In a similar way, the molar absorptivities of the complex $Pd(TDPA)_2$ were deduced from solutions with $C_{TDPA} : C_{Pd} \geqslant 2$. Now, all the metal would be complexed and the $Pd(TDPA)_2$ species would predominate, in which case eqn (2) is obtained:

$$A_{exp} - \varepsilon_{TDPA}(C_{TDPA} - 2C_{Pd}) = A_2 = \varepsilon_{Pd(TDPA)_2}C_{Pd}. \quad (2)$$

The molar absorptivities, $\varepsilon_{Pd(TDPA)}$ and $\varepsilon_{Pd(TDPA)_2}$, were found by plotting A_1 vs C_{TDPA} and A_2 vs C_{Pd}, respectively (Fig. 3 and Table 3). The molar absorptivities of the Pd–DTDPA system (Table 3) were obtained analogously to that of the Pd–TDPA system by eqns (3) and (4):

$$A_{exp} - \varepsilon_{Pd}(C_{Pd} - 2C_{DTDPA}) = A_3 = \varepsilon_{Pd_2(DTDPA)}C_{DTDPA}, \quad (3)$$

$$A_{exp} - \varepsilon_{DTDPA}(C_{DTDPA} - C_{Pd}) = A_4 = \varepsilon_{Pd(DTDPA)}C_{Pd}. \quad (4)$$

Numerical methods. The LETAGROP computer program (spectrophotometric version SPEFO[17]) was used to treat experimental data (absorbances

Table 2. Calculated molar absorptivities (l mol^{-1} cm^{-1}) of TDPA, DTDPA and palladium in acid perchlorate medium with an ionic strength of 0.5 M $(Na^+, H^+)ClO_4^-$

	Wavelength (nm)									
	225	230	240	247	260	267	270	275	330	340
ε_{Pd}	1057	535	169	149	108	106	64	64	34	34
ε_{TDPA}	332	197	60	NC[a]	NC	NC	NA[b]	NA	NA	NA
ε_{DTDPA}	NC	NC	NC	410	304	231	NC	NC	NA	NA

[a] Not calculated.
[b] No absorbance.

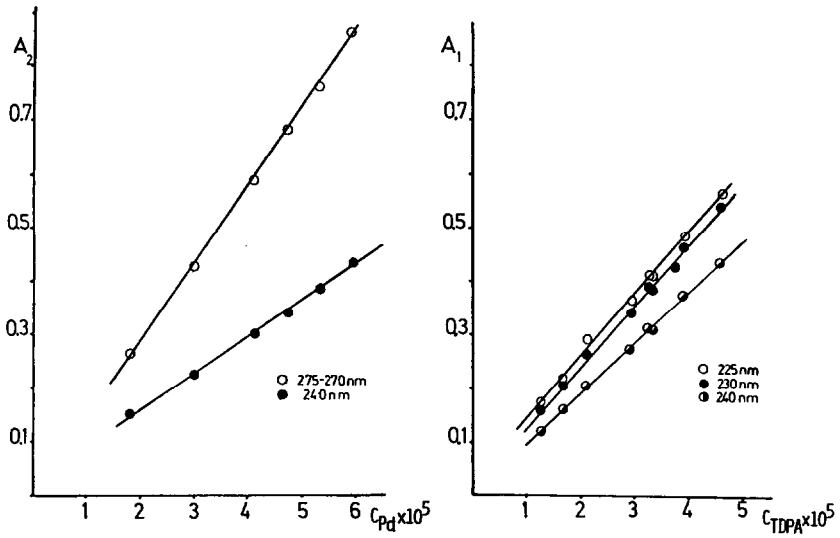


Fig. 3. Graphics to calculate molar absorptivities of Pd(TDPA) at 225, 230 and 240 nm, and $Pd(TDPA)_2$ species at 240 and 275 nm.

and concentrations of the metal, hydrogen and ligands). The minimized function was:

$$U = \sum_{1}^{NP} \sum_{1}^{NW} (A_{calc} - A_{exp})^2, \qquad (5)$$

where NP and NW are the number of experimental points and wavelengths, respectively, and $A_{calc} - A_{exp}$ the difference between the theoretical absorbance calculated by the program from the proposed model and the measured experimental absorbance. The molar absorptivities, previously calculated by graphical methods, were the initial input values; this was followed by the refinement of the equilibrium constants with fixed molar absorptivities. The output was a set of initial constants, which were recalculated in a final cycle by minimizing both the constants and the molar absorptivities. The computer treatment was simultaneously applied at five wavelengths to the experimental data of Table 1. The final computer values of the constants and molar absorptivities are listed in Tables 4 and 3, respectively. The overall formation constants for the system $pPd^{2+} + qH^+ + rL^{2-} \rightleftarrows Pd_pH_qL_r^{(2p+q-2r)+}$ are expressed as log $(\beta_{pqr} \pm 3\sigma_\beta)$ where σ is the standard deviation. If 3σ is greater than 0.20 then the program writes the maximum value of log $(\beta \pm 3\sigma)$. Other models (2:2, 2:4 and 4:2) for both systems were tried but did not improve the U function, and as a result were rejected.

Table 3 shows agreement between numerical and graphical methods except for the polynuclear complex of DTDPA. This difference can be explained by looking at Fig. 4 which corresponds to the species distribution diagrams calculated by the computer program HALTAFALL.[18] The species Pd(DTDPA) is always present in the metal concentration range studied and in consequence its absorbance can not be neglected as it was assumed in the graphical calculation. The diagram for the TDPA complexes is independent of the free concentration of palladium in solution while that of DTDPA depends on the metal because a polynuclear complex, $Pd_2(DTDPA)$, is present.

The stepwise constants (K_i) listed in Table 4 have been calculated from the overall constants (Table 4) and the ligand protonation constants.[10] These K_i values are greater than those of the corresponding complexes of d^{10} metal ions, e.g. Ag(I) and Hg(II), and divalent cations, e.g. Cu(II), Ni(II), Cd(II)...[11,19-21] due to the high affinity between sulphur atoms (soft ligands) and palladium(II) (soft cation).

In the experimental hydrogen concentration ($pC_H = 1.3$) the ligands are totally protonated (more than 99.9%) and the palladium site reaction with hydroxide ion, if we follow Baes and Mesmer,[22] is small in these conditions [log $\alpha_{Pd(OH)} = 0.04$]. The number of hydrogens associated to a given complex can not be directly ascertained because absorbance variations were not observed in the pH range 1–3 which was fixed to minimize the hydroxospecies of palladium. Although, the comparison between silver(I) complexes of TDPA and DTDPA[11,21] and palladium(II) complexes of the present work admits as a conclusion that the ligands are totally protonated, as in the case of silver, and can be represented as $Pd_i(H_2L)_j^{2i+}$. Some data can be given to explain this similarity. The mononuclear complexes of the

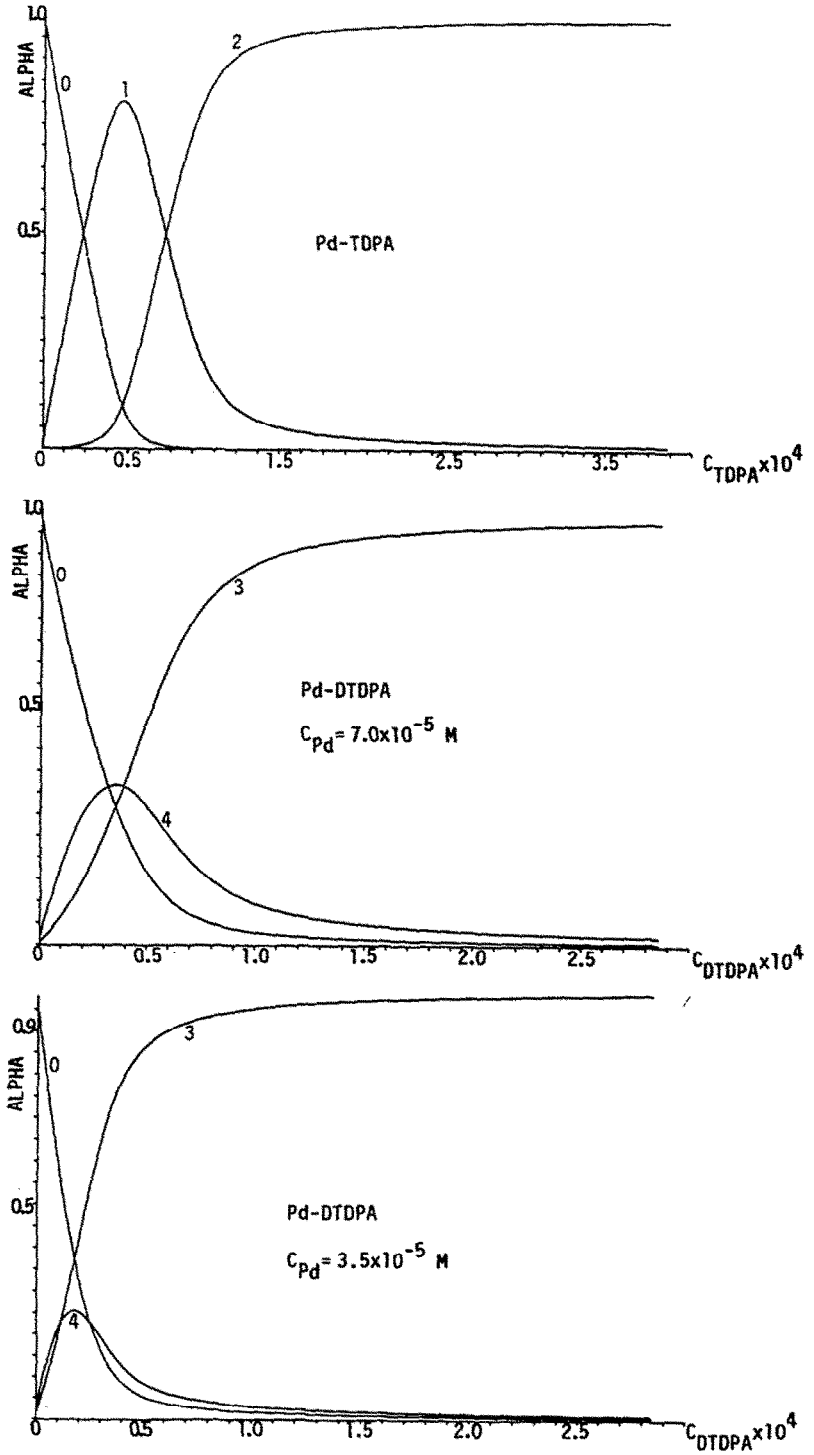


Fig. 4. Species distribution diagrams of Pd–TDPA and Pd–DTDPA systems calculated by the HALTAFALL program: (0) Pd, (1) Pd(TDPA), (2) $Pd(TDPA)_2$, (3) Pd(DTDPA), and (4) $Pd_2(DTDPA)$.

Table 3. Values of molar absorptivities (l mol^{-1} cm^{-1}) found in graphical and numerical methods (final values are those from LETAGROP program)

		Wavelength (nm)				
TDPA		225	230	240	270	275
$\varepsilon_{Pd(TDPA)}$	Graphical	11,498	11,145	9106	NC[a]	1635
	Computer	12,423±68	11,836±57	9625±39	2225±39	1497±45
	% difference	8.0	6.2	5.7		8.4
$\varepsilon_{Pd(TDPA)_2}$	Graphical	NC	NC	6789	14,296	14,291
	Computer	7207±76	6954±64	7123±48	14,624±36	14,461±50
	% difference			4.9	2.3	1.2
		247	260	267	330	340
DTDPA						
$\varepsilon_{Pd(DTDPA)}$	Graphical	9243	9885	9806	7127	6858
	Computer	9260±27	9863±26	9742±25	7117±39	6899±38
	% difference	0.2	0.2	0.7	0.1	0.6
$\varepsilon_{Pd_2(DTDPA)}$	Graphical	11,400	11,250	11,350	3800	3300
	Computer	15,901±302	15,279±290	14,843±435	NA[b]	NA
	% difference	28.3	26.4	23.5		

[a] Not calculated.
[b] No absorbance.

final models proposed coincide with those previously found for silver(I).[11,21] The possibility of polynuclear species for both palladium(II) with ligands containing disulphide groups and silver(I) with dithiopropanoic acid has already been pointed out;[11,23] in this case, the polynuclear 2:1 Pd–DTDPA complex would agree with it. Table 4 shows that the logarithmic difference between the constants of the mononuclear 1:1 and 1:2 Pd–TDPA complexes is 1.82 while for the silver system it was 1.11;[11] then, by following Arhland's theory, this value, smaller than 2, would indicate there is no d_π–d_π bonding between palladium and sulphur. There is also agreement if TDPA and DTDPA mononuclear 1:1 complexes are compared for a particular metal ion system; these differences,

Table 4. Final values of overall complex equilibrium constants [$\log(\beta \pm 3\sigma)$] obtained with the LETAGROP program [$I = 0.5$ M (Na^+, H^+)ClO_4^-]: the other constants (K) are calculated from β_{pqr} and overall ligand protonation constants (β_2^H)

$$pPd^{2+} + qH^+ + rL^{2-} \rightleftarrows Pd_pH_qL_r^{(2p+q-2r)+}, \quad \beta_{pqr} = \frac{[Pd_pH_qL_r^{(2p+q-2r)+}]}{[Pd^{2+}]^p[H^+]^q[L^{2-}]^r}$$

	TDPA	DTDPA
$\log \beta_{121}$	16.71±0.19	15.25±0.14
$\log \beta_{142}$	31.60, max 31.81	
$\log \beta_{221}$		19.67, max 19.89
Sig Y	0.010	0.009
U_{min}	1.38×10^{-2}	2.57×10^{-2}
$\log\left[K^{H_2L}_{Pd(H_2L)} = \frac{\beta_{121}}{\beta_2^H}\right]$	7.40	5.92
$\log\left[K^{Pd(H_2L)}_{Pd(H_2L)_2} = \frac{\beta_{142}}{\beta_{121}\beta_2^H}\right]$	5.58	
$\log\left[K^{H_2L}_{Pd_2(H_2L)} = \frac{\beta_{221}}{\beta_2^H}\right]$		10.34

expressed in logarithmic units, are 1.48 (Table 4) and 1.26[24] for palladium(II) and silver(I) complexes, respectively. The stepwise constant of $Pd(TDPA)_2$ is 1.82 logarithmic units smaller than that of the first complex Pd(TDPA), and would be explained by steric hindrance when a second bulky molecule of the ligand approximates the Pd(TDPA) species. The trend is always that the constants from TDPA species are greater than those similar to DTDPA.

Taking into account all previous considerations and keeping in mind the analogous behaviour of both ligands with respect to silver(I) and palladium(II), it can be assumed that, under the experimental conditions, the metal–ligand coordination seems to occur mainly through the sulphur donor atoms, where the remaining carboxylic groups are protonated and practically without any interaction with the metal ion.

REFERENCES

1. Yu. A. Zolotov, O. M. Petrukhin, G. I. Malofeeva, E. V. Marcheva, O. A. Shiryaeva, V. A. Shestakov, V. G. Miskar'yants, V. I. Nefedov, Yu. E. Murinov and Yu. E. Nikitin, *Anal. Chim. Acta* 1983, **148**, 135.
2. L. R. M. Pitombo and E. De Oliveira, *Anal. Chim. Acta* 1977, **101**, 177.
3. F. R. Hartley, *Coord. Chem. Rev.* 1981, **35**, 143.
4. A. Napoli, *Ann. Chim. (Rome)* 1976, **66**, 529.
5. L. R. M. Pitombo and G. Oliveira, *Anal. Chim. Acta* 1975, **75**, 391.
6. O. Procházková, J. Podlahová and J. Podlaha, *Coll. Czech. Chem. Commun.* 1973, **38**, 1128.
7. J. Einar and S. Per, *Anal. Chim. Acta* 1971, **53**, 309.
8. H. N. Hughes, *Coord. Chem. Rev.* 1981, **37**, 308.
9. K. Prout and S. Hernández, *Acta Cryst.* 1982, **B38**, 338.
10. J. Marco, T. Tornos, S. Hernández and H. Iturriaga, *An. Quím.* 1984, **B80**, 506.
11. S. Hernández and H. Iturriaga, *An. Quím.* 1985, **B81**, 41.
12. *Some Laboratory Methods.* Mimeograph, Department of Inorganic Chemistry, Royal Institute of Technology, Stockholm (1959).
13. K. Burger and D. Dyrssen, *Acta Chem. Scand.* 1963, **17**, 1489.
14. P. Job, *Ann. Chim.* 1928, **9**, 113.
15. J. H. Yoe and A. L. Jones, *Ind. Eng. Chem. Anal. Ed.* 1944, **16**, 111.
16. F. R. Hartley, C. Burgess and R. M. Alcock, *Solution Equilibria*, 1st Edn, p. 313. Ellis Horwood, Chichester (1980).
17. L. G. Sillén and B. Warnqvist, *Arkiv Kemi* 1969, **31**, 315.
18. N. Ingri, W. Kakolowicz, L. G. Sillén and B. Warnqvist, *Talanta* 1967, **14**, 1261.
19. F. J. C. Rossotti and R. J. Whewell, *J. Chem. Soc., Dalton Trans.* 1979, 257.
20. R. Aruga, *J. Inorg. Nucl. Chem.* 1979, **41**, 849.
21. D. K. Laing and L. D. Petit, *J. Chem. Soc., Dalton Trans.* 1975, 2297.
22. Ch. F. Baes and R. E. Mesmer, *The Hydrolysis of Cations*, p. 264. John Wiley, New York (1976).
23. H. Lam-Thanh and S. Fermandjian, *J. Chim. Phys. Phys.-Chim. Biol.* 1977, **74**, 361.
24. S. Ahrland, J. Chatt, N. R. Davies and A. A. Williams, *J. Chem. Soc.* 1958, 276.

Polyhedron Vol. 5, No. 11, pp. 1785–1789, 1986
Printed in Great Britain

0277–5387/86 $3.00+.00
Pergamon Journals Ltd

UNEXPECTED PREPARATION AND X-RAY CRYSTAL STRUCTURE OF THE DINUCLEAR COMPLEX $Mo_2(\mu\text{-}P(O)(OCH_3)_2)_2(CO)_4(P(OCH_3)_3)_2(CF_3COO)_2$

SAMIR ARABI,*† CHANTAL BERTHELOT and JEAN-PIERRE BARRY

Département de Chimie, Université de Sherbrooke, Sherbrooke, Québec J1K 2R1, Canada

NICHOLAS J. TAYLOR

Chemistry Department, University of Waterloo, Waterloo, Ontario N2L 3G1, Canada

and

BRUNO CHAUDRET*

Laboratoire de Chimie de Coordination du CNRS, Unité n° 8241 liée par convention à l'Université Paul Sabatier, 205 route de Narbonne, 31400 Toulouse, France

(*Received* 25 *November* 1985; *accepted* 4 *March* 1986)

Abstract—Prolonged reaction of CF_3COOH with $Mo(CO)_3(P(OCH_3)_3)_3$ in CH_2Cl_2 yields the dimer $[Mo(CO)_2(\mu(O)P(OCH_3)_2)P(OCH_3)_3CF_3COO]_2$ in low yield. The complex has been characterized by the usual spectroscopic methods and by an X-ray crystal structure determination. The molybdenum atoms are linked by two O–P bridges, the six-membered dimetallacycle adopting a twisted-boat conformation. Each molybdenum is seven-coordinated and has a capped trigonal prism geometry, the capping position being occupied by an oxygen atom of the bridging $OP(OCH_3)_2$ group. A mechanism similar to the well-known Michaelis–Arbuzov rearrangement is proposed and substantiated by the concomitant apparition of CF_3COOCH_3 during the reaction.

Protonation of zero-valent molybdenum complexes is a well-documented method for the preparation of heptacoordinate molybdenum hydrido complexes. In previous studies we have shown that the reaction of $Mo(CO)_2(PR_3)_4$ ($R = CH_3$) produced the cations $[MoH(CO)_2(PR_3)_4]^+$.[1] However, in the case of $Mo(CO)_3(PR_3)_3$, the reaction is highly dependent on the nature of the R group. When R = Me, $[MoH(CO)_3(PMe_3)_3]^+CF_3COO^-$ is obtained first, and a longer reaction time leads to $Mo(CO)_2(PMe_3)_3(CF_3COO)_2$, a heptacoordinated complex containing two monodentate trifluoroacetate ligands.[2] In the case of the more bulky R = Et, dissociation of a phosphine occurs to give $Mo(CO)_2(PEt_3)_2(CF_3COO)_2$, which contains one monodentate and one bidentate trifluoroacetate group.[3] Furthermore, the protonation of $Mo(P(OCH_3)_3)_6$ was first shown to produce $[MoH(P(OCH)_3)_6]^+$,[4] but only in low yield, the major product of the reaction being a complex containing a dimethoxyphosphino group $[Mo(P(OCH_3)_2)(P(OCH_3)_3)_5]^+$.[5] In this paper, we describe the results of the protonation of $Mo(CO)_3(P(OCH_3)_3)_3$ and the unexpected formation of a new heptacoordinate dinuclear complex.

RESULTS AND DISCUSSION

The reaction of $Mo(CO)_3(P(OCH_3)_3)_3$ with excess CF_3COOH in CH_2Cl_2 produced a yellow solution from which, by precipitation with methanol and recrystallization, we could isolate a low

* Authors to whom correspondence should be addressed.

† Present address: c/o Dr B. Chaudret, Laboratoire de Chimie de Coordination du CNRS, Unité n° 8241 liée par convention à l'Université Paul Sabatier, 205 route de Narbonne, 31400 Toulouse, France.

yield (*ca* 10%) of yellow crystals analyzing for $Mo_2(CO)_4(P(O)(OCH_3)_2)_2(P(OCH_3)_3)_2(CF_3COO)_2$. The IR spectrum showed four bands at 1960(m), 1890(s), 1865(m) and 1610(w) cm^{-1}. The latter was attributed to the chelating trifluoroacetato ligands. The ^1H NMR spectrum only shows two doublets in a 2:3 ratio at δ 3.59 (J_{PH} 11.5 Hz) and 3.82 ppm (J_{PH} 12 Hz). Finally, the ^{31}P NMR spectrum consists of two doublets in a 1:1 ratio at δ 176.18 and 136.50 ppm (J_{PP} 50.3 Hz). Since these data did not allow an unambiguous proposition of structure for the complex, an X-ray crystal structure determination was undertaken. The results are shown in Fig. 1 and Tables 1 and 2.

The complex is a centrosymmetric dimer containing two heptacoordinated molybdenum units linked by two R_2P–O bridges. The geometry around each molybdenum is that of a capped trigonal prism.[6] The capping position is occupied by O(3)′, the oxygen atom of the bridging R_2PO group. The capped quadrilateral face contains the CF_3COO^- ion acting as a bidentate group [O(9) and O(10)], one CO ligand [C(2)] and one R_2PO group [P(1)]. The remaining edge contains one CO [C(1)] and one $P(OCH_3)_3$ [P(2)] molecule. The two coordinated phosphorus groups on each molybdenum atom are *cis* to one another in agreement with the low P–P coupling constant observed by ^{31}P NMR. The conformation of the dimetallacycle (—Mo—P—O—)$_2$ is that of a twisted boat. The bond lengths are all in the usual range except for Mo—O(9) and Mo—O(10) which are significantly longer than other known Mo—O distances (usually in the range 2.09–2.15 Å),[7] probably indicating a weakly bonded trifluoroacetato group. There is no significant difference between the Mo—P(1) and the Mo—P(2) bond [2.420(1) and 2.402(1) Å, respectively]. The bridging P—O distance [P(1)—O(3)] is shorter than other phosphite P—O bonds [1.526(3) Å vs 1.57–1.59 Å], suggesting that the bond has a significant π-bond character as in related complexes.[8,9] Finally, the Mo–Mo distance is very long [4.563(1) Å] and precludes any kind of metal–metal interaction. This type of bridging R_2PO group is not very usual and so far examples have been found only in manganese, rhenium and platinum chemistry.[10] In molybdenum chemistry, this structure can be related to that of other heptacoordinate dimers bridged by oxygen-containing ligands such as the carbonato-bridged complex $[Mo(\mu\text{-}CO_3)(CO)(PMe_2Ph)_3]_2$[11] (Mo...Mo = 4.95 Å) or the μ-SO_2 derivative $[Mo(\mu\text{-}SO_2)(CO)_2(py)(PPh_3)]_2$.[12]

As a whole, the formation of this complex

Table 1. Bond lengths (Å)

Mo—P(1)	2.420(1)	Mo—P(2)	2.402(1)
Mo—O(3′)	2.094(3)	Mo—O(9)	2.277(4)
Mo—O(10)	2.306(4)	Mo—C(1)	1.942(5)
Mo—C(2)	1.941(5)	Mo...Mo	4.563(1)
P(1)—O(3)	1.526(3)	P(1)—C(4)	1.587(4)
P(1)—O(5)	1.589(4)	P(2)—O(6)	1.583(5)
P(2)—O(7)	1.567(4)	P(2)—O(8)	1.573(5)
C(1)—O(1)	1.147(7)	C(2)—O(2)	1.144(6)
O(4)—C(4)	1.408(8)	O(5)—C(5)	1.466(7)
O(6)—C(6)	1.377(10)	O(7)—C(7)	1.458(8)
O(8)—C(8)	1.412(10)	O(9)—C(9)	1.255(7)
O(10)—C(9)	1.236(7)	C(9)—C(10)	1.543(10)
C(10)—F(1)	1.307(12)	C(10)—F(2)	1.253(12)
C(10)—F(3A)	1.272(13)	C(10)—F(3B)	1.251(11)

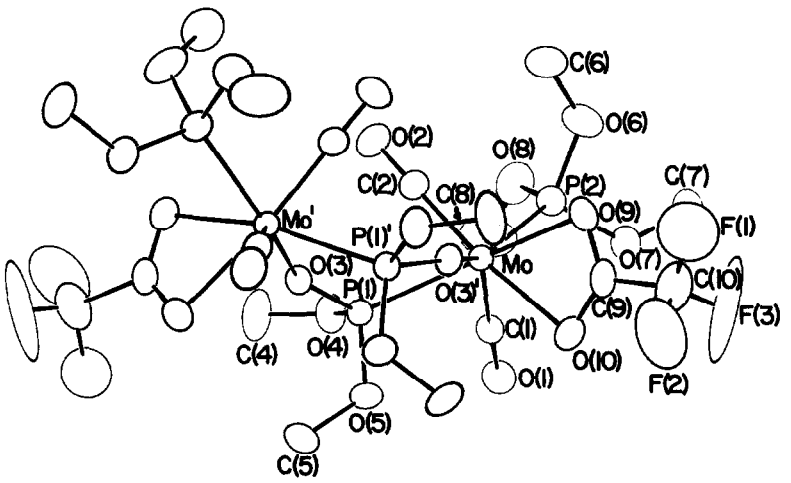


Fig. 1. Molecular structure of $Mo_2(P(O)(OCH_3)_2)_2(CO)_4(P(OCH_3)_3)_2(CF_3COO)_2$showing the atom-numbering scheme.

Table 2. Bond angles (°)

P(1)—Mo—P(2)	125.9(1)	P(1)—Mo—O(3′)	81.1(1)
P(1)—Mo—O(9)	158.1(1)	P(1)—Mo—O(10)	114.5(1)
P(1)—Mo—C(1)	73.8(1)	P(1)—Mo—C(2)	71.9(1)
P(2)—Mo—O(3′)	148.2(1)	P(2)—Mo—O(9)	75.7(1)
P(2)—Mo—O(10)	101.6(1)	P(2)—Mo—C(1)	73.5(1)
P(2)—Mo—C(2)	76.5(1)	O(3′)—Mo—O(9)	77.3(1)
O(3′)—Mo—O(10)	77.3(1)	O(3′)—Mo—C(1)	136.1(1)
O(3′)—Mo—C(2)	100.4(1)	O(9)—Mo—O(10)	57.3(1)
O(9)—Mo—C(1)	120.7(1)	O(9)—Mo—C(2)	115.2(1)
O(10)—Mo—C(1)	81.2(1)	O(10)—Mo—C(2)	172.4(1)
C(1)—Mo—C(2)	105.0(2)	Mo—P(1)—O(3)	116.1(1)
Mo—P(1)—O(4)	113.3(1)	Mo—P(1)—O(5)	107.9(1)
O(3)—P(1)—O(4)	106.1(1)	O(3)—P(1)—O(5)	106.8(1)
O(4)—P(1)—O(5)	106.0(2)	Mo—P(2)—O(6)	115.5(1)
Mo—P(2)—O(7)	111.3(1)	Mo—P(2)—O(8)	120.8(1)
O(6)—P(2)—O(7)	100.7(2)	O(6)—P(2)—O(8)	98.8(2)
O(7)—P(2)—O(8)	107.3(2)	Mo—C(1)—O(1)	173.0(2)
Mo—C(2)—O(2)	179.2(2)	Mo′—O(3)—P(1)	148.1(1)
P(1)—O(4)—C(4)	125.5(3)	P(1)—O(5)—C(5)	121.6(2)
P(2)—O(6)—C(6)	127.8(3)	P(2)—O(7)—C(7)	123.5(3)
P(2)—O(8)—C(8)	125.1(4)	Mo—O(9)—C(9)	89.8(2)
Mo—O(10)—C(9)	89.0(2)	O(9)—C(9)—O(10)	123.8(2)
O(9)—C(9)—C(10)	118.7(3)	C(10)—C(9)—O(10)	117.5(3)
C(9)—C(10)—F(1)	110.8(4)	C(9)—C(10)—F(2)	111.3(4)
C(9)—C(10)—F(3A)	113.0(4)	C(9)—C(10)—F(3B)	110.9(4)
F(1)—C(10)—F(2)	99.0(5)	F(1)—C(10)—F(3A)	128.7(5)
F(1)—C(10)—F(3B)	86.1(5)	F(2)—C(10)—F(3A)	89.0(5)
F(2)—C(10)—F(3B)	132.2(5)	F(3A)—C(10)—F(3B)	54.2(5)

seemed surprising and we tried to elucidate its mechanism. A study by Haines and Nolte[13] has shown that the reaction of $[CpMo(CO)_3]_2$ with excess $P(OCH_3)_3$ led eventually to a 1:1 mixture of $[CpMo(CO)_2(P(OCH_3)_3)(P(O)(OCH_3)_2)]$ and $[CpMo(CH_3)(CO)_2(P(OCH_3)_3)]$ through an ionic derivative $[CpMo(CO)_2(P(OCH_3)_3)_2][CpMo(CO)_3]$. Actually, our mechanism is probably very similar and also similar to the well-known Michaelis–Arbuzov type rearrangement of phosphites in the presence of alkyl halides. Thus in both cases formation of a cationic species containing a phosphorus in a tetrahedral environment is observed followed by rupture of an O—C bond and migration of the alkyl group on the anionic species [eqns (1) and (2), respectively]:

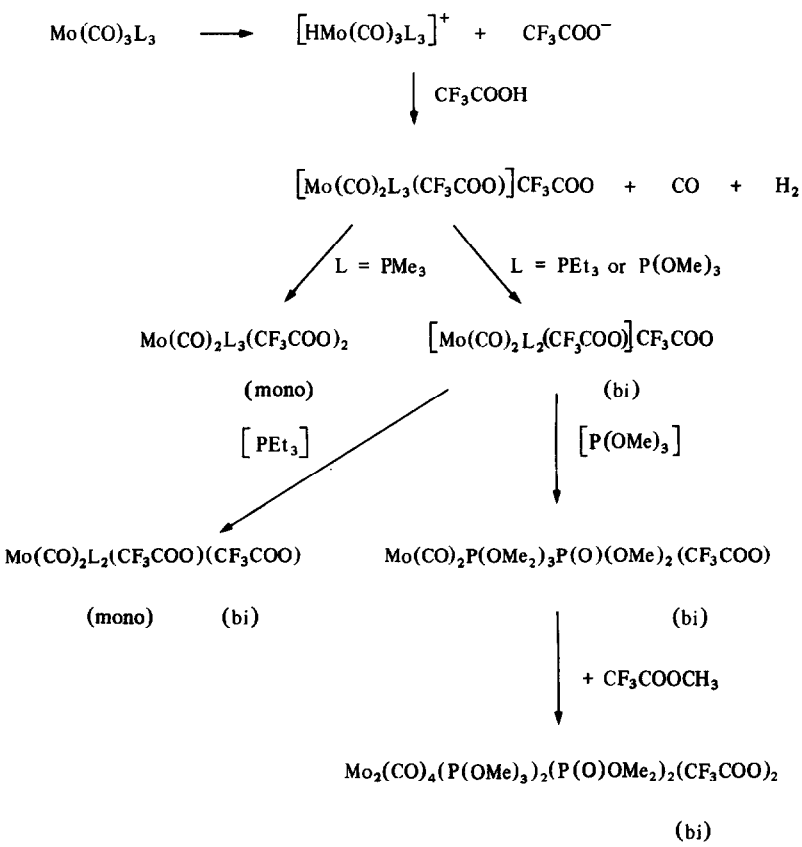
$$[CpMo(CO)_2(P(OR)_3)_2][CpMo(CO)_3] \rightarrow [CpMo(CO)_2(P(OR)_3)(P(O)(OR)_2)] + CpMo(CO)_3R, \quad (1)$$

$$P(OR)_3 + R'X \rightarrow [R'P(OR)_3]X \rightarrow R'P(O)(OR)_2 + RX. \quad (2)$$

Concerning our reaction (Scheme 1) we assume that in the presence of excess CF_3COOH, as for similar complexes with other ligands, formation of a diacetato complex is observed on which one trifluoroacetate could be weakly bonded, thus leading to an ionic species. One methyl group should then transfer to the CF_3COO^- anion and indeed ^1H NMR monitoring of the reaction shows the formation of CF_3COOCH_3. Finally, the complex $Mo(P(O)(OCH_3)_2)(CO)_2(P(OCH_3)_3)(CF_3COO)$ which has eliminated CO {formation of $Mo(CO)_4[P(OCH_3)_3]_2$ is also observed in this reaction} dimerizes in order to achieve an 18-electron configuration around the molybdenum. This type of complex containing weakly bonded trifluoroacetate ligands and easily broken bridges,[14] thus easily producing vacant sites of coordination, can be very important for reactivity and catalytic studies.

EXPERIMENTAL

IR spectra were recorded in solution in CH_2Cl_2 or as Nujol mulls on a Perkin–Elmer 257 grating



Scheme 1. Proposed mechanism for the reactions of $Mo(CO)_3(PR_3)_3$ complexes with CF_3COOH (mono means a monodentate trifluoroacetate group, bi a bidentate trifluoroacetate group).

diffractometer. ^1H and ^{31}P NMR were recorded on a WM250 Bruker (250 and 101.22 MHz, respectively) operating in the Fourier transform mode with TMS and external H_3PO_4 (85% in D_2O) as reference, respectively. All operations were carried out under dry nitrogen and solvents were carefully degassed before use.

Preparation of $Mo_2(\mu\text{-}P(O)(OCH_3)_2)_2(CO)_4(P(OCH_3)_3)_2(CF_3COO)_2$

$Mo(CO)_3(P(OCH_3)_3)_3$ (2 g, 3.63 mmol) was added to a mixture of CF_3COOH (10 cm^3, excess) and CH_2Cl_2 (20 cm^3) and the resulting yellow solution was stirred at room temperature for 24 h. Methanol (20 cm^3) was then added and the mixture was cooled to −18°C, thus producing a yellow precipitate. After filtration, the precipitate was washed several times with methanol and dried *in vacuo*. It was then recrystallized from CH_2Cl_2, affording yellow crystals of the complex (yield *ca* 10%). Occasionally, the first crystalline product obtained in very low yield was $Mo(CO)_4(P(OCH_3)_3)_2$.

Found: C, 21.7; H, 3.0; P, 12.4; F, 11.4%. Calc. for $MoC_9F_3H_{15}O_{10}P_2$: C, 24.0; H, 3.0; P, 12.1; F, 11.2%.

Crystal structure

Crystal data. $Mo_2P_4F_6O_{20}C_{18}H_{30}$, molecular weight = 996.19, orthorhombic, $a = 24.439(3)$ Å, $b = 8.861(1)$ Å, $c = 16.688(2)$ Å, $V = 3613.8(6)$ Å^3, space group *Pbcn* (D_{2h}^{14}—No. 60), $Z = 4$; $\rho_m = 1.83$ g cm^{-3}, $\rho_c = 1.831$ g cm^{-3}; $F(000) = 1984$; $\lambda = 0.71069$ Å; $\mu(\text{Mo-}K_a) = 9.70$ cm^{-1}.

Data collection and solution. Intensity data were collected on a crystal of dimensions $0.31 \times 0.29 \times 0.27$ mm using θ–2θ scans ($3.2 < 2\theta < 52.0°$) with a variable scan speed of 2.93–29.3° min^{-1} and a scan width of 0.8° below $K\alpha_1$, to 0.8° above $K\alpha_2$ on a Syntex $P2_1$ diffractometer. From a total of 3581 measured reflections, 2572 with $I > 3\sigma(I)$ were considered observed and used in the structure solution and refinement. Two standard reflections (040; 1200) monitored every 100 measurements showed only minor fluctuations during data collection. Data were cor-

rected for Lorentz and polarization effects but not for absorption.

The molybdenum atom was located in a Patterson synthesis and the light atoms via a subsequent Fourier map. Refinement of all non-hydrogen atoms with isotropic parameters gave an R value of 0.095 ($R = \Sigma \| F_o| - |F_c\| / \Sigma |F_o|$). Refinement with anisotropic thermal parameters reduced R to 0.042. A difference Fourier synthesis at this stage revealed disorder of the CF_3 group. F(3) was found to be resolvable into two centres while the other fluorine atoms apparently possessed singular sites. Inclusion of the F(3) disorder into the refinement led to convergence at $R = 0.038$ with the weighted residual $R_w = 0.046$ $\{R_w = [\Sigma\ w(|F_o| - |F_c|)^2 / \Sigma\ w(|F_o|)^2]^{1/2}\}$. An empirical weighting scheme of the form $w^{-1} = 2.52 - 0.0225|F_o| + 0.00029|F_o|^2$ was used in the final cycles of refinement. A final difference Fourier synthesis indicated maximum residuals of 0.6 e Å^{-3} in the vicinity of the CF_3 and —OMe groups. Scattering factors were taken from the *International Tables*,[15] including both the real and imaginary components of the anomalous dispersion for molybdenum. Computer programs used have been described elsewhere.[16] Final atomic coordinates and other crystallographic data have been deposited with the Editor and atomic coordinates have been sent to the Cambridge Crystallographic Data Centre.

Acknowledgements—We thank the National Sciences and Engineering Research Council of Canada for financial support (S.A.), the University of Waterloo Structure Service and Dr R. Pince for helpful discussions.

REFERENCES

1. S. Arabi, R. Mathieu and R. Poilblanc, *J. Organomet. Chem.* 1976, **104**, 323.
2. A. L. Beauchamp, F. Belanger-Gariepy and S. Arabi, *Inorg. Chem.* 1985, **24**, 1860.
3. A. L. Beauchamp, F. Belanger-Gariepy and S. Arabi, unpublished results.
4. R. Mathieu and R. Poilblanc, *C. R. Acad. Sci., Ser. C* 1974, **279**, 1113.
5. E. L. Muetterties, J. F. Kirner, W. J. Evans, P. L. Watson, S. Abdel-Meguid, I. Tavanaiepour and V. W. Day, *Proc. Natl Acad. Sci. U.S.A.* 1978, **75**, 1056.
6. See, for example: M. G. B. Drew, *Prog. Inorg. Chem.* 1977, **23**, 67; and D. L. Kepert, *Prog. Inorg. Chem.* 1979, **25**, 41.
7. F. A. Cotton, M. Extine and L. D. Gage, *Inorg. Chem.* 1978, **17**, 172.
8. G. Mundig, B. Schilling, M. Weishaupt, E. Lindner and J. Strähle, *Z. Anorg. Allg. Chem.* 1977, **437**, 169.
9. S. Hoehne, E. Lindner and B. Shilling, *J. Organomet. Chem.* 1977, **139**, 315.
10. For a recent review on this type of complexes, see B. Walther, *Coord. Chem. Rev.* 1984, **60**, 67 (and references therein).
11. J. Chatt, M. Kubota, G. J. Leigh, M. C. March, R. Mason and D. J. Yarrow, *J. Chem. Soc., Chem. Commun.* 1974, 1033.
12. G. J. Kubas, G. D. Jarvinen and R. R. Ryan, *J. Am. Chem. Soc.* 1983, **105**, 1883.
13. R. J. Haines and C. R. Nolte, *J. Organomet. Chem.* 1970, **24**, 725.
14. J. Chatt and B. T. Heaton, *J. Chem. Soc. A* 1968, 2745.
15. *International Tables for X-ray Crystallography*, Vol. 4. Kynoch Press, Birmingham (1974).
16. A. J. Carty, G. N. Mott, N. J. Taylor and J. E. Yule, *J. Am. Chem. Soc.* 1978, **100**, 3051.

Polyhedron Vol. 5, No. 11, pp. 1791–1797, 1986
Printed in Great Britain

0277–5387/86 $3.00+.00
Pergamon Journals Ltd

BONDING IN CLUSTERS—VIII.* ELECTRONIC STRUCTURE OF *CLOSO*-SIX-APEX AND *NIDO*-FIVE-APEX IRON CARBONYL CARBIDE AND NITRIDE CLUSTERS

PAUL BRINT,† KIERAN O'CUILL and TREVOR R. SPALDING

Department of Chemistry, University College, Cork, Ireland

(*Received* 29 *August* 1985; *accepted* 11 *March* 1986)

Abstract—An electronic structure of *closo*-six-apex metal carbonyl clusters is proposed, based on a comparison with Stone's description of *closo*-borane clusters. From this, and by comparison with B_5H_9, a description of the occupied cluster orbitals of *nido*-five-apex metal carbonyl clusters is proposed and found to agree well with calculations on $Fe_5(CO)_{15}C$ and $Fe_5H(CO)_{14}N$. The photoelectron spectrum of the nitride is presented. The role of the interstitial atom and the chemical stabilities of the compounds are discussed.

The existence of metal carbonyl clusters with geometries analogous to borane clusters has been well rationalized in a phenomenological manner by Wade's rules[1] and the "isolobal–isoelectronic" description of Hoffmann and Mingos.[2] For example Wade's rules state that the $Fe(CO)_3$ group can replace a BH group in a borane cluster without changing the cluster geometry, and the Hoffmann–Mingos description shows that these two groups are "isolobal–isoelectronic" in the manner shown in Fig. 1. The BH group has three "atomic" orbitals (AOs) and two electrons available for cluster bonding, the $Fe(CO)_3$ group has three similarly oriented orbitals and two electrons not accounted for by carbonyl bonding or metal lone pairs. On the basis of these "rules" the observed octahedral arrangements of metal atoms in $[Fe_6(CO)_{16}C]^{2-}$ or $Co_6(CO)_{16}$ can be compared with *closo*-$B_6H_6^{2-}$, and the square-based pyramidal arrangement in $M_5(CO)_{15}C$ (M = Fe, Ru or Os) with *nido*-B_5H_9.

In this paper we consider the application of Stone's theoretical description[3] of the electronic structure of *closo*-boranes to analogous metal clusters. This is not a phenomenological description and counts among its successes the first *a priori* explanation of the triangular faced polyhedral geometries of the $B_nH_n^{2-}$ anions stabilized by the occupation of $n+1$ cluster-bonding molecular orbitals (MOs). As Stone's theory may justifiably be considered as the basis of the phenomenological descriptions, it should, by implication, be useful in analogous metal clusters. We investigated this by replacing the BH groups used in Stone's discussion with metal carbonyl groups and then tested the results by comparison with self-consistent charge calculations and the photoelectron spectrum of $Fe_5(H)(CO)_{14}N$. We are particularly interested in the role of the interstitial main-group atom found in many clusters since it appears to be significant in the stability of the clusters.

Stone has demonstrated that for $B_nH_n^{2-}$ the basis set of $3n$ AOs [two tangential (π) and one radial (σ) per BH group (Fig. 1)] generate three groups of n MOs. These are separable in the limit of spherical symmetry to which all *closo*-borane geometries

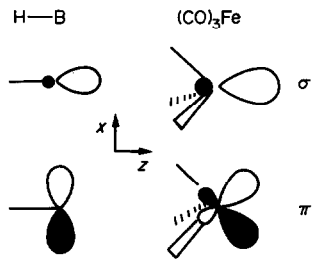


Fig. 1. Isolobal atomic orbitals of the BH and $Fe(CO)_3$ moieties.

* For Part VII see Ref. 13.

† Author to whom correspondence should be addressed.

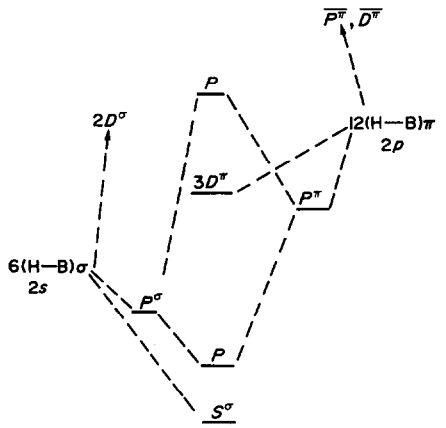


Fig. 2. Schematic of the MO diagram of $B_6H_6^{2-}$.

approximate, hence the tangential/radial labels. The n radial AOs produce n MOs with spherical harmonic properties which are labelled $S^\sigma, P^\sigma, D^\sigma \ldots$ in order of increasing energy (the spherical degeneracy is usually lifted by the molecular symmetry). The $2n$ tangential AOs produce two groups of n MOs, both with tensor harmonic properties but differing in parity, labelled P^π, $D^\pi, \ldots$, and $\overline{P^\pi}$, $\overline{D^\pi}$. . . . One major distinction is that the radial AOs have a predominantly boron $2s$ composition and are therefore lower in energy than the tangential AOs which are almost pure boron $2p$. This leads to the MO diagram for $B_6H_6^{2-}$ shown in Fig. 2. The extent of P^σ–P^π mixing in the symmetry of the anion is a matter of debate[4] but is not critical in the following argument. The seven occupied cluster MOs of the $B_6H_6^{2-}$ anion are S^σ, $3P$, $3D^\pi$. Stone developed energy equations for each type of MO that showed that the orbitals are most stable when the geometry of the cluster is a triangular faced polyhedron.

EXPERIMENTAL

$Fe_5(CO)_{15}C$[5] and $Fe_5(H)(CO)_{14}N$[6] were prepared by literature methods and identified by their IR and mass spectra. The photoelectron spectrum of $Fe_5(H)(CO)_{14}N$ was measured on an apparatus described previously.[7] The solid was introduced into the ionization region and heated to 90°C, at which temperature the vapour pressure was sufficient to give a count rate of 1500 counts s^{-1}. The spectrum was calibrated using the known ionizations of N_2 and H_2O (introduced with the sample). The IR spectrum of the sample was unchanged after recovery at room temperature and therefore decomposition was assumed to be insignificant. [Attempts to measure the spectra of $Fe_5(CO)_{15}C$, $Os_5(CO)_{15}C$ and $Os_6(CO)_{17}C$ all failed as the room-temperature vapour pressure was too small and slight heating led to rapid decomposition in each case.]

All calculations were performed using Hoffmann's FORTICON 8 program extended to accept the large number of AOs involved.[8] The geometries used were symmetrized geometries based on average experimental bond lengths and angles.[6,9] This resulted in relative dispositions of the carbonyl ligands which were different to the experimental ones but this was necessary in order to simplify the assignment of the MOs. Calculations with geometries approaching the experimental ones produced insignificant changes in orbital energies and suggest that symmetrization is not an important source of error.

RESULTS AND DISCUSSION

Attempts to construct a diagram similar to Fig. 2 for a *closo*-six-apex metal carbonyl cluster, e.g. "$[Fe_6(CO)_{18}]^{2-}$", are immediately complicated by the composition of the $Fe(CO)_3$ AOs of Fig. 1. The σ- and π-symmetry type orbitals have a predominantly iron $3d$ composition and should therefore have similar energies. Mingos has shown[10] that the calculation gives the orbital energy of the σ-lobe as higher than that of the π-lobes. This is the reverse of the BH order. One would therefore construct a diagram such as Fig. 3(a) for this compound, noting that the energy spread over the seven orbitals is small. Educing reasons why the unfavourable AO energies should produce the required occupied MOs is a matter of tentative guess-work but could be based on the possibly greater overlap of the radial lobes than of the tangential ones. Conversely, this is probably a good argument for the non-existence of "$[Fe_6(CO)_{18}]^{2-}$". One has however to account for the existence of the isoelectronic clusters $Co_6(CO)_{16}$, $[Co_6(CO)_{15}]^{2-}$ and $[Co_6(CO)_{14}]^{4-}$ which have the expected octahedron of cobalt atoms.[11]

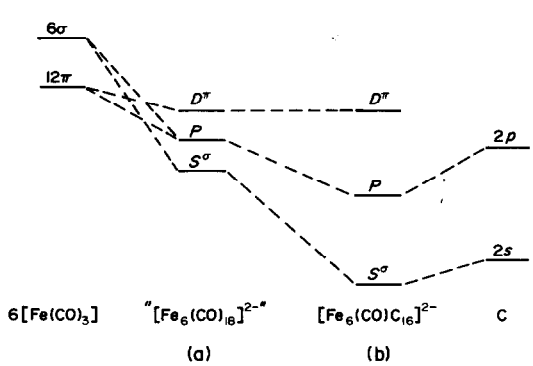


Fig. 3.

Extended Hückel calculations on the $M(CO)_3$ group (M = Mn, Fe or Co) show that the σ–π-lobe energy separation is 2.09, 1.92 and 1.21 eV in that order and, therefore, the $Co(CO)_3$ unit is a much better starting point for achieving an MO diagram such as Fig. 3(a) than the $Fe(CO)_3$ unit. In Mingos's extended Hückel[12] calculation on $[Co_6(CO)_{14}]^{4-}$ the seven cluster-bonding orbitals are identifiable in the group of high-energy occupied MOs and are all within 1 eV of the highest-energy MO (HOMO).

The MOs of Fig. 3(a) can be made to resemble those of Fig. 2 more closely by the introduction of an interstitial atom with a corresponding reduction of the number of carbonyl ligands, e.g. the carbon atom in $Fe_6(CO)_{16}C^{2-}$. The symmetries of the AOs of the interstitial atom allow interaction only with the S^σ and P MOs of the metal carbonyl cluster. This should result in the MO diagram of Fig. 3(b), with a stable bonding S^σ MO predominantly on the carbon atom, and a stabilized set of P-orbitals. The actual energy and composition of these latter MOs are unpredictable at this level of description. The P^σ/P^π composition of the metal carbonyl P-orbitals is unknown as is the relative energy of the carbon atom $2p$ orbitals.

One immediate experimental corollary of Fig. 3 is the different stability and chemical reactivity of metal clusters with and without interstitial atoms. If a perturbation can displace one or more of the cluster-bonding MOs to the virtual-orbital set, particularly one of the S^σ, P orbitals which we have shown[13] are the more important bonding orbitals of the boranes, then the cluster will open up and become labile, losing its closed deltahedral geometry. This is far more probable for clusters without interstitial atoms and such clusters are consistently less stable and more reactive than those with interstitial atoms. Some of the above discussion has been addressed at a qualitative level by Wade.[14]

It is the utility of Fig. 3 that we now wish to investigate through calculations and spectroscopic work on *nido*-five-apex iron carbide and nitride clusters. As these compounds are analogous to *nido*-B_5H_9 we first briefly review the cluster-bonding MOs of the borane. The B_5H_9 geometry is related to $B_6H_6^{2-}$ by deletion of one of the apices of the octahedron. It also has the same number of cluster-bonding MOs. Figure 4 shows the MOs of both molecules calculated using the MNDO method.[4] The energy separations of the three types of orbitals are large. Stone's labels S^σ, P and D^π are clearly valid for B_5H_9, particularly if the bridging hydrogens are ignored. Only the P_z-orbital is seriously affected by apex deletion and has become extensively mixed with a P^π-orbital. We expect the

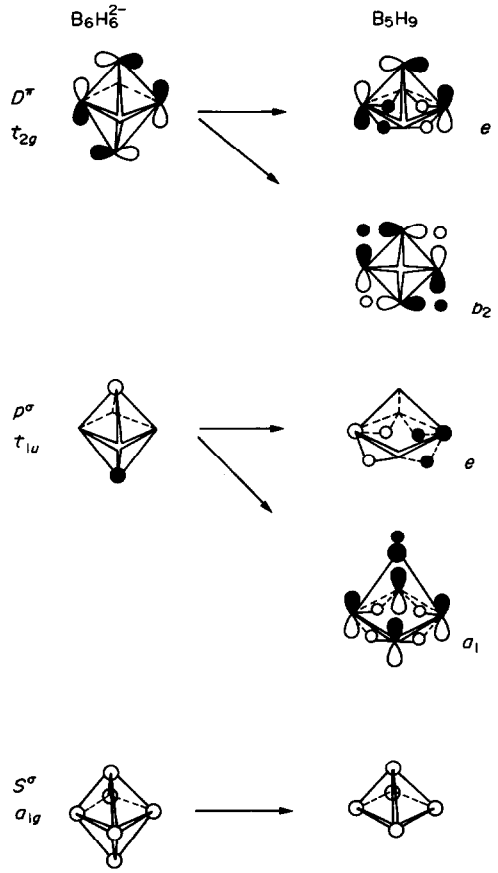


Fig. 4. Correlation of the cluster-bonding orbitals of $B_6H_6^{2-}$ and B_5H_9.

orbitals of $Fe_5(CO)_{15}C$ and $Fe_5(H)(CO)_{14}N$ to resemble these orbitals, together with a significant contribution from the basal carbon or nitrogen atom to the S^σ and P MOs.

A self-consistent charge calculation was performed on $Fe_5(CO)_{15}C$ in the C_s-symmetry shown in Fig. 5. This was necessary in order to simplify the assignment of the MOs. It is worth noting that the molecule has 97 occupied valence MOs: 15 Fe "lone pairs" which include any Fe → CO π^*-back-bonding, and 75 carbonyl orbitals (these can be subdivided into 15 5σ which include Fe ← CO σ-donation, 30 of type 1π, and 15 each from $4\sigma^*$ and 3σ), and the seven cluster orbitals. The calculation shows the 18 HOMOs to be 40–60% localized on the metal atoms, whilst only four lower-energy orbitals are more than 15% metal-localized (*vide infra*). The C_s-symmetry is only a small perturbation to the C_{4v} metal atom framework for these orbitals and the symmetries of the 18 orbitals are exactly those expected from the 15 lone-pair orbitals and the three D^π cluster orbitals. Figure 5 shows the energy spread of these orbitals. The non-degenerate orbitals are given their C_s labels (it is impossible in

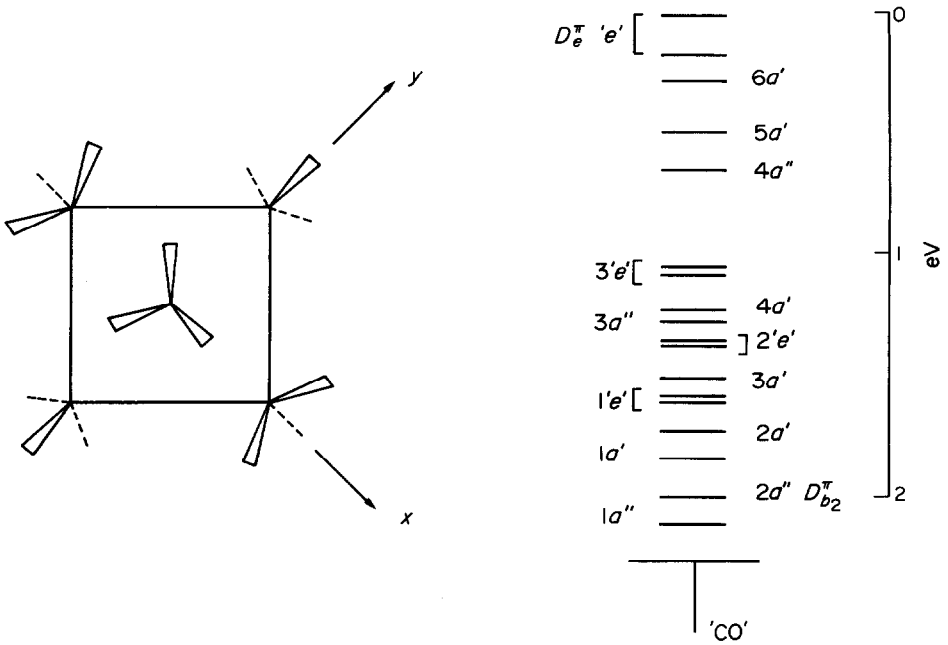


Fig. 5. Geometry of $Fe_5(CO)_{15}C$ used in calculation and the energy separations and assignments of the 18 HOMOs calculated.

a number of cases to identify their C_{4v} parentage) and the four C_{4v} degenerate pairs are labelled '*e*' (and transform as two *a'* in C_s) as these are least perturbed by the lower symmetry. Inspection of the composition allows the clear assignment of the cluster-bonding orbitals indicated in Fig. 5, and illustrated in Fig. 6. Comparison of the D_e^π and $D_{b_2}^\pi$ of Fig. 6 with those of B_5H_9 shows that the borane comparison is valid through to the composition of the orbitals. The D^π-orbitals have contributions from atoms not involved in the borane orbitals, arising from mixing with lone pairs of the same symmetry, particularly those perpendicular to the Fe–C direction. Such orbitals are labelled D^δ in Stone's description[3] and should be non-bonding. However the mixing has the effect of dèstabilizing the D_e^π pair, causing them to be the HOMOs of the molecule, and stabilizing the $D_{b_2}^\pi$ by antibonding and bonding interactions, respectively. The D^π labels are based on majority composition but are not unique. Clearly some lone-pair orbitals (particularly 3'*e'* and 4*a''*) have D^π character. Calculations on $Fe_5(CO)_{15}C$ in geometries closer to experimental enhance the mixing and it is impossible to assign even majority D^π or lone-pair character to individual orbitals.

Hoffmann[5] has reported an energy level diagram for "$[Ru_6(CO)_{18}]^{2-}$" and $[Ru_6(CO)_{16}C]^{2-}$ similar to Fig. 3, and determined using extended Hückel calculations. The orbitals corresponding to S^σ and *P* orbitals are not stabilized to anything like the extent that we find for $Fe_5(CO)_{15}C$. This is a consequence of the lack of charge-iteration in his calculation which we have previously shown[16] is necessary to account reasonably for metal–main-group atom interactions.

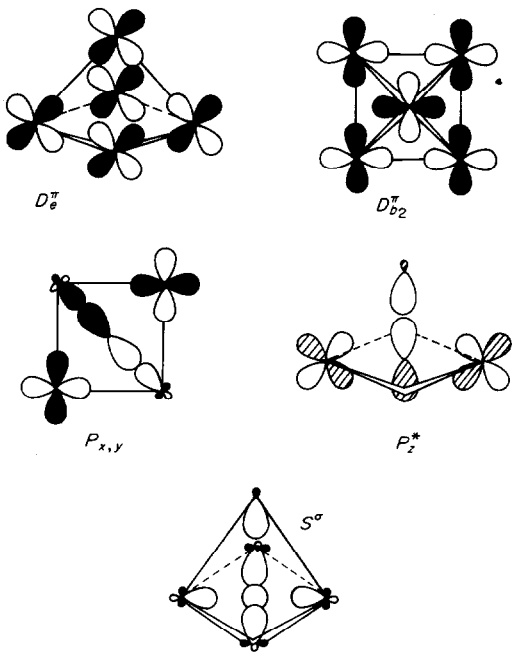


Fig. 6. Major components of the cluster-bonding orbitals of $Fe_5(CO)_{15}C$. * Represents a section through the *xz* plane; a similar contribution occurs in the *yz* plane (not shown).

Figure 7 shows a schematic of all the valence energy levels of $Fe_5(CO)_{15}C$ and $Fe_5(H)(CO)_{14}N$. The 18 orbitals discussed above are followed by three blocks of carbonyl orbitals as shown. The three P and the S^σ cluster orbitals are easily identified at 7 and 20 eV below the HOMOs as they have large contributions from the basal carbon atom (60%) and the metal atoms (25% $P_{x,y}$, and 30% P_z and S^σ), and are shown in Fig. 6. The comparison of these orbitals with the related MOs of B_5H_9 is remarkably good. The metal σ hybrids ($3d_{z^2}$, $4s$, $4p_z$) substitute for the boron $2s$ orbital and the component of $P_{x,y}$ from the bridging hydrogens of B_5H_9 is supplied by the basal metal atoms not directly interacting with the carbon $2p$ orbital. Again the P_z-orbital is the one least like its *closo* precursor and is mixed with a P^π-orbital on the basal metal atoms. The carbon $2s$ and $2p$ contributions to these four orbitals are exactly those expected from the discussion of Stone's theory above. These four orbitals are insensitive to changes of the geometry of the carbonyl ligands unlike the D^π-orbitals. Provided the square-based pyramidal geometry of the metal atoms is maintained the orbitals have the composition shown.

In a similar manner a calculation on $Fe_5(H)(CO)_{14}N$ in a geometry very close to the experimental one shows that the lower symmetry completely mixes the D^π and lone-pair orbitals so that no assignment can be made for the top 18 orbitals. The S^σ- and P-orbitals of the nitride are very similar to the carbide ones, only somewhat lower in energy. There appears to be nothing significant about the nature of the basal bridging carbonyls and hydrogen atom of this molecule. Their orbitals are calculated to be mixed with those of the terminal carbonyls, the hydrogen mainly in the (5σ, 1π) group.

Figure 8 shows the photoelectron spectrum of

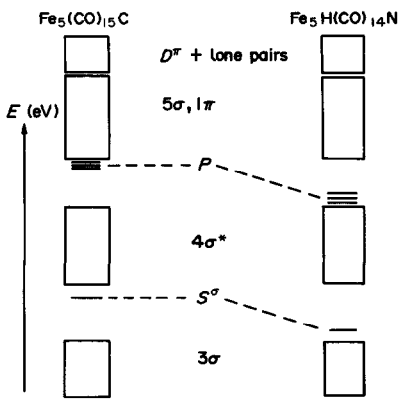


Fig. 7. Schematic of the valence orbitals of $Fe_5(CO)_{15}C$ and $Fe_5(H)(CO)_{14}N$.

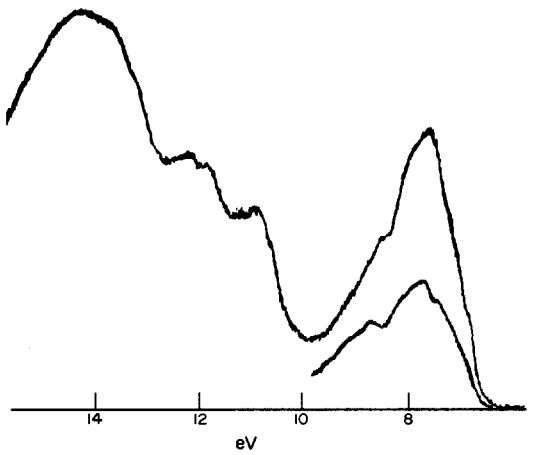


Fig. 8. He(I) photoelectron spectrum of $Fe_5(H)(CO)_{14}N$.

$Fe_5H(CO)_{14}N$. To the authors' knowledge no other molecule containing five metal atoms has been studied by gas-phase PES. The spectrum is remarkably structured for so large a molecule. The low-energy '$3d$' band (6.5–9.5 eV) has a width similar to that predicted by the calculation and is followed by a carbonyl band (10–15 eV) corresponding to the (5σ, 1π) group of MOs. No useful measurements could be made below 17 eV. There is clearly no possibility of identifying individual ionizations in the '$3d$' band. The structure observed in the 10–13-eV region of the carbonyl band is unusual, and could be related to the bridge-bonded carbonyl and hydrogen ligands. Ionizations due to MOs localized on bridging hydrogens have been observed at 12.5 eV[17] but apparently no spectra of molecules with symmetrically bridging carbonyls have been reported and assigned. The spectra of $Fe_2(CO)_6(C_4H_4)$ and $Fe_3(CO)_8(C_4H_4)$, which both contain semi-bridging carbonyls, have been reported.[18] These carbonyls are found to contribute to the HOMOs of the molecules, unlike the above, and also to a number of MOs in the -12 to -13 eV binding-energy region.

The calculations suggest that the D^π-orbitals are very sensitive to the carbonyl position. This is realized in practice as a considerable variety of carbonyl arrangements have been observed. This sensitivity is not surprising as the lone-pair orbitals formed from ($4p$, $3d$) hybridization of opposite phase to the π AOs of Fig. 1 are the ones most likely to provide d–π^* backbonding interaction. Provided the D^π-lone-pair mixing does not displace any D^π component to the virtual-orbital set then none of the cluster-bonding contributions from these orbitals is lost. The energy gap between occupied and virtual orbitals is small. The calculations

predict a HOMO–LUMO gap of 0.8 eV and the absorption spectra of $[Fe_6(CO)_{16}C]^{2-}$ and $Fe_5(CO)_{15}C$ both show electronic absorptions as low as 1 eV in energy. As the low-energy virtual orbitals are calculated to be largely metal-localized the loss of cluster bonding due to mixing of D^{π} with lone pairs is a distinct possibility.

Due to the experimental indistinguishability of D^{π} and lone-pair orbitals, the calculated sensitivity to carbonyl position, and the possibility of mixing with virtual lone-pair orbitals we are of the opinion that the D^{π}-orbitals are probably not very important in determining the strength of the overall cluster bonding. If the D^{π}-orbitals were critical to the structure of the clusters one might expect them to be far less sensitive to rearrangement of the carbonyl ligands than is indicated by the calculations. This observation is in accord with our recent work[13] on *closo*-six-apex borane and carborane clusters where we concluded that the D^{π}-orbitals are very weakly bonding but are important in defining the shape of the molecule, the stability being due essentially to the S^{σ}- and P-orbitals. The structure[20] of $[Co_6(CO)_{14}C]^-$ appears to support this opinion. The cluster has one Co—Co distance (2.96 Å) that is almost too long to be considered as bonding. The D^{π} interactions of this region of the cluster have clearly been disrupted yet the cluster retains a basically octahedral arrangement of metal atoms.

The interaction of S^{σ} and P metal orbitals with the interstitial atom is relevant to earlier work we reported on $Fe_5(CO)_{15}C$ and the related metalloboranes 1- and 2-$Fe(CO)_3B_4H_8$ and 1,2-$Fe_2(CO)_6B_3H_7$.[21] We observed that the radial hybrid ($4s$, $4p_z$, $3d_{z^2}$) metal lobes in the metalloborane molecules were shown to make little contribution to the cluster bonding, whereas they were important in the carbide cluster. The energy separation of this lobe from the boron $2s$ orbital is too large to allow an effective interaction and the metal component of cluster bonding is achieved almost entirely by the H-lobes. In $[Fe_2(CO)_6B_3H_7)]$ there are insufficient boron atoms to construct the S^{σ} and P MOs, and one of the P-orbitals is lost, presumably replaced by a metal–metal σ-bonding orbital constructed from the two metal σ-lobes. This would account for the orientation of the carbonyl ligands more towards the metal–metal axis than the cluster centre.

CONCLUSIONS

The following general statements can be made on the basis of the above discussions, even allowing for the approximate nature of the calculations employed.

(1) Stone's theory and terminology can be transferred from boranes to metal clusters, and underpins the "borane analogy" summarized by Wade's and Hoffmann and Mingos's description of the molecules considered.

(2) The group of metal-localized orbitals at the top of the orbital stack of a metal cluster will contain $4n+1$ orbitals [$3n$ lone pairs$+(n+1)$ cluster orbitals] or $4n-3$ orbitals if the cluster involves an interstitial atom. n is the number of apices of the related *closo*-borane geometry.

(3) Only in highly symmetric metal clusters, of which $Co_6(CO)_{14}^{4-}$ is the only obvious example, could cluster or lone-pair character be clearly distinguishable in this top group of MOs. It is therefore difficult to conceive of any experimental measurement on the valence orbitals to demonstrate the application of Stone's theory to these clusters.

(4) For clusters with an interstitial atom four cluster MOs are low in energy, one (S^{σ}) much lower than the other three (P). These MOs have a large contribution from the interstitial atom and are the major source of stability in such clusters.

(5) Clusters with interstitial atoms should be more likely to have chemistries based on retention of cluster geometry and should be more stable than related clusters without interstitial atoms. This applies equally to *closo*, *nido* or *arachno* systems, but may be more marked in the latter, e.g. there are no *arachno*-Fe_4 compounds known which do not have an interstitial atom.

As a final comment we note that there must be a minimum cluster size capable of accommodating an interstitial atom. Taking main-group atoms as interstitials, the p-orbitals of the atom will be clearly destabilized by too small a cluster, negating the stabilizing interaction discussed above. A *closo*-Fe_5 trigonal bipyramidal cluster would have an Fe—C distance of 147 pm, which is unreasonably small ($r_C = 77$ pm and $r_{Fe} = 112$ pm) whilst for the Fe_6 octahedron the distance is 187 pm {cf. Fe—C lengths in $[Fe_6(CO)_{16}C]^{2-}$ of 189 ± 8 pm}, very close to the optimum. The smallest metal clusters observed of *closo*, *nido* or *arachno* type, e.g. $[Fe_4(CO)_{12}C]^{2-}$, are all based on the octahedron.

REFERENCES

1. K. Wade, *Adv. Inorg. Chem. Radiochem.* 1976, **18**, 1.
2. M. Elian, M. M. L. Chen, D. M. P. Mingos and R. Hoffmann, *Inorg. Chem.* 1976, **15**, 1148.
3. A. J. Stone, *Mol. Phys.* 1980, **41**, 1339; *Inorg. Chem.* 1981, **20**, 563.
4. P. Brint, J. P. Cronin, E. Seward and T. Whelan, *J. Chem. Soc., Dalton Trans.* 1983, 975.

5. M. Tachikawa, R. L. Geerts and E. L. Muetterties, *J. Organomet. Chem.* 1981, **213**, 11.
6. M. Tackikawa, J. Stein, E. L. Muetterties, E. G. Teller, M. A. Beno, E. Gebert and J. M. Williams, *J. Am. Chem. Soc.* 1980, **108**, 6648.
7. B. R. Higginson, D. R. Lloyd, S. Evans and A. F. Orchard, *J. Chem. Soc., Faraday Trans.* II 1975, 1913.
8. J. Howell, A. Rossi, D. Wallace, K. Haraki and R. Hoffmann, *QCPE* 1977, **10**, 344.
9. E. H. Brage, L. F. Dahl, W. Hubel and D. L. Wampler, *J. Am. Chem. Soc.* 1962, **84**, 4633.
10. D. M. P. Mingos, *Adv. Organomet. Chem.* 1977, **15**, 1.
11. V. Albano, P. Chini and V. Scatturin, *J. Organomet. Chem.* 1968, **15**, 423; V. Albano, P. L. Bellon, P. Chini and V. Scatturin, *ibid.* 1969, **16**, 461.
12. D. M. P. Mingos, *J. Chem. Soc., Dalton Trans.* 1974, 133.
13. T. Whelan and P. Brint, *J. Chem. Soc., Faraday Trans.* II 1985, **81**, 267.
14. K. Wade and C. Housecroft, *Gazz. Chim. Ital.* 1980, **87**, 110.
15. S. D. Wijeyesekara and R. Hoffmann, *Organometallics* 1984, **3**, 949.
16. N. C. V. Costa, D. R. Lloyd, P. Brint, T. R. Spalding and W. K. Pelin, *J. Chem. Soc., Dalton Trans.* 1982, 201.
17. J. C. Green, D. M. P. Mingos and E. A. Seddon, *Inorg. Chem.* 1981, **20**, 2595; D. E. Sherwood and M. B. Hall, *Organometallics* 1982, **1**, 1519.
18. M. Casarin, D. Ajo, G. Granozzi, E. Tondello and S. Aime, *Inorg. Chem.* 1985, **24**, 1241.
19. J. C. Green, E. A. Seddon and D. M. P. Mingos, *J. Chem. Soc., Chem. Commun.* 1979, 94.
20. V. G. Albano, P. Chini, G. Ciana, M. Sansoni, D. Strunolo, B. T. Heaton and S. Martinengo, *J. Am. Chem. Soc.* 1976, **98**, 5027.
21. P. Brint, W. K. Pelin and T. R. Spalding, *J. Inorg. Nucl. Chem. Lett.* 1980, **16**, 391; P. Brint and T. R. Spalding, *J. Chem. Soc., Dalton Trans.* 1980, 391.

Polyhedron Vol. 5, No. 11, pp. 1799–1803, 1986
Printed in Great Britain

0277–5387/86 $3.00+.00
Pergamon Journals Ltd

PREPARATION, CHARACTERIZATION AND CRYSTAL STRUCTURE OF *N,N*-DIMETHYLANILINIUM β-OCTAMOLYBDATE DIHYDRATE

P. ROMÁN* and J. M. GUTIÉRREZ-ZORRILLA

Departamento de Química Inorgánica, Universidad del País Vasco, Apartado 644, 48080 Bilbao, Spain

and

M. MARTÍNEZ-RIPOLL and S. GARCÍA-BLANCO

Departamento de Cristalografía, Instituto Rocasolano, CSIC, Serrano 119, 28006 Madrid, Spain

(*Received* 25 *November* 1985; *accepted* 11 *March* 1986)

Abstract—*N,N*-dimethylanilinium β-octamolybdate dihydrate has been synthesized in acidic aqueous solution. The compound has been identified by using TG, DTG, IR and ^{1}H NMR techniques. It crystallizes in the triclinic system, space group $P\bar{1}$, $Z = 1$, $a = 11.755(3)$ Å, $b = 11.836(5)$ Å, $c = 10.498(2)$ Å, $\alpha = 105.29(2)°$, $\beta = 81.56(3)°$, $\gamma = 115.24(3)°$, $V = 1273.4(8)$ Å, $D_o = 2.23(1)$ Mg m^{-3}, $D_x = 2.23$ Mg m^{-3}, $R = 0.029$ and $R_w = 0.032$ for 5259 observed reflexions. Two crystallographically independent $[C_8H_{12}N]^+$ cations, one water molecule and one centrosymmetric β-octamolybdate polyanion are present in the asymmetric unit. Hydrogen bonds of types N—H···O and O—H···O seem to stabilize the structure.

In a previous paper[1] we reported the crystal structure of anilinium β-octamolybdate dihydrate. Anilinium and *N,N*-dimethylanilinium anhydrous salts were first described by Andreu.[2] The study of these compounds is part of a general investigation of anilinium, *N*-alkylanilinium and *N,N*-dialkylanilinium polymolybdates. Some of these salts may play an important role as possible catalysts in redox reactions, and also show photochemical properties.

EXPERIMENTAL

A suspension of MoO_3 (5.0 g) and distilled water (850 cm^3) was stirred and heated, and *N,N*-dimethylanilinium (5.0 cm^3) was added. After evaporating, the resulting slightly turbid solution (pH = 3.5) was cooled and filtered. Crystals of *N,N*-dimethylanilinium octamolybdate dihydrate (**I**) appeared in the solution. The light blue prismatic crystals were washed with ether, ethanol and water, and finally dried in air. They were found to be stable to air, light and X-ray exposure.

Compound **I** appeared to be a dihydrate: Found: Mo, 44.9; C, 22.5; H, 3.0; N, 3.3%; weight loss at 570°C, 32.6%; Calc. for $(C_8H_{12}N)_4Mo_8O_{26}\cdot 2H_2O$: Mo, 44.9; C, 22.5; H, 3.1; N, 3.3%; weight loss at 570°C, 32.6%.

Thermogravimetric analyses were performed on a Perkin–Elmer TGS-2 thermobalance at a heating rate of 5°C min^{-1} in a nitrogen stream under atmospheric pressure. The IR spectra were recorded in KBr pellets on a Beckman IR-4240 spectrophotometer (4000–250 cm^{-1}). ^{1}H NMR spectra were recorded in deuterated DMSO solution using TMS as the internal standard on a Perkin–Elmer R-12 B instrument (60 MHz).

Crystal data are shown in Table 1. Cell parameters were obtained by least-squares fit from 30 Bragg angles measured for both positive and nega-

* Author to whom correspondence should be addressed.

Table 1. Crystal data

Formula	$(C_8H_{12}N)_4[Mo_8O_{26}]\cdot 2H_2O$
M_r	1708.3
Space group	$P\bar{1}$
a (Å)	11.755(3)
b (Å)	11.836(5)
c (Å)	10.498(2)
α (°)	105.29(2)
β (°)	81.56(3)
γ (°)	115.24(3)
V (Å^3)	1273.4(8)
Z	1
D_o (Mg m^{-3})	2.23(1)
D_x (Mg m^{-3})	2.23
μ (cm^{-1})	19.5
Temperature (K)	295
Radiation	λ(Mo-K_α) = 0.71069 Å
Number of independent reflexions	7317
Number of observed reflexions	5259 for $I > 3\sigma(I)$
R and R_w	0.029 and 0.032

tive θ values. 7317 independent reflexions measured up to $\theta = 30°$ on a CAD4 diffractometer with Mo-K_α radiation. There was no absorption correction. 5259 reflexions with $I > 3\sigma(I)$ were considered as observed. Scattering factors for neutral atoms and anomalous dispersion effects for Mo are from *International Tables for X-ray Crystallography*.[3] The structure was refined by full-matrix least-squares analysis using unit weights (H atoms as isotropic fixed contributors). Difference syntheses confirmed the existence of H atoms attached to N and O atoms. The remaining H atoms of the *N,N*-dimethylanilinium cations were located at their expected positions (broad maxima in the $\Delta\rho$ maps). Final-discrepancy indices are given in Table 1.

Final atomic coordinates, isotropic or equivalent

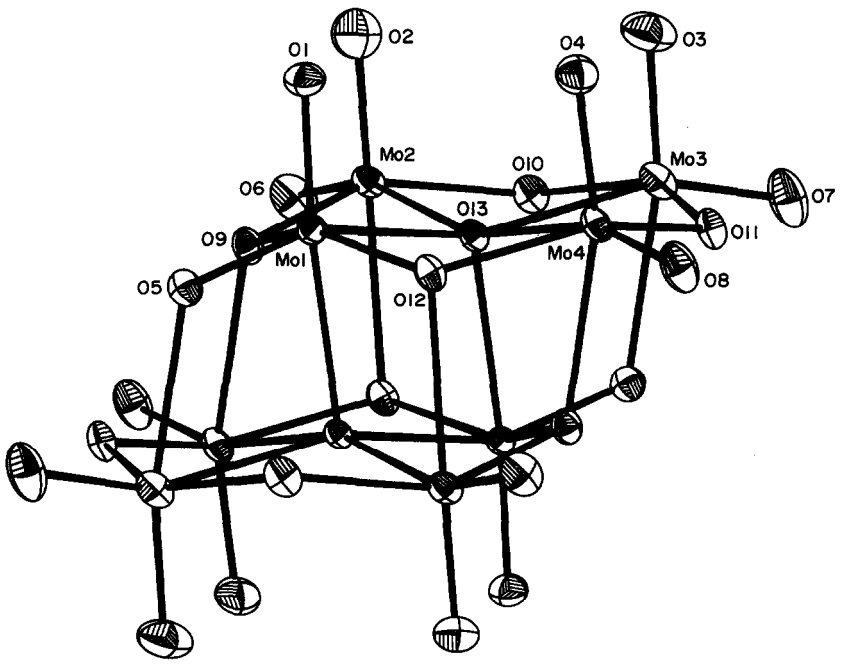


Fig. 1. β-Octamolybdate anion with atom labelling.

isotropic temperature factors, lists of F_o/F_c values, anisotropic thermal parameters for non-H atoms and hydrogen contacts have been deposited with the Editor as supplementary material.*

Most calculations were performed using the XRAY 76 system[4] running on a VAX 11/750 computer.

RESULTS AND DISCUSSION

The thermal decomposition of the compound shows its hydrated state. The two water molecules are lost in one step (70–130°C). There are seven stages in the total thermal decomposition, the final product being identified as MoO_3 by IR and its powder diffraction pattern. The formation of MoO_3 corresponds to the residue weight obtained in the chemical analysis.

N,N-dimethylanilinium octamolybdate dihydrate exhibits a very similar spectrum to anilinium β-octamolybdate dihydrate. Only small differences have been appreciated in the region of 2800 cm^{-1} due to the presence of the methyl groups linked to the N atom, and one band at 1450 cm^{-1} corresponding to C—H bending (methyl groups). The C—N stretching vibrations give two peaks at 1150 and 1200 cm^{-1}.

^1H NMR spectra show a multiplet between 6.3 and 7.2 ppm due to the aromatic protons. There is a signal at 2.8 ppm attributed to the methyl protons. A broad signal at 5.1 ppm is assigned to exchanging protons linked to the N atoms with the water protons.

The structure solution confirms that compound I contains discrete β-$Mo_8O_{26}^{4-}$ anions, $[C_8H_{12}N]^+$ cations and water molecules.

The β-octamolybdate polyanion is built up of eight distorted MoO_6 octahedra sharing edges and corners. A schematic drawing of the polyanion with atom labelling is shown in Fig. 1.

The Mo—O bond lengths within the MoO_6 octahedra are listed in Table 2 together with those from anilinium octamolybdate dihydrate and the idealized polyanion.

The O—O distances and O—Mo—O bond angles are displayed in Table 3. The degree of distortion of MoO_6 octahedra, estimated by eqns (1)–(3) are summarized in Table 3:

$$\Delta_1 = \frac{1}{6}\sum[(R_i - R)/R]^2, \quad (1)$$

Table 2. Mo—O bond lengths (Å) in compound I, anilinium octamolybdate dihydrate and the idealized polyanion

Bond	Compound I	Anilinium salt	Idealized polyanion[a]
Mo1—O1	1.700(3)	1.700(4)	1.70
Mo1—O5	1.760(3)	1.751(3)	1.75
Mo1—O9	1.977(4)	1.943(3)	1.95
Mo1—O12	1.961(3)	1.958(3)	1.95
Mo1—O13	2.135(3)	2.149(2)	2.15
Mo1—O13′	2.360(3)	2.398(3)	2.37
Mo2—O2	1.707(4)	1.710(4)	1.70
Mo2—O6	1.705(5)	1.718(3)	1.71
Mo2—O9	2.019(3)	1.986(2)	2.00
Mo2—O10	1.905(3)	1.890(3)	1.89
Mo3—O13	2.355(4)	2.317(3)	2.32
Mo3—O12′	2.345(3)	2.321(3)	2.34
Mo3—O3	1.703(4)	1.703(4)	1.70
Mo3—O7	1.710(4)	1.692(3)	1.70
Mo3—O10	1.932(4)	1.942(3)	1.93
Mo3—O11	1.928(4)	1.919(3)	1.93
Mo3—O13	2.471(3)	2.501(3)	2.48
Mo3—O5′	2.283(3)	2.322(4)	2.30
Mo4—O4	1.706(4)	1.712(4)	1.70
Mo4—O8	1.705(4)	1.713(3)	1.71
Mo4—O11	1.899(4)	1.872(3)	1.89
Mo4—O12	1.997(3)	2.004(3)	2.00
Mo4—O13	2.342(4)	2.299(3)	2.32
Mo4—O9′	2.420(3)	2.376(3)	2.34

[a] Idealized polyanion (2/*m* symmetry) obtained from octamolybdates with ESDs ⩽ 0.006 Å from Mo—O bond lengths: salts of ammonium,[5] melaminium,[6] di-μ-aqua-tetrakis[μ-(methanol)-(methanol) sodium],[7] 3-ethylpyridinium,[8] 4-ethylpyridinium,[9] 3-methylpyridinium,[10] pyridinium,[11] anilinium[1] and *N,N*,-dimethyl anilinium.

$$\Delta_e = \frac{1}{12}\sum[(D_i - D)/D]^2, \quad (2)$$

$$\Delta_\alpha = \frac{1}{3}\sum[(\alpha_i - 180)/180]^2, \quad (3)$$

where R_i = individual Mo—O distance, R = mean Mo—O distance, D_i = individual O—O distance, D = mean O—O distance, and α_i = individual O—Mo—O_{trans} angle.

Plotting Δ_α vs Δ_e we can obtain the linear-regression formula $\Delta_\alpha = 0.0035 + 0.833\Delta_e$ with a correlation coefficient (r) of 0.993. Mo2, Mo3 and Mo4 octahedra present a similar degree of distortion. The Mo1 octahedron is the least distorted because of its central position in the polyanion.

* Atomic coordinates have also been deposited with the Cambridge Crystallographic Data Centre.

Table 3. O—O distances (Å) and O—Mo—O bond angles (°) (octahedral distortion)

Mo1	O1	O5	O9	O12	O13	O13′
O1		104.7(2)	99.8(2)	101.6(2)	98.8(2)	174.4(2)
O5	2.740(4)		95.6(2)	96.8(2)	156.5(1)	80.8(2)
O9	2.818(6)	2.772(6)		151.6(1)	79.8(1)	79.2(2)
O12	2.843(5)	2.785(4)			78.7(2)	77.6(2)
O13	2.925(5)		2.639(4)	2.601(6)		75.7(2)
O13′		2.708(5)	2.781(4)	2.726(5)	2.765(4)	
Mo2	**O2**	**O6**	**O9**	**O10**	**O13**	**O12′**
O2		104.9(2)	96.5(2)	101.0(2)	93.8(2)	162.9(2)
O6	2.705(7)		100.0(2)	102.1(2)	160.1(2)	90.1(2)
O9	2.788(5)	2.860(6)		147.1(2)	73.8(1)	72.2(2)
O10	2.790(5)	2.810(5)			77.4(2)	83.6(2)
O13	2.999(5)		2.639(4)	2.687(6)		70.9(2)
O12′		2.902(5)	2.584(5)	2.853(4)	2.726(5)	
Mo3	**O3**	**O7**	**O10**	**O11**	**O13**	**O5′**
O3		104.8(2)	97.7(2)	98.2(2)	96.0(2)	165.3(2)
O7	2.703(7)		101.3(2)	104.3(2)	159.2(2)	89.9(2)
O10	2.742(6)	2.819(5)		145.1(2)	74.1(1)	78.1(2)
O11	2.750(6)	2.877(6)			73.6(1)	78.6(2)
O13	3.143(5)		2.687(6)	2.669(4)		69.3(2)
O5′		2.851(5)	2.670(5)	2.681(5)	2.708(5)	
Mo4	**O4**	**O8**	**O11**	**O12**	**O13**	**O9′**
O4		105.4(2)	102.9(2)	97.3(2)	94.9(2)	163.8(2)
O8	2.714(5)		100.8(2)	100.6(2)	159.5(2)	88.0(2)
O11	2.821(6)	2.778(7)		145.3(2)	77.2(2)	82.9(2)
O12	2.787(4)	2.855(4)			73.2(1)	70.9(2)
O13	3.012(6)		2.669(4)	2.601(6)		71.4(2)
.O9′		2.912(6)	2.885(4)	2.584(5)	2.781(5)	

Distortion	Mo1	Mo2	Mo3	Mo4
$\Delta_1 \times 10^4$	126	177	201	196
$\Delta_e \times 10^4$	9	16	22	19
$\Delta_\alpha \times 10^4$	140	182	206	194

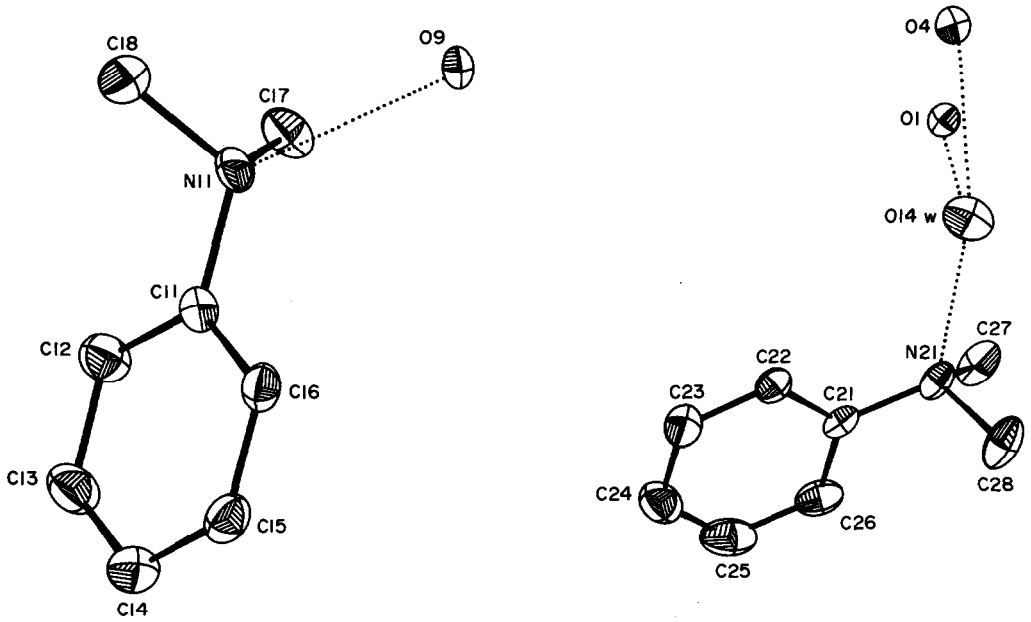


Fig. 2. *N,N*-dimethylanilinium cations showing hydrogen contacts.

Figure 2 shows a schematic drawing of the two independent cations of the structure as well as their proximity to several O atoms of the polyanions and water molecules together with the different hydrogen contacts within the structure. These can be classified in two types: N—H···O (2.97–3.27 Å) and O—H···O (2.68–3.11 Å).[12]

REFERENCES

1. P. Román, J. M. Gutiérrez-Zorrilla, C. Esteban-Calderón, M. Martínez-Ripoll and S. García-Blanco, *Polyhedron* 1985, **4**, 1043.
2. C. Andreu, Thesis, Universidad del País Vasco, Bilbao, Spain (1981).
3. *International Tables for X-ray Crystallography*, Vol. 4, pp. 72–98, and 149. Kynoch Press, Birmingham (1974).
4. J. M. Stewart, *The XRAY 76 System*. Computer Science Center, University of Maryland, College Park, Maryland (1976).
5. H. Vivier, J. Bernard and H. Djomaa, *Rev. Chim. Miner.* 1977, **14**, 584.
6. W. J. Kroenke, J. P. Fackler and A. M. Mazany, *Inorg. Chem.* 1983, **22**, 2412.
7. E. M. McCarron III and R. L. Harlow, *Acta Cryst.* 1984, **C40**, 1140.
8. P. Román, J. Jaud and J. Galy, *Z. Krist.* 1981, **154**, 59.
9. P. Román, M. Martínez-Ripoll and J. Jaud, *Z. Krist.* 1982, **158**, 141.
10. P. Román, M. E. González-Aguado, M. C. Esteban-Calderón, M. Martínez-Ripoll and S. García-Blanco, *Z. Krist.* 1983, **165**, 271.
11. M. C. Esteban-Calderón, M. Martínez-Ripoll, S. García-Blanco and P. Román, *An. Quím.* 1984, **B80**, 470.
12. I. Olovsson and P.-G. Jonsson, in *The Hydrogen Bond* (Edited by P. Schuster, G. Zundel and C. Sandorfy), Vol. 2, p. 395. North-Holland, Amsterdam (1976).

Polyhedron Vol. 5, No. 11, pp. 1805–1813, 1986
Printed in Great Britain

0277–5387/86 $3.00+.00
© 1986 Pergamon Journals Ltd

A NEW TREND IN THE SYNERGISTIC EXTRACTION OF RARE-EARTH(III) COMPLEXES WITH VARIOUS β-DIKETONES AND 1,10-PHENANTHROLINE

SHIGETO NAKAMURA and NOBUO SUZUKI*

Department of Chemistry, Faculty of Science, Tohoku University, Sendai 980, Japan

(*Received* 6 *January* 1986; *accepted* 11 *March* 1986)

Abstract—The synergistic extraction of rare-earth (RE) [La(III), Sm(III), Tb(III) and Lu(III)] complexes, with three β-diketones (HA) [hexafluoroacetylacetone (Hhfa), pivaloyltrifluoroacetone (Hpta) and benzoylacetone] in the presence of a bidentate ligand (S), 1,10-phenanthroline, in benzene was investigated. The general composition of the adducts formed is expressed as $RE(A)_3S$. $RE(A)_3(S)_2$ is also observed in La–Hhfa, La–Hpta and Sm–Hhfa systems. The adduct formation constants $\beta_{s,1}$ and $\beta_{s,2}$ and the synergistic extraction constants $K_{ex,s,1}$ were determined. The trend of these constants is discussed in terms of the RE(III), β-diketone, neutral bidentate ligand and organic solvent.

The well-known synergistic effect in solvent extraction involves the enhancement of the extraction of a metal ion with an acidic chelating agent by the addition of a neutral ligand. Many studies have been carried out on the synergistic extraction using a neutral unidentate ligand, such as tributylphosphate (tbp) or trioctylphosphine oxide (topo). Compared with those, the systematic study of the synergistic extraction system involving a neutral bidentate ligand is sparse. We have investigated the synergistic extraction of bivalent and tervalent metal ions with several β-diketones and different bidentate heterocyclic amines in nonpolar organic solvents.[1–5] In a previous paper, the synergistic extraction of several rare-earth ions [RE(III)] with various β-diketones and 2,2′-bipyridine (bpy) was carried out, and a remarkable enhancement by bpy was observed.[5] Further investigation of the synergistic extraction using other bidentate ligands seemed to be of much interest and necessary to make the specific enhancement more clear.

In the present paper, the synergistic extractions of several RE(III) complexes with hexafluoroacetylacetone (Hhfa), pivaloyltrifluoroacetone (Hpta) and benzoylacetone (Hba) in the presence of 1,10-phenanthroline (phen) in benzene were investigated. This system was expected to show a larger synergistic effect than the bpy system, by analogy with the investigation of Tm(III)–thenoyltrifluoroacetone (Htta)–phen, bpy.[3] The adduct formation constant and extraction constant were determined and discussed together with those in acetylacetone (Hacac)–phen systems.[2,4]

* Author to whom correspondence should be addressed.

EXPERIMENTAL

Materials and apparatus

Radioactive solutions of ^{140}La, ^{153}Sm, ^{160}Tb and ^{177}Lu were prepared as described previously.[4,5] Hhfa was distilled in the presence of P_4O_{10}. Reagent-grade Hba, Hpta and phen were used as obtained. Benzene was stirred with conc. sulfuric acid, washed with water and distilled after drying. Unless otherwise stated, reagents used were of guaranteed reagent grade. The γ-activity of each radioisotope was measured with an NaI(Tl) well-type scintillation detector.

Procedure

An aqueous solution (6 cm^3) containing 10^{-7}–10^{-5} M RE(III) labelled with its radioisotope was placed in a 30-cm^3 centrifuge tube with a ground-glass stopper. In the Hba systems, 2×10^{-3}–2×10^{-2} M sodium citrate was added to prevent hydrolysis. A benzene solution (6 cm^3) containing 10^{-4}–10^{-1} M β-diketone and 10^{-6}–10^{-3} M phen was added and shaken for 1–3 h at 25°C, then centrifuged. An aliquot was taken from each phase, the γ-activity

was measured, and the distribution ratio of the metal was calculated as the radioactivity ratio. The pH of the aqueous phase was adjusted with 5×10^{-3}–10^{-2} M piperazine-*N*,*N*′-bis(2-ethanesulfonic acid) and sodium hydroxide solution, and the equilibrium pH value was measured immediately after shaking. The ion strength was adjusted to 0.1 with sodium perchlorate.

Equilibrium equations

The distribution ratio (D_0) of a tervalent cation (M^{3+}) with a chelating extractant (HA) can be expressed as follows;

$$D_0=\frac{[\overline{MA_3}]}{[M^{3+}]+\sum[MA_n^{3-n}]}=\frac{P_{MA_3}\beta_3[A^-]^3}{1+\sum\beta_n[A^-]^n}, \quad (1)$$

where the bar denotes the organic phase, β_n the formation constant of MA_n^{3-n} in the aqueous phase, P_{MA_3} the partition coefficient of MA_3, and A^- the chelating anion in the aqueous phase. Often the extraction constant (K_{ex}) is given for the overall extraction reaction as:

$$M^{3+}+3\overline{HA}\rightleftharpoons\overline{MA_3}+3H^+,$$

$$K_{ex}=\frac{[\overline{MA_3}][H^+]^3}{[M^{3+}][\overline{HA}]^3}=\left(\frac{K_{HA}}{P_{HA}}\right)^3P_{MA_3}\beta_3, \quad (2)$$

where K_{HA} and P_{HA} denote the acid dissociation constant and the partition coefficient of HA, respectively. In the lower-concentration region for A^-, the intermediate chelates in the aqueous phase can be neglected in eqn (1), and D_0 is related simply to K_{ex} by the following equation:

$$D_0=K_{ex}\left(\frac{P_{HA}}{K_{HA}}\right)^3[A^-]^3. \quad (3)$$

In the synergistic extraction of M^{3+} with HA and a neutral ligand (S) the distribution ratio (D) can be expressed as follows:

$$D=\frac{[\overline{MA_3}]+\sum[\overline{MA_3S_m}]}{[M^{3+}]+\sum[MA_n^{3-n}]}$$

$$=\frac{P_{MA_3}\beta_3[A^-]^3(1+\sum\beta_{s,m}[\bar{S}]^m)}{1+\sum\beta_n[A^-]^n}, \quad (4)$$

where $\beta_{s,m}$ is the adduct formation constant in the organic phase corresponding to the following equilibrium:

$$\overline{MA_3}+m\bar{S}\rightleftharpoons\overline{MA_3S_m},$$

$$\beta_{s,m}=\frac{[\overline{MA_3S_m}]}{[\overline{MA_3}][\bar{S}]^m}. \quad (5)$$

From eqns (1) and (4), the following simple relationship is obtained:

$$D/D_0=1+\sum\beta_{s,m}[\bar{S}]^m. \quad (6)$$

If only MA_3S_m is the dominant species in the organic phase, D/D_0 depends on the mth power of $[\bar{S}]$. When the extraction is made from an aqueous phase containing an auxiliary complexing agent, e.g. the citrate ion in the extraction with Hba, we have to introduce an additional complex formation in eqns (1) and (4), but we finally arrive at the same equation.[5]

The synergistic extraction constant ($K_{ex,s,m}$) is defined by the following equilibrium:

$$M^{3-}+3\overline{HA}+m\bar{S}\rightleftharpoons\overline{MA_3S_m}+3H^+,$$

$$K_{ex,s,m}=\frac{[\overline{MA_3S_m}][H^+]^3}{[M^{3+}][\overline{HA}]^3[\bar{S}]^m}=\left(\frac{K_{HA}}{P_{HA}}\right)^3P_{MA_3}\beta_3\beta_{s,m}. \quad (7)$$

$K_{ex,s,m}$ can be calculated from the following relationship derived from eqns (2) and (7):

$$K_{ex,s,m}=K_{ex}\beta_{s,m}. \quad (8)$$

RESULTS AND DISCUSSION

Synergistic extraction with Hhfa and phen

The synergistic extraction of La(III) with various Hhfa concentrations and a constant phen concentration in benzene at a fixed pH was carried out, and plots of the logarithm of the distribution ratio against the logarithm of the hfa^- concentration are shown in Fig. 1. The equilibrium hfa^- concentration in the aqueous phase was calculated as follows:

$$[A^-]=\frac{C_{HA}}{(P_{HA}+1)[H^+]/K_{HA}+1}, \quad (9)$$

where C_{HA} denotes the initial Hhfa concentration. The literature values of K_{HA} and P_{HA} were adopted, i.e. $\log K_{HA}=-4.46$ and $\log P_{HA}=-1.91$.[6] A large synergistic enhancement can be observed by comparing the plots of $\log D_0$ in the absence of phen in Fig. 1. The plots for the synergistic extraction system give a straight line with a slope of 3.0. Therefore, it is proved that three molecules of hfa^- participate in the synergistic extraction of La(III).

Plots of $\log D/D_0$ against $\log[\bar{S}]$ in the synergistic extraction of La(III), Sm(III) and Lu(III) with Hhfa and various phen concentrations are shown in Fig. 2. The equilibrium phen concentration in the organic phase was calculated from the following

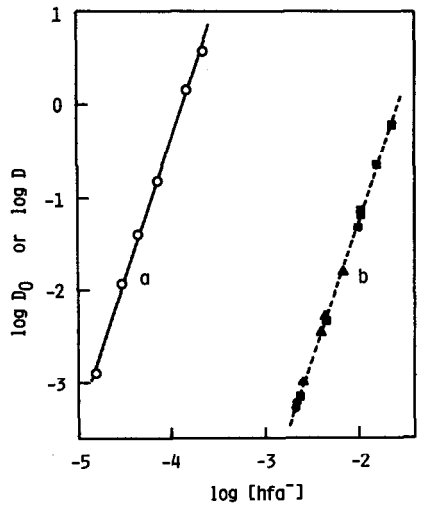


Fig. 1. Distribution ratio of La(III) as a function of hfa^- concentration in the presence and absence of phen in benzene. (a) 2.46×10^{-4} M phen, pH 3.38. (b) Without phen: (■) 10^{-1} M Hhfa, (▲) 3×10^{-2} M Hhfa, and (●) 10^{-2} M Hhfa.[5]

equation:

$$[\bar{S}] = \frac{C_S}{1+(1+[H^+]/K_{HS})/P_S}, \qquad (10)$$

where C_S denotes the initial phen concentration.

The acid dissociation constant of protonated phen (K_{HA}) and the partition coefficient of phen (P_S) were determined photometrically,[2] i.e. $\log K_{HS} = -5.04$ and $\log P_S = 0.78$. The values of D_0 were calculated from eqn (3) using K_{ex} summarized in Table 1. The plots for Lu(III) in Fig. 2 give a straight line with a slope of 1.0, and this shows, from eqn (6), that the chelate : phen mole ratio of the adduct is 1 : 1, and no evidence for the formation of a higher adduct, such as $Lu(hfa)_3(phen)_2$, is observed. The plots for La(III), however, give a straight line with a slope of 2.0, which suggests that a 1 : 2 adduct between the chelate and phen forms in this concentration range for phen. In most synergistic extraction studies of RE(III) with β-diketone and a neutral unidentate ligand, such as the RE(III)–Htta–tbp system,[7] and the La(III), Eu(III), Tb(III), Lu(III)–benzoyltrifluoroacetone (Hbfa)–topo, tbp, hexanol system,[8,9] the dominant species involves three molecules of β-diketone ligand and two molecules of neutral ligand, and the coordination number of the central metal of the adduct seems to be eight, which is confirmed by an X-ray crystallographic study of a similar adduct, $Nd(tta)_3(tppo)_2$ (tppo is triphenylphosphine oxide).[10] If phen acts as a bidentate ligand, the preferential formation of the adduct

Table 1. Extraction constants (K_{ex}) in RE(III)–HA–benzene systems, and adduct formation constants ($\beta_{s,m}$) and synergistic extraction constants ($K_{ex,s,1}$) in RE(III)–HA–phen–benzene systems

HA	RE(III)	Log K_{ex}	Log $\beta_{s,1}$	Log $\beta_{s,2}$[a]	Log $K_{ex,s,1}$
Hhfa	La	−2.91[b]	(9.03)[c]	15.92	(6.12)
	Sm	−1.66[b]	9.76	13.37	8.10
	Lu	−1.20[b]	10.60	—	9.40
Hpta	La	−12.65[b]	8.87	13.06	−3.78
	Sm	−10.06[b]	9.83	—	−0.23
	Lu	−8.39[b]	9.82	—	1.43
Hba	La		7.53	—	
	Sm		7.65	—	
	Tb		7.58	—	
	Lu		6.53	—	
Hacac	La	−20.12[d]	6.76[e]	—	−13.36
	Nd	−18.38[d]	6.84[e]	—	−11.54
	Sm	−17.80[d]	6.86[e]	—	−10.94
	Tb	−16.42[d]	6.63[e]	—	−9.79
	Tm	−15.20[d]	5.84[e]	—	−9.36
	Lu	−14.50[d]	5.27[e]	—	−9.23

[a] A dash denotes that no observation of the adduct formation of $RE(A)_3(phen)_2$ was obtained under the given experimental conditions.

[b] From our previous work.[5]

[c] Calculated from eqn (11).

[d] K_{ex} for Hacac are evaluated from eqn (2) (see text).

[e] From our previous work.[4]

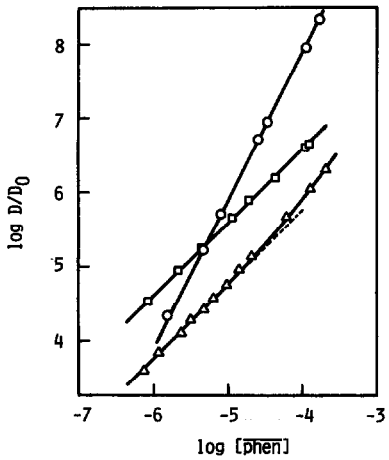


Fig. 2. Effect of phen concentration in benzene on the synergistic extraction of RE(III) with Hhfa ($[Hhfa]_{init} = 10^{-3}$ M): (○) La, pH 3.3; (△) Sm, pH 3.5; and (□) Lu, pH 3.3.

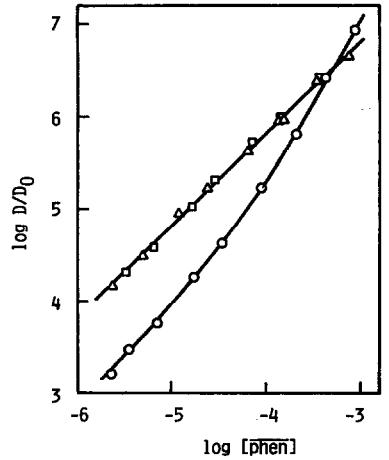


Fig. 3. Effect of phen concentration in benzene on the synergistic extraction of RE(III) with Hpta ($[Hpta]_{init} = 10^{-3}$ M): (○) La, pH 5.4; (△) Sm, pH 4.5; and (□) Lu, pH 4.1.

involving three β-diketone ligands and one phen ligand is understandable. In fact, the same type of adduct was observed in the synergistic extraction of RE(III) with β-diketone and a bidentate ligand, e.g. $RE(acac)_3phen$ (RE = La, Nd, Sm, Tb, Tm or Lu[2,4]) and $Tm(tta)_3S$ (S = phen, bpy or 2,9-dimethyl-1,10-phenanthroline[3]). In the synergistic extraction of La(III) with Hhfa and bpy, however, the possibility of the formation of a higher adduct, such as $La(hfa)_3(bpy)_2$, was also pointed out.[5] The plots for the present La(III)–Hhfa–phen system clearly give a straight line with a slope of 2.0. This is a very interesting result and a typical example of a higher adduct involving an acidic chelating agent and a bidentate ligand, such as $La(hfa)_3(S)_2$, though the coordination stereochemistry cannot be clear.

In Fig. 2, the plots for Sm(III) in the lower-concentration range for phen give a straight line with a slope of 1.0, but those in the higher-concentration range for phen deviate positively from the straight line. This suggests that, in the lower-concentration range for phen, the 1 : 1 adduct between the metal chelate and phen is predominantly formed, and in the higher-concentration range for phen a mixture of the 1 : 1 adduct and a higher adduct (possibly a 1 : 2 adduct) are present. The adduct formation constants, $\beta_{s,1}$ for $RE(hfa)_3phen$ and $\beta_{s,2}$ for $RE(hfa)_3(phen)_2$, are calculated from eqn (6) by the least-squares method and listed in Table 1.

Synergistic extraction with Hpta and phen

The synergistic extraction of La(III), Sm(III) and Lu(III) with Hpta and phen in benzene was carried out and the plots of $\log D/D_0$ against $\log [\overline{phen}]$ are shown in Fig. 3. The values of D_0 were calculated from eqn (3) using K_{ex} values in Table 1, and the quoted values of p_{HA} and K_{HA}, i.e. $\log P_{HA} = 2.15$ and $\log K_{HA} = -7.01$.[6] The plots for Sm(III) and Lu(III) give straight lines with a slope of 1.0, which suggests that a single adduct, $RE(pta)_3phen$, is formed. For La(III), however, the plots give curved lines having two asymptotes with a slope of 1.0 in the lower-concentration region for phen and a slope of 2.0 in the higher-concentration region for phen, corresponding to the formation of $La(pta)_3phen$ and $La(pta)_3(phen)_2$. The adduct formation constant $\beta_{s,1}$ and $\beta_{s,2}$ are listed in Table 1.

Synergistic extraction with Hba and phen

The extraction of La(III), Sm(III), Tb(III) and Lu(III) with Hba in the presence and absence of phen in benzene was carried out, and the plots of $\log D/D_0$ against $\log [\overline{phen}]$ are shown in Fig. 4. These plots for each RE(III) give a straight line with a slope of 1.0, which suggests that only one adduct, $RE(ba)_3phen$, is formed. The adduct formation constants are listed in Table 1.

Comparison of the adduct formation constants

Adduct formation constants involving neutral bidentate ligands are very large, e.g. $\beta_{s,1}$ for Hpta and Hhfa is about 10^9–10^{11}, and $\beta_{s,2}$ for La(III)–Hhfa reaches 10^{16}. Few synergistic extractions with a chelating extractant and a neutral ligand, in which the adduct formation constant exceeds 10^{15}, have been reported.[9,11,12] The $\beta_{s,1}$ and $\beta_{s,2}$ for phen are

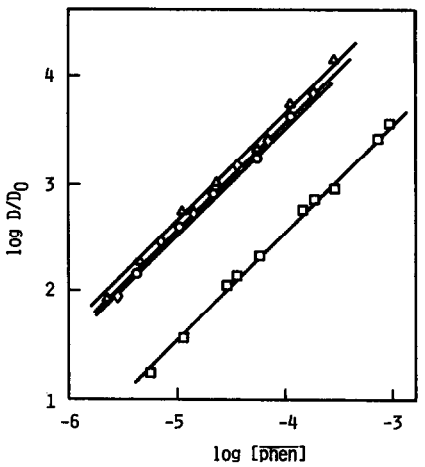


Fig. 4. Effect of phen concentration in benzene on the synergistic extraction of RE(III) with Hba in the presence of citrate: (○) La, 2.7×10^{-2} M Hba, 2×10^{-3} M citrate, pH 9.3; (△) Sm, 2.7×10^{-2} M Hba, 2×10^{-3} M citrate, pH 8.7; (◇) Tb, 2×10^{-2} M Hba, 1×10^{-2} M citrate, pH 8.9; and (□) Lu, 2×10^{-2} M Hba, 2×10^{-2} M citrate, pH 8.9.

larger than those for bpy.[5] In Fig. 5, $\log\beta_{s,1}$ for phen is plotted against $\log\beta_{s,1}$ for bpy in corresponding combinations of RE(III) and β-diketones, together with those in the Hacac systems.[4] These plots indicate a good linear relationship and give a straight line with a slope of 1.02. This relationship can be approximated by the following equation:

$$\log\beta_{s,1}(\text{phen}) = \log\beta_{s,1}(\text{bpy}) + 3.42(\pm0.08). \quad (11)$$

The above relationship may be interpreted as follows. The thermodynamic adduct formation constant ($\beta^o_{s,1}$) can be related to the apparent one ($\beta^x_{s,1}$) by introducing the activity coefficient (γ) of the solute in the organic phase, in terms of the mole fraction scale:

$$\beta^o_{s,1} = \beta^x_{s,1}\frac{\gamma_{MA_3S}}{\gamma_{MA_3}\gamma_S}, \quad (12)$$

where the subscripts MA_3S, MA_3 and S denote adduct, chelate and neutral ligand, respectively. Further, $\beta^o_{s,1}$ can be related to the standard chemical potential (μ^o) of the solute in its pure liquid state:

$$-2.303RT\log\beta^o_{s,1} = \mu^o_{MA_3S} - \mu^o_{MA_3} - \mu^o_S. \quad (13)$$

From eqns (12) and (13), $\beta^x_{s,1}$ can be written as follows:

$$\log\beta^x_{s,1} = -(\mu^o_{MA_3S} - \mu^o_{MA_3} - \mu^o_S)/2.303RT - (\log\gamma_{MA_3S} - \log\gamma_{MA_3} - \log\gamma_S). \quad (14)$$

Here, the adduct formation constant on the mole fraction scale is connected with that on the molar-concentration scale under the assumption that the concentration of each solute is low enough:

$$\beta^x_{s,1} = \beta_{s,1}\frac{1000}{V_o}, \quad (15)$$

where V_o denotes the molar volume of the solvent. Then, from eqns (14) and (15), $\beta_{s,1}$ for phen can be related to that for bpy by the following equation:

$$\log\beta_{s,1}(\text{phen}) = \log\beta_{s,1}(\text{bpy}) + A + B, \quad (16)$$

where:

$$A = (\mu^o_{MA_3bpy} - \mu^o_{MA_3phen})/2.303RT + (\log\gamma_{MA_3bpy} - \log\gamma_{MA_3phen}), \quad (17)$$

$$B = (\mu^o_{phen} - \mu^o_{bpy})/2.303RT + (\log\gamma_{phen} - \log\gamma_{bpy}). \quad (18)$$

From a simple comparison of eqns (11) and (16) we can get the relationship:

$$A + B = 3.42. \quad (19)$$

Here B, as shown in eqn (18), is constant for a given organic solvent and not dependent on the adduct, but substantially A takes different values with different adducts in the same organic solvent. The constant value (3.42) for $A+B$ for two adducts in a given organic solvent suggests that the value of A is negligibly small compared with B or practically constant for these adducts. In eqn (17) the chemical potential of the adducts is not known, but the chemical-potential term of A may take a constant value, and the activity coefficients of the adducts with phen and bpy may be nearly equal, considering that both adducts involve three molecules of the same β-diketone and one molecule of heterocyclic amine with a similar structure.

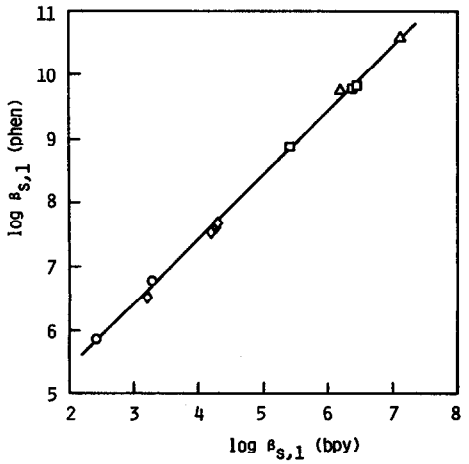


Fig. 5. Correlation of $\log\beta_{s,1}$ between phen and bpy systems: (△) Hhfa, (□) Hpta, (◇) Hba, and (○) Hacac.

The activity of a nonelectrolyte solute (a_c) in an organic solvent can be expressed, based on the regular solution theory,[13] as:

$$\ln a_c = \ln X_c + \frac{V_c}{RT}\phi_o^2(\delta_c - \delta_o)^2, \quad (20)$$

where X, ϕ and δ denote the mole fraction, the volume fraction and the solubility parameter, respectively, and the subscripts c and o the solute and the organic solvent, respectively. When the concentration of solute is very low, ϕ_o is approximately unity. Accordingly, the activity coefficient can be written as follows:

$$\log \gamma_c = \frac{V_c}{2.303RT}(\delta_c - \delta_o)^2. \quad (21)$$

Therefore, the following equation can be obtained:

$$\log \gamma_{MA_3bpy} - \log \gamma_{MA_3phen} = \frac{V_{MA_3bpy}}{2.303RT}(\delta_{MA_3bpy} - \delta_o)^2 - \frac{V_{MA_3phen}}{2.303RT}(\delta_{MA_3phen} - \delta_o)^2. \quad (22)$$

It seems that the value for this equation varies with different solvents. However, in the limiting case, in which V_{MA_3bpy} and δ_{MA_3bpy} are assumed to be equal to V_{MA_3phen} and δ_{MA_3phen}, respectively, the value of eqn (22) is zero. The molar volume of the bpy adduct is close to that of the phen adduct, because the molar volumes of bpy and phen are close to each other (134 cm^3 mol^{-1} for bpy and 142 cm^3 mol^{-1} for phen).[14] The solubility parameters of the phen and bpy adducts may be approximated to each other, considering the similarity in the intermolecular force of the phen adduct and the bpy adduct; hence, the value of eqn (22) will be negligibly small. This means that A takes a constant value governed only by μ^o, and $A+B$ takes a constant value.

The same relationship for eqns (16) and (19) seems to hold good in the Tm(III)–Htta–phen, bpy–benzene system, that is $\log \beta_{s,1} = 9.93$ (phen) and 6.58 (bpy), a difference of 3.35 (close to 3.42), but in another solvent system [Tm(III)–Htta–phen, bpy–cyclohexane] $\log \beta_{s,1} = 11.76$ (phen) and 7.57 (bpy), a difference of 4.19.[3] To understand the solvent effect in eqn (16), the activity coefficient terms in eqns (17) and (18) must be discussed, but, as discussed above, practically the activity coefficient term in eqn (18) is highly dependent on the nature of the solvent. We tried to estimate the activity coefficient of a neutral bidentate ligand in the organic solvent as follows. The partition coefficient of a solute expressed on the mole fraction scale (P_c^x) is related to the activity coefficient of the solute in the organic phase (γ_c) and in the aqueous phase ($\gamma_{c,a}$):

$$P_c^x = \frac{X_c}{X_{c,a}} = \frac{\gamma_{c,a}}{\gamma_c}. \quad (23)$$

From eqns (18) and (23) the following equation is derived:

$$B = (\mu^o_{phen} - \mu^o_{bpy})/2.303RT + (\log \gamma_{phen,a} - \log \gamma_{bpy,a}) + (\log P^x_{bpy} - \log P^x_{phen}). \quad (24)$$

The chemical-potential term is a constant and the activity coefficient terms in the aqueous phase ($\gamma_{phen,a}$ and $\gamma_{bpy,a}$) are also constant; hence, we can derive the same type of equation as eqn (16), including an overall constant (c):

$$\log \beta_{s,1}(phen) = \log \beta_{s,1}(bpy) + (\log P^x_{bpy} - \log P^x_{phen}) + C, \quad (25)$$

where:

$$C = (\mu^o_{MA_3bpy} - \mu^o_{MA_3phen})/2.303RT + (\mu^o_{phen} - \mu^o_{bpy})/2.303RT + (\log \gamma_{phen,a} - \log \gamma_{bpy,a}) = 2.15. \quad (26)$$

The constant C can be simply estimated as 2.15 by subtracting the value of $\log P^x_{bpy} - \log P^x_{phen}$ for benzene, which is determined experimentally,[3] from the constant value of 3.42 in eqn (11). This relationship is expected to apply in many other organic solvent systems which have no specific solute–solvent interaction. That is, the phen adduct formation constant in any organic solvent can be predicted from the bpy adduct formation constant by eqn (25). For example, in a cyclohexane solvent system, eqn (25) can be rewritten as follows by knowing $\log P_{bpy}$ and $\log P_{phen}$:[3]

$$\log \beta_{s,1}(phen) = \log \beta_{s,1}(bpy) + 4.26. \quad (27)$$

The experimental value of $\beta_{s,1}$ in the Tm(III)–Htta–bpy–cyclohexane system is 7.57;[3] hence, $\beta_{s,1}$ for the Tm(III)–Htta–phen–cyclohexane system is calculated as 11.83, which is in good agreement with the experimental value of 11.76.[3]

The value of $\beta_{s,1}$ for phen in the La(III)–Hhfa–benzene system could not be obtained under the present experimental conditions. $\beta_{s,1}$ is estimated from eqn (11) using the experimental $\beta_{s,1}$ for bpy, i.e. $\log \beta_{s,1}(bpy) = 5.61$;[5] hence, $\log \beta_{s,1}$ for phen is calculated as 9.03 (Table 1). The proportion of $La(hfa)_3phen$ to $La(hfa)_3(phen)_2$ in the organic phase can be calculated by using $\beta_{s,1}$ and $\beta_{s,2}$ as

only 10%, even at a concentration of 10^{-6} M phen, which is why $\beta_{s,1}$ cannot be determined experimentally by the present extraction technique.

The logarithmic values of $\beta_{s,1}$ are plotted in order of RE(III) atomic number in Fig. 6. A similar tendency is also observed in the bpy systems.[5] The values of $\beta_{s,1}$ for a given RE with different β-diketones increase in the order Hacac < Hba < Hpta $\leqslant$ Hhfa. This is in accord with the order of K_{HA}, i.e. $10^{-8.88}$ (Hacac)[15] < $10^{-8.39}$ (Hba) < $10^{-7.01}$ (Hpta) < $10^{-4.46}$ (Hhfa),[6] and may be the reverse of the chelate formation constants of RE(III) with these β-diketones, which is also observed in the synergistic extraction system involving a unidentate neutral ligand.[9] As to the central metal, in the Hacac and Hba systems, $\beta_{s,1}$ trends to decrease with increasing RE atomic number, and this tendency has been observed in most of the synergistic extraction studies using a unidentate neutral ligand; e.g. $\beta_{s,2}$ in the RE(III)–Htta–tbp and RE(III)–Hbfa–topo systems.[7-9] On the other hand, in Hpta and Hhfa systems, $\beta_{s,1}$ tends to increase with increasing RE(III) atomic number. How this characteristic trend is governed by the chelating agents is not yet known. This trend cannot be completely elucidated, but seems to be simply explained as follows. A stronger coordination of a chelating ligand ($acac^-$ or ba^-) to the central metal ions, in accordance with a larger chelate formation constant for RE(III) of higher atomic number, accompanies a lesser ability to accept a further addition of a neutral bidentate ligand for a RE(III) chelate of higher atomic number. On the other hand, the RE(III) chelate with hfa^-, with a very weak coordination ability considering the quite large acid dissociation constant of Hhfa, has a residual ability to accept

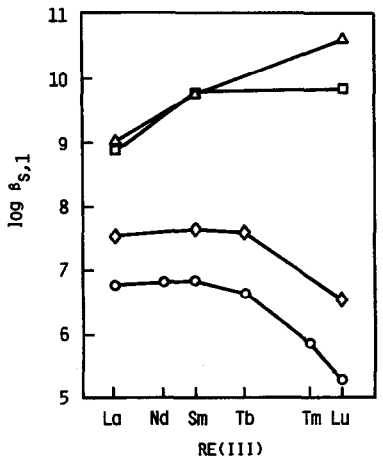


Fig. 6. Plots of adduct formation constants in RE(III)–HA–phen–benzene systems in order of RE atomic number: (△) Hhfa, (□) Hpta, (◇) Hba, and (○) Hacac.

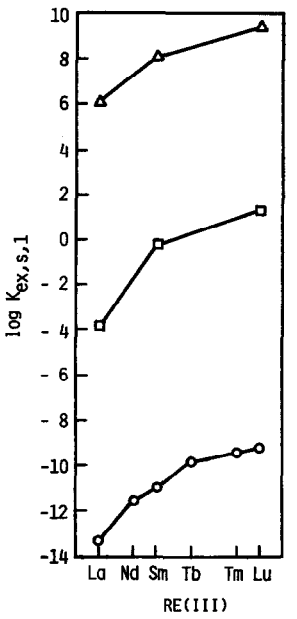


Fig. 7. Plots of synergistic extraction constants in RE–HA–phen systems in order of RE atomic number: (○) Hacac, (□) Hpta, and (△) Hhfa.

further coordination of the quite strong base of a neutral bidentate ligand. The difference between $\log\beta_{s,1}$ for Lu(III) and that for La(III) [$\Delta\log\beta_{s,1}$(Lu–La)] varies with different β-diketones, and its order of magnitude is -1.49 (Hacac) < -1.00 (Hba) < 0.95 (Hpta) < 1.57 (Hhfa), which accords with the order of the acid dissociation constant of β-diketones.

A secondary adduct containing two molecules of phen, $RE(A)_3(phen)_2$, is observed in limited extraction systems such as the La(III)–Hhfa, Sm(III)–Hhfa and La(III)–Hpta systems. $\beta_{s,2}$ for La(III)–Hhfa is larger than that for La(III)–Hpta, but secondary-adduct formation for Sm(III) is observed only in the system involving Hhfa. The secondary adduct seems to be formed in the system involving β-diketones with a larger acid dissociation constant. The successive adduct formation constant ($K_{s,2}$) of $RE(A)_3(phen)_2$ is calculated from the ratio $\beta_{s,2}/\beta_{s,1}$. Log $K_{s,2}$ is 6.89 for $La(hfa)_3(phen)_2$, 3.61 for $Sm(hfa)_3(phen)_2$ and 4.19 for $La(pta)_3(phen)_2$. $K_{s,2}$ is much influenced by the central metal of the adduct, and tends to be smaller the larger the RE atomic number.

Comparison of the synergistic extraction constants

The synergistic extraction constant ($K_{ex,s}$) is often used as a simple measure of the extractability of a metal ion in a synergistic extraction. $K_{ex,s,1}$ calculated from eqn (8) are listed in Table 1 and plotted in order of RE(III) atomic number in Fig.

Table 2. Differences in the logarithmic values of the extraction constants, adduct formation constants and synergistic extraction constants between Lu(III) and La(III) systems

HA	$\Delta \log K_{ex}$(Lu–La)	$\Delta \log \beta_{s,1}$(Lu–La)	$\Delta \log K_{ex,s,1}$(Lu–La)
Hhfa	1.71	1.57	3.28
Hpta	4.26	0.95	5.21
Hacac	5.62	−1.49	4.13

7. For this calculation, K_{ex} in the Hhfa and Hpta systems were the experimental values[5] and K_{ex} in the Hacac system was estimated from eqn (2) using P_{MA_3}[16] and the quoted values of P_{HA}, K_{HA} and β_3: $\log P_{MA_3} = -2.17$ (La), -2.12 (Nd), -1.89 (Sm), -1.60 (Tb), -0.63 (Tm), and -0.32 (Lu);[16] $\log P_{HA} = 0.74$;[17] $\log \beta_3 = 10.91$ (La), 12.60 (Nd), 12.95 (Sm), 14.04 (Tb), 14.29 (Tm), and 14.68 (Lu).[18] The $K_{ex,s,1}$ values for a given metal are in the order Hacac < Hpta < Hhfa. This is understandable as the result of the similar increasing trend of both K_{ex} and $\beta_{s,1}$: Hacac < Hpta < Hhfa. $K_{ex,s,1}$ for each β-diketone increases with increasing RE atomic number. This is a result of the increase in both K_{ex} and $\beta_{s,1}$ in the same way in the Hhfa and Hpta systems. In the Hacac systems, the tendency of $\beta_{s,1}$ reverses, but K_{ex} is quite large, to fully compensate for a small reverse change in $\beta_{s,1}$. Here, the difference between $\log K_{ex,s,1}$ for Lu(III) and that for La(III) can be calculated:

$$\Delta \log K_{ex,s,1}(\text{Lu–La}) = \log K_{ex,s,1}(\text{Lu}) - \log K_{ex,s,1}(\text{La}) = \Delta \log K_{ex}(\text{Lu–La}) + \Delta \log \beta_{s,1}(\text{Lu–La}), \quad (28)$$

where:

$$\Delta \log K_{ex}(\text{Lu–La}) = \log K_{ex}(\text{Lu}) - \log K_{ex}(\text{La}). \quad (29)$$

$\Delta \log K_{ex}$ and $\Delta \log K_{ex,s,1}$ are sometimes taken as the separation factors of two metal ions in an extraction with an acidic chelating agent and a synergistic extraction, respectively. The calculated values of $\Delta \log K_{ex,s,1}$(Lu–La) are listed in Table 2, together with $\Delta \log K_{ex}$(Lu–La) and $\Delta \log \beta_{s,1}$(Lu–La). In the Hacac system, $\Delta \log K_{ex,s,1}$(Lu–La) is smaller than $\Delta \log K_{ex}$(Lu–La), but in the Hpta and Hhfa systems, $\Delta \log K_{ex,s,1}$(Lu–La) are larger than $\Delta \log K_{ex}$(Lu–La). It has been generally believed that synergistic extraction makes the separation of metals worse, compared with extraction with a chelating ligand only. In the Hpta and Hhfa systems involving the bidentate neutral ligand phen, however, the separation factor can be improved by synergistic extraction. This suggests a further possibility of synergism in separation science. $\Delta \log K_{ex,s,1}$ as the sum of $\Delta \log K_{ex}$(Lu–La) and $\Delta \log \beta_{s,1}$(Lu–La) are in the order Hhfa < Hacac < Hpta. This order does not agree with either that of $\Delta \log K_{ex}$(Lu–La) or $\Delta \log \beta_{s,1}$(Lu–La), because the order of $\Delta \log K_{ex}$(Lu–La) is the reverse of that of $\Delta \log \beta_{s,1}$(Lu–La). This means that the theoretical prediction of a synergistic extraction involving an acidic chelating agent and a neutral bidentate ligand is not so easy, and further systematic investigation is required.

Acknowledgement—We thank Dr H. Imura for his encouraging interest and many discussions.

REFERENCES

1 S. Nakamura, H. Imura and N. Suzuki, *J. Radioanal. Nucl. Chem.* 1984, **82**, 33.
2. S. Nakamura, H. Imura and N. Suzuki, *Inorg. Chim. Acta* 1985, **109**, 157.
3. S. Nakamura, H. Imura and N. Suzuki, *Inorg. Chim. Acta* 1985, **110**, 101.
4. S. Nakamura and N. Suzuki, *J. Radioanal. Nucl. Chem.* 1986, **99**, 145.
5. S. Nakamura and N. Suzuki, *Inorg. Chim. Acta* 1986, **114**, 101.
6. T. Sekine, Y. Hasegawa and N. Ihara, *J. Inorg. Nucl. Chem.* 1973, **35**, 3968.
7. L. Farbu, J. Alstad and J. H. Augustson, *J. Inorg. Nucl. Chem.* 1974, **36**, 2091.
8. T. Shigematsu, M. Tabushi, M. Matsui and T. Honjyo, *Bull. Chem. Soc. Jpn* 1967, **40**, 2807.
9. Y. Marcus and A. S. Kertes, *Ion Exchange and Solvent Extraction of Metal Complexes*, p. 815. Wiley Interscience, London (1969).
10. J. G. Leipoldt, L. D. C. Bok, S. E. Laubscher and S. S. Basson, *J. Inorg. Nucl. Chem.* 1975, **37**, 2477.
11. J. Stary and H. Frieser, *Equilibrium Constants of Liquid–Liquid Distribution Reactions, Part 4: Chelating Extractants*. Pergamon Press, Oxford (1978).
12. N. Suzuki, K. Saitoh and H. Watarai, *Solvent Extraction Database, Proceedings of Symposium on Solvent Extraction (Japan)*, 1982, p. 85. Japanese Association of Solvent Extraction; N. Suzuki, K. Saitoh and H. Watarai, *Japan Analyst* 1984, **33**, T52.
13. J. H. Hildebrand and R. L. Scott, *Solubility of Non-electrolytes*. Dover Publications, New York (1964).

14. O. Enea, C. Jolicoeur and L. G. Hepler, *Can. J. Chem.* 1980, **58**, 704.
15. S. Oki, *Bull. Chem. Soc. Jpn* 1965, **38**, 522.
16. N. Suzuki and S. Nakamura, *Inorg. Chim. Acta* 1985, **110**, 243.
17. T. Wakahayashi, S. Oki, T. Omori and N. Suzuki, *J. Inorg. Nucl. Chem.* 1964, **26**, 2255.
18. I. Grenthe and W. C. Fernelius, *J. Am. Chem. Soc.* 1960, **82**, 6258.

Polyhedron Vol. 5, No. 11, pp. 1815–1819, 1986
Printed in Great Britain

0277–5387/86 $3.00+ .00
Pergamon Journals Ltd

FIVE- AND SIX-COORDINATED TRANSITION-METAL MIXED-ANION COMPOUNDS CONTAINING THE STERICALLY CONSTRAINED PYRAZOLE-CONTAINING LIGAND 1,6-BIS(3′,5′-DIMETHYLPYRAZOL-1′-YL)-2,5-DIMETHYL-2,5-DIAZAHEXANE

FRANS PAAP, WILLEM L. DRIESSEN* and JAN REEDIJK

Gorlaeus Laboratories, Department of Chemistry, State University of Leiden, P.O. Box 9502, 2300 RA Leiden, The Netherlands

(*Received* 5 *February* 1986; *accepted* 11 *March* 1986)

Abstract—The dimethylpyrazole derivative of *N*,*N*′-dimethylethylenediamine, viz. 1,6-bis(3′,5′-dimethylpyrazol-1′-yl)-2,5-diazahexane (debd), forms coordination compounds with the transition-metal ions Co(II), Ni(II), Cu(II) and Zn(II) in the presence of a halide and a perchlorate anion of stoichiometry $[M(debd)X(H_2O)_n]ClO_4$ ($n = 0$ or 1). The ligand is always tetradentate. With cobalt and nickel six-coordinate compounds are formed. With copper and zinc five-coordinate compounds are formed. The compounds have been characterized by spectroscopic and magnetic methods (IR, ligand field, ESR and NMR).

Currently, much attention is given to the coordinating behaviour of pyrazole-containing ligands,[1–3] especially in relation to modelling active sites of metalloenzymes.[4–6] To obtain a better understanding of the coordinating possibilities of this type of ligand, we recently reported about a series of metal complexes with the ligand 1,6-bis (3′,5′ - dimethylpyrazol - 1′ - yl) - 2,5 - dimethyl - 2,5 - diazahexane (debd) (Fig. 1).[7] With transition-metal ions in combination with the anions NCS^- and N_3^-, six-coordinated metal compounds of formula $M(debd)X_2$ were formed with the anions in the *cis*-position. With the larger anions Cl^- and Br^- only compounds with the relatively large metal ions Mn^{2+} and Cd^{2+} could be isolated, which most likely originates from steric effects.[7,8]

When using this type of compound as metalloenzyme models, there should be the possibility of coordinating and binding reversibly small ligands, in addition to the larger debd ligand. We therefore extended the earlier investigation of the $[M(debd)]^{2+}$ unit, and tried to coordinate Cl^- and Br^- to other metals than Mn^{2+} and Cd^{2+}, with the aim of obtaining a better insight into the restrictions

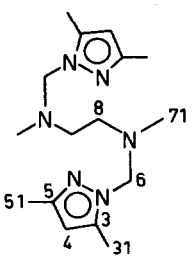


Fig. 1. Schematic drawing of the ligand debd, indicating the numbering used.

of the debd ligand. This paper describes the synthesis and characterization of such compounds: Cu^{2+} and Zn^{2+} yield five-coordinated compounds with only one bound Cl^- and Br^-, whereas Ni^{2+} and Co^{2+} yield six-coordinated compounds, in which water occurs as an additional ligand. Such a water ligand also occurs in the enzymes carboxypeptidase[9] and alcohol dehydrogenase.[10]

EXPERIMENTAL

Starting materials

Commercially available solvents and hydrated metal salts were used. The ligand debd was syn-

* Author to whom correspondence should be addressed.

thesized as described[7,11] by the condensation of *N*-hydroxymethyl-3,5-dimethylpyrazole and the amine *N,N'*-dimethylethylenediamine (Janssen Chimica) using acetonitrile as the solvent. The ligand was obtained as a yellow oil. The purity was checked by NMR. The ligand was used without further purification.

Synthesis of the complexes

The compounds $[MCl(debd)(H_2O)]ClO_4$ (M = Ni or Co) and $[CuX(debd)]ClO_4$ (X = Cl or Br) were synthesized by adding a hot solution of 5 mmol of debd in 15 cm^3 ethanol to a solution of the appropriate metal halide (2.5 mmol) and the appropriate metal perchlorate (2.5 mmol) in 15 cm^3 of hot ethanol. The compounds separated from the solution as microcrystalline material (Ni or Co compounds) or powders (Cu compounds) upon standing. The compounds $[ZnX(debd)]ClO_4$ (X = Cl or Br) were prepared by adding a hot solution of 6 mmol of debd in 15 cm^3 methanol to a hot solution of 3 mmol of $Zn(ClO_4)_2$ and 3 mmol of the appropriate zinc halide in 15 cm^3 of methanol. The compounds crystallized from the solution upon standing. Cu-doped zinc compounds were prepared by adding a small amount of copper salt to the solution of the zinc salts.

CAUTION: perchlorate salts may yield explosive mixtures. Although no accidents concerning perchlorates occurred during this research, perchlorates should only be prepared in small amounts and be handled with adequate care.[12]

Spectroscopic methods

IR spectra (4000–180 cm^{-1}) were recorded on a Perkin–Elmer PE580 instrument, using KBr pellets and Nujol mulls between NaCl discs or polyethene discs (low frequencies).

Electronic spectra were measured on a Perkin–Elmer UV330 instrument, operating in the diffuse-reflectance mode with MgO as a reference. ESR spectra were measured in a Varian E-3 EPR spectrometer, using a 9.5-GHz microwave bridge. The solid, powdered samples were measured at ambient temperature and at 77 K; methanolic solutions were measured as frozen glasses at 77 K.

All NMR spectra were measured in deuterated dmso solutions. Proton NMR spectra were recorded on a JEOL LNM PS100 instrument, operating at 99.5 MHz, externally locked and using TMS as an internal reference. ^{13}C NMR spectra were recorded on a JEOL JEC 980B instrument, operating at 50.1 MHz, using ^2H as an internal lock and dmso as an internal reference (39.500 ppm downfield from TMS).

X-ray powder diffraction patterns were obtained using a Guinier-type camera.

Elemental analyses were performed at the microanalytical laboratory of the University College, Dublin, Republic of Ireland.

Conductivities were measured of 10^{-3} M solutions in CH_3NO_2, using a Seibold LTB conductor.

RESULTS AND DISCUSSION

The compounds, obtained from the reaction between the debd ligand and a 1 : 1 mixture of MCl_2 and $M(ClO_4)_2$ (M = Ni or Co), can be formulated as $[MCl(debd)(H_2O)]ClO_4$. Their IR spectra are practically identical, as well as their X-ray powder diffraction patterns, indicating a very similar structure for both compounds. Their IR spectra are, except for the perchlorate vibrations, remarkably similar to the spectra of the $M(debd)X_2$ compounds,[7] indicating a similar *cis*-symmetrical configuration for the coordinated debd ligand. The electronic spectra show typical octahedral features (see Tables 1 and 4) with ligand field parameters in agreement with an $N_4(Cl)O$ chromophore.[13] The strong, sharp ν(O—H) near 3500 cm^{-1} in the IR spectra strongly suggests the coordination of a water molecule to the metal.[14,15] Vibrations at 222 cm^{-1} (Co) and 238 cm^{-1} (Ni), assigned to the ν(M—Cl) indicate terminal metal–halogen bonds.[16] The magnetic susceptibility, measured down to 4 K (Table 2), shows only a very small temperature dependence, probably originating from zero-field effects. Dimeric structures would be expected to show much stronger effects.[17,18] Even though these data in itself cannot exclude the presence of halogen-bridged dimeric structures, they strongly support the assignment of a monomeric structure to the compounds. The combination of data leads to the conclusion that these compounds have a monomeric, *cis*-octahedral structure with both a water molecule and a chloride ion coordinated to the metal, in addition to the tetradentate debd ligand.

The compounds $[CuCl(debd)]ClO_4$ and $[CuBr(debd)]ClO_4$ should have mutually very similar structures, as can be concluded from their almost identical IR spectra and X-ray powder diffraction patterns. Their conductance values in solution agree with 1 : 1 electrolytes[19] (see Table 1), suggesting the coordination of the halogen anion, and not the perchlorate anion, to the metal ion, as is also seen from the sharp Cl—O vibrations in the IR spectrum. The elemental analysis does not suggest the presence of water, nor is there any indication of coordinated

Table 1. Colours, IR and X-ray types, melting points, molar conductivities and elemental analyses of the debd compounds

Compound	Colour	IR type	X-ray type	Melting point (°C)	Molar conductivity (S mol^{-1} cm^2)
[Co(debd)Cl(H_2O)]ClO_4	Red	I	A	231	
[Ni(debd)Cl(H_2O)]ClO_4	Blue	I	A	283	
[Cu(debd)Cl]ClO_4	Blue	II	B	205	84
[Cu(debd)Br]ClO_4	Green	II	B	201	102
[Zn(debd)Cl]ClO_4	White	III	C	203	88
[Zn(debd)Br]ClO_4	White	III	C	198	86

Elemental analysis found (calc.) (%) for

[Co(debd)Cl(H_2O)]ClO_4: C, 37.4 (37.2); H, 5.9 (5.9); N, 15.7 (16.3); Cl, 13.7 (13.7)
[Cu(debd)Cl]ClO_4: C, 37.9 (38.2); H, 5.9 (5.6); N, 16.6 (16.7); Cl, 14.1 (14.1)
[Zn(debd)Cl]ClO_4: C, 38.0 (38.1); H, 5.7 (5.6); N, 16.9 (16.6); Cl, 13.8 (14.0)

Table 2. Magnetic-susceptibility data of the cobalt and nickel debd compounds

Compound	μ_{10} (BM)	μ_{300} (BM)	θ_{4-80} (K)
[Co(debd)Cl(H_2O)]ClO_4	4.06	4.40	−3 (±1)
[Ni(debd)Cl(H_2O)]ClO_4	3.42	3.09	0.5 (±1)

Table 3. Some IR data of the debd compounds

Compound	ν(M—X) (cm^{-1})	ν(O—H)$_{H_2O}$ (cm^{-1})
[Co(debd)Cl(H_2O)]ClO_4	222	3500
[Ni(debd)Cl(H_2O)]ClO_4	238	3510
[Cu(debd)Cl]ClO_4	298	
[Cu(debd)Br]ClO_4	248	
[Zn(debd)Cl]ClO_4	331	
[Zn(debd)Br]ClO_4	252	

water in the IR spectra. The values for the ν(Cu—X) vibrations (see Table 3) also suggest a five-coordinated structure rather than a six-coordinated structure.[14,16,20] The ESR and ligand field data (Tables 4 and 5) are in agreement with a square pyramidal five-coordinated structure.[21,22] When the steric constraints of the ligand and the known structure of the Cu(debd)$(NCS)_2$ compound[23] are considered, the four nitrogen ligands probably form the basis of the pyramid, with the halide ion on top.

The compounds [ZnCl(debd)]ClO_4 and [ZnBr(debd)]ClO_4 are mutually isostructural, which can be concluded from the similarity of IR spectra and X-ray powder diffraction patterns. Their NMR [^{1}H and ^{13}C (see Table 6)] spectra are also remarkably similar, confirming the structural similarity of the compounds. The elemental analysis does not suggest the presence of water, nor do the ^{1}H NMR spectra show any resonances due to water. The conductivity data suggest 1 : 1 electrolytes[19] (see Table 1), indicating the coordination of the halide anion. These data suggest a five-coordinated structure for the zinc compounds also. The ESR spectrum of the Cu-doped [ZnBr(debd)]ClO_4 compound is of the 'reversed' type,[22,24] indicating a d_{z^2} ground state, and suggesting a trigonal bipyrimidal structure for the zinc compounds. The sterical constraints of the debd ligand, in combination with the simple NMR spectra, suggest a structure similar to the structure of the six-coordinated compounds M(debd)X_2,[7] with the halide occupying one equatorial coordination site.

Concluding remarks

The steric constraints of the debd ligand greatly influence its coordination possibilities. Octahedral, six-coordinated compounds are formed only with a limited combination of metals and anions.[7] The adaptability of the Cu(II) ion allows relief of the steric interaction by elongation of the Cu—N(pyrazole) bonds[23] in the compound Cu(debd)$(NCS)_2$. This flexibility also allows the formation of the described five-coordinated copper compounds. With zinc similar five-coordinated compounds are also formed. With cobalt and nickel, chloride and water are coordinated to the [M(debd)]$^{2+}$ moiety. The bromide analogues could not be isolated, which can be explained by the steric requirements of the ligand (bromide being larger than chloride).

Table 4. Ligand field data of the debd compounds

Compound	σ_1 ($\times 10^3$ cm^{-1})	σ_2 ($\times 10^3$ cm^{-1})	σ_3 ($\times 10^3$ cm^{-1})
[Co(debd)Cl(H_2O)]ClO_4	8.66		19.0
[Ni(debd)Cl(H_2O)]ClO_4	9.50	15.6	25.8
[Cu(debd)Cl]ClO_4	14.1		
[Cu(debd)Br]ClO_4	14.0		

Table 5. ESR data of the debd compounds

	Solid (77 K and room temperature)		MeOH solution (77 K)	
Compound	$g_\perp$	$g_\parallel$ [$A_\parallel$ (G)]	$g_\perp$	$g_\parallel$ [$A_\parallel$ (G)]
[Cu(debd)Cl]ClO_4	2.08		2.06	2.25 (161)
[Cu(debd)Br]ClO_4	2.06	2.16	2.06	2.26 (160)
[Zn(debd)Br]ClO_4 (Cu-doped)	2.00	2.18 (90)		

Table 6. NMR data of the zinc debd compounds[a]

	[Zn(debd)Cl]ClO_4		[Zn(debd)Br]ClO_4		Free ligand	
Proton, carbon	$\delta(^{13}C)$	$\delta(^1H)$	$\delta(^{13}C)$	$\delta(^1H)$	$\delta(^{13}C)$	$\delta(^1H)$
3	141.4		141.5		139.4	
4	107.3	6.11	107.4	6.14	105.1	5.81
5	148.9		148.9	4.77	145.7	
6	67.2	4.75	67.1	2.30	68.7	4.64
8	48.9	2.29	49.1	2.32	51.7	2.59
71	39.3	2.32	39.4	2.30	39.6	2.21
51	13.3	2.29	13.3	2.19	13.4	2.25
31	10.2	2.18	10.2		10.8	2.15

[a] δ in ppm relative to TMS. For ligand numbering, see Fig. 1.

REFERENCES

1. F. B. Hulsbergen, W. L. Driessen, J. Reedijk and G. C. Verschoor, *Inorg. Chim. Acta* 1984, **23**, 3588.
2. J. W. F. M. Schoonhoven, W. L. Driessen, J. Reedijk and G. C. Verschoor, *J. Chem. Soc., Dalton Trans.* 1984, 1053.
3. F. Mani and C. Mealli, *Inorg. Chim. Acta* 1982, **63**, 97.
4. T. N. Sorrell, M. R. Malachowski and D. L. Jameson, *Inorg. Chem.* 1982, **21**, 3250.
5. J. S. Thompson, *J. Am. Chem. Soc.* 1984, **106**, 4057.
6. C. Benelli, I. Bertini, M. Di Vaira and F. Mani, *Inorg. Chem.* 1984, **23**, 1422.
7. F. Paap, W. L. Driessen, J. Reedijk, B. Kojić-Prodić and A. L. Spek, *Inorg. Chim. Acta* 1985, **104**, 55.
8. F. Paap, A. Erdonmez, W. L. Driessen and J. Reedijk, *Acta Cryst.* 1986, **C42**, 783.
9. K. D. Hardman and W. N. Libscomb, *J. Am. Chem. Soc.* 1984, **106**, 463.
10. I. Bertini, M. Gerber, G. Lanini, C. Luchinat, W. Mazet, S. Rawes and M. Zeppezauer, *J. Am. Chem. Soc.* 1984, **106**, 1826.
11. W. L. Driessen, *Recl Trav. Chim. Pays-Bas* 1982, **101**, 441.
12. W. C. Wolsey, *J. Chem. Educ.* 1978, **50**, A355.
13. A. B. P. Lever, *Inorganic Electronic Spectroscopy*, 2nd Edn. Elsevier, Amsterdam (1984).
14. K. Nakamoto, *Infrared and Raman Spectra of Inorganic and Coordination Compounds*, 3rd Edn. Wiley, New York (1978).
15. N. M. Karayannis, C. M. Mikulski, S. D. Sonsino, E. E. Bradshaw and L. L. Pytlewski, *Inorg. Chim. Acta* 1975, **14**, 195.
16. R. J. H. Clark and C. S. Williams, *Inorg. Chem.* 1965, **4**, 350.

17. E. J. Laskowski, R. Felthouse, D. N. Hendrickson and G. J. Long, *Inorg. Chem.* 1976, **15**, 2908.
18. A. P. Ginsburg, R. L. Martin, R. W. Brooks and R. C. Sherwood, *Inorg. Chem.* 1972, **11**, 2884.
19. W. J. Geary, *Coord. Chem. Rev.* 1971, **7**, 81.
20. R. J. H. Clark and C. S. Williams, *Spectrochim. Acta* 1966, **22**, 1081.
21. H. M. J. Hendriks, Thesis, Leiden (1981).
22. B. J. Hathaway and D. E. Billing, *Coord. Chem. Rev.* 1970, **5**, 143.
23. F. Paap, W. L. Driessen, J. Reedijk, M. Dartmann and B. Krebs, *Inorg. Chem.* (in press).
24. C. Goldstein, *Inorg. Chem.* 1984, **23**, 4387.

Polyhedron Vol. 5, No. 11, pp. 1821–1827, 1986
Printed in Great Britain

0277–5387/86 $3.00+.00
Pergamon Journals Ltd

SYNTHESIS AND MOLECULAR STRUCTURE OF THE POLAR, BINUCLEAR COMPLEX, MONOCHLOROTETRA-(6-FLUORO-2-OXOPYRIDINE)DIRUTHENIUM(II,III)

AKHIL R. CHAKRAVARTY, F. ALBERT COTTON* and WILLI SCHWOTZER

Department of Chemistry and Laboratory for Molecular Structure and Bonding, Texas A&M University, College Station, TX 77843, U.S.A.

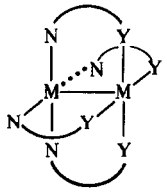
(*Received* 10 *January* 1985; *accepted* 11 *March* 1986)

Abstract—The dark purple title compound was prepared by reaction of $Ru_2Cl(O_2CCH_3)_4$ with molten 6-fluoro-2-hydroxypyrine (Hfhp) in quantitative yield. Crystals of composition $Ru_2Cl(fhp)_4$ were obtained by slow diffusion of hexane into a CH_2Cl_2 solution of the compound. The crystals belong to the tetragonal space group *I4mm* with the following unit-cell dimensions: $a = b = 10.890(2)$ Å, $c = 13.178(4)$ Å, $\alpha = \beta = \gamma = 90.0°$, $V = 1562.8(6)$ Å^3, and $Z = 2$. The $Ru_2Cl(fhp)_4$ molecule, which has crystallographic *4mm* (C_{4v}) symmetry, contains a diruthenium(II,III) unit with a metal–metal bond order of 2.5. The four bridging fhp ligands across the Ru_2 unit are oriented in one direction to form a polar molecule. The coordination spheres of the two ruthenium atoms [Ru(1) and Ru(2)] are $Ru(2)N(1)_4$ and $Ru(1)Cl(1)O(1)_4$, respectively. The axial site on Ru(1) is blocked by four F(1) atoms. The Ru(1)—Ru(2), Ru(2)—Cl(1), Ru(2)—O(1) and Ru(1)—N(1) distances are 2.284(1), 2.427(3), 1.971(2) and 2.089(4) Å, respectively. The electronic spectrum of the compound in CH_2Cl_2 shows two strong bands at 522 nm ($\varepsilon = 4720$ M^{-1} cm^{-1}) and 355 nm ($\varepsilon = 3770$ M^{-1} cm^{-1}). Cyclic voltammetry of $Ru_2Cl(fhp)_4$ in CH_2Cl_2 in the presence of 0.1 M $[N(C_2H_5)_4]ClO_4$ at 100 mV s^{-1} shows two quasireversible metal-centered one-electron oxidation and reduction processes at +1.68 V ($\Delta E_p = 120$ mV) and −0.01 V ($\Delta E_p = 126$ mV), respectively, vs an Ag–AgCl reference electrode.

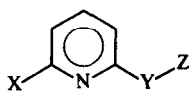
Recent work from this laboratory has shown[1–7] that the formation of a new class of metal–metal multiple bonded complexes of type $M_2(NY)_4$ (**1**), where NY is ligand **2** bridging across the pair of metal atoms, is governed by the presence of a strong axial coordination as well as the bulk of X and Z on the bridging ligand. The discovery of compounds having a polar arrangement of ligands was first reported[1] in 1983 from our laboratory. It was found[1,2] that in $M_2(fhp)_4L$ (M = Cr, Mo, W or Rh; L = THF or Me_2SO) the four bridging fhp ligands are oriented in the same direction. The axial coordination is on to the metal which is bonded to four O atoms. This unprecedented sort of arrangement was surprising because earlier structural studies had shown that a 2:2 (or, rarely, a 3:1) arrangement of ligands occurs in chp and mhp complexes.[7–11]

Subsequent reports[3–6] from this laboratory on

* Author to whom correspondence should be addressed.



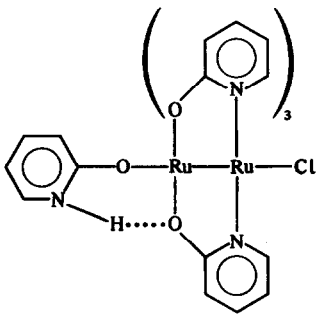
1



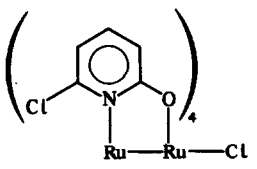
2

X	Y	Z	
H	NH	Ph	PhNHpy
H	O	H	Hhp
F	O	H	Hfhp
Cl	O	H	Hchp
Me	O	H	Hmhp

the diruthenium(II,III) complexes have shown that Hhp, PhNHpy and Hchp ligands also form complexes $Ru_2Cl(hp)_4(Hhp)$ (**3**), $Ru_2Cl(PhNpy)_4$ and $Ru_2Cl(chp)_4$ (**4**) having a polar arrangement of bridging ligands. Our attempts to prepare a polar $Ru_2Cl(mhp)_4$ were unsuccessful, although we were able to prepare a new mixed-ligand complex, $Ru_2Cl(O_2CCH_3)_2(mhp)_2 \cdot 0.5CH_2Cl_2$.[5] The reported[12] structure of $Ru_2(mhp)_4 \cdot CH_2Cl_2$, a diruthenium(II,II) complex, has a 2:2 type of ligand arrangement, but there is no axial ligand.



3



4

Among ligands of type **2**, i.e. 2-hydroxypyridine and its derivatives, the bulk of X plays an important steric role in determining the coordination geometry of the metal atoms. When X = H(Hhp), the axial Cl coordination is on the metal which is coordinated to four nitrogen atoms, thus freeing the other axial site for coordination by a neutral Hhp ligand,[3] which forms a hydrogen bond to one bridging hp ligand. When X = Cl (Hchp), there is a basic change in the deployment of the ligands.[4] Now the axial coordination is to the metal atom bonded to four oxygen atoms, while the other axial site is blocked by four bulky Cl atoms. The presence of four Cl atoms close to each other also causes a twist of the ligand arrangement with an approximate torsion angle of 19°. A similar polar twist is also observed[3] in $Ru_2Cl(PhNpy)_4$. In the situation where X = Me, the polar arrangement of the ligands would result in a considerably greater twist compared to that in $Ru_2Cl(chp)_4$ because of the greater bulk of Me over Cl, and we could not isolate $Ru_2Cl(mhp)_4$.[5] Using Hfhp as a bridging ligand we have prepared the $Ru_2Cl(fhp)_4$ complex. The steric bulk of F lies between that of H and that of Cl, and thus we were interested to learn the extent of twist, if any, and the effect of fhp on the Ru—Ru and Ru—Cl bond lengths in $Ru_2Cl(fhp)_4$.

In this paper we report that we have succeeded with the synthesis and structure of the new diruthenium(II,III) complex, $Ru_2Cl(fhp)_4$, and that it does have a polar arrangement of bridging ligands. The present study is part of our systematic investigations to understand the role of steric and electronic factors responsible in the formation of polar molecules in which two metal atoms are in completely different coordination environments.

EXPERIMENTAL

Materials

$Ru_2Cl(O_2CCH_3)_4$ was prepared by following a literature procedure.[13] The ligand 6-fluoro-2-hydroxypyridine (Hfhp) was kindly supplied by the Dow Chemical Co.

Preparation of $Ru_2Cl(fhp)_4$

A mixture of 0.12 g of $Ru_2Cl(O_2CCH_3)_4$ and 0.50 g of Hfhp was heated at 130°C for 2 h under a dinitrogen atmosphere. The color of the melt changed from brown to deep purple. Excess ligand was removed by sublimation *in vacuo* at 130°C. The purple solid, obtained in quantitative yield, was dissolved in 20 cm^3 of CH_2Cl_2 and the solution filtered. A 5-cm^3 portion of the filtrate was placed in a test tube and 10 cm^3 of hexane was carefully placed on top of the CH_2Cl_2 solution, maintaining as much as possible a distinct interface between the two layers. Slow diffusion of hexane into the CH_2Cl_2 solution gave dark-coloured, large crystals in quantitative yield.

Found: C, 35.2; H, 2.0; N, 8.1%. Calc. for $Ru_2Cl(fhp)_4$: C, 35.0; H, 1.7; N, 8.2%. The compound is soluble in common organic solvents other than hexane. Electronic spectrum in CH_2Cl_2 solvent: λ_{max} = 522 nm (ε = 4720 M^{-1} cm^{-1}), 420 nm (shoulder), and 355 nm (ε = 3770 M^{-1} cm^{-1}).

Measurements

The elemental analysis was obtained from Galbraith Laboratories, Inc. The electronic spectrum was recorded on a Cary 17D spectrophotometer. Electrochemical measurements were carried out in

Table 1. Crystallographic data

Formula	$Ru_2Cl(C_5H_3NOF)_4$
Formula weight	685.93 g mol^{-1}
Space group	*I4mm* (No. 107)
Systematic absences	*hkl*: $h+k+l=2n$, 0*kl* ($k+l=2n$), *hhl* ($l=2n$)
a (Å)	10.890(2)
b (Å)	10.890(2)
c (Å)	13.178(4)
α (°)	90.0
β (°)	90.0
γ (°)	90.0
V (Å^3)	1562.8(6)
Z	2
d_c (g cm^{-3})	1.458
Crystal size (mm)	0.6 × 0.6 × 0.5
μ(Mo-K_α) (cm^{-1})	10.831
Data collection instrument	Nicolet P3
Radiation (monochromated in incident beam)	Mo-K_α ($\lambda_{\bar{a}}$ = 0.71073 Å)
Orientation reflections: No., range (2θ)	25, 20 < 2θ < 30°
Temperature (°C)	22 ± 1
Scan method	ω–2θ
Data collection range [2θ (°)]	4–50
No. of unique data, total with $F_o^2 > 3\sigma(F_o^2)$	409, 394
No. of parameters refined	57
Transmission factors: maximum, minimum (experimental) (%)	96.55, 84.90
R^a	0.0288
R_w^b	0.0383
Quality-of-fit indicator[c]	1.109
Largest shift/esd (final cycle)	0.48
Largest peak (*e* Å^{-3})	0.601

[a] $R = \sum ||F_o| - |F_c|| / \sum |F_o|$.

[b] $R_w = [\sum w(|F_o| - |F_c|)^2 / \sum w|F_o|^2]^{1/2}$; $w = 1/\sigma^2(|F_o|)$.

[c] Quality of fit = $[\sum w(|F_o| - |F_c|)^2 / (N_{obs} - N_{parameters})]^{1/2}$.

CH_2Cl_2 solutions in the presence of 0.2 M tetrabutylammonium perchlorate as a supporting electrolyte under an argon atmosphere with a Bioanalytical Systems, Inc. Model BAS 100 Electrochemical Analyser instrument in connection with a Bausch & Lomb, Houston Instruments Model DMP 40 digital plotter. In a three-electrode cell system, a platinum disk Model BAS MF 2032 and a platinum wire were used as working and auxiliary electrodes, and a BAS MAF 2020 Ag–AgCl was used as reference electrode. All potentials were referenced to the Ag–AgCl electrode at 22 ± 1°C and are uncorrected for junction potentials.

X-ray crystallographic procedures

Pertinent crystallographic data are given in Table 1. The structure of a single crystal of size 0.6 × 0.6 × 0.5 mm, mounted on a glass fiber, was determined by using general procedures prescribed in the literature.[14]* Measurement of the unit-cell constants and data collection were performed on a Nicolet P3 diffractometer equipped with graphite-monochromated Mo-K_α (λ = 0.71073 Å) radiation. Lorentz, polarization and absorption corrections were applied to the data. Systematic absences from the preliminary data collection, which was performed in the 2θ range 20–30°, revealed *I*-center-

* Calculations were done on the VAX-11/780 computer in the Department of Chemistry, Texas A&M University, College Station, Texas with a VAX-SDP software package.

ing, and during subsequent data collection the $h+k+l = 2n$ restriction was applied. There was no decay of the crystal during 12.1 h of exposure time. The systematic absences in the data are consistent with all of the space groups *I*422, *I*4*mm*, $I\bar{4}m2$ (or $I\bar{4}2m$) and *I*4/*mmm*. With $Z = 2$ and the anticipated structure, only *I*4*mm* was acceptable for an ordered structure, and accordingly it was used to begin the process of solving and refining the structure. It proved to be entirely satisfactory and is doubtless correct. The positions of the two ruthenium atoms, one of which was placed at the origin, were obtained from the Patterson function, which along with data set seemed to be more consistent with the space group *I*4*mm*. The remaining non-hydrogen atoms were found using least-square refinements and difference Fourier maps.

The asymmetric unit consists of two metal atoms, one Cl atom, and one fhp ligand. Ru(2) and Cl are at the special position 0, 0, *z*, while all the other atoms are at the special position *x*, *x*, *z*. All the atoms were refined anisotropically and in the last cycle 394 data with $I > 3\sigma(I)$ were used to refine 57 parameters, to final values of $R = 0.0288$ and $R_w = 0.0383$. The final difference Fourier map had the highest peak with 0.60 *e* Å^{-3}.*

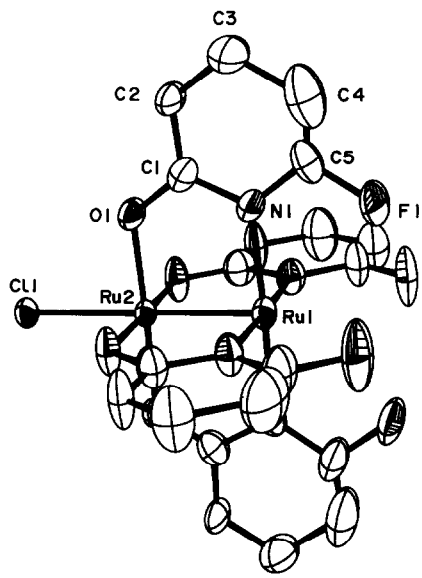


Fig. 1. ORTEP view of $Ru_2Cl(fhp)_4$ molecule with atoms represented by thermal vibration ellipsoids at the 50% level. The atom-labeling scheme in this molecule is defined.

RESULTS

Molecular structure

Selected bond distances and angles are listed in Table 2, and an ORTEP view of the molecule is shown in Fig. 1.

A C_4-axis coincides with the linear Cl(1)—Ru(2)—Ru(1) chain, and there are vertical mirror planes containing the fhp ligands and bisecting the angles between them. Thus, all the atoms belonging to the asymmetric unit lie in one plane, and the molecular symmetry is rigorously 4*mm* (C_{4v}). The molecule has a diruthenium(II,III) unit bridged by four fhp ligands in a fashion that gives rise to a polar arrangement of ligands. The coordination geometry of Ru(2) is octahedral with $Ru(1)O(1)_4Cl(1)$ while the other ruthenium atom, Ru(1), is square pyramidal (virtually octahedral with one empty site) with a $Ru(2)N(1)_4$ coordination sphere. The axial position on this Ru is empty because of the array of four F(1) atoms, which form a square with its plane normal to the Cl(1)—Ru(2)—Ru(1) axis screening this axial site.

The Ru(1)—Ru(2) distance in $Ru_2Cl(fhp)_4$ is 2.284(1) Å. The metal–metal distances found[3–5] in other diruthenium(II,III) complexes having a polar arrangement of ligands show little variation, lying between 2.278 and 2.286 Å. Among diruthenium tetracarboxylates,[15–19] the Ru—Ru distance ranges from 2.248 to 2.292 Å. The longest Ru—Ru bond length of 2.296 Å is known [20] in $Ru_2Cl(4\text{-}Cl\text{-}C_6H_4CONH)_4 \cdot CH_3OH$. The Ru(2)—Cl(1), Ru(2)—O(1) and Ru(1)—N(1) distances in $Ru_2Cl(fhp)_4$ are 2.427(3), 1.971(2) and 2.089(4) Å, respectively. The Ru—Cl distance is quite short compared to those in $Ru_2Cl(O_2CR)_4$, which are typically ~2.55 Å. It is our general observation that, in diruthenium complexes with only one axial site occupied by a Cl atom and the other one empty, the Ru—Cl bond lengths are in the range 2.419–2.443 Å.

Electronic spectra

The visible absorption spectrum of $Ru_2Cl(fhp)_4$ in CH_2Cl_2 displays one strong band at 522 nm ($\varepsilon = 4720$ M^{-1} cm^{-1}). At 355 nm, there is another moderately strong absorption with $\varepsilon = 3770$ M^{-1} cm^{-1}. The shoulder observed at 420 nm is weak. The spectrum is shown in Fig. 2.

Among polar diruthenium(II,III) complexes, the low-energy band position is found to be sen-

* Tables of atomic coordinates, structure factors, anisotropic thermal parameters and a complete list of bond distances and angles have been deposited with the Editor at Queen Mary College and at the Cambridge Crystallographic Data Centre.

Table 2. Selected bond distances (Å) and angles (°) for $Ru_2Cl(fhp)_4$[ab]

Bond distance		Bond angle	
Ru(2)—Ru(1)	2.284(1)	Ru(1)—Ru(2)—Cl(1)	180.0
Ru(2)—Cl(1)	2.427(3)	Ru(1)—Ru(2)—O(1)	90.9(2)
Ru(2)—O(1)	1.971(2)	Ru(2)—Ru(1)—N(1)	88.7(3)
Ru(1)—N(1)	2.089(4)	Cl(1)—Ru(2)—O(1)	89.1(2)
N(1)—C(1)	1.342(14)	O(1)—C(1)—N(1)	119.1(4)
N(1)—C(5)	1.342(11)	F(1)—C(5)—N(1)	109.7(6)
O(1)—C(1)	1.292(12)	F(1)—C(5)—C(4)	121.4(9)
F(1)—C(5)	1.376(11)	N(1)—C(5)—C(4)	129(1)
		Ru(1)—N(1)—C(5)	124.1(7)
		Ru(1)—N(1)—C(1)	118.1(6)
		Ru(2)—O(1)—C(1)	123.2(5)

[a] Numbers in praentheses are estimated standard deviations in the least significant digits.

[b] The distance between the two closest F atoms in 2.939 Å.

sitive to the nature of the bridging ligand. The shift towards higher energy follows the order hp > fhp > chp > mhp > PhNpy. The metal–metal distance increases in the same order. For comparison, the Ru—Ru and Ru—Cl distances in polar diruthenium(II,III) complexes along with their low-energy electronic spectral data are presented in Table 3.

While we observed two bands in the electronic spectrum of $Ru_2Cl(fhp)_4$, the spectra $Ru_2Cl(chp)_4$ and $Ru_2Cl(O_2CCH_3)_2(mhp)_2$ exhibit[4,5] several bands. In $Ru_2Cl(chp)_4$, a low-energy band at 680 nm with $\varepsilon = 980\ M^{-1}\ cm^{-1}$ is present along with three higher-energy shoulders at 440, 380 and 340 nm. The electronic spectrum of the mixed-ligand complex $Ru_2Cl(O_2CCH_3)_2(mhp)_2$ also shows[5] three additional bands and shoulders at 460 nm, 378 nm ($\varepsilon = 1540\ M^{-1}\ cm^{-1}$) and 292 nm ($\varepsilon = 8070\ M^{-1}\ cm^{-1}$).

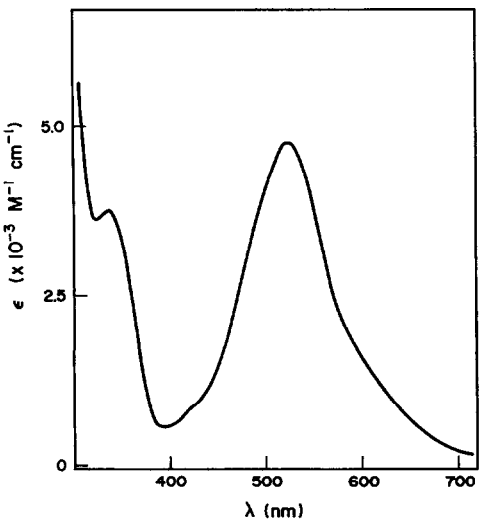


Fig. 2. Electronic spectrum of $Ru_2Cl(fhp)_4$ in CH_2Cl_2.

The diffuse-reflectance spectrum of $Ru_2Cl(O_2CCH_3)_4$ studied by Clark and Franks is known[21] to have a maximum at 21,600 cm^{-1} (*ca* 462 nm). The presence of this band was also observed by Martin *et al.*[19] in the polarized electronic spectra for tetraacetate. From the SCF-Xα-SW calculation done on $[Ru_2(O_2CR)_4]^+$ complexes, Norman *et al.*[22] assigned this band to an allowed $O(\pi) \rightarrow \pi^*(RuRu)$ transition. If we consider that the band observed by us in $Ru_2Cl(O_2CCH_3)_2(mhp)_2$ at 460 nm has the same origin as in tetracarboxylates, the intense lower-energy band could be assigned to the transition involving the bridging mhp ligands and the $\pi^*(RuRu)$. This argument is supported by the presence of only one intense band in the range 480–764 nm having $\varepsilon > 3000\ M^{-1}\ cm^{-1}$ in these polar complexes. The band observed at 17,900 cm^{-1} (*ca* 558 nm) in $Ru_2Cl(O_2CCH_3)_4$ was assigned by Norman *et al.* to a $Cl \rightarrow \pi^*(RuRu)$ or $Cl \rightarrow \sigma^*(RuRu)$ transition. The band observed near 400 nm in the polar complexes could have the same origin. The observed shift of this band position from the tetracarboxylato to these polar compounds could be due to shortening of the Ru—Cl bond in the latter complexes.

Electrochemistry

The electron-transfer behavior of $Ru_2Cl(fhp)_4$ was studied in CH_2Cl_2 solution by cyclic voltam-

Table 3. Comparison of the Ru—Ru and Ru—Cl distances and the band maximas in polar diruthenium(II,III) complexes

Compound	Ru—Ru (Å)	Ru—Cl (Å)	λ_{max} (nm) [ε (M^{-1} cm^{-1})]	Reference
$Ru_2Cl(hp)_4(Hhp)$	2.286(1)	2.558(2)	480 (4690)	3
$Ru_2Cl(fhp)_4$	2.284(1)	2.427(3)	522 (4720)	This work
$Ru_2Cl(chp)_4 \cdot CH_2Cl_2$	2.281(1)	2.443(2)	536 (4740)	4
$Ru_2Cl(O_2CCH_3)_2(mhp)_2 \cdot 0.5CH_2Cl_2$	2.278(2)	2.419(5)	550 (3370)	5
$Ru_2Cl(PhNpy)_4$	2.275(3)	2.437(7)	764 (6910)	3

metry. In the voltage scan range of +2.0 to −2.0 V, two voltammograms were observed at −0.01 and +1.68 V with ΔE_p values of 126 and 120 mV, respectively, at a scan rate of 100 mV s^{-1}. The $i_{p,a}/i_{p,c}$ ratio of the voltammograms equals unity at scan rates of 100–500 mV s^{-1} indicating a quasireversible electron-transfer process. One-electron stoichiometry as well as the nature of the process, as given in eqn (1):

$$[Ru_2Cl(fhp)_4]^+ \underset{-e^-}{\overset{+e^-}{\rightleftharpoons}} Ru_2Cl(fhp)_4$$

$$E_{1/2} = +1.68\ V\ (\Delta E_p = 120\ mV)$$

$$\underset{-e^-}{\overset{+e^-}{\rightleftharpoons}} [Ru_2Cl(fhp)_4]^-, \quad (1)$$

$$E_{1/2} = -0.01\ V\ (\Delta E_p = 126\ mV)$$

were determined by controlled-potential coulometry. Both processes are believed to be metal-centered.

These results, when compared with electrochemical studies done on other polar diruthenium(II,III) species,[6] show that the redox properties of all compounds with 2-hydroxypyridine and its derivatives as bridging ligands tend to be similar. However, a considerable shift towards a lower potential for both the processes occurs on changing ligand coordination from O,N to N,N, e.g. in $Ru_2Cl(PhNpy)_4$ the processes occur at +0.50 V (ΔE_p = 60 mV) and −0.75 V (ΔE_p = 67 mV).

DISCUSSION

With the preparation and structural characterization of $Ru_2Cl(fhp)_4$ we have obtained further experimental evidence to corroborate our previous arguments concerning the reasons why certain binuclear species adopt the completely polar arrangement of ligands. We have argued that for a ligand of type **2** (or any other such as PhNpy, which also would place bulky groups near the axial site on the M_2 core), the 2 : 2 arrangement is disfavored because it prevents the formation of a strong axial ligand bond at *either* end. Indeed, in many cases it would preclude the formation of even weak axial bonds. With the polar arrangement, one strong axial bond can be formed, although, of course, the formation of a second axial bond is then entirely ruled out. A second factor, however, is whether the four blocking groups, X in **2**, can all be accommodated at one end. When X = H there is no problem at all, and it is possible to obtain a compound, **3**, in which the axial Cl ion is bound to the end of the M_2 unit where all of the X groups are. In this case, there is also an axial ligand at the other end that forms a hydrogen bond, and it is likely that the Cl^- ligand is forced to the other end because the hydrogen-bonded ligand has a strong preference for the end where hydrogen bond formation is possible.

In our previous work we next went to the chp ligand, where X is much larger, namely Cl. Here, again, the polar arrangement was adopted (see **4**), but apparently with difficulty, since the Cl...Cl nonbonded contacts are close and seem to induce some twisting about the Ru—Ru axis to yield a slight increase in these distances. At this point, two predictions were implied. (1) If the X groups were to be made even larger, say CH_3 groups, adoption of a polar $Ru_2(NY)_4Cl$ structure could become impossible. (2) If the X groups were to be made somewhat smaller than Cl, say F atoms, then a polar $Ru_2(NY)_4Cl$ structure would be adopted without any twisting. The first of these predictions is of limited usefulness since its verification requires the "proof of a negative", which isn't possible. Nevertheless, its correctness is supported (not proved) by the finding that $Ru_2(O_2CCH_3)_4Cl$ could be converted only to $Ru_2(O_2CCH_3)_2(mhp)_2Cl$, and not all the way to $Ru_2(mhp)_4Cl$.

What we are now reporting is proof of the correctness of the second prediction. We have demonstrated that $Ru_2(fhp)_4Cl$ can be made, that it has the polar structure, and that there is no twist about

the Ru—Ru bond. In fact, in the crystal the angle of twist is rigorously zero.

Acknowledgement—We are grateful to the National Science Foundation for financial support.

REFERENCES

1. F. A. Cotton, L. R. Falvello, S. Han and W. Wang, *Inorg. Chem.* 1983, **22**, 4106.
2. F. A. Cotton, S. Han and W. Wang, *Inorg. Chem.* 1984, **23**, 4762.
3. A. R. Chakravarty, F. A. Cotton and D. A. Tocher, *Inorg. Chem.* 1985, **24**, 172.
4. A. R. Chakravarty, F. A. Cotton and D. A. Tocher, *Inorg. Chem.* 1985, **24**, 1263.
5. A. R. Chakravarty, F. A. Cotton and D. A. Tocher, *Inorg. Chem.* 1985, **24**, 2857.
6. A. R. Chakravarty, F. A. Cotton, D. A. Tocher and J. H. Tocher, *Polyhedron* 1985, **4**, 1475.
7. F. A. Cotton and R. A. Walton, *Multiple Bonds Between Metal Atoms*. Wiley, New York (1982).
8. F. A. Cotton and T. R. Felthouse, *Inorg. Chem.* 1980, **19**, 320.
9. M. Berry, C. D. Garner, I. H. Hillier and W. Clegg, *Inorg. Chim. Acta* 1980, **45**, L209.
10. F. A. Cotton, P. E. Fanwick, R. H. Niswander and J. C. Sekutowski, *J. Am. Chem. Soc.* 1978, **100**, 4725.
11. F. A. Cotton, W. H. Ilsley and W. Kaim, *Inorg. Chem.* 1980, **19**, 1453.
12. W. Clegg, *Acta Cryst.* 1980, **B36**, 3112.
13. T. A. Stephenson and G. Wilkinson, *J. Inorg. Nucl. Chem.* 1966, **28**, 2285.
14. A. Bino, F. A. Cotton and P. E. Fanwick, *Inorg. Chem.* 1979, **18**, 3558; F. A. Cotton, B. A. Frenz, G. Deganello and A. Shaver, *J. Organomet. Chem.* 1973, **50**, 227; A. C. T. North, D. C. Phillips and F. S. Mathews, *Acta Cryst.* 1968, **A24**, 351.
15. T. Togano, M. Mukaida and T. Nomura, *Bull. Chem. Soc. Jpn* 1980, **53**, 2085.
16. M. J. Bennett, K. G. Caulton and F. A. Cotton, *Inorg. Chem.* 1969, **8**, 1.
17. A. Bino, F. A. Cotton and T. R. Felthouse, *Inorg. Chem.* 1979, **18**, 2599.
18. M. Mukaida, T. Nomura and T. Ishimori, *Bull. Chem. Soc. Jpn* 1967, **40**, 2462; 1972, **45**, 2143.
19. D. S. Martin, R. A. Newman and L. M. Vlasnik, *Inorg. Chem.* 1980, **19**, 3404.
20. A. R. Chakravarty, F. A. Cotton and D. A. Tocher, *Polyhedron* 1985, **4**, 1097.
21. R. J. H. Clark and M. L. Franks, *J. Chem. Soc., Dalton Trans.* 1976, 1825.
22. J. G. Norman, G. E. Renzoni and D. A. Case, *J. Am. Chem. Soc.* 1979, **101**, 5256.

Polyhedron Vol. 5, No. 11, pp. 1829–1831, 1986
Printed in Great Britain

0277–5387/86 $3.00+.00
© 1986 Pergamon Journals Ltd

SYNTHESIS AND STRUCTURE OF COBALT(II) SQUARATE CHLORIDE

O. St. C. HEADLEY and L. A. HALL*

Department of Chemistry, University of the West Indies, St. Augustine, Trinidad

(*Received* 25 *February* 1986; *accepted* 24 *March* 1986)

Abstract—Cobalt(II) squarate chloride $[Co(HC_4O_4)(Cl)(C_2H_5OH)]_2 \cdot C_2H_5OH$ has been synthesized by reacting ethanolic solutions of $CoCl_2 \cdot 6H_2O$ and squaric acid in a nitrogen atmosphere. Analysis of the spectroscopic data, magnetic-susceptibility and weight loss measurements suggests that the complex is five-coordinate.

We have recently reported the synthesis of the two five-coordinate squarate complexes, iron(II) and nickel(II) squarate chlorides, from ethanolic solution.[1] We have now synthesized cobalt(II) squarate chloride which is apparently also five-coordinate.

EXPERIMENTAL

Chemicals

Squaric acid was obtained from Aldrich, recrystallized once from water and dried at approximately 100°C. Analar $CoCl_2 \cdot 6H_2O$ obtained from BDH was used as received. Analar grade ethanol (BDH) was redistilled over CaO prior to use.

Preparation of the complex

Squaric acid (0.34 g, 3.0 mmol) was dissolved in 200 cm^3 of hot ethanol through which a continuous stream of dry nitrogen was being passed. Cobalt(II) chloride-6-water (1.20 g, 3.0 mmol) was then dissolved in a similar volume of hot degassed ethanol and the solution quickly added to the squaric acid solution. After mixing, the passage of nitrogen was continued for about 5 min. Following filtration, the purple complex which separated out from a blue solution was transferred to a glass manifold in a nitrogen-filled glove bag. Found: C, 29.4; H, 4.9; Cl, 13.1; Co, 22.0%. Calc. for $C_{14}H_{20}Cl_2Co_2$: C, 30.4; H, 3.6; Cl, 12.8; Co, 21.3%.

* Author to whom correspondence should be addressed.

Instrumentation

The IR spectra were recorded on a Perkin–Elmer model 983 spectrophotometer. Nujol was used as the mulling agent and "saran wrap" as window material for the spectrum between 600 and 180 cm^{-1}. The UV–VIS–NIR reflectance spectra were done on a Varian 2300 spectrophotometer. Magnetic-susceptibility measurements were performed using a Newport magnetic balance. $HgCo(SCN)_4$ was used as the susceptibility standard. The TGA curve was obtained on a Netzsch STA 409 thermogravimetric analyser.

Analyses

The carbon and hydrogen analyses were done by Mikroanalytisches Labor Pascher. Cobalt was determined by atomic absorption spectrophotometry using a Pye–Unicam SP9 spectrophotometer while chlorine was determined gravimetrically.[2]

RESULTS AND DISCUSSION

The UV–VIS–NIR spectrum (Fig. 1) shows bands at 27,000, 13,300–23,300 and 5300–10,000 cm^{-1}. Two weak bands occur at about 4300 and 4700 cm^{-1}. The band between 13,300 and 23,300 has a fine structure in addition to a shoulder at about 14,000 cm^{-1}. These bands can be explained in terms of the energy-level diagram for five-coordinate cobalt(II) obtained by Norgett *et al.*[3] The broad absorption band between 5300 and 10,000

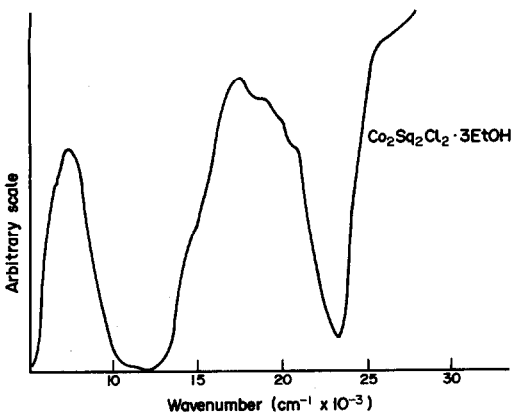


Fig. 1. Electronic spectrum of $Co_2Sq_2Cl_2 \cdot 3EtOH$ ($Sq = C_4O_4H^-$).

cm^{-1} has been assigned to $(e'')^4(e')^3 \rightarrow (e'')^3(e')^4$, while the absorptions between 13,300 and 23,300 cm^{-1} have been assigned to $(e'')^4(e')^3 \rightarrow (e'')^4(e')^2 a_1^1$. The band at 27,000 cm^{-1} has been assigned to the $(e'')^4(e')^3 \rightarrow (e'')^3(e')^3 a_1^1$ transfer. The three bands predicted to occur at about 20,000 cm^{-1} are actually observed in the spectrum of cobalt(II) squarate chloride. These bands make up the fine structure in the 13,300–23,300-cm^{-1} region and occur at 19,100, 19,800 and 20,800 cm^{-1}, respectively. The bands at 14,800 and 17,400 cm^{-1} have been attributed to the one-electron transitions predicted to occur at energies of 16,100 and 18,200 cm^{-1} by Norgett's model. The complex thus appears to be five-coordinate.

In the IR spectrum of cobalt(II) squarate chloride (Table 1), the broad band between 1500 and 1700 cm^{-1} has been assigned to C—C and C—O stretching modes. The peaks at 750, 1100, 1150 and 2250 cm^{-1}, and the band between 2600 and 2700 cm^{-1} are assumed to be absorptions due to squarate since they all appear in the spectrum of squaric acid and/or the squarates.[4-7] The peak at 1800 cm^{-1} is attributed to C=O stretching. The broad band between 3100 and 3600 cm^{-1} is assumed to be due to the O—H stretching of hydrogen-bonded hydroxyl groups from both ethanol and squarate. The peak at 1050 cm^{-1} has been assigned to a C—C—O stretching mode of ethanol while the peak at 875 cm^{-1} is assumed due to be an out-of-plane-bonded deformation. The Co—O stretching gives rise to peaks at 446 and 530 cm^{-1}, respectively.[8] Peaks at 215 and 225 cm^{-1}, and the broad band at 250–300 cm^{-1} have been assumed to be due to bridging chloride.[9]

The following structure is proposed:

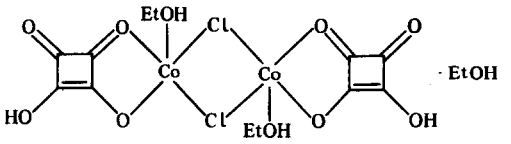


Table 1. IR spectroscopic data for $[Co(HC_4O_4)(Cl)(C_2H_5OH)]_2 \cdot C_2H_5OH$

Frequency[a] (cm^{-1})	Assignment
3100–3600 s, b	O—H stretch
2600–2700 w, b	Overtone and/or combination bands due to squarate
2250 m, sh	Overtone of peak at approximately 1100 cm^{-1}
1800 w, sh	C=O stretch
1500–1700 b	C—C and C—O stretching
1260 m, sh	O—H bending and C—O stretching of the ethanol molecule
1150 vw	Bands due to squarate
1100 s, sh	
1050 m, sh	C—C—O stretching of ethanol molecule
875 m, sh	Out-of-plane O—H bonded deformation
750 s, sh	C—O deformation due to squarate
530, 446 s, sh	M—O stretching
250–300 m, b	M—Cl bridging
225 s, sh	
215 s, sh	

[a] s = strong, sh = sharp, w = weak, vw = very weak, b = broad, and m = medium.

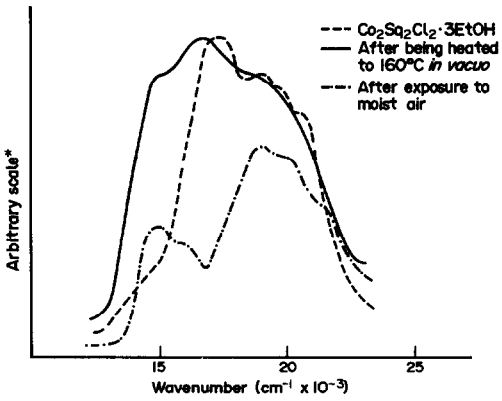


Fig. 2. Changes in the electronic spectra of $Co_2Sq_2Cl_2 \cdot 3EtOH$ due to changes in environment (Sq = $C_4O_4H^-$). * Peak heights are not intended to show relative intensities.

When cobalt(II) squarate chloride is exposed to the atmosphere it turns pink. The UV–VIS spectrum of the exposed complex shows broad bands at 13,300–16,700 and 17,000–23,300 cm^{-1}. The band at 13,300–17,000 cm^{-1} has a fine structure while the band at 17,000–23,300 cm^{-1} has a shoulder on the high-frequency side at about 21,600 cm^{-1}. These bands at 13,300–16,700 and 17,000–23,300 cm^{-1} have been assigned to the $^4T_{1g} \rightarrow {}^4A_{2g}$ and $^4T_{1g}(P)$ transitions of octahedral cobalt(II).

If cobalt(II) squarate chloride is heated *in vacuo* it turns blue. The UV–VIS spectrum of the heated substance has a broad band extending from 12,800 to 23,300 cm^{-1} which, although poorly resolved, has two maxima at 15,600 and 16,700 cm^{-1}, and a shoulder at 18,900 cm^{-1}. This broad band is assumed to be due to the $^4A_2 \rightarrow {}^4T_1(P)$ transition of tetrahedral cobalt(II).

A comparison of the UV–VIS spectra of cobalt(II) squarate chloride before exposure to the atmosphere, after exposure to the atmosphere and after heating at 160°C *in vacuo* is given in Fig. 2. The complex therefore appears to become octahedral on exposure to the atmosphere due to the coordination of water and tetrahedral due to loss of coordinated ethanol when heated *in vacuo*.

The hydrogen analysis of cobalt(II) squarate chloride is about 36% higher than expected and this has been attributed to solvent contamination as was observed for nickel(II) and iron(II) squarate chloride.[1]

The thermal weight loss curve for $[Co(HC_4O_4)(Cl)(C_2H_5OH)]_2 \cdot C_2H_5OH$ shows weight losses of 19.4 and 10.3% at about 180 and 250°C, respectively. This could be interpreted in terms of the sequential loss of the two coordinated ethanol molecules (16.7% calculated) and "lattice" ethanol (8.3% calculated). The differences between the theoretical and experimental weight losses have been assumed to be due to solvent contamination.

Cobalt(II) squarate chloride has a magnetic moment of 5.30 BM. This relatively high value could be due to clathrated solvent molecules.[6] However, high-spin five-coordinate cobalt(II) complexes with square-pyramidal geometry have similar magnetic moments.[10]

REFERENCES

1. O. St. C. Headley and L. Hall, *Polyhedron* 1985, **4**, 1697.
2. A. I. Vogel, *A Textbook of Quantitative Inorganic Analysis*, 3rd Edn, pp. 461 and 462. Longmans, London (1961).
3. M. Norgett, J. Thornley and L. Venanzi, *J. Chem. Soc. A* 1967, 540.
4. N. R. West and Y. Niu, *J. Am. Chem. Soc.* 1963, **85**, 2589.
5. F. G. Baglin and C. B. Rose, *Spectrochim. Acta* 1970, **26A**, 2298.
6. B. C. Gerstein and M. Habenschuss, *J. Appl. Phys.* 1972, **12**, 5155.
7. M. Ito and R. West, *J. Am. Chem. Soc.* 1963, **85**, 1580.
8. D. Adams, *Metal–Ligand and Related Vibrations*, p. 260. Edward Arnold, London (1967).
9. K. Nakamoto, *Infrared Spectra of Inorganic and Coordinated Compounds*, 2nd Edn, pp. 216–218. Wiley Interscience, New York (1970).
10. F. Lions, I. Dance and J. Lewis, *J. Chem. Soc.* 1967, 565.

Polyhedron Vol. 5, No. 11, pp. 1833–1837, 1986
Printed in Great Britain

0277–5387/86 $3.00+.00
Pergamon Journals Ltd

TERTIARY PHOSPHINE BOROHYDRIDO COMPLEXES OF CHROMIUM, TUNGSTEN AND RHENIUM: CRYSTAL STRUCTURE OF *TRANS*-HYDRIDO(η^2-TETRAHYDROBORATO)BIS[1,2-BIS(DIMETHYLPHOSPHINO)ETHANE]CHROMIUM(II)

ANDREW R. BARRON, JULIAN E. SALT and GEOFFREY WILKINSON*

Chemistry Department, Imperial College, London SW7 2AY, U.K.

and

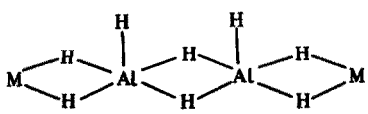
MAJID MOTEVALLI and MICHAEL B. HURSTHOUSE*

Chemistry Department, Queen Mary College, London E1 4NS, U.K.

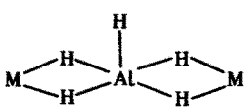
(*Received* 20 *March* 1986; *accepted* 24 *March* 1986)

Abstract—The synthesis of the borohydride complexes $(dmpe)_2CrH(\eta^2\text{-}BH_4)$ (**A**) [dmpe = 1,2-bis(dimethylphosphino)ethane], $(Me_3P)_3WH_3(\eta^2\text{-}BH_4)$ and $(Me_2PhP)_3ReH(\eta^1\text{-}BH_4)(\eta^2\text{-}BH_4)$ are reported. ^1H and ^{31}P NMR spectra show that all the molecules are non-rigid, undergoing metal–hydride exchanges. The heavy-atom structure of **A** has been confirmed by X-ray crystallography.

A variety of transition-metal hydrido aluminohydrides[1] have dimeric structures of types **1** and **2** with five-coordinate Al. Borohydrides where boron is four-coordinate are commonly monomeric with $M(\mu\text{-}H_n)BH_{4-n}$ groups,[2(a)] although bridge groups are known.[2(b)] The patterns of non-rigid behaviour in the two types of complex according to ^1H and ^{31}P NMR spectra also differ considerably. The only borohydrides that have aluminohydride analogues are those of bis(pentamethylcyclopentadienyl)titanium(III)[3] and tris(trimethylphosphine)ruthenium(II).[4] We now report on some other borohydrides whose comparable aluminohydrides have been characterized in order to allow spectroscopic and structural comparison.



1



2

RESULTS AND DISCUSSION

Chromium

The diamagnetic aluminohydride made from $(dmpe)_2CrCl_2$ [dmpe = 1,2-bis(dimethylphosphino)ethane] and $LiAlH_4$ is $[(dmpe)_2HCr(\mu\text{-}H)_2AlH(\mu\text{-}H)]_2$.[5] Interaction of the chloride with an excess of $NaBH_4$ in diethylether–tetrahydrofuran (thf) leads to bright red crystals of $(dmpe)_2HCr(\eta^2\text{-}BH_4)$ (**A**). The IR spectrum shows strong bands typical of terminal B—H groups at 2460 and 2430 cm^{-1}, as well as a band at 2060 cm^{-1} due to Cr—H. A weaker band, *ca* 1650 cm^{-1}, is a bridging hydride stretch. Unlike the aluminohydride the compound is paramagnetic ($\mu_M = 2.49$ BM) with low-spin Cr(II) (d^4). The ^1H NMR spectrum contains many broadened peaks due to the CH_3 and CH_2 protons of dmpe [δ −13.5 ppm (P-C$\underline{H}_2$) and −15.6 ppm (P-C$\underline{H}_3$]; the hydrides appear as three separate peaks at δ −25.5, −29.4 and −33.5 ppm.

* Authors to whom correspondence should be addressed.

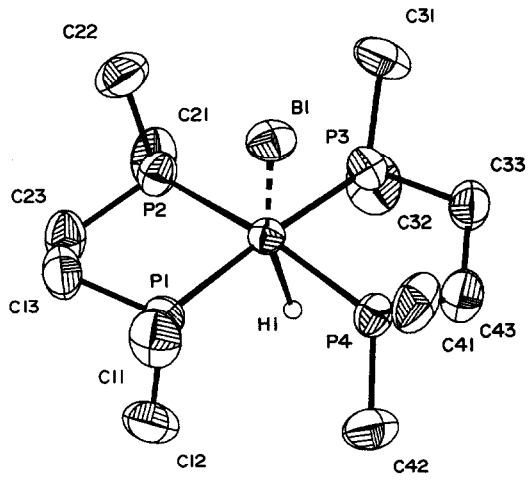


Fig. 1.

The structure of the compound is illustrated in Fig. 1; selected bond lengths and angles are given in Table 1. The BH_4 hydrogens were not located and we presume that this group is disordered with respect to these atoms. The main features of this typical $M(dmpe)_2L_2$ "octahedral" structure are the Cr—P bond lengths, which, at 2.321–2.346(6) Å, lie to the lower end of the range found for other Cr(II) $(dmpe)_2$ complexes,[6] and the slight bending down of the equatorial Cr—P bonds away from the BH_4 group [B...Cr—P = 94.4–97.2(4)°]. Otherwise, the geometry is as expected, with P—Cr—P chelate angles of 83(1)° and P—C distances of 1.82–1.8(2) Å.

Tungsten

The addition of $LiBH_4$ to an ether suspension of $WCl_4(PMe_3)_3$[7] results in a bright orange solution that yields the hexane-soluble $(Me_3P)_3H_3W(BH_4)$ (**B**).

The IR spectrum of the compound clearly shows various stretches due to terminal and bridging hydrides. A strong doublet at *ca* 2450 cm^{-1} [ν(B—H_b)] along with a broad signal at 1800 cm^{-1} [ν(B—H_b)] is indicative of a bidentate borohydride,[3] while a terminal metal hydride stretch at 2060 cm^{-1} is in the region expected for tungsten.[8] Although complex **B** undoubtedly has a geometry around the tungsten similar to that in the aluminohydride $[(Me_3P)_3H_3W(\mu\text{-}H)_2AlH(\mu\text{-}OBu^n)]_2$,[9] the tungsten hydride stretch in the latter is appreciably shifted and appears as part of a strong hydride envelope in the region 1800–1600 cm^{-1}. The remaining IR bands in **B** can be assigned to various phosphine stretches and deformations.

At room temperature the exchange between terminal M—H and bridging M(μ-H)B hydrides occurs rapidly on the NMR time scale. There is a broad singlet at δ −2.33 ppm which, on cooling decoalesces to give two broad signals at δ −0.13 ppm (B—H) and −6.25 ppm [W(μ-H)B].

Whereas in aluminohydrides the exchange between terminal M—H and bridging M(μ-H)Al hydrides is usually facile at room temperature, the equivalent exchange process for the borohydride compound occurs only at about +50°C. The process is typical of borohydride[2,3] with the BH_4 peaks coalescing with the metal hydride resonance (δ −7.80 ppm), to give a broad singlet (−4.62 ppm).

The $^{31}P\text{-}\{^1H\}$ NMR spectrum comprises a singlet with ^{183}W satellites [δ = −21.6 ppm, J(P–^{183}W) = 140 Hz]. When the phosphine protons are selectively decoupled the signal becomes a binomial quartet [J(P–H) = 26.0 Hz], indicating the presence of three terminal metal hydrides. No coupling is observed at room temperature due to the bridging hydrides.

Rhenium

The aluminohydride $[(Me_2PhP)_3H_2Re(\mu\text{-}H)_2Al(\mu\text{-}H)]_2$ has been described.[9] The interaction of $LiBH_4$ with $ReCl_3(PMe_2Ph)_3$ in Et_2O yields the bright orange, hexane soluble complex $(Me_2PhP)_3HRe(BH_4)_2$ (**C**).

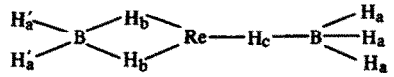
The IR spectrum indicates the presence of two different terminal B—H_t hydride environments: a strong doublet at 2530 cm^{-1} due to B—H_t stretching in a bidentate η^2-BH_4 unit plus a higher-frequency band at 2390 cm^{-1} in the region assigned to η^1-BH_4 terminal B—H_t stretches.[2,3] Two stretches are present in the Re—H stretching region (1960 and 1895 cm^{-1}). However this is not inconsistent with the proposed formulation as two bands are also observed in the complex $(Ph_2MeP)_3HRe(\mu\text{-}H)_3AlMe_2$,[10] which has been crystallographically characterized as having three bridging Re(μ-H)Al hydrides and one terminal Re—H hydride. Two broad peaks in the IR spectrum at 1700 and 1610 cm^{-1} are probably due to bridging hydrides whilst the remaining peaks between 1500 and 400 cm^{-1} are attributed to phosphine vibrations.

In addition to PMe_2Ph bands the ^1H NMR spectrum contains a broad singlet (δ −2.70 ppm), due to the two BH_4 groups, and a quartet [δ −4.60 ppm, J(P–H) = 34.6 Hz] due to the terminal Re—H. As with complex **B** the exchange between metal hydride and borohydride groups occurs only at > 75°C. On cooling to −20°C the BH_4 peak merges with the base line, whilst at −50°C three new peaks appear: a broad singlet at *ca* −1.6 ppm assigned B—H_a (see **3**) and two broad peaks at δ −5.30 and −13.70

Table 1. Selected bond lengths (Å) and bond angles (°) for $(dmpe)_2HCr(\eta^2\text{-}BH_4)$

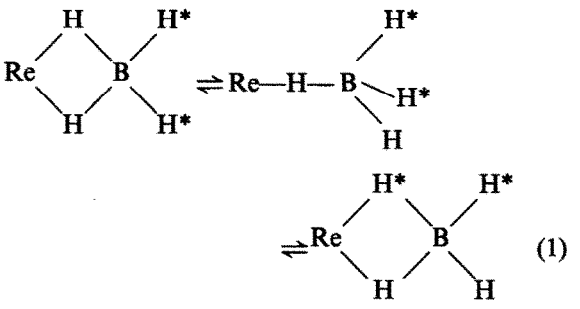
Bond lengths			
P(1)—Cr(1)	2.342(6)	P(2)—Cr(1)	2.346(6)
P(3)—Cr(1)	2.330(6)	P(4)—Cr(1)	2.321(6)
C(11)—P(1)	1.842(20)	C(12)—P(1)	1.821(19)
C(13)—P(1)	1.870(16)	C(21)—P(2)	1.828(18)
C(22)—P(2)	1.819(18)	C(23)—P(2)	1.874(17)
C(31)—P(3)	1.826(19)	C(32)—P(3)	1.855(18)
C(33)—P(3)	1.829(17)	C(41)—P(4)	1.850(19)
C(42)—P(4)	1.834(19)	C(43)—P(4)	1.842(19)
C(23)—C(13)	1.489(22)	C(43)—C(33)	1.524(24)
H(1)—Cr(1)	1.885(120)		
Bond angles			
P(2)—Cr(1)—P(1)	82.5(2)	P(3)—Cr(1)—P(1)	170.0(2)
P(3)—Cr(1)—P(2)	96.2(2)	P(4)—Cr(1)—P(1)	96.1(2)
P(4)—Cr(1)—P(2)	167.2(2)	P(4)—Cr(1)—P(3)	83.0(2)
C(11)—P(1)—Cr(1)	122.5(7)	C(12)—P(1)—Cr(1)	118.9(7)
C(12)—P(1)—C(11)	99.3(9)	C(13)—P(1)—Cr(1)	110.3(6)
C(13)—P(1)—C(11)	101.0(9)	C(13)—P(1)—C(12)	101.4(9)
C(21)—P(2)—Cr(1)	124.0(6)	C(22)—P(2)—Cr(1)	117.1(7)
C(22)—P(2)—C(21)	102.5(9)	C(23)—P(2)—Cr(1)	108.4(6)
C(23)—P(2)—C(21)	98.8(8)	C(23)—P(2)—C(22)	102.8(9)
C(31)—P(3)—Cr(1)	121.3(8)	C(32)—P(3)—Cr(1)	117.7(7)
C(32)—P(3)—C(31)	102.1(10)	C(33)—P(3)—Cr(1)	110.3(6)
C(33)—P(3)—C(31)	100.0(9)	C(33)—P(3)—C(32)	102.6(9)
C(41)—P(4)—Cr(1)	120.1(7)	C(42)—P(4)—Cr(1)	120.9(6)
C(42)—P(4)—C(41)	99.9(8)	C(43)—P(4)—Cr(1)	108.0(6)
C(43)—P(4)—C(41)	102.9(8)	C(43)—P(4)—C(42)	102.6(9)
C(23)—C(13)—P(1)	107.4(11)	C(13)—C(23)—P(2)	110.9(11)
C(43)—C(33)—P(3)	107.5(11)	C(33)—C(43)—P(4)	110.2(13)
H(1)—Cr(1)—P(1)	89.6(36)	H(1)—Cr(1)—P(2)	100.9(35)
H(1)—Cr(1)—P(3)	80.9(36)	H(1)—Cr(1)—P(4)	66.4(35)
H(1)—Cr(1)—B(1)	161.8(34)		

ppm due to $Re(\mu\text{-}H_b)B$ and $Re(\mu\text{-}H_b)B$ hydrides, respectively. The $^{31}P\text{-}\{^1H\}$ NMR spectrum, a singlet at room temperature, splits into a doublet when the phosphine protons are selectively decoupled [δ −24.6 ppm, J(P–H) = 32 Hz].



3

At −50°C the $^{31}P\text{-}\{^1H\}$ spectrum is a doublet and a triplet [δ −22.5 and −24.5 ppm, respectively, J(P–P′) = 10.6 Hz]. Hence it appears that the compound contains both η^1 and η^2 units. This appears to be the first example of this situation in a transition-metal complex. However, examples of complexes containing both η^3 and η^2 units have been reported.[11] The η^1- and η^2-BH_4 groups undergo mutual exchange as well as each having a separate $B\text{—}H_t \rightleftharpoons B\text{—}H_b$ equilibrium. These two exchange processes are probably closely related. If the exchange between bridging and terminal hydrides in the η^2-BH_4 unit involves a unidentate intermediate [eqn (1)]:



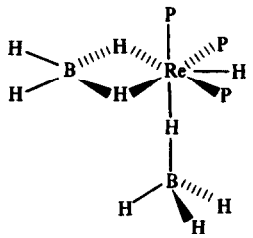
(1)

then the vacant site on the rhenium can be occupied by a hydride from either BH_4 group.

Pathways involving unidentate groups have been used to explain the stereochemical non-rigidity in compounds such as $Al(BH_4)_3$.[12]

The coordinate geometry about rhenium can be described as a pentagonal bipyramid (**4**) with one

phosphine and the unidentate borohydride occupying axial sites.



4

In this conformation the inter-exchange between the two different BH_4^- units can readily occur, whilst the energy required to initiate the exchange with the terminal rhenium hydride is large due to the *equatorial* arrangement.

EXPERIMENTAL

Microanalyses were by Pascher Laboratories, Bonn. Melting points were determined in sealed capillaries and are uncorrected. IR spectra were recorded in the region 4000–400 cm^{-1} on a Perkin–Elmer 683 grating spectrometer in Nujol mulls. NMR spectra were recorded on a JEOL FX90Q spectrometer [δ values in ppm relative to $SiMe_4$ (^1H) and 85% H_3PO_4 external (^{31}P) in d^8-toluene].

All manipulations were carried out under argon. Solvents were distilled and degassed before use.

trans - (*Hydrido*)(η^2 - *tetrahydroborato*)*bis*[1,2 - *bis*(*dimethylphosphino*)*ethane*]*chromium*(II) (A)

Excess solid $NaBH_4$ was added to a solution of $CrCl_2(dmpe)_2$ (0.40 g, 0.94 mmol) in Et_2O–thf (50+40 cm^3) at −78°C. The mixture was warmed slowly and stirred at room temperature for 12 h, when the solution became dark red brown. Removal of solvent and extraction of the brown solid with hexane (40 cm^3), filtration and concentration of the solution, followed by cooling to −20°C gave small red-brown needles which on crystallization from toluene (20 cm^3) gave large red prisms. Yield 0.5 g (60%). M.p. 183°C (decomp.). Required for $C_{12}H_{37}BCrP_4$: C, 39.1; H, 10.0; B, 2.0; P. 33.7%. Found: C, 36.6; H, 9.1; B, 2.98; P, 31.4%.

IR: 2460s, 2430s, 2060m, 1650br.w, 1290m, 1260s, 1200m, 1140m, 1130m, 1120w, 1060s, 950s, 930s, 890w, 860m, 770m, 765m, 730m, 700m, 670w and 650w cm^{-1}.

NMR: ^1H: −13.5 (8H, br.s, P-C$\underline{H}_2$). −15.6 (24H, br.s, P-C$\underline{H}_3$), −25.5, −29.4 and −33.5 [5H, Cr—H, Cr(μ-H)B and B—H].

Trihydrido(η^2 - *tetrahydroborato*)*tris*(*trimethyl* - *phosphine*)*tungsten*(IV) (B)

Solid $WCl_4(PMe_3)_3$ (1.00 g, 1.81 mmol) was added to a suspension of $LiBH_4$ (0.17 g, 7.73 mmol) in Et_2O (50 cm^3) at −78°C and the stirred mixture warmed to room temperature. After stirring for *ca* 6 h the solvent was removed and the red solid extracted with hexane (2 × 3 cm^3). Reduction in volume and cooling (−20°C) yielded orange crystals. Yield 0.41 g (53%). M.p. 180°C (decomp.). Required for $C_9H_{34}BP_3W$: C, 25.1; H, 7.9; B, 2.6; P. 21.6%. Found: C, 24.9; H, 7.8; B, 2.6; P, 22.0%.

IR: 2495s, 2420s, 2060m, 1800br.m, 1410m, 1295m, 1275s, 1140w, 940s, 850s, 800br.m, 915 and 660s cm^{-1}.

NMR: ^1H (298 K): 1.40 [27H, d, J(P–H) = 7.0 Hz, P-C$\underline{H}_3$]; −2.33 [4H, br.s, W(μ-H)B and B—H]; −7.80 (3H, br.s, W—H). ^{31}P–{^1H}: −21.6 [br.s with tungsten satellites, J(P–W) = 140 Hz].

Hydrido bis(η^1,η^2 - *tetrahydroborato*)*tris* (*dimethylphenylphosphine*)*rhenium*(III) (C)

To a cooled (0°C) suspension of $LiBH_4$ (0.20 g, 9.09 mmol) in Et_2O (40 cm^3) was added $ReCl_3(PMe_2Ph)_3$[13] (1.70 g, 2.41 mmol). The mixture was refluxed gently for *ca* 2 h, and the resulting orange solution evaporated *in vacuo*. Extraction of the residue with hexane (3 × 30 cm^3), removal of the solvent and crystallization of the solid from toluene resulted in several batches of bright orange crystals. Yield 1.09 g (72%). M.p. 84°C (decomp.). Required for $C_{24}H_{42}B_2ReP_3$: C, 45.6; H, 6.7; B, 3.5; P, 14.7%. Found: C, 45.0; H, 6.5; B, 3.4; P, 14.5%.

IR: 3080w, 2530s, 2520s, 2405s, 2390s, 1920s, 1850w, 1895w, 1435s, 1405m, 1290s, 1280s, 1100s, 1030m, 940vs, 905s, 860m, 840m, 800m, 750m, 740s, 720m, 700s, 675m, 480m and 415m.

NMR: ^1H (298 K): 7.29 (15H, m, P-C$_6\underline{H}_5$), 1.35 (18H, s, P-C$\underline{H}_3$), −2.70 [8H, br.s, Re(μ-H)B and B—H], −4.60 [1H, q, J(P–H) = 34.6 Hz, Re—H]. ^{31}P–{^1H}: −24.6(s).

Crystallographic studies

Crystals of $CrH(BH_4)(dmpe)_2$ were sealed under argon in thin-walled glass capillaries for X-ray examinations. The orientation matrix, and associated cell dimensions, and intensity data were obtained at 293 K following previously described procedures,[14] using an Enraf–Nonius CAD4 diffractometer operating in the ω–2θ scan mode, and graphite-monochromatized Mo-K_α radiation [λ(Mo-K_α) = 0.71069 Å]. The structure was solved via the heavy-atom method and refined by full-

matrix least squares,[15] with scattering factor data taken from Ref. 16. All non-hydrogen atoms were refined anisotropically. The chromium-bonded hydrogen atom was experimentally located and refined isotropically; hydrogens on the dmpe carbon atoms were inserted in idealized positions (C—H = 0.98 Å) and assigned a fixed U_{iso} of $1.2U_{equ}$ of the parent carbon atom. The BH_4 hydrogens could not be located and were not included.

Crystal data. $C_{12}H_{37}BCrP_4$, molecular weight = 368.13, orthorhombic, $a = 18.290(3)$ Å, $b = 9.299(2)$ Å, $c = 12.374(2)$ Å, $V = 2104.6$ Å space group $Pna2_1$, $d_c = 1.16$ g cm^{-3}, $Z = 4$, μ(Mo-K_α) = 8.17 cm^{-1}, 2245 intensities measured, 1949 unique and 1332 observed [$F_o > 2\sigma(F_o)$]. 167 parameters, $R = 0.56$, $R_\omega = 0.057$, weights = $1/[\sigma^2(F)+0.0002F_o^2]$.

Final atomic parameters, full lists of bond lengths and angles and F_o/F_c values have been deposited as supplementary material with the Editor from whom copies are available on request. Atomic coordinates have also been deposited with the Cambridge Crystallographic Data Centre.

Acknowledgement—We thank the SERC for X-ray facilities and studentships (J.E.S. and A.R.B.).

REFERENCES

1. A. R. Barron and G. Wilkinson, *Polyhedron* (in press).
2. (a) T. J. Marks and J. R. Kolb, *Chem. Rev.* 1977, **77**, 263; (b) D. G. Holah, A. N. Hughes, S. Maciaszek and V. R. Magnuson, *J. Chem. Soc., Chem. Commun.* 1983, 1308; J. C. Vites, C. Eigenbrot and T. P. Fehlner, *J. Am. Chem. Soc.* 1984, **106**, 4633; T. M. Gilbert, F. J. Hollander and R. G. Bergman, *J. Am. Chem. Soc.* 1985, **107**, 3508.
3. V. K. Belsky, A. I. Sizov, B. M. Bulychev and G. L. Soloveichick, *J. Organomet. Chem.* 1985, **280**, 67.
4. J. A. Statler, G. Wilkinson, M. Thornton-Pett and M. B. Hursthouse, *J. Chem. Soc., Dalton Trans.* 1984, 1731.
5. A. R. Barron, J. E. Salt and G. Wilkinson, *J. Chem. Soc., Dalton Trans.* 1986, 1329.
6. J. E. Salt, G. Wilkinson, M. Motevalli and M. B. Hursthouse, *J. Chem. Soc., Dalton Trans.* 1986, 1141.
7. P. R. Sharp, *Organometallics* 1984, **4**, 1217.
8. K. W. Chiu, R. A. Jones, G. Wilkinson, A. M. R. Gales, K. M. A. Malik and M. B. Hursthouse, *J. Chem. Soc., Dalton Trans.* 1981, 1204.
9. A. R. Barron, D. Lyons, G. Wilkinson, A. J. Downes, M. Motevalli and M. B. Hursthouse, *J. Chem. Soc., Dalton Trans.* 1986, 279.
10. W. A. Skupinski, J. C. Huffman, J. W. Bruno and K. G. Caulton, *J. Am. Chem. Soc.* 1984, **106**, 8128.
11. (a) H. J. Wasserman, D. C. Moody and R. R. Ryan, *J. Chem. Soc., Chem. Commun.* 1984, 532; (b) P. P. Charpin, M. Lance, E. Soulie, D. Vigner and H. Marquet-Ellis, *Acta Cryst.* 1985, **C41**, 1723.
12. R. E. Williams, *J. Inorg. Nucl. Chem.* 1961, **20**, 198.
13. J. Chatt, G. J. Leigh, D. M. P. Mingos and R. J. Parke, *J. Chem. Soc. A* 1968, 2636.
14. R. A. Jones, K. M. A. Malik, M. B. Hursthouse and G. Wilkinson, *J. Am. Chem. Soc.* 1979, **101**, 4128.
15. G. M. Sheldrick, *SHELX76*. University of Cambridge, Cambridge (1976).
16. *International Tables for X-ray Crystallography*, Vol. 4. Kynoch Press, Birmingham (1974).

Polyhedron Vol. 5, No. 11, pp. 1839–1844, 1986
Printed in Great Britain

0277–5387/86 $3.00+.00
Pergamon Journals Ltd

CHROMIUM(III)–CITRATE COMPLEXES: A STUDY USING ION EXCHANGE AND ISOTACHOPHORESIS

G. ABBAY and T. W. GILBERT*

Department of Chemistry, University of Cincinnati, Cincinnati, OH 45221, U.S.A.

(*Received* 2 *December* 1985; *accepted* 18 *March* 1986)

Abstract—Aqueous solutions containing equimolar chromium(III) and citric acid at various total concentrations and pH values were fractionated by weak ion exchange on amino-propyl-derivatized silica and by isotachophoresis. The chromium : citrate combining ratios were determined by liquid scintillation spectrometry. Of the approximately 15 solution species formed, the six major species were found to contain chromium and citrate in a ratio of 1 : 1. Possible structures of these complexes are discussed.

Hydroxycarboxylic acids are effective complexing agents for metals and are useful pH buffers. As a result, many industrial and analytical separation processes employ these ligands. Citric acid, because of its high solubility and low cost, is particularly widely used. However, its solution chemistry with metals can be complicated since it is known to form complexes containing metal ions of different identity (heteronuclear or mixed-metal complexes).[1–4] Our initial purpose was to study such complexes using chromatographic techniques. The kinetic inertness provided by the use of chromium(III) as one of the metals should permit separation of the mixed species on the chromatographic time scale. This work is our preliminary study of chromium(III) with citric acid alone.

Although the complexation of chromium(III) with citrate has long been recognized, documentation has been sparse. In all studies to date, chromium(III) has been reported to combine with citrate in a 1 : 1 molar ratio.[1,5,6] In the one attempt made to estimate equilibrium constants of formation, the species CrL, $[Cr(OH)L]^-$ and $[Cr(OH)_2L]^{2-}$ were postulated, where L represents the trivalent citrate anion.[6] Equilibrium measurements alone cannot establish unambiguously whether protons are liberated from water molecules in the inner coordination sphere of the chromium or from the very weak hydroxyl groups (pK *ca* 16) of the citric acid. The involvement of the hydroxyl groups of several hydroxycarboxylic acids through dissociation and coordination to metal ions is now well-established[7,8] and is most likely also occurring here. The only other combining ratio previously demonstrated is that of 2Cr : 1 citrate. However, to form this complex, the presence of a large excess of the weakly binding ligand, acetate, was required.[1] These conditions do not pertain to the present experiments.

Through analogy to the reaction of vanadyl(IV) and copper(II) ions with citric acid which showed the release of four equivalents of protons per citric acid reacted,[9] it was reasoned that the chromium(III) citrate complex should be anionic at pH values greater than 4.5. Preliminary experiments using a polystyrene–DVB anion exchanger (Aminex A-27) showed this to be the case. Five components could be resolved from the reaction mixtures but even at elevated temperatures 4 h were required for the separation. Consequently, it was decided to try a weak amino-bonded silica exchanger which should have faster exchange kinetics and improved resolving power. In addition, for confirmation of results, a capillary isotachophoresis apparatus was constructed and used for the separation of the same reaction mixtures.

EXPERIMENTAL

The chromatographic system consisted of an Altex Model 100A high-pressure pump and a Model 153 UV detector operated at 254 nm with a 0.008-cm^3 flow cell. A Knauer column (250 × 4.6 mm) was slurry packed with 5-μm Spherisorb amino-bonded phase using a Haskel pneumatic

* Author to whom correspondence should be addressed.

pump. Counting experiments using ^{51}Cr tracer and ^{14}C-labeled citric acid were done using a Packard Model 3320 liquid scintillation spectrometer.

Isotachophoresis experiments were done on an instrument constructed using the design principles outlined by Everaerts *et al.*[10] A 30-kV power supply with an associated high-voltage controller were commercial units (Bertan Associates, Model 210-30P). The potential-gradient detector was of new design.[11]

A stock solution of chromium(III) was prepared from hexaquochromium(III) perchlorate (G. F. Smith), assayed, and diluted to 0.30 M. An equimolar stock solution of citric acid was prepared by dissolving AR grade monohydrated crystals in water. Mobile phases were made from sodium perchlorate (AR) and tris(hydroxymethyl)aminomethane (primary standard). They were adjusted as required to specific pH values with perchloric acid and sodium hydroxide using a Beckman Zeromatic pH meter. All solutions were filtered through 0.5-μm Millipore membrane filters.

Two sets of sample solutions were prepared which were equimolar in chromium(III) and citric acid. The first set had different levels of chromium(III) and citric acid (0.0060, 0.060 and 0.30 M) but a constant pH of 5.5. The second set was 0.060 M in chromium and citric acid, but had different pH values (4.5, 5.0, 5.5 and 6.0). Because of the slow substitution kinetics of hexaquochromium(III) ions, the solutions were made up slightly under volume to permit pH adjustment as the reactions proceeded. They were kept in a water bath at 45°C until the desired pH value of each solution could be achieved. After cooling and dilution to final volume, the pH values were checked again. This procedure required from 46 to 60 h in the water bath to accomplish.

RESULTS AND DISCUSSION

The reaction of equimolar solutions of chromium(III) and citric acid results in a mixture of products of unexpected complexity. Depending on the solution and chromatographic conditions, 15 or more species can be resolved. Figure 1 shows a typical chromatogram, and indicates the six major peaks selected for study.

Figure 2 shows the chromatograms obtained at different concentration levels obtained from reacting equimolar quantities of chromium(III) and citric acid at pH 5.5. Three things should be noticed: first, the reaction mixtures are exceedingly complicated. Only chromium(III) perchlorate, citric acid, and a little sodium hydroxide for pH adjustment, were used in their preparation. Even the minor peaks are reproducible from run to run and from preparation to preparation. Second, the later eluting peaks are relatively much favored over the earlier peaks as the overall concentration increases. Finally, the retention times of all the peaks are constant and independent of the overall con-

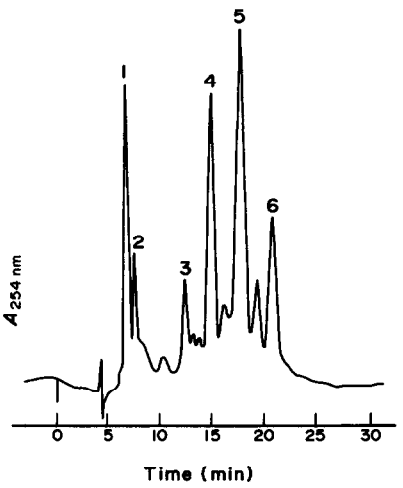


Fig. 1. Anion exchange chromatographic separation of an equimolar reaction mixture of chromium(III) and citric acid at pH 5.5. The numbers indicate the six major peaks chosen for study. Mobile phase: 0.50 M sodium perchlorate, 0.10 M tris buffer. Flow rate 0.90 cm^3 min^{-1}. Sample size 20 mm^3. Detector: UV at 254 nm, 0.16 AUFS.

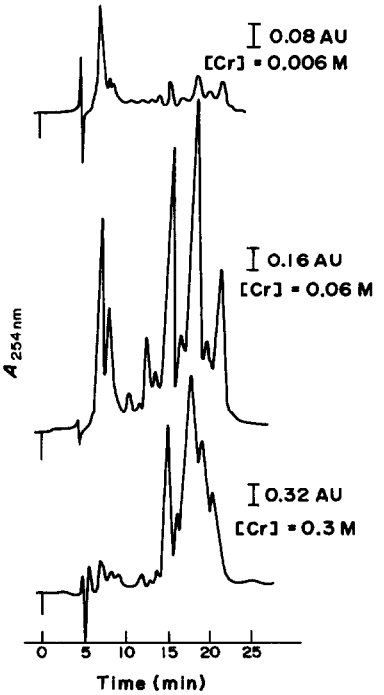


Fig. 2. Effect of overall concentration on peak distribution of equimolar chromium(III)–citrate solutions at pH 5.5. Other conditions as in Fig. 1.

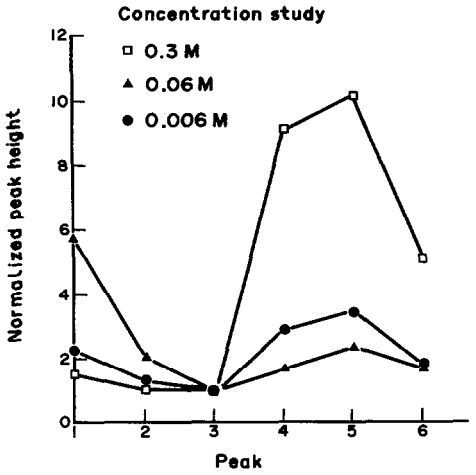


Fig. 3. Normalized relative peak heights as a function of concentration. Data taken from Fig. 2.

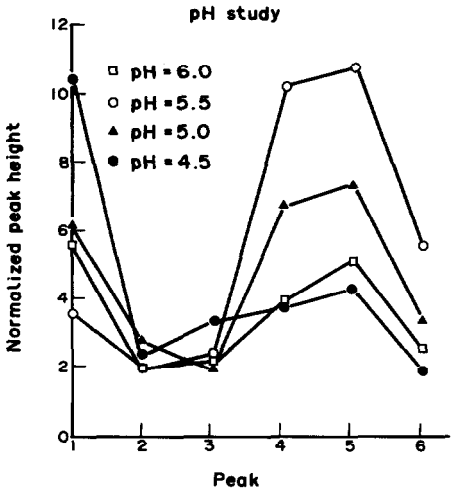


Fig. 5. Normalized relative peak heights as a function of pH. Data taken from Fig. 4.

centration. In order to make direct comparisons of the chromatograms, the peak heights of the six major peaks were normalized to account for the different concentration levels and detector sensitivities employed (Fig. 3).

To study the effect of pH on the yields of the six major solution species, a second set of solutions were prepared and subjected to chromatographic separation. As can be seen from Fig. 4, the same pattern of peaks is obtained in each chromatogram. The retention and the resolution of the peaks decrease as the pH of the solutions increases. This is to be expected, and has nothing to do with the chemistry of the chromium–citrate reaction. It is caused by the decrease in the number of exchange sites of the weak anion exchanger with increasing pH. Again, through a process of normalization of the peak heights to a common exchange capacity of the exchanger, comparisons of the relative amounts of the six peaks can be made (Fig. 5). It can be seen that the first peak eluted is strongly favored at lower pH values, whereas the last three peaks are favored at higher pH values. Peaks 2 and 3 do not seem to be significantly affected.

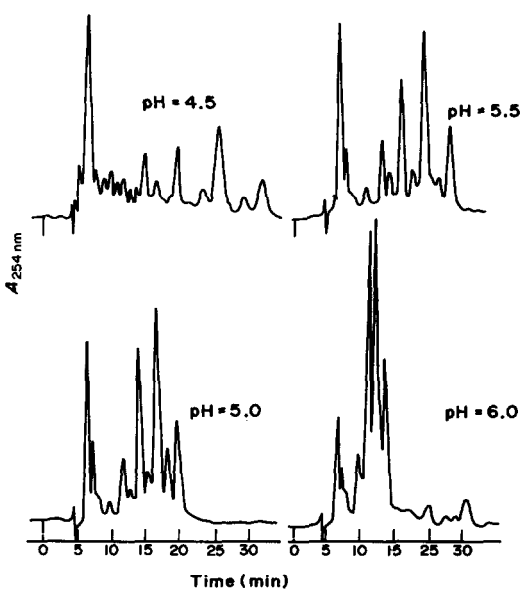


Fig. 4. Effect of pH on peak distribution of equimolar (0.060 M) chromium(III)–citrate solutions. Other conditions as in Fig. 1.

In a series of experiments duplicating the conditions of Fig. 1, ^{51}Cr tracer and ^{14}C-labeled citric acid were incorporated into the reaction mixture. By placing a NaI crystal scintillator flow-through detector in series with the UV detector, a two-channel recording of the chromatographic separation was possible. A chromatogram closely similar to Fig. 1 was obtained from the UV detector, and a second chromatogram from the rate counter showed the same peaks as the UV detector. In addition, the peaks were in the same proportion as in the UV trace. This shows that all the peaks in the chromatogram contain chromium since the crystal was totally unresponsive to ^{14}C, and, further, that the molar absorptivity of the chromium in the separated species is approximately constant.

In another experiment, the six major peaks shown in Fig. 1 were collected as separate fractions, treated with Universal Scintillation Cocktail (Fisher Scientific Co.) and counted with a liquid scintillation spectrometer. It was found that it was not possible to separate completely the emissions of the two isotopes by energy window selection, and so the fractions were counted at 14-day intervals. The activity decreases could be attributed solely to the ^{51}Cr (half-life 27.8 days). A simple calculation from the decay curve then gave the activities of the

Table 1. ^{51}C and ^{14}C activities in separated fractions

Peak No.[a]	Counts per unit time		Normalized counts[b]		Activity ratio
	^{51}Cr	^{14}C	^{51}Cr	^{14}C	(^{51}Cr : ^{14}C)
1	8131	6565	1.57	1.53	1.00 : 0.97
2	5163	4291	1.00	1.00	—
3	5552	4626	1.08	1.08	1.00 : 1.00
4	9109	9092	1.76	2.12	1.00 : 1.20
5	20,373	17,287	3.95	4.03	1.00 : 1.02
6	7707	7099	1.49	1.65	1.00 : 1.11

[a] See Fig. 1 for peak identification.
[b] Peak 2 counts are each assigned to unity.

two isotopes at the time of separation. In Table 1 are shown the counts obtained on each of the fractions corresponding to the six major chromatographic peaks. When the counts are normalized, it is seen that the ratio of chromium to citric acid in each fraction is approximately constant. Since all previous studies have indicated a 1 : 1 combining ratio, it is evident that chromium and citrate are present in this ratio in each one of the species separated.

In order to verify the surprising finding of so many different species formed from so few reactants, another high-performance separation technique was sought. For this product mixture, isotachophoresis seemed the most promising. It differs from chromatography in several important aspects. First, it is a single-phase technique, with no partitioning into or onto a second solid or liquid phase. The basis for separation is totally different; separation is achieved through the differential migration of ionic species according to their effective mobilities in an electric field. If the migrating ions are kinetically inert toward dissociation, then their effective mobilities will be characteristics of the species, and will depend on their charges, solvation and masses. If, in addition, there are present acidic or basic groups which can associate or dissociate, then the effective mobility will be a function of the solution pH as well. When a true isotachophoretic condition is achieved through the appropriate selection of leading and terminating electrolytes and pH, the step heights will be characteristic of the species migrating, and the zone lengths will be proportional to the amounts of the various sample constituents. An important feature of isotachophoresis is that the zone boundaries are self-sharpening. A consequence of this is that the method is useful for minor sample constituents since they are actually concentrated into narrow zones with the same step positions and heights that they would have as major components of the sample.

Figure 6 shows a typical isotachopherogram of an equimolar chromium(III)–citrate mixture. The direct recording of the detector signal (curve A) clearly shows the presence of six major steps. In addition, the derivative trace (curve B) reveals the presence of five or six more zones of minor constituents. It was hoped that the isotachophoretic zones could be correlated one by one with the chromatographic peaks obtained by the ion exchange separation. Unfortunately, our attempts at this were not successful, and only descriptive general conclusions could be reached (*vide infra*). However, it is clear that both separation methods reveal with

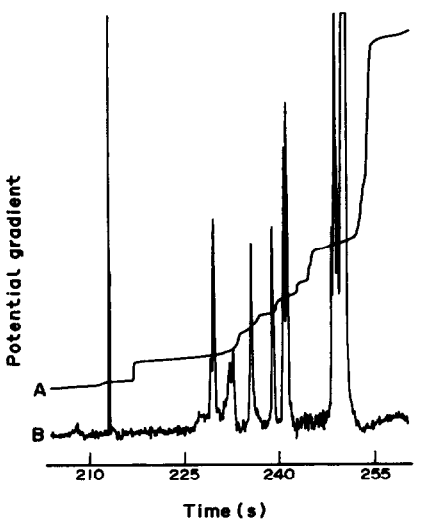


Fig. 6. Isotachopherogram of equimolar (0.024 M) chromium(III)–citrate at pH 5.0. Curve A is the direct signal from the potential gradient detector. Curve B is the electronically obtained and simultaneously recorded derivative of curve A. Curve B is displaced slightly to the left of curve A. For other conditions, see Table 2.

Table 2. Summary of isotachophoresis data on equimolar chromium(III)–citrate mixtures[a]

Concentration of mixture (M)	Sample size (mm^3)	pH[b]	Zones detected	First zone (% of total)	Six major zones (% of total)
0.012	4.0	5.0	14	45	87
0.024	4.0	5.0	11	44	92
0.060	3.0	4.5	9	42	88
0.060	3.0	5.0	10	48	92
0.060	3.0	5.5	8	61	96

[a] Isotachophoresis conditions: leading electrolyte, aniline hydrochloride buffer (0.015 M); trailing electrolyte, caproic acid (0.020 M); electrolysis current, 75 μA; capillary dimensions, 150 mm long × 0.5 mm i.d.

[b] The sample, leading electrolyte, and trailing electrolyte were adjusted to the pH indicated.

comparable efficiency the complicated nature of the reaction of chromium(III) with citric acid.

Table 2 summarizes the results of other isotachophoretic separations of reaction products in which the reactants differed in concentrations and pH values. For reasons related to ionic charge and size, we believe the first isotachophoretic zone is due to a species responsible for one of the later eluting chromatographic peaks. It is seen that both increasing concentration and increasing pH favors its formation. This is the same behavior exhibited by the late eluting chromatographic peaks.

There are many structures for mononuclear and dinuclear complexes of chromium(III) and citric acid which can be drawn exhibiting 1:1 stoichiometry. Some suggestions which seem chemically reasonable and which can be constructed with space-filling molecular models are shown in Fig. 7. The mononuclear structure **I**, as shown, has a net charge of −1. However, simple dissociation of protons from the water molecules in the primary hydration shell could increase the charge. Such differently charged species would not be separable by either technique since they would be in rapid dynamic equilibrium. It is the loss of coordinated water and not the change in protonation which is the slow process.[12] Structure **II** incorporates the dioxo or dihydroxo bridge arrangement which is

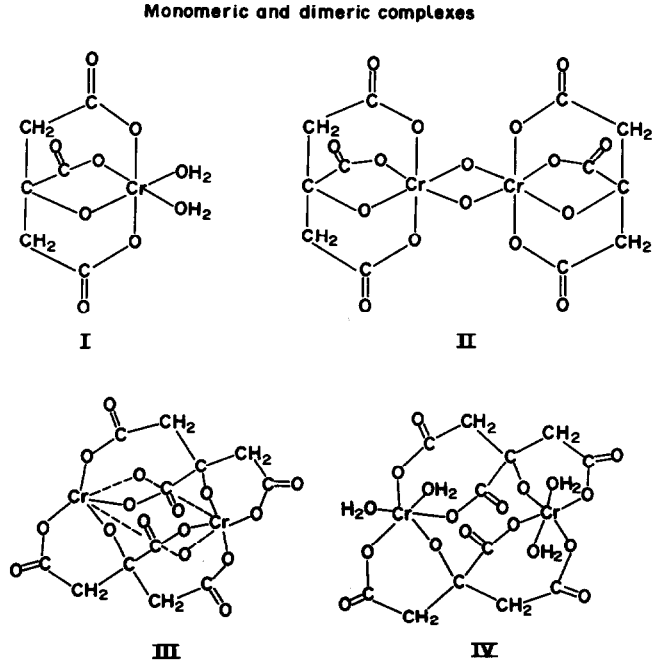


Fig. 7. Postulated structures for chromium(III)–citrate complexes.

well-established in chromium chemistry.[13,14] For the dioxo structure shown, the charge is -6; for the dihydroxo species it would be -4. Again, the protonation equilibria should be rapid and the species inseparable. However, numerous possibilities for isomerization exist which depend on how the citrates coordinate about the chromium nuclei. Structure **III** utilizes only citrate bridges between the chromiums; structure **IV** uses both citrate and oxo bridges. These structures are not written in the belief that these are necessarily the actual species separated in these experiments, but only to indicate how such a complicated mixture could originate. The possibilities for geometric isomers in these structures are many, and it has been shown that geometric isomers of chelated chromium(III) are readily separated by reversed-phase liquid chromatography.[15] Similarly, it would be expected that different spacial geometries would also influence ion exchange partition and effective mobilities.

In conclusion, it should be noted that the results of Tripathy and Patnaik[6] on the formation constants of chromium(III)–citrate complexes were done at a concentration level of about 8 mM in chromium and over a pH range from 3 to 8. Our results clearly show the formation of significant amounts of polynuclear complexes under such conditions. Furthermore, it is uncertain that equilibrium had been achieved since the constants were reported for 25°C and no mention of slow reaction kinetics was made. The constants reported should, therefore, be regarded with great skepticism.

Acknowledgement—This work was supported in part by the National Science Foundation under Grant CHE 77-15319.

REFERENCES

1. T. W. Gilbert and L. Newman, *Anal. Chem.* 1968, **40**, 2123.
2. A. Adin, P. Klotz and L. Newman, *Inorg. Chem.* 1970, **9**, 2499.
3. B. Binder, *Inorg. Chem.* 1971, **10**, 2146.
4. M. M. Petit-Ramel and I. Khalil, *Bull. Soc. Chim. Fr.* 1974, 1259.
5. R. E. Hamm, R. L. Johnson, R. H. Perkins and R. E. Davis, *J. Am. Chem. Soc.* 1958, **80**, 4469.
6. K. K. Tripathy and A. K. Patnaik, *J. Indian Chem. Soc.* 1966, **43**, 772.
7. R. E. Tapscott and R. L. Belford, *Inorg. Chem.* 1967, **6**, 735.
8. R. E. Tapscott and R. L. Belford, *Inorg. Chem.* 1968, **7**, 356.
9. G. Abbay, unpublished experiments.
10. F. M. Everaerts, Th. P. E. M. Verheggen and J. L. Beckers, *Isotachophoresis*. Elsevier, Amsterdam (1976).
11. G. Abbay, T. H. Ridgway, E. Younginger and T. W. Gilbert, submitted for publication.
12. C. Postmus and E. L. King, *J. Am. Chem. Soc.* 1955, **59**, 1208.
13. M. Thompson and R. E. Connick, *Inorg. Chem.* 1981, **20**, 2279.
14. H. Toftlund and J. Springborg, *Chem. Commun.* 1976, 1017.
15. B. Wenclawiak and R. E. Seviers, *Fresenius' Z. Anal. Chem.* 1983, **314**, 682.

Polyhedron Vol. 5, No. 11, pp. 1845–1851, 1986
Printed in Great Britain

0277–5387/86 $3.00+.00
Pergamon Journals Ltd

ON THE EXTRACTION WITH LONG-CHAIN AMINES—XXXVI. EXTRACTION OF Cu(II) FROM CHLORIDE MEDIA

J. COELLO, J. M. MADARIAGA and M. MUHAMMED*

Department of Inorganic Chemistry, The Royal Institute of Technology, S-10044 Stockholm, Sweden

and

M. VALIENTE and H. ITURRIAGA

Departamento de Química Analítica, Universidad Autónoma de Barcelona, Bellaterra, Barcelona, Spain

(*Received* 17 *February* 1986; *accepted* 18 *March* 1986)

Abstract—The extraction of Cu(II) from 5.0 M lithium chloride solutions using tri-*n*-dodecylammonium chloride (TLAHCl) dissolved in toluene was studied at 25°C. The data were treated both graphically, by the normalized-curves methods, and numerically using the LETAGROP–DISTR program. In both cases, the extraction of copper was best explained by the formation of the species $(TLAHCl)_2CuCl_2$ and $(TLAHCl)_5CuCl_2$ in the organic phase. The formation constants for the different species were obtained at different ionic strengths (1.0–5.0 mol dm^{-3}) and correlated using the specific-interaction theory.

The extraction of metals from chloride solutions by long-chain amines has been studied under a great variety of experimental conditions.[1] The extraction of copper by cationic[2–6] and anionic extractants[7–17] from acidic chloride solutions has been studied by several workers, focusing the attention on the speciation in the organic phase and the influence of the chloride ion concentration on the extraction.

The extraction of metals is generally dependent on the composition of the aqueous phase. However, the extraction data for a given system can be used for other aqueous-phase compositions (e.g. different feed solutions) if a correlation of the data to the variation in the aqueous-phase composition could be made. Speciation studies generally consider only the variation of the reacting species, but the presence of non-reacting ions [expressed by the ionic strength (I)] affecting the metal extraction is normally neglected.

Recently, we started a program for a systematic study of the extraction of metals from chloride solutions.[17–19] The extraction of copper from solutions with different chloride concentrations ($[Cl^-] = 1.0$, 2.0 or 3.0 mol dm^{-3}) was reported.[17] The study was extended to include the extraction of copper from solutions with constant I (5.0 mol dm^{-3}) and different chloride concentrations. In the present paper, the work is extended to a chloride concentration of 5.0 mol dm^{-3}.

EXPERIMENTAL

Reagents and solutions

Tri-*n*-dodecylammonium chloride (TLAHCl) was prepared and purified as described in Ref. 20.

Toluene (Merck p.a.) was washed with 0.1 M NaOH, H_2O, 0.1 M HCl and, finally, double distilled water before use.

Copper chloride (Merck p.a.) was purified by recrystallization.

Lithium chloride (Merck p.a.) was recrystallized twice before use as described in Ref. 21.

The organic phase was prepared by dissolving TLAHCl in toluene. The total TLAHCl concentration was varied from 0.05 to 0.265 mol dm^{-3}. The composition of the aqueous phase was $[Cu(II)] = B$ mol dm^{-3}, $[H^+] = A$ mol dm^{-3}, $[Li^+] = 5-2B-A$ mol dm^{-3} and $[Cl^-] = 5.0$ mol dm^{-3}. The total Cu(II) concentration was varied

* Author to whom correspondence should be addressed.

from 0.05 to 0.021 mol dm^{-3}, whereas the hydrogen ion concentration was maintained constant at 10^{-2} mol dm^{-3}.

Distribution measurements

Experiments were carried out at 25°C by shaking equal volumes of both phases using stoppered glass tubes for 3 h. The Cu(II) concentration in the aqueous phase was determined by titrations with EDTA using Fast Sulphon Black as indicator.[22] The organic phase was dissolved in ethanol and the copper was titrated with EDTA using PAN as indicator.[23]

RESULTS AND DISCUSSION

The distribution coefficient of the metal (D) defined as:

$$D = [\text{Cu(II)}]_{org}/[\text{Cu(II)}]_{aq} \quad (1)$$

was determined as a function of the total concentration of TLAHCl at a given total initial Cu(II) concentration in the aqueous phase. The experimental data (log D vs log $[\text{TLAHCl}]_{tot}$) are plotted in Fig. 1. The extraction of Cu(II) can be formally described by the following reaction:

$$n[\text{TLAHCl}]_{org} + Cu^{2+} + 2Cl^- \rightarrow (\text{TLAHCl})_n CuCl_{2org}. \quad (2)$$

In the aqueous phase, the activity coefficients of the different species may be regarded as constant since I was maintained at a constant value. For the organic phase, ideal behaviour is assumed as the concentrations of the reacting species are low. The possible coextraction of water is formally neglected. Experiments using different Cu(II) concentrations indicate the absence of polynuclear complexes in the organic phase.

The equilibrium constant for reaction (2) can be written as:

$$K_n = [(\text{TLAHCl})_n CuCl_2]_{org} [\text{TLAHCl}]_{org}^{-n} [Cl^-]^{-2} [Cu^{2+}]^{-1}. \quad (3)$$

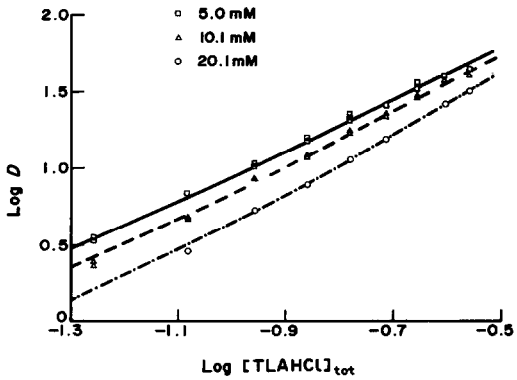


Fig. 1. Experimental points presented as log D vs log-$[\text{TLAHCl}]_{tot}$. Curves are drawn using the constants given in Table 1.

TLAHCl in toluene was found to form trimers:[24]

$$3(\text{TLAHCl})_{org} \rightarrow (\text{TLAHCl})_{3org} \quad (4)$$

and an aggregation constant (log Q) of 2.7 ± 0.1.

The formation constants of the aqueous copper chloride complexes (β_i) are defined as:

$$\beta_i = [CuCl_i^{2-i}][Cu^{2+}]^{-1}[Cl^-]^{-i} \quad (5)$$

and their values at the different Is were calculated from Ref. 25 using the specific-interaction theory. The interaction coefficients used are summarized in Table 1, and the log β_i calculated are given in Table 2.

As $V_{org} = V_{aq}$, the mass balance conditions are:

$$[\text{TLAHCl}]_{tot} = c + 3Qc^3 + \sum nK_n b l^2 c^n, \quad (6)$$

and

$$[\text{Cu(II)}]_{tot} = [\text{Cu(II)}]_{org} + [\text{Cu(II)}]_{aq}, \quad (7)$$

where:

$$[\text{Cu(II)}]_{org} = D(1+D)^{-1}[\text{Cu(II)}]_{tot} = \sum K_n b l^2 c^n, \quad (8)$$

$$[\text{Cu(II)}]_{aq} = (D+1)^{-1}[\text{Cu(II)}]_{tot} = [Cu^{2+}] + \sum [CuCl_i^{2-i}] = b(1 + \sum \beta_i l^i), \quad (9)$$

Table 1. Interaction coefficients (kg mol^{-1}) used in the calculation of log β_i

ε (Cu^{2+}, ClO_4^-) = 0.32[a]	ε ($CuCl^+$, ClO_4^-) = 0.29[b]	ε ($CuCl^+$, Cl^-) = 0.14[c]
ε (Cu^{2+}, Cl^-) = 0.08[a]	ε ($CuCl_3^-$, Na^+) = 0.14[b]	ε ($CuCl_3^-$, Li^+) = 0.29[b]
ε (Cl^-, Na^+) = 0.03[a]	ε ($CuCl_n^{2-}$, Na^+) = 0.22[c]	ε ($CuCl_n^{2-}$, Li^+) = 0.43[b]
ε (Cl^-, Li^+) = 0.10[a]		

[a] Values taken from Ref. 31.

[b] Values taken from Ref. 32, assuming the same values for Cu^{2+} and Zn^{2+}.

[c] Values also taken from Ref. 32, but assumed to be one-half of the related ones.

Table 2. Values of the equilibrium constants for the copper chloro complexes calculated using the specific-interaction theory

I	Log β_1	Log β_2	Log β_3	Log β_4	Log α
5 M ($NaClO_4$)	0.40	0.06	−0.05	−1.60	
5 M (LiCl)	0.17	−0.99	−1.51	−3.04	−1.19
3 M (LiCl)	0.13	−1.60	−1.68	−3.17	−0.77
2 M (LiCl)	0.13	−1.84	−1.71	−3.20	−0.59
1 M (LiCl)	0.19	−1.99	−1.67	−3.18	−0.41

and

$$[Cl^-]_{tot} = [Cl^-]_{aq} + [Cl^-]_m. \quad (10)$$

$[Cl^-]_{tot}$ is the total initial chloride concentration in the aqueous phase, $[Cl^-]_{aq}$ is the total chloride in the aqueous phase at equilibrium, and $[Cl^-]_m$ is the total chloride extracted together with the copper.

It follows that:

$$[Cl^-]_m = 2[(TLAHCl)_nCuCl_2]_{org} = 2[Cu(II)]_{org}, \quad (11)$$

and

$$[Cl^-]_{aq} = l + \sum i[CuCl_i^{2-i}]. \quad (12)$$

b, l and c are the free equilibrium concentrations of Cu^{2+}, Cl^- and TLAHCl, respectively.

Using eqns (1), (8) and (9) D can be written as:

$$D = \sum K_n l^2 c^n (1 + \sum \beta_i l^i)^{-1}. \quad (13)$$

The data were treated using both graphical and numerical methods, for the determination of the extracted copper species and their constants.

Graphical treatment

Assuming that only one species containing copper is formed in the organic phase, eqn (13) could be rewritten as:

$$\log D = \log K_n (1 + \sum \beta_i l^i)^{-1} + N \log c + 2 \log l, \quad (14)$$

and

$$\log D = \log K_n' + N \log c \quad (15)$$

where K_n' is a conditional constant defined by:

$$K_n' = K_n l^2 (1 + \sum \beta_i l^i)^{-1}. \quad (16)$$

Different n values will thus represent different species.

Models with $n = 2$, 3, 4 and 5 were considered. As the total copper concentration is much smaller than total chloride concentration, it is possible to assume, as a first approximation, that the free $[Cl^-]$ (l) is equal to the total chloride. For each case the free [TLAHCl] (c) was calculated using eqns (6) and (8). For the model to be accepted, a plot of $\log D$ vs $\log c$ should yield a straight line with a slope equal to the assumed n. None of the models fulfill this condition. This indicates that more than one species containing copper may be present in the organic phase.

In further treating the data, the variation in free $[Cl^-]$ as a result of copper extraction was considered.

A conditional distribution coefficient (D') may be defined as:

$$D' = D(1 + \sum \beta_i l^i) l^{-2}, \quad (17)$$

and eqn (13) is rewritten as:

$$D' = \sum K_n c^n. \quad (18)$$

Using $[Cu(II)]_{aq}$, $[Cl^-]_{aq}$ can be calculated from eqns (10) and (11). l can be calculated for each point by solving the copper and chloride mass balance equations using the values of the chloro complex formation constants.

In order to determine the free TLAHCl, the term $\sum n K_n b l^2 c^n$ in eqn (6) was estimated using the approximation:

$$\sum n K_n b l^2 c^n \approx \nu \sum K_n b l^2 c^n \approx \nu [Cu(II)]_{org}, \quad (19)$$

where ν is the average number of TLAHCl molecules bound to the metal in the organic phase. In this case, from the slopes obtained in the treatment considering only one species, a value for ν of 3.5 seems acceptable.

The TLAHCl mass balance equation can then be written as:

$$[TLAHCl]_{tot} = c' + 3Qc'^3 + 3.5[Cu(II)]_{org}, \quad (20)$$

where c' is the free ammonium salt concentration.

Assuming two copper-containing species do exist

in the organic phase, eqn (18) can be written as:

$$D' = K_p c'^p + K_s c'^s \quad (p < s), \tag{21}$$

or

$$D'/K_p c'^p = 1 + (K_s c'^{s-p})/K_p. \tag{22}$$

A normalized variable is defined by:

$$V^r = (K_s/K_p)c'^r, \tag{23}$$

where $r = s - p$. The normalized function (Y) is thus obtained:

$$Y = 1 + V^r. \tag{24}$$

By plotting log Y vs log V a set of curves is thus obtained for different r values. Superimposing the plot of log Y vs log V on the experimental curve $\log(D'/c'^p)$ vs $\log c'$, and, with vertical and horizontal translations of the curves, it may be possible to obtain the position of the best fit. By reading off the differences:

$$\log(D'/c'^p) - \log Y = \log K_p \tag{25}$$

and

$$(\log V - \log c') = (\log K_s - \log K_p)/r \tag{26}$$

the values of the formation constants are obtained.

Two different models were considered. First, assuming $p = 3$, c' was calculated using $v = 3.5$. In the second model ($p = 2$) a better fit was obtained. The same graphical treatment was applied to an earlier study.[17] It was found that the data were better explained by the present model. The plots showing the best fits for the different ionic strengths are presented in Fig. 2. A summary of the values of the constants graphically obtained are given in Table 3.

Computer calculations

The experimental data at 5.0 mol dm^{-3} ionic strength were treated by using the LETAGROP–DISTR program.[26] In this treatment the error-square sum defined by eqn (27) is minimized:

$$U = \sum_{N_p} (\log D_{calc} - \log D_{exp})^2. \tag{27}$$

The standard deviation [σ (log D)] is defined as:

$$\sigma(\log D) = (U/N_p)^{1/2}, \tag{28}$$

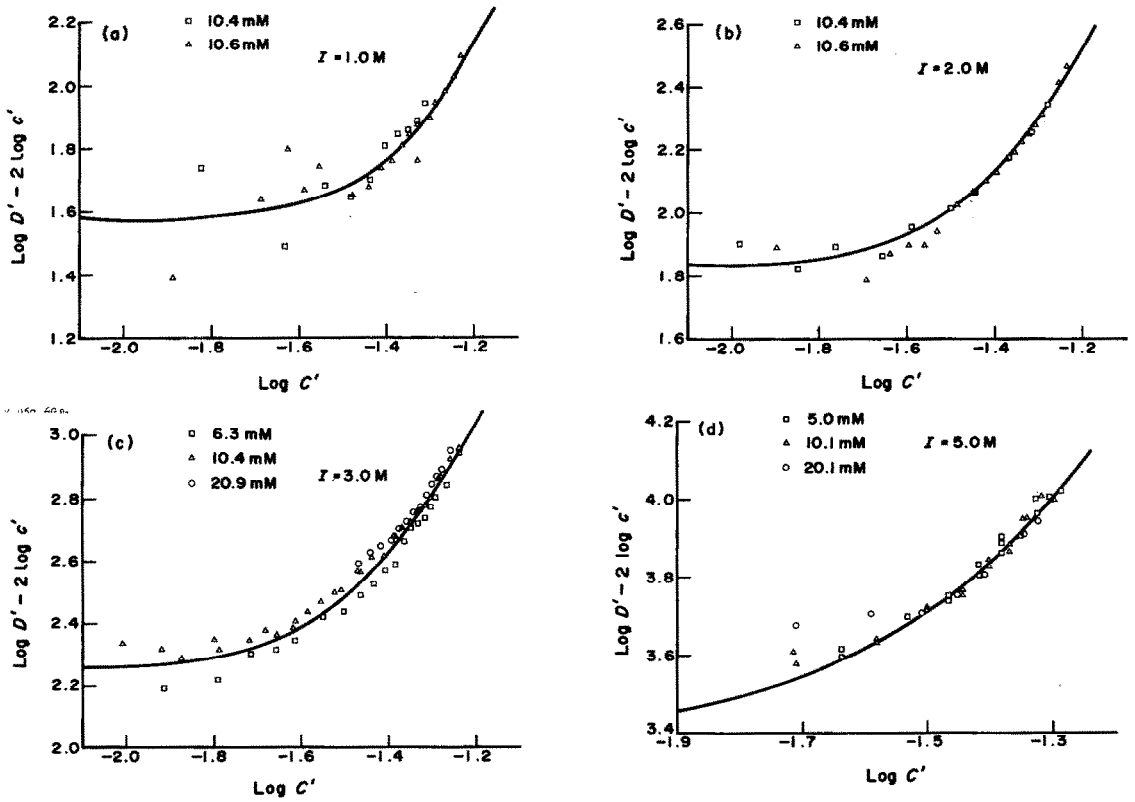


Fig. 2. Plot of $\log D' - 2\log[\text{TLAHCl}]_{free}$ vs $\log[\text{TLAHCl}]_{free}$ calculated from eqn (20) for different ionic strengths (I): (a) $I = 1.0$ M, (b) $I = 2.0$ M, (c) $I = 3.0$ M, and (d) $I = 5.0$ M. The continuous lines are the normalized functions log Y vs log V with $r = 3$. $c' = [\text{TLAHCl}]_{free}$.

Table 3. Formation constants for copper extraction in reaction (2) obtained graphically and numerically, plus values of the conditional extraction constants (molar scale)[a]

I	p q r	Graphical log K_n	LETAGROP–DISTR log K_n	U	$\sigma(\log D)$	Log K'_n
1	2 1 2	1.60	1.61±0.07			1.20±0.07
	5 1 2	5.76	5.73±0.09	0.0274	0.0361	5.32±0.09
2	2 1 2	1.85	1.84±0.03			1.25±0.03
	5 1 2	6.19	6.21±0.05	0.0217	0.0283	5.62±0.05
3	2 1 2	2.28	2.27±0.04			1.50±0.04
	5 1 2	6.80	6.79±0.04	0.0805	0.0363	6.02±0.04
5	2 1 2	3.46	3.43±0.02			2.24±0.02
	5 1 2	7.81	7.83±0.03	0.0160	0.0200	6.64±0.03

[a] Values of the constants are given with $\pm 3\sigma$ (log K).

where N_p is the total number of experimental points used in the calculations.

The model suggested in the earlier study as well as that proposed from the graphical treatment were considered. Other species were also assumed and their effect on the goodness of the fit was examined. The best fit of the data was obtained with the model $(TLAHCl)_2CuCl_{2\,org} + (TLAHCl)_5CuCl_{2\,org}$.

The data of Ref. 17 were also subjected to the computer treatment and the model suggested at 5.0 mol dm^{-3} was also found to give a better fit for the lower chloride concentrations.

The results obtained are summarized in Table 3.

Dependence of K_n *on the ionic strength*

The results of the Cu(II) extraction studies at different Is indicate that the composition of the extracted species is independent of I, whereas the formation constants of the different species vary with I.

In order to correlate the values of the equilibrium constants to I, the specific-interaction theory, developed by Guggenheim[27] and Scatchard,[28] was used. In this approach the activity coefficient (γ_i) of an ion of charge Z_i in a solution of I may be expressed as:

$$\log \gamma_i = -Z_i^2 D(I) + \sum \varepsilon(i,k) m_k. \quad (29)$$

The summation is made over all ions (k) present in the solution at molality m_k. $D(I)$ is the Debye–Hückel term $A\sqrt{I}/(1+1.5\sqrt{I})$, with $A = 0.5107$ at 25°C, while the ε terms, called interaction coefficients, are equal to zero if ions i and k are of the same charge sign.

Assuming ideality in the organic phase, the dependence of β^I on I is given by:

$$\log \beta^I = \log \beta^0 - (\Delta z^2 A\sqrt{I})/(1+1.5\sqrt{I}) + \sum \varepsilon(i,k) I_k, \quad (30)$$

with

$$\Delta z^2 = \sum n_j z_j^2 - \sum p_l z_l^2, \quad (30a)$$

where n_j denotes the stoichiometric coefficients of the reacting ionic species of charge Z_j [Cu^{2+} and Cl^- in eqn (2)], p_l is the coefficient of the ionic species of charge Z_l formed in reaction (2), and β^0 represents the formation constant at zero I in the molal scale.

It is possible to define a conditional constant (K'_n) for reaction (2) that describes the equilibria without taking into account the copper chloro complexes in the aqueous phase:

$$K'_n = K_n \alpha, \quad (31)$$

where α is the fraction of the free copper concentration:

$$[Cu^{2+}] = [Cu(II)]_{tot}\alpha, \quad (32)$$

and

$$\alpha = (1 + \sum \beta_i l^i)^{-1}. \quad (33)$$

The log α values at different Is (on the molar scale) are given in Table 2, and the calculated log k_n are summarized in Table 3.

In this case, for the equilibrium given by eqn (2) the species in the organic phase are non-ionic. It follows that $\Delta z^2 = 6$, and eqn (30) can be written as:

$$\log K_n^{\prime I} + 6A\sqrt{I}/(1+1.5\sqrt{I}) = \log K_n^{\prime 0} + \sum \varepsilon I, \quad (34)$$

where:

$$K_n'^0 = [(TLAHCl)_nCuCl_2]_{org}[Cu^{2+}]^{-1}[Cl^-]^{-2}[TLAHCl]^n_{org}, \quad (35)$$

and

$$\sum \varepsilon = \varepsilon(Cu^{2+}, Cl^-) + 2\varepsilon(Cl^-, Li^+). \quad (36)$$

Plotting $\log K_n'^I + 6D(I)$ vs I a straight line should be obtained with an intercept equal to $\log K_n'^0$ and a value for the slope given by eqn (36).

To correlate the constants it is necessary first to transform them to the molality scale. The concentration C (in mol dm^{-3}) of a solute with molecular weight M_w is expressed in units of molality, knowing the density of the solution (ρ), by using the expression:

$$m = C/(\rho - 10^{-3}CM_w). \quad (37)$$

For the species present in the organic phase, their concentration is very small and the term $10^{-3}CM_w$ is assumed to be negligible, and thus the density of the pure solvent can be used.[29] In the aqueous phase, the density of the solution is considered equal to the density of the ionic medium. The values have been taken from Ref. 30.

The experimental points have been plotted in Fig. 3 and fitted to a straight line with a weight $W = \sigma^{-2}$, where σ is the standard deviation of the extraction constants of reaction (2) given in Table 3. The obtained values of the constants (on the molar scale) are $\log K_2'^0 = 1.97 \pm 0.06$ and $\log K_5'^0 = 6.33 \pm 0.10$.

Slope values [0.31 ± 0.01 for $(TLAHCl)_2CuCl_2$, and 0.32 ± 0.02 for $(TLAHCl)_5CuCl_2$] agree with the ε values tabulated in Ref. 31 and given in Table 1.

The distribution diagram of the different species containing copper is plotted in Fig. 4.

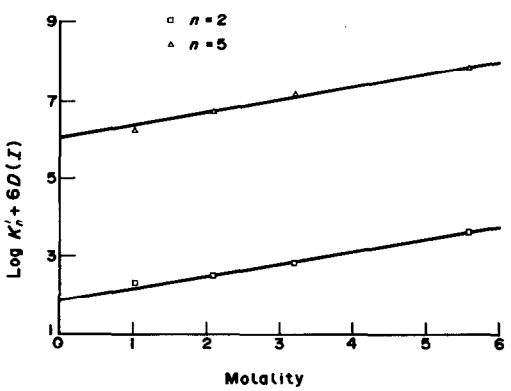


Fig. 3. Plot of $\log K_n' + 6A\sqrt{I}/(1+1.5\sqrt{I})$ [$D(I)$] vs ionic strength. The intercepts are $\log K_2'^0 = 1.89 \pm 0.06$, and $\log K_5^0 = 6.07 \pm 0.10$ (on the molal scale).

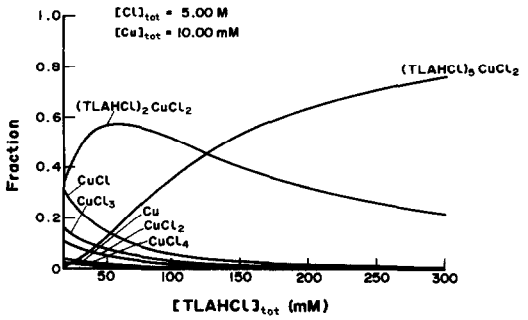


Fig. 4. Distribution of the species containing copper at different $[TLAHCl]_{tot}$.

Acknowledgement—We wish to thank Prof. E. Högfeldt for his suggestions and comments on the manuscript.

REFERENCES

1. Y. Marcus and A. S. Kertes, *Ion Exchange and Solvent Extraction of Metal Complexes*. Wiley Interscience, New York (1969).
2. P. G. Christie, V. I. Lakshmanan and G. Lawson, *Proc. ISEC* 74 (*Lyon*) 1974, **1**, 685.
3. V. I. Lakshmanan, C. J. Lawson and P. S. Nylholm, *Proc. ISEC* 74 (*Lyon*) 1974, **1**, 699.
4. V. I. Lakshmanan and C. J. Lawson, *J. Inorg. Nucl. Chem.* 1974, **37**, 207.
5. H. Eccles, C. J. Lawson and J. Rawlence, *Hydrometallurgy* 1976, **1**, 349.
6. P. G. Christie, V. I. Lakshmanan and G. J. Lawson, *Hydrometallurgy* 1976, **2**, 105.
7. G. Nakagawa, *J. Chem. Soc. Jpn, Pure Chem.* 1960, **81**, 1533.
8. J. Mizumachi, *J. Chem. Soc. Jpn, Pure Chem.* 1962, **83**, 67.
9. S. Lindenbaum and G. E. Boyd, *J. Phys. Chem.* 1963, **67**, 1238.
10. D. F. C. Morris and E. R. Gardner, *Electrochim. Acta* 1963, **8**, 823.
11. Y. Marcus, *Coord. Chem. Rev.* 1967, **2**, 257.
12. F. G. Seeley and D. J. Crouse, *J. Chem. Eng. Data* 1966, **11**, 424.
13. T. Sato and K. Adachi, *J. Inorg. Nucl. Chem.* 1969, **31**, 1395.
14. T. Sato and T. Kato, *J. Inorg. Nucl. Chem.* 1977, **39**, 1205.
15. T. Sato, A. Katsuhiko, K. Toshikazu and N. Takato, *Sep. Sci. Technol.* 1983, **17**, 1565.
16. T. Sato, *J. Appl. Chem. Biotechnol.* 1972, **22**, 1233.
17. M. Valiente and M. Muhammed, *Chem. Scr.* 1984, **23**, 64.
18. M. Aguilar and M. Muhammed, *J. Inorg. Nucl. Chem.* 1976, **38**, 1193.
19. J. Aparicio, M. Valiente and M. Muhammed, *Solvent Extr. Ion Exch.* 1985, **3**, 485.
20. M. Muhammed, J. Szabon and E. Högfeldt, *Chem. Scr.* 1974, **6**, 61.

21. *Some Laboratory Methods.* Mimeograph, Department of Inorganic Chemistry, The Royal Institute of Technology, Stockholm (1959).
22. A. I. Vogel, *A Text Book of Quantitative Inorganic Analysis*, 3rd Edn. Longman, London (1961).
23. G. Schwarzenbach and H. Flashka, *Complexometric Titrations.* Methuen, London (1969).
24. J. Aparacio, J. Coello, L. A. Fernandez and M. Muhammed *Chem. Scr.* (in press).
25. R. W. Rammette and G. Fan, *Inorg. Chem.* 1983, **22**, 3323.
26. D. H. Liem, *Acta Chem. Scand.* 1971, **25**, 1421.
27. E. A. Guggenheim, *Application of Statistical Mechanics.* Clarendon Press, Oxford (1966).
28. G. Scatchard, *Equilibrium in Solution. Surface and Colloid Chemistry.* Harvard University Press, Cambridge, MA (1976).
29. J. A. Riddick and W. B. Bunger, *Organic Solvents.* Wiley Interscience, New York (1970).
30. C. Baes and R. Mesmer, *The Hydrolysis of Cations.* Wiley Interscience, New York (1976).
31. L. Ciavatta, *Ann. Chim. (Rome)* 1980, **70**, 551.
32. J. Aparicio, J. Coello, L. A. Fernandez and M. Muhammed, unpublished data.

Polyhedron Vol. 5, No. 11, pp. 1853–1855, 1986
Printed in Great Britain

0277–5387/86 $3.00+.00
Pergamon Journals Ltd

SYNTHESIS AND CHARACTERISTIC STUDIES OF TIN(II) AND TIN(IV) COMPLEXES OF MACROCYCLIC SCHIFF BASES

ANIL VARSHNEY and J. P. TANDON*

Department of Chemistry, University of Rajasthan, Jaipur 302004, India

(*Received* 30 *January* 1986; *accepted* 18 *March* 1986)

Abstract—Equimolar reactions of tin (II) chloride, tin(IV) chloride or dimethyltin dichloride with macrocyclic Schiff bases lead to the formation of a new series of tin(II) and tin(IV) complexes. An attempt has been made to prove the structures of the resulting complexes on the basis of elemental analysis, conductance measurements, molecular-weight determination, and electronic, IR and multinuclear magnetic resonance (^{1}H, ^{13}C and ^{119}Sn) spectral studies.

Apart from some recent papers dealing with tin(II) and tin(IV) adducts with various crown ethers[1–5] no work has been reported on the tin(II) and tin(IV) macrocyclic Schiff base complexes. In view of this, it was considered of interest to synthesize and characterize tin(II) and tin(IV) derivatives of these ligands, and the results of these investigations are reported in this paper.

EXPERIMENTAL

All the reactions were carried out under an anhydrous and oxygen-free nitrogen atmosphere. Stannous chloride was dehydrated by dissolving it into acetic anhydride.[6] The ligands (2,3,8,9-tetraphenyl-1,4,7,10-tetraazacyclododeca-1,3,7,9-tetraene and 2,3,8,9 - tetraphenyl - 5,12 - dimethyl - 1,4,7,10 - tetraazacyclododeca-1,3,7,9-tetraene) were prepared by mixing ethylenediamine or 1,2-propylenediamine with an alcoholic solution of benzil in a 1 : 1 molar ratio followed by the addition of 6 cm^3 of concentrated hydrochloric acid. The resulting solution was refluxed for about 2 h on a waterbath and kept overnight. A light yellow crystalline solid precipitated out, which was recrystallized from ethanol. The ligands are also soluble in carbon tetrachloride, chloroform, methanol, DMF and DMSO (m.p. 159 and 96°C).

The complexes were analysed as reported earlier[7,8] and the IR spectra were recorded on a Perkin–Elmer 577 IR spectrophotometer in the region 4000–200 cm^{-1} using KBr optics. The electronic spectra (in methanol) were taken on a Toshniwal spectrophotometer. A Perkin–Elmer (Model R-12B) spectrometer was used for obtaining the PMR spectra employing $CDCl_3$ as the solvent and TMS as the internal standard.

Molar-conductance measurements were made in anhydrous dimethylformamide at 36 ± 1°C using a Systronics conductivity bridge Model 305. Molecular-weight determinations were carried out by the Rast Camphor method. ^{13}C and ^{119}Sn NMR spectra were recorded on a 90-MHz JEOL NMR spectrometer using $CHCl_3$ as the solvent, and TMS and TMT as the internal standards.

Synthesis of tin(II) *and tin*(IV) *complexes*

To a weighed amount of tin(II) chloride, tin(IV) chloride or dimethyltin dichloride was added the calculated amount of ethylenediamine or 1,2-propylenediamine and benzil in a 1 : 2 : 2 molar ratio, using tetrahydrofuran or benzene as the reaction medium in an oxygen-free nitrogen atmosphere. The color of the contents immediately changed from light yellow to dark yellow. The solution was stirred using a magnetic stirrer for *ca* 1 h. The excess solvent was removed from the filtrate and the compound was finally dried *in vacuo* at a bath temperature of 40 ± 5°C after being repeatedly washed with dry cyclohexane.

RESULTS AND DISCUSSION

Reactions of tin(II) chloride, tin(IV) chloride and dimethyltin dichloride with ethylenediamine or 1,2-propylenediamine and benzil in a 1 : 2 : 2 molar ratio afford adducts of types $SnCl_2 \cdot L$, $SnCl_4 \cdot L$ and $Me_2SnCl_2 \cdot L$ (L = a macrocyclic Schiff base). These

* Author to whom correspondence should be addressed.

Table 1. Characteristic properties of tin(II) and tin(IV) complexes

No.	Reactants (g)			Yield (%)	Product characteristics (colour and state)	M.p. (°C)	Analysis (%)			Molecular weight	
	Tin compound	Ligand	Molar ratio				Sn Found (calc.)	N Found (calc.)	Cl Found (calc.)	Found	(calc.)
1	$SnCl_2$ (0.246)	$C_{32}H_{28}N_4$ (0.607)	1:1	80	$SnCl_2 \cdot C_{32}H_{28}N_4$ (Red solid)	210	18.0 (18.0)	8.0 (8.5)	10.2 (10.8)	642	(658)
2	$SnCl_2$ (0.623)	$C_{34}H_{32}N_4$ (1.629)	1:1	76	$SnCl_2 \cdot C_{34}H_{32}N_4$ (Yellow solid)	180	16.8 (17.3)	7.9 (8.2)	9.9 (10.3)	661	(686)
3	$SnCl_4$ (0.325)	$C_{32}H_{28}N_4$ (0.583)	1:1	77	$SnCl_4 \cdot C_{32}H_{28}N_4$ (Yellow solid)	290	16.0 (16.3)	7.2 (7.7)	19.0 (19.5)	701	(729)
4	$SnCl_4$ (0.615)	$C_{34}H_{32}N_4$ (1.170)	1:1	78	$SnCl_4 \cdot C_{34}H_{32}N_4$ (Red solid)	280	15.0 (15.7)	7.0 (7.4)	18.3 (18.8)	740	(757)
5	Me_2SnCl_2 (0.813)	$C_{32}H_{28}N_4$ (1.731)	1:1	77	$Me_2SnCl_2 \cdot C_{32}H_{28}N_4$ (Yellow solid)	240	16.9 (17.3)	7.9 (8.1)	10.0 (10.3)	710	(688)
6	Me_2SnCl_2 (0.345)	$C_{34}H_{32}N_4$ (0.778)	1:1	76	$Me_2SnCl_2 \cdot C_{34}H_{32}N_4$ (Yellow solid)	245	16.0 (16.6)	7.2 (7.8)	9.3 (9.9)	691	(716)

adducts are soluble in solvents like methanol, DMSO and chloroform, but insoluble in benzene.

The molar conductance of 10^{-3} M solutions of these adducts in DMF lies in the range 10–20 Ω^{-1} cm^2 mol^{-1}, indicating their non-electrolytic nature. The molecular weights of the adducts determined by the Rast Camphor method correspond with the formula weight, indicating their monomeric nature.

In the electronic spectra of the ligands, a band is observed at *ca* 218 nm, which may be assigned to the "1*B*" band of the phenyl ring. This undergoes a bathochromic shift due to complexation and is observed at *ca* 220 nm in the complexes. Similarly, the ligand chromophore C=N, which absorbs at *ca* 290 nm, shifts to a higher wavelength and is observed at 296 nm. The band in the spectrum of the ligand at *ca* 340 nm is likely to be the secondary band of the benzene and this shifts to 370 nm in the complexes possibly due to polarization of the C=N bond caused by the metal–ligand interaction.

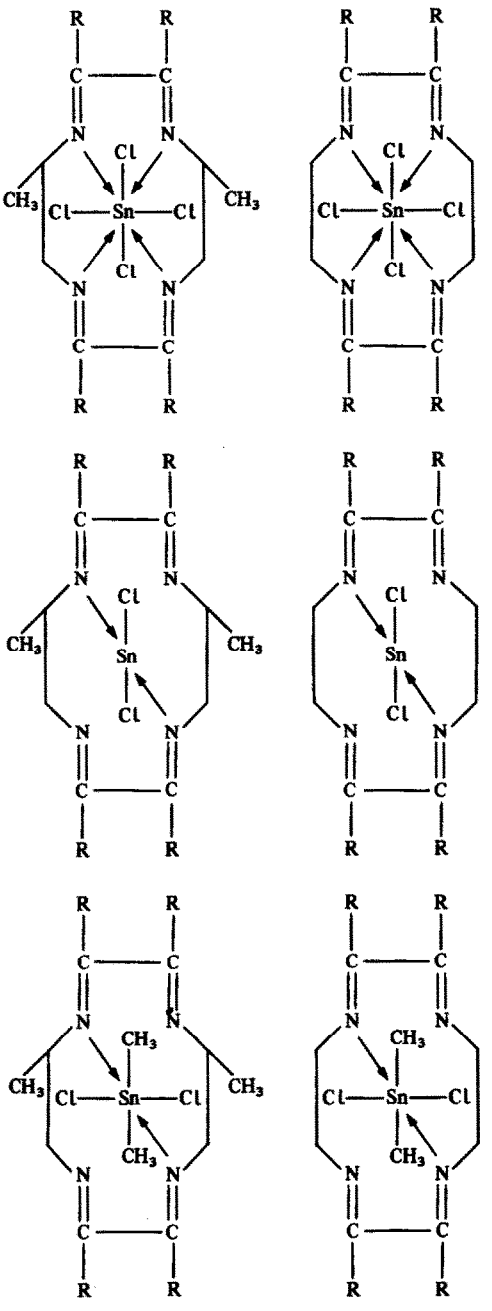
The strong ligand band around 1620 cm^{-1} assignable to C=N is shifted to a higher wavenumber in the spectra of the adducts and this indicates coordination of the ligand through the nitrogen atom of the azomethine group.[9] The new bands around 430 and 600 cm^{-1} in the complexes could be assigned to $\nu(N \rightarrow Sn)$ and $\nu(C—Sn)$,[10] respectively. In the PMR spectra of the adducts in DMSO-d_6, the signals at δ 2.25 and 8.15 ppm have been assigned to methyl and methine protons, respectively. These signals appear downfield compared to the corresponding signals (δ 2.10 and 8.00 ppm) of the ligands, indicating coordination of the ligands to the tin via the azomethine nitrogen. The proton signals due to phenyl groups are observed in the range δ 6.5–7.6 and shift downfield, lending further support to the above mode of coordination.

In the ^{13}C NMR spectra of the ligands, the presence of four signals at δ 167.2, 168.2, 169.5 and 170.2 ppm may be due to all the four azomethine carbons. All these four signals shift downfield (δ 169.2, 170.3, 170.6 and 171.31 ppm, respectively) in the case of tin(IV) chloride adducts, indicating the coordination of all four nitrogens to the tin atom. However, in the case of tin(II) chloride adducts, out of the four signals originally observed, only two signals (δ 167.2 and 169.5 ppm) shift downfield (δ 168.3 and 170.3 ppm), indicating the coordination of only two of these nitrogens to the tin.

The compound $SnCl_4 \cdot C_{34}H_{32}N_4$ gives a sharp signal at δ −638 ppm in the ^{119}Sn NMR spectrum, which is far below the value reported for tin(IV) chloride (δ −150 ppm).[11] On this basis an antiprismatic eight-coordinate structure similar to the tin phthalocyanine system[12] may be proposed for this complex.

The compound $SnCl_2 \cdot C_{34}H_{32}N_4$ gives a sharp signal at δ −576 ppm in the ^{119}Sn NMR spectrum, which is below the reported value for tricoordinated hydrated tin(II) chloride.[13] Therefore, a four-coordinate square pyramidal geometry can be proposed for the resulting tin(II) complex.

Furthermore, the presence of a sharp signal at δ −250 ppm in the ^{119}Sn NMR spectrum of the tin(IV) complex $Me_2SnCl_2 \cdot C_{34}H_{32}N_4$ can be attributed to an octahedral six-coordinate geometry as also reported earlier.[14] On the basis of the above evidence, the following tentative structures can be assigned to these newly synthesized derivatives:



where R = C_6H_5

Acknowledgement—One of us (A.V.) is thankful to the U.G.C., New Delhi, India, for financial assistance.

REFERENCES

1. R. H. Herber and A. E. Smelkinson, *Inorg. Chem.* 1978, **17**, 1023.
2. P. A. Cusack, B. N. Patel and P. J. Smith, *Inorg. Chim. Acta.* 1983, **76**, L21.
3. P. A. Cusack, B. N. Patel, P. J. Smith, D. W. Allen and I. W. Nowell, *J. Chem. Soc., Dalton Trans.* 1984, 1239.
4. G. Valle, A. Cassol and U. Russo, *Inorg. Chim. Acta* 1984, **82**, 81.
5. U. Russo, A. Cassol and A. Silvestri, *J. Organomet. Chem.* 1984, **260**, 69.
6. R. Gull and M. Zeldin, *J. Inorg. Nucl. Chem.* 1975, **37**, 1133.
7. A. Varshney and J. P. Tandon, *Polyhedron* 1985, **4**, 1311.
8. A. Varshney, J. P. Tandon and A. J. Crowe, *Polyhedron* 1986, **5**, 739.
9. A. Varshney and J. P. Tandon, *Indian J. Chem.* 1985, **24A**, 70.
10. A. Saxena and J. P. Tandon, *Polyhedron* 1984, **3**, 681.
11. J. D. Kennedy and W. McFarlane, *Rev. Silicon, Germanium, Tin, Lead Compd* 1974, **3**, 935.
12. W. E. Bennett, *Abstracts, 152nd American Chemical Society National Meeting New York City, September* 1966.
13. P. J. Smith and L. Smith, *Inorg. Chim. Acta Rev.* 1973, **7**, 11.
14. J. D. Kennedy and W. McFarlane, *J. Chem. Soc., Perkin* II 1974, 146.

Polyhedron Vol. 5, No. 11, pp. 1857–1863, 1986
Printed in Great Britain

0277–5387/86 $3.00+.00
Pergamon Journals Ltd

TRANS-BIS(DIFLUOROBORONDIMETHYLGLYOXIMATO) COBALT(III) COMPLEXES CONTAINING IMIDAZOLE AND CHLORIDE OR THIOCYANATE AS AXIAL LIGANDS

JAYANTA K. DAS and KAILASH C. DASH*

Department of Chemistry, Utkal University, Vani Vihar, Bhubaneswar 751004, India

(*Received* 11 *November* 1985; *accepted* 18 *March* 1986)

Abstract—Halo- and pseudohalocobaloxime complexes $[Co(DH)_2(Im)(X)]$ (X = Cl or CNS), containing imidazole (Im) or its derivatives, interact with $BF_3 \cdot Et_2O$ to form a series of cobalt(III) complexes, $[Co(DBF_2)_2(Im)(X)]$, that contain a 14-membered macrocyclic ligand. These light coloured microcrystalline solid complexes, stable under ordinary conditions, were characterized on the basis of elemental analyses, conductivity measurements, electronic, IR, NMR and mass spectra, and thermogravimetric and cyclic voltammetric studies, and are shown to possess a six-coordinated *trans*-octahedral configuration. The mass spectra do not reveal any molecular-ion peak whereas the results of thermolyses reveal the decreased stability of these complexes compared to the corresponding cobaloximes and yield polymeric intermediates, and finally forming Co_3O_4 as the end product. Cyclic voltammetric studies show four reductive waves and an oxidative wave, confirming an oxidation number of III for the central cobalt atom.

The study of macrocyclic-ligand systems is of importance in view of their presence in many biologically significant naturally occurring metal complexes, such as the metallo proteins, vitamin B_{12} and chlorophyll etc. In these macrocyclic complexes both the metal ion and the size of the ring play an important role.[1] Investigation of macrocyclic complexes of cobalt(III) throws light on different aspects of stereochemistry,[2–4] molecular rearrangement and electrochemistry[5,6] etc. In view of the biological significance of imidazole (Im), a fundamental component of enzymes and proteins[7,8] and of cobaloximes, which simulate the reactions of vitamin B_{12} and are of importance in vitamin B_{12} "model chemistry",[9,10] we have been studying the syntheses and the stereochemical as well as biochemical behaviour of Im-containing cobaloxime complexes with the general formulae $[Co(DH)_2(L)(X)]$ (DH = the monoanion of dimethylglyoxime; X = Cl, CNS, CNSe, N_3, ClO_4, BF_4, NO_2, NO_3 etc.; L = Im, benzimidazole and their different substituted derivatives).[11–15] The report of Schrauzer[16] on the reactivity of $BF_3 \cdot Et_2O$ with bis(dimethylglyoximato)nickel(II) $[Ni(DH)_2]$ to form the yellow planar macrocyclic complex bis(difluoroborondimethylglyoximato) nickel(II) $[Ni(DBF_2)_2]$ prompted us to synthesize and elucidate the stereochemistry and stability of six-coordinated cobalt(III) complexes, $[Co(DBF_2)_2(L)(X)]$† (X = Cl or CNS, L = Im or its derivatives), containing a similar 14-membered macrocyclic ligand and resembling the corrin system. These complexes are derived by the reaction of $BF_3 \cdot Et_2O$ with the parent cobaloximes containing an Im base.

EXPERIMENTAL

Materials

Im and its substituted derivatives were used as supplied by M/s BASF, Ludwigshafen, F.R.G. $Co(NO_3)_2 \cdot 6H_2O$, $CoCl_2 \cdot 6H_2O$, KCNS and DH_2

* Author to whom correspondence should be addressed.

† Throughout this paper DH_2 represents neutral dimethylglyoxime and DH^- its monoanion, DBF_2^- represents the monoanion of the macrocylic boronic ester ligand difluoroborondimethylglyoxime (1,8-diboro-1,1,8,8-tetrafluoro-2,7,9,14-tetraoxa-3,6,10,13-tetraaza-4,5,11,12-tetramethyl cyclotetradeca-3,5,10,12-tetraene) and the archaic symbolism CNS indicates only the presence of thiocyanate without specifying its mode of bonding.

were BDH reagents. $BF_3 \cdot Et_2O$ was distilled before use.

Syntheses of cobaloxime complexes

Chloro- and thiocyanatocobaloxime complexes of type $[Co(DH)_2(X)(L)]$ containing Im ligands were synthesized by bubbling air into a mixture of the appropriate cobalt(II) salt, dimethylglyoxime (DH_2) and Im in a ratio of 1:2:2 in EtOH, for a period of 1–6 h, depending on the nature and position of the substituents in the Im ring.[11,15]

Syntheses of macrocyclic complexes, $[Co(DBF_2)_2(X)(L)]$

Difluoroboro-bridged macrocyclic complexes of cobalt(III) were obtained by the reaction of the corresponding cobaloxime complexes in dry ether with freshly distilled boron trifluoride etherate. After completion of the reaction, usually marked by colour change (8–16 h), the reaction vessel was allowed to stand overnight and the product, collected on a glass frit, was washed with ether and dried *in vacuo*. The desired product was purified by recrystallization of the product from hot acetonitrile or a water–alcohol mixture. A typical method of synthesis of one of the complexes is detailed below.

Synthesis of $[Co(DBF_2)_2(Cl)(Im)]$. 0.5 g of the chloro(imidazole)bis(dimethylglyoximato)cobalt(III) complex, $[Co(DH)_2(Cl)(Im)]$, was suspended in 15–20 cm^3 of dry ether to which 1.5–2.0 cm^3 of freshly distilled boron trifluoride etherate was added very slowly with constant stirring. The stirring was continued till a definite colour change from greenish-yellow to light pink was observed, indicating the formation of the difluoroborondimethylglyoxime complex (6 h). However, the process was continued for a further 2 h in order to ensure the completion of the reaction. The reaction mixture was allowed to settle overnight and the product, collected on a sintered glass by filtration, was repeatedly washed with dry ether. The microcrystalline solid product thus obtained was recrystallized from hot acetonitrile. The reaction seems to proceed in the following manner:

$$2CoCl_2 \cdot 6H_2O + 4DH_2 + 4Im + \tfrac{1}{2}O_2 \rightarrow 2[Co(DH)_2(Cl)(Im)] + 2Im \cdot HCl + 13H_2O \quad (1)$$

$$[Co(DH)_2(Cl)(Im)] + 2BF_3 \cdot Et_2O \rightarrow [Co(DBF_2)_2(Cl)(Im)] + 2HF + 2Et_2O. \quad (2)$$

Analyses

Cobalt was estimated volumetrically by the method of Laitenen and Burdett.[17] Chlorine and sulphur were determined gravimetrically as AgCl and $BaSO_4$, respectively, after alkaline oxidative fusion. Microanalytical data of C, H and N were obtained from Inorganic Chemistry Institute, Technical University, Munich, F.R.G.

Electrolytic conductance, and electronic and IR spectra

Electrolytic conductance of the complexes was determined at room temperature in $MeNO_2$ and MeOH solutions (*ca* 10^{-3} M) with an ELICO conductivity bridge type CM 82 and a dip type cell with a cell constant of 0.5. Electronic spectra in dilute MeOH solutions ($\sim 10^{-3}$–10^{-5} M) were recorded in a Varian 634 spectrophotometer, and IR spectra in the 4000–400-cm^{-1} region were recorded as KBr discs or a Nujol mull in a Perkin–Elmer 337 grating spectrometer.

NMR spectra

NMR spectra of the complexes were recorded in CD_3NO_2 and DMSO-d_6 media in a Bruker spectrometer operating at 80.13 MHz.

Thermolysis

Thermal decomposition of the complexes was carried out using a Shimadzu DT 30 instrument which records T, TG and DTA simultaneously with a heating rate of 10°C min^{-1}.

Mass spectra

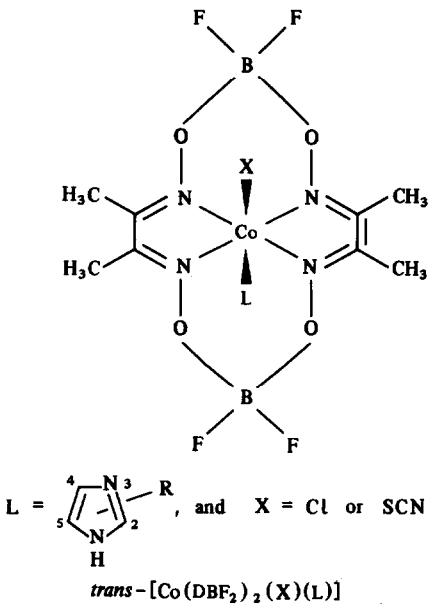
Mass spectra of the compounds were recorded in a Varian CH-7 MAT spectrometer operating at an electron energy of 70 eV. The instrument was maintained at 473 K and the emission current was 300 μA.

Cyclic voltammogram

Cyclic voltammograms of the complexes were run in MeCN using Pt as the working electrode and tetraethyl ammonium perchlorate (TEAP) as the supporting electrolyte, using a PAR model 370-4 electrochemistry system along with a PAR model 174A polarographic analyser, a PAR model 175 Universal programmer and a Houston Instruments RE 0074 XY recorder.

RESULTS AND DISCUSSION

Cobaloxime complexes containing imidazole and chloride or thiocyanate as axial ligands, $[Co(DH)_2(X)(L)]$ (L = Im or a substituted Im, X = Cl or CNS), interact with $BF_3 \cdot Et_2O$ in dry ether to form *trans*-[chloro(imidazole)bis(difluoroborondimethylglyoximato)cobalt(III)] complexes, $[Co(DBF_2)_2(Cl)(L)]$, and *trans*-[thiocyanato(imidazole) bis (difluoroborondimethylglyoximato)cobalt(III)] complexes, $[Co(DBF_2)_2(SCN)(L)]$, where the protons of the $[Co(DH)_2]^+$ moiety are replaced by BF_2 groups (see Scheme 1). These complexes contain the 14-membered tetradentate macrocyclic *N*-donor (N_4) ligand, 1,8-diboro-1,1,8,8-tetrafluoro-2,7,9,14-tetraoxa-3,6,10,13-tetraaza-4,5,11,12-tetramethyl cyclotetradeca-3,5,10,12-tetraene (DBF_2^-) occupying the four planar positions, with the imidazole base and chloride or thiocyanate ion bonded orthogonally. All the complexes reported in this work are presented in Table 1, along with analytical and other characterizing data. The molar-conductance values [Λ_M (Ω^{-1} cm^2 mol^{-1})] in MeOH and $MeNO_2$ at room temperature support the non-ionic nature of the complexes,[17] indicating coordination of Cl^- and SCN^- to the cobalt centre. However, slightly higher values obtained in some cases may be



Scheme 1.

Table 1. Analytical and other characterizing data of *trans*-[A(X)(L)] complexes (A = $[Co(DBF_2)_2]^+$)

Compound[a]	Colour	M.p. (°C)	Analytical data (%)[b] Co	C	H	N	X[c]	Λ_M[d] (Ω^{-1} cm^2 mol^{-1})
[A(Cl)(Im)]	Light pink	192	12.0 (12.1)	27.9 (27.0)	3.6 (3.3)	17.5 (17.2)	6.8 (7.3)	26.3
[A(Cl)(1-MeIm)]	Light yellow	190	12.2 (11.7)	28.2 (28.7)	3.0 (2.6)	16.6 (16.7)	6.6 (7.1)	28.1
[A(Cl)(2-MeIm)]	Light pink	188	12.0 (11.7)	28.8 (28.7)	2.8 (2.6)	16.1 (16.7)	6.8 (7.1)	20.5
[A(Cl)(4-MeIm)]	Light yellow	195	12.0 (11.7)	28.1 (28.7)	2.9 (2.6)	16.9 (16.7)	7.4 (7.1)	22.5
[A(Cl)(1-Vi,2-MeIm)]	Light pink	180	10.8 (11.2)	31.2 (31.8)	3.9 (3.8)	15.6 (15.9)	6.5 (6.7)	49.4
[A(SCN)(Im)]	Yellow	162	11.1 (11.5)	28.0 (28.2)	3.4 (3.1)	19.4 (19.2)	6.2 (6.3)	37.1
[A(SCN)(1-MeIm)]	Yellow	158	11.4 (11.2)	29.8 (29.7)	3.8 (3.4)	18.5 (18.7)	5.9 (6.1)	27.9
[A(SCN)(1-EtIm)]	Yellow	164	10.6 (10.9)	31.4 (31.2)	4.1 (3.7)	18.3 (18.2)	6.2 (5.1)	29.9
[A(SCN)(2-MeIm)]	Yellow	155	11.2 (11.2)	29.2 (29.7)	3.1 (3.4)	18.3 (18.7)	6.7 (6.1)	34.4
[A(SCN)(4-MeIm)]	Yellow	165	10.9 (11.2)	30.6 (29.7)	3.6 (3.4)	19.5 (18.7)	6.5 (6.1)	34.9
[A(SCN)(1-Vi,2-MeIm)]	Yellow	150	10.3 (10.7)	32.2 (32.7)	3.5 (3.6)	17.9 (17.8)	5.2 (5.8)	49.5

[a] Abbreviations: Im = imidazoles, Me = methyl, Et = ethyl, Vi = vinyl.
[b] Theoretical values in parentheses.
[c] X = S for thiocyanato complexes.
[d] At room temperature in an $MeNO_2$ solution. Similar results are obtained in an MeOH solution.

Table 2. Prominent IR bands (cm^{-1}) of *trans*-[A(X)(L)] complexes (A = $[Co(DBF_2)_2]^+$)

Compound	SCN⁻	DBF_2^- group				
	ν(C≡N)	ν(C≡N)	ν(N—O)	ν(B—F)	ν(B—O)	BF_2 deformation vibration
[A(Cl)(Im)]	—	1625	1248, 1116	1020	1200, 835	768, 752
[A(Cl)(1-MeIm)]	—	1615	1245, 1115	1025	1202, 845	764
[A(Cl)(2-MeIm)]	—	1622	1242, 1113	1022	1190, 838	766, 742
[A(Cl)(4-MeIm)]	—	1612	1245, 1108	1020	1195, 842	765
[A(SCN)(Im)]	2112	1602	1250, 1100	1025	1198, 830	756
[A(SCN)(1-MeIm)]	2108	1600	1245, 1108	1022	1190, 832	752
[A(SCN)(2-MeIm)]	2116	1600	1246, 1108	1022	1190, 848	762, 748
[A(SCN)(4-MeIm)]	2118	1610	1248, 1108	1022	1195, 845	760

due to the solvolytic effect of the solvent or due to partial ion-pair formation in solution.

The ligand field spectra of complexes in a MeOH medium are identical to each other and exhibit a peak of weak to moderate intensity at ~ 18,000 cm^{-1} due to the $^1A_{1g} \rightarrow {}^1T_{1g}$ transition, characteristic of a pseudo-octahedral cobalt(III) d^6 system.[18] The more intense band in the 40,500–42,500-cm^{-1} region is attributable to the intraligand $\pi \rightarrow \pi^*$ transition of the coordinated oxime group, whereas an ill-defined shoulder in the 31,000–34,000-cm^{-1} region arises due to the possible $d_\pi(Co) \rightarrow \pi^*(DH^-)$ MLCT transition.[19,20] However, the LMCT band, as seen in the case of the parent cobaloxime complexes,[11,15] is not observed in these macrocyclic complexes.

A systematic investigation of the IR spectra of free DH_2 and chloro- or thiocyanato(imidazole) cobaloximes, and the macrocyclic complexes derived from them, revealed the coordination of difluoroborondimethylglyoximate, an Im ligand and the ambidentate SCN^- group. In these macrocyclic complexes the prominent IR absorption frequencies are located in almost the same position, indicating that variation of the base does not greatly affect the IR spectra. However, variations to a certain extent are observed in the IR frequencies of cobaloximes and the corresponding macrocyclic complexes due to the presence of the BF_2 groups. The difluoroboro-bridged macrocyclic complexes $[Co(DBF_2)_2(X)(L)]$ and $Ni(DBF_2)_2$ do not exhibit any weak band in the 1700–1800-cm^{-1} region characteristic of δ(O—H···O) of the hydrogen bridge in these systems.[21] $BF_3 \cdot Et_2O$, being a more effective reagent for the synthesis of the fully closed $Ni(DBF_2)_2$ complex[22] than BF_4^- ($NaBF_4$),[16] has interacted with the O—H···O group of cobaloximes to form boron-bridged complexes containing the O—BF_2—O group, and this observation also provides further evidence for the presence of a hydrogen bridge in the parent cobaloxime complexes.

The ν(C⋯N) frequency of free DH_2 observed at 1620 cm^{-1} is shifted to a lower wavenumber (1560–1570 cm^{-1}) in the parent cobaloxime complexes, as reported earlier,[11–15] causing a higher conjugation of the dioxime chelate ring, accounting for its increased stability.[23] However, the ν(C⋯N) of the synthesized macrocyclic difluoroborondimethylglyoximato complexes, observed as a sharp and intense band at about 1600–1625 cm^{-1}, is consistent with earlier observations,[24–26] indicating that the CN stretching frequency is less affected in these complexes, and may be due to the attachment of the electronegative fluorine atoms to the electronically poor boron atom. While free DH_2 has no band at ~1240 cm^{-1}, a sharp intense band was observed in $Ni(DH)_2$ and all the cobaloxime complexes at 1240 cm^{-1}, in addition to the band at 1090 cm^{-1} due to the ν(N—O) of the ionized N—OH group of DH_2,[27] indicating the non-equivalent nature of the two N—O bonds.[28] All these difluoroboro-bridged macrocyclic complexes exhibit two bands at ~1240 cm^{-1} and in the 1100–1120-cm^{-1} region due to ν(N—O), the former remaining almost unaffected while the latter experiences a positive shift.

The vibrational spectra of these complexes in the 1200–700-cm^{-1} range demonstrates the presence of the BF_2 group in the 14-membered macrocyclic ring system. All these complexes exhibit an intense band at 1005–1030 cm^{-1}, assignable to the ν(B—F) frequency, and two other bands of reduced intensity at 1190–1200 and 830–850 cm^{-1}, attributable to ν(B—O) vibrations.[16,24] A band of moderate intensity observed at ~750 cm^{-1}, either as a singlet or as an ill-defined doublet, is assigned to the vibration of the —BF_2 group.[29] All these observations indi-

cate the presence of the $[Co(DBF_2)_2]^+$ group in a square plane, making room for the orthogonal coordination of the imidazole base and an anion to the cobalt(III) centre to complete the octahedron. The ν(Co—N) stretching frequencies observed at 515 and 430 cm^{-1} indicate the coordination of the oximate group and the Im base, respectively, to the cobalt(III) ion.[11–15]

The vibrational spectra also helps in deciphering the mode of attachment of the ambidentate CNS^- group.[30,31] The CNS^- group in thiocyanato(imidazole) cobaloxime complexes contains Co—S bonding[11] even though cobalt(III) (a typical hard acid) is expected to coordinate through the *N*-end of the CNS^- group.[31] These macrocyclic complexes containing the thiocyanate ion exhibit a sharp and strong band at about 2100–2120 cm^{-1} due to the ν(C≡N) of the CNS^- group, indicating Co—S bonding. The ν(C—S) is somewhat obscured by the ν(B—O) and the deformation vibration of BF_2. However, the δ(NCS) observed at 450 cm^{-1} further confirms the Co—S bonding. Even though the ν(Co—Cl) has not been located due to the limitations of instrument, the analytical and Λ_M values unambigously prove the coordination of the Cl^- to the Co(III) ion.

NMR spectra

Even though the ^1H NMR chemical shifts of the cobaloxime complexes have established a *trans* structure for the cobaloxime complexes, $[Co(DH)_2(X)(L)]$,[11,13,33–36] not much information is available on the ^1H NMR spectra of the macrocyclic complexes derived from them. The methyl protons of free DH_2 observed as a sharp singlet at 1.98 ppm has undergone a clear downfield shift of about 0.4 ppm in $[Co(DBF_2)_2]^+$ and is now observed at ~ 2.30 ppm as a sharp singlet, characteristic of the four equivalent methyl groups, indicating their *trans* structure. The methyl protons of DH_2 were located in similar position in $Co(DH)_2^+$ complexes containing imidazole and an anion.[33] Thus, the replacement of the oxime protons by $—BF_2$ groups does not affect the original *trans* structure of the parent cobaloximes. The ^1H NMR spectra of uncoordinated Im exhibit two separate signals in an intensity ratio of 1:2 at 7.82 ppm due to H-2 and 7.14 ppm due to H-4 and H-5 protons. On coordination, the equivalence of H-4 and H-5 is lost and two separate signals are observed. These macrocyclic complexes containing an Im ligand show ^1H NMR signals at 7.5, 7.2 and 6.5 ppm due to the H-2, H-4 and H-5 of Im, respectively, indicating its coordination to the metal ion.

The poor solubility of these complexes in suitable solvents precluded the measurement of good-quality ^{13}C NMR spectra.

Cyclic voltammetric studies

Even though polarographic reductions of cobaloxime complexes have been reported[9,10,37,38] the electrochemical oxidation has received much less attention,[39] and more so in the case of the difluoroborondimethylglyoximate cobalt(III) complexes, $[Co(DBF_2)_2]^+$. The electrochemical behaviour of a series of the cobalt(III) macrocyclic complexes containing imidazole and the SCN^- group as axial ligands have been investigated by cyclic vol-

Table 3. Proton chemical shifts of *trans*-[A(X)(L)] complexes[a] (A = $[Co(DBF_2)_2]^+$)

Compound	DBF_2^- protons	Imidazole proton			
	—CH_3 group	H-2	H-4	H-5	R
Imidazole[b]	—	7.82	7.14	7.14	—
Dimethylglyoxime[b]	1.98	—	—	—	—
[A(Cl)(Im)][c]	2.30	7.50	7.02	6.75	—
[A(Cl)(1-MeIm)][c]	2.48	7.52	7.05	6.60	3.75 (1-Me)
[A(Cl)(2-MeIm)][c]	2.36	—	7.78	6.95	2.31 (2-Me)
[A(Cl)(4-MeIm)][c]	2.28	7.35	—	6.75	2.75 (4-Me)
[A(SCN)(Im)][d]	2.32	7.55	7.15	6.68	—
[A(SCN)(1-MeIm)][d]	2.30	7.50	7.22	6.56	3.65 (1-Me)
[A(SCN)(2-MeIm)][d]	2.34	—	7.65	6.87	2.38 (2-Me)

[a] All values in ppm downfield to TMS.
[b] Measurements in DMF-d_7 at ambient room temperature.
[c] Measurements in DMSO-d_6.
[d] Measurements in CD_3NO_2.

Table 4. Cyclic voltammetric peak potential [V(SCE)] data[a] of [A(SCN)(L)] complexes in acetonitrile (A = $[Co(DBF_2)_2]^+$) using platinum as the working electrode

Compound	Positive side of SCE (oxidation)			Negative side of SCE (reduction)		
	E_{pa} (V)	E_{pc} (V)	E^o_{298} (V)	E_{pc} (V)	E_{pa} (V)	E^o_{298} (V)
[A(SCN)(Im)]	1.32	1.23	1.275	−0.62	−0.53	−0.58
				−0.92	−0.80	−0.86
				−1.20	−1.09	−1.15
				—	—	—
[A(SCN)(1-MeIm)]	1.30	1.20	1.25	−0.59	−0.46	−0.53
				−0.92	−0.76	−0.84
				−1.20	−1.08	−1.14
				—	—	—
[A(SCN)(2-MeIm)]	1.20	1.07	1.135	−0.56	−0.30	−0.43
				−0.86	−0.73	−0.81
				−1.18	−1.02	−1.10
				−1.97	−1.86	−1.92
[A(SCN)(4-MeIm)]	1.02	0.94	0.98	—	—	—
				−0.84	−0.74	−0.79
				−1.19	−1.12	−1.15
				−1.82	−1.26	−1.54

[a] Conditions are as follows: scan rate, 0.05 V s^{-1}; solute concentration, $\sim 3.0 \times 10^{-3}$ M; supporting electrolyte, TEAP: the reported E_{pc} values are uncorrected for junction potentials.

tammetric studies in acetonitrile solution using TEAP as the supporting electrolyte and the results are shown in Table 4, and Figs 1 and 2. Invariably all these complexes exhibit three or four reductive responses on the negative side of the saturated calomel electrode (SCE) under identical conditions in contrast to our earlier observation of five reductive waves for azido(imidazole) cobaloxime complexes.[40] The first three reductions may be due to the reduction of cobalt(III) → cobalt(II), cobalt(II) → cobalt(I), and cobalt(I) → cobalt(0), whereas the fourth one corresponds to the reduction of the ligand.[10] The reductions of these complexes which take place at a lower potential may be due to the presence of the —BF_2 group in close proximity to the metal centre. However, all these observations clearly indicate the existence of cobalt

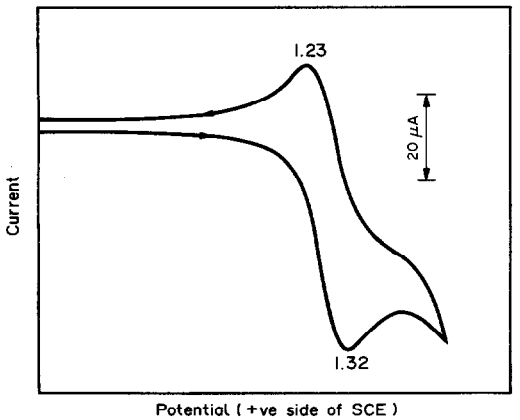


Fig. 1. Cyclic voltammogram of *trans*-$[Co(DBF_2)_2(SCN)(Im)]$ in acetonitrile solution (positive side of SCE).

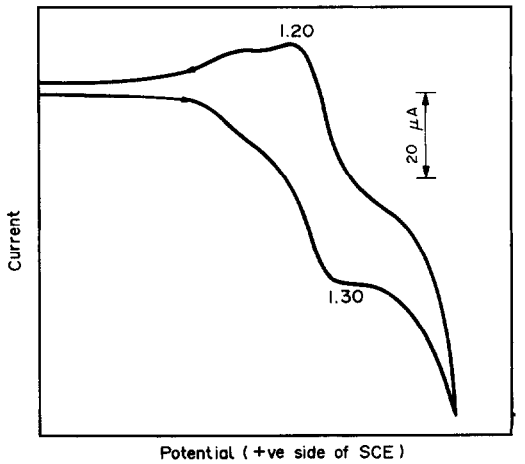


Fig. 2. Cyclic voltammogram of *trans*-$[Co(DBF_2)_2(SCN)(1\text{-MeIm})]$ in acetonitrile solution (positive side of SCE).

in the III state unlike the presence of cobalt(II) in the alkylcobaloxime complexes.[10] Just like azido-(imidazole) cobaloximes,[40] all these complexes record a reversible oxidative peak at about +1.0 V (Pt electrode) which may be due[41] to the one-electron oxidation of cobalt(III) → cobalt(IV).

Mass spectra and thermal analyses

A comparative investigation of the mass spectral studies of free DH_2, $Ni(DH)_2$ and $[Co(DBF_2)_2(Cl)(Im)]$ was made to gain information about the stability and the metal–ligand interactions in these complexes. It reveals that molecular-ion peaks are observed for both DH_2 and $Ni(DH)_2$, but not for the macrocyclic complex, just like the precursor cobaloxime complexes,[42] indicating the comparable stability of the parent cobaloximes and the derived macrocyclic complexes. However, the thermal-decomposition studies establish the lower thermal stability of these complexes relative to the parent cobaloximes. All these macrocyclic complexes on heating decompose, giving polymeric intermediates, and finally forming Co_3O_4 as the ultimate end product.

Acknowledgements—We are thankful to Prof. Dr H. Schumann, Technical University, Berlin, F.R.G., for ^1H NMR spectra, Priv.-Doz. Dr H. H. Karsch, Technical University, Munich, F.R.G., for microanalyses and Prof. A. Chakravorty and Mr B. K. Ghosh of Indian Association for Cultivation of Sciences, Jadavpur, India, for recording cyclic voltammograms. One of us (KCD) thanks the UGC, New Delhi, for a National Fellowship. JKD thanks the UGC, New Delhi, for a Teacher Fellowship, and the Government of Orissa for leave of absence.

REFERENCES

1. L. Y. Martin, Y. Hung, S. C. Jackels, A. M. Tait and D. H. Busch, *J. Am. Chem. Soc.* 1977, **99**, 4029.
2. A. Eschenomoser, *Q. Rev.* 1970, **24**, 366.
3. C. K. Poon and M. L. Tobe, *J. Chem. Soc. A* 1967, 2069.
4. C. K. Poon and M. L. Tobe, *J. Chem. Soc. A* 1968, 1549.
5. G. A. Zakrzewski, C. A. Ghilardi and E. C. Lingafelter, *J. Am. Chem. Soc.* 1971, **93**, 4411.
6. L. Y. Martin, L. J. Dehayes, L. J. Zomba and D. H. Busch, *J. Am. Chem. Soc.* 1974, **96**, 4046.
7. R. J. Sundburg and R. B. Martin, *Chem. Rev.* 1974, **74**, 471.
8. E. Baraniak, H. C. Freemann, T. M. James and C. E. Hockolds, *J. Chem. Soc. A* 1970, 2558.
9. G. N. Schrauzer and G. Klatel, *Angew. Chem.* 1965, **77**, 180.
10. G. N. Schrauzer and R. J. Windgassen, *J. Am. Chem. Soc.* 1966, **88**, 3738.
11. J. K. Das and K. C. Dash, *Polyhedron* 1985, **4**, 1109.
12. J. K. Das and K. C. Dash, *Synth. React. Inorg. Met.-Org. Chem.* 1985, **15**, 839.
13. J. K. Das and K. C. Dash, *Indian J. Chem.* 1985, **24A**, 387.
14. J. K. Das and K. C. Dash, *Transition Met. Chem.* (in press).
15. J. K. Das and K. C. Dash, *Proc. Natl Acad. Sci., India* 1986, **56**(I)A, 14.
16. G. N. Schrauzer, *Chem. Ber.* 1962, **95**, 1438.
17. W. J. Geary, *Coord. Chem. Rev.* 1971, **7**, 81.
18. A. B. P. Lever, *Inorganic Electronic Spectroscopy*. Elsevier, Amsterdam (1968).
19. Y. Yamano, I. Masuda and K. Shimura, *Bull. Chem. Soc. Jpn* 1967, **44**, 1581.
20. J. Chakrabarty, K. B. Naik and B. Sahoo, *Indian J. Chem.* 1982, **21A**, 1103.
21. R. D. Gillard and G. Wilkinson, *J. Chem. Soc.* 1963, 6041.
22. J. E. Parks, B. E. Wagner and R. H. Holm, *Inorg. Chem.* 1971, **10**, 2472.
23. K. Burger, I. Ruff and F. Ruff, *J. Inorg. Nucl. Chem.* 1965, **27**, 179.
24. S. C. Jackels and N. J. Rose, *Inorg. Chem.* 1973, **12**, 1232.
25. T. Sasaki and F. Matsunaga, *Bull. Chem. Soc. Jpn* 1969, **42**, 1308.
26. J. Chakrabarty and B. Sahoo, *Indian J. Chem.* 1982, **21A**, 48.
27. R. Blinc and D. Hadzi, *J. Chem. Soc.* 1958, 4536.
28. *Tables of Interatomic Distances*. Chemical Society, London (1958).
29. V. I. Spitsyn, I. D. Kolli, E. A. Ballabanova and O. N. Mironinko, *Russ. J. Inorg. Chem.* 1975, **20**, 29.
30. R. A. Bailey, S. L. Kozak, T. W. Michelsen and W. N. Mills, *Coord. Chem. Rev.* 1971, **6**, 407.
31. J. L. Burmeister, *Coord. Chem. Rev.* 1966, **1**, 205.
32. R. G. Pearson, *J. Am. Chem. Soc.* 1963, **85**, 3533.
33. J. K. Das and K. C. Dash, *Indian J. Chem.* 1985, **24A**, 696.
34. W. C. Trogler, R. C. Stewart, L. A. Epps and L. G. Marzilli, *Inorg. Chem.* 1974, **13**, 1564.
35. L. A. Epps and L. G. Marzilli, *Inorg. Chem.* 1973, **12**, 1514.
36. H. A. O. Hill and K. G. Morallee, *J. Chem. Soc. A* 1969, 554.
37. G. Costa, G. Mestroni, A. Puxeddu and E. Resenhofer, *J. Chem. Soc. A* 1970, 2870.
38. Y. Hohokabe and N. Yamazuki, *Bull. Chem. Soc. Jpn* 1971, **44**, 1563.
39. G. Costa, *Pure Appl. Chem.* 1972, **30**, 335.
40. J. K. Das, V. Chakravorty and K. C. Dash, *Transition Met. Chem.* 1986, **11**, 170.
41. J. Topich and J. Halpern, *Inorg. Chem.* 1979, **18**, 1339.
42. J. K. Das, V. Chakravorty and K. C. Dash, *Thermochim. Acta* 1986, **97**, 303.

Polyhedron Vol. 5, No. 11, pp. 1865–1866, 1986
Printed in Great Britain

0277–5387/86 $3.00+.00
Pergamon Journals Ltd

ELECTROCHEMICAL REACTIONS OF SOME POLYHYDRIC ALCOHOLS AT A COPPER ANODE

J. S. BANAIT* and P. K. PAHIL

Chemistry Department, Punjabi University, Patiala 147002, India

(*Received* 6 *November* 1985; *accepted* 18 *March* 1986)

Abstract—The reactions of some polyhydric alcohols have been carried out at a copper anode and the reaction products have been identified by chemical analysis and IR spectral studies. All the reactions have been found to yield copper(II) glycolates with almost 100% current efficiency.

Though electrochemical methods have been used extensively in synthetic organic chemistry,[1–5] little efforts have been made in applying this technique for the synthesis of inorganic and organometallic compounds in spite of the fact that electrochemical properties of such compounds have been widely studied.[6–8] In this report the reactions of ethylene glycol, glycerol, 1,2-propandiol, phloroglucinol and 2-mercaptoethanol at a copper anode are described.

EXPERIMENTAL

Material and equipment

N,N-dimethylformamide (DMF) was distilled and dried over molecular sieves, and was used as solvent in these electrochemical studies. Ethylene glycol, glycerol, 1,2-propandiol, phloroglucinol and 2-mercaptoethanol were used as supplied. Tetrabutylammonium chloride (Bu_4NCl) (Reidel Pure) was dried under reduced pressure and elevated temperature, and was used as a supporting electrolyte.

An H-type electrolysis cell made of Pyrex glass was used to carry out the electrochemical reactions. The cathode and anode compartments were separated from each other by a sintered disc of G-3 porosity. Volume of one of the compartments was almost 3 times that of the other one.

Platinum foil (1 × 1 cm) was used as a cathode. A thick layer of copper had been deposited electrochemically[9] on a sheet of copper (5 × 5 × 0.2 cm) in order to ensure the purity of the anode material.

Direct current was obtained with the help of a Toshniwal electrophoresis power supply.

The solution of the polyhydric alcohol (5 g) in 250 cm^3 of DMF was taken in the electrolysis cell. A copper plate freshly electroplated with copper was dipped in the larger compartment and platinum foil in the other one. Necessary connections were made with the power supply and potential across the electrodes was than adjusted so that a current of about 20 mA passed through the cell. The electrolytic cell can be represented as:

$$Pt^{(-)}|DMF+R(YH)_n+Bu_4NCl|Cu^{(+)} \quad (1)$$

where $Pt^{(-)}$ is the platinum cathode, $Cu^{(+)}$ is the copper anode, and $R(YH)_n$ is the polyhydric alcohol/thiol, i.e. Y represents oxygen or sulphur atom in $R(YH)_n$. Electrolysis was carried out for 6 h. A green coloured solid separated out in the anode compartment which was filtered, washed repeatedly with dry ether, and dried *in vacuo*.

IR spectra of the products were scanned on a Beckman IR-20 spectrophotometer in Nujol using sodium chloride plates in the region 4000–600 cm^{-1} and polythene plates in the region 600–200 cm^{-1}.

Copper contents in the products were estimated volumetrically.[9]

RESULTS AND DISCUSSION

Solutions of ethylene glycol, glycerol, 1,2-propandiol, phloroglucinol and 2-mercaptoethanol have been electrolyzed at a sufficiently high potential so that a current of about 20 mA passes through the solution. The electrolytic characteristics have been summarized in Table 1.

* Author to whom correspondence should be addressed.

Table 1. Electrolytic characteristics, and analytical and other relevant data of the electrolysis processes

Polyhydric alcohol	Potential (V)	Product	Colour	Current efficiency [eq (Faraday)$^{-1}$]	Percentage of copper	
					Found	Required
Ethylene glycol	15	$C_2H_4O_2Cu$	Bluish green	0.95	51.0	51.4
Glycerol	15	$C_3H_6O_3Cu$	Bluish green	1.00	41.2	41.4
1,2-Propandiol	10	$C_6H_6O_2Cu$	Parrot green	0.98	46.6	46.2
Phloroglucinol	10	$C_6H_4O_3Cu$	Dark green	0.95	33.3	33.9
2-Mercaptoethanol	10	$C_2H_4(O)SCu$	Brownish green	0.98	44.7	45.5

The products of the electrochemical reactions are insoluble in most of the commonly used organic solvents, and are also hygroscopic. The copper contents in these compounds (determined volumetrically) correspond to the respective copper(II) glycolates of these polyhydric alcohols. All the relevant data are recorded in Table 1.

IR spectral data of the products recorded in the 4000–200 cm^{-1} region reveal that all the compounds of polyhydric alcohols show characteristic absorption bands in the 1020–1060 and 520–560 cm^{-1} regions, which correspond to ν(C—O) and ν(Cu—O) stretching frequencies, respectively.[10,11] The IR spectrum of the copper(II) compound of 2-mercaptoethanol shows absorption bands at 1040, 550, 650 and 315 cm^{-1}, which are due to ν(C—O), ν(Cu—O), ν(C—S) and ν(Cu—S) stretching modes, respectively.[10–13] The IR data, therefore, confirm that the products of the present electrochemical reactions are copper(II) glycolates/thiolates, and thus support the analytical data.

Current efficiencies of these reactions have also been determined and are recorded in Table 1. Perusal of Table 1 reveals that the current efficiencies of all these systems vary from 0.95 to 1.00 eq (Faraday)$^{-1}$ showing thereby that the reactions leading to the formation of copper(II) glycolates are the predominant reactions of these systems. The reaction scheme can be written as:

At the cathode:

$$R(YH)_n + 2e^- \rightarrow (YH)_{n-2}RY^{2-} + H_2(g). \quad (2)$$

At the anode:

$$(YH)_{n-2}RY^{2-} + Cu^{(+)} \rightarrow [(YH)_{n-2}RY_2]Cu + 2e^-, \quad (3)$$

where $(YH)_{n-2}RY^{2-}$ is the dianion of the polyhydric alcohol/thiol.

In recent years, the use of pure metals as reagents has increased through the development of the vapour-phase synthetic technique, which of course needs very sophisticated apparatus and the reaction is carried out at a very high temperature. In contrast, these electrochemical reactions have been carried out at room temperature with all the advantages of using routine laboratory apparatus and metals as reagents.

Such high values of current efficiencies, the use of simple laboratory apparatus and reagents, and, moreover, a direct method[13] compared to the usual synthetic method suggest that these electrochemical methods can be commercially used for the preparation of copper(II) glycolates/thiolates.

REFERENCES

1. M. J. Allen, *Organic Electrode Processes*. Chapman & Hall, London (1956).
2. W. M. Clark, *Oxidation and Reduction Potentials of Organic Systems*. Robert E. Krieger, New York (1972).
3. M. M. Baizer (Ed.), *Organic Electrochemistry*. Marcel Dekker, New York (1973).
4. N. L. Weinberg (Ed.), *Techniques of Electro-organic Synthesis*. Wiley Interscience, New York (1975).
5. L. Eberson and H. Schaffer, *Topics of Current Chemistry*, No. 21. Springer, Berlin (1971).
6. R. G. Jones and H. Gilman, *Chem. Rev.* 1954, **54**, 835.
7. B. L. Laure and C. D. Schmulback, *Prog. Inorg. Chem.* 1971, **14**, 65.
8. P. N. Gupta and S. A. Bhat, *J. Electrochem. Soc. India* 1982, **31(4)**, 171.
9. A. I. Vogel, *A Text Book of Quantitative Inorganic Analysis*. Longmans, London (1961).
10. C. H. Brubaker, Jr and M. Nicholas, *J. Inorg. Nucl. Chem.* 1965, **27**, 59.
11. R. W. Adams, C. G. Barraclough, R. L. Martin and G. Winter, *Aust. J. Chem.* 1967, **20**, 2351.
12. F. F. Said and D. G. Tuck, *Inorg. Chim. Acta* 1982, **59**, 1.
13. D. C. Bradley, R. C. Mehrotra and D. P. Gaur, *Metal Alkoxides*. Academic Press, New York (1978).

Polyhedron Vol. 5, No. 11, pp. 1867–1872, 1986
Printed in Great Britain

0277–5387/86 $3.00+.00
© 1986 Pergamon Journals Ltd

SPECTRAL STUDIES ON THE MAGNETICALLY ANOMALOUS Ni(II) COMPLEXES OF SUBSTITUTED PHENYLAZO-2,4-DINITROSORESORCINOL COMPOUNDS

MAMDOUH S. MASOUD,* ALI EL-DISSOUKY and ENAS E. GHATWARY

Chemistry Department, Faculty of Science, Alexandria, Egypt

(*Received* 12 *September* 1985; *accepted after revision* 28 *May* 1986)

Abstract—Hydrated Ni(II) chloride reacts with new substituted phenylazo-2,4-dinitrosoresorcinol ligands to give complexes with stoichiometry $[NiCl_nL(H_2O)]$ ($n=0$ or 1, and L is the anion of the ligand). These complexes have room-temperature μ_{eff} in the 1.77–2.66-BM/Ni range. The planar $\rightleftharpoons$ tetrahedral equilibrium for these complexes is proved by electronic spectral studies either in a Nujol mull or in a 1,2-dichloroethane solvent. The ligation properties of these complexes by the Lewis bases pyridine or 2-picoline point to the formation of a distorted octahedral configuration. The calculated ligand field parameters are related to the electronic characters of the ligands and the Lewis bases. The IR spectra show that all the titled ligands (except the *o*-carboxy compound) are monobasic bidentate, coordinated to the nickel ion *via* the enolized phenolic oxygen and the azo-nitrogen atoms. The *o*-carboxy compound acts as dibasic tridentate in the coordination.

In view of the role played by nitroso complexes in body systems, delineation of the nature of the metal binding and stereochemistry in nitroso complexes seems to be interesting.[1] The azo compounds have also gained much attention because of their use as models of biological systems.[2] In our laboratory, the coordinating behaviour and chemical equilibria of some nitroso[3–8] and azo[9–14] compounds have been investigated in depth. However, no structural chemistry and coordinating studies have been reported for ligands containing both azo and nitroso functional groups. The major interests of this paper are: (i) the synthesis of new substituted phenylazo-2,4-dinitrosoresorcinol (**I**) ligands, (ii) the synthesis of Ni(II) complexes derived from these ligands, (iii) assigning the stereochemistry of the complexes based on the electronic-spectra and magnetic-susceptibility measurements, and (iv) knowing the mode of bonding in these complexes from the IR spectral data.

*Author to whom correspondence should be addressed.

EXPERIMENTAL

Preparation of the organic ligands

2,4-Dinitrosoresorcinol was prepared according to the method outlined by Orndorff and Nichols.[15] I were obtained by direct diazotization of the aniline derivatives (*o*-toluidine, *o*-chloroaniline, *o*-aminobenzoic acid, *m*-toluidine, *m*-chloroaniline and *m*-nitroaniline), followed by coupling with 2,4-dinitrosoresorcinol. The compounds were characterized by their elemental analyses given in Table 1.

Preparation of the Ni(II) *complexes*

These were prepared according to the general method, viz.: to a suspension of 0.025 mol of the ligand in 50 cm^3 absolute ethanol, 0.01 mol of hydrated $NiCl_2$ in 20 cm^3 absolute ethanol was added. The reaction mixture was refluxed with stirring for 6–8 h. On cooling the polycrystalline solid precipitated in each case was filtered off, washed several times with ethanol followed by ether, and dried *in vacuo* over P_4O_{10}.

The nickel content was determined by the

Table 1. Analytical data of substituted phenylazo-2,4-dinitrosoresorcinol ligands and their Ni(II) complexes

Compound	% calculated (% found)				
	C	H	N	Cl	Ni
o-Carboxyphenylazo-2,4-dinitrosoresorcinol (H_2L_1)	49.4 (49.1)	2.5 (2.5)	17.7 (17.9)		
o-Chlorophenylazo-2,4-dinitrosoresorcinol (HL_2)	47.1 (46.8)	2.3 (2.3)	18.3 (18.4)		
o-Tolylazo-2,4-dinitrosoresorcinol (HL_3)	54.5 (54.6)	3.5 (3.4)	19.6 (19.6)		
m-Chlorophenylazo-2,4 dinitrosoresorcinol (HL_4)	47.1 (46.9)	2.3 (2.1)	18.3 (18.4		
m-Tolylazo-2,4-dinitrosoresorcinol (HL_5)	54.5 (54.4)	3.5 (3.4)	19.6 (19.8)		
m-Nitrophenylazo-2,4-dinitrosoresorcinol (HL_6)	45.4 (45.1)	2.2 (2.1)	22.1 (22.0)		
$[NiL_1(H_2O)]$	39.7 (39.4)	2.5 (2.5)	14.3 (14.1)		14.9 (15.0)
$[NiClL_2(H_2O)]$	37.6 (37.3)	2.3 (2.4)	14.6 (14.6)	17.0 (16.9)	15.3 (15.4)
$[NiClL_3(H_2O)$	39.2 (39.0)	3.0 (3.0)	14.1 (13.9)	8.9 (9.0)	14.7 (14.7)
$[NiClL_4(H_2O)]$	37.6 (37.3)	2.3 (2.3)	14.6 (14.6)	17.0 (16.8)	15.3 (15.4)
$[NiClL_5(H_2O)]$	39.2 (39.0)	3.0 (3.0)	14.1 (13.9)	8.9 (9.0)	14.7 (14.7)
$[NiClL_6(H_2O)]$	33.5 (33.2)	2.1 (2.1)	16.3 (16.2)	8.3 (8.3)	13.7 (13.7)

complexometric-titration procedure.[16] Carbon, nitrogen, hydrogen and chloride contents were estimated at the Microanalytical Laboratory at Cairo University, Cairo, Egypt. The data are collected in Table 1.

Physical measurements

The diffuse-reflectance and solution spectra were recorded using a CARY 14 spectrophotometer. Magnetic measurements were carried out using the Gouy method.[17] The KBr IR spectra were made with Unicam SP 1025 and SP 3-100 spectrophotometers equipped with NaCl prisms.

RESULTS AND DISCUSSION

The interaction of **I** with hydrated $NiCl_2$ in ethanol gave complexes of stoichiometry $[NiCl_nL(H_2O)]$ ($n = 0$ or 1, and L is the anion of the ligand). The complexes are brown or brownish red in colour. They are stable in air and are partially soluble in water and in most organic solvents but freely soluble in Lewis bases such as pyridine and 2-picoline.

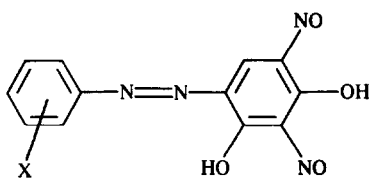
The room-temperature μ_{eff} of all the complexes exhibit anomalous values in the range 1.77–2.66 BM (Table 2). These values are lower than those for octahedral, tetrahedral or high-spin five-coordinate Ni(II) complexes. They may be consistent with those of low-spin five-coordinate Ni(II) complexes. Bis-halo-bisphosphino and bis(salicylaldiminato)nickel(II) complexes with anomalous magnetic moments exist in a planar–tetrahedral mixture in the solid state and/or in solution.[18] It was proved that several four-coordinated Ni(II) complexes give a diamagnetic–paramagnetic mixture in the same crystalline solid.[19] This was referred to the change in the effective ligand field acting on Ni(II) by melting, grinding or dissolving the complexes.[20] Accordingly, the Ni(II) complexes under investigation can be assumed to exist in a mixture in the solid state.

The solid-reflectance and 1,2-dichloroethane solution spectra of the prepared Ni(II) complexes were recorded in the 5000–30,000-cm^{-1} range. The

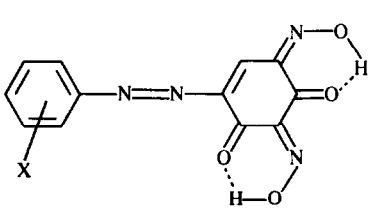
Table 2. Magnetic and electronic spectral data of Ni(II) complexes

Compound[a]	State[b]	μ_{eff} (BM)	ε_{max}	N_t	$\bar{\nu}$ (cm^{-1})			
$[NiL_1(H_2O)]$	Solid	1.77	9	29	5270	6750	18,960	
	$C_2H_4Cl_2$				5200	6740	18,980	
	Py				9780	9980	11,790	15,430
							15,620	23,250
	2-Pic				9140	9650	12,070	15,140
							15,480	23,050
$[NiClL_2(H_2O)]$	Solid	2.42	23	54	5020	6800	18,530	
	$C_2H_4Cl_2$				5010	6805	18,530	
	Py				9830	11,960	15,440	15,890
							24,800	
	2-Pic				9470	11,980	15,020	15,670
							23,700	
$[NiClL_3(H_2O)]$	Solid	2.37	22	52	5130	6790	18,840	
	$C_2H_4Cl_2$				5100	6700	18,860	
	Py				10,500	12,490	15,230	15,990
							24,990	
	2-Pic				9300	9930	12,800	15,240
							15,540	23,120
$[NiClL_4(H_2O)]$	Solid	2.58	26	61	5270	6870	18.370	
	$C_2H_4Cl_2$				5250	6860	18,400	
	Py				9640	10,380	11,675	15,320
							15,880	24,350
	2-Pic				8970	9980	11,800	15,060
							15,480	23,890
$[NiClL_5(H_2O)]$	Solid	2.56	25	60	5240	6830	18,410	
	$C_2H_4Cl_2$				5220	6825	18,420	
	Py				9640	11,690	15,040	15,460
							23,670	
	2-Pic				8680	9690	11,090	14,900
							15,180	23,420
$[NiClL_6(H_2O)]$	Solid	2.66	27	65	5300	6900	18,250	
	$C_2H_4Cl_2$				5270	6880	18,300	
	Py				9750	10,500	12,970	15,690
							16,080	24,380
	2-Pic				9370	9950	12,990	15,380
							15,980	23,260

[a]For L_1–L_6 see Table 1.
[b]Py = pyridine, and 2-Pic = 2-picoline.



I



II

X = *o*-COOH, *o*-Cl, *o*-CH_3, *m*-Cl, *m*-CH_3 or *m*-NO_2

data are summarized in Table 2. The solid spectra are identical to those obtained for the solutions and exhibit bands in the 5000–5300- $[\nu_1(^3T_1 \rightarrow {}^3T_2)]$, 6750–6900- $[\nu_2(^3T_1 \rightarrow {}^3A_2)]$ and 18,000–19,000-cm^{-1} regions. These spectral data are very similar to those of square planar–tetrahedral configurations[21–23] in either the solid state or solution. The second band is for an idealized tetrahedral symmetry. The third band can be attributed to a composite of the tetrahedral $\nu^3[^3T_1 \rightarrow {}^3T_1(P)]$ transition and the lowest-energy spin-allowed transition of the planar isomer, presumably the $^1A_{1g} \rightarrow {}^1B_{1g}$ transition. The existence of the planar transitional band together with those of tetrahedral geometry were made evident by comparison with the spectra of similar complexes.[20–24] The following equation[21] is applied:

$$N_t = 100\mu_{obs}^2/3.3,$$

where N_t is % tetrahedral, μ_{obs} is the measured effective magnetic moment and 3.3 is the value of the magnetic moment for standard tetrahedral Ni(II) complexes. The N_t values are given in Table 2, where the effect of the substituents on the stereochemistry of the complexes is shown. For the *o*-substituents, the N_t value increases in the sequence: -Cl > $-CH_3$ > -COOH. This could be explained by the steric, electronic requirement and/or their chelating properties. The lower N_t value of the tridentate *o*-carboxy-containing complex can be related to its strong steric requirement enhancing the existence of the planar form. The order of increasing N_t value for the *m*-substituents follows the order: $-NO_2$ > -Cl > $-CH_3$. The N_t values are used to calculate the molar extinction coefficient of the tetrahedral geometry in the 6720–6900-cm^{-1} region where the planar molecules do not absorb. This is done by using the following equation:[21]

$$N_t = 100\varepsilon_{max}^{max}/42,$$

where the integer 42 is the molar extinction coefficient of the peak around 6700–6950 cm^{-1} for the pure pseudo-tetrahedral Ni(II) complexes. The ε values are in the order *m*-NO_2 > *m*-Cl > *m*-CH_3 > *o*-Cl > *o*-CH_3 > *o*-COOH. This is the same sequence as for N_t. The data are summarized in Table 2. Accordingly, the significant property of the ligand fields is the existence of a well-defined trend in the energies of ν_2 and the planar component of ν_3. This is related to the electronic requirements of their positions and the relative percent of the isomers are varied. The data are collected in Table 2 with a direct relation between ν_2 and N_t from one side and an inverse relation between ν_3 and N_t from the other side. The ν_3 combination bands provide a measure of the frequency trend of the planar *d–d* transition for the following reasons: (i) the intensity increases as N_t decreases, and (ii) the trend in ν_3 energies is opposite to that in ν_2.

The electronic spectra of the Ni(II) complexes in solutions in the Lewis bases pyridine or 2-picoline are given in Table 2. The spectra of all complexes are quite different from those recorded in either 1,2-dichloroethane or by solid reflectance. This indicates a strong interaction with the Lewis base

Table 3. Ligand field parameters of Ni(II) complexes[a]

Compound[b]	Solvent[c]	ν_1	ν_2	ν_3	$\frac{\nu_2}{\nu_1}$	Dq	B'[d]	β	$\frac{Dq}{B'}$
$[NiL_1(H_2O)]$	Py	9780	15,525	23,250	1.57	978	629	0.61	1.55
	2-Pic	9395	15,310	23,050	1.63	939	678	0.69	1.39
$[NiClL_2(H_2O)]$	Py	9830	15,665	24,800	1.59	983	732	0.71	1.34
	2-Pic	9470	15,345	23,700	1.62	947	709	0.68	1.34
$[NiClL_3(H_2O)]$	Py	10,500	15,610	24,990	1.49	1050	607	0.59	1.73
	2-Pic	9615	15,390	23,120	1.60	962	644	0.63	1.49
$[NiClL_4(H_2O)]$	Py	10,000	15,600	24,350	1.56	1000	663	0.64	1.51
	2-Pic	9475	15,260	23,890	1.61	948	716	0.69	1.32
$[NiClL_5(H_2O)]$	Py	9640	15,250	23,670	1.58	964	667	0.65	1.45
	2-Pic	9185	15,040	23,420	1.63	919	727	0.71	1.26
$[NiClL_6(H_2O)]$	Py	10,125	15,885	24,380	1.56	1013	659	0.64	1.54
	2-Pic	9660	15,680	23,260	1.62	966	664	0.65	1.45

[a] In cm^{-1}.
[b] For L_1–L_6 see Table 1.
[c] Abbreviations as in Table 2.
[d] B_o for the free Ni(II) ion = 1030 cm^{-1}.

molecules. All spectra consist of four major bands with maxima at 9185–10,500, 11,000–13,000, 15,000–15,400 and 23,000–24,400 cm^{-1}. These are consistent for tetragonally distorted octahedral Ni(II) complexes.[25,26] The bands at 9185–10,500, 15,000–15,400 and 23,000–24,400 cm^{-1} are assigned to $\nu_1[^3A_{2g} \rightarrow {}^3T_{2g}(P)]$, $\nu_2[^3A_{2g} \rightarrow {}^3T_{1g}(F)]$ and $^3A_{2g} \rightarrow {}^3T_{1g}(P)$ transitions, respectively. In this symmetry, two spin-forbidden transitional bands may be observed and assigned to $^3A_{2g} \rightarrow {}^1E_g(D)$ and $^3A_{2g} \rightarrow {}^1E_g(G)$ transitions. Therefore, the band in the 11,000–13,000-cm^{-1} region could be assigned to the spin-forbidden transitions. Furthermore, the observed splitting in the ν_2 and ν_3 absorption bands suggests the presence of a distortion of the idealized symmetry.[27] The calculated ligand field parameters are given in Table 3. The Dq values for the Ni(II) complexes under investigation lie in the 918.5–1050-cm^{-1} region, indicating an intermediate ligand field position of our ligands in the nephelauxetic series [the Dq values found in octahedral Ni(II) complexes[27] vary between 6400 and 12,700 cm^{-1}]. The values of B' for all the adduct complexes are in the 629–731-cm^{-1} region, lower than that of the free Ni(II) ion (1030 cm^{-1}). The reduction in the B' values could be taken as a criterion for the amount of covalency in these complexes. This could also be explained on the basis that the e_g-electrons are σ-antibonding and spend some time on the ligand. The t_{2g}-electrons may become π-bonding or antibonding, and will also spend some of its time on the ligand. Such delocalization will increase the mean distance between the d-electrons and thereby reduce the value of B'. The ratio $\beta = B'/B_o$ is used to indicate the amount of reduction of B_o (for the free ion). According to the values of β given in Table 3, a covalent-character bonding in our complexes can

Table 4. Main IR bands (cm^{-1}) of the substituted phenylazo-2,4-dinitrosoresorcinol ligands and their Ni(II) complexes[a]

Compound[b]	ν(OH)	ν(N=N)	ν(NOH)	ν(C=O)	ν(C=N)	δ(NO_{bend})	ν(NO)
H_2L_1	3460b	1480m	980m	1685s	1600m	885m	
			920w	1655s	1570m	870w	
HL_2	3520b	1483m	940s	1640s	1595s	862m	1442m
	3315b	1468w				821w	
	3072m						
HL_3	3531b	1485m	959m	1695s	1600s	842m	
	3422m			1664s			
	3187m						
	3928m						
HL_4	3516b	1480m	995m	1690s	1595s	848m	
	3390m		964m	1664s			
	3156m						
HL_5	3418b	1480m	960m	1645s	1600m	876m	
					1578m	834m	
HL_6	3495b	1533m	991m	1631s	1595s	894m	
	3281b		917w			874w	
	3091m						
$[NiL_1(H_2O)]$	3530b	1530m	990m	1695s	1610m	880s	
				1670s			
				1625m			
$[NiClL_2(H_2O)]$	3400b	1525m	980m	1610s	1595s	830m	1425m
	3090m		940w				
$[NiClL_3(H_2O)]$	3315b	1517m	970m	1670s	1591s	832m	1458m
				1635m			1416w
$[NiClL_4(H_2O)]$	3390b	1525s	982m	1680s	1587s	894m	1483m
				1625s		847m	1426w
$[NiClL_5(H_2O)]$	3405b	1508m	958w	1620s	1585s	845m	
				1605m		818w	
$[NiClL_6(H_2O)]$	3380b	1540m	935m	1645m	1600m	880m	
						810w	

[a]s = strong, m = medium, w = weak, and b = broad.

[b]For H_2L_1 etc. see Table 1.

be assumed (ionic ligands form complexes with β values very close to the unity). From the Dq, B' and β values, our ligands can be arranged in the order: *o*-Cl > *m*-CH_3 > *m*-Cl > *o*-COOH > *o*-CH_3 > *m*-NO_2 with the same Lewis base.

IR spectra

The ligands gave characteristic spectral regions as follows:

(i) 3531–2938 cm^{-1} due to the intramolecular hydrogen-bonded OH group overlapping with oximic OH stretching.[28] Such a region is due to a hydrogen-bonding effect or water molecules (Table 4).

(ii) 1695–1611 cm^{-1} due to ν(C=O), absent in all complexes.

(iii) 1600–1570 cm^{-1} due to free ν(N=N), affected on complexation, i.e. the azo group contributes in the structure of the complex compound.

(iv) 990–950 cm^{-1} due to ν(=NOH). This in turn verifies the phenomenon of tautomerism.

(v) 950–860 cm^{-1} due to hydrogen bonding. This finding is parallel to that present in the stretching spectral region. Therefore, structure **II** could be assumed for these ligands.

For the carboxy system, the following are noticed:

(i) A strong and broad band at 3460 cm^{-1} is present due to the presence of intramolecular O···H—O between the —C=O and —COOH of one molecule and the —OH group of another.

(ii) The presence of band (i) beside that in the range 980–870 cm^{-1} is assigned to intramolecular bonds between the —C=O and —OH of the oxime. The presence of strong bands at 1570–1430 cm^{-1} could be used to assign the presence of the azo group in an azobenzene-like structure in a *trans* configuration.[29] This region is affected on complexation, i.e. the azo group takes part in the complex compound. The absence of bands in the free ligand at 1490 and 1400 cm^{-1} is due to the lack of N=O. The carboxylate radical is identified by the presence of two bands at 1685 and 1655 cm^{-1} (a strong and weak feature, respectively), due to ν(C=O) and $\nu_{asym}(COO^-)$, in turn. The first is absent and the second is red-shifted on complexation.

Generally, the bidentate nature for all the ligands—except that of the carboxy ligands—is based on the interaction of the azo and phenolic oxygen with nickel. The carboxy ligands are tridentate, i.e. the azo, hydroxy and carboxy groups all attach to Ni(II).

REFERENCES

1. C. L. Walters, *Chem. Br.* 1977, **13**, 140.
2. S. Patai, *The Chemistry of Hydrazo, Azo and Azoxy Groups*, Part I. Wiley, New York (1975).
3. M. S. Masoud, A. M. Khalil and I. Abdel-Gawad, *Indian J. Chem.* 1977, **15A**, 468.
4. M. S. Masoud, T. M. Salem and M. El-Essawi, *Monatsch. Chem.* 1978, **109**, 221.
5. M. S. Masoud, M. M. Osman and H. El-Naggar, *Z. Anal. Chem.* 1978, **289**, 207.
6. M. S. Masoud, T. M. Salem and M. El-Essawi, *J. Chem. Eng. Data* 1978, **23**, 12.
7. M. S. Masoud and S. A. Ghonaim, *Pol. J. Chem.* 1980, **54**, 651.
8. M. S. Masoud, T. M. Salem and M. El-Essawi, *Synth. React. Inorg. Met–Org. Chem.* 1983, **13**, 79.
9. M. S. Masoud, A. M. Kaddah, A. M. Khalil and N. I. Tawfik, *Indian J. Chem.* 1979, **17A**, 502.
10. M. S. Masoud and F. M. El-Zawawy, *Talanta* 1980, **27**, 766.
11. M. S. Masoud, M. M. Osman, T. M. Salem and E. A. Khalil, *Indian J. Chem.* 1981, **20A**, 584.
12. M. S. Goher, M. S. Masoud and A. M. Heiba, *Pol. J. Chem.* 1981, **55**, 1491.
13. M. S. Masoud, T. M. Salem and M. A. El-Henawi, *Indian J. Chem.* 1981, **20A**, 297.
14. M. S. Masoud, S. A. Abou Ali, G. Y. Ali and M. El-Dessouky, *J. Chem. Eng. Data* 1983, **28**, 297.
15. W. K. Orndorff and M. L. Nichols, *J. Am. Chem. Soc.* 1923, **45**, 1636.
16. G. Scharzenbach, In *Complexometric Titrations* (Translated by H. Irving). Methuen, London (1959).
17. B. N. Figgis and R. S. Nyholm, *J. Chem. Soc.* 1959, 331.
18. B. T. Kilbourn and H. M. Pawwll, *J. Chem. Soc. A* 1970, 1688.
19. L. Sacconi, R. Cini, M. Ciampolini and F. Maggo, *J. Am. Chem. Soc.* 1960, **82**, 3487.
20. A. El-Dissouky, M. M. Abou-Sekkina and A. Z. El-Sonbati, *Acta Chim. Hung.* 1983, **114**, 29.
21. L. Sacconi, M. Ciampolini and N. Nardi, *J. Am. Chem. Soc.* 1964, **86**, 819.
22. A. El-Dissouky, G. B. Mohamed and L. S. Refaat, *Transition Met. Chem.* 1984, **9**, 23.
23. A. El-Dissouky and L. S. Refaat, *Inorg. Chim. Acta* 1984, **87**, 213.
24. A. El-Dissouky, M. M. Abou-Sekkina, M. El-Kersh and A. Z. El-Sonbati, *Transition Met. Chem.* 1984, **9**, 372.
25. M. F. El-Shazly, T. M. Salem, A. El-Dissouky and A. M. Hindawey, *Inorg. Chim. Acta* 1977, **25**, 55.
26. M. M. Abou-Sekkina, A. El-Dissouky and M. M. Osman, *Thermochim. Acta* 1982, **55**, 231.
27. A. B. P. Lever, *Inorganic Electronic Spectroscopy*, p. 317. Elsevier, Amsterdam (1968).
28. P. Ball, *Acta Chem. Scand.* 1958, **12**, 1777.
29. K. Kubler and W. Luttke, *Z. Electrochim.* 1960, **64**, 650.

Polyhedron Vol. 5, No. 11, pp. 1873–1879, 1986
Printed in Great Britain

0277–5387/86 $3.00+.00
© 1986 Pergamon Journals Ltd

ELUCIDATION OF STRUCTURES OF *NIDO*-7-CB_8H_{12} AND $B_9H_{12}^-$ BY TWO-DIMENSIONAL ^{11}B–^{11}B NMR SPECTROSCOPY

S. HEŘMÁNEK,* J. FUSEK, B. ŠTÍBR, J. PLEŠEK and T. JELÍNEK

Institute of Inorganic Chemistry, Czechoslovak Academy of Sciences, 250 68 Řež near Prague, Czechoslovakia

(*Received* 6 *December* 1985; *accepted after revision* 28 *May* 1986)

Abstract—The product of the thermal decomposition of 4-CB_8H_{14} is, according to two-dimensional (2-D) ^{11}B–^{11}B NMR spectroscopy, 7-CB_8H_{12}. An analogous structure stems from the 2-D NMR for $B_9H_{12}^-$. A new approach to the estimation of distribution of bonds in borane skeletons is proposed on the grounds of positions of individual signals in the given ^{11}B NMR spectrum and documented in the distribution of bonding electrons in $B_9H_{12}^-$ and 7-CB_8H_{12}.

In earlier papers[1,2] we have described a pyrolytic preparation of a new *nido*-CB_8H_{12} carbaborane (**1**) from 4-CB_8H_{14}. The ^{11}B and ^1H NMR spectra (^{11}B, 32.1-MHz; ^1H, 100-MHz) offered two possible structures [**2** and **3** (Fig. 1)] exhibiting five ^{11}B signals of relative areas 1:2:2:2:1 and two types of H-bridges of relative intensity 2:1. Structure **2** was consistent with the ease of dehydrogenation while structure **3** corresponded to the character of the ^{11}B NMR spectrum in the light of our ^{11}B NMR empirical rules.[3] A definite decision was believed to require an x-ray diffraction study. The importance of a solution of this problem was enhanced by finding that the carbaborane discussed (**1**) has a ^{11}B NMR spectrum similar in character to that of the isoelectronic $B_9H_{12}^-$ anion (**4**).[1] This "^{11}B NMR isospectrality"[4] indicated that both compounds are structurally very similar, and for both the distribution of H-bridges as in **3** and **4** was preferred.[1]

EXPERIMENTAL

The measured 7-CB_8H_{12} and $B_9H_{12}N(CH_3)_4$ compounds were prepared according to the literature[2] and Ref. 5, respectively.

NMR spectra were measured using a Varian XL-200 NMR spectrometer (^{11}B, 64.184-MHz; ^1H, 200-MHz). The locked spectra of **1** were recorded in $CDCl_3$, and those of $B_9H_{12}N(CH_3)_4$ in CD_3COCD_3. Referencing was to an external $BF_3 \cdot O(C_2H_5)_2$ for ^{11}B and an internal TMS for ^1H.

For two-dimensional (2-D) ^{11}B–^{11}B NMR spectroscopy, the COSY pulse sequence was used to generate the t_1, t_2 matrix (512 × 512 for **1** and 256 × 256 for **4**). The spectra were obtained utilizing a standard Varian XL-200 software "HOMCOR" pulsed sequence. For **1** the following acquisition parameters were used: acquisition time (AT) = 0.051 s, relaxation delay (D1) = 0.2 s, sweep width (SW) = 5000 Hz, number of transitions (NT) = 32; $B_9H_{12}^-$: AT = 0.032 s, D1 = 0.2 s, SW = 4000 Hz, NT = 32. The resulting COSY spectra were line-narrowed (using resolution enhancement = 0.003 and apodization function = 0.01), symmetrized, and recorded using a Nicolet Zeta 1553 plotter.

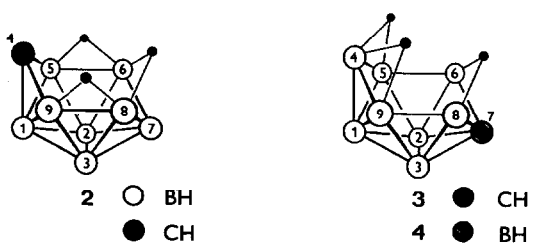


Fig. 1. Structure of CB_8H_{12} and $B_9H_{12}^-$: (a) proposed structure of **2**, and (b) proposed and found structures of 7-CB_8H_{12} (**3**) and $B_9H_{12}^-$ (**4**).

*Author to whom correspondence should be addressed.

RESULTS AND DISCUSSION

CB_8H_{12}

With the introduction of 2-D ^{11}B–^{11}B NMR spectroscopy[6] the above-mentioned problem was simplified to searching for the presence or absence of an interaction (i.e. of a cross-peak) between two atoms both represented by signals of intensity 1 at 6.46 and −54.43 ppm. As shown in Fig. 2, their cross-peak is unambiguously present, which confirms both the formerly preferred[1] rearranged structure **3** and the importance of the ^{11}B NMR empirical rules.[3]

Structure **3** was further confirmed by a detailed NMR study of **1** (shown in Fig. 3). Selective ^1H decoupling by the frequency corresponding to an H-bridge of intensity 1 (−5.5 ppm) unequivocally demonstrated the loss of μH coupling at B(6,8) (Fig. 3c) while the selective ^1H decoupling by the frequency of the H-bridge of intensity 2 (at −3.1 ppm) resulted in a simultaneous loss of μH coupling at B(5,9) and B(4) (Fig. 3d). A distinct μH splitting of the B(6,8) signal at −27.57 is also in agreement with the "μH rule", according to which this phenomenon is observed with signals of B atoms which bear μH, and are either joined to a C-vertex[7] or are connected with an adjacent B atom by a classical B—B bond. The ^{11}B NMR characteristics and the assignment of all signals are summarized in Table 1.

In the pyrolysis of 4-CB_8H_{14}, deuterated to a great extent in the 2,3- and partly in the 6,8-positions, a derivative of **3**, deuterated partially in positions B(1,2,3,6,8) was obtained. This denied the mechanism based on a rotation of the inner B(1,2,3) triangle[1] and another rearrangement mechanism has to be proposed.

$B_9H_{12}^-$

Under similar conditions to **1**, a 2-D ^{11}B–^{11}B NMR spectrum of the isoelectronic $B_9H_{12}^-$ anion was obtained (Fig. 4), which enabled us to propose structure **4** and make a complete ^{11}B signal

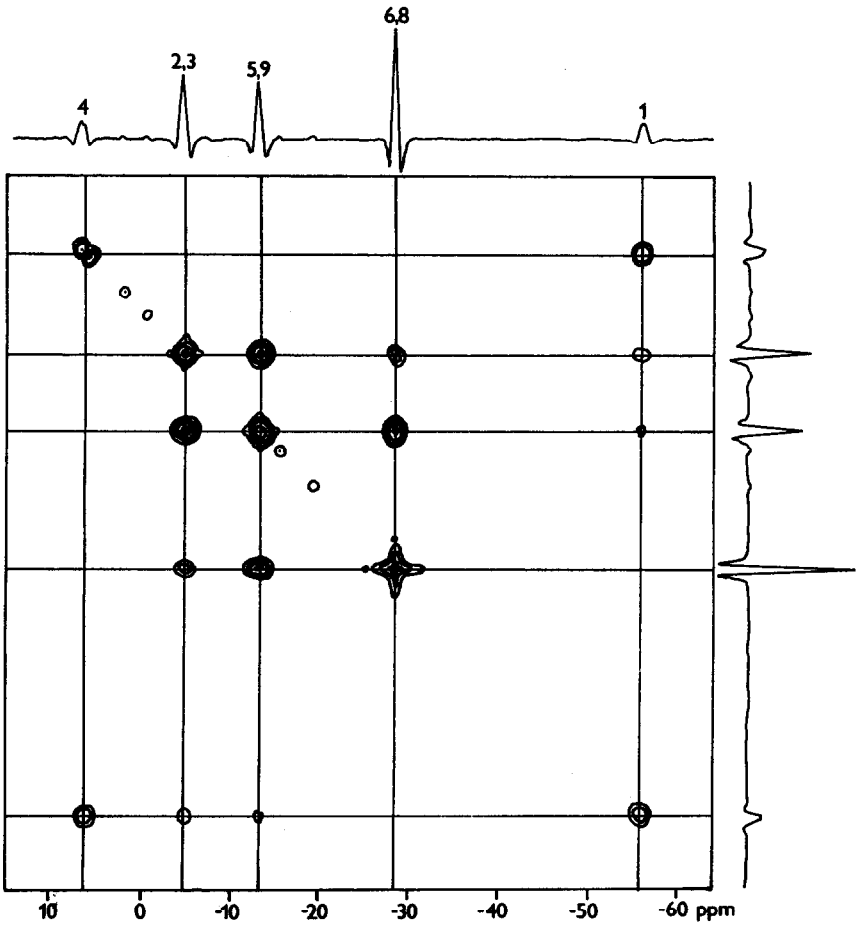


Fig. 2. ^1H-decoupled 2-D ^{11}B–^{11}B and one-dimensional FT NMR spectra of 7-CB_8H_{12} in $CDCl_3$.

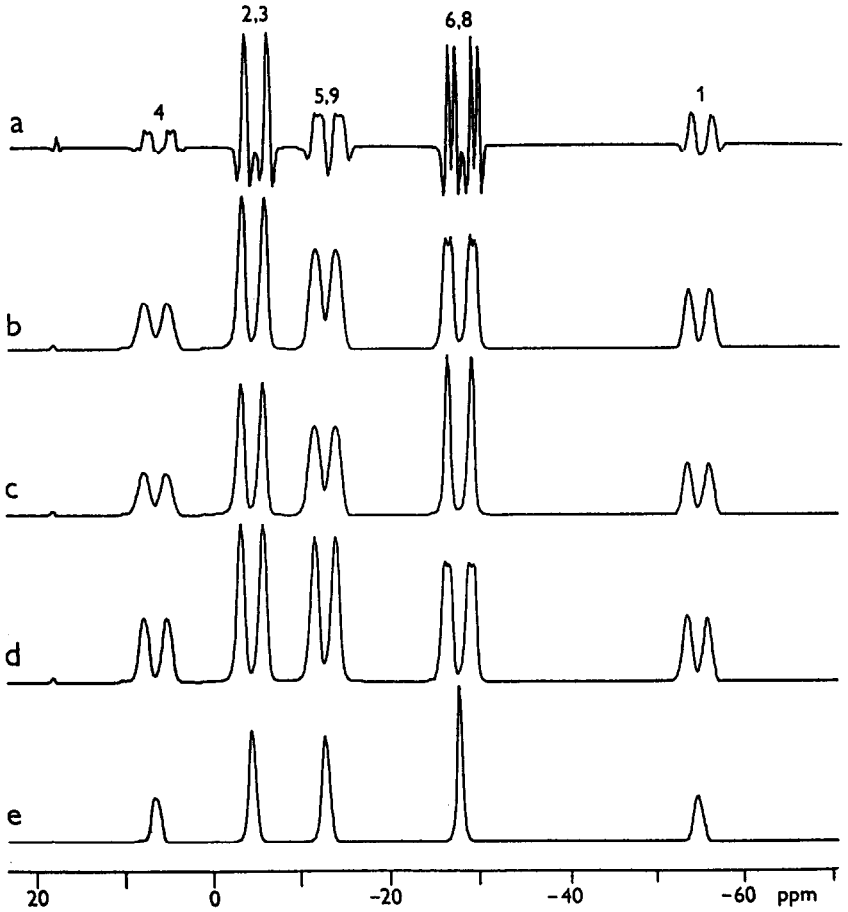


Fig. 3. ^{11}B NMR spectra of 7-CB_8H_{12}: (a) undecoupled and line-narrowed, (b) undecoupled, (c) selectively μH (−5.5 ppm) decoupled, (d) selectively 2μH (−3.1 ppm) decoupled, and (e) ^1H-decoupled.

Table 1. ^{11}B NMR (64.18-MHz) characteristics of $B_9H_{12}N(CH_3)_4$ in CD_3COCD_3 and of 7-CB_8H_{12} in $CDCl_3$ ($\Delta = \delta_3 - \delta_4$)

	$B_9H_{12}^-$		7-CB_8H_{12}			
B	δ (ppm)	J (Hz)	δ	J	Δ	Relation to 7-C
7	−10.47		–	–		
2,3	−10.47	137	−4.34	163	6.13	Vicinal
5,9	−14.74		−12.67	154	2.07	*Meta*
4	−16.24	175, 49	6.46	143, 40	22.70	Antipodal
6,8	−35.00	148	−27.57	173, 47	7.43	Vicinal
1	−52.74	153	−54.43	160	−1.69	*Meta*

assignment (Table 1). The ^{11}B NMR spectrum of **4** is almost identical with that of Siedle *et al.*[8] measured in CD_3CN. The structure **4** determined in this work substantiated the Coordination Number Pattern Recognition Theory of Williams, who preferred structure **4** on those grounds.[9]

A graphical correlation of ^{11}B NMR spectra[10] of the $B_9H_{12}^-$ and 7-CB_8H_{12} *nido* compounds (Fig. 5) indicates an observable vicinal shift of ^{11}B signals of the adjacent B(2,3) and B(6,8) atoms, and an

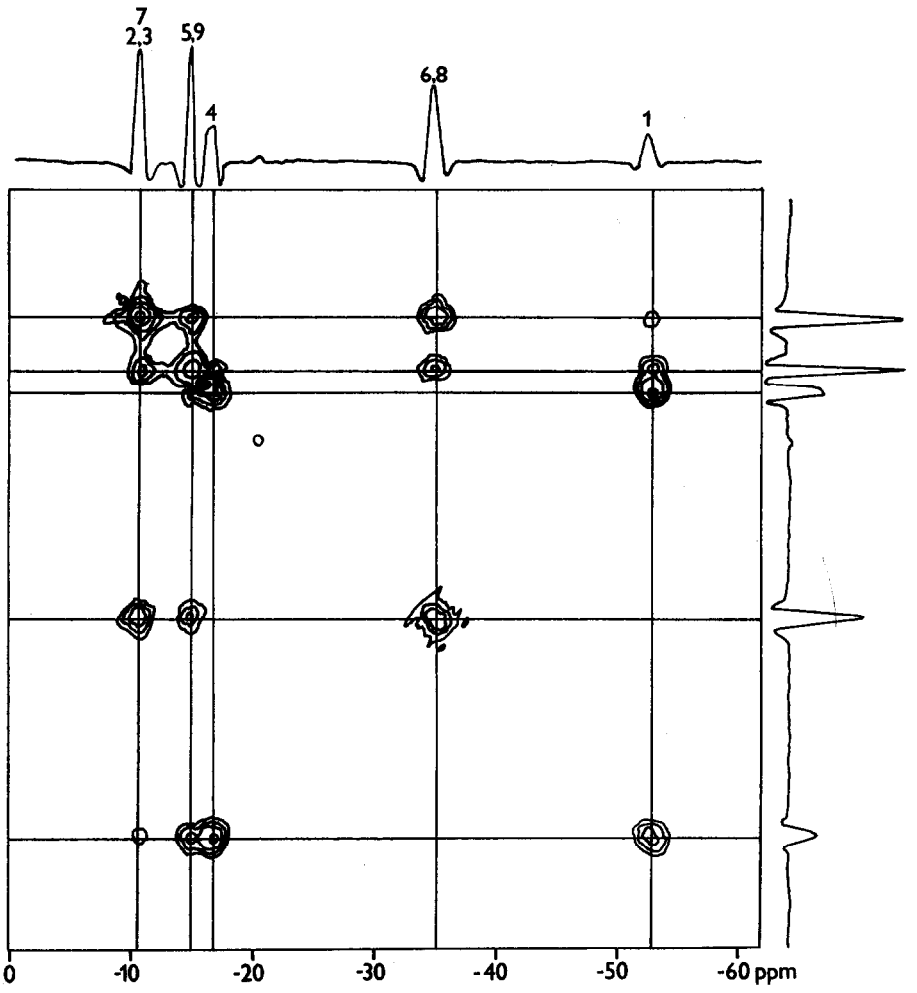


Fig. 4. ^{1}H-decoupled 2-D ^{11}B–^{11}B and one-dimensional FT NMR spectra of $B_9H_{12}N(CH_3)_4$ in CD_3COCD_3.

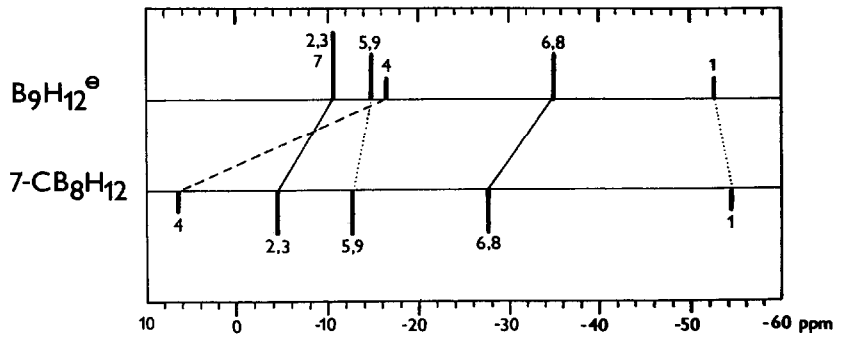


Fig. 5. Schematic demonstration of changes in ^{11}B chemical shifts evoked by substituting B for C in position 7 in $B_9H_{12}^-$: (——) vicinal, (····) *meta*, and (– – – –) antipodal shift.

outstanding antipodal shift (23.7 ppm) of the opposite B(4) atom caused by the partially positive C-vertex.[10]

Distribution of bonds in $B_9H_{12}^-$ *and* 7-CB_8H_{12}

Nido boranes and their derivatives can be described by a set of styx formulae[11] composed of H-bridges (s), three-center (t) and classical (y) bonds, and of *endo*-hydrogens (x). The isoelectronic $B_9H_{12}^-$ and 7-CB_8H_{12} compounds discussed can be expressed by two distinct tautomeric styx formulae [3530 (**5** and **6**) and 2621 (**7**)], differing in number of B—H—B bridges and BH_2 groups. Each tautomeric formula is, moreover, a hybrid of many canonical resonance formulae, differing in the dislocation of styx-given bonds. From all these, three representative formulae (**5**–**7**) were elected to show possible boundary arrangements in particular parts of these skeletons (Fig. 6).

Up to now, the choice of optimum formulae was a matter of quantum chemical calculations based on X-ray structural analysis. In the case of $B_9H_{12}^-$ these attempts were unsuccessful due to the disorder of the measured crystals.[8] Difficulties in obtaining suitable crystals, long-term measuring and computing, and further complications were the reason why a new approach was looked for.

Almost 10 years ago, a series of empirical rules was presented[3,12] which give a mutual relationship of the ^{11}B NMR chemical shift of an observed B* atom with the position of the center of a bond connecting two adjacent skeletal atoms. It was stated that "shielding" increases (or, probably better, paramagnetic deshielding decreases) in the order shown in Fig. 7.

A tight relation between the ^{11}B chemical shift of a given skeletal atom and the distribution of bonding electrons in front or behind the imaginary connecting line of a couple of adjacent skeletal atoms is illustrated for three compounds [$B_{10}H_{14}$ (**9**), 4,6-$C_2B_7H_{13}$ (**10**) and 4-$(CH_3)_2SB_9H_{13}$ (**11**)] (Fig. 8) which have marked parts of the molecule analogous with those in **3** or **4**. These three compounds were elected due to the correct assignment of all signals (see values in ppm) and a very probable distribution of bonds in **9** and **10**, estimated by quantum chemical calculations and visualized by fractional bonds.

A confrontation of ^{11}B chemical shifts of the key atoms B(1) (−16.24 ppm) and B(4) (−52.74 ppm) in $B_9H_{12}^-$ with chemical shifts of B atoms enclosed in dashed boxes for compounds **9** and **10** allows one to prefer a classical B—B bond (see **5** and **7**) to two partial three-center bonds (**6**) between B(1) and B(4). Similarly, the chemical shift of −10.47 ppm of

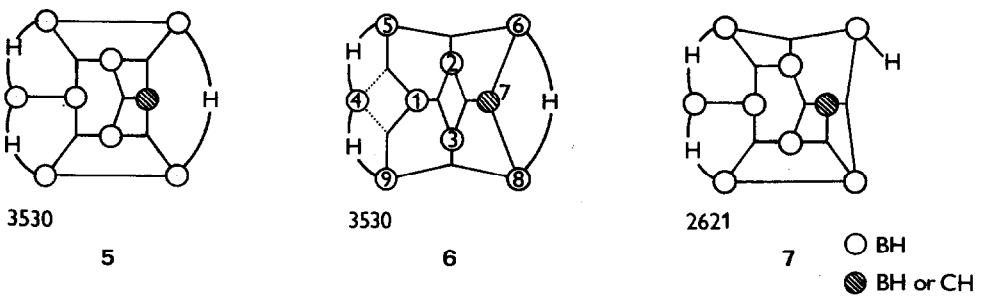


Fig. 6. Selected representative valence structures of $B_9H_{12}^-$ and 7-CB_8H_{12}.

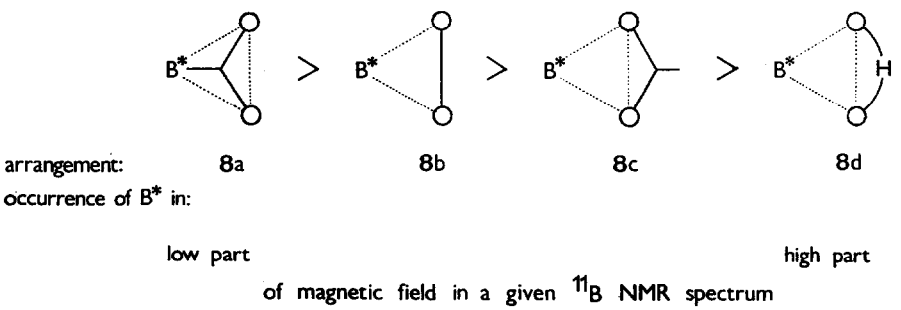


Fig. 7. Relation between the position of the B* signal in a given ^{11}B NMR spectrum and the location of the center of bonding electrons connecting two neighboring atoms (○). Individual bond arrangements are ordered according to the decreasing deshielding of B*.

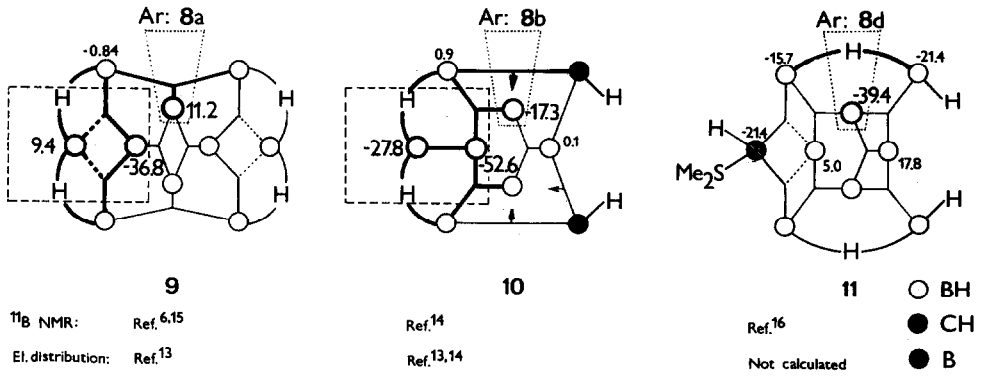


Fig. 8. Bonding schemes of $B_{10}H_{14}$ (**9**), 4,6-$C_2B_7H_{13}$ (**10**) and 4-$(CH_3)_2SB_9H_{13}$ (**11**). Bond arrangements (Ar) governing ^{11}B chemical shifts of particular atoms are marked by bold contours, and are enclosed in dashed or dotted boxes.

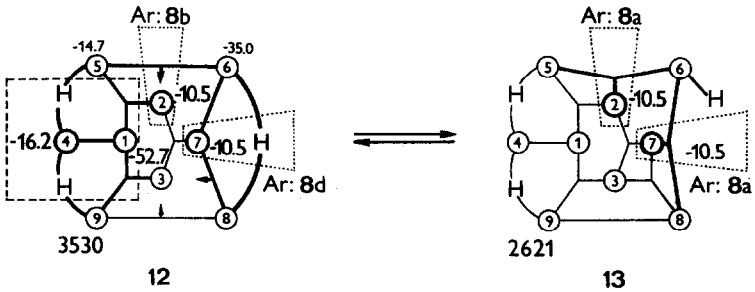


Fig. 9. Distribution of bonding electrons in $B_9H_{12}^-$ deduced from the ^{11}B chemical shifts of B(1,2,4,7) atoms. The analogous distribution is expected for 7-CB_8H_{12}.

the B(2,3) atoms, and its occurrence in the low part of the given spectrum favors a hybrid of a three-center bond and a classical bond in the areas B(2,5,6) and B(3,8,9) (cf. dotted boxes in **9** and **10**). The presence of a B—H—B bridge between B(6) and B(8) is controversial [cf. the relatively low δ value (-10.47 ppm) of the B(7) atom]. This seeming discrepancy can be easily explained by assuming an alternating occurrence of the B—H—B bridge and BH_2 group in this area, i.e. the existence of both tautomers (**12** and **13**) in equilibrium and, consequently, alternating arrangements (**8d** and **8a**) at B(7), averaging a generally high shift (**8d**) (-40 ± 10 ppm) and a low shift (**8a**) (10 ± 10 ppm) to the average value of -10.5 ppm. The tautomers **12** and **13** are expressed by localized valence structures composed of fraction bonds distributed in such a manner as to reflect ^{11}B chemical shifts of individual B atoms and their bonding surroundings (Fig. 9).

With the 7-CB_8H_{12} carborane, taking into account changes brought about by the effect of the 7-C heteroatom (see Fig. 5), we can consider its ^{11}B NMR spectrum to be analogous to that of $B_9H_{12}^-$. For 7-CB_8H_{12} a $BH_2 \rightleftharpoons$B—H—B tautomerism is also present, stemming from the relative low ^{13}C δ value of 31.06 ppm, which corresponds to a ^{11}B δ value of *ca.* -20 ppm.[15] On the grounds of the relationships discussed a tautomerism of structures **12** and **13** with a 7-C vertex is proposed.

CONCLUSIONS

(i) The thermal origin of 7-CB_8H_{12}, leading to a transformation of the four- to the five-coordinated carbon vertex, supports the idea that the thermodynamically best isomers are those "with bridge hydrogens in optimal positions and carbons in next best positions"[9] (Williams' rules 2 and 3).

(ii) This work substantiated the preference for a five-membered face with *nido* nine-vertex borane and heteroborane compounds.

(iii) This study has confirmed a tight relationship between the location of bonding electrons and the chemical shift of individual vertex atoms.

(iv) A new approach to the estimation of a distribution of bonding electrons in the framework of borane and heteroborane molecules, based on argument (iii), is proposed.

Acknowledgements—We thank Drs J. Schraml and V. Blechta for very valuable help concerning the preparation of 2-D measurements.

REFERENCES

1. K. Baše, S. Heřmánek and B. Štíbr, *Chem. Ind. (London)* 1977, 951.
2. K. Baše, B. Štíbr, J. Dolanský and J. Duben, *Collect. Czech. Chem. Commun.* 1981, **46**, 2345.
3. S. Heřmánek and J. Plešek, *Z. Anorg. Allg. Chem.* 1974, **409**, 115.
4. J. Plešek, S. Heřmánek and Z. Janoušek, *Collect. Czech. Chem. Commun.* 1977, **42**, 785.
5. B. M. Graybill, J. K. Ruff and M. F. Hawthorne, *J. Am. Chem. Soc.* 1961, **83**, 2669.
6. T. L. Venable, W. C. Hutton and R. N. Grimes, *J. Am. Chem. Soc.* 1984, **106**, 29.
7. J. Plešek, B. Štíbr and S. Heřmánek, *Chem. Ind. (London)* 1974, 662.
8. A. R. Siedle, G. M. Bodner, A. R. Garber and L. J. Todd, *Inorg. Chem.* 1974, **13**, 1756.
9. R. E. Williams, In *Advances in Inorganic Chemistry and Radiochemistry* (Edited by H. J. Emeléus and A. G. Sharpe), Vol. 18, pp. 67–181. Academic Press, New York (1976).
10. S. Heřmánek, V. Gregor, B. Štíbr, J. Plešek, Z. Janoušek and V. A. Antonovich, *Collect. Czech. Chem. Commun.* 1976, **41**, 1492.
11. W. N. Lipscomb, *Boron Hydrides*, pp. 27–78. W. A. Benjamin, New York (1963).
12. S. Heřmánek, J. Plešek and B. Štíbr, IIIrd International Meeting on Boron Compounds, 5–9 July 1976, Munich, Ettal, Abstract No. 52.
13. J. H. Hall, Jr, D. A. Dixon, T. A. Halgren, L. D. Brown and W. N. Lipscomb, *J. Am. Chem. Soc.* 1975, **97**, 4202.
14. J. Dolanský, S. Heřmánek and R. Zahradník, *Collect. Czech. Chem. Commun.* 1981, **46**, 2479.
15. S. Heřmánek, unpublished results.
16. G. M. Bodner, F. R. Scholer, L. J. Todd, L. E. Senor and J. C. Carter, *Inorg. Chem.* 1971, **10**, 942.

Polyhedron Vol. 5, No. 11, pp. 1881–1883, 1986
Printed in Great Britain

0277-5387/86 $3.00+.00
© 1986 Pergamon Journals Ltd

A FACILE SYNTHESIS AND PROPERTIES OF QUINONE FROM A POLYVALENT PORPHYRIN, TETRAKIS(3,5-DI-*TERT*-BUTYL-4-HYDROXYPHENYL)PORPHYRIN

TOSHIHIKO OZAWA* and AKIRA HANAKI

National Institute of Radiological Sciences, 9-1, Anagawa-4-chome, Chiba-shi 260, Japan

(*Received* 3 *March* 1986; *accepted* 28 *May* 1986)

Abstract—The quinone 5,15-di-(3,5-di-*tert*-butyl-4-hydroxyphenyl)-10,20-di-(3,5-di-*tert*-butyl-4-quinomethane)porpho-10,20-dimethene (**2**) was obtained in high yield by the oxidation of the polyvalent porphyrin tetrakis(3,5-di-*tert*-butyl-4-hydroxyphenyl)porphyrin (**1**) with an Mn^{2+}–O_2 system in dimethylformamide. **2** was reduced to **1** by ascorbic acid or hydroquinone.

In a preceding paper,[1] we described how the polyvalent porphyrin tetrakis(3,5-di-*tert*-butyl-4-hydroxyphenyl)porphyrin (**1**) was oxidized by the superoxide ion (O_2^-) to give the corresponding quinone, 5,15-di-(3,5-di-*tert*-butyl-4-hydroxyphenyl)-10,20-di-(3,5-di-*tert*-butyl-4-quinomethene)porpho-10,20-dimethene (**2**). Further, Milgrom[2] reported that **2** was obtained by aerial oxidation of **1** in basic solutions. However, the yield of **2** was somewhat low in both systems (50.1 and 60%, respectively). Then, we tried to obtain **2** in high yield and found that the Mn^{2+}–O_2 system is suitable for preparing **2** in extremely high yield. Furthermore, it is of interest that the oxidation product, **2**, is very stable, whereas other porphyrins, such as tetraphenylporphyrin and hydroxyporphyrin, undergo further redox or ring-opening reactions during oxidation steps.[3,4] Traylor *et al.*[5,6] reported that **2** is reduced quantitatively to **1** in chloroform ($CHCl_3$) by stannous chloride or aqueous sodium dithionite but not reduced by *p*-cresol and other phenols. We intended to examine the reduction of **2** by use of some organic reducing agents and found that ascorbic acid and hydroquinone can reduce **2** to **1**. We report these results in this paper.

*Author to whom correspondence should be addressed.

EXPERIMENTAL

Materials

1 was prepared as described previously.[1] $CuCl_2 \cdot 2H_2O$, $FeCl_3$, $MnCl_2 \cdot 2H_2O$ and $CoCl_2$ were obtained from Wako Pure Chemical Industries Ltd. Potassium superoxide was purchased from Alfa Products, Inc. Dicyclohexyl-18-crown-6 was purchased from Nippon Soda Ltd and used without further purification. L-Ascorbic acid and hydroquinone were obtained from Wako Pure Chemical Industries Ltd and Nakarai Chemicals Ltd, respectively, and used as received. α-Tocopherol (vitamin E) was purchased from Aldrich. Other reagents were commercially available. $CHCl_3$ was distilled and passed through a neutral alumina column prior to use. Other solvents were distilled prior to use.

Spectral measurements

Visible absorption spectra were recorded at room temperature with a Union Giken SM-401 spectrophotometer. ESR spectra were obtained at room temperature or at 77 K with a JEOL-PE-1X (X-band) ESR spectrometer with 100-kHz field modulation. ESR parameters were obtained by comparison with 1,1-diphenyl-2-picrylhydrazyl ($g = 2.0036$) and a standard Mn^{2+}–MgO

Table 1. Reaction mode of **1** with some metal ions

Valence change	Reduction potential[a] (V)	Reaction mode
$Cu(II)+e^- \rightarrow Cu(I)$	0.153	Incorporation
$Fe(III)+e^- \rightarrow Fe(II)$	0.77	Incorporation
$Mn(III)+e^- \rightarrow Mn(II)$	1.51	Oxidation
$Co(III)+e^- \rightarrow Co(II)$	1.842	Incorporation

[a]Reference 11.

powdered marker. IR spectra were recorded on a JASCO IRA-1 IR spectrometer. The ^1H NMR spectra were recorded on a JEOL JNM-FX-100 spectrometer in $CDCl_3$ solution with tetramethylsilane as an internal standard.

Synthesis of **2**

2 was prepared by the oxidation method using Mn^{2+}–O_2 as follows: **1**[7-9] (0.944 g, 0.84 mmol) was dissolved in 200 cm^3 of dimethylformamide (DMF) and the solution was heated to flux. $MnCl_2 \cdot 2H_2O$ (0.664 g, 4.1 mmol) was added to this refluxing solution and the reaction mixture was further refluxed for 15 min. The formation of **2** was checked spectrophotometrically. After completion of the reaction, the reaction mixtures were evaporated to dryness by a rotary evaporator and the residues were dissolved in a minimum amount of $CHCl_3$. This solution was placed on a column packed with dry activated alumina (neutral, Woelm) and chromatographed with $CHCl_3$ as eluant. The first eluate, a reddish fraction, was the unreacted **1**, and the second purple eluate was collected and concentrated to dryness. The residue was recrystallized from $CHCl_3$–petroleum ether (b.p. 60–70°C) to give dark-green microcrystals. The yield was 0.899 g (95.2%, based on porphyrin). Found: C, 75.9; H, 8.3; N, 5.1%. Calc. for $C_{76}H_{92}N_4O_4 \cdot 4H_2O$: C, 76.2; H, 8.4; N, 4.7%. M.p. > 300°C. Their spectroscopic data were identical to those of **2**.[1,2,5] ^1H NMR ($CDCl_3$): δ (ppm) 1.35 (s, *m*-^{t}Bu); 6.71 (s, *p*-OH); 7.40 (s, *o*-H); and 8.92 (s, pyrrole H). IR ($CHCl_3$) (cm^{-1}): 3700 and 3520 (OH), and 1600–1610 cm^{-1} (carbonyl C=O). Visible ($CHCl_3$): 522 nm (log ε = 5.09).

RESULTS AND DISCUSSION

2 was almost quantitatively prepared from the oxidation of **1** by Mn^{2+}–O_2 in DMF in comparison with the oxidation by superoxide ion in dimethyl sulphoxide[1] or aerial oxidation in basic solutions.[2] That is, the yield of **2** was 95.2% in the Mn^{2+}–O_2 oxidation, 50.1% in the superoxide oxidation and 60% in the aerial oxidation, respectively. Other metal ions such as Fe^{3+}, Cu^{2+} and Co^{2+} did not oxidize **1** in air, but were incorporated into **1** to yield the corresponding metalloporphyrins.[10] These results may be explained by the reduction potentials of metal ions (Table 1).[11] Both Cu^{2+} and Fe^{3+} ions having low reduction potentials cannot oxidize **1** and are incorporated into the cavity of **1**. The Co^{2+} ion is hardly oxidized by O_2 to the Co^{3+} ion which has a high reduction potential and is incorporated into the cavity of **1**. On the other hand, since in basic

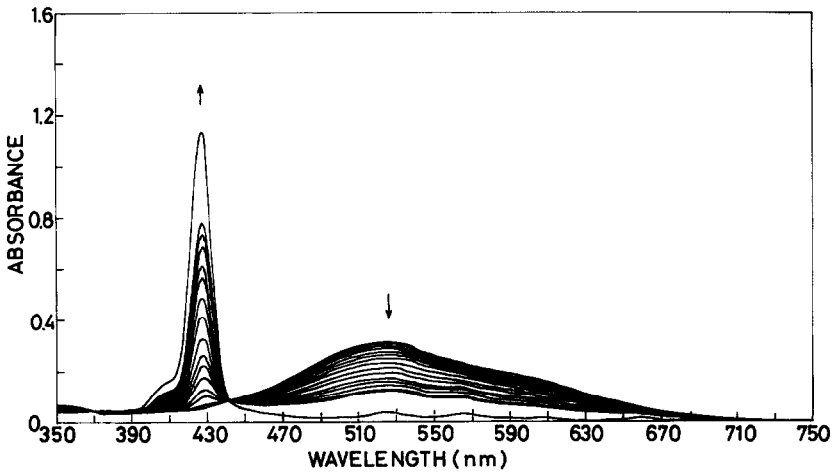
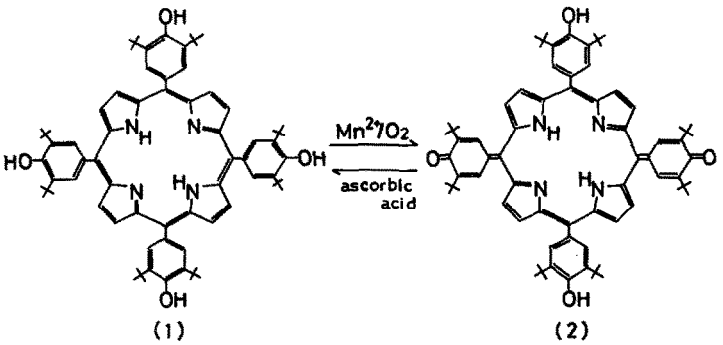


Fig. 1. Visible spectral changes accompanying the reduction of **2** to **1** by ascorbic acid in $CHCl_3$ solution at 25°C. Concentrations: **2** = 2.57×10^{-6} mol dm^{-3}, and ascorbic acid = 1.87×10^{-5} mol dm^{-3}. Time after mixing (min): 0, 5, 10, 20, 30, 40, 60, 90, 120, 150, 180, 210, 240 and 270. The final spectrum was recorded after 20 h.



Scheme 1.

media Mn^{2+} ion is easily oxidized by O_2 to the Mn^{3+} ion, which has a high reduction potential,[12] the Mn^{3+} ion formed from the oxidation of the Mn^{2+} ion by O_2 in DMF can oxidize **1** to give **2**. From these results, it is indicated that the Mn^{2+} ion is a suitable reagent for preparing a high yield of **2** in basic media such as DMF.

2 shows a very broad absorption spectrum (λ_{max} = 522 nm, $\log \varepsilon = 5.09$) in $CHCl_3$. When ascorbic acid in ethyl alcohol–H_2O (9:1) was added to a $CHCl_3$ solution of **2**, spectral changes were observed as shown in Fig. 1. The final spectrum showed five absorption bands (λ_{max} = 427, 525, 563, 606 and 658 nm) and was identical with that of **1** in $CHCl_3$. This result indicates that **2** can be reduced by ascorbic acid to **1**.

The same spectral changes were observed upon the reaction of hydroquinone with **2**, although its reaction rate was slower than that between **2** and ascorbic acid. α-Tocopherol (vitamin E) which is known to act as an antioxidant in living organs did not reduce **2**. Traylor *et al.*[5,6] reported that **2** is reduced by stannous chloride or sodium dithionite but not reduced by *p*-cresol and other phenols. These results suggest that **2** has less oxidizing ability.

In the reaction of **2** with ascorbic acid, the reaction shown in Scheme 1 may be assumed.

Both the semiquinone radical and the ascorbic acid free radical,[13,14] which are anticipated as reaction intermediates, could not be detected by ESR spectrometry. This result suggests that the reduction of **2** does not involve the formation of stable semiquinone radicals or, if the semiquinone radical could be formed, its lifetime should be too short to be detected by ESR spectrometry.

We are now further investigating the reductions of **2** by other organic or inorganic substrates.

REFERENCES

1. T. Ozawa and A. Hanaki, *Inorg. Chim. Acta* 1985, **108**, L11.
2. L. R. Milgrom, *Tetrahedron* 1983, **47**, 3895.
3. P. S. Clezy, In *The Porphyrins* (Edited by D. Dolphin), Vol. 2, pp. 103–130. Academic Press, New York (1978).
4. J.-H. Fuhrhop and S. Besecke, *Angew. Chem., Int. Ed. Engl.* 1974, **13**, 150.
5. T. G. Traylor, K. B. Nolan and R. Hildreth, *J. Am. Chem. Soc.* 1983, **105**, 6149.
6. T. G. Traylor, K. Nolan, R. Hildreth and T. A. Evans, *Heterocycles* 1984, **21**, 249.
7. G. M. Badger, R. A. Jones and R. L. Lawlett, *Aust. J. Chem.* 1964, **17**, 1028.
8. A. L. W. Shorey, C. Lorberau, S. S. Eaton and G. R. Eaton, *J. Org. Chem.* 1980, **45**, 4296.
9. T. A. Evans, G. Srivasta, D. T. Sawyer and T. G. Traylor, *Inorg. Chem.* 1985, **24**, 4733.
10. T. Ozawa and A. Hanaki, to be submitted for publication.
11. W. M. Latimer, *Oxidation Potentials*, 2nd Edn. Prentice-Hall, Englewood Cliffs, NJ (1952).
12. F. A. Cotton and G. Wilkinson, *Advanced Inorganic Chemistry*, 3rd Edn, p. 846. Wiley Interscience, New York (1972).
13. I. Yamazaki and L. H. Piette, *Biochim. Biophys. Acta* 1961, **50**, 62.
14. Y. Kirino and T. Kwan, *Chem. Pharm. Bull.* 1971, **19**, 831.

Polyhedron Vol. 5, No. 11, pp. 1885–1890, 1986
Printed in Great Britain

0277–5387/86 $3.00+.00
© 1986 Pergamon Journals Ltd

OPTICALLY ACTIVE COBALT(III) COMPLEXES OF 1,4,8,11-TETRAAZACYCLOTETRADECANE COORDINATED IN A FOLDED CONFIGURATION

MATSUO NONOYAMA,* TAKAKO YAMAGUCHI and HIDEKO KIMIJIRI

Department of Chemistry, Faculty of Science, Nagoya University, Chikusa, Nagoya 464, Japan

(*Received* 11 *March* 1986; *accepted* 28 *May* 1986)

Abstract—Some optically active cobalt(III) complexes of 1,4,8,11-tetraazacyclotetradecane (L) coordinated in a folded (*cis*) configuration, $[CoL(XY)]^{n+}$ [XY = (*R*)-propylenediamine ($n = 3$), (*S*)-alanine ($n = 2$) or acetylacetone ($n = 2$)], have been prepared and separated into isomers by column chromatography. These complexes are characterized spectroscopically and absolute configurations are assumed based on the circular-dichroism spectra.

A wealth of investigations have been carried out for complexes of tetraazamacrocycles but only a small part of the investigations participates in complexes coordinated with tetraazamacrocycles in a folded (*cis*) configuration.[1] Optically active complexes of the folded tetraazamacrocycles have been studied quite sparingly.[2,3] 1,4,8,11-Tetraazacyclotetradecane (cyclam), one of the most widely used tetraazamacrocycles coordinated in a folded configuration, exists in two enantiomers.[3,4] Configurational chirality results from an alternating displacement of five- and six-membered chelate rings around a central metal ion, but it is impossible to assign a simple Δ or Λ description to either enantiomer. The secondary nitrogen atoms are chiral and can be described in terms of *R* or *S* (Fig. 1). In a preliminary paper,[5] we have reported on an optically active complex, $[Co(en)(cyclam)]^{3+}$ (en = ethylenediamine), and in this paper we describe some new optically active cobalt(III) complexes coordinated with cyclam in a folded (*cis*) configuration.

RESULTS AND DISCUSSION

Reactions of *trans*-$[CoCl_2(cyclam)]Cl$ with bidentate ligands (XY) [XY = (*R*)-propylenediamine (pn), (*S*)-alanine (ala) or acetylacetone (Hacac)] in hot dimethylsulfoxide gave $[Co(XY)(cyclam)]^{n+}$ complexes. Isomers of the pn and ala complexes were separated by chromatography on an SP Sephadex C-25 column[6] with an aqueous solution of disodium hydrogen phosphate as an eluent (Table 1, where abbreviations for the complexes are given). The acac complex was optically resolved also by chromatography with an aqueous solution of sodium antimony tartrate as an eluent (Table 1). By this method $[Co(en)(cyclam)]^{3+}$ was previously resolved.[5]

The chemical shifts of methyl groups in the ^1H NMR spectra are given in Table 1. Two isomers (P+) and (P−) can not be distinguished by the ^1H

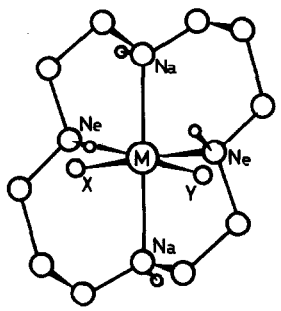


Fig. 1. Structure of Λ(en) and Δ(tn) (*RRRR*, *δδ*)-[Co(XY)(cyclam)]. Λ(en) and Δ(tn) represent, respectively, the chirality with respect to the pair of en or tn rings of cyclam, *R* the chirality of N atoms, and *δ* a *gauche* conformation of en rings (tn = trimethylenediamine). The structure of the Δ(en) and Λ(tn) (*SSSS*, *λλ*)-isomers is just the mirror image of the one shown.

*Author to whom correspondence should be addressed.

Table 1. Yields, analytical results and ^{1}H NMR of the complexes

Complex[a]	Yield[b] (%)	Analysis: found (calc.) (%) C	H	N	$\delta(CH_3)$[c] (ppm) [J (Hz)]
(P−) $(-)_D$-$[Co(pn)L]Cl_3\cdot 2H_2O$	31	32.9 (32.8)	7.7 (8.0)	17.7 (17.7)	1.51d (5.8)
(P+) $(+)_D$-$[Co(pn)L](ClO_4)_3$	2	25.1 (24.7)	5.5 (5.4)	13.4 (13.3)	1.45d (5.5)
(A−) $(-)_D$-$[Co(ala)L](ClO_4)_2$	14	28.3 (28.6)	5.5 (5.5)	12.6 (12.8)	1.53d (7.2)
(A+) $(+)_D$-$[Co(ala)L](ClO_4)_2$	20	28.3 (28.6)	5.5 (5.5)	12.7 (12.8)	1.53d (6.9)
(C+) $(+)_D$-$[Co(acac)L](ClO_4)_2\cdot H_2O$	14	31.2 (31.3)	5.8 (5.8)	9.6 (9.7)	2.21s [d]
(C−) $(-)_D$-$[Co(acac)L](ClO_4)_2\cdot H_2O$	13	31.3 (31.3)	5.7 (5.8)	9.7 (9.7)	2.21s [d]

[a] L = cyclam.
[b] Isolated yields.
[c] In D_2O solutions (chemical shifts are given vs sodium trimethylsilylpropionate). d = doublet, and s = singlet.
[d] The signal of the methine proton of acac is at 5.87s ppm.

Table 2. ^{13}C NMR spectra of the complexes in D_2O solutions

Complex[a]	$\delta(^{13}C)$ (ppm) from TMS					
(P−) $(-)_D$-$[Co(pn)L]Cl_3\cdot 2H_2O$	17.93	22.03	44.78	49.46	50.53	50.68
	51.02	51.12	55.02	55.11	55.41	55.55
(P+) $(+)_D$-$[Co(pn)L](ClO_4)_3$	17.93	20.07	45.32	45.47	50.10	50.73
	54.53	54.92				
(A−) $(-)_D$-$[Co(ala)L](ClO_4)_2$	19.55	22.43	22.84	45.94	48.96	50.17
	50.61	50.84	54.66	54.78	186.34	
(A+) $(+)_D$-$[Co(ala)L](ClO_4)_2$	19.26	22.49	45.38	46.23	48.55	50.14
	50.26	50.49	55.01	55.72	185.87	
(C+) $(+)_D$-$[Co(acac)L](ClO_4)_2\cdot H_2O$	22.72	27.30	45.15	48.38	48.96	54.01
	100.57	192.34				
(E+) $(+)_D$-$[Co(en)L]Cl_3\cdot 1\frac{1}{4}H_2O$	22.12	45.12	45.86	49.75	50.97	55.41

[a] L = cyclam.

NMR spectra. To identify the isomers, the ^{13}C NMR spectra were measured (Table 2). The numbers of ^{13}C signals are small for (E+) and (C+), and this consists with the presence of a two-fold axis in these complexes. The spectra are in agreement with the proposed structure (Fig. 1) and the bidentate ligands are shown to be coordinated in the usual manner.

The pn and en complexes are pink despite a CoN_6 chromophore and the ala complex with a $CoON_5$ chromophore is red. These colours are different from those of $[Co(en)_3]^{3+}$ and $[Co(ala)(en)_2]^{2+}$, respectively, with the same chromophore. The absorption spectral patterns of the cyclam complexes are very similar to those of the corresponding bis(ethylenediamine) complexes, $[Co(XY)(en)_2]^{n+}$ (Table 3), but the following two points should be noted. Substitution of the $(en)_2$ part by cyclam results in a lowering of the energies ($\tilde{\nu}_{max}$) of the *d–d* transitions, and in a significant enhancement of the molar extinction coefficients ($\log \varepsilon$). The first point is in contrast with the fact that the ligand field of a secondary amino group is usually stronger than that of a primary one.[7] The weakened ligand field of cyclam compared with that of the $(en)_2$ part should be caused by distortions of an octahedral ligand field: connection of the $(en)_2$ part with two trimethylene chains produces strains and crowds around a central metal ion if cyclam adopts a folded configuration, as revealed for

Table 3. Absorption (AB) and CD spectra of the complexes [in aqueous solutions ($\tilde{\nu}$ in $10^3\,cm^{-1}$)]

Complex[a]	AB $\tilde{\nu}_{max}$ (log ε)	CD $\tilde{\nu}_{ext}$	CD (Δε)
(P−) $(-)_D$-[Co(pn)L]$Cl_3 \cdot 2H_2O$	20.3 (2.16)	19.0 (−1.31)	21.3 (+2.42)
	28.2 (2.14)	28.5 (−0.33)	
	42.5 (4.36)	38.8 (−6.07)	44.2 (+15.02)
(P+) $(+)_D$-[Co(pn)L]$(ClO_4)_3$	20.3 (2.14)	19.1 (+0.89)	21.3 (−1.04)
	28.2 (2.12)	29.1 (+0.18)	
	42.6 (4.37)	39.5 (+8.35)	44.5 (−7.27)
(A−) $(-)_D$-[Co(ala)L]$(ClO_4)_2$	19.5 (2.22)	18.4 (−1.47)	20.4 (+1.82)
	27.7 (2.21)	28.6 (−0.25)	
	42.2 (4.37)	39.6 (−9.79)	44.8 (+13.01)
(A+) $(+)_D$-[Co(ala)L]$(ClO_4)_2$	19.6 (2.22)	18.6 (+1.21)	21.0 (−2.03)
	27.6 (2.23)	25.8 (−0.14)	29.1 (+0.11)
		33.7 (−0.06)	
	42.4 (4.36)	39.7 (+8.60)	45.5 (−16.35)
(C+) $(+)_D$-[Co(acac)L]$(ClO_4)_2 \cdot H_2O$	19.2 (2.32)	18.0 (+1.15)	20.1 (−1.71)
	27.0sh[b]	24.3 (−0.56)	
	30.4 (3.50)	31.3 (+4.20)	36.7 (+7.21)
	42.7 (4.50)	39.5 (−14.71)	48.5 (+10.24)
(E+) $(+)_D$-[Co(en)L]$Cl_3 \cdot 1\frac{1}{4}H_2O$[c]	20.3 (2.16)	19.0 (+1.09)	21.2 (−1.81)
	28.3 (2.15)	28.5 (+0.25)	
	42.5 (4.34)	39.1 (+7.40)	44.6 (−11.72)
$(+)_D$-$[Co(en)_3]^{3+}$[d]	21.3 (1.92)	20.3 (+1.89)	23.7 (−0.17)
	29.4 (1.87)	28.5 (+0.25)	
	48.1 (4.18)	47.2 (−31)	
$(+)_D$-$[Co(ala)(en)_2]^{2+}$[e]	20.5 (2.00)	19.9 (+2.56)	22.8 (−0.27)
	28.7 (2.04)	27.0 (+0.07)	30.8 (+0.08)
	46.6 (4.33)	47.5 (−30.83)	
$(+)_D$-$[Co(acac)(en)_2]^{2+}$[f]	20.1 (2.14)	20.2 (+2.4)	
	26sh	26.8 (−1.3)	
	30.9 (3.62)	31.0 (−10)	
	37sh	35.7 (−3)	
	42sh	40.8 (−11)	50.6 (+20)

[a] L = cyclam.
[b] sh = shoulder.
[c] M. Nonoyama and O. Hirai, *Inorg. Chim. Acta* 1981, **54**, L283.
[d] S. F. Mason and P. J. Peart, *J. Chem. Soc., Dalton Trans.* 1977, 937.
[e] C. T. Liu and B. E. Douglas, *Inorg. Chem.* 1964, **3**, 1356.
[f] L. J. Boucher, *Inorg. Chim. Acta* 1972, **6**, 29.

$[Co(en)(cyclam)]^{3+}$ by X-ray analysis[4] (an axial N_a—Co—N_a bond angle of 173° is reported). The distortions should also be reflected in the higher molar extinction coefficients. Similar complexes of a smaller-size macrocycle, $[Co(XY)(cyclen)]^{n+}$ (cyclen = 1,4,7,10-tetraazacyclododecane), have higher molar extinction coefficients and lower-energy *d–d* transitions than the corresponding cyclam ones.[8] More pronounced distortions in $[Co(XY)(cyclen)]^{n+}$ [where the $(en)_2$ part is connected with two ethylene chains] have been shown by X-ray analysis.[9,10]

It is interesting to compare the electronic spectra of the cyclam complexes with those of an unsaturated analogue, for instance 5,12-dimethyl-1,4,8,11-tetraazacyclotetradeca-4,11-diene (L1). The L1 complexes with en, ala and acac show ν_{max} of *d–d* transitions at higher energies, which are nearly comparable with those of the $(en)_2$ analogues.[11] L1 is more compact due to the presence of unsaturated C=N bonds. In the cyclam complexes there are more non-bonding intra- and inter-chelate ring repulsions, which may characterize in part the spectral properties.

All the complexes are chiral and their circular-dichroism (CD) spectra are measured (Table 3, Figs

2 and 3). The CD spectra of the two isomers (P+) and (P−) are roughly opposite in pattern, suggesting that the two are pseudoenantiomers. The pattern of (P+) is very similar to that of (E+). The absolute configuration of (E+) was previously assumed to be Λ(en) (Fig. 1, XY = en).[5] The absolute configuration of (P+) is, therefore, Λ(en). The marked difference in intensity of the CD spectra of (P+) and (P−) is explained as follows.

A preferred λ-conformation of (*R*)-pn shows a CD spectrum due to a vicinal effect {for instance, $[Co(pn)(NH_3)_4]^{3+}$ shows ν_{ext} at 19.3 ($\Delta\varepsilon = -0.063$) and 21.7 $(+0.34)\times 10^3\,cm^{-1}$ in the first *d–d* transition region (Fig. 2)}.[12] This interferes in the CD spectra caused by a chiral Δ(en) or Λ(en) configuration of the fragment "[Co(XY)(cyclam)]". The CD spectra of the fragment can, roughly, be estimated by that of (E+) since an en chelate ring is usually flexible in solution. For the (P+) isomer, assumed to have a Λ(en) configuration, the vicinal effect of (*R*)-pn acts in a contradictory way (Fig. 2) (the vicinal CD spectrum of (*R*)-pn is reversed in sign compared with the CD spectrum of (E+)[5] and should reduce the intensity of the spectrum of (P+)). For (P−), on the contrary, the vicinal CD is additive to the CD spectrum of (E−) [the spectrum of (E−) is just the mirror image of that of (E+)] and then the spectrum of (P−) is enhanced.

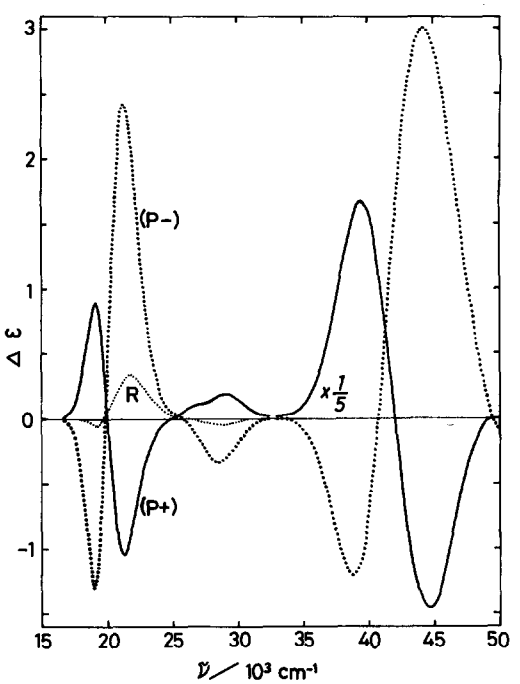


Fig. 2. CD spectra of: (P+) $(+)_D$-[Co(pn)(cyclam)] $(ClO_4)_3$, (P−) $(-)_D$-[Co(pn)(cyclam)]$Cl_3\cdot 3H_2O$ and (R) $[Co(R\text{-pn})(NH_3)_4]^{3+}$ in H_2O.

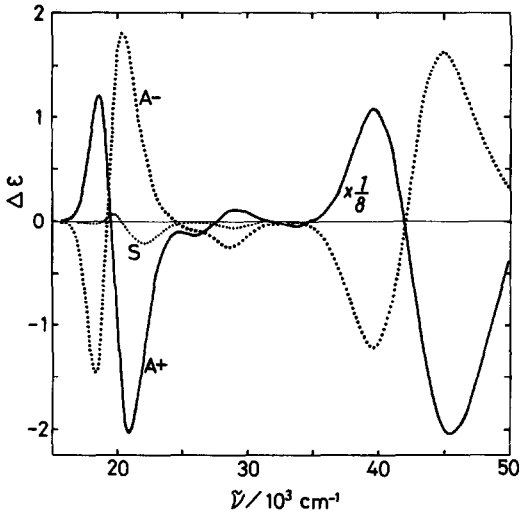


Fig. 3. CD spectra of: (A+) $(+)_D$-[Co(ala)(cyclam)] $(ClO_4)_2$, (A−) $(-)_D$-[Co(ala)(cyclam)]$(ClO_4)_2$ and (S) $[Co(S\text{-ala})(NH_3)_4]^{2+}$ in H_2O.

The two five-membered chelate rings of Λ(en)-[Co(XY)(cyclam)] [where the chirality of all the secondary amino groups is *R* (Fig. 1)] adopt a δ *gauche* conformation as revealed by X-ray structural analysis.[4] The chelate ring of (*R*)-pn is usually fixed to a λ-conformation due to a preferred equatorial orientation of the methyl substituent. For the (P+) [Λ(en)] isomer, therefore, the three five-membered chelate rings are in a set of λδδ conformations, that is, an *ob* lel_2 set, and the (P−) [Δ(en)] isomer has a set of λλλ conformations (lel_3). The lel_3 set is the most stable in energy.[13] The difference in energy between (P−) and (P+) is reflected in the formation ratio (P−)/(P+) (85/15). The assignment of Λ(en) to (P+) is compatible with these observations.

The CD spectra of (A+) and (A−) are also of pseudoenantiomers and that of (A+) is similar in pattern to that of (E+) suggesting a similar absolute configuration [Λ(en)] for (A+). The different intensity of the CD spectra between (A+) and (A−) can be explained similarly as for the case of (P+) and (P−), considering the vicinal CD spectrum of (*S*)-ala {the spectrum of [Co(ala)$(NH_3)_4]^{2+}$ is given in Fig. 3}.[14] A preferred equatorial orientation of a methyl substituent results in a δ-conformation of the chelate ring of (*S*)-ala, although less packered than that of pn.[13] (A+) is shown to exist in a Λ(en) [δδδ (lel_3)] configuration, while (A−) is Δ(en) [δλλ (*ob* lel_2)]. This may reflect the slightly preferred formation of (A+) [the formation ratio (A+)/(A−) = 57/43].

In the first *d–d* transition region, the CD spectral pattern of (C+) is similar to that of (E+) and Λ(en)

is tentatively assigned to (C+), but, in the UV region, there are absorptions due to an acac ligand and the CD pattern in this region can not be simply compared with that of (E+) or (A+). In the CD spectra of $[Co(XY)(cyclam)]^{n+}$ the higher-energy component {corresponding to the A_2-component of $[Co(en)_3]^{3+}$} of the first *d–d* transition ($^1A_{1g} \rightarrow {}^1T_{1g}$ in O_h) is intensified compared with that of the corresponding $[Co(XY)(en)_2]^{n+}$ (Table 3). The differences are considered to originate in part from the presence of extra six-membered chelate rings and of chiral amino groups in cyclam. The above discussion is based on the assumption that the CD spectra are, to a first approximation, caused only by five-membered chelate rings in a *gauche* conformation, and that contributions from six-membered rings in a chair conformation are, compared to those of five-membered ones, sufficiently small to be ignored. We expect that the chiral structures of these complexes of cyclam will be confirmed by X-ray structural analysis.

EXPERIMENTAL

Measurements

Measurements were carried out by methods reported previously.[8] ^{13}C NMR spectra were recorded on a JNM FX-100 spectrometer and dioxane was used as an internal standard (δ = 67.8 ppm). Chemical shifts were given relative to tetramethylsilane (TMS).

Preparation

(P+) $(+)_D$-$[Co(pn)(cyclam)](ClO_4)_3$ *and* (P−) $(-)_D$-$[Co(pn)(cyclam)]Cl_3 \cdot 2H_2O$. To a hot dimethylsulfoxide solution (30 cm^3) of 1.5 mmol of (*R*)-pn·2HCl and 3.0 mmol of 1,8-diazabicyclo-(5.4.0)-7-undecene (DBU) was added 1.0 mmol of *trans*-$[CoCl_2(cyclam)]Cl$ and the mixture was heated on a steam bath for several minutes until the complex had reacted to give an orange-red solution. The solution was diluted with 100 cm^3 of 0.01 M hydrochloric acid and adsorbed on a short column of SP Sephadex C-25. The column was washed with 0.1 M hydrochloric acid and eluted with 1.0 M hydrochloric acid. The eluant was evaporated and, in order to separate isomers, readsorbed on a column (150 cm × 3 cm ϕ) of SP Sephadex C-25. The column was developed with a 0.2 M aqueous solution of disodium hydrogenphosphate to give two pink-orange bands; the former one was more deeply coloured. The two bands were collected separately and diluted with water (10 times the volume of the eluant of the respective band). The diluted solutions were adsorbed on a short column of SP Sephadex C-25 and washed sufficiently with 0.03 M hydrochloric acid. The column was eluted with 1 M hydrochloric acid and concentrated to a small volume. From the first band, upon addition of ethanol, pink $(-)_D$-$[Co(pn)(cyclam)]Cl_3 \cdot 2H_2O$ was obtained. From the latter band, upon addition of lithium perchlorate (1 mmol) followed by ethanol, pink $(+)_D$-$[Co(pn)(cyclam)](ClO_4)_3$ was obtained. The relative yield of $(-)_D/(+)_D$ was about 85/15.

(A−) $(-)_D$- and (A+) $(+)_D$-$[Co(ala)(cyclam)](ClO_4)_2$. To a hot dimethylsulfoxide solution (40 cm^3) of 2 mmol of (*S*)-ala and 2 mmol of DBU was added 1 mmol of *trans*-$[CoCl_2(cyclam)]Cl$ and the mixture was heated for about 10 min on a steam bath with occasional stirring until the complex had reacted. The resultant red solution was treated as above and the short column used first was washed and eluted, respectively, with 0.1 and 1.0 M aqueous solutions of lithium chloride. Upon development two red bands appeared and then each eluant was diluted with water (30 times the volume of the respective eluant). The column used last was washed as above with 0.01 M aqueous solution of lithium chloride and eluted with a 1.0 M aqueous solution of lithium perchlorate. Addition of ethanol to the concentrated eluants gave the red $(-)_D$-isomer (from the former band) and the $(+)_D$-isomer (from the latter band). The formation ratio $(-)_D/(+)_D$ was about 43/57.

(C+) $(+)_D$- *and* (C−) $(-)_D$-$[Co(acac)(cyclam)](ClO_4)_2$. This complex was prepared similarly to $[Co(ala)(cyclam)]^{2+}$ by using acetylacetone instead of ala and, for optical resolution, this was adsorbed on a column (150 cm × 3 cm ϕ) of SP Sephadex C-25. The column was eluted with a 0.15 M aqueous solution of sodium antimony tartrate to give two slightly overlapping red bands. The overlapping part was subjected to rechromatography. The front and rear parts were treated as for $[Co(ala)(cyclam)]^{2+}$. From the front part the red $(+)_D$-isomer and, from the rear, the $(-)_D$-isomer were obtained.

(E+) $(+)_D$-$[Co(en)(cyclam)]Cl_3 \cdot 1\frac{1}{4}H_2O$. This[5] was prepared by a method similar to that for $[Co(pn)(cyclam)]^{3+}$ by using en instead of pn·2HCl and DBU, and optically resolved similarly to $[Co(acac)(cyclam)]^{2+}$.

Acknowledgement—We wish to thank the Ministry of Education, Science, and Culture for Scientific Research Grant-in-Aid No. 60540390.

REFERENCES

1. G. A. Melson (Ed.), *Coordination Chemistry of Macrocyclic Compounds*. Plenum Press, New York (1979).
2. D. A. House and V. McKee, *Inorg. Chem.* 1984, **23**, 4234.
3. J. Cragel and B. E. Douglas, *Inorg. Chim. Acta* 1974, **10**, 33.
4. T. F. Lai and C. K. Poon, *Inorg. Chem.* 1976, **15**, 1562.
5. M. Nonoyama and O. Hirai, *Inorg. Chim. Acta* 1981, **54**, L283.
6. Y. Yoshikawa and K. Yamasaki, *Coord. Chem. Rev.* 1979, **28**, 205.
7. V. J. Thöm, J. C. A. Boeyens, G. J. McDougall and R. D. Hancock, *J. Am. Chem. Soc.* 1984, **106**, 3198.
8. M. Nonoyama and T. Kurimoto, *Polyhedron* 1985, **4**, 471.
9. N. Matsumoto, A. Hirano, T. Hara and A. Ohyoshi, *J. Chem. Soc., Dalton Trans.* 1983, 2405.
10. Y. Iitaka, M. Shina and E. Kimura, *Inorg. Chem.* 1974, **13**, 2886.
11. M. A. Ali, R. W. Hay and G. A. Lawrance, *Inorg. Chim. Acta* 1983, **70**, 65.
12. M. Kunimatsu, H. Kanno, M. Kojima and J. Fujita, *Bull. Chem. Soc. Jpn* 1980, **53**, 1571.
13. M. Shibata, *Modern Syntheses of Cobalt*(III) *Complexes*, p. 69. Springer, Berlin (1983).
14. J. Fujita, T. Yasui and Y. Shimura, *Bull. Chem. Soc. Jpn* 1965, **38**, 654.

Polyhedron Vol. 5, No. 11, pp. 1891–1893, 1986
Printed in Great Britain

0277-5387/86 $3.00+.00
Pergamon Journals Ltd

COMMUNICATION

SYNTHESIS, CHARACTERIZATION AND REACTIVITY OF SOME RHENIUM PHOSPHITE COMPLEXES

LARRY F. RHODES and KENNETH G. CAULTON

Department of Chemistry, Indiana University, Bloomington, IN 47405, U.S.A.

and

WITOLD K. RYBAK* and JÓZEF J. ZIÓŁKOWSKI*

Institute of Chemistry, University of Wrocław, 50-383 Wrocław, Poland

(*Received* 14 *January* 1986; *accepted* 7 *May* 1986)

Abstract—The preparation and characterization of some Re(III), Re(IV) and Re(V) chloro phosphite complexes are reported. Both Re(III) and Re(IV) complexes react with sodium borohydride, yielding the corresponding polyhydrides, $ReH_5[P(OEt)_3]_3$ and $ReH_7[P(OEt)_3]_2$. The thermal and photochemical reactivity of these complexes is described.

The chemistry of rhenium phosphine complexes is well developed but the chemistry of the analogous rhenium phosphite complexes is a relatively unexplored area. To date, there have been only a few reports in the literature concerning rhenium phosphites.[1] Different reactivities of metal phosphite complexes relative to the phosphine analogs as a result of different electronic and steric properties[2] have prompted us to pursue the synthesis of these rhenium compounds. In this paper the improved synthesis of $ReCl_3[P(OEt)_3]_3$ (**3**) as well as several new rhenium triethyl phosphite compounds are reported (Scheme 1).

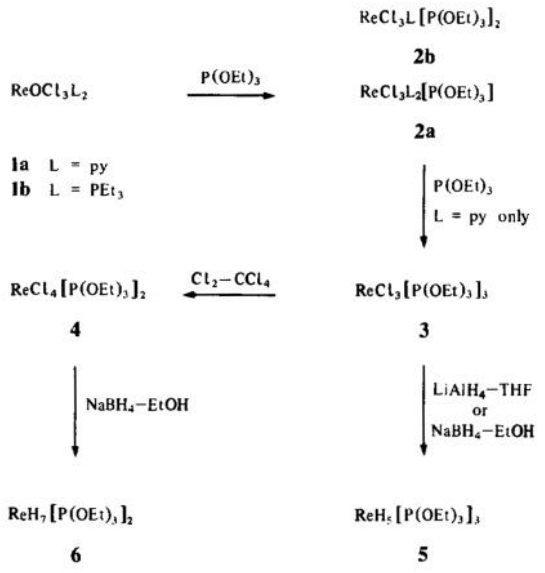
In a preliminary account the synthesis of **3**, starting from $ReOCl_3(PPh_3)_2$ was reported.[3] However, chromatographic isolation of **3** often resulted in lower yield, because of its sensitivity to air in solution.† Thus an alternative synthetic method was sought. It was found that the reaction of $ReOCl_3py_2^{1(a)}$ (**1a**) and excess $P(OEt)_3$ in boiling benzene gave high reproducible yields of **3** *without chromatographic separation*.‡ Shorter reaction times (about 15 h) yielded the partially substituted *trans*, *mer*-$ReCl_3py_2[P(OEt)_3]$ (**2a**) shown in Scheme 1. Spectroscopic data are consistent with the assigned geometry.§ Similarly the synthesis of **3** was attempted using *cis*-$ReOCl_3(PEt_3)_2^4$ (**1b**) since the volatility of the byproduct ($OPEt_3$) should also facilitate the separation of **3**. After 4.5 h of reflux in benzene an eight-fold excess of $P(OEt)_3$ reacts with

*Authors to whom correspondence should be addressed.

†Preliminary data suggest that **3** reacts with O_2 in hexane to form blue crystals of $ReOCl_3[P(OEt)_3]_2$. IR (Nujol mull): 975 cm^{-1}. Calc. for $C_{12}H_{30}O_7Cl_3P_2Re$: C, 22.5; H, 4.7; Cl, 16.6; P, 9.7%. Found: C, 22.1; H, 4.3; Cl, 16.5; P, 10.0%.

‡**1a** (1.4 g, 30 mmol) was refluxed in benzene (30 cm^3) with a 20-fold excess of $P(OEt)_3$ under N_2 for 36 h. The yellow solution was evaporated to dryness and additionally vacuum (8×10^{-3} hPa) dried overnight. The solid (**3**) was recrystallized from a hexane–pentane solution (yield 87%).

§IR (Nujol): ν(Re—Cl) (cm^{-1}) 307s, 267m and 250m. ^1H NMR ($CDCl_3$, 25°C): δ (TMS) (ppm) 3.05 (t, J = 7 Hz, 9H, CH_3); 4.06 (t, J = 7.7 Hz, 2H, py); 4.94 (d, J = 5.9 Hz, 4H, py); 10.15 (q, J = 7 Hz, 6H, CH_2); and 17.28 (t, J = 6.8 Hz, 4H, py).



Scheme 1. Synthesis of rhenium phosphite compounds.

1b to form *cis*, *mer*-$ReCl_3(PEt_3)[P(OEt)_3]_2$ (**2b**).* Surprisingly, even after prolonged reflux (48 h) in benzene with an excess of $P(OEt)_3$, no further phosphine substitution of **2b** is observed (^1H NMR). Most probably, the extent of these substitution reactions is controlled both by electronic effects and the geometry of the reacting complexes. These newly synthesized Re(III) complexes (**2a** and **b**) exhibit the expected contact-shifted signals in the ^1H NMR spectrum as a result of the temperature-independent paramagnetism.[5]

It has been shown that Re(III) chloro phosphines can be oxidized easily to Re(IV) complexes by treatment with chlorine.[6] A similar chemistry was observed when **3** reacted with Cl_2 in CCl_4.† Spectroscopic data suggest the formation of *trans*-$ReCl_4[P(OEt)_3]_2$ (**4**) in this reaction.

The successful isolation and characterisation of the chloro phosphite complexes (**3** and **4**) provided a unique opportunity to prepare the corresponding hydrido phosphite complexes of rhenium, and to compare their reactivity with well-known phosphine analogs. A general procedure[7] can be applied for the preparation of these polyhydrides. The pentahydride $ReH_5[P(OEt)_3]_3$ (**5**)‡ can be synthesized from **3** by treatment with $LiAlH_4$ in the THF, or with $NaBH_4$ in EtOH at ambient temperature. From **4**, $ReH_7[P(OEt)_3]_2$ (**6**)§ can be obtained by means of $NaBH_4$ treatment in EtOH at room temperature (see Scheme 1). In both cases the reaction mixtures were stirred until the characteristic colours of **3** (yellow) and **4** (red) disappeared, leaving a colourless slurry. The solvent was then removed *in vacuo* and the polyhydride was extracted into benzene from the solid residue. The two polyhydride products (**5** and **6**) are to our knowledge the first examples of high oxidation state rhenium hydride phosphites.

The photochemistry of $ReH_5(PMe_2Ph)_3$ has been well characterized.[8] The reactive intermediate was determined, via isolation of reaction products and laser flash photolysis, to be the unsaturated $ReH_5(PMe_2Ph)_2$.[8(c)] A similar chemistry was expected from **5**. However, being thermally unreactive (65°C, 12 h in C_6D_6) as its phosphine analog, the photolysis of **5** in benzene-d_6 solution also showed no net reaction after 8 h.‖ Likewise, photolysis in the presence of eight molar equivalents of PEt_3 in benzene gave no net reaction (^1H NMR). On the contrary, the thermal chemistry of **6** follows the typical reactivity patterns observed in other heptahydride rhenium compounds.[9] Thus, heating a C_6D_6 solution of **6** results in H/D exchange (^1H NMR) as well as in a growth of the new hydride quintet [$\delta -6.8$, $J(P-H) = 8.6$ Hz], indicative of the formation of $Re_2H_8[P(OEt)_3]_4$.[8(a)] This type of reactivity suggests the transient character for $ReH_5[P(OEt)_3]_2$.

The lack of an observable reactivity during the photolysis of **5** and thermal reactivity of **6** is astonishing, especially since both precursors should generate the same transient species, $ReH_5[P(OEt)_2]_2$. The obvious difference between **5** and **6**

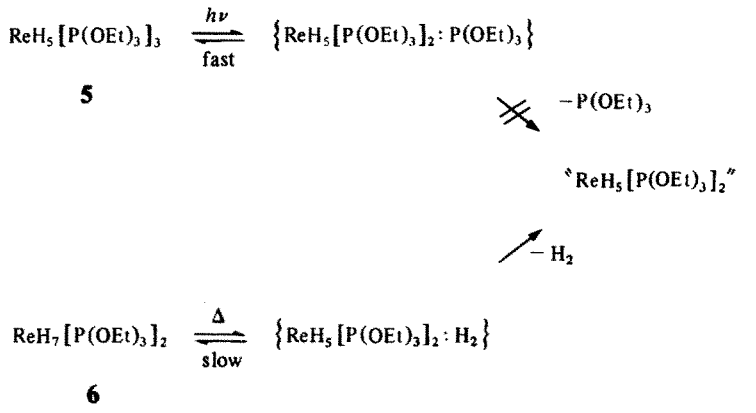
*IR (Nujol): ν(Re—Cl) (cm^{-1}) 311s, 283m and 257m. ^1H NMR (C_6H_6): δ (ppm) 2.33 and 2.79 (t and t, J = 7 Hz, 9H and 9H, CH_3); 7.0 and 10.74 (q and q, J = 7 Hz, 6H and 6H, CH_2) [indicating a non-equivalent $P(OEt)_3$]; 5.5 (q, J = 7.2 Hz, 6H, CH_2); and 8.0 (t, J = 7.2 Hz, 9H, CH_3).

†Chlorine gas was slowly bubbled through a CCl_4 solution of **3** (0.5 g) for 1 h. To the resulting red solution a small amount of MeOH was added and red crystals were isolated after cooling down to −20°C (yield 50%). The high solubility of **4** precludes further isolation. Calc. for $C_{12}H_{30}O_6Cl_4P_2Re$: C, 21.2; H, 4.6; Cl, 21.5%. Found: C, 22.0; H, 5.0; Cl, 21.7%. IR (KBr): ν(Re—Cl) (cm^{-1}) 325s. ^1H NMR (C_6D_6): δ (ppm) 1.21 (br.s, 3H, CH_3); and 14.28 (br.s, 2H, CH_2).

‡IR (Nujol): ν(Re—H) (cm^{-1}) 1975 br.vw, and 1900 br.w. ^1H NMR (C_6D_6): δ (ppm) 4.068 (m, 18H, CH_2); 1.211 (t, J = 6.9 Hz, 27H, CH_3); and −7.225 (q, J_{PH} = 17 Hz, 5H); $^{31}P-\{^1H\}$ NMR: δ (H_3PO_4) − 105.73 (s); $^{31}P-\{^1H_{CH}\}$ − 105.73 (sextet).

§^1H NMR (C_6D_6): (ppm) 3.912 (ddq, 12H, CH_2); 1.053 (t, 18H, CH_3); and −6.212 (t, J_{PH} = 17 Hz, 7H); $^{31}P-\{^1H\}$ NMR: − 109.7 (s); $^{31}P-\{^1H_{CH}\}$ − 109.7 (octet).

‖250-W medium-pressure Hanovia Hg lamp, and Pyrex filter.



Scheme 2. Curly brackets indicate species in solvent cage.

is the type of ligand extruded from the coordination sphere of the metal complex. With the available data it can be concluded that, in the photochemical case, a back-reaction with photoextruded $P(OEt)_3$ is favoured over a reaction with added substrate (C_6D_6 or PEt_3). In the thermal case (**6**), further reaction with added substrate is observed (H/D exchange and dimerization) (see Scheme 2). It seems that the observed reactivity is dependent upon the rate of diffusion of the extruded ligand [$P(OEt)_3$ or H_2] out of the solvent cage, thereby allowing "naked" $ReH_5[P(OEt)_3]_2$ to react with additional reagents.

REFERENCES

1. (a) H. W. Choi and E. L. Muetterties, *J. Am. Chem. Soc.* 1982, **104**, 152; (b) N. P. Johnson and M. E. L. Pickford, *J. Chem. Soc., Dalton Trans.* 1976, 950; (c) M. Freni and P. Romiti, *Inorg. Nucl. Chem. Lett.* 1970, **6**, 167 (and references therein); (d) M. Freni and V. Valenti, *Gazz. Chim. Ital.* 1960, **90**, 1436.
2. C. A. Tolman, *Chem. Rev.* 1977, **77**, 313.
3. W. K. Rybak and J. J. Ziółkowski, *Polyhedron* 1983, **2**, 541.
4. M. A. Green, Ph.D. thesis, Indiana University (1982).
5. (a) E. W. Randall and D. Shaw, *Mol. Phys.* 1965, **10**, 41; (b) J. Chatt, G. J. Leigh, D. M. P. Mingos, E. W. Randall and D. Shaw, *J. Chem. Soc., Chem. Commun.* 1968, 419.
6. J. Chatt, G. J. Leigh, D. M. P. Mingos and R. J. Paske, *J. Chem. Soc. A* 1968, 2636.
7. G. G. Hlatky and R. H. Crabtree, *Coord. Chem. Rev.* 1985, **65**, 1.
8. M. A. Green, J. C. Huffman and K. G. Caulton, *J. Am. Chem. Soc.* 1981, **103**, 695; (b) M. A. Green, J. C. Huffman, K. G. Caulton, W. K. Rybak and J. J. Ziółkowski, *J. Organomet. Chem.* 1981, **218**, C39; (c) S. Muralidharan, G. Ferraudi, M. A. Green and K. G. Caulton, *ibid.* 1983, **244**, 47; (d) M. C. L. Trimachi, M. A. Green, J. C. Huffman and K. G. Caulton, *Organometallics* 1985, **4**, 514; (d) D. A. Roberts and G. L. Geoffroy, *J. Organomet. Chem.* 1981, **214**, 221.
9. (a) J. Chatt and R. S. Coffey, *J. Chem. Soc. A* 1969, 1963; (b) D. Baudry, M. Ephritikhine, H. Felkin and J. Zakrzewski, *J. Chem. Soc., Chem. Commun.* 1982, 1235; (c) E. H. K. Zeiher, D. G. DeWitt and K. G. Caulton, *J. Am. Chem. Soc.* 1984, **106**, 7006.

Polyhedron Vol. 5, No. 11, pp. 1895–1896, 1986
Pergamon Journals Ltd. Printed in Great Britain

ANNOUNCEMENTS

FIFTH INTERNATIONAL SYMPOSIUM ON PLATINUM AND OTHER METAL COORDINATION COMPOUNDS IN CANCER CHEMOTHERAPY

The University of Padua, Faculty of Pharmacy and Consiglio Nazionale delle Ricerche are organizing this Symposium which will be held at Hotel Sheraton Orologio, Abano Terme, Padua, Italy (29 June–2 July 1987).

Scientific program

The following provisional topics are expected:

Session A: Biochemistry of platinum complexes in cancer chemotherapy.

Session B: Pharmacological mechanisms of cisplatinum action.

Session C: Clinical applications of platinum complexes.

Session D: Advances in antitumor research with non-platinum complexes.

Session E: Development of new metal coordination compounds: synthesis and characterization.

Session F: Toxicology of metal coordination complexes as antitumor agents.

Presentation

The conference will have the following format:
(1) Plenary and session lectures.
(2) Regular papers.
(3) Poster sessions.

Language

The official language of the conference will be *English.*

Public information

The proceedings of the conference will be published in a special volume to appear after the closing of the Symposium by *Martinus Nijhoff, Boston.* A collection of abstracts will be circulated during the Symposium.

Registration fee

(1) Active participants: U.S. $270.
(2) Non-active participants: U.S. $100.

The registration fee for active participants will cover coffees and lunches throughout the Symposium, the social dinner, the sightseeing tour, and publication of the Volume of Proceedings.

The non-active participants will be offered the social dinner and the sightseeing tour to the countryside.

For further information contact: P. Uguagliati, Dipartamento Scienze Farmaceutiche, Via Marzolo, 5, 35131 Padua, Italy.

7th FECHEM CONFERENCE ON ORGANOMETALLIC CHEMISTRY

This Conference will be held in Toledo, Spain (31 August–5 September 1987).

Scope

The Conference will be concerned with all aspects of synthesis, structure and applications of organometallic compounds. The scientific programme will include invited plenary lectures and poster sessions.

The number of Conference participants will be limited according to FECHEM rules.

Location

The Conference will be held in Toledo which is easily accessible from Madrid (70 km) by bus or train. Regular public buses connect Barajas Airport with bus and train terminals in Madrid.

Polyhedron Vol. 5, No. 11, pp. 1895–1896, 1986
Pergamon Journals Ltd. Printed in Great Britain

ANNOUNCEMENTS

FIFTH INTERNATIONAL SYMPOSIUM ON PLATINUM AND OTHER METAL COORDINATION COMPOUNDS IN CANCER CHEMOTHERAPY

The University of Padua, Faculty of Pharmacy and Consiglio Nazionale delle Ricerche are organizing this Symposium which will be held at Hotel Sheraton Orologio, Abano Terme, Padua, Italy (29 June–2 July 1987).

Scientific program

The following provisional topics are expected:

Session A: Biochemistry of platinum complexes in cancer chemotherapy.

Session B: Pharmacological mechanisms of cisplatinum action.

Session C: Clinical applications of platinum complexes.

Session D: Advances in antitumor research with non-platinum complexes.

Session E: Development of new metal coordination compounds: synthesis and characterization.

Session F: Toxicology of metal coordination complexes as antitumor agents.

Presentation

The conference will have the following format:
(1) Plenary and session lectures.
(2) Regular papers.
(3) Poster sessions.

Language

The official language of the conference will be *English.*

Public information

The proceedings of the conference will be published in a special volume to appear after the closing of the Symposium by *Martinus Nijhoff, Boston.* A collection of abstracts will be circulated during the Symposium.

Registration fee

(1) Active participants: U.S. $270.
(2) Non-active participants: U.S. $100.

The registration fee for active participants will cover coffees and lunches throughout the Symposium, the social dinner, the sightseeing tour, and publication of the Volume of Proceedings.

The non-active participants will be offered the social dinner and the sightseeing tour to the countryside.

For further information contact: P. Uguagliati, Dipartamento Scienze Farmaceutiche, Via Marzolo, 5, 35131 Padua, Italy.

7th FECHEM CONFERENCE ON ORGANOMETALLIC CHEMISTRY

This Conference will be held in Toledo, Spain (31 August–5 September 1987).

Scope

The Conference will be concerned with all aspects of synthesis, structure and applications of organometallic compounds. The scientific programme will include invited plenary lectures and poster sessions.

The number of Conference participants will be limited according to FECHEM rules.

Location

The Conference will be held in Toledo which is easily accessible from Madrid (70 km) by bus or train. Regular public buses connect Barajas Airport with bus and train terminals in Madrid.

Accommodation

Student rooms will be available for triple, double or single occupancy at "Convento de S. Juan de la Penitencia" and "Castillo de S. Servando". Rooms will also be reserved at various hotels.

Fees

The price will be 30,000 Pes. including: registration, lodging in student rooms, meals and social activities.

Extra payment will be required for hotel lodging.

Polyhedron Vol. 5, No. 12, pp. 1897–1915, 1986
Printed in Great Britain

0277–5387/86 $5.00+.00
Pergamon Journals Ltd

POLYHEDRON REPORT NUMBER 17

TRANSITION-METAL ALUMINOHYDRIDE COMPLEXES

ANDREW R. BARRON and GEOFFREY WILKINSON*

Department of Chemistry, Imperial College of Science and Technology, London SW7 2AY, U.K.

CONTENTS

1. INTRODUCTION 1897
2. RANGE OF ALUMINOHYDRIDE COMPLEXES 1897
3. SYNTHESIS OF ALUMINOHYDRIDE COMPLEXES 1899
4. VIBRATIONAL SPECTROSCOPY 1900
5. ESR STUDIES 1900
6. NMR SPECTROSCOPY 1902
7. FLUXIONAL BEHAVIOUR 1903
8. X-RAY STRUCTURAL STUDIES OF METAL ALUMINOHYDRIDE COMPLEXES 1905
9. REACTION CHEMISTRY OF ALUMINOHYDRIDE COMPLEXES. 1910

1. INTRODUCTION

The tetrahydroaluminate ion, AlH_4^-, has been used widely as a reducing agent in organic chemistry.[1–3] The Li^+ and Na^+ salts are the most common in use, but other ionic group I and II metal tetrahydroaluminates have been made.[4] Until recently there have been few examples of transition-metal aluminohydride† complexes reported in the literature, in contrast to the wide range of transition-metal borohydride complexes.[5] This is unexpected in light of the extensive use of $MAlH_4$ (M = Na or Li) in the synthesis of transition-metal hydrides,[6,7] e.g. eqns (1) and (2):

$$(\eta^5\text{-}C_5H_5)Ru(PPh_3)_2Cl \xrightarrow{LiAlH_4,\ Et_2O} (\eta^5\text{-}C_5H_5)Ru(PPh_3)_2H,^{8} \quad (1)$$

$$ReOCl_3(PPh_3)_2 \xrightarrow[MeOH]{LiAlH_4,\ thf} ReH_7(PPh_3)_2,^{9} \quad (2)$$

as well as their use as cocatalysts with early transition-metal halides and complex halides, in catalytic hydrogenation and in polymerization.[10,11]

This review reports recent advances in the field of covalent transition-metal aluminohydrides, and compares their structure and chemistry, where relevant, to that of analogous borohydride complexes.

2. RANGE OF ALUMINOHYDRIDE COMPLEXES

The majority of known transition-metal aluminohydride complexes (Table 1) are stabilized by tertiary phosphines (both uni- and bidentate) or by η^5-cyclopentdienyl ligands (including those with alkyl substituents). However, only a few metal aluminohydrides, $[M(AlH_4)_n]$, have been reported[12] and their structures have yet to be confirmed by X-ray crystallography.

* Author to whom correspondence should be addressed.

† The term aluminohydride has been adopted throughout this article so as to include all complexes with the $M(\mu\text{-}H)_2Al$ unit and not just those of AlH_4^-. Where aluminohydride complexes contain hydrides terminal to the metal, besides any bridges to aluminium, these are called alumino-polyhydrides.

Table 1. Transition-metal aluminohydride complexes[a]

Metal	Compound[b]	Reference[c]	Method of characterization[d]
Y	$[Cp_2YAlH_4 \cdot NEt_3]_2$	13	IR, X-ray
	$[Cp_2YAlH_4 \cdot OEt_2]_2$	13	IR
	$[Cp_2YAlH_4 \cdot thf]_2$	13, 14	IR, X-ray
	$[Cp_2YAlH_4]_2OEt_2$	13	IR, X-ray
	$[Cp_2YAlH_4]_2$	15	IR
	$Y(AlH_4)_3$	16	
Ti	$[Cp_2TiAlH_4]_n$	17	IR, ESR
	$Cp_2TiAlH_2Cl_2 \cdot OEt_2$	18	IR, X-ray
	$Cp_2TiAlH_2Cl_2 \cdot NEt_3$	19	IR
	$[(Cp–Cp)TiAlH_4]_n$	20	
	$[Cp_2TiAlH_4]_2$tmeda	21	X-ray
	$[Cp_2TiAlH_4(C_5H_4)Ti(Cp)H]_2$	22	X-ray
	$[Cp^*_2TiAlH_4]_2$	23	X-ray
	$[Cp^*_2Ti]AlH_5$	23	X-ray
	$Ti(AlH_4)_4$	16	
Zr	$[Cp_2Zr(H)AlH_4]_2$	24	IR
V	$[Cp_2VAlH_4]_2 \cdot OEt_2$	25	
	$[Cp_2V]_2AlH_2Cl \cdot OEt_2$	25	
Nb	$Cp_2NbAlH_2Et_2$	26	NMR
	$[Cp_2NbAlH_4]_n$	26	NMR
	$Nb(AlH_4)_5$	16	
Ta	$(dmpe)_2TaAlH_2(OC_2H_4OMe)_2$	27	IR, NMR, X-ray
	$[Cp'_2TaAlH_4]_2$	28	IR, NMR
Cr	$[(dmpe)_2HCrAlH_4]_2$	29	IR, NMR
Mo	$Cp_2MoAlH_2R_3$		
	(R = Me, Et or Ph)	30	NMR
	$[(Me_3P)_4HMoAlH_4]_2$	29	NMR
W	$Cp_2WAlH_3R_3$		
	(R = Et or Ph)	30	NMR
	$Cp_2WAlH_2Me_3$	30, 31	NMR, X-ray
	$[(Me_3P)_4HWAlH_4]_2$	29	IR, NMR
	$[(Me_3P)_4ClWAlH_4]_2$	29	IR, NMR
	$[(Me_3P)_3H_3WAlH_4]_2$	32	IR, NMR
	$[(Me_3P)_3H_3WAlH_3OBu^n]_2$	32	IR, NMR, X-ray
	$[(Me_3P)_3H_3W]_2AlH_5$	32, 33	IR, NMR, X-ray
Mn	$[(dmpe)_2MnAlH_4]_2$	34, 35	IR, NMR, X-ray
Re	$[(Me_2PhP)_3H_2ReAlH_4]_2$	32	IR, NMR
	$[(Me_2PhP)_3H_2ReAlH_3OBu^n]_2$	32	IR, NMR
	$(Ph_2MeP)_3HReAlH_3Me_2$	36	IR, NMR, X-ray
	$(Me_2PhP)_3HReAlH_3Me_2$	36	IR, NMR
	$(Ph_2MeP)_2H_4ReAlH_2Me_2$	36	IR, NMR
	$(Me_2PhP)_2H_4ReAlH_2Me_2$	36	IR, NMR
Fe	$Fe(AlH_4)_2$	16	
Ru	$[(L)_3HRuAlH_4]_2$		
	(L = PMe_3, $EtPh_2P$ or PPh_3)	37	IR, NMR
	$[(Me_3P)_3HRu]_2AlH_5$	37	IR, NMR
Os	$[L_3HOsAlH_4]_2$		
	(L = PMe_3 or PPh_3)	37	IR, NMR
Ni	$(^nBu_3P)_2NiAlH_2Et_2$	38	ESR

[a] Cp = η^5-C_5H_5, Cp–Cp = $CH_2(\eta^5$-$C_5H_4)_2$, Cp* = η^5-C_5Me_5, Cp′ = η^5-C_5H_4Me, dmpe = 1,2,-bis(dimethylphosphino)ethane; tmeda = tetramethylethylenediamine.

[b] No structural data are implied by the given formula.

[c] The references chosen are those containing synthetic and spectroscopic details.

[d] Elemental analysis is assumed for all isolable products.

The complexes so far characterized are of the *d*-group transition elements but lanthanide and actinide complexes should be capable of existence.

3. SYNTHESIS OF ALUMINOHYDRIDE COMPLEXES

The synthesis of transition-metal aluminohydrides is most readily accomplished by the reaction of a metal halide complex with $LiAlH_4$ in ethers. Reduction of the metal may also occur as in eqn (3):

$$(\eta^5\text{-}C_5H_5)_2Nb(IV)Cl_2 \xrightarrow[Et_2O]{LiAlH_4} (\eta^5\text{-}C_5H_5)_2Nb(III)AlH_4.^{26} \quad (3)$$

If the number of halides replaced is greater than one, and no reduction of the metal occurs then an aluminohydride, containing terminal metal hydrides, as well as those bridging to aluminium, may be formed [eqn (4)]:

$$(Me_3P)_4Ru(II)Cl_2 \xrightarrow[Et_2O]{LiAlH_4} [(Me_3P)_3HRu(II)(\mu\text{-}H)_2Al(H)(\mu\text{-}H)]_2.^{37} \quad (4)$$

In this case insoluble AlH_3 is formed along with LiCl as products.

The actual mechanism for the formation of co-ordinated AlH_4^- complexes may not be simply a substitution of halide for AlH_4^-. From calorimetric and ESR studies Bulychev *et al.*[17] have proposed a mechanism for the formation of $(\eta^5\text{-}C_5H_5)_2Ti(\mu\text{-}H)_2AlH_2$ from $(\eta^5\text{-}C_5H_5)_2TiCl_2$ which involves the formation of various species containing halides attached to the aluminium atom, e.g. $[(\eta^5\text{-}C_5H_5)_2Ti(\mu\text{-}H)_2AlHCl]_2$. Such species can be trapped by addition of MeCN and isolation of the resulting imine complex.[28]

The choice of solvent has been found to be very important in determining the final product. Thus reactions may proceed in thf but not in Et_2O [eqns (5) and (6)]:

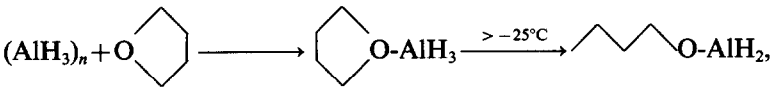
$$(Me_3P)_4OsCl_2 \xrightarrow[Et_2O]{LiAlH_4} \quad (5)$$

$$(Me_3P)_4OsCl_2 \xrightarrow[thf]{LiAlH_4} [(Me_3P)_3HOs(AlH_4)]_2.^{37} \quad (6)$$

However, in certain cases the aluminohydride reacts with thf to produce bridging *n*-butoxo groups, contained in an $Al(\mu\text{-}OBu^n)_2Al$ unit [eqn (7)]:

$$[(Me_3P)_3H_3WAlH_4]_2 \xrightarrow{thf} [(Me_3P)_3H_3W(AlH_3OBu^n)]_2.^{32} \quad (7)$$

The interaction of AlH_3 with thf has been known for some time[39] [eqn (8)]:



(8)

and leads to a source of *n*-butoxo groups via ring cleavage.

The use of aluminium alkyl hydrides or alkoxyhydrides has also been successful in the formation of the $M(\mu\text{-}H)_2Al$ unit [eqns (9) and (10)]:

$$(\eta^5\text{-}C_5H_5)_2NbCl_2 \xrightarrow{LiAlH_2Et_2} (\eta^5\text{-}C_5H_5)_2NbH_2AlEt_2, \quad (9)$$

$$(dmpe)_2TaCl_2 \xrightarrow{LiAlH_2(OC_2H_4OMe)_2} [(dmpe)_2TaH_2Al(O(CH_2)_2OMe)_2]_2.^{27} \quad (10)$$

Where a suitable halide starting material is unavailable, the exchange of a BH_4^- group by an AlH_4^- group can lead to an aluminohydride [eqn (11)]:

$$(\eta^5\text{-}C_5Me_5)_2TiBH_4 \xrightarrow{LiAlH_4} [(\eta^5\text{-}C_5Me_5)_2TiAlH_4]_2.^{23} \quad (11)$$

Alternatively, instead of $LiAlH_4$, $(AlH_3)_n$ can be used with a metal halide to produce the

$M(\mu\text{-}H)_2Al$ unit [eqn (12)]:

$$(\eta^5\text{-}C_5H_5)_2TiCl_2 \xrightarrow[Et_2O]{AlH_3} (\eta^5\text{-}C_5H_5)_2Ti(\mu\text{-}H)_2AlCl_2 \cdot OEt_2.^{18} \quad (12)$$

Recently, borohydrides have been synthesized by the addition to metal polyhydrides of BH_3.[40] Although no "AlH_4^-" complexes have been made by this route,[30] several $M(\mu\text{-}H)_nAlMe_2$ complexes have been synthesized from the addition of $AlMe_3$ to rhenium polyhydrides[36] [eqn (13)]:

$$(Me_2PhP)_2ReH_7 + AlMe_3 \longrightarrow (Me_2PhP)_2H_4Re(\mu\text{-}H)_2AlMe_2 + CH_4.^{36} \quad (13)$$

Hydrolysis of these aluminohydrides results in the formation of the original polyhydride. It may be possible to use AlH_3 to produce an aluminohydride from easily obtainable polyhydrides.

Trialkylaluminium compounds are well known as Lewis acids,[42] and will coordinate with donors such as amines, phosphines, ethers and thioethers.[42] Similarly, the Lewis case nature of certain metal hydrides facilitates the synthesis of a series of aluminohydrides[30,31] [eqn (14)]:

$$(\eta^5\text{-}C_5H_5)_2WH_2 + AlMe_3 \longrightarrow [(\eta^5\text{-}C_5H_5)_2W(\mu\text{-}H)_2AlMe_3]. \quad (14)$$

As with borohydrides, the stability of aluminohydrides with respect to thermal decomposition is most likely both thermodynamic and kinetic. This includes the stability of the complex with respect to a metal hydride and aluminium trihydride,† i.e. eqn (15):

$$M^{n+}AlH_4^- \longrightarrow M^{n+}H^- + AlH_3. \quad (15)$$

Bulky or chelating ligands may be used to impede the decomposition process.[38]

4. VIBRATIONAL SPECTROSCOPY

IR and Raman spectroscopy have been widely used in the assignment of the structure of many transition-metal borohydrides.[5]

For aluminohydrides it is more difficult to assign the IR bands due to hydride-containing ligands because of serious overlapping of different stretches. In general, for terminal transition-metal hydrides ν(M—H) appear in the range 1500–2100 cm^{-1},[7] whilst bridging hydrides are in the 1550–1650 cm^{-1} range (M—H—M).

Terminal Al—H stretches can vary in position, 1700–1850 cm^{-1} [ν(Al—H)] being common.[19] Bridging $M(\mu\text{-}H)Al$ stretching frequencies depend on the transition metal present, and, because of this, the values quoted in the literature vary widely from *ca* 1200 cm^{-1}[19] to as high as *ca* 1800 cm^{-1}.[36] It has also been noted[19] that more than one stretch is associated with the $Ti(\mu\text{-}H)_2Al$ unit, e.g. $[(\eta^5\text{-}C_5H_5)_2Ti(\mu\text{-}H)_2AlHCl \cdot Et_2O]$[19] {1150 and 1250 cm^{-1} [$\nu(TiH_2Al)$], and 1340 sh and 1470 sh cm^{-1} [ν(TiHAl)]}. Even in complexes containing only bridging $M(\mu\text{-}H)Al$ hydrides more than one peak has been observed, e.g. in $[(dmpe)_2Ta(\mu\text{-}H)_2Al(OC_2H_4OMe)(\mu\text{-}OC_2H_4OMe)]_2$[27] (1605 and 1646 cm^{-1}). The reason for the multiplicity of bridging hydride stretches may be allied to the asymmetrical nature of the hydride bridge, as found by X-ray crystallography (Section 8).

The IR spectrum is thus very difficult to assign, although the hydride envelope is very characteristic compared with metal hydrides.[6] For the present, IR spectra must be used in conjunction with other techniques to assign the structure of many aluminohydrides.

5. ESR STUDIES

The majority of known aluminohydrides are diamagnetic, making NMR spectroscopy (where solubility and stability permits) the most convenient method of study (see Section 6). However, the most widely studied system has been the paramagnetic titanium(III) species obtained from the reaction of $[(\eta^5\text{-}C_5H_5)_2TiCl]_2$ with $LiAlH_4$.[17,42]

† The reaction of $(dmpe)_2FeCl_2$ with two equivalents of $LiAlH_4$ in Et_2O results, at low temperature, in a yellow aluminohydride, characterized by its IR spectrum, but on warming the solution becomes colourless and only the dihydride $(dmpe)_2FeH_2$ can be isolated.[28]

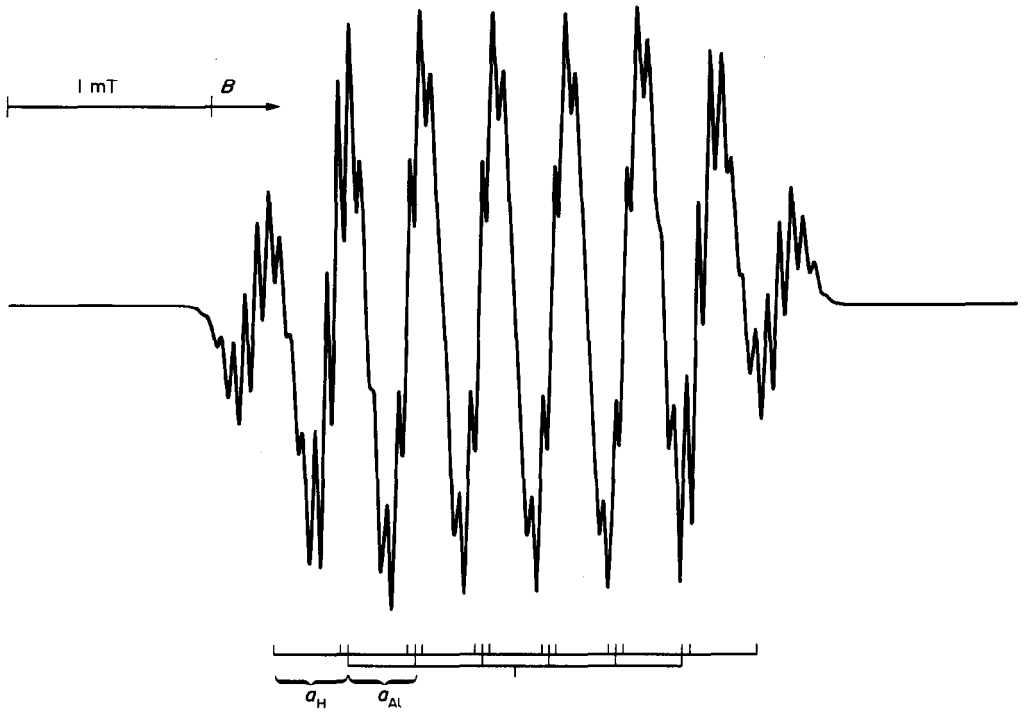
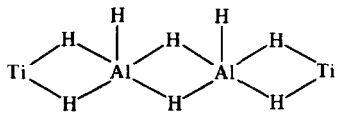


Fig. 1. Computer-simulated ESR spectrum of $(\eta^5\text{-}C_5H_5)_2Ti(AlH_4)$ (using data obtained from Ref. 44) $a_{Al} = 0.36$ mT, $a_H = 0.40$ mT, and $a_{H(Cp)} = 0.056$ mT.

Early studies on what was considered to be $(\eta^5\text{-}C_5H_5)_2TiAlH_4$ showed a single signal ($g = 1.979$) coupled to the ^{27}Al nucleus ($I = \frac{5}{2}$)[43] with the hyperfine coupling due to two protons just discernable as 1:2:1 triplets. High-resolution spectra showed this coupling clearly (Fig. 1), as well as super-hyperfine splitting due to interaction with the nuclear spins of the cyclopentadienyl protons.[44,45]

ESR has also been used as a probe in the study of unisolable intermediates in the formation of $(\eta^5\text{-}C_5H_5)_2TiAlH_4$.[42,46]

On isotopic substitution of H by D there is a broadening in the spectra at room temperature;[45] however, no explanation was given. In the light of recent X-ray crystallographic studies[23,32,35] it is reasonable to propose a dimeric structure containing a bridging $Ti(\mu\text{-}H)_2Al(H)(\mu\text{-}H)_2Al(H)(\mu\text{-}H)_2Ti$ unit (**1**)



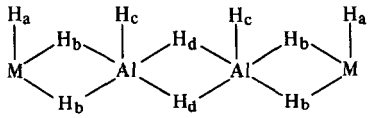
1

A distorted trigonal bipyramidal geometry around the aluminium is most probable (see Section 8), with one bridging $Ti(\mu\text{-}H)Al$ hydride axial and the other equatorial.[23,32,35] At room temperature the bridging $Al(\mu\text{-}H)Al$ and terminal Al—H hydrides would be fluxional[33] (see Section 7). This exchange process would alter the bridging $Ti(\mu\text{-}H)Al$ environments from axial to equatorial, and vice versa. In a given conformation the coupling constants due to the $Ti(\mu\text{-}H)Al$ hydrides would not be identical ($a_{Heq} \neq a_{Hax}$). On passing to the other conformations these coupling constants would be exchanged. Such a process would obviously be affected by replacement of hydrogen by deuterium and result in a broadening of the signal, as is observed.[43]

ESR has been useful in studying some unisolable aluminohydride complexes such as $\{(n\text{-}C_4H_9)_3P\}_2Ni(\mu\text{-}H)_2Al(C_2H_5)_2$,[38] whose structure has been proposed on the basis of the observed spectrum.

6. NMR SPECTROSCOPY

Transition-metal hydride resonances in the hydride region normally lie to high field of Me_4Si (δ 0 to -30 ppm). This has been attributed to strong shielding of the ^1H nuclear by *d*-electrons of the metal.[47] In aluminohydrides the terminal M—H_a resonances, where present (for labelling see **2**) do indeed appear to be in this region, as do the bridging M(μ-H_b)Al resonances (Fig. 2).



2

The latter appear upfield of the former. The shift in general is dependent on the number of transition-metal *d*-electrons (the greater the number the higher field the signal).

Where aluminohydrides contain phosphorus donor ligands the hydride signal is spin–spin coupled to the ^{31}P nucleus. Since these compounds are generally non-rigid at room temperature (see Section 7) a binomial multiplet of $n+1$ lines, due to n phosphines bound to the metal, results.

Any terminal Al—H_c and Al(μ-H_d)Al resonances present appear at δ 4–6 ppm as a very broad singlets (Fig. 2), sometimes the line width is such that the signals may be lost in the base line.[26] The broadening of all hydride peaks is most probably ascribed to the large quadrupole moment of ^{27}Al.

The fluctional behaviour of the hydrides will be discussed later (Section 7).

NMR spectroscopy also makes it possible to determine the hydride multiplicity in an aluminohydride where there are terminal metal hydrides present, i.e. alumino-polyhydrides. Two general methods can be used. It is possible to integrate and compare the area of the hydride resonance with that of the ligand protons. However, there are two drawbacks to this method: (1) the relaxation time of the hydride may be different from those of the ligand protons, thus reducing the accuracy of the integration; and (2) the aluminohydride may be hydrolysed by any residual moisture in the deuterated solvent to give a polyhydride [see Section 9(ii)]. Although the M—H signal will be at a different shift from that in the aluminohydride, the signal due to the ligand will not vary greatly, thus making the integration difficult to measure accurately.

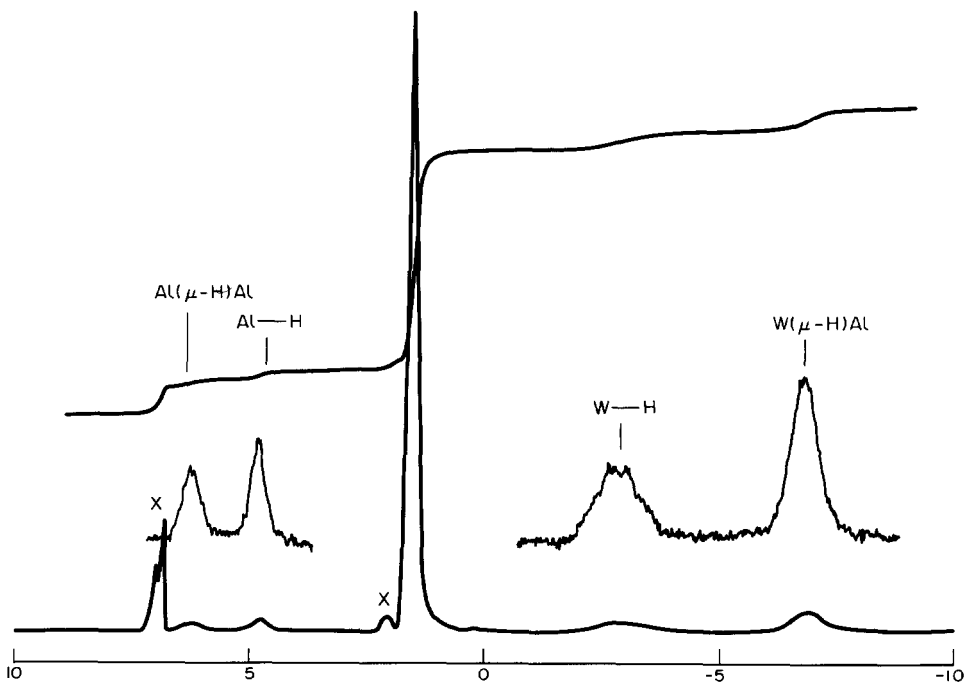


Fig. 2. ^1H NMR spectrum (203 K) of $[(Me_3P)_3H_3W(\mu\text{-}H)_2Al(H)(\mu\text{-}H)]_2$. X denotes peak due to the solvent, d^8-toluene.

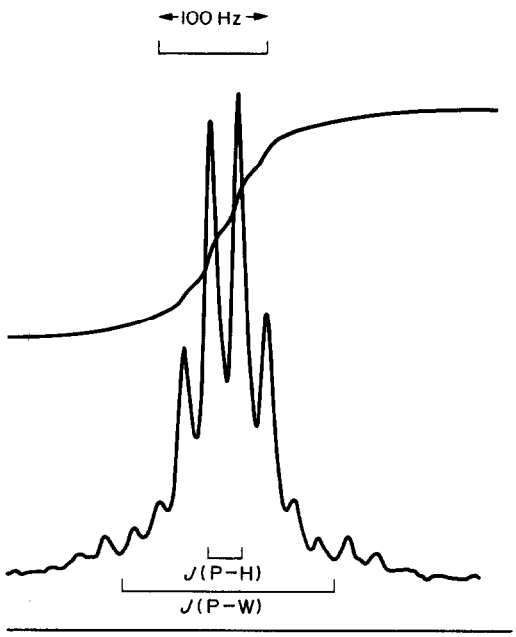


Fig. 3. ^{31}P NMR spectrum of $[(Me_3P)_3H_3W(\mu\text{-}H)_2Al(H)(\mu\text{-}H)]_2$ with only the phosphine P—$C\underline{H}_3$ protons decoupled. J(P–H) = 25.4 Hz, and J(P–W) = 199.4 Hz.

When phosphorus donors are present, the ^{31}P NMR spectrum is a more reliable method for the determination of hydride multiplicity. On selective decoupling the phosphine protons only the M—H and M(μ-H)Al hydrides will interact with the phosphorus nuclei, thus giving a multplet of $n+1$ lines (for n hydrides) (Fig. 3). This is in contrast to borohydrides where no coupling is observed for the bridging M(μ-H)B hydrides. The multiplet may not in fact be binomial, depending on the stereochemistry of the metal and its fluxional behaviour.[37]

A further tool in the structural characterization of aluminohydrides has been the use of ^{27}Al NMR spectroscopy. Although ^{27}Al possesses a large quadrupole moment[48] narrow lines in the NMR spectra can be obtained. The line width depends on the geometry of the substituents around the aluminium nucleus. X-ray crystallography indicates that the aluminium centres have a five-coordinate distorted trigonal bipyramidal geometry.[23,33] Given the low symmetry, large line widths would be expected and are indeed found.[32,37] Only relatively few five-coordinate aluminium species are known; of these a series of alkoxy-aluminium compounds have ^{27}Al NMR spectra[47] of comparable position and line width. All the complexes so far studied have given broad singlets in the region 50–70 ppm with line widths of 4000–5000 Hz. It is interesting to note that the AlH_5^- complexes such as $[(Me_3P)_3H_3W]_2AlH_5$[33] have similar positions and line widths, suggesting that the aluminiums in the M(μ-H)$_2$Al(H)(μ-H)$_2$Al(H)(μ-H)$_2$M unit do not interact with each other's quadrupole moment.

7. FLUXIONAL BEHAVIOUR

The fluxional behaviour of transition-metal borohydrides has been well studied by NMR spectroscopy.[5] At room temperature the bridging M(μ-H)B and terminal B—H hydrides commonly undergo rapid intramolecular exchange, but seldom undergo exchange with any transition-metal terminal M—H hydrides that may also be present in the molecules. Exchange has been observed, but only at elevated temperature, e.g. in $RuH(BH_4)(PMe_3)_3$[50] and $OsH_3(BH_4)(PR_3)_2$ (R = c-C_5H_9).[51]

By contrast the terminal M—H_a and bridging M(μ-H_b)Al hydrogen atoms (see **2** for labelling) in aluminohydrides undergo exchange at room temperature. Using NMR spectroscopy this exchange can be studied (Fig. 4). From the low-temperature NMR data the activation energy can be calculated[32,37] the magnitude of which is dependent upon the environment around the metal centre[32] and whether any rearrangement of the ancillary ligands is required.[37] A *fac* arrangement around the

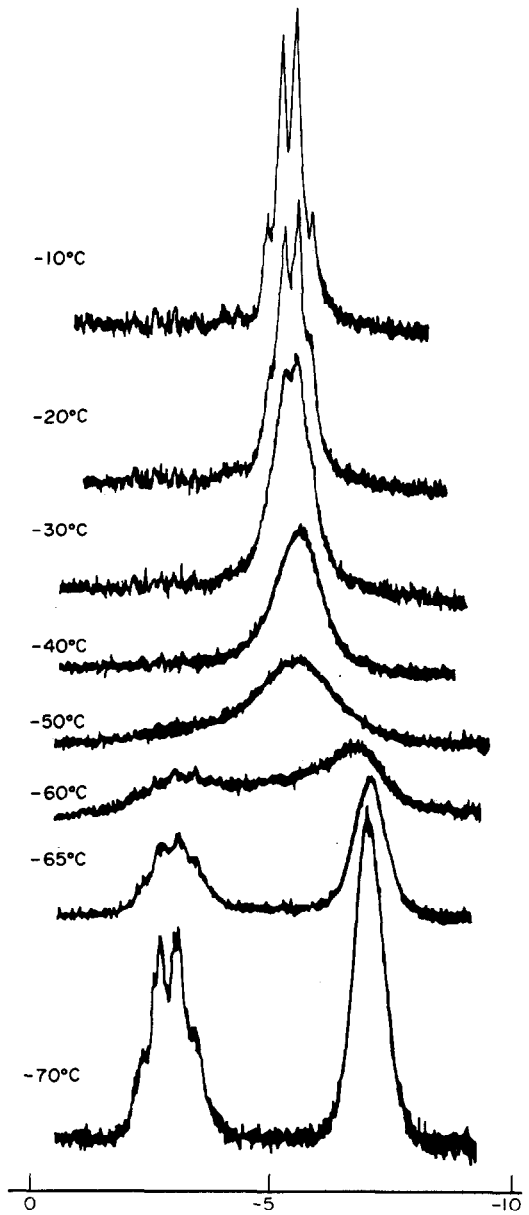


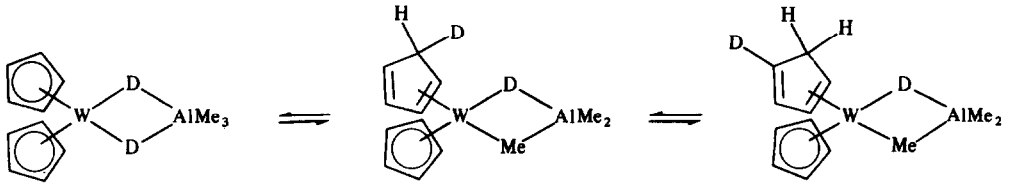
Fig. 4. Variable-temperature ^{1}H NMR spectra of $[(Me_3P)_3W(\mu\text{-}H)_2AlH(\mu\text{-}OBu^n)]_2$ over the region 0 to -10 ppm vs Me_4Si in d^8-toluene solvent.[52]

transition metal, as in *fac*-$[(Me_3P)_3HRu(\mu\text{-}H)_2Al(H)(\mu\text{-}H)]_2$,[37] allows for a very labile M—H_a and M(μ-H_b)Al exchange, which appears equally rapid in complexes with bulkier phosphines.[37] A consequence of this is that the aluminohydride may adopt a different stereochemistry around the metal, in contrast to the analogous borohydride[29,37] so as to accommodate this exchange process.

The dimeric nature of most aluminohydrides allows for an exchange between terminal Al—H_c and bridging Al(μ-H_d)Al hydrides (no analogous exchange in borohydrides has been reported). The activation energy of this exchange process (*ca* 50 kJ mol^{-1}) appears to be independent of the sterochemistry around the metal and is readily stopped at low temperature. As yet no mechanism has been proposed.

Where cyclopentadienyl ligands are used to stabilize aluminohydrides a third type of exchange is observed. That is, between the bridging M(μ-H)Al and cyclopentadienyl ring hydrides. A study of the deuterated complexes show that isotopic scrambling occurs.[26,28] Bruno *et al.*[31] have proposed a

mechanism involving hydride transfer from the metal to the cyclopentadienyl ring [eqn (16)]:



(16)

However, the analogous exchange observed in $(\eta^5\text{-}C_5H_5)_2M(BH_4)$ complexes[53] suggests that a hydrogen is transferred from the ring to the transition metal and from there onto the boron.

NMR experiments involving line broadening have been used to estimate the energy and rate of the exchange for borohydrides. However, no line broadening is observed in the complexes $(\eta^5\text{-}C_5H_5)_2NbAlD_4$[26]† and $[(\eta^5\text{-}C_5H_4Me)_2Ta(\mu\text{-}D)_2Al(D)(\mu\text{-}D)]_2$,[28] although it has been noted that thf slows the rate of exchange, perhaps by blocking the vacant sites on the aluminium or metal.

8. X-RAY STRUCTURAL STUDIES OF METAL ALUMINOHYDRIDES

A knowledge of the structure and configuration of a series of compounds contributes immensely to an understanding of their physical and chemical properties. Unfortunately for transition-metal aluminohydrides and hydrides in general, the most common solid-state structural technique, single-crystal X-ray diffraction, may not allow hydrogen atoms to be accurately located except in special cases. This is because the magnitude of X-ray scattering is approximately proportional to the square of the atomic number of the atoms in the compound.

Whereas borohydrides have been studied by a variety of structural techniques, including gas-phase electron diffraction,[54] single-crystal neutron diffraction,[55] broad-line nuclear magnetic resonance,[56] as well as X-ray diffraction.

The study of aluminohydrides, which are not volatile, has so far been confined to X-ray diffraction. The crystal structure of $LiAlH_4$, as determined by X-ray diffraction,[57] shows the aluminium to be four-coordinate with a tetrahedral arrangement of four hydrides (Fig. 5). These hydrides can be divided into two types μ_2- (bridging one lithium and one aluminium) and μ_3-

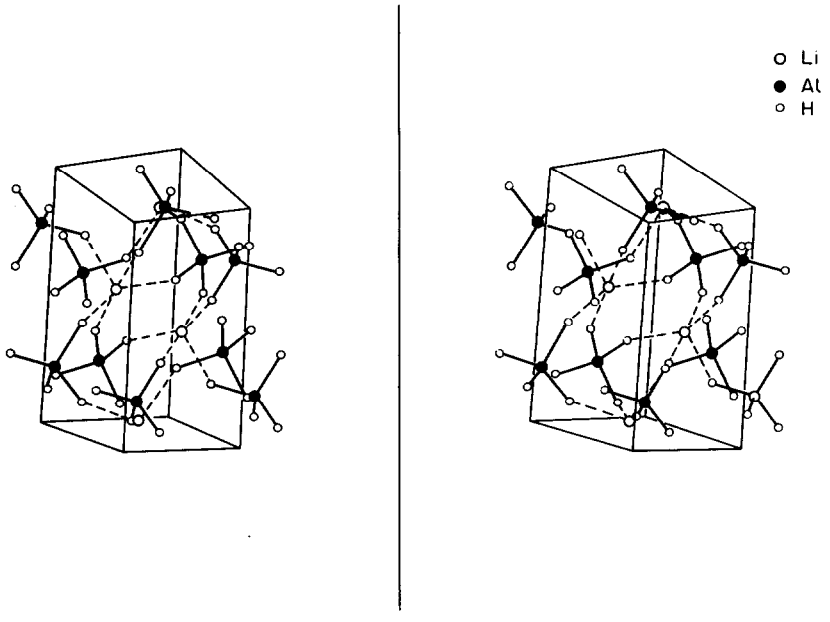


Fig. 5. Stereo pair view (*ca* along *c*) of unit cell of $LiAlH_4$: *a*-axis horizontal and *b*-axis vertical. The μ_3-hydrides are on the *b*- and *c*-faces (coordinates obtained from Ref. 57).

† Although this complex was formulated[26] from ^1H NMR spectroscopy to be monomeric it is undoubtedly isostructural with the dimeric tantalum complex.[28]

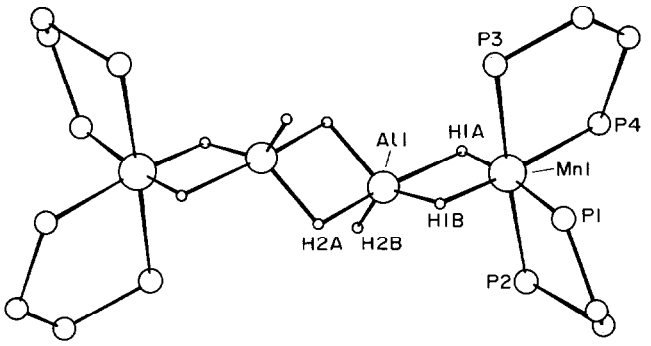
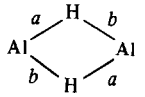


Fig. 6. Structure of $[(dmpe)_2Mn(\mu\text{-}H)_2Al(H)(\mu\text{-}H)]_2$. The methyl groups and methylene protons have been omitted for clarity (coordinates obtained from Ref. 35).

(bridging two lithiums and one aluminium). The Al—H bond distances vary between 1.516(27) and 1.578(26) Å.

The tetrahedral geometry around boron, as present in KBH_4,[58] is maintained throughout transition-metal borohydride chemistry. This does not, however, appear to be the case for aluminohydrides where a four-coordinate complex is the exception.

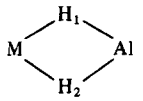
The first tetrahydridoaluminate complex to be crystallographically characterized, $[(dmpe)_2Mn(\mu\text{-}H)_2Al(H)(\mu\text{-}H)]_2$,[34,35] was found to be a centrosymmetric dimer containing a $Mn(\mu\text{-}H)_2AlH(\mu\text{-}H)_2Al(H)(\mu\text{-}H)_2M_2$ core (Fig. 6). The aluminium atoms adopt distorted trigonal bipyramidal geometries, with one bridging $Al(\mu\text{-}H)Al$ and one bridging $Mn(\mu\text{-}H)Al$ hydride occupying the axial positions around each aluminium. The Mn—H distances in the $Mn(\mu\text{-}H)_2Al$ unit are equal, and shorter than the two Al—H distances. The central $Al(\mu\text{-}H)_2Al$ unit is assymetric with the long and short distances differing by about 0.3 Å (**3**)



3

	a (Å)	*b* (Å)
$[(dmpe)_2Mn(\mu\text{-}H)_2Al(H)(\mu\text{-}H)]_2$	1.510(30)	1.804(28)
$[(C_5Me_5)_2Ti(\mu\text{-}H)_2Al(H)(\mu\text{-}H)]_2$	1.56(1)	1.94(1)

The asymmetry of the $Al(\mu\text{-}H)_2Al$ unit has also been observed in the complex $[(\eta^5\text{-}C_5Me_5)_2Ti(\mu\text{-}H)_2Al(H)(\mu\text{-}H)]_2$.[23] The coordination geometry around the aluminium is again distorted trigonal bipyramidal (Fig. 7). However, unlike the manganese complex the $Ti(\mu\text{-}H)_2Al$ unit is asymmetric (**4**) with one hydrogen nearer the aluminium than the other. As with the majority of bis-η^5-cyclopentadienyl complexes of titanium, the geometry is pseudo tetrahedral, with the aluminium atom located on the C_2-axis of the "sandwich".



4

	M—H_1 (Å)	M—H_2 (Å)	Al—H_1 (Å)	Al—H_2 (Å)
$[(C_5Me_5)_2Ti(\mu\text{-}H)_2Al(H)(\mu\text{-}H)]_2$	1.92(1)	1.86(1)	1.63(1)	1.70(1)
$[(Me_3P)_3H_3W]_2AlH_5$	1.771(61)	1.653(82)	2.020(61)	1.802(80)

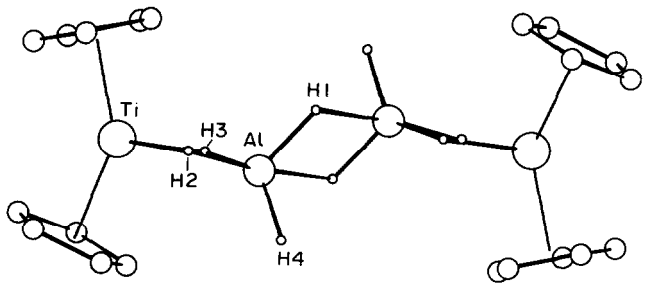
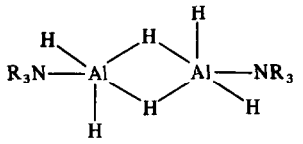


Fig. 7. Molecular structure of $[(\eta^5\text{-}C_5Me_5)_2Ti(\mu\text{-}H)_2Al(H)(\mu\text{-}H)]_2$ using the atom coordinates of Ref. 23. The methyl groups have been omitted for clarity.

The bridging $M(\mu\text{-}H)_2Al(H)(\mu\text{-}H)_2Al(H)(\mu\text{-}H)_2M$ unit found in these compounds is similar to those proposed for the amine adducts of AlH_3[59] (**5**), and appears to be a common feature of aluminohydride complexes.[29,37]

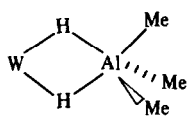


5

When a chelating amine such as tetramethylethylenediamine (tmeda) forms adducts with AlH_3 an infinite chain structure is found to be of preference,[60] each "link" consisting of an $-\{AlH_3(tmeda)\}-$ unit. Bulychev *et al.*[21] have reported the X-ray crystal structure of the complex $[(\eta^5\text{-}C_5H_5)_2Ti(\mu\text{-}H)_2AlH_2]_2 \cdot \mu\text{-tmeda}$ (Fig. 8), where two $(\eta^5\text{-}C_5H_5)_2TiH_2AlH_2$ moieties are bonded via a bidentate tmeda ligand by donor–acceptor N–Al bonds. The coordination polyhedron at the aluminium is distorted trigonal bipyramidal with the nitrogen and one of the bridging $Ti(\mu\text{-}H)Al$ hydrides occupy axial positions on each aluminium.

The similarity of these transition-metal aluminohydrides to alanes suggests that, whereas it is correct to consider transition-metal borohydrides as consisting of L_nM^+ and BH_4^- moieties, similar models for aluminium analogues are not as accurate. It may be wiser to consider the complexes as being derived from a donor–acceptor complex of $L_nM\text{-}H$ and AlH_3, rather than L_nM^+ and AlH_4^-.

This Lewis acid–base representation is substantiated by the complex $(\eta^5\text{-}C_5H_5)_2W(\mu\text{-}H)_2AlMe_3$,[31] whose structure consists of the basic $(\eta^5\text{-}C_5H_5)_2WH_2$ unit coordinating to the Lewis acid $AlMe_3$ (**6**)



6

Dimers may also be formed with bridging alkoxides, in an $Al(\mu\text{-}OR)_2Al$ unit. The complex $[(dmpe)_2Ta(\mu\text{-}H)_2Al(OC_2H_4OMe)(\mu\text{-}OC_2H_4OMe)]_2$[27] contains both terminal Al–OR and bridging $Al(\mu\text{-}$

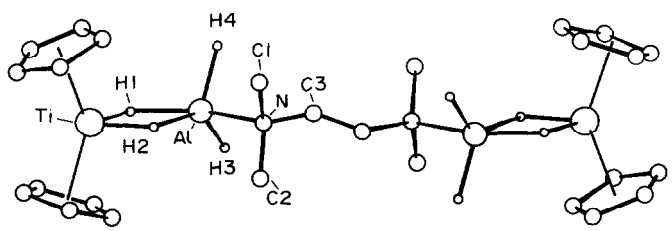


Fig. 8. Molecular structure of $[(\eta^5\text{-}C_5H_5)_2Ti(\mu\text{-}H)_2AlH_2]_2 \cdot$ tmeda. The organic H atoms have been omitted for clarity (coordinates from Ref. 21).

OR)Al groups (R = CH_2CH_2OMe). Interestingly the Ta atom adopts a distorted square-based pyramidal coordination with the four phosphorus atoms forming the basal plane while a $(\mu\text{-H})_2Al$ unit occupies the apex. This is in contrast to the closely related manganese complex, $[(dmpe)_2Mn(\mu\text{-H})_2Al(H)(\mu\text{-H})]_2$,[34,35] where the stereochemistry around the manganese is octahedral. The angle between the normal to the P_4 plane and the Ta–Al vector is 16.1°, suggesting that the $Ta(\mu\text{-H})_2Al$ unit is not planar as is the case for the manganese[35] and titanium[23] complexes. Steric factors could account for the change in stereochemistry. Certainly, steric hindrance caused by bridging *n*-butoxide groups in the complex $[(Me_3P)_3H_3W(\mu\text{-H})_2Al(H)(\mu\text{-OBu}^n)]_2$[32] is the probable reason for the adoption of a pseudo *cis* geometry, as opposed to the *trans* geometry found in other complexes[23,34] (**7**):



7

Compounds with alkyl groups on the aluminium do not show any ability to dimerize and remain as monomers. The X-ray crystal structure of $(MePh_2P)_2H_4Re(\mu\text{-H})_2AlMe_2$[36] has been determined and reveals a planar P_2ReAl (Fig. 9) framework with vertical (non-crystallographic) C_2-symmetry. The aluminium atom lies on the C_2-axis, similar to that found in $[(\eta^5\text{-}C_5Me_5)_2Ti(\mu\text{-H})_2Al(H)(\mu\text{-H})]_2$.[23] Of the six metal-bound hydrogen atoms found, two are unequivocally terminal to rhenium, and the remaining four hydrides are in the Re... Al internuclear region. However, these four can be subdivided into two pairs, two with short distances to Al [1.79(8) and 2.02(12) Å], and the other two with long non-bonding distances to Al [2.50(8) and 2.22(9) Å]. The latter are comparable to the non-bonding distance between the aluminium and the hydrogen atom in the $AlMe_2$ group [2.63(23)–2.62(14) Å].

From this result it is proposed that the aluminium is bound to the rhenium by two bridging hydrides. The aluminium adopts a tetrahedral geometry, with the MeAlMe plane being close to perpendicular (98.2°) to the H–Re–H plane.

In the closely related complex $[(Ph_2MeP)_3HRe(\mu\text{-H})_3AlMe_2]$[36] the aluminium is five-coordinate with three bridging $Re(\mu\text{-H})Al$ hydrides (Fig. 10) off-set from the Re... Al vector. The $Re(\mu\text{-H})_3Al$ bridge is entirely asymmetric with one hydride being equidistant from the aluminium and rhenium [Re—H = 1.73(5) Å, Al—H = 1.76(5) Å] atoms, the others being closer to the rhenium (Re—H_{av} = 1.54 Å, Al—H_{av} = 2.02 Å).

All the structures so far discussed have a transition metal/aluminium ratio of 1. However, the complex $[(Me_3P)_3H_3W(\mu\text{-H})_2Al(H)(\mu\text{-H})_2WH_3(PMe_3)_3]$[33] contains two tungsten atoms, bridged by a single aluminium (Fig. 11), in what can be regarded as a bis-adduct of the Lewis acid AlH_3 with $WH_4(PMe_3)_3$, or with equal validity two $[WH_3(PMe_3)_3]^-$ units joined by a bridging AlH_5^- unit. The asymmetric $W(\mu\text{-H})_2Al$ units (**4**) are near to being planar whilst the geometry around the aluminium approximates quite well to a trigonal bipyramid.

It is likely that the third hydride bridge occurs in order to enable the aluminium to become pentacoordinate. However, the complex $(Me_3P)_3H_2W(\mu\text{-H})_3AlCl_2(NMe_3)$[28] contains a symmetrical $(\mu\text{-H})_3$ bridge (see **8**) but here the aluminium is six-coordinate octahedral, no doubt a reflection of the greater electron-withdrawing effect of the two chlorides.

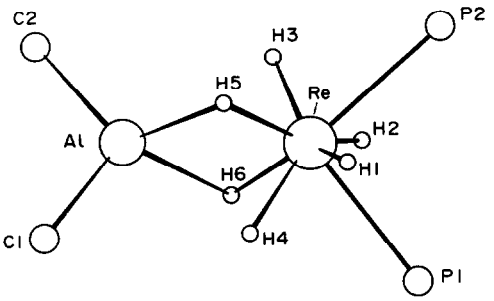


Fig. 9. Molecular structure of $(Ph_2Me)_2H_4Re(\mu\text{-H})_2AlMe_2$ using the atomic coordinates of Ref. 36. The methyl H atoms, as well as the organic groups attached to phosphorus, have been omitted for clarity.

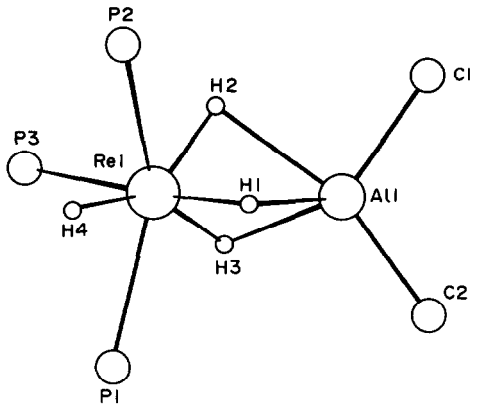
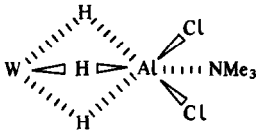


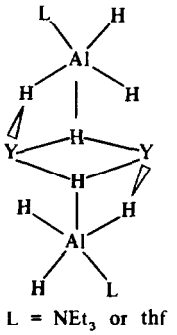
Fig. 10. Molecular structure of $(Ph_2MeP)_3HRe(\mu\text{-}H)_3AlMe_2$ (atomic coordinates from Ref. 36). Methyl hydrogens and organic groups attached to phosphorus have been omitted.



8

A complex with a similar bridge $[(\eta^5\text{-}C_5Me_5)_2Ti(\mu\text{-}H)_2Al(H)(\mu\text{-}H)_2Ti(\eta^5\text{-}C_5Me_5)_2]$[23] has also been reported.

A series of aluminohydride complexes of yttrium,[13,14] $\{[(\eta^5\text{-}C_5H_5)_2Y(\mu_3\text{-}H)][(\mu\text{-}H)AlH_2L]\}_2$ (L = thf or NEt_3) have been synthesized and their structures solved by X-ray crystallography (**9**).



9

These compounds were reported to be "the first representatives of aluminium hydride compounds involving three-coordinate hydrogen atoms". However, it should be noted that similar bridging hydrides have been found in $LiAlH_4$ (Fig. 5). Each $(\eta^5\text{-}C_5H_5)_2Y$ sandwich is bridged by two μ_3-hydrides to two aluminiums. Each aluminium is linked to one of the yttriums by a μ_2-hydride. The yttrium and aluminium atoms are coplanar, along the bisecting plane of the $(\eta^5\text{-}C_5H_5)_2Y$ wedge.

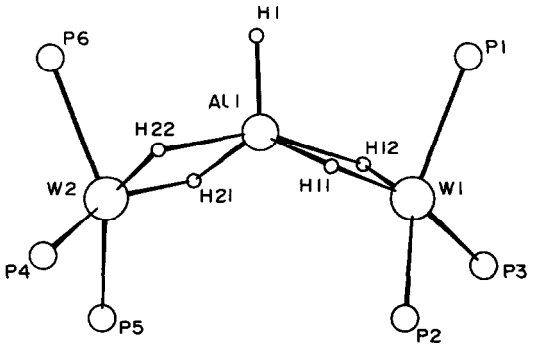
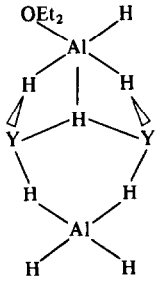


Fig. 11. Structure of $[(Me_3P)_3H_3W]_2AlH_5$. Only the hydrogens attached to Al (terminal and bridging) have been located with reasonable certainty.

As is common, the aluminium is a distorted trigonal bipyramid, with the axial position occupied by the solvent molecule and the μ_3-hydride.

The monosolvated complex $[(\eta^5\text{-}C_5H_5)_2YAlH_4]_2 \cdot OEt_2$[13] is of interest because it contains both four- and five-coordinated aluminiums (**10**). The four-coordinate geometry is a distorted tetrahedron with two of the hydrides bridging to different yttriums. The five-coordinate aluminium exists as the expected trigonal bipyramidal geometry.



10

These yttrium complexes are best considered as alane adducts of $[(\eta^5\text{-}C_5H_5)_2Y(\mu\text{-}H)]_2$. This representation is supported by the formation of an alane adduct of $[(\eta^5\text{-}C_5H_5)_2Y(\mu\text{-}Cl)]_2$[61] containing $Y(\mu\text{-}H)Al$ bridges linking alternate aluminium and yttrium fragments in an infinite chain.

The structural properties of aluminohydrides thus differ substantially from those of analogous borohydrides in several ways; whereas borohydrides are four-coordinate and tetrahedral, the majority of aluminohydrides are five-coordinate with trigonal bipyramidal aluminium. This ability of aluminium to become five-coordinate most probably arises from hybridization, involving one of the low lying 3*d* orbitals, along with the 3*s* and 3*p* orbitals. To achieve five-coordination the aluminohydrides are required to form dimers with a metal/aluminium ratio of either 1 or 2.

Borohydrides have been found to have a variety of bridges $[M(\mu\text{-}H)_nB$ ($n = 1$, 2 or 3)], but aluminohydrides are mainly bridged by two $M(\mu\text{-}H)Al$ units, even when "spare" terminal M—H hydrides are present.[32] The only case for three bridging hydrides is when the compound is precluded from forming a dimer by terminal alkyl groups.[36] The hydrides in the $M(\mu\text{-}H)_2Al$ bridge are asymmetric, reflecting the difference between axial and equatorial sites on the aluminium, as opposed to equivalent sides on the tetrahedral borohydrides.

9. REACTION CHEMISTRY OF ALUMINOHYDRIDES

Although several trends can be found the study of the reactivity of transition-metal aluminohydrides is in its infancy.

(i) *Thermal degradation*

When the complex $[(\eta^5\text{-}C_5Me_5)_2Ti(\mu\text{-}H)_2AlH(\mu\text{-}H)]_2$[23] is stored for any length of time in solution decomposition occurs to give the complex $[(\eta^5\text{-}C_5Me_5)_2Ti]_2AlH_5$[23] along with aluminium and hydrogen. A similar reaction is observed when the complex $[(Me_3P)_3H_3W(\mu\text{-}H)_2Al(H)(\mu\text{-}H)]_2$ is refluxed in hexane for a few hours, the product being $[(Me_3P)_3H_3WAlH_5$.[32] The proposed mechanism for the decomposition of the titanium complex [eqn (17)] would seem to be stoichiometric:

$$[(\eta^5\text{-}C_5Me_5)_2Ti(\mu\text{-}H)_2Al(H)(\mu\text{-}H)]_2 \rightarrow [(\eta^5\text{-}C_5Me_5)_2Ti]_2AlH_5 + Al + \tfrac{3}{2}H_2. \quad (17)$$

However, NMR studies[28] of the decomposition of the tungsten compound indicate that the reaction is far more complicated.

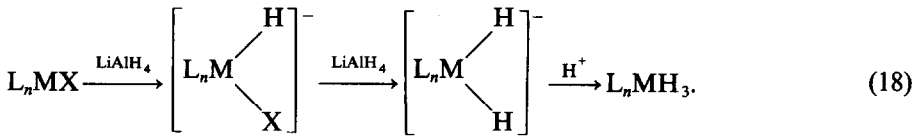
If the unsubstituted cyclopentadienyl complex is used further decomposition occurs with recombination of basic hydride hydrogens and acidic protons of the Cp rings to give a polycyclic complex, $[(\eta^5\text{-}C_5H_5)_2Ti(\mu\text{-}H)_2Al(\mu\text{-}H)(\eta^1:\eta^5\text{-}C_5H_4)TiCp(\mu\text{-}H)]_2$,[22] whose structure has been found by X-ray crystallography.

(ii) *Hydrolysis*

In general the aluminohydride complexes are moisture-sensitive, yielding on hydrolysis the

appropriate polyhydride.[29,32,36] Thus the addition of MeOH or H_2O to a diethyl ether solution of $[(dmpe)_2HCr(\mu\text{-}H)_2Al(H)(\mu\text{-}H)]_2$[29] yields the polyhydride $(dmpe)_2CrH_4$.[62]

$LiAlH_4$ has been widely used in the synthesis of transition-metal polyhydrides.[6] Often the formal oxidation state of the metal in the product is higher than in the starting material, usually a halide. That is, there is an apparent oxidation by what is normally regarded as a reducing agent. Davies *et al.*[63] attempted to explain this by the mechanism of eqn (18):



$$L_nMX \xrightarrow{LiAlH_4} \left[L_nM(H)(X)\right]^- \xrightarrow{LiAlH_4} \left[L_nM(H)_2\right]^- \xrightarrow{H^+} L_nMH_3. \quad (18)$$

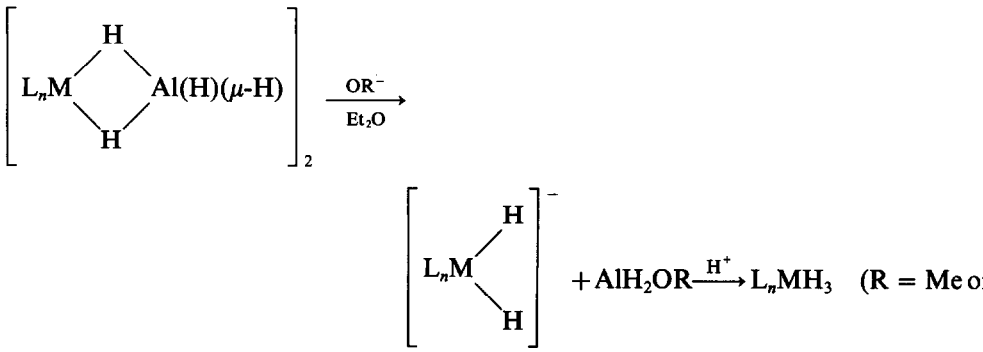
However, in the light of hydrolysis studies on aluminohydrides,[29] is appears that these are, in fact, intermediates in the synthesis of polyhydrides as in eqn (19):

$$L_nMX \xrightarrow{LiAlH_4} [L_nM(\mu\text{-}H)_2Al(H)(\mu\text{-}H)]_2 \xrightarrow{H_2O} L_nMH_3. \quad (19)$$

The formation, prior to hydrolysis, of yellow solutions in the synthesis of $IrH_5(PR_3)_3$[64] and of orange solutions in the synthesis of $[(\eta^5\text{-}C_5H_4Me)_2TaH_3]$[65] have been noted but without comment on the possibility of intermediate aluminium-containing species. In some cases (e.g. the tantalum one) the oxidation state of the metal is the same both in the starting material and the product. Two possibilities can be considered: (a) direct attack of H^- on L_nMCl_m with no formation of an aluminohydride, or (b) reduction of the metal halide complex to give an aluminohydride followed by oxidation during hydrolysis. The reaction of $TaCl_5$ with two equivalents of LiC_5H_4Me followed by addition of three equivalents of $LiAlH_4$ yields $[(\eta^5\text{-}C_5H_4Me)_2Ta(III)(\mu\text{-}H)_5Al(H)(\mu\text{-}H)]_2$: hydrolysis of this complex then gives the trihydride.[28]

The actual mechanism for the hydrolysis of the aluminohydride is as yet not certain. Deuteration studies indicate that the $M(\mu\text{-}H)_2Al$ bridge is cleaved either symmetrically,[29,32] i.e. one hydride is retained on the transition metal and one on the aluminium, or asymmetrically,[26,28] i.e. both hydrides are retained on the transition metal.

The asymmetric cleavage may result from initial nucleophilic attack on the five-coordinate aluminium atom followed by protonation of the resulting hydrido anion [eqn (20)]:



$$\left[L_nM(H)_2Al(H)(\mu\text{-}H)\right]_2 \xrightarrow[Et_2O]{OR^-} \left[L_nM(H)_2\right]^- + AlH_2OR \xrightarrow{H^+} L_nMH_3 \quad (R = Me \text{ or } H). \quad (20)$$

(iii) *Reaction with Lewis bases*

There is a wide variety of aluminium–nitrogen complexes[41] formed via Lewis acid–base interactions. Whereas borohydrides readily react with simple trialkyl amines, NR_3, no such reaction has been observed for aluminohydrides.[27,28] However, if a chelating amine such as tmeda is used the reactivity is increased.

Addition to tmeda to a toluene solution of $[(\eta^5\text{-}C_5H_5)_2TiAlH_4]_n$ yields the bridged species $[(C_5H_5)_2TiAlH_4]_2\mu$-tmeda.[21] In other cases the insoluble adduct $(tmeda \cdot AlH_3)$ is produced along with an aluminohydride containing a single AlH_5^{2-}-bridge between two transition-metal units[32,37] [eqn(21)]:

$$[(Me_3P)_3HRu(\mu\text{-}H)_2Al(H)(\mu\text{-}H)]_2 \xrightarrow[Et_2O]{tmeda} [AlH_3 \cdot tmeda]_n + [(Me_3P)_3HRu]_2AlH_5.[38] \quad (21)$$

(iv) *Reaction with organo* C≡N *and* C=N *bonds*

The reduction of organic nitriles with $LiAlH_4$ has been widely used in organic synthesis.[66]

Interaction of MeCN with $[(Me_3P)_3H_3W(\mu\text{-}H)_2Al(H)(\mu\text{-}H)]_2$ yields the imine-bridged complex $[(Me_3P)_3H_3W(\mu\text{-}H)_2Al(H)(\mu\text{-}N{=}CH{-}Me)]_2$[28] containing a four-membered Al–N ring system. On hydrolysis acetaldehyde is liberated along with $(Me_3P)_3WH_6$.

Interestingly, the complex $[(Me_3P)_3H_3W]_2AlH_5$ does not react with nitriles even at elevated temperatures, suggesting that it is the bridging $Al(\mu\text{-}H)Al$ hydrides that become incorporated into the imine.

The reaction of imines (R'N=CHR) with a WCl_6–$LiAlH_4$ mixture yields a mixture of tertiary and secondary amines,[67] but the authors have not considered an aluminohydride intermediate in the proposed mechanism.

(v) *Reaction with lithium alkyls*

Addition of alkyllithium reagents to $[(Me_3P)_3H_3W(\mu\text{-}H)_2Al(H)(\mu\text{-}H)]_2$ yields the polyhydride anion $\{[(Me_3P)_3WH_5]Li\}_4$.[68]

The aluminohydride acts in an analogous way to $AlH_3 \cdot NR_3$[69] [eqn (22)] with attack by the nucleophile at the unsaturated five-coordinate aluminium:

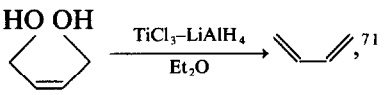
$$AlH_3 \cdot NR_3 + LiR \rightarrow AlH_2R \cdot NR_3 + LiH. \tag{22}$$

(vi) *Uses in catalysis*

Although so far studies on reactions of isolated aluminohydrides are few, their *in situ* use in catalytic systems has been known for some time.

Mixtures of titanium halides ($TiCl_4$ and $TiCl_3$) with aluminium hydride species have been successfully used as Ziegler–Natta catalysts in the polymerization of alkenes,[10,11] as well as in a range of other organic transformations [eqns (23) and (24)]:

$$2R_2C{=}O \xrightarrow[Et_2O]{TiCl_3\text{–}LiAlH_4} R_2C{=}CR_2,^{70} \tag{23}$$



,[71] (24)

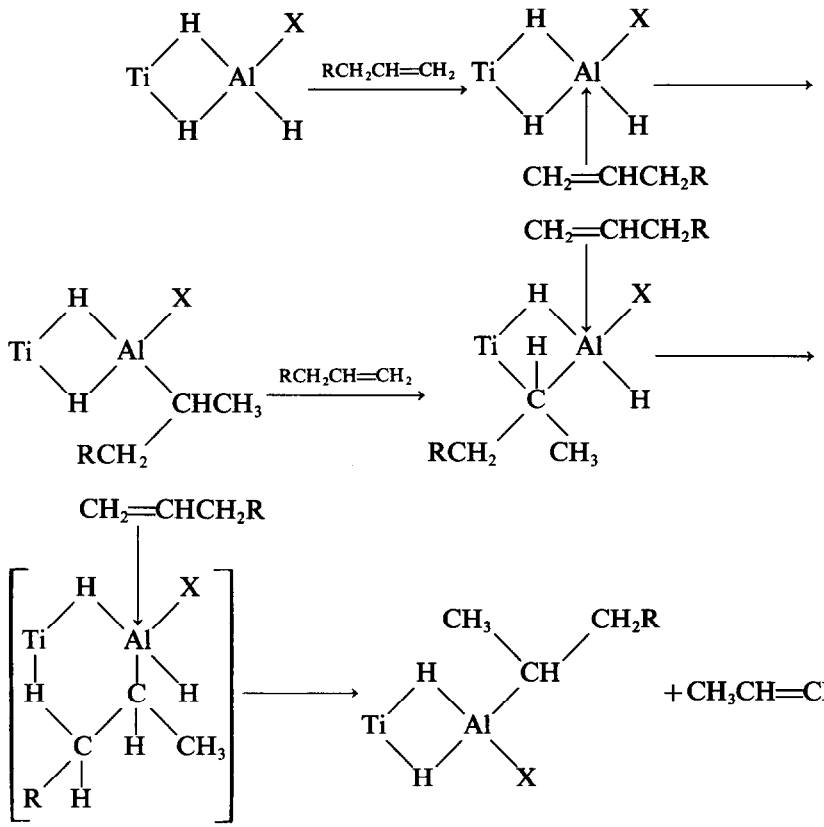
although little is known of the exact nature of the catalytic intermediates.

Mixtures of $[(\eta^5\text{-}C_5H_5)TiCl]_2$ and $LiAlH_4$ have been used for a variety of catalytic processes. With a Ti/Al ratio of 1 [i.e. a complex formulated as "$Cp_2Ti(\mu\text{-}H)_2AlH_2$"] the maximum activity for the isomerization of α-olefins is observed and for which a mechanism involving the coordination of the olefin to the coordinatively unsaturated aluminium atom has been proposed[72] [eqn (25)].

It should be noted that all these studies *assume a monomeric structure*; however in the light of crystallographic results discussed above, the active species may be dimeric.[23] If this is the case the aluminium is still unsaturated (maximum coordination 6[41]) and so this mechanism is still feasible.

Using a Ti/Al ratio of 2[73] the catalytic system can be used to hydrogenate α-olefins as well as cyclohexene and benzene.[74] ESR data suggest that the reactive species is a complex of the formula $[(\eta^5\text{-}C_5H_5)_2Ti]_2AlH_4X$ (X = hal or H).[10] This has been confirmed by studying the catalytic and spectroscopic properties of the crystallographically characterized complex $[(\eta^5\text{-}C_5Me_5)_2Ti]_2AlH_5$.[23]

It should be noted that other aluminohydrides have shown little or no ability to act as catalysts.[27,28]



(25)

Acknowledgements—We thank Majid Motevalli and Michael B. Hurthouse for their help with the crystallographic diagrams and the S.E.R.C. for a studentship (A.R.B.).

REFERENCES

1. J. S. Pizey, *Lithium Aluminium Hydride*. Horwood–Wiley, Chichester (1977).
2. A. Streitweiser and G. H. Heathcock, *Introduction to Organic Chemistry*, Macmillan, London (1976).
3. E. R. H. Walker, *Chem. Soc. Rev.* 1976, **5**, 23.
4. (a) A. B. Goel, *Indian J. Chem., Sect. A* 1978, **16**, 491; (b) L. I. Zakharkin and V. V. Gavrilenko, *J. Gen. Chem. USSR* (Eng. Transl.) 1962, **32**, 688; (c) E. Wiberg and R. Bauen, *Z. Naturforsch.* 1952, **76A**, 131.
5. T. J. Marks and J. R. Kolb, *Chem. Rev.* 1977, **77**, 263 (and references therein).
6. G. G. Hlatky and R. H. Crabtree, *Coord. Chem. Rev.* 1985, **65**, 1.
7. H. D. Kaesz and R. B. Saillant, *Chem. Rev.* 1972, **72**, 231.
8. T. Blackmore, M. I. Bruce and F. G. A. Stone, *J. Chem. Soc. A* 1971, 2376.
9. J. Chatt and R. S. Coffey, *J. Chem. Soc. A* 1969, 1963.
10. E. V. Evdokimova, B. M. Bulychev and G. L. Soloveichik, *Kinet. Katal.* 1981, **22**, 170.
11. P. C. Wailes, R. S. P. Coutts and H. Weigold, *Organometallic Chemistry of Titanium, Zirconium and Hafnium*. Academic Press, New York (1974).
12. M. E. Kost and A. I. Golovanova, *Izd. Akad. Nauk SSSR, Neorg. Mater.* 1978, **14**, 1732.
13. V. K. Bel'skii, A. B. Erofeev, B. M. Bulychev and G. L. Soloveichik, *J. Organomet. Chem.* 1984, **265**, 123.
14. V. K. Bel'skii, B. M. Bulychev, A. B. Erofeev and G. L. Soloveichik, *J. Organomet. Chem.* 1984, **268**, 707.
15. A. B. Erofeev, G. L. Soloveichik, B. M. Bulychev and V. B. Polyakova, *Koord. Khim.* 1983, **9**, 190.
16. M. E. Kost and A. I. Golovanova, *Izv. Akad. Nauk SSSR, Neorg. Mater.* 1978, **14**, 1732.
17. B. M. Bulychev, S. E. Tokaveva, G. L. Soloveichik and E. V. Erdokimova, *J. Organomet. Chem.* 1979, **179**, 263.
18. E. B. Lobkovskii, G. L. Soloveichik, B. M. Bulychev, R. G. Gew and Y. T. Struchkov, *J. Organomet. Chem.* 1984, **270**, 45.
19. B. M. Bulychev, A. L. Kostenko, G. L. Soloveichik and V. B. Polyakov, *Transition Met. Chem.* 1981, **6**, 240.
20. A. I. Sizov and B. M. Bulychev, *Zh. Neorg. Khim.* 1981, **26**, 2652.

21. E. B. Lobkovskii, G. L. Soloveichik, A. I. Sisov, B. M. Bulychev, A. I. Gusev and N. I. Kivillova, *J. Organomet. Chem.* 1984, **265**, 167.
22. E. B. Lobkovskii, G. L. Soloveichik, A. I. Sizov and B. M. Bulychev, *J. Organomet. Chem.* 1985, **280**, 53.
23. V. K. Bel'skii, A. I. Sizov, B. M. Bulychev and G. L. Soloveichik, *J. Organomet. Chem.* 1985, **280**, 67.
24. P. C. Wailes and H. Weigold, *J. Organomet. Chem.* 1970, **24**, 405.
25. A. B. Erofeev, B. M. Bulychev and G. L. Soloveichik, *Zh. Neorg. Khim.* 1980, **25**, 2634.
26. J. A. Labringer and K. S. Wong, *J. Organomet. Chem.* 1979, **170**, 373.
27. T. J. McMeese, S. S. Wreford and B. M. Foxman, *J. Chem. Soc., Chem. Commun.* 1978, 500.
28. A. R. Barron, Thesis, University of London (1986).
29. A. R. Barron, J. Salt and G. Wilkinson, *J. Chem. Soc., Dalton Trans.* 1986, 1329.
30. V. A. Stow and B. S. Thomas, *Can. J. Chem.* 1971, **49**, 2504.
31. J. W. Bruno, J. C. Huffman and K. G. Caulton, *J. Am. Chem. Soc.* 1984, **106**, 444.
32. A. R. Barron, D. Lyons, G. Wilkinson, M. Motevalli, A. Downes and M. B. Hursthouse, *J. Chem. Soc., Dalton Trans.* 1986, 279.
33. A. R. Barron, M. Motevalli, M. B. Hursthouse and G. Wilkinson, *J. Chem. Soc., Chem. Commun.* 1985, 664.
34. G. S. Girolami, G. Wilkinson, M. Thornton-Pett and M. B. Hursthouse, *J. Am. Chem. Soc.* 1983, **105**, 6752.
35. C. G. Howard, G. S. Girolami, G. Wilkinson, M. Thornton-Pett and M. B. Hursthouse, *J. Chem. Soc., Dalton Trans.* 1985, 921.
36. W. A. Skupinski, J. C. Huffman, J. W. Bruno and K. G. Caulton, *J. Am. Chem. Soc.* 1984, **106**, 8128.
37. A. R. Barron and G. Wilkinson, *J. Chem. Soc., Dalton Trans.* 1986, 287.
38. V. V. Saraev, F. K. Schmidt, V. A. Gruznykh, L. V. Mironova and T. I. Bakunina, *Koord. Khim.* 1979, **5**, 897.
39. E. Wiberg and E. Amberger, *Hydrides of the Main Groups I–IV*, p. 403. Elsevier, New York (1971).
40. P. W. Frost, J. A. K. Howard and J. L. Spencer, *J. Chem. Soc., Chem. Commun.* 1984, 1362.
41. F. A. Cotton and G. Wilkinson, *Advanced Inorganic Chemistry*, 4th edn. Wiley, New York (1980).
42. B. M. Bulychev, *Izd. Akad. Nauk SSSR, Neorg. Mater.* 1978, **14**, 1735.
43. G. Henrici-Olivé and S. Olivé, *J. Organomet. Chem.* 1970, **23**, 155.
44. K. Mach and H. Antropiusova, *J. Organomet. Chem.* 1983, **248**, 287.
45. J. Myall, J. G. Kenworthy and M. C. R. Symons, *J. Chem. Soc. A* 1971, 1020.
46. B. M. Bulychev, S. E. Tokareva, G. L. Soloveichik and E. V. Erdokimova, *J. Organomet. Chem.* 1979, **179**, 263.
47. (a) A. D. Buckingham and P. J. Stephens, *J. Chem. Soc.* 1964, 2747; (b) P. W. Atkins, J. C. Green and M. L. H. Green, *J. Chem. Soc. A* 1968, 2275.
48. R. K. Harris and B. E. Mann, *N.M.R. and the Periodic Table*. Academic Press, London (1978).
49. (a) R. Berun, A. Rufinska, H. Lehmkuhl, E. Janssen and C. Kruger, *Angew. Chem., Int. Ed. Engl.* 1983, **22**, 779; (b) G. Van Koten, *Organometallics* 1985, **4**, 170.
50. J. A. Statler, G. Wilkinson, M. Thornton-Pett and M. B. Hursthouse, *J. Chem. Soc., Dalton Trans.* 1984, 1731.
51. P. W. Frost, J. A. K. Howard and J. L. Spencer, *J. Chem. Soc., Chem. Commun.* 1984, 1362.
52. D. Lyons, thesis, University of London (1983).
53. T. J. Marks and J. R. Kolb, *J. Am. Chem. Soc.* 1975, **97**, 3397; R. A. Hoffman and S. Forsen, *Prog. Nucl. Magn. Reson. Spectrosc.* 1966, **1**, 173.
54. A. Almenningen, G. Gunderson and A. Haaland, *Acta Chem. Scand.* 1968, **22**, 328.
55. E. R. Bernstein, W. C. Manulton, T. A. Keiderling, S. J. La Placa, S. J. Lippard and J. J. Mayente, *Inorg. Chem.* 1972, **11**, 3009.
56. T. J. Marks and J. R. Kolb, *J. Am. Chem. Soc.* 1975, **97**, 27.
57. N. Sklar and B. Post, *Inorg. Chem.* 1967, **6**, 669.
58. E. R. Peterson, *Diss. Abstr.* 1965, **25**, 5588.
59. J. K. Ruff and M. F. Hawthorne, *J. Am. Chem. Soc.* 1960, **82**, 2141.
60. G. J. Palenik, *Acta Cryst.* 1964, **17**, 1573.
61. E. B. Lobkovski, G. L. Soloveichik, A. B. Erofeev, B. M. Bulychev and V. K. Bel'skii, *J. Organomet. Chem.* 1982, **255**, 151.
62. J. E. Salt, G. S. Girolami, G. Wilkinson, M. Motevalli, M. Thornton-Pett and M. B. Hursthouse, *J. Chem. Soc., Dalton Trans.* 1985, 685.
63. G. J. Baird, S. G. Davies, S. D. Moon, S. J. Simpson and R. H. Jones, *J. Chem. Soc., Dalton Trans.* 1985, 1479.
64. J. Chatt, R. S. Coffey and B. L. Shaw, *J. Chem. Soc. A* 1965, 7391.
65. G. W. Parshall and V. Klabunde, *J. Am. Chem. Soc.* 1972, **94**, 9081.
66. H. C. Brown and C. P. Garg, *J. Am. Chem. Soc.* 1964, **86**, 1085.

67. T. Ikariya, Y. Ishikana, K. Hirani and S. Yoshikana, *J. Organomet. Chem.* 1985, **288**, 311.
68. A. R. Barron, M. Motevalli, M. B. Hursthouse and G. Wilkinson, *J. Chem. Soc., Chem. Commun.* 1986, 81.
69. F. M. Peters, B. Bartocha and A. J. Bilbo, *Can. J. Chem.* 1963, **41**, 105; J. K. Ruff, *J. Am. Chem. Soc.* 1961, **83**, 1798.
70. R. Davis, M. Malinowski, I. Westdorp and N. Y. Geise, *J. Org. Chem.* 1982, **47**, 248.
71. H. M. Walborsky and H. H. Wüst, *J. Am. Chem. Soc.* 1982, **104**, 5807.
72. B. M. Bulychev, E. V. Erdokimova, A. I. Sizov and G. L. Soloveichik, *J. Organomet. Chem.* 1982, **239**, 313.
73. E. V. Erdokimova, G. L. Soloveichik and B. M. Bulychev, *Kinet. Katal.* 1982, **23**, 1109.
74. (a) K. N. Semenenko, B. M. Bulychev and G. L. Soloveichik, *Chem. Abstr.* 1976, **85**, 159376d; (b) B. M. Bulychev and E. V. Erdokimova, *Chem. Abstr.* 1982, **97**, 109604d.

Polyhedron Vol. 5, No. 12, pp. 1917–1920, 1986
Printed in Great Britain

0277-5387/86 $3.00+.00
Pergamon Journals Ltd

SELECTIVE REAGENTS FOR SOLVENT EXTRACTION OF METALS—III. PICOLINIC ACIDS

BJÖRN ELMAN,* A. G. SVERKER HÖGBERG† and CHRISTINA MOBERG*

Royal Institute of Technology, Department of Organic Chemistry,
S-100 44 Stockholm, Sweden

and

MAMOUN MUHAMMED

Royal Institute of Technology, Department of Inorganic Chemistry,
S-100 44 Stockholm, Sweden

(*Received* 3 *October* 1985; *accepted* 11 *November* 1985)

Abstract—Alkyl-substituted pyridine-2-carboxylic acids have been found to be efficient reagents for the extraction of Cu^{2+}, Fe^{3+}, Co^{2+} and Ni^{2+} from aqueous sulfate solutions at pH 1.7. The effects of the position and the nature of the substituent are discussed.

Considerable attention has been devoted to the development of chelating agents for liquid–liquid extraction of metal ions.[1–3] In particular, reagents capable of extracting base metals at low pH conditions are of great interest for the recovery of metals from acidic leach solutions.

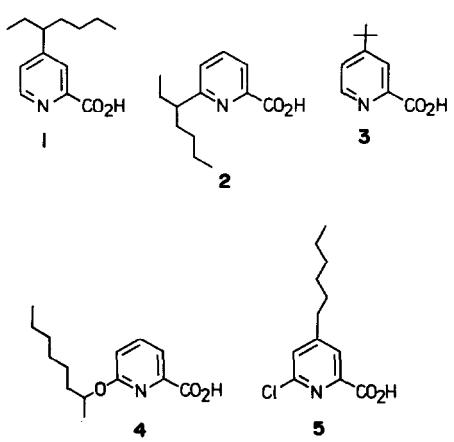
We have recently reported on the syntheses and extracting properties of substituted quinoline-2-carboxylic acids.[4,5] Since pyridine-2-carboxylic acid, picolinic acid, also forms stable complexes with a variety of metal ions,[6] we prepared substituted pyridine-2-carboxylic acids to investigate their extracting properties, and herewith the results of this investigation are described.

RESULTS

Reagent **1**, 4-(3-heptyl)pyridine-2-carboxylic acid, was prepared, along with the isomer 6-(3-heptyl)pyridine-2-carboxylic acid (**2**), by radical alkylation[7] of 2-cyanopyridine with 2-ethylhexanoic acid, followed by hydrolysis. Compound **1** is stable under acidic conditions—no degradation was observed during 60 days at pH 1. It is essentially insoluble in water but is readily soluble in various organic solvents (37.5 g of **1** can be dissolved in 100 ml of Shellsol A + 20% decanol).

The reagents were tested for their ability to extract Cu^{2+}, Zn^{2+}, Ni^{2+}, Co^{2+}, Fe^{2+}, Cd^{2+}, Fe^{3+} and K^+ from aqueous sulfate solutions of mixtures of metal ions into an organic phase. The results are reported as $pH_{1/2}$ values (Table 1), which were calculated from the concentrations of metal ions measured by atomic absorption spectrophotometric analysis of the aqueous phase after extraction.

Inspection of Table 1 reveals that compound **1** is an effective reagent for the extraction of Cu^{2+} and Fe^{3+} in particular but also for Ni^{2+} and Co^{2+} at low pH. A slightly higher affinity for Ni^{2+} than for



*Authors to whom correspondence should be addressed.
†Present address: Boliden Kemi AB, Box 902, S-25109 Helsingborg, Sweden.

Co^{2+} is shown. The Ni^{2+}–Co^{2+} selectivity can be increased slightly by using a 2:1 mixture of 2-ethylhexanoic oxime[8] and **1** in toluene. This mixture extracts 100% of Ni^{2+} and 25% of Co^{2+} at pH 1.83.

The 6-substituted isomer **2** is much less efficient, extracting only minor amounts of all metal ions, with the exception of Cu^{2+}, at pH values below 2.5 ($pH_{1/2}$ for Cu^{2+} is 2.0). Reagent **3**, however, which was prepared analogously to **1**, showed extracting properties (Table 1) similar to those of **1**.

Compounds **4** and **5** were also tested as reagents for extraction of metal ions into a chloroform phase. Neither reagent extracted metal ions below pH 2. For solutions with pH values between 2 and 3, Cu^{2+} was extracted; the $pH_{1/2}$ values for Cu^{2+} were 3.1 and 2.4 for **4** and **5**, respectively.

Measurements were made of the distribution of metal ions at pH 2 between an aqueous phase containing varying concentrations of a single metal ion (Cu^{2+}, Fe^{3+}, Fe^{2+}, Ni^{2+}, Co^{2+} or Zn^{2+}) and an organic phase of equal volume containing **1**. Using a 5% solution of reagent **1** in Shellsol A+20% decanol as a modifier, maximum loadings of 8.4, 4.5, 3.6 and 4.5 g metal dm^{-3} of Cu^{2+}, Zn^{2+}, Fe^{2+} and Fe^{3+}, respectively, were obtained. A third phase formed when Ni^{2+} and Co^{2+} were extracted from concentrated solutions (>*ca* 3.9 and 4.8 g metal dm^{-3}, respectively). In chloroform, about the same loadings of Ni^{2+} and Co^{2+} could be obtained, but the distributions of metal ions between the two phases were somewhat less favorable.

The rates of the extraction of Cu^{2+}, Fe^{3+} and Zn^{2+} from 2 mM aqueous solutions of single metal sulfates at pH 2 by reagent **1** in an equal volume of chloroform were determined by measuring the concentrations of metal ions in the aqueous phase at intervals. From this data it was concluded that 98% of Cu^{2+} was extracted within 1 min, while $t_{1/2}$ for Zn^{2+} was *ca* 0.8 min and for Fe^{3+} *ca* 1 min.

Ligand **1** could be regenerated from the Zn^{2+} and Cu^{2+} complexes by treatment with 1 and 4 M H_2SO_4, respectively.

Table 1.

	Reagent[a]				
	1	**2**	**3**	**4**	**5**
Cu^{2+}	<0.8	2.0	0.3	3.1	2.4
Zn^{2+}	2.1	[b]	2.4	[b]	[b]
Ni^{2+}	1.2	[b]	1.5	[b]	[b]
Co^{2+}	1.7	[b]	2.2	[b]	[b]
Fe^{2+}	1.9	[b]	2.5	[b]	[b]
Fe^{3+}	<0.9	[b]	<0.8	[b]	2.6
Cd^{2+}	2.5	[b]	[b]	[b]	[b]
K^{+}	[b]	[b]	[b]	[b]	[b]

[a]The extractions were performed with equal volumes of an aqueous phase containing initially 2 mM metal sulfates and a 20 mM chloroform solution of the reagent.

[b]Less than *ca* 5% extraction at pH 2 corresponding to $pH_{1/2} > 2.8$ for divalent metal ions.

DISCUSSION

Pyridine-2-carboxylic acid forms stable complexes with a variety of metal ions. Because the parent compound is water soluble, it cannot be used as a reagent for liquid–liquid extraction. Introduction of a lipophilic group to the molecule provides a more suitable reagent. With a heptyl chain or even a tertiary butyl group as the lipophilic substituent, a reagent with the desired properties was achieved. Attempts to prepare picolinic acids with longer chains resulted in considerably lower yields. Therefore, these products were not tested.

The position of the lipophilic group on the pyridine nucleus is important, as shown by the different extraction performances of the isomers **1** and **2**. The poor extracting ability of **2** compared to **1** is probably due to steric hindrance in the complexing region. The electronic nature of the substituent also seems to be of importance since compound **4** extracts less Cu^{2+} than **2**. This effect may, at least in part, be due to a reduced electron donor ability of the nitrogen atom caused by the electron-withdrawing alkoxy substituent. The same effect may also explain the poor extracting properties of **5**.

Several reagents have recently been developed for liquid–liquid extraction of Ni^{2+} and Co^{2+}.[8–12] These reagents are usually only efficient at conditions above pH 2 however. The reagent reported here can be used for the efficient extraction of these two metal ions at lower pH, though it is not useful for separation of the two ions. We have recently found that the selectivity of quinoline-2-carboxylic acids for different metal ions is greatly influenced by the electronic and steric nature and the position of the substituents,[4] and it can therefore be expected that the same factors are operative among pyridine-2-carboxylic acids. We are currently studying such effects, particularly on the Ni^{2+}–Co^{2+} selectivity.

EXPERIMENTAL

Instrumentation

All melting points are uncorrected. IR spectra were recorded on a Perkin–Elmer 257 spectrometer and mass spectra were run on an LKB 9000 spectrometer. NMR spectra were recorded on a Bruker

WP 200 spectrometer at 200 MHz and on a Varian EM 360 instrument at 60 MHz. A Perkin–Elmer 603 atomic absorption spectrophotometer was used for metal determinations.

Elemental analyses were performed by Mikro Kemi AB in Uppsala and are within 0.4%.

Preparation of substituted picolinic acids

1 *and* **2**. $(NH_4)_2S_2O_8$ (28.85 mmol) in water (40 cm^3) was added over 15 min to a mixture of 2-cyanopyridine (19.23 mmol), 2-ethylhexanoic acid (96.15 mmol), $AgNO_3$ (1.923 mmol) and 1 M H_2SO_4 (58 cm^3) at 70°C. After stirring for 3 h at 70°C the mixture was poured into ice-water, neutralized with 25% NH_3 (40 cm^3) and extracted with CH_2Cl_2 (2×100 cm^3). The organic phase was washed with 5% NaOH (100 cm^3) and dried ($MgSO_4$). Evaporation afforded 3.56 g of crude product which was chromatographed on silica gel (235 g) with CH_2Cl_2 as the mobile phase to give 2-cyano-4-(3-heptyl)pyridine (59%) and 2-cyano-6-(3-heptyl)pyridine (11%). Alternatively, the cyanopyridines could be separated by crystallization from diethyl ether–petroleum ether. 2-Cyano-4-(3-heptyl)pyridine: IR (film): 3050, 2960–2850, 2230 and 1595 cm^{-1}. NMR (CCl_4): δ 0.6–1.0 (6H, *m*, CH_3), 1.0–2.0 (8H, *m*, CH_2), 2.65 [1H, *tt*, $J = 6$ Hz, C*H*(Et)Bu], 7.3 (1H, *dd*, $J = 5$ and 2 Hz, 5-pyridyl), 7.5 (1H, *s*, 3-pyridyl) and 8.55 (1H, *d*, $J = 5$ Hz, 6-pyridyl). Analysis: C, H and N. 2-Cyano-6-(3-heptyl)pyridine—IR (film): 3050, 2960–2850, 2230 and 1590 cm^{-1}. NMR (CCl_4): δ 0.6–1.0 (6H, *m*, CH_3), 1.0–2.0 (8H, *m*, CH_2), 2.65 [1H, *tt*, $J = 6$ Hz, C*H*(Et)Bu], 7.25 (1H, *dd*, $J = 9$ and 2 Hz, 5-pyridyl) and 7.35–7.9 (2H, *m*). Analysis: C, H and N.

2-Cyano-4-(3-heptyl)pyridine (9.32 mmol) and KOH (93.2 mmol) were reacted in ethylene glycol (50 cm^3) at 130°C. After 3 days, the pH was adjusted to 3 and the mixture extracted with $CHCl_3$ (3×50 cm^3). The organic phase was washed with H_2O (2×100 cm^3), dried ($MgSO_4$) and the solvent evaporated to give the product (**1**) as a yellow oil that slowly crystallized (84%, m.p. 100.5–102.5°C). IR (KBr): 3420, 3050, 2960–2850, 2600–2300, 1700 and 1600 cm^{-1}. MS *m/z* (rel. int.): 222(0.5), 221(0.5), 150(62), 146(44), 132(32), 118(36), 106(38), 104(34), 29(42), 28(100) and 27(32). ^{1}H NMR [$(CD_3)_2CO$]: δ 0.6–1.0 (6H, *m*, CH_3), 1.0–1.4 (4H, *m*, CH_2), 1.4–1.9 (4H, *m*, CH_2), 2.4–2.95 (1H, *m*, CH-py), 7.5 (1H, *dd*, $J = 6$ and 2 Hz), 8.0 (1H, *d*, $J = 2$ Hz), 8.65 (1H, *d*, $J = 6$ Hz) and 9.5 (1H, *s*, OH). Analysis: C, H and N.

2-Cyano-6-(3-heptyl)pyridine was hydrolysed in the same manner to give **2**.

4-t-*Butylpyridine*-2-*carboxylic acid* (**3**). This compound was prepared the same way as **1** from 2,2-dimethylpropionic acid and 2-cyanopyridine, followed by hydrolysis (33% overall yield). M.p. 90–91°C. IR (KBr): 2960, 1720 and 1600 cm^{-1}. MS *m/z* (rel. int.): 164(43), 135(100), 120(52), 118(33) and 28(40).

2-(2-*Carboxy*-6-*pyridyloxy*)*octane* (**4**). This compound was prepared by reaction of 2-cyano-6-chloropyridine (1.33 g, 9.6 mmol) with 2-octanol (1.24 g, 9.6 mmol) in monoglyme (50 cm^3) in the presence of NaH (0.46 g, 19.1 mmol) at 80°C for 1.5 h. Addition of water, extraction with diethyl ether and flash chromatography [ethyl acetate–petroleum ether (7 : 93)] gave 2-(6-cyano-2-pyridyloxy)octane (55%), which was hydrolysed (KOH–EtOH–H_2O, 80°C, 24 h) to give **4** (93%). IR (film): 3300, 2960–2850 and 1710 cm^{-1}. MS *m/z* (rel. int.): 251(3), 140(100). ^{1}H NMR (CCl_4): δ 0.6–1.95 (16H, *m*), 5.20 [1H, *m*, OC*H*(CH_3)C_6H_{13}], 6.75–7.0 (1H, *m*, 5-pyridyl), 7.65–7.85 (2H, *m*, 3- and 4-pyridyl) and 10.5 (1H, *s*, OH).

6-*Chloro*-4-(n-*hexyl*)*pyridine*-2-*carboxylic acid* (**5**). 4-(*n*-Hexyl)-pyridine, obtained from 4-picolyl lithium and 1-bromopentane, was treated with sodium amide followed by HCl–$NaNO_2$ to give 4-(*n*-hexyl)-2-chloropyridine. This product was treated with 3-chloroperbenzoic acid to give the *N*-oxide, which was reacted with $(CH_3)_2SO_4$ followed by NaCN and the product finally hydrolysed to give **3**. IR (KBr): 3400–3100, 3060, 2960–2850, 1725 and 1600 cm^{-1}. MS *m/z* (rel. int.): 243(31), 241(67), 171(80), 153(80), 142(30), 140(100), 127(42), 125(37), 43(100), 41(80) and 17(90). ^{1}H NMR ($CDCl_3$): δ 0.7–1.0 (3H, *m*, CH_3), 1.0–2.0 (8H, *m*, CH_2), 2.7 (2H, *t*, $J = 7$ Hz, CH_2-py), 7.4 (1H, *s*, 5-pyridyl), 8.0 (1H, *s*, 3-pyridyl) and 9.85 (1H, *s*, OH). Analysis: C, H and N.

Metal extraction tests

Aqueous solutions of mixtures of metal sulfates (Cu^{2+}, Zn^{2+}, Ni^{2+}, Co^{2+} and Fe^{2+}, or Cu^{2+}, Zn^{2+}, Ni^{2+}, Co^{2+} and Cd^{2+}, or Cu^{2+}, Zn^{2+}, Fe^{3+}, Cd^{2+} and K^+), *ca* 2 mM in each metal ion, at pH *ca* 2 or 4 were agitated with equal volumes of 20 mM organic solutions of the appropriate reagent until equilibrium was reached. The two phases were then separated by centrifugation and the amount of metal present in the aqueous phase was determined by atomic absorption spectrophotometry.

Acknowledgements—All metal extraction tests were performed by Ms Kerstin Högberg at the Department of Inorganic Chemistry, Royal Institute of Technology. This work was supported by the Swedish Board for Technical Development.

REFERENCES

1. M. J. Hudson, *Hydrometallurgy* 1982, **9**, 149.
2. F. Habashi, *C & En* 1982, 46.
3. A. R. Burkin, *Chem. Ind. (London)* 1983, 690.
4. A. G. S. Högberg, K. Madan, C. Moberg, B. Sjöberg, M. Weber and M. Muhammed, *Polyhedron* 1985, **4**, 971.
5. B. Elman, A. G. S. Högberg, M. Weber and M. Muhammed, *Polyhedron* 1985, **4**, 1197.
6. K. Suzuki, M. Yasuda and K. Yamasaki, *J. Phys. Chem.* 1957, **61**, 229.
7. F. Minisci, R. Bernardi, F. Bertini, R. Galli and M. Perchinummo, *Tetrahedron* 1971, **27**, 3575.
8. J. S. Preston, *Hydrometallurgy* 1983, **11**, 105.
9. R. R. Grinstead, In *Proceedings of the International Solvent Extraction Conference ISEC 80, Liège, Belgium* (1980).
10. J. E. Barnes, J. H. Setchfield and G. O. R. Williams, *J. Inorg. Nucl. Chem.* 1976, **38**, 1065.
11. J. S. Preston, *Hydrometallurgy* 1982, **9**, 115.
12. D. B. Dreisinger and W. C. Cooper, *Hydrometallurgy* 1984, **12**, 1.

Polyhedron Vol. 5, No. 12, pp. 1921–1926, 1986
Printed in Great Britain

0277–5387/86 $3.00+.00
Pergamon Journals Ltd

SYNTHESIS AND REACTIONS OF 4-VINYL PYRIDINE DERIVATIVES OF RUTHENIUM(II)*

SARADA GOPINATHAN, I. R. UNNI and C. GOPINATHAN†

Inorganic Chemistry Division, National Chemical Laboratory, Poona 411008, India

(*Received* 12 *September* 1985; *accepted after revision* 27 *January* 1986)

Abstract—4-Vinyl pyridine (4-Vp) reacts with $RuHClCO(PPh_3)_3$ (I) in THF to give $RuHClCO(PPh_3)_2$(4-Vp) (II), which reacts with sodium derivatives of bidentate chelating ligands to afford substitution products, $[RuH(CO)(PPh_3)_2(L)]$. The bidentate ligands used are 2-hydroxybenzaldehyde, 2-hydroxy-3-methoxybenzaldehyde, trifluorothenoylacetone and 8-hydroxyquinoline. Insertion reactions of the Ru—H bond of II with activated olefins such as acrylonitrile [giving $RuCl(CO)(CH_3CHCN)(PPh_3)_2$(4-Vp)], 2-vinyl pyridine, dimethyl fumarate and monobromodiethyl fumarate have been carried out to obtain chelated Ru–C bonded complexes. $RuCl_2(PPh_3)_3$ reacts with an excess of 4-Vp to give an octahedral ruthenium addition complex containing two vinyl pyridine ligands. The dimer $[RuClCO(CH_3CHCN)(PPh_3)$(4-Vp)$]_2$ is obtained by the reaction of $[RuClCO(CH_3CHCN)(PPh_3)_2]_2$ with an excess of 4-Vp. Stereochemical assignments have been made for these new complexes on the basis of IR and ^1H NMR data.

Substitution reactions of carbonylchlorohydridotris(triphenylphosphine)ruthenium(II) (I) with ligands like phosphines, phosphites, phosphinites and phosphonates have been studied by various workers,[1,2] but there have been no reports regarding reactions using nitrogen bases. It has been observed that because of the strong *trans* bond weakening effect of the hydride ligand, complex I readily undergoes substitution at the *trans* site with the above bases, giving neutral monosubstituted products. Douglas and Shaw[3] have observed that no detectable displacement of phosphine took place even when an excess of 4-methyl pyridine was added to a complex similar to I. In continuation of our work on reactions of ruthenium hydrido complexes,[4,5] we now report a new range of ruthenium(II) complexes containing 4-vinyl pyridine.

EXPERIMENTAL

The ruthenium complex $[RuHCl(CO)(PPh_3)_3]$ (I) was prepared as described by Robinson *et al.*[6] The organic ligands were commercially available and their purities checked. Solvents were freshly distilled after careful drying and degassed prior to use. Reactions were performed under nitrogen and worked up *in vacuo* or under nitrogen. Elemental analyses were done by the microanalysis group of the laboratory. IR spectra were taken in Nujol mulls, KBr pellets or in chloroform solution in a Perkin–Elmer 599 grating spectrophotometer. ^1H NMR spectra were recorded in $CDCl_3$ on Varian FT 80A and Bruker WH 90 spectrometers.

(*a*) *Carbonylchlorohydrido bis(triphenylphosphine)*4-*vinyl pyridine ruthenium* (II)

Freshly distilled 4-vinyl pyridine (0.21 g, 2mmol) was added to a suspension of I (0.238 g, 0.25 mmol) in THF (20 cm^3) in a Schlenk tube. The solution was magnetically stirred at 25°C for 24 h to obtain a light brown precipitate. This was filtered through a sintered glass disc in air and washed with hexane (10 cm^3, 3 times) and kept *in vacuo* at 1 mm pressure for 2 h. Yield 0.155 g (78%).

(*b*) *Carbonylhydrido(salicylaldehydato)bis(triphenylphosphine) ruthenium*

To a suspension of sodium salicylaldehyde [prepared from salicylaldehyde (0.037 g, 0.3 mmol) and oil-free sodium hydride (0.008 g, 0.33 mmol)] in THF (30 cm^3) was added II (0.2 g, 0.25 mmol), and the mixture was stirred for 12 h at 25°C, after which the solvent was removed under reduced pressure.

* NCL Communication No. 3811.

† Author to whom correspondence should be addressed.

The residue was extracted with benzene, centrifuged, and the solvent again removed under reduced pressure. The mass was washed with hexane (10 cm^3, 3 times), crystallized from a benzene–hexane [1 : 1 (v/v)] mixture and dried at 0.1 mm pressure for 2 h. The yellow microcrystalline solid weighed 0.12 g (78%). Other chelated ruthenium derivatives have been prepared similarly.

(*c*) *Carbonylchloro*(1 - *cyanoethyl*) *bis*(*triphenylphosphine*)4-*vinyl pyridineruthenium*

Freshly distilled acrylonitrile (0.106 g, 2 mmol) was added to a suspension of **II** (0.2 g, 0.25 mmol) in THF (30 cm^3), and the mixture was magnetically stirred at 25°C for 24 h. The resulting clear brown solution was evaporated to dryness *in vacuo* and the mass thus obtained was washed 3 times with small lots of hexane and the solid crystallized from a benzene–hexane mixture. Yield 0.17 g (82%).

(*d*) *Carbonylchloro - bis*(*triphenylphosphine*)2 - (2′ - *pyridyl*)*ethyl ruthenium*

To a suspension of **II** (0.2 g, 0.25 mmol) in THF (30 cm^3) was added 2-vinyl pyridine (0.105 g, 1 mmol), and the mixture stirred for 14 h and processed to obtain a light green crystalline solid. Yield 0.17 g (85%). Reactions with fumarates have been carried out similarly.

(*e*) *Carbonylchlorodithioformato - bis*(*triphenylphosphine*)*ruthenium*

To a suspension of **II** (0.2 g, 0.25 mmol) in benzene (20 cm^3) was added carbon disulphide (5 ml) and the mixture was kept at room temperature for 24 h. The yellow crystals separated were filtered, dried *in vacuo* and recrystallized from a dichloromethane–hexane mixture. Yield 0.15 g (78%).

(*f*) *Carbonylchloro*(1 - *cyanoethyl*)*triphenylphosphine*)4-*vinyl pyridineruthenium dimer*

$[RuCl(CO)(CH_3CHCN)(PPh_3)_2]$ (0.19 g, 0.25 mmol) was suspended in THF (25 cm^3) and was reacted with 4-vinyl pyridine (0.105 g, 1 mmol) by stirring at room temperature for 24 h. The red solution obtained was processed as in (c) to obtain a dark red crystalline solid. Yield 0.12 g (83%).

(*g*) *Dichloro - bis*(*triphenylphosphine*)*bis*(4 - *vinyl pyridine*)*ruthenium*

To a suspension of $RuCl_2(PPh_3)_3$ (0.19 g, 0.25 mmol) in benzene (30 cm^3) was added an excess of 4-vinyl pyridine (0.22 g, 2 mmol), the mixture was stirred for 24 h at ambient temperature, and then refluxed for 4 h to obtain a clear red solution. It was then processed as in (c) to get a red microcrystalline solid. Yield 0.21 g (93%).

RESULTS AND DISCUSSION

The hydrido complex **I** reacts smoothly with 4-vinyl pyridine (freshly distilled, monomer) in THF at ambient temperature to afford the neutral monosubstituted product **II**. This colourless microcrystalline solid is stable towards air, is soluble in chloroform and dichloromethane, and insoluble in hexane (Table 1).

The IR spectrum of compound **II** shows a strong band at 1900 cm^{-1} due to $\nu(C{\equiv}O)$ and a medium-intensity band at 1990 cm^{-1} arising from $\nu(Ru{-}H)$ (Table 2). In the starting hydrido complex (**I**) the corresponding vibrations are at 1922 and 2020 cm^{-1}, respectively.[6] Low-frequency shifts are expected when triphenylphosphine situated *trans* to the hydrido ligand is substituted by a strong σ-donating ligand like 4-vinyl pyridine having little π-accepting ability. The coordination of the ligand to ruthenium is through its nitrogen lone pair and not through the vinylic π-system as seen from the vinylic CH and CH_2 out-of-plane deformations at 995 and 935 cm^{-1}, respectively.[7]

The high-field proton NMR spectrum of the compound comprises a triplet centred at δ −13.52 [$^2J(PH)_{cis}$ = 20 Hz], which suggests that the hydride is *cis* to two equivalent phosphorus atoms as shown in Fig. 1.

The chlorine substitution in complex **II** has been carried out using the sodium derivatives of bidentate ligands like 2-hydroxybenzaldehyde (salicylaldehyde), 3-methoxy-2-hydroxybenzaldehyde (*o*-vanillin), 8-hydroxyquinoline (oxine) and trifluorothenoylacetone in THF medium. The chelated derivatives are obtained in good yield by the elimination of chlorine and 4-vinyl pyridine (Table 1):

$$RuHCl(CO)(PPh_3)_2(4\text{-}Vp) + NaL \rightarrow RuH(CO)(PPh_3)_2(L) + NaCl + 4\text{-}Vp.$$

These are freely soluble in benzene and chloroform,

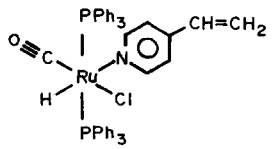


Fig. 1.

Table 1. New ruthenium(II) complexes

S. No.	Compound[a]	M.p. (°C)	Colour	% analysis: found (calc.) C	H	P
1	$[RuClH(CO)(PPh_3)_2(4\text{-}Vp)]$	199	Colourless	66.8 (66.4)	4.9 (4.8)	7.8 (7.8)
2	$[RuH(Sal)(CO)(PPh_3)_2]$	110	Yellow	68.1 (68.1)	4.7 (4.7)	7.9 (8.0)
3	$[RuH(o\text{-}Vanil)(CO)(PPh_3)_2]$	155	Brown	67.1 (67.1)	4.7 (4.8)	7.6 (7.7)
4	$[RuH(Oxine)(CO)(PPh_3)_2]$	230	Brown	69.1 (69.2)	4.7 (4.7)	7.7 (7.8)
5	$[RuH(Tftac)(CO)(PPh_3)_2]$	106	Orange	61.8 (61.7)	4.1 (4.0)	7.0 (7.1)
6	$[RuCl(CH_3CHCN)(CO)(PPh_3)_2(4\text{-}Vp)]$	155	Brown	66.4 (66.6)	4.9 (4.9)	7.2 (7.3)
7	$[RuCl(CHCO_2Me)(CH_2COOMe)(CO)(PPh_3)_2]$	172	Green	61.8 (61.9)	4.8 (4.7)	7.4 (7.4)
8	$[RuCl(CHCO_2Et)(CHBrCOOEt)(CO)(PPh_3)_2]$	113	Green	57.3 (57.4)	4.6 (5.5)	6.5 (6.6)
9	$[RuCl(2\text{-}Ep)(CO)(PPh_3)_2]$	170	Green	66.8 (66.4)	5.0 (4.8)	7.7 (7.8)
10	$[RuCl(S_2CH)(CO)(PPh_3)_2]$	223	Yellow	59.5 (59.6)	4.1 (4.1)	8.0 (8.1)
11	$[RuCl(CH_3CHCN)(CO)(PPh_3)(4\text{-}Vp)]_2$	140	Red	59.4 (59.4)	4.3 (4.5)	5.4 (5.3)
12	$[RuCl_2(PPh_3)_2(4\text{-}Vp)_2]$	220	Red	66.3 (66.2)	4.8 (4.9)	7.0 (6.8)

[a] Abbreviations: 4-Vp, 4-vinyl pyridine; Sal-H, salicylaldehyde; *o*-Vanil-H, *o*-vanillin; Oxine-H, 8-hydroxyquinoline; Tftac-H, trifluorothenoylacetone; 2-Ep, 2-ethyl pyridine; PPh_3, triphenylphosphine.

and insoluble in hexane; but the solution stability is poor in all cases. The same products were obtained by the reaction of $[RuHCl(CO)(PPh_3)_3]$ with the sodium salts of the respective bidentate ligands.

The IR spectra of the chelated complexes (Table 2) show clearly that the ligands are coordinated. The $\nu(C{\equiv}O)$ has been shifted to a higher frequency except in the case of 8-hydroxyquinoline derivative, suggesting less electron density at ruthenium atom as a result of chelate formation. There is not a considerable change in the ν(Ru—H) mode.

^{1}H NMR spectra (Table 2) of these derivatives exhibit triplets due to coupling of the Ru—H proton with two *cis* phosphorus atoms. Two triplets of equal intensity having very similar chemical shifts are observed for the complexes suggesting the existence of two isomers. Separation of these isomers was attempted by column chromatography using a variety of elutants. The yellow fraction obtained by elution with benzene gave similar ^{1}H NMR signals as the unchromatographed starting material, suggesting that the isomers are not resolved probably because of their very close R_f values. Attempts to elute out the isomers using other solvents also failed. The two isomers can have the structures shown in Fig. 2(a) and (b). However, in the case of the 8-hydroxyquinoline derivative, the resonance due to the Ru—H proton in the major isomer is at δ −9.85 (80%) and the minor isomer at δ −14.85 (20%). The resonance at δ −9.85 arises from the structure (Fig. 3) as the σ-donating oxine nitrogen is *trans* to the π-acceptor carbonyl ligand. This is in good agreement with the reduction in $\nu(C{\equiv}O)$ in this complex.

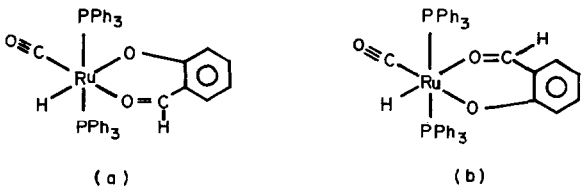


Fig. 2.

Complex II has been reacted with activated olefins in THF at ambient temperature to give Ru–C-bonded mononuclear insertion compounds. The olefins used are acrylonitrile, dimethyl fumarate and bromodiethyl fumarate. Acrylic esters did not yield any pure isolable product:

$$[RuHCl(CO)(PPh_3)_2(4\text{-}Vp)] + CH_2{=}CHCN \rightarrow [RuCl(CO)(CH_3CHCN)(PPh_3)_2] + 4\text{-}Vp.$$

The IR spectrum of the 1-cyanoethylruthenium complex lacks a ν(Ru—H) mode at 1990 cm^{-1} and shows a strong band at 1925 cm^{-1} due to the terminal carbonyl group. The ν(CN) is at 2230 cm^{-1}, confirming the non-involvement of a nitrile group in coordination. The vinylic $\delta(CH_2)$ is at 935 cm^{-1} as in the starting hydrido complex.[5] The ^{1}H NMR spectrum shows two doublets due to methyl resonance at δ 0.17 and 0.43 [^3J(HH) = 8 Hz] with

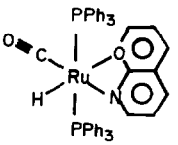


Fig. 3.

Table 2. IR (ν in cm^{-1}) and proton NMR (δ in ppm) data of new ruthenium(II) complexes

S. No.	Compound	ν(C≡O)	ν(Ru—H)	ν(C=O)/(C=N)	ν(Ru—H)	Other NMR resonances
1	$[RuClH(CO)(PPh_3)_2(4\text{-}Vp)]$	1900	1990	—	−13.52 t	5.4–6.9 [$\delta(CH_2{=}CH)$]
2	$[RuH(Sal)(CO)(PPh_3)_2]$	1915	1990	1615	−14.31 t −14.34 t	8.2 d [δ(CH)]
3	$[RuH(o\text{-}Vanil)(CO)(PPh_3)_2]$	1920	1990	1605	−14.11 t −14.15 t	3.52 [$\delta(OCH_3)$], 8.28 d [δ(CH)]
4	$[RuH(Oxine)(CO)(PPh_3)_2]$	1900	1955	1570	−9.85 t −14.85 t	—
5	$[RuH(Tftac)(CO)(PPh_3)_2]$	1930	1970	1600	−14.24 t −13.53 t	—
6	$[RuCl(CH_3CHCN)(CO)(PPh_3)_2(4\text{-}Vp)]$	1925	—	2230	—	0.17 d [$\delta(CH_3)$], 0.43 d [$\delta(CH_3)$], 2.43 m [δ(CH)], 5.4–6.7 [$\delta(CH_2{=}CH)$ (major)], 5.41–6.83 [$\delta(CH_2{=}CH)$ (minor)]
7	$[RuCl(CHCO_2Me)(CH_2COOMe)(CO)(PPh_3)_2]$	1930	—	1620, 1660	—	3.03 [$\delta(OCH_3)$], 3.77 [$\delta(OCH_3)$], 3.87 [$\delta(OCH_3)$]
8	$[RuCl(CHCO_2Et)(CHBrCOOEt)(CO)(PPh_3)_2]$	1935	—	1615, 1720	—	1.33 dt [$\delta(CH_3)$], 4.3 dq [$\delta(OCH_2)$], 6.44 [δ(CH—Ru)], 6.6 [δ(CH—Br)]
9	$[RuCl(2\text{-}Ep)(CO)(PPh_3)_2]$	1915	—	—	—	1.8 t [$\delta(CH_2{-}Ru)$], 2.6 t [$\delta(CH_2)$]
10	$[RuCl(S_2CH)(CO)(PPh_3)_2]$	1945	—	—	—	11.88 [$\delta(S_2CH)$], ^4J(PH) = 8 Hz
11	$[RuCl(CH_3CHCN)(CO)(PPh_3)(4\text{-}Vp)]_2$	1920	—	2200	—	0.4 d [$\delta(CH_3)$], 0.63 d [$\delta(CH_3)$], 5.4–6.9 [$\delta(CH_2{=}CH)$]
12	$[RuCl_2(PPh_3)_2(4\text{-}Vp)_2]$	—	—	—	—	5.3–6.7 [$\delta(CH_2{=}CH)$]

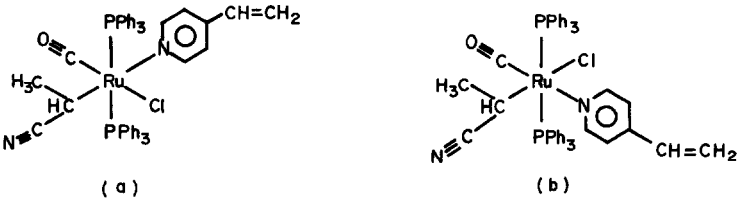


Fig. 4.

relative intensities of 2:1, suggesting the presence of two isomers. A high-field shift for methyl protons is expected when a strong σ-donating nitrogen is situated at the *trans* position. The tertiary methine proton, $\rangle$CH, resonates at δ 2.43 as a multiplet. The δ values for vinylic protons of major and minor isomers are well separated and they resonate between δ 5.4 and 6.7. All these data suggest the stereochemistry of the complex shown in Fig. 4.

2-Vinyl pyridine adds to the Ru—H bond in **II** to give the compound $[RuCl(CO)(CH_2CH_2C_5H_4N)(PPh_3)_2]$ with the elimination of 4-vinyl pyridine. The same compound has been synthesized by Hiraki *et al.*[8] by the reaction of **I** with 2-vinyl pyridine [reported: m.p. 170°C, ν(C≡O) 1908 cm^{-1}, chemical shift δ 1.8 t, 2.6 t for CH_2] and on the basis of IR and NMR data the stereochemistry is suggested to be as shown in Fig. 5.

The hydrido complex **(II)** reacts with carbon disulphide in a benzene medium at ambient temperature to yield the insertion product $[RuCl(CO)(S_2CH)(PPh_3)_2]$ as an air-stable yellow-crystalline solid; 4-vinyl pyridine is eliminated.

$$[RuHCl(CO)(PPh_3)_2(4\text{-Vp})] + CS_2 \rightarrow [RuCl(CO)(S_2CH)(PPh_3)_2] + 4\text{-Vp}.$$

When the same reaction is carried out in refluxing benzene (7 h), a red product which is a 1:1 mixture of two isomers, as seen from the ^1H NMR spectrum, was obtained. Fractional crystallization of the product separated the less soluble yellow isomer. From the mother liquor pure isomers could not be obtained even by using chromatographic techniques.

The IR spectrum of the yellow product shows bands at 1235 and 930 cm^{-1}, attributable to δ(HCS) and $\nu_{as}(CS_2)$, respectively, which suggests the presence of a chelated dithio ligand.[9,10] The ^1H NMR spectrum comprises a triplet at δ 11.88 [^4J(PH) ~ 8 Hz] due to the coupling of a dithioformate proton (S_2CH) with *trans* phosphorus nuclei. The following structure (Fig. 6) is proposed; an X-ray crystal study is underway.

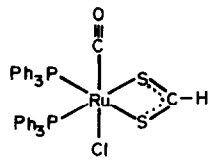


Fig. 6.

This compound has been found to be identical with that prepared by Robinson and Sahajpal[11] by the insertion reaction of $[RuHCl(CO)(PPh_3)_3]$ with carbon disulphide in refluxing benzene for 30 min [reported: m.p. 214–216°C, ν(C≡O) 1958 cm^{-1}, $\nu(S_2CH)$ 1230 and 920 cm^{-1}, chemical shift δ 11.87 t, $^4J(PH)_{trans} = 8$ Hz].

Ligand substitution reaction of the dimer $[RuCl(CO)(CH_3CHCN)(PPh_3)_2]_2$[8] with excess 4-vinyl pyridine yields the monosubstituted dimeric derivative $[RuCl(CO)(CH_3CHCN)(PPh_3)(4\text{-Vp})]_2$. The IR spectrum of the dimer shows ν(CN) at 2200 cm^{-1} and ν(C≡O) at 1920 cm^{-1}. The ^1H NMR spectrum comprises two doublets due to methyl protons, which suggests the presence of isomers.

$RuCl_2(PPh_3)_2$ reacts with excess 4-vinyl pyridine in refluxing benzene to afford the red air-stable compound $[RuCl_2(PPh_3)_2(4\text{-Vp})_2]$. The IR spectrum shows bands characteristic of 4-vinyl pyridine. In the lower-frequency region two weak bands observed at 350 and 330 cm^{-1} suggest *cis* coordination of chlorine atoms to ruthenium as shown in Fig. 7.

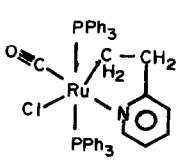


Fig. 5.

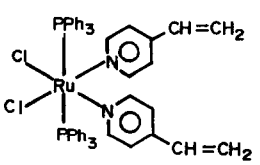


Fig. 7.

REFERENCES

1. C. L. Creswell, S. D. Robinson and A. Sahajpal, *Polyhedron* 1983, **2**, 517.
2. J. W. Gilje, R. Schumtzler, W. S. Sheldrick and V. Wray, *Polyhedron* 1983, **2**, 603.
3. P. G. Douglas and B. L. Shaw, *J. Chem. Soc. A* 1970, 556.
4. K. Joseph, S. Gopinathan and C. Gopinathan, *Synth. React. Inorg. Met–Org. Chem.* 1984, **14**, 1005.
5. S. Gopinathan, K. Joseph and C. Gopinathan, *J. Organomet. Chem.* 1984, **269**, 273.
6. N. Ahmad, J. J. Levison, S. D. Robinson and M. F. Uttley, In *Inorganic Syntheses* (Edited by G. W. Parshall), Vol. 15, p. 48. McGraw-Hill, New York (1974).
7. S. J. Bryan, P. G. Huggett and K. Wade, *Coord. Chem. Rev.* 1982, **44**, 149.
8. K. Hiraki, Y. Sasada and T. Kitamura, *Chem. Lett.* 1980, 449.
9. I. S. Butler and A. E. Fenster, *J. Organomet. Chem.* 1974, **66**, 161.
10. F. W. Einstein, E. Enwall, N. Filtcroft and J. M. Leach, *J. Inorg. Nucl. Chem.* 1972, **34**, 885.
11. S. D. Robinson and A. Sahajpal, *Inorg. Chem.* 1977, **16**, 2718.

Polyhedron Vol. 5, No. 12, pp. 1927–1930, 1986
Printed in Great Britain

0277–5387/86 $3.00+.00
© 1986 Pergamon Journals Ltd

2-MERCAPTO-5-METHYL-1,3,4-THIADIAZOLE AS A LIGAND IN Ru(III), Rh(III), Os(III) AND Ir(III) TRICHLORIDE COMPLEXES

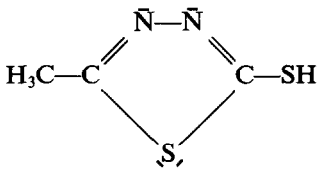
A. C. FABRETTI* and A. GIUSTI

Department of Chemistry, University of Modena, 41100 Modena, Italy

(*Received* 3 *March* 1986; *accepted* 24 *March* 1986)

Abstract—Some 2-mercapto-5-methyl-1,3,4-thiadiazole complexes of Rh(III), Ir(III), Ru(III) and Os(III) have been prepared and characterized by chemical-analysis, conductometric, room-temperature magnetic-moment, electronic, IR, EPR and thermogravimetric measurements. From the magnetic properties it was derived that the above ligand forms low-spin complexes with all the metal ions. The position and multiplicity of the metal–halogen stretching modes in the far-IR region have been investigated. The wavelengths of the principal electronic absorption peaks have been accounted for in terms of the crystal field theory and the various parameters have been calculated.

As a part of a series of investigations into the behaviour of heterocyclic ligands[1] we have considered 2-mercapto-5-methyl-1,3,4-thiadiazole (mttz) which has, besides the three-heteroatoms of the five-membered ring, another potential binding site such as the exocyclic sulphur atom. These ligands exist in —N=C—SH or —NH—C=S forms, exhibiting a thiol⇔thione equilibrium. However, we have established that the thione form dominates in the solid state. The coordination compounds of this ligand with some metal of the VIII group, such as Ru(III), Rh(III), Os(III) and Ir(III), have been prepared and studied



EXPERIMENTAL

Preparation of the complexes

The mttz derivatives were prepared by reaction of an ethanolic–hydrochloric solution of the metal chloride with an ethanolic solution of the ligand in an M : L ratio of 1 : 3. The same result was obtained without HCl.

Any attempt to prepare inner complexes in basic media caused the precipitation of the metal hydroxide.

Analysis

Carbon, nitrogen, sulphur and hydrogen were determined using a Carlo-Erba 1106 analyser.

The electrical conductances of the complexes were measured in DMF. The IR spectra were recorded with a Perkin–Elmer 180 spectrophotometer as KBr disks or Nujol mulls on polyethylene. The electronic spectra were recorded with a Shimadzu MPS 50L spectrometer either in DMF or in the solid state. EPR spectra were recorded at X-band frequencies on a Varian E-9 spectrometer at room and liquid-nitrogen temperatures on the powdered samples. The TGA and DTG measurements were carried out on a Mettler TA 3000 system; a scan rate of 10°C min^{-1} was used.

RESULTS AND DISCUSSION

The new compounds prepared in the present investigation are listed in Table 1.

The molar conductances in 10^{-3} M DMF solution are in the 15–24 Ω^{-1} mol^{-1} cm^2 range indicating the nonelectrolytic nature of the compounds.

* Author to whom correspondence should be addressed.

Table 1. Analytical data for the complexes

Compound	Colour	Found (calc.) (%) N	C	H	S	H_2O
$RhLCl_3 \cdot H_2O$	Orange	7.8 (7.8)	10.1 (10.1)	1.5 (1.6)	18.2 (17.8)	4.2 (4.0)
$IrLCl_3 \cdot H_2O$	Mustard	6.1 (6.2)	8.0 (8.0)	1.2 (1.3)	13.8 (14.3)	4.9 (5.0)
$RuL_{2.5}Cl_3$	Black	13.0 (13.0)	17.0 (16.8)	2.0 (1.9)	30.1 (29.8)	
$OsL_{2.5}Cl_3$	Brown	11.5 (11.2)	14.6 (14.4)	1.5 (1.6)	25.3 (25.6)	

This is consistent with the stoichiometry assumed for the complexes on the basis of analytical data. The rhodium and iridium complexes are diamagnetic while the ruthenium and osmium complexes have magnetic moments at room temperature of 1.6 and 1.5 BM, respectively. These values are slightly below the spin-only value. The EPR spectra of the powdered mttz ruthenium and osmium complexes consist in each case of a single broad signal with a peak-to-peak separation of about 1000 G either at room or liquid-nitrogen temperature, proving that the metals are in the oxidation state III. No detailed analysis of any spectrum is possible. The g_o values are 2.112 and 2.135 for ruthenium and osmium complexes, respectively.

IR spectra

The ligand mttz does not show any ν(SH) band in the 2600–2500-cm^{-1} region, in which this stretching frequency is generally expected.[2]

In order to verify the thioketo form of the ligand deuteration of the molecule has been carried out by refluxing for several hours and evaporating to dryness from a CH_3OD solution. Of the four ligand bands at 3120(sh), 3050(s), 2975(m) and 2865(s) cm^{-1} three are still present in the deuterated form at 3055(mw), 2980(w) and 2875(m) cm^{-1}, and may be assigned to ν(CH) modes, while a new very strong polyhumped band centred at 2260(vs) cm^{-1} is assignable to the ν(ND) mode, the corresponding ν(NH) band at 3120 cm^{-1} disappears, giving a ν(NH)/ν(ND) ratio of 1.38. Other bands sensitive to deuteration [1448(vs), 973(m) and 763(vs) cm^{-1}, which shift, respectively, to 1342(vs), 930(s), and 557 (vs) and 529 (s) cm^{-1}] are principally NH and ND vibrational bands.

It may therefore be concluded that the ligand is mainly in the thioketo form.

The ν(NH) frequency and the other NH vibration bands of the ligand remain practically unchanged upon complexation; this result excludes a NH coordination of the ligand to the metal ion.

The ligand band at 1550(sm) cm^{-1}, which shows only a very small frequency decrease on deuteration to 1540(ms) cm^{-1} and may be assigned mainly to a ν(C=N) mode, is shifted to 1542–1538 cm^{-1} in the complexes. This small frequency lowering should indicate a weak coordination of the ligand in the complexes though the unprotonated nitrogen atom. In the case of ruthenium and osmium derivatives a shoulder at 1550 cm^{-1} is still present in the spectra. This should mean a double behaviour of the ligands in the cited complexes. On the contrary, the ligand band at 1268(vs) cm^{-1} to which an important ν(C—N) contribution may be assigned[2] increases to 1295–1305 cm^{-1} in the complexes in agreement with the electronic shift $HN\overset{\curvearrowright}{-}C\overset{\curvearrowright}{=}S \rightarrow M$ due to a coordination of the ligand through its thiocarbonylic sulphur atom. Consequently some frequencies lowering are observed in the complexes for the bands in the 1070–760-cm^{-1} region [1070(vs) → 1043–1050(vs) and 763(vs) → 755–758(s)], in which a ν(C=S) contribution may be located.

In the far-IR spectra five new bands are located in the 348–248-cm^{-1} region which can be assigned to ν(M—Cl), ν(MS) and ν(MN) vibrations in agreement with data of other similar compounds.[4–6]

The sixth new band at 223(m) cm^{-1} for rhodium and iridium derivatives can be attributed to a M—OH_2 vibration mode (Table 2).

Visible spectra

Almost the same spectra for the complexes are found either in DMF solution or in Nujol mulls.

The rhodium mttz complex shows two bands at 19.6 and 24.4 kK, expected for spin-allowed transitions to the $t_{2g}^5 e_g^1$ configuration. The ligand field bands are large but not obscured by charge-transfer absorptions. The $10Dq$ and B' values, as calculated from the position of these bands by means of the following equations[7]—$\nu_1 = \Delta - 4B' + 86(B')^2/\Delta$ and $\nu_2 = \Delta + 12B' + 2(B')^2/\Delta$—are reported in Table 2 and are well within those found for other trivalent rhodium complexes.[4,5,8–11]

These bands are in the wavelength range expected for chromophores containing S, N, Cl and O.

Table 2. Significant IR bands (cm^{-1}) for the complexes

	ν(OH)	ν(M—Cl)	ν(M—S)	ν(M—L)
$RhLCl_3 \cdot H_2O$	3440s	329s, 303m, 297m	347sh	275m 223m
$IrLCl_3 \cdot H_2O$	3415s	320s, 304s, 280sh	348sh	262 m 223m
$RuL_{2.5}Cl_3$		319s, 289s, 278s	362m	248sh
$OsL_{2.5}Cl_3$		330sh, 309sh, 280s	373m	248sh

Table 3. Electronic spectra and ligand field parameters (kK) of low-spin metal(III) complexes

	$^1A_{1g} \rightarrow {}^1T_{1g}$	$\rightarrow {}^1T_{2g}$	$\rightarrow {}^3T_{1g}$	ν_1/ν_2	Δ	B'	β					
$RhLCl_3 \cdot H_2O$	19.6	25.0	14.9	1.27	20.5	0.373	0.52					
$IrLCl_3 \cdot H_2O$	22.0	28.5	16.4	1.29	23.0	0.453	0.69					
	$^2T_{2g} \rightarrow {}^4T_{1g}$	$\rightarrow {}^4T_{2g}$	$\rightarrow {}^2A_{2g}, {}^2T_{1g}$	$\rightarrow {}^2E_g$		$\rightarrow {}^2T_{1g}, {}^2T_{2g}$		$\rightarrow {}^2A_{1g}$		B	C	$10Dq$
				Obs.	Calc.	Obs.	Calc.	Obs.	Calc.			
$RuL_{2.5}Cl_3$	15.4	19.4	21.5	24.5	25.9	28.6	28.5	32.2	31.0	0.500	1.530	24.0
$OsL_{2.5}Cl_3$	17.9	20.8	23.8	27.8	27.1	29.4	28.9	32.5	30.7	0.363	1.604	26.1

As for the iridium complex the two observed absorption bands are in the range expected for the two spin-allowed transition ν_1 and ν_2, from the ground state $^1A_{1g}$ (Table 3). The band at 16.4 kK (14.9 kK for the rhodium complex) can be attributed to the spin-forbidden $^1A_{1g} \rightarrow {}^3T_{1g}$ transition.[8,10,12,13]

The B' values are of the order of 0.52 and 0.69% of the free ion values in the rhodium and iridium derivatives, respectively, suggesting a considerable orbital overlap with a strong covalency in the metal–ligand σ-bond.

In the spectra of $Ru(mttz)_{2.5}Cl_3$ complex six maxima or shoulders are present; the low intensity of these transitions suggests that they are crystal field transitions and they appear to be characteristic of octahedral complexes of ruthenium(III).[14,15] The two broad low-intensity bands at 15.4 and 19.4 kK are assigned to the spin-forbidden transitions, while the remaining bands are assigned to transitions to doublet states.

On the basis of the following energy levels for low-spin d^5 ions in an octahedral environment:[15]

$^2T_2$	t^5	0
$^4T_1$	t^4e	$10Dq-5B-4C$
$^4T_2$	t^4e	$10Dq+3B-4C$
$^6A_1$	t^3e^2	$20Dq-15B-10C$
$^2A_2, {}^2T_1$	t^4e	$10Dq-2B-C$
^2E	t^4e	$10Dq+7B-C$
$^2T_1, {}^2T_2$	t^4e	$10Dq+12B-C$
$^2A_1$	t^4e	$10Dq+17B-C$

The assignments are given in the Table 3 together with the parameters $10Dq$, B and C.

It is not possible to measure the intensity of the $^2T_2(t^5) \rightarrow {}^6A_1(t^3e^2)$ transition because it corresponds to the highly forbidden transition of the double-electron excitation ($\Delta S = +2$).

As shown in Table 2, the calculated energies for the excited configuration $t_{2g}^4 e_g^1$ fall in the same region as the observed transitions, supporting the suggested configuration.

As for the Os(III) derivative the metal is in a t_{2g}^5-configuration; the two bands at lower wavenumbers are assigned to the two spin-forbidden transition $^2T_2 \rightarrow {}^4T_1$ and $^2T_2 \rightarrow {}^4T_2$ (Table 3). The low-intensity bands between 23.8 and 32.5 kK are transitions from the ground state to doublet states $t_{2g}^4 e_g^1$. These transitions are characteristic of Os(III) octahedral complexes.

The relative low magnetic moments of Ru(III) and Os(III) derivatives at room temperature are probably due to some electron exchange between metal ions though a bridging ligand molecule.

Thermal behaviour of the complexes

The thermogravimetric analysis shows in the case of rhodium and iridium compounds a weight loss in the range 50–140°C (Table 1) due to water molecules. Over 140°C the compounds begin to decompose, leaving M_2O_3 as decomposition products.

REFERENCES

1. A. Benedetti, P. G. DeBenedetti, A. C. Fabretti, G. C. Franchini and C. Gatti, *Transition Met. Chem.* 1984, **9**, 457.
2. C. N. R. Rao, *Chemical Applications of Infrared Spectroscopy*, p. 297. Academic Press, New York (1963).
3. A. C. Fabretti, G. C. Franchini and G. Peyronel, *Spectrochim. Acta* 1980, **36A**, 517.
4. E. Bertelli, C. Preti and G. Tosi, *J. Inorg. Nucl. Chem.* 1975, **37**, 1421.
5. C. Preti and G. Tosi, *J. Coord. Chem.* 1977, **7**, 35.
6. C. Preti and G. Tosi, *J. Coord. Chem.* 1978, **8**, 15.
7. C. K. Jorgensen, *Prog. Inorg. Chem.* 1962, **4**, 73.
8. C. K. Kalia and A. Chakravarty, *Inorg. Chem.* 1969, **8**, 2586.
9. C. K. Jorgensen, *Acta Chem. Scand.* 1956, **10**, 500.
10. C. K. Jorgensen, *Absorption Spectra and Chemical Bonding in Complexes*. Pergamon Press, Oxford (1964).
11. C. J. Ballhausen, *Introduction to Ligand Field Theory*. McGraw-Hill, New York (1962).
12. R. A. Bauer and F. Basolo, *Inorg. Chem.* 1969, **8**, 2231.
13. J. A. Broomhead and W. Grumley, *Inorg. Chem.* 1971, **10**, 2002.
14. R. W. Olliff and A. L. Odell, *J. Chem. Soc.* 1964, 2467.
15. D. S. McClure, *Solid State Phys.* 1959, **9**, 399.

Polyhedron Vol. 5, No. 12, pp. 1931–1933, 1986
Printed in Great Britain

0277–5387/86 $3.00+.00
Pergamon Journals Ltd

REACTIONS OF DITHIOCARBAMATES OF DIMOLYBDENUM—II. REACTION OF MOLYBDENUM ACETATE WITH TWO EQUIVALENTS OF DITHIOCARBAMATE

D. M. BAIRD* and S. D. CROLL

Department of Chemistry, Western Illinois University, Macomb, IL 61455, U.S.A.

(*Received* 17 *February* 1986; *accepted after revision* 1 *May* 1986)

Abstract—Reaction of molybdenum acetate with two equivalents of sodium diethyl dithiocarbamate in methanol results in the tetrakis-substituted $Mo_2(dtc)_4$ (dtc = dithiocarbamate). Exposure of this product to the atmosphere produces $Mo_2O_3(dtc)_4$.

Recently we reported the structure of $Mo_2(Pdtc)_2(OAc)_2TPPO$ (Pdtc = pyrroledithiocarbamate, TPPO = triphenylphosphineoxide).[1] This compound was obtained from reaction of molybdenum acetate with four equivalents of Pdtc. The product of this reaction was later reacted with TPPO in benzene in order to produce higher-quality crystals. A major feature of the structure was the fact that only two of the acetates had been replaced by dithiocarbamates. In addition this was the first example of a dimolybdenum complex with bridging dithiocarbamates.

When four equivalents of dialkyldithiocarbamate are reacted with molybdenum acetate $Mo_2(dtc)_4$ is formed.[2,3] This compound probably has the molybdenum acetate structure with all four of the dithiocarbamates bridging the quadruply bonded dimolybdenum unit. This species, however, rearranges to form an unusual complex in which two of the dithiocarbamate ligands have been reduced by the molybdenum atoms, producing two bridging sulfides and two thiocarboxamide groups (Fig. 1).[3,4]

The structure of $Mo_2(Pdtc)_2(OAc)_2$ led us to wonder what the structure of a complex with two dialkyldithiocarbamates and two acetates would be. Would the two dithiocarbamates simply act as bridging ligands to give a product analogous to the product obtained when pyrroledithiocarbamate was used or would the two dithiocarbamates be reduced and give a product with two bridging sulfides, two thiocarboxamides and two bidentate acetates (see Fig. 2)?

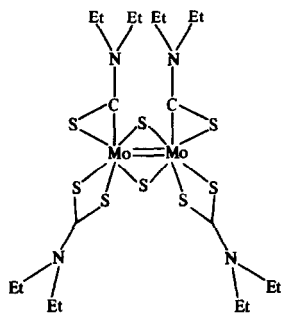


Fig. 1.

The results of a study of reaction (1), that is the reaction of molybdenum acetate with two equivalents of diethyl dithiocarbamate, are presented in this paper.

$$Mo_2(OAc)_4 + 2Na(dtc) \rightarrow Mo_2(dtc)_4 + \tfrac{1}{2}Mo_2(OAc)_4. \quad (1)$$

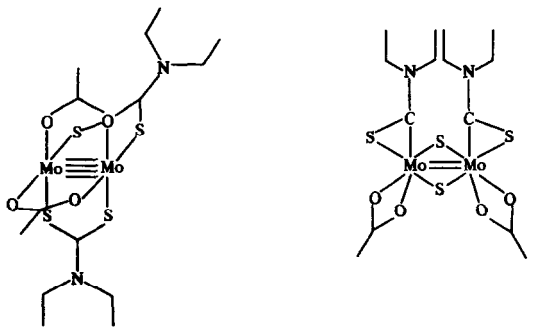


Fig. 2.

* Author to whom correspondence should be addressed.

EXPERIMENTAL

Materials and methods

Molybdenum acetate was prepared by the method of Wilkinson.[5] Sodium diethyldithiocarbamate tris hydrate was purchased from Fisher Chemical Co. and was used as received. All reactions were performed under an Ar atmosphere using standard Schlenk techniques. Methanol was dried by refluxing over calcium sulfate for 2 h. It was then distilled onto fresh calcium sulfate, where it was stored.

Spectroscopic measurements

Electronic absorption spectra were recorded on a Hitachi 100A spectrophotometer or a Perkin–Elmer 552, in methylene chloride solutions. IR spectra were obtained on a Perkin–Elmer 621 spectrophotometer as KBr pellets which were prepared under inert conditions. NMR were taken on a JOEL 90 in $DCCl_3$.

Reactions

In a typical reaction molybdenum acetate was added to two equivalents of sodium diethyldithiocarbamate which had been dissolved is dry degassed methanol according to reaction (1). A green precipitate formed immediately. After stirring the mixture for about 30 min the green material was filtered under Ar. The material was then left with the filter system open to the atmosphere overnight. The contact with air produced $Mo_2O_3(dtc)_4$.

RESULTS

Upon reaction of molybdenum acetate with two equivalents of sodium diethyldithiocarbamate in dry degassed methanol a green precipitate forms immediately. Unreacted molybdenum acetate is visible in the mixture and upon filtration. The conditions used here are the same as those that have been used to produce $Mo_2(dtc)_4$ in other laboratories.[2–4] The green precipitate formed in reaction (1) reacts with even the smallest traces of oxygen to form a purple $Mo_2O_3^{4+}$ complex. This latter reaction is so facile that it was difficult to perform analyses on the green species. As a result the green compound was allowed to react slowly with air and analyses were performed on the purple species. Solution samples were prepared by dissolving the purple compound and then filtering out unreacted $Mo_2(OAc)_4$. It was assumed that if the green complex had the formula $Mo_2(dtc)_2(OAc)_2$ then the purple species would be $Mo_2O_3(OAc)_2(dtc)_2$ by analogy with the reaction of $Mo_2(dtc)_4$ with oxygen, which has been reported to produce $Mo_2O_3(dtc)_4$.[2,3]

IR, electronic-absorption and NMR analyses of the purple complex obtained from reaction (1) showed it to be $Mo_2O_3(dtc)_4$. In each case spectra were identical to those obtained from an authentic sample of $Mo_2O_3(dtc)_4$ prepared by the method of Newton.[6] The NMR spectrum of the purple complex showed only resonances from the ethyl groups of the dithiocarbamates. The possibility of acetate resonance lies under these ethyl resonances can be ruled out by the integration which shows a 1 : 1.48 ratio of ethyl $-CH_3$ ($\delta = 1.295$) to ethyl $-CH_2$ ($\delta = 3.857$) protons. This compares with a theoretical ratio of 1 : 1.5. The IR spectrum of the purple species obtained from reaction (1) is identical to the IR spectrum of the authentic $Mo_2O_3(dtc)_4$ compound. This is particularly important for the 1500–1600-cm^{-1} region, where acetate vibrational frequencies may be observed. The electronic-absorption spectra of $Mo_2O_3(dtc)_4$ from both sources show bands at 380 and 510 nm. The source of these bands has been discussed.[6,7]

DISCUSSION

These results suggest that either a dimolybdenum species which has had one or two acetates replaced by a dialkyldithiocarbamate is more reactive to substitution by a further dithiocarbamate than molybdenum acetate itself or precipitation of $Mo_2(dtc)_4$ drives the equilibria in Scheme 1 toward that complex.

$$Mo_2(OAc)_4 + dtc^- \rightleftarrows Mo_2(OAc)_3(dtc) + OAc^-,$$

$$Mo_2(OAc)_3(dtc) + dtc^- \rightleftarrows Mo_2(OAc)_2(dtc)_2 + OAc^-,$$

$$Mo_2(OAc)_2(dtc)_2 + dtc^- \rightleftarrows Mo_2(OAc)(dtc)_3 + OAc^-,$$

$$Mo_2(OAc)(dtc)_3 + dtc^- \rightleftarrows Mo_2(dtc)_4 + OAc^-.$$

Scheme 1.

In either case it becomes difficult to isolate our target product, $Mo_2(OAc)_2(dtc)_2$. It seems unlikely at this point that an equilibrium control of the product is involved since $Mo_2(OAc)_4$ is not very soluble in methanol. During the reaction yellow $Mo_2(OAc)_4$ crystals are always visible. There is no evidence that the $Mo_2(OAc)_4$ has gone into solution and come back out. That is, much of the $Mo_2(OAc)_4$ is never involved in the reaction scheme.

In conclusion we have shown that the reaction of $Mo_2(OAc)_4$ with two equivalents of dialkyldithiocarbamate in methanol produces $Mo_2(dtc)_4$, which, upon exposure to air, gives $Mo_2O_3(dtc)_4$. We are initiating a study of the kinetics of this reaction system in order to determine

if the product is obtained due to an increased lability of acetates on a dimolybdenum unit that has already been substituted with dithiocarbamate.

Acknowledgements—DMB wishes to acknowledge the Research Corp. and the Western Illinois University Research Council for support of this work.

REFERENCES

1. D. M. Baird, P. E. Fanwick and T. Barwick, *Inorg. Chem.* 1985, **24**, 3753.
2. P. Vella and J. Zubieta, *J. Inorg. Nucl. Chem.* 1978, **40**, 477.
3. D. F. Steele and T. A. Stephenson, *Inorg. Nucl. Chem. Lett.* 1973, **9**, 777.
4. L. Ricard, J. Estienne and R. Weiss, *Inorg. Chem.* 1974, **13**, 2745.
5. G. Wilkinson and Z. Dori, *Inorg. Synth.* 1969, 87.
6. W. E. Newton, J. L. Corbin, D. C. Bravard, J. E. Searles and J. W. McDonald, *Inorg. Chem.* 1974, **13**, 1100.
7. G. J.-J. Chen, J. W. McDonald, D. C. Bravard and W. E. Newton, *Inorg. Chem.* 1985, **24**, 2327.

Polyhedron Vol. 5, No. 12, pp. 1935–1939, 1986
Printed in Great Britain

0277–5387/86 $3.00+.00
Pergamon Journals Ltd

^{133}Cs NMR STUDY OF THE CRYPTAND-222–Cs^+ COMPLEX IN BINARY SOLVENT MIXTURES

GHOLAMHOSSEIN ROUNAGHI and ALEXANDER I. POPOV*

Department of Chemistry, Michigan State University, East Lansing, MI 48824, U.S.A.

(*Received* 9 *January* 1986; *accepted after revision* 1 *May* 1986)

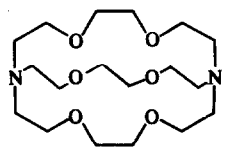
Abstract—The formation constants of the cryptand-222 complex with the cesium ion were studied by ^{133}Cs NMR measurements in four binary solvent systems: acetone–dimethylsulfoxide (Me_2CO–Me_2SO), acetonitrile (MeCN)–Me_2SO, propylene carbonate(PC)–Me_2SO and PC–dimethylformamide (DMF). In the neat solvents the formation constant increases in the order Me_2SO < DMF < Me_2CO < PC < MeCN, which is the inverse order of their solvating abilities as given by the Gutmann donor number. In binary mixtures the stabilities varied monotonically with the composition. As expected, there is no correlation between the stabilities of the complexes and the dielectric constant of the medium. It seems that, for aprotic solvents with similar Pearson basicities and in the absence of ion pair formation, the donor ability of a binary solvent mixture can be qualitatively predicted from the donicities of the two solvents and the composition of the mixture.

In recent years it has become abundantly clear that solvent properties exert a very significant influence on the thermodynamics and kinetics of all reactions in solutions and, in particular, on the complexation reaction between a metal ion and a neutral or a charged ligand. At least two solvent properties play a particularly important role, the solvating ability *vis-à-vis* the metal ion *and* the ligand, and the dielectric constant which influences not only the coulombic forces between the ion and a charged ligand but also may complicate the system by promoting competition from ion pair formation.

While the dielectric constant of a solvent is a readily measured quantity, its donor properties are evaluated much less readily. A number of empirical scales have been proposed,[1] each with its own set of advantages and disadvantages. However, until our fundamental knowledge of the liquid state improves dramatically, we have to rely on empirical approaches for the estimation of the solvating power of solvents.

In a case of alkali ion complexes with macrocyclic ligands (crown ethers and cryptands) the Gutmann donicity scale[2] is particularly useful,[3] provided the dielectric constant of the solvent is high enough to prevent ion pair formation and that, in the case of alkali cations, the solvents are not "soft" bases.[4] With the above provisos, the stability constant is an inverse function of the donor number.[3,4]

In a previous paper[5] we reported a study of the Cs^+ ion complexes with the crown ethers dibenzo-21-crown-7 and dibenzo-24-crown-8 in several mixed solvents. It was of interest to us to extend these studies to cesium cryptates where the interaction between the cation and the ligand is much stronger and, therefore, the influence of the solvent may be less apparent. The work described below involved a study of the Cs^+ ion complex with cryptand-222 (C222) (**1**) which was selected as the probe since the behavior of this complex in neat solvents is rather well-known. A total of four binary systems and five organic solvents, acetone (AC), acetonitrile (AN), dimethylformamide (DMF), dimethylsulfoxide (DMSO) and propylene carbonate (PC), were used. These solvents were selected so as to give a respectable range of donicities and yet with sufficiently high dielectric constants as to avoid ion pair formation. All of these solvents can be classified as "hard" bases.



1

* Author to whom correspondence should be addressed.

EXPERIMENTAL

The macrobicyclic ligand C222 (E.M. Laboratories, Inc.) was purified by two recrystallizations from *n*-hexane and then vacuum dried for several ways. Cesium thiocyanate (Rocky Mountain Research, Inc.) was recrystallized from methanol and dried *in vacuo* at 50°C for 48 h. After drying, it was stored in a vacuum desiccator over granulated barium oxide.

AC (Fisher Scientific Co.), DMSO (Fisher), PC (Aldrich) and AN (Mallinckrodt) were purified and dried by previously outlined procedures.[5] DMF (Mallinckrodt) was refluxed over night under reduced pressure over calcium hydride, then fractionally distilled; the middle 60% fraction of the distillate was further dried over freshly activated molecular sieves (Linde type 4 A). Karl Fischer titration, and gas chromatography (in the case of AC) showed the water content of all of the solvents to be less than 100 ppm.

Most ^{133}Cs NMR measurements were carried out on a Bruker WH-180 spectrometer in the Fourier transform mode at a field of 42.3 kG and a frequency of 23.62 MHz. Some of the data were obtained with a Varian DA-60 spectrometer with a multinuclear probe at a field of 14.09 kG and 7.87 Mz. The details are given in a previous paper.[5]

In all cases the exchange of the Cs^+ ion between the complexed and the free sites was fast at the temperature and the frequency of the measurement. Assuming that only the 1 : 1 complex is formed, the population-averaged chemical shift is given by:

$$\delta_{obs} = \delta_f X_f + \delta_c X_c, \quad (1)$$

where δ_f and δ_c are the resonances corresponding to the free and the complexed Cs^+ ion, respectively, and X_f and X_c are the corresponding mole fractions of the two species. Equation (1) is combined with the equilibrium constant expression to yield:[6]

$$\delta_{obs} = [(KC_M - KC_L - 1) + (K^2C_L^2 + K^2C_M^2 - 2K^2C_LC_M + 2KC_M + 2KC_L + 1)^{1/2}]\left(\frac{\delta_f - \delta_c}{2KC_M}\right) + \delta_c. \quad (2)$$

C_M and C_L are the *total* concentrations of the metal ion and the ligand, respectively, and K is the formation constant.

Our procedure involves substitution of the experimental parameters, δ_{obs}, δ_f, C_M and C_L, into the equation, and varying K and δ_c until the calculated chemical shifts correspond, within experimental error, to the measured values. A nonlinear least-squares curve-fitting program KINFIT[7] was used for the calculations.

RESULTS AND DISCUSSION

Complexation of the cesium ion with C222 was studied in AC–DMSO, AN–DMSO, PC–DMSO and PC–DMF binary systems at the probe temperature (32°C). As an example, results obtained in the PC–DMF system are shown in Fig. 1 and the data are shown in Table 1. A similar behavior was observed in other systems, i.e. as the mole fraction of AC, AN and PC is increased in the AC–DMSO, PC–DMSO and AN–DMSO mixtures, the plots show a more pronounced curvature, indicating the formation of a more stable complex.

The values of the formation constants of the complex in the neat solvents are given in Table 2. The data obtained in the mixed solvents are summarized in Table 3. These data show, for example, that the values of the stability constants increase as the concentration of DMSO and DMF in binary mixtures is lowered. In strongly solvating solvents, such as DMSO and DMF, complex formation is rather scant, while in solvents with medium donicities, such as AC, PC and AN, a more stable complex is formed. These results parallel the behavior observed by Mei *et al.*[3] for cesium ion complexes with cryptands in various neat nonaqueous solvents. From these data it is seen that the solvating ability, as defined by Gutmann, agrees well with the behavior of the Cs^+ ion cryptate in various mixed nonaqueous solvents.

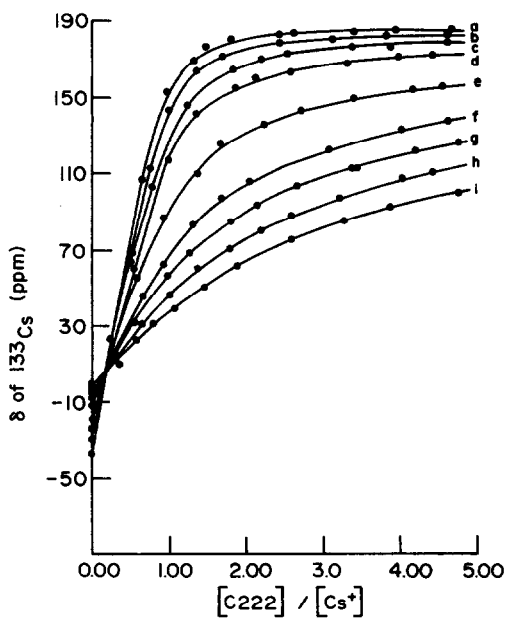


Fig. 1. ^{133}Cs chemical shifts vs [C222]/[Cs^+] mole ratio in the DMF–PC system: mol % PC = (a) 100, (b) 89.2, (c) 78.5, (d) 68.1, (e) 47.7, (f), 28.1, (g) 18.6, (h) 9.2, and (i) 0.0.

Table 1. Mole ratio–chemical-shift data for CsSCN (0.005 M) in the presence of C222 in DMF–PC systems at 32°C

Pure DMF		90% DMF–10% PC		80% DMF–20% PC		70% DMF–30% PC	
L/Cs^+	δ (ppm)	L/Cs^+	δ (ppm)	L/Cs^+	δ (ppm)	L/Cs^+	δ (ppm)
0.00	−1.5	0.00	−3.0	0.00	−5.1	0.00	−7.5
0.33	9.6	0.31	14.3	0.24	11.3	0.26	15.0
0.57	23.1	0.63	30.8	0.55	32.3	0.64	45.6
0.80	30.9	1.00	45.7	0.98	56.5	0.92	61.8
1.08	39.2	1.39	60.0	1.27	68.0	1.32	82.4
1.47	50.5	1.80	70.7	1.82	84.7	1.68	97.0
1.88	61.1	2.20	79.9	2.14	93.7	2.04	106.1
2.59	76.0	2.59	87.9	2.65	103.5	2.44	115.0
3.29	85.1	3.22	98.0	3.39	112.7	3.08	123.3
3.88	92.2	4.04	106.9	4.22	121.4	4.04	132.3
4.78	99.2	4.45	109.3	4.78	125.5	4.62	137.1

50% DMF–50% PC		30% DMF–70% PC		20% DMF–80% PC		10% DMF–90% PC		Pure PC	
L/Cs^+	δ (ppm)	L/Cs^+	δ (ppm)	L/Cs^+	δ (ppm)	L/Cs^+	δ (ppm)	L/Cs^+	δ (ppm)
0.00	−12.7	0.00	−20.0	0.00	−24.1	0.00	−29.3	0.00	−37.1
0.24	15.5	0.26	21.2	0.26	23.9	0.22	23.0	0.20	14.9
0.57	55.3	0.54	60.0	0.60	69.2	0.48	69.2	0.65	106.4
0.92	86.0	0.98	116.8	0.78	103.4	0.74	113.5	0.98	152.4
1.35	109.9	1.36	141.7	1.22	145.4	1.00	143.8	1.33	168.7
1.49	124.7	1.86	155.1	1.84	164.4	1.36	163.9	1.49	176.4
2.24	135.9	2.12	159.5	2.20	170.2	1.70	171.5	1.84	180.0
2.71	143.2	2.58	163.2	2.54	172.4	2.44	178.5	2.45	182.3
3.41	148.0	3.32	167.3	3.38	175.8	3.24	180.4	2.63	182.5
4.18	153.1	3.98	170.0	3.90	175.9	3.86	181.6	3.41	183.6
4.57	155.2	4.44	170.7	4.64	177.2	4.64	182.1	3.96	184.1
								4.69	184.5

The limiting chemical shifts of the cesium–cryptate complex depends on the composition of the mixed solvents. It can be concluded, therefore, that the Cs^+ inside the C222 cavity is not completely shielded from the influence of the medium, and that there is still some direct contact between the solvent molecule and the cation. The crystal structure of the C222 · Cs^+ complex showed that the Cs^+ ion is slightly larger than the equilibrium size of the ligand cavity.[8] When the ligand penetrates the cavity it somewhat distorts the ligand. ^{133}Cs NMR studies on this complex in a variety of solvents showed[3,9] that, at room temperature, the cation does not completely penetrate the ligand cavity and forms an "exclusive" complex where a portion of the complexed cation is exposed to the solvent and, therefore, its ^{133}Cs resonance is solvent-dependent.

Table 2. Formation constants of the C222 · Cs^+ complex in neat solvents at 32°C

Solvent	Dipole moment	Donor number[a]	Log K_f
AC	20.7	17	3.75
DMSO	46.7	29.8	1.19
AN	38	14.1	4.71
PC	64.4	15.1	3.90
DMF	36.7	26.6	2.00

[a] Reference 2.

The variations of the formation constants of the C222 · Cs^+ complex as a function of solvent composition in AC–DMSO, AN–DMSO, PC–DMSO and PC–DMF mixtures are shown in Figs 2 and 3. It is interesting to note that in AC–DMSO solutions the variation of the stability constants of the cesium–cryptate complex with the solvent composition is not significant at low AC concentration (from 0 to ~15 mol % AC), suggesting that in these

Table 3. Log formation constants and limiting chemical shifts for the C222·Cs^+ complex in different binary media at 32±1°C[a]

Medium	Log K_f	Complex
AC–DMSO: mol % AC		
100	3.75±0.02	191.1±0.1
94.8	3.28±0.01	187.2±0.2
84.5	2.80±0.01	176.8±0.3
74.3	2.41±0.02	156.7±1.0
49.1	1.80±0.01	155.7±1.5
24.3	1.38±0.04	163.5±7.7
14.6	1.31±0.03	156.1±3.8
4.9	1.25±0.04	143.7±6.0
0.00	1.19±0.02	154.2±3.4
AN–DMSO: mol % AN		
100	4.71±0.06	206.0±0.3
84.4	3.27±0.02	193.9±0.2
66.9	2.52±0.03	179.4±1.6
47.4	2.05±0.03	167.4±3.0
25.2	1.68±0.02	148.0±3.0
PC–DMSO: mol % PC		
100	3.90±0.01	186.0±0.1
77.1	3.09±0.07	173.7±1.3
55.8	2.36±0.02	170.8±1.2
35.9	1.94±0.01	159.4±1.2
17.4	1.55±0.04	155.6±5.6
PC–DMF: mol % PC		
100	3.90±0.01	186.0±0.1
89.2	3.65±0.02	184.8±0.2
78.5	3.45±0.03	181.1±0.4
68.1	3.19±0.01	178.0±0.3
47.7	2.80±0.03	169.6±1.2
28.1	2.45±0.01	163.8±1.0
18.6	2.29±0.01	159.8±0.8
9.2	2.14±0.02	154.8±1.9
0.00	2.00±0.02	150.1±3.0

[a] 0.005 M CsSCN in all cases.

solutions the metal ion, and possibly the ligand, are solvated only by DMSO. At higher contents of the AC, however, there is a substantial increase in the formation constants. It seems reasonable to assume that upon addition of more AC to the system, the DMSO molecules in the first solvation shell of the Cs^+ ion are gradually replaced by the AC molecules. Since AC is a much weaker solvating solvent than DMSO, the stability of the complex is enhanced by a diminished competition of the solvent for the metal ion.

The above results indicate that the concept of solvent donicity and the predictive ability of the donor numbers holds true at least for the binary solvent systems we investigated. It seems likely that the above generalization will hold in other solvent systems with similar properties, e.g. acid–base

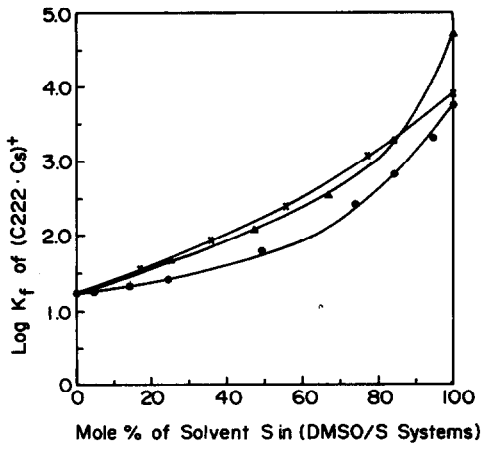


Fig. 2. Variation of the stability constant of the C222·Cs^+ complex with solvent composition in DMSO–S systems: (▲) S = AN, (×) S = PC, and (●) S = AC.

character, hydrogen-bonding ability and large enough values of dielectric constants to prevent a significant amount of ion pairing. It should be noted, however, that many systems are complicated by the solvation of the ligand. This ligand–solvent interaction can have a sizable effect on the stability constants of complexes.[10] It is obvious, however, that much additional work is needed to elucidate the behavior of solvent mixtures.

Acknowledgement—We gratefully acknowledge the support of this work by the National Science Foundation Grant CHE-8515474.

REFERENCES

1. T. R. Griffiths and D. C. Pugh, *Coord. Chem. Rev.* 1979, **29**, 129.

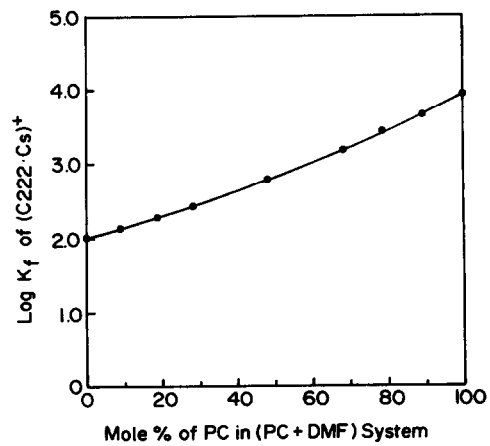


Fig. 3. Variation of the stability constant of the C222·Cs^+ complex with solvent composition in DMF–PC mixture.

2. V. Gutmann and E. Wychera, *Inorg. Nucl. Chem. Lett.* 1966, **21**, 257; V. Gutmann, *Coordination Chemistry in Nonaqueous Solvents*. Springer, Vienna (1968).
3. E. Mei, L. Liu, J. L. Dye and A. I. Popov, *J. Solution Chem.* 1977, **6**, 771.
4. M. Shamsipur, G. Rounaghi and A. I. Popov, *J. Solution Chem.* 1980, **9**, 701.
5. G. Rounaghi and A. I. Popov, *Polyhedron* 1986, **5**, 1329.
6. E. T. Roach, P. R. Handy and A. I. Popov, *Inorg. Nucl. Chem. Lett.* 1973, **9**, 359.
7. V. A. Nicely and J. L. Dye, *J. Chem. Educ.* 1971, **48**, 443.
8. D. Moras, B. Metz and R. Weiss, *Acta Cryst.* 1973, **B29**, 388.
9. E. Mei, A. I. Popov and J. L. Dye, *J. Am. Chem. Soc.* 1977, **99**, 6532.
10. P. A. Mosier-Boss and A. I. Popov, *J. Am. Chem. Soc.* 1985, **107**, 6168.

Polyhedron Vol. 5, No. 12, pp. 1941–1945, 1986
Printed in Great Britain

0277–5387/86 $3.00+.00
© 1986 Pergamon Journals Ltd

TRIMETALLIC COMPLEXES OF FERROCENYLENE BIS[MERCURY(II)THIOCYANATE]

P. P. SINGH* and D. S. GUPTA

Department of Chemistry, M.L.K. College, Balrampur 271201, India

(*Received* 20 *August* 1985; *accepted after revision* 7 *May* 1986)

Abstract—$[Fe(C_5H_4HgSCN)_2M(NCS)_2]$ complexes were prepared by reacting ferrocenylene bis[mercury(II)thiocyanate] with $M(NCS)_2$ [M = Co(II), Ni(II), Cu(II) or Zn(II)]. Their adducts of general formula $[Fe(C_5H_4HgSCN)_2M(NCS)_2L]$ were prepared by reacting ferrocenylene bis[mercury(II)thiocyanate] and $M(NCS)_2L_2$ (L = morph or en). All compounds were characterized by elemental analyses, and molar-conductance, IR and electronic spectral studies. These studies indicated that the geometry around the metal is tetrahedral for cobalt and zinc, and octahedral for nickel and copper. Both types of complex have a thiocyanate-bridged structure.

Ferrocene derivatives have been used as ligands towards certain metal ions. The resulting complexes have two different metals.[1,2] Bimetallic complexes having moieties other than ferrocene have also been reported.[3] In this paper we present a new series of complexes containing three different metals by involving ferrocenylene bis[mercury(II)thiocyanate] (FBMT).

EXPERIMENTAL

Reagent grade solvents were purified before use. $M(NCS)_2$ (M = Co, Ni, Cu or Zn) were prepared by reacting their respective nitrates with KNCS in ethanol. $M(NCS)_2L_2$ [L = morph or en] were prepared by direct reaction of morph or en with $M(NCS)_2$ in ethanol. Morph, en and dimethylsulphoxide (DMSO) were used from fresh bottles FBMT was prepared by mercuration of ferrocene as described below.

Preparation of FBMT

To a solution of ferrocene (18.4 g, 0.1 mol) in benzene (96 cm^3), a solution of mercuric acetate (32.8 g, 0.1 mol) in methanol (360 cm^3) was added drop by drop over a period of 1 h with continuous stirring. The stirring was further continued for 0.5 h. To this solution a solution of KNCS (9.7 g, 0.1 mol) in distilled water (10 cm^3) was added and stirred for 0.5 h. An orange yellow precipitate was obtained which was filtered through a Buchner funnel, washed with petroleum ether and dried *in vacuo*. This compound was a mixture of ferrocenyl mercury thiocyanate (FMT) and FBMT. From the mixture FBMT was separated by Soxhlet extraction using 1,2-dichloroethane as solvent. The extraction was repeated with 1,2-dichloroethane 7 or 8 times till the extract became colourless. On vacuum evaporation of the extract impure FMT was obtained. The residue was FBMT, which was purified by dissolving in DMSO, followed by addition of water. The compound was filtered, washed with petroleum ether and dried *in vacuo*. The purity of the compound was tested by elemental analyses and IR spectral measurements. The FBMT so obtained was used as ligand.

FBMT: m.p. 145°C (d). Found: N, 4.0; S, 9.1; Hg, 56.9%. Calc.: N, 4.0; S, 9.1; Hg, 57.1%.

Preparation of complexes

$[Fe(C_5H_4HgSCN)_2M(NCS)_2L_x]$ *adducts* [M = Co(II), Ni(II), Cu(II) *or* Zn(II); L = 2*morph or en*]. $[Fe(C_5H_4HgSCN)_2]$ (1 mmol) was dissolved in 30 cm^3 of DMSO and the solution was diluted with 100 cm^3 of acetone. To this solution, 1 mmol solution of $M(NCS)_2 \cdot 2L$ in 25 cm^3 acetone was added and stirred for 36 h. Solid compound was formed in each case, which was filtered, washed with acetone and dried *in vacuo*. The complexes were purified by dissolving in DMSO and isolating them by addition of water.

* Author to whom correspondence should be addressed.

$[Fe(C_5H_4HgSCN)_2M(NCS)_2]$: *Lewis acids* (M = Co *or* Ni). The compounds were prepared by heating the morpholine complexes $[Fe(C_5H_4HgSCN)_2 M(NCS)_2(morph)_2]$ *in vacuo* for about 80 h at 60°C. The morpholine was given off leaving behind the compounds of general formula $[Fe(C_5H_4HgSCN)_2M(NCS)_2]$. The compounds were purified by first dissolving in acetone and isolating them by addition of petroleum ether.

$[Fe(C_5H_4HgSCN)_2M(NCS)_2$ (M = Cu *or* Zn). 0.7 g of FBMT was dissolved in 30 cm^3 of DMSO and diluted with 100 cm^3 of ethanol. To this solution a solution of an equimolar quantity of $M(NCS)_2$ in 25 cm^3 of acetone was added and stirred for 36 h. Solid compound was formed in each case, which was filtered, washed with acetone and dried *in vacuo*. The compounds were recrystallized from an acetone–ethanol mixture.

Analyses of the complexes

The complexes were analysed for cobalt as anthranilate, nickel as dimethylglyoximate, sulphur as sulphate and mercury as sulphide, gravimetrically. Nitrogen was estimated by the semimicro Kjeldahl's method. Analytical results are presented in Table 1.

Physical measurements

The molar conductances of the complexes were measured in DMSO using a Philips conductivity bridge model PR-9500. Electronic spectra were recorded as Nujol mulls or in DMSO (solution phase) on a Pye–Unicam SP-5-500 spectrophotometer in the range 250–999 nm. IR spectra were recorded as Nujol mulls or KBr pellets on a Pye–Unicam SP-3-300 spectrophotometer in the range 4000–200 cm^{-1}. The molecular weights were determined by the cryoscopic method using DMSO.

RESULTS AND DISCUSSION

The IR spectra of FBMT were recorded in Nujol and DMSO. The mull spectra show the presence of three bands at 2190, 2120 and 2100 cm^{-1} in the ν(C—N) region, two bands at 730 and 720 cm^{-1} in the ν(C—S) region and two bands at 460 and 410 cm^{-1} in the δ(NCS) region. In solution phase only two bands at 2120 and 2100 cm^{-1} are observed, and the band at 2190 cm^{-1} disappears. This shows that FBMT is a dimer like CH_3HgSCN in the solid phase[4] through bridging as shown in Fig. 1. In the solution phase the bridge is ruptured and it becomes a monomer as shown below.

Lewis acids

On reaction with $M(NCS)_2$ FBMT forms complexes of general formula $[Fe(C_5H_4HgSCN)_2 M(NCS)_2]$. These complexes have been referred to as Lewis acids. The IR spectra indicate that the ν(C—N) stretching band moves from 2120 in FBMT to 2190 cm^{-1} in the Lewis acid. The ν(C—S) and δ(NCS) bands change their positions to 790 and 480 cm^{-1}, respectively. The positions of these bands are indicative of the presence of bridging thiocyanate group.[3] A band is also observed in the region 2070 cm^{-1} which is assigned to *N*-bonded terminal thiocyanate arising from M—NCS.[5] These changes indicate that the thiocyanate of FBMT becomes bridged by coordination through its free *N*-end to the M of $M(NCS)_2$. The electronic spectral data as presented in Table 2 indicate that cobalt is in tetrahedral and the nickel is in octahedral geometry in their Lewis acids. The octahedral geometry in case of the nickel Lewis acid is perhaps acquired by axial coordination of thiocyanate group of other molecule of adjacent layer.[7] Copper perhaps also acquires octahedral geometry through similar axial coordination in its Lewis acid. The IR spectra of the zinc Lewis acid have close similarity with the cobalt Lewis acid. The zinc has also a preference for tetrahedral geometry; hence it can be presumed that the geometry around this metal is also tetrahedral. The molar-conductance data show that they are non-conducting in nature. On the basis of the above results the following structures (Figs 2 and 3) can be proposed

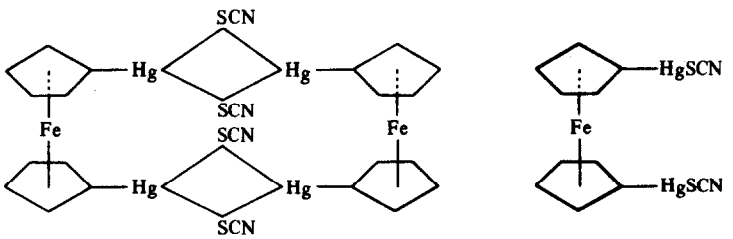


Fig. 1.

Table 1. Analytical data of the complexes

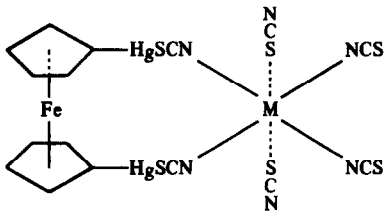
Complex	Colour	D.T.[a] (°C)	% sulphur		% mercury		% metal		% nitrogen		Molar conductance (cm^{-1} mhos mol^{-1}) $M/1024$	Molecular wt	
			Calc.	Obs.	Calc.	Obs.	Calc.	Obs.	Calc.	Obs.		Calc.	Obs.
Lewis acids													
$[Fe(C_5H_4HgSCN)_2Co(NCS)_2]$	Blue	230	14.6	14.2	45.7	43.0	6.6	6.5	6.4	6.3	58.6	—	—
$[Fe(C_5H_4HgSCN)_2Ni(NCS)_2]$	Yellowish green	240	14.6	14.5	45.7	44.9	6.6	6.6	6.4	6.3	70.3	—	—
$[Fe(C_5H_4HgSCN)_2Cu(NCS)_2]$	Light green	150	14.5	14.4	45.4	44.2	7.1	7.2	6.4	6.3	30.6	—	—
$[Fe(C_5H_4HgSCN)_2Zn(NCS)_2]$	Dirty white	178	14.5	14.5	45.3	45.3	7.4	7.2	6.3	6.3	48.4	—	—
Adducts													
$[Fe(C_5H_4HgSCN)_2Co(NCS)_2$2morph]	Dirty green	185	12.2	12.2	38.2	37.4	5.5	5.5	8.0	8.0	63.2	1048	1152
$[Fe(C_5H_4HgSCN)_2Ni(NCS)_2$2morph]	Mustard	213	12.2	12.2	38.2	37.6	5.5	5.4	8.0	7.9	77.4	1048	1140
$[Fe(C_5H_4HgSCN)_2Ni(NCS)_2$en]	Dirty yellow	188	13.7	13.5	42.8	41.8	6.2	6.2	9.0	8.7	71.4	934	890
$[Fe(C_5H_4HgSCN)_2Cu(NCS)_2$2morph]	Greenish yellow	160	12.2	12.1	38.0	37.7	6.0	5.9	8.0	7.7	38.7	1053	978
$[Fe(C_5H_4HgSCN)_2Cu(NCS)_2$en]	Dirty yellow	180	13.6	13.5	42.6	42.1	6.7	6.5	8.9	8.7	48.7	939	—
$[Fe(C_5H_4HgSCN)_2Zn(NCS)_2$2morph]	Pale yellow	155	12.1	12.1	37.9	37.0	6.2	5.9	8.0	7.7	54.0	1055	—
$[Fe(C_5H_4HgSCN)_2Zn(NCS)_2$en]	Pale yellow	145	13.6	13.6	42.5	41.9	6.9	6.7	8.9	8.8	76.5	941	1020

[a] Decomposition temperature.

Table 2. IR and electronic spectral bands with parameters

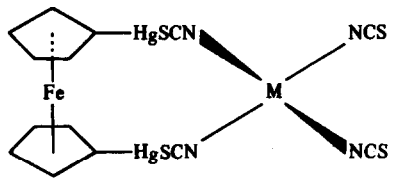
Complexes	IR spectral bands[a]					Electronic spectral bands and parameters					
	ν(C—N) (cm^{-1})	ν(C—S) (cm^{-1})	δ(NCS) (cm^{-1})	ν[M(NCS)] (cm^{-1})	ν(N—H) (cm^{-1})	ν_3 (cm^{-1})	ν_2 (cm^{-1})	ν_1 (cm^{-1})	Dq (cm^{-1})	B' (cm^{-1})	β
Ligand											
$[Fe(C_5H_4HgSCN)_2]$ (solid phase)	2190(w) 2120(s) 2100(s)	730(s) 720(s)	460(s) 410(sh)	—	—	—	—	—	—	—	—
$[Fe(C_5H_4HgSCN)_2]$ (solution phase)	2120(s) 2070(m)	740(s) 720(s)	450(s) 420(m)	—	—	—	—	—	—	—	—
Lewis acids											
$[Fe(C_5H_4HgSCN)_2Co(NCS)_2]$	2190(s) 2120(s)	790(s) 760(w)	480(sh) 460(s)	320(s) 295(s)	—	17,500	10,600	—	541	796	0.77
$[Fe(C_5H_4HgSCN)_2Ni(NCS)_2]$	2170(w) 2100(s)	780(s) 760(s)	470(s) 450(s)	260(s) 240(sh)	—	27,800	16,600	10,400	1020	906	0.87
$[Fe(C_5H_4HgSCN)_2Cu(NCS)_2]$	2180(s) 2100(m)	760(s) 740(s)	480(w) 440(s)	265(s) 245(m)	—	—	—	—	—	—	—
$[Fe(C_5H_4HgSCN)_2Zn(NCS)_2]$	2160(sh) 2100(s)	770(m) 740(s)	470(s) 450(s)	225(s) 280(m)	—	—	—	—	—	—	—
Adducts											
$[Fe(C_5H_4HgSCN)_2Co(NCS)_2$2morph]	2160(s) 2115(s)	730(m) 705(m)	490(s) 440(sh)	285(m) 260(m)	3310	20,200	15,900	8500	842	917	0.94
$[Fe(C_5H_4HgSCN)_2Ni(NCS)_2$2morph]	2160(s) 2140(sh)	770(s) 730(sh)	460(sh) 430(s)	265(m) 250(s)	3305	26,300	16,400	10,500	1033	781	0.76
$[Fe(C_5H_4HgSCN)_2Ni(NCS)_2$en]	2150(s) 2090(sh)	720(m) 700(m)	485(m)	270(s) 245(m)	3445	27,000	16,700	10,440	1043	827	0.80
$[Fe(C_5H_4HgSCN)_2Cu(NCS)_2$2morph]	2175(s) 2090(sh)	770(s) 730(m)	475(s) 420(sh)	255(s) 235(m)	3330	—	—	—	—	—	—
$[Fe(C_5H_4HgSCN)_2Cu(NCS)_2$en]	2185(s) 2090(m)	760(m) 730(m)	475(m)	270(m) 255(s)	3435	—	—	—	—	—	—
$[Fe(C_5H_4HgSCN)_2Zn(NCS)_2$2morph]	2180(s) 2100(sh)	730(sh) 705(s)	440(s) 425(m)	280(s) 265(m)	3400	—	—	—	—	—	—
$[Fe(C_5H_4HgSCN)_2Zn(NCS)_2$en]	2185(s) 2105(s)	720(s)	490(m) 450(m)	290(m) 255(m)	3430	—	—	—	—	—	—

[a] s = strong, sh = shoulder, m = medium, w = weak.



M = Ni(II) or Cu(II)

Fig. 2.



M = Co(II) or Zn(II)

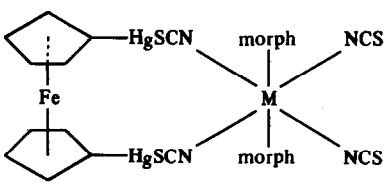
Fig. 3.

for the Lewis acids. Since a single crystal could not be grown the proposed structures are tentative.

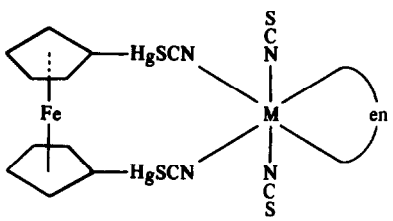
Adducts $[Fe(C_5H_4HgSCN)_2M(NCS)_2L_x$ (L = *morph or en*, x = 1 *or* 2)

FBMT on reaction with $M(NCS)_2L_2$ forms adducts of general formula $[Fe(C_5H_4HgSCN)_2 M(NCS)_2L_x$. The IR spectra of these adducts show that there is no significant change in the positions of ν(C—N), ν(C—S) and δ(NCS) on adduct formation as compared to the Lewis acid. However, a negative shift in the position of ν(M—NCS) is observed when M is cobalt and zinc. This change in ν(M—NCS) is on account of change in geometry of the metal ions from tetrahedral to octahedral. It has earlier been observed that a change in geometry causes a negative shift in the ν(M—NCS) band.[8,9] The geometry around nickel and copper remains the same on adduct formation, hence the changes in the positions of ν(M—NCS) in these cases are insignificant. This shows that the basic structure of the Lewis acid is retained and the change is only in the coordination geometry. The electronic spectral data are presented in Table 2.

The spectral band positions and spectral parameters favour octahedral geometry around cobalt and nickel. Since the infrared spectra of the complexes of zinc and copper have close similarity with cobalt and nickel complexes, it has been presumed that they too have octahedral geometry around M. All the adducts are non-conducting in DMSO solution. On the basis of the above studies the following structures (**IIIa** and **IIIb**) can be proposed for the adducts.



IIIa



IIIb

Acknowledgement—We are grateful to CSIR, New Delhi, for providing financial assistance.

REFERENCES

1. L. Wolf and H. Henning, *Z. Anorg. Chem.* 1965, **341**, 1.
2. E. J. Olszewski and D. F. Martin, *J. Organomet. Chem.* 1966, **5**, 203.
3. P. P. Singh, *Coord. Chem. Rev.* 1980, **32**, 33.
4. R. P. J. Cooney and J. R. Hall, *Aust. J. Chem.* 1969, **22**, 2117.
5. A. Sabitini and I. Bertini, *Inorg. Chem.* 1965, **4**, 1655.
6. Y. Tanabe and S. Sugano, *J. Phys. Soc. Jpn* 1954, **9**, 753.
7. D. Forster and D. M. L. Goodgame, *Inorg. Chem.* 1965, **4**, 715.
8. R. J. H. Clark and C. S. Williams, *Spectrochim. Acta* 1966, **22**, 1081.
9. R. Makhija, L. Pazdernika and R. Rivest, *Can. J. Chem.* 1973, **51**, 2987.

Polyhedron Vol. 5, No. 12, pp. 1947–1952, 1986
Printed in Great Britain

0277–5387/86 $3.00+.00
© 1986 Pergamon Journals Ltd

TERNARY COMPLEXES OF 5′-CYTIDINE MONOPHOSPHATE AND CYTOSINE WITH SOME BIOLOGICALLY IMPORTANT SECONDARY LIGANDS

PULIMAMIDI RABINDRA REDDY* and B. MADHUSUDHAN REDDY

Department of Chemistry, Osmania University, Hyderabad 500007, India

(*Received* 30 *October* 1985; *accepted after revision* 7 *May* 1986)

Abstract—Potentiometric equilibrium measurements have been made at 35°C for the interaction of 5′-cytidine monophosphate and Cu(II), Ni(II), Zn(II), Co(II), Mn(II), Mg(II) and Ca(II) with biologically important secondary ligands (glycine, oxalic acid, histidine and histamine) in a 1:1:1 ratio. Similar studies with cytosine were carried out for comparison. For the above systems, the ternary complexes are found to be more stable than the corresponding binary complexes. The Δ log K values for 1:1:1 complexes of metal–5′-cytidine monophosphate (or cytosine) with aromatic ligands are more positive compared to the corresponding complexes with aliphatic ligands. This is explained in terms of "stacking phenomenon" that occur between the two aromatic moieties of the primary and secondary ligands in solution.

Nucleotides contain a heterocyclic nitrogenase base (either purine or pyrimidine derivative), a pentose sugar and the phosphate moiety. Because of the presence of these three components, which offer a large number of potential binding sites for metal coordination, the study of metal interactions with these molecules becomes very important and interesting from the view point of a bioinorganic chemist. A large number of papers have appeared on metal–nucleotide complexes[1–15] to explore the nature of the bonding. One method of approach is the study of ternary complexes of these molecules especially with biologically important ligands, as these systems mimic many biological reactions.

The ternary complexes of pyrimidine nucleotides are less known compared to purine nucleotides. The solid dimeric and polymeric complexes of uridine 5′-monophosphate[16,17] and cytidine-5′-monophosphate[18–20] (5′-CMP) were reported earlier. However, in solution only the ternary complexes of 5′-CMP with Ni(II) and L-tryptopan were reported.[11] In view of this we have undertaken a detailed investigation of the interaction of 5′-CMP with various divalent metal ions and biologically important ligands (glycine, oxalic acid, histidine and histamine). We have also studied the similar interactions with cytosine, the simplest example of metal–nucleic base interactions, for comparison. These studies we hope will help in the correct assignment of the coordination sites on nucleic acid components in the absence and presence of the phosphate residue, which adds a new dimension to the metal-bonding concept.

*Author to whom correspondence should be addressed.

EXPERIMENTAL

5′-CMP, cytosine, glycine, histidine and histamine were obtained from Sigma Chemical Co. (U.S.A.) and oxalic acid from Fluka (Switzerland). Transition and alkaline earth metal ions were of AnalaR grade and were standardized volumetrically by titration with disodium salt of EDTA in the presence of a suitable indicator as outlined by Schwarzenbach.[21] Carbonate-free sodium hydroxide was prepared by the method of Schwarzenbach and Biedermann.[22]

The experimental conditions and procedures in this work were similar to those described in our earlier publication.[23]

CALCULATIONS AND RESULTS

Dissociation constants

The acid dissociation constants of the 5′-CMP, cytosine, glycine, oxalic acid, histidine and his-

tamine were calculated by the usual algebraic method.

Formation constants

To calculate the stability constants of the ternary complexes of Ni(II), Zn(II) and Co(II) with 5′-CMP and histidine in a 1 : 1 : 1 ratio the following equations were employed [eqns (1)–(12)] (charges are omitted for clarity):

$$M+H_2L+H_2A \rightleftharpoons MLA+4H^+, \quad (1)$$

together with the related equilibria:

$$M+L+A \overset{K^M_{MLA}}{\rightleftharpoons} MLA, \quad (2)$$

$$K^M_{MLA} = \frac{[MLA]}{[M][L][A]}, \quad (3)$$

$$[L] = \frac{\alpha Q}{XQ+YP}, \quad (4)$$

$$[A] = \frac{\alpha P}{XQ+YP}, \quad (5)$$

$$[M] = [A]P \quad \text{or} \quad [L]Q, \quad (6)$$

$$[MLA] = T_M - [M], \quad (7)$$

$$\alpha = (4-m)T_L - [H^+] + [OH^-], \quad (8)$$

$$Q = \frac{[H^+]^2}{K_aK_{2a}} + \frac{[H^+]}{K_{2a}} + 1 \quad (9)$$

$$Y = \frac{4[H^+]^2}{K_aK_{2a}} + \frac{3[H^+]}{K_{2a}} + 2 \quad (10)$$

using K_a and K_{2a} of 5′-CMP,

$$P = \frac{[H^+]^2}{K_aK_{2a}} + \frac{[H^+]}{K_{2a}} + 1 \quad (11)$$

$$X = \frac{4[H^+]^2}{K_aK_{2a}} + \frac{3[H^+]}{K_{2a}} + 2 \quad (12)$$

using K_a and K_{2a} of histidine.

These equations [(1)–(12)] were also employed to calculate the stability constants of the ternary complexes of Ni(II), Zn(II) and Co(II) with 5′-CMP and histamine in a 1 : 1 : 1 ratio.

To calculate the stability constants of the ternary complexes of Cu(II), Ni(II), Zn(II), Co(II), Mn(II), Mg(II) and Ca(II) with 5′-CMP and oxalic acid the following equations were used:

$$M+H_2L+H_2A \rightleftharpoons MHLA+3H^+ \quad (13)$$

together with the related equilibria:

$$M+HL+A \overset{K^M_{M(HL)A}}{\rightleftharpoons} MHLA, \quad (14)$$

$$K^M_{M(HL)A} = \frac{[MHLA]}{[M][HL][A]}. \quad (15)$$

The calculation of the constant $K^M_{M(HL)A}$ was done by the method described in our earlier publication.[24] These equations [(13)–(15)] were also employed to calculate the stability constants of Cu(II), Mg(II), Mn(II) and Ca(II) with 5′-CMP and histidine or histamine in the buffer region between $m = 0$ and $m = 3$.

In order to calculate the stability constants of Cu(II), Ni(II), Zn(II), Co(II), Mn(II), Mg(II) and Ca(II) with 5′-CMP and glycine in a 1 : 1 : 1 ratio the following equations were used:

$$M+H_2L+H_2A \rightleftharpoons M(HL)(HA)+2H^+ \quad (16)$$

together with the related equilibria:

$$M+HL+HA \rightleftharpoons M(HL)(HA), \quad (17)$$

$$K^M_{M(HL)(HA)} = \frac{[M(HL)(HA)]}{[M][HL][HA]}, \quad (18)$$

where HL is the monoanion of 5′-CMP and HA is neutral glycine.

The calculation of the constants $K^M_{M(HL)(HA)}$ was done by the equations given in our previous paper.[24] These equations were also employed to calculate the stability constants of Cu(II), Ni(II) and Co(II) with 5′-CMP and glycine in a 1 : 1 : 1 ratio in the buffer region between $m = 2$ and $m = 4$.

For the ternary metal(II) ion–5′-CMP–oxalic acid complexes in the buffer region between $m = 3$ and $m = 4$ the following equations were used:

$$M(HL)A \rightleftharpoons MLA+H^+, \quad (19)$$

together with the related equilibria:

$$M+L+A \overset{K^{M(HL)A}_{MLA}}{\rightleftharpoons} MLA, \quad (20)$$

$$K^{M(HL)A}_{MLA} = \frac{T_M - [M]}{[M][L]}. \quad (21)$$

$K^{M(HL)A}_{MLA}$ was calculated by the equations given in our earlier paper.[25] These equations [(19)–(21)] were also employed for Zn(II), Mn(II), Mg(II) and Ca(II) with 5′-CMP and glycine in a 1 : 1 : 1 ratio in the buffer region between $m = 2$ and $m = 3$, and also for Cu(II), Mn(II), Mg(II) and Ca(II) with 5′-CMP and histidine or histamine in a 1 : 1 : 1 ratio in the region between $m = 3$ and $m = 4$.

All the above calculations were done by a CASIO PB 100 Personel Computer with suitable programmes.

DISCUSSION

The proton dissociation constants of the ligands 5′-CMP, cytosine, glycine, oxalic acid, histidine and histamine are presented in Table 1.

Table 2 presents the stability constants of ternary

Table 1. Acid dissociation constants of the ligands; temp. 35°C, $\mu = 0.10$ mol dm^{-3} (KNO_3)

Ligand	pK_a	pK_{2a}
5′-CMP	4.40±0.03	6.56±0.03
Cytosine	4.67±0.02	—
Glycine	2.33±0.02	9.75±0.02
Oxalic acid	2.18±0.05	4.20±0.05
Histidine	6.00±0.04	9.00±0.04
Histamine	5.87±0.04	9.63±0.04

complexes of cytosine with glycine, oxalic acid and histamine. Table 3 gives the ternary complexes of 5′-CMP with glycine, oxalic acid, histamine and histidine. Among the ternary complexes of divalent metal ions and cytosine [only Cu(II) constants can be compared] the following order is observed with various secondary ligands: histidine[26] > histamine > glycine > oxalic acid. This is in accordance with the aromaticity and the nature of the donor atoms of these ligands.[25,27–29]

It is important here to mention briefly the various factors that influence the formation of ternary complexes in solution. In ternary systems the interligand interactions have been found to be most effective in deciding the stability of the ternary complexes along with other factors like the nature of the metal ion, the geometry of the metal complex and the solvent effects, etc. However, it should be mentioned here that these interactions (interligand) are highly specific and selective. The effects of charge neutralization, the π-accepting capacity of the secondary ligand and the stacking interactions are usually quantified in terms of $\Delta \log K$. $\Delta \log K$ is the difference between the overall 1 : 1 : 1 ternary complexes

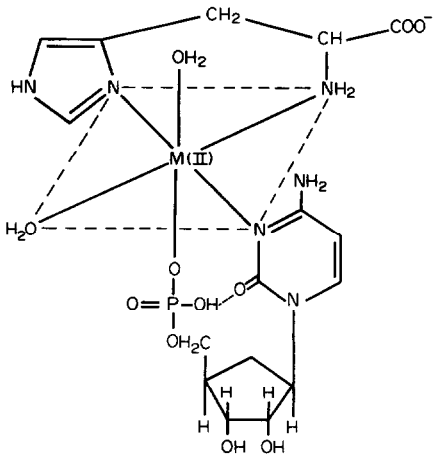


Fig. 1. Tentative structure of M(II) : 5′-CMP : histidine (1 : 1 : 1) illustrating the histamine-like coordination and stacking interaction.

and the corresponding 1 : 1 binary complexes. Since $\Delta \log K$ is derived from two different constants it is also a constant but varies with temperature like any other constant. The $\Delta \log K$ values for the various systems studied are given in Table 4.

It can be seen from the Table 4 that the $\Delta \log K$ values are positive for all the systems. First, let us compare the $\Delta \log K$ values for the systems where interligand interactions are absent (glycine and oxalic acid systems of cytosine). The corresponding values with 5′-CMP could not be computed owing to the formation of different types of complexes in binary and ternary systems. The $\Delta \log K$ values for Cu(II)–cytosine–glycine are more positive than for the Cu(II)–cytosine–oxalic acid complexes; for the rest of the metal ions the data could not be computed. This is due to the involvement of mixed

Table 2. Stability constants[a] of ternary complexes of cytosine (H_2L) with glycine, oxalic acid and histamine (H_2A); temp. 35°C, $\mu = 0.10$ mol dm^{-3} (KNO_3)

Metal ion (II)	Metal : cytosine[b] (1 : 1) log K^{M}_{MHL}	Metal : cytosine : glycine (1 : 1 : 1) log $K^{M}_{M(HL)(HA)}$	log $K^{M(HL)(HA)}_{M(HL)A}$	log $K^{M}_{M(HL)A}$	Metal : cytosine : oxalic acid (1 : 1 : 1) log $K^{M}_{M(HL)A}$	Metal : cytosine : histamine (1 : 1 : 1) log $K^{M}_{M(HL)(HA)}$	log $K^{M(HL)(HA)}_{M(HL)A}$	log $K^{M}_{M(HL)A}$
Cu	2.73	—	—	12.94	10.07	—	—	13.59
Ni	2.23	8.53	5.99	—	9.45	—	—	11.45
Zn	2.31	8.61	5.70	—	9.21	—	—	11.05
Co	2.31	8.53	5.23	—	9.15	—	—	11.13
Mn	—	8.05	4.10	—	9.07	7.63	3.45	—
Mg	1.76	8.29	3.30	—	8.07	6.91	3.06	—
Ca	2.14	8.22	3.40	—	8.49	7.21	3.22	—

[a]Deviations are omitted for clarity.
[b]From Ref. 34.

Table 3. Stability constants[a] of ternary complexes of 5′-CMP (H_2L) with glycine, oxalic acid, histamine and histidine (H_2A); temp. 35°C, μ = 0.10 mol dm^{-3} (KNO_3)

Metal ion (II)	M:5′-CMP[b] (1:1)	M:5′-CMP:glycine (1:1:1)			M:5′-CMP:oxalic acid (1:1:1)		M:5′-CMP:histamine (1:1:1)			M:5′-CMP:histidine (1:1:1)	
	$\log K^{M}_{ML}$	$K^{M}_{(HL)(HA)}$	$K^{M(HL)(HA)}_{ML(HA)}$	$K^{M(HL)(HA)}_{MLA}$	$K^{M}_{M(HL)A}$	$K^{M(HL)A}_{MLA}$	$K^{M}_{ML(HA)}$	$K^{ML(HA)}_{MLA}$	K^{M}_{MLA}	$K^{M}_{ML(HA)}$	$K^{M(HL)}_{MLA}$	K^{M}_{MLA}
Cu	3.22	6.67	—	11.93	7.78	4.11	10.62	6.45	—	9.76	6.72	—
Ni	3.01	6.17	—	9.25	7.09	3.81	—	—	15.12	—	—	16.37
Zn	2.91	5.80	2.69	—	6.80	2.96	—	—	13.98	—	—	14.05
Co	2.83	6.12	—	8.49	7.10	3.70	—	—	14.08	—	—	14.27
Mn	2.77	5.64	2.65	—	6.61	3.66	6.49	3.84	—	6.00	3.14	—
Mg	2.82	5.86	1.40	—	6.36	2.72	5.31	2.36	—	5.27	2.87	—
Ca	2.39	5.87	2.62	—	6.40	—	5.57	2.63	—	5.43	3.02	—

[a]Deviations are omitted for clarity.
[b]From Ref. 35.

donor atoms in metal coordination in the case of glycine system (enhancement of stability on coordination with mixed N/O atoms compared to pure O/O and N/N atoms). Similar results were also reported for other related systems.[24,28,30] This is further supported by electrostatic molecular potential calculations.[31] In the case of systems where interligand interactions are expected (histidine and histamine systems of cytosine and 5′-CMP), the Δ log K values of histidine are less positive than the corresponding values of histamine for all the metal ions with cytosine as well as 5′-CMP. This trend is exactly the reverse of that observed in their respective binary complexes. In 1:1 complexes histidine forms more stable complexes than histamine as it is known to behave as a terdentate ligand. However, in ternary complexes the data suggest that histidine is acting as a bidentate ligand. Then the interesting question that arises is which is the donor group that is not involved in metal binding in ternary system. It is likely that the histidine may act in a histamine-like manner involving amino and imidazole groups for metal-bonding and hydrogen-bond type of interaction between the histidine C(=O)—O and the —NH_2 of 5′-CMP takes place. As a result the C(=O)—O group is kept away from the metal. Although we do not have definite evidence for this, similar observations were made earlier in the case of metal–ATP–histidine[32] and metal–cytidine–histidine complexes.[25] Such an interaction is known to disfavour the formation of ternary complexes in solution by an entropy factor as the ligands become more rigid as a consequence of a bridge between two non-coordinating groups (amino and carboxylate groups), and also due to the different degrees of solvent interaction with the metal ion. This may be the reason for the less positive values of Δ log K in histidine complexes compared to the histamine in both cytosine and 5′-CMP systems.

It is of interest and important here to compare the Δ log K values of cytosine and 5′-CMP systems (histidine and histamine) with that of cytidine.[25] The Δ log K values of 5′-CMP are more positive, followed by cytidine and cytosine. Higher values in the case of the 5′-CMP system are due to the presence of the phosphate moiety, which is the strongest donor group. The more positive values of cytidine compared to cytosine may be due to the presence of an additional donor atom in the latter which may exert an influence on the donor atom which is being chelated and this accounts for its lower stability. The magnitudes of Δ log K values of all the systems indicate that the stacking interaction, which is

Table 4. Δ log K values for various metal–ligand systems in solution; temp. = 35°C, μ = 0.10 mol dm^{-3} (KNO_3)

Metal ion (II)	M : cytosine : glycine (1 : 1 : 1)	M : cytosine : oxalic acid (1 : 1 : 1)	M : cytosine : histamine (1 : 1 : 1)	M : cytosine : histamine[a] (1 : 1 : 1)	M : 5′-CMP : histidine (1 : 1 : 1)	M : 5′-CMP : histamine (1 : 1 : 1)
Cu	+1.60	+1.18	+1.88	+0.51	—	—
Ni	—	+1.99	+2.86	+1.16	+4.94	+5.75
Zn	—	+1.59	+2.63	+1.26	+4.79	+4.96
Co	—	+1.87	+2.84	+1.45	+4.44	+5.27
Mn	—	+1.74	+2.42	—	—	—
Mg	—	+1.66	+2.71	+0.01	—	—
Ca	—	+1.50	+2.75	+0.01	—	—

[a]From Ref. 26.

expected to occur between the pyrimidine ring of the primary ligand and imidazole ring of the secondary ligands, is most effective for accounting the extra stability found in ternary systems.

Based on the above conclusions we propose Fig. 1 as the structure for metal–5′-CMP–histidine. This structure allows: (i) minimum steric hindrance between two ligands, and (ii) there is a hydrogen-type bonding between the OH of phosphate and the C(2)—O of the imidazole ring. The stacking is possible as both the ligands are only two bond distances apart. Though many studies in solution favoured the phosphate group rather than the purine or pyrimidine base as the primary metal-binding site, the simultaneous binding of a metal ion to base and phosphate was reported for the modified mononucleotides of transfer RNA.[33] Consequently, we have also involved N(3) along with phosphate oxygen in metal bonding as it allows the required stacking interaction.

Acknowledgement—Financial support from CSIR, New Delhi, is gratefully acknowledged.

REFERENCES

1. M. M. T. Khan and P. R. Reddy, *J. Inorg. Nucl. Chem.* 1973, **35**, 2813.
2. M. M. T. Khan and P. R. Reddy, *J. Inorg. Nucl. Chem.* 1973, **35**, 2821.
3. M. M. T. Khan and P. R. Reddy, *J. Inorg. Nucl. Chem.* 1975, **37**, 771.
4. M. M. T. Khan and P. R. Reddy, *J. Inorg. Nucl. Chem.* 1976, **38**, 1234.
5. W. Wallas, *Acta Chem. Scand.* 1958, **12**, 528.
6. L. G. Marzilli, T. J. Kistenmacher and G. L. Eichhorn, In *Metal Ions in Biology* (Edited by T. G. Spiro), Chap. 5 (and references therein). John Wiley, New York (1980).
7. P. R. Reddy, K. V. Reddy and M. M. T. Khan, *Indian J. Chem.* 1983, **22A**, 959.
8. R. W. Gillert and R. Bau, In *Metal Ions in Biological Systems* (Edited by H. Sigel), Chap. 1, p. 8. Marcel Dekker, New York (1979).
9. R. B. Martin and Y. H. Mariam, In *Metal Ions in Biological Systems* (Edited by H. Sigel), Chap. 2, p. 8. Marcel Dekker, New York (1979).
10. W. D. Wilson, B. L. Heyl, P. R. Reddy and L. G. Marzilli, *Inorg. Chem.* 1982, **21**, 2527.
11. J. B. Orenberg, B. E. Fischer and H. Sigel, *J. Inorg. Nucl. Chem.* 1980, **42**, 785.
12. K. H. Scheller, F. Hofstetter, P. R. Mitchell, B. Prijs and H. Sigel, *J. Am. Chem. Soc.* 1981, **103**, 247.
13. M. M. T. Khan and A. E. Martell, *J. Am. Chem. Soc.* 1966, **88**, 668.
14. M. M. T. Khan and P. R. Reddy, *J. Inorg. Nucl. Chem.* 1972, **34**, 967.
15. H. Sigel and P. Chandri, *J. Am. Chem. Soc.* 1977, **99**, 3142.
16. B. E. Fischer and R. Bau, *Inorg. Chem.* 1978, **17**, 27; *J. Chem. Soc., Chem. Commun.* 1977, 272.
17. B. A. Cartwright, D. M. L. Goodgame, I. Jeeves and A. C. Skapski, *Biochim. Biophys. Acta* 1977, **195**, 477.
18. S. Lovie and R. Bau, *J. Am. Chem. Soc.* 1977, **99**, 3874.
19. G. R. Clark and J. D. Orbell, *J. Chem. Soc., Chem. Commun.* 1975, 697; *Acta Cryst.* 1978, **B34**, 1815.
20. K. Aoki, *Biochim. Biophys. Acta* 1976, **447**, 379.
21. G. Schwarzenbach, *Complexometric Titrations*, p. 77. Interscience, New York (1977).
22. G. Schwarzenbach and R. Biedermann, *Helv. Chim. Acta* 1948, **31**, 311.
23. P. R. Reddy, K. Venugopal Reddy and M. M. T. Khan, *J. Inorg. Nucl. Chem.* 1976, **38**, 1923.
24. P. R. Reddy, K. Venugopal Reddy and M. M. T. Khan, *J. Inorg. Nucl. Chem.* 1979, **41**, 423.
25. P. R. Reddy and V. B. M. Rao, *Polyhedron* 1985, **4**, 1603.
26. M. M. T. Khan and S. Satyanarayana, *Indian J. Chem.* 1983, **22A**, 584.
27. P. R. Reddy, M. H. Reddy and K. V. Reddy, *Inorg. Chem.* 1984, **23**, 974.
28. P. R. Reddy and M. H. Reddy, *Polyhedron* 1983, **2**, 1171.

29. P. R. Reddy and M. H. Reddy, *J. Chem. Soc., Dalton Trans.* 1985, 239.
30. G. Ostacoli, In *Bioenergetics and Thermodynamics. Model Systems* (Edited by A. Braibanti), p. 181. D. Reidel, Dordrecht (1980).
31. R. Bonaccorsi, A. Pullman, E. Scrocco and J. Tomasi, *Theor. Chim. Acta* 1972, **24**, 51.
32. G. Arena, R. Coll, V. Cucinolta, S. Musumeci, E. Rizzarelli and S. Sammaratano, *J. Chem. Soc., Dalton Trans.* 1984, 1651.
33. P. R. Reddy, W. D. Hamill, Jr, G. B. Chheda and M. P. Schweizer, *Biochemistry* 1981, **20**, 4979.
34. M. M. T. Khan and M. S. Jyothi, *Indian J. Chem.* 1977, **15A**, 1002.
35. P. R. Reddy and B. M. Reddy, *Proc. Nat. Acad. Sci.* 1985, **8**, 7.

Polyhedron Vol. 5, No. 12, pp. 1953–1956, 1986
Printed in Great Britain

0277–5387/86 $3.00+.00
Pergamon Journals Ltd

VIBRATIONAL SPECTRUM OF $[(CD_3)_3S]I$ AND NORMAL COORDINATE CALCULATIONS FOR $[(CH_3)_3S]^+$ AND $[(CD_3)_3S]^+$ CATIONS

KOYO AIDA, SHIN KUSAKA, TAKASHI UEDA,* HISASHI SHIBUYA† and YOSHIKA IMAI‡

Department of Engineering Science, Faculty of Engineering,
Tohoku University, Sendai 980, Japan

(*Received* 6 *January* 1986; *accepted* 7 *May* 1986)

Abstract—IR (4000–30 cm^{-1}) and Raman (4000–0 cm^{-1}) spectra of $[(CD_3)_3S]I$ have been observed, together with those of $[(CH_3)_3S]I$. By assuming a C_{3v} molecular symmetry for the cations $[(CH_3)_3S]^+$ and $[(CD_3)_3S]^+$, all the active fundamentals of $[(CD_3)_3S]^+$ have been assigned and normal coordinate calculations have been carried out by a symmetry force field for $[(CH_3)_3S]^+$ and $[(CD_3)_3S]^+$. The strength of the S—C and C—H bonds in the compound has been compared with that in dimethyl sulfide by using their valence stretching force constants.

During the course of a vibrational spectroscopic study on dimethyl sulfide–boron trihalide adducts,[1] we were interested in the extent to which the bond strength of the ligand is influenced by adduct formation. It is of interest to investigate such influence encountered in other dimethyl sulfide adducts. Dimethyl sulfide reacts with some alkyl halides to form sulfonium compounds. The sulfonium compound contains a sulfonium ion which can be regarded as an adduct between a carbonium ion and dimethyl sulfide. Therefore, the study has now been extended to trimethylsulfonium iodide which is one of the simplest sulfonium compounds.

Although the vibrational spectra of trimethylsulfonium halide have been observed by Creighton *et al.*,[2] no vibrational spectra of the deuterated compounds have been reported. They also carried out the normal coordinate calculations, without the data of the isotopic compounds. However, in order to obtain more reliable force constants, the calculations should be made including the data of isotopic molecules. In this paper we report the vibrational spectra of $[(CD_3)_3S]^+$ and the normal coordinate calculations for $[(CH_3)_3S]^+$ and $[(CD_3)_3S]^+$. Since the trimethylsulfonium iodide is easily prepared and the spectra of sulfonium compounds do not depend on an anion, with a few exceptions, no study has been made on other trimethylsulfonium compounds in this work.

EXPERIMENTAL

Trimethylsulfonium iodide was prepared by the reaction of dimethyl sulfide with methyl iodide in a sealed glass tube at room temperature. The white solid was deposited after a day. The crude compound was recrystallized from ethanol and dried over P_4O_{10} *in vacuo*: m.p. 209.5–212°C (lit.[2] 211–212.5°C). The deuterated compound was prepared in the same manner using $(CD_3)_2S$ and CD_3I: m.p. 209–211°C.

IR (4000–400 cm^{-1}) and far-IR (400–30 cm^{-1}) spectra were recorded on Hitachi 345 and Hitachi FIS-III spectrophotometers, respectively. The spectra were observed in Nujol and hexachlorobutadiene mulls.

Raman spectra (4000–0 cm^{-1}) were recorded in the solid state on a JEOL-JRS-S1 spectrophotometer equipped with an He–Ne laser. The spectra were also measured in aqueous solutions in order to obtain qualitative polarizations.

*Present address: Supply Product Division, Ricoh Company Ltd, Numazu, Shizuoka 410, Japan.

†Present address: General Sekiyu K. K. Sakai Refinery, Sakai, Osaka 592, Japan.

‡Author to whom correspondence should be addressed.

RESULTS AND DISCUSSION

The crystal structure for the compound was examined by an X-ray diffraction method.[3] Though the study had revealed that the SC_3 skeleton has a C_{3v} symmetry, no information about the configuration of the methyl groups was obtained owing to the low X-ray scattering power of a hydrogen atom. We assumed that each methyl group is staggered to the neighbouring C—S bonds for the free sulfonium ion. Therefore its overall symmetry is also C_{3v}. Under this symmetry, 33 normal vibrations divide into $7a_1+4a_2+11e$. The a_1 and e modes are active in both the IR and Raman spectra and the a_2 modes inactive in both.

No discussion about the vibrational spectra and the assignments for the light compound seems to be necessary, since they were almost the same as those reported by Creighton *et al.*[2]

Table 1 shows the observed IR and Raman frequencies and their assignments for $[(CD_3)_3S]^+$. The assignments of the fundamentals were made by taking into consideration those of $(CD_3)_2S$[4] and $(CD_3)_3P$.[5] Trimethylphosphine is isoelectronic with the trimethylsulfonium ion. But there is also no need to discuss them except for the modes which are observed below 400 cm^{-1}.

Three modes (a_1 and e SC_3 deformations and an e methyl torsion) are expected to be observed below 400 cm^{-1}. We have observed three Raman bands at 269, 243 and 153 cm^{-1} in the solution spectrum. Though the correct polarization measurement for the band at 269 cm^{-1} is difficult owing to the overlap of the band at 243 cm^{-1}, the 269-cm^{-1} band

Table 1. Observed vibrational frequencies (cm^{-1}) for $[(CD_3)_3S]I$

IR	Raman		
solid	solid	soln	Proposed assignment
3267 w			2251+1030 = 3281
3241 w			2251+997 = 3248
3074 vw			2251+825 = 3076
2251 s	2251 m	2270 m	CD_3 asym. str. (ν_1, ν_{12}, ν_{13})
2241 w	2242 m		
2113 w	2116 s	2138 s,p	CD_3 sym. str. (ν_2, ν_{14})
1966 w			990×2 = 1980
1816 vw			997+825 = 1822
1741 vw			1037+710 = 1747
1704 w			997+710 = 1707 1037+669 = 1706
1663 w			847+825 = 1672
1347 vw			669×2 = 1338
1269 w			997+273 = 1270 1037+234 = 1275
1037 s	1036 w	1034 m	CD_3 asym. def. (ν_3, ν_{15}, ν_{16})
1030 m	1021 m		
997 w	996 vw		CD_3 sym. def. (ν_4, ν_{17})
990 w			
847 m	840 sh	846 m,p	CD_3 rock (ν_5)
825 s	832 m	834 m	CD_3 rock (ν_{18})
710 m	715 m	715 w	CD_3 rock (ν_{19})
669 m	675 vs	685 s,dp	CS_3 str. (ν_{20})
593 m	601 vs	608 vs,p	CS_3 str. (ν_6)
273 w	271 m	269 sh,p(?)	CSC def. (ν_7)
238 w	243 s	243 s	CSC def. (ν_{21})
195 w	185 w	153 vw	CD_3 torsion (ν_{22})
91 s			lattice mode
79 s			lattice mode
64 s			lattice mode

w = weak, s = strong, vw = very weak, vs = very strong, m = medium, sh = shoulder, p = polarized, dp = depolarized, asym. = asymmetric, sym. = symmetric, str. = stretch, def. = deformation.

seems to be polarized. Therefore, we assigned the band to the a_1 SC_3 deformation (ν_7). Thus the 243- and 153-cm^{-1} bands should be due to the e modes. Considering their intensity and the assignments for the light compound, we assigned the 243-cm^{-1} band to the e SC_3 deformation (ν_{21}) and the 153-cm^{-1} to the e torsion (ν_{22}). For $[(CH_3)_3S]I$ the former mode was observed at 284 cm^{-1} and the latter at 209 cm^{-1} in the solution Raman spectrum. The ratio 209/153 is 1.37 which is close to that expected for the methyl torsion, while 284/243 is 1.17 which is too small for the torsion.

The normal coordinate calculations were performed for the a_1 and e modes using programs designed by Watari.[6] Molecular parameters used here were based on the X-ray data,[3] except for those of methyl group which were assumed: r(C—S) = 1.83 Å, r(C—H) = 1.093 Å, $\angle CSC = 103°$, $\angle SCH = \angle HCH = 109°28'$. The least-squares refinements were carried out in terms of the symmetry force constants, which were fitted to the observed fundamental frequencies, for the two isotropic molecules, simultaneously. The observed frequencies used in the calculation were obtained from the Raman spectra for the aqueous solution except for ν_{18} for $[(CH_3)_3S]^+$ and ν_4 and ν_{17} for $[(CD_3)_3S]^+$. ν_{18} for $[(CH_3)_3S]^+$ was obtained from the IR spectrum and ν_4 and ν_{17} from the Raman spectrum in the solid.

Table 2. Description of the symmetry coordinates for trimethylsulfonium ion

Vibrational mode	Coordinate		
	A_1	A_2	E
CH_3 or CD_3 asym. str.	S_1	S_8	S_{12}, S_{13}
CH_3 or CD_3 sym. str.	S_2		S_{14}
CH_3 or CD_3 asym. def.	S_3	S_9	S_{15}, S_{16}
CH_3 or CD_3 sym. def.	S_4		S_{17}
CH_3 or CD_3 rocking	S_5	S_{10}	S_{18}, S_{19}
SC_3 str.	S_6		S_{20}
SC_3 def.	S_7		S_{21}
CH_3 or CD_3 torsion		S_{11}	S_{22}

Table 2 shows the description of the symmetry coordinate which needs in order to describe the potential energy distributions. Table 3 shows the observed and calculated frequencies and potential energy distributions for $[(CH_3)_3S]^+$ and $[(CD_3)_3S]^+$. The average errors between the observed and calculated frequencies are 0.70 and 0.54% for a_1 and e modes, respectively. The proposed assignments for $[(CH_3)_3S]^+$ and $[(CD_3)_3S]^+$ are supported by the potential energy distribution shown in Table 3. Table 4 shows symmetry force constants from the last cycle in the least-squares refinement, together with their statistical errors.

Table 3. Observed and calculated frequencies (cm^{-1}) and potential energy distributions for the cations $[(CH_3)_3S]^+$ and $[(CD_3)_3S]^+$

No.	$[(CH_3)_3S]^+$			$[(CD_3)_3S]^+$		
	Obs.[a]	Calc.	PED[b]	Obs.[a]	Calc.	PED[b]
ν_1	3022	3029	$100S_1$	2270	2260	$98S_1$
ν_2	2932	2933	$99S_2$	2138	2136	$96S_2$
ν_3	1421	1427	$87S_3$ $12S_5$	1034	1024	$92S_3$
ν_4	1318	1320	$87S_4$ $11S_2$	996	994	$79S_4$ $13S_2$
ν_5	1050	1059	$84S_5$ $12S_3$	846	832	$81S_5$
ν_6	655	659	$94S_6$	608	603	$89S_6$
ν_7	312	309	$93S_7$	269	274	$91S_7$
ν_{12}	3022	3031	$88S_{12}$ $12S_{13}$	2270	2257	$75S_{12}$ $24S_{13}$
ν_{13}	3022	3029	$88S_{13}$ $12S_{12}$	2270	2261	$75S_{13}$ $24S_{12}$
ν_{14}	2932	2933	$99S_{14}$	2138	2136	$96S_{14}$
ν_{15}	1421	1426	$93S_{15}$	1034	1027	$92S_{15}$
ν_{16}	1421	1428	$87S_{16}$ $13S_{18}$	1034	1024	$88S_{16}$
ν_{17}	1318	1321	$88S_{17}$ $10S_{14}$	996	992	$78S_{17}$ $13S_{14}$
ν_{18}	1060	1060	$84S_{18}$ $12S_{16}$	834	835	$73S_{18}$ $15S_{20}$
ν_{19}	942	944	$93S_{19}$	715	714	$80S_{19}$ $11S_{20}$
ν_{20}	734	740	$94S_{20}$	685	675	$68S_{20}$ $17S_{19}$ $14S_{18}$
ν_{21}	284	281	$95S_{21}$	243	246	$93S_{21}$
ν_{22}	209	211	$98S_{22}$	153	151	$99S_{22}$

[a] See the test.

[b] Values less than 10% in magnitude are omitted.

Table 4. Symmetry force constants and their statistical errors[a]

	Constant	$F(\sigma)$		Constant	$F(\sigma)$
$F_{1,1}$	4.877	0.030	$F_{12,12}$	4.885	0.031
$F_{2,2}$	4.757	0.157	$F_{13,13}$	4.876	0.031
$F_{3,3}$	0.505	0.008	$F_{14,14}$	4.764	0.128
$F_{4,4}$	0.599	0.047	$F_{15,15}$	0.514	0.006
$F_{5,5}$	0.752	0.016	$F_{16,16}$	0.504	0.006
$F_{6,6}$	3.031	0.087	$F_{17,17}$	0.602	0.038
$F_{7,7}$	1.275	0.078	$F_{18,18}$	0.767	0.012
$F_{2,4}$	−0.421	0.182	$F_{19,19}$	0.621	0.013
$F_{4,6}$	−0.330	0.096	$F_{20,20}$	3.134	0.074
			$F_{21,21}$	0.955	0.051
			$F_{22,22}$	0.081	0.007
			$F_{14,17}$	−0.414	0.149
			$F_{17,20}$	−0.365	0.073

[a]The stretching force constants are given in N cm^{-1}, the deformation force constants in 10^{-16} N cm rad^{-2}, and the stretching–deformation interaction constants in 10^{-8} rad^{-1}. The subscript number i in $F_{i,i}$ (diagonal element) corresponds with that in S_i in Table 2. $F(\sigma)$ means the statistical error.

The S—C and C—H valence stretching force constants were 3.1 ± 0.06 and 4.8 ± 0.035 N cm^{-1}, respectively. These were calculated from the symmetry force constants in Table 4. The S—C force constant is slightly smaller than that of dimethyl sulfide reported by Levin and Pearce;[7] 3.4 ± 0.08 N cm^{-1}, while the C—H force constant is slightly larger than 4.7 ± 0.05 N cm^{-1} [7] in dimethyl sulfide. Though many investigators reported the force constants of dimethyl sulfide, it seems to be reasonable to be compared with Levin–Pearce's force constants, because the force constants were calculated by using a valence force field and their statistical errors were also reported. These force constants show that upon adduct formation the S—C bond of dimethyl sulfide is weakened but the C—H bond strengthened, indicating that adduct formation influences the C—H bonds as well as the C—S bonds. For the C—S bonds, this is consistent with what might be expected from their bond distances; 1.83 Å in trimethylsulfonium iodide,[3] 1.802 Å in dimethyl sulfide.[8]

Acknowledgements—This work was partly supported by a grant from the Tohoku Industrial Association to which our thanks are due. One of the authors (Y.I.) thanks Associated Prof. M. Tanaka for his kind help in making the computer programs accessible from a TSS (time sharing system) terminal, and for permitting the use of the terminal.

REFERENCES

1. Unpublished work.
2. J. A. Creighton, J. H. S. Green, D. J. Harrison and S. M. Waller, *Spectrochim. Acta* 1967, **23A**, 2973.
3. D. E. Zuccaro and J. D. McCullough, *Z. Krist.* 1959, **112**, 401.
4. J. P. Perchard, M. T. Forel and M. L. Josien, *J. Chim. Phys.* 1964, **61**, 645.
5. H. Rojhantalab, J. W. Nibler and C. J. Wilkins, *Spectrochim. Acta* 1976, **32A**, 519.
6. F. Watari, *J. Phys. Chem.* 1980, **84**, 448.
7. I. W. Levin and R. A. R. Pearce, In *Vibrational Spectra and Structure* (Edited by J. R. Durig), Vol. 4, p. 101. Elsevier, Amsterdam (1975).
8. L. Pierce and M. Hayashi, *J. Chem. Phys.* 1961, **35**, 479.

Polyhedron Vol. 5, No. 12, pp. 1957–1963, 1986
Printed in Great Britain

0277–5387/86 $3.00+.00
Pergamon Journals Ltd

SPECTROSCOPIC *CIS*-INFLUENCES IN OCTAHEDRAL TIN(IV) *MESO*-TETRAPHENYLPORPHYRIN COMPLEXES

DENNIS P. ARNOLD

Chemistry Department, Queensland Institute of Technology, G.P.O. Box 2434, Brisbane 4001, Australia

(*Received* 6 *January* 1986; *accepted* 7 *May* 1986)

Abstract—Visible absorption and ^{1}H NMR spectra have been measured for a series of octahedral tin(IV) porphyrin complexes Sn(TPP)X_2, where TPP is *meso*-tetraphenylporphyrin and X is Cl, OH, OMe, OAc, NO_3, ClO_4, Br, I, NCS and OC_6H_4-*p*-Me. The tin–proton coupling constants to the β-pyrrole protons decrease from 19.2 Hz (X = ClO_4) to 9.9 Hz (X = OMe), and for the oxygen-bound ligands, correlate well with the basicity of the ligands. The halides do not fit this relationship, perhaps because of π-bonding effects. The chemical shifts of the β-protons also depend on the nature of X, and vary from 9.35 (X = ClO_4) to 9.04 (X = OC_6H_4-*p*-Me) ppm. Increasing basicity of X causes red shifts in the visible spectra, as well as a decrease in the molar absorption coefficient ratio ($\varepsilon_\beta/\varepsilon_\alpha$) for the visible absorption bands. Tin–proton coupling constants for the axial ligands OH, OMe and OAc are reported. The complex Sn(TPP)$(ClO_4)_2$ exhibits unusual NMR behaviour in $CDCl_3$ solutions, possibly due to self-aggregation.

NMR spectra of diamagnetic metalloporphyrins containing spin-$\frac{1}{2}$ magnetically active metal ions have been exploited to a limited extent in structural and reactivity studies. Various data for thallium(III),[1–3] mercury(II),[3] phosphorus(V),[4] platinum(II)[5–7] and tin(IV)[8–11] complexes of octaethylporphyrin (OEP) and tetraphenylporphyrin (TPP) have been published, including some metal–^{1}H and metal–^{13}C coupling constants. Some data have also been forthcoming on the NMR properties of proton-bearing axial ligands in tin(IV) complexes,[8–11] including interesting long-range couplings between axial OH protons and ^{13}C nuclei on the porphyrin periphery.[8] Studies of five-coordinate indium(III) porphyrins have revealed correlations between the donor strengths of axial ligands and electro- and spectrochemical properties,[12] although the absence of a spin-$\frac{1}{2}$ isotope necessarily restricted the NMR data to chemical shifts.

The present study was undertaken to evaluate the utility of coupling constants involving ^{117}Sn and ^{119}Sn in studies of the chemistry of these metalloporphyrins, in particular with respect to the reactions of axial ligands. In this paper, the syntheses, visible absorption and ^{1}H NMR spectra of a series of octahedral Sn(IV) TPP complexes (Fig. 1) are reported, and correlations between spectroscopic properties and the nature of the axial ligands are discussed.

RESULTS AND DISCUSSION

IR spectra

Complexes containing IR-active axial ligands exhibited the expected bands in solid-state spectra (Table 1). The hydroxo ligands in **2** were identified by a weak, sharp doublet at 3590 and 3610 cm^{-1}.[8] The low frequency of the ν(CN) band in the spectrum of **9** suggests that the thiocyanate ligands are N-bound.[13] NMR data support this conclusion (see below).

The situation with the O-bound ligands in complexes **3**, **5** and **6** is less clear. It appears that, especially for **3**, both unidentate and bidentate ligands are present in the solid state. In Zr(OEP)$(OAc)_2$, bands at 1560, 1460 and 690 cm^{-1} were assigned to chelating acetates, while in Sn(OEP)$(OAc)_2$, bands at 1640 and 1380 cm^{-1} indicated unidentate ligands.[14] Intermediate coordination has been found crystallographically for In(OEP)(OAc) which absorbs at 1570 and 1405 cm^{-1}.[15]

Table 1. Visible absorption and selected IR data for $Sn(TPP)X_2$ complexes

Axial ligand	IR data for axial ligands	Visible absorption data: λ_{max} nm ($\varepsilon \times 10^{-3}$)				
		B(0,0) (Soret)	*Q*(2,0)	*Q*(1,0)(β)	*Q*(0,0)(α)	$\varepsilon_\beta/\varepsilon_\alpha$
ClO_4[a]	1135, 1095, 1030 s, br, 920 m, 618 m	424 (520)	513 (3.1)	552 (20.3)	591 (8.5)	2.39
NO_3[b]	1515 s, 1380 s, br, 1275 s, br, 958 s, br	423 (606)	514 (3.3)	553 (22.7)	593 (8.4)	2.70
OAc[b]	1660 s, 1560 m, br, 1465 m, 1275 s, br	425 (555)	518 (3.1)	557 (19.9)	596 (8.5)	2.34
NCS[a]	1998 vs, 845 w	425 (598)	519 (3.6)	559 (19.4)	598 (11.2)	1.73
OMe		427 (30.1)[c]	520 (0.17)[c]	559 (1.00)[c]	598 (0.60)[c]	1.67
OH[a]	3610 vw, 3590 vw	426 (636)	521 (3.6)	560 (21.7)	600 (13.2)	1.64
Cl		427 (691)	520 (3.9)	561 (21.0)	600 (13.1)	1.60
OC_6H_4Me[a]	1252 s, br	425 (575)	522 (3.7)	561 (19.0)	601 (10.4)	1.82
Br		429 (617)	525 (3.5)	565 (19.8)	605 (14.6)	1.36
I[d]		428 (13.5)[c]	530 (0.24)[c]	568 (1.00)[c]	614 (0.8)[c]	1.25

[a]IR in Nujol mull.
[b]IR in KBr disc.
[c]ε given relative to *Q*(1,0) band.
[d]All bands broad, shoulders at *ca* 434 and 604 nm.

Complex **3** shows bands for both types (Table 2), while the NMR spectrum of a solution of the same material showed only single Sn-porphyrin and acetate methyl signals. The situation for the dinitrato analogue (**5**) is similarly ambiguous from the IR spectrum.[13] A poorly resolved envelope of bands from 1135 to 960 cm^{-1} for **6** is consistent with O-bound perchlorate ligands.[13–16]

Visible absorption spectra

The spectra (Table 1) of all the complexes except (**8**) are typical of Sn(IV) porphyrins, and exhibit the "normal" type of metalloporphyrin spectrum.[17] The compounds are displayed in Table 1 in order of increasing red shift of the α band. The other bands show a similar trend, although shifts for the

Table 2. Selected ^1H chemical shifts[a] and Sn–H coupling constants (Hz) for $Sn(TPP)X_2$ complexes

Axial ligand	Pyrrole β-H resonance		Axial ligand resonances	
	δ	^4J(Sn–H)[b]	δ	*J*(Sn–H)
ClO_4	9.35	19.2		
NO_3	9.28	17.5		
NCS	9.24	16.0		
Cl	9.18 (9.20)[c]	15.2 (15.5)[c]		
Br	9.18	15.2		
OAc	9.14	14.5	−0.96	3.6 (^4J)[b]
I	9.13	13.7		
OC_6H_4Me	9.04	12.0	1.68 (*p*-Me) 1.72 (2′, 6′), 5.42 (3′, 5′)[d]	Not observed
OH	9.14 (9.12)[c]	10.4 (9.5)[c]	−7.55 br (−7.46)[c]	*ca* 36 (^2J)[b] (37)[c]
OMe	9.08	9.9	−2.04	70.3 [$^3J(^{119}Sn–H)$] 67.1 [$^3J(^{117}Sn–H)$]

[a]In ppm relative to $CHCl_3$ at 7.24. Protons of the *meso*-phenyl groups appeared in all complexes as two multiplets centred at *ca* 8.3 (ortho) and 7.8 (meta, para).
[b]Separate couplings to ^{119}Sn and ^{117}Sn not resolved, average value given.
[c]Literature values.[8]
[d]AA′XX′; doublet separation 8.1 Hz.

Soret band are very small. Gouterman *et al.*[18] studied a smaller series of Sn(etioporphyrin-I)X_2 complexes (X = F, OCOPh, OH, Cl, Br, I) and found a similar red shift of the α band. The complex (**8**) is somewhat unstable in $CHCl_3$ solution, but it is clear that it exhibits an unusual spectrum, in that the bands are all broadened and have reduced ε_{max} compared with the other compounds. Both the instability and the spectral differences were noted for Sn(Etio-I)I_2, and to a lesser extent for Sn(Etio-I)Br_2.[18] The red shift for **8** is such that the solid appears almost black and thin films of the solution are greenish, while all the others appear red, purple or violet.

The second parameter which changes significantly over the series is the ratio of the molar absorption coefficients for the β and α bands ($\varepsilon_\beta/\varepsilon_\alpha$). A general relationship between red shift and decreasing ratio is clear, but the trend is not smooth. With the exception of X = ClO_4, the O-donors show a rough dependence of $\varepsilon_\beta/\varepsilon_\alpha$ on the strength of their conjugate acids. As discussed under NMR spectra below, the positions of the halides are exceptional. The behaviour of complex **6** may reflect aggregation (see below). The limit of these trends is probably Sn(TPP)$(CH_2SiMe_3)_2$ reported by Pommier *et al.*[10] The powerful σ-donor ligands cause a red shift of the α band to 660 nm, and a reduction of $\varepsilon_\beta/\varepsilon_\alpha$ to *ca* 0.5. A parallel series of TPP complexes is In(TPP)R, where R was varied from ClO_4 through Cl and increasingly basic alkyl groups to *t*-butyl.[12] The α-band shifted from 595 to 639 nm, and $\varepsilon_\beta/\varepsilon_\alpha$ decreased from 1.94 to 0.72. A striking difference appears, however, on perusal of the data for the electron-rich macrocycles OEP and Etio-I. The same red shift trend is evident in In(OEP)R, but the effect on $\varepsilon_\beta/\varepsilon_\alpha$ is large, and in the opposite sense to that the TPP series, viz. 0.96 (ClO_4) to 3.78 (t-Bu).[12] This reversal is also present in Sn(Etio-I)X_2, for which the ratio changes from 0.87(X = F) to 1.77(X = I),[18] and in Tl(OEP)X_2, where $\varepsilon_\beta/\varepsilon_\alpha$ varies from 1.18 (X = $OCOCF_3$) to 1.54 (X = CN).[1] Such an inversion has been noted before in comparisons of OEP and TPP complexes for different metal ions. A high value of $\varepsilon_\beta/\varepsilon_\alpha$ for TPP complexes generally indicates more stable metal ion coordination, as expected in this series for weaker donors such as NO_3, whereas the opposite is found for OEP complexes.[19] A theoretical explanation has apparently not yet been advanced.

^1H NMR spectra

The relevant ^1H data for complexes **1–10** are displayed in Table 2, together with comparable literature data. The spectra are typical of TPP metal

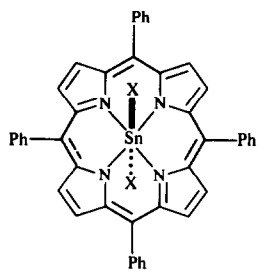
Formula	Number in text	X
	**1**	Cl
	2	OH
	3	OAc
	4	OMe
	5	NO_3
	6	ClO_4
	7	Br
	8	I
	9	NCS
	10	OC_6H_4-*p*-Me

Fig. 1. Structures of Sn(TPP)X_2 complexes.

complexes, consisting of singlet β-pyrrole resonances at lowest field, the *meso*-phenyl groups in the normal regions of 8.3 and 7.8 ppm, and signals for proton-containing axial ligands at high field. The β-pyrrole and axial ligand (X = OH, OMe, OAc) signals are flanked by Sn satellites due to coupling with ^{119}Sn and ^{117}Sn (spin-$\frac{1}{2}$, abundances 8.6 and 7.6%, respectively). Although the ^1H spectra of various Sn(IV) porphyrin complexes, e.g. Sn(OEP)X_2 (X = Cl, OMe, OPh, OAc)[9,20,21] and Sn(TPP)X_2 (X = Cl, OH)[8] have been reported, Sn—H coupling information has been unavailable until recently,[8] presumably because of signal-to-noise problems. With the advent of high-field FT instruments, such information is now accessible even for very insoluble complexes.

Sn–H coupling constants

The compounds are listed in Table 2 in order of decreasing magnitude of ^4J(Sn–H) for the β-pyrrole signals. Individual couplings to ^{119}Sn and ^{117}Sn were not resolved so average values are given. If only O-bound ligands are considered, it is apparent that a representative selection of such ligands is present, spanning a wide range of donor abilities. Moreover, the coupling constants for this smaller set show a good correlation ($r = 0.991$, $n = 6$) with the pK_as of the conjugate acids[22] of the ligands (Fig. 2). This dependence may be useful in structural assignment and reactivity studies. The halides, however, do not fit this correlation, although they span a very small pK_a range, and changes in J are small. The difference in ^4J(Sn–H) for two of the complexes, i.e. **1** and **2**, has been recorded by Milgrom and Sheppard.[8] The larger value of J for X = Cl was attributed to the tendency of that ligand to engage in p_π–d_π bonding, which causes an increase in σ-overlap in the Sn–N bonds.[8] However, ^4J(Sn–H) for **8** (X = I) is slightly less than that for **1**, while the effects of π-bonding would be expected to be greater, since the 5*p* orbitals of I should be more compatible with the empty Sn 5*d*

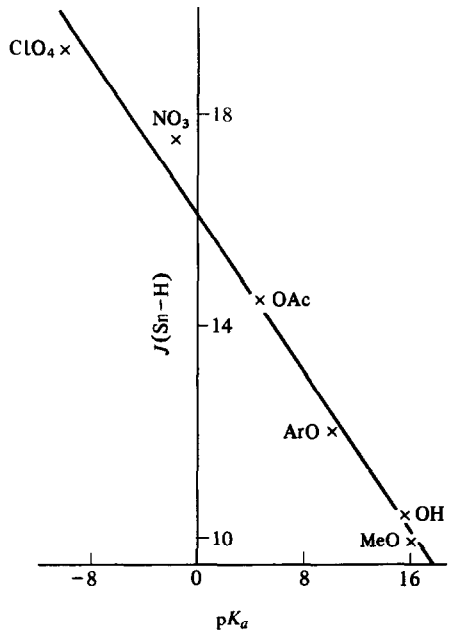


Fig. 2. Dependence of ^4J(Sn–H) (Hz) for β-pyrrole protons in Sn(TPP)X_2 complexes on the pK_a of the conjugate acids HX.

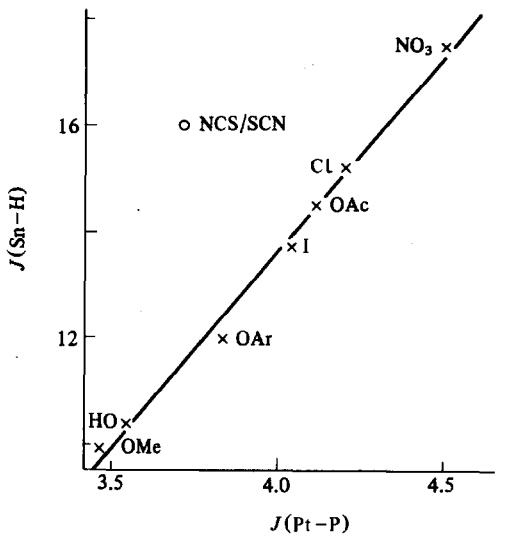


Fig. 3. Plot of ^4J(Sn–H) (Hz) for β-pyrrole protons in Sn(TPP)X_2 complexes vs ^1J(Pt–P) (kHz) in PtX(Me)(dppe) complexes [from Ref. 23, in which ArO = *p*-(MeO)C_6H_4O]. (NCS/SCN point not included in linear-regression analysis.)

orbitals than are the 3*p* orbitals of Cl. It appears, therefore, that both increased π-donation (e.g. for the halides) and increased σ-donation (for the oxygen ligands) cause a weakening of the Sn–N bonds, which is transmitted to the peripheral protons, thus decreasing ^4J(Sn–H). Transmission of electronic effects to the β-pyrrole protons in TPP complexes has been attributed mainly to contact interactions between the electrons of the σ-bonds in the macrocycle.[1-7]

Where the two series have ligands X in common, a surprising correlation ($r = 0.996$, $n = 7$) (Fig. 3) exists between ^4J(Sn–H) in Sn(TPP)X_2 and ^1J(Pt–P)(*trans* to X) in PtX(Me)(dppe) [dppe = 1,2-bis(diphenylphosphino)ethane].[23] A naive inference is that these ligands in two completely different families of compounds are exerting similar influences on very different coupling constant types. Here the *cis*-influence in the Sn(IV) series operates in the same sense as the *trans*-influence in the Pt(II) series, which is often not the case when comparisons are made within a single type of complex, e.g. [Pt(Ar)$(PEt_3)_3$]BF_4.[24] While very little can be concluded from such an obscure comparison, perhaps the σ-transmission arguments above are reinforced by it. Interestingly, the thiocyanate point lies well off the line, suggesting again that it is N-bonded in **9**, since it has been convincingly argued that it is S-bonded in the Pt series.[23]

β-Pyrrole chemical shifts

These chemical shifts show a similar dependence on ligand basicity, with weaker bases causing downfield shifts. A plot of ^4J(Sn–H) against δ (Fig. 4) indicates a good correlation ($r = 0.993$, $n = 8$), if the points for X = OH and OMe are excluded. Since the *J* values for these complexes fit well with the pK_a dependence, these chemical shifts seem anomalous. Literature data for X = OH are closely comparable with the present ones.[8] Inclusion of the β-pyrrole chemical shift for Sn(TPP)$(CH_2CH_3)_2$, *ca* 8.8 ppm,[11] indicates a continuation of the upfield shift for even more basic ligands. A similar dependence on the base strength of X has been reported for the chemical shifts of the β-pyrrole protons in In(TPP)X and the *meso*-protons in In(OEP)X complexes.[12]

Other NMR data

The protons in axial ligands appear at high field because of their location within the shielding zone of the macrocycle. Such chemical shifts for phenoxy, acetoxy and methoxy protons have been observed for Sn(OEP)X_2 complexes,[9] but Sn–H coupling constants were not reported. Recently, both δ and *J*(Sn–H) data were given for (**2**).[8] The trend of ^3J(Sn–H) > ^2J(Sn–H) > ^4J(Sn–H) evident in the series is similar to that observed for organotin(IV) compounds.[25] The OH ligand is subject to proton exchange with water, since marked broad-

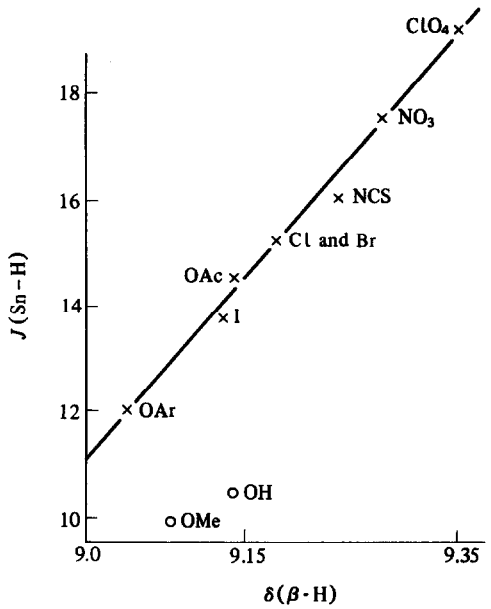


Fig. 4. Plot of ^4J(Sn–H) (Hz) vs chemical shift [δ (ppm)] for β-pyrrole protons in Sn(TPP)X_2 complexes. (OH and OMe points not included in linear-regression analysis.)

ening and a downfield shift occur when the $CDCl_3$ is not specially dried.

Complex **6** exhibits unusual behaviour in $CDCl_3$ solutions which is not apparent for any of the other compounds. A fresh solution of **6** in $CDCl_3$ shows two sets of peaks. The data in Table 2 refer to one set, which remains sharp. The other signals ($\delta_{pyrrole}$ 9.13, ^4J(Sn–H) = 13.5 Hz, δ_{ortho} 8.1, $\delta_{meta,para}$ 7.75) are broader. On standing for less than 24 h, a purple precipitate appears, accompanied by the loss of these broad peaks. The peaks assigned to the monomeric complex (**6**), whose δ and J values are internally consistent with those of the rest of the series, gradually disappear as precipitation continues. In acetone-d_6 and pyridine-d_5 solutions, single species exhibiting sharp peaks are present (δ 9.56, J = 18.0 Hz and δ 9.35, J = 13.2 Hz, respectively), and no precipitation occurs over many days. The precipitate can be dissolved in acetone to give a solution whose visible spectrum is virtually identical with that of the original solid **6** in acetone. Washing the precipitate with $CHCl_3$ slowly dissolves some of it, producing a spectrum very similar to that of the supernatant in $CDCl_3$. This behaviour seems consistent with aggregation in the weakly polar solvent, which does not occur in acetone or pyridine. Perhaps intermolecular perchlorate bridges are formed, leading to oligomerization. These phenomena are under investigation.

EXPERIMENTAL

General

^{1}H NMR spectra were recorded on the Bruker CXP-300 F.T. instrument at the Brisbane NMR Centre, Griffith University, using $CDCl_3$ as solvent. Preliminary spectra were obtained on a Varian EM-360 spectrometer. UV–visible spectra were recorded on a Varian DMS-100 spectrometer in $CHCl_3$ solutions. IR spectra were obtained on a Jasco IR-810 instrument in either Nujol mulls or KBr pellets. Microanalyses were carried out by the Microanalytical Service, University of Queensland. The ligand *meso*-tetraphenylporphyrin (TPP) was prepared and purified ("chlorin-free") by the literature method.[26] Inorganic salts were A.R. grade.

Preparations of Sn(TPP)X_2

X = Cl. This complex was prepared according to the literature[27] and recrystallized from $CHCl_3$–hexane to yield violet crystals.

X = OH. A solution of Sn(TPP)Cl_2 (100 mg) in CH_2Cl_2 (10 cm^3) was stirred with basic alumina (Woelm, activity IV, 2 g) for 15 min. The suspension was filtered through a short column of the same alumina, eluting with CH_2Cl_2. The major red–purple band was collected and concentrated, and then hexane was added to yield maroon microcrystals (70 mg, 73%), which were dried at 70°C under vacuum (< 1 mmHg).

X = OMe. A suspension of Sn(TTP)Cl_2 (50 mg) in dry $CHCl_3$–MeOH [1 : 1 (v/v), 10 cm^3) was stirred under dry N_2 with basic alumina (Woelm, activity IV, 1 g). After 10 min, the suspension was percolated through a short column of the same alumina, eluting with dry MeOH. The major band was collected, concentrated and cooled to yield the product as maroon microcrystals (25 mg, 50%), which were dried under vacuum at room temperature and stored in a desiccator. This material was shown to be >95% pure by ^{1}H NMR.

X = OAc. A mixture of Sn(TPP)Cl_2 (110 mg), AgOAc (130 mg) and glacial acetic acid (25 cm^3) was heated under reflux for 3 h, filtered while hot, then left at room temperature for 3 days. White crystals of excess AgOAc were removed by filtration, then the volume was reduced and hexane was added to yield shiny purple crystals, shown by NMR to be contaminated with acetic acid. Grinding and vacuum drying (70°C, < 1 mmHg) gave a maroon powder, which was recrystallized from CH_2Cl_2–hexane to yield shiny violet prisms. (Found: C = 67.7, H = 4.1, N = 6.5.

$C_{48}H_{34}N_4O_4Sn$ requires C = 67.9, H = 4.0, N = 6.6%.)

X = NO_3. A mixture of $Sn(TPP)Cl_2$ (70 mg) and $AgNO_3$ (70 mg) was refluxed in dry benzene (25 cm^3) for 3 h. Precipitated AgCl was removed by filtration, the solution was evaporated to dryness, and the residue was recrystallized from $CHCl_3$–hexane to give purple microcrystals in nearly quantitative yield. Recrystallization from CH_2Cl_2–hexane gave shiny purple prisms. (Found: C = 62.2, H = 3.4, N = 9.7. $C_{44}H_{28}N_6O_6Sn$ requires C = 61.8, H = 3.3, N = 9.8%.)

X = ClO_4. A solution of $Sn(TPP)Cl_2$ (80 mg) in dry benzene (10 cm^3) was stirred at 55°C. A solution of $AgClO_4$ (82 mg) in dry benzene (3 cm^3) was added, and stirring was continued at 55°C for 30 min. The purple complex and AgCl precipitated, leaving a bluish-purple supernatant. All solids were collected by filtration, then the porphyrinic materials were extracted by washing the residue with successive small portions of boiling $CHCl_3$, and filtering the resulting solution through Celite. Hexane was added and the solution concentrated to yield violet prisms (64 mg, 69%). Recrystallization from CH_2Cl_2–hexane gave maroon microcrystals. (Found: C = 56.7, H = 3.2, N = 5.8. $C_{44}H_{28}Cl_2N_4O_8Sn$ requires C = 56.8, H = 3.0, N = 6.0%.)

X = Br. A solution of $Sn(TPP)(ClO_4)_2$ (33 mg) in acetone (10 cm^3) was treated with LiBr (30 mg). The purple precipitate was collected after 30 min stirring, washed with acetone and dried. Recrystallization from CH_2Cl_2–hexane gave violet prisms (20 mg, 63%). (Found: C = 59.3, H = 3.2, N = 6.2. $C_{44}H_{28}Br_2N_4Sn$ requires C = 59.3, H = 3.2, N = 6.3%.)

X = I. A solution of $Sn(TPP)(ClO_4)_2$ (30 mg) in acetone (5 cm^3) was treated with KI (20 mg). Sparkling black prisms (21 mg, 66%) were formed directly from the reaction mixture, and were collected, washed with acetone and dried. Recrystallization from CH_2Cl_2–hexane gave very dark green crystals with a purple reflectance. (Found: C = 54.7, H = 2.9, N = 5.9. $C_{44}H_{28}I_2N_4Sn$ requires C = 53.6, H = 2.9, N = 5.7%.)

X = NCS. A solution of $Sn(TPP)(ClO_4)_2$ (30 mg) in acetone (5 cm^3) was treated with KSCN (20 mg). The mixture was stirred for 30 min, then filtered to yield purple crystals which were washed with acetone and dried (15 mg, 55%). Recrystallization from CH_2Cl_2–hexane gave glistening purple prisms. (Found: C = 63.7, 65.9; H = 3.2, 3.5; N = 9.6, 9.3. $C_{46}H_{28}N_6O_2Sn$ requires C = 65.7, H = 3.3, N = 9.9%.)

X = OC_6H_4-*p*-Me. A mixture of $Sn(TPP)(OH)_2$ (26 mg), *p*-cresol (20 mg) and benzene (5 cm^3) was stirred and refluxed for 1 h. The solvent was removed by distillation then the product was dissolved in CH_2Cl_2 and precipitated with hexane (19 mg, 59%). Recrystallization from CH_2Cl_2–hexane gave dark maroon microcrystals. [Found: C = 72.8, H = 4.4, N = 5.9. $C_{58}H_{42}O_2N_4Sn$ requires C = 73.7, H = 4.5, N = 5.9%.)

Acknowledgements—I thank Mr P. Comino and Dr P. Barron for assistance with the NMR spectrometer.

REFERENCES

1. R. J. Abraham, G. H. Barnett and K. M. Smith, *J. Chem. Soc., Perkin Trans. I.* 1973, 2142.
2. R. J. Abraham, G. E. Hawkes and K. M. Smith, *J. Chem. Soc., Perkin Trans. II.* 1974, 627.
3. R. J. Abraham, G. E. Hawkes, M. F. Hudson and K. M. Smith, *J. Chem. Soc., Perkin Trans. II.* 1975, 204.
4. C. A. Marrese and C. J. Carrano, *Inorg. Chem.* 1983, **22**, 1858.
5. J. W. Buchler and L. Puppe, *Liebig's Ann. Chem.* 1974, 1046.
6. L. R. Milgrom, *Polyhedron* 1984, **3**, 879.
7. L. R. Milgrom, *Polyhedron* 1985, **4**, 1279.
8. L. R. Milgrom and R. N. Sheppard, *J. Chem. Soc., Chem. Commun.* 1985, 351.
9. J. W. Buchler, L. Puppe, K. Rohbock and H. H. Schneehage, *Chem. Ber.* 1973, **106**, 2710.
10. C. Cloutour, D. Lafargue, J. A. Richards and J.-C. Pommier, *J. Organomet. Chem.* 1977, **137**, 157.
11. C. Cloutour, C. Debaig-Valade, C. Gacherieu and J.-C. Pommier, *J. Organomet. Chem.* 1984, **269**, 239.
12. K. M. Kadish, B. Boisselier-Cocolios, P. Cocolios and R. Guilard, *Inorg. Chem.* 1985, **24**, 2139.
13. K. Nakamoto, *Infrared and Raman Spectra of Inorganic and Coordination Compounds*, 3rd Ed. Wiley Interscience, N.Y. (1978).
14. J. W. Buchler, In *Porphyrins and Metalloporphyrins* (Edited by K. M. Smith), p. 222. Elsevier, Amsterdam (1975).
15. P. Cocolios, R. Guilard, D. Bayeul and C. Lecomte, *Inorg. Chem.* 1985, **24**, 2058.
16. K. M. Kadish, J. L. Cornillon, P. Cocolios, A. Tabard and R. Guilard, *Inorg. Chem.* 1985, **24**, 3645.
17. J. W. Buchler, In *The Porphyrins* (Edited by D. Dolphin), Vol. I, p. 415. Academic Press, N.Y. (1979).
18. M. Gouterman, F. P. Schwarz, P. D. Smith and D. Dolphin, *J. Chem. Phys.* 1973, **59**, 676.
19. J. W. Buchler, Ref. 14, p. 204.
20. J.-H. Fuhrhop, *Z. Naturforsch.* 1970, **25B**, 255.
21. D. J. Whitten, J. C. Yau and F. A. Carrol, *J. Am. Chem. Soc.* 1971, **93**, 2291.
22. J. March, *Advanced Organic Chemistry*, 2nd Ed., p. 227 and references therein. McGraw-Hill, Tokyo (1977).
23. T. G. Appleton and M. A. Bennett, *Inorg. Chem.* 1978, **17**, 738.

24. D. P. Arnold and M. A. Bennett, *Inorg. Chem.* 1984, **23**, 2117.
25. R. C. Poller, *The Chemistry of Organotin Compounds*, p. 240. Academic Press, N.Y. (1970).
26. G. H. Barnett, M. F. Hudson and K. M. Smith, *J. Chem. Soc., Perkin Trans. I.* 1975, 1401.
27. P. Rothemund and A. R. Menotti, *J. Am. Chem. Soc.* 1948, **70**, 1808.

Polyhedron Vol. 5, No. 12, pp. 1965–1968, 1986
Printed in Great Britain

0277–5387/86 $3.00+.00
Pergamon Journals Ltd

KINETICS OF FORMATION OF INTERMEDIATES IN SILVER ION ASSISTED AQUATIONS

HERVINE MILLER

Chemistry Department, University of the West Indies, Cave Hill, Barbados

(*Received* 31 *January* 1986; *accepted* 7 *May* 1986)

Abstract—There is kinetic evidence for the formation of $[Co(NH_3)_5NCSAg_3]^{5+}$ in the interaction of $[Co(NH_3)_5NCS]^{2+}$ with Ag^+ in aqueous solution, with pseudo-first-order formation rate constant $k = 0.158\ s^{-1}$ for the forward reaction in the following equation at 25°C and $[Ag^+]$ in the range $1.23–5.0 \times 10^{-2}$ mol dm^{-3} and 0.10 ionic strength ($NaClO_4$):

$$[Co(NH_3)_5NCSAg_2]^{4+} + Ag^+ \xrightarrow{k} [Co(NH_3)_5NCSAg_3]^{5+}.$$

Additionally, the formation constant, β_2, for $[Co(NH_3)_5NCSAg_2]^{4+}$ has been determined to be $\log \beta_2 = 4.717$. For the $[Rh(NH_3)_5I]^{2+}$–Ag^+ reaction there is evidence of an outer-sphere interaction with rate constants of $k_2 = 670\ dm^3\ mol^{-1}\ s^{-1}$ at 25°C and 0.10 ionic strength. This outer-sphere species undergoes further reaction to give the silver ion containing intermediates of the aquation reactions.

As part of the study of the silver ion assisted aquation of pentaammine metal(III) complexes, it seemed worthwhile to examine whether rates of formation of the intermediates in these reactions could be measured by conventional stopped-flow techniques. Evidence for the existence of species of the type $\{[M(NH_3)_5X]_mAg_n\}^{(m+n)+}$, where M = Cr(III), Co(III) or Rh(III); X = I^- or NCS^-; $m = 1$ or 2; and $n = 1$, 2 or 3, had previously been obtained from spectrophotometric,[1,2] potentiometric[2,3] and kinetic[4,5] studies, all of which indicated a stepwise complex formation. For Cr(III)[6] and Co(III)[1] solids having $m = 1$ and $n = 1$ or 2 have been isolated and characterized but analogous Rh(III) compounds have not been isolated to date. The stability constants, K_1, for the 1:1 adducts are of the order of $\log K_1 = 3.0$[3] and the rates of aquation for the pure pentaammine and its silver adducts are negligible at room temperatures.

Kinetics of the reactions of $[Co(NH_3)_5NCS]^{2+}$ and $[Rh(NH_3)_5I]^{2+}$ with silver ions in aqueous solution were examined at 25°C and the results are herein reported.

EXPERIMENTAL

Analytical-grade reagents and deionized or double-distilled (all-glass) water, as solvent, were used throughout. Acidopentaammine complexes and silver and sodium perchlorate solutions were prepared as previously reported.[1,2]

The drive syringes of a Durrum stopped-flow spectrophotometer were filled with reaction solutions of composition as follows.

Solution 1: $AgClO_4$ (variable concentration), $HClO_4$ to pH ~3 and $NaClO_4$ to ionic strength 0.10. Solutions were filtered using Millipore 0.45-μm filter disc together with a Millipore Swinney adapter to remove any traces of colloidal silver chloride.

Solution 2: pentaammine (fixed concentration), $HClO_4$ to pH ~3 and $NaClO_4$ to ionic strength 0.10, such that on 1:1 dilution the reaction mixture had the desired $[Ag^+]$ and [pentaammine].

The solutions and the reaction chamber were thermostatted at 25.0°C in diffuse light or near darkness. Concentrations of pentaammine were chosen such that absorbance at the monitoring wavelength was *ca* 0.5.

Photometric adjustments were made with solution 1 as blank and the reactions were monitored at 263 nm and 255 nm for $[Co(NH_3)_5NCS]^{2+}$ and $[Rh(NH_3)_5I]^{2+}$, respectively. At these wavelengths the difference between the spectra of the pure pentaammine solutions and of those containing silver ions was optimum. Typical absorb-

ance changes for the concentrations used were 0.03–0.05 units.

Multiple determinations of the absorbance vs time plots were done at each silver ion concentration and an average taken by superimposing the oscilliscope traces. For the $[Rh(NH_3)_5I]^{2+}$ reaction a few determinations were done at the same temperature using a modified Zeiss PMQII spectrophotometer[7] to confirm that the stopped-flow apparatus had not produced spurious results. In addition, by measuring the absorbance, A_∞, corresponding to the infinity values of the first and subsequent reactions which take place the spectra of the intermediates could be obtained. Wavelength was varied from 250 to 325 nm with Ag^+ solution used as reference solution for the photometric adjustments. A new reaction run was done at each wavelength.

All component parts of the stopped-flow system had to be thoroughly cleaned with EDTA, followed by repeated rinsings with water, so as to desorb any silver ions. Failure to do this or to reduce the amount of light reaching the apparatus resulted in the well-known photochemical changes of the silver solution and "blackening" of the equipment. This risk of damage to expensive equipment severely limited the scope of this study.

RESULTS AND DISCUSSION

Figure 1 shows a typical oscilloscope trace for the reaction of $[Co(NH_3)_5NCS]^{2+}$ with silver ions and represents not less than eight superimposed plots of absorbance vs time. Data from such plots yielded good first order kinetics

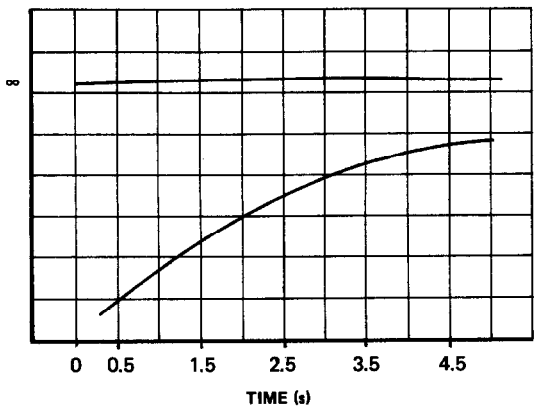


Fig. 1. Typical oscilloscope trace of absorbance vs time for the $[Co(NH_3)_5NCS]^{2+}$–Ag^+ reaction. $[Ag^+]_{total} = 1.25 \times 10^{-2}$ mol dm^{-3}. $[Co(NH_3)_5NCS^{2+}]_{total} = 2.5 \times 10^{-4}$ mol dm^{-3}.

Table 1. Observed rate constants, k_{obs}, for the $[Co(NH_3)_5NCS]^{2+}$–Ag^+ interaction at 25°C and 0.10 ionic strength ($NaClO_4$)

$10^2[Ag^+]^a$ (mol dm^{-3})	1.23	2.48	3.73	4.98
$10^2 k_{obs}$ (s^{-1})	3.5	6.1	7.2	8.3

[a]Corrected for complete formation of $[Co(NH_3)_5NCSAg]^{3+}$.

over more than three half-lives. The pseudo-first-order rate constants, k_{obs}, in Table 1 for $[Co(NH_3)_5NCS]^{2+} = 2.50 \times 10^{-4}$ mol dm^{-3} and $[Ag^+]_{total} = 1.25\text{–}5.0 \times 10^{-2}$ mol dm^{-3} are reproducible to within 2%.

Under the reaction conditions, $[Ag^+] \gg [Co(NH_3)_5NCS]^{2+}$, it is assumed that $[Co(NH_3)_5NCSAg]^{3+}$ is completely formed within the mixing time given its known formation constant, $\log K_1 = 3.350$[3] and the concentration of the reacting species. From previous[1] spectrophotometric data under similar conditions, complexes $\{[Co(NH_3)_5NCS]_mAg_n\}^{(2m+n)+}$ formed would be expected to have values of $m = 1$ and $n > 2$ and, by analogy with the Ag^+–SCN^- system, n should not exceed 4. On the basis of these observations the formation of $[Co(NH_3)_5NCSAg_3]^{5+}$ is postulated as follows:

$$[(NH_3)_5CoNCSAg]^{3+} + Ag^+ \overset{K_2}{\rightleftharpoons} [(NH_3)_5CoNCSAg_2]^{4+} \text{ (fast)}, \quad (1)$$

$$[(NH_3)_5CoNCSAg_2]^{4+} + Ag^+ \overset{k}{\rightleftharpoons} [(NH_3)_5CoNCSAg_3]^{5+} \text{ (slow)}. \quad (2)$$

For this reaction scheme the observed pseudo-first-order rate constants, k_{obs}, would be given by eqn (4)

$$k_{obs} = \frac{kK_2[Ag^+]}{1 + K_2[Ag^+]}. \quad (3)$$

The predicted linearity of the $1/k_{obs}$ vs $1/[Ag^+]$ plots has been observed and linear regression analysis of the data yields values of $k = 0.158$ s^{-1} and $K_2 = 23.3$ dm^3 mol^{-1}. This leads to a value of $\log \beta_{12} = 4.717$, where $\beta_{12} = K_1K_2$, for the overall stability constant of $[Co(NH_3)_5NCSAg_2]^{4+}$ which has been isolated as the nitrate.[1] This value is several orders or magnitude lower than for similar Hg^{2+} complexes,[8] as is the trend when Ag^+ and Hg^{2+} values have been compared for similar reactions.

For $[Rh(NH_3)_5I]^{2+}$ the reaction with Ag^+ under

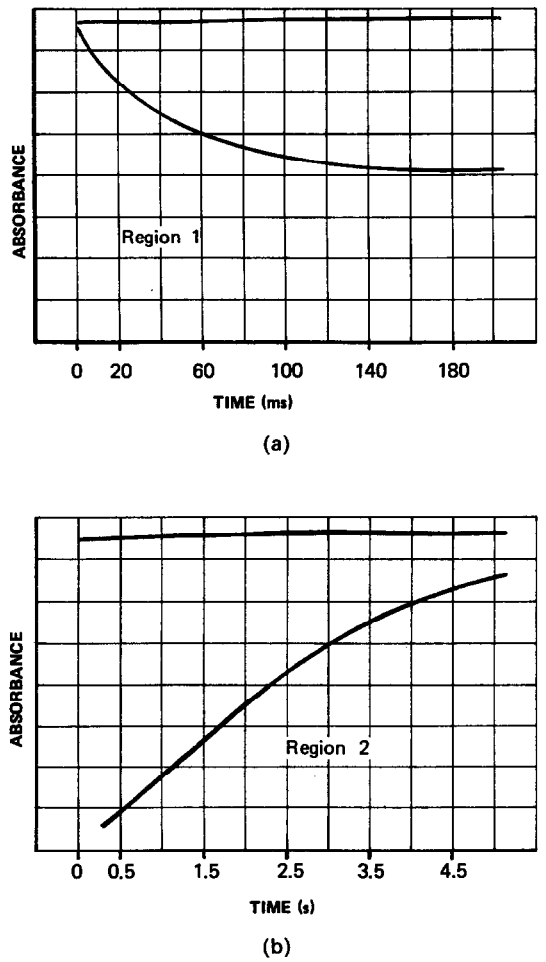


Fig. 2. Typical oscilloscope traces of absorbance vs time for the $[Rh(NH_3)_5I]^{2+}$–Ag^+ reaction. $[Ag^+]_{total} = 1.25 \times 10^{-2}$ mol dm^{-3}. $[Rh(NH_3)_5I^{2+}]_{total} = 8.0 \times 10^{-5}$ mol dm^{-3}.

similar conditions is more complex. The absorbance vs time plots seem to be divisible into two regions as in Fig. 2 which shows typical oscilloscope traces for this reaction. Good first-order kinetics were observed for both regions 1 and 2 and the pseudo-first-order rate constants k and k' respectively are in Table 2 for $[Rh(NH_3)_5I^{2+}] = 8.0 \times 10^{-5}$ mol dm^{-3} and $[Ag^+] = 0.50$–5.0×10^{-2} mol dm^{-3}. The rate constants are reproducible to better than 5%. The data for region 1 show that k varies linearly with Ag^+ over the range studied, thus indicating a true bimolecular association with second-order rate constant, k_2, of 670 dm^3 mol^{-1} s^{-1}. Such a value may result from an outer-sphere interaction of the two cations. This interpretation of the experimental data is based on the observed decrease in absorbance and a comparison with other bimolecular association reactions for example Cr^{2+}–V^{2+} charge-transfer reactions[9] for which the second-order rate constants are lower and $\sim 1.2 \times 10^2$ dm^3 mol^{-1} s^{-1}. The more favourable charge product of +2 for the Ag^+–$Rh(NH_3)_5I^{2+}$ interaction may account for this higher value of k_2. Furthermore, associations of this type are well-known precursors in many substitution and redox reactions and represent the first relaxation process in the formation of the intermediate species. The interaction of the iodine atom with Ag^+ should increase the Rh—I bond distance in the reactant and lead to the observed decrease in the absorbance of the charge-transfer bands. Supporting evidence is obtained from A_∞ vs wavelength plots which showed a small shift to longer wavelength with a broad maximum at *ca* 283 nm, indicating that the intermediate at this stage is different from those previously reported[2] as Ag^+-containing species.

Table 2. Observed rate constants for the $[Rh(NH_3)_5I]^{2+}$–Ag^+ interaction at 25°C and 0.10 ionic strength ($NaClO_4$)

10^2[Ag][a] (mol dm^{-3})	Region 1 k (s^{-1})	Region 2 k' (s^{-1})
0.50	20.0	0.243
1.25	23.9	0.260
2.50	34.3	0.160
5.00	49.8	0.124

[a]Initial $[Ag^+]$.

For region 2 a two-fold decrease of the pseudo-first-order rate constant, k', with the 10-fold increase in $[Ag^+]$, is observed, but no detailed mechanistic evaluation is possible with this limited data. However, these reactions must lead to complexes of the type $[Rh(NH_3)_5IAg_n]^{n+2}$ (n = 1, 2 or 3) as these are thermodynamic products of the interaction. Under the reaction conditions complexes should have all three values of n.[2]

There is evidence to support these complex species as the intermediates in the silver ion assisted aquation of $[Rh(NH_3)_5I]^{2+}$. For example, Boyce *et al.*[5] reported data (Table 9) which show good linear free energy correlation between the aquation rate contants, k_n, and the formation constants, K_n, of these complexes. If it is assumed, as suggested[10] for metal ion assisted aquations, that the formation constants, K', for the leaving groups [eqn (4)] are related to those for the reacting complexes [eqn (5)]:

$$[Ag_{n-1}I]^{(n-2)+} + Ag^+ \overset{K'}{\rightleftharpoons} [Ag_nI]^{(n-1)+}, \quad (4)$$

$$[Rh(NH_3)_5IAg_{n-1}]^{n+1} + Ag^+ \overset{K_n}{\rightleftharpoons} [Rh(NH_3)_5IAg_n]^{n+2}, \quad (5)$$

by eqn (6):

$$K_n = b + mK' \quad (6)$$

and that b is sufficiently small to allow for the approximation in eqn (7) to be valid:

$$K_n = mK' \quad (7)$$

then the data of Boyce *et al.*[5] are well reproduced by eqn (8):

$$\log k_n = 1.52 + 1.37 \mathrm{p}K_n \quad (8)$$

with standard deviations of 0.026 an 0.030 in slope and intercept, respectively. A slope > 1 is indicative of a dissociative mechanism often encountered for other Rh(III) equations.

It is, therefore, reasonable to assume that the outer-sphere complex, initially formed, rearranges or reacts further with Ag^+ to give such intermediates, the spectra of which corresponds to those in other studies.[2]

REFERENCES

1. G. C. Lalor and H. Miller, *J. Inorg. Nucl. Chem.* 1975, **37**, 307.
2. G. C. Lalor and H. Miller, *Rev. Latinoamer. Quim.* 1976, **7**, 102.
3. G. C. Lalor and H. Miller, *J. Inorg. Nucl. Chem.* 1975, **37**, 1832.
4. G. C. Lalor and H. Miller, *J. Inorg. Nucl. Chem.* 1978, **40**, 305.
5. C. StC. Boyce, G. C. Lalor and H. Miller, *J. Inorg. Nucl. Chem.* 1979, **41**, 857.
6. H. Miller, *Polyhedron* 1985, **4**, 1659.
7. G. C. Lalor, *Lab. Practice* 1971, **19**, 607.
8. (a) L. C. Falk and R. G. Linck, *Inorg. Chem.* 1971, **10**, 215; (b) A. Pfeil, T. P. Dasgupta, D. A. Palmer and H. Kelm, *Inorg. Chim. Acta* 1980, **44**, L23.
9. F. Basolo and R. G. Pearson, *Mechanism of Inorganic Reaction*, 2nd Edn, p. 481. John Wiley, New York (1967).
10. I. V. Kozhevnikov and E. S. Rudakov, *Inorg. Nucl. Chem. Lett.* 1972, **8**, 571.

Polyhedron Vol. 5, No. 12, pp. 1969–1974, 1986
Printed in Great Britain

0277–5387/86 $3.00+.00
Pergamon Journals Ltd

X-RAY PHOTOELECTRON SPECTROSCOPY OF SOME Co(II) DITHIOCARBAMATES

GIOVANNI POLZONETTI*

Department of Chemistry, University "La Sapienza", P. le A. Moro, 5, 00185 Rome, Italy

and

CARLO PRETI and GIUSEPPE TOSI

Department of Chemistry, University of Modena, Via G. Campi, 183, 41100 Modena, Italy

(*Received* 17 *February* 1986; *accepted* 7 *May* 1986)

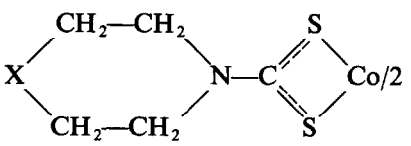
Abstract—The X-ray photoelectron spectra of a series of Co(II) dithiocarbamate complexes have been studied. Data confirmed the substantial identity of the electronic structure of the chromophores throughout the series, and Co2$P_{3/2}$ BE values of 780.1 eV are in good agreement with the expectation on the base of Feltham–Brant scale. Shake-up satellites associated with the Co2$P_{3/2}$ photoelectron line have been investigated and compared with magnetic moments.

Application of X-ray photoelectron spectroscopy (XPS) to the investigation of the electronic structure of molecules has become a widely accepted technique. The transition metals as a group show such interesting properties as variable valence, paramagnetism and a highly diverse stereochemistry. Hence, they are ideally suited for XPS studies by probing directly the electronic environment of transition metal or ion.

Dithiocarbamate have properties which make them useful in applications including vulcanization accelerators, fungicides and pesticides among others.[1]

Several structural studies of metal dithiocarbamates have been published.[2–4] It has been recognized that the ligand forms a four membered chelate ring with delocalization of electrons over the S_2CN moiety. X-ray photoelectron spectroscopy has not been used as much as other techniques to investigate metal dithiocarbamates. Jørgensen and Berthou[5] reported data for Cu(II) and Ni(II) dithiocarbamate. Perry and Geanangel[6] reported about tin diethyl- and dimethyl dithiocarbamates. Frost *et al.*[7] studied several diethyldithiocarbamates giving particular emphasis to the satellite structure. Best *et al.*[8] investigated sulfur behaviour in Fe, Mo diethyl- and Co(III) dimethyldithiocarbamates. Van Attekum and Trooster[9] studied the X-ray induced decomposition of gold (III) dimethyl- and *n*-propyl dithiocarbamates. Walton[10] reviewed the sulfur behaviour in the metal dithiocarbamates among others. Chang and Cheng[11] examined the Cu(II), Pb(II) and Sn(IV) diethyldithiocarbamates reporting a procedure to decompose the C1*S* signal into three components in order to get a more accurate spectra calibration.

More recently Payne *et al.*[12,13] and Liesegang and Lee[14] reported data on IR–XPS chemical shifts correlations for eleven disubstituted Cu(II) and Ni(II) dithiocarbamates in which they found strong effects of the substituents on the binding energies, specially for sulfur, attributing its changes to the reverse movement of electronic charge towards the S atom. With the aim of correlating XPS spectra with chemical properties, and following a systematic XPS investigation of metal dithiocarbamates, we already examined a series of Cu(II) and Ni(II) dithiocarbamates.[15,16] In the present work we extended our study to the series of quadratic complexes of Co(II), **1**,



(1)

*Author to whom correspondence should be addressed.

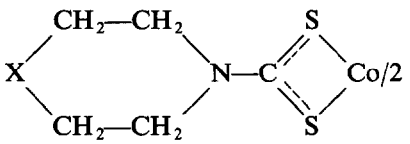
where

X = CH_2, NH, NCH_3, O, S, CH–Ph or N–Ph.

EXPERIMENTAL

Synthesis

The cobalt(II) complexes:



where X = CH_2 (piperidinedithiocarbamate = Pipdtc),
HN (piperazinedithiocarbamate = Pzdtc),
CH_3N (*N*-methylpiperazinedithiocarbamate = Mepzdtc),
O (morpholinedithiocarbamate = Morphdtc),
S (thiomorpholinedithiocarbamate = Timdtc),
C_6H_5—CH (4-phenylpiperidinedithiocarbamate = 4Ph-pipdtc),
C_6H_5—N (phenylpiperazinedithiocarbamate = Ph-N-pzdtc)

were prepared and purified, according to previous literature reports, by some of us[17–20] and on the basis of their properties were classified as low spin Co(II) compounds.

Spectral measurements

The X-ray photoelectron spectra were measured using a VG ESCA-3 MKI spectrometer employing $AlK_{\alpha 1,2}$ X-rays ($h\nu$ = 1486.6 *eV*). Samples were deposited as thin powder films on gold bearing plates, whose $Au4f_{7/2}$ signal at 84.0 eV was used as reference. Samples proved to be essentially stable under X-rays (typical power 12 kV × 10 mA). Vacuum in the analysis chamber was typically 1×10^{-9} torr, and the resolution was about 1.6 eV on the $Au4f_{7/2}$ line. Gaussian curve fitting was performed by computer program. Quantitative evaluation of atomic ratios, in the XPS sampling layer, was achieved by analysis of the XPS signal intensity of solid Co(II) dithiocarbamates and by using the Scofield's atomic cross-sections values[21] together with the $E_k^{1/2}$ dependence of mean free-path values and $E_k^{-1/2}$ dependence of luminosity factors. As the sensitivity factors gave results not in agreement with the nominal formulas, further measurements were performed on two standard compounds: $CoSO_4$ and $[Co(NH_3)_5CO_3]NO_3$, and a factor of 1.6 was found to adjust the sensitivity factors for S, N, C and O with respect to Co, giving results in agreement with the expected composition. The application of this factor 1.6 to the dithiocarbamate compounds gave good quantitative values, within the usual range of ±20%.

No attempts were made to clean the sample, by ion bombardment, in order to avoid decomposition.

The referencing procedure based on Cl*S* of contamination carbon taken at 285.0 eV[22] cannot be applied here in a simple way, as we have described previously,[15,16] due to the fact that position and shape of the Cl*S* signal vary according to the different kind of C atoms present in the ligands. A significant assignment can be obtained only identifying the actual Cl*S* components and assigning them to a consistent and transferable scheme like that reported in Table 1. The same procedure was used by Chang and Cheng.[11]

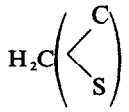
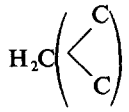
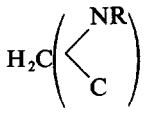
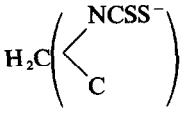
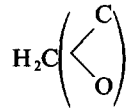
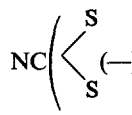
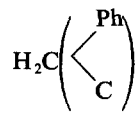
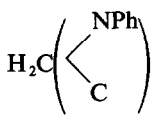
RESULTS

The data obtained in the present study are summarized in Table 2 and typical spectra are reported in Fig. 1. To our knowledge this is the first investigation of Co(II) dithiocarbamates. Frost *et al.*[7] studied the octahedral diamagnetic Co(III) diethyldithiocarbamate complex and Best *et al.*[8] reported about sulfur for the same Co(III) complex. The former authors found for $Co2p_{3/2}$ and S2*p* lines the presence of weak satellites at 5.2 eV and 6.0 eV, respectively, attributable to shake-up process, they noted also that the Co spin-orbit splitting ($2P_{1/2}$, $2P_{3/2}$) of 14.9 eV was in agreement with that measured for diamagnetic Co(III) compounds.

In this work, the low spin Co(II) compounds show intense broad additional lines to higher binding energy of the $Co2p_{1/2}$, $2P_{3/2}$ lines attributable to shake-up process. These satellites are separated by 6.3 ± 0.1 eV (ΔE) from the parent peaks throughout the series of Co(II) compounds, shift of comparable magnitude with the Frost *et al.*[7] value for Co(III) diethyl derivative of 5.2 ± 0.3 eV. Co2*p* additional lines are broad and their intensity, along the series, falls between 12.7 and 44.5% of the total intensity of $Co2p_{3/2}$ signal. It is most notable that they occur with significant intensity only in the case of the paramagnetic cobalt(II) complexes. In our case, for instance, I_{sat} for $Co(Timdtc)_2$ is about 20.5% of the total intensity of $Co2p_{3/2}$, whilst for the analogous Co(III) compound $Co(Timdtc)_3$, we found $I_{sat} \sim 1.4\%$ probably due to some impurity of Co(II) on the surface.

Moreover, for the same two compounds, the $2p_{1/2}$, $2p_{3/2}$ energy separation observed is close to 16.0 eV for the paramagnetic cobalt(II) whilst the diamagnetic cobalt(III) complex shows a separation of only 15.0 eV in agreement with the literature reports.[7,23–25]

Table 1. XPS BE values of Cl*S* for different C environments (eV)

	284.3
	284.3
Contamination	285.0
	285.0
Phenyl	285.0
	285.7
	286.0
	286.3
	284.3
	284.5

Several authors[7,23-30] suggest that satellites depend on whether the central metal atom has unpaired electrons or not and Borod'ko *et al.*[26] suggest that satellite intensities correlate with the spin density on the Co atoms in paramagnetic species or, less accurately, with the magnetic moments. More recently however, Perera *et al.*[31] reported that a strong shake-up satellite is favored by two factors: "(a) the amounts of charge transferred from the ligand to the metal and (b) whether or not the central ion component of the mainly ligand orbital is small before ionization".

Moreover, they pointed out also that the most important requirement for the presence of satellites in the photoelectron spectra of transition metal compounds is an incompletely filled 3*d* subshell, it does not matter whether the compound is paramagnetic or diamagnetic.

A tentative correlation between magnetic moments values (μ) and Co2$p_{3/2}$ satellites did not give very good results. Co(Pipdtc)$_2$ for instance shows an intensity of satellites (I_{sat}) too high with respect to the others, and in the meantime Co(4PhPipdtc)$_2$ and Co(PhNPzdtc)$_2$ show an I_{sat} too low. This might be perhaps due to the different amount of the surface contamination of Co(III) species, which can be caused by oxidation of Co(II) complexes or formed during the preparation. These surface contamination can reduce the satellite lines in intensity.

In a previous paper[15] we found a good relationship between I_{sat} and magnetic moment values for a series of Cu(II) dithiocarbamates. The spectra for Cu2$p_{3/2}$ showed satellites whose intensity throughout the series varied between 17 and 23% of the total intensity ($I_{sat} + I_{main\ peak}$), and their position was about 10.5 eV higher BE than the main 2*p* line, that is in good agreement with the Frost *et al.*[7] data for Cu(II) diethyldithiocarbamate. It is not in agreement with Payne *et al.*[13] who studied a series of Cu(II) dithiocarbamates and did not find any satellites structure for Cu2$p_{3/2}$.

For the Co complexes, additional signals were also observed for S2*p* lines at about 6.6 eV from the main line, like those we already observed for Cu(II) and Ni(II) dithiocarbamates;[15,16] Frost *et al.*[7] attributed these peaks to shake-up satellites. However, an alternative interpretation is that some of these "satellites" might be due to the formation of small amounts of high oxidation state sulfur contaminations.

The electronic structure of the central metal chromophores [CoS_4] appears, on XPS evidence, substantially similar for all the Co(II) dithiocarbamates investigated here, and practically independent on the nature of the remote substituent X. As it can be seen from Table 2, binding energies do not vary largely and are essentially stable throughout the series of planar Co(II) compounds studied.

The Co2$p_{3/2}$ signals fall at 780.1 $\pm$ 0.2 eV for all the investigated Co(II) compounds, a value which is in good agreement with the predicted value (779.6 eV) of the additive ligand contribution model by Feltham and Brant.[32] The BE value for S2*p* fall at 162.0 $\pm$ 0.2 eV throughout the series; this value is within the values reported by Walton (161.7–162.9)[10] and indicates the absence of any strong effect due to the remote substituent X. The sulfur BE value is lower than the average values reported for the analogous Cu(II) and Ni(II) dithio-

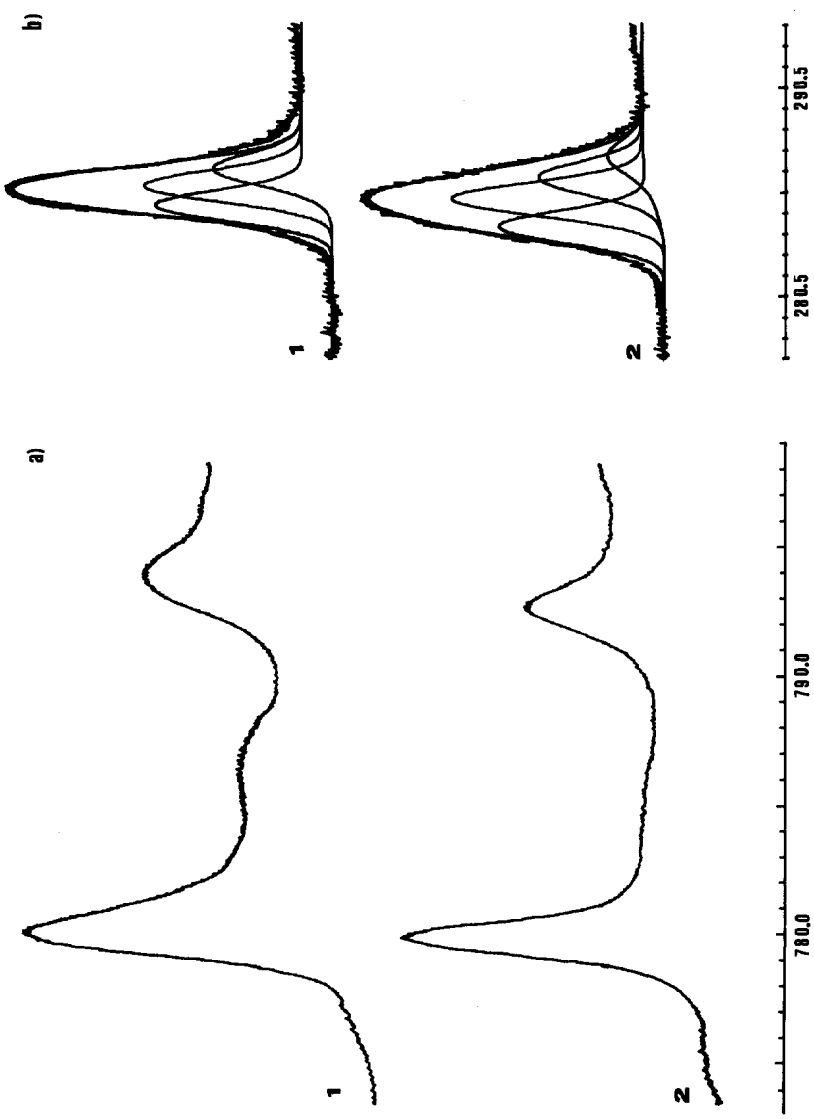


Fig. 1. (a) XPS spectra in the Co2*p* region for (1) $Co(Timdtc)_2$ and (2) $Co(Timdtc)_3$. (b) Gaussian decomposition of the C1*S* bands of (1) $Co(Pzdtc)_2$ and (2) $Co(PhNpzdtc)_2$.

Table 2. BEs (FWHM)[a] and ΔE in eV: intensities (10^3 counts s^{-1}), and number of atoms[b]

Compound	$Co2p_{3/2}$	$Co2p_{3/2}$ Sat.	S2p	N1S	C1S	C1S Components	O1S	μ
$Co(Pipdtc)_2$	780.0 (2.3)	$\Delta E = 6.2$	160.0 (2.8)	399.7 (2.3)	284.9 (2.9)	284.3 (50.7%)	531.5 (2.9)	
	22.1	44.5%[c]	23.3	15.5	58.1	285.6 (33.6%)	9.8	2.00
	1.0		2.7	1.9	11.2	286.5 (15.6%)	2.0	
$Co(Pzdtc)_2$	780.0 (2.4)	$\Delta E = 6.3$	161.8 (3.0)	399.6 (2.8)	285.5 (2.8)	284.8 (39.2%)	531.5 (3.0)	
	29.0	28.95%	26.4	24.3	45.1	285.7 (39.2%)	25.8	2.5
	1.0		4.2	3.7	12.2	286.5 (21.6%)	2.1	
$Co(Mepzdtc)_2$	780.2 (2.2)	$\Delta E = 6.2$	162.0 (2.7)	399.6 (2.5)	285.7 (2.6)	284.9 (29.2%)	531.7 (2.7)	
	22.5	17.8%	24.5	25.2	60.1	285.8 (47.4%)	10.0	1.60
	1.0		5.0	4.7	20.9	286.9 (23.4%)	1.1	
$Co(Morphdtc)_2$	780.1 (2.2)	$\Delta E = 6.3$	162.0 (2.8)	400.0 (2.1)	286.0 (2.4)	285.4 (34.8%)	532.6 (2.7)	
	30.2	16.8%	31.6	14.5	54.5	286.3 (49.1%)	40.8	2.08
	1.0		4.7	2.0	13.7	287.1 (16.1%)	3.5	
$Co(Timdtc)_2$	780.1 (2.5)	$\Delta E = 6.1$	162.3 (3.3)	399.7 (2.3)	284.9 (2.9)	284.0 (31.0%)	531.3 (3.0)	
	28.8	20.5%	42.9	12.5	47.3	285.0 (45.5%)	15.8	2.03
	1.0		6.8	1.9	12.5	286.0 (23.5%)	1.1	
$Co(4Phpipdtc)_2$	780.0 (2.3)	$\Delta E = 6.4$	161.9 (2.5)	399.8 (2.2)	284.6 (2.6)	284.7 (50.0%)	531.4 (3.0)	
	16.3	13.7%	17.9	9.6	76.3	283.8 (26.1%)	7.8	2.30
						285.9 (18.3%)		
	1.0		5.0	2.5	35.6	286.6 (5.6%)	1.1	
$Co(PhNpzdtc)_2$	780.3 (2.3)	$\Delta E = 6.5$	162.3 (2.6)	399.6 (2.3)	285.2 (3.3)	285.1 (39.8%)	531.6 (2.8)	
	16.1	12.7%	19.5	19.7	69.4	283.8 (31.9%)	9.2	
						286.1 (21.2%)		2.14
	1.0		5.6	5.0	33.1	287.1 (7.1%)	1.2	

[a] Full width at half maximum.
[b] Referred to 1.00 Co atom.
[c] Relative satellite intensity with respect to the total area of both satellite and the main $Co2p_{3/2}$ line.

carbamates[15,16] (162.0 against 162.2 and 162.5, respectively). The N1*S* BE value of 399.8 ± 0.2 eV is the same already reported for Cu(II) and Ni(II) dithiocarbamates[15,16] and confirms the insensitivity of the electronic structure of the bonding functions to the groups substituted in X position.

These findings and those already reported for the Ni(II) and Cu(II) series of dithiocarbamates[15,16] are not in agreement with Payne *et al.*[13] who studied Ni(II) and Cu(II) dithiocarbamates and reported that by substituting CH_2 with O in remote position of the ligand (e.g. by substituting piperidinedithiocarbamate with morpholinedithiocarbamate) the BE shift (ΔE_b) was: (a) 1.24 eV for Cu2$p_{3/2}$, 1.18 eV for S2*p* and (b) 1.43 eV for Ni2$p_{3/2}$, 2.96 for S2*p*, 1.4 for N1*S* for the copper and the nickel series, respectively.

We would not expect such a binding energy shift for such a substitution.

REFERENCES

1. C. D. Thorn and R. A. Ludwing, *The Dithiocarbamates and Related Compounds*. Elsevier, Amsterdam (1962).
2. R. Eisenberg, *Prog. Inorg. Chem.* 1970, **12,** 295.
3. D. Couconvanis and J. P. Fackler, *J. Inorg. Chem.* 1967, **6,** 2047.
4. M. Bonamico, G. Dessy, A. Mugnoli, A. Vaciago and L. Zambonelli, *Acta Cryst.* 1965, **19**, 868.
5. C. K. Jørgensen and M. Berthou, *Mat. Fis. Medd. Danske Vidensk. Selskab.* 1972, **38,** N. 15.
6. D. Perry and R. A. Geanangel, *Inorg. Chim. Acta* 1975, **13,** 185.
7. D. C. Frost, C. A. McDowell and R. L. Tapping, *J. Electron Spectrosc. Relat. Phen.* 1975, **7,** 297.
8. S. A. Best, P. Brant, R. D. Feltham, T. B. Rauchfuss, D. M. Roundhill and R. A. Walton, *Inorg. Chem.* 1977, **16,** 1976.
9. P. M. Th. M. Van Attekum and J. M. Trooster, *J. Chem. Soc. Dalton Trans.* 1980, 201
10. R. A. Walton, *Coord. Chem. Rev.* 1980, **31,** 183.
11. Hoo-pin Chang and K. L. Cheng, *Spectrosc. Letts* 1981, **14,** 795.
12. R. Payne, R. J. Magee and J. Liesegang, *Chem. Phys. Letts* 1982, **93**, 103.
13. R. Payne, R. J. Magee and J. Liesegang, *J. Electron Spectrosc. Relat. Phen.* 1985, **35,** 113.
14. J. Liesegang and A. R. Lee, *J. Electron Spectrosc. Relat. Phen.* 1985, **35,** 101.
15. C. Furlani, G. Polzonetti, C. Preti and G. Tosi, *Inorg. Chim. Acta* 1983, **73,** 105.
16. C. Furlani, G. Polzonetti, C. Preti and G. Tosi, *Gazz. Chim. Ital.* 1983, **113,** 609.
17. C. Preti and G. Tosi, *J. Inorg. Nucl. Chem.* 1976, **38,** 1746.
18. G. Marcotrigiano, G. C. Pellacani and C. Preti, *J. Inorg. Nucl. Chem.* 1974, **36,** 3709.
19. G. Arovamudan, D. M. Brown and D. Ventkappayya, *J. Chem. Soc. A* 1971, 2744.
20. A. C. Fabretti, F. Forghieri, A. Giusti, C. Preti and G. Tosi, *Inorg. Chim. Acta* 1984, **86,** 127.
21. J. H. Scofield, *J. Electron Spectrosc. Relat. Phen.* 1976, **8,** 129.
22. P. Swift, *Surf. Interface Anal.* 1982, **4,** 77.
23. D. C. Frost, C. A. McDowell and I. S. Woolsey, *Chem. Phys. Letts* 1972, **17,** 320.
24. D. Briggs and V. A. Gibson, *Chem. Phys. Letts*, 1974, **25,** 493.
25. D. C. Frost, C. A. McDowell and I. S. Woolsey, *Mol. Phys.* 1974, **27,** 1473.
26. Yu. G. Borod'ko, S. Vetchinkin, S. L. Zimont, I. N. Ivleva and Yu. M. Shul'ga, *Chem. Phys. Letts* 1976, **42,** 264.
27. L. Yin, I. Adler, T. Tsang, L. J. Matienzo and S. O. Grim, *Chem. Phys. Letts* 1974, **24,** 81.
28. D. C. Frost, C. A. McDowell and R. L. Tapping, *J. Electron Spectrosc. Relat. Phen.* 1975, **6**, 347.
29. L. J. Matienzo, L. I. Yin, S. O. Grim and W. E. Swartz, Jr, *Inorg. Chem.* 1973, **12**, 2762.
30. G. A. Vernon, G. Stucky and T. A. Carlson, *Inorg. Chem.* 1976, **15,** 278.
31. J. S. H. Q. Perera, D. C. Frost and C. A. McDowell, *J. Chem. Phys.* 1980, **72,** 5151.
32. R. D. Feltham and P. Brant, *J. Am. Chem. Soc.* 1982, **104,** 641.

Polyhedron Vol. 5, No. 12, pp. 1975–1982, 1986
Printed in Great Britain

0277–5387/86 $3.00+.00
© 1986 Pergamon Journals Ltd

ELECTROCHEMISTRY OF RHENIUM(V) COMPLEXES WITH BIDENTATE–BIDENTATE AND TRIDENTATE–BIDENTATE SCHIFF BASE LIGANDS

RENATO SEEBER

Dipartimento di Chimica, Università di Siena, Pian dei Mantellini 44, 53100 Siena, Italy

GIAN ANTONIO MAZZOCCHIN

Dipartimento di Spettroscopia ed Elettrochimica, Università di Venezia, Dorsoduro 2137, 30123 Venezia, Italy

and

ULDERICO MAZZI,* FIORENZO REFOSCO and FRANCESCO TISATO

Istituto di Chimica e Tecnologia dei Radioelementi del C.N.R., Area della Ricerca, Corso Stati Uniti 4, 35100 Padova, Italy

(*Received* 24 *February* 1986; *accepted* 7 *May* 1986)

Abstract—The cathodic and anodic behaviour of rhenium(V) complexes, characterized by the ReO^{3+} core, with bidentate and tridentate Schiff base ligands, has been studied in acetonitrile solvent. Cyclic voltammetry and controlled potential coulometry were the main electroanalytical techniques employed to define the electrode processes. Electrolyses were also carried out with the aim to identify the nature of the reduced and oxidized products. In particular, it was possible to isolate and characterize new rhenium(VI) complexes, containing the group ReO^{4+}, and the possibility of obtaining stable rhenium(IV) complexes has also been proved.

Our previous electrochemical studies have been devoted to complexes of rhenium in oxidation states ranging from +1 to +4.[1–3] Oxidizing or reducing these compounds, containing ligands such as carbon monoxide and different phosphines, we were able to prepare and characterize unusual rhenium compounds, as well as to define the electrode mechanisms through which they are formed. Since rhenium is known to assume a wide range of possible oxidation states (from −1 to +7) our attention has now turned toward complexes with the metal in higher oxidation states. In addition to the interest of the chemistry of the complexes of this metal, a further appealing aspect lies in the growing importance of ^{99m}Tc in nuclear medicine; our previous electrochemical studies on complexes of rhenium and technetium[1–6] have allowed us to draw out useful comparisons, as well as to gain, on the basis of the studies on the complexes of the first metal, important suggestions on the properties of those of the latter element.

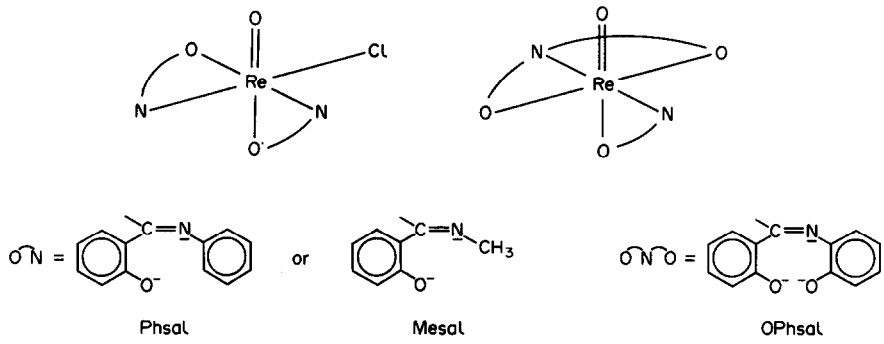
Relatively simple procedures are requested to synthesize rhenium(V) complexes containing the ReO^{3+} core; this atomic group involves specific interesting chemical properties and the resulting complexes exhibit quite satisfactory stability.[7–10] We report here electrochemical studies on Schiff base rhenium(V) complexes of the type $[ReOCl(BSB)_2]$ and [ReO(TSB)(BSB)] where BSB = *N*-methylsalicylideneiminate or *N*-phenylsalicylideneiminate and TSB = *N*-(2-oxidophenyl)salicylideneiminate.

Our aim is to elucidate both anodic and cathodic electrode mechanisms, as well as to characterize the final electrolysis products in which ReO^{2+} or ReO^{4+} cores may be present.

EXPERIMENTAL

Acetonitrile (MeCN) (Fluka-Burdick & Jackson, distilled in glass) was used without further puri-

* Author to whom correspondence should be addressed.



Scheme 1.

fication, storing it under nitrogen on 0.3 nm molecular sieves (Union Carbide).

$NaClO_4$ supporting electrolyte was prepared by neutralizing $HClO_4$ with Na_2CO_3; then it was twice crystallized from hot water and dried at 110°C. $[NEt_4]ClO_4$(TEAP)(C. Erba) supporting electrolyte was dried in a vacuum oven at 50°C and used without further purification.

99.99% pure nitrogen was bubbled through the solutions before the electrochemical tests, in order to remove oxygen.

The synthesis of the studied complexes has been described elsewhere.[7,8,10]

In the voltammetric tests the polarizing unit was a PAR 170 Electrochemistry System; voltammograms were recorded either with a Linseis LY 1800 pen recorder or with a Hewlett-Packard 1223 A storage oscilloscope, depending on the potential scan rate. The stationary working electrode was either a platinum disc (geometrical area of about 5 mm^2) or a gold sphere freshly covered with mercury; they both were surrounded by a platinum spiral counter electrode; the saturated calomel electrode—reference electrode—was connected with the working electrode compartment through a salt bridge ending in a Luggin capillary.

In the controlled potential electrolyses an AMEL model 552 potentiostat with an associated AMEL model 558 coulometer were used; these tests were carried out in an H-shaped cell with anodic and cathodic compartments separated from each other by a sintered glass disc. A platinum gauze was used as working electrode while the auxiliary electrode was a mercury pool.

In the voltammetric as well as in the coulometric experiments, TEAP was used as supporting electrolyte. $NaClO_4$ was employed in exhaustive electrolyses performed with the aim to recover the reduction or oxidation products.

All electrochemical measurements were carried out at 25 ± 0.1°C. The reference electrode was an aqueous saturated calomel electrode (SCE); however, after performing the voltammetric tests, biscyclopentadienyl iron(*II*) was added to the solutions in order to refer the calculated $E'_{1/2}$ to $E'_{1/2}$ of this "internal reference" redox couple. In this way, the measured quantity results are unaffected by variable liquid junction potential at the aqueous–organic solvents interface.

In order to isolate the electrolysis products, namely the cathodic reduction products, different procedures were followed for the different compounds. In particular, the solutions after reduction of $[ReOCl(BSB)_2]$ complexes were dried removing MeCN solvent under reduced pressure and the resulting solids were washed with $CHCl_3$ to solubilize the rhenium complexes; after filtering, this last solvent was also removed and the pure solid was analyzed by elemental analysis, IR spectroscopy and magnetic moment measurement. All these recovery procedures were performed carefully avoiding the presence of oxygen and by using deaerated solvents. A similar procedure was followed for the reduction products of [ReO(TSB)(BSB)]; however, it was observed that decomposition and/or reoxidation of the electrolysis products could be avoided only if the solid obtained after removal of MeCN was treated with a very small amount of a protic solvent, typically ethanol.

IR spectra were recorded on a Perkin-Elmer model 580B spectrometer. Magnetic moment measurements were performed with an Oxford Instrument.

RESULTS AND DISCUSSION

$[ReOCl(BSB)_2]$

Cathodic behaviour. Figure 1 reports the voltammetric behaviour of the complex $[ReOCl(Phsal)_2]$ in acetonitrile solution. A first reversible elec-

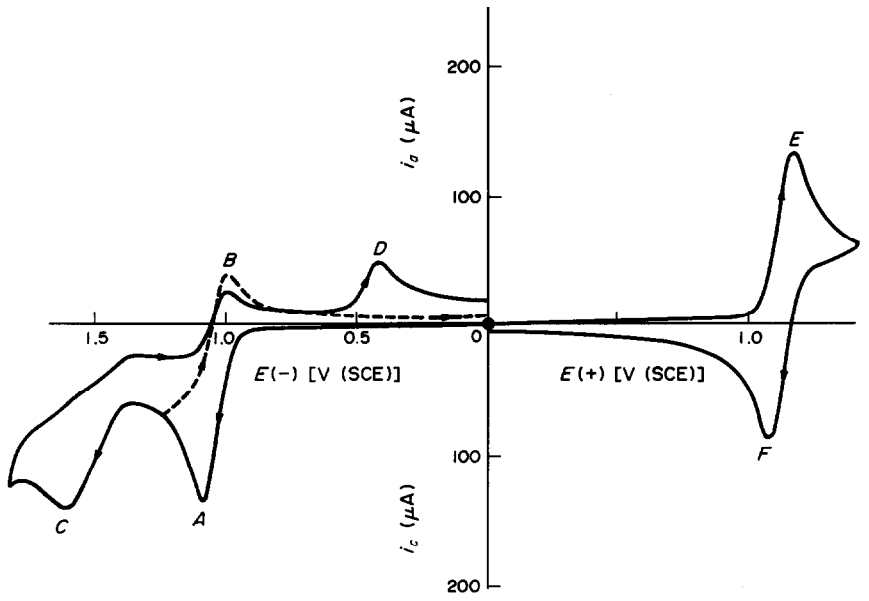


Fig. 1. Cyclic voltammograms recorded on a 4.9×10^{-3} M [ReOCl(Phsal)$_2$], 0.1 M TEAP, and MeCN solution. Platinum working microelectrode; potential scan rate, 0.2 V s^{-1}. (●) Starting potential.

trode reduction leads to a species which is stable enough on the short voltammetric time scale (the ratio of backward to forward peak currents relative to the peaks system A–B is always quite near to one). Exhaustive coulometric electrolyses at peak A lead to a consumption of 1 mol of electrons per mole of starting compound. Voltammetric curves recorded on the electrolysed solutions show a further reduction peak at potential values quite near those of peak C; in addition, the reduced complex is oxidizable at an anodic peak, rather low in height, which corresponds to peak D of Fig. 1, but no peak is recorded at the potential of peak B.

Oxidizing the reduced solutions at a potential only just less cathodic than those where oxidation of the starting complex occurs, this last can be regenerated with a good yield (*ca.* 60–70%).

The analysis of the reduced solutions reveals the presence of free chloride ions; accordingly, performing electrolyses using $NaClO_4$ as supporting electrolyte, NaCl is precipitated. Moreover, from these solutions the reduced rhenium complex can be recovered and characterized following the procedure described above. The elemental analysis data are as follows (found: C, 52.4; H, 3.4; N, 4.8. Calc. for $C_{26}H_{20}ReN_2O_3$: C, 52.5; H, 3.4; N, 4.7%). Two most significant data can be drawn from the IR spectra. The ν(Re—Cl) absorption, located at 311 cm^{-1} in the spectrum of the starting complexes, is now absent, in agreement with the presence of free chloride ions in the reduced solution. On the contrary the ν(Re=O) is still present, at a wavenumber value quite close to that for the starting complex (960 cm^{-1}). Magnetic susceptibility measurements on solid samples at room temperature lead to $\mu_{eff.} = 1.96$ B.M., in agreement with a d^3 configuration in a square pyramidal environment, as reported by Hoffman *et al.*[11]

The compound is soluble in EtOH, CH_2Cl_2, $CHCl_3$ and MeCN, and insoluble in Et_2O and C_6H_6. However, it slowly decomposes in chlorinated solvents and no physico-chemical measurements could be performed on these solutions.

Accordingly with the reported data the more probable configuration can be the one in Fig. 2. The stereochemical position of the two bidentate Schiff base in the horizontal square pyramidal plane can be deduced from the possible reaction mechanism leading to the product. In fact after the electrode reaction the chlorine atom is the most probable leaving group. The substitution with the phenolic oxygen of the ligand allows the formation of the product without the detaching of the whole ligand and consequently the reproduction of the starting compound both by electrochemical and chemical oxidation.

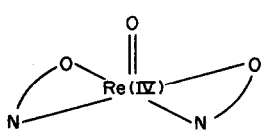


Fig. 2. Schematic drawing of the rhenium(IV) compound obtained by cathodic reduction of [ReOCl(Phsal)$_2$]. $\widehat{NO}$ = Phsal.

On the basis of these findings, the electrode reduction mechanism at peak A can be summarized as follows:

$$[ReOCl(Phsal)_2] + e^- \rightleftarrows [ReOCl(Phsal)_2]^- \quad (1)$$

$$[ReOCl(Phsal)_2]^- \rightarrow [ReO(Phsal)_2] + Cl^- \quad (2)$$

Since oxidation of $[ReO(Phsal)_2]$ to the starting compound requires the uptake of a chloride ion in a 1 : 1 ratio, it is reasonable that the regeneration of $[ReOCl(Phsal)_2]$ can occur only with a non-quantitative yield. The slowness of the chemical reaction following the reduction charge transfer step allows the evaluation of $E'_{1/2}$ for the couple $[ReOCl(Phsal)_2]/[ReOCl(Phsal)_2]^-$, which results equal to -1.43 V (referred to $E'_{1/2}$ of the ferricinium ion/ferrocene couple).

As to the electrode process occurring at peak C, it involves the uptake of one further electron, but this reduction is followed by irreversible decomposition reactions leading to products which could not be identified.

$[ReOCl(Mesal)_2]$ exhibits an electrochemical behaviour which is only qualitatively similar to that of the corresponding Phsal complex. In fact, the cathodic reduction of $[ReOCl(Mesal)_2]$ shows some significant differences; as to the voltammetric behaviour, the anodic peak directly associated to the first cathodic one does not result, at any potential scan rate, as high as required for a backward to the forward peak-currents-ratio equal to one. In particular, this ratio increases increasing the potential scan rate, reaching unity only for a high enough value of this experimental parameter. Also in this case, in controlled potential coulometries at potentials of the first reduction peak, 1 mol of electrons per mole of starting complex is spent, and chloride ions are present in the solution. The voltammograms of these electrolyzed solutions show that the product can be further reduced corresponding to a peak with $(E_p)_c \simeq -1.55$ V vs SCE and oxidized at a peak ($(E_p)_a \simeq +0.6$ V vs SCE) with a small directly associated cathodic peak. Also in this case we have tried to isolate the reduction product following the same procedure, but when $CHCl_3$ is used it is quickly converted to the starting complex. Nevertheless, since after reduction insoluble NaCl is recovered, also in this case the same reduction mechanism, previously outlined for $[ReOCl(Phsal)_2]$, can be hypothesized, even if the voltammetric data agree with a faster release of the chloride ion by the electrogenerated anionic species. On the basis of the trend of the backward to forward peak currents ratio at varying the potential scan rate,[12] a half-life time of about 0.2 s (at 25 ± 0.1°C) can be evaluated for the directly electrogenerated species. Cyclic voltammograms recorded at high enough potential scan rate, allow us to calculate $E'_{1/2}$, $[ReOCl(Mesal)_2]/[ReOCl(Mesal)_2]^- = -1.54$ V (vs $E'_{1/2}$ of the couple ferricinium ion/ferrocene).

As to the reduction and oxidation processes this reduced compound undergoes, while its further reduction, involving the consumption of 1 mol of electrons per mole of starting complex, does not lead to any stable rhenium complex, electrode oxidation at a potential of $+0.7$ V vs SCE allows one to regenerate the starting compound at a yield higher than 60%. It must be taken into account that the presence in the solution of free chloride ions, which strongly adsorb on the platinum electrode surface, prevents the recording of completely reliable voltammetric curves in the anodic potential region, as well as carrying out satisfactory electrolysis tests at those potentials.

As regards the electrode reduction of both the studied $[ReOCl(BSB)_2]$ complexes, completely similar results are obtained by using a mercury microelectrode, with respect to both shape and location of the cathodic voltammetric peaks, as well as to the trend of the peak currents ratio at varying the potential sweep rate. These facts allow us to conclude that the charge transfer occurs via an outer sphere electrode mechanism.[13]

Anodic behaviour. As shown in Fig. 1, $[ReOCl(Phsal)_2]$ undergoes a reversible electrode oxidation. Controlled potential coulometries reveal it is a one-electron oxidation; furthermore, the charge transfer is not complicated by any following chemical reaction, neither on the voltammetric nor on the exhaustive electrolysis time scale. In fact, the ratio between backward and forward peak currents is equal to one for any potential scan rate and, even more significantly, cyclic voltammetry after exhaustive oxidation shows the same reversible peaks system (see Fig. 3). Of course, peak F is first recorded in a forward cathodic scan starting at a potential of about $+1.5$ V vs SCE and peak E is recorded as an associated peak if the potential scan direction is reversed after traversing peak F. If, on the contrary, the cathodic scan goes on, the peaks systems reported in the cathodic potentials region of Fig. 1 are recorded, suggesting that the starting complex is regenerated at the potentials of peak F. Accordingly, exhaustively reducing, at the potentials of peak F, solutions of $[ReOCl(Phsal)_2]$ previously oxidized at peak E, the starting compound is regenerated with a yield very near 100%.

Quite a similar behaviour is exhibited by the compound $[ReOCl(Mesal)_2]$, as regards both voltammetric and coulometric–voltammetric results.

These findings allow us to propose a method to prepare via electrochemical procedures stable

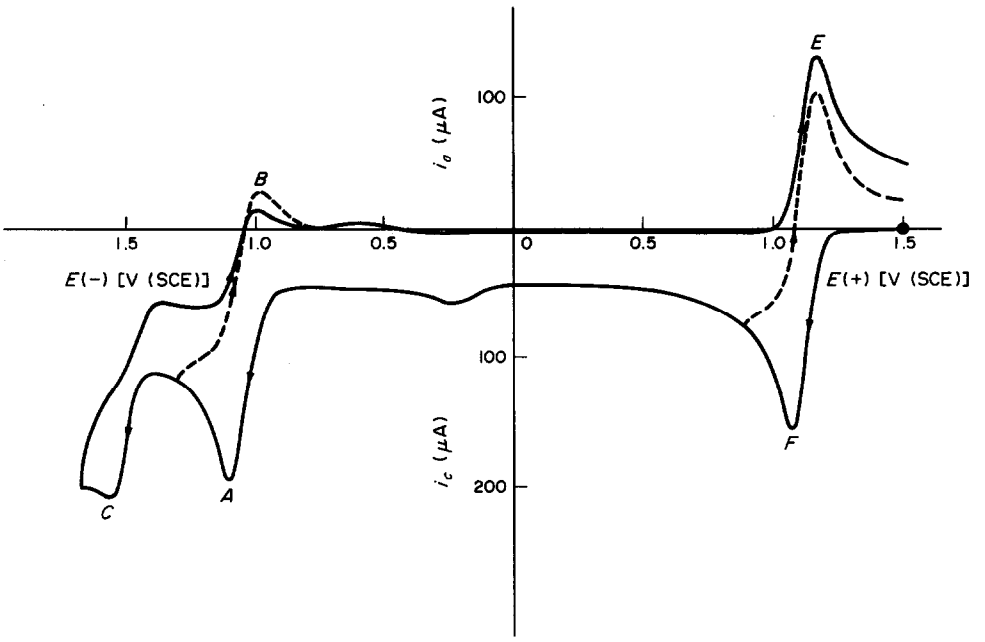


Fig. 3. Cyclic voltammograms recorded on a 4.9×10^{-3} M [ReOCl(Phsal)$_2$] solution, previously oxidized exhaustively in correspondence to peak E of the curve in Fig. 1. Same experimental conditions as for the voltammograms in Fig. 1. (●) Starting potential.

rhenium(VI) complexes containing the ReO^{4+} core.

On the basis of the voltammetric tests the following $E'_{1/2}$ values can be calculated: $E'_{1/2}$, $[ReOCl(Phsal)_2]^+/[ReOCl(Phsal)_2] = +0.76$ V; $E'_{1/2}$ $[ReOCl(Mesal)_2]^+/[ReOCl(Mesal)_2] = +0.67$ V (vs $E'_{1/2}$ of the couple ferricinium ion/ferrocene).

[ReO(TSB)(BSB)]

Cathodic behaviour. Figure 4 illustrates the voltammetric behaviour of [ReO(OPhsal)(Phsal)] in acetonitrile solution. It is evident that no anodic response directly associated to the cathodic peak A can be recorded at the potential scan rate employed to draw the figure (0.2 V s^{-1}). Only at sweep rates higher than 2 V s^{-1} the peak attributable to the oxidation of the species primarily formed at the electrode can be noted, with a relative height progressively increasing at increasing the scan rate. On the basis of the dependence on this last experimental parameter of the ratio $(i_p)_{backward}/(i_p)_{forward}$, of the results of a series of voltammetric measurements

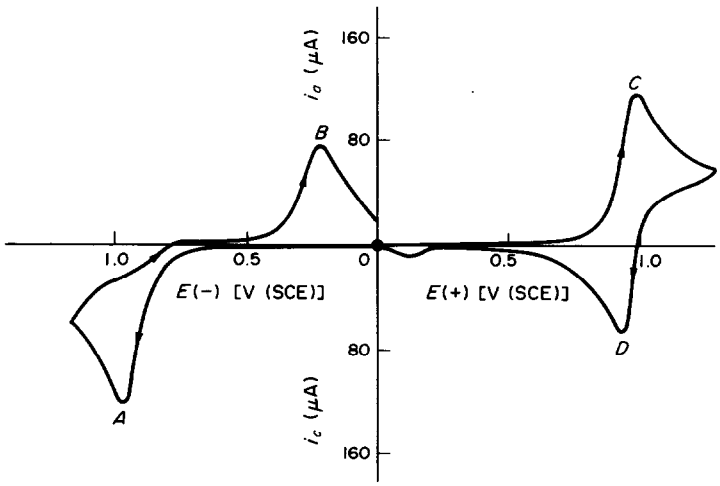


Fig. 4. Cyclic voltammograms recorded on a 4.5×10^{-3} M [ReO(OPhsal)(Phsal)], 0.1 M TEAP, and MeCN solution. Platinum working microelectrode; potential scan rate, 0.2 V s^{-1}. (●) Starting potential.

with different depolarizer concentrations, of chronoamperometric tests and, finally, of the coulometric datum (1 mol of electrons per mole of electrolyzed compound is spent), it is possible to conclude that the electrode reduction consists in an EC mechanism, were a one-electron reversible charge transfer is followed by a first order irreversible chemical reaction. The cyclic voltammetric curves at different potential scan rates allow us to estimate a half-life time of about 25 ms for the short-lived electrogenerated species. The $E'_{1/2}$ value of the couple [ReO(OPhsal)(Phsal)]/[ReO(OPhsal)(Phsal)]$^-$ can be estimated only approximately ($\simeq -1.33$ vs $E'_{1/2}$ of the couple ferricinium ion/ferrocene).

Voltammetric curves recorded on the exhaustively electrolyzed solutions appear as those shown in Fig. 5. During a sweep starting at the potential of the electrolyses performed, peak B is recorded. By switching the potential after traversing this anodic peak, peak A, attributable to the reduction of the complex [ReO(OPhsal)(Phsal)], is recorded. If, on the contrary, the anodic sweep continues towards more positive potentials, the same peaks (system C/D) recorded on solutions of the starting complex, can be noted. Accordingly, electrolysing the reduced solutions at a potential of 0.0 V vs SCE, the starting complex is quantitatively regenerated through the consumption of 1 mol of electrons per mole of compound.

Solutions of the starting compound were also exhaustively reduced in order to identify the final electrolysis products. As we have already mentioned in the Experimental section, through the usual procedure involving dissolution of the reduction product in $CHCl_3$, even if it was carried out in carefully deoxygenated media, we did not manage to avoid that the compound partially decomposed and partially regenerated the starting complex. However, the product was stabilized by treating it with ethanol. Recalling that the voltammetric results suggest that the primary reduction product, [ReO(OPhsal)(Phsal)]$^-$, undergoes a fast chemical reaction leading to a complex that, by oxidation regenerates the starting compound, we can suppose that the chemical reaction consists in the release by the metal centre of one phenolic site of the tridentate ligand, as a consequence of the reduced positive charge on rhenium. On the other hand if, through electrode oxidation, we increase back the rhenium oxidation state, the initial situation is re-established. In this context, the role of the protic solvent in stabilizing the reduction product may consist in the protonation of the free phenolic site. Accordingly, the solubility of the product in MeCN results is noticeably lower after protonation.

The elemental analysis data are as follows (found: C, 44.9; H, 2.7; N, 3.9. Calc. for

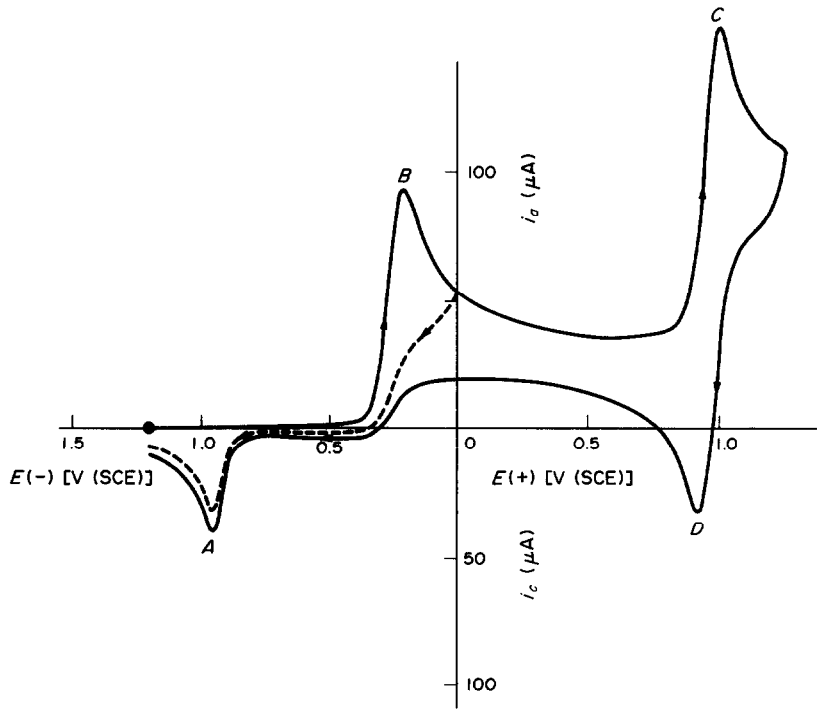


Fig. 5. Cyclic voltammograms recorded on a 4.5×10^{-3} M [ReO(OPhsal)(Phsal)] solution, previously reduced exhaustively at peak A of the curve in Fig. 4. Same experimental conditions as for the voltammograms in Fig. 4. (●) Starting potential.

$C_{26}H_{20}ReN_2O_4$: C, 51.1; H, 3.3; N, 4.6%). The compound could not be further purified owing to the continuous transformation back to the starting complex. For this reason the elemental analyses are not in agreement with the formulation but the C:N:H ratio are consistent with the presence of two ligands in the product and presumably the impurities are due to inorganic compounds.

IR spectra of the recovered reduction products show a significant lowering of the wavenumber of the ν(Re=O) absorption (a shift of about 50 cm^{-1}). This result is in apparent disagreement with that obtained on the reduction product of [ReOCl(Phsal)$_2$], but a weakening of the Re=O bond can be explained assuming the formation of an intramolecular hydrogen bond.

On these bases, and considering, as reported above, only the leaving of the phenolic groups, we propose the formulation reported in Fig. 6 for the product of the [ReO(OPhsal)(Phsal)] reduction.

The compound is soluble in EtOH, MeOH and MeCN and insoluble in Et_2O and pentane; moreover, it easily regenerates the starting complex in CH_2Cl_2, $CHCl_3$, C_6H_6 and acetone.

The results obtained with the complex [ReO (OPhsal)(Mesal)] are only qualitatively similar. Apart from the exact values of the potentials at which the different peaks are recorded, Fig. 4 is still useful to discuss the electrochemical behaviour of this compound. The main differences lie in the lower stability of the electrogenerated species [ReOCl (OPhsal)(Mesal)]$^-$ (half-life time of about 5 ms), and in the value of $E^r_{1/2}$ for the couple [ReO (OPhsal)(Mesal)]/[ReO(OPhsal)(Mesal)]$^-$, which resulted equal to about -1.37 V (vs $E^r_{1/2}$ of the couple ferricinium ion/ferrocene).

Also in this case the reduced solution can be reoxidized at a potential noticeably anodic in respect to the potentials of the cathodic peak (see, qualitatively, peak B in Fig. 5), regenerating quantitatively the starting complex.

The recovery of the reduction product has been more difficult in respect to the corresponding Phsal complex, because it exhibits a marked tendency to regenerate the starting compound if only small traces of oxidizing agents such as oxygen or water, are present. It was only possible to recover a mixture of starting complex and reduced product. IR spectra of this mixture show a first ν(Re=O) band at 924 cm^{-1}, attributable to the reduction product and a second ν(Re=O) band at 957 cm^{-1}, due to the starting complex. The formulation of this compound can be assumed as reported in Fig. 6 by analogy with the previous one.

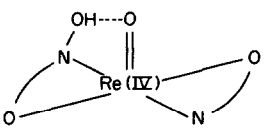


Fig. 6. Proposed scheme for the rhenium(IV) molecule obtained by cathodic reduction of [ReO(OPhsal)(Phsal)], after treatment with ethanol. $\widehat{NO}$ = Phsal and $\widehat{ONOH}$ = HOPhsal.

Also for these tridentate–bidentate compounds, completely similar results are obtained using mercury as the working electrode material.

Anodic behaviour. As Fig. 4 shows for the complex [ReO(OPhsal)(Phsal)], both the [ReO(TSB) (BSB)] compounds undergo reversible oxidation. The oxidized species are stable on the voltametric time scale, so much so that backward to forward peak ratios equal unity also at the lowest (50 mV s^{-1}) potential scan rate used. Controlled potential electrolyses allows one to ascertain that the electrode processes involve a one-electron charge-transfer; however the oxidized species are not stable at the longer electrolysis times and voltammetric tests after electrolyses do not show the peak system C/D giving any interesting information about the presence in the solution of some particular rhenium complex either. Many attempts to recover the oxidation products have been performed. Unfortunately, even if different procedures have been tried, a brown oil was always obtained and all attempts to obtain crystalline products has failed.

On the basis of the voltammetric data it is possible to evaluate $E^r_{1/2}$, [ReO(OPhsal)(Phsal)]$^+$/[ReO(OPhsal)(Phsal)] = +0.57 V, and $E^r_{1/2}$, [ReO (OPhsal)(Mesal)]$^+$/[ReO(OPhsal)(Mesal)] = +0.53 V (vs $E^r_{1/2}$ of the couple ferricinium ion/ferrocene).

As a final consideration, let us observe that the relative values of the $E^r_{1/2}$ calculated for the eight redox couples identified result in agreement with the different electron withdrawing effects of methyl and phenyl groups. In fact, both as regard [ReOCl(BSB)$_2$] and [ReO(TSB)(BSB)], the resulting $E^r_{1/2}$ values for neutral/anionic and cationic/neutral redox couples are more positive for BSB = Phsal than for BSB = Mesal.

From the recovery products point of view, the complexes have shown the presence of Re=O oxo moiety. This fact is particularly important if it is considered that the Re=O group was found in the same complex with rhenium atom in three different oxidation states: VI, V and IV.

To date the principal example of the ReO^{4+} core was given by the complex $[ReOCl_5]^-$ [14,15] and in a few of its substitution products.[16] The ReO^{2+} core was never clearly authenticated.

In particular the oxo oxygen in the fourth oxi-

dation state was always considered bound to a hydrogen atom, for example in the $[Re(OH)Cl_3(PEt_2Ph)_2]$ compound reported by Duatti *et al.*[17] and the formal oxidation state of oxogroup was −1. Concerning the $[ReO(BSB)_2]$ complexes, only phenyl protons can interact with the oxo group, while in the case of [ReO(TSB)(BSB)] complexes a phenolic hydrogen can bind Re=O; however, in both cases oxo group is considered in −2 formal oxidation state.

REFERENCES

1. R. Seeber, G. A. Mazzocchin, E. Roncari and U. Mazzi, *Transition Met. Chem.* 1981, **6**, 123.
2. E. Roncari, U. Mazzi, R. Seeber and P. Zanello, *J. Electroanal. Chem.* 1982, **132**, 221.
3. R. Seeber, G. A. Mazzocchin, U. Mazzi, E. Roncari and F. Refosco, *Transition Met. Chem.* 1984, **9**, 315.
4. G. A. Mazzocchin, R. Seeber, U. Mazzi and E. Roncari, *Inorg. Chim. Acta* 1978, **29**, 1.
5. G. A. Mazzocchin, R. Seeber, U. Mazzi and E. Roncari, *Inorg. Chim. Acta* 1978, **29**, 5.
6. U. Mazzi, E. Roncari, R. Seeber and G. A. Mazzocchin, *Inorg. Chim. Acta* 1980, **41**, 95.
7. U. Mazzi, E. Roncari, R. Rossi, V. Bertolasi, O. Traverso and L. Magon, *Transition Met. Chem.* 1980, **5**, 289.
8. A. Marchi, A. Duatti, R. Rossi, L. Magon, U. Mazzi and A. Pasquetto, *Inorg. Chim. Acta* 1984, **81**, 15.
9. U. Mazzi, F. Refosco, G. Bandoli and M. Nicolini, *Transition Met. Chem.* 1985, **10**, 121.
10. U. Mazzi, F. Refosco, F. Tisato, G. Bandoli and M. Nicolini, *J. Chem. Soc., Dalton Trans.* 1986, 1623.
11. R. Hoffman, M. M. L. Chen, M. Elian, A. R. Rossi and D. M. P. Mingos, *Inorg. Chem.* 1974, **13**, 2666.
12. R. S. Nicholson and I. Shain, *Analyt. Chem.* 1964, **36**, 706.
13. V. I. Kravtsov, *J. Electroanal. Chem.* 1976, **69**, 125.
14. T. Lis and B. Jezowska-Trzebiatowska, *Acta Cryst.* 1982, **B33**, 1248.
15. B. J. Brisdon and D. A. Edwards, *Inorg. Chem.* 1968, **7**, 1897.
16. G. Rouschias, *Chem. Rev.* 1974, **74**, 531.
17. M. Sacerdoti, V. Bertolasi, G. Gilli and A. Duatti, *Acta Cryst.* 1982, **B38**, 96.

Polyhedron Vol. 5, No. 12, pp. 1983–1986, 1986
Printed in Great Britain

0277–5387/86 $3.00+.00
© 1986 Pergamon Journals Ltd

PYROPHTHALONE AND ITS DERIVATIVES AS LIGANDS—I. MODE OF COORDINATION—FORMATION OF ISOMERIC IMINOPYROPHTHALONE COMPLEXES

M. MITEWA and P. R. BONTCHEV*

Department of Chemistry, University of Sofia, 1126 Sofia, Bulgaria

M. KASHCHIEVA and S. MINCHEV

High Pedagogical Institute, Shoumen, Bulgaria

V. BARDAROV

Institute of Hygiene and Occupational Health, Sofia, Bulgaria

and

G. WERNER

Department of Chemistry, Karl Marx University, Leipzig, G.D.R.

(*Received* 25 *March* 1986; *accepted* 7 *May* 1986)

Abstract—The complex formation of Co(II), Ni(II), Zn(II) with aminopyrophthalone was studied by means of electronic, IR, EPR and ^{1}H–NMR spectroscopy. It was established that with Co(II) and Ni(II) two isomeric complexes are formed in contrast to Zn(II) and Cu(II) complex formation. On the basis of the spectral data obtained the coordination mode and structure of the complex species are assumed.

We have already studied the complexation properties of some derivatives of 1,3-indandione, namely of 2-(2-pyridyl)-1,3-indandione or pyrophthalone (PPH), 2-(2-quinolyl)-1,3-indandione or quinophthalone (QPH) and 3-amino-2-(2-pyridyl)-indenone or iminopyrophthalone (IPH) towards some transition metal ions.[1–3] These ligands are used as dyes, organic semiconductors, and anti-inflammatory and anaesthetic agents.[4–8] The structure of the pyrophthalone and iminopyrophthalone complexes with Cu(II)—one of the most important biometals, was studied in detail.[1,2] In the present paper the results obtained for the Co(II), Ni(II) and Zn(II) complexes of iminopyrophthalone are reported, emphasizing mainly the mode of coordination of the ligand.

EXPERIMENTAL

The electronic and IR spectra were obtained on recording spectrometers "Specord UV–vis", "Specord 71 IR", VEB Carl Zeiss-Jena and Perkin-Elmer 983 (CsI discs, spectral range 4000–200 cm^{-1}). The EPR spectra were recorded on X-band EPR-spectrometer ERS-220 (G.D.R.), the ^{1}H–NMR on FT–NMR spectrometer "Bruker WP-200". The HPLC experiments were performed on Perkin-Elmer LC system consisting of a series of four solvent delivery system connected with 8-μl flow cell of 550 SE UV–Vis spectrometer.

Synthetic procedures

IPH was obtained and purified as described previously.[1] The complexes $Co(IP)_2$, $Ni(IP)_2$ and $Zn(IP)_2$ were obtained in slightly acidic medium (pH ~ 4–5) mixing ethanolic solution of IPH (5×10^{-3} M) with water solution of the corresponding metal salt [$M''Cl_2$ or $M''(NO_3)_2$] at 40°C (metal to ligand ratio 1 : 2). The corresponding complexes were precipitated after careful neutralization of the solution with 0.1 M NaOH. The products

* Author to whom correspondence should be addressed

Table 1. Analytical and electronic spectral data

Comp.	% N calc.	% N found	% Me[a] calc.	% Me[a] found	λ_{max},[b] nm
IPH	12.6	12.8 12.7			333; 352
$Co(IP)_2$	11.2	10.9 10.8	11.7	11.4	330; 350; 398
$Ni(IP)_2$	11.2	10.9 10.8	11.7	11.5	336; 348
$Zn(IP)_2$	11.0	11.5 11.6	12.9	12.4	336; 348; 380

[a] Average of three measurements.
[b] Solvent acetonitrile (An).

were filtered off, washed with ethanol and dried for a week over P_2O_5 under low pressure.

Analytical data

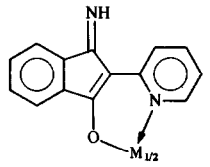
Elemental analysis of N was provided according to Kjeldahl (treatment for 12 h). Nickel and zinc were determined complexometrically at pH 10 and indicators murexide for nickel and eriochrom T for zinc after ashing the sample and dissolving the residue in HNO_3 (2:1). Cobalt was determined photometrically with nitroso-R-salt at $\lambda = 500$ nm after wet oxidative destruction of the sample with conc. HNO_3, evaporation near dryness and dissolving the residue in water.

RESULTS AND DISCUSSION

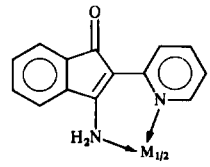
The analytical data obtained show that the complexes thus formed have a metal to ligand ratio of 1:2. Their formation is connected with the appearance of a new band in the visible spectra of the complexes (see Table 1).

In order to obtain some structural information IR, EPR and ^{1}H–NMR investigations were provided. In Table 2 the IR data obtained for the complexes studied together with that for $Cu(IP)_2$[1] are presented.

It is evident that the IR spectral data for $Zn(IP)_2$ are very similar to that of $Cu(IP)_2$, showing a similarity of their mode of coordination as well. For $Cu(IP)_2$ chelation through enolic oxygen and nitrogen atom from the pyridyl ring (str. I) has been found. By means of EPR and magnetic susceptibility data a depressed tetrahedral or rhombic symmetry with slightly mis-aligned tetragonal axes was assumed.[1,2]



I



II

The IR data for the Co(II) and Ni(II) complexes show the simultaneous presence of carbonyl, imino- and amino (ν^s and ν^{as}) vibrations. Therefore simultaneous formation of two isomeric complexes (str. I and II) of Co(II) and Ni(II) should be assumed. These results are in agreement with the HPLC and ^{1}H–NMR data obtained. The chromatograms of Cu(II) and Zn(II) complexes show one single peak, while these of Co(II) and Ni(II) complexes show two peaks (Fig. 1), thus suggesting the presence of two isomeric species.

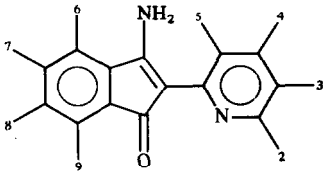
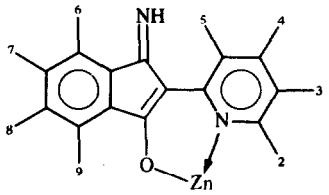
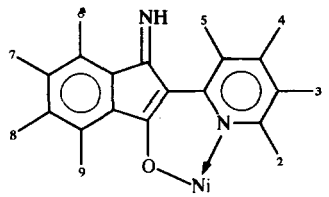
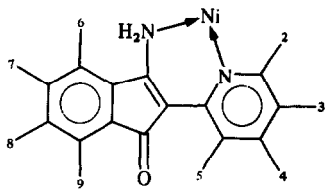
The ^{1}H–NMR data obtained for $Ni(IP)_2$ and $Zn(IP)_2$ in the range 0–20 ppm together with that

Table 2. Selected IR data for IPH and its complexes

IPH (cm^{-1})	$Co(IP)_2$ (cm^{-1})	$Ni(IP)_2$ (cm^{-1})	$Cu(IP)_2$ (cm^{-1})	$Zn(IP)_2$ (cm^{-1})	Assignment
1500 s	1480 s	1475 s	1488 s	1490 s	Vibrations of the phthalone system[8]
1515 s	—	—	—	1535 s	
—	1565 s	1565 s	1552 s	1555 s	
1590 s	—	1595 s	—	1575 m	
1620 s	1610 s	1620 sh	1602 s	1610 m	
—	1650 m	1640 sh	1650 m	1640 m	$\nu_{C=N}$[1,9]
1730 m	1728 m	1725 s	—	—	$\nu_{C=O}$[1]
3150 m	3230 br	3200 br	—	—	$\nu^s_{NH_2}$[1,10]
3320 m	3430 br	3400 v.br	—	—	$\nu^{as}_{NH_2}$[1,10]
—	3240 w	3280 w	3280 m	3290 m	$\nu_{=NH}$[1,9]

s ≡ strong; m ≡ medium; w ≡ weak; br ≡ broad; v.br ≡ very broad; sh ≡ shoulder.

Table 3. ^{1}H-NMR data (solvent DMSO-d_6)

Compound	H_2	H_3	H_4	H_5	$H_{6/9}$		$H_{7/8}$	NH_2	=NH
	d 8.39 8.43	tr 6.96 7.00 7.03	q 7.82 7.80 7.78 7.76	d 8.45 8.47	m 7.70		m 7.74	d 9.26 10.23	—
	d 9.08 9.12	tr 6.92 6.94 6.98	d 7.78 7.79	s 8.30	H_6 d 7.70 7.71	H_9 s 8.93	m 7.50	—	s 10.1
	s 9.22	s 6.96	s 7.74	s 8.41	s 7.64	s 9.80	s 7.32	—	s 10.2
	s 9.22	s 6.96	s 7.74	s 8.41	s 7.64	s 9.58	s 7.39	d 14.4 14.88	—

s ≡ singlet, d ≡ doublet, tr ≡ triplet, q ≡ quartet, m ≡ multiplet.

of IPH were assigned[1] and summarized in Table 3. They are also consistent with the conclusions made above.

The comparison of IPH and $Zn(IP)_2$ spectra indicates on the Zn(II) chelation through enolic oxygen and nitrogen from pyridyl ring. In $Zn(IP)_2$ spectrum instead of NH_2 doublet at 9.26 and 10.23 ppm[1] a new peak at 10.1 ppm due to =NH group appears. The doublet of H_2 proton is strongly shifted and the multiplet due to $H_{6/9}$ protons is affected as well, namely a doublet at 7.70 ppm is observed, assigned to the H_6 proton and the new peak at 8.93 ppm should be assigned to the H_9 proton. The shifts of the H_2 and H_9 protons signals indicates the coordination of Zn(II) to the neighbouring N- and O-atoms respectively.

In the $Ni(IP)_2$ spectrum a greater number of signals is observed. A new low-field doublet (14.4 and 14.9 ppm) is present due most probably to coordinated NH_2 group and an =NH singlet is also observed indicating the presence of the other isomer. In this case the H_2 proton neighbouring the pyridyl nitrogen is also shifted as well as the signals due to H_5 and H_9. For H_9 two different peaks are observed, due most probably to the H_9 protons of the two isomers.

The EPR study of the $Co(IP)_2$ complex [powder sample, diamagnetically diluted with $Zn(IP)_2$] in the range 700–5700 Oe at −190°C showed that only one almost isotropic singlet line ($g = 2.002 \pm 0.001$) was observed, thus proving the oxidation state +2 for the complex. According to the literature data[11] the EPR results show that for the $Co(IP)_2$ complex a planar structure seems more likely than a tetrahedral one.

The fact that Co(II) and Ni(II) are forming two isomeric complexes with IPH in contrast to Cu(II) and Zn(II) is rather surprising taking into account the very close values of their ionic radii.[12] Most probably the simultaneous formation of the two

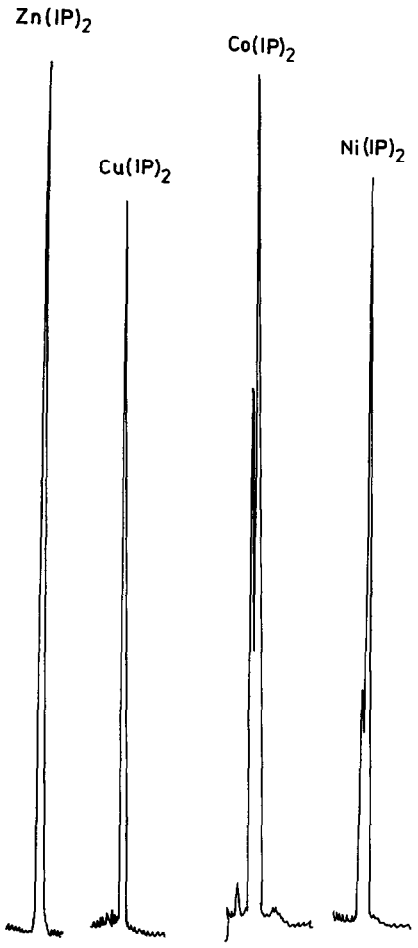


Fig. 1. HPLC data. PE—analytical column (25 cm × 4.6 mm). HC—ODS (10 μ), isocratic separation with mobile phase An : water (60% : 40%), 1 ml/min. Spectrophotometric detection at λ = 210 nm.

different types of complexes with Co(II) and Ni(II) is due to a proper steric orientation and energy level of the nitrogen atom orbitals of NH_2 group, for which overlapping with *d*-orbitals only of Co(II) and Ni(II) is possible.

REFERENCES

1. P. R. Bontchev, M. Mitewa, S. Minshev, M. Kashchieva and D. Mechandjiev, *J. Prakt. Chem.* 1983, **325**, 803.
2. M. Mitewa, P. R. Bontchev, A. Malinovski, M. Kashchieva and S. Minchev, *C. r. Acad. Bulg. Sci.* 1983, **36**, 1311.
3. M. Mitewa, P. R. Bontchev, V. Enchev, S. Minchev and M. Kashchieva, *J. Prakt. Chem.* 1985, **327**, 516.
4. B. K. Manukian and A. Mangini, *Chimia* 1970, **24**, 382.
5. M. Tomanek-Kunitzer, F.R.D.-patent No. 1265582 (1968).
6. J. Ploquin, L. Sparfel, G. le Bant, L. Welin, I. Y. Petit and N. Henry, *Chim. Ther.* 1973, 350.
7. G. le Bant, L. Sparfel, J. Ploquin, I. Y. Petit, N. Henry and L. Welin, *Bull. Soc. Pharm. de l'Ouest* 1973, **15**, 43.
8. I. J. Neiland and J. J. Katzen, *Khim. Geterozikl. Soed.* 1975, 435.
9. J. F. Freimanis and G. J. Vanag, *J. Obsch. Khim.* 1964, **34**, 452.
10. K. Nakamoto, *Infrared and Raman Spectra of Inorganic and Coordination Compounds*, 3rd edn. Wiley Interscience, New York (1978).
11. H. A. Kuska and M. T. Rogers, *Electron Spin Resonance of First Row Transition Metal Complex Ion.* Wiley Interscience, New York (1968).
12. L. Ahrens, *Geochim. Cosmochim. Acta* 1952, **2**, 155.

Polyhedron Vol. 5, No. 12, pp. 1987–1990, 1986
Printed in Great Britain

0277-5387/86 $3.00+.00
© 1986 Pergamon Journals Ltd

SYNTHESIS AND CRYSTAL STRUCTURE OF A NEW NICKEL(II)–TERPYRIDINE COMPLEX: [Ni(terpy)(NO_2)(ONO)(H_2O)]

ROBERTO CORTES, M. ISABEL ARRIORTUA, TEOFILO ROJO,* XAVIER SOLANS† and DANIEL BELTRAN‡

Departamentos de Química (Inorgánica) y Cristalografía, Universidad del País Vasco, Aptdo. 644, 48080 Bilbao, Spain

(*Received* 28 *January* 1986; *accepted* 7 *May* 1986)

Abstract—The compounds Ni(terpy)$Cl_2 \cdot 3H_2O$ and $NaNO_2$ react readily in aqueous solution to give the complex [Ni(terpy)(NO_2)(ONO)(H_2O)], which has been structurally characterized by an X-ray diffraction study. The hexacoordinate nickel atom bonds to three nitrogen atoms of the terpyridine ligand, to a "nitro" group, to a "nitrite" group and to a water molecule. Distortion from an octahedron to a trigonal prism, for the complex, has been evaluated. An infrared study of the complex has been carried out and shows bands of nitro and nitrite coordination. Magnetic study reveals a Curie–Weiss behavior, giving an effective magnetic moment at room temperature 3.12 B.M.

The nitrite group is unusual because of the number of different ways in which it can coordinate to a metal.[1] As a monodentate ligand it can bond via either nitrogen or oxygen, while as a bidentate ligand it can chelate or bridge either via nitrogen and oxygen or via a single oxygen atom. The factors influencing the type of nitrite coordination adopted are often delicately balanced.

The ligand 2,2′:6′,2″-terpyridine(terpy) forms two types of complexes when it reacts with one bivalent transition metal in 1:1 ratio, M(terpy)X_2 and [M(terpy)X]Y (X, Y = (pseudo)halide or counterion). The former leads to discrete monomeric molecules,[2,3] while the latter gives rise to polynuclear species in which the X atom acts as a bridging ligand, causing magnetic interactions.[4]

In recent years the work carried out in our laboratories has been based on the coordination studies of both types of complex to explain their physical properties. Only one structure of a monoterpyridine nickel(II) complex has been reported so far.[5]

In order to advance this work we have studied this Ni–nitrite complex.

RESULTS AND DISCUSSION

The crystal consists of single molecules with an hexacoordinate stereochemistry around the nickel atom, resulting from bonding to a quasi-planar tridentate ligand, to a "nitro" group, to a "nitrite" group and to a water molecule. The results of the single crystal X-ray diffraction study are summarized in Table 1 and the molecular structure is shown in Fig. 1.

The main distortions from octahedral geometry are caused by the tridentate ligand which subtends angles at nickel of 77.8 and 78.1°. Intermolecular hydrogen bonds are present in the compound [O(w)—H(w)...O1($-x$, $1-y$, $-z$) 2.84(3) Å, H(w)..O1 2.00(4) Å, ∠O(w)—H(w)...O1 179.46°; O(w)—H(w)′...O4($-x$, $1-y$, $1-z$) 2.85(6) Å, H(w)′...O4 2.09(6) Å, ∠O(w)—H(w)′...O4 162.79°].

Values obtained for bond distances and angles in the terpy ligand are in good agreement with those in the literature.[6,7]

It could be expected that the N—O bond distance in the nitrite involving the oxygen atom closer to the metal increases in length, while for the less strongly bonded oxygen it decreases.[1] On the con-

* Author to whom correspondence should be addressed.
† Departamento Cristalografía y Mineralogía, Universidad de Barcelona, Spain.
‡ Departamento Química Inorgánica, Universidad de Valencia, Spain.

Table 1. Selected internuclear distances (Å) and angles (°) for $[Ni(C_{15}H_{11}N_3)(NO_2)(ONO)(H_2O)]$ with estimated standard deviations in parentheses

Ni—N(1)	2.108(3)	N(2)—C(6)	1.346(4)
Ni—N(2)	2.005(3)	N(2)—C(10)	1.333(4)
Ni—N(3)	2.113(3)	N(3)—C(11)	1.345(4)
Ni—N(4)	2.092(3)	N(3)—C(15)	1.349(4)
Ni—O(w)	2.064(2)	N(4)—O(1)	1.247(4)
Ni—O(3)	2.078(3)	N(4)—O(2)	1.237(3)
N(1)—C(1)	1.341(4)	N(5)—O(3)	1.203(4)
N(1)—C(5)	1.351(4)	N(5)—O(4)	1.242(4)
N(1)—Ni—N(2)	77.8(1)	Ni—N(1)—C(1)	127.0(2)
N(1)—Ni—N(3)	155.9(1)	C(1)—N(1)—C(5)	118.3(3)
N(1)—Ni—N(4)	89.5(1)	Ni—N(2)—C(6)	119.3(2)
N(1)—Ni—O(w)	101.1(1)	Ni—N(2)—C(10)	119.1(2)
N(2)—Ni—N(3)	78.1(1)	C(6)—N(2)—C(10)	121.6(3)
N(2)—Ni—N(4)	93.0(1)	Ni—N(3)—C(15)	114.1(2)
N(2)—Ni—O(w)	177.7(1)	C(11)—N(3)—C(15)	118.1(3)
N(3)—Ni—N(4)	93.1(1)	Ni—N(4)—O(1)	122.5(2)
N(3)—Ni—O(w)	102.9(1)	Ni—N(4)—O(2)	120.3(2)
N(4)—Ni—O(3)	173.9(1)	O(1)—N(4)—O(2)	117.3(3)
N(4)—Ni—O(w)	89.1(1)	O(3)—N(5)—O(4)	116.6(3)
O(3)—Ni—N(1)	94.1(1)	Ni—O(3)—N(5)	120.8(2)
O(3)—Ni—N(2)	92.5(1)	N(1)—C(1)—C(2)	122.8(4)
O(3)—Ni—N(3)	85.5(1)	N(2)—C(6)—C(5)	113.3(3)
O(3)—Ni—O(w)	85.4(1)	N(3)—C(11)—C(10)	115.0(3)

trary, the observed N—O bond distance for the metal bonded oxygen is 1.203(4) Å while for the other is 1.242(4) Å.

This can probably be explained on the basis of intermolecular hydrogen bonds between the water molecule and the free oxygen of the nitrite group.

Distortion from an octahedron to a trigonal prism (Δ) for the complex has been examined using the Muetterties and Guggenberger description[8] by comparison of the observed dihedral angles (δ) formed by the normal to adjacent polytopal faces with those of the ideal octahedron ($\Delta = 0$) (see Table 2); the value $\Delta = 0.09$ indicates that the $[NiN_4O_2]$ polyhedron is close to octahedral.

The infrared spectrum of the complex, pelleted in KBr, has been recorded in the hope that the

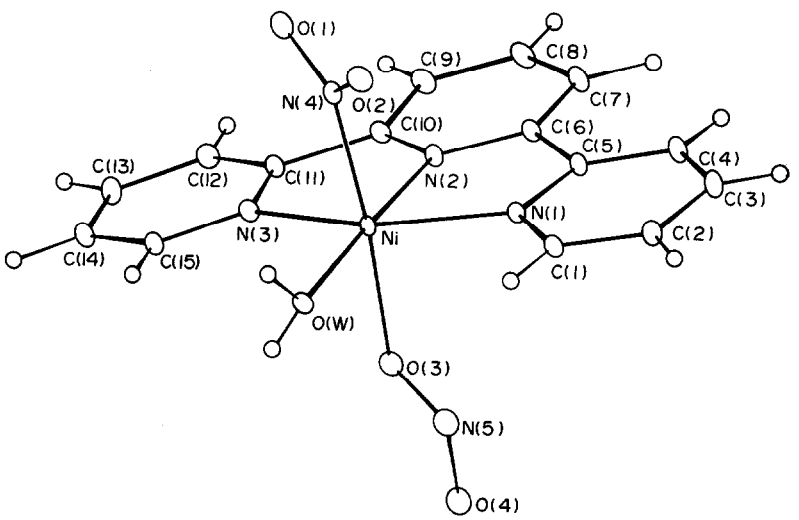


Fig. 1. Molecular structure of the complex Ni(terpy)$(NO_2)(ONO)(H_2O)$ showing the atom-numbering scheme.

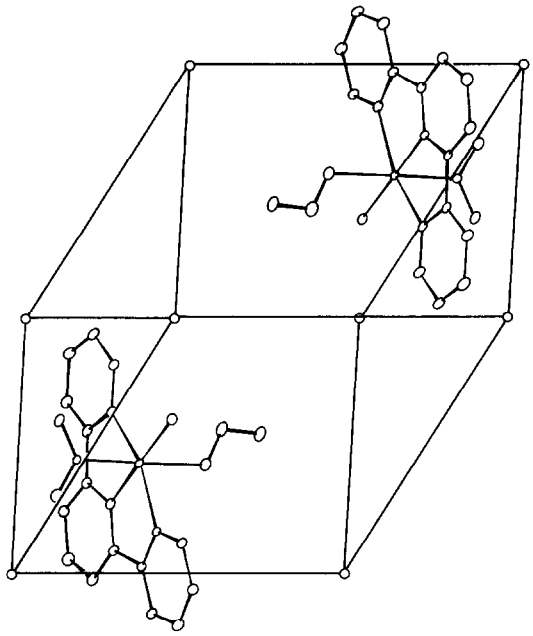


Fig. 2.

"nitrite" and "nitro" peaks could be identified and used for the study of the relationship between the vibrational frequencies and the internal geometry of the nitrite ion.

The general effect of coordination via nitrogen is to raise the frequency of both $\nu_{as}(NO_2)$ and $\nu_s(NO_2)$ from the free ion values of 1328 cm^{-1} and 1260 cm^{-1} respectively. Coordination via oxygen may be expected to raise the frequency of $\nu_{as}(NO_2)$ and to lower that of $\nu_s(NO_2)$.[1]

The IR spectrum of Ni(terpy)(NO_2)(ONO)(H_2O) in the N—O stretching region has two bands due to nitro group at 1303 $cm^{-1}(\nu_{as})$ and 1274 $cm^{-1}(\nu_s)$; bands at 1358 $cm^{-1}(\nu_{as})$ and 1128 $cm^{-1}(\nu_s)$ may be attributed to "nitrite" group.[9]

Table 2. Distortion Δ^a of the $[NiN_4O_2]$ polyhedron

Dihedral angle	Polyhedron: Octahedron (°)	Polyhedron: NiN_4O_2 (°)	Polyhedron: Trigonal prism (°)
δb_1	70.5	59.4[N(4)—O(w)—N(3)—O(3)]	0
$\delta b_1'$	70.5	56.9[N(1)—N(4)—N(2)—N(3)]	0
$\delta b_1''$	70.5	69.4[O(w)—N(1)—O(3)—N(2)]	0
δb_2	70.5	78.7[O(3)—N(1)—N(2)—N(4)]	120
$\delta b_2'$	70.5	82.8[N(1)—O(3)—O(w)—N(3)]	120
$\delta b_2''$	70.5	73.0[N(2)—N(4)—N(3)—O(w)]	120
δ_1	70.5	63.9[N(4)—N(1)—O(w)—O(3)]	90
δ_2	70.5	76.8[O(3)—N(2)—N(3)—N(4)]	90
δ_3	70.5	73.7[N(2)—N(1)—N(4)—O(w)]	90
δ_4	70.5	74.9[O(w)—O(3)—N(3)—N(2)]	90
δ_5	70.5	82.9[N(1)—O(w)—N(4)—N(3)]	90
δ_6	70.5	55.4[N(1)—N(2)—O(3)—N(3)]	90
Δ	0	0.09	1

[a] Δ is calculated using the following formula:

$$\Delta = \sum \frac{[\delta b_1 - \delta b_{1\,oct}]}{846} + \sum \frac{[\delta b_2 - \delta b_{2\,oct}]}{594} + \sum \frac{[\delta_i - \delta_{oct}]}{234}.$$

Susceptibility measurements over a temperature range 77–300 K obey the Curie–Weiss law. The effective magnetic moment at room temperature is 3.12 B.M.

EXPERIMENTAL

Synthesis of the complex

[Ni(terpy)(NO_2)(ONO)(H_2O)] was prepared by mixing the complex Ni(terpy)$Cl_2 \cdot 3H_2O$, synthesized by us,[10] with an excess of sodium nitrite in aqueous solutions. Red crystals of the compound were obtained by slow evaporation of this solution, and then washed with acetone and dried *in vacuo*. The red colour may be indicative of nitro-coordination for nickel(II) complex. (Found: C, 45.0; H, 3.4; N, 17.5. $NiC_{15}H_{11}N_3N_2O_4H_2O$ requires C, 44.8; H, 3.2; N, 17.4%.)

Crystal structure determination

Crystals grow as red needles from aqueous medium. Diffracted intensities were collected at room temperature on a Phillips PW 1100 four-circle diffractometer using a crystal of dimensions $0.08 \times 0.02 \times 0.42$ mm.

Of the total 2777 reflections, measured to $2\theta \leqslant 50$ ($\omega - 2\theta$ scans) 2087 had $I \geqslant 2.5\sigma(I)$, and only these were used in the refinement of the structure after the data had been corrected for Lorentz and polarization effects, not for absorption.

Crystal data. Ni($C_{15}H_{11}N_3$)(NO_2)(ONO)(H_2O), $M = 402.1$, triclinic, $a = 9.079(2)$, $b = 9.430(2)$, $c = 10.683(3)$ Å, $\alpha = 76.61(3)$, $\beta = 70.73(2)$, $\gamma = 68.02(2)°$, $U = 794.5(3)$ Å^3, space group: $P\bar{1}$, $Z = 2$, $D_x = 1.68$ g cm^{-3}, $F(000) = 410$, Mo-K_α X-radiation (graphite monochromated), $\lambda = 0.7106$ Å, μ(Mo-K_α) = 12.63 cm^{-1}.

The structure was solved by direct methods, using the 1980 version of MULTAN. It was refined isotropically and also anisotropically using the program SHELX 76.[11] The positions of the hydrogen atoms were determined from the difference Fourier synthesis.

Refinement converged at $R = 0.030$ ($Rw = 0.031$) with a weighting scheme of the form $w = [\sigma^2(F_0) + 0.00035(F_0)^2]^{-1}$ giving a satisfactory weight analysis. A final electron density difference synthesis showed no peaks >0.3 e Å^{-3}. All computations were carried out on an IBM 3083 computer. Atomic scattering factors and anomalous dispersions corrections were taken from Ref. 12. The atomic coordinates of this work are available on request from the Editor and have also been deposited with the Cambridge Crystallographic Data Centre.

Magnetic measurements

Magnetic susceptibility measurements were performed with a Faraday type magnetic microbalance between 77–300 K.

Acknowledgement—This work was supported in part by the grant 2930/84 from the C.A.I.C.Y.T., which we gratefully acknowledge.

REFERENCES

1. M. A. Hitchman and G. Rowbottom, *Coord. Chem. Rev.* 1982, **40**, 55.
2. T. Rojo, M. Vlasse and D. Beltran-Porter, *Acta Cryst.* 1983, **C39**, 194.
3. J. M. Savariault, T. Rojo, M. I. Arriortua and J. Galy, *C. r. Acad. Sci. Paris* 1983, **297**, 895.
4. T. Rojo, J. Darriet, J. M. Dance and D. Beltran-Porter, *Inorg. Chim. Acta* 1982, **64**, 1105.
5. R. Cortés, M. I. Arriortua, T. Rojo, X. Solans, C. Miravitlles and D. Beltran, *Acta Cryst.* in press.
6. D. L. Kepert, E. S. Kucharski and A. H. White, *J. Chem. Soc. Dalton Trans.* 1980, 1932.
7. M. Vlasse, T. Rojo and D. Beltran-Porter, *Acta Cryst.* 1983, **C39**, 560.
8. E. L. Muetterties and L. J. Guggenberger, *J. Am. Chem. Soc.* 1974, **96**, 1748.
9. D. M. L. Goodgame, *Inorg. Chem.* 1967, **6**, 815.
10. R. Cortés, M. I. Arriortua, J. L. Mesa and T. Rojo, *J. Appl. Cryst.* 1985, **18**, 366.
11. G. M. Sheldrick, SHELX76. Program for crystal structure determination. University of Cambridge, U.K. (1976).
12. *International Tables for X-ray Crystallography*, Vol. 4. Kynoch Press. Birmingham (1974).

Polyhedron Vol. 5, No. 12, pp. 1991–1995, 1986
Printed in Great Britain

0277–5387/86 $3.00+.00
Pergamon Journals Ltd

THE NITROSATION OF ANILINE WITH $Zn(py)_2(ONO)_2$

ANNA G. McKENNA* and JAMES C. FANNING†
Department of Chemistry and Geology, Clemson University, Clemson, SC 29634, U.S.A.

(*Received* 27 *January* 1986; *accepted* 8 *May* 1986)

Abstract—Diazoaminobenzene (DAAB) formed slowly when aniline was reacted with $Zn(py)_2(ONO)_2$ in dichloroethane at 60°. The rate of reaction was followed by measuring the DAAB concentration spectrophotometrically at 353 nm. Complex concentrations ranged from 5 to 30 mM, while those of aniline were from 100 to 900 mM. The kinetic data were explained by a mechanism involving a pre-equilibrium, wherein aniline displaced a nitrite ion from the zinc complex. This was followed by a slow reaction of the free nitrite ion with the solvent, forming a highly reactive nitrosating species.

It has been previously communicated that metal nitrite complexes with O-bound nitrite, the nitrito form, are capable of efficiently nitrosating secondary amines in organic solvents.[1] In an attempt to show that the reaction also occurs with primary amines, dinitritobis(pyridine)zinc, $Zn(py)_2(ONO)_2$, was reacted with aniline at 60° in dichloroethane (DCE) under a nitrogen atmosphere and in the absence of light. The reaction which slowly produced the intensely colored N-coupled diazoaminobenzene (DAAB), $C_6H_5N{=}NN(H)C_6H_5$, was followed spectrophotometrically. The Zn complex was used since it has the potential to form nitrito complexes in solution. In the solid state the nitrite groups are bound in a bidentate manner.[2] In solution, one end of the nitrite might be expected to be displaced from the labile Zn(II) ion. The complex dissolved readily in DCE and was colorless. Also, the Zn(II) ion was felt to be less likely to bind to the azo product than transition metal ions and thus not change the character of the reaction as it proceeded.

EXPERIMENTAL

$Zn(py)_2(ONO)_2$ was prepared according to the procedure of Goodgame *et al.*[2] and gave satisfactory analysis. The aniline and DCE were distilled prior to use and protected from moisture and light.

For the nitrosation reactions, 50 cm^3 of the complex solution were transferred to a 75 cm^3 two neck flask. Twenty-five cm^3 of the aniline solution were placed in a vented dropping funnel. The dropping funnel was inserted into one neck of the flask and a stopcock into the other neck. The system was purged with nitrogen and the complex solution heated in a constant temperature bath for 15 min before adding the amine solution. The reaction was carried out in a nitrogen atmosphere and protected from light. Under a stream of nitrogen, the stopcock was removed and a septum inserted. Fractions of 50 to 200 μl were removed at various times, diluted to 2 cm^3 and the visible spectra measured. A Bausch and Lomb Spectronic 2000 was used for these measurements.

A 50 cm^3 solution, 3.0 mM in complex and 80.0 mM in aniline, was allowed to stand for 3 h at 60°. The solution was then shaken with conc. aqueous NH_3 to destroy the complex, followed by dilute HCl to remove the amine and pyridine. After washing the organic layer, drying it and removing the DCE under vacuum, the infrared, ultraviolet–visible, and mass spectral properties of the product were obtained. They matched those of DAAB synthesized by the method of Vogel.[3] In DCE, DAAB has an absorption band at 353 nm (ε 20,000 cm^{-1} M^{-1}) and obeys the Beer–Lambert law over the concentration range used in these experiments. The 353 nm band did not shift during the reaction, indicating that no rearrangement occurred to form p-aminoazobenzene (4-(phenylazo)-benzenamine) which absorbs at 384 nm. p-Aminoazobenzene was synthesized from DAAB by heating it in aqueous acid.[3]

* Present address: College of St. Benedict, Saint Joseph, MN 56374, U.S.A.
† Author to whom correspondence should be addressed.

RESULTS AND DISCUSSION

The nitrosation reaction was carried out at complex concentrations ranging from 5 to 30 mM and over an aniline concentration range of 100 to 900 mM. Figure 1 shows the concentration of DAAB vs time for a 30 mM $Zn(py)_2(ONO)_2$/600 mM aniline solution with added DAAB (2.1 mM) and without it. The curves are essentially parallel for over 300 min showing that no significant decomposition of DAAB occurred during the early part of the reaction. For this reason most of the kinetic runs were followed for about 300 min. Attempts to obtain the theoretical yield of DAAB were unsuccessful, probably because of DAAB decomposition.

The overall reaction for the formation of DAAB in the early stages can be considered to be:

$$Zn(py)_2(ONO)_2 + 2C_6H_5NH_2 \rightarrow Zn(py)_2(ONO)(OH) + C_6H_5N_2N(H)C_6H_5 + H_2O.$$

No evidence for the zinc product exists and it is quite probable that one or both pys are exchanged with the excess aniline. As the reaction proceeds both nitrites probably react; however, DAAB may decompose or convert to p-aminoazobenzene. The 30 mM $Zn(py)_2(ONO)_2$/600 mM aniline reaction after 27 h showed spectrophotometric evidence of a 47% conversion of total nitrite into DAAB.

A mechanism which is able to explain the kinetic data is as follows:

$$MX + A = MA + X \quad \text{pre-equilibrium, } K \quad (1)$$

$$X + \text{solvent} \rightarrow B \quad \text{slow step, } k \quad (2)$$

$$B + A \rightarrow \text{DAAB} + \text{other products} \quad \text{fast} \quad (3)$$

Step (1) involves the reactant complex (MX) with a substitutionally labile nitrite (X), displaced by the amine (A) in a rapidly established pre-equilibrium having an equilibrium constant, K. The nitrite then reacts with solvent in a pseudo-first order slow step with a rate constant, k, to produce an intermediate (B). B reacts with amine to produce, in a series of fast reactions, DAAB and other products. From the relationship

$$-\frac{d[MX]}{dt} = \frac{d[X]}{dt} = -k[X] = -\frac{kK[MX][A]}{[MA]} \quad (4)$$

and the assumptions that $[A] \sim [A]_0$, the initial amine concentration, and that the initial MX concentration, $[MX]_0$, is equal to the sum of the concentrations of MX and MA, eqn (5) may be derived.

$$[MX]_0 \ln\left(\frac{[MX]}{[MX]_0}\right) + [MX]_0 - [MX] = -kK[A]_0 t. \quad (5)$$

Initially $[MX] = [MX]_0 - [\text{DAAB}] - [X]$; however, as [DAAB] increases,

$$[MX] \sim [MX]_0 - [\text{DAAB}]. \quad (6)$$

Substituting (6) into (5) gives

$$[MX]_0 \ln\left(1 - \frac{[\text{DAAB}]}{[MX]_0}\right) + [\text{DAAB}] = -kK[A]_0 t. \quad (7)$$

Thus a graph of the left side of eqn (7) vs time should result in a straight line with a slope of $-kK[A]_0$ after the reaction has proceeded for a given period of time.

The plots of eqn (7) for solutions with an initial aniline concentration of 600 mM and zinc complex concentrations of 5.2, 11, 20 and 30 mM are shown in Fig. 2. At the lower concentrations a longer time was required to reach the linear region of the reaction. The slopes of the linear region are approximately equal [average value: $(-1.18 \pm 0.08) \times 10^{-4}$ mM s^{-1}]. Table 1 gives the slopes for each experiment. The slopes from the experiments where the initial zinc complex concentration is 11 mM are shown plotted against the initial aniline concentrations in Fig. 3. An approximate linear relationship results (slope: -1.67×10^{-7} s^{-1}; intercept: 8.8×10^{-6}; correlation coefficient: 0.95) with a

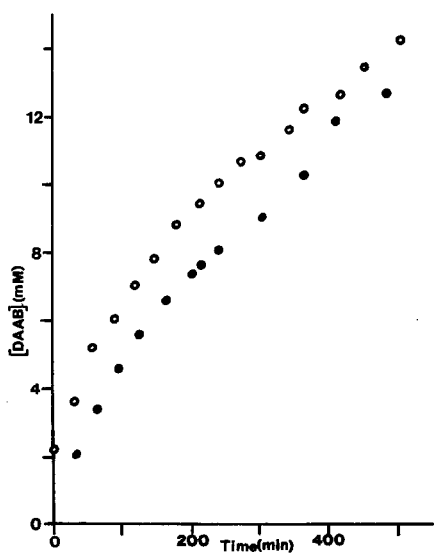


Fig. 1. The concentration of DAAB vs time (min) for the reaction of 30.0 mM $Zn(py)_2(ONO)_2$ and 600 mM aniline at 60° in DCE with added (2.1 mM) DAAB (○) and without added DAAB (●).

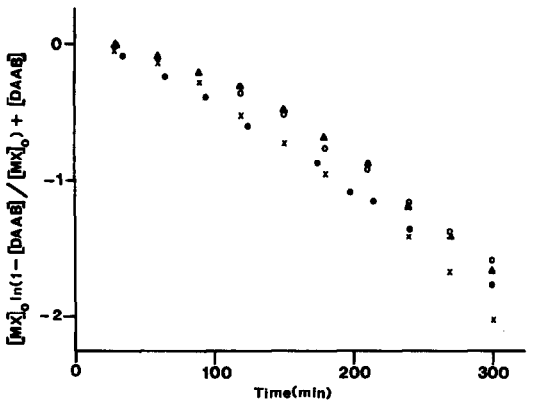


Fig. 2. The function,

$$[MX]_0 \ln\left(1-\frac{[\text{DAAB}]}{[MX]_0}\right)+[\text{DAAB}],$$

vs time (min) for the experiments with 600 mM aniline and 30 (●, A); 20 (×, C); 11 (○, D); and 5.2 mM (△, F) $Zn(py)_2(ONO)_2$ nitrosation reactions. Letters refer to experiments listed in Table 1.

near zero intercept. Because of the relatively long time (>60 min) required to reach the linear region of the reaction with low concentrations of aniline and complex, the slopes for these concentrations were somewhat inexact.

An initial slope method was also used to examine the kinetics. If it is assumed that $[A] \sim [A]_0$ and, for the initial stages, that $[MA] = [X] = \sqrt{K[MX]_0[A]_0}$, then using eqn (4), a first-order relationship results

$$\frac{d[MX]}{dt} = -kK^{1/2}\sqrt{\left(\frac{[A]_0}{[MX]_0}\right)}[MX].$$

Therefore, the experimental initial first-order rate constant

$$k_e = kK^{1/2}\sqrt{\left(\frac{[A]_0}{[MX]_0}\right)}$$

or

$$\ln(k_e) = 0.5\ln\left(\frac{[A]_0}{[MX]_0}\right)+\ln(kK^{1/2}).$$

To obtain k_e, $\ln([MX]_0-[\text{DAAB}])$ vs time plots were made and the initial slope, equal to k_e, determined. The k_e values are given in Table 1.

A log–log plot of k_e vs $[A]_0/[MX]_0$ is shown in Fig. 4. An increase in k_e with an increase in the ratio was found. The slope of the best line drawn through the points is 0.46 ± 0.11 (90% confidence limit). Thus, the expected slope of 0.5 is well within this limit. The intercept is -12.07 which makes $kK^{1/2}$ equal to 5.7×10^{-6}. Using this value and the slope of the line in Fig. 3 (-1.67×10^{-7}), equal to $-kK$, allows a rough calculation of K (9×10^{-4}) and k (2×10^{-4} s^{-1}).

The excess aniline in each solution is expected to produce partial, if not total, substitution of the two pyridines bound to the labile zinc ion. An estimate of the amount of *bis*-aniline complex may be made

Table 1. Results of the reaction of $Zn(py)_2(ONO)_2$ with aniline in 1,2-dichloroethane

Expts	$[Zn(py)_2(ONO)_2]_0$[a] (mM)	$[\text{Aniline}]_0$[a] (mM)	Slope × 10^5[b] (±1.1 mM s^{-1})	$k_e\times10^5$[c] (±0.5 s^{-1})
A	30	600	10.8	2.7
B	30[d]	600	10.7	2.3
C	20	600	12.8	3.2
D	11	600	11.0	3.8
E	5.0	600	12.8	4.8
F	5.2	600	12.5	5.2
G	11	100	1.3	2.0
H	11	100	0.7	1.2
I	11[e]	300	6.0	2.2
J	11	300	4.0	2.5
K	11	450	4.8	2.8
L	11	900	13.8	4.2
M	11[f]	600	22.5	8.0

[a] Initial concentrations.
[b] Slope of eqn (7) plot (see text).
[c] Initial first-order rate constant.
[d] 2.1 mM diazoaminobenzene present at start of reaction.
[e] Complex solution allowed to stand 24 h at 60° prior to adding aniline.
[f] Solvent saturated with water.

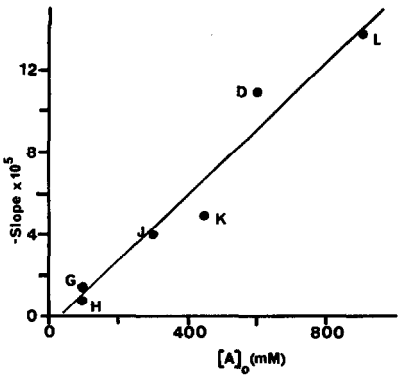


Fig. 3. The slopes of the

$$[MX]_0 \ln\left(1-\frac{[\text{DAAB}]}{[MX]_0}\right)+[\text{DAAB}]$$

vs time plots for the experiments with 11 mM $Zn(py)_2(ONO)_2$ plotted against the initial aniline concentrations. The least-squares line is shown. Letters refer to experiments listed in Table 1.

if the equilibrium constant for the reaction:

$$ZnL(py)_2^n + 2A = ZnL(A)_2^n + 2py$$

is known. It may be calculated from stability constant data. Such data are not available for the nitrite complex used in this study; however, data are available for two very different zinc complexes and the calculated equilibrium constant values are quite similar. When L is the acetylacetonate anion; n, zero; and the solvent benzene at 20°, the equilibrium constant is 1.2×10^{-2}.[4] When L is $(H_2O)_x$; n, +2; and a 30° aqueous solution with an ionic strength of 0.1 is used, the equilibrium constant is 8×10^{-3}.[5]

Assuming a value of 1×10^{-2} for the equilibrium

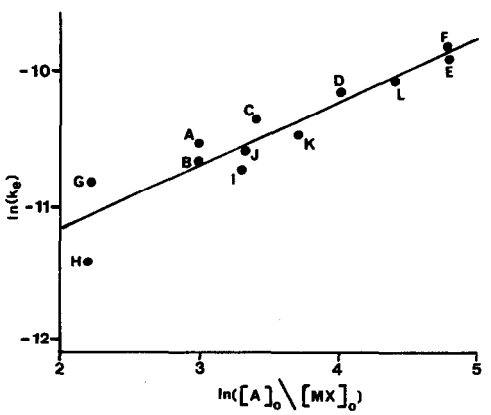


Fig. 4. $\ln(k_e)$ vs $\ln([A]_0/[MX]_0)$ for the $Zn(py)_2(ONO)_2$/aniline reactions given in Table 1. $[A]_0$ and $[MX]_0$ are the initial aniline and zinc complex concentrations and k_e is the initial first-order rate constant. The least-squares line is shown. Letters refer to experiments listed in Table 1.

constant when $Zn(py)_2(ONO)_2$ has both pyridines replaced by aniline, the per cent of *bis*-aniline product was calculated for the solutions with the highest aniline/complex ratio (expts E and F) and the lowest ratio (expts G and H). Experiments E and F with 5 mM complex and 600 mM aniline would have 97% *bis*-aniline product; while expts G and H with 11 mM complex and 100 mM aniline would have 45% *bis* product.

Thus, it appears that for most of the solutions, the *bis*-aniline complex is a major, if not predominant, reactant species in solution. If the $[A]_0$ values were adjusted by subtracting $2[M]_0$, the slopes and correlation coefficients of the lines shown in Figs 3 and 4 were unaffected.

At this time we believe the free nitrite ion leads to the eventual production of DAAB. Ongoing work in our laboratory and other work[6] has shown that nitrite salts in DCE and dichloromethane react with the solvent to produce, as yet, an unidentified product which appears to have a high nitrosating potential. The product is probably a nitrite ester, RONO, resulting from the substitution of a chloride by a nitrite on a solvent molecule.[6]

The bound nitrite does not appear to have appreciable reactivity with the solvent. Heating an 11 mM zinc complex solution at 60° for 24 h prior to making it 300 mM in aniline results in only small changes in the eqn (7) slope and k_e (expt. I) compared to a solution with comparable concentrations and reacted in the normal manner (expt. J).

The kinetic data were examined in detail with a number of models which involved the direct nitrosation of aniline by the zinc nitrite complex. The models considered varying amounts of pyridine substitution by aniline and aniline displacement of one end of the bidentate nitrite. Most of the models predicted that the complex would react with first order kinetics and that the aniline would have an order dependent on the model. Since an excess of aniline was used for the experiments, the data were treated with first order kinetics, and second order as well, but to no avail. These models were unable to explain all of the collected data. Only the solvent reaction model presented here was able to give a complete explanation. We are now seeking a solvent for the complex which would not participate in the nitrosation reaction and would allow the complex to serve as a direct nitrosating agent of amines.

The nitrito complex, $Co(NH_3)_5ONO^{2+}$ has been shown to nitrosate water[7] and azide ions[8] in aqueous solution. The inert complex is considered to be the active nitrosating agent for the azide ions and not involve the solvent.

The primary *N*-nitrosamine, $C_6H_5N(H)NO$, is expected to be formed as part of eqn (3). Reactions

leading to the formation of the diazonium product, DAAB, from the nitrosamine are fast even at temperatures well below 60°. Aziz *et al.*[9] have discussed recently the nitrosation of aniline by N_2O_4 and have outlined a nitrosation pathway producing the diazonium ion, $C_6H_5N_2^+$. DAAB forms by the attack of this ion on an aniline molecule.

The 60° reaction temperature was the optimum temperature for this study. Both decreasing and increasing the temperature by 10° showed a sharp decrease in the rate of DAAB production. At 70° considerable DAAB decomposition occurred.

The presence of water in the DCE resulted in an increase in rate (expt. M). Since water is a product of the reaction, it should cause an increase in rate as the reaction proceeds.

Acknowledgements—The authors would like to thank Dr. Larry Keefer of the National Cancer Institute, Frederick, Maryland for very helpful discussions and Dr. H. Garth Spencer of Clemson University's Department of Chemistry and Geology for his advice concerning the nitrosation kinetics.

REFERENCES

1. A. F. Croisy, J. C. Fanning, L. K. Keefer, B. W. Slavin and S.-J. Uhm, *IARC Sci. Publ.* 1980, No. 31, 83–93.
2. D. M. L. Goodgame, M. A. Hitchman and D. F. Marsham, *J. Chem. Soc. A* 1980, 1933.
3. A. I. Vogel, *Practical Organic Chemistry*, third edn., p. 622. Longman, London (1956).
4. M. Studnickova-Valentova and M. Branc, *Colln Czech. Chem. Commun.* 1975, **40**, 2025.
5. *Stability Constants of Metal-Ion Complexes*, Supplement No. 1, Special Publication No. 25, The Chemical Society, London (1971).
6. L. K. Keefer, in *N-Nitrosamines* (Edited by J.-P. Anselme), ACS Symp. Series, No. 101, pp. 91–108. American Chemical Society, Washington, D.C. (1979).
7. D. C. Klimek, B. Grossman and A. Haim, *Inorg. Chem.* 1972, **11**, 2382.
8. F. Seel and D. Meyer, *Z. Anorg. Allg. Chem.* 1974, **408**, 283; 1961, **308**, 305.
9. A. Aziz, M. Hoharum and M. I. Khahi, *J. Chem. Soc. Faraday Trans.* 1981, **77**, 1737 and references therein.

Polyhedron Vol. 5, No. 12, pp. 1997–2000, 1986
Printed in Great Britain

0277–5387/86 $3.00+.00
© 1986 Pergamon Journals Ltd

SYNTHESIS OF SODIUM ZIRCONIUM PHOSPHATES

DOMINIQUE P. VLIERS, WILFRIED J. MORTIER and ROBERT A. SCHOONHEYDT*

Laboratorium voor Oppervlaktechemie, K. U. Leuven, Kard. Mercierlaan 92, B3030 Heverlee, Belgium

(*Received* 20 *August* 1985; *accepted after revision* 8 *May* 1986)

Abstract—$Zr(O_3PONa)_2 \cdot nH_2O$ can be prepared as a single crystalline phase by direct precipitation in the presence of HF. This material is a powder. When a single crystal of α-HZrP is exchanged with Na^+, $Zr(O_3PONa)_2 \cdot nH_2O$ is obtained as a powder-like crystal. The zero level Weissenberg photograph shows a monoclinic symmetry; the unit cell ($a = 0.900$ nm, $b = 1.059$ nm, $c = 2.210$ nm and $\beta = 117.12°$) contains eight formula units $Zr(O_3PONa)_2 \cdot 3H_2O$. This is doubled with respect to α-HZrP.

Crystalline $Zr(O_3POH)_2 \cdot H_2O$ (α-HZrP) is the most important member of the acid salts of quadrivalent metals. It is used as an ion exchanger.[1,2] When the proton is exchanged by transition metals a heterogeneous catalyst is produced.[3–5] When it is exchanged by organic cations stable aqueous suspensions can be prepared, which open new ways for applications.[6,7]

A limitation to the extension of our knowledge about zirconium phosphates is the lack of accurate structural data. A detailed structure has been published for α-HZrP.[8] Half exchanged and fully exchanged alkali metal zirconium phosphates are only known as powders.[9–11] In this note we describe our efforts to obtain single crystals of $Zr(O_3PONa)_2 \cdot nH_2O$ and their characterization.

EXPERIMENTAL

Direct precipitation

The precipitation of sodium exchanged α-zirconium phosphate was based on the HF method for the synthesis of α-HZrP.[12] 4.2 g $ZrOCl_2 \cdot 8H_2O$, 3 g NaCl and 3 or 4 cm^3 HF 40% are dissolved in 27 or 26 cm^3 water respectively. The HF/Zr molar ratio is 5.2 and 6.9 respectively. To this solution 11.6, 23.2 or 116 g $Na_2HPO_4 \cdot 2H_2O$, dissolved in 100 cm^3 water, was added to obtain a P/Zr molar ratio of 5, 10 or 50 respectively. P stands for sodium phosphate. The reaction mixture was stirred on a waterbath at 330–335 K for 2 weeks. The reaction product was washed with water and freeze-dried.

To prepare large crystals the temperature of the reaction mixture with HF/Zr = 5.2 and P/Zr = 50 was increased from 325 to 360 K at a rate of 2° per day and kept at 360 K for 1 week.

In a second set of synthesis reactions $NaH_2PO_4 \cdot 2H_2O$ was used instead of $Na_2HPO_4 \cdot 2H_2O$. 10.2 g or 20.4 g $NaH_2PO_4 \cdot 2H_2O$, dissolved in 100 cm^3 water, were added to the solution of $ZrOCl_2$, HF and NaCl. The P/Zr ratio was 5 or 10 respectively. These reaction products were air-dried instead of freeze-dried.

Ion exchange

Large α-HZrP crystals (particle size of about 1 mm) were synthesized as described by Alberti *et al.*[13] 0.5 g of these α-HZrP crystals were equilibrated with 100 cm^3 NaCl 0.1 M and 40 cm^3 NaOH 0.1 M for 2 weeks. The exchanged crystals were air-dried. The best crystal out of about 30 examined under microscope was used for single crystal X-ray analysis.

Crystalline α-HZrP powder was prepared by direct precipitation as described by Alberti and Torracca.[12] The sodium-exchange was performed in the same way as for the large α-HZrP crystals. Part of the exchanged powder was freeze-dried, the other part was air-dried. These samples were used as references for the NaZrPs formed by direct precipitation.

* Author to whom correspondence should be addressed.

Techniques

X-ray powder diffraction (XRD) patterns (Ni-filtered Cu K_α radiation) were obtained with a modified Siemens type F diffractometer [automated and equipped with a position-sensitive detector (M. Braun)]. The X-ray patterns of the synthesized or ion-exchanged products were identified by comparison with published spectra.[9,14,15]

Oscillation and zero level Weissenberg photographs were taken from several α-HZrP and NaZrP crystals (plates with mean size approximately 0.2 mm).

RESULTS AND DISCUSSION

Direct preparation of $Zr(O_3PONa)_2 \cdot nH_2O$

Large single crystals of α-HZrP can be prepared in the presence of HF because the slow decomposition of $ZrF_n^{(4-n)+}$ is the rate-determing step. When the same synthesis conditions are applied with NaH_2PO_4 or Na_2HPO_4 instead of H_3PO_4 the crystalline phases given in Table 1 are obtained. These are present as powders. In no case did we obtain large crystals. The XRD patterns of the samples 1, 3, 4 and 7 (Table 1) are given in Fig. 1 as examples together with the patterns of $Zr(O_3PONa)_2 \cdot H_2O$ and $Zr(O_3PONa)_2 \cdot 3H_2O$, obtained by Na^+-exchange of α-HZrP powder.

With Na_2HPO_4 pure phases of $Zr(O_3PONa)_2 \cdot nH_2O$ are obtained with HF/Zr and P/Zr ratios of 5.2 and 10 to 50 respectively. At lower P/Zr ratios or higher HF/Zr ratios mixtures of phases or zirconium fluorides are obtained. With NaH_2PO_4 no pure single phase could be isolated.

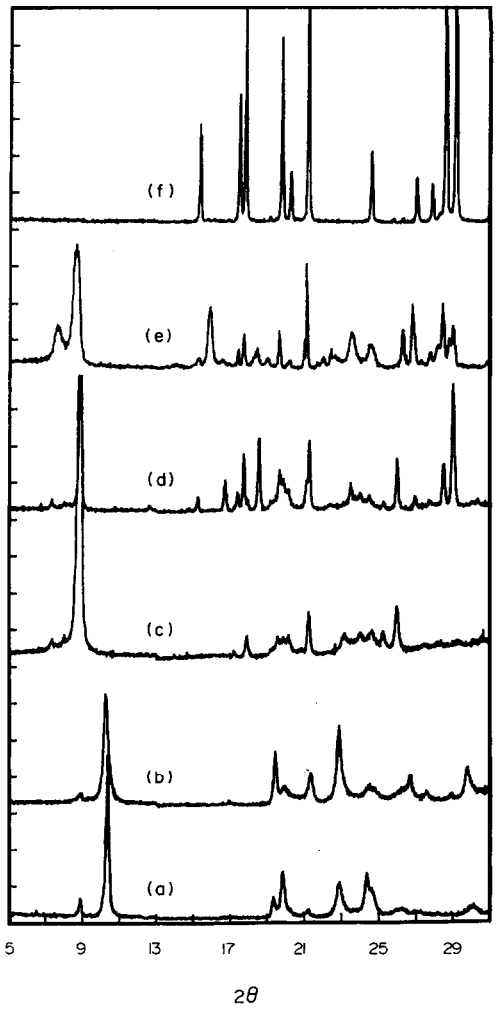


Fig. 1. XRD patterns of $Zr(O_3PONa)_2 \cdot H_2O$ (a), sample No. 3 (b), $Zr(O_3PONa)_2 \cdot 3H_2O$ (c), sample No. 1 (d), sample No. 7 (e) and sample No. 4 (f).

Table 1. Reaction products obtained by direct precipitation from a solution with given reagent concentrations

Sample No.	P[a] source	Zr(IV) (M)	HF (M)	P (M)	Product
1	$Na_2HPO_4 \cdot 2H_2O$	0.10	0.52	0.5	D,[b] β-$Na_5Zr_2F_{13}$
2		0.10	0.52	1.0	E
3		0.10	0.52	5.0	E
4		0.10	0.69	0.5	β-$Na_5Zr_2F_{13}$
5		0.10	0.69	1.0	Na_3ZrF_7
6	$NaH_2PO_4 \cdot 2H_2O$	0.10	0.52	0.5	D, A, Na_3ZrF_7
7		0.10	0.52	1.0	D, A, β-$Na_5Zr_2F_{13}$

[a] P stands for sodium phosphate.

[b] The phases are identified by letters as defined in Ref. 9. A stands for $Zr(O_3PONa)(O_3POH) \cdot 5H_3O$. D stands for $Zr(O_3PONa)_2 \cdot 3H_2O$. E stands for $Zr(O_3PONa)_2 \cdot H_2O$.

The failure to obtain large single crystals can be attributed to the following two reasons.

(1) The interlayer distance of $Zr(O_3PONa)_2 \cdot H_2O$ is 1.18 nm (as derived from the supposed d_{002} reflections in the XRD patterns[9]). This is too large for efficient interlayer cohesion. Cleavage of α-HZrP crystals during the exchange with Na^+ was indeed observed by Alberti *et al.*[13]

(2) The maximum concentration of an aqueous solution of sodium phosphates is 5 M, i.e. only half of the concentration of phosphoric acid needed to obtain large single crystals of α-HZrP[13] (the crystal size increased with increasing phosphoric acid concentration).

Ion-exchanged $Zr(O_3PONa)_2 \cdot 3H_2O$

Single crystals of α-HZrP were ion-exchanged with Na^+ as described in the experimental section. The oscillation photograph parallel to the *b*-axis of a single crystal of $Zr(O_3PONa)_2 \cdot 3H_2O$ is shown in Fig. 2.

A first observation is a deterioration of the diffraction pattern, which could be expected already from a visual inspection of the crystal which is no longer transparent. In view of the pronounced disintegration of the crystals upon exchange, the oscillation photograph shown in Fig. 2 is consistent with a diffraction pattern of domains which are more or less oriented in a parallel fashion. This is also evident on the Weissenberg photograph. A second observation is a doubling of the *b*-axis. Although the most intense spots are still those of the original α-HZrP material (figure not shown), weak but definite spots consisting of *h*,*k*/2,*l* lines emerge, indicating a doubling of the *b*-axis.

The unit cell parameters could be derived from the Weissenberg photograph (Table 2) and the *a*-axis was chosen so as to coincide with the original *a*-axis. This is reasonable in view of the fact that the zirconium phosphate layers will be less affected than the interlayer spacing. (The original *b*-axis was indeed still predominant although symmetry lowering is obvious and no indication was found for a doubling of the *a*-axis.) The *c*-axis was chosen so as to reproduce the d_{001} spacing observed in the XRD patterns (Fig. 1c) (*i.e.* $c \sin \beta$).

It is remarkable that the widening of the diffraction spots is anisotropic: only the *b*-axis is affected. The structural changes due to K^+-exchange ($ZrHK(PO_4)_2$[16]) are indeed restricted to a shift of the layers along the *b*-axis (apart of course from a swelling due to the intercalation of the cations).

From the available information on systematic extinctions, the probable spacegroup is $P2_1/c$, such as was found also for all other structures investigated: [$ZrKH(PO_4)_2$[16] and $Zr(O_3PONH_4)_2$[17]].

The resulting unit cell volume, *V*, of $Zr(O_3PONa)_2 \cdot$

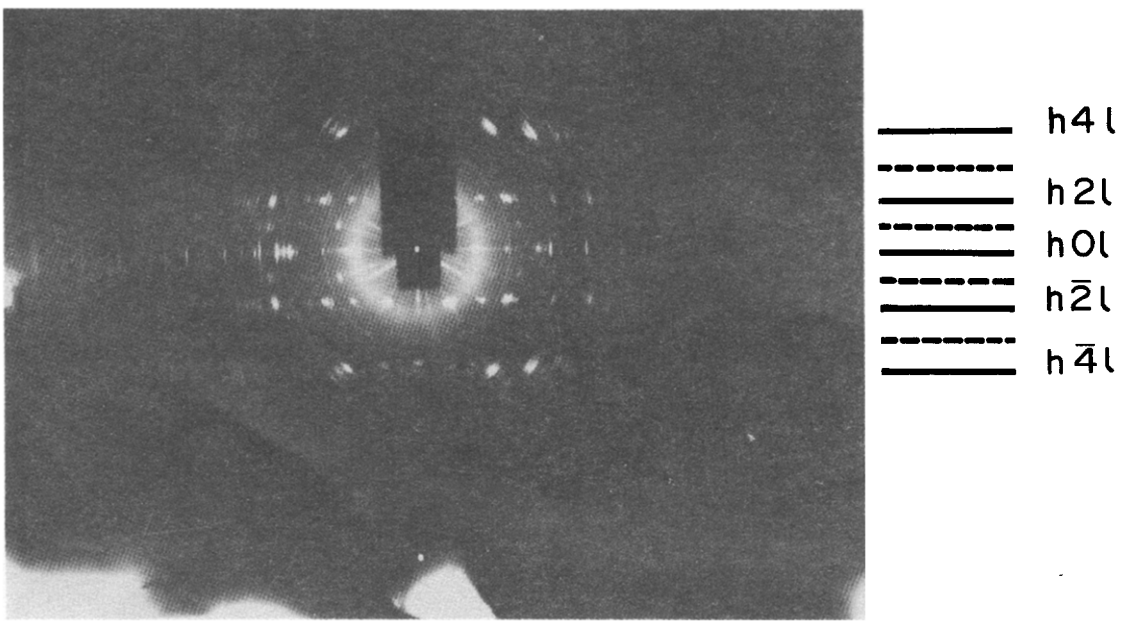


Fig. 2. Oscillation photograph of a single crystal of $Zr(O_3PONa)_2 \cdot 3H_2O$.

Table 2. Unit cell dimensions of zirconium phosphates

	$Zr(O_3PONa)_2 \cdot 3H_2O$	α-HZrP[8]
a, nm	0.900	0.9060
b, nm	1.059	0.5297
c, nm	2.210	1.5414
β, deg	117.12	101.71
V, nm^3	1.875	0.7243

$3H_2O$ is more than doubled with respect to the unit cell volume of α-HZrP (Table 2). The unit cell possesses eight formula units $Zr(O_3PONa)_2 \cdot 3H_2O$ or $Z = 8$ and, to be compatible with the symmetry, four non-equivalent phosphate groups must be present in the asymmetric unit.

Acknowledgement—W.J.M. and R.A.S. acknowledge a permanent research position as senior research associate of the National Fund of Scientific Research (Belgium).

REFERENCES

1. A. Clearfield and J. A. Stynes, *J. Inorg. Nucl. Chem.* 1964, **26**, 117.
2. A. Clearfield (ed.), *Inorganic Ion Exchange Materials*. CRC Press, Boca Raton, Florida (1982).
3. A. Clearfield and S. P. Pack, *J. Catal.* 1978, **51**, 431.
4. T. Hattori, H. Hanai and Y. Murakami, *J. Catal.* 1979, **56**, 294.
5. Y. Izumi and Y. Mizutani, *Bull. Chem. Soc. Jpn* 1979, **52**, 3065.
6. G. Alberti and U. Constantino, European Patent Application, 1983, EP 0 094 919 A2.
7. G. Alberti, M. Casciola and U. Costantino, *J. Colloid and Interface Sci.* 1985, **107**, 257.
8. J. M. Troup and A. Clearfield, *Inorg. Chem.* 1977, **16**, 3311.
9. A. Clearfield, W. L. Duax, A. S. Medina, G. P. Smith and J. R. Thomas, *J. Phys. Chem.* 1969, **73**, 3424.
10. A. Clearfield, W. L. Duax, J. M. Garces and A. S. Medina, *J. Inorg. Nucl. Chem.* 1972, **34**, 329.
11. A. Clearfield, S. P. Pack and J. M. Troup, *J. Inorg. Nucl. Chem.* 1977, **39**, 1437.
12. G. Alberti and E. Torracca, *J. Inorg. Nucl. Chem.* 1968, **30**, 317.
13. G. Alberti, U. Costantino and R. Giullietti, *J. Inorg. Nucl. Chem.* 1980, **40**, 1062.
14. L. A. Harris, *Acta Cryst.* 1959, **12**, 172.
15. R. E. Thoma, H. Insely, H. A. Friedman and G. M. Herbert, *J. Chem. Engng Data* 1965, **10**, 219.
16. A. Clearfield, L. B. McCuster and P. R. Rudolf, *Inorg. Chem.* 1984, **23**, 2679.
17. A. Clearfield and J. M. Troup, *J. Phys. Chem.* 1973, **77**, 243.

Polyhedron Vol. 5, No. 12, pp. 2001–2003, 1986
Printed in Great Britain

0277–5387/86 $3.00+.00
Pergamon Journals Ltd

UNEXPECTED REACTION OF SULFUR DICHLORIDE WITH [Cr(CO)$_5$THF]: A Cr(III) PRODUCT WITHOUT CARBON MONOXIDE AS LIGAND

CARLOS DÍAZ

Universidad de Chile, Facultad de Ciencias, Casilla 653, Santiago, Chile

(*Received* 20 *August* 1985; *accepted after revision* 8 *May* 1986)

Abstract—The reaction of SCl_2 with the complex Cr(CO)$_5$THF produces a solid which does not contain carbonyl groups. Elemental analysis, IR and diffuse reflectance spectra as well as magnetic and chemical properties and deuterium substitution experiment suggest the formula [Cr(H_2O)(THF)(SCl_2)Cl_3]·2THF.

It is well-known that the reaction of the complex [Cr(CO)$_5$THF], photochemically generated, with neutral ligands L gives rise to the formation of monosubstituted complex [Cr(CO)$_5$L].[1–3] This method has been especially useful in the synthesis of the [M(CO)$_5$L] complexes with L = sulfur(II) ligand.[4] The reaction of [Cr(CO)$_5$THF] with sulfur dichloride yielded a product which contained no carbon monoxide ligand, and the details of this reaction are reported here.

RESULTS AND DISCUSSION

Although all results are consequent with the formulation [Cr(H_2O)(THF)(SCl_2)Cl_3]·2THF for the product of the reaction of SCl_2 with [Cr(CO)$_5$THF] a definitive determination of the structure of complex by a crystal X-ray analysis was not possible because the insolubility or decomposition of the compound in organic solvent precluded the growing of a suitable single crystal.

The addition of sulfur dichloride to a tetrahydrofuran solution of [Cr(CO)$_5$THF] gave a pink–violet solid whose IR spectra showed no carbonyl bands but surprisingly did show the characteristic bands of coordinated water.

In Table 1 are shown the frequencies observed for this compound. In addition to the three fundamental modes of the water molecule in the spectra are observed the typical—and expected—rocking and wagging modes of coordinated H_2O.[5,6] The Cr—OH_2 stretching frequency is assigned at 490 cm^{-1}, according with the frequencies observed in other chromium–water compounds.[5]

The presence of the coordinated water is confirmed by the use of heavy water in the THF at the

Table 1. Infrared spectra of Cr[(H_2O)(THF)(SCl_2)Cl_3]·2THF (A) and its deuterated (D_2O) analogue (B)

(A)	(B)	Assignment[a]
3290 (vs)		ν(O—H)
	2410, 2340	ν(O—D)
2970 m		THF, $\nu(CH_2)$
2940 m sh		
2903 m sh		
2878 w sh		
1615 st		δ(O—H)
	1110	δ(O—D)
1455 m		THF, $\rho(CH_2)$ sciss
1360 w		THF, $\rho(CH_2)$ wag
1339 m		
1285 w		
1255 w		
1180 w		THF, $\rho(CH_2)$ twist
1039 m		THF,[b] ν(C—O—C)$_{as}$
1008 st		THF, ν(C—O—C)$_{as}$
940 m		THF,[b] ν(C—O—C)$_s$
920 m		
855 vs		THF, ν(C—O—C)$_s$
800 w		ρ rock (H_2O)
680 w sh		ρ wag (H_2O)
490–510		ν(S—Cl)
440 m		ν(Cr—OH_2)
330 st		ν(Cr—Cl), ν(Cr—S)
310 m sh		
290 m sh		

[a] See text.
[b] Tetrahydrofuran uncoordinated.

start. In this case the bands at 3290 (νOH) and 1610 (δOH) shifted to 2410, 2340 and 1110 cm^{-1} respectively on deuteration (see Table 1). The ratios of the frequencies are very close to the expected value of $(\nu_H/\nu_D)^{1/2} = 1.41$.

Also in the spectra are observed the bands of tetrahydrofuran coordinated. The frequencies corresponding to ν(C—O—C)$_{as}$ and ν(C—O—C)$_s$ in free tetrahydrofuran are lowered 61 and 56 cm^{-1} respectively by coordination, behavior characteristic of this ligand linked to $CrCl_3$.[7,8]

A thermogravimetric analysis of the complex agree with the formulation suggested, containing THF solvation molecules. The weight-loss curve reveals that the tetrahydrofuran began to escape at 60°C, behavior typical of organic solvate molecules.*

Because THF and water do not absorb in the 650–200 range, the broad band at 510–490 cm^{-1} may be assigned to SCl_2 modes; e.g. $[PdCl_2(SCl_2)_2]$ 510–530 cm^{-1},[9] $[N(SCl)_2][Re_2Cl_9]$ 512, 494 cm^{-1},[10] $[TaCl_5 \cdot NSCl]$ 493 cm^{-1},[11] $[N(SCl)_2][NbCl_6]$ 514, 492,[11] $[SCl_3][AlCl_4]$ 516, 530 cm^{-1}.[12] The band at 330 cm^{-1} with shoulders at 310 and 290 cm^{-1} can be attributed to Cr—Cl stretching vibrations and Cr—S stretching vibration, by comparison with the assignment for the following complexes: $CrCl_3$, 315 cm^{-1}; $CrCl_3(THF)_3$ 369, 340, 311 cm^{-1} and $CrCl_3 \cdot (Py)_3$ 364, 341, 307 cm^{-1}.[13] The Cr—S stretching vibration occurs at 310–360 cm^{-1}.[14]

The magnetic moment of the complex is 3.87 B.M. which is close to the spin-only value for three unpaired electrons, and typical of Cr(III) complexes.

The electronic spectra of the complex, obtained by diffuse reflectance (Fig. 1), show three ligand-field bands (one with splitting). The energies and relative intensity of these bands is similar to that found in Cr(III) complexes with a nearly regular octahedral stereochemistry, but belonging strictly to lower symmetry.[15]

Although the complex has four different types of ligand and hence should have a symmetry lower than D_{4h} or C_{4v}, it can be treated as approximately belonging to D_{4h} (with two chlorides in *trans* position) if each different ligand, SCl_2, H_2O, THF and Cl can be averaged in considering the ligand fields.[15] Following this analysis the bands have been assigned in terms of D_{4h} nomenclature (see Fig. 1).

Further the similar spectral and magnetic data of the complex with those for $CrCl_3$[16] and other

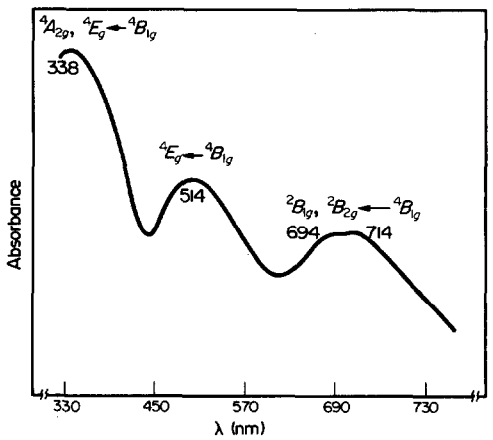


Fig. 1. Reflectance diffuse absorption spectra of $[Cr(H_2O)(THF)(SCl_2)Cl_3] \cdot 2THF$.

$[CrCl_3L_2]_2$ complexes[13] support the presence of three chloride coordinated to chromium(III). In spite of the nucleophilic characteristic expected from the lone pair on sulfur and chlorine atoms of SCl_2 only a reduced number of unstable adducts $AlCl_3 \cdot SCl_2$, $FeCl_3 \cdot SCl_2$ and $SbCl_5 \cdot SCl_2$ are known.[18] Recently iridium, platinum, palladium and osmium complexes with SCl_2 as ligand have been reported.[9]

The formulation of a Cr(III) complex from the hexacarbonylchromium(0) can be understood if we consider a possible oxidation of Cr(0) with the chlorine, presumably formed in the disproportionation of SCl_2.[19] Moreover this could explain the coordination of chloride toward chromium.

EXPERIMENTAL

$Cr(CO)_6$ (Aldrich) was used without prior purification. Sulfur dichloride (Fluka) was distilled with a few drops of PCl_3 prior to use, and the fraction boiling at 58–60°C collected. Tetrahydrofuran was dried with sodium. IR and diffuse reflectance spectra were obtained by using the Perkin–Elmer 621 and Pye–Unicam SP 1800 spectrophotometers respectively. Magnetic moment was measured in a Cahn Ventron model RTS apparatus by the Faraday method. Correction for the diamagnetism of the ligand was made by using Pascal's constants. Reactions were done in a N_2 atmosphere.

Reaction of $[Cr(CO)_5THF]$ with SCl_2. A solution of 1 g of $Cr(CO)_6$ in ca. 60 cm^3 THF was irradiated (UV lamp, Hanau, medium pressure, 150 W) for 100 min at room temperature.[4] Then, a solution of 3.2 g of SCl_2 was added dropwise and the mixture stirred for 30 min. Immediately carbon monoxide was evolved. Solvent was then evaporated under reduced pressure leaving behind a pink–violet solid. This was dried *in vacuo* for 3 h and stored in a

* Unfortunately no other information was obtained from the thermal decomposition weight-loss curve because a horizontal weight level was not observed.

Schlenk apparatus under argon. The compound is hygroscopic and has a pungent odor. In organic solvents it is insoluble or decomposes. m.p. 124–125°C. Found: C, 29.5; H, 5.2; S, 5.6; Cr, 10.8. Calc. for $C_{12}H_{26}O_4Cl_5SCr$; C, 30.2; H, 5.4; S, 6.7; Cr, 10.9%. Chromium analyses were done by oxidation of sample with HNO_3 followed by oxidation of the solution to $Cr_2O_7^{2-}$ with $NaBiO_3$ and titration with Fe^{2+}.

The presence of sulfur dichloride in the complex is confirmed by the reaction of the Cr(III)—SCl_2 compound with copper perchlorate hexahydrate in acetonitrile to give the $[Cu(CH_3CN)_2]ClO_4$. This redox reaction is characteristic for SCl_2 and other sulfur(II) compounds.[17]

Reaction of $[Cr(H_2O)(THF)(SCl_2)Cl_3]\cdot 2THF$ with $Cu(ClO_4)_2\cdot 6H_2O$. 0.14 g of the Cr(III) complex in CH_3CN, was added dropwise over 0.42 g of the copper salt in the same solvent, with stirring and ambient temperature. A small amount of green solid formed, was filtered and by evaporation of the solvent the white crystalline complex $[Cu(CH_3CN)_4]ClO_4$ was obtained, and identified by IR.[17]

Acknowledgement—To Departamento de Investigación y Bibliotecas de la Universidad de Chile for financial support of this work.

REFERENCES

1. W. Strohmeier and F. J. Müller, *Chem. Ber.* 1969, **102**, 3608.
2. W. Strohmeier, *Angew. Chem., Int. Ed.* 1964, **3**, 730.
3. E. W. Ainscough, F. J. Birch and A. M. Brodie, *Inorg. Chim. Acta* 1976, **20**, 187.
4. C. Díaz and G. González, *Inorg. Chim. Acta* 1984, **85**, 61.
5. K. Nakamoto, *Infrared Spectra of Inorganic and Coordination Compounds*. Wiley (1980).
6. G. Percy and S. Stenton, *J. Chem. Soc. Dalton Trans.* 1976, 1466.
7. L. Benner and C. A. Root, *Inorg. Chem.* 1972, **11**, 652.
8. G. M. Barrow and S. Searles, *J. Am. Chem. Soc.* 1953, **75**, 1175.
9. N. I. Timoschenko, S. V. Volkov and Z. A. Fokina, *Rev. Chim. Miner.* 1983, **20**, 776.
10. H. G. Hauck, P. Klingelhöfer, V. Müller and K. Dehnicke, *Z. Anorg. Allg. Chem.* 1984, **510**, 180.
11. J. Hanich and K. Dehnicke, *Z. Naturforsch* 1984, **39B**, 1467.
12. H. E. Doorenbo, J. C. Evans and R. D. Kagel, *J. Phys. Chem.* 1970, **74**, 3385.
13. M. A. Bennett, R. J. H. Clark and A. D. J. Goodwin, *J. Chem. Soc. A* 1970, 541.
14. D. A. Adams, *Metal-Ligand and Related Vibrations*. E. Arnold (1967).
15. J. R. Perumareddi, *Coord. Chem. Rev.* 1969, **4**, 73.
16. A. B. P. Lever, *Inorganic Electronic Spectroscopy*. Elsevier (1968).
17. C. Díaz, *Polyhedron* 1985, **4**, 1269.
18. S. N. Nabi and M. A. Khaleque, *J. Chem. Soc.* 1965, 3626.
19. D. N. Harpp, K. Steliou and T. M. Chan, *J. Am. Chem. Soc.* 1978, **100**, 1222.

Polyhedron Vol. 5, No. 12, pp. 2005–2011, 1986
Printed in Great Britain

0277–5387/86 $3.00+.00
© 1986 Pergamon Journals Ltd

A COMPARATIVE STUDY OF THE STRUCTURES, NMR PROPERTIES AND MAGNETIC BEHAVIOUR OF COMPLEXES OF COBALT(II) WITH OCTAMETHYLPYROPHOSPHORAMIDE AND NONAMETHYLIMIDODIPHOSPHORAMIDE

F. BENABICHA,* A. COURTOIS,* J. J. DELPUECH,†‡ E. ELKAÏM,* J. HUBSCH,* L. RODEHÜSER† and P. RUBINI†

*Laboratoire de Cristallographie et de Minéralogie, U.A.CNRS No. 809 and †Laboratoire d'Étude des Solutions Organiques et Colloïdales, U.A.CNRS No. 406, Faculté des Sciences, Université de Nancy I, B.P. No. 239, F-54506 Vandoeuvre-lès-Nancy Cedex, France

(*Received* 9 *December* 1985; *accepted* 8 *May* 1986)

Abstract—The structure of the complex $Co(NIPA)_3(ClO_4)_2$ has been determined by X-ray diffraction analysis and found to be very close to that of the corresponding OMPA complex. The magnetic susceptibilities of the OMPA and NIPA complexes have been measured by a thermomagnetic method and have allowed the calculation of $\chi_\parallel$ and $\chi_\perp$, the susceptibilities along the principal axes of the complexes. The magnetic properties of the isomorphous nickel compounds have been studied for comparison. Results give evidence for the greater magnetic anisotropy of the NIPA complexes.

In an earlier publication[1] we reported the results of a NMR study on stereochemically non-rigid paramagnetic tris-chelate complexes of cobalt(II) with the two ligands: octamethylpyrophosphoramide [OMPA: $(NMe_2)_2P(O)OP(O)(NMe_2)_2$] and nonamethylimidodiphosphoramide [NIPA: $(NMe_2)_2P(O)NMeP(O)(NMe_2)_2$]. These complexes, studied as perchlorate salts dissolved in a solvent mixture of deuterated nitromethane and dichloromethane, exhibit two signals corresponding to the terminal *N*-methyl groups. This inequivalence is due to the D_3 symmetry of the complexes in which these two substituents occupy diastereotopic positions. In spite of a very similar structure of the ligands which differ only by the bridging group between the phosphorus atoms, the chemical shifts of the proton NMR spectra were found quite different. For example, at −36°C, the values are 12.69 and −8.87 ppm for $Co(OMPA)_3^{2+}$ against 18.65 and −19.47 ppm for $Co(NIPA)_3^{2+}$.

As the chemical shifts depend essentially on dipolar interactions between the electron spin of the metal ion and the nuclear spin of the observed nuclei, they are governed by two factors, a geometrical one and a magnetic one. The former term is related to the positions of the hydrogen atoms in the complex and the latter to the difference of magnetic susceptibilities $\chi_\parallel$ and $\chi_\perp$ along the principal axes of the complex (C_3 and C_2 respectively). In our previous study, we assumed that the structures of the two complexes were strictly identical on the basis of powder diagram studies[2,3] which indicated isomorphous compounds. We therefore concluded that the observed differences between the chemical shifts were due to a variation of the magnetic anisotropies on going from one complex to another. Considering the similar structure of the ligands, these results seemed rather surprising. We therefore decided to reexamine the complete geometry of $Co(NIPA)_3(ClO_4)_2$ by X-ray diffraction on a single crystal to verify if minor variations in the structure could account for the observed phenomena. In addition magnetic measurements were performed on these and the corresponding nickel(II) compounds to complete the study.

EXPERIMENTAL

Materials

The complexes $Co(NIPA)_3(ClO_4)_2$, $Co(OMPA)_3(ClO_4)_2$, $Ni(NIPA)_3(ClO_4)_2$ and $Ni(OMPA)_3(ClO_4)_2$

‡ Author to whom correspondence should be addressed.

were prepared as described before.[1,2,4] Crystals of the NIPA complex were obtained by recrystallization from an anhydrous acetone solution.

All manipulations were carried out under purified argon in a glove box because of the hygroscopic character of the compounds. The crystal of $Co(NIPA)_3(ClO_4)_2$ was sealed in a Lindeman glass capillary for the crystallographic study. $Ni(NIPA)_3(ClO_4)_2$ powder was put in a tight box between two beryllium windows for the crystallographic data collection.

Magnetic measurements

Thermomagnetic measurements for the complexes $Co(NIPA)_3(ClO_4)_2$, $Co(OMPA)_3(ClO_4)_2$, $Ni(NIPA)_3(ClO_4)_2$ and $Ni(OMPA)_3(ClO_4)_2$ were performed between 4.2 and 300 K in a S.Q.U.I.D. magnetometer (SHE, minimum detectable magnetization: 2×10^{-8} emu) and in a vibrating sample magnetometer (PAR, minimum detectable magnetization: 5×10^{-5} emu). The sample was warmed up in an applied field of 10 kOe and the susceptibility was recorded as a function of temperature.

Susceptibility data are reported on a molar basis in c.g.s. units. Effective moments as well as the molar magnetizations are given in Bohr magnetons:

$$M = \chi_m H/N\beta$$

where N is Avogadro's number, χ_m the molar susceptibility, H the applied field and β is the Bohr magneton. The data are corrected for the diamagnetism of the sample holder and that of the ligand.

Crystallographic measurements

The data for the compounds as well as the experimental and refinement parameters are given in Table 1.

$Co(NIPA)_3(ClO_4)_2$. The crystal of $Co(NIPA)_3(ClO_4)_2$ was a hexagonal prism elongated along the [001] crystallographic axis. Cell dimensions were adjusted by a least-squares procedure applied to the setting angles of 25 reflections measured with the indicated diffractometer with graphite-monochromated CuK_α radiation at room temperature. A correction was applied to the data according to the linear decrease of the three standards. Empirical absorption corrections were calculated by using the program DIFABS.[5]

Table 1. Experimental data and refinement parameters

	$Co(NIPA)_3(ClO_4)_2$	$Ni(NIPA)_3(ClO_4)_2$
State	Single crystal	Powder
Cryst. system	Trigonal	Trigonal
Space group	$P\bar{3}c1$	$P\bar{3}c1$
a, Å	12.974(2)	12.78(2)
c, Å	18.439(3)	18.22(4)
V, Å^3	2687.7	2577
Z	2	2
ρ_{calc}, g cm^{-3}	1.43	—
Cryst. dimensions	$0.15 \times 0.20 \times 0.45$ mm^3	—
Colour	Pink	Yellow
Diffractometer	CAD4-F Nonius	CGR θ60
Radiation	$CuK\alpha(\lambda = 1.5418$ Å)	$CuK\alpha$
Scan procedure	$\theta, 2\theta$	—
θ range	$1° < \theta < 75°$	$2° < \theta < 20°$
Collected reflections	1916	19 (from 47 contributing reflections)
Reflections in refinement	$941(I > 3\sigma(I))$	19
Reference reflections	3, every 2 h (8% decay)	—
Checking of the crystal alignment	Every 50 reflections	—
Corrections	Lorentz and polarization, empirical absorption correction $0.19 < A < 1.98$	Lorentz and polarization, no absorption correction
Residual factors	$R_F = 4.8\%$, $R_{wF} = 5.8\%$	$R_I = 7\%$

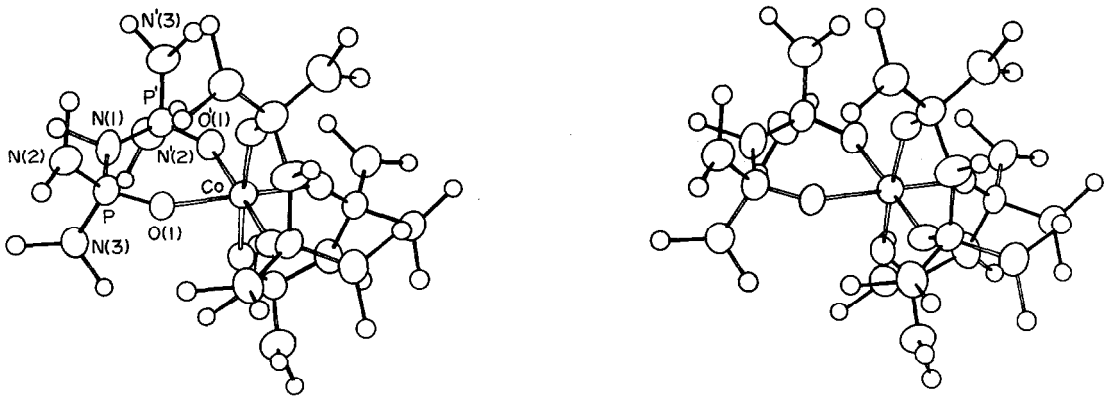


Fig. 1. Stereoscopic ORTEP[12] view of the complex $Co(NIPA)_3(ClO_4)_2$.

$Ni(NIPA)_3(ClO_4)_2$. The box containing the powder was rotated to minimize the effects of possible preferred orientation. Diffraction data were collected on the diffractometer with quartz-monochromated CuK_α radiation at room temperature. The observed reflections may be indexed with a trigonal cell similar to that of $Co(NIPA)_3(ClO_4)_2$. Cell dimensions were adjusted by a least-squares procedure[6] applied to all the measured reflections. Intensities were recorded on paper and measured by planimetry. The 19 observed peaks are stemming from 47 non zero reflections measured until $2\theta = 41°$.

Solution and refinement of structures

$Co(NIPA)_3(ClO_4)_2$. The cobalt and phosphorus atoms were located from Patterson maps. These atoms are found on the same sites as those in the Co—OMPA complex structure.[7] Therefore we placed the other atoms in the cell correspondingly. The carbon bound to the central nitrogen was located by difference Fourier synthesis. The positions of hydrogens were calculated after checking on difference Fourier maps.

N(1) and C(1) are located on a C_2 axis, an incompatible symmetry for a methyl group. Therefore we must attribute a half multiplicity to the three hydrogens H(Cl). The fit is good ($R < 5\%$) for the centrosymmetric hypothesis $P\bar{3}c1$. Taking into account that the absorption corrections are not perfect, we think it is not reasonable to choose the $P\bar{3}c1$ group without the C_2 axis leading to a non-statistic interpretation. Moreover, the zero-moment test of Howells *et al.*[8] shows a typical centric distribution.

Difference maps obtained with all atoms except the perchlorate oxygens had areas of residual electron density corresponding to more than one ClO_4 tetrahedron. However it was impossible to refine some of these positions without observing an unacceptable increase of their thermal parameters. Therefore we decided to place only the O(2)–O(3) tetrahedron for which the disorder is expressed by somewhat anisotropic thermal parameters.

A full-matrix least-squares refinement[9] [on $\Sigma w(\Delta F)^2$] including a weighting scheme, $w = 1/(\sigma^2(F_0) + 0.0016F^2)$, converged to $R = 0.048$ and $R_w = 0.052$ with anisotropic thermal parameters for non-H atoms and isotropic temperature factors (equivalent to those of bonded atoms) for hydrogens. Atomic scattering factors were taken from the *International Tables for X-ray Crystallography*.[10]

Final positional and thermal parameters and a list of calculated and observed factors have been deposited as supplementary data with the Editor, from whom copies are available on request.*

$Ni(NIPA)_3(ClO_4)_2$. At first, all the atoms were located in the corresponding sites of the Co—NIPA structure with isotropic thermal parameters equal to those of the latter. Taking into account the restricted number of independent data, we only refined the positions of atoms of the chelate ring by a least-squares procedure[11] which minimizes the quantity $U = \Sigma(I_0 - I_c)^2$. When several reflections overlapped, the sum of their intensities was taken as a unique value. The refinement is checked by the decrease of U and yielded $R = \Sigma(I_0 - I_c)/\Sigma I_0 = 7\%$. The positions of refined atoms and a list of calculated and observed intensities are available as supplementary data.

RESULTS AND DISCUSSION

Structures

The geometry of $Co(NIPA)_3(ClO_4)_2$ including the atomic numbering scheme of one ligand is illustrated by the stereoscopic ORTEP view[12] of Fig. 1.

* Atomic coordinates have also been deposited with the Cambridge Crystallographic Data Centre.

Table 2. Bond lengths in the complex $Co(NIPA)_3(ClO_4)_2$

Atom 1	Atom 2	Distance	Atom 1	Atom 2	Distance	Atom 1	Atom 2	Distance
Co	O(1)	2.084(3)	O(1)	N(1)	2.597(6)	N(2)	C(3)	1.433(8)
Cl	O(2)	1.307(11)	O(1)	N(2)	2.659(4)	N(2)	C(4)	3.027(8)
Cl	O(3)	1.339(6)	O(1)	N(3)	2.521(6)	N(3)	C(1)	3.250(6)
P	O(1)	1.471(4)	O(1)	C(5)	2.912(7)	N(3)	C(2)	3.015(7)
P	N(1)	1.678(3)	O(2)	O(3)	2.155(11)	N(3)	C(4)	1.468(8)
P	N(2)	1.634(3)	N(1)	N(2)	2.580(4)	N(3)	C(5)	1.468(6)
P	N(3)	1.616(5)	N(1)	N(3)	2.730(5)	C(1)	C(3)	3.166(8)
P	C(1)	2.685(7)	N(1)	C(1)	1.491(10)	C(2)	C(3)	2.441(9)
P	C(2)	2.681(5)	N(1)	C(3)	2.943(6)	C(2)	C(4)	3.218(10)
P	C(3)	2.679(6)	N(2)	N(3)	2.567(5)	C(4)	C(5)	2.462(8)
P	C(4)	2.739(7)	N(2)	C(1)	2.976(6)			
P	C(5)	2.656(5)	N(2)	C(2)	1.477(7)			

Table 3. Distances and angles for the complexes $Co(OMPA)_3(ClO_4)_2$, $Co(NIPA)_3(ClO_4)_2$ and $Ni(NIPA)_3(ClO_4)_2$

	$Co(OMPA)_3(ClO_4)_2$[a]	$Co(NIPA)_3(ClO_4)_2$	$Ni(NIPA)_3(ClO_4)_2$
M—O(1)	2.084(3) Å	2.084(3) Å	2.21(5) Å
P—O(1)	1.476(5) Å	1.471(4) Å	1.49(5) Å
P—N(1)	1.606(3) Å	1.678(3) Å	1.66(5) Å
P—N(2)	1.602(4) Å	1.634(3) Å	1.54(2) Å
P—N(3)	1.610(5) Å	1.616(5) Å	1.70(4) Å
O(1)—M—O′(1)	92.1(1)°	92.20(10)°	93(2)°
O(1)—M—O″(1)	91.7(1)°	92.21(8)°	91(3)°
O(1)—M—O‴(1)	90.8(1)°	92.13(8)°	97(2)°
P—N(1)—P′	134.6(3)°	128.6(3)°	117(4)°

[a] Ref. 7.

For greater clarity, the methyl groups are plotted as small spheres. Table 2 summarizes bond lengths and angles. The cobalt ion is octahedrally surrounded by six oxygen atoms stemming from three ligands related by a C_3 axis. The O—Co—O angles in Table 3 indicate small deviations from octahedral geometry. Each ligand presents a *cis* conformation [dihedral angle O(1)—P—P′/P—P′—O′(1) = 3.1°] contrary to the free ligand NIPA in the solid state.[13] The O, P and N atoms of each chelate ring are almost coplanar, the Co^{2+} ion being situated in the plane (Table 4) corroborating infrared and Raman measurements.[2] Least-squares planes calculations show that all nitrogen atoms have a trigonal planar hybridization.

The results of the crystallographic study about $Ni(NIPA)_3(ClO_4)_2$ are not significantly different from those of $Co(NIPA)_3(ClO_4)_2$ (see comparison of distances in Table 3 taking into account the standard deviations). Therefore we can consider that the two structures are isomorphous.

Table 3 also compares distances and angles in the complexes $Co(NIPA)_3(ClO_4)_2$ and $Co(OMPA)_3(ClO_4)_2$. Co—O,P—O lengths and O—Co—O angles are very similar. Obviously distances and angles concerning the central atoms of the chelate ring [N(1) for NIPA and O(2) for OMPA] are clearly different.

Table 4. Deviations of the different atoms of the chelate ring from the least-squares plane in the complex $Co(NIPA)_3(ClO_4)_2$

Atom	d (Å)
O(1)	−0.022(3)
P	0.021(1)
N(1)	0.0
P′	−0.021(1)
O′(1)	0.022(3)
Co	0.0

Therefore we conclude that the environment of the metal ion (Co or Ni) is very similar in the two considered complexes.

Magnetic measurements

Once the exact structure of the NIPA complex had been established we could recalculate the geometrical term $\langle(3\cos^2\theta-1)/r^3\rangle$ for the hydrogen atoms of the N-methyl groups, in the same way as for the OMPA complex, θ representing the angle between the C_3 axis and the vector connecting the cation to the observed atom and r being the distance between them. Following the method described in Ref. 1, we could subsequently determine the contribution of the pseudo-contact shifts δ_{pc} to the total chemical shift δ_p. From the knowledge of δ_{pc}, we could compute $\Delta\chi$, the difference between the magnetic susceptibilities along the $C_2(\chi_\perp)$ and $C_3(\chi_\parallel)$ axes respectively, according to the relation:

$$\delta_{pc} = (\chi_\parallel - \chi_\perp)\left\langle \frac{3\cos^2\theta-1}{r^3} \right\rangle.$$

The results are summarized in Table 5 and show a good agreement with those obtained previously. This study confirms our earlier conclusion that the OMPA complex is magnetically by far less anisotropic than the NIPA complex. (For example, at −36°C, $\Delta\chi = 5.31\times10^{-3}$ and 10.80×10^{-3} Å^3 for the complexes of OMPA and NIPA respectively.)

Table 5. Mean magnetic susceptibilities $\langle\chi\rangle$ and differences $\Delta\chi$ between transverse ($\chi_\perp$) and longitudinal ($\chi_\parallel$) magnetic susceptibilities (in 10^{-3} Å^3) for the complex $Co(NIPA)_3(ClO_4)_2$ as well as $\chi_\parallel$ and $\chi_\perp$, at different temperatures, calculated from the NMR results of Ref. 1 and the crystallographic data and magnetic measurements of this work

T (K)	$\langle\chi\rangle$	$\Delta\chi$	$\chi_\parallel$	$\chi_\perp$
194.5	18.93	14.95	8.96	23.91
222	16.28	12.37	8.04	20.41
230	15.63	11.46	7.99	19.45
237	15.10	10.80	7.90	18.70
247	14.39	10.12	7.64	17.76

This trend is not actually reflected by the values of magnetic moments measured by Joesten *et al.*[14] for the OMPA complex (5.24 B.M.) and by the authors for Co—NIPA (5.08 B.M.). Since these measurements had been made at room temperature only, we decided to determine them more accurately by thermomagnetic analysis. Plots of the reciprocal molar susceptibility, χ_m^{-1}, and effective magnetic moments, μ_{eff}, vs temperature are shown in Fig. 2(a) and (b), the arrows indicating the corresponding

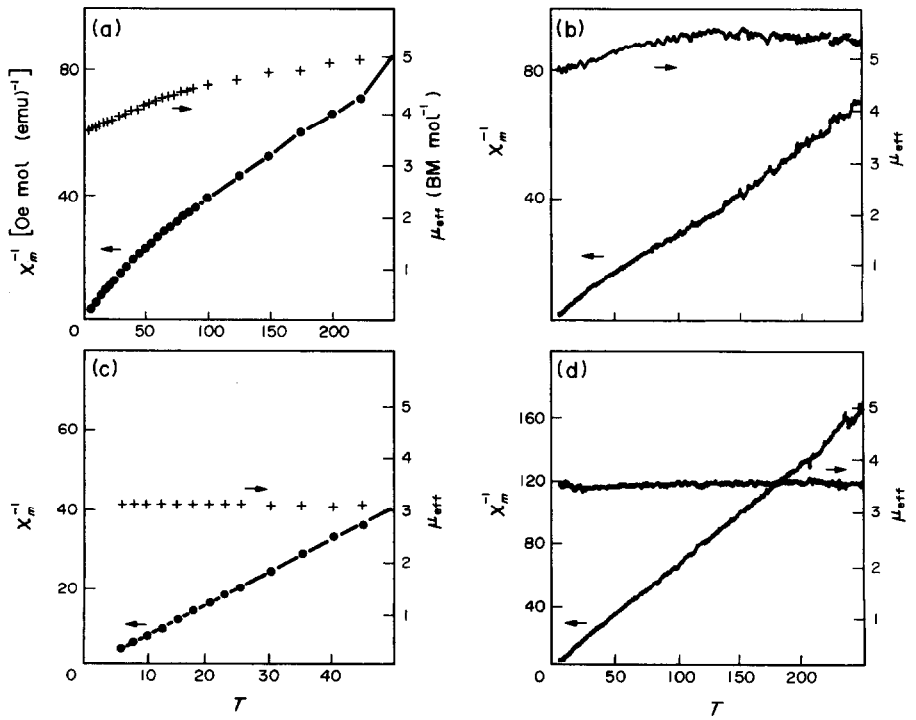


Fig. 2. Plots of χ_m^{-1} and μ_{eff} vs temperature (T) for $Co(OMPA)_3(ClO_4)_2$ (a), $Co(NIPA)_3(ClO_4)_2$ (b), $Ni(OMPA)_3(ClO_4)_2$ (c), and $Ni(NIPA)_3(ClO_4)_2$ (d). The arrows designate the corresponding axes. (Values corrected for T.I.P. terms.)

axes. μ_{eff} was calculated from the relation:

$$\mu_{eff}^2 = \frac{3k}{N\beta^2}\chi_m T = 8\chi_m T$$

where k is the Boltzmann constant.

For these complexes, the inverse magnetic susceptibility vs temperature curve presents a curvature towards the T axis and does not follow a Curie law. The effective magnetic moment calculated for the Co—NIPA complex, is at any temperature greater than that of the OMPA compound. It tends towards a maximum of 5.5 B.M. above 125 K and is nearly constant at higher temperatures. For the Co—OMPA complex, the effective magnetic moment reaches a maximum of 5.1 B.M. at about 240 K.

In our previous publication[1] we had used a single value of $\langle\chi\rangle$ determined at 300 K, and assumed that the product $\langle\chi\rangle \cdot T$ was constant at different temperatures. On the base of the results mentioned above, we decided to recalculate $\chi_\perp$ and $\chi_\parallel$ from the relations $\Delta\chi = \chi_\perp - \chi_\parallel$ and $\langle\chi\rangle = (\chi_\parallel + 2\chi_\perp)/3$ for each temperature of the NMR experiments of Ref. 1. The results are shown in Tables 5 and 6. The magnetic susceptibilities along the C_3 axis are found very similar whereas those perpendicular to it differ significantly.

The magnetic behaviour found for these Co complexes is characteristic for the $^4T_{1g}$ ground term and that for the complexes of OMPA and NIPA with the Ni^{2+} ion is characteristic for the $^3A_{2g}$ ground term, as shown in Fig. 2(c) and (d).

In the case of these nickel chelates, the variation of the magnetic susceptibility with temperature follows practically a Curie law. An additional small constant T.I.P. (Temperature Independent Paramagnetism) is due to a contribution from the A_{2g} term and related to the energy separation $10D_q$ between the $^3A_{2g}$ and $^3T_{1g}$ levels by the equation[15]

$$\chi_{T.I.P.} = 8N\beta^2/|10D_q|.$$

Table 6. Mean magnetic susceptibilities $\langle\chi\rangle$ and differences $\Delta\chi$ between transverse ($\chi_\perp$) and longitudinal ($\chi_\parallel$) magnetic susceptibilities, as well as $\chi_\parallel$ and $\chi_\perp$ (in 10^{-3} Å^3) for the complex $Co(OMPA)_3(ClO_4)_2$ at different temperatures, calculated from the NMR results of Ref. 1 and the magnetic measurements of this work

T (K)	$\langle\chi\rangle$	$\Delta\chi$	$\chi_\parallel$	$\chi_\perp$
190.5	14.31	5.39	10.72	16.11
208	13.36	5.46	9.72	15.18
221	12.76	5.46	9.12	14.58
237	12.10	5.31	8.56	13.87
252	11.56	5.07	8.18	13.25

To estimate this contribution, we measured the diamagnetism of NIPA alone and that of the sample holder. The data were corrected for these diamagnetic contributions.

The experimental susceptibilities were fitted according to:

$$\chi = \frac{C}{T} + \chi_{T.I.P.}$$

The values for $\chi_{T.I.P.}$ calculated in this way are 280×10^{-6} e.m.u. mol^{-1} for $Ni(OMPA)_3(ClO_4)_2$ and 288×10^{-6} e.m.u. mol^{-1} for $Ni(NIPA)_3(ClO_4)_2$. The corresponding results for D_q are approximately 746 cm^{-1} and 724 cm$^{-1} \pm 40$ cm^{-1}, respectively. They agree with the values determined spectrophotometrically by Joesten *et al.*[4,14], e.g. 726 (or 731, Ref. 16) and 727 cm^{-1}.

A difference in the magnetic behaviour of the NIPA complex compared to the corresponding OMPA compound however, is also verified in this case of magnetically "normal" complexes. Temperature independent values of μ_{eff} can be obtained for the nickel compounds: 3.14 B.M. for $Ni(OMPA)_3(ClO_4)_2$ and 3.45 B.M. for $Ni(NIPA)_3(ClO_4)_2$ (compared to 3.26 B.M. determined by Joesten *et al.*[14]). The corresponding g values are 2.22 and 2.44. On the base of powder diffraction data,[2,16] it can be ascertained that the two nickel compounds are of nearly identical structure and that they are both in turn very close to the corresponding cobalt complexes (cf. Table 3).

CONCLUSION

The results of these studies confirm our previous hypothesis concerning the different magnetic properties of OMPA complexes compared to NIPA compounds although their structures are very similar as verified by X-ray diffraction analysis. We had noticed also that the complexes of the two ligands did not show the same behaviour as far as the intra and intermolecular exchange reactions are concerned, the OMPA being much more labile than NIPA. Thermodynamic stabilities, too, differ significantly between complexes of a given ion with the two ligands.[17] These facts could be explained either by a difference in the nature of the metal–ligand bonds (i.e. a more important electron delocalization in the case of OMPA)—although contradictory to the observation of rigorously the same metal–oxygen distances in the two cobalt complexes—or, the distance of closest approach being limited by the crowding of ligands around the ion, by a different charge-distribution in the ligands, leading to a stronger interaction with the cation in the case of NIPA.

REFERENCES

1. P. R. Rubini, Z. Poaty, J. C. Boubel, L. Rodehüser and J. J. Delpuech. *Inorg. Chem.* 1983, **22**, 1295.
2. M. W. G. de Bolster and W. L. Groeneveld, *Rec. Trav. Chim.* 1972, **91**, 171.
3. P. T. Miller, P. G. Lenhert and M. D. Joesten, *Inorg. Chem.* 1972, **11**, 2221.
4. K. T. Lannert and M. D. Joesten, *Inorg. Chem.* 1968, **7**, 2048.
5. N. Walker and D. Stuart, *Acta Cryst.* 1983, **A39**, 158.
6. A. A. Cox, A program for least-squares refinement of unit cell dimensions. The City University, London (1967).
7. M. D. Joesten, M. S. Hussain and P. G. Lenhert, *Inorg. Chem.* 1970, **9**, 151.
8. E. R. Howells, D. C. Phillips and D. Rogers, *Acta Cryst.* 1950, **3**, 210.
9. B. A. Frenz, *Structure Determination Package.* Enraf-Nonius, Delft, The Netherlands.
10. *International Tables for X-ray Crystallography*, Vol. IV. Kynoch Press, Birmingham (1974).
11. A. Courtois, A program for least-squares refinement of crystal structures from powder data. Laboratoire de Cristallographie, Université de Nancy I, Nancy, France (1973).
12. C. K. Johnson, ORTEP II, Report ORNL-3794, revised Oak Ridge National Laboratory, Tennessee (1971).
13. K. Bokolo, A. Courtois, J. J. Delpuech, E. Elkaïm, J. Protas, D. Rinaldi, L. Rodehüser and P. Rubini, *J. Am. Chem. Soc.* 1984, **106**, 6333.
14. M. D. Joesten and K. M. Nykerk, *Inorg. Chem.* 1964, **3**, 548.
15. B. N. Figgis, *Introduction to Ligand Fields.* Interscience, New York (1966).
16. R. A. Palmer and C. R. Taylor, *Inorg. Chem.* 1971, **10**, 2546.
17. Unpublished results.

Polyhedron Vol. 5, No. 12, pp. 2013–2020, 1986
Printed in Great Britain

0277-5387/86 $3.00+.00
© 1986 Pergamon Journals Ltd

BIS[BIS{(DIPHENYLPHOSPHINYL)METHYL}ETHYL PHOSPHINATE]BIS(ETHANOL) COPPER(II) PERCHLORATE: SYNTHESIS, CRYSTAL AND MOLECULAR STRUCTURE

MARIJA HERCEG,* PAVICA BRONZAN-PLANINIĆ, HENRIKA MEIDER and BORIS MATKOVIĆ

"Rudjer Bošković" Institute, 41001 Zagreb, Croatia, Yugoslavia

(*Received* 6 *January* 1986; *accepted* 8 *May* 1986)

Abstract—Bis[bis{(diphenylphosphinyl)methyl}ethyl phosphinate]bis(ethanol) metal(II) perchlorate complexes, where metal = Co, Ni or Cu, have been prepared by the reaction of metal perchlorates and bis[(diphenylphosphinyl)methyl]ethyl phosphinate, (RPOEt), in absolute ethanol. The crystal structure of the copper complex is triclinic, space group $P\bar{1}$, $a = 13.688(7)$ Å, $b = 14.424(10)$ Å, $c = 9.865(2)$ Å, $\alpha = 110.43(4)°$, $\beta = 90.13(2)°$, $\gamma = 115.54(4)°$, $V = 1619.8$ Å^3, $Z = 1$ and refined to $R = 0.048$ ($R_w = 0.057$). The structure consists of complex cations surrounded by perchlorate anions. Two RPOEt ligands and two ethanols are coordinated to the copper atom situated at the centre of symmetry 0, 0, 0. The RPOEt ligand is bidentate [Cu—O distances 1.969(4) Å, 2.312(4) Å], but the third oxygen atom from phosphoryl bonds is hydrogen bonded [2.669(6) Å], to the oxygen atom of ethanol molecule coordinated to the copper at 1.988(4) Å. The conformations of the ligand and chelate rings, magnetic data, molar conductance values, infrared and electronic spectra are given.

The synthesis of some cobalt(II), nickel(II) and copper(II) perchlorate[1] and chloride [2,3] complexes with tripod organophosphorus compounds, was reported previously. The types of ligands, together with their abbreviations, are portrayed in Scheme 1.

The preparation of ligands RPOEt, RPPh and RPOH was reported before.[4,5] Bis[(diphenylphosphinyl)methyl]ethyl phosphinate (RPOEt) is the ligand studied in the present work. It has three phosphoryl groups bridged by methylene groups. Another ligand consisting of three phosphoryl groups bridged by methylimido groups is dodecamethyl diimidotriphosphoramide, named TRIPA, $[(CH_3)_2N]_2P(O) \cdot NCH_3 \cdot [(CH_3)_2N]P(O) \cdot NCH_3 \cdot P(O)[(CH_3)_2N]_2$.[6–8] In the complexes: $[Er(TRIPA)_2(NO_3)](NO_3)_2$ and $[Ca(TRIPA)(NO_3)_2(H_2O)]$ TRIPA acts as tridentate ligand.[8]

The ligands RPOEt, RPPh and RPOH are potentially tridentate too. Conformation analyses revealed that RPPh acts preferentially as a bidentate ligand, but the possibility that this ligand is a tridentate complexing agent was not excluded.[9] No structure of any complex with RPOEt, RPPh and RPOH has been reported yet.

Formulae of investigated complexes are: $[Co(RPOEt)_2(C_2H_5OH)_2](ClO_4)_2$, $[Ni(RPOEt)_2(C_2H_5OH)_2](ClO_4)_2$ and $[Cu(RPOEt)_2(C_2H_5OH)_2](ClO_4)_2$. These compounds were characterized by chemical analysis, infrared and electronic spectra, magnetic and conductivity measurements. X-ray structure determination has been carried out on $[Cu(RPOEt)_2(C_2H_5OH)_2](ClO_4)_2$.

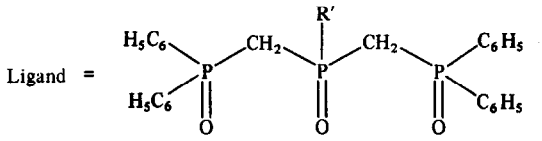
EXPERIMENTAL

The ligand, bis[(diphenylphosphinyl)methyl] ethyl phosphinate (RPOEt) was prepared according to the literature data.[5]

For conductivity measurements nitrobenzene was purified by the method of Taylor and Kraus.[10] All other solvents were analytical grade reagents dried over molecular sieves without further purification.

Physical measurements and the instrumentation employed have been already described.[1] The correction for the diamagnetism of the ligand was made with the use of Pascal's constants.[11] All physical

* Author to whom correspondence should be addressed.



$(C_{26}P_3O_3H_{24}R')$

If R′ is OC_2H_5, the ligand is bis[(diphenylphosphinyl)methyl]ethyl phosphinate (RPOEt)

If R′ is C_6H_5, the ligand is bis[(diphenylphosphinyl)methyl]phenylphosphine oxide (RPPh)

If R′ is OH, the ligand is bis[(diphenylphosphinyl)methyl]phosphinic acid (RPOH)

Scheme 1.

measurements were carried out immediately after recrystallization.

Preparation of complexes

The complexes $[M(RPOEt)_2(C_2H_5OH)_2](ClO_4)_2$ (M = Co, Ni, Cu) were obtained by the reaction of metal(II) perchlorate and ligand, both dissolved in absolute ethanol and mixed together in a molar ratio of 1:2. As all three complexes were obtained exactly in the same manner, only detailed preparation of $[Cu(RPOEt)_2(C_2H_5OH)_2](ClO_4)_2$ is given: 0.371 g $Cu(ClO_4)_2 \cdot 6H_2O$ (1 mmol) was dissolved in 4 cm^3 of hot absolute ethanol, filtered and added slowly into a hot, filtered solution of 1.054 g RPOEt (2 mmol) in 10 cm^3 abs. ethanol. After one day the product was filtered and washed with absolute ethanol and diethylether. The complexes were recrystallized by dissolving in hot 96% ethanol. The solution was refluxed for an hour, filtered and allowed to stand in a covered beaker for 2 days. The crystals were then collected by filtration and washed with small portions of abs. ethanol. The yield was about 80%. Found: Cu, 4.4; P, 13.4; Cl, 5.2. Calc. for $[Cu(RPOEt)_2(C_2H_5OH)_2](ClO_4)_2$: Cu, 4.5; P, 13.3; Cl, 5.1%. Found: Co, 4.2; P, 13.3; Cl, 5.1. Calc. for $[Co(RPOEt)_2(C_2H_5OH)_2](ClO_4)_2$: Co, 4.0; P, 13.3; Cl, 5.1%. Found: Ni, 4.1; P, 13.5; Cl, 5.1. Calc. for $[Ni(RPOEt)_2(C_2H_5OH)_2](ClO_4)_2$: Ni, 4.2; P, 13.3; Cl, 5.1%.

Crystallography

Pale bluish, almost colourless crystals of $[Cu(RPOEt)_2(C_2H_5OH)_2](ClO_4)_2$, suitable for crystallographic study, were obtained by slow careful cooling of a hot 96% ethanolic solution of the recrystallized complex. Pink crystals of the corresponding cobalt complex and greenish crystals of Ni complex obtained in the same way, were not large enough for crystallographic study. However, X-ray powder patterns of the three compounds are similar and indicate a close structural relationship.

The crystals are unstable and were kept in a desiccator over ethyl alcohol. Crystallographic parameters are given in Table 1. Three-dimensional intensity data were collected at room temperature with a Philips PW 1100 diffractometer. As a check on the stability of diffractometer and of the crystal three standard reflections ($00\bar{1}$; $\bar{1}11$; $\bar{2}2\bar{2}$) were monitored periodically. The intensities were corrected with ZOAK program[12] for Lorentz and polarization effects.

The structure was solved by vector and difference Fourier methods. The calculations included both f' and f'' for anomalous dispersion effects of Cu, Cl, P, O and C atoms.[13] The positions of H atoms were calculated from geometrical criteria and included in the structure factor calculations at the end of isotropic refinement. They were given the calculated isotropic temperature factors $B(H) = 1.6B(C) - 2$. Neither positional nor temperature parameters were refined for H atoms. All non-hydrogen atoms were refined anisotropically. The function minimized in least-squares refinement was $w(|F_0| - |F_c|)^2$. The weighting function applied was $w = 1/\sigma^2(F_0)$, a weighting scheme of type 9 from the XRAY system.[14] The scattering factors of Cromer and Mann[15] were used for non-H and those of Stewart *et al.*[16] for H atoms. The final residuals are $R = 0.048$, $R_w = 0.057$. The goodness of fit dropped from $S = 1.531$ to $S = 1.007$ by applying scale factor for weights, SCALWT = 0.43.[14] The largest shift/error in the final cycle is 0.48. Calculations were performed on a Univac 1100 computer at the University Computing Centre, Zagreb with XRAY 76 system.[14] Final positional and thermal parameters and structure factors have been deposited as supplementary material.

RESULTS AND DISCUSSION

Description of the structure

Figure 1 is an ORTEP plot of the structure with atom numbering scheme. Selected bond distances

Table 1. Crystallographic parameters

Formula	$C_{60}H_{70}O_{18}P_6Cl_2Cu$	$C_{60}H_{70}O_{18}P_6Cl_2Co$
Formula weight	1399.5	1394.9
Space group	$P\bar{1}$	$P\bar{1}$
a (Å)	13.688(7)	13.753(4)
b (Å)	14.424(10)	14.449(5)
c (Å)	9.865(2)	9.860(4)
α (°)	110.43(4)	110.65(3)
β (°)	90.13(2)	90.12(3)
γ (°)	115.54(2)	115.71(4)
V (Å^3)	1619.8	1623.8
Z	1	1
D_c (g cm^{-3})	1.435	1.426
D_0 (g cm^{-3})	1.38 (pycnometer, decalin as liquid)	
$F(0, 0, 0)$	727	725
μ (cm^{-1})	6.4	39.8
λ (Å)	0.7107	1.5418
Data collection instrument	Philips PW 1100	Philips PW 1100
Orientation reflections		
No., range, 2θ°	22, 4–16	18, 10–25
Crystal size (mm)	$0.4 \times 0.16 \times 0.06$	
Scan method	θ–2θ	
Data collection range, 2θ°	4–60	
No. of unique data measured	3970	
Total with $F_0^2 \geqslant 3\sigma F_0^2$	3640	
No. of parameters refined	394	
R	0.048	
R_w	0.057	

and bond angles are given in Tables 2 and 3, respectively; C—C distances and C—C—C angles in peripheral phenyl rings are available as supplementary material.*

The structure consists of complex cations surrounded by perchlorate anions. Two RPOEt ligands and two ethanols are coordinated to the copper atom. The polyhedron around the copper is tetrahedrally distorted octahedron. The RPOEt ligand is bidentate, but the third phosphoryl oxygen atom is hydrogen bonded to the oxygen atom of ethanol molecule coordinated to the copper.

One terminal and the central P=O group of RPOEt ligand are coordinated to the copper at two unequal distances [1.969(4) and 2.312(4) Å] thus permitting an extended conformation of the ligand, with the torsion angle about one of the central bonds, C(91)—P(3), of 171.9(3)°, the O(1)—Cu—O(3) chelate angle of 90.0(1)° and O(1)···O(3) bite of 3.036(4) Å. The conformation about the other central bond, P(3)—C(93), is gauche, with a torsion angle −78.6(4)°, the O(3)···O(5) distance is 3.269(5) Å and the P(1)—P(3)—P(5) virtual angle is 120.14(6)°. The valence angle on the bridging carbon atom which is involved in the six-membered chelate ring, P(1)—C(91)—P(3) is larger than the corresponding angle in the non coordinated part of the ligand, P(3)—C(93)—P(5), 113.9(3),° vs 112.1(3)°. The

* Supplementary material, available from the Editor, includes: tables of atom parameters, equivalent isotropic and anisotropic temperature factors, observed and calculated structure factors, bond distances and angles within peripheral phenyl rings and those including hydrogen atoms, as well as equations of least-squares planes. Atomic coordinates have also been deposited with the Cambridge Crystallographic Data Centre.

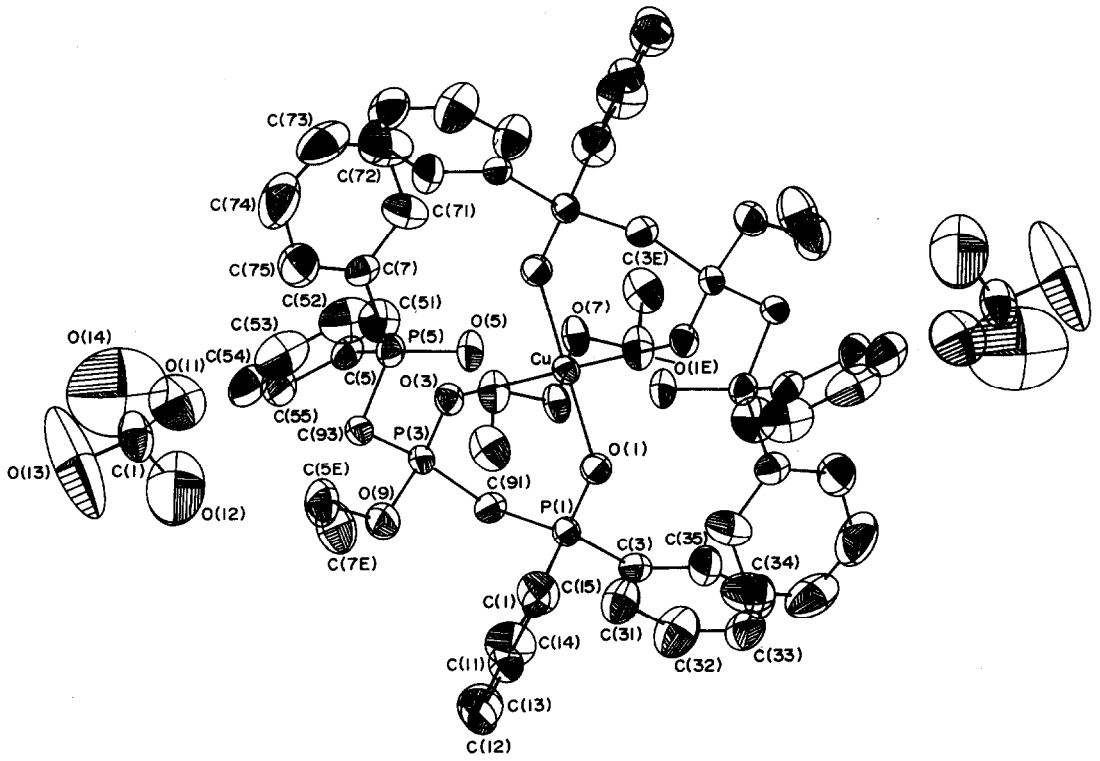


Fig. 1. Molecular geometry and atom-labelling scheme for the molecule $[Cu(RPOEt)_2(C_2H_5OH)_2](ClO_4)_2$.

intracation hydrogen bond, O(5)···H—O(7) of 2.669(6) Å with H—O(7) of 1.092(4) Å and the angle on H of 179.6(2)° may be responsible for this.

Taking into account the O(5)···H—O(7) hydrogen bond, there are two chelate rings in one asymmetric unit, around the copper atom. The conformation of the six-membered Cu—O(1)—P(1)—C(91)—P(3)—O(3) ring may be described following Cremer and Pople[17] by the amplitude of pucker $Q = 0.633(4)$ Å and pseudorotational phase angles $\varphi = 176.4(3)°$ and $\theta = 78.5(3)°$. P(1) and O(3) lie on one side and O(1) and P(3) on the other side of the least-squares plane through the P(3), O(3), O(1), P(1) atoms of the ring. The deviation of ring atoms from this plane is −0.009(2) Å for P(1); 0.009(2) Å for P(3), 0.030(4) Å for O(1) and −0.029(4) Å for O(3).[18] Cu and C(91) are well above the plane, 0.337(2) Å and 0.689(5) Å respectively. After Boeyens[19] this conformation is near boat $B_{4,1}$ ($\varphi = 180.0°$, $\theta = 90.0°$). The torsion angles are given in Table 4.

Table 2. Some important bond distances (Å)

Cu—O(1)	1.969(4)	P(1)—O(1)	1.496(5)
Cu—O(3)	2.312(4)	P(1)—C(91)	1.796(5)
Cu—O(7)	1.988(4)	P(1)—C(1)	1.782(6)
O(7)—C(1E)	1.448(5)	P(1)—C(3)	1.796(4)
O(9)—C(5E)	1.476(6)	P(3)—O(3)	1.475(5)
C(1E)—C(3E)	1.490(9)	P(3)—O(9)	1.568(4)
C(5E)—C(7E)	1.468(11)	P(3)—C(91)	1.808(4)
Cl(1)—O(11)	1.370(9)	P(3)—C(93)	1.798(6)
Cl(1)—O(12)	1.345(10)	P(5)—O(5)	1.492(3)
Cl(1)—O(13)	1.320(10)	P(5)—C(93)	1.809(6)
Cl(1)—O(14)	1.332(14)	P(5)—C(5)	1.794(7)
		P(5)—C(7)	1.791(6)

The second ring could be considered as eight membered, Cu—O(3)—P(3)—C(93)—P(5)—O(5)···H—O(7), or seven membered if geometrically determined H atom is excluded. This seven membered ring is rather puckered. There is a significant deviation of the ring atoms from the least-squares plane through the O(5), O(7), Cu and O(3) atoms of the ring. The atom O(5) is 0.028(5) Å, Cu 0.015(3) Å on one side and the atom O(7) is 0.047(5) Å, O(3) 0.026(5) Å on the other side of the plane. The other ring atoms are P(3) 1.046(3) Å, C(93) 0.493(6) Å above and P(5) 0.463(3) Å below the plane. Torsion angles are given in Table 4. The O(3)···O(7) bite distance is 2.948(5) Å and the corresponding angle on the copper atom is 86.2(1)°. The longest copper–

Table 3. Some important bond angles (deg)[a]

O(1)—Cu—O(3)	90.0(1)	C(91)—P(3)—C(93)	105.7(3)
O(1)—Cu—O(3)′	90.0(1)	O(5)—P(5)—C(93)	112.1(2)
O(1)—Cu—O(7)	92.2(2)	O(5)—P(5)—C(5)	110.9(2)
O(1)—Cu—O(7)′	87.8(2)	O(5)—P(5)—C(7)	110.8(3)
O(3)—Cu—O(7)	86.2(1)	C(93)—P(5)—C(5)	105.7(3)
O(3)—Cu—O(7)′	93.8(1)	C(93)—P(5)—C(7)	109.2(3)
O(1)—P(1)—C(91)	112.6(2)	C(5)—P(5)—C(7)	107.9(3)
O(1)—P(1)—C(1)	112.1(3)	P(3)—O(9)—C(5E)	119.3(4)
O(1)—P(1)—C(3)	110.2(2)	O(9)—C(5E)—C(7E)	109.8(5)
C(91)—P(1)—C(1)	106.1(3)	Cu—O(7)—C(1E)	125.0(3)
C(91)—P(1)—C(3)	108.1(3)	O(7)—C(1E)—C(3E)	110.5(4)
C(1)—P(1)—C(3)	107.4(2)	O(11)—Cl(1)—O(12)	109.6(5)
O(3)—P(3)—O(9)	115.5(2)	O(11)—Cl(1)—O(13)	113.5(6)
O(3)—P(3)—C(91)	113.6(2)	O(11)—Cl(1)—O(14)	111.0(9)
O(3)—P(3)—C(93)	112.4(2)	O(12)—Cl(1)—O(13)	110.9(8)
O(9)—P(3)—C(91)	102.8(2)	O(12)—Cl(1)—O(14)	105.7(8)
O(9)—P(3)—C(93)	105.7(2)	O(13)—Cl(1)—O(14)	105.8(8)

[a] The atoms marked with a prime correspond to positions obtained by using the transformation $-x, -y, -z$.

oxygen bond distance [2.312(4) Å] involves the central phosphoryl bond which is the shortest one [1.475(5) Å]. The two peripheral phosphoryl bonds are equal, 1.496(5) and 1.492(3) Å. The bond distances and angles of the ligand (Tables 2 and 3) are close to the values found before in the crystal structures of diphenylphosphinic acid,[20] diphenylthiophospinic acid,[21] sodium salt of monomethyl ester of fosfomycin,[22] or sodium salts of bis(diphenylphosphinyl) methane.[23,24] The smooth differences in P—C bonds along the backbone of the ligand (Table 2) seem to have similar causes as, for instance, the differences in P—O bonds along the backbone of $P_3O_{10}^{5-}$ anion in the crystal structures of condensed triphosphates or the differences in $P—N_{bridge}$ bonds in TRIPA · H_2O (Table 5).

As is usual in phosphine oxides and related compounds, distortion of phosphorus coordination tetrahedra is observed i.e. the $C_{sp^3}—P—C_{sp^3}$ angle decreases to 105.7(3)° while O=P—O angle increases to 115.5(2)°. The two angles involving oxygen from the ethoxy group, $O—P—C_{sp^3}$ are quite different, 102.8(2)° vs 105.7(2)°.

All three oxygen atoms from P=O groups lie on the same side of the plane through the three phosphorus atoms at various distances, O(1) at −1.489(5) Å, O(3) at −1.473(5) Å and O(5) at −0.399(5) Å, with O(1)···O(3) and O(3)···O(5)

Table 4. Torsion angles (deg)

6-membered chelate ring		7-membered ring	
Cu—O(1)—P(1)—C(91)	13.9(4)	Cu—O(3)—P(3)—C(93)	−130.6(2)
O(1)—P(1)—C(91)—P(3)	−51.2(4)	O(3)—P(3)—C(93)—P(5)	45.9(3)
P(1)—C(91)—P(3)—O(3)	48.1(4)	P(3)—C(93)—P(5)—O(5)	34.1(4)
C(91)—P(3)—O(3)—Cu	−10.6(4)	C(93)—P(5)—O(5)···O(7)	−68.3(4)
P(3)—O(3)—Cu—O(1)	−18.4(3)	P(5)—O(5)···O(7)—Cu	30.7(4)
O(3)—Cu—O(1)—P(1)	16.9(3)	O(5)···O(7)—Cu—O(3)	−3.9(2)
		O(7)—Cu—O(3)—P(3)	73.8(3)
RPOEt ligand			
C(1)—P(1)—C(91)—P(3)	71.8(4)	C(91)—P(3)—C(93)—P(5)	−78.6(4)
C(3)—P(1)—C(91)—P(3)	−173.2(3)	P(3)—C(93)—P(5)—C(5)	155.0(3)
P(1)—C(91)—P(3)—C(93)	171.9(3)	P(3)—C(93)—P(5)—C(7)	−89.1(3)
P(1)—C(91)—P(3)—P(9)	−77.4(4)		

Table 5. Bond distances and angles along the backbone of the ligands $P_3O_{10}^{5-}$, TRIPA and RPOEt

Compound	Longer P—X_{bridge}[a] bonds (Å)	Shorter P—X_{bridge} bonds (Å)	P—X_{bridge}—P angles (deg)	Ref.
$Na_5P_3O_{10}\cdot 6H_2O$	1.67(1) 1.67(1)	1.60(1) 1.60(1)	124.4(1) 123.4(1)	25
$Na_3MnP_3O_{10}\cdot 12H_2O$[b]	1.619(5) 1.629(8)	1.588(4) 1.591(5)	135.5(4) 133.4(4)	26
$Na_3CuP_3O_{10}\cdot 12H_2O$[b]	1.629(3) 1.629(3)	1.578(3) 1.590(3)	133.3(2) 132.5(2)	27
$Na_3CdP_3O_{10}\cdot 12H_2O$[b]	1.640(5) 1.620(5)	1.593(5) 1.599(5)	135.2(3) 136.8(3)	28
$TRIPA\cdot H_2O$	1.689(2) 1.695(2)	1.671(2) 1.667(2)	126.6(1) 125.8(1)	29
$[Cu(RPOEt)_2(C_2H_5OH)_2](ClO_4)_2$	1.808(4) 1.809(6)	1.796(5) 1.798(6)	113.9(3) 112.1(3)	this paper

[a] *X* is O, N or C.
[b] Mn, Cu and Cd compounds seem to be isostructural.

distances of 3.036(4) Å and 3.269(5) Å, respectively. The plane through phenyl ring C(1) to C(15) is almost parallel to the plane through O(3) P(3), O(9) [dihedral angle of 4.7(3)°], and perpendicular to the plane through P(1), P(3), P(5) [dihedral angle of 89.5(2)°]. The acute angle between the plane through phenyl ring C(3) to C(35) and the plane through C(1) to C(15) is 73.9(2)°. The plane through the phenyl ring C(5) to C(55) is roughly parallel to the plane through O(5), O(7), O(3), Cu, O(3)′, O(7)′, O(5)′ [Table 3, dihedral angle of 9.3(2)°]. The acute angle between the plane through phenyl ring C(7) to C(75) and the plane through C(5) to C(55) is 74.4(3)°.

The cation–anion interactions seem to be rather weak. Cation–anion distances shorter than 3.6 Å are given in Table 6.

Physical properties

Magnetic data of the cobalt(II) and nickel(II) complexes (Table 7) are indicative of spin-free octahedral compounds. The effective moment of the copper(II) complexes is more or less independent of the stereochemistry.

Molar conductance values observed (Table 7) are close to those expected for 2 : 1 electrolytes.

The intensity, position and shape of the absorption bands in the electronic spectra (Table 7) are typical of octahedral cobalt(II) and nickel(II) complexes. The broad asymmetric band in the near IR region in the spectrum of copper(II) complex appearing at 855 nm can be compared with the spectra of known tetragonally distorted octahedral copper(II) complexes.

Infrared spectral data (Table 8) are in good agreement with the X-ray structural determinations. The most important absorption bands in the spectra of the ligand and its complexes in the range of 4000–620 cm^{-1} are those of P═O, than OH and C—O vibrations from the coordinated ethanol and of ClO_4-ion vibrations. The spectrum of the ligand exhibits three strong absorption bands assigned to P═O stretching vibrations. The maximum at 1245

Table 6. Cation–anion distances[a] (Å)

O(11)···C(53)^{I}	3.373(15)	O(12)···C(93)	3.562(11)
O(11)···C(5E)	3.515(9)	O(13)···C(31)^{II}	3.446(13)
O(11)···C(75)	3.518(11)	O(13)···C(14)^{III}	3.523(10)
O(12)···C(93)^{II}	3.410(14)	O(13)···C(91)^{II}	3.584(16)
O(12)···C(91)^{II}	3.490(14)	O(14)···C(11)^{II}	3.456(19)

[a] Key: (I) $x, y, 1+z$; (II) $-x, 1-y, -z$; (III) $-x, 1-y, 1-z$.

Table 7. Electronic spectra, conductometric and magnetic measurements

Compound	Colour	λ_{max}[a] (nm)	Λ[b] (cm^2 ohm^{-1} mol^{-1})	μ_{eff} (B.M.)
$[Cu(RPOEt)_2(C_2H_5OH)_2](ClO_4)_2$	white	855	46.56	1.95
$[Ni(RPOEt)_2(C_2H_5OH)_2](ClO_4)_2$	greenish	413, 780, 1420	46.86	3.32
$[Co[RPOEt)_2(C_2H_5OH)_2](ClO_4)_2$	pink	480, 530	46.92	4.92

[a] Recorded as nujol mulls.
[b] Measured in 10^{-3} M nitrobenzene solutions, at 295 K.

Table 8. Main IR vibrational bands (cm^{-1}) and relative assignments

Compound	ν(P=O)	ν(O—H) (coordinated ethanol)	ν(C—O)	$\nu(ClO_4^-)$
RPOEt	1245s, sp 1220s, sp 1190s, sp			
$[Cu(RPOEt)_2(C_2H_5OH)_2](ClO_4)_2$	1210s, sp 1178s, sp 1162s, sp	3030m	1040m 1015m	1090vs 935w 625m
$[Co(RPOEt)_2(C_2H_5OH)_2](ClO_4)_2$	1200s, sp 1180s, sp 1165s, sp	3130m	1047m 1015m	1090vs 935w 625m
$[Ni(RPOEt)_2(C_2H_5OH)_2](ClO_4)_2$	1198s, sp 1180s, sp 1170s, sp	3130m	1047m 1015m	1090vs 935w 625m

cm^{-1} assigned to the P=O stretching vibration of the central phosphoryl group, and the maximum appearing at 1220 cm^{-1} are shifted to lower wave numbers (1210–1162 cm^{-1}). Data observed indicate that in all isolated metal complexes the central P=O group as well as one of the exterior P=O groups are involved in complex formation. Positions of the maxima of the central P=O group vibrations indicate stronger bonding of the ligand to the cobalt(II) and nickel(II) than to the copper(II) ion. The maximum assigned to P—OC_2H_5 vibrations appearing in the spectrum of the ligand RPOEt at 1035 cm^{-1} is not shifted in the spectra of the complexes. That means that this group is not

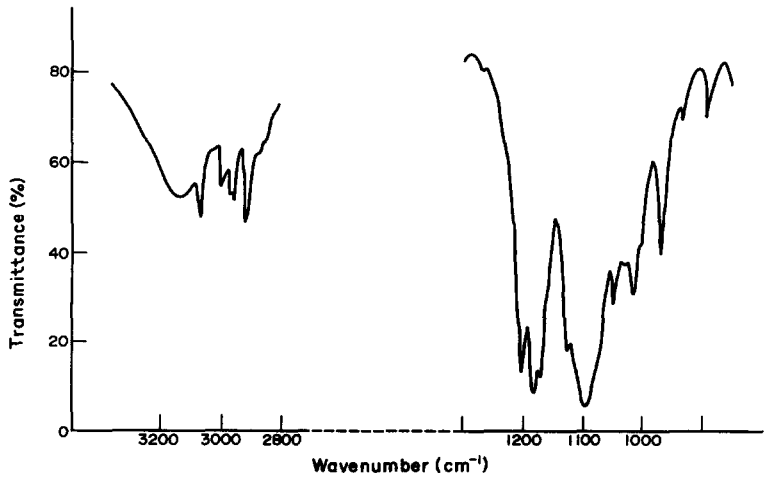


Fig. 2. IR absorption spectrum of $[Co(RPOEt)_2(C_2H_5OH)_2](ClO_4)_2$.

involved in complex formation. Maxima of the OH vibrations assigned to the coordinated ethanol indicate stronger coordination of ethanol in the copper(II) (3030 cm^{-1}) than in the nickel(II) and cobalt(II) (3130 cm^{-1}) complexes. The weaker coordination of ethanol in the cobalt(II) and nickel(II) complexes is the reason for the rather high instability of these complexes and the faster replacement of ethanol by water than in the case of the copper(II) compound. The most important absorption bands of $[Co(RPOEt)_2(C_2H_5OH)_2](ClO_4)_2$ are presented in Fig. 2.

Acknowledgements—This work was supported by grant from the Foundation of Scientific Research of SR Croatia. We thank Dr Tonči Balić-Žunić for conducting some of the preliminary studies and Mr Milenko Bruvo for collecting the data on Philips PW 1100 diffractometer at University of Zagreb.

REFERENCES

1. P. Bronzan-Planinić and H. Meider, *Polyhedron* 1983, **2**, 69.
2. P. Bronzan-Planinić and H. Meider, *Croat. Chem. Acta* 1984, **57**, 477.
3. E. I. Sinyavskaja, S. A. Pisareva, N. I. Cokur, T. I. Ignatjeva and M. P. Komarova, *Z. Neorg. Khim.* 1981, 26, 1274.
4. L. Maier, *Helv. Chim. Acta* 1969, **52**, 827.
5. T. Ya. Medved, Yu. M. Polikarpov, S. A. Pisareva, E. I. Matrosov and M. I. Kabachnik, *Izv. Akad. Nauk SSSR, Ser. Khim.* 1968, 2062.
6. M. W. G. De Bolster, J. Den Heijer and W. L. Groeneveld, *Z. Naturforsch.* 1972, **27b**, 1324.
7. R. P. Scholer, *Inorg. Chim. Acta* 1979, **35**, 79.
8. J. C. P. M. Lapidaire, Ph.D. Thesis, Rijksuniversiteit, Leiden, The Netherlands (1982).
9. A. P. Baranov, V. G. Dashevskii, T. Ya. Medved and M. I. Kabachnik, *Teor. Eksp. Khim.* 1979, **15**, 514.
10. E. G. Taylor and C. A. Kraus, *J. Am. Chem. Soc.* 1947, **69**, 1731.
11. A. Earnshaw, *Introduction to Magnetochemistry*. Academic Press, London (1968).
12. I. Vicković, The ZOAK program—a version of November 1975. Laboratory of General and Inorganic Chemistry, Faculty of Science, The University of Zagreb.
13. D. T. Cromer and D. Liberman, *J. Chem. Phys.* 1970, **53**, 1891.
14. J. M. Stewart, P. A. Machin, C. W. Dickinson, H. L. Ammon, H. Heck and H. Flack, XRAY 76 System. Technical Report TR-446. Computer Science Center, University of Maryland, College Park, Maryland (1976).
15. D. T. Cromer and J. B. Mann, *Acta Cryst., Cryst. Phys. Diffr., Theor. Gen. Cryst.* 1968, **A24**, 321.
16. R. F. Stewart, E. R. Davidson and W. T. Simpson, *J. Chem. Phys.* 1965, **42**, 3175.
17. D. Cremer and J. A. Pople, *J. Am. Chem. Soc.* 1975, **97**, 1354.
18. M. Nardelli, A. Musatti, P. Domiano and G. Andreetti, *Ric. Sci., Rend., Ser. A* 1965, **8**, 807.
19. J. C. A. Boeyens, *J. Cryst. Molec. Struct.* 1978, **8**, 317.
20. D. Fenske, R. Mattes, J. Löns and K. F. Tebbe, *Chem. Ber.* 1973, **106**, 1139.
21. R. Mattes and D. Rühl, *Acta Cryst.* 1984, **C40**, 106.
22. A. Perales, M. Martinez-Ripoll and J. Fayos, *Acta Cryst.* 1984, **C40**, 357.
23. W. Hewertson, B. T. Kilbourn and R. H. B. Mais, *J. Chem. Soc. Chem. Commun.* 1970, 952.
24. A. E. Kalinin, V. G. Andrianov and Ya. T. Struchkov, *Z. Struct. Khim.* 1976, **17**, 153.
25. D. M. Wiench, M. Jansen and R. Hoppe, *Z. Anorg. Allg. Chem.* 1982, **488**, 80.
26. M. Herceg, *Second European Crystallographic Meeting*, Keszthely, Hungary (1974); M. Herceg, J. Fischer, A. Mitschler and M. Šljukić, *Proc. 15th ICCC*, Moscow, U.S.S.R., Vol. 1, p. 41 (1973).
27. O. Jouini, M. Dabbabi, M. T. Averbuch-Pouchot, A. Durif and J. C. Guitel, *Acta Cryst.* 1984, **C40**, 728.
28. V. Lutsko and G. Johansson, *Acta Chem. Scand.* 1984, **A38**, 415.
29. J. C. P. M. Lapidaire and A. J. De Kok, *Z. Naturforsch.* 1980, **35b**, 1203.

Polyhedron Vol. 5, No. 12, pp. 2021–2031, 1986
Printed in Great Britain

0277–5387/86 $3.00+.00
© 1986 Pergamon Journals Ltd

SYNTHESIS, PROPERTIES AND STRUCTURES OF THE TWO "ELECTRON RICH" COBALT–SULPHUR CLUSTERS $[Co_6(\mu_3\text{-}S)_8(PEt_3)_6]^{1+,0}$

FRANCO CECCONI, CARLO A. GHILARDI,* STEFANO MIDOLLINI and ANNABELLA ORLANDINI

Istituto per lo Studio della Stereochimica ed Energetica dei Composti di Coordinazione, C.N.R., Via Guerrazzi, 27-50132 Firenze, Italy

and

PIERO ZANELLO

Dipartimento di Chimica, Università di Siena, Pian dei Mantellini 44, 53100 Siena, Italy

(*Received* 23 *January* 1986; *accepted* 8 *May* 1986)

Abstract—The reaction of hydrogen sulphide with $[Co(H_2O)_6](BF_4)_2$ and triethylphosphine in the presence of sodium tetraphenylborate or tetrabutylammonium hexafluorophosphate gave the paramagnetic clusters $[Co_6(\mu_3\text{-}S)_8(PEt_3)_6](Y)$ ($Y = BPh_4$, (**1**), PF_6, (**2**)). These compounds can be easily reduced by sodium naphthalenide to the diamagnetic species $[Co_6(\mu_3\text{-}S)_8(PEt_3)_6]\cdot 2C_4H_8O$ (**3**). The molecular structures of **1** and **3** have been established by single-crystal X-ray diffraction methods. Crystal data: (**1**) space group $P\bar{1}$, $a = 19.481(9)$, $b = 15.562(7)$, $c = 12.390(6)$ Å, $\alpha = 92.70(8)$, $\beta = 94.50(7)$, $\gamma = 94.10(9)°$, $Z = 2$, (**3**) space group $R\bar{3}$, $a = 11.780(6)$ Å, $\alpha = 92.50(7)°$, $Z = 1$. Both structures were solved by the heavy atom method and refined by full-matrix least-squares techniques to the conventional R factors values of 0.050 for **1** and 0.044 for **3** on the basis of 4251 and 1918 observed reflections, respectively. The two clusters $[Co_6(\mu_3\text{-}S)_8(PEt_3)_6]^{1+,0}$ are isostructural, the inner core consisting of an octahedron of cobalt atoms with all the faces symmetrically capped by triply bridging sulphur atoms. Each metal centre is additionally linked to a triethylphosphine group so that each cobalt atom is co-ordinated by four sulphur atoms and one phosphorus in a distorted square pyramidal environment. The addition of one electron whilst leaving unchanged the geometry of the inner framework, induces small changes in the structural parameters, the average Co—Co and Co—P distances being 2.794 (3) and 2.162 (2) Å for **1** and 2.817 (3) and 2.138 (2) Å for **3** respectively. Electrochemistry in non-aqueous solvents shows the electron-transfer sequence

$$[Co_6S_8(PEt_3)_6]^0 \underset{+e^-}{\overset{-e^-}{\rightleftharpoons}} [Co_6S_8(PEt_3)_6]^+ \underset{+e^-}{\overset{-e^-}{\rightleftharpoons}} [Co_6S_8(PEt_3)_6]^{2+} \underset{+e^-}{\overset{-e^-}{\rightleftharpoons}} [Co_6S_8(PEt_3)_6]^{3+}.$$

The tricationic species is stable only in the short time of cyclic voltammetric tests.

In recent years polynuclear metal-sulphide complexes have attracted great interest, owing to their importance both in industrial and enzymatic catalysis.

On the one hand, metal-sulphur-clusters could be regarded as models for heterogeneous metal-sulphide catalysts[1,2] and on the other hand it is well known that it is mainly of electron transfer the biological function of the iron-sulphur proteins, which, as electron carriers, satisfy electron supply or removal in the enzymatic catalysis.[3]

Electrochemistry of metal-sulphur clusters can play an important role in determining both ther-

* Author to whom correspondence should be addressed.

modynamic and kinetic aspects of their redox changes. For instance, in order to model iron-sulphur compounds able to mimic iron-sulphur proteins a great deal of study has been devoted to test the ability of these compounds to undergo one-electron charge transfers, and to compare the relevant redox potentials with those of iron proteins.[4]

Holm *et al.* succeeded in the synthesis of iron-sulphur clusters through the "spontaneous self-assembly" reactions, from mixture of appropriate reactants.[5] Later such strategy appeared suited for the synthesis of other systems.[6]

Recently, we succeeded in the synthesis of unprecedented metal sulphur clusters such as $[Ni_9(\mu_4\text{-}S)_3(\mu_3\text{-}S)_6(PEt_3)_6](BPh_4)_2$[7] and $[Fe_6(\mu_3\text{-}S)_8(PEt_3)_6](BPh_4)_2$[8] by the reaction of H_2S with nickel(II) or iron(II) ions in the presence of monotertiary phosphines. The first complex, which is diamagnetic, has a confacial bioctahedral skeleton, whereas the second, which is paramagnetic with six unpaired electrons in the cluster unit, at room temperature, has an octahedral face-capped geometry. Interestingly these two geometries are closely related to the structures present in some molybdenum chalcogenide crystal noteworthy for their particular electron conductor ability (Chevrel phases).[9]

In this paper we report the synthesis, the single-crystal X-ray structure determinations and the electrochemical properties of the cobalt clusters $[Co_6(\mu_3\text{-}S)_8(PEt_3)_6](BPh_4)$ (**1**) and $[Co_6(\mu_3\text{-}S)_8(PEt_3)_6]\cdot 2C_4H_8O$ (**3**).

Preliminary reports of this work have been already published.[10,11]

EXPERIMENTAL

Chemicals were generally used as purchased. Tetrahydrofuran was distilled over $LiAlH_4$ under nitrogen. Commercial grade dichloromethane, benzene, absolute ethanol and *n*-butanol were used without purification.

Synthesis of $[Co_6(\mu_3\text{-}S)_8(PEt_3)_6](BPh_4)$ (1)

A deoxygenated solution of $[Co(H_2O)_6](BF_4)_2$ (0.68 g, 2 mmol) in 20 cm^3 of ethanol was added to a deoxygenated solution of PEt_3 (0.71 g, 6 mmol) in 30 cm^3 of dichloromethane, under a nitrogen atmosphere and hydrogen sulphide was bubbled through, at room temperature, for 10 min. The resulting dark-brown solution was stirred overnight under a slight stream of nitrogen; then sodium tetraphenylborate (0.34 g, 1 mmol) was added. The solution was filtered and the filtrate was evaporated in air, at room temperature. After ca. 12 h dark brown crystals together with colourless crystals and a dark powder separated. This material was filtered and treated with boiling benzene (ca. 200 cm^3) in which only the brown crystals dissolved. The resulting solution was filtered and 20 cm^3 of *n*-butanol was added. By slow evaporation of the solvent in air, at room temperature, large dark brown crystals precipitated; they were collected on a filter, washed with *n*-butanol and then with petroleum ether and dried *in vacuo*; yield 0.17 g (31%). Found: C, 43.8; H, 7.1; Co, 21.3; S, 15.5. Calc. for $C_{60}H_{110}BCo_6P_6S_8$: C, 44.0; H, 6.8; Co, 21.6; S, 15.7%.

Synthesis of $[Co_6(\mu_3\text{-}S)_8(PEt_3)_6](PF_6)$ (2)

A deoxygenated solution of $[Co(H_2O)_6](BF_4)_2$ (0.68 g, 2 mmol) in 20 cm^3 of *n*-butanol was added to a deoxygenated solution of PEt_3 (0.71 g, 6 mmol) in 30 cm^3 of acetone, under a nitrogen atmosphere and hydrogen sulphide was bubbled through, at room temperature for 10 min. The resulting dark-brown solution was stirred overnight under a slight stream of nitrogen; then tetrabutylammonium hexafluorophosphate (0.39 g, 1 mmol) was added. The solution was filtered and the filtrate was evaporated in air, at room temperature until dark brown crystals separated. These were filtered and recrystallized from methylene chloride and *n*-butanol. Large dark brown crystals were obtained, which were collected in a filter, washed with *n*-butanol, and then with petroleum ether and dried *in vacuo*; yield 0.095 g (21%). Found: C, 29.3; H, 6.3; Co, 23.7. Calc. for $C_{36}H_{90}Co_6F_6P_7S_8$: C, 29.5; H, 6.2; Co, 24.1%.

Synthesis of $[Co_6(\mu_3\text{-}S)_8(PEt_3)_6]\cdot 2C_4H_8O$ (3)

Sodium naphthalenide (0.025 g, 0.16 mmol) in 15 cm^3 of thf was added to a solution of $[Co_6(\mu_3\text{-}S)_8(PEt_3)_6]BPh_4$ (0.2 g, 0.12 mmol) in 30 cm^3 of thf with stirring, at room temperature. Then the solution was allowed to stand and crystals, rapidly formed (10 min), were isolated; yield 0.15 g (86%). Found: C, 36.5; H, 7.5; Co, 23.7. Calc. for $C_{44}H_{106}Co_6O_2P_6S_8$: C, 36.1; H, 7.3; Co, 24.2%.

Physical methods

Conductivity and magnetic susceptibilities measurements were carried out by previously described methods.[12]

Electrochemistry

Acetonitrile and dichloromethane solvents (Burdik and Jackson, distilled in glass, UV grade) were

used as received. Tetraethylammonium perchlorate (Carlo Erba) and tetrabutylammonium perchlorate (Fluka) supporting electrolytes were dried in a vacuum oven and used without further purification. Bis(η-cyclopentadienyl)iron(II) (Alfa Products) was used as purchased. Extra pure nitrogen was used to remove oxygen from tested solutions. Electrochemical techniques were carried out using a PAR model 170 Electrochemistry System as polarizing unity; the recording device for potential scan rates higher than 0.5 V s^{-1} was a Hewlett–Packard model 1123 A storage oscilloscope. Cyclic voltammetry and chronoamperometry were performed both with a gold sphere working microelectrode freshly covered with a thin mercury layer, and with a platinum sphere working microelectrode; the working electrode was surrounded by a platinum-spiral counter-electrode. The potential of the working microelectrode was probed by a Luggin capillary reference electrode compartment. Controlled potential coulometric tests were performed in a H-shaped cell with anodic and cathodic compartments separated by a sintered glass disc. The working macroelectrode was either a mercury pool or a platinum gauze. A mercury pool was used as counter electrode. In these tests an Amel potentiostat model 551, with an associated coulometer Amel integrator model 558, were used. In all electrochemical tests an aqueous saturated calomel electrode (SCE) was used as reference electrode. The temperature was controlled at 20 ± 0.1°C.

X-ray data collection

Diffraction data were collected at room temperature on a Philips PW 1100 automatic diffractometer. Unit cell parameters for compound **1** and **3** were determined from the least squares refinement of the setting angles of 20 and 24 accurately centred reflections, respectively. Crystal data and data collection details are reported in Table 1. After cor-

Table 1. Crystal data and data collection details

	1	**2**
Formula	$C_{60}H_{110}BCo_6P_6S_8$	$C_{44}H_{106}Co_6O_2P_6S_8$
Mol. wt.	1638.3	1463.3
Space group	$P\bar{1}$	$R\bar{3}$
a, Å	19.481 (9)	11.780 (6)
b, Å	15.562 (7)	
c, Å	12.390 (6)	
α, deg	92.70 (8)	92.50 (7)
β, deg	94.50 (7)	
γ, deg	94.10 (9)	
V, Å^3	3729.8	1629.9
Z	2	1
$d_{calc.}$, g cm^{-3}	1.458	1.490
T of data coll., K	295	295
Colour	Dark brown	Dark brown
Habit	Parallelepiped	Cube
Dimensions, mm	$0.05 \times 0.22 \times 0.50$	$0.20 \times 0.20 \times 0.20$
Linear abs coeff, cm^{-1}	16.8	19.1
Transmission factors	0.70–0.92	0.65–0.74
Diffractometer	Philips PW 1100	Philips PW 1100
Radiation, Å	Mo Kα ($\lambda = 0.7107$)	Mo Kα ($\lambda = 0.7107$)
Monochromator	Graphite	Graphite
Method	$\omega - 2\theta$	$\omega - 2\theta$
Scan speed, deg/s	0.07	0.06
Scan width, deg	$0.7 + 0.69 \tan\theta$	$0.7 + 0.69 \tan\theta$
Bkgd time	Half the scan time	Half the scan time
Stds	3 every 120 min	3 every 120 min
Max dev stds, %	± 1	± 1
2θ limits, deg	$5 \leqslant 2\theta \leqslant 40$	$5 \leqslant 2\theta \leqslant 60$
Data collected	$\pm h, \pm k, +l$	$\pm h, \pm k, \pm l$ ($h \geqslant k \geqslant l$)
No. of total data	6942	3465
No. of data used [$I \geqslant 3\sigma(I)$]	4251	1918
Final No. of variables	381	72
R, R_w	0.050, 0.051	0.044, 0.045

rection for background the intensities were assigned standard deviations calculated by using for the instability factor k the value of 0.03.[13] Intensity data were corrected for Lorentz and polarization effects and for absorption.[14]

Solution and refinement of the structures

All the calculations were carried out on a SEL 32/77 computer by using the SHELX-76[14] and ORTEP[15] programs. Atomic scattering factors of the appropriate neutral atoms were taken from ref. 16 for the non-hydrogen atoms and from ref. 17 for hydrogen atoms. Both the $\Delta f'$ and $\Delta f''$ components of anomalous dispersion were included for all non-hydrogen atoms.[18] The refinement was based on F_0, the function minimized being $\Sigma w(|F_0|-|F_c|)^2$, where $w = 1/\sigma^2(F_0)$. The structure of both compounds was solved by the heavy atom method. Several Fourier maps revealed all the non hydrogen atoms and for compound **3** the disordered solvating tetrahydrofuran molecule. Full-matrix least-squares refinements were carried out by using anisotropic thermal parameters only for cobalt, sulphur and phosphorus. The phenyl rings of the tetraphenylborate were treated as rigid groups. The hydrogen atoms were introduced in calculated positions but not refined. The tetrahydrofuran molecule was refined as rigid group with population parameter of 1/3. The refinement converged at R and R_w factors value of 0.050 and 0.051 for **1** and 0.044 and 0.045 for **3** respectively. R and R_w are defined as $\Sigma||F_0|-|F_c||/\Sigma|F_0|$ and $[\Sigma w(|F_0|-|F_c|)^2/\Sigma w|F_0|^2]^{1/2}$. Final difference Fourier maps did not show any feature. Final atomic coordinates for both compounds, tables of thermal parameters and lists of F_0/F_c have been deposited with the Editor as supplementary material.*

RESULTS AND DISCUSSION

Synthesis

The reaction of H_2S with $[Co(H_2O)_6]^{2+}$, in the presence of PEt_3 (Co/P $\cong$ 1/3), at room temperature, affords the cluster ion $[Co_6(\mu_3\text{-}S)_8(PEt_3)_6]^+$ which can be isolated as tetraphenylborate **1** or hexafluorophosphate **2** salt. A large excess of PEt_3, with respect to the stoichiometry of the final product, is necessary in order to prevent the precipitation of the binary cobalt sulphide. The reaction occurs in air, the initial stage being carried out under a nitrogen atmosphere only to prevent the phosphine oxidation.

At the end of the reaction the metal atoms are formally oxidized, the cobalt mean oxidation state being +2.83. A similar formal oxidation was previously observed during the formation of the clusters $[Ni_9(\mu_4\text{-}S)_3(\mu_3\text{-}S)_6(PEt_3)_6]^{2+}$ and $[Fe_6(\mu_3\text{-}S)_8(PEt_3)_6]^{2+}$ with final mean oxidation states of +2.22 and +3.0 for nickel and iron respectively.

Unfortunately we were not able to identify all of the reaction products and the oxidant.

The complex **1** can be easily reduced in thf solution by sodium naphthalenide to form the uncharged species $[Co_6(\mu_3\text{-}S)_8(PEt_3)_6]\cdot 2C_4H_8O$, **3** (Scheme 1).

$$[Co_6(\mu_3\text{-}S)_8(PEt_3)_6]^+ + NaC_{10}H_8 \rightarrow [Co_6(\mu_3\text{-}S)_8(PEt_3)_6] + Na^+ + C_{10}H_8$$

Scheme 1.

The clusters **1** and **2** are air stable both in the solid state and in solution. They are very soluble in polar organic solvents such as acetone, dichloromethane, nitroethane, in which they behave as 1 : 1 electrolytes. **1** is also soluble in warm benzene. The complex **3**, which is practically insoluble in the common organic solvents, is indefinitely stable under nitrogen.

The complex **1** and **2** are paramagnetic with bulk magnetic moments of 2.10 and 2.14 μ_B *per* cluster unit, at room temperature, respectively. This result, which indicates one unpaired electron for the cluster agrees with the presence of an odd total electrons number in the cation. The uncharged cluster is diamagnetic.

Description of the structures

Compound **1** is constructed of discrete $[Co_6(\mu_3\text{-}S)_8(PEt_3)_6]^+$ cations and $[BPh_4]^-$ anions. Figure 1 shows a perspective view of the cation and selected bond distances and angles are reported in Tables 2 and 3. Compound **3** consists of discrete cluster units with interspersed molecules of tetrahydrofuran. Table 4 lists selected bond distances and angles of the uncharged species, while Fig. 2 shows the inner core of **1** and **3**.

The structure determination has shown that both the monopositive and the neutral species retain the same $M_6S_8P_6$ framework as the previously described iron derivative $[Fe_6(\mu_3\text{-}S)_8(PEt_3)_6]^{2+}$.[8] The inner core of the two clusters consists of an octahedron of cobalt atoms with all the faces symmetrically capped by triply-bridging sulphur atoms. Moreover

* Atomic coordinates have also been deposited with the Cambridge Crystallographic Data Centre.

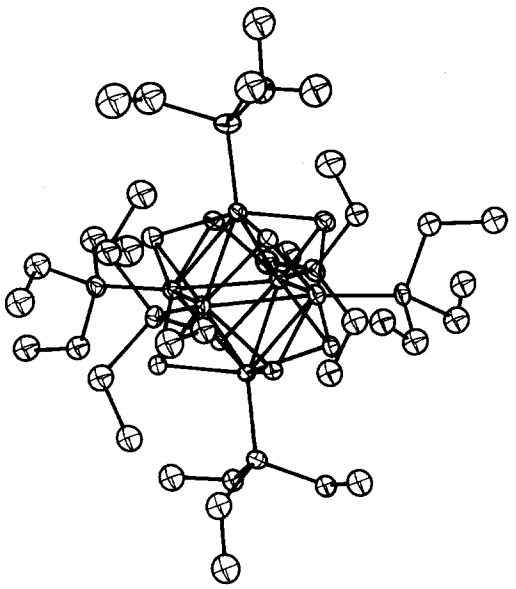


Fig. 1. Perspective view of the cluster cation $[Co_6(\mu_3\text{-}S)_8(PEt_3)_6]^+$. ORTEP drawing with 30% probability ellipsoids.

Table 2. Selected bond distances (Å) with estimated standard deviations for $[Co_6(\mu_3\text{-}S)_8(PEt_3)_6]BPh_4$

		Co—Co	
Co1—Co2	2.790 (2)	Co2—Co6	2.802 (2)
Co1—Co3	2.800 (2)	Co3—Co4	2.794 (2)
Co1—Co4	2.771 (2)	Co3—Co6	2.786 (2)
Co1—Co5	2.808 (2)	Co4—Co5	2.804 (2)
Co2—Co3	2.793 (2)	Co4—Co6	2.783 (2)
Co2—Co5	2.796 (2)	Co5—Co6	2.800 (2)
mean	2.794 (3)[a]		
		Co—μ_3—S	
Co1—S1	2.214 (4)	Co4—S2	2.221 (4)
Co1—S2	2.227 (4)	Co4—S3	2.244 (4)
Co1—S3	2.228 (4)	Co4—S6	2.244 (4)
Co1—S4	2.243 (4)	Co4—S7	2.234 (4)
Co2—S1	2.210 (4)	Co5—S3	2.250 (4)
Co2—S4	2.251 (4)	Co5—S4	2.233 (4)
Co2—S5	2.249 (4)	Co5—S7	2.226 (4)
Co2—S8	2.228 (4)	Co5—S8	2.238 (4)
Co3—S1	2.218 (4)	Co6—S5	2.230 (4)
Co3—S2	2.226 (4)	Co6—S6	2.237 (4)
Co3—S5	2.238 (4)	Co6—S7	2.226 (4)
Co3—S6	2.234 (4)	Co6—S8	2.257 (4)
mean	2.234 (4)		
		Co—P	
Co1—P1	2.165 (4)	Co4—P4	2.160 (4)
Co2—P2	2.161 (4)	Co5—P5	2.170 (4)
Co3—P3	2.161 (4)	Co6—P6	2.158 (4)
mean	2.162 (2)		
		S···S	
S1···S2	3.072 (4)	S3···S7	3.105 (4)
S1···S4	3.101 (4)	S4···S8	3.108 (4)
S1···S5	3.106 (4)	S5···S6	3.108 (4)
S2···S3	3.119 (4)	S5···S8	3.093 (4)
S2···S6	3.084 (4)	S6···S7	3.115 (4)
S3···S4	3.083 (4)	S7···S8	3.116 (4)
mean	3.101 (4)		

[a] The estimated errors on the means were calculated according to the formula $[\Sigma_n(d_n-d)^2/n(n-1)]^{1/2}$.

each metal atom is linked to a triethylphosphine group along the body diagonal of the octahedron. Each metal atom is therefore surrounded by four sulphur and one phosphorus atom in a distorted square pyramidal environment and it is additionally linked to other four metal atoms. Alternatively the Co_6S_8 unit may be described as a cube of sulphur atoms with the metal atoms in the face centred positions.

The monocation has no crystallographic symmetry imposed, however the deviations of the M_6 unit from a regular octahedron are small. As a matter of fact no systematic distortions are present: the Co—Co distances range from 2.771 (2) to 2.808 (2) Å and the Co—Co—Co angles, which fall in the ranges 59.2 (1)–60.5 (1)° and 89.4 (1)–90.6 (1)° are very close to the values of 60.0 and 90.0 for perfect octahedral symmetry. The crystallographic symmetry of the neutral species is C_{3i} and in this case the deviations of the inner core from the O_h symmetry are even smaller, the Co—Co—Co angles being equal within the experimental errors to the ideal values.

The comparison of the geometries of the monocharged and neutral derivatives shows a small difference in the average Co—Co distance which goes from 2.794 (3) to 2.817 (2) Å. Moreover the Co—S distances in **1** and **3** are equal within the experimental errors, while the Co—P bond distance in the neutral species is shorter, 2.138 (2) Å, than that in the monocation, 2.162 (2) Å (av). No other features or distortions are observed between the two cluster units.

Therefore the addition of one electron, whilst leaving unchanged the geometry of the inner framework, induces small variation in the metal–metal interactions and in the Co—P distances, but does not affect the metal sulphur bonds, which are the actual stabilizing factors of the metal framework.[7] In this connection it is noteworthy that the values of the Co—Co distances are rather long if compared with those reported for other cobalt clusters[6,19,20] and may be related to the high valence electron numbers (97 and 98) of these cobalt clusters. Indeed

the class of the well-known octahedral carbonyl clusters possesses an electronic configuration of 86 valence electrons.[21] A fully comparable value of Co—Co distance, 2.811 (1) Å, was found for $[Co_6(\mu_3\text{-}S)_8(CO)_6]$ which is isoelectronic with **3**.[22]

Of great interest is also the comparison of these

Table 3. Selected bond angles (°) with estimated standard deviations for $[Co_6(\mu_3\text{-}S)_8(PEt_3)_6]BPh_4$

Co2—Co1—Co3	60.0 (1)	Co1—Co5—Co2	59.7 (1)
Co2—Co1—Co4	90.2 (1)	Co1—Co5—Co4	59.2 (1)
Co2—Co1—Co5	59.9 (1)	Co1—Co5—Co6	89.4 (1)
Co3—Co1—Co4	60.2 (1)	Co2—Co5—Co4	89.4 (1)
Co3—Co1—Co5	90.2 (1)	Co2—Co5—Co6	60.1 (1)
Co4—Co1—Co5	60.3 (1)	Co4—Co5—Co6	59.6 (1)
S1—Co1—S2	87.6 (1)	S3—Co5—S4	86.9 (1)
S1—Co1—S3	158.2 (1)	S3—Co5—S7	87.9 (1)
S1—Co1—S4	88.2 (1)	S3—Co5—S8	157.6 (1)
S2—Co1—S3	88.9 (1)	S4—Co5—S7	157.7 (1)
S2—Co1—S4	158.2 (1)	S4—Co5—S8	88.1 (1)
S3—Co1—S4	87.2 (1)	S7—Co5—S8	88.5 (1)
P1—Co1—S1	98.9 (1)	P5—Co5—S3	104.2 (1)
P1—Co1—S2	101.6 (1)	P5—Co5—S4	102.8 (1)
P1—Co1—S3	102.9 (1)	P5—Co5—S7	99.5 (1)
P1—Co1—S4	100.2 (1)	P5—Co5—S8	98.2 (1)
Co1—Co2—Co3	60.2 (1)	Co2—Co6—Co3	60.0 (1)
Co1—Co2—Co5	60.3 (1)	Co2—Co6—Co4	89.7 (1)
Co1—Co2—Co6	89.7 (1)	Co2—Co6—Co5	59.9 (1)
Co3—Co2—Co5	90.6 (1)	Co3—Co6—Co4	60.2 (1)
Co3—Co2—Co6	59.7 (1)	Co3—Co6—Co5	90.6 (1)
Co5—Co2—Co6	60.0 (1)	Co4—Co6—Co5	60.3 (1)
S1—Co2—S4	88.1 (1)	S5—Co6—S6	88.2 (1)
S1—Co2—S5	88.3 (1)	S5—Co6—S7	158.4 (1)
S1—Co2—S8	158.1 (1)	S5—Co6—S8	87.2 (1)
S4—Co2—S5	158.0 (1)	S6—Co6—S7	88.5 (1)
S4—Co2—S8	87.9 (1)	S6—Co6—S8	158.2 (1)
S5—Co2—S8	87.4 (1)	S7—Co6—S8	88.1 (1)
P2—Co2—S1	98.5 (1)	P6—Co6—S5	101.5 (1)
P2—Co2—S4	102.9 (1)	P6—Co6—S6	97.9 (1)
P2—Co2—S5	99.0 (1)	P6—Co6—S7	100.0 (1)
P2—Co2—S8	103.4 (1)	P6—Co6—S8	103.9 (1)
Co1—Co3—Co2	59.9 (1)	Co1—S1—Co2	78.2 (1)
Co1—Co3—Co4	59.4 (1)	Co1—S1—Co3	78.3 (1)
Co1—Co3—Co6	89.8 (1)	Co2—S1—Co3	78.2 (1)
Co2—Co3—Co4	89.7 (1)		
Co2—Co3—Co6	60.3 (1)	Co1—S2—Co3	77.9 (1)
Co4—Co3—Co6	59.8 (1)	Co1—S2—Co4	77.1 (1)
		Co3—S2—Co4	77.9 (1)
S1—Co3—S2	87.5 (1)		
S1—Co3—S5	88.4 (1)	Co1—S3—Co4	76.6 (1)
S1—Co3—S6	157.5 (1)	Co1—S3—Co5	77.7 (1)
S2—Co3—S5	157.8 (1)	Co4—S3—Co5	77.2 (1)
S2—Co3—S6	87.5 (1)		
S5—Co3—S6	88.1 (1)	Co1—S4—Co2	76.8 (1)
P3—Co3—S1	99.2 (1)	Co1—S4—Co5	77.7 (1)
P3—Co3—S2	97.2 (1)	Co2—S4—Co5	77.2 (1)
P3—Co3—S5	105.0 (1)		
P3—Co3—S6	103.1 (1)		

Table 3—*contd.*

Co1—Co4—Co3	60.4 (1)	Co2—S5—Co3	77.0 (1)
Co1—Co4—Co5	60.5 (1)	Co2—S5—Co6	77.4 (1)
Co1—Co4—Co6	90.4 (1)	Co3—S5—Co6	77.1 (1)
Co3—Co4—Co5	90.4 (1)		
Co3—Co4—Co6	59.9 (1)	Co3—S6—Co4	77.2 (1)
Co5—Co4—Co6	60.1 (1)	Co3—S6—Co6	77.1 (1)
		Co4—S6—Co6	76.8 (1)
S2—Co4—S3	88.6 (1)		
S2—Co4—S6	87.4 (1)	Co4—S7—Co5	77.9 (1)
S2—Co4—S7	158.1 (1)	Co4—S7—Co6	77.2 (1)
S3—Co4—S6	158.7 (1)	Co5—S7—Co6	77.9 (1)
S3—Co4—S7	87.8 (1)		
S6—Co4—S7	88.2 (1)	Co2—S8—Co5	77.5 (1)
P4—Co4—S2	100.7 (1)	Co2—S8—Co6	77.3 (1)
P4—Co4—S3	98.3 (1)	Co5—S8—Co6	77.0 (1)
P4—Co4—S6	103.1 (1)		
P4—Co4—S7	101.2 (1)		

two electron rich clusters with the isostructural iron parent compound $[Fe_6(\mu_3\text{-}S)_8(PEt_3)_6]^{2+}$, which possesses 90 valence electrons. In the latter compound the metal–metal distance decreases together with the number of electrons to the value of 2.617 (6) Å. Besides shorter metal–metal distances the iron cluster displays longer M–L distances, Fe—S = 2.247 (1) (av) and Fe—P = 2.293 (6) (av) Å, indi-

Table 4. Selected bond distances (Å) and angles (°) with estimated standard deviations for $[Co_6(\mu_3\text{-}S)_8(PEt_3)_6]\cdot 2C_4H_8O$

		Co—Co	
Co—Co^a	2.814 (1)	Co—Co^b	2.819 (1)
mean	2.817 (3)		
		Co—μ_3—S	
Co—S1	2.243 (2)	Co—S2^a	2.222 (2)
Co—S2	2.229 (2)	Co—S2^c	2.237 (2)
mean	2.233 (5)		
		Co—P	
Co—P	2.138 (2)		
		S···S	
S1—S2	3.095 (2)	S2—S2^c	3.095 (2)
Co^a—Co—Co^b	90.0	Co^a—Co—Co^c	60.1 (1)
Co^a—Co—Co^d	60.0	Co^b—Co—Co^c	59.9 (1)
S1—Co—S2	87.6 (1)	S2^a—Co—S2^c	87.9 (1)
S1—Co—S2^a	87.7 (1)	P—Co—S1	103.3 (1)
S1—Co—S2^c	157.1 (1)	P—Co—S2	103.8 (1)
S2—Co—S2^a	157.0 (1)	P—Co—S2^a	99.2 (1)
S2—Co—S2^c	87.7 (1)	P—Co—S2^c	99.6 (1)
Co—S1—Co^a	77.7 (1)	Co—S2—Co^b	78.3 (1)
Co—S2—Co^d	78.4 (1)	Co^b—S2—Co^d	78.4 (1)

Subscripts refer to the following equivalent positions: $^a z, x, y$; $^b -z, -x, -y$; $^c -y, -z, -x$; $^d y, z, x$.

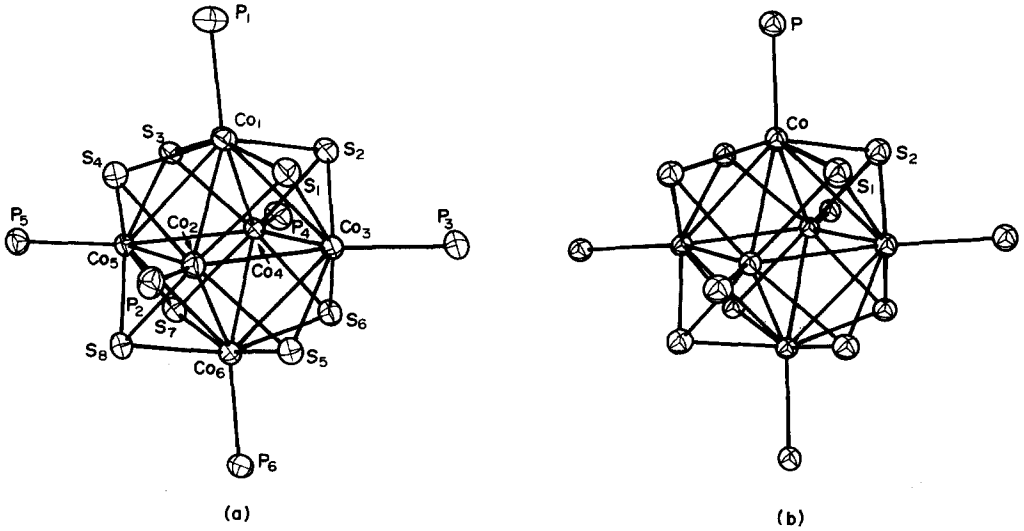


Fig. 2. Perspective view of the inner core of the cluster cation $[Co_6(\mu_3\text{-}S)_8(PEt_3)_6]^+$ (a) and the cluster molecule $[Co_6(\mu_3\text{-}S)_8(PEt_3)_6]$ (b). ORTEP drawing with 30% probability ellipsoids.

cating that the increase of the total electron number results in a lengthening of the metal–metal distances with a parallel decrease of the M–P distances and to a lesser extent of the M–S ones. A larger sensitivity to the redox changes has been found for the terminal Co—S distances than for the bridging ones in $[Co_8S_6(SPh)_8]^{-4,-5}$ [6] in which the metal and sulphur positions are reversed with respect to those in **1** and **3**.

Other changes in the structural parameters associated with the variation of the electron numbers are reported in Table 5: all the reported mean structural parameters vary monotonically, with the number of electrons. Augmenting the electron density the separations between the metals in *trans* positions become larger in such a way that the metal atoms lying at the face centred positions of the sulphur cubes are pushed out, the deviations of the metal atoms from the S_4 planes going from 0.27 to 0.45 Å. Moreover the triply-bridging sulphur becomes more flat, the M–S–M average angle going from 71.2 (1)° to 78.2 (2)° and the average S–S edge going from 3.154(8) to 3.095 (2) Å.

The concomitance of the above changes is such that, augmenting the number of electrons, the M_6S_8 becomes more similar to a ball than to a cube encompassing an octahedron.

Electrochemistry

The electrochemical behaviour of the polinuclear monocation (**1**) has been studied by cyclic voltammetry. The relevant responses at a platinum

Table 5. Mean structural parameters within the isostructural series $[M_6(\mu_3\text{-}S)_8(PEt_3)_6]^n$ ($n = 2+, 1+, 0$)

	$[Fe_6(\mu_3\text{-}S)_8(PEt_3)_6]^{2+\,a}$	$[Co_6(\mu_3\text{-}S)_8(PEt_3)_6]^{1+\,b}$	$[Co_6(\mu_3\text{-}S)_8(PEt_3)_6]^{b}$
M–M, Å	2.617 (6)	2.794 (3)	2.817 (3)
M–S, Å	2.247 (1)	2.234 (4)	2.233 (5)
M–P, Å	2.293 (6)	2.162 (2)	2.138 (2)
M···M, Å	3.701 (14)	3.951 (10)	3.983 (1)
S···S, Å	3.154 (8)	3.101 (4)	3.095 (2)
M–S–M, deg	71.2 (1)	77.4 (1)	78.2 (2)
Displacements of the metal atoms from the S_4 planes, Å	0.27–0.29	0.42–0.43	0.45

[a] Data from ref. 8.
[b] This work.

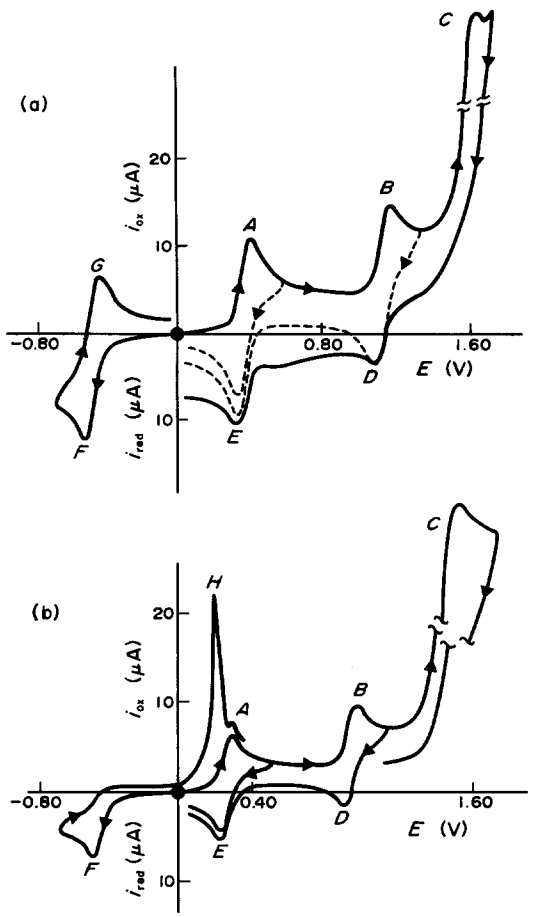


Fig. 3. Cyclic voltammetric responses of: (a) $[Co_6(\mu_3\text{-}S)_8(PEt_3)_6](PF_6)$ (6.9×10^{-4} mol dm^{-3}) and $(NBu_4)(ClO_4)$ (0.1 mol dm^{-3}) in CH_2Cl_2 solvent, and (b) $[Co_6(\mu_3\text{-}S)_8(PEt_3)_6](PF_6)$ (4.3×10^{-4} mol dm^{-3}) and $(NEt_4)(ClO_4)$ (0.1 mol dm^{-3}) in MeCN solvent. Platinum working microelectrode scan rate 0.2 V s^{-1}. (●) Starting potential.

electrode both in CH_2Cl_2 and MeCN solutions are shown in Fig. 3.

As it can be seen the cluster gives rise to three oxidation and one reduction processes in both solvents, the only significant difference being the insolubility in MeCN of the product electrogenerated in correspondence of peak F, which is desorbed and reoxidized at the potentials of peak H, well anodic with respect to the potentials of peak G recorded in CH_2Cl_2 solvent. Controlled potential coulometric experiments showed that both the anodic process occurring at peak A and the cathodic one occurring at peak F involve the consumption of 1 mol of electrons per mole of starting compound. On the contrary in the electrolysis directly performed at potentials of peak B, the anodic current abruptly falls after the consumption of 2 mol of electrons per mole of starting compound, but it remains significantly higher than the background current up to the overall consumption of 4 mol of electrons per mole of starting compound. Finally coulometric experiments in correspondence to peak C in MeCN solvent, where the solvent discharge does not interfere, show the consumption of a number of electrons higher than 30 per molecule of the starting compound.

The analysis of cyclic voltammetric responses with scan rate[23] varying from 0.02 to 100 V s^{-1} showed the following features. The anodic process occurring at peak A involves an uncomplicated one-electron reversible charge transfer, which slightly departs from reversibility criteria only at scan rates higher than 5 V s^{-1}, probably because of some uncompensated solution resistance; in fact ΔE_p gradually increases from the theoretical value of 59 to 90 mV in the scan rate range 5–100 V s^{-1}. On the basis of its peak height, also the anodic process occurring at peak B involves a one-electron charge transfer in the cyclic voltammetric time scale; however, in the scan rate range 0.02–1 V s^{-1}, the diagnostic parameters i_{pc}/i_{pa}, which is lower than unity, and $i_{pa}/v^{1/2}$, which decreases, show it to be complicated by following chemical reactions, while at scan rates higher than 1 V s^{-1} it appears as an uncomplicated one-electron reversible charge transfer slightly departing from reversibility at scan rates higher than 5 V s^{-1}. On the other hand potential-step chronoamperometric experiments in the time range 0.002–3 s reveal this anodic process to be a one-electron charge transfer up to 2 s (i.e. $i \times t^{1/2}$ is constant), then the number of electrons involved increases. In summary, all voltammetric data indicate that the second anodic process can be described according to a complicated electrode mechanism in which more than one chemical reactions are interposed between more than two one-electron charge transfer (ECEC...); however in the cyclic voltammetric time scale the first coupled chemical reaction is enough slow that the electrode mechanism can be considered to approach a more simple EC mechanism.

The anodic process occurring at peak C is a multi-electron charge transfer (its peak height is seven times higher than that of peak A or B), totally irreversible in character.

Finally the cathodic process occurring at peak F in CH_2Cl_2 solvent, involves an uncomplicated one-electron charge transfer, having a degree of reversibility lower than the first two anodic processes. In fact ΔE_p gradually increases from 86 to 200 mV in the scan rate 0.02–100 V s^{-1}.

The whole of electrochemical data have to be interpreted in these terms: (i) the peak system A/E is due to the reversible oxidation of the monocation

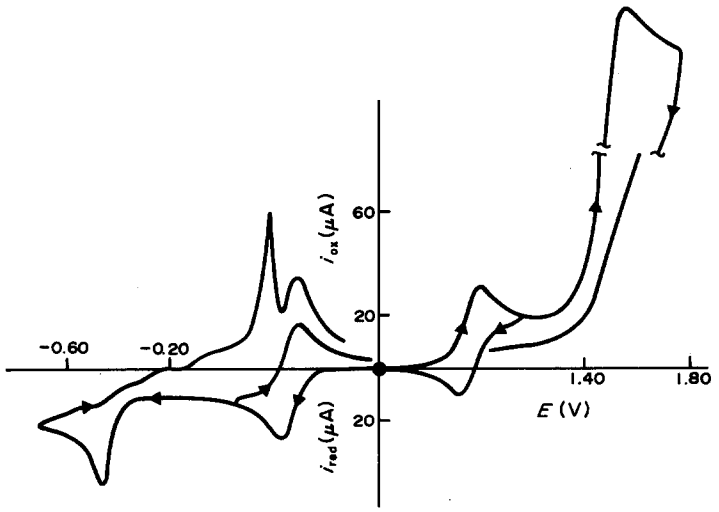


Fig. 4. Cyclic voltammogram at a platinum microelectrode recorded on a MeCN solution of $[Co_6(\mu_3\text{-}S)_8(PEt_3)_6](PF_6)$ (2.38×10^{-5} mol) containing $(NEt_4)(ClO_4)$ (0.1 mol dm^{-3}) after exhaustive electrolysis at +0.5 V (2.3 C spent) at a platinum working macroelectrode. Scan rate 0.2 V s^{-1}. (●) Starting potential.

cluster to the corresponding dication (1+/2+). As it can be seen from Fig. 4 this dication is a quite stable product; (ii) the peak system B/D is due to the reversible oxidation of the cluster dication to the corresponding trication (2+/3+), which however is stable only on the short times of the cyclic voltammetric test. In fact, assuming that the first chemical reaction coupled to the 2+/3+ charge transfer (very likely the decomposition of the trication cluster) is an irreversible first-order chemical reaction, it is possible to evaluate, by the method of Nicholson and Shain,[24] an half-life of about 5 s for the electrogenerated trication; (iii) peak C is likely due to the anodic oxidation of the triethylphosphine ligand. In fact free PEt_3 oxidizes irreversibly at $E_p = +1.34$ V in MeCN/$(NEt_4)(ClO_4)$ (0.1 mol dm^{-3}) solution; and (iv) the peak system F/G (or F/H) is due to the reversible reduction of the starting polinuclear monocation to the corresponding neutral form (1+/0), previously obtained by chemical reduction.

Table 6 summarizes the redox potentials of the cluster under study in the two employed solvents. In order to eliminate variable diffusion potentials arising at the aqueous/non-aqueous interface of the aqueous reference electrode, and in the attempt to make comparable the potential data in different solvents, we used ferrocene as an internal standard,[25] so that potentials vs the solvent-independent ferrocenium/ferrocene couple are also reported. It must however be taken into account that the ferrocenium/ferrocene couple is also nominally independent from the solvent, in fact it shows a formal electrode potential, $E^{\circ\prime}$, of +0.49 V in CH_2Cl_2, and of +0.40 V in MeCN. Therefore a shift in potential values of about 0.1 V towards more negative values is expected in passing from CH_2Cl_2 to MeCN. As it can be seen the shift is higher for what concerns the 2+/3+ couple.

Since thermodynamic redox potentials are directly related to the relative energies of the HOMO/LUMO levels, it can be speculated that in CH_2Cl_2 solvent the difference in energy between the HOMO and LUMO levels is of about 82 kJ mol^{-1} for the monocation cluster, as well as of about 105 kJ mol^{-1} for the dication cluster. In MeCN the difference is of about 91 kJ mol^{-1} for the dication, clearly indicating that the solvation terms involved in HOMO/LUMO levels[26] are different for the two solvents here used, so making this type of calculations a useful, but rough estimate of the involved orbital energies. A comparison with the

Table 6. Formal electrode potential (in V vs SCE) for the electron transfer series exhibited by $[Co_6(\mu_3\text{-}S)_8(PEt_3)_6]^+$. Potential values in parentheses refer to the ferrocenium/ferrocene couple

Solvent	1+/0	1+/2+	2+/3+
CH_2Cl_2	−0.48	+0.37	+1.13
	(−0.97)	(−0.12)	(+0.64)
MeCN	−0.51[a]	+0.25	+0.95
	(+0.89[a])	(−0.13)	(+0.57)

[a] Peak potential value at 0.2 V s^{-1}.

redox chemistry of the very similar cluster $[Co_8S_6(SPh)_8]^{-}$[46] in MeCN solvent is shown in Scheme 2.

$$[Co_8S_6(SPh)_8]^{5-} \underset{}{\overset{-1.12\,V}{\rightleftharpoons}} [Co_8S_6(SPh)_8]^{4-}$$

$$\overset{-0.52\,V}{\rightleftharpoons} [Co_8S_6(SPh)_8]^{3-}$$

$$[Co_6S_8(PEt_3)_6]^{0} \overset{\sim -0.5\,V}{\rightleftharpoons} [Co_6S_8(PEt_3)_6]^{+}$$

$$\overset{+0.25\,V}{\rightleftharpoons} [Co_6S_8(PEt_3)_6]^{2+}$$

$$\overset{+0.95\,V}{\rightleftharpoons} [Co_6S_8](PEt_3)_6]^{3+}$$

Scheme 2.

A first glance indicates that the Co_6S_8 core offers a more rich availability of one-electron charge transfers than the Co_8S_6 core. The relevant redox potentials are shifted towards more positive values, probably because of the presence of terminal uncharged triethylphosphine groups in the title compound with respect to the negatively charged benzene thiolate groups in $[Co_8S_6(SPh)_8]^{4-}$.

In spite of the electrochemical stability of the dipositive species we were unable so far to isolate it in the solid state.

Acknowledgement—Thanks are due to Mr. F. Nuzzi for microanalyses.

REFERENCES

1. O. Weisser and S. Landa, in *Sulphide Catalysts: Their Properties and Applications*. Pergamon Press, Oxford (1973).
2. B. Bogdanovic, P. Göttsch and M. Rubach, *J. Mol. Catal.* 1981, **11**, 135.
3. J. M. Berg and R. H. Holm, in *Iron–Sulfur Proteins* (Edited by T. G. Spiro), Vol. 4. Wiley, New York (1982).
4. T. Toan, B. K. Teo, J. A. Ferguson, T. J. Meyer and L. F. Dahl, *J. Am. Chem. Soc.* 1977, **99**, 408; M. G. Kanatzidis, W. R. Hagen, W. R. Dunham, R. K. Lester and D. Coucouvanis, *J. Am. Chem. Soc.* 1985, **107**, 953 and references therein; W. E. Cleland Jr. and B. A. Averill, *Inorg. Chem.* 1984, **23**, 4192 and references therein; K. S. Hagen, A. D. Watson and R. H. Holm, *J. Am. Chem. Soc.* 1983, **105**, 3905 and references therein; G. J. Kubas and P. J. Vergamini, *Inorg. Chem.* 1981, **20**, 2667; A. L. Balch, *J. Am. Chem. Soc.* 1969, **91**, 6962.
5. R. H. Holm, *Chem. Soc. Rev.* 1981, **10**, 455.
6. G. Christou, K. S. Hagen, J. K. Bashkin and R. H. Holm, *Inorg. Chem.* 1985, **24**, 1010.
7. F. Cecconi, C. A. Ghilardi and S. Midollini, *Inorg. Chem.* 1983, **22**, 3802.
8. A. Agresti, M. Bacci, F. Cecconi, C. A. Ghilardi and S. Midollini, *Inorg. Chem.* 1985, **24**, 689.
9. R. Chevrel, M. Sergent and M. J. Prigent, *Mat. Res. Bull.* 1974, **9**, 1487, A. Gruttner, K. Yvon, R. Chevrel, M. Potel, M. Sergent and B. Seeber, *Acta Cryst.* 1979, **B35**, 285.
10. F. Cecconi, C. A. Ghilardi and S. Midollini, *Inorg. Chim. Acta* 1981, **64**, L47.
11. F. Cecconi, C. A. Ghilardi, S. Midollini and A. Orlandini, *Inorg. Chim. Acta* 1983, **76**, L183.
12. I. Bertini, F. Mani and L. Sacconi, *Inorg. Chem.* 1968, **7**, 1417.
13. P. W. R. Corfiled, R. J. Deodens and J. A. Ibers, *Inorg. Chem.* 1976, **6**, 197.
14. G. M. Sheldrick, *System of Computing Programs*. University of Cambridge, Cambridge, U.K. (1976).
15. C. K. Johnson, Oak Ridge National Laboratory Report ORNL (U.S.) 1976, ORNL-5138.
16. *International Tables for X-ray Crystallography*, Vol. IV, p. 99. Kynoch Press, Birmingham, U.K. (1974).
17. R. F. Stewart, E. R. Davidson and W. T. Simpson, *J. Chem. Phys.* 1965, **42**, 3175.
18. *International Tables for X-ray Crystallography*, Vol. IV, p. 149. Kynoch Press, Birmingham, U.K. (1974).
19. C. H. Wei and L. F. Dahl, *Cryst. Struct. Commun.* 1975, **4**, 583.
20. V. G. Albano, P. L. Bellon, P. Chini and F. Scatturin, *J. Organomet. Chem.* 1969, **16**, 461.
21. D. M. P. Mingos, *J. Chem. Soc. Dalton Trans.* 1974, 133; J. W. Lauher, *J. Am. Chem. Soc.* 1978, **100**, 5305; B. K. Teo, *Inorg. Chem.* 1984, **23**, 1215.
22. G. Gervasio, R. Rossetti, P. L. Stanghellini and G. Bor, *Inorg. Chim. Acta* 1984, **83**, L9.
23. E. R. Brown and R. F. Large, in *Techniques of Chemistry*, Part IIA (Edited by A. Weissberger), Chapter VI. Wiley Interscience, New York (1971).
24. R. S. Nicholson and I. Shain, *Analyt. Chem.* 1964, **36**, 706.
25. R. R. Gagnè, C. A. Kowal and G. C. Lisensky, *Inorg. Chem.* 1980, **19**, 2855.
26. F. D. Saeva and G. R. Olin, *J. Am. Chem. Soc.* 1980, **102**, 299.

Polyhedron Vol. 5, No. 12, pp. 2033–2038, 1986
Printed in Great Britain

0277–5387/86 $3.00+.00
© 1986 Pergamon Journals Ltd

SYNTHESIS AND RESONANCE RAMAN STUDY OF CONDUCTIVE IODINATED MATERIALS DERIVED FROM [M(dmit)(phen)] COMPLEXES [M = Pd(II), Pt(II)]

R. VICENTE and J. RIBAS*

Departament de Química Inorgànica, Facultat de Química, Universitat de Barcelona, Diagonal 647, 08028 Barcelona, Spain

and

C. SOURISSEAU

Laboratoire de Spectroscopie Infrarouge, U.A. 124 CNRS, Université de Bordeaux I, 351 Cours de la Libération, 33405 Talence Cedex, France

(*Received* 24 *January* 1986 ; *accepted* 8 *May* 1986)

Abstract—The synthesis and characterization of the [M(dmit)(phen)] complexes [M = Pd(II), Pt(II); H_2dmit = 4,5-dimercapto-1,3-dithiole-2-thione; phen = 1,10-phenanthroline) and of the iodinated [M(dmit)(phen)]I compounds are described. The conductivity of [M(dmit)(phen)] increases upon oxidation by a factor of 10^6, and is ca. 5×10^{-3} $ohm^{-1}\,cm^{-1}$ for the [M(dmit)(phen)]I compounds. The nature of the iodine species in these solids is determined by UV–visible and resonance Raman spectroscopies. The only polyiodide present is I_3^- and, thus, the charge distribution can be expressed as $[M(dmit)(phen)]^{0.33+}[I_3^-]_{0.33}$.

One of the strategies which can be employed for synthesizing highly conductive low-dimensional materials derives from the observation that halogenation of certain solids greatly increases their electrical conductivity. An extraordinary large variety of such conductive halogenated, and especially iodinated, materials has been studied,[1,2] including organic systems, transition metal complexes and polymers.

In these materials, iodine species reported to exist are I_2, I^-, I_3^- and I_5^-. Since the first Raman spectroscopic studies by Kiefer and Bernstein,[3] and Kaya and coworkers[4] on I_3^- species dissolved in methanol, this technique has been widely used[5–13] in the study of this anion for the following reasons :

(i) The existence of intense allowed electronic transition of the type $\sigma \rightarrow \sigma^*$ and/or $\pi \rightarrow \sigma^*$ gives rise to resonance Raman spectra which are greatly enhanced, by excitation in the visible, and generally characterized by a very intense ν_1 mode ($\nu_{sym}I_3^-$) and the activity of a $n\nu_1$ overtone progression.

(ii) Less intense additional signals observed in ordinary Raman and resonance Raman conditions have found various structural interpretations and have also been assigned to vibrational modes of several I_4^{2-}, I_5^- or I_6^{2-} polyiodides. However, the asymmetric linear configuration $C_{\infty v}$ seems now well established for I_3^- in solution.

(iii) The formation and the existence of I_3^- species in iodinated compounds, such as conductive complexes,[1,2,10,11] are clearly evidenced by resonance Raman scattering spectra, in spite of their very dark colour. In this respect, I_2 (ca. 210–180 cm^{-1}) and I_3^- (116–106 cm^{-1}) species are clearly discriminated by vibrational spectroscopy.

In the course of previous investigations on highly conductive bis(dithiolato) metal complexes[14] we have prepared mixed-ligand mononuclear complexes of the type [M(dmit)(Phos)$_2$] (M = Ni(II), Pd(II), Pt(II)); H_2dmit = 4,5-dimercapto-1,3-dithiole-2-thione; (Phos)$_2$ = dppe or $(PPh_3)_2$.[15] Several

* Author to whom correspondence should be addressed.

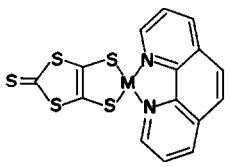


Fig. 1. [M(dmit)(phen)] complexes.

attempts to oxidize these complexes with iodine or bromine have failed to produce any conductive materials. This was probably due to steric effects of the $(Phos)_2$ ligands, precluding the stacking of the molecules. For example, in the crystal structure of [Pt(dmit)(dppe)] the Pt atom displays a distorted square planar configuration but there is no close stacking of the molecules.[16]

In order to circumvent this difficulty, we have studied the effect of replacing in such $[M(dmit)L_2]$ complexes the $(Phos)_2$ ligand by more planar bidentate ligands such as 2,2′-bipyridine[17] and 1,10-phenanthroline (phen). We report here the synthesis and characterization of the [M(dmit)(phen)] complexes [M = Pd(II), Pt(II)] (Fig. 1) and of the conductive [M(dmit)(phen)]I derived compounds, and the results of a resonance Raman study of these iodinated materials.

EXPERIMENTAL

(1) *Starting materials*

The benzoil salt $dmit(COPh)_2$ is prepared following the method of Steimecke and coworkers.[18] $[PdCl_2(phen)]$ and $[PtCl_2(phen)]$ were prepared following ref. 19. All reactions were carried out under inert atmosphere conditions unless otherwise stated. C, H, N analyses were carried out on a Carlo Erba instrument.

(2) *Synthesis of the* [M(dmit)(phen)] *complexes* [M = Pd(II), Pt(II)]

The $dmit^{2-}$ anion is generated in solution by reaction of $dmit(COPh)_2$ with 2 mol equivalent of sodium methoxide at room temperature. To the resulting solution is added 1 mol equivalent of the appropriate $[MCl_2(phen)]$ solid complex, and the solution refluxed for 5 h. A brown-to-reddish microcrystalline powder precipitates from the reaction mixture and after cooling is collected by filtering, washed with ethanol and dried under vacuum over silicagel. Yields were ca. 60%. Both compounds are insoluble in most common organic solvents but DMF, in which they are slightly soluble, precluding further purification by recrystallization. Analytical data are gathered in Table 1.

(3) *Iodine oxidation and synthesis of* [M(dmit)(phen)]I *compounds* [M = Pd(II), Pt(II)]

These compounds were prepared by mixing a solution of iodine in DMF (two-fold excess) with a solution-slurry of the corresponding [M(dmit)(phen)] complex in DMF. After stirring the reaction mixture for 30 min, the resulting dark brown precipitate is filtered out, and washed with methanol, hexane and, finally, several times with CCl_4 until no traces of iodine could be detected in the washing solvent. The solid was finally dried under vacuum. Yields were ca. 70%. Analytical data are gathered in Table 1.

(4) *Physical measurements*

IR spectra (4000–600 cm^{-1}) were recorded as KBr pellets with a Beckman IR-20A spectrophotometer. UV–visible spectra were recorded as KBr pellets with a 5230-UV Beckman spectro-

Table 1. Elemental analysis of [M(dmit)(phen)] and [M(dmit)(phen)]I complexes

Compound	Element	C%	H%	N%	I%
[Pd(dmit)(phen)]	Calc.	37.3	1.7	5.8	
	Found	37.1	1.6	5.6	
[Pt(dmit)(phen)]	Calc.	31.5	1.4	4.9	
	Found	31.8	1.4	4.7	
[Pd(dmit)(phen)]I	Calc.	29.5	1.3	4.6	20.8
	Found	29.8	1.2	4.5	19.9
[Pt(dmit)(phen)]I	Calc.	25.8	1.1	4.0	18.2
	Found	25.5	1.0	4.1	18.6

photometer. Electrical conductivities were estimated on compressed pellets as described in ref. 20.

Low frequency (10–650 cm^{-1}) resonance Raman spectra were obtained using a Coderg T800 triple monochromathor and a Spectra Physics Argon (5145 Å, model 171) or Krypton (6471 Å, model 2020) Laser. The detector was a RCA/C 31034 photomultiplier coupled with a photon counting device. Low excitation Laser powers were used ($P_0 \leqslant 60$ mW) because of the strong absorption of the compounds in this wavelength range (see electronic absorption spectra). The compounds were grinded as solid polycrystalline mixtures in KCl (ca. 6% w/w) and the samples were attached to rapidly rotating discs (ca. 2000 rpm) in order to avoid any local heating: under these conditions no decomposition was observed over long periods. The asymmetry of the Raman lines was checked by varying the amplification ratio and the spectral resolutions (between 1.6 and 3 cm^{-1}).

RESULTS AND DISCUSSION

The [M(dmit)(phen)] complexes [M = Pd(II), Pt(II)] were obtained by reaction of the corresponding [MCl_2(phen)] with the $dmit^{2-}$ anion generated in solution from [dmit($COPh)_2$] and methanolate. These complexes were characterized by elemental analysis (Table 1) and IR spectroscopy. Most of the observed IR bands are due to the coordinated ligands. The most characteristic absorptions, observed between 1500 and 1400 cm^{-1}, 840cm^{-1} and 700 cm^{-1} in the spectra of [M(dmit)(phen)] are mainly ring vibrations similar to corresponding bands of the coordinated 1,10-phenanthroline in [MCl_2(phen)].[21] On the other hand, new strong bands at ca. 1050 and 1030 cm^{-1} appear in the spectra of the [M(dmit)(phen)] complexes and are easily assigned to the typical ν(C⋯S) stretching frequencies of the dmit ligand.[15,18,22]

The [M(dmit)(phen)] complexes are slightly soluble in DMF. Reaction of a solution-slurry of these complexes with iodine dissolved in DMF yields the corresponding [M(dmit)(phen)]I compounds. The stoichiometry of both compounds is assigned from elemental analysis data (Table 1). Very little information can be gained from the IR spectra of these iodinated materials which show very few intense and broad bands (Fig. 2). However, the broad absorption bands near 1100 and 1250 cm^{-1} are similar to those observed in a number of other conductive systems.[23,24] Such features in the IR spectra of narrow band semiconductor or metallic materials, should be explicitly attributed to electron–molecular vibration interaction and not generically to an electron–phonon interaction.[24]

As a matter of fact, the [M(dmit)(phen)]I compounds exhibit a fairly high compaction powder conductivity at room temperature: ca. 5×10^{-3} $ohm^{-1}\,cm^{-1}$. The conductivity of the corresponding [M(dmit)(phen)] starting complexes being lower than 10^{-9} $ohm^{-1}\,cm^{-1}$, this means that iodination results in an increase of the conductivity by a factor of at least 10.[6]

It can be inferred from the conductivity increase and the peculiar features of the IR spectra that iodination of [M(dmit)(phen)] leads to partially oxidized materials. A first indication on the nature of the iodine species present in these solids and, hence, the degree of the charge transfer can be found in the UV–visible spectra: it is known that the intense absorption maximum for a chain of I_3^- ions is in the 550 nm region,[1,25] whereas chains of I_5^- give rise to an absorption maximum at ca. 700 nm.[1,26] In

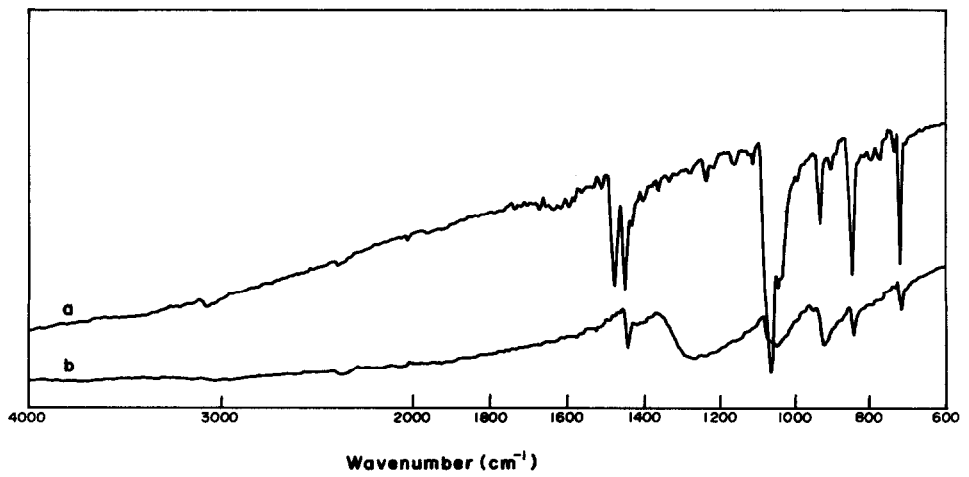


Fig. 2. IR spectra of: (a) [Pt(dmit)(phen)], and (b) [Pt(dmit)(phen)]I.

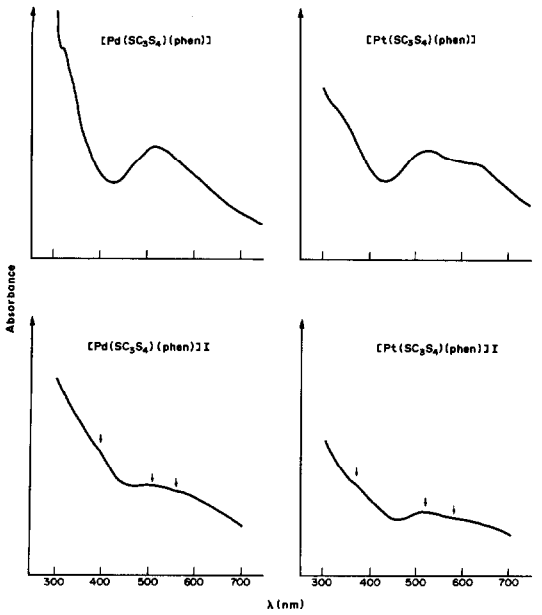


Fig. 3. UV–vis absorption spectra (KBr pellets) of [M(dmit)(phen)] and [M(dmit)(phen)]I compounds (M = Pd or Pt) (dmit = SC_3S_4).

our case (Fig. 3), whereas the unoxidized [M(dmit)(phen)] complexes exhibit weak d–d absorptions at ca. 520 and 325 nm for M = Pd and ca. 625, 530 and 325 nm for M = Pt, the oxidized [Pd(dmit)(phen)]I compound exhibits broad intense absorption at ca. 510 nm with shoulders at ca. 550 and 400 nm. Likewise the [Pt(dmit)(phen)]I compound exhibit a very broad asymmetric absorption maximum centred at ca. 525 nm with shoulders at ca. 575 and 375 nm. These observations agree with those previously reported for [M(dmit)(bipy)]I[17] and are consistent with the presence of I_3^- species in the studied compounds.

A definitive answer to this question is given by resonance Raman spectroscopy.

The Raman spectra of both platinum and palladium complexes are quite similar and only those obtained for the platinum complex are shown in Fig. 4. All the observed band-wavenumbers and proposed assignments are gathered in Table 2, together with their relative intensities and band-widths (FWHM).

The spectra exhibit essentially a very intense band at 105 cm^{-1}, characteristic of the $\nu_1(\Sigma^+)$ mode of I_3^- species and some weaker and broader progressions $n \times \nu_1$ of this mode as far as $n = 6$. Using the classical expressions $\nu(n)/n = (\omega e + \omega eXe) + \omega eXe \times n$ and the plots of $\nu(n)/n$ vs n, where n is the vibrational quantum number, the following spectroscopic constants have been estimated, $\omega e = 104.8\ cm^{-1}$ and $\omega eXe \simeq +0.4\ cm^{-1}$ (Fig. 5). These values are in agreement with those reported in several previous studies.[3–7]

It is noteworthy that weaker additional signals are also detected at 52 cm^{-1} (lattice mode), 148 cm^{-1} (ν_3, Σ^+), 170 cm^{-1} ($2 \times \nu_2$) and 254 cm^{-1} ($\nu_1 + \nu_3$) while the high frequency mode at 514 cm^{-1} is likely to be due to the stretching ν(C=S) mode of the $SC_3S_4^{2-}$ ligand. The very low intensity of the

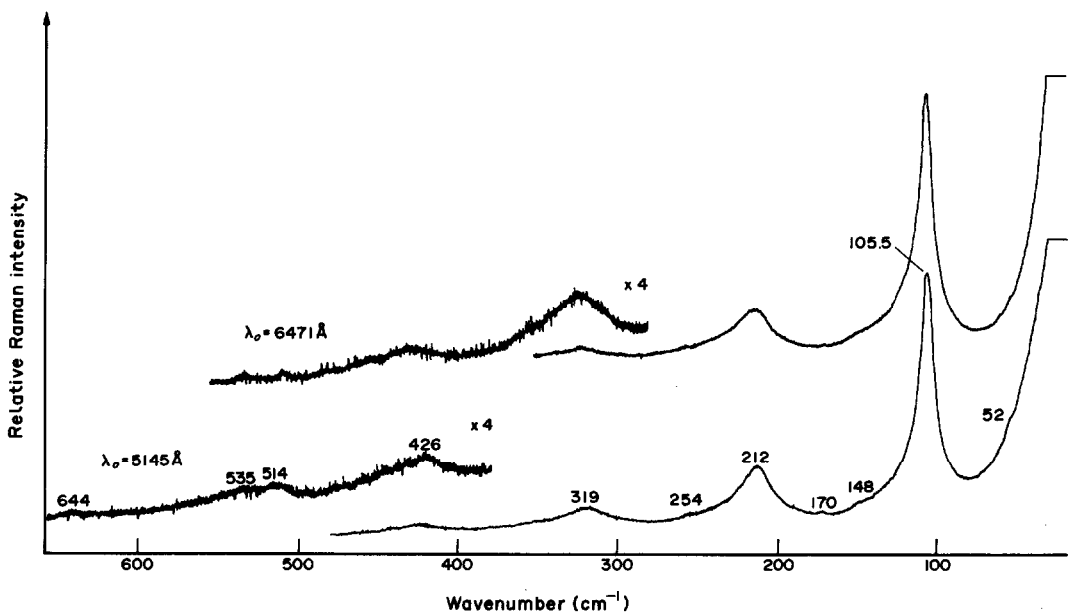


Fig. 4. Resonance Raman spectra of solid mixtures in KCl [5–6% (w/w)] of [Pt(dmit)(phen)]I using 60-mW incident laser radiations for 6471- and 5145-Å lines.

Table 2. Resonance Raman band wavenumbers (cm^{-1}) and assignments for [M(dmit)(phen)]I (M = Pd, Pt) at 300 K

[Pt(dmit)(phen)]$(I_3)_{0.33}$			[Pd(dmit)(phen)]$(I_3)_{0.33}$			
ν (cm^{-1})	$\Delta\nu_{1/2}$ (cm^{-1})	Intensity	ν (cm^{-1})	$\Delta\nu_{1/2}$ (cm^{-1})	Intensity	Assignment
52	—	vw	52	—	vw	Lattice mode
105.5	11	100	105.5	11	100	ν_1 ($\nu_{sym}I_3^-$)
148	—	w	148	—	w	ν_3 ($\nu_{asym}I_3^-$)
170	—	vw	170	—	vw	$2\nu_2$ ($2\times\delta I_3^-$)
212	24	24	212	25	24	$2\times\nu_1$
254	—	vw	254	—	vw	$\nu_1+\nu_3$
319	38	8	319	39	8.5	$3\times\nu_1$
426	46	3	427	46	3	$4\times\nu_1$
514	—	3	514	—	3	ν(C═S)
535	—	w	535	—	w	$5\times\nu_1$
644	—	vw	644	—	vw	$6\times\nu_1$

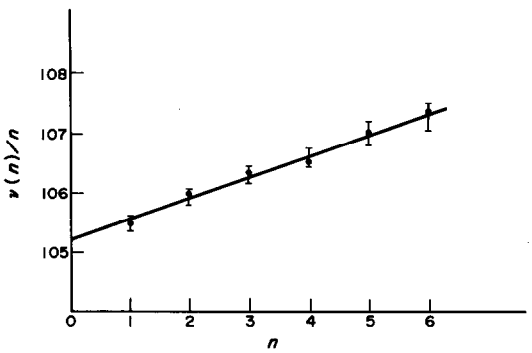


Fig. 5. Plot of $\nu(n)/n$ vs n obtained from the $n\nu_1$ overtone progression of the I_3^- species.

ν_3 mode for both exciting radiations used indicates that the I_3^- species have probably a nearly symmetric linear structure. At this point, these resonance Raman results confirm that I_3^- is the only polyiodide present in these partially oxydized compounds. Finally, large broadenings of the bands due to the overtones and asymmetric profiles are clearly evidenced on the recorded spectra even using high resolution conditions. This must reflect coupling to lattice modes or vibrational dephasing. Assuming linear coupling to lattice modes, we would expect a linear dependence on the linewidth on n,[5] whereas vibrational dephasing would introduce a n^2 dependence.[27] Our results indicate a behaviour roughly linear upon n, confirming the large contribution of the first mechanism.[5,8] Nevertheless, "hot band" processes may also make a significant contribution since the profiles are always asymmetric on the high frequency side ($\omega eXe > 0$)[17,28] and the asymmetries generally disappear when cooling the samples to 20–10 K.[5,8]

Acknowledgements—Financial Assistance from the University of Barcelona and the Generalitat of Catalunya (CIRIT) is gratefully acknowledged. The authors wish to thank R. Cavagnat for efficient technical assistance in the recording of resonance Raman spectra.

REFERENCES

1. T. J. Marks and D. W. Kalina, in *Extended Linear Chain Compounds* (Edited by J. S. Miller), Vol. 1, pp. 197–331. Plenum Press, New York (1982).
2. P. Coppens, *Ibid.* Vol. 1, pp. 33–356 (1982).
3. W. Kiefer and H. J. Bernstein, *Chem. Phys. Lett.* 1972, **16**, 5.
4. K. Kaya, N. Mikami, Y. Ugadawa and M. Ito, *Chem. Phys. Lett.* 1972, **16**, 151.
5. T. P. Martin, *Phys. Rev.* 1976, **B13**, 3617.
6. J. C. Rubin and D. Sala, *J. Raman Spectrosc.* 1981, **11**, 320.
7. L. Andrew, E. S. Prochaska and A. Loewenschuss, *Inorg. Chem.* 1980, **19**, 463.
8. M. R. Mohammad and W. F. Sherman, *J. Molec. Struct.* 1984, **115**, 27.
9. K. R. Loos and A. C. Jones, *J. Phys. Chem.* 1974, **78**, 2306 and references therein.
10. J. L. Petersen, C. S. Schramm, D. R. Stojakovic, B. M. Hoffman and T. J. Marks, *J. Am. Chem. Soc.* 1977, **99**, 286 and references therein.
11. P. J. Trotter and P. A. White, *Appl. Spectrosc.* 1978, **32**, 323.
12. F. Inagaki, I. Harada, T. Shimananchi and M. Tasumi, *Bull. Soc. Chim. Jpn* 1972, **45**, 3384.
13. A. G. Maki and R. Forneris, *Spectrochim. Acta* 1967, **23A**, 867.
14. J. Ribas and P. Cassoux, *C. r. Hbd. Séanc. Acad. Sci. Paris* 1981, **II293**, 287; J. Ribas and R. Vicente, *Ann.*

Quim. 1985, **B81**, 190; R. Vicente, J. Ribas, P. Cassoux and L. Valade, *Synth. Met.* 1986, **13**, 265.
15. R. Vicente, J. Ribas and P. Cassoux, *Nouv. J. Chim.* 1984, **8**, 653.
16. R. Vicente, J. Ribas, X. Solans, M. Font-Altaba and P. Cassoux, unpublished results.
17. R. Vicente, J. Ribas, P. Cassoux and C. Sourisseau, *Synth. Met.* 1986, **15**, 79.
18. G. Steimecke, H. J. Seiler, R. Kirmse and E. Hoyer, *Phosphorus Sulphur* 1979, **7**, 49; G. Steimecke, Ph.D. Thesis, Leipzig, G.D.R. (1977).
19. S. E. Livingstone, *J. Proc. R. Soc. New South Wales* 1952, **85**, 151; F. A. Palocsay and J. V. Rend, *Inorg. Chem.* 1969, **8**, 524.
20. P. Lacroix, O. Kahn, A. Gleizes, L. Valade and P. Cassoux, *Nouv. J. Chim.* 1984, **8**, 643.
21. A. A. Schilt and R. C. Taylor, *J. Inorg. Nucl. Chem.* 1959, **9**, 211; R. G. Inskeep, *J. Inorg. Nucl. Chem.* 1962, **24**, 763.
22. R. R. Schumaker and E. M. Engler, *J. Am. Chem. Soc.* 1977, **99**, 5521; H. Poleschner, W. John, G. Kempe, E. Hoyer and E. Fanghänel, *Z. Chem.* 1978, **18**, 345.
23. B. N. Diel, T. Inabe, N. K. Jaggi, J. W. Lyding, O. Schneider, M. Hanack, C. R. Kannewurf, T. J. Marks and L. H. Schwartz, *J. Am. Chem. Soc.* 1984, **106**, 3207 and references therein.
24. V. A. Starodub, V. N. Baumer, I. M. Guelle, F. Golovkina, V. G. Alyoshin, V. V. Nemoshkalenko and A. I. Senkiewicz, *Synth. Met.* 1983, **5**, 101.
25. J. M. Redy, K. Knox and M. B. Robin, *J. Chem. Phys.* 1964, **40**, 1082 and refs 5e and 49 in 1.
26. References 5e, 8a and 50 in 1.
27. A. H. Zewail and D. J. Diestler, *Chem. Phys. Lett.* 1979, **65**, 37.
28. A. D. Bandrak, K. D. Tuong, C. Carlone and S. Jandl, *Chem. Phys. Lett.* 1983, **95**, 78.

Polyhedron Vol. 5, No. 12, pp. 2039–2045, 1986
Printed in Great Britain

0277–5387/86 $3.00+.00
© 1986 Pergamon Journals Ltd

EXTRACTION OF CADMIUM(II) BY ORGANOPHOSPHORUS COMPOUNDS

I. CASAS, N. MIRALLES, A. SASTRE* and M. AGUILAR

Departament de Química, Escola Tècnica Superior d'Enginyers Industrials de Barcelona, Universitat Politècnica de Catalunya, Diagonal 647, 08028 Barcelona, Spain

(*Received* 19 *February* 1986; *accepted* 8 *May* 1986)

Abstract—The extraction of cadmium(II) by di-(2-ethylhexyl) phosphoric acid dissolved in tetradecane from aqueous chloride and perchlorate solutions has been studied at 25°C. The distribution of the metal has been determined as a function of metal and DEHPA concentrations. Distribution data have been treated both graphically and numerically using the program LETAGROP-DISTR (*Acta Chem. Scand.* 1971, **25**, 1521) and the composition of the extracted species into the organic phase has been determined. The extraction constants for these species are given in Table 1.

This work is part of a series dealing with the extraction of divalent metal ions by organophosphorus extractants dissolved in commercial diluents.[2,3] The aim of this work is to investigate the different systems and describe them in terms of species and equilibrium constants, in order to establish if speciation in the organic phase may be utilized to design metal separation methods.[4]

The extraction of cadmium(II) by di-(2-ethylhexyl) phosphoric acid (henceforth DEHPA in the text and HA in formulas) has been studied under a great variety of experimental conditions. Most of the work is connected with the separation of cadmium and zinc in different media[5–8] and less emphasis has been placed on equilibrium studies. It seems from these studies that extraction reaction models proposed by different authors do not agree with each other—probably because of different experimental conditions.

Thus, while Grimm and Kolarik[9] found the species $CdA_2(HA)_3$ in the extraction of cadmium(II) from chloride solutions by DEHPA dissolved in *n*-dodecane, Rice *et al.*[5] studied the extraction of Zn(II), Cd(II) and Hg(II) from sulphate solution by different extractants and reported species of composition $MA_2(HA)_2$ in organic phase, even though data for cadmium do not exactly fit the proposed model. According to these authors this may probably be due to the polymerization reactions, or else perhaps due to activity coefficient variations.

On the other hand Baes[10] in a review on the extraction of metal ions by dialkylphosphoric acid gives some constants for the extraction of $CdA_2(HA)_2$ in different diluents, although these constants were estimated from the work of several investigators and corrected for toluene as solvent.

All these results make us think that new distribution data may contribute to the clarification of the uncertainties in the composition of Cd–DEHPA-extracted species at low metal loading, as well as give new information on organophosphorus extractants.

Under these circumstances, a detailed study of the extraction of Cd(II) by DEHPA in tetradecane is undertaken. The object of this is to describe the metal extraction in terms of species and extraction constants.

EXPERIMENTAL

Reagents

Di-(2-ethylhexyl) phosphoric acid (DEHPA = HA)—supplied by BDH. Its purity was determined by potentiometric titration in an 80% ethanol solution of the acid with NaOH 0.1 mol dm^{-3} using Gran plots.[11] Purity was found to be 98.2%

Tetradecane—supplied by PETRESA, is a commercial hydrocarbon of the following characteristics:

* Author to whom correspondence should be addressed.

Density at 15°C	0.768
Aromatic content, ppm	215
Water content, ppm	50 max.
Boiling point at 760 mmHg	253.7°C.
Distribution (%)	
C_{13}	1.2
C_{14}	98.2
C_{15}	0.1.

Tetradecane was washed with NaOH 0.1 mol dm^{-3}, distilled water, HCl 0.1 mol dm^{-3} and finally distilled water until no evidence of chloride ions in the aqueous solution.

Sodium chloride and sodium perchlorate—used as ionic medium, were prepared as described in ref. 12.

Perchloric acid and hydrochloric acid.—Merck p.a. were used without further purification. A stock solution of both acids was prepared and standardized against HgO and NaI.[13]

Cadmium perchlorate—was prepared from cadmium oxide (Probus p.a.) and perchloric acid (Merck p.a.) as described in ref. 14. The cadmium concentration of the stock solution was determined by complexometric titration with EDTA using eriochrome black T as indicator.[15] The perchlorate concentration of the stock solution was determined as described elsewhere.[3]

Cadmium chloride—Merck p.a. was used without further purification. A stock solution was prepared and analysed as cadmium perchlorate.

Extraction procedure

All experiments were carried out at 25°C. The phases in contact had the following composition:

Aqueous phase:	
$(Na^+, H^+, Cd^{2+})ClO_4^-$	1.0 mol dm^{-3}
$(Na^+, H^+, Cd^{2+})ClO_4^-$	0.1 mol dm^{-3}
$(Na^+, H^+, Cd^{2+})Cl^-$	0.1 mol dm^{-3}
Organic phase:	DEHPA in tetradecane.

The extractant concentrations were varied from 0.010 to 0.150 mol dm^{-3}.

Volumes (15 cm^3) of each phase was shaken out mechanically in stoppered glass tubes for 30 min. This time was enough to reach equilibrium and the tubes were then centrifuged.

Metal content in both phases were determined by atomic absorption spectrometry or by complexometric titration with EDTA. The metal in organic phase was stripped from an aliquot by dilute nitric acid and determined in the same way.

RESULTS

The distribution coefficient of cadmium(II) between the organic and aqueous phases was obtained directly as the ratio of the total cadmium concentration in both phases

$$D = \frac{[Cd(II)]_{(org)}}{[Cd(II)]_{(aq)}}. \quad (1)$$

When only DEHPA was present in the initial organic phase, values of D were determined as a function of both the total concentration of DEHPA and pH, for different total concentrations of metal in either chloride or perchlorate media.

The results are plotted in Figs 1 and 2 as $\log D - 2pH$ *vs* total DEHPA concentration for different ionic media.

Treatment of data

Graphical treatment. The extraction of cadmium with cationic extractant (DEHPA) may be described by the following general reaction

$$Cd^{2+} + mHA_{(org)} \rightarrow CdA_2(HA)_{m-2} + 2H^+ \quad (2)$$

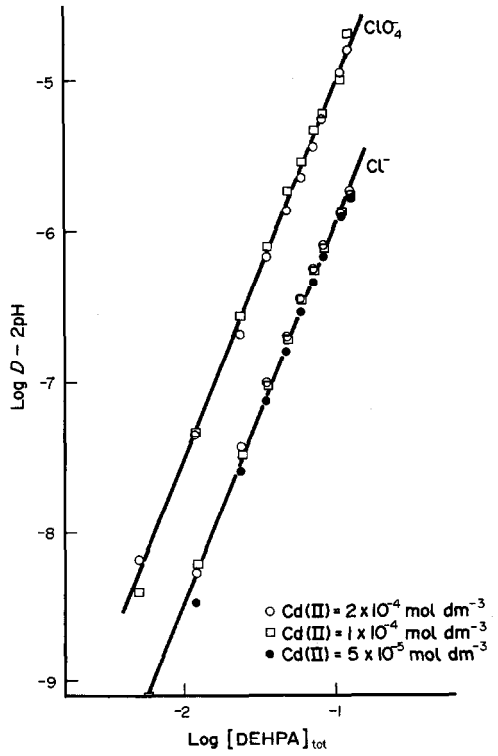


Fig. 1. $\log D - 2pH$ plotted as a function of the total DEHPA concentration in tetradecane at 0.1 mol dm^{-3} ionic strength in chloride and perchlorate media. The full-drawn lines have been calculated using the constants given in Tables 1 and 2.

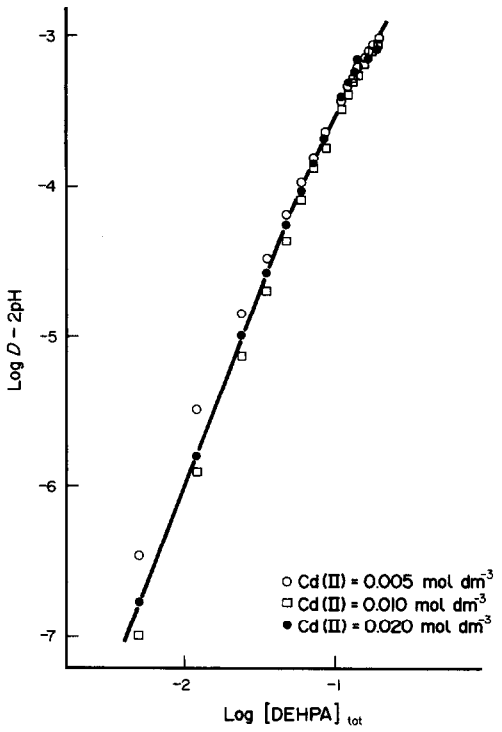


Fig. 2. Log $D-2$pH plotted as a function of the total DEHPA concentration in tetradecane at 1.0 mol dm^{-3} ionic strength in perchlorate medium. The full-drawn lines have been calculated using the constants given in Tables 1 and 2.

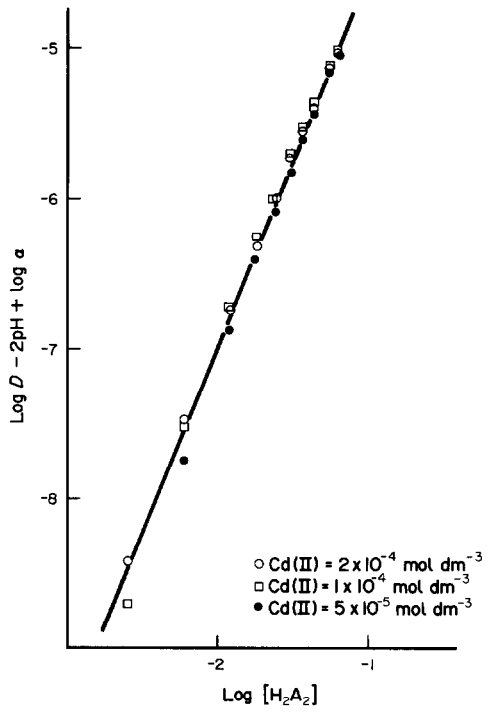


Fig. 3. Log $D-2$pH$+\log\alpha$ plotted as a function of free DEHPA concentration in tetradecane at 0.1 mol dm^{-3} ionic strength in chloride medium. The curve has been calculated from eqn (14) with $m = 4$ or 5, and $L = 0.01$.

where HA refers to di-(2-ethylhexyl) phosphoric acid and β_{1m} is the formation constant, defined by

$$\beta_{1m} = \frac{[CdA_2(HA)_{m-2}]_{(org)}[H^+]^2}{[Cd^{2+}][HA]^m_{(org)}}. \qquad (3)$$

Polynuclear cadmium(II) complexes in the organic phase have been excluded because plots log $D-2$pH$+\log\alpha$ *vs* log $[H_2A_2]$ are independent of cadmium concentration (Figs 3–5).

As a starting model, taking into account the previous findings for similar systems,[3] two species of the type $CdA_2(HA)_2$ and $CdA_2(HA)_3$ may be assumed.

Then the distribution coefficient becomes

$$D = \frac{[CdA_2(HA)_2]_{(org)} + [CdA_2(HA)_3]_{(org)}}{[Cd(II)]_{(aq)}}$$

$$= \frac{[HA]^2_{(org)}\beta_{14}[H^+]^{-2} + [HA]^3_{(org)}\beta_{15}[H^+]^{-2}}{\alpha} \qquad (4)$$

where α is the ratio $[Cd(II)]_{(aq)}/[Cd^{2+}]$.

Since no complexes are formed between cadmium and perchlorate ions, $\alpha = 1$ in this ionic medium.

In chloride solutions α can be written as

$$\alpha = 1 + \beta_1[Cl^-] \qquad (5)$$

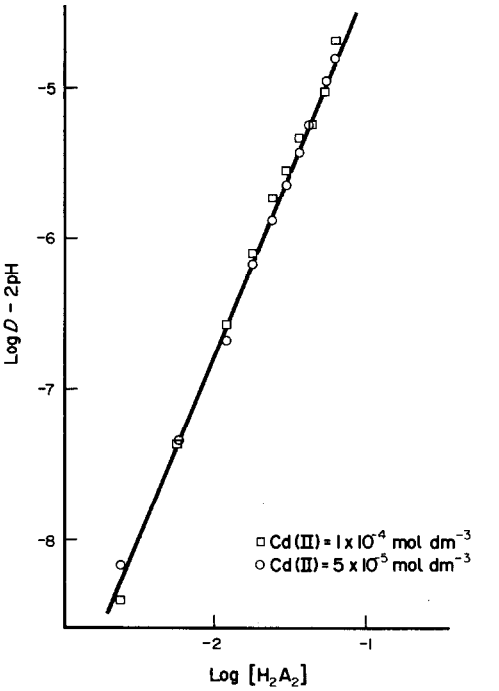


Fig. 4. Log $D-2$pH plotted as a function of free DEHPA concentration in tetradecane at 0.1 mol dm^{-3} ionic strength in perchlorate medium. The curve has been calculated from eqn (14) with $m = 4$ or 5, and $L = 0.01$.

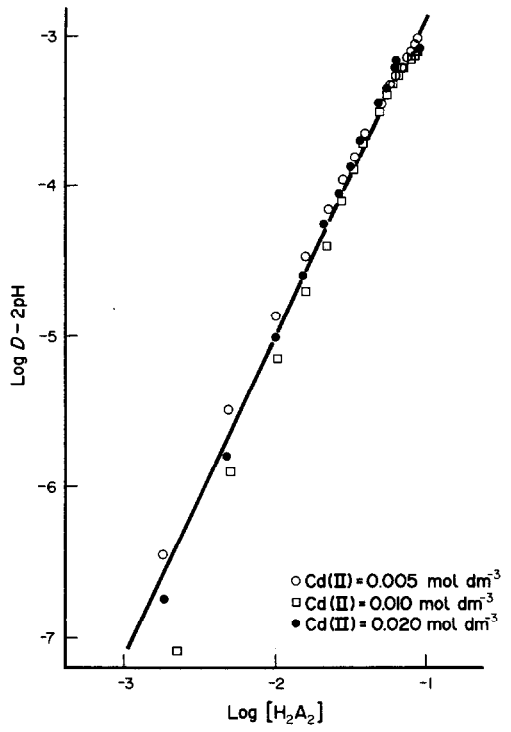


Fig. 5. Log $D-2$pH plotted as a function of free DEHPA concentration in tetradecane at 1.0 mol dm^{-3} ionic strength in perchlorate medium. The curve has been calculated from eqn (14) with $m = 4$ or 5, and $L = 0.2$.

where β_1 is the formation constant of the cadmium–chloride complex. The value of β_1 was taken from ref. 16.

Considering the dimerization equilibrium of DEHPA represented by

$$2HA_{(org)} \rightleftharpoons H_2A_{2(org)} \tag{6}$$

$$K_D = \frac{[H_2A_2]_{(org)}}{[HA]^2_{(org)}}. \tag{7}$$

Equation (4) becomes

$$D\alpha[H^+]^2 = \beta_{14}K_D^{-2}[H_2A_2]^2_{(org)} + \beta_{15}K_D^{-5/2}[H_2A_2]^{5/2}_{(org)} \tag{8}$$

in which D is expressed as a function of the dimer concentration. The K_D value was taken from ref. 17.

$[H_2A_2]_{(org)}$ values may be calculated from the mass action law

$$[HA]_{tot} = 2[H_2A_2]_{(org)} + [H_2A_2]^{1/2}_{(org)}K_D^{-1/2} + m[Cd(II)]_{(org)} + [HA]_{(aq)}. \tag{9}$$

Considering the high value of K_D and the low water solubility of DEHPA, values of $[H_2A_2]_{(org)}$ can be calculated for different m, as

$$[H_2A_2]_{(org)} = \frac{[HA]_{tot}}{2} - \frac{mD}{2(1+D)}[Cd(II)]_{tot}. \tag{10}$$

Two new variables u, Y and a parameter L may be defined as

$$u = \beta_{15}^{2/5}K_D^{-1}[H_2A_2]_{(org)} \tag{11}$$

$$L = \beta_{14}\beta_{15}^{-4/5} \tag{12}$$

$$Y = D\alpha[H^+]^2. \tag{13}$$

Substituting in eqn (8), we get

$$Y = Lu^2 + u^{5/2}. \tag{14}$$

By means of eqn (14), a set of curves of $\log Y = f(\log u)$ were constructed for different L values and were compared to the experimental $(\log D - 2\text{pH} + \log\alpha) = f(\log [H_2A_2]_{(org)})$ curves for perchlorate and chloride media. Thus, by superimposing these curves on the theoretical model function, a position was found by lateral translation along the abscissa, where the experimental curves coincide with one of the theoretical curves.

By reading off the difference

$$\log u - \log [H_2A_2]_{(org)} = 2/5 \log \beta_{15} - \log K_D \tag{15}$$

$\log \beta_{15}$ was determined.

The best fit was found for $L = 0.2$ in perchlorate 1.0 mol dm^{-3} and $L = 0.01$ for perchlorate and chloride 0.1 mol dm^{-3} (Figs 3–5), and β_{14} was then calculated using eqn (12). The results are given in Table 1.

Theoretical functions were also constructed on the assumption of the existence of the species with $m = p$ and $m = p+1$ (p = 2–5) but the fit to the experimental curve was not acceptable.

Numerical treatment. A refinement of the model obtained was performed using the program LETAGROP-DISTR.[1] In this program, the

Table 1. Survey of the extraction constants determined by different methods

Method of calculation	$\log \beta_{14}$	$\log \beta_{15}$
Perchlorate solution 1.0 M		
GRAPHICAL	8.2	11.1
LETAGROP-DISTR	8.22±0.14	11.12±0.19
Perchlorate solution 0.1 M		
GRAPHICAL	6.0	10.0
LETAGROP-DISTR	5.71max6.23	9.90±0.11
Chloride solution 0.1 M		
GRAPHICAL	5.9	9.8
LETAGROP-DISTR	5.80±0.22	9.70±0.04

Table 2. Equilibrium constants used in this work

Reaction	Constants	Ref.
$2HA_{(org)} = H_2A_{2(org)}$	5.01×10^4	17
$HA_{(aq)} = HA_{(org)}$	2.00×10^3	17
$HA_{(aq)} = A^-_{(aq)} + H^+_{(aq)}$	1.91×10^{-2}	18

Table 3. Some details of the calculation with LETAGROP-DISTR

Species	U	$\sigma(\log D)$	Rejected species
Perchlorate media 1.0 M			
$CdA_2(HA)_2$	0.134	0.066	—
$CdA_2(HA)_3$	0.432	0.115	—
$CdA_2(HA)_2$			
$CdA_2(HA)_3$	0.075	0.050	—
CdA_2			
CdA_2HA			
$CdA_2(HA)_2$			CdA_2
$CdA_2(HA)_3$	0.075	0.050	CdA_2HA
CdA_2HA			
$CdA_2(HA)_2$			
$CdA_2(HA)_3$	0.075	0.050	CdA_2HA
Perchlorate media 0.1 M			
$CdA_2(HA)_2$	0.348	0.152	—
$CdA_2(HA)_3$	0.027	0.043	—
$CdA_2(HA)_2$			
$CdA_2(HA)_3$	0.023	0.040	—
CdA_2			
$CdA_2(HA)_2$			
$CdA_2(HA)_3$	0.023	0.040	CdA_2
CdA_2			
CdA_2HA			
$CdA_2(HA)_2$			CdA_2
$CdA_2(HA)_3$	0.023	0.040	CdA_2HA
Chloride media 0.1 M			
$CdA_2(HA)_2$	0.343	0.143	—
$CdA_2(HA)_3$	0.018	0.033	—
$CdA_2(HA)_2$			
$CdA_2(HA)_3$	0.011	0.027	—
CdA_2			
$CdA_2(HA)_2$			
$CdA_2(HA)_3$	0.011	0.027	CdA_2
CdA_2			
CdA_2HA			
$CdA_2(HA)_2$			CdA_2
$CdA_2(HA)_3$	0.011	0.027	CdA_2HA

Species rejected when $\beta_1 = 0$.

computer searches for the best set of formation constants that would minimize the error square sum, defined by

$$U = \sum (\log D_{exp} - \log D_{calc})^2 \qquad (16)$$

where D_{exp} is the distribution ratio of cadmium determined experimentally and D_{calc} is the calculated D value obtained by solving the mass balance equations, assuming a certain set of species and constants. The program also calculates the standard deviation $\sigma(\log D)$, defined by

$$\sigma(\log D) = \left[\sum \frac{(\log D_{exp} - \log D_{calc})^2}{N_p}\right]^{1/2}. \qquad (17)$$

The equilibrium constants for the different DEHPA species in the two-phase system used in the present work are given in Table 2. The calculations were performed in two steps. First, the model and the constants β_{14}, β_{15} obtained from graphical treatment were used as starting values and U was then calculated and minimized. Furthermore, several other calculations with LETAGROP-DISTR were carried out, in order to investigate the possibility of finding other sets of complexes which could improve the fit of the experimental data.

The results are given in Table 3. The values of the minimum U and the standard deviation $\sigma(\log D)$ are shown for each set tried. The lowest error squares sum was obtained for the model $CdA_2(HA)_2$ and $CdA_2(HA)_3$ derived graphically in both chloride and perchlorate media.

Finally, the distribution of cadmium in organic phase between the two species $CdA_2(HA)_2$ and $CdA_2(HA)_3$ have been calculated with the program HALTAFALL[22] using the constants given in Table 1.

CONCLUSIONS

The results of the present work, summarized in Table 1, indicate that the extraction of Cd(II) from different media (Cl^-, ClO_4^-) may be explained assuming the formation in the organic phase of two species of composition $CdA_2(HA)_2$ and $CdA_2(HA)_3$. This conclusion may explain the observed fractionary slope (2.4) for both chloride and perchlorate media in the plots $\log D - 2pH + \log \alpha$ *vs* $\log [H_2A_2]$ at low Cd/DEHPA ratio where the predominant species is $CdA_2(HA)_3$ (Figs 3, 4). As the ratio Cd/DEHPA increases, slope tends to approximate to 2 and the predominance of the species $CdA_2(HA)_2$ seems to be evident (Fig. 5).

As seen in Fig. 6, the species $CdA_2(HA)_3$ becomes predominant for Cd/DEHPA < 0.1, while for ratio

Table 4. The equilibrium constants for $CdA_2(HA)_2$ and $CdA_2(HA)_3$ found in the literature

Solvent	Medium	log K_1	log β_{14}	log K_2	log β_{15}	Ref.
Amsco 80-125	NO_3^-	−1.8	7.6	—	—	10, 19
Toluene[a]	NO_3^-	−2.4	7.0	—	—	10
Toluene	Cl^-	−3.75	5.67	—	—	10, 20
Dodecane[b]	NO_3^-	—	—	−1.65	10.1	9
Tetradecane	ClO_4^-	—	5.71max6.23	—	9.90±0.11	this work
Tetradecane[c]	Cl^-	—	5.08±0.22	—	9.00±0.04	this work

K_1 and K_2 are the formation constants of $CdA_2(HA)_2$ and $CdA_2(HA)_3$ defined by

$$K_1 = \frac{[CdA_2(HA)_2]_{org}[H^+]^2}{[Zn^{2+}][H_2A_2]^2_{org}} \quad \text{and} \quad K_2 = \frac{[CdA_2(HA)_3]_{org}[H^+]^2}{[Zn^{2+}][H_2A_2]^{2.5}_{org}}$$

respectively, and β_{14} and β_{15} are the formation constants of reaction (2) calculated from expression $\beta_{14} = K_D^2 K_1$ and $\beta_{15} = K_D^{2.5} K_2$.

[a] Corrected and standardized value per toluene as solvent.[10]

[b] Tentatively acceptable value of the constant reviewed by Kolarik.[21]

[c] Conditional constants.

Cd/DEHPA > 0.1 the predominant species in organic phase is $CdA_2(HA)_2$.

In this sense the reaction model and constants in Table 1 represent a more complete description and in certain ways may unify the results of some other authors.[5,9,10] Finally, although information on extraction constants for this system is scarce, constants quoted in Table 1 seem to be within the broad range of values given in the literature (Table 4).

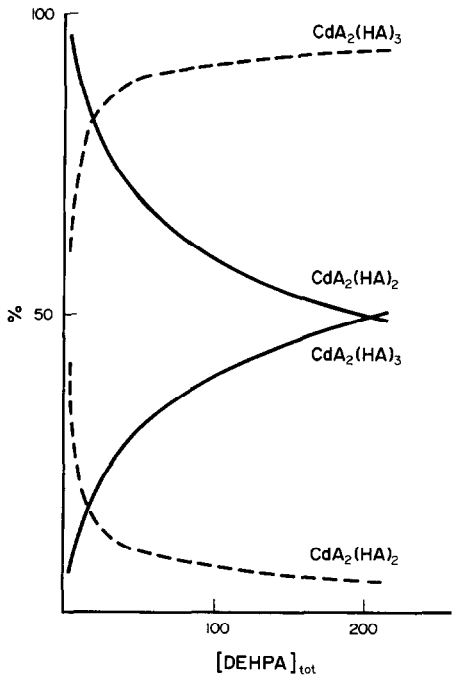


Fig. 6. Fraction of $CdA_2(HA)_2$ and $CdA_2(HA)_3$ plotted as a function of the total DEHPA concentration in organic phase: (----) Cd/DEHPA > 0.1, and (·····) Cd/DEHPA < 0.1.

REFERENCES

1. D. H. Liem, *Acta Chem. Scand.* 1971, **25**, 1521.
2. A. M. Sastre, N. Miralles and M. Aguilar, *Chem. Scripta* 1984, **24**, 44.
3. A. M. Sastre and M. Muhammed, *Hydrometallurgy* 1984, **12**, 177.
4. M. Muhammed and A. M. Sastre, *Proc. Symp. on Ion Exchange and Solvent Extraction*, II-49, Oslo (1982).
5. N. M. Rice and M. R. Smith, *J. Appl. Chem. Biotechnol.* 1975, **25**, 379.
6. N. M. Rice and M. R. Smith, *Can. Met. Q.* 1973, **12**, 341.
7. J. Shibata and S. Nishimura, *Trans. JIM* 1977, **18**, 794.
8. Z. Kolarik and R. Grimm, *J. Inorg. Nucl. Chem.* 1976, **38**, 1721.
9. R. Grimm and Z. Kolarik, *J. Inorg. Nucl. Chem.* 1974, **36**, 189.
10. C. F. Baes, *J. Inorg. Nucl. Chem.* 1962, **24**, 707.
11. G. Gran, *Analyst* 1952, **77**, 661.
12. Some Laboratory Methods in Current Use at the Department of Inorganic Chemistry, The Royal Institute of Technology, Mimeograph (1959).
13. A. I. Vogel, *Textbook of Quantitative Inorganic Analysis*, 4th edn. Longmans, London (1964).
14. G. Biederman and L. Ciavatta, *Acta Chem. Scand.* 1962, **16**, 1785.
15. G. Schwarzenbach and H. A. Flashka, *Complex Titrations*. Methuen, London (1969).
16. M. H. Hutchinson and W. C. E. Higginson, *J. Chem. Soc. Dalton Trans.* 1973, 1247.

17. Z. Kolarik, *Coll. Czech. Chem. Commun.* 1967, **32**, 311.
18. V. C. Smelov and V. P. Janin, *Radiokhimiya* 1969, **11**, 415.
19. E. Lamb, *Report ORNL CF-60-6-135*, 1960, 5.
20. R. Kimura, *Bull. Chem. Soc. Jpn* 1960, **33**, 1038.
21. Z. Kolarik, *Pure Appl. Chem.* 1980, **54**, 2593.
22. N. Ingri, W. Kakotowicz, L. G. Sillen and B. Warnquist, *Talanta* 1967, **14**, 1261.

Polyhedron Vol. 5, No. 12, pp. 2047–2049, 1986
Printed in Great Britain

0277–5387/86 $3.00+.00
© 1986 Pergamon Journals Ltd

PREPARATION AND METAL-ADSORPTION PROPERTIES OF POLYSTYRENE RESINS FUNCTIONALIZED WITH MULTIDENTATE LIGANDS HAVING NITROGEN AND SULFUR DONOR SETS

MASATO NISHIZAWA, TOSHIRO YOKOYAMA, TETSUO KIMURA and TOSHISHIGE M. SUZUKI*

Government Industrial Research Institute, Tohoku 4-2-1 Nigatake, Sendai 983, Japan

(*Received* 26 *February* 1986; *accepted* 8 *May* 1986)

Abstract—*N*-Mercaptoethylated derivatives of macroporous polystyrene resins functionalized with diethylenetriamine or pyridylamines have been synthesized. The resin with higher sulfur content reveals better selectivity toward 'soft' metal ions. Concentration of Ag(I) and Hg(II) has been examined by the column containing the present chelating resins.

Chelating polymer resins involving sulfur donor atoms have attracted much attention from the analytical and environmental points of view because of their high selectivity toward heavy metal ions.[1] Recently we have synthesized the chelating resins in which various amines are immobilized onto crosslinked polystyrene beads.[2,3] The aminated resins were found to be convenient substrates for the preparation of multidentate *N*-derivatives particularly when the ligand contains the primary amino groups.[4,5] *N*-Mercaptoethylated derivatives of poly(ethylene-grafted-styrene) have been prepared and the complexation properties examined.[1a] This paper describes the mercaptoethylation of the polymer-bound diethylenetiramine (dien) or pyridylamines where amino and imino nitrogens are available for the *N*-substitution, respectively. The adsorption characteristics of the resins for heavy metal ions and the column concentration of Ag(I) and Hg(II) have been examined.

EXPERIMENTAL

Materials

Macroporous styrene–10%-divinylbenzene copolymer beads (60–100 mesh, Mitsubishi Chemical Co.) were used as the polymer matrix. The surface area and the mean pore radius of the resin are 7.5 $m^2 g^{-1}$ and 720 Å, respectively. The beads were chloromethylated (Cl: 17.5%) followed by functionalization with dien or pyridylamines as described in the literature.[2–4]

Resin **1**. Resin beads containing dien (17 g, 0.05 mol of dien) were swollen in toluene (60 cm^3) and heated to 60°C. While stirring, ethylenesulfide (12.5 g, 0.21 mol) in toluene (40 cm^3) were added over 20 min. A few drops of *n*-butanethiol were added to each toluene solution in order to avoid the polymerization of ethylenesulfide.[6] The reaction mixture was heated at 120°C for 6 h, then filtered. The resin beads were washed successively with toluene, ethanol and diethyl ether and dried *in vacuo* at 50°C. Yield: 27.8 g.

Resins **2** *and* **3**. These were obtained using a similar procedure with much longer reaction time (30 h) to that for the resin **1** using the resins functionalized with *N*-[2-(2-pyridyl)ethyl]ethylenediamine and 2-pyridylmethylamine, respectively.

Equilibrium adsorption capacity

Typically, 100 mg of dry resin was added to 100 cm^3 of metal ion solution of various pH and the mixture was shaken at room temperature. After equilibrium was attained, the concentration of the remaining metal ion in the supernatant was analyzed by atomic absorption spectroscopy.

Column breakthrough experiment

Resin **1** was swollen with water and poured onto a glass column. Then about 500 ppm of metal ion

* Author to whom correspondence should be addressed.

solution [Ag(I) or Hg(II)] of appropriate pH were passed through the column continuously at a rate of 1.5 $cm^3 min^{-1}$. The effluent was fractionated into 15-cm^3 portions and the amount of metal ion was determined. The adsorbed Ag(I) and Hg(II) were released from the resin by elution with 3% thiourea in 2 mol dm^{-3} of sulfuric acid and 2 mol dm^{-3} of hydrochloric acid, respectively.

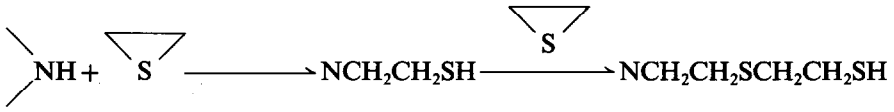
Measurements

Metal ion concentration was determined with a Shimadzu atomic absorption/flame photometer model AA-610S. The analysis of Hg(II) was carried out with a Hiranuma HG-1 flameless atomic absorption apparatus.

RESULTS AND DISCUSSION

Preparation and characterization of the resins

The analytical data of the resins are summarized in Table 1. Total sulfur content in resin **1** is approximately equal to that of the calculated value assuming that each of the dien moiety has reacted with 4 moles of ethylenesulfide. The parent dien-bound resin contains free amino groups since the ligand is linked to polymer uniquely through the imino nitrogen.[3,4] Therefore two sets of the amino groups in each dien unit can be available for the *N*-substitution. The iodometric titration[1b] demonstrated that resin **1** contains *ca* 3.7 mmol of thiol (—SH) group per gram of the resin which corresponds to approximately 60% of the total sulfur in the resin. This indicates that some of the sulfur atoms are not present in the form of a thiol group probably because successive reactions took place at the thiol terminal in the resin as shown below.



A similar procedure for the preparation of resin **1** was applied to the resins functionalized with pyridylamines in which imino nitrogens are available for the *N*-substitution. The lower sulfur content in the resulting resins may be attributed to the unfavourable steric environment around the imino nitrogens. It has been pointed out that the yields of this type of reactions are affected by the presence of bulky substituents on the nitrogen atom.[7] Imino groups in the pyridylamine-bound resins locate between bulky polymer matrix and pyridyl group, and hence access of ethylenesulfide would be restricted.

Equilibrium adsorption capacity

Figures 1 and 2 show the equilibrium adsorption capacity *vs* pH profiles for resins **1** and **2**. Resin **1** does not show clear pH dependence on the adsorption capacity in the pH range 1–8 irrespective of the metal ions examined. The resin prefers to associate with heavy metal ions such as Ag(I), Hg(II) and Mo(VI) while it has lower affinity for the common

Table 1. Analytical data of the chelating resins

Resin	Parent resin	N content %N (mmol g^{-1})	S content %S (mmol g^{-1})
1	PS-CH_2-N($CH_2CH_2NH_2$)$_2$	6.4 (4.6)	21.7 (6.8)
2	PS-CH_2-$NHCH_2CH_2NHCH_2CH_2$-(pyridyl)	7.4 (5.3)	5.4 (1.7)
3	PS-CH_2NHCH_2-(pyridyl)	7.2 (5.1)	3.0 (0.9)

PS = polystyrene resin.

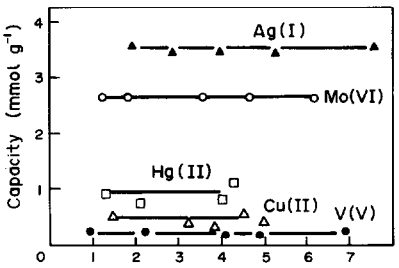


Fig. 1. Equilibrium adsorption capacity of resin **1** as a function of pH.

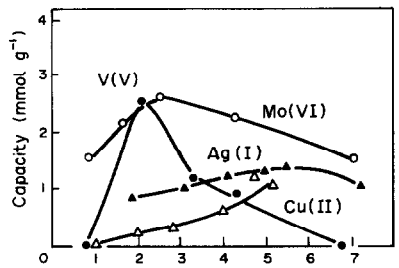


Fig. 2. Equilibrium adsorption capacity of resin **2** as a function of pH.

metal ions including alkaline, alkaline earth ions, Ni(II), Co(II), Fe(II) and Zn(II). The capacity for Ag(I) is nearly equal to the thiol content estimated by iodometry indicating that each thiol group coordinates to Ag(I) in a 1 : 1 molar ratio. The adsorbed Ag(I) and Hg(II) were released almost quantitatively from the resin by elution with acidic thiourea solution. The resin showed reproducible capacity upon several adsorption and regeneration cycles. On the contrary, when alkaline solution was employed to release metal ions, as in the case of Mo(VI), gradual oxidation of thiol group to disulfide took place.[8] However the resin capacity was restored upon treatment with a reducing agent such as $NaHSO_3$ solution.

Resin **2** whose sulfur/nitrogen ratio is much lower than resin **1** showed rather distinct pH dependence for the adsorption capacity. Lowering of sulfur content coincides with the decrease in Ag(I) capacity and increase in Cu(II) capacity. It seems that the adsorption characteristics of the resin **2** are much like the parent aminated resin due to low reaction conversion.

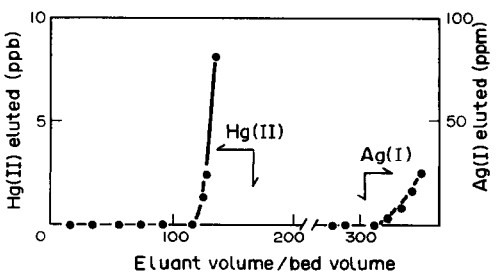


Fig. 3. Column adsorption of Hg(II) or Ag(I) using resin **1**. Breakthrough profiles were obtained in the separated experiments.

Column adsorption of Hg(II) and Ag(I)

Resin **1** has been applied to the adsorption of Hg(II) and Ag(I) by column operation since the adsorption rates for these metal ions are sufficiently rapid, i.e. equilibrium was attained within 30 min under batchwise procedure. Macroporous resins have numerous pores inside the beads which allow facile diffusion of metal ions into the polymer matrix.

When the Hg(II) solution (500 ppm, pH = 3.5) containing a seawater level of sodium chloride was passed through the column of resin **1** (⌀1.3 × 7.5 cm, 5 g), no detectable amount of Hg(II) was found in the eluate until the breakthrough point (Fig. 3). The amount of Hg(II) adsorbed at the breakthrough point was 0.54 mmol per gram of resin. A similar procedure using the column (⌀1.0 × 4.9 cm, 2 g) was applied to the solution containing 500 ppm of Ag(I) (pH = 4.1). About 300 bed volumes of the feed solution could be passed through the column without any leakage of Ag(I) into the effluent. The capacity at the breakthrough point was found to be 2.5 mmol per gram of resin. The adsorbed ions were recovered in a concentrated form on elution with acidic thiourea solution and the regenerated column could be used repeatedly.

REFERENCES

1. (a) T. Saegusa, S. Kobayashi, M. Hayashi and A. Yamada, *Polym. J.* 1978, **10**, 403; (b) H. Egawa, Y. Jogo and H. Maeda, *Nippon Kagaku.* 1979, 1760; (c) A. Deratani and B. Sebille, *Macromol. Chem.* 1981, **182**, 1875; (d) A. Deratani and B. Sebille, *Anal. Chem.* 1981, **53**, 1742; (e) C. Y. Liu and P. J. Sun, *Talanta* 1984, **31**, 353.
2. T. Yokoyama, A. Kikuchi, T. Kimura and T. M. Suzuki, *Bull. Chem. Soc. Jpn* 1983, **56**, 463.
3. T. M. Suzuki and T. Yokoyama, *Polyhedron* 1983, **2**, 127.
4. T. M. Suzuki and T. Yokoyama, *Polyhedron* 1984, **3**, 939.
5. M. Nishizawa, T. Yokoyama, T. Kimura and T. M. Suzuki, *Bull. Chem. Soc. Jpn* 1984, **57**, 2859.
6. U.S. Patent 2,185,660; *Chem. Abstr.* 1940, **34**, 2865.
7. H. R. Snyder, J. M. Stewart and J. B. Ziegler, *J. Am. Chem. Soc.* 1947, **69**, 2672.
8. H. Gilman, M. A. Plunkett, L. Tolman, L. Fullhart and H. S. Broadbent, *J. Am. Chem. Soc.* 1945, **67**, 1845.

Polyhedron Vol. 5, No. 12, pp. 2051–2057, 1986
Printed in Great Britain

0277–5387/86 $3.00+.00
© 1986 Pergamon Journals Ltd

STUDIES ON SPIROBORATE COMPLEXES—I. A NEW SYNTHESIS OF BIS-CATECHOL SPIROBORATE AND ITS ANALOGS USING 2-AMINO-4-METHYLPYRIDINE BORANE

YOSHIHISA OKAMOTO* and TOSHIO KINOSHITA

School of Pharmaceutical Sciences, Kitasato University, 5-9-1 Shirokane, Minato-ku, Tokyo 108, Japan

and

YUKA TAKEI and YOSHIO MATSUMOTO

Department of Chemistry, Faculty of Hygienic Sciences, Kitasato University, 1-15-1 Kitasato, Sagamihara-shi, Kanagawa-ken 228, Japan

(*Received* 3 *March* 1986; *accepted* 8 *May* 1986)

Abstract—A new synthesis of bis-catechol spiroborate and its analogs are described. Not only five- but also six- and seven-membered spiroborates are obtained. The reaction mechanisms are also discussed.

The reaction of boric acid or borate salts with diols has directed chemists' attention to examine stereochemical and structural problems of the diols, and to evaluate the equilibrium constants for a number of diol–boric acid reactions.[1–4] As Scheme I shows, the reaction system frequently involves complicated equilibria between several types of compounds such as the cyclic ester (**1**) and ionized, strongly acidic complexes in which one boron atom is associated with one (**2**) or two (**3**) molecules of the diol.[1,3,5,6] A type of compound (**4**) can also be formed directly from the diol and boric acid.[7] In general, the use of excess amounts of boric acid gave **1** and **2**, whereas the use of excess amounts of diol gave **3** and **4**, predominantly.[7] When boric acid and a diol are used in equimolecular amounts under alkaline conditions, very often **2** can be isolated in crystalline form from water,[7] except for pinacol as a diol which gives a type of compound **3**.[8]

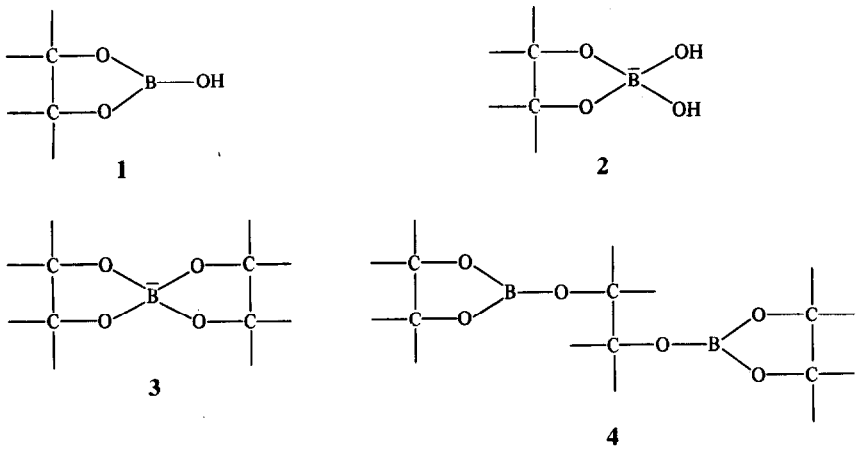
Böeseken[1] and Meulenhoff[9] synthesized bis-catechol spiroborate complexes such as **6**, **7a** and **7b** from the reaction of catechol (**5a**) with potassium borate, and the reaction of **5a** with boric acid and aniline or pyridine in molar ratio of 2 : 1, and 2 : 1 : 1, respectively (Scheme II). However, some of catechols such as pyrogallol (**5b**) and 2,3-dihydroxybenzaldehyde (**5d**) cannot give compounds of type **7** by Meulenhoff's method, and some of the compounds such as 2,2′-dihydroxydiphenyl are insoluble in water. Since there are no reports on preparation of such bis-catechol spiroborate complexes using amine borane, we report here a new method for synthesizing bis-catechol spiroborate (**9a**) and its analogs in organic solvents using 2-amino-4-methylpyridine borane (Scheme III).

EXPERIMENTAL

Melting points were determined by using a Yamato Scientific stirred liquid apparatus and are uncorrected. PMR spectra were run on a Varian EM-90 (90 MHz) spectrometer with $(CD_3)_2SO$ as the solvent and $(CH_3)_4Si$ as the internal standard. Elementary analyses (C, H, N) of all compounds described here were performed on a Perkin–Elmer 240B instrument.

Bis-catechol spiroborate (**9a**)—A solution of 2-amino-4-methylpyridine borane (**8**, 0.6 g, 4.9 mmol) in 10 cm^3 of triethyl orthoformate was added to a solution of catechol (0.5 g, 4.54 mmol) in 10 cm^3 of triethyl orthoformate with stirring. After 2 min, precipitates were filtered off, and washed with ether to give a pure **9a** in 73% yield, m.p. 207–209°C (decomp.). Found: C, 64.4; H, 5.1; N, 8.3%. Calc.

* Author to whom correspondence should be addressed.



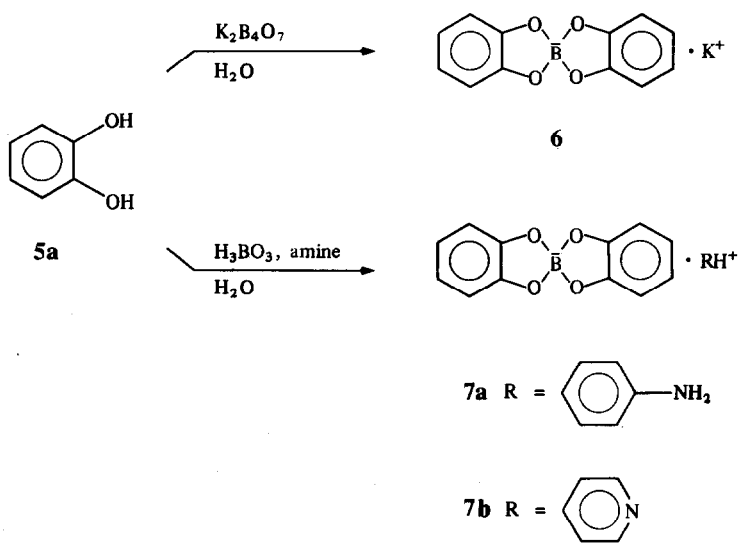
Scheme I.

for $C_{18}H_{17}BN_2O_4$: C, 64.3; H, 5.1; N, 8.3%. PMR: δ 2.30 (3H, s, CH_3), 6.47 (8H, s, benzene), 6.67 (1H, d, 5-H of pyridine ring), 6.70 (1H, s, 3-H of pyridine ring), 7.73 (3H, b, NH_2 and $\overset{+}{N}H$), 7.78 (1H, d, 6-H of pyridine ring).

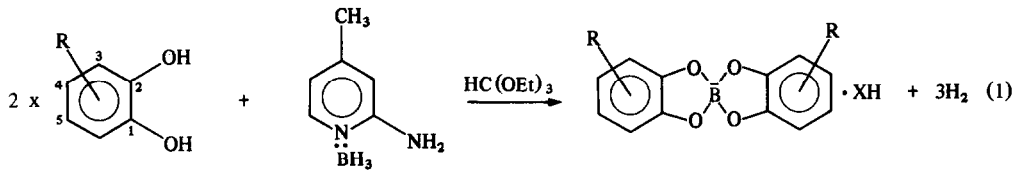
Bis-pyrogallol spiroborate (**9b**)—A solution of **8** (0.4 g, 3.28 mmol) in 10 cm^3 of triethyl orthoformate was added to a solution of pyrogallol (0.5 g, 3.96 mmol) in 10 cm^3 of triethyl orthoformate with stirring. After 1 min, precipitates were filtered off and washed with chloroform to give pure **9b** in 89% yield, m.p. 84–85°C(decomp.). Found: C, 52.2; H, 4.1; N, 6.9%. Calc. for $C_{18}H_{17}BN_2O_6 \cdot CHCl_3$: C, 51.9; H, 4.1; N, 6.6%. PMR: δ 2.27 (3H, s, CH_3), 6.00–6.70 (8H, m, benzene and 3(5)-H of pyridine ring), 7.40 (5H, b, OH, NH_2 and $\overset{+}{N}H$), 7.78 (1H, d, 6-H of pyridine ring).

Bis(3,4-*dihydroxytoluene*) *spiroborate* (**9c**)—A solution of **8** (0.5 g, 4.10 mmol) in 10 cm^3 of triethyl orthoformate was added to a solution of 3,4-dihydroxytoluene (0.5 g, 4.03 mmol) in 10 cm^3 of triethyl orthoformate with stirring. After 2 min, precipitates were filtered off and washed with carbon tetrachloride to give pure **9c** in 55% yield, m.p. 209–211°C(decomp.). Found: C, 66.1; H, 5.9; N, 7.8%. Calc. for $C_{20}H_{21}BN_2O_4$: C, 66.0; H, 5.8; N, 7.7%. PMR: δ 2.15 (6H, s, CH_3 of benzene ring), 2.30 (3H, s, CH_3 of pyridine ring), 6.28 (6H, s, benzene), 6.67 (1H, d, 5-H of pyridine ring), 6.70 (1H, s, 3-H of pyridine ring), 7.70 (3H, b, NH_2 and $\overset{+}{N}H$), 7.77 (1H, d, 6-H of pyridine ring).

Bis(2,3-*dihydroxybenzaldehyde*) *spiroborate* (**9d**)—To a solution of 2,3-dihydroxybenzaldehyde (1 g, 7.24 mmol) in 50 cm^3 of ether was added trimethyl borate (0.4 g, 3.85 mmol) and the mixture was stirred for 3 min. A solution of 2-amino-4-methylpyridine (0.4 g, 3.70 mmol) in 10 cm^3 ether was added to the above solution with stirring. After



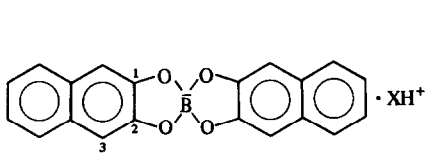
Scheme II.



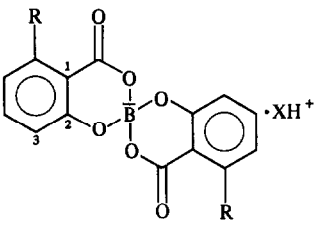
5a R = H
5b R = 3-OH
5c R = 4-CH_3
5d R = 3-CHO

8

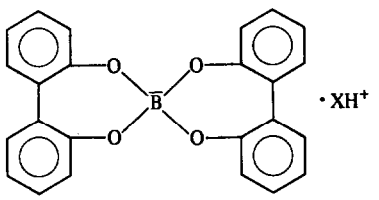
9a R = H
9b R = 3-OH
9c R = 4-CH_3
9d R = 3-CHO
9e R = 3-CH_2OH
X = 2-amino-4-methylpyridine



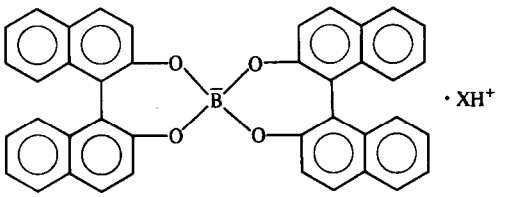
10



11a R = H
11b R = OH



12



25

Scheme III.

30 min, precipitates were filtered off to give 0.92 g of a pure **9d**. When the filtrate was allowed to stand overnight, 0.11 g of the pure **9d** was obtained. Total yield, 1.03 g (73%), m.p. 176°C(decomp.). Found: C, 60.6; H, 4.4; N, 7.0%. Calc. for $C_{20}H_{17}BN_2O_6 \cdot 1/3H_2O$: C, 60.3; H, 4.5; N, 7.0%. PMR: δ 2.30 (3H, s, CH_3), 6.47–7.07 (8H, m, benzene and 3(5)-H of pyridine ring), 7.70 (3H, b, NH_2 and $\overset{+}{N}H$), 7.75 (1H, d, 6-H of pyridine ring), 10.20 (2H, s, CHO).

Bis(2,3-*dihydroxybenzylalcohol*) *spiroborate* (**9e**)—Amine borane **8** (2 g, 16.4 mmol) was gradually added to a solution of 2,3-dihydroxybenzaldehyde (2 g, 14.5 mmol) in 50 cm^3 of chloroform with stirring. The mixture was stirred at room temperature overnight. Precipitates were filtered off, and dried to give pure **9e** in 83% yield, m.p. 111–112°C(decomp.). Found: C, 59.6; H, 5.3; N, 6.9%. Calc. for $C_{20}H_{21}BN_2O_6 \cdot 1/3H_2O$: C, 59.7; H, 5.4; N, 7.0%. PMR: δ 2.33 (3H, s, CH_3), 4.43 (2H, s, CH_2), 5.40–8.40 (5H, b, OH, NH_2 and $\overset{+}{N}H$), 6.30–6.80 (8H, m, benzene and 3(5)-H of pyridine ring), 7.77 (1H, d, 6-H of pyridine ring).

Bis(2,3-*dihydroxynaphthalene*) *spiroborate* (**10**)—A solution of **8** (0.2 g, 1.85 mmol) in 10 cm^3 of triethyl orthoformate was added to a solution of 2,3-dihydroxynaphthalene (0.2 g, 1.25 mmol) in 10 cm^3 of triethyl orthoformate with stirring. After 40 min, precipitates were filtered off and washed with chloroform to give pure **10** in 78% yield, m.p. 248–250°C(decomp.). Found: C, 69.0, 5.1; N, 6.2%. Calc. for $C_{26}H_{21}BN_2O_4 \cdot H_2O$: C, 68.7; H, 5.1; N, 6.2%. PMR: δ 2.28 (3H, s, CH_3), 6.60–8.00 (18H, m, all protons except for methyl protons).

Bis(*salicylic acid*) *spiroborate* (**11a**)—A solution of **8** (0.9 g, 7.4 mmol) in 36 cm^3 of triethyl orthoformate was added to a solution of salicylic acid (1.5 g, 7.4 mmol) in 36 cm^3 of triethyl orthoformate with stirring. After 10 min, precipitates were filtered off and washed with carbon tetrachloride to give

pure **11a** in 36% yield, m.p. 176–178°C(decomp.). Found: C, 60.4; H, 4.2; N, 6.9%. Calc. for $C_{20}H_{17}BN_2O_6 \cdot 1/3H_2O$: C, 60.3; H, 4.5; N, 7.0%. PMR: δ 2.30 (3H, s, CH_3), 6.70 (1H, d, 5-H of pyridine ring), 6.73 (1H, s, 3-H of pyridine ring), 6.80 (2H, d, 3-H of benzene ring), 6.87 (2H, t, 5-H of benzene ring), 7.43 (2H, dt, 4-H of benzene ring), 7.77 (2H, b, NH_2), 7.80 (2H, dd, 6-H of benzene ring), 7.80 (1H, d, 6-H of pyridine ring), 13.00 (1H, b, $\overset{+}{N}H$).

Bis(2,6-dihydroxybenzoic acid) spiroborate (**11b**)—To a solution of **8** (0.2 g, 1.64 mmol) in 10 cm^3 of triethyl orthoformate was added 2,6-dihydroxybenzoic acid (0.25 g, 1.62 mmol) with stirring. After 30 min, precipitates were filtered off and washed with carbon tetrachloride to give pure **11b** in 70% yield, m.p. 239–240°C(decomp.). Found: C, 54.8; H, 4.0; N, 6.4%. Calc. for $C_{20}H_{17}BN_2O_8 \cdot 3/4H_2O$: C, 54.9; H, 4.3; N, 6.4%. PMR: δ 2.30 (3H, s, CH_3), 6.28 (2H, d, 3-H of benzene ring), 6.32 (2H, d, 5-H of benzene ring), 6.70 (1H, d, 5-H of pyridine ring), 6.73 (1H, d, 3-H of pyridine ring), 7.30 (2H, t, 4-H of benzene ring), 7.77 (2H, b, NH_2), 7.80 (1H, d, 6-H of pyridine ring), 11.67 (2H, s, OH), 13.00 (1H, b, $\overset{+}{N}H$).

Bis(2,2′-dihydroxydiphenyl) spiroborate (**12**)—A solution of **8** (0.5 g, 4.1 mmol) in 10 cm^3 of triethyl orthoformate was added to a solution of 2,2′-dihydroxydiphenyl (0.5 g, 2.69 mmol) in 10 cm^3 of triethyl orthoformate with stirring. After 3 min, precipitates were filtered off, and washed with carbon tetrachloride to give pure **12** in 92% yield, m.p. 246–248°C(decomp.). Found: C, 73.7; H, 5.2; N, 5.9%. Calc. for $C_{30}H_{25}BN_2O_4$: C, 73.8; H, 5.2; N, 5.7%. PMR: δ 2.23 (3H, s, CH_3), 6.60 (1H, d, 5-H of pyridine ring), 6.63 (1H, s, 3-H of pyridine ring), 6.77–7.43 (16H, m, benzene), 7.60 (3H, b, NH_2 and $\overset{+}{N}H$), 7.67 (1H, d, 6-H of pyridine ring).

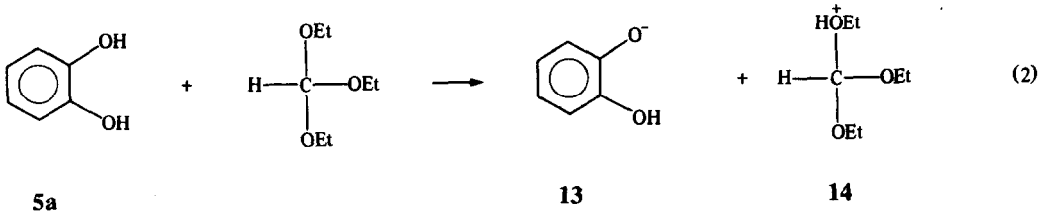
RESULTS AND DISCUSSION

When 2-amino-4-methylpyridine borane (**8**) was reacted with **5a** for a few minutes in chloroform in the presence of triethyl orthoformate, **9a** was precipitated. The use of excess amounts of the amine borane in this reaction gave **9a** in a better yield. Since the oxygen atoms of **9a** originate in **5a**, types of compounds **1** and **2** which are often associated with **3** in boric acid–diol equilibria can never be formed. The compound **9a** was entirely the same one as that obtained by Meulenhoff's method. Similarly, compounds **9b**, **9c** and bis(2,3-dihydroxynaphthalene) spiroborate (**10**) were obtained from **5b**, **5c** and 2,3-dihydroxynaphthalene, respectively. It is worth noting that these reactions were subjected to the presence of the orthoester. Namely, when **5a** was treated with **8** in chloroform for 1 h, no reaction occurred, however, when triethyl orthoformate was added to the above mixed solution (or was used as a solvent), **9a** was soon precipitated. These results indicate that the initiation of the reaction is due to taking up the phenolic proton of **5a** by the orthoester. We propose the reaction mechanisms in Scheme IV. Since ethanol was not detected in the reaction by mass analyses, the role of the orthoester might be that of the Lewis base as shown in eqn (2). Although solvents such as ether, acetal and tetrahydrofuran (THF) might be thought of as the Lewis bases in these reactions, they did not afford these spirane types of complexes. This fact indicates that these solvents cannot take up a proton from the weak acid to produce a catechol anion **13**. The anion **13** would react with the amine borane **8** to give **15** which readily cyclizes to catechol borane (**16**) with liberation of hydrogen gas. The compound **16** would react with **5a** to yield a spirane type acid (**17**) which can form **9a** with 2-amino-4-methylpyridine. The overall reaction is summarized in eqn (1). Since it is known that *o*-aminophenol in place of **5a** readily affords **18**[10] by the reaction with **16** which was readily available through the rapid reaction of **5a** with borane in THF,[11] eqn (6) would be reasonable.

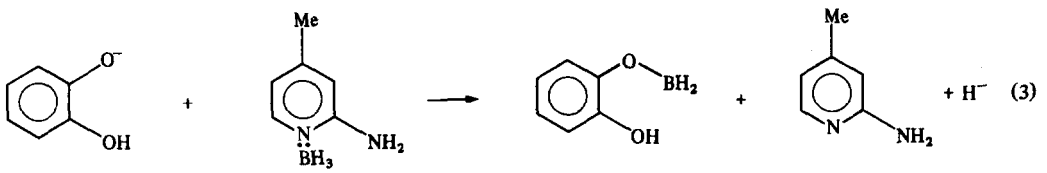
Although an orthoester was essential for eqn (1), there was one exception where **5d** was reacted with **8** in chloroform to give a reduced spiroborate (**9e**) as shown in Scheme V. The initial step of the reaction would be in the reduction of the aldehyde group which takes up a proton from the hydroxy group and a hydrogen anion from **8** to afford **19**. The reduced compound **19** would readily form compound **20**, then, **9e** was obtained through reactions [eqns (9)–(13)] like those described in Scheme IV. Compound **9d** was obtained by the reaction of **5d** with trimethyl borate and 2-amino-4-methylpyridine.

Our method was used to synthesize other spiroborates (**10**, **11a**, **11b** and **12**) from the corresponding diols. The structures of all compounds obtained here were determined by proton magnetic resonance (PMR), but the optical resolution was not done for the racemic spiroborates. Isolation of **12** is specially interesting because a boron-assisted synthesis of the macrocyclic host molecules containing convergent hydroxy groups (**24**) has recently been reported where the key intermediates were assumed to be as in structure **23** but they had not been isolated (Scheme VI).[12]

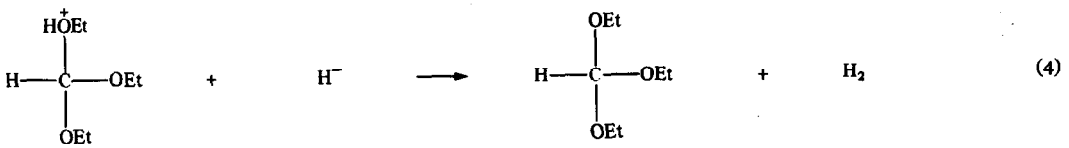
Recently, R(+)- and S(−)-1,1′-bi-2-naphthol have been recognized to be effective constituents of a chiral hydride reagent exemplified by Noyori's



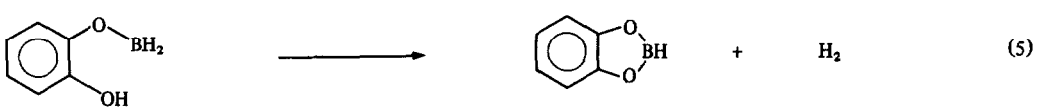
5a 13 14 (2)



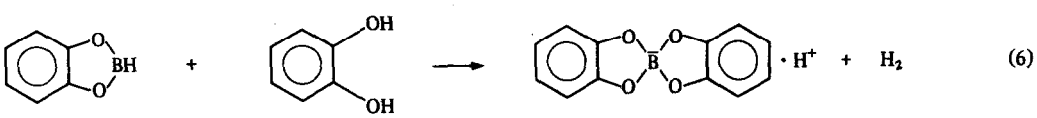
13 8 15 (3)



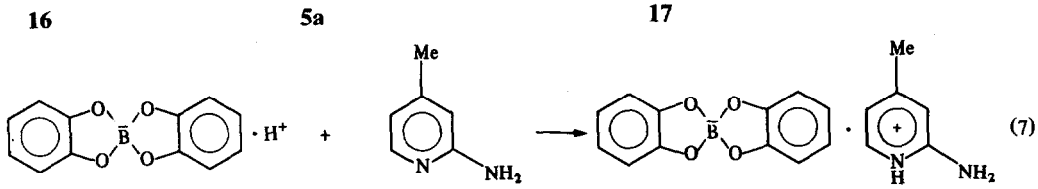
14 (4)



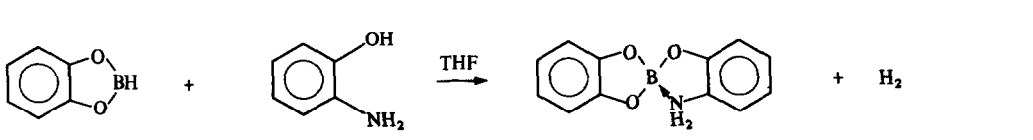
15 16 (5)



16 5a 17 (6)

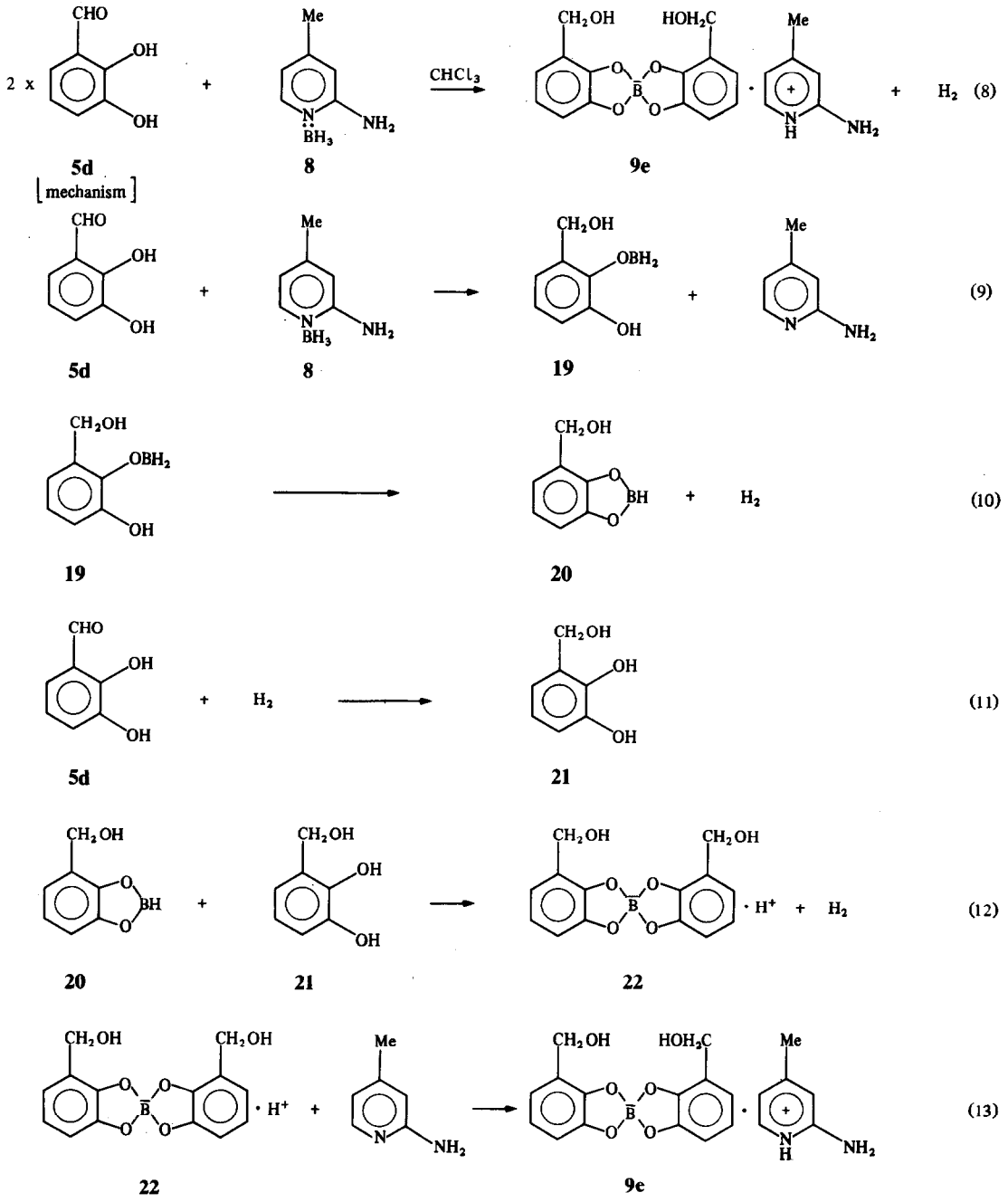


17 9a (7)

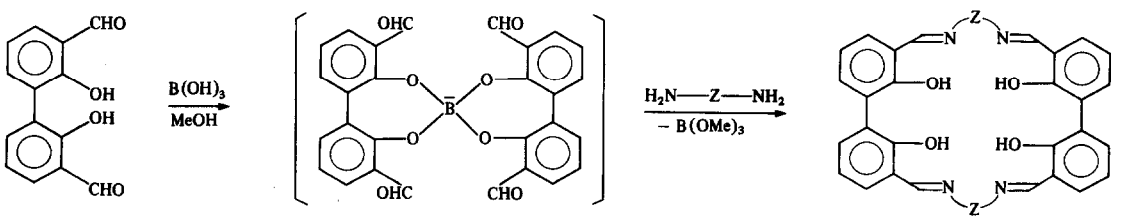


16 18

Scheme IV.



Scheme V.



Scheme VI.

BINAL-H,[13] and a new microbial resolution of the racemic binaphthols has been reported[14] instead of a classical tedious resolution method.[15] On the other hand, since there is a possibility of producing a spiroborate (**25**) as a type of R(+)·B·R(+) or S(−)·B·S(−) complex by the reaction of **8** with the corresponding racemic binaphthols, we attempted to isolate **25**, however, the 2-amino-4-methylpyridinium salt of the binaphthol was obtained instead. This result indicates that the dihedral angle of the diol and the distance between the two oxygen atoms of the binaphthol in the solvent are outside the requirements for the formation of the spiroborate, namely 0° to 60° for the angle and 2.2 to 2.5 Å for the distance.[16]

In conclusion, 2-amino-4-methylpyridine borane (**8**) which is stable and readily prepared in aqueous media[17] was found to be a useful alternative to boric acid to produce spiroborate complexes in organic solvents without yielding types of compounds **1**, **2** and **4**.

REFERENCES

1. J. Böeseken, *Adv. Carbohydrate Chem.* 1949, **4**, 189.
2. G. L. Roy, A. L. LaFerriere and J. O. Edwards, *J. Inorg. Nucl. Chem.* 1957, **4**, 106.
3. P. H. Hermans, *Z. Anorg. Allg. Chem.* 1925, **142**, 83.
4. A. B. Foster, *Adv. Carbohydrate Chem.* 1957, **12**, 81.
5. N. Vermaas, *Rec. Trav. Chim.* 1932, **51**, 67.
6. H. S. Isbell, J. F. Brewster, N. B. Holt and H. J. Frush, *J. Res. Nat. Bur. Stand.* 1948, **40**, 129.
7. J. Dale, *J. Chem. Soc.* 1961, 910.
8. J. Dale, *J. Chem. Soc.* 1961, 922.
9. J. Meulenhoff, *Z. Anorg. Allg. Chem.* 1925, **142**, 373.
10. H. R. Morales, H. Tlahuext, F. Santiesteban and R. Contreras, *Spectrochim. Acta* 1984, **40A**, 855.
11. H. C. Brown and S. K. Gupta, *J. Am. Chem. Soc.* 1971, **93**, 1816.
12. W. Moneta, P. Baret and J.-L. Pierre, *J. Chem. Soc., Chem. Commun.* 1985, 899.
13. R. Noyori, I. Tomino, Y. Tanimoto and M. Nishizawa, *J. Am. Chem. Soc.* 1984, **106**, 6709.
14. Y. Fujimoto, H. Iwadate and N. Ikekawa, *J. Chem. Soc., Chem. Commun.* 1985, 1333; S.-H. Wu, L.-Q. Zhang, C.-S. Chen, G. Girdaukas and C. J. Sih, *Tetrahedron Lett.* 1985, **26**, 4323.
15. J. Jacques, C. Fouquey and R. Viterbo, *Tetrahedron Lett.* 1971, 4617; E. P. Kyba, G. W. Gokel, F. de Jong, K. Koga, L. R. Sousa, M. G. Siegel, L. Kaplan, G. D. Y. Sogah and D. J. Cram, *J. Org. Chem.* 1977, **42**, 4173.
16. T. E. Acree, *Adv. Chem. Ser., Carbohydrates in Solution* 1973, **117**, 208.
17. Y. Okamoto, T. Osawa and T. Kinoshita, *Synthesis* 1982, 462.

Polyhedron Vol. 5, No. 12, pp. 2059–2061, 1986
Printed in Great Britain

0277–5387/86 $3.00+.00
© 1986 Pergamon Journals Ltd

THE PAIRING PRINCIPLE IN TENSOR SURFACE HARMONIC THEORY: DEFINITION OF A GENERAL CLASS OF *N*-ATOM *POLAR DELTAHEDRA* WITH *N* SKELETAL ELECTRON PAIRS

R. L. JOHNSTON and D. M. P. MINGOS*

Inorganic Chemistry Laboratory, University of Oxford, South Parks Road, Oxford OX1 3QR, U.K.

(*Received* 20 *March* 1986; *accepted* 8 *May* 1986)

Abstract—A general group theoretical criterion, based on the Pairing Principle in Stone's Tensor Surface Harmonic Theory, is presented for *polar deltahedra* with $3p+1$ ($p = 1, 2, 3, \ldots, X$) atoms and belonging to the C_3, C_{3v}, T and T_d point groups. These clusters are characterised by N ($N = 3p+1$) skeletal bonding molecular orbitals and examples of such clusters with $N = 4$, 7 and 10 atoms are discussed. This treatment follows on from the group theoretical analysis presented by Fowler, but the *polar deltahedral* generalisation follows from a group theoretical restriction not previously recognised.

In a recent paper Fowler[1] described a theoretical analysis for high nuclearity deltahedral boranes B_NH_N ($N > 12$) and confirmed Lipscomb's[2] earlier conclusion that a certain number of these molecules should be characterised by N rather than the usual $N+1$ skeletal electron pairs.[3] Fowler showed that these unconventional deltahedra did not represent accidental departures from the $N+1$ skeletal electron pair rule,[3] but formed the basis of a more general pattern. Within the framework of Stone's Tensor Surface Harmonic Theory[4] and utilising some elegant group theoretical methods developed by Ceulemans[5] and Quinn,[6] Fowler[1] concluded that the unconventional electron counts arose because the polyhedra belonged to the C_3, C_{3v}, T and T_d point groups and discussed some specific examples with 16, 19 and 22 boron atoms.

It is the purpose of this paper to demonstrate that the examples discussed by Fowler[1] form part of a wider pattern arising from a further group theoretical restriction which applies to this specific class of deltahedron. Furthermore, the conclusions we have arrived at are corroborated by some structurally characterised examples of lower nuclearity metallaboranes.[7]

Fowler[1] has concluded that a group theoretical criterion for symmetry-induced departures from the $N+1$ skeletal electron pair rule arises for clusters where the irreducible representations spanned by the L^π and $\bar{L}^\pi$ tangential molecular orbitals contain an odd number of self-conjugate E representations. He showed that this arises for *closo* clusters in just two cases:

(1) T or T_d clusters with an odd number of sets of four equivalent cage atoms.
(2) C_m or C_{mv} ($m \geqslant 3$) clusters with an odd number of cage atoms on the C_m axis.

It is not, however, geometrically feasible to have a *closo*-deltahedron with an odd number of cage atoms on the principal rotation axis C_m with $m > 3$, because square, pentagonal and higher faces would be generated. For $m > 3$ the polyhedra are actually *nido* and fit the rule with their well-known count of $(N+2)$ skeletal electron pairs. Only when $m = 3$ does the principal axis also pass through a triangular face and we define such polyhedra as *polar deltahedra* (see Fig. 1 for examples). If the principal axis bisects a deltahedral edge the point group is restricted to C_{2v}, C_2 or C_s and the L^π and $\bar{L}^\pi$ orbitals do not contain E representations so that the group theoretical criterion arising from the pairing principle cannot be rigorously applied.

In a C_3 or C_{3v} deltahedron there are p sets (layers) of symmetry-related atoms lying in planes perpendicular to the C_3 axis, consequently the total

* Author to whom correspondence should be addressed.

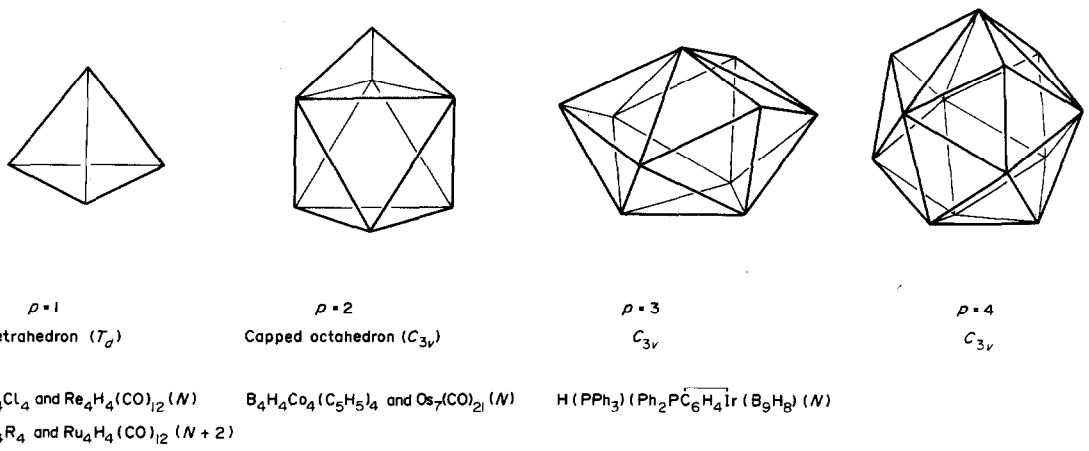


Fig. 1. Examples of polar deltahedral clusters with either N or $N+2$ skeletal bonding molecular orbitals.

number of atoms in *polar deltahedra* must be $3p+1$. The higher symmetry T or T_d possibilities arise from the occurrence of three additional threefold symmetry axes, but those deltahedra with anomalous electron pairs (N or $N+2$ skeletal electron pairs) also possess $3p+1$ atoms (one atom on each of these axes) and so may be classified as *polar deltahedra*. There is therefore a general class of *polar deltahedra* with $N = 3p+1$ atoms which are characterised by N bonding skeletal molecular orbitals.

Fowler[1] has discussed some examples of hypothetical boranes, with 16 ($p = 5$, T_d), 19 ($p = 6$, C_{3v}) and 22 ($p = 7$, T_d) atoms, which have N bonding skeletal molecular orbitals in agreement with his analysis. In Fig. 1 we illustrate examples of lower nuclearity *polar deltahedra* with $3p+1$ atoms which emerge as a result of our more general treatment. The occurrence of N (or $N+2$) electron pairs in the tetrahedron ($p = 1$) has been discussed by Fowler,[1] the capped octahedron ($p = 2$) is not known for B_NH_N but the *isolobal* analogue $[Co_3(\eta^5\text{-}C_5H_5)_3B_4H_4]$, studied by Grimes,[8] has the predicted geometry. Similarly for 10-atom clusters ($p = 3$) metalloboranes and metallocarboranes with 10 skeletal electron pairs have been reported by Greenwood and Kennedy[9] and described by Baker[10] as *hyper-closo*. For $p = 4$ the C_{3v} geometry has not been observed to date but molecular orbital calculations indicate the likelihood of a C_{3v} cluster with 13 skeletal electron pairs[11] (Lipscomb's calculations[2] on an alternative C_{2v} structure predict the usual ($N+1 = 14$) skeletal electron pair count).

This group theoretically based rule for *polar deltahedra* can be derived simply for axial point groups in the following manner. For each of the p triangles of symmetry-related atoms, the L^σ orbitals give rise to A_1 and E irreducible representations. The L^σ orbitals of a cluster belonging to an axial point group can be obtained by combining the L^σ orbitals of its constituent orbits (i.e. sets of symmetry-related atoms).[6] Quinn has also shown that the π_θ components of L^π and $\bar{L}^\pi$ can be derived by using the L^σ orbitals as generator functions with a basis set of p_θ^π orbitals rather than radial orbitals. In group theoretical terms this corresponds to the direct product:

$$\Gamma_{\pi_\theta} = \Gamma_\sigma \otimes \Gamma_z.$$

The π_φ components are generated by taking the π_θ components and rotating the p orbitals on each atom by 90° (in the same sense) about a radial vector. This process corresponds to the action of the parity inversion operator. This operator ($\hat{\varepsilon}$) belongs to the irreducible representation (Γ_u°) which is antisymmetric with respect to all improper rotations (including inversion and reflections) of the point group. In axial point groups the symmetry of the parity inversion operator is given by the direct product

$$\Gamma_u^\circ = \Gamma_z \otimes \Gamma_{R_z}.$$

Thus the component is obtained from the L orbitals by taking the following direct product:

$$\Gamma_{\pi_\varphi} = \{\Gamma_\sigma \otimes \Gamma_z\} \otimes \{\Gamma_z \otimes \Gamma_{R_z}\} = \Gamma_\sigma \otimes \Gamma_{R_z}$$

(in terms of Stone's Tensor Surface Harmonic Theory this is not surprising since the component p^φ atomic orbitals are defined such that their positive lobes follow the direction of R_z). A summary of this information is shown below

$$\begin{array}{ccc} \{\Gamma_\sigma\}L^\sigma & \xrightarrow{\otimes\Gamma_z} & (L^\pi/\bar{L}^\pi)_\theta\{\Gamma_{\pi_\theta}\} \\ & \searrow^{\otimes\Gamma_{R_z}} & \downarrow \hat{\varepsilon} \otimes \Gamma_u^\circ \\ & & (\bar{L}^\pi/L^\pi)_\varphi\{\Gamma_{\pi_\varphi}\}. \end{array}$$

In the C_{3v} point group $\Gamma_z = A_1$ and $\Gamma_{R_z} = A_2$, for axial groups in general Γ_z and Γ_{R_z} are one-dimensional. Since $E \otimes A_1$ or $E \otimes A_2 = E$ then for every E function in L^σ there will be one in L^π and one in $\bar{L}^\pi$. The total number of E representations in the $L^\pi/\bar{L}^\pi$ orbitals is therefore even ($2p$). When considering polyhedra with vertices lying on the C_3 axis the above method for generating $L^\pi/\bar{L}^\pi$ orbitals does not work because at the poles of a sphere an atomic p_z orbital has pure radial rather than tangential orientation (at any other position it can be resolved into radial and tangential components). To get round this problem it is merely necessary to work out the π orbitals for the non-polar structure and add the orbitals of the polar atoms. For one polar atom in C_{3v} symmetry the p^π atomic orbitals (p_x and p_y) transform as E so the *polar deltahedron* possesses in total an odd number ($2p+1$) of E representations in the $L^\pi/\bar{L}^\pi$ orbitals. As Fowler has pointed out[1] this results in an equal number (p) of bonding (L^π) and antibonding ($\bar{L}^\pi$) E functions and one self-conjugate ($L^\pi/\bar{L}^\pi$) E set which is roughly non-bonding. Occupation of these latter orbitals would lead to a cluster with ($N+2$) skeletal electron pairs but usually they are unoccupied and an N skeletal electron pair count is observed.

The arguments presented above may readily be extended to other types of polyhedra belonging to axial point groups. In general if a (*non-polar*) polyhedron belongs to an axial point group and its L^σ orbitals contain a certain number (X) of E representations then the $L^\pi/\bar{L}^\pi$ set of orbitals will contain an even number ($2X$) of E functions. Introducing one atom on the principal rotation axis (thereby generating a *polar* polyhedron) will result in an odd number ($2X+1$) of Es, one of which will be a non-bonding $L^\pi/\bar{L}^\pi$ pair. The introduction of a second atom on the principal rotation axis generates a *bipolar* polyhedron which again has an even number ($2X+2$) of Es which, for deltahedra, again split into bonding (L^π) and antibonding ($\bar{L}^\pi$) sets.

Acknowledgements—The S.E.R.C. is thanked for financial support and Dr P. W. Fowler for many helpful comments.

REFERENCES

1. P. W. Fowler, *Polyhedron* 1985, **4**, 2051.
2. L. D. Brown and W. N. Lipscomb, *Inorg. Chem.* 1977, **16**, 2989; J. Bicerano, D. S. Marynick and W. N. Lipscomb, *Inorg. Chem.* 1978, **17**, 2041, 3443.
3. K. Wade, *Adv. Inorg. Chem. Radiochem.* 1976, **18**, 1; D. M. P. Mingos, *Nature Phys. Sci. (London)* 1972, **236**, 99.
4. A. J. Stone, *Mol. Phys.* 1980, **41**, 1339; A. J. Stone, *Inorg. Chem.* 1981, **20**, 563; A. J. Stone and M. J. Alderton, *Inorg. Chem.* 1982, **21**, 2297; A. J. Stone, *Polyhedron* 1984, **3**, 1299.
5. A. Ceulemens, *Mol. Phys.* 1985, **54**, 161.
6. D. B. Redmond, C. M. Quinn and J. G. R. McKiernan, *J. Chem. Soc., Faraday Trans.* 1983, **79**, 1791.
7. R. N. Grimes (Ed.), *Metal Interactions with Boron Clusters*. Plenum Press, New York (1982).
8. J. R. Pipal and R. N. Grimes, *Inorg. Chem.* 1977, **16**, 3255.
9. N. N. Greenwood, *Pure Appl. Chem.* 1983, **55**, 77, 1415; J. Bould, N. N. Greenwood, J. D. Kennedy and W. S. McDonald, *J. Chem. Soc., Chem. Commun.* 1982, 465; J. Bould, J. E. Crook, N. N. Greenwood, J. D. Kennedy and W. S. McDonald, *J. Chem. Soc., Chem. Commun.* 1982, 346.
10. R. T. Baker, *Inorg. Chem.* 1986, **25**, 109. See also J. D. Kennedy, *Inorg. Chem.* 1986, **25**, 111; R. L. Johnston and D. M. P. Mingos, *Inorg. Chem.* 1986, **25**, 3321.
11. R. L. Johnston and D. M. P. Mingos, unpublished results.

Polyhedron Vol. 5, No. 12, pp. 2063–2067, 1986
Printed in Great Britain.

0277–5387/86 $3.00+.00
Pergamon Journals Ltd

COMPLEXES OF NITRILOTRIMETHYLPHOSPHONIC ACID WITH COBALT, NICKEL, COPPER AND ZINC

IVAN LUKEŠ,* DANA REJŠKOVÁ, ROMAN ODVÁRKO and PAVEL VOJTÍŠEK

Department of Inorganic Chemistry, Charles University, 128 40 Prague 2, Czechoslovakia

(*Received* 25 *October* 1985; *accepted after revision* 13 *May* 1986)

Abstract—Substances of the types MH_4ntmp, $Mg_3[M(Hntmp)]_2$, M_2H_2ntmp and $Mg[M_2(Hntmp)]_2$, where M = Co, Ni, Cu, Zn and $H_6ntmp = N[CH_2PO(OH)_2]_3$ were prepared. The sodium and cesium salts of the $[Co(Hntmp)]^{3-}$ complexes were also prepared. The IR and electronic spectra and the experimental magnetic susceptibilities indicate that these are high-spin complexes. The coordination surroundings of the central atom consist of a highly distorted octahedron of the ligand oxygen atoms. The nitrogen atom is not coordinated to the central atom.

Aminoalkylphosphonic acids are interesting as analogues of natural amino acids and as chelating agents. Therefore, we have studied the preparation and the properties of the complexes of the transition metals with nitrilotrimethylphosphonic acid $N[CH_2P(O)(OH)_2]_3$ (denoted as H_6ntmp, Fig. 1). This substance has a betain structure both in solution and in the solid state.[1–6] The dissociation constants have been determined pH-metrically[7–9] and are somewhat dependent on the H_6ntmp concentration in dilute solution.[9] Complex compounds of H_6ntmp have only been studied in solution. Morozova *et al.*[10] studied the formation of 1 : 1 complexes pH-metrically and spectrophotometrically. This type of complex is formed even in acidic media, where the logarithms of the stability constants for the formation of the species $[M(H_3ntmp)]^-$ range from 4.79 to 6.35. However, only the stability constants for the formation of the complex species $[M(ntmp)]^{4-}$ (M = Co, Ni, Cu, Zn) are higher than or comparable with those for analogous complexes of nitrilotriacetic acid.[11] The preparation and a study of the H_6ntmp complexes with cobalt, nickel, copper and zinc are dealt with in the present paper.

EXPERIMENTAL

The IR spectra were obtained on a Perkin–Elmer 225 instrument in the ranges 400–4000 cm^{-1} in a Nujol mull and 2000–4000 cm^{-1} in hexachlorobutadiene. The magnetic susceptibility was measured at 298 K using the Faraday method, on a balance calibrated with cupric sulphate pentahydrate and sodium chloride. The diffusion reflectance spectra of the solid substances were obtained on a VSU-2 instrument (Zeiss, Jena) in the range 200–1200 nm, using magnesium oxide as the reference substance. The absorption electronic spectra of aqueous solutions of the substances were obtained using a Unicam SP 800 and VSU-2 instrument, from 250 to 400 nm at a concentration of 0.003 M and from 400 to 1100 nm at concentrations from 0.005 to 0.01 M, depending on the solubility of the test compounds, using 5-cm cells.

Orientative X-ray powder patterns were obtained using the Debye–Scherrer method and a Mikrometa 2 instrument (Chirana).

In the substances prepared, the alkali metals were determined by atomic absorption spectrometry, magnesium and the transition metal were determined chelatometrically after sample combustion and dissolution of the residue in hydrochloric acid; nitrogen was determined as NH_3 by distillation on mineralization of the sample. The water was determined from the weight loss from 50 to 200°C.

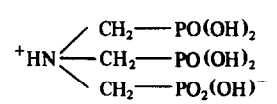


Fig. 1. Nitrilotrimethylphosphonic acid.

* Author to whom correspondence should be addressed.

Preparations

H_6ntmp. The preparation of Moedritzer and Irani[12] was used and the product was isolated after crystallization from aqueous solution. The acid readily forms supersaturated oily solutions and thus the crystallization ability was tested frequently in samples taken during evaporation of the solution. The product was recrystallized in the same way from an aqueous solution.

Na_6ntmp·$3H_2O$. To a solution of 0.01 mol of H_6ntmp in 100 cm^3 water, 0.1 mol NaOH and 200 cm^3 methanol was added, thus precipitating an oily solution that was transferred to a flask, covered with 200 cm^3 methanol and refluxed. The product separated gradually in the form of small crystals that were filtered off and washed with ethanol and ether.

MH_4ntmp. Freshly precipitated and washed transition metal hydroxide (0.03 mol) was dissolved in a solution of 10 g H_6ntmp in 150 cm^3 water. The solution obtained was transferred to four times as large a volume of ethanol. The precipitate separated was filtered off, washed several times with ethanol and ether and dried over silica gel.

$Mg_3[M(Hntmp)]_2 \cdot 16H_2O$. Small crystals separated spontaneously on neutralization of a MH_4ntmp solution with sodium hydroxide to pH = 8 followed by the addition of a stoichiometric amount of $Mg(ClO_4)_2$. Only $Mg_3[Ni(Hntmp)]_2 \cdot 18H_2O$ was precipitated with methanol as above.

$Na_3[Co(Hntmp)] \cdot 6H_2O$ and $Cs_3[Co(Hntmp)] \cdot 4H_2O$. A CoH_4ntmp solution was neutralized with NaOH or $CsCO_3$ to pH 7.5–8, evaporating the solution in the air to obtain a highly viscous oil and covering the oil several times with ethanol and spreading it in a mortar. A fine product separated that was washed with ethanol and dried over silica gel.

M_2H_2ntmp. To a solution of 0.07 moles of H_6ntmp in 50 cm^3 water a suspension of the appropriate hydroxide in 200 cm^3 water was added. The hydroxide amount was stoichiometric, only a 50% excess of $Ni(OH)_2$ had to be added. On mild heating and dissolution of the hydroxide a fine product separated, was filtered off and washed with ethanol and ether.

$Mg[M_2Hntmp]_2$. Under the same conditions as M_2H_2ntmp, but the stoichiometric amount of $Mg(ClO_4)_2$ dissolved in 20 cm^3 H_2O, was added before heating the solution.

The results of analyses of the compounds prepared are given in Table 1.

RESULTS AND DISCUSSION

Nitrilotrimethylphosphonic acid forms 1 : 1 and 1 : 2 complexes with the studied metals. Complexes

Table 1. Analytical and magnetic data

Compound	% Found (calc.) Co, Ni, Cu, Zn	N	Mg, Na, Cs	H_2O	μ_{eff} (BM)
H_6ntmp		4.7 (4.7)			
Na_6ntmp·$3H_2O$		2.9 (2.9)	29.3 (28.5)	11.8 (10.2)	
CoH_4ntmp·$4H_2O$	13.8 (13.8)	3.2 (3.3)		17.3 (17.6)	4.89
Na_3[Co(Hntmp)]·$6H_2O$	11.2 (11.4)	2.7 (2.6)	13.2 (13.0)	20.5 (19.2)	5.29
Cs_3[Co(Hntmp)]·$4H_2O$	7.1 (7.0)	1.6 (1.7)	47.3 (47.3)	8.7 (9.6)	4.55
Mg_3[Co(Hntmp)]$_2$·$16H_2O$	11.0 (11.1)	2.5 (2.6)	6.9 (6.8)	26.7 (27.3)	4.79
Co_2H_2ntmp·$6H_2O$	22.8 (22.6)	2.7 (2.7)		21.3 (19.9)	4.68
Mg[Co_2(Hntmp)]$_2$·$9.5H_2O$	24.0 (23.1)	2.8 (2.7)	2.4 (2.3)	16.9 (16.7)	4.91
NiH_4ntmp·$5H_2O$	13.1 (13.2)	3.1 (3.1)		20.5 (20.3)	3.24
Mg_3[Ni(Hntmp)]$_2$·$18H_2O$	10.7 (10.6)	2.5 (2.5)	6.6 (6.6)	29.3 (29.2)	3.18
Ni_2H_2ntmp·$6H_2O$	22.2 (22.5)	2.7 (2.7)		21.0 (20.2)	3.12
Mg[Ni_2(Hntmp)]$_2$·$22H_2O$	18.7 (18.9)	2.2 (2.2)	1.9 (2.0)	31.6 (31.8)	3.08
CuH_4ntmp·$4H_2O$	14.8 (14.7)	3.3 (3.2)		16.6 (16.8)	1.98
Mg_3[Cu(Hntmp)]$_2$·$16H_2O$	11.7 (11.8)	2.6 (2.6)	6.6 (6.8)	26.4 (27.1)	1.93
Cu_2H_2ntmp·$10H_2O$	21.1 (21.1)	2.3 (2.3)		30.1 (30.1)	1.89
Mg[Cu_2(Hntmp)]$_2$·$18H_2O$	21.1 (21.3)	2.4 (2.3)	2.0 (2.0)	27.0 (27.0)	1.87
ZnH_4ntmp·$2H_2O$	16.6 (16.4)	3.5 (3.5)		8.8 (8.5)	
Mg_3[Zn(Hntmp)]$_2$·$16H_2O$	12.1 (12.1)	2.6 (2.6)	6.7 (6.8)	26.4 (26.8)	
Zn_2H_2ntmp·$2H_2O$	28.1 (28.3)	3.0 (3.0)		8.1 (8.2)	
Mg[Zn_2(Hntmp)]$_2$·$10H_2O$	24.7 (24.8)	2.6 (2.7)	2.3 (2.3)	16.8 (17.4)	

of the MH_4ntmp type are readily soluble in water and can be precipitated by methanol. We tried to prepare alkaline salts of the $[M(ntmp)]^{4-}$ type, especially those of $CoH_4ntmp \cdot 4H_2O$. The salts $Na_3[Co(Hntmp)] \cdot 6H_2O$ and $Cs_3[Co(Hntmp)] \cdot 4H_2O$ were prepared by precipitation with ethanol. The analogous lithium salt could not be prepared in this way. In contrast to $CoH_4ntmp \cdot 4H_2O$, the above substances are only sparingly soluble after drying. The substances precipitated appear as X-ray amorphous. Magnesium was found to be the most advantageous external cation, probably because of its relatively weak complexes with the ligand.[13,14] The complexes $Mg_3[MHntmp]_2 \cdot 16H_2O$ crystallized from the solution, except for the Ni complex that contained 18 molecules of water. The X-ray powder patterns indicate that these substances are isostructural. The test complexes with the ligand-to-metal ratio equal to 1:2 are very poorly soluble in water and precipitate spontaneously. No pH region has been found with the 1:1 and 1:2 complexes, from which complexes $[Mntmp]^{4-}$ or $[M_2ntmp]^{2-}$, i.e. the complexes in which the last hydrogen atom is substituted, could be isolated. Complexes of the types $[MHntmp]^{3-}$ or $[M_2Hntmp]^{-}$ were always obtained (at pH < 10) or hydroxy complexes of various compositions resulted at pH > 10.

The IR spectra of the substances prepared were measured in the range 400–4000 cm^{-1}. The absorption bands have a dominant character in a region 900–1200 cm^{-1}. The bands are listed in Table 2, together with the assignment. According to the literature[9,15–18] the spectra are consistent with oxygen coordination to the metals.

The calculated effective magnetic moments are given in Table 1 for the prepared complexes of cobalt, nickel and copper and demonstrate that these are high-spin complexes.

The electronic absorption spectra of the copper complexes correspond very well to the appropriate diffuse reflectance spectra (Table 3). A broad absorption band was always found, corresponding to the transition, $\nu_1(^2T_{2g} \leftarrow {}^2E_g)$ with assumed coordination number of six. Although the band is very wide, it can be found that the band maximum for the $[Cu(Hntmp)]^{3-}$ complex type is shifted by about 500 cm^{-1} toward lower values with respect to that for the $[Cu_2(Hntmp)]^{-}$ complex type. A shoulder was found in the visible region, which is apparently connected with the complex character of the absorption band for the ν_1 transition.

With the nickel complexes, the electronic and diffusion reflectance spectra are also in good agreement, are given in Table 3 and suggest a coordination number of six. A shoulder was observed in a region 16,900–17,200 cm^{-1} for the substances $NiH_4ntmp \cdot 5H_2O$ and $Mg_3[Ni(Hntmp)]_2 \cdot 18H_2O$, which apparently corresponds to the spin-forbidden transition $^1T_{1g} \leftarrow {}^3A_{2g}$.

The character of the electronic absorption and reflectance spectra of the cobalt complexes is the

Table 2. Bands (cm^{-1}) in the IR spectra of the stretching vibrations of phosphonic group

	ν_sP(OH)	$\nu_s(PO_2)$	$\nu_{as}(PO_2)$
$CoH_4ntmp \cdot 4H_2O$	940	1075	1170
$NiH_4ntmp \cdot 5H_2O$	932	1059, 1069	1169
$CuH_4ntmp \cdot 4H_2O$	937	1054, 1073	1154
$ZnH_4ntmp \cdot 2H_2O$	947	1052, 1089	1162
	$\nu_s(PO_3)$	$\nu_{as}(PO_3)$	
Na_6ntmp	970, 990	1100	
$Na[Co(Hntmp)] \cdot 6H_2O$	975	1050 (1070)	1115
$Cs_3[Co(Hntmp)] \cdot 4H_2O$	955, 970	1035 (1070)	1110
$Mg_3[Co(Hntmp)]_2 \cdot 16H_2O$	958, 980	1050	1110
$Mg_3[Ni(Hntmp)]_2 \cdot 18H_2O$	981	1073	1110
$Mg_3[Zn(Hntmp)]_2 \cdot 16H_2O$	995	1048	1110
$Mg_3[Cu(Hntmp)]_2 \cdot 16H_2O$	986	1056	1110
$Mg[Co_2(Hntmp)]_2 \cdot 9.5H_2O$	950, 982	1045	1110
$Mg[Ni_2(Hntmp)]_2 \cdot 22H_2O$	975, 1005	1060	1110
$Mg[Zn_2(Hntmp)]_2 \cdot 10H_2O$	918, 958	1045	1110
$Mg[Cu_2(Hntmp)]_2 \cdot 18H_2O$	947, 995	1058	1110
$Co_2H_2ntmp \cdot 6H_2O$	935, 975	1040, 1075	1140
$Ni_2H_2ntmp \cdot 6H_2O$	952, 998	1076	1140
$Zn_2H_2ntmp \cdot 2H_2O$	927, 949	1026	1120
$Cu_2H_2ntmp \cdot 10H_2O$	950, 1000	1064	1150

Table 3. Ligand-field spectral data (10^3 cm^{-1}). Transmittance (reflectance)

Compound					
$CoH_4ntmp \cdot 4H_2O$	(7.8)	11.8	(13.5)sh	18.9 (18.9)	20.4sh
$Na_3[Co(Hntmp)] \cdot 6H_2O$	(8.7)	12.5 (11.8)b	(16.1)sh	18.9 (17.7)	
$Cs_3[Co(Hntmp)] \cdot 4H_2O$	(9.7)	12.5 (11.5)b		18.9 (17.7)	
$Mg_3[Co(Hntmp)]_2 \cdot 16H_2O$		12.5 (12.3)	(15.9)sh	18.9 (18.2)	
$Co_2H_2ntmp \cdot 6H_2O$	(8.3)	11.9 (11.4)b	(15.6)sh	18.9 (18.5)	
$Mg[Co_2(Hntmp)]_2 \cdot 9.5H_2O$	(8.3–10.0)	(11.4)b	(16.6)sh	(18.5)	(26.3)sh
$NiH_4ntmp \cdot 5H_2O$	(8.3)	12.8 (12.8)		16.9 (16.9)sh	25.0 (24.4)
$Mg_3[Ni(Hntmp)]_2 \cdot 18H_2O$	(8.3)	13.9 (13.9)		16.9 (17.2)sh	25.0 (25.0)
$Ni_2H_2ntmp \cdot 6H_2O$	(8.3)	13.3 (13.2)			24.4 (24.4)
$Mg[Ni_2(Hntmp)]_2 \cdot 22H_2O$	(8.3)	13.3 (13.2)			24.4 (24.4)
$CuH_4ntmp \cdot 4H_2O$		11.0–11.6b (11.4)		16.4 (16.4)sh	
$Mg_3[Cu(Hntmp)]_2 \cdot 16H_2O$		11.1–11.5b (11.6)		16.1 (16.1)sh	
$Cu_2H_2ntmp \cdot 10H_2O$		11.4–12.2b (11.9)			
$Mg[Cu_2(Hntmp)]_2 \cdot 18H_2O$		11.4–12.0b (11.9)			

same, except for the spectrum of $CoH_4ntmp \cdot 4H_2O$. The diffusion reflectance spectrum of this compound (Fig. 2 bottom) is typical of a cobalt compound with octahedral surroundings.[19,20] In the electronic absorption spectrum and in the spectra of all the other cobalt complexes an absorption band appears in the region 12,500–11,800 cm^{-1}, which might suggest a coordination number of five (Fig. 2 and Table 3). The coordination surroundings of cobalt would be a trigonal bipyramid and the band would correspond to the $E' \leftarrow A'$ transition, or a tetragonal pyramid and the band would correspond to a transition from the ground state to the B_1 state, as, for example, in phosphinate complexes of cobalt.[21] It is difficult to establish the coordination surroundings of cobalt on the basis of these spectra, as the symmetries of a distorted octahedron in one direction and of a tetragonal pyramid are the same.

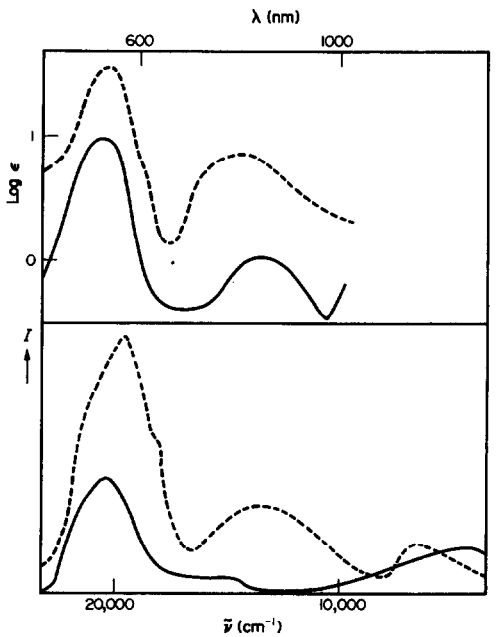


Fig. 2. Electronic absorption spectra (upper part) and diffusion reflectance spectra (lower part) of $CoH_4(ntmp) \cdot 4H_2O$ (full curve) and $Na_3[Co(Hntmp)] \cdot 6H_2O$ (broken curve).

If a justified assumption is adopted that the complexes of the $Mg_3[M(Hntmp)]_2 \cdot 16H_2O$ type are isostructural and the spectrum of $Mg_3[Cu(Hntmp)]_2 \cdot 16H_2O$, as well as those of the other complexes of copper and nickel, suggest a coordination number of six for the central atom, then the coordination number of cobalt in the studied complexes is probably also six.

The band at 8300 cm^{-1} in the diffusion reflectance spectra of the nickel complexes and the wide absorption band in the region 11,000–12,000 cm^{-1} of the copper complexes directly correspond to a value of $10Dq$. For the cobalt complexes the value, $10Dq$, was calculated according to Reedijk[22] and amounts on average to 8880 cm^{-1}. The f_L parameter, calculated from the above values for H_6ntmp, amounts to 0.98 (Co complexes); 1.00 (Ni complexes) and 1.03 (Cu complexes) and thus is comparable with the value given for H_2O.

It follows from the complex stoichiometry and from the IR spectra that the nitrogen atom is not coordinated to the central atom. The coordination surroundings are apparently a strongly distorted octahedron of oxygen atoms, which can be expected in view of the bond angles and bonding distances in the ligand alone. During the thermal decomposition

which was used to determine the water present it has been found that the studied substances are dehydrated in a single step below 100°C. In the IR spectra there is neither splitting nor a shift of the band of deformation vibration of water molecules. Hence it can be assumed that the surroundings of the central atom consist solely of the oxygen atoms of the phosphonic groups. However, coordination of water cannot be excluded with the complexes of the $[M_2(Hntmp)]^-$ type, in view of the stoichiometry.

The poor solubility of the M_2Hntmp complexes, all the prepared magnesium salts and the relatively poor solubility of the isolated $Na_3[Co(Hntmp)]\cdot 6H_2O$ complexes suggest that these substances have a polymeric character in the solid state.

REFERENCES

1. A. J. Kireva and N. M. Dyatlova, *Zh. Neorg. Khim.* 1971, **16**, 557.
2. N. M. Dyatlova and B. W. Zhabanov, *Zh. Fiz. Khim.* 1969, **43**, 744.
3. N. M. Dyatlova, M. I. Kabachnik and T. Ya. Medved, *Dokl. Akad. Nauk SSSR* 1965, **161**, 607.
4. A. E. Martell, R. J. Motekaitis, A. R. Fried, J. S. Wilson and D. T. McMillan, *Can. J. Chem.* 1965, **53**, 3471.
5. J. J. Daly and P. J. Wheatley, *J. Chem. Soc. A* 1967, 212.
6. J. Barycki, P. Mastalerr and H. Raatajczak, *Rocz. Chem.* 1971, **45**, 557.
7. R. P. Carter, R. L. Carrol and R. R. Irani, *Inorg. Chem.* 1967, **6**, 936.
8. H. S. Hendrickson, *Anal. Chem.* 1967, **39**, 998.
9. L. V. Nikitina, A. I. Grigoreyev and N. M. Dyatlova, *Zh. Obshch. Khim.* 1974, **44**, 1598.
10. S. Morozova, L. V. Nikitina, N. M. Dyatlova and G. V. Serebrgakova, *Zh. Neorg. Khim.* 1975, **20**, 413.
11. G. Schwarzenbach and R. Gut, *Helv. Chim. Acta* 1956, **34**, 1589.
12. K. Moedritzer and R. R. Irani, *J. Org. Chem.* 1966, **31**, 160.
13. L. V. Nikitina, A. I. Griforeyev and N. M. Dyatlova, *Zh. Obshch. Khim.* 1974, **44**, 1669.
14. L. V. Nikitina, N. F. Shugal, A. I. Grigoryev and N. M. Dyatlova, *Zh. Obshch. Khim.* 1975, **45**, 552.
15. N. Palta, B. V. Rao, S. N. Dubey and D. M. Puri, *Polyhedron* 1984, **3**, 527.
16. K. Nakamoto, J. Morimato and A. E. Martell, *J. Am. Chem. Soc.* 1963, **85**, 309.
17. K. Nakamoto, *Infrared Spectra of Inorganic and Coordination Compounds*, pp. 117, 239. Wiley, New York (1970).
18. K. Nakamoto and P. J. McCarthy, *Spectroscopy and Structure of Metal Chelate Compounds*, p. 187. Wiley, New York (1968).
19. A. B. Lever, *Inorganic Electronic Spectroscopy*, p. 491. Elsevier, Amsterdam (1984).
20. L. Banci, A. Bencini, C. Benelli, D. Gatteschi and C. Zanchini, *Struct. Bond.* 1982, **52**, 37.
21. M. W. G. de Bolster and R. J. Jans, *Z. Anorg. Allg. Chem.* 1982, **488**, 207.
22. J. Reedijk, W. L. Drissen and W. L. Grosneweld, *Rec. Trav. Chim.* 1969, **88**, 1095.

Polyhedron Vol. 5, No. 12, pp. 2069–2074, 1986
Printed in Great Britain

0277–5387/86 $3.00+.00
Pergamon Journals Ltd

TUNGSTEN–MANNITOL AND SORBITOL COMPLEXES: STRUCTURAL CHARACTERIZATION BY IR AND CARBON-13 NUCLEAR MAGNETIC RESONANCE SPECTROSCOPY

E. LLOPIS,* J. A. RAMIREZ and A. CERVILLA

Departamento de Química Inorgánica, Facultad de Químicas, Universidad de Valencia, Dr. Moliner, 50, Burjassot, Valencia, Spain

(*Received* 10 *December* 1985; *accepted after revision* 13 *May* 1986)

Abstract—Polarimetric and spectrophotometric studies of the mannitol–tungsten(VI) system show the formation of three stable complexes. Their stoichiometries, degrees of condensation and interconversion equilibria have been studied. The structure of these compounds has been investigated by ^{13}C NMR spectroscopy in aqueous solution and by IR spectroscopy in the solid state for the two species stable at pH < 7.

Although the literature contains sufficient information to establish that tungstates and molybdates interact with mannitol, or its isomer sorbitol, to form a stable species of stoichiometric ratio metal : ligand = 2 in approximately aqueous neutral solutions, no other reliable conclusions can be inferred from the reported results since there are many disagreements among them.[1–6]

We have shown in a previous publication the number, composition, degree of condensation and stability of the complex species formed between tungstate ions and sorbitol.[7]

According to Weigel *et al.*[8] for the 2 : 1 complex, the speculative structure given is a cyclic one which has a μ-oxo bond and a symmetrically bridged sorbitol molecule coordinated to each tungsten atom by two α-CHOH groups.

The main purpose of this paper has been the study in solution of the complexes which mannitol forms, in order to see whether the change of the ligand conformation has any influence on the formation of these species; this paper also deals with the structural study of these complexes by ^{13}C NMR spectroscopy. It has been possible in the same way to isolate the dinuclear species in a solid state and this has allowed its characterization by IR spectroscopy.

* Author to whom correspondence should be addressed.

EXPERIMENTAL

$Na_2[W_2O_3(OH)_4(C_6H_{10}O_6)]$ *synthesis*

An aqueous solution containing the stoichiometric amounts of Na_2WO_4 and mannitol (0.5 mol dm^{-3} in mannitol) was acidified with $HClO_4$ at pH = 6.0. Addition of acetone to the solution produces the formation of a syrup at the bottom of the flask. This syrup was decanted and washed with warm absolute ethanol becoming a white powder which was dried in a dessicator over H_2SO_4(c).

Found: C, 10.1; W, 53.6%. Calc.: C, 10.1; W, 45.3%.

$Na[W_2O_3(OH)(C_6H_{11}O_6)_2]$ *synthesis*

To an aqueous solution containing Na_2WO_4, mannitol and $HClO_4$ in 1 : 1.5 : 1.5 ratio, respectively (1 mol dm^{-3} in Na_2WO_4), acetone was added and a syrup obtained that, after dehydration with absolute ethanol, was dried (lightly protected) in a dessicator over H_2SO_4(c).

Found: C, 17.4; W, 42.5%. Calc.: C, 17.7; W, 45.3%.

The rotatory power of the samples was measured with a Perkin–Elmer 141 digital photoelectric polarimeter; measurement accuracy was $\pm 0.002°$. The cell was thermostatically set at 25°C and had a length of 10 ± 0.02 cm. The measurements were

taken at five different wavelengths (589, 578, 546, 436 and 365 nm) and all these results were comparable.

The pH of the samples was measured with a Radiometer pH-meter 82 with a pH accuracy of ± 0.01. All the samples were prepared to be 1 mol dm^{-3} in $NaClO_4$ and the pH was adjusted to the required value adding the proper amounts of concentrated NaOH and/or $HClO_4$ (70%). Specific conditions of the samples are indicated in the text.

The ^{13}C NMR spectra were recorded using a Bruker AC-200 spectrometer at an operating frequency of 50.32 MHz. This instrument was also used to record 200 MHz ^1H NMR spectra.

RESULTS AND DISCUSSION

The procedures used, in the polarimetric and spectrophotometric study,[9] have been similar to the ones previously described.[7,10,11]

Table 1 summarizes the rotatory power values in the course of the acidification of a solution 0.38 mol dm^{-3} in D(−)mannitol with $HClO_4$ ($\hat{D}_{mann}$). These values are essentially independent of the pH, but they are greatly modified by addition of Na_2WO_4 1.9×10^{-2} mol dm^{-3} to the solution of D(−)mannitol, ($\hat{D}_{mann/W}$), (|Mann|/|W(VI)| = 20). The rotatory powers due to the excess of mannitol are superimposed on the values of $\hat{D}_{mann/W}$, and we can consider that the difference $\Delta\hat{D} = \hat{D}_{mann/W} - \hat{D}_{mann}$ represents the change in the rotatory power with pH produced by the complexes (Fig. 1).

Table 1. Rotatory power values (degrees) for a solution 0.38 mol in D(−)mannitol in presence (a) or absence (b) of Na_2WO_4 1.9×10^{-2} mol dm^{-3}. $\Delta\hat{D} = \hat{D}_{mann/W} - \hat{D}_{mann}$, $\lambda = 365$ nm, ionic strength in all samples $NaClO_4$ 1 mol dm^{-3}

pH	(a) $\hat{D}_{mann/W}$	(b) $\hat{D}_{mann}$	$\Delta\hat{D}$
11.25	−0.395	−0.444	0.049
10.50	−0.210	−0.320	0.082
9.53	−0.194	−0.288	0.094
8.39	−0.193	−0.287	0.094
8.13	−0.195	−0.286	0.091
7.83	−0.196	−0.286	0.090
7.42	−0.200	−0.285	0.085
6.10	−0.200	−0.283	0.083
4.30	−0.200	−0.283	0.083
2.80	−0.198	−0.280	0.082
1.76	−0.186	−0.279	0.093
1.53	−0.170	−0.279	0.109
1.32	−0.163	−0.279	0.116
1.22	−0.155	−0.279	0.124
1.01	−0.153	−0.278	0.125
0.95	−0.153	−0.278	0.125

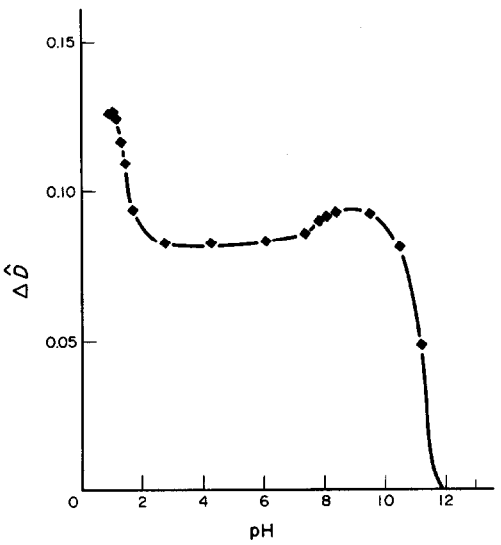


Fig. 1. Optical-activity variations as a function of pH. Excess of D(−)mannitol. $[Na_2WO_4] = 1.9 \times 10^{-2}$ mol dm^{-3}. [Mannitol] = 0.38 mol dm^{-3}. $\lambda = 365$ nm.

The existence of four breaks in curve $\Delta\hat{D}$ *vs* pH at pH = 12.0, 9.0, 5.0 and 1.0 suggests the presence of three different complex species.

From Fig. 1 values, acid equivalents needed to form every complex species, from mannitol and tungstate ions, as well as their condensation degree can be deduced.[10] On the other hand, application of the generalized Asmus and molar-ratio methods[12,13] at each pH break where only one complex species is assumed to be present, allowed a simultaneous calculation of complex composition, condensation degree and stability constant.

The above results suggest the following complexation equilibria, which agrees with those reported for the tungsten(VI)–sorbitol system[7]

$12 > pH > 9.0$

$$WO_4^{2-} + 2C_6H_{14}O_6 + H_2O \rightleftarrows [WO(OH)(C_6H_{12}O_6)_2]^- + OH^- + 2H_2O$$

$9.0 > pH > 7.0$

$$\{[WO(OH)(C_6H_{12}O_6)_2]^- + OH^-\} + H^+ + \tfrac{1}{2}H_2O \rightleftarrows [W_2O_3(OH)_4(C_6H_{10}O_6)]^{2-} + \tfrac{3}{2}C_6H_{14}O_6$$

$3.0 > pH > 1.0$

$$[W_2O_3(OH)_4(C_6H_{14}O_6)]^{2-} + C_6H_{14}O_6 + H^+ \rightleftarrows [W_2O_3(OH)(C_6H_{11}O_6)_2]^- + 3H_2O.$$

The proposed formulations are based on structural information in the literature and in previous works on related tungsten(VI) and molybdenum(VI) compounds.[11,14,15]

It should be noted that formation of $[W_2O_3(OH)L_2]^{3-}$ only occurs if an excess of mannitol is present since, in a very acidic medium, the condensation equilibria of uncomplexed tungsten(VI) are strongly favoured.

Structural characterization

At high pH values (pH > 9.0), tungstate ion forms, mainly, a stable 1 : 2 complex

$$WO_4^{2-} + 2C_6H_{14}O_6 + H_2O \rightleftarrows [WO(OH)(C_6H_{12}O_6)_2]^- + OH^- + 2H_2O.$$

Therefore consistent with this equilibrium, the addition of sorbitol or mannitol to a solution containing WO_4^{2-} produces an increase in the pH.

The apparent stability constant of this complex has been evaluated, and a large ligand : tungsten(VI) ratio is needed to displace its formation equilibrium towards complete complex formation. That is why we think that all attempts at isolation in a pure state have been unsuccessful.

Figure 2 displays ^{13}C NMR spectrum of a solution of Na_2WO_4 0.5 mol dm^{-3} and sorbitol 2.5 mol dm^{-3} at pH = 9.5. In the presence of free sorbitol, the spectrum shows sharp and well-resolved resonances for both the bound and the free ligand, which indicates that an intermolecular exchange, if its exists, must be slow on an NMR scale.

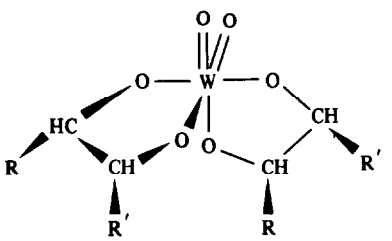
The ^{13}C NMR signals of primary C—OH groups are found between 61 and 64 ppm and, therefore, we can suppose that they are uncoordinated. Downfield, three ^{13}C signals of secondary carbon atoms appear to be shifted about 10 ppm with respect to those of the free ligand.

For sorbitol, as a polyol having an asymmetric configuration, one signal for each carbon atom should be expected, being the ^{13}C signal of secondary C atoms located between 68 and 73 ppm. In this region, the complex species only shows a signal which is of the highest intensity.

The spectral behaviour found for this species allows us to conclude, thus, that there are only two C—OH secondary groups bonded to tungsten(VI), which causes a downfield shift in their resonances, being in agreement with other previous results.[16]

Another important fact to be pointed out concerning this spectrum is that one of two C—OH coordinated group resonances is found to be split into a doublet, which is interpreted as being due to the presence of two environments not magnetically equivalent for the sorbitol coordinated CHOH groups.

The foregoing features, usually observed for other *cis*-MO_2L_2 complexes [M = W(VI) of Mo(VI) and L being a single deprotonated chelating oxo-ligand] prompt us to propose the following structure for the complex species stable at higher pH.



I

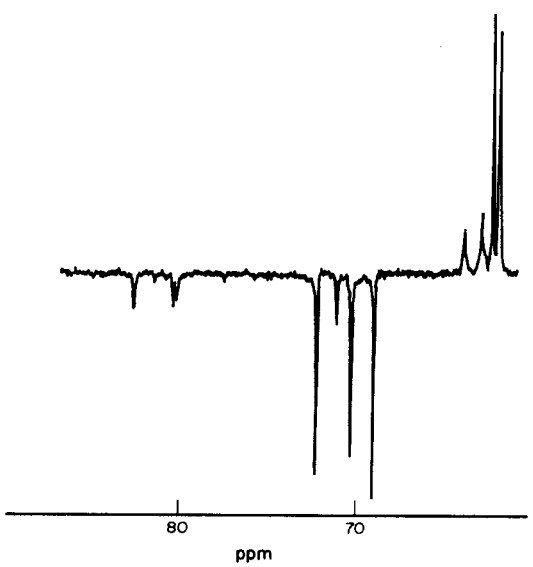


Fig. 2. DEPT ^{13}C NMR spectrum of 0.5 mol dm^{-3} Na_2WO_4 and 2.5 mol dm^{-3} sorbitol at pH = 9.5.

In contrast to $[WO(OH)L_2]^{2-}$, the formation reaction of the complex species $[W_2O_3(OH)_4(C_6H_{10}O_6)]^{2-}$ has a higher stability constant, and proceeds smoothly giving this species in a pure form and a good yield.

We have, thus, prepared the $Na_2[W_2O_3(OH)_4(C_6H_{10}O_6)]$ complex and observed that the IR spectrum of the solid (KBr pellet) (Fig. 3a), in the 900 cm^{-1} region, shows two strong bands at 910 and 955 cm^{-1} which indicate the presence of *cis*-WO_2 groups.[17,18] Besides these absorbances, the broad band at 660 cm^{-1} might be assigned to the stretching antisymmetric vibrations of the W—O_b—W group,[11] and the other band at 400 cm^{-1} can be assigned to a W—O_b—W symmetric bond.[19,20]

On the other hand, a solution of this complex species [for sorbitol–tungsten(VI) system] gives rise to the room temperature ^{13}C NMR spectrum shown in Fig. 4a. The number of signals which appear

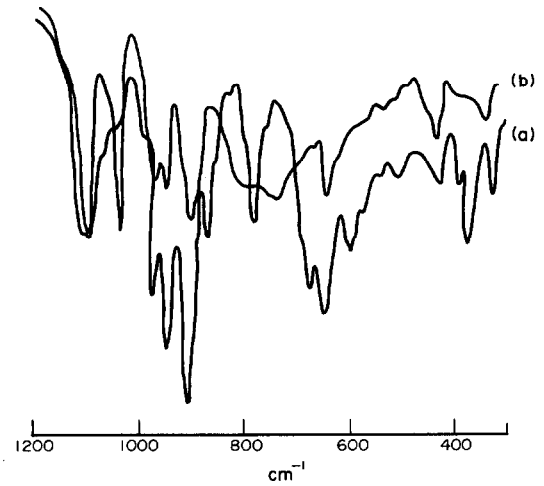
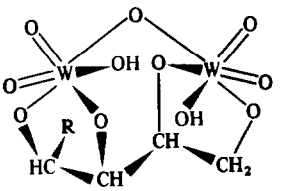


Fig. 3. IR spectra (KBr pellet) of: (a) $Na_2[W_2O_3(OH)_4(C_6H_{10}O_6)]$, and (b) $Na[W_2O_3(OH)(C_6H_{11}O_6)]$.

clearly shows the presence of two different isomers in solution, and their chemical shifts indicate that there is only a CH_2OH and a CHOH group uncoordinated in each isomer. In Table 2 we show the chemical shifts of fee and complexed ligands at different pH values.

We have observed that D-mannitol, D-sorbitol and D-gluconic acid (in excess of metal) show the same ^{13}C NMR spectrum, corresponding to the existence of two similar isomers, while adonitol (a polyol with a different conformation) is only able to form a single isomer for the complex species stable at these pH values ($3 < pH < 7$).

These observations mentioned above lead us to propose, as a more likely structure in solution, one of the structures proposed by Angus (tetrytol system C-1, C-2, C-3 and C-4), but with an alcoxy coordination in trans position to the μ-oxo bond (II).[21]



II

Table 2. ^{13}C NMR chemical shifts from tungsten(VI)–mannitol and sorbitol complexes

pH	Free ligand				Complexed ligand						
	CHOH			CH_2OH	HCOM			CHOH		H_2COM	CH_2OH
1.00	72.29	70.66	69.05	62.28	78.34	76.59	75.68	70.94			62.72
		70.56		61.97							62.64
1.00[a]		70.40	68.80	62.67	79.07	76.34	—	69.43			61.96
											62.09
1.50	72.13	70.60	68.88	62.17	78.36	76.51	75.56	71.18			62.65
		70.54		61.96							62.49
					88.88	80.05		76.93	72.68	70.05	61.56
2.50[a]		70.33	68.71	62.57	89.62	80.02	79.00	76.28	70.81	69.99	—
					88.80					68.01	62.21
3.50	72.20	70.54	68.97	62.60	88.91	80.10		77.06	72.72	70.00	61.50
		70.47		61.91							
4.15[a]		70.52	68.90	62.78	89.83	80.22	79.22	76.43	71.00	70.19	62.40
					89.01					68.20	
6.00					89.72	80.02			72.43	70.04	62.00
					88.98	80.17	—	77.13	72.78	67.97	61.54
7.00	72.12	70.52	68.91	62.16	89.62	80.16	79.86	76.98	72.68	70.01	—
		70.48		61.93	88.89	80.06			72.47	67.90	61.49
7.10[a]		70.24	68.57	62.49	89.57	78.87	78.96	76.23	—	67.99	62.12
					88.67					69.89	—
9.00						82.88	80.75		71.26		63.99
							80.21				62.86
9.20	72.28	70.78	69.00	62.30		83.01	80.93		71.39		64.16
		70.65		62.09			80.35				63.05
9.50	72.42	70.41	69.12	62.34		83.03	80.56		71.28		63.88
		70.48		62.00		—	80.77				62.98

[a] Signals from free and complexed mannitol.

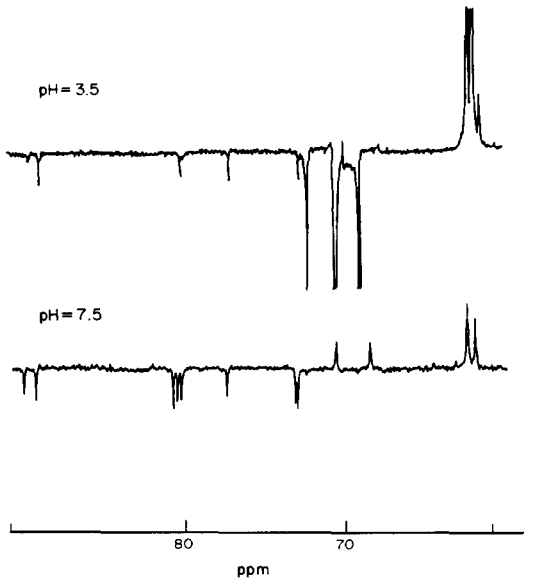


Fig. 4. DEPT ^{13}C NMR spectra of tungsten(VI)–sorbitol system in excess of ligand (pH = 3.5) and in excess of metal (pH = 7.5).

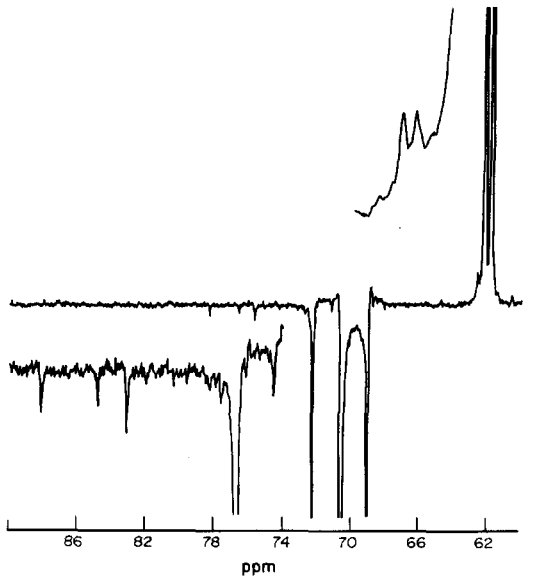
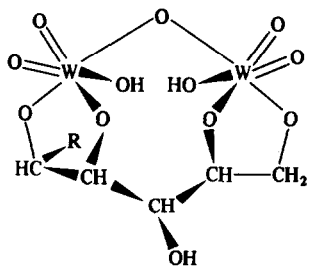


Fig. 5. DEPT ^{13}C NMR spectrum of 0.25 mol dm^{-3} Na_2WO_4 and 2.5 mol dm^{-3} sorbitol at pH = 1.0.

Concerning the structure of the second isomer, in spite of the fact that different signals are observed for each isomer at pH = 7.0 whose intensities are not temperature-dependent ($0°C < T < 90°C$), only the signals from one of these isomers are detected when the pH decreases because the signal intensities for the second isomer becomes very weak (Fig. 4).

That is why we have considered that the ligand has a different coordination to the metal in each isomer, the interconversion process being unlikely. Therefore, the second isomer for the mannitol and sorbitol complexes at this pH will be one where the ligand molecule will be coordinated by the same hydroxy terminal group (C-1) and three different CHOH groups, probably through C-2, C-4 and C-5 (III).



III

Concerning the third complex species, it has also been possible to isolate its sodium salt, which displays the IR spectrum shown in Fig. 3b. The WO_t region is similar to that found for the 2 : 1 species, but it also shows a new intense band at 1040 cm^{-1}. Bands at 1000–1100 cm^{-1} are described in a great number of complexes with hydroxo bridges[22,23] and, therefore, lead us to suggest the conversion of the M—O—M bond in a double M—O—M bridge, one of which must be protonated.

This structural change might explain the change in the stoichiometric ratio (from 2 : 1 to 2 : 2). In fact, it becomes reasonable to assume that the cyclic structure of the 2 : 1 complex is not compatible with the formation of a new μ-hydroxo bond which could agree with that a tricoordination of mannitol or sorbitol molecule to each tungsten(VI) center became easier.

This last consideration was fully corroborated in the ^{13}C NMR spectrum displayed by the complex species stable at lower pH (Fig. 5). In this spectrum, only three of the six signals expected for a coordinated sorbitol molecule are downfield shifted, whilst the other set of three resonances (one of a carbinol group and two of the terminal CH_2OH groups) are very close to the resonances of the analog groups in the free ligand, suggesting that these alcoholic groups are not coordinated.

All those results can be extended to mannitol complexes.

Acknowledgement—The authors wish to thank Mª José Viqueira for her help in the English correction of the manuscript.

REFERENCES

1. M. Mikesova and M. Bartusek, *Collect. Chem. Commun.* 1978, **43**, 1867.

2. S. A. Barke, E. J. Bourne, A. B. Foster and R. B. Ward, *Nature* 1957, **179**, 262.
3. H. Frey, *Ann. Chim.* 1943, **18**, 1.
4. R. A. Chalmers and A. G. Sinclair, *J. Inorg. Nucl. Chem.* 1967, **29**, 2065.
5. L. Petterson, *Acta Chem. Scand.* 1972, **26**, 4067.
6. G. Spaccu and E. Popper, *Z. Phys. Chem.* 1939, **B41**, 112.
7. A. Cervilla, J. A. Ramirez and A. Beltran-Porter, *Trans. Met. Chem.* 1983, **8**, 21.
8. J. Angus, E. J. Bourne and H. Weigel, *J. Chem. Soc.* 1965, 21.
9. E. Llopis, Doctoral Thesis, University of Valencia, Spain (1985).
10. A. Beltran, A. Cervilla and J. Beltran, *J. Inorg. Nucl. Chem.* 1981, **43**, 1337.
11. A. Beltran, F. Caturla, A. Cervilla and J. Beltran, *J. Inorg. Nucl. Chem.* 1981, **43**, 3277.
12. A. Beltran-Porter and J. A. Ramirez, *Can. J. Chem.* 1983, **61**, 1100.
13. A. Beltran-Porter, D. Beltran-Porter, A. Cervilla and J. A. Ramirez, *Talanta* 1983, **30**, 124.
14. B. Spivak, and Z. Dori, *Coord. Chem. Rev.* 1975, **17**, 99.
15. A. Beltran-Porter, A. Cervilla, F. Caturla and B. Segura, *Trans. Met. Chem.* 1983, **8**, 222.
16. A. Cervilla, J. A. Ramirez and E. Llopis, *Trans. Met. Chem.* (in press).
17. R. J. Butcher, H. K. J. Powell, C. J. Wilkins and S. Hian Yong, *J. Chem. Soc., Dalton Trans.* 1976, 356.
18. Y. A. Buslaev and R. L. Davidovich, *Russ. J. Inorg. Chem.* 1968, **13**, 656.
19. M. Cousins and M. L. H. Green, *J. Chem. Soc.* 1963, 889.
20. R. M. Wing and K. P. Callahan, *Inorg. Chem.* 1969, **8**, 871.
21. M. A. Freeman, D. R. van der Vaart, F. A. Shultz and C. N. Reilley, *J. Coord. Chem.* 1981, **11**, 81.
22. K. Nakamoto, *Infrared Spectra of Inorganic and Coordination Compounds*. Wiley, New York (1963).
23. J. R. Ferraro and W. R. Walker, *Inorg. Chem.* 1965, **4**, 1382.

Polyhedron Vol. 5, No. 12, pp. 2075–2080, 1986
Printed in Great Britain

0277–5387/86 $3.00+.00
Pergamon Journals Ltd

REACTIONS AND X-RAY CRYSTAL STRUCTURE OF (3-CYANO-2,4-PENTANEDIONATO-*N*)PENTAAMMINECOBALT(III) PERCHLORATE CHLORIDE DIHYDRATE

R. J. BALAHURA,* G. FERGUSON, A. JOHNSTON and B. L. RUHL

Guelph-Waterloo Centre for Graduate Work in Chemistry, Department of Chemistry and Biochemistry, University of Guelph, Guelph, Ontario, Canada N1G 2W1

(*Received* 18 *November* 1985; *accepted after revision* 19 *May* 1986)

Abstract—The pentaamminecobalt(III) complex with the 3-cyano-2,4-pentanedionate anion coordinated through the nitrile nitrogen has been characterized by X-ray crystallography. The crystals of $[(NH_3)_5CoNCacac](Cl)(ClO_4)\cdot 2H_2O$ are triclinic, space group $P\bar{1}$, $a = 10.245(2)$ Å, $b = 14.071(4)$ Å, $c = 6.971(2)$ Å, $\alpha = 90.03(3)°$, $\beta = 109.86(2)°$, $\gamma = 108.91(2)°$, $V = 887.1$ Å^3, $Z = 2$, $D_c = 1.64$ g cm^{-3}, $F(000) = 456$, Mo–K_α radiation, $\lambda = 0.71069$ Å, μ(Mo–K_α) = 12.7 cm^{-1}. The structure was determined by the heavy-atom method, and refined by block-diagonal least-squares calculations, $R = 0.0537$, $R_w = 0.0607$, for 2499 observed reflections. Principal dimensions are: Co—N(NH_3) *trans* to $NCacac^-$ 1.940(5), other Co—N(NH_3) 1.967(2), Co—N($NCacac^-$) 1.911(5) Å. The pendant acac moiety is best described in terms of a delocalized bond network with, for example, C—C distances in the range 1.44–1.52(1) Å. Several reactions involving this free acac group are also described including the preparation and characterization of the dimeric species pentaamminecobalt(III) - μ - (3 - cyano - 2,4 - pentanedionato) - bis(propylenediamine) cobalt(III) perchlorate.

Most metal acetylacetone (2,4-pentanedione, Hacac), complexes involve coordination of the ligand as the enolate ion to form a six-membered ring.[1] However, there are examples where the metal is bonded directly to the methine carbon leaving a pendant acac moiety.[2] Metals forming these types of complexes are second and third row transition metals, in particular platinum. Potassium chlorobis(acetylacetonato)platinate(II), contains both a bidentate chelated acac group and a methine carbon-bonded ligand.[3] For the latter arrangement, the 'free' acac is a potential donor for other metal ions.

We have been interested in metal complexes with pendant groups capable of strong interaction with redox metal ions for mechanistic studies.[4] To this end we have selectively coordinated potential chelating agents via a monodentate substituent.[5,6] For example, 3-cyano-2,4-pentanedione has been bonded to cobalt(III) through the nitrile nitrogen leaving the pendant acac available to chelate to other metal ions.[6] The structure and reactivity of this unique complex are of considerable interest in this regard. In this paper we report the X-ray crystal structure of (3-cyano-2,4-pentanedionato-*N*)-pentaamminecobalt(III) perchlorate chloride dihydrate, $[(NH_3)_5CoNCacac](Cl)(ClO_4)\cdot 2H_2O$.

Several examples of the reactivity of the pendant acac in the complex are also given.

EXPERIMENTAL

The title complex was prepared as described previously as were solutions for kinetic studies.[6]

Synthesis of pentaamminecobalt(III) - μ - (3 - *cyano* - 2,4 - *pentanedionato*) - *bis*(*propylenediamine*) *cobalt*(III) *perchlorate*, $[(NH_3)_5CoNCacacCo(tn)_2](ClO_4)_5$

Aquahydroxybis (propylenediamine) cobalt (III) perchlorate,[7] 0.074 g, and (3-cyano-2,4-pentane-

* Author to whom correspondence should be addressed.

dionato-*N*)pentaamminecobalt(III) perchlorate, 0.072 g, were dissolved in 20 cm^3 H_2O and 3 drops of concentrated perchloric acid added. The solution was stirred for 24 h at room temperature, diluted to 500 cm^3 with water and charged onto a weak acid CM–Sephadex cation exchange column. Elution with increasing concentrations of NaCl removed unreacted starting material and slowly moved a 5+ ion down the column. This species was removed from the column and isolated as the perchlorate salt.

Found: C, 14.7; H, 4.3; N, 14.4%. Calc. for $Co_2C_{12}H_{41}O_{22}N_{10}Cl_5$: C, 14.8; H, 4.2; N, 14.4%.

Infrared: $\nu_{C\equiv N} = 2240\ cm^{-1}$.

^1H NMR: *cis*-NH_3, 4.09 δ (12 H); *trans*-NH_3, 3.68 δ (3H); propylenediamine NH protons, 5.34, 5.10, 4.75, 4.57 δ (8H); propylenediamine CH protons, 2.56–1.74 δ (12H); CH_3, 2.42 δ (6H).

Kinetic studies

The reduction reactions were carried out on a Durrum Model D-110 stopped flow spectrophotometer. All reagents were handled and mixed using standard syringe techniques. The reactions were carried out under pseudo-first-order conditions (reductant in greater than 10-fold excess over oxidant). Absorbance-time data were collected and displayed using a DASAR analog–digital data storage and retrieval system (American Instruments Co.). Rate constants were obtained directly from the exponential decay traces by matching this curve with a curve generated by an exponential curve simulator. Agreement between these values and rate constants obtained from a plot of $\log(A_t - A_\infty)$ *vs* time was within 1% (A_t and A_∞ are the absorbances at time t and after the reaction was complete).

Physical measurements

Infrared spectra were obtained using a Beckman Model IR-12 spectrophotometer using KBr pellets. Proton magnetic resonance spectra were recorded with a Bruker AM-250 spectrometer.

X-ray studies

Crystal data. $C_6H_{21}CoN_6O_2 \cdot Cl \cdot ClO_4 \cdot 2H_2O$, $M = 439.14$. Triclinic, $a = 10.245(2)$ Å, $b = 14.071(4)$ Å, $c = 6.971(2)$ Å, $\alpha = 90.03(3)°$, $\beta = 109.86(2)°$, $\gamma = 108.91(2)°$, $V = 887.1$ Å^3, $Z = 2$, $D_c = 1.64\ g\ cm^{-3}$, $F(000) = 456$, Mo–K_α radiation, $\lambda = 0.71069$ Å, μ(Mo–K_α) = 12.7 cm^{-1}, Space group $P\bar{1}$.

Structure determination and refinement

Accurate cell parameters were obtained by a least-squares refinement of the setting angles of 25 reflections (with θ in the range 10–15°) measured on a Enraf–Nonius CAD4 diffractometer. Intensity data were collected by the $\omega/2\theta$ method with a small ($0.23 \times 0.38 \times 0.08$ mm) crystal to a maximum θ of 25°, and 3110 unique data were obtained. After corrections for Lorentz and polarization effects the data with $I > 3\sigma(I)$ (2499) were labelled observed and used in structure solution and refinement.

The coordinates of the Co atom were obtained from an analysis of a three-dimensional Patterson function. The remaining non-hydrogen atoms were located in the subsequent heavy-atom phased Fourier summations. It was clear from intermediate difference maps that one of the waters of hydration was disordered over two sites and this was allowed for. Refinement was by block-diagonal least-squares calculations,[8] initially with isotropic and then with anisotropic thermal parameters. A difference map computed at an intermediate stage in the refinement revealed maxima in positions expected for all the hydrogen atoms, except those in the disordered water molecule; these were then allowed for in geometrically idealized positions (C—H = 1.08 Å) and included but not refined in the final rounds of calculations. In the refinement cycles a weighting scheme of the form $w = 1/[\sigma^2 F]$ was employed. The scattering factors were taken from refs 9 and 10, and allowance was made for anomalous dispersion.[11] Refinement converged with $R = 0.0537$ and $R' = \Sigma w\Delta^2/\Sigma wF_0^2 = 0.0607$ for the 2499 observed reflections. A final difference map showed some peaks (maximum $0.69e$ Å^{-3}) near the low occupancy oxygen atom. Figure 1 is a perspective view of the cation with our numbering scheme. Final coordinates for the non-hydrogen atoms, lists of anisotropic thermal parameters, calculated hydrogen coordinates, and hydrogen-bond distances involving the ions and water molecules, together with observed and calculated structure factors have been deposited as supplementary material with the Editor, from whom copies are available on request. Atomic coordinates have also been deposited with the Cambridge Crystallographic Data Centre.

RESULTS AND DISCUSSION

The dimensions in the cation in $[(NH_3)_5CoN\text{-}Cacac](Cl)(ClO_4) \cdot 2H_2O$ are listed in Table 1. The crystallographic analysis demonstrates that the $[(NH_3)_5CoNCacac]^{2+}$ cation is composed of an octahedrally coordinated cobalt atom bonded to

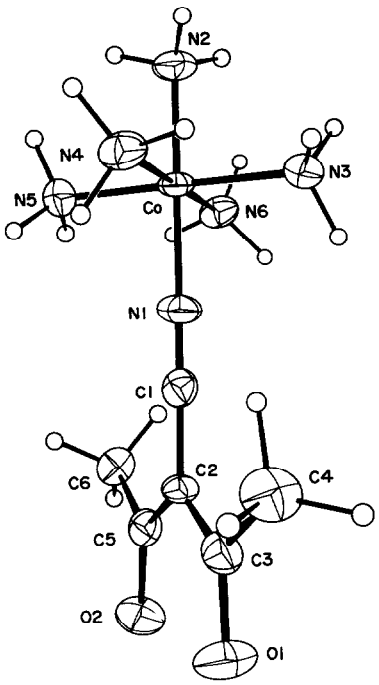


Fig. 1. An ORTEP view of the $[(NH_3)_5CoNCacac]^{2+}$ cation with our numbering scheme; ellipsoids are at the 50% level except for hydrogens which are shown as spheres of an arbitrary size.

five NH_3 ligands with *cis* N—Co—N angles of 89.0°–91.3(2)°. The sixth position is occupied by the nitrile coordinated $NCacac^-$ moiety, with *cis* N—Co—N angles of 89.2°–90.3(2)°.

The Co—N(NH_3) bonds range in length from 1.940(5) to 1.968(5) Å, with the Co—N bond [1.940(5) Å] *trans* to the $NCacac^-$ moiety significantly shorter than the *cis* Co—N bonds [average = 1.967(2) Å]. The average value for the *cis* Co—N bond length agrees well with distances found in other cobalt–ammine complexes, e.g. Co—N = 1.968 Å for $Co(NH_3)_6^{3+}$.[12]

The shortening of the *trans* Co—N bond seen in the present work has been observed for a few other complexes,[13–15] notably for *sp* or sp^2 hybridized nitrogen donor ligands. In the complex $[(NH_3)_5CoNCCo(CN)_5]$ this effect has been interpreted as being due to donation of metal $d\pi$ electrons into the vacant π^*2p nitrogen orbital on the cyano ligands,[13] shifting the metal electron cloud away from the *trans* NH_3 ligand and thereby minimizing repulsion.

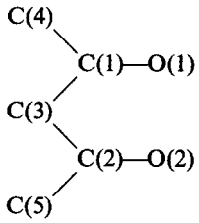
The cobalt–nitrile bond length of 1.911(5) Å is significantly shorter than the Co—NH_3 bond lengths, which is expected due to the *sp* hybridization of the nitrogen atom, in comparison to sp^3

Table 1. Interatomic bond distances (Å) and cation bond angles (degrees) for $[(NH_3)_5CoNCacac](Cl)(ClO_4)\cdot 2H_2O$[a,b]

(a) Distances from cobalt			
Co—N(1)	1.911(5)	Co—N(4)	1.968(5)
Co—N(2)	1.940(5)	Co—N(5)	1.966(5)
Co—N(3)	1.966(5)	Co—N(6)	1.967(5)
(b) Distances in 3-cyano-2,4-pentanedionate ligand			
N(1)—C(1)	1.153(7)	C(3)—O(1)	1.236(7)
C(1)—C(2)	1.405(8)	C(3)—C(4)	1.521(8)
C(2)—C(3)	1.435(9)	C(5)—O(2)	1.260(7)
C(2)—C(5)	1.459(8)	C(5)—C(6)	1.486(9)
(c) Bond angles			
N(1)—Co—N(2)	178.7(2)	N(4)—Co—N(6)	179.3(2)
N(1)—Co—N(3)	90.3(2)	N(5)—Co—N(6)	91.3(2)
N(1)—Co—N(4)	89.8(2)	Co—N(1)—C(1)	179.0(5)
N(1)—Co—N(5)	89.2(2)	N(1)—C(1)—C(2)	179.5(6)
N(1)—Co—N(6)	89.6(2)	C(1)—C(2)—C(3)	118.6(5)
N(2)—Co—N(3)	90.5(2)	C(3)—C(2)—C(5)	125.6(5)
N(2)—Co—N(4)	91.3(2)	C(2)—C(3)—O(1)	123.0(5)
N(2)—Co—N(5)	90.0(2)	C(2)—C(3)—C(4)	119.6(5)
N(2)—Co—N(6)	89.4(2)	O(1)—C(3)—C(4)	117.5(6)
N(3)—Co—N(4)	90.6(2)	C(1)—C(2)—C(5)	115.9(5)
N(3)—Co—N(5)	179.4(2)	C(2)—C(5)—O(2)	121.0(5)
N(3)—Co—N(6)	89.0(2)	C(2)—C(5)—C(6)	120.2(5)
N(4)—Co—N(5)	89.1(2)	O(2)—C(5)—C(6)	118.8(5)

[a] Estimated standard deviations of last digit in parentheses.
[b] For numbering scheme see Fig. 1.

Table 2. Selected bond lengths in metal acetylacetonate complexes[a]



Bond	$K[Pt(acac)_2Cl]$ [b]	$K[Pt(acac)_2Cl]$ [c]	$[(NH_3)_5CoNCacac]^{2+}$	$Co(acac)_3$[d]
C(1)—O(1)	1.21(2)	1.26(3)	1.236(7)	1.252–1.294
C(2)—O(2)	1.19(3)	1.35(2)	1.260(7)	(1.268 avg)
C(2)—C(3)	1.53(3)	1.38(3)	1.459(8)	1.357–1.398
C(1)—C(3)	1.54(3)	1.44(3)	1.435(9)	(1.382 avg)
C(1)—C(4)	1.52(3)	1.45(3)	1.486(9)	1.51–1.58
C(2)—C(5)	1.53(3)	1.53(3)	1.521(8)	(1.544 avg)

[a] Numbering scheme according to the structure; bond lengths in Å.
[b] Monodentate carbon bonded acac, ref. 3.
[c] Bidentate oxygen bonded acac, ref. 3.
[d] Ref. 16.

hybridization for the NH_3 ligands. This value compares well with the value reported for $(NH_3)_5CoNCCo(CN)_5$ of 1.920(3) Å.[13] The Co—N(1)—C(1) angle of 179.0(5)° indicates linear coordination of the NCacac ligand, and the N(1)—C(1) bond length of 1.153(7) Å is in accord with accepted values.[13]

Other bond lengths in the $NCacac^-$ ligand, along with parameters for other metal–acac complexes are summarized in Table 2. The carbonyl bond lengths in $NCacac^-$ are significantly longer than those for typical C=O bonds, and are close to the range of C=O bond lengths found in metal(acac) complexes.[16] The crystal structure of $K[Pt(acac)_2Cl]$,[3] which contains both pendant acac (methine carbon σ-bonded to Pt) and bidentate chelated acac groups, indicates that the pendant β-diketone is best represented as a keto-type structure containing single C—C and double C=O bonds (loss of delocalization). This is definitely not the case for the $NCacac^-$ ligand, as comparison of bond lengths in Table 2 indicates that the $NCacac^-$ moiety is best described in terms of a delocalized bond network, as in $Co(acac)_3$.[16] The values obtained for the methine C–carbonyl C bond lengths are intermediate between those reported for $M(acac)_3$-type complexes and the σ-bonded structure in $K[Pt(acac)_2Cl]$. A bond order greater than 1 is evident, however delocalization is not to the same degree as in $Co(acac)_3$.

The methine carbon–nitrile carbon bond length C(1)—C(2) in $NCacac^-$ [1.405(8) Å] is significantly shorter than typical carbon–carbon single bonds (1.51–1.54 Å), indicating that delocalization extends into this bond as well. This conjugated system should provide a facile pathway for electron transfer *via* π^* orbitals.

The 'bite' size, or oxygen–oxygen distance, was found to be 2.778(3) Å, which is in the middle of the range found for $M(III)(acac)_3$ complexes (M = Al, Co, Mn, Cr, Fe and V).[16]

The bonding of metal ions to the pendant keto acac group in $[Pt(acac)_2Cl]^-$ indicates that the M—O bonds in the binuclear species were weaker than typical M—O bonds in enol coordinated species.[17] Although a limited amount of π-electron delocalization is present, the bonding in the binuclear complex still involves keto coordination.

For $[(NH_3)_5CoNCacac]^{2+}$, the favourable bite size, combined with the 'enol' nature of the β-diketone, implies that metal coordination to the remote linkage may dominate in the reactions of the complex.

It has been shown that the reduction of $[(NH_3)_5CoNCacac]^{2+}$ by chromium(II) occurs by an inner-sphere mechanism where the reductant attacks at the free acac grouping.[6] The mechanism predicts that addition of non-reducing metal ions should inhibit the reduction due to competition for the chelating β-diketone moiety between reductant and the added metal ion. This prediction was investigated for the reduction of the complex by chro-

Table 3. Kinetic data for the Cr(II) reduction of $[(NH_3)_5CoNCacac]^{2+}$ in the presence of added M^{n+} [a,b]

M^{2+}	$[M^{n+}]$ (mol dm^{-3})	k_{obsd} (s^{-1})	K_M (dm^3 mol^{-1})
—	—	136	—
Co^{2+}	0.0245	124	24±2
	0.074	96	
	0.1213	84	
	0.1273	83	
Zn^{2+}	0.0245	128	9±1
	0.074	118	
	0.1213	115	
	0.1273	110	
	0.285	90	
Ni^{2+}	0.0245	135	—
	0.1213	144	
	0.1273	138	
Mn^{2+}	0.1213	125	3±1
Ba^{2+}	0.1213	139	—

[a] Temperature = 25°C, Ionic strength = 1.00 mol dm^{-3} ($LiClO_4$).

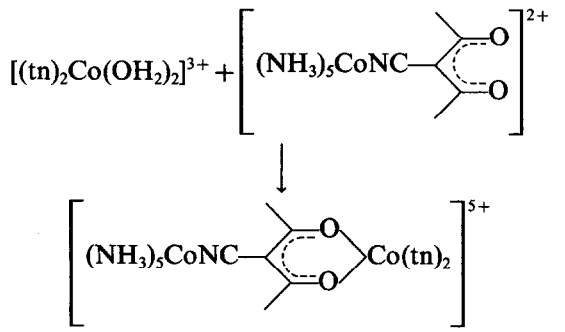
[b] $[H^+] = 0.12$ mol dm^{-3}, $[Cr^{2+}] = 0.01335$ mol dm^{-3}, $[Co(III)] = 2.5 \times 10^{-4}$ mol dm^{-3}.

mium(II) in the presence of Ba^{2+}, Ni^{2+}, Mn^{2+}, Zn^{2+} and Co^{2+}. The data are given in Table 3. The data are consistent with the mechanism outlined in Scheme 1. The following rate equation can be derived from Scheme 1:

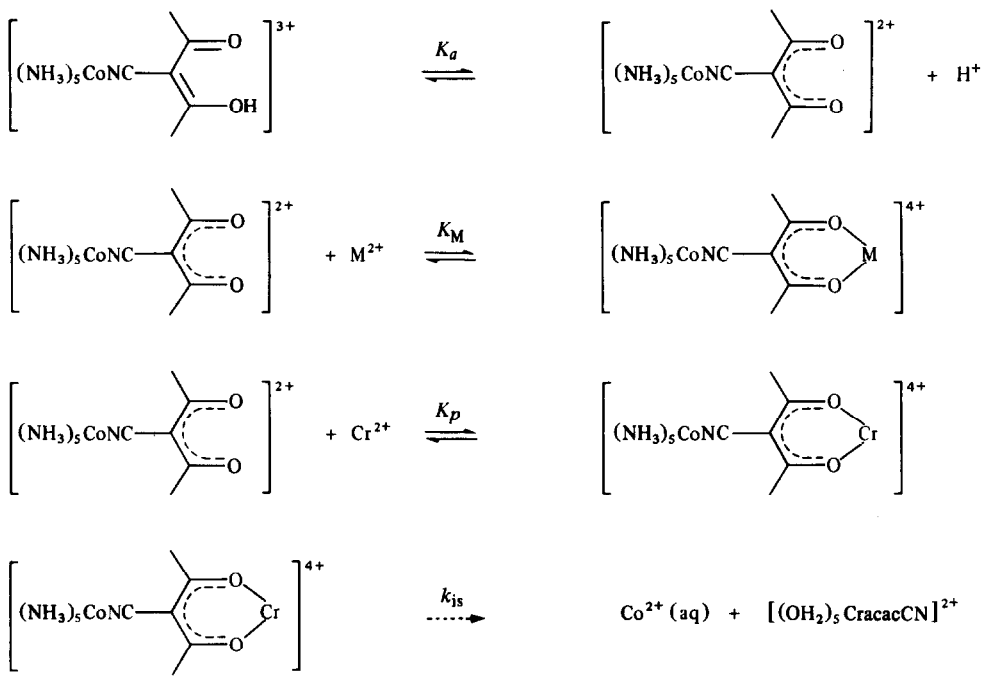
$$k_{obsd} = \frac{k_{is}K_p[Cr^{2+}]}{1+[H^+]K_a^{-1}+K_p[Cr^{2+}]+K_M[M^{2+}]}.$$

A plot of k_{obsd}^{-1} *vs* $[M^{2+}]$ at constant $[Cr^{2+}]$ and constant $[H^+]$ gave the expected linear plots with constant intercept and varying slopes. The values of K_M obtained from these plots are also collected in Table 3. Thus the kinetic data are also consistent with the existence of a reactive pendant acac group.

Finally, we have also shown that the parent complex can be used to prepare dimeric species. The reaction below



occurs readily in dilute acid due to the lability of the water molecules in $(tn)_2Co(OH_2)_2^{3+}$ [7,18] and the chelating ability of the free acac. The nitrile stretching frequency (2240 cm^{-1}) of the dimer shows the expected shift to higher frequency [19] when compared to that for the free ligand ($\nu_{C\equiv N}$ = 2225 cm^{-1}) or



Scheme 1.

uncomplexed nitrile in the complex $en_2Coacac–CN^{2+}$ ($\nu_{C\equiv N} = 2220\ cm^{-1}$). The NMR spectrum of the dimer in Me_2SO-d_6 shows *cis*- and *trans*-NH_3 peaks (4.09 and 3.68δ, respectively) similar to those found in $(NH_3)_5CoNCacac^{2+}$ (3.90 and 3.60δ, respectively). Also the methyl peaks in the dimer occur at 2.42δ indicating that the acac moiety is chelated as in the $en_2Coacac–CN^{2+}$ complex (2.50δ).[6]

Acknowledgement—The authors wish to thank the Natural Sciences and Engineering Research Council of Canada for financial support of this work.

REFERENCES

1. D. W. Thompson, *Struct. Bond.* 1971, **9**, 27.
2. D. Gibson, *Coord. Chem. Rev.* 1969, **4**, 225.
3. R. Mason, G. B. Robertson and P. J. Pauling, *J. Chem. Soc. (A)* 1969, 485.
4. A. J. Johnston, Ph.D. Thesis, University of Guelph (1983).
5. C. Alexander, University of Guelph, private communication.
6. R. J. Balahura and A. J. Johnston, *Inorg. Chem.* 1983, **22**, 3309.
7. I. R. Jonasson, S. F. Lincoln and D. R. Stranks, *Aust. J. Chem.* 1970, **23**, 2267.
8. E. J. Gabe, A. C. Larson, Y. Wong and F. L. Lee, *The NRC Crystal Structure Programs*, National Research Council Laboratories, Ottawa, Canada, K1A 0R6 (1981).
9. D. T. Cromer and J. B. Mann, *Acta Cryst.* 1968, **A24**, 321.
10. R. F. Stewart, E. R. Davidson and W. T. Simpson, *J. Chem. Phys.* 1965, **42**, 3175.
11. D. T. Cromer and D. J. Liberman, *J. Chem. Phys.* 1970, **53**, 1891.
12. P. W. Meek and J. A. Ibers, *Inorg. Chem.* 1970, **9**, 465.
13. B.-C. Wang, W. P. Schaefer and R. E. Marsh, *Inorg. Chem.* 1971, **10**, 1492.
14. C. B. Storm, C. M. Freeman, R. J. Butcher, A. H. Turner, N. S. Rowan, F. O. Johnson and E. Sinn, *Inorg. Chem.* 1983, **22**, 678.
15. W. P. Schaefer, *Inorg. Chem.* 1968, **7**, 725.
16. P. K. Hon and C. E. Pfluger, *J. Coord. Chem.* 1973, **3**, 67.
17. Y. Nakamura and K. Nakamoto, *Inorg. Chem.* 1975, **14**, 63.
18. I. R. Jonasson, R. S. Murray, D. R. Stranks and J. K. Yandell, *Proc. 12th Int. Conf. Coord. Chem.* (Sydney), 1969, 32.
19. H. J. Coerver and C. Curran, *J. Am. Chem. Soc.* 1958, **80**, 3522.

Polyhedron Vol. 5, No. 12, pp. 2081–2091, 1986
Printed in Great Britain

0277–5387/86 $3.00+.00
© 1986 Pergamon Journals Ltd

STUDIES OF π-BONDING PERTURBATION IN THE TUNGSTEN–NITROGEN MULTIPLE BOND OF ISOPROPYLIMIDO TUNGSTEN(VI) COMPLEXES: THE CRYSTAL AND MOLECULAR STRUCTURES OF $[W(NCHMe_2)Cl_4]_2 \cdot C_6H_6$ AND $[W(NCHMe_2)Cl_5][NEt_4]$

BARRY R. ASHCROFT, GEORGE R. CLARK, ALASTAIR J. NIELSON* and CLIFTON E. F. RICKARD

Department of Chemistry, Auckland University, Private Bag, Auckland, New Zealand

(*Received* 11 *March* 1986; *accepted* 19 *May* 1986)

Abstract—^{13}C NMR chemical shift data for the α-carbon (δ_α) of a variety of tungsten isopropylimido complexes indicate that the extent to which the nitrogen lone pair participates in multiple bonding to tungsten depends on the form of the complex and the ligands involved. The structures of $[W(NCHMe_2)Cl_4]_2 \cdot C_6H_6$ (**1a**) and $[W(NCHMe_2)Cl_5][NEt_4]$ (**7**) which show widely different δ_α values, have been determined by single-crystal X-ray diffraction methods. Crystals of **1a** are triclinic space group $P\bar{1}$, with $a = 6.394(2)$, $b = 8.890(3)$, $c = 11.205(2)$ Å and $\alpha = 109.95(2)°$, $\beta = 98.91(2)°$, $\gamma = 93.96(2)°$; crystals of **7** are orthorhombic, space group *Pnma*, with $a = 13.667(5)$, $b = 15.152(2)$, $c = 9.432(2)$ Å. Both structures were solved by Patterson and Fourier methods and refined to an R value of 0.050 for 1325 observed data of **1a** and to an R value of 0.050 for the 1157 observed data of **7**. Complex **1a** is dimeric with a W—N bond length of 1.697(12) Å and complex **7** is monomeric with a longer W—N bond length of 1.763(16) Å. Comparison of the W—Cl bond lengths and correlations with π-bonding to make an 18-electron count, indicates that the W—N bond lengths differ in the two complexes as a result of overall π-bonding requirements.

The multiple bond of organoimido complexes (M≡NR)[1] has not shown the diversity of reactions exhibited by the related alkylidene and alkylidyne complexes (M=CHR and M≡CR)[2] and in general is comparatively unreactive. Electrophilic activity has been observed to occur for osmium organoimido complexes where the amination of olefins is now well known[3] and also in the reactions of $Cr(N\text{-}t\text{-}Bu)_2(OSiMe_3)_2$ with Ph_2Zn.[4] Nucleophilic activity has been identified in the reaction of M≡NR complexes with PhCHO to give M=O complexes and PhCH=NR[5] while $Mo(NPh)_2(S_2CNEt_2)_2$ reacts with MeBr to give $Mo(NPh)Br_2(S_2CNEt_2)_2$.[6] These reactions have mainly been identified by analysis of the organic products produced but some examples of the intermediate complexes are now emerging. The alkanolaminato osmium(VI) complex $Os_2O_4(OCMe_2CH_2NBu^t)_2$ has recently been characterised by X-ray crystallography[7] as have the amido complexes $[W_2(NHPh)_2(\mu\text{-pinacol})(pinacol)_4]$[8] and $[W(NCMe_3)(NHCMe_3)_2(benzopinacol)]$,[9] which result from protonation of an imido function.

One approach taken to increase the nucleophilicity of the imido nitrogen has been the preparation of complexes in which the maximum electron count can exceed 18 electrons, either by placing a strongly competitive π-donating ligand *trans* to the imido function as in the case of $[Re(NPhCH_3)(OEt)(S_2CNMe_2)_2]$[10] or by introducing a second imido function which is forced to act essentially as a two-electron donor (i.e. M=N̈R) as in the case of $[Mo(NPh)_2(S_2CNEt_2)_2]$.[11] Alternatively, ^{13}C NMR investigations of a series of d^0 *t*-butylimido complexes have shown that on changing the metal, the charge on the imido nitrogen atom decreases on proceeding upwards and to the right of the transition metal series.[12]

In view of these studies we were interested in

* Author to whom correspondence should be addressed.

preparing complexes of tungsten(VI) in which the reactivity of the imido ligand might be enhanced. We report here results of studies in which ligands other than the organoimido function are varied and the effect on the W—N linkage examined by ^{13}C NMR spectroscopy and X-ray crystallography.

EXPERIMENTAL

$WOCl_4$ was prepared by reaction of WO_3 with thionyl chloride[20] and trimethylphosphine by a literature method.[21] Trityl ethoxide was obtained by refluxing trityl chloride with ethanol and triethylamine in benzene and recrystallising the product from petroleum ether at −20°C. Tetraethyl ammonium chloride, sodium acetate and diethyldithiocarbamate were dried at 100°C *in vacuo* for 24 h and stored in Schlenk tubes under dry nitrogen. Lithium *t*-butoxide was prepared from *t*-butanol and *n*-butyllithium in petroleum ether. Propionitrile was dried over and distilled from calcium hydride. Petroleum ether (b.p. range 40–60°C), toluene, benzene and diethyl ether were distilled over sodium wire and dichloromethane over calcium hydride. All distillations were carried out under N_2 treated to remove oxygen and water, as were manipulations using bench-top, air-sensitive techniques.[22] IR spectra were recorded on a Perkin–Elmer 597 spectrometer, ^1H NMR on a Varian T60 Model spectrometer and ^{13}C NMR spectra on a JEOL FX60 spectrometer. Analytical data were obtained by Professor A. D. Campbell and associates, University of Otago, New Zealand. Melting points were determined in sealed tubes under N_2 on an electrothermal melting point apparatus and are uncorrected.

Hexachloro - di - μ - chlorobis(isopropylimido)ditungsten(VI) (1)

Iso-propylisocyanate (1.65 cm^3, 17.0 mmol) was added to tungsten oxytetrachloride (5.7 g, 16.7 mmol) in benzene (90 cm^3) and the resulting red solution refluxed overnight, after which it was filtered while hot and the volume reduced to *ca* 30 cm^3. On standing the product formed as orange–red crystals which were filtered, washed with cold benzene (2 × 10 cm^3) and dried *in vacuo* whereupon crystallinity was lost. The air-sensitive complex may be stored under nitrogen for several months without decomposition but traces of moisture cause the formation of a blue colouration. M.p. 158–160°C.

IR (Nujol) bands at 1650w, 1580m, 1240s, 1230s, 1150m, 1150m, 1070s, 930m, 935s, 880s, 860s, 810s, 680w, 610m, 540s, 480s, 400s, 370s, 330s, 300s, 280s; (KEL-F) 2900w, 2250w, 1570w cm^{-1}.

Tetrachloropropionitrile(isopropylimido)tungsten (VI) (2)

Propionitrile (35 cm^3) was added to hexachloro-di-μ-chlorobis(isopropylimido)ditungsten(VI) (1.2 g, 1.6 mmol) and the mixture stirred for 2 h. The orange solution was filtered, the volume reduced to *ca* 3 cm^3 and on standing at −20°C the complex formed as orange crystals which were filtered off and dried *in vacuo*. M.p. 179–183°.

IR (Nujol) bands at 2280m, 1460s, 1418m, 1364m, 1305m, 1270s, 1155w, 1110w, 1074m, 845w, 780w, 724w, 620w, 565m, 330s cm^{-1}.

Triphenylcarbonium tetrachloroethoxy(isopropylimido)tungsten(VI) (3)

Trityl ethoxide (0.5 g, 1.73 mmol) in dichloromethane (30 cm^3) was added to hexachloro-di-μ-chlorobis(isopropylimido)ditungsten(VI) (0.66 g, 8.6 mmol) suspended in dichloromethane and the mixture was stirred for 4 h. The yellow–orange solution was filtered and the solvent removed to give the complex as a gum which failed to solidify on continuous washing with petroleum ether and drying *in vacuo*. The complex was characterised by ^1H and ^{13}C NMR spectroscopy (see Table 2). Λ_m(MeCN) 107.3 ohm^{-1} cm^2 mol^{-1}.

IR (smear) bands at 3020s, 2990s, 2950s, 1575s, 1475s, 1440s, 1280m, 1350m, 1308w, 1260m, 1200m, 1180m, 1150m, 1070s, 1024s, 975s, 860s, 805s, 750s, 690s, 660s, 620s, 504w, 455w, 320s cm^{-1}.

Chlorotris(diethyldithiocarbamate)isopropylimidotungsten(VI) (4)

A suspension of sodium diethyldithiocarbamate (2.36 g, 13.8 mmol) in dichloromethane (80 cm^3) was added to a solution of hexachloro-di-μ-chlorobis(isopropylimido)ditungsten(VI) (1.32 g, 1.72 mmol) in dichloromethane (50 cm^3) and the mixture was stirred for 15 h. The yellow solution was filtered and the solvent removed to give a yellow gum which failed to solidify on extensive washing with petroleum ether. The complex was characterised by NMR spectroscopy (see Table 2).

IR (smear) bands at 3375m, 3175w, 2960s, 2920s, 2860s, 2800s, 2715m, 2620m, 2530m, 2445m, 2350w, 2220w, 2100w, 2010w, 1980w, 1920w, 1830w, 1770w, 1620m, 1580m, 1560s, 1540s, 1410s, 1380s, 1345s, 1300s, 1260s, 1220s, 1200s, 1140s, 1110m, 1090s, 1070s, 1010s, 980s, 920s, 855s, 835s, 790s, 735s, 705m, 670w, 610m, 595m, 570s, 560s, 520w, 495m, 465w, 440m, 420m, 400m, 380s, 365s,

340m, 330w, 315w, 300w, 295s, 265m, 260s, 240m cm^{-1}.

Triphenylcarbonium pentachloro(isopropylimido)tungstate(VI) (**5**)

Trityl chloride (0.44 g, 1.57 mmol) in dichloromethane (30 cm^3) was added to isopropylimidotungsten tetrachloride dimer (0.6 g, 0.78 mmol) and the mixture was stirred for 3 h. The red solution was filtered and the solvent removed to give a red gummy material which was continuously washed with petroleum ether, dried *in vacuo* and ground with a spatula until the complex was obtained as a yellow–brown powder. Λ_m(MeCN) 103.6 ohm^{-1} cm^2 mol^{-1}.

IR (Nujol) bands at 1660m, 1460s, 1445s, 1290m, 1270m, 1160m, 1100w, 1070w, 1025w, 980m, 870m, 820m, 750m, 735m, 692m, 660m, 618m, 608m, 568w, 504w, 460w, 400m, 310s, 280m cm^{-1}.

Chlorobisacetato-di-μ-acetatobis(isopropylimido)ditungsten(VI) (**6**)

Benzene (120 cm^3) was added to isopropylimido tungsten tetrachloride dimer(1.1 g, 1.44 mmol) and sodium acetate (1.0 g, 12.2 mmol) and the mixture was stirred for 4 h and then left to stand for 2 h. The solution was filtered and the solvent removed giving a yellow gum which failed to solidify on extensive washing with petroleum ether. The complex was characterised by NMR spectroscopy (see Table 2). It did not mull in Nujol or KEL-F.

Tetraethylammonium pentachloro(isopropylimido)tungstate(VI) (**7**)

Tetraethylammonium chloride (0.30 g, 1.8 mmol) in dichloromethane (30 cm^3) was added to hexachloro-di-μ-chlorobis(isopropylimido)ditungsten-(VI) (1.4 g, 1.8 mmol) in dichloromethane (60 cm^3) and the solution stirred for 2 h. The red solution was filtered and the solvent removed *in vacuo* leaving a red crystalline solid which was recrystallised from dichloromethane giving the complex as large red prisms. M.p. 154°C.

IR (Nujol) bands at 1360s, 1255s, 1210w, 1160s, 1150m, 1110w, 1070w, 1050w, 995s, 920w, 900w, 860w, 810w, 780s, 680w, 650w, 630w, 610m, 575m, 510w, 460w, 400w, 375w, 350m, 320s, 310s, 300s, 290s, 280m, 240s; (KEL-F) 2925w, 2270w, 1510w, 1460m, 1450w, 1430m, 1390m, 1370m, 1350m cm^{-1}.

Dichloro(isopropylimido)tris(trimethylphosphine)tungsten(IV) (**8**)

Isopropylimido tungsten tetrachloride dimer (1.2 g, 1.6 mmol) in benzene (100 cm^3) was added to a benzene solution (100 cm^3) of trimethylphosphine (1 cm^3, 9 mmol) and sodium–mercury amalgam (0.16 g sodium, 7 mmol; 50 g mercury) and the mixture stirred for 4 h. The blue solution was filtered from the spent amalgam, the solvent removed and the resulting solid taken up in toluene. Reducing the volume to *ca* 15 cm^3 and cooling to −20°C gave the complex as a purple crystalline solid. M.p. 118–120°C.

IR (Nujol) bands at 1410m, 1305m, 1300m, 1270s, 1260s, 1150w, 1110m, 1090m, 1070m, 1010m, 970s, 945s, 850m, 820m, 800s, 705m, 665s, 610w, 540w, 470w, 400w, 385w, 370m, 345s, 335m, 330m, 290w, 270s, 255m; (KEL-F) 2960s, 2900s, 2850m, 1450w, 1410s cm^{-1}.

Tris(t-butoxy)chloro(isopropylimido)tungsten(VI) (**9**)

Lithium *t*-butoxide (1.75 g, 22 mmol) in diethyl ether (30 cm^3) was added to a solution of isopropylimido tungsten tetrachloride (2.0 g, 2.0 mmol) in diethyl ether (40 cm^3) and the mixture was stirred for 12 h. The solution was filtered from the precipitated lithium chloride and the solvent removed to give a pale yellow crystalline solid which was extracted with petroleum ether (50 cm^3). After filtering, the volume was reduced to *ca* 5 cm^3 and the solution allowed to stand giving the complex as a colourless crystalline solid which was filtered off, washed with petroleum ether cooled to dry-ice temperature and dried *in vacuo*. M.p. 187°C decomp.

IR (Nujol) bands at 1650m, 1630m, 1610s, 1520m, 1500m, 1390m, 1260w, 1210m, 1160m, 1090w, 1020m, 950s, 935s, 900s, 860s, 840s, 820w, 800w, 660s, 575m, 480s, 465s, 410m, 365s, 340m, 260w; (KEL-F) 1455s, 1430w, 1390m, 1375s, 1365s cm^{-1}.

Tetraphenylarsonium pentachloro(isopropylimido)tungstate(VI) (**10**)

Tetraphenylarsonium chloride (1.39 g, 3.3 mmol) in dichloromethane (50 cm^3) was added to hexachloro-di-μ-chlorobis(isopropylimido)ditungsten-(VI) (1.2 g, 1.57 mmol) and the mixture was stirred for 2 h. The resulting red solution was filtered and the solvent removed to give the complex as an orange–red flaky solid which was washed several times with petroleum ether and dried *in vacuo*.

M.p. 45–50°C. The complex did not mull in Nujol or KEL-F.

Crystallographic studies

Single crystals of $[W(NCHMe_2)Cl_4]_2 \cdot C_6H_6$ (**1a**) (grown from benzene solution) and $[W(NCHMe_2)Cl_5][NEt_4]$ (**7**) (grown from dichloromethane) were sealed under nitrogen in glass capillaries and mounted on an Enraf–Nonius CAD-4 diffractometer.

Crystal data. Compound **1a**: $C_6H_{14}Cl_8N_2W \cdot C_6H_6$, $M = 843.63$, triclinic $a = 6.394(2)$, $b = 8.890(3)$, $c = 11.205(2)$ Å, $\alpha = 109.95(2)$, $\beta = 98.91(2)$, $\gamma = 93.96(2)°$, $U = 586.32$ Å^3; space group $P\bar{1}$, $Z = 1$, $D_c = 2.389$ g cm^{-3}, $F(000) = 390$, μ(Mo–K_α) = 112.7 cm^{-1}.

Crystal data. Compound **7**: $C_{11}H_{27}Cl_5N_2W$, M = 548.50, orthorhombic, $a = 13.667(5)$, $b = 15.152(2)$, $c = 9.432(2)$ Å, $U = 1953.10$ Å^3; space group *Pnma*, $Z = 4$, $D_c = 1.865$ g cm^{-3}, $F(000) = 1064$, μ(Mo–K_α) = 69.2 cm^{-1}.

Data collection. Accurate unit cell dimensions were determined by least-squares fits to the observed setting angles of 25 reflections using Mo–K_α radiation (Zr filter for $[W(NCHMe_2)Cl_4]_2 \cdot C_6H_6$, graphite monochromator for $[W(NCHMe_2)Cl_5][NEt_4]$).

Intensity data collections employed the $2\theta/\omega$ scan technique with a total background/peak count time ratio of 1/2. Reflections were counted for either 60 s or else until $\sigma(I)/I$ was 0.022 or 0.020 for the two compounds, respectively.[23] Measured data: compound **1a**, 2199 reflections ($\theta_{max} = 25°$), compound **7**, 2200 reflections ($\theta_{max} = 25°$). The intensities of three standard reflections were remeasured systematically throughout the data collections, and these showed isotropic declines to 0.35 and 0.71 of their initial values. The data were corrected for Lorentz, polarisation, crystal decay and absorption.[24]

Structure solutions and refinements. Both structures were solved by Patterson and Fourier methods and refined by the full-matrix least-squares technique.[25] The function minimised was $\sum w(|F_o| - |F_c|)^2$. Atomic scattering factors and dispersion corrections were for neutral atoms. After initial isotropic refinement, anisotropic thermal parameters were refined for the heavier atoms. In complex **7** the cation nitrogen atom occupies a crystallographic centre of symmetry with the β-carbons being related in pairs through the centre. The α-carbons are statistically disordered such that the cation spends half its time in one orientation, half its time in the alternative orientation, whilst maintaining common positions for the nitrogen and four outer carbon atoms. Such a model enables a very satisfactory refinement to be carried out in the centrosymmetric space group *Pnma*. Final residuals R and R_w were 0.050 and 0.053 for both the 1325 observed data [$I > 3\sigma(I)$] of compound **1a** and the 1157 observed data [$I > 2.5\sigma(I)$] of compound **7**.

Final atomic co-ordinates for both complexes, tables of thermal parameters, and listings of observed and calculated structure factors have been deposited with the Editor as supplementary material.*

RESULTS AND DISCUSSION

Preparation of complexes

To make ^{13}C NMR spectral comparisons with the range of known *t*-butylimido complexes we required $[W(NCMe_3)Cl_4]_2$, however, the general procedure for preparing organoimido complexes of tungsten(VI) by reacting alkylisocyanates with $[WOCl_4]$ fails with *t*-butylisocyanate.[13] We have thus restricted our studies to isopropylimido complexes, the preparation of $[W(NCHMe_2)Cl_4]_2$ (**1**) being straightforward. The preparative methods used are similar to those employed for phenylimido complexes of tungsten(VI)[13] and are shown in Fig. 1. Analytical data are contained in Table 1.

Several of the complexes persisted as gummy materials or did not analyse satisfactorily so that characterisation was made by NMR spectroscopy (Table 2). For example, reaction of **1** with eight equivalents of sodium acetate led to a green oil, the main component of which was identified as $[W(NCHMe_2)(\mu\text{-}OAc)(OAc)_2Cl]_2$ (**6**) from the presence in the ^1H NMR spectrum of three acetate group methyl resonances, a doublet for the isopropyl methyl groups and the isopropylimido methine proton septet at the characteristic shift of 6.05 ppm. In the ^{13}C NMR spectrum the isopropyl methine and methyl carbons appeared at 65.5 and 23.8 ppm, respectively, three acetate group methyl resonances were present at 22.4, 23.1 and 24.1 ppm, while there were three acetate group quaternaries at 170, 172 and 181.0 ppm, the latter resonance being in the vicinity of that characteristic of bridging acetate ligands.[14]

Reaction of **1** with eight equivalents of NaS_2CNEt_2 similarly gave an oil characterised as $[W(NCHMe_2)Cl(S_2CNEt_2)_3]_x$ (**4**) on the basis of

* Atom co-ordinates for these structures have also been deposited with the Cambridge Crystallographic Data Centre for inclusion in their data base. Copies are available on request from the Editor at Queen Mary College.

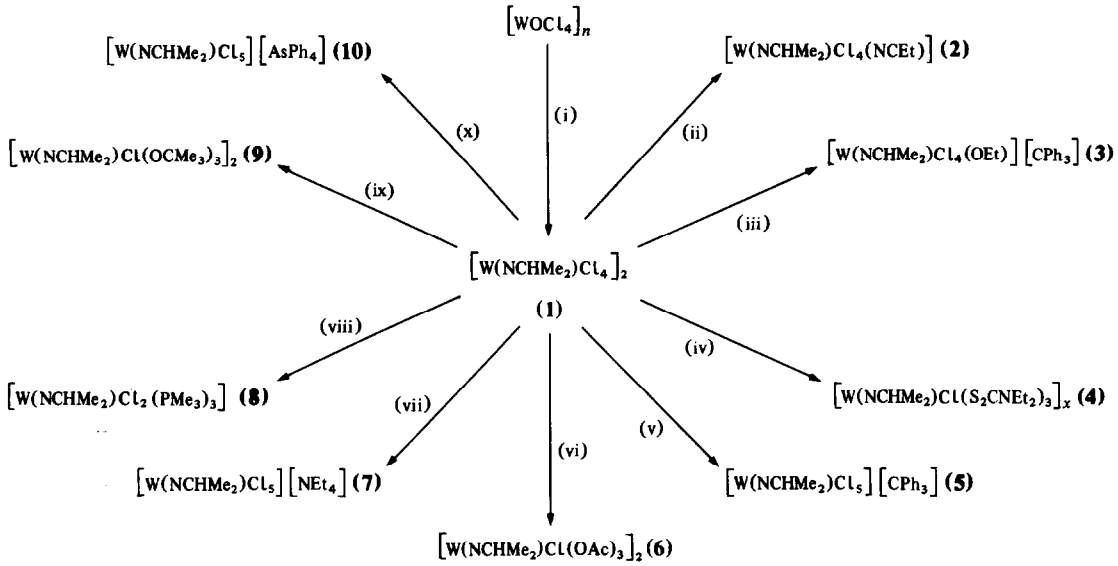


Fig. 1. (i) Me_2CHNCO–benzene; (ii) EtCN; (iii) Ph_3COEt–CH_2Cl_2; (iv) NaS_2CNEt_2–CH_2Cl_2; (v) Ph_3CCl–CH_2Cl_2; (vi) NaOAc–benzene; (vii) Et_4NCl–CH_2Cl_2; (viii) Na–Hg amalgam, PMe_3 and benzene; (ix) $LiOCMe_3$–diethyl ether; and (x) Ph_4AsCl–CH_2Cl_2.

methine, methylene and methyl group proton resonances in the ratio of 1 : 12 : 24. The ^{13}C NMR spectrum suggested the presence of two species, there being two isopropylimido CH resonances and two sets of dithiocarbamate quaternary carbons. The two terminal quaternaries of each species appear at 192.8 and 196.9 ppm while two further resonances at 196.0 and 200.3 ppm are assigned to chelating or bridging dithiocarbamate ligands. Structures **4a** and **4b** are proposed on the basis of these features.

We were also interested in preparing complexes that given sufficient electron density on the imido nitrogen atom might react further to form amido complexes by the following reaction sequence:

$$[W(NCHMe_2)Cl_4]_2 + 2R{-}X \rightarrow 2[W(NCHMe_2)Cl_4X][R] \rightarrow [W(NCHMe_2R)Cl_4X].$$

Isopropylimido tungsten tetrachloride is surprisingly inert to a range of alkyl halides but the trityl

Table 1. Physical data

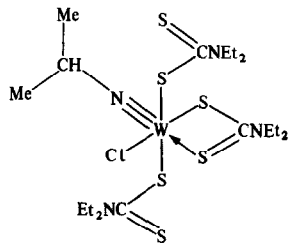
Complex	Colour	M.p.[a] (°C)	Analytical data C	H	N
$[W(NCHMe_2)Cl_4]_2$ (1)	orange	158–160	9.4 (9.4)	2.1 (1.9)	3.3 (3.7)
$[W(NCHMe_2)Cl_4(NCEt)]$ (2)	red	179–183	16.5 (14.1)	2.8 (2.8)	6.0 (6.6)
$[W(NCHMe_2)Cl_5][CPh_3]\cdot CH_2Cl_2$ (5)[b]	yellow–brown	102–106	36.6 (37.0)	3.3 (3.2)	1.5 (1.9)
$[W(NCHMe_2)Cl_5][NEt_4]$ (7)	red	154	24.1 (24.1)	5.0 (5.1)	5.1 (5.1)
$[W(NCHMe_2)Cl_2(PMe_3)_3]$ (8)	purple	118–120	27.0 (26.7)	6.4 (6.3)	2.3 (2.6)
$[W(NCHMe_2)Cl(OCMe_3)_3]_2$ (9)	colourless	187(d)	36.3 (36.5)	6.9 (6.9)	3.1 (2.5)
$[W(NCHMe_2)Cl_5][AsPh_4]$ (10)	orange	45–50	40.6 (40.5)	4.0 (3.4)	1.6 (1.8)

[a] Decomposition points in parentheses.
[b] CH_2Cl_2 verified by ^1H NMR spectrum.

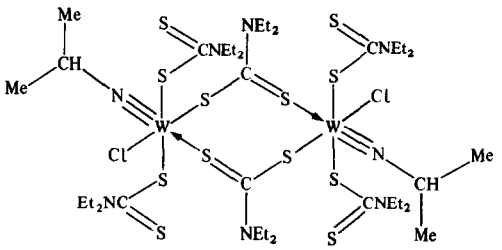
Table 2. NMR spectra

Complex	^{13}C NMR spectra[a]				^{1}H NMR spectra[a,b]		
	δ_α	δ_β	Δ	Others	CH	Me_2	Others
$[W(NCHMe_2)Cl_4]_2$ (1)	71.6	23.2	48.4	—	7.05	1.72	—
$[W(NCHMe_2)Cl_4(NCEt)]$ (2)	68.4	23.1	45.3	9.4 (CH_3) 11.7 (CH_2) 122.3 (NC)	7.08	1.68	1.46 (t, 3H, CH_3) 2.78 (q, 2H, CH_2)
$[W(NCHMe_2)Cl_4(OEt)][CPh_3]$ (3)[c]	67.3	22.8	44.5	22.8 (CH_3) 84.1 (CH_2) 128.1, 130.0, 131.5, 144.3 (CPh_3)[d]	6.64	1.30–1.89(b)	1.30–1.80 (obscured t, 3H, CH_3) 5.42 (q, 2H, OCH_2) 7.40 (s, 15H, CPh_3)
$[W(NCHMe_2)Cl(S_2CNEt_2)_3]_x$ (4)[c]	66.6, 64.4	21.9, 20.3	44.7, 44.1	11.5, 12.5 (CH_3) 43.4, 44.1, 44.4, 45.4, 46.9, 49.7 (CH_2) 193.8, 196.0, 196.9, 200.3 (CS_2)	4.50	1.50 (obscured)	1.10–1.72 (m, 18H, CH_3) 3.42–4.20 (m, 12H, CH_2)
$[W(NCHMe_2)Cl_5][CPh_3]$ (5)	66.0	23.4	42.6	129.7, 138.6, 141.3 (CPh_3)[g]	7.10 (obscured)	1.63	7.30–8.20 (m, 15H, CPh_3)
$[W(NCHMe_2)Cl(OAc)_3]_2$ (6)[c]	65.6	23.8	41.8	22.4, 23.1, 24.1 (CH_3) 171.0, 172.5, (O_2C, terminal ligand) 181.4 (O_2C, bridging ligand)	6.0	1.30	2.10, 2.15, 2.25 (3, 9H, $3CH_3$)
$[W(NCHMe_2)Cl_5][NEt_4]$ (7)	64.6	23.8	40.8	8.2 (CH_3) 53.3, 53.5, 53.7 (triplet, CH_2)	6.60	1.65	1.40–1.50 (m, 12H, $4CH_3$) 3.10–3.64 (m, 8H, $4CH_2$)
$[W(NCHMe_2)Cl_2(PMe_3)_3]$ (8)[c]	64.3, 63.0	20.9	43.4, 42.1 (41.3, 40.0)[f]	17.2 (very broad, PMe_3)	[g]	1.12	1.56–1.85 (m, 27H, $3PMe_3$)
$[W(NHCMe_2)Cl(OCMe_3)_3]_2$ (9)	63.9	23.4	40.5	3.4 (CH_3) 79.4 (OC)	5.10	1.35	1.4 (s, 27H, $3Me_3$)
$[W(NCHMe_2)Cl_5][AsPh_4]$ (10)	63.8	23.7	40.1	120.3, 129.4, 130.1, 131.2, 133.0, 134.9 142.3 ($AsPh_4$)	7.1 (obscured)	1.55	7.4–8.2 (m, 20H, $AsPh_4$)

[a] Spectra obtained in $CDCl_3$, values ppm from TMS.
[b] b = broad, m = multiplet, q = quartet, s = singlet, t = triplet.
[c] Complexes characterised by NMR spectra.
[d] Trityl cation quaternary carbon not observed after acquisition times used.
[e] Tungsten(IV) complex. Peaks broad due to slight paramagnetism.
[f] Δ value calculated using average of δ_β values for other complexes (23.0).
[g] CH resonance not observed.



4a



4b

complexes $[W(NCHMe_2)Cl_4X][CPh_3]$ (X = Cl, OEt) (**5** and **3**) were readily formed but persisted as dichloromethane solvates. The complexes are 1 : 1 electrolytes in acetonitrile although the conductance values lie slightly outside the recognised lower limit. Ethoxy complex (**3**) failed to form a solid and was characterised by ^1H NMR spectroscopy, the salient features being the isopropylimido group methine proton resonance at 6.64 ppm and the ethoxide CH_2 quartet at 5.42 ppm. Both complexes apparently react further in solution but we have not yet been able to gain reliable evidence for transformation of either to an amido complex.

NMR spectra

^1H and ^{13}C NMR spectral details for the complexes are contained in Table 2. In the ^1H NMR spectra the imido ligand methine proton occurs in the region 4.5 to 7.1 ppm but as these protons may be influenced by environmental effects related to the different supporting ligands, interpretation of the shifts is not meaningful. In general however the protons are more shielded when the complexes contain oxygen or sulphur donors.

Table 2 shows the complexes arranged in descending order of the isopropylimido ligand ^{13}C NMR spectrum α-carbon resonance, relative to TMS. ^{13}C NMR studies for *t*-butylimido complexes of a range of metals[12] have shown that decreasing electron density on the nitrogen atom causes a downfield shift of the α-carbon resonance and an upfield shift for the β-carbon, the difference between the two, Δ ($\Delta = \delta_\alpha - \delta_\beta$), being used as an experimental probe for electron density on nitrogen. For the present complexes where only tungsten metal-centres are present, the position of the α-carbon resonance is used for this purpose as within experimental error the δ_α values follow the trend downwards.

The δ_α values indicate that the nitrogen lone pair participates in multiple bonding to tungsten to the greatest extent in $[W(NCHMe_2)Cl_4]_2$ (**1**). Thus the complex might be expected to show electrophilic reactivity at nitrogen with a progressive trend towards nucleophilic activity for the other complexes down the table. We note, however, that in comparison with the various *t*-butylimido complexes reported,[12] the Δ (40.1) value for $[W(NCHMe_2)Cl_5][AsPh_4]$ (**10**) compares with that of $[OsO(NBu^t)_3]$ (40.1) so that the anionic tungsten complex would still be regarded as being essentially electrophilic.

As an additional probe of small changes in electron density between nitrogen and tungsten we have obtained the methine C–H coupling constant for two complexes with widely differing δ_α values in view of the magnitude of J_{CH} for the α-carbon of substituted alkyl organic compounds being dependent on substituent electronegativity.[15] For $[W(NCHMe_2)Cl_4]_2$ (**1**) and $[W(NCHMe_2)Cl_5][NEt_4]$ (**7**), the J_{CH} values at 144.5 and 141.0 Hz, respectively, are much larger than J_{CH} for isopropylamine at 124.5 Hz, but the difference between complexes, although small, does indicate that polarisation of the W—N bond is slightly greater in the dimer. The J_{CH} values obtained compare with CH_3OH at 141.0 Hz, CH_3OPh at 143.0 Hz and CH_3NO_2 at 146.7 Hz.[15]

In order to relate ^{13}C NMR features to structural aspects, X-ray crystal structure determinations were carried out on $[W(NCHMe_2)Cl_4]_2 \cdot C_6H_6$ (**1a**) and $[W(NCHMe_2)Cl_5][NEt_4]$ (**7**).

X-ray crystallography studies

The X-ray crystal structure of $[W(NCHMe_2)Cl_4]_2 \cdot C_6H_6$ (**1a**) shows the molecule to be a dimer in which the two halves are centrosymmetrically related. Each tungsten atom adopts a distorted octahedral co-ordination geometry, consisting of three terminal chlorine atoms with a fourth chlorine forming a bridge between the two tungsten atoms. The isopropylimido ligand is terminal and lies *trans* to one of the chlorine bridges. A view of the molecule is shown in Fig. 2. Bond distances and angles are given in Table 3.

The isopropylimido ligand is essentially linear with a W—N—C(1) bond angle of 171.5(4)°. The

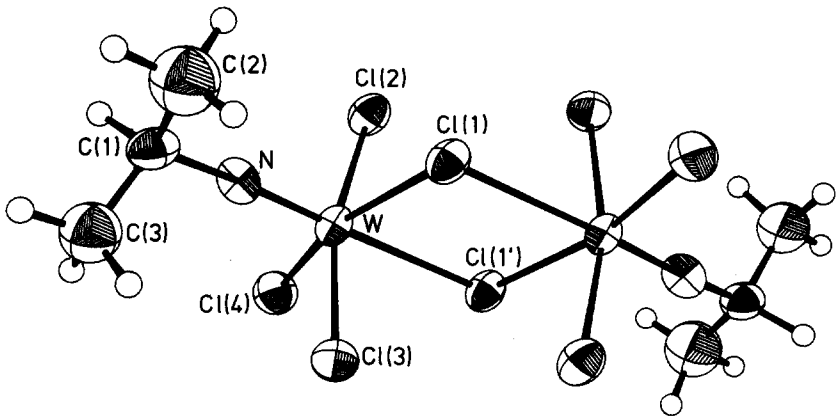


Fig. 2. $[W(NCHMe_2)Cl_4]_2$ molecule. Thermal ellipsoids have been drawn at the 50% probability level.

short W—N bond distance of 1.697(12) Å is not significantly different from the value of 1.71 Å predicted for a W—N bond acting as a four-electron donor (W≡NR).[1] The bridging chlorides are unsymmetrical in that W—Cl(1) is 2.418(4) Å whereas W—Cl(1′) is 2.736(5) Å. Since Cl(1′) is situated *trans* to the imido function, the lengthening of W—Cl(1′) is most likely due to a very strong *trans*-influence associated with the multiple bonding between tungsten and nitrogen.[13] The terminal W—Cl bond distances range from 2.285(4) to 2.310(4) Å.

Distortion from octahedral geometry in the molecule arises from chlorine atoms (1)–(4) being displaced away from the imido group, the mean N—W—Cl(*n*) angle (*n* = 1–4) being 97.8°. The tungsten atom lies 0.32 Å from the plane made by these four chlorine atoms.

The crystal structure of **7** consists of discrete tetraethylammonium cations and complex anions. The anion is monomeric with a distorted octahedral geometry. The molecule is shown in Fig. 3 and bond distances and angles shown in Table 4.

The isopropylimido ligand is again essentially linear with a W—N—C bond angle of 174.4(16)° while the W—N(1) bond length of 1.763(16) is significantly longer than that found for the parent dimer and slightly longer than those found for other organoimido complexes in which the W—N bonds are considered to have bond orders of less than 3.[1,8,13,16,17] The W—Cl bond lengths in the equatorial plane range from 2.346(3) to 2.357(5) Å while the

Table 3. Selected bond lengths and angles for $[W(NCHMe_2)Cl_4]_2 \cdot C_6H_6$

Bond length (Å)			
W—N	1.697(12)	W—Cl(3)	2.307(4)
W—Cl(1)	2.418(4)	W—Cl(4)	2.285(4)
W—Cl(1′)	2.736(5)	N—C(1)	1.45(2)
W—Cl(2)	2.310(4)	W···W′	4.008(1)
Bond angle (degrees)			
W—N—C(1)	171.5(9)	Cl(1)—W—Cl(4)	162.95(14)
Cl(1)—W—N	95.6(4)	Cl(1′)—W—Cl(2)	83.91(13)
Cl(2)—W—N	99.0(4)	Cl(1′)—W—Cl(3)	81.62(13)
Cl(3)—W—N	95.1(4)	Cl(1′)—W—Cl(4)	84.92(13)
Cl(4)—W—N	101.4(4)	Cl(2)—W—Cl(3)	165.18(14)
Cl(1′)—W—N	172.9(6)	Cl(2)—W—Cl(4)	90.48(15)
Cl(1)—W—Cl(1′)	78.08(13)	Cl(3)—W—Cl(4)	91.39(15)
Cl(1)—W—Cl(2)	86.47(13)	W—Cl(1)—W′	101.92(10)
Cl(1)—W—Cl(3)	87.44(14)		

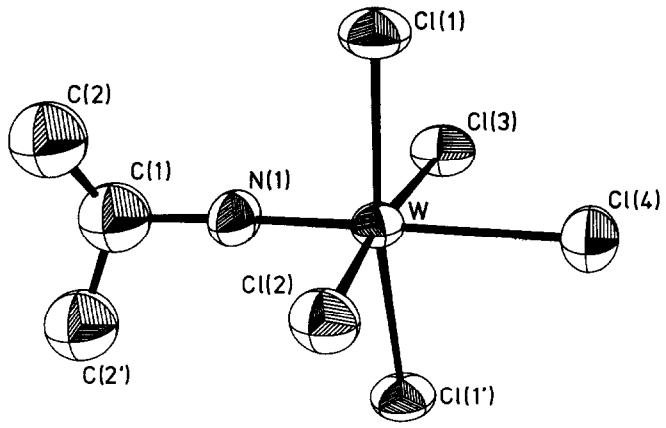


Fig. 3. $[W(NCHMe_2)Cl_5]$ anion. Thermal ellipsoids have been drawn at the 50% probability level.

W—Cl bond *trans* to the imido function is long at 2.462(5) Å. The octahedron is less distorted than in the dimer with the average of the angles between nitrogen, tungsten and the four equatorial chlorines being 93.6°. The tungsten atom lies 0.15 Å from the plane made by these four chlorine atoms.

The main point of interest in the two structures is the difference in the W—N bond lengths which at 1.697(12) and 1.763(16) differ by 0.066 Å which is at least 4 standard deviations. However the W—N—C bond angles at 171.5(9)° and 174.4(16)° are not significantly different, being essentially linear, so that the differences in bond lengths can apparently be accommodated without effecting a major change in the hybridisation state of nitrogen. By contrast in $[Mo(NPh)_2(S_2CNEt_2)_2]$[11] where one Mo—N bond is long [1.789(4) Å] and is associated with a Mo—N—C bond angle of 139.4(4)° a bond order of about 2.3 is implied but in $[\{W(NPh)(OCMe_3)_2\}_2(\mu\text{-}O)(\mu\text{-}OCMe_3)_2]$[17] a bond order of about 2.8 is suggested for a W—N bond length and W—N—C bond angle of 1.737(5) Å and 165.3(5)°, respectively. In the $[W(NCHMe_2)Cl_5]$ anion however, the W—N bond is lengthened to 1.763(16) Å without significant change to the W—N—C bond angle.

The W—N bond lengths observed in the present complexes may be explained in terms of the 18-electron rule when bonding of the other ligands is also taken into account. In the dimeric complex the bond lengths associated with the bridging chloride [2.418(4) and 2.736(5) Å] are consistent with Cl(1) acting as a one-electron donor to W and a two-electron donor to W′. The Cl(1)—W′ bond length is extremely long, as is the equivalent W—Cl(1′) bond length so that the bonding between the two halves of the molecule is weak. Assuming however that Cl(1) acts as a one- and two-electron donor to the respective tungsten atoms, the remaining terminal chlorides are one-electron donors and the

Table 4. Selected bond lengths and angles for $[W(NCHMe_2)Cl_5][NEt_4]$

	Bond length (Å)		
W—N(1)	1.763(16)	W—Cl(2)	2.356(5)
W—Cl(1)	2.346(3)	W—Cl(3)	2.357(5)
W—Cl(1′)	2.346(3)	W—Cl(4)	2.462(5)
	Bond angle (degrees)		
W—N(1)—C(1)	174.4(16)	Cl(2)—W—Cl(3)	172.5(2)
Cl(1)—W—Cl(1′)	172.9(1)	Cl(2)—W—Cl(4)	85.8(2)
Cl(1)—W—Cl(2)	89.9(1)	Cl(2)—W—N(1)	92.3(6)
Cl(1)—W—Cl(3)	89.6(1)	Cl(3)—W—Cl(4)	86.7(2)
Cl(1)—W—Cl(4)	86.5(1)	Cl(3)—W—N(1)	95.2(6)
Cl(1)—W—N(1)	93.5(1)	Cl(4)—W—N(1)	178.1(6)

imido group acts as a four-electron donor, then the electron count for the complex is 16.

Consideration of the terminal W—Cl bond lengths indicates that the two extra electrons needed to complete an 18-electron count, arise mainly from a π-contribution at Cl(4) [the W—Cl(4) bond length at 2.285(4) Å is similar to the terminal W—Cl bond lengths in $[WOCl_4]_x$[18] at 2.28 Å where an extra electron from each chlorine atom or more realistically a series of Cl⇌W—Cl canonicals involving π-bonding, is needed to achieve 18 electrons]. The contribution lies to a lesser extent from Cl(2) and Cl(3) [W—Cl bond lengths 2.310(4) and 2.307(4) Å, respectively]. The W—Cl(4) bond length also indicates that chlorine is better able to participate in π-bonding to the metal when it lies *trans* to Cl(1) in which minimal π-bonding to W occurs. As such, Cl(4) does not have to compete for π-bonding orbitals as do Cl(2) and Cl(3). Of the ligands capable of π-bonding, the imido nitrogen is apparently best able to supply electrons and this is reflected by the shortened W—N bond length [1.697(12) Å] which is similar to the predicted value of 1.71 Å for a four-electron donor.[1]

In the case of the anionic complex, more chlorine ligands are available to participate in π-bonding and this appears to relieve the need for the imido ligand to act strictly as a four-electron donor. The W—Cl(4) bond length at 2.462(5) Å is considerably longer than those in the equatorial plane as a result of the imido group *trans* influence so that little π-bonding is expected from this ligand. The remaining W—Cl bond lengths range from 2.346(3) to 2.357(5) Å, all being shorter than that found for chlorine acting as a one-electron donor in the dimeric complex, so that they represent the average of the canonicals contributing to π-bonding.

CONCLUSION

Correlation of an 18-electron count with structural details thus indicates that changes in the W—N bond length between the two complexes results mainly from overall π-bonding requirements rather than a competitive π-bonding situation *trans* to the imido function. While there are differences in the shift of the α-carbon ^{13}C NMR resonances of the imido ligands for all the complexes these can also be expected to relate to π-bonding capabilities of the other ligands present. For example, from inspections of the decreasing δ_α values in Table 1, $[W(NCHMe_2)Cl_4(NCEt)]$ (**2**), with more terminal chlorine ligands, has a lesser need for W—N π-bonding than does $[W(NCHMe_2)Cl_4]_2$ (**1**). $[W(NCHMe_2)Cl(OCMe_3)_3]_2$ (**9**) lies at the lower end of the table as the alkoxide ligand is a better π-bonding ligand than chlorine.[19] Interestingly, $[W(NCHMe_2)Cl_4(OEt)][CPh_3]$ (**3**) in which the ethoxide ligand is expected to lie *trans* to the imido function and therefore compete for π-bonding orbitals, is intermediate in the list, so that the nitrogen lone pair is not free to interact with the carbocation and otherwise produce the amido complex, $[W(NCHMe_2CPh_3)Cl_4(OEt)]$.

REFERENCES

1. W. A. Nugent and B. L. Haymore, *Coord. Chem. Rev.* 1980, **31**, 123.
2. R. R. Schrock, *Science* 1983, **219**, 13.
3. A. O. Chong, K. Oshima and K. B. Sharpless, *J. Am. Chem. Soc.* 1977, **99**, 3420.
4. W. A. Nugent and R. L. Harlow, *J. Am. Chem. Soc.* 1980, **102**, 1759.
5. W. A. Nugent and R. L. Harlow, *Abstracts, 179th National Meeting of the American Chemical Society*, Houston, TX, No. PETR-26 (March 1980).
6. E. A. Maatta and R. A. D. Wentworth, *Inorg. Chem.* 1979, **18**, 2409.
7. W. P. Griffith, N. T. McManus, A. C. Skapski and A. J. Nielson, *Inorg. Chim. Acta* 1985, **103**, L5.
8. P. A. Bates, A. J. Nielson and J. M. Waters, *Polyhedron* 1985, **4**, 999.
9. D. M.-T. Chan, W. C. Fultz, W. A. Nugent, D. C. Roe and T. H. Tulip, *J. Am. Chem. Soc.* 1985, **107**, 251.
10. G. V. Goeden and B. L. Haymore, *Inorg. Chem.* 1983, **22**, 157.
11. B. L. Haymore, E. A. Maatta and R. A. D. Wentworth, *J. Am. Chem. Soc.* 1979, **101**, 2063.
12. W. A. Nugent, R. J. McKinney, R. V. Kasowski and F. A. Van-Catledge, *Inorg. Chim. Acta* 1982, **65**, L91.
13. D. C. Bradley, M. B. Hursthouse, K. M. A. Malik, A. J. Nielson and R. L. Short, *J. Chem. Soc., Dalton Trans.* 1983, 2651.
14. A. J. Nielson, *Transition Met. Chem.* 1981, **6**, 180.
15. J. B. Stothers, *Carbon-13 NMR Spectroscopy*, p. 337. Academic Press, New York (1972); G. C. Levey, R. L. Lichter and G. L. Nelson, *Carbon-13 Nuclear Magnetic Resonance Spectroscopy*, 2nd edn, p. 68. Wiley, New York (1980).
16. A. J. Nielson, J. M. Waters and D. C. Bradley, *Polyhedron* 1985, **4**, 285.
17. F. A. Cotton and E. S. Shamshoum, *J. Am. Chem. Soc.* 1984, **106**, 3222.
18. Von H. Hess and H. Hortung, *Z. Anorg. Allg. Chem.* 1966, **344**, 157.
19. M. H. Chisholm, *Polyhedron* 1981, **2**, 681.
20. R. Colton and I. B. Tonkins, *Aust. J. Chem.* 1965, **18**, 447.
21. W. Wolfsberger and H. Schmidbaur, *Synth. React. Inorg. Metal-Org. Chem.* 1974, **4**, 149.
22. A. J. Nielson, *Chem. N.Z.* 1985, **49**, 11.

23. $\sigma(I) = (20.1166/NPI)\sqrt{C+4B}$, where the constant term in the maximum possible scan rate, *NPI* is the ratio of the maximum possible scan rate to the scan rate for the measurement, C = total counts, B = total background.
24. Empirical absorption corrections using azimuthal scan data, A. C. T. North, D. C. Phillips and F. Scott Mathews, *Acta Cryst.* 1968, **A24**, 351.
25. Computing was carried out using the SDP suite of programs on a PDP-11 computer and SHELX-76 on an IBM 4341 computer.

Polyhedron Vol. 5, No. 12, pp. 2093–2096, 1986
Printed in Great Britain

0277–5387/86 $3.00+.00
© 1986 Pergamon Journals Ltd

CRYSTAL AND MOLECULAR STRUCTURES OF TWO EUROPIUM(III) NITRATE COMPLEXES WITH TRIPHENYLPHOSPHINE OXIDE

G. VALLE*

Centro di studi sui Biopolimeri del C.N.R., Via Marzolo 1, 35131 Padova, Italy

and

G. CASOTTO, P. L. ZANONATO and B. ZARLI*

Dipartimento di Chimica Inorganica, Metallorganica ed Analitica, Universita' di Padova, Via Loredan 4, 35131 Padova, Italy

(*Received* 17 *March* 1986; *accepted* 19 *May* 1986)

Abstract—The X-ray structures of the complexes $Eu(NO_3)_3(Ph_3PO)_3(acetone)_2$ (**A**) (Ph_3PO = triphenylphosphine oxide) and $Eu(NO_3)_3(Ph_3PO)_2(ethanol)$ (**B**) have been solved by the heavy-atom method, by using the three-dimensional Patterson–Fourier synthesis. The crystals are both monoclinic and belong to the space group $P2_1/n$, with $Z = 4$. The cell dimensions are: $a = 27.825(4)$ Å, $b = 19.422(4)$ Å, $c = 11.238(2)$ Å, $\beta = 94.9(3)°$ for **A**; and $a = 22.193(4)$ Å, $b = 10.866(2)$ Å, $c = 17.101(3)$ Å, $\beta = 105.6(3)°$ for **B**. In both complexes the europium(III) ion is ennea-coordinated to three chelate nitrate groups and three oxygens of the Ph_3PO ligands for **A** and two of the Ph_3PO and one of the ethanol for **B**. The acetone molecules of **A** are outside the coordination sphere of the metal and disordered.

A wide interest has been shown concerning the complexes formed by europium(III), together with the other lanthanides, and various monodentate neutral ligands with O as the donor atom.[1–14] These simple ligands have been proved to be very useful in the study of the different coordination geometries which are possible for this ion, because compounds with many stoicheiometries can be obtained, depending upon the reaction conditions. Different compounds are obtained according to the binding ability of the anion and the solvent, and the experimental procedure itself. On the basis of IR, electronic and fluorescence spectra, coordination numbers and idealized geometries around the metal center have been proposed,[10,15–23] whereas few X-ray structures have been reported in the literature to support the spectroscopic results.[24–27] It therefore seemed interesting to have a series of these simple compounds for a complete study of their characteristics, and of the electronic and structural properties by absorption, fluorescence and Mössbauer effect spectroscopies, and, when feasible, by X-ray structure determinations. The goal of this research is an attempt to rationalize the effects leading to one of the various possible geometries. Therefore, several europium(III) nitrate complexes with triphenylphosphine oxide (Ph_3PO) of triphenylarsine oxide have been prepared. The use of the nitrate group as an anion is due to its good bidentate ligand behavior, and to its small bite that allows us to consider it as occupying a single coordination position. The phosphine and arsine oxides have been chosen because of the great binding ability of the O atom toward the lanthanides, enhanced by the strong electric dipole of the P–O or As–O moieties. We now report on the X-ray single-crystal structures of two of these complexes, namely $Eu(NO_3)_3(Ph_3PO)_3(acetone)_2$ (**A**) and $Eu(NO_3)_3(Ph_3PO)_2(ethanol)$ (**B**), that have characteristics typical of the whole series.

* Author to whom correspondence should be addressed.

EXPERIMENTAL

The complexes were prepared as previously reported.[1] Recrystallization from acetone and ethanol, respectively, yielded crystals which were suitable for the X-ray analysis.

Crystal data

A: $EuC_{60}H_{57}N_3O_{14}P_3$, monoclinic, space group = $P2_1/n$, $a = 27.825(4)$ Å, $b = 19.422(4)$ Å, $c = 11.238(2)$ Å, $\beta = 94.9(3)°$, $U = 6050.6(5)$ Å^3, $Z = 4$, $F(000) = 2632$, $D_c = 1.415$ g cm^{-3}, $D_m = 1.40$ g cm^{-3}, $\mu = 16.1$ cm^{-1}, $M = 1289.01$.

B: $EuC_{38}H_{36}N_3O_{12}P_2$, monoclinic, space group = $P2_1/n$, $a = 22.193(4)$ Å, $b = 10.866(2)$ Å, $c = 17.101(3)$ Å, $\beta = 105.6(3)°$, $U = 3972.0(8)$ Å^3, $Z = 4$, $F(000) = 1896$, $D_c = 1.572$ g cm^{-3}, $D_m = 1.56$ g cm^{-3}, $\mu = 16.0$ cm^{-1}, $M = 940.63$.

All the data were collected on a Philips PW 1100 four-circle diffractometer at room temperature in the range $2° < 2\theta < 50°$, with graphite-monochromatized Mo-K_α radiation ($\lambda = 0.71069$ Å). For complex **A**, 11,174 reflections were measured, of which 10,607 were unique ($R_{int} = 0.017$), and 4774, considered observed following the criterion $I > 3.5\sigma(I)$, were used in the subsequent calculations. For complex **B** 7233 reflections were measured, of which 6994 were unique ($R_{int} = 0.06$) and 5625 were considered observed [$I > 3\sigma(I)$].

Both structures were solved using the heavy-atom block-diagonal least-squares refinement based on F and the function $\sum w[|F_o|-|F_c|]^2$, in which $w = 1$, was minimized. The SHELX-76 program and its scattering factors for C, N, O and P atoms were used in the refinement;[28] scattering factor data for Eu were taken from Ref. 29. In structure **A** only Eu and P atoms, and in structure **B** also N and O atoms were refined anisotropically. The final R factor for complex **A** is 0.129 and for complex **B** 0.0436. The very high R value for **A** is attributed to the large disorder of the phenyl groups and the acetone molecules.

Distances and angles between the metal center and atoms forming the coordination polyhedra are reported in Table 4; the fractional atomic coordinates, thermal parameters, and the observed and calculated structure factors have been deposited as supplementary data with Editor, from whom copies are available on request.* Perspective views of the two structures, along with the atom-numbering scheme, are shown in Figs 1 and 2.

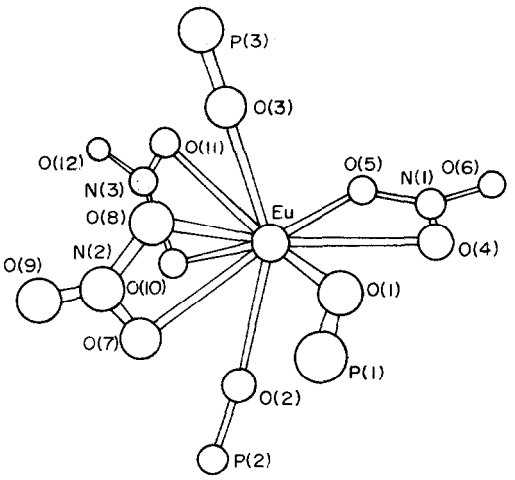


Fig. 1. Perspective view of the molecule $Eu(NO_3)_3(Ph_3PO)_3$ along with the atom-numbering scheme.

RESULTS AND DISCUSSION

The structures of both complexes are rather similar to each other: the europium(III) center is surrounded by nine O atoms, six from the three nitrate groups and three from the monodentate ligands. The nitrate groups are all bidentate as in other complexes of the 4*f* transition elements,[30–36] and as already suggested by the IR spectra.[1] The average O (nitrate)—Eu bond distances are 2.497 Å for complex **A** and 2.500 Å for complex **B**, and the O—Eu—O bond angles range between 50 and 52°, values that are close to those of related compounds.[25,26] The coordination sphere in complex **A** is completed by three phosphine oxide molecules,

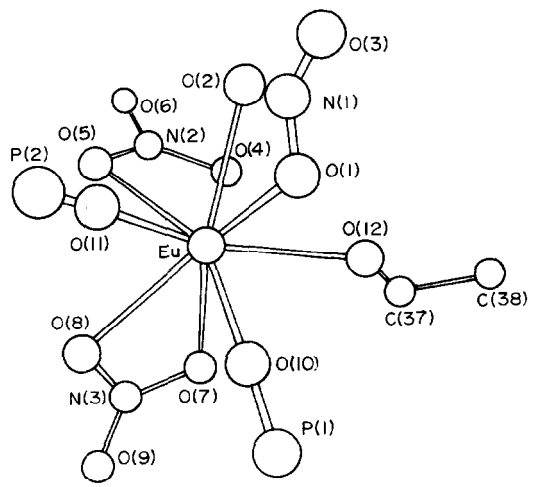


Fig. 2. Perspective view of the molecule $Eu(NO_3)_3(Ph_3PO)_2$(ethanol) along with the atom-numbering scheme.

* Atomic coordinates have also been deposited with the Cambridge Crystallographic Data Centre.

while in complex **B** one of the ligands has been substituted by an ethanol molecule [the acetone molecules are not bonded to the europium(III) ion, the Eu—O (acetone) distances being over 4.0 Å]. The polyhedron surrounding the europium(III) ion does not conform to any of the common geometries found in nine-coordinate lanthanide complexes, viz. tricapped trigonal prism and monocapped square antiprism. If the nitrate groups are considered as occupying a single coordination site, the geometry of the resulting polyhedron, formed now by the three O atoms from the monodentate ligands and by three N atoms, is a highly distorted octahedron where the angles between opposite ligands range from about 151° for O—Eu—O to 176° for N—Eu—N (Table 1). The bidentate nitrate groups may be considered as symmetrically bonded to the europium(III) ion because the Eu—O bond distances differ by less than 0.10 Å from each other. For complex **A** the N—O (bonded) distance seems to be identical to the N–O (non-bonded) distance, while in complex **B** it is slightly longer as already found in other symmetrically bidentate nitrate groups.[25] The O—N—O interbond angle involving both coordinated O atoms is smaller than 120° (average values are 116 and 117°, respectively) and the other two angles are correspondingly larger (121 and 122°). The Eu—O—P bond angles on the O

Table 1. Bond lengths (Å) and angles (°) with σ in parentheses

$Eu(NO_3)_3(Ph_3PO)_3(acetone)_2$		$Eu(NO_3)_3(Ph_3PO)_2(ethanol)$	
	Eu—O (ligand)		
Eu—O(1)	2.35(2)	Eu—O(12)	2.443(5)
Eu—O(2)	2.26(3)	Eu—O(10)	2.312(4)
Eu—O(3)	2.38(2)	Eu—O(11)	2.296(3)
	Eu—O (nitrate)		
Eu—O(4)	2.58(3)	Eu—O(1)	2.532(5)
Eu—O(5)	2.58(3)	Eu—O(2)	2.504(8)
Eu—O(7)	2.49(3)	Eu—O(7)	2.469(4)
Eu—O(8)	2.39(3)	Eu—O(8)	2.502(6)
Eu—O(10)	2.48(3)	Eu—O(4)	2.497(5)
Eu—O(11)	2.46(4)	Eu—O(5)	2.499(5)
	Angles centered on Eu		
	Both oxygens from the same nitrate		
O(4)—Eu—O(5)	52(1)	O(1)—Eu—O(2)	50.6(1)
O(7)—Eu—O(8)	50(1)	O(7)—Eu—O(8)	51.2(2)
O(10)—Eu—O(11)	50(1)	O(4)—Eu—O(5)	50.9(2)
	Oxygens of the ligands		
O(2)—Eu—O(3)	152(1)	O(11)—Eu—O(12)	150.6(2)
O(1)—Eu—O(2)	91(1)	O(10)—Eu—O(12)	79.4(2)
O(1)—Eu—O(3)	91(1)	O(10)—Eu—O(11)	90.3(2)
	N—Eu—N		
N(1)—Eu—N(2)	176(1)	N(1)—Eu—N(3)	176.0(2)
N(1)—Eu—N(3)	93(1)	N(1)—Eu—N(2)	97.6(2)
N(2)—Eu—N(3)	82(1)	N(2)—Eu—N(3)	86.4(2)
	N—Eu—O (ligand)		
N(1)—Eu—O(1)	101(1)	N(1)—Eu—O(10)	101.2(2)
N(1)—Eu—O(2)	100(1)	N(1)—Eu—O(12)	77.8(2)
N(1)—Eu—O(3)	107(1)	N(1)—Eu—O(11)	77.3(2)
N(2)—Eu—O(1)	83(1)	N(3)—Eu—O(10)	75.0(2)
N(2)—Eu—O(2)	80(1)	N(3)—Eu—O(12)	102.5(2)
N(2)—Eu—O(3)	71(1)	N(3)—Eu—O(11)	101.2(2)
N(3)—Eu—O(1)	165(1)	N(2)—Eu—O(10)	159.7(2)
N(3)—Eu—O(2)	90(1)	N(2)—Eu—O(12)	97.2(2)
N(3)—Eu—O(3)	82(1)	N(2)—Eu—O(11)	101.5(2)

atom vary from 144 to 171°, with values similar to those already found for uranyl complexes with Ph_3PO or triphenylarsine oxide.[37] It may be interesting to note that the values of this angle are widespread in the first complex (144, 163 and 171°) and much less in the second one (164 and 168°) which is also much less crowded for the substitution of a phosphine oxide molecule by an ethanol molecule.

Acknowledgement—Financial support from the M.P.I., Italy, is gratefully acknowledged.

REFERENCES

1. D. R. Cousins and F. A. Hart, *J. Inorg. Nucl. Chem.* 1981, **29**, 1745.
2. D. R. Cousins and F. A. Hart, *J. Inorg. Nucl. Chem.* 1967, **29**, 2965.
3. E. Giesbrecht and L. B. Zinner, *Inorg. Nucl. Chem. Lett.* 1969, **5**, 575.
4. J. I. Donoghue, E. Fernandez, J. A. McMillan and D. A. Peters, *J. Inorg. Nucl. Chem.* 1969, **34**, 1431.
5. J. T. Donoghue and D. A. Peters, *J. Inorg. Nucl. Chem.* 1969, **34**, 467.
6. L. B. Zinner and G. Vicentini, *Inorg. Chim. Acta* 1975, **15**, 235.
7. E. Giesbrecht and M. Kawashita, *J. Inorg. Nucl. Chem.* 1970, **32**, 2461.
8. M. K. Kuya and O. A. Serra, *J. Coord. Chem.* 1980, **10**, 13.
9. A. Seminara and E. Rizzarelli, *Inorg. Chim. Acta* 1980, **40**, 249.
10. C. H. Harrison and W. H. Watson, *J. Inorg. Nucl. Chem.* 1970, **32**, 2255.
11. A. Musumeci and A. Seminara, *Inorg. Chim. Acta* 1981, **54**, L81.
12. L. B. Zinner and G. Vicentini, *J. Inorg. Nucl. Chem.* 1975, **37**, 1999.
13. M. K. Kuya, O. A. Serra and V. K. L. Osorio, *J. Inorg. Nucl. Chem.* 1975, **37**, 1998.
14. O. A. Serra, M. Perrier, V. K. L. Osorio and Y. Kawano, *Inorg. Chim. Acta* 1976, **17**, 135.
15. E. Butter and W. Seifert, *Z. Anorg. Allg. Chem.* 1969, **368**, 134.
16. R. P. Scholer and A. E. Merbach, *Inorg. Chim. Acta* 1975, **15**, 15.
17. S. P. Sinha, *Z. Anorg. Allg. Chem.* 1977, **434**, 277.
18. D. X. West and R. E. Kohrman, *J. Inorg. Nucl. Chem.* 1979, **41**, 1569.
19. L. R. F. DeCarvalho, G. Vicentini and K. Zinner, *J. Inorg. Nucl. Chem.* 1981, **43**, 1088.
20. A. Musumeci, R. P. Bonomo and A. Seminara, *Inorg. Chim. Acta* 1980, **45**, L169.
21. L. R. F. DeCarvalho and G. Vicentini, *J. Coord. Chem.* 1981, **11**, 67.
22. A. Musumeci, R. P. Bonomo, V. Cucinotta and A. Seminara, *Inorg. Chim. Acta* 1982, **59**, 133.
23. A. Seminara and A. Musumeci, *Inorg. Chim. Acta* 1984, **95**, 291.
24. W. H. Watson, R. J. Williams and N. R. Stemple, *J. Inorg. Nucl. Chem.* 1972, **34**, 501.
25. C. Chieh, G. E. Toogood, T. D. Boyle and C. M. Burgess, *Acta Cryst.* 1976, **B32**, 1008.
26. J. C. G. Bunzli and B. Klein, *J. Inorg. Nucl. Chem.* 1980, **42**, 1307.
27. D. L. Kepert, J. M. Patrick and A. H. White, *Aust. J. Chem.* 1983, **36**, 477.
28. G. Sheldrick, *"SHELX 76" System of Computing Programs.* University of Cambridge, Cambridge (1976).
29. *International Tables for X-ray Crystallography*, 2nd Edn, Vol. 4, p. 99. Kynoch Press, Birmingham (1974).
30. L. A. Aslanov, L. I. Soleva and M. A. Porai-Koshits, *Zh. Strukt. Khim.* 1972, **13**, 1101.
31. L. A. Aslanov, L. I. Soleva and M. A. Porai-Koshits, *Zh. Strukt. Khim.* 1973, **14**, 1064.
32. K. K. Bhandary and H. Manohar, *Acta Cryst.* 1973, **B29**, 1093.
33. K. K. Bhandary, H. Manohar and K. Venkatesan, *J. Chem. Soc., Dalton Trans.* 1975, 288.
34. K. K. Bhandary, H. Manohar and K. Venkatesan, *Acta Cryst.* 1976, **B32**, 861.
35. B. Eriksson, L. O. Larsson, L. Ninisto and J. Valkonen, *Inorg. Chem.* 1980, **19**, 1207.
36. M. deMatheus, J. L. Brianso', X. Solans, G. Germain and J. P. Declercq, *Z. Krist.* 1983, **165**, 233.
37. G. Bombieri, U. Croatto, E. Forsellini, B. Zarli and R. Graziani, *J. Chem. Soc., Dalton Trans.* 1972, 560 (and references therein).

Polyhedron Vol. 5, No. 12, pp. 2097–2100, 1986
Printed in Great Britain

0277–5387/86 $3.00+.00
© 1986 Pergamon Journals Ltd

POTENTIOMETRIC DETERMINATION OF STABILITY CONSTANTS OF INORGANIC CYCLOPHOSPHATE COMPLEXES WITH COPPER(II), CADMIUM(II) AND LEAD(II) IONS

GENICHIRO KURA

Department of Chemistry, Fukuoka University of Education, Akama, Munakata, Fukuoka 811-41, Japan

(*Received* 24 *April* 1986; *accepted* 28 *May* 1986)

Abstract—The stability constants of the complexes of cyclophosphate anions and copper(II), cadmium(II) and lead(II) ions were determined by potentiometry with the use of ion-selective electrodes. For each metal ion, the stability constant of the 1 : 1 complex increases linearly with the charge on the phosphate ion. For the same cyclophosphate ion, the stability constants also increase with increase in the crystal radii of the cation, i.e. in the order: $Cu^{2+} < Cd^{2+} < Pb^{2+}$. These results suggest that the complex formed is a typical outer-sphere type based on electrostatic forces.

Of the inorganic condensed phosphates, cyclophosphates ranging from the trimeric anion, $P_3O_9^{3-}$, through the octametric anion, $P_8O_{24}^{8-}$, with cyclic structures are very interesting electrolytes, since they have a high negative charge on their relatively compact structure.[1] These phosphates are stable for the hydrolysis reaction at ordinary temperatures in slightly acidic or basic aqueous solutions.[2–5] Protonation of cyclophosphates has been neglected provided the hydrogen ion concentration of the solutions is low,[6] and so the treatment of these cyclophosphates is easier than that of other condensed phosphates.

The interaction of cyclophosphates and several cations has already been reported by the author.[6–9] The property of the interaction was considered to be ascribed to the electrostatic force between highly negatively charged phosphate anions and cations. In this study, we have determined the stability constants of the complexes of cyclo-tri-, cyclo-tetra-, cyclo-hexa- and cyclo-octaphosphate and copper(II), cadmium(II) and lead(II) ions by potentiometry with the use of ion-selective electrodes. The mechanism of the complex formation is discussed.

In this paper, cyclophosphates are abbreviated as P_{nm}, where n is the degree of polymerization.

EXPERIMENTAL

Reagents

A standard solution of copper(II) perchlorate was prepared from copper(II) carbonate hydroxide and perchloric acid. Stock solutions of cadmium(II) and lead(II) ions were prepared from the nitrates of reagent grade.

Cyclophosphates were prepared by the usual methods[2,5] and their purity was checked by liquid chromatography.[5]

The other chemicals used in this study were reagent grade and commercially available.

The concentrations of the stock solution of the metal ions were determined by complexometric titration with EDTA.

Apparatus

Potential measurements were made with the Orion Ion Meter Model 801. As ion-selective electrodes, the Orion Model 94-29A, 94-48A and 94-82A were used for copper(II), cadmium(II) and lead(II) ion measurements, respectively. The Orion Model 90-01-00 reference electrode was also used for all potential measurements.

Procedure

The potential was measured at 25±0.1°C in a thermostatted vessel and the pH of the test solution was adjusted to 4 with $HClO_4$. The ionic strength (I) of the test solutions was adjusted by adding $NaClO_4$ as follows: $I = 0.4$ for P_{3m}, $I = 0.3$ for P_{4m}, and $I = 0.1$ for P_{6m} and P_{8m}. The concentration range of the total phosphate and metal ion in the test solutions are given below:

$[M^{2+}]_t$: 2.9×10^{-4}–1.9×10^{-2} M for the P_{3m} and P_{4m} systems, and 2.9×10^{-5}–1.9×10^{-3} M for the P_{6m} and P_{8m} systems.

$[P]_t$: 5.0×10^{-2}–3.3×10^{-2} M for the P_{3m} system, 1.3×10^{-2}–2.0×10^{-2} M for the P_{4m} system, and 6.7×10^{-4}–1.0×10^{-3} M for the P_{6m} and P_{8m} systems.

Before activity measurements the ion-selective electrodes were aged in the metal ion solution of the prescribed concentration for several hours. The electrode systems were standardized before and after each experiment using several metal ion solutions of various concentrations which covered the concentration range of interest.

For the determination of the free metal ion concentration, a titration method was applied and standardization of the electrodes was first carried out by adding metal ion to aqueous solutions free from cyclophosphates. The I of both solutions was adjusted to the prescribed values.

RESULTS AND DISCUSSION

The potential reading of the ion meter can be converted to the concentration of the metal ions when the I of the test solution is known. However, the I of the solution cannot be calculated unless the stability constant of the complex formed is determined.

This problem was solved by successive approximations as follows. At first, the I of the test solution was adjusted to an approximate value designed by adding the supporting electrolyte, and the potential was measured and converted to the free metal ion concentration by assuming that I was constant. Thus, the average number of metal ions bound to one cyclophosphate anion ($\bar{n}$) was determined, and from the formation curve thus obtained approximate stability constants were calculated and refined. Next, I was adjusted rather accurately to a constant value designed by adding the supporting electrolyte to the test solution by the calculation based on the stability constants determined above, and $\bar{n}$ was again measured. The I of the systems calculated using the stability constants finally determined agreed very closely with the prescribed value. The above two-step measurements were satisfactory for the purpose of determining the accurate stability constants.

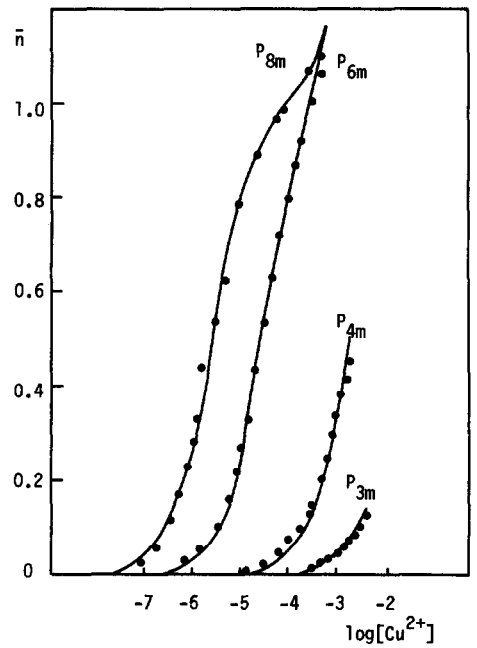


Fig. 1. Formation curve for the Cu^{2+}–P_{nm} system.

If a cyclophosphate anion and a metal ion are denoted as P^{m-} and M^{2+}, respectively, for the complex formation reaction

$$nM^{2+} + P^{m-} \rightleftarrows M_nP^{2n-m} \qquad (1)$$

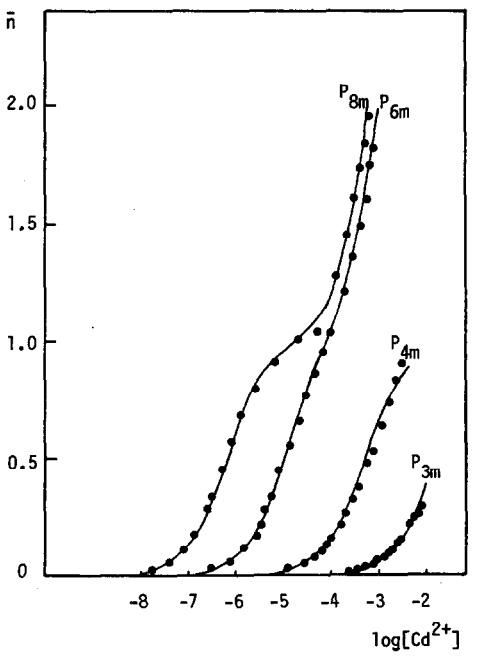


Fig. 2. Formation curve for the Cd^{2+}–P_{nm} system.

Table 1. Stability constants of cyclophosphate complexes with Cu^{2+}, Cd^{2+} and Pb^{2+} ions at 25°C

	P_{3m}	P_{4m}	P_{6m}			P_{8m}		
	Log β_1	Log β_1	Log β_1	Log β_2	Log β_3	Log β_1	Log β_2	Log β_3
Cu^{2+}	1.6	2.7	4.5	7.1		5.6	8.1	
Cd^{2+}	1.8	3.3	5.0	8.3	11.1	6.2	9.6	12.6
Pb^{2+}	2.8	4.5	7.5	12.1	15.3	7.5	12.1	15.3

$\bar{n}$ can be presented as:

$$\bar{n} = \frac{[M^{2+}]_t - [M^{2+}]_{free}}{[P]_t}, \quad (2)$$

where $[M^{2+}]_t$, $[M^{2+}]_{free}$ and $[P]_t$ denote the total metal, free metal and total cyclophosphate concentration, respectively. The formation curves for the copper(II), cadmium(II) and lead(II) ion systems are shown in Figs 1–3. From these formation curves, we have determined accurate stability constants by combining the half-$\bar{n}$ method and successive approximations.

For cyclo-tri- and cyclo-tetraphosphate complexes, $\bar{n}$ is lower than 1 for all metal ions, then only 1 : 1 complex formation was assumed and the stability constant β_1 was directly calculated using the following equation:

$$\beta_1 = \frac{\bar{n}}{(1-\bar{n})[Cu^{2+}]_{free}}. \quad (3)$$

For the Cu^{2+}–P_{6m} and Cu^{2+}–P_{8m} systems, the formation of a 2:1 [copper(II):cyclophosphate ratio] complex was assumed. For the Cd^{2+}–P_{6m}, Cd^{2+}–P_{8m}, and Pb^{2+}–P_{6m} and Pb^{2+}–P_{8m} systems, the maximum number of metal ions bound to one cyclophosphate anion was assumed to be 3.

The stability constants obtained are shown in Table 1. The solid lines in Figs 1–3 are drawn using the calculation based on the stability constants in Table 1, and other points are experimentally obtained. The coincidence of both is satisfactory.

For each cyclophosphate, $\log \beta_1$ values, which are plotted in Fig. 4, increase almost linearly with their negative charge. Complex formation of cyclophosphate anion with these bivalent cations is thought to be ascribed to the electrostatic interaction. For the same cyclophosphate anion, the stability constant increases in the order: Cu^{2+} (0.72 Å) < Cd^{2+} (0.97 Å) < Pb^{2+} (1.20 Å). This order is in accord with the increase in the crystal radii. This result is compatible with a complex formation of outer-sphere type based on the electrostatic force.

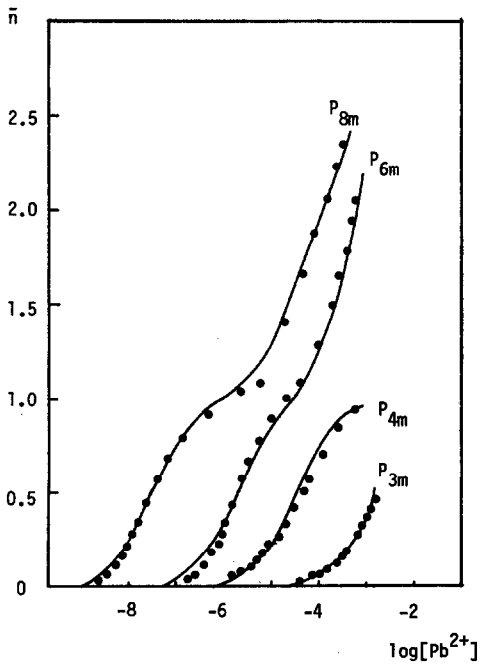


Fig. 3. Formation curve for the Pb^{2+}–P_{nm} system.

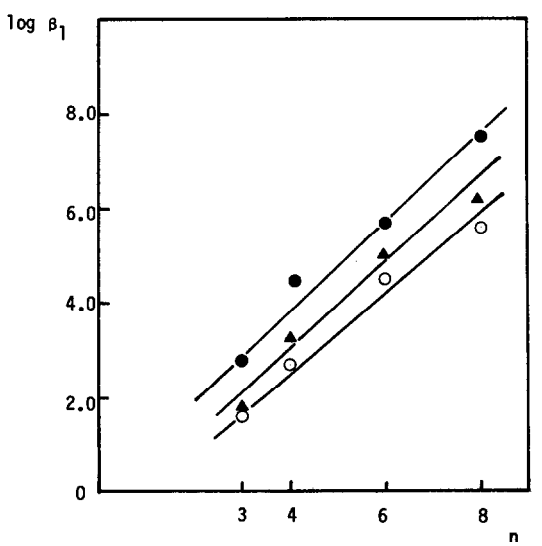


Fig. 4. Variation of stability constant with anion charge: (●) Pb^{2+}–P_{nm}, (▲) Cd^{2+}–P_{nm}, and (○) Cu^{2+}–P_{nm}.

REFERENCES

1. J. R. Van Wazer, *Phosphorus and Its Compounds*. Interscience, New York (1958).
2. G. Kura, *J. Chromatogr.* 1981, **211**, 87.
3. G. Kura, T. Nakashima and F. Oshima, *J. Chromatogr.* 1981, **219**, 385.
4. G. Kura, *J. Chromarogr.* 1982, **246**, 73.
5. G. Kura, *Bull. Chem. Soc. Jpn* 1983, **56**, 3769.
6. G. Kura and S. Ohashi, *J. Inorg. Nucl. Chem.* 1976, **38**, 1151.
7. G. Kura and S. Ohashi, *J. Inorg. Nucl. Chem.* 1972, **34**, 3899.
8. G. Kura, S. Ohashi and S. Kura, *J. Inorg. Nucl. Chem.* 1974, **36**, 1605.
9. M. Koganemura, H. Waki, S. Ohashi and G. Kura, *J. Inorg. Nucl. Chem.* 1979, **41**, 1457.

Polyhedron Vol. 5, No. 12, pp. 2101–2105, 1986
Printed in Great Britain.

0277-5387/86 $3.00 + .00
© 1986 Pergamon Journals Ltd.

SPECTROPHOTOMETRIC DETERMINATION OF FORMATION CONSTANTS OF VARIOUS TYPES OF COMPLEXES BY USE OF ANOTHER COMPETING LIGAND

EMIKO OHYOSHI

Yatsushiro National College of Technology, Hirayamashinmachi 2627, Yatsushiro, Kumamoto, 866, Japan

(*Received* 20 *May* 1986; *accepted* 23 *June* 1986)

Abstract—A method has been developed for determining the formation constants of various colored complexes, ML and ML_2, and their protonated forms, spectrophotometrically, by measuring the absorbance of all forms of the colored complexes in the absence and presence of another ligand, Y, which forms the colorless complex MY, with a known formation constant. This method is based on the competition between the two ligands, L and Y, for the metal ion. An experimental test has been done for the Zn(II)–4-(2-pyridylazo)resorcinol (PAR) (H_2L) system by using nitrilotriacetic acid (NTA) as another ligand, Y. The results showed that the concentrations of PAR used were suitable for the study of 1:2 complexes, ZnL_2, ZnL(HL) and $Zn(HL)_2$, but were too high to study the 1:1 complexes. With the aid of the formation constants of ZnL and ZnHL determined previously, the experimental data gave an approximate value for the formation constant of ZnY (Y = NTA) which agreed with the published value.

When a metal simultaneously forms various colored complexes involving protonated species, it is very difficult to estimate each species by spectrophotometry. A recent study[1] showed that the estimation of the free-ligand concentration spectrophotometrically can be used to evaluate the formation constants of both protonated and normal complexes. This method, however, is limited to the 1:1 complexes. To study a system involving 1:2 complexes, the ligand concentration must be used in large excess over the metal, and all the metal ions would thus form the colored complexes. When another ligand with which the metal forms a colorless complex having a known formation constant is added to such a system, the absorbance due to the colored complexes decreases as a result of competition between the two ligands. By measuring this decrease, which corresponds to the amount of the colorless complex, we can evaluate the equilibrium concentrations of both colored and colorless complexes, which would enable us to estimate the free metal ion concentration. Therefore, the principle seems to be analogous to that of the cation exchange method (the use of another ligand in place of the cation exchange resin) which has been useful for the analysis of various complex species.[2–5] Hughes and Martell[6] have described a method using another competing metal for determining relative stability constants by spectrophotometric determination of the positions of exchange equilibria. However, it is applicable only to a system of 1:1 complexes with a known molar absorptivity.

In this study, a spectrophotometric method has been developed for determining the formation constants of various types of colored complexes without a knowledge of any molar absorptivities by the use of another competing ligand, and applied to the Zn(II) and 4-(2-pyridylazo)resorcinol (PAR) (H_2L) system. The procedure is more rapid and simple compared to the cation exchange method.

CALCULATION OF COMPLEX FORMATION CONSTANTS

When a metal, M, reacts with a reagent, H_2L, like PAR, at relatively low pH, possible forms of the colored complexes are MHL, ML, $M(HL)_2$, M(HL)L and ML_2 (the charges are omitted for simplicity). Under conditions where the concentration of the ligand (C_L) is in large excess over that

of the metal (C_M), all the metal would be complexed. Then:

$$C_M = [MHL] + [ML] + [M(HL)_2] + [M(HL)L] + [ML_2]. \quad (1)$$

When another ligand, Y, which forms the colorless complex MY, is added to such a solution, it displaces the ligands HL and L, and the total amount of the colored complexes decreases. If we can assume that no mixed-ligand complexes are formed (this assumption will be tested later), the concentration of MY is given by:

$$[MY] = C_M - ([MHL] + [ML] + [M(HL)_2] + [M(HL)L] + [ML_2]). \quad (2)$$

Since the total amount of the colored complexes can be estimated spectrophotometrically, the relative amounts of the colorless complex and the colored complexes (all forms) at equilibrium are given by measuring the absorbance at the peak of the colored complexes before and after addition of Y, A_t and A, as follows:

$$[MY]/([MHL] + [ML] + [M(HL)_2] + [M(HL)L] + [ML_2]) = (A_t - A)/(A - A_o), \quad (3)$$

where A_o is the absorbance of the free colored ligand at the peak of the colored complexes. Using the formation constants of all the complexes, K_{MHL}, K_{ML}, $K_{M(HL)_2}$, $K_{M(HL)L}$, K_{ML_2} and K_{MY}, the dissociation constants of H_2L and HL, K_1 and K_2, and the α coefficient,[7] $\alpha_L = [L']/[L] \simeq C_L/[L]$, where [L'] is free ligand not combined with any metal (in this case $[L'] \simeq C_L$ since $C_M \ll C_L$), eqn (3) is expressed as:

$$K_{MY}[Y]/\{(K_{MHL}K_1[H] + K_{ML}K_1K_2)C_L/(\alpha_L K_1K_2) + (K_{M(HL)_2}K_1^2[H]^2 + K_{M(HL)L}K_1^2K_2[H] + K_{ML_2}K_1^2K_2^2)C_L^2/(\alpha_L K_1K_2)^2\} = (A_t - A)/(A - A_o). \quad (4)$$

It can be seen from eqn (4) that the ratio $(A_t - A)/(A - A_o)$ should be proportional to [Y] at constant pH and C_L. This linear relation can be used to prove the assumption that no mixed-ligand complexes are formed. The slope, s_1, should be given as a function of C_L or pH. When s_1 is determined at different C_L keeping pH constant, the quantity $1/(s_1C_L)$ can be expressed as a function of C_L:

$$1/(s_1C_L) = \{(K_{MHL}K_1[H] + K_{ML}K_1K_2)/(\alpha_L K_1K_2) + (K_{M(HL)_2}K_1^2[H]^2 + K_{M(HL)L}K_1^2K_2[H] + K_{ML_2}K_1^2K_2^2)C_L/(\alpha_L K_1K_2)^2\}/K_{MY}. \quad (5)$$

According to eqn (5), a plot of $1/(s_1C_L)$ vs C_L should be linear with an intercept of $(K_{MHL}K_1[H] + K_{M(HL)_2}K_1^2[H]^2 + K_{M(HL)L}K_1^2K_2[H] + K_{ML_2}K_1^2K_2^2)/(K_{MY}\alpha_L^2K_1^2K_2^2)(s_2)$. The products of $\alpha_L K_1K_2$ and y_1, and of $(\alpha_L K_1K_2)^2$ and s_2 are both given as a function of pH:

$$\alpha_L K_1K_2y_1 = (K_{MHL}K_1[H] + K_{ML}K_1K_2)/K_{MY}, \quad (6)$$

$$(\alpha_L K_1K_2)^2s_2 = (K_{M(HL)_2}K_1^2[H]^2 + K_{M(HL)L}K_1^2K_2[H] + K_{ML_2}K_1^2K_2^2)/K_{MY}. \quad (7)$$

Hence, with a knowledge of K_{MY} we can determine the formation constants of various complexes by evaluating y_1 and s_2 at different pH values. The K_{MHL} and K_{ML} values are obtained from the slope and intercept of the plot of eqn (6). The plot of eqn (7) at low values of [H] should be linear to yield K_{ML_2} as the intercept (y_2). Subtracting this intercept, y_2, from $(\alpha_L K_1K_2)^2s_2$ and dividing it by [H], we obtain:

$$\{(\alpha_L K_1K_2)^2s_2 - y_2\}/[H] = (K_{M(HL)_2}K_1^2[H] + K_{M(HL)L}K_1^2K_2)/K_{MY}. \quad (8)$$

The plot of the left-hand side of eqn (8) vs [H] gives $K_{M(HL)_2}$ and $K_{M(HL)L}$ as the slope and intercept, respectively. In this experiment, we used PAR and nitrilotriacetic acid (NTA) as the ligands H_2L and Y, respectively.

EXPERIMENTAL

Materials

All chemicals used were of reagent grade. PAR was obtained from Dojindo Chemical Co., and its

purity was checked by using thin-layer chromatography.[8] Weighed quantities of PAR and NTA were dissolved in a small volume of 1.0 M NaOH and diluted with distilled water to prepare the stock solutions of PAR (1.0×10^{-2} M) and NTA ($2.5–5.0 \times 10^{-3}$ M). A Zn(II) solution having a concentration of about 0.01 M was prepared from nitrate and standardized by EDTA titration using xylenol orange as an indicator. Sodium diethylbarbiturate and sodium nitrate were used to maintain the pH at 6.5–8 and the ionic strength at 0.1, respectively.

Procedure

An aliquot of 1.0×10^{-3} M Zn(II) solution was added using a microliter pipet to 10 cm^3 of buffered PAR solution ($5–11 \times 10^{-5}$ M), to give concentrations of $3–5 \times 10^{-6}$ M. The NTA solution was then added in small aliquots, $20–50 \times 10^{-3}$ cm^3 each. The absorbance at 500 nm (λ_{max} of the Zn–PAR is 493 nm, at which we observed a larger contribution of the free PAR absorption peak at 415 nm) was measured before any addition of the substance (A_o) and then after each addition of the metal (A_t) and the NTA solution (A) by using a Shimadzu UV-260 spectrophotometer. The variation in the absorbance due to the free PAR (415 nm) was also measured to evaluate [L′] at equilibrium, which is more accurate than C_L for using in calculation.

RESULTS AND DISCUSSION

The experiments were carried out under conditions where $C_L \gg C_M$ (L = PAR, M = Zn). The absorbance due to the Zn–PAR complex at 500 nm, $A_t - A_o$ was not varied with increasing C_L at constant pH to show all the metal ions being complexes. The apparent molar absorptivity ($\varepsilon_{Zn\text{-}PAR}$) [$= (A_t - A_o)/C_M$], which was confirmed to be unchanged with varying C_M ($3–5 \times 10^{-6}$ M), gradually decreased with decreasing pH from 8.3×10^4 (pH = 7.92) to 5.5×10^4 (pH = 5.52), suggesting that protonation of the Zn–PAR complex occurred. To analyse these complex species we used another competing ligand, NTA (Y) and studied the effect on the complexation equilibria between Zn(II) and PAR. As shown in Table 1, the absorbance due to the Zn–PAR complex (500 nm) decreases with increasing concentrations of NTA (C_Y) which is related to [Y] by the equation: $[Y] = K^H_{HY}(C_Y - [MY])/[H]$, where $K^H_{HY} = [H][Y]/[HY] = 10^{-9.719}$ and $[MY] = C_M(A_t - A)/(A_t - A_o)$. At the same time, the free PAR absorption peak (415 nm) was observed to increase. From the variation in these two peaks at relatively high pH, we concluded that only the reaction: $ZnL_2 + Y = ZnY + 2L'$ took place, i.e. no formation of the mixed-ligand complex, ZnLY, which was the assumption made in deriving equations. This was also proved by the fact that the linear character of the plots according to eqn (4) (a constant value of the slope s_1 given in Table 1) was obtained at constant pH and C_L.

Using the slope s_1, determined at different C_L, keeping pH constant, we plot the quantity $1/(s_1C_L)$ vs C_L [eqn (5)] as shown in Fig. 1. All the plots yield a linear relationship with a very small intercept (y_1), indicating that almost all the complexes have a 1:2 metal:ligand ratio under the conditions studied. Hence, both K_{MHL} and K_{ML} could not accurately be evaluated in this experiment. However, the y_1 values obtained at relatively low pH were used to test the validity of this method. According to eqn (6), with a knowledge of K_{MHL}, K^1_{ML}, K_1 and K^{10}_2, and the use of y_1 values in Fig. 1(b), we obtained values of log K_{MY} ranging from 10.3 to 10.5, which agreed with the published value of 10.44.[9] It is noted that the slope increases to a great extent with

Table 1. Effect of another competing ligand, NTA (Y), on the Zn(II)–PAR system

C_M ($\times 10^6$ M)	C_Y ($\times 10^6$ M)	[Y] ($\times 10^8$ M)	A (500 nm)	$(A_t - A)/(A - A_o)$	s_1 ($\times 10^{-5}$)
		pH = 7.92, $C_L = 7.3 \times 10^{-5}$ M			
0	0	0	0.154 (A_o)		
4	0	0	0.483 (A_t)		
4	20	31	0.418	0.25	8.0
4	40	63	0.372	0.51	8.1
		pH = 7.00, $C_L = 6.5 \times 10^{-5}$ M			
0	0	0	0.178 (A_o)		
4	0	0	0.446 (A_t)		
4	5	0.77	0.376	0.35	460
4	10	1.61	0.330	0.76	470

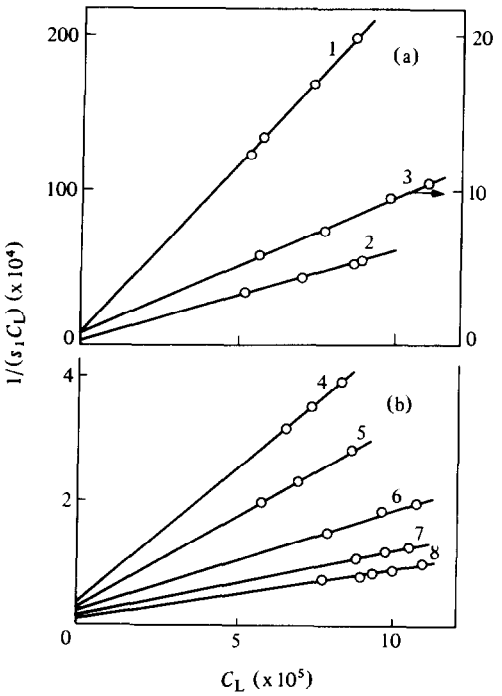


Fig. 1. Plots according to eqn (5) at different pH values: pH 7.92 (1), 7.63 (2), 7.18 (3), 7.00 (4), 6.89 (5), 6.73 (6), 6.60 (7), and 6.52 (8).

increasing pH, suggesting that the stability of ML_2 is much larger than that of M(HL)L or $M(HL)_2$.

To study the protonation of the complex species with increasing [H], we tried to plot the product of the slope of each line (s_2) in Fig. 1 and $(\alpha_L K_1 K_2)^2$ against [H] according to eqn (7) (curve a in Fig. 2). The slope of the plot is nearly constant at low values of [H], where ML_2 and M(HL)L are present, and then gradually increases with increasing [H], indicating that formation of $M(HL)_2$ occurs. With a knowledge of K_{MY}, $K_{MY} = 10^{10.44}$,[9] K_{ML_2} could be calculated from the intercept of the linear portion of the plot (curve a). With the use of this intercept (y_2) the plot of eqn (8) yields line b in Fig. 2. By using the linear-squares method $K_{M(HL)L}$ and $K_{M(HL)_2}$ were obtained from the intercept and slope of line b. With these values the protonation constants of ML_2 and M(HL)L, $K^H_{M(HL)L}$ and $K^H_{M(HL)_2}$, were calculated by the following equations:

$$K^H_{M(HL)L} = [M(HL)L]/([ML_2][H]) = K_{M(HL)L}/(K_{ML_2}K_2), \quad (9)$$

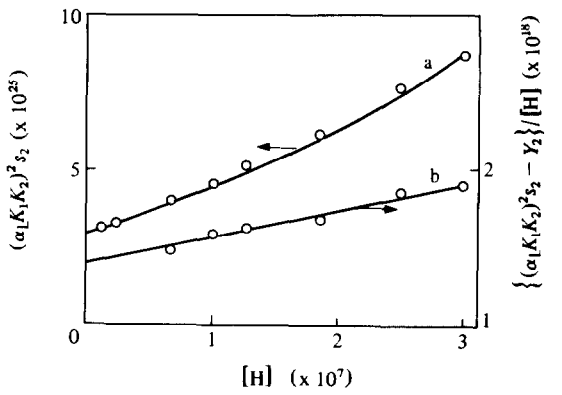


Fig. 2. Plots according to eqn (7) (a) and eqn (8) (b).

$$K^H_{M(HL)_2} = [M(HL)_2]/([M(HL)L][H]) = K_{M(HL)_2}/(K_{M(HL)L}K_2). \quad (10)$$

In Table 2, all the constants obtained are listed together with those in the literature.

From Table 2, it can be seen that the value for the protonation constant of ML_2 reported by Tanaka *et al.*[11] is much larger than ours. They measured the absorbance of a 1:2 Zn–PAR complex (at 495 nm) as a function of pH and evaluated the protonation constants and molar absorptivities of various species by means of curve fitting. The apparent molar absorptivity at 495 nm obtained in this experiment was 8.3×10^4 at pH 7.92 and 8.0×10^4 at pH 7.63. These values agreed well with the reported value of 8.1×10^4 at pH 8 in borate buffer.[12] Therefore, their evaluation for the molar absorptivity of ML_2 ($\varepsilon_{ML_2} = 9.58 \times 10^4$) seems to be too large. Another problem is that under their experimental conditions ($C_L = 7.50 \times 10^{-6}$ M) it must be considered that, with decreasing pH, transformation of the 1:2 to the 1:1 complex as well as their protonation occurs. This would result in a larger decrease in absorbance at 495 nm with decreasing pH from 8 to 7 as compared with our results ($C_L > 5 \times 10^{-5}$ M in this experiment). They assumed that protonation of a 1:2 complex only occurred, and this would make the value of $K^H_{M(HL)L}$ large.

In conclusion, this method is applicable to a study of the formation of various colored complexes without a knowledge of any molar absorptivities.

Table 2. Formation and protonation constants of Zn(II)–PAR complexes (0.1 M $NaNO_3$, 25°C)

	$\log K_{M(HL)_2}$	$\log K_{M(HL)L}$	$\log K_{ML_2}$	$\log K^H_{M(HL)_2}$	$\log K^H_{M(HL)L}$
This work	9.66 ± 0.08	15.89 ± 0.04	21.52 ± 0.03	6.07 ± 0.12	6.67 ± 0.07
Reference 11			22.2 ± 0.2	6.45 ± 0.05	7.55 ± 0.05

REFERENCES

1. E. Ohyoshi, *Anal. Chem.* 1983, **55,** 2404.
2. E. Ohyoshi and A. Ohyoshi, *J. Inorg. Nucl. Chem.* 1971, **33,** 4265.
3. A. Ohyoshi, E. Ohyoshi, H. Ono and S. Yamakawa, *J. Inorg. Nucl. Chem.* 1972, **34,** 1955.
4. E. Ohyoshi, J. Oda and A. Ohyoshi, *Bull. Chem. Soc. Jpn* 1975, **48,** 227.
5. E. Ohyoshi and A. Ohyoshi, *Bull. Chem. Soc. Jpn* 1980, **53,** 805.
6. V. L. Hughes and A. E. Martell, *J. Phys. Chem.* 1953, **57,** 694.
7. A. Ringbom, *Complexation in Analytical Chemistry.* Interscience, New York (1963).
8. F. H. Pollard, G. Nickless, T. J. Samuelson and R. G. Anderson, *J. Chromatogr.* 1964, **16,** 231.
9. H. M. N. H. Irving and M. G. Miles, *J. Chem. Soc. A* 1966, 727.
10. W. J. Geary, G. Nickless and F. H. Pollard, *Anal. Chim. Acta* 1962, **27,** 71.
11. M. Tanaka, S. Funahashi and K. Shirai, *Inorg. Chem.* 1968, **7,** 573.
12. S. Ahrland and R. G. Herman, *Anal. Chem.* 1975, **47,** 2422.

Polyhedron Vol. 5, No. 12, pp. 2107–2108, 1986
Printed in Great Britain

0277-5387/86 $3.00+.00
© 1986 Pergamon Journals Ltd.

SYNTHESIS OF Tc(IV) ALCOHOLATO COMPLEXES WITH METHANOL, ETHYLENEGLYCOL AND 1,2,4-BUTANETRIOL

R. ALBERTO, G. ANDEREGG* and K. MAY

Laboratorium für Anorganische Chemie, ETH Zürich, CH-8092 Zürich, Switzerland

(*Received* 25 *June* 1986; *accepted* 7 *July* 1986)

Abstract—The preparation of three Tc(IV) alcoholato complexes: $K_2[^{99}Tc(OMe)_6]$, $K_2[^{99}Tc(glyc)_3]\cdot 3C_2H_5OH$ ($H_2glyc = CH_2OHCH_2OH$), and $K_2[^{99}Tc(butri)_2]\cdot CH_3OH$ ($H_3butri = CH_2OHCHOHCH_2CH_2OH$) is described.

Among the Tc(IV) hexahalogenocomplexes, $K_2[TcBr_6]$ shows, in contrast to $K_2[TcF_6]$ and $K_2[TcCl_6]$, an unexpectedly high solubility in methanol. The reason seems to be a partial substitution of bromide by methoxide (MeO^-) and pH measurements in water-free MeOH gave an acidic pH, according to the following equation

$$(TcBr_6]^{2-} + nCH_3OH \xrightarrow{\text{methanol}} [Tc(OCH_3)_nBr_{6-n}]^{2-} + nH^+ + nBr^- \quad (1)$$

Since Tc(IV) prefers oxygen as a donor atom, it should be possible to obtain bromide-free complex salts.

EXPERIMENTAL

KOMe was prepared by direct reaction of elemental potassium with MeOH. Solutions of KOMe in MeOH have a long shelf-life. MeOH was therefore evaporated *in vacuo* immediately prior to use.

Synthesis of $K_2[Tc(IV)(OMe)_6]$ **(I)**

$$[TcBr_6]^{2-} + 6MeO^- \xrightarrow{\text{methanol}} [Tc(OMe)_6]^{2-} + 6Br^-$$

320 mg $K_2[TcBr_6]$ (0.5 mmol) in 10 cm^3 of MeOH were added dropwise to 490 mg KOMe (7 mmol) under nitrogen. The solution discolored completely within 10 min. KBr precipitated during the evaporation to a total volume of 2 cm^3. The KBr (97%) was filtered and washed with several drops of cold MeOH. In the filtrate the solvent was removed first by a stream of dry nitrogen and then *in vacuo*. The remaining white powder was treated twice with 1 cm^3 of *t*-butanol (*t*-BuOH) to remove the excess of KOMe. The residue was washed with another portion of *t*-BuOH then with CH_3CN and dried *in vacuo*. 124 mg of a pale greenish salt was obtained. Found: K, 22.1; Tc, 26.9. Calc. for **I**: K, 21.5; Tc, 27.2%.

The ratio MeO/Tc was determined by complete hydrolysis of the complex and acidimetric titration of the obtained hydroxyl ions and was found to be 5.97. The complex is soluble in MeOH and EtOH, insoluble in other common organic solvents, it decomposes rapidly in aqueous solution, if the pH < 12 but it is stable for several days if the pH > 12. In the air, the complex changes into a red species which in turn is oxidized to pertechnetate. For this reason, an R_f value in CH_3CN–H_2O (2.5:1 v/v) could not be determined.

Synthesis of $K_2[Tc(IV)(glyc)_3]\cdot 3C_2H_5OH$ **(II)** ($glyc = OCH_2CH_2O$)

220 mg of **I** and 1.5 cm^3 of freshly distilled ethyleneglycol were mixed and transferred into an ultrasonic vibrator and **I** dissolved slowly. The substitution of MeO^- by glycolate can be scanned by paper chromatography. The educt remains at the starting point and the product shows an R_f value of 0.2. After 24 h the excess ethyleneglycol was removed by high vacuum distillation. The intense hygroscopic nature of the remaining greenish salt was attributed to missing alcohol molecules

*Author to whom correspondence should be addressed.

in the unitary crystal cell. Recrystallization from CH_3CN–EtOH (3:1 v/v) yielded 185 mg (62%) of a colorless non-hygroscopic salt. Found: K, 15.4; Tc, 19.3; C, 28.8; H, 6.1. Calc. for **II**: K, 15.8; Tc, 20.0; C, 29.1; H, 6.1%.

Synthesis of $K_2[Tc(IV)(butri)_2]\cdot CH_3OH$ **(III)** (butri = 1,2,4-*butanetriolate*)

200 mg of **I** (0.55 mmol) and 2 cm^3 of 1,2,4-butanetriol were treated as described for **II**. The resulting solution was mixed with 1 cm^3 of *t*-BuOH and left to stand overnight. The white powder which settled was filtered off and recrystallized from CH_3CN–MeOH (3:1 v/v) giving 160 mg of a white non-hygroscopic salt. Found: K, 18.1; Tc, 23.5; C, 26.2; H, 4.3. Calc. for **III**: K, 18.8; Tc, 23.8; C, 26.0; H, 4.4%.

Spectroscopic properties of the complexes:

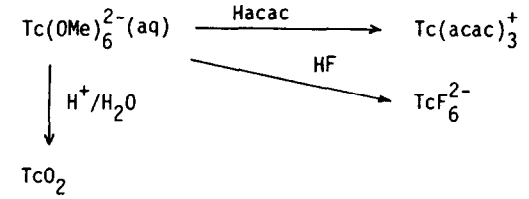
	UV–(abs MeOH)	IR (TcO-st)(KBr)
$Tc(OMe)_6^{2-}$	$\lambda_{max} = 274$ nm	IR: $\nu = 450\ cm^{-1}$
$Tc(glyc)_3^{2-}$	$\lambda_{max} = 270$ nm	IR: $\nu = 455\ cm^{-1}$
$Tc(butri)_2^{2-}$	$\lambda_{max} = 267$ nm	IR: $\nu = 460\ cm^{-1}$

The IR band at 450 cm^{-1} can be assigned to a Tc—O stretching frequency. It lies between that of Tc—F—st (574 cm^{-1}) and that of Tc—Cl—st (330 cm^{-1}).[1] Moreover, the IR spectra agree with those of the corresponding alcohols.

DISCUSSION

It has long been known that most metal centers with significant A-character form binary complexes with alcoholates.[2–4] The feasibility of synthesizing such complexes with Tc(IV) also indicates that Tc(IV) shows a similar behavior.

It was not possible to grow crystals suitable for X-ray studies. The proof that Tc is in the +IV oxidation state had to be obtained indirectly from chemical measurements including elemental analysis. We have also synthesized known Tc(IV) complexes using **I** as starting material. The scheme below illustrates the complexes,[5,6] all of which could be produced in good yields (Hacac = acetylacetone).



As mentioned earlier, the complexes are soluble in MeOH and EtOH. **I** is stable in aqueous solution at pH > 12, **II** for pH > 10–11, and **III** for pH > 8–9. Below these limits the rate of hydrolysis increases with decreasing pH. Hydrolysis can be prevented by adding a strong ligand. This provides a useful method of synthesizing new Tc(IV) complexes directly from aqueous solution. The question arises as to the nature of the coordination of complexes **II** and **III**. It is theoretically possible, that the alcohols of crystallization are coordinated while the multidentate ligands are partially protonated and not fully coordinated. This question can be answered from a thermodynamic point of view. The significantly higher stability of **II** and **III** with respect to hydrolysis cannot be explained in the absence of chelating effects. If in these cases unidentate ligands were coordinated, hydrolysis should take place under the same conditions as for **I**.

Acknowledgements—The authors thank the Stiftung Entwicklungsfonds für Seltene Metalle and the Eidg. Institut für Reaktorforschung, Würenlingen, for financial support (R.A.) of these investigations.

REFERENCES

1. C. K. Jørgensen and K. Schwochau, *Z. Naturforsch.* 1965, **20A**, 65.
2. F. Bischoff and H. Adkins, *J. Am. Chem. Soc.* 1924, **46**, 256.
3. D. C. Bradley, W. Wardlaw and A. Whitley, *J. Chem. Soc.* 1955, 726.
4. D. C. Bradley, W. Wardlaw and R. K. Multani, *J. Chem. Soc.* 1958, 126.
5. M. J. Abrams, A. Davison, A. G. Jones and C. E. Costello, *Inorg. Chim. Acta* 1983, **L235**, 77.
6. R. Alberto and G. Anderegg, *Polyhedron* 1985, **4**, 1067.

Polyhedron Vol. 5, No. 12, pp. 2109–2111, 1986
Printed in Great Britain.

0277–5387/86 $3.00 + .00
© 1986 Pergamon Journals Ltd.

COMMUNICATION

CRYSTAL STRUCTURE OF SODIUM IODIDE · (DIGLYME): AN UNPRECEDENTED BRIDGING ROLE FOR DIGLYME

ROBERT E. MULVEY*

Chemistry Department, Durham University, South Road, Durham DH1 3LE, U.K.

WILLIAM CLEGG*

Department of Inorganic Chemistry, The University, Newcastle upon Tyne NE1 7RU, U.K.

and

DONALD BARR and RONALD SNAITH

Department of Pure and Applied Chemistry, Strathclyde University, 295 Cathedral St., Glasgow G1 1XL, U.K.

(*Received* 18 *April* 1986; *accepted* 23 *June* 1986)

Abstract—The diglyme adduct of sodium iodide, $NaI \cdot (CH_3OCH_2CH_2)_2O$, has been structurally characterized by X-ray diffraction. It forms infinite zig-zag chains which, unlike most complexes of the salt, retain Na—I bonds. In addition, diglyme molecules bridge pairs of Na atoms through four-co-ordinate O atoms, so representing a new role for this neutral oxygen donor.

Diglyme · {di-(2-methoxyethyl)ether [$(CH_3OCH_2CH_2)_2O$]}, a high-temperature ether solvent (b.p. 162°C) which was first prepared in 1925,[1] has for many years been widely employed in both organic and inorganic synthesis.[2] A powerful sequestering agent, it is very effective in solvating cations of sodium salts, a property which facilitates reactions of "ionic" compounds in non-polar media. Research chemists engaged in structural studies of transition-metal species have found diglyme to be a particularly useful solvent as it frequently gives rise to stable, crystalline complexes: crystal structures of diglyme-containing Ti, Cr, Zr, Mo and W systems have been reported recently in the literature.[3–7]

In the course of seeking a mixed-metal cluster of Li and Na we have synthesized (unintentionally) NaI · diglyme, which to the best of our knowledge has never been previously isolated. Surprisingly, no diglyme adduct of a sodium salt (or indeed of a *simple* salt of any other alkali metal) appears to have been structurally determined by X-ray diffraction. Therefore we have carried out a structure analysis of the title compound.

EXPERIMENTAL

The method which produced NaI · diglyme was explored with a view to incorporating sodium into a lithium imide cluster, specifically the trigonal antiprismatic hexamer $[LiN{=}C(Ph)Bu^t]_6$,[8] which is readily accessible from equimolar proportions of LiPh and $Bu^tC{\equiv}N$. Accordingly, LiPh (5.0 cm^3 of a 2 M solution in ether–cyclohexane, 10.0 mmol) was added dropwise to a chilled mixture of NaI (0.5 g, 3.3 mmol) and diglyme (8.0 cm^3, 56.0 mmol) in a Schlenk tube under an atmosphere of dry, oxygen-free nitrogen. Following a vigorous reaction $Bu^tC{\equiv}N$ (1.1 cm^3, 10.0 mmol) was added, generating a crimson solution. Cooling to 0°C afforded highly moisture-sensitive, colourless, needle-like crystals, identified as $NaI \cdot (CH_3OCH_2CH_2)_2O$, m.p. 78°C; cf. NaI itself,

*Authors to whom correspondence should be addressed.

661°C. (Found: C, 25.7; H, 5.0; Li, 0.0; I, 43.8; Na, 8.1%. $C_6H_{14}INaO_3$ requires: C, 25.4; H, 4.9; I, 44.7; Na, 8.1; O, 16.9%.) A second product, an orange solid, has not yet been characterized.

A subsequent attempt to prepare the complex directly from anhydrous NaI and diglyme proved successful, although the crystals obtained were of an inferior quality. To effect complete dissolution of the salt a 10-fold excess of hot diglyme (80°C) was required. The complex was rapidly precipitated, however, when the solution was agitated or cooled by a few degrees.

Crystallography

$C_6H_{14}INaO_3$, $M = 284.1$, orthorhombic, *Fddd*, $a = 7.9147(3)$ Å, $b = 23.1492(7)$ Å, $c = 23.7448(8)$ Å, $V = 4350.5$ Å^3, $Z = 16$, $D_c = 1.735$ g cm^{-3}, $F(000) = 2208$, $\mu = 2.92$ mm^{-1} for Mo-$K\alpha$ radiation ($\lambda = 0.71073$ Å). Of 1179 reflections measured with a Siemens AED2 diffractometer at 293 K ($2\theta_{max} = 50°$), and corrected for absorption by semi-empirical methods, 966 were unique ($R_{int} = 0.016$), and 762 with $F > 4\sigma(F)$ were used for structure determination by Patterson and difference syntheses.[9] Blocked-cascade refinement to minimize $w\Delta^2$ [$\Delta = |F_o| - |F_c|$; $w^{-1} = \sigma^2(F)$] with anisotropic thermal parameters for non-H atoms, constrained H atoms [C—H = 0.96 Å, H—C—H = 109.5°, $U(H) = 1.2U_{eq}(C)$] and an extinction correction $F_c' = F_c/(1 + xF_c^2/\sin 2\theta)^{1/4}$ [$x = 4.0(2) \times 10^{-7}$] gave $R = 0.025$, $R' = (\Sigma w\Delta^2/\Sigma wF_o^2)^{1/2} = 0.024$, a satisfactory analysis of variance, and no significant features in a final-difference map. Tables of atomic co-ordinates and other crystallographic data have been deposited with the Editor and the Cambridge Crystallographic Data Centre.

RESULTS AND DISCUSSION

The molecular structure consists of polymeric chains (viewed end-on in Fig. 1) of NaI·diglyme units. These chains are built-up in a zig-zag arrangement (Fig. 2). Sets of parallel two-fold axes of symmetry pass through the I and O(1) atoms, with a second, perpendicular set passing through the Na atoms, both sets being perpendicular to the chain direction. Table 1 gives the important bond lengths and angles. The Na—I bonds are marginally shorter in length [3.164(1) Å] than the closest Na—I distances in the salt itself (3.231 Å),[10] reflecting the lower co-ordination state of the I atoms in the diglyme complex (i.e. 2 vs 6). The fact that Na—I bonds are retained at all is highly surprising. Normally complexation results in "solvent-separated"

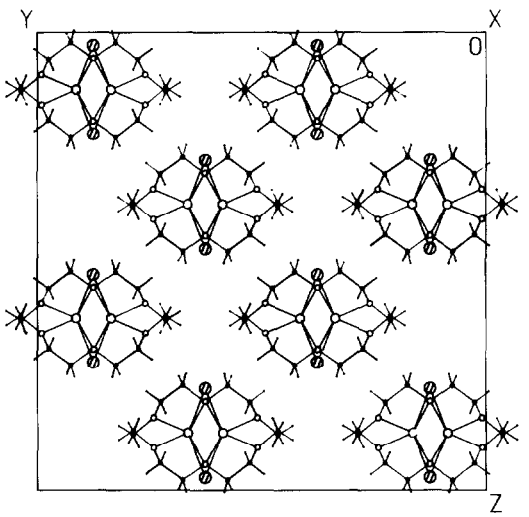


Fig. 1. Projection of NaI diglyme along the *x*-axis: large dots, C; small dots, H; small circles, O; large circles, Na; shaded circles, I.

Table 1. Bond lengths (Å) and angles (°)[a]

Na—I	3.164(1)	Na—O(1)	2.714(2)
Na—O(2)	2.427(3)	O(1)—C(1)	1.432(4)
O(2)—C(2)	1.427(5)	O(2)—C(3)	1.423(6)
C(1)—C(2)	1.481(6)		
Na—I—Na(a)	86.8(1)	I—Na—O(1)	83.3(1)
I—Na—O(2)	93.7(1)	O(1)—Na—O(2)	67.5(1)
I—Na—I(b)	146.8(1)	O(1)—Na—I(b)	85.8(1)
O(2)—Na—I(b)	110.7(1)	O(1)—Na—O(1b)	141.1(1)
O(2)—Na—O(1b)	150.6(1)	O(2)—Na—O(2b)	85.4(2)
Na—O(1)—C(1)	100.5(2)	Na—O(1)—Na(a)	106.5(1)
C(1)—O(1)—Na(a)	119.7(2)	C(1)—O(1)—C(1a)	110.8(4)
Na—O(2)—C(2)	117.0(2)	Na—O(2)—C(3)	120.1(3)
C(2)—O(2)—C(3)	110.8(3)	O(1)—C(1)—C(2)	109.8(3)
O(2)—C(2)—C(1)	109.7(3)		

[a]Symmetry operators: (a) $\frac{3}{4} - x, \frac{3}{4} - y, z$; and (b) $\frac{1}{4} - x, y, \frac{5}{4} - z$.

ion pairs, particularly with chelating ligands like diglyme but even in the case of ligands with only one co-ordinatively active atom; X-ray structure analyses of tris(acetone)– and tris(methanol)–Na^+I^-[11,12] exemplify this point. Our structure is more akin to that of $NaI\cdot(H_2O)_2$.[13] This complex consists of sheets composed of an hexagonal array of octahedrally co-ordinated Na atoms, with each Na being linked to its three neighbouring Na atoms by a centro-symmetric pair of I atoms [at interatomic distances of 3.210(6) and 3.260(11) Å] or water molecules. The environment of the metal atoms in NaI·diglyme (Fig. 2) is likewise octahedral; two opposite sites are occupied by I atoms while oxygens from independent diglyme molecules participate in two terminal bonds to each Na. To complete the six-fold co-ordination arrangement, however, the central O atoms [O(1)] of the diglyme molecules *bridge* between pairs of Na atoms. This is the first example of μ_2-bonding involving diglyme. In common with *neutral* oxygen donors in general, diglyme usually attaches terminally, through 3-co-ordinate O atoms, to metal atoms. Examples are (diglyme)Cd[$Mn(CO)_5$]$_2$,[14] (μ_3-N_2)(η^5:η^5-$C_{10}H_8$)(η-C_5H_5)$_2$Ti$_2$[(η^1:η^5-C_5H_4)(η-C_5H_5)$_3$Ti$_2$] · [(η-C_5H_5)$_2$(diglyme)Ti] · diglyme[15] and $Mo_2(O_2CC_6H_5)_4\cdot 2$(diglyme),[16] where the ether functions as a tri-, bi- and monodentate ligand, respectively. A comparison can be made between the Na—O bridge bonds in this system and those in "washing-soda", which is composed of $[Na_2(H_2O)_{10}]^{2+}$ and CO_3^{2-} ions. In the cations, two sodium–water octahedra share an edge making eight terminal and four bridging Na—O bonds (range of lengths: in the former, 2.39–2.51 Å; in the latter, 2.31–2.49 Å).[17] The interatomic distances in the diglyme complex, refined to a final R value of 0.025 (cf. 0.18 in the decahydrate), provide a more precise comparison of the different types of Na—O bond, as those in a bridging mode are distinctly longer [2.714(2) Å] than those in a terminal arrangement [2.427(3) Å]. Finally, it should be noted that the title compound as isolated is insoluble in hydrocarbon solvents but is soluble in diglyme itself. The conclusion drawn is that excess of a strongly coordinating solvent such as diglyme cleaves the polymeric chains and presumably breaks all metal–halogen bonds, separating the metal ions to give $Na(diglyme)_x^+ \ldots I^-$ solution species.

Acknowledgements—We thank the SERC for financial support including a research grant towards crystallographic apparatus, and Professor K. Wade for helpful discussion.

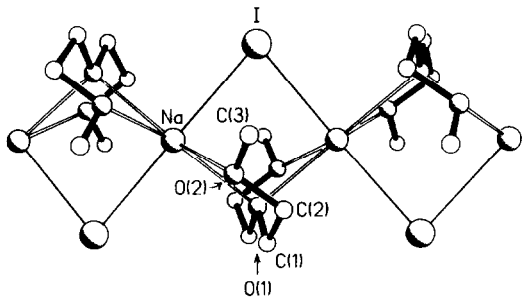


Fig. 2. Part of the zig-zag chain structure. H atoms have been omitted for clarity.

REFERENCES

1. L. H. Cretcher and W. H. Pittenger, *J. Am. Chem. Soc.* 1925, **47,** 163.
2. L. F. Fieser and M. Fieser, *Reagents for Organic Synthesis*, Vol. 1, p. 255. John Wiley, New York (1967) and later volumes. M. Szwarc (Ed.), *Ions and Ion Pairs in Organic Reactions*, Vol. 1, p. 115, Wiley Interscience, New York (1972). F. A. Cotton and G. Wilkinson, *Advanced Inorganic Chemistry*, 4th Edn, p. 264, Wiley Interscience, New York (1980).
3. M. G. B. Drew and J. A. Hutton, *J. Chem. Soc., Dalton Trans.* 1978, 1176.
4. F. A. Cotton, R. H. Niswander and J. C. Sekutowski, *Inorg. Chem.* 1979, **18,** 1152.
5. N. E. Schore, S. J. Young, M. M. Olmstead and P. Hofmann, *Organometallics* 1983, **2,** 1769.
6. F. A. Cotton and G. N. Mott, *Inorg. Chim. Acta* 1983, **70,** 159.
7. A. P. Sattelberger, K. W. McLaughlin and J. C. Huffman, *J. Am. Chem. Soc.* 1981, **103,** 2880.
8. D. Barr, W. Clegg, R. E. Mulvey, R. Snaith and K. Wade, *J. Chem. Soc., Chem. Commun.* 1986 295.
9. G. M. Sheldrick, *SHELXTL*: an integrated system for solving, refining and displaying crystal structures from diffraction data, Revision 5, University of Göttingen (1985).
10. A. F. Wells, *Structural Inorganic Chemistry*, 5th Edn, p. 444. Oxford Science Publications, Clarendon Press, Oxford (1984).
11. P. Piret, Y. Gobillon and M. van Meerssche, *Bull. Soc. Chim. Fr.* 1963, 205.
12. P. Piret and C. Mesureur, *J. Chim. Phys. Phys.-Chim. Biol.* 1965, **62,** 287.
13. J. Verbist, P. Piret and M. van Meerssche, *Bull. Soc. Fr. Mineral. Crist.* 1970, **93,** 509.
14. W. Clegg and P. J. Wheatley, *J. Chem. Soc., Dalton Trans.* 1974, 424.
15. G. P. Pez, P. Apgar and R. K. Crissey, *J. Am. Chem. Soc.* 1982, **104,** 482.
16. D. M. Collins, F. A. Cotton and C. A. Murillo, *Inorg. Chem.* 1976, **15,** 2950.
17. T. Taga, *Acta Cryst.* 1969, **B25,** 2656.

Polyhedron Vol. 5, No. 12, pp. 2113–2115, 1986
Printed in Great Britain

0277-5387/86 $3.00+.00
© 1986 Pergamon Journals Ltd.

COMMUNICATION

VARIATION OF ACTIVATION VOLUMES FOR AQUATION OF CHLOROAMINECOBALT(III) COMPLEXES

GEOFFREY A. LAWRANCE

Department of Chemistry, The University of Newcastle, New South Wales 2308, Australia

(*Received* 6 *June* 1986; *accepted* 23 *June* 1986)

Abstract—Activation volumes for aquation of *cis*-$[Co(en)_2(NO_2)Cl]^+$, *trans*-$[Co(en)_2(CN)Cl]^+$, *cis*-α- and *cis*-β-$[Co(trien)Cl_2]^+$ have been determined, and are compared with values reported for a range of chloroaminecobalt(III) complexes. Variation of reported $\Delta V^{\neq}$ in terms of, particularly, solvation effects is discussed.

The mechanistic value of measured activation volume ($\Delta V^{\neq}_{exp}$) in reactions of coordination complexes has been the basis for extensive study.[1–6] At least for reactions involving exchanges of small neutral molecules, interpretation of $\Delta V^{\neq}_{exp}$ in terms of volume changes arising from displacement of particles at the active site seems relatively straightforward.[6] This is because motions of small neutral molecules should not involve any large changes in solvation from precursor to transition state. If we assign to the experimental activation volume separate contributions from intrinsic displacement ($\Delta V^{\neq}_{intr}$) and solvation ($\Delta V^{\neq}_{solv}$) terms, where the former term carries the mechanistically significant information, it becomes clear that interpretation of $\Delta V^{\neq}_{exp}$ values depends on small $\Delta V^{\neq}_{solv}$ components or at least an understanding of the significance of this term in various circumstances.

With ionic leaving groups, a dissociative transition state may involve formation of, or substantial motion towards formation of, a new charge centre. In polar solvents, significant electrostriction of the new charge centre with concomitant changes in molar volumes of participating solvent molecules will occur. The result is seen experimentally as a negative contribution to $\Delta V^{\neq}_{exp}$. Variation in $\Delta V^{\neq}_{exp}$ from +1.2 to −9.9 to −18.5 $cm^3 mol^{-1}$ for $[Co(NH_3)_5L]^{n+}$ hydrolysis[7,8] as L varies from OH_2 to Cl^- to SO_4^{2-} can be used to illustrate the role of electrostriction. While these complexes aquate by essentially the same mechanism, clearly $\Delta V^{\neq}_{exp}$ alone is not mechanistically definitive, being masked by solvent electrostriction terms in the latter two examples.

The significance of the problem can be gauged further by the observation that $\Delta V^{\neq}_{exp}$ for chloride aquation from a range of cobalt(III) amines vary between −10 and +11 $cm^3 mol^{-1}$.[1,8,13] Here, differences must lie not just with the central metal ion or leaving group but also with the non-leaving groups and overall charge. We have been working to extend the number of such examples for which $\Delta V^{\neq}_{exp}$ have been measured. Recently, $\Delta V^{\neq}_{exp}$ for aquation of $[Co(NH_3)_5Cl]^{2+}$, *trans*-$[Co(NH_3)_4(NH_2CH_3)Cl]^{2+}$ and $[Co(NH_2CH_3)_5Cl]^{2+}$ were compared.[13] It was found that $\Delta V^{\neq}_{exp}$ becomes more positive with increasing molar volume of the cation. Here, we report $\Delta V^{\neq}_{exp}$ for several other chloroaminecobalt(III) complexes, and examine the overall trend.

With stereochemically unconfined cobalt(III) complexes, isomerization can accompany spontaneous aquation,[14] which can make interpretation of $\Delta V^{\neq}_{exp}$ more difficult. The complexes *cis*-$[Co(en)_2(NO_2)Cl]^+$, *trans*-$[Co(en)_2(CN)Cl]^+$ and *cis*-$[Co(trien)Cl_2]^+$ were chosen for study because they are reported to undergo aquation with retention of configuration.[5–7] Hydrolyses were followed in 0.1 M $HClO_4$ on a Varian 635 spectrophotometer fitted with a high-pressure cell at a fixed wavelength and a constant temperature. Minor enhancement of observed rate constants with increased pressure were observed in all cases. Results $\{10^4 k_{obs}$ (s^{-1}) [*P*(bar)]} obtained were as follows: *cis*-$[Co(en)_2(NO_2)Cl]^+$: 3.63 ± 0.10(1), 3.78 ± 0.20 (345), 3.92 ± 0.15(690), 4.03 ± 0.10(1035), 4.23 ± 0.05 (1380); *trans*-$[Co(en)_2(CN)Cl]^+$: *cis*-α-3.10 ± 0.09(1), 3.16 ± 0.07(345), 3.20 ± 0.10(690), 3.36 ± 0.16

(1035), 3.45 ± 0.10(1380); *cis*-α-$[Co(trien)Cl_2]^+$:1.89 ± 0.06(1), 2.01 ± 0.13(345), *cis*-β-[2.19 ± 0.11(690), 2.33 ± 0.06(1035), 2.50 ± 0.10(1380). Further, aquation of *cis*-β-$[Co(trien)Cl_2]^+$ was reexamined, since deviation from first-order behaviour was more substantial than expected in the initial study,[11] limiting accuracy of determined k_{obs}. The revised results, using a different sample of complex, which yields a different $\Delta V^{\neq}_{exp}$, are for *cis*-β-$[Co(trien)Cl_2]^+$: 14.7 ± 0.4(1), 15.0 ± 0.3 (345), 15.5 ± 0.4(690), 16.1 ± 0.4(1035), 16.4 ± 0.3 (1380). Experiments were conducted at 35, 35, 27 and 25°C, respectively. Activation volumes for complexes were calculated in the usual manner,[5] and are included in Table 1, along with activation enthalpy and entropy values previously determined, and data for similar complexes.

Although in all cases chloride aquation from cobalt(III) is occurring, with the consequent expectation of a basic mechanistic constancy, it is clear from data in Table 1 that both $\Delta V^{\neq}_{exp}$ and $\Delta S^{\neq}_{exp}$ vary appreciably. Since a strictly limiting dissociative character is unlikely,[14] variations could in part reflect differing Co^{3+}–Cl^- separation in the transition state, which would affect both $\Delta V^{\neq}_{intr}$ and $\Delta V^{\neq}_{solv}$ terms. In any case, the sensitivity to particularly non-leaving groups is apparent. Variation in the series *trans*-$[Co(en)_2(X)Cl]^+$ is notable, since $\Delta V^{\neq}_{exp}$ changes with *trans*-X group from +11 cm^3 mol^{-1} (X = Cl^-) to +0.7 cm^3 mol^{-1} (X = N_3^-) to −2.0 cm^3 mol^{-1} (X = CN^-). At least for the first two, aquation occurs with some isomerization.[14] Since isomerization reactions alone in cobalt(III) chemistry can exhibit large positive $\Delta V^{\neq}_{exp}$,[18] variations observed may reflect the amount of rearrangement in the transition-state formation. The extent of bond stretching necessary to reach the transition state for aquation reactions in complexes where chelate rings exist may differ from the situation with simple ammines if molecular relaxation and rearrangement to permit a choice of geometry in the successor are involved in part in the activation process for aquation.

Except for $[Co(tren)Cl_2]^+$ and $[Co(dtcd)(N_3)Cl]^+$, all complexes show a quite close linear relationship between $\Delta V^{\neq}_{exp}$ and $\Delta S^{\neq}_{exp}$. For the $[Co(tren)Cl_2]^+$ ion, the first hydrolysis is a composite reaction since two non-equivalent sites exist, one of which may be especially labile;[19] observed $\Delta V^{\neq}_{exp}$ in this case may be less accessible to interpretation. Alone amongst the complexes, aquation of $[Co(dtcd)(N_3)Cl]^+$ involves loss from a large substituted and unsaturated macrocyclic complex, which may represent a special situation.[10] Since intrinsic and electrostrictive effects should usually contribute in a like sense to $\Delta V^{\neq}_{exp}$ and $\Delta S^{\neq}_{exp}$, a correlation between these terms is not unexpected, and has been addressed previously.[20] One interpretation of the significantly positive $\Delta V^{\neq}_{exp}$ for $[Co(tren)Cl_2]^+$ and $[Co(dtcd)(N_3)Cl]^+$ could be to assert a significant shift towards a limiting dissociative mechanism in these cases. However, there seems no special case for this assertion at least with the *trans*-$[Co(en)_2Cl_2]^+$ ion, where $\Delta V^{\neq}_{exp}$ is also large and positive;[9] thus it may not be an acceptable interpretation in general.

Reactions of cobalt(III) complexes in acid, while believed to be dissociative in nature, have rarely been considered to involve a limiting mechanism. Lifetimes of any intermediates are probably in no more than the picosecond range, which should not permit complete solvent reorganization in the activation process itself. Varying the non-leaving groups may vary the lifetime of the activated

Table 1. Activation parameters for aquation of chloroaminecobalt(III) complexes

Complex[a]	$k^{25°C}$ (s^{-1})	$\Delta H^{\neq}$ (kJ mol^{-1})	$\Delta S^{\neq}$ (J K^{-1} mol^{-1})	$\Delta V^{\neq}$ (cm^3 mol^{-1})	Reference
$[Co(NH_3)_5Cl]^{2+}$	1.7×10^{-6}	93 (± 1)	−44 (± 3)	−9.9 (± 0.5)	8
trans-$[Co(NH_3)_4(NH_2CH_3)Cl]^{2+}$	1.1×10^{-5}	95 (± 2)	−19 (± 6)	−4.6 (± 0.5)	13
$[Co(NH_2CH_3)_5Cl]^{2+}$	4.0×10^{-5}	95 (± 1.5)	−10 (± 4)	−2.3 (± 0.4)	13
cis-α-$[Co(trien)Cl_2]^+$	1.6×10^{-4}	90 (± 1.7)	−24 (± 6)	−5.0 (± 0.4)	[b], 17
cis-β-$[Co(trien)Cl_2)^+$	1.5×10^{-3}	88 (± 1.7)	−11 (± 6)	−2.0 (± 0.6)	[b], 17
cis-$[Co(tren)Cl_2]^+$	3.0×10^{-3}	74 (± 2)	−45 (± 6)	+7.3 (± 0.4)	11
cis-$[Co(en)_2(NO_2)Cl]^+$	1.2×10^{-4}	90 (± 0.5)	−17 (± 2)	−2.9 (± 0.3)	[b], 15
trans-$[Co(en)_2Cl_2]^+$	3.1×10^{-5}	115 (± 5)	+56 (± 15)	+11.0 (± 0.6)	9, 23
trans-$[Co(en)_2(CN)Cl]^+$	7.8×10^{-5}	94 (± 0.6)	−9 (± 2)	−2.0 (± 0.4)	[b], 16
trans-$[Co(en)_2(N_3)Cl]^+$	2.2×10^{-4}	93 (± 4)	+2 (± 11)	+0.7 (± 0.1)	12, 24
trans-$[Co(dtcd)(N_3)Cl]^+$	4.6×10^{-4}	77 (± 2)	−51 (± 6)	+8.3 (± 0.4)	10

[a]en = ethane-1,2-diamine, trien = 1,8-diamino-3,6-diazaoctane, tren = *N*,*N*′-bis(2-aminoethyl)ethane-1,2-diamine, and dtcd = 5,12-dimethyl-1,4,8,11-tetraazacyclotetradeca-4,11-diene.

[b]This work.

groups may vary the lifetime of the activated complex a little. In a timescale regime where solvent reorganization may be occurring at a more "leisurely" pace, the actual progress to, and "resting" period in, the transition state for a particular molecule may markedly affect the $\Delta V^{\neq}_{solv}$ component of $\Delta V^{\neq}_{exp}$ when displacement of ionic groups is involved. An increase (in a positive sense) in $\Delta V^{\neq}_{exp}$ as the size of the cation increases or the type of ligands vary may then reflect a small change in either the amount of bond extension in forming the transition state or its lifetime, or both. No abrupt change in mechanism need be considered.

Complexes with markedly positive $\Delta V^{\neq}_{exp}$, such as $[Co(en)_2Cl_2]^+$, may involve more substantial rearrangement in forming the transition state, with electrostriction of new charge centres being offset by displacement of electrostricted water molecules into the bulk solvent by motions of the non-leaving groups. There may be a prospect for examining this concept. It is known, for example, that solvolysis of $[Co(NH_3)_5(OCH\cdot N(CH_3)_2)]^{3+}$ in H_2O or $OCH\cdot N(CH_3)_2$ yields essentially identical $\Delta V^{\neq}_{exp}$,[21] perhaps indicative of small $\Delta V^{\neq}_{solv}$ contributions to $\Delta V^{\neq}_{exp}$. However, isomerizations of $[Co(en)_2(X)(OH_2)]^{2+}$ complexes, even from H_2O to D_2O as solvent,[22] show differences in $\Delta V^{\neq}_{exp}$ which probably relate to variations in $\Delta V^{\neq}_{solv}$. Variations in $\Delta V^{\neq}_{exp}$ for *trans*-$[Co(en)_2Cl_2]^+$ solvolysis compared with those for *trans*-$[Co(en)_2(CN)Cl]^+$, for example, may probe the comparative roles of $\Delta V^{\neq}_{solv}$ terms in each case. It is clear that a greater understanding of the part played by solvation terms is important for a more detailed interpretation of $\Delta V^{\neq}_{exp}$ when ionic leaving groups are involved.

REFERENCES

1. T. W. Swaddle, *Coord. Chem. Rev.* 1974, **14,** 217.
2. D. R. Stranks, *Pure Appl. Chem.* 1974, **38,** 303.
3. T. Asano and W. T. le Noble, *Chem. Rev.* 1978, **78,** 407.
4. D. A. Palmer and H. Kelm, In *High Pressure Chemistry* (Edited by H. Kelm), p. 435. Reidel, Dordrecht (1978).
5. G. A. Lawrance and D. R. Stranks, *Acc. Chem. Res.* 1979, **11,** 403.
6. A. E. Merbach, *Pure Appl. Chem.* 1982, **54,** 1479.
7. H. R. Hunt and H. Taube, *J. Am. Chem. Soc.* 1958, **80,** 2642.
8. W. E. Jones, L. R. Carey and T. W. Swaddle, *Can. J. Chem.* 1972, **50,** 2739.
9. H. Lentz and S. O. Oh, *High Temp.–High Pressures* 1975, **7,** 91.
10. G. A. Lawrance and S. Suvachittanont, *Aust. J. Chem.* 1980, **33,** 327.
11. G. A. Lawrance, *Inorg. Chim. Acta* 1980, **45,** L275.
12. Y. Kitamura, S. Nariyuki and T. Kondo, *Bull. Chem. Soc. Jpn* 1984, **57,** 285.
13. G. A. Lawrance, K. Schneider and R. van Eldik, *Inorg. Chem.* 1984, **23,** 3922.
14. W. G. Jackson and A. M. Sargeson, *Inorg. Chem.* 1978, **17,** 1348.
15. S. Asperger and C. K. Ingold, *J. Chem. Soc.* 1956, 2862.
16. S. C. Chan and M. L. Tobe, *J. Chem. Soc.* 1963, 514.
17. A. M. Sargeson and G. H. Searle, *Inorg. Chem.* 1967, **6,** 2172.
18. G. A. Lawrance and S. Suvachittanont, *J. Coord. Chem.* 1979, **9,** 13.
19. S. K. Madan and J. Peone, Jr., *Inorg. Chem.* 1967, **6,** 464.
20. M. V. Twigg, *Inorg. Chim. Acta* 1977, **24,** L84.
21. G. A. Lawrance, *Inorg. Chem.* 1982, **21,** 3687; S. D. Ho, M. J. Sisley and T. W. Swaddle, *Can. J. Chem.* 1978, **56,** 2609.
22. G. A. Lawrance, *Aust. J. Chem.* 1980, **33,** 1649.
23. R. G. Pearson, C. R. Boston and F. Basolo, *J. Am. Chem. Soc.* 1953, **75,** 3089.
24. P. J. Staples and M. L. Tobe, *J. Chem. Soc.* 1960, 4803.

Polyhedron Vol. 5, No. 12, pp. 2117–2118, 1986
Printed in Great Britain.

0277–5387/86 $3.00 + .00
© 1986 Pergamon Journals Ltd.

COMMUNICATION

A NOVEL PALLADIUM-INDUCED EPIMERIZATION OF STEROID ALCOHOLS—A SINGLE-STEP SYNTHESIS OF EPIMERIC ALCOHOLS

B. M. CHOUDARY

Regional Research Laboratory, Hyderabad 500007, India

(*Received* 13 *May* 1986; *accepted* 23 *June* 1986)

Abstract—The epimerization of steroid alcohols is induced by the $Pd(PPh_3)_4$–*p*-benzoquinone system. A convenient method for the synthesis of epicholesterol is described.

A transannular 1,5-hydride shift via palladium complex has been proposed in the reaction of cyclohexylmethylmercury chloride with $PdCl_2$ in the presence of the $CuCl_2$–HOAc system to give 1-chloro-4-methylcyclohexane.[1] In the Wacker reaction, the oxidation of ethylene to acetaldehyde, a 1,2-hydride shift via a palladium complex, was visualized.[2] The palladium-catalysed oxidation of secondary alcohols[3] in the presence of bromobenzene could be explained by an hydride shift from alkoxy to phenyl moiety in the transient complex based on the mechanism reported in the reduction of arylhalides by sodium methoxide.[4] Palladium is also known to isomerize[5] and invert[6] allylacetates.

This communication reports the epimerization of steroid alcohols in a single step induced by the $Pd(PPh_3)_4$–*p*-benzoquinone system. The Δ^5-steroid alcohols give selectively epimeric alcohols [eqn (1); Table 1, entries 1–4] while saturated alcohols give ketones apart from corresponding epimeric alcohols [eqn (2); Table 1, entries 5 and 6].

Similarly, *trans*-4-*t*-butylcyclohexanol, a monocyclic alcohol (entry 7) is isomerized into *cis*-4-butylcyclohexanol. Incidentally, this is a convenient method for the synthesis of epicholesterol in reasonable yields as against the tedious multistep synthesis reported earlier,[7] and is the first report of the epimerization of alcohols induced by $Pd(PPh_3)_4$–*p*-benzoquinone.

EXPERIMENTAL

Measurements and materials

Spectra were recorded on Perkin–Elmer (IR), Varian A-60 (NMR) and RMU 6 (mass) spectrometers. All solvents were dried by standard procedures.

Epimerization of steroid alcohols

Clear solutions of $Pd(PPh_3)_4$ (0.004 mmol) in *m*-xylene (3 cm^3) and *p*-benzoquinone (0.008 mmol) in *m*-xylene (3 $cm)^3$ were separately injected through

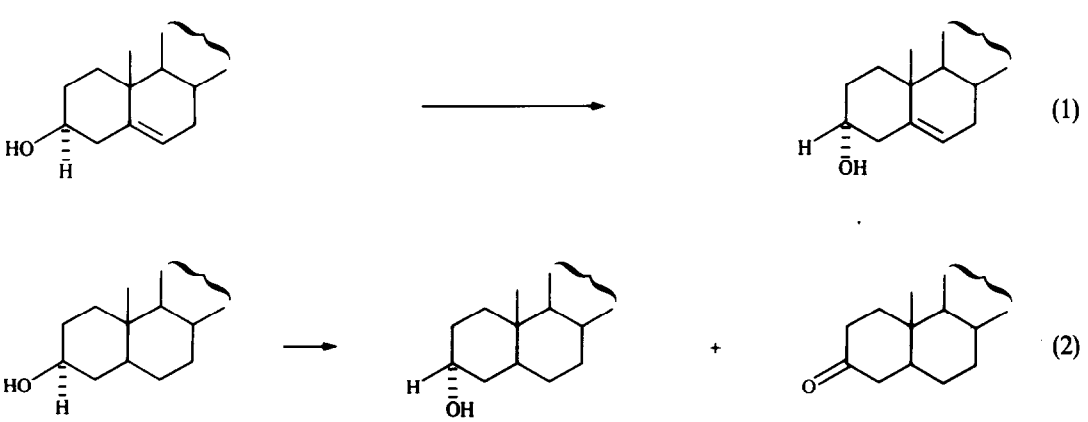


Table 1. Epimerization of steroid alcohols[a]

Entry	Compound	Epimeric alcohol [isolated yield (%)]	Ketone (isolated yield (%)]
1	Cholesterol	Epicholesterol (40) (50)[b]	
2	Stigmast-5-en-3β-ol	Stigmast-5-en-3-α-ol (34)	
3	Diosgenin	Epidiosgenin (15)	
4	Epicholesterol	Cholesterol (24)	
5	Cholestanol	Epicholestanol (36)	Cholestan-3-one (25)
6	Epiandrosterone	Androsterone (33)	Androstan-3,17-dione (15)
7	*trans*-4-*t*-Butylcyclohexanol	*cis*-4-*t*-Butylcyclohexanol (15)	4-*t*-Butylcyclohexanone (8)

[a]All reactions were carried out under the following conditions: substrate, 0.4 mmol, $Pd(PPh_3)_4$, 0.004 mmol, *p*-benzoquinone, 0.008 mmol (entries 1–4), 0.400 mmol (entries 5–7); reaction time, 6 h; and solvent, *p*-xylene under reflux.

[b]Yield based on ^1H NMR.

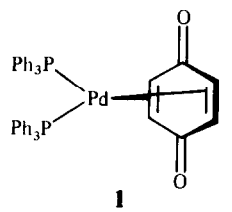
a septum into a nitrogen-purged R.B. flask equipped with a magnetic stirrer and a condenser. Cholesterol (0.40 mmol) in *m*-xylene (5.0 cm^3) was injected to the homogeneous catalytic system and the reaction mixture was heated to reflux for 6 h under a nitrogen atmosphere. Then the reaction mixture was cooled, filtered and evaporated to dryness *in vacuo*. The residue was chromatographed to isolate pure compounds.

RESULTS AND DISCUSSION

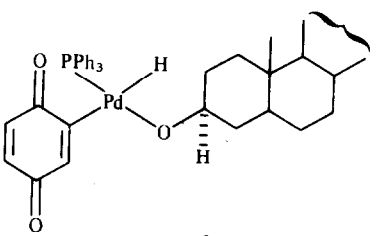
The isolated yields of epimeric alcohols are given in Table 1. The products are well characterized by m.p., ^1H NMR, IR, and mass spectra, and compared with authentic samples.

The bidentate *p*-benzoquinone–$Pd(PPh_3)_4$ complex[8] (**1**) which is expected to form *in situ* may be a real catalytic species in this system since no epimerization occurs in the absence of *p*-benzoquinone. Moreover the isolation of hydroquinone and ketone from a reaction medium involving epimerization of saturated alcohols which is due to the transfer of hydrogen from steroid alcohol to *p*-benzoquinone demonstrates that the *p*-benzoquinone is part of the catalytic system. This reaction required excess *p*-benzoquinone since it acts also as a hydrogen acceptor and is converted into hydroquinone, while the catalytic amount of *p*-benzoquinone is sufficient for epimerization of Δ^5-steroid alcohols. A trace of palladium metal is deposited during the reaction. The epimerization reaction of cholesterol which gives a 1:1 epimeric ratio did not proceed further on continuation of the reaction. The epimerization may have involved hydride inversion by the activation of the carbinyl proton induced by palladium in the intermediate hydridoalkoxypalladium(II) (**2**) which can be formed from the reaction of **1** with a secondary steroid alcohol.

The hydroxyl inversion can be ruled out in view of the formation of a ketone as a side product in



1



2

saturated sterols and the absence of diene formation in unsaturated Δ^5-sterols, which is a homoallyl alcohol. The diene is formed in the epimerization reaction of allyl acetate.[6] However, further work to understand the mechanism is under progress.

Acknowledgements—I thank Drs G. S. Sidhu and M. Pardhasaradhi for their encouragement and helpful discussions.

REFERENCES

1. A. Heumann and J. E. Backvail, *Angew. Chem., Int. Ed. Engl.* 1985, **24**, 107.
2. J. Smidt, *Chem. Ind. (London)* 1962, 54.
3. Y. Tamaru, Y. Yamamoto, Y. Yamada and Z. I. Yoshida, *Tetrahedron Lett.* 1979, 1401.
4. A. Zask and P. J. Helquist, *J. Org. Chem.* 1978, **43**, 1619.
5. L. E. Overman and F. M. Knoll, *Tetrahedron Lett.* 1979, 321.
6. B. M. Trost, T. R. Verhoeven and J. M. Fortunak, *Tetrahedron Lett.* 1979, 2301.
7. L. P. L. Piacenza, *J. Org. Chem.* 1977, **42**, 3778.
8. S. Takahashi and N. Hagihara, *Nippon Kagaku Zasshi* 1967, **88**, 1306; *Chem. Abstr.* 1968, **69**, 27514g.

Polyhedron Vol. 5, No. 12, pp. 2119–2120, 1986
Printed in Great Britain

0277-5387/86 $3.00+.00
Pergamon Journals Ltd.

COMMUNICATION

PHOTOCHEMICAL DECOMPOSITION OF THE $CS_2N_3^-$ ION

M. F. F. LEITE MANZANO*

Departamento de Química, Universidade Federal de São Carlos, SP, Brazil

E. TFOUNI

Departamento de Química, FFCL de Ribeirão Preto—USP, SP, Brazil

and

D. W. FRANCO

IFQSC, USP, São Carlos, Brazil

(*Received* 28 *August* 1985; *accepted after revision* 27 *June* 1986)

Abstract—The pseudo-halide 1, 2, 3, 4-thiatriazol-5-thiolate, in the anion and acid forms, undergoes photochemical decomposition with the formation of sulfur, nitrogen and the thiocyanate anion, with quantum yields (ϕ_{313}) of 0.13 and 0.26 for the acid and anion forms, respectively.

The synthesis,[1] analytical applications,[2] coordinative abilities,[3] oxidation reactions[4] and quantum mechanic calculations[5] for the pseudo-halide 1,2,3,4-thiatriazol-5-thiolate anion, $CS_2N_3^-$, have been already reported.

In the course of an investigation of the chemical properties of thiatriazol ring, we describe the photochemical decomposition of the $CS_2N_3^-$ and HCS_2N_3 systems.

EXPERIMENTAL

$NaCS_2N_3$ was synthesized and standardized as described previously.[1] For the photolysis studies, $NaCS_2N_3$ aqueous solutions at different hydrogen ion concentrations were irradiated at 313 nm with light of 1.58×10^{-7} Einsteins min^{-1}. The intensity of the light source was measured using ferrioxalate actinometry.[6]

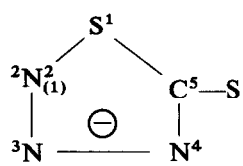
After 3 min of irradiation the solutions exhibit some turbidity, probably due to the formation of colloidal sulphur. Thus, only solutions irradiated for less than 2 min were analysed for the calculation of quantum yields.

Photolysis as monitored spectrophotometrically at 313 nm. At each pH, different samples were irradiated for 15, 30, 45, 60 and 120 s each. Quantum yields were plotted vs % reaction, and extrapolated back to 0% reaction to obtain the reported quantum yield values.

RESULTS AND DISCUSSION

The absorption band[2,5] of the acid, at 313 nm, is due to a π–π^* transition ($4a''$–$5a''$). For the anion, the absorption maximum at 313 nm is assumed[2,5] to be a combination of $n \rightarrow \pi^*$ with π–π^* transitions ($12'$–$5a''$ and $4a''$–$5a''$, respectively).

Continuous photolysis of aqueous solutions of the acid and of the anion with light of 313 nm leads to the photochemical decomposition of the ring,[1,2,4,7] according to:



(1)

*Author to whom correspondence should be addressed.

The quantum yields for reaction (1) at several hydrogen ion concentrations are listed in Table 1. Since the pK_a for HCS_2N_3 is 1.5,[1] at pH values higher than 3.0 only the $CS_2N_3^-$ form is present, and in a 1.0 M $HClO_4$ solution more than 96% of the pseudo-halide is present as HCS_2N_3.

In the absence of light, the $NaCS_2N_3$ solutions are more stable than the corresponding HCS_2N_3 ones. In fact, quantum mechanical calculations[5] showed that the anion $CS_2N_3^-$ is more stable than HCS_2N_3 by 29 kcal mol^{-1}. However, under irradiation, the anion is more unstable than the acid, as indicated by the quantum yields of 0.13 and 0.26 for HCS_2N_3 and $CS_2N_3^-$, respectively.

The decomposition of the 1,2,3,4-thiatriazol ring is not a simple process. The bond orders in the ground state show a low bond order value (0.06) for the N(2)—N(3) bond in the thiatriazol ring. However, the bond orders or electron densities in the excited states of HCS_2N_3 and $CS_2N_3^-$ are not known, not allowing the identification of the first bond break in the ring.

Table 1. Quantum yields for the reaction[a]

$$CS_2N_3^- \xrightarrow{h\nu} N_2 + S + SCN^-$$

pH	0.0[b]	0.5	1.0	3.0	4.6	5.2	11.8
ϕ	0.13[c]	0.19	0.26	0.27	0.26	0.27	0.27

[a] μ = 1.0 M, $NaClO_4$, 25°C. Each ϕ value is a mean of four independent determinations with agreement better than 96%.

[b] 1.0 M $HClO_4$.

[c] Refers to the acid form.

Studies on the degradation of the thiatriazol ring as an alternative synthetic route[8] for isothiocyanate synthesis are in progress and will be reported later.

Acknowledgements—We are greatly indebted to the following foundations for financial support: Conselho Nacional de Desenvolvimento Científico e Tecnológico (CNPq) and Fundação de Amparo à Pesquisa do Estado de São Paulo.

REFERENCES

1. E. F. A. Neves and D. W. Franco, *J. Inorg. Nucl. Chem.* 1974, **36,** 3851.
2. E. F. A. Neves and D. W. Franco, *Talanta* 1979, **26,** 81.
3. E. F. A. Neaves, N. Milken and D. W. Franco, *J. Inorg. Nucl. Chem.* 1981, **43,** 2081 (and references therein).
4. E. F. A. Neves, W. L. Polito, V. L. Moraes and D. W. Franco, *Talanta* 1981, **28,** 867 (and references therein).
5. M. Conti, D. W. Franco and M. Trsic, *Inorg. Chim. Acta* 1986, **113,** 71.
6. C. G. Hatchard and C. A. Parker, *Proc. R. Soc. London, Ser. A* 1956, **235,** 518.
7. P. Suppan, *Principles of Photochemistry.* Bartholomew Press, London (1973).
8. G. La Monica, G. Ardizzoia, S. Cenini and F. Porta, *J. Organomet. Chem.* 1984, **273,** 263.

Polyhedron Vol. 5, No. 12, pp. 2121–2122, 1986
Printed in Great Britain

0277–5387/86 $3.00+.00
© 1986 Pergamon Journals Ltd.

COMMUNICATION

SYNTHESIS AND X-RAY STRUCTURE OF THE Mo(VI) SPECIES $Mo_4O_{12}(C_{12}H_{30}N_4S_2)_2(C_3H_7ON)_n$ ($n \approx 2$)

MICHAEL B. HURSTHOUSE and RICHARD L. SHORT

Department of Chemistry, Queen Mary College, London E1 4NS, U.K.

and

BRIAN PIGGOTT,* ALAN TUCKER and SWEE FATT WONG

Department of Chemistry, The Hatfield Polytechnic, Hatfield AL10 9AB, U.K.

(*Received* 2 *June* 1986; *accepted* 27 *June* 1986)

Abstract—Dissolution of $Mo_2O_5((CH_3)_2NCH_2CH_2NHCH_2CH_2S)_2$ in dimethylformamide results in the formation of a species without coordinated sulphur, as indicated by ^{95}Mo NMR spectroscopy. Subsequent crystallization of this solution yielded the compound $Mo_4O_{12}(C_{12}H_{30}N_4S_2)_2(C_3H_7ON)_2$ which X-ray crystallography shows to consist of a novel Mo_4O_{12} core, containing an eight-membered Mo_4O_4 ring with the two pairs of diagonal molybdenum atoms linked by disulphido-containing groups.

An X-ray structure analysis of the compound $[Mo_2O_5(Me_2NCH_2CH_2NHCH_2CH_2S)_2]$ showed it to contain the $Mo_2O_5^{2+}$ core with six-coordination about each Mo(VI) atom being completed by 2N and 1S donors.[1] This structure is very similar to that reported earlier for $[Mo_2O_5(Me_2NCH_2CH_2NHCH_2CMe_2S)_2]$.[2]

Since we are interested in the ^{95}Mo NMR spectra of $Mo_2O_5^{2+}$ species, we have recorded the spectra of these two compounds in dimethylformamide (DMF). In each case, signals were observed at approximately 330 and 125 ppm. The signal at 330 ppm we assigned to the $Mo_2O_5L_2$ species, where L is $(Me_2NCH_2CH_2NHCH_2CH_2S^-)$ or $(Me_2NCH_2CH_2NHCH_2CMe_2S^-)$. The signal at 125 ppm was presumed to indicate the presence of a second species, which we accordingly attempted to isolate. After repeated attempts we were successful in obtaining a white, crystalline air-sensitive product from a DMF solution of $Mo_2O_5(Me_2NCH_2CH_2NHCH_2CH_2S)_2$.

A subsequent X-ray study of these crystals revealed a novel structural type based on an eight-membered Mo_4O_4 ring.† The structure found is shown in the Fig. 1. The two bridging oxygens at each molybdenum are *cis* to each other, with distorted octahedral geometry being completed by two *cis* terminal oxo atoms and two *cis* amine nitrogen atoms. The Mo—O bond lengths in the ring alternate, with values of 1.80–1.81(1) and 2.11–2.13(1) Å, respectively, the longer ones being *trans* to terminal oxo functions. The corresponding bonds in the starting material are equal at 1.91 Å and

*Author to whom correspondence should be addressed at: 4 Coach Drive, Hitchin, Herts SG4 9AP.

†Crystal data: $C_{24}H_{60}N_8O_{12}S_4Mo_4(C_3H_7ON)_n$, $M_4 = 1310.99$ for $n = 2$, triclinic, space group $P\bar{1}$, $a = 12.219(2)$ Å, $b = 16.627(3)$ Å, $c = 16.847(3)$ Å, $\alpha = 60.13(1)°$, $\beta = 77.21(1)°$, $\gamma = 73.19(1)°$, $U = 2828.9$ Å^3, $Z = 2$, $D_c = 1.539$ g cm^{-3}, Mo-K_α radiation, $\lambda = 0.71069$ Å, μ(Mo-K_α) = 9.7 cm^{-1}.

The structure was solved by direct methods and refined by least squares to $R = 0.049$ for 4636 reflections with $I > 2\sigma(I)$, and with all non-hydrogen atoms in the complex anisotropic and hydrogens included in calculated positions. Atoms of the solvent molecules, which occupy three sites at approx. 70% were refined isotropically.

Tables of atomic positional and thermal parameters, bond lengths and angles and F_o/F_c values have been deposited as supplementary data with the Editor, from whom copies are available on request. Atomic coordinates have also been deposited with the Cambridge Crystallographic Data Centre.

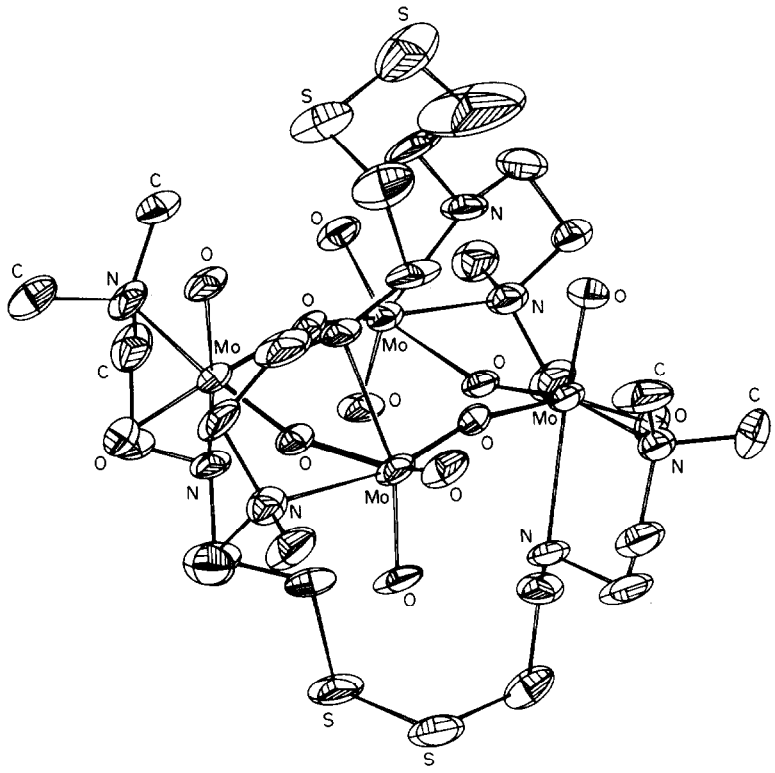


Fig. 1. Structure of the complex $Mo_4O_{12}(C_{12}H_{30}N_4S_2)_2$ Significant bond lengths (Å) are: Mo—O (bridge) = 1.80–1.81(1) (short), and 2.11–2.13(1) (long); Mo—O(oxo) = 1.71–1.73(1), and Mo—N 2.34–2.39(2).

neither of them are *trans* to a terminal oxygen.[1]

A further interesting feature of the molecule is the form of the organic ligands. Instead of these being tridentate NNS donors, as in the starting material,[1] they are now NN donors, with the displaced thiolate ends linking to form disulphide bridges. The two ligands present each connect pairs of diagonally related Mo atoms.

The structure of the title compound is loosely related to those of two other MoO ring species, the tetranuclear anion $[Mo_4O_8(OMe)_2(NNPh_4)]^{2-}$[3] and its related complex $[Mo_8O_{20}(NNPh)_6]^{4-}$[4] The former comprises a ring containing two MoO_2 and two $Mo(NNPh)_2$ units linked by Mo—O—Mo bridges, with two methoxy bridges between the $Mo(NNPh)_2$ metal atoms, whilst the latter can be described as a crown of six oxo-bridged molybdenum centres, alternately $[MoO_4]^{2-}$ and $[Mo(NNPh)_2]^{2+}$ moieties, capped above and below by oxomolybdate fragments.

Acknowledgement—We thank the SERC for support of this work.

REFERENCES

1. K. Gebreyes, S. N. Shaikh and J. Zubieta, *Acta Cryst.* 1985, **C41**, 871.
2. C. P. Marabella, J. H. Enemark, K. F. Miller, A. E. Bruce, N. Pariyadath, J. L. Corbin and E. I. Stiefel, *Inorg. Chem.* 1983, **22**, 3456.
3. T.-C. Hsieh and J. Zubieta, *Inorg. Chem.* 1985, **24**, 1287.
4. T.-C. Hsieh and J. Zubieta, *J. Chem. Soc., Chem. Commun.* 1985, 1749.

Polyhedron Vol. 5, No. 12, pp. 2123–2125, 1986
Printed in Great Britain

0277–5387/86 $3.00+.00
© 1086 Pergamon Journals Ltd.

COMMUNICATION

A CONVENIENT SYNTHESIS OF $Fe(CO)_2(\eta^2\text{-}S_2CNMe_2)_2$ AND $Fe(\eta^2\text{-}S_2CNMe_2)_2$ FROM THE MONODENTATE DITHIOCARBAMATO DERIVATIVE, $[(\eta^5\text{-}C_5H_5)(CO)_3W(\eta^1\text{-}SCSNMe_2)]$ AND $Fe_2(CO)_9$

SALIL K. JHA, B. H. S. THIMMAPPA and PRADEEP MATHUR*

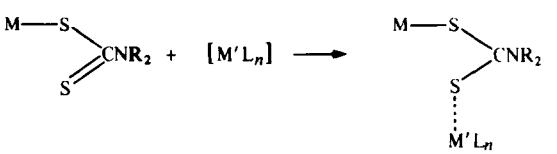
Department of Chemistry, Indian Institute of Technology, Powai, Bombay 400076, India

(*Received* 12 *May* 1986; *accepted* 7 *July* 1986)

Abstract—A high yield synthesis of the carbonyl dithiocarbamato derivative $Fe(CO)_2(\eta^2\text{-}S_2CNMe_2)_2$ and $Fe(\eta^2\text{-}S_2CNMe_2)_2$ by photolysis with visible light of solutions containing $Fe_2(CO)_9$ or $Fe_3(CO)_{12}$ and $[(\eta^5\text{-}C_5H_5)(CO)_3W(\eta^1\text{-}SCSNMe_2)]$ is reported.

The chemistry of carbonyl dithiocarbamate complexes has generated considerable interest lately.[1] Derivatives of the form $(CO)_nM(dtc)_m$ with M = Rh, $n = 2$, $m = 1$; M = Fe, $n = 2$, $m = 2$; M = Mn, $n = 4$, $m = 1$; dtc = dialkyldithiocarbamate, have been prepared by reacting the sodium salts of dialkyldithiocarbamates with metal carbonyl halides or by oxidation of the metal carbonyls with tetraalkylthiocarbamoyl disulphides.[2] Other methods for the preparation of dithiocarbamate complexes include using trimethyltin thiocarbamates,[3] CS_2–CO_2 exchange on the carbamate derivatives,[4] or by reacting carbamoyl complexes of transition metals with CS_2.[5] Although most syntheses result in the dithiocarbamato ligand acting in a bidentate manner, several reports have appeared in the literature recently giving methods for preparing complexes containing monodentate dithiocarbamato ligands.[6–9]

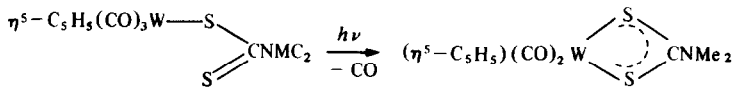
We have been interested in investigating the reactivity of the uncoordinated sulphur atom towards additional transition metal centres (Scheme 1). The complex $[(\eta^5\text{-}C_5H_5)(CO)_3WSC(\text{—}S)NMe_2]$ (**I**), is a suitable candidate for such an investigation because: (i) it can be conveniently synthesized in good yields by irradiating with visible light solutions containing $[\eta^5\text{-}C_5H_5(CO)_3W]_2$ and tetramethylthiuram disulphide (tmtd);[6] and (ii) the dtc ligand maintains the monodentate mode of bonding unless heated strongly or photolysed with UV irradiation, which leads to formation of the dicarbonyl chelate (**II**) (Scheme 2).



Scheme 1. Reactivity of uncoordinated sulphur atom of η^1-dithiocarbamate ligand towards transition-metal centres.

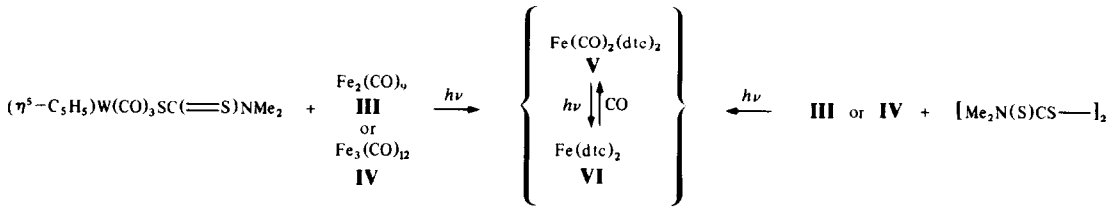
We report here our findings on the reaction of (**I**) with iron carbonyl fragments $Fe(CO)_x$ generated from $Fe_2(CO)_9$ (**III**) or $Fe_3(CO)_{12}$ (**IV**) (Scheme 3). When oxygen-free toluene solutions containing **I** and **III** are irradiated with visible light under a nitrogen stream, the colour of the solution changes from orange-red to dark brown. From the photolysed solution, after column chromatography, two products have been isolated and identified on the basis of IR, NMR, UV spectra and microanalytical data as $Fe(CO)_2(\eta^2\text{-dtc})_2$ (**V**) and $Fe(\eta^2\text{-dtc})_2$ (**VI**).[2] Interestingly, Abrahamson and Freeman[6] have reported the formation of **I** from $Fe(dtc)_3$ and $[\eta^5\text{-}C_5H_5(CO)_3W]_2$. In our reaction, even after prolonged photolysis, $Fe(\eta^2\text{-dtc})_3$ is not obtained and at the end of the photolysis there is no evidence of any unreacted **I**. Irradiation of solutions

*Author to whom correspondence should be addressed.



I II

Scheme 2. Conversion of monodentate dithiocarbamato derivative (I) to the dicarbonyl chelate (II).



Scheme 3. Photolytic synthesis of $Fe(CO)_2(dtc)_2$ (V) and $Fe(dtc)_2$ (VI).

containing I and IV also yielded V and VI. There is no observable reaction between the bidentate chelate derivative $[Cp(CO)_2W(\eta^2\text{-}S_2CNMe_2)]$ and $Fe_2(CO)_9$ or $Fe_3(CO)_{12}$. The special reactivity of the monodentate dithiocarbamate ligand makes complex I a useful starting material for carbonyl dithiocarbamato derivatives; the generality of this transmetallation type of reaction is currently being investigated with other binary carbonyl complexes. We have also synthesized the dithiocarbamato derivatives V and VI by photolysing with visible light solutions containing either III or IV with tetramethylthiuram disulphide.

Pure V, on photolysis with visible light forms VI, which readily adds CO at room temperature to give V quantitatively. Thus, in the above reaction V is probably the initial product formed, but loses CO under the reaction conditions and forms VI.

The very mild conditions of our reactions appear to be advantageous, giving high yields of the carbonyl dithiocarbamato complexes and an improvement on earlier reported methods.

EXPERIMENTAL

All reactions were routinely performed under an inert atmosphere of argon using standard Schlenk techniques. The solvents were dried and distilled prior to use. IR spectra were recorded on a Perkin–Elmer 681 spectrophotometer and calibrated against polystyrene. NMR spectra were recorded on Hitachi T-60, and UV spectra on a Shimadzu 260 spectrophotometer.

Photolysis of $[(\eta^5\text{-}C_5H_5)(CO)_3W(\eta^1\text{-}SCSNMe_2)]$ *and* $Fe_2(CO)_9$

A mixture of diironnonacarbonyl (0.2 g 0.55 mmol) and $(\eta^5\text{-}C_5H_5)(CO)_3W(\eta^1\text{-}SCSNMe_2)$ (0.25 g 0.55 mmol) in 60 cm^3 of toluene solvent was irradiated with visible light for 2 h. The solvent was removed *in vacuo* and the dark brown residue was put on a silica gel column. Elution with petroleum ether–dichloromethane (50:50) gave a red-brown band identified as $Fe(\eta^2\text{-dtc})_2(CO)_2$, yield = 60%; IR (KBr): ν(CO) 1970 cm^{-1}, 2040 cm^{-1}, ν(CN) 1535 cm^{-1}, ν(CS) 995 cm^{-1}; NMR ($CDCl_3$): δ 3.28, 3.20; $\lambda_{max}(CH_2Cl_2)$: 236.8, 274.8, 383 nm. Further elution with neat dichloromethane gave the dark brown $Fe(\eta^2\text{-dtc})_2$, yield = 30%; IR (KBr): ν(CN) 1530 cm^{-1}, ν(CS) 990 cm^{-1}; NMR ($CDCl_3$): δ 3.60; $\lambda_{max}(CH_2Cl_2)$: 231, 256, 343 nm. Both complexes gave satisfactory, C, H, and N microanalysis results.

The photolysis of I and $Fe_3(CO)_{12}$ was carried out similarly to obtain $Fe(CO)_2(\eta^2\text{-dtc})_2$ and $Fe(\eta^2\text{-dtc})_2$ in yields of 60 and 30%, respectively, after 2 h. Prolonged photolysis in either reaction resulted in quantitative formation of only $Fe(\eta^2\text{-dtc})_2$ which converted back to $Fe(CO)_2(\eta^2\text{-dtc})_2$ quantitatively when a toluene solution of $Fe(\eta^2\text{-dtc})_2$ was bubbled with carbonmonoxide for 1 h.

Photolysis of $Fe_2(CO)_9$ *and tetramethylthiuram disulphide (tmtd)*

A mixture of diironnonacarbonyl (0.15 g 0.41 mmol) and tetramethylthiuram disulphide (0.1 g 0.41 mmol) in 70 cm^3 of toluene solvent was

irradiated with visible light for 0.5 h. Removal of solvent *in vacuo* and chromatographic work up as above gave $Fe(CO)_2(\eta^2\text{-dtc})_2$ and $Fe(\eta^2\text{-dtc})_2$ in yields of 66 and 30%, respectively.

The reaction of $Fe_3(CO)_{12}$ and tmtd was carried out similarly to give $Fe(CO)_2(\eta^2\text{-dtc})_2$ and $Fe(\eta^2\text{-dtc})_2$ in similar yields.

REFERENCES

1. (a) E. C. Alyea, G. Ferguson, M. Parvez and A. Somogyvari, *Polyhedron* 1985, **4,** 783; (b) T. Tetsumi, M. Sumi, M. Tanaka and T. Shono, *Polyhedron* 1985, **4,** 1439; (c) S. J. N. Burgmayer and J. L. Templeton, *Inorg. Chem.* 1985, **24,** 2224; (d) M. C. W. Mak, K. S. Jasion and C. Chieb, *Inorg. Chem.* 1985, **24,** 1587; (e) M. A. Bennett and I. W. Boyd, *J. Organomet. Chem.* 1985, **290,** 165.
2. F. A. Cotton and J. A. McCleverty, *Inorg. Chem.* 1964, **3,** 1398.
3. (a) K. R. M. Sringster, D. L. Greene and B. J. McCormick, *Inorg. Chim. Acta* 1977, **23,** 13; (b) E. W. Abel and M. O. Dunster, *J. Chem. Soc. Dalton Trans.* 1973, 98; (c) C. O. Connor, J. D. Gilbert and G. Wilkinson, *J. Chem. Soc. A* 1969, 84; (d) K. Tanaka, Y. Miya-Uchi and T. Tanaka, *Inorg. Chem.* 1975, **14,** 1545.
4. G. LaMonica, S. Cenini, F. Porta and M. Pizzotti, *J. Chem. Soc., Dalton Trans.* 1976, 1777.
5. L. Busetto, A. Palazzi and V. Foliadas, *Inorg. Chim. Acta* 1980, **40,** 147.
6. H. B. Abrahamson and M. L. Freeman, *Organometallics* 1983, **2,** 679.
7. G. Nagao, K. Tanaka and T. Tanaka, *Inorg. Chim. Acta* 1980, **42,** 43.
8. O. Catheline, E. Romain and D. Astrue, *Inorg. Chem.* 1984, **23,** 4508.
9. (a) M. Moran and I. Cuadrado, *J. Organomet. Chem.* 1985, **295,** 353; (b) C. G. Young, S. A. Roberts and J. H. Enemark, *Inorg. Chim. Acta* 1986, **114,** L-7.

Polyhedron Vol. 5, No. 12, pp. 2127–2128, 1986
Pergamon Journals Ltd. Printed in Great Britain

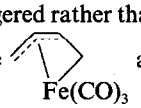
BOOK REVIEW

Gmelin Handbook of Inorganic Chemistry. Fe—Organoiron Compounds, Part A8, Ferrocene 8. Springer, Berlin, 1986. ISBN 3-540-93527-4, xiii+419 pp., DM1552. **Part B9, Mononuclear Compounds 9.** Springer, Berlin, 1985. ISBN 3-540-93522-3, ix+286 pp., DM1064. **Part B10, Mononuclear Compounds 10.** Springer, Berlin, 1986. ISBN 3-540-93523-1, ix+361 pp., DM1356. **Part C7, Polynuclear Compounds 7.** Springer, Berlin, 1986. ISBN 3-540-93530-4, xii+410 pp., DM 1488.

The burgeoning organometallic chemistry of iron has been treated well by Gmelin. Unlike any other metal, it has been granted more than one series—series A is devoted to ferrocene and its derivatives, series B to the other mononuclear compounds, and series C to polynuclear iron compounds—totalling in all 27 volumes.

Volume A8 is dedicated to disubstituted ferrocene derivatives with C-, H- and O-containing substituents. Like the other volumes, it contains useful tabulations of recent reviews. Its first 50 pp. are devoted to 1,1′-diacetyl ferrocene; the thoroughness of the Gmelin treatment is illustrated by the two closely packed pages comparing preparative routes, and the subsequent page devoted to its purification. Over 30 references are cited for its melting point. ^{1}H, ^{13}C and ^{57}Fe NMR data; Mössbauer, IR and Raman, electronic, MCD and photoelectron spectra are given, as well as crystallographic data; just as useful is the section on the reaction chemistry of diacetyl ferrocene. One section that this reviewer found particularly interesting detailed catalytic applications. Similarly, dipping into the subsequent sections (100 pp.) on other 1,1-disubstituted ferrocenes, one finds that compounds of this type have been used as polymerization catalysts, polymer stabilizers, ingredients for photosensitive photoimaging materials, treatments for iron-deficiency anaemia, and as antiknock agents. Later sections treat the 1,2- and 1,3-compounds (where two substituents co-exist on one ring), carboxylic acid, ester and acyl chloride derivatives, finishing with heterocyclic compounds with oxygen as the heteroatom. The volume concludes with a formula index covering Vols A7 (which initiated the coverage of disubstituted ferrocenes) and A8, the present one.

Volume B9 covers organometallic compounds of type $^{4}LFe(CO)_3$, in which the ligand forms four iron–carbon bonds and has ring systems with seven–nine member atoms. It begins with the seven-membered heterocyclic systems, where the N-containing heterocycles are azepines and diazepines, the less common oxygen analogues the oxepines, and one example of a B-containing ring. Much more important are the systems based on cycloheptadiene. As usual, detailed data are presented, in accessible and logical tabular form, for these and derivatives of cycloheptatriene, which are discussed subsequently. The complex structural and reaction chemistry of these complexes is clarified by the usual lucid structural diagrams. A further 90 pp. are devoted to the chemistry of the derivatives of cyclooctadiene, cyclooctatriene and cyclooctatetraene systems, as well as those of larger ring systems. Cyclooctatetraene iron tricarbonyl receives thorough treatment, including some 3 pp. discussing its NMR spectra.

Volume B10 (which includes empirical formula and ligand formula indexes to Vols B8–B10) takes on the story with complexes of trimethylene methane (and derivatives thereof): σ,π-allyl and σ,σ,π-allyl ligands. The trimethylenemethane complexes exemplified by the type $[(CH_2)_3C]Fe(CO)_3$ have attractive "piano-stool"-type structures adopting the staggered rather than the eclipsed configuration. Allyls of type  are considered next: these involve both σ- and π-bonding of the allyl moiety, either cyclic or acyclic. As usual, spectroscopic data are clearly tabulated and known molecular structures represented. The four much rarer σ,σ,π-allyls are also included. Next, consideration is given to compounds where more than one hydrocarbon "fragment" is present in the organometallic molecule. Several of the few known have not been isolated but postulated from spectroscopic data. Also included are the ferrocene analogues involving phosphole and arsole ligands, the sandwich structure having been established for molecules such as $[cyclo\text{-}PC_4H_2(CH_3)_2]_2Fe$. Slightly more complex are the diene complexes of type $(1,3\text{-diene})_2Fe \cdot L$ (where $L = PR_3$, pyridine etc.) and the analogous compounds with $L = CO$, many of which have been prepared by matrix cocondensation methods.

Volume C7 appears out of sequence, before C6, which will deal with trinuclear-type compounds up to $Fe_3(CO)_{11}$ with monodentate ligands. C7 begins with a 100 pp. devoted to $Fe_3(CO)_{12}$, commencing with a very useful survey of routes to the preparation and formation of $Fe_3(CO)_{12}$. The lengthy history of the structural determination and the IR spectra, including the controversial nature of the solution species, are discussed, along with other spectroscopic results. The reaction chemistry is broken into sections treating, successively, its reactions with elements, inorganic compounds, organic and organometallic compounds. An interesting little section deals with uses of $Fe_3(CO)_{12}$ in organic synthesis, followed by a consideration of catalytic and other uses. The next three sections of the book are concerned with compounds containing the Fe_3 unit with ligands bound, respectively, through two, three and four carbon atoms, and are relatively brief. Over 30 pp. are devoted, however, to the

many triiron compounds containing C_5-rings. What is interesting (to this reviewer) is the number of syntheses where $Fe_2(CO)_9$ and other Fe_2 compounds can be used as starting materials for the synthesis of Fe_3 derivatives, here and elsewhere. This part of the book is brought to a close with the compounds of ligands binding through six or more carbon atoms, and a number of compounds of undefined structure.

The subsequent 150 pp. are devoted to compounds with four iron atoms. It begins with a most useful survey of relevant literature (like the other volumes to at least 1984) and a synopsis of theoretical considerations underlying the bonding in the compounds. The system adopted for classification of the tetranuclear clusters is based on the number of Fe—Fe bonds, the doyen being the salts of $[Fe_4(CO)_{13}]^{2-}$, first prepared by Hieber around 1930. Another important class are the clusters $[(C_5H_5)Fe(CO)]_4^n$ ($n = -1, 0, +1$ or $+2$), with the faultless serendipitous pedigree (for organometallics) of an accidental discovery; next come the clusters with a $Fe_4E(CO)_{12}$ "butterfly" core (E = C, N, B or NC) and Fe_4MC (M = metal) cores. The clusters with four Fe—Fe bonds come next, exemplified by $Fe_4(CO)_{12}(PMe_3)_2$. Here, as elsewhere in the volume, a good deal of use is made of simplified structural diagrams in the tables of data which makes it very easy to identify individual compounds and relate them to others. Subsequent sections deal with compounds with three, two, one and no Fe—Fe bonds including the $[(C_5H_5)FeS]_4$ clusters, which are ferredoxin models. Pentanuclear compounds, best known as $Fe_5C(CO)_{15}$, hexanuclear and octanuclear derivatives follow on, completing the volume, which has both empirical formula and ligand formula indexes. (Compounds with more than eight iron atoms will be treated in Vol. C6.)

All four volumes reduce a considerable bulk of information to intelligibility and a large degree of digestibility. Though not a first choice for a rapid literature search, Gmelin remains unrivalled as a means of easy access to all published data on an individual compound. Many workers could use a period spent reading one of these volumes as a springboard to a new project.

SIMON COTTON

Stanground School
Peterborough
Cambs. PE7 3BY, U.K.

Polyhedron Vol. 5, No. 12, p. 2129, 1986
Pergamon Journals Ltd. Printed in Great Britain

ANNOUNCEMENT

POLYHEDRON PUBLICATION AWARD

Pergamon Journals Ltd is pleased to announce the award annually of a cash prize of $1000 for the best paper published in *Polyhedron*.

The award will be made to the authors of the original research paper (not including *Polyhedron* Reports) judged to be the best on the basis of scientific originality, significance, clarity and style of presentation. The first award will be made for a paper published in Volume 6, 1987. Members of the Editorial Board will each be invited to nominate two papers for the award and the final selection will be made by an anonymous committee appointed by the Editors who themselves will not be eligible for the award.

The recipient of the first award will be notified early in 1988.